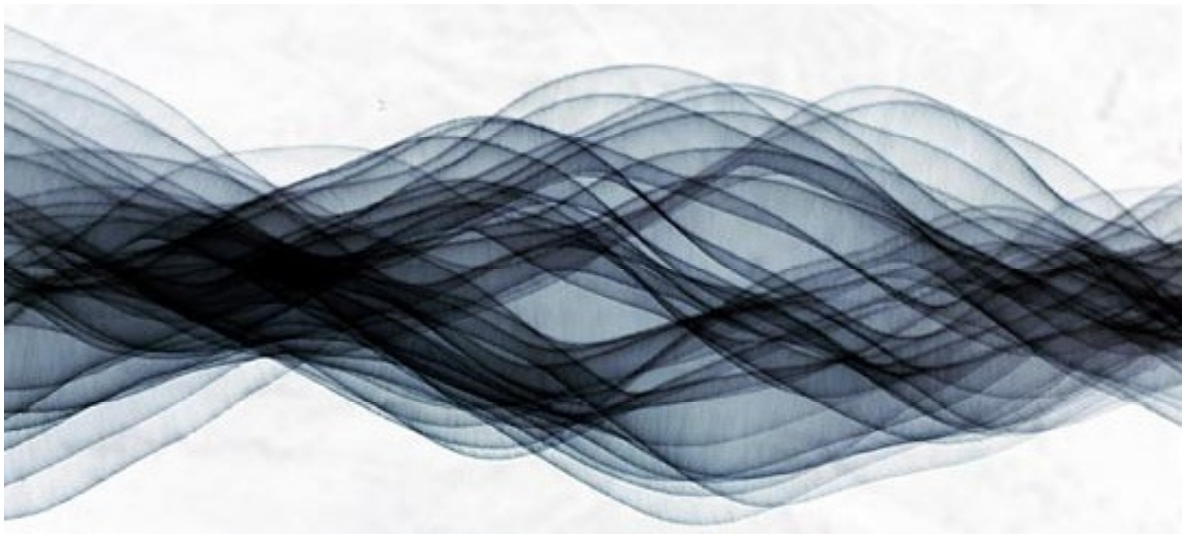

Graduate courses in Physics

Physics

Ph.W. Courteille
Universidade de São Paulo
Instituto de Física de São Carlos
26/10/2023

2

.

.

Preface

Script with subjects and exercises for graduation in Physics relevant to the courses of the IFSC: FCM0501 (Física I para físicos), FCM0101 (Física I para engenheiros e matemáticos), FFI0405 (Física Geral I para engenheiros e matemáticos), FCM0200 (Física Básica I para engenheiros e matemáticos).

Information and announcements regarding the course will be published on the website:
http://www.ifsc.usp.br/ strontium/ − > Teaching − > FFI0132

The following literature is recommended for preparation and further reading:

Ph.W. Courteille, script on *Optical spectroscopy: A practical course* (2020)

Ph.W. Courteille, script on *Electrodynamics: Electricity, magnetism, and radiation* (2020)

Ph.W. Courteille, script on *Quantum mechanics applied to atomic and molecular physics* (2020)

H.J. Pain, *The Physics of Vibrations and Waves*

Zilio & Bagnato, *Apostila do Curso de Física, Mecânica, calor e ondas*

H. Moyses Nussensveig, Curso de Física Básica 2, *Fluidos, oscilações, ondas & calor*

J.B. Marion, *Classical Eletromagnetic Radiation*, Dover (2012)

W.K.H. Panofsky and M. Phillips, *Classical Electricity and Magnetism*, Dover (2012)

J.J. Jackson, *Classical electrodynamics*, John Wiley & Sons (1999)

D.J. Griffiths, *Introduction to Electrodynamics*, Cambridge University Press (2017)

J.R. Reitz, F.J. Milford, R.W. Christy, *Foundation of electromagnetic theory*

M. Born, *Principles of Optics*, 6^{th}ed. Pergamon Press New York (1980)

P. Horowitz and W. Hill, *The Art of Electronics*, Cambridge University Press (2001)

U. Tietze & Ch. Schenk, *Halbleiterschaltungstechnik*, Springer-Verlag (1978)

W.R. Theis, *Grundzüge der Quantentheorie*, Teubner (1985)

H.J. Metcalf, P. van der Straten, *Laser Cooling and Trapping*, Graduate Texts in Contemporary Physics, Springer (1999)

J. Weiner and P-T. Ho, *Light-Matter Interaction: Fundamentals and Applications*, Springer-Verlag, Berlin (2003)

Ch.J. Foot, *Atomic physics*, (Oxford Master Series in Atomic, Optical and Laser Physics, 2005)

R. Loudon, *The quantum theory of light*, Oxford Science Publications, Oxford (1973)

Ch.C. Gerry and P.L. Knight, *Introductory Quantum Optics*, Cambridge University Press (2005)

P. Meystre and M. Sargent III, *Elements of Quantum Optics*, Springer-Verlag, Berlin (1990)

I.I. Sobelman, *Atomic Spectra and Radiative Transitions*, Springer Verlag, Berlin (1977)

M. Weissbluth, *Photon-Atom Interactions* (Academic Press, Boston, 1989)

C. Cohen-Tannoudji, B. Diu, F. Laloe, *Quantum mechanics, vol. 1*, Wiley Interscience

D.J. Griffiths, *Introduction to Quantum mechanics*, Pearson Education Limited (2014)

L.I. Schiff, *Quantum mechanics*, McGraw-Hill Book Company (1968)

J.J. Sakurai, J.J. Napolitano, *Modern Quantum Mechanics*, 2^{nd} ed., Springer (2011)

P.W. Atkins and R.S. Friedman, *Molecular Quantum Mechanics*, (3^{rd} ed. Oxford University (2001)

I.N. Levine, *Quantum Chemistry*, Allyn and Bacon, 7^{th} ed. Pearson (1983)

H.A. Bethe, R. Jackiw, *Intermediate Quantum Mechanics*, 3^{rd} ed. Taylor & Francis (1997)

J.I. Steinfeld, *Molecules and Radiation*, The MIT Press, Cambridge (2005)

A. Corney, *Atomic and Laser Spectroscopy*, Clarendon Press, Oxford (1977)

B.H. Bransden, C.J. Joachain, *Physics of Atoms and Molecules*, John Wiley & Sons (1983)

Content

Part I

Classical Mechanics

Chapter 1

Foundations and mathematical tools

1.1 General considerations on physics

Before starting the course let us make some general comments on physics [1].

1.1.1 Definition of physics

1.1.1.1 Why to study physics?

The best motivation to study physics is certainly the desire to unravel the mysteries of the universe. The desire may be driven by curiosity (where are we coming from and where are we going) or by necessity, to improve our living conditions or to survive critical situations ("we've gonna have to science the shit out of this [Matt Damon]").

Even if, during the studies or practicing research, curiosity is not always satisfied and many questions remain open, physicists are often confronted with fundamental questions.

1.1.1.2 What is the purpose of physics?

- Technology
- Understanding the world, curiosity leading to sometimes unexpected applications
- The reward of the study is a better appreciation of the simplicity, beauty, and harmony of the laws of nature.

1.1.1.3 Theory and reality

Since ancient Greece philosophers and scientists have been wondering about what is out there and how much of it the human mind can grasp. How does our image of the universe connect to reality? How much of reality can we learn through observation?

"Quantum phenomena do not occur in a Hilbert space. They occur in a laboratory [Asher Peres]"

[1] See [961], Cap. 1.

"It doesn't matter how beautiful your theory is, it doesn't matter how smart you are. If it doesn't agree with experiment, it's wrong" [Richard P. Feynman].

1.1.1.4 The scientific method, physics and mathematics

Observation and experimentation as well as abstraction and induction.

- Abstraction of inessential effects
- Physical laws and theories (reduction of a large number of phenomena to a few laws, predictive power)
- Domains of restricted validity (new theories contain the old ones in some limit, even if the basic concepts may differ radically)
- Ancient theories have their right to be (e.g. because of their simplicity, they can be derived from a more general theory following well-defined procedures).

1.1.1.5 Relationship between physics and mathematics

Although mathematics is the most important tool in physics, these two sciences are fundamentally different. According to *Carl Friedrich von Weizsäcker* mathematics is a *structural science* while physics is a *natural science* [1345, 1346]. The mathematical method is deductive. A mathematical theory is good when it is complete and intrinsically without controversy, it cannot be *correct*. It is not more than a tool and does not contain *reality*. For instance, axiomatic geometry remains valid, when the words 'point, straight, plane' are replaced by 'table, cup, chair'. The method of mathematics is deductive.

In contrast, physics is a *natural science*. A physical theory is good when it is *true*, which means that it describes the universe as correctly as possible. The central activity of a physicist is to *measure* [2]. The physicist makes hypotheses that he formulates as theories, but he must verify their correctness experimentally, otherwise the theory is of no use. The physicist already has in his mind an image of how the universe works (which may or may not be correct), and this image guides his intuition in the formulation of new better theories or improved measurement techniques. According to *Karl Popper*, in contrast to pseudo-science and religious beliefs, a physical theory or model must be *falsifiable*, i.e. its correctness must be verifiable through experimentation. It is good practice to incorporate into a scientific model conjectures about its range of validity (e.g. sufficiently low velocities, small masses, or high energies). Within its range of validity the model should be universal, i.e. always and everywhere make correct predictions in the outcome of experiments. A single negative experiment is sufficient to falsify the model. A scientific model must provide recipes allowing for its falsification by experiment or at least allow for them to be formulated. An good example is Einstein's hidden variables assumption. At the beginning the debate appeared as purely metaphysical. Only Bell's proposal how to test the assumption by measurement turned it into a scientific theory, which finally was falsified experimentally. This shows that the whole art of a physicist consists in constructing meaningful

[2] 'Quantum phenomena do not occur in Hilbert space, they occur in laboratory' [A. Peres].

experiments. The biggest task of theory is to allow questions to be asked. Measuring means: asking the *right question*. A right question is a question with possible answers, called *observables*.

1.1.1.6 Relationship between physics and other sciences

- Chemistry and molecular biology

1.1.1.7 Plato, Newton, Leibniz, Kant, Einstein and Bohr

What is first ideas or phenomena? Plato, Newton, Kant and Einstein would perhaps say: ideas. Leibniz and Bohr: phenomena.

However, Plato has a lot say about quantum mechanics, dialectic approach, the part and the whole. Also the cave parabola seems to indicate that Plato would support the relativity of perceptions.

1.1.1.8 Space and time

The discussion of the role of *space* and *time* in physics is best started with the controverse between Newton and Leibniz. Newton imagined space and time as a Cartesian space. Space and time are basically different from all other quantities: They are dimensions, they are the recipient in which all processes occur, To say it with Kant, 'die Gefäße unserer Erkenntnis, unseres Denkens'. *Leibniz* had another vision. He asked what a space with nothing in it might look like, what a time with nothing happening might look like. Space and time are no observables, but rather *distance* between objects or duration between events. They have no physical reality by themselves. They are nothing more than mathematical concepts, dimensions in which things may be displaced and evolve.

Time may be defined through processes which are, to the best of our knowledge, periodic, i.e. repetitive, like the oscillations of a pendulum. But we might also understand time as a measure for the frequency of any events, e.g. collisions between any two atoms in a gas. Then time runs fast if a lot happens, but slowly if nothing happens. Time then goes with the inverse of temperature.

1.1.1.9 Before the big bang

The basic process in modern physics is a collision. Every interaction force is mediated by particles. These particles collide with other particles and exchange energy, momentum and other features. The fundamental nature of the collision process leads us to define time as the inverse of the collision rate.

In this light, the question about the beginning of the universe or what was before the *big bang* might be a silly one, like to ask about the start point of a sphere. If with the density in the early universe the temperature diverges, so does the time. Time steps have to be chosen shorter and shorter as one approaches the big bang, without ever reaching the limit.

This implies that causality is interrupted, there is no point in asking about the before of the universe, may not even its origin.

1.1.1.10 The arrow of time

Aging seems to be a macroscopic phenomenon. It comes into play at the interface between the microscopic and macroscopic world. Classically at the boundary of kinetic theory and thermodynamics, i.e. via the second law of thermodynamics [951]. Modern theories pin it down to decoherence phenomena [1004].

Causality in chaos science: *weak causality*: Same causes have same effects.

strong causality: Similar causes have similar effects.

Not the physical laws are subject to *indeterminism*, but the quantum states cannot be characterized better than permitted by the uncertainty relation.

1.1.2 Structure of physics

1.1.2.1 Orders of magnitude, significant number of digits

The objects of physical science are measurable quantities or *observables*, which (at least in classical physics) correspond to *real* numbers. Even though complex numbers are sometimes used to represent physical quantities, only their real parts are associated with physical reality.

Many physical quantities have wide ranges of possible values (time, distances, ..), and many values are little known (for example, the number of stars in the universe. No physical quantity can be measured with absolute certainty. That is, when presenting the result of measurements, we always need to specify the estimated uncertainty or error. For example, a measurement of a mathematical constant may yield $\pi = 3.14159 \pm 0.00002$. Obviously, it is meaningless to specify a value with a higher precision as the uncertainty or to specify the uncertainty itself by more than 1 (or at most 2) digits. Hence, we always use the same number of *significant digits* for the value and its uncertainty, that is, the same number of digits behind the decimal point. If the quantity depends on several quantities, the significant digit is given by the quantity with the smallest precision.

The uncertainty of a measurement of a quantity m is a complicated issue because, in order to quantify it, in principle we would need a more precise measurement to compare with. However, what we always can do is repeat the measurement N times (if possible varying the conditions) and to calculate the mean value,

$$\bar{m} = \tfrac{1}{N} \sum_k m_k \tag{1.1}$$

of the individual measurement outcomes m_k, as well as the standard deviation,

$$\Delta m = \sqrt{\frac{1}{N-1} \sum_k (m_k - \bar{m})^2} \ . \tag{1.2}$$

The physical quantity is then specified as,

$$m = \bar{m} \pm \Delta m \ . \tag{1.3}$$

This uncertainty grasps *stochastic (or random) errors* due to an imperfect realization of the measurement limiting the *precision*. On the other hand, a conceptual flaw

of the design of the measurement apparatus can lead to deviations, which often are unknown. These are called *systematic errors* and limit the *accuracy* of the apparatus, as illustrated in Fig. 1.1.

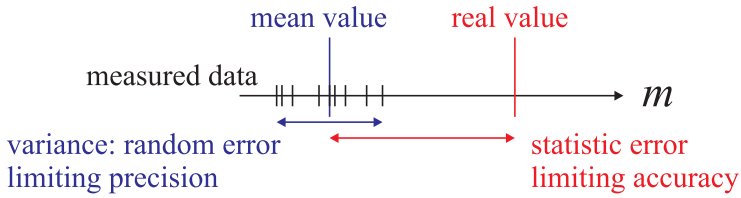

Figure 1.1: Illustration of stochastic and systematic errors in a measurement of a quantity m.

1.1.2.2 Units

Physical quantities *always* consist of a number and a unit forming an inseparable entity. For example, a mass can be specified by the assertion,

$$m = 2\,\mathrm{kg}\ , \tag{1.4}$$

stating that a particular object I have in mind and that I will call henceforward by the name m has a mass of 2 kg. Note that every equation represents an assertion, that is either a *definition* or a *verifiable statement*, which we assume to be true if not otherwise stated. For example, the sentence

$$2\,\mathrm{kg}\cdot 2\,\mathrm{m/s}^2 = 4\,\mathrm{N} \tag{1.5}$$

is a verifiable statement that we find to be correct [3]. In contrast, the statement

$$2\ \cdot 2 = 4\,\mathrm{N} \tag{1.6}$$

is false and the statement

$$2\ \cdot 2 = 4 \tag{1.7}$$

is physically meaningless.

Measuring means determining the numerical value of a physical quantity, but this is only possible with respect to a reference value. For example, distances are compared to the circumference of the Earth, times with the duration of the day. In practice, it is more convenient to choose as reference value the unitary value. For example, we will consider the distance

$$d = 1\,\mathrm{m}\ , \tag{1.8}$$

as our reference distance, which in turn is related to a (previously determined) Earth circumference by a fixed numerical factor of 1:40 000 000. In this sense, measurement always means comparison with a reference that we will call *standard*.

[3] A practical issue of consequently using units is that they allow us to quickly check whether a formula is false. If a formula represented by an equation exhibits different units on both sides, it must obviously be wrong.

1.1.2.3 Linearization of functions, graphical representation

The linearization of exponential, logarithmic and polynomial functions facilitates their graphical representation and the determination of constants,

$$\begin{aligned} y &= ax + b \\ \lg y &= ax + b \quad \Longrightarrow \quad y = 10^{ax+b} = BA^x \\ y &= a \lg x + b \\ \lg y &= a \lg x + b \quad \Longrightarrow \quad y = 10^{a \lg x + b} = Bx^a \end{aligned} \tag{1.9}$$

where we defined $B \equiv 10^b$ and $A \equiv 10^a$. See Fig. 1.2.

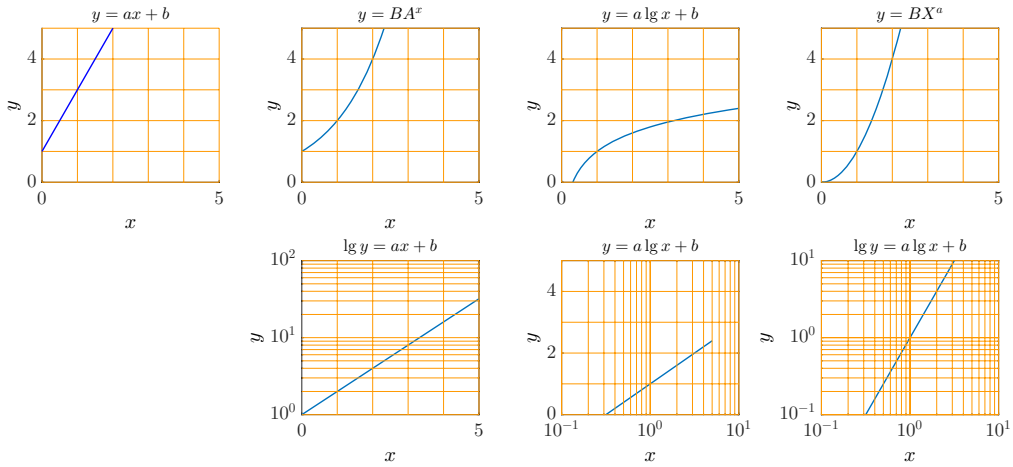

Figure 1.2: Original and linearized curved.

1.1.2.4 Length measurements

- Historical standards $1\,\mathrm{m} = 1\ 650\ 763.73 \lambda_{Kr86}$ and $c = 299\ 792\ 458\,\mathrm{m/s}$.
- Measurement of Eratosthenes 300 AC.

1.1.2.5 Coordinate systems

- Cartesian or polar coordinates for two or three dimensions.
- The latitude is easy to measure ($\lambda = 90° - \angle(norte - zenit)$), but the longitude is difficult (needs very precise clocks).

1.1.2.6 Time measurements

Absolute space and time do not exist. According to the restricted and the general theory of relativity they are interconnected by velocity and they depend on the presence of mass. But even in a more metaphysical sense one may wonder with Gottfried

Leibniz about the meaning of space with nothing inside and of time with nothing happening. Indeed, our practical approach to the measurement of time is based on the observation of recurrent phenomena that we think of being periodic, such as a day on Earth, the dripping of a water pipe, or the oscillation of a pendulum or of an atomic excitation. Assuming the time intervals separating the recurrent phenomena as being all the same, we build a ruler for time which we call clock (see Sec. 36.5).

Historically, the development of ever precise clocks has been motivated by navigation. Indeed, 1 minute of inaccuracy in the clock generates an uncertainty of 28 km in global positioning. And this motivation still prevails nowadays although, meanwhile, atomic clocks have uncertainties of below 10^{-16}.

Apart from periodic processes, time measurement can also be done by exponential processes, such as radioactive decay. This method is commonly used in radioactive dating. Do the Excs. 1.1.3.1 to 1.1.3.5.

1.1.2.7 The international system of units

Not every physical quantity needs to have its own standard. Often it is easier to quantify this quantity by measuring other physical quantities to which it is related in a simple way. For example, instead of measuring a *distance* by comparing it to the Earth circumference it may be easier to measure the *time* needed by a beam of light to cover this distance. In this sense, all physical quantities have been traced back by simple relationships to a small number of so-called *basic units*. Today, seven basic units are officially recognized as such by the international Conférence Générale des Poids et mesures (CGPM): the second (unit symbol 's') as a measure of time, the meter (unit symbol 'm') as a measure of distance, the kilogram (unit symbol 'kg') as a measure of mass, the Ampère (unit symbol 'A') as a measure of electrical current, the Kelvin (unit symbol 'K') as a measure of temperature, the mol (unit symbol 'mol') as a measure of molar mass, and the candela (unit symbol 'cd') as a measure of luminosity [4].

By decision of the 26^e CPGM in 2018 [5], all basic units are related to the most fundamental unit, the second, for which the most precise measurement tools are available. Measurements of all other units are traced back to time measurements using simple relationships and *natural constants* [6]:

[4] Note that, the molar mass and the luminosity are not fundamental in a strict sense, and only appear in the SI-system, because they are convenient for the communities of chemistry and illumination industry. After all, industrial and practical life applications are a main motivation for standardization (see Quantum Science Seminar talk by William Phillips).

[5] SI-Brochure.

[6] So, in a sense, 'time' is the only remaining fundamental quantity.

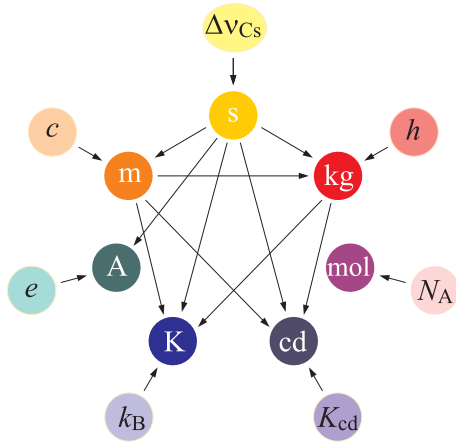

Figure 1.3: SI unit system.

base unit	relationship	definition
time	t	$1\,\mathrm{s} = \frac{9\ 192\ 631\ 770}{\Delta\nu_{Cs}}$
distance	$d = ct$	$1\,\mathrm{m} = \frac{c}{299\ 792\ 458}\,1\,\mathrm{s}$
mass	$m = \frac{h\nu}{c^2}$	$1\,\mathrm{kg} = \frac{(299\ 792\ 458)^2}{c^2}\frac{h}{6.626\ 070\ 15\times10^{-34}}\ \frac{1}{1\,\mathrm{s}}$
electric current	$I = \dot{Q}$	$1\,\mathrm{A} = \frac{e}{1.602\ 176\ 634\times10^{-19}}\ \frac{1}{1\,\mathrm{s}}$
temperature	$T = \frac{h\nu}{k_B}$	$1\,\mathrm{K} = \frac{c^2}{(299\ 792\ 458)^2}\frac{1.308\ 649\times10^{-23}}{k_B}\ 1\,\mathrm{kg}$
molar mass	$T = \frac{mc^2}{k_B}$	$1\,\mathrm{mol} = \frac{6.022\ 140\ 76\times10^{23}}{N_A}$
luminosity		$1\,\mathrm{cd}$

These natural constants are the transition frequency of cesium atoms Δ_{Cs}, the velocity of light c, Planck's constant h, the elementary charge e, Boltzmann's constant k_B, and Avogadro's constant N_A. The natural constants are considered as fixed and exact. Hence, any improved measurement of the velocity of light will not result in a more precise value of c, but in an improved definition of the meter.

1.1.3 Exercises

1.1.3.1 Ex: Mean value and standard deviation

The surface area of a house plant is measured by 10 people finding different values. Determine the mean and standard deviation of the measurement. How many measurements are in the confidence interval, that is, within the standard deviation?

person	measured value [m^2]
1	99.9
2	76
3	96.0
4	100
5	101.2
6	99.9
7	110
8	96.0
9	100.4
10	101.6

Solution: *The average value of the measurements is,*

$$\bar{A} = \frac{1}{10}\sum_{i=1}^{10} A_i = 98.1 \ .$$

The standard deviation is,

$$\bar{\sigma} = \sqrt{\frac{1}{10}\sum_{i=1}^{10}(A_i - \bar{A})} \simeq 8.22 \ .$$

Therefore, all measurements between $98.10 + 8.22 = 106.32$ *and* $98.1 - 8.22 = 89.88$ *fall within the confidence interval.*

1.1.3.2 Ex: Circumference of the Earth

In the 3rd century BC, the Greek Eratosthenes measured the circumference of the Earth by comparing the angles between the sun's rays and the vertical at noon in two different places. In Siena he measured 0° and in Alexandria, which is 785 km north of Siena, he measured 7.2°. What is the circumference he found?

Solution: *With* $s = 785$ *km and* $\theta = 7.2°$ *we find,*

$$\frac{s}{2\pi R} = \frac{\theta}{360°} \ .$$

Hence, $2\pi R = 39250\,\text{km}$.

1.1.3.3 Ex: Radioactive dating with ^{40}K

A chemical analysis of a 1 g rock sample reveals the presence of $m_K = 4.21 \cdot 10^{-2}$ g potassium (^{39}K+^{40}K) and $m_A = 9.02 \cdot 10^{-7}$ g argon (^{40}A). How old is the rock? **Help:** The current relative abundance is 1 atom of ^{40}K for every 8400 atoms of ^{39}K.

Only 12% of ^{40}K desintegrate into ^{40}A, the rest into ^{40}Ca. The decay time of ^{40}K is $t_{1/2} = 1.3 \cdot 10^9$ a.

Solution: *The amounts of potassium and argon correspond to,*

$$N_K = \frac{m_K}{u_K} = \frac{4.21 \cdot 10^{-2}\,\mathrm{g}}{39.1u} = 6.48 \cdot 10^{20}$$
$$N_A = \frac{m_A}{u_A} = \frac{9.02 \cdot 10^{-7}}{39.95u} = 1.36 \cdot 10^{16} \ .$$

Given the relative abundance, the current number of atoms of ^{40}K in the sample is,

$$N_{K40}^{actual} = \frac{N_K}{8400} \ .$$

The number of ^{40}K that disintegrated is,

$$N_{K40}^{desint} = \frac{100 N_A}{12} \ ,$$

and the initial number of ^{40}K number was,

$$N_{K40}^{initial} = N_{K40} + N_{K40}^{desint} \ .$$

So the rock age is,

$$t = t_{1/2} \log_2 \frac{N_{K40}^{initial}}{N_{K40}^{actual}} = 3.5 \cdot 10^9\,\mathrm{a} \ .$$

1.1.3.4 Ex: Paramecia

A biologist analyzes the behavior of a paramecium. Make a position versus time diagram and determine the average speed.

tempo [s]	posição [cm]
0	2
10.5	2.1
12	96.0
23	100
40	101.6

Solution: *The animal covers a distance of* 101.6 cm *in* 40 *seconds. With that we get the average speed,*

$$\bar{v} = \frac{101.6\,\mathrm{m}}{40\,\mathrm{s}} = 2.54\,\mathrm{cm/s} \ .$$

1.1.3.5 Ex: Spirograph

Find the parametrization of the curves produced by a spirograph.

Solution:

1.2 Basics mathematical notions, vector analysis

We will not spend time on mathematical fundamentals, such as notions of vectors and matrices, one-dimensional derivatives and integers, complex numbers, and differential equations. Students who have doubts should try to solve the exercises of Chapter 1 of the Handbook by Zilio and Bagnato.

1.2.1 Scalars, vectors and matrices

1.2.2 Exercises

1.2.2.1 Ex: Vectors

A room has the dimensions $3 \times 4 \times 5\,\mathrm{m}^3$. A fly departs from one of its corners and flies to the diametrically opposite corner. What is the absolute value of the displacement? Could its trajectory be less than this displacement? Choose a convenient coordinate system and express the displacement in vector form.

Solution: *see Zilio & Bagnato, Apostila: Física I: Mecânica, calor e ondas*

1.2.2.2 Ex: Vectors

Consider the vectors $\mathbf{x} = x_1\hat{\mathbf{e}}_1 + x_2\hat{\mathbf{e}}_2 + x_3\hat{\mathbf{e}}_3$ and $\mathbf{y} = y_1\hat{\mathbf{e}}_1 + y_2\hat{\mathbf{e}}_2 + y_3\hat{\mathbf{e}}_3$. Calculate $|\mathbf{x}|$, $\mathbf{x} \cdot \mathbf{y}$ and $\mathbf{x} \times \mathbf{y}$.

Solution:

1.2.2.3 Ex: Vectors

Can we combine two vectors with different absolute values and have a resulting vector with zero length? How about 3 vectors?

Solution: *see Zilio & Bagnato, Apostila: Física I: Mecânica, calor e ondas*

1.2.2.4 Ex: Vectors

Consider a moving body whose position vector is given (in cm) by $\mathbf{r} = 3\hat{\mathbf{e}}_x \cos\omega t + 4\hat{\mathbf{e}}_y \sin\omega t$.
a. Display in a scaled graph $\mathbf{r}$ at a given time t;

b. after a small time interval Δt show the new vector $\mathbf{r}$ on the same graph;
c. calculate the displacement $\Delta\mathbf{s} = \mathbf{r}(t + \Delta t) - \mathbf{r}(t)$ suffered by the body during the interval Δt;
d. calculate $\mathbf{v} = \Delta\mathbf{s}/\Delta t$ and check its orientation for $\omega t = 0,\ \pi/2,\ \pi,\ 3\pi/2$;
e. calculate $\mathbf{r} \cdot \mathbf{v}$ and discuss the result;
f. calculate $\mathbf{r} \times \mathbf{v}$ and discuss the result.

Solution: *see Zilio & Bagnato, Apostila: Física I: Mecânica, calor e ondas*

1.2.2.5 Ex: Vectors

Show that the magnitude of the sum of two vectors $\mathbf{a}$ and $\mathbf{b}$ is always within the limits,

$$||\mathbf{a}| - |\mathbf{b}|| \leq |\mathbf{a} + \mathbf{b}| \leq |\mathbf{a}| + |\mathbf{b}| \ .$$

Solution: *Calculating the square of the terms,*

$$(|\mathbf{a}| - |\mathbf{b}|)^2 \leq (\mathbf{a} + \mathbf{b})^2 \leq (|\mathbf{a}| + |\mathbf{b}|)^2 \ ,$$

we get,

$$-|\mathbf{a}||\mathbf{b}| \leq |\mathbf{a}||\mathbf{b}| \cos\theta \leq |\mathbf{a}||\mathbf{b}| \ .$$

1.2.2.6 Ex: Vector product

Invent a method based on the cross product to calculate the area enclosed by a path delimited by the points $A \to B \to C$....

Solution: *The area is given by,*

$$F = \tfrac{1}{2}(\overrightarrow{AB} \times \overrightarrow{AC} + \overrightarrow{AC} \times \overrightarrow{AD} + \overrightarrow{AB} \times \overrightarrow{AC} + ...) \ .$$

For convex paths, all components are positive. For partially concave paths, some components can be negative.

1.2.2.7 Ex: Matrix multiplication

Determine the products of the following matrices,

$$\begin{pmatrix} 1 & a \\ 0 & 1 \end{pmatrix}\begin{pmatrix} 1 & 0 \\ b & 1 \end{pmatrix} \quad , \quad \begin{pmatrix} 1 & 0 \\ b & 1 \end{pmatrix}\begin{pmatrix} 1 & a \\ 0 & 1 \end{pmatrix} \quad , \quad \begin{pmatrix} 4 & 3 \\ 2 & 2 \\ 7 & -5 \end{pmatrix}\begin{pmatrix} 1 & 2 & 3 & 4 \\ 5 & 6 & 7 & 8 \end{pmatrix} \ .$$

Solution: *trivial*

1.2.2.8 Ex: Matrix multiplication

Consider the matrices A and B and the column vector $\mathbf{x}$ given by,

$$A = \begin{pmatrix} 0 & 1 & 0 \\ 1 & 1 & 0 \\ 0 & 1 & 1 \end{pmatrix} \quad , \quad B = \begin{pmatrix} -1 & -5 & 8 \\ 2 & 1 & 0 \\ 1 & 4 & 6 \end{pmatrix} \quad , \quad \vec{x} = \begin{pmatrix} 1 \\ 0 \\ 0 \end{pmatrix} \ .$$

a. Calculate the vector $\mathbf{y} = A(B\mathbf{x})$.
b. Show that for arbitrary matrices A and B and vectors $\mathbf{x}$ holds $A(B\mathbf{x}) = (AB)\mathbf{x}$.
c. Let A be an arbitrary matrix with A_{ij} elements. The conjugate matrix of A^t is defined by $(A^t)_{ij} = A_{ji}$; that is, the column indexes i and those of the row j are exchanged. Show,

$$(AB)^t = B^t A^t \ .$$

Solution: *a. We calculate,*

$$\begin{pmatrix} 0 & 1 & 0 \\ 1 & 1 & 0 \\ 0 & 1 & 1 \end{pmatrix} \begin{pmatrix} -1 & -5 & 8 \\ 2 & 1 & 0 \\ 1 & 4 & 6 \end{pmatrix} \begin{pmatrix} 1 \\ 0 \\ 0 \end{pmatrix} = \begin{pmatrix} 2 \\ 1 \\ 3 \end{pmatrix} \ .$$

b. We calculate,

$$\begin{aligned}
(AB)\mathbf{x} &= \begin{pmatrix} a_{11} & a_{12} & a_{13} \\ a_{21} & a_{22} & a_{23} \\ a_{31} & a_{32} & a_{33} \end{pmatrix} \begin{pmatrix} b_{11} & b_{12} & b_{13} \\ b_{21} & b_{22} & b_{23} \\ b_{31} & b_{32} & b_{33} \end{pmatrix} \begin{pmatrix} x_1 \\ x_2 \\ x_3 \end{pmatrix} \\
&= \begin{pmatrix} a_{11}b_{11} + a_{12}b_{21} + a_{13}b_{31} & a_{11}b_{12} + a_{12}b_{22} + a_{13}b_{32} & a_{11}b_{13} + a_{12}b_{23} + a_{13}b_{33} \\ a_{21}b_{11} + a_{22}b_{21} + a_{23}b_{31} & a_{21}b_{12} + a_{22}b_{22} + a_{23}b_{32} & a_{21}b_{13} + a_{22}b_{23} + a_{23}b_{33} \\ a_{31}b_{11} + a_{32}b_{21} + a_{33}b_{31} & a_{31}b_{12} + a_{32}b_{22} + a_{33}b_{32} & a_{31}b_{13} + a_{32}b_{23} + a_{33}b_{33} \end{pmatrix} \begin{pmatrix} x_1 \\ x_2 \\ x_3 \end{pmatrix} \\
&= \begin{pmatrix} (a_{11}b_{11} + a_{12}b_{21} + a_{13}b_{31})\,x_1 + (a_{11}b_{12} + a_{12}b_{22} + a_{13}b_{32})\,x_2 + (a_{11}b_{13} + a_{12}b_{23} + a_{13}b_{33})\,x_3 \\ (a_{21}b_{11} + a_{22}b_{21} + a_{23}b_{31})\,x_1 + (a_{21}b_{12} + a_{22}b_{22} + a_{23}b_{32})\,x_2 + (a_{21}b_{13} + a_{22}b_{23} + a_{23}b_{33})\,x_3 \\ (a_{31}b_{11} + a_{32}b_{21} + a_{33}b_{31})\,x_1 + (a_{31}b_{12} + a_{32}b_{22} + a_{33}b_{32})\,x_2 + (a_{31}b_{13} + a_{32}b_{23} + a_{33}b_{33})\,x_3 \end{pmatrix} \\
&= \begin{pmatrix} a_{11} & a_{12} & a_{13} \\ a_{21} & a_{22} & a_{23} \\ a_{31} & a_{32} & a_{33} \end{pmatrix} \begin{pmatrix} b_{11}x_1 + b_{12}x_2 + b_{13}x_3 \\ b_{21}x_1 + b_{22}x_2 + b_{23}x_3 \\ b_{31}x_1 + b_{32}x_2 + b_{33}x_3 \end{pmatrix} = A(B\mathbf{x})
\end{aligned}$$

c. We calculate,

$$\begin{aligned}
(AB)^t &= \left[\begin{pmatrix} a_{11} & a_{12} & a_{13} \\ a_{21} & a_{22} & a_{23} \\ a_{31} & a_{32} & a_{33} \end{pmatrix} \begin{pmatrix} b_{11} & b_{12} & b_{13} \\ b_{21} & b_{22} & b_{23} \\ b_{31} & b_{32} & b_{33} \end{pmatrix} \right]^t \\
&= \begin{pmatrix} a_{11}b_{11} + a_{12}b_{21} + a_{13}b_{31} & a_{11}b_{12} + a_{12}b_{22} + a_{13}b_{32} & a_{11}b_{13} + a_{12}b_{23} + a_{13}b_{33} \\ a_{21}b_{11} + a_{22}b_{21} + a_{23}b_{31} & a_{21}b_{12} + a_{22}b_{22} + a_{23}b_{32} & a_{21}b_{13} + a_{22}b_{23} + a_{23}b_{33} \\ a_{31}b_{11} + a_{32}b_{21} + a_{33}b_{31} & a_{31}b_{12} + a_{32}b_{22} + a_{33}b_{32} & a_{31}b_{13} + a_{32}b_{23} + a_{33}b_{33} \end{pmatrix}^t \\
&= \begin{pmatrix} a_{11}b_{11} + a_{12}b_{21} + a_{13}b_{31} & a_{21}b_{11} + a_{22}b_{21} + a_{23}b_{31} & a_{31}b_{11} + a_{32}b_{21} + a_{33}b_{31} \\ a_{11}b_{12} + a_{12}b_{22} + a_{13}b_{32} & a_{21}b_{12} + a_{22}b_{22} + a_{23}b_{32} & a_{31}b_{12} + a_{32}b_{22} + a_{33}b_{32} \\ a_{11}b_{13} + a_{12}b_{23} + a_{13}b_{33} & a_{21}b_{13} + a_{22}b_{23} + a_{23}b_{33} & a_{31}b_{13} + a_{32}b_{23} + a_{33}b_{33} \end{pmatrix} \\
&= \begin{pmatrix} b_{11} & b_{21} & b_{31} \\ b_{12} & b_{22} & b_{32} \\ b_{13} & b_{23} & b_{33} \end{pmatrix} \begin{pmatrix} a_{11} & a_{21} & a_{31} \\ a_{12} & a_{22} & a_{32} \\ a_{13} & a_{23} & a_{33} \end{pmatrix} \\
&= \begin{pmatrix} b_{11} & b_{12} & b_{13} \\ b_{21} & b_{22} & b_{23} \\ b_{31} & b_{32} & b_{33} \end{pmatrix}^t \begin{pmatrix} a_{11} & a_{12} & a_{13} \\ a_{21} & a_{22} & a_{23} \\ a_{31} & a_{32} & a_{33} \end{pmatrix}^t = B^t A^t \ .
\end{aligned}$$

1.3 Infinitesimal calculus

Several physical quantities are related by derivatives or integrals.

1.3.1 Derivation

1.3.2 Integration

1.3.3 Exercises

1.3.3.1 Ex: Derivatives

We know that $(\sin x)' = \cos x$ and $(\cos x)' = -\sin x$. Use this notion to calculate:

a. $(\arccos x)'$,
b. $(\arctan x)'$.

Derive by x:

c. $y = (x^3 + 2)\cos x^2$,
d. $y = \dfrac{x^2 + 1}{\sin \ \ln x}$.

Calculate the derivatives of,

e. $f(x) = 5 \ x \ e^{ax} \ \sin x$,
f. $f(t) = \dfrac{a^t}{\sin t}$,
g. $f(z) = \ln \dfrac{1 - z^2}{1 + z^2}$.

Solution: *Deriving by x*

c. $y' = 3x^2 \cos x^2 - 2x\left(x^3 + 2\right)\sin x^2$
d. $y' = \dfrac{2x}{\sin(\ln x)} - \dfrac{x^2 + 1}{\sin^2 \ln x}\dfrac{\cos \ln x}{x}$.

The derivatives are

e. $f(x) = 5e^{ax}\sin x + 5xe^{ax}(\sin x)\, a + 5xe^{ax}\cos x$
f. $f(t) = -a^t \dfrac{\ln a \sin t - \cos t}{-1 + \cos^2 t}$
h. $f(z) = \dfrac{4z}{z^4 - 1}$.

1.3.3.2 Ex: Curves discussion

Consider the parable $y = 2x^2 + x - 3$.
a. Using the concept of the derivative, find the position x_0 that corresponds to the extreme (maximum or minimum);

b. Substitute the value of x_0 in the parabola equation to find the value of y_0;
c. Calculate the squares to find the vertex points x_0 and y_0;
d. Find the points at which the parable crosses the axis x;
e. Sketch the parable (graphic with few details);
f. Using integration, find the area under the parable between the points 1 and 2.

Solution: *see Zilio & Bagnato, Apostila: Física I: Mecânica, calor e ondas*

1.3.3.3 Ex: Integrals

Calculate the following indefinite integrals,

$$\text{a.} \quad \int 3x \; dx \;,$$
$$\text{b.} \quad \int (7x^2 + 4x^3 - 2) \; dx \;,$$

and the definite integrals,

$$\text{c.} \quad \int_0^{\pi} (3\sin x + \cos x) \; dx \;,$$
$$\text{d.} \quad \int_{-1}^{1} (5 + 2x^2) \; dx \;,$$
$$\text{e.} \quad \int_0^{1} e^{2x} \; dx \;,$$
$$\text{f.} \quad \int_0^{\pi/4} \sin x \cos x \; dx \;.$$

Solution: *see Zilio & Bagnato, Apostila: Física I: Mecânica, calor e ondas*

1.3.3.4 Ex: Integrals

Find a suitable substitution to solve the following integrals,

a. $\int dt \;\; \sin(\omega t + \alpha)$ b. $\int dx \; \frac{2x}{\sqrt{1+x^2}}$

c. $\int dx \; x^2 \ln x$ d. $\int_0^{\pi/3} d\phi \; \frac{\sin\phi}{\sqrt{1+\cos\phi}}$

Calculate by partial integration,

e. $\int dx \; (x+2)^2 \ln x$ f. $\int dx \; xe^{-x}$

g. $\int dx \; x^2 \ln x$ h. $\int_0^1 dx \; x\sqrt{1+x}$

Calculate,

i. $\int \frac{dx}{x(\ln x)^3}$ j. $\int dx\ \frac{\sin 2x}{1-\cos 2x}$

Find a serial expansion around the position $x = 0$ for,

k. $\int_0^1 dx\ e^{-x^2}$ l. $\int_0^\pi dx\ \frac{\sin x}{x}$

Solution:

a. $$\int \sin(\omega t + \alpha)dt = -\frac{\cos(\omega t + \alpha)}{\omega}$$

b. $$\int \frac{2x}{\sqrt{1+x^2}}dx = 2\sqrt{(1+x^2)}$$

c. $$\int x^2 \ln x dx = \frac{1}{3}x^3 \ln x - \frac{1}{9}x^3$$

d. $$\int_0^{\pi/3} \frac{\sin\phi}{\sqrt{1+\cos\phi}}d\phi = -2\sqrt{(1+\cos\phi)}\Big|_0^{\pi/3} = \left(2-\sqrt{3}\right)\sqrt{2}$$

e. $$\int (x+2)^2 \ln x dx = \left(\frac{1}{3}x^2 + 2x + 4\right) x\ln x - \left(\frac{1}{9}x^2 + x + 4\right)x$$

f. $$\int xe^{-x}dx = -(x+1)e^{-x}$$

g. $$\int x^2 \ln x dx = \frac{1}{3}x^3 \ln x - \frac{1}{9}x^3$$

h. $$\int_0^1 x\sqrt{1+x}dx = -\frac{2}{3}\left(\sqrt{(1+x)}\right)^3 + \frac{2}{5}\left(\sqrt{(1+x)}\right)^5\Big|_0^1 = \frac{4}{15}(\sqrt{2}+1)$$

i. $$\int \frac{dx}{x(\ln x)^3} = -\frac{1}{2\ln^2 x}$$

j. $$\int \frac{\sin 2x}{1-\cos 2x}dx = \frac{1}{2}\ln(1-\cos 2x)$$

k. $$\int \frac{x}{e^x}dx = -(x+1)e^{-x}$$

l. $$\int_0^1 e^{-x^2}dx = \int_0^1 \sum_{n=0}^{\infty}\frac{(-1)^n x^{2n}}{n!}dx = \sum_{n=0}^{\infty}\frac{(-1)^n}{n!}\frac{x^{2n+1}}{2n+1}\Big|_0^1$$
$$= \sum_{n=0}^{\infty}\frac{(-1)^n}{n!}\frac{1}{2n+1}$$

m. $$\int_0^\pi \frac{\sin\phi}{\phi}d\phi = \int_0^\pi \sum_{n=0}^{\infty}\frac{(-1)^n\phi^{2n}}{(2n+1)!}d\phi = \sum_{n=0}^{\infty}\frac{(-1)^n\phi^{2n+1}}{(2n+1)!(2n+1)}\Big|_0^\pi$$
$$= \sum_{n=0}^{\infty}\frac{(-1)^n\pi^{2n+1}}{(2n+1)!(2n+1)}$$

1.3.3.5 Ex: Numerical integration for pedestrians

Consider the differential equation for the mass-spring system $\ddot{x} = -\omega^2 x$ with $\omega = 2\pi \cdot 1\ \mathrm{s}^{-1}$.
a. Determine the equivalent system of coupled first-order differential equations.
b. Calculate using the Euler procedure the numerical solution of this system for the initial conditions, $x(t = 0) = 1$ m and $v(t = 0) = 0$ for the two time intervals of $\Delta t = 0.1$ s. Compare the result with the exact solution.
c. Repeat the calculation of (b) with four time intervals of $\Delta t = 0.05$ s.
d. Use the second-order Runge-Kutta procedure with two time intervals of $\Delta t = 0.1$ s.

Figure 1.4: Runge-Kutta procedure.

Solution: *a.* $y_1(t) = x(t)$, $y_2(t) = \dot{x}(t) = v(t) \Rightarrow \dot{y}_2(t) = -\omega^2 x(t)$, $\dot{y}_1(t) = y_2(t)$
$f_1(t) = y_2(t)$, $f_2 = -\omega^2 y_1(t)$

b. Euler, $\Delta t = 0.1$

t (s)	*0*	*0.1*	*0.2*
x (m)	*1.0*	*1.0*	*0.605*
v (m/s)	*0.0*	*-3.948*	*-7.896*

c. Euler, $\Delta t = 0.05$

t (s)	*0*	*0.05*	*0.1*	*0.15*	*0.2*
x (m)	*1.0*	*1.0*	*0.901*	*0.704*	*0.418*
v (m/s)	*0.0*	*-1.974*	*-3.948*	*-5.727*	*-7.116*

d. Runge-Kutta of second-order

t (s)	*0*	*0.1*	*0.2*
x (m)	*1.0*	*0.803*	*0.249*
v (m/s)	*0.0*	*-3.948*	*-6.337*

$$y_1(t+h) = y_1(t) + \Delta t \cdot y_2(t) - \tfrac{(\Delta t)^2}{2}\omega^2 y_1(t)$$
$$y_2(t+h) = y_2(t) - \Delta t\omega^2 \cdot y_1(t) - \tfrac{(\Delta t)^2}{2}\omega^2 y_2(t)$$

1.3.3.6 Ex: Taylor series

Expand the function

$$f(x) = \frac{1}{\sqrt{1+x}}$$

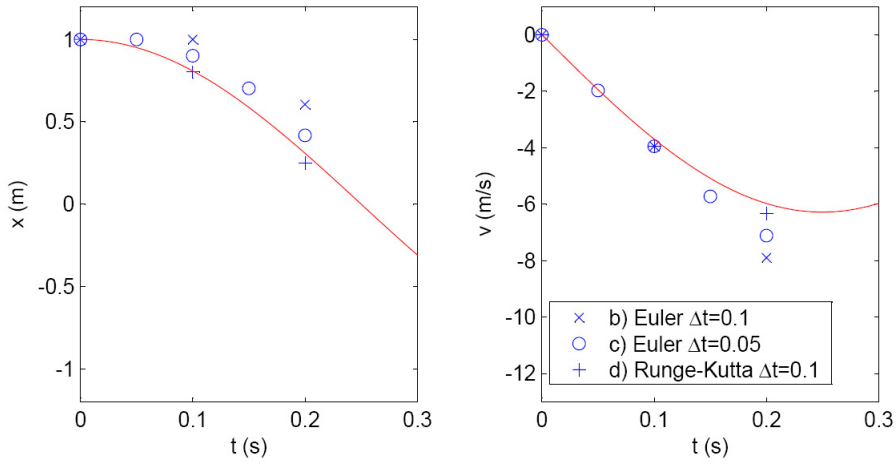

Figure 1.5: Runge-Kutta procedure.

in a Taylor series around the position $x = 0$. To do this, calculate the derivatives at least until third order and try to find the general law indicating how to find the series coefficients. Draw the function and the Taylor approximations.

Solution:

1.3.3.7 Ex: Partial derivatives

Be $r(x_1, x_2, x_3) = \sqrt{x_1^2 + x_2^2 + x_3^2}$. Find the first two partial derivatives and show by explicit calculation, that

$$\text{a.} \quad \frac{\partial^2 r}{\partial x_i \partial x_j} = \frac{\partial^2 r}{\partial x_j \partial x_i} \qquad \text{and} \qquad \text{b.} \quad \sum_{i=1}^{3} \frac{\partial^2}{\partial x_i^2}\left(\frac{1}{r}\right) = 0 \ .$$

Solution: *a. The first derivative is,*

$$\frac{\partial}{\partial x_i} r(x_1, x_2, x_3) = \frac{x_i}{r} \ ,$$

and the second,

$$\frac{\partial^2}{\partial x_i \partial x_j} r(x_1, x_2, x_3) = -\frac{x_i x_j}{r^3} + \delta_{ij} \frac{1}{r} \ .$$

With that, (a) it is already proven.
b. Now,

$$\sum_{i=1}^{3}\frac{\partial^2}{\partial x_i^2}\left(\frac{1}{r}\right)=\sum_{i=1}^{3}\frac{\partial}{\partial x_i}\left(\frac{-1}{r^2}\frac{\partial r}{\partial x_i}\right)=-\sum_{i=1}^{3}\left(\frac{\partial^2}{\partial x_i^2}\frac{1}{r^2}-\frac{2}{r^3}\left(\frac{\partial r}{\partial x_i}\right)^2\right)$$
$$=-\sum_{i=1}^{3}\left(-\frac{x_i^2}{r^5}+\frac{1}{r^3}-\frac{2}{r^3}\left(\frac{x_i}{r}\right)^2\right)$$
$$=-\sum_{i=1}^{3}\left(-3\frac{x_i^2}{r^5}+\frac{1}{r^3}\right)=-\frac{3}{r^3}+\frac{3}{r^5}\sum_{i=1}^{3}(x_i^2)=0\ .$$

1.4 Complex numbers

The imaginary unit is defined as,

$$\boxed{\imath\equiv\sqrt{-1}}\ . \tag{1.10}$$

From this follows a number of arithmetic rules that are studied in the following exercises.

1.4.1 Basic rules

real part, imaginary part, absolute value

1.4.2 The complex plane

the Euler formulae

1.4.3 Complex numbers in physics

1.4.4 Exercises

1.4.4.1 Ex: Complex numbers

Solve the following equations,

$$\frac{z}{1+\imath}-\frac{z}{1-\imath}=1+(z-\bar{z})\sin(\pi+\imath\ln 3)\quad,\quad -2\imath z=\frac{1+\bar{z}}{1+\imath}\ .$$

Calculate the absolute value, the real part and the imaginary part of,

$$\frac{2\imath-1}{\imath-2}\quad,\quad(1+2\imath)^3\quad,\quad\frac{3\imath}{\imath-\sqrt{3}}\ .$$

Solution: *a. We have,*

$$\sin(\pi + \imath \ln 3) = \sin\pi \cosh \ln 3 + \imath \cos\pi \sinh \ln 3 = -\imath \sinh \ln 3$$
$$= -\imath \frac{e^{\ln 3} - e^{-\ln 3}}{2} = -\imath \frac{3 - 1/3}{2} = -\imath \frac{4}{3} \ .$$

On the other side we have,

$$\frac{z}{1+\imath} - \frac{z}{1-\imath} = \frac{z(1-\imath) - z(1+\imath)}{(1-\imath)(1+\imath)} = -\imath z \ .$$

With that and after having entered $z = a + ib$ the equation to solve simplifies to,

$$-\imath a + b = -\imath z = \frac{z}{1+\imath} - \frac{z}{1-\imath}$$
$$= 1 + (z - \bar{z}) \sin(\pi + \imath \ln 3) = 1 + 2\imath b \left(-\imath \frac{4}{3}\right) = 1 + b\frac{8}{3} \ .$$

The comparison of real and imaginary parts gives,

$$a = 0 \qquad \textit{and} \qquad b = -\frac{3}{5} \ .$$

b. Multiplying the equation to solve with $1 + \imath$ gives,

$$-2\imath z + 2z = 1 + \bar{z} \ .$$

Inserting $z = a + \imath b$ gives,

$$2\imath(b - a) + 2(a + b) = 1 + a - \imath b \ .$$

The comparison of real and imaginary parts gives,

$$2(a + b) = 1 + a \qquad \textit{and} \qquad 2(b - a) = -b \ .$$

Solving the system of equations finally gives $a = 3$ and $b = 2$.
c. We have,

$$\left|\frac{2\imath - 1}{\imath - 2}\right| = \frac{2\imath - 1}{\imath - 2}\frac{-2\imath - 1}{-\imath - 2} = 1$$
$$\mathfrak{Re}\ \frac{2\imath - 1}{\imath - 2} = \frac{1}{2}\left(\frac{2\imath - 1}{\imath - 2} + \frac{-2\imath - 1}{-\imath - 2}\right) = \frac{4}{5}$$
$$\mathfrak{Im}\ \frac{2\imath - 1}{\imath - 2} = \frac{1}{2\imath}\left(\frac{2\imath - 1}{\imath - 2} - \frac{-2\imath - 1}{-\imath - 2}\right) = -\frac{3}{5} \ .$$

Also, we get for the absolute value, $|(1+2i)^3| = 5\sqrt{5}$, for the real part, $\mathfrak{Re}\ [(1+2i)^3] = -11$, and for the imaginary part, $\mathfrak{Im}\ [(1+2i)^3] = -2$. Also,

$$\left|\frac{3\imath}{\imath - \sqrt{3}}\right| = \frac{3}{2} \quad , \quad \mathfrak{Re}\ \left[\frac{3\imath}{\imath - \sqrt{3}}\right] = \frac{3}{4} \quad , \quad \mathfrak{Im}\ \left[\frac{3\imath}{\imath - \sqrt{3}}\right] = -\frac{3}{4}\sqrt{3} \ .$$

1.4.4.2 Ex: Complex numbers

Let $z = a + \imath b$ be a complex number. Calculate the real part and the imaginary part of the following expressions: $\sin z$, $z^2 - \bar{z}^2$, $\frac{z+\imath}{\bar{z}-\imath}$.

Solution: *a.*

$$\begin{aligned}\sin z &= \frac{1}{2\imath}(e^{\imath z} - e^{-\imath z}) = \frac{1}{2\imath}\left(e^{\imath(a+\imath b)} - e^{-\imath(a+\imath b)}\right) = \frac{1}{2\imath}\left(e^{\imath a}e^{-b} - e^{-\imath a}e^{b}\right)\\ &= \frac{1}{2\imath}\left(\left[\cos a + \imath \sin a\right]e^{-b} - \left[\cos a - \imath \sin a\right]e^{b}\right)\\ &= \frac{1}{2}\sin a(e^b + e^{-b}) + \frac{\imath}{2}\cos a(e^b - e^{-b}) = \sin a \cosh b + \imath \cos a \sinh b\end{aligned}$$

b.

$$z^2 - \bar{z}^2 = (a+\imath b)^2 - (a-\imath b)^2 = a^2 + 2\imath ab - b^2 - (a^2 - 2\imath ab - b^2) = 4\imath ab$$

c.

$$\frac{z+\imath}{\bar{z}-\imath} = \frac{a+\imath(b+1)}{a-\imath(b+1)} = \frac{a+\imath(b+1)}{a-\imath(b+1)}\frac{a+\imath(b+1)}{a+\imath(b+1)} = \frac{a^2-(b+1)^2}{a^2+(b+1)^2} + \imath\frac{2a(b+1)}{a^2+(b+1)^2}$$

1.4.4.3 Ex: Complex numbers

Solves the following equation by $z \in \mathbb{C}$:

$$-\bar{z} = \frac{1-z}{\imath - 1} + \ln(43)\cdot\sin\left(\frac{\pi}{\imath+1} + \frac{\pi}{\imath-1}\right) - \frac{e^{-\imath\frac{5}{4}\pi}}{\sqrt{2}}\ .$$

Solution: *Complex equation*

$$\begin{aligned}-\bar{z} &= \frac{1-z}{\imath-1} + \ln(43)\cdot\sin\underbrace{\left(\frac{\pi}{\imath+1} + \frac{\pi}{\imath-1}\right)}_{=\frac{2\pi\imath}{-2}} - \frac{e^{-\imath\frac{5}{4}\pi}}{\sqrt{2}}\\ &\Leftrightarrow -\bar{z} = \frac{1-z}{\imath-1} + 0 - \frac{\imath}{\imath-1}\\ &\Leftrightarrow -\bar{z}(\imath-1) = 1 - z - \imath\\ &\Rightarrow -(a-\imath b)(\imath-1) = 1 - (a+\imath b) - \imath\\ &\Leftrightarrow -a\imath - b + a - \imath b = 1 - a - \imath b - \imath\\ &\Leftrightarrow -a\imath - b + 2a = 1 - \imath\\ &\Rightarrow \begin{pmatrix}-b+2a\\ -a\end{pmatrix} = \begin{pmatrix}1\\-1\end{pmatrix}\\ &\Rightarrow a = 1, b = 1 \Rightarrow z = \imath + 1\ .\end{aligned}$$

1.4.4.4 Ex: Complex numbers

Be $z_1 = 4 + 7\imath,\ z_2 = 3 - 9\imath$. Calculate

a. $z_1 + z_2$ e $z_1 - z_2$
b. $z_1 \cdot z_2$
c. z_1^2 e z_2^3
d. $|z_1|$ e $|z_2|$
e. z_1/z_2 .

Now be $z = x + \imath y$. Calculate the real and imaginary part of the expression,

$$\frac{z}{1+2z} \ .$$

Finally, we consider two complex numbers z_1 and z_2. Show that $(z_1 z_2)^* = z_1^* z_2^*$, where z^* is the conjugate complex number of z.

Solution:

1.4.4.5 Ex: Complex numbers

Be

$$z_1 = 1 - \imath\sqrt{3} \quad , \quad z_2 = \frac{1}{2\sqrt{2}} + \imath\frac{\sqrt{2}}{4} \quad , \quad z_3 = -\imath \ ,$$

a. Represent $z_{1,2,3}$ in a polar form $z_{1,2,3} = r_{1,2,3} e^{\imath\phi_{1,2,3}}$.
b. Are the angles $\phi_{1,2,3}$ determined unambiguous? What values are possible?
c. Now, calculate,

$$\sqrt{z_1} \quad , \quad \sqrt[3]{z_2} \quad , \quad \sqrt[4]{z_3} \ .$$

Show how the different possible values of ϕ lead to an ambiguity of the roots.

Solution:

1.5 Differential equations

1.5.1 First order differential equations

The solution is usually an exponential function.

1.5.2 Second order differential equations

Oscillations are processes described by second-order differential equations. We now consider the second-order linear differential equation with constant coefficients:

$$z''(x) + \alpha z'(x) + \beta z(x) = f(x) \ , \tag{1.11}$$

where $z, f : \mathcal{R} \to \mathcal{C}$, com $\alpha, \beta \in \mathcal{C}$.

The homogeneous equation $f \equiv 0$ is always solved by a linear combination of two solutions of the form $z_{1,2}(x) = e^{\lambda_{1,2}x}$ or $z_1(x) = e^{\lambda_1 x}$, $z_2(x) = xe^{\lambda_1 x}$. To show this, we consider two solutions z_1 and z_2 of the homogeneous differential equation, i.e. for $f = 0$, then $z''_{1,2}(x) + \alpha z'_{1,2}(x) + \beta z_{1,2}(x) = 0$. Now we insert the linear combination $Az_1 + Bz_2$ into the differential equation:

$$(Az_1 + Bz_2)'' + \alpha(Az_1 + Bz_2)' + \beta(Az_1 + Bz_2) = 0 \ . \tag{1.12}$$

Arranging,

$$(Az_1'' + \alpha Az_1' + \beta Az_1) + (Bz_2'' + \alpha Bz_2' + \beta Bz_2) = 0 \ . \tag{1.13}$$

The two parentheses must disappear separately. By inserting the ansatz $e^{\lambda x}$ into the homogeneous differential equation, we get,

$$\begin{aligned}(e^{\lambda x})'' + \alpha(e^{\lambda x})' + \beta(e^{\lambda x}) &= 0\\ \lambda^2 e^{\lambda x''} + \lambda\alpha e^{\lambda x} + \beta e^{\lambda x} &= 0\\ \lambda^2 + \lambda\alpha + \beta &= 0 \ .\end{aligned}$$

The characteristic polynomial has two solutions,

$$\lambda_{1,2} = -\frac{\alpha}{2} \pm \sqrt{\frac{\alpha^2}{4} - \beta} \ .$$

Depending on the values of the coefficients α and β the root can be real, zero, or imaginary. For real $\lambda_{1,2}$, the solutions $e^{\lambda x}$ describe an exponential increase or a decay. For zero roots we obtain the aperiodic limit case. For imaginary $\lambda_{1,2}$ we get a vibration.

The inhomogeneous equation, $f \neq 0$, can always be solved by the solutions mentioned above plus a particular solution $z_f(x)$.

1.5.3 Exercises

1.5.3.1 Ex: Exponential law

The value of a coin is divided by two each day. Derive the exponential law allowing to predict the value of the currency at any future date.

Solution: *The value of the currency decreases regularly, which means,*

$$dV = -\alpha dt V(t) \ .$$

This gives,

$$\frac{dV}{V} = -\alpha dt \ ,$$

or

$$V = V_0 e^{-\alpha dt} \ ,$$

with $\alpha = 2d^{-1}$ *and* $\Delta t = 1d$.

1.5.3.2 Ex: First order differential equation

A differential equation of order n is usually an equation between the first n derivatives from a function, the function itself, and its independent variables with the form $F(x, y(x), y'(x), ..., y^{(n)}(x)) = 0$. The initial conditions $(y^{(n-1)}(x_0) = y_0^{(n-1)}, ..., y(x_0) = y_0)$ must be specified to obtain an unambiguous solution. A particular case are first-order equations of the form $y'(x) + f(x)g(y(x)) = 0$ with $y(x_0) = y_0$.
a. Show that the general solution of this equation is given by $\int_{y_0}^{y} \frac{d\tilde{y}}{g(\tilde{y})} = -\int_{x_0}^{x} f(\tilde{x})d\tilde{x}$.
b. Solve the following equations:

$$y'(x) + \cos 2y \cos x = 0 \qquad \text{with} \qquad y(0) = \pi/4$$
$$\log y'(x)x + y + x^2 = 0 \qquad \text{with} \qquad y(\infty) = 0 \ .$$

Does each initial condition make sense?
c. Show that homogeneous linear first-order differential equations $y'(x)+f(x)y(x) = 0$ (with $y(x_0) = y_0$) belong to the class specified above. Find the general solution. $\left(y(x) = y_0 e^{-\int_{x_0}^{x} f(x)dx}\right)$.

Solution: *a. Rephrasing the equation* $y'(x) + f(x)g(y(x)) = 0$

$$\frac{y'}{g(y)} = -f(x)$$
$$\int_{y_0}^{y} \frac{d\tilde{y}}{g(\tilde{y})} = -\int_{x_0}^{x} f(\tilde{x})d\tilde{x} \ .$$

b. Rephrasing the equation $y' + \cos^2 y \cos x = 0$

$$\frac{y'}{\cos^2 y} = -\cos x$$
$$\int_{y_0}^{y} \frac{dy}{\cos^2 y} = -\int_{x_0}^{x} \cos x dx$$
$$\int_{y_0}^{y} \frac{dy}{\cos^2 y} = -\sin x + \sin x_0 \ .$$

Rephrasing the equation $\ln \frac{y'}{x} + y + x^2 = 0$

$$\frac{y'}{x} = e^{-y-x^2}$$
$$\int_{y_0}^{y} \tilde{y} e^{\tilde{y}} d\tilde{y} = \int_{x_0}^{x} \tilde{x} e^{-\tilde{x}^2} d\tilde{x}$$
$$ye^y|_{y_0}^{y} - \int_{y_0}^{y} e^y dy = \frac{1}{2}\int_{x_0^2}^{x^2} e^{-\xi} d\xi$$
$$(1-y)e^y = (1-y_0)e^{y_0} + \frac{1}{2}(e^{-x^2} - e^{-x_0^2}) \ .$$

Inserting the initial conditions $y(\infty) = 0$,

$$y_0 = -\frac{1}{2}e^{-x_0^2 - y_0} - e^{-y_0} + 1 \ ,$$

gives the solution,

$$(1-y)e^y = 1 + \frac{1}{2}e^{-x^2} \ .$$

The right side is always positive. Therefore, only initial conditions $y > 0$ are relevant.
c.

$$\begin{aligned} y'(x) + f(x)y(x) &= 0 \\ \int \frac{dy(x)}{y(x)} &= -\int f(x)dx \\ y &= y_0 e^{-\int f(x)dx} \ . \end{aligned}$$

1.5.3.3 Ex: Bernoulli's differential equation

Consider the equation,

$$y' = ay + by^\alpha \ ,$$

with $a, b \in \mathbb{R}$, $\alpha \neq 0, 1$ and the initial conditions $x_0 = 0$ and $y_0 = \left(\frac{1-b}{a}\right)^{1/(1-\alpha)}$. Find the solution $y(x)$.
Help: Transform the nonlinear differential equation into a first order linear differential equation by the substitution $y = z^{1/(1-\alpha)}$.

Solution: *With the given substitution we obtain,*

$$\frac{1}{1-\alpha} z^{\alpha/(1-\alpha)} z' = a z^{1/(1-\alpha)} + b z^{\alpha/(1-\alpha)} \ .$$

With that follows,

$$\frac{z'}{1-\alpha} = az + b \quad \Rightarrow \quad z' = (az+b)(1-\alpha) \ .$$

Separation of variables,

$$\begin{aligned} \frac{dz}{az+b} = (1-\alpha)dx \quad &\Rightarrow \quad \int_{z_0}^{z} \frac{d\tilde{z}}{a\tilde{z}+b} = (1-\alpha)\int_{x_0}^{x} d\tilde{x} \\ &\Rightarrow \frac{1}{a}\ln(a\tilde{z}+b)\Big|_{z_0}^{z} = (1-\alpha)(x-x_0) \\ &\Rightarrow \ln(az+b) = \ln(az_0+b) + a(1-\alpha)(x-x_0) \ . \end{aligned}$$

Inserting the initial conditions,

$$\ln(az+b) = a(1-\alpha)x \Rightarrow z(x) = \frac{1}{a}\left[e^{a(1-\alpha)x} - b\right] \ .$$

Finally,

$$y(x) = \left\{\frac{1}{a}\left[e^{a(1-\alpha)x} - b\right]\right\}^{1/(1-\alpha)} \ .$$

1.5.3.4 Ex: Ellipse

An ellipse is the set of all points C satisfying the condition $\overline{AC} + \overline{BC} = 2a$, where the two focal points A and B are at a given distance $2e$.
a. Show that this definition is equivalent to the ellipse equation of the form,

$$\frac{x^2}{a^2} + \frac{y^2}{b^2} = 1 \ ,$$

where a and b are the large and small half-axes. How does e depend on a de b?
b. Show that the ellipse equation is given in plane polar coordinates by,

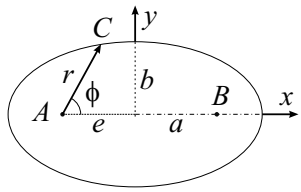

Figure 1.6: Ellipse.

$$r = \frac{P}{1 - \epsilon \cos\phi} \ .$$

Determine the eccentricity ϵ and the parameter P as a function of a and b.

Solution: *a. We have the conditions* $\overline{AC} + \overline{BC} = 2a$, $\overline{AB} = 2e$ *and* $\overline{AC} = r$. *By the Pythagorean theorem we have therefore,*

$$y^2 = \overline{AC}^2 - \left(\tfrac{1}{2}\overline{AB} + x\right)^2 = \overline{BC}^2 - \left(\tfrac{1}{2}\overline{AB} - x\right)^2 \ , \tag{1.14}$$

resp.

$$y^2 = r^2 - (e+x)^2 = (2a - r)^2 - (e - x)^2 \ . \tag{1.15}$$

Solving the second equation (1.15) by r *we obtain,*

$$r = a + e\frac{x}{a} \ . \tag{1.16}$$

Substituting into the first equation (1.15) we obtain,

$$\begin{aligned} y^2 &= \left(a + e\frac{x}{a}\right)^2 - (e+x)^2 \\ &= a^2 - e^2 - x^2 + e^2\frac{x^2}{a^2} \ . \end{aligned} \tag{1.17}$$

For $x = 0$ *holds* $y = b$, *hence,*

$$e^2 = a^2 - b^2 \ . \tag{1.18}$$

Inserting in Eq. (1.17) we finally get the ellipse equation,

$$\frac{x^2}{a^2} + \frac{y^2}{b^2} = 1 \ . \tag{1.19}$$

b. According to the drawing,

$$\begin{aligned} r\sin\phi &= y \\ r\cos\phi &= x + e \ . \end{aligned} \tag{1.20}$$

Inserting into the ellipse equation (1.19) yields,

$$\begin{aligned} \frac{(r\cos\phi - e)^2}{a^2} + \frac{r^2\sin^2\phi}{b^2} &= 1 \\ b^2r^2\cos^2\phi - b^2 2er\cos\phi + b^2e^2 + a^2r^2\sin^2\phi &= a^2b^2 \\ a^2r^2 - 2b^2er\cos\phi - e^2r^2\cos^2\phi &= b^4 \ . \end{aligned} \tag{1.21}$$

Introducing the parameter $P \equiv b^2/a$ and the eccentricity $\epsilon \equiv \sqrt{a^2 - b^2}/a$,

$$r^2 = P^2 + 2P\varepsilon r\cos\phi + \varepsilon^2 r^2\cos^2\phi = (P + \varepsilon r\cos\phi)^2 \ . \tag{1.22}$$

Finally,

$$r = \frac{P}{1 - \varepsilon\cos\phi} \ . \tag{1.23}$$

1.5.3.5 Ex: Binomial- and Poisson distribution

Show that from the binomial distribution,

$$P(n) = \frac{N!}{n!\,(N-n)!}\ p^n\ (1-p)^{N-n} \ .$$

follows the Poisson distribution,

$$P(n) = \frac{\alpha^n}{n!}e^{-\alpha} \qquad \text{with} \quad \alpha \equiv \bar{n} \equiv N\ p \ ,$$

in the limit $p \ll 1$ and $n \ll N$. Use the approximation formulas $\log(1-p) \simeq -p$ and $\frac{N!}{(N-n)!} \simeq N^n$. Can you justify the approximation formulas?

Solution: *The first approximation formula follows the Taylor expansion, the second follows from,*

$$\frac{N!}{(N-n)!} \equiv \prod_{j=0}^{n-1}(N-j) \simeq_{n\ll N} \prod_{j=0}^{n-1} N \equiv N^n \ .$$

Hence, $(1-p)^{N-n} = \exp\left(log(1-p)^{N-n}\right) = \exp(N-n)\log(1-p) \simeq \exp(-N\,p) = \exp(-\alpha)$. For this, $\frac{N!}{(N-n)!}\ p^n \simeq N^n\ p^n = \alpha^n$.

1.5.3.6 Ex: Second order differential equations

Find the general solutions $z(x)$ of the following equations:
a. $7z'' - 2\imath\sqrt{3}z' - 3z = 6$
b. $z'' - 10z' + 9z = 9x$.

Solution: *a. Inserting the ansatz* $z(x) = e^{\lambda x}$ *in the homogeneous differential equation,* $7z'' - 2\imath\sqrt{3}z' - 3z = 0$*, we obtain,*

$$\begin{aligned} 7\lambda^2 e^{\lambda x} - 2\imath\sqrt{3}\lambda e^{\lambda x} - 3e^{\lambda x} &= 0 \\ 7\lambda^2 - 2\imath\sqrt{3}\lambda - 3 &= 0 \ , \end{aligned}$$

and therefore the characteristic polynomial,

$$\lambda_{1,2} = \frac{\imath\sqrt{3}}{7} \pm \sqrt{\frac{-3}{49} + \frac{3}{7}} \ .$$

It is appropriate to search as a particular inhomogeneous solution $z_{inh}(x)$ *of the differential equation* $7z'' - 2\imath\sqrt{3}z' - 3z = 6$ *a function whose first and second derivatives disappear* ($z'' = 0 = z'$)*, that is, a solution of the equation,*

$$-3z_{inh} = 6 \ .$$

We can easily see that

$$z(x) = z_{hmg}(x) + z_{inh}(x) = Ae^{\lambda_1 x} + Be^{\lambda_2 x} - 2$$

solves the inhomogeneous equation.
b. Inserting the ansatz $z(x) = e^{\lambda x}$ *in the homogeneous differential equation,* $z'' - 10z' + 9z = 0$*, we obtain,*

$$\begin{aligned} \lambda^2 e^{\lambda x} - 10\lambda e^{\lambda x} + 9e^{\lambda x} &= 0 \\ \lambda^2 - 10\lambda + 9 &= 0 \ . \end{aligned}$$

and therefore the characteristic polynomial,

$$\lambda_{1,2} = 5 \pm \sqrt{25 - 9} = 1 ou\ 9 \ .$$

As a particular inhomogeneous solution of the differential equation $z'' - 10z' + 9z = 9x$ *we insert a first order polynomial, whose second derivative disappears,* $z_{inh}(x) \equiv x + a$*. Inserting in the differential equation,*

$$\begin{aligned} z''_{inh} - 10z'_{inh} + 9z_{inh} &= 9x \\ -10 + 9(x + a) &= 9x \\ a &= \frac{10}{9} \ . \end{aligned}$$

We can easily see that,

$$z(x) = z_{hmg}(x) + z_{inh}(x) = Ae^{x} + Be^{9x} + x + \frac{10}{9}$$

solves the inhomogeneous equation.

1.5.3.7 Ex: Second order differential equations

Given is a second order linear differential equation with constant coefficients: $z''(x) + \alpha z'(x) + \beta z(x) = f(x)$, where $z,\ f\colon \mathbb{R} \to \mathbb{C}$, $\alpha,\ \beta \in \mathbb{C}$. Show that
a. for the case $f(x) = \gamma x^n$ an ansatz $z_f(x) = \sum_{k=0}^{n} a_k x^k$ solves the inhomogeneous equation, where $\gamma, a_k \in \mathbb{C}$;
b. for the case, that $f(x)$ can be expanded in a Taylor series around the point x_0, the ansatz $z_f(x) = \sum_{k=0}^{\infty} a_k (x - x_0)^k$, $\gamma, a_k \in \mathbb{C}$, solves the inhomogeneous equation. Use linearity and the result of (a).
c. for the case $f(x) = \gamma x^n e^{\delta x}$ an ansatz $z_f(x) = e^{\delta x} \sum_{k=0}^{n} a_k x^k$ solves the inhomogeneous equation, where $\gamma\ ,\ \delta\ ,\ a_k \in \mathbb{C}$.

Solution: *a. Inserting the ansatz in the differential equation we obtain,*

$$\sum_{k=2}^{n} a_k k(k-1) x^{k-2} + \alpha \sum_{k=1}^{n} a_k k x^{k-1} + \beta \sum_{k=0}^{n} a_k x^k = \gamma x^n \ .$$

The terms proportional to x^k must disappear separately, such that the coefficients can be determined iteratively,

$$\begin{aligned} \beta a_n &= \gamma \\ \beta a_{n-1} &= -n\alpha a_n \\ \beta a_k &= -(k+1)\alpha a_{k+1} - (k+2)(k+1) a_{k+2} \ , \end{aligned}$$

for $k = n-2, .., 0$.
b. For each term of the Taylor expansion $\propto x_n$ we can find a solution as done in item (a). Using the linearity it is clear that for the expansion we have as a solution the linear combination of these partial solutions.
c.

1.5.3.8 Ex: Population explosion

Develop a model for population explosion.

Solution: *Discretize,*

$$\begin{aligned} a_k^{60} &= a_{k-1}^{40} - a_{k-1}^{60} \\ a_k^{40} &= a_{k-1}^{20} - a_{k-1}^{40} \\ a_k^{20} &= a_{k-1}^{0} - a_{k-1}^{20} \\ a_k^{0} &= \eta a_k^{20} \ . \end{aligned}$$

Total population,

$$\begin{aligned} \sum_j a_k^j &= \eta a_k^{20} + a_{k-1}^0 - a_{k-1}^{20} + a_{k-1}^{20} - a_{k-1}^{40} + a_{k-1}^{40} - a_{k-1}^{60} \\ &= \eta a_k^{20} + a_{k-1}^0 - a_{k-1}^{60} \ . \end{aligned}$$

Solve numerically

$$\begin{pmatrix} a_k^0 \\ a_k^{20} \\ a_k^{40} \\ a_k^{60} \end{pmatrix} = \begin{pmatrix} \eta & 0 & 0 & 0 \\ 1 & -1 & 0 & 0 \\ 0 & 1 & -1 & 0 \\ 0 & 0 & 1 & -1 \end{pmatrix} \begin{pmatrix} a_{k-1}^0 \\ a_{k-1}^{20} \\ a_{k-1}^{40} \\ a_{k-1}^{60} \end{pmatrix} .$$

1.5.3.9 Ex: Population explosion

Develop a model for the Wuhan virus pandemia.

Solution:

1.6 Vector analysis

1.6.1 Vector algebra

Let us start with a little revision of vector algebra. A vector is a physical quantity composed of a value, a direction and a unit. For example, $\mathbf{v}$ could be the velocity of a body measured in meters per second traveling in northbound direction. Mathematically, vectors form a *vector space*, that is, an algebraic construct characterized by the existence of several operations defined by the following laws.

The addition of vectors is a *commutative* and *associative* operation, that is,

$$\mathbf{a}+\mathbf{b}=\mathbf{b}+\mathbf{a} \quad \text{and} \quad (\mathbf{a}+\mathbf{b})+\mathbf{c}=\mathbf{a}+(\mathbf{b}+\mathbf{c}) \ . \tag{1.24}$$

The multiplication with a scalar is *commutative* and *distributive*,

$$\lambda\mathbf{a}=\mathbf{a}\lambda \quad \text{and} \quad \lambda(\mathbf{a}+\mathbf{b})=\lambda\mathbf{a}+\lambda\mathbf{b} \ . \tag{1.25}$$

The scalar product of two vectors defined by,

$$\boxed{\mathbf{a}\cdot\mathbf{b}\equiv ab\cos\theta} \ , \tag{1.26}$$

where θ is the angle between the two vectors, is *commutative* and *distributive*, but not *associative*,

$$\mathbf{a}\cdot\mathbf{b}=\mathbf{b}\cdot\mathbf{a} \quad \text{and} \quad \mathbf{a}\cdot(\mathbf{b}+\mathbf{c})=\mathbf{a}\cdot\mathbf{b}+\mathbf{a}\cdot\mathbf{c} \quad \text{and} \quad (\mathbf{a}\cdot\mathbf{b})\mathbf{b}\neq\mathbf{a}(\mathbf{b}\cdot\mathbf{c}) \ . \tag{1.27}$$

Finally, the vector product defined by,

$$\boxed{\mathbf{a}\times\mathbf{b}\equiv ab\hat{\mathbf{e}}_n\sin\theta} \ , \tag{1.28}$$

where θ is the angle between the two vectors and $\hat{\mathbf{e}}_n$ a unit vector pointing in the direction perpendicular to $\mathbf{a}$ and $\mathbf{b}$, is *distributive*, but neither *commutative* nor *associative*,

$$\begin{aligned} \mathbf{a}\times\mathbf{b}=-\mathbf{b}\times\mathbf{a}\neq\mathbf{b}\times\mathbf{a} \quad &\text{and} \quad \mathbf{a}\times(\mathbf{b}+\mathbf{c})=\mathbf{a}\times\mathbf{b}+\mathbf{a}\times\mathbf{c} \\ &\text{and} \quad (\mathbf{a}\times\mathbf{b})\times\mathbf{c}\neq\mathbf{a}\times(\mathbf{b}\times\mathbf{c}) \ . \end{aligned} \tag{1.29}$$

Once we have chosen a basis, that is, a set of three linearly independent vectors, we can also express the vectors in terms of their components in this basis. The most common basis is the Cartesian coordinate system characterized by three fixed and orthogonal vectors, $\hat{\mathbf{e}}_x$, $\hat{\mathbf{e}}_y$, and $\hat{\mathbf{e}}_z$, such that each vector can be decomposed as,

$$\mathbf{a} = a_x\hat{\mathbf{e}}_x + a_y\hat{\mathbf{e}}_y + a_z\hat{\mathbf{e}}_z \ . \tag{1.30}$$

In this representation the operations on the vector space defined above read,

$$\begin{aligned} \mathbf{a}+\mathbf{b} &= (a_x+b_x)\hat{\mathbf{e}}_x + (a_y+b_y)\hat{\mathbf{e}}_y + (a_z+b_z)\hat{\mathbf{e}}_z \\ \lambda\mathbf{a} &= \lambda a_x\hat{\mathbf{e}}_x + \lambda a_y\hat{\mathbf{e}}_y + \lambda a_z\hat{\mathbf{e}}_z \\ \mathbf{a}\cdot\mathbf{b} &= a_xb_x + a_yb_y + a_zb_z \\ \mathbf{a}\times\mathbf{b} &= \begin{pmatrix} a_yb_z - a_zb_y \\ a_zb_x - a_xb_z \\ a_xb_y - a_yb_z \end{pmatrix} \ . \end{aligned} \tag{1.31}$$

Combinations of scalar and vector products can be used to calculate other geometric quantities. An example is the *scalar triple product* defined by $\mathbf{a}\cdot(\mathbf{b}\times\mathbf{c})$ and satisfying the following permutation rules,

$$\mathbf{a}\cdot(\mathbf{b}\times\mathbf{c}) = \mathbf{c}\cdot(\mathbf{a}\times\mathbf{b}) = -\mathbf{c}\cdot(\mathbf{b}\times\mathbf{a}) = (\mathbf{a}\times\mathbf{b})\cdot\mathbf{c} \ . \tag{1.32}$$

Its absolute value $|\mathbf{a}\cdot(\mathbf{b}\times\mathbf{c})|$ has the meaning of the volume of the parallelepiped spanned by the three vectors. The *vector triple product* defined by $\mathbf{a}\times(\mathbf{b}\times\mathbf{c})$ can be simplified,

$$\mathbf{a}\times(\mathbf{b}\times\mathbf{c}) = \mathbf{b}(\mathbf{a}\cdot\mathbf{c}) - \mathbf{c}(\mathbf{a}\cdot\mathbf{b}) \ . \tag{1.33}$$

We verify the commutativity and the distributivity of the scalar and vector triple products in Exc. 1.6.3.1, and we train them more in Excs. 1.6.3.2 to 1.6.3.4.

1.6.2 Transformation of vectors

Of course, the definition of the vector as quantity characterized by a magnitude and a direction is unequivocal, for example, the speed $\mathbf{v}$ of a car on a road. Nevertheless, the representation of the vector depends on the orientation of the Cartesian coordinate system, which is totally arbitrary. For example, a vector given by $\mathbf{r} = x\hat{\mathbf{e}}_x + y\hat{\mathbf{e}}_r + z\hat{\mathbf{e}}_z$ in one system will be described by $\mathbf{r} = x'\hat{\mathbf{e}}'_x + y'\hat{\mathbf{e}}'_y + z'\hat{\mathbf{e}}'_z$ in another system.

The behavior of vectors under transformations of coordinate systems is a very important characteristic of physical quantities and of theories governing their dynamics. For example, while classical mechanics is defined by the Galilei transform, relativistic mechanics is defined by the Lorentz transform, and we will see later that electrodynamics is incompatible with the Galilei transform. In Excs. 1.6.3.5 to 1.6.3.12 we practice the calculus with rotation matrices [7].

There are basically two things that can be done with vectors in space: *translations* and *rotations*. Both will be discussed in the following.

[7] Note that the procedure is different from the one used in quantum mechanics, where any transformation needs to be described by unitary operations.

1.6.2.1 Translations

Translations are simply performed by adding a vector to all position vectors,

$$\mathbf{r}' = \mathcal{T}_{tr}\mathbf{r} = \mathbf{r} + \mathbf{a} \ . \tag{1.34}$$

1.6.2.2 Rotations

If the two systems are simply rotated with respect to each other, we have [8],

$$\mathbf{r}' = \begin{pmatrix} x' \\ y' \\ z' \end{pmatrix} = \mathcal{T}_{rt}\mathbf{r} = \begin{pmatrix} R_{xx} & R_{xy} & R_{xz} \\ R_{yx} & R_{yy} & R_{yz} \\ R_{zx} & R_{zy} & R_{zz} \end{pmatrix} \begin{pmatrix} x \\ y \\ z \end{pmatrix} = \mathcal{R}\mathbf{r} \ , \tag{1.35}$$

or [9],

$$\boxed{r'_k = \sum_l R_{kl} r_l} \ . \tag{1.36}$$

Example 1 (*Rotation about the z-axis*): For example, for a rotation around the z-axis by an angle of ϕ we get,

$$\begin{pmatrix} x' \\ y' \\ z' \end{pmatrix} = \begin{pmatrix} \cos\phi & \sin\phi & 0 \\ -\sin\phi & \cos\phi & 0 \\ 0 & 0 & 1 \end{pmatrix} \begin{pmatrix} x \\ y \\ z \end{pmatrix} \ .$$

Rotation matrices $\mathcal{R}$ must satisfy the following requirements:

- The transformation preserves the lengths and orientations of vectors and the angles between vectors. That is, the scalar product satisfies $\mathcal{R}\mathbf{r}_2 \cdot \mathcal{R}\mathbf{r}_2 = \mathbf{r}_1 \cdot \mathbf{r}_2$.
- The transformation is orthogonal, $\mathcal{R}^{-1} = \mathcal{R}^\dagger$, and unitary, $\det \mathcal{R} = 1$.

1.6.3 Exercises

1.6.3.1 Ex: Vector algebra

a. Show that scalar and vector products are distributive.
b. Find out whether the vector product is associative.

Solution: *a. Distributivity of the scalar product,*

$$\mathbf{a} \cdot (\mathbf{b} + \mathbf{c}) = ... = \mathbf{a} \cdot \mathbf{b} + \mathbf{a} \cdot \mathbf{c}$$

Distributivity of the vector product,

$$\mathbf{a} \times (\mathbf{b} + \mathbf{c}) = ... = \mathbf{a} \times \mathbf{b} + \mathbf{a} \times \mathbf{c}$$

[8] By $\mathcal{T}$ we denote operations or prescriptions, while $\mathcal{R}$ is a rotation matrix.
[9] We note here that a tensor of two dimensions transforms like,

$$T'_{kl} = \sum_{l,k} R_{km} R_{ln} T_{mn} \ .$$

b. Associativity of the vector product,

$$\mathbf{a} \times (\mathbf{b} \times \mathbf{c}) = ... = (\mathbf{a} \times \mathbf{b}) \times \mathbf{c} \ .$$

1.6.3.2 Ex: Vector algebra

a. Consider a unit cube with one corner fixed at the origin and generated by the vectors, $\mathbf{a} = (1, 0, 0)$, $\mathbf{b} = (0, 1, 0)$ and $\mathbf{c} = (0, 0, 1)$. Determine the angle between the diagonals passing through the center of the cube.
b. Consider the plane containing the points $\mathbf{a}$, $\mathbf{b}$, and $\mathbf{c}$ giving in (a). Use the vector product to calculate the normal vector of this plane.

Solution: *a. We choose the diagonals* $\mathbf{d}_1 = (1, 1, 1) - (0, 0, 0)$ *and* $\mathbf{d}_2 = (1, 0, 0) - (0, 1, 1)$ *and we get the scalar product,*

$$\mathbf{d}_1 \cdot \mathbf{d}_2 = -1 = d_1 d_2 \cos\theta \ .$$

With $d_1 = d_2 = \sqrt{3}$*, we find* $\theta = 109.47°$*.*
b. We choose two vectors of the plane, $\mathbf{d}_1 = \mathbf{a} - \mathbf{b}$ *and* $\mathbf{d}_2 = \mathbf{a} - \mathbf{c}$ *and we calculate the vector product,*

$$\mathbf{d}_1 \times \mathbf{d}_2 = (\mathbf{a} - \mathbf{b}) \times (\mathbf{a} - \mathbf{c}) = \begin{pmatrix} 1 \\ -1 \\ 0 \end{pmatrix} \times \begin{pmatrix} 1 \\ 0 \\ -1 \end{pmatrix} = \begin{pmatrix} 1 \\ 1 \\ 1 \end{pmatrix} \ .$$

1.6.3.3 Ex: Vector algebra

a. Prove the rule $\mathbf{a} \times (\mathbf{b} \times \mathbf{c}) = \mathbf{b}(\mathbf{a} \cdot \mathbf{c}) - \mathbf{c}(\mathbf{a} \cdot \mathbf{b})$ writing both sides in component form.
b. Prove $\mathbf{a} \times (\mathbf{b} \times \mathbf{c}) + \mathbf{b} \times (\mathbf{c} \times \mathbf{a}) + \mathbf{c} \times (\mathbf{a} \times \mathbf{b})$. Under what conditions holds $\mathbf{a} \times (\mathbf{b} \times \mathbf{c}) = (\mathbf{a} \times \mathbf{b}) \times \mathbf{c}$?

Solution: *a.*
b. Obviously when $\mathbf{a} = \mathbf{c}$*, since,*

$$\mathbf{a} \times (\mathbf{b} \times \mathbf{a}) = -(\mathbf{b} \times \mathbf{a}) \times \mathbf{a} = (\mathbf{a} \times \mathbf{b}) \times \mathbf{a} \ .$$

1.6.3.4 Ex: Vector algebra

a. Two vectors point from the origin to points $\mathbf{r} = (2, 8, 7)$ and $\mathbf{r}' = (4, 6, 8)$. Determine the distance between the points.

Solution: *The distance is,* $|\mathbf{r} - \mathbf{r}'| = \sqrt{(2-4)^2 + (8-6)^2 + (7-8)^2} = 3$.

1.6.3.5 Ex: Rotation of the coordinate system

a. Show that the two-dimensional rotation matrix

$$\begin{pmatrix} \cos\phi & \sin\phi \\ -\sin\phi & \cos\phi \end{pmatrix}$$

preserves the scalar product, that is, $a'_x b'_x + a'_y b'_y = a_x b_x + a_y b_y$.
b. What are the constraints for the elements R_{ij} of the three-dimensional rotation matrix to preserve the length of an arbitrary vector under transformation?

Solution: *a. We have*

$$\begin{aligned} \mathbf{a}' \cdot \mathbf{b}' &= \begin{pmatrix} \cos & \sin \\ -\sin & \cos \end{pmatrix} \begin{pmatrix} a_x \\ a_y \end{pmatrix} \begin{pmatrix} \cos & \sin \\ -\sin & \cos \end{pmatrix} \begin{pmatrix} b_x \\ b_y \end{pmatrix} \\ &= \begin{pmatrix} a_x \cos + a_y \sin \\ -a_x \sin + a_y \cos \end{pmatrix} \begin{pmatrix} b_x \cos + b_y \sin \\ -b_x \sin + b_y \cos \end{pmatrix} = \ldots = a_x b_x + a_y b_y \ . \end{aligned}$$

b. First we consider a two-dimensional matrix. As the condition,

$$a'^2_x + a'^2_y = (R_{xx} a_x + R_{xy} a_y)^2 + (R_{yx} a_x + R_{yy} a_y)^2 = a_x^2 + a_y^2$$

needs to be satisfied for all a_x and a_y, the terms proportional to a_x^2, a_y^2 and $a_x a_y$ must zero separately:

$$\begin{aligned} a_x^2 &\longmapsto R_{xx}^2 + R_{yx}^2 = 1 \\ a_y^2 &\longmapsto R_{xy}^2 + R_{yy}^2 = 1 \\ a_x a_y &\longmapsto R_{xx} R_{xy} + R_{yx} R_{yy} = 0 \ , \end{aligned}$$

what is satisfied by $R_{xx} = R_{yy} = \cos\phi$ and $R_{xy} = -R_{yx} = \sin\phi$. In three dimensions,

$(R_{xx} a_x + R_{xy} a_y + R_{xz} a_z)^2 + (R_{yx} a_x + R_{yy} a_y + R_{yz} a_z)^2 + (R_{zx} a_x + R_{zy} a_y + R_{zz} a_z)^2$
$= a_x^2 + a_y^2 + a_z^2$

gives,

$$\begin{aligned} a_x^2 &\longmapsto R_{xx}^2 + R_{yx}^2 + R_{zx}^2 = 1 = \sum_k R_{kx} \\ a_y^2 &\longmapsto R_{xy}^2 + R_{yy}^2 + R_{zy}^2 = 1 = \sum_k R_{ky} \\ a_z^2 &\longmapsto R_{xz}^2 + R_{yz}^2 + R_{zz}^2 = 1 = \sum_k R_{kz} \\ a_x a_y &\longmapsto R_{xx} R_{xy} + R_{yx} R_{yy} + R_{zx} R_{zy} = 0 = \sum_k R_{kx} R_{ky} \\ a_x a_z &\longmapsto R_{xx} R_{xz} + R_{yx} R_{yz} + R_{zx} R_{zz} = 0 = \sum_k R_{kx} R_{kz} \\ a_y a_z &\longmapsto R_{xy} R_{xz} + R_{yy} R_{yz} + R_{zy} R_{zz} = 0 = \sum_k R_{ky} R_{kz} \ . \end{aligned}$$

1.6.3.6 Ex: Rotation of the coordinate system

Find the matrix describing a rotation of 120° around the axis $\vec{\omega} = (1,1,1)$.

Solution: *Two procedures are possible. The first is to satisfy the conditions for R to be a rotation matrix, as shown in Exc. 1.6.3.5, and impose the additional conditions that $\omega = (1,1,1)$ stays still and that any vector orthogonal to ω, for exemple, $a = (1,-1,0)$ makes a rotation of 120°,*

$$\begin{pmatrix} R_{xx} & R_{xy} & R_{xz} \\ R_{yx} & R_{yy} & R_{yz} \\ R_{zx} & R_{zy} & R_{zz} \end{pmatrix} \begin{pmatrix} 1 \\ 1 \\ 1 \end{pmatrix} = \begin{pmatrix} R_{xx}+R_{xy}+R_{xz} \\ R_{yx}+R_{yy}+R_{yz} \\ R_{zx}+R_{zy}+R_{zz} \end{pmatrix} = \begin{pmatrix} 1 \\ 1 \\ 1 \end{pmatrix} .$$

The second procedure is to rotate the axis $\omega = (1,1,1)$ towards $\hat{\mathbf{e}}_z$ using rotations around the $\hat{\mathbf{e}}_z$ and then $\hat{\mathbf{e}}_y$-axes, to apply the desired rotation of 120°, and finally come back. With MAPLE it is easy to verify that the matrix,

$$M = \begin{pmatrix} \cos(-\phi) & \sin(-\phi) & 0 \\ -\sin(-\phi) & \cos(-\phi) & 0 \\ 0 & 0 & 1 \end{pmatrix} \begin{pmatrix} \cos(-\alpha) & 0 & \sin(-\alpha) \\ 0 & 1 & 0 \\ -\sin(-\alpha) & 0 & \cos(-\alpha) \end{pmatrix} \begin{pmatrix} \cos\beta & \sin\beta & 0 \\ -\sin\beta & \cos\beta & 0 \\ 0 & 1 & \end{pmatrix} \begin{pmatrix} \cos\alpha & 0 & \sin\alpha \\ 0 & 1 & 0 \\ -\sin\alpha & 0 & \cos\alpha \end{pmatrix} \begin{pmatrix} \cos\phi & \sin\phi & 0 \\ -\sin\phi & \cos\phi & 0 \\ 0 & 0 & 1 \end{pmatrix}$$

with $\phi = \frac{\pi}{4}$ and $\alpha = \arctan\frac{1}{\sqrt{2}}$ meets the requirement,

$$\begin{pmatrix} 1 \\ 1 \\ 1 \end{pmatrix} = M \begin{pmatrix} 1 \\ 1 \\ 1 \end{pmatrix} .$$

Calculating the sinus and cosinus of the angles, including the angle $\beta = \frac{2\pi}{3}$,

$$\begin{aligned} &\cos\phi = \cos\tfrac{\pi}{4} = \sqrt{\tfrac{1}{2}} = \sin\phi \\ &\cos\alpha = \cos\arctan\sqrt{\tfrac{1}{2}} = \cos\arcsin\sqrt{\tfrac{1}{3}} = \sqrt{\tfrac{1}{3}} \quad , \quad \sin\alpha = \sqrt{\tfrac{2}{3}} \\ &\cos\beta = \cos\tfrac{2\pi}{3} = -\tfrac{1}{2} \quad , \quad \sin\beta = \tfrac{\sqrt{3}}{2} . \end{aligned}$$

With these angles we find the rotation matrix about an axis ω,

$$M = \begin{pmatrix} \frac{1}{3}+\frac{2}{3}\cos\beta & \frac{1}{3}+\frac{1}{3}\sqrt{3}\sin\beta-\frac{1}{3}\cos\beta & \frac{1}{3}-\frac{1}{3}\sqrt{3}\sin\beta-\frac{1}{3}\cos\beta \\ \frac{1}{3}-\frac{1}{3}\sqrt{3}\sin\beta-\frac{1}{3}\cos\beta & \frac{1}{3}+\frac{2}{3}\cos\beta & \frac{1}{3}+\frac{1}{3}\sqrt{3}\sin\beta-\frac{1}{3}\cos\beta \\ \frac{1}{3}+\frac{1}{3}\sqrt{3}\sin\beta-\frac{1}{3}\cos\beta & \frac{1}{3}-\frac{1}{3}\sqrt{3}\sin\beta-\frac{1}{3}\cos\beta & \frac{1}{3}+\frac{2}{3}\cos\beta \end{pmatrix} = \begin{pmatrix} 0 & 1 & 0 \\ 0 & 0 & 1 \\ 1 & 0 & 0 \end{pmatrix} .$$

A third procedure is to define a coordinate system with z as the axis of rotation, for example,

$$\mathbf{a} = \tfrac{1}{2}(1,-1,0) \quad , \quad \mathbf{b} = \tfrac{1}{6}(1,1,-2) \quad , \quad \omega = \tfrac{1}{3}(1,1,1) ,$$

checking that $\mathbf{a}\times\mathbf{b} = \vec{\omega}$. The transformation matrix between these coordinate systems is,

$$\mathcal{R}_t = \begin{pmatrix} \hat{\mathbf{e}}_x\cdot\mathbf{a} & \hat{\mathbf{e}}_x\cdot\mathbf{b} & \hat{\mathbf{e}}_x\cdot\vec{\omega} \\ \hat{\mathbf{e}}_y\cdot\mathbf{a} & \hat{\mathbf{e}}_y\cdot\mathbf{b} & \hat{\mathbf{e}}_y\cdot\vec{\omega} \\ \hat{\mathbf{e}}_z\cdot\mathbf{a} & \hat{\mathbf{e}}_z\cdot\mathbf{b} & \hat{\mathbf{e}}_z\cdot\vec{\omega} \end{pmatrix} .$$

Now just concatenate these arrays.

1.6.3.7 Ex: Rotation of the coordinate system

Consider the transformation that corresponds to an inversion of the components of the vector $\mathbf{r} \longrightarrow -\mathbf{r}$ and find out, how the vector product and the triple scalar product transform under inversion.

Solution: *The vector product transform as,*

$$(-\mathbf{r}_1) \times (-\mathbf{r}_2) = \mathbf{r}_1 \times \mathbf{r}_2 \ .$$

That is, the resulting vector is not inverted. *Therefore, it is also called* pseudo-vector. *Examples are torque* $\mathbf{r} \times \mathbf{P}$ *and the Lorentz force* $e\mathbf{v} \times \mathbf{B}$. *The triple scalar product becomes,*

$$(-\mathbf{r}_1) \cdot [(-\mathbf{r}_2) \times (-\mathbf{r}_3)] = -\mathbf{r}_1 \cdot (\mathbf{r}_2 \times \mathbf{r}_3) \ .$$

That is, the resulting scalar is inverted. *This is why it is also called* pseudo-scalar.

1.6.3.8 Ex: Rotation matrices

Show that the scalar product $\mathbf{a} \cdot \mathbf{b}$ and the angle α between the two vectors are preserved when we rotate the two vectors by an angle θ around any axis.

Solution: *Treating the two vectors as matrices,* $\mathbf{a} = A$ *and* $\mathbf{b} = B$, *we write the scalar product as,* $\mathbf{a} \cdot \mathbf{b} = A^\dagger B$. *Now, since the rotation matrix must satisfy,* $\mathcal{R}^\dagger = \mathcal{R}^{-1}$,

$$A^\dagger \cdot B = A^\dagger \mathcal{R}^\dagger \mathcal{R} B = (\mathcal{R}A)^\dagger \mathcal{R} B \ .$$

Alternative solution: *We chose the orthonormal base in such a way that an arbitrary* rotation *be described as a rotation around the axis. z:*

$$\mathcal{R} = \begin{pmatrix} \cos\theta & \sin\theta & 0 \\ -\sin\theta & \cos\theta & 0 \\ 0 & 0 & 1 \end{pmatrix} \ .$$

Thereby,

$$\begin{aligned} \mathcal{R}\mathbf{a} \cdot \mathcal{R}\mathbf{b} &= \left[\begin{pmatrix} \cos\theta & \sin\theta & 0 \\ -\sin\theta & \cos\theta & 0 \\ 0 & 0 & 1 \end{pmatrix} \begin{pmatrix} a_1 \\ a_2 \\ a_3 \end{pmatrix} \right]^t \begin{pmatrix} \cos\theta & \sin\theta & 0 \\ -\sin\theta & \cos\theta & 0 \\ 0 & 0 & 1 \end{pmatrix} \begin{pmatrix} b_1 \\ b_2 \\ b_3 \end{pmatrix} \\ &= (a_1 \cos\theta + a_2 \sin\theta)(b_1 \cos\theta + b_2 \sin\theta) \\ &\quad + (-a_1 \sin\theta + a_2 \cos\theta)(-b_1 \sin\theta + b_2 \cos\theta) + a_3 b_3 \\ &= a_1 b_1 + a_2 b_2 + a_3 b_3 = \mathbf{a} \cdot \mathbf{b} \ . \end{aligned}$$

The absolute value is,

$$\begin{aligned} |\mathcal{R}\mathbf{a}| &= \left\| \begin{pmatrix} \cos\theta & \sin\theta & 0 \\ -\sin\theta & \cos\theta & 0 \\ 0 & 0 & 1 \end{pmatrix} \begin{pmatrix} a_1 \\ a_2 \\ a_3 \end{pmatrix} \right\| \\ &= \sqrt{|a_1 \cos\theta + a_2 \sin\theta|^2 + |-a_1 \sin\theta + a_2 \cos\theta|^2 + |a_3|^2} = \sqrt{(a_2^2 + a_1^2 + a_3^2)} = |\mathbf{a}| \ . \end{aligned}$$

The angle should be maintained as,

$$|\mathcal{R}\mathbf{a}|^2 \cos\alpha = \mathcal{R}\mathbf{a}\cdot\mathcal{R}\mathbf{a} = \mathbf{a}\cdot\mathbf{a} = |\mathbf{a}|^2\cos\alpha \ .$$

1.6.3.9 Ex: Rotation matrices

Consider the matrix,

$$\mathcal{R} = \frac{1}{2}\begin{pmatrix} \sqrt{2} & \sqrt{2} & 0 \\ -1 & 1 & \sqrt{2} \\ 1 & -1 & \sqrt{2} \end{pmatrix} \ .$$

a. Show that $\mathcal{R}$ is a rotation matrix.
b. Determine the axis of rotation.
Help: The rotation axis $\mathbf{a}$ stays invariant under rotation: $\mathcal{R}\mathbf{a} = \mathbf{a}$. Use this condition.
c. Determine the rotation angle.
Help: Consider for this a vector that is perpendicular to $\mathbf{a}$.

Solution: *a. Rotation matrices are unitary operations maintaining orientation, i.e.,* $\det\mathcal{R} = +1$ *and* $\mathcal{R}^T\mathcal{R} = 1$,

$$\det\mathcal{R} = \frac{1}{2^3}\det\begin{pmatrix} \sqrt{2} & \sqrt{2} & 0 \\ -1 & 1 & \sqrt{2} \\ 1 & -1 & \sqrt{2} \end{pmatrix} = 1$$

$$\mathcal{R}^T\mathcal{R} = \frac{1}{2^2}\begin{pmatrix} \sqrt{2} & -1 & 1 \\ \sqrt{2} & 1 & -1 \\ 0 & \sqrt{2} & \sqrt{2} \end{pmatrix}\begin{pmatrix} \sqrt{2} & \sqrt{2} & 0 \\ -1 & 1 & \sqrt{2} \\ 1 & -1 & \sqrt{2} \end{pmatrix} = 1 \ .$$

b. We have,

$$\mathcal{R}\mathbf{a} = \frac{1}{2}\begin{pmatrix} \sqrt{2} & \sqrt{2} & 0 \\ -1 & 1 & \sqrt{2} \\ 1 & -1 & \sqrt{2} \end{pmatrix}\begin{pmatrix} x \\ y \\ z \end{pmatrix} = \begin{pmatrix} \frac{1}{2}\sqrt{2}x + \frac{1}{2}\sqrt{2}y \\ -\frac{1}{2}x + \frac{1}{2}y + \frac{1}{2}\sqrt{2}z \\ \frac{1}{2}x - \frac{1}{2}y + \frac{1}{2}\sqrt{2}z \end{pmatrix} = \begin{pmatrix} x \\ y \\ z \end{pmatrix} = \mathbf{a} \ .$$

The resolution of the system of linear equations gives $y = (\sqrt{2}-1)x$ *and* $z = x$. *The axis of rotation, i.e.* the eigenvector of the rotation *is* $\mathbf{a} = \frac{1}{\sqrt{5-2\sqrt{2}}}\begin{pmatrix} 1 \\ \sqrt{2}-1 \\ 1 \end{pmatrix}$.

c. We choose a test vector $\mathbf{b}$ *perpendicular to* $\mathbf{a}$. *E.g.* $\mathbf{b} = \begin{pmatrix} 2 \\ 0 \\ -2 \end{pmatrix}$. *The rotation* $\mathcal{R}$

applied to $\mathbf{b}$ *gives,* $\mathbf{c} = \mathcal{R}\mathbf{b} \begin{pmatrix} \sqrt{2} \\ -1-\sqrt{2} \\ 1-\sqrt{2} \end{pmatrix}$,

$$|\mathbf{c}| = |\mathbf{b}| = \sqrt{8}$$
$$\mathbf{bc} = 4\sqrt{2} - 2 = |\mathbf{b}||\mathbf{c}| \cos\alpha = 8\cos\alpha \ .$$

with that, follow, $\cos\alpha = \frac{1}{\sqrt{2}} - \frac{1}{4} \simeq 0.4571$. *Therefore, the rotation angle is* $\alpha \simeq 62.8°$.

1.6.3.10 Ex: Rotation matrices

A rotation by an angle ϕ around the z-axis is described by the rotation matrix $\mathcal{R}_z(\phi)$ with,

$$\mathcal{R}_z(\phi) = \begin{pmatrix} \cos\phi & \sin\phi & 0 \\ -\sin\phi & \cos\phi & 0 \\ 0 & 0 & 1 \end{pmatrix} \ .$$

a. Show by an explicit calculation that inverse matrix satisfies, $\mathcal{R}_z^{-1}(\phi) = \mathcal{R}_z(-\phi) = \mathcal{R}_z^t(\phi)$.
b. Show, $\mathcal{R}_z(\phi_1)\mathcal{R}_z(\phi_2) = \mathcal{R}_z(\phi_1+\phi_2) = \mathcal{R}_z(\phi_2)\mathcal{R}_z(\phi_1)$.
c. Show, $[\mathcal{R}_z(\phi_1)\mathcal{R}_z(\phi_2)]^t = \mathcal{R}_z^t(\phi_2)\mathcal{R}_z^t(\phi_1)$.

Solution: *a. Rotation matrices are unitary. Therefore, the inverse matrix is equal to the transposed matrix. The transposed matrix is easily obtained by inversion of the sign of the angle* ϕ.
b. This can be done with MAPLE. We find that,

$$\begin{aligned} \mathcal{R}_z(\phi_1)\mathcal{R}z(\phi_2) &= \begin{pmatrix} \cos\phi_1 & \sin\phi_1 & 0 \\ -\sin\phi_1 & \cos\phi_1 & 0 \\ 0 & 0 & 1 \end{pmatrix} \begin{pmatrix} \cos\phi_2 & \sin\phi_2 & 0 \\ -\sin\phi_2 & \cos\phi_2 & 0 \\ 0 & 0 & 1 \end{pmatrix} \\ &= \begin{pmatrix} \cos\phi_1\cos\phi_2 - \sin\phi_1\sin\phi_2 & \cos\phi_1\sin\phi_2 + \sin\phi_1\cos\phi_2 & 0 \\ -\sin\phi_1\cos\phi_2 - \cos\phi_1\sin\phi_2 & \cos\phi_1\cos\phi_2 - \sin\phi_1\sin\phi_2 & 0 \\ 0 & 0 & 1 \end{pmatrix} \\ &= \begin{pmatrix} \cos(\phi_1+\phi_2) & \sin(\phi_1+\phi_2) & 0 \\ -\sin(\phi_1+\phi_2) & \cos(\phi_1+\phi_2) & 0 \\ 0 & 0 & 1 \end{pmatrix} = \mathcal{R}_z(\phi_1+\phi_2) = \mathcal{R}_z(\phi_2)\mathcal{R}_z(\phi_1) \ . \end{aligned}$$

1.6.3.11 Ex: Rotation matrices

a. Be given the basis $(\hat{\mathbf{e}}_x, \hat{\mathbf{e}}_y, \hat{\mathbf{e}}_z)$ in Cartesian coordinates. Determine the transformation matrices for cylindrical basis $(\hat{\mathbf{e}}_\rho, \hat{\mathbf{e}}_\varphi, \hat{\mathbf{e}}_z)$ and the spherical basis $(\hat{\mathbf{e}}_r, \hat{\mathbf{e}}_\theta, \hat{\mathbf{e}}_\varphi)$ and their inverse matrices.

b. For both cases transform the force fields,

$$\mathbf{F}_1 = -\kappa \begin{pmatrix} x \\ y \\ z \end{pmatrix} \qquad \mathbf{F}_2 = \gamma \begin{pmatrix} y \\ -x \\ 0 \end{pmatrix} \qquad \mathbf{F}_3 = \delta \begin{pmatrix} -\frac{xz}{\sqrt{x^2+y^2}} \\ -\frac{y\ z}{\sqrt{x^2+y^2}} \\ \sqrt{x^2+y^2} \end{pmatrix} .$$

c. Show generally that for rotation matrices, the vectors that correspond to the columns of the matrices are mutually orthogonal. The same holds for rows of the matrices. Use the relationship, $A^t A = A A^t = 1$.

Solution: *a. The matrices consisting of the basis vectors are in Cartesian coordinates,*

$$\mathcal{R}_{ka} = \begin{pmatrix} \hat{\mathbf{e}}_x, & \hat{\mathbf{e}}_y, & \hat{\mathbf{e}}_z \end{pmatrix} = \begin{pmatrix} 1 & 0 & 0 \\ 0 & 1 & 0 \\ 0 & 0 & 1 \end{pmatrix} ,$$

in cylindrical coordinates,

$$\begin{aligned} \mathbf{r}_{zy} &= \begin{pmatrix} \hat{\mathbf{e}}_\rho, & \hat{\mathbf{e}}_\phi, & \hat{\mathbf{e}}_z \end{pmatrix} \\ &= \begin{pmatrix} \hat{\mathbf{e}}_x \cos\phi + \hat{\mathbf{e}}_y \sin\phi, & -\hat{\mathbf{e}}_x \sin\phi + \hat{\mathbf{e}}_y \cos\phi, & \hat{\mathbf{e}}_z \end{pmatrix} = \begin{pmatrix} \cos\phi & -\sin\phi & 0 \\ \sin\phi & \cos\phi & 0 \\ 0 & 0 & 1 \end{pmatrix} , \end{aligned}$$

and in spherical coordinates,

$$\begin{aligned} \mathcal{R}_{ku} &= \begin{pmatrix} \hat{\mathbf{e}}_r, & \hat{\mathbf{e}}_\theta, & \hat{\mathbf{e}}_\phi \end{pmatrix} \\ &= \begin{pmatrix} \hat{\mathbf{e}}_x \sin\theta\cos\phi + \hat{\mathbf{e}}_y \sin\theta\sin\phi + \hat{\mathbf{e}}_z \cos\theta \\ \hat{\mathbf{e}}_x \cos\theta\cos\phi + \hat{\mathbf{e}}_y \cos\theta\sin\phi - \hat{\mathbf{e}}_z \sin\theta \\ -\hat{\mathbf{e}}_x \sin\theta + \hat{\mathbf{e}}_y \cos\theta \end{pmatrix}^T \\ &= \begin{pmatrix} \sin\theta\cos\phi & \cos\theta\cos\phi & -\sin\theta \\ \sin\theta\sin\phi & \cos\theta\sin\phi & \cos\theta \\ \cos\theta & -\sin\theta & 0 \end{pmatrix} \end{aligned}$$

they are precisely the transformation matrices. Inverse transformations simply follow as transpositions of unitary matrices, $\mathcal{R}^{-1} = \mathcal{R}^T$.
b. Transforming force fields is easy with MAPLE.
c. The condition for a rotation matrix is,

$$1 = \mathcal{R}^T\mathcal{R} = \begin{pmatrix} a & b & c \\ d & f & g \\ h & k & l \end{pmatrix}^T \begin{pmatrix} a & b & c \\ d & f & g \\ h & k & l \end{pmatrix} = \begin{pmatrix} a^2+d^2+h^2 & ab+df+hk & ac+dg+hl \\ ab+df+hk & b^2+f^2+k^2 & bc+fg+kl \\ ac+dg+hl & bc+fg+kl & c^2+g^2+l^2 \end{pmatrix} .$$

That is, equivalent to the requirement, that the column vectors are mutually orthogonal,

$$\begin{pmatrix} a \\ d \\ h \end{pmatrix} \begin{pmatrix} b \\ f \\ k \end{pmatrix} = \begin{pmatrix} a \\ d \\ h \end{pmatrix} \begin{pmatrix} c \\ g \\ l \end{pmatrix} = \begin{pmatrix} b \\ f \\ k \end{pmatrix} \begin{pmatrix} c \\ g \\ l \end{pmatrix} = 0 .$$

1.6.3.12 Ex: Rotation of the coordinate system

Here, we want to rotate a rod around several axes and determine, whether its final orientation depends on the rotation path. We know that the matrix

$$\mathcal{R}_z(\alpha) = \begin{pmatrix} \cos\alpha & \sin\alpha & 0 \\ -\sin\alpha & \cos\alpha & 0 \\ 0 & 0 & 1 \end{pmatrix}$$

describes the transformation of a vector under rotation of the coordinate system by an angle α around the axis z.
a. Show that corresponding rotations around the x-axis, respectively, the y-axis are given by,

$$\mathcal{R}_x(\alpha) = \begin{pmatrix} 1 & 0 & 0 \\ 0 & \cos\alpha & \sin\alpha \\ 0 & -\sin\alpha & \cos\alpha \end{pmatrix} \quad , \quad \mathcal{R}_y(\alpha) = \begin{pmatrix} \cos\alpha & 0 & -\sin\alpha \\ 0 & 1 & 0 \\ \sin\alpha & 0 & \cos\alpha \end{pmatrix} .$$

b. Show that a rotation of the coordinate system around the y-axis by an angle $\alpha = \pi/2$ leads to the same result as a rotation around the z-axis by the angle $\pi/2$ followed by a rotation around x by the angle $\pi/2$ followed by a rotation around z by the angle $3\pi/2$.

Solution: *a. All rotation matrices are unitary,* $\det \mathcal{R}(\alpha) = 1$, $R^{-1}(\alpha) = \mathcal{R}^t(\alpha)$. *The matrix* $\mathcal{R}_x(\alpha)$ *leaves the* x*-component of the vector unchanged, the matrix* $R^y(\alpha)$ *leaves the* y*-component unchanged,*

$$\mathcal{R}_x(\alpha) = \begin{pmatrix} 1 & 0 & 0 \\ 0 & \cos\alpha & \sin\alpha \\ 0 & -\sin\alpha & \cos\alpha \end{pmatrix} \begin{pmatrix} a \\ b \\ c \end{pmatrix} = \begin{pmatrix} a \\ b\cos\alpha + c\sin\alpha \\ -b\sin\alpha + c\cos\alpha \end{pmatrix}$$

$$\mathcal{R}_y(\alpha) = \begin{pmatrix} \cos\alpha & 0 & -\sin\alpha \\ 0 & 1 & 0 \\ \sin\alpha & 0 & \cos\alpha \end{pmatrix} \begin{pmatrix} a \\ b \\ c \end{pmatrix} = \begin{pmatrix} a\cos\alpha - c\sin\alpha \\ b \\ a\sin\alpha + c\cos\alpha \end{pmatrix} .$$

b. We have,

$$\mathcal{R}_z(3\pi/2)\mathcal{R}_x(\pi/2)\mathcal{R}_z(\pi/2) = \begin{pmatrix} 0 & -1 & 0 \\ 1 & 0 & 0 \\ 0 & 0 & 1 \end{pmatrix} \begin{pmatrix} 1 & 0 & 0 \\ 0 & 0 & 1 \\ 0 & -1 & 0 \end{pmatrix} \begin{pmatrix} 0 & 1 & 0 \\ -1 & 0 & 0 \\ 0 & 0 & 1 \end{pmatrix}$$
$$= \begin{pmatrix} 0 & 0 & -1 \\ 0 & 1 & 0 \\ 1 & 0 & 0 \end{pmatrix} = \mathcal{R}_y(\pi/2) .$$

1.7 Further reading

H.M. Nussenzveig, Edgar Blucher (2013), *Curso de Física Básica: Mecânica - vol 1* [961]ISBN

C.F. von Weizsäcker, München (1971), *Einheit der Natur* [1345]ISBN

C.F. von Weizsäcker, München (2006), *Aufbau der Physik* [1346]ISBN

Chapter 2

Dynamics of point masses

2.1 Motion of point masses

2.1.1 One-dimensional motion

Among the various movements that we will study, the one-dimensional motion is the simplest, because all vector quantities that describe the motion are parallel. Since the motion occurs in only one dimension, only one coordinate is required to specify the position of a body at each instant of time [1].

2.1.1.1 Velocity

The rate of change of the spatial coordinates of a body is called *velocity*. It can be characterized by specifying the body's position in a time table, as shown below (stroboscopic measurement) or by a graph, as shown in Fig. 2.1.

t [s]	x [m]	v [m/s]
0	0	-
1	0.4	0.4
2	0.6	0.1
3	0.7	0.06
4	0.8	0.07

The velocity averaged over a time interval $[t_1, t_2]$,

$$\bar{v} = \frac{x(t_2) - x(t_1)}{t_2 - t_1} \ , \tag{2.1}$$

is the angular coefficient of the slope connecting the points $(x(t_1), t_1)$ and $(x(t_2), t_2)$ of the curve (see Fig. 2.1).

A motion is called *uniform* when the velocity is constant,

$$x(t) = x_0 + v(t - t_0) \ . \tag{2.2}$$

For non-uniform (e.g. accelerated) motion the instantaneous velocity is calculated via,

$$\boxed{v(t) = \lim_{\Delta t \to 0} \frac{x(t + \Delta t) - x(t)}{\Delta t} \equiv \frac{dx(t)}{dt} \equiv \dot{x}(t)} \ . \tag{2.3}$$

[1] See [Cap. 2, Moyses] [Cap. 2, Zilio & Bagnato].

For example, the function $y(t) = -10\,\mathrm{m/s^2}\cdot t^2 + 5\,\mathrm{m/s}\cdot t + 2\,\mathrm{m}$ parametrizes a trajectory taken by a uniform motion [2].

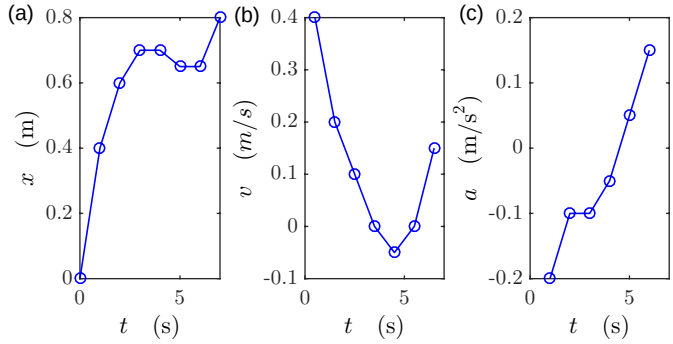

Figure 2.1: Graphical representation of the motion specified in the table. (a) Instantaneous position, (b) velocity, and (c) acceleration.

Inverse problem: Draw a graph $t \mapsto v$ and measure the area underneath:

$$x(t_2) - x(t_1) = \int_{t_1}^{t_2} v(t)dt \ . \tag{2.4}$$

2.1.1.2 Acceleration

The rate of change of the instantaneous velocity of a body is called *acceleration*. Analogous to the velocity it can be characterized by specifying the body's velocity in a time table or a graph.

Acceleration can be progressive or backward, leading to deceleration. The instantaneous acceleration is calculated via,

$$\boxed{a(t) = \lim_{\Delta t \to 0} \frac{v(t+\Delta t) - v(t)}{\Delta t} \equiv \frac{dv(t)}{dt} \equiv \dot{v}(t)} \ . \tag{2.5}$$

Inverse problem: Draw a graph $t \mapsto a$ and measure the area underneath:

$$v(t_2) - v(t_1) = \int_{t_1}^{t_2} a(t)dt \ , \tag{2.6}$$

yielding [3],

$$x(t) = x(t_0) + \int_{t_0}^{t} v(t')dt' = x(t_0) + \int_{t_0}^{t} \left[v(t_0) + \int_{t_0}^{t'} a(t'')dt'' \right] dt' \tag{2.7}$$

$$= x(t_0) + v(t_0)(t - t_0) + \int_{t_0}^{t} \int_{t_0}^{t'} a(t'')dt''dt' \ . \tag{2.8}$$

One-dimensional motion will be studied in Excs. 2.1.4.1 to 2.1.4.11.

[2] Why do we have to write the units?
[3] Galileo.

2.1.2 Motion in two and three dimensions

2.1.2.1 Description in terms of coordinates

Under normal circumstances, space is three-dimensional, and so is the motion of a body through it. Hence, we need three coordinates to specify the position of a body at a given time, and knowing the time-dependence of the three coordinates we can parametrized the body's motion through space. Luckily, specifying a coordinate system we can reduce a bi- or (tri-)dimensional motion into two (three) one-dimensional motions.

That is to say, the physical quantities position, velocity, and force are vector quantities consistent, in fact, of three values. In this sense, they are fundamentally different from scalar quantities, such as time, temperature, or volume [4]. Using the basis,

$$\hat{\mathbf{e}}_x \equiv \begin{pmatrix} 1 \\ 0 \end{pmatrix} \qquad \text{and} \qquad \hat{\mathbf{e}}_y \equiv \begin{pmatrix} 0 \\ 1 \end{pmatrix} \ , \tag{2.9}$$

called *Cartesian basis*, we write the vector velocity,

$$\mathbf{v}(t) = \frac{d\mathbf{r}(t)}{dt} = \dot{x}(t)\hat{\mathbf{e}}_x + \dot{y}(t)\hat{\mathbf{e}}_y = \begin{pmatrix} v_x(t) \\ v_y(t) \end{pmatrix} \ , \tag{2.10}$$

and the vector acceleration,

$$\mathbf{a}(t) = \frac{d\mathbf{v}(t)}{dt} = \dot{v}_x(t)\hat{\mathbf{e}}_x + \dot{v}_y(t)\hat{\mathbf{e}}_y = \begin{pmatrix} a_x(t) \\ a_y(t) \end{pmatrix} \ . \tag{2.11}$$

2.1.2.2 Uniformly accelerated movement by gravitation

The differential equations (2.3) or (2.5) are insufficient to determine the trajectory of a body. We additionally need to specify initial conditions. For a n-dimensional motion, we need $2n$ initial conditions.

Example 2 (*Motion due to terrestrial gravitation*): The acceleration of a body in the Earth's gravitational field is,

$$\mathbf{a}(t) = const = \Big(0, -g\Big) \ . \tag{2.12}$$

With arbitrary initial conditions, $\mathbf{r}(t_0) = \mathbf{r}_0$ and $\mathbf{v}(t_0) = \mathbf{v}_0$ we find,

$$\mathbf{v}(t) = \mathbf{v}_0 + \mathbf{a}(t - t_0) \tag{2.13}$$

and,

$$\mathbf{v}(t) = \mathbf{v}_0 + \mathbf{a}(t - t_0) \qquad \text{and} \qquad \mathbf{r}(t) = \mathbf{r}_0 + \mathbf{v}_0(t - t_0) + \tfrac{1}{2}\mathbf{a}(t - t_0)^2 \ . \tag{2.14}$$

Elimination time in these two equations,

$$y - y_0 = \frac{v_{0y}}{v_{0x}}(x - x_0) + \frac{a}{2}(x - x_0)^2 \ . \tag{2.15}$$

[4] Rules of how to use vectors (length, scalar product, and vector product.

Example 3 (*Motion of a projectile subject to gravity*): We identify the motion as being two-dimensional. Hence, an appropriate choice of the coordinate system allows us to eliminate one coordinate and to restrict to two coordinates that we will call $\hat{\mathbf{e}}_x$ and e_y. We choose the initial conditions as $\mathbf{r}(t_0) = (0, 0)$ and $\mathbf{v}(t_0) = v_0 \begin{pmatrix} \cos\theta \\ \sin\theta \end{pmatrix}$. The equations of motion are then,

$$\mathbf{r}(t) = \begin{pmatrix} v_0 t \cos\theta \\ v_0 t \sin\theta - \frac{1}{2} g t^2 \end{pmatrix} . \tag{2.16}$$

Elimination time in the two equations (2.16),

$$y = x \tan\theta - \frac{g x^2}{2 v_0^2 \cos^2\theta} . \tag{2.17}$$

We my now use this equation to calculate the maximum height and the maximum range of the throw.

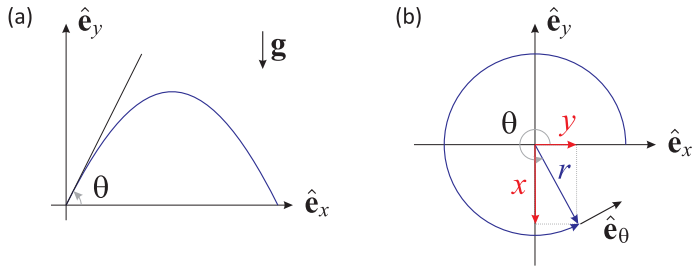

Figure 2.2: (a) Ballistic trajectory in the field of gravity. (b) Circular motion in Cartesian and polar coordinates.

Note that two movements $x(t)$ and $y(t)$ can be coupled by other physical effect, such as via the friction exerted by air.

2.1.2.3 Circular motion and polar coordinates

When we called a movement one, two, or three-dimensional, what we really meant is the number of scalar differential equations needed to describe it. Strictly speaking, however, any movement of a point mass is described by a curve in space, which is a one-dimensional object. Consequently, in the examples 4 and 3 we were able to replace the two differential equations parametrized in time $\{x(t), y(t)\}$ by a single one for $y(x)$ by eliminating time [5].

Sometimes the number of differential equations needed to describe a motion can be reduced without having to eliminate time by a proper choice of the coordinate system, which is better adapted to the symmetry of the motion. Until now we only used Cartesian coordinates (2.9). A nice example for this is the *circular motion*

[5] Note that time is automatically reintroduced in the equations once we calculate velocities by derivating coordinates.

defined by $|\mathbf{r}| = r = const$. Let us define two new coordinates oriented along the instantaneous position and the instantaneous velocity of the body,

$$\boxed{\hat{\mathbf{e}}_r(t) \equiv \frac{\mathbf{r}(t)}{r} \qquad \text{and} \qquad \hat{\mathbf{e}}_\theta(t) \equiv \frac{\mathbf{v}(t)}{v(t)}} \ . \tag{2.18}$$

We note that (for a circular motion) the new coordinates, called *polar coordinates*, are orthogonal but not fixed in space: they rotate along the circle together with the body.

The constancy of the radius $r^2 = x(t)^2 + y(t)^2$, however, implies that we may, choosing the Cartesian coordinate system such as to satisfy the initial condition $x(0) = r$, define two new variables $\{r, \theta(t)\}$ one of which is constant and the other time-dependent, such that,

$$\mathbf{r}(t) = \begin{pmatrix} x(t) \\ y(t) \end{pmatrix} = r \begin{pmatrix} \cos\theta(t) \\ \sin\theta(t) \end{pmatrix} = r\hat{\mathbf{e}}_r(t) \ , \tag{2.19}$$

for the velocity,

$$\mathbf{v}(t) = \frac{d\mathbf{r}(t)}{dt} = \begin{pmatrix} v_x(t) \\ v_y(t) \end{pmatrix} = r \begin{pmatrix} -\dot{\theta}(t)\sin\theta(t) \\ \dot{\theta}(t)\cos\theta(t) \end{pmatrix} = \dot{\theta}(t) \begin{pmatrix} -y(t) \\ x(t) \end{pmatrix} = v(t)\hat{\mathbf{e}}_\theta(t) \ , \tag{2.20}$$

and for the acceleration,

$$\mathbf{a}(t) = \frac{d\mathbf{v}(t)}{dt} = r \begin{pmatrix} -\ddot{\theta}(t)\sin\theta(t) - \dot{\theta}(t)^2\cos\theta(t) \\ \ddot{\theta}(t)\cos\theta(t) - \dot{\theta}(t)^2\sin\theta(t) \end{pmatrix} = -r\dot{\theta}(t)^2\hat{\mathbf{e}}_r + r\ddot{\theta}(t)\hat{\mathbf{e}}_\theta(t) \ . \tag{2.21}$$

That is, the acceleration is composed of a tangential and a normal component,

$$\mathbf{a}(t) \cdot \hat{\mathbf{e}}_\theta(t) = r\ddot{\theta}(t) \qquad \text{and} \qquad \mathbf{a}(t) \cdot \hat{\mathbf{e}}_r = -r\dot{\theta}(t)^2 \ . \tag{2.22}$$

The circular motion is called *uniform* when $|\mathbf{v}| = v = const$. Then, $\ddot{\theta} = 0$ and $\dot{\theta} \equiv \omega = const$, and the above formulas simplify accordingly. Then $\theta = \theta_0 + \omega(t - t_0)$ and, using $\omega \equiv v/r$, we get for the arc traveled by the body,

$$s(t) = r\theta(t) = s_0 + v(t - t_0) \ . \tag{2.23}$$

Motion in one and two dimensions will be studied in Excs. 2.1.4.12 to 2.1.4.12.

2.1.3 Newton's laws

Newton formulated the following fundamental laws of classical mechanics:

i. Principle of inertia (without forces objects move with uniform velocity)

ii. $F = ma$

iii. Reaction principle (actio = reaction)

iv. Forces can be added (corollary)

Their interpretation is that: (i) In the absence of forces linear momentum is conserved; systems not subject to external forces (called *inertial systems*) are equivalent, e.g. there no way to decide an absolute speed from with in a system. (ii) Forces generate a change of linear momentum leading to an acceleration $\sum_k \mathbf{F}_k = m\dot{\mathbf{v}}$.

Newton's laws have a wide range of applications. Formulated for fixed masses, they can nevertheless be generalized to variable masses,

$$\boxed{\mathbf{F} = \dot{\mathbf{p}} = m\dot{\mathbf{v}} + \mathbf{v}\dot{m}} \ . \tag{2.24}$$

2.1.4 Exercises

2.1.4.1 Ex: Overtaking

A car travels at a constant safety distance of 40 m behind a truck (length: 25 m) at 80 km/h . To overtake, he accelerates with $a = 1.3\,\mathrm{m/s^2}$ to $v = 100\,\mathrm{km/h}$. How long is the overtaking time and the path length if the safety distance at the time of reentering the drive lane is 40 m?

Solution: *Be x the location of the car and $z(t) = 80\,\mathrm{km/h}\cdot t$ the location of the truck. Before the overtaking manoeuvre, at the time t_0,*

$$\begin{aligned} x(t_0) - z(t_0) &= -40\,\mathrm{m} \\ \dot{x}(t_0) - \dot{z}(t_0) &= 0 \ . \end{aligned}$$

From then until the time t_1 of reaching the maximum speed $x(t) = 100\,\mathrm{km/h}$ we have,

$$\begin{aligned} \ddot{x}(t) - \ddot{z}(t) &= 1.3\,\mathrm{m/s^2} \\ \dot{x}(t) - \dot{z}(t) &= 1.3\,\mathrm{m/s^2}\cdot(t - t_0) \\ x(t) - z(t) &= 1.3\,\mathrm{m/s^2}\cdot\frac{(t-t_0)^2}{2} - 40\,\mathrm{m} \ . \end{aligned}$$

The maximum speed is reached after the time

$$t_1 - t_0 = \frac{\dot{x}(t_1) - \dot{x}(t_0)}{a} = 4.3\,\mathrm{s}$$

At this time, the distance from the truck is,

$$x(t_1) - z(t_1) = 1.3\,\mathrm{m/s^2}\cdot\frac{(t_1-t_0)^2}{2} - 40\,\mathrm{m} = -28\,\mathrm{m} \ .$$

Now the car is traveling at a constant speed up to the time t_2. It must hold,

$$x(t_2) - z(t_2) = [\dot{x}(t_1) - \dot{z}(t_1)]\cdot(t_2 - t_1) - 28\,\mathrm{m} = 40\,\mathrm{m} + 25\,\mathrm{m} \ .$$

From this we calculate the time $t_2 - t_1 = 16.7\,\mathrm{s}$, hence, in total,

$$t_2 - t_0 = 21\,\mathrm{s}$$

The distance covered is the distance covered by the truck plus the acquired lead,

$$x(t) = 40\,\mathrm{m} + 40\,\mathrm{m} + 25\,\mathrm{m} + 80\,\mathrm{km/h}\cdot 21\,\mathrm{s} = 572\,\mathrm{m} \ .$$

2.1.4.2 Ex: Skater

A roller skater who moves at a constant speed of 10 m/s overtakes a jogger. After 5 minutes she passes a snack bar, where she takes a break for 2 minutes. Then she drives back at the same speed and meets the jogger after another 3 minutes. How fast does the jogger run?

Solution: *First, we calculate the distance traveled by the roller skater to the snack bar:* $s = vt = 10\,\mathrm{m/s} \times 5\,\mathrm{min}$. *She meets the jogger after* $5 + 2 + 3 = 10\,\mathrm{min}$, *when the jogger has traveled* $10\,\mathrm{m/s} \times 5\,\mathrm{min} - 10\,\mathrm{m/s} \times 3\,\mathrm{min} = 1200\,\mathrm{m}$. *The jogger therefore needs* $10\,\mathrm{min}$ *for* $1200\,\mathrm{m}$, *from this follows for his speed* $v = s/t = 1200\,\mathrm{m}\,/600\,\mathrm{s} = 2\,\mathrm{m/s}$.

2.1.4.3 Ex: Thieves

Two bank robbers on the run have to walk $s = 10\,\mathrm{km}$ to the rescue border, but only have one bike without luggage rack. They therefore decide to proceed as follows: Robber A drives 500 m ahead, leaves the bike and continues. Robber B goes up to the bike, sits on, drives past Robber A and continues 500 m. Then he in turn leaves the bike. In this way the robbers take turns up to the border. Assume the robbers are 6 km/h on foot and 20 km/h on bike.
a. Is this a good idea? Are the robbers really faster? If so, calculate the time saved.
b. How often do they have to change?

Solution: *a. Robber B overtakes robber A for the first time after* 1 km. *This is clear for reasons of symmetry (time inversion invariance), but can also be calculated in detail. In order to overcome the* 10 km *they have to make 10 partial trips.*
b. For a partial trip the robbers need the time $t = 500\,\mathrm{m}\left(\frac{1}{v_{rad}} + \frac{1}{v_{fus}}\right) = 0.1083\,\mathrm{h}$. *Hence, for the entire route 1.083 h. This is faster than on foot (*1.666 h*), but slower than by bike (*0.5 h*). All in all, these robbers seem to be smart and should rather earn their living as an mathematician rather than robbing banks.*

2.1.4.4 Ex: One-dimensional movement

A large jet plane must reach a speed of 500 km/h in order to take off, and has an acceleration of $4\,\mathrm{m/s^2}$. How long does it take for the plane to take off and how far does it have to run on the runway?

Solution: *The speed is given by* $v = at$. *Therefore,*

$$t = \frac{v}{a} = \frac{500}{3.6 \cdot 4}\,\mathrm{s} = 33.7\,\mathrm{m} \ .$$

The distance is,

$$x = \frac{a}{2}t^2 = \frac{4}{2} \cdot 33.7^2\,\mathrm{m} = 2270\,\mathrm{m} \ .$$

2.1.4.5 Ex: One-dimensional movement

A particle, initially at rest at the origin, moves for 10 s on a straight line, with increasing acceleration according to the law, $a = bt$, where t is time and $b = 0.5\,\mathrm{m/s^3}$. Plot the velocity v and the position x of the particle as a function of time. What is the analytical expression for $v(t)$?

Solution: *With the initial condition $x_0 = 0$ e $v_0 = 0$, the expressions are,*

$$v(t) = v_0 + \int_0^t a(t_1)dt_1 = \frac{b}{2}t^2$$
$$x(t) = x_0 + \int_0^t v(t_1)dt_1 = \frac{b}{6}t^3 \ .$$

2.1.4.6 Ex: One-dimensional movement

A projectile of mass m is ejected at the initial velocity v_0 vertically from a catapult.
a. Calculate the maximum height that the projectile reaches without considering the air resistance.
b. Now, we consider air resistance given by Stokes' friction law. Write down the equation of motion for this case.
c. Show that the equation of motion is solved by $v = e^{-\gamma t/m}\left(\frac{mg}{\gamma} + v_0\right) - \frac{mg}{\gamma}$.
d. Determine the time t_m when the projectile is at its maximum point from $v(t_m) = 0$.
e. What is the maximum height $s(t_m)$?

Solution: *a. The equation of motion, $ma = -mg$, has the solution, $v = v_0 - gt$. The maximum point, $v = 0$, is reached when $t_m = \frac{v_0}{g}$. So the maximum height is,*

$$s = v_0 t_m - \frac{g}{2}t_m^2 = v_0\frac{v_0}{g} - \frac{g}{2}\left(\frac{v_0}{g}\right)^2 = \frac{v_0^2}{2g} \ .$$

b. With friction we have, $ma = -mg - \gamma v$.
c. To solve this we separate the variables,

$$dt = \frac{-mdv}{mg + \gamma v}$$
$$\Leftrightarrow \quad t = -m\int_{v_0}^{v}\frac{dv}{mg+\gamma v} = -\frac{m}{\gamma}\int_{mg+\gamma v_0}^{mg+\gamma v}\frac{d\zeta}{\zeta} = -\frac{m}{\gamma}\ln\left(\frac{mg+\gamma v}{mg+\gamma v_0}\right) \ .$$

Hence,

$$v = e^{-\gamma t/m}\left(\frac{mg}{\gamma} + v_0\right) - \frac{mg}{\gamma} \simeq \left(1 - \frac{\gamma t}{m}\right)\left(\frac{mg}{\gamma} + v_0\right) - \frac{mg}{\gamma} = v_0 - gt - \frac{\gamma v_0 t}{m} \ .$$

d. Now $v(t_m) = 0$ leads to,

$$t_m = -\frac{m}{\gamma}\ln\frac{1}{1+\gamma v_0/mg} \simeq -\frac{m}{\gamma}\left(-\frac{\gamma v_0}{mg} + \frac{\gamma^2 v_0^2}{2m^2g^2}\right) = \frac{v_0}{g}\left(1 - \frac{\gamma v_0}{mg}\right) \ .$$

e. Finally,

$$\begin{aligned} s(t_m) &= \int_0^{t_m} v dt = -e^{-\gamma t_m/m}\frac{m}{\gamma}\left(\frac{mg}{\gamma}+v_0\right) - \frac{mg}{\gamma}t_m + \frac{m}{\gamma}\left(\frac{mg}{\gamma}+v_0\right) \\ &= -\frac{1}{1+\gamma v_0/mg}\frac{m}{\gamma}\left(\frac{mg}{\gamma}+v_0\right) - \frac{mg}{\gamma}\left(-\frac{m}{\gamma}\ln\frac{1}{1+\gamma v_0/mg}\right) + \frac{m}{\gamma}\left(\frac{mg}{\gamma}+v_0\right) \\ &= \frac{mv_0}{\gamma} + \frac{m^2 g}{\gamma^2}\ln\frac{1}{1+\gamma v_0/mg} \\ &\simeq \frac{mv_0}{\gamma} + \frac{m^2 g}{\gamma^2}\left(-\frac{\gamma v_0}{mg} + \frac{\gamma^2 v_0^2}{2m^2 g^2} - \frac{\gamma^3 v_0^3}{3m^3 g^3}\right) = \frac{v_0^2}{2g}\left(1-\frac{\gamma v_0}{3mg}\right) . \end{aligned}$$

2.1.4.7 Ex: Acceleration

A possible method to measure the acceleration of gravity g is to launch a ball upwards in an evacuated tube and accurately measure the instants t_1 and t_2 of its passage (on its way up and down) across a given height z. Show that:

$$g = \frac{2z}{t_1 t_2} .$$

Solution: *The motion equation is,*

$$s(t) = \frac{g}{2}t^2 + v_0 t .$$

We know two points of the trajectory:

$$\frac{g}{2}t_1^2 + v_0 t_1 = z = \frac{g}{2}t_2^2 + v_0 t_2 .$$

Hence,

$$\begin{aligned} g &= \frac{2z}{t_1^2} - \frac{2v_0}{t_1} \qquad \textit{and} \qquad v_0 = \frac{z}{t_2} - \frac{g}{2}t_2 \\ g &= \frac{2z}{t_1^2} - \frac{2}{t_1}\left(\frac{z}{t_2} - \frac{g}{2}t_2\right) \\ g &= \frac{-2z}{t_1 t_2} . \end{aligned}$$

2.1.4.8 Ex: Acceleration

You want to train to be a juggler, keeping two balls in the air throwing them to a maximum height of 2 m. How often and how fast and how fast do you have to throw

the balls up?

Solution: *The equation of motion is,*

$$s(t) = \frac{g}{2}t^2 + v_0 t \ .$$

We know two points of the trajectory,

$$0 = -\frac{g}{2}t^2 + v_0 t \qquad \textit{and} \qquad y_m = -\frac{g}{2}\left(\frac{t}{2}\right)^2 + v_0\frac{t}{2} \ .$$

Hence,

$$v_0 = \frac{g}{2}t \qquad \textit{and} \qquad y_m = -\frac{g}{2}\left(\frac{t}{2}\right)^2 + \frac{g}{2}t\frac{t}{2} = \frac{g}{8}t^2$$

$$t = \sqrt{\frac{8y_m}{g}} \simeq 1.3\,\mathrm{s} \qquad \textit{and} \qquad v_0 = \frac{g}{2}\sqrt{\frac{8y_m}{g}} = \sqrt{2gy_m} \simeq 6.3\,\mathrm{m/s} \ .$$

With two balls this time has to be divided by 2.

2.1.4.9 Ex: Acceleration

A racing car can be accelerated from 0 to 100 km/h in 4 s. Compare the corresponding mean acceleration with the acceleration of gravity. If the acceleration is constant, how far does the car travel until it reaches 100 km/h?

Solution: *The average acceleration is,*

$$a = \frac{100\,\mathrm{km/h} - 0\,\mathrm{km/h}}{4\,\mathrm{s} - 0\,\mathrm{s}} \simeq 7\,\mathrm{m/s^2} \simeq 0.7g \ .$$

The distance traveled is,

$$s = \frac{a}{2}t^2 \simeq 55.5\,\mathrm{m} \ .$$

2.1.4.10 Ex: Optical cooling

Atoms of a gas (rubidium-87) are irradiated by a laser beam. Each photon transfers the moment $\Delta p = h/\lambda$, where $\lambda = 780\,\mathrm{nm}$ is the wavelength of the light and $h = 6.626 \cdot 10^{-34}\,\mathrm{Js}$. The mass of a rubidium atom is $m = 87 \cdot 1.66 \cdot 10^{-27}\,\mathrm{kg}$. The scattering rate is $\Gamma = 3.8 \cdot 10^7\,\mathrm{s^{-1}}$. What is the acceleration? Compare with the Earth's gravitational acceleration.

Solution: $a = \frac{F}{m} = \frac{1}{m}\frac{d}{dt}p = \frac{1}{m}\Gamma\Delta p \simeq 220000\,\mathrm{m/s^2} \simeq 22600\ g.$

2.1.4.11 Ex: Free fall

A stone falls from a balloon vertically ascending at a speed of $v_0 = 20\,\mathrm{m/s}$.
a. Calculate the speed of the stone after 10 s.
b. Calculate the distance covered by the stone in 10 s.
c. Solve the same problem with a balloon descending at the same speed.

Solution: *Upper signs refer to the ascending balloon and lower signs for the descending.*
a. The speed after 10 s *follows from,*

$$v(t) = -gt \pm v(0)$$

with $v(10\,\mathrm{s}) = -98.1\,\mathrm{m/s} \pm 20\,\mathrm{m/s} = -78.1\,\mathrm{m/s}$, *resp.* $-118.1\,\mathrm{m/s}$.
b. The distance traveled after the position where it left the balloon is,

$$s(t) = -\frac{g}{2}t^2 \pm v(0)t \ ,$$

hence $s(10\,\mathrm{s}) = -9.81 \cdot 50\,\mathrm{m} \pm 200\,\mathrm{m} = -290.5\,\mathrm{m}$ *resp.* $-690.5\,\mathrm{m}$.

2.1.4.12 Ex: Two-dimensional movement

A hose, with the nozzle 1.5 m above ground, is pointed upwards at an angle of 30° with the floor. The water jet hits a flower bed 15 m away.
a. At what velocity does the jet come out of the hose?
b. What is its maximum height.

Solution: *The equations of motion are,*

$$x = v_0 t \cos\alpha \qquad (\textit{and} \qquad y = -\frac{g}{2}t^2 + v_0 t \sin\alpha + y_0 \ .$$

with $\alpha = 30°$, $(t_0, x_0, y_0) = (0, 0, 1.5\,\mathrm{m})$ *and* $(t_1, x_1, y_1) = (t_1, 15\,\mathrm{m}, 0)$. *Substituting* t,

$$\begin{aligned} x_1 &= v_0 t_1 \cos\alpha \\ 0 &= -\frac{g}{2}\left(\frac{x_1}{v_0\cos\alpha}\right)^2 + x_1\tan\alpha + y_0 \\ v_0 &= \frac{x_1}{\cos\alpha}\sqrt{\frac{g}{2}\frac{1}{x_1\tan\alpha + y_0}} \simeq 12\,\mathrm{m/s} \ . \end{aligned}$$

To find the maximum height, we seek the minimum speed,

$$\begin{aligned} 0 = \dot{y} &= -gt_2 + v_0\sin\alpha \\ t_2 &= \frac{v_0}{g}\sin\alpha \\ y_2 &= -\frac{g}{2}t_2^2 + v_0 t_2 \sin\alpha + y_0 = \frac{v_0^2}{2g}\sin^2\alpha + y_0 \simeq 3.3\,\mathrm{m} \ . \end{aligned}$$

2.1.4.13 Ex: Potential

The following force field is given: $\mathbf{F}(\mathbf{r}) = \begin{pmatrix} -2axyz^2 + by^2 \\ -ax^2z^2 + 2bxy \\ -2ax^2yz \end{pmatrix}$. Determine the corresponding potential $V(\mathbf{r})$. Determine the work required to bring a point mass from $\begin{pmatrix} -1 \\ -1 \\ -1 \end{pmatrix}$ to $\begin{pmatrix} 1 \\ 1 \\ 1 \end{pmatrix}$.

Solution: *The potential follows from integrating* $\mathbf{F} = -\nabla\phi$ *in the individual components,*

$$\begin{aligned} -\phi &= -ax^2yz^2 + bxy^2 + A_x(y,z) \\ &= -ax^2yz^2 + bxy^2 + A_y(x,z) \\ &= -ax^2yz^2 + A_z(x,y) \ . \end{aligned}$$

Hence, $A_x(y,z) = A_y(x,z) = A_z(x,y) - bxy^2 \equiv B$*, such that* $\phi = ax^2yz^2 - bxy^2 - B$*. The work is,*

$$\phi(\mathbf{r}_2) - \phi(\mathbf{r}_1) = \left(ax_2^2y_2z_2^2 - bx_2y_2^2 - B\right) - \left(ax_1^2y_1z_1^2 - bx_1y_1^2 - B\right) = 2a - 2b \ .$$

2.1.4.14 Ex: Shot put

A shot put is able to throw a 7.257 kg ball at an initial speed of $v_0 = 15\,\mathrm{m/s}$. What is the maximum range w he can achieve with such a throw? How much further could he throw the ball (at the same initial speed) if it were half as heavy? How much further could he throw the ball if he were on the moon? Note: The lunar attraction is $g_M = 1.62\,\mathrm{m/s^2}$.

Solution: *The ballistic parabola is described by,*

$$\mathbf{r}(t) = \begin{pmatrix} v_0 t\cos\alpha \\ v_0 t\sin\alpha - \frac{g}{2}t^2 \end{pmatrix} \equiv \begin{pmatrix} w \\ 0 \end{pmatrix} \ .$$

The throw range is maximum if $\frac{dw}{d\alpha} = \frac{2v_0^2}{g}\left(\cos^2\alpha - \sin\alpha^2\right) \equiv 0$*, hence, when* $\sin\alpha = \cos\alpha$*, or when* $\alpha = \pi/4$*. So the throw range is* $w = v_0 t_m \cos\alpha = v_0 \frac{2v_0\sin\alpha}{g}\cos\alpha = \frac{v_0^2}{g} = 22.9\,\mathrm{m}$*. The throw distance does not depend on the mass of the ball. On the moon the range would be* $w = 138.9\,\mathrm{m}$*.*

2.1.4.15 Ex: Shot put

In a shot put, a ball with the initial speed $v_0 = 10\,\mathrm{m/s}$ is thrown at a height of $h = 2\,\mathrm{m}$ above ground at an angle of 35°.

a. Calculate the throw distance of the ball.
b. At what speed and at what angle does the ball hit the ground?
c. Calculate the maximum throw height and the time when it is reached?
d. What condition must the throw angle fulfill for maximum throw range? At what angle is the maximum throw range reached in the special case $h = 0\,\mathrm{m}$?

Solution: *a. Equation of motion*

$$\begin{aligned} x &= v_0 t \cos\alpha \\ y &= v_0 t \sin\alpha - \frac{g}{2}t^2 + y_0 \equiv 0 \ . \end{aligned}$$

Boundary condition

$$\begin{aligned} 0 \equiv t_1^2 - \frac{2v_0 t_1}{g}\sin\alpha + \left(\frac{v_0}{g}\sin\alpha\right)^2 - \sqrt{\left(\frac{v_0}{g}\sin\alpha\right)^2 + \frac{2}{g}y_0}^2 \\ t_1 = \frac{v_0}{g}\sin\alpha \pm \sqrt{\left(\frac{v_0}{g}\sin\alpha\right)^2 + \frac{2}{g}y_0} = 1.45\,\mathrm{s} \\ x_1 = v_0 t_1 \cos\alpha = 11.9\,\mathrm{m} \ . \end{aligned}$$

b. Impact,

$$v(t_1) = \sqrt{\dot{x}(t_1)^2 + \dot{y}(t_1)^2} = \sqrt{v_0^2\cos^2\alpha + (v_0\sin\alpha - g t_1)^2} = 11.8\,\mathrm{m/s} \ ,$$

and

$$\alpha = \arctan\frac{\dot{y}(t_1)}{\dot{x}(t_1)} = 56^\circ \ .$$

c. Maximum height

$$\begin{aligned} 0 \equiv \dot{y} &= v_0\sin\alpha - g t_2 \\ t_2 &= \frac{v_0\sin\alpha}{g} = 0.6\,\mathrm{s} \\ y(t_2) &= v_0 t_2 \sin\alpha - \frac{g}{2}t_2^2 + y_0 = 3.7\,\mathrm{m} \ . \end{aligned}$$

d. Starting altitude $y_0 = h$, altitude of impact y. $v_\perp = v_0\sin\alpha$, $v_\parallel = v_0\cos\alpha$.

$$\begin{aligned} \textit{Total time of flight:} \quad & t = \frac{v_\perp + \sqrt{v_\perp^2 + 2g(y_0 - y)}}{g} \\ \textit{Throw range:} \quad & x = v_\parallel \cdot t. \\ \textit{Maximum:} \quad & 0 \equiv \partial_\alpha x = \frac{v_0^2}{g}\partial_\alpha\left(\cos\alpha\sin\alpha + \cos\alpha\sqrt{\sin^2\alpha + \frac{2g}{v_0^2}(y_0 - y)}\right). \end{aligned}$$

Hence,

$$\cos^2\alpha\left(1 + \frac{\sin\alpha}{\sqrt{\sin^2\alpha + \frac{2g(y_0-y)}{v_0^2}}}\right) = \sin^2\alpha\left(1 + \sqrt{\sin^2\alpha + \frac{2g(y_0-y)}{v_0^2}}\right).$$

A special case is obtained for $y_0 - y = 0$:

$$0 = \frac{4v_0^2}{g}(\cos^2\alpha - \frac{1}{2}) \Rightarrow \alpha = \pi/4 \ .$$

2.1.4.16 Ex: Rocket in the homogeneous field of gravitation

A rocket moves in the homogeneous field of gravity vertically upwards. Reactor gas is ejected at a constant rate $\gamma = \left|\frac{dm}{dt}\right| = const$ and with the velocity v_g. Describe the recoil of the rocket exerted by the ejected gas using $\mathbf{F} = \frac{dm}{dt}\mathbf{v}_g$ or exploiting the momentum conservation law for infinitesimal changes of m (occurring with the velocity v_g) and of v_{rocket}.

Solution: *The mass and speed of the rocket depend on time. At each instant, the force*

$$F = \frac{d}{dt}(mv) = \frac{dm}{dt}v_g + m\frac{dv}{dt} = -mg$$

acts on the rocket. By separating the variables

$$v_g \int \frac{dm}{m} + v = -\int g dt \ ,$$

and finally

$$v(t) - v_0 = v_g \ln\frac{m_0}{m(t)} - gt \ .$$

2.2 Kinetic and potential energy

2.2.1 Conservative potentials

Newton's axioms tell us that the reason for acceleration are forces, but they do not explain the origin of the forces. In our daily experience the forces seem to arise either from contact between bodies, i.e. collisions, or from action at a distance, as in the case of gravity or electromagnetism. In the latter case, the force exerted on a body may or may not depend on its position.

Newton realized the existence of a vertical force field called gravity, which appears to be homogeneous, that is, $F(y) = F = mgy$, where $g = 9.81\,\mathrm{m/s^2}$ is called *gravitational acceleration*.

> **Example 4 (*Ball rolling on a slope*):** Throwing a mass into a rising slope, we experimentally notice that the height over ground Δy the mass reaches when coming to rest only depends on its initial velocity but not on the path. We also notice that this height satisfies,
>
> $$\Delta y \propto v^2 \ . \tag{2.25}$$
>
> Furthermore, we measure the proportionality factor to be $1/2g$.

Hence, in the homogeneous field of gravity,

$$F\Delta y = mg\Delta y = \frac{m}{2}v^2 \ . \tag{2.26}$$

We call the quantity on the right-hand side the *kinetic energy* of the mass while moving at a velocity v at ground height. The left-hand side quantity, attributed to the mass having climbed the slope to height Δy and been stopped to zero velocity, is termed *potential energy* of gravitation. Repeating the experiment for various types of slopes with various inclinations which may even vary along the slope, we verify that the final height does not depend on the trajectory of the mass, that we may parametrize as $t \to \mathbf{s}(\mathbf{t})$. That is,

$$\int_{init}^{final} \mathbf{F} \cdot d\mathbf{s} = const = V(y_{final}) - V(y_{init}) \ , \tag{2.27}$$

or for a closed path,

$$\oint \mathbf{F} \cdot d\mathbf{s} = 0 \ . \tag{2.28}$$

Only this fact allows us to attribute the potential energy solely to the mass and not to the force field. We will see later that this is only true for particular force fields (e.g. homogeneous or radial fields) and in the absence of friction. We will call force fields having this property *conservative*. The above integral equation can be cast into a differential version,

$$\boxed{\nabla \times \mathbf{F}(\mathbf{r}) = 0 \qquad \text{such that} \qquad \mathbf{F}(\mathbf{r}) = -\nabla V(\mathbf{r})} \ , \tag{2.29}$$

provided, of course, that such a unique conservative potential exists.

2.2.2 Conservation of energy

2.2.3 Translations and rotations of point masses, Galilei boost

The *Galilei transform* to an inertial system moving with velocity $\mathbf{u}$ is defined by,

$$\begin{aligned} t &\to t' = t \\ \mathbf{x} &\to \mathbf{x}' = \mathbf{x} + \mathbf{u}t \ . \end{aligned} \tag{2.30}$$

2.2.3.1 Galilei invariance

Consider a set of interacting particles, $m\dot{v}_i = -\nabla_{\mathbf{x}_i} \sum_j V_{ij}(|\mathbf{x}_i - \mathbf{x}_j|)$. This equation has obviously a Galilei-invariant form. In contrast, the wave equation $\nabla_r^2\psi - \frac{1}{c^2}\frac{\partial^2\psi}{\partial t^2} = 0$ has not, because,

$$\left.\frac{\partial}{\partial t'}\right|_{r'=const} = \left.\frac{\partial}{\partial t}\right|_{r=const} - \mathbf{u} \cdot \nabla_r \ . \tag{2.31}$$

Do the Exc. 2.2.4.1.

2.2.4 Exercises

2.2.4.1 Ex: Galilei transform

A train runs at a constant speed v_0. Inside the train, from a height h_0 a ball of mass m is released.
a. Calculate the ball's trajectory as seen by an observer traveling on the train.
b. Calculate the ball's trajectory as seen by an observer outside the train.
c. Now, the train is uniformly decelerated from the moment on when the ball is released. Calculate the trajectory of the ball as seen by an observer i. traveling on the train and ii. outside the train.

Solution: *a. The observer on the train finds,*

$$\mathbf{r}_1(t) = (h_0 - \tfrac{g}{2}t^2)\hat{\mathbf{e}}_y \ .$$

b. The outside observer finds,

$$\mathbf{r}_2(t) = (h_0 - \tfrac{g}{2}t^2)\hat{\mathbf{e}}_y + v_0 t\hat{\mathbf{e}}_x \ .$$

c. The deceleration be $a_0 < 0$. The observer on the train finds a horizontal accelerating force,

$$\mathbf{r}_1(t) = (h_0 - \tfrac{g}{2}t^2)\hat{\mathbf{e}}_y + \tfrac{a_0}{2}t^2\hat{\mathbf{e}}_x \ .$$

d. The outside observer finds the same trajectory as before,

$$\mathbf{r}_2(t) = (h_0 - \tfrac{g}{2}t^2)\hat{\mathbf{e}}_y + v_0 t\hat{\mathbf{e}}_x \ .$$

2.2.4.2 Ex: Energy conservation in free fall

Consider the free fall of a mass m from the height h.
a. Write down the kinetic energy and the potential energy of the mass as functions of $z(t)$ respectively $\dot{z}(t)$.
b. Calculate $z(t)$ by integrating the energy conservation law for the initial conditions $\dot{z}(t=0) = 0$. To do this, derive from $\dot{z}(t)$ an equation of the form $\dot{z} = f(z)$ and integrate this equation after separating the variables.

Solution: *a. The potential energy is $E_{pot}(z,\dot{z}) = mgz$, the kinetic energy is $E_{kin}(z,\dot{z}) = \frac{1}{2}m\dot{z}^2$.*
b. The energy is conserved, $E(z,\dot{z}) = \frac{1}{2}m\dot{z}^2 + mgz = const.$ If $z(0) = 0$ and $\dot{z}(0) = 0$, we can let $E = 0$. The equation of motion is $\dot{z} = \sqrt{-2gz}$, where $z < 0$. Now,

$$\frac{dz}{\sqrt{-2gz}} = dt$$

$$\int_{z(0)}^{z(t)} \frac{dz'}{\sqrt{-2gz'}} = \int_0^t dt'$$

$$\frac{1}{\sqrt{2g}}\left[-2\sqrt{-z(t)} + 2\sqrt{-z(0)}\right] = t \ .$$

Finally, we get $z(t) = -\frac{1}{2}gt^2$.

2.2.4.3 Ex: Ski jumping with salto

Two skiers go down a slope on different routes. Calculate the final speed and the arrival time for the two trajectories sketched on the graph by solid and dashed lines.

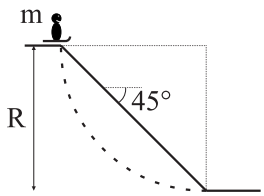

Figure 2.3: Scheme of the ramp.

Solution: *a. We parametrize the trajectory of a body descending a slope of height* h *inclined by an angle* $\theta = \pi/4$ *as,*

$$\mathbf{r}(\xi) = h\begin{pmatrix}1-\xi\\1-\xi\end{pmatrix} \qquad \textit{such that} \qquad \mathbf{v} = -h\dot{\xi}\begin{pmatrix}1\\1\end{pmatrix} \ ,$$

where $\xi \in [0,1]$ *and choosing the origin of the coordinates at the basis of the slope. Energy is conserved,* $\frac{m}{2}v_x^2 + \frac{m}{2}v_y^2 + mgy = mgh$*, with the initial energy* $E_{pot} = mgh$*. We derive,*

$$v^2 = v_x^2 + v_y^2 = 2h^2\dot{\xi}^2 = 2g(h-y) = 2gh\xi$$

That is, we know the speed at each point,

$$v = \sqrt{2gh\xi} \ .$$

The speed does not depend on the trajectory, but only on the height of the slope. But to find $\xi(t)$*, we must solve the differential equation,*

$$\dot{\xi}^2 = \frac{g}{h}\xi$$

or the integral

$$\int_0^\xi \frac{d\xi}{\sqrt{\xi}} = 2\sqrt{\xi} = \sqrt{\frac{g}{h}}t \ .$$

That is, $\xi = \frac{g}{4R}t^2$ *b. We parametrize the trajectory of a body descending a circle segment of* R *as,*

$$\mathbf{r}(\xi) = h\begin{pmatrix}\cos\xi\\1-\sin\xi\end{pmatrix} \qquad \textit{such that} \qquad \vec{v} = -h\dot{\xi}\begin{pmatrix}\sin\xi\\\cos\xi\end{pmatrix} \ ,$$

where $\xi \in [0, \pi/2]$ and choosing the origin of the coordinates at the basis of the circle segment. Energy is conserved, $\frac{m}{2}v_x^2 + \frac{m}{2}v_y^2 + mgy = mgh$, with the initial energy $E_{pot} = mgh$. We derive,

$$v^2 = v_x^2 + v_y^2 = h^2\dot{\xi}^2 = 2g(h-y) = 2gh\sin\xi \ .$$

That is, we know the speed at each point,

$$v = \sqrt{2gh\sin\xi} \ .$$

The speed does not depend on the trajectory, but only on the height of the slope. But to find $\alpha(t)$, we must solve the differential equation,

$$\dot{\xi} = \sqrt{\frac{2g}{h}\sin\xi}$$

or the elliptic integral,

$$\int_0^\xi \frac{d\xi}{\sqrt{\sin\xi}} = \sqrt{\frac{2g}{h}}t \ .$$

c. We parametrize the trajectory of a body descending a parabola defined by,

$$\mathbf{r}(\xi) = h\begin{pmatrix} 1-\xi \\ (1-\xi)^2 \end{pmatrix} \qquad \textit{such that} \qquad \vec{v} = -h\dot{\xi}\begin{pmatrix} 1 \\ 2(1-\xi) \end{pmatrix} \ ,$$

where $\xi \in [0, 1]$ and choosing the origin of the coordinates at the basis of the circle segment. Energy is conserved, $\frac{m}{2}v_x^2 + \frac{m}{2}v_y^2 + mgy = mgh$, with the initial energy $E_{pot} = mgh$. We derive,

$$v^2 = v_x^2 + v_y^2 = h^2\dot{\xi}^2[1 + 4(1-\xi)^2] = 2g(h-y) = 2gh[1-(1-\xi)^2] \ .$$

That is, we know the speed at each point,

$$v = \xi\sqrt{2gh} \ .$$

The speed does not depend on the trajectory, but only on the height of the slope. But to find $\xi(t)$, we must solve the differential equation,

$$\dot{\xi} = \sqrt{\frac{2g}{h}}\sqrt{\frac{1-(1-\xi)^2}{1+4(1-\xi)^2}}$$

or the elliptic integral,

$$\int_0^\xi \sqrt{\frac{1+4(1-\xi)^2}{1-(1-\xi)^2}}d\xi = \sqrt{\frac{2g}{h}}dt \ .$$

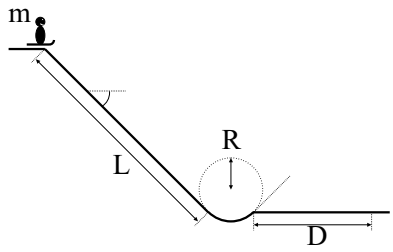

Figure 2.4: Scheme of the ramp.

2.2.4.4 Ex: Ski jumping with salto

A skier with a body weight of 75 kg descends an $L = 50\,\mathrm{m}$ high ski jump with a -100% gradient. At the lower end the ski jump merges into a trough, the curvature of which is described by a circle with radius $R = 10\,\mathrm{m}$. At an inclination of 100%, the trough suddenly merges into a horizontal plane. Friction is neglected. What is the minimum weight the skis must bear before they break? How far does the skier fly over the plane D?

Solution: *On the descent, the skier converts the potential energy* $E_{pot} = mgh = mgL\sin 45^\circ$ *into kinetic energy* $E_{kin} = E_{pot} = \frac{m}{2}\mathbf{v}^2$. *The initial speed when jumping off the trough is thus,*

$$\mathbf{v}(0) = \sqrt{\frac{E_{kin}}{m}} \begin{pmatrix} 1 \\ 1 \end{pmatrix} .$$

The ballistic parabola is given by,

$$\mathbf{x}(t) = \begin{pmatrix} v_{x0}t \\ v_{y0}t - \frac{g}{2}t^2 \end{pmatrix} \equiv \begin{pmatrix} v_{x0}t \\ 0 \end{pmatrix} .$$

Hence,

$$t = \frac{2v_{y0}}{g} ,$$

so the range of the jump is $D = \frac{2v_{x0}v_{y0}}{g} = \frac{2E_{kin}}{mg} = 2h \approx 70.7\,\mathrm{m}$. *The height difference between the position of the take-off and the lowest point of the trough is* $R - R\cos 45^\circ \approx 2.9\,\mathrm{m}$. *That is why the maximum speed of the skier is,*

$$v_m = \sqrt{\frac{2E_{kin}}{m}} = \sqrt{\frac{2mgh'}{m}} = \sqrt{2g\left(L\sin 45^\circ + R - R\cos 45^\circ\right)} .$$

Inside the circular trough at the lowest point of the ski jump the centrifugal force is,

$$F_z = m\omega^2 R = m\frac{v_m^2}{R} .$$

Together with the skier's weight, the skis have to withstand a load of up to,

$$\begin{aligned} m' &= m + \frac{F_z}{g} = m + \frac{mv_m^2}{gR} \\ &= m\left(2 + \frac{2L}{R}\sin 45^\circ - \cos 45^\circ\right) = 8.36\,\mathrm{m} \approx 630\,\mathrm{kg} \ . \end{aligned}$$

2.2.4.5 Ex: Ski jumping with salto

A skier goes down a slide. The work exerted by the gravitational field on the skier is,

$$W = \int_{s_0}^{s_1} \mathbf{F} \cdot d\vec{s} = \int_0^x F_s \sqrt{1 + y''} dx \ .$$

Now we consider three different slides:
a. The slide is described by the function $y(x) = \sqrt{h^2 - x^2}$ with $dy/dx = -x/\sqrt{h^2 - x^2} = -x/y$. We also know,

$$F_s(x) = (-mg\hat{\mathbf{e}}_y) \cdot (-\hat{\mathbf{e}}_\theta) = mg\cos\theta \ .$$

Therefore, we can simplify the integral with $x = h\cos\theta$ and $y = h\sin\theta$,

$$\begin{aligned} W &= mg\cos\theta \int_0^x \frac{xdx}{\sqrt{h^2 - x^2}} = mg\int_0^x \frac{xdx}{y} = -mg\int_h^{\sqrt{h^2-x^2}} dy \\ &= mg(h - \sqrt{h^2 - x^2}) = mg(h - y) = \frac{m}{2}v^2 \ . \end{aligned}$$

b. The slide is described by the function $y(x) = (h - x)^2$ with $dy/dx = -2(h - x)$. We also know,

$$F_s(x) = -mg\sin\theta = -mg\frac{\tan\theta}{\sqrt{1 + \tan^2\theta}} = -mg\frac{y'}{\sqrt{1 + y'^2}} \ .$$

So we can simplify the integral,

$$W = -mg\int_0^x \frac{y'}{\sqrt{1 + y'^2}}\sqrt{1 + y'^2}dx = -mg\int_0^x y'dx = -mg\int_h^y dy = mg(h - y) = \frac{m}{2}v^2 \ .$$

c. The slide is described by the function $y(x) = h - \sqrt{h^2 - (x - h)^2}$. With $dy/dx = \frac{-(x-h)}{\sqrt{h^2-(x-h)^2}}$. We also know,

$$F_s(x) = -mg\sin\theta = -mg\frac{\tan\theta}{\sqrt{1 + \tan^2\theta}} = -mg\frac{y'}{\sqrt{1 + y''}} \ .$$

So we can simplify the integral,

$$W = -mg\int_0^x \frac{y'}{\sqrt{1 + y''}}\sqrt{1 + y'^2}dx = -mg\int_0^x y'dx = -mg\int_h^y dy = mg(h - y) = \frac{m}{2}v^2 \ .$$

Solution:

2.2.4.6 Ex: Looping

A body starts at speed $v_0 = 0$ from point A and slides without friction on a slope (see figure). At point B the slope becomes a circle of radius R.
a. What is the speed at points B and C of the circle?
b. What is the maximum fraction R/h to prevent the body from falling at point B?
c. What is the minimum speed at point B to prevent the body from falling?

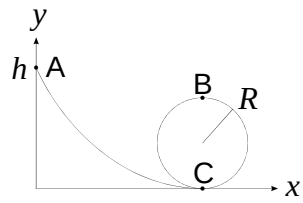

Figure 2.5: Looping.

Solution: *a. Energy conservation* $\frac{m}{2}v_C^2 = mgh$ *yields,*

$$v_C = \sqrt{2gh} \ .$$

Energy conservation $\frac{m}{2}v_B^2 + 2mgR = mgh$ *yields,*

$$v_B = \sqrt{2gh - 4gR} \ .$$

b. The centrifugal force must be greater than the gravitation force, that is, $m\frac{v_B^2}{R} > mg$. *Substitution of* v_B *leads to,*

$$\frac{R}{h} > \frac{2}{5} \ .$$

c. Energy conservation $\frac{m}{2}v_B^2 + 2mgR = \frac{m}{2}v_C^2$ *yields, after resolution by* v_B *and substitution in the condition* $m\frac{v_B^2}{R} > mg$,

$$v_C > \sqrt{5gR} \ .$$

2.2.4.7 Ex: Forces

A body of mass m moves under the influence of three forces:

$$\begin{aligned}
\mathbf{F}_1(\mathbf{r}) &= (\alpha \cos \omega(x+y), -\beta(y+y_0)^2, \gamma(z+z_0)^2) \\
\mathbf{F}_2(\mathbf{r}) &= (\alpha \sin \omega x \sin \omega y, \beta(y-y_0)^2, -\gamma(z-z_0)^2) \\
\mathbf{F}_3(\mathbf{r}) &= (\alpha \cos(\omega x + \pi) \cos \omega y, 3\beta y y_0, \gamma z_0(z_0 - 4z)) \ .
\end{aligned}$$

The body is at $t = 0$ at the point $\mathbf{r}(0)$ with velocity $\mathbf{v}(0)$. What is the absolute value of the body's velocity $|\mathbf{v}(t)|$ after a time t when it is at the point $\mathbf{r}(t)$?

Solution: *The force*

$$\mathbf{F} = \begin{pmatrix} \alpha\cos\omega(x+y) \\ -\beta(y+y_0)^2 \\ \gamma(z+z_0)^2 \end{pmatrix} + \begin{pmatrix} \alpha\sin\omega x\sin\omega y \\ \beta(y-y_0)^2 \\ -\gamma(z-z_0)^2 \end{pmatrix} + \begin{pmatrix} \alpha\cos(\omega x+\pi)\cos\omega y \\ 3\beta y y_0 \\ \gamma z_0(z_0-4z) \end{pmatrix}$$

can be simplified to,

$$\begin{pmatrix} m\ddot{x} \\ m\ddot{y} \\ m\ddot{z} \end{pmatrix} = \begin{pmatrix} 0 \\ -\beta y y_0 \\ \gamma z_0^2 \end{pmatrix} .$$

Then the velocities in x and z-direction are, respectively, $\dot{x} = v_{x0}$ and $\dot{z} = \frac{\gamma z_0^2}{m}t + v_{z0}$. For the y-direction we get a vibration,

$$y = \frac{v_{y0}}{\omega}\sin\omega t + y_0\cos\omega t \quad \textit{with} \quad \omega = \sqrt{\frac{\beta y_0}{m}} ,$$

satisfying the boundary conditions $y(0) = y_0$ and $\dot{y}(0) = v_{y0}$. Finally, the absolute value of the speed is,

$$|\mathbf{v}| = \sqrt{v_x^2 + v_y^2 + v_z^2} = \sqrt{v_{x0}^2 + (v_{y0}\cos\omega t - y_0\omega\sin\omega t)^2 + \left(\frac{\gamma z_0^2}{m}t + v_{z0}\right)^2} .$$

2.2.4.8 Ex: Pushed inclined plane

A 45° wedge is pushed over a table with constant acceleration a. A cuboid of mass m slides on the wedge without friction. At the time $t = 0$ the cuboid is at a height h and, like the cuboid, at rest.
a. Give the acceleration $\mathbf{a}(t)$ and speed $\mathbf{v}(t)$ as a function of time.
b. Give kinetic and potential energy of the cuboid as a function of time. Does energy conservation hold?

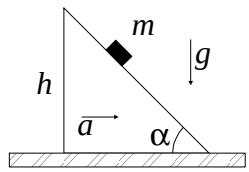

Figure 2.6: Pushed inclined plane.

Solution: *a. The weight $\mathbf{F}_g = -mg\hat{\mathbf{e}}_y$ and the force due to the acceleration of the wedge $\mathbf{F}_a = ma\hat{\mathbf{e}}_x$ act on the cuboid. Let $\hat{\mathbf{e}}_f = \hat{\mathbf{e}}_x\cos\alpha - \hat{\mathbf{e}}_y\sin\alpha$ be the unit vector of the surface of the wedge and $\hat{\mathbf{e}}_n = \hat{\mathbf{e}}_x = \sin\alpha + \hat{\mathbf{e}}_y\cos\alpha$ the normal of the surface. As*

long as the cuboid adheres to the surface of the wedge, we only need to consider the projection of gravity on the surface and the projection of the acceleration of the wedge on the normal,

$$\begin{aligned} m\frac{d^2}{dt^2}\mathbf{r} &= (\mathbf{F}_g \cdot \hat{\mathbf{e}}_f)\hat{\mathbf{e}}_f + (\mathbf{F}_a \cdot \hat{\mathbf{e}}_n)\hat{\mathbf{e}}_n \\ &= [-mg\hat{\mathbf{e}}_y \cdot (\hat{\mathbf{e}}_x \cos\alpha - \hat{\mathbf{e}}_y \sin\alpha)]\,(\hat{\mathbf{e}}_x \cos\alpha - \hat{\mathbf{e}}_y \sin\alpha) + [ma\hat{\mathbf{e}}_x \cdot (\hat{\mathbf{e}}_x \cos\alpha + \hat{\mathbf{e}}_y \sin\alpha)]\,(\hat{\mathbf{e}}_x \cos \\ &= m\begin{pmatrix} g\sin\alpha\cos\alpha + a\cos\alpha\cos\alpha \\ -g\sin\alpha\sin\alpha + a\cos\alpha\sin\alpha \end{pmatrix} \overset{\alpha=45^\circ}{\longrightarrow} \frac{m}{2}\begin{pmatrix} g+a \\ -g+a \end{pmatrix} \\ m\frac{d}{dt}\mathbf{r} &= \frac{m}{2}\begin{pmatrix} g+a \\ -g+a \end{pmatrix} t \\ m\mathbf{r} &= \frac{m}{4}\begin{pmatrix} g+a \\ -g+a \end{pmatrix} t^2 + \begin{pmatrix} 0 \\ h \end{pmatrix} \ . \end{aligned}$$

b. The energy,

$$\begin{aligned} E = T + V &= \frac{m}{2}v^2 + mgy(t) = \frac{m}{2}(\dot{x}(t)^2 + \dot{y}(t)^2) + mg\dot{y}(t) \\ &= \frac{m}{2}\frac{1}{2}(a^2+g^2) + mg\frac{1}{2}\frac{1}{2}(a-g)t^2 + mgh = \frac{m}{4}(a^2+ag)t^2 + mgh \end{aligned}$$

is not conserved,

$$\frac{dE}{dt} = \frac{m}{2}(a^2+ag)t \neq 0$$

for $a \neq 0$.

2.2.4.9 Ex: Bungee jump

An organizer is offering bungee jumps from a bridge of height H. First of all, a student (body length h, mass m) wants to jump upside down from a standing position. The rope (spring constant C) is tied to him exactly in the middle of the body. Help the operator with his calculations.
a. By what length a_0 is the rope stretched when the student is hanging on the rope at rest?
b. How long is the rope to be dimensioned so that the student can just touch the surface of the water flowing under the bridge with his head? Take into account (a) calculated pre-stretch of the rope. (Numerical values: $H = 100\,\mathrm{m}$, $h = 1.90\,\mathrm{m}$, $m = 50\,\mathrm{kg}$, $C = 50\,\mathrm{N/m}$)

Solution: *Let l_0 be the length of the unstretched rope and S the total stretch.*
a. The rope elongation at rest results from $|\mathbf{F}| = Cx$ that is $mg = Ca_0$ yielding,

$$a_0 = \frac{mg}{C} = 9.81\,\mathrm{m} \ .$$

b. The following applies to the lengths $H - \frac{h}{2} = l_0 + a_0 + x$. We seek for $l_0 = H - \frac{h}{2} - (a_0 + x) = H - \frac{h}{2} - s$. s results from the equilibrium between potential energy

and elongation energy of the elastic rope $mgH = \frac{1}{2}Cs^2$. *Hence,*

$$s = \sqrt{\frac{2mgH}{C}} = 44.29\,\mathrm{m} \ .$$

Therefore $l_0 = 54.76\,\mathrm{m}$ *and* $x = s - a_0 = 34.48\,\mathrm{m}$.

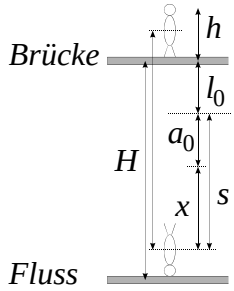

Figure 2.7: Scheme of the arrangement.

2.2.4.10 Ex: Body sliding from a cylinder with friction

A body bound to move with friction on a cylinder of radius R is released at an angle θ_0 with zero velocity.
a. What is the maximum coefficient of static friction μ_e allowed for the body to slide?
b. Once the body starts to slide, the friction is dominated by the dynamic friction coefficient μ_d. What is the work done until the body reaches the horizontal position ($\theta = 0°$)?
c. What is the final velocity?

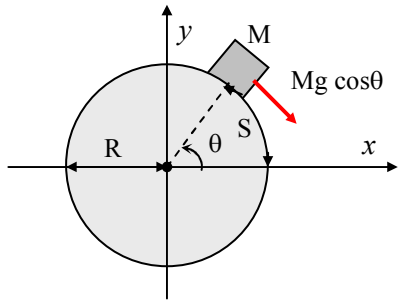

Figure 2.8: Body sliding from a cylinder with friction.

Solution: *a. The tension due to the pressure of the body on the cylinder depends on its position,*

$$\mathbf{N} = mg\sin\theta \ .$$

So the friction force is,

$$\mathbf{F}_{at} = -\mu_e \mathbf{N} = -\mu_e mg \sin\theta \ .$$

To allow the body to slide, we need at least,

$$0 < F_{gr} + F_{at} = mg\cos\theta_0 - \mu_e mg \sin\theta_0 \ .$$

That is, $\mu_e < \cot\theta_0$.
b. In the case of sliding, the work performed is,

$$W = \int_{s_0}^{s_1} (\mathbf{F}_{gr} + F_{at}) d\vec{s} = -\int_{\theta_0}^{0} (mg\cos\theta \mathbf{F}_{gr} - \mu_d mg \sin\theta) R d\theta \ .$$

with $ds = -Rd\theta$. *Hence,*

$$W = -Rmg(-\sin\theta_0 + \mu_d - \mu_d \cos\theta_0) = \frac{m}{2} v^2 \ .$$

c. And from this we get the velocity,

$$v = \sqrt{2Rg(\sin\theta_0 - \mu_d + \mu_d \cos\theta_0)} \ .$$

2.2.4.11 Ex: Bodies sliding down a slope

Two children are descending with an interval of 2 s a 4 m high frictionless slide ending in a horizontal plane. What is the final distance between them?

Solution: *The final velocity of children is,*

$$v = \sqrt{2gh} \ .$$

Therefore, the distance is $d = vt = t\sqrt{2gh} = 17.7\,\mathrm{m}$.

2.2.4.12 Ex: Energy conservation in the harmonic oscillator

Consider a mass of $m = 0.1\,\mathrm{kg}$ that vibrates on a spring with the spring constant $C = 10\,\mathrm{N/m}$. The maximum deflection A around the rest position of the spring is 10 cm.
a. At what frequency does the mass vibrate?
b. Give the potential and the kinetic energy of the mass as a function of the displacement $x(t)$ resp. $\dot{x}(t)$.
c. Derive the equation of motion for the deflection from the energy theorem. The initial condition is chosen so that at time $t = 0$ the mass is at the zero crossing ($x(0) = 0$) and has maximum speed. First help: Integrate using the *variable separation* method. Second help: $\int \frac{dx}{\sqrt{a^2 - x^2}} = \arcsin\frac{x}{a}$.

Solution: *a. The force equation is* $m\ddot{x} = -Cx$. *Hence, the mass vibrates with the frequency* $\omega/2\pi = \frac{1}{2\pi}\sqrt{C/m} \approx 0.16\ s^{-1}$.
b. The potential energy is $E_{pot}(x) = \frac{C}{2}x^2$, *the kinetic energy is* $E_{kin}(\dot{x}) = \frac{1}{2}m\dot{x}^2$.
c. The energy remains constant, $E = \frac{1}{2}m\dot{x}^2 + \frac{C}{2}x^2 = \frac{C}{2}A^2$. *Hence,*

$$\frac{dx}{\sqrt{C/m}\sqrt{A^2 - x^2}} = dt$$
$$\int_{x(0)}^{x(t)} \frac{dx'}{\sqrt{C/m}\sqrt{A^2 - x'^2}} = \int_0^t dt'$$
$$\frac{1}{\sqrt{C/m}} \arcsin \frac{x'}{A}\bigg|_0^{x(t)} = t\ .$$

Finally we get $x = A \sin \sqrt{C/m}t$.

2.2.4.13 Ex: Anharmonic potential

A mass m moves in a potential $V(x)$, which has a minimum at $V(0) = 0$ for $x = 0$ and a first maximum at x_M. At time $t = 0$ the mass is at point $x = 0$. The initial speed is chosen so that, when it reaches the maximum of the potential at x_M its velocity is zero. Calculate for the two cases $V(x) = \alpha x^2 - \beta x^4$ and $V(x) = \lambda(1 - \cos^2 \kappa x)$:
a. the coordinates of the maximum x_M and $V(x_M)$;
b. with the help of the energy conservation law the total energy E;
c. the implicit equation of motion $t = g(x)$ or, if possible, the explicit one $x = f(t)$;
How long does the mass take to reach the point x_M. Justify the result by physical arguments.

Solution: *a. For the first potential there are extrema when* $\frac{d}{dx}V(x) = 2\alpha x - 4\beta x^3 = 0$, *that is,* $x = 0$ *as well as* $x = \pm\sqrt{\frac{\alpha}{2\beta}}$. *Because of* $\frac{d^2}{dx^2}V(x) = 2\alpha - 12\beta x^2$ *there is a minimum at* $x = 0$ *if* $\alpha > 0$. *There are maxima at* $x = \pm\sqrt{\frac{\alpha}{2\beta}}$ *if* $\alpha > 0$. *For the second potential* $\frac{d}{dx}V(x) = 2\lambda \cos \kappa x \sin \kappa x = 0$, *that is, there is a minimum at* $x = 0$. *There are maxima at* $x = \pm\frac{\pi}{2\kappa}$.
b. The energy is for both potentials,

$$E = \frac{m}{2}v^2 + \alpha x^2 - \beta x^4 = \alpha\frac{\alpha}{2\beta} - \beta\frac{\alpha^2}{4\beta^2} = \frac{\alpha^2}{4\beta}$$
$$E = \frac{m}{2}v^2 + \lambda(1 - \cos^2 \kappa x) = \lambda(1 - \cos^2 \kappa x_M) = \lambda\ .$$

c. The equation of motion results from the energy theorem. For the first potential,

$$\begin{aligned}
\dot{x} &= \sqrt{\frac{2\alpha^2}{4m\beta} - \frac{2\alpha}{m}x^2 + \frac{2\beta}{m}x^4} \\
dt &= \sqrt{\frac{4m\beta}{2}}\frac{dx}{\sqrt{\alpha^2 - 4\alpha\beta x^2 + 4\beta^2 x^4}} = \frac{\sqrt{2m\beta}dx}{\alpha - 2\beta x^2} \\
t &= \sqrt{2m\beta}\int \frac{dx}{\alpha - 2\beta x^2} = \frac{1}{\sqrt{2\alpha\beta}}\,arctanh\; x\sqrt{\frac{2\beta}{\alpha}} \\
x &= \sqrt{\frac{\alpha}{2\beta}}\tanh t\sqrt{2\alpha\beta}\ .
\end{aligned}$$

Hence, $t = \frac{1}{\sqrt{2\alpha\beta}}\,arctanh\; x\sqrt{\frac{2\beta}{\alpha}} \overset{x\to x_M}{\longrightarrow} \infty$. *For the second potential,*

$$\begin{aligned}
\dot{x} &= \sqrt{\frac{2\lambda}{m}}\cos\kappa x \\
dt &= \sqrt{\frac{m}{2\lambda}}\frac{dx}{\cos\kappa x} \\
t &= \sqrt{\frac{m}{2\lambda}}\int \frac{dx}{\cos\kappa x} = \sqrt{\frac{m}{2\lambda}}\frac{\ln(1+\sin\kappa x) - \ln(\cos\kappa x)}{\kappa} \\
e^{\sqrt{\frac{2\lambda}{m}}\kappa t} &= \frac{1+\sin\kappa x}{\cos\kappa x} \\
x &= \frac{1}{\kappa}\,\mathrm{arcsin}\tanh\sqrt{\frac{2\lambda\kappa^2}{m}}t\ .
\end{aligned}$$

Hence, $t = \sqrt{\frac{m}{2\lambda}}\frac{\ln 2 - \ln 0}{\kappa} \overset{x\to x_M}{\longrightarrow} \infty$. *In both cases, the mass takes an infinitely long time to reach the maximum. This is because the maximum is an unstable point. If the mass sits up there and* $v = 0$*, it is not accelerated.*

2.2.4.14 Ex: Anharmonic potential

A particle with the mass $m = 1.4 \times 10^{-25}\,\mathrm{kg}$ moves along the positive x-axis. A constant force directed towards the origin of the coordinate system of $B = 10^{-23}\,\mathrm{N}$ and a repulsive force of A/x^2 act on the particle, whereby $A = 10^{-35}\,\mathrm{Nm}^2$.
a. Calculate the potential energy function $V(x)$.
b. Sketch the energy as a function of the location x when the maximum kinetic energy is $T_0 = 10^{-28}\,\mathrm{J}$.
c. Determine the equilibrium position x_0 (force $F(x_0) = 0$) and the turning points (velocity $\dot{x} = 0$).
d. How large is the frequency of small vibrations around x_0?

Solution: *The force is,*

$$F = \frac{A}{x^2} - B\ .$$

The equilibrium position is at $F(x_0) = 0$, *also* $x_0 = \sqrt{A/B} \approx 1\,\mu\text{m}$. *The potential is,*

$$V = \frac{A}{x} + Bx \ .$$

The Taylor expansion around the equilibrium position is,

$$\begin{aligned} V &= V(x_0) + V'(x_0)(x - x_0) + V''(x_0)\frac{(x - x_0)^2}{2!} + ... \\ &\simeq \frac{A}{x_0} + Bx_0 + \left(-\frac{A}{x_0^2} + B\right)(x - x_0) + \frac{A}{x_0^3}(x - x_0)^2 \\ &= const + \frac{A}{x_0^3}\tilde{x}^2 \ . \end{aligned}$$

The frequency of small vibrations is therefore,

$$\omega = \sqrt{\frac{2}{m}\frac{A}{x_0^3}} \approx 2\pi \times 2\,\text{kHz} \ .$$

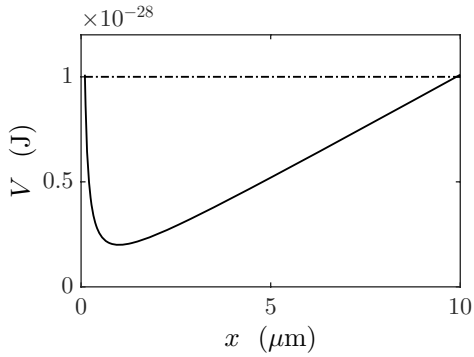

Figure 2.9: Anharmonic potential.

2.2.4.15 Ex: Free flight with friction

A body of mass m starts to fall at time $t = 0$ and point $z = 0$ with the initial velocity $\mathbf{v} = v_0\hat{\mathbf{e}}_z$ in the homogeneous terrestrial field of gravity (the z-axis is directed downwards). Its movement in the atmosphere is subject to Newton's friction force, $\mathbf{F}_R = -\alpha v\mathbf{v}$. We are considering only the movement along the z-axis.
a. What is the equation of motion for the body?
b. How should v_0 be chosen to obtain a movement with constant speed? v
c. Now, let the initial velocity v_0 be zero. Calculate the relationship between the falling distance z and the maximum reached velocity. **Help:** Use the method of separating the variables and, for that, write the equation of motion in the form $dz = f(v)dv$. Use the following result: $\int \frac{x}{a^2 - x^2}dx = -0.5\ln(a^2 - x^2)$.)

d. After which falling distance does the body reach 50 % of the maximum speed?

Solution: *a. The equation of motion is* $m\ddot{z} + \alpha v^2 = mg$.
b. For acceleration to end, we need $\ddot{z} = 0$. *From this follows* $v_0 = \sqrt{\frac{mg}{\alpha}}$.
c. The equation of motion can be written in the form,

$$dt = \frac{mdv}{mg - \alpha v^2}$$

The differential dt *can be replaced by* $v = \frac{dz}{dt}$, *giving,*

$$dz = \frac{mvdv}{mg - \alpha v^2} \ .$$

Hence,

$$z = \frac{m}{\alpha}\int_0^v \frac{vdv}{mg/\alpha - v^2} = -\frac{m}{2\alpha}\ln\left(\frac{mg}{\alpha} - v^2\right)\Big|_0^v = -\frac{m}{2\alpha}\ln\left(1 - \frac{\alpha}{mg}v^2\right) \ .$$

We can also integrate the differential, dt,

$$t = \frac{m}{\alpha}\int_0^v \frac{dv}{mg/\alpha - v^2} = \frac{m}{2\alpha}\ln\pm\frac{mg/\alpha + v}{mg/\alpha - v}\Big|_0^v = \frac{m}{2\alpha}\ln\frac{mg/\alpha + v}{mg/\alpha - v} \ .$$

d. The maximum speed is reached for $z \to \infty$. *The logarithm*

$$z = \infty = -\frac{m}{2\alpha}\ln\left(1 - \frac{\alpha}{mg}v_m^2\right) \ .$$

diverges, when $v_m = \sqrt{\frac{mg}{\alpha}}$. *The body reaches 50 % of its maximum speed at the position,*

$$z = -\frac{m}{2\alpha}\ln\left(1 - \frac{\alpha}{mg}\left(\frac{v_m}{2}\right)^2\right) = -\frac{m}{2\alpha}\ln\left(1 - \frac{1}{4}\right) = \frac{m}{2\alpha}0.2877 \ .$$

2.2.4.16 Ex: Free flight with friction numerically

Here, we want to solve Exc. 2.2.4.15 numerically. A body of mass $m = 1\,\text{kg}$ begins to fall at time $t = 0$ at point $z = 0$ with the initial velocity $\mathbf{v} = v_0\hat{\mathbf{e}}_z$ in the homogeneous gravitational field of the Earth (the z-axis is directed downwards). When moving in the atmosphere, it is subject to Newton's friction force $\mathbf{F}_R = -\alpha v\mathbf{v}$ with $\alpha = 0.01\,\text{kg/m}$. We are considering only the movement along the z-axis.
a. What is the equation of motion for the body?
b. Calculate the trajectory of the body by numerically integrating the equation of motion with the Euler method. Use different starting velocities v_0. Choose v_0 such that, at the beginning, the movement has constant v?

Solution: *a. The equation of motion is* $m\ddot{z} + \alpha v^2 = mg$. *It can be rewritten into the following system of equations:*

$$\dot{v} = -\frac{\alpha}{m}v^2 + g$$
$$\dot{z} = v \ .$$

b. Speed and location are after a small time interval dt,

$$v(t+dt) = v(t) + dt \ \left(g - \frac{\alpha}{m}v(t)^2\right)$$
$$z(t+dt) = z(t) + dt \ v \ .$$

One can now discretize by $t_k \equiv t + kdt$, $z_k \equiv z(t+t_k)$ *and* $v_k \equiv v(t_k)$ *and solve the system of equations iteratively.*

$$v_{k+1} = v_k + dt \ \left(g - \frac{\alpha}{m}v_k^2\right)$$
$$z_{k+1} = z_k + dt \ v_k \ .$$

The movement is constant from the beginning if $v_0 = \sqrt{mg/\alpha} \approx 31.3209$.

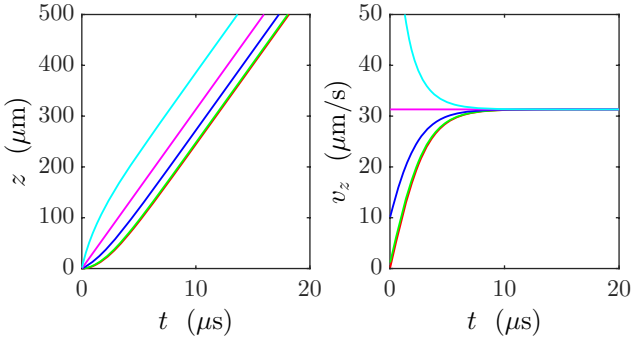

Figure 2.10: Trajectory and speed for a free fall with friction for different initial velocities $v_0 = 0, 1, 10, 31.3209, 100$. Here $dt = 0.02\,\mathrm{s}$.

2.2.4.17 Ex: Parachutist with resistance (Möllemanns Rechenaufgabe)

A skydiver exits his plane in 2000 m. Unfortunately, he forgot to put on his parachute. Suppose that air resistance can be described by Stokes friction with the friction coefficient $k = 0.05\,\mathrm{s}^{-1}$.
a. Calculate the parachutist's maximum speed.
b. What would be the total time T of the skydiver's flight if the friction was negligible?
c. What is the distance between the skydiver and the ground at time T in case the friction is not negligible.

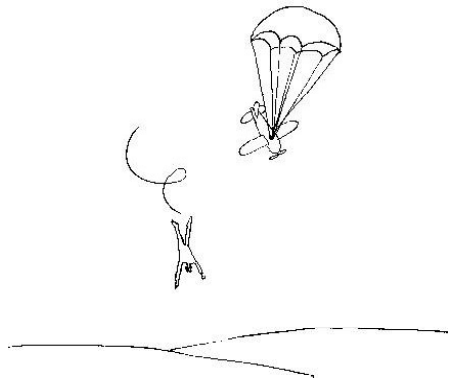

Figure 2.11: Parachutist with resistance.

Solution: *Gravity acts along* $\hat{\mathbf{e}}_z$*. The equation of motion is now,*

$$m\ddot{z} + mk\dot{z} - mg = 0 \ .$$

After separating the variables,

$$dt = \frac{dv}{g - kv} \ .$$

The solution is,

$$t = \int_0^t t dt = \int_0^v \frac{dv}{g - kv} = -\frac{1}{k}\left[\ln(g - kv)\right]_0^v = -\frac{1}{k}\ln\left(\frac{g - kv}{g}\right)$$
$$v = \frac{g}{k}(1 - e^{-kt}) \ .$$

The maximum speed is $v_\infty = \frac{g}{k} \approx \frac{9.81\,\mathrm{m/s^2}}{0.05\,\mathrm{Ns/m}} = 196\,\mathrm{m/s}$*. The flight time without friction follows from* $h = \frac{g}{2}t^2$ *para* $t = \sqrt{\frac{2h}{g}} = 20.2\,\mathrm{s}$*. The falling distance with friction is,*

$$z(T) = \int_0^T v dt = \frac{g}{k}\int_0^T (1 - e^{-kT}) dt = \frac{g}{k}\left[T + \frac{1}{k}e^{-kT}\right]_0^T = \frac{g}{k}\left[T - \frac{1}{k}(1 - e^{-kT})\right] \ .$$

Hence, the rest of the way is $h - z(T) \approx 533\,\mathrm{m}$*. An estimate with Taylor expansion gives,*

$$h - z(T) = \frac{g}{2}t^2 - \frac{g}{k}\left[t - \frac{1}{k}\left(1 - 1 + kt - \frac{1}{2}k^2t^2 + \frac{1}{6}k^3t^3\right)\right] \simeq \frac{g}{6}kt^3 \approx 674\,\mathrm{m/s} \ .$$

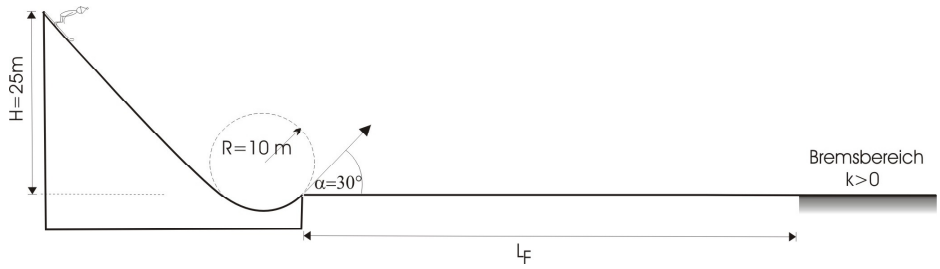

Figure 2.12: Oblique throw with friction.

2.2.4.18 Ex: Oblique throw with friction

You built a ski jumping tower, and now you have to create the associated slope. It consists of an inclined plane and a circular arc with radius $R = 10\,\mathrm{m}$ connected to it. The point of take-off is at ground level, and the tangent to the arc and the surface of the ground enclose an angle of $\alpha = 30°$. The ski ramp is frictionless and there is no friction by air resistance during the flight. Now, the braking area behind the desired flight path L_F, that causes a friction force $F_R = -k \cdot v$, needs to be engineered. The jumper has a mass of $m = 80\,\mathrm{kg}$.
a. At what distance L_F must the braking area begin so that the jumper arrives directly at the braking area for a height of the tower of $H = 25\,\mathrm{m}$?
b. What acceleration does the ski jumper experience in the lowest point of the tower (inside the circular path) in addition to the normal gravitational acceleration?
c. As soon as he arrives at the braking area, the frictional force acts and slows down the jumper. How large must the friction coefficient be chosen so that the ski jumper comes to a standstill in less than 6 s? A residual speed of less than 1 cm/s is defined as a standstill. To do this, set up the differential equation and solve it.

Solution: *a. Starting speed at the time of take-off:* $E_{kin} = E_{pot}$:

$$\frac{1}{2}mv^2 = mgH \Rightarrow v = \sqrt{2gH}$$
$$v_x = v\cos\alpha = \sqrt{2gH}\cos\alpha$$
$$v_x = v\cos\alpha = \sqrt{2gH}\sin\alpha \ .$$

Flight time t_F *until touch-down:*

$$0 = v_y t_F - \frac{1}{2}gt_F^2 \Rightarrow t_F = \frac{2v_y}{g} = \frac{2\sqrt{2gH}\sin\alpha}{g} \ .$$

Flight distance,

$$L_F = v_x \cdot t_F = \sqrt{2gH}\cos\alpha \cdot \frac{2\sqrt{2gH}\sin\alpha}{g} = 4H\sin\alpha\cdot\cos\alpha \simeq 43.3\,\mathrm{m} \ .$$

b. The lowest point is lower than 0 m*:*

$$H' = H + h' \qquad with \qquad h' = R\cdot(1-\cos(30°)) \simeq 1.34\,\mathrm{m} \Rightarrow v = \sqrt{2gH'} \simeq 25.6\,\mathrm{m/s} \ .$$

The centrifugal force at this speed is:

$$m \cdot a = \frac{mv^2}{R} \Rightarrow a = \frac{2gH'}{R} = 2g(H/R + \cos\alpha) \simeq 66\,\mathrm{m/s^2} \simeq 6.7g \ .$$

c. Only $v_x(t=0) \simeq 22.15\,\mathrm{m/s}$ *need to be decelerated.*

$$\dot{v}_x = -\frac{F_R}{m} = -\frac{k}{m}v_x \Leftrightarrow \frac{dv_x}{dt} = -\frac{k}{m}v_x$$

such that,

$$\frac{dv_x}{v_x} = -\frac{k}{m}dt \Rightarrow \int_{v_{x0}}^{v_x} \frac{dv'_x}{v'_x} = -\frac{k}{m}\int_0^t dt' \Rightarrow k = \frac{m}{t}\ln\left(\frac{v_{x0}}{v_x}\right) \ .$$

With $t = 6\,\mathrm{s}$, $v_x = 0.01\,\mathrm{m/s}$ *and* $v_{x0} = v_x(t=0) = 22.15\,\mathrm{m/s}$ *we obtain* $k = 102.7\,\mathrm{kg/s^2}$.

2.2.4.19 Ex: Oblique throw with friction

A soccer ball with a mass of 1 kg is shot at an initial speed v_0. In addition to the force of gravity, the Stokes force acts on the ball $\mathbf{F}_R = -km\mathbf{v}$.
a. Set up the equations of motion.
b. Solve the equations of motion for $x(t)$ and $y(t)$.
c. Show by a Taylor expansion of the solutions $x(t)$ and $y(t)$ that for $\beta \to 0$ follows the solution of the frictionless oblique throw.
d. Give an equation for the flight time T_{max} and determine the range x_{max}.
Note: Note that the general solution of the inhomogeneous differential equation consists of the general solution of the homogeneous and a particular solution of the inhomogeneous differential equation. Determine the constants from the boundary conditions.

Solution: *a. The equation of motion is* $m\ddot{\mathbf{r}} + \beta\dot{\mathbf{r}} - m\mathbf{g} = 0$. *In component notation,*

$$m\ddot{x} + \beta\dot{x} = 0 \qquad \textit{and} \qquad m\ddot{y} + \beta\dot{y} + mg = 0 \ .$$

b. The equation for vertical movement can be solved by separating the variables,

$$dt = \frac{d\dot{y}}{-\beta\dot{y}/m - g}$$

$$t = \frac{m}{-\beta}\int_{\dot{y}_0}^{\dot{y}} \frac{d\dot{y}}{\dot{y} + mg/\beta} = -\frac{m}{\beta}\ln\left(\dot{y} + mg/\beta\right) + \frac{m}{\beta}\ln\left(\dot{y}_0 + mg/\beta\right) = -\frac{m}{\beta}\ln\frac{\dot{y} + mg/\beta}{\dot{y}_0 + mg/\beta}$$

$$\dot{y} = \left(\dot{y}_0 + mg/\beta\right)e^{-\beta t/m} - mg/\beta$$

$$y = \left(\dot{y}_0 + mg/\beta\right)\int_0^t e^{-\beta t/m}dt - \int_0^t mg/\beta dt = \left(\dot{y}_0 + \frac{mg}{\beta}\right)\frac{m}{\beta}\left(1 - e^{-\beta t/m}\right) - \frac{mgt}{\beta} \ .$$

The solution for horizontal movement is analog for $g = 0$,

$$x = \frac{m\dot{x}_0}{\beta}(1 - e^{-\beta t/m}) \ .$$

c. Taylor expansion of $y(t)$ yields,

$$y = \left(\dot{y}_0 + \frac{mg}{\beta}\right)\frac{m}{\beta}\left(1 - 1 + \frac{\beta}{m}t - \frac{\beta^2}{2m^2}t^2 + \frac{\beta^3}{6m^3}t^3 - ...\right) - \frac{mgt}{\beta} \overset{\beta\to 0}{\longrightarrow} \dot{y}_0 t - \frac{g}{2}t^2 \ ,$$

and analogously for x.
d. The flight time follows from,

$$y = 0 = \left(\dot{y}_0 + \frac{mg}{\beta}\right)\frac{m}{\beta}\left(1 - e^{-\beta t_m/m}\right) - \frac{mgt_m}{\beta} \ .$$

The equation cannot be explicitly resolved by t. We can solve it numerically or graphically, or we can develop the exponential function into a Taylor series,

$$\left(\dot{y}_0 + \frac{mg}{\beta}\right)\frac{m}{\beta}\left(1 - \left[1 - \frac{\beta t}{m} + \frac{1}{2}\left(\frac{\beta t_m}{m}\right)^2 - ...\right]\right) = \frac{mgt_m}{\beta}$$

$$t_m \simeq \frac{2}{1 + gm/\beta\dot{y}_0} \ .$$

The reach is then $x_m = x(t_m)$.

2.2.4.20 Ex: Oscillations and static friction

A wooden block vibrates smoothly on a horizontal spring with an oscillation period of $T = 1.2\,\mathrm{s}$. A second block of wood lies on top of the first, the coefficient of static friction between the two blocks being $\mu_H = 0.25$. The static friction is caused by the

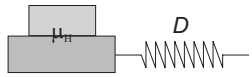

Figure 2.13: Oscillations and static friction.

surface roughness of the two blocks and depends on the mass m of the upper block like $F_H = \mu_H mg$.
a. Will the wooden block slip, if the amplitude of the vibration is 1 cm?
b. Determine the largest allowable vibration amplitude for the wooden block not to slip.

Solution: *The following applies to the period and angular frequency of the harmonic oscillation $T = 2\pi\sqrt{m/D}$ and $\omega_0 = \sqrt{D/m}$,*

$$x(t) = x_0\cos\omega_0 t \quad , \quad \dot{x}(t) = -x_0\omega_0\sin\omega_0 t \quad , \quad \ddot{x}(t) = -x_0\omega_0^2\cos\omega 0t \ .$$

Hence,

$$\ddot{x}_{max} = -x_0\frac{D}{m} = x_0(2\pi/T)^2 \ .$$

a. With $x_0 = 1\,\mathrm{cm}$ we find $\ddot{x}_{max} = 0.274\,\mathrm{m/s^2}$. The static friction is $F_H = \mu_H mg$. In the event of slipping, must apply,

$$F = m\ddot{x} > F_H \qquad \Rightarrow \qquad \ddot{x} > 0.25\cdot g \simeq 2.45\,\mathrm{m/s^2} \equiv a_{crit} \ .$$

Hence, the block does not slip.
b. $x_{max} = a_{crit}(T/(2\pi))^2 = 8.95\,\mathrm{cm}$. *For* $x > 8.95\,\mathrm{cm}$ *the block will slip.*

2.2.4.21 Ex: Stokes' friction

In viscous media (fluids, gases) a velocity-dependent force F_R acts opposite to the movement of a body. For laminar flows, $F_R = Cv$ with a constant C, which in the case of a sphere of radius r has the value $C = 6\pi\eta r$, where η is the viscosity of the medium.
a. Emperor Charlemagne (year 742-814) is upset, because the Saxon Duke Widukind does let himself be subdued. Out of frustration, he threw his golden sphere, symbol of his kingdom (radius $r = 8\,\mathrm{cm}$, density $\rho = 3.19\,\mathrm{g/cm^3}$) into the Rhine. Establish the equation of motion for the sphere in the water and solve it with the initial values $x(t = 0) = 0\,\mathrm{m}$, $v(t = 0) = 0\,\mathrm{m/s}$. How fast does the golden sphere descend to the bottom? Despise buoyancy. The viscosity of water is $\eta_{H_2O} = 1.7 \cdot 10^{-3}\,\mathrm{Ns/m^2}$.
b. If Charlemagne had launched the sphere from the Lorelei rock (height 125 m above the Rhine), how big would the difference in velocity be due to Stokes friction at the moment of impact on the Rhine's surface compared to the frictionless case? Solve the equation of motion of the sphere with the viscosity of the air $\eta_{\mathrm{ar}} = 1.7 \cdot 10^{-5}\,\mathrm{Ns/m^2}$.

Solution: *a. The equation of motion is,*

$$ma = -C_{ag}v - mg \ .$$

Separating the variables,

$$dt = -\frac{mdv}{C_{ag}v + mg} \ .$$

Integrating,

$$t = -\frac{m}{C_{ag}} \ln \frac{C_{ag}v + mg}{C_{ag}v_0 + mg} \ ,$$

or

$$v = \frac{mg}{C_{ag}} e^{-C_{ag}t/m} - \frac{mg}{C_{ag}} \ .$$

With the initial speed $v_0 = 0$ *and the mass* $m = \frac{4\pi}{3} r^3 \rho \simeq 6.8\,\mathrm{kg}$ *we get the maximum speed* $v_{max} = -mg/C_{ag} \simeq 26\,\mathrm{kg/s}$.
b. Without friction the speed of the sphere after a drop of 125 m *would be,*

$$v = \sqrt{2gh} \simeq 50\,\mathrm{m/s} \ .$$

With friction we need to calculate the fall time,

$$0 = \frac{mg}{C_{ar}} \int_0^{t_q} (e^{-C_{ar}t_q/m} - 1)dt = -\frac{m^2 g}{C_{ar}^2} \left(e^{-C_{ar}t_q/m} - \frac{C_{ar}t_q}{m} \right) \ .$$

giving $t_q \simeq ....$ *Now, we can calculate the final speed by,*

$$v = \frac{mg}{C_{ar}} e^{-C_{ar}t_q/m} - \frac{mg}{C_{ar}} \simeq ... \ .$$

2.2.4.22 Ex: Newton's friction

A sports car feels air resistance of the form $F_R = -b \cdot v^2$ as well as a rolling frictional force independent on the velocity F_{rol}. Derive an equation for the power needed to maintain a high velocity v. Assume realistic values for the constants and the sports car's power, and calculate the maximum possible resulting speed. Justify your choice of values!

Solution: *The car's engine must exert an accelerating force F_{mot} to keep the car moving,*

$$ma = F_{mot} - bv^2 - F_{rol} = 0 \ .$$

Let's assume that the car has the power $P = 100\,\mathrm{kW}$. We get,

$$P = F_{mot}v = (bv^2 + F_{rol})v \ .$$

We also assume that air resistance limits the speed to $v_{max} = 300\,\mathrm{km/h}$ disregarding rolling friction. Hence,

$$P \simeq bv_{max}^3 \ ,$$

giving $b \simeq 0.17\,\mathrm{kg\ s/m}$. On the other hand, we can assume that the rolling friction also limits the speed to $v_{max} = 300\,\mathrm{km/h}$ neglecting air resistance. So,

$$P \simeq F_{rol}v_{max} \ ,$$

giving $F_{rol} \simeq 1200\,\mathrm{N}$. We must now solve the second cubic equation.

2.2.4.23 Ex: Mass sliding with friction

What is the energy expenditure for a body of mass m sliding over and decelerated by a horizontal plane with the dynamic friction coefficient μ_d.

Solution: *The friction force is,*

$$F_{at} = -\mu_d N = -\mu_d mg \ .$$

The work is,

$$W = \int_{s_i}^{s_f} F_{at}ds = E_{kin,f} - E_{kin,i}$$
$$-\mu_d mg\Delta s = \frac{m}{2}v^2 - \frac{m}{2}v_0^2 \ .$$

2.2.4.24 Ex: One-dimensional movement

The driver of a train moving with speed v_1, sees, at a distance d ahead of him, a freight train moving in the same direction with speed v_2. He applies the brakes, transmitting the acceleration $-a$ to the train. Show that if: $d > (v_1 - v_2)^2/2a$, there will be no

collision and if $d < (v_1 - v_2)^2/2a$ there will be a collision.

Solution: *The trajectories of the two trains are described by,*

$$x_1 = v_1 t \qquad \text{and} \qquad x_2 = d + v_2 t - \tfrac{a}{2} t^2 \ .$$

The condition for collision, $x_1 = x_2$, requires,

$$\tfrac{a}{2} t^2 + (v_1 - v_2)t - d = 0 \ .$$

That is, the collision occurs at time,

$$t = -\frac{(v_1 - v_2)}{a} \pm \sqrt{\frac{(v_1 - v_2)^2}{a^2} - \frac{2d}{a}} \ .$$

There will be no collision when the root becomes imaginary, that is when $d > (v_1 - v_2)^2/2a$.

2.2.4.25 Ex: One-dimensional movement

Drops of water fall from a shower onto the floor 2 m below. The drops fall at regular intervals and when the first one hits the ground, the fourth is starting to fall. Determine the position of all the drops at the instant when one of them hits the floor.

Solution: *The time for a drop to fall to the ground is given by,*

$$h = \frac{g}{2} \Delta t_4^2 \ .$$

For 4 drops, time is divided by 3. So,

$$y_1 = h - \frac{g}{2}\left(\frac{3\Delta t_4}{3}\right)^2 = h - \frac{9h}{9} = 0\,\text{m} \quad , \quad y_2 = h - \frac{g}{2}\left(\frac{2\Delta t_4}{3}\right)^2 = h - \frac{4h}{9} = \tfrac{10}{9}\,\text{m} \ ,$$

$$y_3 = h - \frac{g}{2}\left(\frac{1\Delta t_4}{3}\right)^2 = h - \frac{h}{9} = \tfrac{16}{9}\,\text{m} \quad , \quad y_4 = h - \frac{g}{2}\left(\frac{0\Delta t_4}{3}\right)^2 = h = 2\,\text{m} \ .$$

2.2.4.26 Ex: One-dimensional movement

The position of a particle that moves along the x-axis depends on time according to the equation: $x = at^2 - bt^3$, x in cm, t in s.
a. At what point is x maximum?
b. What is the speed and at what moment is it zero?
c. What is the acceleration and at what time is it zero?

Solution: *See [1435].*

2.2.4.27 Ex: One-dimensional movement

A plane with speed v_0 lands on an aircraft carrier with negative acceleration $a = -A\sqrt{t}$. What is the minimum required length of the runway?

Solution: *The plane's speed at the end of the runway is given by,*

$$v = v_0 + \int_0^{t_f} a\ dt = v_0 - A\int_0^{t_f} t^{1/2}\ dt = v_0 - A\frac{2}{3}t_f^{3/2} = 0\ .$$

The position is, inserting $t_f = \left(\frac{3v_0}{2A}\right)^{2/3}$,

$$x = \int_0^{t_f} v\ dt = \int_0^{t_f}\left(v_0 - A\frac{2}{3}t^{3/2}\right)\ dt = v_0 t_f - A\frac{2}{3}\frac{2}{5}t_f^{5/2} = \frac{3v_0}{5}\left(\frac{3v_0}{2A}\right)^{2/3}\ .$$

2.2.4.28 Ex: One-dimensional movement

Two bodies are located at the origin of the x-axis when $t = 0\,\mathrm{s}$. Body A has a constant speed of $2\,\mathrm{m/s}$. Body B is initially at rest but subject to a constant acceleration of $1\,\mathrm{m/s^2}$.
a. Represent schematically, in the same graph, the positions of bodies A and B as a function of time.
b. What is the time of collision?
c. What is the position x when the collision will occur?
d. What is the speed of body B at the time of collision?
e. At what time will the velocities of the two bodies be equal?

Solution: *a. The trajectories of the bodies are given by,*

$$x_a = v_a t$$
$$x_b = \frac{a}{2}t^2\ .$$

b. They meet when $x_a = x_b$*, that is, at time* $t_e = \frac{2v_a}{a} = 4\,\mathrm{s}$.
c. The position of the bodies at this time is $x_a(t_e) = v_a t_e = 8\,\mathrm{m}$.
d. The speed of body B is $v_b = at_e = 4\,\mathrm{m/s}$.
e. From the condition $v_a = v_b = at_v$ *we obtain* $t_v = \frac{v_a}{a} = 2\,\mathrm{s}$.

2.2.4.29 Ex: Cylinder rolling without sliding

Consider a cylinder of radius R rolling without sliding on a horizontal plane. The center of mass of the cylinder is accelerated.
a. What is the angular acceleration of the cylinder?
b. What is the rotation angle β of the cylinder as a function of time?

Solution:

2.2.4.30 Ex: Relative velocity of rotating bodies

Two bodies A and B are in uniform circular movements of concentric trajectories with radii r_a and r_b and angular velocities ω_a and ω_b. Determine the relative speed between the two bodies.

Solution:

2.2.4.31 Ex: Acceleration of a sliding body

Determine the acceleration of a body that slides along the thread of a screw with step h and radius R. Disregard friction and consider the body to have started from rest.

Solution:

2.2.4.32 Ex: Ballistics

To launch a ball from ground over a wall of height H located at a distance S (see figure), what is the lowest initial speed with which the ball has to be launched?

Solution:

2.2.4.33 Ex: Ballistics

A bullet is fired from a cannon with speed v_0. Determine the geometric region where the bullet will certainly not hit the ground.

Solution:

2.2.4.34 Ex: Ballistics

An inclined plane forms an angle α with the xy-plane, as shown in the figure. A body is launched with speed v_0, forming an angle with the y-axis. Disregarding friction calculate: x_{max}, z_{max} and the time it takes for the projectile to return to the y-axis.

Solution:

2.2.4.35 Ex: Ballistics

A stone is launched at an initial speed of 20 m/s. Knowing that it stayed for 2 s in the air, calculate:
a. the launch angle (with respect to the horizontal), b. the maximum height reached,
c. the reach,
d. another launch angle for which the stone will have the same range. (In this case

the time will be different from 2 s).

Solution:

2.2.4.36 Ex: Translation with / without friction

A body is moved with speed $v = 5\,\mathrm{m/s}$ over a horizontal plane without friction. Suddenly he encounters another plane (also without friction) inclined by an angle $\theta = 30°$ and having a height of $H = 0.8\,\mathrm{m}$, as shown in the figure.
a. At what distance d from the end of the inclined plane will the body fall?
b. What is the maximum height that the body will reach

Solution:

2.2.4.37 Ex: Collision

A small body is launched from the origin with speed $v_0 = 100/\sqrt{3}\,\mathrm{m/s}$ under an angle $\theta = 60°$ with the horizontal. Another body is launched 1 second later, at the same speed v_0, but horizontally and from a height H, as shown in the figure. Suppose there is a collision between the two bodies and that $g = 10\,\mathrm{m/s^2}$. a. At what time does the collision occur?
b. How high should H be for the collision to occur?
c. What are the x and y coordinates of the collision?

Solution:

2.2.4.38 Ex: Ballistics

A small body is launched from the origin with speed v_0 under an angle θ with the horizontal. Another body is launched with the same speed v_0, but horizontally and from a height H, as shown in the figure. What should be the value of H such that they reach the same point on the x-axis?

Solution:

2.2.4.39 Ex: Ballistics

a. Show that the movement of a projectile launched with v_0 and θ is described by the parabola: $y(x) = \frac{v_{0y}^2}{2g} - \frac{g}{2}\left(\frac{x}{v_{0x}} - \frac{v_{0y}}{g}\right)^2$, with $v_{0x} = v_0\cos\theta$ and $v_{0y} = v_0\sin\theta$.
b. Find the angle α that the trajectory forms with the horizontal for any x ($\tan\alpha = dy/dx$),
c. Find x_{max} corresponding to the top of the trajectory ($\tan\alpha = 0$).
d. Find the reach R by letting $\alpha = \pi - \theta$.

Solution:

2.2.4.40 Ex: Coupled masses

a. Find the angle θ for the left figure so that the system remains at rest. Disregard friction.
b. Find the ratio between the masses M_1 and M_2 such that the system remains at rest in the right figure. Disregard friction.

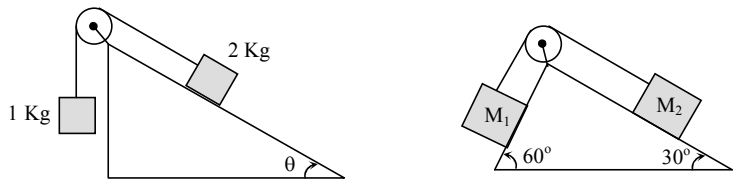

Figure 2.14: Coupled masses.

Solution: *a. Equilibrium,*

$$a_1 = -m_1 g \equiv a_2 = -m_2 g \sin\theta \ .$$

Hence,

$$\theta = \arcsin \frac{m_1}{m_2} = \arcsin \frac{1}{2} = 30^\circ \ .$$

b. Equilibrium

$$a_1 = -m_1 g \sin\theta_1 \equiv a_2 = -m_2 g \sin\theta_2 \ .$$

Hence,

$$\frac{m_2}{m_1} = \frac{\sin\theta_1}{\sin\theta_2} = \frac{1}{\sqrt{3}} \ .$$

2.2.4.41 Ex: Coupled masses

a. Find the acceleration of the 2 kg body shown in the left figure.
b. Find the mass of body A such that the acceleration of body B in the right figure is zero.

Solution: *a. We know that the acceleration of the pulley, $a_{12} = -a_5$, is given by,*

$$a_5 = -g\frac{m_5 - (m_1 + m_2)}{m_5 + (m_1 + m_2)} = -\frac{g}{4} \ .$$

Also,

$$a_2 = (-g + a_5)\frac{m_2 - m_1}{m_1 + m_2} - a_5 = -\frac{g}{6} \ .$$

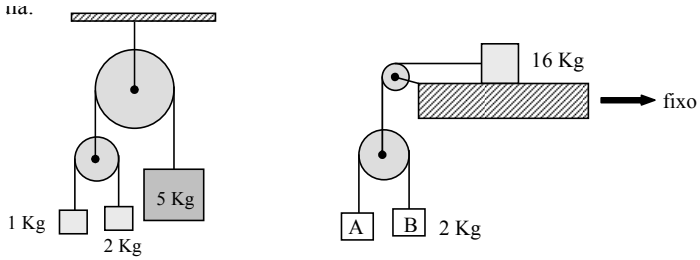

Figure 2.15: Coupled masses.

This does not agree with the template [1435]: $a_2 = \frac{2}{15}g$.
b. We know that the acceleration of the pulley, $a_{AB} = -a_{16}$*, is given by,*

$$(m_A + m_B + m_{16})a_{16} = (m_A + m_B)g \ .$$

Hence,

$$a_{16} = \frac{m_A + m_B}{m_A + m_B + m_{16}}g \ .$$

Also,

$$0 = a_B = (-g + a_{16})\frac{m_B - m_A}{m_B + m_A} - a_{16}$$

or equivalently,

$$-2a_{16} = a_A = (-g + a_{16})\frac{m_A - m_B}{m_B + m_A} - a_{16} \ .$$

Inserting in the equation for a_B *the expression for* a_{16}*, we get*

$$0 = -g\frac{-m_{16}m_A + m_{16}m_B + m_A^2 + 2m_Am_B + m_B^2}{(m_A + m_B + m_{16})(m_A + m_B)}$$

which is only satisfied when the numerator is zero:

$$m_A = \frac{m_{16}}{2} - m_B \pm \sqrt{m_{16}\left(\frac{m_{16}}{4} - 2m_B\right)} = 6\,\text{kg} \ .$$

This does not agree with the template [1435]: $m_A = 4kg$.

2.2.4.42 Ex: Frictionless pulley

A string of length L and linear mass density λ passes through a pulley without friction. It is released from rest, with a length x pending on one side and $L - x$ on the other.
a. determine the acceleration as a function of x;
b. for which situation is the acceleration zero?

Solution: *a. We have,*

$$a = \frac{\int_0^x \lambda ds - \int_0^{L-x} \lambda ds}{\int_0^L \lambda ds}g = \left(\frac{2x}{L} - 1\right)g \ .$$

b. $x = \frac{L}{2}$.

2.2.4.43 Ex: Coupled bodies

In the system shown in the figure, find:
a. the acceleration of the total system and
b. the force on the rope at point A.

Solution:

2.2.4.44 Ex: Coupled bodies

N bodies connected to each other by massless strings are pulled on a ramp by means of a force F. Calculate the tension in the rope connected to the i-th body.

Solution:

2.2.4.45 Ex: Coupled bodies

Consider the conical pendulum shown in the figure, where the string connecting the mass M to point O has no mass.
a. find the angle θ as a function of the velocity of mass M,
b. find the tension in the string at point O.

Solution:

2.2.4.46 Ex: Coupled bodies without friction

A body of mass M is hung by an ideal string over a triangular block of angle θ, as shown in the figure. In the absence of friction between the blocks, we ask what is the maximum acceleration that can be given to the system such that the body M remains in contact with the triangular block. In this case, what is the tension in the rope? If the system is moving at a constant speed, what is the value of the tension in the rope and of the normal?

Solution:

2.3 Friction

Stokes friction $F_{frc} \propto -v$ and *Newton friction* $F_{frc} \propto -v^2$.

2.3.0.1 Ex: Coupled masses with friction

In the system exhibited in the figure body A slides on a surface with a friction coefficient μ. The ropes and pulleys have no mass.
a. find the accelerations of blocks A and B;
b. find the tension in the rope connected to body A.

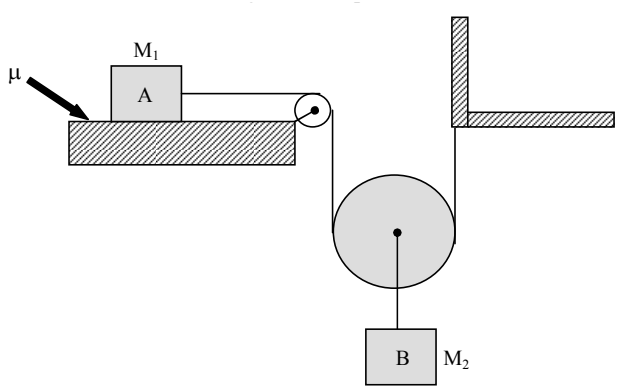

Figure 2.16: Coupled masses with friction.

Solution: *a. We use the energy conservation law:*

$$\frac{M_1}{2}v_1^2 + \frac{M_2}{2}v_2^2 + M_2 g x_2 = -\mu M_1 g x_1 \ ,$$

with the derivative,

$$\frac{M_1}{2}2v_1\dot{v}_1 + \frac{M_2}{2}2v_2\dot{v}_2 + M_2 g\dot{x}_2 = -\mu M_1 g\dot{x}_1 \ .$$

The geometry of the problem shows, that $x_1 = -2x_2$. Therefore,

$$\frac{M_1}{2}2v_1\dot{v}_1 + \frac{M_2}{4}v_1\dot{v}_1 - \frac{M_2}{2}g\dot{x}_1 = -\mu M_1 g\dot{x}_1$$
$$M_1 a_1 + \frac{M_2}{4}a_1 - \frac{M_2}{2}g = -\mu M_1 g \ .$$

Hence,

$$a_1 = 2a_2 = 2g\frac{M_2 - 2\mu M_1}{M_2 + 4M_1} \ .$$

b. The stresses are,

$$T_2 = \frac{1}{2}M_2(g - a_2) = \frac{1}{2}M_2\left(g - g\frac{M_2 - 2\mu M_1}{M_2 + 4M_1}\right) = gM_1M_2\frac{2+\mu}{M_2 + 4M_1}$$
$$T_1 = T_3 = \tfrac{1}{2}T_2 \ .$$

where T_3 is the tension in the rope between the pulleys.
Alternatively, we can establish the equations of motion,

$$\begin{aligned} M_1 a_1 &= -F_{at} + T_1 \\ M_2 a_2 &= M_2 g - T_2 \\ F_{at} &= \mu M g \\ a_1 &= 2a + 2 \ , \end{aligned}$$

This system of equations can be solved by giving the same results.

2.3.0.2 Ex: Inclined plane with and without friction

a. Given the angle θ of an inclined plane without friction, what is the acceleration a_R such that the block of mass m shown in the figure does not slide?
b. If the inclined plane had a friction coefficient μ, what would be the maximum and minimum accelerations such that the block does not slide?

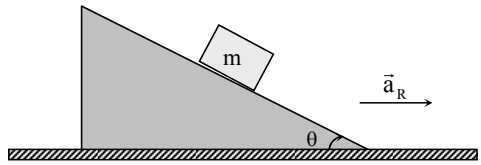

Figure 2.17: Inclined plane.

Solution: *a. Without friction, the projections of the forces on the inclined axis must cancel:*

$$a_R \cos\theta = g \sin\theta \ .$$

In this case, $N = mg\cos\theta$.
b. Along the inclined axis the balance of forces demands,

$$mg\sin\theta - ma_R\cos\theta \mp \mu_e N = 0 \ ,$$

where the upper sign indicates an upward frictional force (case of sliding downward) and the lower sign indicates a downward frictional force (case of sliding upward). In the normal direction to the inclined axis we have,

$$-mg\cos\theta + ma_R\sin\theta + N = 0 \ .$$

Hence,

$$mg\sin\theta - ma_R\cos\theta \mp \mu_e mg\cos\theta \pm \mu_e ma_R\sin\theta = 0 \ ,$$

which gives,

$$a_R = g\frac{\sin\theta \mp \mu_e\cos\theta}{\cos\theta \mp \mu_e\sin\theta} \ .$$

2.3.0.3 Ex: Static friction

a. The system shown in the figure is friction-free. Determine the value of the force F such that body A does not descend or rise.
b. If there were a static friction μ between the surfaces of the blocks, what would be the maximum and minimum values of forces such that body A does not fall or rise?

Solution:

2.3.0.4 Ex: Viscous medium

A body with initial velocity v_0 penetrates a medium that produces a viscous force given by (a) $F = -b\sqrt{v}$ and (b) $F = -cv^2$. Determine the maximum distance that the body penetrates into this medium for both cases.

Solution: *a. The equation of motion,*

$$ma = m\frac{dv}{dt} = -b\sqrt{v} \ ,$$

can be written,

$$v^{-1/2}dv = -\frac{b}{m}dt \ .$$

Integration,

$$\int_{v_0}^{v} v^{-1/2}dv = -\frac{b}{m}\int_0^t dt \ ,$$

gives the velocity,

$$v = \left(v_0^{1/2} - \frac{b}{2m}t\right)^2 \ .$$

The body stops, whenv $= 0$*, isto é* $t_0 = \frac{2m}{b}v_0^{1/2}$*. At this moment, the path taken is,*

$$s_0 = \int_0^{t_0} vdt = v_0 t_0 - v_0^{1/2}\frac{b}{2m}t_0^2 + \frac{b^2}{12m^2}t_0^3 = \frac{2}{3}v_0^{\frac{3}{2}}\frac{m}{b} \ .$$

b. The equation of motion,

$$ma = m\frac{dv}{dt} = -bv^2$$

can be written,

$$v^{-2}dv = -\frac{b}{m}dt \ .$$

Integration,

$$\int_{v_0}^{v} v^{-2}dv = -\frac{b}{m}\int_0^t dt$$

gives the velocity,

$$v = \frac{1}{v_0^{-1} + \frac{b}{m}t} \ .$$

Using the substitution,

$$u = v_0^{-1} + \frac{b}{m}t \qquad with \qquad \frac{du}{dt} = \frac{b}{m} \ .$$

The path taken is,

$$s = \int_0^t \frac{1}{v_0^{-1} + \frac{b}{m}t} dt = \frac{m}{b} \int_{v_0^{-1}}^{v_0^{-1} + \frac{b}{m}t} \frac{du}{u} = \frac{m}{b} \ln\left(1 + v_0 \frac{b}{m}t\right) \ .$$

That is, the body penetrates the medium without limitation.

2.3.0.5 Ex: Inclined plane with friction

The system shown in the figure employs pulleys without mass. Find the acceleration of each block and the tension in the string.

Solution:

2.3.0.6 Ex: Coupled bodies subject to friction

In the system shown in the figure, the block is in contact with the horizontal surface without friction and subject to a force F. There is a static friction μ between this block and block A in such a way that there is no relative movement between the three blocks forming the system. Calculate: (a) The angle, (b) The tension in the string, and (c) the minimum μ.

Solution:

2.3.0.7 Ex: Body subject to friction

A block of mass M rests on a table with a static friction coefficient μ_e. A force F is applied to the block so as to form an angle θ with the horizontal, as shown in the figure. Assuming that the block is always on the verge of sliding,
a. what is the angle θ that allows the applied force to be minimal, and
b. in this case, what will be the value of the force F_{min}?

Solution:

2.3.0.8 Ex: Coupled bodies with friction

A block of mass M_1 is on top of another block of mass M_2, which slides over the floor, as shown in the figure. The static friction between the two blocks is μ_e and the kinetic friction between block 2 and the ground is μ_c. a. Determine the maximum force F that can be applied to block 2 without block 1 sliding over it.

b. If the force is increased such that M_1 starts to slide, and the kinetic friction between the blocks is also μ_c, what will be the acceleration of each mass?

Solution:

2.3.0.9 Ex: Coupled bodies with friction

A block of mass M is located on top of another block of the same mass, on a flat plane inclined by an angle θ, as shown in the figure. The static friction between the two blocks is μ, and between the lower block and the plane it is zero.
a. Determine the maximum force F that can be applied to the upper block without sliding over the lower block.
b. In this case, what will be the acceleration of the total system?

Solution:

2.3.0.10 Ex: Inclined plane with friction

A body of mass m is located on a triangular block of angle θ and mass M, as shown in the figure. There is no friction between the triangular block and the ground, and static friction coefficient between the two blocks is μ.
a. What is the maximum horizontal force F that can be applied to the block m such that it does not slide over the wedge?
b. What is the value of normal in this situation?

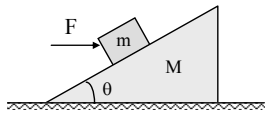

Figure 2.18: Inclined plane.

Solution: *a. We have the following equations. The acceleration of the system is* $(M+m)a = F$*, the friction in the static limit is* $F_{at} = \mu_e N$*, and the mass weight* m *produces a normal tension* N *and a friction force* F_{at}*, such that,*

$$N\cos\theta - F_{at}\sin\theta - mg = 0 \ .$$

The tangential force is

$$F_t = F\cos\theta - mg\sin\theta - F_{at} \ ,$$

and the normal force is,

$$F_n = -F\sin\theta - mg\cos\theta + N \ .$$

Thus, the horizontal acceleration of the mass m *is,*

$$ma = F_t\cos\theta - F_n\sin\theta = (F\cos\theta - mg\sin\theta - F_a)\cos\theta - (-F\sin\theta - mg\cos\theta + N)\sin\theta \ ,$$

which gives,

$$F = \frac{M+m}{M}(\mu_e + \tan\theta)N\cos\theta \ .$$

Solving the equation of balance between weight and friction for N and inserting into the equation above, we finally find,

$$F = mg\frac{M+m}{M}\frac{\tan\theta + \mu_e}{1-\mu_e\tan\theta} \ .$$

b. Solving the first equation for N, we obtain,

$$N = \frac{mg}{\cos\theta - \mu_e\sin\theta} \ .$$

2.3.0.11 Ex: Potential energy

A body is accelerated uniformly from rest until it reaches the speed v_f in time t_f. Show that the instantaneous power delivered to the body is:

$$P(t) = mv_f^2\frac{t}{t_f^2} \ .$$

Solution: *The final speed is,*

$$v_f = at_f \ .$$

With that, we can calculate the instantaneous power:

$$\dot{W} = \frac{d}{dt}\int_0^s Fds = F\frac{d}{dt}s = F\frac{d}{dt}\frac{a}{2}t^2 = Fat = \frac{mv_f^2}{t_f^2}t \ .$$

2.3.0.12 Ex: Body subject to friction

Consider the system sketched in the figure, where the force F is constant and the planes have a dynamic friction coefficient μ. Calculate the total work performed by the forces acting on the system when it moves an infinitesimal distance Δx.

Solution:

2.3.0.13 Ex: Lennard-Jones potential

Consider the Lennard-Jones potential commonly used as the interaction energy between two atoms forming a molecule:

$$U(r) = C\left[\left(\frac{r_0}{r}\right)^{12} - 2\left(\frac{r_0}{r}\right)^{6}\right] \ .$$

a. Draw $U(r)$ as a function of r.
b. Show that the minimum energy (equilibrium position) is at r_0.
c. Find the force between atoms as a function of r.
d. What is the energy required to separate the atoms that form the molecule?

Solution: *b. The derivative of the potential must zero:*

$$0 = \frac{dU(r)}{dr} = C\frac{d}{dr}\left[\left(\frac{r_0}{r}\right)^{12} - 2\left(\frac{r_0}{r}\right)^{6}\right] = C\left[\frac{-12}{r}\left(\frac{r_0}{r}\right)^{12} - 2\frac{-6}{r}\left(\frac{r_0}{r}\right)^{6}\right] .$$

c. The force is,

$$F = -\frac{dU(r)}{dr} = 12C\left[\frac{-1}{r}\left(\frac{r_0}{r}\right)^{12} + \frac{1}{r}\left(\frac{r_0}{r}\right)^{6}\right] .$$

d. The energy is,

$$E_{ion} = \int_{r_0}^{\infty} F dr = U(r_0) - U_\infty = C .$$

2.3.0.14 Ex: Pendulum

A pendulum of mass m and length l is released from the point $\theta = 60°$ from rest, as shown in the figure. Upon reaching the vertical position $\theta = 0°$, the pendulum string encounters a nail fixed at a distance d from the ceiling. Find the minimum distance d for the mass m to rotate around the nail.

Solution:

2.3.0.15 Ex: Body in a circular truss

A body of mass m moves within a vertical circular rail of radius R (see figure). When m is at the lowest position its speed is v_0.
a. What is the minimum value of v_0 such that the body goes through the entire track?
b. If v_0 were 78% of the value determined in (a), the body would go up the rail up the point P, where it will lose contact with the rail. Find the coordinate θ of this point.

Solution:

2.3.0.16 Ex: Body in a potential

A body of mass M, subject to a potential $U(x) = -\cos \pi x$, is released at the origin ($x = 0$) with speed v_0.
a. Sketch the potential in the region $-1 \leq x \leq 1$.
b. Find the force $F(x)$ acting on the body.
c. What is the maximum speed v_0 that can be imparted to the body in such a way

that it is confined to the region $-1 \leq x \leq 1$?

Solution:

2.3.0.17 Ex: Roller coaster with looping

A mass m slides without friction along the roller coaster shown in the figure. The circular part has radius R and the mass departs from rest at point B, at the height h measured with respect to relation to the base of the tracks.
a. What is the kinetic energy of m at the point P?
b. What is the acceleration of m at point P assuming that the mass remains on the track?
c. What is the lowest value of h for m to perform the circular motion?
d. For a value of h greater than this minimum, write down the expression for the normal force exerted by the track on the mass.

Solution:

2.3.0.18 Ex: Body on an inclined plane

A 2 kg body is released on an inclined plane from a point where it elongates by 4 m a spring having the constant spring constant of $k = 100\,\mathrm{N/m}$. The spring is fixed parallel to the plane, inclined by $\theta = 30°$ (see figure).
a. Calculate the maximum compression of the spring assuming that its mass be negligible;
b. Calculate the maximum compression of the spring when the inclined plane exerts friction, the friction coefficient between it and the body being equal to 0.2);
c. In the case (b), what is the height that the body reaches on its way back upward?

Solution:

2.3.0.19 Ex: Bodies climbing a slope

Two bodies propagating at the same speed v on a horizontal plane have a distance of d. After having climbed a high slope h, what will be the distance between them?

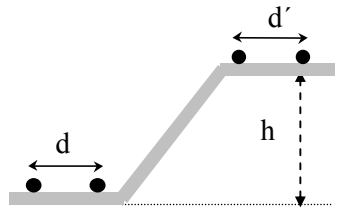

Figure 2.19: Bodies climbing a slope.

Solution: *The velocity of the bodies in the upper plane, v_s, is given by,*

$$\frac{m}{2}v^2 - \frac{m}{2}v_s^2 = mgh \ .$$

As the trajectories of the bodies are the same, we have,

$$d_s = \frac{v_s}{v}d = d\sqrt{1 - \frac{2gh}{v^2}} \ .$$

2.3.1 Exercises

2.4 Many-body systems

2.4.1 Balance of forces

2.4.2 Center-of-mass

2.4.3 Collisions and conservation of linear momentum

2.4.3.1 Binary elastic collisions and molecule formation

Binary collisions between atoms are always *elastic*. To see this, we set up the conservation laws for energy and momentum allowing for an inelastic lost of kinetic energy ΔE:

$$\boxed{\frac{p_{i1}^2}{2m} + \frac{p_{i2}^2}{2m} = \frac{p_{f1}^2}{2m} + \frac{p_{f2}^2}{2m} + \Delta E \quad \text{and} \quad \mathbf{p}_{i1} + \mathbf{p}_{i2} = \mathbf{p}_{f1} + \mathbf{p}_{f2}} \ . \tag{2.32}$$

Without loss of generality we may transform in to the center-of-mass system, where $\mathbf{p}'_{i1} + \mathbf{p}'_{i2} = 0 = \mathbf{p}'_{f1} + \mathbf{p}'_{f2}$. Inserting this into the law of energy conservation,

$$m\Delta E = p'^2_{i1} - p'^2_{f1} \ . \tag{2.33}$$

So, obviously, if no energy can be dissipated, e.g. into internal atomic excitations, the kinetic energy must remain unchanged.

Without loss of generality we may transform into the inertial system, where $\mathbf{p}''_{i2} = 0$. Inserting this into the conservation laws,

$$\frac{p''^2_{i1}}{2m} = \frac{p''^2_{f1}}{2m} + \frac{p''^2_{f2}}{2m} + \Delta E \quad \text{and} \quad \mathbf{p}''_{i1} = \mathbf{p}''_{f1} + \mathbf{p}''_{f2} \ . \tag{2.34}$$

Now substituting $\mathbf{p}_{i1}$ in the energy conservation law,

$$m\Delta E = \mathbf{p}''_{f1} \cdot \mathbf{p}''_{f2} \ . \tag{2.35}$$

So, if no energy can be dissipated, the atoms move in orthogonal directions after the collision.

Can two colliding atoms form a molecule? The laws of energy and momentum conservation require,

$$\frac{\mathbf{p}_1^2}{2m} + \frac{\mathbf{p}_2^2}{2m} = \frac{\mathbf{p}_{12}^2}{m} + \Delta E \qquad \text{and} \qquad \mathbf{p}_1 + \mathbf{p}_2 = \mathbf{p}_{12} \ . \tag{2.36}$$

In the center-of-mass inertial system, we have,

$$2\frac{\mathbf{p}_1''}{2m} = \Delta E \qquad \text{and} \qquad \mathbf{p}_1' + \mathbf{p}_2' = 0 = \mathbf{p}_{12}' \ . \tag{2.37}$$

That is, a molecule can only be formed if the collision is inelastic ($\Delta E \neq 0$), which is only possible if there is an excited internal state having exactly the energy ΔE.

2.4.4 Exercises

2.4.4.1 Ex: Mass hanging at a gallow

The mass M is hanging from a string attached to a vertical mast and attached to a boom, so that the angle becomes $\alpha = 90°$, as indicated in the figure. With $h = 1\,\mathrm{m}$, $l = 1\,\mathrm{m}$ and $m = 1\,\mathrm{kg}$, calculate the tension in the wire.

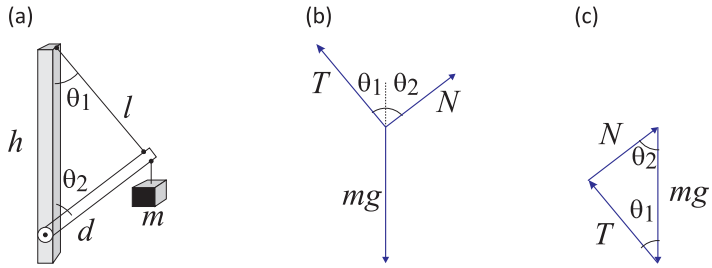

Figure 2.20: (a) Mass hanging at a gallow. (b,c) Alternative force diagrams.

Solution: *The balance of forces requires for the tensions acting on the wire (T) and the boom (N),*

$$0 = T\sin\theta_1 - N\sin\theta_2$$
$$mg = T\cos\theta_1 + N\cos\theta_2 \ .$$

Multiplying the first equation by $\cos\theta_2$ *and the second by* $\sin\theta_2$ *and adding the results,*

$$T = \frac{mg\sin\theta_2}{\sin\theta_2\cos\theta_1 + \sin\theta_1\cos\theta_2} \ .$$

For arbitrary triangles hold the trigonometric relationships,

$$l^2 + h^2 - 2hl\cos\theta_1 = d^2 \qquad \text{and} \qquad d^2 + h^2 - 2hd\cos\theta_2 = l^2 \ .$$

Inserting in the above equation for T we get,

$$T = mg\frac{\sqrt{1-\left(\frac{d^2+h^2-l^2}{2hd}\right))^2}}{\frac{l^2+h^2-d^2}{2hl}\sqrt{1-\left(\frac{d^2+h^2-l^2}{2hd}\right)^2} + \frac{d^2+h^2-l^2}{2hd}\sqrt{1-\left(\frac{l^2+h^2-d^2}{2hl}\right)^2}} = mg\frac{l}{h} = 9.81\,\mathrm{N} \ .$$

2.4.4.2 Ex: Three blocks

Determine the equilibrium situation of the system sketched in the figure.

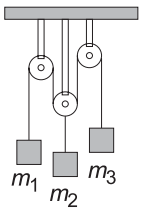

Figure 2.21: Scheme of the system.

Solution: *The solution is,*

$$(m_1 + m_2 + m_3)a = m_1 g \pm m_2 g - m_3 g \ .$$

2.4.4.3 Ex: Balance of forces on the inclined plane

One body with the mass 8 kg and a second body with the mass 10 kg connected by a wire slide without friction each one on an inclined plane. The wire runs without friction over a block, as shown in the diagram.
a. In which direction will the bodies move?
b. Calculate the acceleration of the bodies.
c. Now the two bodies are replaced by other bodies with the masses m_1 and m_2, such that there is no more acceleration, that is, the bodies are at rest. What should the ratio of the mass m_1 and m_2 be?

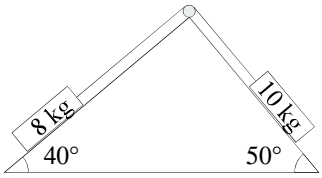

Figure 2.22: Inclined plane.

Solution: *a. The* 10 kg *body pulls the* 8 kg *body over the block.*

b. The forces acting on the bodies m_l and m_r are,

$$(m_l + m_r)a = m_l g \sin\alpha_l - m_r g \sin\alpha_r$$
$$a = g\frac{m_l \sin\alpha_l - m_r \sin\alpha_r}{m_l + m_r} = g\frac{8\sin\left(\pi\frac{40}{180}\right) - 10\sin\left(\pi\frac{50}{180}\right)}{8+10} = 1.37\,\mathrm{m/s^2} \ .$$

c. Equilibrium is reached when,

$$0 = g\frac{m_l \sin\alpha_l - m_r \sin\alpha_r}{m_l + m_r}$$
$$\frac{m_l}{m_r} = \frac{\sin\alpha_r}{\sin\alpha_l} = \frac{\sin\left(\pi\frac{50}{180}\right)}{\sin\left(\pi\frac{40}{180}\right)} \simeq 1.15 \ .$$

2.4.4.4 Ex: Balance of forces on the arc

Two spheres of mass m_1 and $m_2 = 2m_1$ connected by a rope of length L are located on both sides of a wall with a semicircular cross-sectional area (see figure). The diameter of the circular arc is $2R$.

a. At what horizontal distance x from the center of the wall must the spheres be in

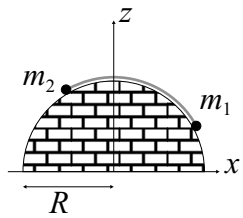

Figure 2.23: Balance of forces on the arc.

order to avoid acceleration? Assume $L = \pi R/2$.

b. Set up the equation of motion.

c. Now assume that the rope is so short that the sine expressions can be replaced by their first-order Taylor expansion. Solve the equation of motion in this approximation. Assume that at $t = 0$ the balls are the same height.

Solution: *a. The forces acting on the spheres are due to gravity $F_k(x) = m_k g \sin\alpha_k$, where the angles α_k are taken with respect to the vertical. With the boundary condition $\alpha_1 + \alpha_2 = \frac{L}{R}$ is the balance equation is,*

$$m_1 g \sin\alpha_1 = m_2 g \sin\alpha_2 \quad \Rightarrow \quad \sin\alpha_1 = \frac{m_2}{m_1}\sin\left(\frac{L}{R} - \alpha_1\right) \quad \Rightarrow \quad \tan\alpha_1 = 2 = \frac{1}{\tan\alpha_2} \ .$$

The angles between the vertical and the locations of the masses are $\alpha_1 = 63.4°$ and $\alpha_2 = 26.6°$. The distances are $x_1 = \cos\alpha_1 = 0.45R$ resp. $x_2 = 0.89R$.

b. The acceleration force is $(m_1+m_2)a(t) = (m_1+m_2)R\ddot{\alpha}_1(t)$. *Hence, the equation of motion is,*

$$(m_1+m_2)R\ddot{\alpha}_1(t) = m_1 g\sin\alpha_1(t) - m_2 g\sin\left(\frac{L}{R}-\alpha_1(t)\right)$$
$$\Rightarrow \quad \ddot{\alpha}_1(t) - \frac{g}{3R}\sin\alpha_1(t) + \frac{2g}{3R}\sin\left(\frac{L}{R}-\alpha_1(t)\right) = 0 \ .$$

c. From the approximate equation of motion, $\ddot{\alpha}_1(t) - \frac{g}{R}\alpha_1(t) = -\frac{2gL}{3R^2}$ *one obtains the characteristic equation with the ansatz,* $\alpha_1 = Ae^{\lambda t} + C$,

$$\lambda^2 Ae^{\lambda t} - \frac{g}{R}\left(Ae^{\lambda t}+C\right) = -\frac{2gL}{3R^2} \ .$$

It follows $C = \frac{2L}{3R}$ *and* $\lambda = \pm\sqrt{\frac{g}{R}}$. *The solution is now,* $\alpha_1 = Ae^{\sqrt{\frac{g}{R}}t} + Be^{-\sqrt{\frac{g}{R}}t} + \frac{2L}{3R}$. *From the initial condition* $\alpha_1(0) = \frac{2L}{3R}$ *follows,*

$$\alpha_1 = 2\sinh\sqrt{\frac{g}{R}} + \frac{2L}{3R} \ .$$

2.4.4.5 Ex: Relative and center of mass coordinates

Consider two mass m_1 and m_2 at the positions $\mathbf{r}_1$ and $\mathbf{r}_2$.
a. Calculate the vector $\mathbf{r}$ of the center of mass and express the vectors $\mathbf{r}_1$ and $\mathbf{r}_2$ as a function of the vector $\mathbf{r}$ and the relative vector $\mathbf{r} \equiv= \mathbf{r}_2 - \mathbf{r}_1$.
b. Show that the vector is on the line connecting the masses m_1 and m_2. (**Help:** Parametrize the direct path from $\mathbf{r}_1$ to $\mathbf{r}_2$ and show, that $\mathbf{r}$ is a point on that path.)
c. Suppose that there are no external forces acting on the two masses and that only the gravitational force between them is present. Also suppose that each mass moves on a circle around the center of mass. Assume equilibrium between the gravitational attraction and the centripetal force for the two masses. Compare with the corresponding equation of motion for the relative coordinate (reduced mass).
d. Consider as an example the two-body system composed of the Earth and the Moon ($m_E = 5.974\times10^{24}\,\mathrm{kg}$, $m_M = 7.35\times10^{22}\,\mathrm{kg}$, $r = 384000\,\mathrm{km}$). What is the distance d from the center of mass of this system from the center of the Earth?
e. What is the error in calculating the period T of a revolution of the Moon around the Earth, when the Earth's movement is neglected, that is, when the origin of the coordinates is identified with the center of the Earth?

Solution: *a. The total momentum is additive. We define the vector of the center of mass* $\mathbf{r}$, *such that* $P = M\dot{\mathbf{r}} = (m_1+m_2)\dot{\mathbf{r}} \equiv m_1\dot{\mathbf{r}}_1 + m_2\dot{\mathbf{r}}_2 = \mathbf{p}_1 + \mathbf{p}_2$. *Then,*

$$\mathbf{r} = \frac{m_1\mathbf{r}_1 + m_2\mathbf{r}_2}{M} \ .$$

With $\mathbf{r} = \mathbf{r}_2 - \mathbf{r}_1$ *the individual coordinates are expressed by,*

$$\mathbf{r}_1 = \mathbf{r} - \frac{m_2}{M}\mathbf{r} \qquad \textit{and} \qquad \mathbf{r}_2 = \mathbf{r} + \frac{m_1}{M}\mathbf{r} \ .$$

b. The connecting line is given by,

$$\mathbf{r}(s) = \mathbf{r}_1 + s(\mathbf{r}_2 - \mathbf{r}_1) \ .$$

For $s = m_2/M$ we obtain,

$$\mathbf{r}(s) = \left(1 - \frac{m_2}{M}\right)\mathbf{r}_1 + \frac{m_2}{M}\mathbf{r}_2 = \frac{m_1}{M}\mathbf{r}_1 + \frac{m_2}{M}\mathbf{r}_2 = \mathbf{r} \ .$$

c. The centripetal force on m_1 respectively m_2 is,

$$m_1\omega^2|\mathbf{r}_1 - \mathbf{r}| = \frac{Gm_1m_2}{r^2} \qquad \textit{resp.} \qquad m_2\omega^2|\mathbf{r}_2 - \mathbf{r}| = \frac{Gm_1m_2}{r^2} \ .$$

After replacing the individual coordinates,

$$\frac{m_1m_2}{M}\omega^2 r = \frac{Gm_1m_2}{r^2} \ .$$

Follows the equation of motion,

$$\dot{\varphi} = \omega^2 = \frac{GM}{r^3} \ .$$

The equation of motion of the relative coordinate is, $\mu\frac{d^2\mathbf{r}}{dt^2} = -\frac{Gm_1m_2}{r^3}\mathbf{r}$, with reduced mass $\mu = m_1m_2/M$. The derivatives of the position vector are,

$$\begin{aligned}
\mathbf{r} &= r\hat{\mathbf{e}}_r(t) = r\hat{\mathbf{e}}_x\cos\varphi(t) + r\hat{\mathbf{e}}_y\sin\varphi(t) \\
\frac{d\mathbf{r}}{dt} &= -r\dot{\varphi}\hat{\mathbf{e}}_x\sin\varphi + r\dot{\varphi}\hat{\mathbf{e}}_y\cos\varphi = -r\dot{\varphi}\hat{\mathbf{e}}_\varphi \\
\frac{d^2\mathbf{r}}{dt^2} &= -r\dot{\varphi}^2\hat{\mathbf{e}}_x\cos\varphi - r\dot{\varphi}^2\hat{\mathbf{e}}_y\sin\varphi - r\ddot{\varphi}\hat{\mathbf{e}}_x\sin\varphi + r\ddot{\varphi}\hat{\mathbf{e}}_y\cos\varphi = -r\dot{\varphi}^2\hat{\mathbf{e}}_r \ .
\end{aligned}$$

So the equation of motion,$\mu r\dot{\varphi}^2 = \frac{Gm_1m_2}{r^2}$ is identical with the one derived above.
d. For the Earth-Moon system, the modulus of the center of mass vector is, according to (a), with $m_1 = m_E$ and $m_2 = m_M$

$$|\mathbf{r} - \mathbf{r}_E| = \frac{m_M}{M}r = \frac{7.35\times10^{22}}{5.974\times10^{24} + 7.35\times10^{22}} \times 384000\,\text{km} = 4667\,\text{km} \ .$$

Thus, it stays within the volume of the Earth.
e. The rotation frequency is, following (c) $\omega = \sqrt{\frac{GM}{r^3}}$. The approximated rotation frequency is given by $m_{2M}\omega_n^2 r = \frac{Gm_Em_M}{r^2}$. Hence, $\omega_n = \sqrt{\frac{Gm_E}{r^3}}$. That is,

$$\frac{\omega_n}{\omega} = \sqrt{\frac{m_E}{M}} = \sqrt{\frac{5.974\times10^{24}}{5.974\times10^{24} + 7.35\times10^{22}}} = 0.9939 \ .$$

The error is 0.6%.

2.4.4.6 Ex: Why Paddy's Not at Work Today (Pat Cooksey)

Identify the movement described in the following song and calculate the total time of the event assuming that each floor is 3 m high, Paddy weighs 70 kg and the pile of bricks 100 kg.

Dear Sir I write this note to inform you of my plight
And at the time of writing I am not a pretty sight
My body is all black and blue, my face a deathly gray
I write this note to tell why Paddy's not at work today

While working on the fourteenth floor, some bricks I had to clear
And to throw them down from off the top seemed quite a good idea
But the gaffer wasn't very pleased, he was an awful sod
He said I had to cart them down the ladder in me hod.

Well clearing all those bricks by hand, it seemed so very slow
So I hoisted up a barrel and secured the rope below
But in my haste to do the job, I was too blind to see
That a barrel full of building bricks is heavier than me.

So when I had untied the rope, the barrel fell like lead
And clinging tightly to the rope I started up instead
I took off like a rocket and to my dismay I found
That half way up I met the bloody barrel coming down.

Well the barrel broke my shoulder as on to the ground it sped
And when I reached the top I banged the pulley with me head
I held on tight, though numb with shock from this almighty blow
And the barrel spilled out half its load fourteen floors below

Now when those building bricks fell from the barrel to the floor
I then outweighed the barrel so I started down once more
I held on tightly to the rope as I flew to the ground
And I landed on those building bricks that were scattered all around.

Now as I lay there on the deck I thought I'd passed the worst
But when the barrel reached the top, that's when the bottom burst
A shower of bricks came down on me, I knew I had no hope
In all of this confusion, I let go the bloody rope.

The barrel being heavier, it started down once more
And landed right on top of me as I lay on the floor
It broke three ribs and my left arm, and I can only say
That I hope you'll understand why Paddy's not at work today.

Solution:

2.4.4.7 Ex: Superposition of forces

A climber wants to climb a mountain. He weighs with all its equipment 90 kg. He has a cable with a tensile strength of 100 kg. For safety reasons, he uses two ropes fixed at a distance of 10 m at the same height of the wall. He pulls upwards in a way to be always at an equal distance from the two fixing points. Will the ropes hold or will he fall? If so, at what point?

Solution: *Be $d = 10\,\mathrm{m}$ the distance from the fixing points and $-h$ the height difference between the fixing point and the climber. The force due to the climber's weight is,*

$$\mathbf{G} = -mg\hat{\mathbf{e}}_y = \mathbf{F}_+ + \mathbf{F}_- \ .$$

On both cables the acting forces are $\mathbf{F}_\pm = x \begin{pmatrix} \mp d/2 \\ -h \\ 0 \end{pmatrix}$. *From this follows* $x = \frac{mg}{2h}$. *The value of the stresses acting on the cables must be less than* $F_{mx} = 100\,\mathrm{kg}$, *so* $F_\pm = \frac{mg}{2h}\sqrt{d^2/4 + h^2} < F_{mx}$. *From this follows,*

$$h > \frac{d/2}{\sqrt{\left(\frac{2F_{mx}}{mg}\right)^2 - 1}} = \frac{10\,\mathrm{m}/2}{\sqrt{\left(\frac{2\cdot 100}{90}\right)^2 - 1}} \simeq 2.5\,\mathrm{m} \ .$$

2.4.4.8 Ex: Mobile sports field

Two athletes play with a heavy medicine ball ($m = 4\,\mathrm{kg}$) on a moving platform without friction. They are at a distance of $L = 10\,\mathrm{m}$. In the middle between them there is an elastic net with spring constant $D = 800\,\mathrm{N/m}$. The left athlete throws the ball at a speed of $v_B = 8\,\mathrm{m/s}$ parallel to the Earth's surface.

a. What is the velocity of the platform together with the athletes (total mass

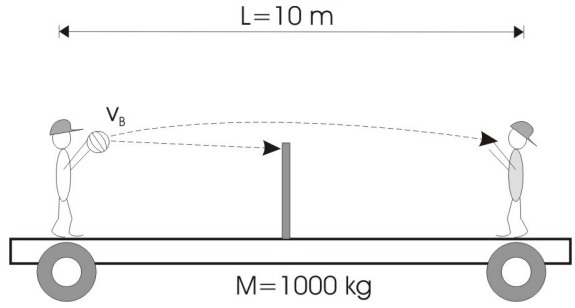

Figure 2.24: Scheme of the system.

$M = 1000\,\mathrm{kg}$), after the moment when the ball leaves the athlete's hand? Suppose the athletes to be firmly connected to the ground.
b. The ball reaches the athlete to the right who catches it. What is the distance covered by the platform?
c. Now, suppose that the ball is blocked by the net. What is the maximum deflection of the net? How is the speed profile of the platform from the moment on when the ball is released?

Solution: *a. Momentum conservation requests,*

$$m \cdot v_B = M \cdot v_W \Leftrightarrow v_W = \frac{m}{M}\, v_B = 3.2\,\mathrm{cm/s}$$

b. Total flight duration $t_w = L/v_R = 1.245\,\mathrm{s}$. *Traveled distance* $L_W = v_W \cdot t_W \simeq \mathrm{cm}$.
c. Relative velocity ball-net $v_R = v_B + v_W = 8.032\,\mathrm{m/s}$. *Energy conservation:*

$$\frac{1}{2} m v_R^2 = \frac{1}{2} D x_{max}^2 \Leftrightarrow x_{max} = \sqrt{\frac{m v_R^2}{D}} \simeq 56.8\,\mathrm{cm}\ .$$

Velocity profile for the platform: Oscillation during half a period $T/2 = \pi\sqrt{m/D}$*:*

$$v_W(t) = \begin{cases} \frac{m}{M} v_B & t < \frac{L/2}{v_R} \simeq 0.62\,\mathrm{s} \\ \frac{m}{M} v_B \cdot (1 - \sin(\sqrt{m/D}t)) & \frac{L/2}{v_R} \simeq 0.62\,\mathrm{s} < t < \frac{L/2}{v_R} + \pi\sqrt{\frac{m}{D}} \simeq 0.94\,\mathrm{s} \\ -\frac{m}{M} v_B & t > \frac{L/2}{v_R} + \pi\sqrt{\frac{m}{D}} \simeq 0.94\,\mathrm{s} \end{cases}$$

2.4.4.9 Ex: Firework ratchet

A firework ratchet is launched vertically up to a height of 50 m (along the z-axis). At the apex of the parabolic trajectory, the ratchet explodes in three parts with masses $m_1 = 200\,\mathrm{g}$, $m_2 = 300\,\mathrm{g}$ and $m_3 = 400\,\mathrm{g}$. The energy liberated by the explosion (200 J) is converted into kinetic energy for the three fragments. Assume that the resulting momenta are on a single horizontal line (along the x-axis). How long after the explosion and at what positions do the fragments hit the ground in the case that the larger fragment receives the same energy than the sum of the energy of the smaller fragments?
How will the results change when the masses m_1 and m_2 stay the same, but the larger fragment has the mass $m_3 = 500\,\mathrm{g}$?

Solution: *Total fall time:* $t = \sqrt{2s/g} = \sqrt{100/9.81}\,\mathrm{s} \simeq 3.2\,\mathrm{s}$.

$$\begin{aligned} &\textit{momentum conservation:} && p_1 + p_2 + p_3 = 0\ , \\ &\textit{energy conservation:} && \frac{p_1^2}{2m_1} + \frac{p_2^2}{2m_2} + \frac{p_3^2}{2m_3} = E_0\ . \end{aligned}$$

With $\frac{p_3^2}{2m_3} = E_0/2 \Rightarrow p_3 = \sqrt{E_0 m_3}$ *follows,*

$$p_1 + p_2 + \sqrt{E_0 m_3} = 0 \Rightarrow p_1 = -(p_2 + \sqrt{E_0 m_3})\ .$$

Now,

$$\Rightarrow \frac{(-\sqrt{E_0 m_3} - p_2)^2}{2m_1} + \frac{p_2^2}{2m_2} = E_0/2 \Rightarrow p_{2\pm} = \pm \frac{\sqrt{E_0 m_2}(\sqrt{m_1}\sqrt{m_1 + m_2 - m_3} \mp \sqrt{m_2 m_3})}{m_1 + m_2} \ .$$

Because of the two possibilities for the sign of p_2 there are two configurations:

	p_1 *(kg·m/s)*	p_2	p_3	v_1 *(m/s)*	v_2	v_3	x_1 *(m)*	x_2	x_3
p_{2+}	*-5.77*	*-3.17*	*8.94*	*-28.8*	*-10.6*	*22.4*	*-92.1*	*-33.8*	*71.4*
p_{2-}	*-1.39*	*-7.56*	*8.94*	*-6.9*	*-25.2*	*22.4*	*-22.1*	*-80.4*	*71.4*

When the largest mass is $m_3 = 500\,\mathrm{g}$, it is equal to the sum of the others. In this case, $v_3 = v_{cm,1+2}$.

2.4.4.10 Ex: Ballistic pendulum

We measure the speed of a bullet by a ballistic pendulum. The pendulum, suspended on a wire (length $L = 2\,\mathrm{m}$, mass $M = 4\,\mathrm{kg}$) is moved due to the collision. Determine from the maximum horizontal displacement ($y = 10\,\mathrm{cm}$) the velocity of the pendulum after the collision and the velocity of the bullet (mass $m = 0.1\,\mathrm{kg}$).

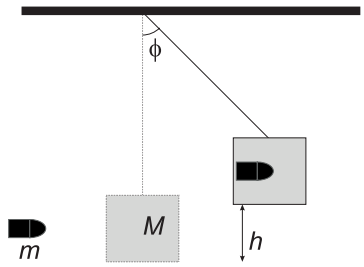

Figure 2.25: Ballistic pendulum.

Solution: *Momentum conservation requires equal linear momenta of the bullet p_{bal} before and of the pendulum p_{pen} after the collision. Therefore,*

$$m v_{bal} = (M + m) v_{pen} \ .$$

On the other hand, kinetic energy is not conserved,

$$T_{bal} = \frac{m}{2} v_{bal}^2 \neq \frac{m^2}{2(M+m)} v_{bal}^2 = \frac{M+m}{2} \frac{m^2}{(M+m)^2} v_{bal}^2 = \frac{M+m}{2} v_{pen}^2 = T_{pen} \ .$$

The energy $\Delta E = T_{bal} - T_{pen} = \frac{mM}{2(M+m)} v_{bal}^2$ must therefore be dissipated. Energy conservation after the collision requires,

$$(M + m) g h = \frac{M+m}{2} v_{pen}^2 \ .$$

Therefore, the velocity of the bullet is,

$$v_{bal} = \frac{M+m}{m} v_{pen} = \frac{M+m}{m}\sqrt{2gh}\ .$$

For the pendulum holds, $y = L\sin\theta$ *e* $h + L\cos\theta = L$*. Solving by* h*, we find,*

$$h = L - L\sqrt{1 - \frac{y^2}{L^2}} \simeq \frac{1}{2L}y^2$$

for small oscillations. Finally,

$$v_{bal} = \frac{M+m}{m} y\sqrt{\frac{g}{L}} \approx 9\,\mathrm{m/s}\ .$$

2.4.4.11 Ex: Central collision in a train station

A wagon of mass m_1 collides elastically with another wagon at rest of mass m_2. What is the relation between the masses m_1 and m_2, if after the collision
a. the wagons have the same velocity in opposite directions,
b. m_2 is three times the velocity of m_1 in the same direction,
c. m_1 is repelled with a third of the initial velocity?

Solution: *a. The condition is,*

$$v_1' = \frac{m_1 - m_2}{m_1 + m_2} v_1 + \frac{2m_2}{m_1 + m_2} \cdot 0 \stackrel{!}{=} -v_2' = -\frac{m_2 - m_1}{m_1 + m_2} \cdot 0 - \frac{2m_1}{m_1 + m_2} v_1$$

hence,

$$\Rightarrow m_1 - m_2 = -2m_1 \Leftrightarrow m_2 = 3m_1$$

b. The condition is,

$$3 \cdot v_1' = 3\frac{m_1 - m_2}{m_1 + m_2} v_1 + \frac{3 \cdot 2m_2}{m_1 + m_2} \cdot 0 \stackrel{!}{=} v_2' = \frac{m_2 - m_1}{m_1 + m_2} \cdot 0 - \frac{2m_1}{m_1 + m_2} v_1$$

hence,

$$\Rightarrow 3(m_1 - m_2) = 2m_1 \Leftrightarrow m_1 = 3m_2$$

c. The condition is,

$$v_1' = \frac{m_1 - m_2}{m_1 + m_2} v_1 + \frac{2m_2}{m_1 + m_2} \cdot 0 \stackrel{!}{=} -\frac{1}{3} v_1'$$

hence,

$$\Rightarrow m_1 - m_2 = -\frac{1}{3}(m_1 + m_2) \Leftrightarrow \frac{4}{3}m_1 = \frac{2}{3}m_2 \Leftrightarrow 2m_1 = m_2$$

2.4.4.12 Ex: (In-) elastic collision

A billiard ball with the speed $\mathbf{v}_{1i} = v_0\hat{\mathbf{e}}_x$ hits a second one initially at rest. Due to the collision the first ball changes the speed to $\mathbf{v}_{1f} = \frac{2v_0}{3}(\hat{\mathbf{e}}_x\cos\theta + \hat{\mathbf{e}}_y\sin\theta)$, where $\theta = 45°$.
a. Determine the speed of the second ball, $\mathbf{v}_{2f}$, after the collision.
b. Calculate the dissipated energy and determine if shock whether elastic or inelastic.

Solution: *a. With the conservation of linear momentum,*

$$\begin{aligned} m\mathbf{v}_{1i} &= m\mathbf{v}_{1f} + m\mathbf{v}_{2f} \\ \Leftrightarrow \quad \begin{pmatrix} v_0 \\ 0 \end{pmatrix} &= \begin{pmatrix} \frac{2v_0}{3}\cos\theta + v_{2fx} \\ \frac{2v_0}{3}\sin\theta + v_{2fy} \end{pmatrix} \\ \Leftrightarrow \mathbf{v}_{2f} = \begin{pmatrix} v_{2fx} \\ v_{2fy} \end{pmatrix} &= v_0 \begin{pmatrix} 1 - \frac{2}{3}\cos\theta \\ \frac{2}{3}\sin\theta \end{pmatrix} = v_0 \begin{pmatrix} 1 - \frac{\sqrt{2}}{3} \\ \frac{\sqrt{2}}{3} \end{pmatrix} . \end{aligned}$$

b. The difference between the kinetic energies before and after shock is,

$$\begin{aligned} E_{diss} = E_i - E_f &= \frac{m}{2}v_{1i}^2 - \frac{m}{2}v_{1f}^2 - \frac{m}{2}v_{2f}^2 = \frac{m}{2}v_0^2\left(1 - \tfrac{2^2}{3^2} - (1 - \tfrac{\sqrt{2}}{3})^2 - (\tfrac{\sqrt{2}}{3})^2\right) \\ &= \frac{6\sqrt{2} - 8}{9}E_i \simeq 0.054E_i > 0 . \end{aligned}$$

The shock is partially inelastic.

2.4.4.13 Ex: Variable mass

A wagon of mass M initially at rest is filled with fuel representing half of its mass. The fuel is now horizontally ejected at a constant rate γ and a constant speed v_c, thus propelling the car in the opposite direction. What is the final speed of the wagon when the fuel is completely consumed?

Solution: *The equation of motion is,*

$$F = \frac{d}{dt}(mv) = m\frac{dv}{dt} + v_c\frac{dm}{dt} = 0 .$$

Separating the variables

$$\int_0^{v_f} dv = -v_c\int_M^{M/2}\frac{dm}{m} ,$$

giving

$$v_f = -v_c\ln\tfrac{1}{2} \simeq 0.7v_c .$$

2.4.4.14 Ex: Mass sliding down a movable wedge

A block of mass m rests on a wedge of mass M and angle θ, which is placed on a horizontal surface. Releasing the system from rest, with the body at a height h, determine the speed of the wedge when the block touches the ground. All surfaces are free from friction.

Solution: *We use the principle of energy and momentum conservation,*

$$mgh = \frac{m}{2}v^2 + \frac{M}{2}V^2 \qquad \textit{and} \qquad 0 = mv_x + MV_x \qquad \textit{and} \qquad \frac{-v_y}{v_x - V_x} = \tan\theta \ .$$

We insert the second and third equation into the first,

$$mgh = \frac{m}{2}v_x^2+\frac{m}{2}v_y^2+\frac{M}{2}V_x^2 = \frac{m}{2}v_x^2+\frac{m}{2}(v_x-V_x)^2\tan^2\theta+\frac{M}{2}V_x^2 = \frac{M^2}{2m}V_x^2+\frac{m}{2}(-\frac{M}{m}V_x-V_x)^2\tan^2\theta+$$

This gives,

$$V_x = \sqrt{\frac{2gh}{\left(1+\frac{M}{m}\right)\frac{M}{m}+(1+\frac{M}{m})^2\tan^2\theta}} = \sqrt{\frac{2gh\cos^2\theta}{\left(1+\frac{M}{m}\right)\left(\frac{M}{m}+\sin^2\theta\right)}} \ .$$

2.4.4.15 Ex: Vertical collision

A body of mass $M = 400\,\mathrm{g}$ is released from rest from a height of $h = 10\,\mathrm{m}$ with respect to the Earth's surface. Simultaneously, a bullet of mass $m = 100\,\mathrm{g}$ is fired vertically from the surface with the speed $v_0 = 10\,\mathrm{m/s}$. Knowing that somewhere in the trajectory the masses collide and merge, we ask how long it takes for the masses to fall from the moment when M is released.

Solution: *The masses meet at the height*

$$Y_1 = Y_0 - \frac{g}{2}t_1^2 \equiv y_1 = v_0 t_1 - \frac{g}{2}t_1^2$$

and time

$$t_1 = \frac{y_0}{v_0} = 1\,\mathrm{s} \ ,$$

yielding

$$\begin{aligned} y_1 &= y_0 - \frac{g y_0^2}{2v_0^2} = 5.1\,\mathrm{m} \\ V_1 &= \dot{Y}_1 = -gt_1 = -g\frac{y_0}{v_0} = -9.8\,\mathrm{m/s} \\ v_1 &= \dot{y}_1 = v_0 - gt_1 = v_0 - g\frac{y_0}{v_0} = 0.2\,\mathrm{m/s} \ . \end{aligned}$$

Momentum conservation requires,

$$MV_1 + mv_1 = (M+m)v_2 \ .$$

So the speed of the combined masses is,

$$v_2 = \frac{MV_1 + mv_1}{M+m} = -7.8\,\mathrm{m/s} \ ,$$

at the height

$$y_2 = y_1 + v_2 t_2 - \frac{g}{2} t_2^2 \equiv 0 \ ,$$

and time

$$t_2 = \frac{v_2}{g} \pm \sqrt{\frac{v_2^2}{g^2} + \frac{2}{g} y_1} = 0.49\,\mathrm{m/s} \ .$$

The total time is,

$$t_{tot} = t + t_2 = 1.49\,\mathrm{m/s} \ .$$

2.4.4.16 Ex: Variable mass

An open freight car weighs 10 tons and is sliding on a frictionless track with a speed of 60 cm/s. Heavy rain suddenly starts and the drops fall vertically with a velocity v_0 with respect to the ground. How fast is the wagon after collecting 500 kg of water?

Solution: *The equation of motion is,*

$$ma = m\frac{dv}{dt} = -\frac{dm}{dt} v \ .$$

Hence,

$$\int_{v_0}^{v_f} \frac{dv}{v} = -\int_{m_0}^{m_f} \frac{dm}{m}$$
$$\ln \frac{v_f}{v_0} = \ln \frac{m_0}{m_f} \ .$$

Finally,

$$v_f = v_0 \frac{m_0}{m_f} = 57.14\,\mathrm{cm/s} \ .$$

2.4.4.17 Ex: Variable mass

An hourglass is placed on a scale plate. Initially ($t = 0$), all the sand is at rest in the upper container of the hourglass. The sand falls into the lower container at a rate $\lambda = -dm/dt$. Prepare a graph of the reading on the scale for $t \geq 0$.

Solution: *The weight of the hourglass only varies when it starts to pour sand and when it ends doing it. In the interval between these moments, the part of the sand that is in free flight does not contribute to the weight, such that the weight is less.*

The graph shows a rapid and linear initial decrease from the initial weight to a lower weight. Then the weight remains constant for a long time until it comes to the point where it increases again linearly to the initial value.
To calculate the stationary reading, that is, $\dot{x}_{scale} = 0$, we write,

$$0 = ma_{scale} = -mg - \dot{m}u_{top} + \dot{m}u_{bottom} - kx \ ,$$

where the coordinate x represents the reading of the scale. The velocity of sand leaving the upper container is $\dot{x}_{top} = 0$ and the velocity of sand entering the lower container is $\dot{x}_{bottom} = gt = \sqrt{2sg}$, where s is the vertical distance between the containers. With this,

$$x = -\frac{m}{k}g - \lambda\sqrt{2sg} \ .$$

2.4.4.18 Ex: Variable mass

A raindrop of initial mass M_0 starts to fall from rest. Assuming that the drop gains mass as it passes through the clouds at a rate proportional to the product of mass by velocity ($dm/dt = Kmv$), calculate the velocity $v(t)$. Neglect air resistance.

Solution: *The equation of motion is,*

$$ma = m\dot{v} = -mg + \dot{m}v = mg + (Kmv)v \ ,$$

or

$$\frac{dv}{dt} = -g + Kv^2 \ .$$

Hence,

$$-\int_0^t dt = \frac{1}{g}\int_0^v \frac{dv}{1 - \frac{K}{g}v^2} \ ,$$

with the solution,

$$-t = \frac{1}{g}\sqrt{\frac{g}{K}}\, artanh\left(\sqrt{\frac{K}{g}}v\right) \ .$$

Finally,

$$v = \sqrt{\frac{g}{K}}\tanh(\sqrt{Kg}t) \ .$$

2.4.4.19 Ex: Variable mass

A toy rocket has a carcass that weighs 100 g and an initial amount of fuel of 400 g. The velocity relative to the rocket with which the fuel comes out is 100 m/s and the rate at which it is burned is 100 m/s. Assuming it takes off from the Earth's surface ($g = 10\,\mathrm{m/s^2}$ constant) with zero initial velocity, what maximum velocity will it

reach?

Solution: *We have the relative velocity of the fuel of the rocket* $u = 100\,\mathrm{m/s}$ *and the fuel expense rate of* $\dot{m} = -100\,\mathrm{g/s}$*, the initial weight* $m = 500\,\mathrm{g}$ *and the final weight* $m_f = 100\,\mathrm{g}$*. The equation of motion is,*

$$ma = m\frac{dv}{dt} = -mg + \dot{m}u \ .$$

The mass varies as $m(t) = m_i - \dot{m}t$ *until it reaches the point* $m(t) = m_f$*, which happens at time* $t = (m_i - m_f)/\dot{m}$*. Thereby,*

$$\int_0^v dv = \int_0^{(m_i-m_f)/\dot{m}} \left(-g + \frac{\dot{m}u}{m_i - \dot{m}t}\right) dt \ .$$

The speed is,

$$\begin{aligned} v &= -g\frac{m_i - m_f}{\dot{m}} + u\dot{m}\int_0^{(m_i-m_f)/\dot{m}} \frac{dt}{m_i - \dot{m}t} = -g\frac{m_i - m_f}{\dot{m}} - u\int_{m_i}^{m_f}\frac{dz}{z} \\ &= -g\frac{m_i - m_f}{\dot{m}} - u\ln\frac{m_f}{m_i} = (-40 + 100)\,\mathrm{m/s}\ln 5 = 120\,\mathrm{m/s} \ . \end{aligned}$$

This is different from the template: $61.6\,\mathrm{m/s}$*, which is false!*

2.4.4.20 Ex: Variable mass

Calculate the power required to lift a rope vertically, initially completely wound on the ground, at a constant speed v_0. The linear mass density of the rope is λ.

Solution: *The length of the raised part of the string grows as* $y = v_0 t$ *until the time* $t_f = L/v_0$*. The power required,*

$$P = F \cdot v_0 = m(t)gv_0 = \lambda L(t)gv_0 = \lambda v_0 t g v_0 \ ,$$

grows linearly until it's maximum at time t_f*,*

$$P = \lambda L g v_0 = Mgv_0 \ .$$

2.4.4.21 Ex: Collision of two masses

Two trolleys with masses m_1 and m_2 and speeds v_1 and v_2 collide elastically (energy is conserved). Knowing that the momentum of the system is preserved during the collision, calculate the speeds of the cars after the crash.

Solution: *Conservation of energy and momentum,*

$$\begin{aligned} \frac{m_1}{2}v_{1i}^2 + \frac{m_2}{2}v_{2i}^2 &= \frac{m_1}{2}v_{1f}^2 + \frac{m_2}{2}v_{2f}^2 \\ m_1 v_{1i} + m_2 v_{2i} &= m_1 v_{1f} + m_2 v_{2f} \ . \end{aligned}$$

Inserting the second in the first equation, thus eliminating v_{2f}, we get,

$$m_1 v_{1i}^2 + m_2 v_{2i}^2 = m_1 v_{1f}^2 + \tfrac{1}{m_2}\left(m_1 v_{1i} + m_2 v_{2i} - m_1 v_{1f}\right)^2 \ ,$$

and

$$0 = \tfrac{m_1}{m_2}(m_1+m_2)v_{1f}^2 - 2\tfrac{m_1}{m_2}(m_1 v_{1i}+m_2 v_{2i})v_{1f} - m_1 v_{1i}^2 - m_2 v_{2i}^2 + \tfrac{1}{m_2}(m_1 v_{1i}+m_2 v_{2i})^2 \ ,$$

and

$$\begin{aligned} 0 &= v_{1f}^2 - 2\frac{m_1 v_{1i} + m_2 v_{2i}}{m_1+m_2} v_{1f} - \frac{m_2(m_1 v_{1i}^2 + m_2 v_{2i}^2)}{m_1(m_1+m_2)} + \frac{(m_1 v_{1i} + m_2 v_{2i})^2}{m_1(m_1+m_2)} \\ &= \left(v_{1f} - \frac{m_1 v_{1i} + m_2 v_{2i}}{m_1+m_2}\right)^2 - \sqrt{\left(\frac{m_1 v_{1i} + m_2 v_{2i}}{m_1+m_2}\right)^2 + \frac{m_2(m_1 v_{1i}^2 + m_2 v_{2i}^2)}{m_1(m_1+m_2)} - \frac{(m_1 v_{1i} + m_2 v_{2i})^2}{m_1(m_1+m_2)}}^2 \\ &= \left(v_{1f} - \frac{m_1 v_{1i} + m_2 v_{2i}}{m_1+m_2}\right)^2 - \left(m_2 \frac{v_{1i} - v_{2i}}{m_1+m_2}\right)^2 \ . \end{aligned}$$

Finally,

$$\begin{aligned} v_{1f} &= \frac{m_1 v_{1i} + m_2 v_{2i} \pm m_2 v_{1i} \mp m_2 v_{2i}}{m_1+m_2} \\ &= v_{1i}, \frac{(m_1 - m_2)\, v_{1i} + 2 m_2 v_{2i}}{m_1+m_2} \ , \end{aligned}$$

and for symmetry reasons,

$$v_{2f} = v_{2i}, \frac{(m_2 - m_1) v_{2i} + 2 m_1 v_{1i}}{m_1+m_2} \ .$$

2.4.4.22 Ex: Collision of two masses

Two balls A and B of different masses collide. A is initially at rest and B has the velocity v. After the shock, B has a speed of $v/2$ and moves perpendicular to the direction of the initial movement. Determine the direction of A's movement after the collision. What is the change in energy due to the collision?

Solution: *Momentum conservation requires,*

$$\begin{pmatrix} m_B v \\ 0 \end{pmatrix} = \begin{pmatrix} m_A v_{Ax} \\ m_A v_{Ay} + m_B \frac{v}{2} \end{pmatrix} \ .$$

Therefore, the direction is given by,

$$\tan\theta_A = \frac{v_{Ax}}{v_{Ay}} = \frac{1}{2} \ .$$

Energy conservation requires,

$$\frac{m_B}{2} v^2 = \frac{m_A}{2} v_A^2 + \frac{m_B}{2}\left(\frac{v}{2}\right)^2 \ .$$

Therefore, energy expenditure is,

$$\Delta E_{kin} = \frac{m_A}{2}(v_{Ax}^2 + v_{Ay}^2) + \frac{m_B}{2}\left(\frac{v}{2}\right)^2 - \frac{m_B}{2}v^2$$
$$= \frac{m_A}{2}\left(\frac{m_B^2}{m_A^2}v^2 + \frac{m_B^2}{4m_A^2}v^2\right) + \frac{m_B}{2}\left(\frac{v}{2}\right)^2 - \frac{m_B}{2}v^2 = -\frac{m_B}{2}v^2\frac{3m_A - 5m_B}{4m_A} \ .$$

2.4.4.23 Ex: Collision of two masses

A bullet of mass m is fired with the velocity v against a ballistic pendulum of mass M. The bullet passes through the pendulum and emerges with the velocity $v/4$.
a. calculate the maximum height of the oscillating pendulum,
b. calculate the energy dissipated when the bullet passes through the pendulum.

Solution: *a. Momentum conservation during the collision,*

$$mv = Mv_M + m\frac{v}{4} \qquad \Longrightarrow \qquad v_M = \frac{3m}{4M}v \ .$$

Energy conservation of the accelerated pendulum,

$$\frac{M}{2}v_M^2 = Mgh \qquad \Longrightarrow \qquad h = \frac{v_M^2}{2g} = \frac{1}{2g}\left(\frac{3m}{4M}v\right)^2 = \frac{9m^2}{32gM^2}v^2 \ .$$

b. Energy conservation during the collision,

$$\frac{m}{2}v^2 = Mgh + \frac{m}{2}\left(\frac{v}{4}\right)^2 + E_{diss}$$
$$\Longrightarrow E_{diss} = \frac{m}{2}v^2 - Mgh - \frac{m}{2}\left(\frac{v}{4}\right)^2 = \frac{15m}{32}v^2 - Mg\frac{9m^2}{32gM^2}v^2 = \left(\frac{15}{16} - \frac{9m}{16M}\right)\frac{m}{2}v^2 \ .$$

2.5 Further reading

H.M. Nussenzveig, Edgar Blucher (2013), *Curso de Física Básica: Mecânica - vol 1* [961]ISBN

phet, *Interactive Simulations for Science and Math* http

sofisica, *Material de apoio didático* http

Chapter 3

Rotations and dynamics of rigid bodies

So far we have considered the translation dynamics of point masses. Obviously, point masses, unlike extended rigid bodies, cannot rotate.

3.1 Rotation about a fixed axis

Summary of common transformations,

operation	action on position	on momentum
translation	$\mathcal{T}_{tr}\mathbf{r} = \mathbf{r} + \mathbf{a}$	$\mathcal{T}_{tr}\mathbf{p} = \mathbf{p}$
kick	$\mathcal{T}_{kc}\mathbf{r} = \mathbf{r}$	$\mathcal{T}_{kc}\mathbf{p} = \mathbf{p} + m\mathbf{v}$
rotation	$\mathcal{T}_{rt}\mathbf{r} = e^{\vec{\alpha}\times}\mathbf{r}$	$\mathcal{T}_{rt}\mathbf{p} = e^{\vec{\alpha}\times}\mathbf{p}$
Galilei boost	$\mathcal{T}_{G}\mathbf{r} = \mathbf{r} + \mathbf{v}t$	$\mathcal{T}_{G}\mathbf{p} = \mathbf{p} + m\mathbf{v}$
transform to accelerated frame	$\mathcal{T}_{ac}\mathbf{r} = \mathbf{r}$	$\mathcal{T}_{ac}\mathbf{p} = \mathbf{p} + m\mathbf{g}t$
transform to rotating frame	$\mathcal{T}_{ar}\mathbf{r} = e^{\vec{\omega}t\times}\mathbf{r}$	$\mathcal{T}_{ar}\mathbf{p} = e^{\vec{\omega}t\times}\mathbf{p}$

Let us have a closer look at the rotation operator defined by,

$$\boxed{\mathcal{T}_{rt}\mathbf{r} = e^{\vec{\alpha}\times}\mathbf{r}}\ . \tag{3.1}$$

It can be expanded as,

$$\begin{aligned}\mathcal{T}_{rt}\mathbf{r} = \sum_n \frac{(\vec{\alpha}\times)^n}{n!}\mathbf{r} &= \mathbf{r} + \vec{\alpha}\times\mathbf{r} + \tfrac{1}{2}\vec{\alpha}\times(\vec{\alpha}\times\mathbf{r}) + ... \\ &= \hat{\mathbf{e}}_\alpha(\hat{\mathbf{e}}_\alpha\cdot\mathbf{r}) + \hat{\mathbf{e}}_\alpha\times\mathbf{r}\sin\alpha - \hat{\mathbf{e}}_\alpha\times(\hat{\mathbf{e}}_\alpha\times\mathbf{r})\cos\alpha\ .\end{aligned} \tag{3.2}$$

Choosing the rotation angle along Cartesian coordinates, we find matrix representations of the rotations transformations. For, $\vec{\alpha} = \alpha\hat{\mathbf{e}}_x$,

$$\mathcal{T}_{rt}\mathbf{r} = x\hat{\mathbf{e}}_x + (y\hat{\mathbf{e}}_z - z\hat{\mathbf{e}}_y)\sin\alpha + (y\hat{\mathbf{e}}_y + z\hat{\mathbf{e}}_z)\cos\alpha = R_x\mathbf{r} \tag{3.3}$$

$$\text{with}\qquad R_x = \begin{pmatrix}1 & 0 & 0\\ 0 & \cos\alpha & -\sin\alpha\\ 0 & \sin\alpha & \cos\alpha\end{pmatrix}\ ,$$

for, $\vec{\alpha} = \alpha\hat{\mathbf{e}}_y$,

$$\mathcal{T}_{rt}\mathbf{r} = y\hat{\mathbf{e}}_y + (z\hat{\mathbf{e}}_x - x\hat{\mathbf{e}}_z)\sin\alpha + (x\hat{\mathbf{e}}_x + z\hat{\mathbf{e}}_z)\cos\alpha = R_y\mathbf{r} \tag{3.4}$$
$$\text{with} \qquad R_y = \begin{pmatrix} \cos\alpha & 0 & -\sin\alpha \\ 0 & 1 & 0 \\ \sin\alpha & 0 & \cos\alpha \end{pmatrix} ,$$

and for, $\vec{\alpha} = \alpha\hat{\mathbf{e}}_z$,

$$\mathcal{T}_{rt}\mathbf{r} = z\hat{\mathbf{e}}_z + (x\hat{\mathbf{e}}_y - y\hat{\mathbf{e}}_x)\sin\alpha - \hat{\mathbf{e}}_z \times (\hat{\mathbf{e}}_z \times \mathbf{r})\cos\alpha = R_z\mathbf{r} \tag{3.5}$$
$$\text{with} \qquad R_z = \begin{pmatrix} \cos\alpha & -\sin\alpha & 0 \\ \sin\alpha & \cos\alpha & 0 \\ 0 & 0 & 1 \end{pmatrix} .$$

Furthermore, since the vectors $\hat{\mathbf{e}}_\alpha$, $\hat{\mathbf{e}}_\alpha \times \mathbf{p}$, and $\hat{\mathbf{e}}_\alpha \times (\hat{\mathbf{e}}_\alpha \times \mathbf{p})$ in Eq. (3.2) obviously form an orthogonal coordinate system, we find defining $\gamma \equiv \angle(\hat{\mathbf{e}}_\alpha, \mathbf{p})$,

$$\begin{aligned} \mathcal{T}_{rt}(e^{\vec{\alpha}\times}\mathbf{p})^2 &= [\hat{\mathbf{e}}_\alpha(\hat{\mathbf{e}}_\alpha \cdot \mathbf{p}) + \hat{\mathbf{e}}_\alpha \times \mathbf{p}\sin\alpha\hat{\mathbf{e}}_\alpha \times (\hat{\mathbf{e}}_\alpha \times \mathbf{p})\cos\alpha]^2 \\ &= [\hat{\mathbf{e}}_\alpha(\hat{\mathbf{e}}_\alpha \cdot \mathbf{p})]^2 + [\hat{\mathbf{e}}_\alpha \times \mathbf{p}\sin\alpha]^2 + [\hat{\mathbf{e}}_\alpha \times (\hat{\mathbf{e}}_\alpha \times \mathbf{p})\cos\alpha]^2 \\ &= \mathbf{p}^2\cos^2\gamma + \mathbf{p}^2\sin^2\alpha\sin^2\gamma + \mathbf{p}^2\cos^2\alpha\sin^2\gamma = \mathbf{p}^2 , \end{aligned} \tag{3.6}$$

that the kinetic energy and the potential energy in radial potentials is invariant to rotation,

$$\mathcal{T}_{rt}\left(\frac{\mathbf{p}^2}{2m} + V(|\mathbf{r}|)\right) = \frac{\mathbf{p}^2}{2m} + V(|\mathbf{r}|) . \tag{3.7}$$

3.1.1 Transformation into a rotating system

Transformation into a rotating system,

$$\frac{d}{dt}T_{ar}\mathbf{r} = e^{\vec{\omega}t\times}\frac{d}{dt}\mathbf{r} + \left(\frac{d}{dt}e^{\vec{\omega}t\times}\right)\mathbf{r} = \left(\frac{d}{dt} + \vec{\omega}\times\right)T_{ar}\mathbf{r} , \tag{3.8}$$

from which we deduce the rule,

$$\boxed{\left\{\frac{d}{dt}\right\}_{lab} = \left\{\frac{d}{dt}\right\}_{rot} + \vec{\omega}\times} . \tag{3.9}$$

Use this expression to resolve Exc. 3.1.4.1 to 3.1.4.4.

3.1.2 Inertial forces in the rotating system

Coriolis force, .

3.1.3 Inertial forces in the linearly accelerated system

3.1.4 Exercises

3.1.4.1 Ex: Rotating coordinate systems

A body of mass m is thrown horizontally at a velocity v_0 in the x-direction in the homogeneous gravitational field of the Earth. (Gravity towards $-z$). The rotation of the Earth is not taken into account.
a. Give the solution $\mathbf{r}(t)$ of the equation of motion.
b. Transform the solution into a coordinate system that rotates around the z-axis at the angular velocity ω.
c. Set up the equation of motion in the rotating system and show that the transformed path from (b) satisfies it.

Solution: *a. Path,*

$$\mathbf{r}(t) = \begin{pmatrix} v_0 t \\ 0 \\ -\frac{1}{2} g t^2 \end{pmatrix} .$$

b. The rotation is performed by,

$$R_z = \begin{pmatrix} \cos\omega t & \sin\omega t & 0 \\ -\sin\omega t & \cos\omega t & 0 \\ 0 & 0 & 1 \end{pmatrix} ,$$

so that,

$$\mathbf{r}'(t) = R_z \mathbf{r}(t) = \begin{pmatrix} v_0 t \cos\omega t \\ -v_0 t \sin\omega t \\ -\frac{1}{2} g t^2 \end{pmatrix} .$$

c. It must hold,

$$\frac{d^2}{dt^2}\mathbf{r}' = \mathbf{g}' - \vec{\omega} \times (\vec{\omega} \times \mathbf{r}') - 2\vec{\omega} \times \frac{d}{dt}\mathbf{r}' .$$

with $\mathbf{g}' = \mathbf{r} - (g\hat{\mathbf{e}}_z) = -g\hat{\mathbf{e}}_z$ *and* $\vec{\omega} = \omega\hat{\mathbf{e}}_z$. *This is valid because of (calculate with MAPLE),*

$$\frac{d}{dt}\mathbf{r}' = \begin{pmatrix} -\omega v_0 t \sin\omega t + v_0 \cos\omega t \\ -\omega v_0 t \cos\omega t - v_0 \sin\omega t \\ -gt \end{pmatrix}$$

$$\frac{d^2}{dt^2}\mathbf{r}' = \frac{d}{dt}\begin{pmatrix} -\omega^2 v_0 t \cos\omega t - 2\omega v_0 \sin\omega t \\ \omega^2 v_0 t \sin\omega t - 2\omega v_0 \cos\omega t \\ -g \end{pmatrix}$$

$$\vec{\omega} \times (\vec{\omega} \times \mathbf{r}') = \begin{pmatrix} -\omega^2 v_0 t \cos\omega t \\ \omega^2 v_0 t \sin\omega t \\ 0 \end{pmatrix}$$

$$\vec{\omega} \times \frac{d}{dt}\mathbf{r}' = \begin{pmatrix} \omega^2 v_0 t \cos\omega t + \omega v_0 \sin\omega t \\ -\omega^2 v_0 t \sin\omega t + \omega v_0 \cos\omega t \\ 0 \end{pmatrix} .$$

3.1.4.2 Ex: Rotating vulture

Consider two Cartesian coordinate systems that are identical at time $t = 0$. One rotates around the z-axis at a constant angular velocity ω, while the laboratory system is at rest. On the x-axis of this rotating system, a vulture moves from the coordinate origin (at time $t = 0$) at a constant speed v.
a. Calculate the vectors of the vulture's position and velocity in the rotating coordinate system.
b. Calculate the Cartesian coordinates of the vulture in the laboratory system and from this the velocity in the laboratory system.
c. Calculate directly the velocity observed in the laboratory system using the relationship (3.9).

Solution: *a. The location in the rotating coordinate system is* $\mathbf{r}(t) = vt\hat{\mathbf{e}}_{x,rot}$. *The velocity* $\mathbf{v}_R = v\hat{\mathbf{e}}_{x,rot}$.
b. The location in the laboratory system is,

$$\mathbf{r}(t) = vt \begin{pmatrix} \cos\phi \\ \sin\phi \\ 0 \end{pmatrix}$$

with $\phi = \omega t$. *The velocity is,*

$$\dot{\mathbf{r}}(t) = v \begin{pmatrix} \cos\phi \\ \sin\phi \\ 0 \end{pmatrix} + vt\omega \begin{pmatrix} -\sin\phi \\ \cos\phi \\ 0 \end{pmatrix}$$

with $|v| = \sqrt{v^2 + (\omega v t)^2}$.
c. The velocity observed in the laboratory system is,

$$\begin{aligned}\mathbf{v}_{lab} &= v\hat{\mathbf{e}}_r + \vec{\omega} \times r\hat{\mathbf{e}}_r = v\hat{\mathbf{e}}_r + \omega v t \hat{\mathbf{e}}_\phi \\ &= v\hat{\mathbf{e}}_{x,rot} + \omega v t \hat{\mathbf{e}}_{y,rot} = v \begin{pmatrix} \cos\phi \\ \sin\phi \\ 0 \end{pmatrix} + vt\omega \begin{pmatrix} -\sin\phi \\ \cos\phi \\ 0 \end{pmatrix} .\end{aligned}$$

$|v_{lab}|$ *is obviously independent of the chosen basic system.*

3.1.4.3 Ex: Rotating system

Consider a rotating coordinate system, which at time $t = 0$ coincides with the lab system, but rotates relative to the lab system with angular velocity $\omega = 2\pi/T$, $T = 10\,\mathrm{s}$, around the z-axis. In this coordinate system the rotation of a mass point be given by the vector,

$$\mathbf{r}' = \begin{pmatrix} a \\ a \\ 0 \end{pmatrix} .$$

a. Determine the position vector of this point with respect to the laboratory coordinate system.
b. Consider the position vector at time $t = 5\,\mathrm{s}$ and determine its velocity measured in the rotating system and in the laboratory system.

Solution: *a. We have,*

$$\mathbf{r}(t) = \mathcal{R}_z(\omega t)\mathbf{r}' = \begin{pmatrix} \cos\omega t & \sin\omega t & 0 \\ -\sin\omega t & \cos\omega t & 0 \\ 0 & 0 & 1 \end{pmatrix} \begin{pmatrix} a \\ a \\ 0 \end{pmatrix} = \begin{pmatrix} a\cos\omega t + a\sin\omega t \\ -a\sin\omega t + a\cos\omega t \\ 0 \end{pmatrix} .$$

b. We have,

$$\mathbf{r}(5\,\mathrm{s}) = \begin{pmatrix} a\cos 2\pi\frac{t}{T} + a\sin 2\pi\frac{t}{T} \\ -a\sin 2\pi\frac{t}{T} + a\cos 2\pi\frac{t}{T} \\ 0 \end{pmatrix} = \begin{pmatrix} a\cos\pi + a\sin\pi \\ -a\sin\pi + a\cos\pi \\ 0 \end{pmatrix} = \begin{pmatrix} -a \\ -a \\ 0 \end{pmatrix} .$$

And,

$$\mathbf{v}'(t) = \left\{\frac{d\mathbf{r}}{dt}\right\}_{rot} = \begin{pmatrix} -a\omega\sin\omega t + a\omega\cos\omega t \\ -a\omega\cos\omega t - a\omega\sin\omega t \\ 0 \end{pmatrix}$$

$$|\mathbf{v}'(t)| = a\omega\sqrt{(|-\sin\omega t + \cos\omega t|^2 + |-\cos\omega t - \sin\omega t|^2)} = \tfrac{2\pi}{T}\sqrt{2}a = a \cdot 0.89 \;\; 1/\mathrm{s}$$

$$\mathbf{v}(t) = \left\{\frac{d\mathbf{r}}{dt}\right\}_{lab} = \left\{\frac{d\mathbf{r}}{dt}\right\}_{rot} + \vec{\omega} \times \mathbf{r} = a\omega \begin{pmatrix} -\sin\omega t + \cos\omega t - (-\sin\omega t + \cos\omega t) \\ -\cos\omega t - \sin\omega t + (\cos\omega t + \sin\omega t) \\ 0 \end{pmatrix} = \begin{pmatrix} 0 \\ 0 \\ 0 \end{pmatrix}$$

$$\|\mathbf{v}'(t)\| = 0 .$$

3.1.4.4 Ex: Rotating system

Consider two coordinate systems, both with their origin at the center of the Earth and their z-axis parallel to the Earth's rotation axis. The rotating system rotates with the Earth, while the laboratory system is fixed to the solar system. An airplane moves at a constant velocity v relative to the Earth's surface on a direct trajectory from the north pole to the equator, where it arrives after a time $\tau = 12\,\mathrm{h}$. What is the velocity of the plane (as a function of time) seen by the lab system?

Solution: *The transformation from the laboratory to rotating system is described by,*

$$\mathcal{R}_z(\omega t) = \begin{pmatrix} \cos\omega t & \sin\omega t & 0 \\ -\sin\omega t & \cos\omega t & 0 \\ 0 & 0 & 1 \end{pmatrix} ,$$

where $\omega = 2\pi/48$ h. In the rotating system it is parametrized by,

$$\mathbf{r}'(t) = \begin{pmatrix} R\sin\Omega t \\ 0 \\ R\cos\Omega t \end{pmatrix} ,$$

where $\Omega = \frac{1}{2}\pi/12$ h$= \frac{1}{2}\omega$. In the rotating system the speed is,

$$\mathbf{v}'(t) = \frac{d}{dt}\mathbf{r}'(t) = \begin{pmatrix} \Omega R\cos\Omega t \\ 0 \\ -\Omega R\sin\Omega t \end{pmatrix} ,$$

with the absolute value $|\mathbf{v}'(t)| = \Omega R$. In the laboratory system the trajectory is,

$$\mathbf{r}(t) = R^z(-\omega t)\mathbf{r}'(t) = \begin{pmatrix} R\sin\Omega t\cos\omega t \\ R\sin\Omega t\sin\omega t \\ R\cos\Omega t \end{pmatrix}$$

and the speed,

$$\mathbf{v}(t) = \frac{d}{dt}\mathbf{r}(t) = \begin{pmatrix} \Omega R\cos\Omega t\cos\omega t - \omega R\sin\Omega t\sin\omega t \\ \Omega R\cos\Omega t\sin\omega t + \omega R\sin\Omega t\cos\omega t \\ -\Omega R\sin\Omega t \end{pmatrix} .$$

Alternatively we can write,

$$\begin{aligned}\mathbf{v}(t) &= \frac{d}{dt}\mathbf{r}(t)\\ &= \frac{d}{dt}[R^z(-\omega t)\mathbf{r}'(t)]\\ &= R^z(-\omega t)\frac{d}{dt}\mathbf{r}'(t) + \left[\frac{d}{dt}R^z(-\omega t)\right]\mathbf{r}'(t)\\ &= R^z(-\omega t)\frac{d}{dt}\mathbf{r}'(t) + R^z(-\omega t)\left[\vec{\omega}\times\mathbf{r}'(t)\right]\\ &= R^z(-\omega t)\frac{d}{dt}\mathbf{r}'(t) + \vec{\omega}\times R^z(-\omega t)\mathbf{r}'(t)\\ &= R^z(-\omega t)\mathbf{v}'(t) + \vec{\omega}\times\mathbf{r}(t)\ .\end{aligned}$$

We easily check,

$$\begin{aligned}\mathcal{R}_z(-\omega t)\mathbf{v}'(t) + \vec{\omega}\times\mathbf{r}(t) &= \begin{pmatrix}\cos\omega t & -\sin\omega t & 0\\ \sin\omega t & \cos\omega t & 0\\ 0 & 0 & 1\end{pmatrix}\begin{pmatrix}\Omega R\cos\Omega t\\ 0\\ -\Omega R\sin\Omega t\end{pmatrix} + \begin{pmatrix}0\\0\\\omega\end{pmatrix}\times\begin{pmatrix}R\sin\Omega t\cos\omega t\\ R\sin\Omega t\sin\omega t\\ R\cos\Omega t\end{pmatrix}\\ &= \begin{pmatrix}\Omega R\cos\Omega t\cos\omega t - \omega R\sin\Omega t\sin\omega t\\ \Omega R\cos\Omega t\sin\omega t + \omega R\sin\Omega t\cos\omega t\\ -\Omega R\sin\Omega t\end{pmatrix}\ .\end{aligned}$$

The value after 12 h *is* $|\mathbf{v}(t)| = \sqrt{\omega^2R^2\sin^2\Omega t + v_0^2} = \sqrt{\omega^2R^2\sin^2\frac{1}{2}\pi + (\Omega R)^2} = R\sqrt{\omega^2+\Omega^2} = R\sqrt{\omega^2+(\frac{1}{2}\omega)^2} = 6730\,\text{km}\cdot\frac{2\pi}{24\,\text{h}}\sqrt{\frac{5}{4}} = 547\,\text{m/s}$.

3.1.4.5 Ex: Inertial forces

A car travels at a speed $v = 100\,\text{km/h}$ from São Carlos (latitude $\theta = -22°$) to Ribeirão Preto, which is north of São Carlos.
a. Calculate the value of the Coriolis acceleration. In which direction is the car deviated?
b. Calculate the centrifugal force knowing that the radius of the Earth is 6370 km.

Solution: *a. The Coriolis force is*

$$\vec{a}_{Cor} = -2\vec{\omega}\times\mathbf{v} = -2\hat{\mathbf{e}}_\phi\frac{2\pi}{T_{dia}}v\sin\theta = 1.5\cdot10^{-4}g\hat{\mathbf{e}}_\phi\ .$$

Deviation to the left.
b. The centrifugal force is,

$$\vec{a}_{cen} = -2\vec{\omega}\times(\vec{\omega}\times\mathbf{r}) = -2\hat{\mathbf{e}}_\rho\omega^2R\sin(90°-\theta) = 2\hat{\mathbf{e}}_\rho\left(\frac{2\pi}{T_{dia}}\right)^2R\cos\theta = 6.4\cdot10^{-3}\,\text{g}\ .$$

3.1.4.6 Ex: Foucault's pendulum

A pendulum of mass $m = 7\,\mathrm{kg}$ and length $L = 6\,\mathrm{m}$ is deflected by the angle $\beta = 4°$ and then released. The experiment takes place at a latitude of $\Phi = 51°$ north.
a. How strong is the Coriolis force when passing through the rest position?
b. What is the radius of curvature r of the projection of the pendulum's path onto the horizontal base at the rest point?
c. How long is the oscillation period T of a full rotation of the pendulum plane in the lab frame?

Solution: *a. The velocity v_0 of the pendulum at zero crossing is, with the help of the energy conservation law, given by,*

$$\frac{m}{2}v_0^2 = mgl(1-\cos\beta)$$

or

$$v_0 = \sqrt{2gl(1-\cos\beta)}\ .$$

Hence,

$$F_C = 2mv_0\omega' = 2m\sqrt{2gl(1-\cos\beta)}\omega'\ .$$

The effective component ω' of the angular velocity at the location of the latitude Φ is,

$$\omega' = \frac{2\pi}{d^*}\sin\Phi\ ,$$

where $d^* = 86164\,\mathrm{s}$ is the duration of a sidereal day, which is slightly different from $d = 24\cdot 3600\,\mathrm{s} = 86400\,\mathrm{s}$. Therefore follows for the Coriolis force at zero crossing,

$$F_C = \frac{4\pi m}{d^*}\sin\Phi\sqrt{2gl(1-\cos\beta)} \approx 4.25\cdot 10^{-4}\,\mathrm{N}\ .$$

b. The Coriolis force is equal to the centrifugal force of the horizontal movement, i.e.,

$$F_C = 2mv_0\omega' = F_Z = \frac{m}{r}v_0^2\ .$$

From this we calculate the radius of curvature to be,

$$r = \frac{v_0}{2\omega'} = \frac{d^*}{4\pi\sin\Phi}\sqrt{2gl(1-\cos\beta)} \approx 5\,\mathrm{km}\ .$$

c. One gets a full turn for $T = d^*/\sin\Phi \approx 30.8\,\mathrm{h}$.

3.1.4.7 Ex: Earth rotation

a. A car with the mass $m = 1000\,\mathrm{kg}$ stands on the equator of the Earth. What is the total force acting on the car, and in which direction does it point? Assume the Earth to be a sphere with radius $R_{earth} = 6370\,\mathrm{km}$. The angular velocity is $\omega_{earth} = 7.27\cdot 10^{-5}\,\mathrm{s^{-1}}$.
b. Now the car is traveling eastwards at a speed $v = 100\,\mathrm{km/h}$ along the equator. What total force is acting on it, and which direction does this force have?

Figure 3.1: Earth rotation.

c. How fast would the car have to travel eastwards along the equator to lift off the surface of the Earth?

Solution: *a. When the car is stands still, only gravity and centrifugal force act on it,* $\mathbf{F}_g = -mg\hat{\mathbf{e}}_r$ *and*

$$\mathbf{F}_Z = -m\vec{\omega} \times (\vec{\omega} \times \mathbf{r}) = -m[\vec{\omega} \cdot (\vec{\omega} \cdot \mathbf{r}) - \mathbf{r} \cdot (\vec{\omega} \cdot \vec{\omega})] = m\omega^2 r\hat{\mathbf{e}}_r \ .$$

That is, all in all,

$$\mathbf{F}_{ges} = (-mg + m\omega^2 r)\hat{\mathbf{e}}_r \ .$$

b. Now, three forces act along the equator in an eastward direction $\mathbf{F}_g = -mg\hat{\mathbf{e}}_r$, $\mathbf{F}_Z = +m\left(\frac{v^2}{R} + \omega^2 R\right)\hat{\mathbf{e}}_r$, $\mathbf{F}_C = +2m\omega v\hat{\mathbf{e}}_r$. *It should be noted here, that the centrifugal acceleration is increased when traveling in the east direction, since the Earth also rotates in the east direction. So overall,*

$$\mathbf{F}_{ges} = m\left(-g + \frac{v^2}{R} + \omega^2 R + 2\omega v\right)\hat{\mathbf{e}}_r \ .$$

c. For the car to take off, the sum of all forces acting on it must disappear, i.e.,

$$-mg + m\left(\omega^2 R + \frac{v^2}{R}\right) + 2m\omega v = 0 \ .$$

Resolved by the speed v *we get,*

$$v = -R\omega \pm \sqrt{Rg} \ .$$

Hence, $v_{West} = -8.37\,\mathrm{km/s}$ *and* $v_{Ost} = 7.44\,\mathrm{km/s}$.

3.1.4.8 Ex: Spinning top in a horizontal plane

Discuss the spinning top on a horizontal plane. What happens when the plane is inclined?

Solution:

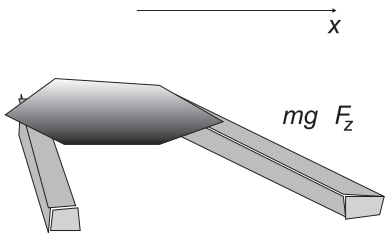

Figure 3.2: Spinning top.

3.1.4.9 Ex: Inertial forces

a. Calculate the correction for the weight of a mass m at rest at the equator due to centrifugal force. Does the centrifugal force modify the falling time for a mass released at a height above the Earth?
b. What are the value and orientation of the Coriolis acceleration acting on a body at the north pole moving with the speed $v = 100\,\mathrm{m/s}$ to the south?
c. Calculate the deviation due to the Coriolis force for a body falling at the equator from a height of $h = 100\,\mathrm{m}$.

Solution: *a. With* $\omega = \frac{2\pi}{1\,\mathrm{d}}$ *we find,*

$$\mathbf{F}_{centr} = -m\vec{\omega} \times (\vec{\omega} \times \mathbf{r}) = m\omega^2 r\hat{\mathbf{e}}_r \ .$$

This gives, $\Delta g = 0.0034\,\mathrm{g}$. *However, the force does not act on free masses.*
b. With $\omega = \frac{2\pi}{1\,\mathrm{d}}$

$$\mathbf{F}_{Cor} = -2m\vec{\omega} \times \mathbf{v} = -2m\omega v\hat{\mathbf{e}}_\phi \ .$$

The force acts towards east and has the value $a_{Cor} = 0.015\,\mathrm{m/s}$.
c. The Coriolis force can be approximated (the deviation from the vertical path is negligible),

$$\mathbf{F}_{Cor} = -2m\vec{\omega} \times \vec{v} \simeq m\vec{a}_{Cor}$$

with $a_{Cor} = 2\omega v_{grv}$. *The fall time and the instantaneous speed are,*

$$t_1 = \sqrt{\frac{2h}{g}} \qquad \textit{and} \qquad v_{grv} = gt \ .$$

So, we get the speed,

$$v_{Cor} = \int_0^t a_{Cor}dt = \int_0^t 2\omega g t dt = 2\omega g\frac{t^2}{2}$$

and the deviation,

$$s_{Cor} = \int_0^{t_1} v_{Cor}dt = \frac{1}{3}\omega g t_1^3 \ .$$

3.1.4.10 Ex: Carousel

A vertical bar rotates around the z-axis at a constant angular velocity ω. A thread of length l is attached to the upper end of the rod, while a mass m is attached to the other end of the thread.
a. Find the tension that acts on the thread.
b. Find the angle between thread and bar in equilibrium.

Solution: *Gravity is* $\mathbf{F}_g = -mg\hat{\mathbf{e}}_z$*, the centrifugal force is* $\mathbf{F}_z = -m\vec{\omega} \times (\vec{\omega} \times \mathbf{r})$ *and the tension of the thread is* $\mathbf{F}_T = -T\sin\phi\hat{\mathbf{e}}_x + T\cos\phi\hat{\mathbf{e}}_z$*. With,*

$$\mathbf{r} = l[\sin\phi\hat{\mathbf{e}}_x + (1-\cos\phi)\hat{\mathbf{e}}_z] \ ,$$

follows,

$$\mathbf{F}_g = m\omega^2 l\sin\phi\hat{\mathbf{e}}_x \ .$$

In equilibrium of forces,

$$0 = -mg\hat{\mathbf{e}}_z + m\omega^2 l\sin\phi\hat{\mathbf{e}}_x - T\sin\phi\hat{\mathbf{e}}_x + T\cos\phi\hat{\mathbf{e}}_z \ .$$

The equations for the components are,

$$m\omega^2 l\sin\phi - T\sin\phi = 0 \qquad \textit{and} \qquad T\cos\phi - mg = 0 \ .$$

One solution to the first equation is $\sin\phi = 0$*, when the centrifugal force vanishes. Otherwise we find,*

$$T = m\omega^2 l \qquad \textit{and} \qquad \cos\phi = \frac{g}{\omega^2 l} \ .$$

3.1.4.11 Ex: Yo-yo

A yo-yo with radius R and thickness D is accelerated in the field of terrestrial attraction.
a. Determine the inertial moments with respect to the yo-yo's symmetry axis and to the instantaneous point of suspension on the string.
b. Calculate the torque and write down the equation for the rotational motion.
c. From the equation of motion, calculate the angular and linear accelerations, the angular and linear velocities, and the angular momentum.

Solution: *a. The mass of the yo-yo is,*

$$M = \int dm = \rho\pi R^2 D \ .$$

The inertial moment with respect to the axis of symmetry is,

$$I_{cm} = \int r^2 dm = \frac{M}{2}R^2 \ .$$

The inertial moment with respect to the suspension point is,

$$I = I_{cm} + MR^2 = \frac{3M}{2}R^2 \ .$$

b. The equation of motion is,

$$\begin{aligned} I\vec{\alpha} = \vec{\tau} &= \mathbf{r} \times \mathbf{F} \\ \Leftrightarrow \quad \frac{3M}{2}R^2\alpha &= RMg \ . \end{aligned}$$

c. So we have,

$$\begin{aligned} \alpha &= \frac{2g}{3R} \quad , \quad a = R\alpha = \frac{2g}{3} \\ \omega &= \int \alpha dt = \frac{2g}{3R}t \quad , \quad v = R\alpha = \frac{2g}{3}t \\ L &= I\omega = \frac{3M}{2}R^2\frac{2g}{3R}t = MgRt = \tau t \ . \end{aligned}$$

Alternatively it is possible to use energy conservation,

$$\begin{aligned} \tfrac{d}{dt}Mgh &= \tfrac{d}{dt}\tfrac{1}{2}I\omega^2 \\ \Rightarrow Mgv &= \tfrac{1}{2}I2\omega\dot{\omega} \\ \Rightarrow MgR &= I\alpha \\ \Rightarrow \frac{2g}{3R} &= \alpha \ . \end{aligned}$$

3.1.4.12 Ex: Deviation to the east

An object is thrown up vertically at the initial speed v_0. Determine the east deflection based on the Earth's rotation as a function of latitude.

Solution: *The coordinate system is placed in the starting point of the movement so that the initial conditions are:* $\mathbf{r}(0) = 0$ *und* $\mathbf{v}(0) = z0\hat{\mathbf{e}}_z$. *z points up, y to the east and x to the south. For the eastward movement we have,*

$$\dot{y} = -2\omega(x\cos\lambda + z\sin\lambda) \ .$$

The southward movement of the body is negligible. Likewise the effect of the eastward deviation on z. We get the movement of free fall,

$$z = \frac{g}{2}t^2 + v_0 t \ .$$

Inserting into the eastward deviation,

$$\dot{y} = -2\omega\left(\frac{g}{2}t^2 + v_0 t\right)\sin\lambda \ .$$

Hence, the eastward deviation points in western direction:

$$y = 2\omega \left(\frac{g}{6} t^3 - \frac{v_0}{2} \right) \sin\lambda \ .$$

3.1.4.13 Ex: Coriolis force

A body falls in free fall at the equator of the Earth from a height of $h = 100\,\mathrm{m}$. At the beginning of the movement ($t = 0$) the body rests at the height h. Air friction is neglected. The centrifugal acceleration is already taken into account in the value of the gravitational acceleration $g = 9.81\,\mathrm{m/s^{-2}}$ relative to the Earth's surface.
a. Set up the equations of motion. Show that the path lies in a plane. What is its spatial location?
b. Solve the differential equations by combining the remaining components of $\mathbf{r}(t)$ into a complex variable $u(t)$. Pay attention to the initial conditions!
c. Give the solution $\mathbf{r}(t)$ and then approximate for small ωt (ω being the angular velocity of the Earth's rotation). Why is this approximation justified?
d. What is the distance from the real point of impact to the point that would be reached without the action of the Coriolis force? In which direction is the body deviated?

Solution: *a. In the Earth-bound system (x to the east, y to the north, z upwards):*

$$\ddot{\mathbf{r}}(t) = \mathbf{g} - 2\vec{\omega} \times \dot{\mathbf{r}}(t) - \vec{\omega} \times (\vec{\omega} \times \mathbf{r}(t)) \qquad \textit{with} \qquad \mathbf{g} = -g\hat{\mathbf{e}}_z \qquad \textit{with} \qquad \vec{\omega} = \omega \hat{\mathbf{e}}_y \ .$$

From the initial condition $\mathbf{r}(0) = h\hat{\mathbf{e}}_z$ and $\dot{\mathbf{r}}(0) = 0$ follows $\hat{\mathbf{e}}_y \cdot \mathbf{r}(t) = 0$. So the movement only takes place in the (x, z) plane.
b. In component notation,

$$\ddot{x} = -2\omega\dot{z} + \omega^2 x \qquad \textit{and} \qquad \ddot{z} = -g + 2\omega\dot{x} + \omega^2 z \ ,$$

where $\omega = \frac{2\pi}{24\,\mathrm{h}} = 7.3 \cdot 10^{-5}\,\mathrm{s^{-1}}$. Via $u(t) = z(t) + \imath x(t)$ with $u(0) = h$ and $\dot{u}(0) = 0$ one gets the complex differential equation,

$$\ddot{u} + 2\imath\omega\dot{u} - \omega^2 u = -g \ ,$$

with the particular solution $u_{part} = g/\omega^2$. The homogeneous ansatz $u_{hom} \sim e^{\lambda t}$ provides the characteristic equation $\lambda^2 + 2\imath\omega\lambda - \omega^2 = 0$ with the solution $\lambda = -\imath\omega$. From this follows,

$$\begin{aligned} u(t) &= g/\omega^2 + (A + Bt)e^{-\imath\omega t} \qquad \textit{and} \qquad \dot{u}(t) &&= [B - \imath\omega(A + Bt)]e^{-\imath\omega t} \\ \Rightarrow \quad A &= h - g/\omega^2 \qquad \textit{and} \qquad B &&= \imath\omega A = \imath\omega(h - g/\omega^2) \ . \end{aligned}$$

Finally,

$$u(t) = g/\omega^2 + (h - g/\omega^2)(1 + \imath\omega t)e^{-\imath\omega t} \ .$$

c. The real components,

$$\begin{aligned} z(t) &= g/\omega^2 + (h - g/\omega^2)[\cos\omega t + \omega t \sin\omega t] \\ x(t) &= (h - g/\omega^2)[-\sin\omega t + \omega t \cos\omega t] \end{aligned}$$

with the expansion of $\omega t \ll 1$*:*

$$\cos\omega t + \omega t \sin\omega t = 1 + \frac{1}{2}\omega^2 t^2 + \mathcal{O}(\omega^4 t^4)$$
$$-\sin\omega t + \omega t \cos\omega t = -\frac{1}{3}\omega^3 t^3 + \mathcal{O}(\omega^5 t^5) \ ,$$

become,

$$z(t) \approx h - \frac{1}{2}gt^2 \qquad \textit{and} \qquad x(t) \approx \frac{1}{3}g\omega t^3$$

d. Drop time T *and deviation* $x(T)$*:*

$$T = \sqrt{\frac{2h}{g}} = 4.5\,\mathrm{s} \qquad \textit{and} \qquad x(T) = \frac{1}{3}g\omega T^3 = 2.2\,\mathrm{cm} \ .$$

Note: *If we omit the terms* $\mathcal{O}(\omega^2)$ *from the equations of motion, the DEq system can be solved trivially.*

3.1.4.14 Ex: Coriolis force

A penguin with the mass m is located directly at the South Pole and begins to slide horizontally at the initial velocity v on the ice. The ice slows him down with the force $\mathbf{F} = -\gamma\mathbf{v}$.
a. Write down the equations of motion in a coordinate system originating at the south pole, which rotates with the Earth.
Note: Place the x-axis in the direction of the penguin's initial velocity and combine the variables x and y to a complex variable $z = x + \imath y$. Neglect the curvature of the Earth. b. Calculate the end position of the penguin on the assumption that the

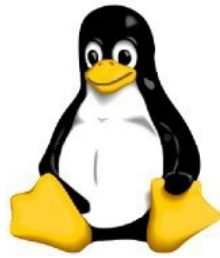

Figure 3.3: Coriolis force.

rotation speed of the earth ω is small enough to neglect quadratic terms $\propto \omega^2$ in the equations of motion or in their solution.

Solution: *a. In the rotating system* $\vec{\omega} = (0, 0, \omega)$ *the equation of motion is,*

$$\ddot{r}' = -\frac{\gamma}{m}\mathbf{r} \ .$$

Hence, in the lab system,

$$\left(\frac{d}{dt}-\vec{\omega}\times\right)\left(\frac{d}{dt}-\vec{\omega}\times\right)\mathbf{r}=-\frac{\gamma}{m}\mathbf{r}\ .$$

From this follows,

$$\mathbf{r}-2\vec{\omega}\times\mathbf{r}+\vec{\omega}\times(\vec{\omega}\times\mathbf{r})=-\frac{\gamma}{m}\mathbf{r}\ .$$

For the x- resp. y-components the equations of motion are,

$$\begin{aligned}\ddot{x}&=-\frac{\gamma}{m}\dot{x}+\omega^2x-2\omega\dot{y}\\ \ddot{y}&=-\frac{\gamma}{m}\dot{y}+\omega^2y+2\omega\dot{x}\ ,\end{aligned}$$

wheres the second and third terms represent centripetal and Coriolis force, $z=x+\imath y$, hence,

$$\begin{aligned}\ddot{z}&=-\tilde{\gamma}\dot{z}+\omega^2z+2\imath\omega\dot{z}\qquad z=Ce^{\lambda t}\\ \lambda^2&=-\tilde{\gamma}\lambda+\omega^2+2\imath\omega\lambda\qquad z=Ae^{\lambda_1 t}+Be^{\lambda_2 t}\\ \lambda_{1,2}&=\frac{-\tilde{\gamma}+2\imath\ \omega\pm\sqrt{\tilde{\gamma}^2-4\imath\tilde{\gamma}\omega}}{2}\ ,\end{aligned}$$

where $\tilde{\gamma}=\gamma/m$. $x=\mathfrak{Re}\ z$ and $y=\mathfrak{Im}\ z$ will be damped sine/cosine.
b. The equation resp. solution will be,

$$\begin{aligned}\ddot{z}&=-\tilde{\gamma}\dot{z}+2\imath\omega\dot{z}\qquad z=Ce^{\lambda t}\\ \lambda^2&=-\tilde{\gamma}\lambda+2\imath\omega\lambda\qquad z=Ae^{\lambda_1 t}+Be^{\lambda_2 t}\\ \lambda_{1,2}&=\frac{-\tilde{\gamma}+2\imath\omega\pm(\tilde{\gamma}-2\imath\omega)}{2}\to\lambda_1=0\quad\lambda_2=-\tilde{\gamma}+2\imath\omega\ .\end{aligned}$$

The initial conditions $z(0)=0$, $\dot{z}(0)=v$ lead to,

$$B=-A=\frac{v}{-\tilde{\gamma}+2\imath\omega}\simeq-v\frac{\tilde{\gamma}+2\imath\omega}{\tilde{\gamma}^2}+O(\omega^2)\ .$$

For large t we have $e^{-\tilde{\gamma}t}\ll 1$ and $z\simeq A=v/\tilde{\gamma}+2\imath v\omega/\tilde{\gamma}$ such that $x(\infty)=mv/\gamma$, $y(\infty)=2mv\ \omega/\gamma$.

3.1.4.15 Ex: Center of mass

You have three rectangular blocks of same heights and depths, but with different lengths and different masses. You want to build an inclined tower with them. Determine experimentally or theoretically how to stack the blocks so that the top block overhangs as much as possible. What is the most favorable order in the case of same masses but different lengths? What is the most advantageous order in the case of same lengths but different masses?

Solution: *Let x_{sj} be the center-of-masses points of the individual blocks. In order for the uppermost block $j = 3$ to remain on the middle block $j = 2$, the following must apply,*

$$\frac{m_3(x_{s3} - x_{s2})}{m_3} < \frac{1}{2}L_2 \ .$$

The following must apply so that the two upper blocks remain on the lower block $j = 1$,

$$\frac{m_2\,(x_{s2} - x_{s1}) + m_3\,(x_{s3} - x_{s1})}{m_2 + m_3} < \frac{1}{2}L_1 \ .$$

Let the origin be fixed by $x_{s1} = 0$. Then by eliminating x_{s2} we get from (1) and (2),

$$x_{s3} < \frac{L_1}{2} + \frac{m_2}{m_2 + m_3}\frac{L_2}{2} \ .$$

So the overhang is,

$$\ddot{u} = x_{s3} + \frac{L_3}{2} < \frac{L_1}{2} + \frac{m_2}{m_2 + m_3}\frac{L_2}{2} + \frac{L_3}{2} \ .$$

In the case of equal lengths,

$$\ddot{u} < L\left(1 + \frac{1}{2}\frac{m_2}{m_2 + m_3}\right) \ ,$$

it makes sense to put the light mass on top of the heavy one, $m_3 < m_2$. In the case of equal masses,

$$\ddot{u} < \frac{L_1}{2} + \frac{L_2}{4} + \frac{L_3}{2} \ ,$$

it makes sense to put the longer block on top of the shorter one, $L_3 > L_2$.

3.1.4.16 Ex: Inclined pyramid

Five identical point masses m are arranged at the corners of an oblique pyramid with the height H and a square base area $F = a^2$, i.e. they are located at $(x, y, z) = (\pm a/2, \pm a/2, 0)$ and $(b, 0, H)$. What is the maximum lateral displacement b of the top of the pyramid so that the pyramid does not tip out of the horizontal xy-plane?

Solution: *The mass of the pyramid is $M = 5m$. The center of gravity vector of a discrete mass distribution is given by,*

$$\mathbf{S} = \frac{\sum m_j \mathbf{r}_j}{\sum m_j} \ .$$

For the given pyramid,

$$\mathbf{S} = \frac{1}{M}\sum_{j=1}^{5} m\mathbf{r}_j = \frac{1}{M}\left(m(H\hat{\mathbf{e}}_z + b\hat{\mathbf{e}}_x) + m\sum_{j=1}^{4}\mathbf{r}_j\right) = \frac{1}{M}m(H\hat{\mathbf{e}}_z + b\hat{\mathbf{e}}_x) = \frac{H\hat{\mathbf{e}}_z + b\hat{\mathbf{e}}_x}{5} \ .$$

Now the axis is tilted from the center of the base to the top of the pyramid by an angle α. It falls over when $\mathbf{S}\hat{\mathbf{e}}_x > \frac{a}{2}$, hence,

$$\frac{H\hat{\mathbf{e}}_z + b\hat{\mathbf{e}}_x}{5}\hat{\mathbf{e}}_x > \frac{a}{2} \ ,$$

hence $b > 2.5a$.

3.1.4.17 Ex: Inclined cone

A rigid cone with a homogeneous mass distribution has the height H and a base area with a radius R. How far can you tilt the cone before it falls over?

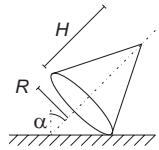

Figure 3.4: Inclined cone.

Solution: *The mass of the cone is,*

$$m = \rho_0 \int_{cone} d^3\mathbf{r} = \rho_0 \int_0^H \int_0^{2\pi} \int_0^{R-Rz/H} \rho d\rho d\phi dz = 2\pi\rho_0 \int_0^H \int_0^{R-Rz/H} \rho d\rho dz$$
$$= 2\pi\rho_0 \int_0^H \frac{(R-Rz/H)^2}{2} dz = 2\pi\rho_0 R^2 \left[\frac{z}{2} - \frac{z^2}{2H} + \frac{z^3}{6h^2}\right]_0^H = \frac{\pi}{3}\rho_0 R^2 H \ .$$

The center of gravity vector of a continuous mass distribution $\rho(\mathbf{r})$ is given by,

$$\mathbf{S} = \frac{\int \rho(\mathbf{r})\mathbf{r}d^3\mathbf{r}}{\int \rho(\mathbf{r})d^3\mathbf{r}} \ .$$

For a homogeneous cone,

$$\mathbf{S} = \frac{\rho_0}{m}\int_{cone} \mathbf{r}d^3\mathbf{r} = \frac{\rho_0}{m}\int_0^H \int_0^{2\pi} \int_0^{R-Rz/H} \begin{pmatrix} \rho\cos\phi \\ \rho\sin\phi \\ z \end{pmatrix} \rho d\rho d\phi dz$$

$$= 2\pi\frac{\rho_0}{m}\int_0^H \begin{pmatrix} 0 \\ 0 \\ z \end{pmatrix} \int_0^{R-Rz/H} \rho d\rho dz = 2\pi\frac{\rho_0}{m}\hat{\mathbf{e}}_z \int_0^H z\frac{(R-Rz/H)^2}{2} dz$$

$$= 2\pi\frac{\rho_0}{m}R^2\hat{\mathbf{e}}_z \left[\frac{z^2}{4} - \frac{2z^3}{6H} + \frac{R^2z^4}{8H^2}\right]_0^H = \frac{\pi}{12}\frac{\rho_0}{m}R^2H^2\hat{\mathbf{e}}_z = \frac{H}{4}\hat{\mathbf{e}}_z \ .$$

Now the cone is tilted by the angle α. It falls over when $S\sin\alpha > R\cos\alpha$, hence,

$$\arctan\alpha > \frac{H}{4R} \ .$$

3.1.4.18 Ex: Angular momentum of the Earth

a. Calculate the angular momentum of the Earth's rotation around its center of mass (mass $M = 5.97 \times 10^{24}\,\mathrm{kg}$, radius $R = 6370\,\mathrm{km}$).
b. Compare this with the angular momentum of the Earth's rotation around the sun (distance between Sun and Earth $D = 150 \times 10^{9}\,\mathrm{km}$).

Solution: *a. The angular momentum is,*

$$\mathbf{L} = I\vec{\omega} \ .$$

With the inertial moment $I = \frac{2}{5}MR^2$ *we obtain,*

$$L = I\omega = \frac{2}{5}MR^2\frac{2\pi}{60\cdot 60\cdot 24\,\mathrm{s}} = 7.0\cdot 10^{33}\,\mathrm{kg\ m^2\,s^{-1}} \ .$$

b. The inertial moment is now $I = MD^2$*. Hence,*

$$L = I\omega = MD^2\frac{2\pi}{60\cdot 60\cdot 24\cdot 365\,\mathrm{s}} = 4.8\cdot 10^{31}\,\mathrm{kg\ m^2\,s^{-1}} \ .$$

3.1.4.19 Ex: Inertial moment

a. Calculate the mass of a cone with homogeneous density (height H and a base radius R).
b. Calculate the cone's inertial moment with respect to the symmetry axis.
c. The cone now rotates with the frequency ω around an axis displaced by a distance R parallel to the symmetry axis. How to calculate the angular momentum?

Solution: *a. The cone mass is,*

$$\begin{aligned} M &= \int dm = \rho\int_0^{2\pi}\int_0^{H}\int_0^{R-zR/H} r dr dz d\phi = 2\pi\rho\int_0^{H}\tfrac{1}{2}\left(R-\frac{R}{H}z\right)^2 dz \\ &= -2\pi\rho\frac{H}{R}\int_R^0 \tfrac{1}{2}\zeta^2 d\zeta = \pi\rho\frac{H}{R}\frac{1}{3}R^3 = \frac{\pi\rho}{3}HR^2 \ . \end{aligned}$$

b. The inertial moment is,

$$\begin{aligned} I_{cm} &= \int dm = \rho\int_0^{2\pi}\int_0^{H}\int_0^{R-zR/H} r^2 r dr dz d\phi = 2\pi\rho\int_0^{H}\tfrac{1}{4}\left(R-\frac{R}{H}z\right)^4 dz \\ &= -2\pi\rho\frac{H}{R}\int_R^0 \tfrac{1}{4}\zeta^4 d\zeta = \frac{\pi}{2}\rho\frac{H}{R}\frac{1}{5}R^5 = \frac{3}{10}MR^2 \ . \end{aligned}$$

c. The angular momentum is,

$$L = I\omega = (I_{cm} + MR^2)\omega = \frac{13}{10}MR^2 \ .$$

3.1.4.20 Ex: Glass of beer

A cylindrical glass of beer (height $H = 18\,\text{cm}$, diameter $D = 6\,\text{cm}$, mass $m_G = 0.5\,\text{kg}$, the bottom is without mass) has, when empty, its center of mass exactly halfway up. Obviously, it is there too, when the glass is filled with beer (density $\rho = 1000\,\text{kg/m}^3$) up to the upper limit. Down to which height h do you have to drink the beer for the center of mass to be at its lowest height?

Solution: *Be h the wanted height of beer. Then the beer mass is,*

$$m_B = \frac{\pi D^2}{4} h\rho \ .$$

The center of mass of the beer is at $h/2$, that of the glass at $H/2$. The total center of mass is at,

$$S = \frac{\frac{H}{2}m_G + \frac{h}{2}m_B}{m_G + m_B} = \frac{\frac{H}{2}m_G + \frac{h}{2}\frac{\pi D^2}{4}h\rho}{m_G + \frac{\pi D^2}{4}h\rho} = \frac{4Hm_G + \pi D^2\rho h^2}{8m_G + 2\pi D^2\rho h} \ .$$

With $dS/dh = 0$ we find,

$$\begin{aligned} 2\pi D^2\rho h\left(8m_G + 2\pi D^2\rho h\right) - \left(4Hm_G + \pi D^2\rho h^2\right)2\pi D^2\rho &= 0 \\ 2\pi^2 D^4\rho^2 h^2 + 16\pi m_G\rho D^2 h - 8\pi m_G\rho D^2 H &= 0 \\ h^2 + \frac{8m_G}{\pi D^2\rho}h - \frac{4m_G}{\pi D^2\rho}H &= 0 \\ h = -\frac{4m_G}{\pi D^2\rho} + \frac{4m_G}{\pi D^2\rho}\sqrt{1 + \frac{\pi D^2\rho H}{4m_G}} &> 0 \ . \end{aligned}$$

Therefore, the height is $h = 7.44\,\text{cm}$.

3.1.4.21 Ex: Inertial moment

Consider a flat symmetrical triangle with surface density σ and corner length a. Fix the coordinate system such that the triangle is given by the corners $A = (0, \frac{a}{2})$, $B = (0, -\frac{a}{2})$ e $C = (\frac{a\sqrt{3}}{2}, 0)$.
a. Calculate the mass of the triangle.
b. Calculate the center of mass.
c. Calculate the inertial moment with respect to an axis normal to the surface through the center of mass of the triangle.

Solution: *a. The mass is,*

$$M = 2\sigma\int_0^{a/2}\int_0^{\sqrt{3}(a/2-y)} dxdy = 2\sigma\int_0^{a/2}\sqrt{3}\left(\tfrac{a}{2} - y\right)dy = 2\sigma\sqrt{3}\left[\tfrac{a}{2}y - \tfrac{1}{2}y^2\right]_0^{a/2} = \sigma\sqrt{3}\frac{a^2}{4} \ .$$

b. The center of mass is given by,

$$x_{cm} = \frac{\int\int \sigma x dxdy}{\int\int \sigma dxdy} = \frac{1}{M} 2\sigma \int_0^{a/2} \int_0^{\sqrt{3}(a/2-y)} x dxdy = \frac{2\sigma}{M} \int_0^{a/2} \tfrac{1}{2}\sqrt{3}^2 \left(\tfrac{a}{2} - y\right)^2 dy$$
$$= \frac{3\sigma}{M} \frac{1}{24} a^3 = \frac{a}{2\sqrt{3}}$$
$$y_{cm} = 0 \ .$$

c. The inertial moment with respect to an axis crossing the origin is,

$$I_0 = \int r^2 dm = 2\sigma \int_0^{a/2} \int_0^{\sqrt{3}(a/2-y)} (x^2+y^2) dxdy = 2\sigma \int_0^{a/2} \left[\tfrac{1}{3}\sqrt{3}^3 (\tfrac{a}{2}-y)^3 + \sqrt{3}(\tfrac{a}{2}-y)y^2\right] dy$$
$$= 2\sigma\sqrt{3} \int_0^{a/2} \left[(\tfrac{a}{2}-y)^3 + (\tfrac{a}{2}-y)y^2\right] dy = \tfrac{2\sigma\sqrt{3}}{48} a^4 = \tfrac{M}{6} a^2 \ .$$

And the inertial moment with respect to an axis crossing the center of mass is,

$$I = I_{cm} + I_0 = M \left(\frac{a}{2\sqrt{3}}\right)^2 + \tfrac{M}{6} a^2 = \frac{M}{4} a^2 \ .$$

3.1.4.22 Ex: Inertial moment

Consider a flat arc segment with surface density σ, radius R, and angle ϕ. Fix the coordinate system at the center of the arc such that the axis of symmetry is x.
a. Calculate the mass of the segment.
b. Calculate the center of mass.
c. Calculate the inertial moment with respect to a normal axis at the surface through the center of mass of the segment.

Solution: *a. The mass is,*

$$M = \sigma \int_{-\phi/2}^{\phi/2} \int_0^R r dr d\phi = \sigma \frac{R^2}{2} \phi \ .$$

b. The center of mass is given by,

$$x_{cm} = \frac{\int\int \sigma x dxdy}{\int\int \sigma dxdy} = \frac{\sigma}{M} \int_{-\phi/2}^{\phi/2} \int_0^R x r dr d\phi = \frac{\sigma}{M} \int_{-\phi/2}^{\phi/2} \int_0^R r^2 \cos\phi dr d\phi = \frac{\sigma}{M} \frac{R^3}{3} \int_{-\phi/2}^{\phi/2} \cos\phi d\phi$$
$$= \frac{2\sigma}{3M} R^3 \sin\frac{\phi}{2} = \frac{4R}{3\phi} \sin\frac{\phi}{2}$$
$$y_{cm} = 0 \ .$$

c. The inertial moment with respect to an axis crossing a corner is,

$$I_0 = \int r^2 dm = \sigma \int_{-\phi/2}^{\phi/2} \int_0^R r^3 dr d\phi = \sigma \frac{R^4}{4} \phi = \frac{M}{2} R^2 \ .$$

And the inertial moment with respect to an axis crossing the center of mass is,

$$I = I_{cm} + I_0 = Mx_{cm}^2 + \frac{M}{2}R^2 = M\left(\frac{4R}{3\phi}\sin\frac{\phi}{2}\right)^2 + \frac{M}{2}R^2 = \frac{M}{2}R^2\left[1 + \frac{32}{9\phi^2}\sin^2\tfrac{\phi}{2}\right] .$$

3.1.4.23 Ex: Inertial tensor

Calculate the moment of inertia of a homogeneous hollow cylinder with mass m, length L, outer radius R, and inner radius r.

Solution: *The mass of the hollow cylinder is,*

$$m = \pi\varrho_0 L(R^2 - r^2) .$$

The inertia tensor is for continuous systems given by,

$$I_{ij} = \int_V \varrho(\mathbf{r})\left[\delta_{ij}\mathbf{r}^2 - x_i x_j\right] dV .$$

So for a hollow cylinder with length L, outer radius R, and inner radius r,

$$\begin{aligned} I_{33} &= \varrho_0 \int_{hollow\ \ cylinder} \left(x^2 + y^2\right) dV = \varrho_0 \int_0^{2\pi}\int_{-L/2}^{L/2}\int_r^R \rho^2 \rho d\rho dz d\phi \\ &= \pi\varrho_0 L\frac{R^4 - r^4}{2} = \frac{m}{2}(R^2 + r^2) . \end{aligned}$$

For I_{11} and I_{22} one gets,

$$\begin{aligned} I_{11} + I_{22} &= \varrho_0 \int_{hollow\ \ cylinder} \left(x^2 + y^2 + 2z^2\right) dV = I_{33} + 2\varrho_0 \int_0^{2\pi}\int_{-L/2}^{L/2}\int_r^R z^2 \rho d\rho dz d\phi \\ &= \frac{m}{2}(R^2 + r^2) + \frac{m}{6}L^2 = 2I_{11} = 2I_{22} . \end{aligned}$$

For the non-diagonal elements one gets,

$$I_{i\neq j} = \int_V \rho(\mathbf{r}) x_i x_j dV = \rho\int_{-d/2}^{d/2} x_i x_j dx_i dx_j dx_k = 0 .$$

3.1.4.24 Ex: Inertial tensor

Determine the tensor of inertia for
a. a tetrahedron in which the mass is distributed equally between the corner points in a coordinate system in which the z-axis passes through the center of opposite edges;
b. of the tetrahedron in a coordinate system in which the z-axis passes through one of its corners and through its center of gravity.

Solution:

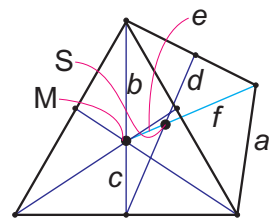

Tetraeder. If the tetrahedron has the edge length of a, then the distance of the center M of a facet from a corner of the same facet is $b = \frac{a}{2\cos 30^\circ} = a\frac{\sqrt{3}}{3}$. *The distance of the center of a facet to an edge of the same facet is* $c = \frac{a}{2}\tan 30^\circ = a\frac{\sqrt{3}}{6}$. *The distance of the center of gravity of the tetrahedron from the edges is* $d = \frac{1}{2}\sqrt{(b+c)^2 - \frac{a^2}{4}} = a\frac{\sqrt{2}}{4}$. *The distance of the center of gravity to the center of the facets is* $e = \sqrt{d^2 - c^2} = \frac{a}{2\sqrt{6}}$. *The distance of the corners from the center of gravity is* $f = \sqrt{d^2 + \frac{a^2}{4}} = \frac{a}{2}\sqrt{\frac{3}{2}}$, *such that for every corner* α *holds* $\mathbf{r}_\alpha^2 = \frac{3}{8}a^2$.
The inertial tensor is for point-like systems,

$$I_{ij} = \sum_\alpha m_\alpha \left(\delta_{ij}\mathbf{r}_\alpha^2 - x_\alpha^{(i)} x_\alpha^{(j)}\right) = \begin{pmatrix} \sum_\alpha m_\alpha \left(\mathbf{r}_\alpha^2 - x_\alpha^2\right) & -\sum_\alpha m_\alpha x_a y_\alpha & -\sum_\alpha m_\alpha x_a z_\alpha \\ -\sum_\alpha m_\alpha x_a y_\alpha & \sum_\alpha m_\alpha \left(\mathbf{r}_\alpha^2 - y_\alpha^2\right) & -\sum_\alpha m_\alpha y_a z_\alpha \\ -\sum_\alpha m_\alpha x_a z_\alpha & -\sum_\alpha m_\alpha y_a z_\alpha & \sum_\alpha m_\alpha \left(\mathbf{r}_\alpha^2 - z_\alpha^2\right) \end{pmatrix} .$$

a. Placing the coordinate system so that the z-axis cuts two opposite edges in their center and the x-axis runs parallel to one of the edges, then the points of the tetrahedron are at $(\pm a/2, 0, d)$ *and* $(0, \pm a/2, -d)$,

$$I = m\begin{pmatrix} 4\frac{3a^2}{8} - \frac{a^2}{4} - \frac{a^2}{4} - 0 - 0 & 0 & 0 \\ 0 & 4\frac{3a^2}{8} - 0 - 0 - \frac{a^2}{4} - \frac{a^2}{4} & 0 \\ 0 & 0 & 4\frac{3a^2}{8} - \frac{a^2}{8} - \frac{a^2}{8} - \frac{a^2}{8} - \frac{a^2}{8} \end{pmatrix} = ma^2\mathbf{1}_3 .$$

b. Placing the coordinate system so that the z-axis goes through one corner of the tetrahedron and through its center of gravity and the x-axis points towards a second corner, then the points of the tetrahedron at $(0, 0, f)$, $(0, b, -e)$ *and* $(\pm a/2, -c, -e)$,

$$I = m\begin{pmatrix} 4\frac{3a^2}{8} - 0 - 0 - \frac{a^2}{4} - \frac{a^2}{4} & -0 - 0 + \frac{ac}{2} - \frac{ac}{2} & -0 - 0 + \frac{ae}{2} - \frac{ae}{2} \\ -0 - 0 + \frac{ac}{2} - \frac{ac}{2} & 4\frac{3a^2}{8} - 0 - b^2 - c^2 - c^2 & -0 + be - ce + ce \\ -0 - 0 + \frac{ae}{2} - \frac{ae}{2} & -0 + be - ce + ce & 4\frac{3a^2}{8} - f^2 - e^2 - e^2 - e^2 \end{pmatrix} = ma^2\mathbf{1}_3 .$$

One could have come up with it straight away, since the matrix must emerge from that of part (b) by rotation, but the unit matrix is equal into itself when it rotates, $D^t E_3 D = E_3$.

3.1.4.25 Ex: Inertial tensor

Two balls of different radii $R_1 > R_2$ and same homogeneous mass density ρ are welded together at their point of contact. Derive the moment of inertia of each individual sphere (axis of rotation through the center).
a. Where is the center-of-mass of the total system?
b. Calculate the main moments of inertia of the total system with regard to its center of gravity. **Note:** Use Steiner's theorem.

Solution: *It doesn't matter about which axis the ball is rotated; we take the z-axis.*

$$I = \int_{ball} \rho(x^2+y^2)dV = \rho \int_0^R r^2 dr \int_0^\pi \sin\theta d\theta \int_0^{2\pi} d\phi \left(r^2 \sin^2\theta \cos^2\phi + r^2 \sin\theta^2 \sin^2\phi\right)$$
$$= 2\pi\rho \frac{1}{5} R^5 \int_0^\theta d\theta \sin^3\theta = 2\pi\rho \frac{1}{5} R^5 \frac{4}{3} \ .$$

The last integral can be solved by partial integration. So the moment of inertia is, $I = \frac{8}{15}\pi\rho R^5$. *With* $\rho = M/V = M/(\frac{4}{3}\pi R^3)$ *one gets* $I = \frac{2}{5}MR^2$.
a. The center of gravity vector of the system is,

$$\mathbf{S} = \frac{M_1\mathbf{r}_1 + M_2\mathbf{r}_2}{M_1+M_2} \ .$$

The center of gravity is on the connecting line between the individual centers of the spheres. If we now place the coordinate origin in the center of sphere 1 and, for example, the x-axis along the vector connecting the two centers of the spheres, only the x-component of $\mathbf{S} \neq 0$, *namely,*

$$S_x = \frac{M_2}{M_1+M_2}(R_1+R_2) \ .$$

This shows that the center of gravity seen from the center of sphere 1 is at $\frac{M_2}{M_1+M_2}$ *of the connecting line.*
b. Let us rotate the system around an axis $\hat{\omega}$ *that goes through the center of sphere 1. Then the moment of inertia about this axis is calculated according to Steiner's theorem to* $I_\omega = I_\omega^{SP} + Mb^2$. *Note that we are looking for* I_ω^{SP}. *On the other hand, the moment of inertia when rotating around this axis is also equal to the sum of the moment of inertia of ball 1 when rotating around its center plus the moment of inertia of ball 2 when rotating around the axis through ball 1. So:*

$$I_\omega = \frac{2}{5}MR_1^2 + I_{\omega,K_2}$$

We can now calculate again I_{ω,K_2} *using the Steiner theorem:*

$$I_{\omega,K_2} = \frac{2}{5}M_2R_2^2 + M_2(R_1+R_2)^2 \ .$$

Inserting we get,

$$I_\omega = \frac{2}{5}M_1R_1^2 + I_{\omega,K_2} = \frac{2}{5}M_1R_1^2 + \frac{2}{5}M_2R_2^2 + M_2(R_1+R_2)^2$$
$$I_\omega = I_\omega^{SP} + Mb^2 = I_\omega^{SP} + (M_1+M_2)\left(\frac{M_2}{M_1+M_2}(R_1+R_2)\right)^2 \ .$$

This we can now solve by

$$I_\omega^{SP} = I_\omega - (M_1+M_2)b^2 = \frac{2}{5}M_1R_1^2 + \frac{2}{5}M_2R_2^2 + M_2(R_1+R_2)^2 - \frac{M_2}{M_1+M_2}(R_1+R_2)^2$$

The second main moment of inertia is identical to the one just calculated and the third (axis of rotation through both spherical centers) is additively composed of the individual moments of inertia of the spheres for rotations around their centers.

3.1.4.26 Ex: Rolling movement

A cylinder of mass m with radius R rolls over the ski jump shown in the figure, which has a gradient of -173% (i.e. $\tan\alpha = -1.73$). After having left the ski jump at a height of $h = H/2$, he falls in the Earth's gravity field. Compare the flight distance with the case in which the cylinder does not roll, but slides smoothly over the hill.

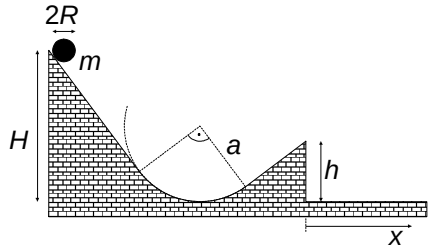

Figure 3.5: Rolling movement.

Solution: *In the event of rolling, the potential energy is converted into kinetic and rotational energy,*

$$\frac{m}{2}v^2 + \frac{I_z}{2}\omega^2 = mg(H-h) \ .$$

With $\omega = v/R$ and $I_z = mR^2/2$ one get at the take-off position $v_0 = \sqrt{\frac{4}{3}g(H-h)}$. The rotational energy is lost.
When sliding, the kinetic energy is greater at the take-off position,

$$\frac{m}{2}v^2 = mg(H-h) \ ,$$

because no rotational energy is generated, so $v_0 = \sqrt{2g(H-h)}$.
The slope angle of the ski jump is at the take-off position $\alpha + 90° = 30°$, such that,

$$\dot{x}_0 = v_0\cos(\alpha+90) = \frac{\sqrt{3}}{2}v_0 \qquad \textit{and} \qquad \dot{y}_0 = v_0\sin(\alpha+90) = \frac{1}{2}v_0 \ .$$

The flight time is given by,

$$y(t) = -\frac{g}{2}t^2 + \dot{y}_0 t + h = 0 \qquad \textit{respectively} \qquad t = \frac{1}{g}\left(\dot{y}_0 + \sqrt{\dot{y}_0^2 + 2gh}\right) \ .$$

The flight distance is then $x(t) = \dot{x}_0 t$. With $\eta = 4/3$ for the rolling motion and $\eta = 2$ for the sliding motion we can write,

$$\begin{aligned}
&x(t) = \dot{x}_0 t \\
&= \sqrt{\eta g(H-h)}\cos(\alpha+90)\tfrac{1}{g}\left(\sqrt{\eta g(H-h)}\sin(\alpha+90°) + \sqrt{\eta g(H-h)\sin(\alpha+90°)^2 + 2gh}\right) \\
&= \sqrt{\eta g\left(H-\frac{H}{2}\right)}\frac{\sqrt{3}}{2}\frac{1}{g}\left(\sqrt{\eta g\left(H-\frac{H}{2}\right)}\frac{1}{2} + \sqrt{\eta g\left(H-\frac{H}{2}\right)\frac{1}{4} + 2g\frac{H}{2}}\right) \\
&= \frac{\sqrt{3}H}{8}\left(\eta + \sqrt{\eta^2+8\eta}\right) \ .
\end{aligned}$$

The ratio is,

$$\frac{x_{roll}(t)}{x_{slide}(t)} = \frac{\frac{4}{3} + \sqrt{\left(\frac{4}{3}\right)^2 + 8 \cdot \frac{4}{3}}}{2 + \sqrt{2^2 + 8 \cdot 2}} = \frac{2}{3}\frac{1+\sqrt{7}}{1+\sqrt{5}} \simeq 0.75 \ .$$

3.1.4.27 Ex: Accelerated rotational movement

A mass $m = 1\,\mathrm{kg}$ is hanging on a light cord, which is wound on a $d = 2\,\mathrm{cm}$ thick wheel with the radius $r = 10\,\mathrm{cm}$. The wheel has a homogeneously distributed mass of $M = 10\,\mathrm{kg}$ and rotates without friction.
a. Determine the tensile force in the cord.
b. Determine the acceleration of the mass.

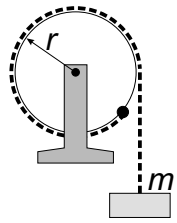

Figure 3.6: Accelerated rotational movement.

Solution: *a. The force of the weight force and the acceleration work to pull the mass m downwards, $m\mathbf{a} = m\mathbf{g} + \mathbf{Z}$. The tensile force in the cord is therefore of an amount $Z = mg - ma$.*
b. The torque is $\mathbf{D} = \frac{d}{dt}\mathbf{L}$. Hence, $\mathbf{r} \times \vec{Z} = I\frac{d}{dt}\vec{\omega}$.
Now we have $Zr = I\dot{\omega} = I\frac{d}{dt}\frac{v}{r} = I\frac{a}{r}$. Hence, $a = \frac{Zr^2}{I}$.
Now $mg - Z = m\frac{Zr^2}{I}$, also $Z = \frac{mg}{1+mr^2/I}$ respectively $a = \frac{mgr^2}{I+mr^2)}$.
The following applies to the wheel (solid cylinder): $I = \frac{1}{2}Mr^2$, thus the acceleration of the mass is $a = \frac{mgr^2}{\frac{1}{2}Mr^2+mr^2} = \frac{2m}{M+2m}g$.
c. Be H the height of the wheel axle, h the initial height of the mass m, $z(t)$ the time-dependent height of the mass.
Conservation of energy requires: $MgH + mgh = MgH + \frac{1}{2}I\omega(t)^2 + mgz(t) + mv^2(t)$.
thus $mg(h - z(t)) = \frac{1}{4}Mr^2\omega^2(t) + \frac{1}{2}mv^2(t)$.
We have $\omega = d\phi(t)/dt$ and $dz/dt = v(t) = rd\phi/dt = r\omega(t)$.
also $mg(h - z) = \frac{1}{4}Mv^2 + \frac{1}{2}mv^2 = \frac{M+2m}{4}\left(\frac{dz}{dt}\right)^2$.
Separation of the variables: $\sqrt{\frac{4mg}{M+2m}}dt = \frac{dz}{\sqrt{h-z}}$.
Integration: $\sqrt{\frac{4mg}{M+2m}}t = \left[-2\sqrt{h-\tilde{z}}\right]_z^h = 2\sqrt{h-z}$, also $z(t) = h - \frac{4mg}{M+2m}t^2 = h - t^2 0.8175\,\mathrm{m/s^2}$ and $a(t) = -\frac{2m}{M+2m}g$.

3.1.4.28 Ex: Hovering dumbbell

A dumbbell rotates at the angular velocity ω around a rotation axis that passes through its center of gravity and forms an angle α with the axis connecting the masses (see figure).
a. Calculate the angular momentum vector of the barbell in the co-rotating coordinate system.
b. How does the angular momentum behave in a non-rotating coordinate system?
c. Calculate the torque that must act so that the angular velocity remains constant.

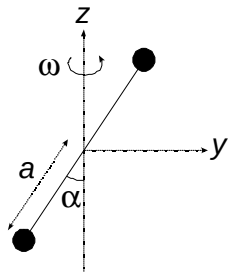

Figure 3.7: Hovering dumbbell.

Solution: *a. The angular momentum vector of the dumbbell in the co-rotating coordinate system is,*

$$\mathbf{L} = I\vec{\omega} = I \begin{pmatrix} 0 \\ 0 \\ \omega \end{pmatrix}$$

$$\mathbf{r}_i = \begin{pmatrix} 0 \\ \pm a \sin\alpha \\ \pm a \cos\alpha \end{pmatrix}$$

$$I_{zx} = 0 \quad , \quad I_{zy} = -2ma^2 \sin\alpha\cos\alpha \quad , \quad I_{zz} = 2ma^2 \sin^2\alpha \ .$$

Hence,

$$\mathbf{L} = \begin{pmatrix} 0 \\ -2ma^2\omega \sin\alpha\cos\alpha \\ 2ma^2\omega \sin^2\alpha \end{pmatrix} \ .$$

b. The angular momentum in a non-rotating coordinate system is,

$$\mathbf{L}_{lab} = \begin{pmatrix} \cos\omega t & -\sin\omega t & 0 \\ \sin\omega t & \cos\omega t & 0 \\ 0 & 0 & 1 \end{pmatrix} \mathbf{L} = 2ma^2\omega \sin\alpha \begin{pmatrix} \cos\alpha \sin\omega t \\ -\cos\alpha\cos\omega t \\ \sin\alpha \end{pmatrix} \ .$$

c. The torque is,

$$\mathbf{N} = \frac{d\mathbf{L}}{dt} = \omega^2 2\omega^2 ma^2 \sin\alpha\cos\alpha \begin{pmatrix} \cos\omega t \\ \sin\omega t \\ 0 \end{pmatrix} .$$

3.1.4.29 Ex: Hovering cross

Four masses of equal weight m are connected to each other in the manner shown by a rigid cross. The mass of the connecting rods is negligible. The cross rotates at a constant angular velocity ω around an axis of rotation that lies in its plane, passes through its center of gravity and forms an angle α with its long axis.
a. Calculate the inertia tensor I of the body in the co-rotating system. b. First

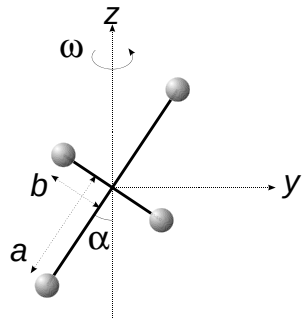

Figure 3.8: Hovering cross.

calculate the angular momentum $\mathbf{L}$ in the co-rotating system using the relationship $\mathbf{L} = I\vec{\omega}$, where $\vec{\omega} = (0, 0, \omega)$ is invariant under rotation around the z-axis. Then transform $\mathbf{L}$ back into the laboratory system.
c. Calculate the torque that must act so that the angular velocity remains constant.

Solution: *a. The angular momentum vector of the dumbbell in the co-rotating coordinate system is,* $\mathbf{L} = I\vec{\omega} = I\omega\hat{\mathbf{e}}_z$. *The masses are at the positions,*

$$\mathbf{r}_{1,2} = \begin{pmatrix} 0 \\ \pm a\sin\alpha \\ \pm a\cos\alpha \end{pmatrix} \qquad \textit{and} \qquad \mathbf{r}_{3,4} = \begin{pmatrix} 0 \\ \mp b\cos\alpha \\ \pm b\sin\alpha \end{pmatrix} .$$

Only the last column of the tensor of inertia is interesting. The components are,

$$\begin{aligned} I_{zx} &= 0 \\ I_{zy} &= -2ma^2 \sin\alpha\cos\alpha - 2mb^2 \sin\alpha\cos\alpha \\ I_{zz} &= 2ma^2 \sin^2\alpha + 2mb^2 \cos\alpha \ . \end{aligned}$$

b. Hence,

$$\mathbf{L} = \begin{pmatrix} 0 \\ -2m\omega \sin\alpha \cos\alpha (a^2 + b^2) \\ 2m\omega (a^2 \sin^2\alpha + b^2 \cos^2\alpha) \end{pmatrix} .$$

The angular momentum in a non-rotating coordinate system is,

$$\mathbf{L}_{lab} = \begin{pmatrix} \cos\omega t & -\sin\omega t & 0 \\ \sin\omega t & \cos\omega t & 0 \\ 0 & 0 & 1 \end{pmatrix} \mathbf{L} = 2m\omega \begin{pmatrix} \sin\alpha\cos\alpha \sin\omega t (a^2 + b^2) \\ -\sin\alpha\cos\alpha\cos\omega t \left(a^2 + b^2\right) \\ a^2 \sin^2\alpha + b^2 \cos^2\alpha \end{pmatrix} .$$

c. The torque is,

$$\mathbf{N} = \frac{d\mathbf{L}}{dt} = 2m\omega^2 \sin\alpha\cos\alpha (a^2 + b^2) \begin{pmatrix} \cos\omega t \\ \sin\omega t \\ 0 \end{pmatrix} .$$

3.1.4.30 Ex: A farmer on a ladder

A farmer of mass $M = 90\,\mathrm{kg}$ harvests apples climbing a ladder (length $L = 10\,\mathrm{m}$, mass $m = 30\,\mathrm{kg}$) leaning at an angle $\phi = 60°$ against a branch relative to the Earth's surface. While harvesting the highest apples at the top, the branch suddenly breaks away. In his fear, the farmer clings to the ladder. The system ladder-farmer now falls down with the ladder base remaining fixed. Neglect the spatial expansion of the farmer. The ladder can be viewed as a one-dimensional rod.
a. Show that the moment of inertia I_{LB} of the ladder-farmer system for a rotation around the ladder base point can be given as $I_{LB} = \left(\frac{m}{3} + M\right) L^2$.
b. At what speed v_1 does the farmer reach the surface of the Earth?
c. At the instant when the branches break, in his shock the farmer drops an apple. At what speed v_2 does the apple reach the surface of the Earth?
d. Would the farmer fall more slowly when letting the ladder go at the moment when the branch breaks?

Solution: *a. The moment of inertia of a bar orthogonal to its length is,*

$$I_L = \int r^2 dm = \int \rho(\mathbf{r}) r^2 d^3 r = \rho_0 \int_0^L r^2 dr = \rho_0 \frac{L^3}{3} = m\frac{L^2}{3} .$$

The farmer is located at a distance L from the pivot. Hence, according to Steiner's theorem, $I_B = ML^2$. Overall,

$$I_{LB} = I_L + I_B = \left(\frac{m}{3} + M\right) L^2 .$$

b. The potential energy of the farmer is $E_{pot,B} = MgL\sin\phi$, the energy of the ladder $E_{pot,L} = \frac{m}{2} gL\sin\phi$ is converted into rotational energy when falling, $E_{rot} = \frac{I}{2}\omega^2$. Hence,

$$\frac{I}{2}\omega^2 = \left(\frac{m}{2} + M\right) gL\sin\phi .$$

Thus,

$$v_1 = \omega L = L\sqrt{\frac{2\,(m/2+M)\,gL\sin\phi}{I}} = \sqrt{\frac{m/2+M}{m/3+M}2gL\sin\phi} =$$

c. The speed follows from equating $E_{pot} = \frac{m_A}{2}L\sin\phi$ *and* $E_{kin} = \frac{m_A}{2}v_2^2$

$$m_A gL\sin\phi = \frac{m_A}{2}v_2^2 \ .$$

Hence,

$$v_2 = \sqrt{2gL\sin\phi} =$$

d. Because of

$$v_1 = \sqrt{\frac{m/2+M}{m/3+M}2gL\sin\phi} > \sqrt{2gL\sin\phi} = v_2$$

it actually falls more slowly.

3.1.4.31 Ex: Angular momentum

A thin bar of length L and mass M is suspended at one end thus forming a physical pendulum.
a. I calculate the inertial moment of the bar.
b. Now, the pendulum is tilted a little. Calculate the torque as a function of the angle of inclination.
c. For very small angles θ holds the approximation $\sin\theta \simeq \theta$. Use this approach to establish the equation of motion.

Solution: *a. Be* $\lambda = M/L$ *the linear mass density of the bar. The inertial moment is,*

$$I = \int r^2 dm = \lambda\int_0^L z^2 dz = \frac{\lambda}{3}L^3 = \frac{M}{3}L^2 \ .$$

b. The torque is,

$$I\ddot{\vec{\theta}} = \tau = \mathbf{L}\times M\mathbf{g} = LMg\sin(180^\circ-\theta) = LMg\sin\theta \ .$$

c. The equation of motion is,

$$\ddot{\theta} \simeq \frac{LMg}{I}\theta = \frac{3g}{L}\theta \ .$$

3.1.4.32 Ex: Accelerated pendulum

A pendulum of length R is suspended in a car which is uniformly accelerated with the acceleration a.
a. Calculate the angle of the pendulum's displacement.

b. Calculate the torque exerted by the accelerating force of the car.
c. What is the torque exerted by the weight in this situation?
d. Calculates the ratio of the torques. Justify the obtained result.

Solution: *a. The angle is given by,*

$$\tan\theta = \frac{a}{g} \ .$$

b. The torque due to the acceleration of the car is,

$$|\vec{\tau}_a| = |\mathbf{r}\times\mathbf{F}| = Rma\sin(90^\circ - \theta) = Rma\cos\theta = Rma\frac{1}{\sqrt{1+\tan\theta^2}} = Rma\frac{1}{\sqrt{1+\frac{a^2}{g^2}}} = Rm\frac{1}{\sqrt{\frac{1}{a^2}+\frac{1}{g^2}}}$$

c. The torque due to the gravitational acceleration is,

$$|\vec{\tau}_g| = |\mathbf{r}\times\mathbf{F}| = Rmg\sin\theta = Rmg\frac{1}{\sqrt{1+1/\tan\theta^2}}$$
$$= Rmg\frac{1}{\sqrt{1+\frac{g^2}{a^2}}} = Rm\frac{1}{\sqrt{\frac{1}{g^2}+\frac{1}{a^2}}} \ .$$

d. The ratio is,

$$\frac{|\vec{\tau}_a|}{|\vec{\tau}_a|} = \frac{Rma\cos\theta}{Rmg\sin\theta} = \frac{a}{g\tan\theta} = 1.$$

That's because the pendulum is in balance.

3.1.4.33 Ex: Rotating disc

A round disk of mass M with radius R is rotatably mounted about a vertical axis passing through its center. A spring of negligible mass with the spring constant κ is attached to the disc tangentially to the edge. The spring, which is initially fully compressed by the length d, represents a launching device for a ball of mass m. The disk rests until the ball is released being ejected horizontally by the spring. Calculate the angular velocity of the disk after the ejection.
Help: Use the angular momentum and energy conservation laws.

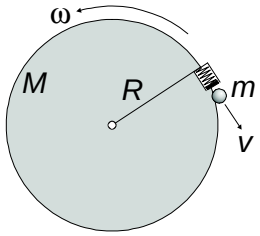

Figure 3.9: Rotating disc.

Solution: *The moment of inertia of the disc is* $I_{disc} = \frac{1}{2}MR^2$. *Conservation of angular momentum requires,* $0 = \mathbf{L}_{disc} + \mathbf{L}_{sphere}$, *hence,*

$$0 = I\vec{\omega} + \mathbf{r} \times \mathbf{p}_{sphere} \ ,$$

resp.

$$p_{sphere} = -\frac{I\omega}{R\sin\alpha} = -\frac{I\omega}{R} \ .$$

Conservation of energy requires $E_{spring} = E_{sphere} + E_{disc}$, *also*

$$\frac{\kappa}{2}d^2 = \frac{1}{2m}p_{sphere}^2 + \frac{I}{2}\omega^2 \ .$$

Substitution of p_{sphere} *yields,*

$$\frac{\kappa}{2}d^2 = \frac{1}{2m}\left(\frac{I\omega}{R}\right)^2 + \frac{I}{2}\omega^2 \ ,$$

and resolved after ω

$$\omega = \sqrt{\frac{\kappa d^2}{I^2/mR^2 + I}} = \frac{2d}{R}\sqrt{\frac{\kappa m}{M^2 + 2mM}} \ .$$

3.1.4.34 Ex: Billiard

A resting billiard ball with radius r is played with a horizontal queue, which gives it an impulse $\Delta p = F\Delta t$. The queue hits the ball at a height h above the table. How does the initial angular velocity ω of the sphere depend on Δp and h? **Help:** The ball rolls without slipping.

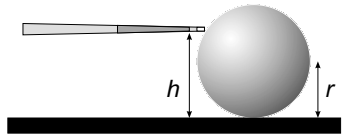

Figure 3.10: Billiard.

Solution: *The moment of inertia of the sphere is* $I_\omega = \frac{2}{5}mr^2$. *The angular momentum is* $\mathbf{L} = \mathbf{r} \times \Delta\mathbf{p} = I_\omega\omega$. *Hence,*

$$\omega = \frac{r\Delta p\sin\phi}{I_\omega} \ ,$$

where $\sin\phi = \frac{h-r}{r}$. *With* $v_0 = \Delta p/m$ *we get,*

$$\omega = \frac{rmv_0}{\frac{2}{5}mr^2}\frac{h-r}{r} = \frac{5}{2}v_0\frac{h-r}{r^2} \ .$$

3.1.4.35 Ex: Rotating and propagating arc

Calculate the angular momentum of an arc (a) rotating around its center of mass, (b) rotating around a peripheral point, and (c) rolling without friction on a surface.

Solution: *a. The inertial moment of the arc is $I_{cm} = MR^2$. The angular momentum of the mass distribution m in the center of mass system (cm) is,*

$$\mathbf{L}_m^{(cm)} = \sum_i \vec{x}_i \times m_i \mathbf{u}_i = \sum_i m_i R u \hat{\mathbf{e}} a_\omega = MR^2 \vec{\omega}_{cm} = I\vec{\omega}_{cm} \ .$$

Considering the same rotation from the point of view of a point O located away from the center of mass,

$$\begin{aligned}\mathbf{L}^{(O)} &= \sum_i \mathbf{r}_i \times m_i \mathbf{v}_i = \sum_i (\mathbf{r}_{cm} + \vec{x}_i) \times m_i (\mathbf{v}_{cm} + \mathbf{u}_i) \\ &= \sum_i m_i \mathbf{r}_{cm} \times \mathbf{v}_{cm} + m_i \mathbf{r}_{cm} \times \mathbf{u}_i + m_i \vec{x}_i \times \mathbf{v}_{cm} + m_i \vec{x}_i \times \mathbf{u}_i \\ &= M\mathbf{r}_{cm} \times \mathbf{v}_{cm} + m_i \mathbf{r}_{cm} \times \mathbf{u}_i + m_i \vec{x}_i \times \mathbf{v}_{cm} + m_i \vec{x}_i \times \mathbf{u}_i = \mathbf{L}_M^{(O)} + 0 + 0 + \mathbf{L}_m^{(cm)} \ ,\end{aligned}$$

with $M = \sum_i m_i$. As the arc does not move its center of mass, $\mathbf{L}_M^{(O)} = 0$, and

$$\mathbf{L}^{(O)} = \mathbf{L}_m^{(cm)} \ .$$

b. Now we assume that the arc moves with angular velocity ω_{cm} around a peripheral point. In the center of mass system the arc still rotates in the same way as in (a) producing an angular momentum $\mathbf{L}_m^{(cm)}$. But in addition the center of mass rotates with the same angular velocity ω_{cm}, producing an angular momentum $\mathbf{r}_{cm} \times \mathbf{p}_{cm}$,

$$\mathbf{L}^{(O)} = \mathbf{r}_{cm} \times \mathbf{p}_{cm} + \mathbf{L}_m^{(cm)} = MRv_{cm}\hat{\mathbf{e}}_\omega + I\vec{\omega}_{cm} = 2MR^2\vec{\omega}_{cm} \ .$$

We would have reached the same conclusion using Steiner's theorem, $I_O = I_{cm} + MR^2$,

$$\mathbf{L}^{(O)} = I_{(O)}\vec{\omega}_{cm} = (I_{cm} + MR^2)\vec{\omega}_{cm} = 2MR^2\vec{\omega}_{cm} \ .$$

c. Now we assume that the arc's center of mass moves with velocity $v_{cm} = R\omega_{cm}$ on a straight line, such that the circumference is in phase with a tangential surface,

$$\mathbf{L}^{(O)} = \mathbf{r}_{cm} \times \vec{p}_{cm} + \mathbf{L}_m^{(cm)} = Mbv_{cm}\hat{\mathbf{e}}_\omega + I\vec{\omega}_{cm} = MR^2\vec{\omega}_{cm} + I\vec{\omega}_{cm} = 2MR^2\vec{\omega}_{cm} \ ,$$

where $b = R$ is the impact parameter. It is interesting that this gives the same result as in (b). This can be understood, because the propagation on the surface can be seen in each infinitesimal instant as a rotation around the support point.

3.2 The rigid body

In mechanics a rigid body is defined as a system of masses whose mutual distances are kept fixed during any motion. The rigid bodies of practical interest are generally

extended over macroscopic volumes and form a (quasi-)continuous mass distribution. The motion of large rigid bodies is more complicated than the motion of a point mass, since in addition to the translational motion, there may be rotations about one or more axes. The dynamics of both types of motion can clearly be separated in rigid bodies.

3.2.1 Translations and rotations: linear and angular momentum

The translational motion of a rigid body of mass M is fully described by the evolution of the coordinates and the velocity of its center-of-mass. In fact, one can assimilate the translation dynamics of the body with the whole mass M being concentrated in the center-of-mass. The total momentum $\mathbf{p}$ of the body is,

$$\mathbf{p} = m\mathbf{v} \ , \tag{3.10}$$

where $\mathbf{v}$ is the velocity of the center-of-mass. The equation that determines the translational dynamics is Newton's second law,

$$\mathbf{F}_{ext} = \frac{d\mathbf{p}}{dt} \ , \tag{3.11}$$

where $\mathbf{F}_{ext}$ is the vectorial sum of external forces acting on the body. When no external forces act, the amount of translational motion of the rigid body is conserved. Similarly, the translational kinetic and the gravitational potential energies of the rigid body can be evaluated by simply considering, respectively, the velocity and height H of the center-of-mass with respect to a reference level of potential energy:

$$E_{kin} = \frac{M}{2}v^2 \qquad \text{and} \qquad E_{grv} = MgH \ . \tag{3.12}$$

The (pure) rotation of a rigid body about its center-of-mass also contains kinetic energy. The quantity representing the amount of rotational motion of a rigid body is the rotational angular momentum. For simplicity, we will assume that the rotation occurs about an axis passing through the center-of-mass of the body, and that the body is symmetric around that axis. In this situation, the angular momentum reads,

$$\mathbf{L} = I\vec{\omega} \ , \tag{3.13}$$

where $\vec{\omega}$ is the angular velocity and I the moment of inertia of the rigid body with respect to the rotation axis. The moment of inertia is obtained by summing for the entire body over the contributions of the products between the elementary mass fragments δm_i and the square of their distances d_i^2 from the rotation axis,

$$I = \sum_i d_i^2 \delta m_i \ . \tag{3.14}$$

For an extensive body of volume V and density ρ, the sum in this equation is expressed as an integral along the infinitesimal mass elements $dm = \rho dV$,

$$I - \int_V d^2 \rho dV \ . \tag{3.15}$$

3.2.2 Rotational energy and moment of inertia

The equation that determines the dynamics of rotation is a consequence of Newton's second law, and results in,

$$\tau_{ext} = \frac{d\mathbf{L}}{dt} \ . \tag{3.16}$$

where τ_{ext} is the vectorial sum over the torques exerted by each external force acting on the body,

$$\tau_{ext} = \sum_i \mathbf{r}_i \times \mathbf{F}_{ext,i} \ . \tag{3.17}$$

In this expression, $\mathbf{r}_i$ is the vector indicating the point of application of the force $\mathbf{F}_{ext,i}$ on the body, measured with respect to the center-of-mass. When the total external torque is zero, the angular momentum of the rigid body is conserved. The kinetic energy associated with the rotation of the rigid body is given by the expression,

$$E_{rot} = \frac{I}{2}\omega^2 \ . \tag{3.18}$$

Example 5 (*Cylinder on a slope*): A cylinder of radius R rolls down a slope of inclination θ. We have $h = z\sin\theta$ and $v = R\omega$. Energy conservation means, $mgh = \frac{m}{2}v^2 + \frac{I}{2}\omega^2$, hence,

$$v = \sqrt{\frac{2gh}{1 + I/mR^2}} \ . \tag{3.19}$$

For a plain cylinder we know $I = \frac{m}{2}R^2$ and for a hollow one we know $I = \frac{m}{2}(R^2+r^2)$. This means, plain cylinders will always reach the same final velocity,

$$v = \sqrt{\frac{4gh}{3}} \ , \tag{3.20}$$

while hollow cylinders will be slower,

$$v = \sqrt{\frac{4gh}{3 + r^2/R^2}} \ . \tag{3.21}$$

3.2.3 Rotation dynamics about a fixed axis

3.2.4 Static equilibrium of a rigid body

3.2.5 Constant acceleration

3.2.6 Exercises

3.2.6.1 Ex: Inertial momentum

Calculate the moment of inertia of a quadrilateral of point masses in relation to the axes shown in the figure.

Solution: *Regarding axis 1 we have,*

$$I_1 = 2\tfrac{a^2}{4}m + 2\tfrac{a^2}{4}2m = \tfrac{3}{2}a^2 m \ .$$

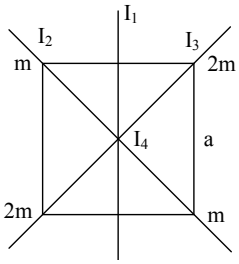

Figure 3.11: Inertial momentum.

Regarding axis 2 we have,

$$I_2 = 2\frac{a^2}{4}2m = 2a^2m \ .$$

Regarding axis 3 we have,

$$I_3 = 2\frac{a^2}{4}m = a^2m \ .$$

Regarding axis 4 we have,

$$I_4 = 2\frac{a^2}{2}m + 2\frac{a^2}{2}2m = 3a^2m \ .$$

3.2.6.2 Ex: Inertial momentum

A disc of radius R and surface mass density σ has a circular hole of radius r at a distance a from the center of the disc. Calculate the moments of inertia with respect to the axes 1, 2 and 3, as shown in the figure.

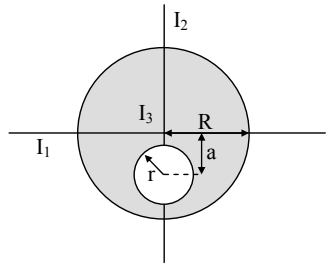

Figure 3.12: Inertial momentum.

Solution: *The moment of inertia of a disk of mass $M = \pi R^2\sigma$ with respect to an axis within the plane through the center of mass is,*

$$I_d = \int \rho^2 dm = \sigma \int_{-R}^{R}\int_{-\sqrt{R^2-z^2}}^{\sqrt{R^2-z^2}} \rho^2 d\rho dz = \sigma \int_{-R}^{R} \frac{\rho^3}{3}\Big|_{-\sqrt{R^2-z^2}}^{\sqrt{R^2-z^2}} dz$$
$$= \frac{2\sigma}{3}\int_{-R}^{R} \sqrt{R^2-z^2}^3 dz = \sigma\frac{\pi}{4}R^4 = M\frac{R^2}{4} \ .$$

So we have with respect to the axis 1,

$$I_1 = M\frac{R^2}{4} - \left(m\frac{r^2}{4} + ma^2\right) \ ,$$

where M is the mass of the disk without a hole and m is the mass that is missing from the hole. Regarding axis 2 we have,

$$I_2 = M\frac{R^2}{4} - m\frac{r^2}{4}.$$

The moment of inertia of the disk with respect to an axis within normal to the plane crossing the center of mass is,

$$I_n = \int \rho^2 dm = \sigma \int_0^{2\pi}\int_0^R \rho^2 \rho d\rho d\phi = 2\pi\sigma \left.\frac{\rho^4}{4}\right|_0^R = M\frac{R^2}{2} \ .$$

Hence, we have with respect to the axis 3,

$$I_3 = M\frac{R^2}{2} - \left(m\frac{r^2}{2} + ma^2\right) \ .$$

3.2.6.3 Ex: Inertial momentum

Calculate the moment of inertia of a sphere of mass M and radius R with respect to an axis passing through the center of mass.

Solution: *As the volume of the sphere is $V = \frac{4}{3}\pi R^3$, we get with $\rho^2 \equiv x^2 + y^2$,*

$$I = \int \rho^2 dm = \frac{M}{V}\int_V \rho^2 d^3r = \frac{M}{V}\int_0^{2\pi}\int_0^R\int_0^{\sqrt{R^2-z^2}} \rho^2 \rho d\rho dz d\phi = \frac{M}{V}\int_0^R \left[\frac{2\pi}{4}\rho^4\right]_0^{\sqrt{R^2-z^2}} dz$$
$$= \frac{M}{V}\frac{2\pi}{4}\int_0^R (R^2 - z^2)dz = \frac{3M}{4\pi R^3}\frac{2\pi}{4}\left[R^2 z - \tfrac{1}{3}z^3\right]_0^R = \frac{2MR^2}{5} \ .$$

3.2.6.4 Ex: Inertial momentum of a slender bar

A thin bar of mass M and length L makes an angle θ with the y-axis, as shown in the figure.
a. Calculate the moment of inertia for rotation about the axis;
b. Calculate the moment of inertia for rotation around an axis parallel to y and passing through the center of mass.

Solution: *a. With the mass distribution $dm = \lambda dl$ we have,*

$$I_a = \int r^2 dm = \lambda \int_0^L (l\sin\theta)^2 dl = \frac{\lambda L^3}{3}\sin^2\theta = \frac{ML^2}{3}\sin^2\theta \ .$$

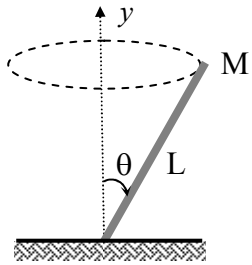

Figure 3.13: Slender bar.

b. We laso have,

$$I_b = I_a - M\left(\frac{L}{2}\sin\theta\right)^2 = \frac{ML^2}{12}\sin^2\theta \ ,$$

or alternatively

$$I_b = \int r^2 dm = \lambda \int_{-L/2}^{L/2} (l\sin\theta)^2 dl = \frac{\lambda}{3} 2\left(\frac{L}{2}\right)^3 \sin^2\theta = \frac{ML^2}{12}\sin^2\theta \ .$$

3.3 Angular momentum

3.3.1 Torque and angular momentum of a particle system

3.3.1.1 Steiner's theorem

The angular momentum I_ω of a rigid body with respect to a rotation axis $\hat{\mathbf{e}}_\omega$ can be divided into $I_\omega = I_\omega^{SP} + Mb^2$. Here, I_ω^{SP} is the inertial moment of the body with respect to the rotation axis $\hat{\mathbf{e}}_{0\omega}$, which is parallel to $\hat{\mathbf{e}}_\omega$ and traverses the center-of-mass of the body, M is the mass of the body, and b is the distance from the rotation axis. This is *Steiner's theorem*.

To demonstrate Steiner's theorem, we consider the vector of a mass point α of the rigid body a first time in the coordinate system, whose origin lies on the axis $\hat{\mathbf{e}}_\omega$, and which we call $\mathbf{r}_\alpha$. A second time we describe this mass point in the coordinate system, whose origin lies in the center-of-mass, and which we call $\mathbf{r}$. The vector of the position of the mass α in the center-of-mass system be described by ρ_α. With this nomenclature,

$$\mathbf{r}_\alpha = \mathbf{r} + \vec{\rho}_\alpha \ .$$

The moment of inertia with respect to the $\hat{\mathbf{e}}_\omega$-axis is then,

$$\begin{aligned} I_\omega &= \sum_\alpha m_\alpha \left(\mathbf{r}_\alpha^2 - (\mathbf{r}_\alpha \cdot \hat{\mathbf{e}}_\omega)\right) \\ &= \sum_\alpha m_\alpha \left[(\mathbf{r} + \vec{\rho}_\alpha)^2 - ((\mathbf{r} + \vec{\rho}_\alpha) \cdot \hat{\mathbf{e}}_\omega)^2\right] \\ &= \sum_\alpha m_\alpha \left[(\mathbf{r}^2 + 2\mathbf{r}\vec{\rho}_\alpha + \vec{\rho}_\alpha^2 - (\mathbf{r} \cdot \hat{\mathbf{e}}_\omega)^2 - 2(\mathbf{r} \cdot \hat{\mathbf{e}}_\omega)(\vec{\rho}_\alpha \cdot \hat{\mathbf{e}}_\omega) - (\vec{\rho}_\alpha \cdot \hat{\mathbf{e}}_\omega)^2\right] \\ &= MR^2 + 0 + \sum_\alpha m_\alpha \vec{\rho}_\alpha^2 - M\,(\mathbf{r} \cdot \hat{\mathbf{e}}_\omega)^2 - 0 - \sum_\alpha m_\alpha\,(\vec{\rho}_\alpha \cdot \hat{\mathbf{e}}_\omega)^2 \\ &= I_\omega^{SP} + Mb^2 \ . \end{aligned}$$

The zeros of the fourth line come from $\sum_\alpha m_\alpha \vec{\rho}_\alpha = 0$, because the left side just corresponds to the center-of-mass vector multiplied with the total mass, but which has in the center-of-mass system the value $\mathbf{r} = 0$.

3.3.2 Rotational work-energy relation

3.3.3 Conservation of angular momentum

Like the conservation law for linear momentum, the conservation law for angular momentum is universal. It holds for a rotational collision,

$$(I_1 + I_2)\omega = I_1\omega_1 + I_2\omega_2 \ . \tag{3.22}$$

On the other side, non-rotational energy is not conserved in a rotational collision, $E_{rot} < E_{rot,1} + E_{rot,2}$, because part of the energy can be dissipated:

$$E_{rot,1} + E_{rot,2} - E_{rot} = \frac{I_1}{2}\omega_1^2 + \frac{I_2}{2}\omega_2^2 - \frac{I_1 + I_2}{2}\omega^2 = \frac{-I_1 I_2}{2(I_1 + I_2)}(\omega_1 - \omega_2)^2 \ . \tag{3.23}$$

3.3.4 Combination of translation and rotation

Example 6 (*Gyroscope*): The angular momentum due to the rotation of a wheel is,

$$\mathbf{L}_\omega = I_\omega^{(cm)}\vec{\omega} \ .$$

for a disk-shaped wheel the inertial moment $I_\omega^{(cm)}$ about an axis of rotation $\vec{\omega}$ crossing the center-of-mass is,

$$I_\omega^{(cm)} = \frac{M}{2}R^2 \ .$$

The force of gravitation,

$$\mathbf{F}_g = m\mathbf{g}$$

produces a torque,

$$\vec{\tau}_g = \mathbf{D} \times \mathbf{F}_g = Dmg\hat{\mathbf{e}}_\phi \sin\theta \ .$$

Initially, the rotation axis of the disk is horizontal $\theta = 0$. Due to the torque the shaft tilts downward thus forcing the angular momentum to shift to $\mathbf{L}_\omega + d\mathbf{L}_\omega$ with the velocity,

$$\tfrac{d\mathbf{L}_\omega}{dt} = \vec{\tau}_g \ .$$

How can the system react to compensate for this change of $\mathbf{L}_\omega$?
The *total angular momentum in the direction* $\mathbf{g}$ *must be conserved*, as there is no external torque in it. Fortunately, there is another possible movement that can generate an angular momentum: the rotation around the point of support O with the angular velocity $\vec{\Omega}$:

$$const = \mathbf{L}_{tot} = \mathbf{L}_\omega + \mathbf{L}_\Omega \qquad \text{or} \qquad \frac{d\mathbf{L}_\omega}{dt} = -\frac{d\mathbf{L}_\Omega}{dt} \ .$$

That is, we have a torque $\vec{\tau}_\Omega = \frac{d\mathbf{L}_\Omega}{dt}$. Hence, $|\tau_\omega| = |\tau_\Omega|$, but since the orientation of $\mathbf{L}_\Omega$ is vertically fixed, the orientation of $\vec{\tau}_\Omega$ is also vertical, which corresponds to an azimuthal force. Thus, instead of an inclination of the rotation axis $\mathbf{L}_\omega$, we get an *azimuthal* shift by an angle,

$$d\vec{\phi} = \frac{d\mathbf{L}_\Omega}{L_\omega \sin\theta} = \frac{d\mathbf{L}_\omega}{L_\omega \sin\theta} = \frac{\vec{\tau}_g dt}{I_\omega^{(cm)} \omega \sin\theta} = \frac{Dm(-\mathbf{g})\sin\theta dt}{I_\omega^{(cm)} \omega \sin\theta} = -\frac{Dm\mathbf{g}dt}{I_\omega^{(cm)}\omega} \ .$$

The frequency of this *precession* movement,

$$\vec{\Omega} = \frac{d\vec{\phi}}{dt} \ ,$$

produces an angular momentum,

$$\mathbf{L}_\Omega = M\mathbf{D} \times \mathbf{v}_\Omega = MD^2\vec{\Omega} = I_\Omega^{(O)}\vec{\Omega} \ .$$

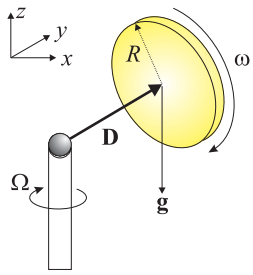

Figure 3.14: Rotating wheel supported on one end of its axis.

Now, the precession modifies the direction of the angular momentum in the plane,

$$\mathbf{L}_\omega = L_\omega \hat{\mathbf{e}}_\phi \ ,$$

with $\hat{\mathbf{e}}_\phi = \hat{\mathbf{e}}_x \cos\Omega t + \hat{\mathbf{e}}_y \sin\Omega t$. Hence,

$$\dot{\mathbf{L}} = L\vec{\Omega} = \vec{\tau}_\omega = L\frac{-Dm\mathbf{g}dt}{I_\omega^{(cm)}\omega} = -Dm\mathbf{g} = \mathbf{D} \times \mathbf{F} \ .$$

Finally, we find a force exactly compensating gravity,

$$\mathbf{F} = -m\mathbf{g} \ .$$

3.3.5 Exercises

3.3.5.1 Ex: Statics of a ladder

A ladder of mass M and length L leans on a frictionless wall and and stands on a floor with friction μ (see figure). Knowing that the angle between the ladder and the wall is 45°, what should be the force on a rope tied in the middle of the stairs so that it does not fall?

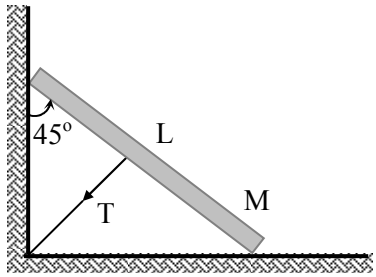

Figure 3.15: Statics of a ladder.

Solution: *The equations of motion are,*

$$\begin{aligned} 0 &= Mg + T\cos\theta - N_2 \\ 0 &= F_{at} + T\sin\theta - N_1 \\ 0 &= \tau_0 + \tau_T - \tau_1 \end{aligned}$$

where $F_{at} = \mu N_2$ *and,*

$$\begin{aligned} \tau_0 &= |\mathbf{r} \times M\mathbf{g}| = \frac{L}{2} Mg \sin(\theta + 90^\circ) \\ \tau_T &= |\mathbf{r} \times \vec{T}| = \frac{L}{2} T \sin\alpha \\ \tau_1 &= |\mathbf{r} \times N_1| = L N_1 \sin(180^\circ - \theta) \ . \end{aligned}$$

For $\theta = 45^\circ$ *we have* $\alpha = 90^\circ$*, and the equations of motion become,*

$$\begin{aligned} 0 &= Mg + \frac{T}{\sqrt{2}} - N_2 \\ 0 &= F_{at} + \frac{T}{\sqrt{2}} - N_1 \\ 0 &= \frac{L}{2}\frac{Mg}{\sqrt{2}} + \frac{L}{2} T - L\frac{N_1}{\sqrt{2}} \ . \end{aligned}$$

Eliminating N_2 and then N_1

$$\begin{aligned} 0 &= Mg + \frac{T}{\sqrt{2}} - \frac{F_{at}}{\mu} = Mg + \frac{T}{\sqrt{2}} - \frac{1}{\mu}\left(N_1 - \frac{T}{\sqrt{2}}\right) \\ &= Mg + \frac{T}{\sqrt{2}} - \frac{1}{\mu}\left(\left[\frac{1}{2}Mg + \frac{1}{\sqrt{2}}T\right] - \frac{T}{\sqrt{2}}\right) = Mg + \frac{T}{\sqrt{2}} - \frac{1}{2\mu}Mg \\ T &= \frac{\mu^{-1} - \sqrt{2}}{\sqrt{2}}Mg \ . \end{aligned}$$

3.3.5.2 Ex: Statics of a ladder

A ladder of mass M and length L leans against wall and stands on the floor (both without friction) such as to form an angle θ with the wall, as shown in the figure. A rope tied at a height of H (parallel to the floor) keeps the ladder at rest. Calculate:
a. the tension in the rope;
b. the maximum height H_{max} at which equilibrium is possible;
c. the angular acceleration at the instant this rope is cut.

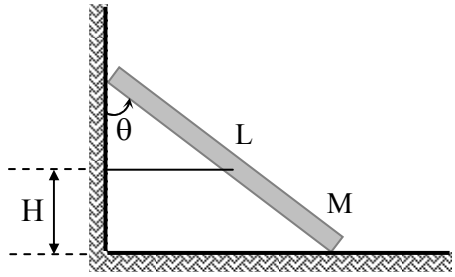

Figure 3.16: Statics of a ladder.

Solution: *a. Since the body is in equilibrium, all forces and all torques must compensate, $\sum \mathbf{F} = 0$ and $\sum \vec{\tau} = 0$. Let $\mathbf{N}_1$ and $\mathbf{N}_2$ be the pressures acting in normal direction on the wall and the floor, respectively. $\mathbf{T}$ is the tension in the string. We place the origin at the support point of the ladder on the wall. We can then express the distance between this point and the point of attachment of the rope by,*

$$x = \frac{L\cos\theta - H}{\cos\theta} \ .$$

We now have,

$$\begin{aligned} N_2 - Mg &= 0 \\ N_1 - T &= 0 \\ LN_2\sin\theta - xT\cos\theta - \tfrac{L}{2}Mg\sin\theta &= 0 \ , \end{aligned}$$

torque around the support point. Replacing the pressures,

$$LMg\sin\theta - (L\cos\theta - H)T - \tfrac{L}{2}Mg\sin\theta = 0$$
$$\Rightarrow T = \frac{1}{2}\frac{LMg\sin\theta}{L\cos\theta - H} \ .$$

b. This depends on the resistance of the rope, because when H rises, approaching $L\cos\theta$, the tension diverges.
c. The angular acceleration if the string is cut, that is if $T = 0$, is given by,

$$I\vec{\alpha} = \sum \vec{\tau} = LN_2\sin\theta - \tfrac{L}{2}Mg\sin\theta \ .$$

with the moment of inertia being $I = ML^2/3$, we have

$$\alpha = \frac{1}{I}\frac{L}{2}Mg\sin\theta = \frac{3}{2}\frac{g\sin\theta}{L} \ .$$

3.3.5.3 Ex: Statics of a ladder

A Λ-shaped ladder of mass $2M$ mass is opened to form an angle θ. What should be the coefficient of static friction with the floor so that it doesn't fall? (see figure).

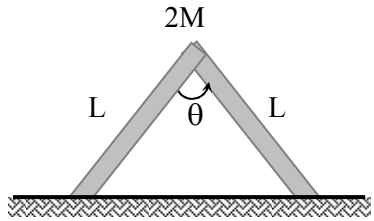

Figure 3.17: Statics of a ladder.

Solution: *Since the body is in equilibrium, all forces and all torques must compensate, $\sum \mathbf{F} = 0$ and $\sum \vec{\tau} = 0$. Instead of considering the ladder as open, since the problem is symmetrical, we can consider half the ladder leaning against a wall at an angle $\theta/2$. Let $\mathbf{N}_1$ and $\mathbf{N}_2$ be the normal pressures on the wall and floor, respectively, and $F_{at} = \mu N_2$ the friction force on the floor. With that we have,*

$$N_2 - Mg = 0$$
$$N_1 - F_{at} = 0$$
$$\tfrac{L}{2}Mg\sin\tfrac{\theta}{2} - LF_{at}\cos\tfrac{\theta}{2} = 0 \ ,$$

because the friction force compensates the pressure on the wall, and the torque exerted by the weight compensates the torque exerted by the friction. Therefore,

$$\mu = \tfrac{1}{2}\tan\tfrac{\theta}{2} \ .$$

3.3.5.4 Ex: Statics of a ladder

A painter of mass M stands at the top of a Λ-shaped ladder of negligible weight (length of each side: L) that rests on an extremely smooth floor M. There is a crossbar at half height that prevents the ladder from opening. The vertex angle is θ. What is the force on the crossbar?

Solution: *Since the body is in equilibrium, all forces and all torques must compensate,* $\sum \mathbf{F} = 0$ *and* $\sum \vec{\tau} = 0$. *Instead of considering the ladder as open, as the problem is symmetrical, we can consider half the ladder leaning against a wall at an angle* $\theta/2$. *Let* $\mathbf{N}_1$ *and* $\mathbf{N}_2$ *be the normal pressures to the wall and floor, respectively. For the system to be in balance, we have*

$$\begin{aligned} N_1 - T &= 0 \\ N_2 - \tfrac{1}{2}Mg &= 0 \\ LN_2 \sin\tfrac{\theta}{2} - \tfrac{L}{2}N_1 \cos\tfrac{\theta}{2} &= 0 \ , \end{aligned}$$

because the pressure on the 'wall' is compensated by the tension in the rope, the weight exerts a pressure on the floor, and the torque due to the weight is compensated by the torque exerted by the rope. So the tension in the crossbar is,

$$T = Mg \tan\tfrac{\theta}{2} \ .$$

3.3.5.5 Ex: Statics of a ladder

A bar of length L and mass M is placed over a hole, as shown in the figure. What must be the friction coefficient for the bar to stay at rest?

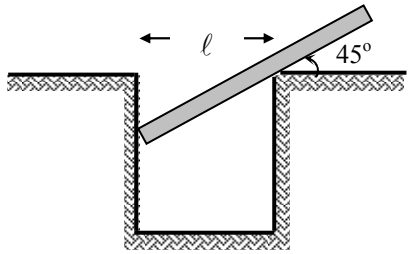

Figure 3.18: Statics of a ladder.

Solution: *In addition to the weight* Mg, *the following forces act on the center of mass: the tension at the right edge of the hole* $T_x = T\sin\theta$ *and* $T_y = T\cos\theta$, *the tension* $N = -T_x$, *and the friction* $F_{at} = \mu N$ *at the left edge of the hole. For The acceleration we write,*

$$0 = Ma = Mg - T_y - F_{at} = Mg - N\cot\theta - \mu N \ .$$

The bar can rotate around the right support point. Two forces act vertically, the weight acts on the center of mass located at a distance $d_1 = \frac{\ell}{\cos\theta} - L$ *from the rotation axis, and the friction acts on the left end of the bar at a distance* $d_2 = \frac{\ell}{\cos\theta}$ *of the rotation axis. This produces a torque:*

$$\begin{aligned} 0 = I\alpha &= |\mathbf{d}_1 \times M\mathbf{g}| + |\mathbf{d}_2 \times \mathbf{F}_{at}| \\ &= \left(\frac{\ell}{\cos\theta} - L\right) Mg\sin\theta - \frac{\ell}{\cos\theta}\mu N\sin\theta = \ell Mg\tan\theta - LMg\sin\theta - \ell\mu N\tan\theta \ . \end{aligned}$$

Solving the equation for the acceleration by N*,*

$$N = \frac{Mg}{\mu + \cot\theta} \ ,$$

and inserting into the equation for the torque we get,

$$0 = \ell Mg\tan\theta - LMg\sin\theta - \ell\mu\tan\theta\frac{Mg}{\mu + \cot\theta} \ ,$$

or solving for μ*,*

$$\mu = \left(\frac{1}{1 - L/\ell\sqrt{2}} - 1\right)^{-1} \ .$$

3.3.5.6 Ex: Torque on a block

On a smooth surface, a cubic block of size L and mass M slides with speed v (see figure). At a certain point, the cube hits a small obstacle. How fast should the velocity v of the block be in order to rotate around this point?

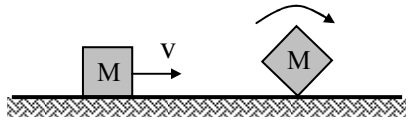

Figure 3.19: Torque on a block.

Solution: *The kinetic energy of the block is given by* $K = \frac{1}{2}Mv^2$ *before the crash. As the movement does not dissipate energy, we have energy conservation. At the instant when the cube is starting to rotate, we have only gravitational potential energy. So* $K = U$*, where* U *is the gravitational potential energy of the cube when it is going to fall to its other side. The difference in the height of the center of mass in the stable and labile position is,*

$$h = \frac{\sqrt{2}}{2}L - \frac{L}{2} = (\sqrt{2} - 1)\frac{L}{2} \ .$$

Hence,

$$\tfrac{1}{2}Mv_0^2 = Mgh = Mg(\sqrt{2}-1)\frac{L}{2}$$
$$\Rightarrow v_0 = \sqrt{Lg(\sqrt{2}-1)}\ .$$

That is, v_0 is the velocity necessary for the rotating cube to stop with the diagonal being vertical. So any velocity $v > v_0$ makes the cube flip over.

3.3.5.7 Ex: Falling rod

At the end of a rod of length L the negligible mass is placed a mass M. The system is released from vertical under the action of gravity. What is the equation that describes the angle $\theta(t)$ (see the figure)?

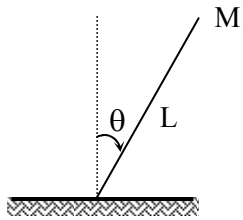

Figure 3.20: Falling rod.

Solution: *The inertial moment of the rod is $I = ML^2$. In the case of friction, the rod falls rotating around the point of the plane, supporting the lower end of the rod. Hence,*

$$I\alpha = |\mathbf{L} \times M\mathbf{g}| = LMg\sin\theta\ ,$$

and finally,

$$\ddot{\theta} = \frac{g}{L}\sin\theta\ .$$

Without friction, the rod rotates around its center of mass. Its acceleration is partially compensated by a stress $N = Mg\sin\theta$ exerted by the plane:

$$Ma = Mg - N\ .$$

Therefore, the angular acceleration is given by,

$$I\alpha = |\mathbf{L} \times M\mathbf{g}| + |\frac{\mathbf{L}}{2} \times \mathbf{N}| = LMg\sin\theta - \frac{L}{2}Mg\sin^2\theta\ .$$

Finally,

$$\ddot{\theta} = \frac{g}{L}\sin\theta - \frac{g}{2L}\sin^2\theta\ ,$$

and the acceleration is,

$$a = g - g\sin\theta\ ,$$

until the point, wave the bar suddenly encounters the plane.

3.3.5.8 Ex: Rotating arc

An arc of radius R, which rotates with angular velocity ω_0, is placed on a rough horizontal surface, as shown in the figure, the speed of its center of mass being zero. Determine the speed of the center of mass after slipping has ceased.

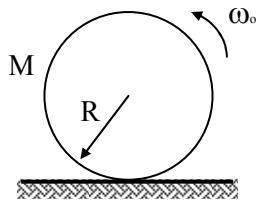

Figure 3.21: Rotating arc.

Solution: *The inertial moment of the arc is $I = MR^2$. The angular momentum at the center of mass before contact is,*

$$\mathbf{L}_{cm,i} = I\vec{\omega}_0 = MR^2\vec{\omega}_0 \ .$$

After contact between the arc and the rough surface, the arc starts to rotate around the contact point. The angular momentum is,

$$\mathbf{L}_f = \mathbf{L}_{cm,f} + \mathbf{r} \times \vec{p}_{cm}$$
$$L_f = \tilde{I}\omega + Rp_{cm}$$

with $\tilde{I} = I + MR^2$. As the bow does not slide, $R\omega = v_{cm}$, and

$$L_f = \tilde{I}\frac{v_{cm}}{R} + MRv_{cm} = 2MR^2\frac{v_{cm}}{R} + MRv_{cm} \ .$$

Since the angular momentum is conserved, $L_f = L_{cm,i}$, we obtain,

$$2MR^2\frac{v_{cm}}{R} + MRv_{cm} = MR^2\omega_0 \ ,$$

and finally,

$$v_{cm} = \frac{1}{3}R\omega_0 \ .$$

3.3.5.9 Ex: Angular momentum

The integral of the torque with respect to time is called the angular momentum. Starting from the relationship $\vec{\tau} = d\mathbf{L}/dt$, show that the impulse is the variation of the angular momentum.

Solution: *We have,*

$$\int_{t_1}^{t_2} \vec{\tau} dt = \int_{t_1}^{t_2} \frac{d\mathbf{L}}{dt} dt = \mathbf{L}(t_2) - \mathbf{L}(t_1) \ .$$

3.3.5.10 Ex: Billiard

A billiard ball initially at rest receives an instant boost from a cue. The cue is kept horizontal at a distance h from the center. The ball leaves with speed v_0 and the final speed is $9v_0/7$. Show that $h = 4R/5$, where R is the radius of the sphere.

Solution: *We divide the problem into three phases. The first (A) refers to the instant when the ball receives the kick, the second (B) refers to the instant immediately after the kick, when the ball acquires the speed v_0 and slides over the table, and the third (C) when the ball, after sliding a certain distance on the table, has speed v and rolls on the table without sliding. The translation movement in (B) is the result of the momentum transfer (ΔP, where P is the linear momentum of the ball) due to the force F applied in (A),*

$$\begin{aligned} \Delta P = P_B - P_A = Mv_0 - 0 = F\Delta t \\ F\Delta t = Mv_0 \ . \end{aligned}$$

The same analysis can be done for the rotation movement of the ball, where L is the angular movement, I is the moment of inertia, and ω_0 is the initial angular velocity of the ball:

$$\begin{aligned} \Delta L = L_B - L_A = I\omega_0 - 0 = \tau\Delta t \\ \frac{2MR^2}{5}\omega_0 = -Fh\Delta t \\ F\Delta t = -\frac{2MR^2}{5h}\omega_0 \ . \end{aligned}$$

The negative sign that appears in the last equation refers to the direction of the torque that the force F exerts on the ball. Equating the two equations for $F\Delta t$,

$$\begin{aligned} Mv_0 = -\frac{2MR^2}{5h}\omega_0 \\ \Longrightarrow \omega_0 = -\frac{5hv_0}{2R^2} \ . \end{aligned}$$

Now let's analyze the translation of the ball from state (B) to state (C):

$$\begin{aligned} \sum F = Ma_x \\ a_x = \frac{F}{M} \ . \end{aligned}$$

Movement from (B) to (C):

$$v_x = v_{x0} + a_x t \ .$$

The v_x speed was given in the statement of the problem:

$$\begin{aligned} \frac{9}{7}v_0 &= v_0 + \frac{F}{M}t \\ \Longrightarrow Ft &= \frac{2}{7}Mv_0 \ . \end{aligned}$$

Now let's analyze the rotation of the ball from state (B) to state (C):

$$\begin{aligned} \sum \tau_z &= I\alpha_z \\ FR &= \frac{2MR^2}{5}\alpha \\ \alpha &= \frac{5F}{2MR} \ . \end{aligned}$$

Rotation from (B) to (C):

$$\begin{aligned} \omega_z &= \omega_{z_0} + \alpha_z t \\ \Longrightarrow \frac{-9v_0}{7R} &= -\frac{5hv_0}{2R^2} + \frac{5F}{2MR}t \\ \Longrightarrow Ft &= Mv_0\left(\frac{h}{R} - \frac{18}{35}\right) \ . \end{aligned}$$

Equating the equations for the quantity Ft we obtain,

$$\frac{2}{7}Mv_0 = Mv_0\left(\frac{h}{R} - \frac{18}{25}\right) \ ,$$

and finally, $h = \frac{4}{5}R$.

3.3.5.11 Ex: Bohr's atom

Niels Bohr postulated that a rotating mechanical system can only have angular momentum with multiple values of a constant $\hbar$, called Planck's constant $\hbar = h/2\pi = 1.054 \times 10^{-34}$ Js, that is: $L = I\omega = n\hbar$, being n a positive integer or zero.
a. Show that with this postulate, the energy of a rotor can only acquire discrete, that is, quantized values.
b. Consider a mass m forced to rotate on a circle of radius R (e.g. hydrogen atom). What are the possible values for the angular velocity considering Bohr's postulate?
c. What kinetic energy values can the atom adopt?

Solution: *a. The possible energies of the quantized rotor are,*

$$E_{rot} = \frac{I}{2}\omega^2 = \frac{1}{2}L\omega = \frac{1}{2}n\hbar\omega \ .$$

b. Inserting the inertial moment of the electron $I = mR^2$ in the rotational energy, we have,

$$\omega = \frac{n\hbar}{mR^2} \ .$$

c. The kinetic energy is,

$$E_{kin} = \frac{m}{2}R^2\omega^2 = \frac{m}{2}R^2\left(\frac{n\hbar}{mR^2}\right)^2 = \frac{1}{2m}\frac{n^2\hbar^2}{R^2} \ .$$

3.3.5.12 Ex: Earth rotation

Many of the great rivers flow into the equatorial region carrying sandy sediments. What effect does this have on the Earth's rotation?

Solution: *They transfer mass to regions further from the Earth's rotation axis and thus increase the moment of inertia. Since rotational energy must be preserved,*

$$\frac{I_1}{2}\omega_1^2 = E_{rot} = \frac{I_2}{2}\omega_2^2 \ ,$$

the frequency of the Earth's rotation decreases.

3.3.5.13 Ex: Cylinder rolling on an inclined plane

A cylinder of mass M and radius R rotates without sliding on a horizontal plane. The speed of the center of mass is v. It encounters a plane with a tilt angle θ in front of it, as shown in the figure.
b. What were the linear and angular momenta when the cylinder meets the inclined plane?
c. How long does the cylinder take to reach the maximum height, and to what height does it rise on the inclined plane?
d. In this position, what was the change in angular momentum?

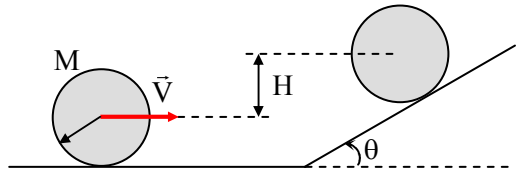

Figure 3.22: Cylinder rolling on an inclined plane.

Solution: *a. We assume the cylinder to meet the inclination as a fully elastic shock.*

In this case, the momenta due to the shock are,

$$\mathbf{I}_p = \int_{t_1}^{t_2} \mathbf{F} dt = \vec{p}_2 - \vec{p}_1 = \begin{pmatrix} mv_0 \\ 0 \end{pmatrix} - \begin{pmatrix} mv_0 \cos\theta \\ mv_0 \sin\theta \end{pmatrix}$$
$$\mathbf{I}_L = \int_{t_1}^{t_2} \vec{\tau} dt = \mathbf{L}_2 - \mathbf{L}_1 = 0 \ .$$

b. The only torque is due to friction. So the equations of motion are,

$$I\vec{\alpha} = \vec{\tau} = \mathbf{r} \times \mathbf{F}_{at}$$
$$Ma_{cm} = Mg\sin\theta - F_{at} \ .$$

Since the cylinder does not slide, $\alpha = \frac{a_{cm}}{R}$, and with the inertial moment, $I = \frac{M}{2}R^2\alpha$, we have,

$$a_{cm} = g\sin\theta - \frac{F_{at}}{M} = g\sin\theta - \frac{I\alpha}{MR} = g\sin\theta - \frac{\frac{M}{2}R^2\alpha}{MR} = g\sin\theta - \frac{1}{2}R\frac{a_{cm}}{R} = \frac{2}{3}g\sin\theta \ .$$

The body comes to a halt, when $0 = v_{cm} = v_0 - a_{cm}t = v_0 - \frac{2}{3}gt\sin\theta$, that is, at the time,

$$t = \frac{3v_0}{2g\sin\theta}$$

at the height,

$$H = s\sin\theta = \left(v_0 t - \frac{a_{cm}}{2}t^2\right)\sin\theta = \frac{3v_0^2}{4g} \ .$$

c. The initial angular momentum was,

$$\mathbf{L} = \mathbf{r}_0 \times \vec{p}_0 + I\vec{\omega}_0$$
$$L = MRv_0 + \frac{M}{2}R^2\omega_0 = \frac{3M}{2}Rv_0$$

and after stopping at the time H is $L = 0$.
d. The dissipated energy is,

$$E_{diss} = E_{pot} - E_{kin} + E_{rot} = MgH - \frac{M}{2}v_0^2 - \frac{M}{2}\omega_0^2 r^2 = -\frac{M}{4}v_0^2 \ .$$

3.3.5.14 Ex: Disc pushed by a mass

A disk of mass M and radius R can move around an axis passing through its center of mass, as shown in the figure. A particle of mass M as well follows a linear path with velocity v_i and impact parameter $d = R/2$ relative to the center-of-mass point. When it hits the disk it undergoes a deflection of 90° and has its velocity changed to $v_f = v_i/2$.
a. What is the angular velocity of the disc after the collision?
b. What is the energy dissipated in the collision?

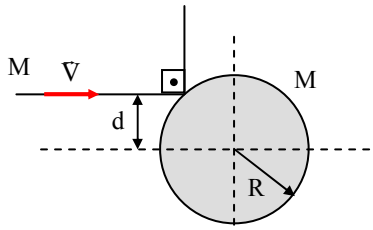

Figure 3.23: Disc pushed by a mass.

Solution: *a. Using the impact parameters $d_i = R/2 = d_f$ and the inertial moment of the disk $I = \frac{M}{2}R^2$ we have the initial angular momentum,*

$$\mathbf{L}_i = \mathbf{r} \times M\mathbf{v}_i = rMv_i\hat{\mathbf{e}}_\theta \sin\phi = Mv_i d_i \hat{\mathbf{e}}_\theta = Mv_i \tfrac{1}{2}R\hat{\mathbf{e}}_\theta \ .$$

In the same way we obtain for the final angular momentum,

$$\mathbf{L}_f = Mv_f d_f \hat{\mathbf{e}}_\theta + I\vec{\omega}_f = \left(Mv_f \tfrac{1}{2}R + \tfrac{M}{2}R^2\omega_f\right)\hat{\mathbf{e}}_\theta \ .$$

The momenta are equal, giving

$$Mv_i \tfrac{1}{2}R = M2v_i\sqrt{3}\tfrac{1}{2}R + \frac{M}{2}R^2\omega_f \ ,$$

and finally,

$$\omega_f = \frac{v_i}{2R} \ .$$

b. The dissipated energy is,

$$E_{diss} = \frac{M}{2}v_f^2 + \frac{I}{2}\omega_f^2 - \frac{M}{2}v_i^2 = \frac{M}{2}\left(\frac{v_i}{2}\right)^2 + \frac{1}{2}\frac{M}{2}R^2\frac{v_i^2}{4R^2} - \frac{M}{2}v_i^2 = -\frac{5}{8}\frac{M}{2}v_i^2 \ .$$

3.3.5.15 Ex: Disc pushed by a mass

A disc of mass $2m$ and radius R rests on an extremely smooth horizontal table. A bullet of mass m, speed v_0 and impact parameter R hits the disc and chokes it (see figure). Calculate:
a. The angular velocity of the system right after the collision;
b. The center-of-mass velocity after the collision;
c. The energy dissipated in the collision.

Solution: *a. Using the inertial moment of the disk $I = mR^2$ we have the initial angular momentum,*

$$\mathbf{L}_i = \mathbf{r} \times m\mathbf{v}_0 = rmv_0\hat{\mathbf{e}}_\theta \sin\phi = mv_0 R\hat{\mathbf{e}}_\theta \ .$$

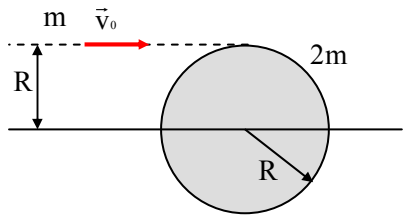

Figure 3.24: Disc pushed by a mass.

The final angular momentum is,

$$\mathbf{L}_j = I\omega\hat{\mathbf{e}}_\theta \ .$$

The moments are equal, giving

$$\omega = \frac{mv_0R}{I} = \frac{v_0}{R} \ .$$

b. The speed of the center of mass after the collision is given by the conservation of linear momentum,

$$\vec{p}_i = mv_0\hat{\mathbf{e}}_x = \vec{p}_f = (2m+m)v_f\hat{\mathbf{e}}_x \ .$$

Hence,

$$v_f = \frac{v_0}{3} \ .$$

c. The energy dissipated in the collision is,

$$E_{diss} = \frac{m}{2}v_f^2 + \frac{I}{2}\omega_f^2 - \frac{2m+m}{2}v_0^2 = \frac{1}{9}\frac{m}{2}v_0^2 + \frac{1}{9}\frac{mR^2}{2}\left(\frac{v_0^2}{R^2}\right) - \frac{m}{2}v_0^2 = \frac{m}{2}v_0^2\frac{-7}{9} \ .$$

3.3.5.16 Ex: Billiard

A billiard ball initially at rest receives an sudden impulse from a cue, which forms an angle with the horizontal, as shown in the figure. The ball leaves with initial velocity v_0 and at the end of the movement it is at rest.
a. Determine the angle θ for this to happen.
b. What is the initial angular velocity of the ball?
c. What is the energy dissipated during the movement?

Solution: *a. The inertial moment of the ball is $I_{cm} = \frac{2}{5}MR^2$. After the momentum, the ball's center of mass has the linear momentum,*

$$p_x = Mv_0 = p\cos\theta \ .$$

As the cue hits the ball at an angle θ, the other component of the impulse generates an angular momentum,

$$L = I_{cm}\omega_0 = Rp_y = RMv_0\sin\theta \ .$$

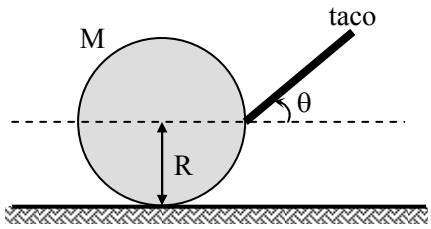

Figure 3.25: Billiard.

Therefore, the initial velocity of the ball is,

$$\omega_0 = \frac{RMv_0 \sin\theta}{I_{cm}} = \frac{5v_0 \sin\theta}{2R} \ .$$

b. Now, we have a movement combining translation and rotation,

$$\begin{aligned} Ma &= -F_{at} \\ I\alpha &= \tau = RF_{at} \ , \end{aligned}$$

where the inertial moment needs to be taken with respect to the instantaneous rotation axis that is in the plane,

$$I = I_{cm} + MR^2 \ .$$

Integrating the equations we get,

$$\begin{aligned} 0 = v &= v_0 + at = v_0 - \frac{F_{at}}{M}t \\ 0 = \omega &= \omega_0 + \alpha t = \omega_0 - \frac{RF_{at}}{I}t \end{aligned}$$

eliminating, $F_{at}t$,

$$\begin{aligned} Mv_0 = \frac{I\omega_0}{R} = \frac{I_{cm} + MR^2}{R}\frac{5v_0 \sin\theta}{2R} = \frac{\frac{2}{5}MR^2 + MR^2}{R}\frac{5v_0 \sin\theta}{2R} = \frac{7M}{2}v_0 \sin\theta \\ \theta = \arcsin\tfrac{2}{7} = 16.6^\circ \ . \end{aligned}$$

c. The energy is totally dissipated,

$$E_{diss} = 0 - \frac{M}{2}v_0^2 - \frac{M}{2}R^2\omega_0^2 \ .$$

3.3.5.17 Ex: Horizontal pendulum with variable length

A particle of mass m is attached to the end of a wire and follows a circular path of radius r on a horizontal table without friction. The wire passes through a hole in the table and the other end is initially fixed. In this situation, the initial radius is r_0 and

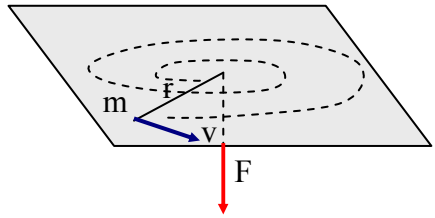

Figure 3.26: Horizontal pendulum with variable length.

the initial angular velocity is ω_0. The wire is then slowly pulled in order to reduce the radius of the circular path, as shown in the figure.
a. How will the angular velocity vary as a function of r?
b. What work has to be done to bring the particle to the radius $r_0/2$?

Solution: *a. The inertial moment is* $I = mr_0^2$. *As the angular momentum is conserved, we have,*

$$L = I\omega = mr^2\omega = mr_0^2\omega_0 = I_0\omega_0 = L_0 \ .$$

Hence,

$$\omega = \frac{r_0^2}{r^2}\omega_0 \ .$$

b. The work is,

$$W = \int \mathbf{F}\cdot d\mathbf{S} = \int_{r_0}^{r_0/2} m\omega^2 r dr = \int_{r_0}^{r_0/2} m\frac{r_0^4}{r^4}\omega_0^2 r dr$$
$$= m\omega_0^2 r_0^4\left(\frac{-1}{2(r_0/2)^2} + \frac{1}{2r_0^2}\right) = \frac{-3m}{2}\omega_0^2\frac{r_0^4}{r_0^2} \ .$$

3.3.5.18 Ex: Cylinder rolling on an inclined plane

Consider a cylinder of mass M and radius R descending an inclined plane of angle θ without sliding. Calculate the acceleration of the center of mass and the friction force acting on the cylinder.

Solution: *We have the equations of motion,*

$$Ma = Mg\sin\theta - F_{at}$$
$$I\alpha = \tau_{at} = RF_{at} \ ,$$

with $I = \frac{M}{2}R^2$. *As the cylinder does not slide, we have,*

$$a = R\alpha \ .$$

Inserting the linear and rotational accelerations,

$$g\sin\theta - \frac{F_{at}}{M} = R\frac{RF_{at}}{I} \ ,$$

giving the friction,

$$F_{at} = \frac{M}{3} g \sin\theta \ .$$

Now we can calculate the acceleration of the center of mass,

$$a = \frac{2}{3} g \sin\theta \ .$$

Calculating the total energy,

$$E = Mgh - \frac{M}{2}v^2 + \frac{M}{2}R^2\omega^2 = -Mg\sin\theta\frac{a}{2}t^2 + M(at)^2 = \frac{1}{9}Mg^2t^2\sin^2\theta \ ,$$

we find that it increases over time, which is strange.
Alternatively, we can consider the movement as a rotation around the support point. Regarding this point, the cylinder's moment of inertia is,

$$I = \frac{M}{2}R^2 + MR^2 \ ,$$

following Steiner's law. Therefore,

$$I\vec{\alpha} = \vec{\tau} = \mathbf{r} \times M\mathbf{g} \ .$$

That is,

$$a = R\alpha = \frac{R}{I}RMg\sin\theta = \frac{2}{3}g\sin\theta \ .$$

3.3.5.19 Ex: Billiard

A billiard ball of mass M and radius R ($I = \frac{2}{5}MR^2$ slides without rotating with speed v_0 on a frictionless table. Suddenly it encounters a part of table with friction and after some time is running without sliding.
a. Calculate the final speed of the ball.
b. What is the energy dissipated in the process?

Solution: *a. We have the equations of motion,*

$$I\alpha = \tau = RF_{at} = R\mu Mg$$
$$Ma = -F_{at} = -\mu Mg \ ,$$

with $I = \frac{2}{5}MR^2$. The speed of the ball will decrease while the angular velocity will increase,

$$v = v_0 + at = v_0 - \mu gt$$
$$\omega = \omega_0 + \alpha t = \frac{R\mu Mg}{I}t = \frac{5\mu g}{2R}t \ ,$$

up to the moment T_e, when the ball does not slide any more, that is,

$$v(t_e) = R\omega(t_e) \ .$$

In this case, we find,

$$t_e = \frac{2v_0}{7\mu g} \qquad \textit{and} \qquad v_e = \frac{5v_0}{7} \ .$$

b. The dissipated energy is,

$$E_{diss} = \frac{m}{2}v_0^2 - \frac{m}{2}v_e^2 - \frac{I}{2}\omega^2 = \frac{M}{2}v_0^2\left(1 - \frac{25}{49} - \frac{2}{5}\right) \approx 0.09\frac{m}{2}v_0^2 \ .$$

3.3.5.20 Ex: Shock and conservation laws

In an experiment Maxwell's wheel was used to determine the moment of inertia I of a body of mass $m = 1490\,\mathrm{g}$. The axis of the body around which it spins during the fall has a radius of $r = 0.6\,\mathrm{cm}$ (the mass of the axis is included in the mass m of the body). See figure below. Measurements of the fall time t_b were made for various heights h, and the data are given in the table below. The moment of inertia I is given by the expression,

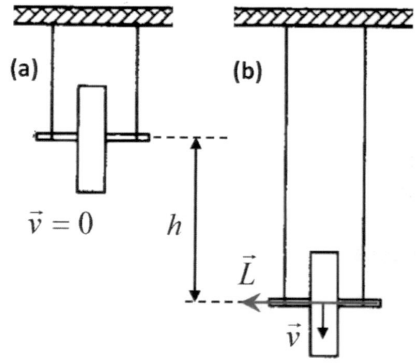

$$I = \left(\frac{gt_b^2}{2h} - 1\right) mr^2 \ ,$$

which implies the following relationship between h and t_b,

$$h = \alpha t_b^2 \qquad \text{where} \qquad \alpha = \frac{g}{2}\frac{mr^2}{I + mr^2} \ .$$

a. Using a double logarithmic paper draw the graph $\log h \times \log t_b$. Choose the line that best approximates the data and determine its angular and linear coefficients. From them determine (i) The power law of t_b in the expression $h = \alpha t_b^{\beta}$ and (ii) The value of α and from it the value of I.
b. Using a millimetric paper draw the graph $h \times t_b^2$, and from the slope α determine the value of I again. Compare the results.

h (cm)	t_b (s)
10	1.2
20	1.8
30	2.1
40	2.5
50	2.8
60	3.0
70	3.3
80	3.6
90	3.7

Solution: *a. From the graph we obtain the slope,*

$$\beta = \frac{\lg h_2 - \lg h_1}{\lg t_{b2} - \lg t_{b1}} \approx 2$$

and the linear coefficient,

$$\alpha = 10^{\lg h_3 - \beta \lg t_{b3}} = 6.5\,\mathrm{cm/s^2} \ .$$

With that we calculate,

$$I = mr^2 \left(\frac{g}{2\alpha} - 1\right) = 0.004\,\mathrm{kg\ m^2} \ .$$

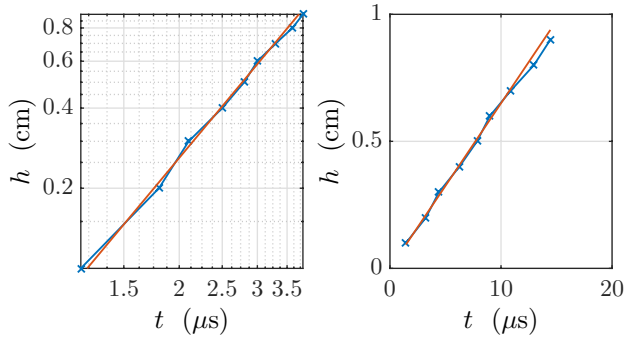

Figure 3.27:

b. From the graph we obtain the slope

$$\alpha = \frac{h_2 - h_1}{t_{b2}^2 - t_{b1}^2} \approx 6.5\,\mathrm{cm/s^2} \ .$$

With that we calculate,

$$I = \frac{g}{2}\frac{mr^2}{\alpha} - mr^2 = 0.004\,\mathrm{kg\ m^2} \ .$$

3.4 Further reading

H.M. Nussenzveig, Edgar Blucher (2013), *Curso de Física Básica: Mecânica - vol 1* [961]ISBN

Chapter 4

Vibrations

Vibrations are periodic processes, that is, processes that repeat themselves after a given time interval. After a time called *period*, the system under consideration returns to the same state in which it was initially. There innumerable examples for periodic processes, such as the motion of a seesaw, oceanic tides, electronic $L-C$ circuits, alternating current or rotations like that of the Earth around the Sun. Thus, vibrations are among the most fundamental processes in all domains of physics. A lecture version of this chapter can be found at (watch talk).

4.1 Free periodic motion

A movement is considered as free, when apart from a *restoring force*, that is a force working to counteract the displacement, there are no other forces accelerating or slowing down the motion.

4.1.1 Clocks

Periodic motions are used to *measure time*. Assuming a given process to be truly periodic, we can inversely *postulate* that the time interval within which this process occurs is constant. This interval is used to define a *unit of time*. For example, the 'day' is defined as the interval that the Earth needs to complete a rotation about its axis. The 'second' is defined as the 86400-th fraction of this period. Taking the second inversely as the base unit, we can define the day as the time interval needed for a periodic process taking 1 s to occur 86400 times. That is, we count the number of times ν that this process occurs within a day and calculate the duration of a day through,

$$\Delta T = \frac{1}{\nu} \, . \tag{4.1}$$

In real life, vibrations are subject to perturbations, just like all physical processes. These perturbations may afflict the periodicity and falsify the measurement of time. For example, the oceanic tides, which depend on the rotation of the moon around the Earth, can influence the Earth's own rotation. One of the challenges of *metrology*, which is the science dealing with issues related to the measurement of time, is to identify processes in nature that are likely to be insensitive to external perturbations. Nowadays, the most stable known periodic processes are vibrations of electrons within atoms. Therefore, the international time is defined by an atomic clock based on

cesium: The 'official' second is the time interval in which the state of an electron oscillates 9192631770 times when the hyperfine structure of a cesium atom is excited by a microwave.

The unit of time is,

$$\text{unit}(T) = \text{s} \ . \tag{4.2}$$

A *frequency* is defined as the number of processes that occur within one second. We use the unit,

$$\text{unit}(\nu) = \text{Hz} \ . \tag{4.3}$$

Often, to simplify mathematical formulas, we will use the derived quantity of the *angular frequency* also called *angular velocity*,

$$\omega \equiv 2\pi\nu \ . \tag{4.4}$$

It has the unit,

$$\text{unit}(\omega) = \text{rad/s} \neq \text{Hz} \ . \tag{4.5}$$

It is important not to use the unit 'Hertz' for angular frequencies in order to avoid confusion.

4.1.2 Periodic trajectories

Many periodic processes are based on repetitive trajectories of particles or bodies. As an example, let us the movement of a body in a box shown in Fig. 4.1. When the body encounters a wall, it is elastically reflected thereby maintaining its velocity but reversing the direction of propagation. Clearly, the velocity is the derivative of the position,

$$v(t) = \dot{x}(t) \ . \tag{4.6}$$

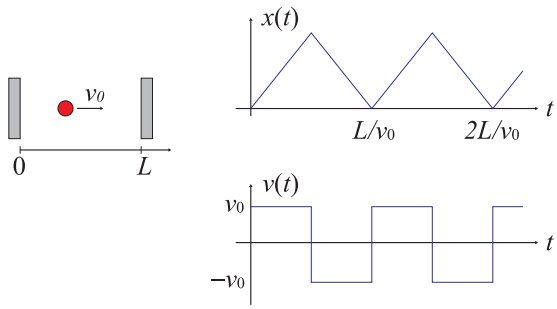

Figure 4.1: Trajectory of a body in a rectangular box. Upper trace: instantaneous position. Lower trace: instantaneous velocity.

To fully describe the trajectory of a body and to identify, when the trajectory repeats, two parameters are needed. Specifying, for example, the time evolution of position $x(t)$ and velocity $v(t)$, we can search for time intervals T after which,

$$x(t_0 + T) = x(t_0) \qquad \text{and} \qquad v(t_0 + T) = v(t_0) \ . \tag{4.7}$$

Obviously, as seen in Fig. 4.1, it is not enough just to look for the time when $x(t_0 + T) = x(t_0)$.

4.1.3 Simple harmonic motion

The simplest motion imaginable is the harmonic oscillation described by,

$$x(t) = A\cos(\omega_0 t - \phi) \ , \tag{4.8}$$

and exhibit in Fig. 4.2. A is the *amplitude* of the motion, such that $2A$ is the distance between the two turning points. $T = 2\pi/\omega_0$ is the oscillation period, since,

$$\cos[\omega_0(t+T) - \phi] = \cos[\omega_0 t + 2\pi - \phi] = \cos[\omega_0 t - \phi] \ . \tag{4.9}$$

ϕ is a *phase shift* describing the time delay $t = \phi/\omega_0$ for the oscillation to reach the turning point.

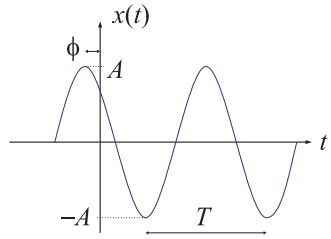

Figure 4.2: Illustration of the cosenus function with the amplitude A, the period T and the phase being negative for this graph $\phi < 0$.

The velocity and acceleration follow from,

$$v(t) = \dot{x}(t) = -\omega_0 A\sin(\omega_0 t - \phi) \qquad \text{and} \qquad a(t) = \dot{v}(t) = -\omega_0^2 A\cos(\omega_0 t - \phi) \ . \tag{4.10}$$

with this we can, using Newton's law, calculate the force necessary to sustain the oscillation of the body,

$$F(t) = ma(t) = -m\omega_0^2 A\cos(\omega_0 t - \phi) = -m\omega_0^2 x(t) \equiv kx(t) \ . \tag{4.11}$$

That is, in the presence of a force, which is proportional to the displacement but with the opposite direction, $F \propto -x$, we expect a sinusoidal solution. The proportionality constant k is called *spring constant*. Obviously the oscillation frequency is independent of amplitude and phase,

$$\omega_0 = \sqrt{k/m} \ . \tag{4.12}$$

Solve Exc. 4.1.10.1 and 4.1.10.2.

Example 7 (*Harmonic vibration*):

- Suspended spring-mass system, pendulums with various masses and lengths of wire, oscilloscope and function generator, water recipient with a floating body.

4.1.4 The spring-mass system

Let us now discuss a possible experimental realization of a sinusoidal vibration. Fig. 4.3 illustrates the spring-mass system consisting of a mass horizontally fixed to a spring. This system has a resting position, which we can set to the point $x = 0$, where no forces act on the mass. When elongated or compressed, the spring exerts a restoring force on the mass working to bring the mass back into its resting position,

$$F_{restore} = -kx \ . \tag{4.13}$$

This so-called *Hooke's law* holds for reasonably small elongations. The spring coefficient k is a characteristic of the spring.

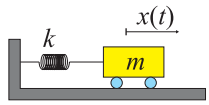

Figure 4.3: Illustration of the spring-mass system.

The oscillation frequency of the spring-mass system is determined by the spring coefficient and the mass, but the phase and the amplitude of the oscillation are parameters, that depend on the way the spring-mass is excited. Knowing the position and velocity of the oscillation at a given time, that is, the initial conditions of the motion, we can determine the amplitude and phase. To see this, we expand the general formula for a sinusoidal oscillation,

$$x(t) = A\cos(\omega_0 t - \phi) = A\cos(\omega_0 t)\cos\phi + A\sin(\omega_0 t)\sin\phi \tag{4.14}$$

and calculate the derivative,

$$v(t) = -A\omega_0\cos\phi\sin(\omega_0 t) + A\omega_0\sin\phi\cos(\omega_0 t) \ . \tag{4.15}$$

With the initial conditions $x(0) = x_0$ and $v(0) = v_0$ we get,

$$A\cos\phi = x_0 \qquad \text{and} \qquad A\omega_0\sin\phi = v_0 \ . \tag{4.16}$$

Hence,

$$x(t) = x_0\cos(\omega_0 t) + \frac{v_0}{\omega_0}\sin(\omega_0 t) \ . \tag{4.17}$$

Solve the Excs. 4.1.10.3, 4.1.10.4, 4.1.10.5, and 4.1.10.6.

4.1.5 Energy conservation

Considerations of *energy conservation* can often help solving mechanical problems. The kinetic energy due to the movement of the mass m is,

$$E_{kin} = \tfrac{m}{2}v^2 \ , \tag{4.18}$$

and the potential energy due to the restoring force is,

$$E_{pot} = -\int_0^x F dx' = -\int_0^x -kx' dx' = \tfrac{k}{2}x^2 \ . \tag{4.19}$$

The total energy must be conserved:

$$E = E_{kin} + E_{pot} = \frac{m}{2}v^2 + \frac{k}{2}x^2 = const \ , \tag{4.20}$$

but is continuously transformed between kinetic energy and potential energy. This is illustrated on the left-hand side of the Fig. 4.4.

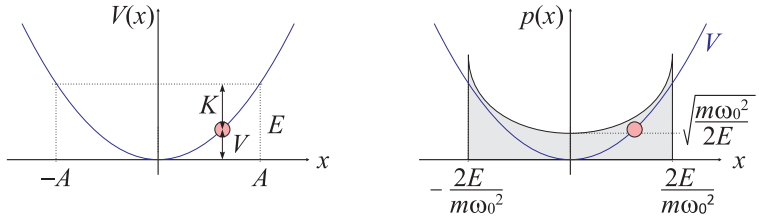

Figure 4.4: (Left) Energy conservation in the spring-mass system showing the kinetic energy K, the potential energy V, and the total energy E. (Right) Probability density of finding the oscillator in position x.

Example 8 (*Probability distribution in the harmonic oscillator*): Let us now use the principle of energy conservation to calculate the probability of finding the oscillating mass next to a given displacement x. For this, we solve the last equation by the velocity,

$$v = \frac{dx}{dt} = \sqrt{\frac{2}{m}E - \frac{k}{m}x^2} = \omega_0\sqrt{\frac{2E}{m\omega_0^2} - x^2} \ , \tag{4.21}$$

or

$$\frac{dx}{\sqrt{\frac{2E}{m\omega_0^2} - x^2}} = \omega_0 dt \ . \tag{4.22}$$

The probability of finding the mass within a given time interval dt is,

$$p(t)dt = \frac{dt}{T} = \frac{\omega_0}{2\pi}dt = \frac{dx}{2\pi\sqrt{\frac{2E}{m\omega_0^2} - x^2}} = \tilde{p}(x)dx \ . \tag{4.23}$$

Hence,

$$\tilde{p}(x) = \frac{1}{2\pi\sqrt{\frac{2E}{m\omega_0^2} - x^2}} \tag{4.24}$$

is the probability density of finding in the mass at the position $x(t)$. Using $\int \frac{dx}{\sqrt{a^2-x^2}} = \arcsin\frac{x}{a}$ with $x_0 = \sqrt{\frac{2E}{m\omega_0^2}}$ we verify,

$$2\int_{-x_0}^{x_0}\tilde{p}(x)dx = \frac{1}{\pi}\left[\arcsin\frac{x}{\sqrt{\frac{2E}{m\omega_0^2}}}\right]_{-x_0}^{x_0} = \frac{2}{\pi}\arcsin\frac{x_0}{\sqrt{\frac{2E}{m\omega_0^2}}} = \frac{2}{\pi}\arcsin 1 = 1 \ . \tag{4.25}$$

The probability density is shown on the right side of Fig. 4.4 [1].

[1] To understand the difference between the probability densities $p(t)$ and $\tilde{p}(x)$ we imagine the following experiments: We divide the period T into equal intervals dt and take a series of photos, all with the same exposure time dt. To understand the meaning of $p(t)$, we throw a random number to choose one of the photos. Each photo has the same probability dt/T to be chosen and, of course, $\int_0^T p(t)dt = 1$. To understand the meaning of $\tilde{p}(x)$, we identify the position of the oscillator in each photo and plot it in a histogram. This histogram is reproduced by $\tilde{p}(x)$.

4.1.6 The spring-mass system with gravity

When a mass is suspended vertically to a spring, as shown on the left-hand side of Fig. 4.5, the gravitational force acts on the mass in addition to the restoring force. This can be expressed by the following balance of forces,

$$ma = -ky - mg \ , \tag{4.26}$$

letting the y-axis be positive in the direction opposite to gravitation. Replacing $\tilde{y}' \equiv y - y_0$ with $y_0 \equiv -\frac{mg}{k}$, we obtain,

$$m\tilde{a} = -k\tilde{y} \ . \tag{4.27}$$

Therefore, the movement is the same as in the absence of gravitation, but around an equilibrium point shifted downward by y_0.

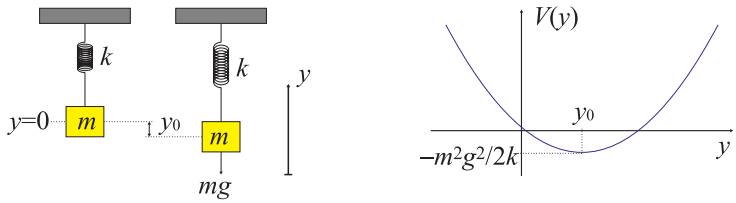

Figure 4.5: Left: Vertical spring-mass system. Right: Conservation of energy in the spring-mass system with gravity.

Energy conservation is now generalized to,

$$E = E_{kin} + E_{mol} + E_{grv} = \tfrac{m}{2}v^2 + \tfrac{k}{2}y^2 + mgy = const \ , \tag{4.28}$$

the potential energy being,

$$\begin{aligned} E_{pot} = E_{mol} + E_{grv} &= \tfrac{k}{2}y^2 + mgy \\ &= \tfrac{k}{2}(y - y_0)^2 + \tfrac{k}{2}2y_0y - \tfrac{k}{2}y_0^2 + mgy = \tfrac{k}{2}(y - y_0)^2 - \frac{m^2g^2}{2k} \ . \end{aligned} \tag{4.29}$$

The right-hand side of Fig. 4.5 illustrates the conservation of energy in the spring-mass system with gravity. See Excs. 4.1.10.7, 4.1.10.8, 4.1.10.9, and 4.1.10.10.

4.1.7 The pendulum

The pendulum is another system which oscillates in the gravitational field. In the following, we will distinguish three different types of pendulums. In the *ideal pendulum* the mass of the oscillating body is all concentrated in one point and the oscillations have small amplitudes. In the *physical pendulum* the mass of the body is distributed over a finite spatial region. And *mathematical pendulum* is a point mass oscillating with a large amplitude and therefore subject to a nonlinear restoring force.

Figure 4.6: Physical pendulum.

4.1.7.1 The ideal pendulum

The *ideal pendulum* is schematized on the left side of Fig. 4.6. As the centrifugal force is compensated for by the traction of the wire supporting the mass, the acceleration force ma is solely due to the perpendicular projection $-mg\sin\theta$ on the wire. For small amplitudes, $\sin\theta \simeq \theta$, such that [2],

$$ma \simeq -mg\theta \ . \tag{4.30}$$

The tangential acceleration is now,

$$a = \dot{v} = \ddot{s} = \frac{d}{dt}\theta L = L\ddot{\theta} \ . \tag{4.31}$$

Thus,

$$\ddot{\theta} + \frac{g}{L}\theta \simeq 0 \ . \tag{4.32}$$

This equation has the same structure as that of the already studied spring-mass system $\ddot{x} + \frac{k}{m}x = 0$. Therefore, we can deduce that the ideal pendulum oscillates with the frequency,

$$\omega_0 = \sqrt{\frac{g}{L}} \ , \tag{4.33}$$

only that the oscillating degree of freedom is an angle rather than a spatial shift. It is interesting to note that the oscillation frequency is independent of the mass. See Exc. 4.1.10.11.

4.1.7.2 The physical pendulum

We consider an irregular body suspended at a point P as schematized on the right-hand side of Fig. 4.6. The center-of-mass be displaced from the suspension point by a distance D. This system represents the *physical pendulum*. Gravitation exerts a torque $\vec{\tau}$ on the center-of-mass,

$$\vec{\tau} = \mathbf{D} \times m\mathbf{g} \qquad \text{with} \qquad \tau = I\ddot{\theta} \ , \tag{4.34}$$

where I is the moment of inertia of the body for rotations about the suspension axis. Like this,

$$I\ddot{\theta} = -Dmg\sin\theta \ . \tag{4.35}$$

[2]The equation of motion can be derived from the Hamiltonian $H = \frac{L_\theta^2}{2ml^2} + mgl\cos\theta$ using $\dot{\theta} = \partial H/\partial \mathbf{L}_\theta$ and $\dot{L_\theta} = -\partial H/\partial\theta$, where L_θ is the angular momentum.

Considering once more small angles, $\sin\theta \simeq \theta$, we obtain,

$$\ddot{\theta} + \omega_0^2 \theta \simeq 0 \qquad \text{with} \qquad \omega_0 \equiv \sqrt{\frac{Dmg}{I}} \ . \tag{4.36}$$

It is worth mentioning that the inertial moment of a body whose mass is concentrated in a point at a distance D from the suspension point follows *Steiner's law*,

$$I = mD^2 \ . \tag{4.37}$$

With this we recover the expression of the ideal pendulum,

$$\omega_0 = \sqrt{\frac{Dmg}{mD^2}} = \sqrt{\frac{g}{D}} \ . \tag{4.38}$$

4.1.7.3 The mathematical pendulum

The equation describing the mathematical pendulum (see Fig. 4.6) has already been derived but, differently from what we did before, here we will not apply the small angle approximation,

$$\ddot{\theta} = -\frac{g}{L}\sin\theta = -\omega_0^2 \sin\theta \ . \tag{4.39}$$

Energy conservation can be formulated as follows:

$$\begin{aligned} 0 = \frac{dE}{dt} &= \frac{d}{dt}(E_{rot} + E_{pot}) = \frac{d}{dt}\frac{I}{2}\dot{\theta}^2 + \frac{d}{dt}mgL(1-\cos\theta) \\ &= \frac{I}{2}2\dot{\theta}\ddot{\theta} + mgL\dot{\theta}\sin\theta \simeq \dot{\theta}(I\ddot{\theta} + mgL\theta) \ . \end{aligned} \tag{4.40}$$

Thus, we obtain the same differential equation,

$$\ddot{\theta} + \frac{mgL}{I}\theta = 0 \ . \tag{4.41}$$

Example 9 (*Simulation of an anharmonic pendulum*): When the anharmonicity is not negligible, it is impossible to solve the differential equation analytically. We must resort to numerical simulations. The simplest procedure is an iteration of the type,

$$\begin{aligned} \theta(t+dt) &= \theta(t) + dt\dot{\theta} = \theta(t) + dt\omega \\ \omega(t+dt) &= \omega(t) + dt\dot{\omega} = \omega(t) - dt\omega_0 \sin\theta \ . \end{aligned}$$

Fig. 4.7(a) shows the temporal dephasing of the oscillation caused by the anharmonicity as compared to the harmonic oscillation. Fig. 4.7(b) shows the orbits $\theta(t) \longmapsto \omega(t)$ in the phase space.

4.1.8 The spring-cylinder system

Another example of an oscillating system is shown in Fig. 4.8. The inertial moment of the cylinder is $I = \frac{M}{2}R^2$. The spring exerts the force,

$$F_{mol} = -kx \ . \tag{4.42}$$

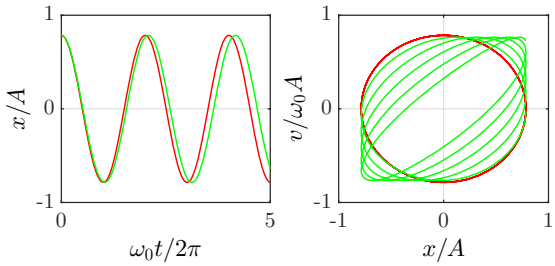

Figure 4.7: (code) Diffusion due to anharmonicities (a) in time and (b) in phase space. The red curves show the harmonic approximation.

Therefore, we have the equations of motion,

$$M\ddot{x} = F_{mol} - F_{at} \qquad (4.43)$$
$$I\ddot{\theta} = -RF_{at} \ .$$

If the wheel does not slip, we can eliminate the friction using $x = R\omega$, and we obtain,

$$I\ddot{\theta} = I\frac{\ddot{x}}{R} = \frac{M}{2}R^2\frac{\ddot{x}}{R} = -RF_{at} = -R(-kx - M\ddot{x}) \ . \qquad (4.44)$$

Resolving by $\ddot{x}$,

$$\ddot{x} + \frac{2k}{3M}x = 0 \ . \qquad (4.45)$$

The frequency is,

$$\omega_0 = \sqrt{\frac{2k}{3M}} \ . \qquad (4.46)$$

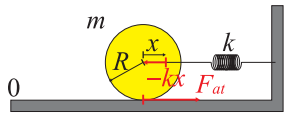

Figure 4.8: The spring-cylinder system.

4.1.9 Two-body oscillation

We now consider the oscillations of two bodies m_1 and m_2 located at the positions x_1 and x_2 and interconnected by a spring k, as shown in Fig. 4.9. The free length, that is, the distance at which the spring exerts no forces on the masses, is ℓ. The forces grow with the stretch $x \equiv x_2 - x_1 - \ell$ of the spring, such that $x > 0$ when the spring is stretched and $x < 0$ when it is compressed. Thereby,

$$m_1\ddot{x}_1 = kx \qquad \text{and} \qquad m_2\ddot{x}_2 = -kx \ . \qquad (4.47)$$

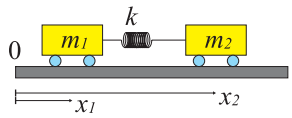

Figure 4.9: Two bodies in relative vibration.

Adding these equations,

$$m_1\ddot{x}_1 + m_2\ddot{x}_2 \equiv (m_1 + m_2)\ddot{x}_{cm} = 0 \ . \tag{4.48}$$

Dividing the equations by the masses and subtracting them,

$$\ddot{x}_1 - \ddot{x}_2 = -k\left(\frac{1}{m_1} + \frac{1}{m_2}\right)x = \ddot{x}_{rel} = -\frac{k}{\mu}x = \omega_0 x \ , \tag{4.49}$$

where $\omega_0^2 = k/\mu$ and $\mu^{-1} \equiv m_1^{-1} + m_2^{-1}$ is called the *reduced mass*. The introduction of the reduced mass turns the oscillator consisting of two bodies equivalent to a system consisting of only one mass and one spring, but with an increased vibration frequency,

$$\omega_\mu = \sqrt{\frac{k}{\mu}} = \sqrt{2\frac{k}{m}} \ . \tag{4.50}$$

This system represents an important model for the description of *molecular vibration*. Note that for $m_1 \longrightarrow \infty$ we restore the known situation of a spring-mass system fixed to a wall.

4.1.10 Exercises

4.1.10.1 Ex: Zenith in São Carlos

Knowing that the latitude of the Sun in the tropics of Capricorn is $\alpha_{trop} = 23°$ calculate at what time of the year the sun is vertical at noon in São Carlos, SP, Brazil.

Solution: *The zenith of the sun oscillates sinusoidally with a period of one year and an amplitude α_{trop}. Hence,*

$$\alpha(t) = \alpha_{trop}\cos\frac{2\pi t}{365\,\mathrm{d}} \ .$$

The sun is vertical in São Carlos ($\alpha_{sc} = 21.92°$) when $\alpha(t) = \alpha_{sc}$, that is,

$$\alpha_{trop}\cos\frac{2\pi t}{365\,\mathrm{d}} = \alpha_{sc} \ .$$

or

$$t = \frac{365\,\mathrm{d}}{2\pi}\arccos\frac{\alpha_{SC}}{\alpha_{WK}} = 17.9\,\mathrm{d} \ .$$

4.1.10.2 Ex: Length of days on Earth

Calculate the length of a day on Earth as a function of the location's longitude ϕ and latitude θ and of the season of the year.

Solution: *We set the z-axis to coincide with the axis of Earth, so that a location on Earth is specified by,*

$$\mathbf{r} = r \begin{pmatrix} \cos\theta\cos\phi \\ \cos\theta\sin\phi \\ \sin\theta \end{pmatrix} ,$$

with $\phi = 2\pi t/24\,\mathrm{h}$, θ, *and* $R = 6370\,\mathrm{km}$. *The coordinate of the Sun is parameterized as,*

$$\mathbf{R} = R \begin{pmatrix} \cos\alpha \\ 0 \\ \sin\alpha \end{pmatrix} ,$$

with $R = 1.59 \cdot 10^9\,\mathrm{km}$ *and the inclination of the Earth's axis,*

$$\alpha = \alpha_0 \sin\tfrac{2\pi t}{365\,\mathrm{d}} ,$$

with $\alpha_0 = 23^\circ$. *The condition* $\mathbf{r}\cdot\mathbf{R} = 0$ *yields,*

$$\Delta t = \frac{24\,\mathrm{h}}{2\pi}\Delta\phi = \frac{24\,\mathrm{h}}{\pi}\arccos(-tan\theta\tan\alpha) .$$

For example, for Quimper located at $\theta = 48^\circ$, *we get on the 21-th of June* $\Delta t = 15\,\mathrm{h}\,45\,\mathrm{min}$ *and on the 21-th of December* $\Delta t = 8\,\mathrm{h}\,15\,\mathrm{min}$. *For Nice located at* $\theta = 43^\circ$, *we get in summer* $\Delta t = 15\,\mathrm{h}\,6\,\mathrm{min}$ *and in winter* $\Delta t = 8\,\mathrm{h}\,53\,\mathrm{min}$.

4.1.10.3 Ex: Swing modes

In the systems shown in the figure there is no friction between the surfaces of the bodies and floor, and the springs have negligible mass. Find the natural oscillation frequencies.

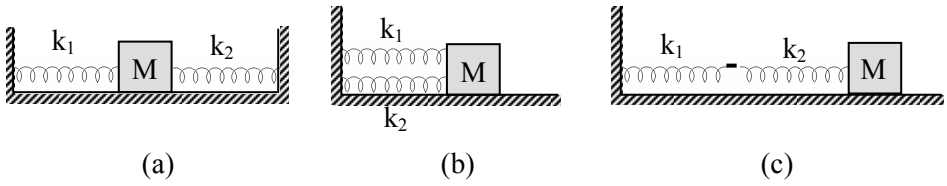

Figure 4.10: Swing modes.

Solution: *a. Be* x_1 *and* x_2 *the independent rest positions of the two springs, such that the independent restorative forces are,*

$$F_1 = -k_1(x - x_1) \qquad and \qquad -F_2 = -k_2(x_2 - x) .$$

The resting position of the springs acting jointly x_0 follows from,

$$0 = F_1 + F_2 = -k_1(x_0 - x_1) - k_2(x_0 - x_2) \ ,$$

giving,

$$x_0 = \frac{k_1 x_1 + k_2 x_2}{k_1 + k_2} \ .$$

The equation of motion is now,

$$M\ddot{x} = F_1 + F_2 = -k_1(x_0 - x_1) - k_2(x_0 - x_2) = -(k_1 + k_2)(x - x_0) \ .$$

Hence,

$$\omega_0 = \sqrt{\frac{k_1 + k_2}{M}} \ .$$

b. The same argument can be used to treat springs in parallel. We have $k = k_1 + k_2$, hence,

$$\omega_0 = \sqrt{\frac{k_1 + k_2}{M}}.$$

c. For springs in series the derivation is more complicated. We call y and y_1, respectively, the current position and the resting position of the connection point between the springs and x and x_2, respectively, the current position and the resting position of the mass. Since the connection point has no mass, we have an equilibrium between the forces exerted by the two springs,

$$0 = F_1 + F_2 = -k_1(y - y_1) + k_2(x - x_2 - y + y_1) \ ,$$

yielding,

$$y - y_1 = \frac{k_2}{k_1 + k_2}(x - x_2) \ .$$

The equation of motion is now,

$$M\ddot{x} = F_M = -F_2 = -k_2(x - x_2 - y + y_1) = -\frac{k_1 k_2}{k_1 + k_2}(x - x_2) \ .$$

Hence, $k = (k_1^{-1} + k_2^{-1})^{-1}$ and,

$$\omega_0 = \sqrt{\frac{(k_1^{-1} + k_2^{-1})^{-1}}{M}} \ .$$

4.1.10.4 Ex: Coupled springs

A mass m is suspended within a horizontal ring of radius $R = 1\,\mathrm{m}$ by three springs with the constants $D_1 = 0.1\,\mathrm{kg/m}$, $D_2 = 0.2\,\mathrm{N/m}$, and $D_3 = 0.3\,\mathrm{N/m}$. The suspension points of the springs on the ring have the same mutual distances. Determine the equilibrium position of the mass assuming that the springs' extensions at rest range is 0.

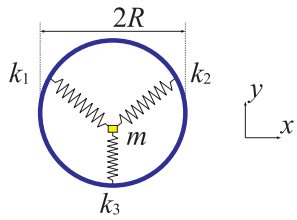

Figure 4.11: Coupled springs.

Solution: *We choose the origin of the coordinate system at the center of the ring and the equilibrium position at* $\mathbf{r}$*. Then the forces are balanced holds* $\mathbf{F}_1 + \mathbf{F}_2 + \mathbf{F}_3 = 0$*. Following the scheme the suspension points are at,*

$$\mathbf{a}_1 = R\begin{pmatrix} -\frac{1}{2}\sqrt{3} \\ \frac{1}{2} \end{pmatrix} \quad , \quad \mathbf{a}_2 = R\begin{pmatrix} \frac{1}{2}\sqrt{3} \\ \frac{1}{2} \end{pmatrix} \quad , \quad \mathbf{a}_3 = R\begin{pmatrix} 0 \\ -1 \end{pmatrix} \ ,$$

where $a_1 = a_2 = a_3$*. Hence,* $-k_1(\mathbf{a}_1 - \mathbf{r}) - k_2(\mathbf{a}_2 - \mathbf{r}) - k_3(\mathbf{a}_3 - \mathbf{r}) = 0$*. Finally we get for the components,*

$$x_0 = \frac{k_1 - k_2}{k_1 + k_2 + k_3}\frac{R}{2}\sqrt{3} \quad , \quad y_0 = \frac{k_1 + k_2 - 2k_3}{k_1 + k_2 + k_3}\frac{R}{2} \ .$$

The equations of motion are, letting the springs be equal, $k_1 = k_2 = k_3$*,*

$$m\ddot{x} = -k\left(x + \tfrac{R}{2}\sqrt{3}\right) - k\left(x - \tfrac{R}{2}\sqrt{3}\right) - kx = -3kx$$
$$m\ddot{y} = -k\left(y - \tfrac{R}{2}\right) - k\left(y - \tfrac{R}{2}\right) - k\left(y + R\right) = -3ky \ .$$

4.1.10.5 Ex: Coupled springs

A mass m is suspended by four springs with the constants k_n, as shown in the figure. Determine the equilibrium position of the mass. Assume the ideal case of ideally compressible springs.

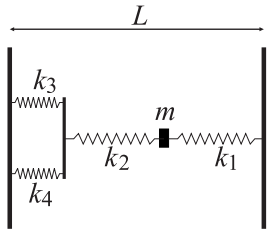

Figure 4.12: Coupled springs.

Solution: *Springs are arbitrarily compressible, i.e., $F_n = -k_n a_n$. Following the scheme, both the mass m and the connecting plate between the springs are in equilibrium, that is, $F_{34} = F_2 = F_1$. Since the springs k_3 and k_4 are mounted in parallel, their total spring constant is additive. Hence we have $(k_3 + k_4)a_3 = k_2 a_2 = k_1 a_1$. Using the condition that the sum of the individual displacements of the spring is $a_1 + a_2 + a_3 = L$, we obtain:*

$$a_1 = \frac{L}{1 + k_1/k_2 + k_1/(k_3 + k_4)} \ .$$

4.1.10.6 Ex: Coupled springs

Calculate the resulting spring constants for the constructions shown in the scheme. Individual springs are arbitrarily compressible with spring constants D_k.

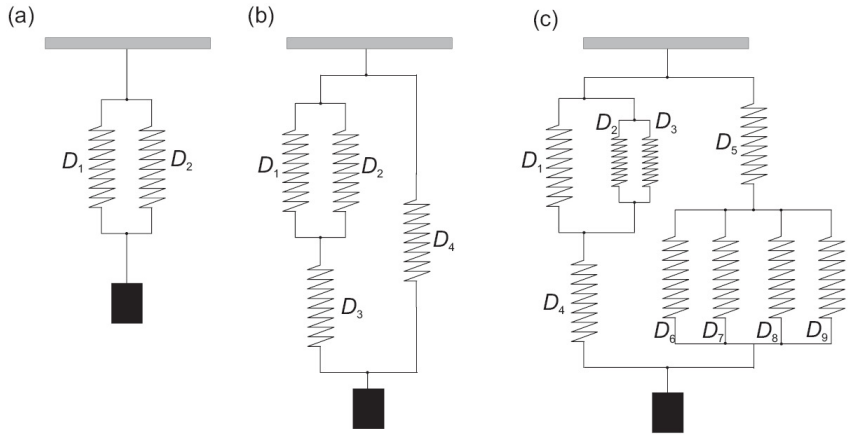

Figure 4.13: Coupled springs.

Solution: *For a spring assembly in series we have the two equations,*

$$mg - D_1 x_1 = 0 \qquad \textit{and} \qquad mg - D_2(x_2 - x_1) = 0 \ .$$

Hence,

$$x_2 = \frac{D_1 + D_2}{D_2} x_1 = \frac{D_1 + D_2}{D_1 D_2} mg \ ,$$

or

$$D_{tot} = \left(\frac{1}{D_1} + \frac{1}{D_2} \right)^{-1} \ .$$

And analogously for a parallel assembly we have the equation

$$mg - D_1 x - D_2 x = 0 \ .$$

Hence,

$$D_{tot} = D_1 + D_2 \ .$$

By applying these rules to the shown assemblies, we get
a. $D = D_1 + D_2$
b. $D = \left(\frac{1}{D_1+D_2} + \frac{1}{D_3}\right)^{-1} + D_4$
c. $D = \left(\frac{1}{D_1+D_2+D_3} + \frac{1}{D_4}\right)^{-1} + \left(\frac{1}{D_5} + \frac{1}{D_6+D_7+D_8+D_9}\right)^{-1}$

4.1.10.7 Ex: Spring-mass system

A body of unknown mass hangs at the end of a spring, which is neither stretched nor compressed, and is released from rest at a certain moment. The body drops a distance y_1 until it rests for the first time after the release. Calculate the period of oscillatory motion.

Solution: *Since the mass is released at rest, it will periodically return to the starting point. By conservation of energy the falling distance is twice the oscillation amplitude, which is equal to the resting position in the gravitational field,*

$$y_1 = 2y_0 = \tfrac{mg}{2k} \ .$$

So the oscillation frequency is,

$$\omega_0 = \sqrt{\frac{k}{m}} = \frac{2g}{y_1} \ .$$

4.1.10.8 Ex: Spring-mass system

A body of $m = 1.5\,\mathrm{kg}$ stretches a spring by $y_0 = 2.8\,\mathrm{cm}$ from its natural length when being at rest. Now, we let it swing at this spring with an amplitude of $y_m = 2.2\,\mathrm{cm}$.
a. Calculate total energy of the system.
b. Calculate the gravitational potential energy at the body's lower turning point.
c. Calculate the potential energy of the spring at the body's lower turning point.
d. What is the maximum kinetic energy of the body (when $U = 0$ is the point where the spring is at equilibrium).

Solution: *a. Since the stretch of the spring corresponds to* $y_0 = -\frac{mg}{k}$*, we can calculate the spring constant,*

$$k = \frac{mg}{-y_0} = 526\,\mathrm{N/m} \ ,$$

and the oscillation frequency is,

$$\omega_0 = \sqrt{\frac{k}{m}} \ .$$

So we can describe the motion by the function,

$$y(t) = y_m \cos \omega_0 t + y_0 \ .$$

The total energy at the upper turning point is,

$$E = E_{mol} + E_{grv} = \frac{k}{2}(y_m + y_0)^2 + mg(y_m + y_0) = -0.079\,\mathrm{J} \ .$$

b. The gravitational potential energy at the lower turning point is

$$E_{grv} = mg(-y_m + y_0) = -0.74\,\mathrm{J} \ .$$

c. The total potential energy at the lower turning point is equal to the total energy (a), because the kinetic energy disappears.
d. The instantaneous velocity being,

$$v(t) = -y_m \omega_0 \sin \omega_0 t \ ,$$

the maximum kinetic energy is,

$$E_{kin} = \frac{m}{2} y_m^2 \omega_0^2 = 0.13\,\mathrm{J} \ .$$

The figure shows the energy conservation using the expressions of the formula (4.28). The red line shows the temporal transformation of kinetic energy, the green line of the spring, the blue of gravitation, the cyan of the potential, and black of the total energy.

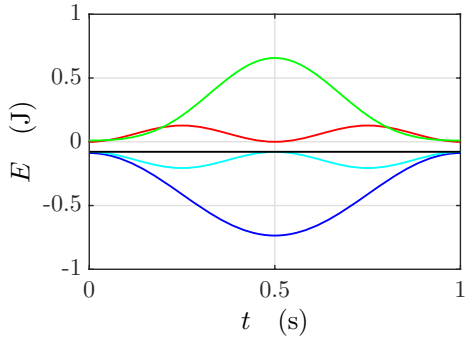

Figure 4.14: Spring-mass system.

4.1.10.9 Ex: U-shaped water tube

Consider a U-shaped tube filled with water. The total length of the water column is L. Exerting pressure on one tube outlet the column is incited to perform oscillations. Calculate the period of the oscillation.

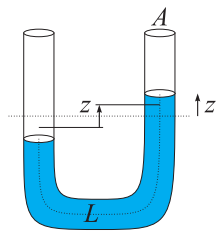

Figure 4.15: U-shaped water tube.

Solution: *If A is the cross section, the total mass of the water is $M = \rho V = \rho AL$, where ρ is the density of water. When the column moves at velocity v, it has kinetic energy,*

$$E_{kin} = \frac{M}{2} v^2 \ .$$

To put the mass $M_z = \rho V_z = \rho Az$ above the resting level of the water, such that the center of mass is a distance z above the low level, we need to provide the work,

$$-W = gM_z z = g\rho Az^2 = E_{pot} \ .$$

Energy conservation requires,

$$E = E_{kin} + E_{pot} = \frac{\rho AL}{2}\dot{z}^2 + g\rho Az^2 = \frac{M}{2}\dot{z}^2 + \frac{2gM}{2L}z^2 = const.$$

Hence, comparing the coefficient of the potential energy with $\frac{M}{2}\omega_0^2$,

$$\omega_0 = \sqrt{\frac{2g}{L}} \ .$$

4.1.10.10 Ex: Buoy in the sea

A hollow cylindrical buoy with cross-sectional area A and mass M floats in the sea so that the axis of symmetry is aligned with gravitation. An albatross of mass m sitting on the buoy waits until time $t = 0$ and takes off. With which frequency and amplitude does the buoy oscillate if friction can be neglected? Derive the equation of motion and the complete solution.

Solution: *The upward buoyant force of the water is,*

$$F_a = \sigma Agz \ ,$$

with the water density $\sigma = 1\,\mathrm{kg/l}$ and the immersion depth of the buoy z. Following Archimedes' law the buoy is at balance at the depth z_0, when $F_a - (M + m)g = 0$, that is, when,

$$-\sigma Az_0 g = (M + m)g \ .$$

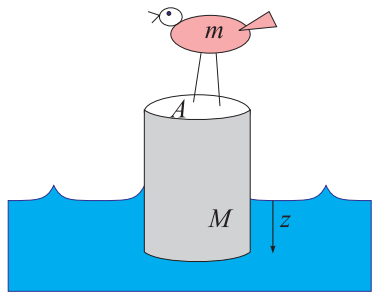

Figure 4.16: Fluctuating buoy.

From this we derive an immersion depth with albatross of $z_0 = \frac{M+m}{\sigma A}$. *When the albatross takes off, the weight decreases and we get an acceleration,* $M\ddot{z} = -\sigma A z g - Mg$ *com* $z(0) = z_0$. *That is, the equation of motion is,*

$$\ddot{z} + \frac{\sigma A g}{M} z = -g \ .$$

Hence, the vibration frequency is $\omega = \sqrt{\frac{\sigma A g}{M}}$. *To make this inhomogeneous differential equation a homogeneous one, we make, as in the case of the spring-mass in the gravitational field, the substitution,* $\tilde{z} = z + \frac{M}{\sigma A}$. *With that we get,*

$$\ddot{\tilde{z}} + \frac{\sigma A g}{M} \tilde{z} = 0 \ .$$

The general solution of this equation is $\tilde{z} = C \sin \omega t + D \cos \omega t$, *such that,*

$$z = C \sin \omega t + D \cos \omega t - \frac{M}{\sigma A} \ .$$

With the known initial conditions we have,

$$\begin{aligned} z(0) = z_0 &= C \sin \omega t + D \cos \omega t - \frac{M}{\sigma A} = D - \frac{M}{\sigma A} \\ \dot{z}(0) = 0 &= \omega C \cos \omega t - \omega D \sin \omega t = \omega C \ , \end{aligned}$$

and we can calculate the vibration amplitude, $D = z_0 + \frac{M}{\sigma A} = -\frac{m}{\sigma A}$. *Hence, the complete solution is,*

$$z = -\frac{m}{\sigma A} \cos \omega t - \frac{M}{\sigma A} \ .$$

4.1.10.11 Ex: Complicated pendulum oscillation

At a distance of $d = 30\,\text{cm}$ below the suspension point of a pendulum with the length $l_1 = 50\,\text{cm}$ there is a fixed pin S on which the wire suspending the pendulum temporarily bends during vibration. How many vibrations does the pendulum perform

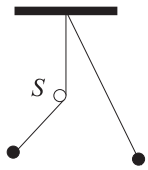

Figure 4.17: Mathematical pendulum.

per minute?

Solution: *We have half vibrations for two different wire lengths, l_1 and $l_2 = l_1 - d$. We know,*

$$\omega_{1,2} = \sqrt{\frac{g}{l_{1,2}}} \qquad \textit{and} \qquad T_{1,2} = \frac{2\pi}{\omega_{1,2}} \ .$$

Thereby,

$$f = \frac{1}{T} = \frac{1}{T_1/2 + T_2/2} = \frac{\sqrt{g}}{\pi(\sqrt{l_1} + \sqrt{l_2})} \approx 51.8\,\mathrm{min}^{-1} \ .$$

4.1.10.12 Ex: Physical pendulum

Calculate the oscillation frequency of a thin bar of mass m and length L suspended at one end.

Solution: *The inertial moment of a thin bar is,*

$$I = \tfrac{1}{3} m L^2 \ .$$

The center-of-mass is in the middle of the bar, $L = 2D$. Hence,

$$\omega_0 = \sqrt{\frac{Dmg}{I}} = \sqrt{\frac{3g}{2L}} \ .$$

4.1.10.13 Ex: Physical pendulum

An irregularly shaped flat body has the mass $m = 3.2\,\mathrm{kg}$ and is hung on a massless rod with adjustable length, which is free to swing in the plane of the body itself. When the rod's length is $L_1 = 1.0\,\mathrm{m}$, the period of the pendulum is $t_1 = 2.6\,\mathrm{s}$. When the rod is shortened to $L_2 = 0.8\,\mathrm{m}$, the period decreases to $t_2 = 2.5\,\mathrm{s}$. What is the period of the oscillation when the length is $L_3 = 0.5\,\mathrm{m}$?

Solution: *Knowing that the period is proportional to the root of the distance between the point of suspension and the center of gravity of the body, $t_k = C\sqrt{L_k}$ with a constant C, we have*

$$t_1 = C\sqrt{\Delta L + L_1} \qquad , \qquad t_2 = C\sqrt{\Delta L + L_2} \ ,$$

where ΔL is the distance between the center of gravity of the body and the attachment point on the rod. With this,

$$C = \sqrt{\frac{t_2^2 - t_1^2}{L_2 - L_1}} \quad , \qquad \Delta L = \frac{t_1^2}{C^2} - L_1 \ ,$$

and

$$t_3 = C\sqrt{\Delta L + L_3} = \sqrt{t_1^2 + (t_2^2 - t_1^2)\frac{L_3 - L_1}{L_2 - L_1}} = 2.34\,\mathrm{s} \ .$$

4.1.10.14 Ex: Physical pendulum

A physical pendulum of mass M consists of a homogeneous cube with the edge length d. As shown in the figure, the pendulum is hung without friction on a horizontal rotation axis.
a. Determine the inertial momentum about the rotation axis using Steiner's theorem.
b. The pendulum now performs small oscillations around its resting position. Determine the angular momentum.
c. Give the equation of motion for small pendulum amplitudes ϕ around its resting position and the oscillation period.

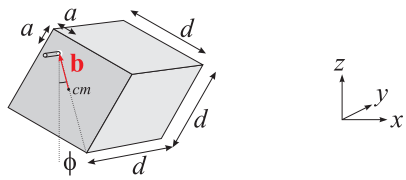

Figure 4.18: Physical pendulum.

Solution: *a. We calculate the tensor of inertia I_{ij} for a coordinate system in the center of the cube:*

$$I_{ij} = \int_V \rho(\mathbf{r}) \left[\delta_{ij} \sum_{\alpha=1}^{3} x_\alpha^2 - x_i x_j \right] dV \ .$$

Hence,

$$\begin{aligned} I_{11} &= \int_V \rho(\vec{r}) \left[x_1^2 + x_2^2 + x_3^2 - x_1 x_1 \right] dV = \rho \int_{-d/2}^{d/2} (x_2^2 + x_3^2) dx_1 dx_2 dx_3 \\ &= \frac{\rho d^5}{6} = \frac{M d^2}{6} = I_{22} = I_{33} \\ I_{\imath \neq j} &= \int_V \rho(\mathbf{r}) x_i x_j dV = \rho \int_{-d/2}^{d/2} x_i x_j dx_i dx_j dx_k = 0 \ . \end{aligned}$$

Thus, I^{CM} adopts the form:

$$I^{CM} = \begin{pmatrix} Md^2/6 & 0 & 0 \\ 0 & Md^2/6 & 0 \\ 0 & 0 & Md^2/6 \end{pmatrix} .$$

Now we nail the cube to the wall. Here, the vertical distance b from the new axis of rotation $\vec{\omega} = \omega\hat{\mathbf{e}}_3$ until the center of mass is given by,

$$\mathbf{b} = \sqrt{2}\left(\frac{d}{2} - a\right)\hat{\mathbf{e}}_b \ .$$

$\hat{\mathbf{e}}_b$ shows from the origin of the new coordinate system (around which the rotation occurs) to the origin of the old coordinate system (the center-of-mass system), $\hat{\mathbf{e}}_b = -\hat{\mathbf{e}}_1 \sin\phi - \hat{\mathbf{e}}_2 \cos\phi$. With Steiner's theorem, $I_\omega = I^{CM}_{\omega_0} + Mb^2$, we get the inertial moment regarding the new rotation axis $I_\omega = 2M\left(\frac{1}{3}d^2 - da + a^2\right)$. The torque is,

$$\mathbf{D} = \frac{\partial}{\partial t}\mathbf{L} = \frac{\partial}{\partial t} I\vec{\omega} = I_\omega \ddot{\phi}\hat{\mathbf{e}}_3 \ .$$

The force of gravitational attraction $F_g = -Mg\hat{e}_2$ cause, when displaced from the rest position, a torque,

$$\mathbf{D} = \mathbf{b} \times \mathbf{F}_g = -b\hat{\mathbf{e}}_b \times Mg\hat{\mathbf{e}}_2 = bMg \sin\phi \hat{\mathbf{e}}_3 \ .$$

Where ϕ is the angle between $\vec{b}$ and the axis $\hat{\mathbf{e}}_2$, that is, the direction of gravitational attraction. Since the torque has to be conserved ($\frac{\partial}{\partial t}\mathbf{L} = 0$), the sum of the torques must be zero,

$$0 = I_\omega \ddot{\phi} + bMg \sin\phi \ .$$

Solving the differential equation for small $\phi(t)$ gives the period T as,

$$T = 2\pi\sqrt{\frac{I_\omega}{bMg}} \ .$$

4.1.10.15 Ex: Physical pendulum on a spiral spring

Consider a beam of mass $m = 1\,\mathrm{kg}$ with the dimensions $(a, b, c) = (3\,\mathrm{cm}, 3\,\mathrm{cm}, 8\,\mathrm{cm})$. The beam is rotatable about an axis through the point A. At point B, at a distance r from point A, the beam is fixed to a spiral spring exerting the retroactive force $\mathbf{F}_R = D\vec{\phi}$ with $D = 100\,\mathrm{N/m}$. Determine the differential equation of motion and solve it. Determine the period of the oscillation.

Solution: *The retroactive force exerts a torque $|\mathbf{M}| = |\mathbf{r} \times \mathbf{F}_R| = rD\phi$. The torque due to the inertia of the mass is $\mathbf{M}_T = I\vec{\omega}$. With that the equation of motion gets,*

$$I\ddot{\phi} + rF_R\phi = 0 \ .$$

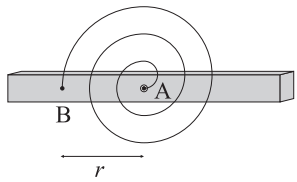

Figure 4.19: Physical pendulum on a spiral spring.

The inertial moment of the beam is,

$$I_\omega = \frac{1}{V}\int_{viga} \varrho(\mathbf{r})(y^2+z^2)d^3r = \frac{\varrho_0}{V}\int_{-c/2}^{c/2}\int_{-b/2}^{b/2}\int_{-a/2}^{a/2}(y^2+z^2)dxdydz$$
$$= \frac{\varrho_0 abc}{12V}(a^2+c^2) = \frac{\varrho_0}{6}(a^2+c^2)\ ,$$

The rest is trivial.

4.1.10.16 Ex: Accelerated pendulum

A simple pendulum of length L is attached to a cart that slides without friction downward an plane inclined by an angle α with respect to the horizontal. Determine the oscillation period of the pendulum on the cart.

Solution: *The force accelerating the car is,*

$$\mathbf{F}_{car} = m\mathbf{a} \qquad with \qquad a = g\sin\alpha\ .$$

The effective force acting on the pendulum suspended inside the cart is,

$$\mathbf{F}_{eff} = m\mathbf{g} - m\mathbf{a} \qquad with \qquad F_{eff} = gm\cos\alpha\ .$$

where $\mathbf{a}$ *is the acceleration of the cart along the plane. Hence, the pendulum's oscillation frequency is,*

$$\omega_0 = \sqrt{\frac{g_{eff}}{L}} = \sqrt{\frac{g\cos\alpha}{L}}\ .$$

4.1.10.17 Ex: Accelerated pendulum

a. A pendulum of length L and mass M is suspended from the roof of a wagon horizontally accelerated with the acceleration a_{ext}. Find the equilibrium position of the pendulum. Determine the oscillation frequency for small oscillations and derive the differential equation of motion for an observer sitting in the wagon. (Note that you cannot assume small displacements, if the acceleration a_{ext} is large.)
b. In the same wagon there is a mass m connected to the front wall by a spring k. Find the equilibrium position of the mass. Determine the oscillation frequency and

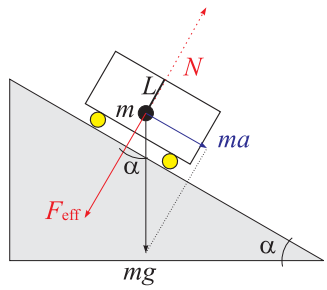

Figure 4.20: Accelerated pendulum.

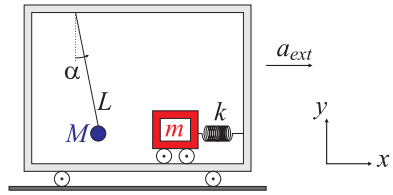

Figure 4.21: Accelerated pendulum.

derive the differential motion equation for an observer sitting in the wagon.

Solution: *a. Effective acceleration is,*

$$a_{ef} = \sqrt{g^2 + a^2} \ .$$

Hence the frequency for small amplitudes is,

$$\omega_0 = \sqrt{\frac{a_{ef}}{L}} = \sqrt{\frac{\sqrt{g^2 + a^2}}{L}} \ .$$

We derive the equation of motion in the sketched Cartesian system, where $x = L\sin\alpha$ *and* $y = -L\cos\alpha$*. Here, Newton's equation* $m\ddot{\vec{x}} = m\vec{g} + m\vec{a}$ *becomes,*

$$mL\begin{pmatrix}\ddot{\alpha}\cos\alpha - \dot{\alpha}^2\sin\alpha \\ \ddot{\alpha}\sin\alpha + \dot{\alpha}^2\cos\alpha\end{pmatrix} = m\begin{pmatrix}\ddot{x} \\ \ddot{y}\end{pmatrix} = mg\sin\alpha\begin{pmatrix}-\cos\alpha \\ -\sin\alpha\end{pmatrix} + \begin{pmatrix}ma \\ 0\end{pmatrix} \ .$$

Calculating $m\ddot{x}\cos\alpha + m\ddot{y}\sin\alpha$ *we find,*

$$\ddot{\alpha} = -\frac{g}{L}\sin\alpha + \frac{a}{L}\cos\alpha \ .$$

To find the oscillation frequency, we need to put this equation into a form $\ddot{\alpha} = -A\sin(\alpha - \phi) = A\cos\phi\sin\alpha - A\sin\phi\cos\alpha$*. By comparison,*

$$A\cos\phi = -\frac{g}{L} \quad , \quad A\sin\phi = -\frac{a}{L} \ ,$$

or

$$A = \sqrt{\frac{g^2 + a^2}{L^2}} \quad , \quad \tan\phi = \frac{a}{g} \ .$$

Hence,

$$\ddot{\alpha} = -\frac{\sqrt{g^2+a^2}}{L}\sin(\alpha - \arctan\tfrac{a}{g}) \simeq -\frac{\sqrt{g^2+a^2}}{L}(\alpha - \arctan\tfrac{a}{g}) \ ,$$

confirming the effective acceleration. Still, we transform to the variable $\tilde{\alpha} \equiv \alpha - \arctan\frac{a}{g}$,

$$\ddot{\tilde{\alpha}} = -\frac{\sqrt{g^2+a^2}}{L}\sin(\tilde{\alpha}) \ .$$

b. The equation $m\mathbf{x} = m\mathbf{g} + m\mathbf{a}$ *becomes,*

$$m\ddot{x} = -kx + ma \ .$$

Substituting $\tilde{x} = x - \frac{ma}{k}$,

$$m\ddot{x} = -k\left(\tilde{x} + \frac{ma}{k}\right) + ma = -k\tilde{x} = m\ddot{\tilde{x}} \ .$$

4.1.10.18 Ex: Oscillation of a rolling cylinder

Consider a cylinder secured by two springs that rotates without sliding, as shown in the figure. Calculate the frequency for small oscillations of the system.

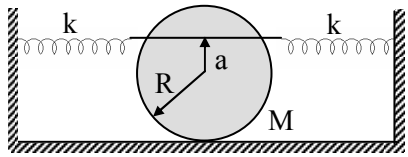

Figure 4.22: Rolling cylinder.

Solution: *The inertial moment is* $I = \frac{M}{2}R^2$. *The springs exert the forces,*

$$F_{mol} = -kx + k(L - x) \ .$$

Hence we have the equations of motion,

$$M\ddot{x} = F_{mol} - F_{at}$$
$$I\ddot{\theta} = I\frac{\ddot{x}}{R} = dF_{mol} - RF_{at} \ .$$

Using $x = R\omega$ *and eliminating the friction, we get,*

$$I\ddot{\theta} = I\frac{\ddot{x}}{R} = \frac{M}{2}R^2\frac{\ddot{x}}{R} = dF - RF_{at} = d[-kx + k(L-x)] - R[-kx + k(L-x) - M\ddot{x}] \ .$$

Solving by $\ddot{x}$,

$$\ddot{x} + \frac{2k}{M}\left(1 + \frac{d}{R}\right)(2x - L) = 0 \ .$$

The frequency is,

$$\omega_0 = \sqrt{\frac{4k}{M}\left(1 - \frac{d}{R}\right)} \ .$$

4.1.10.19 Ex: Rocking chair

Consider a thin rod of mass M and length $2L$ leaning on its center-of-mass, as shown in the figure. It is attached at both ends by springs of constants k. Calculate the angular frequency for small oscillations of the system.

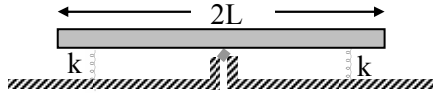

Figure 4.23: Rocking chair.

Solution: *The moment of inertia is $I = \frac{1}{3}ML^2$. The equation of motion is,*

$$I\vec{\alpha} = \vec{\tau} = \mathbf{L} \times \mathbf{F}_{ml} + (-\mathbf{L}) \times \mathbf{F}_{ml} = \mathbf{L} \times (-k\mathbf{x}) + (-\mathbf{L}) \times k\mathbf{x} \ .$$

Hence,

$$\frac{1}{3}MR^2\ddot{\theta} = -2Lkx = -2Lk\ell\theta$$
$$\ddot{\theta} + \frac{6k}{M}\theta = 0$$
$$\omega_0 = \sqrt{\frac{6k}{M}} \ .$$

4.1.10.20 Ex: Rotational oscillation of a disk

Consider a disk of mass M and radius R ($I = \frac{1}{2}MR^2$) that can rotate around the polar axis. A body of mass $m$hangs at an ideal rope that runs through the disk (without slipping) and is attached to a wall by a spring of constant k, as shown in the figure. Calculate the natural oscillation frequency of the system.

Solution: *The angular acceleration of the disc M the inertial moment of which is $I = \frac{M}{2}R^2$, is given by,*

$$\frac{M}{2}R^2\vec{\alpha} = I\vec{\alpha} = \vec{\tau}_m + \vec{\tau}_k = \mathbf{R} \times m\mathbf{g} - \mathbf{R} \times k\mathbf{x} = (Rmg - Rkx)\hat{\mathbf{e}}_\theta \ .$$

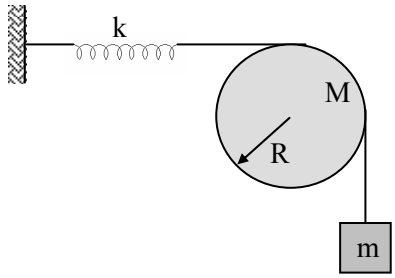

Figure 4.24: Rotational oscillation of a disk.

As the body does not slide, the angle of the disc is linked to the mass displacement, $x = R\theta$. *We get,*

$$\alpha = \ddot{\theta} = \frac{2mg - 2kx}{MR} = \frac{2mg}{MR} + \frac{2k}{M}\theta \ .$$

Substituting $\theta \equiv \tilde{\theta} - \frac{mg}{kR}$*:*

$$\ddot{\tilde{\theta}} = \frac{2mg}{MR} - \frac{2k}{M}\left(\tilde{\theta} - \frac{mg}{kR}\right) = -\frac{2k}{M}\tilde{\theta} \ .$$

That is, we have a harmonic oscillation around the angle $\theta_0 = \frac{mg}{kR}$ *with frequency* $\omega_0 = \sqrt{\frac{2k}{M}}$.

4.1.10.21 Ex: Oscillation of a half cylinder

Consider a massive, homogeneous half-cylinder of mass M and radius R resting on a horizontal surface. If one side of this solid is slightly pushed down and released, it will swing around its equilibrium position. Determine the period of this oscillation.

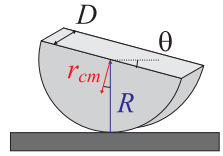

Figure 4.25: Oscillation of a half cylinder.

Solution: *The mass of the half cylinder is,*

$$M = \int dm = \rho_0 \int_0^D \int_0^\pi \int_0^R \rho_0 r dr d\theta dz = \rho_0 \pi D \tfrac{R^2}{2} \ .$$

The moment of inertia about the symmetry axis of the cylinder, if it were complete, would be,

$$I_0 = \int r^2 dm = \rho_0 \int_0^D \int_0^\pi \int_0^R r^2 \rho_0 r dr d\theta dz = \rho_0 \pi D \tfrac{R^4}{4} = MR^2/2 \ .$$

Following Steiner's theorem the moment of inertia with respect to support point of the half-cylinder is,

$$I = I_0 + MR^2 = \tfrac{3}{2}MR^2 \ .$$

We calculate the center-of-mass of a half cylinder lying on its flat side. The definition of the center-of-mass is,

$$\mathbf{r}_{cm} = \frac{1}{M}\int \mathbf{r} dm \ .$$

For symmetry reasons $x_{cm} = 0$. Also,

$$y_{cm} = \frac{\rho_0}{M}\int_0^D \int_0^R \int_{-\sqrt{R^2-y^2}}^{\sqrt{R^2-y^2}} y dx dy dz = \frac{\rho_0 D}{M}\int_0^R 2y\sqrt{R^2-y^2}dy = \frac{\rho_0 D}{M}\int_0^{R^2} \sqrt{R^2-u}du$$
$$= -\frac{2}{3}\frac{\rho_0 D}{M}(R^2-u)^{\frac{3}{2}}\Big|_0^{R^2} = \frac{2}{3}R^3\frac{\rho_0 D}{M} = \frac{4R}{3\pi} \ .$$

Let θ be the angle of oscillation. Seen from the support point the center-of-mass is at,

$$\mathbf{r} = \begin{pmatrix} 0 \\ R \\ 0 \end{pmatrix} - \begin{pmatrix} y_{cm}\sin\theta \\ y_{cm}\cos\theta \\ 0 \end{pmatrix} \ .$$

The equation of motion is,

$$m\ddot{x} = -F_{at}...$$
$$I\ddot{\theta} = \vec{\tau} = \mathbf{r}\times\vec{F} = \begin{pmatrix} -y_{cm}\sin\theta \\ R - y_{cm}\cos\theta \\ 0 \end{pmatrix} \times \begin{pmatrix} 0 \\ -gM \\ 0 \end{pmatrix} = -y_{cm}gM\hat{e}_z\sin\theta$$
$$\ddot{\theta} = -\frac{y_{cm}gM}{I}\sin\theta = -\frac{\frac{4R}{3\pi}gM}{\frac{3}{2}MR^2}\sin\theta = -\frac{8g}{9\pi R}\sin\theta \ .$$

Hence, the period of oscillation is,

$$T = \frac{2\pi}{\omega} = \frac{2\pi}{\sqrt{\frac{8g}{9\pi R}}} = \sqrt{\frac{9\pi^3}{2}}\sqrt{\frac{R}{g}} \approx 7.78\sqrt{R/g} \ .$$

4.1.10.22 Ex: Pendulum coupled to a spring

Consider a simple pendulum of mass m and length L, connected to a spring of constant k, as shown in the figure. Calculate the frequency of the system for small oscillation amplitudes.

Solution: *The inertial moment is $I = ML^2$. The equation of motion is,*

$$I\vec{\alpha} = \vec{\tau} = \vec{L}\times M\vec{g} + \vec{a}\times\vec{F}_{ml} \ .$$

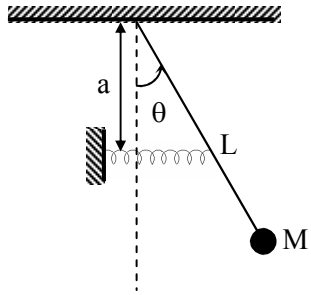

Figure 4.26: Pendulum coupled to a spring.

Hence,

$$ML^2\ddot{\theta} = -LMg\sin\theta - akx = -LMg\sin\theta - aka\theta$$
$$0 = \ddot{\theta} + \frac{g}{L}\sin\theta + \frac{ka^2}{ML^2}\theta \simeq \ddot{\theta} + \left(\frac{g}{L} + \frac{ka^2}{ML^2}\right)\theta$$
$$\omega_0 = \sqrt{\frac{g}{L} + \frac{ka^2}{ML^2}}\ .$$

4.1.10.23 Ex: Pendulum carousel

A mass m is hung by a rope of length l on a carousel with the radius R. The pendulum performs small amplitude oscillations in the direction of the rotation axis of the carousel. How does the period of oscillation depend on the rotation speed of the carousel?

Solution: *The retroactive force is,*

$$F_R = -mg\sin\phi + \frac{mv^2}{R'}\cos\phi\ .$$

We have $v(x) = (R+x)\omega = (R + l\sin\phi)\omega$ *and* $R' = R + x$. *Hece,*

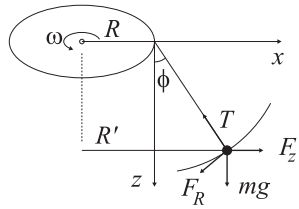

Figure 4.27: Pendulum carousel.

$$F_R = -mg\sin\phi + m\omega^2(R + l\sin\phi)\cos\phi\ .$$

The equation of motion, hence, is,

$$m\ddot{s} = -mg\sin\phi + m\omega^2(R + l\sin\phi)\cos\phi \ .$$

Since $s = l\phi$, $\ddot{s} = l\ddot{\phi}$, *follows* $l\ddot{\phi} = -g\sin\phi + \omega^2(R + l\sin\phi)\cos\phi$ *or,*

$$\ddot{\phi} + \frac{g}{l}\sin\phi - \omega^2\left(\frac{R}{l} + \sin\phi\right)\cos\phi = 0 \ .$$

For small displacements we have, $\cos\phi \approx 1$ *and* $\sin\phi \approx \phi$, *d.h.*

$$\ddot{\phi} + \left(\frac{g}{l} - \omega^2\right) - \omega^2\frac{R}{l} = 0 \ .$$

The solution of the homogeneous differential equation is,

$$\phi_h = \sin\sqrt{\frac{g}{l} - \omega^2}t$$

A particular solution of the inhomogeneous differential equation is,

$$\phi_i = \frac{\omega^2(R/l)}{g/l - \omega^2}$$

The total solution is $\phi = \phi_h + \phi_i$. *The oscillation period is,*

$$T = \frac{2\pi}{\sqrt{g/l - \omega^2}}$$

For large angular velocities, $\omega = \sqrt{g/l}$, *the period of oscillation tends to infinity because the centrifugal force dominates.*

4.2 Superposition of periodic movements

Several movements that we already know can be understood as superpositions of periodic movements in different directions and, possibly, with different phases. Example are the circular or elliptical motion of a planet around the sun or the Lissajous figures. In these cases, the motion must be described by vectors, $\mathbf{r}(t) \equiv (x(t), y(t))$. It is also possible to imagine superpositions of periodic movements in the same degree of freedom. The movement of the membrane of a loudspeaker or musical instruments usually vibrates harmonically, but follows a *superposition* of harmonic oscillations. According to the *superposition principle*, we will take the resultant of several harmonic vibrations as the sum of the individual vibrations.

4.2.1 Rotations and complex notation

We now consider a uniform circular motion. The radius of the circle being R, the motion is completely described by the angle $\theta(t)$ which grows uniformly,

$$\theta = \omega t + \alpha \ . \tag{4.51}$$

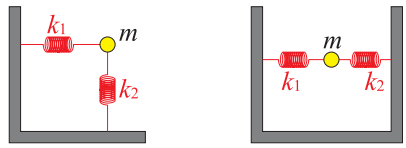

Figure 4.28: Superposition of vibrations in different (left) and equal (right) degrees of freedom.

The projections of the movement in x and y are,

$$x(t) = A\cos\theta \qquad \text{and} \qquad y(t) = A\sin\theta\ . \tag{4.52}$$

Thus, we can affirm $x(t) = y(t + \pi/2)$, that is, the projections have a mutual phase shift of $\pi/2$.

The circular motion can be represented in the complex plane using the imaginary unit $i \equiv \sqrt{-1}$ and Euler's relationship $e^{\imath\theta} = \cos\theta + \imath\sin\theta$, as illustrated in Fig. 4.29.[3,4] With $r = Ae^{\imath\theta}$ we obtain $x = A\mathfrak{Re}\ e^{\imath\theta}$ and $\imath y = A\mathfrak{Im}\ e^{\imath\theta}$ and $r = x + \imath y$.

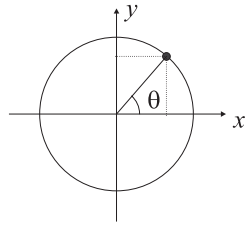

Figure 4.29: Circular motion in the complex plane.

We will use the complex notation extensively, as it greatly facilitates the calculation.

4.2.2 Lissajous figures

Other periodic movements in the two-dimensional plane are possible, when the movements in x and y have different phases or frequencies. These are called *Lissajous figures*.

We consider a body subject to two harmonic movements in orthogonal directions:

$$x(t) = A_x\cos(\omega_x t + \varphi_x) \qquad \text{and} \qquad y(t) = A_y\cos(\omega_y t + \varphi_y)\ . \tag{4.53}$$

When ω_x/ω_y is a rational number, the curve is closed and the motion repeats after equal time periods. The upper charts in Fig. 4.30 show trajectories of the body for $\omega_x/\omega_y = 1/2,\ 1/3$, and $2/3$, letting $A_x = A_y$ and $\varphi_x = \varphi_y$. The lower charts in Fig. 4.30 show trajectories for $\omega_x/\omega_y = 1/2,\ 1/3$, letting $\varphi_x - \varphi_y = 0,\ \pi/4$, and $\pi/2$.

Example 10 (*Lissajous figures*):

[3] The Euler relation can easily be derived by Taylor expansion.

[4] To check your notions on complex numbers do the exercises in Chp. 1 of the Book of A.P. French.

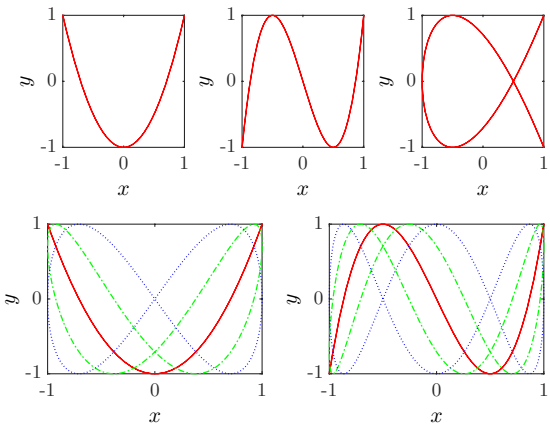

Figure 4.30: (code) Trajectories of a body oscillating with different frequencies in two dimensions.

- Connect two function generators to the two channels of an oscilloscope in x-y.
- MATLAB simulation.

.

4.2.3 Vibrations with equal frequencies superposed in one dimension

Vibratory movements can overlap. The result can be described as a sum,

$$\begin{aligned} x(t) &= x_1(t) + x_2(t) = A_1\cos(\omega t + \alpha_1) + A_2\cos(\omega t + \alpha_2) \\ &= \mathrm{Re}[A_1 e^{\imath(\omega t+\alpha_1)} + A_2 e^{\imath(\omega t+\alpha_2)}] = \mathrm{Re}e^{\imath\omega t}[A_1 e^{\imath\alpha_1} + A_2 e^{\imath\alpha_2}] \ . \end{aligned} \tag{4.54}$$

That is, the new motion is a cosine vibration, $x(t) = A\cos\omega t$, with the phase,

$$\tan\alpha = \frac{\mathrm{Im}\ x(0)}{\mathrm{Re}\ x(0)} = \frac{\mathrm{Im}(A_1 e^{\imath\alpha_1} + A_2 e^{\imath\alpha_2})}{\mathrm{Re}(A_1 e^{\imath\alpha_1} + A_2 e^{\imath\alpha_2})} = \frac{A_1\sin\alpha_1 + A_2\sin\alpha_2}{A_1\cos\alpha_1 + A_2\cos\alpha_2} \ , \tag{4.55}$$

and the amplitude,

$$A = |A_1 e^{\imath\alpha_1} + A_2 e^{\imath\alpha_2}| = \sqrt{A_1^2 + A_2^2 + 2A_1A_2\cos(\alpha_1 - \alpha_2)} \ . \tag{4.56}$$

We consider the case $A_1 = A_2$,

$$\tan\alpha = \frac{\sin\alpha_1 + \sin\alpha_2}{\cos\alpha_1 + \cos\alpha_2} \quad , \quad A = 2A\cos\frac{\alpha_1 - \alpha_2}{2} \ . \tag{4.57}$$

The cases $\alpha_1 = \alpha_2$ or $\alpha_2 = 0$ further simplify the result.

4.2.4 Frequency beat

Vibratory movements with different frequencies can overlap. The result can be described as a sum,

$$x(t) = x_1(t) + x_2(t) = A_1 \cos \omega_1 t + A_2 \cos \omega_2 t = \mathfrak{Re}\left[A_1 e^{\imath\omega_1 t} + A_2 e^{\imath\omega_2 t}\right] . \tag{4.58}$$

Considering the case $A_1 = A_2$ we obtain,

$$\begin{aligned} x(t) &= A\mathfrak{Re}\left[e^{\imath\omega_1 t} + e^{\imath\omega_2 t}\right] \\ &= A\mathfrak{Re}\left[e^{\imath(\omega_1+\omega_2)t/2} e^{\imath(\omega_1-\omega_2)t/2} + e^{\imath(\omega_1+\omega_2)t/2} e^{-\imath(\omega_1-\omega_2)t/2}\right] \\ &= A\mathfrak{Re}\; e^{\imath(\omega_1+\omega_2)t/2} 2\cos\frac{(\omega_1-\omega_2)t}{2} \\ &= 2A\cos\frac{(\omega_1+\omega_2)t}{2}\cos\frac{(\omega_1-\omega_2)t}{2} \; . \end{aligned} \tag{4.59}$$

Example 11 (*Amplitude modulation*): An important example is the amplitude modulation of radiofrequency signals.

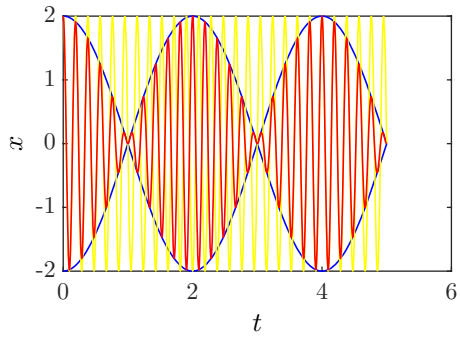

Figure 4.31: (code) Illustration of the beating of two frequencies $\nu_1 = 5.5\,\text{Hz}$ and $\nu_2 = 5\,\text{Hz}$ showing the perceived vibration (red), the vibration with the frequency $(\nu_1 + \nu_2)/2$ (blue), and the vibration with frequency $(\nu_1 - \nu_2)/2$ (yellow).

Example 12 (*Visualization of beat frequencies on an oscilloscope*):

- Connect two function generators to the two channels of an oscilloscope and add the channels.
- MATLAB simulation.
- Modulate one signal by another in a frequency mixer.

.

4.2.5 Amplitude and frequency modulation

Radio frequencies above 300 kHz can easily be emitted and received by antennas, while audio frequencies are below 20 kHz. However, radio frequencies can be used as carriers for audio frequencies. This can be done by modulating the audio signal

on the *amplitude* of the carrier () before sending the carrier frequency. The receiver retrieves the audio signal by demodulating the carrier. Therefore, audio signals can be transmitted by electromagnetic waves. Another technique consists in modulating the *frequency* of these waves (). We will now calculate the spectrum of these two modulations using complex notation and show how to demodulate the encoded audio signals by multiplication with a local oscillator corresponding to the carrier wave.

4.2.5.1 AM

Let ω and Ω be the frequencies of the carrier wave and the modulation, respectively. We can describe the amplitude modulation by,

$$U(t) = (1 + S(t)) \cos \omega t \ . \tag{4.60}$$

After the receiver has registered this signal, we demodulate it by multiplying it with $\cos \omega t$:

$$U(t) \cos \omega t = (1 + S(t)) \cos^2 \omega t = (1 + S(t)) \left(\tfrac{1}{2} + \tfrac{1}{2} \cos 2\omega t\right) \ . \tag{4.61}$$

We purify this signal passing it through a low-pass filter eliminating the rapid oscillations:

$$U(t) \cos \omega t \longrightarrow \tfrac{1}{2}(1 + S(t)) \ . \tag{4.62}$$

We retrieve the original signal $S(t)$.

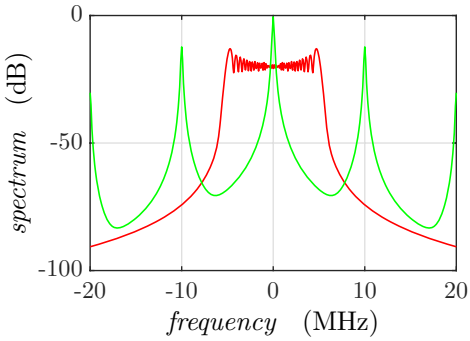

Figure 4.32: (code) Modulation signal.

4.2.5.2 FM

We can describe the frequency modulation by,

$$U(t) = e^{\imath(\omega t + N \sin \Omega t)} = e^{\imath \omega t} \sum_{k=-\infty}^{\infty} \mathcal{J}_k(N) e^{\imath k \Omega t} \ . \tag{4.63}$$

The modulation of the carrier wave generates sidebands. This can be seen by expanding the signal carrying the phase modulation into a Fourier series,

$$e^{\imath \omega t} \sum_{k=-\infty}^{\infty} \mathcal{J}_k(\beta) e^{\imath k \Omega t} \simeq e^{\imath \omega t} + \mathcal{J}_1(N) e^{\imath \omega t + \imath \Omega t} + \mathcal{J}_{-1}(N) e^{\imath \omega t - \imath \Omega t} \tag{4.64}$$

when the *modulation index* N is small. Here, $J_{-k}(N) = (-1)^k J_k(N)$ are the Bessel functions.

The spectrum of a signal with PM modulation consists of discrete lines, called sidebands, whose amplitudes are given by Bessel functions,

$$S(\omega) = \sum_{k=-\infty}^{\infty} |\mathcal{J}_k(N)|^2 \delta(\omega + k\Omega) \ . \tag{4.65}$$

In real systems, the frequency bands have finite widths β due to frequency noise or to the finite resolution of the detectors,

$$S(\omega) = \sum_{k=-\infty}^{\infty} |\mathcal{J}_k(N)|^2 \frac{N^2}{(\omega - k\Omega)^2 + N^2} \ . \tag{4.66}$$

Example 13 (*Frequency spectrum*):

- Modulate the frequency of a VCO.
- Show in the spectrum analyzer the transition to sidebands.

.

4.2.6 Exercises

4.2.6.1 Ex: Amplitude modulation

Consider a carrier wave of $\omega/2\pi = 1$ MHz frequency whose amplitude is modulated by an acoustic signal of $\Omega/2\pi = 1\,\text{kHz}$: $U(t) = A\cos\Omega t\cos\omega t$. To demodulate the signal, multiply the received wave $U(t)$ by the carrier radiofrequency. Interpret the result.

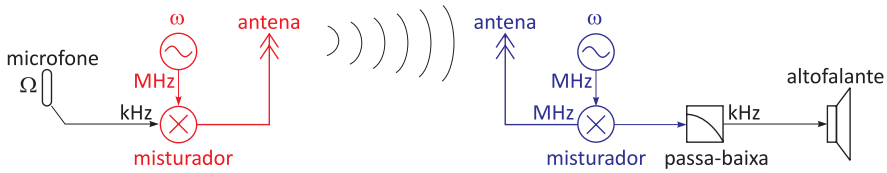

Figure 4.33: Illustration of radiofrequency signal transmission.

Solution: *The demodulated signal is,*

$$S(t)\cos\omega t = A\cos\omega t\cos\Omega t\cos\omega t = \tfrac{1}{4}A\cos[(2\omega - \Omega)t] + \tfrac{1}{4}A\cos[(2\omega + \Omega)t] + \tfrac{1}{2}A\cos\Omega t \ .$$

The first two terms oscillate with high frequency and can be eliminated by a low-pass filter. The third term oscillates precisely with the frequency of the wanted signal Ω.

4.3 Damped and forced vibrations

Frequently, vibrations are exposed to external perturbations. For example, damping forces due to friction exerted by the medium in which vibration takes place work to waste and dissipate the energy of the oscillation and, therefore, to reduce the amplitude of the oscillation. In contrast, periodic forces can pump energy into the oscillator system and excite vibrations.

4.3.1 Damped vibration and friction

Let us first deal with damping by forces named *Stokes friction*, that is, forces which are proportional to the velocity of the oscillating mass and contrary to the direction of motion, $F_{frc} = -bv$, where b is the friction coefficient. With this additional term, the equation of motion is,

$$ma = -bv - kx \ . \tag{4.67}$$

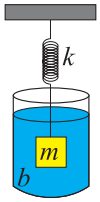

Figure 4.34: Oscillation damped by a viscous medium.

The calculation of the *damped oscillator* can be greatly simplified by the use of complex numbers by making the ansatz,

$$x(t) = Ae^{\lambda t} \ , \tag{4.68}$$

where λ is a complex number. We get,

$$m\lambda^2 + b\lambda + k = 0 \ , \tag{4.69}$$

giving the characteristic equation,

$$\lambda = -\gamma \pm \sqrt{\gamma^2 - \omega_0^2} \ , \tag{4.70}$$

with

$$\omega_0 = \sqrt{\frac{k}{m}} \qquad \text{and} \qquad \gamma = \frac{b}{2m} \ . \tag{4.71}$$

The friction determines the damping behavior. We distinguish three cases discussed in the following sections.

4.3.1.1 Overdamped case

In the overdamped case, for $\omega_0 < \gamma$, there are two real solutions $\lambda = -\gamma \pm \kappa$ with $\kappa \equiv \sqrt{\gamma^2 - \omega_0^2}$ for the characteristic equation, giving,

$$x(t) = e^{-\gamma t}(Ae^{-\kappa t} + Be^{\kappa t}) \ . \tag{4.72}$$

Choosing the initial conditions,

$$\begin{aligned} x_0 = x(0) &= e^{-\gamma t}(Ae^{-\kappa t} + Be^{\kappa t}) = A + B \\ 0 = v(0) &= -A(\gamma+\kappa)e^{-(\gamma+\kappa)t} - B(\gamma-\kappa)e^{-(\gamma-\kappa)t} = -A(\gamma+\kappa) - B(\gamma-\kappa) \ , \end{aligned} \tag{4.73}$$

we determine the amplitudes,

$$A = \frac{x_0}{2}\left(1 - \frac{\gamma}{\kappa}\right) \qquad \text{and} \qquad B = \frac{x_0}{2}\left(1 + \frac{\gamma}{\kappa}\right) \ . \tag{4.74}$$

Finally, the solution is [5],

$$x(t) = x_0 e^{-\gamma t}\left[\cosh \kappa t + \frac{\gamma}{\kappa}\sinh \kappa t\right] \ . \tag{4.75}$$

4.3.1.2 Underdamped case

In the underdamped case, for $\omega_0 > \gamma$, we have two complex solutions $\lambda = -\gamma \pm \imath\omega$ with $\omega \equiv \sqrt{\omega_0^2 - \gamma^2}$, giving,

$$x(t) = e^{-\gamma t}(Ae^{\imath\omega t} + Be^{-\imath\omega t}) \ . \tag{4.76}$$

Choosing the initial conditions,

$$\begin{aligned} x_0 = x(0) &= e^{-\gamma t}(Ae^{\imath\omega t} + Be^{-\imath\omega t}) = A + B \\ 0 = v(0) &= -A(\gamma-\imath\omega)e^{-(\gamma-\imath\omega)t} - B(\gamma+\imath\omega)e^{-(\gamma+\imath\omega)t} = -A(\gamma-\imath\omega) - B(\gamma+\imath\omega) \ , \end{aligned} \tag{4.77}$$

we determine the amplitudes,

$$A = \frac{x_0}{2}\left(1 + \frac{\gamma}{\imath\omega}\right) \qquad \text{and} \qquad B = \frac{x_0}{2}\left(1 - \frac{\gamma}{\imath\omega}\right) \ . \tag{4.78}$$

Finally, the solution is [6],

$$x(t) = x_0 e^{-\gamma t}\left[\cos \omega t + \frac{\gamma}{\omega}\sin \omega t\right] \ . \tag{4.79}$$

[5] Note that for super-strong damping, we have $\kappa \simeq \gamma$ and therefore,

$$x(t) = Ae^{-2\gamma t} + B \ .$$

, This is nothing more than the solution of the equation of motion without restoring force, $ma = -bv$.

[6] Note that, for very weak damping, we have $\gamma \simeq 0$ and $\omega \simeq \omega_0$ and hence,

$$x(t) = Ae^{\imath\omega_0 t} + Be^{-\imath\omega_0 t} \ .$$

This is nothing more than the solution of the frictionless equation of motion, $ma = -kx$.

4.3.1.3 Critically damped case

In the critically damped case, for $\omega_0 = \gamma$, there is only one solution $\lambda = -\gamma$, giving

$$x(t) = Ae^{-\gamma t} \ . \tag{4.80}$$

Since one solution is not sufficient to solve a second order differential equation, we need to look for another linearly independent solution. We can try another ansatz,

$$x(t) = Bte^{\lambda t} \ , \tag{4.81}$$

resulting in the characteristic equation,

$$m(\lambda^2 te^{\lambda t} + 2\lambda e^{\lambda t}) + b(\lambda te^{\lambda t} + e^{\lambda t}) + kte^{\lambda t} = 0 \ . \tag{4.82}$$

The terms in $e^{\lambda t}$ and $te^{\lambda t}$ should disappear separately, giving,

$$2m\lambda + b = 0 \quad \text{and} \quad m\lambda^2 t + b\lambda t + kt = 0 \quad \Longrightarrow \quad \lambda = -\frac{b}{2m} = -\gamma = -\omega_0 \ . \tag{4.83}$$

Finally, the solution is,

$$x(t) = (A + Bt)e^{-\gamma t} \ . \tag{4.84}$$

Choosing the initial conditions,

$$\begin{aligned} x_0 = x(0) &= (A + Bt)e^{-\gamma t} = A \\ 0 = v(0) &= (-\gamma A - \gamma Bt + B)e^{-\gamma t} = -\gamma A + B \ , \end{aligned} \tag{4.85}$$

we determine the amplitudes,

$$A = x_0 \qquad \text{and} \qquad B = \gamma x_0 \ . \tag{4.86}$$

Finally, the solution is,

$$x(t) = x_0(1 + \gamma t)e^{-\gamma t} \ . \tag{4.87}$$

Fig. 4.35 illustrates the damping of the oscillation for various friction rates γ.

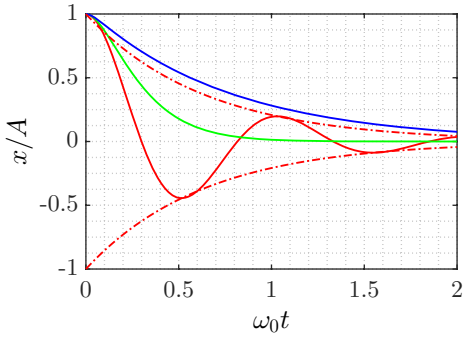

Figure 4.35: (code) Damped oscillation for $\omega_0 = 10\,\mathrm{s}^{-1}$ and $\gamma = 2.5\,\mathrm{s}^{-1}$ (red), $10\,\mathrm{s}^{-1}$ (green), and $25\,\mathrm{s}^{-1}$ (blue).

The critical friction coefficient generates a damped movement without any 'overshoot', since the velocity $\dot{x}(t)$ only disappears for $t = 0$.

4.3.1.4 Quality factor and energy loss

For a harmonic oscillation we establish the balance of energies,

$$\begin{aligned} E &= \frac{m}{2}v^2 + \frac{k}{2}x^2 \\ &= \frac{m}{2}\left(A\imath\omega_0 e^{\imath\omega_0 t} - B\imath\omega_0 e^{-\imath\omega_0 t}\right)^2 + \frac{m}{2}\omega_0^2\left(Ae^{\imath\omega_0 t} + Be^{-\imath\omega_0 t}\right)^2 = 2m\omega_0^2 AB \ . \end{aligned} \tag{4.88}$$

Now, for an underdamped oscillation we replace the amplitudes by $A \to Ae^{-\gamma t}$ and $B \to Be^{-\gamma t}$, such that,

$$E(t) = 2m\omega_0^2 ABe^{-2\gamma t} \ . \tag{4.89}$$

Obviously, the energy is decreasing at the rate 2γ.

We define the *quality factor* as the number of radians that the damped system oscillates before its energy falls to e^{-1},

$$Q = \frac{\omega}{2\gamma} = \frac{\omega m}{b} \simeq \frac{\omega_0 m}{b} \ . \tag{4.90}$$

Comparing the initial energy with the energy remaining after one cycle,

$$\frac{E}{\Delta E} = \frac{E(0)}{E(0) - E(2\pi/\omega)} = \frac{1}{1 - e^{-4\pi\gamma/\omega}} \simeq \frac{\omega}{4\pi\gamma} \ , \tag{4.91}$$

we find that the quantity,

$$\frac{Q}{2\pi} = \frac{E}{\Delta E} \tag{4.92}$$

represents a measure for the energy dissipation.

4.3.2 Forced vibration and resonance

We have seen that a damped oscillator loses its energy over time. To sustain the oscillation, it is necessary to provide energy. The simplest way to do this, is to force the oscillator to oscillate at a frequency ω by applying an external force $F_0 \cos\omega t$. The question now is, what will be the amplitude of the oscillation and its phase with respect to the phase of the applied force. We begin by establishing the equation of motion,

$$ma + bv + m\omega_0^2 x = F_0 \cos\omega t \ . \tag{4.93}$$

The calculation can be greatly simplified by the use of complex numbers. We write the differential equation as,

$$ma + bv + m\omega_0^2 x = F_0 e^{\imath\omega t} \ , \tag{4.94}$$

making the ansatz $x(t) = Ae^{\imath\omega t - \imath\delta}$, yielding

$$-\omega^2 Ae^{\imath\omega t - \imath\delta} m + \imath\omega b Ae^{\imath\omega t - \imath\delta} + m\omega_0^2 Ae^{\imath\omega t - \imath\delta} = F_0 e^{\imath\omega t} \ . \tag{4.95}$$

We rewrite this formula,

$$e^{\imath\delta} = A\frac{m(\omega_0^2 - \omega^2) + \imath b\omega}{F_0} \ . \tag{4.96}$$

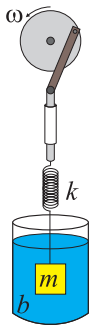

Figure 4.36: Forced oscillation damped by a viscous medium.

Immediately we get the solutions,

$$\tan\delta = \frac{\sin\delta}{\cos\delta} = \frac{\mathfrak{Im}\; e^{\imath\delta}}{\mathrm{Re}e^{\imath\delta}} = \frac{b\omega}{m(\omega_0^2-\omega^2)} \tag{4.97}$$
$$A = \left|Ae^{-\imath\delta}\right| = \left|\frac{F_0}{m(\omega_0^2-\omega^2)+\imath\omega b}\right| = \frac{F_0}{\sqrt{m^2(\omega_0^2-\omega^2)^2+b^2\omega^2}} \ .$$

The frequency response (spectrum) of the oscillator to the periodic excitation is illustrated in Fig. 4.37. We see that, when we increase the friction, we decrease the height and increase the width of the spectrum $|A(\omega)|$. Fig. 4.37(b) shows that, increasing the excitation frequency, the oscillation undergoes a phase shift of π.

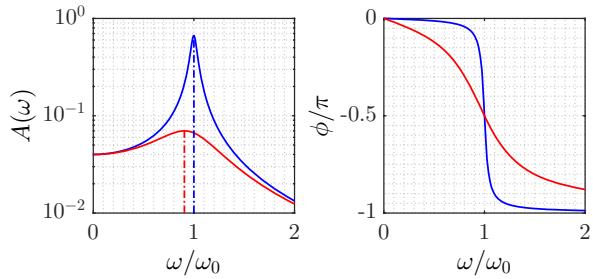

Figure 4.37: (code) Frequency response of the amplitude and phase of the oscillator for a force of $F_0 = 1\,\mathrm{N}$, a mass of $m = 1\,\mathrm{kg}$, a resonance frequency of $\omega_0 = (2\pi)\ 5\,\mathrm{Hz}$, and a friction coefficient of $b = 0.5$ (blue) or $b = 1$ (red).

We now ask, at what excitation frequency ω the oscillator responds with maximum amplitude,

$$0 = \frac{d}{d\omega_m}A(\omega_m) = F_0\omega_m\frac{2m^2\omega_0^2 - 2m^2\omega_m^2 - b^2}{(m^2\omega_0^4 - 2m^2\omega_0^2\omega_m^2 + m^2\omega_m^4 + b^2\omega_m^2)^{\frac{3}{2}}} \ . \tag{4.98}$$

The numerator disappears for,

$$\omega_m = \sqrt{\omega_0^2 - \frac{b^2}{2m^2}} \ , \tag{4.99}$$

and the amplitude becomes,

$$A_m = \frac{F_0}{b\sqrt{\omega_0^2 - \frac{b^2}{4m^2}}} \ . \tag{4.100}$$

4.3.2.1 Quality factor

For weak damping $\gamma \ll \omega_0$ and small detunings, $|\omega - \omega_0| \ll \omega_0$, we can approximate the expression for the spectrum by,

$$A(\omega) \simeq \left| \frac{F_0}{m} \frac{1}{2\omega_0(\omega_0 - \omega) + \imath\omega_0 \frac{b}{m}} \right| = \left| \frac{F_0}{2m\omega_0} \frac{1}{\omega - \omega_0 - \imath\gamma} \right| \ .$$

This function corresponds to a Lorentzian profile with the width FWHM $\Delta\omega = 2\gamma$. The *quality factor* defined in the section discussing the damped oscillator measures the quality of the resonance,

$$Q = \frac{\omega}{2\gamma} = \frac{\omega}{\Delta\omega} \ . \tag{4.101}$$

Example 14 (*Harmonic vibration*):

- Construct a L-C-circuit, excite it by a function generator by making a frequency ramp, and show the resonance on the oscilloscope. It works with a coil of $N = 12$ turns, of length $\ell = 6\,\text{cm}$ and of radius $r = 1.4\,\text{cm}$, giving $L = 1.4\,\mu\text{H}$. We can also set $R = 2.2\,\Omega$ and $C = 100\,\text{nF}$, giving $\omega_0 = 9.4\,\text{MHz}$.

4.3.3 Exercises

4.3.3.1 Ex: Resolution of the damped oscillator equation

Solve the damped oscillator equation for $4km > b^2$ using the ansatz $x(t) = Ae^{-\gamma t}\cos\omega t$.

Solution: *To determine the frequency of the damped oscillation described by this equation, we choose the function,*

$$x(t) = Ae^{-\gamma t}\cos\omega t$$

with the derivatives:

$$v(t) = -\gamma Ae^{-\gamma t}\cos\omega t - \omega Ae^{-\gamma t}\sin\omega t$$
$$a(t) = (\gamma^2 - \omega^2)Ae^{-\gamma t}\cos\omega t + 2\gamma\omega Ae^{-\gamma t}\sin\omega t \ .$$

Entering the differential equation and collecting the cos and sin terms separately:

$$(\gamma^2 - \omega^2) - \gamma\frac{b}{m} + \frac{k}{m} = 0 \qquad \text{and} \qquad 2\gamma\omega - \omega\frac{b}{m} = 0$$
$$\gamma = \frac{b}{2m} \qquad \text{and} \qquad \omega = \sqrt{\gamma^2 - \gamma\frac{b}{m} + \frac{k}{m}} = \sqrt{\omega_0^2 - \frac{b^2}{4m^2}}$$

com $\omega_0 \equiv \sqrt{k/m}$.

4.3.3.2 Ex: Damped oscillation

In a damped oscillation the oscillation period is $T = 1\,\mathrm{s}$. The ratio between two consecutive amplitudes is 2. Despite the large damping, the deviation of the period T_0 compared to the undamped oscillation is small. Calculate the deviation.

Solution: *The oscillation is described by,*

$$x(t) = Ae^{-\gamma t}\cos\omega t \ ,$$

with $\omega = 2\pi/T$. Hence, the condition $x(0) = 2x(T)$ gives,

$$A = 2Ae^{-\gamma T} \qquad or \qquad \gamma = \frac{\ln 2}{T} = 0.6931\,\mathrm{s}^{-1} \ .$$

This gives the frequency of the undamped oscillation,

$$\omega_0 = \sqrt{\omega^2 - \gamma^2} = (2\pi)\ 0.9939\,\mathrm{s}^{-1} \ ,$$

and the deviation,

$$\Delta T = T - T_0 = 2\pi\left(\frac{1}{\omega} - \frac{1}{\omega_0}\right) = 0.0061\,\mathrm{s} \ .$$

4.3.3.3 Ex: Damped physical pendulum

The physical pendulum shown in the figure consists of a disk of mass M and radius R suspended on an axes parallel to the symmetry axis of the disk and passing the edge of the disk.
a. Calculate the inertial momentum of the disk, $I = \int_V r^2 dm$, with respect to the suspension axes.
b. Derive the equation of motion by considering a weak Stokes damping due to friction proportional to the angular velocity and by approximating for small amplitude oscillations.
c. What is the natural oscillation frequency of the pendulum (without friction)? How to calculate the oscillation frequency considering friction?
d. Write down the solution of the equation of motion for the initial situation $\phi(0) = 0$ and $\dot{\phi}(0) = \dot{\phi}_0$.

Solution: *a. The mass of the cylinder is,*

$$M = \int_V \rho_0 dm = \rho_0 \int_0^L \int_0^{2\pi} \int_0^R r dr d\phi dz = \rho_0 \pi R^2 L \ .$$

The moment of inertia for a rotation around the center-of-mass is,

$$I_{cm} = \int_V \rho_0 r^2 dm = \rho_0 \int_0^L \int_0^{2\pi} \int_0^R r^2 r dr d\phi dz = \rho_0 \pi L \frac{R^4}{2} = \frac{M}{2} R^2 \ .$$

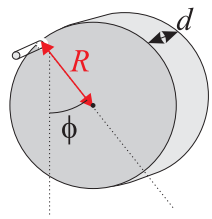

Figure 4.38: Damped physical pendulum.

The moment of inertia for a rotation about the distant axis is,

$$I = I_{cm} + MR^2 = \frac{3M}{2}R^2 \ .$$

b. The equation of motion is,

$$I\alpha = |\vec{R} \times \vec{\tau}| = -MgR\sin\theta - b\dot{\theta} \ ,$$

or, considering small amplitude oscillations,

$$\ddot{\theta} + \frac{2b}{3MR^2}\dot{\theta} + \frac{2g}{3R}\theta = 0 \ .$$

c. The frequency without friction is,

$$\omega_0 = \sqrt{\frac{2g}{3R}} \ ,$$

the damping coefficient is,

$$\gamma = \frac{b}{3MR^2} \ ,$$

and the frequency with friction is,

$$\omega = \sqrt{\omega_0^2 - \gamma^2} = \sqrt{\omega_0^2 - \frac{b^2}{9M^2R^4}} \ .$$

d. Making the ansatz $\phi(t) = e^{-\gamma t}(Ae^{\imath\omega t} + Be^{-\imath\omega t})$, we obtain,

$$\begin{aligned} \phi(0) &= 0 = A + B \\ \dot{\phi}(0) &= \dot{\phi}_0 = (\imath\omega - \gamma)A + (-\imath\omega - \gamma)B \ . \end{aligned}$$

Hence,

$$A = -B = \frac{\dot{\phi}_0}{2\imath\omega} \ ,$$

and finally,

$$\phi(t) = e^{-\gamma t}\left(\frac{\dot{\phi}_0}{2\imath\omega}e^{\imath\omega t} - \frac{\dot{\phi}_0}{2\imath\omega}e^{-\imath\omega t}\right) = \frac{\dot{\phi}_0}{\omega}e^{-\gamma t}\sin\omega t \ .$$

4.3.3.4 Ex: Pendulum with friction

Jane has prepared dinner and Tarzan (80 kg) and Cheeta (40 kg) must return home. The house is in a tree at a height of 10 m, so that both must swing home on a (massless) rope hanging from $l = 100\,\mathrm{m}$ high tree. Tarzan grabs the rope at the height of its center-of-mass $h = 1.2\,\mathrm{m}$ above ground, Cheeta because of its height is smaller at 0.8 m above ground. With what initial speed both need to grab the rope to reach the platform of the house with their feet. Consider Stokes' friction force, $F_R = C \cdot v$ with $C = 4{\cdot}10^{-4}\,\mathrm{Ns/m}$ (Tarzan) respectively, $C = 2{\cdot}10^{-4}\,\mathrm{Ns/m}$ (Cheeta). Why is this force different for the two? Treat the oscillating motion as small displacement. Determine whether the vibration is weakly damped. Do you think Jane will have dinner alone?

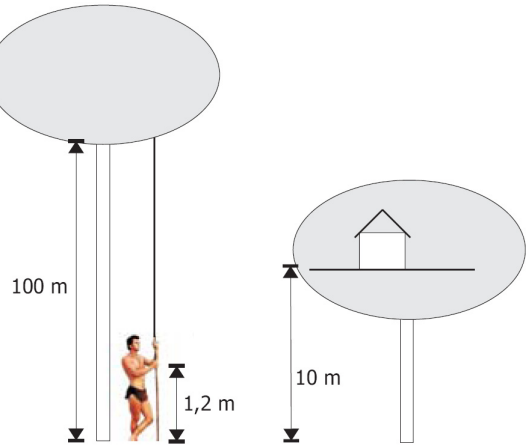

Figure 4.39: Pendulum with friction.

Solution: *The effective length of the rope is* $l = 100\,\mathrm{m} - h$. *Hence,*

$$x = l\phi \qquad \Rightarrow \qquad \dot{x} = l\dot{\phi} \qquad \text{and} \qquad \ddot{x} = l\ddot{\phi}\ .$$

Maximum displacement required for feet to reach the house floor,

$$x_{goal} = \sqrt{(100\,\mathrm{m})^2 - (95\,\mathrm{m})^2} = 31.2\,\mathrm{m}$$
$$\Rightarrow \phi_{goal} = \arctan(31.2\ \mathrm{m}/100\,\mathrm{m}) \simeq 0.3061\ .$$

Since $\sin(0.3061) \simeq 0.3014$, *the assumption of weak damping is justified,*

$$\ddot{\phi} + \frac{C}{m}\dot{\phi} + \frac{g}{l}\sin\phi = 0\ .$$

With the ansatz $\phi(t) = E^{\lambda t}$ *we get the equation,*

$$\lambda = -\frac{C}{2m} \pm \sqrt{\left(\frac{C}{2m}\right)^2 - \frac{g}{l}}\ .$$

Testing the damping force, e.g.,

$$\delta^2 \equiv \frac{C^2}{4m^2} = \frac{4 \cdot 10^{-4}\,\mathrm{Ns/m}}{4 \cdot 80\,\mathrm{kg}} \simeq 3 \cdot 10^{-8}\ \frac{1}{s^2} \ll \frac{g}{l} \simeq 0.1\ \frac{1}{\mathrm{s}^2}$$
$$\lambda_{1,2} = -\delta \pm \imath\sqrt{\frac{g}{l} - \delta^2} = -\delta \pm \imath\omega_1$$

with $\omega_1 = \sqrt{\omega_0^2 - \delta^2}$ *and* $\omega_0 = \sqrt{g}l$. *The general solution for the displacement* $x(t)$ *with the amplitude* A *is,*

$$x(t) = A \cdot e^{-\delta t} \cdot \cos(\omega_1 t + \phi_0)\ .$$

With the boundary condition $x(t=0) = 0$ *we obtain* $\Phi_0 = -\pi/2$ *and,*

$$x(t) = A \cdot e^{-\delta t} \cdot \sin(\omega_1 t)\ .$$

Reaching the required height is conditioned to $x(t = \frac{2\pi}{\omega_1}) = x_{goal}$, *Hence,*

$$A = x_{goal} \cdot e^{2\pi\delta/\omega_1}\ .$$

The required initial speed follows with

$$\dot{x}(t) = -\delta A e^{-\delta t}\sin(\omega_1 t) + \omega_1 A e^{-\delta t}\cos(\omega_1 t)\ ,$$

yielding,

$$\dot{x}(t=0) = \omega_1 A = \omega_1 \cdot x_{goal} \cdot e^{2\pi\frac{\delta}{\omega_1}}\ .$$

Substitution of numerical values for Tarzan and Cheeta gives the following values,

$$\dot{x}_{Tarzan}(t=0) \simeq 9.84\,\mathrm{m/s} \simeq 35.4\,\mathrm{km/h} \qquad \textit{and} \qquad \dot{x}_{Cheeta}(t=0) \simeq 9.81\,\mathrm{m/s} \simeq 35.3\,\mathrm{km/h}\ .$$

Jane should have dinner alone, if they can't reach the speed of athletes like Michael Johnson: 10.35 m/s.

4.3.3.5 Ex: Resolution of the forced oscillator equation

Solve the forced oscillator equation using the ansatz $x(t) = A\cos(\omega t - \delta)$.

Solution: *Inserting the ansatz* $x(t) = A\cos(\omega t - \delta)$ *into the differential equation we get,*

$$-\omega^2 mA\cos(\omega t - \delta) - \omega bA\sin(\omega t - \delta) + m\omega_0^2 A\cos(\omega t - \delta) = F_0\cos\omega t\ .$$

Using the trigonometric rules,

$$\cos(\omega t - \delta) = \cos\omega t\cos\delta + \sin\omega t\sin\delta$$
$$\sin(\omega t - \delta) = \sin\omega t\cos\delta - \cos\omega t\sin\delta$$

we obtain,

$$-\omega^2 mA\left[\cos\omega t\cos\delta+\sin\omega t\sin\delta\right]-\omega bA\left[\sin\omega t\cos\delta-\cos\omega t\sin\delta\right]$$
$$+m\omega_0^2 A\left[\cos\omega t\cos\delta+\sin\omega t\sin\delta\right]=F_0\cos\omega t\ .$$

This equation must be valid for $t=\omega\pi/2$ and for $t=0$. That is, we get two equations,

$$-\omega bA\cos\delta+m\left(\omega_0^2-\omega^2\right)A\sin\delta=0$$
$$\omega bA\sin\delta+m\left(\omega_0^2-\omega^2\right)A\cos\delta=F_0$$

or

$$\tan\delta=\frac{b\omega}{m(\omega_0^2-\omega^2)}$$
$$A=\frac{F_0}{\omega b\sin\delta+m(\omega_0^2-\omega^2)\cos\delta}\ .$$

To solve the second equation we derive the following trigonometric rules

$$\tan\delta=\frac{\sin\delta}{\cos\delta}=\frac{\sin\delta}{\sqrt{1-\sin^2\delta}}=\frac{1}{\sqrt{\frac{1}{\sin^2\delta}-1}}\qquad\Longrightarrow\qquad\sin\delta=\sqrt{\frac{1}{1+\frac{1}{\tan^2\delta}}}$$
$$\tan\delta=\frac{\sin\delta}{\cos\delta}=\frac{\sqrt{1-\cos^2\delta}}{\cos\delta}=\sqrt{\frac{1}{\cos^2\delta}-1}\qquad\Longrightarrow\qquad\cos\delta=\frac{1}{\sqrt{1+\tan^2\delta}}\ .$$

With this we can calculate:

$$A=\frac{F_0}{\omega b\sqrt{\frac{1}{1+\frac{1}{\tan^2 x}}}+m(\omega_0^2-\omega^2)\frac{1}{\sqrt{1+\tan^2\delta}}}$$
$$=\frac{F_0}{\omega b\sqrt{\frac{1}{1+\frac{1}{\left(\frac{b\omega}{m(\omega_0^2-\omega^2)}\right)^2}}}+m(\omega_0^2-\omega^2)\frac{1}{\sqrt{1+\left(\frac{b\omega}{m(\omega_0^2-\omega^2)}\right)^2}}}=\frac{F_0}{\sqrt{m^2(\omega_0^2-\omega^2)^2+b^2\omega^2}}\ .$$

4.3.3.6 Ex: Oscillation with coercive force

On a body of mass m along the x-axis act a force proportional to the displacement $F_h=-\kappa x$ and a Stokes friction force $F_R=-\gamma\dot{x}$. A time-dependent force is switched on at time $t=0$, while the body rests at the position $x=0$. The force increases linearly over time until it suddenly disappears at time $t=T$. Determine the work that the external force has done up this time. Consider the various solutions of the equation of motion resulting from the various combinations of κ and γ.

Solution: *The particular solution can be found by the ansatz $x_p(t)=be^{-t/\tau}$ with $b=\beta\tau^2/(m-\gamma\tau+\kappa\tau^2)$. Depending on whether $\gamma^2-4\kappa m>,=,<0$ we have for a. $\gamma^2-4\kappa m\equiv\Gamma^2>0$*

$$x(t)=e^{-\frac{\gamma t}{2m}}\left(Ae^{-\frac{\Gamma t}{2m}}+Be^{\frac{\Gamma t}{2m}}\right)+\frac{\beta\tau^2 m\ e^{-\frac{t}{\tau}}}{(m-\frac{\gamma\tau}{2})^2-\frac{\Gamma^2\tau^2}{4}}\ ;$$

for b. $\gamma^2 - 4\kappa m = 0$

$$x(t) = e^{-\frac{\gamma t}{2m}}(A + Bt) + \frac{\beta\tau^2 m\, e^{-\frac{t}{\tau}}}{(m - \frac{\gamma\tau}{2})^2} \; ;$$

for c. $\kappa m - \gamma^2 \equiv \Omega^2 > 0$

$$x(t) = e^{-\frac{\gamma t}{2m}}\left(A\cos\frac{\Omega t}{2m} + B\sin\frac{\Omega t}{2m}\right) + \frac{\beta\tau^2 m\, e^{-\frac{t}{\tau}}}{(m - \frac{\gamma\tau}{2})^2 + \frac{\Omega^2\tau^2}{4}} \; .$$

Through the boundary conditions $x(0) = 0$, $\dot{x}(0) = 0$ *we can determine* A, B. *Furthermore, we immediately see that* $x(\infty) = 0$, $\dot{x}(\infty) = 0$ *for all of the above mentioned solutions. Since the work of the two non-conservative forces equals the difference between the kinetic energy and the work for conservative forces, that is,* $A = 0$, *the entire work of* $F(t)$ *has been dissipated by* F_R.

4.3.3.7 Ex: Oscillation with coercive force

You want to measure the friction coefficient γ of a sphere (mass $m = 10\,\text{kg}$, diameter $d = 10\,\text{cm}$) in water. To do this, you let the sphere oscillate on a spring (spring constant $k = 100\,\text{N/m}$) in a water bath exciting the oscillation by a periodic force, $F(t) = F_0\cos\omega t$. By varying the excitation frequency ω until observing the maximum oscillation amplitude, you measure the resonance frequency $\omega_w = 2\pi\cdot 1\,\text{Hz}$. Now, you let the water out of the tub and repeat the measurement finding $\omega_0 = 2\pi\cdot 2\,\text{Hz}$.
a. Determine the resting position of the mass in water and air.
b. Establish the differential equation of motion. Assume that the weight of the sphere in water is reduced by the buoyancy $V\rho_{wat}g$, where V is the volume of the sphere and ρ_{wat} the density of the water.
c. What is the value of γ?

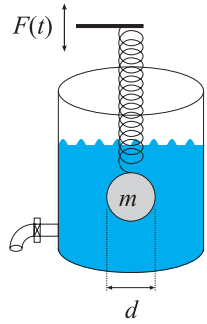

Figure 4.40: Driven pendulum.

Solution: *a. The differential equation is,*

$$m\ddot{x} + \gamma\dot{x} + Dx = mg - V\rho_{was}g + F_0\cos\omega t \; .$$

b. The resting position of the mass in air is $x_l = \frac{mg}{D} \simeq 0.98\,\mathrm{m}$ *and in water* $x_w = z + \frac{m - V\rho_{was}}{D} g \simeq 0.57\,\mathrm{m}$. *This ansatz leads to the known differential equation,*

$$m\ddot{z} + \gamma\dot{z} + Dz = F_0 \cos\omega t \ .$$

c. The resonance frequencies with and without friction are related by,

$$\omega_w = \sqrt{\omega_0^2 - \frac{\gamma^2}{2m^2}} \ .$$

Hence, $\gamma = m\sqrt{2\omega_0^2 - 2\omega_w^2} \simeq 154\,\mathrm{kg/s}$.

4.3.3.8 Ex: Electronic oscillator circuit

The instantaneous current $I(t)$ in an L-R-C-circuit (inductance of a coil, ohmic resistance and capacitance in series) excited by an alternating voltage source $U(t) = U_0 \cos\omega t$ satisfies the following differential equation,

$$L\dot{I} + RI + C^{-1}\int_0^t I dt' = U_0 \sin\omega t \ .$$

a. Derive the equation for the moving charge $\dot{Q} = I$, compare the obtained equation with that of the damped and forced spring-mass oscillator and determine the solution for the current.
b. Determine the resonance frequency ω_0 of the circuit.
c. Determine the quality factor Q of the circuit. How you can increase Q without changing the resonance frequency?

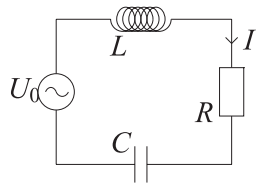

Figure 4.41: Line filter.

Solution: *a. The equation of motion of the damped and forced spring mass system is,*

$$ma + bv + kx = F_0 \cos\omega t \ .$$

The solutions are,

$$\tan\delta = \frac{\sin\delta}{\cos\delta} = \frac{Im\ e^{\imath\delta}}{Re\ e^{\imath\delta}} = \frac{R\omega}{L(\omega_0^2 - \omega^2)}$$
$$A = \left|Ae^{-\imath\delta}\right| = \left|\frac{U_0\omega}{L(\omega_0^2 - \omega^2) + \imath\omega R}\right| = \frac{U_0\omega}{\sqrt{L^2(\omega_0^2 - \omega^2)^2 + R^2\omega^2}} \ .$$

b. The natural frequency is,

$$\omega_0 = \frac{1}{\sqrt{LC}} \ .$$

c. Quality factor can be increased by decreasing strength R,

$$Q = \frac{1}{R}\sqrt{\frac{L}{C}} \ .$$

4.3.3.9 Ex: Electronic oscillator circuit

A voltage $U(t)$ is known to produce in an coil of inductance L the current $I_L = L^{-1}\int_0^{t'} U dt$, in an ohmic resistance R the current $I_R = R^{-1}U$, and in a capacitor of capacitance C the current $I = C\dot{U}$. In the parallel L-R-C circuit shown in the figure, at each instant of time the sum of the currents I_L, I_R and I_C must compensate the current $I_F(t) = I_0 e^{i\omega t}$ supplied by an alternating current source, while the voltage $U(t)$ is the same across all components.
a. Derive the differential equation for the derivative of the voltage $\dot{U}$.
b. What would be the oscillation frequency of the current without source ($I_0 = 0$) and without resistance ($R = \infty$)?
c. What would be the oscillation frequency of the current without source ($I_0 = 0$) but with resistance ($R \neq \infty$)?
d. Doing the ansatz $U(t) = U_0 e^{\imath\omega t + \imath\phi}$ derive the characteristic equation.
e. Use the characteristic equation to calculate the impedance defined by $Z \equiv |U_0/I_0|$ and the phase ϕ of the current oscillation as a function of the frequency ω. Prepare qualitative sketches of functions $Z(\omega)$ and $\phi(\omega)$.

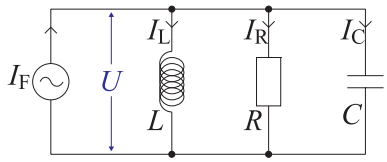

Figure 4.42: Notch filter.

Solution: *a. The equation of motion of the damped and forced system is,*

$$I_L + I_R + I_C = L^{-1}\int_0^{t'} U dt + R^{-1}U + C\dot{U} = I_0 e^{\imath\omega t} = I_F \ ,$$

or

$$L^{-1}U + R^{-1}\dot{U} + C\ddot{U} = \imath\omega I_0 e^{\imath\omega t} \ .$$

b. Without source and without resistance the differential equation would be,

$$\ddot{U} + (LC)^{-1}U = 0 \ .$$

Therefore, the natural frequency would be,

$$\omega_0 = \frac{1}{\sqrt{LC}} \ .$$

c. Without source but with resistance the differential equation would be,

$$\ddot{U} + (RC)^{-1}\dot{U} + (LC)^{-1}U = 0 \ .$$

Therefore, the oscillation frequency would be,

$$\omega_\gamma = \sqrt{\omega_0^2 - \gamma^2} \ ,$$

com $2\gamma \equiv (RC)^{-1}$.
d. Inserting the ansatz $U = U_0 e^{\imath\omega t + \imath\phi}$,

$$L^{-1}U_0 e^{\imath\phi} + \imath\omega R^{-1}U_0 e^{\imath\phi} - \omega^2 C U_0 e^{\imath\phi} = \imath\omega I_0 \ ,$$

or

$$-\omega U_0 + 2i\gamma\omega U_0 + \omega_0^2 U_0 = \imath e^{-\imath\phi}\omega I_0/C \ .$$

e. The solutions are,

$$Z \equiv \frac{U_0}{I_0}e^{\imath\phi} = \frac{\imath\omega}{L^{-1} + \imath\omega R^{-1} - \omega^2 C} = \frac{1}{R^{-1} + \imath[\omega C - 1/(\omega L)]} = \frac{\imath\omega/C}{\omega_0^2 - \omega^2 + 2\imath\gamma\omega} \ ,$$

$$|Z| = \left|\frac{U_0}{I_0}\right| = \frac{1}{\sqrt{R^{-2} + [\omega C - 1/(\omega L)]^2}} = \frac{\omega^2/C}{\sqrt{(\omega^2 - \omega_0^2)^2 + 4\gamma^2\omega^2}}$$

$$\tan\phi = \frac{Im\ Z}{Re\ Z} = \frac{-[\omega C - 1/(\omega L)]}{R^{-1}} = R/(\omega L) - \omega RC = \frac{\omega_0^2 - \omega^2}{2\gamma\omega} \ .$$

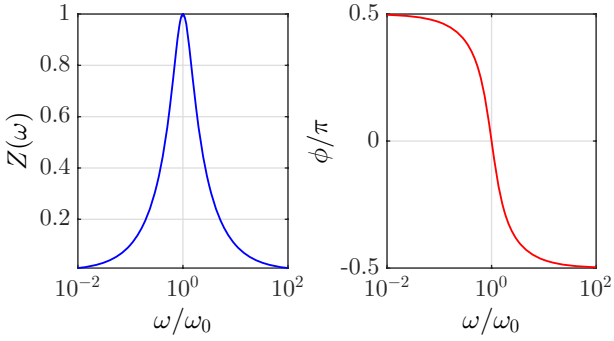

Figure 4.43: Bode diagram of the notch filter.

4.3.3.10 Ex: Lorentz model of light-atom interaction

The Lorentz model describes the interaction of an electron attached to an atom with an incident light beam as a damped oscillator. The electron's binding to the nucleus is taken into account by a restoring force $-\omega_0^2 x$. The decay of the excited state with the rate Γ is the reason for the damping force $-m\Gamma\dot{x}$. And the excitation is produced by the Lorentz force exerted by the electrical component of the light beam, $e\mathcal{E}_0 e^{\imath\omega t}$, where e is the charge of the electron. Establish the differential equation and calculate the amplitude of electron's oscillation as a function of the excitation frequency.

Solution: *The differential equation is,*

$$m\ddot{x} + m\Gamma\dot{x} + m\omega_0^2 x = e\mathcal{E}_0 e^{\imath\omega t} \ .$$

The ansatz $x \equiv x_0 e^{\imath\omega t}$ *leads to the oscillation amplitude,*

$$x_0(\omega) = \left| \frac{e\mathcal{E}_0}{m} \frac{1}{\omega_0^2 - \omega^2 - \imath\Gamma\omega} \right| \ .$$

For small detunings $\delta = \omega - \omega_0 \ll \omega$ *vale*

$$x_0(\omega) \simeq \frac{e\mathcal{E}_0}{m} \left| \frac{1}{2\omega_0(\omega_0 - \omega) + \imath\Gamma\omega_0} \right| = \frac{e\mathcal{E}_0}{m\omega_0} \left| \frac{1}{\delta - \imath\frac{\Gamma}{2}} \right| \ .$$

We also have,

$$\phi(\omega) = \frac{\mathfrak{Im}\ \alpha}{\mathfrak{Re}\ \alpha} = \frac{-\gamma\omega^2}{\omega^2 - \omega_0^2} \xrightarrow{\omega \to \omega_0} \frac{\gamma}{2\Delta} \ .$$

4.3.3.11 Ex: Lorentz model of light-atom interaction

a. Electric fields $\mathcal{E}$ exert on electric charges q the Coulomb force $F = q\mathcal{E}$. Write the differential equation for the undamped motion of an electron (charge $-e$, mass m) harmonically bound to its nucleus under the influence of an alternating electric field, $\mathcal{E} = \mathcal{E}_0 \sin\omega t$.
b. Show that the general solution can be written as,

$$x(t) = \frac{-e\mathcal{E}_0 \sin\omega t}{m(\omega_0^2 - \omega^2)} + A\cos\omega_0 t + B\sin\omega_0 t \ .$$

c. Write the solution in terms of the initial conditions $x(0) = 0 = \dot{x}(0)$.

Solution: *a. The differential equation is,*

$$m\ddot{x} + m\omega_0^2 x = -e\mathcal{E}\sin\omega t \ .$$

b. Entering the solution into the differential equation makes it easy to verify that the solution satisfies the differential equation.
c. Entering the initial conditions,

$$x(0) = A = 0 \qquad , \qquad \dot{x}(0) = \frac{-e\omega\mathcal{E}}{m(\omega_0^2 - \omega^2)} + B\omega_0 = 0 \ .$$

Hence,

$$x(t) = \frac{e\mathcal{E}}{m(\omega_0^2 - \omega^2)} \left(\frac{\omega}{\omega_0} \sin \omega_0 t - \sin \omega t \right) \ .$$

4.4 Coupled oscillations and normal modes

So far we have discussed the behavior of isolated oscillators. Energy losses or gains were described in a bulk way via a coupling to an external reservoir without structure of its own. However, the reservoir often has vibrational degrees of freedom, as well, and can dump (or supply) energy. This usually happens when neighboring oscillators share a rigid, massive, or sturdy medium. The transfer of energy to neighboring oscillators is the key ingredient for any oscillatory propagation of energy called *wave*.

4.4.1 Two coupled oscillators

To discuss the *coupling between oscillators* at the most fundamental level, we consider two ideal and identical pendulums (length L and mass m) coupled by a spring of constant k, as shown in Fig. 4.44. The differential equations of motion for the angles

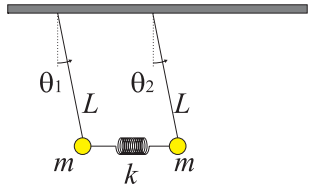

Figure 4.44: Two coupled pendulums.

θ_1 and θ_2 are,

$$\begin{aligned} mL\ddot{\theta}_1 &= -mg \sin\theta_1 - k(x_1 - x_2) \\ mL\ddot{\theta}_2 &= -mg \sin\theta_2 - k(x_2 - x_1) \ , \end{aligned} \tag{4.102}$$

with $x_j = L \sin\theta_j$. For small oscillations we have, therefore,

$$\begin{aligned} \ddot{\theta}_1 &= -\tfrac{g}{L} \sin\theta_1 - \tfrac{k}{m}(\sin\theta_1 - \sin\theta_2) \simeq -(\tfrac{g}{L} + \tfrac{k}{m})\theta_1 + \tfrac{k}{m}\theta_2 \\ \ddot{\theta}_2 &= -\tfrac{g}{L} \sin\theta_2 - \tfrac{k}{m}(\sin\theta_2 - \sin\theta_1) \simeq -(\tfrac{g}{L} + \tfrac{k}{m})\theta_2 + \tfrac{k}{m}\theta_1 \ . \end{aligned} \tag{4.103}$$

We define the normal coordinates of the vibration $\aleph \equiv \frac{1}{\sqrt{2}}(\theta_1 - \theta_2)$ and $\Psi \equiv \frac{1}{\sqrt{2}}(\theta_1 + \theta_2)$. We find the differential equations for $\aleph$ and Ψ by adding and subtracting the equations of motion,

$$\ddot{\theta}_1 + \ddot{\theta}_2 \simeq -\tfrac{g}{L}(\theta_1 + \theta_2) \qquad \text{and} \qquad \ddot{\theta}_1 - \ddot{\theta}_2 \simeq -(\tfrac{g}{L} + \tfrac{2k}{m})(\theta_1 - \theta_2) \ ,$$

or,

$$\ddot{\Psi} + \omega_\Psi^2 \Psi = 0 \qquad \text{and} \qquad \ddot{\aleph} + \omega_\aleph^2 \aleph = 0$$

using the angular frequencies of the vibrational normal modes,

$$\omega_\Psi = \sqrt{\frac{g}{L}} \quad \text{and} \quad \omega_\aleph = \sqrt{\frac{g}{L} + \frac{2k}{m}} \ .$$

4.4.2 Normal modes

Thus, the normal coordinates Ψ and $\aleph$ allow a description of the motion by decoupled linear differential equations. A vibration involving only one *normal coordinate* is called *normal mode*. In this mode all the components participating in the oscillation oscillate at the same frequency.

The importance of the normal modes is they are totally independent, that is, they never exchange energy and they can be pumped separately. Therefore, the total energy of the system can be expressed as the sum of terms containing the squares of the normal coordinates (potential energy) and their first derivatives (kinetic energy). Every independent path by which a system can gain energy is called *degree of freedom* and has an associated normal coordinate. For example, an isolated harmonic oscillator has two degrees of freedom, as it can gain potential or kinetic energy and two normal coordinates, x and v. And the coupled oscillator system,

$$E_\aleph = a\dot{\aleph}^2 + b\aleph^2 \quad \text{and} \quad E_\Psi = a\dot{\Psi}^2 + b\Psi^2 \ , \tag{4.104}$$

has four degrees of freedom.[7]

Every movement of the system can be represented by a superposition of normal modes,

$$\aleph = \tfrac{1}{\sqrt{2}}(\theta_1 - \theta_2) = \aleph_0 \cos(\omega_\aleph t + \phi_\aleph) \quad \text{and} \quad \Psi = \tfrac{1}{\sqrt{2}}(\theta_1 + \theta_2) = \Psi_0 \cos(\omega_\Psi t + \phi_\Psi) \ . \tag{4.105}$$

Choosing $\sqrt{2}A = \aleph_0 = \Psi_0$ and $\phi_\aleph = \phi_\Psi = 0$,

$$\begin{aligned} \theta_1 &= \tfrac{1}{\sqrt{2}}(\Psi + \aleph) = A\cos\omega_\aleph t + A\cos\omega_\Psi t = 2A\cos\tfrac{(\omega_\Psi - \omega_\aleph)t}{2}\cos\tfrac{(\omega_\Psi + \omega_\aleph)t}{2} \\ \theta_2 &= \tfrac{1}{\sqrt{2}}(\Psi - \aleph) = A\cos\omega_\aleph t - A\cos\omega_\Psi t = 2A\sin\tfrac{(\omega_\Psi - \omega_\aleph)t}{2}\sin\tfrac{(\omega_\Psi + \omega_\aleph)t}{2} \ . \end{aligned} \tag{4.106}$$

The oscillation shows the behavior of a frequency beat [8].

Example 15 (*Normal modes*):

- Two pendulums suspended on a movable horizontal bar which, in turn, is suspended by two wires to a rigid ceiling. Show (anti-)symmetric modes and their different exposure to damping of the motion of the bar.

4.4.3 Normal modes in large systems

There are techniques for solving systems many coupled oscillator. Let us consider, for example, a chain of $n = 1, ..., N$ oscillators coupled by springs. We have,

[7] Note that the motion of a single pendulum is a movement in two Cartesian dimensions and therefore would have four degrees of freedom. However, the joint action of gravity and the tension of the wire constrains the movement into one dimension thus freezing two degrees of freedom.

[8] Normal modes are observed in the molecular vibrations of H_2O and CO_2 (see Pain).

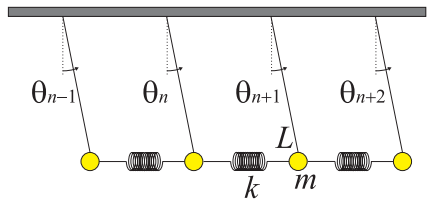

Figure 4.45: Array of coupled pendulums.

$$\ddot{\theta}_n = -\frac{g}{l}\theta_n - \frac{k}{m}(\theta_n - \theta_{n+1}) - \frac{k}{m}(\theta_n - \theta_{n-1}) \ . \tag{4.107}$$

Inserting the ansatz $\theta_n \equiv A_n e^{i\omega t}$, we obtain

$$\omega^2 A_n = \omega_0^2 A_n + \beta^2(A_n - A_{n+1}) + \beta^2(A_n - A_{n-1}) \ , \tag{4.108}$$

using the abbreviations $\omega_0^2 = g/l$ and $\beta^2 = k/m$. Defining the vector $\vec{A} \equiv (\cdots A_n \cdots)$ and the matrix,

$$\hat{M} \equiv \begin{pmatrix} \omega_0^2+\beta^2 & -\beta^2 & & & & & \\ -\beta^2 & \ddots & \ddots & & & & \\ & \ddots & \omega_0^2+2\beta^2 & -\beta^2 & & & \\ & & -\beta^2 & \omega_0^2+2\beta^2 & \ddots & & \\ & & & \ddots & \ddots & -\beta^2 & \\ & & & & -\beta^2 & \omega_0^2+\beta^2 \end{pmatrix} \ , \tag{4.109}$$

we put the characteristic equation into a form called an eigenvalue equation,

$$\hat{M}\vec{A} = \omega^2 \vec{A} \ . \tag{4.110}$$

The matrix $\hat{M}$ is characterized by the fact that it contains on its diagonal the energy of each individual oscillator (that is, $\omega_0^2 + 2\beta^2$ when the oscillator is in the middle of the chain, and $\omega_0^2 + \beta^2$) at the two ends of the chain). On the secondary diagonals (that is, at the positions $M_{n,n\pm1}$) are the coupling energies between two oscillators n and $n \pm 1$. A normal mode of the system corresponds to an *eigenvector* of the matrix $\hat{M}$, and the natural frequency of this mode corresponds to the respective *eigenvalue*.

The equation (4.110) has non-trivial solutions only, when the determinant of the matrix $\hat{M} - \omega^2$ vanishes. The eigenvalues are those ω^2 which satisfy this requirement,

$$\det(\hat{M} - \omega^2 \mathbf{1}) = 0 \ . \tag{4.111}$$

4.4.4 Dissipation in coupled oscillator systems

We now extend the system of two coupled pendulums to include damping. Assuming that the movement of the pendulum is subject to damping,

$$\begin{aligned} \ddot{\theta}_1 &= -\Gamma\dot{\theta}_1 - \tfrac{g}{L}\theta_1 - \tfrac{k}{m}(\theta_1 - \theta_2) \\ \ddot{\theta}_2 &= -\Gamma\dot{\theta}_2 - \tfrac{g}{L}\theta_2 - \tfrac{k}{m}(\theta_2 - \theta_1) \ , \end{aligned} \tag{4.112}$$

giving the collective modes,

$$\begin{aligned} \ddot{\Psi} &= \ddot{\theta}_1 + \ddot{\theta}_2 = -\Gamma\dot{\Psi} - \tfrac{g}{L}\Psi \\ \ddot{\aleph} &= \ddot{\theta}_1 - \ddot{\theta}_2 = -\Gamma\dot{\aleph} - \left(\tfrac{g}{L} + \tfrac{2k}{m}\right)\aleph \ . \end{aligned} \tag{4.113}$$

Assuming that the movement of the spring (not the movement of the pendulums) is subject to damping,

$$\begin{aligned} \ddot{\theta}_1 &= -\tfrac{g}{L}\theta_1 - \tfrac{k}{m}(\theta_1 - \theta_2) - \Gamma(\dot{\theta}_1 - \dot{\theta}_2) \\ \ddot{\theta}_2 &= -\tfrac{g}{L}\theta_2 - \tfrac{k}{m}(\theta_2 - \theta_1) - \Gamma(\dot{\theta}_2 - \dot{\theta}_1) \ , \end{aligned} \tag{4.114}$$

giving the collective modes

$$\begin{aligned} \ddot{\Psi} &= \ddot{\theta}_1 + \ddot{\theta}_2 = -\tfrac{g}{L}\Psi \\ \ddot{\aleph} &= \ddot{\theta}_1 - \ddot{\theta}_2 = -\left(\tfrac{g}{L} + \tfrac{2k}{m}\right)\aleph - 2\Gamma\dot{\aleph} \ . \end{aligned} \tag{4.115}$$

Thus, the anti-symmetric mode Ψ is free from damping, while the symmetric mode $\aleph$ damps out twice as fast. Therefore, Ψ is called the *subradiant* mode and $\aleph$ the *superradiant* mode.

4.4.5 Exercises

4.4.5.1 Ex: Energy of normal modes

Verify that the total energy of a system of two coupled oscillators is equal to the sum of the energies of the normal modes.

Solution: *We have,*

$$\begin{aligned} E_{tot} &= E_{kin,1} + E_{pot,1} + E_{kin,2} + E_{pot,2} + E_{cpl} \\ &= \tfrac{m}{2}v_1^2 + \tfrac{mg}{2L}x_1^2 + \tfrac{m}{2}v_2^2 + \tfrac{mg}{2L}x_2^2 + \tfrac{k}{2}(x_1 - x_2)^2 \\ &= \tfrac{m}{2}(L\dot{\theta}_1)^2 + \tfrac{mg}{2L}(L\theta_1)^2 + \tfrac{m}{2}(L\dot{\theta}_2)^2 + \tfrac{mg}{2L}(L\theta_2)^2 + \tfrac{k}{2}L^2(\theta_1 - \theta_2)^2 \\ &= \tfrac{m}{2}(L\dot{\Psi})^2 + \tfrac{m}{2}gL\Psi^2 + \tfrac{m}{2}(L\dot{\aleph})^2 + \tfrac{m}{2}gL\aleph^2 + kL^2\aleph^2 \\ &= \tfrac{m}{2}(L\dot{\Psi})^2 + \tfrac{m}{2}\omega_\Psi^2(L\Psi)^2 + \tfrac{m}{2}(L\dot{\aleph})^2 + \tfrac{m}{2}\omega_\aleph^2(L\aleph)^2 = E_\Psi + E_\aleph \ . \end{aligned}$$

4.4.5.2 Ex: Normal modes of two spring-coupled masses

Consider two different masses m_1 and m_2 coupled by a spring k.
a. Determine the equation of motion and the characteristic equation for each mass.
b. Write the characteristic equations in matrix form: $\hat{M}\vec{a} = \omega^2\vec{a}$, where $\vec{a} \equiv (a_1, a_2)$ and a_j are the amplitude of the oscillations and calculate the two eigenvalues of the matrix.
c. Calculate the normal modes, that is, the eigenvectors solving the equation $\hat{M}\vec{a} = \omega_k^2\vec{a}$ for each eigenvalue.

d. Derive the differential equations of the center-of-mass motion and the relative motion. Compare the result with the normal modes.

Solution: *a. For a chain of two masses we have,*

$$m_1\ddot{x}_1 = -k(x_1 - x_2) \qquad , \qquad m_2\ddot{x}_2 = -k(x_2 - x_1) \ .$$

Doing the ansatz $x_n = a_n e^{i\omega t}$ *and with the abbreviation* $\omega_j \equiv \frac{k}{m_j}$ *we get the characteristic equations,*

$$-\omega^2 a_1 = -\omega_1^2(a_1 - a_2) \qquad , \qquad -\omega^2 a_2 = -\omega_2^2(a_2 - a_1) \ .$$

b. The matrix form of the characteristic equations is,

$$\begin{pmatrix} \omega_1^2 & -\omega_1^2 \\ -\omega_2^2 & \omega_2^2 \end{pmatrix} \begin{pmatrix} a_1 \\ a_2 \end{pmatrix} = \omega^2 \begin{pmatrix} a_1 \\ a_2 \end{pmatrix} \ .$$

Solving,

$$0 = \det(\hat{M} - \omega^2 \mathbf{1}) = -\omega_1^2\omega^2 - \omega^2\omega_2^2 + \omega^4 = \omega^2(\omega^2 - \omega_1^2 - \omega_2^2) \ ,$$

we get the eigenvalues $\omega = 0$ *and* $\omega = \sqrt{\omega_1^2 + \omega_2^2}$.
c. The first eigenvector is obtained by,

$$\hat{M}\vec{a} = \begin{pmatrix} \omega_1^2 a_1 - \omega_1^2 a_2 \\ -\omega_2^2 a_1 + \omega_2^2 a_2 \end{pmatrix} = 0 \cdot \begin{pmatrix} a_1 \\ a_2 \end{pmatrix} = \omega^2 \vec{a} \ ,$$

which is only possible when $a_1 = a_2$. *For the second eigenvalue,*

$$\hat{M}\vec{a} = \begin{pmatrix} \omega_1^2 a_1 - \omega_1^2 a_2 \\ -\omega_2^2 a_1 + \omega_2^2 a_2 \end{pmatrix} = (\omega_1^2 + \omega_2^2) \begin{pmatrix} a_1 \\ a_2 \end{pmatrix} = \omega^2 \vec{a} \ ,$$

which implies $\omega_1^2 a_2 = -\omega_2^2 a_1$. *Therefore, the normal modes are,*

$$\vec{a} = \begin{pmatrix} 1 \\ 1 \end{pmatrix} \qquad \textit{and} \qquad \vec{a} = \frac{1}{\sqrt{\omega_1^4 + \omega_2^4}} \begin{pmatrix} \omega_1^2 \\ -\omega_2^2 \end{pmatrix} \ .$$

d. The center of mass is at the position $x_{cm} = \frac{m_1 x_1 + m_2 x_2}{m_1 + m_2}$. *We call* $x_{rl} = x_1 - x_2$ *the relative coordinate. The equations are,*

$$\ddot{x}_{cm} = \frac{m_1\ddot{x}_1 + m_2\ddot{x}_2}{m_1 + m_2} = \frac{-k(x_1 - x_2) - k(x_2 - x_1)}{m_1 + m_2} = 0$$

$$\ddot{x}_{rl} = \ddot{x}_1 - \ddot{x}_2 = -\frac{k}{m_1}(x_1 - x_2) + \frac{k}{m_2}(x_2 - x_1) = -\frac{k}{\mu}(x_1 - x_2) = -(\omega_1^2 + \omega_2^2)(x_1 - x_2) \ ,$$

with $\mu^{-1} \equiv m_1^{-1} + m_2^{-1}$. *The first mode corresponds to a translation without vibration, the second to an anti-symmetrical vibration without translation around the center-of-mass. This corresponds to the results obtained by the reduced mass method.*

4.4.5.3 Ex: Spring-coupled chain of masses

Consider a chain of spring-coupled masses.
a. Determine the equation of motion and the characteristic equation for each mass.
b. Calculate the normal modes for a chain consisting of three masses.

Solution: *a. For each mass we have,*

$$m\ddot{x}_n = -k(x_n - x_{n-1}) - k(x_n - x_{n+1}) \ .$$

Making the ansatz $x_n = A_n e^{\imath\omega t}$ *we get the characteristic equation,*

$$-\omega^2 A_n = -\omega_0^2(A_n - A_{n-1}) - \omega_0^2(A_n - A_{n+1}) \ .$$

In matrix notation,

$$\begin{pmatrix} \omega_0^2 & -\omega_0^2 & 0 & 0 & 0 \\ -\omega_0^2 & 2\omega_0^2 & -\omega_0^2 & 0 & 0 \\ 0 & -\omega_0^2 & \ddots & \ddots & 0 \\ 0 & 0 & \ddots & 2\omega_0^2 & -\omega_0^2 \\ 0 & 0 & 0 & -\omega_0^2 & \omega_0^2 \end{pmatrix} \ .$$

b. For a chain of three masses we have,

$$\begin{pmatrix} \omega_0^2 & -\omega_0^2 & 0 \\ -\omega_0^2 & 2\omega_0^2 & -\omega_0^2 \\ 0 & -\omega_0^2 & \omega_0 \end{pmatrix} \ .$$

To find the eigenvalues, we solve,

$$0 = \det[\hat{M} - \lambda\mathbf{1}]] = -3\omega_0^4\lambda + 4\omega_0^2\lambda^2 - \lambda^3 = -\lambda(\lambda - \omega_0)(\lambda - 3\omega_0^2) \ ,$$

giving the eigenvalues, $\lambda = 0$, $\lambda = \omega_0^2$, *and* $\lambda = 3\omega_0^2$. *To find the eigenvectors, we do* $\hat{M}\vec{a} = 0\vec{a}$ *with* $\vec{a} \equiv (a_1, a_2, a_3)$, *yielding,*

$$a_1 = a_2 = a_3 \ ,$$

and therefore the eigenvector,

$$\vec{a} = \frac{1}{\sqrt{3}} \begin{pmatrix} 1 \\ 1 \\ 1 \end{pmatrix} \ .$$

For the second eigenvector, we do $\hat{M}\vec{a} = \omega_0^2\vec{a}$ *yielding,*

$$a_2 = 0 \quad , \quad a_3 = -a_1 \ ,$$

and therefore the eigenvector,

$$\vec{a} = \frac{1}{\sqrt{3}} \begin{pmatrix} 1 \\ 0 \\ -1 \end{pmatrix} \ .$$

For the third eigenvector, we do $\hat{M}\vec{a} = 3\omega_0^2\vec{a}$ *yielding,*

$$a_1 - a_2 = 3a_1 \quad , \quad a_1 - a_2 = 3a_1 \quad , \quad -a_2 + a_3 = 3a_3 \ ,$$

or

$$a_1 = a_3 = -\tfrac{1}{2}a_2 \quad , \quad a_2 = a_2 \ ,$$

and therefore the eigenvector,

$$\vec{a} = \frac{1}{\sqrt{3}}\begin{pmatrix} -\frac{1}{2}a_2 \\ a_2 \\ -\frac{1}{2}a_2 \end{pmatrix} / \frac{a_2}{\sqrt{2}} = \sqrt{\frac{2}{3}}\begin{pmatrix} -\frac{1}{2} \\ 1 \\ -\frac{1}{2} \end{pmatrix} \ .$$

4.4.5.4 Ex: Normal modes of CO_2

We consider the carbon dioxide molecule CO_2, for which we make a spring-mass model with three masses coupled by k springs in a linear chain. Calculate the frequencies of the normal modes and the eigenvectors of the vibrations.

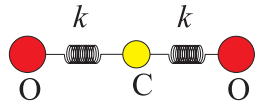

Figure 4.46: Normal modes of CO_2.

Solution: *The differential equations are*

$$\begin{aligned} m_O\ddot{x}_1 &= -k(x_1 - x_2) \\ m_C\ddot{x}_2 &= -k(x_2 - x_1) - k(x_2 - x_3) \\ m_O\ddot{x}_3 &= -k(x_3 - x_2) \ . \end{aligned}$$

With the ansatz $x_n = A_n e^{i\omega t}$ *and the abbreviations* $\omega_O \equiv \sqrt{\frac{k}{m_O}}$ *and* $\omega_C \equiv \sqrt{\frac{k}{m_C}}$ *we get the characteristic equations,*

$$\begin{aligned} \omega^2 A_1 &= \omega_O^2(A_1 - A_2) \\ \omega^2 A_2 &= \omega_C^2(A_2 - A_1) + \omega_C^2(A_2 - A_3) \\ \omega^2 A_3 &= \omega_O^2(A_3 - A_2) \ . \end{aligned}$$

Introducing the matrix and the vector,

$$M \equiv \begin{pmatrix} \omega_O^2 & -\omega_O^2 & 0 \\ -\omega_C^2 & 2\omega_C^2 & -\omega_C^2 \\ 0 & -\omega_O^2 & \omega_O^2 \end{pmatrix} \quad \text{and} \quad \vec{A} \equiv \begin{pmatrix} A_1 \\ A_2 \\ A_3 \end{pmatrix} \ ,$$

the equation takes the form of an eigenvalue equation,

$$M\vec{A} = \omega^2\vec{A} \ .$$

The frequencies of the normal modes are the eigenvalues of the matrix,

$$\begin{aligned} 0 = \det[M - \omega^2 E_3] &= -2\omega_O^2\omega_C^2\omega^2 - \omega_O^4\omega^2 + 2\omega_O^2\omega^4 + 2\omega^4\omega_C^2 - \omega^6 \\ &= -\omega^2(\omega^2 - \omega_O^2 - 2\omega_C^2)(\omega^2 - \omega_O^2) \ . \end{aligned}$$

Entering the eigenvalue $\omega = 0$ in the eigenvalue equation gives,

$$A_1 = A_2 = A_3 \qquad \textit{and hence} \qquad \vec{A} = \begin{pmatrix} 1 \\ 1 \\ 1 \end{pmatrix} \ .$$

Entering the eigenvalue $\omega = \omega_O$ in the eigenvalue equation we get,

$$A_2 = 0 \quad , \quad A_1 = -A_3 \qquad \textit{and hence} \qquad \vec{A} = \begin{pmatrix} 1 \\ 0 \\ -1 \end{pmatrix} \ .$$

Entering the eigenvalue $\omega = \sqrt{\omega_O^2 + 2\omega_C^2}$ in the eigenvalue equation we get,

$$2\omega_C^2 A_1 = -\omega_O^2 A_2 = 2\omega_C^2 A_3 \qquad \textit{and hence} \qquad \vec{A} = \begin{pmatrix} 1 \\ -2\omega_C^2/\omega_O^2 \\ 1 \end{pmatrix} \ .$$

4.4.5.5 Ex: Three coupled pendulums

Determine the frequencies of the oscillation modes of a chain of three spring-coupled pendulums.

Solution: *In the example of three oscillators we have,*

$$\begin{pmatrix} \omega_0^2 + \beta^2 & \beta^2 & 0 \\ \beta^2 & \omega_0^2 + 2\beta^2 & \beta^2 \\ 0 & \beta^2 & \omega_0^2 + \beta^2 \end{pmatrix} \begin{pmatrix} A_1 \\ A_2 \\ A_3 \end{pmatrix} = 0 \ .$$

The matrix eigenvectors and eigenvalues are:

$$\begin{aligned} (1,1,1) \quad & \textit{for} \quad \omega^2 = \omega_0^2 \\ (1,0,-1) \quad & \textit{for} \quad \omega^2 = \omega_0^2 + \beta^2 \\ (1,-2,1) \quad & \textit{for} \quad \omega^2 = \omega_0^2 + 3\beta^2 \ . \end{aligned}$$

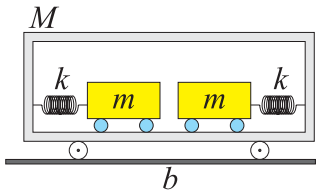

Figure 4.47: Super- and subradiant pendulums.

4.4.5.6 Ex: Super- and subradiance

We consider three carts attached by springs (spring constant k), as shown in the figure. The inner carts have mass m and are subject to damping by friction with the coefficient γ. The outer cart has mass M and friction Γ.
a. Establish the equations of motion of the three carts.
b. Discuss the case $M \to 0$.

Solution: *a. The equations of motion of these three carts are,*

$$\begin{aligned} m\ddot{x}_1 &= -k(x_1 - x_2) - \gamma\dot{x}_1 \\ M\ddot{x}_2 &= -k(x_2 - x_1) - k(x_2 - x_3) - \Gamma\dot{x}_2 \\ m\ddot{x}_3 &= -k(x_3 - x_2) - \gamma\dot{x}_3 \ . \end{aligned}$$

b. Para $M \to 0$,

$$\begin{aligned} m\ddot{x}_1 &= -kx_1 + \tfrac{1}{2}kx_1 + \tfrac{1}{2}kx_3 - \tfrac{1}{2}\Gamma\dot{x}_2 - \gamma\dot{x}_1 \\ kx_2 &= \tfrac{1}{2}kx_1 + \tfrac{1}{2}kx_3 - \tfrac{1}{2}\Gamma\dot{x}_2 \\ m\ddot{x}_3 &= -kx_3 + \tfrac{1}{2}kx_1 + \tfrac{1}{2}kx_3 - \tfrac{1}{2}\Gamma\dot{x}_2 - \gamma\dot{x}_3 \ . \end{aligned}$$

Substituting,

$$\begin{aligned} m\ddot{x}_1 &= -\tfrac{1}{2}k(x_1 - x_3) - \tfrac{1}{2}\Gamma\dot{x}_2 - \gamma\dot{x}_1 \\ m\ddot{x}_3 &= -\tfrac{1}{2}k(x_3 - x_1) - \tfrac{1}{2}\Gamma\dot{x}_2 - \gamma\dot{x}_3 \ . \end{aligned}$$

Considering the normal modes,

$$m\ddot{\Psi} = -\Gamma\dot{x}_2 - \gamma\dot{\Psi} \qquad , \qquad m\ddot{\aleph} = -k\aleph - \gamma\dot{\aleph} \ .$$

Obviously, in the absence of dissipation γ in the movement of the individual oscillators, we have two modes. One of the modes, called Ψ, is subject to dissipation Γ linked to the coupling between the oscillators. This mode is called superradiant, as it delivers its energy quickly to the environment. The other mode, called $\aleph$, is free of dissipation and is therefore called subradiant.

4.5 Further reading

H.M. Nussenzveig, Edgar Blucher (2014), *Curso de Física Básica: Fluidos, Vibrações e Ondas, Calor - vol 2* [962]ISBN

Chapter 5

Waves

While in *vibrating* bodies the motion and the energy are localized in space, *waves* do propagate and carry energy to other places. In fact, waves represent the most important mechanism for transporting and exchanging energy and information. We can understand a wave as a perturbation propagating through an elastic material medium. In some cases, however, e.g. for electromagnetic waves, the propagation of the wave is due to a self-sustained oscillation between two forms of energy (electric and magnetic) without the need of a material medium. Here, is a classification of the most common types of waves: A lecture version of this chapter can be found at

Table 5.1: *Types of waves.*

wave	pulse	sound	sound	surface	light	de Broglie
medium	string	air	crystal	fluid	vacuum	particle
polarize	trans.	long.	trans./long.	long.	trans.	long.
transform	Galilei	Galilei	Galilei	Galilei	Lorentz	Galilei
wave eq.	Helmholtz	Helmholtz	Helmholtz	Helmholtz	Helmholtz	Schrödinger

(watch talk).

5.1 Propagation of waves

There are several types of wave that we will classify according to the propagation medium and to the polarization, that is, we will distinguish longitudinal and transverse waves. There are media only supporting transverse waves (strings, water surfaces). Others only withstand longitudinal waves (sound in fluid media). Finally, there are media supporting both (sound in solids, electromagnetic waves).

The simplest example of a pulse is a local deformation of a string, as shown in Fig. 5.1. The pulse travels to one end of the string by a motion called *propagation*. The propagation is not conditioned to any transport of mass, but all the particles of the system go back to their original positions after the passage of the pulse. However, there is energy transport along the string, since each of its portions suffers an increase in kinetic and potential energy during the passage of the pulse.

In general, the pulse broadens during propagation, an effect called *dispersion*. To simplify the problem let us, as a first approximation neglect the dispersion and

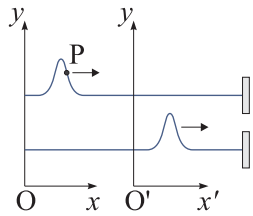

Figure 5.1: Pulse propagation along a rope.

suppose that the pulse does not change its shape,

$$Y(x,t) = f(x - vt) \ , \tag{5.1}$$

where the propagation velocity is positive when the pulse propagates in the direction of the positive x-axis.

The behavior of the pulse at the end of the rope depends on its fixation. Attached to a wall, the reflected pulse has opposite propagation amplitude and direction,

$$Y_{rfl}(x,t) = -f(x + vt) \ . \tag{5.2}$$

Fixed to another rope, the pulse will be partially reflected and partially transmitted.

5.1.1 Transverse waves, propagation of pulses on a rope

Pulses on a rope are examples for transverse waves. The speed at which the pulse propagates on a rope depends essentially on the properties of the string, that is, its mass density μ and the applied tension T, but not on the pulse amplitude. We take a small length element dx of the string with mass $dm = \mu dx$ and consider a pulse traveling with velocity v, as shown in Fig. 5.1.

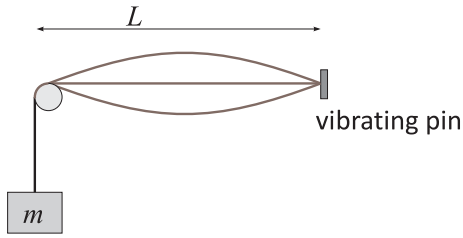

Figure 5.2: Mass element of a rope upon a passage of a pulse.

The vertical force due to the difference of tensions is,

$$F_y = T \sin\theta(x + dx) - T \sin\theta(x) \ . \tag{5.3}$$

Assuming $\theta(x)$ small, such that $\sin\theta(x) \simeq \tan\theta(x) = \frac{dY}{dx}$,

$$F_y = T \left(\frac{dY}{dx}\right)_{x+dx} - T \left(\frac{dY}{dx}\right)_x = T \frac{\partial^2 Y}{\partial x^2} dx \ . \tag{5.4}$$

On the other hand, applying Newton's second law to this string element, we find,

$$F_y = dm\frac{\partial^2 Y}{\partial t^2} \ . \tag{5.5}$$

Thus,

$$\frac{\partial^2 Y}{\partial x^2} = \frac{\mu}{T}\frac{\partial^2 Y}{\partial t^2} \ . \tag{5.6}$$

This equation is called *wave equation* and fully describes the propagation of the pulse on the string. Since $Y = f(x - vt)$ depends on both x and t, the derivatives that appear in the equation are partial, that is, one derives with respect to one variable keeping the other constant. To find the velocity, we write,

$$\frac{\partial^2 Y}{\partial t^2} = \frac{\partial}{\partial t}\left(\frac{\partial x}{\partial t}\frac{\partial Y}{\partial x}\right) = v\frac{\partial}{\partial t}\left(\frac{\partial Y}{\partial x}\right) = v\frac{\partial}{\partial x}\left(\frac{\partial Y}{\partial t}\right) = v\frac{\partial}{\partial x}\left(\frac{\partial x}{\partial t}\frac{\partial Y}{\partial x}\right) = v^2\frac{\partial Y^2}{\partial x^2} \ , \tag{5.7}$$

and compare the second relation with the wave equation, finding,

$$v = \sqrt{\frac{T}{\mu}} \ . \tag{5.8}$$

Example 16 (*Reflection of pulses on a rope*):

- Excite a pulse on a rope fixed to the wall (i) directly or (ii) through a thinner rope.

5.1.2 Longitudinal waves, propagation of sonar pulses in a tube

Acoustic pulses are examples for longitudinal waves. They are due to a process of compression and decompression of a gaseous medium (such as air), liquid or even solid. Let us consider an oscillating piston inside a tube (cross section A) filled with air of mass density ρ_0, as shown in Fig. 5.3. When the piston moves, it causes a local pressure increase. We want to find the velocity v at which the compression travels along the tube.

As shown in Fig. 5.3, the piston causes a negative pressure gradient along the tube giving rise to an unbalanced force which accelerates mass elements of air to the right. To simplify the situation let us assume that the piston is moved with velocity u within a time interval Δt compressing the volume of the tube by a value

$$\Delta V = -Au\Delta t \ . \tag{5.9}$$

During this time, the piston accelerates a mass $m = \rho_0 V$ of air within a volume V given by the propagation velocity v of the pulse along the tube,

$$V = Av\Delta t \ . \tag{5.10}$$

The mass within this volume receives a momentum,

$$F\Delta t = mu \ . \tag{5.11}$$

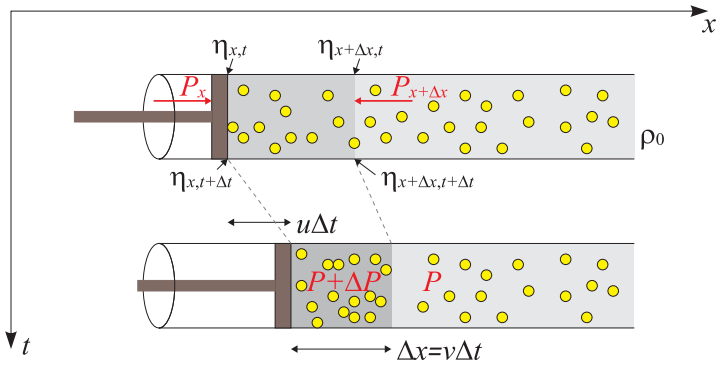

Figure 5.3: Sound waves produced by a swinging piston.

The pressure difference inside and outside the volume V causes a pressure imbalance,

$$F = A\Delta P \ . \tag{5.12}$$

With these relations we can calculate the *compressibility* of the gas,

$$\frac{1}{\kappa} \equiv -\frac{\Delta P}{\Delta V/V} = \frac{F/A}{u/v} = \frac{mu/A\Delta t}{u/v} = \frac{\rho_0 V v}{A\Delta t} = \rho_0 v^2 \ , \tag{5.13}$$

we obtain the propagation velocity of the pulse in the gas,

$$v = \sqrt{\frac{1}{\kappa\rho_0}} \ . \tag{5.14}$$

Thus, the velocity of sound propagation depends critically on the material medium. We have $v_{ar} = 331\,\mathrm{m/s}$, $v_{H_2} = 1286\,\mathrm{m/s}$, $v_{H_2O} = 331\,\mathrm{m/s}$, $v_{rubber} = 54\,\mathrm{m/s}$, and $v_{Al} = 5100\,\mathrm{m/s}$.

To derive the equation of motion, we consider a thin gas element with thickness Δx and mass $m = \rho_0 A\Delta x$ subject to a difference of pressure on both sides of,

$$P_x - P_{x+\Delta x} = -\frac{\partial P_x}{\partial x}\Delta x = -\frac{\partial}{\partial x}(P_0 + \Delta P)\Delta x = -\frac{\partial \Delta P}{\partial x}\Delta x \ , \tag{5.15}$$

where we subtracted the background pressure P_0 assumed to be constant. This pressure difference creates a force $F = A(P_x - P_{x+\Delta x})$ accelerating the gas element following Newton's law, $F = m\ddot{\eta}$, where $\eta(x)$ is the displacement of the element, such that,

$$\frac{\partial \eta}{\partial x} = \frac{\Delta V}{V} \tag{5.16}$$

and the compression (see Fig. 5.3). We therefore obtain,

$$\rho_0 \Delta x \frac{\partial^2 \eta}{\partial t^2} = \frac{F}{A} = -\frac{\partial \Delta P}{\partial x}\Delta x \ . \tag{5.17}$$

Substituting ΔP by the relationship (5.13),

$$\rho_0 \frac{\partial^2 \eta}{\partial t^2} = -\frac{\partial}{\partial x}\left(-\frac{1}{\kappa}\frac{\partial \eta}{\partial x}\right) = \frac{1}{\kappa}\frac{\partial^2 \eta}{\partial x^2} \ , \tag{5.18}$$

which gives the wave equation. Solve Excs. 5.1.7.1, 5.1.7.2, and 5.1.7.3.

5.1.3 Electromagnetic waves

Electromagnetic waves are in several aspects different from mechanical longitudinal or transverse waves. For example, they do not need a propagation medium, but move through the vacuum at an extremely high speed. The speed of light, $c = 299792458\,\mathrm{m/s}$ exactly, is so high, that the laws of classical mechanics are no longer valid, but must be replaced by relativistic laws. And since there is no propagation medium, with respect to vacuum all inertial systems are equivalent, which will have important consequences for the Doppler effect. We will show that the electromagnetic wave equation almost comes out as a corollary of the theory of special relativity.

Electromagnetic waves always arise when a charge changes position. In this way the theory of electromagnetic waves is also a consequence of the theory electromagnetism, which is contained in Maxwell's equations. We will introduce here, without derivation, the wave equation for the electric and magnetic fields.

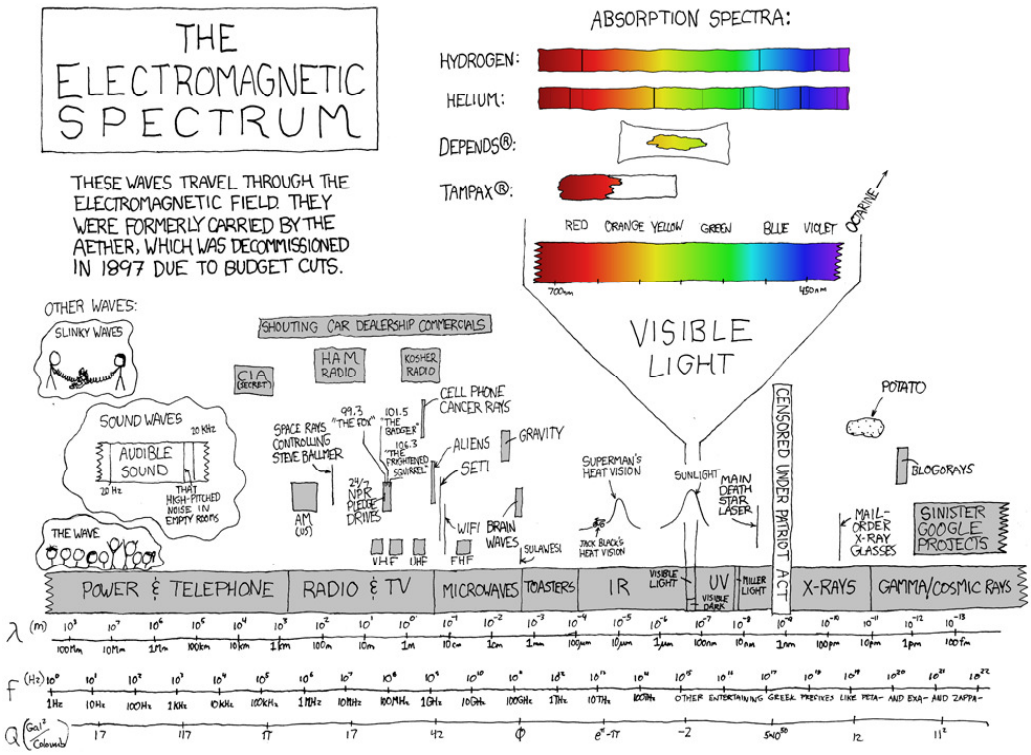

Figure 5.4: The electromagnetic spectrum.

5.1.3.1 Helmholtz equation

We have already seen how the periodic conversion between kinetic and potential energy in a pendulum can propagate in space when the pendulum is coupled to other pendulums attached to each other in a chain, and that this model explains the propagation of a pulse on the string. We also discussed how electrical and magnetic

energy can be interconverted in an electronic L-C-circuit with a capacitor storing electrical energy and an inductance (a coil) storing magnetic energy. The law of electrodynamics describing the transformation of electric field variations into magnetic energy is *Ampère's law*, and the law describing the transformation of magnetic field variations into electric energy is *Faraday's law*,

$$\frac{\partial \vec{\mathcal{E}}}{\partial t} \curvearrowright \vec{\mathcal{B}}(t) \quad , \quad \frac{\partial \vec{\mathcal{B}}}{\partial t} \curvearrowright -\vec{\mathcal{E}}(t) \ . \tag{5.19}$$

Extending the circuit L-C to a chain, it is possible to show that the electromagnetic oscillation propagates along the chain. This model describes well the propagation of electromagnetic energy along a coaxial cable or the propagation of light in free space.

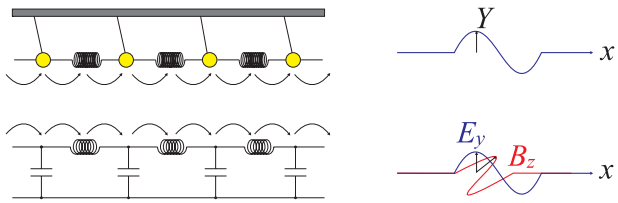

Figure 5.5: Analogy between the propagation of mechanical waves (above) and electromagnetic waves (below).

The *electrical energy* stored in the capacitor and the *magnetic energy* stored in the coil are given by,

$$E_{ele} = \tfrac{\varepsilon_0}{2}|\vec{\mathcal{E}}|^2 \quad , \quad E_{mag} = \tfrac{1}{2\mu_0}|\vec{\mathcal{B}}|^2 \ , \tag{5.20}$$

where the constants $\varepsilon_0 = 8.854 \cdot 10^{-12}\,\mathrm{As/Vm}$ and $\mu_0 = 4\pi \cdot 10^{-7}\,\mathrm{Vs/Am}$ are called *permittivity* and *permeability* of the vacuum. By analogy with the waves on a string, we can write the wave equations (called *Helmholtz equations*) for plane electromagnetic waves propagating along the x-axis,

$$\frac{\partial^2 \mathcal{E}_y}{\partial t^2} = \frac{1}{\varepsilon_0 \mu_0}\frac{\partial^2 \mathcal{E}_y}{\partial x^2} \quad , \quad \frac{\partial^2 \mathcal{B}_z}{\partial t^2} = \frac{1}{\varepsilon_0 \mu_0}\frac{\partial^2 \mathcal{B}_z}{\partial x^2} \ . \tag{5.21}$$

The formal derivation must be made from the *Maxwell equations*, which are the fundamental equations of the theory of electrodynamics. Here, we only note that,

- electromagnetic waves (in free space) are transverse;
- the electric field vector, the magnetic field vector, and the direction of propagation are orthogonal;
- the propagation velocity is the speed of light, because $c^2 = 1/\varepsilon_0\mu_0$.

5.1.3.2 Radiation intensity

In electrodynamic theory the energy flux is calculated by the *Poynting vector*,

$$\vec{S}(\mathbf{r}, t) = \tfrac{1}{\mu_0}\vec{\mathcal{E}}(\mathbf{r}, t) \times \vec{\mathcal{B}}(\mathbf{r}, t) \ . \tag{5.22}$$

The absolute value is the intensity of the light field,

$$I(\mathbf{r}, t) = |\mathbf{S}(\mathbf{r}, t)| \ . \tag{5.23}$$

5.1.4 Harmonic waves

In general, a light field is a superposition of many waves with many different frequencies and polarizations and propagating in many directions. The laser is an exception. Being monochromatic, polarized, directional, and coherent, it is very close to the ideal of an *harmonic wave*, that is, a wave described by the function,

$$Y(x, t) = Y_0 \cos(kx - \omega_0 t) \ , \tag{5.24}$$

where $\omega_0 = 2\pi\nu$ is the angular frequency of the oscillation and $k = 2\pi/\lambda$ the wavevector. By inserting this function into the *wave equation*,

$$\frac{\partial^2 Y}{\partial t^2} = c^2 \frac{\partial Y^2}{\partial x^2} \ , \tag{5.25}$$

where we now call c the propagation velocity of the harmonic wave, we verify the *dispersion relation*,

$$\omega = ck \ . \tag{5.26}$$

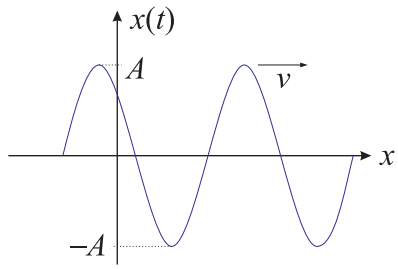

Figure 5.6: Illustration of a harmonic wave.

Often, the propagation velocity is independent of the wavelength, $c(k) = const$. In this case, a wave composed of several waves with different wavevectors k propagates without dispersing, that is, without changing its shape. In other cases, when $c(k) \neq const$, the wave deforms along its path.

5.1.5 Wave packets

Since the wave equation (5.25) is linear, the superposition principle is valid, that is, if Y_1 and Y_2 are solutions, then $\alpha Y_1 + \beta Y_2$ also is. More generally, we can say that, if $A(k)e^{\imath(kx-\omega t)}$ is a solution satisfying the wave equation for any k, then obviously,

$$Y(x, t) = \int_{-\infty}^{\infty} A(k) e^{\imath(kx-\omega t)} dk \ , \tag{5.27}$$

is. This means that the displacement $Y(x)$ and the distribution of amplitudes $A(k)$ are related by Fourier transform, $Y(x,t) = e^{-i\omega t}\mathcal{F}A(k)$.

Assuming a Gaussian distribution of wavevectors characterized by the width [1] Δk, $A(k) = e^{-(k-k_0)^2/2\Delta k^2}$, we obtain as solution for the wave equation,

$$\begin{aligned} Y(x,t) &= \int_{-\infty}^{\infty} e^{-(k-k_0)^2/2\Delta k^2} e^{\imath(kx-\omega t)} dk \qquad (5.28) \\ &= e^{\imath(k_0 x-\omega t)} \int_{-\infty}^{\infty} e^{-q^2/2\Delta k^2} e^{\imath q x} dq = \sqrt{2\pi k} e^{-\Delta k^2 x^2/2} e^{\imath(k_0 x-\omega t)} \ . \end{aligned}$$

This solution of the wave equation describes an *wave packet* with a Gaussian envelope [2], that is, a localized perturbation, as we discussed at the initial example of a pulse propagating on a string. Obviously, other distributions of wavevectors are possible.

Note that the width of the distribution of wavevectors, Δk, and that of the spatial distribution, $\Delta x \equiv 1/\Delta k$ satisfy a relation called *Fourier's theorem*,

$$\Delta x \Delta k = 1 \ , \qquad (5.29)$$

which in quantum mechanics turns into *Heisenberg's uncertainty relation*: The broader a wavevector distribution, the narrower the spatial distribution, and vice versa. In the limit of a sinusoidal wave described by a single wavevector, we expect a infinite spatial extension of the wave.

5.1.6 Dispersion

We consider a superposition of two waves,

$$\begin{aligned} Y_1(x,t) + Y_2(x,t) &= a\cos(k_1 x - \omega_1 t) + a\cos(k_2 x - \omega_2 t) \qquad (5.30) \\ &= 2a\cos\left[\tfrac{(k_1-k_2)x}{2} - \tfrac{(\omega_1-\omega_2)t}{2}\right] \cos\left[\tfrac{(k_1+k_2)x}{2} - \tfrac{(\omega_1+\omega_2)t}{2}\right] \ . \end{aligned}$$

The resulting wave can be regarded as a wave of frequency $\frac{1}{2}(\omega_1+\omega_2)t$ and wavelength $\frac{1}{2}(k_1+k_2)$, whose amplitude is modulated by an envelope of frequency $\frac{1}{2}(\omega_1-\omega_2)t$ and wavelength $\frac{1}{2}(k_1-k_2)x$.

In the absence of dispersion the *phase velocities* of the two waves and the propagation velocity of the envelope, called *group velocity*, are equal,

$$c = \frac{\omega_1}{k_1} = \frac{\omega_2}{k_2} = \frac{\omega_1-\omega_2}{k_1-k_2} = \frac{\Delta\omega}{\Delta k} = v_g \ . \qquad (5.31)$$

[1] Δk is half the *total* Gaussian width at *rms* (root-mean-square) height, that is, at $1/\sqrt{e}$ of the maximum.

[2] The definition of the Fourier transform in one dimension is,

$$Y(x) = \mathcal{F}A(k) \equiv \tfrac{1}{\sqrt{2\pi}} \int_{-\infty}^{\infty} A(k) e^{\imath kx} dk \ .$$

For the Gaussian function we have,

$$\begin{aligned} Y(x) &= \tfrac{1}{\sqrt{2\pi}} \int_{-\infty}^{\infty} e^{-ak^2} e^{\imath kx} dk = \tfrac{1}{\sqrt{2\pi}} e^{-x^2/4a} \int_{-\infty}^{\infty} e^{-a(k-ix/2a)^2} dk \\ &= \tfrac{1}{\sqrt{2\pi}} e^{-x^2/4a} \int_{-\infty}^{\infty} e^{-aq^2} dq = \tfrac{1}{\sqrt{2a}} e^{-x^2/4a} \ . \end{aligned}$$

However, the phase velocities of the two harmonic waves can also be different, such that the frequency depends on the wavelength, $\omega = \omega(k)$. In this case, the phase velocity also varies with the wavelength,

$$v_g = \frac{d\omega}{dk} = \frac{d}{dk}(kc) = c + k\frac{dc}{dk} \ . \tag{5.32}$$

Often this variation is not very strong, such that it is possible to expand,

$$\omega(k) = \omega_0 + \left.\frac{d\omega}{dk}\right|_{k_0} \cdot (k-k_0) + \frac{1}{2}\left.\frac{d^2\omega}{dk^2}\right|_{k_0} \cdot (k-k_0)^2 \equiv \omega_0 + v_g(k-k_0) + \beta(k-k_0)^2 \ . \tag{5.33}$$

In general we have, $v_g < c$, a situation that is called *normal dispersion*. But there are examples of *abnormal dispersion*, where $v_g > c$, e.g. close to resonances or with matter waves characterized by a quadratic dispersion relation $\hbar\omega = (\hbar k)^2/2m$.

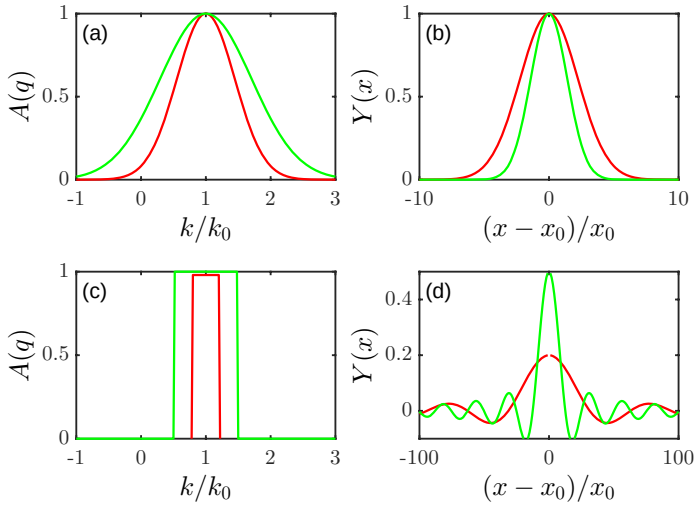

Figure 5.7: (code) Gaussian (upper graphs) and rectangular (lower graphs) distribution of amplitudes in momentum space (left) and in position space (right).

5.1.6.1 Rectangular wave packet with linear dispersion

As an example, we determine the shape of the wavepacket for a rectangular amplitude distribution, $A(k) = A_0\chi_{[k_0-\Delta k/2, k_0+\Delta k/2]}$, subject to linear dispersion (expansion up

to the linear term in Eq. (5.33)). By the Fourier theorem,

$$Y(x,t) = \int_{-\infty}^{\infty} A(k) e^{\imath(kx-\omega t)} dk = A_0 \int_{k_0-\Delta k/2}^{k_0+\Delta k/2} e^{\imath(kx-\omega_0 t + \frac{d\omega}{dk}\big|_{k_0}(k-k_0)t)} dk \tag{5.34}$$

$$= A_0 e^{\imath(k_0 x-\omega_0 t)} \int_{k_0-\Delta k/2}^{k_0+\Delta k/2} e^{\imath(k-k_0)\left(x-\frac{d\omega}{dk}\big|_{k_0} t\right)} dk$$

$$= A_0 e^{\imath(k_0 x-\omega_0 t)} \int_{-\Delta k/2}^{\Delta k/2} e^{\imath k\left(x-\frac{d\omega}{dk}\big|_{k_0} t\right)} dk = A_0 e^{\imath(k_0 x-\omega_0 t)} \int_{-\Delta k/2}^{\Delta k/2} e^{\imath k u} dk$$

$$= A_0 e^{\imath(k_0 x-\omega_0 t)} \frac{e^{\imath\Delta k/2 u} - e^{-i\Delta k/2 u}}{\imath u} = 2A_0 e^{\imath(k_0 x-\omega_0 t)} \frac{\sin\frac{u\Delta k}{2}}{u} \equiv A(x,t) e^{\imath(k_0 x-\omega_0 t)} .$$

With the abbreviation $u \equiv x - \frac{d\omega}{dk}\big|_{k_0} t = x - v_g t$ the interpretation of the group velocity becomes obvious,

$$v_g \equiv \left.\frac{d\omega}{dk}\right|_{k_0} t . \tag{5.35}$$

The envelope has the shape of a 'sinc' function, such that the intensity of the wave is,

$$|Y(x,t)|^2 = A_0 \Delta k \ \mathrm{sinc}\left[\tfrac{\Delta k}{2}(x-v_g t)\right] . \tag{5.36}$$

Obviously, the *wavepacket* is localized in space. It moves at group velocity, but does not diffuse.

5.1.6.2 Dispersion of a Gaussian wave packet subject to quadratic dispersion

Quadratic dispersion leads to a spreading of the wavepackets. We show this at the example of the Gaussian wavepacket $A(k) = e^{-\alpha(k-k_0)^2}$, expanding the dispersion relation (5.33) up to the quadratic term. By the Fourier theorem,

$$Y(x,t) = \int_{-\infty}^{\infty} A(k) e^{\imath(kx-\omega t)} dk = A_0 e^{\imath(k_0 x-\omega_0 t)} \int_{-\infty}^{\infty} e^{\imath(k-k_0)(x-v_g t)-(\alpha+i\beta t)(k-k_0)^2} dk$$

$$= A_0 e^{\imath(k_0 x-\omega_0 t)} \int_{-\infty}^{\infty} e^{\imath k(x-v_g t)-(\alpha+i\beta t)k^2} dk$$

$$\equiv A_0 e^{\imath(k_0 x-\omega_0 t)} \int_{-\infty}^{\infty} e^{\imath k u - v k^2} dk = A_0 \sqrt{\tfrac{\pi}{v}} e^{\imath(k_0 x-\omega_0 t)} e^{-u^2/4v} . \tag{5.37}$$

The absolute square of this solution describes the spatial energy distribution of the wavepacket,

$$|Y(x,t)|^2 = A_0^2 \frac{\pi}{\sqrt{v v^*}} e^{-u^2/4v - u^2/4v^*} = A_0^2 \frac{\pi}{x_0\sqrt{\alpha/2}} e^{-(x-v_g t)^2/x_0^2} , \tag{5.38}$$

with $x_0 \equiv \sqrt{2\alpha}\sqrt{1+\frac{\beta^2}{\alpha^2}t^2}$. Obviously, for long times the pulse spreads out at constant speed. Since the constant α gives the initial width of the pulse, we realize that an initially compressed pulse spreads faster. Therefore, the angular coefficient of the dispersion relation determines the group velocity, while the curvature determines the spreading speed (dispersion).

5.1.7 Exercises

5.1.7.1 Ex: Speed of sound

A person drops a stone from the top of a bridge and hears the sound of the stone hitting the water after $t = 4\,\mathrm{s}$.
a. Estimate the distance between the bridge and the water level, assuming that the propagation time of sound is negligible.
b. Improve the estimate by taking into account the finite speed of sound.

Solution: *a. The height would be* $h = \frac{g}{2}t^2 = 78.48\,\mathrm{m}$.
b. We know $h = \frac{g}{2}t_{cai}^2 = c_{som}(t - t_{cai})$. *Hence,*

$$t_{fall} = -\frac{c_{sound}}{g} \pm \frac{c_{sound}}{g}\sqrt{1 + \frac{2gt}{c_{sound}}} = 3.79\,\mathrm{s} \ ,$$

and $h = 70.55\,\mathrm{m}$.

5.1.7.2 Ex: Distance of a lightning

An approximate method for estimating the distance of a lightning consists in starting to count the seconds when the lightning stroke and stop counting when the thunder arrives. The number of seconds counted divided by 3 gives the distance from the lightning in kilometers. Estimate accuracy of this procedure.

Solution:

5.1.7.3 Ex: Speed of sound

A student in her room listens to the radio broadcasting a nearby football game. She is 1.6 km south of the field. On the radio, the student hears the noise generated by an electromagnetic pulse caused by a lightning strike. Two seconds later she hears the noise of thunder on the radio which was captured by the microphone of the football field. Four seconds after hearing the noise on the radio, she hears the noise of the thunder directly. Where did the lightning strike in relation to the soccer field?

Solution:

5.1.7.4 Ex: Absence of dispersion in sound

Discuss the experimental evidence that leads us to assume that the speed of sound in the audible range must be the same at all wavelengths.

Solution: *If there were dispersion, high and low sounds would be desynchronized (e.g., at a public concert). The noise of explosions noise would be quickly attenuated.*

5.1.7.5 Ex: Optical dispersion

a. While vacuum is strictly dispersionless, the refractive index of air depends on the wavelength of light λ, on temperature T in $^\circ$ C and on the atmospheric pressure P in mbar like,

$$n_s = 1 + 10^{-8}\left(8342.13 + \frac{2406030}{130 - 10^{12}/\lambda^2} + \frac{15997}{38.9 - 10^{12}/\lambda^2}\right)$$
$$n = 1 + (n_s - 1)\frac{0.00185097P}{1 + 0.003661T} \ .$$

Calculate the dispersion of air within range $\lambda_1 = 400\,\text{nm}$ and $\lambda_2 = 800\,\text{nm}$.
b. Using Snell's law,

$$\frac{n_1}{n_2} = \frac{\sin\alpha_2}{\alpha_1} \ ,$$

calculate the angular dispersion $d\alpha_{ar}/d\lambda$ of a beam of light at the interface between vacuum and atmospheric air for $P = 1013\,\text{mbar}$ and $T = 25^\circ$ C around $\lambda = 500\,\text{nm}$.

Solution: *We have,*

$$\frac{d\alpha_{ar}}{d\lambda} = \frac{d}{d\lambda}\arcsin\frac{\sin\alpha_{vac}}{n} = \ .$$

5.1.7.6 Ex: Dispersion near an atomic resonance

Near an atomic resonance ω_0 the refractive index can be approximated by,

$$n = 1 - \frac{\alpha}{\omega^2 - \omega_0^2} \ ,$$

where the polarizability of the gas α is a constant. Calculate the group velocity $v_g(\omega_l)$ of a laser wave packet passing through a gas of these atoms as a function of the laser frequency ω_l. Approximate $|\omega - \omega_0| \ll \omega_0$. Make a qualitative chart of $n(\omega_l)$, $k(\omega_l)$, of the phase velocity $v_f(\omega_l)$, and of the group velocity $v_g(\omega_l)$.

Solution: *Expressing k by ω,*

$$k = \frac{\omega n(\omega)}{c} = \frac{\omega}{c}\left(1 - \frac{\alpha}{\omega^2 - \omega_0^2}\right)$$

we can calculate the phase velocity by,

$$v_f = \frac{c}{n} = \frac{c}{1 - \frac{\alpha}{\omega^2 - \omega_0^2}} \ .$$

we can calculate the group velocity by,

$$v_g = \left.\frac{d\omega}{dk}\right|_{k=k_l} = \frac{1}{\left.\frac{dk}{d\omega}\right|_{\omega=\omega_l}} = \frac{1}{\left.\frac{d}{d\omega}\frac{\omega n(k)}{c}\right|_{\omega=\omega_l}} = \frac{1}{\left.\frac{d}{d\omega}\frac{\omega}{c}\left(1 - \frac{\alpha}{\omega^2-\omega_0^2}\right)\right|_{\omega=\omega_l}}$$
$$= \frac{c}{1 + \alpha\frac{\omega_l^2 + \omega_0^2}{(\omega_l^2 - \omega_0^2)^2}} = \frac{c}{n - (n-1)\frac{2\omega^2}{\omega^2 - \omega_0^2}} \ .$$

For $\omega \simeq \omega_0$ we can approximate,

$$v_g = \frac{c}{1 + \frac{\alpha}{2(\omega_l - \omega_0)^2}} \ .$$

Alternatively, approximating $\omega \simeq \omega_0$ we can calculate,

$$k \simeq \frac{\omega}{c}\left(1 - \frac{\alpha}{2\omega_0(\omega - \omega_0)}\right) \ ,$$

and express ω by k,

$$\omega = \tfrac{1}{2}\left(\omega_0 + \tfrac{\alpha}{2\omega_0} + ck\right) \pm \sqrt{\tfrac{1}{4}\left(\omega_0 + \tfrac{\alpha}{2\omega_0} + ck\right)^2 - ck\omega_0} \ ,$$

giving,

$$v_g = \left.\frac{d\omega}{dk}\right|_{k=k_l} = \tfrac{c}{2} \pm \tfrac{c}{2} \frac{-\omega_0 + \frac{\alpha}{2\omega_0} + ck_l}{\sqrt{\left(\omega_0 + \frac{\alpha}{2\omega_0} + ck_l\right)^2 - 4ck_l\omega_0}} \ .$$

The graph shows the approximation as points in magenta. Similarly, we can show

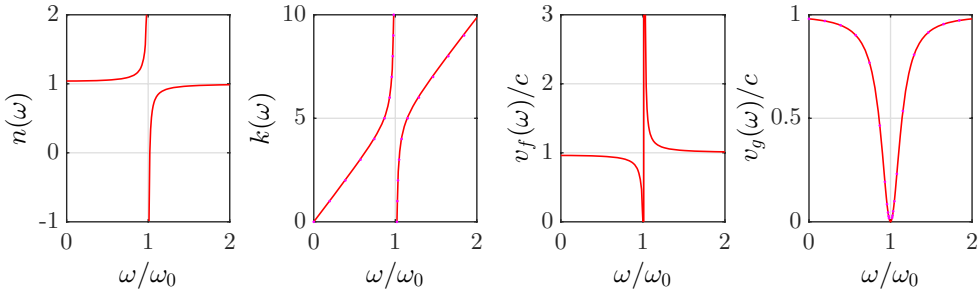

Figure 5.8: Dispersion near an atomic resonance.

that for $n(\omega) = 1 + \frac{\alpha}{1+(\omega-\omega_0)^2/\Gamma^2}$ group velocity is,

$$v_g = \frac{c}{n - (n-1)\frac{2\omega^2(\omega-\omega_0)}{\Gamma^2+(\omega-\omega_0)^2}} \ ,$$

and for $n(\omega) = 1 + \alpha e^{-(\omega-\omega_0)^2/\Gamma^2}$ the group velocity is,

$$v_g = \frac{c}{n - (n-1)\frac{2\omega(\omega-\omega_0)}{\Gamma^2}} \ .$$

5.1.7.7 Ex: Group velocity near a broad transition

The refractive index of a dilute gas (density ρ) of atoms excited by a light beam of frequency ω near a transition (resonant frequency ω_0 and width Γ) can be approximated

by,

$$n = \sqrt{1 - \frac{4\pi\rho\Gamma}{k_0^3(2\Delta + \imath\Gamma)}} \simeq 1 - \frac{2\pi\rho\Gamma}{k_0^3(2\Delta + \imath\Gamma)} \ ,$$

where $ck_0 = \omega_0$ and $\Delta \equiv \omega - \omega_0$. Calculate the group velocity near resonance.

Solution: *The real part is,*

$$n_r = \mathfrak{Re}\ n = 1 - \frac{4\pi\rho\Gamma\Delta}{k_0^3(4\Delta^2 + \Gamma^2)} \ .$$

The group velocity is,

$$v_g = \frac{1}{\frac{dk}{d\omega}\Big|_{\omega=\bar{\omega}}} = \frac{1}{\frac{d}{d\omega}\frac{\omega n(k)}{c}\Big|_{\omega=\bar{\omega}}} = \frac{1}{\frac{d}{d\omega}\left(\frac{\omega}{c} - \frac{\omega}{c}\frac{4\pi\rho\Gamma\Delta}{k_0^3(4\Delta^2+\Gamma^2)}\right)\Big|_{\omega=\bar{\omega}}}$$
$$= \frac{c}{1 - \frac{4\pi\rho\Gamma}{k_0^3}\frac{-4\omega_0(\omega-\omega_0)^2+(2\omega-\omega_0)\Gamma^2}{[4(\omega-\omega_0)^2+\Gamma^2]^2}\Big|_{\omega=\bar{\omega}}} \ .$$

The profile of the group velocity shows two poles.

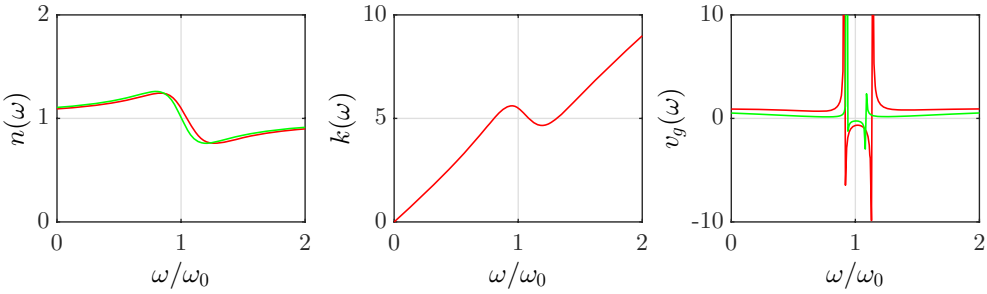

Figure 5.9: Group velocity near a broad transition.

5.1.7.8 Ex: Dispersion in a metal

The dispersion ratio in metals can be approximated by,

$$n^2(\omega) = 1 + \omega_p^2\left(\frac{f_e}{-\omega^2 - \imath\gamma_e\omega} + \sum_j \frac{f_j}{\omega_{0j}^2 - \omega^2 - \imath\gamma_j\omega}\right) \ ,$$

where ω_p is called the plasma frequency and f_e and f_j are constants. Calculate the group velocity $v_g(\omega)$.

Solution:

5.2 The Doppler effect

5.2.1 Sonic Doppler effect

Waves propagate from a source to an listener within an elastic material medium with the propagation velocity v. So far, we assumed the source, the medium, and the listener at rest. The question now is, what happens when one of these three components gets in motion.

5.2.1.1 Source in motion

We imagine a source emitting signals at frequency f_0. Within the time of a period $T = \frac{1}{f_0}$ these pulses travel a distance,

$$\lambda = vT = \frac{v}{f_0} \ , \tag{5.39}$$

within the medium. While the source is at rest, the distance between the pulses is λ. However, when the source moves in the propagation direction of the pulses, a resting listener judges that the pulses are emitted within the medium at reduced distances Δx, as shown in Fig. 5.10,

$$\Delta x = \lambda - u_s T \ . \tag{5.40}$$

A listener now receives the pulses at the increased frequency of,

$$f = \frac{v}{\Delta x} = \frac{v}{\lambda - u_s T} = \frac{v f_0}{v - u_s} = \frac{f_0}{1 - u_s/v} \ . \tag{5.41}$$

This effect is called *sonic Doppler effect*. For small velocities we can expand,

$$f = \frac{f_0}{1 \mp u_s/v} \simeq f_0 \left(1 \pm \frac{u_s}{v}\right) \ , \tag{5.42}$$

where the upper (lower) signals apply, when the source approaches (moves away from) the listener.

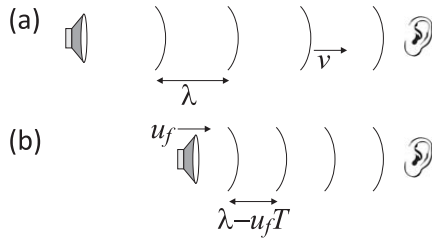

Figure 5.10: Doppler effect due to a motion of the source. In (a) the source is at rest, in (b) it moves toward the listener.

5.2.1.2 Listener in motion

Again, we consider the same source emitting signals at frequency f_0. While the source is at rest, the distance between the pulses is λ. However, when the listener is approaching the source, as shown in Fig. 5.11, pulses are recorded by the listener in a shorter time intervals,

$$T = \frac{\lambda}{v + u_r} = \frac{1}{f} \ . \tag{5.43}$$

That is, the listener measures a larger number of pulses,

$$f = f_0 \left(1 \pm \frac{u_r}{v}\right) \ , \tag{5.44}$$

where the upper (lower) signs apply, when the receiver approaches (moves away from) the source.

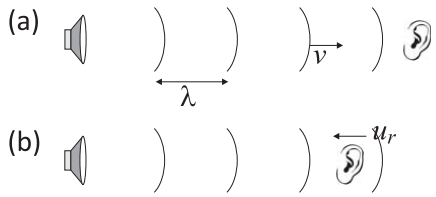

Figure 5.11: Doppler effect due to a motion of the listener. In (a) the listener is at rest, in (b) it moves toward the source.

5.2.1.3 Moving medium

We can combine the two Doppler effects into a single expression,

$$f = f_0 \frac{v^2 - \mathbf{v} \cdot \mathbf{u}_r}{v^2 - \mathbf{v} \cdot \mathbf{u}_s} \ . \tag{5.45}$$

The cases discussed above refer to the source or the listener being in motion *with respect to the medium carrying the wave* considered at rest. If the medium is moving at a velocity u_m, e.g. due to a wind moving the air, the velocities of the source and the listener with respect to the medium are modified, $u_s \to u_s - u_m$ and $u_r \to u_r - u_m$, such that,

$$f = f_0 \frac{1 - (u_r - u_m)/v}{1 - (u_s - u_m)/v} \ . \tag{5.46}$$

The same result is obtained by a transformation of the propagation velocity of the sound, $v \to v + u_m$.

5.2.2 Wave equation under Galilei transformation

The Galilei transformation says, that we obtain the function describing the motion in the system S' simply by substituting $x \to x'$ and $t \to t'$ with [3],

$$\begin{aligned} t' \equiv t \quad &\text{and} \quad x' \equiv x - ut \quad \text{or} \\ t \equiv t' \quad &\text{and} \quad x \equiv x' + ut \ , \end{aligned} \tag{5.47}$$

which implies,

$$v' = \frac{\partial x'}{\partial t'} = \frac{\partial x}{\partial t} - u = v - u \ . \tag{5.48}$$

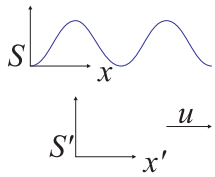

Figure 5.12: Wave in the inertial system S seen by an observer moving at the velocity u in the system S'.

Newton's classical mechanics is *Galilei invariant*, which means that fundamental equations of the type,

$$m\dot{v}_i = -\nabla_{x_i} \sum_j V_{ij}(|x_i - x_j|) \ , \tag{5.49}$$

do not change their form under *Galilei transform*. In contrast, the wave equation is not Galilei invariant. To see this, we consider a wave in the inertial system S being at rest with respect to the propagation medium. The wave is described by $Y(x,t)$ and satisfies the wave equation,

$$\frac{\partial^2 Y(x,t)}{\partial t^2} = c^2 \frac{\partial^2 Y(x,t)}{\partial x^2} \ . \tag{5.50}$$

An observer be in the inertial system S' moving with respect to S with velocity u, such that $x' = x - ut$. The question now is, what is the equation of motion for this wave described by $Y'(x',t')$, that is, we want to check the validity of,

$$\frac{\partial^2 Y'(x',t')}{\partial t'^2} \stackrel{?}{=} c^2 \frac{\partial^2 Y'(x',t')}{\partial x'^2} \ . \tag{5.51}$$

For example, the wave $Y(x,t) = \sin k(x - ct)$ traveling to the right is perceived in the system S', also traveling to the right, as $Y'(x',t') = \sin k[x' - (c-u)t'] = Y(x,t)$. Hence,

$$Y'(x',t') = Y(x,t) \ , \tag{5.52}$$

[3] Note that the Galilei transform,

$$\begin{pmatrix} ct' \\ x' \end{pmatrix} = G \begin{pmatrix} ct \\ x \end{pmatrix} \qquad \text{with} \qquad G \equiv \begin{pmatrix} 1 & 0 \\ -\beta & 1 \end{pmatrix}$$

is unitary because $\det G = 1$.

that is, we expect that the laws valid in S are also valid in S'. We calculate the partial derivatives,

$$\frac{\partial Y'(x',t')}{\partial t'} = \frac{\partial Y(x,t)}{\partial t'} = \frac{\partial t}{\partial t'}\left.\frac{\partial Y(x,t)}{\partial t}\right|_{x=const} + \frac{\partial x}{\partial t'}\left.\frac{\partial Y(x,t)}{\partial x}\right|_{t=const} = \frac{\partial Y(x,t)}{\partial t} + u\frac{\partial Y(x,t)}{\partial x}$$
$$\frac{\partial Y'(x',t')}{\partial x'} = \frac{\partial Y(x,t)}{\partial x'} = \frac{\partial t}{\partial x'}\left.\frac{\partial Y(x,t)}{\partial t}\right|_{x=const} + \frac{\partial x}{\partial x'}\left.\frac{\partial Y(x,t)}{\partial x}\right|_{t=const} = \frac{\partial Y(x,t)}{\partial x} \ . \quad (5.53)$$

Therefore, we come to the conclusion that in the system propagating with the wave, the wave equation is modified,

$$\begin{aligned}\frac{\partial^2 Y'(x',t')}{\partial t'^2} &= \frac{\partial^2 Y(x,t)}{\partial t^2} + 2u\frac{\partial^2 Y(x,t)}{\partial t\partial x} + u^2\frac{\partial^2 Y(x,t)}{\partial x^2} \\ &= c^2\frac{\partial^2 Y(x,t)}{\partial x^2} + 2u\frac{\partial^2 Y(x,t)}{\partial t\partial x} + u^2\frac{\partial^2 Y(x,t)}{\partial x^2} \\ &= (c^2+u^2)\frac{\partial^2 Y(x,t)}{\partial x^2} + 2u\frac{\partial^2 Y(x,t)}{\partial t\partial x} = (c^2-u^2)\frac{\partial^2 Y'(x',t')}{\partial x'^2} + 2u\frac{\partial^2 Y'(x',t')}{\partial t'\partial x'} \ .\end{aligned} \quad (5.54)$$

Only in cases, where the wavefunction can be written as $Y(x,t) = f(x-ct) = f(x'-(c-u)t') = f'(x'-ct') = Y'(x',t')$, do we obtain a wave equation similar to the one of the system S, but with the modified propagation velocity,

$$\begin{aligned}\frac{\partial^2 f'(x'-ct')}{\partial t'^2} &= (c^2-u^2)\frac{\partial^2 f'(x'-ct')}{\partial x'^2} + 2u\frac{\partial^2 f'(x'-ct')}{\partial x'\partial t'} \\ &= (c^2-u^2)\frac{\partial^2 f'(x'-ct')}{\partial x'^2} + 2u\frac{\partial^2 f(x'-(c-u)t')}{\partial x'\partial t'} \\ &= (c^2-u^2)\frac{\partial^2 f'(x'-ct')}{\partial x'^2} - 2u(c-u)\frac{\partial^2 f'(x'-ct')}{\partial x'^2} = (c-u)^2\frac{\partial^2 f'(x'-ct')}{\partial x'^2} \ .\end{aligned} \quad (5.55)$$

The observation that the wave equation is not Galilei-invariant expresses the fact that there is a preferential system for the wave to propagate, which is simply the system in which the propagation medium is at rest. Only in this inertial system will a spherical wave propagate isotropically.

Example 17 (*Wave equation under Galilei transformation*): We now verify the validity of the wave equation in the propagating system S' using the example of a sine wave,

$$\begin{aligned}&(c^2-u^2)\frac{\partial^2 \sin k[x'-(c-u)t']}{\partial x'^2} + 2u\frac{\partial^2 \sin k[x'-(c-u)t']}{\partial x'\partial t'} \\ &= -k^2(c^2-u^2)\sin k[x'-(c-u)t'] + 2uk^2(c-u)\sin k[x'-(c-u)t'] \\ &= -k^2(c-u)^2\sin k[x'-(c-u)t'] = \frac{\partial^2 \sin k[x'-(c-u)t']}{\partial t'^2} \ .\end{aligned}$$

5.2.3 Wave equation under Lorentz transformation

The question now is, how about electromagnetic waves which, as we have already noted and as has been verified by the famous Michelson experiment, survive without any medium. If there is no propagation medium, all inertial systems should be

equivalent and the wave equation should be the same in all systems, as well as the propagation velocity, i.e. the speed of light. These were the consideration of *Henry Poincaré*. To resolve the problem we need another transformation than the one of *Galileo Galilei*. Who found it first was *Hendrik Antoon Lorentz*, however the biggest intellectual challenge was to accept all the consequences that this transformation bears. It was *Albert Einstein* who accepted the challenge and created a new mechanics called *relativistic mechanics*. As the wave equation for electromagnetic waves, called the *Helmholtz equation*, is a direct consequence of Maxwell's theory, it is not surprising that the relativistic theory is not only compatible with the electrodynamic theory, but provides a deeper understanding of it.

We begin by making the ansatz of a general transformation interconnecting the temporal and spatial coordinates by four unknown parameters, γ, $\tilde{\gamma}$, β, and $\tilde{\beta}$,

$$ct = \gamma(ct' + \beta x') \qquad \text{and} \qquad x = \tilde{\gamma}(x' + \tilde{\beta}ct') \; . \tag{5.56}$$

The same calculation made for the Galilei transform now gives the first derivatives,

$$\frac{\partial Y'(x',t')}{c\partial t'} = \frac{\partial Y(x,t)}{c\partial t'} = \frac{\partial t}{\partial t'}\,\frac{\partial Y(x,t)}{c\partial t}\bigg|_{x=const} + \frac{\partial x}{c\partial t'}\,\frac{\partial Y(x,t)}{\partial x}\bigg|_{t=const} = \gamma\frac{\partial Y(x,t)}{c\partial t} + \tilde{\gamma}\tilde{\beta}\frac{\partial Y(x,t)}{\partial x} \tag{5.57}$$

$$\frac{\partial Y'(x',t')}{\partial x'} = \frac{\partial Y(x,t)}{\partial x'} = \frac{\partial ct}{\partial x'}\,\frac{\partial Y(x,t)}{c\partial t}\bigg|_{x=const} + \frac{\partial x}{\partial x'}\,\frac{\partial Y(x,t)}{\partial x}\bigg|_{t=const} = \gamma\beta\frac{\partial Y(x,t)}{c\partial t} + \tilde{\gamma}\frac{\partial Y(x,t)}{\partial x} \; .$$

The second derivatives and the application of the wave equation in the system S give,

$$\begin{aligned}
\frac{\partial^2 Y'(x',t')}{c^2\partial t'^2} &= \gamma^2\frac{\partial^2 Y(x,t)}{c^2\partial t^2} + 2\gamma\tilde{\gamma}\tilde{\beta}\frac{\partial^2 Y(x,t)}{c\partial t\partial x} + (\tilde{\gamma}\tilde{\beta})^2\frac{\partial^2 Y(x,t)}{\partial x^2} \\
&= \gamma^2\frac{\partial^2 Y(x,t)}{\partial x^2} + 2\gamma\tilde{\gamma}\tilde{\beta}\frac{\partial^2 Y(x,t)}{c\partial t\partial x} + (\tilde{\gamma}\tilde{\beta})^2\frac{\partial^2 Y(x,t)}{c^2\partial t^2} \\
&= (\gamma\beta)^2\frac{\partial^2 Y(x,t)}{c^2\partial t^2} + 2\gamma\tilde{\gamma}\beta\frac{\partial^2 Y(x,t)}{c\partial t\partial x} + \tilde{\gamma}^2\frac{\partial^2 Y(x,t)}{\partial x^2} = \frac{\partial^2 Y(x',t')}{\partial x'^2} \; .
\end{aligned} \tag{5.58}$$

That is, the wave equation in the system S' has the same form [4]. Thus, the requirement of invariance of the wave equation allows to affirm,

$$\gamma = \tilde{\gamma} \qquad \text{and} \qquad (\gamma\beta)^2 = (\tilde{\gamma}\tilde{\beta})^2 \qquad \text{and} \qquad \beta = \tilde{\beta} \; . \tag{5.59}$$

In addition, the transformation

$$\begin{pmatrix} ct' \\ x' \end{pmatrix} = L\begin{pmatrix} ct \\ x \end{pmatrix} \qquad \text{with} \qquad L \equiv \begin{pmatrix} \gamma & \gamma\beta \\ \gamma\beta & \gamma \end{pmatrix} \tag{5.60}$$

has to be unitary, that is,

$$1 = \det L = \gamma\tilde{\gamma} - \gamma\tilde{\gamma}\beta\tilde{\beta} = \gamma^2(1-\beta^2) \; , \tag{5.61}$$

[4] Note that the calculus is dramatically simplified using the covariant formalism of 4-dimensional *space-time vectors* introduced by *Hermann Minkowski* and *Gregory Ricci-Curbastro*.

which allows to relate the parameters γ and β by,

$$\gamma = \frac{1}{\sqrt{1-\beta^2}} \ . \tag{5.62}$$

Finally and obviously, we expect to recover the Galilei transform at low velocities,

$$ct = \gamma(ct' + \beta x') \to ct \qquad \text{and} \qquad x = \gamma(x' + \beta ct') \to x + ut \ . \tag{5.63}$$

That is, the limit is obtained by $\gamma \to 1$ and $\gamma\beta c \to u$, such that,

$$\beta = \frac{u}{c} \ . \tag{5.64}$$

such that the *Lorentz transform* from one inertial system S to another system S' is,

$$\begin{aligned} t' &= \gamma\left(t - \tfrac{u}{c^2}x\right) \qquad \text{and} \qquad x' = \gamma(x - ut) \qquad \text{or} \\ t &= \gamma\left(t' + \tfrac{u}{c^2}x'\right) \qquad \text{and} \qquad x = \gamma(x' + ut') \ . \end{aligned} \tag{5.65}$$

5.2.4 Relativistic Doppler effect

We have seen at the example of sonic waves, that the magnitude of the Doppler effect depends on who moves with respect to the medium, whether it is the source or the listener. Electromagnetic waves, however, propagate in empty space, hence there is no material medium or wind. According to Einstein's theory of relativity, there is no absolute motion and the propagation velocity of light is the same for all inertial systems. Therefore, the theory of the sonic Doppler effect can not apply to electromagnetic waves. To deal with the Doppler effect of light, we need to talk a little about time dilation.

5.2.4.1 Dilation of time

We consider a clock flying through the lab S with the velocity v. The clock produces regular time intervals for which we measure in the lab the duration $t_2 - t_1$. The spatio-temporal points are Lorentz-transformed to the system S' in which the clock is at rest by,

$$\begin{pmatrix} ct'_j \\ z'_j \end{pmatrix} = \begin{pmatrix} \gamma ct_j - \gamma\beta z_j \\ -\gamma\beta ct_j + \gamma z_j \end{pmatrix} \ . \tag{5.66}$$

Hence,

$$\begin{aligned} t'_2 - t'_1 &= \gamma t_2 - \gamma\beta\frac{z_2}{c} - \gamma t_1 + \gamma\beta\frac{z_1}{c} \\ &= \gamma t_2 - \beta\left(\frac{z'}{c} + \gamma\beta t_2\right) - \gamma t_1 + \beta\left(\frac{z'}{c} + \gamma\beta t_1\right) = \gamma^{-1}(t_2 - t_1) \ . \end{aligned} \tag{5.67}$$

Consequently, in the lab the time interval seems longer than in the resting system.

Example 18 (*Doppler effect on a moving laser*): Coming back to the Doppler effect we now consider a light source flying through the lab S, for example, a laser operating at a frequency ω', which is well defined by an atomic

transition of the active medium. A spectrometer installed in the same resting system S' as the laser will measure just this frequency. Now we ask ourselves, what frequency would a spectrometer installed in the lab measure. The classical response has been derived for a moving sound source,

$$\omega = \omega' - ku = \omega' - \frac{\omega}{c}u = \frac{\omega'}{1+\frac{u}{c}} \ , \tag{5.68}$$

with $k = \omega/c$. But now, because of time dilation, we need to multiply by γ,

$$\omega = \frac{\gamma^{-1}\omega'}{1+\frac{u}{c}} = \sqrt{\frac{1-\beta}{1+\beta}}\omega' \simeq \omega'\left(1 \pm \frac{u}{c} + \frac{u^2}{2c^2}\right) \ . \tag{5.69}$$

5.2.5 Exercises

5.2.5.1 Ex: Sonic Doppler effect

A speaker hanging from a wire of length $L = 1\,\mathrm{m}$ oscillates with a maximum angle of $\theta_m = 10°$ and emits a sound of $\nu = 440\,\mathrm{Hz}$.
a. What is the frequency of oscillation of the pendulum?
b. What is the energy $E_{cin} + E_{pot}$ of the oscillation?
c. What is the maximum oscillation speed?
d. What are the minimum and maximum frequencies of the sound perceived by a stationary receiver.

Solution: *a. The pendulum's oscillation frequency is,*

$$\omega = \sqrt{\frac{g}{L}} = 2\pi \cdot 0.5\,\mathrm{Hz} \ .$$

b. The energy of the oscillation is,

$$E_{cin} + E_{pot} = \tfrac{m}{2}v^2 + mg(L - L\cos\theta) = \tfrac{m}{2}v_m^2 = mg(L - L\cos\theta_m) = 0.149\,\mathrm{J} \ .$$

c. Therefore, the maximum speed of the speaker is,

$$v_m = \sqrt{2gL(1-\cos\theta_m)} = 54.6\,\mathrm{cm/s} \ .$$

d. The speed of sound being $v_s = 340\,\mathrm{m/s}$, the minimum and maximum sound frequencies are,

$$\nu_r = \nu_f \frac{v_s}{v_s \pm v_m} = 440\,\mathrm{Hz} \ \ \frac{340}{340 \pm 0.3} = 439.3 \ (440.7)\,\mathrm{m/s} \ .$$

5.2.5.2 Ex: Sonic Doppler effect

Two identical speakers uniformly emit sound waves of $f = 680\,\text{Hz}$. The audio power of each speaker is $P = 1\,\text{mW}$. A point P is $r_1 = 2.0\,\text{m}$ away from one device and $r_2 = 3.0\,\text{m}$ from the other.
a. Calculate the intensities I_1 and I_2 of the sound from each speaker separately at the P.
b. If the emission of the speakers were coherent and in phase, what would be the sound intensity in P?
c. If the emission of the speakers were coherent with a phase difference of 180°, what would be the sound intensity in P?
d. If the speaker output were incoherent, what would be the sound intensity in P?

Solution: *a. First speaker (distance r_1):*

$$I_1 = \frac{P}{4\pi r_1^2} = 19.9\,\mu\text{W/m}^2 \ .$$

Second speaker (distance r_2):

$$I_2 = \frac{P}{4\pi r_2^2} = 8.849\,\mu\text{W/m}^2 \ .$$

b. Knowing that the frequency is constant, and that the intensity I is proportional to the square of the amplitude A, it is possible to calculate the intensity when the interference is fully constructive (intensity is maximum) by: $A = C\sqrt{I}$. Since the frequency is constant, C will be the same value at any given point. Adding the amplitudes, we get,

$$\sqrt{I_{max}} = A/C = \sqrt{I_1} + \sqrt{I_2}$$
$$I_{max} = (\sqrt{I_1} + \sqrt{I_2})^2 = 55.3\,\mu\text{W/m}^2 \ .$$

c. Same as for the previous item, however, knowing that in totally destructive interference, the intensity is minimal and its amplitudes are subtracted, we get,

$$\sqrt{I_{min}} = A/C = \sqrt{I_1} - \sqrt{I_2}$$
$$I_{min} = (\sqrt{I_1} - \sqrt{I_2})^2 = 2.21\,\mu\text{W/m}^2 \ .$$

d. Knowing that these are incoherent waves, we just add the intensities:

$$I = I_1 + I_2 = 19.9\,\mu\text{W/m}^2 + 8.849\,\mu\text{W/m}^2 = 28.7\,\mu\text{W/m}^2 \ .$$

5.2.5.3 Ex: Sonic Doppler effect

Suppose that a source of sound and a listener are both at rest, but the medium is moving relative to this frame. Will there be any variation in the frequency heard by

the observer?

Solution: *No, because within the inertial system moving together with the medium the frequency would actually be shifted up (down) when the medium moves in the direction opposite (parallel) to the vector pointing from the source to observer. But this effect is compensated by the opposite effect upon sound reception by the listener, who hears the frequency lower (higher) when the medium moves in the opposite (parallel) direction.*

5.2.5.4 Ex: Sonic Doppler effect

Consider a source that emits waves of frequency f_{fnt} moving at velocity v_{fnt} on the x-axis. Consider an observer moving with velocity v_{obs} also on the x-axis. What will be the frequency perceived by the observer? Call the wave propagation velocity of c.

Solution: *Be x_{fnt} the position of the sound source and $v_{fnt} > 0$ its speed relative to the x-axis. The wavelength produced by the source in a medium is given by,*

$$\lambda_{med} = \lambda_{fnt}\left(1 - \frac{v_{fnt}}{c}\right) = \frac{c}{f_{fnt}}\left(1 - \frac{v_{fnt}}{c}\right) \ ,$$

where $c > 0$ in the region $x > x_{fnt}$ and $c < 0$ in the region $x < x_{fnt}$. Now, an observer in the region $x > x_{fnt}$ that moves with speed v_{obs} relative to the x-axis probes this wavelength with frequency,

$$\begin{aligned} f_{obs} &= \frac{c - v_{obs}}{\lambda_{med}} = \frac{c - v_{obs}}{\frac{c}{f_{fnt}}\left(1 - \frac{v_{fnt}}{c}\right)} = f_{fnt}\frac{1 - \frac{v_{obs}}{c}}{1 - \frac{v_{fnt}}{c}} \\ &\simeq f_{fnt}\left(1 - \frac{v_{obs}}{c}\right)\left(1 + \frac{v_{fnt}}{c}\right) = f_{fnt}\left(1 - \frac{v_{obs} - v_{fnt}}{c} - \frac{v_{obs}v_{fnt}}{c}\right) \\ &\simeq f_{fnt}\left(1 - \frac{v_{obs} - v_{fnt}}{c}\right) \ . \end{aligned}$$

5.2.5.5 Ex: Sonic Doppler effect

Two trains travel on rails in opposite directions at velocities of the same magnitude. One of them is whistling. The whistle frequency perceived by a passenger on the other train ranges from 348 Hz when approaching to 259 Hz when moving away.
a. What is the velocity of the trains.
b. What is the frequency of the whistle.

Solution: *a.* 90 km/h,
b. 300 Hz.

5.2.5.6 Ex: Sonic Doppler effect

On a mountain road, while approaching a vertical wall which the road will surround, a driver is honking his horn. The echo from the wall interferes with the sound of the horn, producing 5 beats per second. Knowing that the frequency of the horn is 200 Hz, what is the speed of the car?

Solution: 15 km/h.

5.2.5.7 Ex: Sonic Doppler effect

A fixed sound source emits a sound of frequency ν_0. The sound is reflected by a fast approaching object (velocity u). The reflected echo returns to the source, where it interferes with the emitted waves giving rise to frequent beats $\Delta\nu$. Show that it is possible to determine the amplitude of the velocity of the moving object $|u|$ as a function of $\Delta\nu$, of ν_0, and of the speed of sound c.

Solution: $|u| = \frac{\nu\Delta\nu}{2\nu_0+\Delta\nu}$.

5.2.5.8 Ex: Sonic Doppler effect

Two cars (1 and 2) drive in opposite directions on a road, with velocities of amplitudes v_1 and v_2. Car 1 travels against the wind, whose velocity is V. At sight of car 2 the driver of car 1 presses his horn, whose frequency is ν_0. The speed of sound in motionless air is c. What is the frequency ν of the horn sound perceived by the driver of car 2? What is the frequency ν' heard by the driver of a car 3 traveling in the same direction as car 1 and at the same speed?

Solution: $\nu = \nu_0 \frac{c-V+v_2}{c-V-v_1}$; $\nu' = \nu_0$.

5.2.5.9 Ex: Sonic Doppler effect

A physicist is molested by a fly orbiting his head. Since he is also a musician, he realizes that the sound of the buzz varies by one pitch. Calculate the speed of the fly.

Solution:

5.2.5.10 Ex: Doppler effect

a. In a storm with wind velocity v a speaker well attached to the ground makes a sound of frequency f_0. How do you calculate the frequency recorded by a microphone taken by the wind and driven away from the speaker at the speed u?
b. Verify your answer in (a) by comparing the three cases (i) $u = 0$, (ii) $u = v$, and (iii) $v = 0$ with the cases of a moving source or receiver.

Solution: *a. In the system where the air is at rest the speaker is moving away with the speed v. Therefore, the frequency that would be perceived by a listener moving along with the wind is,*

$$f_{medium} = \frac{f_0}{1+v/c} \ .$$

In the system where the air is at rest the microphone is moving away in the same direction as the speaker with the speed $u - v < 0$. Hence,

$$f_{micro} = f_{medium}\left(1 - \frac{u-v}{c}\right) = f_0 \frac{1-(u-v)/c}{1+v/c} = f_0\left(1 + \frac{-u/c}{1+v/c}\right) \ .$$

Alternatively, we calculate the Doppler shift first disregarding the wind,

$$f_{rep} = f_0\left(1 - \frac{u}{c}\right) \ ,$$

and transforming to the wind system by, $c \to c+v$, giving the same result,

$$f = f_0\left(1 - \frac{u}{c+v}\right) \ .$$

b. (i) With the microphone fixed to the ground $u = 0$, we observe $f = f_0$.
(ii) In case where the microphone reaches the wind speed, $u = v$, we observe $f = f_0 \frac{1}{1+v/c}$, which is the Doppler effect of a moving source.
(iii) Without wind $v = 0$ but with a microphone velocity u we observe $f = f_0\left(1 - \frac{u}{c}\right)$, which is the Doppler of a moving receiver.

5.2.5.11 Ex: Sonic Doppler effect

A citizen of São Carlos is molested by a Tucano airplane operated by the Academia das Forças Aéreas de Pirassununga. He notices that while the airplane realizes looping on top of his head, the emitted sounds varies by up to an octave. Estimate the airplane's velocity.

Solution: *Assuming for simplicity that the airplane moves with uniform velocity on a straight line passing near by the citizen, we calculate for the maximum and minimum velocities $\pm u_s$ with respect to the observer,*

$$f_0\left(1 + \frac{u_s}{v}\right) = 2f_0\left(1 - \frac{u_s}{v}\right) \ ,$$

from which we obtain $u_s = \frac{v}{3}$ independently of the emitted sound frequency.

5.3 Interference

The superposition of two counterpropagating waves can generate a *standing wave*. In these waves the oscillation amplitude depends on the position, but there is no energy transport.

5.3.1 Standing waves

We consider two waves $Y_\pm(x,t) = A\cos(kx \mp \omega t + \phi)$ propagating in opposite directions. In the case of a string this situation can be realized, e.g. by exciting a wave $Y_-(x,t)$ propagating in $-x$ direction, reflecting it subsequently at the end of the string ($x = 0$), and letting the wave $Y_+(x,t)$ propagate back in x direction,

$$Y(x,t) = Y_-(x,t) + Y_-(x,t) = A\cos(kx + \omega t) \pm A\cos(kx - \omega t) \ . \tag{5.70}$$

The sign of the reflected wave depends on how the end of the string is attached. If the end is fixed, the reflected wave inverts its amplitude. If it is free to move, the amplitude remains unaltered.

Let L be the length of the rope. The boundary conditions can be formulated as follows: When one end is clamped, the oscillation amplitude must be zero at this end,

$$Y(0,t) = 0 \qquad \text{or} \qquad Y(L,t) = 0 \ . \tag{5.71}$$

When one end is loose, the amplitude of oscillation must be maximum,

$$Y(0,t) = A \qquad \text{or} \qquad Y(L,t) = A \ . \tag{5.72}$$

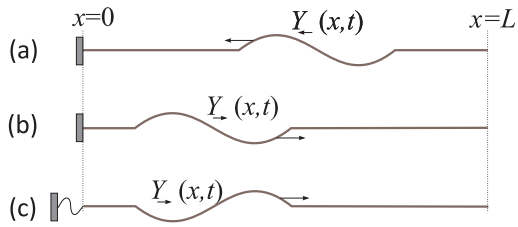

Figure 5.13: Superposition of a left-bound wave (a) with a wave reflected at a clamped end (b) or a loose end (c).

5.3.1.1 Rope with two ends fastened

In case that the two ends of the rope are clamped, we can simplify the superposition (5.70),

$$Y(x,t) = A\cos(kx + \omega t) - A\cos(kx - \omega t) = 2\sin kx \sin \omega t \ . \tag{5.73}$$

The boundary condition, $Y(L,t) = 0$, requires,

$$kL = \frac{2\pi L}{\lambda} = n\pi \ , \tag{5.74}$$

for a natural number n. This means that for a given length L and a given propagation velocity v, we can only excite oscillations satisfying,

$$\lambda = \frac{2L}{n} \qquad \text{and} \qquad \nu = \frac{v}{\lambda} = n\frac{v}{2L} \ . \tag{5.75}$$

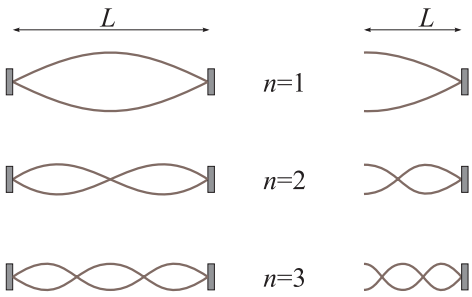

Figure 5.14: Vibration modes of a string fot (left) both ends tight up and (right) for one loose end.

5.3.1.2 Rope with one free end

In case that the end of the string at $x = 0$ is loose, we can simplify the superposition (5.70),

$$Y(x,t) = A\cos(kx + \omega t) + A\cos(kx - \omega t) = 2\cos kx \cos \omega t \ . \tag{5.76}$$

The boundary condition, $Y(L,t) = 0$, requires,

$$\phi = \tfrac{\pi}{2} \qquad \text{and} \qquad kL = \frac{2\pi L}{\lambda} = \left(n - \tfrac{1}{2}\right)\pi \ , \tag{5.77}$$

for a natural number n. This means that for a given length L and a given propagation velocity v, we can only excite oscillations satisfying,

$$\lambda = \frac{2L}{n - \frac{1}{2}} \qquad \text{and} \qquad \nu = \frac{v}{\lambda} = \left(n - \tfrac{1}{2}\right)\frac{v}{2L} \ . \tag{5.78}$$

Example 19 (*Stationary sound wave*):

- Exciting a stationary sound wave in a bottle.
- Exciting a standing sound wave on a guitar string.

5.3.2 Interferometry

5.3.2.1 Phase matching of two laser beams

When phase-matching two plane waves $\mathcal{E}_1 = Ae^{\imath\omega_1 t}$ and $\mathcal{E}_2 = Ae^{\imath\omega_2 t}$ on a photodiode, such that their wavevectors are parallel, the photodiode generates a *beat signal*,

$$I = |E_1 + E_2|^2 = AB[2 + 2\cos(\omega_1 - i\omega_2)t] \ . \tag{5.79}$$

In order to get a high signal contrast, a good phase-matching is important. It is particularly important to adjust the wavevectors to be absolutely parallel. In practice, however, this can be tricky, as the laser beams are frequently not plane waves, but have a finite diameter and radius of curvature.

Example 20 (*Laser interferometry*):

- Construct Michelson and Mach-Zehnder laser interferometers with one mirror mounted on a piezo. Show interference rings.

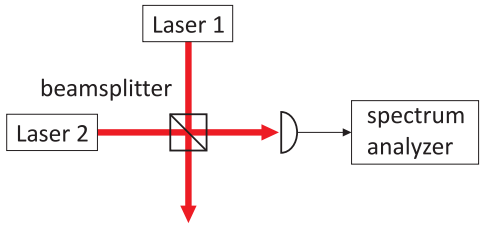

Figure 5.15: Principle of a beat frequency measurement.

5.3.3 Diffraction

According to the Huygens principle, each point P_z within a slit emits a spherical wave reaching a given point P_k of the screen with a phase lag corresponding to the distance, as shown in Fig. 5.16,

$$r_{12} = \overline{P_\eta P_y} = \sqrt{(y-\eta)^2 + z^2} \ . \tag{5.80}$$

Thus, the phase difference between this ray and a ray coming out of the origin (which we place somewhere on the optical axis) is,

$$\phi = k\Delta r_{12} = k(\sqrt{(y-\eta)^2+z^2} - \sqrt{y^2+z^2}) \simeq -\frac{ky\eta}{\sqrt{y^2+z^2}} \simeq -\frac{ky\eta}{z} \equiv q\eta \ , \tag{5.81}$$

with $q = k\sin\alpha = ky/z$. If $A(\eta)$ is the amplitude of the excitation at the point η of the slit, then $B(y) = \frac{1}{z}e^{\imath\phi}$ is the amplitude at point y of the screen. Adding the contributions of all points,

$$B(q) = \sum_z e^{\imath\phi(y,z)} \to \int A(\eta) e^{\imath q\eta} d\eta \ . \tag{5.82}$$

We see that the amplitude distribution on the screen $B(y)$ is nothing more than the Fourier transform of the amplitude distribution $A(\eta)$ within the slit, regardless of the shape of the slit.

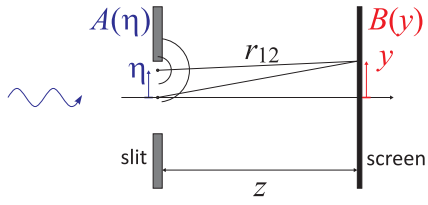

Figure 5.16: Fraunhofer diffraction at the slit.

The theory can be extended to 2D and 3D geometries, for example, a distribution of point-like scatterers within a given volume.

5.3.3.1 Single slit

As an example, we calculate the interference pattern behind a single slit. The Fourier transform of $A(\eta) = \chi_{[-d/2,d/2]}$ is,

$$B(q) = \int_{-d/2}^{d/2} e^{\imath q\eta} d\eta = \left. \frac{e^{\imath q\eta}}{\imath q} \right|_{-d/2}^{d/2} = d \frac{\sin \frac{1}{2} qd}{\frac{1}{2} qd} \ . \tag{5.83}$$

The intensity is $I(q) = c\varepsilon_0 |B(q)|^2$.

5.3.3.2 Diffraction grating

We now calculate the interference pattern behind a diffraction grating with $N = 1000$ infinitely thin slits aligned within one millimeter. The Fourier transform of $A(\eta) = \sum_{n=1}^{N} \chi_{[(n-1)d,(n-1)d+\Delta d]}$ is,

$$\begin{aligned} B(q) = \sum_{n=1}^{N} \int_{(n-1)d}^{(n-1)d+\Delta d} e^{\imath q\eta} d\eta = \frac{e^{\imath q\Delta d} - 1}{\imath q} \sum_{n=1}^{N} e^{\imath (n-1) qd} \\ \simeq \Delta d \sum_{n=0}^{N} e^{\imath nqd} = \Delta d \frac{1 - e^{\imath Nqd}}{1 - e^{\imath qd}} \ , \end{aligned} \tag{5.84}$$

where we approximated for $q\Delta d \ll 1$. For $N \to \infty$ we can approximate further,

$$B(q) = \frac{\Delta d}{1 - e^{\imath qd}} \ . \tag{5.85}$$

This is the *Airy function*, which is zero everywhere except at points where $qd = 2n\pi$. The intensity is,

$$I(q) = c\varepsilon_0 |B(q)|^2 = c\varepsilon_0 \frac{\Delta d^2}{2 - 2\cos qd} = c\varepsilon_0 \left(\frac{\Delta d}{2 \sin \frac{qd}{2}} \right)^2 \ . \tag{5.86}$$

The grating constant is $d = 0.001\,\text{mm}$. The resulting pattern can be interpreted as arising from a regular chain of antennas emitting synchronously. With a large number of point antennas, the chain emits in very well-defined directions. In addition, the direction can be controlled by arranging for a well-defined phase shift between the fields driving neighboring antennas.

5.3.4 Plane and spherical waves

In three dimensions the wave equation takes the form,

$$0 = \Box E \equiv \left(\frac{1}{c^2} \frac{\partial}{\partial t} - \nabla^2 \right) E \ . \tag{5.87}$$

In Cartesian coordinates, this gives,

$$0 = \left(\frac{1}{c^2} \frac{\partial^2}{\partial t^2} - \frac{\partial^2}{\partial x^2} - \frac{\partial^2}{\partial y^2} - \frac{\partial^2}{\partial z^2} \right) E \ . \tag{5.88}$$

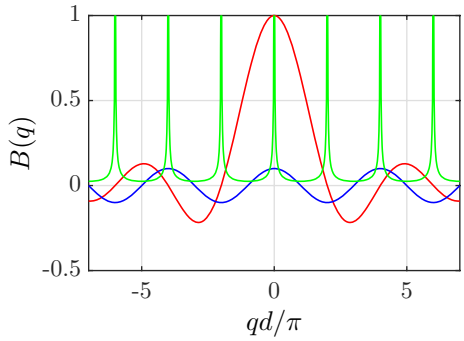

Figure 5.17: (code) Intensity distribution behind a diffraction grating for a single slit (red), a double slit (blue), and an infinite diffraction grating (green).

Plane waves, that is, waves described by the function,

$$Y(\vec{r},t) = Y_0 \sin(\vec{k}\cdot\vec{r} - \omega t) \ , \tag{5.89}$$

satisfy the wave equation if,

$$0 = -\frac{\omega^2}{c^2} + k_x^2 + k_y^2 + k_z^2 = -\frac{\omega}{c^2} + \vec{k}^2 \ . \tag{5.90}$$

5.3.4.1 Spherical waves

Spherical waves, that is, waves described by the function,

$$Y(\mathbf{r},t) = f(r)\sin(kr - \omega t) \ , \tag{5.91}$$

also satisfy the wave equation, provided the function $f(r)$ satisfies certain conditions. To find these conditions we use the representation of the *Laplace operator* in spherical coordinates,

$$\nabla^2 = \frac{1}{r}\frac{\partial^2}{\partial r^2}r + \frac{1}{r^2\sin\theta}\frac{\partial}{\partial\theta}\left(\sin\theta\frac{\partial}{\partial\theta}\right) + \frac{1}{r^2\sin^2\theta}\frac{\partial^2}{\partial\phi^2} \ , \tag{5.92}$$

and insert the ansatz for $Y(\mathbf{r},t)$ into the wave equation. We have on one hand,

$$\frac{1}{c^2}\frac{d^2}{dt^2}(f\sin) = -\frac{\omega^2}{c^2} f\sin \ . \tag{5.93}$$

On the other hand,

$$\begin{aligned}\frac{1}{r}\frac{d^2}{dr^2}(rf\sin) &= \frac{1}{r}\frac{d}{dr}[f\sin + rf'\sin + krf\cos] \\ &= f''\sin + \frac{2f'}{r}\sin - k^2 f\sin + \frac{2k}{r}f\cos + 2kf'\cos \ ,\end{aligned} \tag{5.94}$$

such that,

$$0 = \Box f\sin = -\left(f'' + \frac{2f'}{r}\right)\sin - 2k\left(f' + \frac{f}{r}\right)\cos \ . \tag{5.95}$$

Thus the function f must satisfy the radial differential equation,

$$rf' + f = 0 \ . \tag{5.96}$$

This equation can be easily solved with the result $f(r) = r^{-1}$.

5.3.5 Formation of light beams

We consider monochromatic waves with frequency ω. Other waveforms can be synthesized by superpositions of waves with different frequencies. We also restrict to scalar waves. In fact, electromagnetic light fields are vectorial, however, close to the axis of an optical beam the fields are practically uniformly polarized, and representing the amplitude of the field by a scalar wave is an excellent approximation. The field amplitude $\psi(\mathbf{r}, t)$ is governed by the following scalar wave equation,

$$\nabla^2\psi = \frac{1}{c^2}\frac{\partial^2\psi}{\partial t^2} \ . \tag{5.97}$$

We let ψ be of the form,

$$\psi(\mathbf{r}, t) = A(\mathbf{r})e^{\imath[\phi(\mathbf{r})-\omega t]} \ , \tag{5.98}$$

where A and ϕ are real functions of space. A is the *amplitude*, and the exponent is called the *phase* of the wave. In this form, it is implied that abrupt spatial or temporal variations are contained in the phase. The surface obtained by fixing the phase equal to a constant,

$$\phi(\mathbf{r}) - \omega t = const \tag{5.99}$$

is called *wave front* or *phase front*. The fast motion associated with a wave can be followed through the propagation of a particular wavefront. The interference between two waves is formed by the fronts of the two waves. The speed at which a particular wavefront is moving is called *phase velocity*. Suppose we follow a particular wavefront at the moment t: At time $t + \Delta t$, the phase front will have moved to another surface. A point $\mathbf{r}$ on the original surface will have moved to another point $\mathbf{r} + \Delta\mathbf{r}$ [see Fig. 5.18(a)]:

$$\phi(\mathbf{r} + \Delta\mathbf{r}) - \omega(t + \Delta t) = \phi(\mathbf{r}) - \omega t = const \tag{5.100}$$

Expanding $\phi(\mathbf{r} + \Delta\mathbf{r}) \simeq \phi(\mathbf{r}) + \nabla\phi(\mathbf{r})\Delta\mathbf{r}$, we obtain,

$$\nabla\phi(\mathbf{r})\Delta\mathbf{r} = -\omega t \ . \tag{5.101}$$

$\nabla\phi(\mathbf{r})$ is orthogonal to the phase front and is called the *wavevector*. $\Delta\mathbf{r}$ is smallest in the direction $\nabla\phi$, and the wavefront propagates with the velocity,

$$\frac{|\Delta\mathbf{r}|}{\Delta t} = \frac{\omega}{|\nabla\phi(\mathbf{r})|} \ . \tag{5.102}$$

which is the *phase velocity*. The phase velocity can vary from point to point in space.

Example 21 (*Phase velocity of a superposition of two plane waves*): The superposition of two plane waves with wavevectors $\mathbf{k}_{1,2} = k\hat{\mathbf{e}}_z\cos\theta \pm k\hat{\mathbf{e}}_x\sin\theta$ is described by,

$$\psi(\mathbf{r}, t) = A_0e^{\imath(\mathbf{k}_1\cdot\mathbf{r}-\omega t)} + A_0e^{\imath(\mathbf{k}_2\cdot\mathbf{r}-\omega t)} = 2A_0\cos(kx\sin\theta)e^{\imath(kz\cos\theta-\omega t)} \ . \tag{5.103}$$

The phase front of this wave is a plane with normal vectors pointing along the z-axis, as illustrated in Fig. 5.18(b), and the phase velocity is now $\omega/k\cos\theta = c/\cos\theta > c$.

5.3.5.1 Beam formation by superposition of plane waves

Plane waves extend throughout the space and are uniform in transverse direction, whereas an *optical beam* is confined in transverse direction. However, as we saw in the last example, by superposing two plane waves, a resulting wave can be obtained which varies sinusoidally in transverse direction. By extrapolating this concept to superpositions of many plane waves, it is possible to construct by interference arbitrary transverse amplitude distributions. The propagation of a confined wave is the essence of *diffraction theory*. A particular case is the Gaussian beam. For mathematical simplicity and ease of visualization let us restrict ourselves to waves in two dimensions in the x-z plane. Only in the final phase will we present the complete results for three-dimensional Gaussian beams.

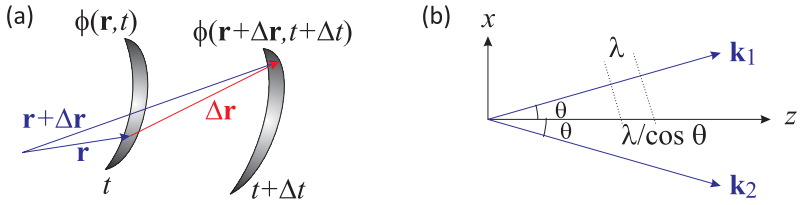

Figure 5.18: Superposition of two plane waves. The phase velocity along the direction z is higher than c, the speed of light, because in one period, the wavefront of each partial wave propagates over a distance λ, but along the z axis over a distance of $\lambda/\cos\theta$.

Before going into detailed calculations, we consider the last example again. The transverse standing wave resulting from the superposition of two plane waves, each one propagating at an angle θ with respect to the z-axis has a spatial frequency $k\sin\theta \simeq k\theta$ for small θ. We now come to a very important property of wave diffraction. Suppose that, in order to confine the wave in transverse direction, we continue adding plane waves, each one propagating at a different small angle θ, so that the amplitude adds constructively within the range $|x| < \Delta x$ and destructively out of it. By the uncertainty principle that results from the Fourier analysis and applies to this case,

$$\Delta(k\theta)\Delta x \gtrsim 1 \ . \tag{5.104}$$

That is, to confine a beam inside a width of Δx, it requires a distribution of plane waves in an angular spreading of at least $\lambda/2\pi\Delta x$. The angular spreading means that the beam will eventually diverge with an angle $\Delta\theta$.

5.3.5.2 Fresnel integrals and beam propagation

Let us now superpose plane waves in a way to form a beam. Each partial wave propagates under some angle θ with respect to the z-axis and has an amplitude

$A(\theta)d\theta$, so that the resulting wave (omitting the harmonic temporal variation) is,

$$\psi(x,z) = \int d\theta A(\theta) e^{\imath kx \sin\theta + \imath kz\cos\theta} \ . \tag{5.105}$$

In the so-called *paraxial approximation*, $A(\theta)$ is significant only within a small angular interval close to zero. This means that, according to Eq. (5.104), the transverse dimension of the beam is large in comparison to the wavelength. Expanding the trigonometric functions up the order θ^2,

$$\psi(x,z) \simeq \int d\theta A(\theta) e^{\imath kx\theta + \imath kz(1-\theta^2/2)} = e^{\imath kz} \int d\theta A(\theta) e^{\imath kx\theta - ikz\theta^2/2} \ . \tag{5.106}$$

This wave can be considered as a plane wave, $e^{\imath kz}$, modulated by the integral of (5.106). The expression (5.106) completely describes the propagation of the wave, provided that the wave is known at some point, say $z = 0$. In fact, at $z = 0$, the expression (5.106) for $\psi_0(x) \equiv \psi(x,0)$ is a Fourier transform, whose inverse yields the angular distribution,

$$A(\theta) = \frac{k}{2\pi} \int d\xi \psi_0(\xi) e^{-\imath k\xi\theta} \ . \tag{5.107}$$

Substitution of $A(\theta)$ back into Eq. (5.106) gives,

$$\psi_z(x) \equiv \psi(x,z) = \frac{k}{2\pi} e^{\imath kz} \int d\theta \int d\xi \psi_0(\xi) e^{\imath(k\theta x - k\theta\xi - kz\theta^2/2)} \ . \tag{5.108}$$

From here on, in order to emphasize the different roles played by the transverse coordinates x and y, we will label the axial position z as an index to the wave function.

We can first integrate over θ via a quadratic extension of the exponent. The result,

$$\frac{k}{2\pi} e^{\imath kz} \int d\theta e^{\imath(k\theta x - k\theta\xi - kz\theta^2/2)} = \sqrt{\frac{k}{2\pi\imath z}} e^{\imath k(z + (x-\xi)^2/2z} \equiv h_z(x-\xi) \ , \tag{5.109}$$

gives us the field at the position z as an integral over ξ of the field in $z = 0$, $\psi_0(\xi)$. The expression (5.109) is called *impulse response*, *kernel*, *propagator*, or *Green's function*, depending on the context. Carry out the integral (5.109) in Exc. 5.3.6.17.

The kernel has very simple physical interpretations: It is the field at point (x,z) generated by a point source with unitary amplitude located in $(\xi,0)$. In the same time, it is a (two-dimensional) spherical wave in a paraxial form. To see this, we write the field of a two-dimensional spherical wave (i.e. a circular wave) with its center in $(\xi,0)$ as,

$$\sqrt{\frac{1}{r}} e^{\imath kr} \ , \tag{5.110}$$

where $r = \sqrt{(x-\xi)^2 + z^2}$. (Instead of $1/r$ as in three dimensions, the amplitude decreases as $\sqrt{1/r}$ in two dimensions.) Near the z-axis, we approximate $r \simeq z + (x-\xi)^2/2z$, and the spherical wave becomes,

$$\sqrt{\frac{1}{z}} e^{\imath k[z + (x-\xi)^2/2z]} \ , \tag{5.111}$$

which is the same expression as $h_z(x-\xi)$ in Eq. (5.109). Note that the quadratic term in $x-\xi$ can become considerable in comparison with the wavelength. Eq. (5.106) now becomes,

$$\boxed{\psi_z(x) = \int h_z(x-\xi)\psi_0(\xi)d\xi = \sqrt{\frac{k}{2\pi\imath z}}e^{\imath kz}\int e^{\imath k(x-\xi)^2/2z}\psi_0(\xi)d\xi} \ . \tag{5.112}$$

We will call this integral the *Fresnel integral*. It is the mathematical expression of the *Huygens principle*: The field in (x,z) is the sum of all spherical waves centered on all previous points $(\xi,0)$ weighed with the respective field amplitude $\psi_0(\xi)$ [1204].

The expressions (5.106) and (5.112) represent two equivalent ways to calculate wave propagation. Eq. (5.106) calculates the wave from the angular distribution of its plane wave components. When the angular distribution is of Hermite-Gaussian type, a Gaussian beam results. In contrast, Eq. (5.112) computes the wave at a point z from the field at an initial point $z=0$. This is the traditional theory of Fresnel diffraction. Here, also a Gaussian beam results when ψ_0 is Hermite-Gaussian.

To deepen our understanding of beam propagation let us introduce the important concept of *near field* and *far field*. By 'near field' we mean a distance z sufficiently small to be allowed to neglect the quadratic term in the exponent of Eq. (5.106),

$$k\theta^2 z \ll 1 \ . \tag{5.113}$$

Then the near field, in zero-order approximation, is precisely the field at $z=0$ multiplied with propagation phase factor $e^{\imath kz}$,

$$\psi_z(x) \simeq e^{\imath kz}\int d\theta A(\theta)e^{\imath kz\theta} = e^{\imath kz}\psi_0(x) \ , \tag{5.114}$$

where the second equation follows from Eq. (5.107). Let us now examine the first-order correction and define 'near' more precisely.

The question is, what is the maximum angle of θ allowed in (5.113)? It is not $\pi/2$, but rather, it is the range of angles over which $A(\theta)$ is significantly different from zero. This angular range $\Delta\theta$ is related to the range of transverse distance Δx via the Fourier transform (5.104), so that,

$$\frac{\pi\Delta x^2}{\lambda} \gg z/2 \ . \tag{5.115}$$

The quantity on the left side, called the *Rayleigh range*, is the demarcation between the near and far field regimes. A simple physical interpretation for this quantity will be given below.

Let us now investigate the 'far field' regime of large z having a closer look at Eq. (5.112). When ψ_0 is confined to Δx, and if z is sufficiently large for the quadratic factor to be,

$$k\xi^2/2z \ll 1 \ , \tag{5.116}$$

or

$$\frac{\pi\Delta x^2}{\lambda} \ll z \ , \tag{5.117}$$

then it can be ignored, and the integral becomes,

$$\psi(x,z) \simeq \sqrt{\frac{k}{\imath 2\pi z}} e^{\imath k(z+x^2/2z)} \int e^{-\imath k x\xi/z} \psi_0(\xi) d\xi \ . \tag{5.118}$$

We see that the amplitude of the far field is given by the amplitude of the Fourier transform of the field at $z = 0$ except for a quadratic phase factor $kx^2/(2z)$ [5]

Let us go back to the near field and calculate the first-order correction. For small $z = \Delta z$, we can expand the exponent in equation (5.106),

$$\begin{aligned} \psi_z(x) &\simeq e^{\imath k\Delta z} \int d\theta A(\theta) \left(1 - \imath k \frac{\theta^2}{2} \Delta z\right) e^{\imath k\theta x} \\ &= e^{\imath k\Delta z} \psi_0(x) - e^{\imath k\Delta z} \frac{\imath k\Delta z}{2} \int d\theta A(\theta) \theta^2 e^{\imath k\theta x} \ . \end{aligned} \tag{5.119}$$

The last integral is,

$$\int d\theta A(\theta) \theta^2 e^{\imath k\theta x} = -\frac{1}{k^2} \frac{\partial^2}{\partial x^2} \int d\theta A(\theta) e^{\imath k\theta x} = -\frac{1}{k^2} \frac{\partial^2 \psi_0(x)}{\partial x^2} \ , \tag{5.120}$$

Such that close to $z = 0$, we get,

$$\psi_z(x) \simeq e^{\imath k\Delta z} \left[\psi(x,0) + \frac{\imath \Delta z}{2k} \frac{\partial^2 \psi(x,0)}{\partial x^2}\right] \ . \tag{5.121}$$

Note that the first-order correction is in quadrature with the zero-order term (5.114) (if ψ_0 is real), which means that the correction is in the phase, not in the amplitude. The second derivative can be seen as a diffusion operator [6], and it is this phase diffusion, which is the cause of phenomenon of *diffraction*.

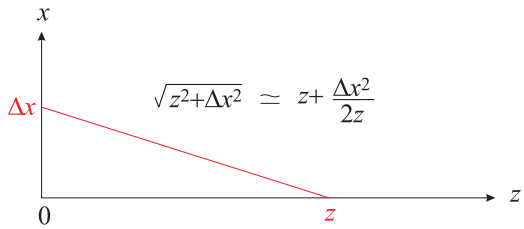

Figure 5.19: Illustration of the Rayleigh range: The distance from $(0,0)$ to $(0,z)$ is z. The distance from $(0,\Delta x)$ to $(0,z)$ is approximately $z + \Delta x^2/(2z)$. The difference is $\Delta x^2/(2z)$. Thus, a wave coming from $(0,0)$ and a wave coming from $(0,\Delta x)$ will acquire a phase difference of $k\Delta x^2/(2z)$ when they reach $(0,z)$. The phase difference is equal to 1 when z equals the Rayleigh range. The phase difference is insignificant in the far field, but significant in the near field.

We can generalize a little more: Suppose we write ψ as a plane wave $e^{\imath kz}$ modulated by a function with slow variation $u(x,z)$,

$$\psi_z(x) \equiv u_z(x) e^{\imath kz} \ , \tag{5.122}$$

[5] In fact, the phase factor can be circumvented by choosing z equal to a focal length f of a lens.

[6] This is because the second derivative of a Gaussian function is negative in the center and positive in the wings, so that when added to the original function, the distribution is reduced in the center and increased in the wings.

then

$$u_{\Delta z}(x) - u_0(x) = \frac{\imath \Delta z}{2k} \frac{\partial^2 u_0(x)}{\partial x^2} \ . \tag{5.123}$$

We derived this relation for a particular point on the z-axis, $z = 0$. However, there is no particular need to choose this point, and the relationship applies to any z. Thus, letting $\Delta z \to 0$, we get,

$$2ik \frac{\partial u}{\partial z} + \frac{\partial^2 u}{\partial x^2} = 0 \ . \tag{5.124}$$

This equation is called *paraxial wave equation*. It is an approximate form of the scalar wave equation and has the same form as the Schrödinger equation for a free particle. The equation can be generalized to three dimensions by a similar derivation:

$$\boxed{2\imath k \frac{\partial u}{\partial z} + \frac{\partial^2 u}{\partial x^2} + \frac{\partial^2 u}{\partial y^2} = 0} \ . \tag{5.125}$$

The *Fresnel integral is the solution of the paraxial wave equation* with a boundary condition for ψ at $z = 0$. We will show in Sec. 18.4.3 that a three-dimensional wave can be constructed from two-dimensional waves [1364]. The resulting Fresnel integral in three dimensions is,

$$\boxed{\psi_z(x,y) = \frac{e^{\imath kz}}{\imath \lambda z} \int e^{\imath k(x-\xi)^2/2z} e^{\imath k(y-\eta)^2/2z} \psi_0(\xi,\eta) d\xi d\eta} \ , \tag{5.126}$$

where $\psi_0(x,y)$ is the distribution of the field amplitude at $z = 0$. Note that, as required by energy conservation, in three dimensions the field decays like $1/z$ and not like $\sqrt{1/z}$, as it does in two dimensions. Note also that the pulse response in three dimensions is essentially the product of two two-dimensional pulse responses.

5.3.5.3 Application of Fresnel diffraction theory

The Fresnel diffraction integral, Eq. (5.112), can be applied in various situations illustrating its use and the difference between wave optics and geometric optics. Examples are the diffraction through a slit, the pin-hole camera, the focusing of a thin lens, etc. [1364].

Near-field diffraction (also called *Fresnel diffraction*) and far-field diffraction (also called *Fraunhofer diffraction*) are often distinguished by a quantity called the *Fresnel number*,

$$F \equiv \frac{a^2}{z\lambda} \ , \tag{5.127}$$

where a is the size of the beam (or *aperture*). The near field zone is defined by $F \gtrsim 1$, whereas in the far field zone, $F \ll 1$. For a Gaussian beam, letting $a = \sqrt{\pi} w_0$, we recover the Rayleigh length condition for Fresnel diffraction $z \lesssim z_R$, respectively Fraunhofer diffraction, $z \gg z_R$.

5.3.6 Exercises

5.3.6.1 Ex: Waves on a rope

A string with linear mass density μ is attached at two points distant by $L = 1\,\mathrm{m}$. A mass of $m = 1\,\mathrm{kg}$ is attached to one end of the string that goes over a pulley, as shown in the figure. Excited by a vibrating pin with frequency $f = 1\,\mathrm{kHz}$ the string performs transverse vibrations with the wavelength $\lambda = 2L$.
a. Calculate the sound velocity.
b. Now the mass is replaced by a mass $m' = 4m$. Calculate the new sound velocity.
c. Assuming the sound velocity, how often should the pin excite the string to observe the third oscillation mode (three anti-nodes)?

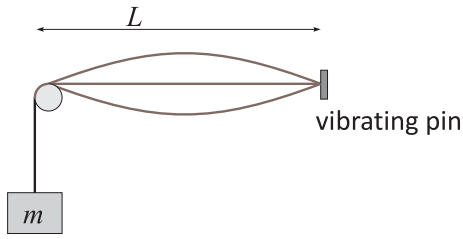

Figure 5.20: Waves on a rope.

Solution: *a. We have,*

$$v = \lambda_n f_n = \frac{2L}{n} f_n \ .$$

Hence, $v_1 = 2Lf_1 = 2\,\mathrm{km/s}$.
b. We have,

$$v' = \sqrt{\frac{m'g}{\mu}} = 2v \ .$$

Hence, $v_1' = 4\,\mathrm{km/s}$.
c. To calculate the new frequency,

$$v' = \lambda_3 f_3 = \frac{2L}{3} f_3 \ .$$

Hence, $f_3 = \frac{3v_1'}{2L} = 6\,\mathrm{kHz}$.

5.3.6.2 Ex: Optical cavity

Optical cavities consist of two light reflecting mirrors. Standing light waves must satisfy the condition that the electric and magnetic fields vanish on the mirror surfaces. What is the frequency difference between two consecutive modes of a of length $L = 10\,\mathrm{cm}$?

Solution: *The free spectral range is,*

$$\delta_{fsr} = \frac{c}{2L} = 1.5\,\mathrm{GHz} \ .$$

5.3.6.3 Ex: Waves on a rope

A string vibrates according to the equation $y(x,t) = 15\sin\frac{\pi x}{4\,\mathrm{cm}}\cos(30\,\mathrm{s}^{-1}\,\pi t)$.
a. What is the velocity of a string element at the position $x = 2\,\mathrm{cm}$ at the instant of time $t = 2\,\mathrm{s}$?
b. What is the propagation speed of this wave?

Solution: *a. In this position there is a node. Therefore,*

$$\dot{y}(x,t) = (-30\pi)15\sin\frac{\pi x}{4}\sin(30\pi t) = 0 \ .$$

b. Since it is a standing wave, it does not propagate.

5.3.6.4 Ex: Violin

The length of a violin string is $L = 50\,\mathrm{cm}$, and its mass is $m = 2.0\,\mathrm{g}$. When it is attached at the ends, the string can emit the a'-pitch ('la') corresponding to 440 Hz. Where should a finger be placed so that the emitted sound is the c"-pitch ('do') at 528 Hz?

Solution: *The mass density is,*

$$\mu = \frac{m}{L} = 4\,\mathrm{g/m} \ .$$

For a given string, the fundamental frequency only depends on its length. Hence, the frequencies 440 Hz *and* 528 Hz*,*

$$f_1 = \frac{1}{2L_1}\sqrt{\frac{T}{\mu}} \quad , \quad f_2 = \frac{1}{2L_2}\sqrt{\frac{T}{\mu}} \ ,$$

are related by,

$$L_2 = L_1\frac{f_1}{f_2} = 20\,\mathrm{cm}\,\frac{440}{528} \ .$$

5.3.6.5 Ex: Sound waves

The air column inside a closed tube, filled with a gas whose characteristic sound velocity is v_s, is excited by a speaker vibrating at the frequency f. Gradually increasing the frequency of the speaker one observes that the tube emits a sound at $f = 440\,\text{Hz}$ and the next time at 660 Hz.
a. What is the length of the tube?
b. What is the speed of sound?

Solution: *a. We have,*

$$v_s = \lambda_n f_n = \frac{2L}{n} f_n = \frac{2L}{n+1} f_{n+1} \ ,$$

with $f_n = 440\,\text{Hz}$ *and* $f_{n+1} = 610\,\text{Hz}$. *Hence,*

$$\Delta f = f_{n+1} - f_n = \frac{n+1}{2L} v_s - \frac{n}{2L} v_s = \frac{v_s}{2L} \ .$$

Finally, $L = \frac{v_s}{2\Delta f} = 1\,\text{m}$.
b. We also know,

$$n = \frac{f_n}{f_{n+1} - f_n} = 2 \ .$$

Hence, $v_s = \lambda_n f_n = \frac{2L}{n} f_n = 440\,\text{m/s}$.

5.3.6.6 Ex: Sound in a bottle

An experimenter blows into a bottle partially filled with water producing a sound of 1000 Hz. After drinking some of the water until the level decreased by 5 cm he is able to produce a sound at 630 Hz. Determine the possible values for the speed of sound knowing that the vibration of the air column inside the bottle should have a node at the end which is in contact with water and an anti-node at the mouth of the bottle. Comparing the result to the known value for the speed of sound in air, what is the excited vibration mode?

Solution: *We know* $c = \lambda_n \nu_n$ *and,*

$$(\tfrac{1}{4} + \tfrac{n}{2})\lambda_n = L_n \ ,$$

for $n = 0, 1, 2, ..,$ *where* L_n *is the height of the air column. Therefore,*

$$c = \frac{2\Delta L}{(n + \frac{1}{2})(\frac{1}{\nu_1} - \frac{1}{\nu_2})} \ .$$

With $n = 0$ *we have* $c = 340\,\text{Hz}$, *what is the known sound velocity. Hence, the fundamental mode is excited.*

5.3.6.7 Ex: Sonic waves in a tube

The figure shows a rod fixed at its center to a vibrator. A disc attached to the end of the rod penetrates a glass tube filled with a gas and where cork dust had been deposited. At the other end of the tube there is a movable piston. When producing longitudinal vibrations at the rod, we note that for certain positions of the movable piston, the cork dust forms a pattern of node and anti-nodes. Knowing for one of the positions of the piston the distance d between the anti-nodes and the frequency f of the vibration, show that the speed of sound in the gas is $v = 2fd$. This is called Kundt's method for determining the speed of sound in a gas.

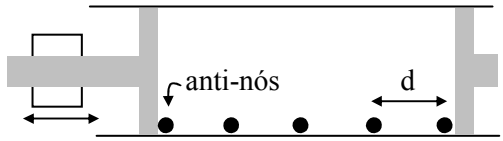

Figure 5.21: Sonic waves in a tube.

Solution:

5.3.6.8 Ex: Sound filter

A tube can act as an acoustic filter discriminating various sound frequencies crossing it from its own frequencies. A car muffler is an application example.
a. Explain how this filter works.
b. Determine the 'cut-off' frequency below which sound is not transmitted.

Solution:

5.3.6.9 Ex: Snell's law

Derive Snell's law from Huygens principle.

Solution:

5.3.6.10 Ex: Surface gravitational waves, capillary waves

Dependence of the propagation velocity on the height of the water column.

Solution:

5.3.6.11 Ex: Propagating standing wave

Consider two propagating waves $\mathcal{E}_\pm(x,t)$ with equal amplitudes and slightly different frequencies $\omega_\pm$ propagating in opposite directions along the x-axis.
a. Show that, approximating $k_+ \simeq k_-$, at each instant of time the interference pattern along the x-axis forms a standing wave.
b. Determine the group velocity of this wave.

Solution: *a. We have,*

$$\begin{aligned}|e^{\imath(k_+x-\omega_+t)} + e^{\imath(-k_-x-\omega_-t)}| &= |e^{\imath\omega_+(x/c-t)} + e^{\imath\omega_-(-x/c-t)}| \\ &= \sqrt{2+2\cos[\omega_+(x/c-t)-\omega_-(-x/c-t)]} \\ &= 2\cos\left[\tfrac{\omega_++\omega_-}{2c}x - \tfrac{\omega_+-\omega_-}{2}t\right] \simeq 2\cos\left[kx - \tfrac{\omega_+-\omega_-}{2}t\right] \ .\end{aligned}$$

In real notation [7] *defining*

$$a+b = k_+x-\omega_+t \quad , \quad a-b = -k_-x-\omega_-t \ ,$$

or

$$a = \tfrac{k_+-k_-}{2}x - \tfrac{\omega_++\omega_-}{2}t \quad , \quad b = \tfrac{k_++k_-}{2}x - \tfrac{\omega_+-\omega_-}{2}t$$

we can write,

$$\begin{aligned}\cos(k_+x-\omega_+t)+\cos(-k_-x-\omega_-t) &= \cos(a+b)+\cos(a-b) = 2\cos a\cos b \\ &= 2\cos\left(\tfrac{k_+-k_-}{2}x - \tfrac{\omega_++\omega_-}{2}t\right)\cos\left(\tfrac{k_++k_-}{2}x - \tfrac{\omega_+-\omega_-}{2}t\right) \\ &\simeq 2\cos\left(\tfrac{k_+-k_-}{2}x - \omega t\right)\cos\left(kx - \tfrac{\omega_+-\omega_-}{2}t\right) \ .\end{aligned}$$

b. Interference produces a standing wave that moves slowly with the group velocity, $v_g = \frac{\omega_1-\omega_2}{k}$.

5.3.6.12 Ex: Mach-Zehnder and Michelson-interferometer

Interferometers are devices that allow the comparison of distances via the propagation time of waves taking different paths. The interferometers outlined in the figures are based on beam splitters that divide and recombine a wave described by $I_n(x,t) = A_n\cos(kx-\omega t)$. Determine the amplitude of the signal at the position of the beam splitter recombining the waves as a function of a variation $\Delta x = 4\pi/k$ of the length of the second interferometer arm.

Solution: *Be* $I_0(0,t) = e^{\imath(kx-\omega t)} = e^{-\imath\omega t}$ *the signal immediately in front of the first beam splitter. Immediately behind it we have two waves* $I_{1,2}(0,t) = 2^{-1/2}e^{\imath(kx-\omega t)} =$

[7] We note,

$$\begin{aligned}|z_1+z_2|^2 = |z_1|^2+|z_2|^2+z_1z_2^*+z_1^*z_2 = x_1^2+y_1^2+x_2^2+y_2^2+2x_1x_2+2y_1y_2 &= (x_1+x_2)^2+(y_1+y_2)^2 \\ &= |\mathrm{Re}z_1+\mathrm{Re}z_2|^2+|\mathrm{Im}z_1+\mathrm{Im}z_2|^2 \ .\end{aligned}$$

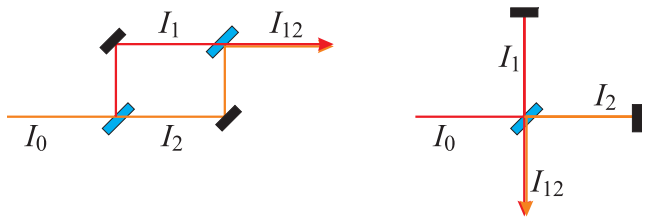

Figure 5.22: Mach-Zehnder and Michelson-interferometer.

$2^{-1/2}e^{-\imath\omega t}$. *With the interferometer arm lengths* $d_{1,2}$ *we have, just in front of the second separator, the signals* $I_{1,2}(d_{1,2},t) = 2^{-1/2}e^{\imath(kd_{1,2}-\omega t)}$. *Immediately behind it we have the recombined wave,*

$$I_s(t) = 2^{-1/2}e^{\imath(kd_1-\omega t)} + 2^{-1/2}e^{\imath(kd_2-\omega t)} = 2^{1/2}\cos k(d_1+d_2)e^{-\imath\omega t} \ .$$

That is, after the second beam splitter the signal oscillates with an amplitude that depends on the length difference of the interferometer arms like $\cos k(d_1+d_2)$.

5.3.6.13 Ex: Multiple interference in optical cavities

An optical beam splitter is a mirror with partial transmission and partial reflection,

$$\mathcal{E}_r(x,t) = \pm r\mathcal{E}_0(x,t) \quad , \quad \mathcal{E}_t(x,t) = t\mathcal{E}_0(x,t) \ .$$

The reflection signal depends on the direction of incidence, because reflection at a denser medium introduces a phase shift of π. Using this rules derive for a set of two mirrors r_1 and r_2 separated by a distance L the field $\mathcal{E}_{cav}$ between the mirrors as a function of the wave vector of the incident field $\mathcal{E}_{in}$. Also calculate the amplitudes of the transmitted and reflected light. Calculate the phase shifts between the transmitted (reflected) light and the incident light. Interpret the results.

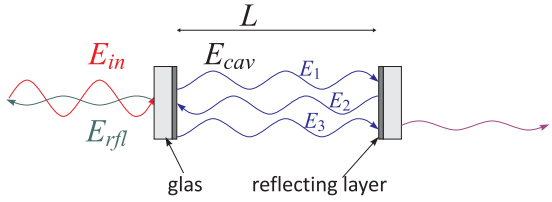

Figure 5.23: Optical cavity.

Solution: *The wave is reflected several times. For the field within the cavity we find, using* $r_j = 1 - t_j$,

$$\mathcal{E}_{cav}(x) = \mathcal{E}_{in}t_1\sum_n\left[(r_1r_2)^n e^{\imath k[2nL+x]} - r_2(r_1r_2)^n e^{\imath k[(2n+2)L-x]}\right] = \mathcal{E}_{in}t_1\frac{e^{\imath kx} - r_2e^{\imath k(2L-x)}}{1-r_1r_2e^{\imath k2L}} \ ,$$

using the Fourier expansion of $(1-s)^{-1} = \sum_n s^n$. *The reflected and transmitted fields are,*

$$\mathcal{E}_{rfl} = r_1 \mathcal{E}_{in} + \mathcal{E}_{in} \sum_{n=0}^{\infty} t_1(-r_2)(r_1 r_2)^n t_1 e^{\imath k 2(n+1)L} = \mathcal{E}_{in}\left(r_1 - \frac{e^{\imath k 2L} t_1^2 r_2}{1 - r_1 r_2 e^{2\imath k L}}\right)$$

$$\mathcal{E}_{trns} = \mathcal{E}_{in} \sum_{n=0}^{\infty} t_1 (r_1 r_2)^n t_2 e^{\imath k(2n+1)L} = \mathcal{E}_{in} \frac{t_1 t_2 e^{\imath k L}}{1 - r_1 r_2 e^{2\imath k L}} \ .$$

The phase shift is calculated by,

$$\phi = \arctan \frac{\mathfrak{Im}\ \mathcal{E}}{\mathfrak{Re}\ \mathcal{E}} \ .$$

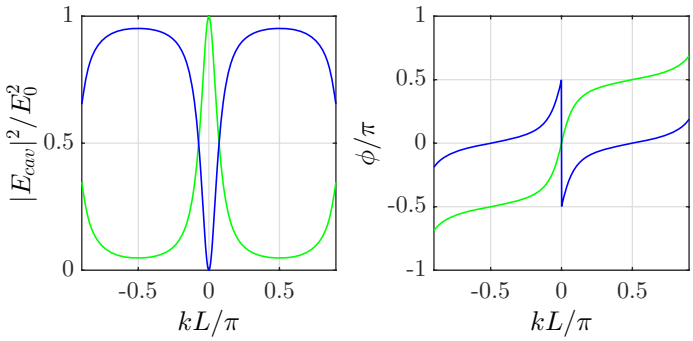

Figure 5.24: Optical cavity.

5.3.6.14 Ex: Double slit

Calculate the interference pattern behind a double slit.

Solution: *The Fourier transform of* $A(z) = \chi_{[-d/2-\Delta d,-d/2]} + \chi_{[d/2,d/2+\Delta d]}$ *is,*

$$\begin{aligned} B(q) &= \int_{-d/2-\Delta d}^{-d/2} e^{\imath q z} dz + \int_{d/2}^{d/2+\Delta d} e^{\imath q z} dz \\ &= \frac{e^{-iqd/2}}{\imath q}(1 - e^{-iq\Delta d}) + \frac{e^{\imath q d/2}}{\imath q}(e^{\imath q \Delta d} - 1) \simeq 2\Delta d \cos \tfrac{1}{2} q d \ . \end{aligned}$$

The intensity is $I(q) = c\varepsilon_0 |B(q)|^2$.

5.3.6.15 Ex: Spherical waves

Show that spherical waves given by $Y(\mathbf{r}, t) = \frac{Y_0}{kr} \sin(kr - \omega t)$ satisfy the 3D wave equation. Use Cartesian coordinates.

Solution: *We proceed in Cartesian coordinates. On one hand, we have,*

$$\frac{1}{c^2}\frac{d^2}{dt^2}\frac{\sin(kr-\omega t)}{kr} = -\frac{\omega^2}{c^2}\frac{\sin}{kr} \ .$$

On the othe hand,

$$\begin{aligned}\frac{d^2}{dx^2}\frac{\sin(kr-\omega t)}{kr} &= \frac{d^2}{dx^2}\frac{\sin(k\sqrt{x^2+y^2+z^2}-\omega t)}{k\sqrt{x^2+y^2+z^2}} \\ &= \frac{k^2r^2x^2\sin -3x^2\sin +r^2\sin -3kx^2r\cos +kr^3\cos}{kr^5} \ ,\end{aligned}$$

such that,

$$\nabla^2\frac{\sin(kr-\omega t)}{kr} = \frac{k^2r^4\sin -3r^2\sin +3r^2\sin -3kr^3\cos +3kr^3\cos}{kr^5} = \frac{k^2\sin}{kr} \ .$$

In spherical coordinates the task is trivial.

5.3.6.16 Ex: Interference in spherical waves

Two spherical waves are generated at positions $\mathbf{r}_\pm = \pm R\hat{\mathbf{e}}_z$. Determine surfaces of destructive interference for these waves.

Solution: *Destructive interference occurs when*

$$\begin{aligned}&\cos[k|\mathbf{r}-\mathbf{r}_+|-\omega t]+\cos[k|\mathbf{r}-\mathbf{r}_-|-\omega t] \\ &\qquad = 2\cos\frac{k|\mathbf{r}-\mathbf{r}_+|+k|\mathbf{r}-\mathbf{r}_-|-2\omega t}{2}\cos\frac{k|\mathbf{r}-\mathbf{r}_+|-k|\mathbf{r}-\mathbf{r}_-|}{2} = 0\end{aligned}$$

at all times. This requires,

$$|\mathbf{r}-\mathbf{r}_+|-|\mathbf{r}-\mathbf{r}_-| = \left(n+\tfrac{1}{2}\right)\lambda \ ,$$

for integer n. This means that for a distant observation point, $r \gg R$,

$$\begin{aligned}\left(n+\tfrac{1}{2}\right)\lambda &= \sqrt{r^2+R^2-2R\mathbf{r}\hat{\mathbf{e}}_z}-\sqrt{r^2+R^2+2R\mathbf{r}\hat{\mathbf{e}}_z} \\ &= r\sqrt{1+\frac{R^2}{r^2}-\frac{2Rz}{r^2}}-r\sqrt{1+\frac{R^2}{r^2}+\frac{2Rz}{r^2}} \simeq -2R\cos\theta \ .\end{aligned}$$

Constructive interference lines are obtained similarly.

5.3.6.17 Ex: Green's function

Calculate the integral Eq. (5.109).

Solution: *We have,*

$$\int d\theta e^{\imath(kx\theta - kx'\theta - kz\theta^2/2)} = \int d\theta e^{\imath k[(x-x')\theta - z\theta^2/2]} = \int d\theta e^{\imath k\left[\frac{(x-x')^2}{2z} - \frac{z}{2}\left(\theta - \frac{x-x'}{z}\right)^2\right]}$$
$$= e^{\imath k\frac{(x-x')^2}{2z}} \int d\theta' e^{-\frac{\imath kz}{2}\theta'^2} = e^{\imath k\frac{(x-x')^2}{2z}} \sqrt{\frac{2}{\imath kz}} \int d\tilde{\theta} e^{-\tilde{\theta}^2} = e^{\imath k\frac{(x-x')^2}{2z}} \sqrt{\frac{2\pi}{\imath kz}} \ .$$

5.4 Fourier analysis

Every periodic function $f(\xi) = f(\xi + 2\pi)$ can be decomposed into a series of harmonic vibrations. This is the *Fourier theorem*,

$$\boxed{f(\xi) = \frac{a_0}{2} + \sum_{n=1}^{\infty}(a_n \cos n\xi + b_n \sin n\xi)} \ . \tag{5.128}$$

To determine the coefficients, we calculate,

$$\int_0^{2\pi} f(\xi)d\xi = \int_0^{2\pi} \left[\frac{a_0}{2} + \sum_{m=1}^{\infty} a_m \cos m\xi + b_m \sin m\xi\right] d\xi = \pi a_0 \tag{5.129}$$
$$\int_0^{2\pi} f(\xi)\cos k\xi d\xi = \int_0^{2\pi} \left[\frac{a_0}{2} + \sum_{m=1}^{\infty} a_m \cos m\xi + b_m \sin m\xi\right] \cos n\xi d\xi = \pi a_n$$
$$\int_0^{2\pi} f(\xi)\sin k\xi d\xi = \int_0^{2\pi} \left[\frac{a_0}{2} + \sum_{m=1}^{\infty} a_m \cos m\xi + b_m \sin m\xi\right] \sin n\xi d\xi = \pi b_n \ ,$$

using the rules,

$$\int_0^{2\pi} \cos n\xi \cos m\xi d\xi = \int_0^{2\pi} \sin n\xi \sin m\xi d\xi = \pi\delta_{n,m} \quad \text{and} \quad \int_0^{2\pi} \cos n\xi \sin m\xi dx = 0 \ . \tag{5.130}$$

We can use these equations to calculate the Fourier expansion. To simplify the calculations, it is useful to consider the symmetry of the periodic function, since if $f(\xi) = f(-\xi)$, we can neglect all the coefficients b_n, and if $f(\xi) = -f(-\xi)$, we can neglect the coefficients b_n [8]

[8] Alternatively we can write the theorem as,

$$f(\xi) = \sum_{n=-\infty}^{\infty} d_n e^{\imath n\xi} \ ,$$

determining the coefficients as,

$$\int_{-\pi}^{\pi} f(\xi)e^{-\imath k\xi}d\xi = \int_{-\pi}^{\pi} f(\xi)e^{-\imath k\xi}d\xi \sum_{n=-\infty}^{\infty} d_n e^{\imath n\xi}d\xi = 2\pi d_n \ ,$$

with,

$$2d_n = a_n - \imath b_n \quad \text{for} \quad n \geq 0 \quad \text{and} \quad 2d_n = a_{-n} + \imath b_{-n} \quad \text{for} \quad n < 0 \ .$$

Example 22 (*Frequency spectrum and low-pass filter*):

- Show the spectrum of a rectangular signal on an oscilloscope and on an spectrum analyzer.
- Show the same spectrum filtered by a low pass filter.

.

5.4.1 Expansion of vibrations

Interpreting $\xi \equiv \omega t$ as time, we can apply the Fourier theorem (5.128) on temporal signals, $S(t) = f(\omega t)$, where ω is the angular frequency,

$$S(t) = f(\omega t) = \frac{a_0}{2} + \sum_{n=1}^{\infty} (a_n \cos n\omega t + b_n \sin n\omega t) \ , \tag{5.131}$$

with,

$$a_0 = \frac{\omega}{\pi} \int_0^{2\pi/\omega} S(t) dt \qquad \text{and} \qquad a_n = \frac{\omega}{\pi} \int_0^{2\pi/\omega} S(t) \cos n\omega t dt \tag{5.132}$$
$$\text{and} \qquad b_n = \frac{\omega}{\pi} \int_0^{2\pi/\omega} S(t) \sin n\omega t dt \ .$$

The representation of the coefficients a_n and b_n as functions of the number n is called *harmonic spectrum*. As we mentioned earlier, the spectrum of a sound is what determines the timbre. The total *harmonic distortion* is defined by,

$$k \equiv \frac{\sum_{n=2}^{\infty} (a_n + b_n)}{\sum_{n=1}^{\infty} (a_n + b_n)} \ . \tag{5.133}$$

Radiofrequency circuits such as HiFi amplifiers are characterized by their transmission fidelity, that is, the absence of harmonic distortion in the amplification of each harmonic coefficient.

5.4.1.1 Expansion of a triangular signal

We consider a *triangular signal* given by [9],

$$S(t) = \begin{cases} \omega t \\ \pi - \omega t \end{cases} \qquad \text{for} \qquad \begin{array}{l} 0 < \omega t < \frac{\pi}{2} \\ \frac{\pi}{2} < \omega t < \pi \end{array} \ . \tag{5.134}$$

We calculate the coefficients, $a_0 = 0$, because the signal is symmetric about the t-axis (it has no offset), and $a_n = 0$, because the signal has the symmetry $S(t) = -S(-t)$. Also,

$$b_n = \frac{2\omega}{\pi} \int_0^{\pi/2\omega} \omega t \sin n\omega t dt + \frac{2\omega}{\pi} \int_{\pi/2\omega}^{\pi/\omega} (\pi - \omega t) \sin n\omega t dt = \frac{4}{\pi} \frac{\sin \frac{1}{2}\pi n}{n^2} \ , \tag{5.135}$$

[9] Note that the function $S(t) = \frac{\pi}{2} - \left(\frac{\pi}{2} - \omega t\right) \frac{\cos \omega t}{|\cos \omega t|}$, which describes the same triangular signal, it is easier to program in numerical softwares.

with the consequence,

$$S(t) = \frac{4}{\pi} \sum_{n=1,3,\ldots} \frac{(-1)^{(n-1)/2}}{n^2} \sin n\omega t \ . \tag{5.136}$$

5.4.2 Theory of harmony

Non-linearities in oscillating systems can excite harmonic frequencies f_n, that is, multiples of the fundamental frequency $f_n = (n+1)f$. These are the components of the Fourier series.

All musical instruments produce harmonics. This is what makes the timbre of the instrument. When we play several notes together, we perceive the octave interval as pleasant. This is, because all the harmonics of a pitch and of its octave coincide.

- harmonic pitch, well-tempered chromatic scale, flat ♭, sharp ♯, ♮, musical clef, tuning fork $f_{a'} = 440\,\mathrm{Hz}$

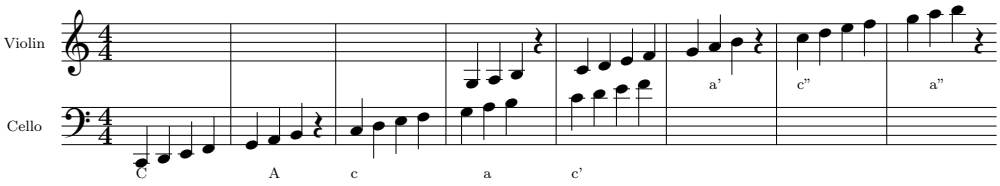

Figure 5.25: (code) Ladder of pitches over 3 octaves. Pitches can be generated in MATLAB. A sample program can be downloaded by clicking on the link.

In the *well-tempered* tonality the interval of a *octave* is divided into 12 intervals,

$$n \in [\mathrm{a}, \mathrm{a\#}, \mathrm{h}, \mathrm{c}, \mathrm{c\#}, \mathrm{d}, \mathrm{d\#}, \mathrm{e}, \mathrm{f}, \mathrm{f\#}, \mathrm{g}, \mathrm{g\#}] \ . \tag{5.137}$$

Defining *normal tuning* as,

$$f_a = 440\,\mathrm{Hz} \ , \tag{5.138}$$

the pitches correspond to the frequencies,

$$f_n = 2^{n/12} f_a \ . \tag{5.139}$$

For example, we calculate the frequency of the 'd',

$$f_d = 2^{-7/12} f_a = 391.9954\,\mathrm{Hz} \ . \tag{5.140}$$

Thus, all notes are logarithmically equidistant:

$$\mathrm{lb}\ f_{n+1} - \mathrm{lb}\ f_n = \mathrm{lb}\ (2^{(n+1)/12} f_{la}) - \mathrm{lb}\ (2^{n/12} f_{la}) = 1 \tag{5.141}$$

$$\frac{f_{n+1}}{f_n} = \frac{2^{(n+1)/12} f_{la}}{2^{n/12} f_{la}} = 2^{1/12} \ . \tag{5.142}$$

Why are there just 12 pitches? Several instruments have more than one resonator emitting sound, e.g. the violoncello has 4 strings, c, g, d', and a'. Each string is detuned by a *quint* from the next string, that is,

$$3f_c = 2f_g \qquad \text{and} \qquad 3f_g = 2f_{d'} \qquad \text{and} \qquad 3f_{d'} = 2f_{a'} \ . \tag{5.143}$$

Each string has its own series of harmonics. The timbre of the instrument appears more pleasant, when the harmonics of the various strings coincide. Let us now check, whether our definition of logarithmically equidistant pitches satisfies this condition,

$$3f_d = 3 \cdot 2^{-7/12} f_a = 2.0023 f_a \neq 2f_a \ . \tag{5.144}$$

Thus, harmonic tuning is not perfect, but quite close to the well-tempered tuning. In Exc. 5.4.6.5 we show that, nevertheless, the discrepancy is able to produce nasty beat notes.

The guitar, which is tuned in *quart*s,

$$4f_c = 3f_{fa} \ , \tag{5.145}$$

has the same problem [10],

$$4f_c = 4 \cdot 2^{-5/12} f_f = 2.9966 f_f \neq 3f_f \ . \tag{5.146}$$

Resolve the Excs. 5.4.6.6, 5.4.6.7 and 5.4.6.8.

5.4.3 Expansion of waves

Interpreting $\xi \equiv kx$ as position, we can apply the Fourier theorem (5.128) to standing waves, $Y(x) = f(kx)$, where $k = 2\pi/k$ is the wavevector.

5.4.4 Normal modes in continuous systems at the example of a string

We will now apply the Fourier expansion to calculate the normal modes of a vibrating string. Depending on which mode of oscillation is excited, the displacement of the string is given by,

$$Y_n(x,t) = (A_n \cos \omega_n t + B_n \sin \omega_n t) \sin \tfrac{\omega_n x}{c} \ , \tag{5.147}$$

where $\omega_n = n\pi c/l$ is the frequency of the *normal mode*. An arbitrary vibration can be decomposed as superpositions of these modes,

$$Y(x,t) = \sum_n Y_n(x,t) \ . \tag{5.148}$$

As an initial condition we assume that the string is at a position $Y(x,0) = Y_0(x)$ with the velocity $V(x,0) = V_0(x)$ at all points. Then,

$$Y_0(x) = \sum_n Y_n(x,0) = \sum_n A_n \sin \tfrac{\omega_n x}{c} \tag{5.149}$$

$$\text{and} \qquad V_0(x) = \sum_n \frac{d}{dt} Y_n(x,0) = \sum_n \omega_n B_n \sin \tfrac{\omega_n x}{c} \ .$$

[10] Include Matlab sound examples here!

We find the amplitudes by calculating the integrals,

$$\frac{2}{l}\int_0^l Y_0(x)\sin\tfrac{\omega_n x}{c}dx = \frac{2}{l}\sum_m A_m\int_0^l \sin\tfrac{m\pi x}{l}\sin\tfrac{n\pi x}{l}dx = A_n \tag{5.150}$$
$$\frac{2}{l}\int_0^l V_0(x)\sin\tfrac{\omega_n x}{c}dx = \frac{2}{l}\int_0^l \sum_m \omega_n B_m \sin\tfrac{m\pi x}{l}\sin\tfrac{n\pi x}{l}dx = \omega_n B_n \ .$$

We now assume that the rope is initially excited by a triangular deformation, that is, we pull the rope in its middle up to a distance d and let go. That is, the initial conditions are given by,

$$V_0(x) = 0 \qquad \text{and} \qquad \frac{\pi}{2d}Y_0(x) = \begin{cases} \frac{\pi x}{l} \\ \frac{\pi(l-x)}{l} \end{cases} \qquad \text{for} \qquad \begin{array}{l} 0 < \frac{\pi x}{l} < \frac{\pi}{2} \\ \frac{\pi}{2} < \frac{\pi x}{l} < \pi \end{array} \ . \tag{5.151}$$

We can compare this function with the triangle function Eq. (5.134) and make the same Fourier expansion as in (5.136),

$$\frac{\pi}{2d}Y_0(x) = \frac{4}{\pi}\sum_{n=1,3,\ldots}\frac{(-1)^{(n-1)/2}}{n^2}\sin\tfrac{n\pi x}{l} \ . \tag{5.152}$$

Comparing this expansion with (5.149), we find $B_n = 0$ and,

$$\sum_m A_m \sin\tfrac{\omega_m x}{c} = Y_0(x) = \frac{2d}{\pi}\frac{4}{\pi}\sum_{n=1,3,\ldots}\frac{(-1)^{(n-1)/2}}{n^2}\sin\tfrac{n\pi x}{l} \ . \tag{5.153}$$

yielding for odd coefficients $m = 1, 3, ..,$

$$A_n = \frac{8d}{n^2\pi^2}(-1)^{(n-1)/2} \ . \tag{5.154}$$

Thus, the vibration of the string is completely described by,

$$Y(x,t) = \frac{8d}{\pi^2}\sum_{n=1,3,\ldots}\frac{(-1)^{(n-1)/2}}{n^2}\cos\omega_n t\sin\tfrac{\omega_n x}{c} \ . \tag{5.155}$$

The energy is the sum of the energies of all normal modes,

$$E = \sum_{n=1,3,\ldots}\frac{m}{4}\omega_n^2 A_n^2 = \sum_{n=1,3,\ldots}\tfrac{m}{4}\left(\frac{n\pi c}{l}\right)^2\left(\frac{8d}{n^2\pi^2}\right)^2 = \sum_{n=1,3,\ldots} m\frac{16d^2c^2}{n^2\pi^2 l^2} = \frac{2md^2c^2}{l^2} \ , \tag{5.156}$$

knowing $\sum_{n=1,3,\ldots}\frac{1}{n^2} = \frac{\pi^2}{8}$.

5.4.5 Waves in crystalline lattices

The sound may propagate in a crystalline lattice, for example a metal or a crystal, by means of longitudinal or transverse vibrations. To understand the propagation of longitudinal vibrations in a monoatomic lattice, we consider the model of a chain of

N masses coupled by springs. The treatment for transverse vibrations is analogous. As we have shown in previous sections, the movement of each mass is described by the differential equation,

$$\ddot{x}_n = \omega_0^2(x_n - x_{n-1}) + \omega_0^2(x_n - x_{n+1}) \ , \tag{5.157}$$

with $n = 1, .., N$. Making the ansatz $x_n = A_n e^{-\imath\omega t}$, we obtain the characteristic equation,

$$\omega^2 A_n = \omega_0^2(A_n - A_{n-1}) + \omega_0^2(A_n - A_{n+1}) \ . \tag{5.158}$$

When we hit one of the oscillators of a linear chain, we excite a wave that propagates along the chain. Therefore, it is reasonable to guess $A_n = Ae^{\imath nka}$ for the displacements of the oscillators, where $a \equiv x_{n+1} - x_n$ is the lattice constant. We obtain,

$$\omega^2 = \omega_0^2(1 - e^{-ika}) + \omega_0^2(1 - e^{\imath ka}) = 2\omega_0^2(1 - \cos ka) = 4\omega_0^2 \sin^2 \frac{ka}{2} \ . \tag{5.159}$$

The dispersion relation is shown in Fig. 5.26. Obviously, in the limit of long waves, $ka \ll 1$, the relation can be approximated by,

$$\omega = 2\omega_0 \left| \sin \frac{ka}{2} \right| \simeq \omega_0 ka \equiv ck \ , \tag{5.160}$$

where c is the propagation velocity of the wave. This relation is linear, thus reproducing the situation of acoustic waves.

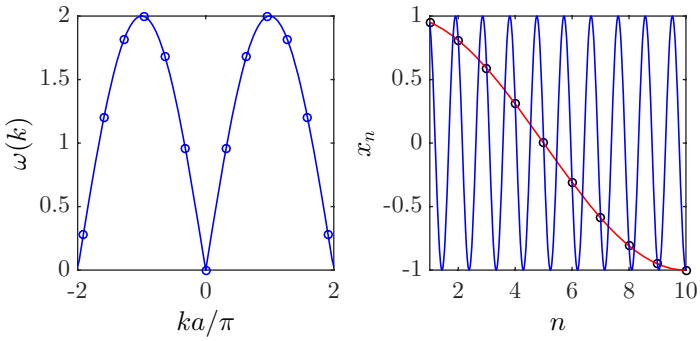

Figure 5.26: (code) Dispersion relation of a one-dimensional crystalline lattice consisting of 20 atoms.

The displacements of individual oscillators are now,

$$x_n(t) = na + Ae^{\imath nka - \imath\omega t} \ . \tag{5.161}$$

We need now to discuss, what are the possible values for k. First, since by adding 2π to the value ka we get the same result, we may concentrate on the region $-\pi < ka < \pi$, called the first *Brillouin zone*. And since the crystal is symmetric (we can reverse the

order of all oscillators), we can assume cyclic boundary conditions, $e^{\imath nka} = e^{\imath(N-n)ka}$, such that $(N-2n)ka/2\pi$ is an arbitrary integer number for any n, for example $n = 0$,

$$k = \frac{2\pi}{Na} \cdot \ell \ , \tag{5.162}$$

for $\ell \in \mathbb{N}$. To stay within the Brillouin zone, we set $\ell = -\frac{N}{2}, .., \frac{N}{2}$. That is, we have N possible values, which corresponds to just half the number of degrees of freedom.

Let us consider particular solutions. In the center of the Brillouin zone, $k = 0$ we have,

$$x_n(t) = na + Ae^{\imath\omega t} \ , \tag{5.163}$$

which corresponds to an in-phase oscillation of all oscillators. On the edge of the Brillouin zone, $k = \pm\pi/a$,

$$x_n(t) = na + A(-1)^n e^{\imath\omega t} \ , \tag{5.164}$$

which corresponds to a movement, where consecutive oscillators oscillate in anti-phase.

5.4.5.1 Waves in diatomic crystalline lattices

Many lattices are diatomic, that is, made of two species of atoms with different masses. For example, the NaCl salt crystal is a lattice alternating Na^+ and Cl^- ions. In analogy with the monoatomic lattice we establish the equations of motion,

$$\begin{aligned} \ddot{x}_n &= -\omega_x^2(x_n - y_{n-1}) - \omega_x^2(x_n - y_n) \\ \ddot{y}_n &= -\omega_y^2(y_n - x_{n+1}) - \omega_y^2(y_n - x_n) \ , \end{aligned} \tag{5.165}$$

with $\omega_{x,y} \equiv \sqrt{k/m_{x,y}}$. Inserting the ansätze $x_n = Ae^{\imath(nka-\omega t)}$ and $y_n = Be^{\imath(nka-\omega t)}$, we find the equations,

$$\begin{aligned} -\omega^2 A &= -\omega_x^2(2A - Be^{-\imath ka} - B) \\ -\omega^2 B &= -\omega_y^2(2B - Ae^{\imath ka} - A) \ , \end{aligned} \tag{5.166}$$

or,

$$\begin{pmatrix} 2\omega_x^2 - \omega^2 & -\omega_x^2(1 + e^{-ika}) \\ -\omega_y^2(1 + e^{\imath ka}) & 2\omega_y^2 - \omega^2 \end{pmatrix} \begin{pmatrix} A \\ B \end{pmatrix} = 0 \ . \tag{5.167}$$

The characteristic equation is,

$$0 = \det \hat{M} = (2\omega_x^2 - \omega^2)(2\omega_y^2 - \omega^2) - \omega_x^2(1 - e^{-\imath ka})\omega_y^2(1 - e^{\imath ka}) \ , \tag{5.168}$$

with the solution,

$$\omega^2 = \omega_x^2 + \omega_y^2 \pm \sqrt{\omega_x^4 + \omega_y^4 + 2\omega_x^2\omega_y^2 \cos ka} \ . \tag{5.169}$$

For $ka \ll 1$ we can approximate,

$$\begin{aligned} \omega^2 &\simeq \omega_x^2 + \omega_y^2 \pm \sqrt{(\omega_x^2 + \omega_y^2)^2 - \omega_x^2\omega_y^2 k^2 a^2} \\ &\simeq 2(\omega_x^2 + \omega_y^2) \quad , \quad \omega_x^2\omega_y^2 k^2 a^2 \ . \end{aligned} \tag{5.170}$$

The first eigenvalue is called the *optical branch* and the second the *acoustic branch*. The optical branch corresponds to an anti-phase motion of the atoms of the species x and y. This motion can be excited by light fields. The acoustic branch corresponds to an in-phase motion of the atoms.

In contrast, for $ka \simeq \pm\pi/a$ we obtain,

$$\omega^2 = \omega_x^2 \quad , \quad \omega_y^2 \ . \tag{5.171}$$

In these solutions either atom x oscillates while y stays at rest, or the opposite.

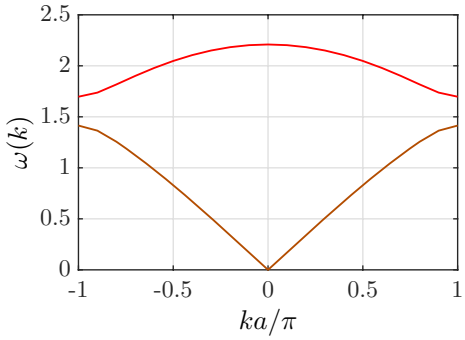

Figure 5.27: (code) Dispersion relation in a one-dimensional lattice showing in blue the optical branch and in green the acoustic branch.

5.4.6 Exercises

5.4.6.1 Ex: Fourier expansion

Expand the function $f(\xi) = \sin^3 \xi$ in a Fourier series.

Solution: *Trigonometric rules allow us to calculate,*

$$f(\xi) = \sin^3 \xi = \tfrac{3}{4} \sin \xi - \tfrac{1}{4} \sin 3\xi \ .$$

But the same result can be obtained by Fourier expansion. For symmetry reasons it is clear that $a_0 = 0 = a_n$. The coefficients,

$$b_n = \frac{1}{\sqrt{\pi}} \int_{-\pi}^{\pi} \sin^3 \xi \sin n\xi d\xi = \frac{12 \sin n\pi}{n^4 - 10n^2 + 9}$$

only do not disappear for $n = 1$ and $n = 3$. The graph on the left of the figure shows the two expansion terms separately, while the graph on the right shows the sum $f(\alpha)$.

5.4.6.2 Ex: Fourier expansion of sea waves

Surface waves on the sea are often better described by the function $f(x,t) = (kx - 2n\pi)^2$ inside the intervals $x \in [(2n-1)\pi/k, (2n+1)\pi/k]$ com $n \in \mathbb{N}$. Expands the

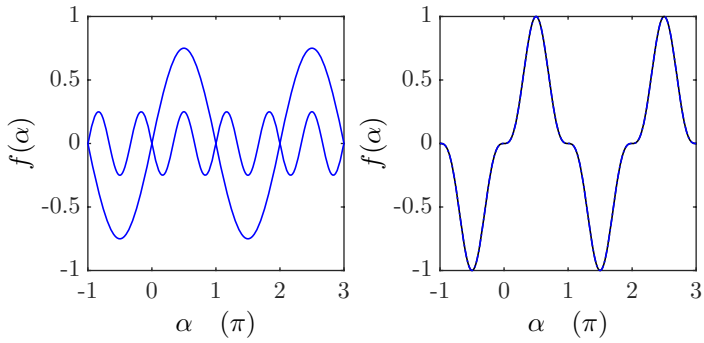

Figure 5.28: (code)

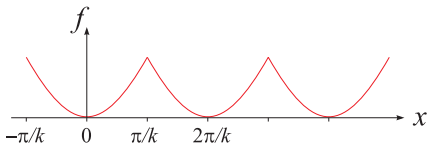

Figure 5.29: (code)

wave in a spatial Fourier series. Use the formula $\int z^2\cos(bz)dz = \frac{1}{b^3}[(b^2z^2-2)\sin bz + 2bz\cos bz]$.

Solution: *The coefficients of expansion are,*

$$a_0 = \frac{1}{\pi}\int_{-\pi}^{\pi} f(x)d(kx) = \frac{1}{\pi}\int_{-\pi}^{\pi}(kx)^2 d(kx) = \frac{u^3}{3\pi}\Big|_{-\pi}^{\pi} = \frac{2\pi^2}{3}$$

$$a_n = \frac{1}{\pi}\int_{-\pi}^{\pi} f(x)\cos nkx d(kx) = \frac{1}{\pi}\int_{-\pi}^{\pi}(kx)^2\cos nkx d(kx)$$

$$= \frac{1}{n^3}[(n^2z^2-2)\sin nz + 2nz\cos nz]\Big|_{-\pi}^{\pi} = \frac{4\cos n\pi}{n^2}$$

$$b_n = \frac{1}{\pi}\int_{-\pi}^{\pi} f(x)\sin nkx d(kx) = 0$$

$$f(x) = \frac{a_0}{2} + \sum_{n=1}^{\infty}(a_n\cos nkx + b_n\sin nkx) = \frac{\pi^2}{3} + 4\sum_{n=1}^{\infty}\frac{(-1)^n}{n^2}\cos nkx\ .$$

Note that the function can be parametrized as $f(x) = (mod(kx-\pi, 2\pi)-\pi)^2$ *for numerical treatment.*

5.4.6.3 Ex: Fourier expansion of a rectified signal

An alternating electric current can be turned into a signal of half-cycles, $f(t) = |\cos\frac{\omega t}{2}|$, by a diode rectifier bridge. Expand this signal into a temporal Fourier series. Use the formula $\int\cos(az)\cos(bz)dz = \frac{\sin[(a-b)z]}{2(a-b)} + \frac{\sin[(a+b)z]}{2(a+b)}$.

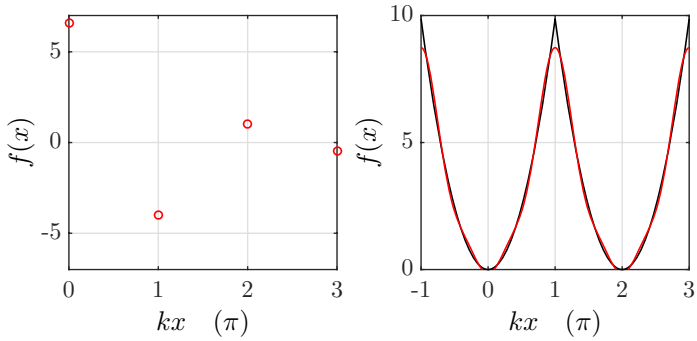

Figure 5.30: (code)

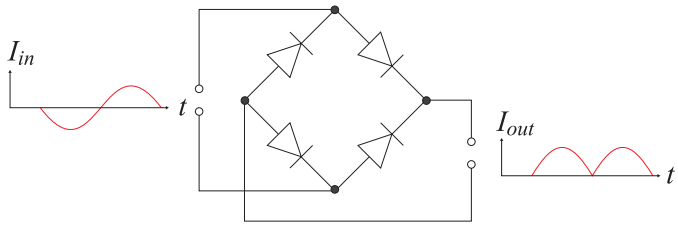

Figure 5.31: Fourier expansion of a rectified signal.

Solution: *The expansion coefficients are,*

$$a_0 = \frac{1}{\pi}\int_{-\pi}^{\pi} f(t)d(\omega t) = \frac{1}{\pi}\int_{-\pi}^{\pi} \cos\tfrac{\omega t}{2} d(\omega t) = \frac{2}{\pi}\int_{-\pi/2}^{\pi/2} \cos u du = \frac{2}{\pi}\sin u\Big|_{-\pi/2}^{\pi/2} = \frac{4}{\pi}$$

$$a_n = \frac{1}{\pi}\int_{-\pi}^{\pi} f(t)\cos\omega t d(\omega t) = \frac{1}{\pi}\int_{-\pi}^{\pi} \cos\tfrac{\omega t}{2}\cos nkt d(\omega t) = \frac{1}{\pi}\int_{-\pi}^{\pi} \cos\tfrac{z}{2}\cos nz dz = -\frac{4}{\pi}\frac{\cos\pi n}{4n^2-1}$$

$$b_n = \frac{1}{\pi}\int_{-\pi}^{\pi} f(t)\sin n\omega t d(\omega t) = 0$$

$$f(x) = \frac{a_0}{2} + \sum_{n=1}^{\infty}(a_n\cos n\omega t + b_n \sin n\omega t) = \frac{2}{\pi} + \frac{4}{\pi}\sum_{n=1}^{\infty}\frac{(-1)^n}{4n^2-1}\cos n\omega t\ .$$

The graph on the left of the figure shows Fourier components, while the graph on the right shows the original function $f(t)$ as well as the expanded function up to third order.

5.4.6.4 Ex: Action of a low pass filter on a spectrum

One method of creating a sinusoidal signal in electronics consist in first creating a rectangular signal via a switching circuit and then pass this signal through a low-pass filter by cutting off the harmonics. Simulate this procedure using the Fourier transform method starting from the rectangular signal $S(t) = \sin\omega t/|\sin\omega t|$ with

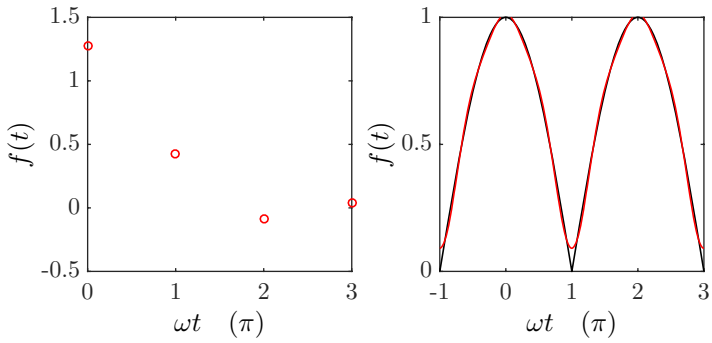

Figure 5.32: (code)

$\omega/2\pi = 1\,\mathrm{kHz}$ and using a low pass filter, such as $F(\omega) = 1/\left(1+(\omega/\omega_g)^2\right)$, where the cut-off frequency is, $\omega_g/2\pi = 1\,\mathrm{kHz}$. Evaluate the harmonic distortion of the rectangular signal and the filtered signal.

Solution: *For the function $S(t)$ we calculate the coefficients,*

$$a_0 = \frac{\omega}{\pi}\int_0^{2\pi/\omega} \frac{\sin\omega t}{|\sin\omega t|}dt = 0 \quad , \quad a_n = \frac{\omega}{\pi}\int_0^{2\pi/\omega} \frac{\sin\omega t}{|\sin\omega t|}\cos n\omega t dt = 0 \quad ,$$

$$b_n = \frac{\omega}{\pi}\int_0^{2\pi/\omega} \frac{\sin\omega t}{|\sin\omega t|}\sin n\omega t dt = \frac{2}{\pi}\int_0^{\pi}\sin n\alpha d\alpha = -\frac{2}{\pi}\frac{\cos\pi n - 1}{n} = \frac{2}{n\pi}[1-(-1)^n] \ ,$$

with the consequence,

$$S(t) = \frac{2}{\pi}\sum_{n=1,3,\ldots}\frac{\sin n\omega t}{n} \ .$$

Graph (a) shows the amplitudes b_n and graph (b) the approximation by the Fourier series to orders 1, 2, and 20 (red). Attenuating the amplitudes as,

$$\tilde{b}_n = \frac{b_n}{1+(n\omega/\omega_g)^2} \ ,$$

we have,

$$S(t) = \frac{2}{\pi}\sum_{n=1,3,\ldots}\frac{1}{n}\frac{\sin n\omega t}{1+(n\omega/\omega_g)^2} \ .$$

Graph (c) shows the amplitudes attenuated by the filter $\tilde{b}_n$ and graph (d) the Fourier series approximation to orders 1, 2 and 20 (red). Obviously, the filtered signal is almost sinusoidal. A higher order filter can improve the result. Calculating the harmonic distortion of the numerically filtered rectangular signal gives $k \approx 0.1466$. For a second order filter of type $1/\left(1+(\omega/\omega_g)^4\right)$, we obtain $k \approx 0.0018$.

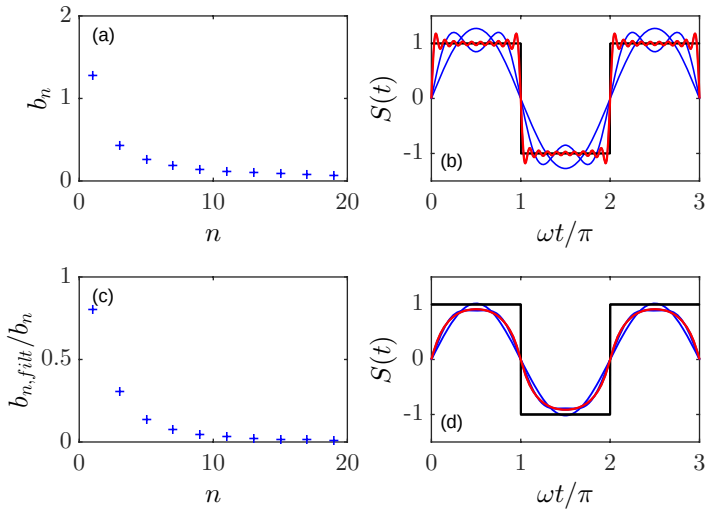

Figure 5.33: (code)

5.4.6.5 Ex: Tuning a violin

What would be the beat frequency between the pitches $3f_{c'}$ and $2f_{g'}$ if the strings were tuned logarithmically equidistant.

Solution: *It would be,*

$$\begin{aligned}\Delta f \equiv 3f_c - 2f_g &= 3\cdot 2^{-9/12} f_a - 2\cdot 2^{-2/12} f_a \\ &= (3\cdot 2^{-9/12} - 2\cdot 2^{-2/12}) f_a = 0.002\ f_a = 0.8858\,\text{Hz}\ ,\end{aligned}$$

which is enough to be nasty.

5.4.6.6 Ex: String instruments

Imagine a string instrument with 12 strings tuned in quints. How far would be the highest string from a harmonic of the lowest one.

Solution: *We find* $2^7 - (3/2)^1 2 \simeq 1.7\,\text{Hz}$.

5.4.6.7 Ex: String instruments

Prepare a list comparing the harmonics up to ninth order in the harmonic and in the tempered scale.

Solution: *The comparison is listed in the following table:*

harmonic scale f_n	*tempered scale* $\tilde{f}_n$	$(f_n - \tilde{f}_n)/f_n$
$1f = 2^0 \cdot f$		0
$2f = 2^1 \cdot 2f$		0
$3f = 2^1 \cdot \frac{3}{2}f$	$\simeq 2^1 \cdot 2^{7/12} \cdot f = 2.9966f$	0.11%
$4f = 2^2 \cdot f$		0
$5f = 2^2 \cdot \frac{5}{4}f$	$\simeq 2^2 \cdot 2^{4/12} \cdot f = 5.0397f$	−0.79%
$6f = 2^2 \cdot \frac{3}{2}f$	$\simeq 2^2 \cdot 2^{7/12} \cdot f = 5.9932f$	0.11%
$7f = 2^2 \cdot \frac{7}{4}f$	$\simeq 2^2 \cdot 2^{10/12} \cdot f = 7.1272f$	−1.82%
$8f = 2^3 \cdot f$		0
$9f = 2^3 \cdot \frac{9}{8}f$	$\simeq 2^3 \cdot 2^{2/12} \cdot f = 8.9797f$	0.23%

5.4.6.8 Ex: Frequency beating of sound waves

To tune a violin a musician first tunes the a-string ('la') at $f_a = 440\,\text{Hz}$ and then plays two neighboring strings, paying attention to the frequency beats. When playing the a- and the e-string ('mi'), the violinist hears a beat frequency of 3 Hz, and he notes that this frequency increases as the tension of the e-string increases. (The e-string is tuned to $f_e = 660\,\text{Hz}$.)
a. Why is there a beat when the two strings are played simultaneously?
b. What is the vibration frequency of the e-string when the beat frequency it generates together with the a-string is 3 Hz?
c. If the tension on the e-string is 80 N for a beat frequency of 3 Hz, what tension corresponds to a perfect tuning of the string?

Solution:

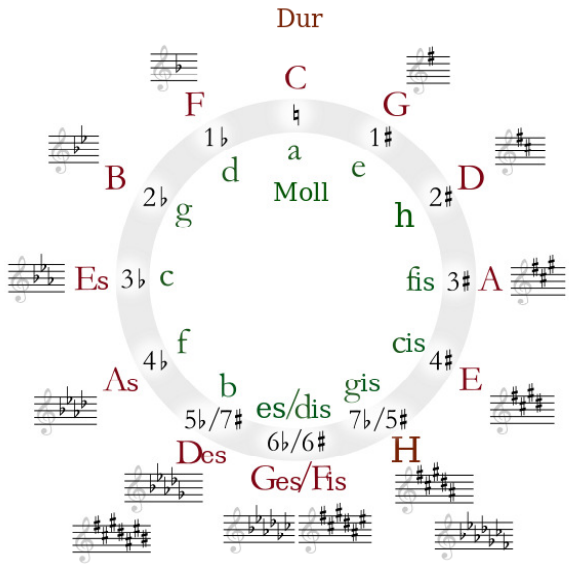

Figure 5.34: Circulo de quintas.

5.4.6.9 Ex: Frequency beating of sound waves

A violinist tries to tune the strings of his instrument.
a. Comparing the a-string ('la') to a tuning fork ($\nu_{dia} = 440\,\text{Hz}$), he hears a beat with the frequency 1 Hz. By increasing the tension on the rope, the beat frequency increases. What was the frequency of the 'a'-string before the tension increased?
b. After having adjusted the a-string the violinist wants to tune the d-string ('re'). He realizes that the second harmonic $3\nu_d$ produces with the first harmonic of the a-string ($2\nu_a$) a beat of 1 Hz. Decreasing the tension of the d-string the beat disappears. What was the initial frequency of the d-string and by what percentage does the violinist need to decrease the tension of the string?

Solution: *a. The beat frequency is,*

$$\tfrac{1}{2}(\nu_{frk} - \nu_a) = \pm 1\,\text{Hz} \ .$$

Since $\nu_a \propto \sqrt{F_T}$ and noting that, by increasing the voltage, an increase in the beat frequency is observed, we conclude $\nu_a > \nu_{frk}$. Hence, $\nu_a = 402\,\text{Hz}$.
b. We know

$$\tfrac{1}{2}(3\nu_d - 2\nu_a) = \pm 1\,\text{Hz} \ .$$

Since by decreasing the tension (and therefore the frequency) of the d-string the harmonic frequencies coincide, we deduce,

$$\nu_d = \tfrac{2}{3}\nu_a + \tfrac{2}{3}\,\text{Hz} = 294\,\text{Hz} \ .$$

After tuning we have $\nu'_d = \frac{2}{3}\nu_a = 293.3\,\text{Hz}$. Hence,

$$\frac{F_T/\mu}{F'_T/\mu} = \left(\frac{\nu_d}{\nu'_d}\right)^2 = \left(\frac{293.3}{294}\right)^2 = 99.6\% \ .$$

5.4.6.10 Ex: Normal modes on a string

A stretched wire of mass m, length L, and tension T is triggered by two sources, one at each end. Both sources have the same frequency ν and amplitude A, but are out of phase by exactly 180° with respect to each other. (At each end there is an anti-node.) What is the lowest possible value of ω consistent with the stationary vibrations of the wire?

Solution: *It is $\lambda = 2L$ and hence,*

$$\omega = 2\pi\frac{c}{\lambda} = 2\pi\frac{\sqrt{T/\mu}}{2L} = 2\pi\frac{\sqrt{TL/m}}{2L} = \pi\sqrt{\frac{T}{Lm}} \ .$$

5.4.6.11 Ex: Normal modes on a string

a. Find the total vibration energy of a wire of length L fixed at both ends and oscillating in its n-th characteristic mode with amplitude A. The tension on the wire is T, and its total mass is M. (**Suggestion:** Consider the integrated kinetic energy at the instant when the wire is straight.)
b. Calculate the total vibration energy of the same wire vibrating in the following superposition of normal modes:

$$Y(x,t) = A_1 \sin \tfrac{\pi x}{L} \cos \omega_1 t + A_3 \sin \tfrac{3\pi x}{L} \cos(\omega_3 t - \tfrac{\pi}{4}) \ .$$

You should be able to verify that it is the sum of the energies of the two modes taken separately.

Solution: *a. The function describing the n-th mode can be written as,*

$$Y(x,t) = \sin \frac{n\pi x}{L} \cos \omega_n t \ .$$

The kinetic energy of each mass element of the wire is,

$$\frac{d}{dt} Y(x,t) = -A_1 \omega_n \sin \frac{n\pi x}{L} \sin \omega_n t \ .$$

At the moments when the rope is stretched, $\omega_n t = \pi/2 + N\pi$, the energy is,

$$\frac{d}{dt} Y(x,t) = -A_1 \omega_n \sin \frac{n\pi x}{L} \ .$$

The spatial integral gives the total energy,

$$E = \int_0^L \frac{m/L}{2} \left(\frac{d}{dt} Y(x,t) \right)^2 dx = A_1^2 \omega_1^2 \frac{m}{2L} \frac{L}{n\pi} \int_0^{n\pi} \sin^2 \xi d\xi = A_1^2 \omega_1^2 \frac{m}{2L} \frac{n\pi}{2} = A_1^2 \frac{m\omega_n^2}{4} \ .$$

With

$$\omega_n = 2\pi \frac{c}{\lambda_n} = 2\pi \frac{\sqrt{T/(m/L)}}{2L/n} = \pi \sqrt{\frac{Tn^2}{mL}} \ ,$$

we have,

$$E = \frac{A_1^2 n^2 \pi^2 T}{4L} \ .$$

b. We consider the stationary wave at time, $t = 0$. At this instant, ...

5.4.6.12 Ex: Normal modes on a string

A wire of length L is attached at both ends under a tension T. The wire is pulled sideways by a distance h from its center, such that the rope adopts a triangular shape, and the it is released.
a. What is the energy of the subsequent oscillations. **Suggestion**: Consider the work that needs to be done against the tension to give the wire its initial deformation, and suppose that the tension remains unchanged upon a slight increase of its length

caused by transverse the displacements.
b. How many times will the triangular shape reappear?

Solution: *a. The work is,*

$$W = \int_0^h F dh' = 2\int_0^h T\sin\alpha dh' = 2T\int_0^h \frac{h'dh'}{\sqrt{h'^2+(L/2)^2}} = LT\int_0^{2h/L} \frac{zdz}{\sqrt{z^2+1}}$$
$$= LT\left(\sqrt{1+\left(\frac{2h}{L}\right)^2}-1\right) \simeq \frac{2h^2T}{L} \ .$$

b. Periodicity is given by the fundamental vibration.

5.4.6.13 Ex: Waves on a rope

A string with linear mass density μ is attached at two points distant from each other by $L = 1\,\text{m}$. A mass $m = 1\,\text{kg}$ is now attached to one end of the rope that goes through a pulley, as shown in the figure. Excited by a vibrating pin with frequency $f = 1\,\text{kHz}$ the string performs transverse vibrations with wavelength $\lambda = 2L$.
a. Calculate the propagation velocity of the wave.
b. At what frequency should the pin excite the rope to observe the third oscillation mode (three anti-nodes)?
c. Now the mass is doubled. Calculate the new speed of sound.
d. How should the mass be chosen to obtain a fundamental mode frequency equal to the frequency of the third mode calculated in (b)?

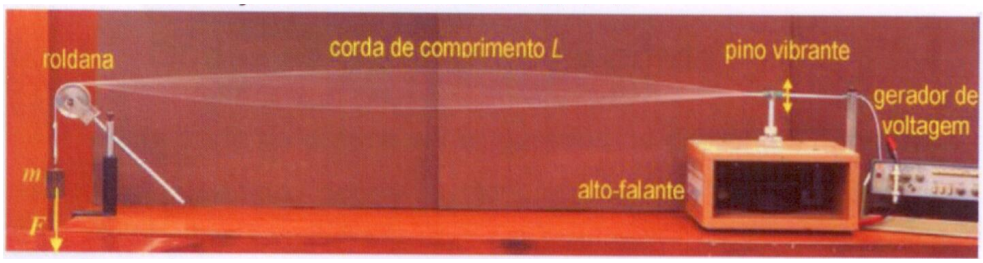

Figure 5.35: Waves on a rope.

Solution: *a. We have,*

$$v = \lambda_n f_n = \frac{2L}{n} f_n \ .$$

Hence, $v_1 = 2Lf_1 = 2\,\text{km/s}$.
b. To calculate the frequency, we let,

$$v' = \lambda_3 f_3 = \frac{2L}{3} f_3 \ .$$

Hence, $f_3 = \frac{3v_1'}{2L} = 3\,\mathrm{kHz}$.
c. We have,

$$v' = \sqrt{\frac{m'g}{\mu}} = \sqrt{2}\sqrt{\frac{mg}{\mu}} = \sqrt{2}v \ .$$

Hence, $v_1' = 2.82\,\mathrm{km/s}$.
d. We have,

$$3 = \frac{v'}{v} = \sqrt{\frac{m'g}{\mu}\frac{\mu}{mg}} = \sqrt{\frac{m'}{m}} \ .$$

Hence, $m' = 9m \approx 9\,\mathrm{kg}$.

5.5 Matter waves

Quantum mechanics tells us that light sometimes behaves like particles and matter like waves. Letting us guide by this analogy we will, in the following, guess the fundamental equations of motion for the propagation of matter waves from a comparison of the respective dispersion relations of light and massive particles.

5.5.1 Dispersion relation and Schrödinger's equation

On one hand, the propagation light is (in the vacuum) is described by the dispersion relation $\omega = ck$ or,

$$\omega^2 - c^2k^2 = 0 \ . \tag{5.172}$$

Since light is a wave it can, in the most general form, be described by a wavepacket, $A(\mathbf{r},t) = \int e^{\imath(\mathbf{k}\cdot\mathbf{r}-\omega t)}a(\mathbf{k})d^3k$. It is easy to verify that the *wave equation*,

$$\frac{\partial^2}{\partial t^2}A - c^2\nabla^2 A = 0 \ , \tag{5.173}$$

reproduces the dispersion relation.

On the other hand, slow massive particles possess the kinetic energy,

$$E = \frac{p^2}{2m} \ . \tag{5.174}$$

With de Broglie's hypothesis that even a massive particle has wavelength, we can try an *ansatz* [11] for a wave equation satisfying the dispersion relation (5.174). From Planck's formula, $E = \hbar\omega$, and the formula of *Louis de Broglie*, $\mathbf{p} = \hbar\mathbf{k}$, describing the particle by a wavepacket not being subject to external forces $\psi(\mathbf{r},t) = \int e^{\imath(\mathbf{k}\cdot\mathbf{r}-\omega t)}\phi(\mathbf{k})d^3k$, it is easy to verify that the differential equation,

$$\imath\hbar\frac{\partial}{\partial t}\psi = \left(-\frac{\hbar^2}{2m}\nabla^2\right)\psi \ , \tag{5.175}$$

[11] Kick, work hypothesis, guess.

reproduces the dispersion relation. If the particle is subject to a potential, its total energy is $E = \mathbf{p}^2/2m + V(\mathbf{r}, t)$. This dispersion relation corresponds to the famous *Schrödinger equation*,

$$\imath\hbar\frac{\partial}{\partial t}\psi = \left(-\frac{\hbar^2}{2m}\Delta + V(r,t)\right)\psi \ . \tag{5.176}$$

Since we accept that light particles and lenses behave like a wave, to calculate their trajectories, we must determine the potential landscape $V(\mathbf{r})$ in which this particle moves before solving the Schrödinger equation. This is the role of *wave mechanics*, which is one of the formulations of quantum mechanics.

5.5.1.1 Scalar waves and vectorial waves

The electromagnetic field is a *vector field*, since $\vec{\mathcal{E}}(\mathbf{r}, t)$ and $\vec{\mathcal{B}}(\mathbf{r}, t)$ are vectors. Therefore, it has a polarization. In contrast, the field of matter $\psi(\mathbf{r}, t)$ is a *scalar field* and therefore does not have the degree of freedom of polarization, in analogy with sound. This has important consequences, for example, the fact that two collinear light fields with orthogonal polarizations do not interfere has no analogue with matter wave fields.

5.5.2 Matter waves

Broglie's formula assigns a wave to each body, The wavelength decreases as the velocity of the particle grows. The necessity to describe a massive particle as a matter wave depends on the relationship between its Broglie wavelength and other characteristic quantities of the system under consideration. If the wavelength is large, we expect typical interference phenomena for waves; if the wavelength is small, the particle will behave like a mass, which is perfectly localized in space and incapable of interfering.

Characteristic features of the system may be, for example, the presence of a narrow slit diffracting the Broglie wave of an atom or an electron passing through it. Another characteristic feature is the average distance between several atoms. In fact, when an atomic gas is so cold, that is, composed of atoms so slow, that the Broglie wavelength of the atoms is longer than the average distance, then the atoms interfere with each other. In the case of bosonic atoms, the interference will be constructive, resulting in a matter wave of gigantic amplitude. This phenomenon is called Bose-Einstein condensation [12].

Before calculating the temperature required for this phenomenon to happen, we need to inform the reader, that the interatomic distance can not be compressed arbitrarily, because below distances of typically $\bar{d} = 1\ \mu$m, the gas tends to form molecules. For the Broglie waves of different atoms to interfere, the wavelength must be longer. The average velocity of the atoms in a gas of temperature T is given by,

$$\frac{m}{2}\bar{v}^2 = \frac{k_B}{2}T \ .$$

Therefore, the temperature of the gas must be,

$$T = \frac{m\bar{v}^2}{k_B} = \frac{\bar{p}^2}{k_B m} = \frac{\hbar^2\bar{k}^2}{k_B m} = \frac{4\pi^2\hbar^2}{k_B m\lambda_{dB}^2} < \frac{h^2}{k_B m d^2} \ .$$

[12] See script on *Quantum mechanics* (2023).

For rubidium atoms of mass $m = 87u$ we calculate $T < 200\,\text{nm}$.

The development of powerful experimental techniques allowed in 1995 the cooling of rubidium gases down to such low temperatures and the experimental realization of Bose-Einstein condensates, that is, matter waves made up of 10^6 atoms. See Exc. 5.5.3.1.

5.5.3 Exercises

5.5.3.1 Ex: Interference in Bose-Einstein condensates

Calculate the periodicity of the interference pattern of two Bose-Einstein condensates supposed to have intrinsic temperatures $T = 0$ interpenetrating at a relative velocity $v = 1\,\text{mm/s}$.

Solution: *The periodicity is* $d = \frac{\lambda_{dB}}{2} = \frac{2\pi}{2k} = \frac{2\pi\hbar}{2mv} = 2.3\,\mu\text{m}$.

5.6 Further reading

H.M. Nussenzveig, Edgar Blucher (2014), *Curso de Física Básica: Fluidos, Vibrações e Ondas, Calor - vol 2* [962]ISBN

Chapter 6

Gravitation

6.1 Planetary orbits

6.1.1 Kopernicus' laws

Nicolaus Copernicus published in 1543 his book *De revolutionibus orbium coelestium* in which he states:

1. The planetary orbit is a circle with epicycles.
2. The Sun is approximately at the center of the orbit.
3. The speed of the planet in the main orbit is constant.

Despite being correct in saying that the planets revolved around the Sun, Copernicus was incorrect in defining their orbits. It was Kepler who correctly defined the orbit of planets as follows:

1. The planetary orbit is not a circle with epicycles, but an ellipse.
2. The Sun is not at the center but at a focal point of the elliptical orbit.
3. Neither the linear speed nor the angular speed of the planet in the orbit is constant, but the area speed is constant.

6.1.2 Kepler's laws

Kepler's laws of planetary motion, published by *Johannes Kepler* between 1609 and 1619, describe the orbits of planets around the Sun:

1. The orbit of a planet is an ellipse with the Sun at one of the two foci.
2. A line segment joining a planet and the Sun sweeps out equal areas during equal intervals of time.
3. The square of a planet's orbital period is proportional to the cube of the length of the semi-major axis of its orbit.

The elliptical orbits of planets were indicated by calculations of the orbit of Mars. From this, Kepler inferred that other bodies in the Solar System, including those farther away from the Sun, also have elliptical orbits. The second law helps to establish

that when a planet is closer to the Sun, it travels faster. The third law expresses that the farther a planet is from the Sun, the slower its orbital speed, and vice versa. *Isaac Newton* showed in 1687 that relationships like Kepler's would apply in the Solar System as a consequence of his own laws of motion and law of universal gravitation. Do the Excs. 6.1.3.1, 6.1.3.2, and 6.1.3.3.

The eccentricity of the orbit of the Earth makes the time from the March equinox to the September equinox, around 186 days, unequal to the time from the September equinox to the March equinox, around 179 days. A diameter would cut the orbit into equal parts, but the plane through the Sun parallel to the equator of the Earth cuts the orbit into two parts with areas in a 186 to 179 ratio, so the eccentricity of the orbit of the Earth is approximately,

$$e \approx \frac{\pi}{4}\frac{186-179}{186+179} \approx 0.015 \ , \tag{6.1}$$

which is close to the correct value (0.016710218). The accuracy of this calculation requires that the two dates chosen be along the elliptical orbit's minor axis and that the midpoints of each half be along the major axis. As the two dates chosen here are equinoxes, this will be correct when perihelion, the date the Earth is closest to the Sun, falls on a solstice. The current perihelion, near January 4, is fairly close to the solstice of December 21 or 22.

6.1.3 Exercises

6.1.3.1 Ex: Kepler orbits

The moon moves in a good approximation on a circular path with radius $R = 384000\,\mathrm{km}$ around the Earth. Assume that the Earth's mass would suddenly decrease.
a. How much would the mass have to decrease so that the moon could escape the Earth?
b. How would the moon's orbit change if the mass decreased by a factor of 3, 2 or 1.5?

Solution: *a. The total energy of the moon rotation is negative,*

$$E = E_{kin} + E_{pot} = \frac{m_{☾}}{2}v_0^2 - \frac{\gamma_N M_{♁} m_{☾}}{r_0} = -\frac{m_{☾}}{2}v_0^2 = -\frac{\gamma_N M_{♁} m_{☾}}{2r_0} \ .$$

After the loss of mass, the Earth has the mass $\tilde{M}_{♁}$ and the moon has the energy,

$$\tilde{E} = \frac{m_{☾}}{2}v_0^2 - \frac{\gamma_N \tilde{M}_{♁} m_{☾}}{r_0} = \frac{\gamma_N (M_{♁}/2 - \tilde{M}_{♁}) m_{☾}}{r_0} \ .$$

In order to escape from Earth, the total energy must be positive. I.e. the mass of the Earth must be reduced to less than half, $M_{♁} > 2\tilde{M}_{♁}$.
b. The path of the moon is described by a conic section,

$$r = \frac{P}{1-\varepsilon\cos\phi} \quad \textit{and} \quad P = \frac{L^2}{\alpha m_{☾}} \quad \textit{and} \quad \varepsilon = \frac{C}{\alpha m} = \sqrt{1 + \frac{2L^2}{\alpha^2 m}(E_{kin}+E_{pot})} \ ,$$

where $\alpha = \gamma_N M_{\sun} m_{\moon}$ and the angular momentum of the moon is $L = m_{\moon}\,\omega r_0^2$. The half parameter and the eccentricity are,

$$P = \frac{\omega^2 r_0^4}{\gamma_N M_{\sun}} = r_0$$
$$\varepsilon = \sqrt{1 + \frac{2L^2}{\alpha^2 m_{\moon}}(E_{kin} + E_{pot})} = \sqrt{1 + \frac{2r_0}{\gamma_N M_{\sun} m_{\moon}}\left(-\frac{\gamma_N M_{\sun} m_{\moon}}{2r_0}\right)} = 0\ .$$

I.e. the moon initially describes a circular orbit. After the mass reduction, the total energy changes,

$$\varepsilon = \sqrt{1 + \frac{2r_0}{\gamma_N M_{\sun} m_{\moon}}\left(\frac{\gamma_N (M_{\sun}/2 - \tilde{M}_{\sun}) m_{\moon}}{r_0}\right)} = \sqrt{2 - \frac{2\tilde{M}_{\sun}}{M_{\sun}}}\ .$$

The eccentricity becomes $\varepsilon = 1$ if the reduced mass is $\tilde{M}_{\sun} = M_{\sun}/2$. The lunar orbit then becomes a parabola. The eccentricity becomes $\varepsilon > 1$ if the mass reduction is larger. The lunar orbit then becomes the hyperbola.

6.1.3.2 Ex: Kepler orbits of missiles

Consider an object of mass $m \ll M_{\earth}$ which is launched at an initial velocity $\mathbf{v}_0$ (at an angle θ relative to the Earth's surface). We neglects any friction.
a. What possible trajectories can the object move on? How does the type of trajectory depend on the conservation parameters?
b. Calculate the maximum speed that the object may have to move on a closed trajectory. Does this speed depend on θ? Does the projectile always fall back to Earth when the path is closed?
c. Neglecting the Earth's rotation calculate the flight distance of the projectile above the Earth's surface for velocities below the above-mentioned limit velocity.
Help: Set the center of the Earth in the focal point of the Kepler orbit.

Solution: *a. The projectile can move on ellipses, parabolas or hyperbolas, depending on the initial velocity. The equation of motion is that of a conic section,*

$$r = \frac{P}{1 - \epsilon\cos\phi}\ ,$$

where $\epsilon = \sqrt{1 + \frac{2l^2}{\alpha^2 m}E}$. The conservation parameters are the total energy $E = \frac{m}{2}v^2 - \frac{\alpha}{r}$ and the angular momentum l. For the projectile to move on a closed path, the eccentricity must be $\epsilon < 1$, i.e. $mv^2/2 < \alpha/r$. Otherwise it moves on hyperbolas or a parabola.
b. The escape speed is when $R_{\earth} = 6370\,\mathrm{km}$ is the Earth's radius and $M_{\earth} = 6\times10^{24}\,\mathrm{kg}$ its mass,

$$v_f = \sqrt{\frac{2\alpha}{mR_{\earth}}} = \sqrt{\frac{2\gamma_N M_{\earth}}{R_{\earth}}} \approx 11.2\,\mathrm{km/s}\ .$$

It does not depend on the launch angle θ.
c. According to the sketch, $\theta = 90° - \phi$. Hence, the length of the geodesic $L = \frac{\phi}{2\pi} 2\pi R_{\oplus} = (90° - \theta) R_{\oplus}$.

6.1.3.3 Ex: Halley's Comet

The comet Haley moves like a planet on an elliptical orbit around the sun. Its orbital period is 75 years and the closest distance to the sun is 0.5 AE. (One astronomical unit is the distance from the Earth to the sun, assuming that the orbit of the Earth around the sun is a circular orbit.)
a. Use this information to calculate the value for the major semi-axis a and the minor semi-axis b of the comet's orbit in astronomical units. Use this to determine the eccentricity ε of the orbit.
b. What is the maximum distance of the comet from the sun?
c. Calculate the minimum and maximum speed of the comet on its orbit.

Solution:
We have $T = 75\,\mathrm{a}$, $T_{\oplus} = 1\,\mathrm{a}$, $d = 0.5\,\mathrm{AE}$ and $d_E = 1\,\mathrm{AE} = a_E$.
a. According to Kepler's 3rd law,

$$\frac{T^2}{a^3} = \frac{T_{\oplus}^2}{a_E^3} = \frac{(1\,\mathrm{a})^2}{(1\,\mathrm{AE})^3} = const\ .$$

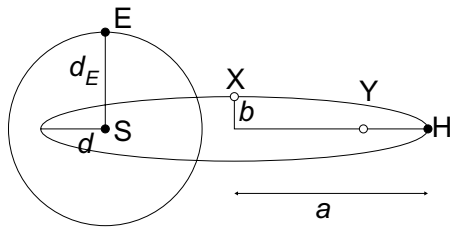

From this follows

$$a = \sqrt[3]{\frac{(1\,\mathrm{AE})^3}{(1\,\mathrm{a})^2}(75\,\mathrm{a})^2} \simeq 17.78\,\mathrm{AE}\ .$$

From the ellipse construction follows,

$$\begin{aligned} \bar{SX} + \bar{XY} = 2\bar{SX} &= 2a \\ \Rightarrow \bar{SX} &= a = \sqrt{b^2 + (a-d)^2} \\ \Rightarrow b &= \sqrt{a^2 - (a-d)^2} = \sqrt{2ad - d^2} \simeq 4.19\,\mathrm{AE}\ . \end{aligned}$$

b. The maximum distance is at the far end of the major semi-axis,

$$r_{\max} = 2a - d = 35.06\,\mathrm{AE}\ .$$

c. The change in the swept area is,

$$\frac{dA}{dt} = \frac{1}{2}\left|\mathbf{r} \times \frac{d\mathbf{r}}{dt}\right| = \frac{1}{2}|\mathbf{r} \times \mathbf{r}| = \frac{|\mathbf{l}|}{2m} = \frac{A_{ges}}{T} = \frac{\pi ab}{T} = const\ .$$

Since we have at the locations of maximum and minimum distance, or minimum and maximum speed $\mathbf{r} \perp \mathbf{v}$,

$$\frac{dA}{dt} = \frac{1}{2} rv = \frac{\pi ab}{T} = const\ .$$

From which follows,

$$v_{\min} = \frac{2\pi ab}{T r_{\max}} \simeq 0.178 \ \text{AE/a} \qquad \textit{and} \qquad v_{\max} = \frac{2\pi ab}{T r_{\min}} \simeq 12.48 \ \text{AE/a} \ .$$

6.2 Newton's law

Newton's law of *gravity* about the force between two massive bodies,

$$\mathbf{F} = -\nabla V(r) \ . \tag{6.2}$$

can be deduced from a conservative central potential,

$$\boxed{V(r) = \frac{\gamma_N M m}{r}} \ . \tag{6.3}$$

If $M = M_{♁}$ is the mass of the Earth, a test mass m close to the surface ($r_{♁} \approx 6378\,\text{km}$) will be accelerated by,

$$g = \frac{F}{m} = -\frac{\partial}{\partial r}\frac{\gamma_N M_{♁}}{r}\bigg|_{r=R_{♁}} = \frac{\gamma_N M_{♁}}{R_{♁}^2} = 9.81\,\text{m/s}^2 \ . \tag{6.4}$$

with Newton's constant,

$$\boxed{\gamma_N = 6.67 \cdot 10^{-11}\,\text{m}^3/\text{kg s}^2} \ . \tag{6.5}$$

6.2.1 Cosmic velocities

6.2.1.1 First cosmic velocity

The first *cosmic velocity* is defined as the velocity that a body must have in order to circle the center of the Earth on an orbit with the Earth's radius. We calculate this velocity from the condition that the centripetal force be equal to the centrifugal force,

$$\frac{m v_1^2}{r_{♁}} = \gamma_N \frac{m M_{♁}}{r_{♁}^2} \qquad \Rightarrow \qquad v_1 = \sqrt{\frac{\gamma_N M_{♁}}{r_{♁}}} \ , \tag{6.6}$$

yielding $v_1 \approx 7.91\,\text{km/s} = 2.84 \cdot 10^4\,\text{km/h}$. In Exc. 6.2.3.1 we estimate the mass of the milky way galaxy from the velocity of the sun and its distance from the galaxy's center. In Exc. 6.2.3.2 we compare the heights of stationary orbits around the Earth and the moon.

Example 23 (*Angular velocity of a satellite*): Here, we calculate the velocity of a satellite on a circular orbit at a height of 400 km above the Earth's surface,

$$v_1 = \sqrt{\frac{\gamma_N M_{♁}}{r_{♁} + h}} \ ,$$

yielding $v_1 \approx 7.66\,\text{km/s} = 2.76 \cdot 10^4\,\text{km/h}$.

6.2.1.2 Escape velocity

The *escape velocity* or second cosmic velocity is the velocity that a body must have to be able to leave the Earth's gravity field completely. We calculate the second cosmic speed for the Earth from,

$$E_{kin} = \frac{m}{2}v_2^2 = \text{final} - \text{initial energy in the limit final energy } \to 0 \ . \tag{6.7}$$

Hence,

$$E_{kin} = 0 - \left(-\gamma_N \frac{mM_{\text{♁}}}{r_{\text{♁}}}\right) \qquad \Rightarrow \qquad v_2 = \sqrt{\frac{2\gamma_N M_{\text{♁}}}{r_{\text{♁}}}} = v_1\sqrt{2} \ , \tag{6.8}$$

yielding $v_2 \approx 11.2\,\text{km/s} = 4.03 \cdot 10^4\,\text{km/h}$. Apparently, the cosmic velocities v_1 and v_2 are related. In Exc. 6.2.3.3 and 6.2.3.4 we calculate cosmic velocities for, respectively, Earth and the comet Tschurjumow-Gerasimenko.

> **Example 24 (*Escape velocity for a satellite*):** The escape velocity for a satellite that is in a 400 km high orbit above the Earth's surface is $v_2 \approx 10.83\,\text{km/s} = 3.90 \cdot 10^4\,\text{km/h}$.

6.2.2 Deriving Kepler's laws from Newton's laws

6.2.2.1 Kepler's first law

The orbits are ellipses, with focal points F1 and F2 for the first planet and F1 and F3 for the second planet. The Sun is placed at focal point F1. The two shaded sectors A1 and A2 have the same surface area and the time for planet 1 to cover segment A1 is equal to the time to cover segment A2. The total orbit times for planet 1 and planet 2 have a ratio $(a_1/a_2)^{3/2}$.

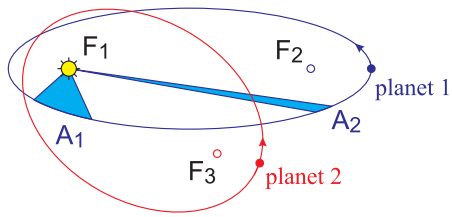

Figure 6.1: Illustration of Kepler's three laws with two planetary orbits.

6.2.2.2 Kepler's second law

The area swept by the planet's trajectory in infinitesimal time steps is,

$$A(t, t+dt) = \tfrac{1}{2}|\mathbf{r}(t) \times \dot{\mathbf{r}}(t)|dt = \tfrac{L}{2m}dt \ .$$

Since central potentials preserve angular momentum,

$$\dot{\mathbf{L}} = \frac{d}{dt}m\mathbf{r} \times \mathbf{p} = m(\dot{\mathbf{r}} \times \dot{\mathbf{r}} + \mathbf{r} \times \ddot{\mathbf{r}}) = m\mathbf{r} \times \ddot{\mathbf{r}} = -\mathbf{r} \times \nabla V(r) = -\mathbf{r} \times \frac{\partial V(r)}{\partial r}\hat{\mathbf{e}}_r = \mathbf{0} \ ,$$

for a given time difference $dt = t_1 - t_0$ the swept area is the same. Angular momentum is a constant of motion, $\dot{\mathbf{L}} = 0$, for central potentials.

6.2.2.3 Kepler's third law

6.2.3 Exercises

6.2.3.1 Ex: Mass of the Milky Way

Estimate the total mass of our galaxy (the milky way) using the parameters of the orbits of the sun (and the solar system) around the center of the galaxy. Assume that the major part of the mass of our galaxy is in the form of a uniform sphere (bulge). The speed of the sun on its way around the center of the galaxy is approximately $v = 250\,\mathrm{km/h}$, the distance of the sun from the center of the galaxy is approximately $r = 28000\,\mathrm{ly}$ (light years). To how many stars like our sun does this correspond to?

Solution: *We use Newton's second law, $F = ma$, with a as centripetal acceleration, $a = v^2/r$, and F as the general law of gravity:*

$$\gamma_N \frac{Mm}{r^2} = m\frac{v^2}{r} \ ,$$

where M is the mass of the galaxy and m is the mass of our sun or the solar system. As a solution we get,

$$M = \frac{rv^2}{\gamma_N} \approx 3 \cdot 10^{41}\,\mathrm{kg} \ .$$

In terms of number of stars like our sun ($M_\odot = 2.0 \cdot 10^{30}\,\mathrm{kg}$) we get about 10^{11} stars.

6.2.3.2 Ex: Gravitation on Earth and Moon

How high are the orbits of 'geo-stationary' and 'lunar-stationary' satellites?

Solution: *The equilibrium position r of 'planeto-stationary' orbits results from,*

$$\frac{mv_1^2}{r} = \gamma_N \frac{mM}{r^2} \qquad \textit{with} \qquad v_1 = \frac{2\pi r}{T} \ ,$$

with T the period for a revolution of the planet around itself. Form this,

$$r = \sqrt[3]{\gamma_N \frac{M}{4\pi^2} T^2} \ .$$

For the Earth with $M = M_\oplus = 5.97 \cdot 10^{24}\,\mathrm{kg}$ and $T = 1\,\mathrm{d}$ we get $r = 42200\,\mathrm{km}$. For the Moon with $M_\leftmoon = 7.35 \cdot 10^{22}\,\mathrm{kg}$ and $T = 27.3\,\mathrm{d}$ we get $r = 88400\,\mathrm{km}$.

6.2.3.3 Ex: Cosmic velocities

a. How long is the orbital period T of a 1 t satellite on a circular orbit at a height of 20 km around the Earth? How long is the orbital period T of the Earth around the sun (the mass of the sun is 3.334×10^5 times larger than that of the Earth)? At what distance from Earth is the orbit of a satellite geostationary?
b. Calculate the escape velocity from Earth (or cosmic speed) for a person weighing 75 kg.

Solution: *a. The satellite is on a stable orbit when the centrifugal force is compensated by gravity,*

$$m\omega^2 r = \frac{\gamma_N M m}{r^2}$$

$$T = \frac{2\pi}{\omega} = 2\pi\sqrt{\frac{r^3}{\gamma_N M}} \ .$$

With $r = 6370\,\mathrm{km} + 20\,\mathrm{km}$, $M = 5.97 \times 10^{24}\,\mathrm{kg}$ *we get* $T = 1.4128\,\mathrm{h}$. *The calculation bill with* $r = 1.496 \times 10^8\,\mathrm{km}$ *and* $M = 1.99 \times 10^{30}\,\mathrm{kg}$ *yields the sidereal year* $T = 365.2364\,\mathrm{d}$. *A geostationary orbit is obtained for* $T = \mathrm{d}$, *hence,*

$$r = (\gamma_N M)^{1/3} \left(\frac{T}{2\pi}\right)^{2/3} \approx 42270\,\mathrm{km} \ .$$

b. The initial kinetic energy compensates for the potential difference, if

$$\frac{m}{2}v^2 = \frac{\gamma_N M m}{r} - \frac{\gamma_N M m}{\infty} \ ,$$

where r *is the earth's radius. So* $v = \sqrt{2\gamma_N M/r} \approx 11.2\,\mathrm{km/s}$.

6.2.3.4 Ex: Tschurjumow-Gerasimenko

The satellite Rosetta of the ESA ($m_{sat} = 3000\,\mathrm{kg}$) was placed on an orbit of the comet Tschurjumow-Gerasimenko (mass $m_{TG} = 3.14 \cdot 10^{12}\,\mathrm{kg}$, diameter $d_{TG} = 4\,\mathrm{km}$).
a. For the satellite to orbit the comet once a terrestrial day, what is the required height of the orbit?
b. What is the escape velocity from the comet's surface?

Solution: *a. Equilibrium between the gravitational force and the centrifugal force requires,*

$$F = \gamma_N \frac{m_{TG} m_{sat}}{h^2} = m_{sat}\omega^2 h \ .$$

Hence,

$$h = \left(\gamma_N \frac{m_{TG}}{\omega^2}\right)^{1/3} = \left(\gamma_N \frac{m_{TG}}{4\pi^2} T^2\right)^{1/3} = 3.4\,\mathrm{km} \ .$$

Thus, the satellite should fly $1.4\,\mathrm{km}$ *above the comet's surface.*
b. The escape velocity is given by,

$$\gamma_N \frac{m_{TG} m}{d_{TG}/2} = \frac{m}{2} v_{esc}^2 \ .$$

Hence,

$$v_{esc} = \sqrt{\frac{4\gamma_N m_{TG}}{d_{TG}}} = 45\,\mathrm{cm/s} \ .$$

6.3 Gravitational potential

For an arbitrary mass distribution $\rho(\mathbf{r})$ the *gravitational potential* acting on a test mass m can be calculated from,

$$\boxed{V(\mathbf{r}) = -\gamma_N m \int_{\mathbb{R}^3} \frac{\rho(\mathbf{r}')}{|\mathbf{r}-\mathbf{r}'|} d^3r'} \ . \tag{6.9}$$

For a point-mass with mass M located at the origin, $\mathbf{r}' = 0$, we parametrize $\rho(\mathbf{r}') = M\delta^3(\mathbf{r}')$, and recover Newton's law,

$$V(\mathbf{r}) = -\gamma_N \frac{Mm}{r} \ . \tag{6.10}$$

The gravitational potential being conservative, trajectories of test masses can simply be derived by solving the equation of motion,

$$\boxed{m\ddot{\mathbf{r}} = -\nabla V(\mathbf{r}) = \gamma_N m \int_{\mathbb{R}^3} \rho(\mathbf{r}') \frac{\mathbf{r}-\mathbf{r}'}{|\mathbf{r}-\mathbf{r}'|^3} d^3r'} \ . \tag{6.11}$$

If in practice analytic solution are beyond reach, numerical procedure are always possible.

Example 25 (*Gravitational potential in- and outside a homogeneous sphere*): In this example we will calculate the gravitational force that a particle of mass m is subjected to when placed inside a homogeneous sphere of radius R at a distance r from its center.
The potential exerted by a mass distribution with the density $\rho(\mathbf{r}')$ on a particle of mass m located at the position $\mathbf{r}$ is,

$$V(\mathbf{r}) = -\int \rho(\mathbf{r}') \frac{\gamma_N m}{|\mathbf{r}-\mathbf{r}'|} d^3r' = -\int_{sphere} \rho_0 \frac{\gamma_N m}{|\mathbf{r}-\mathbf{r}'|} r'^2 \sin\theta' dr' d\theta' d\phi' \ . \tag{6.12}$$

Substituting,

$$\xi \equiv |\mathbf{r}-\mathbf{r}'| = \sqrt{r^2 + r'^2 - 2rr'\cos\theta'} \tag{6.13}$$
$$\frac{d\xi}{d\theta'} = \frac{rr'\sin\theta'}{\xi} \ ,$$

we obtain,

$$V(\mathbf{r}) = -\int_{sphere} \rho_0 \frac{\gamma_N m r'}{r} d\xi dr' d\phi' = \frac{2\pi\rho_0\gamma_N m}{r} \int_0^R \int_{\xi_{\min}}^{\xi_{\max}} r' d\xi dr' \ . \tag{6.14}$$

The integration limits follow from the values adopted by ξ for $\theta = 0$ resp. $\theta = \pi$. For $r \leq R$ we have that r' is always greater than r. Hence, $\xi = r' - r, .., r' + r$. For $R \leq r$ we have that r' is always smaller than r. Hence, $\xi = r - r', .., r' + r$.

$$V(\mathbf{r}) = -\frac{2\pi\rho_0\gamma_N m}{r} \begin{cases} \int_r^R 2rr'dr' + \int_0^r 2r'^2 dr' \\ \int_0^R 2r'^2 dr' \end{cases} \quad \text{for} \quad \begin{cases} r \leq R \\ R \leq r \end{cases} . \tag{6.15}$$

With the sphere's mass,

$$M = \frac{4\pi\rho_0 R^3}{3} , \tag{6.16}$$

the potential becomes,

$$\begin{aligned} V(\mathbf{r}) &= -2\pi\rho_0\gamma_N m \left(R^2 - \frac{1}{3}r^2\right)\theta(R-r) - 2\pi\rho_0\gamma_N m\frac{2R^3}{3r}\theta(r-R) \\ &= -\gamma_N Mm\left(\frac{3}{2R} - \frac{r^2}{2R^3}\right)\theta(R-r) - \gamma_N Mm\frac{1}{r}\theta(r-R) . \end{aligned} \tag{6.17}$$

The force can be calculated using the gradient in spherical coordinates,

$$\begin{aligned} \mathbf{F} &= -\nabla V(\mathbf{r}) = -\hat{\mathbf{e}}_r\frac{\partial}{\partial r}V(\mathbf{r}) \\ &= -\hat{\mathbf{e}}_r\gamma_N Mm\frac{r}{R^3}\theta(R-r) - \hat{\mathbf{e}}_r\gamma_N Mm\frac{1}{r^2}\theta(r-R) . \end{aligned} \tag{6.18}$$

The gravitational acceleration is often specified in units of *Gal* after *Galilei*, where $1\,\text{Gal} \equiv 1\,\text{cm/s}^2$.

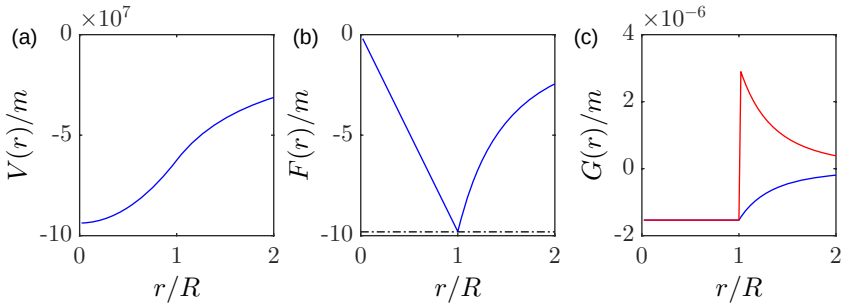

Figure 6.2: (code) Gravity in- and outside of Earth. (a) Gravitational potential, (b) gravitational force, and (c) radial (blue) and transverse (red) gravity gradient.

The above example shows that

1. outside a spherical mass distribution the gravitational potential can simply be replaced by that of a point mass sitting at the center of the mass distribution;
2. the superposition principle,

$$\boxed{V_{\rho_1+\rho_2}(\mathbf{r}) = V_{\rho_1}(\mathbf{r}) + V_{\rho_2}(\mathbf{r})} , \tag{6.19}$$

allows us to described the impact of mass cavities via simple subtraction

In classical mechanics we often describe gravity as a homogenous force field, which can be derived from a potential scaling linearly with the height above normal ground,

$$V(h) = mgh \ . \tag{6.20}$$

Obviously, this is approximation obtained by linearizing the gravitational potential on the Earth's surface. From Newton's law,

$$V(\mathbf{r}) = -\frac{\gamma_N M m}{r} \ , \tag{6.21}$$

using the Taylor expansion:

$$V(\mathbf{r}+\mathbf{h}) = e^{\mathbf{h}\cdot\nabla_\mathbf{r}} V(\mathbf{r}) = \sum_{\nu=0}^{\infty} \frac{(\mathbf{h}\cdot\nabla_\mathbf{r})^\nu}{\nu!} V(\mathbf{r}) = V(\mathbf{r}) + (\mathbf{h}\cdot\nabla_\mathbf{r})V(\mathbf{r}) + \frac{1}{2}(\mathbf{h}\cdot\nabla_\mathbf{r})(\mathbf{h}\cdot\nabla_\mathbf{r})V(\mathbf{r}) \ , \tag{6.22}$$

we get,

$$V(\mathbf{r}+\mathbf{h}) \simeq V(\mathbf{r}) + h\frac{\gamma_N M m}{r^2} = V(\mathbf{r}) + hgm \ . \tag{6.23}$$

In Exc. 6.3.5.1 we derive an expression generalizing Eq. (6.17) to arbitrary isotropic gravitational potentials. In Excs. 6.3.5.2, 6.3.5.3, 6.3.5.4, and 6.3.5.5 we calculate the potentials for other isotropic mass distributions. In Exc. 6.3.5.6 we use the superposition principle to calculate the potential generated by a spherical cavity inside a homogeneous sphere. In Excs. 6.3.5.7, 6.3.5.8, and 6.3.5.9 we calculate potentials generated by non-spherical density distributions. In Excs. 6.3.5.10, 6.3.5.11, and 6.3.5.12 we apply the results derived for the Earth's inner gravitational potential to derive possible trajectories through boreholes traversing the Earth.

6.3.1 Rotation and divergence of gravitational force fields

The rotation and divergence of gravitational force fields are,

$$\begin{aligned} \nabla^2 V(\mathbf{r}) = \nabla\cdot\mathbf{F}(\mathbf{r}) &= -4\pi\gamma_N m\rho(\mathbf{r}) \\ \nabla\times\mathbf{F}(\mathbf{r}) &= 0 \ . \end{aligned} \tag{6.24}$$

The integral formulation of Eq. (6.24) reads,

$$\oint_{\partial V} \mathbf{F}\cdot d\mathbf{S} = -4\pi\gamma_N M m \ , \tag{6.25}$$

with $M = \oint_{\partial V} \rho(\mathbf{r}) d^3r$.

The interpretation of these expressions are:

- The Poisson equation relates the divergence of the force field directly to the density distribution.
- The divergence is nothing else than the diagonal of gravity gradient defined in Sec. 6.3.2.
- For being conservative, gravitational potentials are rotation-free.

- The integral over a closed surface is proportional to the enclosed mass.

The Lagrangian density for Newtonian gravity is,

$$\mathcal{L}(\mathbf{r},t) = -\rho(\mathbf{r},t) - \tfrac{1}{8\pi\gamma_N}[\nabla V(\mathbf{r},t)]^2 \ . \tag{6.26}$$

Applying the Hamitonian principle to this Lagrangian one recovers the Poisson equation for gravity.

6.3.2 Gravity gradients

The *gravity gradient* is a tensor defined as the second derivative of the potential,

$$\boxed{G_{kl}(\mathbf{r}) = G_{lk}(\mathbf{r}) = \frac{\partial g_l(\mathbf{r})}{\partial x_k} = \frac{1}{m}\frac{\partial F_l(\mathbf{r})}{\partial x_k} = -\frac{1}{m}\frac{\partial}{\partial x_k}\frac{\partial V(\mathbf{r})}{\partial x_l}} \ . \tag{6.27}$$

Inserting the potential (6.9) we obtain,

$$\begin{aligned} G_{kl}(\mathbf{r}) &= -\frac{1}{m}\frac{\partial}{\partial x_k}\frac{\partial V(\mathbf{r})}{\partial x_l} = \gamma_N \int_{R^3} \rho(\mathbf{r}')\frac{\partial}{\partial x_k}\frac{\partial}{\partial x_l}\frac{1}{|\mathbf{r}-\mathbf{r}'|}d^3r' \qquad (6.28)\\ &= \gamma_N \int_{R^3} \frac{\rho(\mathbf{r}')}{|\mathbf{r}-\mathbf{r}'|^5}\begin{pmatrix} 3(x-x')^2-(\mathbf{r}-\mathbf{r}')^2 & 3(x-x')(y-y') & 3(x-x')(z-z') \\ 3(x-x')(y-y') & 3(y-y')^2-(\mathbf{r}-\mathbf{r}')^2 & 3(y-y')(z-z') \\ 3(x-x')(z-z') & 3(y-y')(z-z') & 3(z-z')^2-(\mathbf{r}-\mathbf{r}')^2 \end{pmatrix} d^3r' \\ &= \gamma_N \int_{R^3} \frac{\rho(\mathbf{r}')}{|\mathbf{r}-\mathbf{r}'|^3} K_{kl}(\mathbf{r}-\mathbf{r}')d^3r' \ , \end{aligned}$$

defining the kernel,

$$K_{kl}(\mathbf{r}-\mathbf{r}') \equiv \frac{3(x_k-x'_k)(x_l-x'_l)-\delta_{kl}(\mathbf{r}-\mathbf{r}')^2}{|\mathbf{r}-\mathbf{r}'|^2} \ . \tag{6.29}$$

For example, for the gravitational potential generated by a point mass,

$$V(r) = \gamma_N \frac{Mm}{r} = \gamma_N \frac{Mm}{\sqrt{x^2+y^2+z^2}} \ , \tag{6.30}$$

we find,

$$\begin{aligned} G_{kl}(\mathbf{r}) = -\frac{1}{m}\frac{\partial}{\partial x_k}\frac{\partial V(\mathbf{r})}{\partial x_l} &= \frac{\gamma_N M}{r^5}\begin{pmatrix} 3x^2-r^2 & 3xy & 3xz \\ 3xy & 3y^2-r^2 & 3yz \\ 3xz & 3yz & 3z^2-r^2 \end{pmatrix} \qquad (6.31)\\ &= \frac{\gamma_N M}{r^5}(3x_k x_l - r^2\delta_{kl}) \ . \end{aligned}$$

Gravity gradients are often given in units of *Eotvos* after *Eötvös*, where 1 Eotvos = $10^{-9}\,\mathrm{s}^{-2}$. In Exc. 6.3.5.13 we calculate the gravity gradient tensor of Earth (modeled as an idealized sphere) at the north-pole.

Example 26 (*Gravitational curvature in- and outside a homogeneous sphere*): The gravitational potential an force in- and outside a homogeneous sphere have been calculated in the example 25. Using the result we derive the gravity gradient,

$$
\begin{aligned}
G_{kl}(\mathbf{r}) &= -\frac{1}{m}\frac{\partial}{\partial x_k}\frac{\partial}{\partial x_l}V(\mathbf{r}) \qquad (6.32)\\
&= -\frac{\gamma_N M}{R^3}\begin{pmatrix}1&0&0\\0&1&0\\0&0&1\end{pmatrix}\theta(R-r) + \frac{\gamma_N M}{r^5}\begin{pmatrix}3x^2-r^2 & 3xy & 3xz\\ 3xy & 3y^2-r^2 & 3yz\\ 3xz & 3yz & 3z^2-r^2\end{pmatrix}\theta(r-R)\\
&= -\frac{\gamma_N M}{R^3}\delta_{kl}\theta(R-r) - \frac{\gamma_N M}{r^3}\left(\delta_{kl}-\frac{3x_k x_l}{r^2}\right)\theta(r-R)\ .
\end{aligned}
$$

The example 25 revealed that neither the potential nor the force are discontinuous at the sphere's surface. In contrast, the radial component of the curvature $G_{k=l}(r=R)$ is discontinuous at the north pole, while the transverse components $G_{k\neq l}(r=R)$ stay continuous, which is obviously due to the isotropic symmetry of the potential. To see this better, let us move along the symmetry axis setting $\mathbf{r} = r\hat{\mathbf{e}}_z$,

$$
G_{kl}(r\hat{\mathbf{e}}_z) = -\frac{\gamma_N M}{R^3}\begin{pmatrix}1&0&0\\0&1&0\\0&0&1\end{pmatrix}\theta(R-r) - \frac{\gamma_N M}{r^3}\begin{pmatrix}1&0&0\\0&1&0\\0&0&-2\end{pmatrix}\theta(r-R)\ . \qquad (6.33)
$$

Applying this results to Earth, be find inside Earth a constant gravity gradient of $-\gamma_N M_{\oplus}/R_{\oplus}^3 = 1.54\cdot 10^{-6}\,\mathrm{s}^{-2}$.

6.3.2.1 Gravimetry and gravity gradiometry

Gravity-gradiometers measure spatial variations of the gravitational acceleration. Being obtained as second derivatives of the gravitational potential, they are more sensitive to local mass variations, as nearly homogeneous large scale contributions to the acceleration are removed. For this reason, gravity-gradiometers need to be less accurate, provided they are sensitive enough. In Exc. 6.3.5.14 we estimate the sensitivity of modern gravimeters.

Example 27 (*Gravitation in- and outside a massive shell*): The calculations of examples 25 and 26 can be generalized for a homogenous massive shell with density ρ_1, inner radius R_i, and outer radius R_0. In Exc. 6.3.5.2 we show that the gravitational potential is,

$$
\begin{aligned}
V(\mathbf{r}) = -2\pi\rho_1\gamma_N m\,\big[&(R_o^2-R_i^2)\theta(R_i-r) \qquad (6.34)\\
&+\left(R_o^2-\frac{r^2}{3}-\frac{2R_o^3}{3r}\right)\theta(r-R_i)\theta(R_o-r) + \frac{2(R_o^3-R_i^3)}{3r}\theta(r-R_o)\Big]\ ,
\end{aligned}
$$

the gravitational force,

$$
\begin{aligned}
\mathbf{F}(\mathbf{r} = -\nabla V(\mathbf{r}) &= -\hat{\mathbf{e}}_r\frac{\partial}{\partial r}V(\mathbf{r}) \qquad (6.35)\\
&= \hat{\mathbf{e}}_r\frac{4\pi\rho_1\gamma_N m}{3}\left[\left(-r+\frac{R_o^3}{r^2}\right)\theta(r-R_i)\theta(R_o-r) - \frac{R_o^3-R_i^3}{r^2}\theta(r-R_o)\right]\ ,
\end{aligned}
$$

and the gravity gradient,

$$G_{kl}(\mathbf{r}) = -\frac{1}{m}\frac{\partial}{\partial x_k}\frac{\partial}{\partial x_l}V(\mathbf{r}) \tag{6.36}$$
$$= -\frac{4\pi\rho_1\gamma_N}{3}\left[\left(\delta_{kl} - \frac{R_i^3}{r^3}\left(\delta_{kl} - \frac{3x_k x_l}{r^2}\right)\right)\theta(r-R_i)\theta(R_o-r) + \frac{R_o^3 - R_i^3}{r^3}\left(\delta_{kl} - \frac{3x_k x_l}{r^2}\right)\theta(r-R_o)\right] .$$

For $R_i \to 0$ we recover the results of example 26. Particularly along the symmetry axis,

$$G_{zz}(\mathbf{r}) = -\frac{4\pi\rho_1\gamma_N}{3}\left[\left(1 + \frac{2R_i^3}{r^3}\right)\theta(r-R_i)\theta(R_o-r) - 2\frac{R_o^3 - R_i^3}{r^3}\theta(r-R_o)\right] . \tag{6.37}$$

6.3.3 Constants of motion

Trajectories can also be derive exploiting constants of motion. In Excs. 6.3.5.18 to 6.3.5.23 we calculate trajectories of bodies under the influence of gravity.

6.3.4 The virial law

The virial law states,

$$\boxed{\overline{T} = -\overline{\frac{1}{2}\sum_i \mathbf{F}_i\mathbf{r}_i}} . \tag{6.38}$$

For potentials of the form $V(r) = \alpha r^k$ we have,

$$\mathbf{F} = -\nabla V = -k\alpha r^{k-1}\hat{\mathbf{e}}_r . \tag{6.39}$$

Thus $\overline{T}$ and $\overline{V}$ related via,

$$\overline{T} = -\overline{\frac{1}{2}\sum_i \mathbf{F}_i\mathbf{r}_i} = \frac{k}{2}\overline{\sum_i \alpha r_i^{k-1}\hat{\mathbf{e}}_{r_i}\cdot\mathbf{r}_i} = \frac{k}{2}\overline{\sum_i \alpha r_i^k} = \frac{k}{2}\overline{V} . \tag{6.40}$$

In Exc. 6.3.5.24 we apply the virial law to a spring pendulum.

Example 28 (*The virial law for the harmonic potential and for* $1/r$*-potentials*): The special case $k = 2$ yields,

$$V(r) = \alpha r^2 \Rightarrow \overline{T} = \overline{V} , \tag{6.41}$$

and corresponds to a harmonic oscillator with $\alpha = \frac{1}{2}m\omega_0^2$.
The special case $k = -1$ yields,

$$V(r) = \frac{\alpha}{r} \Rightarrow \overline{T} = -\frac{1}{2}\overline{V} , \tag{6.42}$$

and corresponds to a Coulomb potential with $\alpha = \frac{q_1 q_2}{4\pi\epsilon_0}$, respectively a gravitational potential with $\alpha = -\gamma_N Mm$.
In the case of the gravitational potential, for positive total energy, we get,

$$E = \overline{T} + \overline{V} > 0 \qquad \overline{T} = -\tfrac{1}{2}\overline{V} \Rightarrow E = \tfrac{1}{2}\overline{V} > 0 \Rightarrow Mm < 0 . \tag{6.43}$$

Thus,

$$\overline{T} = \frac{1}{2} m \overline{v^2} = -\frac{1}{2}\overline{V} < 0 \Rightarrow m < 0 \tag{6.44}$$

This leads to the demand for negative masses, which is not sensible. The virial theorem can only apply to bound systems with $E < 0$.

6.3.5 Exercises

6.3.5.1 Ex: Arbitrary isotropic mass density distributions

a. Generalize the calculation of gravitational potentials and forces exhibited in example 24 to arbitrary, but isotropic mass density distributions $\rho(\mathbf{r}') = \rho(r')$.
b. Study the case of a sharp edge, $\rho(r') \equiv \rho(r')\theta(R - r')$.
c. Study the case of a homogeneous distribution, $\rho(r') \equiv \rho_0\theta(R - r')$, for a sphere with total mass M.
d. Study the case of a parabolic distribution, $\rho(r') \equiv \rho_0 \left(1 - \frac{r'^2}{R^2}\right) \theta(R - r')$, for a sphere with total mass M.

Solution: *a. The potential is,*

$$\begin{aligned} V(\mathbf{r}) &= -\int_{\mathbb{R}^3} \rho(r') \frac{\gamma_N m}{|\mathbf{r} - \mathbf{r}'|} d^3r' = -\int_{\mathbb{R}^3} \rho(r') \frac{\gamma_N m}{|\mathbf{r} - \mathbf{r}'|} r'^2 \sin\theta' dr' d\theta' d\phi' \\ &= -2\pi\gamma_N m \int_0^\infty \rho(r') r'^2 \int_0^\pi \frac{\sin\theta'}{\sqrt{r^2 + r'^2 - 2rr'\cos\theta'}} d\theta' dr' \ . \end{aligned}$$

The solution of the angular integral is,

$$\begin{aligned} \int_0^\pi \frac{\sin\theta'}{\sqrt{r^2 + r'^2 - 2rr'\cos\theta'}} d\theta' &= \frac{r\left[1 + \text{sign}(r' - r)\right] + r'\left[1 - \text{sign}(r' - r)\right]}{rr'} \\ &= \begin{cases} \frac{2}{r} \\ \frac{2}{r'} \end{cases} \quad for \quad \begin{cases} r' < r \\ r' > r \end{cases} . \end{aligned}$$

With this,

$$V(r) = -4\pi\gamma_N m \left(\int_0^r \rho(r') \frac{r'^2}{r} dr' + \int_r^\infty \rho(r') r' dr' \right) \ ,$$

or,

$$\boxed{V(r) = -4\pi\gamma_N m \left(\int_0^r \rho(r') \left(\frac{r'^2}{r} - r' \right) dr' + \int_0^\infty \rho(r') r' dr' \right)} \ . \tag{6.45}$$

The force follows from, $\mathbf{F}(\mathbf{r}) = -\nabla V(\mathbf{r}) = -\hat{\mathbf{e}}_r \partial_r V(r)$*, yielding,*

$$\boxed{F(r) = -\frac{\partial V(r)}{\partial r} = 4\pi\gamma_N m \frac{\partial}{\partial r} \int_0^r \rho(r') \left(\frac{r'^2}{r} - r' \right) dr'} \ . \tag{6.46}$$

b. Assuming a sharp edge, $\rho(r') \equiv \rho(r')\theta(R - r')$*, such that,*

$$M = 4\pi \int_0^R \rho(r') r'^2 dr' \ ,$$

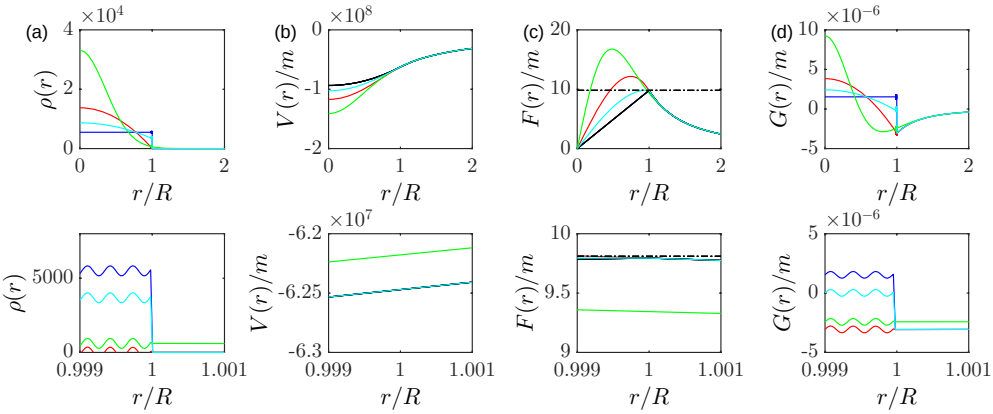

Figure 6.3: (code) (a) Radial density distributions, (b) potentials, (c) forces, and (d) gravity gradients for (blue) a homogeneous sphere, (red) a parabolic density distribution, (green) a Gaussian density distribution, and (cyan) a homogeneous density distribution with a superposed radial density modulation. The mass and the radius of the sphere are taken from Earth.

we get,

$$V(r) = -4\pi\gamma_N m \left(\int_0^r \rho(r')\theta(R-r')\frac{r'^2}{r}dr' + \int_r^\infty \rho(r')\theta(R-r')r'dr' \right)$$
$$= -4\pi\gamma_N m \begin{cases} \int_0^r \rho(r')\frac{r'^2}{r}dr' + \int_r^R \rho(r')r'dr' & for \quad r<R \\ \int_0^R \rho(r')\frac{r'^2}{r}dr' & \quad r>R \end{cases} .$$

The force is now,

$$F(r) = -\frac{\partial V(r)}{\partial r}$$
$$= -4\pi\gamma_N m \begin{cases} \int_0^r \rho(r')r'^2dr' \frac{\partial}{\partial r}\frac{1}{r} + \frac{1}{r}\frac{\partial}{\partial r}\int_0^r \rho(r')r'^2dr' - \rho(r)r & for \quad r<R \\ \int_0^R \rho(r')r'^2dr' \frac{\partial}{\partial r}\frac{1}{r} & \quad r>R \end{cases}$$
$$= -4\pi\gamma_N m \begin{cases} -\frac{1}{r^2}\int_0^r \rho(r')r'^2dr' & for \quad r<R \\ -\frac{1}{r^2}\int_0^R \rho(r')r'^2dr' & \quad r>R \end{cases} .$$

c. Assuming a homogeneous density distribution, $\rho(r') \equiv \rho_0\theta(R-r')$, such that,

$$M = 4\pi\rho_0 \int_0^R r'^2dr' = \frac{4\pi}{3}R^3\rho_0 ,$$

we get,

$$V(r) = -\gamma_N M m \begin{cases} \frac{3}{2R} - \frac{r^2}{2R^3} & for \quad r<R \\ \frac{1}{r} & \quad r>R \end{cases} .$$

The force is now,

$$F(r) = \gamma_N M m \begin{cases} \frac{r}{R^3} & for \quad r<R \\ \frac{1}{r^2} & \quad r>R \end{cases} .$$

d. Assuming a parabolic density distribution, $\rho(r') \equiv \frac{15M}{8\pi R^3}\left(1-\frac{r'^2}{R^2}\right)\theta(R-r')$*, such that,*

$$M = 4\pi\int_0^\infty \rho(r')r'^2dr' = 4\pi\rho_0\int_0^R\left(1-\frac{r'^2}{R^2}\right)r'^2dr' = \frac{8\pi R^3\rho_0}{15}\ ,$$

we get,

$$V(r) = -4\pi\gamma_N m\frac{15M}{8\pi R^3}\begin{cases}\int_0^r\left(1-\frac{r'^2}{R^2}\right)\frac{r'^2}{r}dr' + \int_r^R\left(1-\frac{r'^2}{R^2}\right)r'dr' & for \quad r<R\\ \int_0^R\left(1-\frac{r'^2}{R^2}\right)\frac{r'^2}{r}dr' & \quad r>R\end{cases}$$

$$= -\frac{15\gamma_N Mm}{2R^3}\begin{cases}\int_0^r\left(1-\frac{r'^2}{R^2}\right)\frac{r'^2}{r}dr' + \int_r^R\left(1-\frac{r'^2}{R^2}\right)r'dr' & for \quad r<R\\ \int_0^R\left(1-\frac{r'^2}{R^2}\right)\frac{r'^2}{r}dr' & \quad r>R\end{cases}\ .$$

6.3.5.2 Ex: Gravitational potential of a spherical shell

Consider a spherical shell with an inner radius a and an outer radius b.
a. Calculate the gravitational potential inside the sphere, inside the shell material and outside the sphere. (**Help:** Substitute the distance between the test particle m and a point of the mass distribution and make a case distinction for the integration limits for this distance variable.)
b. Calculate the force on a test particle.
c. Specify now for a massive sphere.
d. Specify for a very thin spherical shell.

Solution: *a. The potential exerted by a mass distribution with density* $\rho(\mathbf{r}')$ *on a particle of mass* m *located at the position* $\mathbf{r}$ *is,*

$$V(\mathbf{r}) = -\int\rho(\mathbf{r}')\frac{\gamma_N m}{|\mathbf{r}-\mathbf{r}'|}d^3\mathbf{r}' = -\int_{shell}\rho_0\frac{\gamma_N m}{|\mathbf{r}-\mathbf{r}'|}r'^2\sin\theta' dr'd\theta'd\phi'\ .$$

Substituting,

$$R \equiv |\mathbf{r}-\mathbf{r}'| = \sqrt{r^2+r'^2-2rr'\cos\theta'}$$
$$\frac{dR}{d\theta'} = \frac{rr'\sin\theta'}{R}\ ,$$

we obtain

$$V(\mathbf{r}) = -\int_{shell}\rho_0\frac{\gamma_N mr'}{r}dRdr'd\phi' = \frac{2\pi\rho_0\gamma_N m}{r}\int_a^b\int_{R_{\min}}^{R_{\max}}r'dRdr'\ .$$

The integration limits follow from the values adopted by R *for* $\theta = 0$ *respectively* $\theta = \pi$*. For* $r \le a$ *we have that* r' *is always larger than* r*. Therefore,* $R = r'-r,..,r'+r$*. For* $b \le r$ *we have that* r' *is always less than* r*. Hence,* $R = r-r',..,r'+r$*.*

$$V(\mathbf{r}) = -\frac{2\pi\rho_0\gamma_N m}{r}\begin{cases}\int_a^b 2rr'dr' & \quad r\le a\\ \int_r^b 2rr'dr' + \int_a^r 2r'^2dr' & for \quad a\le r\le b\\ \int_a^b 2r'^2dr' & \quad b\le r\end{cases}\ .$$

The result is,

$$V(\mathbf{r}) = -2\pi\rho_0\gamma_N m \begin{cases} b^2 - a^2 \\ b^2 - \frac{1}{3}r^2 - \frac{2}{3}\frac{a^3}{r} \\ \frac{2}{3}\frac{b^3-a^3}{r} \end{cases} \quad for \quad \begin{cases} r \le a \\ a \le r \le b \\ b \le r \end{cases} .$$

b. The force follows from,

$$\mathbf{F} = -\nabla V(\mathbf{r}) = \hat{\mathbf{e}}_r \frac{\partial}{\partial r} V(\mathbf{r}) = \hat{\mathbf{e}}_r 2\pi\rho_0\gamma_N m \begin{cases} 0 \\ \frac{2}{3}\frac{a^3}{r^2} - \frac{2}{3}r \\ -\frac{2}{3}\frac{b^3-a^3}{r^2} \end{cases} \quad for \quad \begin{cases} r \le a \\ a \le r \le b \\ b \le r \end{cases} .$$

c. Applying the result for the potential to a massive sphere ($a = 0$ and $M = \rho_0 V = \rho_0 \frac{4\pi b^3}{3}$) we have,

$$V(\mathbf{r}) = -\frac{\gamma_N M m}{r} \begin{cases} \frac{3r}{2b} - \frac{r^3}{2b^3} \\ 1 \end{cases} \quad for \quad \begin{cases} r \le b \\ b \le r \end{cases} .$$

Applying the result for the force to a massive sphere,

$$\mathbf{F} = -\hat{\mathbf{e}}_r \frac{\gamma_N M m}{r^2} \begin{cases} \frac{M_r}{M} \\ 1 \end{cases} \quad for \quad \begin{cases} r \le b \\ b \le r \end{cases} ,$$

where $M_r \equiv 4\pi\rho_0 r^3/3$.
d. We now calculate the potential for a thin shell, $\rho(\mathbf{r}') = \rho_0 = \sigma_0\delta(r' - b)$ and $M = \sigma_0 4\pi b^2$. We have,

$$\begin{aligned} V(\mathbf{r}) &= -\frac{2\pi\rho_0\gamma_N m}{r} \begin{cases} \int_0^b 2rr'dr' \\ \int_0^b 2r'^2 dr' \end{cases} \quad for \quad \begin{cases} r \le b \\ b \le r \end{cases} \\ &= -\frac{2\pi\sigma_0 b^2\gamma_N m}{r} \begin{cases} 2br \\ 2b^2 \end{cases} \quad for \quad \begin{cases} r \le b \\ b \le r \end{cases} \\ &= -\frac{\gamma_N M m}{r} \begin{cases} \frac{r}{b} \\ 1 \end{cases} \quad for \quad \begin{cases} r \le b \\ b \le r \end{cases} . \end{aligned}$$

Applying the result of force to a thin shell,

$$\mathbf{F} = -\hat{\mathbf{e}}_r \frac{\gamma_N M m}{r^2} \begin{cases} 0 \\ 1 \end{cases} \quad for \quad \begin{cases} r \le b \\ b \le r \end{cases} .$$

6.3.5.3 Ex: Two concentric shells

Let us consider two concentric spherical shells of uniform density with masses M_1 and M_2. Calculate the force on a particle of mass m placed (a) inside the inner shell, (b) outside the inner but inside the outer shell, and (c) outside the outer sphere.

Solution:

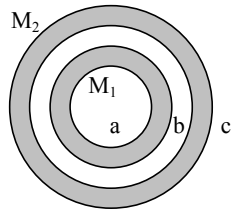

Figure 6.4:

6.3.5.4 Ex: Gravity influenced by a thin surface layer

Model the Earth as a homogeneous sphere of mass density ρ_0 isotropically covered by a $\Delta R = 1\text{m}$ thick homogeneous layer with different density ρ_1. How does the gravitational potential depend on the ratio ρ_1/ρ_0?

Solution: *Understanding Earth as a homogeneous sphere, the gravitational potential, force, and curvature are known. Hence, we may restrict to calculating these fields for a shell of positive or negative mass, whose fields will add to that of the homogeneous Earth. Also, as shown in the example 3, only the radial component of the gravity gradient is discontinuous at density boundaries such as the sphere's surface. Hence, we may concentrate our analysis on this component. The mass of the Earth*

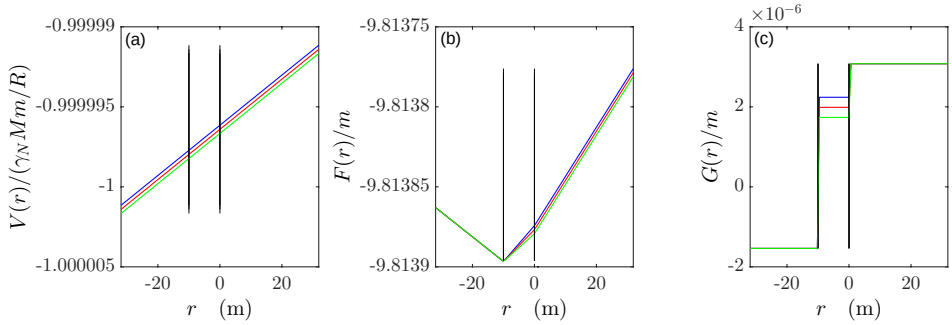

Figure 6.5: (code) Gravity gradient within a thin surface layer.

M without the layer is,

$$M = \frac{4\pi\rho_0 R^3}{3} \ .$$

The potentials generated by the Earth and the outer shell are, respectively, at a location r outside Earth are,

$$V_{\overset{\star}{\circ}}(\mathbf{r}) = -2\pi\rho_0\gamma_N m\frac{2}{3}\frac{R^3}{r}\hat{\mathbf{e}}_r$$
$$V_{\bigcirc}(\mathbf{r}) = -2\pi\rho_1\gamma_N m\frac{2}{3}\frac{(R+\Delta R)^3 - R^3}{r}\hat{\mathbf{e}}_r \ .$$

Adding both,

$$V_{\oplus}(\mathbf{r}) + V_{\bigcirc}(\mathbf{r}) = -\frac{4\pi\gamma_N m}{3}\hat{\mathbf{e}}_r\left(\rho_0\frac{R^3}{r} + \rho_1\frac{(R+\Delta R)^3 - R^3}{r}\right)$$
$$\simeq -\gamma_N M m\frac{\hat{\mathbf{e}}_r}{r}\left(1 + \frac{\rho_1}{\rho_0}\frac{3\Delta R}{R}\right) \ .$$

Setting $r \equiv R + \Delta R$*,*

$$V_{\oplus}(\mathbf{r}) + V_{\bigcirc}(\mathbf{r}) \simeq -\gamma_N M m\frac{\hat{\mathbf{e}}_r}{R+\Delta R}\left(1 + \frac{\rho_1}{\rho_0}\frac{3\Delta R}{R}\right) \ .$$

The dependency on the surface density is,

$$\frac{\partial[V_{\oplus}(\mathbf{r}) + V_{\bigcirc}(\mathbf{r})]}{V_{\oplus}(\mathbf{r})\partial\rho_1}\Delta\rho_1 = -\frac{3\Delta R}{R}\frac{\Delta\rho_1}{\rho_0} \approx \frac{3\cdot 1\,\mathrm{m}}{6378\,\mathrm{km}}\frac{\Delta\rho_1}{\rho_0} \approx -4.7\times 10^{-7}\frac{\Delta\rho_1}{\rho_0} \ .$$

The mean density and gravity gradient of Earth are,

$$\rho_{\oplus} = \frac{3M_{\oplus}}{4\pi R_{\oplus}^3} \approx 5450\,\mathrm{kg/m^3} \qquad \textit{and} \qquad \frac{4\pi\rho_{\oplus}\gamma_N}{3} = \frac{\gamma_N M_{\oplus}}{R_{\oplus}^3} \approx 1.54\cdot 10^{-6}\,\mathrm{s^{-2}} \ .$$

Hence, it seems that, if local gravity is uncertain, this will cause an offset, but the depth-dependence of the gravity gradient should still depend on ρ_1*.*

6.3.5.5 Ex: Gravitational force inside a shell

Show through geometric arguments that a particle of mass m placed inside a spherical shell of uniform mass density is subject to zero force, regardless of the position of the particle. What would happen if the surface mass density was not constant?

Solution: *Using spherical coordinates, we can divide the spherical shell into mass elements* $dm = \sigma R^2\sin\theta d\theta d\phi$*, such that,*

$$\int dm = \int_0^{2\pi}\int_0^{\pi}\sigma R^2\sin\theta' d\theta' d\phi' = 4\pi R^2\sigma = M \ .$$

Each mass element generates a gravitational field at the position $\mathbf{r}$ *within the shell of*

$$\mathbf{g}(\mathbf{r}) = -\frac{\gamma_N M}{r^2}\hat{\mathbf{e}}_r \ .$$

Therefore, for each mass element centered at the position θ', ϕ' *there is an element centered at the opposite position* $\pi-\theta', \pi+\phi'$ *having the same solid angle and exerting a force of equal intensity but opposite direction.*

6.3.5.6 Ex: Gravitational potential of a massive sphere with spherical cavity

A spherical cavity is machined into in a lead sphere of radius R such that its surface touches the outer surface of the massive sphere and passes through the its center. The primitive mass of the lead sphere is M. What will be the force that the sphere with the cavity will exert on a mass m at a distance z from the center of the outer sphere, when the mass and the centers of the sphere and the cavity are aligned?

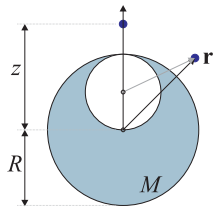

Figure 6.6: Scheme of the problem.

Solution: *The gravitational potential is given by,*

$$V(\mathbf{r}) = -\gamma_N \rho_0 m \int_{constr} \frac{dV'}{|\mathbf{r}-\mathbf{r}'|} = V_{outer-sphere}(\mathbf{r}) - V_{inner-cavity}(\mathbf{r}) \ .$$

Defining the mass of the outer sphere and the mass missing in the inner sphere,

$$M_o = \frac{4\pi}{3}\rho_0 R^3 \quad , \quad M_i = \frac{4\pi}{3}\rho_0 \left(\frac{R}{2}\right)^3 = \frac{M_o}{8} \ ,$$

we get, using the results (6.16),

$$V_{outer-sphere}(\mathbf{r}) = \begin{cases} -\gamma_N \frac{M_o m}{R}\left(\frac{3}{2} - \frac{r^2}{2R^2}\right)\hat{\mathbf{e}}_r & for\ r \le R \\ -\gamma_N \frac{M_o m}{r}\hat{\mathbf{e}}_r & for\ r \ge R \end{cases}$$

$$V_{inner-cavity}(\mathbf{r}) = \begin{cases} -\gamma_N \frac{M_i m}{R/2}\left(\frac{3}{2} - \frac{|\mathbf{r}-\frac{R}{2}\hat{\mathbf{e}}_z|^2}{2(R/2)^2}\right)\hat{\mathbf{e}}_r & for\ |\mathbf{r}-\frac{R}{2}\hat{\mathbf{e}}_z| \le \frac{R}{2} \\ -\gamma_N \frac{M_i m}{|\mathbf{r}-\frac{R}{2}\hat{\mathbf{e}}_z|}\hat{\mathbf{e}}_r & for\ |\mathbf{r}-\frac{R}{2}\hat{\mathbf{e}}_z| \ge \frac{R}{2} \end{cases} .$$

Along the z-axis, $\mathbf{r} = z\hat{\mathbf{e}}_z$*, the formulas simplify to,*

$$V_{outer-sphere}(0,0,z) = \begin{cases} -\gamma_N \frac{M_o m}{2R}\left(3 - \frac{z^2}{R^2}\right)\hat{\mathbf{e}}_z & for\ |z| \le R \\ -\gamma_N \frac{M_o m}{|z|}\hat{\mathbf{e}}_z & for\ |z| \ge R \end{cases}$$

$$V_{inner-cavity}(0,0,z) = \begin{cases} -\gamma_N \frac{M_o m}{8R}\left(3 - \frac{|z-\frac{R}{2}|^2}{(R/2)^2}\right)\hat{\mathbf{e}}_z & for\ |z-\frac{R}{2}| \le \frac{R}{2} \\ -\gamma_N \frac{M_o m}{8|z-\frac{R}{2}|}\hat{\mathbf{e}}_z & for\ |z-\frac{R}{2}| \ge \frac{R}{2} \end{cases} .$$

Particular solutions are found for $z = 0$*,*

$$V(0,0,z=0) = -\gamma_N \frac{5M_o m}{4R}\hat{\mathbf{e}}_z \ .$$

For $z = +R$ we have,

$$V(0,0,z=+R) = -\gamma_N \frac{3M_o m}{4R}\hat{\mathbf{e}}_z \ .$$

For $z = -R$ we have,

$$V(0,0,z=-R) = -\gamma_N \frac{11M_o m}{12R}\hat{\mathbf{e}}_z \ ,$$

and finally for $z \to \pm\infty$,

$$V(0,0,z\to\pm\infty) = -\gamma_N M_o m\hat{\mathbf{e}}_z \left(\frac{1}{|z|} - \frac{1}{8|z-\frac{R}{2}|}\right) \simeq -\gamma_N \frac{7M_o m}{8z}\hat{\mathbf{e}}_z \ .$$

6.3.5.7 Ex: Gravitational potential of a disk

Calculate the potential of a homogeneous thin disc with the surface density $\sigma = M/\pi R^2 = \rho dz$ along the axis of symmetry and the gravitational force it exerts on a mass m.
Help: When integrating over the thickness a of the disk, use the relation: $\int_0^d zf(z')dz' = f(0)dz$.

Solution: *The potential of a mass distribution $\rho(\mathbf{r}')$ acting on a test mass m located at the position $\mathbf{r}$ is,*

$$\begin{aligned} V(\mathbf{r}) &= -\int_{disk} \rho(\mathbf{r}')\frac{\gamma_N m}{|\mathbf{r}-\mathbf{r}'|}d^3\mathbf{r}' \\ &= -\gamma_N m\int_0^a\int_0^R\int_0^{2\pi} \rho_0 \frac{1}{\sqrt{(r-r')^2+(z-z')^2}} r'dr'dz'd\phi' \ . \end{aligned}$$

Now be $\mathbf{r} = z\hat{\mathbf{e}}_z$.

$$\begin{aligned} V(z) &= -2\pi\gamma_N m\rho_0 \int_0^a\int_0^R \frac{1}{\sqrt{r''+(z-z')^2}} r'dr'dz' \\ &= -2\pi\gamma_N m\rho_0 \int_0^a \left(\sqrt{R^2+(z-z')^2} - (z-z')\right)dz' \ . \end{aligned}$$

For a thin disk $\rho(z) \simeq \rho_0 a\delta(z)$,

$$V(z) = -2\pi\gamma_N m\rho_0 a(\sqrt{R^2+z^2} - z) \ .$$

The force is,

$$F = -\frac{d}{dz}V(z) = 2\pi\gamma_N m\rho_0 a\left(\frac{z}{\sqrt{R^2+z^2}} - 1\right) \ .$$

6.3.5.8 Ex: Gravitational force of a ring

Calculate the gravitational force of a ring of linear mass density $\lambda = M/2\pi R = \rho dRdz$ on the symmetry axis.
Help: When integrating on the thickness of the ring, use the relations: $\int_0^{dz} f(z')dz' = f(0)dz$ and $\int_R^{R+dR} f(r')dr' = f(R)dR$.

Solution: *The gravitational potential of a ring around the axis of symmetry* $\hat{\mathbf{e}}_z$ *is,*

$$V(\mathbf{r}) = -\int_{ring} \frac{\gamma_N m}{|\mathbf{r}-\mathbf{r}'|}\rho(\mathbf{r}')dV' = -\gamma_N M \int_{ring} \frac{1}{|\mathbf{r}-\mathbf{r}'|}\rho(\mathbf{r}')r'dr'dz'd\phi'$$
$$= -\gamma_N m\rho RdRdz \int_0^{2\pi} \frac{1}{\left|\begin{pmatrix}x\\y\\z\end{pmatrix} - \begin{pmatrix}R\cos\phi'\\R\sin\phi'\\0\end{pmatrix}\right|} d\phi' \ .$$

For a test mass m *located on the symmetry axis,* $\mathbf{r} = z\hat{\mathbf{e}}_z$*,*

$$V(\mathbf{r}) = -\gamma_N m\lambda R \int_0^{2\pi} \frac{1}{\left|\begin{pmatrix}0\\0\\z\end{pmatrix} - \begin{pmatrix}R\cos\phi'\\R\sin\phi'\\0\end{pmatrix}\right|} d\phi'$$
$$= -\gamma_N m\lambda R \int_0^{2\pi} \frac{1}{\sqrt{R^2\cos^2\phi' + R^2\sin^2\phi' + z^2}} d\phi'$$
$$= -\gamma_N m\lambda R \int_0^{2\pi} \frac{1}{\sqrt{R^2+z^2}} d\phi' = -2\pi\gamma_N m\lambda R \frac{1}{\sqrt{R^2+z^2}} = -\frac{\gamma_N Mm}{\sqrt{R^2+z^2}} \ .$$

The gradient gives the force, $\mathbf{F}(\mathbf{r}) = -\nabla V(\mathbf{r})$*, or,*

$$F_z = -\frac{\partial V}{\partial z} = -\frac{d}{dz}\frac{\gamma_N Mm}{\sqrt{R^2+z^2}} = -\frac{\gamma_N Mm}{s^3}z = -\frac{\gamma_N Mm}{s^2}\cos\alpha \ .$$

6.3.5.9 Ex: Gravitational oscillation through a ring

Consider a heavy ring of mass M and radius R and a particle of mass m placed in its center. What is the frequency for small amplitude oscillations in the direction perpendicular to the plane of the ring?

Solution: *The gravitational potential of a ring around the symmetry axis* $\hat{\mathbf{e}}_z$ *is,*

$$V(\mathbf{r}) = \int_{ring} \frac{\gamma_N m}{|\mathbf{r}-\mathbf{r}'|}\rho(\mathbf{r}')dV' = \gamma_N m \int_{ring} \frac{\lambda\delta(z')\delta(r'-R')}{\left|\begin{pmatrix}x\\y\\z\end{pmatrix} - \begin{pmatrix}r'\cos\phi'\\r'\sin\phi'\\z'\end{pmatrix}\right|} r'dr'd\phi'dz'$$

$$= \gamma_N mR \int_{ring} \frac{\lambda}{\left|\begin{pmatrix}x\\y\\z\end{pmatrix} - \begin{pmatrix}R\cos\phi'\\R\sin\phi'\\0\end{pmatrix}\right|} d\phi' \ .$$

For a test mass m *located on the symmetry axis,* $\mathbf{r} = z\hat{\mathbf{e}}_z$*,*

$$V(\mathbf{r}) = \gamma_N mR \int_{ring} \frac{\lambda}{\left|\begin{pmatrix}0\\0\\z\end{pmatrix} - \begin{pmatrix}R\cos\phi'\\R\sin\phi'\\0\end{pmatrix}\right|} d\phi' = \gamma_N mR \int_{ring} \frac{\lambda}{\sqrt{R^2\cos^2\phi' + R^2\sin^2\phi' + z^2}} d\phi'$$

$$= \gamma_N mR \int_{ring} \frac{\lambda}{\sqrt{R^2+z^2}} d\phi' = 2\pi\gamma_N mR \frac{\lambda}{\sqrt{R^2+z^2}} = \frac{\gamma_N Mm}{\sqrt{R^2+z^2}} \ .$$

The gradient gives force,

$$\mathbf{F}(\mathbf{r}) = -\nabla V(\mathbf{r})$$

$$F_z = -\frac{\partial V}{\partial z} = -\frac{d}{dz}\frac{\gamma_N Mm}{\sqrt{R^2+z^2}} = -\frac{\gamma_N Mm}{s^3} z = m\ddot{z} \ .$$

Therefore, the frequency of small oscillations will be,

$$\omega = \sqrt{\frac{\gamma_N M}{s^3}} \ .$$

6.3.5.10 Ex: Intraplanetary oscillation

A body of mass m is placed at a distance r_0 from the center of a planet of mass M and radius R.
a. Calculate the potential energy for $0 \leq r \leq \infty$. Suppose that the mass density of the planet is uniform and that the mass m can move within it through a tunnel. Consider $V(\infty) = 0$. Calculate the velocity as a function of r for $r < R$ knowing that $V(r_0) = 0$.

Solution: *Within the planet the gravitational force is*

$$F = \frac{\gamma_N Mmr}{R^3} = m\ddot{r} \ .$$

Following Hooke's law the proportionality $F \propto r$ *produces a harmonic movement,*

$$r = r_0 \sin\omega t \qquad , \qquad v = \omega v_0 \cos\omega t \ ,$$

with

$$\omega = \sqrt{\frac{\gamma_N M}{s^3}} \ .$$

6.3.5.11 Ex: Shortcut avoiding the Earth's center

Show that in a tunnel dug through the Earth (not necessarily along a diameter) the movement of an object will be harmonic.

Solution: *Within a massive sphere the gravitational force is,*

$$\mathbf{F} = \frac{\gamma_N M m r}{b^3} \hat{\mathbf{e}}_r \ .$$

Following Hooke's law the proportionality $F \propto r$ produces a harmonic movement.

6.3.5.12 Ex: Shortcut through the Earth

a. Two innovative companies make suggestions on how to get mail to New Zealand as quickly as possible. One company suggests drilling a hole through the Earth, placing the mail in a fireproof box and allowing it to swing through the hole (smoothly) through the center of the Earth so that it can be easily received by the recipient in New Zealand. The other company wants to shoot the mail in a very low orbit of only 1 m above the surface of the Earth at the first cosmic speed (smoothly) to New Zealand, where it should then be caught by a correspondingly soft pillow. Which of these two suggestions (if they were feasible) would get the mail faster to destination?
b. Assume that the well was planned incorrectly and that the hole missed the center of the earth by 100 km. What does the equation of motion look like?
Help: The mass distribution of the earth can be assumed to be homogeneous. Earth rotation and friction effects are neglected.

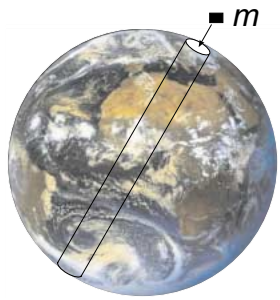

Figure 6.7:

Solution: *a. Let m be the mass of mail. For the first company,*

$$\frac{mv_1^2}{r_{\oplus}} = \gamma_N \frac{mM_{\oplus}}{r_{\oplus}^2} \qquad \Rightarrow \qquad v_1 = \sqrt{\frac{\gamma_N M_{\oplus}}{r_{\oplus}}} \qquad \Rightarrow \qquad t_1 = \frac{\frac{1}{2}U_{\oplus}}{v_1} = \frac{\pi r_{\oplus}}{\sqrt{\frac{\gamma_N M_{\oplus}}{r_{\oplus}}}} \ .$$

Inserting numbers, $v_1 \approx 7.91\,\mathrm{km/s}$. Now,

$$t_1 = \frac{\frac{1}{2} \cdot U_{\oplus}}{v_1} = \frac{\pi r_{\oplus}}{\sqrt{\frac{\gamma_N M_{\oplus}}{r_{\oplus}}}} \ ,$$

yielding, $t_1 \approx 42.3\,\mathrm{min}$.
For the second company: For $r < r_{\oplus}$ the force law applies,

$$F(r) = -\gamma_N \ \frac{Mm}{r_{\oplus}} \ r \ ,$$

thus the force is analogous to that of a spring,

$$F(r) = -Dr \qquad with \qquad D = g \ \frac{M_{\oplus} m}{r_{\oplus}^3} \ .$$

The movement is a harmonic vibration of the frequency,

$$\omega = \sqrt{D/m} = \sqrt{\frac{\gamma_N M_{\oplus}}{R_{\oplus}^3}} \ .$$

Postal delivery corresponds to half an oscillation period,

$$t_2 = \frac{T}{2} = \frac{\pi}{\omega} = \pi r_{Earth} \sqrt{r_{\oplus}/(\gamma_N \cdot M_{\oplus})} \ ,$$

and is just as long as the way taking the orbit.
b. .

6.3.5.13 Ex: Gravity gradient caused by underground cavities

In this exercise we discuss whether gravity gradiometry can identify the presence of underground cavities. We proceed in steps:
a. Assuming a homogeneous density distribution for Earth, calculate the gravity gradient tensor at the north-pole.
b. How does the tensor change in the presence of a point-like mass $M_1 = 10\,\mathrm{tons}$ located at a distance $d = 1\,\mathrm{m}$ in southern direction.
c. Describe the underground cavity by a spherical void centered at 1 m below the north-pole's surface at having a radius such that the missing mass corresponds to 10 tons of Earth material.

Solution: *a. We assume an isotropic mass density distribution for Earth and set the origin in the north-pole. The potential then reads,*

$$V(\mathbf{r}) = \gamma_N M m \left(\frac{3}{2R} - \frac{|\mathbf{r} + R\hat{\mathbf{e}}_z|^2}{2R^3} \right) \theta(-r) + \gamma_N M m \frac{1}{|\mathbf{r} + R\hat{\mathbf{e}}_z|} \theta(r) \ .$$

Since $\mathbf{r} = 0$ *at the north-pole, the gravity gradient is,*

$$\begin{aligned} G(\mathbf{r}) &= \frac{\gamma_N M}{R^3} \begin{pmatrix} -1 & 0 & 0 \\ 0 & -1 & 0 \\ 0 & 0 & 1 \end{pmatrix} \theta(-r) \\ &\quad + \frac{\gamma_N M}{|\mathbf{r} + R\hat{\mathbf{e}}_z|^5} \begin{pmatrix} 2x^2 - y^2 - (z+R)^2 & 3xy & 3x(z+R) \\ 3xy & 2y^2 - (z+R)^2 - x^2 & 3y(z+R) \\ 3x(z+R) & 3y(z+R) & 2(z+R)^2 - x^2 - y^2 \end{pmatrix} \theta(r) \\ &\longrightarrow \frac{\gamma_N M}{R^3} \begin{pmatrix} -1 & 0 & 0 \\ 0 & -1 & 0 \\ 0 & 0 & 2 \end{pmatrix} \theta(r) + \frac{\gamma_N M}{R^3} \begin{pmatrix} -1 & 0 & 0 \\ 0 & -1 & 0 \\ 0 & 0 & 2 \end{pmatrix} \theta(-r) \ , \end{aligned}$$

or,

$$G_{kl}(0) = \frac{\gamma_N M}{R^3} (1 - 3\theta(r)\delta_{kz})\delta_{kl} \ ,$$

with $R = 6378\,\mathrm{km}$.
b. For the additional potential we perform an analogous calculation,

$$\begin{aligned} G_1(\mathbf{r}) &= \frac{\gamma_N M_1}{|\mathbf{r} + d\hat{\mathbf{e}}_x|^5} \begin{pmatrix} 2(x+d)^2 - y^2 - z^2 & 3(x+d)y & 3(x+d)z \\ 3(x+d)y & 2y^2 - z^2 - (x+d)^2 & 3yz \\ 3(x+d)z & 3yz & 2z^2 - (x+d)^2 - y^2 \end{pmatrix} \\ &\longrightarrow \frac{\gamma_N M_1}{d^3} \begin{pmatrix} 2 & 0 & 0 \\ 0 & -1 & 0 \\ 0 & 0 & -1 \end{pmatrix} \ , \end{aligned}$$

with $d = 1\,\mathrm{m}$. *A direct comparison shows,*

$$\frac{\gamma_N M}{R^3} \approx 1.5 \cdot 10^{-6}\,\mathrm{s}^{-2} \qquad \textit{and} \qquad \frac{\gamma_N M_1}{d^3} \approx 6.7 \times 10^{-7}\,\mathrm{s}^{-2} \ .$$

That is, a gravity gradiometer which is capable of measuring the inhomogeneity of a 'perfect' Earth is not far from being able to detect inhomogeneities caused by heavy local masses.
c. The absence of mass can be treated in the same way as the presence. That is, we can apply the results of (a) and (b) for a 'negative' mass M_1 *distributed over spherical cavity of radius,*

$$R_1 = \left(\frac{3M_1}{4\pi\rho_{\odot}} \right)^{1/3} = R_{\odot} \left(\frac{M_1}{M_{\odot}} \right)^{1/3} \approx 0.76\,\mathrm{m} \ .$$

6.3.5.14 Ex: Gravity gradient upon horizontal density modulation

A gravimeter and a gravity gradiometer are hovering at a distance z over a flat surface infinitely extended in x and y. The surface has a thickness b and a horizontal density modulation in x-direction: $\rho_1(\mathbf{r}') = \rho_1(x')\theta(b+z')\theta(-z')$. Calculate the gravitational potential, force, and gradients. Consider the particular case of a localized density modulation: $\rho_1(x') = \rho_1\theta(x')\theta(a-x')$.

Solution: *As the mass distribution is infinite, the potential will naturally diverge. On the other hand, the force is finite,*

$$\begin{aligned}\mathbf{F}(\mathbf{r}) &= -\gamma_N \int_{-\infty}^{\infty} \rho_1(x') \int_{-b}^{0}\int_{-\infty}^{\infty} \frac{\mathbf{r}-\mathbf{r}'}{\sqrt{(x-x')^2+y'^2+(z-z')^2}^3} dy'dz'dx' \\ &= -\gamma_N \int_{-\infty}^{\infty} \rho_1(x') \begin{pmatrix} 2\arctan\frac{b+z}{x-x'} - 2\arctan\frac{z}{x-x'} \\ 0 \\ \ln\frac{(x-x')^2+(z+b)^2}{(x-x')^2+z^2} \end{pmatrix} dx' \ .\end{aligned}$$

The gravity gradient is,

$$\begin{aligned}G_{kl}(\mathbf{r}) &= \frac{1}{m}\frac{\partial F_l(\mathbf{r})}{\partial x_k} \\ &= \gamma_N \int \rho_1(x') \int_{-b}^{0}\int_{-\infty}^{\infty} \frac{1}{\sqrt{(x-x')^2+y'^2+(z-z')^2}^5} \times \\ &\quad \times \begin{pmatrix} 2(x-x')^2-y'^2-(z-z')^2 & 0 & 3(x-x')(z-z') \\ 0 & 0 & 0 \\ 3(x-x')(z-z') & 0 & 2(z-z')^2-(x-x')^2-y'^2 \end{pmatrix} dy'dz'dx' \\ &= \gamma_N \int \frac{2b\rho_1(x')}{[(x-x')^2+z^2][(x-x')^2+(z+b)^2]} \begin{pmatrix} (x-x')^2-z(z+b) & 0 & (x-x')(2z+b) \\ 0 & 0 & 0 \\ (x-x')(2z+b) & 0 & -(x-x')^2+z(z+b)^2 \end{pmatrix} dx' \ .\end{aligned}$$

If the gravimeter or the gravity gradiometer are hovering at a small distance $z \ll b$ close to the surface, the force becomes,

$$\mathbf{F}(x,0,0) \xrightarrow{z\ll b} -\gamma_N \int_{-\infty}^{\infty} \rho_1(x') \begin{pmatrix} 2\arctan\frac{b}{x-x'} \\ 0 \\ \ln\left(1+\left(\frac{b}{x-x'}\right)^2\right) \end{pmatrix} dx' \ ,$$

and the gradients,

$$G_{kl}(x,0,0) \xrightarrow{z\ll b} 2\gamma_N b \int_{-\infty}^{\infty} \frac{\rho_1(x')}{(x-x')^2+b^2} dx' \begin{pmatrix} 1 & 0 & \frac{b}{x-x'} \\ 0 & 0 & 0 \\ \frac{b}{x-x'} & 0 & -1 \end{pmatrix} \ .$$

Assuming a limited density fluctuation $\rho_1(x') = \rho_1\theta(x')\theta(a-x')$, the force reads,

$$\mathbf{F}(x,0,0) = -\gamma_N\rho_1 \begin{pmatrix} 2a\arctan\frac{b}{x-a} - 2x\arctan\frac{ab}{x(x-a)+b^2} + b\ln\frac{x^2+b^2}{(x-a)^2+b^2} \\ 0 \\ x\ln\frac{(x^2+b^2)(x-a)^2}{x^2[(x-a)^2+b^2]} + a\ln\left(1+\frac{b^2}{(x-a)^2}\right) + 2b\arctan\frac{ab}{x(x-a)+b^2} \end{pmatrix} \ ,$$

and the gradients (using $\arctan x \pm \arctan y = \arctan \frac{x \pm y}{1 \mp xy}$*),*

$$G_{kl}(x,0,0) = 2\gamma_N \rho_1 \begin{pmatrix} \arctan \frac{ab}{x(x-a)+b^2} & 0 & \frac{1}{2}\ln\frac{(x-a)^2+b^2}{x^2+b^2} - \ln\frac{x-a}{x} \\ 0 & 0 & 0 \\ \frac{1}{2}\ln\frac{(x-a)^2+b^2}{x^2+b^2} - \ln\frac{x-a}{x} & 0 & -\arctan\frac{ab}{x(x-a)+b^2} \end{pmatrix} .$$

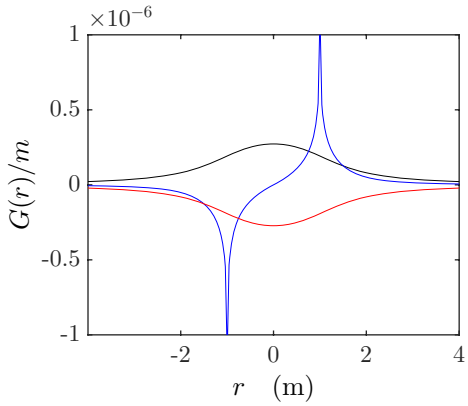

Figure 6.8: (code) Gravity gradients due to a 1 m deep and 1 m large mass of density $\rho_1 = 1300$ kg/cm^3: (black) horizontal gradient upon horizontal displacement G_{xx}, (red) vertical gradient upon vertical displacement G_{zz}, and (blue) horizontal gradient upon vertical displacement G_{xz}, and vice versa.

6.3.5.15 Ex: Gravity gradients

a. Modern commercial gravity gradiometers can measure acceleration gradients on the order of $|\nabla a| \approx 10^{-5}\,\mathrm{s}^{-2}$. Compare with the gravity gradient on the Earth's surface. What is the smallest height difference detectable by a state of the art gradiometer?
b. Calculate the gravity gradient caused by a massive sphere of mass $m_{sphere} = 10\,\mathrm{t}$ at $d = 1\,\mathrm{m}$ distance?
c. The French company μQuans offers atomic quantum gravimeters with guaranteed sensitivities of $50\,\mu\mathrm{Gal}/\sqrt{\mathrm{Hz}}$ at a cycling frequency of 2 Hz. Assuming the Earth as a homogeneous sphere, for how long must the signal be integrated to be able to measure a 1 cm height variation over the Earth's surface.
d. For how long must the signal be integrated to be able to measure a gravity variation caused by a 10 t mass at 1 m distance.

Solution: *a. From Newton's law,*

$$g = \frac{F}{m} = \frac{\gamma_N M_{\odot}}{r^2} ,$$

where $M_{\oplus}$ is the mass of the Earth and r the distance from the center of the Earth. We calculate,

$$\frac{\nabla g}{g} = \frac{\partial g}{g \partial r} \nabla r = \frac{-2\gamma_N M_{\oplus}}{g r^3} \hat{\mathbf{e}}_r = \frac{-2}{r} \hat{\mathbf{e}}_r \ .$$

This yields at the surface of the Earth ($r = R_{\oplus}$),

$$\frac{\partial g}{g \partial R} = \frac{-2}{R_{\oplus}} \approx -3 \cdot 10^{-7}\,\mathrm{m}^{-1} \ ,$$

or,

$$\frac{\partial g}{\partial R} = \frac{-2g}{R_{\oplus}} \approx -3 \cdot 10^{-6}\,\mathrm{s}^{-2} \ .$$

So, with state-of-the-art gravity gradiometers we can measure the variation of g due to height changes of about $3\,\mathrm{m}$.
b. The same calculation as in (a) yields,

$$a_d = \frac{\gamma_N m_{sphere}}{d^2} \ ,$$

and,

$$\frac{\partial a}{\partial d} = \frac{-2\gamma_N m_{sphere}}{d^3} \approx -1.33 \cdot 10^{-6}\,\mathrm{s}^{-2} \ .$$

c. As we have seen, the gravitational acceleration on Earth is,

$$\frac{\partial g}{\partial R} \approx -3 \cdot 10^{-6}\,\mathrm{s}^{-2} = -3\,\mu\mathrm{Gal/cm} \ .$$

with the gravimeter's sensitivity of,

$$s \equiv \Delta g \sqrt{\tau} = \frac{50\,\mu\mathrm{Gal}}{\sqrt{\mathrm{Hz}}} \ ,$$

it should be possible to detect a $\Delta R = 1\,\mathrm{cm}$ elevation in

$$\tau = \left(s \frac{\Delta R}{\Delta g} \frac{1}{\Delta R} \right)^2 = \left(\frac{50\,\mu\mathrm{Gal}}{\sqrt{\mathrm{Hz}}} \ \frac{\mathrm{cm}}{3.1\,\mu\mathrm{Gal}} \ \frac{1}{1\,\mathrm{cm}} \right)^2 \approx 260\,\mathrm{s} = 4.3\,\mathrm{min} \ .$$

d. The same calculations as in (c) yields,

$$\tau = \left(s \frac{\Delta R}{\Delta g} \frac{1}{\Delta R} \right)^2 = \left(\frac{50\,\mu\mathrm{Gal}}{\sqrt{\mathrm{Hz}}} \ \frac{\mathrm{cm}}{1.3\,\mu\mathrm{Gal}} \ \frac{1}{1\,\mathrm{cm}} \right)^2 \approx \left(\frac{50}{1.3} \right)^2 = 24.6\,\mathrm{min} \ .$$

6.3.5.16 Ex: Acceleration of a mass subject to a circular motion in an inhomogeneous force field

Commercial *Gravity Gradient Instruments* (GGI) are based on accelerometers mounted on the border of a disk of radius R rotating at a frequency ω. Let us suppose that the disk's rotation axis is the z-axis and that is located inside an inhomogeneous force

field (e.g. gravity) characterized by its gradient tensor (assumed to be constant over time and over the length scale of R).
a. Calculate the time-dependent acceleration recorded by the accelerometer in radial direction.
b. The voltage signal delivered by the accelerometer is now added to one delivered by a second accelerometer sitting on the opposite side of the disk.
c. Finally, the signals are demodulated at 2ω and time-averaged over a period $2\pi/\omega$.

Solution: *The Taylor expansion of gravitational potential can be written,*

$$\begin{aligned} V(\mathbf{r}+\mathbf{R}) &= \exp(\mathbf{R}\cdot\nabla_{\mathbf{r}})V(\mathbf{R}) = V(\mathbf{r}) + (\mathbf{R}\cdot\nabla_{\mathbf{r}})V(\mathbf{r}) + \tfrac{1}{2}(\mathbf{R}\cdot\nabla_{\mathbf{r}})(\mathbf{R}\cdot\nabla_{\mathbf{r}})V(\mathbf{r}) + ... \\ &= V(\mathbf{r}) + \tfrac{1}{2}\sum_{k=1} R_k \frac{\partial V(\mathbf{r})}{\partial x_k} + \tfrac{1}{2}\sum_{k,l=1} R_k R_l \frac{\partial^2 V(\mathbf{r})}{\partial x_k \partial x_l} + ... \\ &\equiv V(\mathbf{r}) - \tfrac{m}{2}\sum_{k=1} R_k a_k(\mathbf{r}) - \tfrac{m}{2}\sum_{k,l=1} R_k R_l G_{kl}(\mathbf{r}) + ... \ . \end{aligned}$$

a. Describing the trajectory of an accelerometer by,

$$\mathbf{r}+\mathbf{R}(t) = \mathbf{r} + \begin{pmatrix} R\cos\omega t \\ R\sin\omega t \\ 0 \end{pmatrix} \ ,$$

the acceleration sensed by the rotating mass is just given by the centripetal force,

$$\mathbf{a}_{rot}(t) = -\omega^2 \mathbf{R}(t) \ ,$$

exerted by the coercive force imposed by the disk, plus possible stationary external force gradients,

$$\begin{aligned} \mathbf{a}_{grd}(t) = \mathbf{a}_{grd}(\mathbf{r}+\mathbf{R}(t)) &= \begin{pmatrix} a_{x,grd}(x+X(t), y+Y(t), z+Z(t)) \\ a_{y,grd}(x+X(t), y+Y(t), z+Z(t)) \\ a_{z,grd}(x+X(t), y+Y(t), z+Z(t)) \end{pmatrix} \\ &= \begin{pmatrix} a_{x,grd}(\mathbf{r}) + X\left.\frac{\partial a_{x,grd}}{\partial x}\right|_{X=0} + Y\left.\frac{\partial a_{x,grd}}{\partial y}\right|_{Y=0} + Z\left.\frac{\partial a_{x,grd}}{\partial z}\right|_{Z=0} \\ a_{y,grd}(\mathbf{r}) + X\left.\frac{\partial a_{y,grd}}{\partial x}\right|_{X=0} + Y\left.\frac{\partial a_{y,grd}}{\partial y}\right|_{Y=0} + Z\left.\frac{\partial a_{y,grd}}{\partial z}\right|_{Z=0} \\ a_{z,grd}(\mathbf{r}) + X\left.\frac{\partial a_{z,grd}}{\partial x}\right|_{X=0} + Y\left.\frac{\partial a_{z,grd}}{\partial y}\right|_{Y=0} + Z\left.\frac{\partial a_{z,grd}}{\partial z}\right|_{Z=0} \end{pmatrix} \quad with \quad G_{kl} \equiv \left.\frac{\partial a_{k,grd}}{\partial x_l}\right|_{X_l=0} \\ &= \begin{pmatrix} a_{x,grd}(\mathbf{r}) + XG_{xx}(\mathbf{r}) + YG_{xy}(\mathbf{r}) + ZG_{xz}(\mathbf{r}) \\ a_{y,grd}(\mathbf{r}) + XG_{yx}(\mathbf{r}) + YG_{yy}(\mathbf{r}) + ZG_{yz}(\mathbf{r}) \\ a_{z,grd}(\mathbf{r}) + XG_{zx}(\mathbf{r}) + YG_{zy}(\mathbf{r}) + ZG_{zz}(\mathbf{r}) \end{pmatrix} \\ &= \begin{pmatrix} a_{x,grd}(\mathbf{r}) + RG_{xx}(\mathbf{r})\cos\omega t + RG_{xy}(\mathbf{r})\sin\omega t \\ a_{y,grd}(\mathbf{r}) + RG_{yx}(\mathbf{r})\cos\omega t + RG_{yy}(\mathbf{r})\sin\omega t \\ a_{z,grd}(\mathbf{r}) + RG_{zx}(\mathbf{r})\cos\omega t + RG_{zy}(\mathbf{r})\sin\omega t \end{pmatrix} \ . \end{aligned}$$

Now, we assume that the mass be in fact an accelerometer oriented such that it measures only the radial component of the acceleration (simplifying the notation by drop-

ping the $(\mathbf{r})$*-dependence),*

$$\begin{aligned} a_r(t) &= [\mathbf{a}_{rot}(t) + \mathbf{a}_{grd}(t)] \cdot \mathbf{R}(t) \\ &= -\omega^2 R^2 + \begin{pmatrix} a_{x,grd} + RG_{xx}\cos\omega t + RG_{xy}\sin\omega t \\ a_{y,grd} + RG_{yx}\cos\omega t + RG_{yy}\sin\omega t \\ a_{z,grd} + RG_{zx}\cos\omega t + RG_{zy}\sin\omega t \end{pmatrix} \cdot \begin{pmatrix} R\cos\omega t \\ R\sin\omega t \\ 0 \end{pmatrix} \\ &= -\omega^2 R^2 + a_{x,grd} R\cos\omega t + a_{y,grd} R\sin\omega t + \\ &+ \tfrac{1}{2}R^2\left[G_{xx} + G_{yy} + (G_{xx} - G_{yy})\cos 2\omega t + (G_{xy} + G_{yx})\sin 2\omega t\right] \ . \end{aligned}$$

b. Now, we assume that on the opposite side of the disk there is a second accelerometer delivering a signal shifted by $\omega t \longrightarrow \omega t + \pi$*. The sum of both cancels the terms oscillating at* ω*,*

$$a'_r(t) = -2\omega^2 R^2 + R^2\left[G_{xx} + G_{yy} + (G_{xx} - G_{yy})\cos 2\omega t + (G_{xy} + G_{yx})\sin 2\omega t\right] \ .$$

c. The signals are demodulated at 2ω *and time-averaged over a period* $2\pi/\omega$*,*

$$\begin{aligned} &\overline{a'_r(t)\sin 2\omega t} \\ &= \frac{\omega}{2\pi}\int_0^{2\pi/\omega} R^2\left[G_{xx} + G_{yy} + (G_{xx} - G_{yy})\cos 2\omega t + (G_{xy} + G_{yx})\sin 2\omega t\right]\sin 2\omega t dt \\ &= R^2 G_{xy} \\ &\overline{a'_r(t)\cos 2\omega t} \\ &= \frac{\omega}{2\pi}\int_0^{2\pi/\omega} R^2\left[G_{xx} + G_{yy} + (G_{xx} - G_{yy})\cos 2\omega t + (G_{xy} + G_{yx})\sin 2\omega t\right]\cos 2\omega t dt \\ &= \tfrac{1}{2}R^2(G_{xx} - G_{yy}) \ . \end{aligned}$$

The GGI thus delivers the components $G_{xy}(\mathbf{r})$ *and* $G_{xx}(\mathbf{r}) - G_{yy}(\mathbf{r})$ *of the gravity gradient tensor as it is moved through space* $\mathbf{r}$*.*

6.3.5.17 Ex: Angular momentum in spherical coordinates

a. Calculate the acceleration, the angular momentum, and its derivative in spherical coordinates using the result of Exc. 12.3.8.6.
b. Set $\theta = \frac{\pi}{2}$ in all expressions.
c. Derive the equation of motion for a central potential.

Solution: *a. The expressions for position, velocity, and acceleration found in Exc. 12.3.8.6 are,*

$$\begin{aligned} \mathbf{r} &= r\hat{\mathbf{e}}_r \\ \mathbf{v} &= \dot{\mathbf{r}} = \dot{r}\hat{\mathbf{e}}_r + r\dot{\theta}\hat{\mathbf{e}}_\theta + \dot{\phi}r\sin\theta\hat{\mathbf{e}}_\phi \\ \mathbf{a} &= \ddot{\mathbf{r}} = (\ddot{r} - r\dot{\theta}^2 - \dot{\phi}^2 r\sin^2\theta)\hat{\mathbf{e}}_r \\ &\quad + (2\dot{r}\dot{\theta} + r\ddot{\theta} - \dot{\phi}^2 r\sin\theta\cos\theta)\hat{\mathbf{e}}_\theta \\ &\quad + (2\dot{\phi}\dot{r}\sin\theta + 2\dot{\phi}r\dot{\theta}\cos\theta + \ddot{\phi}r\sin\theta)\hat{\mathbf{e}}_\phi \ . \end{aligned}$$

The angular momentum and its derivative follow immediately,

$$\begin{aligned}\mathbf{L} &= \mathbf{r}\times\mathbf{p} = mr(-r\dot\theta\hat{\mathbf{e}}_\phi + \dot\phi r\sin\theta\hat{\mathbf{e}}_\theta)\\ \dot{\mathbf{L}} &= \mathbf{r}\times\dot{\mathbf{p}}\\ &= -mr(2\dot r\dot\theta + r\ddot\theta - \dot\phi^2 r\sin\theta\cos\theta)\hat{\mathbf{e}}_\phi + (2\dot\phi\dot r\sin\theta + 2\dot\phi r\dot\theta\cos\theta + \ddot\phi r\sin\theta)\hat{\mathbf{e}}_\theta\ .\end{aligned}$$

b. With $\theta = \frac{\pi}{2}$ the expressions simplify to,

$$\begin{aligned}\mathbf{r} &= r\hat{\mathbf{e}}_r\\ \mathbf{v} &= \dot r\hat{\mathbf{e}}_r + \dot\phi r\hat{\mathbf{e}}_\phi\\ \mathbf{a} &= (\ddot r - \dot\phi^2 r)\hat{\mathbf{e}}_r + (2\dot\phi\dot r + \ddot\phi r)\hat{\mathbf{e}}_\phi\\ \mathbf{L} &= m\omega r^2\hat{\mathbf{e}}_\theta\\ \dot{\mathbf{L}} &= \mathbf{r}\times\dot{\mathbf{p}} = (2\dot\phi\dot r + \ddot\phi r)\hat{\mathbf{e}}_\theta = (\hat{\mathbf{e}}_\phi\cdot\mathbf{a})\hat{\mathbf{e}}_\theta\ .\end{aligned}$$

c. In a central potential $V(r)$, Newton's law reads,

$$\begin{aligned}m\mathbf{a} &= -\nabla V(r)\\ &= -\left(\hat{\mathbf{e}}_r\frac{\partial}{\partial r} + \hat{\mathbf{e}}_\theta\frac{1}{r}\frac{\partial}{\partial\theta} + \hat{\mathbf{e}}_\phi\frac{1}{r\sin\theta}\frac{\partial}{\partial\phi}\right)V(r) = -\hat{\mathbf{e}}_r\frac{\partial V}{\partial r}\ .\end{aligned}$$

Hence for $\theta = \frac{\pi}{2}$,

$$\begin{aligned}a_r &= \ddot r = -\frac{\partial V}{m\partial r} + \dot\phi^2 r = -\frac{\partial V_{eff}}{m\partial r} \qquad \textit{with} \qquad V_{eff}(r) = V(r) + \frac{m}{2}\omega^2 r^2\\ a_\phi &= \ddot\phi = -\frac{2\dot\phi\dot r}{r} = -\frac{2\omega\dot r}{r}\\ a_\theta &= \ddot\theta = 0\ .\end{aligned}$$

We finally find $\mathbf{L} = m\omega r^2\hat{\mathbf{e}}_\theta$ and $\dot{\mathbf{L}} = 0$.

6.3.5.18 Ex: Scattering at a central force, angular momentum

Consider the scattering of a particle of mass M at an attractive central force field $\mathbf{F}(\mathbf{r}) = -\frac{\alpha}{r^2}\hat{\mathbf{e}}_r$ with $\alpha > 0$. Far from the force center the velocity of the particle is given by v_∞. The asymptotic distance perpendicular to the velocity for very large distances from the force center is called the impact parameter b.
a. Determine the relationship between the impact parameter b and the angular momentum L of the particle.
b. The path of the particle has the shape of a conic section, which in plane polar coordinates can be parametrized by $r = P/(1-\epsilon\cos\phi)$. Find ϵ and P as a function of b, v_∞, M and α. c. Find an expression for $\sin(\theta/2)$. Here, θ is the scattering angle between the asymptotic orbits of the particle, i.e. the paths of the incoming and outgoing particles for large distances from the force center.
d. How does θ for constant v_∞ depend on the impact parameter b? Discuss the special cases $b = 0$ and $b \to \infty$.

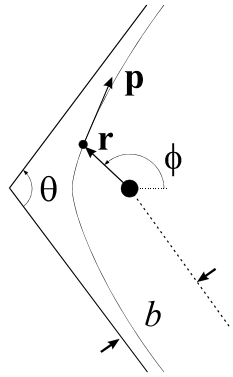

Figure 6.9:

Solution: *a. The angular momentum is in a central potential* $\mathbf{L} = \mathbf{r} \times \mathbf{p} = rp\hat{\mathbf{e}}_z \sin\beta$ *s a constant of motion. For* $t \to -\infty$ *we have* $\beta = \phi$ *and* $r \sin\phi = b$*. So,*

$$\mathbf{L} = mv_\infty b\hat{\mathbf{e}}_z \ .$$

b. The force field is,

$$\mathbf{F} = \dot{\mathbf{p}} = -\nabla V = \nabla\frac{\alpha}{r} = -\frac{\alpha}{r^3}\mathbf{r} \ .$$

We can now show,

$$\begin{aligned}\frac{d}{dt}(\mathbf{p}\times\mathbf{L}) = \dot{\mathbf{p}}\times\mathbf{L} &= -\frac{\alpha}{r^3}\mathbf{r}\times(\mathbf{r}\times\mathbf{p}) \\ &= -\frac{\alpha}{r^3}\left[\mathbf{r}(\mathbf{r}\cdot\mathbf{p}) - \mathbf{p}(\mathbf{r}\cdot\mathbf{r})\right] = m\alpha\left[\frac{\mathbf{v}}{r} - \frac{\mathbf{r}(\mathbf{r}\cdot\mathbf{v})}{r^3}\right] = \frac{d}{dt}m\alpha\frac{\mathbf{r}}{r} \ .\end{aligned}$$

Integration provides a constant of motion, the Lenz vector $\mathbf{C} = m\alpha\frac{\mathbf{r}}{r} - \mathbf{p}\times\mathbf{L}$*,*

$$\begin{aligned}\mathbf{r}\cdot(\mathbf{p}\times\mathbf{L}) &= \alpha\frac{\mathbf{r}}{r} - \mathbf{r}\cdot\mathbf{C} \\ L^2 &= m\alpha r - rC\cos\phi \\ \frac{L^2}{m\alpha - C\cos\phi} = r &= \frac{P}{1-\varepsilon\cos\phi} \ .\end{aligned}$$

So by comparison with the ellipse equation,

$$P = \frac{L^2}{\alpha m} = \frac{b^2v_\infty^2m^2}{\alpha m} \qquad \textit{and} \qquad \varepsilon = \frac{C}{\alpha m} \ .$$

For the absolute value of Lenz's vector C *one gets,*

$$\begin{aligned}C^2 &= m^2\alpha^2 + p^2L^2 - 2m\alpha\cdot\frac{\mathbf{r}}{r}(\mathbf{p}\times\mathbf{L}) = m^2\alpha^2 + p^2L^2 - 2m\alpha L^2\frac{1}{r} \\ &= m^2\alpha^2 + 2mL^2\left(\frac{p^2}{2m} - \frac{\alpha}{r}\right) = m^2\alpha^2 + 2mL^2(E_{kin} + E_{pot}) \\ &= m^2\alpha^2 + m^2L^2v_\infty^2 = m^2\alpha^2 + m^4v_\infty^4b^2 \ ,\end{aligned}$$

since $E = E_{kin} + E_{pot} = \frac{m}{2}v_\infty^2$ *is another constant of motion. In the end,*

$$\varepsilon^2 = 1 + \frac{m^2 v_\infty^4 b^2}{\alpha^2} \ .$$

c. Consider the ellipse equation $r(\phi) = \frac{P}{1-\varepsilon\cos\phi}$ *for* $r \to \pm\infty$,

$$1 - \varepsilon\cos\phi_\infty = 0 \ .$$

It follows,

$$\theta = \phi_{-\infty} + \phi_\infty = 2\arccos\frac{1}{\varepsilon}$$

$$\sin\theta/2 = \sin\arccos\frac{1}{\varepsilon} = \sqrt{1-1/\varepsilon^2} = \sqrt{\frac{\frac{m^2v_\infty^4 b^2}{\alpha^2}}{1+\frac{m^2v_\infty^4 b^2}{\alpha^2}}} = \sqrt{\frac{\kappa^2}{1+\kappa^2}} \ .$$

with the abbreviation $\kappa \equiv \frac{mv_\infty^2 b}{\alpha}$.
d. Given v_∞ *we have that* $\kappa \propto b$. *For the case Fall* $b \to 0$ *we have that* $\theta = 0$, *i.e. the particle is reflected. In the case of* $b \to \infty$, $\theta = \pi$, *i.e. there is no deviation.*

6.3.5.19 Ex: Gravitational force, trajectory

The trajectory of the Kepler problem can be derived from the integral expression:

$$\varphi(r) = \varphi_0 + \int_{r_0}^{r} \frac{l\,dr}{r^2\sqrt{2m(E+\frac{\alpha}{r}) - \frac{l^2}{r^2}}} \ .$$

Here E is the total energy, $\alpha = \gamma_N mM$ and $l = mr^2\dot{\varphi}$. We also introduce the quantities:

$$p = \frac{l^2}{m\alpha} \qquad \text{and} \qquad \varepsilon = \sqrt{1+\frac{2El^2}{m\alpha^2}} \ .$$

a. Convince yourself that, with the substitution $\xi = (p/r - 1)/\varepsilon$, the integral expression can be written in the form:

$$\varphi(r) = \varphi_0 - \int_{\frac{1}{\varepsilon}(\frac{p}{r_0}-1)}^{\frac{1}{\varepsilon}(\frac{p}{r}-1)} \frac{d\xi}{\sqrt{1-\xi^2}} \ .$$

b. Show with the help of energy conservation that the minimum distance from the force center is determined by $r_{\min} = \frac{p}{1+\varepsilon}$ for all values of E.
c. Show that the trajectories for $\varphi_0 = \pi$ and $r = r_{\min}$ are $r(\varphi) = \frac{p}{1-\varepsilon\,\cos\varphi}$, where $\int dx/\sqrt{1-x^2} = \arcsin x$.
d. Confirm that for elliptical trajectories ($0 \le \varepsilon < 1$ and $p = b^2/a^2$ where $a(b)$, the major semi-axis follows Kepler's 3rd law. Use the area theorem.

Solution: *a. The integral can be rewritten with the following substitutions: With* $u = 1/v$ *that is* $\frac{dr}{r^2} = -du$*, we get,*

$$-l \int_{1/r_0}^{1/r} \frac{du}{\sqrt{2mE + 2m\alpha u - l^2 u^2}} \ .$$

With $x = Pu$ *and* $P = l^2/m\alpha$ *we get,*

$$-\int \frac{dx}{\sqrt{2El^2/m\alpha^2 + 2x - x^2}} \ .$$

With $y = x - 1$ *we get,*

$$-\int \frac{dy}{\sqrt{2El^2/m\alpha^2 + 1 - y^2}} \ .$$

With $\xi = y/\epsilon$ *and* $\epsilon = \sqrt{1 + \frac{2El^2}{m\alpha^2}}$ *we get,*

$$-\int \frac{d\xi}{\sqrt{1 - \xi^2}} \ .$$

This results in,

$$\phi = -\int_{\xi_0=(P/r_0-1)/\epsilon}^{\xi=(P/r-1)/\epsilon} \frac{d\xi}{\sqrt{1 - \xi^2}} + \phi_0 \ .$$

b.Energy conservation with $\dot{r} = 0$ *(turning points):*

$$E = \frac{l^2}{2mr^2} - \frac{\alpha}{r} \ ,$$

with $u = 1/r$ *and* $P = l^2/m\alpha$ *follows* $Pu^2 - 2u = 2E/\alpha$*. The solution to this is,*

$$u_{1,2} = \frac{2 \pm \sqrt{4 + 4\frac{2PE}{\alpha}}}{2P} = \frac{1 \pm \varepsilon}{P} \ .$$

The minimum value for r *corresponds to a maximum value of* u*:*

$$\text{for } \varepsilon < 1 \quad , \quad u_{\max} = \frac{1+\varepsilon}{P} \text{ follows } r_{\min} = \frac{P}{1+\varepsilon}$$
$$\text{for } \varepsilon \geq 1 \quad , \quad u_{\max} = \frac{1+\varepsilon}{P} > 0 \text{ follows } r_{\min} = \frac{P}{1+\varepsilon} \ .$$

c. For the integral expression we get $\phi = \arccos\xi + \phi_0 - \arccos\xi_0$*. Insert for* $\phi_0 = \pi$ *the value* $r_0 = r_{\min}$ *and hence* $\xi_0 = \frac{P/r_0-1}{\varepsilon} = 1$*:*

$$\phi = \arccos\xi + \pi - \arccos 1 \ .$$

Follows $\xi = \frac{P/r-1}{\varepsilon} = \cos(\phi - \pi) = -\cos\phi$ *and hence* $r = \frac{P}{1-\varepsilon\cos\phi}$.
d. With the area theorem,

$$\frac{l}{2m} = \frac{\text{total area}}{T} = \frac{\pi ab}{T} \ ,$$

$$\frac{T^2}{a^3} = \frac{4m^2\pi^2 b^2}{l^2 a} \ ,$$

with $P = \frac{b^2}{a} = \frac{l^2}{m\alpha}$

$$\frac{T^2}{a^3} = \frac{4m^2\pi^2 P}{e^2} = \frac{4m\pi^2}{\alpha} = \frac{4\pi^2}{\gamma_N M} = const \ .$$

6.3.5.20 Ex: Central force, trajectory

Consider two masses m_1 and m_2 located at $\mathbf{r}_1$ and $\mathbf{r}_2$. There is an attractive force between them of the amount $F(\mathbf{r}_1, \mathbf{r}_2) = 2\lambda/|\mathbf{r}_1 - \mathbf{r}_2|^3$ ($\lambda > 0$).
a. Specify the angular momentum of the relative motion $\mathbf{l}$ and the energy conservation as a function of $\mathbf{r}$, $\mathbf{p}$ and the reduced mass μ, whereby we may designate by $E > 0$ the total energy of the system.
b. At the time $t = 0$ we let the relative distance of both particles be $r_{\min}$, the relative velocity in the direction of r be zero and $\varphi(r_{\min}) = 0$. Determine the relationship between $r_{\min}$, E, l, λ and μ. Is it possible to eliminate l and λ from the energy conservation law? Calculate the function $r(t)$.
c. Express $\frac{d}{d\varphi} r(\varphi) = \dot{r}/\dot{\varphi}$ as a function of E, l, r and $r_{\min}$ and calculate the trajectory $r(\varphi)$.

Solution: *a. We have,*

$$E = \frac{1}{2}\mu\dot{r}^2 + \frac{l^2}{2\mu r^2} + \frac{\lambda}{r^2} \ .$$

b. From (a) follows with $\dot{r}(r_{\min}) = 0$,

$$\begin{aligned} \frac{\mu}{2}\dot{r}^2 + \frac{l^2}{2\mu r^2} + \frac{\lambda}{r^2} = E = \frac{l^2}{2\mu r_{\min}^2} + \frac{\lambda}{r_{\min}^2} \\ \Rightarrow \frac{l^2}{2\mu} + \lambda = E r_{\min}^2 \\ \Rightarrow E = \frac{\mu}{2}\dot{r}^2 + E\frac{r_{\min}^2}{r^2} \ . \end{aligned}$$

Separation of variables and integration provides,

$$\begin{aligned} \frac{dr}{dt} &= \sqrt{\frac{2E}{\mu}} \frac{1}{r} \sqrt{r^2 - r_{\min}^2} \\ \Rightarrow \int \frac{r dr}{\sqrt{r^2 - r_{\min}^2}} &= \int \sqrt{\frac{2E}{\mu}} dt \\ \Rightarrow r(t) &= \sqrt{r_{\min}^2 + \frac{2E}{\mu} t^2} \ . \end{aligned}$$

c. We have,

$$\frac{dr(\varphi)}{d\varphi} = \frac{\dot{r}}{\dot{\varphi}} = \frac{r^2}{l}\sqrt{2\mu E\left(1 - \frac{r_{\min}^2}{r^2}\right)} \ .$$

Separation of variables and integration provides,

$$\int \frac{dr(\varphi)}{r\sqrt{r^2 - r_{\min}^2}} = \int \frac{\sqrt{2\mu E}}{l} d\varphi$$

$$\Rightarrow -\frac{1}{r_{\min}} \arctan \frac{r_{\min}}{\sqrt{r^2 - r_{\min}^2}} = \frac{\sqrt{2\mu E}}{l}\varphi$$

$$\Rightarrow r = \sqrt{r_{\min}^2 + \frac{r_{\min}^2}{\tan^2\left(\frac{-\sqrt{2\mu E}}{l} r_{\min}\varphi\right)}} = \frac{r_{\min}}{\sin\left(\frac{-\sqrt{2\mu E}}{l} r_{\min}\varphi\right)} = \frac{-r_{\min}}{\sin\left(\varphi\sqrt{1 + \frac{2\mu\lambda}{l^2}}\right)} \ .$$

Hence,

$$r(\varphi) = \frac{r_{\min}}{\cos\Omega\varphi} \ .$$

6.3.5.21 Ex: Ballistic movement

Consider the movement of an intercontinental missile launched at an inclination of θ_0, as shown in the figure, with speed v_0, in the indicated position. Calculate the body's trajectory.

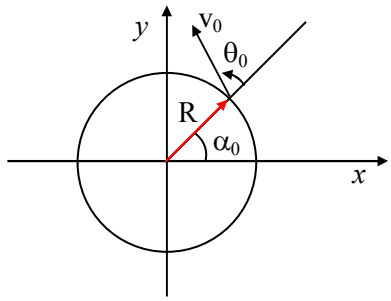

Figure 6.10:

Solution:

6.3.5.22 Ex: Rotation of three bodies

Three identical bodies of mass M are located at the vertices of an equilateral triangle with border length L. How fast should they move, if they all rotate under the influence of mutual gravity, on a circular orbit that circumscribes the triangle always kept

equilateral?

Solution: *With the distance r of each body from the center of origin, the distance between the bodies is $L = 2r\cos\frac{60^\circ}{2} = r\sqrt{3}$. The centripetal force that must act on one of the three masses is,*

$$\mathbf{F}_1 = -\frac{Mv^2}{r}\hat{\mathbf{e}}_r \ .$$

The gravitational force between two bodies is

$$\mathbf{F}_{12} = -\frac{\gamma_N MM}{L^2}\hat{\mathbf{e}}_{12} \ .$$

Equilibrium demands $\mathbf{F}_1 = \mathbf{F}_{12} + \mathbf{F}_{13}$. Hence,

$$-\frac{Mv^2}{r} = -2\frac{\gamma_N MM}{L^2}\cos\tfrac{60^\circ}{2} \ ,$$

Which gives,

$$v = \sqrt{\frac{\gamma_N M}{L}} \ .$$

6.3.5.23 Ex: Rotation of two bodies

Consider two masses m and $2m$ with gravitational attraction. At what angular velocity should they rotate so that the distance d between them is constant?

Solution: *Both masses revolve around the center of mass located at the point,*

$$0 = \mathbf{r}_{cm} = \frac{m\mathbf{r}_m + 2m\mathbf{r}_{2m}}{m+2m} = \frac{1}{3}(\mathbf{r}_m + 2\mathbf{r}_{2m}) \ .$$

Hence, $\mathbf{r}_m = -2\mathbf{r}_{2m}$, or with $d = r_m + r_{2m}$ we have $d = 3r_{2m} = \frac{3}{2}r_m$. Force equilibrium requests,

$$\frac{mv_m^2}{r_m} = \frac{\gamma_N m2m}{d^2} = \frac{2mv_{2m}^2}{r_{2m}} \ ,$$

which gives,

$$\frac{3v_m^2}{2d} = \frac{\gamma_N 2m}{d^2} = \frac{6v_{2m}^2}{d} \ ,$$

and finally,

$$v_m = 2v_{2m} = \sqrt{\frac{4\gamma_N m}{3d}} \ .$$

6.3.5.24 Ex: The virial law

Consider a mathematical spring pendulum with $D = 100\,\mathrm{N/m}$ and an attached mass of $m = 100\,\mathrm{g}$. The average kinetic energy of the pendulum be $\overline{T} = 0.5\,\mathrm{J}$. What is the mean deflection $\overline{x}$ and the mean quadratic deflection $\overline{x^2}$?

Solution: *For $\overline{x}$, integration over a period of oscillation $T = (2\pi\omega_0)^{-1}$ yields,*

$$\overline{x} = \frac{1}{T}\int_0^T A \cdot \sin(2\pi\omega_0 t + \phi) = 0 \ .$$

For $\overline{x^2}$, with $E = \overline{T} + \overline{V}$, we deduce,

$$\overline{T} = \overline{V} = E/2 \qquad \Rightarrow \qquad \frac{1}{2}m\omega_0^2\overline{x^2} = E/2 \qquad \Rightarrow \qquad \overline{x^2} = \frac{E}{m\omega_0^2} = \frac{E}{D} \ ,$$

with $\omega_0 = \sqrt{D/m}$. With $E = 2\overline{T} = 1\,\mathrm{J}$ we get $\overline{x^2} = 0.01\,\mathrm{m}^2$ resp. $\sqrt{\overline{x^2}} = 10\,\mathrm{cm}$. Specifying the mass is not required.

6.4 Outlook on general relativity

The fundamental idea of *general relativity* is the *equivalence* of inert and heavy mass. While special relativity follows from Lorentz invariance, general relativity follows from Lorentz boost invariance, see also Secs. 12.4.3 and 20.5.

Example 29 (*Relativistic correction to Newton's law*): .

6.4.1 Gravitational red-shift

The *gravitational red-shift* $\Delta\omega$ suffered by a clock of mass m can be estimated from (see Sec.36.5.2),

$$\boxed{\hbar\Delta\omega = m\Delta\tfrac{V(\mathbf{r})}{m}} \ , \tag{6.47}$$

where $\Delta V(\mathbf{r})$ is the gravitational potential difference with and without a nearby heavy mass. The mass of the clock is a measure of its pace: $m = E/c^2 = \hbar\omega/c^2$. For instance, on the surface of Earth we get,

$$\hbar\Delta\omega = mg\Delta z = \frac{E}{c^2}g\Delta z = \frac{\hbar\omega}{c^2}g\Delta z \ . \tag{6.48}$$

Hence,

$$\frac{\Delta\omega}{\omega} = \frac{g}{c^2}\Delta z \simeq \Delta z \cdot 10^{-16}\,\mathrm{m}^{-1} \ . \tag{6.49}$$

6.4.2 Exercises

6.5 Further reading

H.M. Nussenzveig, Edgar Blucher (2013), *Curso de Física Básica: Mecânica - vol 1* [961]ISBN

Chapter 7

Classical mechanics

7.1 The Lagrange formalism

Lagrange function $L = T - V$ with holonomic constraints, $F_i(r_1, r_2, r_3) = A = const$ with $i \in [1, .., e]$,

$$\frac{\delta L}{\delta r_j} + \sum_{i=1}^{e} \lambda_i \frac{\partial F_i}{\partial r_j} = 0 \ . \tag{7.1}$$

with

$$\frac{\delta L}{\delta r_j} \equiv \frac{\partial L}{\partial r_j} - \frac{d}{dt}\frac{\partial L}{\partial \dot{r}_j} \ . \tag{7.2}$$

7.1.1 Exercises

7.1.1.1 Ex: Rigid bodies

Two point masses m and M ($m \neq M$) are connected to the ends of a massless wire of length l, which passes through a hole in a horizontal table; m moves without friction on the table while M does it vertically under the joint action of gravity and tension of the wire (disregard also the friction between the wire and the hole).
a. What initial speed must be given to m in order for M to remain at rest below the table surface?
b. Knowing that the system's Lagrangian is $\mathcal{L} = \frac{1}{2}(m+M)\dot{r}^2 + \frac{1}{2}mr^2\dot{\theta}^2 - Mg(r-l)$, get the equations of motion.
c. Get the conserved quantities and explain the physical meaning of each one.
d. If M were slightly displaced from its vertical position, small oscillations would occur in the system. Calculate the period of these oscillations.

Solution: *a. The balance between centrifugal and gravitational forces requires,*

$$\frac{mv^2}{r} = F_{cp} = T = F_g = Mg \ .$$

Hence,

$$v = \sqrt{\frac{Mgr}{m}} \ .$$

b. Lagrange equations:

$$\frac{\partial \mathcal{L}}{\partial q} = \frac{d}{dt}\frac{\mathcal{L}}{\partial \dot{q}} \ .$$

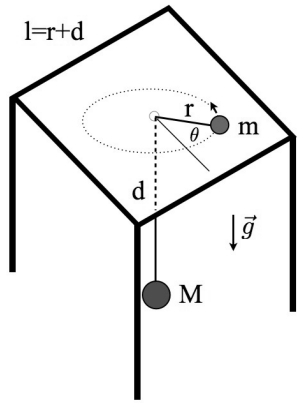

Figure 7.1:

For $q \equiv r$:

$$\frac{\partial \mathcal{L}}{\partial r} = -Mg + mr\dot{\theta}^2 = -Mg + \frac{L^2}{mr^2} = \frac{d}{dt}\frac{\mathcal{L}}{\partial \dot{r}} = (m+M)\ddot{r} \ .$$

where $\mathcal{L} = mr^2\dot{\theta}$ is the angular momentum. For $q \equiv \theta$:

$$\frac{\partial \mathcal{L}}{\partial \theta} = 0 = \frac{d}{dt}\frac{\mathcal{L}}{\partial \dot{\theta}} = \frac{d}{dt}(mr^2\dot{\theta}) \ .$$

In summary, the equations of the movement are:

$$(m+M)\ddot{r} = -Mg + mr\dot{\theta}^2 = -Mg + \frac{L^2}{mr^2}$$
$$\frac{d}{dt}(mr^2\dot{\theta}) = \frac{d}{dt}L = 0 \ .$$

c. Energy,

$$E = T+V = \tfrac{1}{2}(m+M)\dot{r}^2 + \tfrac{1}{2}mr^2\dot{\theta}^2 + Mg(r-l) = \tfrac{1}{2}(m+M)\dot{r}^2 + \frac{L^2}{2mr^2}\dot{\theta}^2 + Mg(r-l) \ .$$

Angular momentum,

$$L = mr^2\dot{\theta} \ .$$

E and L have no explicit dependence on time and are constant.
d. The effective potential is:

$$V_{ef} = Mg(r-l) + \frac{L^2}{2mr^2} \ ,$$

the spring constant is $k = \left.\frac{d^2V_{ef}}{dr^2}\right|_{r_{eq}}$. Calculating the first and second derivatives:

$$\left.\frac{dV_{ef}}{dr}\right|_{r_{eq}} = Mg - \left.\frac{L^2}{mr^3}\right|_{r_{eq}} = 0 \Longrightarrow \ L^2 = Mmgr_{eq}^3$$
$$\left.\frac{d^2V_{ef}}{dr^2}\right|_{r_{eq}} = \left.\frac{3L^2}{mr^4}\right|_{r_{eq}} = \frac{3r_{eq}^3Mmg}{mr_{eq}^4} = \frac{3Mg}{r_{eq}} \ ,$$

we get,

$$T = 2\pi \frac{1}{\sqrt{\frac{h}{M+m}}} = 2\pi \sqrt{\frac{(M+m)r_{eq}}{3Mg}} \ .$$

7.1.1.2 Ex: Trapped particle

A particle of mass m is subject to a one-dimensional potential $V(x) = \frac{1}{2}kx^2 - \frac{k}{4a^2}x^4$, where k and a are positive constants and $-\infty < x < \infty$.
a. Determine the force $F(x)$, obtain the equilibrium points, and determine their nature.
b. Calculate the period of the movement for small oscillations around the stable equilibrium point.
c. Assume that the particle is at rest at the point $x = 0$, and that it receives an impulse that instantly gives it a velocity v oriented in positive x-direction. Discuss what happens in the following cases:
i. $0 < v \leq a\sqrt{k/2m}$,
ii. $v > a\sqrt{k/2m}$.
d. Sketch the system's phase diagram (i.e. $p = m\dot{x}$ vs. x, for $E(x,p) = cte$) for the various types of movement. Indicate clearly the curve that corresponds to the transition between periodic and non-periodic motion, as well as the corresponding energy value.

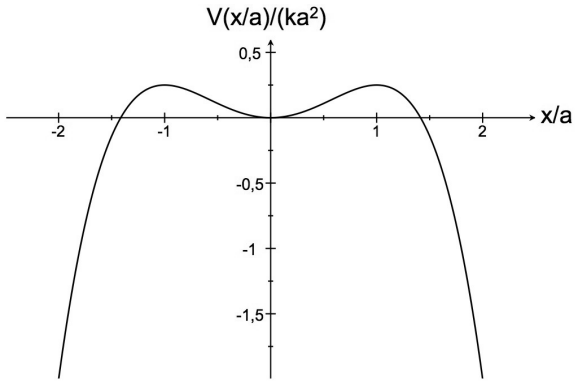

Figure 7.2:

Solution: *a. The force is,*

$$F = -\frac{dV(x)}{dx} = -kx + \frac{k}{a^2}x^3 \ .$$

The equilibrium points are, where the force goes to zero, that is, we have $x = 0$ and $x = \pm a$. As the derivative $D(x) \equiv dF/dx = -k + \frac{k}{a^2}x^2$ is,

$$D(0) < 0 \qquad and \qquad D(\pm a) = 0 \ ,$$

the position $x = 0$ is stable and the points $x = \mp a$ are labile.
b. For small oscillations we can neglect the fourth order of the potential,

$$V(x) \simeq \frac{k}{2}x^2 \ .$$

Hence,

$$\omega = \sqrt{\frac{k}{m}} \ .$$

c. The height of the potential at the points $\pm\alpha$ is,

$$V(\pm a) = \frac{k}{4}a^2 \ .$$

The kinetic energy corresponding to the initial velocity $v_0 = a\sqrt{k/2m}$ is,

$$E_{kin} = \frac{m}{2}v^2 = \frac{m}{2}\frac{ka^2}{2m} = \frac{k}{4}a^2 \ .$$

Therefore, the particle is trapped when $v_0 = a\sqrt{k/2m}$.
d. Phase diagram:

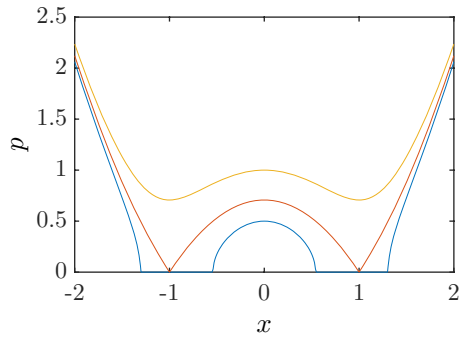

Figure 7.3:

7.1.1.3 Ex: Satellite

An artificial satellite of mass m_1 on an elliptical orbit around the Earth has its maximum and minimum distances from the **surface** of the Earth given by h and H, respectively. It is also known that the maximum approximation occurs over the North Pole. A particle of mass $m_2 = m_1/10$ collides centrally and completely inelastically with the satellite, exactly when it is passing over the North Pole. At the time of the collision, the absolute value of the satellite's speed was v_1 and the particle had the same speed, but in the opposite direction to the satellite. Assume that the Earth is a sphere of uniform density with radius R and mass M; despise air resistance.
a. Obtain the speed v_S of the 'satellite+mass' system after the collision in terms of v_1?

b. Obtain the speed v_1 of the satellite before the collision.
c. Obtain the energy and the angular momentum of the 'satellite+mass' system in terms of quantities that characterize the satellite's movement before the collision (i.e., mass, speed, and position).
d. Obtain the equation for the orbit of the 'satellite+mass' system.

Solution: *a. Moment conservation during the inelastic collision with* $v_2 = -v_1$ *and* $m_2 = m_1/10$

$$(m_1 + m_2)v_S = m_1 v_1 + m_2 v_2$$
$$\Longrightarrow \; v_S = \frac{m_1 - m_2}{m_1 + m_2} v_1 = \frac{0.9}{1.1} v_1 \; .$$

b. Conservation of energy and angular momentum with $r_h = R_T + h$ *and* $r_H = R_T + H$,

$$E \equiv \frac{m_1}{2} v_H^2 - \frac{GM_T m_1}{r_H} = \frac{m_1}{2} v_h^2 - \frac{GM_T m_1}{r_h}$$
$$L \equiv m_1 r_H v_H = m_1 r_h v_h \; .$$

Solving the second equation by v_H *and replacing in the first,*

$$\left(\frac{r_h}{r_H} v_h\right)^2 - \frac{2GM_T}{r_H} = v_h^2 - \frac{2GM_T}{r_h}$$
$$\Longrightarrow \; v_h = \sqrt{\frac{2GM_T r_H}{r_h(r_h + r_H)}} \; .$$

c. Energy at the instant after the collision,

$$E_S = \frac{m_1 + m_2}{2} v_S^2 - \frac{GM_T(m_1 + m_2)}{r_h} = \frac{(m_1 - m_2)^2}{2(m_1 + m_2)} v_1^2 - \frac{GM_T(m_1 + m_2)}{r_h} \; .$$

Angular momentum,

$$\vec{L}_S = (m_1 + m_2)\vec{r}_h \times \vec{v}_S = (m_1 + m_2) r_h \frac{m_1 - m_2}{m_1 + m_2} v_1 \hat{e}_L = (m_1 - m_2) r_h v_1 \hat{e}_L = \tfrac{9}{10}\vec{L} \; ,$$

d. The equation for the orbit is, according to the problem,

$$r(\phi) = \frac{p}{1 + \epsilon \cos\phi} \qquad \textit{where} \qquad p = \frac{L^2}{GM_T m} \qquad \textit{and} \qquad \epsilon = \sqrt{1 + \frac{2EL^2}{(GM_T)^2 m}} \; .$$

Substituting E_S, L_S, *and* m_S *we obtain the orbit equation after the collision. The orbit remains bound* ($E_S < 0$), *i.e. like an ellipse with the center of the Earth in one of the foci.*

7.1.1.4 Ex: Rigid bodies

A simple pendulum consists of a particle of mass m suspended by an inextensible wire of length a and with negligible mass. Its suspension point is connected to a support

that moves horizontally without friction, as shown in the figure. Suppose that the support is small enough and that the pendulum moves only in the vertical plane. Using as generalized coordinates x and θ, where x is the horizontal position of the support and θ the angular displacement of the pendulum, as shown in the figure. The movement of the system is described by the Lagrangian:

$$\mathcal{L} = \frac{m}{2}\dot{x}^2 + \frac{m}{2}\left(a^2\dot{\theta}^2 + 2a\dot{x}\dot{\theta}\cos\theta\right) + mga\cos\theta \ .$$

a. Get the equation of motion for the coordinate θ.
b. Assuming that the angular displacements are small and that the movement of the support is harmonic and described by $x(t) = x_0\cos\omega t$, obtain the general solution $\theta(t)$ of the equation of motion for the coordinate θ.
c. In the case of the previous item, obtain the resonance frequency ω_R.
d. Write down the general solution for $\theta(t)$, when the initial conditions are $\theta(0) = 0$ and $\dot{\theta}(0) = 0$ and the support moves with the frequency $\omega < \omega_R$.

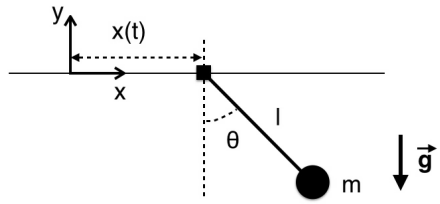

Figure 7.4:

Solution: *a. Inserting $\mathcal{L}$ into the Lagrange equation,*

$$\frac{d}{dt}\frac{\partial\mathcal{L}}{\partial\dot{\theta}} - \frac{\partial\mathcal{L}}{\partial\theta} = 0$$

gives

$$\begin{aligned}
&\frac{d}{dt}\left(ml^2\dot{\theta} + ml\dot{x}\cos\theta\right) - \left(-ml\dot{x}\dot{\theta}\sin\theta - mgl\sin\theta\right) \\
&= ml^2\ddot{\theta} + ml\ddot{x}\cos\theta - ml\dot{x}\dot{\theta}\sin\theta + ml\dot{x}\dot{\theta}\sin\theta + mgl\sin\theta \\
&= ml^2\ddot{\theta} + ml\ddot{x}\cos\theta + mgl\sin\theta = 0 \ ,
\end{aligned}$$

or

$$\ddot{\theta} + \frac{\ddot{x}}{l}\cos\theta + \frac{g}{l}\sin\theta = 0 \ .$$

b. In the limit of small oscillations, $\cos \to 1$ *and* $\sin \to \theta$*. This simplifies the equation of motion to,*

$$\ddot{\theta} + \frac{g}{l}\theta = -\frac{\ddot{x}}{l} \ .$$

Inserting $\ddot{x}(t) = -x_0\omega^2\cos\omega t$ *and defining* $\omega_0 = \sqrt{g/l}$*, we obtain the equation of motion for this particular movement of the support in the limit of small oscillations,*

$$\ddot{\theta} + \omega_0^2\theta = \frac{1}{l}x_0\omega^2\cos\omega t \ ,$$

whose solution is a superposition of the general homogeneous solution (1) with a particular inhomogeneous solution (2):

$$\theta_g(t) = a\cos\omega_0 t + b\sin\omega_0 t \ ,$$
$$\theta_p(t) = A\cos(\omega t + \delta) \ .$$

Inserting the particular solution into a differential equation,

$$A = \frac{x_0\omega^2}{l|\omega_0^2 - \omega^2|} \ ,$$

with the sign + for $\omega < \omega_0$, i.e. $\delta = 0$ and the sign − for $\omega > \omega_0$, i.e. $\delta = -\pi$. (The sign $\pm$ refers to the phase δ, which in this frictionless case is simply '+' when $\omega_0 > \omega$ and '-' when $\omega_0 < \omega$. Finally,

$$\theta(t) = a\cos\omega_0 t + b\sin\omega_0 t \pm \frac{x_0\omega^2}{l|\omega_0^2 - \omega^2|}\cos(\omega t) \ .$$

c. We have,

$$\omega_R = \omega_0 = \sqrt{g/l} \ .$$

d. With the initial condition $\theta(0) = 0$ we have,

$$\alpha + \frac{x_0\omega^2}{l(\omega_0^2 - \omega^2)} = 0 \ ,$$

that is, $\alpha = -\frac{x_0\omega^2}{l(\omega_0^2-\omega^2)}$. Also,

$$\dot\theta(t) = -\frac{x_0\omega^3\sin\omega t}{l(\omega_0^2 - \omega^2)} - \alpha\omega_0\sin\omega_0 t + b\omega_0\cos\omega_0 t \ .$$

that is $b = 0$. Finally,

$$\theta(t) = -\frac{x_0\omega^2}{l(\omega_0^2 - \omega^2)}(\cos\omega_0 t - \cos\omega t) \ .$$

7.1.1.5 Ex: Tritium atom

A tritium atom can be classically described as a nucleus with an electric charge $+e$, composed of a proton and two neutrons, orbited by an electron of charge $-e$ on a circular orbit of radius r_0. In a process known as β-decay, the nucleus of the tritium atom turns into an ionized helium atom, whose nucleus is composed of two protons and one neutron, emitting a pair of particles that quickly escape from the atomic system. As a consequence the electron suddenly perceives a new situation now orbiting a nucleus of charge $+2e$. The nucleus has a mass large enough to be considered at rest.
a. Obtain the energy E_a of the electron orbital before β-decay.
b. Calculate the energy E_d of the electron after the β- decay and get the ratio

$\rho = E_a/E_d$.
c. Determine the total angular momentum of the electron only as a function of r_0 and the electron mass m_e.
d. Calculate the largest and smallest distances between the electron and the nucleus in the new orbit in terms of r_0.

Solution: *a. The orbit is circular:*

$$\frac{mv_0^2}{r_0} = F_{electrostatic} = \frac{e^2}{4\pi\epsilon_0 r_0^2} \ .$$

Introducing $C = mv_0^2 = \frac{e^2}{4\pi\epsilon_0 r_0}$ *and writing the energy* E_a *of the orbit before the decay:*

$$E_a = \frac{mv_0^2}{2} - \frac{e^2}{4\pi\epsilon_0 r_0} = -\tfrac{1}{2}C \ .$$

b. In the instant the decay occurs, the orbital electron has the velocity v_0*, but its potential energy has suddenly changed to* $\frac{-2e^2}{4\pi\epsilon_0 r_0}$*. Hence.*

$$E_b = \frac{mv_0^2}{2} - \frac{2e^2}{4\pi\epsilon_0 r_0} = -\frac{3}{2}\frac{e^2}{4\pi\epsilon_0 r_0} = -\tfrac{3}{2}C \ .$$

So the ratio is,

$$\rho = E_a/E_d = \frac{1}{3} \ .$$

c. The electron orbital angular momentum is also constant: it has the same value as in the instant when the β*-decay occurred. Writing down the energy conservation:*

$$E_d = -\frac{3}{2}\frac{e^2}{4\pi\epsilon_0 r_0} = -\frac{2e^2}{4\pi\epsilon_0 r_0} + \frac{m\dot{r}^2}{2} + \frac{mr^2\dot{\theta}^2}{2} = -2\frac{e^2}{4\pi\epsilon_0 r_0}\frac{r_0}{r} + \frac{m\dot{r}^2}{2} + \frac{L^2\dot{\theta}^2}{2mr^2} \ .$$

Calculating the angular momentum at the instant of the decay in terms of r_0 *and* m*:*

$$L = mr_0 v_0 = mr_0\sqrt{\frac{1}{r}\frac{e^2}{4\pi\epsilon_0 r_0}} = \sqrt{\frac{me^2 r_0}{4\pi\epsilon_0}} \ ,$$

or also

$$\frac{L^2}{2mr^2} = \frac{1}{2mr^2}\frac{me^2}{4\pi\epsilon_0 r_0}r_0^2 = \frac{1}{2}\frac{e^2}{4\pi\epsilon_0 r_0}\frac{r_0^2}{r^2} = \frac{1}{2}C\frac{r_0^2}{r^2} \ .$$

d. For the points of maximum and minimum approximation, $\dot{r} = 0$*, we get,*

$$-\frac{3}{2}C = -2C\frac{r_0}{r} + \frac{1}{2}\frac{r_0^2}{r^2} \ .$$

Hence,

$$\frac{1}{2}\left(\frac{r_0}{r}\right)^2 - 2\frac{r_0}{r} + \frac{3}{2} = 0 \ ,$$

with the roots:

$$\frac{r_0}{r} = 3 \qquad \textit{and} \qquad \frac{r_0}{r} = 1 \ ,$$

and hence,

$$r_{max} = r_0 \qquad \textit{and} \qquad r_{min} = \frac{1}{3}r_0 \ .$$

7.1.1.6 Ex: Pendulum in a wagon

Consider a mathematical pendulum of mass m and length L suspended in a wagon of mass M initially at rest, as shown in the figure. Derive the equations of motion for the pendulum and the wagon including a friction for the movement of the wagon. Approximate for small oscillation amplitudes.

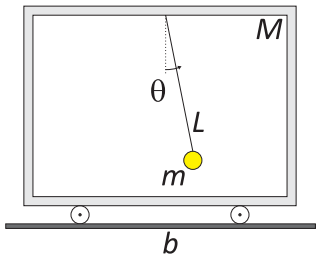

Figure 7.5: Pendulum in a wagon.

Solution: *If X is the position of the wagon, the pendulum position is,*

$$x = L\sin\theta + X \qquad , \qquad y = -L\cos\theta \ .$$

So we have four generalized coordinates, θ, $\dot\theta$, X, and $\dot X$. The kinetic energy of the system is,

$$\begin{aligned} T &= \tfrac{M}{2}\dot X^2 + \tfrac{m}{2}\dot x^2 + \tfrac{m}{2}\dot y^2 \\ &= \tfrac{M}{2}\dot X^2 + \tfrac{m}{2}(\ell\dot\theta\cos\theta + \dot X)^2 + \ell^2\tfrac{m}{2}\dot\theta^2\sin^2\theta \\ &= \tfrac{M}{2}\dot X^2 + \tfrac{m}{2}\ell^2\dot\theta^2 + m\ell\dot X\dot\theta\cos\theta + \tfrac{m}{2}\dot X^2 \ , \end{aligned}$$

and the potential energy,

$$V = mgy = -mg\ell\cos\theta$$

and the Lagrangian $L = T - V$. We calculate,

$$\begin{aligned} \frac{d}{dt}\frac{\partial\mathcal{L}}{\partial\dot\theta} &= \frac{d}{dt}(m\ell^2\dot\theta + m\ell\dot X\cos\theta) = m\ell^2\ddot\theta + m\ell\ddot X\cos\theta - m\ell\dot X\dot\theta\sin\theta \\ \frac{\partial\mathcal{L}}{\partial\theta} &= -m\ell\dot X\dot\theta\sin\theta - mg\ell\sin\theta \\ \frac{d}{dt}\frac{\partial\mathcal{L}}{\partial\dot X} &= \frac{d}{dt}(M\dot X + m\ell\dot\theta\cos\theta + m\dot X) = M\ddot X + m\ell\ddot\theta\cos\theta - m\ell\dot\theta^2\sin\theta + m\ddot X \\ \frac{\partial\mathcal{L}}{\partial X} &= 0 \ . \end{aligned}$$

The Lagrange equations are,

$$\begin{aligned} 0 &= \frac{d}{dt}\frac{\partial\mathcal{L}}{\partial\dot\theta} - \frac{\partial\mathcal{L}}{\partial\theta} = m\ell^2\ddot\theta + m\ell\ddot X\cos\theta + mg\ell\sin\theta \\ 0 &= \frac{d}{dt}\frac{\partial\mathcal{L}}{\partial\dot X} - \frac{\partial\mathcal{L}}{\partial X} = M\ddot X + m\ell\ddot\theta\cos\theta - m\ell\dot\theta^2\sin\theta + m\ddot X - 0 \ . \end{aligned}$$

For small angles,

$$0 = m\ell\ddot{\theta} + m\ddot{X} + mg\theta$$
$$0 = (M+m)\ddot{X} + m\ell\ddot{\theta} - m\ell\dot{\theta}^2\theta \ ,$$

or,

$$\ell\ddot{\theta} = -g\theta - \ddot{X}$$
$$M\ddot{X} = mg\theta + m\ell\dot{\theta}^2\theta \ .$$

The last term corresponds to the centrifugal force and is small for small angles,

$$\ddot{\theta} \simeq -\frac{g}{\ell}\left(1 + \frac{m}{M}\right)\theta \ .$$

7.1.1.7 Ex: Two pendulums in a wagon

Consider two pendulums of mass m and length L suspended inside a wagon of mass M initially at rest, as shown in the figure.
a. Making the approximation for small oscillation amplitudes, derive the equations of motion for each pendulum and for the wagon including a damping due to friction of the moving wagon.
b. Calculate the oscillation frequencies of the collective modes. Which mode is most subject to friction?

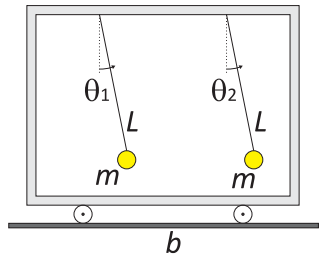

Figure 7.6: Two pendulums in a wagon.

Solution: *a. If X is the position of the wagon, the pendulum positions are,*

$$x_1 = L\sin\theta_1 + X \quad , \quad x_2 = L\sin\theta_2 + X \quad , \quad y_1 = -L\cos\theta_1 \quad , \quad y_2 = -L\cos\theta_2 \ .$$

So we have six generalized coordinates, θ_1, $\dot{\theta}_1$, θ_2, $\dot{\theta}_2$, X and $\dot{X}$. In analogy with the single-pendulum system we calculate,

$$\begin{aligned} T &= \tfrac{M}{2}\dot{X}^2 + \tfrac{m}{2}\dot{x}_1^2 + \tfrac{m}{2}\dot{x}_2^2 + \tfrac{m}{2}\dot{y}_1^2 + \tfrac{m}{2}\dot{y}_2^2 \\ &= \tfrac{M}{2}\dot{X}^2 + \tfrac{m}{2}\ell^2\dot{\theta}_1^2 + m\ell\dot{X}\dot{\theta}_1\cos\theta + \tfrac{m}{2}\ell^2\dot{\theta}_2^2 + m\ell\dot{X}\dot{\theta}_2\cos\theta_2 + m\dot{X}^2 \ , \end{aligned}$$

and the potential energy,

$$V = mgy_1 + mgy_2 = -mg\ell\cos\theta_1 - mg\ell\cos\theta_2$$

and the Lagrangian $\mathcal{L} = T - V$*. We calculate,*

$$\begin{aligned}
\frac{d}{dt}\frac{\partial\mathcal{L}}{\partial\dot\theta_1} &= m\ell^2\ddot\theta_1 + m\ell\ddot X\cos\theta_1 - m\ell\dot X\dot\theta_1\sin\theta_1\\
\frac{\partial\mathcal{L}}{\partial\theta_1} &= -m\ell\dot X\dot\theta\sin\theta_1 - mg\ell\sin\theta_1\\
\frac{d}{dt}\frac{\partial\mathcal{L}}{\partial\dot\theta_2} &= m\ell^2\ddot\theta_2 + m\ell\ddot X\cos\theta_2 - m\ell\dot X\dot\theta_2\sin\theta_2\\
\frac{\partial\mathcal{L}}{\partial\theta_2} &= -m\ell\dot X\dot\theta\sin\theta_2 - mg\ell\sin\theta_2\\
\frac{d}{dt}\frac{\partial\mathcal{L}}{\partial\dot X} &= M\ddot X + m\ell\ddot\theta_1\cos\theta_1 - m\ell\dot\theta_1^2\sin\theta_1 + m\ell\ddot\theta_2\cos\theta_2 - m\ell\dot\theta_2^2\sin\theta_2 + 2m\ddot X\\
\frac{\partial\mathcal{L}}{\partial X} &= 0\ .
\end{aligned}$$

Lagrange's equations become for small angles,

$$\begin{aligned}
0 &= m\ell\ddot\theta_1 + m\ddot X + mg\theta_1\\
0 &= m\ell\ddot\theta_2 + m\ddot X + mg\theta_2\\
0 &= M\ddot X + m\ell\ddot(\theta_1+\theta_2) - m\ell(\dot\theta_1^2\theta_1 + \dot\theta_2^2\theta_2) + 2m\ddot X\ .
\end{aligned}$$

or neglecting non-linear terms,

$$\ddot\Psi = -\frac{g}{\ell}\Psi - \frac{2}{\ell}\ddot X \qquad , \qquad \ddot\aleph = -\frac{g}{\ell}\aleph \qquad , \qquad (M+2m)\ddot X \simeq -m\ell\ddot\Psi\ .$$

or,

$$\ddot\Psi = -\frac{g}{\ell}\left(1+\frac{2m}{M}\right)\Psi \qquad , \qquad \ddot\aleph = -\frac{g}{\ell}\aleph \qquad , \qquad \ddot X = \frac{mg}{M}\Psi\ .$$

b. The frequencies of the normal modes are $\omega = 0$ *for the uniform movement of the entire system,* $\omega = \sqrt{g/\ell}$ *for the oscillation with opposite phases, and* $\omega = \sqrt{\frac{g}{\ell}(1+2m/M)}$ *for the in-phase oscillation.*

7.1.1.8 Ex: Two pendulums in a wagon attached by a spring

Repeat the previous exercise, but now the car is attached to a wall by a spring k.

Solution: *The generalized coordinates and the kinetic energy remain the same, but the potential energy changes to,*

$$V = -mg\ell\cos\theta_1 - mg\ell\cos\theta_2 + \frac{k}{2}X^2\ .$$

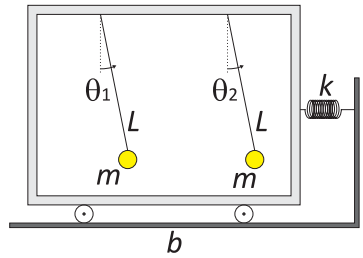

Figure 7.7: Two pendulums in a wagon.

Recalculating the Lagrangian $\mathcal{L} = T - V$ of the car movement,

$$\frac{d}{dt}\frac{\partial \mathcal{L}}{\partial \dot{X}} = M\ddot{X} + m\ell\ddot{\theta}_1\cos\theta_1 - m\ell\dot{\theta}_1^2\sin\theta_1 + m\ell\ddot{\theta}_2\cos\theta_2 - m\ell\dot{\theta}_2^2\sin\theta_2 + 2m\ddot{X}$$
$$\frac{\partial \mathcal{L}}{\partial X} = kX \ .$$

Lagrange's equations become for small angles,

$$0 = m\ell\ddot{\theta}_1 + m\ddot{X} + mg\theta_1$$
$$0 = m\ell\ddot{\theta}_2 + m\ddot{X} + mg\theta_2$$
$$0 = M\ddot{X} + m\ell\ddot{(}\theta_1 + \theta_2) - m\ell(\dot{\theta}_1^2\theta_1 + \dot{\theta}_2^2\theta_2) + 2m\ddot{X} - kX \ .$$

or neglecting non-linear terms,

$$\ddot{\Psi} = -\frac{g}{\ell}\Psi - \frac{2}{\ell}\ddot{X} \quad , \quad \ddot{\aleph} = -\frac{g}{\ell}\aleph \quad , \quad (M+2m)\ddot{X} \simeq -kX - m\ell\ddot{\Psi} \ .$$

or,

$$\ddot{\Psi} = -\frac{g}{\ell}\left(1 + \frac{2m}{M}\right)\Psi + \frac{2k}{M\ell}X \quad , \quad \ddot{\aleph} = -\frac{g}{\ell}\aleph \quad , \quad \ddot{X} = \frac{-k}{M}X + \frac{mg}{M}\Psi \ .$$

7.1.1.9 Ex: Super- and subradiance

We consider two pendulums of mass m and length ℓ suspended on a rod of mass M that itself is suspended to an immobile ceiling by wires of length L, as shown in the figure. Derive the equations for collective modes including damping for small amplitudes.

Solution: *The position of the rod is,*

$$X = L\sin\Theta \quad , \quad Y = -L\cos\Theta \ .$$

The pendulum positions are,

$$x_1 = \ell\sin\theta_1 + L\sin\Theta \quad , \quad y_1 = -\ell\cos\theta_1 - L\cos\Theta$$
$$x_2 = \ell\sin\theta_2 + L\sin\Theta \quad , \quad y_2 = -\ell\cos\theta_2 - L\cos\Theta \ .$$

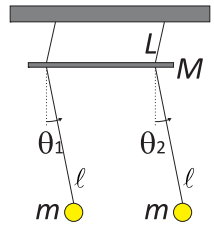

Figure 7.8: Super- and subradiance.

So we have six generalized coordinates, θ_1, $\dot\theta_1$, θ_2, $\dot\theta_2$, Θ e $\dot\Theta$. In analogy with the single-pendulum system we calculate,

$$\begin{aligned}
T &= \tfrac{M}{2}\dot X^2 + \tfrac{M}{2}\dot Y^2 + \tfrac{m}{2}\dot x_1^2 + \tfrac{m}{2}\dot y_1^2 + \tfrac{m}{2}\dot x_2^2 + \tfrac{m}{2}\dot y_2^2 \\
&= \tfrac{3M}{2}L^2\dot\Theta^2 + \tfrac{m}{2}\ell^2\dot\theta_1^2 + mL\ell\dot\theta_1\cos\theta_1\dot\Theta\cos\Theta + mL\ell\dot\theta_1\sin\theta_1\dot\Theta\sin\Theta \\
&\quad + \tfrac{m}{2}\ell^2\dot\theta_2^2 + mL\ell\dot\theta_2\cos\theta_2\dot\Theta\cos\Theta + mL\ell\dot\theta_2\sin\theta_2\dot\Theta\sin\Theta \\
&= \tfrac{3M}{2}L^2\dot\Theta^2 + \tfrac{m}{2}\ell^2\dot\theta_1^2 + mL\ell\dot\theta_1\dot\Theta\cos(\theta_1-\Theta) + \tfrac{m}{2}\ell^2\dot\theta_2^2 + mL\ell\dot\theta_2\dot\Theta\cos(\theta_2-\Theta)\ ,
\end{aligned}$$

and the potential energy,

$$V = mgY + mgy_1 + mgy_2 = -MgL\cos\Theta - mg\ell\cos\theta_1 - mg\ell\cos\theta_2\ .$$

The Lagrangian $\mathcal{L} = T - V$ is,

$$\begin{aligned}
\frac{d}{dt}\frac{\partial\mathcal{L}}{\partial\dot\Theta} &= 3ML^2\ddot\Theta + mL\ell\ddot\theta_1\cos(\theta_1-\Theta) - mL\ell\dot\theta_1(\dot\theta_1-\dot\Theta)\sin(\theta_1-\Theta) \\
&\quad + mL\ell\ddot\theta_2\cos(\theta_2-\Theta) - mL\ell\dot\theta_2(\dot\theta_2-\dot\Theta)\sin(\theta_2-\Theta) \\
\frac{\partial\mathcal{L}}{\partial\Theta} &= mL\ell\dot\theta_1\dot\Theta\sin(\theta_1-\Theta) + mL\ell\dot\theta_2\dot\Theta\sin(\theta_2-\Theta) - MgL\sin\Theta \\
\frac{d}{dt}\frac{\partial\mathcal{L}}{\partial\dot\theta_1} &= m\ell^2\ddot\theta_1 + mL\ell\ddot\Theta\cos(\theta_1-\Theta) - mL\ell\dot\Theta(\dot\theta_1-\dot\Theta)\sin(\theta_1-\Theta) \\
\frac{\partial\mathcal{L}}{\partial\theta_1} &= -mL\ell\dot\theta_1\dot\Theta\sin(\theta_1-\Theta) - mg\ell\sin\theta_1 \\
\frac{d}{dt}\frac{\partial\mathcal{L}}{\partial\dot\theta_2} &= m\ell^2\ddot\theta_2 + mL\ell\ddot\Theta\cos(\theta_2-\Theta) - mL\ell\dot\Theta(\dot\theta_2-\dot\Theta)\sin(\theta_2-\Theta) \\
\frac{\partial\mathcal{L}}{\partial\theta_2} &= -mL\ell\dot\theta_2\dot\Theta\sin(\theta_2-\Theta) - mg\ell\sin\theta_2\ .
\end{aligned}$$

The Lagrange equations are,

$$\begin{aligned}
0 &= 3ML\ddot\Theta + m\ell\ddot\theta_1\cos(\theta_1-\Theta) - m\ell\dot\theta_1^2\sin(\theta_1-\Theta) \\
&\quad + m\ell\ddot\theta_2\cos(\theta_2-\Theta) - m\ell\dot\theta_2^2\sin(\theta_2-\Theta) + Mg\sin\Theta \\
0 &= \ell\ddot\theta_1 + L\ddot\Theta\cos(\theta_1-\Theta) + L\dot\Theta^2\sin(\theta_1-\Theta) + g\sin\theta_1 \\
0 &= \ell\ddot\theta_2 + L\ddot\Theta\cos(\theta_2-\Theta) + L\dot\Theta^2\sin(\theta_2-\Theta) + g\sin\theta_2\ .
\end{aligned}$$

For small angles and neglecting nonlinear terms,

$$\ddot{\Theta} = -\frac{g}{3L}\Theta - \frac{m\ell}{3ML}(\ddot{\theta}_1 + \ddot{\theta}_2) \quad , \quad \ddot{\theta}_1 = -\frac{g}{\ell}\theta_1 - \frac{L}{\ell}\ddot{\Theta} \quad , \quad \ddot{\theta}_2 = -\frac{g}{\ell}\theta_2 - \frac{L}{\ell}\ddot{\Theta} \; .$$

or,

$$\ddot{\Theta} = -\frac{g}{3L}\Theta - \frac{m\ell}{3ML}\ddot{\Psi} \quad , \quad \ddot{\Psi} = -\frac{g}{\ell}\Psi - \frac{2L}{\ell}\ddot{\Theta} \quad , \quad \ddot{\aleph} = -\frac{g}{\ell}\aleph \; ,$$

or,

$$\ddot{\Theta} = -\frac{1}{1-\frac{2m}{3M}}\frac{g}{3L}\Theta - \frac{1}{1-\frac{3M}{2m}}\frac{\ell g}{2L^2}\psi \quad , \quad \ddot{\Psi} = -\frac{1}{1-\frac{2m}{3M}}\frac{g}{L}\psi + \frac{1}{1-\frac{2m}{3M}}\frac{2g}{3\ell}\Theta \quad , \quad \ddot{\aleph} = -\frac{g}{\ell}\aleph \; .$$

7.2 The Euler-Lagrange formalism

7.3 The Hamilton formalism

7.4 The Hamilton-Jacobi formalism

7.5 Further reading

H. Goldstein and C.P. Poole and J.L. Safko, *Classical mechanics* [520]ISBN

Chapter 8

Hydrodynamics

8.1 Foundations

8.1.1 Archimedes' principle, buoyancy

The density of a substance is the quotient between its mass and its volume,

$$\rho \equiv \frac{m}{V} \ . \tag{8.1}$$

Archimedes' principle says that

> A body immersed in a liquid undergoes the action of an upward force, whose absolute value is equal to the weight of the volume of liquid displaced by the body.

Let us consider a liquid, with density ρ, in hydrostatic equilibrium inside a container and highlight a portion of it, with volume V, as shown in Fig. 8.1(a). In order to have hydrostatic equilibrium, it is necessary that the sum over all forces acting on the highlighted volume of liquid be zero. One of these forces is the weight,

$$\mathbf{P} = m\mathbf{g} = \rho V \mathbf{g} \ , \tag{8.2}$$

of the volume V. The other force is the sum $\mathbf{E}$ over all pressure forces that the remaining liquid exerts on the surface of the volume V, Fig. 8.1(b). That is,

$$\mathbf{P} + \mathbf{E} = 0 \ . \tag{8.3}$$

Thus, the force $\mathbf{E}$ which 'pushes' the highlighted portion of liquid, has a magnitude equal to its weight, $E = P = \rho V g$, and is called *buoyancy*.

In case that the highlighted volume V is filled with another body with density ρ' different from that of the liquid ρ, the buoyancy will not change. That is, the buoyancy E will always be the weight of the liquid of density ρ displaced by the body of density ρ' that has been introduced in its interior.

On the other hand, the new weight of the volume is $P' = \rho' m V$. In the case $\rho > \rho'$, the body submerged in the liquid will rise to the surface, since the buoyancy exerted by the liquid will be greater than the weight of the body. Otherwise, when $\rho < \rho'$, the submerged body will sink to the bottom of the container. In both cases, the submerged body will not stay in hydrostatic equilibrium. Resolve the Exc. 8.1.2.1.

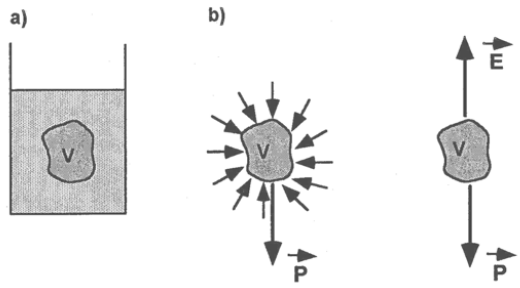

Figure 8.1: Representation of the forces acting on a body submerged in a liquid.

8.1.2 Exercises

8.1.2.1 Ex: Critical buoyancy and Cartesian diver

A balloon is filled at atmospheric pressure with 1 liter of air. An aluminum weight of 1 kg is attached to it. The whole setup is now immersed into water. Calculate the total force acting on the setup as function of the depth of immersion.

Solution: *The buoyancy of the balloon is given by,*

$$B_{bal} = g\rho_{wat}V_{bal} \ ,$$

where the volume of the balloon adjusts to the water pressure at a given depth,

$$pV_{bal} = Nk_BT \ .$$

Assuming a constant water temperature, we find,

$$V_{bal}(z) = \frac{p(0)}{p(z)}V_{bal}(0) \ ,$$

where the underwater pressure is,

$$p(z) = g\rho_{wat}z + p(0) \ .$$

The buoyancy of the aluminum weight is given by,

$$B_{wei} = g\rho_{wat}V_{Al} = m_{wei}g\frac{\rho_{wat}}{\rho_{Al}} \ .$$

It is independent on the depth, because aluminium is incompressible. The total force is now,

$$\begin{aligned} F = B_{bal} + B_{wei} - m_{wei}g &= \frac{g\rho_{wat}}{g\rho_{wat}z + p(0)}p(0)V_{bal}(0) + m_{wei}g\frac{\rho_{wat}}{\rho_{Al}} - m_{wei}g \\ &\simeq \frac{p(0)V_{bal}(0)}{z} - m_{wei}g\left(1 - \frac{\rho_{wat}}{\rho_{Al}}\right) \ , \end{aligned}$$

neglecting the atmospheric pressure $p(0)$. The force balances at $F = 0$ that is

$$z_0 \simeq \frac{p(0)V_{bal}(0)}{m_{wei}g\left(1 - \frac{\rho_{wat}}{\rho_{Al}}\right)} \simeq \frac{p(0)V_{bal}(0)}{m_{wei}g} \ ,$$

neglecting the buoyancy of the weight. Hence,

$$F \simeq p(0)V_{bal}(0)\left(\frac{1}{z} - \frac{1}{z_0}\right) \ .$$

That for z above the critical depth $z_0 \approx 10$ m, the force is directed upward. Else downward.

8.1.2.2 Ex: Buoyancy of a a wooden ball in a liquid

A wooden ball of density m is trapped at depth h in a liquid of density density ρ. Releasing the ball from its position, determine how high above the surface it will float.

Solution:

8.1.2.3 Ex: Buoyancy of oil

Three containers with false bottoms (see figure) were placed in water at the same depth. Filling into the three bottles the same amount of oil, which one of the three bottoms will fall first? Justify!

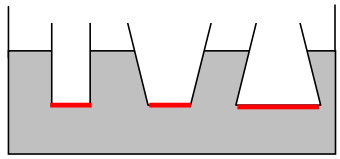

Figure 8.2: Buoyancy of oil.

Solution:

8.1.2.4 Ex: A tank

A lidless rectangular tank, with the dimensions given in the figure, moves with an acceleration a and contains water up to a height of h (when $a = 0$). At what value of the acceleration will the water begin to flow out?

Solution:

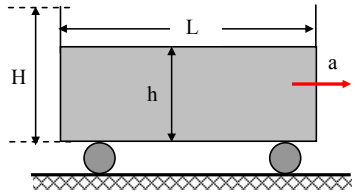

Figure 8.3: Scheme of the tank.

8.1.2.5 Ex: Buoyancy in mercury and water

A cube of a certain material floats in a container containing mercury ($\rho_{Hg} = 13.6\,\mathrm{g/cm^3}$) such that 1/4 of its volume is submerged. Adding enough water to the system to cover the cube ($\rho_{water} = l\,\mathrm{g/cm^3}$), what fraction of its volume will still remain immersed in mercury?

Solution:

8.1.2.6 Ex: Immersion

A board of length L leans on a stone and is partially immersed in water. As the figure shows, a portion of length a is above the support point. Being d is the density of the wood, what portion of the board is submerged?

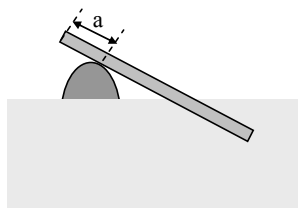

Figure 8.4: Immersion of a stone.

Solution:

8.1.2.7 Ex: Conical container

Milk is placed in a conical container. Over time, occurs at the top the formation of cream, which is less dense. During this process there is no change in volume, that is, h remains constant (see figure). What happens to the pressure at the bottom of the container? Justify your answer.

Solution:

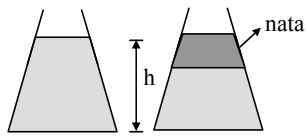

Figure 8.5: Conical container.

8.1.2.8 Ex: Cylindrical can

a. Into a cylindrical can of area A water is poured up to a height of h. Determine the velocity v at which water flows out of a hole of area A located at the bottom. How much water should be added to the can per unit of time such that v is constant?
b. In case that no water is added to the can and the height varies, calculate the flow rate θ as a function of time.

Solution:

8.1.2.9 Ex: Siphon

Via a siphon, water is removed from a container, as shown in the figure. The area of the pipe is constant along its length and the velocity of the surface of the liquid is neglected.
a. What is the water speed at the outlet of the pipe?
b. What is the pressure at the highest point of the siphon?
c. What is the maximum height h at which it is still possible to siphon water?

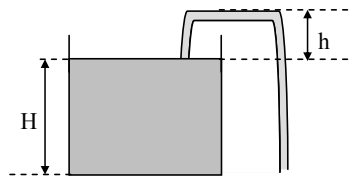

Figure 8.6: Siphon.

Solution:

8.1.2.10 Ex: Water tank

A water tank is mounted on a wagon that can move horizontally without friction (see figure). In the wall of the box there is a hole of area A at a depth H, through which water flows parallel to the horizontal plane. The initial total mass of the system (box, water and wagon) is M_0 and the speed of the water surface is neglected. If the wagon is initially at rest when the hole is opened, what will be the initial acceleration of the

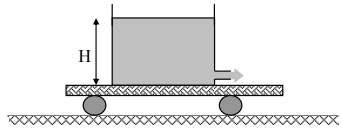

Figure 8.7: Water tank.

system?

Solution:

8.1.2.11 Ex: Water pipe

A water pipe rotates at a speed ω around a vertical axis, as shown in the figure. Calculate the pressure as a function of r, using $P(r = 0) = P_0$.

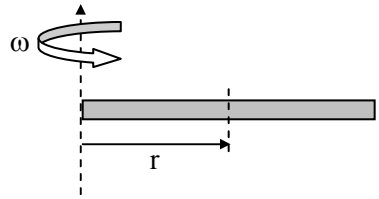

Figure 8.8: Water pipe.

Solution:

8.1.2.12 Ex: Flow meter

A flow meter consists of a conical, vertical glass tube with a metallic sphere of mass m and radius r inside it, as shown in the figure. Calculate the flow of a gas with a given viscosity as a function of the height h. Consider, very small. **Note:** $F_{Stokes} = 6\pi\eta rv$.

Solution:

8.2 Continuity and Navier-Stokes equations

8.3 Further reading

J. Pedlosky (1992), *Geophysical Fluid Dynamics* [1006]ISBN

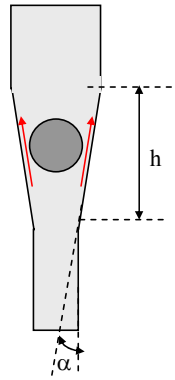

Figure 8.9: Flow meter.

Chapter 9

Thermodynamics and kinetic gas theory

Thermodynamics is a central branch of modern science, and its general laws govern the physical and chemical processes which occur in our world. An important early application of thermodynamics dealt with steam engines (heat engines) in which heat is converted to mechanical energy. Classical thermodynamics was developed in the nineteenth and in the beginning of the twentieth century by Watt, Carnot, Clausius, Joule, von Helmholtz, Lord Kelvin, Nernst, Boltzmann and Gibbs. The so-called First, Second and Third Laws of Thermodynamics were discovered during this period. They set general limits for the conversion of one form of energy, for example heat or chemical energy, to another one, for example mechanical work. One phase in the development of thermodynamics ended with the formulation of statistical thermodynamics by Boltzmann and Gibbs. Statistical thermodynamics is based on the fact that what we experience as heat is actually an outward manifestation of molecular and atomic motion.

Classical thermodynamics has played a dominant role in the development of modern science and technology. In suffers, however, from certain limitations, as it cannot be used for the study of irreversible processes but only for reversible processes and transitions between different states of equilibrium. Many of the most important and interesting processes in nature are irreversible. A good example is provided by living organisms which consume chemical energy in the form of nutrients, perform work and excrete waste as well as give off heat to the surroundings without themselves undergoing changes; they represent what is called a stationary or steady state. The boiling of an egg provides another example, and still another one is, a thermocouple with a cold and a hot junction connected to an electrical measuring instrument.

The first investigator who developed a method for the exact treatment of such problems, for example of the thermocouple, was Onsager. His approach was, however based on assumptions which in principle make it applicable only to systems close to equilibrium. The contribution of Prigogine to thermodynamic theory is his successful extension of it to systems which are far from thermodynamic equilibrium. This is extremely interesting as large differences compared to conditions close to equilibrium had to be expected. Prigogine has demonstrated that a new form of ordered structures can exist under such conditions, and he has given them the name dissipative structures to stress that they only exist in conjunction with their environment.

In the present chapter we will first deal with equilibrium thermodynamics, as well

in the classical as in the quantum regime.

9.1 Equilibrium thermodynamics

9.1.1 Probabilities

Excs. 9.1.5.1 to 9.1.5.8.

9.1.2 Thermal motion

9.1.3 Temperature and Maxwell-Boltzmann distribution

9.1.3.1 Temperature and heat

9.1.3.2 Temperature measurement

Scales of *Celsius*, *Fahrenheit*, and *Kelvin*.

9.1.4 Heat capacity

Heat capacity

9.1.5 Exercises

9.1.5.1 Ex: Probabilities

In a game, 5 ideal dice are rolled.
a. What is the probability that exactly two of these dice show the number one?
b. What is the probability that at least one die shows the number one?

Solution: *a. The probability that exactly two of these dice show the number one is,*

$$P = \binom{5}{2} \frac{1}{6}^2 \left(1 - \frac{1}{6}\right)^{5-2} = \frac{625}{3888} \approx 16\% \ .$$

b. The probability that at least one die shows the number one is,

$$P = 1 - \binom{5}{0} \frac{1}{6}^0 \left(1 - \frac{1}{6}\right)^{5-0} = \frac{4651}{7776} \approx 60\% \ .$$

9.1.5.2 Ex: Probabilities

With what probability have out of
a. 1000 random numbers between 1 and 100 exactly five the value 50;
b. 100 two people on birthday January 1st.

Solution: *a. From the Poisson distribution:*

$$P = \frac{10^n}{n!} e^{-\alpha} = \frac{10^5}{5!} e^{-1000/100} \simeq 0.0378 \ .$$

b. Similarly,

$$P = \frac{10^n}{n!} e^{-\alpha} = \frac{10^2}{2!} e^{-100/365} \simeq 0.0285 \ .$$

9.1.5.3 Ex: Probabilities

What is the probability that you inhale at least one molecule that Julius Caesar exhaled during his last breath (Tu quoque, Brute, fili mi!)? Assume a breathing volume of 3 liters and an atmosphere height of approximately 10 km. Assume the density of the atmosphere is approximately homogeneous.

Solution: *The number of molecules per liter is approximately,*

$$N_L = \frac{pV}{k_B T} \simeq \frac{1013\,\mathrm{hPa} \cdot 10^{-3}\,\mathrm{m}^3}{k_B \cdot 300\,\mathrm{K}} = 2.44 \cdot 10^{22} \ .$$

The number of molecules in the atmosphere is about $N = N_L \cdot V_A/(1\ liter)$, where $V_A \simeq 4\pi R_E^2 h \simeq 1.4 \cdot 10^{44}\,\mathrm{m}^3$. The number of molecules per breath is $A \simeq 8 \cdot 10^{22}$. The probability that no molecule can be found is,

$$P \simeq (1-p)^A = e^{(A \log(1-p))} \simeq e^{(-Ap)} = 1.4 \cdot 10^{-22} \ ,$$

where $p = A/N$ is the probability to find one of Caesar's molecules. Alternatively, the Poisson distribution with $\alpha = A^2/N$ and $n = 0$, $P = e^{-A\ p}$ gives the same result. That means we share each of our breaths with Caesar!

9.1.5.4 Ex: Idiots roulette

A Bavarian, a Swabian and an East Frisian play Russian roulette together, each according to their own rules. The Bavarian inserts two cartridges into the drum of a six-shot revolver, sets the drum in a rapid rotation, aims at his own head and pulls the trigger once. The Swabian puts a cartridge in the revolver and pulls the trigger twice, the East Frisian puts a cartridge in the revolver, pulls the trigger once, turns the drum a second time and pulls the trigger again. What is the chance of survival of the three crazy people?

Solution: *The chance of survival for the Bavarian is $P = \frac{2}{3} = 66\%$, for the Swabian $P = \frac{1}{6} \cdot \frac{1}{6}$, and for the East Frisian $P = \frac{5}{6} \cdot \frac{5}{6} = 69\%$.*

9.1.5.5 Ex: Idiots roulette

A student writes a multiple choice test in physics. It consists of 18 tasks. For each task, only one of the four proposed solutions is correct. Since he does not understand much about the topic, he trusts his luck and checks the possible solutions by chance. What is the probability that the student meets the minimum requirement of 8 correct answers?

Solution: *The probability is,*

$$P = 1 - \sum_{k=0}^{7} \binom{18}{k} \left(\frac{1}{4}\right)^k \left(\frac{3}{4}\right)^{18-k} = 0.057 \ .$$

9.1.5.6 Ex: Probabilities

A slot machine consists of three concentric rings. Each ring is evenly divided into 10 sections and the sections in each ring are continuously labeled with "a" to "j". By pressing the start button, the three rings start to rotate independently. If the luck button is pressed, the rings brake independently of one another and three letters appear side by side in the viewing window. With three ones you win, with two ones there is a free spin.
a. Calculate the probability for one free spin per game.
b. What is the probability of getting exactly 3 free spins in 10 games?
c. What is the probability of winning at least once in 10 games?

Solution: *a. The probability for one "a" is* $p_1 = 0.1$. *The probability to make exactly* m *"a" per game* $W_{3,m} = \binom{3}{m} p_1^k (1-p_1)^{N-k}$. *So the probability for a free spin is,*

$$P_{3,2} = \binom{3}{2} \cdot 0.1^2 \cdot 0.9^1 = 2.7\% \ .$$

b. The probability to find in N *games* k *times exactly two "a" is* $P_{N,k} = \binom{N}{k} W_{3,2}^k (1 - W_{3,2})^{N-k}$. *The probability of getting exactly three free spins in 10 games is thus,*

$$P_{N,k} = \binom{10}{3} 0.027^3 \cdot 0.973^7 = 0.2\% \ .$$

c. The probability for three "a" is $p_3 = 0.1^3 = 0.001$. *So the probability to get in* N *games exactly* k *times this result is* $P_{N,k} = \binom{N}{k} p_3^k (1-p_3)^{N-k}$. *So the probability in* 10 *tries to get* 0 *times this result is,*

$$P_{10,0} = \binom{10}{0} 0.001^0 \cdot 0.999^{10} = 0.999^{10} = 99\% \ .$$

The probability of winning at least once is finally $P_{gewinn} = 1 - P_{10,0} = 1\%$.

9.1.5.7 Ex: Binomial distribution

Two drunks stagger on the x-axis. Starting from the origin, they take a step to the right or to the left with the same probability. The steps take place synchronously, and the steps of both people are the same and constant. Determine the probability that they will meet again after N steps.

Solution: *Let us first consider one drunk. The probability for a step to the left is* $p_l = 0.5$. *If he walks exactly* $N/2$ *steps to the left, it means that he also has to walk* $N/2$ *steps to the right in order to come back. The probability of this is* $P_N(N/2) = \binom{N}{N/2} p_l^{N/2}(1-p_l)^{N-N/2}$.
For two drunks, we can sit in the inertial system of one of them. Then the distance between them either increases by two steps or stays unchanged, both with a probability of 50%. We can therefore take the above solution and replace N *with* $N/2$. *So the solution is,*

$$P_N(N/2) = \binom{2N}{N} p_l^N (1-p_l)^{2N-N} = \frac{(2N)!}{(N!)^2}\frac{1}{2^{2N}} \ .$$

The task can also be solved in the following way. The probability that the drunks change their distance is $p_2 = 0.5$. *The probability that they change their distance* k *times in* N *steps* $P_2 = \binom{N}{k} p_2^k (1-p_2)^{N-k}$. *For each of the routes contained in* P_2 *there are again as many routes back to the original distance of the drunk. The overall probability is* $P_2 \cdot P_2$. *Now, we just have to add up all* k *and get the alternative solution,*

$$P = \frac{1}{2^{2N}} \sum_{k=0}^{N} \binom{N}{k}^2 \ .$$

It turns out that this is identical to the above one, but what remains to be shown!

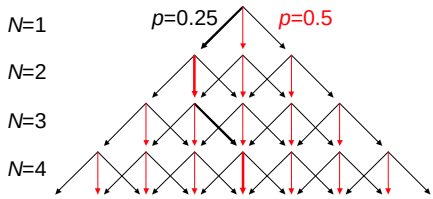

Figure 9.1: Generation of a binomial distribution.

9.1.5.8 Ex: Quantum statistics

n particles are distributed to $N > n$ different cells with the same probability. Calculate the probability:
a. that there is exactly one particle in the first n cells;
b. that there is no cell with more than one particle.
Use the three different assumptions that:
i. the particles are identifiable and arbitrarily many particles can be assigned to each

cell;
ii. the particles are NOT identifiable and arbitrarily many particles can be assigned to each cell;
iii. the particles are NOT identifiable and only a single particle may be assigned to each cell.

Solution: *Be $C(N,n) = N!/(n!(N-n)!)$ the number of different combinations to choose n elements from N, regardless of the order. There are N^n possible cases:*

$$i.\ p_b = \frac{n!}{N^n} \quad , \quad p_a = C(N,n)p_b = \frac{N!}{(N^n(N-n)!)}$$

$$ii.\ p_b = \frac{n!(N-1)!}{(N+n-1)!} \quad , \quad p_a = C(N,n)p_b = \frac{N!(N-1)!}{((N-n)!(N+n-1)!)}$$

$$iii.\ p_a = 1 \quad , \quad p_b = \frac{p_a}{C(N,n)} = \frac{n!(N-n)!}{N!} \ .$$

9.1.5.9 Ex: Velocity distribution

The Maxwellian velocity distribution or Boltzmann distribution of a one-dimensional ideal gas of identical particles of mass m at temperature T is,

$$f(v)dv = \sqrt{\frac{m}{2\pi k_B T}} e^{-mv^2/2k_B T} dv \ .$$

This gives the average kinetic energy for each molecule of $\langle E_{kin} \rangle = \frac{1}{2} k_B T$. According to the equipartition theorem, Maxwell's velocity distribution of a three-dimensional gas is given by $f(v_x)dv_x\ f(v_y)dv_y\ f(v_z)dv_z$.
a. Write down the velocity distribution explicitly and determine the average kinetic energy of a molecule in the three-dimensional gas at temperature T.
Determine the average absolute velocity $\langle v \rangle = \langle |\mathbf{v}| \rangle$ and compare $\langle v \rangle^2$ with $\langle v^2 \rangle$ for the three-dimensional case.
c. What is the number of particles $F(v)dv$ with an absolute velocity $v = |\mathbf{v}|$ in the range v and $v + dv$.
d. Consider a gas made of rubidium atoms ($m = 87 \cdot 1.67 \cdot 10^{-27}\,\mathrm{kg}$) and sketch $F(v)$ for temperatures between 100 K and 300 K.
e. Consider the rubidium gas at room temperature ($T = 300\,\mathrm{K}$). What is the proportion of molecules whose average velocity $\langle v \rangle$ is greater than 1000 m/s?

Solution: *a. The explicit form of the velocity distribution is,*

$$f(v_x)dv_x\ f(v_y)dv_y\ f(v_z)dv_z = \sqrt{\frac{m}{2\pi k_B T}}^3 e^{-m\mathbf{v}^2/2k_B T} d^3\mathbf{v} \ .$$

The mean kinetic energy is,

$$\begin{aligned}
\langle E_3\rangle(|\mathbf{v}|) &= \frac{m}{2}\left\langle \mathbf{v}^2\right\rangle = \int_{-\infty}^{\infty}\frac{m}{2}\mathbf{v}^2 f_3(\mathbf{v})d^3\mathbf{v} \\
&= \int\int\int_{-\infty}^{\infty}\frac{m}{2}\left(v_x^2+v_y^2+v_z^2\right)\left(\frac{m}{2\pi k_BT}\right)^{3/2}\exp\left(-m\frac{v_x^2+v_y^2+v_z^2}{2k_BT}\right)dv_xdv_ydv_z \\
&= \int_0^{2\pi}\int_0^{\pi}\int_0^{\infty}\frac{m}{2}v_r^2\left(\frac{m}{2\pi k_BT}\right)^{3/2}\exp\left(-\frac{mv_r^2}{2k_BT}\right)v_r^2\sin\theta dv_rdv_\theta dv_\phi \\
&= 4\pi\frac{m}{2}\left(\frac{m}{2\pi k_BT}\right)^{3/2}\int_0^{\infty}v_r^4\exp\left(-\frac{mv_r^2}{2k_BT}\right)v_r^2dv_r \\
&= \textit{...(part. integration, surface terms drop out)} \\
&= 4\pi\frac{m}{2}\left(\frac{m}{2\pi k_BT}\right)^{3/2}\frac{3}{8}\sqrt{\pi}\left(\frac{m}{2k_BT}\right)^{-5/2} = \frac{3}{2}k_BT\ .
\end{aligned}$$

Here, one uses,

$$\int_{-\infty}^{\infty}x^ne^{-x^2}dx = \Gamma\left(\tfrac{n+1}{2}\right) = \frac{n-1}{2}\Gamma\left(\tfrac{n-1}{2}\right) \qquad \textit{and} \qquad \Gamma\left(\tfrac{1}{2}\right) = \sqrt{\pi}\ .$$

b. The average absolute velocity is,

$$\begin{aligned}
\langle|\mathbf{v}|\rangle &= \int_{-\infty}^{\infty}vf_3(\mathbf{v})d^3\mathbf{v} \\
&= 4\pi\left(\frac{m}{2\pi k_BT}\right)^{3/2}\int_0^{\infty}v_r\exp\left(-\frac{mv_r^2}{2k_BT}\right)v_r^2dv_r \\
&= \textit{...(part. integration, surface terms drop out)} \\
&= 4\pi\left(\frac{m}{2\pi k_BT}\right)^{3/2}\frac{1}{2}\left(\frac{m}{2k_BT}\right)^{-2} = \sqrt{\frac{8k_BT}{\pi m}}\ .
\end{aligned}$$

Hence,

$$\frac{m}{2}\langle v\rangle^2 = \frac{4}{\pi}k_BT \neq \frac{3}{2}k_BT = \frac{m}{2}\left\langle\vec{v}^2\right\rangle\ .$$

c. The number of particles with absolute velocity in the interval v and $v+dv$ is,

$$F(v)dv = 4\pi v^2 f_3(v)dv\ ,$$

where

$$f_3(v) = \left(\frac{m}{2\pi k_BT}\right)^{3/2}e^{-mv^2/2k_BT}\ .$$

It's easy to verify,

$$\begin{aligned}
\int_0^{\infty}F(v)dv &= 4\pi\left(\frac{m}{2\pi k_BT}\right)^{3/2}\int_0^{\infty}v^2e^{-mv^2/2k_BT}dv \\
&= 4\pi\left(\frac{m}{2\pi k_BT}\right)^{3/2}\left(\frac{2k_BT}{m}\right)^{3/2}\int_0^{\infty}y^2e^{-y^2}dy = 1\ .
\end{aligned}$$

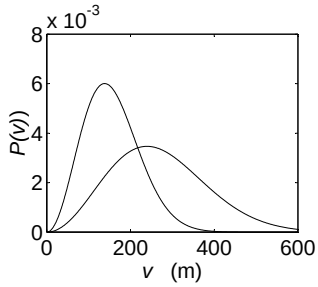

Figure 9.2: Maxwell distribution.

d. Sketch of the distribution function $4\pi v^2 f_3(v)$ *for rubidium atoms:*
e. The definite integral can be traced back by partial integration to,

$$\int_{v_0}^{\infty} F(v)dv = \frac{4}{\sqrt{\pi}} \int_{y_0}^{\infty} y^2 e^{-y^2} dy = \frac{4}{\sqrt{\pi}} \left[-\frac{1}{2} y e^{-y^2} + \frac{1}{4}\sqrt{\pi}\, erf\,(y) \right]_{y_0}^{\infty}$$
$$= 1 - erf\,(y_0) + \frac{2}{\sqrt{\pi}} y_0 e^{-y_0^2} \ .$$

$y_0 = v_0\sqrt{m/2k_BT} \approx 4.18$ *and hence* $\int_{v_0}^{\infty} F(v)dv = 1.251\ 5 \times 10^{-7}$.

9.1.5.10 Ex: Maxwell-Boltzmann distribution

Calculate the number of particles in an ideal homogeneous gas having velocities slower than $2v_{rms}$.

Solution: *With the particle distribution given by,*

$$f(\vec{v}) = \sqrt{\frac{m}{2\pi k_B T}}^3 e^{-m\vec{v}^2/2k_BT} \ ,$$

we can calculate the number of particles,

$$N = 4\pi \int_0^{2v_{rms}} f(v)v^2 dv = \frac{4\pi}{\sqrt{\pi}^3} \int_0^{2v_{rms}} \sqrt{\frac{m}{2k_BT}}^3 e^{-mv^2/2k_BT} v^2 dv = \frac{4}{\sqrt{\pi}} \int_0^{2\zeta_{rms}} e^{-\zeta^2}\zeta^2 d\zeta \ ,$$

using the substitution $\zeta \equiv v\sqrt{m/2k_BT}$. *Since* $v_{rms} = \sqrt{3k_BT/m}$, *we have* $2\zeta_{rms} = \sqrt{6}$. *Using the partial integration rule,* $\int u'v = uv - \int uv'$, *we know,*

$$\int_0^{\sqrt{6}} 1 \cdot e^{-\zeta^2} d\zeta = \zeta \cdot e^{-\zeta^2}\Big|_0^{\sqrt{6}} - \int_0^{\sqrt{6}} \zeta \cdot (-2\zeta) e^{-\zeta^2} d\zeta \ .$$

With this,

$$N = \frac{4}{\sqrt{\pi}} \frac{1}{2} \left[\int_0^{\sqrt{6}} 1 \cdot e^{-\zeta^2} d\zeta - \zeta \cdot e^{-\zeta^2}\Big|_0^{\sqrt{6}} \right] = \frac{4}{\sqrt{\pi}} \frac{1}{2} \left[\int_0^{\sqrt{6}} e^{-\zeta^2} d\zeta - \sqrt{6} e^{-6} \right] = 99.2\% \ .$$

9.1.5.11 Ex: Maxwell-Boltzmann distribution

Using the Maxwell-Boltzmann distribution $f(v)$ and the following formulas, calculate the velocities $\bar{v} \equiv \int_0^\infty v f(v) v^2 dv$ and $v_{rms} \equiv \sqrt{\overline{v^2}}$:

$$\int_0^\infty x^n e^{-x^2} dx = \tfrac{1}{2}\Gamma(\tfrac{n+1}{2}) = \begin{cases} \frac{(2k-1)!!\sqrt{\pi}}{2^{k+1}} & \text{for} \quad n = 2k \\ \frac{k!}{2} & \text{for} \quad n = 2k+1 \end{cases} .$$

Solution:

9.1.5.12 Ex: Mean velocity in a gas

The average velocity of the molecule in an ideal gas is 500 m/s. If the gas maintains the same temperature and the molecular masses are doubled, what will be the new average velocity?

Solution:

9.1.5.13 Ex: Evaporation

a. A three-dimensional homogeneous gas consisting of $N = 10^8$ rubidium atoms (mass $m = 87 \cdot u$) has the temperature $T = 100\,\mu$K. How many atoms are faster on average than $v_1 = 10$ cm/s?
b. Now suppose that all atoms with a velocity $v > v_1$ were suddenly removed. After some time, a new thermal equilibrium is established due to collisions. What is the temperature of the gas now?

Help: Formula for partial integration: $\int y^n e^{-y^2} dy = -\frac{y^{n-1}}{2} e^{-y^2} + \frac{n-1}{2} \int y^{n-2} e^{-y^2} dy$
You can take the value of the error function given by $\text{erf}\,(y_1) \equiv \frac{1}{\sqrt{\pi}} \int_{y_1}^\infty e^{-y^2} dy$ from the sketched curve.

Solution: ***A factor 4 is wrong here, which stems from an originally incorrect normalization of the error function.***
a. The number of particles with absolute velocity $v > v_1 = 10$ cm/s is,

$$N_1 = N \int_{v>v_1} f_3(v) d^3\vec{v} = N \int_0^{2\pi} \int_0^\pi \int_{v_1}^\infty \left(\frac{m}{2\pi k_B T}\right)^{3/2} e^{-mv^2/2k_BT} v^2 \sin\theta dv dv_\theta dv_\phi$$
$$= N 4\pi \left(\frac{m}{2\pi k_B T}\right)^{3/2} \left(\frac{2k_BT}{m}\right)^{3/2} \int_{y_1}^\infty y^2 e^{-y^2} dy ,$$

with $y_1 \equiv v_1\sqrt{m/2k_BT} = 0.10\sqrt{\frac{87\cdot 1.67\cdot 10^{-27}}{2\cdot 1.38\cdot 10^{-23}\cdot 100\cdot 10^{-6}}} \simeq 0.72$. The definite integral can be traced back by partial integration with the definition of the error function (surface

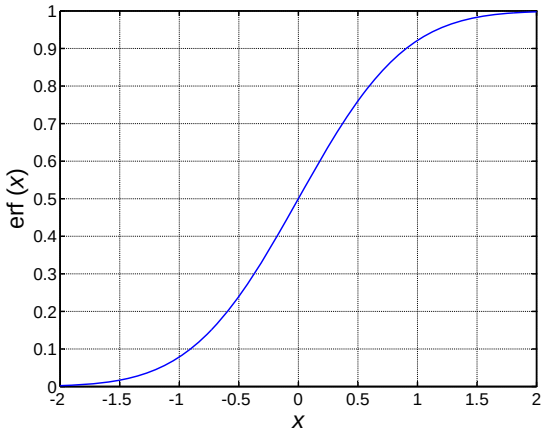

Figure 9.3:

terms are eliminated) to,

$$N_1 = \frac{4N}{\sqrt{\pi}}\int_{y_1}^{\infty} y^2 e^{-y^2} dy = \frac{4N}{\sqrt{\pi}}\left[-\frac{y}{2}e^{-y^2} + \frac{\sqrt{\pi}}{4}\,\mathrm{erf}\,(y)\right]_{y_1}^{\infty}$$
$$= N\left[1 - \mathrm{erf}(y_1) + \frac{2}{\sqrt{\pi}} y_1 e^{-y_1^2}\right] = N\left[1 - \mathrm{erf}(0.72) + \frac{2}{\sqrt{\pi}} 0.72 e^{-0.72^2}\right] \simeq 0.79N \ .$$

b. The total energy is, immediately after removing the fast particles,

$$E = N_1 \int_{v<v_1}^{\infty} \frac{m}{2}\vec{v}^2 f_3(\vec{v}) d^3\vec{v} = N_1 \int_0^{2\pi}\int_0^{\pi}\int_0^{\infty} \frac{m}{2} v^2 \left(\frac{m}{2\pi k_B T}\right)^{3/2} e^{-mv^2/2k_B T} v^2 \sin\theta dv_r dv_\theta dv_\phi$$
$$= N_1 4\pi \frac{m}{2}\left(\frac{m}{2\pi k_B T}\right)^{3/2}\left(\frac{2k_B T}{m}\right)^{5/2}\int_{y_1}^{\infty} y^4 e^{-y^2} dy \ .$$

The definite integral can be traced back by partial integration (surface terms are eliminated) to,

$$E = \frac{4N_1 k_B T}{\sqrt{\pi}}\int_{y_1}^{\infty} y^4 e^{-y^2} dy = \frac{4N_1 k_B T}{\sqrt{\pi}}\left[-\frac{y^3}{2}e^{-y^2}\Big|_{y_1}^{\infty} + \frac{3}{2}\int_{y_1}^{\infty} y^2 e^{-y^2} dy\right]$$
$$= \frac{4N_1 k_B T}{\sqrt{\pi}}\left[\frac{y_1^3}{2}e^{-y_1^2} + \frac{3}{2}\frac{\sqrt{\pi}N_1}{4N}\right] = \frac{4N_1 k_B T}{\sqrt{\pi}}\frac{y_1^3}{2}e^{-y_1^2} + \frac{3N_1^2 k_B T}{2N} \ .$$

After thermalization the kinetic energy is $E_1 = \frac{3N_1}{2}k_B T_1 \equiv E = \frac{4N_1 k_B T}{\sqrt{\pi}}\frac{y_1^3}{2}e^{-y_1^2} + \frac{3N_1^2 k_B T}{2N}$. *From this follows,*

$$T_1 = T\left[\frac{4}{\sqrt{\pi}}\frac{y_1^3}{3}e^{-y_1^2} + \frac{N_1}{N}\right] = T\left[\frac{4}{\sqrt{\pi}}\frac{0.72^3}{3}e^{-0.72^2} + 0.79\right] \simeq 0.96T \ .$$

9.1.5.14 Ex: Trapped gases

The density distribution of a rubidium gas in a three-dimensional harmonic potential can be expressed by,

$$n(\mathbf{r})d^3r = n_0 e^{-U(\mathbf{r})/k_BT} d^3r \ ,$$

where $U(\mathbf{r}) = \frac{m}{2}\omega^2 r^2$. Numerical values: $m = 87 \cdot 1.67 \cdot 10^{-27}$ kg and $\omega = 2\pi \cdot 50$ Hz.
a. Determine the expansion of the gas ($1/e$ width of the distribution) at a given temperature $T = 100$ μK.
b. Determine the maximum density n_0 of the gas when $N = \int n(\mathbf{r})d^3r = 10^8$ is the total number of atoms.
c. The effective volume is defined by $V_{eff} = N/n_0$. How many atoms are in the effective volume?

Solution: *a. The expansion $\bar{r}$ follows with,*

$$\frac{1}{e} = \frac{n(\bar{r})}{n_0} = e^{-m\omega^2\bar{r}^2/2k_BT} \ .$$

With the numerical values $\bar{r} = \sqrt{\frac{2k_BT}{m\omega^2}} = 440$ μm.
b. The maximum density n_0 results from,

$$N = n_0 \int e^{-r^2/\bar{r}^2} d^3r = n_0 \left(\bar{r}\int e^{-x^2}dx\right)^3 = n_0\pi^{3/2}\bar{r}^3 \ .$$

With the numerical values follows $n_0 = \frac{N}{\pi^{3/2}\bar{r}^3} = 2.1 \times 10^{11}$ cm^{-3}.
c. The effective volume is,

$$V_{eff} = \frac{N}{n_0} = \pi^{3/2}\bar{r}^3 \equiv \frac{4\pi}{3}\tilde{r}^3$$
$$\tilde{r} = \bar{r}\sqrt{\pi}\left(\frac{3}{4\pi}\right)^{1/3} \ .$$

So the number of particles is,

$$\begin{aligned} N_{eff} &= \int_{V_{eff}} n(r)d^3r = 4\pi\int_{\tilde{r}} n(r)r^2dr = 4\pi n_0 \int_{\tilde{r}} r^2 e^{-r^2/\bar{r}^2}dr \\ &= 4\pi n_0\left(-\frac{1}{2}\bar{r}^2\tilde{r}e^{-\frac{\tilde{r}^2}{\bar{r}^2}} + \frac{1}{4}\bar{r}^2\bar{r}\sqrt{\pi}\,\mathrm{erf}\left(\frac{\tilde{r}}{\bar{r}}\right)\right) \\ &= N\left(\mathrm{erf}\left(\sqrt{\pi}\left(\frac{3}{4\pi}\right)^{1/3}\right) - \left(\frac{2}{\pi}\right)^{1/3} e^{-\pi\left(\frac{3}{4\pi}\right)^{2/3}}\right) \ . \end{aligned}$$

With the numerical values follows $N = 6.2 \times 10^7$.

9.1.5.15 Ex: Trapped gases

Calculate the internal energy and heat capacity of an ideal gas stored in a harmonic trap and compare the result with a free gas.

Solution: *The normalization condition requires,*

$$\begin{aligned}
1 &= \int\int e^{-\beta\varepsilon-\beta U} d^3\mathbf{k} d^3\mathbf{r} \\
&= \left(\frac{m}{2\pi\hbar}\right)^3 \int\int e^{-\beta\frac{m}{2}v^2-\beta\frac{m}{2}\omega^2 r^2} d^3\mathbf{v} d^3\mathbf{r} \\
&= \left(\frac{m}{2\pi\hbar}\right)^3 \left(\int e^{-\beta\frac{m}{2}v^2} dv \int e^{-\beta\frac{m}{2}\omega^2 r^2} dr\right)^3 \\
&= \left(\frac{m}{2\pi\hbar}\right)^3 \left(\frac{2\pi}{\beta m}\right)^{3/2} \left(\frac{2\pi}{\beta m\omega^2}\right)^{3/2} = \left(\frac{k_B T}{\hbar\omega}\right)^3 .
\end{aligned}$$

The energy is,

$$\begin{aligned}
E(T) &= N\int\int \varepsilon e^{-\beta\varepsilon-\beta U} d^3\mathbf{k} d^3\mathbf{r} \\
&= N\left(\frac{m}{2\pi\hbar}\right)^3 \int\int \frac{m}{2}v^2 e^{-\beta\frac{m}{2}v^2-\beta\frac{m}{2}\omega^2 r^2} d^3\mathbf{v} d^3\mathbf{r} \\
&= N\left(\frac{m}{2\pi\hbar}\right)^3 \int \frac{m}{2}v^2 e^{-\beta\frac{m}{2}v^2} 4\pi v^2 dv \times \left(\int e^{-\beta\frac{m}{2}\omega^2 r^2} dr\right)^3 \\
&= N\left(\frac{m}{2\pi\hbar}\right)^3 4\pi\frac{m}{2}\left(\frac{2}{\beta m}\right)^{5/2} \int u^4 e^{-u^2} du \times \left(\frac{2}{\beta m\omega^2}\right)^{3/2} \left(\int e^{-x^2} dx\right)^3 \\
&= N\left(\frac{m}{2\pi\hbar}\right)^3 4\pi\frac{m}{2}\left(\frac{2}{\beta m}\right)^{5/2} \frac{3}{8}\sqrt{\pi} \times \left(\frac{2}{\beta m\omega^2}\right)^{3/2} \sqrt{\pi}^3 \\
&= \frac{3}{2}Nk_B T\left(\frac{k_B T}{\hbar\omega}\right)^3 = \frac{3}{2}Nk_B T .
\end{aligned}$$

9.1.5.16 Ex: Trapped gases

An ultracold gas made of 10^8 rubidium atoms (mass number 87) is trapped in a three-dimensional potential of the form $U(r) = \frac{m}{2}\omega^2 r^2$ with the oscillation frequencies $\omega/2\pi = 100$ Hz.
a. Assume the spatial distribution function for the atoms to be $n(\mathbf{r}) = n_0 e^{-U(r)/k_B T}$. What is its width at $1/\sqrt{e}$ of the maximum height? How does the width of the distribution function change when the number of atoms is doubled?
b. The trap potential is suddenly switched off. The atoms are robbed of their potential energy, while their kinetic energy leads to the ballistic expansion of the cloud. 20 ms after switching off the trapping potential, a $1/\sqrt{e}$ width of $\bar{r}_a = 0.2$ mm is experimentally measured for the distribution of the expanded atomic cloud. What was the temperature of the atomic cloud in the trap?
Help: Assume that the final size of the atomic cloud is much larger than the size of the trap. Neglect collisions between the atoms.

Solution: *a. The distribution of the atoms in the potential* $U(r) = \frac{m}{2}\omega^2 r^2$ *is,*

$$n(\mathbf{r})d^3r = n_0 e^{-U(r)/k_B T} d^3\mathbf{r} \ .$$

Normalization requires $N = \int n_0 e^{-U(r)/k_B T} d^3r$. *Hence,*

$$n_0 = \frac{N}{\int e^{-U(r)/k_B T} d^3r} = \left(\frac{m\omega^2}{2k_B T}\right)^{3/2} \ .$$

The $1/\sqrt{e}$ *width of the distribution follows from* $n_0/\sqrt{e} = n_0 e^{-U(\bar{r})/k_B T}$ *and reads,*

$$\bar{r} = \sqrt{\frac{k_B T}{m\omega^2}} \ .$$

Obviously, the latitude is independent of the number of atoms.
b. The total energy of the atoms is,

$$E = E_{kin} + E_{pot} = \frac{m}{2}\langle v^2\rangle + \frac{m}{2}\omega^2\langle r^2\rangle \ .$$

After switching off the trap,

$$E = \frac{m}{2}\langle v^2\rangle = \frac{3m}{2}\langle v_x^2\rangle = \frac{3k_B T}{2} \ .$$

After $t = 20$ *ms time-of-flight,*

$$\bar{v}_x = \sqrt{\langle v_x^2\rangle} = \sqrt{\frac{k_B T}{m}} = \frac{\bar{r}_a}{t} \ .$$

Hence,

$$T = \frac{m\bar{r}_a^2}{k_B T^2} \approx 1.05 \ \mu K \ .$$

9.1.5.17 Ex: Heat capacities

The specific heat capacity of air is $c_V = 715\,\mathrm{J\ kg^{-1}\ K^{-1}}$. What is the molar heat capacity? (Air has the relative molecular mass $\mu \approx 29$ and the mass of the H atom is $m_H = 1.67 \cdot 10^{-27}\,\mathrm{kg}$. How many air molecules are there in one kilogram of air?

Solution: *We calculate,*

$$C_V = \frac{\mu c_V}{1000} = 20.735 \ ,$$

and

$$N = N_A \frac{1000}{29} = 6 \cdot 10^{23} \cdot \frac{1000}{29} \ ,$$

or

$$N = \frac{1}{\mu m_H} = 2.06 \cdot 10^{25} \ .$$

9.2 The ideal gas

9.2.1 Equation of state for an ideal gas

The most famous equation of state is based on observations of *Boyle*, *Mariotte* and *Gay-Lussac*:

$$\boxed{pV = Nk_BT} \,. \tag{9.1}$$

9.2.2 Applications of the ideal gas law

The gas thermometer and the barometric formula are examples of the numerous applications of the ideal gas law (see Excs. 9.2.5.1 and 9.2.5.2).

9.2.2.1 The barometric formula

Excs. 9.2.5.3 and 9.2.5.4.

9.2.3 The vacuum

Vacuum pumps

9.2.4 Pressure measurement

9.2.5 Exercises

9.2.5.1 Ex: Gas thermometer

A gas thermometer filled with an ideal gas and working at a constant volume is calibrated on the one hand in dry ice (carbon dioxide in its solid state at a temperature of -80.0° C) and on the other hand in boiling alcohol (78.0° C). At these respective temperatures, the pressure in the gas thermometer is 0.900 bar or 1.635 bar. At absolute zero, the gas in the thermometer is still gaseous, but the pressure has dropped to 0.000 bar.
a. At what $^\circ$ C is the absolute zero?
b. What is the pressure at the freezing point of water and what is it at the boiling point?

Solution: *a. From the ideal gas formula we have,*

$$\begin{aligned} \frac{V}{V_0} &= \frac{T}{T_0}\frac{p_0}{p} \\ \Rightarrow \frac{p_0}{T_0} &= \frac{\Delta p}{\Delta T} = \frac{1.635\,\text{bar} - 0.9\,\text{bar}}{78^\circ\,\text{C} - (-80^\circ\,\text{C})} \approx 4.652 \cdot 10^{-3}\frac{\text{bar}}{^\circ\,\text{C}} \,. \end{aligned}$$

In order to lower the pressure by another 0.9 bar at $T = -80\,$C, the temperature has to be reduced further by $\Delta T = \frac{0.9\ bar}{4.652 \cdot 10^{-3}\frac{\text{bar}}{\text{C}}} = 193.47\ C$. The absolute zero point is therefore at $T = -80^\circ C - 193.47^\circ\,\text{C} = -273.47^\circ\,\text{C} \equiv 0\,\text{K}$.

b. We have,

$$p(0^\circ\,\mathrm{C}) = p(273.47\,\mathrm{K}) = 4.652 \cdot 10^{-3}\frac{\mathrm{bar}}{K} \cdot 273.47\,\mathrm{K} = 1.272\,\mathrm{bar}$$
$$p(100^\circ\,\mathrm{C}) = p(373.47\,\mathrm{K}) = 4.652 \cdot 10^{-3}\frac{\mathrm{bar}}{K} \cdot 373.47\,\mathrm{K} = 1.737\,\mathrm{bar}\ .$$

9.2.5.2 Ex: Gas thermometer

A gas thermometer "a" is connected to a second gas thermometer "b", which is kept in a water bath at a constant temperature. The connecting capillary has a cross-sectional area A and is filled with mercury ($\rho = 13.5$ g/cm^3). At the same temperature T_0 in the two thermometers, the mercury level in both capillaries is the same. Now the gas in thermometer "a" is heated by ΔT. This increases the pressure p_a and thus the volume $V_a \to V_a + \Delta V$. The mercury column is displaced accordingly.
a. What is the relationship between the volume increase ΔV and the temperature increase ΔT in this setup?
b. To simplify, assume that the volumes $V_a = V_b = V_0$ and thus the particle numbers $N_a = N_b = N_0$ are the same. How much has the temperature of the gas in thermometer "a" increased if the following conditions exist in the coupled thermometer: $N_0 = 10^{22}$, $h = 5$ mm, $T_0 = 300$ K, $V_0 = 1000$ cm^3, $A = 1$ cm^2?

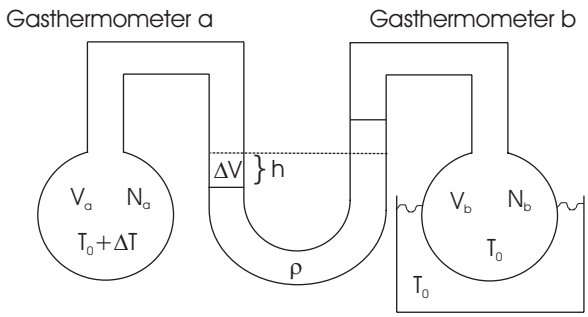

Figure 9.4: Gas thermometer.

Solution: *a. First we consider both thermometers at the same temperature and without displacement of the mercury column:* $p_a = p_b$*, the following also applies* $p_a V_a = T_0 N_a k_B$ *and* $p_b V_b = T_0 N_b k_B \Rightarrow V_a = V_b \frac{N_a}{N_b}$.
Now with increasing temperature in thermometer "a": $T_a \to T_a + \Delta T = T'_a \Rightarrow p'_a T'_a = T'_a N_a k_B \Leftrightarrow p'_a(V_a + \Delta V) = (T_0 + \Delta T) N_a k_B \Rightarrow p'_a = \frac{(T_0+\Delta T) N_a k_B}{V_a + \Delta V}$.
The following applies to thermometer "b": $p'_b(V_b - \Delta V) = T_0 N_b k_B \Rightarrow p'_b = \frac{T_0 N_b k_B}{V_b - \Delta V}$.
In equilibrium, we have, $p'_a = 2\rho g h + p'_b$ *(double height* h *of the mercury column relative to zero displacement):* $\frac{T_+ \Delta T}{V_a + \Delta V} N_a k_B = 2\rho g h + \frac{T_0 N_b k_B}{V_b - \Delta V}$.
The temperature increase will then be $\Delta T = \left(2\rho g h + \frac{T_0 N_b k_B}{V_b - \Delta V}\right) \frac{V_a + \Delta V}{N_a k_B} - T_0$.

b. For $N_a = N_b = N_0$ and $V_a = V_b = V_0$ the equation simplifies to $\Delta T = 2\rho hg\frac{V_0+\Delta V}{N_0 k_B} + \left(\frac{V_0+\Delta V}{V_0-\Delta V} - 1\right) T_0$. For the given values we get $\Delta T \approx 9.9$ K.

9.2.5.3 Ex: Barometric formula

The barometric height formula is usually derived assuming constant temperature. Now suppose that the temperature depends on the height h above the surface of the Earth according to the relationship $T = T_0/(1 + \alpha h)$.
a. Show that the pressure p then must satisfy the following differential equation,

$$\frac{dp}{dh} = -\frac{mg}{k_B T_0}(1 + \alpha h)p \ .$$

b. Find the solution to this differential equation. What is the sign of the constant α? Is the pressure at a fixed height larger or smaller than the value resulting from the height formula at a fixed temperature?

Solution: *a. The additional pressure exerted by the part of the air column within the height difference Δh onto the surface F is,*

$$\Delta p = -\frac{mgN_{\Delta h}}{F} = -\frac{mg\rho\Delta V}{\Delta V/\Delta h} = -mg\frac{N}{V}\Delta h \ .$$

For an ideal gas applies $pV = Nk_BT$. Hence,

$$\Delta p = -mg\frac{p}{\kappa_B T}\Delta h = -mg\frac{p}{\kappa_B T_0}(1 + \alpha h)\Delta h \ .$$

b. By separating the variables,

$$\begin{aligned} \frac{dp}{p} &= -\frac{mg}{k_B T_0}\,(1 + \alpha h)\,dh \\ \ln p - \ln p_0 &= -\frac{mg}{k_B T_0}\left(h + \frac{\alpha}{2}h^2\right) \\ p &= p_0 e^{-\frac{mg}{k_B T_0}\left(h+\frac{\alpha}{2}h^2\right)} \ . \end{aligned}$$

For the temperature to decrease we must have $\alpha > 0$. But then the pressure is lower than estimated with the corresponding barometric height formula at constant temperature.

9.2.5.4 Ex: Barometric formula

The air pressure p at a height h is equal to the weight $m \cdot g$ of the air column, which at this height rests on an (imaginary) horizontal base divided by the base area A of the column ($m = m(h)$: mass of the air column, neglect the curvature of the Earth and the height dependence of the temperature). Therefore, we have for the change dp of the pressure upon a small change of height dh, with the local density $\rho = \rho(h)$:

$$dp = \frac{g\ dm}{A} = \frac{g\rho dV}{A} = -g\rho dh \ . \tag{9.2}$$

Here $dV = -A\ dh$ is the change in volume of the air column (located above the base). The air should be treated approximately as a substance with a uniform molar mass M.
a. Show with the help of the ideal gas equation that Eq. (9.2) can be cast into the form $dp = -k\ \rho\ dh$ under the given conditions with the constant k. Which is the expression for k?
b. So what is the integral relationship $p = p(h)$? At what height h is the air pressure at $T = 273\,\mathrm{K}$ and $M = 29\,\mathrm{g/mol}$ only half the size of $p(0)$?
c. To what fraction is the air pressure on the Mont Blanc (4794 m) and the Mount Everest (8848 m) at $T = 273\,\mathrm{K}$ reduced compared to $p(0)$ at sea level? How big is the pressure difference Δp compared to normal zero on the Tübingen market place ($h = 341\,\mathrm{m}$)?

Solution: *a. We have $dp = -g\ \rho\ dh$. To link the density ρ with the pressure p, we use the relationship valid for the one-component system: $\rho = \frac{mass}{volume} = \frac{mass}{molar\ mass} \cdot \frac{molar\ mass}{volume} = M \cdot c$. In addition, the ideal gas equation provides a link between c and p: $p = RTc$ or $c = p/(RT)$. Using these two relationships,*

$$dp = \frac{gM}{RT} p\ dh = -k\ p\ dh \quad \Leftrightarrow \quad \frac{dp}{dh} = -k\ p\ , \tag{9.3}$$

where $k = \frac{gM}{RT}$. Since the temperature should be constant, k is constant.
b. According to Eq. (9.3) the change in pressure with the height is proportional to the pressure. So we obtain as an integral solution,

$$p = p(0)\ \exp(-k\ h) = p(0)\ \exp\left(-\frac{Mg}{RT} h\right)\ . \tag{9.4}$$

$h = 0$ denotes the height of the sea level. At the half-value $h_{1/2}$, the pressure is only half the size of $p(0)$. According to Eq. (9.3)(a): $\frac{1}{2} = exp(-k \cdot h_{1/2})$. Then $h_{1/2} = \frac{\ln 2}{k} = \ln 2 \frac{RT}{Mg}$. Inserting the specified values we find $h \approx 5500\,\mathrm{m}$. c. From Eq. (9.4),

$$\frac{p}{p(0)} = \exp\left(-\frac{\ln 2}{h_{1/2}} h\right)\ .$$

lt

Mont Blanc	4794 m	*0.55*
Mount Everest	8848 m	*0.33*
market place Tü	341 m	*0.96*

9.3 Entropy and the second law of thermodynamics

9.3.1 Kinetic theory

Following Maxwell (1859) we will now develop a microscopic theory. Let us consider a cubic box with volume V and surface A with N particles inside. The particles undergo elastic collisions, but they will not interact, as we suppose the *gas to be ideal.*

We also disregard external forces. However, we only consider the x-direction. We divide the particles into i classes of velocities v_i. The momentum transferred when a particle encounters the wall of the box is $\Delta p_{xi} = 2mv_{xi}$. The number of encounters of this wall in a time interval Δt is,

$$\frac{1}{2}\frac{N_i}{V}\ Av_{xi}\Delta t\ . \tag{9.5}$$

The total change of momentum is,

$$I = 2mv_{xi} \times \frac{1}{2}\frac{N_i}{V}\ Av_{xi}\Delta t = \frac{N_i m v_{xi}^2 A\Delta t}{V}\ . \tag{9.6}$$

The pressure is,

$$P_i = \frac{I}{A\Delta t} = \frac{N_i m v_{xi}^2}{V}\ . \tag{9.7}$$

Hence,

$$P = \sum_i P_i = \frac{m}{V}\sum_i N_i m v_{xi}^2 \equiv \frac{m}{V}\bar{v_x^2} = \frac{N}{3V}m\bar{v^2} = \frac{2}{3}N\bar{E_{kin}}\ . \tag{9.8}$$

With the ideal gas law $P = Nk_BT$. (Compare Tipler Cap. 8-1 and see Exc. 9.3.5.1).

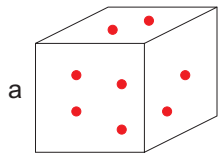

Figure 9.5: Box with N molecules.

9.3.2 Thermal expansion

9.3.3 Heat and work

9.3.4 Heat transport

9.3.5 Exercises

9.3.5.1 Ex: Kinetic pressure

A closed box with end face A and side length L is divided into two equal halves by a movable plate (see figure). Both halves contain one mole of helium under a pressure of p_0. The movable plate is now shifted to the right by the distance x. The shift takes place at constant temperature $T = 20°\text{C}$.
a. Give the volume of the right or left sub-box as a function of x. Give the pressure in the right or left sub-box as a function of x.
b. Calculate the work W that needs to be done to move the plate from $x = 0$ to $x = L/4$. Specify W in joules.

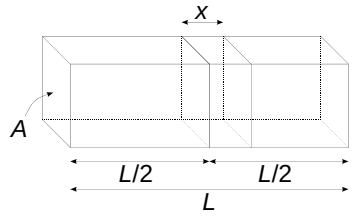

Figure 9.6: Ideal gas in a box.

Solution: *a. For the volumes holds,*

$$V_l = A\left(\frac{L}{2} + x\right) \qquad \textit{and} \qquad V_r = A\left(\frac{L}{2} - x\right) \ .$$

For the pressure we know, $pV = Nk_BT$*, where* N *and* T *are constant. So*

$$p_l = p_0\frac{V_0}{V_l} = p_0\frac{AL/2}{A\,(L/2+x)} = p_0\frac{L}{L+2x} \qquad \textit{and} \qquad V_r = p_0\frac{L}{L-2x} \ .$$

b. The gas on the left exerts the force $F_l = p_lA$ *on the plate in positive* x *direction. The gas on the right* $F_r = -p_rA$*. So the work that has to be done is,*

$$\begin{aligned} W &= -\int_0^{L/4}(F_l + F_r)dx = -A\int_0^{L/4}\left(p_0\frac{L}{L+2x} - p_0\frac{L}{L-2x}\right)dx \\ &= \frac{LAp_0}{2}\ln\frac{4}{3} \ . \end{aligned}$$

Now, we get, $W = p_0V_0\ln\frac{4}{3} = Nk_BT\ln\frac{4}{3} = 1mol{\cdot}6.022{\cdot}10^{23}\ mol^{-1}{\cdot}1.38{\cdot}10^{-23}\ J/K{\cdot}293\ K{\cdot}\ln\frac{4}{3} = 700\ J.$

9.3.5.2 Ex: Bi-metal

Two bars of different materials, with lengths, Young's modules and thermal expansion coefficients given respectively by L_1, L_2, Y_1, Y_2, α_1, and α_2, are pinched between two walls, as shown in the figure. Calculate the distance travelled by the junction point of the bars when the system is heated by an amount ΔT. What is the tension on the bars?

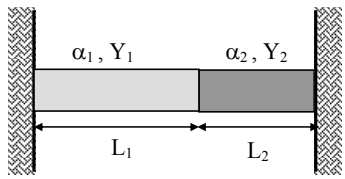

Figure 9.7:

Solution:

9.3.5.3 Ex: Bi-metal

In the sketched construction two thin metal strips with different linear expansion coefficients (aluminium and copper) $\alpha_{Al} = 24 \cdot 10^{-6}$ K^{-1} and $\alpha_{Cu} = 17 \cdot 10^{-6}$ K^{-1} are connected to each other by bars so that they have a fixed distance $d = 1$ mm. When the temperature increases, the two strips expand so that they form circular segments with different radii, as shown in the figure. An angle of the circle segment of $\phi = 1°$ is measured. How big is the temperature increase?

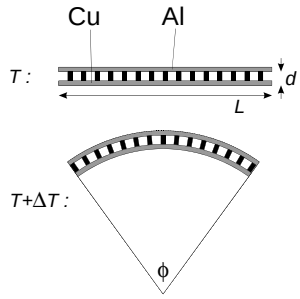

Figure 9.8: Bimetal.

Solution: *For the individual strips holds,*

$$(L + \alpha_{Al}\Delta T L) = \phi(r + d)$$
$$(L + \alpha_{Cu}\Delta T L) = \phi r \ .$$

Therefore,

$$(\alpha_{Al} - \alpha_{Cu})\Delta T L) = \phi d \ .$$

The temperature change is therefore $\Delta T = \frac{\phi d}{L(\alpha_{Al} - \alpha_{Cu})} \approx 25 \ K.$

9.3.5.4 Ex: Linear expansion

The length of a 10 cm long spacer made of quartz glass with linear expansion coefficient $\alpha_1 = -1$ cm/m/°C is to be kept constant by using a spacer made of Invar steel with a linear expansion coefficient $\alpha_1 = 10$ cm/m/°C. How long must the spacer be?

Solution: *Banane.*

9.4 Ideal gas thermodynamics

9.4.1 Heat capacity

9.4.2 Types of expansions

9.4.3 Adiabaticity coefficient

An *adiabatic process* in thermodynamics is a process, in which the system does not exchange heat with the environment. To verify how the pressure and volume of an ideal gas vary during an adiabatic process we need two ingredients. First, the equation of state of an ideal gas, that is,

$$pV = nRT = Nk_BT \ , \tag{9.9}$$

where n is the number of moles of gas, N is the number of molecules of gas, R is the gas constant, and k_B the Boltzmann constant, that is, $Nk_B = nR$ or $R = N_Ak$, where N_A is Avogadro's number. The other ingredient is the *equipartition theorem*, which says that in an ideal gas in equilibrium at temperature T (in Kelvin), the average energy of each molecule per degree of freedom is,

$$\tfrac{1}{2}k_BT \ . \tag{9.10}$$

That is, the total energy of the gas is,

$$U = \tfrac{f}{2}Nk_BT = \tfrac{f}{2}nRT \ , \tag{9.11}$$

where f is the number of degrees of freedom of the gas molecule (accessible at that temperature). In an adiabatic process there is no heat exchange, and therefore energy conservation claims, that the energy variation dU must be equal to the (negative) work dW realized by the gas, that is,

$$dU + dW = 0 \ . \tag{9.12}$$

From (9.11) we have:

$$dU = \tfrac{f}{2}nRdT = -dW = -pdV \ . \tag{9.13}$$

From (9.9) we have:

$$Vdp + pdV = nRdT \ . \tag{9.14}$$

Hence,

$$\tfrac{f}{2}(Vdp + pdV) = -pdV \ , \tag{9.15}$$

yielding,

$$\tfrac{f}{2}Vdp = \left(1 + \tfrac{f}{2}\right)pdV \ . \tag{9.16}$$

Defining,

$$\gamma \equiv \frac{f+2}{f} \ , \tag{9.17}$$

we get,

$$Vdp = -\gamma pdV \ , \tag{9.18}$$

yielding,

$$\frac{dp}{p} = -\gamma \frac{dV}{V} \ , \tag{9.19}$$

yielding,

$$d\ln P = -d\ln V^{\gamma} \ . \tag{9.20}$$

That is,

$$d[\ln(pV^{\gamma})] = 0 \ . \tag{9.21}$$

Hence,

$$pV^{\gamma} = const. \tag{9.22}$$

The heat capacity is defined as the ratio between the absorbed heat and the rise in temperature, i.e.,

$$\Delta Q = C\Delta T \ . \tag{9.23}$$

For a process where the volume is maintained constant the gas does not perform work, and the heat is only used to increase the energy. From (3) we have:

$$\Delta Q = \tfrac{f}{2} \ . \tag{9.24}$$

Therefore, the heat capacity, at constant volume, is,

$$C_V = \tfrac{f}{2} nR \ . \tag{9.25}$$

If the process is done at constant pressure, then the heat is used to change the energy and also to perform work, that is:

$$\Delta Q = \Delta U + \Delta W \ . \tag{9.26}$$

From (1) we have that at constant pressure,

$$p\Delta V = nRT\Delta T \ . \tag{9.27}$$

Hence,

$$\Delta Q = \tfrac{f}{2} nR\Delta T + nR\Delta T = \left(1 + \tfrac{f}{2}\right) \ . \tag{9.28}$$

and

$$C_p = \left(1 + \tfrac{f}{2}\right) nR \ . \tag{9.29}$$

We conclude, then,

$$\frac{C_p}{C_V} = \gamma \qquad \text{and} \qquad C_p - C_V = nR \ . \tag{9.30}$$

Since the specific heat can be obtained from the heat capacity simply by dividing by the mass, the ratio of the specific heat at constant pressure and to the specific heat at constant volume is also equal to the constant γ, that is, $\gamma = c_p/c_V$.

9.4.3.1 The Cléments-Desormes method

The specific heat of solids and liquids is usually measured with samples under atmospheric conditions and without control of the volume of the material. For this reason, these are specific heats measured at constant pressure: c_P. To measure the heat capacity of gases, it is much simpler to work with the gas contained in a rigid recipient, such as a glass bulb with little thermal expansion within the temperature range of the experiment. Then, the measured value is the specific heat at constant volume c_V. The value c_P of a gas is larger than c_V, because in the experiment, at constant pressure, the heat delivered to the material also causes an expansion of the gas, which means that part of that energy has been converted into work and not into an increase the body's thermal energy. The ratio between specific heats at constant pressure and volume, $\gamma = c_p/c_v$, is a value that often appears in the description of thermodynamic processes in gases. This ratio can be measured by isobaric and isochoric processes, respectively measuring c_p and c_v. The first experiment to measure the factor γ in gases was performed in 1819 by *Desormes* and *Clément*. The method consists of applying to a (ideal) gas, a sequence of two processes illustrated in Fig. 9.9: an adiabatic expansion from state (1) to (2), and isochoric heating from (2) to (3). In the initial equilibrium state (1), a certain amount of moles of gas n are at a pressure P_1 above atmospheric pressure with the volume V_1, and a temperature T_1 equal to room temperature. An adiabatic expansion is performed to state (2) with pressure P_2 equal to atmospheric pressure, volume V_2, and temperature T_2 lower than room temperature. Immediately an isochoric heating is carried out toward the state (3), at room temperature, for T_1, and pressure P_3.

To calculate the factor γ of the gas, we consider the relation between P and V in the course of an adiabatic process: $pV^\gamma = const.$. Thus, we can write,

$$p_1 V_1^\gamma = p_2 V_2^\gamma \ . \tag{9.31}$$

From this relation, it is possible to write the factor γ as in Fig. 9.9 for the gas process realized by the Cléments-Desormes experiment: between the initial state (1) and (2) the process is adiabatic. Between (2) and (3) it is isochoric. In order to obtain the result only in terms of pressures and not volumes which, in practice, are more difficult to measure accurately, we can now consider the isochoric process (2) to (3) imposing the condition that states (1) and (3) lie on the same isothermal curve with temperature T_1 (see Exc. 9.4.5.30).

9.4.3.2 Rüchardt's method

Rüchardt's method is discussed in Exc. 9.4.5.20.

9.4.4 Cyclic processes and thermal machines

Thermal machines are based on cyclic processes. Examples are the Carnot cycle, the *Otto cycle*, or the *Diesel cycle*.

9.4.4.1 Carnot cycle

A *Carnot cycle* is an ideal thermodynamic cycle providing, by Carnot's theorem, an upper limit on the efficiency of any classical thermodynamic engine during the

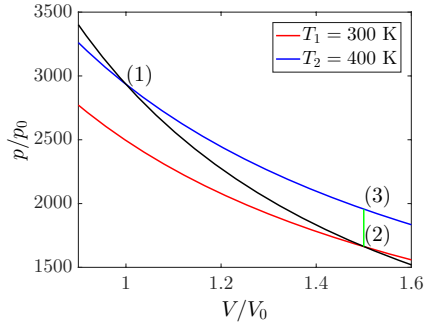

Figure 9.9: Clément-Desormes cyclic process.

conversion of heat into work, or conversely, the efficiency of a refrigeration system in creating a temperature difference through the application of work to the system.

In a Carnot cycle, an engine transfers energy in the form of heat between two thermal reservoirs at temperatures T_{hot} and T_{cold}, and a part of this transferred energy is converted to the work done by the system. The cycle is reversible and hence isentropic. In other words, entropy is conserved; it is only transferred between the thermal reservoirs. When work is applied to the system, heat moves from the cold to hot reservoir, which is exploited in *heat pumps* and *refrigerators*, depending on whether the heat increase of the hot reservoir is exploited or the heat decrease of the cold reservoir. When heat moves from the hot to the cold reservoir, the system applies work to the environment, which can be exploited in *heat engines*.

The work W done by the system or engine to the environment per Carnot cycle depends on the temperatures of the thermal reservoirs and the entropy transferred from the hot reservoir to the system ΔS per cycle such as,

$$W = (T_{hot} - T_{cold})\Delta S = (T_{hot} - T_{cold})\frac{Q_{hot}}{T_{hot}} \ , \tag{9.32}$$

where Q_{hot} is heat transferred from the hot reservoir to the system per cycle.

To calculate the yield of the Carnot cycle (see Fig. 9.10) we ...

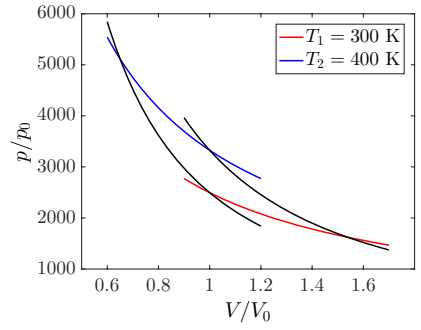

Figure 9.10:

9.4.5 Exercises

9.4.5.1 Ex: Depth gauge

You want to build a depth gauge for diving operations and take advantage of the compressibility of air. To do this, you take a glass cylinder with a movable flask (volume $V = A \cdot x$, footprint A) and a millimeter scale located in the flask. To what water depth h can the device deliver the targeted measuring accuracy of ± 1 m, if the piston position x can be read with an accuracy of ± 1 mm and $x(p_0) = 0.2$ m at the water surface?

Solution: *For $h = 0$ m the pressure is $p = p_0 = 10^5$ Pa and $x = x_0 = 0.2$ m. According to Boyle-Mariotte: $(p_0 + \rho g h) \cdot A \cdot x = p_0 \cdot A \cdot x_0$. $\Rightarrow h = a \cdot \frac{x_0 - x}{x}$ with $a = \frac{p_0}{\rho g} = 10.2$ m. $\Rightarrow \frac{\Delta h}{\Delta x} \approx \frac{\partial h}{\partial x} = -a\frac{x_0}{x^2} < 0$. $\Rightarrow x \approx \sqrt{a x_0 \left|\frac{\Delta x}{\Delta h}\right|}$.*
With $\Delta x = 1$ mm and $\Delta h = 1$ m we get $x = 4.52$ cm and accordingly $h = 35$ m. The device is accurate to a depth of $h = 35$ m to 1 m.

9.4.5.2 Ex: Tramway

A tram with mass $m_B = 12500$ kg brakes from a speed $v = 57.6$ km/h to standstill. What is the temperature of the eight cast iron brake blocks when the mass of each block is 9.0 kg and 60% of the kinetic energy flows into the heating of the blocks?

Solution: *The amount of heat flowing into the brake padsis $Q = 0.6 \cdot 0.5 \cdot m_B v^2 = 960$ kJ. The mass of an Fe atom is 56 u and with the rule of Dulong-Petit follows $c_{Fe} = \frac{24.9}{56}\ \frac{J}{g \cdot K} \approx 0.445\ \frac{J}{g \cdot K}$. The mass of all brake blocks is $M = 8 \cdot 9$ kg= 72 kg, such that we expect a temperature increase of $\Delta T = \frac{Q}{M \cdot c_{Fe}} = \frac{960\ kJ}{72\ kg \cdot 0.445\ \frac{J}{g \cdot K}} \approx 30$ K.*

9.4.5.3 Ex: Heat capacities

a. Two gas containers are brought into thermal contact. They contain gases with the temperatures T_1 and T_2, as well as the heat capacities C_1 and C_2. The thermal capacity of the containers is negligible. What is the temperature of the gases after an equilibrium has been reached?
b. Now consider the temperature equilibrium of three containers, each with 100 g of the gas H_2 at the temperature $T_{H_2} = 10$ C, 50 g of the gas He at the temperature $T_{He} = 15$ C, and 200 g of the gas N_2 at temperature $T_{N_2} = 20$ C. What is the final temperature?

Solution: *a. The temperature is,*

$$T_m = \frac{C_1 T_1 + C_2 T_2}{C_1 + C_2}\ ,$$

because the heat delivered by gas 1 $\Delta Q = C_1(T_1 - t_m) = -C_2(T_2 - T_m)$ must be absorbed by gas 2.

b. The molar heat capacities are $\tilde{C} = N_A \frac{\bar{f}}{2} k_B$*, hence,*

$$\tilde{C}_{H_2} = \tilde{C}_{N_2} = N_A \frac{5}{2} k_B = 20.8\,\mathrm{J/K\ mol} \qquad \textit{and} \qquad \tilde{C}_{He} = N_A \frac{3}{2} k_B = 12.5\,\mathrm{J/K\ mol}\ .$$

The specific heat capacities are $c = \tilde{C}/(m\ N_A)$*, hence,*

$$c_{H_2} = \frac{5}{2}\frac{k_B}{2u} \simeq 10393\,\mathrm{J/K\ kg} \qquad \textit{and} \qquad c_{He} = \frac{3}{2}\frac{k_B}{2u} \simeq 3118\,\mathrm{J/K\ kg}$$
$$\textit{and} \qquad c_{N_2} = \frac{5}{2}\frac{k_B}{14u} \simeq 742\,\mathrm{J/K\ kg}\ .$$

If M *is the total mass of the gases, then the actual heat capacities are* $C = cM$*, hence,*

$$C_{H_2} = 0.1 \cdot 10393\,\mathrm{J/K} \qquad \textit{and} \qquad C_{He} = 0.05 \cdot 3118\,\mathrm{J/K} \qquad \textit{and} \qquad C_{N_2} = 0.2 \cdot 742\,\mathrm{J/K}\ .$$

The temperature is finally,

$$T_m = \frac{C_{H_2} T_{H_2} + C_{He} T_{He} + C_{N_2} T_{N_2}}{C_{H_2} + C_{He} + C_{N_2}} = 11.7\,\mathrm{C}\ .$$

9.4.5.4 Ex: Calorimetry

a. A calorimeter initially contains a volume of $V_1 = 100$ ml of water in thermal equilibrium with the calorimeter at temperature $T_1 = 15°\mathrm{C}$. Now we add a volume $V_2 = 100$ ml of water at temperature $T_2 = 40°\mathrm{C}$. After reaching thermal equilibrium again, the temperature becomes $T_f = 25°\mathrm{C}$. What is the thermal capacity of the calorimeter?
b. Starting from the final condition of the previous item, we add to the calorimeter a metallic body with mass $m_3 = 80$ kg and temperature $T_3 = 90°\mathrm{C}$. After reaching thermal equilibrium again, the temperature becomes $T_{ff} = 35°\mathrm{C}$. What is the specific heat of the body?

Solution: *a. The thermal capacity of the calorimeter is,*

$$C = m_2 c_a \frac{T_2 - T_f}{T_f - T_1} - m_1 c_a = 100\ g{\cdot}1\ cal/g\ ^\circ C{\cdot}\frac{40-25}{25-15} - 100\ g{\cdot}1\ cal/g\ ^\circ C = 50\ cal/^\circ C\,.$$

b. The specific heat of the body is,

$$c_3 = \frac{(m_1+m_2)c_a + C}{m_3}\frac{T_{ff} - T_f}{T_3 - T_{ff}} = \frac{200\ g \cdot 1\ cal/g\ ^\circ C + 50\ cal/^\circ C}{80\ g}\frac{35-25}{90-35} = 0.5682\ cal/g\ ^\circ C\,.$$

9.4.5.5 Ex: Calorimeter for mixtures

The specific heat capacity of platinum c_{Pt} is to be measured with a mixing calorimeter. For this purpose, a platinum body is heated to 100 °C and then thrown into water of 20 °C. To simplify the evaluation, the mass of the water is chosen to be that of the platinum body. The heat absorption of the calorimeter body should be neglected. The specific heat capacity of water is $c_{\mathrm{H_2O}} = 4.19$ J/(g K), the relative atomic mass of platinum is $m_{\mathrm{Pt}} = 195$ u, the linear expansion coefficient $\alpha = 9.0 \cdot 10^{-6}$ K^{-1}.
a. The mixing temperature is 22.41 °C. What value follows for c_{Pt}?
b. What is the value for c_{Pt} when applying the Dulong-Petit rule?
c. The platinum body and the water have the same mass. What is the ratio of the number of platinum atoms to the number of water molecules?
d. How many degrees does the platinum body have to be heated to increase its volume by 1 %?

Solution: *a. We have,*

$$\Delta Q = m_{H_2O} c_{H_2O} \Delta T_{H_2O} + m_{Pt} c_{Pt} \Delta T_{Pt} = 0 \ .$$

The following also applies $m_{H_2O} = m_{Pt}$. Then follows,

$$\Rightarrow c_{Pt} = -c_{H2_O} \frac{\Delta T_{H_2O}}{\Delta T_{Pt}} \ .$$

With $T_{H_2O} = 2.41$ K, $T_{Pt} = -77.59$ K and $c_{H_2O} = 4.19$ J/(g·K) we get $c_{Pt} = 0.130$ J/(g·K).
b. Dulong-Petit: $C_{mol} = 24.9$ J/mol·K $\Rightarrow c_{Pt} = \frac{24.9}{195} \frac{J}{g \cdot K} \approx 0.128 \frac{J}{g \cdot K}$
c. Mass of a H_2O-molecule: $m_{H_2O} = 18$ u, mass of a platinum atom: $m_{Pt} = 195$ u, $N_{H_2O} \cdot m_{H_2O} = M_{H_2O} = M_{Pt} = N_{Pt} \cdot m_{Pt} \Rightarrow \frac{N_{Pt}}{N_{H_2O}} = \frac{18}{195} \approx \frac{0.092}{1}$
d. $L' = (1 + \alpha \cdot \Delta T)L \Rightarrow V' = L'^3 = (1 + \alpha \cdot \Delta T)^3 L^3 = (1 + \alpha \cdot \Delta T)^3 V = 1,01 \cdot V$ $\Rightarrow \Delta T = \frac{\sqrt[3]{1.01} - 1}{\alpha} \approx 370$ K.

9.4.5.6 Ex: Calorimeter for mixtures

The equation of state of an ideal gas $pV = Nk_BT$ applies and the energy is given as $E = C_V T$.
a. Show that for the entropy change of an ideal gas from state A with temperature T_A and volume V_A to state B with temperature T_B and volume V_B holds: $\Delta S = C_V \log(T_B/T_A) + Nk_B \log(V_B/V_A)$.
b. Two insulated containers with the same volume $V = 10$ cm^3, the same pressure $p = 1$ bar and the same temperature $T = 100°$ C are filled with nitrogen and oxygen, respectively. Determine the change in entropy when connecting the containers so that the gases can mix.

Solution: *a. The 1st law of thermodynamics states $\delta Q = dE - \delta W = C_V dT + pdV$. With that and with the ideal gas equation $p = Nk_B \frac{T}{V}$ on gets,*

$$dS = \frac{\delta Q}{T} = \frac{C_V dT + pdV}{T} = C_V \frac{dT}{T} + Nk_B \frac{dV}{V} \ .$$

Hence, we get the entropy change

$$\Delta S = S_B - S_A = \int_{S_A}^{S_B} dS = C_V \int_{T_A}^{T_B} \frac{dT}{T} + Nk_B \int_{V_A}^{V_B} \frac{dV}{V} = C_V \ln \frac{T_B}{T_A} + Nk_B \ln \frac{V_B}{V_A} \ .$$

b. The ideal gas equation $\frac{pV}{T} = Nk_B$ *tells us that with identical pressure, volume and temperature the particle numbers must also be identical, i.e.* $N = N_{O_2} = N_{N_2}$*. Since both gases are diatomic,* $E_{O_2} = E_{N_2} = \frac{f}{2} Nk_B T = C_V T$ *with* $5 = f = f_{O_2} = f_{N_2}$ *degrees of freedom, i.e. the internal energies are identical as are the specific heats. Now if the gases mix, we have,*

$$\Delta Q = 0 = \Delta W \Rightarrow \Delta E = 0 \ ,$$

since the thermal insulation of the containers impedes any exchange of thermal energy with the surroundings. Likewise, no work is done by simply bringing the containers together and removing the partition. The internal energies of the two gases are also the same, so that the two gas components also do not exchange energy. On the other hand, $\Delta E = 0$ *means that the temperature does not change,* $T = constant = T_A = T_B$*. Each of the two gas components* O_2 *and* N_2 *sees its volume doubled,* $V_A \equiv V \to 2V \equiv V_B$*. So with equation (3)*

$$\Delta S_{O_2} = \Delta S_{N_2} = C_V \ln \frac{T_B}{T_A} + Nk_B \ln \frac{V_B}{V_A} = Nk_B \ln 2 \ .$$

Finally, $\Delta S = \Delta S_{O_2} + \Delta S_{N_2} = Nk_B 2 \ln 2$*.*
Note: *The formula (3) respectively (4) apply provided that the particle number* N *of the ideal gas under consideration is maintained constant. If* N *were also to change, the formula receives an additional term that takes this change in particle number into account. Assuming that in subtask (b) the two gases are identical, then the simple addition of the individual entropy change leads to a wrong result. Because of the indistinguishability,* $\Delta S = 0$*, since the probability to find a particle before and after does not change. One could consider the entropy change if the gas is first in* V *with particle number* N *and then in* $2V$ *with particle number* $2N$*. But that would require the extended formula.*

9.4.5.7 Ex: Partial pressures

A closed cylindrical reservoir with the base area $S = 10$ cm^2 is kept at a constant temperature $T = 27°$C. It is divided in two volumes by an airtight mobile disk with the mass $m = 10$ kg. The upper volume V_{O_2} contains $\eta_{O_2} = 1$ mol of oxygen, the lower volume V_{N_2} contains the same amount of nitrogen. Due to its weight the disc finds an equilibrium position when the lower volume is $V_{N_2} = 10$ l.
a. What are the masses m_{O_2} and m_{N_2} of the gases?
b. What are the pressures P_{O_2} and P_{N_2}?
c. What is the upper volume V_{O_2}?
d. What are the densities n_{O_2} and n_{N_2}?
e. Now the disc has a hole, so that the gases can mix and the disc falls to the bottom of the reservoir. What is the final pressure of the mixture?

Solution: *a. The numbers of particles in the gases are equal,*

$$N_{O_2} = \eta_{O_2} N_A = \eta_{N_2} N_A = N_{N_2} = N \ .$$

Therefore, the masses are,

$$m_{O_2} = N \cdot 16u = 16 \ g \qquad and \qquad m_{N_2} = N \cdot 14u = 14 \ g \ .$$

b. The disc presses on the lower volume with the pressure mg/S. The pressures on the volumes are therefore related by $p_{O_2} + \frac{mg}{S} = p_{N_2}$. The pressure in the lower volume is,

$$P_{N_2} = \frac{N k_B T}{V_{N_2}} = 2.5 \ bar \ .$$

The pressure in the upper volume is,

$$P_{O_2} = P_{N_2} - \frac{mg}{S} = 1.5 \ bar \ .$$

c. Now we can calculate the upper volume

$$V_{O_2} = \frac{N k_B T}{P_{O_2}} = 16.5 \ l \ .$$

d. The densities are

$$n_{O_2} = \frac{N}{V_{O_2}} = \frac{P_{O_2}}{k_B T} = 6.0 \cdot 10^{25} \ m^{-3} \qquad and \qquad n_{N_2} = \frac{N}{V_{N_2}} = \frac{P_{N_2}}{k_B T} = 3.6 \cdot 10^{25} \ m^{-3} \ .$$

e. The total pressure is the sum of the partial pressures, $P = P_{O_2} + P_{N_2}$. Knowing the total volume of the reservoir, $\tilde{V} = V_{O_2} + V_{N_2}$ and the ideal gas law we have,

$$\tilde{P} = \tilde{P}_{O_2} + \tilde{P}_{N_2} = \frac{N k_B T}{\tilde{V}} + \frac{N k_B T}{\tilde{V}} = \frac{2 N k_B T}{V_{O_2} + V_{N_2}} = 1.9 \ bar \ .$$

9.4.5.8 Ex: Ideal gas

A diver is at a water depth of h_0 and breathes air from a compressed air bottle. When exhaling, he creates (spherical) air bubbles with the volume V_0. Assume that the surface water temperature is T_1 and decreases evenly to a depth of h_0 by an amount of temperature α per meter.
a. Assume a constant water density ρ and calculate the pressure p depending on the water depth at an atmospheric pressure p_1. b. Calculate the volume of the bubbles as a function of water depth. How big is the volume just below the water surface? Why is it important for the diver to exhale continuously as he ascends?
Numerical values: Water depth $h_0 = 40$ m, $V_0 = 1$ cm^3, $T_1 = 20°$C, $\alpha = 0.2°$C/m, $\rho = 1$ kg/l, and $p_1 = 1013$ hPa.

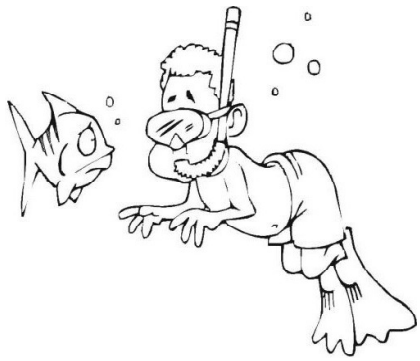

Figure 9.11: Ideal gas in a box.

Solution: *a. The pressure in a water column of depth is h,*

$$p = p_0 + \frac{mg}{A} = p_0 + \frac{\rho V g}{A} = p_0 + \frac{\rho A h g}{A} = p_0 + \rho h g \ .$$

b. The temperature is,

$$T = T_0 - \alpha h \ .$$

According to the ideal gas law, $pV = Nk_BT$, we get,

$$V(h) = \frac{p_{40}V_{40}}{Nk_BT_{40}}\frac{Nk_BT(h)}{p(h)} = V_{40}\frac{p_{40}}{p}\frac{T}{T_{40}} = V_{40}\frac{p_0 + \rho h_{40} g}{p_0 + \rho h g}\frac{T_0 - \alpha h}{T_0 - \alpha h_{40}} \approx V_{40}\frac{h_{40}}{h}\frac{T_0 - \alpha h}{T_0 - \alpha h_{40}} \ .$$

The result is $V_1/V_0 \simeq 5$. The air in the lungs expands. If the diver does not exhale, the alveoli may burst.

9.4.5.9 Ex: Simple model for a solid

Consider a system of N atomic particles at a temperature T. The individual atoms can only be in one of two states. Either in state "0" at the energy $\epsilon_0 = 0$ or in state "1" at energy $\epsilon_1 = \epsilon$. Apart from this energy ϵ_i, the atoms have no kinetic or other energies.
a. Determine the probability w_i that a certain atom is in state i. Note: The distribution is a Boltzmann distribution. How should the normalization be chosen?
b. Determine the statistical mean $\bar{\epsilon}$ for the energy of an atom. What is the expression for the total energy E of N atoms? Which values result for $k_BT = \epsilon$?
c. Calculate the population probability w_j to find a certain atom at the energy ϵ if for temperatures satisfy: $k_BT_j = 0.1 \cdot j \cdot \epsilon$ für $j = 1, 2, 3, 4$. Also calculate the energy E_j of the entire system at these temperatures.
d. Find an expression for the heat capacity c of this N atom system. Note: For this system, the total energy is identical to the thermal energy.
e. Calculate the heat capacities c_j especially for the temperatures T_j from subtask (a). What does this result have to do with 'freezing degrees of freedom'?

Solution: *a. The probability of finding a certain atom in state i is*

$$w_0 = \frac{1}{1+e^{-\epsilon/k_BT}} \qquad \textit{and} \qquad w_0 = \frac{e^{-\epsilon/k_BT}}{1+e^{-\epsilon/k_BT}} \ .$$

b. The statistical mean is,

$$\bar{\epsilon} = 0w_0 + \epsilon w_1 = \epsilon \frac{e^{-\epsilon/k_BT}}{1+e^{-\epsilon/k_BT}} = \epsilon \frac{e^{-1}}{1+e^{-1}} = 027\epsilon \ .$$

The total energy is,

$$E = N\bar{\epsilon} \ .$$

c. The occupation probabilities for the different temperatures are $w_1 = 0.000045$, $w_2 = 0.0067$, $w_3 = 0.03445$, *and* $w_4 = 0.0758$.
d. The heat capacity is,

$$C = \frac{dE}{dT} = N\epsilon \frac{dw_1}{dT} = N\epsilon \frac{de^{-\epsilon/k_BT}}{dT} \frac{d}{dx}\frac{x}{1+x} = Nk_B \frac{\epsilon^2}{(k_BT)^2} \frac{e^{-\epsilon/k_BT}}{(1+e^{-\epsilon/k_BT})^2} \ .$$

e. The associated heat capacities are $C/NK_B = 0.0045$,

$$E = N\bar{\epsilon} \ .$$

Beware: *The model is nonsensical for* $k_BT > \epsilon/2$. *Then several levels are required.*

9.4.5.10 Ex: 1. law of thermodynamics

In a thermally insulated container there is one mole of air at the temperature $T = 400$ K. Now, it is reversibly compressed, doing the work $W = 1.987$ cal. Calculate the ratio V_f/V_i between the final and initial volume. Assume that the air behaves like an ideal gas and that the container itself does not absorb heat from the air.

Solution: *Conversion to Joule:* $1\ cal = 4.187\ J$. *The differential work is for adiabatic processes* $dW = -pdV$. *With the ideal gas equation,* $pV = \nu RT$, *we can substitute the pressure,* $dW = -\frac{\nu RT}{V}dV$, *or,*

$$W = -\nu RT \int \frac{dV}{V} = -\nu RT(\ln V_f - \ln V_i) = -\nu RT \ln \frac{V_f}{V_i} \ .$$

So We get,

$$\frac{V_f}{V_i} = e^{-W/\nu N_A k_B T} \simeq 0.9977 \ .$$

9.4.5.11 Ex: Energy of air

Calculate the kinetic energy as well as the average molecular velocity in 1 kg of air (main components N_2, O_2) at $T = 300$ K. Help: $E_{kin} = Q = m \cdot c \cdot T$; specific heat $c = f/2 \cdot R$.

Solution: $Q = 2.13 \cdot 10^5\ J$ *and* $v = 505.6\ m/s$

9.4.5.12 Ex: Gas compression

Calculate the temperature change resulting from *adiabatic* compression of an ideal gas of volume $V(T_1)$ to $V(T_2) = V(T_1)/10$.
Compare this with the temperature change through an analog *isobaric* compression of an equally ideal gas. **Note:** $\kappa = c_p/c_v = 1.4$ (for air), $T_1 = 293$ K.

Solution: *The following applies to adiabatic compression,* $p_1 V_1^\kappa = p_2 V_2^\kappa$. *Hence,*

$$\Delta T = T_2 - T_1 = \frac{p_2 V_2}{N k_B} - T_1 = \frac{p_1 V_1}{N k_B} \frac{V_1^{\kappa-1}}{V_2^{\kappa-1}} - T_1 = T_1 10^{\kappa-1} - T_1 = \left(10^{1.4-1} - 1\right) \cdot 293\ K \simeq 442.98\ K\,.$$

Mistake!!!??? The expected result is $\Delta T_{adiabatisch} = +460\ K$.
The following applies to isobaric compression $\frac{V_1}{T_1} = \frac{V_2}{T_2}$. *Hence,*

$$\Delta T = T_2 - T_1 = \frac{V_2}{V_1} T_1 - T_1 = \left(\frac{V_2}{V_1} - 1\right) T_1 = \left(\frac{1}{10} - 1\right) \cdot 293\ K \simeq -263.7\ K\,.$$

9.4.5.13 Ex: Gas compression

An oxygen bottle with the volume $V_2 = 40$ l contains a filling ex works that would have the volume $V_1 = 6$ m^3 at atmospheric pressure $p_1 = 101$ kPa. The bottle, which has been emptied to atmospheric pressure, is refilled at a constant temperature of $T_1 = 18°$C. What mechanical work W must be added to the gas to compress it isothermally from p_1 to the filling pressure?

Solution: *The particle number* $N = \frac{pV}{k_B T}$ *is constant, because* pV *is constant. The work follows from* $\delta W = pdV$,

$$W = \int_{V_1}^{V_2} p dV = \int_{V_1}^{V_2} \frac{N k_B T \cdot dV}{V} = p_1 V_1 \int_{V_1}^{V_2} \frac{dV}{V} = p_1 V_1 \left(\ln V_2 - \ln V_1\right)$$
$$= 101000 \cdot 6 \cdot \ln \frac{0.04}{6}\ J = -3.036\ MJ\,.$$

9.4.5.14 Ex: Gas expansion

1 kmol of nitrogen under normal conditions ($p_0 = 1.01 \cdot 10^5$ Pa, $T = 0°$C) adiabatically expands from V_1 to $V_2 = 5 \cdot V_1$. Calculate the change in the internal energy of the gas and the amount of work the gas does as it expands.

Solution: *The adiabatic coefficient is,*

$$\kappa = \frac{c_p}{c_V} = \frac{\tilde{f}+1}{\tilde{f}} = \frac{3.5}{2.5} = 1.4 \ .$$

Adiabatic expansion means,

$$pV^\kappa = \frac{Nk_BTV^\kappa}{V} = const \ .$$

So because of $dU = pdV = -\delta W$ the work is,

$$\begin{aligned}
\Delta W &= \int_{V_1}^{V_2} \frac{Nk_BT}{V}\frac{V^\kappa}{V^\kappa}dV = \frac{Nk_BT}{V}V^\kappa \int_{V_1}^{V_2}\frac{dV}{V^\kappa} \\
&= Nk_BTV^{\kappa-1}\left(\frac{-1}{(\kappa-1)V_2^{\kappa-1}} - \frac{-1}{(\kappa-1)V_1^{\kappa-1}}\right) \\
&= \frac{Nk_BT_1}{\kappa-1}\left(1-\frac{1}{5^{\kappa-1}}\right) = \frac{1\ kmol\cdot N_Ak_B\cdot 273.15\ K}{\kappa-1}\left(1-\frac{1}{5^{\kappa-1}}\right) \\
&= \frac{1000\cdot 8.31\cdot 273.15}{0.4}\left(1-\frac{1}{5^{0.4}}\right)\ J = 2.7\,\text{MJ} \ .
\end{aligned}$$

The change in internal energy is therefore $dU = -2.7$ MJ.

9.4.5.15 Ex: 1. law of thermodynamics

In a thermally insulated container B there are n mol of an ideal gas and a body K with the heat capacity C. Specify the relationship between pressure p and volume V, whereby the change in V is carried out so slowly that the following always applies to body and gas: $T_K = T_G$.
Note: Body and gas exchange heat. Assume that the container itself does not take heat from the gas or the body.

Solution: *Because the gas only gives away heat to the body, the 1st law gives for an infinitesimal variation of the state of the gas:*

$$dU = nC_V dT = \delta Q|_{\text{G}} - pdV \qquad \delta Q|_{\text{G}} = -\delta Q|_{\text{K}} = -CdT \ .$$

It follows,

$$dT = -\frac{p}{C+nC_V}(p\ dV) \ .$$

In addition, by differentiating the equation of state,

$$dT = \frac{1}{nR}(p\ dV + V\ dp) \ .$$

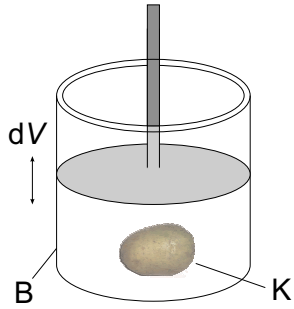

Figure 9.12: Potato.

Equating the results gives,

$$(\kappa+1)pdV+\kappa V dp=0\ , \qquad \kappa=\frac{C_V+C/n}{R}\ .$$

Now we integrate

$$p\ V^{\tilde{\gamma}}=\text{const.} \qquad \tilde{\gamma}=1+\frac{1}{\kappa}=\frac{C_p+C/n}{C_V+C/n}\ .$$

9.4.5.16 Ex: 1. law of thermodynamics

In a thermally insulated container there is one mole of air at temperature $T = 400$ K. It is compressed very slowly (reversibly) while doing the work $W = 1.987$ cal on it. Calculate the behavior of the ratio V_f/V_i between the end and start volume. Assume that the air behaves like an ideal gas and that the container itself does not absorb heat from the air.

Solution: *Conversion to Joule: 1 cal=4.187 J. The differential work for adiabatic processes is $dW = -pdV$. With the ideal gas equation, $pV = \nu RT$, we can substitute the pressure, $dW = -\frac{\nu RT}{V}dV$. Or*

$$W=-\nu RT\int\frac{dV}{V}=-\nu RT(\ln V_f-\ln V_i)=-\nu RT\ln\frac{V_f}{V_i}\ .$$

So we get,

$$\frac{V_f}{V_i}=e^{-W/\nu N_A k_B T}\approx 0.9977\ .$$

9.4.5.17 Ex: 1. law of thermodynamics

A container with 1 mol helium and a container of the same size with 1 mol nitrogen are both heated with the same heating power $W = 10$ W.

a. Calculate how long it takes to warm up the containers from $T_1 = 20°\text{C}$ to $T_2 = 100°\text{C}$, if the thermal capacity of the container is 10 J/K.
b. How long does it take to warm up to 1000°C assuming that the vibrational degrees freedom of N_2 molecules can be excited above 500°C? Neglect heat loss.

Solution: *The thermal energy of a mole is* $Q = \frac{f}{2}RT$.
a. For helium, $f = 3 \Rightarrow Q = \frac{3}{3}RT$. *The heating energy is then* $W = 10 \cdot t\ J = \frac{3}{2}R(100-20)\ K + 10\ J/K \cdot 80\ K$, *where the last term takes into account the heating of the container. With* $R = 8.3\ J(K{\cdot}mol)$ *follows,*

$$t = \frac{120 \cdot 8.31 + 800}{10}\ s = 180\ s = 3\ min\ .$$

For N_2 *molecules above* $T = 300\ K$ *holds,* $f = 5$*:* $t = \frac{200 \cdot 8.31 + 800}{10}\ s = 246\ s = 4.1\ min.$
b. The heating to 1000° C lasts for helium,

$$t = \frac{980 \cdot 3R/2 + 9800}{10}\ s \approx 2200\ s \approx 37\ min\ .$$

For N_2 *between 20-500° we got* $f = 5$, *for* $T > 500°$ *we got* $f = 7$.
Hence,

$$t = \frac{480 \cdot 8.31 \cdot 5/2 + 500R \cdot 7/2 + 9800}{10}\ s = 3431\ s = 57.2\ min\ .$$

9.4.5.18 Ex: 2. law of thermodynamics

A thermally insulated container with a total volume of 10 l is separated into two equal parts by a disc. In each part there are 10 mol of an ideal atomic gas. In one part the gas has the temperature $T_1 = 300$ K, in the other the temperature $T_2 = 400$ K. Calculate the change in the total entropy of the system ΔS in the event that:
a. the disc does not insulate heat;
b. a small hole opens in the disc through which the gases can mix slowly and which at the end closes again;
c. the disc is suddenly removed and then put back in after some time without any work being done.
In all three cases there we wait for equilibrium to establish.

Solution: *In general, we have,*

$$dS = \frac{\delta Q}{T} = C_p \frac{dT}{T}\ .$$

Hence, for finite processes $i \to f$ *we get,*

$$\Delta S = \int C_p \frac{dT}{T} = C_p \ln \frac{T_f}{T_i}\ .$$

For the given example the initial and final states are the same in all three cases. The entropy change in the overall system is the sum of the changes for the two subsystems, the volumes of which do not change. The final temperature $(T_1 + T_2)/2$ *is:*

$$\Delta S_T = \Delta S_1 + \Delta S_2 = \frac{3}{2} N k_B \left(\log \frac{T_1 + T_2}{2T_1} + \log \frac{T_1 + T_2}{2T_2} \right) = 0.06 \ cal/K \ .$$

9.4.5.19 Ex: 2. law of thermodynamics

A heat engine works between two heat sources with temperatures $T_2 > T_1$. If we take away the heat $\mathcal{Q}$ from the second heat source, what is the maximum and minimum work $\mathcal{L}_{\mathcal{M}}$ and $\mathcal{L}_{\Updownarrow}$ that the heating machine can do? What could the corresponding processes look like?

Solution:

9.4.5.20 Ex: Rüchardt's calorimetric method

A mono-atomic ideal gas with the adiabatic coefficient $\kappa = 1.4$ is in a thermally insulated bottle with a long neck. The total volume of the bottle and the neck is $V_0 = 10$ l. At the beginning there is atmospheric pressure. A thermally insulating ball with mass $m = 20$ g is now inserted into the neck (precision tube with a diameter of $d = 16$ mm), which hermetically seals the bottle to the outside. The ball can move smoothly.
a. Determine the equilibrium position of the ball. What is the pressure and volume in the part of the bottle sealed by the ball?
b. The ball is now pushed down slightly from the equilibrium position and then released. With what period τ does the ball vibrate.
Help: Relate the instantaneous pressure p in the bottle to small volume changes ΔV and linearize the expression using a Taylor expansion.

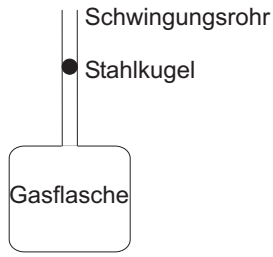

Figure 9.13:

Solution: *a. In equilibrium* $F_{atmos} + mg = F_{pressure}$ *applies. With the pipe cross*

section $A = \frac{1}{4}\pi d^2 = 201\ mm^3$, the pressure exerted on the air volume under the sphere is $p_1 = p_0 + \frac{mg}{A} = 1023\ hPa$. The volume results from the adiabatic equation,

$$p_1 V_1^\kappa = p_0 V_0^\kappa \ ,$$

giving $V_1 = V_0 \left(\frac{p_0}{p_1}\right)^{1/\kappa} = 9.93\ l$. Hence, the equilibrium position $\Delta x = \frac{V_0 - V_1}{A} = 0.35\ m$ below the top of the tube.
b. In Rüchardt's experimental set-up, adiabatic changes in the state of a given gas volume are caused by rapid alternation of compression and expansion by dropping a steel ball into a precision tube above the gas volume, so that it then carries out harmonic vibrations on the gas cushion. Again, the weight and buoyancy act on the ball,

$$F = ma(t) = F_{atmos} + mg - F_{druck} = p_0 A + mg - (p_1 - \Delta p)A = A\Delta p \ .$$

Again, we get for the adiabatic compression, $pV^\kappa = p_1 V_1^\kappa$. Hence, the instantaneous pressure is,

$$p = \frac{p_1 V_1^\kappa}{(V_1 + \Delta V)^\kappa} \simeq p_1 V_1^\kappa \left(\frac{1}{V_1^\kappa} - \frac{\kappa}{V_1^{\kappa+1}}\Delta V\right) = p_1 - \frac{\kappa p_1}{V_1}\Delta V = p_1 + \Delta p \ .$$

By inserting $\Delta V = A\Delta x$ we get from the force equation,

$$ma = A\Delta p = -A\frac{\kappa p_1}{V_1}\Delta V = -A\frac{\kappa p_1}{V_1}A\Delta x$$

the vibration equation,

$$\Delta\ddot{x} + \kappa\frac{p_1 A^2}{mV_1}\cdot\Delta x = 0 \ .$$

The period of the oscillation is $\tau = 2\pi/\omega$ with $\omega = \sqrt{\frac{A^2\kappa p_1}{mV_1}} = 2\pi\cdot 0.86\ Hz$.

9.4.5.21 Ex: Specific heat

The specific heat for an isobaric transformation is defined as $C_p = R + C_V$. A mass of $m = 10$ g of nitrogen is heated at constant pressure $p = 2$ atm and an initial temperature of $T_a = 20°$ C until its volume increases by 20%. Calculate the initial volume V, the final temperature T_e, and the heat supplied Q.

Solution: *$m_{N_2} = 10\ g$ then $N_{N_2} = m_{N_2}/28u$ and $T_a = 20°C$ and $p = 2\ atm = 2\cdot 0.981\ bar$*
a. We get,

$$V_a = \frac{N_{N_2} k_B T_a}{p} = \frac{m_{N_2} k_B T_a}{p28u} = 0.0044\ m^3 = 4.4\ l \ .$$

b. The ideal gas law holds at the beginning and at the end,

$$pV_a = N_{N_2} k_B T_a$$
$$pV_e = N_{N_2} k_B T_e \ .$$

We know, $V_e = 1.2V_a$, so the end temperature is $T_e = 1.2T_a = 1.2{\cdot}293.15^\circ C = 78.63^\circ C$.
c. The heat supplied is,

$$\begin{aligned}\delta Q &= C_V dT + pdV \\ &= C_p dT = N_{N_2} k_B \left(\frac{\tilde{f}}{2} + 1\right) dT \ .\end{aligned}$$

With 3 translational and 2 rotational degrees of freedom $\tilde{f} = 5$, so $\delta Q = 3.5 N_{N_2} k_B dT = 208\ J$.

9.4.5.22 Ex: Specific heat

Calculate the specific heat per mol of an ideal gas for a reversible process according to the law $pV^k =$ constant with $k \in \mathbb{R}$. Can such specific heat be negative? Justify the result.

Solution: *It is not necessary to consider exactly one mole of an ideal gas. We may simply replace the particle number N with the particle number N_A in a mol. We consider an ideal gas with N particles. From the ideal gas equation $\frac{pV}{T} = Nk_B$ and the process with $pV^k = const$ follows,*

$$Nk_B = \frac{pV}{T} = pV^k \frac{V^{1-k}}{T} = const \frac{V^{1-k}}{T} \ .$$

Hence, $\frac{V^{1-k}}{T} = const$.
For the case $k = 1$ this results in $T = const$, i.e. the process is carried out isothermally. Here, the definition of the specific heat $C \equiv \frac{\delta Q}{dT} = \frac{\Delta Q}{\Delta T}$ is meaningless.
Let us now consider the case $k \neq 1$. From $\frac{V^{1-k}}{T} = const$ we get,

$$\frac{V}{T^{1/(1-k)}} \equiv c_0 = \ const \ .$$

Hence, $V = c_0 T^{1/(1-k)}$, which leads us to the following derivation,

$$\frac{dV}{dT} = c_0 \frac{1}{1-k} T^{1/(1-k)-1} \ .$$

The 1st law of thermodynamics $\delta Q = dE - \delta W = C_V dT + pdV$ leads us to the specific heat using equation (2),

$$C = \frac{\delta Q}{dT} = C_V + p\frac{dV}{dT} = C_V + pc_0 \frac{1}{1-k} T^{1/(1-k)-1} = C_V + \frac{1}{1-k}\frac{pV}{T} = C_V + \frac{1}{1-k} Nk_B \ .$$

At the penultimate equal sign, we replaced the constant c_0 with equation (1), and we used the ideal gas equation for the last equal sign. For processes according to the law $pV^k = const$, the specific heat $C \equiv C(k)$ is given by,

$$C \equiv C(k) = C_V + \frac{1}{1-k} Nk_B = Nk_B \left(\frac{f}{2} + \frac{1}{1-k}\right) \ ,$$

as a function of the real number $k \neq 1$ of the process, whereby we used $C_V = \frac{f}{2} N k_B$ (with $f = 3, 5, ...$). We saw above that the specific heat cannot be defined for the isothermal process (with $k = 1$). In fact, it is not even a sensible quantity in the borderline process $k \to 1$, because

$$\lim_{k \searrow 1} \frac{1}{1-k} = -\infty \quad , \quad \lim_{k \nearrow 1} \frac{1}{1-k} = +\infty \ .$$

The specific heat can also become negative: We find exactly,

$$\begin{aligned} &C \equiv C(k) < 0 \quad \textit{for} \quad 1 < k < 2/f + 1 \ , \\ &C \equiv C(k) = 0 \quad \textit{for} \quad k = 2/f + 1 \ , \\ &C \equiv C(k) > 0 \quad \textit{for} \quad k > 2/f + 1 \quad \textit{or} \quad k < 1 \ . \end{aligned}$$

9.4.5.23 Ex: Expansion of a gas

One mole of a simple ideal gas, defined by $u = cRT$, $pv = RT$, is contained in a container of initial volume v_0 and pressure p_0. The gas expands from that initial state to the state corresponding to a final volume $2v_0$, through several different processes. Determine the work W done by the gas and the heat Q received by the gas for each of these processes. Final answers should be given only in terms of (v_0, p_0) and the constant c.
a. Free expansion: also determine the temperature variation ΔT.
b. Isentropic expansion: also obtain the final pressure p_f, using the fact that in this process for an ideal gas $pv^\gamma = constant$, where $\gamma = (c+1)/c$.
c. Isobaric quasi-static expansion.
d. Isothermal quasi-static expansion.
Formulas of thermodynamics:

$$\begin{aligned} \Delta u &= Q - W \\ W &= \int p dV \\ dU &= TdS - pdV + \mu dN \\ \beta &\equiv \frac{1}{k_B T} \\ Z &\equiv e^{-\beta F} = \sum_n e^{-\beta E_n} \\ P_n &= e^{-\beta E_n}/Z \\ U &\equiv \langle E_n \rangle = \sum_n E_n P_n \\ f &= u - TS \ . \end{aligned}$$

Solution: *a. For free expansion, we know* $Q = W = 0$. *Therefore,*

$$\Delta u = cR\Delta T = 0 \ ,$$

with the result, $\Delta T = 0$.
b. This process being isentropic, we have $p_f v_f^\gamma = p_i v_i^\gamma$. *Hence,*

$$p_f = p_i(v_i/v_f)^{1+1/c} = p_0(1/2)^{1+1/c} \ .$$

Since an isentropic process is also quasi-static adiabatic, $Q = 0$, *and*

$$W = -\Delta u = -(u_f - u_i) = -cR(T_f - T_i) = -(cp_f v_f - cp_i v_i) = -cp_0 v_0[(\tfrac{1}{2})^{1/c} - 1] \ .$$

Alternative solution: *Starting from* $p(v) = p_0(v_0/v)^{1+1/c}$, *we obtain,*

$$W = \int_{v_i=v_0}^{v_f=v_0} p(v)dv = -[cp_0 v_0 \tfrac{v_0}{v}^{1/c}]_{v_0}^{2v_0} = -cp_0 v_0[\left(\tfrac{1}{2}\right)^{1/c} - 1] \ .$$

c. We know $W = \int_{v_i=v_0}^{v_f=2v_0} p_0 dv = p_0 v_0$. *With that, we derive,*

$$\begin{aligned} Q = \Delta u + W = \Delta u + p_0\Delta v = u_f - u_i + p_0(v_f - v_i) = cR(T_f - T_i) + p_0(v_f - v_i) \\ = cp_0(v_f - v_i) + p_0(v_f - v_i) = (c+1)p_0(v_f - v_i) = (c+1)p_0 v_0 \ . \end{aligned}$$

d. We have $RT_0 = p_0 v_0 = const$ *throughout the isothermal process. Now,*

$$p(v) = RT_0/v = p_0 v_0/v$$

$$W = \int_{v_i=v_0}^{v_f=2v_0} p(v)dv = p_0 v_0[\ln v]_{v_0}^{2v_0} = p_0 v_0 \ln 2 \ .$$

With $\Delta u = cR\Delta T = Q - W = 0$ *we obtain* $Q = W = p_0 v_0 \ln 2$.

9.4.5.24 Ex: Calorimeter

a. A calorimeter initially contains 100 ml of water in thermal equilibrium with the calorimeter at a temperature of $T_1 = 20°$. Now, an amount of 150 ml of water with the temperature $T_2 = 70°$ is added. After reaching thermal equilibrium again, the temperature becomes $T_f = 45°$. Knowing the specific heat of water, $c_a = 4.186$ J/gK, calculate the thermal capacity of the calorimeter.
b. Now we put into the same calorimeter (filled with 250 ml of water at temperature $T_f = 45°$) additionally a metallic body with the mass $m_3 = 200$ g and temperature $T_3 = 50°$. After reaching thermal equilibrium again, the temperature becomes $T_{ff} = 41°$. Calculate specific heat of the body.

Solution: *a. The thermal capacity of the calorimeter is,*

$$C = m_2 c_a \frac{T_2 - T_f}{T_f - T_1} - m_1 c_a = \left(150 \cdot 4.186 \cdot \frac{70 - 40}{40 - 20} - 100 \cdot 4.186\right) \ J/K = 209 \ J/K \ .$$

b. The specific heat of the body is,

$$c_3 = \frac{[(m_1 + m_2)c_a + C](T_{ff} - T_f)}{m_3(T_3 - T_{ff})} = \frac{[250 \cdot 4.186 + 209](41 - 40)}{200 \cdot (50 - 41)} = 0.698 \ J/gK \ .$$

9.4.5.25 Ex: Measurement of latent heat upon water condensation

A calorimeter with thermal capacity $C = 209$ J/K initially contains 250 ml of water in thermal equilibrium at a temperature of $T_1 = 20°$. Now, an amount of 40 ml of water vapor is added. After reaching thermal equilibrium again, the temperature is $T_f = 92°$. Calculate the latent heat of water condensation.

Solution: *The latent heat of water condensation isfound to be,*

$$L_c = \frac{(m_1 c_a + C)(T_1 - T_f)}{m_2} + c_a(T_c - T_f) = \frac{(250 \cdot 4.186 + 209)(20 - 92)}{40} + 4.186 \cdot (100 - 92)$$
$$= -2226 \ J/g \ .$$

9.4.5.26 Ex: Latent heat in a sauna

A Finnish sauna is heated to 90°C. To increase the thermal conductivity of the air, you put 1 liter of water at a temperature of 20°C in the oven container, where the water is evaporated. How does the temperature of the sauna evolve?

Solution:

9.4.5.27 Ex: Adiabatic expansion

a. During the adiabatic expansion of a gas the pressure P and the volume V of the gas satisfy the relationship $PV^\gamma = \alpha$, where α is a constant, and γ is the factor of the gas that gives the ratio between the specific heats at constant pressure and volume, i.e. $\gamma = c_P/c_V$. A gas was placed in a cylinder with a movable (frictionless) plunger completely insulated from the external environment. The assembly makes it possible to measure the volume and pressure of the gas during its expansion and the experimental values obtained are given in the table below.
a. From the values in the table below, and using the least squares method, determine the gas factor and the constant α. (**Hint:** to obtain a linear relationship, take $x = \log V$ and $y = \log P$.).
b. Determine, through the method of least squares, the uncertainties in the values obtained for γ and α.
c. Using a log×log paper, prepare a graph P×V and determine the values of γ and α. Compare with the results obtained by the least squares method.
Notes: When displaying the values of γ and α, be sure to indicate the units in which they are expressed.
Display the values of S_x, S_y, S_{x2} and S_{xy} used in the least squares method calculations.

V (litros)	P (atm)
40	1.20
41	1.16
43	1.10
44	1.05
46	0.98
47	0.96
49	0.90
50	0.87

Solution: *a. We initially calculate,*

V *(litros)*	P *(atm)*	$\lg V$ *(ltr)*	$\lg P$ *(atm)*
40	*1.20*	*1.6021*	*0.0792*
41	*1.16*	*1.6128*	*0.0645*
43	*1.10*	*1.6335*	*0.0414*
44	*1.05*	*1.6435*	*0.0212*
46	*0.98*	*1.6628*	*-0.0088*
47	*0.96*	*1.6721*	*-0.0177*
49	*0.90*	*1.6902*	*-0.0458*
50	*0.87*	*1.6990*	*-0.0605*

With $x \equiv \lg V$ *e* $y \equiv \lg P$*, we get,*

$$y = ax + b = -\gamma x + \lg \alpha \ .$$

We calculate $N = 8$ *and,*

$$S_x = \sum_{i=1}^{N} x_i = 13.2158 \quad , \quad S_y = \sum_{i=1}^{N} y_i = 0.0735$$

$$S_{x^2} = \sum_{i=1}^{N} x_i^2 = 21.8408 \quad , \quad S_{xy} = \sum_{i=1}^{N} x_i y_i = 0.1089$$

$$D = N S_{x^2} - S_x^2 = 0.0691$$

$$a = \frac{N S_{xy} - S_x S_y}{D} = -1.4441 \quad , \quad b = \frac{S_y S_{x^2} - S_{xy} S_x}{D} = 2.3949$$

$$\Delta y = \sqrt{\frac{\sum_{i=1}^{N} (a x_i + b - y_i)^2)}{N-2}} = 0.0955$$

$$\Delta a = \Delta y \sqrt{\frac{N}{D}} = 1.0281 \quad , \quad \Delta b = \Delta y \sqrt{\frac{S_{x^2}}{D}} = 1.6987 \ .$$

With that we find,

$$\gamma = -a = 1.44 \quad , \quad \alpha = 10^b = 248$$

$$\Delta\gamma = \Delta a = 1.03 \quad , \quad \Delta\alpha = 10^b \ln 10 \Delta b = 971 \ .$$

Consider a set of N *pairs of experimental data* (x_i, y_i)*, where the values* x_i *are*

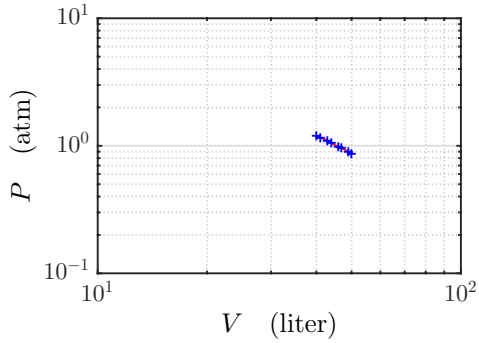

Figure 9.14: Adiabatic expansion.

assigned to the independent variable and y_i to the dependent variable. Assuming that the relationship $y(x)$ is considered as linear, i.e.,

$$y = ax + b \ .$$

the least squares method provides the values for the slope a and the linear term b for the line that best approximates the experimental data. The expressions of the line coefficients and their respective uncertainties are:

$$a = \frac{NS_{xy} - S_x S_y}{D} \quad , \quad \Delta a = \Delta y \sqrt{\frac{N}{D}}$$
$$b = \frac{S_y S_{x^2} - S_{xy} S_x}{D} \quad , \quad \Delta b = \Delta y \sqrt{\frac{S_{x^2}}{D}} \ ,$$

where,

$$S_x = \sum_{i=1}^{N} x_i \quad , \quad S_y = \sum_{i=1}^{N} y_i$$
$$S_{x^2} = \sum_{i=1}^{N} x_i^2 \quad , \quad S_{xy} = \sum_{i=1}^{N} x_i y_i$$

and

$$\Delta y = \sqrt{\frac{\sum_{i=1}^{N} (ax_i + b - y_i)^2)}{N-2}} \quad , \quad D = NS_{x^2} - S_x^2 \ .$$

9.4.5.28 Ex: Adiabatic expansion

A diatomic gas is initially maintained at a pressure of $P_i = 4000$ hPa in a piston of volume $V_i = 1$ l at temperature $T_i = 100°$C. Now the gas pressure forces the piston to move until it reaches half the pressure. Considering the expansion as an adiabatic

process
a. calculate the number of moles η inside the piston;
b. calculate the thermal capacity at constant volume C_V of the gas;
c. calculate thermal capacity at constant pressure C_P;
d. calculate the adiabatic coefficient γ;
e. calculate the final volume of the piston;
f. calculate the final temperature of the gas;
g. calculate the work done by the gas on the piston.
h. Now, the gas cools down gradually while the piston is held fix. Calculate the pressure P_r when the temperature reached $T_r = 20°\text{C}$.

Solution: *a. We have* $\eta = \frac{P_i V_i}{RT_i} = \frac{4\cdot 10^5 \cdot 10^{-3}}{8.31\cdot 293.15}\ mol = 0.16\ mol$;
b. As the gas is diatomic, $C_V = \frac{5}{2}\eta R = 3.4\ J/K$.
c. Similarly, $C_P = \frac{7}{2}\eta R = 4.8\ J/K$.
d. The adiabatic coefficient is, $\gamma = \frac{7}{5} = 1.4$.
e. For adiabatic expansion, $PV^\gamma = const$. *Hence,*

$$V_f = V_i \left(\frac{P_i}{P_f}\right)^\gamma = 10^{-3}\ m^3 \cdot 2^{1.4} = 2.6\ l.$$

f. The final temperature is,

$$T_f = \frac{P_f V_f}{\eta R} = \frac{2\cdot 10^5 \cdot 2.6\cdot 10^{-3}}{8.31\cdot 0.16} = 117.8°\,C\ .$$

g. The work is,

$$\delta W = dE_{int} = C_V dT = \frac{5}{2}\eta R(T_f - T_i) = \frac{5}{2}\cdot 0.16\cdot 8.31\cdot (117.8 - 20) = 325\ J\ .$$

h. The pressure is,

$$P_r = \frac{\eta R T_r}{V_f} = \frac{0.16\cdot 8.31\cdot 293.15}{2.6\cdot 10^{-3}} = 1500\ hPa\ .$$

9.4.5.29 Ex: Cyclic process

A and B be two states of an ideal gas with the same temperature T, but different pressures and volumes. Show explicitly that $\Delta Q/T$ remains the same, regardless of whether we go from A to B via a reversible isothermal process or first with a reversible isobaric process and then with a reversible isochoric process.

Solution: *We denote by* P_A *and* V_A *the pressure and volume of state A, analogously* p_B *and* V_B *of state B. Since both states have the same temperature* $T_A = T_B = T_0$, *it follows from the ideal gas equation that,*

$$p_A V_A = N k_B T_0 = p_B V_B \Rightarrow \frac{p_B}{p_A} = \frac{V_A}{V_B}\ .$$

Isothermal process: *Since* $T = T_0 = const$, *we get* $\Delta E = 0$. *With the 1st law of thermodynamics* $\delta Q = -\delta W = pdV$. *Use the ideal gas equation,* $p = N k_B \frac{T}{V}$ *brings*

us to,,

$$dS = \frac{\delta Q}{T} = \frac{pdV}{T} = Nk_B \frac{dV}{V} \ ,$$

Hence,

$$\Delta S_{it} = \int_{S_A}^{S_B} dS = Nk_B \int_{V_A}^{V_B} \frac{dV}{V} = Nk_B \ln \frac{V_B}{V_A} \ .$$

The index "it" at the entropy change ΔS_{it} means "isothermal". Analogously below, the index "ib" means "isobar" and "ic" means "isochor".
***Isobaric + isochoric process**: $(p_A, V_A) \stackrel{isobar}{\longrightarrow} (p_A, V_B) \stackrel{isochor}{\longrightarrow} (p_B, V_B)$. Here, the temperature changes in each of the two processes T.*
First the isobaric process $(p_A, V_A) \stackrel{isobar}{\longrightarrow} (p_A, V_B)$. The ideal gas equation provides,

$$T = \frac{p_A}{Nk_B} V \Rightarrow dT = \frac{p_A}{Nk_B} dV \ .$$

Replacing dT in the 1st law, $\delta Q = dE - \delta W = C_V dT + p_A dV$, and T in $dS = \frac{\Delta Q}{T}$, we get the relation,

$$dS = \frac{\delta Q}{T} = \frac{1}{T}(C_V dT + p_A dV) = (C_V + Nk_B)\frac{dV}{V} \ .$$

Hence,

$$\Delta S_{ib} = (C_V + Nk_B) \int_{V_A}^{V_B} \frac{dV}{V} = (C_V + Nk_B) \ln \frac{V_B}{V_A} \ .$$

Now the following isochore process control: $(p_A, V_B) \stackrel{isochor}{\longrightarrow} (p_B, V_B)$. The ideal gas equation provides,

$$T = \frac{V_B}{Nk_B} p \Rightarrow dT = \frac{V_B}{Nk_B} dp \ .$$

Because of $\Delta V = 0$ the 1st law is reduced to $\delta Q = dE = C_V dT$. Hence,

$$dS = \frac{\delta Q}{T} = C_V \frac{dT}{T} = C_V \frac{dp}{p} \ .$$

This leads to,

$$\Delta S_{ic} = C_V \int_{p_B}^{p_A} \frac{dp}{p} = C_V \ln \frac{p_B}{pA} = -C_V \ln \frac{V_B}{V_A} \ ,$$

where we used equation (3) for the last equal sign. Overall, we get the entropy change,

$$\Delta S_{ib+ic} = \Delta S_{ib} + \Delta S_{ic} = Nk_B \ln \frac{V_B}{V_A} = \Delta S_{it} \ ,$$

which corresponds to the change in entropy deduced for the isothermal process ΔS_{it} [see equation (4)].

9.4.5.30 Ex: Clément-Desormes cyclic process

An ideal gas with N atoms and the heat capacities $C_V = \frac{3}{2}Nk_B$ and $C_p = \frac{5}{2}Nk_B$ goes through the cycle shown in the figure: First an isotherm from "1" to "2", then an isobar from "2" to "3" and finally an isochore from "3" to "1". For the starting point "1", the temperature T_1 and the volume V_1 are known, for "2" V_2 is given.
a. Calculate the work done and the heat input for all three steps of the cycle.
b. Calculate the efficiency η of the process as a function of V_1 and V_2 respectively T_1 and T_3. Calculate the total changes of internal energy and entropy (see Fig. 9.9).

Solution: *a. For the different ways we get,*

$$
\begin{aligned}
1 \to 2: \quad & \Delta Q = \Delta A = \int_{V_1}^{V_2} p \, dV = Nk_B T_1 \log \frac{V_2}{V_1} \\
2 \to 3: \quad & \Delta Q = \frac{5}{2} N \; k_B \Delta T = -\frac{5}{2} Nk_B T_1 \left(1 - \frac{V_1}{V_2}\right) \; , \\
& \Delta A = p_2 \Delta V = -Nk_B T_1 \left(1 - \frac{V_1}{V_2}\right) \\
3 \to 1: \quad & \Delta Q = \frac{3}{2} N \; k_B \Delta T = \frac{3}{2} Nk_B T_1 \left(1 - \frac{V_1}{V_2}\right) \; , \\
& \Delta A = 0 \; .
\end{aligned}
$$

b. We get,

$$
\begin{aligned}
\eta &= \frac{A_{1\to2} + A_{2\to3}}{Q_{1\to2} + Q_{3\to1}} = \frac{Q_{1\to2} + Q_{2\to3} + Q_{3\to1}}{Q_{1\to2} + Q_{3\to1}} = 1 + \frac{Q_{2\to3}}{Q_{1\to2} + Q_{3\to1}} \\
&= 1 - \frac{5(V_2 - V_1)}{2V_2 \log \frac{V_2}{V_1} + 3(V_2 - V_1)} = \frac{2V_2 \log \frac{V_2}{V_1} - 2(V_2 - V_1)}{2V_2 \log \frac{V_2}{V_1} + 3(V_2 - V_1)} \\
&= 1 - \frac{5(T_1 - T_3)}{2T_1 \log \frac{T_1}{T_3} + 3(T_1 - T_3)} = \frac{2T_1 \log \frac{T_1}{T_3} - 2(T_1 - T_3)}{2T_1 \log \frac{T_1}{T_3} + 3(T_1 - T_3)} \\
\Delta S &= \Delta E = 0 \; .
\end{aligned}
$$

9.4.5.31 Ex: Cyclic process

An ideal gas with N atoms and the heat capacities $C_V = \frac{3}{2}Nk_B$ and $C_p = \frac{5}{2}Nk_B$ goes through the cycle shown in the figure. For the starting point 1 its pressure p_1, volume V_1, and thus also the temperature T_1 are known.
a. Calculate p_2, T_2, p_3 and T_3, if $V_2 = V_3 = 3V_1$.
b. For all 3 steps of the cycle, calculate the work done on the gas ΔW, the heat supplied ΔQ, and the internal energy ΔE, as well as the change in entropy ΔS.

Solution: *a. For the isothermal process* $1 \to 2$ *we know* $p_1 V_1 = p_2 V_2 = 3p_2 V_1$. *Hence,*

$$
p_2 = p_1/3 \qquad \textit{and} \qquad T_2 = T_1 \; .
$$

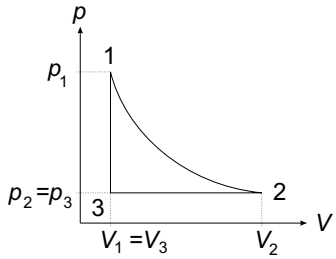

Figure 9.15:

For the adiabatic process $3 \to 1$ *we know* $p_1V_1^\kappa = p_3V_3^\kappa = p_3V_1^\kappa \cdot 3^{5/3}$ *with* $\kappa \equiv C_p/C_V = 5/3$. *Hence,*

$$p_3 = p_1/3^{5/3} \ .$$

Furthermore, $p_3V_3/p_1V_1 = T_3/T_1$. *Hence,*

$$T_3 = \frac{p_1 3V_1}{3^{5/3}p_1V_1}T_1 = \frac{3}{3^{5/3}}T_1 \ .$$

b. For the isothermal process $1 \to 2$ *we know* $\Delta E = \Delta Q + \Delta W = 0$. *Hence,*

$$\Delta W = -\int pdV = -\int_{V_1}^{V_2} Nk_BT_1\frac{dV}{V} = -Nk_BT_1 \ln\frac{V_2}{V_1} = -Nk_BT_1 \ln 3 \ .$$

Thus, the heat is $\Delta Q = -\Delta W$ *and the entropy* $\Delta S = \frac{1}{T_1}\Delta Q = Nk_B \ln 3$.
For the isochoric process $2 \to 3$ *we know* $\Delta W = 0$ *and hence* $\Delta Q = \Delta E = C_V\Delta T = \frac{3}{2}Nk_B(T_3 - T_1) = -\frac{3}{2}Nk_BT_1(1 - 3^{-2/3})$. *Hence,*

$$\Delta S = \int \frac{\delta Q}{T} = C_V\int_{T_1}^{T_3}\frac{dT}{T} = \frac{3}{2}Nk_B \ln\frac{T_3}{T_1} = \frac{3}{2}Nk_B \ln\frac{1}{3^{2/3}} = -Nk_N \ln 3 = \Delta S_{1-2} \ .$$

For the adiabatic process $3 \to 1$ *we know* $\Delta Q = 0 = \Delta S$. *Hence* $\Delta E = \Delta W = C_V(T_1 - T_3) = \frac{3}{2}Nk_BT(1 - 3^{-2/3})$.

9.4.5.32 Ex: Cyclic process

In a heat power machine (illustrated in Fig. 9.16), the working gas (helium) is sealed off in a cylinder by a movable piston. The gas is alternately heated and cooled from the outside. The piston moves back and forth periodically and drives a shaft. The initial state is: $p = 0.2 \cdot 10^6$ Pa, $V = 150\,\mathrm{cm}^3$, $T = 300$ K.
a. Calculate the mass of the enclosed helium and the adiabaticity coefficient.
b. During a complete work cycle, the gas undergoes the following changes in its state:
$1 \to 2$ isochoric heating to 600 K,
$2 \to 3$ isothermal expansion to twice the volume,
$3 \to 4$ isochoric cooling to the initial temperature,
$4 \to 1$ isothermal compression to initial volume.

Calculate the respective pressures and illustrate the cyclic process in a $p-V$ diagram.
c. Calculate the total mechanical work.
d. Calculate the efficiency η of the engine as a ratio of the amount of useful work to the total amount of work.

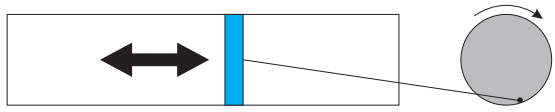

Figure 9.16: Heat power engine

Solution: *a. The mass of helium is $m_{He} = 4u$. Hence, the enclosed mass is,*

$$m = N m_{He} = \frac{pV}{k_B T} m_{He} = x\,\mathrm{kg} \ .$$

The adiabaticity coefficient for the one-atomic gas is,

$$\gamma = \frac{f+1}{f} = 4/3 \ .$$

b. The pressures are... Fig. 9.17 shows the cyclic process.
c. $\Delta W = 20.8$ J.
d. $\eta = 24\%$.

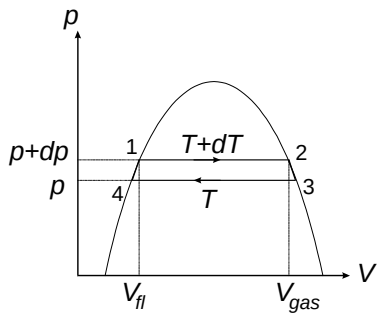

Figure 9.17: Cyclic process of a heat power engine.

9.4.5.33 Ex: Cyclic process

An engine, whose four work steps consist of two isothermal and two isochoric processes, runs at a speed of $N = 500\ \mathrm{min}^{-1}$. There is $\nu = 0.5$ mol of an ideal, monoatomic gas in the volume of the engine. The parameters for the individually labeled working steps are $T_1 = 50°\mathrm{C}$, $p_1 = 2.0$ bar, and $p_2 = 5.0$ bar.
a. Determine the volumes $V_1 = V_2$ and $V_3 = V_4$, the pressure p_4, and the temperature T_2.

b. What efficiency η does the cycle have?
c. How high is the net power P of the engine?

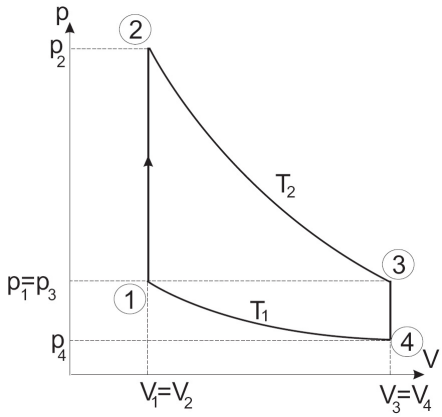

Figure 9.18:

Solution: *a.* $V_1 = 6.7\ dm^3$, $V_3 = 16.75\ dm^3$, $T_2 = 807\ K$, $p_4 = 0.8\ bar$.
b. The efficiency is, $\eta = 0.6 = 60\ \%$.
c. To calculate the engine power $P = \frac{\Delta W_{ges}}{t}$ *we need the work done in the compression and the decompression phase respectively* $W_2 = \nu R T_2 \ln \frac{V_1}{V_3} = -3074\ J$ *respectively* $W_1 = \nu R T_1 \ln \frac{V_3}{V_1} = 1230\ J$. $W_{ges} = W_1 + W_2 = 1817\ J \Rightarrow P = \frac{1843\ J}{0.12\ s} = 15.4\ kJ$.

9.4.5.34 Ex: Particle collisions with a container

How many particle collisions Z does a wall surface $A = 1\ \mathrm{dm}^2$ experience in $\Delta t = 1$ s at $T = 298$ K and $p = 1$ bar through the particles of an ideal gas, if $\langle |v_x| \rangle$, the mean value of the particle velocity in the x direction, has the value 330 m/s?
Hint: Imagine a cuboid box in an xyz coordinate system and assume the wall surface of interest as one of the cuboid surfaces perpendicular to the x-axis. The width of the box is Δx, so its volume is $V = A \cdot \Delta x$. There is a simple relationship for the mean number $\langle \nu_x \rangle$ of impacts that a single particle does exert on the wall within a time Δt depending on Δx, Δt and $\langle |v_x| \rangle$. To get Z you have to consider that the gas contains N particles.

Solution: *Between the impacts on the right wall, the particle has to cross the box once in both directions. The distance covered is* $2\Delta x$. *The average number* $\langle \nu_x \rangle$ *of the impacts that a single particle exerts on the wall results from the average distance* $\langle |v_x| > \cdot \Delta t$ *covered within the time interval* Δt *divided by this distance* $2\Delta x$*:*

$$\langle \nu_x \rangle = \frac{\Delta t \cdot \langle |v_x| >}{2\Delta x} \ .$$

The average number Z of impacts on the wall caused by N particles is therefore,

$$Z = N \cdot \langle \nu_x \rangle = \frac{N\ \Delta t \cdot \langle |v_x| \rangle}{2\Delta x}\ .$$

With $\Delta x = V/A$ and $V = \frac{N\ k_B\ T}{p}$ follows,

$$Z = \frac{\Delta t \cdot < |v_x| > \cdot A \cdot p}{2k_B T} = \frac{10^5\ Nm^{-2} \cdot 1\ s \cdot 330\ ms^{-1} \cdot 0.01\ m^2}{2 \cdot 1.38 \cdot 10^{-23} Nm \cdot K^{-1} \cdot 298\ K} \approx 4 \cdot 10^{25}\ .$$

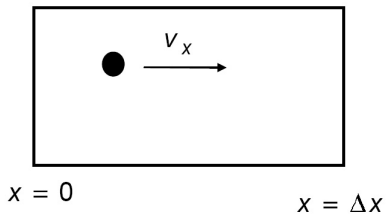

Figure 9.19:

9.4.5.35 Ex: Entropy changes

a. What entropy increase results when 200 g of (liquid) water at 0°C and 200 g water at 90°C are mixed at constant pressure in a heat-insulated recipient? The molar heat c_p of the water should be 75.5 J/(mol K) regardless of the temperature.
b. 1 dm^3 helium at $p_0 = 1$ bar and $T_0 = 0$°C are heated to the temperature $T = 500$ K. How big is the change in entropy upon isochoric and isobaric heating?

Solution: *a. Since S is a state variable, it does not matter which way the temperature equilibration takes place. Because of the path-independence of the entropy one can imagine the mixing process such that the two water portions are brought from their respective initial temperatures to the end temperature as homogeneous phases "1" and "2". The differential entropy change of the individual phases is given by $dS = C_p\ d\ln T$. So we get,*

$$\Delta S = \Delta S_1 + \Delta S_2 = C_P \int_{T_{1,0}}^{T_m} d\ln T + C_P \int_{T_{2,0}}^{T_m} d\ln T = C_P \ln \frac{T_m^2}{T_{1,0} T_{2,0}}\ .$$

From this, $\Delta S \approx 17.0\ J/K$, where $C_p = \nu \cdot c_p = 11.111\ mol \cdot 75.5\ J/(mol\ K)$ and $T_m = 45°\,C = 319\ K$.
b. The entropy change upon isobaric heating from $T_0 = 273\ K$ to $T_1 = 500\ K$ is,

$$\Delta S_{isobar} = \nu \left(C_V \ln \frac{T_1}{T_0} + R \ln \frac{V_1}{V_0} \right)\ ,$$

where $\nu = 1/22.4$ is the molar fraction. Because of $V_1/V_0 = T_1/T_0$ for $p =$const and with $C_P = R + C_V$ we get:

$\Delta S_{isobar} = \nu C_p \ln \frac{T_1}{T_0}$ *with* $C_p = 21$ *J/(K·mol). From this* $\Delta S_{isobar} = \frac{21}{22.4} \ln \frac{500}{273} = 0.58$ *J/K.*
Isochoric heating: $\Delta S_{isochor} = \nu C_v \ln \frac{T_1}{T_0}$ *with* $C_v = 12.7$ *J/(K mol)*$= 0.34$ *J/K.*

9.4.5.36 Ex: Material parameters

The compressibility κ, the thermal expansion coefficient α, and the stress coefficient β are important material parameters. In the case of a single substance system, they are defined by,

$$\kappa = -\frac{1}{V}\left.\frac{\partial V}{\partial p}\right|_{n,T} \qquad \alpha = \frac{1}{V}\left.\frac{\partial V}{\partial T}\right|_{n,p} \qquad \beta = \frac{1}{p}\left.\frac{\partial p}{\partial T}\right|_{n,V} .$$

Here n is the number of moles.
a. Show that these relationships can be rewritten, using the molar volume v, to,

$$\kappa = -\frac{1}{v}\left.\frac{\partial v}{\partial p}\right|_{T} \qquad \alpha = \frac{1}{v}\left.\frac{\partial v}{\partial T}\right|_{p} \qquad \beta = \frac{1}{p}\left.\frac{\partial p}{\partial T}\right|_{v} .$$

b. Use the total differential of $V = V(T, p, n)$ to show that, in general,

$$\beta = \frac{\alpha}{\kappa p} .$$

c. Calculate κ, α and β for an ideal gas as functions of p and T. Show that the relationship from (b) is also fulfilled.

Solution: *a. Relationship between volume* V *and molar volume* v*:* $V = n\ v$.

$$\kappa = -\frac{1}{V}\left.\frac{\partial V}{\partial p}\right|_{n,T} = -\frac{1}{n\ v}\left.\frac{\partial (n\ v)}{\partial p}\right|_{n,T} = -\frac{1}{n\ v} n \left.\frac{\partial v}{\partial p}\right|_{n,T} = -\frac{1}{v}\left.\frac{\partial v}{\partial p}\right|_{n,T} .$$

Analogously for α*. For* $p = p(T, v)$*:*

$$dp = \left.\frac{\partial p}{\partial T}\right|_{v} dT + \left.\frac{\partial p}{\partial v}\right|_{T} dv .$$

Constant v *can be achieved by keeping* V *and* n *constant. So:*

$$\left.\frac{\partial p}{\partial T}\right|_{v} = \left.\frac{\partial p}{\partial T}\right|_{n,V} .$$

From this follows (as requested):

$$\beta = \frac{1}{p}\left.\frac{\partial p}{\partial T}\right|_{n,V} = \frac{1}{p}\left.\frac{\partial p}{\partial T}\right|_{v} .$$

b. Total differential of V*:*

$$dV = \frac{\partial V}{\partial T} dT + \frac{\partial V}{\partial p} dp + \frac{\partial V}{\partial n} dn$$

can be rewritten with α and κ:

$$dV = V\ \alpha\ dT - V\ \kappa\ dp + \frac{\partial V}{\partial n} dn\ .$$

If V and n are constant,

$$0 = V(\alpha\ dT - \kappa\ dp)$$

with $dp = \left.\frac{\partial p}{\partial T}\right|_{n,V} dT$. Hence:

$$0 = V\left[\alpha - \kappa\ \left.\frac{\partial p}{\partial T}\right|_{n,V}\right]\ dT\ .$$

At $V, dT \neq 0$ follows,

$$\alpha - \kappa\ \left.\frac{\partial p}{\partial T}\right|_{n,V} = 0\ .$$

This leads to the wanted relationship.
c. With $v = R\ T/p$ follows,

$$\kappa = -\frac{1}{v}\left.\frac{\partial v}{\partial p}\right|_T = -\frac{p}{RT}\left(R\ T\frac{-1}{p^2}\right) = \frac{1}{p}$$
$$\alpha = \frac{1}{v}\left.\frac{\partial v}{\partial T}\right|_p = \frac{p}{R\ T}\frac{R}{p} = \frac{1}{T}$$
$$\beta = \frac{1}{p}\left.\frac{\partial p}{\partial T}\right|_v = \frac{v}{R\ T}\frac{R}{v} = \frac{1}{T}\ .$$

9.4.5.37 Ex: A lake in winter

How long does it take at an air temperature of $-6°$C to form a 4 cm thick layer of ice on the surface of a lake (thermal conductivity of ice: $\kappa = 1.7 \cdot 10^{-2}$ J/(s cm K); density of ice: $\rho = 0.92$ g/cm^3; amount of heat that must be dissipated to form 1 g of ice: 335 J)
Note: First consider a layer of ice of thickness z, and then think about how much heat has to be dissipated from the lake in order to to form additional layer of thickness dz.

Solution: *Consider a layer of ice of thickness z. To form the next layer of ice of thickness dz, heat must be transported outside through the initial layer. The amount of heat that must be dissipated to form an additional layer of thickness dz and area A is,*

$$dQ_1 = Q_0 \cdot dM = Q_0 \cdot \rho \cdot A \cdot dz$$

with $Q_0 = 335$ J. The amount of heat that can be dissipated in time dt through the layer of ice z is,

$$dQ_2 = -\frac{\kappa\ A\ \Delta T}{z} \cdot dt\ .$$

The ice forms at $T = 0°C \Rightarrow \Delta T = -6\ K$. dQ_1 *and* dQ_2 *must be the same,*

$$\Rightarrow Q_0\ \rho\ A\ dz = -\frac{\kappa\ A\ \Delta T}{z} \Leftrightarrow dt = -\frac{Q_0\ \rho}{\kappa\ \Delta T} z\ dz\ .$$

Integration on both sides yields,

$$\int_0^t dt' = -\frac{Q_0\ \rho}{\kappa\ \Delta T} \int_0^d z\ dz\ ,$$

hence,

$$\Rightarrow t = -\frac{Q_0\ \rho}{\kappa\ \Delta T} \cdot \frac{d^2}{2} \Rightarrow \frac{335\ J/g \cdot 0.92\ g/cm^3}{1.7 \cdot 10^{-2} J/(s{\cdot}cm{\cdot}K) \cdot 6\ K} \cdot \frac{1}{2} \cdot 16\ cm^2 \approx 2.417{\cdot}10^4\ s \approx 6h\,43min\,.$$

9.4.5.38 Ex: Clausius-Clapeyron relationship

Show that the *Clausius-Clapeyron* equation,

$$\frac{dp}{dT} = \frac{L}{T(V_{gas} - V_{fl})}$$

can also be derived via a cycle analogous to Carnot's cycle. The working fluid is an evaporating liquid, and the efficiency of this fictitious machine is dT/T, because the temperature difference between the two isotherms is dT. From the heat Q used in the evaporation and the work done $\oint pdV$, which are related on one hand to the latent heat L and on the other to the volume difference of V_{fl} and V_{gas}, results the rise in vapor pressure dp/dt.

Solution: *We know,* $W = \int pdV \approx dp(V_{gas} - V_{fl})$, $\frac{W}{Q} = \eta = \frac{dT}{T}$, *and* $Q \equiv L$. *From this follows,* $\frac{dp}{dT} = \frac{L}{T(V_{gas} - V_{fl})}$.

9.4.5.39 Ex: Hydrogen concentration in a metal

The concentration of hydrogen c_H, which is dissolved in a metal in the form of H atoms, depends on the pressure p of the H_2 gas around the metal. Determine the relationship between concentration and pressure!
Hint: In equilibrium the chemical reaction $H_2 = 2H$ is determined by $\mu_{H_2} = 2\mu_H$, where $\mu_{H_2} = k_B T \ln p + \chi_{H_2}(T)$. Consult the textbooks to find a suitable ansatz for the chemical potential of a substance (and thus also for atomic hydrogen) in dilute solution.

Solution: *The relation* $\mu_{H_2} = k_B T \ln p + \chi_{H_2}$, *in a solid corresponds to* $p_H \hat{=} c_H$. *Furthermore,* $\mu_H = k_B T \ln c_H + \chi_H$. *In equilibrium be* $\mu_{H_2} = 2\mu_H$, *follows,*

$$\frac{1}{2} \ln p + \frac{\chi_{H_2}}{2k_B T} = \ln c_H + \frac{\chi_H}{k_B T}\ ,$$

follows,

$$c_H = p^{1/2} e^{(\chi_{H_2} - 2\chi_H)/2k_B T} \ .$$

9.4.5.40 Ex: Heat power engine and heat pump

Consider a heat power engine and a heat pump based on the Carnot cycle. Calculate the efficiency and the generated, respectively, consumed power ad a function of the temperature difference between the hot and the cold bath.

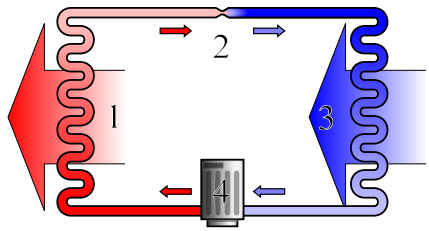

Figure 9.20: Principle of a heat pump.

Solution:

9.4.5.41 Ex: Heat capacity

When drilling a brass block of 500 g ($c = 0.1$ cal/g°C), a power of 300 W is provided for 2 minutes. What is the temperature rise of the block if 75% of the heat generated warms it up? What happens to the remaining 25%?

Solution:

9.4.5.42 Ex: Specific heat

Suppose the specific heat of a body varies with temperature according to the expression $c = A + BT^2$, where A and B are constant and T given in °C. Compare the average value of c between $T = 0$ and $T = T_1$ with its value at $T_1/2$.

Solution:

9.4.5.43 Ex: Thermal expansion

Consider a solid body with momentum of inertia I. Show that due to a small temperature variation ΔT, this momentum varies by $\Delta I = 2\alpha \Delta T$, where α is the linear expansion coefficient. With this result, calculate how much the period of a physical

pendulum varies when subject to a temperature variation ΔT.

Solution:

9.4.5.44 Ex: Thermal conduction

Show that the thermal current in a substance of conductivity K located between the surfaces of two concentric spheres is given by:

$$\frac{dQ}{dt} = H = (T_1 - T_2)\frac{4\pi k r_1 r_2}{r_2 - r_1} \ ,$$

where r_1 and r_2 are respectively the radii of the inner and outer surfaces and $T_1 > T_2$.

Solution:

9.4.5.45 Ex: Thermal work

A thermodynamic system is brought from an initial state A to another B and then brought back to A via the point C, as illustrated in the diagram in the figure. Calculate the work done by the system to complete the entire cycle.

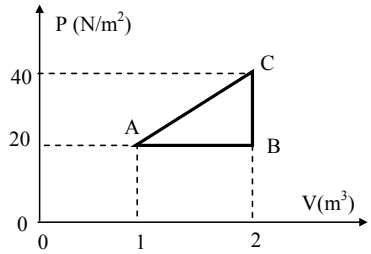

Figure 9.21:

Solution:

9.4.5.46 Ex: Thermal expansion

A bar with thermal expansion coefficient α and Young's modulus Y $\left(\frac{F}{A} = Y\frac{\Delta L}{L}\right)$ is stuck between two walls, as shown in the figure. Calculate the stress in the bar when the temperature is increased by ΔT.

Solution:

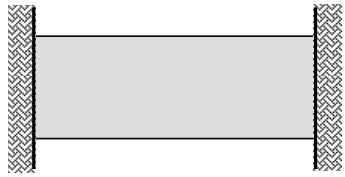

Figure 9.22:

9.4.5.47 Ex: Latent heat

How much heat is needed to transform 1 g of ice at $-10°$C ($c_{gelo} = 0.55$ cal/g°C, $L_f = 80$ cal/g) in a vapor at 100°C ($L_V = 540$ cal/g)?

Solution:

9.4.5.48 Ex: Heat capacity

A metal bar ($C = 0.2$ cal/g°C) at 100°C is placed on a large block of ice at 0°C. What is the mass of the bar if, when the system reaches thermal equilibrium, 500 g of ice have melted?

Solution:

9.4.5.49 Ex: Latent heat

An ice block is placed at $-20°$C in an airtight container together with 200 g of water vapor at 100°C. If the mass of the ice is 500 g, what will be the final temperature of the system?

Solution:

9.4.5.50 Ex: Thermal conduction

Find the temperature gradient and thermal current in a bar of conductivity K, length L and irregular cross section, as shown in the figure.

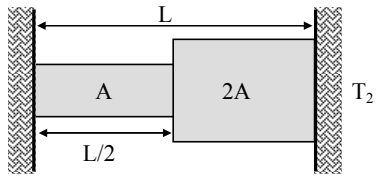

Figure 9.23:

Solution:

9.4.5.51 Ex: Volumetric expansion of an ideal gas

Calculate the volumetric expansion coefficient of an ideal gas at constant pressure.

Solution:

9.4.5.52 Ex: Adiabatic expansion

Calculate the volumetric expansion coefficient of an ideal gas during an adiabatic expansion.

Solution:

9.4.5.53 Ex: Compressibility of an ideal gas

Calculate the compressibility $\left(\kappa = \frac{1}{V}\frac{dV}{dP}\right)_T$ of an ideal gas.

Solution:

9.4.5.54 Ex: Adiabatic expansion

An ideal gas, initially at pressure P_1 and volume V_1, expands adiabatically to pressure P_2 and volume V_2. Show that the work done is $W = (P_1V_1 - P_2V_2)/(\gamma - 1)$, where $\gamma = C_p/C_V$.

Solution:

9.4.5.55 Ex: The Otto cycle

Calculate the yield ($\eta = W/Q$, Q_1 =heat received by the system) of the Otto cycle (see figure).

Solution:

9.4.5.56 Ex: Specific heat at constant volume / pressure

Explain why the specific heat at constant volume is less than the specific heat at constant pressure.

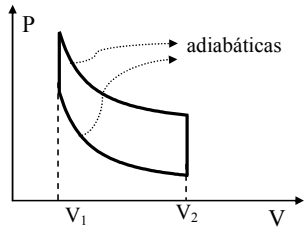

Figure 9.24:

Solution:

9.4.5.57 Ex: Adiabatic coefficient

Show that for a diatomic gas $\gamma = \frac{C_p}{C_V} = \frac{7}{5}$.

Solution:

9.4.5.58 Ex: Thermal cycle

Consider the thermal cycle shown in the figure.
a. Calculate the heat supplied to the system in the isothermal branch $1 \to 2$,
b. Calculate the work in the isobaric branch $2 \to 3$ and
c. Calculate the heat supplied to the system in the isochoric branch $3 \to 1$.

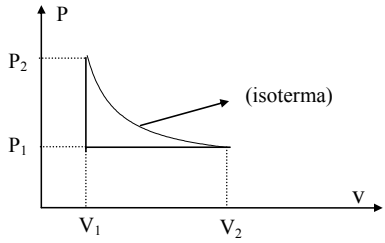

Figure 9.25:

Solution:

9.5 Free energy and enthalpy

9.5.1 Equation of state of the real gas

In reality interparticle interactions increase the effective pressure and the finite size of the molecules reduces the effective volume. In the van der Waals model the ideal gas equation is generalized to,

$$(p + p^*)(V - V^*) = Nk_BT \ , \tag{9.33}$$

with $p^* \propto (N/N_A)^2/V^2$ and V^*. Real gases are studied in Excs. 9.5.5.1 to 9.5.5.4.

9.5.1.1 Joule-Thompson process

In thermodynamics, the *Joule-Thompson effect* describes the temperature change of a real gas or liquid (as differentiated from an ideal gas) when it is forced through a valve or porous plug while keeping it insulated so that no heat is exchanged with the environment (see Exc. 9.5.5.5).

9.5.2 Phase transitions

9.5.2.1 Liquid-gas phase transition

9.5.3 Solutions

9.5.4 Osmotic pressure

9.5.5 Exercises

9.5.5.1 Ex: Real gas

Here we study a *real gas*. The state equation for a real gas according to van der Waals is,

$$\left(p + \frac{a}{V^2}\right)(V - b) = Nk_BT \ .$$

a. Why is the critical point for the liquid-gas phase transition defined by to the conditions,

$$\frac{dp}{dV} = \frac{d^2p}{dV^2} = 0 \ ?$$

b. Show that the temperature of the critical point T_c and the volume of the system at the critical point V_c are linked to the material constants a and b by the relationships:

$$k_BT_c = \frac{8a}{27Nb} \qquad \text{and} \qquad V_c = 3b \ .$$

c.How to calculate the pressure at the critical point as a function of a and b?
d. For CO_2 the values $a = 3.6 \cdot 10^{-6}$ bar m^6 mol^{-2} and $b = 4.3 \cdot 10^{-5}$ m^3 mol^{-1} are suitable parameters of the van der Waals equation. Consider a mole of CO_2 and calculate the values for the critical point V_c, T_c and p_c.

Solution: *a. The critical point corresponds to a saddle point in the pV-diagram.*
b. We have,

$$\begin{aligned} p(V) &= \frac{Nk_BT}{V-b} - \frac{a}{V^2} \\ \frac{dp}{dV} &= -\frac{Nk_BT}{(V-b)^2} + \frac{2a}{V^3} \\ \frac{d^2p}{dV^2} &= \frac{2Nk_BT}{(V-b)^3} - \frac{6a}{V^4} \ . \end{aligned}$$

Inserting the specified relations between T_c and V_c and the material constants yields, for the second and third equations,

$$\begin{aligned} \frac{dp}{dV} &= -\frac{8aN}{27Nb4b^2} + \frac{2a}{27b^3} = 0 \\ \frac{d^2p}{dV^2} &= \frac{2N8a}{27b8b^3} - \frac{6a}{81b^4} = 0 \ . \end{aligned}$$

c. The pressure is at the critical point is,

$$p = \frac{N8a}{27Nb2b} - \frac{a}{9b^2} = \frac{a}{27b^2} \ .$$

d. The values for T_c and p_c are,

$$\begin{aligned} V_c &= 3 \cdot 4.3 \cdot 10^{-5} \ m^3 mol^{-1} \cdot 1 \ mol = 12.9 \cdot 10^{-5} \ m^3 \\ T_c &= \frac{8 \cdot 3.6 \cdot 10^{-6}}{27 N_A k_B \cdot 4.3 \cdot 10^{-5}} \cdot 10^5 \ J \ m^{-3} = 298.5 \ K \\ p_c &= \frac{3.6 \cdot 10^{-5}}{27 \cdot 4.3^2 \cdot 10^{-10}} \ bar = 72.1 \ bar \ . \end{aligned}$$

9.5.5.2 Ex: Real gas

One mole of a real gas satisfies the Dieterici equation of state (an alternative to the van der Waals equation),

$$pe^{\alpha/(N_A k_B TV)}(V-\beta) = N_A k_B T \ ,$$

where are α and β parameters.
a. In what units α and β have to be specified? What sign do you expect for each parameter?
b. Express the parameters of the critical point T_c and V_c by α and β.
c. What arises for $p_c V_c / N_A k_B T_c$?

Solution:

9.5.5.3 Ex: Real gas

The pressure p of a dense gas behaves as a function of temperature T and molar volume v according to the following state equation,

$$p = \frac{RT}{v} - \frac{a}{v^2} \ ,$$

where a is a positive constant and R is the universal gas constant.
a. Use the identity,

$$\left(\frac{\partial u}{\partial v}\right)_T = T\left(\frac{\partial p}{\partial T}\right)_v - p$$

to determine the molar energy u as a function of v.
b. Assuming that $c_v = (\partial u/\partial T)_v$ be constant and equal to c, find u as a function of T and v.
c. In a free gas expansion, does the temperature rise or fall? Take into account that in a free expansion u remains invariant and v grows. Determine ΔT for a small variation Δv of the molar volume.
d. Demonstrate the identity in item (a).

Solution: *a. From the equation of state we obtain,*

$$\frac{\partial p}{\partial T} = \frac{R}{v}$$

which, replaced in the identity, gives,

$$\frac{\partial u}{\partial v} = T\frac{R}{v} - p = \frac{a}{v^2} \ .$$

Integrating,

$$u = -\frac{a}{v} + K(T)$$

where $K(T)$ depends only on T.
b. Differentiating the above expression

$$c_v = \frac{\partial u}{\partial T} = K'(T) = c \ .$$

Integrating $K(T) = cT + K_0$. Hence,

$$u = -\frac{a}{v} + cT + K_0 \ .$$

c. As u is constant, the expression above says that, if v grows then T decreases. Keeping u constant, the expression above says that,

$$c\frac{dT}{dv} = \frac{a}{v^2} \ .$$

Hence,

$$\Delta T = \frac{dT}{dv}\Delta v = \frac{a}{cv^2}\Delta v \ .$$

d. From $du = Tds - pdv$ we get,

$$\left(\frac{\partial u}{\partial v}\right)_T = T\left(\frac{\partial s}{\partial v}\right)_T - p \ .$$

Using the Maxwell relation,

$$\left(\frac{\partial s}{\partial v}\right)_T = \left(\frac{\partial p}{\partial T}\right)_v$$

we obtain the identity.

9.5.5.4 Ex: Isothermal expansion

Calculate the work done during isothermal expansion from V_1 to V_2 of a real gas.

Solution:

9.5.5.5 Ex: Joule-Thomson process

Here we study the *Joule-Thomson effect*. A gas is forced under constant pressure p_1 from a container B1 through a porous partition into a container B2 with constant pressure $p_2 < p_1$. The constancy of the pressures in the containers is ensured by increasing or decreasing their volumes. Finally, it is assumed that the gas is adiabatically isolated from the environment and therefore only exchanges with it energy in the form of work.
a. Show that the enthalpy H remains constant in both recipients during this process.
b. Show that,

$$\left(\frac{\partial T}{\partial p}\right)_H = \frac{1}{C_p}\left(T\frac{\partial V}{\partial T}_p - V\right)$$

and calculate $\left(\frac{\partial T}{\partial p}\right)_H$ explicitly for an ideal gas.
c. For a real gas, the so-called inversion curve $p(T)$ defined by $\left(\frac{\partial T}{\partial p}\right)_H$ is obtained in the pT-plane. Physically interpret the areas above and below this curve. Calculate the inversion curve for the van der Waals gas using the thermal equation of state for real gases.
d. Discuss the behavior of entropy in this process.

Solution:

9.6 Canonical formulation of thermodynamics

The state of stationary thermodynamic systems may ne expressed by equations of state interrelating thermodynamic potentials:

$$f(x_1, ..x_q) = 0 \ . \tag{9.34}$$

The most current *thermodynamic variables* in a *grand canonical ensemble* are the temperature T, the entropy S, the pressure $-P$, the volume V, the particle number N, and the chemical potential μ. The pressure and volume may be replaced by other mechanical variables.

9.6.1 The laws of thermodynamics

There are four fundamental truths in thermodynamics:

- 0. The zeroth law affirms that two systems each one in thermal equilibrium with a third are in equilibrium themselves.
- 1. The first law states that the total energy is conserved $dU = \delta Q + dW$.
- 2. The second law states that heat flows from hot to cold places, i.e. the entropy of closed systems goes always increasing, $dS \geq 0$.
- 3. The third law that for $T \to 0$, the entropy difference between systems connected by a reversible process vanishes, $dS \to 0$. This last law has its origins in quantum mechanics.

9.6.2 Thermodynamic potentials

The main thermodynamic potentials are the total energy E, the heat W, the Helmholtz free energy F, the Gibbs free energy G, the free enthalpy H, and the grand potential W:

$$\boxed{\begin{array}{lll} E = TS - PV + \mu N & \text{and} & dE = TdS - PdV + \mu dN \\ H = TS + \mu N & \text{and} & dH = TdS + VdP + \mu dN \\ F = -PV + \mu N & \text{and} & dF = -SdT - PdV + \mu dN \\ W = PV & \text{and} & dW = -SdT - PdV - Nd\mu \\ G = \mu N & \text{and} & dG = -SdT + VdP - Nd\mu \\ Q = H & \text{and} & dQ = TdS \end{array}} \tag{9.35}$$

From that follow the conditional derivatives of the thermodynamic potentials and other quantities, like the *heat capacity*:

$$\begin{aligned} C_V &= \left(\frac{\partial E}{\partial T}\right)_{N,V} = T\left(\frac{\partial S}{\partial T}\right)_{\mu,V} \\ C_P &= \left(\frac{\partial E}{\partial T}\right)_{N,P} . \end{aligned} \tag{9.36}$$

Therefore, all thermodynamic quantities may be calculated from a few basic formulae:

$$TS(T) = E - \sum\nolimits_j k_B T \ln\left[1 - \exp(-\beta E_j)\right] . \tag{9.37}$$

9.6.3 Exercises

9.6.3.1 Ex: Legendre transform

Legendre transform.

Solution:

9.7 Thermodynamic phase transitions

9.7.1 The balance of transitions

The equilibrium of a chemical reaction may be on the left or right side.

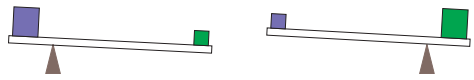

Figure 9.26: The equilibrium of a chemical reaction may be on the left or right side.

9.7.2 Solid-liquid-vapor

In the case of the *liquid-vapor transition* the two phases are only quantitatively distinct, but have the same symmetry. Therefore, a discontinuity of the thermodynamic potentials is required to reveal the phase transition.

In the case of the *solid-liquid transition* the two phases are qualitatively distinct due to different symmetries. We do not need a discontinuity to distinguish the phases. Landau's theory holds for this class of transitions. It establishes a relationship between symmetry considerations and physical characteristics by introducing the notion of the *order parameter* and *free energy*.

9.7.3 Classification of phase transitions

The old *Ehrenfest classification* [641] calls a phase transition of n^{th} order if the derivative $\partial^n \mu / \partial T^n$ is discontinuous. Thus BEC of a trapped ideal gas is a first-order phase transition, because the chemical potential suddenly changes its slope at T_c.

The modern *Landau classification* distinguishes two types of phase transitions in homogeneous systems: First-order phase transitions exhibit a discontinuity in the order parameter, while for continuous phase transitions the order parameter does not make jumps.

First order phase transitions are characterized by 1. equilibrium between phases (liquid-gas, liquid-solid), 2. discontinuous entropy, therefore latent heat, 3. at least one derivative of a thermodynamic potential is discontinuous. **The two phases coexist at the transition point.** E.g. at $T = 0°C$ in a closed system water and ice coexist.

Continuous phase transitions are characterized by 1. no equilibrium, 2. no latent heat, but often discontinuous heat capacity, 3. first order derivatives are all continuous, but second order is discontinuous. **There is no phase coexistence at the critical point**. E.g. at $T = T_c$ there no condensate; only below T_c.

9.7.3.1 Bose-Einstein condensation

Is the observed phase transition in trapped gases really Bose-Einstein condensation? A homogeneous gas has strong fluctuations near T_c that can heavily be influenced by interactions, which could result in phase domains. In contrast, a trapped gas is quite robust near T_c due to the modification of the density of states for small energies by the trapping potential, which make the interaction less important (see stabilization of attractive gases). However, T_c is not precisely defined and far from T_c interactions become very important (Thomas-Fermi limit).

The dynamics of phase transition is rules by a competition between internal energy which tries to minimize itself and entropy which tries to maximize itself. Here are a few examples.

9.8 Quantum statistics

9.8.1 Maxwell-Boltzmann, Bose-Einstein and Fermi-Dirac distribution

9.8.1.1 Black-body radiation

The Bose-Einstein and the Fermi-Dirac distribution both have many applications in quantum mechanics, e.g. for the explanation of the blackbody radiation, the heat capacity of metals, the laser, the Bose-Einstein condensation, and much more. In fact, these distributions must be used whenever quantum statistical effects are important. Here, we will only focus on two examples, one for each type of distribution: We will discuss the blackbody radiation using the Bose-Einstein distribution and an ideal ultra-cold trapped fermion gas with the Fermi-Dirac distribution.

9.8.1.2 Ultra-cold ideal fermion gas

To address this problem, before we study the effects of quantum statistics, we begin by identifying the geometric constraints. Many properties can be understood by calculating the density-of-states $g(\epsilon)$ defined by,

$$\int g(\epsilon)d\epsilon = \frac{1}{(2\pi)^3}\int d^3\mathbf{x}d^3\mathbf{k} = \frac{(2m)^{3/2}}{(2\pi)^2\hbar^3}\int d^3\mathbf{x}d\epsilon\sqrt{\epsilon - U(\mathbf{r})}\ . \tag{9.38}$$

For example, for a box, $U(\mathbf{x}) = -U_0\chi(|\mathbf{x}| > a)$, we get $g(\epsilon) = ...$ For a harmonic oscillator, $U(\mathbf{x}) = \frac{m}{2}\omega^2|\mathbf{x}|^2$, we get $g(\epsilon) = \epsilon^2/2\hbar^2\omega^2$.

Now, the Fermi-Dirac distribution,

$$N = \int \frac{g(\epsilon)}{e^{\beta(\epsilon-\mu)}+1}\ . \tag{9.39}$$

gives the chemical potential.

We can now calculate all thermodynamic potentials, e.g.,

$$E = \frac{\int \epsilon g(\epsilon) f_{FD}(\epsilon)}{\int g(\epsilon) f_{FD}(\epsilon)} \ . \tag{9.40}$$

Same for BEC.

9.8.2 Bose-Einstein condensation

Start calculating the density of states on a box potential, $\rho(\epsilon)d\epsilon = \frac{4\pi V}{h^3}(2m^3)^{1/2}\epsilon^{1/2}d\epsilon$, N and E are

$$\begin{aligned} N &= \int_0^\infty f_{BE}\rho d\epsilon = V\lambda_{th}^{-3} g_{3/2}(e^{-\mu}) \\ E &= \int_0^\infty \epsilon f_{BE}\rho d\epsilon = V\lambda_{th}^{-3}\frac{3k_BT}{2} g_{5/2}(e^{-\mu}) \\ &= \frac{3}{2}k_BT\left(1 - 2^{-5/2}n\lambda_{th}^3\right) + \dots \ , \end{aligned} \tag{9.41}$$

where $\lambda_{th} = \sqrt{2\pi\hbar^2/mk_BT}$ is the *thermal de Broglie wavelength*. Bose gases have a lower pressure then classically predicted.

9.8.3 Fermi degeneracy

A completely analogous treatment to the Bose-gas yield for the case of fermion

$$E = \frac{3}{2}k_BTN\left(1 + 2^{-5/2}n\lambda_{th}^3\right) + \dots \ . \tag{9.42}$$

Bosonic ^{4}He has a very different behavior than fermionic ^{3}He. It stays gaseous at very low temperatures and becomes a Fermi gas before becoming fluid. Fermi gases have a higher pressure then classically predicted.

Electrons in a solid are characterized by a high density and a low mass. Hence, $n\lambda_{th}^3 \approx 10^3$. The interelectronic repulsion is canceled by atomic attraction, so that they may be considered an ideal gas. For the density of states we get the same formula as for bosons in a box multiplied with the factor 2 to account for the spin degree of freedom. Thus, from

$$N = \int_0^{E_F} \rho f_{FD} d\epsilon \ , \tag{9.43}$$

we derive the Fermi energy $E_F = \frac{h^2}{8m}(3N/\pi V)(2/3)$. The free electron gas is deep in the Fermi regime, the classical statistics may only be used at temperatures above $T > 10^5$ K. Hence the energy is temperature-independent and the heat capacity vanishes, *i.e.* the electron gas does not contribute to the heat capacity of a metal. It is only at very low temperatures of a few K, when the heat capacity of the atomic lattice drops due to the underlying bosonic statistics, that the electrons contribute.

Now, make the metallic box potential having a finite depth. An electron can then leave the metal, if it surmounts the *exit work* $W = -V_{min} - E_F \simeq 10$ eV, which is the

difference between the potential depth and the Fermi energy. At high temperatures, the tail of the Fermi-Dirac distribution can leak into the unbound regime, which gives rise to *thermoionic emission*. This feature explains the existence of *contact potentials*: Metals with different W and E_F brought into contact exchange charges until their Fermi level is at same height.

9.8.3.1 Phase space quantization

If *phase space* was not quantized, the cells' size could be chosen so small that they admit at most one particle. Then quantum statistics would not apply, the system would be classical.

9.8.4 Microcanonical ensembles

To obtain the partition function in the *microcanonical ensemble*, we proceed as follows. Bosons have anti-symmetric wavefunctions, Fermions have symmetric ones. Boltzmann particles (called boltzons here for simplicity) have all wavefunctions as eigenfunctions. In the limit of high temperatures all particles behave like boltzons. Discretize the one-particle energies in small cells labeled i of constant energy e_i. Let n_i be their number and g_i their degeneracy. For bosons, each level g_k can hold arbitrarily many of the n_i particles:

$$W_{\{n_i\}} = \prod_i \binom{n_i + g_i - 1}{n_i} \,. \tag{9.44}$$

For boltzons, each level g_k can hold ni particles:

$$W_{\{n_i\}} = \prod_i \frac{g_i^{n_i}}{n_i!} \,. \tag{9.45}$$

For fermions, each level g_k can hold at most one of the n_i particles:

$$W_{\{n_i\}} = \prod_i \binom{g_i}{n_i} \,. \tag{9.46}$$

Using the Laguerre variation principle with $W_{\{n_i\}} = \max\{W_{\{n_i\}}\}$ one can show:

$$\bar{n}_{n_i} = \frac{g_i}{z^{-1}\exp(\beta e_i) + a} \,, \tag{9.47}$$

where $a = +1$ for fermions, $a = -1$ for bosons, and $a = 0$ for boltzons. z and b follow from the boundary conditions:

$$N = \sum_i n_i \qquad \text{and} \qquad E = \sum_i e_i \,. \tag{9.48}$$

From $W_{\{n_i\}}$ the thermodynamic potentials can be calculated. E.g. the entropy reads $S = k_B \ln W_{\{n_i\}} = \sum_i n_i \ln(g_i/\bar{n}_i - a) - a g_i \ln(1 - a\bar{n}_i/g_i)\}$.

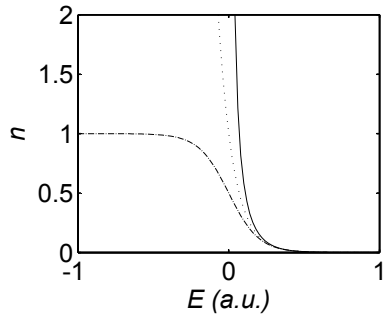

Figure 9.27: Quantum statistic weight for fermions (dash-dotted line), bosons (solid line) and boltzons (dotted line).

9.8.5 Detailed balance

Quantum statistical (anti-)symmetrization of the wavefunction of a cold system leads to Bose-enhancement(Pauli blocking). Take a state $\Psi = \psi_\alpha(1)\psi_\beta(2)$ and symmetrize it to $\Psi s, a = 2^{-1/2}[\psi_\alpha(1)\psi_\beta(2) \pm \psi_\alpha(2)\psi_\beta(1)]$. Now assume the single particle wavefunction overlap, $\alpha = \beta$, then $|\Psi|^2 = (s+1)\ |\psi_\alpha(1)|^2|\psi_\beta(2)|^2$, where $s = 0$ for boltzons, $s = 1$ for bosons, and $s = -1$ for fermions. Generalized to arbitrary numbers of particles we state: *If n bosons(fermions) are in state Ψ, the probability for another bosons(fermions) to joint this state is $1 \pm n$ times the probability without quantum statistics.*

An alternative intuitive derivation of the quantum statistical distribution function is based on the postulate of *detailed balance*, claiming that *equality of the rates $W_{12\to34}$ for two particles to change their states and the rate for the inverse process $W_{34\to12}$ is a sufficient condition for thermal equilibrium*,

$$\begin{aligned} W_{12\to34} &= |M_{12,34}|^2 n_1 n_2 (1+sn_3)(1+sn_4) \\ W_{34\to12} &= |M_{12,34}|^2 n_3 n_4 (1+sn_1)(1+sn_2)\ . \end{aligned} \tag{9.49}$$

Hence,

$$\frac{n_1}{1+sn_1} + \frac{n_2}{1+sn_2} = \frac{n_3}{1+sn_3} + \frac{n_4}{1+sn_4}\ . \tag{9.50}$$

Energy conservation requires

$$E_1 + E_2 = E_3 + E_4\ . \tag{9.51}$$

For a macrocanonic ensemble in thermal equilibrium

$$f(E_i) = n_i\ . \tag{9.52}$$

To satisfy Eqs. (9.50) and (9.51) f must have the functional form

$$f(E_i) = \frac{1}{e^{\beta(E_i-\mu)} \mp s}\ . \tag{9.53}$$

The Bose-Einstein distribution follows directly from the assumption of stimulated emission *bosonic stimulation*.

The Maxwell velocity distribution in a gas in a special application of the Boltzmann distribution.

9.8.6 Canonical ensembles

In order to calculate the density of states, state equation, mean values in the grand *canonical ensemble*, we start from the partition sum (upper signs for fermions and lower signs for bosons):

$$Tr\rho = \prod_{\mathbf{p}} \left(1 + ze^{-\beta e_p}\right)^{\pm 1} \quad . \tag{9.54}$$

Internal energy with fixed volume is proportional to the pressure. For large systems (thermodynamic limit) the sum may be replaced by an integral $\sum_{\mathbf{p}} \overset{N\to\infty}{\longrightarrow} V/h^3 \int d^3\mathbf{p}$, and the integral may be expressed by the Riemann zeta-function (see Sec. (??)). The terms in {} brackets only hold for Bosons, because the integral diverges otherwise. The thermodynamic potentials are

$$\begin{aligned}
n_{\mathbf{p}} &= -\frac{1}{\beta}\frac{\partial}{\partial e_{\mathbf{p}}} \ln Tr\rho = \frac{z\exp(-\beta e_{\mathbf{p}})}{1 \pm z\exp(-\beta e_{\mathbf{p}})} \qquad (9.55)\\
\frac{PV}{k_BT} &= \ln Tr\rho = \sum_{\mathbf{p}} \ln\left(1 \pm z\exp(-\beta e_{\mathbf{p}})\right) \overset{N\to\infty}{\longrightarrow} \frac{V}{\lambda_{dB}^3} g_{5/2}^{(\pm)}(z) - \{N\ln(1-z)\}\\
N &= z\frac{\partial}{\partial z}\ln Tr\rho = \sum_{\mathbf{p}} n_{\mathbf{p}} \overset{N\to\infty}{\longrightarrow} \frac{V}{\lambda_{dB}^3} g_{3/2}^{(\pm)}(z) + \{\frac{N}{1-z}\} \qquad \text{gives the chemical potential}\\
\frac{E}{N} &= -\frac{\partial}{\partial\beta}\ln Tr\rho = \sum_{\mathbf{p}} n_{\mathbf{p}} e_{\mathbf{p}} \overset{N\to\infty}{\longrightarrow} \frac{3k_BTV}{2\lambda_{dB}^3} g_{5/2}^{(\pm)}(z) \approx \frac{3PV}{2}\\
\frac{S}{k_BN} &= \ln Tr\rho = \beta E - N\ln z \overset{N\to\infty}{\longrightarrow} \frac{5V}{2\lambda_{dB}^3} g_{5/2}^{(\pm)}(z) - \{\ln z\} \overset{T\to 0}{\longrightarrow} 0\\
\frac{C_V}{k_BN} &= \left(\frac{\partial E}{\partial\left(k_BT\right)}\right)_{N,V} \overset{N\to\infty}{\longrightarrow} \frac{15V}{4\lambda_{dB}^3} g_{5/2}^{(\pm)}(z) - \left\{\frac{9Ng_{3/2}^{(\pm)}(z)}{4g_{1/2}^{(\pm)}(z)}\right\} \overset{T\to 0}{\longrightarrow} 0\\
\frac{G}{Nk_BT} &= \ln z \ .
\end{aligned}$$

The Bose-Einstein phase transition occurs at some critical temperature T_c. At high temperature $T > T_c$ the ground state population vanishes. At low temperature $T < T_c$, we have to substitute in the above equations z by 1. Since $g_{3/2}$ is limited for $z = 0..1$ the population bilance must be equilibrated by an additional term describing the ground state population:

$$\begin{aligned}
\frac{N}{V} &= \left\{\begin{array}{ll} \frac{g_{3/2}^{(\pm)}(1)}{\lambda_{dB}^3} + \frac{N_0}{V} & \text{for} \quad T \le T_c \\ \frac{g_{3/2}^{(\pm)}(z)}{\lambda_{dB}^3} & \text{for} \quad T \ge T_c \end{array}\right\} \qquad (9.56)\\
\frac{P}{k_BT} &= \left\{\begin{array}{ll} \frac{g_{5/2}^{(\pm)}(1)}{\lambda_{dB}^3} & \text{for} \quad T \le T_c \\ \frac{g_{5/2}^{(\pm)}(z)}{\lambda_{dB}^3} & \text{for} \quad T \ge T_c \end{array}\right\}
\end{aligned}$$

State equation in the Bose-gas phase:

$$\frac{P}{k_BT} = \frac{N}{V}\frac{g_{5/2}^{(\pm)}(z)}{g_{3/2}^{(\pm)}(z)} \ . \tag{9.57}$$

In the classical limit and we get the ideal gas equation:

$$\frac{P}{k_B T} = \frac{N}{V} \ . \tag{9.58}$$

The state equation in the Bose-condensat phase follows directly from equation (II.2.3):

$$\frac{N_0}{N} = 1 - \left(\frac{T}{T_c}\right)^{3/2} \ . \tag{9.59}$$

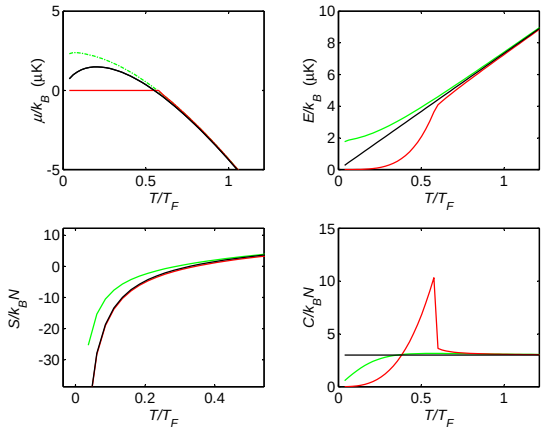

Figure 9.28: Thermodynamic potentials for fermion, bosons and boltzons.

9.8.6.1 Micro- and macrocanonical Bose-condensates

The question which *canonical ensemble* is the correct assumption depends on the experimental situation. The question is particularly interesting in the context of Bose-Einstein condensation: Here it is related to the question which state better describes a BEC: A Fock or a Glauber state.

The condensates experimentally produced in alkali gases consisted of relatively small atom numbers between 1000 to 10^7, so that the validity of the thermodynamic approximation and the use of the density of states approach has been questioned [551]. Also, the decision whether to use the grand canonical, the canonical or the micro-canonical ensemble for calculating the thermodynamic quantities noticeably influences the results. Herzog and Olshanii [615] have shown that for small atom numbers on the order of 100 the canonical and grand canonical statistics lead to predictions on the condensed fraction that differ by up to 10%. On the other hand, they give the same results if the particle numbers are large. Which canonical statistics is more appropriate is not a trivial question and depends on the experimental setup and in particular on the time scale of the measurements. If we look at the sample for short times, the number of condensed atoms will be fixed, and we can assume a canonical ensemble. For longer times, however, the atom number may be an equilibrium parameter depending on the contact of the sample with a reservoir, and the grand canonical statistics is better suited.

9.8.7 Photons

9.8.7.1 Blackbody radiation

The chemical potential is the equilibrium parameter for the particle number. Since, photons are massless and can be created or annihilated in the vacuum, the chemical potential must vanish $\mu = 0$. The Boson number is determined in the case of photons by other thermodynamic quantities like temperature or volume. Blackbody radiation is independent of the walls if the volume is sufficiently large, and only depends on the temperature T. We can therefore freely fix the boundary conditions, f.e.

$$\mathbf{k} = 2\pi/L \cdot \mathbf{n} \qquad \text{where} \qquad n_x, n_y, n_z \in N \ . \tag{9.60}$$

Allowed momentum on a sphere:

$$V/(2\pi)^3 \cdot 4\pi k^2 dk \ . \tag{9.61}$$

For larger volumes:

$$\begin{aligned}
&\sum\nolimits_{\mathbf{p}} \longrightarrow \frac{V}{h^3}\int d^3\mathbf{p} && (9.62)\\
&Z = \frac{1}{1-e^{-\beta\hbar\omega}} \\
&Tr\rho = \sum\nolimits_{\mathbf{k},\kappa} \exp(-\beta E_{\{\mathbf{k},\kappa\}}) = \prod\nolimits_{\mathbf{k},\kappa} \frac{1}{1-e^{-\beta\hbar\omega}} \\
&\langle n_{\mathbf{k}}\rangle = -\frac{1}{\beta}\frac{\partial}{\partial\hbar\omega}\ln Tr\rho = \frac{2}{e^{\beta\hbar\omega}-1} \qquad \text{for the two polarizations} \\
&\rho = \sum\nolimits_n |n\rangle\langle\rho\rangle\langle n| = \sum_n |n\rangle \frac{\langle n\rangle}{(1+\langle n\rangle)^{n+1}}\langle n| = \\
&E = -\frac{\partial}{\partial\beta}\ln Tr\rho = \sum\nolimits_{\mathbf{k},\kappa} \hbar\omega\langle n_{\mathbf{k}}\rangle = 3PV \ .
\end{aligned}$$

9.8.8 Statistical density

There are three possible ensembles that deal with a system of colliding particles depending on the specific boundary conditions. In the microcanonical ensemble

$$\rho_{mn} = \left\{ \begin{matrix} C\cdot\delta_{mn} & \text{for} & E < E_n < E+\Delta & \text{and} & H|\psi_n\rangle = E|\psi_n\rangle \\ & & 0 \quad \text{else} & & \end{matrix} \right\} \ . \tag{9.63}$$

It follows:

$$\rho = \sum_{E<E_n<E+\Delta} |\psi_n\rangle\langle\psi_n| \ . \tag{9.64}$$

Connected to the thermodynamics via $S(E,V) = k_B \log Tr\rho$. After that in almost complete analogy to classical mechanics. In the canonical ensemble, the temperature is an equilibrium parameter.

$$\rho_{mn} = \delta_{mn}\exp(-\beta E_n) \qquad \text{com} \qquad \beta = 1/k_B T \ . \tag{9.65}$$

It follows:

$$1\rho = \exp(-\beta H) \sum_n |\psi_n\rangle\langle\psi_n| \ . \tag{9.66}$$

In the grand canonical ensemble, the temperature and chemical potential are equilibrium parameters.

$$1\rho_{mn} = \exp(-\beta E_n - \mu N) \ . \tag{9.67}$$

It follows:

$$1\rho = \exp(-\beta H - \mu N) \qquad \text{com} \qquad [H, N] = 0 \ . \tag{9.68}$$

9.8.8.1 Calculating thermodynamic systems

The density operator depends on $\varrho = \varrho(\mathbf{1})$ for a microcanonical ensemble, $\varrho = \varrho(\mathbf{1}, E)$ for a canonical ensemble, $\varrho = \varrho(\mathbf{1}, E, N)$ for a grand canonical ensemble, $\varrho = \varrho(\mathbf{1}, E, N, V)$ for a macrocanonical ensemble. The variables on which the density operator does not depend, $\langle\mathbf{1}\rangle, \langle E\rangle, \langle N\rangle, \langle V\rangle$, are fixed for the system,

$$\delta\left(S + k_B\left[(\ln Z - 1)\langle\mathbf{1}\rangle - \beta\langle E\rangle + \beta\mu\langle N\rangle - \beta p\langle V\rangle\right]\right) = 0 \ . \tag{9.69}$$

The thermodynamic quantities follow from equations like

$$dS_{rev} = k_B\beta(\beta dE - \mu dN + pdV) \leq 0 \ . \tag{9.70}$$

Other thermodynamic potentials may be defined via Legendre transformations.

How to calculate thermodynamical systems? Chose the ensemble that applies to the problem, $\varrho = e^{-\beta\cdots}/Z$ and the respective potential P with its thermodynamic relation. Express the dynamic variables a_i via the state sum $Z = \text{Tr } e^{-\beta\cdots}$ and the natural variables n_i by $a_i = (\partial P/\partial n_i)_{a_k, a_l}$. Now express the other potentials via the state sum and the natural variables by $P' = P + a_i n_i$. Express the second derivatives and all other thermodynamic quantities by Z and n_i. Calculate the state sum explicitly, and finally substitute Z everywhere.

9.8.9 Heat capacity measurement

According to the theory of an ideal Bose gas trapped in a harmonic potential the temperature dependence of the heat capacity at the threshold to condensation can easily be obtained as follows. The condensed fraction determines the chemical potential through:

$$N = N_0 + \left(\frac{k_B T}{\hbar\omega}\right)^3 g_3(z) \ , \tag{9.71}$$

where $z(T) = \exp(\mu/k_B T)$ for a grand canonical ensemble and g_n denotes the Riemann zeta function. The condensed fraction vanishes above the critical temperature, the chemical potential vanishes below the critical temperature. $(k_B T/\hbar\omega)^3 = 2\pi(a_{trap}/\lambda_{dB})^3$ denotes the normalized volume of a phase space cell. Knowing $z(T)$ from equation (9.71), we can calculate the total energy, the heat capacity and all the other thermodynamic potentials:

$$C_N = 12 k_B \left(\frac{k_B T}{\hbar\omega}\right)^3 g_4(z) - 9 k_B N \frac{g_3(z)}{g_2(z)} \ . \tag{9.72}$$

The considerable interest in the measurement of thermodynamic quantities of a BEC is motivated by its departure from ideal gas behavior (equations (??) and (9.72)). Indeed, the abrupt discontinuous change in the heat capacity at the phase transition to BEC, expected for ideal gases, is smeared out by atomic collisions [72]. Deviations due to atomic interactions and the finite number of particles [551] should even show up in the temperature dependent measurement of the condensed fraction as it is done by simple time-of-flight analysis. But experimental uncertainties until now prohibited a quantitative investigation [580]. A measurement of the release energy has been performed in Ref. [417].

A possible approach is the in-situ analysis of the cloud's shape while it is trapped. The shape of its condensed fraction reveals its chemical potential which in turn determines the excitation energies and populations of the thermal part of the gas [380].

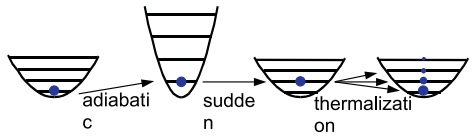

Figure 9.29: Population variation during a slow adiabatic compression followed by a sudden non-adiabatic decompression.

The basic idea consists of applying an adiabatic change followed by a sudden change in the curvature of the trapping potential (Fig. 9.29) in such a way, that the particle number remains constant, the temperature changes in a controllable and predictable way, but the populations are redistributed over the excited energy levels. We take pictures of the trapped cloud just before and after the trap manipulation and analyze them to extract the energy change. The heat capacity can then directly be calculated according to its definition:

$$C_N = \left(\frac{\partial U}{\partial T}\right)_N \quad . \tag{9.73}$$

In the following, we will discuss the steps in more detail. During the slow adiabatic compression the temperature of the trapped cloud will gradually increase like $T' = T\omega'/\omega$, but the population distribution of the energy levels will not. This can be seen from the phase space density, $r = g_3(z)$, that should remain unchanged under adiabatic variations of the trapping potential. In contrast, the sudden switching from ω' back to w will first create a population imbalance (that can even be an inversion). Elastic collisions between the atoms then will rethermalize the sample at the same temperature T. We calibrate the temperature change to the amount of compression and evaluate the heatcapacity:

$$C_N \approx \frac{U' - U}{T' - T} = \frac{1}{T}\frac{U' - U}{\omega'/\omega - 1} \quad . \tag{9.74}$$

The adiabatic compression should be slow, the sudden switching should be fast compared to the trap secular frequencies. The shape of a partially condensed gas is determined by the geometry of the trapping potential ω_r, ω_z, the number of condensed

atoms N_0 and the equilibrium temperature T. One way to measure the energy distribution is to fit the recorded shape of a trapped cloud with calculated wavefunctions for the ground and excited states:

$$n(\mathbf{r}) = |\psi_0(\mathbf{r})|^2 + \sum_j N_j |\psi_j(\mathbf{r})|^2 \ . \tag{9.75}$$

The sum of the particle distribution functions N_j gives the total atom number, the sum of the energy eigenvalues belonging to the wavefunction weigthed with the population distribution (that depends on the temperature) gives the total energy:

$$N = \sum_j N_j \qquad , \qquad U = \sum_j N_j E_j \ . \tag{9.76}$$

The fitting procedure using equation ((??)) consists of several steps. We assume the validity of the two-gas model [380] stating, that the shape of the condensed cloud is (almost) not affected by the thermal cloud. Knowing the condensed atom number, we can solve the Gross-Pitaevski equation and calculate the chemical potential of the trapped cloud. We employ the method of steepest descent [320]

$$\left[-\frac{\hbar^2}{2m}\Delta + V_{trp}(\mathbf{r}) + g|\psi_0(\mathbf{r})|^2 \right] \psi_0(\mathbf{r}) = \mu \psi_0(\mathbf{r}) \ . \tag{9.77}$$

Within this two-gas model, we can now consider the thermal atoms to be moving in an effective potential, that consists of the trapping potential modified by the presence of the condensate $V_{eff}(\mathbf{r}) = V_{trap}(\mathbf{r}) + g|\psi_0(\mathbf{r})|^2$. We can therefore set up and solve a Schrödinger equation eigenvalue problem:

$$\left[-\frac{\hbar^2}{2m}\Delta + V_{eff}(\mathbf{r}) \right]_j \psi_j(\mathbf{r}) = E_j \psi_j(\mathbf{r}) \ . \tag{9.78}$$

As soon as we found the eigenvalues E_j and the eigenfunctions ψ_j, we can determine the population distribution N_j by fitting the measured shape of the total cloud to equation (9.75) and calculate the total energy according to equation (9.76) and the heat capacity according to equation (9.72). Of course, the fitting is only precise if few excited states are populated.

This procedure requires a high resolution power of the imaging system, since typical wavefunction sizes ($N \gg 100000$, $(\nu_{ax}\nu_{rad}^2)^{1/3} \gg 80$ Hz) are on the order of a few 10 mm. In our actual setup the resolution would be diffraction limited to 6mm. We plan to drastically increase the resolution by placing an achromat inside the vacuum chamber close to the atomic cloud. This should allow us to resolve the shapes of the condensed and thermal clouds. Furthermore, we need to set up a nondestructive dispersive imaging system as has been demonstrated by [34].

Experimentally, it is easier to perform Time-Of-Flight (TOF) measurements where the cloud is allowed to freely expand until the spatial distribution of the cloud becomes negligible compared to the expanded velocity distribution. Of course this method is destructive and therefore the adiabatic-sudden change in the trapping potential, meant to calibrate the temperature scale and maintain a fix atom number during the measurement, makes no sense anymore.

The informations about the cloud that follow immediately from TOF measurements are the following: The total number of atoms N is extracted from a calibrated measurement of the integrated counts of missing photons in the probe beam shadow. Since the thermal part and the condensed part are well separated in the expanded cloud we can separately determine the number of condensed atoms N_c. Finally, we can fit the temperature T from the thermal cloud in the far wings, where to a good approximation, the equipartition theorem guaranties a Gaussian distribution:

$$n(E) = \frac{1}{\exp((E-\mu)/k_B T) - 1} \approx (N - N_0) \exp\left(\frac{-p^2}{2m}\right) . \tag{9.79}$$

With these data we can plot the condensed fraction N_c/N versus the reduced temperature $T/T_c(N)$, where $k_B T_c = \hbar\omega \left(N/g_3(1)\right)^{1/3}$ [301] and compare with theory [580]. But the data contain some more information, because we know the absolute value of the condensed atom number N_c. This enables us to calculate the chemical potential by numerically solving the Gross-Pitaevski equation (9.77). Then we can calculate the quasi-particle excitation spectrum according to equation (9.78). Assuming thermal equilibrium we know:

$$N_j = \frac{1}{\exp((E_j - \mu)/k_B T) - 1} , \tag{9.80}$$

and are able to calculate the total energy and the heat capacity from equation (9.75). It is obvious that this method requires much more input from theory and can barely be considered an experimental test of the thermodynamics of ideal gases. For that reason, we opt for the first method.

9.8.9.1 Adiabatic compression

Adiabaticity of a process means reversibility, while tha atom number is unchanged $N = const$ and, hence, constant entropy $S - const$. This implies an unchanged population distribution $n_j = const$ and $\beta\varepsilon_j/T = const$ also we get $\beta\mu, \beta U = const$. Furthermore, the phase space density keeps unchanged $\rho = const$. The process of adiabatically compressing a harmonic trap therefore changes the temperature like $T' = T\omega'/\omega$. This is valid above and below the transition point. The measure is repeated twice: With and without adiabatic-sudden variation. The heat capacity then follows from equation...

9.9 Out-of-equilibrium thermodynamics

9.9.1 Boltzmann's transport equation

Until now we have only treated systems in thermal equilibrium. However many systems are not stable, they drift or oscillate. Even if they are stable, this stability is sometimes only ensured by a continuous feeding with external energy or entropy, which is balanced by some dissipation mechanism. Non-equilibrium systems are difficult to treat.

9.9.1.1 H-theorem

Boltzmann's *H-theorem* is concerned with the tendency of non-equilibrium systems to return to equilibrium. The basic idea is that the fundamental process in gases are collisions. They introduce randomness into the evolution, which breaks the time-reversal symmetry. Other processes may have similar effects. The main point is that a very precisely defined input channel couples to a continuum of output channels, so that the equilibrium lies on the side of the larger mode volume (see Fig. (??)).

9.9.2 Stoßzahlansatz

Consider a gas with velocity distribution f. The *Boltzmann Stoßzahlansatz* reads,

$$\frac{\partial f}{\partial t} = \mathbf{v}\frac{\partial f}{\partial \mathbf{x}} + \left(\frac{\partial f}{\partial t}\right)_{coll} . \tag{9.81}$$

A general rate equation for may write,

$$\frac{d\varrho}{dt} = \frac{\partial \varrho}{\partial t} + \mathbf{v}\nabla_r + \mathbf{a}\nabla_v = R^+ - R^- . \tag{9.82}$$

For constant entropy increase $dS/dt \geq 0$, we get,

$$\frac{d\varrho}{dt} = \sum_{z'} \left(W_{zz'}\varrho_{z'} - W_{z'z}\varrho_z\right) . \tag{9.83}$$

And finally follows the *Boltzmann transport equation*,

$$\frac{d\varrho}{dt} = \int |\mathbf{v}-\mathbf{v}'|\sigma(\mathbf{v},\mathbf{v}'\to\mathbf{u},\mathbf{u}')\left[\varrho(t,\mathbf{r},\mathbf{u})\varrho(t,\mathbf{r},\mathbf{u}') - \varrho(t,\mathbf{r},\mathbf{v})\varrho(t,\mathbf{r},\mathbf{v}')\right] d^3\mathbf{v}'d^3\mathbf{u}d^3\mathbf{u}' , \tag{9.84}$$

which holds for binary collisions disregarding inner degrees of freedom, container walls, molecular chaos, and so on. For a free gas consisting of a single particle species, $dS/dt = 0$, the Liouville equation holds,

$$\frac{d\varrho}{dt} = 0 , \tag{9.85}$$

which yields,

$$\varrho(t,\mathbf{r},\mathbf{u}) = C(t,\mathbf{r})\exp\frac{\left[\mathbf{v}-\mathbf{v}_0(t,\mathbf{r})\right]^2}{-A(t,\mathbf{r})} , \tag{9.86}$$

and from which follows the *Maxwell-Boltzmann distribution*,

$$\varrho(\mathbf{v}) = \left(\frac{3}{2\pi\Delta v^2}\right)^{3/2}\exp -\frac{3[\mathbf{v}-\langle\mathbf{v}\rangle]^2}{2\Delta v^2} . \tag{9.87}$$

9.9.2.1 H quantity and entropy

From the Boltzmann Stoßzahlansatz is it possible to find for the quantity,

$$H \equiv \int f\ \ln f\ d^3\mathbf{p} , \tag{9.88}$$

the inequality,

$$\frac{dH}{dt} \leq 0 \ . \tag{9.89}$$

The equality holds for equilibrium.

It can be shown,

$$S = -k_B H \ . \tag{9.90}$$

Therefore the H quantity is nothing else than the entropy. Due to the derivation from the Stoßzahlansatz, this equation gives a definition of entropy for non-equilibrium systems.

9.9.2.2 Entropy problem

The H theorem is not generally true as is clear from *Loschmidt's reversibility paradox*. This illustrates a certain contradiction between classical mechanics and thermodynamics. Consider the diffusion of a drop of ink in a glass of water. From the point of view of mechanics the process is deterministic, thus our knowledge of the state of the system stays constant, (information) entropy must be constant as well, which is contradicted by thermodynamics.

The solution lies in the unprecisely known initial conditions, in particular in quantum systems due to the Heisenberg uncertainty. The H theorem only makes sense if it is understood in terms of its statistical nature: For equilibrium systems the most probable state is the one with maximum entropy. For non-equilibrium systems we have an overwhelming probability for an increasing entropy, but a decrease is not excluded.

9.9.3 H theorem and Fokker-Planck equation

An H theorem can be derived from *Fokker-Planck equations* [1200]. The H quantity is then the non-equilibrium analog to the Helmholtz free energy,

$$F = U - TS \tag{9.91}$$

$$H = U/D - S \ . \tag{9.92}$$

9.9.4 Irreversibility

Thermodynamics separates into two regimes: Of a *reversible process* and an *irreversible process*. Reversible processes are those, whose trajectories in parameter space can be reverse by inverting the signs of heat exchange Q, mass exchange m and work W. For systems in equilibrium, phase transitions are in general reversible by appropriately tuning some control parameter. For systems far from equilibrium, irreversible *temporal phase transition* may occur. However this classification is phenomenological and insufficient to make the connection to mechanics, in contrast to equilibrium thermodynamics which has been traced back to statistical physics.

For equilibrium statistical mechanics it is the interaction among the degrees of freedom which permits to approach equilibrium. This view coincides with modern views of the role of decoherence. The final (steady) state exhibits no macroscopic dynamics and is in a situation called *detailed balance*. In contrast a flux of energy or

matter may result in the emergence of *spatial patterns* of *rhythmic phenomena*. The transition to ordered structures requires a instabilities, i.e. a critical distance from equilibrium and nonlinear kinetics.

For any change of the state of a system the entropy behaves like,

$$dS = d_e S + d_i S \ , \tag{9.93}$$

where $d_e S$ is the entropy exchange with the external world and $d_i S \geq 0$ the internal *entropy production*. This shows that the entropy of a system can be lowered if $d_e S < 0$. The thermodynamics of irreversible processes exhibits linear and nonlinear phenomena. For small (linear) deviations from equilibrium the steady state of a system is characterized by a *minimum entropy production*. This is however *not* generally the case far from equilibrium. This rule is analogous to the change of internal energy,

$$dU = dQ + dW \ , \tag{9.94}$$

where dQ denotes the heat exchanged with the external world and dW the reversible work applied to the system.

9.9.4.1 Application to the Kuramoto model

According to Prigogine the transition to a dissipative structure is governed by a thermodynamic stability criterion involving excess entropy production. The excess entropy is the amount of dissipation introduced by the disturbance causing the instability. From the above it becomes clear how it is possible that CARL creates order, i.e. lowers entropy: the dissipative force constitutes a large entropy reservoir to which the system may deliver excess entropy.

For Bénard structures and surface waves there is no intrinsic length scale on which the order is expected. In contrast CARL bunching occurs on the order of an optical wavelength. The microsystems are the atoms, the macrosystem is the light.

At first glance the *Kuramoto model* produces order without apparent dissipative force: Universally coupled pendulum exhibit synchronization, i.e., the entropy of the system is reduced. Since the dynamics is deterministic and thus reversible, one would expect no entropy production or reduction. This is however incorrect, the Kuramoto model inherently contains assumptions, which are equivalent to dissipation. This is seen from the derivation of the equations governing weakly coupled pendulum. In fact the Kuramoto does not describe coupled *pendulum* but *pendulum clocks*, i.e. limit cycle oscillations sustained by an external force.

A thermodynamic treatment of the Kuramoto model establishing a link between the Prigogine and Haken point of view is given by Shiino [1200]. The non-equilibrium phase transition can also be of first-order.

[S.W. Koch, 'Dynamics of first-order phase transitions in equilibrium and nonequilibrium systems.', Springer, Lecture Notes in Physics]

9.9.5 Dissipative structures and synergetics

9.9.5.1 Prigogine's approach

Consider a system that exits far from thermodynamic equilibrium (see thermodynamics), hence efficiently dissipates the heat generated to sustain it, and has the capacity

of changing to higher levels of orderliness (see self-organization). According to Prigogine, systems contain subsystems that continuously fluctuate. At times a single fluctuation or a combination of them may become so magnified by possible feedback, that it shatters the preexisting organization. At such revolutionary moments or "bifurcation points", it is impossible to determine in advance whether the system will disintegrate into "chaos" or leap to a new, more differentiated, higher level of "order". The latter case defines the *dissipative structure* so termed because they need more energy to sustain them than the simpler structures they replace and are limited in growth by the amount of heat they are able to disperse [1057].

Quite generally it is possible in principle to distinguish between two types of structures: equilibrium structures, which can exist as isolated systems (for example crystals), and dissipative structures, which can only exist in symbiosis with their surroundings. Dissipative structures display two types of behaviour: close to equilibrium their order tends to be destroyed but far from equilibrium order can be maintained and new structures be formed.

The probability for order to arise from disorder is infinitesimal according to the laws of chance. The formation of ordered, dissipative systems demonstrates, however, that it is possible to create order from disorder. The description of these structures have led to many fundamental discoveries and applications in diverse fields of human endeavour, not only in chemistry. In the last few years applications in biology have been dominating but the theory of dissipative structures has also been used to describe phenomena in social systems [1250, 950].

9.9.5.2 Minimum entropy production

Far from equilibrium nonlinear effects in the rate equations get important. This implies the possibility of multiple solutions, each one with different regions of stability. Transitions from one solution to another occur as phase transitions. In the linear regime with one thermodynamic force held fixed (e.g. temperature gradients) the stable state is a steady-state with *minimum entropy production* and it is *unique*. We say the state lies on the thermodynamic branch. Moving away from the linear regime the thermodynamic branch gets unstable. A *linear stability analysis* can tell when the system gets unstable, but it cannot predict where the system is going to go. At some point a non-equilibrium phase transition occurs often accompanied by dramatic macroscopic changes. The new state is characterized by an order parameter. Even if the boundary condition is held fixed and the steady state in the linear regime is homogeneous, the new state can exhibit oscillations in space and time. The symmetry is broken. The new state has more structure (less symmetry). This requires a steady flow of matter or energy, i.e. entropy production to maintain it.

In my words, Prigogine has in mind that a pumped system develops internal invisible coherence. At some point it has to release it (what entropy/coherence) in a kind of temporal phase transition, where the system has two choices: either turn into chaos or develop a higher order. The state of higher order (or lower symmetry) is called dissipative structure.

9.9.5.3 Criticism

Ilya Prigogine coined the phrase *dissipative structures* as a name for the patterns which self-organize in far-from-equilibrium dissipative systems. Dissipation inspires the wrath of the moralist and the envy of most others; for the physicist, however, it is merely faintly depressing. We call something dissipative if it looses energy to waste-heat. (Technically: if volume in the phase space is not conserved.) The famous Second Law of Thermodynamics amounts to saying that, if something is isolated from the rest of the world, it will dissipate all the free energy it has. Equivalently, it maximizes its entropy. Thermal equilibrium is the state of maximum entropy.

If something is (in a well-defined sense) near thermal equilibrium, one can show that its behavior is governed by linear differential equations (hence the name 'linear thermodynamics' for the appropriate body of theory), and that left to itself it will approach equilibrium exponentially (hence the somewhat more common name 'irreversible thermodynamics'). Here we are guided, not by the entropy, but by 'entropy production', the rate of increase in entropy. Since, once we reach equilibrium, the entropy cannot increase (by definition), the entropy production at equilibrium is zero, and the entropy production is always decreasing (the 'principle of minimum entropy production').

In general, however, things are not well-isolated from the rest of the world. If energy arrives from the outside as quickly as it is dissipated, even bodies in the linear regime can be kept away from equilibrium. (Hence various creationist arguments about the Second Law are worthless: neither living things nor the Earth are well-isolated from the rest of the universe, as may be observed every day at sunrise.) Thus dissipation, and why dissipative systems are not necessarily dull as dish-water. So you can have structures in dissipative systems, and there's no reason not to call them "dissipative structures", though it's not obvious that there are many interesting generalizations about them.

"Far-from-equilibrium" means that your system is so far from its thermal equilibrium that the linear laws I mentioned a moment ago no longer apply; non-linear terms become important. The only general rule about the solution to non-linear differential equations is that there are no general rules; hence the interest in the subject. (Cf. Chaos and non-linear dynamics.) This is not good news, of course, if what you want to do is extend thermodynamics to the far-from-equilibrium case. But, one might suppose, matters are not totally hopeless; we aren't talking about just any arbitrary system of equations, but the particular ones important in thermodynamics; perhaps there is some general principle (like those of maximum entropy, or minimum entropy production) which can guide us to solutions. What Prigogine claims to have done is to have found, if not another extremum principle, then at least an inequality (a "universal evolution criterion"), and to have used it to work out the theory of dissipative structures, according to which patterns are supposed to form when the uniform, uninteresting 'thermodynamic branch' of the system becomes unstable. The math for all this is analogous to that of equilibrium phase transitions with 'broken symmetry', where, again, a uniform state becomes unstable, forcing the system into a patterned, coherent one to minimize free energy. Even without Prigogine's claims that this theory is Very Significant to biology and social science, even without the philosophical and cultural importance he claims for it, this would be very interesting, and the big question is whether he's right, i.e. whether and to what the theory applies.

The authors compare symmetry-breaking in thermodynamic equilibrium systems (leading to phase change) and in systems far from equilibrium (leading to dissipative structures). They conclude that the only similarity between the two is their ability to lead to the emergent property of spatial variation from a homogeneous background. There is a well-developed theory for the equilibrium case involving the order parameter concept, which leads to a strong correlation of the order parameter over macroscopic distances in the broken symmetry phase (as exists, for example, in a ferromagnetic domain). This correlation endows the structure with a self-scaled stability, rigidity, autonomy or permanence. In contrast, the authors assert that there is no developed theory of dissipative structures (despite claims to the contrary) and that perhaps there are no stable dissipative structures at all! Symmetry-breaking effects such as vortices and convection cells in fluids — effects that result from dynamic instability bifurcations — are considered to be unstable and transitory, rather than stable dissipative structures. Thus, the authors do not believe that speculation about dissipative structures and their broken symmetries can, at present, be relevant to questions of the origin and persistence of life.

Prigogine and his school have made a series of attempts to build an analogy between these dissipative far-from-equilibrium systems which form patterns and the Landau free energy and its dependence on the order parameter, which leads to the important properties of equilibrium broken symmetry systems. The attempt is to generalize the principle of maximum entropy production, which holds near equilibrium in steady-state dissipative systems, and to find some kind of dissipation function whose extremum determines the state. As far as we can see, in the few cases in which this idea can be given concrete meaning, it is simply incorrect [773]. In any case, it is clearly out of context in relation to the observed chaotic behavior of real dissipative systems.

9.9.5.4 Haken's approach

The *synergetics* is the theory of cooperation, i.e. the theory of the behavior of coupled systems and in particular of *self-organization* [571].

Equilibrium phase transitions (liquid-solid, ferromagnetic, BEC,...) occur by temperature reduction. The less symmetric (or broken) phase, i.e. the phase with more structure is at lower temperature. This is not generally the case, e.g. living systems tend to die at low temperatures. (The universe will die the 'Kältetod' [Boltzmann, Helmholtz, Clausius]. Did the big bang really have lower entropy, than the today's universe?) Such systems are characterised by a steady flow of energy or matter.

The dynamic systems exhibit transition from disorder to order *analogous* to phase transitions. Those temporal transitions can be understood in the following way. Any system has fluctuations. By continuously emitting small subsystems (fluctuations) out of its equilibrium, the system probes the range of possible motional states it can possibly adopt. If the current state of the system is not stable, a fluctuation may trigger a collective instability. More and more subsystems are slaved into the collective motion. If several instabilities occur simultaneously, often only the fittest survives. This is called *mode competition* (see superradiance) and often leads to *symmetry breaking*. A mode is called *order parameter* if it slaves subsystems.

Eventually the driven system may find to a dynamically stable state (see Paul-

traps). Too strong thermodynamic forcing may lead to *turbulence* or *deterministic chaos*.

Note that one may influence which modes survives by external forces. Furthermore, one may speed up the instability by the application of noise (see *stochastic resonance*).

9.9.5.5 Feedback principle

According to Dawson [332] the state of macroscopic systems made of coupled microscopic subsystems subjected to noise not only is the statistical manifestation of the interacting subsystems as suggested by Boltzmann, but also prescribes the environment felt by the subsystem. This provides a positive feedback: Random perturbation of the microsystems are compensated for and the macrosystem exhibits a coherent self-regulated behaviour. However in special circumstances microscopic fluctuations can become amplified by collective action and become important on a macroscopic scale, then termed *critical phenomena*. The distinction between macro- and microsystems breaks down, if the macrosystem gets intrinsically stochastic itself. The role of critical phenomena is ideally studied with bistable systems. It is reminiscent to *stochastic resonance*s.

Feedback is an essential ingredient. It leads to a cyclic causality. Examples are the problem of the hen and the egg, and the self-generated CARL wave. It is very similar to *Darwinism*, the cyclic recurrence of randomness and necessity, of fluctuation and competition, of mutation and selection.

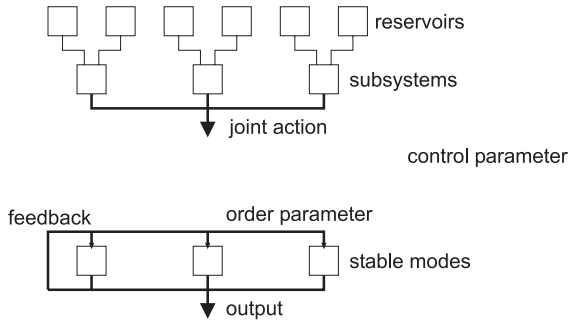

Figure 9.30: Principle of synergetics.

9.9.5.6 Comparison to Prigogine

Prigogine correctly identifies the role of fluctuations.

However he does not rely on feedback. He rather tries to find universal rules based on entropy, i.e. the principle of minimum excess entropy production. Synergetics goes beyond dissipative structures.

9.9.5.7 Example: Bénard instability

Examples range from physical instabilities, autocatalytic chemical reactions to biological, evolutionary, social and economic systems.

The most well-known dissipative structure is perhaps the so-called *Bénard instability*. This is formed when a layer of liquid is heated from below. At a given temperature heat conduction starts to occur predominantly through convection, and it can be observed that regularly spaced, *convection* cells are formed in the layer of liquid. This structure is wholly dependent on the supply of heat and disappears when this ceases. The form of the structures may vary from vertical rolls (distorted to hexagons due to surface tension in the liquid) to concentric rings or spirals. This depends on the exact form of the thermodynamic force, i.e. of the heat gradients.

9.9.5.8 Example: Surface waves

Waves are typically associated with perturbations that propagate in a system and transfer the energy of the system. Wave dynamics is possible both in conservative and dissipative (active) systems. Physical models of nonlinear waves are derived to simplify a complicated system of primary equations in a number of approximations. The same equations at the leading order describe main effects such as nonlinearity, dispersion, diffraction, diffusion, damping and driven forces, and resonances that determine wave propagation.

Oceanic waves generated by wind can reach anomalous high amplitudes in 10-20 meters. Such a giant *surface wave* are called a *freak wave* or *rogue wave*. They are formed as a result of a nonlinear interaction of multiple spectral components of the wave perturbations that propagate with different group velocities. The physical model for freak waves is based in the weak amplitude approximation on the *nonlinear Schrödinger equation* (NLS)

Refs: [http://dmpeli.math.mcmaster.ca/ResearchProjects/ResearchPage4.html].

9.9.5.9 Example: Faraday crispations in fluids

The undulation of the free surface of a viscous fluid in container under vertical vibration is known as *Faraday crispation*. The forced surface waves, which form many interesting *spatio-temporal dissipative structures*, oscillate at a frequency half the forcing frequency. In presence of large dissipation in a thin layer of viscous fluid, the surface crispation may be synchronous with forcing [432, 122, 434, 759, 936, 243].

9.9.5.10 Example: Predator-prey model

The Lotka-Volterra or *predator-prey model* is an example for a temporal oscillation. The populations of predators and prey interdepend via

$$\begin{aligned} \dot{N}_{py} &= \varepsilon_{py} N_{py} - \gamma_{pr} N_{pd} N_{py} \\ \dot{N}_{pd} &= -\varepsilon_{pd} N_{pd} + \gamma_{pd} N_{py} N_{pd} \ . \end{aligned} \tag{9.95}$$

9.9.5.11 Example: Physiology

Kelso's experiment of finger waved in parallel driven by a metronom. Passed a certain critical frequency the fingers are waves in the antiparallel mode. The transition is a phase transition. Amputierte Tausendfüssler spontaneously change their motion

pattern: to insect-like for 6 legs left, dog-like for 4 legs left. The movement is not controlled/programmed by brain, but self-organised via Rückenmark.

The brain exhibits self-organization on many different levels. Firing neurons synchronize, synapses tentatively establish new connections which are only confirmed and reinforced if frequently used. The brain thus resembles much more a dynamically moving system than a computer. Cognition and understanding seems to work like self-organization. Perception is an external control parameter which is only received and processed if it fits into an existing frame. If it doesn't it may still trigger a new idea, a though fluctuation, which can change the state of mind to a new one, if the new state appears to be more consistent or satisfying. The idea takes on the role as order parameter, the brain cell is slaved.

9.9.5.12 Example: Social systems

Static systems are often more unstable than dynamic systems if subject to external forcing. E.g. democracies which are based on an institutionalised permanent revolution can be more robust than dictatures.

9.9.5.13 Example: Laser

The laser is an open system far from equilibrium, because it is coupled to systems with different temperatures. The inversion corresponds to $T < 0$. On the other hand the the emitted photons coupled to ambient atoms at temperatures $T \ll \hbar\omega/k_B$, i.e. $T \approx 0$. Nevertheless, Haken has shown that the laser exhibits all features of a standard equilibrium phase transition.

In particular the equations describing a homogeneously broadened, unidirectional, single mode ring laser are mathematically equivalent to those describing the Bénard instability.

The conversion from a low quality microscopic form of energy (heat, chemical affinity) to a high quality macroscopic form (electricity, work) requires energy itself.

9.9.5.14 Example: CARL

Is a self-organizing system by feedback. As compared to biological systems or even Bénard instabilities, CARL is **very simple**. CARL is **of course** nonlinear: every degrees of freedom is a nonlinear function of the others.

9.9.5.15 Example: Vortex patterns

However there is another example for phase transitions in BECs: The transition from one vortex pattern to another has been classified as a first-order phase transition. But it seems to me that this is rather a non-equilibrium phase transition. I think, *vortex pattern* are *dissipative structures*. They decay by losing the vortices one by one due to relaxation into thermal excitations. On the other hand, vortex pattern are formed by a dissipative force: stirring up a condensate. In fact, an irreversible process is necessary to form a vortex: The BEC is excited by stirring (Dalibard's method) and *decays* into the vortex state. The is perhaps not true even for Cornells method, where the vortex is formed by engineering of the BEC phase.

Vortex pattern are unstable, they have a limited lifetime. It might however be possible to stabilize them have a continuous stirring. This would be a true dissipative structure: A stirring force relying on friction on one hand, diffusion by thermal decay on the other.

9.9.6 Friction and diffusion

Friction and diffusion arise from coupling to a reservoir. Friction comes from coupling to a 0-temperature reservoir, diffusion to a reservoir at finite temperature. For example the decay of a cavity (friction) can be described by coupling to the external vacuum. However if the vacuum contains blackbody radiation, $T > 0$, photons may be coupled in which leads to diffusion.

9.9.7 Non-equilibrium quantum phase transitions

It might be interesting to look out for nonequilibrium quantum phase transitions. However, those are difficults to imagine. Mott-transitions are clearly in some kind of equilibrium (not really a thermal one). They are reversible via a control parameter. They do not require the feeding with energy or entropy, i.e. heating. Clearly, entropy is and must remain zero at $T = 0$.

9.9.8 Fluctuation-dissipation theorem

In statistical physics, the *fluctuation-dissipation theorem* is derived from the assumption that the response of a system in thermodynamic equilibrium to a small external perturbation is the same as its response to a spontaneous fluctuation. There is therefore a direct relation between the fluctuation properties of the thermodynamic system and its linear response properties.

For example, Einstein in his 1905 paper on Brownian motion noted that the same random forces which cause the erratic motion of a particle in Brownian motion would also cause drag if the particle were pulled through the fluid. In other words, the fluctuation of the particle at rest has the same origin as the dissipative frictional force one must do work against, if one tries to perturb the system in a particular direction. From this observation he was able to use statistical mechanics to derive a previously unexpected connection, the Einstein-Smoluchowski relation: $D = \mu k_B T$, linking the diffusion constant D and the mobility of the particles μ (i.e. the ratio of the particle's terminal drift velocity to an applied force, $\mu = vd/F$).

The fluctuation-dissipation theorem can be used to give an explicit relationship between molecular dynamics at thermal equilibrium, and the macroscopic response that is observed in a dynamic measurement. It thus allows molecular scale models (microscopic models) to be used quantitatively to predict material properties in the context of linear response theory.

The essence of fluctuation-dissipation theorem is that it relates equilibrium fluctuations to out-of-equilibrium quantities, like noise power is related to resistance. The theorem is based on fields that are weak relative to the potential of molecular interaction so that rates of relaxation are not affected by the applied field. 'Out-of-equilibrium' in the above sentence should be understood as close to equilibrium or stationary states.

9.9.9 Long-range interactions

Having been pioneered in astrophysics (e.g. in the formation of coherent structures like galaxies and stars), long-range interactions also play a role in plasma physics, hydrodynamics (e.g. jets, vortices like the gulf stream or the Jupiter vortex), systems with dipolar interactions, cold and ultracold gases, clusters and even in some nuclear systems. Today the most promising systems to experimentally study long-range interactions are atomic gases with electromagnetic interactions. However, those are mostly quantum systems. And one is still far from discerning which properties are genuinely ascribable to long-range interactions (whether fundamental or effective).

Systems with *long-range interaction* can behave very differently from systems with *short-range interaction*. The most prominent features are ensemble inequivalence and negative specific heat.[1] The dynamical aspects of the approach of long-range interacting systems to equilibrium is not yet well understood. The statistical physics has to learn in this domain. In particular, if the interacting particles are microscopic objects with quantized degrees of freedom or quantum statistical constraints.

A short-range interacting system is always [229]

- additive, i.e. the total energy of two parts of a system is $E_1 + E_2$, because the interaction energy between the parts E_{12} is negligibly small (is decreases like the surface-to-volume ratio like $N^{2-\alpha/3}$ for an interaction potential $V(R) \propto R^{-\alpha}$);
- having *extensive thermodynamical potentials* (e.g. energy, free energy, entropy, Gibbs free energy,...), i.e. for given values of the *intensive thermodynamical parameters* (e.g. n, T, p,...) they are proportional to N;
- rapid to find to equilibrium (non-equilibrium states are unstable);
- homogeneous at equilibrium (in the absence of external fields).
- having equivalent micro- and macrocanonical ensembles (i.e. the same values for the thermodynamic potentials are calculated for both situations).

In contrast a long-range interacting system

- is not additive;
- has extensive thermodynamical potentials;
- has non-equilibrium situations lasting for macroscopic times (the metastable states represent local extrema of thermodynamic potentials, the evolution towards other non-equilibrium states is driven by mean-field fluctuations);
- is inhomogeneous at all scales;
- exhibits strange concepts like negative specific heat $C = (\partial E/\partial T) < 0$;
- has non-equivalent micro- and macrocanonical ensembles (probably, one has to pick the appropriate ensemble depending on the experimental condition, i.e. isolated system or system held at a fixed temperature);

[1] A specific statistical ensemble is obtained by keeping two out of four (for a 1 component gas) thermodynamic parameters fixed (p, V, T, N).

- exhibits ergodicity breaking;
- shows non-equilibrium phase transitions.

Interaction potentials are short-range if $\int_{R_0}^{\infty} V(\vec{R}) d^3\vec{R} < \infty$. Alternatively, interaction potentials are short-range if there exist constants $C > 0$ and $R_0 > 0$ for which, $|V(\mathbf{r})| = C/|\mathbf{r}|^{\alpha}$ for all $|\mathbf{r}| > R_0$, where $\alpha > 3d$ and d is the dimensionality of the system. The main long-range forces of interest are gravitation and electro-magnetic forces, e.g. Coulomb repulsion and radiation pressure.

$\alpha < 3$ $E_{12} \propto N^{2-\alpha/3}$
$\alpha = 3$ $E_{12} \propto N \ln N$
$3 < \alpha < 4$ $E_{12} \propto N^{2-\alpha/3}$
$\alpha = 4$ $E_{12} \propto N^{2/3} \ln N$
$4 < \alpha$ $E_{12} \propto N^{2/3}$

One distinguishes between continuous and lattice systems.
Long-range interaction is a prerequisite of CARL and self-organization.

9.9.9.1 Negative specific heat

In macrocanonical ensembles the specific heat does not get negative, only in microcanonical ensembles, i.e. in systems isolated from heat baths.

Self-gravitating systems can have *negative specific heat*. According to the virial theorem the energy of such a system is $0 > E = Ekin + E_{pot} = -E_{kin} = \frac{m}{2}\langle v^2 \rangle = \frac{3}{2} k_B T$. For a gravitationally bound two-body system this is easy to see (see Aufgabensammlung zu Integrierter Kurs Physik I, "Keplerbahnen"). Hence, increasing T reduces E. Negative specific heat is usually connected to astrophysical long-range interactions, like self-gravitating clouds, and applies more to equilibrium situations. There is probably no chance of seeing it with CARL. The molasses CARL is best described by a macrocanonical ensemble, since the atoms are not isolated, but connected to a heat bath. The system is completely described by a set of Langevin equations [**?**].

9.9.9.2 Small systems

A short-range interacting *small system* can exhibit similar features as long-range interaction systems, in particular *non-additivity* [**?**]. A small system is defined by the fact, that the range of its interaction is similar to the system's size. As an example one may consider an ultracold atomic gas near a Feshbach resonance. The power law of the interaction potential does not change, but the scattering length can be as large as the atomic cloud.

9.10 Further reading

H.M. Nussenzveig, Edgar Blucher (2014), *Curso de Fisica Basica: Fluidos, Vibrações e Ondas, Calor - vol 2* [962]$_{\text{ISBN}}$

P.H. Chavanis, *Dynamics and thermodynamics of systems with long-range interactions: interpretation of the different functional* [**?**]$_{\text{DOI}}$

A. Giansanti, *Thermodynamics of Small Systems* [?]DOI

Chapter 10

Structure of matter

10.1 High energy physics

10.1.1 Nuclear models

There is a new force coming into play, which act between nucleons. Nuclear models are complicated, several models are used to explain the various features. The energy scale is MeV, hence at room temperature the nuclei are in their ground state. However inside stars or in the history of the universe, excited states play an important role.

α scattering reveals deviation from the Coulombian law for collision parameters below 10 fm, indicates the typical size of a nucleus. The nuclear force which helds together the nucleons is short ranged (2 fm), its energy about 10 times larger than the Coulomb repulsion at typical internucleon distances. The force is charge independent, but depends on the nuclear spin. The Yukawa potential is,

$$V(r) = -g^2 \frac{e^{-r/r_0}}{r} \ , \tag{10.1}$$

with $r_0 = \hbar m_\pi c$

The hyperfine structure in atomic spectra tells the total nuclear spin, which is on the order $\mu \simeq \mu_K \equiv \pi\hbar e/2m_p$. The angular moment μ can be parallel or anti-parallel to the spin I. All nucleons have spin 1/2. If $A = N + Z$ is even/odd, I is integer/half-integer.

Neutrons can be detected by sending them onto a parafine sheet, from which they expel protons into a Geiger counter.

Irregularities in the hyperfine structure (deviations from the Landé interval rule) point to non-spherical nuclear charge distributions giving rise a quadrupole moment.

While α scattering reveals the nuclear mass density, electron scattering tells the electric charge distribution (like in an electron microscope). The first minimum of the diffraction pattern $\theta \simeq \lambda/r$ follows from the electron de Broglie wavelength and the charge radius. Such study confirm the following empirical formula for the charge density

$$\rho(r) = \frac{\rho(0)}{1 + e^{(r-a)/b}} \ , \tag{10.2}$$

where $a \approx A^{1/3} \times 1.07\,\text{fm}$ and $b \approx 0.55\,\text{fm}$. This shows that $\rho(r)$ is flat in the center and has a radius $r_{1/2} \propto A^{1/3}$. The mass and the charge densities are related by $Z\rho_m(r) \simeq A\rho(r)$.

10.1.1.1 Mass defect

The atomic mass unit is $u \equiv 12^{-1} m(^{12}\mathrm{C})$. Deviation of measured atomic masses from integer $m(X)/u$ is due to isotope mixtures. Nuclear reactions $a + A \to B + b$ (e.g. $\alpha + {}^{14}\mathrm{N} \to {}^{17}\mathrm{O} + p$) conserve relativistic energy,

$$K_a + m_a c^2 + m_A c^2 = K_B + m_B c^2 + K_b + m_b c^2 \ . \tag{10.3}$$

The Q value of the reaction is $Q = K_B - K_b - K_a = (m_a + m_A - m_B - m_b)c^2$. Measure the kinetic energies K_b and K_a, express K_B via the scattering angle θ using momentum conservation.

The mass of a nucleus is less than the sum of its components. The difference is the nuclear binding energy or defect mass $\Delta m(X) = \Delta E/c^2 = Z m_p + N m_n - m(X)$. Hence, a neutron capture (if it is possible) liberates electromagnetic energy. The defect mass per nucleon rapidly increases from H to Ca and then slowly drops for higher nuclear masses. The behavior is explained by the Weizsäcker droplet model. According to this the absolute nuclear ground state is around Ca ($Z = 40$), and all other nuclei are metastable, i.e. would ultimately decay into Ca is a proper mechanism was at hand.

For example, the energy balance for nuclear fission converting ${}^{238}\mathrm{U} \to {}^{119}\mathrm{X}$ is $2 \times 119 \times 8.5\,\mathrm{MeV} - 238 \times 7.6\,\mathrm{MeV} = 210\,\mathrm{MeV}$, which goes into kinetic, i.e. thermal energy. Similar considerations hold for fusion and radioactive decay processes. Another example is the capture of a neutron by ${}^{235}\mathrm{U}$, which liberates $m({}^{235}\mathrm{U}) + m_p - m({}^{236}\mathrm{U}) = 6.6\,\mathrm{MeV}$. This energy excites nuclear shape oscillations, which may then induce a fission process. In contrast, for ${}^{238}\mathrm{U}$ the liberated energy is only 5 MeV, which is not enough to excite an oscillation, so that the fission process is inhibited.

10.1.1.2 Droplet nuclear model

The droplet model compares the nucleus with a drop of an incompressible liquid: The density is constant as well as the exit work for evaporation, i.e. the binding energy per nucleon. The analogy is expressed in the following semi-empirical defect mass formula. The mass difference of the nucleus and the sum of its components $B(Z,N) = N m_n + Z m_p - m_{nucl}$ is according to *Weizsäcker's droplet model* approximately,

$$B(Z,A) = 14.1A - 13A^{2/3} - 0.595\frac{Z^2}{A^{1/3}} - 19\frac{(Z-N)^2}{A} + 33.5\frac{1}{A^{3/4}} \times \begin{cases} -1 \text{ for uneven } Z,N \\ 1 \text{ for even } Z,N \\ 0 \text{ else} \end{cases} \tag{10.4}$$

The first (volume) term expressed the constance of B/A, i.e. the nucleus matter is distributed rather homogeneously. The second (surface) term corrects, i.e. lowers the binding energy for anisotropies near the surface of the nucleus. The third (Coulomb) term describes the fact that Coulomb repulsion tends to lower the density of the protons, which reduces their contribution to the binding energy. The forth (symmetry) term accounts for the observation that light nuclei with $Z \simeq N$ have larger binding energies.

For heavy nuclei $N \gtrsim Z$. This is because of Coulomb repulsion more neutrons are necessary to dilute protons than neutrons. The fifth (pairing) term expresses

the tendency of the nucleons to pair with other nucleons of the same species. The maximum of $B(Z, A)$ traces stable regimes in the isotope table.

10.1.1.3 Fermi gas model

Assuming that the nucleons move independently in a square well potential made out of the mean-field of the nucleons, we obtain Weisskopf's Fermi gas model. The Fermi energy of the ground state nuclei is estimated via $A = \int_0^{E_F} \rho(E)n(E)dE$. The potential depth is simply $B + E_F$. In this model it becomes clear, why $Z \simeq N$ is energetically favorable, or when Coulomb repulsion increases the level spacing $N \gtrsim Z$.

10.1.1.4 Shell model and collective model

The binding energy exhibits more feature not explained by the droplet model, such as the existence of magical numbers for A around which the binding energy is particularly high: 2,8,10,... This suggests the existence of a shell structure. The formal approach, somewhat analogous to the Hartree treatment of the electron shell of the atoms, is to set up multiparticle Schrödinger equation and to solve by self-consistently adjustment of the potential shape and the excitation levels. In this picture, the magical number are due to a shell structure, where the energies of the shells are interchanges, because they are shifted by strong nuclear spin-orbit interactions.

The model can also predict to some extend the nuclear spins, which predominantly result from jj coupling. In contrast to the electron shell, where Coulomb repulsion favors $\uparrow\uparrow\uparrow$ states according Hund's rule, in nuclei the Coulomb attraction favors $\uparrow\downarrow$ pairing.

The shell model treats individual nucleons, while the droplet model describes collective effects. There are models trying to include collective effects in the shell model by allowing for anisotropic mean-field potentials. Collective motion of nucleons will then lead to time-dependent shape distortions of $V(\mathbf{r})$. E.g. a nucleon with a large orbital momentum moving around the nuclear surface like a protuberance drags other nucleons thus forming a collective tide wave. Such models can quantitatively explain nuclear quadrupole moments and collective rotations and vibrations. See the analogy to the nonlinear Schrödinger equation in collective oscillations in gaseous Bose-condensates.

The optical model is another generalization of the shell model.

10.1.2 Radioactive decay

10.1.2.1 α-decay

Nuclei can mutate via fission, fusion or radioactive α, β or γ-decay. The α-decay consists in the emission of ${}^4He$ particles. The nuclei resulting from α-decay can decay themselves, and so on until a stable isotope is reached. Hence, there are 4 possible decay families, whose fathers are long-lived ($T_{1/2} \approx 10^{10}$ a) radioactive isotopes: $4n \rightarrow^{233} Th$, $4n + 1 \rightarrow^{237} Np$, $4n + 2 \rightarrow^{238} U$, and $4n + 3 \rightarrow^{235} U$. The released energy $\Delta E = m(Z, A) - m(Z - 2, A - 4) - m(\alpha)$ is mainly Coulombian, since the sum of the volume terms is nearly unchanged. It can be determined by measuring the kinetic energy of the α particles.

The potential seen by an α particle has an attractive square well shape inside the nucleus surrounded by a Coulombian repulsive barrier. In a nucleus which is excited into a shape resonance, an α particle may tunnel through this barrier with a rate R, $dN = -NRdt$. The half decay lifetime is $T_{1/2} = \ln 2/R$.

A decay family in a dynamic equilibrium is characterized by $N_k R_k = N_l R_l$, which is found by solving coupled differential equations in steady-state. This allows for some amount of natural abundance even of very short-lived isotopes ($T_{1/2} \approx 1\,\mu s$).

Fathers of a decay family have low decay energies, which makes them stable. For $Z < 80$ the nuclei are stable anyway. In contrast to other small particles, ^4He has a strong defect mass per nucleon. This makes it favorable to emit α particles. However, other heavier particles can be emitted, as in the fission process. The heavier the particles the more Coulomb energy can be released, which makes fission processes take over beyond $A > 100$.

The product of nuclear reactions generally end up in excited states.

Note the tendency to liberate low-quality (kinetic/thermal) energy having high entropy.

Radioactive α-decay families would always maintain the same $Z - N$, which is unfavorable for heavy nuclei. The β-decay converts protons into neutrons (and vice versa) by the emission or capture of electrons or positrons. Note that this decay does not lead to a change of the decay family. The β-decay is directed into the directions toward the stability region $N \gtrsim Z$. Thus an α-decay is often followed by an electron emission or a positron capture to reduce Z and increase N. The energy balance is $\Delta E = m(Z, A) - m(Z \pm 1, A) \pm m_e$.

10.1.2.2 β-decay

β-emission yields a continuous spectrum. Since the electron takes all the kinetic energy, the nucleus being to heavy, one could expect a single narrow peak in the spectrum. Furthermore, angular momentum is not conserved by the creation of an electron. This led Pauli to postulate the existence of (anti-)neutrinos in reactions like $^A X^Z \rightarrow^A X^{Z+1} + e^- + \bar{\nu}_e$. The neutrino spin is 1/2 and it has no charge. The neutrino mass is 0, in order to allow for the electron taking all the decay energy.

Gamov-Teller selection rules for β-decay: $\Delta i = 0$ and conserved parity. The β-decay results from a new force, the weak interaction. Its range is so short that neutrinos traverse stars without interactions. Nevertheless, neutrinos have been detected via the process $\bar{\nu} +^1 \mathrm{H} \rightarrow n + \bar{e}$, where the positrons can be detected in scintillation chambers, because they also sense the electro-magnetic interaction.

Wu observed that nuclei with aligned dipolar magnetic moments preferentially emit β-radiation into one direction, the one with clockwise heliticity, i.e. the process is not invariant under mirroring (three mirrors make a parity transformation). This implies that the weak interaction does not conserve parity. The spin of a neutrino is $\mathbf{L}_\nu \uparrow\downarrow \mathbf{k}$ and for an anti-neutrino $\mathbf{L}_{\bar{\nu}} \uparrow\uparrow \mathbf{k}$, hence there is a $\mathbf{L}_\nu \mathbf{k}$ interaction. The weak interaction is the only one to be sensitive to heliticity.

A *well-defined heliticity requires vanishing rest mass*, i.e. light velocity for the particles. Otherwise an inertial system could be found, where the momentum $\mathbf{k}$ is inverted and thus, for a given angular momentum, the helicitity.

10.1.2.3 γ-decay

Subsequently to nuclear reactions (β-decay, n-capture,...) excited nuclear states with typically $E > 10^{-2}$ can be populated. Those may decay via emission of γ-radiation thus yielding excitation spectra, which are probed via electrons produced by photo-effect, Compton scattering or pair-production. In contrast to the optical regime, where M1 radiation is suppressed by $(v/c)^2 \simeq 10^{-4}$ and E2 radiation by $(a_B/\lambda)^2 \simeq 10^{-6}$, multipolar transitions are more likely especially at high γ energies. Collisional deexcitation is inhibit by the Coulomb barrier surrounding the nuclei. The selection rules are $|I_f - I_i| \leq L \leq I_f + I_i$ and $\Delta P = (-1)^L$ for electric and $(-1)^{L+1}$ for magnetic radiation. $\Delta I = 0$ is forbidden, because photons carry away 1 unit of angular momentum.

10.1.2.4 Nuclear conversion

γ-decay can be accompanied by emission of groups of monoenergetic electrons. This occurs if the γ-photon is reabsorbed by electrons of the inner shells (K, L, M,...) of the atomic electrons. The rate for this process adds up to the normal γ-decay, $R_\gamma + (\alpha_K + \alpha_L + ..)R_\gamma$.

Mössbauer effect (see Sec. 38.3.3).

10.1.3 Nuclear reactions

10.1.3.1 Nuclear conversion

Until we considered spontaneous nuclear decay. Now let us discuss nuclear reactions. The balance of an equilibrated nuclear reaction tells the masses of the participating nuclei. Any reaction must conserve the following quantities: Relativistic energies, momentum, angular momentum, charge, parity (if the weak force is not involved) and the baryon number.

The p-capture is a process, which can be studied in particle accelerators. If a p has sufficient energy to cross the Coulomb barrier, its de Broglie wave is larger than the range of the nuclear force, but smaller than the size of the nucleus. If it collides with a nucleon, it may loose sufficient energy to be reflected from the potential walls. It then collides again with other nucleons, until the energy is uniformly distributed, so that for no single nucleon the energy is sufficient to escape. However, fluctuations may impart sufficient energy to individual nucleons. Preferentially neutrons, which do not sense the Coulomb barrier may then evaporate. The remaining excitation is dissipate via γ-emission. p-capture followed by n-emission ($d +^A \mathrm{X} \rightarrow^A \mathrm{Y} + \alpha$ or $p +^A \mathrm{X} \rightarrow^A \mathrm{Y} + n$) in nuclear power plants often generates β-active isotope, which are precious side-products used for radioactive tracing, etc..

The differential cross section $d\sigma/d\Omega$ is Coulombian at low scattering angles θ. At large θ, where the nuclear potential comes into play, interference effects result in an oscillatory behavior of $(d\sigma/d\Omega)(\theta)$.

The *shape resonances* are due to constructive interference of incident and reflected de Broglie waves. How about Feshbach resonances?

n scattering can probe resonances of composite nuclei. The resonances are described by the *Breit-Wigner formula* for the total cross-section, which holds for every

damped oscillation,

$$\sigma_r(E) = \frac{\lambda^2}{4\pi} \frac{\Gamma_n \Gamma_r}{(E - E_i)^2 + \Gamma^2/4} \ll \pi r_{nucl}^2 \ . \tag{10.5}$$

This is similar to the optical cross section, where $\lambda^2/2\pi \ll \pi a_B^2$.

10.1.3.2 Fission

Hahn and Strassman discovered that the reaction $n + {}^{238}\mathrm{U} \to \mathrm{X} + \mathrm{Y} + n + n + .. + \Delta E$ liberates 200 MeV plus 2 or 3 neutrons, which is 10^6 times more than for a chemical reaction. In this process as long as the products X and Y are closer than the radius of the target nucleus, the energy increases with their distance, because the surface increases. Triggered by collective vibrations leading to shape oscillations the products may eventually separate. From this point on the surface terms are constant, but the products are strongly accelerated by Coulomb repulsion. I.e. the fission slightly increases the surface energy, but strongly minimizes the Coulomb energy. Since for the target $N \gtrsim Z$, 2 or 3 neutrons must be reemitted ($\approx$ MeV) to approach the $N \simeq Z$ regime for the products.

The lifetime for spontaneous fission is 10^{16} a, but it can be induced by slow n. To moderate the neutrons graphite (^{12}C) or heavy water (D_2O) is used, or light water (H_2O) in combination with enriched ^{235}U. The moderation increases the de Broglie wavelength of the neutrons and thus the cross section for capture. In practice, it is tuned such that exactly 1 out of the 2 to 3 emitted neutrons is captured to induce the next fission. The reaction products are decelerated by reactor materials, which heat up and drive gas turbines.

Fast breeder reactors are based on the process $n + {}^{238}\mathrm{U} \to {}^{239}\mathrm{U} \to {}^{239}\mathrm{Pu} + 2e^-$. The product ^{239}Pu now fissions upon n capture similar to ^{235}U.

10.1.3.3 Fusion

While fission is driven by the desire to reduce Coulomb energy, fusion reduces surface energy. The problem is that the collision partners must override the Coulomb barrier at 1 MeV ($= 10^{10}$ K). In the sun the rate for this becomes noticeable above $T > 10^8$ K. Fusion reactors must compensate their limited resources by more efficient rates, i.e. higher temperatures $T > 10^9$ K.

Fusion is the basic process in the creation of all elements up to Fe. All starts with the *big bang*, a kind of neutron star, where the following processes were in equilibrium

$$\begin{aligned} n &\to p + e + \bar{\nu} \\ \bar{\nu} + p &\to p + \bar{e} \\ p + n &\to p + n + \gamma \\ e + \bar{e} &\to \gamma + \gamma \\ \gamma &\to e + \bar{e} \ . \end{aligned} \tag{10.6}$$

Doppler recoil expands this soup, until it gets transparent for the γ, which subsist today as the 3 K blackbody radiation. Now starts the He-cycle producing the 10%

helium in the actual universe,

$$\begin{aligned} p + n &\to \mathrm{D} + \gamma \\ \mathrm{D} + \mathrm{D} &\to^3 \mathrm{He} + n \\ \mathrm{D} + \mathrm{D} &\to \mathrm{D} + p \\ \mathrm{D} + p &\to^4 \mathrm{He} + n \ . \end{aligned} \tag{10.7}$$

The 90% hydrogen are formed through β-decay of n.

Mass fluctuations now trigger agglomerations, where the temperature rises to $T > 10^5\,\mathrm{K}$, forming a proton electron plasma. Beyond $T > 10^7\,\mathrm{K}$ fusion sets in in the *pp*-cycle,

$$\begin{aligned} p + p &\to \mathrm{D} + \bar{e} + \nu + 0.42\,\mathrm{MeV} \\ p + D &\to^3 \mathrm{He} + \gamma + 0.55\,\mathrm{MeV} \\ {}^3\mathrm{He} + {}^3\mathrm{He} &\to^4 \mathrm{He} + p + p + 12.9\,\mathrm{MeV} \ . \end{aligned} \tag{10.8}$$

If the star heats up to $T > 10^8$ K, the carbon-cycle

$$\begin{aligned} {}^4\mathrm{He} + {}^4\mathrm{He} &\to^8 \mathrm{Be} \\ {}^4\mathrm{He} + {}^8\mathrm{Be} &\to^{12} \mathrm{C} \end{aligned} \tag{10.9}$$

become likely, the second one by a collision resonance-enhanced three-body collision. Once enough carbon has been produced, it catalyses the formation of N and O.

Note that our sun has not yet reached the carbon-cycle. All heavier elements in our solar system are remainders from a previous generation of stars. As the star contracts, more Ne and Mg is formed. At $T > 10^9\,\mathrm{K}$ the Coulomb barrier to the formation of Fe can be overruled. But convection between the elements formed in the core and the outer region, in which the *pp*-cycle is still active is needed to form Na. Elements beyond $A > 60$ cannot be formed by fusion. However, together with n-capture and β-decay elements can be formed up to ^{209}Bi. Beyond this n-capture only induces rapid α-decay.

When the hydrogen has been used up, thermal motion cannot counterbalance gravitation. The sun collapses in a few seconds (e.g. in a supernova) expelling an enormous flux of n. This flux may be high enough to allow for the simultaneous capture of several n circumventing the α-decay and thus creating the heavier elements observed in our solar system.

10.1.4 Elementary particles

10.1.4.1 Fundamental forces

At the surface of a nucleus the relative strength of the 4 fundamental forces is $F_{nucl}/F_{elmg}/F_{weak}/F_{grav} = 1 : 10^{-2} : 10^{-12} : 10^{-40}$. The range of the forces is $r_{grav} = r_{elmg} = \infty$, $r_{weak} \ll r_{nucl} \approx 1$ fm. The range is inversely proportional to the mass of the exchange particles (gravitons, photons, pi-mesons and vector bosons).

Transitions emitting photons must occur between states having different angular momentum, because *there are no oscillating monopoles; this is the reason why photons*

must carry away 1 unit of angular momentum. For analogous reasons, gravitons must carry away 2 units of angular momentum, because the *absence of negative gravitational mass renders gravitational dipole oscillations impossible.*

The nuclear force is spin-dependent. This is seen by the fact that the deuteron has as only one bound state a ${}^3S_1$ spin state, while the ${}^1S_0$ is unbound.

conserved quantity	nuclear force	el.mg. force	weak force	gravity
energy	+	+	+	
momentum	+	+	+	
angular momentum	+	+	+	
charge	+	+	+	
# leptons (e and μ)	+	+	+	
# baryons	+	+	+	
isospin **I**	+	−	−	
isospin I_z	+	+	−	
strangeness	+	+	−	
parity (P)	+	+	−	
charge conjugation (C)	+	+	−	
time reversal (T)	+	+	x	
intensity	1	10^{-2}	10^{-12}	10^{-40}
exchange particle	π	γ	?	graviton
mass (MeV)	140	0	$> 10^4$	0
spin	0		1	2
range (fm)	1	∞	$< 10^{-17}$	∞
sign	both	+ or −	?	+

Time reversal symmetry and charge conjugation (i.e. particle antiparticle transformation) are broken by the weak interaction in the (rare) $\mathrm{K_0\bar{K}_0}$ decay, but the CPT symmetry is conserved.

Note that the Schrödinger equation breaks time-reversal symmetry, but its absolute value does not.

10.1.4.2 Mesons

The nuclear force is known to saturate. This suggests that (while it vanishes at distances $r_0 > 2\,\mathrm{fm}$) the nuclear potential is repulsive at short distances $r_0 < 0.5$ fm. Thus every nucleon only interacts with a limited number of neighbors. The nuclear force can be understood as been transmitted by virtual particles, called mesons, carrying momentum. According to Yukawa every nucleon constantly emits and reabsorbes mesons for a short time satisfying $\Delta E \Delta t \sim \hbar$. Within this time the meson could maximally reach a distance $r_0 = c\Delta t = \hbar c/\Delta E = \hbar/m_\pi c$, which is the range of the interaction and the Compton wavelength of the π meson ($m_\pi = 140\,\mathrm{MeV}$). In the presence of another nucleon within this reach, the meson can be reabsorbed by that one. The transferred momentum is largest, when the mesons carry large kinetic energies, which is close to the nuclei.

This is similar to the Coulomb force being mediated by the exchange of virtual photons by electric charges in a second-quantized theory. The range of the Coulomb interaction is infinite, because the photons have no rest mass. I.e. photons with small energies ω can be encountered at very large distances. However, the transferred momentum is largest, when the photons have high energies capable of imparting large recoils, which is close to the charge.

Mesons can be liberated from virtual to real during a collision; they are observed in cosmic rays.

Mesons interconvert protons and neutrons,

$$\begin{aligned} p &\leftrightarrow n + \pi_+ \\ p &\leftrightarrow p + \pi_0 \\ p &\leftrightarrow p + \pi_- \\ n &\leftrightarrow n + \pi_0 \ . \end{aligned} \tag{10.10}$$

They can carry charge, have an intrinsically negative parity and are instable $\pi^0 \rightarrow \gamma + \gamma$ and $\pi^+ \rightarrow \mu^+ + \nu_\mu$.

Mesons are like all exchange particles bosons. They cannot be fermions because the number of fermions is conserved.

Protons *and neutrons* have a charge distribution that can be probed by electron scattering. This is why also the neutron has an electric dipole moment.

10.1.4.3 Muons

Muons are quasi heavy electrons and decay via $\mu^- \rightarrow e^- + \bar{\nu_e} + \nu_\mu$.

Every fermion has its anti-particle. The number of fermions-antifermions is conserved, in particular the lepton numbers and baryon numbers are constant: $\sum L_e = const$, $\sum L_\mu = const$, and $\sum B = const$, where $L_{e^-} = L_{\nu_e} = 1 = -L_{e^+} = -L_{\bar{\nu}_e}$.

10.1.4.4 The particle zoo

Generations of leptons, neutrinos, quarks

$$\begin{bmatrix} e & u \\ \nu_e & d \end{bmatrix} \quad , \quad \begin{bmatrix} \mu & s \\ \nu_\mu & c \end{bmatrix} \quad , \quad \begin{bmatrix} \tau & t \\ \nu_\tau & b \end{bmatrix} \tag{10.11}$$

and their antiparticles.

The quarks do not exist alone, but as *hadrons*, i.e. either antiquark pairs called *mesons* or quark triplets called *baryons*. The most common ones are the π-mesons ($\pi^0 = u\bar{u}?$, $\pi^\pm = u\bar{d}$), the proton ($p = uud$) and the neutron ($p = udd$). The up quark has the charge 2/3, the down quark -1/3.

10.2 Solid state physics

10.2.1 Models for electrons in crystals

10.2.1.1 Types of solids

In contrast to a gas, which in most cases consists of isolated particles, the interparticle interaction plays a dominant role in crystals. Solids, or more specifically crystals, are

classified according to the predominant type of binding. 1. Molecular binding is responsible for the solidification of binary gases like O_2. Here, fluctuating dipole moments inducing dipole moments in neighboring molecules lead to van der Waals attractive forces on the order of $E_{bind} \simeq 10^{-2}\,\mathrm{eV}$ going like r^{-7}. 2. Ionic binding gives rise to periodic structures alternating positive and negative charges, as in NaCl. 3. Covalent binding is directional. This directionality determines the crystalline structure, such as in graphite and diamonds. In those three binding types there are no free electrons and hence no conductance. However, covalently bound crystals can sometimes be semiconductors or transparent. 4. Metallic binding is a limit of covalent binding, in which the valence electrons, which shared by all atoms, overrule the repulsion between the ions. The ionic lattice is immersed in a gas of free electrons. The ions have filled shells and are spherically symmetric. The electrons can easily absorb light, which makes the crystal opaque. The type of binding is studied via X-ray diffraction, via the dielectric properties, etc..

10.2.1.2 Band model

The number of orbitals in the isolated atoms forming the crystal gives the number of states available to the free electron gas. The exchange interaction of the fermionic electrons lifts the degenerescence (generalization of the H_2 molecule) and gives rise to a band structure. The electronic localization determines the width of the band: very delocalized electrons move in large bands. The interatomic distance also influences the band width. The closer the atoms the stronger the interaction, the larger the bands.

Bands connecting to different orbital may finally overlap. Note that the m_l degeneracy is lifted because spherical symmetry is broken by the crystal $[E(3s) \neq E(3p)]$.

10.2.1.3 Electrical conductance

Electrons can only move in presence of a sufficient number of unpopulated states, even under the influence of an external force. If no states are available the crystals becomes isolating. Overlapping filled and empty bands reserve many states and allow for good conductance.

If the Fermi energy E_F lies between a completely filled conducting band and an empty valence band. The crystal is isolating. However, at $T > 0$, if the forbidden band is narrow as in the case of semiconductors (for Si $\Delta E \simeq 1\,\mathrm{eV}$), the gap may be bridged by thermal excitations.

The electrons collide with crystal impurities, defects and phonons. While the velocity of the electrons is about $\bar{v} \simeq 10^7$ cm/s, the short mean free path λ limits the drift velocity to $v_d \simeq 10^{-2}\,\mathrm{cm/s}$. The Lorentz force eE/m accelerates the electrons between successive collisions occurring at a rate $\bar{v}/\lambda$, such that

$$\frac{j}{ne} = v_d = \frac{eE}{m} \times \frac{\lambda}{\bar{v}} \ , \tag{10.12}$$

where j is the current density and ne the charge density. The fact that $\bar{v}$ and λ do not depends on the electric field is known as Ohm's law. The mobility $\mu \equiv v_d/E$ allows to write the electrical conductance as

$$\rho^{-1} = n_- e_- \mu_- + n_+ e_+ \mu_+ \ . \tag{10.13}$$

The value and sign of the Hall coefficient $1/ne$ can be measured by the Hall effect. It is positive if the conductance occurs primarily through holes and negative if it occurs through electrons.

10.2.1.4 Electron gas model

In this model the electrons move in a square well potential, a mean-field approach accounts globally for the periodic lattice of ions and the influence of all other electrons. The density of states and the electron density are the same as for blackbody radiation

$$\rho(\epsilon)d\epsilon = \frac{V(2m^3)^{1/2}}{\pi^2\hbar^3}\sqrt{\epsilon}d\epsilon \ , \tag{10.14}$$
$$n(\epsilon)\rho(\epsilon)d\epsilon = \frac{1}{e^{(\epsilon-\epsilon_F)/k_BT}+1}\rho(\epsilon)d\epsilon \ .$$

The maximum energy at $T = 0$ can be estimated from the quantized energy levels of a square well potential filled with N^2 electrons,

$$E_{max} = \frac{\hbar^2\pi^2}{2mL^2}N^2 = \frac{\hbar^2\pi^2}{2ma^2} \ , \tag{10.15}$$

where a is the lattice constant. This confirms that the width of the bands depends on the interatomic spacing, but not on the number of ions. The electron gas model is good for large overlap of the bands. In the presence of isolated bands $\rho(\epsilon)$ gets more complicated. In particular, if a band edge is reached while filling the potential well with states, $n(\epsilon)\rho(\epsilon)$ reaches a maximum before in drops down to zero.

10.2.1.5 Electrons in a periodic potential

The Bloch model assumes $\psi(x) = u_k(x)e^{\imath kx}$ with $u_k(x) = u_k(x+a)$. The Kronig-Penney model approximates the lattice potential by a periodic array of square well potentials. Bands open at the edges of Brillouin zones thus forming forbidden gaps. The dispersion relation for free particles $E = \hbar\omega = \hbar^2k^2/2m$ with $v = d\omega/dk$ plus a Lorentz force $d\epsilon = e|\mathcal{E}|dx$ yields

$$m^* = \frac{dv}{dt} = e|\mathcal{E}| \tag{10.16}$$
$$\frac{1}{m^*} = \frac{d^2\omega}{dk^2} \ ,$$

For free particles $m_e = m^*$. Without friction the acceleration is constant and, in a lattice m^* goes through apole at the edges of the Brillouin zones due to Bragg reflection. Note that *the momentum beyond π/a, which cannot be given to the electron is transferred to the lattice.* Note also that the density of states goes with the effective mass and is $\propto \rho$. m^* is a material constant (for Fe $m^* \simeq 10m_e$, thus Fe is a poor conductor). ???

10.2.1.6 Semiconductors

There is an intrinsic temperature-dependent conductivity (for Si $\rho(600\,\mathrm{K})/\rho(300\,\mathrm{K}) \approx 10^9$). Extrinsic conductivity can be induced by photoexcitation or doping. E.g. Ar/Ga

in a Ge crystal has one weakly bound electron more/less than required to fit into the lattice. This generates discrete energy levels slightly below the conducting/above the valence band, $min(E_c) - E_n, E_p - max(E_v) \simeq 0.01\,\text{eV}$.

The Fermi energy E_F is the energy, where half of the electrons are below that. In an isolator is between $max(E_v)$ and $min(E_c)$. In the presence of doping E_F is shifted by the additional amount of electrons/holes toward E_n, E_p. If n and p-doped materials are combined, electrons drift from the n to the p region, such as to minimize energy and obtain a uniform E_F across the hole crystal.

Thermally excited electrons may drift and recombine with holes. The junction is maintained by a steady flux in a dynamic equilibrium. An external voltage can higher/lower the barrier, because the potential drops mostly near the junction, where the resistance is highest. In this case the thermal current is not equilibrated, the diode either blocks or opens. The electrons move to try to rectify E_F.

A transistor is a series of junctions in *npn* of *pnp* configuration. The base-emitter current can be used to switch a collector-emitter current by injecting electrons. A tunnel diode acts like a normal diode except that when the bands come closer together within the junction (at low voltages in conduction polarization), electrons may pass by tunneling from the conducting into the valence band. This flow gradually stops when E_F is leveled (for zero voltage). Tunneling currents react much faster than thermal drift currents.

10.2.2 Kondo effect

Magnetic ions dilutely distributed in a non-magnetic metallic crystal can increase resistance at low temperatures. This is due to an exchange interaction between the dipole moments of the 'impurity' ions and the conducting electrons giving rise to an additional scattering mechanism. The magnetization of the e^- in the vicinity of an ion is known as *Friedel interaction* or *RKKY interaction* (Rutherford-Kittel-Kasuya-Yosida) interaction. The effect is known as *Kondo effect*. A similar effect is observed for quantum dots: a spin-entanglement of the electron trapped in the dot with the conducting electrons give rise to an exchange interaction with increases resistance.

10.3 Plasmas

10.3.1 Debye length

Consider a mixture of charges + and −, that is, a *plasma*. Energy seeks to be minimized by local compensation of charge imbalance. However, thermal motion spoils perfect homogeneity. That is, if on the one hand, looking at large scales, the environment seems neutral and homogeneous, at small scales there may be charge imbalances producing potential sites with exponentially decreasing ranges,

$$\frac{1}{\lambda_D} = \frac{1}{\lambda_{D-}} + \frac{1}{\lambda_{D+}} = \frac{ne^2}{\varepsilon_0}\left(\frac{1}{k_B T_+} + \frac{1}{k_B T_-}\right) . \tag{10.17}$$

The *Debye length* naturally enters the thermodynamic description of large systems of mobile charges. We consider a system of 2 different species of charges $q_\pm$ and $n_\pm(\mathbf{r})$ at locations $\mathbf{r}$. According to the so-called *primitive model*, these charges

are distributed in a continuous medium characterized only by its relative static permittivity, ε_r. This distribution of charges through the medium generates an electric potential $\Phi(\mathbf{r})$ that satisfies the *Poisson equation*:

$$\varepsilon\nabla^2\Phi(\mathbf{r}) = -q_+n_+(\mathbf{r}) - q_-n_-(\mathbf{r}) - \rho_E(\mathbf{r}) \ , \tag{10.18}$$

where $\varepsilon \equiv \varepsilon_r\varepsilon_0$, ε_0 is the dielectric constant, and ρ_E is the charge density outside the medium (logically, not spatially).

The mobile charges do not only generate $\Phi(\mathbf{r})$, but also are moved according to the associated Coulomb force, $-q_\pm\nabla\Phi(\mathbf{r})$. Assuming the system to be in thermodynamic equilibrium with a heat reservoir at an absolute temperature T, the concentrations of discrete charges, $n_\pm(\mathbf{r})$, can be considered as thermodynamic averages (ensemble average) and the associated electrical potential as a thermodynamic mean field. With these assumptions, the concentration of species j is described by the Boltzmann distribution,

$$n_\pm(\mathbf{r}) = n_\pm^0 e^{-q_\pm\Phi(\mathbf{r})/k_BT} \ , \tag{10.19}$$

where n_j^0 is the mean field concentration of the charge species j.

Identifying the instantaneous concentrations and the potentials in the Poisson equation with their mean-field counterparts in the Boltzmann distribution, we obtain the Poisson-Boltzmann equation:

$$\varepsilon\nabla^2\Phi(\mathbf{r}) = -q_+n_+^0 e^{-q_+\Phi(\mathbf{r})/k_BT} - q_-n_-^0 e^{-q_-\Phi(\mathbf{r})/k_BT} - \rho_E(\mathbf{r}) \ . \tag{10.20}$$

Solutions of this nonlinear equation are known for simple systems. Solutions for more general systems can be obtained in the high-temperature (or low-coupling) limit, $q_j\Phi(\mathbf{r}) \ll k_BT$, by Taylor expansion of the exponential,

$$e^{-q_\pm\Phi(\mathbf{r})/k_BT} \approx 1 - \frac{q_\pm\Phi(\mathbf{r})}{k_BT} \ . \tag{10.21}$$

This approximation gives the linearized Poisson-Boltzmann equation,

$$\varepsilon\nabla^2\Phi(\mathbf{r}) = \left(\frac{n_+^0q_+^2}{k_BT} + \frac{n_-^0q_-^2}{k_BT}\right)\Phi(\mathbf{r}) - n_+^0q_+ - n_-^0q_- - \rho_e(\mathbf{r}) \tag{10.22}$$

also known as *Debye-Hückel equation*. The second term on the right side disappears for electrically neutral systems. The term in parentheses divided by ε, has the unit $1/\mathrm{m}^2$. By a dimensional analysis, it leads to a definition of a characteristic length scale,

$$\lambda_D = \left(\frac{\varepsilon k_BT}{n_+^0q_+^2 + n_-^0q_-^2}\right)^{1/2} \tag{10.23}$$

usually called *Debye-Hückel length*. Being the only characteristic length scale of the Debye-Hückel equation, λ_D defines the scale of variations in the potential and the concentrations of the charged species. All charged species contribute to the Debye-Hückel length in the same manner regardless of the charge signal. For an electrically neutral system, the Poisson equation is,

$$\nabla^2\Phi(\mathbf{r}) = \lambda_D^{-2}\Phi(\mathbf{r}) - \frac{\rho_e(\mathbf{r})}{\varepsilon} \ . \tag{10.24}$$

To illustrate the Debye shielding, the potential produced by an external point-like charge $\rho_e = Q\delta(\mathbf{r})$ is,

$$\Phi(\mathbf{r}) = \frac{Q}{4\pi\varepsilon r} e^{-r/\lambda_D} \ . \tag{10.25}$$

The bare Coulomb potential is exponentially shielded by the medium over a distance corresponding to the Debye length.

The length of Debye-Hückel can be expressed in terms of the length of Bjerrum λ_B as,

$$\lambda_D = \left(4\pi\lambda_B \sum_{j=1}^{N} n_j^0 \, z_j^2 \right)^{-1/2} \ , \tag{10.26}$$

where $z_j = q_j/e$.

10.3.1.1 Typical values

In plasmas in space, where the electron density is small, the Debye's length can reach macroscopic values.

system	density n_e (m^{-3})	electronic temperature T(K)	magnetic field B(T)	Debye length λ_D(m)
solar core	10^{32}	10^7	–	10^{-11}
Tokamak	10^{20}	10^8	10	10^{-4}
gas discharge	10^{16}	10^4	–	10^{-4}
ionosphere	10^{12}	10^3	10^{-5}	10^{-3}
magnetosphere	10^7	10^7	10^{-8}	10^2
solar wind	10^6	10^5	10^{-9}	10
interstellar medium	10^5	10^4	10^{-10}	10
intergalactic medium	1	10^6	–	10^5

10.3.1.2 Length of Debye in a plasma

In a plasma, the background medium may be treated as the vacuum ($\varepsilon_r = 1$), and the length of Debye is,

$$\lambda_D = \sqrt{\frac{\varepsilon_0 k_B/q_e^2}{n_e/T_e + \sum_j z_j^2 n_j/T_j}} \ , \tag{10.27}$$

where $T_\pm$ are the temperatures of the electrons and ions, n_- is the density of the electrons and n_+ that of the atomic species j, with positive ionic charge $z_+ q_e$. The ion term is often neglected, giving,

$$\lambda_D = \sqrt{\frac{\varepsilon_0 k_B T_e}{n_e q_e^2}} \ , \tag{10.28}$$

although this is valid only, when the mobility of ions is negligible on the time scale of the process.

10.4 Further reading

H.M. Nussenzveig, *Curso de Física Básica: Ótica, Relatividade e Física Quântica (Volume 4)* [964]ISBN

Chapter 11

Appendices to 'Classical Mechanics'

11.1 Constants and units in classical physics

11.1.1 Constants

11.1.1.1 Mathematical constants

π constant	$\pi = 3.1415..$
Euler constant	$e = 2.71828..$

11.1.1.2 Constants of the SI unit system

These numbers of the special adjustment CODATA 2019 were proposed as *exact* values.

frequency of the hyperfine transition of Cs	$\nu = 9\ 192\ 631\ 770\,\mathrm{Hz}$
velocity of light	$c = 299\ 792\ 458\,\mathrm{m/s}$
Planck's constant	$h = 6.626\ 070\ 15 \cdot 10^{-34}\,\mathrm{Js}$
electronic charge	$e = 1.602\ 176\ 634 \times 10^{-19}\,\mathrm{C}$
Boltzmann's constant	$k_B = 1.380\ 649 \times 10^{-23}\,\mathrm{J/K}$
Avogadro's constant	$N_A = 6.022\ 14076 \times 10^{23}\,\mathrm{mol^{-1}}$
Luminous efficiency	$K_{cd} = 683\,\mathrm{lm}$

11.1.1.3 Derived constants

fine-structure constant	$\alpha = e^2/4\pi\varepsilon_0\hbar c \approx 1/137$
vacuum permittivity	$\varepsilon_0 = 1/\mu_0 c^2 = 8.8542 \times 10^{-12}\,\mathrm{As/Vm}$
vacuum permeability	$\mu_0 = 10^{-7}\,\mathrm{Vs/Am}$
Faraday's constant	$F = 96485.309\,\mathrm{C/mol}$
atomic mass unit	$u_A = 1/N_A \times 1\mathrm{g/mol} = 1.6605402 \times 10^{-27}\,\mathrm{kg}$
gas constant	$R = N_A k_B = 8.314510\,\mathrm{L/mol\ K}$
Bohr radius	$a_B = \alpha/4\pi R_\infty = 0.529 \times 10^{-10}\,\mathrm{m}$
Bohr magneton	$\mu_B = e\hbar/2m_e = 9.27 \times 10^{-24}\,\mathrm{J/T}$
classical electron radius	$r_e = \alpha^2 a_B$
Rydberg constant	$R_\infty = m_e c\alpha^2/2h = 13.7\,\mathrm{eV}$
Compton wavelength	$\lambda_C = h/m_e c$
Thomson cross section	$\sigma_e = (8\pi/3)r_e^2$
gravitational constant	$\gamma = 6.67259 \times 10^{-11}\,\mathrm{m^3 kg^{-1} s^{-2}}$

11.1.1.4 Particle constants

electron mass	$m_e = 9.1096 \times 10^{-12}\,\mathrm{kg}$
g-factor of the electron	$g = 2.002\ 319\ 304\ 386$
muon mass	$m_\mu = 105.658389\,\mathrm{MeV}$
proton mass	$m_p = 938.27231\,\mathrm{MeV}$
g-factor of the proton	$g = 5.5858$
neutron mass	$m_p = 939.56563\,\mathrm{MeV}$
g-factor of the neutron	$g = -3.8261$
deuteron mass	$m_d = 1875.61339\,\mathrm{MeV}$

11.1.1.5 Astronomical constants

earth mass	$m_{♁} = 5.9736 \times 10^{24}\,\mathrm{kg}$
earth radius	$R_{♁} = 6370\,\mathrm{km}$
earth gravity	$g_{♁} = 9.80665\,\mathrm{m/s}$
lunar mass	$m_{☾} = 7.348 \times 10^{22}\,\mathrm{kg}$
lunar radius	$R_{☾} = 1740\,\mathrm{km}$
lunar gravity	$g_{☾} = 1.62\,\mathrm{m/s}$
distance earth-moon	$d_{ES} = 384000\,\mathrm{km}$
sun massa	$m_{☼} = 1.99 \times 10^{30}\,\mathrm{kg}$
sun radius	$R_{☼} = 695300\,\mathrm{km}$
sun gravity	$g_{☼} = 273\,\mathrm{m/s}$
distance earth-sun	$d_{ES} = 1.496 \times 10^{8}\,\mathrm{km}$
sinodic day	$d_{syn} = 24\,\mathrm{h}$
sideric day	$d_{syn} = 23.9345\,\mathrm{h} = 23\,\mathrm{h}\,56\,\mathrm{min}\,4\,\mathrm{s}$
sinodic month	$mon_{syn} = 29.530590\,\mathrm{d}$
sideric month	$mon_{sid} = 27.321666\,\mathrm{d}$
sideric year	$a_{syn} = 365.256365\,\mathrm{h} = 365\,\mathrm{d}\,6\,\mathrm{h}\,9\,\mathrm{min}\,10\,\mathrm{s}$
lunar day	$d_{lunar} = 24.8412\,\mathrm{h}$
$\frac{1}{mon_{sid}}$	$= \frac{1}{a_{sid}} + \frac{1}{mon_{syn}}$
$\frac{1}{d_{sid}}$	$= \frac{1}{a_{sid}} + \frac{1}{d_{syn}}$
$\frac{1}{d_{sid}}$	$= \frac{1}{mon_{sid}} + \frac{1}{d_{lunar}}$

11.1.2 Units

charge	Q	basic unit
current	I	A=C/s
voltage	U	V=N/As
polarizability	α_{pol}	$\mathrm{Asm^2/V}$
susceptibility	χ	1
dipolar moment	1 Debye	$= 10^{-27}/2.998\ \mathrm{Cm} = 10^{-19}/c\ \mathrm{Cm^2/s} = 39.36\ ea_B$

11.2 Quantities and formulas in classical mechanics

time	t	basic unit
position	$\mathbf{r}$	basic unit
velocity	$\mathbf{v}$	$\mathbf{v} = \dot{\mathbf{r}}$
acceleration	$\mathbf{a}$	$\mathbf{a} = \dot{\mathbf{v}}$
mass	m	basic unit
linear momentum	$\mathbf{p}$	$\mathbf{p} = m\mathbf{v}$
force	$\mathbf{F}$	$\mathbf{F} = \dot{\mathbf{p}} = m\mathbf{a}$
kinetic energy	E_{kin}	$E_{kin} = \frac{m}{2}v^2$
angle	$\vec{\phi}$	basic unit
angular velocity	$\vec{\omega}$	$\vec{\omega} = \dot{\mathbf{r}}$
angular acceleration	$\vec{\alpha}$	$\vec{\alpha} = \dot{\vec{\omega}}$
inertial moment (continuous density)	I	$I = \int r_\perp^2 dm = \int_V \rho(\mathbf{r})[\mathbf{r}^2 - (\mathbf{r} \cdot \hat{\mathbf{e}}_\omega)]dV$
inertial moment (discrete density)	I	$I = \sum_i m_i r_i^2$
angular momentum	$\mathbf{L}$	$\mathbf{L} = I\vec{\omega} = \mathbf{r} \times \mathbf{p}$
torque	$\vec{\tau}$	$\vec{\tau} = \dot{\mathbf{L}} = I\vec{\alpha} = \mathbf{r} \times \mathbf{F}$
rotational energy	E_{rot}	$E_{rot} = \frac{m}{2}\omega^2 r^2$
potential energy	E_{pot}	$E_{pot}^{grav} = mgh$, $E_{pot}^{sprng} = \frac{k}{2}x^2$
work	W	$W = \int_{s_1}^{s_2} \mathbf{F} \cdot d\mathbf{s}$
power	P	$P = \dot{W}$

11.2.1 Particular forces

gravitation	$F_{grav} = mg$
Hooke's for elastic spring	$F_{mola} = -k\Delta x$
friction	$F_{at} = -\mu N$
Stokes' friction	$F_{fr} = -\gamma v$
Newton's friction	$F_{fr} = -\gamma v^2$

11.2.2 Inertial momentum

Steiner's theorem	$I_{\omega_2} = I_{\omega_1} + md^2$, where d is the distance between parallel axes
theorem of perpendicular axes	$I_z = I_x + I_y$ para $\rho(\mathbf{r}) = \delta(z)\sigma(x,y)$

11.2.3 Inertial forces due to transitions to translated and rotated systems

transformation to an accelerated frame	$\mathbf{F}_{Gal} = -m\mathbf{a}$
centrifugal force	$\mathbf{F}_{cf} = -m\vec{\omega} \times (\vec{\omega} \times \mathbf{r})$
Coriolis force	$\mathbf{F}_{Cor} = -2m\vec{\omega} \times \mathbf{v}$

11.2.4 Conservation laws

energy conservation	$\sum_k E_{kin}^{(ini)} + \sum_k E_{pot}^{(ini)} = \sum_k E_{kin}^{(fin)} + \sum_k E_{pot}^{(fin)}$
linear momentum conservation	$\sum_k \mathbf{p}_k^{(ini)} = \sum_k \mathbf{p}_k^{(fin)}$
angular momentum conservation	$\sum_k \mathbf{L}_k^{(ini)} = \sum_k \mathbf{L}_k^{(fin)}$
definition of the center-of-mass	$\mathbf{r}_{cm} \equiv \frac{\sum_k m_k \mathbf{r}_k}{\sum_k m_k}$

11.2.5 Rigid bodies, minimum required number of equations of motion

1. estimate number of moving masses	m_1, m_2, ...
2. identify possible movement (degree of freedom) for every mass	$v_{1x}, v_{2x}, ...$ $v_{1y}, v_{2y}, ...$ $v_{1z}, v_{2z}, ...$ $\omega_1, \omega_2, ...$
3. write down for every degree of freedom an equation of motion	$m\dot{v}_{kl} = \sum_j F_j$ $I\dot{\omega}_k = \sum_j \tau_j$

11.2.6 Gravitational laws

Newton's law	$\mathbf{F}(\mathbf{r}) = -\frac{GMm}{\lvert\mathbf{R}-\mathbf{r}\rvert^2}\hat{\mathbf{e}}_{Rr} = -\nabla V(\mathbf{r})$
gravitational potential	$V(\mathbf{r}) = -\int \frac{Gm}{\lvert\mathbf{r}-\mathbf{r}'\rvert^2}\rho(\mathbf{r}')dV'$

11.2.7 Volume elements

cartesian coordinates	$dV = dxdydz$
cylindrical coordinates	$dV = \rho d\rho d\phi dz$
spherical coordinates	$dV = r^2 \sin\theta dr d\theta d\phi$

11.2.8 Oscillations $ma + bv + kx = F_0 \cos\omega t$

dissipative motion	$k = 0,\ F_0 = 0$	$x(t) = Ae^{-\gamma t},\ \gamma = \frac{b}{2m}$
harmonic oscillation	$b = 0,\ F_0 = 0$	$x(t) = A\cos(\omega_0 t + \delta),\ \omega_0 = \sqrt{\frac{k}{m}}$
damped oscillation	$F_0 = 0$	$x(t) = Ae^{-\gamma t}\cos(\omega t + \delta),\ \omega = \sqrt{\omega_0^2 - \gamma^2}$
forced oscillation		$x(t) = A\cos(\omega t + \delta)\ ,\ A = \frac{F_0}{\sqrt{m^2(\omega_0^2-\omega^2)^2+b^2\omega^2}}\ ,$ $\tan\delta = \frac{b\omega}{m(\omega_0^2-\omega^2)}$

11.3 Probability distributions

The *binomial distribution* is defined by,

$$B_k^{(n)} = \binom{n}{k} p^k (1-p)^{n-k}\ . \tag{11.1}$$

The *Poisson distribution* is defined by,

$$P_k = \frac{\lambda^k}{k!} e^{-\lambda}\ , \tag{11.2}$$

for large n and small p, we get $B_k^{(n)} \simeq P_k$ with $\lambda = np$.

11.3.1 Some useful formulae

If the limits of two functions tend to 0, $\lim_{t\to t_0} f(t) = 0 = \lim_{t\to t_0} g(t)$ a rule called *l'Hôpital's rule* goes like,

$$\lim_{t\to t_0} \frac{f(t)}{g(t)} = \lim_{t\to t_0} \frac{f'(t)}{g'(t)}\ . \tag{11.3}$$

Part II

Electrodynamics

Chapter 12

Foundations and mathematical tools

The electrodynamic force is one of the four fundamental forces, together with gravitation, the strong nuclear force, and the weak nuclear force. It is a long-range force ($F \propto r^{-2}$) in the same way as gravitation, but unlike nuclear forces, which are short-ranged. Unlike gravitation, it can be attractive or repulsive. The experimentally

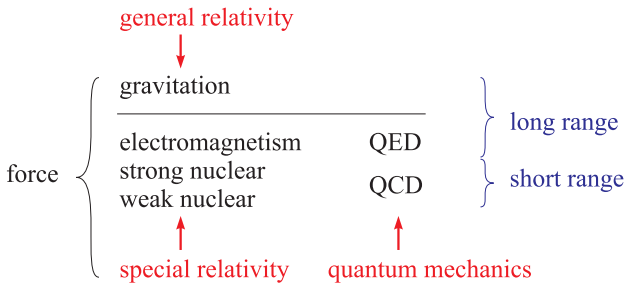

Figure 12.1: The four known fundamental forces.

observed fact, that two spatially separated bodies can exert mutual forces (beyond gravitation), is not explained within classical mechanics. It is necessary to introduce a new degree of freedom called *electric charge* which, to take account of the existence of attractive and repulsive forces, must exist in two different types called positive or negative charges. *Identical charges repel each other, different charges attract each other.* Other observations suggest that the charge is a *conserved and quantized* quantity.

Electrodynamics is an *field theory*, that is, it can describe all electric or magnetic phenomena observed in the following way: Every charge gives rise to a force field, called field electric $\vec{\mathcal{E}}$, which accelerates other charges. But other experimental observations suggest the existence of another force field, called the magnetic field $\vec{\mathcal{B}}$, whose existence is necessary to understand forces only acting on moving charges. That is, the electric and magnetic fields are introduced to explain the forces named after Coulomb and Lorentz,

$$\mathbf{F} = q\vec{\mathcal{E}} + \mathbf{v} \times \vec{\mathcal{B}} \, . \tag{12.1}$$

Thus, fields are quantities distributed in space, which in addition can vary in time,

$$\mathbf{F} = \mathbf{F}(\mathbf{r}, t) \, . \tag{12.2}$$

The concept of a field represents a powerful mathematical tool for describing forces, which are the only observable magnitudes of electromagnetism. That is, we have no sense to *see* the electricity. We can only infer their existence from the observation of forces. On the other hand, the formulation of electrodynamics via vectorial force fields, can be replaced by a description via potentials, which are either scalar or vectorial fields. In many circumstances, potentials facilitate the resolution of electrodynamic problems, but it is important to keep in mind, that potentials are not directly observable.

Maxwell's electrodynamics has a very deep relationship to Einstein's theory of special relativity, such that each theory is conditioned to the validity of the other. The relativistic formulation allows to distill the symmetry inherent to electrodynamics in a highly aesthetic way.

In view of the fundamental role played by scalar and vector fields in electrodynamics, we will start this course the basic mathematical notions of field theory, that is, differential and integral calculus with fields in Cartesian or curvilinear coordinates. We will also have to review basic notions of complex numbers and the Dirac distribution.

12.1 Differential calculus

12.1.1 Scalar and vector fields

The most basic application of vectors is the designation of positions in space, $\mathbf{r} = x\hat{\mathbf{e}}_x + y\hat{\mathbf{e}}_y + z\hat{\mathbf{e}}_z$. But other physical quantities may also depend on the position where they are measured. In case the quantity varying with position is a scalar, $\Phi = \Phi(\mathbf{r})$, we speak of *scalar field*. An example for a scalar field is the temperature distribution across a room. In the case the quantity is a vector, $\mathbf{A} = \mathbf{A}(\mathbf{r})$, we speak of *vector field*. Light propagating through space is an example for a vector field.

A position is generally defined with respect to the center of the coordinate system, called the origin, such that the distance from the center is given by,

$$r \equiv \sqrt{\mathbf{r}\cdot\mathbf{r}} = \sqrt{x^2+y^2+z^2}\ , \tag{12.3}$$

with $\hat{\mathbf{e}}_r$ being a unit vector pointing in the direction of $\mathbf{r}$. In electrodynamics we will often deal with quantities (fields) that depend on the distance between a source located at a position $\mathbf{r}'$ and a detector placed at a position $\mathbf{r}$, such as $\Phi(R) = \Phi(\mathbf{r}-\mathbf{r}')$,

$$\hat{\mathbf{e}}_R = \frac{(x-x')\hat{\mathbf{e}}_x + (y-y')\hat{\mathbf{e}}_y + (z-z')\hat{\mathbf{e}}_z}{\sqrt{(x-x')^2+(y-y')^2+(z-z')^2}}\ . \tag{12.4}$$

12.1.2 The gradient

The derivative of a one-dimensional function $\Phi(x)$ measures, how fast the function changes when we move the position x. That is, when we change x by an amount dx, Φ changes by an amount $d\Phi$ given by,

$$d\Phi = \left(\frac{d\Phi}{dx}\right) dx\ . \tag{12.5}$$

Of course it gets trickier, when Φ is a field depending on three coordinates, because we need to specify in which direction we are changing the position. We have,

$$d\Phi = \left(\frac{\partial\Phi}{\partial x}\right) dx + \left(\frac{\partial\Phi}{\partial y}\right) dy + \left(\frac{\partial\Phi}{\partial z}\right) dz \ . \tag{12.6}$$

This equation resembles the scalar product because,

$$d\Phi = \left(\hat{\mathbf{e}}_x \frac{\partial\Phi}{\partial x} + \hat{\mathbf{e}}_y \frac{\partial\Phi}{\partial y} + \hat{\mathbf{e}}_z \frac{\partial\Phi}{\partial z}\right) \cdot (dx\hat{\mathbf{e}}_x + dy\hat{\mathbf{e}}_y + dz\hat{\mathbf{e}}_z) \equiv \nabla\Phi \cdot d\mathbf{r} \ , \tag{12.7}$$

where we defined a new operator called *nabla*,

$$\nabla \equiv \begin{pmatrix} \partial/\partial x \\ \partial/\partial y \\ \partial/\partial z \end{pmatrix} \ . \tag{12.8}$$

The three-dimensional derivative $\nabla\Phi$ is called the *gradient* of the scalar field Φ,

$$\nabla\Phi(\mathbf{r}) = \hat{\mathbf{e}}_x \frac{\partial\Phi}{\partial x} + \hat{\mathbf{e}}_y \frac{\partial\Phi}{\partial y} + \hat{\mathbf{e}}_z \frac{\partial\Phi}{\partial z} \ , \tag{12.9}$$

and it measures the variation of the value of the field from Φ to $\Phi + d\Phi$, when we move the vector by an infinitesimal amount between two points $\mathbf{r}$ and $\mathbf{r} + d\mathbf{r}$.

We understand the geometric interpretation of the gradient through its formulation as a scalar product:

$$d\Phi = \nabla\Phi \cdot d\mathbf{r} = |\nabla\Phi| \cdot |d\mathbf{r}| \cos\theta \ , \tag{12.10}$$

where θ is the angle between the gradient and the infinitesimal displacement. Now, we fix a *magnitude* of the displacement $|d\mathbf{r}|$ and look for the direction θ in which the variation $d\Phi$ is maximum. Obviously, we find the direction $\theta = 0$, that is, when the gradient points in the same direction as the predefined displacement.

> *The gradient of a scalar field $\Phi(\mathbf{r})$ calculated at a point $\mathbf{r}$ indicates the direction of the greatest field variation from this point, and its absolute value is a measure for the variation.*

The concept of the gradient is easy to understand in a two-dimensional landscape: Imagine being on the slope of a mountain. Depending on the direction in which you are heading and the duration of the journey $d\mathbf{r}$, you will gain or lose a certain amount of potential energy $d\Phi$, which you can calculate by the scalar product $\nabla\Phi \cdot d\mathbf{r}$. If the direction chosen is that indicated by the gradient, you will lose (or gain) a maximum of potential energy. If you choose to go in a direction perpendicular to the gradient, that is, along an equipotential line, the potential energy remains unchanged. This is illustrated in Fig. 12.2.

Let us consider the example of a parabolic field, $\Phi(\mathbf{r}) = -r^2$:

$$\nabla(-r^2) = \begin{pmatrix} -2x \\ -2y \\ -2z \end{pmatrix} = -2\mathbf{r} \ . \tag{12.11}$$

We find that at all points of space the variation is faster in radial direction.

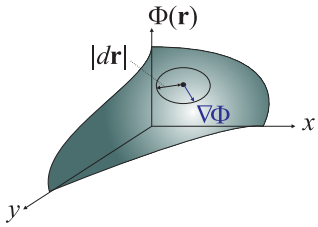

Figure 12.2: The gradient indicates the direction of the largest field variation Φ.

Although the operator ∇ has the shape of a vector, it has no meaning by itself. In fact, it is a *vector operator*, that is, a mathematical *prescription* telling us what to do with the scalar field on which it acts. Nevertheless, it assimilates all the properties of a vector. (We will see in quantum mechanics, that this is more than a coincidence.) Thus, in a way similar as done for the gradient of scalar fields, we can try to apply the ∇ operator on vector fields using the definitions of the scalar and vector products,

$$\text{grad } \Phi(\mathbf{r}) \equiv \nabla\Phi(\mathbf{r}) \quad \text{and} \quad \text{div } \mathbf{A}(\mathbf{r}) \equiv \nabla \cdot \mathbf{A}(\mathbf{r}) \quad \text{and} \quad \text{rot } \mathbf{A}(\mathbf{r}) \equiv \nabla \times \mathbf{A}(\mathbf{r}) \ . \tag{12.12}$$

We practice the calculation with the ∇ operator in the Excs. 12.1.7.1 to 12.1.7.3.

12.1.3 The divergence

Let us now analyze the possible meaning of the expression $\nabla \cdot \mathbf{A}$ called *divergence*. It is easy to show,

$$\nabla \cdot \mathbf{A}(\mathbf{r}) = \frac{\partial A_x}{\partial x} + \frac{\partial A_y}{\partial y} + \frac{\partial A_z}{\partial z} \ . \tag{12.13}$$

Obviously the divergence is a scalar field calculated from a vector field.

> *The divergence measures how much a vector field* $\mathbf{A}(\mathbf{r})$ *spreads out starting from a point* $\mathbf{r}$*. For a given infinitesimal volume it measures the difference between the number of incoming and outgoing field lines.*

Exposed to a field with divergence, an extended distribution of masses will start to concentrate (spread out) in case of a drain (source). The field lines trace the masses trajectories.

> **Example 30 (*Divergence of a radial field*):** We consider the example of the radial field, $\mathbf{A}(\mathbf{r}) = \mathbf{r}$:
>
> $$\nabla \cdot \mathbf{r} = \frac{\partial x}{\partial x} + \frac{\partial y}{\partial y} + \frac{\partial z}{\partial z} = 3 \ . \tag{12.14}$$

12.1.4 The rotation

Let us now examine the possible meaning of the expression $\nabla \times \mathbf{A}$ called *rotation*. It is easy to show,

$$\nabla\times\mathbf{A}(\mathbf{r}) = \begin{vmatrix} \hat{\mathbf{e}}_x & \hat{\mathbf{e}}_y & \hat{\mathbf{e}}_z \\ \partial_x & \partial_y & \partial_z \\ A_x & A_y & A_z \end{vmatrix} = \hat{\mathbf{e}}_x \left(\frac{\partial A_z}{\partial y} - \frac{\partial A_y}{\partial z} \right) + \hat{\mathbf{e}}_y \left(\frac{\partial A_x}{\partial z} - \frac{\partial A_z}{\partial x} \right) + \hat{\mathbf{e}}_z \left(\frac{\partial A_y}{\partial x} - \frac{\partial A_x}{\partial y} \right) . \tag{12.15}$$

Obviously the rotation is a vector field calculated from another vector field.

> *The rotation measures how many of the field lines of a vector field* $\mathbf{A}(\mathbf{r})$ *passing through an infinitesimal volume, return into it.*

Exposed to a field with rotation, an extended distribution of masses will start spinning in closed orbits.

We consider the examples shown in Fig. 12.3. The properties of divergence and rotation are complementary. There are fields exhibiting only one of the properties, or both, or none of them. In cases where there is rotation, it is problematic to specify equipotential lines: Either, the field lines are not orthogonal to the equipotential lines, or they come back.

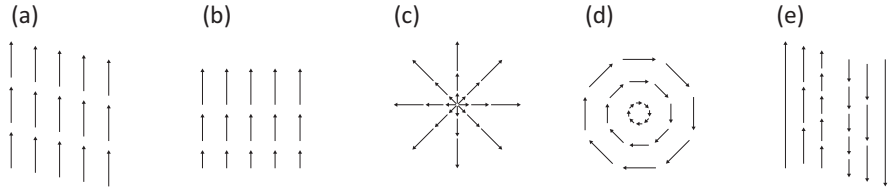

Figure 12.3: (a) Field without divergence, (b) with constant divergence, (c) with radial divergence, (d) with rotation, and (e) with rotation.

Example 31 (*Rotation of a radial field*): We consider the example of a radial field, $\mathbf{A}(\mathbf{r}) = -y\hat{\mathbf{e}}_x + x\hat{\mathbf{e}}_y$:

$$\nabla \times \mathbf{A} = \begin{pmatrix} 0 - \partial_z x \\ \partial_z(-y) - 0 \\ \partial_x x - \partial_y(-y) \end{pmatrix} = 2\hat{\mathbf{e}}_z \ . \tag{12.16}$$

We practice the calculation with divergence and rotation in the Excs. 12.1.7.4 to 12.1.7.7.

12.1.5 Taylor expansion of scalar and vector fields

We know well the Taylor expansion of functions of one variable:

$$\Phi(x+h) = \exp(h\tfrac{d}{dx})\Phi(x) = \sum_{\nu=0}^{\infty} \tfrac{1}{\nu!}(h\tfrac{d}{dx})^\nu \Phi(x) = \Phi(x) + h\Phi'(x) + \tfrac{h}{2}\Phi''(x) + \dots \ . \tag{12.17}$$

The generalization of the expansion to a scalar field, which depends on a vector, is,

$$\Phi(\mathbf{r}+\mathbf{h}) = \exp(\mathbf{h}\cdot\nabla_{\mathbf{r}})\Phi(\mathbf{r}) = \sum_{\nu=0}^{\infty}\frac{1}{\nu!}(\mathbf{h}\cdot\nabla_{\mathbf{r}})^{\nu}\Phi(\mathbf{r}) \tag{12.18}$$
$$= \Phi(\mathbf{r}) + (\mathbf{h}\cdot\nabla_{\mathbf{r}})\Phi(\mathbf{r}) + \tfrac{1}{2}(\mathbf{h}\cdot\nabla_{\mathbf{r}})(\mathbf{h}\cdot\nabla_{\mathbf{r}})\Phi(\mathbf{r}) + \dots\ .$$

We see that the operator $\nabla_{\mathbf{r}}$ generates a translation. We study the Taylor expansion of scalar fields in Exc. 12.1.7.8.

The generalization of the gradient of a vector field is the Jacobian,

$$\mathbf{A} = \begin{pmatrix} A_1 \\ \vdots \\ A_n \end{pmatrix} \qquad \Longrightarrow \qquad J[\mathbf{A}] = \begin{pmatrix} \frac{\partial A_1}{\partial x_1} & \dots & \frac{\partial A_1}{\partial x_n} \\ \vdots & \ddots & \vdots \\ \frac{\partial A_n}{\partial x_1} & \dots & \frac{\partial A_n}{\partial x_n} \end{pmatrix} . \tag{12.19}$$

Therefore, the generalization of the expansion to a vector field is,

$$\mathbf{A}(\mathbf{r}+\mathbf{h}) = \exp(\mathbf{h}\cdot\nabla_{\mathbf{r}})\mathbf{A}(\mathbf{r}) = \mathbf{A}(\mathbf{r}) + \begin{pmatrix} (\mathbf{h}\cdot\nabla_{\mathbf{r}})A_1 \\ \vdots \\ (\mathbf{h}\cdot\nabla_{\mathbf{r}})A_n \end{pmatrix} + \dots \tag{12.20}$$
$$= \mathbf{A}(\mathbf{r}) + \begin{pmatrix} h_1\frac{\partial F_1}{\partial x_1} + \dots + h_n\frac{\partial F_1}{\partial x_n} \\ \vdots \\ h_1\frac{\partial F_n}{\partial x_1} + \dots + h_n\frac{\partial F_n}{\partial x_n} \end{pmatrix} + \dots = \mathbf{A}(\mathbf{r}) + J[\mathbf{A}]\mathbf{h} + \dots\ .$$

12.1.6 Rules for calculation with derivatives

In total there are four possible ways of defining products involving scalar and vector fields, $\Phi\Psi$, $\Phi\mathbf{A}$, $\mathbf{A}\cdot\mathbf{B}$, and $\mathbf{A}\times\mathbf{B}$, and six product rules to calculate the following expressions,

$$\nabla(\Phi\Psi) \quad , \quad \nabla(\mathbf{A}\cdot\mathbf{B}) \quad , \quad \nabla\cdot(\Phi\mathbf{A}) \quad , \quad \nabla\cdot(\mathbf{A}\times\mathbf{B}) \quad , \quad \nabla\times(\Phi\mathbf{A}) \quad , \quad \nabla\times(\mathbf{A}\times\mathbf{B})\ . \tag{12.21}$$

Second derivatives can also be defined in six different combinations,

$$\nabla\cdot(\nabla\phi) \quad , \quad \nabla\times(\nabla\phi) \quad , \quad \nabla(\nabla\cdot\mathbf{A}) \quad , \quad \nabla\cdot(\nabla\times\mathbf{A}) \quad , \quad \nabla\times(\nabla\times\mathbf{A})\ . \tag{12.22}$$

As these rules are used frequently, we summarized them in Secs. 21.6.1 and 21.6.2.

The rules can be derived componentwise from scalar product rules. Very useful tools for this are the *Kronecker symbol* and the *Levi-Civita tensor*. Let us consider a Cartesian coordinate system $i = 1, 2, 3$. The coordinates in this system are x_i and the derivatives $\partial_i \equiv \frac{\partial}{\partial x_i}$. The Kronecker symbol is defined by,

$$\delta_{mn} = \begin{cases} 1 & \text{for } m = n \\ 0 & \text{else} \end{cases} . \tag{12.23}$$

The Levi-Civita tensor is defined by,

$$\epsilon_{kmn} = \begin{cases} 1 & \text{when } (kmn) \text{ is an even permutation of } (123) \\ -1 & \text{when } (kmn) \text{ is an odd permutation of } (123) \\ 0 & \text{when at least two indices are identical} \end{cases} . \tag{12.24}$$

Adopting Einstein's summing convention, we automatically take the sum of an expression over all indexes appearing twice. For example, the scalar product can be written,

$$\mathbf{A} \cdot \mathbf{B} = \sum_i A_i B_i \equiv A_i B_i \ . \tag{12.25}$$

For the vector product we obtain,

$$(\mathbf{A} \times \mathbf{B})_k \equiv \epsilon_{kmn} A_m B_n \ . \tag{12.26}$$

Other examples will be discussed in the Excs. 12.1.7.9 to 12.1.7.11.

12.1.7 Exercises

12.1.7.1 Ex: Differential operators

Find the gradients of the following scalar fields:
a. $\Phi(\mathbf{r}) = x^2 + y^3 + z^4$,
b. $\Phi(\mathbf{r}) = x^2 y^3 z^4$,
c. $\Phi(\mathbf{r}) = e^x \sin y \ln z$.

Solution: *a.* $\nabla\Phi(\mathbf{r}) = 2x\hat{\mathbf{e}}_x + 3y^2\hat{\mathbf{e}}_y + 4z^3\hat{\mathbf{e}}_z$,
b. $\nabla\Phi(\mathbf{r}) = 2xy^3z^4\hat{\mathbf{e}}_x + 3x^2y^2z^4\hat{\mathbf{e}}_y + 4x^2y^3z^3\hat{\mathbf{e}}_z$,
c. $\nabla\Phi(\mathbf{r}) = e^x \sin y \ln z \hat{\mathbf{e}}_x + e^x \cos y \ln z \hat{\mathbf{e}}_y + \frac{e^x \sin y}{z}\hat{\mathbf{e}}_z$.

12.1.7.2 Ex: 2D landscape

A 2D landscape is parametrized by $h(x, y) = 10(2xy - 3x^2 - 4y^2 - 18x + 28y + 12)$.
a. Where is mountain top?
b. What is its height?

Solution: *a. The gradient is,*

$$\nabla h(x, y) = \begin{pmatrix} 20y - 60x - 180 \\ 20x - 80y + 280 \end{pmatrix} = 0 \ ,$$

yielding $x = -2$ *and* $y = 3$.
b. The height is,

$$h(-2, 3) = 720 \ .$$

12.1.7.3 Ex: Differential operators

Calculate $\nabla_{\mathbf{r}'}|\mathbf{r}-\mathbf{r}'|^n$.

Solution: *With*

$$\begin{aligned}\frac{\partial}{\partial x'}&[(x-x')^2+(y-y')^2+(z-z)^2]^{n/2}\\ &=\frac{n}{2}[(x-x')^2+(y-y')^2+(z-z')^2]^{n/2-1}2(x-x')(-1)\\ &=-n|\mathbf{r}-\mathbf{r}'|^{n-2}(x-x')\ .\end{aligned}$$

With this,

$$\nabla(\mathbf{r}-\mathbf{r}')^n=-n|\mathbf{r}-\mathbf{r}'|^{n-2}(\mathbf{r}-\mathbf{r}')\ .$$

12.1.7.4 Ex: Differential operators

Calculate the divergence and the rotation of the vector field $\mathbf{A}=e^{-x^2y}\hat{\mathbf{e}}_x+\frac{z}{1+y^2}\hat{\mathbf{e}}_y+x\hat{\mathbf{e}}_z$ at the position $(0,1,1)$.

Solution: *With Maple*

$$\nabla\cdot\mathbf{A}=-2xye^{-x^2y}-2\frac{z}{(1+y^2)^2}y\ .$$

At the given point the divergence is $\nabla\cdot\mathbf{A}(0,1,1)=-0.5$. *In addition we find,*

$$\nabla\times\mathbf{A}=\begin{pmatrix}-\frac{1}{1+y^2}\\ -1\\ x^2e^{-x^2y}\end{pmatrix}\ .$$

At the given point the rotation is $\nabla\times\mathbf{A}(0,1,1)=(-\frac{1}{2},-1,0)$.

12.1.7.5 Ex: Sources and vertices

a. Determine the divergence and the rotation of the vector field $\mathbf{A}=A_x\hat{\mathbf{e}}_x+A_y\hat{\mathbf{e}}_y+A_z\hat{\mathbf{e}}_z$.
b. Calculate for the following fields the sources and vortices:

$$\begin{aligned}\mathbf{A}_1&=-y\hat{\mathbf{e}}_x+x\hat{\mathbf{e}}_y \quad,\quad \mathbf{A}_2=+y\hat{\mathbf{e}}_x+x\hat{\mathbf{e}}_y\ ,\\ \mathbf{A}_3&=+x\hat{\mathbf{e}}_x+y\hat{\mathbf{e}}_y \quad,\quad \mathbf{A}_4=+x\hat{\mathbf{e}}_x+x\hat{\mathbf{e}}_y\ .\end{aligned}$$

c. Make a graphic illustration of the fields and give a geometric interpretation of div and rot.

Solution: *a. Easy.*
b. The solutions are:

$$\begin{aligned}
\nabla \cdot \mathbf{A}_1 = 0 \quad &, \quad \nabla \times \mathbf{A}_1 = 2\hat{\mathbf{e}}_z \ , \\
\nabla \cdot \mathbf{A}_2 = 0 \quad &, \quad \nabla \times \mathbf{A}_2 = 0 \ , \\
\nabla \cdot \mathbf{A}_3 = 2 \quad &, \quad \nabla \times \mathbf{A}_3 = 0 \ , \\
\nabla \cdot \mathbf{A}_4 = 1 \quad &, \quad \nabla \times \mathbf{A}_4 = \hat{\mathbf{e}}_z \ .
\end{aligned}$$

c. Graphical illustration:

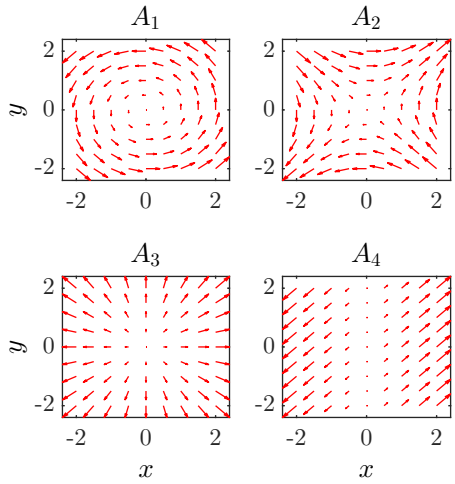

Figure 12.4: Illustration of Sources and vertices.

12.1.7.6 Ex: Sources and vertices

Calculate the divergence $\nabla \cdot \frac{\mathbf{r}}{r^3}$.

Solution: *With*

$$\frac{\partial}{\partial x}\frac{x}{(x^2+y^2+z^2)^{3/2}} = -\frac{2x^2-y^2-z^2}{(x^2+y^2+z^2)^{5/2}} \ ,$$

we obtain,

$$\nabla \cdot \frac{r}{r^3} = -\frac{2x^2-y^2-z^2}{r^5} - \frac{2y^2-z^2-x^2}{r^5} - \frac{2z^2-x^2-y^2}{r^5} = 0 \ .$$

12.1.7.7 Ex: Chain rule for functions of vector field

Apply the chain rule to the gradient of a scalar function of a vector field: $\nabla\phi(\mathbf{E}(\mathbf{r}))$. Use the rule to calculate $\nabla\sqrt{a\mathbf{r}^2}$.

Solution: *By components we have,*

$$\frac{d\phi(E_x,E_y,E_z)}{dx} = \frac{\partial\phi}{\partial E_x}\frac{\partial E_x}{\partial x} + \frac{\partial\phi}{\partial E_y}\frac{\partial E_y}{\partial x} + \frac{\partial\phi}{\partial E_z}\frac{\partial E_z}{\partial x} = \nabla_E\phi\cdot\frac{\partial}{\partial x}\mathbf{E} \ .$$

Hence,

$$\nabla\phi(\mathbf{E}(\mathbf{r})) = \sum_k \frac{\partial\phi}{\partial E_k}\nabla E_k \ .$$

For the given function,

$$\nabla\sqrt{a\mathbf{r}^2} = \sum_k \frac{\partial\sqrt{a\mathbf{r}^2}}{\partial(ax_k^2)}\nabla(ax_k^2) = \sum_k \frac{1}{2\sqrt{a\mathbf{r}^2}}2ax_k\hat{\mathbf{e}}_k = \sqrt{a}\hat{\mathbf{e}}_r \ .$$

12.1.7.8 Ex: Taylor expansion in 3D

Consider the function,

$$f(\mathbf{x}) = \frac{1}{|\mathbf{d}-\mathbf{x}|} \ .$$

Calculate the Taylor expansion in x of this function in Cartesian coordinates at the position $x = 0$ (in all three spatial coordinates) up to second-order.

Solution: *In general we have,*

$$f(\mathbf{x}) = f|_{\mathbf{x}=0} + \left.\frac{\partial f}{\partial x_i}\right|_{\mathbf{x}=0} x_i + \frac{1}{2}\left.\frac{\partial^2 f}{\partial x_i x_j}\right|_{\mathbf{x}=0} x_i x_j + O(|\mathbf{x}|^3) \ ,$$

where we add over equal indices.
In 0. order,

$$f|_{\mathbf{x}=0} = \frac{1}{|\mathbf{d}|} \ .$$

In 1. order,

$$\left[\frac{\partial}{\partial x_i}[(d_1-x_1)^2+(d_2-x_2)^2+(d_3-x_3)^2]^{-1/2}\right]_{\mathbf{x}=0}$$
$$= \left[\frac{d_i-x_i}{[(d_1-x_1)^2+(d_2-x_2)^2+(d_3-x_3)^2]^{3/2}}\right]_{\mathbf{x}=0} = \frac{d_i}{|\mathbf{d}|^3} \ .$$

So we get in first order,

$$\left.\frac{\partial f}{\partial x_i}\right|_{\mathbf{x}=0} x_i = \frac{\mathbf{d}\cdot\mathbf{x}}{|\mathbf{d}|^3} \ .$$

In 2. order for $i \neq j$,

$$\left[\frac{\partial}{\partial x_j}\frac{d_i-x_i}{|\mathbf{d}-\mathbf{x}|^3}\right]_{\mathbf{x}=0} = \left[\frac{\frac{\partial(d_i-x_i)}{\partial x_j}|\mathbf{d}-\mathbf{x}|^3 - (d_i-x_i)\frac{\partial}{\partial x_j}|\mathbf{d}-\mathbf{x}|^3}{|\mathbf{d}-\mathbf{x}|^6}\right]_{\mathbf{x}=0}$$
$$= \left[\frac{3(d_i-x_i)(d_j-x_j)}{|\mathbf{d}-\mathbf{x}|^5}\right]_{\mathbf{x}=0} = 3\frac{d_i d_j}{|\mathbf{d}|^5} \ .$$

In 2. order for $i = j$,

$$\left[\frac{\frac{\partial(d_i-x_i)}{\partial x_i}|\mathbf{d}-\mathbf{x}|^3-(d_i-x_i)\frac{\partial}{\partial x_i}|\mathbf{d}-\mathbf{x}|^3}{|\mathbf{d}-\mathbf{x}|^6}\right]_{\mathbf{x}=0} = \left[\frac{-|\mathbf{d}-\mathbf{x}|^3+(d_i-x_i)3(d_i-x_i)|\mathbf{d}-\mathbf{x}|}{|\mathbf{d}-\mathbf{x}|^6}\right]_{\mathbf{x}=0}$$
$$= \frac{1}{|\mathbf{d}|^5}(3d_i^2-|\mathbf{d}|^2) \ .$$

So we get in second order,

$$\frac{1}{2}\frac{\partial^2 f}{\partial x_i x_j}\Big|_{\mathbf{x}=0} x_i x_j = \frac{3}{2}\frac{d_i d_j}{|\mathbf{d}|^5}x_i x_j + \frac{3}{2}\frac{d_i^2}{|\mathbf{d}|^5}x_i^2 - \frac{1}{2}\frac{1}{|\mathbf{d}|^3}x_i^2 = \frac{3}{2|\mathbf{d}|^5}\sum_{i,j} d_i d_j x_i x_j - \frac{1}{2|\mathbf{d}|^3}\sum_i x_i^2 \ .$$

12.1.7.9 Ex: Levi-Civita tensor

Prove the following relationships for the Kronecker symbol and the Levi-Civita tensor by distinguishing the cases in the indices,
a. $\epsilon_{ijk}\delta_{ij} = 0$,
b. $\epsilon_{ijk}\epsilon_{ijk} = 6$,
d. $\epsilon_{ijk}\epsilon_{imn} = \delta_{jm}\delta_{kn} - \delta_{jn}\delta_{km}$,
c. $\epsilon_{ijk}\epsilon_{ijn} = 2\delta_{kn}$.

Solution: *a. We sum over i and j. Therefore, we can rename these indexes. Now, $\delta_{ij}$is obviously symmetric about permutation, but ϵ_{ijk} is antisymmetric. With that we get,*

$$\begin{aligned} \epsilon_{ijk}\delta_{ij} &= \epsilon_{jik}\delta_{ji} && \text{(rename)} \\ &= -\epsilon_{ijk}\delta_{ij} && \text{(symmetries)} \\ &= 0 \ . \end{aligned}$$

Here we must take into account that $\delta_{jj} = \sum_j \delta_{jj} = 3$.
b. This immediately follows from (b), letting $i = l$ and summing over i.
c. Summing over the i index, which appears twice. j, k, l, m they are fixed indices. Due to tensor properties ϵ the only terms they don't zero are for $j \neq k \neq i$ as well as $l \neq m \neq i$. Therefore, only one i can contribute from the sum and, in addition, it has to be $j = l$ and $k = m$ or $j = m$ and $k = l$. In the first case we get $+1$, in the second (since we must exchange l and m) -1. With this, we immediately prove the statement.
d. Using the result (c) we have,

$$\epsilon_{ijk}\epsilon_{ljk} = \epsilon_{kij}\epsilon_{klj} = \delta_{il}\delta_{jj} - \delta_{ij}\delta jl = 3\delta_{il} - 1\delta_{il} = 2\delta_{il} \ .$$

12.1.7.10 Ex: Levi-Civita tensor

Let the vectors $\mathbf{A}$, $\mathbf{B}$, $\mathbf{C}$, and $\mathbf{D} \in \mathbb{R}^3$ be given. Using the Kronecker Symbol and the Levi-Civita Tensor
a. show $\{\mathbf{A} \times \mathbf{B}\}_i = \epsilon_{ijk} A_j B_k$;
b. prove the relationship, $(\mathbf{A} \times \mathbf{B}) \cdot \mathbf{C} = (\mathbf{B} \times \mathbf{C}) \cdot \mathbf{A} = (\mathbf{C} \times \mathbf{A}) \cdot \mathbf{B}$; c. Using the formulas of (b) derive the following rules of calculation:

i. $(\mathbf{A} \times \mathbf{B})^2 = \mathbf{A}^2\mathbf{B}^2 - (\mathbf{A} \cdot \mathbf{B})^2$
ii. $(\mathbf{A} \times \mathbf{B}) \cdot (\mathbf{C} \times \mathbf{D}) = (\mathbf{A} \cdot \mathbf{C})(\mathbf{B} \cdot \mathbf{D}) - (\mathbf{A} \cdot \mathbf{D})(\mathbf{B} \cdot \mathbf{C})$;

d. prove that:

i. $(\mathbf{A} \times \mathbf{B}) \cdot [(\mathbf{B} \times \mathbf{C}) \times (\mathbf{C} \times \mathbf{A})] = [\mathbf{A} \cdot (\mathbf{B} \times \mathbf{C})]^2$
ii. $\mathbf{A} \times (\mathbf{B} \times \mathbf{C}) + \mathbf{B} \times (\mathbf{C} \times \mathbf{A}) + \mathbf{C} \times (\mathbf{A} \times \mathbf{B}) = 0$.

Solution: *a. Since the indices j and k appear twice, we take the sum applying the Einstein convention. Without restricting generality we choose, $i = 1$. Due to the properties of the ϵ-tensor we get non-zeroing terms just for $j = 2$ and $k = 3$ as well as for $j = 3$ and $k = 2$. In the first case, we have an even permutation of $1, 2, 3$, in the second an odd. We get immediately,*

$$\{\mathbf{A} \times \mathbf{B}\}_1 = A_2 B_3 - A_3 B_2 \ .$$

Analogously we get,

$$\{\mathbf{A} \times \mathbf{B}\}_2 = A_3 B_1 - A_1 B_3$$
$$\{\mathbf{A} \times \mathbf{B}\}_3 = A_1 B_2 - A_2 B_1 \ .$$

b. We have,

$$\epsilon_{ijk} A_j B_k C_i = \epsilon_{jki} B_k C_i A_j = \epsilon_{kij} C_i A_j B_k \ .$$

c.i. Vide (c.ii).
c.ii. We have,

$$\epsilon_{ijk} A_i B_j \epsilon_{lmk} C_l D_m = A_i B_j C_l D_m (\delta_{il}\delta_{jm} - \delta_{im}\delta_{jl}) = A_i C_i B_j D_j - A_i D_i B_j C_j \ .$$

d.i. We have,

$$\epsilon_{ijk} A_i B_j \epsilon_{lmh} B_l C_m \epsilon_{npq} C_n A_p \epsilon_{hqk} = \epsilon_{lmh}\epsilon_{npq}(\delta_{ih}\delta_{jq} - \delta_{iq}\delta_{jh}) A_i B_j B_l C_m C_n A_p \ .$$

We have,

$$= \epsilon_{lmi} B_l C_m A_i \epsilon_{npj} C_n A_p B_j - \epsilon_{npi} A_i C_n A_p \epsilon_{lmj} B_l C_m B_j = \epsilon_{lmi} B_l C_m A_i \epsilon_{npj} C_n A_p B_j \ .$$

d.ii. We have,

$$\epsilon_{ijk}\epsilon_{lmj}(A_i B_l C_m + B_i C_l A_m + C_i A_l B_m) = (\delta_{lk}\delta_{mi} - \delta_{li}\delta_{mk})(A_i B_l C_m + B_i C_l A_m + C_i A_l B_m) = 0 \ .$$

12.1.7.11 Ex: Levi-Civita tensor and vector tautologies

Be Ψ and Φ scalar fields and $\mathbf{A}$, $\mathbf{B}$, $\mathbf{C}$, and $\mathbf{D}$ vector fields. Show the following identities with the help of the Kronecker symbol.:
a. $\mathbf{A}\cdot(\mathbf{B}\times\mathbf{C})=\mathbf{B}\cdot(\mathbf{C}\times\mathbf{A})$,
b. $(\mathbf{A}\times\mathbf{B})\cdot(\mathbf{C}\times\mathbf{D})=(\mathbf{A}\cdot\mathbf{C})(\mathbf{B}\cdot\mathbf{D})-(\mathbf{B}\cdot\mathbf{C})(\mathbf{A}\cdot\mathbf{D})$,
c. $(\mathbf{A}\times\mathbf{B})\times(\mathbf{C}\times\mathbf{D})=((\mathbf{A}\times\mathbf{B})\cdot\mathbf{D})\mathbf{C}-((\mathbf{A}\times\mathbf{B})\cdot\mathbf{C})\mathbf{D}$,
d. $\nabla(\Phi\Psi)=\Phi\nabla\Psi+\Psi\nabla\Phi$,
e. $\nabla\times(\Phi\mathbf{A})=(\nabla\Phi)\times\mathbf{A}+\Phi\nabla\times\mathbf{A}$,
f. $\nabla\times(\mathbf{A}\times\mathbf{B})=(\mathbf{B}\cdot\nabla)\mathbf{A}-(\mathbf{A}\cdot\nabla)\mathbf{B}+\mathbf{A}(\nabla\cdot\mathbf{B})-\mathbf{B}(\nabla\cdot\mathbf{A})$,
g. $\nabla(\mathbf{A}\cdot\mathbf{B})=\mathbf{A}\times(\nabla\times\mathbf{B})+\mathbf{B}\times(\nabla\times\mathbf{A})+(\mathbf{A}\cdot\nabla)\mathbf{B}+(\mathbf{B}\cdot\nabla)\mathbf{A}$,
h. $\nabla\cdot(\nabla\Phi)=\Delta\Phi$,
i. $\mathbf{A}\cdot(\nabla\Phi)=(\mathbf{A}\cdot\nabla)\Phi$,
j. $\mathbf{A}\times(\nabla\Phi)=(\mathbf{A}\times\nabla)\Phi$.
k. $\nabla\cdot(\mathbf{A}\times\mathbf{B})=\mathbf{B}\cdot(\nabla\times\mathbf{A})-\mathbf{A}\cdot(\nabla\times\mathbf{B})$,
l. $\nabla(\Psi\mathbf{A})=\mathbf{A}\cdot\nabla\Psi+\Psi\nabla\cdot\mathbf{A}$,
m. $\nabla\cdot(\Psi\nabla\Psi)=\Psi\Delta\Psi+(\nabla\Psi)^2$
n. $\nabla\cdot(\mathbf{A}\times\mathbf{B})=\mathbf{B}\cdot(\nabla\times\mathbf{A})-\mathbf{A}\cdot(\nabla\times\mathbf{B})$,
o. $\nabla\cdot(\nabla\times\mathbf{A})=0$,
p. $\nabla\times(\nabla\Phi)=0$,
q. $\nabla\times(\nabla\times\mathbf{A})=\nabla(\nabla\cdot\mathbf{A})-\nabla^2\mathbf{A}$.

Solution: *a. We have,*

$$\mathbf{A}\cdot(\mathbf{B}\times\mathbf{C})=...=\mathbf{B}\cdot(\mathbf{C}\times\mathbf{A})$$

b. We have,

$$\begin{aligned}(\mathbf{A}\times\mathbf{B})\cdot(\mathbf{C}\times\mathbf{D})&=(\mathbf{A}\times\mathbf{B})_i(\mathbf{C}\times\mathbf{D})_i\\&=\epsilon_{ijk}\epsilon_{ilm}A_jB_kC_lD_m\\&=(\delta_{jl}\delta_{km}-\delta_{jm}\delta_{kl})A_jB_kC_lD_m\\&=A_jC_jB_kD_k-A_jD_jB_kC_k=(\mathbf{A}\cdot\mathbf{C})(\mathbf{B}\cdot\mathbf{D})-(\mathbf{A}\cdot\mathbf{D})(\mathbf{B}\cdot\mathbf{C})\ .\end{aligned}$$

c. We have,

$$\begin{aligned}\{(\mathbf{A}\times\mathbf{B})\times(\mathbf{C}\times\mathbf{D})\}_i&=\epsilon_{ijk}(\mathbf{A}\times\mathbf{B})_j(\mathbf{C}\times\mathbf{D})_k\\&=\epsilon_{ijk}\epsilon_{jlm}\epsilon_{krs}A_lB_mC_rD_s=\epsilon_{kij}\epsilon_{krs}\epsilon_{jlm}A_lB_mC_rD_s\\&=(\delta_{ir}\delta_{js}-\delta_{is}\delta_{jr})\epsilon_{jlm}A_lB_mC_rD_s\\&=C_iD_j\epsilon_{jlm}A_lB_m-D_iC_j\epsilon_{jlm}A_lB_m\\&=C_i(\mathbf{D}\cdot(\mathbf{A}\times\mathbf{B}))-D_i(\mathbf{C}\cdot(\mathbf{A}\times\mathbf{B}))\\&=C_i(\mathbf{A}\cdot(\mathbf{B}\times\mathbf{D}))-D_i(\mathbf{A}\cdot(\mathbf{B}\times\mathbf{C}))\ ,\end{aligned}$$

where we use in the last line the cyclic permutativity of the triple product.
d. We have,

$$\nabla(\Phi\Psi)=...=\Phi\nabla\Psi+\Psi\nabla\Phi\ .$$

e. We have,

$$\nabla\times(\Phi\mathbf{A})=...=(\nabla\phi)\times\mathbf{A}+\Phi\nabla\times\mathbf{A}\ .$$

f. Here we have,

$$\begin{aligned}\{\nabla\times(\mathbf{A}\times\mathbf{B})\}_i &= \epsilon_{ijk}\partial_j(\mathbf{A}\times\mathbf{B})_k = \epsilon_{ijk}\epsilon_{klm}\partial_j A_l B_m \\ &= (\delta_{il}\delta_{jm}-\delta_{im}\delta_{lj})\partial_j A_l B_m \qquad (T15b)\\ &= \partial_j A_i B_j - \partial_j A_j B_i \\ &= B_j(\partial_j A_i) + A_i(\partial_j B_j) - B_i(\partial_j A_j) - A_j(\partial_j B_i) \\ &= \{\mathbf{A}(\nabla\cdot\mathbf{B}) - \mathbf{B}(\nabla\cdot\mathbf{A}) + (\mathbf{B}\cdot\nabla)\mathbf{A} - (\mathbf{A}\cdot\nabla)\mathbf{B}\}_i \ .\end{aligned}$$

g. We have,

$$\nabla(\mathbf{A}\cdot\mathbf{B}) = ... = \mathbf{A}\times(\nabla\times\mathbf{B}) + \mathbf{B}\times(\nabla\times\mathbf{A}) + (\mathbf{A}\cdot\nabla)\mathbf{B} + (\mathbf{B}\cdot\nabla)\mathbf{A} \ .$$

h. We have,

$$\nabla\cdot(\nabla\Phi) = ... = \Delta\Phi \ .$$

i. We have,

$$\mathbf{A}\cdot(\nabla\Phi) = ... = (\mathbf{A}\cdot\nabla)\Phi \ .$$

j. We have,

$$\mathbf{A}\times(\nabla\Phi) = ... = (\mathbf{A}\times\nabla)\Phi \ .$$

k. We get,

$$\begin{aligned}\nabla\cdot(\mathbf{A}\times\mathbf{B}) &= \epsilon_{ijk}\partial_i A_j B_k = \epsilon_{ijk}(B_k(\partial_i A_j) + A_j(\partial_i B_k)) \\ &= B_k\epsilon_{kij}\partial_i A_j - A_j\epsilon_{jik}\partial_i B_k \\ &= \mathbf{B}\cdot(\nabla\times\mathbf{A}) - \mathbf{A}\cdot(\nabla\times\mathbf{B}) \ .\end{aligned}$$

l. We have,

$$\nabla\cdot(\Psi\mathbf{A}) = \partial_k(\Psi\mathbf{A})_k = \partial_k\Psi A_k = \Psi\partial_k A_k + A_k\partial_k\Psi = \Psi(\nabla\cdot\mathbf{A}) + \mathbf{A}\cdot(\nabla\Psi) \ .$$

m.

n. We have,

$$\begin{aligned}\nabla\cdot(\mathbf{A}\times\mathbf{B}) &= \partial_k(\mathbf{A}\times\mathbf{B})_k = \partial_k\varepsilon_{kmn}a_m b_n = \varepsilon_{nkm}b_n\partial_k a_m - a_m\varepsilon_{mkn}\partial_k b_n \\ &= b_n(\nabla\times\mathbf{A})_n - a_m(\nabla\times\mathbf{B})_m = \mathbf{B}(\nabla\times\mathbf{A}) - \mathbf{A}(\nabla\times\mathbf{B}) \ .\end{aligned}$$

o. We obtain consecutively,

$$\begin{aligned}\nabla\cdot(\nabla\times\mathbf{A}) &= \partial_i\epsilon_{ijk}\partial_j A_k = \epsilon_{ijk}\partial_i\partial_j A_k \\ &= \epsilon_{jik}\partial_j\partial_i A_k && \text{(rename)}\\ &= -\epsilon_{ijk}\partial_i\partial_j A_k && \text{(symmetry)}\\ &= 0 \ .\end{aligned}$$

where we used in the penultimate line, that we can exchange partial derivatives.
p. Here we obtain,

$$\begin{aligned}\{\nabla\times(\nabla\Phi)\}_i &= \epsilon_{ijk}\partial_j\partial_k\Phi \\ &= \epsilon_{ikj}\partial_k\partial_j\Phi && \text{(rename)}\\ &= -\epsilon_{ijk}\partial_j\partial_k\Phi && \text{(symmetry)}\\ &= 0 \ ,\end{aligned}$$

where we once again use the interchangeability of partial derivatives.
q. Vale

$$\begin{aligned}\{\nabla\times(\nabla\times\mathbf{A})\}_i &= \epsilon_{ijk}\partial_j\{\nabla\times\mathbf{A}\}_k\\ &= \epsilon_{ijk}\epsilon_{klm}\partial_j\partial_l A_m\\ &= (\delta_{il}\delta_{jm}-\delta_{im}\delta_{jl})\partial_j\partial_l A_m \qquad (Exc.\ 12.1.7.10(b))\\ &= \partial_i\partial_j A_j-\partial_j\partial_j A_i\\ &= (\nabla)_i(\nabla\cdot\mathbf{A})-\nabla^2 A_i\ .\end{aligned}$$

What was to prove.

12.2 Integral calculus

Three types of integrals are often used in electrodynamics, the *path integral*, the *surface integral*, and the *volume integral*.

12.2.1 Path integral

The path integral is defined on a trajectory $\mathcal{C}(\mathbf{a},\mathbf{b})$ through a (scalar or vector) field linking a start point $\mathbf{a}$ to an end point $\mathbf{b}$. While following the path point by point, incrementing the infinitesimal displacement vector $d\mathbf{l}$ (see Fig. 12.5), we evaluate the local value and the direction of the field, multiply it with $d\mathbf{l}$, and sum it up,

$$\int_{\mathcal{C}(\mathbf{a},\mathbf{b})}\Phi d\mathbf{l}\quad,\quad\int_{\mathcal{C}(\mathbf{a},\mathbf{b})}\mathbf{A}\cdot d\mathbf{l}\ . \tag{12.27}$$

Note that in case of a vector field, the integral is taken over the scalar product between the local field vector and the path element. The work exerted by a force field, $W\equiv\int\mathbf{F}\cdot\mathbf{l}$ is an example. For a path through a field crossing all force lines under right angle, the path integral zeroes, meaning that no work is accumulated.

Depending on the properties of the field, the integral may only depend on the points $\mathbf{a}$ and $\mathbf{b}$ and not on the path $\mathcal{C}$ chosen to go from one to the other. In this case, we say that the vector field is *conservative*, but this is not always the case. Choosing $\mathbf{a}=\mathbf{b}$ we get a closed path, which can be thought of as delimiting a surface in 3D space. We use the notation,

$$\oint_{\partial\mathcal{S}}\mathbf{A}\cdot d\mathbf{l}\ , \tag{12.28}$$

where the symbol ∂S suggests, that the path goes along the edge of the surface S.

In practice, it is often useful to find a parametrization $\mathbf{l}(t)$ for the path with a parameter (e.g. time) defined over $t\in[0,1]$. It allows us to calculate explicitly,

$$\int_{\mathcal{C}(\mathbf{a},\mathbf{b})}\nabla\Phi\cdot d\mathbf{l}=\int_0^1\nabla\Phi(\mathbf{r})\cdot\frac{d\mathbf{l}(t)}{dt}dt\ . \tag{12.29}$$

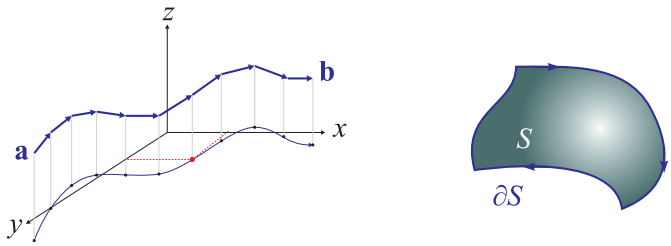

Figure 12.5: Integrating along a path in three-dimensional space.

Example 32 (*Path integral*): As an example, we will calculate the integral along the path parametrized by $\mathbf{l}(t) = \hat{\mathbf{e}}_x \cos t + \hat{\mathbf{e}}_y \sin t$, which is a unit circle around the origin, inside the field $\mathbf{A}(\mathbf{r}) = -y\hat{\mathbf{e}}_x + x\hat{\mathbf{e}}_y$:

$$\oint \mathbf{A} \cdot d\mathbf{l} = \int_0^{2\pi} (-y\hat{\mathbf{e}}_x + x\hat{\mathbf{e}}_y) \cdot \frac{dl}{dt} dt \tag{12.30}$$
$$= \int_0^{2\pi} (-\hat{\mathbf{e}}_x \sin t + \hat{\mathbf{e}}_y \cos t) \left(\hat{\mathbf{e}}_x \frac{d\cos t}{dt} + \hat{\mathbf{e}}_y \frac{d\sin t}{dt} \right) dt = \int_0^{2\pi} (\sin^2 t + \cos^2 t) dt = 2\pi \ .$$

We calculate other examples of path integrals in the Excs. 12.2.7.1 to 12.2.7.4.

12.2.2 Surface integral

The surface integral is defined on a surface $\mathcal{S}$, which can be folded in three-dimensional space. The surface is parceled into infinitesimal areas $d\mathbf{S}$, the local value and the direction of the field are evaluated, multiplied with $d\mathbf{S}$, and summed up,

$$\int_{\mathcal{S}} \Phi d\mathbf{S} \quad , \quad \int_{\mathcal{S}} \mathbf{A} \cdot d\mathbf{S} \ . \tag{12.31}$$

The vector of the area $d\mathbf{S}$ is the local normal vector. In case of the vector field, the integral is taken over the scalar product between the field and the local area. The flux, that is the field lines crossing a surface, $\Psi \equiv \int \mathbf{E} \cdot d\mathbf{S}$ it is an example. The normal vector of the surface of a volume is usually taken as pointing *out of the volume*. For example, a surface element of the x-y plane can be written $d\mathbf{S} = \hat{\mathbf{e}}_z dxdy$ in Cartesian coordinates. For curved surfaces or in curvilinear coordinates the expression will be more complicated.

Often we consider closed surfaces, which can be considered as delimiting a volume in 3D space. We use the notation,

$$\oint_{\partial\mathcal{V}} \mathbf{A} \cdot d\mathbf{S} \ , \tag{12.32}$$

where the symbol $\partial\mathcal{V}$ suggests that the surface encloses the volume $\mathcal{V}$.

Example 33 (*Flow of a field*): As an example, we calculate the field flux

$\mathbf{A} = -y\hat{\mathbf{e}}_x + x^2 y\hat{\mathbf{e}}_y$ through the unit cube:

$$\begin{aligned}\oint_{cubo} \mathbf{A}\cdot dS &= \int_{-1}^{1}\int_{-1}^{1} \mathbf{A}|_{z=1}\hat{\mathbf{e}}_z dxdy + \int_{-1}^{1}\int_{-1}^{1} \mathbf{A}|_{z=-1}(-\hat{\mathbf{e}}_z) dxdy + \int_{-1}^{1}\int_{-1}^{1} \mathbf{A}|_{x=1}\hat{\mathbf{e}}_x dydz \\ &+ \int_{-1}^{1}\int_{-1}^{1} \mathbf{A}|_{x=-1} dydz + \int_{-1}^{1}\int_{-1}^{1} \mathbf{A}|_{y=1}\hat{\mathbf{e}}_y dzdx + \int_{-1}^{1}\int_{-1}^{1} \mathbf{A}|_{y=-1}(-\hat{\mathbf{e}}_y) dzdx \\ &= 0 + 0 + \int_{-1}^{1}\int_{-1}^{1} (-y) dydz + \int_{-1}^{1}\int_{-1}^{1} y dydz + \int_{-1}^{1}\int_{-1}^{1} x^2 dzdx + \int_{-1}^{1}\int_{-1}^{1} x^2 dzdx \\ &= \frac{8}{3}\ . \end{aligned} \tag{12.33}$$

We calculate other examples of surface integrals in Excs. 12.2.7.5 to 12.2.7.8.

12.2.3 Volume integral

The volume integral defined by,

$$\int_{\mathcal{V}} \Phi dV \quad , \quad \int_{\mathcal{V}} \mathbf{A} dV\ . \tag{12.34}$$

In the case of a vector field, we simply write: $\hat{\mathbf{e}}_x \int A_x dV + \hat{\mathbf{e}}_y \int A_y dV + \hat{\mathbf{e}}_z \int A_z dV$.

Example 34 (*Integral de volume*): As an example, we calculate the mass of a cube with homogeneous density ρ_0:

$$m = \int_{-a/2}^{a/2}\int_{-a/2}^{a/2}\int_{-a/2}^{a/2} \rho_0 dxdydz = a^3\rho_0\ . \tag{12.35}$$

We calculate another example of a volume integral in Exc. 12.2.7.9.

12.2.4 Fundamental theorem for gradients

The fundamental theorem of infinitesimal calculus says,

$$\int_{f_a}^{f_b} df = \int_a^b F(x)dx = f(b) - f(a) \qquad \text{or} \qquad df = F(x)dx\ , \tag{12.36}$$

for $F(x) = \frac{df}{dx}$. That is, derivation and integration are inverse operations.

Now in vector analysis, as explained above, we know three different types of derivatives. For each one we need to formulate the fundamental theorem in a specific way. For gradients,

$$\boxed{\int_{\mathcal{C}(\mathbf{a},\mathbf{b})} \nabla\Phi\cdot d\mathbf{l} = \Phi(\mathbf{b}) - \Phi(\mathbf{a})} \qquad \text{or} \qquad d\Phi = \nabla\Phi\cdot d\mathbf{l}\ . \tag{12.37}$$

Since the right-hand side does not depend on the path $\mathcal{C}$, the integral of the gradient can not either. As a consequence,

$$\boxed{\oint_{\mathcal{C}} \nabla\Phi\cdot d\mathbf{l} = 0}\ . \tag{12.38}$$

The geometric interpretation of the fundamental theorem for gradients is simple: Climbing a mountain following a path step by step and gaining at each step the potential energy $d\Phi = \nabla\Phi dx$, we accumulate between the end and the start point of the path the energy $\Phi(\mathbf{b}) - \Phi(\mathbf{a})$. Path independence is an inherent property of gradients.

Example 35 (*Fundamental theorem for gradients*): Let us consider the following example. To travel inside the potential $\Phi(\mathbf{r}) = xy^2$ between the points $\mathbf{r}_1 = (0,0,0)$ and $\mathbf{r}_2 = (2,1,0)$, we can choose between several paths, f.ex. $\mathbf{l}_1(t) = \hat{\mathbf{e}}_x 2t + \hat{\mathbf{e}}_y t$ or $\mathbf{l}_2(t) = \hat{\mathbf{e}}_x 2t + \hat{\mathbf{e}}_y t^2$ with $t \in [0,1]$. In both cases we gain the same potential energy $\Phi(\mathbf{r}_2) - \Phi(\mathbf{r}_1) = 2$:

$$\int_{\mathcal{C}(\mathbf{r}_1,\mathbf{r}_2)} \nabla\Phi \cdot d\mathbf{l}_1 = \int_0^1 (\hat{\mathbf{e}}_x y^2 + \hat{\mathbf{e}}_y 2xy) \cdot (\hat{\mathbf{e}}_x 2 + \hat{\mathbf{e}}_y) dt = \int_0^1 (2t^2 + 4t^2) dt = 2 \tag{12.39}$$

$$\int_{\mathcal{C}(\mathbf{r}_1,\mathbf{r}_2)} \nabla\Phi \cdot d\mathbf{l}_2 = \int_0^1 (\hat{\mathbf{e}}_x y^2 + \hat{\mathbf{e}}_y 2xy) \cdot (\hat{\mathbf{e}}_x 2 + \hat{\mathbf{e}}_y 2t) dt = \int_0^1 (2t^4 + 8t^4) dt = 2 \; .$$

An example for the application of the fundamental theorem for gradients is discussed in Exc. 12.2.7.10.

12.2.5 Stokes' theorem

Stokes' theorem allows us *to convert a surface integral into a path integral* provided the field to be integrated can be expressed as a rotation,

$$\boxed{\int_{\mathcal{S}} (\nabla \times \mathbf{A}) \cdot d\mathbf{S} = \oint_{\partial\mathcal{S}} \mathbf{A} \cdot d\mathbf{l}} \; . \tag{12.40}$$

To find a geometric interpretation we remember that the rotation measures the *twist* of a field $\mathbf{A}$. The integral over the rotation within a given surface (or, more precisely, the flux of the rotation through this surface) measures the total amount of vorticity. A rotating region is like a *kitchen beater* stirring the surface of an incompressible liquid: The more beaters are in the area, the more the liquid will be moved along the edges of the area. Instead of measuring the number of beaters (left-hand side of the theorem (12.40)), we can also walk along the edge of the area and measure the flux along the rim (right-hand side of the theorem (12.40)).

An interesting consequence of Stokes' theorem is that the path integral is independent of the shape of the surface. That is, if the field to be integrated can be expressed bin terms of a rotation, we can deform the surface (without touching the edge) without changing the twist of the field,

$$\boxed{\oint_{\mathcal{S}} (\nabla \times \mathbf{A}) \cdot d\mathbf{S} = 0} \; . \tag{12.41}$$

This is analogous to the corollary obtained for gradients (12.38).

Example 36 (*Teorema de Stokes*): Consider the following example. A field be given by, $\mathbf{A} = -y\hat{\mathbf{e}}_x + x\hat{\mathbf{e}}_y$, such that $\nabla \times \mathbf{A} = 2\hat{\mathbf{e}}_z$. The surface be a disk of

radius R enclosed by a circular path parametrized by, $\mathbf{l} = \begin{pmatrix} R\cos\omega t \\ R\sin\omega t \\ 0 \end{pmatrix}$. Then,

$$\oint_{circle} \mathbf{A}\cdot dl = \int_0^{2\pi} \mathbf{A}\cdot \dot{l}dt = \int_0^{2\pi/\omega} \begin{pmatrix} -y \\ x \\ 0 \end{pmatrix} \cdot \begin{pmatrix} -R\omega\sin\omega t \\ R\omega\cos\omega t \\ 0 \end{pmatrix} dt = 2\pi R^2$$

$$\int_{disk} (\nabla\times\mathbf{A})\cdot dS = \int_{disk} \begin{pmatrix} 0 \\ 0 \\ 2 \end{pmatrix} \hat{\mathbf{e}}_z d\mathbf{A} = 2\int_{disk} dA = 2\pi R^2 \ .$$

In the Excs. 12.2.7.11 and 12.2.7.12 we show applications of Stokes' theorem.

12.2.6 Gauß' theorem

Gauß theorem allows us *to convert a volume integral into a surface integral* provided the field to be integrated can be expressed by a divergence,

$$\boxed{\int_{\mathcal{V}} (\nabla\cdot\mathbf{A})\cdot dV = \oint_{\partial\mathcal{V}} \mathbf{A}\cdot d\mathbf{S}} \ . \tag{12.42}$$

To find a geometric interpretation we remember that the divergence measures the *expansion* force of the field $\mathbf{A}$. The integral over the divergence within a given volume measures the total amount of expansion. A divergent region with is like a tap releasing an incompressible liquid: The more taps are in the volume, the more liquid will be expelled by the edges of the volume. Instead of measuring the number of taps (left-hand side of the theorem (12.42)), we can also bypass the volume by measuring the flux through the surface (right-hand side of the theorem (12.42)).

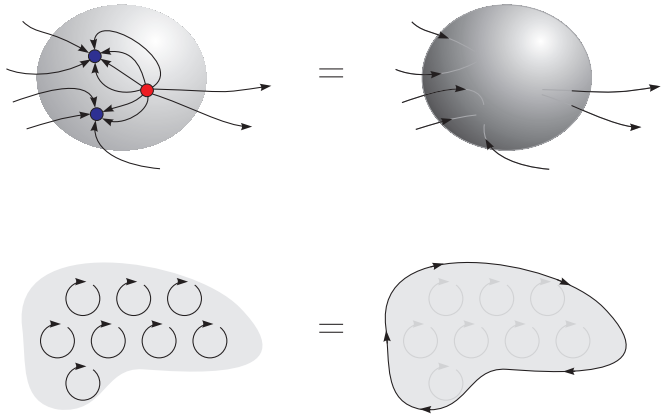

Figure 12.6: Illustration of the theorems of Gauß (above) and Stokes (below).

Example 37 (*Gauß theorem*): Consider the following example. A field be given by, $\mathbf{A} = \mathbf{r}$, such that $\nabla \cdot \mathbf{A} = 3$. The volume be a sphere of radius R enclosed by a surface. So:

$$\oint_{sphericalsurface} \mathbf{A} \cdot d\mathbf{S} = \int_{sphericalsurface} \mathbf{r} \cdot \hat{\mathbf{e}}_r dS = rr^2 \int_0^{2\pi} \int_0^{\pi} \sin\theta d\theta d\phi = 4\pi R^3$$

$$\int_{sphere} (\nabla \cdot A) dV = \int_{sphere} 3dV = 3\frac{4\pi}{3} R^3 = 4\pi R^3 \ .$$

In the Excs. 12.2.7.13 to 12.2.7.16 we show applications of Gauß' theorem.

The theorems of Stokes and Gauß are often used in the context of cylindrical or spherical coordinates. Therefore, we will postpone the presentation of further examples, until we have discussed curvilinear coordinates.

12.2.7 Exercises

12.2.7.1 Ex: Path integral and work

Be the field electric $\mathbf{A}(\mathbf{r}) = E_0 z \hat{\mathbf{e}}_z$ be given. A charge $+q$ be shifted on a straight line from the point $(0,0,0)$ to the point $(1,1,1)$.
a. Write down parametrization for the trajectory.
b. Calculate the work spent on this charge explicitly along the path integral $W = q \int \mathbf{E}(\mathbf{r}) \cdot d\mathbf{r}$.
c. Calculate the work via the potential ϕ.

Solution: *a. One possible parametrization is,*

$$\mathbf{x}(t) = \begin{pmatrix} t \\ t \\ t \end{pmatrix} \qquad with \qquad t \in [0,1] \ .$$

b. The line integral within this parametrization is given by:

$$W = qE_0 \int_0^1 \begin{pmatrix} 0 \\ 0 \\ z(t) \end{pmatrix} \cdot \begin{pmatrix} t \\ t \\ t \end{pmatrix} dt = qE_0 \int_0^1 t dt = \frac{1}{2} qE_0 \ .$$

c. A potential, which corresponds to the field $\mathbf{E}(\mathbf{r})$*, is given by,*

$$\phi(\mathbf{r}) = -\frac{E_0}{2} z^2 \qquad since \qquad -\nabla\phi(\mathbf{r}) = -\begin{pmatrix} d/dx \\ d/dy \\ d/dz \end{pmatrix} \phi(\mathbf{r}) = E_0 z \hat{\mathbf{e}}_z \ .$$

The work is given by,

$$W = -q\phi(\mathbf{r} = (1,1,1)) + q\phi(\mathbf{r} = (0,0,0)) = \frac{1}{2} qE_0 \ .$$

12.2.7.2 Ex: Path integral and work

Consider a field $\mathbf{E}$ depending on z in the following way $\mathbf{E} = E_0 z\hat{\mathbf{e}}_z$. A charge q is moved on a spiral-shaped trajectory $\mathbf{r}(t)$ with radius R,

$$\mathbf{r}(t) = \begin{pmatrix} R\cos t \\ R\sin t \\ \frac{h}{6\pi}t \end{pmatrix}$$

between $z = 0$ until $z = h$. Make a scheme of $\mathbf{r}(t)$. Calculate work made on the charge explicitly via a path integral $W = q\int \mathbf{E}\cdot d\mathbf{r}$. How can we calculate work more easily?

Solution: *Explicitly,*

$$W = q\int \mathbf{E}\cdot d\mathbf{r} = q\int_0^{6\pi} E_0\frac{h}{6\pi}t\hat{\mathbf{e}}_z \begin{pmatrix} 0 \\ 0 \\ h/6\pi \end{pmatrix} dt = \frac{1}{2}qE_0h_2 \ .$$

A integral sobre o potential $\phi = -\frac{E_0}{2}z_2$,

$$W = q(\phi(1) - \phi(2)) = q\left(+\frac{E_0}{2}h_2\right) \ .$$

12.2.7.3 Ex: Path integral and work

Calculate the path integral in the field $\Phi = x^2\hat{\mathbf{e}}_x + 2yz\hat{\mathbf{e}}_y + y^2\hat{\mathbf{e}}_z$ from the origin to the point $(1,1,1)$ on three different paths:
a. For the path $(0,0,0) \longrightarrow (1,0,0) \longrightarrow (1,1,0) \longrightarrow (1,1,1)$;
b. for the path $(0,0,0) \longrightarrow (0,0,1) \longrightarrow (0,1,1) \longrightarrow (1,1,1)$;
c. and on a straight line.

Solution:

12.2.7.4 Ex: Curve parametrization

The movement of a mass point is given in Cartesian coordinates by the vector $\mathbf{r}(t) = (\rho\cos\phi(t), \rho\sin\phi(t), z_0)$ with $\rho = vt$ and $\phi = \omega t + \phi_0$. What is the geometric figure dashed by the movement? Express the speed $\dot{\mathbf{r}}(t)$ and the acceleration $\ddot{\mathbf{r}}(t)$ in Cartesian coordinates. Calculate $|\mathbf{r}(t)|^2$, $|\dot{\mathbf{r}}(t)|^2$,$\mathbf{r}(t)\cdot\ddot{\mathbf{r}}(t)$ and $\mathbf{r}(t)\times\dot{\mathbf{r}}(t)$.

Solution: *We have,*

$$\mathbf{r}(t) = \begin{pmatrix} vt\cos(\omega t + \phi_0) \\ vt\sin(\omega t + \phi_0) \\ z_0 \end{pmatrix} \ ,$$

from which follows,

$$\dot{\mathbf{r}}(t) = v \begin{pmatrix} \cos(\omega t + \phi_0) - \omega t \sin(\omega t + \phi_0) \\ \sin(\omega t + \phi_0) + \omega t \cos(\omega t + \phi_0) \\ 0 \end{pmatrix} ,$$

and

$$\ddot{\mathbf{r}}(t) = v\omega \begin{pmatrix} -2\sin(\omega t + \phi_0) - \omega t \cos(\omega t + \phi_0) \\ 2\cos(\omega t + \phi_0) - \omega t \sin(\omega t + \phi_0) \\ 0 \end{pmatrix} .$$

We also calculate the scalar products,

$$|\mathbf{r}(t)|^2 = v^2 t^2 + z_0^2 \qquad \textit{and} \qquad |\dot{\mathbf{r}}(t)|^2 = v^2\omega^2 t^2 + v^2 ,$$

as well as,

$$\mathbf{r}(t) \cdot \ddot{\mathbf{r}}(t) = v^2 t \qquad \textit{and} \qquad \mathbf{r}(t) \times \dot{\mathbf{r}}(t) = v \begin{pmatrix} -z_0 \sin(\omega t + \phi_0) + z_0 \omega t \cos(\omega t + \phi_0) \\ z_0 \cos(\omega t + \phi_0) - z_0 \omega t \sin(\omega t + \phi_0) \\ v\omega t^2 \end{pmatrix} .$$

12.2.7.5 Ex: Surface integrals

Given be the vector field $\mathbf{A} = zy\hat{\mathbf{e}}_x + y^3 \sin^2 x \hat{\mathbf{e}}_y + xy^2 e^z \hat{\mathbf{e}}_z$. Calculate the integrals $\int \mathbf{A} \cdot d\mathbf{F}$ over the triangle $(0,0,0) \to (0,3,0) \to (0,0,3) \to (0,0,0)$, and over the rectangle $(2,2,0) \to (2,4,0) \to (4,4,0) \to (4,2,0) \to (2,2,0)$.

Solution: *The unit vector of the square points into $\hat{\mathbf{e}}_z$-direction, so with the help of MAPLE,*

$$\int \mathbf{A} \cdot d\mathbf{F} = \int_2^4 dx \int_2^4 dy \; xy^2 = 112 .$$

The unit vector of the triangle points into $\hat{\mathbf{e}}_x$-direction, hence,

$$\int \mathbf{A} \cdot d\mathbf{F} = \int_0^3 dz \int_0^{3-z} dy \; yz = \int_0^3 dz \; \frac{(3-z)^2 z}{2} = \frac{27}{8} .$$

12.2.7.6 Ex: Surface integrals

Calculate the integral over a closed surface
a. of the field $\mathbf{A} = \mathbf{r}$ over the cube $0 \le x \le 1$, $0 \le y \le 1$, $0 \le z \le 1$ e
b. of the field $\mathbf{A} = \rho \mathbf{E}_\rho$ over the radial surface of the cylinder $0 \le z \le 1$, $0 \le \rho \le 1$.

Solution: *a. Surface integral of the cube,*

$$\oint_{cube} \mathbf{r}\cdot d\mathbf{S} = \oint_{cube} \begin{pmatrix} x \\ y \\ z \end{pmatrix} \begin{pmatrix} dS_x \\ dS_y \\ dS_z \end{pmatrix} = \int_0^1 xdydz\Big|_{x=0}^{x=1} + \int_0^1 ydzdx\Big|_{x=0}^{x=1} + \int_0^1 zdxdy\Big|_{x=0}^{x=1}$$
$$= 3\int_0^1 1dy \int_0^1 1dz = 3 \ .$$

b. Parametrization of the cylinder with radius $\rho = R$

$$\mathbf{F} = \left\{ \mathbf{r} = \begin{pmatrix} R\cos\phi \\ R\sin\phi \\ z \end{pmatrix} \right\} \quad , \quad z = [0,1] \quad , \quad \phi = [0, 2\pi] \ .$$

Two linearly independent vectors in directions tangential to the surface are,

$$d\mathbf{F}_z = \frac{\partial \mathbf{r}}{\partial z} dz = \hat{\mathbf{e}}_z dz \qquad \textit{and} \qquad d\mathbf{F}_\phi = \frac{\partial \mathbf{r}}{\partial \phi} d\phi = R\hat{\mathbf{e}}_\phi d\phi \ .$$

With this the area element becomes,

$$d\mathbf{F} = d\mathbf{F}_\phi \times d\mathbf{S}_z = R\hat{\mathbf{e}}_\phi d\phi \times \hat{\mathbf{e}}_z dz = R\hat{\mathbf{e}}_\rho d\phi dz \ .$$

The surface integral of the cylinder is now,

$$\oint_{cylinder} \rho\hat{\mathbf{e}}_\rho d\mathbf{S} = \oint_{cylinder} \rho\hat{\mathbf{e}}_\rho R\hat{\mathbf{e}}_\rho d\phi dz = 2\pi R^2 = 2\pi \ .$$

Alternatively, we can express the divergence in cylindrical coordinates,

$$\nabla\mathbf{v} = \frac{1}{\rho}\frac{\partial}{\partial\rho}(\rho v_\rho) + \frac{1}{\rho}\frac{\partial}{\partial\phi} v_\phi + \frac{\partial}{\partial z} v_z$$

and use Gauß's theorem,

$$\oint_{cylinder} \rho\hat{\mathbf{e}}_\rho d\mathbf{F} = \int \nabla(\rho\hat{\mathbf{e}}_\rho) dV = \int \frac{1}{\rho}\frac{\partial}{\partial\rho}(\rho\rho) d\phi\rho d\rho dz = \int 2\rho d\phi d\rho dz = 2\pi \int 2\rho d\rho = 2\pi \ .$$

12.2.7.7 Ex: Surface integrals

Calculate for the vector field $\mathbf{A}(\mathbf{r}) = c\mathbf{r}$ with c =constant the surface integral

$$I = \int_F \mathbf{A}(\mathbf{r}) \times d\mathbf{S}$$

a. over the surface of a sphere (radius R, center in the origin of coordinates)
b. over the surface of a cylinder (radius R, length L).

Solution: *a. To the surface of the sphere holds* $d\mathbf{F} = R^2 \sin\theta d\theta d\phi \mathbf{E}_r$. *Also, holds* $\mathbf{A} = c\mathbf{r}$ *and hence* $\mathbf{A} \times d\mathbf{F} \sim \mathbf{E}_r \times \mathbf{E}_r = 0$. *Thus,* $I = 0$.
b. For the radial surface of the cylinder $d\mathbf{F} = Rd\varphi dz\mathbf{E}_\rho$. *For the axial surfaces,*

$$F_\pm = \{\mathbf{r} = (\rho\cos\varphi, \rho\sin\varphi, \pm L/2), \text{ where } 0 \le \rho \le R, \text{ and } 0 \le \varphi \le 2\pi\} \ .$$

So here we have,

$$\begin{aligned} d\mathbf{F} &= \left(\frac{\partial \mathbf{r}}{\partial \rho} \times \frac{\partial \mathbf{r}}{\partial \varphi}\right) d\rho d\varphi \\ &= (\cos\varphi, \sin\varphi, 0) \times (-\rho\sin\varphi, \rho\cos\varphi, 0) d\rho d\varphi \\ &= \rho d\rho d\phi \mathbf{E}_z \end{aligned}$$

Following a general convention the normal vector of closed surfaces $d\mathbf{F}$ *points outside. We get,*

$$\begin{aligned} I &= \int_F \mathbf{A} \times d\mathbf{F} = c \int_F (\rho\mathbf{E}_\rho + z\mathbf{E}_z) \times d\mathbf{F} \\ &= c \int_{S_{rad}} Rd\varphi dz(\rho\mathbf{E}_\rho + z\mathbf{E}_z) \times \mathbf{E}_\rho + c \int_{S_{ax}+L/2} d\rho d\varphi\rho(\rho\mathbf{E}_\rho + z\mathbf{E}_z) \times \mathbf{E}_z \\ &\quad - c \int_{S_{ax}-L/2} d\rho d\varphi\rho(\rho\mathbf{E}_\rho + z\mathbf{E}_z) \times \mathbf{E}_z \\ &= cR \int_0^{2\pi} d\varphi \int_{-L/2}^{L/2} dz z\mathbf{E}_\varphi + c \int_0^R d\rho \int_0^{2\pi} d\varphi\rho^2(-\mathbf{E}_\varphi) - c \int_0^R d\rho \int_0^{2\pi} d\varphi\rho^2(-\mathbf{E}_\varphi) \ . \end{aligned}$$

Only that now,

$$\int_0^{2\pi} d\varphi \mathbf{E}_\varphi = \int_0^{2\pi} d\varphi(-\sin\varphi, \cos\varphi, 0) = 0 \ .$$

So here we also get, $I = 0$.

12.2.7.8 Ex: Surface integrals

Prove the relationship:

$$t_{ij} \equiv \int_{O(a)} d\mathbf{f} x_i x_j = \frac{4\pi}{3} a^4 \delta_{ij} \ ,$$

where $i, j = 1, 2, 3$, $x_1 = x$, $x_2 = y$, $x_3 = z$, and the integral has to be calculated on the surface of a sphere with radius a.

Solution: *The area element on the sphere's surface is* $d\mathbf{f} = a^2 d\phi d\theta \sin\theta$. *Also, on the surface of the sphere we have* $x = a\sin\theta\cos\phi$, $y = a\sin\theta\sin\phi$ *and* $z = a\cos\theta$. *With*

$$\int_0^{2\pi} d\phi \sin\phi = \int_0^{2\pi} d\phi \cos\phi = \int_0^{2\pi} d\phi \sin\phi\cos\phi = 0 \ ,$$

we get immediately that the integral zeroes for $i \neq j$. *For* $i = j = 1$ *we obtain,*

$$\begin{aligned} t_{11} &= a^4 \int_0^{2\pi} d\phi \cos^2\phi \int_0^{\pi} d\theta \sin^3\theta \\ &= \pi a^4 \int_{-1}^{+1} dx(1-x^2) = \frac{4\pi}{3}a^4 \ . \end{aligned}$$

In the same way for $i = j = 2$,

$$t_{22} = a^4 \int_0^{2\pi} d\phi \sin^2\phi \int_0^{\pi} d\theta \sin^3\theta = \frac{4\pi}{3}a^4 \ .$$

Finally, for $i = j = 3$

$$t_{33} = 2\pi a^4 \int_{-1}^{+1} dx x^2 = \frac{4\pi}{3}a^4 \ .$$

This was the statement.

12.2.7.9 Ex: Volume integrals

Calculate the volume integral of the function $\Phi = z^2$ over the tetrahedron with the corners in $(0,0,0)$, $(1,0,0)$, $(0,1,0)$, and $(0,0,1)$.

Solution:

12.2.7.10 Ex: Fundamental theorem for gradients

What is the energy gain within the potential $\Phi(\mathbf{r}) = \Phi_0 \frac{\sin kr}{kr}$ along a path keeping a constant distance from the origin.

Solution: *Obviously it's 0.*

12.2.7.11 Ex: Stokes integral theorem

Calculate for following field,

$$\mathbf{A}(\mathbf{r}) = \begin{pmatrix} yz \\ azx \\ xy \end{pmatrix}$$

using Stokes' law the path integral $\oint \mathbf{A} \cdot \mathbf{r}$ for an integration along a circle with radius R around the z-axis at the position $z = h$.

Solution: *The path integral is,*

$$\int_{\partial S} \mathbf{A} \cdot \mathbf{r} = \int_S (\nabla \times \mathbf{A}) \cdot d\mathbf{F} = \int_0^{2\pi} \int_0^R \rho \begin{pmatrix} \partial_y xy - \partial_z axz \\ \partial_z yz - \partial_x xy \\ \partial_x axz - \partial_y yz \end{pmatrix} \hat{\mathbf{e}}_z d\rho d\varphi$$

$$= \int_0^{2\pi} \int_0^R \rho(az - z) d\rho d\varphi = \int_0^{2\pi} (a-1)(\tfrac{1}{2} z R^2) d\varphi = 2\pi(a-1)\tfrac{1}{2} z R^2 \underbrace{=}_{h=z} \tfrac{a-1}{\pi} h R^2 \ .$$

12.2.7.12 Ex: Stokes integral theorem

Calculate the integral $\oint_{\mathcal{C}} x(\hat{\mathbf{e}}_x + \hat{\mathbf{e}}_y)\ d\mathbf{r}$, where $\mathcal{C}$ be the unit circle in the x-y-plane.

Solution: *We have,*

$$\oint_{circumference} x(\hat{\mathbf{e}}_x + \hat{\mathbf{e}}_y)\ d\mathbf{r} = \int_{\mathcal{S}} rot\ x(\hat{\mathbf{e}}_x + \hat{\mathbf{e}}_y)\ d\mathbf{S} = \int_{\mathcal{C}} \hat{\mathbf{e}}_z d\mathbf{S} = \pi \ .$$

12.2.7.13 Ex: Gauß integral theorem

Calculate the flux of the vector field $\mathbf{A}(\mathbf{r}) = \mathbf{r}$ through a sphere with radius R
a. by the surface integral and
b. with the help of Gauß's theorem for the volume integral over the divergence.

Solution: *The surface integral is,*

$$\oint_{\partial V} \mathbf{A} \cdot d\mathbf{F} = \oint_{\partial V} \mathbf{r} \left(\hat{\mathbf{e}}_r - \frac{1}{r} \frac{\partial r}{\partial \theta} \hat{\mathbf{e}}_\theta - \frac{1}{r} \frac{1}{\sin\theta} \frac{\partial r}{\partial \phi} \hat{\mathbf{e}}_\phi \right) r^2 \sin\theta d\theta d\phi = \oint r^3 \sin\theta d\theta d\phi = 4\pi R^3 \ .$$

The volume integral is,

$$\int_V \nabla \cdot \mathbf{A} dV = \int_V 3 dV = 4\pi R^3 \ .$$

12.2.7.14 Ex: Gauß integral theorem

Let F be the surface of an arbitrary volume V. Determine for $\mathbf{A}(x_1, x_2, x_3) = (ax_1, bx_2, cx_3)$ the validity of the relationship,

$$\oint_F d\mathbf{F} \cdot \mathbf{A} = (a+b+c)V \ .$$

Solution: *Vale, pois de* $\nabla \cdot \mathbf{A} = a+b+c$ *segue* $\oint_F d\mathbf{F} \cdot \mathbf{A} = \int_V \nabla \cdot \mathbf{A} = (a+b+c)V$.

12.2.7.15 Ex: Gauß integral theorem

Be a a scalar field and $\mathbf{B}$ a vector field. Show,

$$\int_V d^3\mathbf{r}\ \mathbf{B} \cdot \nabla a = \int_{O(V)} a\mathbf{B}\ \cdot\ d\mathbf{F} - \int_V d^3\mathbf{r}\ a\nabla \cdot \mathbf{B} \ .$$

Solution: *Using the Gauß theorem and the chain rule we obtain for an arbitrary volume* V *and its surface* $O(V)$*:*

$$\int_{O(V)} a\mathbf{B}\ \cdot d\mathbf{F} = \int_V d^3\mathbf{r}\ \nabla \cdot\ (a\mathbf{B}) = \int_V (\mathbf{B} \cdot \nabla a + a\nabla \cdot \mathbf{B})\, d^3\mathbf{r}$$

From this follows immediately,

$$\int_V d^3\mathbf{r}\ \mathbf{B} \cdot \nabla a = \int_{O(V)} a\mathbf{B} \cdot d\mathbf{F} - \int_V d^3\mathbf{r}\ a\nabla \cdot \mathbf{B} \ .$$

12.2.7.16 Ex: Gauß integral theorem

Calculate the integral $\oint_{\mathcal{C}} x(\hat{\mathbf{e}}_x + \hat{\mathbf{e}}_y) \cdot d\mathbf{r}$ about a unitary circular path $\mathcal{C}$ along the equator and the integral $\oint_{\mathcal{F}} x(\hat{\mathbf{e}}_x + \hat{\mathbf{e}}_y) \cdot d\mathbf{F}$, where $\mathcal{F}$ be the surface of a unit sphere.

Solution: *Using Gauß law,*

$$\oint_{surface} x(\hat{\mathbf{e}}_x + \hat{\mathbf{e}}_y)\ d\mathbf{F} = \int_{volume} div\ x(\hat{\mathbf{e}}_x + \hat{\mathbf{e}}_y)\ dV = \int_{surface} dV = \frac{4\pi}{3} \ .$$

Using Stokes Law,

$$\oint_{circumference} x(\hat{\mathbf{e}}_x + \hat{\mathbf{e}}_y)\ d\mathbf{r} = \int_{area} rot\ x(\hat{\mathbf{e}}_x + \hat{\mathbf{e}}_y)\ d\mathbf{F} = \int_F \hat{\mathbf{e}}_z d\mathbf{F} = \pi \ .$$

12.3 Curvilinear coordinates

The most commonly used coordinate systems are Cartesian, cylindrical and spherical. Cylindrical coordinates are expressed in terms of Cartesian coordinates by,

$$\begin{pmatrix} x \\ y \\ z \end{pmatrix} = \begin{pmatrix} \rho\cos\phi \\ \rho\sin\phi \\ z \end{pmatrix} \quad . \tag{12.43}$$

And spherical coordinates are expressed in terms of Cartesian coordinates by,

$$\begin{pmatrix} x \\ y \\ z \end{pmatrix} = \begin{pmatrix} r\sin\theta\cos\phi \\ r\sin\theta\sin\phi \\ r\cos\theta \end{pmatrix} \quad . \tag{12.44}$$

The task now is to express the differential elements (that is, line, surface and volume elements), as well as differential operators (that is, the gradient, divergent and rotation) and the Laplacian in term of curvilinear coordinates.

Let us first consider the general case. The transformation from a Cartesian coordinate system (x, y, z) into a general, curvilinear system (u, v, w) is given by,

$$\mathbf{r} \equiv \begin{pmatrix} x(u,v,w) \\ y(u,v,w) \\ z(u,v,w) \end{pmatrix} \quad . \tag{12.45}$$

The change $d_u\mathbf{r}$ resulting from a small variation du is then $d_u\mathbf{r} = \frac{\partial \mathbf{r}}{\partial u}du$ and occurs in the direction of the new unit vector $\hat{\mathbf{e}}_u$. The unit vectors of the new system, therefore, can be written as,

$$\hat{\mathbf{e}}_u = U(u,v,w)\frac{\partial \mathbf{r}}{\partial u} \quad , \quad \hat{\mathbf{e}}_v = V(u,v,w)\frac{\partial \mathbf{r}}{\partial v} \quad , \quad \hat{\mathbf{e}}_w = W(u,v,w)\frac{\partial \mathbf{r}}{\partial w} \ , \tag{12.46}$$

where

$$U = \left|\frac{\partial \mathbf{r}}{\partial u}\right|^{-1} \quad , \quad V = \left|\frac{\partial \mathbf{r}}{\partial v}\right|^{-1} \quad , \quad W = \left|\frac{\partial \mathbf{r}}{\partial w}\right|^{-1} \quad . \tag{12.47}$$

In the Excs. 12.3.8.1 we study transformations into cylindrical and spherical coordinates.

12.3.1 Differential elements in curvilinear coordinates

In the following we restrict ourselves to orthogonal coordinates, where the unit vectors are perpendicular. In this case, the total differential $d\mathbf{r}$ has the form,

$$d\mathbf{r} = \frac{\partial \mathbf{r}}{\partial u}du + \frac{\partial \mathbf{r}}{\partial v}dv + \frac{\partial \mathbf{r}}{\partial w}dw = \hat{\mathbf{e}}_u\frac{du}{U} + \hat{\mathbf{e}}_v\frac{dv}{V} + \hat{\mathbf{e}}_w\frac{dw}{W} \ , \tag{12.48}$$

and has the length,

$$|d\mathbf{r}|^2 = \left(\frac{du}{U}\right)^2 + \left(\frac{dv}{V}\right)^2 + \left(\frac{dw}{W}\right)^2 \ . \tag{12.49}$$

The volume element is,

$$d\tau = ds_u ds_v ds_w \ . \tag{12.50}$$

12.3.2 Gradient in curvilinear coordinates

We can now express the gradient of a scalar field Φ in orthogonal curvilinear coordinates,

$$\text{grad } \Phi = \nabla\Phi = f_u \hat{\mathbf{e}}_u + f_v \hat{\mathbf{e}}_v + f_w \hat{\mathbf{e}}_w \ , \tag{12.51}$$

where the f_i are functions which have yet to be determined. To this end we compare the coefficients of the expressions,

$$d\Phi = \frac{\partial\Phi}{\partial u}du + \frac{\partial\Phi}{\partial v}dv + \frac{\partial\Phi}{\partial w}dw \ , \tag{12.52}$$

and, inserting (12.48) and (12.51),

$$d\Phi = d\mathbf{r}\cdot\nabla\Phi = \frac{f_u}{U}du + \frac{f_v}{V}dv + \frac{f_w}{W}dw \ . \tag{12.53}$$

We obtain,

$$\nabla\Phi = \left(U\frac{\partial\Phi}{\partial u}\right)\hat{\mathbf{e}}_u + \left(V\frac{\partial\Phi}{\partial v}\right)\hat{\mathbf{e}}_v + \left(W\frac{\partial\Phi}{\partial w}\right)\hat{\mathbf{e}}_w \ . \tag{12.54}$$

12.3.3 Divergence in curvilinear coordinates

Now we will show how to express the divergence of a vector field $\mathbf{A}$ in orthogonal curvilinear coordinates,

$$\text{div } \mathbf{A} = \nabla\cdot\mathbf{A} \ . \tag{12.55}$$

The derivation is a bit complicated. We begin by expressing the unit vectors $\hat{\mathbf{e}}_u$, $\hat{\mathbf{e}}_v$, and $\hat{\mathbf{e}}_w$ by the gradients ∇u, ∇v, and ∇w, using the expression for the gradient (12.54),

$$\nabla u = U\hat{\mathbf{e}}_u \quad , \quad \nabla v = V\hat{\mathbf{e}}_v \quad , \quad \nabla w = W\hat{\mathbf{e}}_w \ . \tag{12.56}$$

We now express each unit vector as the vector product of two of these gradients,

$$\begin{aligned} \nabla u\times\nabla v &= UV\ \hat{\mathbf{e}}_u\times\hat{\mathbf{e}}_v = UV\hat{\mathbf{e}}_w \\ \nabla v\times\nabla w &= VW\ \hat{\mathbf{e}}_v\times\hat{\mathbf{e}}_w = VW\hat{\mathbf{e}}_u \\ \nabla w\times\nabla u &= WU\ \hat{\mathbf{e}}_w\times\hat{\mathbf{e}}_u = WU\hat{\mathbf{e}}_v \ . \end{aligned} \tag{12.57}$$

After that we write $\mathbf{A} = a_u\hat{\mathbf{e}}_u + a_v\hat{\mathbf{e}}_v + a_w\hat{\mathbf{e}}_w$ and start considering the first term of the divergence:

$$\begin{aligned}
&\nabla\cdot(a_u\hat{\mathbf{e}}_u) = \nabla\cdot\left(\frac{a_u}{VW}\nabla v\times\nabla w\right) \qquad (12.58)\\
&= (\nabla v\times\nabla w)\cdot\nabla\left(\frac{a_u}{VW}\right) + \frac{a_u}{VW}\nabla\cdot(\nabla v\times\nabla w) \quad \text{using} \quad \nabla\cdot(\alpha\mathbf{A}) = \mathbf{A}\cdot(\nabla\alpha) + \alpha(\nabla\cdot\mathbf{A})\\
&= VW\hat{\mathbf{e}}_u\cdot\left[\hat{\mathbf{e}}_u U\frac{\partial}{\partial u}\left(\frac{a_u}{VW}\right) + \hat{\mathbf{e}}_v V\frac{\partial}{\partial v}\left(\frac{a_v}{VW}\right) + \hat{\mathbf{e}}_w W\frac{\partial}{\partial w}\left(\frac{a_w}{VW}\right)\right]\\
&\quad + \frac{a_u}{VW}\left[\nabla w\cdot(\nabla\times\nabla v) - \nabla v\cdot(\nabla\times\nabla w)\right] \quad \text{using} \quad \nabla\cdot(\mathbf{A}\times\mathbf{B}) = \mathbf{B}\cdot(\nabla\times\mathbf{A}) - \mathbf{A}\cdot(\nabla\times\mathbf{B})\\
&= UVW\frac{\partial}{\partial u}\left(\frac{a_u}{VW}\right) \quad \text{using} \quad \nabla\times(\nabla\alpha) = 0\ .
\end{aligned}$$

Similarly we can show,

$$\nabla\cdot(a_v\hat{\mathbf{e}}_v) = UVW\frac{\partial}{\partial v}\left(\frac{a_v}{UW}\right) \qquad \text{and} \qquad \nabla\cdot(a_w\hat{\mathbf{e}}_w) = UVW\frac{\partial}{\partial w}\left(\frac{a_w}{UV}\right)\ . \qquad (12.59)$$

With this we finally get,

$$\nabla\cdot\mathbf{A} = UVW\left[\frac{\partial}{\partial u}\left(\frac{a_u}{VW}\right) + \frac{\partial}{\partial v}\left(\frac{a_v}{UW}\right) + \frac{\partial}{\partial w}\left(\frac{a_w}{UV}\right)\right]\ . \qquad (12.60)$$

12.3.4 Rotation in curvilinear coordinates

Now we will show how to express the rotation of a vector field $\mathbf{A}$ in orthogonal curvilinear coordinates,

$$\text{rot}\ \mathbf{A} = \nabla\times\mathbf{A}\ . \qquad (12.61)$$

We write again, $\mathbf{A} = a_u\hat{\mathbf{e}}_u + a_v\hat{\mathbf{e}}_v + a_w\hat{\mathbf{e}}_w$ and start considering the first term of the rotation:

$$\begin{aligned}
&\nabla\times(a_u\hat{\mathbf{e}}_u) = \nabla\times\left(\frac{a_u}{U}\nabla u\right) \quad \text{using} \quad (12.56) \qquad (12.62)\\
&= \left(\nabla\frac{a_u}{U}\right)\times\nabla u + \frac{a_u}{U}(\nabla\times\nabla u) \quad \text{using} \quad \nabla\times(\alpha\mathbf{A}) = (\nabla\alpha)\times\mathbf{A} + \alpha(\nabla\times\mathbf{A})\\
&= U\left(\nabla\frac{a_u}{U}\right)\times\hat{\mathbf{e}}_u \quad \text{and} \quad \nabla\times(\nabla\alpha) = 0 \quad \text{using} \quad (12.56)\\
&= U\left[\hat{\mathbf{e}}_u U\frac{\partial}{\partial u}\left(\frac{a_u}{U}\right) + \hat{\mathbf{e}}_v V\frac{\partial}{\partial v}\left(\frac{a_u}{U}\right) + \hat{\mathbf{e}}_w W\frac{\partial}{\partial w}\left(\frac{a_u}{U}\right)\right]\times\hat{\mathbf{e}}_u\\
&= U\left[\hat{\mathbf{e}}_v W\frac{\partial}{\partial w}\left(\frac{a_u}{U}\right) - \hat{\mathbf{e}}_w V\frac{\partial}{\partial v}\left(\frac{a_u}{U}\right)\right]\\
&= UVW\left[\hat{\mathbf{e}}_v\frac{1}{V}\frac{\partial}{\partial w}\left(\frac{a_u}{U}\right) - \hat{\mathbf{e}}_w\frac{1}{W}\frac{\partial}{\partial v}\left(\frac{a_u}{U}\right)\right]\ .
\end{aligned}$$

Similarly we can show,

$$\begin{aligned}
\nabla\times(a_v\hat{\mathbf{e}}_v) &= UVW\left[\hat{\mathbf{e}}_w\frac{1}{W}\frac{\partial}{\partial u}\left(\frac{a_v}{V}\right) - \hat{\mathbf{e}}_u\frac{1}{U}\frac{\partial}{\partial w}\left(\frac{a_v}{V}\right)\right] \qquad (12.63)\\
\nabla\times(a_w\hat{\mathbf{e}}_w) &= UVW\left[\hat{\mathbf{e}}_u\frac{1}{U}\frac{\partial}{\partial v}\left(\frac{a_w}{W}\right) - \hat{\mathbf{e}}_v\frac{1}{V}\frac{\partial}{\partial u}\left(\frac{a_w}{W}\right)\right]\ .
\end{aligned}$$

With this we finally obtain,

$$\nabla \times \mathbf{A} = \hat{\mathbf{e}}_u VW \left[\frac{\partial}{\partial v} \left(\frac{a_w}{W} \right) - \frac{\partial}{\partial w} \left(\frac{a_v}{V} \right) \right] + \hat{\mathbf{e}}_v UW \left[\frac{\partial}{\partial w} \left(\frac{a_u}{U} \right) - \frac{\partial}{\partial u} \left(\frac{a_w}{w} \right) \right] + \hat{\mathbf{e}}_w UV \left[\frac{\partial}{\partial u} \left(\frac{a_v}{V} \right) - \frac{\partial}{\partial v} \left(\frac{a_u}{U} \right) \right] , \tag{12.64}$$

or, written as a determinant,

$$\nabla \times \mathbf{A} = UVW \det \begin{pmatrix} \frac{\hat{\mathbf{e}}_u}{U} & \frac{\hat{\mathbf{e}}_v}{V} & \frac{\hat{\mathbf{e}}_w}{W} \\ \frac{\partial}{\partial u} & \frac{\partial}{\partial v} & \frac{\partial}{\partial w} \\ \frac{a_u}{U} & \frac{a_v}{V} & \frac{a_w}{W} \end{pmatrix} . \tag{12.65}$$

12.3.5 Cylindrical coordinates

Let us now identify the general coordinates u, v, and w with the cylindrical coordinates ρ, θ, and ϕ defined in Eq. (12.43). In Exc. 12.3.8.2 we calculate for the line element,

$$d\mathbf{r} = d\rho \hat{\mathbf{e}}_\rho + \rho d\phi e_\phi + dz \hat{\mathbf{e}}_z , \tag{12.66}$$

the distance element,

$$|d\mathbf{r}|^2 = (d\rho)^2 + (\rho d\phi)^2 + (dz)^2 , \tag{12.67}$$

the surface element given by $z = z(\rho, \phi)$,

$$d\mathbf{s} = \left(-\frac{\partial z}{\partial \rho} \hat{\mathbf{e}}_\rho - \frac{1}{\rho} \frac{\partial z}{\partial \phi} \hat{\mathbf{e}}_\phi + \hat{\mathbf{e}}_z \right) \rho d\rho d\phi , \tag{12.68}$$

and the volume element,

$$d\tau = r dz \phi dr . \tag{12.69}$$

In the Excs. 12.3.8.3 to 12.3.8.5 we calculate, respectively, the gradient,

$$\nabla \Phi = \hat{\mathbf{e}}_\rho \frac{\partial \Phi}{\partial \rho} + \hat{\mathbf{e}}_\phi \frac{1}{\rho} \frac{\partial \Phi}{\partial \phi} + \hat{\mathbf{e}}_z \frac{\partial \Phi}{\partial z} , \tag{12.70}$$

the divergence,

$$\nabla \cdot \mathbf{A} = \frac{1}{\rho} \frac{\partial}{\partial \rho} [\rho \, a_\rho] + \frac{1}{\rho} \frac{\partial}{\partial \phi} [a_\phi] + \frac{\partial}{\partial z} [a_z] , \tag{12.71}$$

the rotation,

$$\nabla \times \mathbf{A} = \hat{\mathbf{e}}_\rho \frac{1}{\rho} \left[\frac{\partial a_z}{\partial \phi} - \rho \frac{\partial a_\phi}{\partial z} \right] + \hat{\mathbf{e}}_\phi \left[\frac{\partial a_\rho}{\partial z} - \frac{\partial a_z}{\partial \rho} \right] + \hat{\mathbf{e}}_z \frac{1}{\rho} \left[\frac{\partial}{\partial \rho} (\rho a_\phi) - \frac{\partial a_\rho}{\partial \phi} \right] \tag{12.72}$$

and the Laplace operator,

$$\Delta \Phi \equiv \nabla \cdot (\nabla \Phi) = \frac{1}{\rho} \frac{\partial}{\partial \rho} \left(\rho \frac{\partial \Phi}{\partial \rho} \right) + \frac{1}{\rho^2} \frac{\partial^2 \Phi}{\partial \phi^2} + \frac{\partial^2 \Phi}{\partial z^2} . \tag{12.73}$$

in cylindrical coordinates.

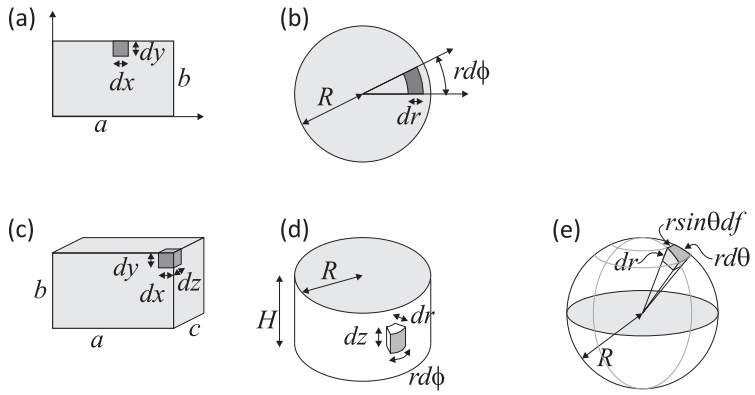

Figure 12.7: Illustration of Cartesian, polar, cylindrical and spherical coordinates.

12.3.6 Spherical coordinates

Let us now identify the general coordinates u, v, and w with the spherical coordinates r, θ, and ϕ defined in Eq. (12.44). In Exc. 12.3.8.2 we calculate for the line element,

$$d\mathbf{r} = dr\hat{\mathbf{e}}_r + rd\theta e_\theta + r\sin\theta d\phi\hat{\mathbf{e}}_\phi \ , \tag{12.74}$$

the distance element,

$$|d\mathbf{r}|^2 = (dr)^2 + (rd\theta)^2 + (r\sin\theta d\phi)^2 \ , \tag{12.75}$$

the surface element given by $r = r(\theta, \phi)$,

$$d\mathbf{s} = \left(\hat{\mathbf{e}}_r - \frac{1}{r}\frac{\partial r}{\partial\theta}\hat{\mathbf{e}}_\theta - \frac{1}{r}\frac{1}{\sin\theta}\frac{\partial r}{\partial\phi}\hat{\mathbf{e}}_\phi\right) r^2\sin\theta d\theta d\phi \ , \tag{12.76}$$

and the volume element,

$$d\tau = ds_u ds_v ds_w = r^2\sin\theta d\theta d\phi dr \ . \tag{12.77}$$

In the Excs. 12.3.8.3 to 12.3.8.5 we calculate, respectively, the gradient,

$$\nabla\Phi = \hat{\mathbf{e}}_r\ \frac{\partial\Phi}{\partial r} + \hat{\mathbf{e}}_\theta\ \frac{1}{r}\ \frac{\partial\Phi}{\partial\theta} + \hat{\mathbf{e}}_\phi\ \frac{1}{r\sin\phi}\ \frac{\partial\Phi}{\partial\phi} \ , \tag{12.78}$$

the divergence,

$$\nabla\cdot\mathbf{A} = \frac{1}{r^2}\frac{\partial}{\partial r}[r^2 a_r] + \frac{1}{r\sin\theta}\frac{\partial}{\partial\theta}[\sin\theta\ a_\theta] + \frac{1}{r\sin\theta}\frac{\partial}{\partial\phi}[a_\phi] \ , \tag{12.79}$$

the rotation,

$$\nabla\times\mathbf{A} = \hat{\mathbf{e}}_r\ \frac{1}{r\sin\theta}\left[\frac{\partial}{\partial\theta}(\sin\theta a_\phi) - \frac{\partial}{\partial\phi}(a_\theta)\right] + \hat{\mathbf{e}}_\theta\ \frac{1}{r\sin\theta}\left[\frac{\partial}{\partial\phi}(a_r) - \sin\theta\frac{\partial}{\partial r}(ra_\phi)\right] + \hat{\mathbf{e}}_\phi\ \frac{1}{r}\left[\frac{\partial}{\partial r}(ra_\theta) - \frac{\partial}{\partial\theta}(a_r)\right] \tag{12.80}$$

and the Laplace operator,

$$\Delta\Phi \equiv \nabla\cdot(\nabla\Phi) = \frac{1}{r^2}\frac{\partial}{\partial r}\left(r^2\frac{\partial\Phi}{\partial r}\right) + \frac{1}{r^2\sin\theta}\frac{\partial}{\partial\theta}\left(\sin\theta\frac{\partial\Phi}{\partial\theta}\right) + \frac{1}{r^2\sin^2\theta}\frac{\partial^2\Phi}{\partial\phi^2}\ , \quad (12.81)$$

in spherical coordinates. We note that the radial part of the Laplace operator can also be written,

$$\frac{1}{r}\frac{\partial^2}{\partial r^2}(r\Phi)\ . \quad (12.82)$$

12.3.7 Differential operators for tensor fields

Until now, we restricted to scalar and vector fields, that is spatially dependent physical quantities such as the temperature or the magnetic field distribution in a room. Some quantities, however, need to be given as matrices or even higher-dimensional objects, for example, gravity gradients or the susceptibility of a crystal. These objects are called tensors. With the definition,

$$\hat{\mathbf{e}}_k \otimes \hat{\mathbf{e}}_l = \hat{\mathbf{e}}_k\hat{\mathbf{e}}_l^\intercal \quad (12.83)$$

we can express a scalar, vector, and second-order tensor as,

$$\Phi \quad , \quad \mathbf{A} = A_k\hat{\mathbf{e}}_k \quad , \quad \mathcal{G} = G_{kl}\hat{\mathbf{e}}_k\otimes\hat{\mathbf{e}}_l\ . \quad (12.84)$$

For instance, in Cartesian coordinates a second-order tensor reads,

$$\mathcal{G} = G_{xx}\hat{\mathbf{e}}_x\hat{\mathbf{e}}_x^\intercal + G_{xy}\hat{\mathbf{e}}_x\hat{\mathbf{e}}_y^\intercal + G_{yx}\hat{\mathbf{e}}_y\hat{\mathbf{e}}_x^\intercal + G_{yy}\hat{\mathbf{e}}_y\hat{\mathbf{e}}_y^\intercal = \begin{pmatrix} G_{xx} & G_{xy}\\ G_{xy} & G_{yy}\end{pmatrix}\ . \quad (12.85)$$

If a tensor $\mathcal{T} = \Phi(\mathbf{r}), \mathbf{A}(\mathbf{r}), \mathcal{G}(\mathbf{r})$ varies in space, we can apply differential operators to it. The gradient $\nabla\mathcal{T}(\mathbf{r})$ of a tensor field in the direction of an arbitrary constant vector $\mathbf{x}$ is defined as,

$$\boxed{\mathbf{x}\cdot\nabla\mathcal{T} = \lim_{\alpha\to 0}\frac{d}{d\alpha}\mathcal{T}(\mathbf{r}+\alpha\mathbf{x})}\ . \quad (12.86)$$

The gradient of a tensor field of order n is a tensor field of order $n+1$. In Cartesian coordinates, $\mathbf{x} = x\hat{\mathbf{e}}_x + y\hat{\mathbf{e}}_y + z\hat{\mathbf{e}}_z$,

$$\nabla\Phi = \hat{\mathbf{e}}_k\frac{\partial}{\partial x_k}\Phi \equiv \Phi_{,k}\hat{\mathbf{e}}_k = \begin{pmatrix}\partial_x\Phi\\ \partial_y\Phi\end{pmatrix} \quad (12.87)$$

$$\nabla\mathbf{A} = \hat{\mathbf{e}}_k\frac{\partial}{\partial x_k}\otimes A_l\hat{\mathbf{e}}_l \equiv A_{,kl}\hat{\mathbf{e}}_k\otimes\hat{\mathbf{e}}_l = \begin{pmatrix}\partial_x A_x & \partial_y A_x\\ \partial_x A_y & \partial_y A_y\end{pmatrix}$$

$$\nabla\mathcal{G} = \hat{\mathbf{e}}_k\frac{\partial}{\partial x_k}\otimes G_{lm}\hat{\mathbf{e}}_l\otimes\hat{\mathbf{e}}_m \equiv G_{,klm}\hat{\mathbf{e}}_k\otimes\hat{\mathbf{e}}_l\otimes\hat{\mathbf{e}}_m = \begin{pmatrix}\partial_x\\ \partial_y\end{pmatrix}\begin{pmatrix}G_{xx} & G_{xy}\\ G_{xy} & G_{yy}\end{pmatrix}\ .$$

The divergence of a tensor field $\mathcal{T}(\mathbf{r})$ is defined using the recursive relation,

$$\begin{aligned}(\nabla\cdot\mathbf{A})\cdot\mathbf{x} &= \text{Tr}\,(\nabla\mathbf{A}) \\ (\nabla\cdot\mathcal{G})\cdot\mathbf{x} &= \nabla\cdot(\mathbf{x}\cdot\mathcal{G}^{\intercal})\ .\end{aligned} \tag{12.88}$$

In Cartesian coordinates the divergence is,

$$\begin{aligned}\nabla\cdot\mathbf{A} &= \hat{\mathbf{e}}_k\frac{\partial}{\partial x_k}\cdot A_l\hat{\mathbf{e}}_l = \frac{\partial A_k}{\partial x_k}\equiv A_{k,k} \\ \nabla\cdot\mathcal{G} &= \hat{\mathbf{e}}_k\frac{\partial}{\partial x_k}\cdot G_{lm}\hat{\mathbf{e}}_l\otimes\hat{\mathbf{e}}_m = \frac{\partial G_{lk}}{\partial x_k}\otimes\hat{\mathbf{e}}_l\equiv G_{lk,k}\hat{\mathbf{e}}_l\ .\end{aligned} \tag{12.89}$$

The curl of an order $n>1$ tensor field $\mathcal{T}(\mathbf{r})$ is also defined using the recursive relation,

$$\begin{aligned}(\nabla\times\mathbf{A})\cdot\mathbf{x} &= \nabla\cdot(\mathbf{A}\times\mathbf{c}) \\ (\nabla\times\mathcal{G})\cdot\mathbf{x} &= \nabla\times(\mathbf{x}\cdot\mathcal{G}^{\intercal})\ ,\end{aligned} \tag{12.90}$$

where c is an arbitrary constant vector. In Cartesian coordinates the divergence the rotation is,

$$\begin{aligned}\nabla\times\mathbf{A} &= \epsilon_{klm}\hat{\mathbf{e}}_k\partial_l A_m \\ \nabla\times\mathcal{G} &= \epsilon_{klm}\hat{\mathbf{e}}_m\otimes\hat{\mathbf{e}}_n\partial_k G_{nl}\ .\end{aligned} \tag{12.91}$$

12.3.8 Exercises

12.3.8.1 Ex: Spherical and cylindrical coordinates

a. Express the cylindrical coordinates ρ, φ, z in terms of the Cartesian ones x, y, z.
b. Express the spherical coordinates r, θ, φ in terms of the Cartesian ones x, y, z.

Solution: *a. We have,*

$$\begin{aligned}r &= \sqrt{x^2+y^2+z^2} \\ \varphi &= \arccos\frac{z}{r} \\ z &= z\ .\end{aligned}$$

b. We have,

$$\begin{aligned}r &= \sqrt{x^2+y^2+z^2} \\ \theta &= \arccos\frac{z}{r} = \arcsin\frac{\sqrt{x^2+y^2}}{r} \\ \varphi &= \arccos\frac{x}{r\sin\theta} = \arccos\frac{x}{\sqrt{x^2+y^2}}\ .\end{aligned}$$

12.3.8.2 Ex: Differential elements in curvilinear coordinates

We have seen in class that the transformation from a Cartesian coordinate system (x, y, z) to another curvilinear and orthogonal system (u, v, w) is given by $\mathbf{r} \equiv (x(u, v, w), y(u, v, w), z(u, v, w))$. Now consider the spherical polar coordinates $\mathbf{r} \equiv (x(r, \theta, \phi), y(r, \theta, \phi), z(r, \theta, \phi)$ defined in class.
a. Calculate the functions U_r, V_θ, W_ϕ defined by,

$$U_r = \left|\frac{\partial \mathbf{r}}{\partial r}\right|^{-1} \quad , \quad V_\theta = \left|\frac{\partial \mathbf{r}}{\partial \theta}\right|^{-1} \quad , \quad W_\phi = \left|\frac{\partial \mathbf{r}}{\partial \phi}\right|^{-1} \ .$$

b. Determine the Cartesian coordinates of the new unit vectors $\hat{\mathbf{e}}_r$, $\hat{\mathbf{e}}_\theta$, $\hat{\mathbf{e}}_\phi$, draw the position of these vectors at a point $\mathbf{r}_0$, and check the orthogonality of the unit vectors. Express the Cartesian unit vectors by the spherical ones.
c. Determine the total differential $d\mathbf{r}$, the line element $(ds)^2 = |d\mathbf{r}|^2$, and the volume element $d\tau = ds_u ds_v ds_w$ in terms of the new coordinates.
d. Repeat steps (a)-(c) for planar polar coordinates.

Solution: *a. We have,*

$$\begin{aligned}
\frac{\partial \mathbf{r}}{\partial r} &= \sin\theta\cos\phi\hat{\mathbf{e}}_x + \sin\theta\sin\phi\hat{\mathbf{e}}_y + \cos\theta\hat{\mathbf{e}}_z \\
\frac{\partial \mathbf{r}}{\partial \theta} &= r\cos\theta\cos\phi\hat{\mathbf{e}}_x + r\cos\theta\sin\phi\hat{\mathbf{e}}_y - r\sin\theta\hat{\mathbf{e}}_z \\
\frac{\partial \mathbf{r}}{\partial \phi} &= -r\sin\theta\sin\phi\hat{\mathbf{e}}_x + r\sin\theta\cos\phi\hat{\mathbf{e}}_y \ .
\end{aligned}$$

From this follows,

$$\begin{aligned}
\frac{1}{U_r} &= \left|\frac{\partial \mathbf{r}}{\partial r}\right| = \sqrt{\sin^2\theta(\cos^2\phi + \sin^2\phi) + \cos^2\theta} = 1 \\
\frac{1}{V_\theta} &= \left|\frac{\partial \mathbf{r}}{\partial \theta}\right| = r\sqrt{\cos^2\theta(\cos^2\phi + \sin^2\phi) + \sin^2\theta} = r \\
\frac{1}{W_\phi} &= \left|\frac{\partial \mathbf{r}}{\partial \phi}\right| = r\sqrt{\sin^2\theta(\cos^2\phi + \sin^2\phi)} = r\sin\theta \ .
\end{aligned}$$

So we have, $U_r = 1$, $V_\theta = \frac{1}{r}$ *and* $W_\phi = \frac{1}{r\sin\theta}$.
b. The unit vectors are,

$$\begin{aligned}
\hat{\mathbf{e}}_r &= U_r\frac{\partial \mathbf{r}}{\partial r} = \hat{\mathbf{e}}_x\sin\theta\cos\phi + \hat{\mathbf{e}}_y\sin\theta\sin\phi + \hat{\mathbf{e}}_z\cos\theta \\
\hat{\mathbf{e}}_\theta &= V_\theta\frac{\partial \mathbf{r}}{\partial \theta} = \hat{\mathbf{e}}_x\cos\theta\cos\phi + \hat{\mathbf{e}}_y\cos\theta\sin\phi - \hat{\mathbf{e}}_z\sin\theta \\
\hat{\mathbf{e}}_\phi &= W_\phi\frac{\partial \mathbf{r}}{\partial \phi} = -\hat{\mathbf{e}}_x\sin\phi + \hat{\mathbf{e}}_y\cos\phi \ .
\end{aligned}$$

It is easy to see that all three unit vectors are orthogonal. Reversing the system of equations, we get,

$$\begin{aligned}\hat{\mathbf{e}}_x &= \hat{\mathbf{e}}_r \sin\theta\cos\phi + \hat{\mathbf{e}}_\theta \cos\theta\cos\phi - \hat{\mathbf{e}}_\phi \sin\phi \\ \hat{\mathbf{e}}_y &= \hat{\mathbf{e}}_r \sin\theta\sin\phi + \hat{\mathbf{e}}_\theta \cos\theta\sin\phi + \hat{\mathbf{e}}_\phi \cos\phi \\ \hat{\mathbf{e}}_z &= \hat{\mathbf{e}}_r \cos\theta - \hat{\mathbf{e}}_\theta \sin\theta \ .\end{aligned}$$

c. The total differential $d\mathbf{r}$ *has the form,*

$$d\mathbf{r} = \hat{\mathbf{e}}_r \frac{dr}{U_r} + \hat{\mathbf{e}}_\theta d\theta V_\theta + \hat{\mathbf{e}}_w \frac{dw}{W_\phi} \ .$$

This makes it easy to show,

$$\begin{aligned}(ds)^2 = |d\mathbf{r}|^2 &= \left(\frac{du}{U}\right)^2 + \left(\frac{dv}{V}\right)^2 + \left(\frac{dw}{W}\right)^2 \\ &= (ds_u)^2 + (ds_v)^2 + (ds_w)^2 \\ &= (dr)^2 + (rd\theta)^2 + (r\sin\theta d\phi)^2 \ .\end{aligned}$$

Now,

$$d\tau = ds_u ds_v ds_w = r^2 \sin\theta d\theta d\phi dr \ .$$

d. This is easy.

12.3.8.3 Ex: Spherical and cylindrical coordinates

Calculate $\nabla\Phi$, $\nabla\cdot\mathbf{A}$, $\nabla\times\mathbf{A}$ and $\Delta\Phi = \nabla\cdot(\nabla\Phi)$
a. in spherical coordinates $(r,\ \theta,\ \phi)$.
b. in cylindrical coordinates $(\rho,\ \phi,\ z)$.

Solution: *a. With Exc. 12.3.8.2(a) segue* $U_r = 1$, $V_\theta = \frac{1}{r}$ *and* $W_\phi = \frac{1}{r\sin\theta}$. *With the results obtained in for arbitrary coordinates we get consecutively:*

$$\nabla\Phi = \hat{\mathbf{e}}_r \ \frac{\partial\Phi}{\partial r} + \hat{\mathbf{e}}_\theta \ \frac{1}{r} \ \frac{\partial\Phi}{\partial\theta} + \hat{\mathbf{e}}_\phi \ \frac{1}{r\sin\phi} \ \frac{\partial\Phi}{\partial\phi} \ ,$$

and

$$\begin{aligned}\nabla\cdot\mathbf{A} &= \frac{1}{r^2\sin\theta}\left(\frac{\partial\Phi}{\partial r}[r^2\sin\theta\ a_r] + \frac{\partial\Phi}{\partial\theta}[r\sin\theta\ a_\theta] + \frac{\partial\Phi}{\partial\phi}[r\ a_\phi\right]) \\ &= \frac{1}{r^2}\frac{\partial\Phi}{\partial r}[r^2 a_r] + \frac{1}{r\sin\theta}\frac{\partial\Phi}{\partial\theta}[\sin\theta\ a_\theta] + \frac{1}{r\sin\theta}\frac{\partial\Phi}{\partial\phi}[a_\phi] \ ,\end{aligned}$$

and also,

$$\nabla\times\mathbf{A} = \frac{1}{r^2\sin\theta} \ \det\begin{pmatrix} \hat{\mathbf{e}}_r & r\hat{\mathbf{e}}_\theta & r\sin\theta\hat{\mathbf{e}}_\phi \\ \frac{\partial}{\partial r} & \frac{\partial}{\partial\theta} & \frac{\partial}{\partial\phi} \\ a_r & ra_\theta & r\sin\theta a_\phi \end{pmatrix} \ ,$$

respectively,

$$\nabla\times\mathbf{A}=\hat{\mathbf{e}}_r\ \frac{1}{r\sin\theta}\left[\frac{\partial\Phi}{\partial\theta}(\sin\theta a_\phi)-\frac{\partial\Phi}{\partial\phi}(a_\theta)\right]+\hat{\mathbf{e}}_\theta\ \frac{1}{r\sin\theta}\left[\frac{\partial\Phi}{\partial\phi}(a_r)-\sin\theta\frac{\partial\Phi}{\partial r}(ra_\phi)\right]$$
$$+\hat{\mathbf{e}}_\phi\ \frac{1}{r}\left[\frac{\partial\Phi}{\partial r}(ra_\theta)-\frac{\partial\Phi}{\partial\theta}(a_r)\right]\ .$$

With the expression for $\nabla\Phi$ *we get immediately,*

$$(\nabla\Phi)_r=\frac{\partial\Phi}{\partial r}\qquad,\qquad(\nabla\Phi)_\theta=\frac{1}{r}\frac{\partial\Phi}{\partial\theta}\qquad,\qquad(\nabla\Phi)_\phi=\frac{1}{r\sin\theta}\frac{\partial\Phi}{\partial\phi}\ ,$$

and

$$\nabla\cdot(\nabla\Phi)=\frac{1}{r^2}\frac{\partial}{\partial r}\left(r^2\frac{\partial\Phi}{\partial r}\right)+\frac{1}{r^2\sin\theta}\frac{\partial}{\partial\theta}\left(\sin\theta\frac{\partial\Phi}{\partial\theta}\right)+\frac{1}{r^2\sin^2\theta}\frac{\partial^2\Phi}{\partial\phi^2}\equiv\Delta\Phi\ .$$

b. The cylindrical coordinates are given by,

$$\mathbf{r}=(x,\ y,\ z)=(\rho\cos\phi,\ \rho\sin\phi,\ z)\ ,$$

From this follows,

$$\frac{\partial\mathbf{r}}{\partial\rho}=\cos\phi\ \hat{\mathbf{e}}_x+\sin\phi\ \hat{\mathbf{e}}_y$$
$$\frac{\partial\mathbf{r}}{\partial\phi}=-\rho\sin\phi\ \hat{\mathbf{e}}_x+\rho\cos\phi\ \hat{\mathbf{e}}_y$$
$$\frac{\partial\mathbf{r}}{\partial z}=\hat{\mathbf{e}}_z\ ,$$

and also,

$${U_\rho}^{-1}=\left|\frac{\partial\mathbf{r}}{\partial\rho}\right|=\sqrt{\cos^2\phi+\sin^2\phi}=1$$
$${V_\phi}^{-1}=\left|\frac{\partial\mathbf{r}}{\partial\phi}\right|=\rho$$
$${W_z}^{-1}=\left|\frac{\partial\mathbf{r}}{\partial z}\right|=1\ .$$

With that we get consecutively,

$$\nabla\Phi=\hat{\mathbf{e}}_\rho\ \frac{\partial\Phi}{\partial\rho}+\hat{\mathbf{e}}_\phi\ \frac{1}{\rho}\ \frac{\partial\Phi}{\partial\phi}+\hat{\mathbf{e}}_z\ \frac{\partial\Phi}{\partial z}\ ,$$

and

$$\nabla\cdot\mathbf{A}=\frac{1}{\rho}\frac{\partial}{\partial\rho}[\rho\ a_\rho]+\frac{1}{\rho}\frac{\partial}{\partial\phi}[a_\phi]+\frac{\partial}{\partial z}[a_z]\ ,$$

and also,

$$\nabla\times\mathbf{A}=\frac{1}{\rho}\ \det\begin{pmatrix}\hat{\mathbf{e}}_\rho & \rho\hat{\mathbf{e}}_\phi & \hat{\mathbf{e}}_z\\ \frac{\partial}{\partial\rho} & \frac{\partial}{\partial\phi} & \frac{\partial}{\partial z}\\ a_\rho & \rho a_\phi & a_z\end{pmatrix}\ ,$$

respectively,

$$\nabla \times \mathbf{A} \;= \hat{\mathbf{e}}_\rho \; \frac{1}{\rho}\left[\frac{\partial a_z}{\partial \phi} - \rho \frac{\partial a_\phi}{\partial z}\right] + \hat{\mathbf{e}}_\phi \; \left[\frac{\partial a_\rho}{\partial z} - \frac{\partial a_z}{\partial \rho}\right] + \hat{\mathbf{e}}_z \; \frac{1}{\rho}\left[\frac{\partial}{\partial \rho}(\rho a_\phi) - \frac{\partial a_\rho}{\partial \phi}\right] \;,$$

and finally,

$$\Delta\Phi = \nabla \cdot (\nabla\Phi) = \frac{1}{\rho}\frac{\partial}{\partial \rho}\left(\rho \frac{\partial \Phi}{\partial \rho}\right) + \frac{1}{\rho^2}\frac{\partial^2 \Phi}{\partial \phi^2} + \frac{\partial^2 \Phi}{\partial z^2} \;.$$

12.3.8.4 Ex: Divergence in curvilinear coordinates

Calculate the divergence of the force field $\mathbf{F}(\mathbf{r}) = \begin{pmatrix} x^2 y \\ 2yz \\ x+z \end{pmatrix}$ (a) in Cartesian and (b) cylindrical coordinates and compare the results.

Solution: *a. In Cartesian coordinates we have* $\nabla \cdot \mathbf{F}(\mathbf{r}) = 2xy + 2z + 1$.
b. The transformation to cylindrical coordinates is defined by

$$\mathbf{r} = \begin{pmatrix} \rho\cos\phi \\ \rho\sin\phi \\ z \end{pmatrix} \;,$$

respectively,

$$\begin{aligned}
\hat{\mathbf{e}}_\rho &\equiv \frac{\partial \mathbf{r}}{\partial r} = \hat{\mathbf{e}}_x \cos\phi + \hat{\mathbf{e}}_y \sin\phi \\
\hat{\mathbf{e}}_\phi &\equiv \frac{1}{r}\frac{\partial \mathbf{r}}{\partial \phi} = -\hat{\mathbf{e}}_x \sin\phi + \hat{\mathbf{e}}_y \cos\phi \\
\hat{\mathbf{e}}_z &\equiv \frac{\partial \mathbf{r}}{\partial z} = \hat{\mathbf{e}}_\rho \times \hat{\mathbf{e}}_\phi \;,
\end{aligned}$$

hence,

$$\begin{aligned}
\hat{\mathbf{e}}_x &= \hat{\mathbf{e}}_\rho \cos\phi - \hat{\mathbf{e}}_\phi \sin\phi \\
\hat{\mathbf{e}}_y &= \hat{\mathbf{e}}_\phi \cos\phi + \hat{\mathbf{e}}_\rho \sin\phi \;.
\end{aligned}$$

The vector field is in cylindrical coordinates,

$$\begin{aligned}
\mathbf{F} &= x^2 y \hat{\mathbf{e}}_x + 2yz\hat{\mathbf{e}}_y + (x+z)\hat{\mathbf{e}}_z \\
&= \hat{\mathbf{e}}_x \rho^3 \cos^2\phi \sin\phi + \hat{\mathbf{e}}_y 2\rho z \sin\phi + \hat{\mathbf{e}}_z(\rho\cos\phi + z) \\
&= (\hat{\mathbf{e}}_\rho \cos\phi - \hat{\mathbf{e}}_\phi \sin\phi)\rho^3 \cos^2\phi \sin\phi + (\hat{\mathbf{e}}_\phi \cos\phi + \hat{\mathbf{e}}_\rho \sin\phi) 2\rho z \sin\phi + \hat{\mathbf{e}}_z(\rho\cos\phi + z) \\
&= \hat{\mathbf{e}}_\rho(\rho^3 \cos^3\phi \sin\phi + 2\rho z \sin^2\phi) + \hat{\mathbf{e}}_\phi(2\rho z \sin\phi\cos\phi - \rho^3 \cos^2\phi \sin^2\phi) + \hat{\mathbf{e}}_z(\rho\cos\phi + z) \;.
\end{aligned}$$

The divergence now is,

$$\nabla\cdot\mathbf{F} = \frac{1}{\rho}\frac{\partial}{\partial\rho}(\rho F_\rho) + \frac{1}{\rho}\frac{\partial}{\partial\phi}F_\phi + \frac{\partial}{\partial z}F_z$$
$$= \frac{1}{\rho}\frac{\partial}{\partial\rho}(\rho^4\cos^3\phi\sin\phi + 2\rho^2 z\sin^2\phi) + \frac{1}{\rho}\frac{\partial}{\partial\phi}(2\rho z\sin\phi\cos\phi - \rho^3\cos^2\phi\sin^2\phi) + \frac{\partial}{\partial z}(\rho\cos\phi + z)$$
$$= (4\rho^2\cos^3\phi\sin\phi + 4z\sin^2\phi) + \left(2z\cos^2\phi - 2z\sin^2\phi + 2\rho^2\cos\phi\sin^3\phi - 2\rho^2\cos^3\phi\sin\phi\right) + 1$$
$$= \frac{4x^3y}{\rho^2} + \frac{4zy^2}{\rho^2} + \frac{2zx^2}{\rho^2} - \frac{2zy^2}{\rho^2} + \frac{2\rho^2xy^3}{\rho^4} - \frac{2\rho^2x^3y}{\rho^4} + 1 = 2xy + 2z + 1\ ,$$

with $\rho^2 = x^2 + y^2$.

12.3.8.5 Ex: Differential operators in curvilinear coordinates

In Cartesian coordinates the differential line element has the form $d\mathbf{r} = \hat{\mathbf{e}}_x dx + \hat{\mathbf{e}}_y dy + \hat{\mathbf{e}}_z dz$ and in arbitrary orthogonal coordinates $d\mathbf{r} = \hat{\mathbf{e}}_1 h_1 dq_1 + \hat{\mathbf{e}}_2 h_2 dq_2 + \hat{\mathbf{e}}_3 h_3 dq_3$ with $\hat{\mathbf{e}}_i = \frac{\partial\mathbf{r}}{\partial q_i}\cdot\left|\frac{\partial\mathbf{r}}{\partial q_i}\right|^{-1}$ and $h_i = \left|\frac{\partial\mathbf{r}}{\partial q_i}\right|$. For spherical coordinates (r,ϕ,θ) we find $h_r = 1, h_\phi = r\sin\theta, h_\theta = r$; for cylindrical coordinates (ρ,ϕ,z) we find $h_\rho = 1, h_\phi = \rho, h_z = 1$.
a. The gradient has the general form,

$$\nabla_i\Phi(\mathbf{r}) = \frac{1}{h_i}\frac{\partial}{\partial q_i}\Phi(\mathbf{r})\ .$$

Determine the gradient in spherical and cylindrical coordinates.
b. The divergence of a vector field $\mathbf{A}$ has the general form,

$$\nabla\cdot\mathbf{A}(\mathbf{r}) = \frac{1}{h_1h_2h_3}\left[\frac{\partial}{\partial q_1}(A_1h_2h_3) + \frac{\partial}{\partial q_2}(A_2h_1h_3) + \frac{\partial}{\partial q_3}(A_3h_1h_2)\right]\ .$$

Determine $\nabla\cdot\mathbf{A}$ in spherical and cylindrical coordinates.
c. Use the results of (a) and (b) to determine the Laplace operator

$$\Delta = \nabla\cdot\nabla$$

in spherical coordinates.

Solution: *For spherical coordinates the coefficients* h_i *are determined from* $\mathbf{r} = \begin{pmatrix} r\sin\theta\cos\phi \\ r\cos\theta\cos\phi \\ r\sin\phi \end{pmatrix}$ *and for cylindrical coordinates from* $\mathbf{r} = \begin{pmatrix} \rho\cos\phi \\ \rho\sin\phi \\ z \end{pmatrix}$.
Gradient in cylindrical coordinates,

$$\nabla\Psi(\rho,\phi,z) = \frac{\partial}{\partial\rho}\Psi(\rho,\phi,z)\hat{\mathbf{e}}_\rho + \frac{1}{\rho}\frac{\partial}{\partial\phi}\Psi(\rho,\phi,z)\hat{\mathbf{e}}_\phi + \frac{\partial}{\partial z}\Psi(\rho,\phi,z)\hat{\mathbf{e}}_z\ .$$

Gradient in spherical coordinates

$$\nabla\Psi(r,\theta,\phi) = \frac{\partial}{\partial r}\Psi(r,\theta,\phi)\hat{\mathbf{e}}_r + \frac{1}{r}\frac{\partial}{\partial\theta}\Psi(r,\theta,\phi)\hat{\mathbf{e}}_\theta + \frac{1}{r\sin\theta}\frac{\partial}{\partial\phi}\Psi(r,\theta,\phi)\hat{\mathbf{e}}_\phi\ .$$

Divergence in cylindrical coordinates,

$$\nabla \cdot \mathbf{A} = \frac{1}{\rho}\frac{\partial}{\partial \rho}(\rho A_\rho) + \frac{1}{\rho}\frac{\partial}{\partial \phi}A_\phi + \frac{\partial}{\partial z}A_z \ .$$

Divergence in spherical coordinate,

$$\nabla \cdot \mathbf{A} = \frac{1}{r^2}\frac{\partial}{\partial r}(r^2 A_r) + \frac{1}{r\sin\theta}\frac{\partial}{\partial \theta}(\sin\theta A_\theta) + \frac{1}{r\sin\theta}\frac{\partial}{\partial \phi}A_\phi \ .$$

Laplace operator in cylindrical coordinates,

$$\Delta = \frac{1}{\rho}\frac{\partial}{\partial \rho}\left(\rho\frac{\partial}{\partial \rho}\right) + \frac{1}{\rho^2}\frac{\partial^2}{\partial \phi^2} + \frac{\partial^2}{\partial z^2} \ .$$

Laplace operator in spherical coordinate,

$$\Delta = \frac{1}{r}\frac{\partial^2}{\partial r^2}r + \frac{1}{r^2\sin\theta}\frac{\partial}{\partial \theta}\left(\sin\theta\frac{\partial}{\partial \theta}\right) + \frac{1}{r^2\sin^2\theta}\frac{\partial^2}{\partial \phi^2} \ .$$

12.3.8.6 Ex: Acceleration in spherical coordinates

In spherical coordinates the velocity vector has the following form,

$$\mathbf{v} = \frac{d\mathbf{r}}{dt} = \dot{r}\hat{\mathbf{e}}_r + r\dot{\theta}\hat{\mathbf{e}}_\theta + \dot{\phi}r\sin\theta\hat{\mathbf{e}}_\phi \ .$$

Calculate the acceleration vector in spherical coordinates. Respect the fact that the basis vectors must also be derived by time.

Solution: *The derivatives of the basis vectors are,*

$$\frac{d}{dt}\hat{\mathbf{e}}_r = \frac{d}{dt}\begin{pmatrix}\sin\theta\cos\phi\\ \sin\theta\sin\phi\\ \cos\theta\end{pmatrix} = \begin{pmatrix}\dot{\theta}\cos\theta\cos\phi - \dot{\phi}\sin\theta\sin\phi\\ \dot{\theta}\cos\theta\sin\phi + \dot{\phi}\sin\theta\cos\phi\\ -\dot{\theta}\sin\theta\end{pmatrix} = \dot{\theta}\hat{\mathbf{e}}_\theta + \dot{\phi}\sin\theta\hat{\mathbf{e}}_\phi$$

$$\frac{d}{dt}\hat{\mathbf{e}}_\theta = \frac{d}{dt}\begin{pmatrix}\cos\theta\cos\phi\\ \cos\theta\sin\phi\\ -\sin\theta\end{pmatrix} = \begin{pmatrix}-\dot{\theta}\sin\theta\cos\phi - \dot{\phi}\cos\theta\sin\phi\\ -\dot{\theta}\sin\theta\sin\phi + \dot{\phi}\cos\theta\cos\phi\\ -\dot{\theta}\cos\theta\end{pmatrix} = -\dot{\theta}\hat{\mathbf{e}}_r + \dot{\phi}\cos\theta\hat{\mathbf{e}}_\phi$$

$$\frac{d}{dt}\hat{\mathbf{e}}_\phi = \frac{d}{dt}\begin{pmatrix}-\sin\phi\\ \cos\phi\\ 0\end{pmatrix} = \begin{pmatrix}-\dot{\phi}\cos\phi\\ -\dot{\phi}\sin\phi\\ 0\end{pmatrix} = -\dot{\phi}\sin\theta\hat{\mathbf{e}}_r - \dot{\phi}\cos\theta\hat{\mathbf{e}}_\theta \ .$$

Hence,

$$\begin{aligned}\mathbf{a} &= \frac{d\mathbf{v}}{dt} = \frac{d^2\mathbf{r}}{dt^2} = \ddot{\mathbf{r}} \\ &= \ddot{r}\hat{\mathbf{e}}_r + \dot{r}\dot{\hat{\mathbf{e}}}_r + \dot{r}\dot{\theta}\hat{\mathbf{e}}_\theta + r\ddot{\theta}\hat{\mathbf{e}}_\theta + r\dot{\theta}\dot{\hat{\mathbf{e}}}_\theta + \ddot{\phi}r\sin\theta\hat{\mathbf{e}}_\phi + \dot{\phi}\dot{r}\sin\theta\hat{\mathbf{e}}_\phi + \dot{\phi}r\dot{\theta}\cos\theta\hat{\mathbf{e}}_\phi + \dot{\phi}r\sin\theta\dot{\hat{\mathbf{e}}}_\phi \ .\end{aligned}$$

Inserting $\dot{\hat{\mathbf{e}}}_r$, $\dot{\hat{\mathbf{e}}}_\theta$ *and* $\dot{\hat{\mathbf{e}}}_\phi$ *gives,*

$$\begin{aligned}\mathbf{a} = &\left(\ddot{r} - r\dot{\theta}^2 - \dot{\phi}^2 r\sin^2\theta\right)\hat{\mathbf{e}}_r \\ &+ \left(2\dot{r}\dot{\theta} + r\ddot{\theta} - \dot{\phi}^2 r\sin\theta\cos\theta\right)\hat{\mathbf{e}}_\theta \\ &+ \left(2\dot{\phi}\dot{r}\sin\theta + 2\dot{\phi}r\dot{\theta}\cos\theta + \ddot{\phi}r\sin\theta\right)\hat{\mathbf{e}}_\phi \ .\end{aligned}$$

12.3.8.7 Ex: Volume element in curvilinear coordinates

a. Calculate the surface of a rectangle with width a and height b in Cartesian coordinates.
b. Calculate the surface of a disk of radius R in polar coordinates.
c. Calculate the volume of a cuboid with dimensions a, b, c in Cartesian coordinates.
d. Calculate the volume of a cylinder with the radius R and height H in cylindrical coordinates.
e. Calculate the volume a sphere with the radius R in spherical coordinates.

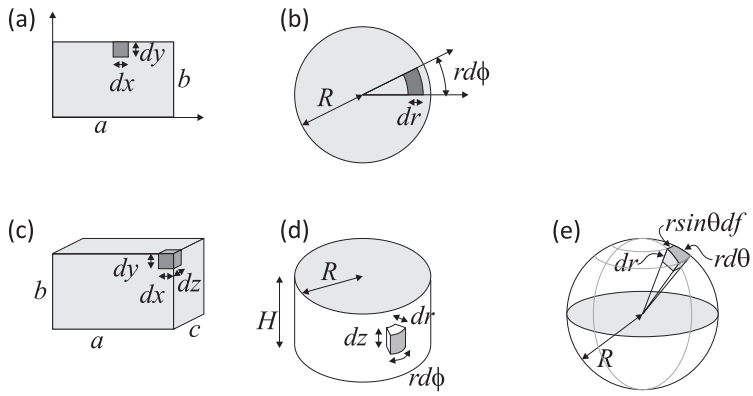

Figure 12.8: Curvilinear coordinates.

Solution: *a. The surface element is,*

$$dS = dxdy \ .$$

With this we calculate the surface of the rectangle,

$$S = \int_{rectangulo} dS = \int_0^a \left(\int_0^b dy\right) dx = \int_0^a dx \int_0^b dy = ab \ .$$

b. The surface element is,

$$dS = rd\phi dr \ .$$

With this we calculate the disk surface,

$$S = \int_{disco} dS = \int_0^R \left(\int_0^{2\pi} r d\phi \right) dr = \int_0^{2\pi} d\phi \int_0^R r dr = 2\pi \frac{R^2}{2} = \pi R^2 \ .$$

c. The volume element is,

$$dV = dxdydz \ .$$

d. The volume element is,

$$dV = rd\phi drdz \ .$$

With this we calculate the cylinder volume,

$$\begin{aligned} V = \int_{cylinder} dV &= \int_0^H \left(\int_0^R \left(\int_0^{2\pi} r d\phi \right) dr \right) dz \\ &= \int_0^{2\pi} d\phi \int_0^R r dr \int_0^H dz = 2\pi \frac{R^2}{2} H = \pi R^2 H \ . \end{aligned}$$

e. The volume element is

$$dV = r^2 \sin\theta d\phi d\theta dr \ .$$

With this we calculate the cylinder volume,

$$\begin{aligned} V = \int_{sphere} dV &= \int_0^\pi \left(\int_0^R \left(\int_0^{2\pi} r \sin\theta d\phi \right) dr \right) r d\theta \\ &= \int_0^{2\pi} d\phi \int_0^R r^2 dr \int_0^\pi \sin\theta d\theta = 2\pi \frac{R^3}{3} 2 = \frac{4\pi}{3} R^3 \ . \end{aligned}$$

12.3.8.8 Ex: Spherical volume

The volume of a body is given by the following formula:

$$V = \int_V 1 \ dV \ .$$

a. Calculate the volume of a 3D-sphere in spherical coordinates.
By the Gauß integral law we can establish a relationship between the volume of the sphere and its surface. (**Help:** For which vector field $\mathbf{A}$ holds: $\nabla \cdot \mathbf{A} = 1$?)
b. Now calculate the volume of the sphere in this sense. You may assume that the surface of the sphere is known.
c. Similarly to the above formula, derive a general relationship between the volume of an n-dimensional hypersphere and its $(n-1)$-dimensional hypersurface. **Help:** Gauß's law holds in arbitrary dimensions with the n-dimensional operator nabla-operator defined by, $\nabla = (\partial/\partial x_1, \ldots, \partial/\partial x_n)$.

Solution: *a. The volume of the sphere is,*

$$V = \int_{sphere} r^2 \sin\theta dr d\theta d\phi = \frac{4\pi}{3} R^3 \ .$$

b. By the law of Gauß,

$$V = \int_{sphere} 1\ dV = \frac{1}{3}\int_V div\ \mathbf{r}\ dV = \frac{1}{3}\oint_{surfaceofsphere} \mathbf{r}d\mathbf{S}$$
$$= \frac{R}{3}\oint_{surfaceofsphere} R^2 d\theta d\phi = \frac{R}{3}\cdot 4\pi R^2\ .$$

c. In n dimensions,

$$V = \int_{hypersphere} 1\ dV = \frac{1}{n}\int_V div\mathbf{r}\ dV = \frac{1}{n}\oint_{surfaceofhypersphere} \mathbf{r}d\mathbf{S}$$
$$= \frac{R}{n}\oint_{surfaceofhypersphere} R^2 d\theta d\phi = \frac{R}{n}\cdot \partial V\ .$$

It i interesting that for $n \to \infty$ the volume of the unitary sphere tends to 0.

12.3.8.9 Ex: Spherical volume

The density distribution of a gas be given by $n(\mathbf{r}) = C^2 - \frac{x^2}{r_0^2} - \frac{y^2}{r_0^2} - \frac{z^2}{r_0^2}$. Determine the constant C in such a way that the density $n(\mathbf{r})$ is normalized to the number of atoms in the gas, i.e., $\int_{\mathcal{V}} n(\mathbf{r})d^3\mathbf{r} = N$, where $\mathcal{V}$ is the volume within which the density is positive, $n(\mathbf{r}) \geq 0$.

Solution: *The volume integral is,*

$$\int_{\mathcal{V}} n(\mathbf{r})d^3\mathbf{r} = \int_{\mathcal{V}} \left(C^2 - \frac{r^2}{r_0^2}\right) d^3\mathbf{r} = 4\pi \int_0^{Cr_0} \left(C^2 - \frac{r^2}{r_0^2}\right) r^2 dr$$
$$= 4\pi \left[\frac{C^2 r^3}{3} - \frac{r^5}{5r_0^2}\right]_0^{Cr_0} = \frac{8\pi C^5 r_0^3}{15} \equiv N\ .$$

With this we get the constant,

$$C = \left(\frac{15N}{8\pi r_0^3}\right)^{1/5}\ .$$

12.3.8.10 Ex: Spherical and cylindrical volume

a. Integrate a circular surface with radius R in Cartesian coordinates and then in polar coordinates.
b. The density distribution of a trapped atomic gas is described by $n(\mathbf{r}) = n_0 e^{-r^2/\bar{r}^2}$, where $n_0 = 10^{13}\,\mathrm{cm}^{-1}$ is the maximum density and $\bar{r} = 100\,\mu\mathrm{m}$ a measure for the extent of the distribution. Calculate the number of atoms $N = \int_{\mathbb{R}^3} n(\mathbf{r})d^3\mathbf{r}$, integrating over Cartesian coordinates and then over polar coordinates.
c. Calculate the density of a homogeneous cylinder of mass 10 kg and length 20 cm by

integrating over its volume..
d. The density distribution of a trapped atomic gas is described by $n(\rho,z) = \max\left\{0, n_0 \cdot \left(1 - \frac{\rho^2}{\rho_m^2} - \frac{z^2}{z_m^2}\right)\right\}$, where $n_0 = 10^{13}\,\mathrm{cm}^{-3}$ is the maximum density and $z_m = 2\rho_m = 100\,\mu\mathrm{m}$ a measure for the extent of the distribution. Calculate the number of atoms by integrating over cylindrical coordinates.

Solution: *a. The surface of the circle is,*

$$S = \int_{circle} d^2r = \int \int_{-\sqrt{R^2-y^2}}^{\sqrt{R^2-y^2}} dxdy = \int 2\sqrt{R^2-y^2}dy = y\sqrt{R^2-y^2} + R^2 \arcsin\frac{y}{R}\Big|_{-R}^{R} = R^2\pi$$

$$S = \int_{circle} d^2r = \int_0^{2\pi}\int_0^R rdrd\phi = 2\pi\frac{R^2}{2} = \pi R^2 \ .$$

b. The number of atoms is,

$$N = \int_{\mathbb{R}^3} n(r)dxdydz = n_0\left(\int_{-\infty}^{\infty} e^{-x^2/\bar{r}^2}dx\right)^3 = n_0\left(\bar{r}\sqrt{\pi}\right)^3$$

$$N = \int_{\mathbb{R}^3} n(r)dr = \int_0^{2\pi}\int_0^{\theta}\int_0^{\infty} n(r)r^2\sin\theta drd\theta d\phi = 4\pi n_0\int_0^{\infty} e^{-r^2/\bar{r}^2}r^2dr$$

$$= 4\pi n_0\left(-\frac{1}{2}\bar{r}^2e^{-r^2/\bar{r}^2}r\Big|_0^{\infty} - \int_0^{\infty} -\frac{1}{2}e^{-r^2/\bar{r}^2}\bar{r}^2dr\right) = \pi n_0\bar{r}^3\sqrt{\pi} \ .$$

Hence, we have $N = 55.7\cdot 10^6$ atoms.
c. The mass is,

$$m = \int_{\mathbb{R}^3}\rho(\vec{r})d^3r = \int_0^h\int_0^{2\pi}\int_0^R \rho_0 rdrd\phi dz = \rho_0\pi h\frac{R^2}{2} = \rho_0 V \ .$$

So the density is, $\rho_0 = \frac{m}{\pi R^2 h} \simeq 6.4\,\mathrm{kg/l}$.
d. The number of atoms is,

$$N = \int_{\mathbb{R}^3} n(\rho,z)d^3r = n_0\int_{n(r)\geq 0}\left(1 - \frac{\rho^2}{\bar{\rho}^2} - \frac{z^2}{\bar{z}^2}\right)\rho d\rho d\phi dz$$

$$= 2\pi n_0\int_{n(r)\geq 0}\left[\frac{\rho^2}{2} - \frac{\rho^4}{4\bar{\rho}^2} - \frac{z^2\rho^2}{2\bar{z}^2}\right]_0^{\bar{\rho}\sqrt{1-z^2/\bar{z}^2}} dz = 2\pi n_0\frac{\bar{\rho}^2}{4}\int_{-\bar{z}}^{\bar{z}}\left(1 - \frac{z^2}{\bar{z}^2}\right)^2 dz$$

$$= 2\pi n_0\frac{\bar{\rho}^2}{4}\left[\frac{1}{5a^4}z^5 - \frac{2}{3}\frac{z^3}{a^2} + z\right]_{-\bar{z}}^{\bar{z}} = 2\pi n_0\frac{\bar{\rho}^2}{4}\frac{16}{15}a = \frac{8\pi}{15}n_0\bar{z}\bar{\rho}^2 \ .$$

Hence, we have $N = 4.2\cdot 10^6$ atoms.

12.3.8.11 Ex: Cylindrical volume

Consider a material (gas or liquid) whose mass density $\rho(\mathbf{r})$ depends on the z-coordinate as follows: $\rho(\mathbf{r}) = \rho_0(1-\alpha z)$. This material is filled into a cylinder (radius R and height c) until the total mass in the cylinder is M. The cylinder stands

in a circular area above the xy in $z = 0$.
a. Calculate the density parameter ρ_0.
b. Calculate vector of center of mass $\mathbf{r}_s$ of the material in the cylinder.
c. Now fill the same material inside a sphere of radius R instead of the cylinder. What are the results in this case if $\alpha = 0.1$ /m, $R = 1$ m, and $M = 10$ kg.
d. A cake of mass M, height h and radius R be cut into fourth equal pieces. Calculate the center of mass of a piece. Calculate the center of mass of the rest of the cake when a piece is taken.

Solution: *a. The total mass integrated over the cylinder is,*

$$M = \int_{cylinder} \rho(\vec{r}) d^3r = \int_0^R \int_0^{2\pi} \int_0^{z_0} \rho_0(1-\alpha z) r dr d\phi dz = \rho_0 2\pi \frac{R^2}{2}\left(z_0 - \frac{\alpha}{2} z_0^2\right) .$$

Therefore, the density parameter is,

$$\rho_0 = \frac{M}{\left(z_0 - \frac{\alpha}{2} z_0^2\right)\pi R^2} = \frac{M}{V}\frac{1}{1-\frac{\alpha}{2}z_0} .$$

b. The center of mass vector is defined by,

$$\vec{r}_s = \frac{1}{M}\int_{cylinder} \vec{r}\rho(\vec{r}) d^3r = (0, 0, z_s) .$$

Hence,

$$z_s = \frac{1}{M}\int_0^R \int_0^{2\pi} \int_0^{z_0} \rho_0 z(1-\alpha z) r dr d\phi dz = \frac{\rho_0}{M}\pi R^2 \left(z_0^2 - \frac{\alpha}{3} z_0^3\right) = z_0 \frac{1-\frac{\alpha}{3}z_0}{1-\frac{\alpha}{2}z_0} .$$

c. For a sphere we calculate in the same way,

$$\begin{aligned} M &= \int_{sphere} \rho(\vec{r}) d^3r = \int_0^{z_0} \int_0^{\sqrt{R^2-(R-z)^2}} \int_0^{2\pi} \rho_0(1-\alpha z) r dr d\phi dz \\ &= 2\pi\rho_0 \int_0^{z_0} \int_0^{\sqrt{R^2-(R-z)^2}} r dr (1-\alpha z) dz = 2\pi\rho_0 \int_0^{z_0} \frac{\sqrt{R^2-(R-z)^2}^2}{2}(1-\alpha z) dz \\ &= 2\pi\rho_0 \int_0^{z_0} \left(\alpha\frac{z^3}{2} - \frac{z^2}{2} - \alpha R z^2 + Rz\right) dz = \pi\rho_0 z_0^2 \left(\frac{\alpha z_0^2}{4} - \frac{z_0}{3} - \frac{2\alpha R z_0}{3} + R\right) . \end{aligned}$$

We easily verify that $\lim_{\alpha\to 0, z_0 \to 2R} M = \frac{4\pi}{3} R^3 \rho_0$. *he center of mass is,*

$$\begin{aligned} \vec{r}_s &= \int_{sphere} \vec{r}\rho(\vec{r}) d^3r = (0, 0, z_s) \\ z_s &= \frac{1}{M}\int_0^{z_0} \int_0^{\sqrt{R^2-(R-z)^2}} \int_0^{2\pi} z\rho_0(1-\alpha z) r dr d\phi dz = \frac{2\pi\rho_0}{M}\int_0^{z_0} \int_0^{\sqrt{R^2-(R-z)^2}} z(1-\alpha z) r dr dz \\ &= \frac{2\pi\rho_0}{M}\int_0^{z_0} \frac{\sqrt{R^2-(R-z)^2}^2}{2} z(1-\alpha z) dz = \frac{2\pi\rho_0}{M}\int_0^{z_0} \left(\alpha\frac{z^4}{2} - \frac{z^3}{2} - \alpha R z^3 + Rz^2\right) dz \\ &= \frac{\pi\rho_0 z^3}{M}\left(\frac{\alpha z_0^2}{5} - \frac{z_0}{4} - \frac{\alpha R z_0}{2} + \frac{2R}{3}\right) = z_0 \frac{\alpha z_0^2/5 - z_0/4 - \alpha R z_0/2 + 2R/3}{\alpha z_0^2/4 - z_0/3 - 2\alpha R z_0/3 + R} . \end{aligned}$$

Once again we can check, $\lim_{\alpha\to 0, z_0\to 2R} z_s = R$.
d. The center of mass of a cake segment is,

$$\vec{r}_s = \frac{\int_{segment}\vec{r}d^3r}{V} = \frac{\int_0^{\phi_0}\int_0^R\int_0^h \vec{r}rdrd\phi dz}{\int_0^{\phi_0}\int_0^R\int_0^h rdrd\phi dz} = \frac{1}{\phi_0 R^2 h/2}\int_0^{\phi_0}\int_0^R\int_0^h \begin{pmatrix} r\cos\phi \\ r\sin\phi \\ z \end{pmatrix} rdrd\phi dz$$

$$= \frac{2}{\phi_0 R^2 h}\begin{pmatrix} \int_0^{\phi_0}\int_0^R\int_0^h r^2\cos\phi drd\phi dz \\ \int_0^{\phi_0}\int_0^R\int_0^h r^2\sin\phi drd\phi dz \\ \int_0^{\phi_0}\int_0^R\int_0^h zrdrd\phi dz \end{pmatrix} = \frac{2}{\phi_0 R^2 h}\begin{pmatrix} \frac{R^3}{3}h\int_0^{\phi_0}\cos\phi d\phi \\ \frac{R^3}{3}h\int_0^{\phi_0}\sin\phi d\phi \\ \frac{R^2h^2}{4}\int_0^{\phi_0} d\phi \end{pmatrix} = \begin{pmatrix} -\frac{2R}{3\phi_0}\sin\phi_0 \\ \frac{2R}{3\phi_0}(\cos\phi_0 - 1) \\ \frac{h}{2} \end{pmatrix} .$$

Since $\int \vec{O}d^3r = V\vec{O}$, *we can without loss of generality place the origin of the coordinate system in the center of the cake.*

12.3.8.12 Ex: Vector potential in curvilinear coordinates

Be given a constant field $\mathbf{B}$ oriented in z-direction. What is the vector potential $\mathbf{A}$ in (a) spherical coordinates, (b) cylindrical coordinates, and (c) Cartesian coordinates? For case (c) also consider the gauge transformation $\mathbf{A}' = \mathbf{A} + \nabla\lambda$ with $\lambda = \pm Bxy/2$.

Solution: *With Stokes' theorem,*

$$\int_F \mathbf{B}\cdot d\mathbf{S} = \int_F (\nabla\times\mathbf{A})\cdot d\mathbf{S} = \int_{R(F)} \mathbf{A}\cdot d\mathbf{S} .$$

Since

$$\mathbf{B} = B\hat{\mathbf{e}}_z ,$$

We chose as integration area a circle with radius ρ *in a plane perpendicular to the* z*-direction at a distance* z *from the origin of our coordinate system. The integration area and the origin then form a cone with the length of the side edges* r *and the half opening angle of the cone* θ.
a. In spherical coordinates $\rho = r\sin\theta$ *is then,*

$$B\pi r^2\sin^2\theta = A_\phi 2\pi r\sin\theta ,$$

that is,

$$\mathbf{A} = A_\phi\hat{\mathbf{e}}_\phi = \frac{B}{2}r\sin\theta\hat{\mathbf{e}}_\phi .$$

b. In cylindrical coordinates we get immediately,

$$B\pi\rho^2 = A_\phi 2\pi\rho ,$$

that is,

$$\mathbf{A} = A_\phi\hat{\mathbf{e}}_\phi = \frac{B}{2}\rho\hat{\mathbf{e}}_\phi .$$

c. For Cartesian coordinates we use the result of (b) with $\rho^2 = x^2 + y^2$ *and insert* $\hat{\mathbf{e}}_\phi$*:*

$$\mathbf{A} = \frac{B}{2}\sqrt{x^2+y^2}\hat{\mathbf{e}}_\phi = \frac{B}{2}\sqrt{x^2+y^2}(-\hat{\mathbf{e}}_x \sin\phi + \hat{\mathbf{e}}_y \cos\phi) = \frac{B}{2}(-y\hat{\mathbf{e}}_x + x\hat{\mathbf{e}}_y) = \frac{B}{2}(-y, x, 0) \ .$$

We now consider the gauge transformation,

$$\mathbf{A}' = \mathbf{A} + \nabla\lambda \ .$$

For

$$\lambda \equiv +\frac{B}{2}xy \ .$$

we obtain,

$$\mathbf{A}' = \frac{B}{2}(-y\hat{\mathbf{e}}_x + x\hat{\mathbf{e}}_y) + \hat{\mathbf{e}}_x\frac{\partial\lambda}{\partial x} + \hat{\mathbf{e}}_y\frac{\partial\lambda}{\partial y} = Bx\hat{\mathbf{e}}_y \ .$$

For

$$\lambda \equiv -\frac{B}{2}xy \ .$$

we get in the same way,

$$\mathbf{A}' = \frac{B}{2}(-y\hat{\mathbf{e}}_x + x\hat{\mathbf{e}}_y) + \hat{\mathbf{e}}_x\frac{\partial\lambda}{\partial x} + \hat{\mathbf{e}}_y\frac{\partial\lambda}{\partial y} = -By\hat{\mathbf{e}}_x \ .$$

12.3.8.13 Ex: Gauß' theorem in curvilinear coordinates

a. Check Gauß' theorem for function $\mathbf{A} = r^2\hat{\mathbf{e}}_r$ using the volume of a sphere of radius R.
b. Do the same for the function $\mathbf{B} = r^{-2}\hat{\mathbf{e}}_r$ and discuss the result.

Solution:

12.3.8.14 Ex: Gauß' theorem in curvilinear coordinates

Calculate the divergence of the function,

$$\mathbf{A} = r\hat{\mathbf{e}}_r \cos\theta + r\hat{\mathbf{e}}_\theta \sin\theta + r\hat{\mathbf{e}}_\varphi \sin\theta\cos\varphi \ .$$

Verify Gauß's theorem for this function using the volume of an inverted semisphere of radius R lying in the x-y-plane.

Solution:

12.3.8.15 Ex: Gauß' theorem in curvilinear coordinates

Calculate the gradient and Laplacian of the function $T = r(\cos\theta + \sin\theta\cos\varphi)$. Check the Laplacian by converting T into Cartesian coordinates. Verify Gauß's theorem using the path $l_1(t) = 2\hat{\mathbf{e}}_x \cos\pi t + 2\hat{\mathbf{e}}_y \sin\pi t$ for $t \in [0, 0.5]$ followed by $l_2(t) = 2\hat{\mathbf{e}}_y \sin\pi t - 2\hat{\mathbf{e}}_z \cos\pi t$ para $t \in [0.5, 1]$.

Solution:

12.3.8.16 Ex: Gauß' theorem in curvilinear coordinates

a. Find the divergence of the function,

$$\mathbf{A} = \rho\hat{\mathbf{e}}_\rho(2 + \sin^2\varphi) + \rho\hat{\mathbf{e}}_\varphi \sin\varphi\cos\varphi + 3z\hat{\mathbf{e}}_z \ .$$

b. Verify Gauß' theorem for this function using a quadrant of cylinder with radius $R = 2$ and height $h = 5$.
c. Find the rotation of $\mathbf{A}$.

Solution:

12.4 Differential geometry in curved space

In previous sections we mainly concentrated on orthogonal coordinate systems, such as Cartesian, cylindrical, or spherical. In cases one has to use non-orthogonal systems the formalism needs to be generalized. For this purpose it is necessary to introduce some new concepts and notations.

Repeat expressions in index formalism *Einstein's sum rule*, $a^n a_n = \sum_a^n a_n$,

$$\boxed{ds^2 = g_{mn} dx^m dx^n} \ . \tag{12.92}$$

12.4.1 Co- and contravariant tensors

A *contravariant* vector or tangent vector (often abbreviated simply as vector, such as a direction vector or velocity vector) has components that contra-vary with a change of basis to compensate. That is, the matrix that transforms the vector components must be the inverse of the matrix that transforms the basis vectors. Examples of contravariant vectors include the position of an object relative to an observer, or any derivative of position with respect to time, including velocity and acceleration. Contravariant components are denoted with upper indices as in,

$$\mathbf{v} = v^i \mathbf{e}_i \ . \tag{12.93}$$

A *covariant* vector or cotangent vector has components that co-vary with a change of basis. That is, the components must be transformed by the same matrix as the

change of basis matrix. Examples of covariant vectors generally appear when taking a gradient of a function. Covariant components are denoted with lower indices as in,

$$\mathbf{w} = w_i \mathbf{e}^i \ . \tag{12.94}$$

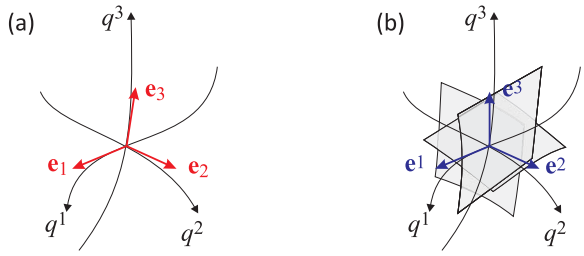

Figure 12.9: (a) Covariant and (b) contravariant basis.

12.4.2 Jacobian for coordinate transformations

The *Jacobian* of a vector field $\mathbf{F}$ is a matrix defined by,

$$\mathbf{J} \equiv \frac{\partial(F_1, .., F_m)}{\partial(x_1, .., x_n)} \equiv \left(\frac{\partial F_m}{\partial x_n} \right) \equiv (J^m_{\ n}) \ . \tag{12.95}$$

We may understand a curvilinear coordinate system $\{x^\mu\}$ as a vector field in Cartesian space $\{x'^\nu\}$,

$$x^\mu = x^\mu(x'^1, .., x'^\nu, .., x'^m) \tag{12.96}$$

for $\mu = 1, .., m$. The Jacobian of this field represents a tool used to transform between the coordinate systems by taking the rate of change of each component of an old basis with respect to each component of a new basis and expressing them as coefficients that make up an old basis. Do the Excs. 12.4.4.2 and 12.4.4.3,

$$\boxed{J^i_{\ j} \equiv \frac{\partial^i x}{\partial x'^j}} \ . \tag{12.97}$$

Example 38 (*Jacobian for polar coordinates*): For example, the Jacobian matrix that transforms polar coordinates to Cartesian coordinates in 2 dimensions is given by,

$$J^i_{\ j} = \begin{pmatrix} \partial_r x & \partial_\theta x \\ \partial_r y & \partial_\theta y \end{pmatrix} = \begin{pmatrix} \cos\theta & r\sin\theta \\ \sin\theta & r\cos\theta \end{pmatrix} \ . \tag{12.98}$$

The components of Cartesian basis vectors can now be written as a linear combination of these coefficients and their corresponding polar bases,

$$\begin{aligned} \hat{\mathbf{e}}_x &= \frac{\partial x}{\partial r}\hat{\mathbf{e}}_r + \frac{\partial x}{\partial \theta}\hat{\mathbf{e}}_\theta = \hat{\mathbf{e}}_r \cos\theta - \hat{\mathbf{e}}_\theta r \sin\theta \\ \hat{\mathbf{e}}_y &= \frac{\partial y}{\partial r}\hat{\mathbf{e}}_r + \frac{\partial y}{\partial \theta}\hat{\mathbf{e}}_\theta = \hat{\mathbf{e}}_r \sin\theta + \hat{\mathbf{e}}_\theta r \cos\theta \ . \end{aligned} \tag{12.99}$$

In the case of relating the Jacobian to the *metric* tensor, the Jacobian can be used to transform the components of one metric to another via the following method,

$$g'_{ij} = \frac{\partial}{\partial x'^i}\frac{\partial}{\partial x'^j} = \left(\frac{\partial x^a}{\partial x'^i}\frac{\partial}{\partial x^a}\right)\left(\frac{\partial x^b}{\partial x'^i}\frac{\partial}{\partial x^b}\right) = \frac{\partial x^a}{\partial x'^i}\frac{\partial x^b}{\partial x'^i}\left(\frac{\partial}{\partial x^a}\frac{\partial}{\partial x^b}\right) = J^a{}_i J^b{}_j g_{ab} \ . \tag{12.100}$$

Knowing this, taking the determinant of the metric g_{ij} requires taking the determinant of the Jacobian matrices and g_{ab} as well,

$$\det g'_{ij} = (\det J^a{}_i)(\det J^b{}_j)(\det g_{ab}) \ . \tag{12.101}$$

Since both Jacobian terms are part of the same matrix and are just written using different indices to differentiate between the components of the old basis,

$$(\det J^a{}_i)(\det J^b{}_j) = (\det J)^2 \ . \tag{12.102}$$

In the case of our old basis being written in Cartesian coordinates,

$$\det g_{ab} = \det \mathbb{I} = 1 \ . \tag{12.103}$$

Therefore the equation of our new transformed metric g_{ij}, simplifies to,

$$\det g_{ij} = (\det J)^2 \quad \Longrightarrow \quad \det J = \sqrt{\det g_{ij}} \ . \tag{12.104}$$

It can be shown that,

$$\frac{d}{dt}\frac{\partial(u,v)}{\partial(x,y)} \equiv \frac{\partial(\frac{d}{dt}u, v)}{\partial(x,y)} + \frac{\partial(u, \frac{d}{dt}v)}{\partial(x,y)} \ . \tag{12.105}$$

The *Hessian* is a square matrix of second-order partial derivatives of a scalar field.

12.4.3 Metric and geodesic equation in Euclidean space

For an arbitrary curvilinear coordinate system u^i we define tangent vectors forming a basis,

$$\mathbf{e}_i = \frac{\partial}{\partial u^i} = \partial_i \ , \tag{12.106}$$

the metric tensor is,

$$g_{ij} \equiv \mathbf{e}_i \cdot \mathbf{e}_j \ . \tag{12.107}$$

See also Secs. 6.4 and 20.5.

12.4.3.1 Metric in spherical coordinates

For spherical coordinates,

$$\mathbf{r} = \begin{pmatrix} x \\ y \\ z \end{pmatrix} = \begin{pmatrix} r\sin\theta\cos\phi \\ r\sin\theta\sin\phi \\ r\cos\theta \end{pmatrix} \quad , \quad \begin{pmatrix} r \\ \theta \\ \phi \end{pmatrix} = \begin{pmatrix} \sqrt{x^2+y^2+z^2} \\ \arccos\frac{z}{\sqrt{x^2+y^2+z^2}} \\ \arctan\frac{y}{x} \end{pmatrix} \ , \tag{12.108}$$

the tangent vectors are,

$$\begin{aligned}
\mathbf{e}_r &= \frac{\partial \mathbf{r}}{\partial r} = \hat{\mathbf{e}}_x \sin\theta\cos\phi + \hat{\mathbf{e}}_y \sin\theta\sin\phi + \hat{\mathbf{e}}_z \cos\theta = \hat{\mathbf{e}}_r \\
\mathbf{e}_\theta &= \frac{\partial \mathbf{r}}{\partial \theta} = r\hat{\mathbf{e}}_x \cos\theta\cos\phi + r\hat{\mathbf{e}}_y \cos\theta\sin\phi - r\hat{\mathbf{e}}_z \sin\theta = r\hat{\mathbf{e}}_\theta \\
\mathbf{e}_\phi &= \frac{\partial \mathbf{r}}{\partial \phi} = -r\sin\theta\hat{\mathbf{e}}_x \sin\phi + r\sin\theta\hat{\mathbf{e}}_y \cos\phi = r\sin\theta\hat{\mathbf{e}}_\phi \ .
\end{aligned} \tag{12.109}$$

Note that, in contrast to the basis vectors $\hat{\mathbf{e}}_i$ the tangent vectors $\mathbf{e}_i$ are not normalized. The spherical metric is,

$$g_{ij} = \frac{\partial x_a}{\partial u^i}\frac{\partial x^a}{\partial u^j} = \begin{pmatrix} \mathbf{e}_r\cdot\mathbf{e}_r & \mathbf{e}_r\cdot\mathbf{e}_\theta & \mathbf{e}_r\cdot\mathbf{e}_\phi \\ \mathbf{e}_\theta\cdot\mathbf{e}_r & \mathbf{e}_\theta\cdot\mathbf{e}_\theta & \mathbf{e}_\theta\cdot\mathbf{e}_\phi \\ \mathbf{e}_\phi\cdot\mathbf{e}_r & \mathbf{e}_\phi\cdot\mathbf{e}_\theta & \mathbf{e}_\phi\cdot\mathbf{e}_\phi \end{pmatrix} = \begin{pmatrix} 1 & 0 & 0 \\ 0 & r^2 & 0 \\ 0 & 0 & r^2\sin^2\theta \end{pmatrix} ,$$

with $x_a = x, y, z$, $u^i = r, \theta, \phi$, and the contra-variant spherical metric being,

$$g^{ij} = \frac{\partial u^i}{\partial x_a}\frac{\partial u^j}{\partial x^a} = \begin{pmatrix} 1 & 0 & 0 \\ 0 & r^{-2} & 0 \\ 0 & 0 & r^{-2}\sin^{-2}\theta \end{pmatrix} . \tag{12.110}$$

we obtain the contra-variant tangent vectors,

$$\begin{aligned}
\mathbf{e}^r &= g^{rr}\mathbf{e}_r = \hat{\mathbf{e}}_x \sin\theta\cos\phi + \hat{\mathbf{e}}_y \sin\theta\sin\phi + \hat{\mathbf{e}}_z \cos\theta = \hat{\mathbf{e}}_r \\
\mathbf{e}^\theta &= g^{\theta\theta}\mathbf{e}_\theta = \frac{1}{r}\hat{\mathbf{e}}_x \cos\theta\cos\phi + \frac{1}{r}\hat{\mathbf{e}}_y \cos\theta\sin\phi - \frac{1}{r}\hat{\mathbf{e}}_z \sin\theta = \frac{1}{r}\hat{\mathbf{e}}_\theta \\
\mathbf{e}^\phi &= g^{\phi\phi}\mathbf{e}_\phi = -\frac{1}{r\sin\theta}\hat{\mathbf{e}}_x \sin\phi + \frac{1}{r\sin\theta}\hat{\mathbf{e}}_y \cos\phi = \frac{1}{r\sin\theta}\hat{\mathbf{e}}_\phi \ .
\end{aligned} \tag{12.111}$$

The diagonal shape of the metrics are comes from the fact that spherical coordinates are orthogonal. In the example 39 we discuss the metric of an non-orthogonal coordinate system.

Example 39 (*Metric in elliptical coordinates*): In contrast to polar, cylindrical, or spherical coordinates, elliptical coordinates given by,

$$\mathbf{r} = \begin{pmatrix} x \\ y \end{pmatrix} = \begin{pmatrix} ar\cos\phi \\ br\sin\phi \end{pmatrix} \quad , \quad \begin{pmatrix} r \\ \phi \end{pmatrix} = \begin{pmatrix} \sqrt{(\frac{x}{a})^2 + (\frac{y}{b})^2} \\ \arctan\frac{ay}{bx} \end{pmatrix} , \tag{12.112}$$

are not orthogonal. The tangent vectors are,

$$\begin{aligned}
\mathbf{e}_r &= \frac{\partial \mathbf{r}}{\partial r} = \hat{\mathbf{e}}_x a\cos\phi + \hat{\mathbf{e}}_y b\sin\phi \\
\mathbf{e}_\phi &= \frac{\partial \mathbf{r}}{\partial \phi} = -\hat{\mathbf{e}}_x ar\sin\phi + \hat{\mathbf{e}}_y br\cos\phi \ .
\end{aligned} \tag{12.113}$$

Note that, in contrast to the basis vectors $\hat{\mathbf{e}}_i$ the tangent vectors $\mathbf{e}_i$ are not normalized. The elliptical metric is,

$$g_{ij} = \frac{\partial x_a}{\partial u^i}\frac{\partial x^a}{\partial u^j} = \begin{pmatrix} \mathbf{e}_r \cdot \mathbf{e}_r & \mathbf{e}_r \cdot \mathbf{e}_\phi \\ \mathbf{e}_\phi \cdot \mathbf{e}_r & \mathbf{e}_\phi \cdot \mathbf{e}_\phi \end{pmatrix} = \begin{pmatrix} a^2\cos^2\phi + b^2\sin^2\phi & (b^2-a^2)r\sin\phi\cos\phi \\ (b^2-a^2)r\sin\phi\cos\phi & (a^2\sin^2\phi + b^2\cos^2\phi)r^2 \end{pmatrix} ,$$

with $x_a = x, y$, $u^i = r, \phi$, and the contra-variant elliptical metric being,

$$g^{ij} = \frac{\partial u^i}{\partial x_a}\frac{\partial u^j}{\partial x^a} = \frac{1}{a^2b^2r^2}\begin{pmatrix} a^2r^2\sin^2\phi + b^2r^2\cos^2\phi & (a^2-b^2)r\sin\phi\cos\phi \\ (a^2-b^2)r\sin\phi\cos\phi & a^2\cos^2\phi + b^2\sin^2\phi) \end{pmatrix} . \tag{12.114}$$

we obtain the cotangent vectors,

$$\begin{aligned} \mathbf{e}^r &= g^{ri}\mathbf{e}_i = g^{rr}\mathbf{e}_r + g^{r\phi}\mathbf{e}_\phi = \hat{\mathbf{e}}_x a^{-1}\cos\phi + \hat{\mathbf{e}}_y b^{-1}\sin\phi \qquad (12.115) \\ \mathbf{e}^\phi &= g^{\phi i}\mathbf{e}_i = g^{\phi r}\mathbf{e}_r + g^{\phi\phi}\mathbf{e}_\phi = -\hat{\mathbf{e}}_x a^{-1}r^{-1}\sin\phi + \hat{\mathbf{e}}_y b^{-1}r^{-1}\cos\phi . \end{aligned}$$

The fact that the metric is not diagonal is due to the elliptical coordinates not being orthogonal. One verifies,

$$\mathbf{e}^r \cdot \mathbf{e}_\phi = 0 = \mathbf{e}_r \cdot \mathbf{e}^\phi \quad , \quad \mathbf{e}^r \cdot \mathbf{e}_r = 1 = \mathbf{e}_\phi \cdot \mathbf{e}^\phi . \tag{12.116}$$

Interestingly, while neither the tangent nor the cotangent vectors are orthogonal, they are mutually orthogonal.

12.4.3.2 Christoffel symbols

The Christoffel symbols are defined by,

$$\Gamma^k_{\ ij} \equiv \frac{\partial \mathbf{e}_i}{\partial x^j}\cdot\mathbf{e}^k . \tag{12.117}$$

They yields for spherical coordinates with $j = r, \theta, \phi$,

$$\Gamma^a_{\ ir} = \begin{pmatrix} 0 & 0 & 0 \\ 0 & r^{-1} & 0 \\ 0 & 0 & r^{-1} \end{pmatrix} \quad , \quad \Gamma^a_{\ i\theta} = \begin{pmatrix} 0 & -r & 0 \\ r^{-1} & 0 & 0 \\ 0 & 0 & -\tan\theta \end{pmatrix} \tag{12.118}$$

$$\Gamma^a_{\ i\phi} = \begin{pmatrix} 0 & 0 & -r\cos^2\theta \\ 0 & r^{-1} & \sin\theta\cos\theta \\ r^{-1} & -\tan\theta & 0 \end{pmatrix} .$$

Do the Exc. 12.4.4.4.

12.4.3.3 Geodesic equation

In differential geometry the *geodesic equation* is a curve representing in some sense the shortest path between two points in a surface, or more generally in a Riemannian manifold. It is a generalization of the notion of a 'straight line'. The geodesic line is obtained by solving the differential equation,

$$\frac{d^2x^k}{ds^2} + \Gamma^k_{\ ab}\frac{dx^a}{ds}\frac{dx^b}{ds} = 0 . \tag{12.119}$$

12.4.4 Exercises

12.4.4.1 Ex: Tensors of rank n

Be given $\mathbf{F} = \mathbf{E} + \imath\mathbf{B}$ and $\mathbf{F}^* = \mathbf{E} - \imath\mathbf{B}$. Identify (in this order) the scalar $\mathbf{F}^* \cdot \mathbf{F}/(8\pi)$, teh vector $\mathbf{F}^* \times \mathbf{F}/(8\pi\imath)$, and the dyade (tensor) $(\mathbf{F}^* \cdot \mathbf{F} + \mathbf{F} \cdot \mathbf{F}^*)/(8\pi)$. What happens to these quantities if we exchange $\mathbf{F}$ for $e^{-\imath\phi}\mathbf{F}$, where ϕ is supposed constant?

Solution: *We get first,*

$$\frac{1}{8\pi}\mathbf{F}^* \cdot \mathbf{F} = \frac{1}{8\pi}(\mathbf{E} - \imath\mathbf{B}) \cdot (\mathbf{E} + \imath\mathbf{B}) = \frac{1}{8\pi}(\mathbf{E}^2 + \mathbf{B}^2) = U \ .$$

Then,

$$\frac{1}{8\pi\imath}\mathbf{F}^* \times \mathbf{F} = \frac{1}{8\pi\imath}(\mathbf{E} - \imath\mathbf{B}) \times (\mathbf{E} + \imath\mathbf{B}) = \frac{1}{4\pi}(\mathbf{E} \times \mathbf{B}) = \frac{1}{c}\mathbf{S} \ .$$

Finally,

$$\begin{aligned}\frac{1}{8\pi}(\mathbf{F}^* \cdot \mathbf{F} + \mathbf{F} \cdot \mathbf{F}^*) &= \frac{1}{8\pi}\left[(\mathbf{E} - \imath\mathbf{B}) \cdot (\mathbf{E} + \imath\mathbf{B}) + (\mathbf{E} + \imath\mathbf{B}) \cdot (\mathbf{E} - i\mathbf{B})\right] \\ &= \frac{1}{8\pi}\left[\mathbf{E} \cdot \mathbf{E} + \imath\mathbf{B} \cdot \mathbf{E} - \imath\mathbf{E} \cdot \mathbf{B} + \mathbf{B} \cdot \mathbf{B} + \mathbf{E} \cdot \mathbf{E} - \imath\mathbf{B} \cdot \mathbf{E} + \imath\mathbf{E} \cdot \mathbf{B} + \mathbf{B} \cdot \mathbf{B}\right] \\ &= \frac{1}{4\pi}(\mathbf{E} \cdot \mathbf{E} + \mathbf{B} \cdot \mathbf{B}) = \overleftrightarrow{T} + U \overleftrightarrow{\mathbf{1}} \ .\end{aligned}$$

Exchanging,

$$\mathbf{F} \to e^{-\imath\phi}\mathbf{F} \qquad \textit{hence} \qquad \mathbf{F}^* \to e^{+\imath\phi}\mathbf{F}^* \ .$$

and we see immediately that all three expressions above are invariant about this transformation.

12.4.4.2 Ex: Jacobian for transformation into curvilinear coordinates

a. Calculate the Jacobian of the transformation from cylindrical coordinates (ρ, z, φ) to Cartesian coordinates (x, y, z).
b. Calculate the Jacobian of the transformation from spherical coordinates (r, θ, φ) to Cartesian coordinates (x, y, z).

Solution: *a. The Jacobian is given by the function* $\mathbf{F} = \mathbf{r}$ *with the components,*

$$\begin{aligned} x &= \rho\cos\varphi \\ y &= \rho\sin\varphi \\ z &= z \ . \end{aligned}$$

The Jacobian of this function is,

$$\mathbf{J}_\mathbf{F}(r, z, \varphi) = \begin{pmatrix} \frac{\partial x}{\partial \rho} & \frac{\partial x}{\partial z} & \frac{\partial x}{\partial \varphi} \\ \frac{\partial y}{\partial \rho} & \frac{\partial y}{\partial z} & \frac{\partial y}{\partial \varphi} \\ \frac{\partial z}{\partial \rho} & \frac{\partial z}{\partial z} & \frac{\partial z}{\partial \varphi} \end{pmatrix} = \begin{pmatrix} \cos\varphi & 0 & -\rho\sin\varphi \\ \sin\varphi & 0 & \rho\cos\varphi \\ 0 & 1 & 0 \end{pmatrix} \ .$$

The determinant is $-\rho$. As an example, the volume element can be expressed as $dV = dxdydz = \rho dr dz d\varphi$. However, this determinant varies with the coordinates.
b. The Jacobian is given by the function $\mathbf{F} = \mathbf{r}$ with the components,

$$\begin{aligned} x &= r\sin\theta\cos\varphi \\ y &= r\sin\theta\sin\varphi \\ z &= r\cos\theta \ . \end{aligned}$$

The Jacobian of this function is,

$$\mathbf{J}_{\mathbf{F}}(r,\theta,\varphi) = \begin{pmatrix} \frac{\partial x}{\partial r} & \frac{\partial x}{\partial \theta} & \frac{\partial x}{\partial \varphi} \\ \frac{\partial y}{\partial r} & \frac{\partial y}{\partial \theta} & \frac{\partial y}{\partial \varphi} \\ \frac{\partial z}{\partial r} & \frac{\partial z}{\partial \theta} & \frac{\partial z}{\partial \varphi} \end{pmatrix} = \begin{pmatrix} \sin\theta\cos\varphi & r\cos\theta\cos\varphi & -r\sin\theta\sin\varphi \\ \sin\theta\sin\varphi & r\cos\theta\sin\varphi & -r\sin\theta\cos\varphi \\ \cos\theta & -r\sin\theta & 0 \end{pmatrix} \ .$$

The determinant is $r^2\sin\theta$. As an example, the volume element can be expressed as $dV = dxdydz = r^2\sin\theta dr d\theta d\varphi$. However, this determinant varies with the coordinates.

12.4.4.3 Ex: Jacobian for Galilei and Lorentz transform

Determine the Jacobean of the Galilei transformation,

$$ct' = ct \quad \text{and} \quad x' = x \quad \text{and} \quad y' = y \quad \text{and} \quad z' = z - \tfrac{u}{c}ct \ ,$$

and the Lorentz transformation,

$$ct' = \gamma(ct - \tfrac{u}{c}x) \quad \text{and} \quad x' = x \quad \text{and} \quad y' = y \quad \text{and} \quad z' = \gamma(z - \tfrac{u}{c}z) \ .$$

Solution: *We have,*

$$G_{\mu\nu} = \frac{\partial x'_\mu}{\partial x_\nu} = \begin{pmatrix} 1 & 0 & 0 & 0 \\ 0 & 1 & 0 & 0 \\ 0 & 0 & 1 & 0 \\ -\frac{u}{c} & 0 & 0 & 1 \end{pmatrix} \quad , \quad \Lambda_{\mu\nu} = \frac{\partial x'_\mu}{\partial x_\nu} = \begin{pmatrix} \gamma & 0 & 0 & -\frac{u}{c}\gamma \\ 0 & 1 & 0 & 0 \\ 0 & 0 & 1 & 0 \\ -\frac{u}{c}\gamma & 0 & 0 & \gamma \end{pmatrix} \ .$$

12.4.4.4 Ex: Christoffel symbols for two-dimensional polar coordinates

Derive the Christoffel symbols for two-dimensional polar coordinates.

Solution: *Polar coordinates are defined by,*

$$\begin{pmatrix} x \\ y \end{pmatrix} = \begin{pmatrix} r\cos\varphi \\ r\sin\varphi \end{pmatrix} \quad , \quad \begin{pmatrix} r \\ \varphi \end{pmatrix} = \begin{pmatrix} \sqrt{x^2+y^2} \\ \arctan\frac{y}{x} \end{pmatrix} \ .$$

From the definition of the Christoffel symbols,

$$\Gamma^m{}_{ab} = \frac{\partial x^m}{\partial u^k}\frac{\partial^2 u^k}{\partial x^a \partial x^b} \ ,$$

we get explicitly,

$$\Gamma^a{}_{br} = \begin{pmatrix} \Gamma^r{}_{rr} & \Gamma^r{}_{\varphi r} \\ \Gamma^\varphi{}_{rr} & \Gamma^\varphi{}_{\varphi r} \end{pmatrix} = \begin{pmatrix} \frac{\partial r}{\partial x}\frac{\partial^2 x}{\partial r^2} + \frac{\partial r}{\partial y}\frac{\partial^2 y}{\partial r^2} & \frac{\partial r}{\partial x}\frac{\partial^2 x}{\partial \varphi \partial r} + \frac{\partial r}{\partial y}\frac{\partial^2 y}{\partial \varphi \partial r} \\ \frac{\partial \varphi}{\partial x}\frac{\partial^2 x}{\partial r^2} + \frac{\partial \varphi}{\partial y}\frac{\partial^2 y}{\partial r^2} & \frac{\partial \varphi}{\partial x}\frac{\partial^2 x}{\partial \varphi \partial r} + \frac{\partial \varphi}{\partial y}\frac{\partial^2 y}{\partial \varphi \partial r} \end{pmatrix} = \begin{pmatrix} 0 & 0 \\ 0 & 0 \end{pmatrix}$$

$$\Gamma^a{}_{b\varphi} = \begin{pmatrix} \Gamma^r{}_{r\varphi} & \Gamma^r{}_{\varphi\varphi} \\ \Gamma^\varphi{}_{r\varphi} & \Gamma^\varphi{}_{\varphi\varphi} \end{pmatrix} = \begin{pmatrix} \frac{\partial r}{\partial x}\frac{\partial^2 x}{\partial r \partial \varphi} + \frac{\partial r}{\partial y}\frac{\partial^2 y}{\partial r \partial \varphi} & \frac{\partial r}{\partial x}\frac{\partial^2 x}{\partial \varphi^2} + \frac{\partial r}{\partial y}\frac{\partial^2 y}{\partial \varphi^2} \\ \frac{\partial \varphi}{\partial x}\frac{\partial^2 x}{\partial r \partial \varphi} + \frac{\partial \varphi}{\partial y}\frac{\partial^2 y}{\partial r \partial \varphi} & \frac{\partial \varphi}{\partial x}\frac{\partial^2 x}{\partial \varphi^2} + \frac{\partial \varphi}{\partial y}\frac{\partial^2 y}{\partial \varphi^2} \end{pmatrix} = \begin{pmatrix} 0 & -r \\ 0 & 0 \end{pmatrix} \ .$$

12.4.4.5 Ex: Distorted polar coordinates

a. Study the coordinate system,

$$\mathbf{r} = \begin{pmatrix} x \\ y \end{pmatrix} = \begin{pmatrix} f(r)\cos\phi \\ g(r)\sin\phi \end{pmatrix}$$

for arbitrary radial functions $f(r)$ and $g(r)$.
b. Consider the particular cases (i) $f = g$ and (ii) $f = ar$ and $g = br$.

Solution: *a. The tangent vectors are,*

$$\mathbf{e}_r = \frac{\partial \mathbf{r}}{\partial r} = \hat{\mathbf{e}}_x f'(r)\cos\phi + \hat{\mathbf{e}}_y g'(r)\sin\phi$$
$$\mathbf{e}_\phi = \frac{\partial \mathbf{r}}{\partial \phi} = -\hat{\mathbf{e}}_x f(r)\sin\phi + \hat{\mathbf{e}}_y g(r)\cos\phi \ ,$$

and the metric,

$$g_{ij} = \begin{pmatrix} f'(r)^2\cos^2\phi + g'(r)^2\sin^2\phi & [g(r)g'(r) - f(r)f'(r)]\sin\phi\cos\phi \\ [g(r)g'(r) - f(r)f'(r)]\sin\phi\cos\phi & f(r)^2\sin^2\phi + g(r)^2\cos^2\phi \end{pmatrix} \ .$$

The determinant of the metric is,

$$\det g_{ij} = \left[f'(r)g(r)\cos^2\phi + f(r)g'(r)\sin^2\phi\right]^2$$

and the inverse metric,

$$g^{ij} = g_{ij}^{-1} = \frac{1}{\det g_{ij}}\begin{pmatrix} f'(r)^2\sin^2\phi + g'(r)^2\cos^2\phi & [f(r)f'(r) - g(r)g'(r)]\sin\phi\cos\phi \\ [f(r)f'(r) - g(r)g'(r)]\sin\phi\cos\phi & f(r)^2\cos^2\phi + g(r)^2\sin^2\phi \end{pmatrix} \ .$$

b. For the case $f = g$ this simplifies to,

$$g_{ij} = \begin{pmatrix} f'(r)^2 & 0 \\ 0 & f(r)^2 \end{pmatrix} \quad , \quad g^{ij} = \begin{pmatrix} f(r)^2 & 0 \\ 0 & f'(r)^2 \end{pmatrix} ,$$

and for the case, $f = ar$ and $g = br$ to,

$$g_{ij} = \begin{pmatrix} a^2\cos^2\phi + b^2\sin^2\phi & (b^2-a^2)r\sin\phi\cos\phi \\ (b^2-a^2)r\sin\phi\cos\phi & (a^2\sin^2\phi + b^2\cos^2\phi)r^2 \end{pmatrix}$$
$$g^{ij} = \begin{pmatrix} a^{-2}\cos^2\phi + b^{-2}\sin^2\phi & (b^{-2}-a^{-2})r^{-1}\sin\phi\cos\phi \\ (b^{-2}-a^{-2})r^{-1}\sin\phi\cos\phi & (a^{-2}\sin^2\phi + b^{-2}\cos^2\phi)r^{-2} \end{pmatrix} .$$

12.4.4.6 Ex: Metric for ellipsoidal coordinates

Generalize the metric for ellipsoidal coordinates.

Solution: *For ellipsoidal coordinates,*

$$\mathbf{r} = \begin{pmatrix} x \\ y \\ z \end{pmatrix} = \begin{pmatrix} ar\sin\theta\cos\phi \\ br\sin\theta\sin\phi \\ cr\cos\theta \end{pmatrix} \quad , \quad \begin{pmatrix} r \\ \theta \\ \phi \end{pmatrix} = \begin{pmatrix} \sqrt{\left(\frac{x}{a}\right)^2 + \left(\frac{y}{b}\right)^2 + \left(\frac{z}{c}\right)^2} \\ \arccos \frac{z/c}{\sqrt{(x/a)^2+(y/b)^2+(z/c)^2}} \\ \arctan \frac{ay}{bx} \end{pmatrix} ,$$

the tangent vectors are,

$$\mathbf{e}_r = \frac{\partial \mathbf{r}}{\partial r} = a\hat{\mathbf{e}}_x \sin\theta\cos\phi + b\hat{\mathbf{e}}_y \sin\theta\sin\phi + c\hat{\mathbf{e}}_z\cos\theta$$
$$\mathbf{e}_\theta = \frac{\partial \mathbf{r}}{\partial \theta} = ar\hat{\mathbf{e}}_x \cos\theta\cos\phi + br\hat{\mathbf{e}}_y \cos\theta\sin\phi - cr\hat{\mathbf{e}}_z\sin\theta$$
$$\mathbf{e}_\phi = \frac{\partial \mathbf{r}}{\partial \phi} = -ar\hat{\mathbf{e}}_x \sin\theta\sin\phi + br\hat{\mathbf{e}}_y \sin\theta\cos\phi \ .$$

Note that, in contrast to the basis vectors $\hat{\mathbf{e}}_i$ the tangent vectors $\mathbf{e}_i$ are not normalized. The ellipsoidal metric is,

$$g_{ij} = \frac{\partial x_a}{\partial u^i}\frac{\partial x^a}{\partial u^j} = \begin{pmatrix} \mathbf{e}_r\cdot\mathbf{e}_r & \mathbf{e}_r\cdot\mathbf{e}_\theta & \mathbf{e}_r\cdot\mathbf{e}_\phi \\ \mathbf{e}_\theta\cdot\mathbf{e}_r & \mathbf{e}_\theta\cdot\mathbf{e}_\theta & \mathbf{e}_\theta\cdot\mathbf{e}_\phi \\ \mathbf{e}_\phi\cdot\mathbf{e}_r & \mathbf{e}_\phi\cdot\mathbf{e}_\theta & \mathbf{e}_\phi\cdot\mathbf{e}_\phi \end{pmatrix}$$
$$= \begin{pmatrix} B_\phi\sin^2\theta + c^2\cos^2\theta & (B_\phi - c^2)r\sin\theta\cos\theta & C_\phi r\sin^2\theta \\ (B_\phi - c^2)r\sin\theta\cos\theta & (B_\phi\cos^2\theta + c^2\sin^2\theta)r^2 & C_\phi r^2\sin\theta\cos\theta \\ C_\phi r\sin^2\theta & C_\phi r^2\sin\theta\cos\theta & A_\phi r^2\sin^2\theta \end{pmatrix} ,$$

with $x_a = x, y, z$, $\xi^i = r, \theta, \phi$ *and with the abbreviations* $A_\phi \equiv a^2 \sin^2\phi + b^2 \cos^2\phi$, $B_\phi \equiv a^2 \cos^2\phi + b^2 \sin^2\phi$, *and* $C_\phi \equiv (b^2 - a^2)\sin\phi\cos\phi$. *The determinant is,*

$$\det g_{ij} = a^2 b^2 c^2 r^4 \sin^2\theta \ .$$

The contra-variant ellipsoidal metric being,

$$g^{ij} = g_{ij}^{-1} = \frac{\partial \xi^i}{\partial x_a}\frac{\partial \xi^j}{\partial x^a}$$

$$= \frac{1}{a^2 b^2 c^2 r^2}\begin{pmatrix} (a^2 b^2 \cos^2\theta + A_\phi c^2 \sin^2\theta) r^2 & (-a^2 b^2 + A_\phi c^2) r \sin\theta\cos\theta & -C_\phi c^2 r \\ (-a^2 b^2 + A_\phi c^2) r \sin\theta\cos\theta & a^2 b^2 \sin^2\theta + A_\phi c^2 \cos^2\theta & -C_\phi c^2 \cot\theta \\ -C_\phi c^2 r & -C_\phi c^2 \cot\theta & \frac{B_\phi c^2}{\sin^2\theta} \end{pmatrix} .$$

we obtain the contra-variant tangent vectors,

$$\begin{aligned} \mathbf{e}^r &= g^{ri}\mathbf{e}_i = \frac{\hat{\mathbf{e}}_x \sin\theta\cos\phi}{a} + \frac{\hat{\mathbf{e}}_y \sin\theta\sin\phi}{b} + \frac{\hat{\mathbf{e}}_z \cos\theta}{c} \\ \mathbf{e}^\theta &= g^{\theta i}\mathbf{e}_i = \frac{\hat{\mathbf{e}}_x \cos\theta\cos\phi}{ar} + \frac{\hat{\mathbf{e}}_y \cos\theta\sin\phi}{br} - \frac{\hat{\mathbf{e}}_z \sin\theta}{cr} \\ \mathbf{e}^\phi &= g^{\phi i}\mathbf{e}_i = -\frac{\hat{\mathbf{e}}_x \sin\phi}{ar\sin\theta} + \frac{\hat{\mathbf{e}}_y \cos\phi}{br\sin\theta} \ . \end{aligned}$$

One verifies,

$$\mathbf{e}^i \cdot \mathbf{e}_j = \delta_{ij} \qquad , \qquad \mathbf{e}^i \cdot \mathbf{e}^j \neq 0, 1 \ ,$$

for $i, j = r, \theta, \phi$.

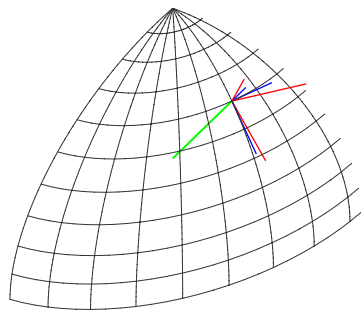

Figure 12.10: (code) Tangent and cotangent coordinates on an ellipsoid.

12.5 Dirac's δ-function

Calculating the divergence of the vector field $\mathbf{A} = \mathbf{r}/r^3$ in spherical coordinates [1],

$$\nabla \cdot \mathbf{A} = \frac{1}{r^2}\frac{\partial}{\partial r}\left(r^2 \frac{1}{r^2}\right) = 0 \ , \tag{12.120}$$

[1] Or in Cartesian coordinates: $\nabla \cdot \mathbf{A} = \frac{\partial}{\partial r^3}\frac{x}{r^3} + \frac{\partial}{\partial r^3}\frac{y}{r^3} + \frac{\partial}{\partial r^3}\frac{z}{r^3} = \frac{3r^3 - 3x^2 r}{r^6} + ... = 0.$

we expect,

$$\int_{sphere} \nabla \cdot \mathbf{A} dV = 0 \ . \tag{12.121}$$

This is surprising, because intuition tells us to expect a huge divergence near the origin. The problem is that the field $\mathbf{A}$ diverges at the origin, which calls for a modification of the expression for the gradient. Gauß' law gives us an indication since, according to this law, the result (12.121) should be equal to the surface integral,

$$\oint_{\partial\ sphere} \mathbf{A} \cdot d\mathbf{S} = \int_0^{2\pi} \int_0^{\pi} \frac{\hat{\mathbf{e}}_r}{R^2} \cdot (R^2 \sin\theta d\theta d\phi \hat{\mathbf{e}}_r) = 4\pi \ . \tag{12.122}$$

As the integral (12.121) contains a divergence within the volume of integration, we conclude that the integral (12.122), which has no divergence within the integration surface is more reliable. Therefore, we look for a function δ satisfying,

$$\int_{sphere} \nabla \cdot \mathbf{A}(\mathbf{r}) dV = \int_{sphere} 4\pi\delta(\mathbf{r}) dV = 4\pi \ , \tag{12.123}$$

that is, a function having the property of killing integrals.

12.5.1 The Dirac function in 1 dimension

In one dimension the *Dirac function* is defined by,

$$\boxed{\delta(x) \equiv \begin{cases} 0 & \text{for} \quad x \neq 0 \\ \infty & \text{for} \quad x = 0 \end{cases}} \ , \tag{12.124}$$

such that,

$$\int_{-\infty}^{\infty} \delta(x) dx = 1 \ . \tag{12.125}$$

The Dirac function can be expressed as the limit of a series of continuous functions,

$$\begin{aligned} \delta(x) &= \lim_{n\to\infty} \frac{n}{\pi} \frac{1}{1+n^2x^2} \\ \delta(x) &= \lim_{n\to\infty} \frac{n}{\pi} \left(\frac{\sin nx}{nx}\right)^2 \\ \delta(x) &= \lim_{n\to\infty} \frac{1}{\pi} \frac{\sin nx}{x} = \lim_{n\to\infty} \frac{1}{2\pi} \int_{-n}^{+n} e^{\imath kx} dk \ . \end{aligned} \tag{12.126}$$

We also note that the Dirac function is even, $\delta(-x) = \delta(x)$, non-linear, $\delta(ax) = \delta(x)/|a|$, and can be interpreted as the derivative of the *Heavyside function*,

$$\int_{-\infty}^{x} \delta(x') dx' = \Theta(x) \qquad \text{or} \qquad \frac{d\Theta}{dx} = \delta(x) \ . \tag{12.127}$$

We will train the calculus with the Dirac function in Excs. 12.5.4.1 to 12.5.4.3.

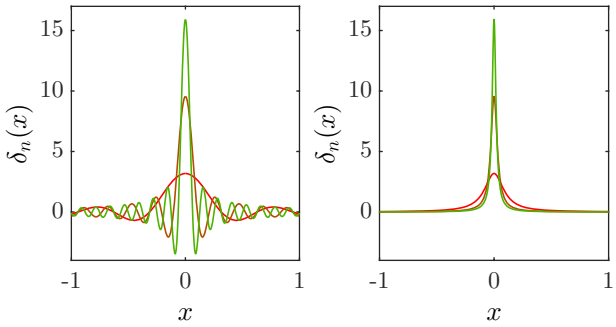

Figure 12.11: (code) Illustration of the function $\frac{1}{\pi}\frac{\sin nx}{x}$ (left) and of the function $\frac{1}{\pi}\frac{n}{1+n^2x^2}$ (right) for various $n \to \infty$.

When the argument of a Dirac function is itself a function $f(x)$, the Dirac is evaluated at each zero-passage of f,

$$\boxed{\int_a^b dx\ g(x)\delta(f(x)) = \int_a^b dx\ g(x)\sum_i \frac{\delta(x-x_i)}{|f'(x_i)|}}\ , \tag{12.128}$$

where $f'(x_i) \neq 0$. We will apply this theorem in Exc. 12.5.4.4.

12.5.2 The Dirac function in 2 and 3 dimensions

In more dimensions the δ-function is often used to parametrize points, paths, or surfaces within a volume. For example, a point charge Q at the position $\mathbf{a}$ can be described by the three-dimensional density distribution,

$$\rho(\mathbf{r}) = Q\delta^3(\mathbf{r}-\mathbf{a}) = Q\delta(x-a_x)\delta(y-a_y)\delta(z-a_z)\ , \tag{12.129}$$

a current I in a circular loop with radius R within the $z=0$ plane generates a current density,

$$\mathbf{j} = I\delta(r-R)\delta(z)\hat{\mathbf{e}}_\phi\ , \tag{12.130}$$

called a *current yarn*. Similarly, a two-dimensional arrangement of charges σ homogeneously distributed over the surface of a sphere with radius R can be described by the three-dimensional density distribution,

$$\rho(\mathbf{r}) = \sigma\delta(r-R)\ . \tag{12.131}$$

Such parametrizations are useful, because they can be applied in fundamental laws of electromagnetism (see Exc. 12.5.4.5).

Example 40 (*Parametrization of a current distribution*): As an example we calculate the current I produced by the distribution (12.130) crossing a rectangular area around the point $\mathbf{r} = R\hat{\mathbf{e}}_x$,

$$\int_{area}\mathbf{j}\cdot d\mathbf{A} = I\int_{R-\Delta x}^{R+\Delta x}\int_{-\Delta z}^{\Delta z}\delta(r-R)\delta(z)\hat{\mathbf{e}}_y d\mathbf{A} = I\int_{r-\Delta x}^{r+\Delta x}\delta(x-R)dx = I\ .$$

Example 41 (*Parametrization of a charge distribution*): In another example we calculate the total charge Q produced by the distribution (12.131),

$$\int_{volume} \rho(\mathbf{r}) dV = \sigma \int_0^{2\pi} \int_0^{\pi} \int_0^{\infty} \delta(r-R) r^2 \sin\theta d\theta d\phi dr = \sigma 4\pi R^2 = Q \ .$$

Example 42 (*Dirac function in Coulomb's Law*): In a third example we show that the field of a point charge, $\varrho(\mathbf{r}) = Q\delta(x)\delta(y)\delta(z)$, can be obtained from Coulomb's law,

$$\vec{\mathcal{E}} = \int \frac{\varrho(\mathbf{r}')}{4\pi\varepsilon_0} \frac{\mathbf{r}-\mathbf{r}'}{|\mathbf{r}-\mathbf{r}'|^3} dV' = \frac{Q}{4\pi\varepsilon_0} \frac{\mathbf{r}}{r^3} \ .$$

12.5.3 Analytical signals

In signal processing theory, an *analytic signal* is a complex-valued function without negative frequency components. The real and imaginary parts of an analytic signal are mutually related by a *Hilbert transform*. Conversely, the analytic representation of a real-valued function is an analytic signal, which comprises the original function and its Hilbert transform. This representation facilitates many mathematical manipulations. The basic idea is that the negative frequency components of the Fourier transform (or spectrum) of a real function are superfluous due to the Hermitian symmetry of such a spectrum. These negative-frequency components can be discarded without loss of information, as long as we are willing to deal with a complex function. This makes certain attributes of the function more accessible, particularly for application in radiofrequency manipulation techniques.

While the manipulated function has no negative frequency components (that is, it is still analytic), the inverse conversion from complex to real is just a matter of discarding the imaginary part. The analytical representation is a generalization of the *phasor* concept: while the phasor is restricted to time-invariant amplitudes, phases and frequencies, the analytic signal allows for temporally variable parameters.

12.5.3.1 Transfer function generating an analytical signal

We consider a real function $s(t)$ with its Fourier transform $S(f)$. Then the transformed function exhibits a Hermitian symmetry about the point $f = 0$, since,

$$S(-f) = S(f)^* \ , \tag{12.132}$$

The function,

$$S_a(f) \equiv \begin{cases} 2S(f) & \text{for } f > 0 \\ S(f) & \text{for } f = 0 \\ 0 & \text{for } f < 0 \end{cases} = S(f) + \text{sgn}(f) S(f) \ , \tag{12.133}$$

where $\mathrm{sgn}(f)$ calculates the sign of f, only contains the non-negative components of $S(f)$. This operation is reversible due to the Hermitian symmetry of $S(f)$:

$$S(f) = \begin{cases} \frac{1}{2}S_a(f) & \text{para } f > 0 \\ S_a(f) & \text{para } f = 0 \\ \frac{1}{2}S_a(-f)^* & \text{para } f < 0 \end{cases} = \tfrac{1}{2}[S_a(f) + S_a(-f)^*] \ . \tag{12.134}$$

The analytical signal of $s(t)$ is the inverse Fourier transform of $S_a(f)$,

$$\begin{aligned} s_a(t) &\equiv \mathcal{F}^{-1}[S_a(f)] = \mathcal{F}^{-1}[S(f) + \mathrm{sgn}(f) \cdot S(f)] \\ &= \mathcal{F}^{-1}[S(f)] + \mathcal{F}^{-1}[\mathrm{sgn}(f)] \star \mathcal{F}^{-1}[S(f)] = s(t) + \imath \left[\tfrac{1}{\pi t} \star s(t)\right] = s(t) + \imath\hat{s}(t) \ , \end{aligned} \tag{12.135}$$

where $\star$ denotes the convolution.

$$\boxed{\hat{s}(t) \equiv \mathcal{H}[s(t)] \equiv \tfrac{1}{\pi t} \star s(t) = \tfrac{1}{\pi}\mathcal{P}\int_{-\infty}^{\infty} \frac{s(\tau)}{t-\tau} d\tau} \ , \tag{12.136}$$

with $\mathcal{P}$ denoting Cauchy's principal value, is the definition of the *Hilbert transform* of $s(t)$ [2].

Example 43 (*Analytical signal of the cosine function*): We consider the signal $s(t) = \cos\omega t$, where $\omega > 0$. Now

$$\begin{aligned} \hat{s}(t) &= \cos(\omega t - \tfrac{\pi}{2}) = \sin\omega t \ , \\ s_a(t) &= s(t) + \imath\hat{s}(t) = \cos\omega t + \imath \sin\omega t = e^{\imath\omega t} \ . \end{aligned}$$

In general, the analytical representation of a simple sinusoidal function is obtained by expressing it in terms of complex exponentials, discarding the negative frequency components, and doubling the positive frequency components, as in the example $s(t) = \cos(\omega t + \theta) = \frac{1}{2}(e^{\imath(\omega t+\theta)} + e^{-\imath(\omega t+\theta)})$. Here, we get directly from Euler's formula,

$$s_a(t) = \begin{cases} e^{\imath(\omega t+\theta)} &= e^{\imath|\omega|t}e^{\imath\theta} & \text{if } \omega > 0 \\ e^{-\imath(\omega t+\theta)} &= e^{\imath|\omega|t}e^{-\imath\theta} & \text{if } \omega < 0 \end{cases} \ .$$

The analytical representation of a sum of sinusoidal functions is the sum of the analytical representations of the individual sinuses.

We note that it is not forbidden to compute $s_a(t)$ for a complex $s(t)$. But this representation may be irreversible, since the original spectrum is usually not symmetric. Therefore, with the exception of the case $s(t) = e^{-\imath\omega t}$ with $\omega > 0$, where,

$$\begin{aligned} \hat{s}(t) &= \imath e^{-\imath\omega t} \\ s_a(t) &= e^{-\imath\omega t} + \imath^2 e^{-\imath\omega t} = e^{-\imath\omega t} - e^{-\imath\omega t} = 0 \ , \end{aligned} \tag{12.137}$$

[2] Also holds,

$$\begin{aligned} \hat{s}(t) &= -\tfrac{1}{\pi}\lim_{\epsilon\to 0}\int_{\epsilon}^{\infty} \frac{s(t+\tau) - s(t-\tau)}{\tau} d\tau \\ \mathcal{H}(\mathcal{H}(s))(t) &= -s(t) \ . \end{aligned}$$

we assume real $s(t)$.

We also note that, since $s(t) = \mathfrak{Re}\,[s_a(t)]$, we can retrieve the negative-frequency components simply by discarding $\mathfrak{Im}\,[s_a(t)]$, which may seem counterintuitive. On the other hand, the conjugate complex part $s_a^*(t)$ contains only the negative-frequency components. Therefore, $s(t) = \mathfrak{Re}\,[s_a^*(t)]$ retrieves the suppressed positive frequency components. In Exc. 12.5.4.7 we calculate the intensity of an electromagnetic wave.

12.5.3.2 Envelope and instantaneous phase

An analytical signal can also be expressed in polar coordinates,

$$s_a(t) = |s_a(t)|e^{\imath\phi(t)} \ , \tag{12.138}$$

in terms of an instantaneous amplitude or *envelope* $|s_a(t)|$ varying with time and an instantaneous phase angle $\phi(t) \equiv \arg[s_a(t)]$. In Fig. 12.12 the blue curve shows $s(t)$ and the red curve shows $|s_a(t)|$.

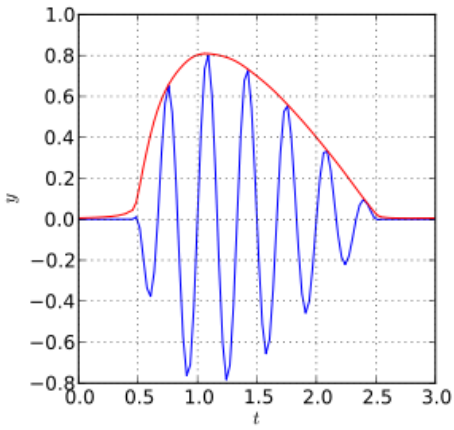

Figure 12.12: Illustration of a function (blue) and the magnitude of its analytical representation (red).

The time derivative of the unwrapped instantaneous phase is the instantaneous angular frequency,

$$\omega(t) \equiv \frac{d\phi(t)}{dt} \ . \tag{12.139}$$

The instantaneous amplitude and the instantaneous phase and frequency are used in some applications to measure and detect local characteristics of the signal or to describe the demodulation of a modulated signal. Polar coordinates conveniently separate amplitude and phase modulation effects.

Analytical signals are often frequency-shifted (down-converted) to 0 Hz, which can create negative (non-symmetric) frequency components:

$$s'_a(t) \equiv s_a(t)e^{-\imath\omega_0 t} = s_m(t)e^{\imath(\phi(t)-\omega_0 t)} \ , \tag{12.140}$$

where ω_0 is an arbitrary reference angular frequency. The function $s'_a(t)$ is called *complex envelope* or 'baseband'. The complex envelope is not unique, but determined

by the choice of ω_0. This concept is often used to deal with band-pass signals. When $s(t)$ is a modulated signal, ω_0 is conveniently chosen as the carrier frequency.

12.5.4 Exercises

12.5.4.1 Ex: Dirac's δ function

a. Calculate $\int_0^\pi d\theta \ \sin^3\theta \ \delta(\cos\theta - \cos\frac{\pi}{3})$.
b. Now, be $\mathbf{r}_0$ a fixed three-dimensional vector with Cartesian coordinates x_0, y_0, and z_0. For the three-dimensional δ-function holds,

$$\int_V f(\mathbf{r})\delta(\mathbf{r}-\mathbf{r}_0)d^3r = \begin{cases} f(\mathbf{r}_0) & \text{if } \mathbf{r}_0 \text{ is within the volume } V \\ 0 & \text{else} \end{cases} .$$

In Cartesian coordinates, $\delta^{(3)}(\mathbf{r}-\mathbf{r}_0) \equiv \delta(x-x_0)\delta(y-y_0)\delta(z-z_0)$. Express $\delta^{(3)}(\mathbf{r}-\mathbf{r}_0)$ in cylindrical coordinates (ρ,φ,z) as a product of three one-dimensional functions δ in $\rho-\rho_0$, $\varphi-\varphi_0$, and $z-z_0$.

Solution: *a. Here, $g(\theta) = \cos\theta - \cos\frac{\pi}{3}$. This function goes through zero within the interval $[0,\pi]$ at position $\theta_1 = \pi/3$. Now, $g'(\theta) = -\sin\theta$ and hence $g'(\theta_1) = -\sin\theta_1$. Consequently, we get,*

$$\int_0^\pi d\theta \sin^3\theta\delta(\cos\theta - \cos\tfrac{\pi}{3}) = \int_0^\pi d\theta \frac{\sin^3\theta}{|\sin\theta_1|}\delta(\theta - \tfrac{\pi}{3}) = \sin^2\theta_1 = \frac{3}{4} .$$

b. In cylindrical coordinates the volume element is, $d^3\mathbf{r} = \rho d\rho d\varphi dz$. We also have, $\mathbf{r} = (x = \rho\cos\varphi\ , y = \rho\sin\varphi\ , z)$ and $\mathbf{r}_0 = (x_0 = \rho_0\cos\varphi_0\ , y_0 = \rho_0\sin\varphi_0\ , z_0)$ Making the ansatz,

$$\delta^{(3)}(\mathbf{r}-\mathbf{r}_0) = f(\rho,\varphi,z)\delta(\rho-\rho_0)\delta(\varphi-\varphi_0)\delta(z-z_0) \ ,$$

we get immediately, (for $\mathbf{r}_0$ in V)

$$\begin{aligned} 1 = \int_V d^3\mathbf{r}\delta^{(3)}(\mathbf{r}-\mathbf{r}_0) &= \int_V d\rho\rho d\varphi dz f(\rho,\varphi,z)\delta(\rho-\rho_0)\delta(\varphi-\varphi_0)\delta(z-z_0) \\ &= \rho_0 f(\rho_0,\varphi_0,z_0) \end{aligned}$$

and hence, $f(\rho_0,\varphi_0,z_0) = \rho_0^{-1}$ respectively,

$$\delta^{(3)}(\mathbf{r}-\mathbf{r}_0) = \frac{1}{\rho_0}\delta(\rho-\rho_0)\delta(\varphi-\varphi_0)\delta(z-z_0) .$$

12.5.4.2 Ex: Dirac's δ function

Calculate the following expressions:
a. $\int_{-1}^{+1} \delta(x)[f(x) - f(0)]\ dx$,
b. $\int_{-1}^{3}(x^3 - x)\sin\left(\frac{\pi}{4}x\right)\delta(x-2)\ dx$,

c. $\int_0^{2\pi} \sin x \ \delta(\cos x) dx$,
d. $\int_{\mathbb{R}^3} \delta(r-R) d^3\mathbf{r}$,
e. $\int_{\mathbb{R}^3} \delta(r-R)\delta(z) d^3\mathbf{r}$,
f. $\int_{-\infty}^{\infty} \left(\frac{d}{dx}\delta(x)\right) f(x) dx$ por integration parcial,
g. $\int_{-\infty}^{\infty} \left(\frac{d^n}{dx^n}\delta(x)\right) f(x) dx$.

Solution: *The solutions are: a.* $\int_{-1}^{+1} \delta(x)[f(x) - f(0)] \ dx = 0$,
b. $\int_{-1}^{3} (x^3 - x) \sin\left(\frac{\pi}{4}x\right) \delta(x-2) \ dx = 6$,
c. $\int_0^{2\pi} \sin x \ \delta(\cos x) dx = \int_0^{2\pi} \sin x \left(\frac{\delta(x-\pi/2)}{1} + \frac{\delta(x-3\pi/2)}{1}\right) dx = 0$,
d. $\int_{\mathbb{R}^3} \delta(r-R) d^3\mathbf{r} = 4\pi R^2$,
e. $\int_{\mathbb{R}^3} \delta(r-R)\delta(z) d^3\mathbf{r} = 2\pi R$,
f. $\int_{-\infty}^{\infty} \left(\frac{d}{dx}\delta(x)\right) f(x) dx = \delta(x) f(x)|_{-\infty}^{\infty} - \int \delta(x) \left(\frac{d}{dx} f(x)\right) dx = -f'(0)$,
g. $\int_{-\infty}^{\infty} \left(\frac{d^n}{dx^n}\delta(x)\right) f(x) dx = (-1)^n f^{(n)}(0)$.

12.5.4.3 Ex: Dirac's δ function

Show,

$$\int_{-\infty}^{\infty} 1 \cdot \hat{f}(k) dk = \int_{-\infty}^{\infty} \hat{1}(x) f(x) dx = 2\pi f(0) \ ,$$

where $\hat{f}(k) \equiv \int_{-\infty}^{\infty} e^{-\imath kx} dx$ is the Fourier transform and $f(x) \equiv \int_{-\infty}^{\infty} e^{\imath kx} dk$ the inverse transform. Also show,

$$\hat{1} = 2\pi\delta(x) \ .$$

Help: $1 = e^{\imath k 0}$.

Solution: *We have,*

$$\int_{-\infty}^{\infty} 1 \cdot \hat{f}(k) dk = \int_{-\infty}^{\infty} \hat{f}(k) e^{ik0} dk = 2\pi f(0) \ ,$$

with the definition of inverse Fourier transformation. We also have,

$$\begin{aligned} \int_{-\infty}^{\infty} 1 \cdot \hat{f}(k) dk &= \int_{-\infty}^{\infty} \int_{-\infty}^{\infty} f(x) e^{-ikx} dx \cdot 1 dk \\ &= \int_{-\infty}^{\infty} \int_{-\infty}^{\infty} 1(k) e^{-ikx} dk f(x) dx = \int_{-\infty}^{\infty} \hat{1}(x) f(x) dx \ . \end{aligned}$$

Comparing these two results,

$$\int_{-\infty}^{\infty} \left(\frac{1}{2\pi}\hat{1}(x)\right) f(x) dx = f(0) \qquad \textit{that is} \qquad \frac{1}{2\pi}\hat{1}(x) = \delta(x) \ .$$

12.5.4.4 Ex: Dirac's δ function

The following properties are, among others, characteristics for Dirac's δ-function,

$$\int_a^b f(x)\delta(x-c)\,dx = \begin{cases} f(c) & \text{if } c \in [a,b] \\ 0 & \text{else} \end{cases} .$$

Being $g(x)$ a function with simple zero passages x_n, that is, $g(x_n) = 0$ and $g'(x_n) \neq 0$, we have

$$\delta(g(x)) = \sum_n \frac{1}{|g'(x_n)|}\delta(x - x_n) .$$

Use these relationships to solve the following integrals,
a. $\int_{-2}^{5} dx\ (x^2 - 5x + 6)\ \delta(x-3)$.
b. $\int_{-\infty}^{\infty} dx\ x^2\ \delta(x^2 - 3x + 2)$.

Solution: *a. 0*
b. We have,

$$\int_{-\infty}^{\infty} dx\ x^2\ \delta(x^2-3x+2) = \int_{-\infty}^{\infty} dx\ x^2\ \left(\frac{\delta(x-1)}{|2x-3|_{x=1}} + \frac{\delta(x-2)}{|2x-3|_{x=2}}\right) = 5 .$$

12.5.4.5 Ex: Dirac's δ function

Demonstrate the following property of the δ-function:

$$\delta(\omega_1 - \omega)\delta(\omega_2 - \omega) = \frac{\delta(\omega_1 - \omega) + \delta(\omega_2 - \omega)}{|\omega_1 - \omega_2|} .$$

Solution:

12.5.4.6 Ex: Parametrization of currents

Parametrize the current density $\mathbf{j}(\mathbf{r}')$ of a current loop
a. in Cartesian coordinates and
b. in spherical coordinates.

Solution: *a. In Cartesian coordinates we make ansatz,* $\mathbf{j}(\mathbf{r}') = \alpha\delta(z')\delta(\rho' - R)\hat{\mathbf{e}}_\phi$. *The normalization condition requires that the integral of* $\mathbf{j}$ *across the surface in the* $y = 0$ *plane for* $x > 0$ *be,*

$$I = \int_{\mathcal{S}} \mathbf{j}(\mathbf{r}') \cdot d\mathbf{S}' = \int_{-\infty}^{\infty}\int_0^{\infty} \alpha\delta(z')\delta(\rho' - R)d\rho' dz' = \alpha ,$$

such that,

$$\mathbf{j}(\mathbf{r}') = I\delta(z')\delta(\rho' - R)\hat{\mathbf{e}}_\phi$$

b. In spherical coordinates we make ansatz, $\mathbf{j}(\mathbf{r}') = \alpha\delta(\theta')\delta(r'-R)\hat{\mathbf{e}}_\phi$. *The normalization condition requires that the integral of* $\mathbf{j}$ *across the surface in the* $y = 0$ *plane for* $x > 0$ *be,*

$$I = \int_{\mathcal{S}} \mathbf{j}(\mathbf{r}') \cdot d\mathbf{S}' = \int_0^\pi \int_0^\infty \alpha\delta(\theta')\delta(r'-R)r'dr'd\theta' = \alpha R \ ,$$

such that,

$$\mathbf{j}(\mathbf{r}') = \frac{I}{R}\delta(\theta')\delta(r'-R)\hat{\mathbf{e}}_\phi \ .$$

Note that for a function $g(x)$ *with simple zero crossings,* $g(x_n) = 0$ *but* $g'(x_n) \neq 0$, *we get* $\delta(g(x)) = \sum_n \frac{1}{|g'(x_n)|}\delta(x - x_n)$. *In our example,*

$$\delta(\cos\theta) = \frac{\delta(\theta - \frac{\pi}{2})}{|-\sin\frac{\pi}{2}|} = \delta(\theta - \tfrac{\pi}{2}) \ .$$

12.5.4.7 Ex: Intensity of an electromagnetic wave

Calculate the intensity of the electromagnetic wave given by (a) $\vec{\mathcal{E}}(\mathbf{r},t) = \vec{\mathcal{E}}_0\cos(kz - \omega t)$ and (b) $\vec{\mathcal{E}}(\mathbf{r},t) = \vec{\mathcal{E}}_0 e^{\imath kz - \imath\omega t}$. Discuss!

Solution: *The magnetic field of the wave is,*

$$\vec{\mathcal{B}} = \tfrac{\mathbf{k}}{\omega} \times \vec{\mathcal{E}}_0\cos(kz - \omega t) \qquad or \qquad \vec{\mathcal{B}} = \tfrac{\mathbf{k}}{\omega} \times \vec{\mathcal{E}}_0 e^{\imath kz - \imath\omega t} \ .$$

With this we calculate the Poynting vector,

$$\mathbf{S} = \vec{\mathcal{E}} \times \vec{\mathcal{B}} = \tfrac{\mathbf{k}}{\omega}\mathcal{E}_0^2\cos^2(kz - \omega t) \qquad or \qquad \mathbf{S} = \tfrac{\mathbf{k}}{\omega}\mathcal{E}_0^2 e^{2\imath kz - 2\imath\omega t} \ .$$

The intensity is now,

$$I = |\mathbf{S}|^2 = \tfrac{1}{c}\mathcal{E}_0^2\cos^2(kz - \omega t) \qquad or \qquad I = \tfrac{1}{c}\mathcal{E}_0^2 \ .$$

The results are different.

12.6 Further reading

J.D. Jackson, *Classical Electrodynamics* [659]ISBN

D.J. Griffiths, *Introduction to Electrodynamics* [545]ISBN

D. Halliday, R. Resnick, and J. Walker, *Fundamentals of Physics* [577]ISBN

H.M. Nussenzveig, *Curso de Física Básica: Eletromagnetismo (Volume 3)* [963]ISBN

Chapter 13

Electrostatics

We have already seen that all electromagnetic phenomena are due to charges, that these charges are quantized and conserved, and that the superposition principle holds for electromagnetic forces. In principle, it should be possible to explain all electromagnetic phenomena by calculation the forces exerted by every charge on every other charge for arbitrary charge distributions. In reality however, the situation is much more complex, because the forces not only depend on the position of the charges, but also on their speed and acceleration. In addition, any information on the actual state of a charge is only transmitted at the finite speed of light, which gives rise to retardation effects.

To simplify the problem we will initially only consider immobile charges. The theory dealing with immobile electric charges is named *electrostatics*. Its fundamental task of electrostatics resides in calculating the force exerted by spatial distributions of charges.

13.1 The electric charge and the Coulomb force

13.1.1 Quantization and conservation of the charge

We know that ordinary matter consists of electrically neutral atoms. An atom, consists of a heavy nucleus and a shell of very light-weighted electrons. The nucleus, in turn, is made up of a number of protons and neutrons. Each proton carries a positive elementary charge $Q = +e$, that is, the charge is quantized in units of e. For an atom to be neutral, the number of electrons (with negative charge $-e$) in the shell must be equal to the number of atoms.

Macroscopic bodies are usually neutral, but that does not mean that positive and negative charges are annihilated. What they can do, is to bunch by equal numbers within restricted regions of space. Then, the forces exerted by the positive and negative charges of a specific region on other far-away charges compensate each other. This effect is called shielding.

Nevertheless, it is possible, exerting work, to separate positive and negative charges, to generate polarizations in dielectric materials or currents in conducting metals, and to perform experiments with electrically charged macroscopic objects.

13.1.2 Coulomb's law

To begin with, we consider a single point charge Q at the position $\mathbf{r}'$ exerting a force on another charge located in $\mathbf{r}$. The so-called *Coulomb force* is,

$$\mathbf{F}_C = \frac{Qq}{4\pi\varepsilon_0}\frac{\mathbf{r}-\mathbf{r}'}{|\mathbf{r}-\mathbf{r}'|^3} \ , \tag{13.1}$$

where ε_0 is a constant called the permittivity of free space. The Coulomb force decreases quadratically with the distance and is directed along the straight line connecting the two charges. Note that the force can be attractive (for $Qq < 0$) or repulsive (for $Qq > 0$). See the Excs. 13.1.3.1 to 13.1.3.22.

According to the *superposition principle* the force acting on the charge is not influenced by the possible existence of other forces, for example, exerted by other charges Q_k located in other positions $\mathbf{r}_k$,

$$\mathbf{F} = \mathbf{F}_1 + \mathbf{F}_2 + ... = \sum_k \frac{Q_k q}{4\pi\varepsilon_0}\frac{\mathbf{r}-\mathbf{r}_k}{|\mathbf{r}-\mathbf{r}_k|^3} \ . \tag{13.2}$$

Introducing an abbreviation,

$$\vec{\mathcal{E}} = \sum_k \frac{Q_k}{4\pi\varepsilon_0}\frac{\mathbf{r}-\mathbf{r}_k}{|\mathbf{r}-\mathbf{r}_k|^3} \ , \tag{13.3}$$

called the *electric field*, we can express the Coulomb force as,

$$\boxed{\mathbf{F}_C = q\vec{\mathcal{E}}} \ . \tag{13.4}$$

Using the Dirac function we can parametrize the distribution of charges by,

$$\varrho(\mathbf{r}) = \sum_k Q_k \delta^3(\mathbf{r}-\mathbf{r}_k) \ . \tag{13.5}$$

The charge of a single electron is small, and often many charges are involved in electrical phenomena. Thus, the discrete character of the charge does not appear, and the charge distribution appears as a smooth distribution of *charge density*, such that,

$$\int_{\mathbb{R}} \varrho(\mathbf{r}')dV' = \int_{\mathbb{R}} \sum_k Q_k \delta^3(\mathbf{r}'-\mathbf{r}_k)dV' = \sum_k Q_k \ . \tag{13.6}$$

With this (fluid model) approximation,

$$\sum_k Q_k ... \longrightarrow \int dV' \varrho(\mathbf{r}') ... \ , \tag{13.7}$$

the *Coulomb law* can be written,

$$\boxed{\vec{\mathcal{E}} = \int \frac{\varrho(\mathbf{r}')}{4\pi\varepsilon_0}\frac{\mathbf{r}-\mathbf{r}'}{|\mathbf{r}-\mathbf{r}'|^3}dV'} \ , \tag{13.8}$$

since by inserting the discrete distribution (13.5) we recover Coulomb's law (13.3).

It is also possible to define from ϱ a two-dimensional *surface charge density* σ or a one-dimensional *linear charge density* λ using the Dirac function. For example, the surface charge density on a spherical shell,

$$\varrho(\mathbf{r}) = \sigma(\theta, \phi)\delta(r - R) \ , \tag{13.9}$$

or the linear charge density on a ring,

$$\varrho(\mathbf{r}) = \lambda(\phi)\delta(r - R)\delta(z) \ . \tag{13.10}$$

Substituting ϱ of the Coulomb law with these expressions, we reduce the dimensionality of the integral. We will study problems related to charge distributions in the Excs. 13.2.4.1 to 13.2.4.12.

13.1.3 Exercises

13.1.3.1 Ex: • Coulomb force

A point charge of $-2.0\,\mu\text{C}$ and a point charge of $4.0\,\mu\text{C}$ are separated by a distance L. Where should a third point charge be placed in order for the electrostatic force on this third charge to be zero?

Solution: ***Gabarite:*** *At a distance equal of* $0.41L$ *from the charge* $-2.0\,\mu\text{C}$ *on side opposite side to the charge* $4.0\,\mu\text{C}$.
The forces must compensate each other, $\mathbf{F}_{13} + \mathbf{F}_{23} = 0$, *giving,*

$$\frac{1}{4\pi\varepsilon_0}\frac{q_1 q_3}{(L+x)^2} = \frac{1}{4\pi\varepsilon_0}\frac{q_2 q_3}{x^2} \ .$$

For $q_1 = 2q_2$ *we get the equation,*

$$x^2 - 2Lx - L^2 = 0 \ ,$$

with the solution,

$$x = L(1 \pm \sqrt{2}) \ .$$

Only the positive sign produces a force minimum, the negative sign corresponds to a maximum.

13.1.3.2 Ex: • Coulomb force

A point particle with a charge of $-1.0\,\mu\text{C}$ is located at the origin; a second point particle with a charge of $2.0\,\mu\text{C}$ is located at $x = 0$, $y = 0.1\,\text{m}$; and a third point particle with a charge of $4.0\,\mu\text{C}$ is located at $x = 0.2\,\text{m}$, $y = 0$. Determine the electrostatic force on each of the three particles.

Solution: *We have,*

$$\mathbf{F}_1 = (0.9\,\text{N})\hat{\mathbf{e}}_x + (1.8\,\text{N})\hat{\mathbf{e}}_y \ ,$$
$$\mathbf{F}_2 = (-1.3\,\text{N})\hat{\mathbf{e}}_x - (1.2\,\text{N})\hat{\mathbf{e}}_y \ , \mathbf{F}_3 = (0.4\,\text{N})\hat{\mathbf{e}}_x - (6.4\,\text{N})\hat{\mathbf{e}}_y \ .$$

13.1.3.3 Ex: • Coulomb force

A point charge of $-5.0\,\mu\text{C}$ is located at $x = 4.0\,\text{m}$, $y = -2.0\,\text{m}$, and a second point charge of $12.0\,\mu\text{C}$ is located at $x = 1.0\,\text{m}$, $y = 2.0\,\text{m}$.
a. Determine the absolute value, the direction and the orientation of the electric field in $x = -1.0\,\text{m}$, $y = 0$.
b. Calculate the absolute value, the direction and the orientation of the electric force acting on an electron placed in the electric field at $x = -1.0\,\text{m}$, $y = 0$.

Solution: *a. We have* $13\,\text{kN/C}$ *at* $230°$.
b. We have $2.1 \cdot 10^{-15}\,\text{N}$ *at* $51°$.

13.1.3.4 Ex: Coulomb force

Imagine an electron near the Earth's surface. At what point should we place a second electron in order for the electrostatic force between the electrons to compensate the gravitational force acting on the first electron?

Solution: *The gravitational force will be compensated by the Coulomb force when* $F_G = m_e g = \frac{1}{4\pi\varepsilon_0}\frac{e^2}{r^2} = F_C$. *Hence,*

$$r = \sqrt{\frac{e^2}{4\pi\varepsilon_0\, m_e g}} = 5\,\text{m} \ .$$

13.1.3.5 Ex: Coulomb force

Three positive point charges Q_1, Q_2, and Q_3 are placed at the corners of an equilateral triangle with the edge length $L = 10\,\text{cm}$. Calculate the value and direction of the force acting on an electron located in the center of the triangle.

Solution: *Following the Coulomb law we have,*

$$\sum_j \mathbf{F}_j = \sum_j \frac{1}{4\pi\varepsilon_0}\frac{Q_j e}{|\mathbf{r}_0 - \mathbf{r}_j|^2}\frac{\mathbf{r}_0 - \mathbf{r}_j}{|\mathbf{r}_0 - \mathbf{r}_j|} \ .$$

Placing the origin in the center, $\mathbf{r}_0 = 0$, *we get,*

$$r_1 = r_2 = r_3 \equiv r \ .$$

Defining h *as the shortest distance between the center and the edges,*

$$\left(\frac{L}{2}\right)^2 + h^2 = r^2 \qquad \textit{and} \qquad (r+h)^2 + \left(\frac{L}{2}\right)^2 = L^2 \ .$$

Solving the second equation by L *and replacing* r *using the first equation,*

$$r + h = \frac{\sqrt{3}}{2}L \qquad \textit{and} \qquad \sqrt{\left(\frac{L}{2}\right)^2 + h^2} + h = \frac{\sqrt{3}}{2}L \ .$$

Solving by h and r,

$$h = \frac{L}{2\sqrt{3}} \qquad \textit{and} \qquad r = \left(\frac{\sqrt{3}L}{2} - \frac{L}{2\sqrt{3}}\right) = \frac{L}{\sqrt{3}} \ .$$

Hence,

$$\begin{aligned}
\mathbf{r}_1 &= -\frac{L}{2}\hat{\mathbf{e}}_x - h\hat{\mathbf{e}}_y = -\frac{L}{2}\hat{\mathbf{e}}_x - \frac{L}{2\sqrt{3}}\hat{\mathbf{e}}_y \ , \\
\mathbf{r}_2 &= \frac{L}{2}\hat{\mathbf{e}}_x - h\hat{\mathbf{e}}_y = \frac{L}{2}\hat{\mathbf{e}}_x - \frac{L}{2\sqrt{3}}\hat{\mathbf{e}}_y \ , \\
\mathbf{r}_3 &= r\hat{\mathbf{e}}_y = \frac{L}{\sqrt{3}}\hat{\mathbf{e}}_y \ .
\end{aligned}$$

Finally,

$$\mathbf{F} = \mathbf{F}_1 + \mathbf{F}_2 + \mathbf{F}_3 = \frac{1}{4\pi\varepsilon_0}\frac{e}{r^3}(Q_1\mathbf{r}_1 + Q_2\mathbf{r}_2 + Q_3\mathbf{r}_3) = \frac{1}{4\pi\varepsilon_0}\frac{3}{2L^2}e\begin{pmatrix} -\sqrt{3}Q_1 + \sqrt{3}Q_2 \\ -Q_1 - Q_2 + 2Q_3 \\ 0 \end{pmatrix} \ .$$

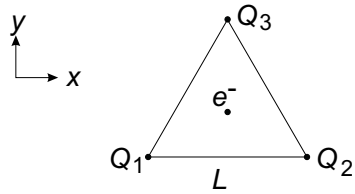

Figure 13.1: Coulomb force.

13.1.3.6 Ex: • Coulomb force

Two particles carrying equal charges q are placed at a mutual distance of $r = 3\,\mathrm{mm}$ and then released. The acceleration of the first particle after having been released is $a_1 = 7\,\mathrm{m/s^2}$, and the acceleration of the second particle is $a_2 = 2\,\mathrm{m/s^2}$. The mass of the first particle is $m_1 = 6 \cdot 10^{-7}\,\mathrm{kg}$.
a. What is the mass of the second particle?
b. What is the charge of the particles?

Solution: *a. The Coulomb force acting on both particles is $F_C = \frac{1}{4\pi\varepsilon_0}\frac{q_1 q_2}{r^2}$, $q_1 = q_2 = q$. Soon after releasing, we have*

$$m_1 a_1 = \frac{1}{4\pi\varepsilon_0}\frac{q}{r^2} = -m_2 a_2 \ .$$

Hence, $m_2 = -m_1 a_1/a_2 = 2.1 \cdot 10^{-6}\,\mathrm{kg}$.
b. In addition, we calculate,

$$q = \sqrt{4\pi\varepsilon_0 r^2 m_1 a_1} = 6.5 \cdot 10^{-11}\,\mathrm{C} = 4 \cdot 10^8\ e\ .$$

13.1.3.7 Ex: • Coulomb force

A small ball of graphite (mass $m = 1\,\mathrm{kg}$) suspended on a wire is touched by an electrically charged plastic stick and picks up 1% of its charge. The result is that the ball is displaced by an angle of 30°, while the stick is held in place at the former position of the ball. The distance between the center of the ball and the end of the stick is 10 cm.
a. Calculate the force exerted by the wire on the ball?
b. Assume that the charge on the stick is fully concentrated at its end. What are the charges on the ball and on the stick?

Solution:

13.1.3.8 Ex: • Acceleration of charges

An electron has an initial velocity of $v_0 = 2 \cdot 10^6\,\mathrm{m/s}$ in $+x$-direction. It enters a region of uniform electric field $\vec{\mathcal{E}} = (300\,\mathrm{N/C})\ \hat{\mathbf{e}}_x$.
a. Determine the acceleration of the electron.
b. How long does it take for the electron to travel a distance of $s = 10.0\,\mathrm{cm}$ along the x-axis towards $+x$ in the region that has field.
c. At what angle and in what direction does the motion of the electron deflect as it travels 10.0 cm in x-direction?

Solution: *a. The acceleration is,*

$$a = \frac{F}{m_e} = \frac{-e\mathcal{E}}{m_e} = -5.28 \cdot 10^{13}\,\mathrm{m/s^2}\ .$$

b. Instantaneous speed is,

$$v = v_0 - at\ .$$

With this we get the traveled distance,

$$s = \int_0^t v dt = v_0 t - \tfrac{a}{2} t^2\ .$$

Hence, the time is,

$$t = \frac{v_0}{a} \pm \sqrt{\frac{v_0^2}{a^2} - \frac{2s}{a}} = 50\,\mathrm{ns}\ .$$

c. The angle is calculated by,

$$\theta = \tan \tfrac{\Delta y}{\Delta x} = 33.4^\circ\ .$$

in $-y$-direction.

13.1.3.9 Ex: • Acceleration of charges

A charged particle of 2.0 g is released from rest in a region that has a uniform electric field, $\vec{\mathcal{E}} = (300\,\mathrm{kN/C})\hat{\mathbf{e}}_x$. After traveling a distance of 0.5 m in this region, the particle has a kinetic energy of 0.12 J. Determine the particle's charge.

Solution: *Putting the formulas together,*

$$v = at \qquad and \qquad s = \tfrac{a}{2}t^2 \ ,$$

we obtain,

$$s = \tfrac{v^2}{2a} \ .$$

The acceleration is,

$$a = \tfrac{F}{m} = \tfrac{qE}{m} \ ,$$

such that the kinetic energy gets,

$$E_{cin} = \tfrac{m}{2}v^2 = \tfrac{m}{2}2as = sqE \ .$$

Finally we get,

$$q = \frac{E_{cin}}{sE} = 800\,\mu\mathrm{C} \ .$$

13.1.3.10 Ex: Charged copper coins

The positive proton charge and the negative electron charge have the same absolute value. Assume that the absolute values would have a relative difference of only 0.0001%. Consider copper coins with $3 \cdot 10^{22}$ atoms. What would be the repulsive force of two coins 1 m apart?
Help: A neutral copper atom contains 29 protons and the same amount of electrons.

Solution: *Each coin has the charge $Q = 29 \cdot 3 \cdot 10^{22} \cdot 0.0001\% \cdot e = 0.14\,\mathrm{C}$. The copper coins repel each other with the electrostatic force,*

$$F_C = \frac{1}{4\pi\varepsilon_0}\frac{Q^2}{r^2} = 1.7 \cdot 10^8\,\mathrm{N} \ .$$

13.1.3.11 Ex: • Weight of the electron

A metal sphere is charged with $Q = +1\,\mu\mathrm{C}$. Determine whether the mass of the sphere increases or decreases due to the charging and calculate the value?

Solution: *Since the sphere is positively charged, the electrons must exit the sphere. Therefore, the sphere loses mass. An electron has the charge* $e = 1.6 \cdot 10^{-19}\,\mathrm{C}$ *and its mass* $m_e = 9.1 \cdot 10^{-31}\,\mathrm{kg}$. *The loss of mass is therefore* $\delta m = \frac{m_e Q}{e} = 5.7 \cdot 10^{-18}\,\mathrm{kg}$, *which is little.*

13.1.3.12 Ex: The hydrogen atom

In the hydrogen atom the typical distance between the positively charged proton and the negatively charged electron is $d \sim 5 \cdot 10^{-11}\,\mathrm{m}$.
a. Calculate the Coulomb force.
b. Compare this force with the gravitational force between the two particles.
c. What should be the speed of the electron around the nucleus to compensate for the gravitational attraction by the centrifugal force?

Solution: *a. Coulomb's force is,*

$$F_C = \frac{1}{4\pi\varepsilon_0}\frac{q_1 q_2}{r^2} = 9.2 \cdot 10^{-8}\,\mathrm{N}\ .$$

b. The gravitational force is,

$$\frac{F_G}{F_C} = \frac{-G\frac{m_1 m_2}{r^2}}{\frac{1}{4\pi\varepsilon_0}\frac{q_1 q_2}{r^2}} = -4\pi\varepsilon_0 G\frac{m_1 m_2}{q_1 q_2} = 4.5 \cdot 10^{-40}\ .$$

Therefore, the ratio is independent of the distance and in addition very small.
c. The balance of forces requires,

$$F_C = \frac{1}{4\pi\varepsilon_0}\frac{q_1 q_2}{r^2} = \frac{mv^2}{r} = F_Z\ ,$$

such that,

$$v = \sqrt{\frac{1}{4\pi\varepsilon_0}\frac{q_1 q_2}{mr}} = 2.25 \cdot 10^6\,\mathrm{m/s} \approx \frac{1}{133}\ c\ .$$

Comment: The ratio of this speed to the speed of light is approximately equal to the fine-structure constant $\alpha \approx \frac{1}{137}$.

13.1.3.13 Ex: Exercise of understanding

Two metallic spheres are placed at a distance d from each other and respectively charged with $+Q$ and $-2Q$.
a. Do spheres attract or repel each other?
b. What happens if we let the spheres contact each other and then put them at the same distance d. How much does the force change?

Solution: *a. Initially, the spheres attract each other, because they are loaded with opposite charges.*
b. When the spheres touch, the charge can flow and will spread evenly over the two

spheres. Therefore, each sphere will have the same charge $-Q/2$, and the spheres will repel each other. While initially the spheres attracted each other with a force proportional to $2Q^2$, now they repel each other with a force proportional to $Q^2/4$. That is, the absolute value of the force decreased by a factor of 8.

13.1.3.14 Ex: • Charged sphere on a spring

A ball with the m is suspended on a spring with the spring constant f.
a. What will be the displacement of the ball due to its weight? What will be the frequency of oscillation?
b. Now the ball is loaded with the charge Q and a second ball with the same charge is approached from below the first ball. Derive the relationship between the position of the first ball z_1 and the position of the second z_2. The position $z_1 = 0$ is the resting position of the spring, that is, the position that the spring would have without suspended mass. CAUTION: you'll get a third order equation in z_1, don't try to solve it!
c. For which position z_2 of the second ball does the first ball stay at the resting position of the spring, that is, for which z_2 do we find $z_1 = 0$ to be solution? Are there any other solutions? What are your interpretations?
d. What is the frequency of oscillation under these conditions, when ball 1 is only slightly displaced around $z_1 = 0$? Use the approximation $\frac{1}{(a-x)^2} \approx \frac{1}{a^2} + \frac{2}{a^3}x$, which holds for $x \ll a$.

Solution: *a. Displacement:*

$$mg = fz_1 \rightarrow z_1 = \frac{mg}{f} \ .$$

Oscillation frequency: in the displaced position z_1 holds:

$$m\ddot{z}_1 = -fz_1 \ .$$

With the ansatz $z_1 = \cos(\omega t)$ follows $\omega = \sqrt{f/m}$. b. Setting the sum of all forces equal to zero:

$$mg - fz_1 - \frac{1}{4\pi\varepsilon_0}\frac{Q^2}{(z_2 - z_1)^2} = 0$$

$$-fz_1^3 + z_1^2(2fz_2 + mg) + z1(-2mgz_2 - fz_2^2) + mgz_2^2 - \frac{1}{4\pi\varepsilon_0}Q^2 = 0 \ .$$

There is a solution $z_1 = 0$, when the constant term disappears, that is, for,

$$mgz_2^2 - \frac{1}{4\pi\varepsilon_0}Q^2 = 0$$

$$z_2 = \frac{Q}{\sqrt{4\pi\varepsilon_0 mg}} \ .$$

We are left with a second order equation. This can have two real solutions, but only one is physically significant: the one where the first ball is below the second. Here, the

spring tries to bounce the first ball upwards, which is prevented by Coulomb's repulsion force exerted by the second ball.
c. The force in the equilibrium position is, with the approximation $z_1 \ll z_2$

$$F(z_1,z_2) \approx mg - fz_1 - \frac{1}{4\pi\varepsilon_0}Q^2(\frac{1}{z_2^2}+\frac{2}{z_2^3}z_1) = mg - \frac{Q^2}{4\pi\varepsilon_0 z_2^2} - (f - \frac{2Q^2}{4\pi\varepsilon_0 z_2^3})z_1$$
$$= mg - \frac{Q^2}{4\pi\varepsilon_0}\frac{4\pi\varepsilon_0 mg}{Q^2} - (f - \frac{2Q^2}{4\pi\varepsilon_0}\frac{(4\pi\varepsilon_0 mg)^{3/2}}{Q^3})z_1 = -(f - \frac{2\sqrt{4\pi\varepsilon_0(mg)^3}}{Q})z_1 \ .$$

Therefore, the new oscillation frequency is,

$$\omega = \sqrt{\frac{1}{m}\left(f - \frac{2\sqrt{4\pi\varepsilon_0(mg)^3}}{Q}\right)} \ .$$

That is, the frequency is less than before.

13.1.3.15 Ex: Stability of a charge distribution

The charge distributions shown in the figure are given. All positive and negative charges have the same absolute value.
a. Determine whether one of these distributions is stable? What happens in different cases?
b. Is it possible to choose the absolute values of the charges in such a way as to make the configurations stable?

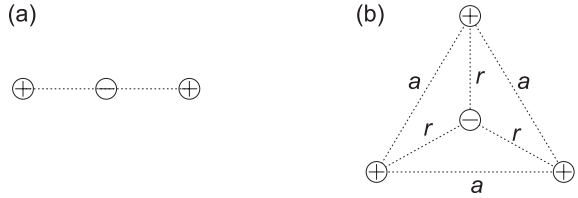

Figure 13.2: Geometry of charge distribution.

Solution: *a. As Coulomb's force falls quadratically with distance and since unequal charges are at twice the distance of equal charges, the two positively charged balls will approach the negative and collide.*
b. Considering the energies we have,$a = \sqrt{3}r$:

$$E = 3 \times \frac{1}{4\pi\varepsilon_0}(2\frac{Q^2}{a} - \frac{Q^2}{r}) = 3 \times \frac{1}{4\pi\varepsilon_0}(2\frac{Q^2}{\sqrt{3}r} - \frac{Q^2}{r}) = 3 \times \frac{Q^2}{4\pi\varepsilon_0 r}(\frac{2}{\sqrt{3}} - 1) \ .$$

Since $\frac{2}{\sqrt{3}} - 1 > 0$, holds $F = -\frac{dE}{dr} > 0$, and so the positive charges will move away from the negative ones.
a. We call the negative charge $-Q_1$ and the two positive charges Q_2,

$$\frac{Q_1 Q_2}{r^2} = \frac{Q_2 Q_2}{(2r)^2} \qquad \textit{such that} \qquad \frac{Q_1}{Q_2} = \frac{1}{4} \ .$$

The outer charges must be four times greater than the inner charges for the force to zero at all distances, that is, to be at equilibrium. However, this equilibrium is unstable, as a small deviation from the correct charges is sufficient to let the system collapse or explode.
b. Analogically with the energy:

$$\frac{Q_1 Q_2}{r} = \frac{2Q_2 Q_2}{\sqrt{3}r} \qquad \textit{such that} \qquad \frac{Q_1}{Q_2} = \frac{2}{\sqrt{3}} \ .$$

The problem here is, that the charge ratio should be irrational. This is not possible because of the charge quantization.

13.1.3.16 Ex: Stability of a charge distribution

Three balls with mass m and each charged with the charge Q are placed in a parabolic bowl. This can be described as a surface in space, where the coordinate z of the surface is given by $z = z(x, y) = A(x^2 + y^2)$. Gravitation shows into $-\hat{\mathbf{e}}_z$ direction. What is the distance the balls adopt, when we set as an additional condition, that all charges are at the same height?

Solution: *The gravitational potential energy is,*

$$W_{gr} = \sum_{k=1}^{3} mgz_k = 3mgz_1 \ .$$

The balls have the same reciprocal distance a_{12} and r_1 from the center of the bowl: $a_{12} = r_1\sqrt{3} = \sqrt{3\,(x_1^2 + y_1^2)}$. Hence,

$$W_{gr} = 3mgA\left(x_1^2 + y_1^2\right) = mgAa_{12}^2 \ .$$

The electrostatic energy is,

$$W_{el} = \frac{1}{2}\sum_{\substack{k,j=1 \\ k\neq j}}^{3} \frac{1}{4\pi\varepsilon_0}\frac{Q^2}{|\mathbf{r}_k - \mathbf{r}_j|} = \frac{1}{2}\frac{1}{4\pi\varepsilon_0}\frac{Q^2}{a_{12}} 3(3-1) = \frac{3}{4\pi\varepsilon_0}\frac{Q^2}{a_{12}} \ .$$

From the minimization condition,

$$0 = \frac{d}{da_{12}}\left(W_{gr} + W_{el}\right) = \frac{d}{da_{12}}\left(mgAa_{12}^2 + \frac{3}{4\pi\varepsilon_0}\frac{Q^2}{a_{12}}\right) = \frac{d}{da_{12}}\left(2mgAa_{12} - \frac{3}{4\pi\varepsilon_0}\frac{Q^2}{a_{12}^2}\right)$$

we have,

$$a_{12} = \left(\frac{3}{8\pi\varepsilon_0}\frac{Q^2}{mgA}\right)^{1/3} \ .$$

The energy then becomes,

$$W_{gr} + W_{el} = \frac{3}{4\pi\varepsilon_0}\frac{Q^2}{a_{12}} + mgAa_{12}^2 = \frac{3}{4\pi\varepsilon_0}\frac{Q^2}{\left(\frac{3}{4\pi\varepsilon_0}\frac{Q^2}{mgA}\right)^{1/3}} + mgA\left(\frac{3}{4\pi\varepsilon_0}\frac{Q^2}{mgA}\right)^{2/3}$$

$$a_{12} = \left(\frac{3}{4\pi\varepsilon_0}\frac{Q^2}{mgA}\right)^{1/3}$$

$$W_{gr} + W_{el} = \left(\frac{3mgAQ^2}{4\pi\varepsilon_0}\right)^{4/3} .$$

Comment: *It is not obvious whether there are other configurations with a charge in the center that would have less energy. Alternatively, we could suspend three balls loaded on a spring.*

13.1.3.17 Ex: Ions in a harmonic potential

Two ions with the positive charge $+e$ are confined to an isotropic harmonic potential. Each ion has the potential energy $U = \frac{1}{2}m\omega^2 r^2$, where r is the distance from the center of the potential. The ions are at rest, only consider two dimensions.
a. What is the distance of the two ions from the center?
b. Calculate the distance for three identical ions.

Solution: *a. The force exerted by the harmonic potential on an ion is,*

$$-\frac{dU}{dr} = -m\omega^2 r .$$

This force must be equalized with the Coulomb force:

$$m\omega^2 r = \frac{1}{4\pi\varepsilon_0}\frac{Q^2}{(2r)^2} \qquad \text{such that} \qquad r = \left(\frac{1}{4\pi\varepsilon_0}\frac{Q^2}{4m\omega^2}\right)^{1/3} .$$

b. With three ions, we must consider that the ions minimize energy by placing themselves in a symmetrical triangle. So the distance between two ions is $a = \sqrt{3}r$. The total energy of the three ions is,

$$E = 3 \times \left(\frac{1}{4\pi\varepsilon_0}\frac{Q^2}{a} + \frac{1}{2}m\omega^2 r^2\right) = \frac{\sqrt{3}}{4\pi\varepsilon_0}\frac{Q^2}{r} + \frac{3}{2}m\omega^2 r^2 .$$

The force is given by,

$$F = -\frac{dE}{dr} = \frac{\sqrt{3}}{4\pi\varepsilon_0}\frac{Q^2}{r^2} - 3m\omega^2 r .$$

From the equilibrium condition, $F = 0$, follows:

$$r = \left(\frac{1}{4\pi\varepsilon_0}\frac{Q^2}{\sqrt{3}m\omega^2}\right)^{1/3} .$$

13.1.3.18 Ex: Spheres on a wire

Two identical spheres with mass $m = 0.1\,\mathrm{kg}$ are suspended at the same point of a ceiling by a 1 m long wire and have the same charge. What is the value of the charge if the two centers of the spheres are 4 cm apart. Use the approximation $\sin\alpha \approx \tan\alpha \approx \alpha$ for small angles α.

Solution: *Each of the two spheres is displaced by* $d = 2\,\mathrm{cm}$ *from the center. The displacement angle is in first order,* $\alpha = d/l$ *with* $l = 1\,\mathrm{m}$ *the wire length. By this displacement the ball is lifted (in first approximation) by a value of* $h = \alpha d$*, hence we have* $h = \frac{d^2}{l}$*. The potential energy of the two balls, therefore, is* $E_{pot} = 2mgh = \frac{2mgd^2}{l}$*. This energy must be matched with the Coulomb potential:*

$$\frac{2mgd^2}{l} = \frac{1}{4\pi\varepsilon_0}\frac{Q^2}{d} \qquad \textit{such that} \qquad Q = \sqrt{\frac{8\pi\varepsilon_0 mgd^3}{l}}\ .$$

Inserting the values we get, $Q = 42\,\mathrm{nC}$.

13.1.3.19 Ex: Oscilloscope

We consider a simple model of an oscilloscope. Inside the device is a Braun tube, inside which electrons are accelerated by a voltage U to a speed v. Then, the electrons fly through the plates of a capacitor and are deflected by the electric field E of the capacitor. (In a real oscilloscope there are two capacitors: one for horizontal deviation and one for vertical.) Behind the capacitor, the electrons fly to a screen, where they produce a bright spot.
a. Calculate the electron velocity v for an accelerating voltage of $U = 1\,\mathrm{kV}$. (Do not consider relativistic effects!)
b. The capacitor has a length of $l = 5$ cm and a distance from the plates of $d = 2\,\mathrm{cm}$. What is the maximum allowable voltage $U_{\max}$ at the capacitor to prevent electrons from hitting one of the capacitor plates? (Electrons enter the capacitor in the center between the plates.)
c. What should be the distance between the plates and the screen (which is 10 cm wide), so that with maximum voltage $U_{\max}$ the entire area of the screen is used?
Comment: Disregard capacitor edge effects!

Solution:

13.1.3.20 Ex: • Electron between charged plates

Between two parallel horizontal plates there is a homogeneous electric field $|\vec{\mathcal{E}}| = 2\cdot 10^3\,\mathrm{N/C}$. The lower plate is charged with a positive charge, the upper plate with a negative, such that the field is oriented upwards. The length of the plates is $L = 10\,\mathrm{cm}$, their distance $d = 2\,\mathrm{cm}$. From the left edge of the bottom plate an electron is shot at an initial velocity $|v_0| = 6\cdot 10^6\,\mathrm{m/s}$ under an angle 45° into the space between the plates.
a. When will the electron hit one of the plates?

b. Which plate is eventually hit and at what horizontal distance from the firing point?

Solution: *a. The electron in the homogeneous field is accelerated downward by the Coulomb force, $m\ddot{y} = -e\mathcal{E}$. The gravitational force is many orders of magnitude weaker. The electron trajectory is given by,*

$$x = v_0 t \cos\alpha \qquad \text{and} \qquad y = -\frac{eE}{2m}t^2 + v_0 t \sin\alpha \ .$$

The electron reaches its maximum height when $\dot{y} = 0$, that is,

$$t_m = \frac{mv_0 \sin\alpha}{e\mathcal{E}} = 12\,\text{ns} \ .$$

At this moment it has reached the height,

$$y_m = -\frac{e\mathcal{E}}{2m}t_m^2 + v_0 t_m \sin\alpha = \frac{mv_0^2 \sin^2\alpha}{2e\mathcal{E}} = 25.7\,\text{cm}$$

and the distance,

$$x_m = v_0 t_m \cos\alpha = 51.1\,\text{cm} \ .$$

That is, at most only the top plate can be reached.
b. The height of the upper plate is reached, when $y = d = -\frac{eE}{2m}t_d^2 + v_0 t_d \sin\alpha$. From this follows,

$$t_d = \frac{mv_0 \sin\alpha}{e\mathcal{E}} \pm \sqrt{\left(\frac{mv_0 \sin\alpha}{eE}\right)^2 - \frac{2md}{e\mathcal{E}}} = 6.4\ ns \quad or \quad 17.7\ ns \ .$$

At the previous instant the distance is $x_d = v_0 t_d = 23.8\,\text{cm}$, that is, the electron can escape.

13.1.3.21 Ex: • The Coulomb-Kepler problem

We consider two particles charged with charges Q_1 and Q_2 and masses $m = m_1 = m_2$ which, for simplicity, can only move along the $\hat{\mathbf{e}}_z$-axis and are subject to mutual Coulomb forces.
a. Derive the differential equations for the positions z_1 and z_2 of the two particles. Reduce the number of variables of the problem by introducing the difference variable $z = z_2 - z_1$ and establish the differential equation for z.
b. The differential equation obtained has the same shape as that of the Kepler problem in mechanics, which, however, is not defined along an axis but on a plane. What are the solutions to Kepler's problem? What important physical quantity does not appear to constrain the freedom of movement to one axis? What would be the impact of this constraint on the solutions to Kepler's problem? What is the additional degree of freedom in the Coulomb-Kepler problem as compared to the Kepler problem?
c. Kepler's differential equation is not easy to solve. Even so, we can learn something by looking at the phase space diagram. For this, we consider two identical particles $Q = Q_1 = Q_2$ and $m = m_1 = m_2$, placed at a distance z_0. What is going to happen?

How will the velocities v_1 and v_2 of the two particles behave with respect to each other? Derive a relationship between the distance z and the velocity v of one of the particles (energy conservation). What is the value of the velocity for $z \to \infty$? Prepare a phase space diagram in (z, v) for three different distances z_0.

Solution: *a. We have,*

$$m\ddot{z}_1(t) = -\frac{Q_1 Q_2}{(z_2(t) - z_1(t))^2} \qquad \textit{and} \qquad m\ddot{z}_2(t) = \frac{Q_1 Q_2}{(z_2(t) - z_1(t))^2} \ ,$$

and with $z = z_2 - z_1$ taking the difference of the two differential equations follows,

$$m\ddot{z}(t) = 2\frac{Q_1 Q_2}{z^2} \ .$$

b. The solutions to Kepler's problem are described by Kepler's three laws. These are,

- *The orbits are ellipses, the center of gravity is in one of the focus of the ellipse.*
- *During same time intervals, a beam sweeps through equal areas.*
- *The squares of the orbital periods of two objects behave like the cubes of the large semi-axes.*

In Kepler's problem, the angular momentum is an important parameter, since it neutralizes attractive gravity, and thus stabilizes the orbit. In just one dimension the angular momentum is zero, therefore, two bodies attract each other without stopping. In the Coulomb-Kepler problem we have the additional freedom, that the force can be repulsive.
c. The two particles will move away from each other without limit. From momentum conservation $mv_1(t) + mv_2(t) = 0$ follows $v_1(t) = -v_2(t)$. Therefore, it is sufficient to analyze only one of the two velocities.
The total energy of the system consists of the potential energy and the kinetic energy of both particles:

$$\begin{aligned} E &= U + T \\ U &= \frac{1}{4\pi\varepsilon_0}\frac{Q^2}{z} \\ T &= \frac{1}{2}mv_1^2 + \frac{1}{2}mv_2^2 = mv^2 \ . \end{aligned}$$

The energy is fixed by the initial conditions $z(0) = z_0$ and $v(0) = 0$:

$$E = \frac{1}{4\pi\varepsilon_0}\frac{Q^2}{z_0} \ .$$

Inserting we get,

$$\frac{1}{4\pi\varepsilon_0}\frac{Q^2}{z_0} = \frac{1}{4\pi\varepsilon_0}\frac{Q^2}{z} + mv^2 \qquad \textit{such that} \qquad v = \sqrt{\frac{1}{4\pi\varepsilon_0 m}\left(\frac{1}{z_0} - \frac{1}{z}\right)} \ .$$

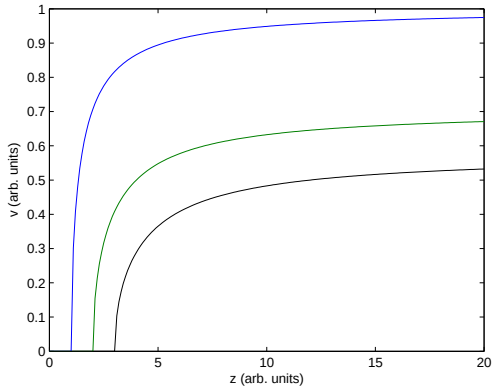

Figure 13.3: Coulomb-Kepler problem.

In the limiting case $z \to \infty$ we get,

$$v_\infty = \sqrt{\frac{1}{4\pi\varepsilon_0 m z_0}} \ .$$

13.1.3.22 Ex: Particle spinning around a charged wire

An infinitely long line uniformly charged with negative charge, has a charge density of λ and is located on the z-axis. A small positively charged particle has mass m and a charge q and is on circular orbit of radius R in the xy-plane centered on the charge line.
a. Deduce an expression for the velocity of the particle.
b. Obtain an expression for the period of the particle's orbit.

Solution: *The field is*

$$\mathcal{E}_r = \frac{1}{2\pi\varepsilon_0}\frac{\lambda}{r} \ .$$

Therefore, force is,

$$F_r = q\mathcal{E}_r = q\frac{1}{2\pi\varepsilon_0}\frac{\lambda}{r} = F_{centr} = m\frac{v^2}{r} \ .$$

With that we get the velocity,

$$v = \sqrt{\frac{1}{2\pi\varepsilon_0}\frac{\lambda q}{m}} \ ,$$

and the period of revolution,

$$T = \frac{2\pi}{\omega} = \frac{2\pi}{v/r} = 2\pi r\sqrt{\frac{2\pi\varepsilon_0 m}{\lambda q}} \ .$$

13.2 Properties of the electric field

In principle the fundamental problem of electrostatics is solved by Coulomb's law. In practice however, the calculation of the electric field generated by a charge distribution can be complicated. On the other hand, electrostatic problems often exhibit symmetries, which allow for their resolution by other techniques avoiding the integrals of Coulomb's law.

13.2.1 Field lines and the electric flux

When we calculate the electric vector field for a charge distribution on a matrix of points in space, we get diagrams like the one shown in Fig. 13.4. The arrows represent, through the lengths of the vectors, the value of the field and, through the orientation of the vector, the direction of the force exerted by the field. The diagram suggests to connect the arrows thus forming lines called *field lines*. These lines are nothing more than the trajectories taken by test charges placed inside the field [1]. Field lines can never intersect (otherwise the direction of force acting on a test charge would be ambiguous) and can never begin or end in free space. They always start from a positive charge and end up in a negative charge.

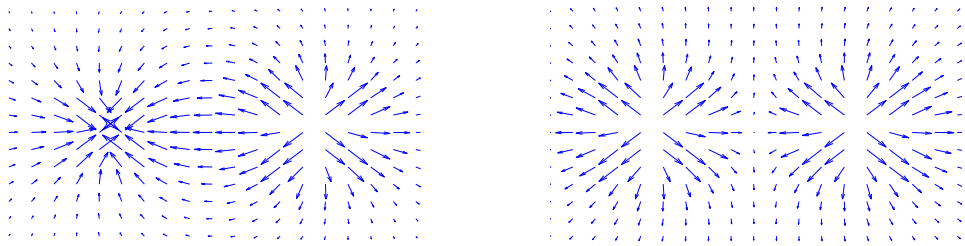

Figure 13.4: Field lines of two equal charges (right) and two opposed charges (left).

The *electric flux* is a measure for the density of field lines crossing a surface. As we have already said, the field line density corresponds to the amplitude of the electric field $\vec{\mathcal{E}}$. The normal vector of the surface $\mathbf{S}$ being locally perpendicular to the plane, we must calculate the flux by taking the integral of the scalar product,

$$\boxed{\Psi_E \equiv \int_{\mathcal{S}} \vec{\mathcal{E}} \cdot d\mathbf{S}} \,. \tag{13.11}$$

Then, instead of illustrating the amplitude of a field through the length of the arrows representing the force exerted on a charge, $\vec{\mathcal{E}} \propto \mathbf{F}$, we can illustrate the amplitude through the local density of lines field, $\vec{\mathcal{E}} \propto \Psi_E$.

The concept of the flux allows us to quantitatively formulate the statement, that field lines can not start or end in free space, but always come out (or penetrate) into charges. For this, we calculate the flux through a sphere around an electric charge q

[1] Note, that the representation by lines (instead of vectors) misses the information about the local field strength. However, this information is still encoded in the local density of the field lines.

located at the origin using Coulomb's law:

$$\oint_{spherical\ surface} \vec{\mathcal{E}} \cdot d\mathbf{S} = \oint_{spherical\ surface} \frac{1}{4\pi\varepsilon_0} \frac{q}{|\mathbf{r}|^2} \hat{\mathbf{e}}_\mathbf{r} \cdot r^2 \sin\theta d\theta d\phi \hat{\mathbf{e}}_\mathbf{r} = \frac{q}{\varepsilon_0} \ . \quad (13.12)$$

With the superposition principle we can generalize this result to arbitrary distributions of charges Q. The so-called *Gauß' law*, or Maxwell's third equation,

$$\boxed{\oint_{\partial\mathcal{V}} \vec{\mathcal{E}} \cdot d\mathbf{S} = \frac{Q}{\varepsilon_0}} \ , \quad (13.13)$$

states, that the number of field lines entering a charge-free volume $\mathcal{V}$ through a closed surface $\partial\mathcal{V}$ must equal the number of lines leaving it. The law also states that *there exist electric charges* acting as sources or drains of field lines. We will resolve flux problems in the Excs. 13.2.4.13 to 13.2.4.29.

13.2.2 Divergence of the electric field and Gauß' law

Gauß' integral theorem (12.42) allows us to rewrite Gauß' law (13.13). On the one hand, we have,

$$\oint_{\partial\mathcal{V}} \vec{\mathcal{E}} \cdot d\mathbf{S} = \int_\mathcal{V} \nabla \cdot \vec{\mathcal{E}} dV \ , \quad (13.14)$$

on the other hand, we can express the total charge inside the volume $\mathcal{V}$ as a sum over the charge distribution,

$$Q = \int_\mathcal{V} \varrho(\mathbf{r}) dV \ . \quad (13.15)$$

comparing the integrands, we obtain the differential form of Gauß' law or Maxwell's third equation:

$$\boxed{\nabla \cdot \vec{\mathcal{E}} = \frac{\varrho}{\varepsilon_0}} \ . \quad (13.16)$$

The Gauß law can also be derived directly from the general Coulomb law: We calculate the divergence of the field of formula (13.8),

$$\begin{aligned} \nabla \cdot \vec{\mathcal{E}} &= \nabla_\mathbf{r} \cdot \int \frac{\varrho(\mathbf{r}')}{4\pi\varepsilon_0} \frac{\mathbf{r}-\mathbf{r}'}{|\mathbf{r}-\mathbf{r}'|^3} dV' = \frac{1}{4\pi\varepsilon_0} \int \varrho(\mathbf{r}') \nabla_\mathbf{r} \cdot \frac{\mathbf{r}-\mathbf{r}'}{|\mathbf{r}-\mathbf{r}'|^3} dV' \quad (13.17) \\ &= \frac{1}{4\pi\varepsilon_0} \int \varrho(\mathbf{r}') 4\pi\delta^3(\mathbf{r}-\mathbf{r}') dV' = \frac{\varrho(\mathbf{r})}{\varepsilon_0} \ . \end{aligned}$$

In the integral form, Gauß' law is very useful for calculating electric fields particularly in situations with a high degree of symmetry. Let us discuss some examples in the following.

Example 44 (*Electric field outside a charged sphere*): We consider a sphere with radius R carrying the total charge Q. Gauß' law says,

$$\oint_{\partial\mathcal{V}} \vec{\mathcal{E}} \cdot d\mathbf{S} = \frac{Q}{\varepsilon_0} \ ,$$

where we choose as volume a sphere with radius $r > R$. At first glance, this does not seem to help much because the field, in which we are interested, is under the integral. But we can explore the symmetry of the system to simplify the integral, since $\vec{\mathcal{E}} = \mathcal{E}\hat{\mathbf{e}}_r$ and $\mathrm{d}\mathbf{S} = dS\hat{\mathbf{e}}_r$, such that we can write the integral,

$$\int_0^{\pi}\int_0^{2\pi} \mathcal{E}r^2 \sin\theta d\theta d\phi = 4\pi r^2 \mathcal{E} = \frac{Q}{\varepsilon_0} \ .$$

Hence,

$$\vec{\mathcal{E}} = \frac{Q}{4\pi\varepsilon_0 r^2}\hat{\mathbf{e}}_r \ .$$

This is precisely Coulomb's law. It is interesting to note that the field does not depend on the distribution ϱ of the charge within the volume. Of course, to take advantage of the symmetry of the system, it is important to choose the adequate volume.

Example 45 (*Box containing an interface*): Let us now give another example of the utility of Gauß' law. We are interested in the electric field generated by an infinitely extended plane carrying a homogeneous surface charge density σ. By symmetry, the $\vec{\mathcal{E}}$-field must cross the plane perpendicularly and have opposite directions above and below the plane. We now imagine a rectangular pill box enclosing a small area of the plane, so that two surfaces of the box (with area S) are parallel to the plane. Inside the box we find the charge,

$$Q = \varepsilon_0 \oint_{\mathcal{S}_{box}} \vec{\mathcal{E}} \cdot d\mathbf{S} = \varepsilon_0 \int_{\mathcal{S}_{upper}} \mathcal{E}dS + \varepsilon_0 \int_{\mathcal{S}_{lower}} \mathcal{E}dS = 2S\mathcal{E} \ .$$

On the other hand, $Q = \int_{\mathcal{V}_{box}} \varrho dV = \sigma S$. Hence,

$$\vec{\mathcal{E}} = \frac{\sigma}{2\varepsilon_0}\hat{\mathbf{n}} \ .$$

It may seem strange that the electric field does not depend on the distance from the plane, but this is due to the fact that the plane is supposed infinite, which is an unrealistic concept. For a limited surface we expect field components not being perpendicular to the interface, which come from the edges of the surface.

13.2.3 Rotation of the electric field and Stokes' law

Stokes' integral theorem (12.40) allows us to rewrite Maxwell's fourth equation(13.23). From

$$\boxed{\oint_{\partial\mathcal{S}} \vec{\mathcal{E}} \cdot d\mathbf{r} = 0} = \int_{\mathcal{S}} (\nabla \times \vec{\mathcal{E}}) \cdot d\mathbf{S} \ , \tag{13.18}$$

we obtain the differential form of Maxwell's second equation:

$$\boxed{\nabla \times \vec{\mathcal{E}} = 0} \ . \tag{13.19}$$

The second Maxwell equation (applied to electrostatics) can also be derived directly from the general Coulomb law: We calculate the rotation of the field of formula (13.3),

$$\nabla \times \vec{\mathcal{E}} = \nabla_{\mathbf{r}} \times \int \frac{\varrho(\mathbf{r}')}{4\pi\varepsilon_0} \frac{\mathbf{r}-\mathbf{r}'}{|\mathbf{r}-\mathbf{r}'|^3} dV' = \frac{1}{4\pi\varepsilon_0} \int \varrho(\mathbf{r}') \nabla_{\mathbf{r}} \times \frac{\mathbf{r}-\mathbf{r}'}{|\mathbf{r}-\mathbf{r}'|^3} dV' = 0 \ . \tag{13.20}$$

The fact that the rotation of any electrostatic field must vanish is a severe constraint. For example, there is no charge distribution leading to a field of the form $\vec{\mathcal{E}} = y\hat{\mathbf{e}}_x$.

A direct consequence of this law is that we can introduce the concept of the potential. This is fundamental, because electrodynamics can be fully formulated in terms of scalar potentials. We will devote the whole next section to electric potentials.

13.2.4 Exercises

13.2.4.1 Ex: Use of Dirac's function in Coulomb's law

Show how the following Coulomb law formulas for one-, two- and three-dimensional density distributions,

$$\vec{\mathcal{E}}(\mathbf{r}) = \frac{1}{4\pi\varepsilon_0}\int_V \frac{\mathbf{r}-\mathbf{r}'}{|\mathbf{r}-\mathbf{r}'|^3}\rho(\mathbf{r}')dV'$$
$$\vec{\mathcal{E}}(\mathbf{r}) = \frac{1}{4\pi\varepsilon_0}\int_A \frac{\mathbf{r}-\mathbf{r}'}{|\mathbf{r}-\mathbf{r}'|^3}\sigma(\mathbf{r}')dA'$$
$$\vec{\mathcal{E}}(\mathbf{r}) = \frac{1}{4\pi\varepsilon_0}\int_C \frac{\mathbf{r}-\mathbf{r}'}{|\mathbf{r}-\mathbf{r}'|^3}\lambda(\mathbf{r}')dC'$$

are linked using Dirac's δ-function, defined by,

$$\delta(x) = \left\{ \begin{array}{ll} \infty & \text{for } x = 0 \\ 0 & \text{for } x \neq 0 \end{array} \right\} \quad \text{such that} \quad \int f(x)\delta(x-a)dx = f(a)\infty\frac{1}{\infty} = f(a)\ .$$

Use the examples of a. A linear charge distribution along the x-axis, given by $\rho(\mathbf{r}') = \lambda(x')\delta(y')\delta(z')$, and b. a surface charge distribution in the $z = 0$ plane, given by$\rho(\mathbf{r}') = \sigma(x', y')\delta(z')$.

Solution: *a. We have*

$$\vec{\mathcal{E}}(\mathbf{r}) = \frac{1}{4\pi\varepsilon_0}\int_V \frac{\mathbf{r}-\mathbf{r}'}{|\mathbf{r}-\mathbf{r}'|^3}\rho(\mathbf{r}')dV' = \frac{1}{4\pi\varepsilon_0}\int_{-\infty}^{\infty}\int_{-\infty}^{\infty}\int_{-\infty}^{\infty}\frac{\mathbf{r}-\mathbf{r}'}{|\mathbf{r}-\mathbf{r}'|^3}\lambda(x')\delta(y')\delta(z')dx'dy'dz'$$
$$= \frac{1}{4\pi\varepsilon_0}\int_{-\infty}^{\infty}\frac{\mathbf{r}-\mathbf{r}'}{|\mathbf{r}-\mathbf{r}'|^3}\lambda(x')dx' = \frac{1}{4\pi\varepsilon_0}\int_{-\infty}^{\infty}\frac{\mathbf{r}-x'\hat{\mathbf{e}}_x}{|\mathbf{r}-x'\hat{\mathbf{e}}_x|^3}\lambda(x')dx'\ .$$

b. We have

$$\vec{\mathcal{E}}(\mathbf{r}) = \frac{1}{4\pi\varepsilon_0}\int_V \frac{\mathbf{r}-\mathbf{r}'}{|\mathbf{r}-\mathbf{r}'|^3}\rho(\mathbf{r}')dV' = \frac{1}{4\pi\varepsilon_0}\int_{-\infty}^{\infty}\int_{-\infty}^{\infty}\int_{-\infty}^{\infty}\frac{\mathbf{r}-\mathbf{r}'}{|\mathbf{r}-\mathbf{r}'|^3}\sigma(x', y')\delta(z')dx'dy'dz'$$
$$= \frac{1}{4\pi\varepsilon_0}\int_{-\infty}^{\infty}\int_{-\infty}^{\infty}\frac{\mathbf{r}-\mathbf{r}'}{|\mathbf{r}-\mathbf{r}'|^3}\sigma(x', y')dx'dy'$$
$$= \frac{1}{4\pi\varepsilon_0}\int_{-\infty}^{\infty}\int_{-\infty}^{\infty}\frac{\mathbf{r}-x'\hat{\mathbf{e}}_x-y'\hat{\mathbf{e}}_y}{|\mathbf{r}-x'\hat{\mathbf{e}}_x-y'\hat{\mathbf{e}}_y|^3}\sigma(x', y')dx'dy'\ .$$

13.2.4.2 Ex: Electric field generated by a linear charge distribution

Calculate the electric field generated by a linear charge distribution. Analyze the field in a remote region.

Solution: *We put the charge distribution $\lambda(x) = Q/L$ along the x-axis and the observation point at $x = 0$. Following Coulomb's law we have,*

$$\vec{\mathcal{E}}(\mathbf{r}) = \frac{1}{4\pi\varepsilon_0}\int_{x_1}^{x_2} \frac{\begin{pmatrix} x \\ y \end{pmatrix} - \begin{pmatrix} x' \\ y' \end{pmatrix}}{\sqrt{(x-x')^2+(y-y')^2}^3}\lambda(x')dx' = \lambda\int_{x_1}^{x_2} \frac{\begin{pmatrix} 0 \\ y \end{pmatrix} - \begin{pmatrix} x' \\ 0 \end{pmatrix}}{\sqrt{x'^2+y^2}^3}dx' \ .$$

Using

$$\int \frac{zdz}{\sqrt{z^2+a^2}^3} = -\frac{1}{\sqrt{z^2+a^2}} \qquad \text{and} \qquad \int \frac{dz}{\sqrt{z^2+a^2}^3} = \frac{z}{a^2\sqrt{z^2+a^2}} \ ,$$

we obtain,

$$\mathcal{E}_x(r) = \frac{\lambda}{4\pi\varepsilon_0}\int_{x_1}^{x_2} \frac{-x'}{\sqrt{x'^2+y^2}^3}dx' = \frac{\lambda}{4\pi\varepsilon_0}\frac{\sqrt{x_1^2+y^2}-\sqrt{x_2^2+y^2}}{\sqrt{x_2^2+y^2}\sqrt{x_1^2+y^2}} = \frac{\lambda}{4\pi\varepsilon_0}\left(\frac{1}{r_2}-\frac{1}{r_1}\right)$$

$$\mathcal{E}_y(r) = \frac{\lambda}{4\pi\varepsilon_0}\int_{x_1}^{x_2} \frac{y}{\sqrt{x'^2+y^2}^3}dx' = \frac{\lambda}{4\pi\varepsilon_0}\frac{x_2\sqrt{x_1^2+y^2}-x_1\sqrt{x_2^2+y^2}}{\sqrt{x_2^2+y^2}y\sqrt{x_1^2+y^2}} = \frac{\lambda}{4\pi\varepsilon_0}\left(\frac{x_2}{yr_2}-\frac{x_1}{yr_1}\right) \ .$$

with the abbreviations $r_k \equiv \sqrt{x_k^2+y^2}$. At long distances along the axis x, $x_1, x_2 \gg L$, we get $\mathcal{E}_y(x) = 0$ for symmetry reasons and

$$\mathcal{E}_x(x) = \frac{\lambda}{4\pi\varepsilon_0}\left(\frac{1}{x_2}-\frac{1}{x_1}\right) = \frac{Q}{4\pi\varepsilon_0 L}\frac{-L}{x_1(x_1+L)} \simeq \frac{-Q}{4\pi\varepsilon_0 x_1^2} \ .$$

At long distances along the y-axis, that is, $y \gg L$, we get $\mathcal{E}_x(x) = 0$ and,

$$\begin{aligned}\mathcal{E}_y(x) &= \frac{\lambda}{4\pi\varepsilon_0}\frac{(x_1+L)\sqrt{x_1^2+y^2}-x_1\sqrt{(x_1+L)^2+y^2}}{\sqrt{x_1^2+y^2}y\sqrt{(x_1+L)^2+y^2}} \\ &\simeq \frac{\lambda}{4\pi\varepsilon_0}\frac{(x_1+L)\sqrt{y^2}-x_1\sqrt{y^2}}{\sqrt{y^2}y\sqrt{y^2}} = \frac{Q}{4\pi\varepsilon_0}\frac{L}{y^2} \ .\end{aligned}$$

For an infinite charge distribution, $x_2 = -x_1 \gg y$,

$$\mathcal{E}_y(x) = \frac{\lambda}{4\pi\varepsilon_0}\frac{x_2\sqrt{x_1^2+y^2}-x_1\sqrt{x_2^2+y^2}}{\sqrt{x_1^2+y^2}y\sqrt{x_2^2+y^2}} = \frac{\lambda}{4\pi\varepsilon_0}\frac{2x_2}{y\sqrt{x_2^2+y^2}} \simeq \frac{\lambda}{2\pi\varepsilon_0}\frac{1}{y} \ .$$

13.2.4.3 Ex: Electric field produced by a charged disc

a. Calculate the electric field along the symmetry axis generated by a thin disk of radius R evenly charged with the charge Q.
b. Discuss the limit $R \to \infty$ assuming that the surface charge density is kept constant.

Solution: *a. The electric field produced by a charged disc is,*

$$\vec{\mathcal{E}}(\mathbf{r}) = \frac{1}{4\pi\varepsilon_0}\int_{disco}\frac{\mathbf{r}-\mathbf{r}'}{|\mathbf{r}-\mathbf{r}'|^3}\rho(\mathbf{r}')r'dr'd\phi'dz'$$

$$= \frac{Q}{4\pi\varepsilon_0\pi R^2}\int_{disco}\frac{\begin{pmatrix}x\\y\\z\end{pmatrix}-\begin{pmatrix}R\cos\phi'\\R\sin\phi'\\0\end{pmatrix}}{\sqrt{(x-r'\cos\phi')^2+(y-r'\sin\phi')^2+z^2}^3}r'dr'd\phi' \ .$$

On the symmetry axis we have $\mathcal{E}_x(z) = \mathcal{E}_y(z) = 0$ *e*

$$\mathcal{E}_z(z) = \frac{Q}{4\pi\varepsilon_0\pi R^2}\int_{disco}\frac{z}{\sqrt{r'^2\cos^2\phi'+r'^2\sin^2\phi'+z^2}^3}r'dr'd\phi'$$

$$= \frac{Q}{4\pi\varepsilon_0\pi R^2}2\pi z\int_0^R\frac{r'}{\sqrt{r'^2+z^2}^3}dr' = \frac{Q}{4\pi\varepsilon_0\pi R^2}2\pi z\int_{z^2}^{R^2+z^2}\frac{u^{-3/2}}{2}du$$

$$= \frac{Q}{4\pi\varepsilon_0\pi R^2}2\pi z\left.\frac{-1}{\sqrt{r'^2+z^2}}\right|_0^R = \frac{Q}{2\pi\varepsilon_0 R^2}\left(\frac{-z}{\sqrt{R^2+z^2}}+\frac{z}{|z|}\right) \ ,$$

with $\int\frac{udu}{\sqrt{u^2+z^2}^3} = -\frac{1}{\sqrt{u^2+z^2}}$.
b. Considering a disk with infinite extension, $R \longrightarrow \infty$*, but with constant charge surface density,* $\sigma \equiv Q/\pi R^2 = const$*, we obtain,*

$$E_z(z) = \frac{\sigma}{2\varepsilon_0}\frac{z}{|z|} \ .$$

That is, the electric field is uniform and opposite on both sides of the disk.

13.2.4.4 Ex: Electric field produced by a spherical layer

A charge q is deposited on a solid conducting sphere of radius R.
a. Parametrize the charge distribution $\rho(\mathbf{r})$.
b. Determine the surface charge density σ on the sphere's surface.
c. Using the Gauß law, $\oint_{\partial V}\vec{\mathcal{E}}(\mathbf{r})\cdot d\mathbf{a} = \frac{Q}{\varepsilon_0}$, calculate the electric field inside and outside the sphere.
d. Using the Coulomb law, $\vec{\mathcal{E}}(\mathbf{r}) = \frac{1}{4\pi\varepsilon_0}\int_A\frac{\mathbf{r}-\mathbf{r}'}{|\mathbf{r}-\mathbf{r}'|^3}\sigma(\mathbf{r}')dA'$ in spherical coordinates,

$$\mathbf{r}' = \begin{pmatrix}R\sin\theta'\cos\phi'\\R\sin\theta'\sin\phi'\\R\sin\theta'\end{pmatrix} \qquad \text{and} \qquad dA' = R^2\sin\theta'd\theta d\phi' \ ,$$

calculate the electric field $E_z(z)$ along the z-axis in- and outside the sphere. Help:

$$\int_{-R}^{R} \frac{z-z'}{\sqrt{z^2-2zz'+R^2}^3} dz' = \begin{cases} \frac{-2R}{z^2} & z < -R \\ 0 & \text{for } -R < z < R \\ \frac{2R}{z^2} & R < z \end{cases} .$$

Solution: *a. The charge density is given by a δ-function: $\rho(\mathbf{r}) = C \cdot \delta^{(3)}(r-R)$, where the constant C must be determined by integration over the entire space. Integrating the density, we hope to obtain the total charge:*

$$\int_V \rho(\mathbf{r}) = C \int_V \delta^{(3)}(r-R) \equiv Q \ .$$

On the other hand, the integral over the δ-function reproduces the total surface:

$$\int_{\partial V} \delta^{(3)}(r-R) = 4\pi R^2 \ .$$

Hence, $C = \frac{Q}{4\pi R^2} = \sigma$ is the surface charge density.
b. The charge will be deposited on the outer surface of the sphere. Thus, the surface charge density is,

$$\sigma = \frac{Q}{4\pi R^2} \ .$$

c. Using the Gauß law,

$$\oint_{\partial V} \vec{\mathcal{E}}(\mathbf{r}) \cdot d\mathbf{a} = E_r 4\pi r^2 = \frac{Q_{inside}}{\varepsilon_0} \ ,$$

we find

$$\vec{\mathcal{E}}(\mathbf{r}) = 0 \ \ for \ \ r < R \ \ and \ \ \vec{\mathcal{E}}(\mathbf{r}) = \frac{Q}{4\pi\varepsilon_0 r^2}\hat{\mathbf{e}}_r \ \ for \ \ r > R \ ,$$

what exactly is Coulomb's law.
d. On the surface σ is constant. Hence,

$$\begin{aligned} \vec{\mathcal{E}}(\mathbf{r}) &= \frac{\sigma}{4\pi\varepsilon_0} \int_A \frac{\mathbf{r}-\mathbf{r}'}{|\mathbf{r}-\mathbf{r}'|^3} dA' = \frac{\sigma}{4\pi\varepsilon_0} \int_A \frac{\mathbf{r}-R\hat{\mathbf{e}}'_r}{|\mathbf{r}-\mathbf{r}'|^3} R^2 \sin\theta' d\theta' d\phi' \\ &= \frac{\sigma R^2}{4\pi\varepsilon_0} \int_A \frac{\begin{pmatrix} 0 \\ 0 \\ z \end{pmatrix} - R \begin{pmatrix} \sin\theta'\cos\phi' \\ \sin\theta'\sin\phi' \\ \cos\theta' \end{pmatrix}}{\sqrt{(x-x')^2+(y-y')^2+(z-z')^2}^3} \sin\theta' d\theta' d\phi' \ . \end{aligned}$$

For the component E_z along the z-axis we have

$$\begin{aligned}\mathcal{E}_z(z) &= \frac{\sigma R^2}{4\pi\varepsilon_0}\int_0^{\pi}\int_0^{2\pi}\frac{z - R\cos\theta'}{\sqrt{(R\sin\theta'\cos\phi')^2 + (R\sin\theta'\sin\phi')^2 + (z - R\cos\theta')^2}^3}\sin\theta' d\theta' d\phi' \\ &= \frac{\sigma R^2}{4\pi\varepsilon_0}2\pi\int_0^{\pi}\frac{z - R\cos\theta'}{\sqrt{(R\sin\theta')^2 + (z - R\cos\theta')^2}^3}\sin\theta' d\theta' \\ &= \frac{Q}{8\pi\varepsilon_0}\int_{-1}^{1}\frac{z - R\cos\theta'}{\sqrt{z^2 - 2Rz\cos\theta' + R^2}^3}d\cos\theta' = \frac{Q}{8\pi\varepsilon_0 R}\int_{-R}^{R}\frac{z - z'}{\sqrt{z^2 - 2zz' + R^2}^3}dz' \ .\end{aligned}$$

Using the formula for calculating the integral, we find,

$$\mathcal{E}_z(z) = \frac{Q}{4\pi\varepsilon_0 z^2}\cdot\begin{cases}-1 & z < -R \\ 0 \quad for & -R < z < R \\ 1 & R < z\end{cases}.$$

13.2.4.5 Ex: Field of a homogeneously charged sphere

Calculate with the Gauß law the electric field of a homogeneously charged sphere (charge Q, radius R)
a. for $r < R$ and
b. for $r \geq R$.

Solution: *For reasons of symmetry the electric field $\vec{\mathcal{E}}$ produced by the charge must show radially outward and the absolute value E can only depend on r. The charge density of the sphere is $\rho(\mathbf{r}) = \rho_0 = \frac{Q}{4\pi R^3/3}$ for $r \leq R$, else $\rho(\mathbf{r}) = 0$. Following the Gauß law we have $\int_{\partial\ subsphere}\vec{\mathcal{E}}\cdot d\mathbf{S} = \frac{1}{\varepsilon_0}\int_{subsphere}\rho(\mathbf{r})d^3r$. Hence, for $r < R$*

$$4\pi r^2\mathcal{E}_r = \frac{\rho_0}{\varepsilon_0}\int_{subsphere} r^2\sin\theta dr d\theta d\phi = \frac{4\pi\rho_0}{3}r^3 \ ,$$

and finally,

$$\mathcal{E}_r = \frac{Q}{4\pi\varepsilon_0 R^3}r \ .$$

For $r \geq R$ we have,

$$4\pi r^2\mathcal{E}_r = \frac{\rho_0}{\varepsilon_0}\int_{sphere} r^2\sin\theta dr d\theta d\phi = \frac{4\pi\rho_0}{3}R^3 \ ,$$

and finally,

$$\mathcal{E}_r = \frac{Q}{4\pi\varepsilon_0 r^2} \ .$$

13.2.4.6 Ex: Field of a charge distribution with spherical symmetry

The electric field generated by a spherically symmetric charge distribution $\rho(r)$ can be given in the form,

$$\vec{\mathcal{E}}(\mathbf{r}) = \frac{\mathbf{r}}{r^3}\, 4\pi \int_0^r dr'\; r'^{\,2}\, \rho(r')\ ,$$

where the origin is in the center of the sphere and $r = |\mathbf{r}|$.
a. Show that $\mathrm{div}\vec{\mathcal{E}} = 4\pi\ \rho$ and $\mathrm{rot}\vec{\mathcal{E}} = 0$.
b. Calculate the field for a sphere of radius R, which is homogeneously charged in the entire volume with the total charge Q.
c. Resolve (b) for a homogeneously charged hollow concentric sphere with inner radius R_i, outer radius R_a and full load Q.
d. Resolve (c) for the case, that the center of the hollow spherical part is displaced by a vector $\mathbf{d}$ with respect to the center of the spherical surface.
Help: The electric field is an additive quantity.

Solution: *a. We have*

$$\nabla\cdot\vec{\mathcal{E}} = \vec{\nabla}\cdot\left[\frac{4\pi}{r^2}\int_0^r dr'\; r'^{\,2}\rho(r')\right]\hat{\mathbf{e}}_r = \frac{1}{r^2}\frac{\partial}{\partial r}\left[r^2\frac{4\pi}{r^2}\int_0^r dr'\; r'^{\,2}\rho(r')\right]$$
$$= \frac{4\pi}{r^2}\frac{\partial}{\partial r}\int_0^r dr'\; r'^{\,2}\rho(r') = \frac{4\pi}{r^2}r^2\rho(r) = 4\pi\rho(r)\ .$$

Vale $\vec{\mathcal{E}} = \hat{\mathbf{e}}_r E_r \equiv \nabla g(r)$. *From this follows immediately,*

$$\vec{\nabla}\times\vec{\mathcal{E}} = \vec{\nabla}\times(\vec{\nabla}g) \equiv 0\ .$$

b. We have,

$$\rho(r) = \begin{cases} \frac{Q}{4\pi R^3/3} & \textit{para } r \le R \\ 0 & \textit{else} \end{cases}\ .$$

Hence,

$$\int_0^r dr'\; r'^2\rho(r') = \begin{cases} \frac{Q}{4\pi R^3/3}\frac{r^3}{3} & \textit{for } r \le R \\ \frac{Q}{4\pi R^3/3}\frac{R^3}{3} & \textit{for } r > R \end{cases}$$

e por isso,

$$\vec{\mathcal{E}}(r) = \hat{\mathbf{e}}_r Q \begin{cases} \frac{r}{R^3} & \textit{for } r \le R \\ \frac{1}{r^2} & \textit{for } r > R \end{cases}\ .$$

c. We have

$$\rho(r) = \begin{cases} 0 & \textit{para } r < R_i \\ \frac{Q}{4\pi(R_a^3 - R_i^3)/3} & \textit{for } R_i \le r \le R_a \\ 0 & \textit{for } r > R_a \end{cases}\ .$$

Hence,

$$\int_0^r dr'\; r'^2\rho(r') = \frac{Q}{4\pi(R_a^3 - R_i^3)/3}\begin{cases} 0 & \textit{for } r < R_i \\ (r^3 - R_i^3)/3 & \textit{para } R_i \le r \le R_a \\ (R_a^3 - R_i^3)/3 & \textit{for } r > R_a \end{cases}$$

and therefore,

$$\vec{\mathcal{E}}(r) = \hat{\mathbf{e}}_r\, Q \begin{cases} 0 & for r < R_i \\ \frac{r^3 - R_i^3}{R_a^3 - R_i^3}\frac{1}{r^2} & for\ R_i \le r \le R_a \\ \frac{1}{r^2} & for\ r > R_a \end{cases} .$$

In the outer region, therefore, we have the same behavior as in (b). Here the field only depends on the total evenly distributed charge Q.
d. We want to place the origin in the center of a large solid *sphere. An arbitrary point* $\mathbf{r}$ *on the surface of the sphere has the vector relative to the center of the small* hollow *sphere* $\mathbf{r}' = \mathbf{r} - \mathbf{d}$. *We let the charge density be,*

$$\rho_1 = \frac{Q}{\frac{4\pi}{3}(R_a^3 - R_i^3)}$$

and use that

$$\vec{\mathcal{E}} = \vec{\mathcal{E}}_{solid\ sphere} - \vec{\mathcal{E}}_{hollow\ sphere} .$$

Now,

$$\vec{\mathcal{E}}_{solid\ sphere} = \frac{\mathbf{r}}{r}\frac{4\pi}{3}\rho_1 \begin{cases} r & for\ r \le R_a \\ \frac{R_a^3}{r^2} & for\ r > R_a \end{cases}$$

and

$$\vec{\mathcal{E}}_{hollow\ sphere} = \frac{\mathbf{r}'}{r'}\frac{4\pi}{3}\rho_1 \begin{cases} r' & for\ r' \le R_i \\ \frac{R_i^3}{r'^2} & for r' > R_i \end{cases} .$$

From this follows immediately,

$$\vec{\mathcal{E}}(\mathbf{r}) = \frac{4\pi}{3}\rho_1 \begin{cases} \mathbf{d} & inside\ the\ hollow\ sphere \\ \mathbf{r} - \frac{\mathbf{r}-\mathbf{d}}{|\mathbf{r}-\mathbf{d}|^3}R_i^3 & within\ the\ shell \\ \frac{\mathbf{r}}{r^3}R_a^3 - \frac{\mathbf{r}-\mathbf{d}}{|\mathbf{r}-\mathbf{d}|^3}R_i^3 & outside \end{cases} .$$

13.2.4.7 Ex: Field of a charge distribution with spherical symmetry

A sphere of radius R is in a vacuum. It is made of a material with a constant permittivity ε and carries the charge q in its center.
a. Calculate the field the electrostatic field $\vec{\mathcal{E}}$ inside and outside the sphere.
b. Calculate the electrostatic potential Φ in the entire space.

Solution:

13.2.4.8 Ex: Charge distribution

We consider the charge density $\rho(\mathbf{r}) = cr\int_0^R dr'\delta(r'-r)$, where $r = |\mathbf{r}|$, $R > 0$ and $c = const$. The total charge be Q.
a. Make a scheme of the function $\rho(\mathbf{r})$. What is the relationship between the constant

c and the total charge Q?
b. Start by showing that the electric field created by a spherically symmetric charge distribution ρ can be written as $\vec{\mathcal{E}}(\mathbf{r}) = \frac{\mathbf{r}}{r^3}\int_0^r dr' r'^2 \frac{1}{\varepsilon_0}\rho(r')$. Here, $\mathbf{r}$ is the vector starting from the origin at the center of symmetry and reaching the surface. Determine the absolute value and direction of the electric field $\vec{\mathcal{E}}(\mathbf{r})$ for $|\mathbf{r}| < R$ and $|\mathbf{r}| > R$ for the given charge distribution. Make a scheme of the profile $|\vec{\mathcal{E}}(\mathbf{r})|$.

Solution: *a. The charge is,*

$$\begin{aligned} Q &= \int \rho(\mathbf{r}) d^3r = 4\pi \int_0^\infty r^2 \rho(r) dr = 4\pi c \int_0^\infty dr\ r^3 \int_0^R dr' \delta(r'-r) \\ &= 4\pi c \int_0^R dr\ r^3 = 4\pi c \frac{R^4}{4} = \pi c R^4 \\ &\Longrightarrow c = \frac{Q}{\pi R^4} \ . \end{aligned}$$

The charge distribution therefore increases linearly with the pitch c between $r = 0$ and $r = R$ and drops to zero for $r > R$.
b. For $\rho(\mathbf{r}) = \rho(r)$ the expression $\vec{\mathcal{E}} = E_r \frac{\mathbf{r}}{r}$ is the volume integral of a sphere with radius r, where the center of the sphere is the center of symmetry,

$$\int_V div\ \vec{\mathcal{E}} d^3r' = \int_V \frac{1}{\varepsilon_0}\rho d^3r' = \frac{4\pi}{\varepsilon_0}\int_0^r \rho(r') r'^2 dr' \ .$$

With Gauß

$$\int_V div\ \vec{\mathcal{E}} d^3r' = \int_{\partial V} \vec{\mathcal{E}} d^2\mathbf{f} = 4\pi r^2 \mathcal{E}_r(r) \ .$$

Follows

$$\begin{aligned} \vec{\mathcal{E}}(\mathbf{r}) &= \frac{1}{\varepsilon_0}\frac{\mathbf{r}}{r^3}\int_0^r dr' r'' \rho(r') = \frac{c}{\varepsilon_0}\frac{\mathbf{r}}{r^3}\int_0^r dr' r''' r' \int_0^R dr'' \delta(r'') - r') \\ &= \begin{cases} \frac{c}{\varepsilon_0}\frac{\mathbf{r}}{r^3}\int_0^r dr' r''' = \frac{Q}{4\pi\varepsilon_0}\hat{\mathbf{e}}_r \frac{r^2}{R^4} & for \quad r \le R \\ \frac{c}{\varepsilon_0}\frac{\mathbf{r}}{r^3}\int_0^R dr' r''' = \frac{Q}{4\pi\varepsilon_0}\hat{\mathbf{e}}_r \frac{1}{r^2} & for \quad r > R \end{cases} . \end{aligned}$$

The amplitude $\mathcal{E}_r$ of the electric field increases between $r = 0$ and R quadratically and then falls as $1/r^2$.

13.2.4.9 Ex: Charge distribution

A thin, square and conductive sheet has $d = 5.0$ m long edges and a charge of $Q = 80\,\mu C$. Assume that the load is evenly distributed on the faces of the sheet.
a. Determine the charge density on each face of the sheet and the electric field in the vicinity of one face.
b. The sheet is placed to the right of an infinite, non-conductive plane charged with the charge density $\sigma_{inf} = 2.0\ \mu C/m^2$, with the faces of the sheet parallel to the plane. Determine the electric field on each face of the sheet and determine the charge density

on each face.

Solution: *a. The charge densities on each side of the sheet are,*

$$\sigma_{esq} = \sigma_{dir} = \frac{Q}{2A} = 1.6\,\mu\text{C/m}^2 \ .$$

With that, we get the fields close to the surfaces,

$$\mathcal{E}_{esq} = -\frac{\sigma_{esq}}{\varepsilon_0} = -181\,\text{kN/C} \qquad \textit{and} \qquad \mathcal{E}_{dir} = \frac{\sigma_{dir}}{\varepsilon_0} = 181\,\text{kN/C} \ .$$

b. The field generated by the infinite plane on its right side is,

$$\mathcal{E}_{inf} = \frac{\sigma_{inf}}{2\varepsilon_0} = 113\,\text{kN/C} \ .$$

Therefore, the total fields on both sides of the sheet are,

$$\mathcal{E}_{esq,x} = \mathcal{E}_{esq} + \mathcal{E}_{inf} = -68\,\text{kN/C} \qquad \textit{and} \qquad \mathcal{E}_{dir,x} = \mathcal{E}_{dir} + \mathcal{E}_{inf} = 294\,\text{kN/C} \ .$$

As the sheet is conductive, the charge densities rearrange themselves like

$$\sigma_{esq,x} = \varepsilon_0 E_{esq,x} = 0.6\,\mu\text{C/m}^2 \qquad \textit{and} \qquad \sigma_{dir,x} = \varepsilon_0 E_{dir,x} = 2.6\,\mu\text{C/m}^2 \ .$$

13.2.4.10 Ex: Charge distribution

A large, flat, non-conductive and non-uniformly charged surface is placed along the $x = 0$ plane. At the origin, the charge density is $\sigma = 3.1\,\mu\text{C/m}^2$. At a short distance from the surface in the positive direction of the x-axis, the x-component of the electric field is $\mathcal{E}_{dir} = 4.65 \cdot 10^5\,\text{N/C}$. What is the value of $\mathcal{E}_x$ a short distance from the surface in the negative direction of the axis x.

Solution: *The discontinuity of the normal of the electric field has to be,*

$$\Delta E_n = \frac{\sigma}{\varepsilon_0} \ .$$

Hence, the field on the left is

$$E_{esq} = E_{dir} - \frac{\sigma}{\varepsilon_0} = -115\,\text{kN/C} \ .$$

The inequality of the fields on the left and right sides comes from the superposition of another electric field due to the uneven distribution of charge on the surface.

13.2.4.11 Ex: Charge distribution

An infinite flat non-conductive blade with surface charge density $\sigma_1 = +3.0\,\mu\text{C/m}^2$ is located in the $y_0 = -0.6\,\text{m}$ plane. A second infinite flat blade with surface charge density of $\sigma_2 = -2.0\,\mu\text{C/m}^2$ is located in the $x_0 = 1.0\,\text{m}$ plane. Finally, a thin

non-conductive spherical shell with radius $R = 1.0\,\mathrm{m}$ and its center in the $z_0 = 0$ plane at the intersection of the two charged blades, has a surface charge density of $\sigma_3 = -3.0\,\mu\mathrm{C/m}^2$. Determine the magnitude, direction, and orientation of the electric field along the x-axis and
a. $x_1 = 0.4\,\mathrm{m}$ and
b. $x_2 = 2.5\,\mathrm{m}$.

Solution: *a. The fields produced by σ_n are,*

$$\vec{\mathcal{E}}_1 = \frac{\sigma_1}{2\varepsilon_0}\frac{y-y_0}{|y-y_0|}\hat{\mathbf{e}}_y \quad , \quad \vec{\mathcal{E}}_2 = \frac{\sigma_2}{2\varepsilon_0}\frac{x-x_0}{|x-x_0|}\hat{\mathbf{e}}_x \quad ,$$
$$\vec{\mathcal{E}}_3 = 0 \;\; for \;\; r < R \;\; and \;\; \frac{\sigma_3 4\pi R^2}{4\pi\varepsilon_0}\frac{1}{r}\hat{\mathbf{e}}_r \;\; for \;\; r > R \;,$$

where $r^2 \equiv (x-x_0)^2 + (y-y_0)^2 + (z-z_0)^2$. The total field is,

$$\vec{\mathcal{E}} = \vec{\mathcal{E}}_1 + \vec{\mathcal{E}}_2 + \vec{\mathcal{E}}_3 \;.$$

We verify that the observation point $\mathbf{r}_1 = (x_1, 0, 0)$ is within the sphere σ_3, $r_1 < R$. Hence,

$$\vec{\mathcal{E}} = \frac{\sigma_1}{2\varepsilon_0}\hat{\mathbf{e}}_y + \frac{\sigma_2}{2\varepsilon_0}(-\hat{\mathbf{e}}_x) + 0 \;,$$

giving $E = \frac{\sqrt{\sigma_1^2+\sigma_2^2}}{2\varepsilon_0} = 204\ kN/C$ and $\theta = \frac{\sigma_1}{\sigma_2} = 56.3°$.
b. We verify that the observation point $\mathbf{r}_2 = (x_2, 0, 0)$ is outside the sphere σ_3, $r_2 > R$. Hence,

$$\vec{\mathcal{E}} = \frac{\sigma_1}{2\varepsilon_0}\hat{\mathbf{e}}_y + \frac{\sigma_2}{2\varepsilon_0}(+\hat{\mathbf{e}}_x) + \frac{\sigma_3}{\varepsilon_0}\frac{R^2}{r_1^2}\hat{\mathbf{e}}_x \;,$$

giving $E = \frac{\sqrt{\sigma_1^2+(\sigma_2+\frac{2R^2}{r_1^2})^2}}{2\varepsilon_0} = 263\ kN/C$ and $\theta = \frac{\sigma_1}{\sigma_2+\frac{2R^2}{r_1}} = 153°$.

13.2.4.12 Ex: Charged sphere

A solid non-conducting sphere with radius $R = 1.0\,\mathrm{cm}$ carries a uniform volumetric charge density. The magnitude of the electric field at a distance $r = 2.0\,\mathrm{cm}$ from the center of the sphere is $\mathcal{E}_r = 1.88 \cdot 10^3\,\mathrm{N/C}$.
a. What is the volumetric charge density of the sphere?
b. Determine the magnitude of the electric field at a distance $d = 5.0\,\mathrm{cm}$ from the center of the sphere.

Solution: *a. Using the Gauß law,*

$$\mathcal{E}_r = \frac{1}{4\pi\varepsilon_0}\frac{Q_{inside}}{r^2} \;,$$

we obtain,

$$Q_{inside} = 4\pi\varepsilon_0 r^2 E_r \;.$$

The density follows from,

$$\rho = \frac{Q_{inside}}{\frac{4\pi}{3}R^3} = \frac{3\varepsilon_0 r^2 \mathcal{E}_r}{R^3} = 2.0\ \mu C\ .$$

b. The electric field at this distance is,

$$\mathcal{E}_d = \frac{1}{4\pi\varepsilon_0}\frac{Q_{inside}}{d^2} = 301.3\,\mathrm{N/C}\ .$$

Gabarite: *a.* $2.0\,\mu\mathrm{C/m^3}$. *b.* $470\,\mathrm{N/C}$.

13.2.4.13 Ex: Electrical flow

A point charge Q is placed in the center of a hypothetical ball with radius R, which on one side is cut at a height h. What is the flow of electric field $\vec{\mathcal{E}}$ through the plane of the cut A illustrated in the figure?

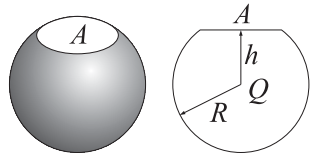

Figure 13.5: Scheme.

Solution: *The electric field is given by,*

$$\vec{\mathcal{E}}(\mathbf{r}) = \frac{1}{4\pi\varepsilon_0}\frac{Q}{r^2}\hat{\mathbf{e}}_r\ .$$

As in a central field without divergence or rotation the flow must be preserved, we can consider instead of the flow through the cut A, a flow through the spherical cap. The flow of the electric field is therefore,

$$\begin{aligned}\Phi &= \int_A \vec{\mathcal{E}}(\mathbf{r}')\cdot d\mathbf{S}' = \int_{\mathcal{S}} \frac{1}{4\pi\varepsilon_0}\frac{Q}{r^2}\hat{\mathbf{e}}_r\cdot d\mathbf{S} = \int_A \frac{1}{4\pi\varepsilon_0}\frac{Q}{R^2}R^2\sin\theta d\theta d\phi \\ &= 2\pi\frac{Q}{4\pi\varepsilon_0}\cos\theta|_{\arccos(h/R)}^{0} = \frac{Q}{2\varepsilon_0}\left(1-\frac{h}{R}\right)\ .\end{aligned}$$

13.2.4.14 Ex: Electrical flow

The cube shown in the figure has an edge length of $d = 1.4\,\mathrm{m}$ and is located inside an electric field.
a. Calculate the electrical flux through the right surface of the cube for an electric field given by $\vec{\mathcal{E}} = -3\,\mathrm{V/m}\cdot\hat{\mathbf{e}}_x + 4\,\mathrm{V/m}\cdot\hat{\mathbf{e}}_z$. What is the total flux across the entire

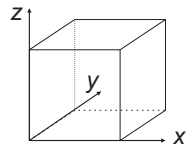

Figure 13.6: Scheme.

surface of the cube?
b. Calculate the total flux across the entire surface of the cube for the electric field $\vec{\mathcal{E}} = -4\,\mathrm{V/m}^2 \cdot \hat{\mathbf{e}}_x + (6\,\mathrm{V/m} + 3\,\mathrm{V/m}^2 \cdot y)\hat{\mathbf{e}}_y$. What charge is contained in the cube?

Solution:

13.2.4.15 Ex: Electrical flow

Calculate the electric field flux $\vec{\mathcal{E}}(\mathbf{r}) = \mathcal{E}_0\hat{\mathbf{e}}_z$ through the semi-sphere with radius R shown in the figure.

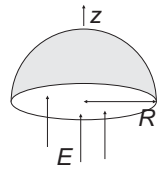

Figure 13.7: Scheme.

Solution: *The surface element in spherical coordinates is,*

$$d\mathbf{a} = R^2 \sin\theta d\theta d\phi \hat{\mathbf{e}}_r \qquad with \qquad \hat{\mathbf{e}}_r = \begin{pmatrix} \sin\theta\cos\phi \\ \sin\theta\sin\phi \\ \cos\theta \end{pmatrix} .$$

The electric field on the surface of the sphere is,

$$\vec{\mathcal{E}} = \mathcal{E}_0 \begin{pmatrix} 0 \\ 0 \\ 1 \end{pmatrix} .$$

The flux through the semi-sphere is therefore,

$$\Psi = R^2 \int_0^{\pi/2} d\theta \sin\theta \int_0^{2\pi} d\phi \mathcal{E}_0 \begin{pmatrix} 0 \\ 0 \\ 1 \end{pmatrix} \cdot \begin{pmatrix} \sin\theta\cos\phi \\ \sin\theta\sin\phi \\ \cos\theta \end{pmatrix} = 2\pi\mathcal{E}_0 R^2 \int_0^{\pi/2} d\theta \sin\theta\cos\theta = \pi\mathcal{E}_0 R^2 .$$

Smart solution: *As the field is homogeneous, the flux* $\int \vec{\mathcal{E}} \cdot d\mathbf{a} = \int E_0 \hat{\mathbf{e}}_z \cdot d\mathbf{a}$ *through the area of the semi-sphere is equal to the flux through a circular surface with the same radius:*

$$\int_{semi-sphere} \vec{\mathcal{E}} \cdot d\mathbf{a} = \int_{circle} \mathcal{E}_0 \hat{\mathbf{e}}_z \cdot \hat{\mathbf{e}}_z dA = \mathcal{E}_0 \pi R^2 \ .$$

13.2.4.16 Ex: Electrical flow

Calculate the flow of the vector field with cylindrical symmetry $\vec{\mathcal{E}}(\mathbf{r}) = \mathcal{E}_0 \hat{\mathbf{e}}_\rho$ through the half cylindrical surface shown in the figure with radius R and length L.

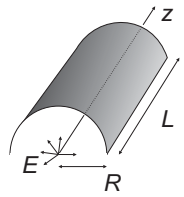

Figure 13.8: Scheme.

Solution: *The surface element is in cylindrical coordinates,*

$$d\mathbf{S} = Rd\phi\hat{\mathbf{e}}_\rho \qquad with \qquad \hat{\mathbf{e}}_\rho = \begin{pmatrix} \cos\phi \\ \sin\phi \\ 0 \end{pmatrix} \ .$$

The flux through the cylinder surface is given by the following expression:

$$\Psi = \int \vec{\mathcal{E}}(\mathbf{r}) \cdot d\mathbf{S} = \int_{\mathcal{S}} E_0 \hat{\mathbf{e}}_\rho \hat{\mathbf{e}}_\rho df = E_0 \pi RL \ .$$

13.2.4.17 Ex: Electric field of a charged sheet

An infinitely extended non-conductive sheet carries a charge with a surface density of $0.1\,\mu C/m^2$ on either side. What is the distance of the equipotential surfaces for a potential difference of 50 V?

Solution: *With* $\rho(\mathbf{r}) = \sigma_0 \delta(z)$ *vale,*

$$\int \mathcal{E}\ df = \oint_{\partial V} \vec{\mathcal{E}}\ d\mathbf{S} = \frac{1}{\varepsilon_0} \int \rho dV = \frac{\sigma_0}{\varepsilon_0} \int dS \ .$$

Follows $\mathcal{E} = \sigma/\varepsilon_0$. *With* $\mathcal{E} = U/d$ *follows* $d = \varepsilon_0 U/\sigma = 4.4\,\text{mm}$.

13.2.4.18 Ex: Electric field between charged planes

Consider two thin, non-conductive planes with infinite length perpendicular to the x-axis and crossing this axis at the positions x_1 and x_2 with $x_1 < x_2$. The planes are uniformly charged with charge densities σ_2. Calculate the electric fields in the three regions $x < x_1$ and $x_1 < x < x_2$ and $x_2 < x$. Discuss the particular cases $\sigma_2 = \sigma_1$ and $\sigma_2 = -\sigma_1$.

Solution: *The fields are,*

$$\mathcal{E}_{esq} = -\frac{\sigma_1}{2\varepsilon_0} - \frac{\sigma_2}{2\varepsilon_0} \quad , \quad \mathcal{E}_{med} = +\frac{\sigma_1}{2\varepsilon_0} - \frac{\sigma_2}{2\varepsilon_0} \quad , \quad \mathcal{E}_{dir} = +\frac{\sigma_1}{2\varepsilon_0} + \frac{\sigma_2}{2\varepsilon_0} \ .$$

For $\sigma_2 = -\sigma_1$, we obtain $\mathcal{E}_{esq} = \mathcal{E}_{dir} = 0$ and $\mathcal{E}_{med} = \sigma_1/\varepsilon_0$.
For $\sigma_2 = \sigma_1$, we obtain $\mathcal{E}_{med} = 0$ and $\mathcal{E}_{esq} = \mathcal{E}_{dir} = \sigma_1/\varepsilon_0$.

13.2.4.19 Ex: Electric field of a photocopier

The electric field just above the surface of the electrically charged drum of a photocopier has the absolute value $2.3 \cdot 10^5\,\mathrm{N/C}$. The drum has a length of 42 cm and a diameter of 12 cm.
a. What is the charge density on the surface supposed conductive?
b. What is the total charge on the drum?
c. Decreasing the drum to 8 cm in order to build a more compact photocopier, the field on the surface must remain the same. What should the charge be in this case?

Solution: *a. For an infinitesimal volume element including a part of the drum's surface we can express the surface density of charges as $\sigma = \varepsilon_0 \mathcal{E} = 2 \cdot 10^{-6}\,\mathrm{C/m^2}$.*
b. For the whole cylinder,

$$\oint_{cylindersurface} \vec{\mathcal{E}}\, d\mathbf{S} = \mathcal{E} \cdot 2\pi RL = \frac{Q}{\varepsilon_0} \ .$$

Follows $Q = \varepsilon_0 E \cdot 2\pi RL = 6.4 \cdot 10^{-7}\,\mathrm{C}$.
c. The charge on the smaller drum should be 12/8=1.5 times less.

13.2.4.20 Ex: Geiger counter

A Geiger-Müller meter consists essentially of a metal tube filled with gas (inner radius r_a) with a thin wire inside (radius r_i). A high voltage is applied between the two. The meter serves, for example, to detect charged particles, which produce pairs of electrons and ions from the gas, which are then extracted by an applied voltage and detected as an electrical signal.
a. Calculate the potential $\phi(r)$, where $\phi(r_a) = 0$ and $\phi(r_i) = U = 1000\,\mathrm{V}$.
b. Be $r_i = 15\,\mu\mathrm{m}$, $r_a = 1\,\mathrm{cm}$. Calculate the strength of the field at the tube's surface.
c. The average free path in the gas is $L = 3\,\mu\mathrm{m}$. At what distance R_I from the wire does an avalanche form, that is, an electron stopped due to a collision is accelerated over a distance L up to the ionization energy $E_I = 5\,\mathrm{eV}$ and, thus, can generate

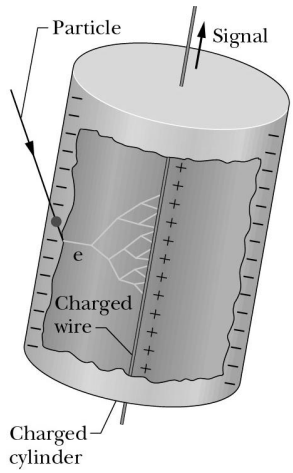

Figure 13.9: Geiger counter.

another electron-ion pair in the subsequent collision?

Solution: *a. The flux through the curved surface of a cylinder with radius r surrounding the wire follows Gauß' law:*

$$\int_{\partial V} \vec{\mathcal{E}} \cdot d\mathbf{S} = \frac{1}{\varepsilon_0} \int_V \rho dV \ .$$

and with that $\mathcal{E} = \frac{Q}{2\pi\varepsilon_0 lr}$ with the charge Q within a segment of the wire of length l. The potential continues follows from the integration of $\vec{\mathcal{E}} = -\vec{\nabla}\Phi$,

$$\Phi = -\int \mathcal{E} dr + C = -\int \frac{Q}{2\pi\varepsilon_0 lr} dr + C = -\frac{Q}{2\pi\varepsilon_0 l} \ln r + C \ .$$

With the boundary condition $\Phi(\mathbf{r})|_{r=r_a} = -\frac{Q}{2\pi\varepsilon_0 l} \ln r_a + C = 0$ segue $\Phi(\mathbf{r}) = \frac{Q}{2\pi\varepsilon_0 l} (\ln r_a - \ln r_i)$. With the boundary condition $\Phi(\mathbf{r})|_{r=r_i} = \frac{Q}{2\pi\varepsilon_0 l}(\ln r_a - \ln r) = U$ segue,

$$\Phi(r) = U \frac{\ln(r_a/r)}{\ln(r_a/r_i)} \ .$$

b. With that we get the field strength on the wire surface,

$$\mathcal{E}(r_i) = \frac{Q}{2\pi\varepsilon_0 l r_i} = \frac{1}{r_i} \frac{U}{\ln \frac{r_a}{r_i}} = 7.2 \cdot 10^4 \, \mathrm{V/cm} \ .$$

c. Avalanches happen at the position R_I,

$$E_I = e\Phi(R_I) - e\Phi(R_I - L) = \frac{eQ}{2\pi\varepsilon_0 l} \ln \frac{R_I - L}{R_I} = eU \frac{\ln \frac{R_I - L}{R_I}}{\ln \frac{r_a}{r_I}} \ .$$

From this,

$$R_I = \frac{L}{1 + \left(\frac{r_a}{r_I}\right)^{E_I/eU}} = 1.5 \, \mathrm{mm} \ .$$

13.2.4.21 Ex: Electrical flow

A thin, non-conductive uniformly charged spherical shell with radius R, has a total positive charge equal to Q. A small piece is removed from the surface.
a. What are the absolute value, the direction and the orientation of the electric field at the center of the void?
b. The piece is placed back into the void. Determine the electrical force exerted on the piece.
c. Using the strength of the force, calculate the electrostatic pressure that tends to expand the sphere.

Solution: *a. The total charge is,*

$$\begin{aligned}\int_{esfer}\rho(\mathbf{r}')dV' &= \int_0^{\pi}\int_0^{2\pi}\int_0^{\infty}\frac{Q}{4\pi R^2}\delta(r'-R)r'^2dr'\sin\theta'd\theta'd\phi' \\ &= 4\pi\int_0^{\infty}\frac{Q}{4\pi R^2}\delta(r'-R)r'^2dr' = Q\ .\end{aligned}$$

The electric field is,

$$\begin{aligned}\vec{\mathcal{E}}(\mathbf{r}) &= \frac{1}{4\pi\varepsilon_0}\int_{sphere}\frac{\mathbf{r}-\mathbf{r}'}{|\mathbf{r}-\mathbf{r}'|^3}\rho(\mathbf{r}')dV' \\ &= \frac{1}{4\pi\varepsilon_0}\int_{d\theta}^{\pi}\int_0^{2\pi}\int_0^{\infty}\frac{\mathbf{r}-\mathbf{r}'}{|\mathbf{r}-\mathbf{r}'|^3}\frac{Q}{4\pi R^2}\delta(r'-R)r'^2dr'\sin\theta'd\theta'd\phi'\ .\end{aligned}$$

At the observation point $\mathbf{r}\equiv R\hat{\mathbf{e}}_z$

$$\vec{\mathcal{E}}(\mathbf{r}) = \frac{1}{4\pi\varepsilon_0}\frac{Q}{4\pi R^2}\int_{d\theta}^{\pi}\int_0^{2\pi}\int_0^{\infty}\frac{R\hat{\mathbf{e}}_z-\mathbf{r}'}{\sqrt{x'^2+y'^2+(R-z')^2}^3}\delta(r'-R)r'^2\sin\theta'd\theta'd\phi'\ ,$$

that is,

$$\begin{aligned}\mathcal{E}_z(R\hat{\mathbf{e}}_z) &= \frac{1}{4\pi\varepsilon_0}\frac{Q}{4\pi R^2}\int_{d\theta}^{\pi}\int_0^{2\pi}\frac{R-R\cos\theta'}{R^3\sqrt{\sin^2\theta'\cos^2\phi'+\sin^2\theta'\sin^2\phi'+(1-\cos\theta')^2}^3}R^2\sin\theta'd\theta'd\phi' \\ &= \frac{1}{4\pi\varepsilon_0}\frac{Q}{4\pi R^2}2\pi\int_{d\theta}^{\pi}\frac{1-\cos\theta'}{\sqrt{\sin^2\theta'+(1-\cos\theta')^2}^3}\sin\theta'd\theta' \\ &= \frac{1}{4\pi\varepsilon_0}\frac{Q}{4\pi R^2}2\pi\int_{d\theta}^{\pi}\frac{\sin\theta'd\theta'}{\sqrt{8}\sqrt{1-\cos\theta'}} = \frac{1}{4\pi\varepsilon_0}\frac{Q}{4\pi R^2}2\pi\left(1-\frac{1}{\sqrt{2}}\sqrt{1-\cos d\theta}\right) \\ &= \frac{1}{4\pi\varepsilon_0}\frac{Q}{2R^2}\left(1-\sin\tfrac{d\theta}{2}\right)\simeq\frac{1}{4\pi\varepsilon_0}\frac{Q}{2R^2}\ .\end{aligned}$$

The force is,

$$\mathbf{F} = Q_{void}\vec{\mathcal{E}} = \frac{\pi a^2Q}{4\pi R^2}E_z\hat{\mathbf{e}}_z = \frac{\pi a^2Q}{4\pi R^2}\frac{1}{4\pi\varepsilon_0}\frac{Q}{2R^2}\hat{\mathbf{e}}_z = \frac{a^2Q^2}{32\pi\varepsilon_0R^4}\hat{\mathbf{e}}_z\ .$$

Alternatively we can subtract the field above the entire sphere $\mathcal{E}_r$ from the field of a disk with radius a at a height h above the disk:

$$\begin{aligned}\mathcal{E}_{sphere} - \mathcal{E}_{disc} &= \frac{1}{4\pi\varepsilon_0}\frac{Q}{R^2} - \frac{\sigma}{2\varepsilon_0}\left(1 - \frac{h}{\sqrt{a^2+h^2}}\right) \\ &= \frac{1}{4\pi\varepsilon_0}\frac{Q}{R^2} - \frac{1}{2\varepsilon_0}\frac{Q}{4\pi R^2}\left(1 - \sin\tfrac{d\theta}{2}\right) \simeq \frac{Q}{8\pi\varepsilon_0 R^2} \ .\end{aligned}$$

Gabarite: *a.* $E = \frac{Q}{8\pi\varepsilon_0 R^2}$, *radially outward. b.* $F = \frac{Q^2 a^2}{32\pi\varepsilon_0 R^4}$, *radially outward. c.* $P = \frac{Q^2}{32\pi^2\varepsilon_0 R^4}$.

13.2.4.22 Ex: Flow through a cone

An imaginary straight circular cone with base angle θ and base radius R is in a charge-free region exposed to a uniform electric field $\vec{\mathcal{E}}$ (the field lines are vertical to the cone axis). What is the ratio between the number of field lines per unit area entering the base and the number of lines per unit area entering the cone's conical surface. Use Gauß's law in your answer.

Solution: *An element of the cone surface is,*

$$dS = \rho d\phi \frac{dz}{\sin\theta} = \left(R - \frac{z}{\tan\theta}\right) d\phi \frac{dz}{\sin\theta} \ .$$

The total surface of the cone is,

$$\begin{aligned}S_{cone} &= \int_0^{2\pi}\int_0^{R\tan\theta}\left(R - \frac{z}{\tan\theta}\right) d\phi\frac{dz}{\sin\theta} = \frac{2\pi}{\sin\theta}\int_0^{R\tan\theta}\left(R - \frac{z}{\tan\theta}\right) dz \\ &= 2\pi\frac{\tan\theta}{\sin\theta}\frac{R^2}{2} = \frac{\pi R^2}{\cos\theta} = \frac{S_{base}}{\cos\theta} \ .\end{aligned}$$

Since the number of field lines crossing S_{base} and S_{cone} is the same, but the areas are different, the number of lines per unit area is $\cos\theta$ times less for S_{cone}.

13.2.4.23 Ex: Flow of a field

Consider the rectangle with the corners,

$$\begin{pmatrix} x_i \\ y_i \\ z_i \end{pmatrix} = \begin{pmatrix} b \\ \frac{a}{\sqrt{2}} \\ 0 \end{pmatrix}, \begin{pmatrix} 0 \\ \frac{a}{\sqrt{2}} \\ 0 \end{pmatrix}, \begin{pmatrix} 0 \\ 0 \\ \frac{a}{\sqrt{2}} \end{pmatrix}, \begin{pmatrix} b \\ 0 \\ \frac{a}{\sqrt{2}} \end{pmatrix}$$

and calculate the flux integral of the field $\mathbf{A}(\mathbf{r})$ through the area $\mathbf{F}$ of the rectangle,

$$\mathbf{A}(\mathbf{r}) = \begin{pmatrix} y^2 \\ 2xy \\ 3z^2 - x^2 \end{pmatrix} \ .$$

Solution: *The solution is,*

$$\int \mathbf{A} \cdot d\mathbf{F} = ab\sqrt{2}\ (\frac{1}{2}a^2 - \frac{1}{3}b^2 + \frac{1}{2\sqrt{2}}ba)$$

.

13.2.4.24 Ex: Flow of a vector field

Calculate the flux of the vector field $\mathbf{A}(\mathbf{r})$ across the surface of a sphere of radius R around the origin of the coordinate system for
a.

$$\mathbf{A}(\mathbf{r}) = 3\frac{\mathbf{r}}{\mathbf{r}^2}\ .$$

b.

$$\mathbf{A}(\mathbf{r}) = \begin{pmatrix} 3z - 2y \\ x + 5z \\ y + x \end{pmatrix}\ .$$

Solution: *We have* $d\mathbf{F} = R^2\ \sin\theta\ d\theta\ d\phi\ \hat{\mathbf{e}}_r$.
a. Hence, $\mathbf{A}(\mathbf{r}) \cdot d\mathbf{F} = 3R\sin\theta d\theta d\phi$ *and therefore,*

$$\int\ \mathbf{A}(\mathbf{r}) \cdot d\mathbf{F} = 12\pi\ R\ .$$

b. Now,

$$\mathbf{A}(\mathbf{r}) = \begin{pmatrix} R(3\cos\theta - 2\sin\theta\sin\phi) \\ R(\sin\theta\cos\phi + 5\cos\theta) \\ R\sin\theta(\sin\phi + \cos\phi) \end{pmatrix}$$

and hence,

$$\mathbf{A}(\mathbf{r}) \cdot d\mathbf{F} = R^3\ (\cos\theta\sin^2\theta(4\cos\phi + 6\sin\phi) - \sin^3\theta\cos\phi\sin\phi)d\theta d\phi\ .$$

Now,

$$\int_0^{2\pi} d\phi \sin\phi = \int_0^{2\pi} d\phi\cos\phi = 0\ ,$$

as well as,

$$\int_0^{2\pi} d\phi \sin\phi\cos\phi = \int_{-1}^{+1} dx\ x = 0\ .$$

Hence follows immediately,

$$\int\ \mathbf{A}(\mathbf{r}) \cdot d\mathbf{F} = 0\ .$$

Alternatively: We immediately see that $\nabla \cdot \mathbf{A} = 0$. *With Gauß' theorem the same result immediately follows.*

13.2.4.25 Ex: Van de Graaff generator

The spherical shell (radius R) of a Van de Graaf generator must be charged until a potential difference of $10^6\,\mathrm{V}$. What should be the minimum diameter of the sphere to avoid lightning discharge?
Help: The field for disruptive discharge in air is $3 \cdot 10^6\,\mathrm{V/m}$.

Solution: *From the Gauß law,*

$$\mathcal{E}_r = \frac{Q}{4\pi\varepsilon_0 r^2} \qquad \textit{and} \qquad \Phi = -\frac{Q}{4\pi\varepsilon_0 r} \ .$$

The potential difference regarding ∞ is,

$$V = \frac{Q}{4\pi\varepsilon_0 R} \ .$$

The electric field on the surface is,

$$R_r = \frac{Q}{4\pi\varepsilon_0 R^2} = \frac{V}{R} \ .$$

from this follows,

$$R = \frac{V}{\mathcal{E}} > \frac{V}{E_{disrp}} = \frac{10^6}{3 \cdot 10^6}\,\mathrm{m} = 33\,\mathrm{cm} \ .$$

13.2.4.26 Ex: Van de Graaff accelerator

Protons are released from rest in a Van de Graaff accelerator system. The protons are initially located at a position where the electrical potential has a value of $5.0\,\mathrm{MV}$, and then, they travel through vacuum to a region where the potential is zero.
a. Determine the final velocity of these electrons.
b. Determine the magnitude of the accelerating electric field if the potential changes uniformly over a distance of $2\,\mathrm{m}$.

Solution: *a.* $3.09 \cdot 10^7\,\mathrm{m/s}$.
b. $2.5\,\mathrm{MV/m}$.

13.2.4.27 Ex: Faraday cage

Show that in a space confined by a grounded surface the electric field must disappear.

Solution: *By the second fundamental law of electrostatics $\nabla \cdot \vec{\mathcal{E}} = \rho/\varepsilon_0$ with $\rho = 0$ and with the field $\vec{\mathcal{E}} = -\nabla\Phi$, follows the Poisson equation,*

$$\Delta\Phi = 0 \ .$$

According to the boundary condition, the surface is at a given potential:

$$\Phi|_{\partial V} = \Phi_0 = const \ .$$

Obviously, $\Phi(\mathbf{r}) \equiv \Phi_0$ *it is a solution. This solution is unequivocal, such that the field is,*

$$\vec{\mathcal{E}} = \nabla \cdot \Phi = 0 \ .$$

13.2.4.28 Ex: Waveguide

The figure shows a portion of the cross section of an infinitely long concentric cable. The inner conductor has a linear charge density of 6 nC/m and the outer conductor has no net charge.
a. Determine the electric field for all values of R, where R is the distance perpendicular to the common axis in the cylindrical system.
b. What are the surface charge densities on the surfaces inside and outside the outer conductor?

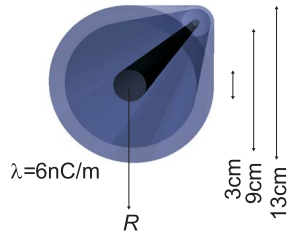

Figure 13.10: Waveguide.

Solution: *a. We imagine an axial cylindrical volume of radius* r *and length* d*. The radial electric field is given by Gauß' law,*

$$\mathcal{E}_R A = \mathcal{E}_R 2\pi d R = \frac{q}{\varepsilon_0} = \frac{\lambda d}{\varepsilon_0} \ .$$

Hence, $E_R = \frac{\lambda}{2\pi\varepsilon_0 R}$*. As the charge goes to the surface of the inner cylinder, we have,*

$$\mathcal{E}_R = 0 \text{ for } R < R_{int} \text{ and } \mathcal{E}_R = \frac{\lambda}{2\pi\varepsilon_0 R} = \frac{1}{R} 107.85\,\mathrm{Nm/C} \text{ for } R_{int} < R < R_{extint}$$

$$\mathcal{E}_R = 0 \text{ for } R_{extint} < R < R_{ext} \text{ and } \mathcal{E}_R = \frac{\lambda_2}{2\pi\varepsilon_0 R} = \frac{1}{R} 107.85\,\mathrm{Nm/C} \text{ for } R < R_{ext} \ .$$

b. With $d\lambda = q = 2\pi r_{int} d\sigma$ *we have,*

$$\sigma_{extint} = \frac{\lambda}{2\pi R_{extint}} = -21.2\,\mathrm{nC/m^2} \text{ and } \sigma_{ext} = \frac{\lambda}{2\pi R_{ext}} = 14.7\,\mathrm{nC/m^2} \ .$$

13.2.4.29 Ex: Fundamental equations of electrostatics

a. Gives the fundamental electrostatic equations in integral and differential form.
b. Gives the fundamental equation in terms of the electrostatic potential.

Solution: *a. In the differential form:*

$$div\ \vec{\mathcal{E}} = \frac{\rho(\mathbf{r})}{\varepsilon_0} \qquad and \qquad rot\ \vec{\mathcal{E}} = 0\ .$$

Using the Gauß', respectively, Stokes theorem we obtain the integral form:

$$\oint_{\partial V} \vec{\mathcal{E}} \cdot d\mathbf{S} = \frac{Q}{\varepsilon_0} \qquad and \qquad \oint_{\partial \mathcal{S}} \vec{\mathcal{E}} \cdot d\mathbf{r} = 0\ .$$

b. For a given charge distribution rho(r) we have:

$$\Phi(\mathbf{r}) = \frac{1}{4\pi\varepsilon_0} \int_V d^3r \frac{\varrho(\mathbf{r}')}{|\mathbf{r} - \mathbf{r}'|}\ .$$

13.3 The scalar electrical potential

We already noted that the electric field generates a force that can accelerate a charge Q along a field line. Therefore, the electric field contains a potential energy which it can convert into kinetic energy by exerting work, $W = \int \mathbf{F} \cdot \mathbf{r} = Q \int \vec{\mathcal{E}} \cdot \mathbf{r}$. The quantity [2],

$$\boxed{\Phi_{\mathbf{a},\mathbf{b}} \equiv \int_{\mathcal{C}_{\mathbf{a},\mathbf{b}}} \vec{\mathcal{E}} \cdot d\mathbf{r}} \tag{13.21}$$

is called the difference of *electric potential* between the points $\mathbf{a}$ and $\mathbf{b}$ connected by a path $\mathcal{C}_{\mathbf{a},\mathbf{b}}$.

Stokes' law (13.18) allows us to state, that the potential difference (13.21) does not depend on the path chosen, because for two different paths $\mathcal{C}$ and $\mathcal{C}'$ between the points $\mathbf{a}$ and $\mathbf{b}$ we have,

$$\int_{\mathcal{C}(\mathbf{a},\mathbf{b})} \vec{\mathcal{E}} \cdot d\mathbf{r} - \int_{\mathcal{C}'(\mathbf{a},\mathbf{b})} \vec{\mathcal{E}} \cdot d\mathbf{r} = 0\ . \tag{13.22}$$

Consequently, the potential defined between a reference point $\mathcal{O}$ and any observation point $\mathbf{r}$ is unambiguous,

$$\Phi(\mathbf{r}) = -\int_{\mathcal{O}}^{\mathbf{r}} \vec{\mathcal{E}} \cdot d\mathbf{r}\ , \tag{13.23}$$

and the potential difference between two points $\mathbf{a}$ and $\mathbf{b}$ is well defined,

$$\Phi(\mathbf{b}) - \Phi(\mathbf{a}) = -\int_{\mathbf{a}}^{\mathbf{b}} \vec{\mathcal{E}} \cdot d\mathbf{r}\ . \tag{13.24}$$

[2] We note that the electric potential is linked to potential energy, but is not the same.

The fundamental theorem for gradients, on the other hand, says that,

$$\Phi(\mathbf{b}) - \Phi(\mathbf{a}) = \int_{\mathbf{a}}^{\mathbf{b}} (\nabla\Phi) \cdot d\mathbf{r} \ . \tag{13.25}$$

These results being valid for any choice of points $\mathbf{a}$ and $\mathbf{b}$, we conclude by comparing these two equations,

$$\boxed{\vec{\mathcal{E}} = -\nabla\Phi} \ . \tag{13.26}$$

Example 46 (*Potential of a point charge*): For an electric field generated by an electric charge e located at the origin we can easily calculate the integral along a path $\mathcal{C}$ between two points a and b using Coulomb's law:

$$\begin{aligned}\int_{\mathcal{C}} \vec{\mathcal{E}} \cdot d\mathbf{r} &= \int_{\mathbf{a}}^{\mathbf{b}} \frac{1}{4\pi\varepsilon_0} \frac{e}{|\mathbf{r}|^2} \hat{\mathbf{e}}_{\mathbf{r}} \cdot (\hat{\mathbf{e}}_{\mathbf{r}} dr + \hat{\mathbf{e}}_\theta r d\theta + \hat{\mathbf{e}}_\phi r \sin\theta d\phi) \\ &= \frac{1}{4\pi\varepsilon_0} \int_{\mathbf{a}}^{\mathbf{b}} \frac{e}{r^2} dr = \frac{1}{4\pi\varepsilon_0} \left(\frac{e}{r_a} - \frac{e}{r_b} \right) \ .\end{aligned}$$

With the superposition principle we can generalize this result for distributions of arbitrary charges Q.

Some comments are appropriate at this point:

- The formulation by the potential (a scalar field) instead of the vector electric field is more compact. It summarized the Coulomb (13.8) law along with the constraint (13.19).
- The reference point $\mathcal{O}$ is arbitrary. Exchanging this reference point by another $\mathcal{O}'$ only adds a global constant to the potential,

$$\Phi'(\mathbf{r}) = -\int_{\mathcal{O}'}^{\mathbf{r}} \vec{\mathcal{E}} \cdot d\mathbf{r} = -\int_{\mathcal{O}'}^{\mathcal{O}} \vec{\mathcal{E}} \cdot d\mathbf{r} - \int_{\mathcal{O}}^{\mathbf{r}} \vec{\mathcal{E}} \cdot d\mathbf{r} = K + \Phi(\mathbf{r}) \ , \tag{13.27}$$

  but does not affect neither the difference of two potentials,

$$\Phi'(\mathbf{b}) - \Phi'(\mathbf{a}) = \Phi(\mathbf{b}) - \Phi(\mathbf{a}) \ , \tag{13.28}$$

  nor the electric field,

$$\nabla\Phi' = \nabla\Phi \ . \tag{13.29}$$

  We conclude that the potential is not a real quantity, but a mathematical trick to simplify our life [3]. Generally, the reference point is placed at infinity, $\mathcal{O} = \infty$, fixing the free choice of the global constant by,

$$\Phi(\infty) \equiv 0 \ . \tag{13.30}$$

- In the same way as the electric field, the electric potential also obeys the superposition principle.

[3] We shall see later that this conclusion must be reviewed in quantum mechanics in the context of the Aharonov-Bohm effect.

13.3.1 The equations of Laplace and Poisson

We already learned the two equations defining the electrostatic field (13.19) and (13.16), that is, $\nabla \times \vec{\mathcal{E}} = 0$ and $\nabla \cdot \vec{\mathcal{E}} = \varrho/\varepsilon_0$. Let us now rewrite these equations for the electric potential,

$$\nabla \times (\nabla \Phi) = 0 \quad , \quad \nabla \cdot \nabla \Phi = \Delta \Phi = -\varrho/\varepsilon_0 \ . \tag{13.31}$$

Thus, the formulation by the potential (13.21) automatically satisfies the requirement (13.22), that the rotation must disappear.

On the other side, we have a second-order differential equation called the *Poisson equation*. In regions with no charge, this equation turns into a *Laplace equation*,

$$\Delta \Phi = 0 \ . \tag{13.32}$$

13.3.2 Potential generated by localized charge distributions

The Poisson equation allows us to reconstruct a charge distribution once its potential is known. However, we usually want to do the opposite. Let us start with a point charge, located at the origin, the potential of which is,

$$\Phi(\mathbf{r}) = -\int \vec{\mathcal{E}} \cdot d\mathbf{r}' = \frac{-1}{4\pi\varepsilon_0} \int \frac{Q}{r'^2} dr' = \frac{1}{4\pi\varepsilon_0} \frac{Q}{r'} \Big|_{\infty}^{\mathbf{r}} = \frac{1}{4\pi\varepsilon_0} \frac{Q}{r} \ . \tag{13.33}$$

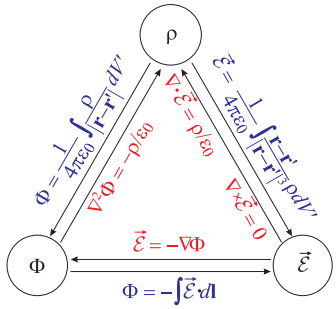

Figure 13.11: The fundamental laws of electrostatics relate the three fundamental quantities, the charge distribution ϱ, the electric field $\vec{\mathcal{E}}$, and the electric potential Φ.

According to the superposition principle, for a discrete distribution of charges Q_k located at the positions $\mathbf{r}_k$,

$$\Phi(\mathbf{r}) = \frac{1}{4\pi\varepsilon_0} \sum_k \frac{Q_k}{|\mathbf{r} - \mathbf{r}_k|} \ . \tag{13.34}$$

Finally, for a continuous distribution $\varrho(\mathbf{r}')$, we obtain the fundamental solution of the electrostatic problem,

$$\boxed{\Phi(\mathbf{r}) = \frac{1}{4\pi\varepsilon_0} \int \frac{dQ'}{|\mathbf{r} - \mathbf{r}'|} = \frac{1}{4\pi\varepsilon_0} \int \frac{\varrho(\mathbf{r}')}{|\mathbf{r} - \mathbf{r}'|} d^3r'} \ . \tag{13.35}$$

From this equation we can derive the Coulomb law (13.8).

Low-dimensional distributions can be treated by suitable parametrization, as in the examples (13.9) and (13.10).

13.3.3 Electrostatic boundary conditions

We have already noticed that the electric field always suffers a discontinuity when passing through a surface charge distribution. To study this, we consider a charged interface traversed by an external electric field $\vec{\mathcal{E}}_{ext}$. Now, we make two thought experiments: (1) We envision a rectangular pill box enclosing a small part of the interface, as shown in Fig. 13.12. The height ϵ of the box is so small that the flux through the sides of the box can be neglected. With this,

$$\oint \vec{\mathcal{E}} \cdot d\mathbf{S} = \tfrac{1}{\varepsilon_0} Q = \tfrac{1}{\varepsilon_0} \sigma S \ , \tag{13.36}$$

where $\vec{\mathcal{E}}$ is the total electric field (that is, the sum of the field generated by the surface charge and field $\vec{\mathcal{E}}_{ext}$). A is the surface of the box. This gives,

$$\mathcal{E}^{\perp}_{top} - \mathcal{E}^{\perp}_{bottom} = \tfrac{1}{\varepsilon_0} \sigma \ . \tag{13.37}$$

(2) We imagine a rectangular surface perpendicular to the interface and cutting through the interface. As shown in Fig. 13.12, the height ϵ of the surface is so small that the potential difference along the vertical branches can be neglected. With this,

$$\oint \vec{\mathcal{E}} \cdot d\mathbf{l} = \int \vec{\mathcal{E}}_{top} \cdot d\mathbf{l} + \int \vec{\mathcal{E}}_{bottom} \cdot d\mathbf{l} = (\vec{\mathcal{E}}_{top} - \vec{\mathcal{E}}_{bottom}) \cdot \mathbf{l} = 0 \ , \tag{13.38}$$

where l is the length of the surface. This gives,

$$\vec{\mathcal{E}}^{\parallel}_{top} = \vec{\mathcal{E}}^{\parallel}_{bottom} \ . \tag{13.39}$$

That is, when traversing a charged interface, only the part of the electric field which is perpendicular to the interface suffers a discontinuity. This simply reflects the fact that the charge generates its own electric field, which is perpendicular to the interface and superposes to the external field.

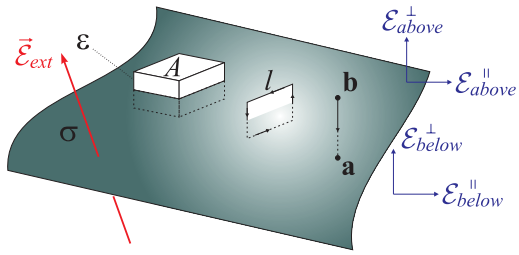

Figure 13.12: Surface S around a box-shaped volume enclosing a small part of the interface, path l around a small area cutting through the interface, and potential difference between two points **a** and **b**.

The potential, on the other hand, is continuous, since the integral between a point **a** above the interface and a point **b** below is,

$$\int_{\mathbf{b}}^{\mathbf{a}} \vec{\mathcal{E}} \cdot d\mathbf{l} = \Phi(\mathbf{b}) - \Phi(\mathbf{a}) \overset{\mathbf{a}\to\mathbf{b}}{\longrightarrow} 0 \ . \tag{13.40}$$

We study the electrostatic boundary conditions in Exc. 13.3.4.18.

13.3.4 Exercises

13.3.4.1 Ex: Earnshaw theorem

Show that the electrostatic potential in free space does not exhibit a maximum. **Comment:** This is why it is not possible to confine charged particles in electrostatic fields.

Solution: *For a charged particle to remain in a stable equilibrium, the force acting on the particle must be repulsive in every direction of space, that is, all field lines must be directed towards the equilibrium point. This is only possible when the divergence of this field is less than zero, that is, this point acts as a sink. However, this is prohibited in free space (that is, inthe absence of charges) by Gauß's law:*

$$\nabla \cdot \mathbf{F} = \nabla \cdot (\nabla \Phi) = \Delta \Phi = 0 \ .$$

An electrostatic force that can be derived from a potential $\Phi(\mathbf{r})$ is always non-divergent, that is, it has neither minimums nor maximums but, at best, saddle points.

13.3.4.2 Ex: Electrical potential between point charges

A point particle with a charge equal to $+2\,\mu$C is fixed at the origin.
a. hat is the electrical potential V at a point 4 m from the origin, considering that $V = 0$ at infinity?
b. How much work must be done to bring a second point charge with a charge of $+3\,\mu$C from infinity to a distance of 4.0 m from the first charge?

Solution: *a.* 4.49 kV
b. 13.5 J

13.3.4.3 Ex: Electrical potential between point charges

Three identical point particles with charge q are located at the corners of an equilateral triangle that is circumscribed in a circle of radius a contained in the plane $z = 0$ and centered at the origin. The values of q and a are $+3.0\,\mu$C and 60 cm, respectively. (Consider that, far from all charges, the potential is zero.)
a. What is the electrical potential at the origin?
b. What is the electrical potential at the point of the z-axis being at $z = a$?
c. How would your responses to the parts (a) and (b) change if the charges q were larger? Explain your answer.

Solution: *a.* 135 kV.
b. 95.3 kV.
c. Since the two field points are equidistant from all points in the circle, the responses to the parts (a) and (b) do not change.

13.3.4.4 Ex: Electrical potential between point charges

Two identical positively charged point particles are fixed to the x-axis at $x = +a$ and $x = -a$.
a. Write down an expression for the electrical potential $V(x)$ as a function of x for all points on the x-axis.
b. Draw $V(x)$ versus x for all points on the x-axis.

Solution: *a.* $V(x) = \frac{1}{4\pi\varepsilon_0}\left(\frac{1}{|x-a|} + \frac{1}{|x+a|}\right)$.

13.3.4.5 Ex: Electrical potential between point charges

The electric field on the x-axis due to a fixed point charge at the origin is given by $\vec{\mathcal{E}} = (b/x^2)\hat{\mathbf{e}}_x$, where $b = 6.0\,\text{kV}\cdot\text{m}$ and $x \neq 0$.
a. Determine the amplitude and sign of the point charge.
b. Determine the potential difference between the points on the x-axis at $x = 1\,\text{m}$ and $x = 2\,\text{m}$. Which of these points is at a higher potential?

Solution: *a.* +668 nC.
b. 3.0 kV. *The point at* $x = 2\,\text{m}$ *is at the highest potential.*

13.3.4.6 Ex: Dielectric disruption of air

Determine the maximum surface charge density σ_{max} that can exist on the surface of any conductor before dielectric discharge in the air occurs.

Solution: $\approx 3 \cdot 10^{-5}\,\text{C/m}^2$.

13.3.4.7 Ex: Potential energy of a charged sphere

a. How much charge is on the surface of an isolated spherical conductor that has a radius of $R = 10.0\,\text{cm}$ and is charged with 2.0 kV?
b. What is the electrostatic potential energy of this conductor? (Consider that the potential is zero far from the sphere.)

Solution: *a.* 22.3 nC,
b. 22.3 μJ.

13.3.4.8 Ex: Energy of a particle in a potential

Four point charges are attached to the vertices of a square centered on the origin. The length of each side of the square is $2a$. The charges are located as follows: $+q$ is in $(-a, +a)$, $+2q$ is in $(+a, +a)$, $-3q$ is in $(+a, -a)$, and $+6q$ is in $(-a, -a)$. A fifth particle with mass m and charge $+q$ is placed at the origin and released from rest. Determine its velocity when it is far from the origin.

Solution: $v = q\sqrt{\frac{6\sqrt{2k}}{ma}} = 2.91q\sqrt{\frac{k}{ma}}$.

13.3.4.9 Ex: Energy of a particle in a potential

Two metallic spheres have radii of 10 cm each. The centers of the two spheres are separated by 50 cm. The spheres are initially neutral, but a charge Q is transferred from one sphere to another, creating a potential difference between them of 100 V. A proton is released from rest at the surface of the positively charged sphere and travels to the negatively charged sphere.
a. What is the kinetic energy once it reaches the negatively charged sphere?
b. At what velocity does it collide with the sphere?

Solution: *a. As the potential difference ΔV is known, it is sufficient to calculate,*

$$U = e\Delta V = 100\,\text{eV} \ .$$

b. With the mass of the proton $m_p = 1.672{\cdot}10^{-27}\,\text{kg}$ and the kinetic energy $U = \frac{m_p}{2}v^2$, we calculate,

$$v = \sqrt{\frac{2U}{m_p}} = 1.38 \cdot 10^5\,\text{m/s} \ .$$

13.3.4.10 Ex: Potential of connected spheres

A spherical conductor of radius R_1 is charged with $V_i = 20\,\text{kV}$. When it is connected through a very thin and long conductive wire to a second very distant spherical conductor, its potential drops to $V_f = 12\,\text{kV}$. What is the radius of the second sphere?

Solution: *We have*

$$V_i = \frac{1}{4\pi\varepsilon_0}\frac{Q}{R_1} \quad , \quad V_f = \frac{1}{4\pi\varepsilon_0}\frac{Q_1}{R_1} = \frac{1}{4\pi\varepsilon_0}\frac{Q_2}{R_2} \quad , \quad Q_1 + Q_2 = Q \ .$$

Solving

$$R_2 = R_1\frac{Q_2}{Q_1} = R_1\frac{Q - Q_1}{Q_1} = R_1\frac{V_i - V_f}{V_f} = R_1\frac{2}{3} \ .$$

13.3.4.11 Ex: Potential of a charged disk

Along the central axis of a uniformly loaded disc, at a point 0.6 m away from the center of the disc, the potential is 80 V and the field intensity is 80 V/m. At a distance of 1.5 m, the potential is 40 V and the electric field strength is 23.5 V/m. (Consider that the potential is very far from the disk). Determine the total charge of the disk.

Solution: 7.1 nC.

13.3.4.12 Ex: Potential of spherical shells

Two conductive concentric spherical shells have equal charges with opposite signs. The inner shell has an external radius a and the charge $+q$; the outer shell has an internal radius b and the charge $-q$. Determine the potential difference $V_a - V_b$ between the shells.

Solution: $V_a - V_b = \frac{q}{4\pi\varepsilon_0}\left(\frac{1}{a} - \frac{1}{b}\right)$.

13.3.4.13 Ex: Electrical potential of a disk

A disk of radius R has a surface charge distribution given by $\sigma = \sigma_0 r^2/R^2$, where σ_0 is a constant and R is the distance from the center of the disk.
a. Determine the total charge on the disk.
b. Find the expression for the electrical potential at a distance z from the center of the disk along the axis that passes through the center of the disk and is perpendicular to its plane.

Solution: *a.* $Q = \frac{1}{2}\pi\sigma_0 R^2$,
b. $V = \frac{\sigma_0}{6\varepsilon_0 R^2}[(R^2 - 2z^2)\sqrt{z^2 + R^2} + 2z^3]$.

13.3.4.14 Ex: Electrical potential of a rod

A stick of length L has a total charge Q evenly distributed along its length. The stick is placed along the x-axis with its center at the origin.
a. What is the electrical potential as a function of the position along the x-axis for $x > L/2$?
b. Show that for $x \gg L/2$, your result reduces to that due to a point charge Q.

Solution: *a.* $V(x) = \frac{Q}{4\pi\varepsilon_0 L}\ln\frac{x+L/2}{x-L/2}$.

13.3.4.15 Ex: Potential of a thin disk

Calculate the electrical potential of a thin disc homogeneously charged with the charge Q along the symmetry axis.

Solution: *The potential that a charge distribution $\varrho(\mathbf{r}')$ exerts on a test charge q located at the position $\mathbf{r}$ is,*

$$\begin{aligned} V(\mathbf{r}) &= -\int_{disc} \frac{1}{4\pi\varepsilon_0}\rho(\mathbf{r}')\frac{q}{|\mathbf{r}-\mathbf{r}'|}d^3r' \\ &= -\frac{q}{4\pi\varepsilon_0}\int_{-a}^{a}\int_0^R\int_0^{2\pi}\rho(z')\frac{1}{\sqrt{(r-r')^2+(z-z')^2}}r'dr'dz'd\phi' \ . \end{aligned}$$

Now let $\mathbf{r} = z\hat{\mathbf{e}}_z$.

$$\begin{aligned} V(z) &= -2\pi\frac{q}{4\pi\varepsilon_0}\int_{-a}^{a}\int_0^R\rho(z')\frac{1}{\sqrt{r'^2+(z-z')^2}}r'dr'dz' \\ &= -2\pi\frac{q}{4\pi\varepsilon_0}\int_{-a}^{a}\rho(z')(\sqrt{R^2+(z-z')^2}-(z-z'))dz' \ . \end{aligned}$$

for a thin disc $\rho(z) \simeq \rho_0\Delta a\delta(z)$

$$\begin{aligned} V(z) &= -2\pi\frac{q}{4\pi\varepsilon_0}\int_{-a}^{a}\rho_0(\sqrt{R^2+(z-z')^2}-(z-z'))\delta(z)\Delta a dz' \\ &= \frac{-q\rho_0}{2\varepsilon_0}[\sqrt{R^2+z^2}-z]\Delta a \ . \end{aligned}$$

The forçe is,

$$F = -\frac{d}{dz}V(z) = 2\pi\frac{q}{4\pi\varepsilon_0}\rho_0\Delta a\left(\frac{z}{\sqrt{R^2+z^2}}-1\right) \ .$$

13.3.4.16 Ex: Electrical potential of four wires

Consider four wires oriented parallel to the z-direction, as shown in the figure. The wires are charged with the charge per unit length q/L.
a. Calculate the electrical potential as a function of x and y.
b. Expand the potential around $x = 0$ and $y = 0$ ($|x|, |y| \ll a$) up to second order. What is the shape of the potential at this point?

Solution: *a. The electrostatic potential is given by* $\Phi(\mathbf{r}) = \frac{1}{4\pi\varepsilon_0}\int\frac{\rho(\mathbf{r}')}{|\mathbf{r}-\mathbf{r}'|}d^3r'$ *with the distribution of* $\rho(\mathbf{r}') = -q\delta(x'-a)\delta(y') + q\delta(x')\delta(y'-a) - q\delta(x'+a)\delta(y') +$

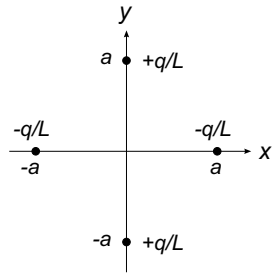

Figure 13.13: Four wires.

$q\delta(x')\delta(y'+a)$. With that, the integral becomes,

$$\begin{aligned}\Phi(\mathbf{r}) &= \frac{q}{4\pi\varepsilon_0}\int\left[\frac{-1}{\sqrt{(x-a)^2+y^2+(z-z')^2}}+\frac{1}{\sqrt{x^2+(y-a)^2+(z-z')^2}}\right.\\ &\left.+\frac{-1}{\sqrt{(x+a)^2+y^2+(z-z')^2}}+\frac{1}{\sqrt{x^2+(y+a)^2+(z-z')^2}}\right]dz'\\ &= \frac{q}{4\pi\varepsilon_0}\ln\frac{\left(z'-z+\sqrt{x^2+(y-a)^2+(z-z')^2}\right)\left(z'-z+\sqrt{x^2+(y+a)^2+(z-z')^2}\right)}{\left(z'-z+\sqrt{(x-a)^2+y^2+(z-z')^2}\right)\left(z'-z+\sqrt{(x+a)^2+y^2+(z-z')^2}\right)}\Bigg|_{-\infty}^{\infty}\\ &= \frac{q}{8\pi\varepsilon_0}\ln\frac{[x^2+(y-a)^2][x^2+(y+a)^2]}{[(x-a)^2+y^2][(x+a)^2+y^2]}\ .\end{aligned}$$

And now??? Alternative solution:
a. We first consider a conductor. The flux through the cylindrical cap with radius r around the wire follows from the Gauß law, $\int_{\partial V}\vec{\mathcal{E}}\cdot\vec{n}d\vec{f}=\frac{1}{\varepsilon_0}\int_V\rho dV$ hence $\mathcal{E}l2\pi r=\frac{1}{\varepsilon_0}Q$, with Q the charge on apiece of wire of length l . With the definition of linear charge density $q=Q/l$ follows: $\mathcal{E}=\frac{2q}{4\pi\varepsilon_0 r}$. For the potential ϕ ($\vec{\mathcal{E}}=-\vec{\nabla}\phi$) we integrate the field and obtain: $\phi=-\frac{2q}{4\pi\varepsilon_0}\ln r$. With four conductors we add the potentials:

$$\begin{aligned}\Phi(\mathbf{r}) &= -\frac{2q}{4\pi\varepsilon_0}\left[-\ln\sqrt{(x-a)^2+y^2}+\ln\sqrt{x^2+(y-a)^2}-\ln\sqrt{(x+a)^2+y^2}+\ln\sqrt{x^2+(y+a)^2}\right]\\ &= \frac{q}{4\pi\varepsilon_0}\ln\frac{[x^2+(y-a)^2][x^2+(y+a)^2]}{[(x-a)^2+y^2][(x+a)^2+y^2]}\ .\end{aligned}$$

b. The expansion up to second order is formally, $\phi(\mathbf{r})=\phi(\mathbf{0})+(\mathbf{r}\nabla)\phi(\mathbf{0})+\frac{1}{2!}(\mathbf{r}\nabla)^2\phi(\mathbf{0})+$ .... We easily get the zero order,

$$\Phi(\mathbf{0})=\frac{q}{4\pi\varepsilon_0}\ln\frac{a^2a^2}{a^2a^2}=0\ .$$

Auxiliary calculation for the first order,

$$\left(x\frac{d}{dx'}+y\frac{d}{dy'}\right)\ln\left[(x'-a)^2+(y'-b)^2\right]=\frac{2x(x'-a)+2y(y'-b)}{(x'-a)^2+(y'-b)^2}\xrightarrow{x',y'=0}\frac{-2ax-2by}{a^2+b^2}$$

With that we get for the first order,

$$(\mathbf{r}\cdot\nabla)\Phi(\mathbf{0}) = \frac{q}{4\pi\varepsilon_0}\left[\frac{-2ay}{a^2}+\frac{2ay}{a^2}-\frac{-2ax}{a^2}-\frac{2ax}{a^2}\right] = 0\ .$$

Auxiliary calculation for the second order,

$$\left(x^2\frac{d^2}{dx''}+2xy\frac{d^2}{dx'dy'}+y^2\frac{d^2}{dy''}\right)\ln[(x'-a)^2+(y'-b)^2]$$
$$= -2x^2\frac{(x'-a)^2-(y'-b)^2}{[(x'-a)^2+(y'-b)^2]^2}-8xy\frac{(x'-a)(y'-b)}{[(x'-a)^2+(y'-b)^2]^2}-2y^2\frac{-(x'-a)^2+(y'-b)^2}{[(x'-a)^2+(y'-b)^2]^2}$$
$$\xrightarrow{x',y'=0}\frac{-2(x^2-y^2)(a^2-b^2)-8xyab}{(a^2+b^2)^2}\ .$$

With that we get for the second order,

$$\frac{1}{2!}(\mathbf{r}\cdot\nabla)^2\phi(\mathbf{0}) = \frac{q}{8\pi\varepsilon_0}\left[\frac{2(x^2-y^2)a^2}{a^4}+\frac{2(x^2-y^2)a^2}{a^4}-\frac{-2(x^2-y^2)a^2}{a^4}-\frac{-2(x^2-y^2)a^2}{a^4}\right]$$
$$= \frac{q}{\pi\varepsilon_0 a^2}(x^2-y^2)\ .$$

Therefore, we obtain a saddle potential.

13.3.4.17 Ex: Stokes law

Consider a thin straight wire of infinite length uniformly charged with linear charge density λ.
a. Parametrize the linear load density using the δ-function.
b. Using Gauss' law, calculate the electric field.
c. Calculate the path integral $\int\vec{\mathcal{E}}\cdot d\mathbf{s}$ for the path parametrized by $\mathbf{s}(t)=\rho(\hat{\mathbf{e}}_x\cos t+\hat{\mathbf{e}}_y\sin t)$ with $t\in[0,2\pi]$.
d. From the electric field obtained in (b) calculate $\nabla\times\vec{\mathcal{E}}$ in Cartesian or cylindrical coordinates.
Help: $\nabla\times\mathbf{S}=\hat{\mathbf{e}}_\rho\ \frac{1}{\rho}\left[\frac{\partial S_z}{\partial\phi}-\rho\frac{\partial S_\phi}{\partial z}\right]+\hat{\mathbf{e}}_\phi\ \left[\frac{\partial S_\rho}{\partial z}-\frac{\partial S_z}{\partial\rho}\right]+\hat{\mathbf{e}}_z\ \frac{1}{\rho}\left[\frac{\partial}{\partial\rho}(\rho S_\phi)-\frac{\partial S_\rho}{\partial\phi}\right]$.

Solution: *a. The linear charge density is,*

$$\varrho(\mathbf{r}) = \lambda\delta(x)\delta(y)\ .$$

b. Gauss' law requires,

$$2\pi\mathcal{E}_\rho\rho\int_{-\infty}^{\infty}dz = \int_0^{2\pi}\int_{-\infty}^{\infty}E_\rho\rho d\phi dz = \oint\vec{\mathcal{E}}\cdot d\mathbf{S} = \int_{\mathbb{R}}\nabla\cdot\vec{\mathcal{E}}dV = \frac{1}{\varepsilon_0}\int\varrho(\mathbf{r})dV$$
$$= \frac{1}{\varepsilon_0}\int_{-\infty}^{\infty}\delta\lambda(x)\delta(y)dV = \frac{1}{\varepsilon_0}\lambda\int_{-\infty}^{\infty}dz\ .$$

Therefore, the electric field is,

$$\vec{\mathcal{E}}_\rho = \frac{\lambda}{2\pi\varepsilon_0\rho}\hat{\mathbf{e}}_\rho = \frac{\lambda}{2\pi\varepsilon_0}\frac{\hat{\mathbf{e}}_x\cos\phi+\hat{\mathbf{e}}_y\sin\phi}{\sqrt{x^2+y^2}}\ .$$

c. The integral yields,

$$\oint \vec{\mathcal{E}} \cdot d\mathbf{s} = \int_0^{2\pi} \frac{\lambda}{2\pi\varepsilon_0\rho} \hat{\mathbf{e}}_\rho \cdot \rho \hat{\mathbf{e}}_\phi d\phi = 0 \ .$$

d. Thus, satisfying Maxwell's law, we obtain in Cartesian coordinates,

$$\nabla \times \vec{\mathcal{E}} = \begin{pmatrix} \partial_y \mathcal{E}_z - \partial_z \mathcal{E}_y \\ \partial_z \mathcal{E}_x - \partial_x \mathcal{E}_z \\ \partial_x \mathcal{E}_y - \partial_y \mathcal{E}_x \end{pmatrix} = \frac{\lambda}{2\pi\varepsilon_0} \begin{pmatrix} 0 \\ 0 \\ \frac{\partial}{\partial x} \frac{\sin\phi}{\sqrt{x^2+y^2}} - \frac{\partial}{\partial y} \frac{\cos\phi}{\sqrt{x^2+y^2}} \end{pmatrix}$$

$$= \frac{\lambda}{2\pi\varepsilon_0} \begin{pmatrix} 0 \\ 0 \\ -\frac{x\sin\phi}{(x^2+y^2)^{\frac{3}{2}}} + \frac{y\cos\phi}{(x^2+y^2)^{\frac{3}{2}}} \end{pmatrix} = \frac{\lambda}{2\pi\varepsilon_0} \begin{pmatrix} 0 \\ 0 \\ -\frac{xy\sin\phi}{\rho^4} + \frac{yx\cos\phi}{\rho^4} \end{pmatrix} = 0 \ .$$

Alternatively, we calculate in spherical coordinates,

$$\nabla \times \vec{\mathcal{E}} = \hat{\mathbf{e}}_\rho \ \frac{1}{\rho} \left[\frac{\partial \mathcal{E}_z}{\partial \phi} - \rho \frac{\partial \mathcal{E}_\phi}{\partial z} \right] = 0 \ .$$

13.3.4.18 Ex: Surface of a conductor

Consider an arbitrary macroscopic conductor whose surface is closed and smooth. Starting from Gauss's law and the electrostatic rotation of the electric field:
a. calculate the electric field inside the conductor;
b. obtain the normal component of the electric field on the outer surface of the conductor in terms of the surface charge density;
c. obtain the tangential component of the electric field on the outer surface of the conductor.

Solution: *a. The electrical charges in the conductor will repel mutually and go to its surface. Tracing a Gaussian surface just below the conductor's surface we see that, in electrostatic equilibrium, there are no charges inside the conductor, such that,*

$$\nabla \cdot \vec{\mathcal{E}} = \rho/\varepsilon_0 = 0 \implies \int_V (\nabla \cdot \vec{\mathcal{E}}) dV = \int_S (\vec{\mathcal{E}} \cdot \hat{n}) dA = \mathcal{E} A \implies \vec{\mathcal{E}} = 0$$

inside the conductor.
b. Consider a Gaussian surface in the shape of a cylinder of infinitesimal height with the top face being outside and the bottom face inside the surface:

$$\nabla \cdot \vec{\mathcal{E}} = \rho/\varepsilon_0 \implies \int_V (\nabla \cdot \vec{\mathcal{E}}) dV = \int_V (\rho/\varepsilon_0) dV \implies \int_S (\vec{\mathcal{E}} \cdot \hat{n}) dA = \int_S (\sigma/\varepsilon_0) dA \implies \vec{\mathcal{E}} \cdot \hat{n} = \sigma/\varepsilon_0 \ ,$$

which is the normal component of the electric field in the vicinity of the surface.
c. Consider a closed, rectangular path γ with infinitesimal height h with one of the

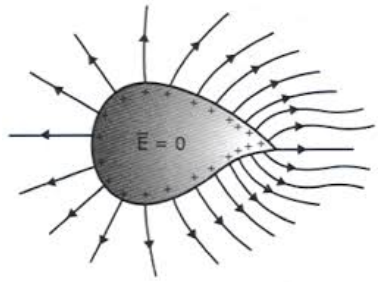

Figure 13.14: Surface of a conductor.

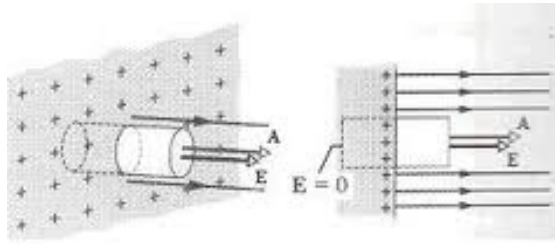

Figure 13.15: Surface of a conductor.

longer path sections L outside and the other inside the surface:

$$\nabla\times\vec{\mathcal{E}}=0 \implies \int_S(\nabla\times\vec{\mathcal{E}})\cdot(\hat{t}\times\hat{n})dA=\oint_\gamma \vec{\mathcal{E}}\cdot d\vec{l}=0 \implies \mathcal{E}_t L+\mathcal{E}_n h-0L-\mathcal{E}_n h=0 \implies \mathcal{E}_t=0\,,$$

which is the tangential component of the electric field in the vicinity of the surface.

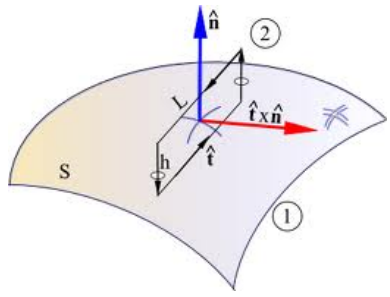

Figure 13.16: Surface of a conductor.

13.4 Electrostatic energy

We calculate the work required to move a test charge q between two points $\mathbf{a}$ and $\mathbf{b}$ within the potential created by a charge distribution,

$$W = -\int_{\mathbf{a}}^{\mathbf{b}} \mathbf{F} \cdot d\mathbf{r} = -q \int_{\mathbf{a}}^{\mathbf{b}} \vec{\mathcal{E}} \cdot d\mathbf{r} = q[\Phi(\mathbf{b}) - \Phi(\mathbf{a})] \ . \tag{13.41}$$

Since the work does not depend on the path, we call the potential *conservative*. Taking the test charge from the reference point to infinity,

$$W = q[\Phi(\mathbf{b}) - \Phi(\infty)] = q\Phi(\mathbf{b}) \ . \tag{13.42}$$

In this sense, the potential is nothing more than the energy per unit of charge q required to take a particle from infinity to a point $\mathbf{r}$.

13.4.1 Energy of a charge distribution

The next question is, what energy is needed to put together a distribution of charges taking them one by one from infinity to predefined points. Every charge Q_k uses an amount of work W_k, only the first charge does not, $W_1 = 0$. Using the abbreviation,

$$W_{k,m} \equiv \frac{1}{4\pi\varepsilon_0} \frac{Q_k Q_m}{|\mathbf{r}_k - \mathbf{r}_m|} \ , \tag{13.43}$$

the work is easily calculated for the second charge, $W_2 = W_{1,2}$. For the third and fourth charge we need *additionally* the amounts of work,

$$W_3 = W_{1,3} + W_{2,3} \qquad \text{and} \qquad W_4 = W_{1,4} + W_{2,4} + W_{3,4} \ . \tag{13.44}$$

The general rule is obvious: For N charges we need in *total* to provide the work,

$$W = \sum_{k=1}^{N} W_k = \sum_{k=1}^{N} \sum_{\substack{m=1 \\ m<k}}^{N} W_{k,m} = \frac{1}{2} \sum_{k=1}^{N} \sum_{\substack{m=1 \\ m\neq k}}^{N} W_{k,m} \ . \tag{13.45}$$

Explicitly, calling Φ the potential created by all charges minus the charge Q_k,

$$\Phi(\mathbf{r}_k) \equiv \sum_{\substack{m=1 \\ m\neq k}}^{N} \frac{1}{4\pi\varepsilon_0} \frac{Q_m}{|\mathbf{r}_k - \mathbf{r}_m|} \ , \tag{13.46}$$

we can write the energy as,

$$W = \tfrac{1}{2} \sum_k Q_k \Phi(\mathbf{r}_k) \ . \tag{13.47}$$

For continuous distributions, this equation turns into,

$$W = \tfrac{1}{2} \int \Phi dQ = \tfrac{1}{2} \int \varrho \Phi dV \ . \tag{13.48}$$

13.4.2 Energy density of an electrostatic field

The energy of a continuous charge distribution can be rewritten using Gauß' law,

$$W = \tfrac{\varepsilon_0}{2} \int (\nabla \cdot \vec{\mathcal{E}}) \Phi dV \ . \tag{13.49}$$

Integration by parts allows transferring the derivative of $\vec{\mathcal{E}}$ to Φ,

$$W = \tfrac{\varepsilon_0}{2} \left[\oint_{\partial \mathcal{V}} \Phi \vec{\mathcal{E}} \cdot d\mathbf{S} - \int_{\mathcal{V}} \vec{\mathcal{E}} \cdot (\nabla \Phi) dV \right] \ . \tag{13.50}$$

The surface integral can be neglected, because we can choose the integration volume arbitrarily large $\mathcal{V}$. Expressing the gradient by the field,

$$W = \tfrac{\varepsilon_0}{2} \int_{\mathcal{V}} \vec{\mathcal{E}}^2 dV = \tfrac{\varepsilon_0}{2} \int_{\mathcal{V}} u dV \ , \tag{13.51}$$

introducing the *energy density*,

$$\boxed{u \equiv \tfrac{\varepsilon_0}{2} \vec{\mathcal{E}}^2} \ . \tag{13.52}$$

Example 47 (*Electrostatic energy of a charged spherical layer*): As an example we calculate the electrostatic energy of a spherical shell of radius R uniformly charged with the total charge Q. Using the formula (13.48) we obtain,

$$W = \frac{1}{2} \int \varrho \Phi dV = \frac{1}{2} \int \frac{Q}{4\pi R^2} \delta(r-R) \Phi R^2 \sin\theta d\theta d\phi dr = \frac{Q}{2} \Phi(R) = \frac{Q}{2} \frac{1}{4\pi\varepsilon_0} \frac{Q}{R} = \frac{Q^2}{8\pi\varepsilon_0} \frac{1}{R} \ .$$

Alternatively, we calculate by the formula (13.51),

$$W = \frac{\varepsilon_0}{2} \int_{\mathbb{R}^3} \vec{\mathcal{E}}^2 dV = \frac{\varepsilon_0}{2} \int_{r \geq R} \left(\frac{1}{4\pi\varepsilon_0} \frac{Q}{R^2} \right)^2 R^2 \sin\theta d\theta d\phi dr = \frac{Q^2}{8\pi\varepsilon_0} \int_R^\infty \frac{1}{R^2} dr = \frac{Q^2}{8\pi\varepsilon_0} \frac{1}{R} \ .$$

1. Comparing the expressions for the electrostatic energy (13.47) and (13.51) [4] we perceive an inconsistency, since the second only allows positive energies, while the former allows positive and negative energies, for example, in the case of two charges with opposed signs aiming to attract each other.

   In fact, both equations are correct, but they describe slightly different situations. Equation (13.47) does not take into account of the work necessary to create these elementary point charges in the first place. In fact, equation (13.51) indicates that the energy of a point charge diverges,

   $$W = \frac{\varepsilon_0}{2} \frac{1}{(4\pi\varepsilon_0)^2} \int_{\mathbb{R}^3} \left(\frac{e}{r^2} \right)^2 r^2 \sin\theta dr d\theta d\phi = \frac{e^2}{8\pi\varepsilon_0} \int_0^\infty \frac{1}{r^2} r^2 \sin\theta dr d\theta d\phi \to \infty \ .$$

   The equation (13.51) is more complete in the sense that it gives the total energy stored in the charge configuration, but the (13.47) is more appropriate when working with point charges, because we then prefer to ignore the part needed

[4] Or equivalently (13.48), which also can not be negative.

for the construction of the electrons. Anyway, we do not know how to create or dismount electrons.

The inconsistency enters the derivation, when we make the transition between the Eqs. (13.47) and (13.48). In the first equation, $\Phi(\mathbf{r}_i)$ represents the potential due to all the other charges except q_i, while in the second $\Phi(\mathbf{r})$ is the total potential. For continuous distributions there is no difference, since the amount of charge at any mathematical point $\mathbf{r}$ is negligible, and its contribution to the potential is zero.

In practice, the divergence does not appear because, when we use Eq. (13.51), generally we consider smooth distributions of charges and not point-like charges.

2. The energy is stored in the entire electrostatic field, that is, we need to integrate over the entire space $\mathbb{R}^3$.

3. The superposition principle is not valid for electrostatic energy, since it is quadratic in the fields, $\int(\vec{\mathcal{E}}_1 + \vec{\mathcal{E}}_2)^2 dV \neq \int(\vec{\mathcal{E}}_1^2 + \vec{\mathcal{E}}_2^2)dV$.

13.4.3 Dielectrics and conductors

In an *insulating* material, such as rubber or glass, all electrons are attached to individual atoms. They can be displaced inside the atom by an external electric field, which creates a polarization of the atom. But they do not move away from the atom. In contrast, in a *conducting* material, such that a metal, one or more electrons per atom can move freely.

What are the characteristics of an ideal conductor?

1. $\vec{\mathcal{E}} = 0$ **inside a conductor.** The electric field inside a conductor must vanish, otherwise there would be forces on the charges working to rearrange them until the forces (and the motion of charges) compensate. In the presence of an external electric field, the charges arrange themselves in such a way as to generate their own field designed to compensate the external field.

2. $\varrho = 0$ **inside a conductor.** Since there is no electric field, Gauß' law prevents residual charges in the interior, since $\varrho = \nabla \cdot \vec{\mathcal{E}}/\varepsilon_0$.

3. **All residual charge is on the surface,** simply because it can not be inside.

4. **Conductor as an equipotential.** As there is no electric field, Stokes' law prevents different potentials because $\Phi(\mathbf{b}) - \Phi(\mathbf{a}) = -\int_{\mathbf{a}}^{\mathbf{b}} \vec{\mathcal{E}} \cdot d\mathbf{r} = 0$.

5. $\vec{\mathcal{E}}$ **is perpendicular to the surface near the surface.** Otherwise, the electric field components parallel to the surface would create forces to rearrange the residual charges until the parallel components disappear. Consequently, electric field lines always meet a conductor orthogonally to the surface $\vec{\mathcal{E}} \perp \partial V$.

13.4.4 Induction of charges (influence)

When we place a charge in front of a neutral conductor we measure an attraction force. The reason is that free charges of the conductor with opposite sign are attracted, while

charges with the same sign are repelled [5]. Now, since the charges with opposite sign are closer to the charge in front than those with the same sign, the attractive force will dominate the repulsive force (see Fig. 13.17 left).

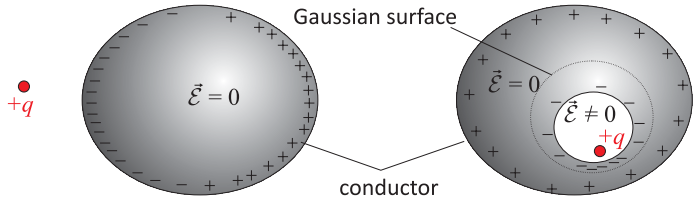

Figure 13.17: Electrostatic induction.

The electric field inside a conductor must vanish, but this only holds for the conductor's bulk material and not necessarily for dielectric impurities or cavities enclosed by the conductor. For example, in the case where there is a charge $+q$ inside a enclosed cavity [see Fig. 13.17(right)], the electric field inside the cavity is clearly nonzero. However, since it must vanish within the conductor, Gauß' law requires that within a volume enclosed by a Gaussian surface, the total charge must be zero. Choosing this Gaussian surface very close to the cavity, we find that a surface charge must have formed at the edges of the cavity, compensating for the charge $+q$ inside the cavity. This charge can only come from the outer surface, which is now charged with the opposite charge, as well. In this way *the charge $+q$ becomes visible from the outside of the conductor.*

The electric field inside a cavity without charges enclosed by a conductor must be zero, because without charges, the field lines could only traverse the cavity. However, the entrance and exit points between the cavity and the conductor are on the same potential, and have no surface charge. This is the principle of *Faraday's cage*, where people inside a conductive cage are shielded and thus protected from electrical phenomena like lightning discharges.

The migration of free excess charges in conductors to the surface is also called *skin effect*: The potential inside the metal the same everywhere, and the electric field disappears $\vec{\mathcal{E}} = 0$.

Example 48 (*Conductors with enclosed cavities*): Two cavities with radii a and b are excavated from a neutral conducting sphere of radius R. In the center of each cavity there be charges, q_a and q_b, respectively.

- The charges on the surfaces of the cavities σ_a and σ_b must be organized such as to shield the charges $q_{a,b}$ in order to prevent the formation of an electric field inside the conductor. If the charges are at the centers of the spheres we simply obtain, $\sigma_a = \frac{q_a}{4\pi a^2}$ and $\sigma_b = \frac{q_b}{4\pi b^2}$. The charges used for shielding are missing from the conductor and must be compensated for by charges of opposite sign. The only place where these opposite charges can accumulate is the outer surface of the conductor. Thus, we have the surface charge $\sigma_R = \frac{-q_a - q_b}{4\pi R^2}$.

[5] That is, the charges in the conductor rearrange to compensate for the electric field created by the charge in front until the total field inside the conductor has vanished.

- The field outside the driver is consequently, $\vec{\mathcal{E}} = \frac{q_a+q_b}{4\pi\varepsilon_0}\frac{\mathbf{r}}{r^3}$, where $\mathbf{r}$ is the point of observation with respect to the center of the conductor.
- Inside each cavity the electric field is determined by Gauß' law, $\vec{\mathcal{E}} = \frac{q_{a,b}}{4\pi\varepsilon_0}\frac{r}{r^3}$, where $\mathbf{r}$ is the observation point respect to the center of the cavity. Note that the surface charge $\sigma_{a,b}$ does not influence the field.
- Since the charges $q_{a,b}$ do not feel external fields, they are not subject to forces.
- Putting a third charge q_c near the conductor, the charge distribution σ_R would change in order to compensate the field within the conductor. Thus, the other quantities determined in (a)-(d) would not change. *The conductor effectively decouples all processes occurring on disconnected surfaces.*

13.4.5 Electrostatic pressure

What is the force exerted by an applied electric field $\vec{\mathcal{E}}_{ext}$ on a charged conductive surface? We know that the surface charge causes a discontinuity of the electric field, so that we need to calculate the force on a surface element dS as the average of the forces acting from above and from below,

$$d\mathbf{F} = dS\frac{\sigma}{2}(\vec{\mathcal{E}}_{top} + \vec{\mathcal{E}}_{bottom}) = \vec{\mathcal{P}}dS \ , \tag{13.53}$$

where $\vec{\mathcal{P}}$ is the *electrostatic pressure* (see Fig. 13.18).

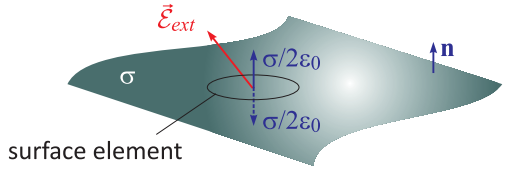

Figure 13.18: Electrostatic pressure exerted by a field $\vec{\mathcal{E}}_{ext}$ on a charged surface element.

In the case of a thin surface, we have,

$$\vec{\mathcal{E}}_{top} = \vec{\mathcal{E}}_{ext} + \frac{\sigma}{2\varepsilon_0}\hat{\mathbf{n}} \quad , \quad \vec{\mathcal{E}}_{bottom} = \vec{\mathcal{E}}_{ext} - \frac{\sigma}{2\varepsilon_0}\hat{\mathbf{n}} \ , \tag{13.54}$$

such that the pressure is,

$$\vec{\mathcal{P}} = \sigma\vec{\mathcal{E}}_{ext} \ . \tag{13.55}$$

In the case of a charged surface of a massive conductor without external field,

$$\vec{\mathcal{E}}_{outside} = \frac{\sigma}{\varepsilon_0}\hat{\mathbf{n}} \quad , \quad \vec{\mathcal{E}}_{inside} = 0 \ , \tag{13.56}$$

such that the pressure is,

$$\vec{\mathcal{P}} = \frac{\sigma}{2}\frac{\sigma}{2\varepsilon_0}\hat{\mathbf{n}} = \frac{\varepsilon_0}{2}\mathcal{E}^2_{outside}\hat{\mathbf{n}} \ . \tag{13.57}$$

That is, even without external field a charged conductor suffers a force trying to push it into the field created by itself, regardless of the sign of the charge. It is interesting to note that this force goes with the square of σ and of $\vec{\mathcal{E}}_{outside}$.

13.4.6 Exercises

13.4.6.1 Ex: Motion of two charges

Two particles with masses m_1 and m_2 and charges $Q_1 > 0$ and $Q_2 > 0$ are placed at a mutual distance d_0 and can move freely in space.
a. What will happen to the particles qualitatively? Which relation holds at all times for the velocities v_1 and v_2 of the two particles?
b. Calculate the velocities of the two particles as a function of their distance and plot the functions $v_1(d)$, respectively $v_2(d)$ (phase space diagrams). What are the velocities reached in the limit $d \to \infty$?

Solution: *a. The charges repel each other. Here, momentum conservation holds,* $m_1 v_1 = -m_2 v_2$.
b. The equation of motion for the distance follows from Coulomb's law, $m_1 \dot{v}_1 = \frac{1}{4\pi\varepsilon_0}\frac{Q_1 Q_2}{|r_1 - r_2|^2} = -m_2 \dot{v}_2$.

$$\ddot{d} = \dot{v}_1 - \dot{v}_2 = \frac{1}{4\pi\varepsilon_0}\left(\frac{1}{m_1} + \frac{1}{m_2}\right)\frac{Q_1 Q_2}{d^2} \ .$$

b. The total energy of the system is composed of the potential energy and the kinetic energy of the two particles:

$$\begin{aligned} E &= T + U \ , \\ U &= \frac{1}{4\pi\varepsilon_0}\frac{Q_1 Q_2}{d} \ , \\ T &= \frac{m_1}{2}v_1^2 + \frac{m_2}{2}v_2^2 \ . \end{aligned}$$

The energy is fixed by the initial conditions $d(0) = d_0$ *and* $v(0) = 0$*:*

$$E = \frac{1}{4\pi\varepsilon_0}\frac{Q_1 Q_2}{d_0} \ .$$

Inserting,

$$\begin{aligned} \frac{m_1}{2}v_1^2 + \frac{m_2}{2}v_2^2 + \frac{1}{4\pi\varepsilon_0}\frac{Q_1 Q_2}{d} &= \frac{1}{4\pi\varepsilon_0}\frac{Q_1 Q_2}{d_0} \\ \Longrightarrow v_1^2\left(\frac{m_1}{2} + \frac{m_1^2}{2m_2}\right) = v_2^2\left(\frac{m_2^2}{2m_1} + \frac{m_2}{2}\right) &= \frac{Q_1 Q_2}{4\pi\varepsilon_0}\left(\frac{1}{d_0} - \frac{1}{d}\right) \\ \Longrightarrow v_k = \sqrt{\frac{Q_1 Q_2}{2\pi\varepsilon_0 m_k^2\left(\frac{1}{m_1} + \frac{1}{m_2}\right)}\left(\frac{1}{d_0} - \frac{1}{d}\right)} \ . \end{aligned}$$

over large distances d

$$v_k \to \frac{1}{m_k}\sqrt{\frac{Q_1 Q_2}{2\pi\varepsilon_0\left(\frac{1}{m_1} + \frac{1}{m_2}\right)}\frac{1}{d_0}} \ .$$

13.4.6.2 Ex: Paul trap

We consider four parallel wires oriented along the z-direction and forming a quadrupolar configuration in the xy-plane, as shown in the figure. The wires are charged with $\pm q$ per unit of length l. Calculate the electrical potential as a function of x and y in the center between the wires and expand around $x = 0$ and $y = 0$ ($|x|, |y| \ll a$) up to second order. What is the shape of the potential at this position? Do you think it is possible to trap a charged particle in this potential?

Solution:

13.4.6.3 Ex: Energy of the electron

Supposing that the charge is homogeneously distributed over a sphere, calculate the *classical electron radius*.

Solution: *We assume that the charge is evenly distributed inside a sphere of radius r_e, $e = \varrho\frac{4\pi}{3}r_e^3$. We try two equivalent calculations:*
a. Using Gauss' law we get for the electric field,

$$\mathcal{E}_{r<r_e} = \frac{\varrho}{3\varepsilon_0}r = \frac{e}{4\pi\varepsilon_0}\frac{r}{r_e^3} \quad , \quad \mathcal{E}_{r>r_e} = \frac{\varrho}{3\varepsilon_0}\frac{r_e^3}{r^2} = \frac{e}{4\pi\varepsilon_0}\frac{1}{r^2} \ .$$

With that, the energy becomes,

$$\mathcal{E}_{ele} = \frac{\varepsilon_0}{2}\int_V |\mathcal{E}_r|^2 dV = \frac{\varepsilon_0}{2}4\pi\int_0^{r_e}\left(\frac{e}{4\pi\varepsilon_0}\frac{r}{r_e^3}\right)^2 r^2 dr + \frac{\varepsilon_0}{2}4\pi\int_{r_e}^{\infty}\left(\frac{e}{4\pi\varepsilon_0}\frac{1}{r^2}\right)^2 r^2 dr = \frac{e^2}{4\pi\varepsilon_0}\frac{3}{5r_e} \ .$$

b. Knowing that the electric field within the homogeneous charge distribution grows linearly with the distance from the origin, we do the following ansatz for the potential, $\Phi(r) = ar^2 + b$. The coefficients are calibrated using the known solutions for the potential and the field on the surface::

$$\Phi(r = r_e) = ar_e^2 + b = \frac{e}{4\pi\varepsilon_0}\frac{1}{r_e} \quad \Longrightarrow \quad b = \frac{e}{4\pi\varepsilon_0}\frac{1}{r_e} - ar_e^2$$
$$\mathcal{E}(r = r_e) = -\frac{d}{dr}\Phi(r_e) = -2ar_e = \frac{e}{4\pi\varepsilon_0}\frac{1}{r_e^2} \quad \Longrightarrow \quad a = -\frac{e}{8\pi\varepsilon_0}\frac{1}{r_e^3} \ .$$

Finally,

$$\Phi(r) = -\frac{e}{8\pi\varepsilon_0}\frac{1}{r_e^3}r^2 + \frac{e}{4\pi\varepsilon_0}\frac{1}{r_e} - ar_e^2 = \frac{e}{4\pi\varepsilon_0 r_e}\left(\frac{3}{2} - \frac{R^2}{2r_e^2}\right) \ .$$

13.4.6.4 Ex: Radius of the electron

a. Try to calculate the electrostatic energy of the field of an electron via,

$$E_F = \int_{\mathbb{R}^3}\frac{\varepsilon_0}{2}\vec{\mathcal{E}}^2(\mathbf{r})\ d^3r$$

What problem appears in the calculation of the radial part of the integral $\int dr$, if the lower limit of integration goes to $r_0 \to 0$?
b. This problem is known as *self-energy divergence*. It is possible to work around this problem, leaving the limits out and choosing the classic electron radius r_0 as the integration limit. The energy E_F of the electric field is then identified with half the energy $E = \frac{1}{2}m_e c^2$ of the electron rest mass m_e. Calculate the classic electron radius!

Solution: *a. We have*

$$\vec{\mathcal{E}} = \frac{1}{4\pi\varepsilon_0}\frac{q}{r^2}\hat{\mathbf{e}}_r \ .$$

With that,

$$E_F = \frac{4\pi\varepsilon_0}{2}\lim_{r_0\to 0}\int_{r_0}^{\infty}\vec{\mathcal{E}}^2(r)r^2dr = \frac{1}{2}\frac{1}{4\pi\varepsilon_0}\lim_{r_0\to 0}\int_{r_0}^{\infty}\frac{q^2}{r^2}dr = \lim_{r_0\to 0}\frac{1}{2}\frac{q^2}{4\pi\varepsilon_0}\frac{1}{r_0} \to \infty \ .$$

b. Equalizing we obtain,

$$\frac{1}{2}\frac{q^2}{4\pi\varepsilon_0}\frac{1}{r_0} = \frac{1}{2}m_e c^2 \ ,$$

and from this,

$$r_0 = \frac{q^2}{4\pi\varepsilon_0 m_e c^2} = 2.82\,\text{fm} \ .$$

13.4.6.5 Ex: Electrostatic energy

a. Write the potential energy of a charge q in an external field $\vec{\mathcal{E}} = -\vec{\nabla}\Phi$?
b. What is the value of the electrostatic energy of N point charges?
c. What is the value of the energy of a charge distribution in the electric field $\vec{\mathcal{E}}(\mathbf{r})$?
d. What are the boundary conditions for the $\vec{\mathcal{E}}$-field on a conductor's surface?
e. Draw the electric field of a point charge q located in front of a metallic plane. What is the induced charge? What is the value of the force on the charge q?

Solution: *a. Electrostatic energy* $W = q\Phi$.
b. Electrostatic energy $W = \frac{1}{2}\sum_{i,k=1;i\neq k}^{N}\frac{q_i q_k}{4\pi\varepsilon_0|\mathbf{r}_i-\mathbf{r}_k|}$.
c. Electrostatic energy $W = \frac{\varepsilon_0}{2}\int d^3r|\vec{\mathcal{E}}(\mathbf{r})|^2$.
d. Boundary conditions on the conductor surface $\vec{\mathcal{E}}_{condutor} = 0$, $\vec{\mathcal{E}}_t = 0$, $\hat{n}\cdot\vec{\mathcal{E}} = \frac{\sigma}{\varepsilon_0}$.
e. The induced charge is $-q$, *the force is,*

$$\mathbf{F} = -\nabla\phi = -\nabla\frac{1}{4\pi\varepsilon}\frac{-q}{|\mathbf{r}+\mathbf{d}|} = \nabla\frac{q}{4\pi\varepsilon}\frac{\mathbf{r}+\mathbf{d}}{|\mathbf{r}+\mathbf{d}|^3}\bigg|_{\mathbf{r}=\mathbf{d}} = \frac{1}{4\pi\varepsilon}\frac{q}{(2d)^2} \ .$$

13.4.6.6 Ex: Electrostatic energy

What is the electrostatic energy of
a. four equal charges Q located at the corners of a tetrahedron with the edge length

d?
b. a dielectric sphere with radius R homogeneously charged with the charge Q? To do this, calculate the electric field inside and outside the sphere using Gauß' law.

Solution: *a. The energy of a charge distribution is,*

$$W = \frac{1}{2}\sum_{\substack{i,k=1\\ i\neq j}}^{N} \frac{1}{4\pi\varepsilon_0}\frac{q_i q_k}{|\mathbf{r}_i - \mathbf{r}_k|} \ .$$

In the equilateral tetrahedron all charges are equidistant, so that,

$$W = \frac{1}{2}\sum_{\substack{i,k=1\\ i\neq j}}^{4} \frac{1}{4\pi\varepsilon_0}\frac{Q^2}{d} = \frac{1}{2}\frac{1}{4\pi\varepsilon_0}\frac{Q^2}{d}4(4-1) = \frac{3}{2\pi\varepsilon_0}\frac{Q^2}{d} \ .$$

b. The energy of a homogeneously charged sphere with radius R follows from,

$$W = \frac{\varepsilon_0}{2}\int_V \vec{\mathcal{E}}^2(\mathbf{r})d^3r = \frac{\varepsilon_0}{2}\int_V \mathcal{E}^2(r)r^2\sin\theta d\theta d\phi dr \ .$$

For reasons of symmetry the electric field must be radial, $\vec{\mathcal{E}}(\mathbf{r}) = E(r)\hat{\mathbf{e}}_r$. The electric field at distance r from the origin follows from the charge inside a sphere having the same radius,

$$Q(r) = \varepsilon_0\int \nabla\vec{\mathcal{E}}\cdot(r')d^3r' = \varepsilon_0\oint \mathcal{E}(r)r^2\sin\theta d\theta d\phi = \varepsilon_0 E(r)4\pi r^2 \ .$$

The field inside and outside the charge distribution is,

$$\mathcal{E}_{in}(r) = \frac{1}{4\pi\varepsilon_0}\frac{Q(r)}{r^2} = \frac{1}{4\pi\varepsilon_0}\frac{Qr}{R^3} \qquad \textit{resp.} \qquad \mathcal{E}_{out}(r) = \frac{1}{4\pi\varepsilon_0}Q\frac{1}{r^2} = \frac{1}{4\pi\varepsilon_0}\frac{Q}{r^2} \ .$$

With that we get the same energy,

$$\begin{aligned} W &= \frac{\varepsilon_0}{2}\int E_{in}^2(r)r^2\sin\theta d\theta d\phi dr + \frac{\varepsilon_0}{2}\int_V E_{out}^2(r)r^2\sin\theta d\theta d\phi dr \\ &= \frac{\varepsilon_0}{2}4\pi\left[\int_{r\le R}\left(\frac{1}{4\pi\varepsilon_0}\frac{Qr}{R^3}\right)^2 r^2dr + \int\left(\frac{1}{4\pi\varepsilon_0}\frac{Q}{r^2}\right)^2 r^2dr\right] \\ &= \frac{1}{2}\frac{Q^2}{4\pi\varepsilon_0}\left(\frac{r^5}{5R^6}\Big|_0^R + \frac{-1}{r}\Big|_R^\infty\right) = \frac{3Q^2}{20\pi\varepsilon_0 R} \ . \end{aligned}$$

13.4.6.7 Ex: Electrostatic energy

a. Eight point charges q are placed in the corners of a cube with the edge length l. Calculate the electrostatic energy of this configuration.

b. A balloon with radius R is charged homogeneously with the charge Q. What is the value of electrostatic energy? What is the force required to inflate the balloon even more, neglecting the elastic force of the balloon?

Solution: *We have for the potential energy of N point charges in their own field:*

$$W_{tot} = \frac{1}{2} \sum_{i,k=1;k\neq i}^{N} \frac{q_i q_k}{4\pi\varepsilon_0 |\mathbf{r}_i - \mathbf{r}_k|} \ .$$

The potential energy of a charge in the given configuration is,

$$W = 3W_{distance\ l} + 3W_{distance\ \sqrt{2}l} + W_{distance\ \sqrt{3}l} = \frac{q^2}{4\pi\varepsilon_0 2}\left(\frac{3}{l} + \frac{3}{\sqrt{2}l} + \frac{1}{\sqrt{3}l}\right)$$
$$= \frac{q^2}{8\pi\varepsilon_0 l}\left(3 + \frac{3}{\sqrt{2}} + \frac{1}{\sqrt{3}}\right) \ .$$

So we get W_{tot}

$$W_{tot} = 8W = \frac{q^2}{\pi\varepsilon_0 l}\left(\frac{3}{l} + \frac{3}{\sqrt{2}l} + \frac{1}{\sqrt{3}l}\right) \approx \frac{5.7q^2}{\pi\varepsilon_0 l} \ .$$

b. With Gauß follows $\mathcal{E} = \frac{Q}{4\pi\varepsilon_0}\frac{1}{r^2}$ for $r > R$ and $\mathcal{E} = 0$ for $r \leq R$. The energy is,

$$E_F = \int dV \frac{\varepsilon_0}{2}\vec{\mathcal{E}}^2(r)dr = 4\pi\frac{\varepsilon_0}{2}\int_0^\infty r^2\mathcal{E}(r)dr = 4\pi\frac{\varepsilon_0}{2}\frac{Q^2}{(4\pi\varepsilon_0)^2}\int_0^\infty r^{-2}dr$$
$$= \frac{Q^2}{8\pi\varepsilon_0}\int_R^\infty r^{-2}dr = \frac{Q^2}{8\pi\varepsilon_0}R^{-1} \ .$$

To increase the radius of the air balloon we must change the energy by $\mathbf{F} = -\nabla E_F$ follows:

$$F = -\frac{d}{dR}E_F = \frac{Q^2}{8\pi\varepsilon_0}\frac{1}{R^2} \ .$$

The force is positive. The air balloon tries to inflate itself!

13.4.6.8 Ex: Charge separation

Two conducting neutral spheres are in contact and attached to insulating rods on a large wooden table. A positively charged stick is brought close to the surface of one of the spheres on the side opposite the point of contact with the other sphere.
a. Describe the charges induced in the two conductive spheres and discuss the charge distribution in both.
b. The two spheres are separated and then the charged stick is taken away. Then, the spheres are separated by a great distance. Discuss the charge distributions on the spheres after they are separated.

Solution: *a. When approaching the positively charged stick, a negative charge is*

induced to the sphere being close to the stick, leaving the more distant sphere positively charged.
b. After separating the spheres and then moving the stick away, the induced charges are evenly distributed in each of the spheres.

13.5 Treatment of boundary conditions and the uniqueness theorem

In practice, the solution of an electrostatic problem, that is, the resolution of the Poisson equation, can be hampered by boundary conditions. For example, charges in front of conducting surfaces induce a redistribution of charges in the conductor which modifies the electric field. The field is unequivocally determined by the charge and the boundary conditions. In this section we will discuss the method of image charges, which is a heuristic model, and the mathematical treatment of boundary conditions.

13.5.1 The method of images charges

One way to simulate boundary conditions is to 'invent' imaginary charges and distribute them in a way that the total field automatically satisfies these boundary conditions. This is usually only helpful when the boundary conditions exhibit a high degree of symmetry. This is the method of the so-called *image charge*s.

The simplest case is that of the point charge Q at a distance d in front of a conductive and grounded plane. By induction the charge will cause a redistribution of charges on the surface of the conductor in such a way, that the field lines cross the surface of the conductor at right angles. But the same boundary conditions can be satisfied by replacing the conductive plane with a second imaginary charge with opposite sign at the position of the image of the first charge regarding the plane as a mirror. From the point of view of the electric field the two configurations are equivalent, but the field is much easier to calculate for a charge and its image using Coulomb's law. See Excs. 13.5.6.1, 13.5.6.2, 13.5.6.3, 13.5.6.4, and 13.5.6.5.

Example 49 (*Induced surface charge*): In the case of the point charge in front of a conducting plane, which is the simplest case imaginable, the boundary conditions are,

$$\Phi(x,y,0)=0 \quad , \quad \Phi(|\mathbf{r}|\gg d)=0 \ ,$$

the potential is,

$$\Phi(\mathbf{r})=\frac{1}{4\pi\varepsilon_0}\left(\frac{Q}{\sqrt{x^2+y^2+(z-d)^2}}+\frac{-Q}{\sqrt{x^2+y^2+(z+d)^2}}\right) \ ,$$

and the field is,

$$\vec{\mathcal{E}}=-\nabla\Phi=\frac{-Q}{4\pi\varepsilon_0}\left(\frac{-1}{\sqrt{x^2+y^2+(z-d)^2}^3}(\hat{\mathbf{e}}_z-\mathbf{r})+\frac{1}{\sqrt{x^2+y^2+(z+d)^2}^3}(\hat{\mathbf{e}}_z+\mathbf{r})\right) .$$

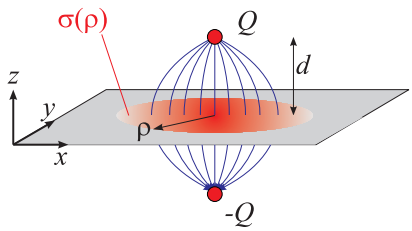

Figure 13.19: Point charge in front of a conductive plane.

We can now calculate the charge distribution on the surface. Gauß' law says,

$$\int_{box} \vec{\mathcal{E}} \cdot d\mathbf{S} = \frac{Q}{\varepsilon_0} = \frac{1}{\varepsilon_0} \int \varrho(\mathbf{r}) dV = \frac{1}{\varepsilon_0} \int \sigma(x,y)\delta(z) dV = \frac{1}{\varepsilon_0} \int \sigma(x,y) dA \ .$$

Therefore, on the surface,

$$\hat{\mathbf{e}}_z \cdot \vec{\mathcal{E}}(x,y,z=0) = \frac{\sigma(x,y)}{\varepsilon_0} \ .$$

Resolving by the charge density,

$$\sigma(x,y) = \varepsilon_0 \hat{\mathbf{e}}_z \cdot \vec{\mathcal{E}}(x,y,z=0) = \frac{-Q}{4\pi} \frac{2}{\sqrt{x^2+y^2+d^2}^3} \ .$$

Also, we can verify that the total surface charge is, $Q_s = -Q$.

13.5.2 Formal solution of the electrostatic problem

The solution of the Laplace equation will, in general, depend on boundary conditions imposed by the geometry of the system. For example, a charge in free space will generate another field than a charge above a conductive surface. The two most common boundary conditions are named after *Dirichlet* and *von Neumann*. The Dirichlet condition fixes the value of the potential on a geometry of surfaces enclosing a volume, $\Phi|_{\partial\mathcal{V}} = \Phi_0$, while the von Neumann condition fixes the value of the potential gradient, $\nabla\Phi|_{\partial\mathcal{V}} = \vec{\mathcal{E}}_0$. Let us discuss these conditions in the following.

Using the following four relationships,

$$\begin{aligned}
&\text{(i)} \quad \nabla^2 \tfrac{1}{4\pi|\mathbf{r}-\mathbf{r}'|} = -\delta(\mathbf{r}-\mathbf{r}') \\
&\text{(ii)} \quad \nabla\cdot(\phi\mathbf{F}) = \phi(\nabla\cdot\mathbf{F}) + (\nabla\phi)\cdot\mathbf{F} \\
&\text{(iii)} \quad \int_{\mathcal{V}} \nabla\cdot\mathbf{F} dV' = \int_{\partial V} \mathbf{F}\cdot d\mathbf{S}' \\
&\text{(iv)} \quad \nabla^2\Phi = -\tfrac{\varrho}{\varepsilon_0} \ ,
\end{aligned} \tag{13.58}$$

we now solve the Poisson equation,

$$\Phi(\mathbf{r}) = \int_{\mathcal{V}} \Phi(\mathbf{r}')\delta(\mathbf{r}-\mathbf{r}')dV' = \tfrac{-1}{4\pi}\int_{\mathcal{V}} \underbrace{\Phi(\mathbf{r}')}_{\phi}\nabla\cdot\underbrace{\left(\nabla\tfrac{1}{|\mathbf{r}-\mathbf{r}'|}\right)}_{\mathbf{F}}dV' \qquad \text{with (i)} \qquad (13.59)$$

$$= \tfrac{1}{4\pi}\int_{\mathcal{V}} \underbrace{\nabla\Phi(\mathbf{r}')}_{\mathbf{F}}\cdot\nabla\underbrace{\tfrac{1}{|\mathbf{r}-\mathbf{r}'|}}_{\phi}dV' - \tfrac{1}{4\pi}\int_{\mathcal{V}}\nabla\cdot\left(\Phi(\mathbf{r}')\nabla\tfrac{1}{|\mathbf{r}-\mathbf{r}'|}\right)dV' \qquad \text{with (ii)}$$

$$= -\tfrac{1}{4\pi}\int_{\mathcal{V}}\tfrac{1}{|\mathbf{r}-\mathbf{r}'|}\nabla\cdot\nabla\Phi(\mathbf{r}')dV' + \tfrac{1}{4\pi}\int_{\mathcal{V}}\nabla\cdot\left(\tfrac{1}{|\mathbf{r}-\mathbf{r}'|}\nabla\Phi(\mathbf{r}')\right)dV' - \tfrac{1}{4\pi}\int_{\mathcal{V}}\nabla\cdot\left(\Phi(\mathbf{r}')\nabla\tfrac{1}{|\mathbf{r}-\mathbf{r}'|}\right)dV' .$$

Finally, using relations (iii and iv), we obtain the final result,

$$\boxed{\Phi(\mathbf{r}) = \tfrac{1}{4\pi\varepsilon_0}\int_{\mathcal{V}}\tfrac{\varrho(\mathbf{r}')}{|\mathbf{r}-\mathbf{r}'|}dV' + \tfrac{1}{4\pi}\oint_{\partial\mathcal{V}}\left(\Phi(\mathbf{r}')\nabla'\tfrac{1}{|\mathbf{r}-\mathbf{r}'|} - \tfrac{1}{|\mathbf{r}-\mathbf{r}'|}\nabla'\Phi(\mathbf{r}')\right)\cdot d\mathbf{S}'}\ , \qquad (13.60)$$

which is an integral version of the Poisson equation. For volumes going to infinity, where the potential disappears, the surface integrals can be neglected, and we get the familiar form of Coulomb's law. For finite volumes, boundary conditions on surfaces can dramatically influence the potential.

Example 50 (*Consistency of Green's relationship*): Obviously, by imposing boundary conditions that coincide with equipotential surfaces of the field created by the charge distribution, the surface terms vanish. Choosing as an example a point charge placed at the origin, $\varrho(\mathbf{r}') = Q\delta^3(\mathbf{r}')$, and inserting its potential,

$$\Phi(\mathbf{r} = R\hat{\mathbf{e}}_r) = \frac{Q}{4\pi\varepsilon_0}\frac{1}{R} = \frac{Q}{4\pi\varepsilon_0}\left.\frac{1}{|\mathbf{r}-\mathbf{r}'|}\right|_{\mathbf{r}\in\partial\mathcal{V}} . \qquad (13.61)$$

in the relationship (13.60), we find that the surface integrals cancel out.

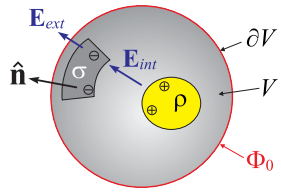

Figure 13.20: Illustration of boundary conditions.

The surface term can be interpreted in terms of a surface charge density, because we know that the normal electric field is discontinuous when crossing a charged sur-

face [6]:

$$\frac{\sigma(\mathbf{r}')}{\varepsilon_0} = -\nabla'\Phi(\mathbf{r}') \cdot \hat{\mathbf{n}} \ . \tag{13.62}$$

We consider the example of a charge distribution, $\varrho(\mathbf{r}')$, surrounded by a surface on which the potential is zero, $\Phi(\mathbf{r}')|_{\partial\mathcal{V}'} = 0$, such that the first surface term of the relation (13.60) fades away. Inserting the expression (13.62) in the second surface term, the relation becomes,

$$\Phi(\mathbf{r}) = \frac{1}{4\pi\varepsilon_0}\int_{\mathcal{V}} \frac{\varrho(\mathbf{r}')}{|\mathbf{r}-\mathbf{a}|} + \frac{1}{4\pi\varepsilon_0}\oint_{\partial\mathcal{V}} \frac{\sigma(\mathbf{r}')}{|\mathbf{r}-\mathbf{r}'|} dS' \ . \tag{13.63}$$

The interpretation of this modified Coulomb law is, that the charge induces a density distribution of surface charges σ within the conducting plane which modifies the electric potential, such that the boundary condition is satisfied.

13.5.3 Green's Function

The function $\frac{1}{4\pi|\mathbf{r}-\mathbf{r}'|}$ not the only one to satisfy the condition (13.58)(i). In fact, there is an entire class of functions called Green functions defined by,

$$\nabla^2 G(\mathbf{r},\mathbf{r}') \equiv -\delta(\mathbf{r}-\mathbf{r}') \ . \tag{13.64}$$

Obviously, for these functions the formula derived in (13.59) will be generalized,

$$\boxed{\Phi(\mathbf{r}) = \tfrac{1}{\varepsilon_0}\int_{\mathcal{V}} \varrho(\mathbf{r}')G(\mathbf{r},\mathbf{r}')dV' + \oint_{\partial\mathcal{V}} (\Phi(\mathbf{r}')\nabla G(\mathbf{r},\mathbf{r}') - G(\mathbf{r},\mathbf{r}')\nabla\Phi(\mathbf{r}')) \cdot d\mathbf{S}'} \ . \tag{13.65}$$

The advantage of the Green function is, that we have the freedom to add any function F,

$$G(\mathbf{r},\mathbf{r}') = \frac{1}{4\pi|\mathbf{r}-\mathbf{r}'|} + F(\mathbf{r},\mathbf{r}') \tag{13.66}$$

satisfying the Laplace equation,

$$\nabla^2 F(\mathbf{r},\mathbf{r}') = 0 \ , \tag{13.67}$$

and the Green function (13.66) will still satisfy the definition (13.64). In particular, we can choose the function F in a way to eliminate one of the two surface integrals in Eq. (13.65) and to obtain an expression only involving Dirichlet's or von Neumann's boundary conditions.

[6] We can derive this considering a thin disk located within the x-y plane and homogeneously charged with the charge density σ_0,

$$\Phi(z\hat{\mathbf{e}}_z) = \frac{1}{4\pi\varepsilon_0}\int_{disco} \frac{\sigma(\mathbf{r}')}{|z\hat{\mathbf{e}}_z - \mathbf{r}'|} dA' = \frac{\sigma_0}{2\varepsilon_0}\int_0^R \frac{1}{\sqrt{r'^2+z^2}} r'dr' = \frac{\sigma_0}{2\varepsilon_0}[\sqrt{R^2+z^2} - z] \ ,$$

and therefore,

$$E_z = -\frac{d\Phi(z\hat{\mathbf{e}}_z)}{dz} = -\frac{\sigma_0}{2\varepsilon_0}\left(\frac{z}{\sqrt{R^2+z^2}} - 1\right) \overset{z\ll R}{\longrightarrow} \frac{\sigma_0}{2\varepsilon_0} \ .$$

13.5.4 Poisson equation with Dirichlet's boundary conditions

The first *uniqueness theorem* proclaims,

> *The solution of the Poisson (or Laplace) equation in a volume $\mathcal{V}$ is uniquely determined, if Φ is specified on the surface of the volume $\partial\mathcal{V}$.*

To prove this theorem, let us specify that the potential adopts the (not necessarily constant) value Φ_0 on the surface and consider two possible solutions of the Laplace equation, Φ_1 and Φ_2. The difference $\Phi_3 \equiv \Phi_1 - \Phi_2$ disappears on the surface, $\Phi_3|_{\partial\mathcal{V}} = 0$, and must also satisfy the Laplace equation: $\nabla^2\Phi_3 = 0$. Now, since the Laplace equation does not allow local maxima or minima [7], Φ_3 must be zero throughout space (see Fig. 13.21 left).

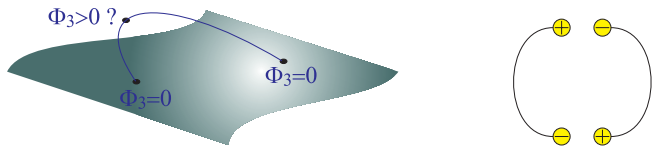

Figure 13.21: Illustration of the uniqueness theorems.

We consider as an example a finite volume V without charges, $\varrho = 0$, surrounded by a conducting border ∂V maintained at a fixed potential, $\Phi(\mathbf{r} \in \partial\mathcal{V}) = \Phi_0 = const.$ This is a typical situation realized, for example, in conductive materials such as metals. Therefore, $\Delta\Phi = 0$ within the volume. A possible trivial solution of the Laplace equation is, $\Phi(\mathbf{r}) = \Phi_0$. The uniqueness theorem now tells us that this is the *unique* solution.

To implement this theorem we choose the following boundary conditions,

$$G_D(\mathbf{r}, \mathbf{r}'_{\in\partial\mathcal{V}}) = 0 \ , \tag{13.68}$$

such that the relationship (13.64) becomes,

$$\boxed{\Phi(\mathbf{r}) = \tfrac{1}{\varepsilon_0}\int_{\mathcal{V}} \varrho(\mathbf{r}')G_D(\mathbf{r},\mathbf{r}')dV' + \oint_{\partial\mathcal{V}} \Phi(\mathbf{r}')\nabla' G_D(\mathbf{r},\mathbf{r}')\cdot d\mathbf{S}'} \ . \tag{13.69}$$

Do the Excs. 13.5.6.7, 13.5.6.8, 13.5.6.9, and 13.5.6.10.

13.5.5 Poisson equation with von Neumann's boundary conditions

The second uniqueness theorem proclaims,

> *In a volume $\mathcal{V}$ surrounded by conductors and containing a specified charge density ϱ, the electric field is uniquely determined by the total charge of each conductor.*

[7] For in a hypothetical maximum (minimum) we would have $\nabla^2\Phi_3 < 0$ (> 0).

To prove this theorem, we will consider a sample of conductors i each one carrying the charge Q_i. Assuming that there are two solutions for the electric field between the conductors, $\vec{\mathcal{E}}_1$ and $\vec{\mathcal{E}}_2$, each of these fields must satisfy, $\nabla \cdot \vec{\mathcal{E}}_1 = \nabla \cdot \vec{\mathcal{E}}_2 = Q_i$. The difference $\vec{\mathcal{E}}_3 \equiv \vec{\mathcal{E}}_1 - \vec{\mathcal{E}}_2$ must also satisfy Gauss' law $\nabla \cdot \vec{\mathcal{E}}_3 = 0$. Hence, $\vec{\mathcal{E}}_3$ must be vanish throughout the space (see Fig. 13.21 right) [8].

In the case of von Neumann boundary conditions we choose,

$$\nabla' G_N(\mathbf{r}, \mathbf{r}'_{\in \partial\mathcal{V}}) = -\tfrac{\hat{\mathbf{n}}}{S} \ , \tag{13.70}$$

because we must satisfy the definition (13.60),

$$-1 = \int_{\mathcal{V}} \nabla'^2 G_N(\mathbf{r}, \mathbf{r}') dV' = \oint_{\partial\mathcal{V}} \nabla' G_N(\mathbf{r}, \mathbf{r}') \cdot d\mathbf{S} = \oint_{\partial\mathcal{V}} \tfrac{-\hat{\mathbf{n}}}{S} \cdot d\mathbf{S} \tag{13.71}$$

such that,

$$\boxed{\Phi(\mathbf{r}) = \tfrac{1}{\varepsilon_0} \int_{\mathcal{V}} \varrho(\mathbf{r}') G_N(\mathbf{r}, \mathbf{r}') dV' - \tfrac{1}{A} \oint_{\partial\mathcal{V}} \Phi(\mathbf{r}') dA' - \oint_{\partial\mathcal{V}} G_N(\mathbf{r}, \mathbf{r}') \nabla' \Phi(\mathbf{r}') \cdot d\mathbf{S}'} \ . \tag{13.72}$$

The first surface term is simply the average of the potential over the area of the surface.

13.5.6 Exercises

13.5.6.1 Ex: Mirror charge

A long, thin wire is suspended along the y-direction at a distance $z = d$ parallel to a grounded metal plate located in the $z = 0$-plane. The surface of the wire carries the charge Q/l per unit length.
a. Draw a scheme of the electric field in the semi-space $z > 0$. **Help:** Use the principle of image charges!
b. Calculate the profile of the electric field near the surface of the plate.
c. What is the surface density $\sigma(x, y)$ of charges on the plate surface.
d. What is the charge induced in the plate per unit length in y-direction?
Comment: A similar problem occurs for conductors on printed circuits. The metal plate corresponds to the copper coating on the backside of the circuit board.

Solution: *a. Analogously to a point charge in front of a metallic plate we now expect a mirror wire with the charge $-Q$ in the distance $-d$ from the surface.*
b. The absolute value of the field generated by the wire is at the position $z = +d$,

$$\mathcal{E}_{wire} = \frac{Q}{2\pi\varepsilon_0 l} \frac{1}{\rho} = \frac{Q}{2\pi\varepsilon_0 l} \frac{1}{\sqrt{x^2 + (z-d)^2}}$$

(towards radially away from the wire). Analogously, for the mirror wire at the position $z = -d$,

$$\mathcal{E}_{mirror} = \frac{-Q}{2\pi\varepsilon_0 l} \frac{1}{\sqrt{x^2 + (z+d)^2}} \ .$$

[8] We present here a slightly simplified argumentation. See [545] for a more complete proof.

On the plate surface the field is parallel to $\hat{\mathbf{e}}_z$*. The* x *and* z*-components of the* E *field on the plate surface at the position* $z = 0$ *are,*

$$\mathcal{E}_{wire,x} = |\mathcal{E}_{wire,x}| \sin\phi = |\mathcal{E}_{wire,x}| \frac{x}{\sqrt{x^2+d^2}} = \frac{Q}{2\pi\varepsilon_0 l} \frac{1}{\sqrt{x^2+d^2}} \frac{x}{\sqrt{x^2+d^2}} = \frac{Q}{2\pi\varepsilon_0 l} \frac{x}{x^2+d^2}$$

and

$$\mathcal{E}_{wire,z} = -|\mathcal{E}_{wire,x}| \cos\phi = -|\mathcal{E}_{wire,x}| \frac{d}{\sqrt{x^2+d^2}} = \frac{-Q}{2\pi\varepsilon_0 l} \frac{1}{\sqrt{x^2+d^2}} \frac{d}{\sqrt{x^2+d^2}} = \frac{-Q}{2\pi\varepsilon_0 l} \frac{d}{x^2+d^2} \ .$$

for the mirror wire we have analogously,

$$\mathcal{E}_{wire,x} = \frac{-Q}{2\pi\varepsilon_0 l} \frac{x}{x^2+d^2}$$

and

$$\mathcal{E}_{wire,z} = \frac{-Q}{2\pi\varepsilon_0 l} \frac{d}{x^2+d^2} \ .$$

This means that the x*-component disappears and (for* $z > 0$*),*

$$\mathcal{E}_z = 2\mathcal{E}_{wire,z} = \frac{-Q}{\pi\varepsilon_0 l} \frac{d}{x^2+d^2} \ .$$

c. We use $\rho(x,y,z) = \sigma(x,y)\delta(z)$*. Furthermore, div* $\vec{\mathcal{E}} = \frac{\partial \mathcal{E}_z}{\partial z}$*, because all other components disappear on the surface. Now we place a small box (area* dA *parallel to the surface) such that a piece of the surface is inside. Now,*

$$\frac{1}{\varepsilon_0} \int \varrho(x,y,z) dV = \frac{1}{\varepsilon_0} \int \sigma(x,y) dA \ .$$

Furthermore,

$$\frac{1}{\varepsilon_0} \int_V \varrho dV = \oint_{\partial box} \vec{\mathcal{E}} \cdot d\mathbf{S} = \mathcal{E}_{z,z>0} dS \ .$$

From this follows,

$$\sigma(x,y) = \varepsilon_0 \mathcal{E}_{z,z>0} = -\frac{Qd}{\pi l} \frac{1}{x^2+d^2} \ .$$

d. Integrating over the length l *in* y*-direction and over all values of* x *gives,*

$$Q_{plate} = \int_0^l dy \int_{-\infty}^{\infty} dx \left(\frac{-Qd}{\pi l} \frac{1}{x^2+d^2} \right) = \frac{-Qdl}{\pi l} \int_{-\infty}^{\infty} dx \frac{1}{x^2+d^2} = \frac{-Qdl}{\pi} \frac{1}{d} \arctan\frac{x}{d} \Big|_{-\infty}^{\infty} = -Q \ .$$

13.5.6.2 Ex: Mirror charge

Consider the scheme, illustrated in the figure, of a point charge $+q$ in front of a corner of a grounded wall.
a. Determine the positions and values of the image charges.
b. Calculate the electrostatic potential $\Phi(\mathbf{r})$ in the upper right quadrant.

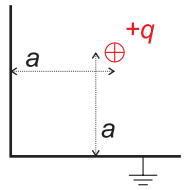

Figure 13.22: Mirror charge.

Solution: *a. There are three image charges,*

$$-q, \begin{pmatrix} -a \\ a \\ 0 \end{pmatrix} \quad , \quad +q, \begin{pmatrix} -a \\ -a \\ 0 \end{pmatrix} \quad , \quad -q, \begin{pmatrix} a \\ -a \\ 0 \end{pmatrix} .$$

b. So we have for $\mathbf{r}$ *in the upper right quadrant:*

$$\Phi(\mathbf{r}) = \frac{q}{4\pi\varepsilon_0}\left[-\frac{1}{\sqrt{(x+a)^2+(y-a)^2+z^2}} + \frac{1}{\sqrt{(x+a)^2+(y+a)^2+z^2}} - \frac{1}{\sqrt{(x-a)^2+(y+a)^2+z^2}} + \frac{1}{\sqrt{(x-a)^2+(y-a)^2+z^2}}\right] .$$

Proof: $\Phi(\mathbf{r}) = 0$ *para* $x = 0$ *ou* $y = 0$.

13.5.6.3 Ex: Mirror charge

Inside a grounded hollow metallic sphere with the inner radius a be a charge $+Q$ at the position $\mathbf{r}_1 = (0, 0, z_1)$. Determine the charge Q' and the position $\mathbf{r}_2$ of an image charge with which it is possible to describe the potential $\Phi(\mathbf{r})$ of the original charge distribution using only the system consisting of the charge and the image charge. Determine $\Phi(\mathbf{r})$.
Help: The position $\mathbf{r}_2$ and the charge Q' are not unambiguously determined. Choose $\mathbf{r}_1 = (0, 0, z_1)$ and $z_2/a = a/z_1$.

Solution: *The boundary condition is* $\Phi(|\mathbf{r}| = a) = 0$. *We now place a charge* Q' *for symmetry reasons at the point* z_2*:*

$$4\pi\varepsilon_0\Phi(\mathbf{r}) = \frac{Q}{|\mathbf{r} - z_1\hat{\mathbf{e}}_z|} + \frac{Q'}{|\mathbf{r} - z_2\hat{\mathbf{e}}_z|}$$

with $\mathbf{r} = r\hat{\mathbf{e}}_r$ *follows from the condition*

$$4\pi\varepsilon_0\Phi(\mathbf{r} = a\hat{\mathbf{e}}_r) = \frac{Q/a}{|\hat{\mathbf{e}}_r - z_1\hat{\mathbf{e}}_z/a|} + \frac{Q'/a}{|\hat{\mathbf{e}}_r - z_2\hat{\mathbf{e}}_z/a|} \equiv 0 .$$

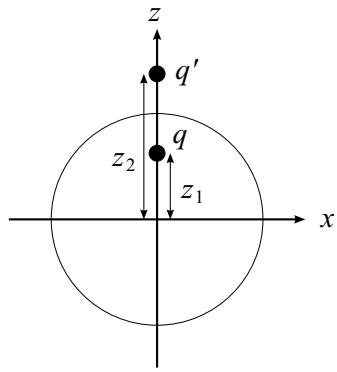

Figure 13.23: Mirror charge.

This is satisfied when

$$Q\sqrt{a^2+z_2^2-az_2\hat{\mathbf{e}}_r\cdot\hat{\mathbf{e}}_z}=-Q'\sqrt{a^2+z_1^2-az_1\hat{\mathbf{e}}_r\cdot\hat{\mathbf{e}}_z}\ .$$

The square gives,

$$Q^2(a^2+z_2^2-az_2\hat{\mathbf{e}}_r\cdot\hat{\mathbf{e}}_z)=Q'^2(a^2+z_1^2-az_1\hat{\mathbf{e}}_r\cdot\hat{\mathbf{e}}_z)Q'Q<0\ .$$

Since this should be satisfied for all angles $\theta=\arccos(\hat{\mathbf{e}}_r\cdot\hat{\mathbf{e}}_z)$,

$$Q^2(-az_2\hat{\mathbf{e}}_r\cdot\hat{\mathbf{e}}_z)=Q''(-az_1\hat{\mathbf{e}}_r\cdot\hat{\mathbf{e}}_z)\qquad\textit{and}\qquad Q^2(a^2+z_2^2)=Q''(a^2+z_1^2)\ ,$$

resp.

$$\frac{Q^2}{Q''}=\frac{z_1}{z_2}=\frac{a^2+z_1^2}{a^2+z_2^2}\ .$$

The second equation gives,

$$z_1a^2+z_1z_2^2-a^2z_2-z_1^2z_2=0\ ,$$

which yields $z_1=a^2/z_2$. *With that we substitute* z_1 *in the first equation,*

$$Q'=\pm Q\frac{z_2}{a}\qquad\textit{and}\qquad Q'Q<0\ .$$

We get a trivial solution for $z_2=z_1$ *and* $Q=-Q'$.

13.5.6.4 Ex: Mirror charge

A conductive surface in the (x,y)-plane has a protrusion in the form of a semi-sphere with radius R. The center of the sphere is in the plane and at the origin of the coordinates. On the symmetry axis $\hat{\mathbf{e}}_z$ at a distance $d>R$ from the plane there is a point charge Q. Determine with the image charge method the potential $\Phi(\mathbf{r})$ and the force $\mathbf{F}$ on the charge Q.

a. To make the surface of the semisphere an equipotential surface ($\Phi \equiv 0$) we need a mirror charge Q_1 on the z-axis at a distance z_1 from the origin. Determine Q_1 and z_1.
b. For the (x, y)-plane to become an equipotential surface as well, we need two more image charges Q_2 and Q_3. Determine the value and position of these charges.
c. With the values and positions of the charges determine: The electrostatic potential $\Phi(\mathbf{r})$ at an arbitrary point $\mathbf{r}$ above the conductive surface, the force $\mathbf{F}$ on the charge Q and its direction (repulsive or attractive).

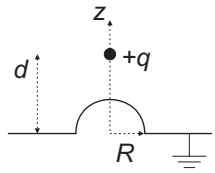

Figure 13.24: Mirror charge.

Solution: *a. The potential must satisfy the boundary condition,*

$$\Phi(\mathbf{r})|_{\mathbf{r}\in spheresurface} = \frac{1}{4\pi\varepsilon_0}\left[\frac{Q}{|\mathbf{r}-z_0\hat{\mathbf{e}}_z|}+\frac{Q_1}{|\mathbf{r}-z_1\hat{\mathbf{e}}_z|}\right]_{\mathbf{r}\in spheresurface} = 0\ .$$

This can be met in a non-trivial way by $z_1 = R^2/z_0$ and $q_1 = -qR/z_0$, since

$$\left[\frac{Q}{|\mathbf{r}-z_0\hat{\mathbf{e}}_z|}+\frac{-qR/z_0}{|\mathbf{r}-\frac{R^2}{z_0}\hat{\mathbf{e}}_z|}\right]_{\mathbf{r}\in spheresurface} = \frac{Q}{\sqrt{X^2+Y^2+(Z-z_0)^2}} - \frac{QR/z_0}{\sqrt{X^2+Y^2+\left(Z-\frac{R^2}{z_0}\right)^2}}$$

$$= \frac{Q}{\sqrt{R^2-2Zz_0+z_0^2}} - \frac{QR}{\sqrt{z_0^2X^2+z_0^2Y^2+z_0^2Z^2-2z_0ZR^2+R^4}} = 0\ .$$

b. The two additional charges must reflect the charges Q and Q_1 in the (x, y)-plane: $z_2 = -z_0$ and $Q_2 = -Q$ and $z_3 = -z_1$ and $Q_3 = -Q_1$.
c. With that we have a complete expression for the potential,

$$\Phi(\mathbf{r}) = \frac{1}{4\pi\varepsilon_0}\sum_{k=0}^{3}\frac{Q_k}{|\mathbf{r}-z_k\hat{\mathbf{e}}_z|} = \frac{Q}{4\pi\varepsilon_0}\left(\frac{1}{|\mathbf{r}-z_0\hat{\mathbf{e}}_z|}-\frac{1}{|\mathbf{r}+z_0\hat{\mathbf{e}}_z|}+\frac{\frac{R}{z_0}}{|\mathbf{r}+\frac{R^2}{z_0}\hat{\mathbf{e}}_z|}-\frac{\frac{R}{z_0}}{|\mathbf{r}-\frac{R^2}{z_0}\hat{\mathbf{e}}_z|}\right)\ .$$

The force acting on the charge follows from the gradient of the field of the three image charges at the position of Q,

$$\mathbf{F}(\mathbf{r}=z_0\hat{\mathbf{e}}_z) = -\nabla\frac{1}{4\pi\varepsilon_0}\sum_{k=1}^{3}\frac{Q_k}{|\mathbf{r}-z_k\hat{\mathbf{e}}_z|}$$

$$= \frac{-Q}{4\pi\varepsilon_0}\hat{\mathbf{e}}_z\left(-\frac{2z_0}{|z_0\hat{\mathbf{e}}_z+z_0\hat{\mathbf{e}}_z|^3}+\frac{\frac{R}{z_0}(z_0+\frac{R^2}{z_0})}{|z_0\hat{\mathbf{e}}_z+\frac{R^2}{z_0}\hat{\mathbf{e}}_z|^3}-\frac{\frac{R}{z_0}(z_0-\frac{R^2}{z_0})}{|z_0\hat{\mathbf{e}}_z-\frac{R^2}{z_0}\hat{\mathbf{e}}_z|^3}\right)$$

$$= \frac{-Q}{4\pi\varepsilon_0}\left(-\frac{1}{4z_0^2}+\frac{Rz_0}{(z_0^2+R^2)^2}-\frac{Rz_0}{(z_0^2-R^2)^2}\right) = \frac{Q}{4\pi\varepsilon_0}\left(\frac{1}{4z_0^2}+\frac{4R^3z_0^3}{(z_0^4-R^4)^2}\right) > 0\ .$$

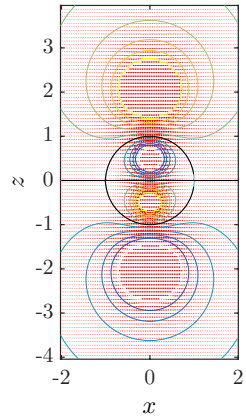

Figure 13.25: Mirror charge.

Therefore, the force is attractive.

13.5.6.5 Ex: Mirror charge

Consider a hollow conducting sphere with radius R whose center is at the origin. At the position with the vector $\mathbf{a}$ ($|\mathbf{a}| > R$) be a point charge q.
a. The sphere is grounded (that is, $\Phi = 0$ at the edge of the hollow sphere). Calculate the potential outside the sphere using the image charge method.
b. Calculate the charge induced on the surface of the sphere.
c. What changes when the sphere is not grounded, but neutral?

Solution:

13.5.6.6 Ex: Point charges in front of a conductor

Consider a point charge Q located at a distance d in front of an infinitely extended conductive plane.
a. Find the parametrization $\varrho(\mathbf{r})$ of the volume charge distribution for the charge and its image.
b. Calculate the potential from the distribution $\varrho(\mathbf{r})$.
c. Calculate the electric field from the distribution $\varrho(\mathbf{r})$.
d. Calculate the surface charge distribution $\sigma(\rho)$ induced in the conductor using Gauss' law.
e. Calculate the potential $\Phi(z)$ along the z-axis from Coulomb's law using the surface charge distribution $\sigma(\rho)$.
f. Compare the result obtained in (e) with the potential produced by the image charge calculated in (b).
Help:: $\int \frac{1}{\sqrt{u^2+a^2}^3} \frac{1}{\sqrt{u^2+b^2}} u du = \frac{1}{a^2-b^2} \sqrt{\frac{u^2+b^2}{u^2+a^2}}$

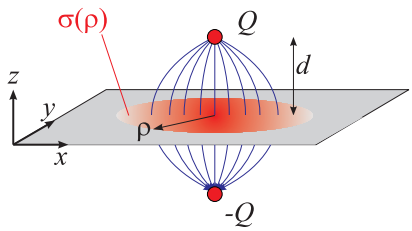

Figure 13.26: Mirror charge.

Solution: *a. We invent a second charge on the other side of the conductive plane, such that the volume charge distribution is,*

$$\varrho(\mathbf{r}) = Q[\delta^3(\mathbf{r} - d\hat{\mathbf{e}}_z) - \delta^3(\mathbf{r} + d\hat{\mathbf{e}}_z)] \ .$$

b. The potential becomes,

$$\begin{aligned}\Phi(\mathbf{r}) &= \frac{1}{4\pi\varepsilon_0}\int_{\mathcal{V}} \frac{\varrho(\mathbf{r}')dV'}{|\mathbf{r}-\mathbf{r}'|} = \frac{1}{4\pi\varepsilon_0}\int_{\mathcal{V}} \frac{Q\left[\delta^3(\mathbf{r} - d\hat{\mathbf{e}}_z) - \delta^3(\mathbf{r} + d\hat{\mathbf{e}}_z)\right]}{|\mathbf{r}-\mathbf{r}'|}dV' \\ &= \frac{1}{4\pi\varepsilon_0}\left(\frac{Q}{|\mathbf{r} - d\hat{\mathbf{e}}_z|} - \frac{Q}{|\mathbf{r} + d\hat{\mathbf{e}}_z|}\right) \ .\end{aligned}$$

c. The field becomes,

$$\vec{\mathcal{E}}(\mathbf{r}) = \frac{1}{4\pi\varepsilon_0}\int_{\mathcal{V}} \frac{\mathbf{r}-\mathbf{r}'}{|\mathbf{r}-\mathbf{r}'|^3}\varrho(\mathbf{r}')dV' = \frac{Q}{4\pi\varepsilon_0}\left(\frac{\mathbf{r} - d\hat{\mathbf{e}}_z}{|\mathbf{r} - d\hat{\mathbf{e}}_z|^3} - \frac{\mathbf{r} + d\hat{\mathbf{e}}_z}{|\mathbf{r} + d\hat{\mathbf{e}}_z|^3}\right) \ .$$

d. With Gauss' law we calculate,

$$\begin{aligned}\frac{1}{\varepsilon_0}\int_0^{2\pi}\int_0^{\infty}\sigma(\rho)\rho d\rho d\phi = \frac{Q}{\varepsilon_0} &= \int_{\mathcal{V}} \nabla\cdot\vec{\mathcal{E}}(\mathbf{r})dV = \oint_{\partial\mathcal{V}} \vec{\mathcal{E}}(\mathbf{r})\cdot d\mathbf{S} \\ &= \frac{Q}{4\pi\varepsilon_0}\int_0^{2\pi}\int_0^{\infty}\left(\frac{\rho\hat{\mathbf{e}}_\rho\cdot\hat{\mathbf{e}}_z - d}{|\rho\hat{\mathbf{e}}_\rho - d\hat{\mathbf{e}}_z|^3} - \frac{\rho\hat{\mathbf{e}}_\rho\cdot\hat{\mathbf{e}}_z + d}{|\rho\hat{\mathbf{e}}_\rho + d\hat{\mathbf{e}}_z|^3}\right)\rho d\rho d\phi \\ &= \frac{Q}{4\pi\varepsilon_0}\int_0^{2\pi}\int_0^{\infty}\left(\frac{-d}{\sqrt{\rho^2+d^2}^3} - \frac{d}{\sqrt{\rho^2+d^2}^3}\right)\rho d\rho d\phi \ ,\end{aligned}$$

such that,

$$\sigma(\rho) = \frac{-2dQ}{4\pi\sqrt{\rho^2+d^2}^3} \ .$$

e. The potential produced by the distribution of surface charge is, for $z \geq 0$,

$$\begin{aligned}\Phi_+(z) &= \frac{1}{4\pi\varepsilon_0}\oint_{\partial V}\frac{\sigma(\mathbf{r}')}{|\mathbf{r}-\mathbf{r}'|}dA' = \frac{1}{4\pi\varepsilon_0}\int_0^{2\pi}\int_0^{\infty}\frac{1}{|z\hat{\mathbf{e}}_z - \mathbf{r}'|}\frac{-2dQ}{4\pi\sqrt{\rho'^2+d^2}^3}\rho' d\rho' d\phi' \\ &= \frac{1}{4\pi\varepsilon_0}\frac{-2dQ}{4\pi}2\pi\int_0^{\infty}\frac{1}{\sqrt{z^2+\rho'^2}}\frac{1}{\sqrt{\rho'^2+d^2}^3}\rho' d\rho' = -\frac{Q}{4\pi\varepsilon_0}\frac{1}{d+z} \ ,\end{aligned}$$

using the given integral formula.
f. From the result obtained in (b) we find the same result for the potential produced by the image load along the z-axis,

$$\Phi(z) = -\frac{1}{4\pi\varepsilon_0}\frac{Q}{|z\hat{\mathbf{e}}_z + d\hat{\mathbf{e}}_z|} = -\frac{1}{4\pi\varepsilon_0}\frac{Q}{|z+d|} \ .$$

13.5.6.7 Ex: Dirichlet boundary conditions by the Green method

Here we want to analyze the problem of a potential in the semi-space defined by $z \geq 0$ with Dirichlet boundary conditions in the $z = 0$-plane and at infinity.
a. Determine the corresponding Greens function.
b. The potential has in the $z = 0$-plane within a circle of radius a the fixed value Φ_0. Outside this circle and on the same plane the potential is $\Phi = 0$. Derive the integral expression for the potential at a point in the upper semi-space with the cylindrical coordinates (ρ, ϕ, z).
c. Now show that the potential along an axis perpendicularly traversing the center of the circle is given by $\Phi(z) = \Phi_0(1 - z/\sqrt{a^2 + z^2})$.

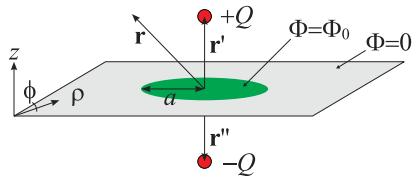

Figure 13.27: Green's function.

Solution: *a. Be* $\mathbf{r} = (x, y, z) = (\rho\cos\varphi, \rho\sin\varphi, z)$ *the position vector of an arbitrary point in the upper semi-space. For the establishment of the Green function, we consider a test charge* $q = +1$ *at a point in the upper semi-space given by the vector* $\mathbf{r}' = (\rho'\cos\varphi', \rho'\sin\varphi', z')$*, together with the corresponding image charge* $q = -1$ *at the* $\mathbf{r}'' = (\rho'\cos\varphi', \rho'\sin\varphi', -z')$ *of the lower semi-space. In this case,*

$$G(\mathbf{r}, \mathbf{r}') = \frac{1}{4\pi|\mathbf{r} - \mathbf{r}'|} - \frac{1}{4\pi|\mathbf{r} - \mathbf{r}''|}$$
$$= \frac{1}{4\pi\sqrt{\rho^2 + \rho'^2 - 2\rho\rho'\cos(\varphi - \varphi') + (z - z')^2}} - \frac{1}{4\pi\sqrt{\rho^2 + \rho'^{\,2} - 2\rho\rho'\cos(\varphi - \varphi') + (z + z')^2}} \ .$$

b. For the Dirichlet boundary problem,

$$\Phi(\mathbf{r}) = -\int_F \Phi(\rho', \varphi', 0)\left(-\frac{\partial G}{\partial z'}\right)_{z'=0} \rho' d\rho' d\varphi'$$
$$= \frac{1}{2\pi}\int_F d\varphi' d\rho' \rho' \Phi(\rho', \varphi', 0)\frac{z}{(\rho^2 + \rho'^2 - 2\rho\rho'\cos(\varphi - \varphi') + z^2)^{3/2}} \ .$$

From this follows,

$$\Phi(\rho,\varphi,z)=\frac{1}{2\pi}\int_0^{2\pi}d\varphi'\int_0^a d\rho'\rho'\frac{\Phi_0 z}{(\rho^2+\rho'^{\,2}-2\rho\rho'\cos(\varphi-\varphi')+z^2)^{3/2}}\ .$$

c. Now we let $\rho=0$ (z-axis). Then,

$$\Phi(0,\varphi,z)=\frac{1}{2\pi}\int_0^{2\pi}d\varphi'\int_0^a d\rho'\rho'\frac{\Phi_0 z}{(\rho'^{\,2}+z^2)^{3/2}}=\Phi_0 z\int_0^a\frac{d\rho'\rho'}{(\rho'^{\,2}+z^2)^{3/2}}$$
$$=\Phi_0 z\left[\frac{-1}{\sqrt{\rho'^{\,2}+z^2}}\right]_{\rho'=0}^{\rho'=a}=\Phi_0 z\left[\frac{1}{z}-\frac{1}{\sqrt{z^2+a^2}}\right]=\Phi_0\left[1-\frac{z}{\sqrt{z^2+a^2}}\right]\ .$$

13.5.6.8 Ex: Conductor plates with mirror charges by the Green method

We consider two flat conductive plates (infinitely extended) with the mutual distance L. Exactly in the middle between the plates there is a point charge $+q$. Use the method of an infinite series of mirror images to calculate the potential between the plates and the force on a plate.

Solution: *We place the z-axis perpendicular to the two conductive plates and through the charge $+q$. At the position of the charge we set $z=0$. The mirror charges must then adopt at $\pm L$ the value $-q$, at $\pm 2L$ the value $+q$, etc. With that, we get for the Green's function (and therefore for the potential),*

$$G=\Phi(x,y,z)=\sum_{m=-\infty}^{m=+\infty}\frac{(-)^m}{\sqrt{x^2+y^2+(z-mL)^2}}$$

The Coulomb force on the right plate is then equal to the sum of the forces exerted by the real charge and the image charges on the left side ($z<0$) on the mirror charges on the right side. For $z\le 0$ we have charges $q(-)^n$ at $z=-Ln$ for $n=0,1,2,....$ For $z>0$ $q(-)^m$ at $z=+Lm$ for $m=1,2,3,....$ For the force between n-th left charge and all the right charges m then holds,

$$F_n=q(-)^n\sum_{m=1}^{\infty}\frac{q(-)^m}{[L(m+n)]^2}$$

With that we get,

$$F=\sum_{n=0}^{\infty}F_n=\sum_{n=0}^{\infty}\sum_{m=1}^{\infty}\frac{q^2(-)^{n+m}}{L^2(m+n)^2}=\frac{q^2}{L^2}\sum_{s=1}^{\infty}\sum_{m=1}^{s}\frac{(-)^s}{s^2}=\frac{q^2}{L^2}\sum_{s=1}^{\infty}\frac{(-)^s}{s}=\frac{q^2}{L^2}\ln 2\ .$$

13.5.6.9 Ex: Hollow sphere by the Green method

We consider an infinitely thin conductive hollow sphere with radius a. In spherical coordinates, the potential on the surface of the sphere is given by $\Phi(a,\theta,\phi)=\Phi_0\cos\theta$.
a. Calculate, using the Green function for the sphere, the potential and the field inside the sphere on the z-axis.
b. Show that $\Phi(r,\theta,\phi)=\Phi_0(r/a)\cos\theta$ is the solution for the interior of the sphere and that $\vec{\mathcal{E}}(\mathbf{r})=-(\Phi_0/a)\hat{\mathbf{e}}_z$.

Solution: *a. Green's function inside the sphere is*

$$G(\mathbf{r},\mathbf{r}')=\frac{1}{4\pi|\mathbf{r}-\mathbf{r}'|}-\frac{a}{4\pi r'|\mathbf{r}-\frac{a^2}{r'^2}\mathbf{r}'|}\ .$$

Letting $\mathbf{r}$ *point in* z*-direction we get,*

$$G=\frac{1}{4\pi\sqrt{r^2+r'^2-2rr'\cos\vartheta'}}-\frac{1}{4\pi\sqrt{\frac{r^2r'^{\ 2}}{a^2}+a^2-2rr'\cos\vartheta'}}\ .$$

So, inside the sphere on the z*-axis,*

$$\Phi_\pm(\mathbf{r})=\pm\int_F\Phi(\mathbf{r}')\frac{\partial G(\mathbf{r},\mathbf{r}')}{\partial r'}\,df'\ .$$

On the other hand,

$$\left.\frac{\partial G(\mathbf{r},\mathbf{r}')}{\partial r'}\right|_{r'=a}=\frac{r^2-a^2}{a\sqrt{r^2+a^2-2ra\cos\vartheta'}^3}\ ,$$

where the $\pm$ *index indicates* r *going to* $\pm z$*. With that we get,*

$$\begin{aligned}\Phi_\pm&=\pm\frac{1}{4\pi}\int_F V_0\cos\vartheta'\frac{r^2-a^2}{a\sqrt{r^2+a^2-2ra\cos\vartheta'}^3}a^2\sin\vartheta'd\vartheta'd\varphi'\\&=\pm\frac{V_0}{2}a(a^2-r^2)\int_{-1}^{+1}\frac{xdx}{(r^2+a^2-2arx)^{3/2}}=\pm\frac{V_0}{2}a(a^2-r^2)\left[\frac{1}{r^2a^2}\frac{-rax+a^2+r^2}{\sqrt{r^2+a^2-2rax}}\right]_{-1}^{+1}\\&=\pm\frac{(a^2-r^2)V_0}{2r^2a}\left[\frac{-ra+a^2+r^2}{a-r}-\frac{ra+a^2+r^2}{a+r}\right]=\pm\frac{r}{a}V_0\ .\end{aligned}$$

Here it is important to have, in both cases, positive roots (for this reason we chose $a-r$ *and not* $r-a$*, which would give the solution in outer space). Since* $\Phi=V_0\cos\vartheta$ *is given, we have that the sign* $+$ *holds for* $\vartheta=0$*, and the sign* $-$ *for* $\vartheta=\pi$*.*
b. We let,

$$\Phi(\mathbf{r})=\frac{V_0}{a}r\cos\vartheta\ ,$$

and hence,

$$\vec{\mathcal{E}}(\mathbf{r})=-\frac{V_0}{a}\hat{\mathbf{e}}_z\ .$$

Here we use the Laplace operator in spherical coordinates. So on the surface of the spheres holds,

$$\Delta\Phi = \frac{1}{r^2}\frac{\partial}{\partial r}\left(r^2\frac{\partial\Phi}{\partial r}\right) + \frac{1}{r^2\sin\vartheta}\frac{\partial}{\partial\vartheta}\left(\sin\vartheta\frac{\partial\Phi}{\partial\vartheta}\right) = \frac{\frac{2V_0}{a}\cos\vartheta}{r} - \frac{\frac{2V_0}{a}\cos\vartheta}{r} = 0 \ .$$

Using the gradient in spherical coordinates and replacing the corresponding unit vectors by Cartesian ones, we obtain immediately,

$$\vec{\mathcal{E}}(\mathbf{r}) = -\frac{V_0}{a}\hat{\mathbf{e}}_z \ .$$

13.5.6.10 Ex: Unambiguity of the solution of the contour problem

Show that with the Dirichlet boundary condition $\Phi(\mathbf{r}) = \Phi_0(\mathbf{r})|_{\in\partial V}$ or the von Neumann boundary condition $\frac{\partial\Phi}{\partial n}\big|_{\partial V} = -\frac{\sigma}{\varepsilon_0}$ within the region of the volume V the potential Φ is unambiguously determined by the Poisson equation $\Delta\Phi = -\frac{1}{\varepsilon_0}\rho(\mathbf{r})$and a constant.

Solution: *Be $\Phi_1(\mathbf{r})$ and $\Phi_2(\mathbf{r})$ solutions of the Poisson equation with*

$$\Phi_1(\mathbf{r}) \equiv \Phi_2(\mathbf{r}) \qquad on \qquad \partial V \ ,$$

respectively

$$\frac{\partial\Phi_1}{\partial n} \equiv \frac{\partial\Phi_2}{\partial n} \qquad on \qquad \partial V \ .$$

For the potential $\Psi(\mathbf{r}) = \Phi_1(\mathbf{r}) - \Phi_2(\mathbf{r})$ then holds $\Delta\Psi \equiv 0$ with

$$\Psi|_{\partial V} \equiv 0 \qquad resp. \qquad \frac{\partial\Psi}{\partial n}\bigg|_{\partial V} \ .$$

We consider,

$$\int_V \nabla(\Psi\nabla\Psi)d^3r = \int_V \Psi\Delta\Psi d^3r + \int_V (\nabla\Psi)\cdot(\nabla\Psi)d^3r = \int_V (\nabla\Psi)\cdot(\nabla\Psi)d^3r \ ,$$

and, with the Gauß theorem,

$$\int_V \nabla(\Psi\nabla\Psi)d^3r = \oint_{\partial V} \Psi(\nabla\Psi)\cdot d\mathbf{F} = 0 \ ,$$

because according to the boundary condition, on the border $\Psi = 0$ (Dirichlet) respectively $\nabla\Psi\cdot d\mathbf{F} = 0$ (von Neumann). But since $(\nabla\Psi)^2 \geq 0$, necessarily everywhere $(\nabla\Psi) = 0$, that is, Ψ must be constant. For the Dirichlet boundary condition, the constant must disappear, because $\Psi|_{\partial V} = 0$, that is,

$$\Phi_1 = \Phi_2 \ .$$

For von Neumann's boundary condition,

$$\Phi_1 = \Phi_2 + const \ .$$

13.6 Solution of the Laplace equation in situations of high symmetry

The Poisson (or Laplace) equation is a second order partial differential equation, which depends on three spatial coordinates. Many situations are characterized by symmetries, which allow us to disregard some spatial dimensions and dramatically simplify the mathematical problem. In the following, we will discuss situations of Cartesian, cylindrical and spherical symmetry.

13.6.1 Variable separation in Cartesian coordinates

In situations where the symmetry of the problem suggests a separation of the Cartesian variables, we can make the ansatz,

$$\Phi(\mathbf{r}) = X(x)Y(y)Z(z) \ . \tag{13.73}$$

In Cartesian coordinates the Laplace equation is written,

$$\left[\frac{\partial^2}{\partial x^2} + \frac{\partial^2}{\partial y^2} + \frac{\partial^2}{\partial z^2}\right]\Phi = 0 \ . \tag{13.74}$$

Inserting the ansatz into the Laplace equation and dividing by Φ,

$$\frac{1}{X}\frac{\partial^2 X}{\partial x^2} + \frac{1}{Y}\frac{\partial^2 Y}{\partial y^2} + \frac{1}{Z}\frac{\partial^2 Z}{\partial z^2} = 0 \ . \tag{13.75}$$

The three terms are functions of different variables and must therefore be constant independently and separately,

$$\frac{1}{X}\frac{\partial^2 X}{\partial x^2} = C_1 \quad , \quad \frac{1}{Y}\frac{\partial^2 Y}{\partial y^2} = C_2 \quad , \quad \frac{1}{Z}\frac{\partial^2 Z}{\partial z^2} = C_3 = -C_1 - C_2 \ . \tag{13.76}$$

The advantage of this procedure is that, the differential equations for the three spatial coordinates being decoupled, we can be solve them separately. In the best case, the field is homogeneous in one of the coordinates, which reduces the dimensionality of the problem.

Example 51 (*Field of a grounded board*): For example, to calculate the field of a plate held at a fixed potential Φ_0 and being infinitely extended in the x-y-plane, we can let $X'(x) = Y'(y) = 0$ and solve the equation,

$$\frac{\partial^2 Z}{\partial z^2} = 0 \ , \tag{13.77}$$

which gives, $\Phi(\mathbf{r}) = Z(z) = Cz + \Phi_0$ and $\vec{\mathcal{E}} = C\hat{\mathbf{e}}_z$. The constants C and Φ_0 must be specified by additional boundary conditions. See Exc. 13.6.4.1.

13.6.2 Variable separation in cylindrical coordinates

In situations where the symmetry of the problem suggests a possible separation of cylindrical variables, we can try the ansatz,

$$\Phi(\mathbf{r}) = R(r)F(\phi)Z(z) \ . \tag{13.78}$$

In cylindrical coordinates the Laplace equation is written,

$$\left[\frac{1}{\rho}\frac{\partial}{\partial\rho}\left(\rho\frac{\partial}{\partial\rho}\right) + \frac{1}{\rho^2}\frac{\partial^2}{\partial\phi^2} + \frac{\partial^2}{\partial z^2}\right]\Phi = 0 \ . \tag{13.79}$$

Inserting the ansatz into the Laplace equation and dividing by Φ,

$$\frac{1}{R\rho}\frac{\partial}{\partial\rho}\left(\rho\frac{\partial R}{\partial\rho}\right) + \frac{1}{F}\frac{\partial^2 F}{\partial\phi^2} + \frac{1}{Z}\frac{\partial^2 Z}{\partial z^2} = 0 \ . \tag{13.80}$$

The three terms are functions of different variables and must therefore be constant separately,

$$\frac{1}{R\rho}\frac{\partial}{\partial\rho}\left(\rho\frac{\partial R}{\partial\rho}\right) = C_1 \quad , \quad \frac{1}{F}\frac{\partial^2 F}{\partial\phi^2} = C_2 \quad , \quad \frac{1}{Z}\frac{\partial^2 Z}{\partial z^2} = C_3 = -C_1 - C_2 \ . \tag{13.81}$$

Example 52 (*Field of a straight wire*): Many geometries have cylindrical symmetry, such that the equations in θ and z become trivial. For example, to calculate the field of a straight and infinite wire maintained at a fixed potential, it is enough to solve a radial differential equation,

$$\frac{\partial}{\partial\rho}\left(\rho\frac{\partial R}{\partial\rho}\right) = 0 \ ,$$

which gives, $\Phi(\mathbf{r}) = R(\rho) = C\ln\rho + \Phi_0$ and $\vec{\mathcal{E}} = C\hat{\mathbf{e}}_\rho/\rho$. The constants C and Φ_0 must be specified by additional boundary conditions.

13.6.3 Variable separation in spherical coordinates

In situations where the symmetry of the problem suggests a possible separation of the spherical variables, we can try the make ansatz,

$$\Phi(\mathbf{r}) = R(r)T(\theta)F(\phi) \ . \tag{13.82}$$

In spherical coordinates the Laplace equation is written,

$$\left[\frac{1}{r^2}\frac{\partial}{\partial r}\left(r^2\frac{\partial}{\partial r}\right) + \frac{1}{r^2\sin\theta}\frac{\partial}{\partial\theta}\left(\sin\theta\frac{\partial}{\partial\theta}\right) + \frac{1}{r^2\sin^2\theta}\frac{\partial^2}{\partial\phi^2}\right]\Phi = 0 \ . \tag{13.83}$$

Inserting the ansatz into the Laplace equation and dividing by Φ,

$$\frac{1}{R}\frac{\partial}{\partial r}\left(r^2\frac{\partial R}{\partial r}\right) + \frac{1}{T\sin\theta}\frac{\partial}{\partial\theta}\left(\sin\theta\frac{\partial T}{\partial\theta}\right) + \frac{1}{Fr^2\sin^2\theta}\frac{\partial^2 F}{\partial\phi^2} = 0 \ . \tag{13.84}$$

The three terms are functions of different variables and must therefore be constant separately,

$$\frac{1}{R}\frac{\partial}{\partial r}\left(r^2\frac{\partial R}{\partial r}\right) = C_1 \quad , \quad \frac{1}{T\sin\theta}\frac{\partial}{\partial\theta}\left(\sin\theta\frac{\partial T}{\partial\theta}\right) = \ell(\ell+1) \tag{13.85}$$
$$\frac{1}{Fr^2\sin^2\theta}\frac{\partial^2 F}{\partial\phi^2} = m = -C_1 - \ell(\ell+1) \ .$$

Example 53 (*Sphere with fixed potential*): Many geometries have spherical symmetry, such that the equations in θ and ϕ become trivial. For example, to calculate the field of a sphere held at a fixed potential, we only have to solve a radial differential equation,

$$\frac{1}{R}\frac{\partial}{\partial r}\left(r^2\frac{\partial R}{\partial r}\right) = 0 \ ,$$

which gives, $\Phi(\mathbf{r}) = R(r) = -C/r + \Phi_0$ and $\vec{\mathcal{E}} = C\hat{\mathbf{e}}_r/r^2$. The constants C and Φ_0 must be specified by additional boundary conditions.

In case of *only azimuthal* symmetry, we have $m = 0$ and $C_1 = -\ell(\ell+1)$. The solutions of the radial equation are simple,

$$R(r) = A_\ell r^\ell + \frac{B_\ell}{r^{\ell+1}} \ . \tag{13.86}$$

The solutions of the angular equation are called *Legendre polynomials*,

$$T(\theta) = P_\ell(\cos\theta) \ . \tag{13.87}$$

They can be derived from the *Rodrigues formula*,

$$P_\ell(z) = \frac{1}{2^\ell \ell!}\left(\frac{d}{dz}\right)^\ell (z^2-1)^\ell \ . \tag{13.88}$$

The first polynomials are,

$$P_0(z) = 1 \quad , \quad P_1(z) = z \quad , \quad P_2(z) = \tfrac{1}{2}(3z^2-1) \quad , \quad P_3(z) = \tfrac{1}{2}(5z^3-3z) \ . \tag{13.89}$$

All in all we get,

$$\boxed{\Phi(\mathbf{r}) = \sum_{\ell=0}^{\infty}\left(A_\ell r^\ell + \frac{B_\ell}{r^{\ell+1}}\right)P_\ell(\cos\theta)} \ . \tag{13.90}$$

Example 54 (*Charged spherical layer*): In this example we consider a spherical shell carrying a surface charge described by $\sigma(\theta)$. The regions $r \le R$ and $r \ge R$ are treated separately. The ansatz (13.90) can not diverge, neither within the sphere where we must let $B_\ell = 0$, nor outside the sphere where we have to let $A_\ell = 0$. On the surface even the potential has to be continuous, such that

$$0 = [\Phi_\ge - \Phi_\le]_{r=R} = \sum_{\ell=0}^{\infty}\frac{B_l}{R^{\ell+1}}P_\ell(\cos\theta) - \sum_{\ell=0}^{\infty}A_\ell R^\ell P_\ell(\cos\theta) \ ,$$

resulting in $B_\ell = A_\ell R^{2\ell+1}$. On the other hand, the electric field is discontinuous,

$$-\frac{\sigma(\theta)}{\varepsilon_0} = \left[\frac{\partial\Phi_>}{\partial r} - \frac{\partial\Phi_<}{\partial r}\right]_{r=R} = \sum_{\ell=0}^{\infty}(2\ell+1)A_\ell R^{\ell-1}P_\ell(\cos\theta) \ .$$

The coefficients are,

$$A_\ell = \frac{1}{2\varepsilon_0 R^{\ell-1}}\int_0^\pi \sigma(\theta)P_\ell(\cos\theta)\sin\theta d\theta \ ,$$

which can be verified from the orthogonality relation,

$$\int_{-1}^{1} P_\ell(z)P_{\ell'}(z)dz = \frac{2\delta_{\ell,\ell'}}{2\ell+1} \ .$$

Particularly for the case $\sigma(\theta) = \sigma_0\cos\theta = \sigma_0 P_1(\cos\theta)$ we obtain,

$$A_\ell = \frac{\sigma_0}{2\varepsilon_0 R^{\ell-1}}\int_0^\pi P_1(z)P_l(z)dz = \frac{\sigma_0}{2\varepsilon_0 R^{\ell-1}}\frac{2}{2\ell+1}\delta_{\ell,1} = \frac{\sigma_0}{3\varepsilon_0}\delta_{\ell,1} \ .$$

Finally,

$$\Phi(\mathbf{r}) = \begin{cases} \frac{\sigma_0}{3\varepsilon_0} r\cos\theta = \frac{\sigma_0}{3\varepsilon_0}\mathbf{r}\cdot\hat{\mathbf{e}}_z & \text{for } \ r \le R \\ \frac{\sigma_0 R^3}{3\varepsilon_0}\frac{1}{r^2}\cos\theta = \frac{\sigma_0 R^3}{3\varepsilon_0}\frac{\mathbf{r}\cdot\hat{\mathbf{e}}_z}{r^3} & \text{for } \ r \ge R \end{cases} \ .$$

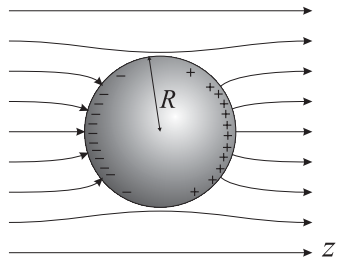

Figure 13.28: Distortion of a homogeneous field by a metallic sphere.

13.6.4 Exercises

13.6.4.1 Ex: Variable separation

Calculate the potential within an infinite rectangular waveguide in the z-direction by solving the Laplace equation using the variable separation method.

Solution: *After separating the variables,* $\Phi(\mathbf{r}) = X(x)Y(y)Z(z)$*, the Laplace equation in Cartesian coordinates becomes,*

$$\frac{1}{X}\frac{\partial^2 X}{\partial x^2} = k^2 \quad , \quad \frac{1}{Y}\frac{\partial^2 Y}{\partial y^2} = -k^2 \quad , \quad \frac{1}{Z}\frac{\partial^2 Z}{\partial z^2} = 0 \ .$$

This gives,

$$X(x) = Ae^{kx} + Be^{-kx} \quad , \quad Y(y) = C\sin ky + D\cos ky \quad , \quad Z(z) = Ez + F \ ,$$

where the amplitudes are fixed by the boundary conditions imposed by the waveguide, for example,

$$\Phi(x,y,z\to\infty)=0 \quad , \quad \Phi(x,y=0,z)=\Phi(x,y=b,z)=0 \quad , \quad \Phi(x=a,y,z)=\Phi(x=-a,y,z)$$

Satisfying the first two conditions,

$$\Phi = 2A\cosh\frac{n\pi x}{b}\sin\frac{n\pi y}{b} \ .$$

To satisfy the third condition we construct a linear combination,

$$\Phi = \sum_{n=1}^{\infty} 2A\cosh\frac{n\pi x}{b}\sin\frac{n\pi y}{b} \ ,$$

postulating,

$$\Phi(a,y,z) = \sum_{n=1}^{\infty} 2A\cosh\frac{n\pi a}{b}\sin\frac{n\pi y}{b} \equiv \Phi_0 \ .$$

It is possible to show by comparison with the Fourier expansion,

$$\Phi(x,y,z) = \frac{4\Phi_0}{\pi}\sum_{n=1,3,5,..}\frac{1}{n}\frac{\cosh n\pi x/b}{\cosh n\pi a/b}\sin\frac{n\pi y}{b} \ .$$

13.6.4.2 Ex: Field of a sphere with a hole

On the surface of a hollow sphere of radius R, from which a cap defined by the opening angle $\theta=\alpha$ was cut out at the north pole, there is a homogeneously distributed surface charge density $Q/4\pi R^2$.
a. Show that the potential within the volume of the sphere can be written in the form,

$$\Phi(r,\theta,\phi) = \frac{Q}{2}\sum_{\ell=0}^{\infty}\frac{1}{2\ell+1}\left[P_{\ell+1}(\cos\alpha)-P_{\ell-1}(\cos\alpha)\right]\ \frac{r^\ell}{R^{\ell+1}}\ P_\ell(\cos\theta)$$

where for $\ell=0$ we have to let $P_{\ell-1}(\cos\alpha)=-1$. What is the shape of the potential outside the hollow sphere?
b. Determine the absolute value and the direction of the electric field at the origin.
c. What potential do we get for $\alpha\to 0$?
Help: Use the following relation for the surface charge density:

$$-\frac{\sigma}{\varepsilon_0} = \left[\frac{\partial\Phi_>}{\partial r}-\frac{\partial\Phi_<}{\partial r}\right]_{r=R} \ ,$$

where the indices $<$ resp. $>$ hold for regions inside resp. outside the sphere. For the integration, the following recursion relation is useful,

$$P_l(x) = \frac{1}{2\ell+1}\left(\frac{dP_{\ell+1}(x)}{dx}-\frac{dP_{\ell-1}(x)}{dx}\right)$$

that holds for $\ell > 0$.

Solution: *a. The solutions inside and outside the hollow sphere must join together in a continuous manner at $r = R$. Therefore, the following Ansätze are valid,*

$$\Phi_>(r,\theta) = \sum_{\ell=0}^{\infty} A_\ell \left(\frac{R}{r}\right)^{\ell+1} P_\ell(\cos\theta) \quad , \quad \Phi_<(r,\theta) = \sum_{\ell=0}^{\infty} A_\ell \left(\frac{r}{R}\right)^{\ell} P_\ell(\cos\theta) \ .$$

Given the surface charge density,

$$\sigma(\cos\theta) = \begin{cases} \frac{Q}{4\pi R^2} & \text{when } \cos\theta < \cos\alpha \\ 0 & \text{else} \end{cases} \ .$$

Now we have Gauß' law,

$$\frac{\sigma}{\varepsilon_0} = \left[\frac{\partial\Phi_<}{\partial r} - \frac{\partial\Phi_>}{\partial r}\right]_{r=R} = \frac{1}{R}\sum_{\ell=0}^{\infty}(2\ell+1)A_\ell P_\ell(\cos\theta) \ .$$

Using the orthogonality of the Legendre polynomials, $(2\ell+1)\int_{-1}^{1} dx P_\ell(x)P_{\ell'}(x) = 2\delta_{\ell,\ell'}$, and the abbreviation $x = \cos\theta$ we apply the operation $\int_{-1}^{1} dx P_{\ell'}(x)...$ to both sides of the last equation,

$$\frac{1}{\varepsilon_0}\int_{-1}^{+1} dx\sigma(x)P_{\ell'}(x) = \frac{Q}{4\pi\varepsilon_0 R^2}\int_{-1}^{\cos\alpha} dx P_{\ell'}(x) = \frac{1}{R}\sum_{\ell=0}^{\infty}(2\ell+1)A_\ell \int_{-1}^{+1} dx P_\ell(x)P_{\ell'}(x) = \frac{2}{R}A_{\ell'} \ .$$

Therefore, we have for the expansion coefficients with the given relationship,

$$\begin{aligned} A_\ell &= \frac{Q}{8\pi\varepsilon_0 R}\int_{-1}^{\cos\alpha} dx P_\ell(x) = \frac{Q}{8\pi\varepsilon_0 R}\frac{1}{2\ell+1}\left[P_{\ell+1}(x) - P_{\ell-1}(x)\right]_{-1}^{\cos\alpha} \\ &= \frac{Q}{8\pi\varepsilon_0 R}\frac{1}{2\ell+1}\left(P_{\ell+1}(\cos\alpha) - P_{\ell-1}(\cos\alpha)\right) \ , \end{aligned}$$

at least for $\ell \neq 0$. But for $\ell = 0$ the integral is trivial: $\int_{-1}^{\cos\alpha} dx P_\ell(x) = \cos\alpha + 1 = P_1(\cos\alpha) - P_{-1}(\cos\alpha)$ with the definition of the problem. Insertion into our original Ansätze immediately gives the potential inside and outside the hollow sphere.
b. We have,

$$\vec{\mathcal{E}} = -\nabla\Phi = -\hat{\mathbf{e}}_r\frac{\partial\Phi}{\partial r} - \hat{\mathbf{e}}_\theta\frac{1}{r}\frac{\partial\Phi}{\partial\theta} + 0 = -\hat{\mathbf{e}}_r\frac{\partial\Phi}{\partial r} + \hat{\mathbf{e}}_\theta\frac{\sin\theta}{r}\frac{\partial\Phi}{\partial\cos\theta} \ .$$

Therefore, we have inside,

$$\vec{\mathcal{E}} = \frac{Q}{8\pi\varepsilon_0}\sum_{\ell=0}^{\infty}\frac{P_{\ell+1}(\cos\alpha) - P_{\ell-1}(\cos\alpha)}{2\ell+1}\frac{r^{\ell-1}}{R^{\ell+1}}\left[-\hat{\mathbf{e}}_r\ell P_\ell(\cos\theta) + \hat{\mathbf{e}}_\theta\sin\theta\frac{dP_\ell(x)}{dx}\right] \ .$$

For $r \to 0$ all terms with the exception of $\ell = 1$ disappear. We therefore have

$$\vec{\mathcal{E}}(\mathbf{r}=0) = \frac{Q}{6R^2}(P_2(\cos\alpha) - P_0(\cos\alpha))(-\hat{\mathbf{e}}_r\cos\theta + \hat{\mathbf{e}}_\theta\sin\theta) \ .$$

Now, $\hat{\mathbf{e}}_r \cos\theta - \hat{\mathbf{e}}_\theta \sin\theta = \hat{\mathbf{e}}_z$, $P_2(\cos\alpha) = (3\cos^2\alpha - 1)/2$ *and* $P_0(\cos\alpha) = 1$. *With that, we get for the electric field at the origin,*

$$\vec{\mathcal{E}}(\mathbf{r}=0) = -\frac{Q}{6R^2}\hat{\mathbf{e}}_z(\frac{3}{2}\cos^2\alpha - \frac{3}{2}) = \frac{Q}{4R^2}\sin^2\alpha\hat{\mathbf{e}}_z \ .$$

c. For $\alpha = 0$ *we have* $\cos\alpha = 1$ *and* $P_\ell(\cos\alpha) = P_\ell(1) = 1$. *With that, in our formulas for the potential, only the terms* $\ell = 0$ *survive:*

$$\Phi_<(\mathbf{r}) = \frac{Q}{4\pi\varepsilon_0 R} \quad , \quad \Phi_>(\mathbf{r}) = \frac{Q}{4\pi\varepsilon_0 r} \ .$$

This is the known result for a closed spherical layer.

13.7 Multipolar expansion

The basic idea of *multipolar expansion* is the approximate description of the potential generated by an arbitrary distribution of charges localized within a volume $\mathcal{V}$. The larger the distance between the observation point and the charge distribution in comparison to the extent of the volume $\mathcal{V}$, the more the potential looks like that of a point charge. The smaller the distance, the more terms (multipole moments) must be taken into account, $\Phi(\mathbf{r}) = \sum_k \Phi_k(\mathbf{r})$. High multipolar orders decay faster (like r^{-k}) with the distance between the observation point and the volume where the charge is concentrated.

We have already seen how to do the Taylor expansion of scalar fields in the formula (12.17) [9]. Here, we want to expand in terms of r^{-1}. We start by expanding the function,

$$\frac{1}{|\mathbf{r}-\mathbf{r}'|} = \frac{1}{r}\sum_{\ell=0}^{\infty}\left(\frac{r'}{r}\right)^\ell P_\ell(\cos\theta') \ , \tag{13.91}$$

where θ' is the angle between $\mathbf{r}$ and $\mathbf{r}'$. Inserting the expansion into Coulomb's law (13.35),

$$\Phi(\mathbf{r}) = \frac{1}{4\pi\varepsilon_0}\int\frac{\varrho(\mathbf{r}')}{|\mathbf{r}-\mathbf{r}'|}d^3r' = \frac{1}{4\pi\varepsilon_0}\sum_{\ell=0}^{\infty}\frac{1}{r^{\ell+1}}\int\varrho(\mathbf{r}')r'^\ell P_\ell(\cos\theta')d^3r' \ . \tag{13.92}$$

Example 55 (*Multipolar expansion by Legendre polynomials*): To discuss the multipolar expansion of the function $\frac{1}{|\mathbf{r}-\mathbf{r}'|}$ we chose the axis $\hat{\mathbf{r}}$ as the symmetry axis, as shown in Fig. 13.29, because in this coordinate system the function has azimuthal symmetry in the variable $\mathbf{r}'$. Therefore, we can apply the solution of the Laplace equation in spherical coordinates derived above,

$$\Phi(\mathbf{r}') = \sum_{\ell=0}^{\infty}\left(A_\ell r'^\ell + \frac{B_\ell}{r'^{\ell+1}}\right)P_\ell(\cos\theta') \ .$$

[9] Using the following property of the Legendre polynomials,

$$\frac{1}{\sqrt{1+\eta(\eta-2z)}} = \sum_\ell \eta^\ell P_\ell(z) \ ,$$

where the left side is called the generating function of the polynomials.

We consider two cases: In a first case in which $r' < r$, for the solution $\Phi(\mathbf{r}')$ to converge, we need to guarantee $B_\ell = 0$ such that,

$$\frac{1}{|\mathbf{r} - \mathbf{r}'|} = \sum_{\ell=0}^{\infty} A_\ell(r) r'^\ell P_\ell(\cos\theta') \ .$$

In the second case in which case $r' > r$, we need to ensure $A_\ell = 0$, such that,

$$\frac{1}{|\mathbf{r} - \mathbf{r}'|} = \sum_{\ell=0}^{\infty} \frac{B_\ell(r)}{r'^{\ell+1}} P_\ell(\cos\theta') \ ,$$

The coefficients $A_\ell(\mathbf{r})$ and $B_\ell(\mathbf{r})$ can not depend on $\mathbf{r}'$. Let us now have a closer look at this second case and rename the variables $\mathbf{r} \leftrightarrow \mathbf{r}'$:

$$\frac{1}{|\mathbf{r}' - \mathbf{r}|} = \sum_{\ell=0}^{\infty} \frac{B_\ell(r')}{r^{\ell+1}} P_\ell(\cos\theta) \ .$$

Comparing this to the first case and using $\theta = -\theta'$ we find,

$$A_\ell(r) r^{\ell+1} = \frac{B_\ell(r')}{r'^\ell} = const = C \ .$$

Hence,

$$\frac{1}{|\mathbf{r} - \mathbf{r}'|} = \sum_{\ell=0}^{\infty} C \frac{r'^\ell}{r^{\ell+1}} P_\ell(\cos\theta') \ .$$

The constant C can be calibrated considering a particular case, for example $\mathbf{r} \parallel \mathbf{r}'$ and $r \gg r'$. In this case, since $P_\ell(1) = 1$, the multipolar expansion,

$$\frac{1}{|\mathbf{r} - \mathbf{r}'|} = \frac{1}{|r - r'|} = \sum_{\ell=0}^{\infty} C \frac{r'^\ell}{r^{\ell+1}} \ ,$$

is nothing more than a Taylor expansion around the point $r - r' \simeq r$.

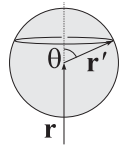

Figure 13.29: In the coordinate system $\hat{\mathbf{r}} = \hat{\mathbf{e}}_z$ the function $|\mathbf{r} - \mathbf{r}'|^{-1}$ has azimuthal symmetry.

13.7.1 The monopole

For $n = 0$ the contribution of the *monopole moment* Q to the potential is,

$$\boxed{\Phi_0(\mathbf{r}) = \frac{Q}{4\pi\varepsilon_0} \frac{1}{r}} \quad \text{where} \quad \boxed{Q = \int_{\mathcal{V}} d^3r' \ \varrho(\mathbf{r}')} \tag{13.93}$$

is just the electric charge.

13.7.2 The dipole

For $n = 1$ the contribution of the *electric dipole moment* $\mathbf{d}$ to the potential follows immediately from formula (13.91),

$$\begin{aligned}\Phi_1(r) &= \tfrac{1}{4\pi\varepsilon_0}\tfrac{1}{r^2}\int \varrho(\mathbf{r}')r' P_1(\cos\theta')d^3r' \\ &= \tfrac{1}{4\pi\varepsilon_0}\tfrac{1}{r^3}\int \varrho(\mathbf{r}')rr'\cos\theta' d^3r' = \tfrac{1}{4\pi\varepsilon_0}\tfrac{\mathbf{r}}{r^3}\cdot\int \varrho(\mathbf{r}')\mathbf{r}' d^3r' \ .\end{aligned}$$

We obtain,

$$\boxed{\Phi_1(\mathbf{r}) = \frac{1}{4\pi\varepsilon_0}\sum_k d_k\frac{x_k}{r^3}} \quad \text{where} \quad \boxed{\mathbf{d} = \int_{\mathcal{V}} d^3r' \ \mathbf{r}'\varrho(\mathbf{r}')} \ . \tag{13.94}$$

13.7.3 The quadrupole

For $n = 2$ the contribution of the *electric quadrupole moment* $q_{i,j}$ to the potential follows immediately from the formula(13.91),

$$\begin{aligned}\Phi_2(r) &= \tfrac{1}{4\pi\varepsilon_0}\tfrac{1}{r^3}\int \varrho(\mathbf{r}')r'^2 P_2(\cos\theta')d^3r' = \tfrac{1}{4\pi\varepsilon_0}\tfrac{1}{r^3}\int \varrho(\mathbf{r}')r'^2\tfrac{3\cos^2\theta'-1}{2}d^3r' \\ &= \tfrac{1}{4\pi\varepsilon_0}\tfrac{1}{2r^5}\int \varrho(\mathbf{r}')(3(\mathbf{r}\cdot\mathbf{r}')^2 - r^2r'^2)d^3r' \\ &= \tfrac{1}{4\pi\varepsilon_0}\tfrac{1}{2r^5}\sum_{k,m}\int \varrho(\mathbf{r}')(3x_kx'_kx_mx'_m - x_kx_mr'^2\delta_{k,m})d^3r' \ .\end{aligned}$$

We obtain,

$$\boxed{\Phi_2(\mathbf{r}) = \frac{1}{4\pi\varepsilon_0}\frac{1}{2}\sum_{k,m} q_{k,m}\frac{x_kx_m}{r^5}} \quad \text{where} \quad \boxed{q_{k,m} = \int_{\mathcal{V}} d^3r' \ (3x'_kx'_m - r'^2\delta_{k,m})\varrho(\mathbf{r}')} \ . \tag{13.95}$$

Example 56 (*Multipole moments of a dipole*): As an example, we consider the simplest dipole, which consists of two charges e and $-e$ separated by a fixed distance a, which we choose parallel to the z-axis. The monopolar moment is,

$$Q = \int d^3r' \ [e\delta(\tfrac{a}{2}\hat{\mathbf{e}}_z - \mathbf{r}') - e\delta(\tfrac{a}{2}\hat{\mathbf{e}}_z + \mathbf{r}')] = 0 \ ,$$

as expected. The dipole moment is,

$$\mathbf{d} = \int d^3r' \ \mathbf{r}'[e\delta(\tfrac{a}{2}\hat{\mathbf{e}}_z - \mathbf{r}') - e\delta(\tfrac{a}{2}\hat{\mathbf{e}}_z + \mathbf{r}')] = ea\begin{pmatrix}0\\0\\1\end{pmatrix} \ ,$$

and the quadrupolar moment is,

$$q_{k,m} = \int d^3r' \ (3x'_k x'_m - r'^2\delta_{km})[e\delta(\tfrac{a}{2}\hat{\mathbf{e}}_z - \mathbf{r}') - e\delta(\tfrac{a}{2}\hat{\mathbf{e}}_z + \mathbf{r}')]$$
$$= \frac{ea^2}{4}\begin{pmatrix} -1 & 0 & 0 \\ 0 & -1 & 0 \\ 0 & 0 & 2 \end{pmatrix} - \frac{ea^2}{4}\begin{pmatrix} -1 & 0 & 0 \\ 0 & -1 & 0 \\ 0 & 0 & 2 \end{pmatrix} = 0 \ .$$

See the Excs. 13.7.5.1 to 13.7.5.10.

Example 57 (*The electric dipole*): The gradient of the potential of a dipole is,

$$\vec{\mathcal{E}}_1 = -\nabla\frac{\mathbf{r}\cdot\mathbf{d}}{4\pi\varepsilon_0 r^3} = \frac{-1}{4\pi\varepsilon_0}\hat{\mathbf{e}}_x\frac{\partial}{\partial x}\frac{xd_x + yd_y + zd_z}{(x^2+y^2+z^2)^{3/2}} + ...$$
$$= \frac{-1}{4\pi\varepsilon_0}\hat{\mathbf{e}}_x\frac{d_x(x^2+y^2+z^2)^{3/2} - (xd_x + yd_y + zd_z)3x(x^2+y^2+z^2)^{1/2}}{(x^2+y^2+z^2)^3} + ...$$
$$= \frac{-1}{4\pi\varepsilon_0}\hat{\mathbf{e}}_x\frac{d_x r^2 - \mathbf{r}\cdot\mathbf{d}3x}{r^5} + ... = \frac{1}{4\pi\varepsilon_0}\frac{3(\hat{\mathbf{e}}_r\cdot\mathbf{d})\hat{\mathbf{e}}_r - \mathbf{d}}{r^3} \ .$$

13.7.4 Expansion into Cartesian coordinates

The multipolar expansion can also be done in Cartesian coordinates by a Taylor series of the Green function [10]. To take this into account, we evaluate the function $G(\mathbf{r},\mathbf{r}') = G(\mathbf{r}-\mathbf{r}')$ around the distance $\mathbf{r}-\mathbf{r}' \simeq \mathbf{r}$,

$$G(\mathbf{r}-\mathbf{r}') = \sum_k \frac{1}{k!}(\mathbf{r}'\cdot\nabla)^k G(\mathbf{r}) = G(\mathbf{r}) + \sum_{k=1} x'_k\frac{\partial}{\partial x_k}G(\mathbf{r}) + \frac{1}{2!}\left(\sum_{k=1}^{3} x'_k\frac{\partial}{\partial x_k}\right)^2 G(\mathbf{r}) + ... \tag{13.96}$$
$$= G(\mathbf{r}) + \sum_{k=1} x'_k\frac{\partial}{\partial x_k}G(\mathbf{r}) + \frac{1}{2!}\sum_{k,m=1}^{3} x'_k x'_m\frac{\partial^2}{\partial x_k\partial x_m}G(\mathbf{r}) + ...$$
$$= G(\mathbf{r}) + \sum_{k=1} x'_k\frac{\partial}{\partial x_k}G(\mathbf{r}) + \frac{1}{6}\sum_{k,m=1}^{3}(3x'_k x'_m - r'^2\delta_{k,m})\frac{\partial^2}{\partial x_k\partial x_m}G(\mathbf{r}) + ...$$

The last transformation is valid if the function G satisfies the Laplace equation, $\nabla^2 G = 0$.

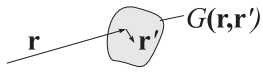

Figure 13.30: Taylor expansion of the Green function around the point $\mathbf{r}-\mathbf{r}' \simeq \mathbf{r}$.

[10] We can imagine the Green function as the potential created by a point-charge distribution, $\varrho(\mathbf{r}') = Q\delta(\mathbf{r}-\mathbf{a})$, since $\Phi(\mathbf{r}) = \int G(\mathbf{r}-\mathbf{r}')\varrho(\mathbf{r}')dV' = QG(\mathbf{r}'-\mathbf{a})$. That is, the multipolar terms come into play due to a small stretching of the charge distribution around the point $\mathbf{r}' = \mathbf{a}$

Example 58 (*Cartesian multipolar expansion*): As an example, we expand the Coulomb potential, $G(\mathbf{r}-\mathbf{r}') = \frac{1}{|\mathbf{r}-\mathbf{r}'|}$. The first derivatives,

$$\frac{\partial}{\partial x_k}\frac{1}{|\mathbf{r}-\mathbf{r}'|} = \frac{x_k - x_k'}{|\mathbf{r}-\mathbf{r}'|^3} \ ,$$

and the second derivatives,

$$\frac{\partial^2}{\partial x_k \partial x_m}\frac{1}{|\mathbf{r}-\mathbf{r}'|} = \frac{3(x_k-x_k')^2 - (\mathbf{r}-\mathbf{r}')^2\delta_{k,m}}{|\mathbf{r}-\mathbf{r}'|^5} \ ,$$

allow us to calculate,

$$\frac{1}{|\mathbf{r}-\mathbf{r}'|} = \frac{1}{r} + \frac{\mathbf{r}\cdot\mathbf{r}'}{r^3} + \frac{1}{6}\sum_{k,m=1}^{3}\frac{3x_kx_m - r^2\delta_{k,m}}{r^5}(3x_k'x_m' - r'^2\delta_{k,m}) \ .$$

The octupolar term of the multipole expansion of the Coulomb potential is,

$$\frac{1}{3!}(\mathbf{r}'\cdot\nabla)^3\frac{1}{r'} = \frac{1}{6}\sum_{k,m,n=1}^{3} x_k'x_m'x_n'\frac{-15x_kx_mx_n + 3r''(x_k\delta_{mn} + x_m\delta_{kn} + x_n\delta_{mk})}{r^7} \ .$$

Inserting this into Coulomb's Law,

$$\Phi(\mathbf{r}) = \frac{1}{4\pi\varepsilon_0}\int\frac{\varrho(\mathbf{r}')}{|\mathbf{r}-\mathbf{r}'|}dV' = \frac{1}{4\pi\varepsilon_0}\left(\frac{1}{r}Q + \frac{\mathbf{r}}{r^3}\cdot\mathbf{d} + \frac{1}{6}\sum_{k,m=1}^{3}\frac{3x_kx_m - r^2\delta_{k,m}}{r^5}q_{k,m} + ...\right) \ ,$$

with the definitions of the multipole moments.

13.7.5 Exercises

13.7.5.1 Ex: Multipoles

A point charge $+2Q$ is at the position $(0,0,a)$ and another charge $+1Q$ at the position $(0,0,-a)$. Calculate a. The monopolar, b. the dipolar, and c. the quadrupolar contribution of the multipolar expansion.

Solution: *a. The charge distribution is parametrized by* $\rho(\mathbf{r}) = 2Q\delta(x)\delta(y)\delta(z-a) + Q\delta(x)\delta(y)\delta(z+a)$. *So, the monopolar moment is,*

$$Q = \int\rho(\mathbf{r})d^3r = 3Q \ .$$

b. The dipole moment is,

$$\begin{aligned}\mathbf{d} &= \int\mathbf{r}\rho(\mathbf{r})d^3r = 2Q\int\mathbf{r}\delta(x)\delta(y)\delta(z-a)d^3r + Q\int\mathbf{r}\delta(x)\delta(y)\delta(z+a)d^3r \\ &= 2Qa\hat{\mathbf{e}}_z + Q(-a)\hat{\mathbf{e}}_z = Qa\hat{\mathbf{e}}_z \ .\end{aligned}$$

c. The quadrupole moment is $q_{ij} = \int\left(3x_ix_j - r^2\delta_{ij}\right)\rho(\mathbf{r})d^3r$. *In particular,*

$$\begin{aligned}q_{11} = q_{22} &= 2Q\int(3x^2-r^2)\delta(x)\delta(y)\delta(z-a)d^3r + Q\int(3x^2-r^2)\delta(x)\delta(y)\delta(z+a)d^3r \\ &= -3Qa^2 \ , \\ q_{33} &= 2Q\int(3z^2-r^2)\delta(x)\delta(y)\delta(z-a)d^3r + Q\int(3z^2-r^2)\delta(x)\delta(y)\delta(z+a)d^3r = 6Qa^2 \ , \\ q_{12} &= 0 \ .\end{aligned}$$

13.7.5.2 Ex: Di- and quadrupolar momenta of spherical charge distributions

Do spherically symmetrical load distributions have dipole or quadrupolar moments? Justify!

Solution: *Spherically symmetrical distributions appear, outside the volume by which they are confined, as point charges and, therefore, can be completely described by the monopolar moment, that is, they have neither dipole nor quadrupolar moment.*

13.7.5.3 Ex: Electric dipole

An electrical dipole consists of two charges of the value $q = 1.5\,\mathrm{nC}$ distant by $a = 6\,\mu\mathrm{m}$.
a. What is the dipole moment?
b. Calculate the dipole potential along the $\hat{\mathbf{e}}_z$ axis of symmetry and in the xy-plane.
c. The dipole is in an $1100\,\mathrm{N/C}$ electric field. What is the difference in potential energies comparing parallel and antiparallel orientations of the dipole.

Solution: *a. With* $\rho(\mathbf{r}) = q\delta(\mathbf{r} - \mathbf{a}/2) - q\delta(\mathbf{r} + \mathbf{a}/2)$ *the charge is,*

$$Q = \int \rho(\mathbf{r}) d^3r = 0 \ .$$

The dipole moment is,

$$\mathbf{a} = \int \mathbf{r}\rho(\mathbf{r}) d^3r = q\mathbf{a} = 9 \cdot 10^{-15}\,\mathrm{Cm} \ .$$

b. The potential is,

$$\Phi(\mathbf{r}) = \frac{1}{4\pi\varepsilon_0} \frac{q}{|\mathbf{r} - \mathbf{a}/2|} - \frac{1}{4\pi\varepsilon_0} \frac{q}{|\mathbf{r} + \mathbf{a}/2|} \ .$$

Along the z-axis we have for $z \notin [-d/2, d/2]$

$$\Phi(0,0,z) = \frac{\pm q}{4\pi\varepsilon_0} \left(\frac{1}{z - a/2} - \frac{1}{z + a/2} \right) = \frac{\pm q}{4\pi\varepsilon_0} \frac{a}{z^2 - a^2/4} \ .$$

Along the z-axis we have for $z \in [-d/2, d/2]$

$$\Phi(0,0,z) = \frac{-q}{4\pi\varepsilon_0} \left(\frac{1}{a/2 - z} - \frac{1}{\sqrt{z + a/2}} \right) = \frac{q}{4\pi\varepsilon_0} \frac{2z}{z^2 - a^2/4} \ .$$

In the x-y-plane we have,

$$\Phi(x,y,0) = \frac{q}{4\pi\varepsilon_0} \left(\frac{1}{\sqrt{x^2 + y^2 + a^2/4}} - \frac{1}{\sqrt{x^2 + y^2 + a^2/4}} \right) = 0 \ .$$

c. The energy of the dipole in the electric field is,

$$E_\pm = -\mathbf{d}\cdot\vec{\mathcal{E}}_\pm = \mp aE \ .$$

With that, the energy difference is $E_+ - E_- = 2aE = 1.8\cdot 10^{-11}\,\mathrm{Cm}$.

13.7.5.4 Ex: Electric dipole

An electric dipole with the moment $\mathbf{d}$ is at the position $\mathbf{r}$. At the origin of the coordinate system there is a point charge e.
a. Calculate the potential energy of the dipole.
b. Calculate the force acting on the dipole.
c. Calculate the force acting on the charge. Is Newton's axiom of mechanics valid: 'actio = reactio'?

Solution: *a. The potential energy of the dipole* $\mathbf{d} = q\mathbf{a}$ *can be calculated from the charge of the dipole in the field of the electron,*

$$\begin{aligned} E_{d,pot} &= \tfrac{1}{2}\int d^3r'\ \rho_d(\mathbf{r}')\Phi_e(\mathbf{r}') = \frac{1}{4\pi\varepsilon_0}\frac{1}{2}\int d^3r'\ \left(q\delta^3(\mathbf{a}/2) - q\delta^3(-\mathbf{a}/2)\right)\frac{e}{|\mathbf{r}'|} \\ &= \frac{1}{4\pi\varepsilon_0}\frac{q}{2}\left(\frac{e}{|\mathbf{a}/2|} - \frac{e}{|-\mathbf{a}/2|}\right) = 0 \ , \end{aligned}$$

or from the charge of the electron e *in the field of the dipole,*

$$\begin{aligned} E_{e,pot} &= \frac{1}{2}\int d^3r'\ \rho_e(\mathbf{r}')\Phi_d(\mathbf{r}') = \frac{1}{4\pi\varepsilon_0}\frac{1}{2}\int d^3r'\ e\delta^3(\mathbf{r})\left(\frac{q}{|\mathbf{r}'-\mathbf{a}/2|} - \frac{q}{|\mathbf{r}'+\mathbf{a}/2|}\right) \\ &= \frac{1}{4\pi\varepsilon_0}\frac{e}{2}\left(\frac{q}{|\mathbf{a}/2|} - \frac{q}{|\mathbf{a}/2|}\right) = 0 \ . \end{aligned}$$

b. The force acting on the dipole follows from $\mathbf{F}_d = -\nabla_{\mathbf{r}} E_{d,pot}|_{\mathbf{r}=0}$, *where*

$$\begin{aligned} E_{d,pot}(\mathbf{r}) &= \frac{1}{2}\int d^3r'\ \rho_d(\mathbf{r}')\Phi_{e,\mathbf{r}}(\mathbf{r}') = \frac{1}{4\pi\varepsilon_0}\frac{1}{2}\int d^3r'\ \left(q\delta^3(\mathbf{r}'-\mathbf{a}/2) - q\delta^3(\mathbf{r}'+\mathbf{a}/2)\right)\frac{e}{|\mathbf{r}'-\mathbf{r}|} \\ &= \frac{1}{4\pi\varepsilon_0}\frac{q}{2}\left(\frac{e}{|\mathbf{a}/2-\mathbf{r}|} - \frac{e}{|-\mathbf{a}/2-\mathbf{r}|}\right) \ . \end{aligned}$$

With this,

$$\mathbf{F}_d = -\frac{1}{4\pi\varepsilon_0}\frac{q}{2}\nabla_{\mathbf{r}}\left[\frac{e}{|\mathbf{a}/2-\mathbf{r}|} - \frac{e}{|-\mathbf{a}/2-\mathbf{r}|}\right]_{\mathbf{r}=0} = \frac{1}{4\pi\varepsilon_0}\frac{q}{2}\left(\frac{e\mathbf{a}/2}{|\mathbf{a}/2|^3} + \frac{e\mathbf{a}/2}{|\mathbf{a}/2|^3}\right) = \frac{1}{\pi\varepsilon_0}\frac{eq}{d^2}\hat{\mathbf{e}}_d \ .$$

c. The force acting on the dipole follows from $\mathbf{F}_e = -\nabla_{\mathbf{r}} E_{e,pot}|_{\mathbf{r}=0}$, *where*

$$\begin{aligned} E_{e,pot}(\mathbf{r}) &= \frac{1}{2}\int d^3r'\ \rho_e(\mathbf{r}')\Phi_{d,\mathbf{r}'}(\mathbf{r}') = \frac{1}{4\pi\varepsilon_0}\frac{1}{2}\int d^3r'\ e\delta^3(\mathbf{r}'+\mathbf{r})\left(\frac{q}{|\mathbf{r}'-\mathbf{a}/2|} - \frac{q}{|\mathbf{r}'+\mathbf{a}/2|}\right) \\ &= \frac{1}{4\pi\varepsilon_0}\frac{e}{2}\left(\frac{q}{|-\mathbf{r}-\mathbf{a}/2|} - \frac{q}{|-\mathbf{r}+\mathbf{a}/2|}\right) \ . \end{aligned}$$

With this,

$$\mathbf{F}_e = -\frac{1}{4\pi\varepsilon_0}\frac{e}{2}\nabla_{\mathbf{r}}\left[\frac{q}{|-\mathbf{r}-\mathbf{a}/2|} - \frac{q}{|-\mathbf{r}+\mathbf{a}/2|}\right]_{\mathbf{r}=0} = \frac{1}{4\pi\varepsilon_0}\frac{e}{2}\left(-\frac{q\mathbf{a}/2}{|\mathbf{a}/2|^3} + \frac{-q\mathbf{a}/2}{|\mathbf{a}/2|^3}\right) = \frac{-1}{\pi\varepsilon_0}\frac{eq}{d^2}\hat{\mathbf{e}}_d \ .$$

Hence, the principle 'actio = reactio' is valid, $\mathbf{F}_d = -\mathbf{F}_e$.

13.7.5.5 Ex: Electric dipole in a field

What is the force acting on an electric dipole $\mathbf{d} = ea \cdot \hat{\mathbf{e}}_r$ at a point $\mathbf{r}$ being aligned along the field lines of an external field produced by a sphere with radius R homogeneously charged with a charge Q?

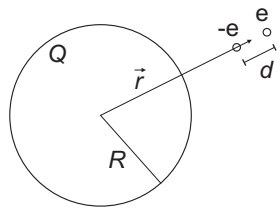

Figure 13.31: Electric dipole in a field.

Solution: *Following Gauß's law,* $\int_{\partial\mathcal{V}} \vec{\mathcal{E}}(\mathbf{r}) \cdot d\mathbf{A} = \frac{1}{\varepsilon_0}\int_{\mathcal{V}} \varrho(\mathbf{r}) d^3r$ *outside the sphere,*

$$\int_{\partial\mathcal{V}} \mathcal{E} dA = \mathcal{E} 4\pi r^2 = \int_{\partial\mathcal{V}} \mathcal{E} dA = \frac{1}{\varepsilon_0} Q$$

and with that,

$$\vec{\mathcal{E}} = \frac{Q}{4\pi\varepsilon_0 r^2}\hat{\mathbf{e}}_r \ .$$

The force now is,

$$\mathbf{F} = e\vec{\mathcal{E}}(\mathbf{r}-\mathbf{a}/2) + e\vec{\mathcal{E}}(\mathbf{r}+\mathbf{a}/2) = \frac{Qe}{4\pi\varepsilon_0}\hat{\mathbf{e}}_r\left(\frac{1}{(r-a/2)^2} - \frac{1}{(r+a/2)^2}\right) \ .$$

for small $d \ll r$ *we can approximate as follows,*

$$\mathbf{F} = \frac{Qe}{4\pi\varepsilon_0}\hat{\mathbf{e}}_r\frac{(r+a/2)^2-(r-a/2)^2}{(r-a/2)^2(r+a/2)^2} \simeq \frac{Qe}{4\pi\varepsilon_0}\hat{\mathbf{e}}_r\frac{2ar}{r^4} \ .$$

This result also follows for small dipolar moments approximating the interaction energy by,

$$W = -\mathbf{d}\cdot\vec{\mathcal{E}} = -ea\hat{\mathbf{e}}_r \cdot \frac{Q}{4\pi\varepsilon_0 r^2}\hat{\mathbf{e}}_r = -\frac{Qea}{4\pi\varepsilon_0 r^2}$$

where we assume, that $\vec{\mathcal{E}}(\mathbf{r}+\mathbf{a}/2) \simeq \vec{\mathcal{E}}(\mathbf{r}-\mathbf{a}/2)$. *The force is finally,*

$$\mathbf{F} = -\nabla W = -\frac{Qea}{2\pi\varepsilon_0 r^3}\hat{\mathbf{e}}_r \ .$$

13.7.5.6 Ex: Electric dipole in a field

Consider a molecule that consists of two rigidly bound masses $m_1 = m_2 = 10^{-25}\,\mathrm{kg}$ at a distance of $a = 10^{-12}\,\mathrm{m}$ and with charges $+e$ resp. $-e$.
a. Calculate the electric dipole moment $\mathbf{d} = d \cdot \hat{\mathbf{e}}_x$ of this charge distribution.
b. Now the molecule is put into rotation by a homogeneous electric field $\vec{\mathcal{E}} = \hat{\mathbf{e}}_z \cdot 100\,\mathrm{V/m}$. Calculate the rotation speed of the molecule as a function of the angle between the dipole moment and the electric field.
Help: The sum of the kinetic and electrostatic energies is conserved during the rotation.

Solution: *a. The dipole moment is,*

$$\mathbf{d} = ea\hat{\mathbf{e}}_x = 1.6 \cdot 10^{-31}\,\mathrm{Cm}\ \ \hat{\mathbf{e}}_x.$$

A homogeneous electric field placed in $\hat{\mathbf{e}}_z$ *direction produces a torque,*

$$\vec{\mathcal{D}} = \left(\mathbf{r} + \frac{\mathbf{a}}{2}\right) \times e\vec{\mathcal{E}} - \left(\mathbf{r} - \frac{\mathbf{a}}{2}\right) \times e\vec{\mathcal{E}} = ea\hat{\mathbf{e}}_x \times \mathcal{E}\hat{\mathbf{e}}_z = -ea\mathcal{E}\hat{\mathbf{e}}_y\ .$$

b. The energy of the dipole in the electric field is,

$$W = -\mathbf{d} \cdot \vec{\mathcal{E}} = -d\mathcal{E}\cos\phi\ .$$

The kinetic energy is,

$$T = \frac{m}{2}v_1^2 + \frac{m}{2}v_2^2 = mv_1^2\ ,$$

since $|v_1| = |v_2|$. *With the angular velocity,*

$$\omega_1 = \frac{v_1}{a/2}$$

the kinetic energy becomes,

$$T = mv_1^2 = m\left(\frac{\omega_1 a}{2}\right)^2\ .$$

At the beginning ($t = 0$) *the electrostatic energy disappears because,* $\phi(0) = 90°$, *and the kinetic energy disappears, because* $v_k(0) = 0$,

$$T(0) + W(0) = 0 = m\left(\frac{\omega_1 a}{2}\right)^2 - d\mathcal{E}\cos\phi\ .$$

Hence,

$$\omega_1^2 = 4\frac{d\mathcal{E}\cos\phi}{ma^2}\ .$$

13.7.5.7 Ex: Dipolar field in two dimensions

Consider two infinitely long parallel conductors with distance d carrying the linear charge density $+\lambda$ resp. $-\lambda$ (charge $\pm Q$ per length l of the conductor). Using the Gauß theorem, first calculate the electric field and the electric potential of one conductor. Then calculate the potential of both conductors by overlapping the individual potentials as a function of the distance r and the angle α (see Fig. 13.32). **Note:** Choose as integration volume a cylinder with length l and radius r along the symmetry axis around the wire. Determine the asymptotic behavior for $r \gg d/2$ and for $r \ll d/2$. To do this, do a Taylor expansion of the expression using: $\ln \frac{1+\epsilon}{1-\epsilon} \approx -2\epsilon + O(\epsilon^3)$. Write the result as a function of the dipole moment $\mathbf{p}$, where $p = |\mathbf{p}| = \lambda d$ is positive and indicates the direction of the dipole moment vector showing from the positive conductor to the negative.

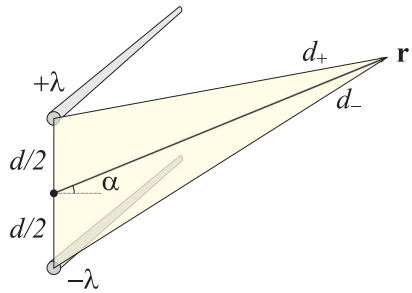

Figure 13.32: Dipolar field.

Solution: *With Gauß' integral theorem,* $\oint_{\partial\mathcal{V}} \vec{\mathcal{E}} \cdot \vec{n} dA = 4\pi \int_{\mathcal{V}} \rho dV$ *follows* $\mathcal{E} l 2\pi r = 4\pi Q$*, with the charge* Q *on a piece of wire of length* l*. With the definition of the linear charge density* $\lambda = Q/l$ *follows,* $\mathcal{E} = \frac{2\lambda}{r}$*. For the potential* Φ *(*$\vec{\mathcal{E}} = -\nabla\Phi$*) we integrate the field and obtain,*

$$\Phi = -2\lambda \ln(r) \ .$$

With two conductors we add the potentials: $\Phi = -2\lambda(\ln(d_+) - \ln(d_-)) = -\lambda \ln \frac{d_+^2}{d_-^2}$*. For* d_+ *and* d_- *we obtain:*

$$d_+^2 = r^2 + a^2 - 2ar\sin\alpha, \qquad \text{and} \qquad d_+^2 = r^2 + a^2 + 2ar\sin\alpha \ ,$$

where we let $a = d/2$*. Therefore, the potential of the two conductors is:*

$$\Phi = -\lambda \ln\left(\frac{1 + \frac{a^2}{r^2} - 2\frac{a}{r}\sin\alpha}{1 + \frac{a^2}{r^2} + 2\frac{a}{r}\sin\alpha}\right) = -\lambda \ln\left(\frac{1 + \frac{r^2}{a^2} - 2\frac{r}{a}\sin\alpha}{1 + \frac{r^2}{a^2} + 2\frac{r}{a}\sin\alpha}\right) \ .$$

For short distances $r/a \ll 1$ *we take the second expression and, neglecting the terms with* r^2/a^2*, we get,*

$$\Phi = 4\lambda \frac{r}{a}\sin\alpha \ .$$

For long distances $r/a \gg 1$ *we take the first term and get analogously,*

$$\Phi = 4\lambda \frac{a}{r}\sin\alpha \ .$$

With $\sin\alpha = -\frac{\mathbf{pr}}{pr}$ *follows for short distances* $\Phi = -2\frac{\mathbf{p}\cdot\mathbf{r}}{a^2}$ *and for long distances* $\Phi = -2\frac{\mathbf{p}\cdot\mathbf{r}}{r^2}$.

13.7.5.8 Ex: Dipolar and quadrupolar fields

Let us consider a system of three point charges aligned to the z-axis. At the positions $z = \pm a$ we have charges $+Q$, at the position $z = 0$ the charge $-2Q$.
a. Determine the charge distribution in terms of the δ-function in Cartesian coordinates.
b. Calculate the electrostatic potential $\Phi(\mathbf{r})$ of this charge distribution and approximate for long distances $|\mathbf{r}| \gg a$. (**Help:** Write the denominators that appear as $\frac{1}{|\mathbf{r}\pm\mathbf{a}|} = \frac{1}{r}\frac{1}{\sqrt{1+x}}$ with $x \equiv \frac{a^2\pm 2\mathbf{a}\cdot\mathbf{r}}{r^2}$ and expand up to second order in a.)
c. Calculate the monopolar moment and the Cartesian components of the dipolar moment and the quadrupolar tensor.
d. Calculate the monopolar, dipolar, and quadrupolar potentials and show that the results coincides with the expansion (b).
e. Now rotate the coordinate system around the x-axis by an angle of 45°. What are the new values for multipolar moments? (**Help:** The quadrupolar tensor is transformed with the rotation matrix λ as $q'_{il} = \lambda_{il} q_{lm} \lambda^{\dagger}_{mj}$).

Solution: *a. The density of charges is,*

$$\varrho(\mathbf{r}) = Q\delta(x)\delta(y)(\delta(z-a) + \delta(z+a) - 2\delta(z)) \ .$$

b. We define the vector $\mathbf{a} \equiv a\hat{\mathbf{e}}_z$. *In this case, we have for the potential at an arbitrary point* $\mathbf{r}$,

$$\Phi(\mathbf{r}) = \frac{1}{4\pi\varepsilon_0}\left(\frac{Q}{|\mathbf{r}-\mathbf{a}|} + \frac{Q}{|\mathbf{r}+\mathbf{a}|} - \frac{2Q}{|\mathbf{r}|}\right) \ .$$

Using the Taylor expansion,

$$\tfrac{1}{\sqrt{1+x}} = 1 - \tfrac{1}{2}x + \tfrac{3}{8}x^2 - \ldots$$

we approximate up to the second order terms in a/r *and we get,*

$$\frac{1}{|\mathbf{r}\pm\mathbf{a}|} = \frac{1}{\sqrt{r^2 + a^2 \pm 2\mathbf{a}\cdot\mathbf{r}}} = \frac{1}{r}\frac{1}{\sqrt{1 + \frac{a^2\pm 2\mathbf{a}\cdot\mathbf{r}}{r^2}}} = \frac{1}{r}\left(1 \mp \frac{\mathbf{a}\cdot\mathbf{r}}{r^2} - \frac{a^2}{2r^2} + \frac{3}{2}\frac{(\mathbf{a}\cdot\mathbf{r})^2}{r^4}\right) + \ldots$$

Follows for the potential,

$$\Phi(\mathbf{r}) \simeq \frac{Q}{4\pi\varepsilon_0}\left(-\frac{2}{r} + \frac{2}{r} + \frac{\mathbf{a}\cdot\mathbf{r}}{r^3} - \frac{\mathbf{a}\cdot\mathbf{r}}{r^3} - \frac{a^2}{r^3} + 3\frac{(\mathbf{a}\cdot\mathbf{r})^2}{r^5}\right) = \frac{Q}{4\pi\varepsilon_0}\left(\frac{3(\mathbf{a}\cdot\mathbf{r})^2}{r^5} - \frac{a^2}{r^3}\right) \ .$$

c. The monopolar moment of this charge distribution is equal to the total charge and therefore obviously equal to 0,

$$Q_{tot} = \int_{\mathbb{R}} \varrho(\mathbf{r}')dV' = 0 \ .$$

For the dipole moment we need to integrate $\rho(\mathbf{r})\mathbf{r}$. The x and y-components of the vector obviously give 0. Now, we consider the z-component. Here we get $Q(a-a-2\cdot 0)=0$,

$$\mathbf{d}=\int_{\mathbb{R}}\mathbf{r}'\varrho(\mathbf{r}')dV'=0\ .$$

Finally, we consider the quadrupolar moment using the general formula,

$$q_{ij}=\int_{\mathbb{R}}(3x_ix_j-r^2\delta_{ij})\varrho(\mathbf{r}')dV'\ .$$

For $i\neq j$ we see immediately, $q_{ij}=0$. For $i=j$ and $i=1$ holds,

$$q_{11}=\int_{\mathbb{R}}(2x^2-y^2-z^2)\varrho(\mathbf{r}')dV'=-2Qa^2$$

in the same way,

$$q_{22}=\int_{\mathbb{R}}(2y^2-x^2-z^2)\varrho(\mathbf{r}')dV'=-2Qa^2$$

and finally,

$$q_{33}=\int_{\mathbb{R}}(2z^2-x^2-y^2)\varrho(\mathbf{r}')dV'=+4Qa^2$$

Hence,

$$(q_{ij})=2Qa^2\begin{pmatrix}-1&0&0\\0&-1&0\\0&0&2\end{pmatrix}\ .$$

d. For the potential follows,

$$\begin{aligned}\Phi(\mathbf{r})&=\tfrac{1}{4\pi\varepsilon_0 r}\sum_i Q_i+\tfrac{1}{4\pi\varepsilon_0 r^3}\sum_i d_ir_i+\tfrac{1}{2}\tfrac{1}{4\pi\varepsilon_0 r^5}\sum_{ij}q_{ij}x_ix_j+\ldots\\&\simeq 0+0+\tfrac{1}{8\pi\varepsilon_0 r^5}2Qa^2(-x^2-y^2+2z^2)=\tfrac{1}{4\pi\varepsilon_0}\tfrac{Qa^2}{r^5}(3z^2-r^2)\ .\end{aligned}$$

e. The matrix describing a rotation around the x-axis is,

$$\begin{pmatrix}x'\\y'\\z'\end{pmatrix}=\begin{pmatrix}1&0&0\\0&\frac{1}{\sqrt{2}}&\frac{1}{\sqrt{2}}\\0&-\frac{1}{\sqrt{2}}&\frac{1}{\sqrt{2}}\end{pmatrix}\begin{pmatrix}x\\y\\z\end{pmatrix}\ ,$$

resp. in a compressed version, $x_i'=\sum_j\lambda_{ij}x_j$. The monopolar moment transforms like a scalar and, therefore, remains unchanged. The dipole moment is like a vector but, as all components in the previous coordinate system are 0, also in the rotated system there is no dipole moment. We need to calculate the quadrupolar tensor. We use now, that λ is an orthogonal transformation, ($det\lambda=1$, $\lambda^{-1}=\lambda^T$), and write,

$$q_{ij}'=\int d^3r'(3x_i'x_j'-r'^2\delta_{ij})=\sum_{lm}\lambda_{il}\lambda_{jm}\int d^3r'(3x_lx_m-r^2\delta_{lm})=\sum_{lm}\lambda_{il}q_{lm}(\lambda^T)_{mj}\ ,$$

where we use that $d^3r' = d^3r$. Inserting the matrix above gives immediately,

$$q' = \begin{pmatrix} 1 & 0 & 0 \\ 0 & \frac{1}{\sqrt{2}} & \frac{1}{\sqrt{2}} \\ 0 & -\frac{1}{\sqrt{2}} & \frac{1}{\sqrt{2}} \end{pmatrix} \begin{pmatrix} -2Qa^2 & 0 & 0 \\ 0 & -2Qa^2 & 0 \\ 0 & 0 & 4Qa^2 \end{pmatrix} \begin{pmatrix} 1 & 0 & 0 \\ 0 & \frac{1}{\sqrt{2}} & \frac{1}{\sqrt{2}} \\ 0 & -\frac{1}{\sqrt{2}} & \frac{1}{\sqrt{2}} \end{pmatrix} = \begin{pmatrix} -2aQ^2 & 0 & 0 \\ 0 & -Qa^2 & 3Qa^2 \\ 0 & 3Qa^2 & 3Qa^2 \end{pmatrix} .$$

13.7.5.9 Ex: Multipoles

The two charge distributions shown in the graph are given.
a. Calculate for both cases first the electrical potential Φ for the distances $r = 2a$, $r = 10a$, and $r = 100a$ for the angles $\alpha = 0°$, $\alpha = 45°$, and $\alpha = 90°$, respectively.
b. The results must now be compared with those of the quadrupolar expansion. What are the monopolar, dipolar and quadrupolar moments for these two geometries? Calculate the monopolar, dipolar and quadrupolar contributions of the electrical potential for the same positions as above. Compare these values with those calculated exactly and identify the dominant contributions.

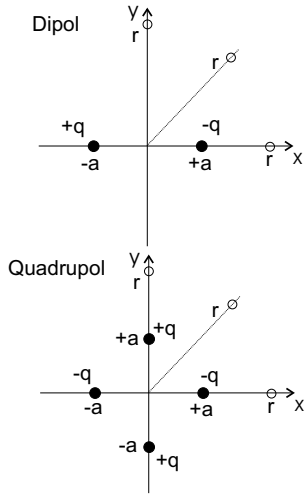

Figure 13.33: Multipoles.

Solution: *We first consider only the superior charge distribution. The potential is,*

$$\Phi = \frac{1}{4\pi\varepsilon_0} \frac{-q}{|\mathbf{r} - \vec{a}|} + \frac{1}{4\pi\varepsilon_0} \frac{q}{|\mathbf{r} + \vec{a}|} .$$

In the given positions with $\alpha = 0°$ we have,

$$\Phi|_{r=na,\alpha=0} = \Phi(na, 0, 0) = \frac{1}{4\pi\varepsilon_0} \frac{-q}{\sqrt{(na-a)^2}} + \frac{1}{4\pi\varepsilon_0} \frac{q}{\sqrt{(na+a)^2}} = \frac{-2q}{4\pi\varepsilon_0 a} \frac{1}{n^2-1}$$

$$\Phi|_{r=2a,\alpha=0} = \frac{-q}{4\pi\varepsilon_0 a} \frac{2}{3} \quad , \quad \Phi|_{r=10a,\alpha=0} = \frac{-q}{4\pi\varepsilon_0 a} \frac{2}{99} \quad , \quad \Phi|_{r=100a,\alpha=0} = \frac{-q}{4\pi\varepsilon_0 a} \frac{2}{9999}$$

with $\alpha = 45^\circ$

$$\Phi|_{r=na,\alpha=45^\circ} = \Phi\left(\frac{na}{\sqrt{2}}, \frac{na}{\sqrt{2}}, 0\right) = \sum_{\pm} \frac{1}{4\pi\varepsilon_0} \frac{\mp q}{\sqrt{(\frac{na}{\sqrt{2}} \mp a)^2 + (\frac{na}{\sqrt{2}})^2}} = \sum_{\pm} \frac{1}{4\pi\varepsilon_0 a} \frac{\mp q}{\sqrt{n^2 \mp \sqrt{2}n + 1}}$$

$$\Phi|_{r=2a,\alpha=0} = \frac{-q}{4\pi\varepsilon_0 a} \cdot 0.32 \quad , \quad \Phi|_{r=10a,\alpha=0} = \frac{-q}{4\pi\varepsilon_0 a} \cdot 0.014 \quad , \quad \Phi|_{r=100a,\alpha=0} = \frac{-q}{4\pi\varepsilon_0 a} \cdot 0.00014$$

with $\alpha = 90^\circ$

$$\Phi|_{r=na,\alpha=90^\circ} = \Phi(0, na, 0) = \frac{1}{4\pi\varepsilon_0} \frac{-q}{\sqrt{(-a)^2 + (na)^2}} + \frac{1}{4\pi\varepsilon_0} \frac{q}{\sqrt{(a)^2 + (na)^2}} = 0 \ .$$

b. With the charge density $\rho(\mathbf{r}) = q[\delta(\mathbf{r}+\vec{a}) - \delta(\mathbf{r}-\vec{a})]$ *the monopolar moment becomes,*

$$Q = \int \rho(\mathbf{r}')d^3r' = q - q = 0 \ .$$

The monopolar part of the potential then is,

$$\Phi_0(\mathbf{r}) = \frac{Q}{4\pi\varepsilon_0} = 0 \ .$$

The dipole moment is,

$$\mathbf{d} = \int \mathbf{r}'\rho(\mathbf{r}')d^3r' = q \int \mathbf{r}'[\delta(\mathbf{r}' + \vec{a}) - \delta(\mathbf{r}' - \vec{a})]d^3r' = -2q\vec{a} \ .$$

The dipolar part of the potential is then,

$$\Phi_1(\mathbf{r}) = \frac{1}{4\pi\varepsilon_0} \frac{\mathbf{r} \cdot \vec{d}}{r^3} = \frac{-2q}{4\pi\varepsilon_0} \frac{\mathbf{r} \cdot \vec{a}}{r^3}.$$

In the given positions with $\alpha = 0^\circ$ *we have,*

$$\Phi_1|_{r=na,\alpha=0} = \frac{-2q}{4\pi\varepsilon_0} \frac{na^2}{(na)^3} = \frac{-q}{4\pi\varepsilon_0 a} \frac{2}{n^2}$$

$$\Phi_1|_{r=2a,\alpha=0} = \frac{-q}{4\pi\varepsilon_0 a} \frac{2}{4} \quad , \quad \Phi_1|_{r=10a,\alpha=0} = \frac{-q}{4\pi\varepsilon_0 a} \frac{2}{100} \quad , \quad \Phi_1|_{r=100a,\alpha=0} = \frac{-q}{4\pi\varepsilon_0 a} \frac{2}{10000}$$

with $\alpha = 45^\circ$

$$\Phi_1|_{r=na,\alpha=45^\circ} = \frac{-2q}{4\pi\varepsilon_0} \frac{(na/\sqrt{2})a}{(na)^3} = \frac{-q}{4\pi\varepsilon_0 a} \frac{\sqrt{2}}{n^2}$$

$$\Phi_1|_{r=2a,\alpha=45^\circ} = \frac{-q \cdot 0.35}{4\pi\varepsilon_0 a} \quad , \quad \Phi_1|_{r=10a,\alpha=0} = \frac{-q \cdot 0.014}{4\pi\varepsilon_0 a} \quad , \quad \Phi_1|_{r=100a,\alpha=0} = \frac{-q \cdot 0.00014}{4\pi\varepsilon_0 a}$$

with $\alpha = 90^\circ$

$$\Phi_1|_{r=na,\alpha=90^\circ} = 0 \ .$$

The quadrupolar moment is,

$$Q_{ij} = \int \rho(\mathbf{r}')[3x'_I x'_j - r''\delta_{ij}]d^3r'$$

$$Q_{11} = \int \rho(\mathbf{r}')[3x''_1 - x''_1 - x''_2]d^3r' = 0 = Q_{22}$$

$$Q_{12} = \int \rho(\mathbf{r}')[3x'_1 x'_2 - x''_1 - x''_2]d^3r' = 0 = Q_{21} \ .$$

The quadrupolar part of the potential then is,

$$\Phi_2(\mathbf{r}) = \frac{1}{4\pi\varepsilon_0}\frac{1}{2}\sum_{ij} Q_{ij}\frac{x_I x_j}{r^5} = 0 \ .$$

Now we consider the distribution of the inferior charges.

13.7.5.10 Ex: Multipoles

Four point charges $+e$ and $-e$ are located at the Cartesian coordinates $(x, y, z) = (0, d, 0), (0, -d, 0), (0, 0, d), (0, 0, -d)$ and four other charges $-e$ at the points $(-d, 0, 0)$, $(-\frac{d}{2}, 0, 0)$, and $(d, 0, 0)$. Calculate the monopolar moment and the Cartesian components of the dipolar and quadrupolar moment of this charge distribution.

Solution:

13.7.5.11 Ex: Multipolar moments of a charge distribution

An ideal hollow sphere with radius R_0 has the surface charge density $\sigma(r, \theta, \phi) = \sigma_0 \cos\theta$ with σ_0 =const. Calculate:
a. The multipolar moments of this charge distribution.
b. The electrostatic potential outside the sphere.

Solution: *a. We have,*

$$\sigma(R_0, \theta, \phi) = \sigma_0 \cos\theta \qquad resp. \qquad \rho(r, \theta, \phi) = \sigma_0 \cos\theta \ \delta(r - R_0) \ .$$

Because of,

$$Y_{10}(\theta, \phi) = \sqrt{\frac{3}{4\pi}}\cos\theta \qquad vale \qquad \rho(r, \theta, \phi) = \sigma_0\delta(r - R_0)\sqrt{\frac{4\pi}{3}}\ Y_{10}(\theta) \ .$$

From this follows

$$\begin{aligned} q_{lm} &\equiv \int_0^{R_0+\epsilon} dr' \int_{(4\pi)} d\Omega' (r')^{l+2} \rho(r', \theta', \phi') Y^*_{lm}(\theta', \phi') \\ &= \sigma_0 \sqrt{\frac{4\pi}{3}} R_0^{l+2} \int_{(4\pi)} d\Omega' Y_{10}(\theta') Y^*_{lm}(\theta', \phi') \\ &= \sigma_0 \sqrt{\frac{4\pi}{3}} R_0^3 \delta_{l1}\delta_{m0} \ . \end{aligned}$$

Therefore, there is only the dipole moment. Defining it as always,

$$P \equiv \sqrt{\frac{4\pi}{3}} q_{10}.$$

we get immediately,

$$P = \left(\frac{4\pi}{3}R_0^3\right)\sigma_0 = V_{sphere}\sigma_0 \ .$$

b. Outside the sphere,

$$\Phi(r,\theta,\phi) = \sum_{l=0}^{\infty}\sum_{m=-l}^{+l} \frac{4\pi}{2l+1}\, q_{lm}\, \frac{Y_{lm}}{r^{l+1}} = \frac{4\pi}{3} R_0^3\, \sigma_0 \sqrt{\frac{4\pi}{3}}\, \frac{Y_{10}(\theta)}{r^2}$$
$$= \frac{4\pi}{3} R_0^3\, \sigma_0\, \frac{\cos\theta}{r^2} = P\, \frac{\cos\theta}{r^2}\ .$$

13.7.5.12 Ex: Multipolar moment of an atomic nucleus

A simple model of a deformed atomic nucleus is a body homogeneously charged with the full charge Ze and being delimited by the quadrupolar surface $R(\theta) = R_0(a(\beta) + \beta Y_{20}(\theta))$. We now assume that the absolute value of the deformation parameter β is very small with respect to 1. For the average radius it is $R_0 = 1.2\ A^{1/3}$ [fm], where A is the number of nucleons present.
a. Visualize the shape of the nucleus.
b. Determine $a(\beta)$ up to second order in β from the request, that the core volume is always $V = 4\pi R_0^3/3$.
c. Calculate the multipolar moments Q_{lm} up to the octupolar term and up to the linear terms in β. Are there any multipolar moments that zero exactly?
d. Calculate also the electrostatic potential also up to linear terms in β.

Solution: *a. We have*

$$Y_{20} = \frac{1}{2}\sqrt{\frac{5}{4\pi}}(3\cos^2\theta - 1)\ .$$

Hence, $Y_{20} = 0$, when $\cos\theta = \pm\frac{1}{\sqrt{3}}$, that is, $\theta \approx 55°$. Depending on whether $\beta > 0$ or $\beta < 0$ we obtain the schemes shown in Fig. 13.34.

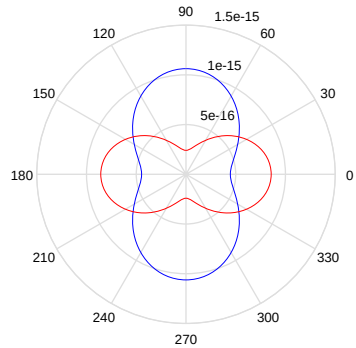

Figure 13.34: Shapes of an atomic nucleus for $\beta > 0$ (blue) and $\beta < 0$ (red).

b. The request reads,

$$V = \frac{4\pi}{3}R_0^3 = \text{const} = \int d\Omega \int_0^{R(\theta)} r^2 dr$$

$$= \int d\Omega \frac{1}{3}R^3(\theta) = \frac{R_0^3}{3}\int d\Omega(a^3 + 3a^2\beta Y_{20} + 3a\beta^2 Y_{20}^2 + O(\beta^3)) = \frac{4\pi}{3}R_0^3(a^3 + \frac{3a\beta^2}{4\pi}) \ .$$

With this we obtain,

$$a = \left(1 - \frac{3\beta^2 a}{4\pi}\right)^{1/3} = 1 - \frac{\beta^2}{4\pi}a + ... \ .$$

resp.

$$a = \frac{1}{1 + \frac{\beta^2}{4\pi}} = 1 - \frac{\beta^2}{4\pi} + ... \ .$$

c. In general we get,

$$q_{lm} = \int_V \rho(\mathbf{r}')(r')^{l+2}Y_{lm}^*(\theta', \phi')dr'd\Omega' \ .$$

Due to the independence on ϕ follows immediately, that all multipolar moments with $m \neq 0$ should disappear. Now,

$$\rho = \frac{3Ze}{4\pi R_0^3} \ .$$

With that, follows for q_{00},

$$q_{00} = \frac{3Ze}{4\pi R_0^3}\int_V \frac{1}{\sqrt{4\pi}}\int d\Omega \int_0^{R(\theta)} drr^2 = \frac{Ze}{\sqrt{4\pi}} \ .$$

With that the monopolar moment becomes,

$$Q_0 \equiv \sqrt{4\pi}q_{00} = Ze \ .$$

In the same way,

$$q_10 = \frac{3Ze}{4\pi R_0^3}\frac{R_0^4}{4}\int d\Omega \left(1 - \frac{\beta^2}{4\pi} + \beta Y_20\right)^4 Y_{10}^* = 0 \ ,$$

since Y_{20} (and hence its powers Y_{20}^k) is an even function of $\cos\theta$, while Y_{10} contains the argument $\cos\theta$ linearly. For the dipole moment follows from that,

$$P \equiv \sqrt{\frac{4\pi}{3}}q_{10} = 0 \ .$$

Furthermore,

$$q_{20} = \frac{3Ze}{4\pi R_0^3}\frac{R_0^5}{5}\int d\Omega(1 + 5\beta Y_{20} + O(\beta^2))Y_{20} = \frac{3Ze}{4\pi}R_0^2\beta \ .$$

resp. for the quadrupolar moment often found in nuclear physics,

$$Q_{20} \equiv \sqrt{\frac{16\pi}{5}} q_{20} = \frac{3Ze}{\sqrt{5\pi}} R_0^2 \beta \ .$$

The octupolar moment $q_{30}$is, on the other hand, equal to 0, since Y_30 is again an odd function in $\cos\theta$.
d. Generally speaking,

$$\Phi(\mathbf{r}) = \sum_{l=0}^{\infty} \sum_{m=-l}^{+l} \frac{4\pi}{2l+1} q_{lm} \frac{Y_{lm}}{r^{l+1}} \ .$$

For our case we get ($m = 0$),

$$\Phi(\mathbf{r}) = \sum_{l=0}^{\infty} q_{l0} \frac{Y_{l0}}{r^{l+1}} = 4\pi q_{00} \frac{1}{\sqrt{4\pi}} \frac{1}{r} + \frac{4\pi}{5} q_{20} \frac{Y_{20}}{r^3} + ... = \frac{Ze}{r} + \frac{3Ze}{5} R_0^2 \beta \frac{Y_{20}}{r^3} \ .$$

13.7.5.13 Ex: Dipole-dipole interaction

a. Consider an electric dipole with dipole moment $\mathbf{d}$. Show that the electric field of the dipole is given by:

$$\vec{\mathcal{E}}(\mathbf{r} = r\hat{\mathbf{e}}_r) = -\frac{1}{4\pi\varepsilon_0} \frac{\mathbf{d} - 3\hat{\mathbf{e}}_r(\hat{\mathbf{e}}_r \cdot \mathbf{d})}{r^3} \ .$$

You may use the expression for a dipole potential.
b. Use this result to calculate the interaction energy U_{12} of two equal dipoles located at a distance d from one another for the dipole configurations shown in the scheme.
Help: To calculate the interaction energy $U_{12}(\mathbf{a})$ between the two dipoles we con-

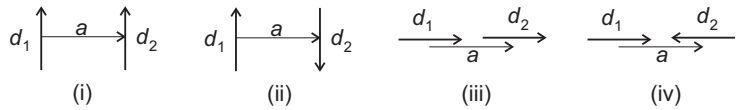

Figure 13.35: Dipole-dipole interaction.

sider the energy of dipole 1 in the electric field of dipole 2. So, $U_{12}(\mathbf{a}) = -\mathbf{d}_1 \vec{\mathcal{E}}_2$. In which configurations do the dipoles attract, in which do they repel each other?
c. A current research area deals with cold dipolar molecules, for example, RbLi molecules having a permanent dipole electrical moment of $d_{RbLi} = 4.3$ Debye. What should be the atomic density n, where $n = a^{-3}$, in order to obtain a dipolar interaction U_0 at least as large as the thermal energy of the molecules? Ultra-cold molecular gases typically have a temperature around 10^{-6} K.

Solution: *The potential of a dipole is,*

$$\Phi(\mathbf{r}) = \frac{1}{4\pi\varepsilon_0} \frac{\mathbf{d} \cdot \mathbf{r}}{r^3} \ .$$

The electric field is given by $\vec{\mathcal{E}} = -\nabla\Phi$. *Derivating,*

$$\begin{aligned}\nabla\Phi &= \frac{-1}{4\pi\varepsilon_0}\left[\frac{(d_x,d_y,d_z)}{r^3} - \frac{3}{2}\frac{\mathbf{d}\cdot\mathbf{r}}{r^5}(2x,2y,2z)\right] \\ &= \frac{-1}{4\pi\varepsilon_0}\left[\frac{\mathbf{d}}{r^3} - 3\frac{\mathbf{d}\cdot\mathbf{r}}{r^5}\mathbf{r}\right] = \frac{-1}{4\pi\varepsilon_0}\frac{\mathbf{d}-3(\mathbf{d}\cdot\hat{\mathbf{e}}_r)\hat{\mathbf{e}}_r}{r^3} \ .\end{aligned}$$

The interaction energy is:

$$-\mathbf{d}_1\cdot\vec{\mathcal{E}}_2 = -\mathbf{d}_1\ \frac{-1}{4\pi\varepsilon_0}\ \frac{\mathbf{d}_2-3(\mathbf{d}_2\cdot\hat{\mathbf{e}}_r)\hat{\mathbf{e}}_r}{a^3} = \frac{-1}{4\pi\varepsilon_0 a^3}\left(\mathbf{d}_1\cdot\mathbf{d}_2 - 3(\mathbf{d}_1\cdot\hat{\mathbf{e}}_r)(\mathbf{d}_2\cdot\hat{\mathbf{e}}_r)\right) \ .$$

Extracting the absolute value of the dipole moment: $\mathbf{d}_i = d\hat{d}_1$*:*

$$U_{12} = \frac{d^2}{4\pi\varepsilon_0 a^3}\left(\hat{d}_1\cdot\hat{d}_2 - 3(\hat{d}_1\cdot\hat{\mathbf{e}}_r)(\hat{d}_2\cdot\hat{\mathbf{e}}_r)\right) \ .$$

b. We define $U_0 \equiv \frac{d^2}{4\pi\varepsilon_0 a^3}$*, so we get for the various configurations:*
i. $U_{12} = U_0(1-3(0)\cdot(0) = U_0 > 0$ *this is repulsive*
ii. $U_{12} = U_0(-1-3(0)\cdot(0) = -U_0 < 0$ *this is attractive*
iii. $U_{12} = U_0(1-3(1)\cdot(1) = -2U_0 < 0$ *this is attractive*
iv. $U_{12} = U_0(-1-3(1)\cdot(-1) = 2U_0 > 0$ *this is repulsive*
c. One Debye corresponds to $3.3\cdot10^{-33}\,\mathrm{cm}$*. Therefore, the RbLi molecule has the dipole moment* $14.2\cdot10^{-33}\,\mathrm{Cm}$*. We get the density from,*

$$\frac{d^2}{4\pi\varepsilon_0 a^3} = k_B T \qquad \textit{and hence} \qquad n = \frac{k_B T 4\pi\varepsilon_0}{d^2} = 7.6\cdot10^{24}\,\mathrm{m^{-3}} \ .$$

13.7.5.14 Ex: Photoelectric effect

During the process described by the photoelectric effect, ultraviolet light can be used to electrically charge a piece of metal.
a. If this light strikes a bar of conductive material electrons, and are ejected with sufficient energy to escape from the surface of the metal, after how much time will the metal have accumulated a charge of $+1.5\,\mathrm{nC}$ if $1.0\cdot10^6$ electrons are ejected per second?
b. If $1.3\,\mathrm{eV}$ is required to eject an electron from the surface, what is the power of the light beam? (Consider the process to be 100% efficient.)

Solution: *a. It will take*

$$\frac{1.5\,\mathrm{nC}}{e\cdot1.0\cdot10^6\,\mathrm{s^{-1}}} = 2.6\,\mathrm{h} \ .$$

b. The required power is

$$1.3\,\mathrm{V}\cdot e\cdot1.0\cdot10^6\,\mathrm{s^{-1}} = 2.1\cdot10^{-13}\,\mathrm{W} \ .$$

13.7.5.15 Ex: Polonium and the use of the Green function

The radioactive metal Polonium (Po), discovered by Marie and Pierre Curie in 1898, crystallizes in a simple cubic lattice (each atom has six neighbors on a regular grid). The nucleus contains 84 protons and the diameter of the atom is approximately $3 \cdot 10^{-8}$ cm. Calculate the distribution of the potential within a primitive cell of a Po crystal traversed by a constant current. Suppose the following model for the crystal: Atomic nuclei (radius $\sim 9 \cdot 10^{-13}$ cm) are at positions $\mathbf{x}'_{\lambda\mu\nu} = (\lambda a + a/2, \mu a + a/2, \nu a + a/2)$ for $\lambda, \mu\nu = 0, \pm 1, \pm 2, ...$, and will be treated as point charges. The electronic shell of a Po atom is represented by charges induced in a grounded conducting cube of size a, in the middle of which is located the positively charged nucleus inducing these charges. Proceed as follows:
a. Start showing that,

$$G(\mathbf{r}, \mathbf{r}') = \frac{32}{\pi a} \sum_{l,m,n=1}^{\infty} \frac{1}{l^2+m^2+n^2} \sin\frac{l\pi x}{a} \sin\frac{l\pi x'}{a} \sin\frac{m\pi y}{a} \sin\frac{m\pi y'}{a} \sin\frac{n\pi z}{a} \sin\frac{n\pi z'}{a} \ ,$$

is the Green function for the Dirichlet contour problem of a cube with edge length a.
b. Calculate the potential in the atom at the position $(a/2, a/2, a/2)$, where we assume for the interior of the cube a charge $\rho(x', y', z') = q\delta(x' - a/2)\delta(y' - a/2)\delta(z' - a/2)$ and that the potential on the six surfaces of the cube adopts the following values: $\Phi(\mathbf{r}') = 0$ on the surface $x' = 0$, $\Phi(\mathbf{r}') = V_0$ on the surface $x' = a$, and $\Phi(\mathbf{r}') = V_0 x'/a$ on the other 4 surfaces $y' = 0,\ y' = a,\ z' = 0,\ z' = a$.
c. Reformulate the term describing the contribution of the surface to the potential using that for $0 < x < \pi$ holds: $1 = (4/\pi)(\sin x + (1/3)\sin 3x + (1/5)\sin 5x + ...)$ and $x = 2(\sin x - (1/2)\sin 2x + (1/3)\sin 3x - (1/4)\sin 4x + ...)$.

Solution: *a. We need to show:*
(i) $G(\mathbf{r}, \mathbf{r}') = G(\mathbf{r}', \mathbf{r})$
(ii) $G(\mathbf{r}, \mathbf{r}' \in$ *peripherical surface*$) = 0$
(iii) $\Delta G(\mathbf{r}, \mathbf{r}') = -4\pi\delta^{(3)}(\mathbf{r} - \mathbf{r}')$
(i) and (ii) they are trivially satisfied. For (iii) we calculate:

$$\begin{aligned}
&\Delta G(\mathbf{r}, \mathbf{r}') \\
&= \frac{32}{\pi a} \sum_{l,m,n=1}^{\infty} \frac{1}{l^2+m^2+n^2} \sin\frac{l\pi x}{a} \sin\frac{l\pi x'}{a} \sin\frac{m\pi y}{a} \sin\frac{m\pi y'}{a} \sin\frac{n\pi z}{a} \sin\frac{n\pi z'}{a} \cdot \frac{\pi^2}{a^2}(-l^2 - m^2 - n^2) \\
&= -4\pi \left(\sqrt{\frac{2}{a}}\right)^6 \sum_{l,m,n=1}^{\infty} \frac{1}{l^2+m^2+n^2} \sin\frac{l\pi x}{a} \sin\frac{l\pi x'}{a} \sin\frac{m\pi y}{a} \sin\frac{m\pi y'}{a} \sin\frac{n\pi z}{a} \sin\frac{n\pi z'}{a} \ .
\end{aligned}$$

Now holds the completeness relation,

$$\sum_{l=1}^{\infty} \sqrt{\frac{2}{a}} \sin\left(\frac{l\pi x}{a}\right) \sin\left(\frac{l\pi x'}{a}\right) = \delta(x - x') \ ,$$

yielding the statement (iii).
b. Vale,

$$\begin{aligned}\Phi(x,y,z) = &\int_V \rho(x',y',z')G(\mathbf{r},\mathbf{r}')dx'dy'dz' \\ &- \frac{1}{4\pi}\int_0^a dy'\int_0^a dz'\Phi(x'=0)\frac{\partial G}{\partial x'}|_{x'=0} - \frac{1}{4\pi}\int_0^a dy'\int_0^a dz'\Phi(x'=a)\frac{\partial G}{\partial x'}|_{x'=a} \\ &- \frac{1}{4\pi}\int_0^a dx'\int_0^a dz'\Phi(y'=0)\frac{\partial G}{\partial y'}|_{y'=0} - \frac{1}{4\pi}\int_0^a dx'\int_0^a dz'\Phi(y'=a)\frac{\partial G}{\partial y'}|_{y'=a} \\ &- \frac{1}{4\pi}\int_0^a dx'\int_0^a dy'\Phi(z'=0)\frac{\partial G}{\partial z'}|_{z'=0} - \frac{1}{4\pi}\int_0^a dx'\int_0^a dy'\Phi(z'=a)\frac{\partial G}{\partial z'}|_{z'=a} \ .\end{aligned}$$

The volume integral gives, after inserting the charge density,

$$\frac{32q}{\pi a}\sum_{l,m,n=1}^{\infty}\frac{(-)^{l+m+n}\sin\left(\frac{(2l+1)\pi x}{a}\right)\sin\left(\frac{(2m+1)\pi y}{a}\right)\sin\left(\frac{(2n+1)\pi z}{a}\right)}{(2l+1)^2+(2m+1)^2+(2n+1)^2} \ .$$

For the surface term we get,

$$\frac{8V_0}{\pi^3}\sum_{l,m,n=1}^{\infty}(-)^{l+1}\frac{(1-(-)^n)(1-(-)^m)}{lmn}\sin\left(\frac{l\pi x}{a}\right)\sin\left(\frac{m\pi y}{a}\right)\sin\left(\frac{n\pi z}{a}\right) \ .$$

With $x=y=z=a/2$ we get from this the desired result.
c. We obtain for the surface term Φ_2, by applying the given formulas on l,m,n inside the cube:

$$\Phi_2(\mathbf{r}) = V_0\frac{x}{a} \ .$$

This is the profile of a potential due to the influence of the constant current toward the negative x-direction, which overlaps with the potential of the crystal.

13.7.5.16 Ex: Electrostatic potential of a hollow sphere via Green function

On the surface of a hollow sphere with radius b without charge there be a certain potential $V(\theta,\phi) = V_0[P_2(\cos\theta) + \alpha P_3(\cos\theta)]$. Calculate the electrostatic potential $\Phi(\mathbf{r})$ inside the sphere.
Help: Green's function for the interior space between two concentric spheres with radii a and b ($a<b$) is,

$$G(\mathbf{r},\mathbf{r}') = \sum_{l=0}^{\infty}\frac{4\pi}{2l+1}\left[1-\left(\frac{a}{b}\right)^{2l+1}\right]\left[r_<^l - \frac{a^{2l+1}}{r_<^{l+1}}\right]\left[\frac{1}{r_>^{l+1}} - \frac{r_>^l}{b^{2l+1}}\right]\sum_{m=-l}^{+l}Y_{lm}(\Omega)Y_{lm}^*(\Omega') \ .$$

where $r_< \equiv \min(|\mathbf{r}|, |\mathbf{r}'|)$ and $r_> \equiv \max(|\mathbf{r}|, |\mathbf{r}'|)$. We also know, $Y_{l0}(\theta, \phi) = \sqrt{(2l+1)/4\pi} P_l(\cos\theta)$.

Solution: *We consider the Green function as given. For the space of a single sphere we set $a = 0$. Hence,*

$$G(\mathbf{r}, \mathbf{r}') = \sum_{l=0}^{\infty} \frac{4\pi}{2l+1} r_<^l \left[\frac{1}{r_>^{l+1}} - \frac{r_>^l}{b^{2l+1}} \right] \sum_{m=-l}^{+l} Y_{lm}(\Omega) Y_{lm}^*(\Omega') \ .$$

The hollow sphere is uncharged. So for all $\mathbf{r}$ in the sphere volume V_K, holds,

$$\int_{V_K} G(\mathbf{r}, \mathbf{r}') \rho(\mathbf{r}') d^3 r' = 0 \ .$$

and therefore,

$$\Phi(\mathbf{r}) = -\frac{1}{4\pi} \int_{O_K} V(\Omega') \left(\frac{\partial G(\mathbf{r}, \mathbf{r}')}{\partial r'} \right)_{r'=b} b^2 d\Omega' \ .$$

where O_K denotes the surface of the sphere. For this surface obviously holds $|\mathbf{r}'| = r_>$ and $|\mathbf{r}| = r_<$, and so we have within the sphere

$$\begin{aligned} \Phi(\mathbf{r}) &= -\frac{1}{4\pi} \int_{(4\pi)} V(\Omega') \sum_{l=0}^{\infty} \frac{4\pi}{2l+1} r^l \left(-\frac{l+1}{b^{l+2}} - \frac{l b^{l-1}}{b^{2l+1}} \right) \sum_{m=-l}^{+l} Y_{lm}(\Omega) Y_{lm}^*(\Omega') b^2 d\Omega' \\ &= \sum_{l=0}^{\infty} \left(\frac{r}{b} \right)^l \sum_{m=-l}^{+l} Y_{lm}(\Omega) \int_{(4\pi)} V(\Omega') Y_{lm}^*(\Omega') d\Omega' \end{aligned}$$

Now,

$$V(\Omega') = V_0 \left(P_2(\cos\theta) + \alpha P_3(\cos\theta) \right) = V_0 \sqrt{4\pi} \left(\frac{Y_{20}(\theta)}{\sqrt{5}} + \frac{\alpha Y_{30}(\theta)}{\sqrt{7}} \right) \ .$$

Using the orthonormality of spherical harmonics,

$$\begin{aligned} \Phi(\mathbf{r}) &= V_0 \sqrt{4\pi} \left[\left(\frac{r}{b} \right)^2 \frac{Y_{20}(\theta)}{\sqrt{5}} + \left(\frac{r}{b} \right)^3 \frac{\alpha Y_{30}(\theta)}{\sqrt{7}} \right] \\ &= V_0 \left(\frac{r}{b} \right)^2 \left[P_2(\cos\theta) + \alpha \left(\frac{r}{b} \right) P_2(\cos\theta) \right] \ . \end{aligned}$$

13.8 Further reading

D.J. Griffiths, *Introduction to Electrodynamics* [545]ISBN

D. Halliday, R. Resnick, and J. Walker, *Fundamentals of Physics* [577]ISBN

H.M. Nussenzveig, *Curso de Física Básica: Eletromagnetismo (Volume 3)* [963]ISBN

Chapter 14

Electrical properties of matter

There are many types of materials, such as solids, liquids, gases, metals, wood or glass, all of which respond differently to applied electric fields. However, most materials can at least roughly be classified into two categories: In materials called *dielectrics* (or insulators) the electrons are strongly bound to the atoms, while in *metals* there are free electrons. Some materials, such as semiconductors, have particular properties, which do not fit into these categories.

Under the influence of electric (or magnetic) forces the electrons can be displaced within a macroscopic body, thus producing a polarization, when the electrons are bound, or a current, when the electrons are free.

14.1 Polarization of dielectrics

Let us first discuss dielectrics. The elementary blocks (molecules) of dielectric materials can react in various ways to applied electric fields, For example, they can be insensitive to electric fields or behave like *permanent dipoles*. Permanent dipoles exist independently of the application of an external field, but generally (without external field) they have random and disorderly orientations. Under the influence of an external field the dipoles will try to reorient themselves, which is called *orientation polarization*.

It is also possible that a material does not have intrinsic dipole moments, but *develops* dipole moments under the action of an external field. In this case we speak of *induced dipoles*. Induced dipoles are formed in the presence of a field displacing bound positive and negative charges in molecules against each other, thus producing a *translation polarization*.

14.1.1 Energy of permanent dipoles

Polar molecules exhibit permanent electric moments. Water is an example or salt Na^+Cl^-. The reason is that halogens, which have a much higher electro-affinity than alkalines, and try to steal electrons from their partner and monopolize the electronic cloud.

The potential energy of a dipole depends on its orientation with respect to the electric field. Using the parametrization $\varrho(\mathbf{r}') = Q[\delta^3(\mathbf{r}' - \frac{\mathbf{a}}{2}) - \delta^3(\mathbf{r}' + \frac{\mathbf{a}}{2})]$, we find

for the interaction energy with a homogeneous field given by $\Phi(\mathbf{r}') = -\mathcal{E}_0 z'$,

$$H_{int} = \int \varrho(\mathbf{r}')\Phi(\mathbf{r}')dV = -Q\mathcal{E}_0 a_z = -\mathbf{d}\cdot\vec{\mathcal{E}}\ . \tag{14.1}$$

Hence [1],

$$\boxed{H_{int} = -\mathbf{d}\cdot\vec{\mathcal{E}}}\ . \tag{14.2}$$

The energy is minimal when $\mathbf{d} \parallel \vec{\mathcal{E}}$.

To calculate the interaction energy between two dipoles $\mathbf{d}_1$ and $\mathbf{d}_2$ we calculate the energy of $\mathbf{d}_1$ within the field created by $\mathbf{d}_2$ (which has been derived in the example 57),

$$H_{int} = -\mathbf{d}_1\cdot\vec{\mathcal{E}}_2 = -\mathbf{d}_1\cdot\frac{1}{4\pi\varepsilon_0}\frac{3(\hat{\mathbf{e}}_r\cdot\mathbf{d}_2)\hat{\mathbf{e}}_r - \mathbf{d}_2}{r^3} = \frac{1}{4\pi\varepsilon_0}\frac{\mathbf{d}_1\cdot\mathbf{d}_2 - 3(\mathbf{d}_1\cdot\hat{\mathbf{e}}_r)(\mathbf{d}_2\cdot\hat{\mathbf{e}}_r)}{r^3}\ . \tag{14.3}$$

14.1.1.1 Alignment of permanent dipoles

In a homogeneous field the force on an (neutral) electric dipole $\mathbf{d} = Q\mathbf{a}$ vanishes, since $\mathbf{F} = Q\vec{\mathcal{E}} + (-Q)\vec{\mathcal{E}} = 0$. However, there will be a torque because,

$$\vec{\tau} = \frac{\mathbf{a}}{2}\times Q\vec{\mathcal{E}} + \frac{-\mathbf{a}}{2}\times(-Q)\vec{\mathcal{E}} = \mathbf{d}\times\vec{\mathcal{E}}\ . \tag{14.4}$$

This means that a freely moving molecule will rotate about its mass center, as illustrated in Fig. 14.1, until (in the presence of dissipation) it finds the orientation with the lowest energy. In this orientation the molecule is aligned to the applied field. See Exc. 14.1.7.1.

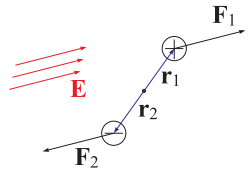

Figure 14.1: Torque on a dipole exerted by an electric field.

In a *non-homogeneous* field, the forces on the charges $\pm Q$ do not compensate [2], $\mathbf{F} = Q\vec{\mathcal{E}}_+ - Q\vec{\mathcal{E}}_- = Q(\mathbf{a}\cdot\nabla)\vec{\mathcal{E}}$. Hence,

$$\boxed{\mathbf{F} = (\mathbf{d}\cdot\nabla)\vec{\mathcal{E}}}\ . \tag{14.5}$$

Placed in front of a conductive surface a dipole feels the forces exerted by the charge of its own image. In Exc. 14.1.7.2 we calculate the torque exerted by a conducting surface on a dipole.

[1] We can also calculate the energy of a dipole in an electric field by the work required to rotate it away from its rest position, $H_{int} = \int\vec{\tau}\cdot d\theta = \int \mathbf{d}\times\vec{\mathcal{E}}d\theta = \int_0^\theta dE\sin\theta d\theta = -dE\cos\theta$.

[2] We note that the force that a field exerts on a dipole can be calculated as a gradient of the interaction energy: $\mathbf{F} = -\nabla H_{int} = \nabla(\mathbf{d}\cdot\vec{\mathcal{E}}) = (\mathbf{d}\cdot\nabla)\vec{\mathcal{E}} + (\vec{\mathcal{E}}\cdot\nabla)\mathbf{d} + (\mathbf{d}\times\nabla)\times\vec{\mathcal{E}} + (\vec{\mathcal{E}}\times\nabla)\times\mathbf{d} = (\mathbf{d}\cdot\nabla)\vec{\mathcal{E}}$.

14.1.2 Induction of dipoles in dielectrics

A priori, neutral non-polar atoms and molecules should not react to applied electric fields. However, the fact that atoms are composed of positive charge distributions (concentrated in a heavy nucleus) and negative ones (concentrated in a light-weighed electron shell), permits a more or less important displacement of these charge distributions with respect to the center-of-mass. Consequently, an electric field *polarizes the atom* and induces an electric dipole moment whose magnitude is approximately proportional to the field,

$$\boxed{\mathbf{d} = \alpha_{pol}\vec{\mathcal{E}}} \ , \tag{14.6}$$

where the constant α_{pol} is called *polarizability*.

> **Example 59 (*Polarizability of a primitive atom*):** In a primitive model we envision an atom as a point-like nucleus carrying the charge $+Q$ surrounded by a uniformly charged electron sphere with radius a carrying the inverse charge $-Q$. In the presence of an external field $\vec{\mathcal{E}}$ the nucleus will be slightly shifted by a distance $\epsilon/2$ to one side and the electron sphere by a distance $-\epsilon/2$ to the opposite side. The polarized atom is in equilibrium, when the field created by the induced dipole $\mathcal{E}_{dp}$ (calculated in Exc. 13.2.4.5) equalizes the external field, i.e.,
>
> $$\mathcal{E}_{dp} = \frac{1}{4\pi\varepsilon_0}\frac{Q\epsilon}{a^3} = \mathcal{E} \ .$$
>
> Hence,
>
> $$\frac{\alpha_{pol}}{4\pi\varepsilon_0} = \frac{d}{4\pi\varepsilon_0\mathcal{E}} = a^3 \approx 0.15 \cdot 10^{-30}\,\mathrm{m}^3 \ ,$$
>
> using for $a = a_B$ the Bohr radius. Despite the simplicity of the model, this results represents a good approximation. A slightly better model is discussed in Exc. 14.1.7.3.

The values for the atomic polarizability range from $\alpha_{pol}/4\pi\varepsilon_0 = 0.205 \cdot 10^{-30}\,\mathrm{m}^3$ for helium to $59.6 \cdot 10^{-30}\,\mathrm{m}^3$ for cesium. This shows that it is far more difficult to polarize atoms with closed electron shells (like noble gases) than atoms with isolated valence electron (such as alkaline atoms). Molecules may react in a more complicated way to the applied fields necessitating an interpretation of the polarizability α_{pol} in terms of a tensor represented by a matrix.

14.1.2.1 Energy of induced dipoles

We now calculate the energy of a polarizable molecule inside an external electric field. We expect two contributions: The first one is the energy W_{ind} stored in the field created by the separation of charges under the action of the external field. The second contribution is the energy H_{int} due to the interaction of the induced dipole with the external field.

W_{ind} is calculated by the work spent on separating the charges. Let e be the valence charge bound to the molecule. The force between this charge and the molecule is described, in first approximation, by a harmonic oscillator with the spring constant k. Inside the electric field, the charge feels the force $e\vec{\mathcal{E}}$, but at the same time the force of the 'molecular spring' goes in the opposite direction. In equilibrium,

$$-k\mathbf{a} + e\vec{\mathcal{E}} = 0 \ . \tag{14.7}$$

To induce this dipole, the electric field must do the work,

$$W_{ind} = \tfrac{1}{2}ka^2 = \tfrac{1}{2}e\mathcal{E}a \ . \tag{14.8}$$

Defining the induced dipole as $\mathbf{d}_{ind} \equiv Ze\mathbf{d}$, we obtain:

$$W_{ind} = \tfrac{1}{2}\mathbf{d}_i \cdot \vec{\mathcal{E}} \ . \tag{14.9}$$

Since the energy of a dipole in an external electric field is, $H_{int} = -\mathbf{d}_i \cdot \vec{\mathcal{E}}$, for the induced dipole we obtain the total energy,

$$H_{tot} = H_{int} + W_{ind} = -\tfrac{1}{2}\mathbf{d}_i \cdot \vec{\mathcal{E}} \ . \tag{14.10}$$

The energy value is less than in the case of a permanent dipole (14.5), since part of the energy had to be spent on creating the dipole in the first place. Expressing the dipole moment by the polarizability (14.6),

$$\boxed{H_{tot} = -\frac{\alpha_{pol}}{2}\vec{\mathcal{E}}^2} \ . \tag{14.11}$$

14.1.3 Macroscopic polarization

With these results we can now describe, what happens to a dielectric material placed in an electric field: If the substance consists of neutral atoms (or non-polar molecules), the field will induce in each particle a small dipole moment pointing in the direction of the field. If the substance consists of polar molecules, each permanent dipole will try to orientate itself along the field [3].

Note that both mechanisms produce the same result: a multitude of small dipoles aligned along the applied field. The sum of the microscopic moments gives rise to a macroscopic *polarization* defined by the sum over all dipole moments,

$$\vec{\mathcal{P}} = \frac{N\mathbf{d}}{V} \ . \tag{14.12}$$

In reality, the two types of polarization are not always well separated, and there are cases where both contribute. Nevertheless, it is usually much easier to rotate a molecule (rotational energy) than to stretch it (vibrational energy). In some (ferro-electric) materials it is possible to freeze the polarization.

14.1.4 Electrostatic field on a polarized or dielectric medium

In this section we will describe the electric field inside a polarized medium forgetting the physical cause of the polarization $\vec{\mathcal{P}}$. The field produced by the polarization (not the external field) can be calculated by the sum of the fields produced by the individual dipoles,

$$\Phi(\mathbf{r}) = \frac{1}{4\pi\varepsilon_0}\sum_k \frac{\mathbf{d}_k \cdot (\mathbf{r}-\mathbf{r}_k)}{|\mathbf{r}-\mathbf{r}_k|^3} \longrightarrow \frac{1}{4\pi\varepsilon_0}\int_{\mathcal{V}} dV' \frac{\vec{\mathcal{P}}(\mathbf{r}')\cdot(\mathbf{r}-\mathbf{r}')}{|\mathbf{r}-\mathbf{r}'|^3} \ , \tag{14.13}$$

[3] Note that thermal motion, particularly at high temperatures, competes with this process, such that the alignment will never be perfect.

introducing the dipole moment distribution $\vec{\mathcal{P}}(\mathbf{r}')$ by $\mathbf{d}_k \to \vec{\mathcal{P}} dV'$. We can rewrite the integral in the form,

$$\Phi(\mathbf{r}) = \frac{1}{4\pi\varepsilon_0}\int_{\mathcal{V}} \vec{\mathcal{P}}(\mathbf{r}')\cdot\nabla'\frac{1}{|\mathbf{r}-\mathbf{r}'|}dV' = \frac{1}{4\pi\varepsilon_0}\left[\int_{\mathcal{V}}\nabla'\cdot\frac{\vec{\mathcal{P}}(\mathbf{r}')}{|\mathbf{r}-\mathbf{r}'|}dV' - \int_{\mathcal{V}}\frac{1}{|\mathbf{r}-\mathbf{r}'|}\nabla'\vec{\mathcal{P}}(\mathbf{r}')dV'\right]$$
$$= \frac{1}{4\pi\varepsilon_0}\oint_{\partial\mathcal{V}}\frac{\vec{\mathcal{P}}(\mathbf{r}')}{|\mathbf{r}-\mathbf{r}'|}dS' - \frac{1}{4\pi\varepsilon_0}\int_{\mathcal{V}}\frac{1}{|\mathbf{r}-\mathbf{r}'|}\nabla'\cdot\vec{\mathcal{P}}(\mathbf{r}')dV' \ . \tag{14.14}$$

Defining,

$$\boxed{\sigma_b \equiv \vec{\mathcal{P}}\cdot\mathbf{n}_S} \quad \text{and} \quad \boxed{\varrho_b \equiv -\nabla\cdot\vec{\mathcal{P}}}\ , \tag{14.15}$$

we obtain

$$\Phi(\mathbf{r}) = \frac{1}{4\pi\varepsilon_0}\oint_{\partial\mathcal{V}}\frac{\sigma_b}{|\mathbf{r}-\mathbf{r}'|}dS' - \frac{1}{4\pi\varepsilon_0}\int_{\mathcal{V}}\frac{\varrho_b}{|\mathbf{r}-\mathbf{r}'|}dV' \ . \tag{14.16}$$

The meaning of this result is that the potential (and therefore the field) of a polarized object is the same as the one produced by a volume distribution ϱ_b plus a surface charge distribution σ_b. The index b indicates the fact that we consider here 'bound charges' (i.e. localized charges). Instead of integrating the field contributions of all individual infinitesimal dipoles, as in Eq. (14.13), we can try to find these bound charges, and then calculate the fields they produce, as we already did in the previous chapter.

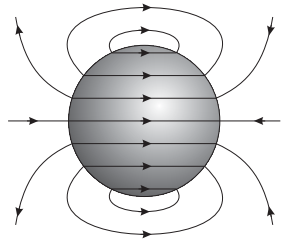

Figure 14.2: Distortion of polarization.

Example 60 (*Microscopic theory of induced dipoles*): As an example we calculate the electric field produced by a homogeneous polarization within a sphere. While the volume charge is zero (otherwise $\vec{\mathcal{P}}$ could not be uniform), the surface charge is $\sigma_b = \vec{\mathcal{P}}\cdot\mathbf{n}_S = \mathcal{P}\cos\theta$. This charge distribution generates a potential which, applying the result derived in example 54, we can write,

$$\Phi(r,\theta) = \begin{cases} \frac{\mathcal{P}}{3\varepsilon_0} r\cos\theta = \frac{1}{4\pi\varepsilon_0}\frac{\mathbf{d}\cdot\mathbf{r}}{R^3} & \text{for} \quad r \le R \\ \frac{\mathcal{P}}{3\varepsilon_0}\frac{R^3}{r^2}\cos\theta = \frac{1}{4\pi\varepsilon_0}\frac{\mathbf{d}\cdot\mathbf{r}}{r^3} & \text{for} \quad r \ge R \end{cases},$$

with $\mathbf{d} = \frac{4\pi}{3}R^3\vec{\mathcal{P}}$. The potential produces a field, which is uniform within the sphere,

$$\vec{\mathcal{E}} = -\nabla\Phi = \begin{cases} -\frac{\mathcal{P}}{3\varepsilon_0}\hat{\mathbf{e}}_z\frac{\partial\Phi}{\partial z} = -\frac{\vec{\mathcal{P}}}{3\varepsilon_0} & \text{for} \quad r \le R \\ \frac{\mathcal{P}}{3\varepsilon_0}\frac{R^3}{r^2}\cos\theta = \frac{1}{4\pi\varepsilon_0}\frac{3(\hat{\mathbf{e}}_r\cdot\mathbf{d})\hat{\mathbf{e}}_r - \mathbf{d}}{r^3} & \text{for} \quad r \ge R \end{cases}.$$

The physical interpretation of the surface charge produced by a uniform polarization is simply a displacement of all the electrons of the body with respect to the positively charged nuclei. Since the electrons remain attached to the nuclei, the volume charge inside the sphere remains neutral. However, the edges of the body accumulate negative charge on one side and positive charge on the other.

14.1.5 Electric displacement

In the previous section we found that the phenomenon of polarization can be understood as being due to a volume charge $\varrho_b = -\nabla \cdot \vec{\mathcal{P}}$ inside the dielectric and a surface charge on the surface of the body $\sigma_b = \vec{\mathcal{P}} \cdot \mathbf{n}_S$. However, many materials have dielectric characteristics and at the same time conductive characteristics, which do not result from a polarization and which we take into account via a distribution of free charges, ϱ_f, the index f indicating 'free charges'.

14.1.5.1 Gauß' Law in dielectric media

Gauß's law can now be generalized for arbitrary media,

$$\varepsilon_0 \nabla \cdot \vec{\mathcal{E}} = \varrho = \varrho_b + \varrho_f = -\nabla \cdot \vec{\mathcal{P}} + \varrho_f \ , \tag{14.17}$$

where $\vec{\mathcal{E}}$ is the total electric field. Defining a new field called the *electric displacement*,

$$\boxed{\vec{\mathcal{D}} \equiv \varepsilon_0 \vec{\mathcal{E}} + \vec{\mathcal{P}}} \ , \tag{14.18}$$

we can now write,

$$\nabla \cdot \vec{\mathcal{D}} = \varrho_f \ . \tag{14.19}$$

The electric displacement is that part of the electric field, which comes only from free charges (which is the part useful for generating currents). We can also define the *electric susceptibility* χ_ε via,

$$\vec{\mathcal{P}} = \varepsilon_0 \chi_\varepsilon \vec{\mathcal{E}} \ , \tag{14.20}$$

or the *permittivity* ε via,

$$\vec{\mathcal{D}} = \varepsilon \vec{\mathcal{E}} = \varepsilon_0 (1 + \chi_\varepsilon) \vec{\mathcal{E}} \ . \tag{14.21}$$

Note that the rotation of the polarization *does not necessarily vanish*, since the susceptibility may depend on position, $\chi_\varepsilon = \chi_\varepsilon(\mathbf{r})$,

$$\nabla \times \vec{\mathcal{D}} = \varepsilon_0 (\nabla \times \vec{\mathcal{E}}) + \nabla \times \vec{\mathcal{P}} = \nabla \times (\varepsilon_0 \chi_\varepsilon \vec{\mathcal{E}}) \neq 0 \ . \tag{14.22}$$

Therefore, $\vec{\mathcal{D}}$ generally can not be derived from a potential, and Coulomb's law is not valid for $\vec{\mathcal{D}}$.

14.1.5.2 Boundary conditions involving dielectrics

The integral version of Gauß's law, $\oint \vec{\mathcal{D}} \cdot d\mathbf{S} = Q_f$, allows us to determine the behavior of the electric displacement near interfaces,

$$\mathcal{D}^\perp_{top} - \mathcal{D}^\perp_{bottom} = \sigma_f \ . \tag{14.23}$$

On the other hand, Stokes' law $\nabla \times \vec{\mathcal{D}} = \varepsilon_0 \nabla \times \vec{\mathcal{E}} + \nabla \times \vec{\mathcal{P}} = \nabla \times \vec{\mathcal{P}}$ yields,

$$\vec{\mathcal{D}}^{\parallel}_{top} - \vec{\mathcal{D}}^{\parallel}_{bottom} = \vec{\mathcal{P}}^{\parallel}_{top} - \vec{\mathcal{P}}^{\parallel}_{bottom} \ . \tag{14.24}$$

This is in contrast to the behavior of the electric $\vec{\mathcal{E}}$ field at interfaces described by Eqs. (13.37) and (13.39).

14.1.6 Electrical susceptibility and permittivity

14.1.6.1 Linear dielectrics

In many materials, as long as the applied electric field is not too strong, the polarization is proportional to the field, $\vec{\mathcal{P}} \propto \vec{\mathcal{E}}$, that is, the electric susceptibility depends on the material's microscopic properties and external factors such as temperature, but not on the applied field, $\chi_\varepsilon \neq \chi_\varepsilon(\vec{\mathcal{E}})$. Hence, linear media can be characterized by a constant,

$$\varepsilon_r \equiv \frac{\varepsilon}{\varepsilon_0} \ , \tag{14.25}$$

called *relative permittivity*.

In *non-linear* media, in contrast, the susceptibility $\chi_\varepsilon(\vec{\mathcal{E}})$ depend on the strength of the electric field. Often the polarization can be expanded in orders of the electric field,

$$\vec{\mathcal{P}}(\vec{\mathcal{E}}) = \varepsilon^{(1)}\vec{\mathcal{E}} + \varepsilon^{(2)}\vec{\mathcal{E}}^2 + \varepsilon^{(3)}\vec{\mathcal{E}}^3 + \dots \ . \tag{14.26}$$

In *anisotropic* materials the situation gets more complicated, because the susceptibility and the permittivity must be understood as tensors,

$$\mathcal{P}_k(\vec{\mathcal{E}}) = \sum_m \varepsilon^{(1)}_{km}\mathcal{E}_m + \sum_{ml} \varepsilon^{(2)}_{kml}\mathcal{E}_m\mathcal{E}_l + \sum_{mlj} \varepsilon^{(3)}_{kmlj}\mathcal{E}_m\mathcal{E}_l\mathcal{E}_j + \dots \ . \tag{14.27}$$

Example 61 (*Microscopic theory of induced dipoles*): We know that an *external electric field* $\vec{\mathcal{E}}_{ext}$ applied to a linear purely dielectric medium generates a *macroscopic polarization* proportional to the field,

$$\vec{\mathcal{P}} = \chi_\varepsilon \varepsilon_0 \vec{\mathcal{E}}_{ext} \ .$$

On the other hand, if the material consists of atoms (or non-polar molecules), the *microscopic dipole moment* induced in each atom is proportional to the *local field*,

$$\mathbf{d}_{ind} = \alpha_{pol}\vec{\mathcal{E}}_{loc} \ .$$

Here, $\vec{\mathcal{E}}_{loc}$ is the *total field* due to the applied field $\vec{\mathcal{E}}_{ext}$ plus the field $\vec{\mathcal{E}}_{self}$ generated by the polarization of the other atoms which are around. The question now is, what is the relationship between the atomic polarizability α_{pol} (characterizing the sample from a microscopic point of view) and the susceptibility χ_e (characterizing the sample from a macroscopic point of view)?

To begin with we consider low densities, in which case it is a good approximation to suppose that the atom does not feel the polarization of its neighbors, that is $\vec{\mathcal{E}}_{loc} \simeq \vec{\mathcal{E}}_{ext}$. We already noticed in Eq. (??) that the polarization is nothing more than the sum over all the dipole moments induced by the local electric field, such that, comparing the last two relations, a first trial would be to affirm,

$$\chi_\varepsilon = \frac{N}{V}\frac{\alpha_{pol}}{\varepsilon_0} \ .$$

But for dense gases, there will be a correction, and the local field will be a superposition of the external field and the field generated by the surrounding dipoles, $\vec{\mathcal{E}}_{loc} = \vec{\mathcal{E}}_{ext} + \vec{\mathcal{E}}_{self}$. To estimate this field, we imagine a single dipole located inside a sphere. The polarization of the surrounding medium is modeled by a surface charge density with the value $\sigma_b \equiv -\mathcal{P}\cos\theta$. The electric field produced by this charge distribution was calculated in example 60: $\vec{\mathcal{E}}_{self} = \vec{\mathcal{P}}/3\varepsilon_0$. With this we calculate,

$$\chi_\varepsilon = \frac{\mathcal{P}}{\varepsilon_0 \mathcal{E}_{ext}} = \frac{\mathcal{P}}{\varepsilon_0(\mathcal{E}_{loc} - \mathcal{E}_{self})} = \frac{\mathcal{P}}{\varepsilon_0(\frac{p_{ind}}{\alpha_{pol}} - \frac{\mathcal{P}}{3\varepsilon_0})} = \frac{N\alpha_{pol}/\varepsilon_0 V}{1 - N\alpha_{pol}/3\varepsilon_0 V} \ . \tag{14.28}$$

This equation is known as *Clausius-Mossotti formula*. The difference between the denominator and 1, called *Lorentz-Lorenz shift*, comes from the energy displacements of the atoms due to the dipole-dipole interactions. At low densities we recover the linear relation. In terms of the relative permittivity we can also write,

$$\frac{\alpha_{pol}}{\varepsilon_0} = \frac{3V}{N}\frac{\varepsilon_r - 1}{\varepsilon_r + 2} \ .$$

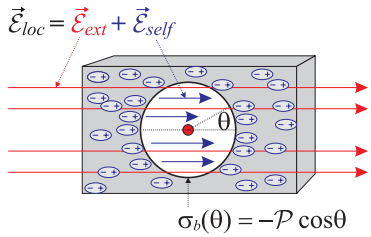

Figure 14.3: The local field $\vec{\mathcal{E}}_{loc}$ is the sum of the external field $\vec{\mathcal{E}}_{ext}$ and the field generated by the polarization $\vec{\mathcal{E}}_{self}$.

14.1.7 Exercises

14.1.7.1 Ex: Torque on dipoles

Calculate the torque on a dipole in front of a conducting surface.

Solution: *The coordinates of the charges of the dipole and its image are,*

$$\mathbf{r}_\pm = \pm\frac{\mathbf{d}}{2} \quad , \quad \mathbf{x}_\pm = -2a\hat{\mathbf{e}}_z \mp \left[\frac{\mathbf{d}}{2} - (\hat{\mathbf{e}}_z \cdot \mathbf{d})\hat{\mathbf{e}}_z\right] \ .$$

With this we calculate the vector products,

$$\mathbf{r}_+ \times \mathbf{x}_\pm = -\mathbf{r}_- \times \mathbf{x}_\pm = (-2a \pm \hat{\mathbf{e}}_z \cdot \mathbf{d})\frac{\mathbf{d}}{2} \times \hat{\mathbf{e}}_z = -\left(a \mp \frac{d}{2}\cos\theta\right) d\sin\theta\hat{\mathbf{e}}_x \ .$$

O torque agora é,

$$
\begin{aligned}
\vec{\tau} &= \mathbf{r}_+ \times Q\vec{\mathcal{E}}(\mathbf{r}_+) + \mathbf{r}_- \times (-Q)\vec{\mathcal{E}}(\mathbf{r}_-) \\
&= \frac{Q^2}{4\pi\varepsilon_0}\left[\mathbf{r}_+ \times \left(\frac{\mathbf{r}_+ - \mathbf{x}_+}{|\mathbf{r}_+ - \mathbf{x}_+|^3} - \frac{\mathbf{r}_+ - \mathbf{x}_-}{|\mathbf{r}_+ - \mathbf{x}_-|^3}\right) - \mathbf{r}_- \times \left(\frac{-\mathbf{r}_+ - \mathbf{x}_+}{|-\mathbf{r}_+ - \mathbf{x}_+|^3} - \frac{-\mathbf{r}_+ - \mathbf{x}_-}{|-\mathbf{r}_+ - \mathbf{x}_-|^3}\right)\right] \\
&= \frac{Q^2}{4\pi\varepsilon_0}\left[\frac{\mathbf{r}_+ \times \mathbf{x}_+}{|\mathbf{d} + (2a - (\hat{\mathbf{e}}_z \cdot \mathbf{d}))\hat{\mathbf{e}}_z|^3} - \frac{\mathbf{r}_+ \times \mathbf{x}_-}{|2a + (\hat{\mathbf{e}}_z \cdot \mathbf{d})|^3} + \frac{\mathbf{r}_+ \times \mathbf{x}_+}{|2a - (\hat{\mathbf{e}}_z \cdot \mathbf{d})|^3} - \frac{\mathbf{r}_+ \times \mathbf{x}_-}{|-\mathbf{d} + (2a + (\hat{\mathbf{e}}_z \cdot \mathbf{d}))\hat{\mathbf{e}}_z|^3}\right] \\
&= \frac{Q^2}{4\pi\varepsilon_0}\left[\frac{-a - \frac{d}{2}\cos\theta}{\sqrt{4a^2 + d^2\sin^2\theta}^3} + \frac{a - \frac{d}{2}\cos\theta}{\sqrt{4a^2 + d^2 + 4ad\cos\theta}^3} + \frac{-a - \frac{d}{2}\cos\theta}{\sqrt{4a^2 + d^2 - 4ad\cos\theta}^3} + \frac{-a + \frac{d}{2}\cos\theta}{\sqrt{4a^2 + d^2\sin^2\theta}^3}\right] d\,s \\
&\simeq \frac{Q^2}{4\pi\varepsilon_0}\left[\frac{a + \frac{z}{2}}{\sqrt{4a^2 + 4az}^3} + \frac{-a + \frac{z}{2}}{\sqrt{4a^2 - 4az}^3} + \frac{-z}{\sqrt{4a^2}^3}\right] d\sin\theta\hat{\mathbf{e}}_x \simeq -\frac{Q^2}{4\pi\varepsilon_0}\frac{3d^2\sin\theta\cos\theta}{8a^3}\hat{\mathbf{e}}_x \ .
\end{aligned}
$$

Assuming $d \ll a$ we disregarded, in the last line, the terms $\propto d^2$ and expanded in

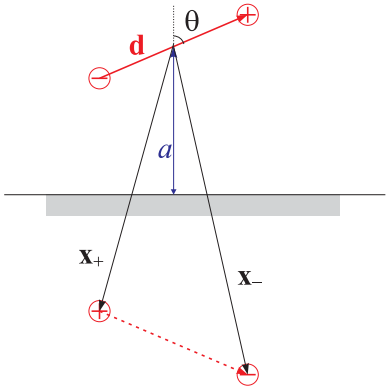

Figure 14.4: Dipoles.

terms of $z \equiv \cos\theta$. In particular, when the dipole is perpendicular to the surface ($\theta \simeq 0$),

$$\vec{\tau}_{perp} = -\frac{Q^2}{4\pi\varepsilon_0}\frac{3d^2}{8a^3}\hat{\mathbf{e}}_x\theta \ .$$

That is, in this position it is in a stable position, because when θ increases ($\theta > 0°$), it receives a torque pushing it backwards. On the other hand, when the dipole is parallel to the surface ($\theta' \equiv \theta - 90° \simeq 0$), we have,

$$\vec{\tau}_{para} \simeq \frac{Q^2}{4\pi\varepsilon_0}\frac{3d^2}{8a^3}\hat{\mathbf{e}}_x\theta' \ .$$

That is, it stays in a labile equilibrium, because when θ' increases ($\theta' > 0°$), it gets a torque pushing it forward.

14.1.7.2 Ex: Torque on dipoles

Consider the configuration of two dipoles shown in the figure and calculate the reciprocal torques.

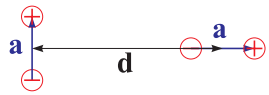

Figure 14.5: Dipoles.

Solution: *a. We put the first dipole in the origin,* $\mathbf{r}_\pm = \pm\frac{d}{2}\hat{\mathbf{e}}_z$*, such that the second is at the coordinates* $\mathbf{x}_\pm = (a+\frac{d}{2})\hat{\mathbf{e}}_x$*. The electric field* $\vec{\mathcal{E}}_\pm$ *generated by the second dipole at the position of the first is,*

$$\vec{\mathcal{E}}(\mathbf{r}_+) = \frac{Q}{4\pi\varepsilon_0}\frac{\frac{d}{2}\hat{\mathbf{e}}_z - (a+\frac{d}{2})\hat{\mathbf{e}}_x}{|\frac{d}{2}\hat{\mathbf{e}}_z - (a+\frac{d}{2})\hat{\mathbf{e}}_x|^3} - \frac{Q}{4\pi\varepsilon_0}\frac{\frac{d}{2}\hat{\mathbf{e}}_z - (a-\frac{d}{2})\hat{\mathbf{e}}_x}{|\frac{d}{2}\hat{\mathbf{e}}_z - (a-\frac{d}{2})\hat{\mathbf{e}}_x|^3}$$
$$\vec{\mathcal{E}}(\mathbf{r}_-) = \frac{Q}{4\pi\varepsilon_0}\frac{-\frac{d}{2}\hat{\mathbf{e}}_z - (a+\frac{d}{2})\hat{\mathbf{e}}_x}{|-\frac{d}{2}\hat{\mathbf{e}}_z - (a+\frac{d}{2})\hat{\mathbf{e}}_x|^3} - \frac{Q}{4\pi\varepsilon_0}\frac{-\frac{d}{2}\hat{\mathbf{e}}_z - (a-\frac{d}{2})\hat{\mathbf{e}}_x}{|-\frac{d}{2}\hat{\mathbf{e}}_z - (a-\frac{d}{2})\hat{\mathbf{e}}_x|^3} \ .$$

The torque now is,

$$\begin{aligned}
\vec{\tau} &= \tfrac{d}{2}\hat{\mathbf{e}}_z \times Q\vec{\mathcal{E}}(\mathbf{r}_+) + (-\tfrac{d}{2}\hat{\mathbf{e}}_z)\times(-Q)\vec{\mathcal{E}}(\mathbf{r}_-) = \frac{Q^2}{4\pi\varepsilon_0}\frac{d}{2}\hat{\mathbf{e}}_z \\
&\times\left(\frac{\frac{d}{2}\hat{\mathbf{e}}_z - (a+\frac{d}{2})\hat{\mathbf{e}}_x}{|\frac{d}{2}\hat{\mathbf{e}}_z - (a+\frac{d}{2})\hat{\mathbf{e}}_x|^3} - \frac{\frac{d}{2}\hat{\mathbf{e}}_z - (a-\frac{d}{2})\hat{\mathbf{e}}_x}{|\frac{d}{2}\hat{\mathbf{e}}_z - (a-\frac{d}{2})\hat{\mathbf{e}}_x|^3} + \frac{-\frac{d}{2}\hat{\mathbf{e}}_z - (a+\frac{d}{2})\hat{\mathbf{e}}_x}{|-\frac{d}{2}\hat{\mathbf{e}}_z - (a+\frac{d}{2})\hat{\mathbf{e}}_x|^3} - \frac{-\frac{d}{2}\hat{\mathbf{e}}_z - (a-\frac{d}{2})\hat{\mathbf{e}}_x}{|-\frac{d}{2}\hat{\mathbf{e}}_z - (a-\frac{d}{2})e_x|^3}\right) \\
&= -\frac{Q^2}{4\pi\varepsilon_0}\frac{d}{2}\left(\frac{a+\frac{d}{2}}{\sqrt{\left(\frac{d}{2}\right)^2+\left(a+\frac{d}{2}\right)^2}^3} - \frac{a-\frac{d}{2}}{\sqrt{\left(\frac{d}{2}\right)^2+\left(a-\frac{d}{2}\right)^2}^3} + \frac{a+\frac{d}{2}}{\sqrt{\left(\frac{d}{2}\right)^2+\left(a+\frac{d}{2}\right)^2}^3} - \frac{a-\frac{d}{2}}{\sqrt{\left(\frac{d}{2}\right)^2+\left(a-\frac{d}{2}\right)^2}^3}\right) \\
&= -\frac{Q^2}{4\pi\varepsilon_0}\frac{d}{2}\left(\frac{2a+d}{\sqrt{\left(\frac{d}{2}\right)^2+\left(a+\frac{d}{2}\right)^2}^3} - \frac{2a-d}{\sqrt{\left(\frac{d}{2}\right)^2+\left(a-\frac{d}{2}\right)^2}^3}\right)\hat{\mathbf{e}}_y \\
&\simeq -\frac{Q^2}{4\pi\varepsilon_0}\frac{d}{2}\left(\frac{2a+d}{a^3} - \frac{2a-d}{a^3}\right)\hat{\mathbf{e}}_y = -\frac{Q^2}{4\pi\varepsilon_0}\frac{d^2}{a^3}\hat{\mathbf{e}}_y \ .
\end{aligned}$$

That is, there exists a torque.
b. Now we put the second dipole at the origin, $\mathbf{r}_\pm = \pm\frac{d}{2}\hat{\mathbf{e}}_z$*, such that the second is at the coordinates ...*

14.1.7.3 Ex: Polarizability of hydrogen

In quantum mechanics we find for the electronic charge distribution in a hydrogen atom,

$$\varrho(r) = \frac{Q}{\pi a_B^3}e^{-2r/a_B} \ .$$

Calculate the polarizability.

Solution: *The electric field of the electronic shell is given by Gauss's law,*

$$\oint \vec{\mathcal{E}}_{ele}\cdot d\mathbf{S} = 4\pi r^2 \mathcal{E}_{ele}(r)$$
$$= \int \frac{\varrho(\mathbf{r}')}{\varepsilon_0} dV' = \frac{1}{\varepsilon_0}\int \frac{Q}{\pi a_B^3} e^{-2r'/a_B} 4\pi r'^2 dr' = \frac{Q}{\varepsilon_0}\left[1 - \left(1 + \frac{2r}{a_B} + \frac{2r^2}{a_B^2}\right) e^{-2r/a_B}\right]$$
$$\simeq \frac{Q}{\varepsilon_0}\left[\frac{4r^3}{3a_B^3} - \frac{2r^4}{a_B^4} + ...\right] .$$

Applying an outer field along the z-axis, in equilibrium position,

$$\frac{Q}{3\pi\varepsilon_0 a_B^3}\mathbf{r} \simeq \vec{\mathcal{E}}_{ele} = \vec{\mathcal{E}}_{ext} = \mathcal{E}_{ext}\hat{\mathbf{e}}_z ,$$

yielding,

$$\mathbf{r} = \frac{3\pi\varepsilon_0 a_B^3}{Q}\mathcal{E}_{ext}\hat{\mathbf{e}}_z .$$

The dipole moment of the electron shell being shifted away from the nucleus is,

$$\mathbf{d} = \int \left[Q\delta^3(\mathbf{r}' - \tfrac{z}{2}\hat{\mathbf{e}}_z) - \varrho(\mathbf{r}' + \tfrac{z}{2}\hat{\mathbf{e}}_z)\right]\mathbf{r}' dV' = \int \left[Q\delta^3(\mathbf{r}' - z\hat{\mathbf{e}}_z) - \varrho(\mathbf{r}')\right](\mathbf{r}' - \tfrac{z}{2}\hat{\mathbf{e}}_z)dV'$$
$$= Q\tfrac{z}{2}\hat{\mathbf{e}}_z - \frac{Q}{\pi a_B^3}\int e^{-2r'/a_B}\mathbf{r}' dV' + \frac{Q}{\pi a_B^3}\tfrac{z}{2}\hat{\mathbf{e}}_z \int e^{-2r'/a_B} dV'$$
$$= Q\tfrac{z}{2}\hat{\mathbf{e}}_z - 0 + \frac{Q}{\pi}\tfrac{z}{2}\hat{\mathbf{e}}_z 4\pi \int_0^\infty u^2 e^{-2u} du = Qz\hat{\mathbf{e}}_z .$$

Finally, the polarizability is,

$$\frac{\alpha_{pol}}{4\pi\varepsilon_0} = \frac{d}{4\pi\varepsilon_0\mathcal{E}_{ext}} = \frac{Qz}{4\pi\varepsilon_0\mathcal{E}_{ext}} = \frac{3}{4}a_B^3 .$$

Alternatively:

$$4\pi r^2\mathcal{E}_{ele}(r) = \frac{Q}{\pi\varepsilon_0 a_B^3}4\pi\int_0^r e^{-2r'/a_B} r'^2 dr' \simeq \frac{Q}{\pi\varepsilon_0 a_B^3}4\pi\int_0^r r'^2 dr' = \frac{Q}{\varepsilon_0 a_B^3}\frac{4r^3}{3} \tag{14.29}$$

gives the same result.

14.1.7.4 Ex: Susceptibility

One liter of water is evaporated in $10\,\mathrm{m}^3$ of dry air at room temperature $T = 300\,\mathrm{K}$.
a. Calculate the dipolar density n of the air. Assume that only the dipolar moments of the evaporated molecules contribute.
b. Determine the susceptibility χ_ε of the air. Use the relation $\mathcal{P} = \varepsilon_0\chi_\varepsilon\mathcal{E}$, as well as Curie's law for the polarization $\mathcal{P}$.

Solution: *a. The number of molecules in* $1\,\mathrm{l} = 1\,\mathrm{kg} = m_0$ *of water, with the molecular mass being* $m_{H_2O} = 18u = 18 \cdot 1.66 \cdot 10^{-27}\,\mathrm{kg}$*, is,*

$$N = \frac{m_0}{m_{H_2O}} = 3.35 \cdot 10^{25} \ .$$

the dipolar density is:

$$n = \frac{N}{V} = 3.35 \cdot 24\,\mathrm{m}^{-3} \ .$$

b. The definition of χ_e *is given by:* $\mathcal{P} = \varepsilon_0 \chi_0 \mathcal{E}$*. With Curie's law:*

$$\vec{\mathcal{P}} = \frac{1}{3} n \frac{\mathbf{d} \cdot \vec{\mathcal{E}}}{k_B T} \mathbf{d} = \frac{1}{3} n \frac{d^2 \mathcal{E}}{k_B T} \hat{\mathbf{e}}_d$$

to d *parallel to* $\mathcal{E}$*. Equalizing,*

$$\varepsilon_0 \chi_0 = \frac{1}{3} n \frac{d^2}{k_B T} = 1.17 \cdot (-3) \ .$$

14.2 Influence of charges and capacitance

We now assume that we have two separate conductors, one carrying the charge $+Q$ and the other $-Q$. Since the potential of each conductor is the same at each point of its body, we can specify a potential difference, called *voltage*, between them,

$$U \equiv \Phi_+ - \Phi_- = -\int_{(-)}^{(+)} \vec{\mathcal{E}} \cdot d\mathbf{l} \ , \tag{14.30}$$

which does not depend on the distribution of the charges throughout the conductors. However, we know from Coulomb's law that the electric field is proportional to the charge Q and from the above equation, also the voltage. The proportionality factor is called *capacitance*,

$$C \equiv \frac{Q}{U} \ . \tag{14.31}$$

14.2.1 Capacitors and storage of electric energy

A device capable of storing charges is called *capacitor*.

> **Example 62 (*Plate capacitor*):** The simplest geometry for a capacitor are two parallel conducting plates (area S) maintained at a distance d. The surface charge distribution $\sigma = Q/S$ produces a field $\mathcal{E} = \sigma/\varepsilon_0$ and a potential difference $U = \mathcal{E}d$, such that,
>
> $$C = \varepsilon_0 \frac{S}{d} \ . \tag{14.32}$$

To charge a capacitor we must bring electrons from the positive side to the negative side of the capacitor. For a single electron, this requires the work

$$\Delta W_e = \int_0^d \mathbf{F} \cdot d\mathbf{r} = ed|\vec{\mathcal{E}}| = eU \ .$$

For a small amount of charge dq,

$$\Delta W_e = \int U \ dQ = \int_0^Q \frac{Q}{C} dQ = \frac{Q^2}{2C} = \frac{1}{2} CU^2 \ .$$

Resolve the Excs. 14.2.2.1-14.2.2.10.

14.2.1.1 Capacitors with dielectrics

In the presence of a dielectric the capacitance increases, $C = \varepsilon_r C_{vac}$. Thus, the field energy also increases by a factor of ε_r.

We consider a capacitor filled with a linear dielectric and charged with the free charge ϱ_f, which generates a voltage U between the electrodes. We want to know the work needed to add a little bit more charge $\delta\varrho_f$ to the volume element dV,

$$\delta W = \int U \ \delta\varrho_f dV \ . \tag{14.33}$$

Now, with Eq. (14.19) we write $\varrho_f = \nabla \cdot \vec{\mathcal{D}}$ and $\delta\varrho_f = \nabla \cdot \delta\vec{\mathcal{D}}$, such that,

$$\delta W = \int_{\mathcal{V}} U \nabla \cdot \delta\vec{\mathcal{D}} dV = \int_{\partial\mathcal{V}} U \ \delta\vec{\mathcal{D}} \cdot d\mathbf{S} - \int_{\mathcal{V}} \delta\vec{\mathcal{D}} \cdot \nabla U dV = \int_{\mathcal{V}} \delta\vec{\mathcal{D}} \cdot \vec{\mathcal{E}} dV \ . \tag{14.34}$$

For a linear dielectric, $\vec{\mathcal{D}} = \varepsilon\vec{\mathcal{E}}$, such that, $\vec{\mathcal{E}} \cdot \delta\vec{\mathcal{D}} = \vec{\mathcal{E}}\varepsilon \cdot \delta\vec{\mathcal{E}} = \frac{1}{2}\delta(\varepsilon E^2) = \frac{1}{2}\delta(\vec{\mathcal{D}} \cdot \vec{\mathcal{E}})$, giving,

$$\delta W = \tfrac{1}{2} \int \delta(\vec{\mathcal{D}} \cdot \vec{\mathcal{E}}) dV \ . \tag{14.35}$$

Finally, to charge the capacitor completely,

$$W = \int \delta W = \tfrac{1}{2} \int \vec{\mathcal{D}} \cdot \vec{\mathcal{E}} = \int u dV \ , \tag{14.36}$$

with the energy density,

$$\boxed{u = \frac{1}{2} \vec{\mathcal{E}} \cdot \vec{\mathcal{D}}} \ . \tag{14.37}$$

Do the Excs. 14.2.2.11-14.2.2.18.

> **Example 63 (*Forces on dielectrics*):** Dielectrics in electric fields are subjected to forces due to the polarization induced in the medium. Let us consider the example of a plate capacitor inside which we insert a dielectric. In the scheme shown in Fig. 14.6 the electric field homogeneously traverses the capacitor and also the dielectric body, such that the forces should disappear. On the other hand, on its edges the dielectric distorts the field, such that forces become possible.

The easiest way to calculate these forces is via the potential energy gradient, $\mathbf{F} = -\nabla W$. If the dielectric body is free to move in x-direction, we have,

$$\mathbf{F} = -\frac{dW}{dx} = -\frac{d}{dx}\frac{Q^2}{2C} = -\frac{d}{dx}\frac{CU^2}{2} \ .$$

We use the first expression, in case the charge on the capacitor is kept constant, and the second, when the voltage on the capacitor is kept constant. Gradually inserting the dielectric, a part of the volume of the capacitor will be empty and another part will be filled with the dielectric medium:

$$C = C_{vac}\frac{x}{a} + C_{vac}\varepsilon_r\frac{a-x}{a} \ .$$

Keeping the charge constant, we get,

$$\mathbf{F} = \frac{Q^2}{2C^2}\frac{dC}{dx} = -\frac{d}{dx}\frac{Q^2}{2(C_{vac}\frac{x}{a} + C_{vac}\varepsilon_r\frac{a-x}{a})} = \frac{Q^2}{2C_{vac}}\frac{-a\chi_\varepsilon}{(a - x\chi_\varepsilon)^2} \ .$$

Since the force is negative, the dielectric is drawn into the capacitor.
The situation is different when we keep the voltage constant, for example, by connecting the capacitor to a battery. In this case we need to use the second expression. However, we must take into account the work UdQ that the battery must do to increase the charge on the capacitor in order to maintain the voltage constant while we increase the capacity via $C_{vac} \to C$,

$$dW = -Fdx + UdQ \ .$$

Hence,

$$F = -\frac{dW}{dx} + U\frac{dQ}{dx} = -\frac{U^2}{2}\frac{dC}{dx} + U^2\frac{dC}{dx} = \frac{Q^2}{2C^2}\frac{dC}{dx} \ ,$$

and we get the same result as in the case where we kept the charge constant.

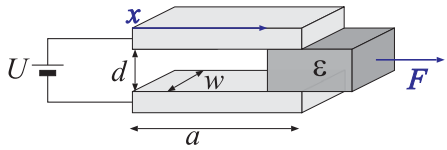

Figure 14.6: Force on the dielectric between the plates of a capacitor.

14.2.1.2 Capacitor circuits

For parallel circuits $C_{tot} = C_1 + C_2$, for circuits in series $C_{tot}^{-1} = C_1^{-1} + C_2^{-1}$. Do the Excs. 14.2.2.19-14.2.2.27.

14.2.2 Exercises

14.2.2.1 Ex: Capacitors

Be given two isolated conductors carrying equal charges but with opposite signs $\pm Q$. The capacity of this configuration is the ratio between the absolute value of the charge of one conductor and the absolute value of the potential difference between the two

conductors. Using Gauß' law calculate the capacity of
a. 2 large parallel plates with area A being at a short distance d;
b. 2 concentric cylindrical conductors (without surfaces at the ends of the cylinders) with radii ρ_1 and ρ_2.
c. 2 concentric spherical surfaces with radii r_1 and r_2.
Help: Choose integration volumes that fits the symmetry of your system.

Solution: *a. Choosing a volume enclosing one of the plates and using Gauß' law:*

$$\frac{Q}{\varepsilon_0} = \int_{\partial V} \vec{\mathcal{E}} \cdot d\mathbf{S} = \int_{\partial V} \mathcal{E}_z \; dxdy = \mathcal{E}_z S \; .$$

The potential difference is,

$$\Phi_1 - \Phi_2 = \int_{plane1}^{plane2} \vec{\mathcal{E}} \cdot d\mathbf{s} = \int_{z_1}^{z_2} \frac{Q}{\varepsilon_0 S} dz = \frac{Q}{\varepsilon_0 A} d \; .$$

Therefore, the capacity is,

$$C = \frac{Q}{|\Phi_1 - \Phi_2|} = \varepsilon_0 \frac{S}{d} \; .$$

b. Choosing a volume enclosing the inner cylinder and using Gauß' law:

$$\frac{Q}{\varepsilon_0} = \int_{\partial V} \vec{\mathcal{E}} \cdot d\mathbf{S} = \int_{\partial V} \mathcal{E}_\rho \; \rho d\phi dz = \mathcal{E}_\rho 2\pi\rho L \; .$$

The potential difference is,

$$\Phi_1 - \Phi_2 = \int_{cilint}^{cilext} \vec{\mathcal{E}} \cdot d\mathbf{l} = \int_{\rho_1}^{\rho_2} \frac{Q}{2\pi\varepsilon_0 L} \frac{1}{\rho} d\rho = \frac{1}{2} \frac{Q}{\pi\varepsilon_0 L} \ln \frac{\rho_2}{\rho_1} \; .$$

Therefore, the capacity is,

$$C = \frac{Q}{|\Phi_1 - \Phi_2|} = \frac{2\pi\varepsilon_0 L}{\ln \rho_2 - \ln \rho_1} \; .$$

c. Choosing a volume enclosing the inner sphere and using Gauß' law:

$$\frac{Q}{\varepsilon_0} = \int_{\partial V} \vec{\mathcal{E}}_\rho \cdot d\mathbf{S} = \int_{\partial V} \mathcal{E}_r \; r^2 \sin\theta d\theta d\phi = \mathcal{E}_r r^2 4\pi \; .$$

The potential difference is,

$$\phi_1 - \phi_2 = \int_{esfint}^{esfext} \vec{\mathcal{E}} \cdot d\mathbf{s} = \int_{r_1}^{r_2} \frac{Q}{4\pi\varepsilon_0 r^2} dr = -\frac{Q}{4\pi\varepsilon_0} \frac{r_1 - r_2}{r_2 r_1} \; .$$

Therefore, the capacity is,

$$C = \frac{Q}{|\phi_1 - \phi_2|} = \frac{4\pi\varepsilon_0 r_2 r_1}{r_2 - r_1} \; .$$

14.2.2.2 Ex: Capacitance of a mercury drop

The capacity of a spherical drop of mercury with radius R is given by $C = 4\pi\varepsilon_0$. Now, two of these drops merge. What is the capacity of this larger drop?

Solution: *The capacity of this larger drop ...*

14.2.2.3 Ex: Charged plates

Consider a thin, very extended metal plate, $d^2 \ll A$, with area A and thickness d carrying the charge Q. Calculate the charge distribution (surface charge density) and the electric field on both sides of the plate neglecting edge effects. How do the charge distribution and the electric field change, when we have two plates instead of one with thickness d at a distance l, one being charged with the charge Q and the other with $-Q$.

Solution:

14.2.2.4 Ex: Plate capacitor

A capacitor is made of two flat metal plates with the surfaces $1\,\mathrm{m}^2$. What should be the distance of the plates to give the capacitor a capacity of $1\,\mathrm{F}$? Is it possible to build such a capacitor?

Solution: *a. From the relationship* $C = \varepsilon_0 \frac{A}{d}$ *It follows that the distance between the plates should be less than* $d = \varepsilon_0 \frac{A}{C} < 8.9\,\mathrm{pm}$*, which is smaller than the atomic radius and therefore impossible.*

14.2.2.5 Ex: Cylindrical capacitor

A cylindrical capacitor is made of two infinitesimally thin coaxial cylindrical surfaces with radii R_1 and R_2. For simplicity, assume that the cylinders are infinitely extended in z-direction. The charge per unit length on the inner cylinder is $+Q/l$, on the outer cylinder $-Q/l$. Calculate the electric field $\vec{\mathcal{E}}(r)$ as a function of the distance r from the symmetry axis for $r \leq R_1$, $R_1 < r < R_2$, and $r \geq R_2$.
Help: Use the symmetry of the problem and Gauß' law.

Solution: *From Gauß' law,* $\int_V \nabla \cdot \vec{\mathcal{E}} d^3\mathbf{r} = \oint_{\partial V} \vec{\mathcal{E}} \cdot d\mathbf{S}$ *together with* $\nabla \cdot \vec{\mathcal{E}} = \varrho/\varepsilon_0$ *gives,*

$$\int_V \varrho d^3\mathbf{r} = \varepsilon_0 \oint_{\partial V} \vec{\mathcal{E}} \cdot d\mathbf{A} \ .$$

Because of the cylindrical symmetry we only need to consider the radial component of the field. We integrate on a cylinder with radius r*. For* $r < R_1$ *we get,*

$$\mathcal{E}_{r<R_1} = 0 \ .$$

for $R_1 < r < R_2$ *we get* $\int_{V_r} \varrho d^3\mathbf{r} = \pi r^2 \varrho L = \frac{Q}{l} L$ *and* $\oint_{\partial V} \vec{\mathcal{E}} \cdot d\mathbf{S} = \mathcal{E}_r \cdot 2\pi r L$. *From this follows,* $\frac{Q}{l} L = \varepsilon_0 \mathcal{E}_r 2\pi r L$, *and finally,*

$$\mathcal{E}_{R_1<r<R_2} = \frac{Q}{2\pi\varepsilon_0 l} \frac{1}{r} \ .$$

for $R_2 < r$ *we get* $Q = 0$, *hence,*

$$\mathcal{E}_{R_2<r} = 0 \ .$$

14.2.2.6 Ex: Cylindrical capacitor (T7)

Two concentric infinitely thin hollow conductive cylinders with radii a and b ($a < b$) and length l are charged with charges $+q$ resp. $-Q$. l is much larger than b, such that border effects are negligible. For symmetry reasons, the electric field can only have one radial component.
a. Write down the charge distribution $\varrho(\mathbf{r})$ in cylindrical coordinates (r, ϕ, z) with the help of the δ-function.
b. Calculate the electric field $\vec{\mathcal{E}}(r, \phi, z)$ in the whole space ($r < a,\ a < r < b,\ b < r$). Use for this the fundamental equations of electrostatics and $\nabla \cdot \vec{\mathcal{E}} = \frac{1}{r} \frac{d}{dr}(eE_r)$. Alternatively, this part can be resolved using Gauß' law.
c. Calculate the potential difference $|\Phi(r = b) - \Phi(r = a)|$ between the two surface of the cylinders. To do this, calculate the line integral $\int \vec{\mathcal{E}} \cdot d\mathbf{r}$ along a suitable path.
d. The capacity C of the device is defined by the absolute value of the ratio between the charge on one cylinder and the potential difference between the cylinders. Calculate the capacity of this 'cylindrical capacitor'.

Solution: *a. We have,*

$$\varrho(r, \phi, z) = \frac{q}{2\pi a l} \delta(r - a) - \frac{q}{2\pi b l} \delta(r - b) \ .$$

Proof:

$$\int\limits_{cil.int} d^3 r \varrho = 2\pi l \int\limits_{a-\varepsilon}^{a+\varepsilon} dr r \varrho = 2\pi a l \frac{q}{2\pi a l} = q \ .$$

b. Using Gauß' faw:

$$\int\limits_{sup.\ cyl.} \vec{\mathcal{E}} \cdot d\vec{f} = 2\pi r l E_r = \int\limits_{vol.\ cyl.} d^3\mathbf{r}\ \nabla \cdot \vec{\mathcal{E}} = 4\pi Q \ ,$$

where Q *is the total charge inside the integration volume. Follows,*

$$\mathcal{E}_r = 0 \qquad for \qquad r < a \qquad and \qquad r > b$$

$$\mathcal{E}_r = \frac{2q}{l} \frac{1}{r} \qquad for \qquad a < r < b \ .$$

Alternatively with Gauß' law,

$$\nabla \cdot \vec{\mathcal{E}} = \frac{1}{r}\frac{d}{dr}(r\mathcal{E}_r) = 4\pi\varrho \ ,$$

and hence,

$$r\mathcal{E}_r|_0^r = 4\pi \int_0^r dr' r' \varrho = \frac{2q}{l}\frac{1}{r} \qquad for \qquad a < r < b \ ,$$

and 0 else.
c. We have,

$$\Delta\Phi = \int_{cyl.int}^{cyl.ext} \vec{\mathcal{E}} \cdot d\mathbf{r} = \int_a^b dr \frac{2q}{lr} = \frac{2q}{l}\ln(\frac{b}{a}) \ .$$

d. We have,

$$C = \frac{q}{\Delta\Phi} = \frac{l}{2}\frac{1}{\ln(\frac{b}{a})} \ .$$

14.2.2.7 Ex: Spherical capacitor

Consider a homogeneously charged ball with radius R_1 and an infinitely thin spherical homogeneously charged shell with radius R_2. The ball has the full charge $+Q$, the shell $-Q$. Calculate the electric field $\vec{\mathcal{E}}(r)$ for $r \leq R_1$, $R_1 < r < R_2$ and $r \geq R_2$.
Help: Use the fact that $\vec{\mathcal{E}}$ must be, for symmetry reasons, radially symmetrical, and depends on the charge density via $\nabla \cdot \vec{\mathcal{E}}(r) = \varrho(r)/\varepsilon_0$. Also use Gauß' law.

Solution: *From the ansatz:*

$$\vec{\mathcal{E}}(\mathbf{r}) = \mathcal{E}(r)\hat{\mathbf{e}}_r \qquad and \qquad d\mathbf{S} = r^2 \sin\theta \ d\theta \ d\phi \ \hat{\mathbf{e}}_r \ .$$

with Gauß:

$$\int_{\partial V} \vec{\mathcal{E}}(\mathbf{r}) \cdot d\mathbf{S} = \frac{1}{\varepsilon_0} \ q(V) \ .$$

For the case $r \leq R_1$:

$$\int \vec{\mathcal{E}} \cdot d\mathbf{S} = \int_{\theta=0}^{\pi}\int_{\phi=0}^{2\pi} \mathcal{E}(r) r^2 \sin\theta d\theta d\phi = 4\pi r^2 E(r) \equiv \frac{1}{\varepsilon_0}Q(r)$$

$Q(r) = \phi V(r)$ *with* $\phi = \frac{Q}{4/3\pi R_1^3}$ *homogeneous charge density, hence* $Q(r) = Q\frac{r^3}{R_1^3}$, *hence* $\mathcal{E}(r) = \frac{Q}{4\pi\varepsilon_0 R_1^3} r$.
For the case $R_1 < r < R_2$:

$$Q(r) = +Q$$

with Gauß $\rightsquigarrow 4\pi r^2 \mathcal{E}(r) = \frac{Q}{\varepsilon_0}$, *hence* $\mathcal{E}(r) = \frac{Q}{4\pi\varepsilon_0}\frac{1}{r^2}$.
For the case $r \leq R_2$:

$$Q = +Q + (-Q) = 0$$

Hence, $\mathcal{E}(r) = 0$.

14.2.2.8 Ex: Thunderstorm

The cloud of a thunderstorm with $17\,\mathrm{km}^2$ of total area floats at a height of $900\,\mathrm{m}$ above the Earth's surface and forms with it a plate capacitor.
a. Calculate the capacity of this plate capacitor (the area to be considered on Earth is equal to that of the cloud).
b. What is the maximum charge of the thundercloud before the capacitor discharges? (The discharge electric field in air is $10^4\,\mathrm{V/cm}$).
c. The capacitor is totally discharged by a lightning, once the critical field strength is reached. What is the current flowing to Earth if the lightning's duration is $1\,\mathrm{ms}$?
d. What power does this correspond to? For how long a power station with a power of $2000\,\mathrm{MW}$ needs to work to produce the energy released by lightning?

Solution:

14.2.2.9 Ex: Spherical capacitor

A spherical capacitor consists of two concentric conducting spheres of radii R_1 and R_2, with $R_1 < R_2$. The inner sphere has a charge $+Q$ and the outer sphere has a charge $-Q$.
a. Calculate the absolute value of the electric field and the energy density as a function of r, where r is the radial distance from the center of the spheres for any r.
b. Determine the capacitance C of the capacitor.
c. Calculate the energy associated with the electric field integrated over a spherical shell of radius r, thickness dr, and volume $4\pi r^2 dr$ located between the conductors. Integrate the obtained expression to find the total energy between the conductors. Give your answer in terms of the charge Q and the capacitance C.

Solution: *a. We have*

$$\vec{\mathcal{E}}(\mathbf{r}) = \mathcal{E}(r)\hat{e}_r \qquad \textit{and} \qquad d\mathbf{F} = r^2 \sin\theta \; d\theta \; d\phi \; \hat{e}_r \; .$$

Gauß' law requires

$$\int_{\partial V} \vec{\mathcal{E}}(\mathbf{r}) \cdot d\mathbf{F} = \frac{1}{\varepsilon_0} \; q(V) \; .$$

That is:

$$\int \vec{\mathcal{E}} d\mathbf{F} = \int_{\theta=0}^{\pi} \int_{\phi=0}^{2\pi} \mathcal{E}(r) r^2 \sin\theta d\theta d\phi = 4\pi r^2 \mathcal{E}(r) \equiv \frac{1}{\varepsilon_0} Q(r) \; ,$$

where $Q(r)$ is the charge concentrated within a sphere with radius r. For $r \leq R_1$, as there is no charge inside the inner sphere, we have,

$$\mathcal{E}(r) = 0 \; .$$

Between the spheres we have

$$\mathcal{E}(r) = \frac{Q}{4\pi\varepsilon_0^2} \; .$$

Outside the outer sphere we have,

$$\mathcal{E}(r) = 0 \ ,$$

because the opposite charges of the spheres compensate. The energy density is,

$$u(r) = \frac{1}{2}\vec{\mathcal{D}} \cdot \vec{\mathcal{E}} = \frac{\varepsilon_0}{2}\mathcal{E}^2 = \frac{Q^2}{32\pi^2\varepsilon_0 r^4} \ .$$

b. The voltage between the spheres is,

$$\Delta V = -\int_{R_1}^{R_2} \mathcal{E}(r)dr = -\frac{Q}{4\pi\varepsilon_0}\int_{R_1}^{R_2}\frac{1}{r^2}dr = \frac{Q}{4\pi\varepsilon_0}\left(\frac{1}{R_2} - \frac{1}{R_1}\right) \ .$$

The capacitance is,

$$C = \frac{Q}{\Delta V} = \frac{4\pi\varepsilon_0}{\frac{1}{R_1} - \frac{1}{R_2}} \ .$$

c. The energy inside a thin layer is given by,

$$\begin{aligned} U &= \int_V u(r)d^3r = \int_0^{2\pi}\int_0^{\pi}\int_r^{r+dr}\frac{Q^2}{32\pi^2\varepsilon_0 r^4}r^2\sin\theta d\phi d\theta dr \\ &= \frac{Q^2}{32\pi^2\varepsilon_0}4\pi\int_r^{r+dr}\frac{1}{r^2}dr = \frac{Q^2}{8\pi\varepsilon_0}\frac{dr}{r} \ . \end{aligned}$$

The total energy between the spheres is,

$$\begin{aligned} U &= \int_V u(r)d^3r = \int_0^{2\pi}\int_0^{\pi}\int_{R_1}^{R_2}\frac{Q^2}{32\pi^2\varepsilon_0 r^4}r^2\sin\theta d\phi d\theta dr \\ &= \frac{Q^2}{32\pi^2\varepsilon_0}4\pi\int_{R_1}^{R_2}\frac{1}{r^2}dr = \frac{Q^2}{8\pi\varepsilon_0}\left.\frac{-1}{r}\right|_{R_1}^{R_2} = \frac{Q^2}{8\pi\varepsilon_0}\left[\frac{1}{R_1} - \frac{1}{R_2}\right] \ . \end{aligned}$$

14.2.2.10 Ex: Lightning rod

The absorption of lightning by a lightning rod can be described by the following model (outlined in the figure): The (x, y) plane of a Cartesian coordinate system divides a half space with the conductivity κ (the soil of the Earth, $z < 0$) from a space with conductivity 0 (air, $z > 0$). In the center of the coordinates is an extremely conductive semispherical electrode connected with the lightning rod of diameter d. Current I can cross the semisphere and enter the conducting half space. For symmetry reasons, the current density may only depend on the distance r from the origin of the coordinates and must be oriented radially: $\mathbf{j} = j_r(r)\hat{\mathbf{e}}_r$. All of the following questions refer to points in the conductive semi-space outside the electrode.
a. Calculate the current density $\mathbf{j}$ as a function of the current amplitude I and the distance r from the source. **Help:** The current flowing from the electrode to the conducting half space must also exit the semisphere K.

b. Determine the electric field $\vec{\mathcal{E}}(\mathbf{r})$.
c. Determine the electrical voltage $U(x, s)$ between two points on the positive x-axis, having the coordinates x and $x + s$, respectively.
d. Determine the voltage U_{tot} for $x = d/2$ and $s \to \infty$. What ohmic resistance can be attributed to the conducting half space?

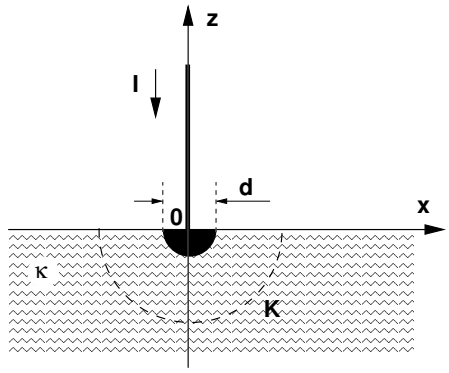

Figure 14.7:

Solution:

14.2.2.11 Ex: Plate capacitor (H13)

An ideal plate capacitor consists of two parallel plates at a distance d. One of the plates, defined by the corners $(0, 0, 0)$, $(a, 0, 0)$, $(a, b, 0)$, and $(0, b, 0)$), be charged with the charge $-Q$, the other plate, defined by the corners $(0, 0, d)$, $(a, 0, d)$, (a, b, d) and $(0, b, d)$, has the charge $+Q$. A part of the intermediate space (up to the surface between the points $(x, 0, 0)$, $(x, b, 0)$, (x, b, d), and $(x, 0, d)$) be filled with a homogeneous dielectric with the dielectric constant ε; the rest of the space between the plates is empty. We assume that a and b are very large, such that border effects can be neglected.
a. Calculate the electric field $\vec{\mathcal{E}}$ and the dielectric displacement $\vec{\mathcal{D}}$ between the plates.
Help: Use $\nabla \times \vec{\mathcal{E}} = 0$ and $\nabla \cdot \vec{\mathcal{D}} = \varrho$. Use surface charge densities.
b. Calculate the energy of the electrostatic field W of this device.
c. What force $F = -dW/dx$ acts on the dielectric for an infinitesimal displacement dx?

Solution: *a. We want to neglect edge effects. The dielectric displacement in the region of the dielectric is given by,*

$$\vec{\mathcal{D}}_1 = \varepsilon \vec{\mathcal{E}}_1 \ .$$

in the remaining region (without dielectric) between the plates by,

$$\vec{\mathcal{D}}_2 = \varepsilon_0 \vec{\mathcal{E}}_2$$

Of course, all of these fields only have the z-component. Now we have,

$$\nabla \times \vec{\mathcal{E}} = 0 \ .$$

Hence, $\mathcal{E}_z$ cannot depend on x nor on y and must be continuous on the boundary surface of the dielectric (in the following, we no longer place the index 'z' to simplify the notation):

$$\mathcal{E}_1 \equiv \mathcal{E}_2 \equiv \mathcal{E} \ .$$

Now we have in the dielectric,

$$\mathcal{D}_1 = \varepsilon \mathcal{E}$$

in the free space between the plates,

$$\mathcal{D}_2 = \varepsilon_0 \mathcal{E}$$

and everywhere,

$$\nabla \cdot \vec{\mathcal{D}} = \varrho \ .$$

Hence,

$$\mathcal{D}_1 = \sigma_1 \qquad \textit{and} \qquad \mathcal{D}_2 = \sigma_2 \ ,$$

where σ_1 resp. σ_2 represent the densities of surface charges. With that we get the full charge,

$$Q = \sigma_1 \ A_1 + \sigma_2 \ A_2 = D_1 A_1 + D_2 A_2 = \mathcal{E}(\varepsilon A_1 + \varepsilon_0 A_2) = \mathcal{E} b(\varepsilon x + \varepsilon_0 a - \varepsilon_0 x) = \mathcal{E} b(\varepsilon_0 a + (\varepsilon - \varepsilon_0)x) \ .$$

resp. for the electric field,

$$\mathcal{E} = \frac{Q}{b(\varepsilon_0 a + [\varepsilon - \varepsilon_0]x)} \ .$$

b. Follows immediately,

$$W = \frac{1}{2} \int d\tau \ \vec{\mathcal{E}} \cdot \vec{\mathcal{D}} = \frac{1}{2}[\mathcal{E}\mathcal{D}_1 A_1 d + \mathcal{E}\mathcal{D}_2 A_2 d] = \frac{1}{2} E^2 d[\varepsilon A_1 + A_2]$$
$$= \frac{1}{2}\mathcal{E}^2 db[\varepsilon_0 a + (\varepsilon - \varepsilon_0)x] = \frac{1}{2} \frac{Q^2 d}{b[\varepsilon_0 a + (\varepsilon - \varepsilon_0)x]} \ .$$

c. The force follows with,

$$F = -\frac{dW}{dx} = \frac{1}{2} \frac{dQ^2(\varepsilon - \varepsilon_0)}{b[a + (\varepsilon - \varepsilon_0)x]^2} \ \geq \ 0 \ .$$

It is oriented in $+x$-direction. The dielectric is therefore dragged to the capacitor.

14.2.2.12 Ex: Spherical capacitor with dielectric (H14)

Two concentric conducting spheres with radii a and b ($a < b$) carry the charges $\pm Q$. Half of the space between the spheres is filled by a dielectric $\varepsilon = const.$
a. Determine the electric field at all points between the spheres.
b. Calculate the surface charge distribution on the inner sphere.
c. Calculate the polarization charge density induced on the surface of the dielectric

at $r = a$.

Solution: *We denote the region between the spheres without dielectric by I, the one with dielectric by I. Without dielectric we have in the intermediate region, $\Phi(r) = \alpha/r + c$. Since the field within the dielectric is also radial, we can use this ansatz in this region as well.*
a. Integration gives immediately,

$$\mathcal{D}_r(r) = \begin{cases} \frac{\alpha}{r^2} & ED\ I\ e \\ \frac{\varepsilon\alpha}{r^2} & ED\ II \end{cases} .$$

The constant α can be determined by Gauß' law:

$$\int\limits_S dS\ \hat{\mathbf{e}}_r \cdot \vec{\mathcal{D}} = 4\pi Q\ ,$$

where Q is the enclosed charge. With that we get,

$$Q = \frac{1}{4\pi}\int\limits_S dS \frac{\alpha}{r^2} + \frac{1}{4\pi}\int\limits_S dS \frac{\varepsilon\alpha}{r^2} = \frac{\varepsilon+1}{2}\alpha\ ,$$

since the integration over the area in both cases gives the same value $4\pi r^2/2$. From this follows for $a < r < b$,

$$\vec{\mathcal{E}}(\mathbf{r}) = \frac{2Q}{\varepsilon+1}\frac{1}{r^2}\hat{\mathbf{e}}_r\ .$$

b. Inside and outside the inner spherical layer we have, $\vec{\mathcal{D}} = 0$, on the surface $\mathcal{D}_r(r = a) = 4\pi\sigma$. Therefore,

$$\sigma = \begin{cases} \frac{1}{\varepsilon+1}\frac{Q}{2\pi a^2} & ED\ I \\ \frac{\varepsilon}{\varepsilon+1}\frac{Q}{2\pi a^2} & ED\ II \end{cases} .$$

c. We have $\mathcal{D}_r = \mathcal{E}_r + 4\pi\sigma_{pol}$. Hence, $\sigma_{pol} = (\mathcal{D}_r - \mathcal{E}_r)/(4\pi) = (\varepsilon - 1)\mathcal{E}_r/4\pi$. Hence,

$$\sigma_{pol} = \begin{cases} 0 & ED\ I \\ \frac{\varepsilon-1}{\varepsilon+1}\frac{Q}{2\pi a^2} & ED\ II \end{cases} .$$

14.2.2.13 Ex: Potential of a charged sphere (T10)

A sphere of radius R be in the vacuum. It consists of a material with the dielectricity constant $\varepsilon = const$ and carries in its center the charge q. Calculate the potential in full space.

Solution: *As there is no surface charge ($\sigma = 0$), a normal component of $\vec{\mathcal{D}}$ is continuous. For $r < R$ we have $\vec{\mathcal{E}}_i = \mathcal{D}_i(r)\vec{\mathcal{E}}_r$. Hence,*

$$\int\limits_{\mathcal{V}(\nabla)} d^3\mathbf{r}\ \nabla \cdot \vec{\mathcal{D}}_i = \int\limits_{O(V(r))} d\mathbf{S} \cdot \vec{\mathcal{D}}_i = \int\limits_{V(r)} d^3\mathbf{r}\ 4\pi\varrho = 4\pi q\ .$$

Integration gives immediately,

$$4\pi r^2 \ \varepsilon \ \mathcal{D}_i(r) = 4\pi q \ ,$$

and hence,

$$\mathcal{D}_i(r) = \frac{q}{\varepsilon r^2} \qquad \textit{well as, obviously} \qquad \mathcal{D}_a(r) = \frac{q}{r^2} \ ,$$

where the index a indicates the region $r > a$. The potential outside the sphere is obviously,

$$\Phi_a(r) = \frac{q}{r} \ .$$

Inside we have,

$$\Phi_i(r) = \frac{q}{R} - \int_R^r \frac{q}{\varepsilon r'^2} dr = \frac{q}{\varepsilon r} + \frac{q}{R}\frac{\varepsilon - 1}{\varepsilon} \ .$$

14.2.2.14 Ex: Plate capacitor with dielectric

We consider two parallel electrodes with area A and distance d (see figure). Calculate the force on the upper electrode in the x-direction, once for constant voltage V_0 and once for constant charge Q for the following two cases:
a. The electrodes are inside a dielectric liquid with permittivity ε;
b. a fixed dielectric with permittivity ε is introduced between capacitor plates. In the residual gap there is no dielectric medium.

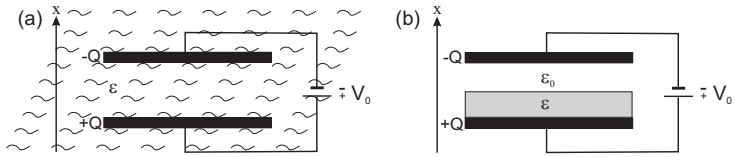

Figure 14.8: Plate capacitor.

Solution: *a. The power of the plate capacitor is (when $Q_1 = -Q_2$)*

$$W = \frac{1}{2}CU^2 = -\frac{1}{2}\frac{Q^2}{C}$$

with $C = \varepsilon_0 \varepsilon \frac{A}{x}$. Now, we have,

$$\mathbf{F}_U = -\nabla W|_{U=const} = -\frac{d}{dx}\frac{1}{2}CU^2 = \frac{1}{2}\varepsilon_0 \varepsilon \frac{A}{x^2}U^2$$

as well as,

$$\mathbf{F}_Q = -\nabla W|_{Q=const} = \frac{d}{dx}\frac{1}{2}\frac{Q^2}{C} = \frac{1}{2}\frac{1}{\varepsilon_0 \varepsilon A}Q^2$$

that is, the force is attractive.
b. As in (a) but with the total capacity of two capacitors in series:

$$C = \frac{1}{\frac{1}{\varepsilon_0 \frac{A}{x-s}} + \frac{1}{\varepsilon_0 \varepsilon \frac{A}{s}}}$$

where x is the distance and s the thickness of the dielectric. Now we have,

$$\mathbf{F}_U = -\frac{d}{dx}\frac{U^2}{2}\frac{1}{\frac{x-s}{\varepsilon_0 A} + \frac{s}{\varepsilon_0 \varepsilon A}} CU^2 = \frac{\varepsilon_0 \varepsilon A U^2}{2}\frac{1}{(\varepsilon(x-s)+s)^2}$$

as well as,

$$\mathbf{F}_Q = \frac{d}{dx}\frac{Q^2}{2}\left(\frac{x-s}{\varepsilon_0 A} + \frac{s}{\varepsilon_0 \varepsilon A}\right) = \frac{Q^2}{2\varepsilon_0 A} \ .$$

14.2.2.15 Ex: Plate capacitor with dielectric

The plate capacitor shown in the figure has a plate surface of $A = 115\,\mathrm{cm}^2$ and a plate distance of $d = 1.24\,\mathrm{cm}$. Between the plates we have the potential difference $U_0 = 85.5\,\mathrm{V}$ produced by a battery. Now, the battery is removed and a dielectric $b = 0.78\,\mathrm{cm}$ thick plate with dielectric constant $\varepsilon = 2.61$ is inserted, as shown in the figure. First calculate
a. capacitance without dielectric and
b. the free charge on the capacitor plates.
c. Now, the dielectric is inserted. Calculate the electric field in the voids and within the dielectric, as well as
d. the potential difference between the plates.
e. What is the capacitance with dielectric?
f. Now assume that the battery remains connected to the capacitor while the dielectric is inserted into the space between the plates. Calculate now the capacitance,
g. the charge on the capacitor plates, and
h. the electric field in the void and inside the dielectric.

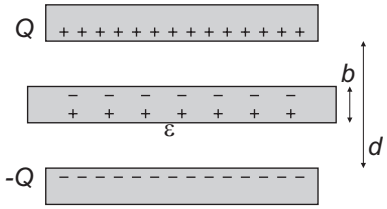

Figure 14.9: Plate capacitor.

Solution: *a. The capacity is,*

$$C = \varepsilon_0 \frac{A}{d} = 8.2\,\mathrm{pF} \ .$$

b. The free charge follows from,

$$Q = CU_0 = 8.2\,\mathrm{pF}\cdot 85.5\,\mathrm{V} = 7\cdot 10^{-10}\,\mathrm{C}\ .$$

c. The electric field in the spaces is,

$$\mathcal{E}_f = \frac{Q}{\varepsilon_0 A} = \frac{7\cdot 10^{-10}\,\mathrm{C}}{\varepsilon_0\cdot 115\,\mathrm{cm}^2} = 68.75\,\mathrm{V/cm}\ .$$

and in the dielectric,

$$E_\varepsilon = \frac{\mathcal{E}_f}{\varepsilon} = \frac{71.25\,\mathrm{V/cm}}{2.61} = 26.34\,\mathrm{V/cm}\ .$$

d. After insertion of the dielectric the potential difference is,

$$U_\varepsilon = \phi_2 - \phi_1 = \int \vec{\mathcal{E}}\cdot d\vec{s} = \mathcal{E}_f(d-b) + \mathcal{E}_\varepsilon b = 71.25\,\mathrm{V/cm}\cdot 0.46\,\mathrm{cm} + 27.30\,\mathrm{V/cm}\cdot 0.78\,\mathrm{cm} = 52.9\,\mathrm{V}\ .$$

e. The capacitance in the dielectric is,

$$C_d = \left(\frac{1}{\varepsilon_0\frac{2A}{(d-b)}} + \frac{1}{\varepsilon_0\varepsilon\frac{A}{b}} + \frac{1}{\varepsilon_0\frac{2A}{(d-b)}}\right)^{-1} = 10.9\,\mathrm{pF}\ .$$

f. If the dielectric is inserted while the battery is connected, the capacity obviously remains unchanged.
g. However, the charge on the capacitor plates is,

$$Q' = C_d U_0 = 10.9\,\mathrm{pF}\cdot 85.5\,\mathrm{V} = 9.3\cdot 10^{-10}\,\mathrm{C}\ .$$

h. The electric field in the empty spaces is,

$$\mathcal{E}_f = \frac{Q'}{\varepsilon_0 A} = \frac{9.3\cdot 10^{-10}\,\mathrm{C}}{\varepsilon_0\cdot 115\,\mathrm{cm}^2} = 91.43\,\mathrm{V/cm}\ .$$

and in the dielectric,

$$\mathcal{E}_\varepsilon = \frac{E_f}{\varepsilon} = \frac{71.25\,\mathrm{V/cm}}{2.61} = 35.03\,\mathrm{V/cm}\ .$$

14.2.2.16 Ex: Plate capacitor with dielectric

Consider a quadratic plate capacitor with edge length l and plate distance d.
a. What is the capacity of the empty capacitor? What is the electrostatic energy when the plates are charged with the charges kept fixed $+Q$ and $-Q$?
b. A dielectric with thickness d, width $L > l$, and dielectric constant ε is now inserted from the side. What is the electrostatic energy as a function of penetration depth x for $0 < x < l$?
c. What is the force acting on the dielectric with function of x for $0 < x < l$?

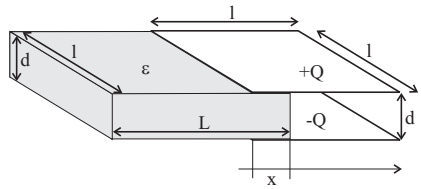

Figure 14.10: Plate capacitor.

Solution: *a. The capacity and energy of the empty capacitor are,*

$$C = \varepsilon_0 \frac{l^2}{d} \ ,$$
$$W = \frac{Q^2}{2C} = \frac{dQ^2}{2\varepsilon_0 l^2} \ .$$

b. Inserting the dielectric we change the capacity and the energy,

$$C_\varepsilon(x) = \varepsilon_0 \frac{l(l-x)}{d} + \varepsilon\varepsilon_0 \frac{lx}{d} = \frac{\varepsilon_0 l}{d}(l + x\varepsilon - x) \ ,$$
$$W = \frac{Q^2}{2C_\varepsilon(x)} = \frac{dQ^2}{2\varepsilon_0 l(l + x\varepsilon - x)} \ .$$

c. On the dielectric acts a force in x-direction,

$$F_x = -\nabla_x W = -\frac{d}{dx}\frac{dQ^2}{2\varepsilon_0 l(l + x\varepsilon - x)} = -\frac{dQ^2}{2\varepsilon_0 l(\varepsilon - 1)} \frac{1}{\left(\frac{l}{\varepsilon - 1} + x\right)^2} \ .$$

14.2.2.17 Ex: Plate capacitor with dielectric

At a plate capacitor consisting of two parallel metal plates of area $0.5\,\mathrm{m}^2$ and distant by $d = 10\,\mathrm{cm}$, there be a voltage of $U_0 = 1000\,\mathrm{V}$.
a. What are the values for the capacitance of the capacity C, the electrical field E between plates, and the charge surface density σ on the plates?
b. A quarter of the capacitor volume is now filled with a dielectric ($\varepsilon = 5$), as shown in the diagram. What is now the capacitance C_g?
Help: We may construct an equivalent circuit diagram by inserting imaginary capacitor plates along equipotential surfaces.

Solution: *a. In a vacuum we have:*

$$C = \varepsilon_0 \frac{A}{d} = 4.43 \cdot 10^{-11} \qquad \textit{and} \qquad \mathcal{E} = \frac{U}{d} = 10^4\,\mathrm{V/m}$$

The surface density of the charge on the capacitor plates is,

$$\sigma = \frac{Q}{A} = \frac{CU}{A} = \varepsilon_0 \frac{U}{d} = \varepsilon_0 \mathcal{E} = 8.85 \cdot 10^{-8}\,\mathrm{C/m}^2 \ .$$

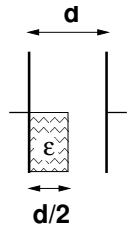

Figure 14.11: Plate capacitor.

b. The equivalent circuit becomes a parallel circuit of the upper half of the capacitor C_1 with the circuit in series of the dielectric quarter C_2 and the empty quarter in the lower half of the capacitor:

$$C_1 = \varepsilon_0 \frac{A/2}{d} = \frac{C}{2} \qquad \textit{and} \qquad C_2 = \varepsilon_0 \varepsilon \frac{A/2}{d/2} = \varepsilon C \qquad \textit{and} \qquad C_3 = \varepsilon_0 \frac{A/2}{d/2} = C \ .$$

With that we get the full capacitance,

$$C_g = C_1 + \frac{C_2 C_3}{C_2 + C_3} = \frac{C}{2} \frac{\varepsilon C}{1+\varepsilon} = \frac{4}{3} C = 5.91 \cdot 10^{-11}\,\mathrm{F} \ .$$

14.2.2.18 Ex: Water capacitor

Consider a plate capacitor (plate distance $d = 20\,\mathrm{cm}$, plate surface area $A = 400\,\mathrm{cm}^2$), which can be half filled with water (dielectric constant $\varepsilon_w = 80.3$). We apply a voltage of $U = 240\,\mathrm{V}$.
a. Calculate the capacitance of the capacitor for the following cases:
i. No water.
ii. The water is perpendicular to the plates..
iii. The water is parallel to the plates.
b. Calculate the charges on the plates for these three cases.
c. Compare the electric field energy of the cases (i) and (iii). From what source does the energy difference come from when the capacitor is filled with water?

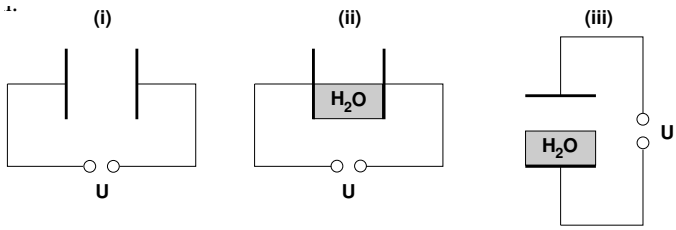

Figure 14.12: Capacitor.

Solution:

14.2.2.19 Ex: Capacitor circuit

The capacitance of the capacitors in the schematic circuit are $C_1 = 10\,\mu\text{F}$, $C_2 = 5\,\mu\text{F}$ and $C_3 = 4\,\mu\text{F}$. The voltage is $U = 100\,\text{V}$.
a. Calculate the total capacitance.
b. Determine for each capacitor the value of the charge, voltage, and stored energy.

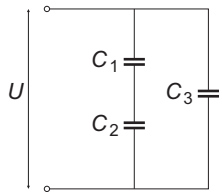

Figure 14.13: Capacitor.

Solution: *a. The total capacitance is,*

$$C = \left(\frac{1}{C_1} + \frac{1}{C_2}\right)^{-1} + C_3 = 7.3\,\mu\text{F} \ .$$

b. From the relationships $U_1 + U_2 = U$ *and* $C_1U_1 = Q_1 = Q_2 = C_2U_2$ *follows,*

$$U_1 = \frac{C_2U}{C_1 + C_2} = 33.3\,\text{V} \qquad \textit{and} \qquad U_2 = \frac{C_1U}{C_1 + C_2} = 66.6\,\text{V} \ .$$

Furthermore,

$$Q_1 = Q_2 = \frac{C_1C_2U}{C_1 + C_2} = (C - C_3)U = 333\,\mu\text{C} \qquad \textit{and} \qquad Q_3 = C_3U = 400\,\mu\text{C} \ ,$$

which shows that $Q = Q_1 + Q_3 = CU = 733\,\text{C}$. *With* $W = \frac{1}{2}CU^2$, *the potential energies are,*

$$W_1 = 5.5\,\text{mJ} \quad , \quad W_2 = 11.1\,\text{mJ} \quad , \quad W_3 = 20\,\text{mJ} \ .$$

The sum of the energies is $W_1 + W_2 + W_3 = \frac{1}{2}CU^2$.

14.2.2.20 Ex: Capacitor circuit

Calculate the total capacitance of the circuits shown in the figure.
a. between the points P1 and P3,
b. between the points P1 and P2.

Solution: *a. Between* P_1 *and* P_3 *the total capacity is:*

$$C_{13} = C + C + \frac{1}{\frac{1}{C} + \frac{1}{C+C}} = \frac{8}{3}C \ .$$

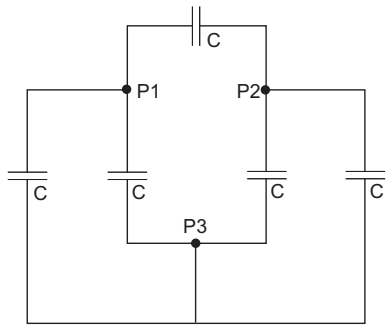

Figure 14.14: Capacitor circuit.

b. Between P_1 and P_2 the total capacity is:

$$C_{12} = C + \frac{1}{\frac{1}{C+C} + \frac{1}{C+C}} = 2C \ .$$

14.2.2.21 Ex: Capacitor circuit

Calculate the total capacitance of the circuits shown in the figure.

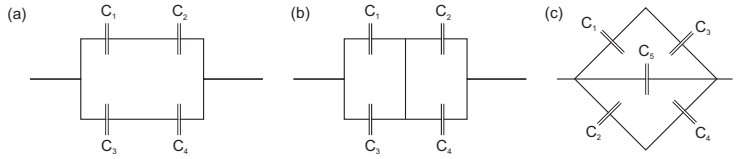

Figure 14.15: Capacitor circuit.

Solution: *a. In circuit in-series the capacities are added reciprocally, in-parallel they are added normally.*

$$C_{tot} = \frac{C_1 C_2}{C_1 + C_2} + \frac{C_3 C_4}{C_3 + C_4} \ .$$

b. Redrawing the circuit we realize that we are dealing with two parallel circuits of capacitors C_1 and C_3, resp., C_2 and C_4 put in series,

$$C_{tot} = \frac{(C_1 + C_3)(C_2 + C_4)}{C_1 + C_3 + C_2 + C_4} \ .$$

c. Redrawing the circuit we realize that the capacitors in series, C_2 and C_4, are paralleled to C_5 and the in-series capacitors C_1 and C_3,

$$C_{tot} = \frac{C_2 C_4}{C_2 + C_4} + C_5 + \frac{C_1 C_3}{C_1 + C_3} \ .$$

14.2.2.22 Ex: Energy in combinations of capacitors

a. Two identical capacitors are connected in parallel. This combination is then connected to the terminals of a battery. How does the total energy stored in the parallel combination of these two capacitors compare to the total energy stored if only one of the capacitors were connected to the terminals of the same battery?
b. Two identical discharged capacitors are connected in series. This combination is then connected to the terminals of a battery. How does the total energy stored in the in-series combination of these two capacitors compare to the total energy stored if only one of the capacitors were connected to the terminals of the same battery?

Solution: *a.* $U_{paralelo} = 2U_{unico}$.
b. $U_{serie} = \frac{1}{2}U_{unico}$

14.2.2.23 Ex: Plate capacitor

An air-filled plate capacitor consists of plates of $2.0\,\mathrm{m}^2$ area separated by 1 mm and is charged with 100 V.
a. What is the electric field between the plates?
b. What is the electrical energy density between the plates?
c. Determine the total energy by multiplying the response to part (b) with the volume between the plates.
d. Determine the capacitance of this arrangement.
e. Calculate the total energy using $U = \frac{1}{2}CV^2$ and compare your answer with the result of part (c).

Solution: *a.* $100\,\mathrm{kV/m}$.
b. $44.3\,\mathrm{mJ/m}^3$.
c. $88.5\,\mu\mathrm{J}$.
d. $17.7\,\mathrm{nF}$.
e. $88.5\,\mu\mathrm{J}$

14.2.2.24 Ex: Combination of capacitors

A $10.0\,\mu\mathrm{F}$ capacitor and a $20.0\,\mu\mathrm{F}$ capacitor are connected in parallel to the terminals of a 6.0 V battery.
a. What is the equivalent capacitance of this combination?
b. What is the potential difference in each capacitor?
c. Determine the charge on each capacitor.
d. Determine the energy stored in each capacitor.

Solution: *a.* $30.0\,\mu\mathrm{F}$.
b. 6.0 V.
c. $Q_{10} = 60\,\mu\mathrm{C}$, $Q_{20} = 120.0\,\mu\mathrm{C}$.
d. $U_{10} = 180\,\mu\mathrm{J}$, $U_{20} = 360\,\mu\mathrm{J}$.

14.2.2.25 Ex: Infinite series of capacitors

What is the equivalent capacitance (in terms of C, which is the capacitance of one of the capacitors) of the infinite chain shown in the figure.

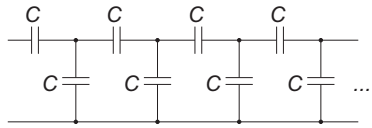

Figure 14.16: Capacitor circuit.

Solution: *The capacitance C_k between the vertical capacitors of one mesh is related to the capacitance C_{k-1} of the previous mesh by,*

$$C_k = C + (C_{k-1} \parallel C) = C + \frac{1}{\frac{1}{C} + \frac{1}{C_{k-1}}} \ .$$

For an infinite succession we can put $C_k = C_{k-1}$, which gives,

$$C_k^2 - CC_k - C^2 = 0 \ ,$$

with the solution,

$$C_k = \frac{C}{2}(1 \pm \sqrt{5}) \ .$$

Therefore, the equivalent capacitance is $C_{eq} = \frac{C}{2}(1 + \sqrt{5})$.

14.2.2.26 Ex: Reconnecting capacitors

A 100 pF capacitor and a 400 pF capacitor are both charged at 2.0 kV. They are then disconnected from the voltage source and connected together, positive plate to positive plate and negative plate to negative plate.
a. Determine the resulting potential difference at each capacitor.
b. Determine the dissipated energy when the connection is made.

Solution: *a.* $V_{100} = V_{400} = 1.2\,\text{kV}$.
b. 640 μJ.

14.2.2.27 Ex: Reconnecting capacitors

A 1.2 μF capacitor is charged at 30 V. After charging the capacitor is disconnected from the voltage source and is connected to the terminals of a second capacitor that had previously been discharged. The final voltage on the 1.2 μF capacitor is 10 V.
a. What is the capacitance of the second capacitor?
b. How much energy was dissipated when the connection was made?

Solution: *a.* 2.4 μF.
b. 0.4 mJ.

14.3 Conduction of current and resistance

To charge a capacitor we need to carry charges to its electrodes. By permitting a displacement of charges we escape, in this section, for the first time from the premises of electrostatics and introduce the concept of a *current* as being due to a movement of charges within a conductor. For now, let us not raise the question, how this current will act on other charges or currents, this subject being discussed in the next chapter.

14.3.1 Motion of charges in dielectrics and conductors

In electrostatics the *electromotive force* accelerating a charge Q is the Coulomb force, $\mathbf{F} = Q\vec{\mathcal{E}}$. Interpreting the current as the sum of the motions v_k of all charges $\sum_k \frac{N_k}{V} Q_k$ within a volume V, we introduce the *current density* in a way analogous to the charge density,

$$\mathbf{j}(\mathbf{r}) = \sum_k \tfrac{N_k Q_k}{V} \mathbf{v}_k \longrightarrow \varrho(\mathbf{r}) \mathbf{v}_{med}(\mathbf{r}) \ , \tag{14.38}$$

where the average is calculated over a small volume. The flow of charges in and out of the volume satisfies the *continuity equation*,

$$\boxed{\nabla \cdot \mathbf{j} + \partial_t \varrho = 0} \ . \tag{14.39}$$

To interpret this equation we consider a volume $\mathcal{V}$ and calculate the flow of charges through the surface of the volume,

$$I \equiv \oint_{\partial \mathcal{V}} \mathbf{j} d\mathbf{S} = \int_{\mathcal{V}} \nabla \cdot \mathbf{j} dV = \int_{\mathcal{V}} \dot{\varrho} dV = \dot{Q} \ . \tag{14.40}$$

That is, the charges passing through the surface must accumulate within the volume. The charge flow I is called *current*.

14.3.2 Ohm's law, stationary currents in continuous media

In the case of free charges inside a conductor, we empirically observe that the electromotive force leads to a stationary current. Obviously, this current depends on the electric field,

$$\mathbf{j} = \mathbf{j}(\vec{\mathcal{E}}) \ , \tag{14.41}$$

despising the magnetic force, which is usually weak. Moreover, we find empirically that the current is often proportional to the field,

$$\boxed{\mathbf{j} = \varsigma \vec{\mathcal{E}}} \ . \tag{14.42}$$

with the *conductivity* ς. This observation is called *Ohm's law*.

We said earlier that $\vec{\mathcal{E}} = 0$ inside a conductor for electrostatic situations, $\mathbf{j} = 0$. This remains valid for perfect conductors, $\vec{\mathcal{E}} = \mathbf{j}/\varsigma = 0$, even when current is flowing.

14.3.2.1 Microscopic view of conduction

Ohm's law may seem surprising, since the current arising from charges accelerated by a potential difference, we would expect that the flow of charges (i.e. the current) should grow in time as the velocity of the charges increases. But in fact, the accelerated electrons often collide with the atoms of the conducting material and are decelerated by the electromotive force $F = m_e a$ or redirected. Moreover, at finite temperature, the thermal velocity of the electrons is very high,

$$v_{term} = \sqrt{\frac{2k_B T}{3m_e}} \approx 6700\,\mathrm{m/s} \ , \tag{14.43}$$

so that the average velocity is constant. The time between two collisions of an electron can be related to its mean free path λ by,

$$t = \frac{\lambda}{v_{term}} \ . \tag{14.44}$$

Now, the average velocity is,

$$v_{med} = \frac{1}{t}\int_0^t v(t')dt' = \frac{at}{2} \ . \tag{14.45}$$

Finally, with n_a molecules per unit volume, each one providing N free electrons, the current density is,

$$\mathbf{j} = n_a N Q \mathbf{v}_{med} = n_a N q \frac{t}{2m_e}\mathbf{F} = n_a N Q \frac{\lambda}{2m_e v_{term}}\mathbf{F} = \frac{n_a N Q^2 \lambda}{2m_e v_{term}}\vec{\mathcal{E}} \ . \tag{14.46}$$

That is, the conductivity can be estimated as,

$$\varsigma = \frac{n_a N Q^2 \lambda}{2m_e v_{term}} \ . \tag{14.47}$$

The *resistivity* is

$$\rho \equiv \frac{1}{\varsigma} \ . \tag{14.48}$$

We note that the resistivity depends on the temperature, $\rho \propto T^{1/2}$.

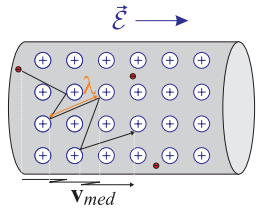

Figure 14.17: Microscopic view of the current.

Example 64 (*Estimation of the average velocity of electrons in a conductor*): Based on Eq. (14.38) we now want to estimate the average propagation velocity of electrons in a copper wire (radius $R = 1\,\text{mm}$) carrying a current of $I = 1\,\text{A}$. With the density of copper of $\rho_m = 8920\,\text{kg/m}^3$, its atomic mass $m_a = 63.5u$ and $N = 1$ valence electron per atom we estimate,

$$v_{med} = \frac{I}{n_a N e \pi R^2} = \frac{Iu}{m_a e \pi R^2} \simeq 8.5\,\text{cm/h} \ .$$

14.3.2.2 Resistors and energy consumption

Let us consider the conductor with the most common geometry: a metallic wire with the shape of a cylinder with cross section S and length L. Applying an electric field, we get,

$$I = \mathbf{j} \cdot \mathbf{S} = \varsigma \vec{\mathcal{E}} \cdot \mathbf{S} = \frac{\varsigma S}{L} U \ , \tag{14.49}$$

where $R = l/\varsigma A$ is called *resistance*. In this form the Ohm's law adopts the following form,

$$\boxed{U = RI} \ . \tag{14.50}$$

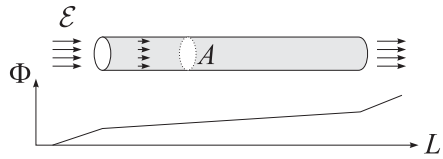

Figure 14.18: Concept of resistance.

A consequence of the frequent collisions of the electrons with the atoms is, that the conductor heats up. The power wasted on a resistance R is,

$$P = VI = RI^2 \ . \tag{14.51}$$

14.3.2.3 Resistor circuits

For parallel circuits $R_{tot}^{-1} = R_1^{-1} + R_2^{-1}$, for circuits in series $R_{tot} = R_1 + R_2$.

14.3.3 Exercises

14.3.3.1 Ex: The α-particle

A beam of α-particles ($q = +2e$), which move with constant kinetic energy $E = 20\,\text{MeV}$, corresponds to a current of $I = 0.25\,\mu\text{A}$. The beam is directed perpendicular to a flat surface.
a. How many α-particles hit the surface in $t = 3\,\text{s}$?
b. How many α-particles are at each instant of time within a $s = 20\,\text{cm}$ long beam segment?

c. What potential difference does an α-particle have to travel to be accelerated from rest to an energy of 20 MeV?

Solution: *a. The number is* $N = It/q = 2.3 \cdot 10^{12}$.
b. The velocity is $v = \sqrt{2E/m} = 3.1 \cdot 10^7$ m/s *for* $m = 4u$. *The time that the particles need to travel the distance is* $t_a = s/v = 6.4$ ns. *Hence, there are* $N_a = It_a/q = 5000$ *particles in this segment.*
c. To reach this energy, a particle must travel the potential difference $U = E/e = 20$ MV.

14.3.3.2 Ex: Electric power

A potential difference of 120 V powers a heater whose resistance is 1 Ω when it is hot.
a. At what rate does this device transform electricity into heat?
b. What is the electricity consumption bill for $t = 5$ h of operation with a price for electricity of $S = 5$ ct/kWh?

Solution: *a. The rate is* $\frac{dE}{dt} = P = \frac{U^2}{R} = 1$ kJ/s.
b. The cost is $K = t\ P\ S = 25.7$ ct.

14.3.3.3 Ex: Ohm's Law and electric Power

By how many degrees does a copper conductor of 100 m in length and 1.2 mm^2 in diameter heat up, when it is traversed for 1 hour by a current of 6 A? Assume the heat is not dissipated and use the following data: specific resistivity: $\rho = 0.02\,\Omega\text{mm}^2/\text{m}$; density: $\rho_{\text{Cu}} = 8.93\,\text{kg/dm}^3$; specific heat capacity: $c_{\text{Cu}} = 389.4\,\text{J/kg K}$.

Solution: *Conductor resistance:*

$$R = \rho\frac{l}{A} = 0.02\ \frac{\Omega\text{mm}^2}{\text{m}}\ .$$

Power spent:

$$P = U\,I = RI^2 = 60\,\text{W}\ .$$

Joule heat produced in 1 h*:*

$$Q = Pt = 216000\,\text{J}\ .$$

Mass of the wire:

$$m_{Cu} = \rho_{Cu}\,V = \rho_{Cu}\,A\,l = 1.0716\,\text{kg}\ .$$

Heating of the wire:

$$Q = c_{Cu}m_{Cu}\Delta T \Rightarrow \Delta T = \frac{Q}{c_{Cu}m_{Cu}} = 518\,\text{K}\ .$$

14.3.3.4 Ex: Continuity equation and conserved quantities

The continuity equation,

$$\dot{\rho} + \nabla \cdot (\vec{v}\rho) = 0 \ ,$$

appears in various areas of physics and describes, for example, the conservation of matter, charge or probability.
a. Explain, based on Gauß' law, the relationship between the continuity equation and charge conservation.
b. Consider a simple mechanical example: A 10 l gas bottle is opened letting gas escape. Determine with the help of the continuity equation after how many minutes half of the gas is gone, if the gas exits at a constant velocity of $v = 1\,\mathrm{m/s}$ and the outlet valve has a cross-sectional area of $A = 10\,\mathrm{mm}^2$?

Solution: *a. Charge conservation requires,*

$$\frac{dQ}{dt} = \int dV \frac{\partial \rho}{\partial t} = -\int dV \nabla \cdot \mathbf{v}\rho = -\int d\mathbf{S} \cdot \mathbf{v}\rho \ .$$

The integral form of the continuity equation holds for any volume V. If within this volume the mass, charge or probability changes, a corresponding quantity must flow across the surface of the volume. This is precisely the conservation.
b. Continuity equation,

$$\frac{dM}{dt} = \int dV \frac{\partial \rho}{\partial t} = -\int dV \nabla \cdot \vec{v}\rho = -\int d\mathbf{S} \cdot \mathbf{v}\rho = -Sv\rho = -Sv\frac{M}{V} \ .$$

Ansatz for the differential equation,

$$M(t) = M_0 e^{-Avt/V} \ .$$

If half of the gas escaped by the time T, then

$$\frac{M(T)}{M_0} = e^{-AvT/V} = \frac{1}{2} \ .$$

Hence,

$$T = \ln 2 \frac{V}{Av} = 690\,\mathrm{s} \ .$$

14.3.3.5 Ex: Drift of electrons in a conducting wire

A gold wire has a circular cross section of 0.1 mm diameter. The ends of this wire are connected to the terminals of a 1.5 V battery. If the wire length is 7.5 cm, how long does it take on average for two electrons leaving the negative terminal of the battery to reach the positive terminal? Consider a resistivity of gold of $2.44 \cdot 10^{-8}\,\Omega\mathrm{m}$.

Solution: 0.86 s.

14.4 The electric circuit

Within a (ideal) conductor potential differences vanish everywhere $\Delta\Phi = 0$, regardless of the conductor's length or shape. In a stationary situations, that is, in the presence of static electric fields, the free electrons of the conductor self-organize their spatial distribution (if necessary by creating local charge imbalances) in order to satisfy this condition. As soon as the condition is satisfied, the movement of charges, necessary for their spatial reorganization, comes to an end.

To sustain a stationary current we need to recycle the electrons, that is, waste the electrons accumulated on the side, where the conductor is connected to the positive potential and provide new electrons on the side, where the conductor is connected to the negative potential. In other words, we need to *close* the circuit by an source-drain device for electrons, called *voltage source* or *current source* depending on the properties of the device.

In addition to the source, there is a wide variety of electronic components capable of manipulating the potential or the current in different ways, such as resistors, capacitors, inductors or transistors. In a circuit, these components are interconnected by conductive wires assumed to be ideal in the sense that they a potential without losses from one component to another.

14.4.1 Kirchhoff's rules

Electrical circuits can be more complicated and consist of several branches. The *mesh rule*,

$$\sum_k U_k = 0 \tag{14.52}$$

and the *node rule*,

$$\sum_k I_k = 0 \ , \tag{14.53}$$

govern the behavior of the potentials and currents in any circuit and serve to analyze its properties.

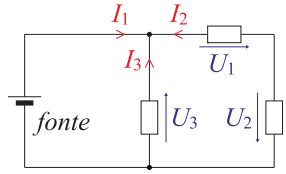

Figure 14.19: Illustration of Kirchhoff mesh and node rules.

Example 65 (*R-C circuit in series*): In addition to the voltage source we got to know two types of elements which can locally influence the voltage or the current: the capacitor and the resistor. The simplest imaginable electrical circuit containing these two components is the *R-C* circuit shown in Fig. 14.20. This circuit can be treated by Kirchhoff's laws,

$$0 = U_F + U_C + U_R \qquad \text{and} \qquad I_F = I_C = I_R \ . \tag{14.54}$$

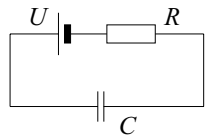

Figure 14.20: Illustration of a R-C-circuit.

Since the current is the same at each point of the circuit, we get the differential equation,

$$0 = U_F + \frac{Q}{C} + RI = U_F + \tfrac{1}{C}\int_0^t I dt' + RI \ , \tag{14.55}$$

which can quickly be solved by imposing the condition that the charge of the capacitor is initially zero,

$$I(t) = I_0(1 - e^{-t/RC}) \ . \tag{14.56}$$

14.4.2 Measuring instruments

Instruments for voltage and current measurement are discussed in the applied undergraduates courses, and we will not repeat this here.

14.4.3 Exercises

14.4.3.1 Ex: Motor starter issues

The starter of a car runs too slow. The mechanic has to decide which part is defective: the motor, the power cord, or the battery. According to the manufacturer's technical instructions, the internal resistance of the $U_0 = 12\,\mathrm{V}$ battery should not exceed $R_{bat} < 0.02\,\Omega$, resistance of the motor must not exceed $R_{mot} < 0.2\,\Omega$, and the resistance of the power cord must not exceed $R_{cab} < 0.04\,\Omega$. Examining the starter motor the mechanic finds a potential difference of 11.4 V at the battery, 3 V in the cable, and a current of 50 A in the starter circuit. Which element of the starter is defective?

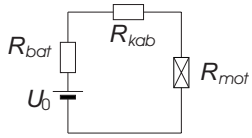

Figure 14.21: Motor starter circuit.

Solution: *The voltage measured on the battery is,*

$$U_{bat} = U_0 - R_{bat}I = (R_{cab} + R_{mot})I \ .$$

That is, the current that must flow is,

$$I = \frac{U_0}{R_{bat} + R_{cab} + R_{mot}} = \frac{12}{0.02 + 0.04 + 0.2} = 46.2\,\Omega \ .$$

The measured resistances are,

$$R'_{bat} = \frac{U_0 - U'_{bat}}{I'} = \frac{12 - 11.4}{50} = 0.012\,\Omega$$
$$R'_{cab} = \frac{U'_{cab}}{I'} = \frac{3\,\mathrm{V}}{50\,\mathrm{A}} = 0.06\,\Omega$$
$$R'_{mot} = \frac{U'_{bat}}{I'} - R'_{cab} = \frac{11.4\,\mathrm{V}}{50\,\mathrm{A}} - 0.06\,\Omega = 0.17\,\Omega \ .$$

Therefore, the cables are defective.

14.4.3.2 Ex: Solar cell

A solar cell generates a voltage of 0.1 V at a resistive load of 500 Ω, but only a voltage of 0.15 V at a resistive load of 1000 Ω. Consider the cell as a *real* voltage source with an internal resistance.
a. What are the internal resistance and unloaded voltage of the cell?
b. Calculate the efficiencies obtained with the two mentioned loads.

Solution: *a. We know,*

$$U_0 - R_i I_1 = R_1 I_1 = U_1 \qquad \textit{and} \qquad U_0 - R_i I_2 = R_2 I_2 = U_2 \ .$$

Hence,

$$U_0 - R_i \frac{U_1}{R_1} = U_1 \qquad \textit{and} \qquad U_0 - R_i \frac{U_2}{R_2} = U_2$$

We obtain,

$$R_i = \frac{U_1 - U_2}{\frac{U_2}{R_2} - \frac{U_1}{R_1}} = 1000\,\Omega \qquad \textit{and} \qquad U_0 = U_1 + \frac{U_1 - U_2}{\frac{U_2}{R_2} - \frac{U_1}{R_1}} \frac{U_1}{R_1} = 0.3\,\mathrm{V}$$

b. Efficiency is defined by,

$$\eta = \frac{P_c}{P_i + P_c} = \frac{R_{1,2} I_{1,2}^2}{R_i I_{1,2}^2 + R_{1,2} I_{1,2}^2} = \frac{R_{1,2}}{R_i + R_{1,2}} \ .$$

Hence, $\eta_1 = 1/3$ and $\eta_2 = 1/2$.

14.4.3.3 Ex: Current and voltage measurement

Circuit (a) shows an arrangement with an amperemeter with internal resistance R_A and a voltmeter with internal resistance R_U to measure resistance R. The value of the resistance follows from $R = U_V/I_R$, where U_V is the value indicated by the voltmeter and I_R the current through the resistance. A part of the current I_A measured by the amperemeter, however, flows through the voltmeter, such that the ratio U_V/I_A of the measured values only indicates an apparent resistance, which we will call R'.
a. How are the true resistance R and the apparent resistance R' interconnected

through the internal resistance R_V voltmeter? How should the internal resistance of the voltmeter be chosen to guarantee that $R' \to R$?
b. With the circuit (b) it is also possible to measure a resistance with an amperemeter and a voltmeter, and also in this case the ratio between the measured values gives only an apparent resistance. How can we determine the true resistance R in this circuit, and how should the internal resistance R_A of the amperemeter be chosen?

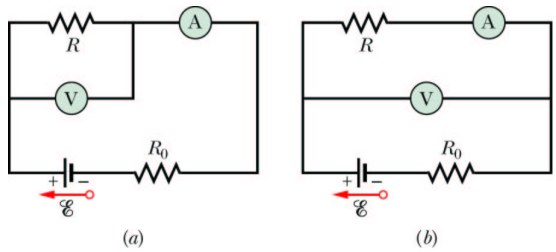

Figure 14.22: Current and voltage measurement.

Solution: *a. With* $U_V = RI_R$, $U_V = R'I_A$, $U_V = R_V I_V$ *and* $I_A = I_R + I_V$ *we have,*

$$R = \frac{U_V}{I_A - I_V} = \frac{U_V}{I_A - \frac{U_V}{R_V}} = \frac{1}{\frac{1}{R'} - \frac{1}{R_V}} \ .$$

For $R_V \to \infty$ *we have* $R' \to R$.
b. With $U_R = RI_A$, $U_V = R'I_A$, $U_A = R_A I_A$ *and* $U_V = U_R + U_A$ *we have,*

$$R = \frac{U_V - U_A}{I_A} = \frac{R'I_A - U_A}{I_A} = R' - R_A \ .$$

For $R_A \to 0$ *for* $R' \to R$.

14.4.3.4 Ex: Real current source

a. How should the internal resistance of a current source R_i be specified in order to obtain a current as independent as possible from the consuming load?
b. You want to run 40 A through an electric coil. The coil has the ohmic resistance of $R = 1\,\Omega$. What should be the internal resistance of the current source in order for a 10% increase in resistance not to change the current by more than 0.1%?

Solution: *a. The current that runs is* $I = U_0/(R_i + R)$. *To prevent that* R *has an influence, we need to let* $R_i \gg R$.
b. We imagine the source as a circuit in series with an ideal voltage source U_0 *and an internal resistance* R_i,

$$U_0 = (R_i + R)I \qquad \text{and} \qquad U_0 = (R_i + R')I' \ ,$$

with $R' = 1.1R$ *and* $I' = 0.99I$ *follows,*

$$R_i = -\frac{RI - R'I'}{I - I'} = -R\frac{1 - \frac{R'I'}{RI}}{1 - \frac{I'}{I}} = 98.9R \ .$$

14.4.3.5 Ex: Real voltage source

A battery can be understood as a real voltage source, consisting of an ideal voltage source U_0 and an internal resistance R_i. The voltage supplied by the battery depends on the consuming load. Which current flows through the resistor R and which voltage U_{out} does the battery supply? How must the resistive load be chosen to maximize the power spent at the ohmic resistor?

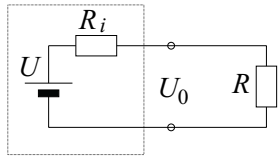

Figure 14.23: Battery.

Solution: *The current through R is,*

$$U_0 = R_{ges} I = (R_i + R) I \quad \Rightarrow \quad I = \frac{U_0}{R_i + R} \ .$$

With Kirchhoff's law:

$$-U_0 + U_R + U_i = -U_0 + RI + R_i I = 0 \quad \Rightarrow \quad I = \frac{U_0}{R_i + R} \ .$$

The voltage U_{out} at the battery is,

$$U_{out} = RI = U_0 \frac{R}{R + R_i} \ .$$

The resistance of the load for which the ohmic power at R is maximum (power matching):

$$P = U_{out} I = U_0 \ \frac{R}{R + R_i} \frac{U_0}{R + R_i} = U_0^2 \ \frac{R}{(R + R_i)^2} \ .$$

Deriving,

$$\frac{dP}{dR} = U_0^2 \ \frac{(R + R_i)^2 - R2(R + R_i)}{(R + R_i)^4} = U_0^2 \ \frac{R^2 + 2RR_i + R_i^2 - 2R^2 - 2RR_i}{(R + R_i)^4}$$
$$= U_0^2 \ \frac{R_i^2 - R^2}{(R + R_i)^4} = 0 \quad \Rightarrow \quad R = R_i \ .$$

Second derivative:

$$\frac{d^2 P}{dR^2} = U_0^2 \ \frac{-2R(R + R_i)^4 - (R_i^2 - R^2)4(R + R_i)^3}{(R + R_i)^8} = U_0^2 \ \frac{-32R^5 - 0}{(2R)^8} = -\frac{U_0^2}{8R^3} < 0$$

for $R_i = R$. Therefore, the power is maximum for $R = R_i$.

14.4.3.6 Ex: Battery circuit

Two batteries 1 and 2 (voltages $U_1 = 2\,\mathrm{V}$ and $U_2 = 0.5\,\mathrm{V}$) and three resistors $R_1 = R_2 = R_3 = 1\,\Omega$ are connected as shown in the figure.
a. What currents flow through the resistors R_1, R_2, and R_3?
b. What is the voltage drop between points A and B?

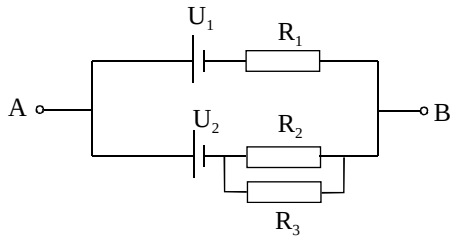

Figure 14.24: Battery circuit.

Solution:

14.4.3.7 Ex: Circuit with battery

Three batteries ($U_1 = 20\,\mathrm{V}$, $U_2 = 5\,\mathrm{V}$, $U_3 = 20\,\mathrm{V}$) each with a finite internal resistance of $0.1\,\Omega$ are connected in parallel. In series with this circuit two resistors are connected ($R_1 = 100\,\Omega$, $R_2 = 200\,\Omega$) (see scheme). What is the electrical voltage at R_1 and R_2?

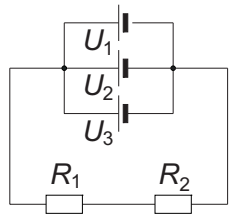

Figure 14.25: Battery circuit.

Solution: *We can imagine each individual battery as being composed by an ideal voltage source U_k and an internal resistance R_{ik}. So the voltage U_k measured at the parallel circuit corresponds to the voltage drop between points a and b: $U_k = U_2 + R_{i2}I_{i2}$. In addition, we have $2I_{i1} = I_{i2}$, since the node law gives at the point the current $I_{i1} + I_{i3} = I_{i2}$ and, for symmetry reasons, also holds $I_{i3} = I_{i1}$. Moreover, the mesh*

law gives,

$$\begin{aligned} -U_1 + R_{i1}I_{i1} + R_{i2}I_{i2} + U_2 = 0 & \\ \Longrightarrow -U_1 + R_{i1}\frac{I_{i2}}{2} + R_{i2}I_{i2} + U_2 = 0 & \\ \Longrightarrow I_{i2}\left(\frac{R_{i1}}{2} + R_{i2}\right) = U_1 - U_2 & \\ \Longrightarrow I_{i2} = 2\frac{U_1 - U_2}{3R_{i2}} \ , & \end{aligned}$$

since $R_{i1} = R_{i2}$. *With that follows* $U_k = U_2 + R_{i2}2\frac{U_1-U_2}{3R_{i2}} = 2U_1 - \frac{1}{3}U_2 = \frac{115}{3}\,\mathrm{V}$. *For the circuit in series we have* $U_k = U_{R1} + U_{R2}$ *and* $\frac{U_{R1}}{U_{R2}} = \frac{R_1}{R_2}$. *Finally,*

$$U_{R1} = \frac{1}{3}\frac{115}{3}\,\mathrm{V} \qquad \textit{and} \qquad U_{R1} = \frac{2}{3}\frac{115}{3}\,\mathrm{V} \ .$$

14.4.3.8 Ex: Kirchhoff's rules

The current circuit shown in the figure consists of voltage sources, $U_1 = 20\,\mathrm{V}$ and $U_2 = 10\,\mathrm{V}$ and resistors, $R_1 = 150\,\Omega$, $R_2 = R_3 = R_5 = 100\,\Omega$, and $R_4 = 50\,\Omega$. What is the current measured by the Ampèremeter A?

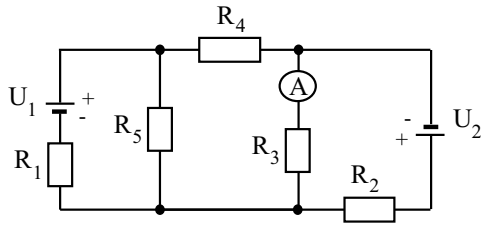

Figure 14.26: Circuits.

Solution:

14.4.3.9 Ex: Kirchhoff's rules

Be given $R_1 = 1\,\Omega$, $R_2 = 2\,\Omega$, as well as $\varepsilon_1 = 2\,\mathrm{V}$ and $\varepsilon_2 = \varepsilon_3 = 4\,\mathrm{V}$.
a. Show that Kirchhoff's node rule for steady currents is a consequence of the continuity equation $\oint \vec{j}d\vec{A} = \frac{dq}{dt}$.
b. Calculate the currents across the three ideal batteries in the circuit shown in figure.
c. Calculate the potential difference between points a and b.

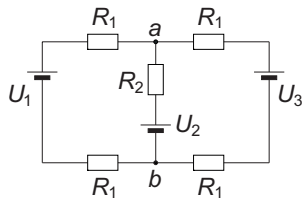

Figure 14.27: Circuits.

Solution: *a. For steady currents we may request:* $\frac{dq}{dt} = 0$. *When several currents parameterized by* $\mathbf{j}_k(\mathbf{r})d\vec{A}_k = I_k$ *combining, follows,*

$$\oint \mathbf{j} d\mathbf{A} = \sum_k I_k = 0 \ .$$

b. We start writing Kirchhoff rules for both nodes and both meshes (node b is redundant):

$$\begin{aligned} -U_1 + R_1 I_1 + R_2 I_2 + U_2 + R_1 I_1 = 0 \\ -U_3 + R_1 I_3 + R_2 I_2 + U_2 + R_1 I_3 = 0 \\ I_1 + I_3 - I_2 = 0 \ . \end{aligned}$$

Eliminating the third equation,

$$\begin{aligned} (2R_1 + R_2)\, I_1 + R_2 I_3 + U_2 - U_1 = 0 \\ R_2 I_1 + (2R_1 + R_2)\, I_3 + U_2 - U_3 = 0 \ . \end{aligned}$$

Solving for I_1 *and* I_3

$$\begin{aligned} I_3 &= -\frac{1}{4} \frac{R_2 U_1 + 2R_1 U_2 - (2R_1 + R_2)\, U_3}{R_1\,(R_1 + R_2)} \\ I_1 &= \frac{1}{4} \frac{(2R_1 + R_2)\, U_1 - 2R_1 U_2 - R_2 U_3}{R_1\,(R_1 + R_2)} \\ I_2 &= \frac{1}{2} \frac{U_1 - 2U_2 + U_3}{R_1 + R_2} \ . \end{aligned}$$

Hence, the currents are $I_1 = -2/3\,\mathrm{A}$, $I_3 = 1/3\,\mathrm{A}$ *and* $I_2 = -1/3\,\mathrm{A}$.
c. The potential difference is,

$$U_{ab} = R_2 I_2 + U_2 = \frac{1}{2} \frac{R_2 U_1 + 2R_1 U_2 + R_2 U_3}{R_1 + R_2} \ .$$

Hence, $U_{ab} = 10/3\,\mathrm{V}$.

14.4.3.10 Ex: Kirchhoff's rules

Consider the following circuit fed by a battery of voltage V. Using Kirchhoff's laws calculate the voltages and currents at the points $P1$ and $P2$. What is the total resistance of this circuit?

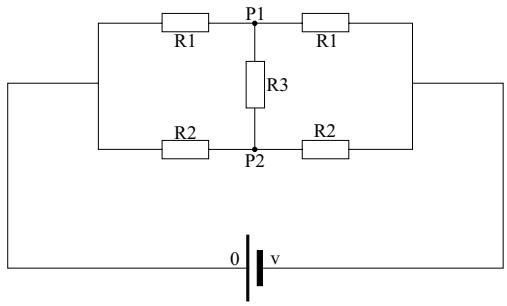

Figure 14.28: Circuits.

Solution: *Applying Kirchhoff's first law to the current at nodes,*

$$\begin{aligned} \textit{(i for the node P1)} \quad & I_{1,l} - I_{1,r} - I_3 = 0 \quad \Rightarrow \quad I_{1,r} = I_{1,l} - I_3 \\ \textit{(ii for the node P2)} \quad & I_{2,l} - I_{2,r} + I_3 = 0 \quad \Rightarrow \quad I_{2,r} = I_{2,l} + I_3 \end{aligned}$$

Applying Kirchhoff's second law to the meshes,

$$\begin{aligned} \textit{(iii for the upper left mesh)} \quad & U_{1,l} + U_3 - U_{2,l} = I_{1,l}R_1 + I_3R_3 - I_{2,l}R_2 = 0 \\ \textit{(iv for the upper right mesh)} \quad & U_{1,r} - U_{2,r} - U_3 = I_{1,r}R_1 - I_{2,r}R_2 - I_3R_3 = 0 \\ \textit{(v for lower mesh)} \quad & U_{2,l} + U_{2,r} - |V| = I_{2,l}R_2 + I_{2,r}R_2 - |V| = 0 \ . \end{aligned}$$

Inserting (i) and (ii) into (iv) we obtain,

$$\textit{(iv')} \quad I_{1,l}R_1 - I_3R_1 - I_{2,l}R_2 - I_3R_2 - I_3R_3 = 0 \ .$$

Subtracting (iii)-(iv') we get,

$$I_3R_1 + I_3R_2 + 2I_3R_3 = R_1 + R_2 + 2R_3)I_3 = 0 \quad \Rightarrow \quad I_3 = 0 \ .$$

Thus, it follows from (i) and (ii),

$$I_{1,r} = I_{1,l} = I_1 \quad \textit{and} \quad I_{2,r} = I_{2,l} = I_2 \ ,$$

and with (v),

$$2I_2R_2 = |V| \quad \Rightarrow \quad I_2 = \frac{|V|}{2R_2}$$

and with (iii):

$$I_1R_1 = I_2R_2 \quad \Rightarrow \quad I_1 = I_2\frac{R_2}{R_1} = \frac{|V|}{2R_1} \ .$$

Using Ohm's law we find the voltages at the resistances,

$$U_{1,l} = U_{1,r} = R_1I_1 = \frac{|V|}{2} \quad \textit{and} \quad U_{2,l} = U_{2,r} = R_2I_2 = \frac{|V|}{2} \ .$$

The voltage at points P1 and P2 is $V/2$, i.e. there is no current I_3 flowing. That is, we have the case of a balanced bridge circuit.

To calculate the total circuit resistance we consider two possibilities of equivalent circuits:
a. Points P1 and P2 staying at the same potential can be short-circuited, giving,

$$R_{ges} = \left(\frac{1}{R_1} + \frac{1}{R_2}\right)^{-1} + \left(\frac{1}{R_1} + \frac{1}{R_2}\right)^{-1} = 2\left(\frac{R_2 + R_1}{R_1 R_2}\right)^{-1} = \frac{2\,R_1\,R_2}{R_1 + R_2}\ .$$

b. Since the current $I_3 = 0$, points P1 and P2 can be separated, giving,

$$R_{ges} = \left(\frac{1}{R_1 + R_1} + \frac{1}{R_2 + R_2}\right)^{-1} = \left(\frac{R_2 + R_1}{2R_1 R_2}\right)^{-1} = \frac{2\ R_1\ R_2}{R_1 + R_2}\ .$$

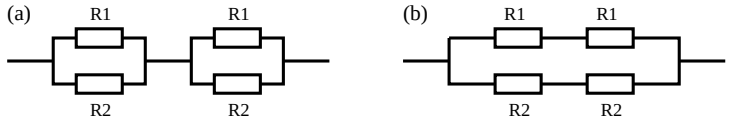

Figure 14.29: Circuits.

14.4.3.11 Ex: Combination of resistors

You have a maximum of 5 resistors of $100\,\Omega$ each. With these try to build circuits having the total resistance of a. $R = 25\,\Omega$, b. $R = 66.\bar{6}\,\Omega$, c. $R = 120\,\Omega$.

Solution: *a. 4 parallel resistors,* $\frac{1}{R_{ges}} = \frac{1}{R} + \frac{1}{R} + \frac{1}{R} + \frac{1}{R} = \frac{4}{R} \ \Rightarrow\ R_{ges} = \frac{R}{4} = 25\,\Omega$
b. 3 resistors, $\frac{1}{R_{ges}} = \frac{1}{R+R} + \frac{1}{R} = \frac{3}{2R} \ \Rightarrow\ R_{ges} = \frac{2}{3}R = 66,\bar{6}\,\Omega$
c. 5 resistors, $\frac{1}{R_{ges}} = \frac{1}{R+R+R} + \frac{1}{R+R} = \frac{5}{6R} \ \Rightarrow\ R_{ges} = \frac{6}{5}R = 120\,\Omega$

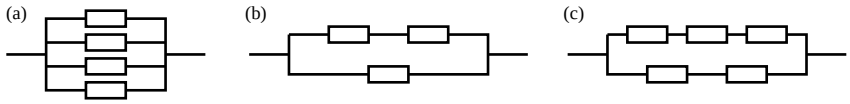

Figure 14.30: Resistors circuits.

14.4.3.12 Ex: Circuit with capacitors and resistors

In the circuit shown in the figure be $R_1 = 600\,\Omega$, $R_2 = 200\,\Omega$, $R_3 = 300\,\Omega$, $C = 20\,\mu\text{F}$, and $U = 12\,\text{V}$.
a. Calculate the voltages measured at the individual resistors and the capacitor as well as the total current I_{ges} when the capacitor is fully charged (stationary case).
b. At time $t = 0$ the switch S is opened. After which time the capacitor voltage drops

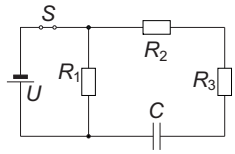

Figure 14.31: Circuits.

to 10 mV?

Solution: *a. When the capacitor is fully charged, no current flows through the resistors R_2 and R_3. The total voltage of* 12 V *drops at the capacitor and the resistor R_1. Through the resistor R_1 goes the current $I = U/R_1 = 20\,\mathrm{mA}$.*
b. When the switch is opened, the capacitor discharges through the circuit in series of all three resistors. Therefore,

$$(R_1 + R_2 + R_3)I = (R_1 + R_2 + R_3)\dot{Q} = U = Q/C \ ,$$

resp.

$$U = U_0 e^{-t/(R_1+R_2+R_3)C} \ .$$

14.4.3.13 Ex: Circuits with resistors and capacitors

Consider the circuit shown in the figure with the following values, $R_1 = R_3 = 100\,\Omega$, $R_2 = R_4 = 200\,\Omega$, $C_1 = C_2 = 10\,\mu\mathrm{F}$, and $U_0 = 20\,\mathrm{V}$.
a. Calculate equivalent resistance and the equivalent capacity of the circuit.
b. At time $t = 0$ the switch S is closed. Find the differential equation for the voltage $U(t)$ at the capacitor C_1 and solve it. When does the voltage drop to $1/e$ of its maximum value?
c. Determine the evolution of the amplitude of the resistor current R_3.

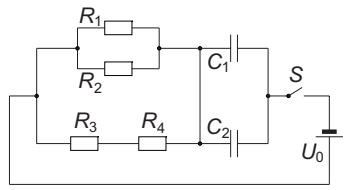

Figure 14.32: Circuits.

Solution: *a. Equivalent resistance,*

$$R_{eq} = \left(\frac{1}{R_1} + \frac{1}{R_2} + \frac{1}{R_3 + R_4}\right)^{-1} \approx 54.5\,\Omega \ .$$

Equivalent capacity,

$$C_{eq} = C_1 + C_2 = 20\,\mu\text{F} \ .$$

b. The mesh rule gives $U_0 = R_{ers}I(t) + U(t)$*, since the voltage in* C_1 *is the same as that in* C_2*. From this follows,*

$$U_0 = R_{eq}\frac{dQ}{dt} + U(t) = R_{ers}C_{ers}\frac{dU(t)}{dt} + U(t) \equiv \frac{1}{M}\frac{dU(t)}{dt} + U(t) \ .$$

Hence, we get the differential equation,

$$\frac{dU(t)}{dt} = MU_0 - MU(t) \ .$$

The solution is obviously, $U(t) = U_0(1 - e^{-Mt})$*. The value* $1/e$ *is reached when* $t = -\frac{1}{M}\ln(1 - 1/e) \approx 0.5\,\text{ms}$*.*
c. With $I(t) = \frac{1}{R_{tot}}[U_0 - U(t)]$ *and the nodes rule,* $I(t) = I_{34} + I_{12}$*, and the mesh rule,* $I_{34}(R_3 + R_4) - I_{12}(R_1 \parallel R_2) = 0$ *, we obtain,*

$$I_1(t) = \frac{R_1 \parallel R_2}{(R_1 \parallel R_2) + R_3 + R_4}I(t) = \frac{R_1 \parallel R_2}{(R_1 \parallel R_2) + R_3 + R_4}U_0 e^{-Mt} \ .$$

14.4.3.14 Ex: Circuits with resistors and capacitors

Calculate the total resistances and capacitances of the following circuits.
Help for (e): Consider the capacitor as a set of capacitors with/without dielectric in series and in parallel.

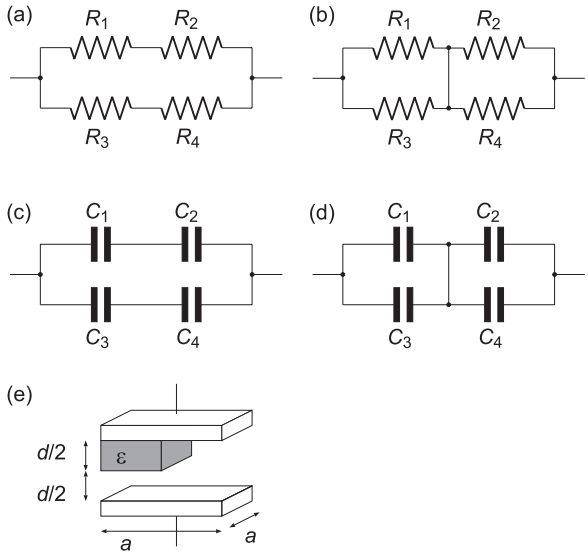

Figure 14.33: Circuits.

Solution: *a.*

$$R = \frac{1}{\frac{1}{R_1+R_2} + \frac{1}{R_3+R_4}} \ .$$

b.

$$R = \frac{1}{\frac{1}{R_1} + \frac{1}{R_2}} + \frac{1}{\frac{1}{R_3} + \frac{1}{R_4}} \ .$$

c.

$$R = \frac{1}{\frac{1}{C_1} + \frac{1}{C_2}} + \frac{1}{\frac{1}{C_3} + \frac{1}{C_4}} \ .$$

d.

$$R = \frac{1}{\frac{1}{C_1+C_2} + \frac{1}{C_3+C_4}} \ .$$

e.

$$C = \varepsilon_0 \frac{a^2/2}{d} + \frac{1}{\frac{1}{\varepsilon_0 \varepsilon \frac{a^2/2}{d}}} + \frac{1}{\varepsilon_0 \frac{a^2/2}{d}} = \varepsilon_0 \frac{a^2}{2d} \frac{2+\varepsilon}{1+\varepsilon} \ .$$

14.4.3.15 Ex: Charging a capacitor

The circuit shown in Fig. 14.20 consists of a voltage source U, a resistance R, and a capacity C. Initially be $U = 0$. From the time $t = 0$ on the voltage source shall give the constant value $U = U_0$. Calculate the time evolution of the current I in the circuit as well as the time evolution of the voltages at the capacitor and at the resistance.
Help: Begin by establishing the differential equation for the current I.

Solution: *Before turning on the source we have $U_0 = U_R = U_C = 0$. Immediately after turning on we have $U_0 = U_R + U_C$. With the current across the resistance $I = U_R/R$ and the capacitor charge $Q_c = CU_C$ we get,*

$$U_0 = RI + \frac{Q}{C} \ .$$

With $I = \dot{Q}_C$ follows,

$$\dot{U}_0 = R\dot{I} + \frac{I}{C} = 0 \ .$$

Finally,

$$\dot{I} = -\frac{1}{RC} I \ ,$$

with the solution $I(t) = I_0 e^{-t/\tau}$ with $\tau = RC$. At time $t = 0$ the capacitor is discharged, so $U_C = 0$. Hence, $U_0 = U_R(t = 0) = RI(t = 0)$ and $I_0 = U_0/R$, hence,

$$I(t) = \frac{U_0}{R} e^{-t/\tau} \ .$$

The resistor voltage drops exponentially, $U(t) = RI(t) = U_0 e^{-t/\tau}$. For the capacitor voltage we have,

$$\dot{U}_C = \frac{I}{C} = \frac{U_0}{RC} e^{-t/\tau}$$
$$\Longrightarrow U_C = \frac{Q}{C} = -\tau \frac{U_0}{RC} e^{-t/\tau} + const = -U_0 e^{-t/\tau} + const \ .$$

At time $t = 0$ holds $U_C = 0$ and with that $const = U_0$, hence U_C goes exponentially from 0 to U_0: $U_C = U_0(1 - e^{-t/\tau}$.

14.4.3.16 Ex: R-C circuit

Consider the electrical circuit shown in the figure with the ideal voltage sources U_k, the resistors R_k, and the capacitor C. Initially the switch C_1 is open.
a. Calculate the charge Q_0 on the capacitor after a long time.
b. Now, the switch is closed. Using Kirchhoff's laws, express the charge on the capacitor as a function of the current I_C across the capacitor and the parameters shown in the figure.
c. Based on the result obtained in (b), calculate the time evolution of the capacitor charge.
d. Indicate the values for $t = 0$ and $t \to \infty$.
e. Discuss the cases (i) $U_2 = U_1$ and (ii) $U_2 = -U_1$.

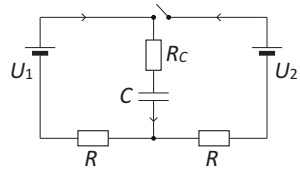

Figure 14.34: Circuits.

Solution: *a. Kirchhoff's node rule for the left mesh gives:*

$$U_1 - \frac{Q_0}{C} - R_C I - RI = 0 \ .$$

In steady state no current is flowing, $I = 0$. Hence,

$$Q_0 = CU_1 \ .$$

b. Now we have two connected meshes. We start writing Kirchhoff's rules for both nodes and both meshes (node b is redundant):

$$U_1 - \frac{Q}{C} - R_C I_C - RI_1 = 0$$
$$U_2 - \frac{Q}{C} - R_C I_C - RI_2 = 0$$
$$I_1 + I_2 - I_C = 0 \ .$$

Adding the first and second equation and replacing the third,

$$0 = U_1 + U_2 - 2\frac{Q}{C} - 2R_C I_C - R(I_1 + I_2) = U_1 + U_2 - 2\frac{Q}{C} - 2R_C I_C - RI_C \ .$$

c. Solving for I_C,

$$\begin{aligned}
(2R_C + R)\frac{dQ}{dt} + 2\frac{Q}{C} &= U_1 + U_2 \\
\tfrac{C}{2}(2R_C + R)\frac{dQ}{\frac{C}{2}(U_1 + U_2) - Q} &= dt \\
-\tfrac{C}{2}(2R_C + R)\ln[\tfrac{C}{2}(U_1 + U_2) - Q]\big|_{Q_0}^{Q(t)} &= t \\
Q(t) &= \tfrac{C}{2}(U_1 + U_2) - [\tfrac{C}{2}(U_1 + U_2) - Q_0]e^{-2t/C(2R_C+R)} \ .
\end{aligned}$$

Substituting $Q_0 = CU_1$, we obtain,

$$Q(t) = \tfrac{C}{2}(U_1 + U_2) + \tfrac{C}{2}(U_1 - U_2)e^{-2t/C(2R_C+R)} \ .$$

d. We have $Q(t = 0) = CU_1$ and $Q(t \to \infty) = \frac{C}{2}(U_1 + U_2)$.
e. For (i) $U_2 = U_1$

$$Q(t) = CU_1 = const \ ,$$

and for (ii) $U_2 = -U_1$

$$Q(t) = CU_1 e^{-2t/C(2R_C+R)} \ .$$

14.4.3.17 Ex: Internal resistance of a battery

A 5 V power supply has an internal resistance of 50 Ω. What is the smallest resistor that can be taken in series with the power source so that the potential drop in the resistor is larger than 4.5 V?

Solution: 0.45 kΩ.

14.4.3.18 Ex: Circuit with two batteries

In the circuit shown in the figure, the batteries have negligible internal resistances. Determine
a. the current in each branch of the circuit
b. the potential difference between the points a and b, and
c. the power supplied by each battery.

Solution: *a. $I_{4\Omega} = 0.667$ A, $I_{3\Omega} = 0.889$ A and $I_{6\Omega} = 1.56$ A.*
b. $V_{ab} = 9.88$ V,
c. $P_{esq} = 8.0$ W, $P_{dir} = 10.7$ W.

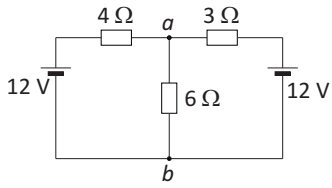

Figure 14.35: Circuits.

14.4.3.19 Ex: Circuit with three batteries

For the circuit shown in the figure, determine the potential difference between the points a and b.

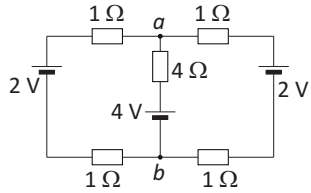

Figure 14.36: Circuits.

Solution: $V_a - V_b = 2.4\,\mathrm{V}$.

14.4.3.20 Ex: Real voltmeter

The voltmeter shown in the figure can be modeled as an *ideal* voltmeter (a voltmeter that has an infinite internal resistance) in parallel with a $10\,\mathrm{M\Omega}$ resistor. Calculate the voltmeter reading when
a. $R = 1.0\,\mathrm{k\Omega}$,
b. $R = 10.0\,\mathrm{k\Omega}$,
c. $R = 1.0\,\mathrm{M\Omega}$,
d. $R = 10.0\,\mathrm{M\Omega}$,
e. $R = 100.0\,\mathrm{M\Omega}$.
f. What is the largest possible value of R if the measured voltage should be within 10% of the *true* voltage (i.e. the voltage drop at R without placing the voltmeter)?

Solution: *a.* $3.33\,\mathrm{V}$,
b. $3.33\,\mathrm{V}$,
c. $3.13\,\mathrm{V}$,
d. $2.00\,\mathrm{V}$,
e. $0.435\,\mathrm{V}$,
f. $R_{max} = 1.67\,\mathrm{M\Omega}$.

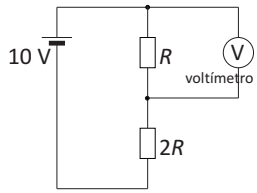

Figure 14.37: Voltmeter.

14.4.3.21 Ex: Circuit with battery and capacitor

The switch shown in the figure is closed after having been open for a long time.
a. What is the initial value of battery current right after the switch S has been closed?
b. What is the battery current a long time after the key has been closed?
c. What are the charges on the capacitor plates a long time after the switch has been closed?
d. Now, the switch S is opened again. What are the charges on the capacitor plates a long time after the switch has been reopened?

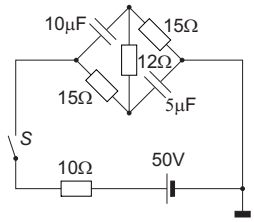

Figure 14.38: Circuits.

Solution: *a.* .

14.4.3.22 Ex: Circuit with battery and capacitor

In the circuit shown in the figure, the capacitor has a capacitance of 2.5 μF and the resistor has a resistance of 0.5 MΩ. Before the switch is closed, the potential drop in capacitor is 12 V, as shown in the figure. The switch S is closed at $t = 0$.
a. What is the current immediately after the switch has been closed?
b. At what instant of time t is the voltage on the capacitor 24 V?

Solution: *a.* 48.0 μA.
b. 0.866 s.

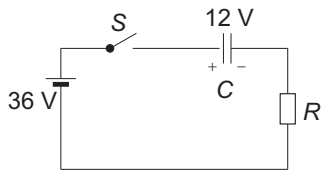

Figure 14.39: Circuits.

14.4.3.23 Ex: Three-phase current

Three-phase current is generated by three potential differences with respect to ground described by,

$$U_n(t) = U_0 \sin(\omega t + n\tfrac{2\pi}{3}) \ ,$$

where $n = 1, 2, 3$ labels the three phases. Assuming $U_0 = 127\,\mathrm{V}$.
a. What is the period-averaged voltage of each phase with respect to ground?
b. What is the period-averaged voltage difference between two phases?
c. What is the amplitude of the voltage difference between two phases?
d. Derive the time-dependent expressions for all currents labeled in Fig. 14.40(a).

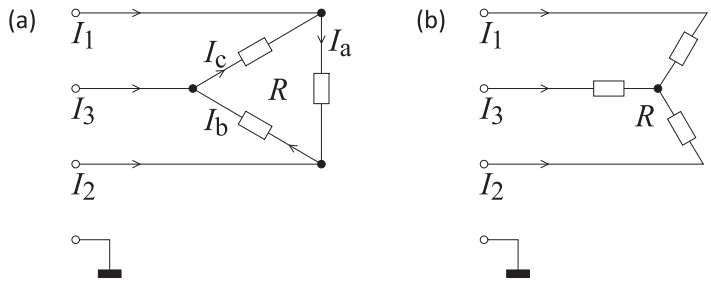

Figure 14.40: (a) Star connection, (b) triangular connection.

Solution: *a. The period-averaged voltage of each phase is,*

$$\bar{U}_n = \sqrt{\frac{\omega}{2\pi}\int_0^{2\pi/\omega} U_n^2(t)dt} = U_0\sqrt{\frac{\omega}{2\pi}\int_0^{2\pi/\omega} \sin^2(\omega t + n\tfrac{2\pi}{3})dt} = \frac{U_0}{\sqrt{2}} \ .$$

b. The period-averaged voltage difference between two phases is,

$$\bar{U}_d = U_0\sqrt{\frac{\omega}{4\pi}\int_0^{4\pi/\omega} \left[\sin(\omega t + \tfrac{2\pi}{3}) - \sin\omega t\right]^2 dt} = \sqrt{\tfrac{3}{2}}U_0 = \sqrt{3}\bar{U}_n \ .$$

c. The voltage difference between two phases is,

$$U(t) = U_0\left[\sin(\omega t + \tfrac{2\pi}{3}) - \sin\omega t\right] = U_0\left(\tfrac{\sqrt{3}}{2}\cos\omega t - \tfrac{3}{2}\sin\omega t\right) = U_0\sqrt{3}\sin(\omega t + \tfrac{5\pi}{6}) \ .$$

Hence, $U_{d0} = \sqrt{3}U_0 = 220\,\mathrm{V}$. *d. Kirchhoff's node rule yields,*

$$I_1 = I_a - I_c \quad , \quad I_2 = I_b - I_a \quad , \quad I_3 = I_c - I_b \ .$$

Resulting in $I_1 + I_2 + I_3 = 0$. *We also know from Kirchhoff's mesh rule,*

$$U_{12} = R_a I_a \quad , \quad U_{23} = R_b I_b \quad , \quad U_{31} = R_c I_c$$

with $U_{mn} = U_m - U_n$. *Hence,*

$$\begin{aligned} I_1 &= \frac{U_{12}}{R_a} - \frac{U_{31}}{R_c} = \frac{U_1 - U_2}{R_a} - \frac{U_3 - U_1}{R_c} \\ &= U_0 \left[\left(\frac{1}{R_a} + \frac{1}{R_c} \right) \sin\left(\omega t + \tfrac{2\pi}{3}\right) - \frac{1}{R_a} \sin\left(\omega t + \tfrac{4\pi}{3}\right) - \frac{1}{R_c} \sin\left(\omega t + \tfrac{6\pi}{3}\right) \right] \end{aligned}$$

etc.. Furthermore,

$$I_a = \frac{U_{12}}{R_a} = \frac{U_1 - U_2}{R_a} = \frac{U_0}{R_a} \left[\sin\left(\omega t + \tfrac{2\pi}{3}\right) - \sin\left(\omega t + \tfrac{4\pi}{3}\right) \right] = \frac{U_0}{R_a} \sqrt{3} \sin\left(\omega t + \tfrac{9\pi}{6}\right)$$

etc..

14.5 Further reading

D.J. Griffiths, *Introduction to Electrodynamics* [545]ISBN

D. Halliday, R. Resnick, and J. Walker, *Fundamentals of Physics* [577]ISBN

H.M. Nussenzveig, *Curso de Física Básica: Eletromagnetismo (Volume 3)* [963]ISBN

Chapter 15

Magnetostatics

Magnetostatics is the theory dealing with stationary currents, the fundamental problem being the calculation of the force exerted by spatial current distributions. Since a current is always due to displacement of charges, it is obviously not stationary in the strict sense. On the other hand, if the charge is transported in such a way that every charge leaving a volume element is immediately replaced by another equivalent charge, the integral over the volume element yields a stationary charge distribution.

15.1 Electric current and the Lorentz force

In the previous chapter we have shown that charges can travel through electric conductors, thus producing currents. We observe experimentally that electrically neutral conductors can exert reciprocal forces. For example, passing currents through two parallel, almost infinitely long thin wires, we find that they attract (repel) each other when their directions are (anti-)parallel. We also observe that a compass needle is deflected near a current-carrying conductor in directions describing concentric circles around the conductor. If the compass needle traces the field lines of a yet unknown field, the force attracting (or repelling) two currents DOES NOT point in the direction of the field lines. These observations show the presence of another phenomenon and another force not explained by Coulomb's law (see Fig. 15.1).

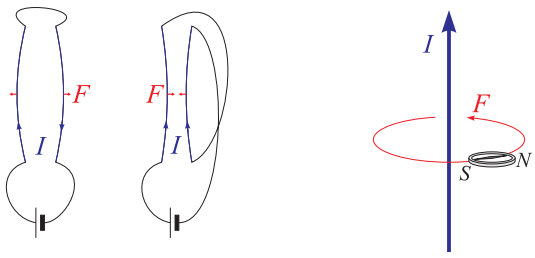

Figure 15.1: Mutual force between two conductors carrying antiparallel and parallel currents. Torque exerted by a current on a compass.

Apparently, the new force is not oriented in the direction of the current I, nor in the direction of the lines described by the compass needle, but perpendicular to the two. To describe this fact, we postulate the existence of a field $\vec{\mathcal{B}}$ called *magnetic*

field, such that the force is described by the vector product,

$$\mathbf{F}_L = I\mathbf{l} \times \vec{\mathcal{B}} \,, \tag{15.1}$$

where $\mathbf{l}$ is an element of the current path. This force is called *Lorentz force*. Note, that this force behaves like a pseudo-vector(see Exc. 1.6.3.7).

In order to analyze this phenomenon from the microscopic point of view, we put forward the hypothesis that the observed force has to do with the *motion* of the charges constituting the current within the postulated magnetic field. We have already introduced in the previous chapter the notion of the *current*, and we connected the current density with the propagation velocity of charges in the Eqs. (14.38) and (14.46),

$$\mathbf{j}(\mathbf{r}') = \varrho(\mathbf{r}')\mathbf{v}' \,. \tag{15.2}$$

With this we get,

$$\begin{aligned} \mathbf{F}_L &= I \int_{\mathcal{C}} d\mathbf{l}' \times \vec{\mathcal{B}} = I \int_{\mathcal{C}} \hat{\mathbf{e}}'_j \times \vec{\mathcal{B}} dl' \\ &= \int_{\mathcal{V}} I\delta^2(\mathbf{r}'_\perp - \mathbf{l}_\perp)\hat{\mathbf{e}}'_j \times \vec{\mathcal{B}} dV' = \int_{\mathcal{V}} \mathbf{j}(\mathbf{r}') \times \vec{\mathcal{B}} dV' = \int_{\mathcal{V}} \varrho(\mathbf{r}')\mathbf{v}' \times \vec{\mathcal{B}}(\mathbf{r}') dV' \,, \end{aligned} \tag{15.3}$$

where we simplified the notation $\mathbf{j}(\mathbf{r}') = I\delta^2(\mathbf{r}'_\perp - \mathbf{l}_\perp)\hat{\mathbf{e}}'_j = I\delta(\hat{\mathbf{e}}_1 \cdot \mathbf{r}' - \hat{\mathbf{e}}_1 \cdot \mathbf{l})\delta(\hat{\mathbf{e}}_2 \cdot \mathbf{r}' - \hat{\mathbf{e}}_2 \cdot \mathbf{l})\hat{\mathbf{e}}'_j$, where $\hat{\mathbf{e}}_{1,2}$ and $\hat{\mathbf{e}}'_j$ are all mutually orthogonal. We conclude,

$$\boxed{\mathbf{F}_L = Q\mathbf{v} \times \vec{\mathcal{B}}} \,. \tag{15.4}$$

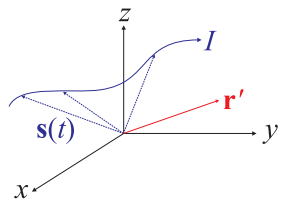

Figure 15.2: Parametrization of a yarn of current using the following recipe: For each point in space $\mathbf{r}' \in \mathbb{R}$ check that this point is also in $\mathbf{r}' \in \mathcal{C}$, that is, whether there exists a t such that $\mathbf{r}' = \mathbf{l}(t)$. At this point determine the direction of the path, $\hat{\mathbf{e}}'_j = d\mathbf{l}/|d\mathbf{l}|$, find two orthogonal unit vectors $\hat{\mathbf{e}}_{1,2}$ and apply the Dirac distribution to these dimensions.

Example 66 (*Cyclotron and synchrotron motion*): A consequence of the fact that, according to (15.4), the force on moving charges is always perpendicular to their velocity is, that their trajectory in a homogeneous magnetic field are *circular*. The centrifugal force compensates for the Lorentz force when,

$$F_L = Qv\mathcal{B} = m\frac{v^2}{R} = F_{cf} \,,$$

which allows to determine the radius R of the circle [1].

This fact is used in particle accelerators called *cyclotrons*, where beams of

[1] This behavior can be observed by injecting a charged particles into a homogeneous magnetic field. Collimated electron beams can be created by an electrode device called the *Wehnelt's cylinder* used in cathode ray tubes called *Braun's tube*.

charged particles are accelerated in by electric fields and deflected by homogeneous magnetic fields located between the regions of acceleration.

An important consequence of the particular form of the Lorentz force is the fact that *magnetic forces do not work*,

$$W_{mg} = \int_{\mathcal{C}} \mathbf{F} \cdot d\mathbf{l} = 0 \ .$$

The direction of motion of a charge can be changed by magnetic fields, but not the absolute value of its velocity. This may seem surprising, as we know that magnets can exert forces of iron bodies.

Example 67 (*Work exerted by magnetic fields*): We consider a conductive wire loop carrying current and being partially immersed in a homogeneous magnetic field, as shown in Fig. 15.3. The device is in equilibrium, when,

$$F = Ia\mathcal{B} = mg \ .$$

When the current exceeds the value $mg/a\mathcal{B}$, a vertical force lifting the device is observed, such that the device gains potential energy,

$$W = Fh \ ,$$

where h is the acquired height. However, the vertical motion corresponds to a current $I\hat{\mathbf{e}}_z$, which creates a force contrary to the current I, such that the battery feeding the wire loop needs to work to maintain the current. The magnetic field only reorients the force into a direction having a parallel component to the horizontal part of the wire loop, thus allowing the battery to work against this force. We shall discuss this from another point of view in context of the Lenz-Faraday law.

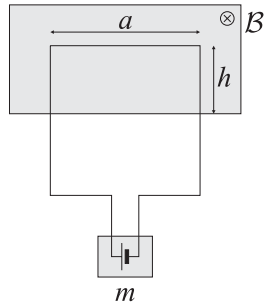

Figure 15.3: Hypothetical device to make the magnetic field work.

15.1.1 The Hall effect

As an example we consider the *Hall effect*: As shown in Fig. 15.4, a current flows to the right through a rectangular rod made of conductive material in the presence of a perpendicular uniform magnetic field $\vec{\mathcal{B}}$. If the mobile charges are positive, they will

be deflected by the magnetic field in downward direction. This deflection results in an accumulation of charges on the upper and lower boundaries of the rod which, in turn, generates an electric Coulomb force counteracting the magnetic force. A balance is reached when the two forces compensate:

$$F_C = Q\mathcal{E} = Q\frac{U_H}{w} = Qv_{med}\mathcal{B} = F_L \ . \tag{15.5}$$

The difference of the electric potentials on the upper and lower boundaries is called *Hall voltage*. The average velocity of the charges can be estimated from Eq. (14.46),

$$v_{med} = \frac{j}{n_a NQ} \ , \tag{15.6}$$

where n_a is the volumetric density of molecules of the rod material, each molecule providing N free electrons. Now, using the dimensions of the rod outlined in Fig. 15.4, we calculate the Hall voltage,

$$U_H = v_{med}\mathcal{B}w = \frac{j}{n_a NQ}\mathcal{B}w = \frac{I\mathcal{B}}{d\ n_a NQ} = A_H\frac{I\mathcal{B}}{d} \ , \tag{15.7}$$

where $A_H = 1/n_a NQ$ is a constant which depends on the rod material.

If the mobile charges were negative, the Hall voltage would change its sign. This fact can be used to identify the sign of free charges in unknown current conductors. Resolve the Excs. 15.1.3.1-15.1.3.13.

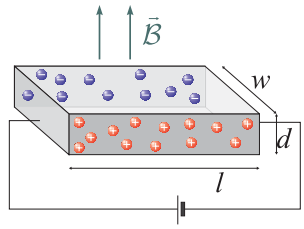

Figure 15.4: Illustration of the Hall Effect.

15.1.2 Biot-Savart's law

In the same way as we parametrize charge distributions (linear, superficial and volumetric) in electrostatics,

$$\sum_k (..)Q_k \longrightarrow \int_{\mathcal{C}} (..)\lambda dl \sim \int_{\mathcal{S}} (..)\sigma dS \sim \int_{\mathcal{V}} (..)\varrho dV \ , \tag{15.8}$$

we can parametrize current distributions (linear, superficial and volumetric) in magnetostatics,

$$\sum_k (..)Q_k\mathbf{v}_k \longrightarrow \int_{\mathcal{C}} (..)\mathbf{I}dl \sim \int_{\mathcal{S}} (..)\vec{\kappa}dS \sim \int_{\mathcal{V}} (..)\mathbf{j}dV \ . \tag{15.9}$$

In electrostatics we had the condition $\dot{\varrho} = 0$, which implies, via the continuity equation (14.39),

$$\nabla \cdot \mathbf{j} = 0 \ . \tag{15.10}$$

In magnetostatics we furthermore demand that $\dot{\mathbf{j}} = 0$.

The equivalent of Coulomb's law in magnetostatics is the Biot-Savart law,

$$\boxed{\vec{\mathcal{B}}(\mathbf{r}) = \frac{\mu_0}{4\pi}\int_{\mathcal{C}} \frac{\mathbf{I}(\mathbf{r}')\times(\mathbf{r}-\mathbf{r}')}{|\mathbf{r}-\mathbf{r}'|^3}dl' = \frac{\mu_0 I}{4\pi}\int_{\mathcal{C}} \frac{d\mathbf{l}'\times(\mathbf{r}-\mathbf{r}')}{|\mathbf{r}-\mathbf{r}'|^3} = \frac{\mu_0}{4\pi}\int_{\mathcal{V}} \mathbf{j}(\mathbf{r}')\times\frac{\mathbf{r}-\mathbf{r}'}{|\mathbf{r}-\mathbf{r}'|^3}dV'} \ . \tag{15.11}$$

Analogously to the way in which we apply Coulomb's law to electrostatics to calculate the electric field produced by charge distributions, we can apply the Biot-Savart's law in magnetostatics to calculate the magnetic field produced by currents.

Example 68 (*Magnetic field of a straight current wire*): We consider an infinitely long and thin wire oriented along the z-axis carrying a current I parametrized by $\mathbf{j}(\mathbf{r}') = \hat{\mathbf{e}}_z I\delta(x')\delta(y')$. Using $\mathbf{r} = \rho\hat{\mathbf{e}}_\rho + z\hat{\mathbf{e}}_z$ and $\mathbf{r}' = z'\hat{\mathbf{e}}_z$ we calculate,

$$\begin{aligned}\vec{\mathcal{B}}(\mathbf{r}) &= \frac{\mu_0 I}{4\pi}\int_{-\infty}^{\infty} dz' \frac{\hat{\mathbf{e}}_z\times(\mathbf{r}-\mathbf{r}')}{|\mathbf{r}-\mathbf{r}'|^3} = \frac{\mu_0 I}{4\pi}\hat{\mathbf{e}}_z\times\rho\hat{\mathbf{e}}_\rho\int_{-\infty}^{\infty}\frac{dz'}{\sqrt{\rho^2+(z-z')^2}^3} \\ &= \frac{\mu_0 I}{4\pi}\hat{\mathbf{e}}_z\times\rho\hat{\mathbf{e}}_\rho\left[\frac{z'}{\rho^2}(\rho^2+z'^2)^{-\frac{1}{2}}\right]_{-\infty}^{\infty} = \frac{\mu_0 I}{4\pi}\hat{\mathbf{e}}_z\times\rho\hat{\mathbf{e}}_\rho\frac{2}{\rho^2} = \frac{\mu_0 I}{2\pi\rho}\hat{\mathbf{e}}_\phi \ .\end{aligned}$$

With this we can now calculate the force exerted by this current on another current I_2 flowing in parallel direction but at a distance ρ:

$$\mathbf{F} = I_2 l\hat{\mathbf{e}}_z\times\vec{\mathcal{B}} = \frac{\mu_0 I I_2 l}{2\pi\rho}(-\hat{\mathbf{e}}_\rho) \ .$$

So the force is attractive.

Example 69 (*Magnetic field of a loop of circular current*): We consider a circular current parametrized by $\mathbf{j}(\mathbf{r}') = \hat{\mathbf{e}}_\phi I\delta(z)\delta(\rho-R)$. Following the Biot-Savart law the generated magnetic field is,

$$\vec{\mathcal{B}}(\mathbf{r}) = \frac{\mu_0}{4\pi}\int_{\mathcal{V}}\frac{\mathbf{j}(\mathbf{r}')\times(\mathbf{r}-\mathbf{r}')}{|\mathbf{r}-\mathbf{r}'|^3}dV' = \frac{\mu_0 I}{4\pi}\oint_{\mathcal{C}}\frac{\hat{\mathbf{e}}_{\phi'}\times(\mathbf{r}-R\hat{\mathbf{e}}_{r'})}{|\mathbf{r}-R\hat{\mathbf{e}}_{r'}|^3}Rd\phi' \ .$$

On the symmetry axis $\mathbf{r} = z\hat{\mathbf{e}}_z$ we get,

$$\begin{aligned}\vec{\mathcal{B}}(z\hat{\mathbf{e}}_z) &= \frac{\mu_0 IR}{4\pi}\oint_{\mathcal{C}}\frac{\hat{\mathbf{e}}_{\phi'}\times(z\hat{\mathbf{e}}_z - R\hat{\mathbf{e}}_{r'})}{\sqrt{R^2\cos^2\phi' + R^2\sin^2\phi' + z^2}^3}d\phi' \\ &= \frac{\mu_0 IR}{4\pi}\oint_{\mathcal{C}}\frac{z\hat{\mathbf{e}}_r + R\hat{\mathbf{e}}_z}{\sqrt{R^2+z^2}^3}d\phi' = \frac{\mu_0 IR^2}{2\sqrt{R^2+z^2}^3}\hat{\mathbf{e}}_z \ ,\end{aligned}$$

where the integral containing the term $z\hat{\mathbf{e}}_r$ vanishes by symmetry.

Resolve the Excs. 15.1.3.14-15.1.3.15.

15.1.3 Exercises

15.1.3.1 Ex: Force on a current conductor

A piece wire having the shape of a semicircle (radius R) congruent to the xy-plane at $z = 0$ is immersed in a homogeneous magnetic $\vec{\mathcal{B}}$-field oriented along $\hat{\mathbf{e}}_z$, as shown in the scheme. Through the wire runs a current I. Calculate the force on the loop and compare it to the force on a piece of straight wire oriented along the y-axis with length $2R$. The current in this wire runs along $\hat{\mathbf{e}}_y$.

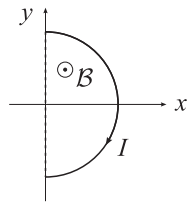

Figure 15.5: Wires.

Solution: *For a small piece of wire holds,*

$$d\mathbf{F} = Id\mathbf{l} \times \vec{\mathcal{B}} \ .$$

The force shows into radial direction and has the absolute value,

$$dF = Idl\mathcal{B} = I\mathcal{B}Rd\phi \ .$$

The component parallel to y is,

$$F_y = \int_{-\pi/2}^{\pi/2} dF \sin\phi = 0 \ .$$

The component parallel to x is,

$$F_x = I\mathcal{B}R \int_{-\pi/2}^{\pi/2} d\phi \cos\phi = 2I\mathcal{B}R \ .$$

This is equal but in opposite direction to the force acting on the piece of wire with length $2R$ toward y (the force on the entire loop is 0, as expected).

15.1.3.2 Ex: Lorentz force

In a wooden cylinder of mass $m = 0.25\,\mathrm{kg}$ and length $L = 10\,\mathrm{cm}$ is wound a 10 turns coil of conducting wire such that the axis of the cylinder is within the plane of the coil. The cylinder is (not slipping) on an plane inclined by $\alpha = 30°$ with respect to the horizontal, so that the plane of the coil is parallel to the inclined plane. The whole setup is subject to a homogeneous vertical magnetic field with the absolute

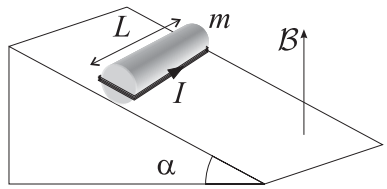

Figure 15.6: Lorentz force.

value $\mathcal{B} = 0.5\,\mathrm{T}$. What should be the minimum current through the coil to prevent the coil from rotating around its center of mass?

Solution: *The weight* $\mathbf{F}_g = -mg\hat{\mathbf{e}}_z$ *exerts a torque around the support point A of the cylinder in the inclined plane. Imagining the cylinder as a mass point concentrated at its center C, we find a torque acting on it,*

$$\vec{\tau}_g = \mathbf{r}_g \times \mathbf{F}_g \ ,$$

where $\mathbf{r}_g = R(\hat{\mathbf{e}}_x \sin\alpha + \hat{\mathbf{e}}_z \cos\alpha)$ *is the vector from A to C and R is the radius of the cylinder. Therefore,*

$$\vec{\tau}_g = -mg\mathbf{r}_g \times \hat{\mathbf{e}}_z = Rmg\hat{\mathbf{e}}_y \sin\alpha \ .$$

The Lorentz forces acting on the front side and the back side of the conductive loop, $\mathbf{F}_\pm = \pm NI\ \mathbf{L} \times \vec{\mathcal{B}} = \pm NILB\hat{\mathbf{e}}_x$*, cause torques,*

$$\vec{\tau}_\pm = \mathbf{r}_\pm \times \mathbf{F}_\pm \ ,$$

where $\mathbf{r}_\pm = \mathbf{r}_g \pm R(\hat{\mathbf{e}}_x \cos\alpha - \hat{\mathbf{e}}_z \sin\alpha) = R(\hat{\mathbf{e}}_x \sin\alpha \pm \hat{\mathbf{e}}_x \cos\alpha + \hat{\mathbf{e}}_z \cos\alpha \mp \hat{\mathbf{e}}_z \sin\alpha)$ *are the vectors of A to the points, where the Lorentz force acts. Therefore,*

$$\begin{aligned}\vec{\tau}_l &= \vec{\tau}_+ + \vec{\tau}_- = NILB(\mathbf{r}_+ - \mathbf{r}_-) \times \hat{\mathbf{e}}_x \\ &= RNILB\hat{\mathbf{e}}_z \times \hat{\mathbf{e}}_x\,[(\cos\alpha - \sin\alpha) - (\cos\alpha + \sin\alpha)] = -R2NILB\hat{\mathbf{e}}_y \sin\alpha \ .\end{aligned}$$

Alternatively, we calculate from magnetic moment, $\mathbf{m} = 2RLNI\hat{\mathbf{e}}_g$*, the torque,*

$$\vec{\tau}_l = \mathbf{m} \times \vec{\mathcal{B}} = -2RLNI\mathcal{B}\sin\alpha \ .$$

To prevent the cylinder from moving, we need $\vec{\mathcal{M}}_g + \vec{\mathcal{M}}_l = 0$*, which means that the current is independent of the slope,*

$$I = \frac{mg}{2NL\mathcal{B}} \ .$$

The current is $I = 2.45\,\mathrm{A}$*.*

15.1.3.3 Ex: Magnetic field mass spectrometer

A spectrometer is used to separate doubly ionized uranium ions of mass $3.92\times10^{-25}\,\mathrm{kg}$ from other similar isotopes. The ions are first accelerated by a potential difference of

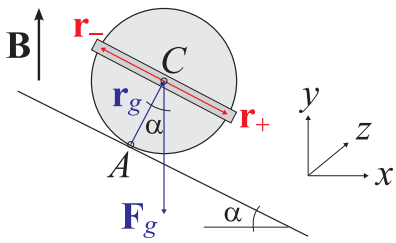

Figure 15.7: Lorentz force.

100 kV and then enter a homogeneous magnetic field, where they are deviated into a circular orbit of radius 1 m. After having covered an angle of 180°, they enter through a 1 mm wide and 1 cm high slit and are accumulated in a collector.
a. Determine the magnetic field of the mass spectrometer from the energy balance of the (individual) ions.
b. The device should be able to separate 100 mg of the desired ions per hour. What should be the intensity of the ionic flux in the beam?
c. What heat is produced in the collector in one hour?

Solution:

15.1.3.4 Ex: Mass spectrometer

In a mass spectrometer, a $^{24}Mg^{+}$ ion has a mass of $3.983 \cdot 10^{-26}$ kg and is accelerated by a potential difference of 2.5 kV. It then enters a region, where it is deflected by a magnetic field of 557 G.
Determine the radius of curvature of the orbits of the ion.
b. What is the difference between the radii of the orbits of the ions ^{26}Mg and ^{24}Mg? Consider a ratio between the masses of 26 : 24.

Solution: *a.* 63.3 cm.
b. 2.58 cm.

15.1.3.5 Ex: Magnetron

A magnetron consists of a diode tube, an anode shaped like a circular cylinder with radius $R_A =$ cm in the center of which the cathode filament is coaxially located. On the glass tube of this diode is a wound cylindrical coil whose axis coincides with the anode. The coil is long enough that the magnetic field along the cathode can be considered homogeneous. The electrons emitted from the cathode wire simultaneously are subject to the electric field between cathode and anode, $U = 1000$ V and the magnetic field $\mathcal{B} = 0.533 \cdot 10^{-2}$ T. The latter has been adjusted so that the electrons barely do not reach the anode. The whole apparatus is basically a velocity filter for electrons and thus a compact version of J.J. Thomson's e/m experiment (1987). From the equation of motion of an electron in the tube, determine the ratio e/m.

Solution:

15.1.3.6 Ex: Conductive copper strips

A copper strip of length $l = 2\,\text{cm}$, width $b = 1\,\text{cm}$, and thickness $d = 150\,\mu\text{m}$ lies within a homogeneous magnetic field $\vec{\mathcal{B}}$ of value $0.65\,\text{T}$, oriented perpendicular to the flat side of the strip. The concentration of free charges in copper is 8.47×10^{28} electrons/m^3. What is the potential difference V across the width of the tape, if it is traversed by a current of $I = 23\,\text{A}$?

Solution: *The Hall voltage is,*

$$U_{Hall} = bE_H = b\frac{1}{en}\frac{I}{bd}\mathcal{B} = \frac{1}{en}\frac{I}{d}\mathcal{B} \simeq 7.3\,\mu\text{V} \quad .$$

15.1.3.7 Ex: Lorentz force

A firm, horizontal, 25 cm long linear wire has a mass of 5 g and is connected to an emf-source via light and flexible wires. A magnetic field of 1.33 T is horizontal and perpendicular to the wire. Determine the current needed for the wire to float, that is, when the wire is released from rest, it remains at rest.

Solution: 1.5 A.

15.1.3.8 Ex: Lorentz force

A current carrying wire is bent in a closed semicircle of radius R in the xy-plane. The wire is inside a uniform magnetic field oriented in $+z$-direction, as shown in the figure. Verify that the force exerted on the ring is zero.

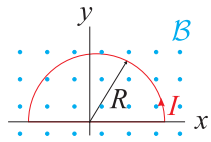

Figure 15.8: Lorentz force.

Solution:

15.1.3.9 Ex: Coulomb and Lorentz force

Two equal point charges are, at some instant of time, located at $(0,0,0)$ and $(0,b,0)$. Both are moving with velocity v in $+x$-direction (consider $v \ll c$). Determine the ratio between the magnitude of the magnetic force and the magnitude of the electric force at each charge.

Solution: *The first charge generates a magnetic field at the position of the second charge which, following the Biot-Savart law, is,*

$$\vec{\mathcal{B}}(\mathbf{b}) = \frac{\mu_0}{4\pi}\frac{q\mathbf{v}\times\mathbf{b}}{b^2} \ .$$

That is,

$$\mathcal{B} = \frac{\mu_0 qv}{4\pi b^2} \ .$$

This produces the Lorentz force,

$$F_L = qv\mathcal{B} = \frac{\mu_0 q^2 v^2}{4\pi b^2} \ .$$

The Coulomb force following Coulomb's law is,

$$F_C = \frac{1}{4\pi\varepsilon_0}\frac{q^2}{b^2} \ .$$

Hence,

$$\frac{F_L}{F_C} = \varepsilon_0\mu_0 c^2 \ .$$

15.1.3.10 Ex: Penning trap

In Penning traps, charged particles move under the influence of a homogeneous magnetic field $\vec{\mathcal{B}} = \mathcal{B}_h\hat{\mathbf{e}}_z$ and a quadrupolar electric field $\vec{\mathcal{E}} = \mathcal{E}_q(\rho\hat{\mathbf{e}}_\rho - 2z\hat{\mathbf{e}}_z)$. On which orbits do the particle move?
Help: Consider the axial and radial movements separately. For the radial motion consider two cases:
1. The influence of the electric field is negligible,
2. centripetal force is negligible.

Solution: *Lorentz force,*

$$\begin{aligned}\mathbf{F} &= Q\vec{\mathcal{E}} + Q\mathbf{v}\times\vec{\mathcal{B}} \\ &= Q\mathcal{E}_q(\rho\hat{\mathbf{e}}_\rho - 2z\hat{\mathbf{e}}_z) + Q\mathbf{v}\times\mathcal{B}_h\hat{\mathbf{e}}_z \\ &= Q\mathcal{E}_q\begin{pmatrix} x \\ y \\ 2z \end{pmatrix} + Q\mathcal{B}_h\begin{pmatrix} v_y \\ -v_x \\ 0 \ . \end{pmatrix}\end{aligned}$$

The linear restoring force in axial direction $F_z = -Q\mathcal{E}_q 2z$ *generates a harmonic oscillation,* $z = z_0 \cos\omega t + \frac{v_0}{\omega}\sin\omega t$ *with the oscillation frequency,*

$$\omega_h = \sqrt{\frac{q}{m} 2\mathcal{E}_q} \ .$$

For the radial motion, we get,

$$m\ddot{x} = Q\mathcal{E}_q x + Q\mathcal{B}_h v_y \qquad \textit{and} \qquad m\ddot{y} = Q\mathcal{E}_q y - Q\mathcal{B}_h v_x \ .$$

Despising the electric field,

$$m\ddot{x} = Q\mathcal{B}_h v_y \qquad \textit{and} \qquad m\ddot{y} = Q\mathcal{B}_h v_x \ .$$

Taking the square gives, $m\ddot{r} = Q\mathcal{B}_h v$ *resp.* $m\omega^2 r = Q\mathcal{B}_h \omega r$*. The particle rotates in the equatorial plane with the cyclotron frequency,*

$$\omega_c = \frac{Q\mathcal{B}_h}{m} \ .$$

Neglecting inertia,

$$0 = Q\mathcal{E}_q x + Q\mathcal{B}_h v_y \qquad \textit{and} \qquad 0 = Q\mathcal{E}_q y - Q\mathcal{B}_h v_x \ .$$

Taking the square gives, $\mathcal{E}_q r = \mathcal{B}_h v$ *resp.* $\mathcal{E}_q r = \mathcal{B}_h \omega r$*. The particle rotates in the equatorial plane with the magnetron frequency of,*

$$\omega_m = \sqrt{\frac{\mathcal{E}_q}{\mathcal{B}_h}} \ .$$

15.1.3.11 Ex: Magnetic trap near a current wire

An infinitely long conducting wire (radius R, axis in z-direction at position $x = y = 0$) carries the current I.
a. Calculate the magnetic field inside and outside the wire.
b. Now a homogeneous magnetic field is added, $\vec{\mathcal{B}}_{apl} = \mathcal{B}_0 \hat{\mathbf{e}}_x$. Calculate the absolute value of the total magnetic field $|\vec{\mathcal{B}}_{tot}|$ inside and outside of wire.
c. Where inside and outside the wire do appear points where $|\vec{\mathcal{B}}_{tot}|$ vanishes? What conditions for the parameters I, R, and $\mathcal{B}_0$ must be met for such points to exist?

Solution: *a. The magnetic field produced by the current is outside the wire,*

$$\vec{\mathcal{B}}_{fio} = \frac{\mu_0 I}{2\pi\rho}\hat{\mathbf{e}}_\phi = \frac{\mu_0 I}{2\pi\rho^2}\begin{pmatrix} -y \\ x \\ 0 \end{pmatrix}$$

and inside,

$$\vec{\mathcal{B}}_{fio} = \frac{\mu_0 I}{2\pi R^2}\rho\hat{\mathbf{e}}_\phi = \frac{\mu_0 I}{2\pi R^2}\begin{pmatrix} -y \\ x \\ 0 \end{pmatrix}$$

b. Total field is outside the wire,

$$|\vec{\mathcal{B}}_{tot}| = \left|\mathcal{B}_0\hat{\mathbf{e}}_x + \frac{\mu_0 I}{2\pi\rho}\hat{\mathbf{e}}_\phi\right| = \left|\left(\mathcal{B}_0 - \frac{\mu_0 I}{2\pi\rho^2}y\right)\hat{\mathbf{e}}_x + \frac{\mu_0 I}{2\pi\rho^2}x\hat{\mathbf{e}}_y\right| = \sqrt{\left(B_0 - \frac{\mu_0 I}{2\pi\rho^2}y\right)^2 + \left(\frac{\mu_0 I}{2\pi\rho^2}x\right)^2}\,.$$

and inside,

$$|\vec{\mathcal{B}}_{tot}| = \left|\mathcal{B}_0\hat{\mathbf{e}}_x + \frac{\mu_0 I}{2\pi R^2}\hat{\mathbf{e}}_\phi\right| = \left|\left(\mathcal{B}_0 - \frac{\mu_0 I}{2\pi R^2}y\right)\hat{\mathbf{e}}_x + \frac{\mu_0 I}{2\pi R^2}x\hat{\mathbf{e}}_y\right| = \sqrt{\left(\mathcal{B}_0 - \frac{\mu_0 I}{2\pi R^2}y\right)^2 + \left(\frac{\mu_0 I}{2\pi R^2}x\right)^2}\,.$$

c. The point outside the wire, where the absolute value vanishes, follows with,

$$\left(\mathcal{B}_0 - \frac{\mu_0 I}{2\pi\rho^2}y\right)^2 + \left(\frac{\mu_0 I}{2\pi\rho^2}x\right)^2 = 0$$

and is at,

$$x = 0 \qquad \textit{and} \qquad \rho = y = \frac{\mu_0 I}{2\pi\mathcal{B}_0}\ .$$

For such points to stay outside the wire, $\rho > R$, we need $\frac{\mu_0 I}{2\pi\mathcal{B}_0} > R$.
The point inside the wire, where the absolute value vanishes, follows with,

$$\left(\mathcal{B}_0 - \frac{\mu_0 I}{2\pi R^2}y\right)^2 + \left(\frac{\mu_0 I}{2\pi R^2}x\right)^2 = 0\ ,$$

and is at,

$$x = 0 \qquad \textit{and} \qquad \rho = y = \frac{2\pi\mathcal{B}_0 R^2}{\mu_0 I}\ .$$

For such points to stay inside the wire, $\rho < R$, we again need $\frac{\mu_0 I}{2\pi\mathcal{B}_0} > R$. That is, once the condition is met, the zero points appear in pairs outside and inside the wire.

15.1.3.12 Ex: Charge in homogeneous fields

A charge e moves in vacuum under the influence of homogeneous fields $\vec{\mathcal{E}}$ and $\vec{\mathcal{B}}$. Suppose that $\vec{\mathcal{E}}\cdot\vec{\mathcal{B}} = 0$ and $\mathbf{v}\cdot\vec{\mathcal{B}} = 0$. At what speed does the charge move without acceleration? What is the absolute value of its speed if $|\vec{\mathcal{E}}| = |\vec{\mathcal{B}}|$?

Solution: *By hypothesis, the electric field $\vec{\mathcal{E}}$ as well as the speed of the charge $\mathbf{v}$ are perpendicular to the magnetic induction. The total force on the charge is,*

$$\mathbf{F} = e\vec{\mathcal{E}} + \frac{e}{c}\mathbf{v}\times\vec{\mathcal{B}}\ .$$

Without acceleration, due to Newton's law, this force must disappear:

$$e\vec{\mathcal{E}} + \frac{e}{c}\mathbf{v} \times \vec{\mathcal{B}} = 0 \ .$$

But that means, that $\vec{\mathcal{E}}$ *and* $\mathbf{v} \times \vec{\mathcal{B}}$ *must be parallel. From this it follows that the velocity must also be perpendicular to the electric field. Since,*

$$\mathbf{v} \cdot \vec{\mathcal{E}} = \mathbf{v} \cdot \vec{\mathcal{B}} = 0 \ .$$

we can write,

$$\mathbf{v} = \lambda \vec{\mathcal{E}} \times \vec{\mathcal{B}} \ .$$

where λ *is a constant. Inserting into the force equation gives,*

$$e\vec{\mathcal{E}} + \frac{e}{c}\lambda(\vec{\mathcal{E}} \times \vec{\mathcal{B}}) \times \vec{\mathcal{B}} = 0 \ .$$

But now we have,

$$(\vec{\mathcal{E}} \times \vec{\mathcal{B}}) \times \vec{\mathcal{B}} = \vec{\mathcal{B}}(\vec{\mathcal{E}} \cdot \vec{\mathcal{B}}) - \vec{\mathcal{E}}(\vec{\mathcal{B}} \cdot \vec{\mathcal{B}}) \ .$$

Since $\vec{\mathcal{E}} \cdot \vec{\mathcal{B}} = 0$ *by hypotheses, immediately follows,*

$$e\vec{\mathcal{E}} - \frac{e}{c}\lambda \mathcal{B}^2 \vec{\mathcal{E}} = 0 \ .$$

where we introduced $\mathcal{B} \equiv |\vec{\mathcal{B}}|$*. With this relationship follows,*

$$\lambda = \frac{c}{\mathcal{B}^2} \ .$$

resp.

$$\mathbf{v} = \frac{c}{\mathcal{B}^2}\vec{\mathcal{E}} \times \vec{\mathcal{B}} \ .$$

For $|\vec{\mathcal{E}}| = |\vec{\mathcal{B}}|$ *we obtain* ($\vec{\mathcal{E}} \cdot \vec{\mathcal{B}} = 0$) $|\vec{\mathcal{E}} \times \vec{\mathcal{B}}| = \mathcal{B}^2$*, and therefore for this particular case,*

$$|\mathbf{v}| = c \ .$$

15.1.3.13 Ex: Rain accelerated by the Earth's magnetic field

Analyze the following train propulsion concept. The train shall be propelled by the magnetic force of the vertical component of the Earth's magnetic field acting on the current-carrying axes of the train. The value of the vertical component of the Earth's magnetic field is 10 μT, the axes have a length of 3 m. The current is fed by the rails and flows from one rail through the conducting wheels and axles to the other rail.
a. What must be the amplitude of the current to generate the modest force of 10 kN on an axis?
b. What is the rate of electric energy loss due to heat production?

Solution: *a. Lorentz's force is* $\mathbf{F} = I\mathbf{l} \times \vec{\mathcal{B}}$*. Therefore, the required current is,*

$$I = \frac{F}{lB} = 333 \cdot 10^6 \,\mathrm{A} \ .$$

b. ???

15.1.3.14 Ex: Biot-Savart law

We consider an infinitely long and thin wire oriented along the z-axis and concentrically embraced by a hollow conductor with radius R and negligible wall thickness. Through the conductor flows the current I_0 and through the wire the current I_1.
a. Calculate based on the Biot-Savart law the magnetic field produced by the inner wire at a distance d from the z-axis.
b. Calculate the force exerted by the magnetic field of the inner wire on a surface element of the current conductor.
c. What is the resulting pressure with $I_1 = -I_0 = 10$ A, $R = 1$ mm?
Help:

$$\int_a^b (c^2 + x^2)^{-\frac{3}{2}} dx = \left[\frac{x}{c^2}(c^2 + x^2)^{-\frac{1}{2}}\right]_a^b$$

Solution: *a. Magnetic field*

$$\vec{\mathcal{B}}(\mathbf{r}) = \frac{\mu_0 I_1}{4\pi} \int_{-\infty}^{\infty} dz' \frac{\hat{\mathbf{e}}_z \times (\mathbf{r} - \mathbf{r}')}{|\mathbf{r} - \mathbf{r}'|^3} \ .$$

With $\mathbf{r} = \mathbf{d} + z\hat{\mathbf{e}}_z$ *and* $\vec{r'} = z'\hat{\mathbf{e}}_z$

$$\begin{aligned}
\vec{\mathcal{B}}(\mathbf{r}) &= \frac{\mu_0 I_1}{4\pi} \hat{\mathbf{e}}_z \times \mathbf{d} \int_{-\infty}^{\infty} dz' (\mathbf{d}^2 + (z - z')^2)^{-3/2} \\
&= \frac{\mu_0 I_1}{4\pi} \hat{\mathbf{e}}_z \times \mathbf{d} \left[\frac{z'}{d^2}(d^2 + z'^2)^{-\frac{1}{2}}\right]_{-\infty}^{\infty} \\
&= \frac{\mu_0 I_1}{4\pi} \hat{\mathbf{e}}_z \times \mathbf{d} \frac{2}{d^2} = \frac{\mu_0 I_1}{2\pi d} \hat{\mathbf{e}}_\phi \ .
\end{aligned}$$

b. Force

$$\begin{aligned}
d\mathbf{F} &= dI_0 dl \hat{\mathbf{e}}_z \times \vec{\mathcal{B}} = -\frac{I_0 d\phi}{2\pi} dl \frac{\mu_0 I_1}{2\pi R} \hat{\mathbf{e}}_\rho \\
&= -\frac{\mu_0 I_0 I_1}{(2\pi R)^2} d\mathbf{S} \ .
\end{aligned}$$

c. Pressure

$$P = \frac{dF}{dA} = -\frac{\mu_0 I_0 I_1}{(2\pi R)^2} \approx 3.183\,\text{Pa} \ .$$

15.1.3.15 Ex: Biot-Savart law

We consider an infinitely long hollow conductor running along the z-axis with finite wall thickness with inner radius $R - \epsilon$ and outer radius $R + \epsilon$. The current density j_0 within the hollow conductor is constant and the total current is I_0.
a. Calculate j_0 from I_0, ϵ, and R.

b. Calculate, based on Ampere's law, the magnetic field produced by the hollow conductor at a distance ρ from the z-axis for $R-\epsilon<\rho<R+\epsilon$.
c. Calculate the resulting force on a volume element of the current-carrying conductor.
d. Integrate the radial force and calculate the limit $\epsilon \to 0$.
e. What is the resulting pressure in $I_0 = 10$ A, $R = 1$ mm? Does the force act inward or outward?

Solution: *a. Current density,*

$$I_0 = j_0\pi[(R+\epsilon)^2-(R-\epsilon)^2] = 4\pi R\epsilon j_0$$
$$j_0 = \frac{I_0}{4\pi R\epsilon}\ .$$

b. Total current within a cylinder of radius ρ,

$$I(\rho) = \pi\left(\rho^2-(R-\epsilon)^2\right)j_0\ .$$

With Ampere's law and making use of the axial symmetry follows for the magnetic field,

$$\vec{\mathcal{B}}(\rho) = \frac{\mu_0}{2\pi\rho}I(\rho)\hat{\mathbf{e}}_\phi = \frac{\mu_0 j_0}{2\rho}\left(\rho^2-(R-\epsilon)^2\right)\hat{\mathbf{e}}_\phi\ .$$

c. Force on the volume element,

$$\begin{aligned} d\vec{F} &= j_0\rho\, d\phi\, d\rho\, dz\, \hat{\mathbf{e}}_z\times\vec{\mathcal{B}}(\rho)\\ &= j_0\rho\, d\phi\, d\rho\, dz\, \hat{\mathbf{e}}_z\times\hat{\mathbf{e}}_\phi\frac{\mu_0 j_0}{2\rho}\left(\rho^2-(R-\epsilon)^2\right)\\ &= -\frac{j_0^2\mu_0}{2}\, d\phi\, d\rho\, dz\, \hat{\mathbf{e}}_\rho\left(\rho^2-(R-\epsilon)^2\right)\ . \end{aligned}$$

d. Integrated force,

$$\int_{R-\epsilon}^{R+\epsilon}(\rho^2-(R-\epsilon)^2)d\rho = \left[\frac{1}{3}\rho^3-\rho(R-\epsilon)^2\right]_{R-\epsilon}^{R+\epsilon}$$
$$= 4R\epsilon^2-\frac{4}{3}\epsilon^3\to 4R\epsilon^2\ .$$

The radially integrated force on a surface element in the limes $\epsilon\to 0$ is,

$$d\vec{F}_A = -2j_0^2\mu_0 R\epsilon^2\, d\phi\, dz\, \hat{\mathbf{e}}_\rho = -2j_0^2\mu_0\epsilon^2 d\mathbf{S} = -\frac{\mu_0 I_0^2}{8\pi^2R^2}d\mathbf{S}\ .$$

e. Pressure,

$$P = -\frac{\mu_0 I_0^2}{8\pi^2R^2}\approx -1.592\,\text{Pa}\ .$$

The force acts inwards, because currents following the same direction attract each other.

15.1.3.16 Ex: Magnetic field of the Earth

The Earth's magnetic field is approximately 0.6 G at the magnetic poles and points vertically downwards at the magnetic pole of the northern hemisphere. If the magnetic field were due to an electric current circulating on a ring with a radius equal to Earth's inner iron core (approximately 1300 km),
a. what would be the required amplitude of the current?
b. What orientation would the current need to have, the same as Earth's rotational motion or the opposite? Justify.

Solution: *a.* 15.5 GA
b. As the Earth's magnetic field points downward at the north pole, the application of the right-hand rule tells us that the current is opposite to the Earth's rotation.

15.1.3.17 Ex: Biot-Savart law

Consider the following device: A current I runs through two identical infinitely thin rings with radius R. The common center of the two rings is at the origin of the coordinates. One ring lies in the xy-plane and the other on the xz-plane.
a. Parametrize the current density $\mathbf{j}$ in spherical coordinates.
b. Show that the $\vec{\mathcal{B}}$ field resulting from this device at source is given by:

$$\vec{\mathcal{B}}(\mathbf{0}) = -\frac{\mu_0 I}{2}\frac{1}{R}\hat{\mathbf{e}}_z - \frac{\mu_0 I}{2}\frac{1}{R}\hat{\mathbf{e}}_y \ .$$

Help: A δ-function in spherical coordinates for the r variable must be multiplied by $\frac{1}{r}$; a δ-function in spherical coordinates for the ϕ variable must be multiplied by $\frac{\pi}{2}$.

Solution: *a. Current density in spherical coordinates:*

$$\mathbf{j} = I\left[\tfrac{1}{r}\delta(r-R)\delta(\theta-\tfrac{\pi}{2})\hat{\mathbf{e}}_\phi + \tfrac{1}{r}\delta(r-R)\frac{\pi}{2}\delta(\phi)\hat{\mathbf{e}}_\phi - \tfrac{1}{r}\delta(r-R)\tfrac{\pi}{2}\delta(\phi-\pi)\hat{\mathbf{e}}_\phi\right] \ .$$

b. Following the law of Biot-Savart:

$$
\begin{aligned}
\vec{\mathcal{B}}(\mathbf{r}) &= \frac{\mu_0}{4\pi}\int_{V'} \nabla \times \frac{\mathbf{j}(\mathbf{r}')}{|\mathbf{r}-\mathbf{r}'|}dV' = \frac{\mu_0}{4\pi}\int_{V'} \frac{(\mathbf{r}-\mathbf{r}')\times \mathbf{j}(\mathbf{r}')}{|\mathbf{r}-\mathbf{r}'|^3}dV' \\
&= \frac{\mu_0}{4\pi}\left[\int_{V'} dV' \frac{\pi}{2}\frac{1}{r'}\delta(r'-R)\delta(\theta'-\tfrac{\pi}{2})\frac{(\mathbf{r}-\mathbf{r}')\times \hat{\mathbf{e}}_\phi}{|\mathbf{r}-\mathbf{r}'|^3} + \int_{V'} dV' \frac{\pi}{2}\frac{1}{r'}\delta(r'-R)\delta(\phi')\frac{(\mathbf{r}-\mathbf{r}')\times \hat{\mathbf{e}}_\theta}{|\mathbf{r}-\mathbf{r}'|^3}\right. \\
&\quad \left. - \int_{V'} dV' \frac{\pi}{2}\frac{1}{r'}\delta(r'-R)\delta(\phi'-\pi)\frac{(\mathbf{r}-\mathbf{r}')\times \hat{\mathbf{e}}_\theta}{|\mathbf{r}-\mathbf{r}'|^3}\right] \\
&= \frac{\mu_0}{4\pi}\left[\int_{V'} dV' \frac{1}{r'}\delta(r'-R)\delta(\theta'-\tfrac{\pi}{2})\frac{\left[\begin{pmatrix}0\\0\\0\end{pmatrix} - \begin{pmatrix}r'\sin\theta'\cos\phi'\\ r'\sin\theta'\sin\phi'\\ r'\cos\theta'\end{pmatrix}\right]\times\begin{pmatrix}-\sin\phi'\\ \cos\phi'\\ 0\end{pmatrix}}{\left|\begin{pmatrix}0\\0\\0\end{pmatrix} - \begin{pmatrix}r'\sin\theta'\cos\phi'\\ r'\sin\theta'\sin\phi'\\ r'\cos\theta'\end{pmatrix}\right|^3}\right. \\
&\quad + \int_{V'} dV' \frac{\pi}{2}\frac{1}{r'}\delta(r'-R)\delta(\phi')\frac{\left[\begin{pmatrix}0\\0\\0\end{pmatrix} - \begin{pmatrix}r'\sin\theta'\cos\phi'\\ r'\sin\theta'\sin\phi'\\ r'\cos\theta'\end{pmatrix}\right]\times\begin{pmatrix}\cos\theta'\cos\phi'\\ \cos\theta'\sin\phi'\\ -\sin\theta'\end{pmatrix}}{\left|\begin{pmatrix}0\\0\\0\end{pmatrix} - \begin{pmatrix}r'\sin\theta'\cos\phi'\\ r'\sin\theta'\sin\phi'\\ r'\cos\theta'\end{pmatrix}\right|^3} \\
&\quad \left. - \int_{V'} dV' \frac{\pi}{2}\frac{1}{r'}\delta(r'-R)\delta(\phi'-\pi)\frac{\left[\begin{pmatrix}0\\0\\0\end{pmatrix} - \begin{pmatrix}r'\sin\theta'\cos\phi'\\ r'\sin\theta'\sin\phi'\\ r'\cos\theta'\end{pmatrix}\right]\times\begin{pmatrix}\cos\theta'\cos\phi'\\ \cos\theta'\sin\phi'\\ -\sin\theta'\end{pmatrix}}{\left|\begin{pmatrix}0\\0\\0\end{pmatrix} - \begin{pmatrix}r'\sin\theta'\cos\phi'\\ r'\sin\theta'\sin\phi'\\ r'\cos\theta'\end{pmatrix}\right|^3}\right] .
\end{aligned}
$$

In the next step we transform the volume element into spherical coordinates and evaluate the δ-function:

$$\begin{aligned}
\vec{\mathcal{B}}(\mathbf{r}) &= \frac{\mu_0}{4\pi}\Big[\int_0^{2\pi} R^2 \sin\left(\theta' = \frac{\pi}{2}\right)\frac{1}{R}d\phi' \frac{\begin{pmatrix}-R\cos\phi'\\-R\sin\phi'\\0\end{pmatrix}\times\begin{pmatrix}-\sin\phi'\\\cos\phi'\\0\end{pmatrix}}{\left[\sqrt{R^2\cos\phi'+R^2\sin\phi'}\right]^3} + \int_0^{\pi} R^2\sin(\theta')\frac{\pi}{2}\frac{1}{R}d\theta' \frac{\begin{pmatrix}-R\sin\theta'\\0\\-R\cos\theta'\end{pmatrix}\times\begin{pmatrix}\cos\theta'\\0\\-\sin\theta'\end{pmatrix}}{\left[\sqrt{R^2\cos\theta'+R^2\sin\theta'}\right]^3} \\
&\quad - \int_0^{\pi} R^2\sin(\theta')\frac{\pi}{2}\frac{1}{R}d\theta' \frac{\begin{pmatrix}+R\sin\theta'\\0\\-R\cos\theta'\end{pmatrix}\times\begin{pmatrix}-\cos\theta'\\0\\-\sin\theta'\end{pmatrix}}{\left[\sqrt{R^2\cos\theta'+R^2\sin\theta'}\right]^3}\Big] \\
&= \frac{\mu_0}{4\pi}R\Big[\int_0^{2\pi} d\phi' \frac{\begin{pmatrix}0\\0\\-R\cos^2\phi'-R\sin^2\phi'\end{pmatrix}}{R^3} + \int_0^{\pi}\frac{\pi}{2}d\phi' \frac{\begin{pmatrix}0\\-R\cos^2\theta'-R\sin^2\theta'\\0\end{pmatrix}}{R^3} - \int_0^{\pi}\frac{\pi}{2}d\phi' \frac{\begin{pmatrix}0\\+R\cos^2\theta'+R\sin^2\theta'\\0\end{pmatrix}}{R^3}\Big] \\
&= \frac{\mu_0}{4\pi}R\Big[2\pi\frac{R}{R^3}(-\hat{\mathbf{e}}_z) + 2\frac{\pi}{2}\frac{R}{R^3}(-\hat{\mathbf{e}}_y) - 2\frac{\pi}{2}\frac{R}{R^3}(\hat{\mathbf{e}}_y)\Big] .
\end{aligned}$$

15.2 Properties of the magnetic field

15.2.1 Field lines and magnetic flux

The *magnetic flux* is introduced in the same way as the electric flux,

$$\boxed{\Psi_M \equiv \int_{\mathcal{S}} \vec{\mathcal{B}}\cdot d\mathbf{S}} \; . \tag{15.12}$$

Resolve the Exc. 15.2.4.1.

15.2.2 Divergence of the magnetic field and Gauß's law

Let us compute the divergence of a magnetic field given by Biot-Savart's law [2],

$$\nabla_r\cdot\vec{\mathcal{B}} = \frac{\mu_0}{4\pi}\int_{\mathcal{V}}[\nabla_r\times\mathbf{j}(\mathbf{r}')]\cdot\frac{\mathbf{r}-\mathbf{r}'}{|\mathbf{r}-\mathbf{r}'|^3}dV' - \frac{\mu_0}{4\pi}\int_{\mathcal{V}}\mathbf{j}(\mathbf{r}')\cdot\left[\nabla_r\times\frac{\mathbf{r}-\mathbf{r}'}{|\mathbf{r}-\mathbf{r}'|^3}\right]dV' = 0 \; , \tag{15.13}$$

since, as we have already shown, the rotation of a Coulombian field is zero. Therefore,

$$\boxed{\nabla\cdot\vec{\mathcal{B}} = 0} \; . \tag{15.14}$$

With Gauß' law we can derive the integral version of this statement,

$$\boxed{\oint_{\partial\mathcal{V}}\vec{\mathcal{B}}\cdot d\mathbf{S} = 0} \; . \tag{15.15}$$

Comparing this equation with the corresponding electrostatic equation (13.13), we deduce the following interpretation: The total magnetic flux Ψ_M across a closed surface

[2] Using the rule $\nabla\cdot(\vec{\mathcal{E}}\times\vec{\mathcal{B}}) = (\nabla\times\vec{\mathcal{E}})\cdot\vec{\mathcal{B}} - \vec{\mathcal{E}}\cdot(\nabla\times\vec{\mathcal{B}})$.

must vanish and can not be changed by *hypothetical magnetic charges*, i.e. *magnetic charges do not exist*!

A direct consequence of this law is that we can introduce the concept of the vector potential, which is fundamental in the sense that it allows us to formulate electrodynamics completely in terms of potentials. We will dedicate the whole next section to magnetic potentials.

15.2.3 Rotation of the magnetic field and Ampère's law

Let us now calculate the rotation of the magnetic field given by Biot-Savart's law [3],

$$\nabla_r \times \vec{\mathcal{B}} = \frac{\mu_0}{4\pi}\int_{\mathcal{V}} -[\mathbf{j}(\mathbf{r}')\cdot\nabla_r]\frac{\mathbf{r}-\mathbf{r}'}{|\mathbf{r}-\mathbf{r}'|^3}dV' + \frac{\mu_0}{4\pi}\int_{\mathcal{V}}\mathbf{j}(\mathbf{r}')\left(\nabla_r\cdot\frac{\mathbf{r}-\mathbf{r}'}{|\mathbf{r}-\mathbf{r}'|^3}\right)dV' \tag{15.16}$$

$$= \frac{\mu_0}{4\pi}\int_{\mathcal{V}}[\mathbf{j}(\mathbf{r}')\cdot\nabla_{r'}]\frac{\mathbf{r}-\mathbf{r}'}{|\mathbf{r}-\mathbf{r}'|^3}dV' + \frac{\mu_0}{4\pi}\int_{\mathcal{V}}\mathbf{j}(\mathbf{r}')4\pi\delta(\mathbf{r}-\mathbf{r}')dV'$$

$$= \frac{\mu_0}{4\pi}\int_{\mathcal{V}}[\mathbf{j}(\mathbf{r}')\cdot\nabla_{r'}]\frac{\mathbf{r}-\mathbf{r}'}{|\mathbf{r}-\mathbf{r}'|^3}dV' + \mu_0\mathbf{j}(\mathbf{r})\ . \tag{15.17}$$

Considering the x-component,

$$(\nabla_r\times\vec{\mathcal{B}})_x = \frac{\mu_0}{4\pi}\int_{\mathcal{V}}\mathbf{j}(\mathbf{r}')\cdot\nabla_{r'}\frac{x-x'}{|\mathbf{r}-\mathbf{r}'|^3} + \mu_0 j_x(\mathbf{r})$$

$$= -\frac{\mu_0}{4\pi}\oint_{\partial\mathcal{V}}\mathbf{j}(\mathbf{r}')\frac{x-x'}{|\mathbf{r}-\mathbf{r}'|^3}d\mathbf{S}' + \frac{\mu_0}{4\pi}\int_{\mathcal{V}}\frac{x-x'}{|\mathbf{r}-\mathbf{r}'|^3}\nabla_{r'}\cdot\mathbf{j}(\mathbf{r}')dV' + \mu_0 j_x(\mathbf{r})\ .$$

The surface integral vanishes when the volume goes to infinity. On the other hand, $\nabla\cdot\mathbf{j} = -\dot{\varrho} = 0$. With this, we obtain,

$$\boxed{\nabla\times\vec{\mathcal{B}} = \mu_0\mathbf{j}}\ . \tag{15.18}$$

The results (15.14) and (15.18) represent parts of Maxwell's first and fourth equations. The equation (15.18) is also called *Ampère's law*. The integral version can be obtained from Stokes' law,

$$\boxed{\oint_{\mathcal{C}}\vec{\mathcal{B}}\cdot d\mathbf{l} = \mu_0 I}\ . \tag{15.19}$$

The interpretation of Ampere's law is, that *every current produces a rotational magnetic field*, that is, a field with closed field lines. Measuring the magnetic field along an closed path we can evaluate the current passing through the surface delimited by the path.

Ampère's law has many applications. Let's discuss some in the next.

Example 70 (*Magnetic field of a straight current-carrying wire*): Let us re-evaluate the example 68 using Ampere's law,

$$\oint\vec{\mathcal{B}}\cdot d\mathbf{l} = B\int_0^{2\pi}\rho d\phi = \mathcal{B}2\pi\rho = \mu_0 I\ .$$

[3] Using the rule $\nabla\times(\vec{\mathcal{E}}\times\vec{\mathcal{B}}) = (\vec{\mathcal{B}}\cdot\nabla)\vec{\mathcal{E}} - (\vec{\mathcal{E}}\cdot\nabla)\vec{\mathcal{B}} + \vec{\mathcal{E}}(\nabla\cdot\vec{\mathcal{B}}) - \vec{\mathcal{B}}(\nabla\cdot\vec{\mathcal{E}})$.

Hence,

$$\mathcal{B} = \frac{\mu_0 I}{2\pi\rho} \ .$$

Example 71 (*Ampère's law*): We can use Ampère's law to show that a locally uniform magnetic field, such as the one shown in Fig. 15.9, is impossible. Let us have a look at the rectangular curve shown by the dashed lines. With the chosen geometry, the curve does not include current,

$$\mu_0 I = 0 \ .$$

On the other hand, the magnetic field accumulated along the curve is,

$$\oint_C \vec{\mathcal{B}} \cdot d\mathbf{l} \neq 0 \ .$$

This is a contradiction. Thus, this example shows that, in the absence of currents, any magnetic field is conservative. We could then define a scalar potential whose gradient would be the magnetic field, but this potential must be *simply connected*, i.e. not be traversed by currents, which limits the practical use of such a potential.

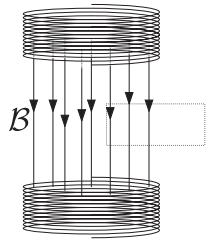

Figure 15.9: Impossibility of a localized homogeneous magnetic field.

Example 72 (*Field of a solenoid*): A solenoid is a very long coil (the distance between two consecutive turns is much smaller than the radius and the total length l of the coil) carrying a current I (see diagram in Fig. 15.10). Ampère's law can be used to easily calculate the magnetic field inside a solenoid composed of N turns,

$$\mathcal{B}dl = \oint_C \vec{\mathcal{B}} \cdot d\mathbf{r} = \mu_0 I \ dN \ .$$

Hence,

$$\mathcal{B} = \mu_0 I \frac{dN}{dl} \ .$$

Resolve the Excs. 15.2.4.2 to 15.2.4.9. In the Excs. 15.2.4.10 to 15.2.4.12 we apply the Biot-Savart law to *Helmholtz coils* and *anti- Helmholtz coils*.

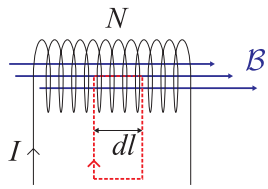

Figure 15.10: Scheme of a solenoid with loop density dN/dl.

15.2.4 Exercises

15.2.4.1 Ex: Magnetic flux

A long solenoid has n turns per unit length, radius R_1, and carries a current I. A circular coil with radius R_2 and N turns is coaxial to the solenoid and is equidistant from its ends.
a. Determine the magnetic flux through the coil if $R_2 < R_1$.
b. Determine the magnetic flux through the coil if $R_2 > R_1$.

Solution: *a.* $\phi_m = \mu_0 n I N \pi R_1^2$.
b. $\phi_m = \mu_0 n I N \pi R_2^2$.

15.2.4.2 Ex: Magnetic field of a conducting ring and Ampère's law

A ring-shaped conducting loop lies in the yz-plane; the loop's symmetry axis is the x-axis. It is traversed by a current I generating on the axis the field $\mathcal{B}_x = \frac{1}{2}\mu_0 I R^2 (x^2+R^2)^{-3/2}$.
a. Calculate the line integral $\int \vec{\mathcal{B}} \cdot d\mathbf{s}$ along the x-axis between $x = -L$ and $x = +L$.
b. Show that for $L \to \infty$ the line integral converges to $\mu_0 I$.
Help: This result can also be obtained with Ampère's law, when we close the integration path through a semicircle with radius L, for which holds $\mathcal{B} \simeq 0$, when L is very large.

Solution: *The line integral is,*

$$\int \vec{\mathcal{B}} \cdot d\mathbf{s} = \frac{\mu_0 I}{2} \int_{-L}^{L} \frac{R^2 \hat{\mathbf{e}}_x}{(x^2+R^2)^{3/2}} \cdot d\mathbf{s} = \frac{\mu_0 I}{2} \int_{-L}^{L} \frac{R^2}{(x^2+R^2)^{3/2}} dx$$
$$= \frac{\mu_0 I}{2} \frac{x}{\sqrt{(x^2+R^2)}}\Bigg|_{-L}^{L} = \frac{\mu_0 I}{2} \frac{2L}{\sqrt{L^2+R^2}} \ .$$

For large distances L,

$$\int \vec{\mathcal{B}} \cdot d\mathbf{s} \longrightarrow \mu_0 I \ .$$

For very large L we can close the integration path,

$$\lim_{L\to\infty} \int \vec{\mathcal{B}} \cdot d\mathbf{s} \simeq \oint \vec{\mathcal{B}} \cdot d\mathbf{s} = \mu_0 I \ ,$$

and obtain Ampere's law.

15.2.4.3 Ex: Biot-Savart's and Ampère's laws

a. Calculate the magnetic field generated by a constant current I on a straight conductor piece of length L.
b. Show that for an infinitely long conductor the Biot-Savart law becomes Ampere's law.

Solution: *a. Following the Biot-Savart,*

$$\vec{\mathcal{B}}(\mathbf{r}) = \frac{\mu_0}{4\pi}\int_{V'}\frac{(\mathbf{r}-\mathbf{r}')\times\mathbf{j}(\mathbf{r}')}{|\mathbf{r}-\mathbf{r}'|^3}d^3\mathbf{r}' \ .$$

With the current wire $\mathbf{j}(\mathbf{r}) = I\hat{\mathbf{e}}_z\delta(x)\delta(y)\theta(-L/2<z<L/2)$ *follows,*

$$\vec{\mathcal{B}}(\mathbf{r}) = \frac{\mu_0 I}{4\pi}(y\hat{\mathbf{e}}_x - x\hat{\mathbf{e}}_y)\int\frac{1}{\sqrt{\rho^2+(z-z')^2}^3}dz' = \frac{\mu_0 I}{4\pi}(y\hat{\mathbf{e}}_x - x\hat{\mathbf{e}}_y)\left.\frac{z'-z}{\rho^2\sqrt{\rho^2+(z-z')^2}}\right|_{-L/2}^{L/2}$$

$$= \frac{\mu_0 I}{4\pi}\frac{y\hat{\mathbf{e}}_x - x\hat{\mathbf{e}}_y}{\rho^2}\left[\frac{L/2-z}{\sqrt{\rho^2+(z-L/2)^2}} + \frac{L/2+z}{\sqrt{\rho^2+(z+L/2)^2}}\right] \ .$$

For long conductor pieces $L\to\infty$,

$$\vec{\mathcal{B}}(\mathbf{r}) \longrightarrow \frac{\mu_0 I}{2\pi}\frac{y\hat{\mathbf{e}}_x - x\hat{\mathbf{e}}_y}{\rho^2} \ .$$

The absolute value is now, $|\vec{\mathcal{B}}(\mathbf{r})| = \frac{\mu_0 I}{2\pi\rho}$. *The magnetic field follows as rotation from the potential vector,* $\vec{\mathcal{B}}(\mathbf{r}) = \nabla\times\mathbf{A}(\mathbf{r}) = \nabla\times\frac{-\mu_0 I}{4\pi}\frac{\hat{\mathbf{e}}_z}{\rho^2}$.

15.2.4.4 Ex: Solenoid

a. To determine the number of turns of a solenoid with diameter $D = 4\,\mathrm{cm}$ and length $L = 10\,\mathrm{cm}$, an experimenter passes a current $I = 1\,\mathrm{A}$ through the coil. He measures the magnetic field $\mathcal{B} = 10\,\mathrm{mT}$. How many windings are there?
b. To confirm it measures the diameter of the copper wire ($d = 1\,\mathrm{mm}$) and ohmic resistance finding $R = 2\,\Omega$. On the internet he finds the resistivity of copper $\rho = 1.7\cdot 10^{-8}\,\Omega\mathrm{m}$.

Solution: *a. The field is*

$$\mathcal{B}(\rho) = \mu_0\frac{N}{L}I \ .$$

Hence, $N = 796$.
b. The resistance is,

$$R = \rho\frac{L}{A} = \rho\frac{N2\pi(D/2)}{\pi(d/2)^2} = 2\ \Omega \ .$$

Hence, $N = 735$.

15.2.4.5 Ex: Toroidal coil

A coil with N turns is arranged in a toroidal form with rotational symmetry around z-axis and has its center at the origin of the coordinates. The coil is densely wound and traversed by a current I (see scheme).
a. Calculate the $\hat{\mathbf{e}}_\phi$-component of the $\vec{\mathcal{B}}$-field for $z = 0$ (xy-plane) as a function of distance ρ from the origin.
b. Determine the $\hat{\mathbf{e}}_\phi$-component of the $\vec{\mathcal{B}}$-field in the entire *inner* space outside the toroid. Draw the $\hat{\mathbf{e}}_\phi$ component as a function of ρ.
c. What should be the value of b, so that $\mathcal{B}_\phi$ is constant within the toroid with an accuracy of $\alpha = 1\%$, when $a = 1\,\text{cm}$? [That is: $\mathcal{B}_\phi(b-a) - \mathcal{B}_\phi(b+a) < \alpha \cdot \mathcal{B}_\phi(b)$]

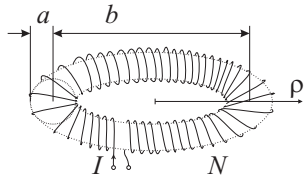

Figure 15.11: Toroidal coil.

Solution: *a. Following Stokes' law:*

$$\oint_C \vec{\mathcal{B}} d\mathbf{s} = N\mu_0 \int \mathbf{j}(\mathbf{r}) d\mathbf{f}$$
$$\mathcal{B}_\phi 2\pi\rho = N\mu_0 I$$
$$\Rightarrow B_\phi = \frac{N\mu_0 I}{2\pi\rho} \qquad para \qquad (b-a) \le \rho \le (b+a)\ ,$$

where the path C is chosen on a circle around the symmetry axis.
b. Outside the torus we have $\mathcal{B}_\phi = 0$ in the entire space. Scheme of the $\mathcal{B}_\phi$-component: $\frac{1}{\rho}$: hyperbolic cut between $b-a$ and $b+a$.
c. $a = 0.01$ m and we need: $\mathcal{B}_\phi(b-a) - \mathcal{B}_\phi(b+a) < \alpha\mathcal{B}_\phi(b)$, hence,

$$\frac{N\mu_0 I}{2\pi}\left(\frac{1}{b-a} - \frac{1}{b+a}\right) < 0.01\frac{N\mu_0 I}{2\pi}\frac{1}{b}$$
$$\frac{1}{b-a} - \frac{1}{b+a} < \alpha\frac{1}{b}$$
$$\Rightarrow 0 < b^2 - \frac{2ab}{\alpha} - a^2$$
$$\Rightarrow b > 200.005\,\text{cm}\ .$$

15.2.4.6 Ex: Toroidal coil

A toroidal coil tightly wound with 1000 turns has an inner radius of 1.0 cm, an outer radius of 2.0 cm, carries a current of 1.5 A. The torus is centered at the origin with

the centers of the individual turns in the $z = 0$ plane. What is the intensity of the magnetic field in the $z = 0$ plane a distance of (a) 1.1 cm and (b) 1.5 cm away from the origin?

Solution: *a.* $\mathcal{B}(1.1\,\mathrm{cm}) = 27.3\,\mathrm{mT}$.
b. $\mathcal{B}(1.5\,\mathrm{cm}) = 20.0\,\mathrm{mT}$

15.2.4.7 Ex: Inhomogeneous current density

The current density on a straight wire of infinite length with the radius R grows linearly from the center outward, $\mathbf{j}(r) = j_0 r\hat{\mathbf{e}}_z$, where $\hat{\mathbf{e}}_z$ shows in the direction of the wire and the total current going through the wire is I.
a. Calculate j_0 as a function of I.
b. Calculate, using Ampere's law, the magnetic field inside and outside the wire.
c. Make a graph of the normalized magnetic field, $\mathcal{B}(r)/\mathcal{B}_R$, versus r/R, where $\mathcal{B}_R \equiv \mu_0 I/2\pi R$.

Solution: *a. The integral of the current density over the surface shall give the total current:*

$$\int_0^{2\pi} r d\phi \int_0^R j_0 r dr = \frac{2\pi}{3} j_0 R^3 = I \ .$$

Hence, $j_0 = \frac{3}{2\pi}\frac{I}{R^3}$.
b. Using Ampère's law we calculate for $r < R$*:*

$$\oint \vec{\mathcal{B}} d\mathbf{l} = 2\pi r \mathcal{B}(r) = \mu_0 \int \mathbf{j} \cdot d\mathbf{S}$$
$$= \mu_0 \frac{3}{2\pi}\frac{I}{R^3} \int_0^{2\pi} r' d\phi \int_0^r r' dr = \mu_0 \frac{3}{2\pi}\frac{I}{R^3} 2\pi \frac{r^3}{3} = \mu_0 I \frac{r^3}{R^3} \ .$$

Hence,

$$\mathcal{B}(r) = \frac{\mu_0}{2\pi} I \frac{r^2}{R^3} \ .$$

In the case $r > R$*, we find again* $\mathcal{B}(r) = \frac{\mu_0}{2\pi}\frac{I}{r}$.
c. The normalized magnetic field starts growing quadratically up to the edge of the conductor, $\frac{\mathcal{B}(r)}{\mathcal{B}_R} = \frac{r^2}{R^2}$*, where it adopts the value* 1*. Then it falls off like,* $\frac{\mathcal{B}(r)}{\mathcal{B}_R} = \frac{R}{r}$.

15.2.4.8 Ex: Magnetic field in a coaxial cable

A coaxial cable consists of an inner conductor with radius R_1 and a cylindrical outer conductor with inner radius R_2 and outer radius R_3. In both conductors flows the same current I in opposite directions. The current densities in each conductor are homogeneous.
a. Calculate the current densities in each conductor.

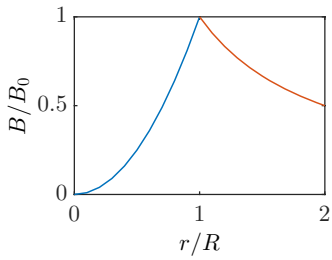

Figure 15.12: Magnetic field.

b. Calculate the magnetic field $\mathcal{B}(r)$ for $r \leq R_1$,
c. for $R_1 \leq r \leq R_2$,
d. for $R_2 \leq r \leq R_3$,
e. for $R_3 \leq r$.

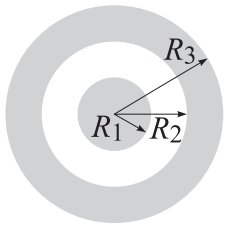

Figure 15.13: Magnetic field in a coaxial cable.

Solution: *a. Current densities in the inner and outer conductors are given by,*

$$j_i = \frac{I}{\pi R_1^2} \qquad \text{and} \qquad j_e = \frac{I}{\pi(R_3^2 - R_2^2)} \ .$$

b. With $\oint \vec{\mathcal{B}} \cdot d\mathbf{l} = \mu_0 \int \mathbf{j} \cdot d\mathbf{S}$ *segue para* $r \leq R_1$,

$$2\pi r \mathcal{B}_b(r) = \mu_0 j_i \pi r^2 = \mu_0 I \frac{r^2}{R_1^2}$$
$$\mathcal{B}_b(r) = \frac{\mu_0 I}{2\pi R_1^2} r \ .$$

c. For $R_1 \leq r \leq R_2$ *we get,*

$$2\pi r \mathcal{B}_c(r) = \mu_0 j_i \pi R_1^2 = \mu_0 I$$
$$\mathcal{B}_c(r) = \frac{\mu_0 I}{2\pi r} \ .$$

d. For $R_2 \leq r \leq R_3$ we get,

$$2\pi r\mathcal{B}_d(r) = \mu_0 j_i \pi R_1^2 - \mu_0 j_a \pi (r^2 - R_2^2) = \mu_0 I - \mu_0 I \frac{r^2 - R_2^2}{R_3^2 - R_2^2}$$
$$B(r)_d = \frac{\mu_0 I}{2\pi r}\left(1 - \frac{r^2 - R_2^2}{R_3^2 - R_2^2}\right) .$$

e. For $R_3 \leq r$ we get,

$$2\pi r\mathcal{B}_e(r) = \mu_0 j_i \pi R^2 - \mu_0 j_e \pi (R_3^2 - R_2^2) = 0$$
$$\mathcal{B}_e(r) = 0 .$$

Note that the magnetic field is continuous at the interfaces: $\mathcal{B}_b(R_1) = \mathcal{B}_c(R_1)$, $\mathcal{B}_c(R_2) = \mathcal{B}_d(R_2)$, and $\mathcal{B}_d(R_3) = \mathcal{B}_e(R_3)$.

15.2.4.9 Ex: Magnetic field of a current conductor

In a straight, infinitely long conductor with circular cross-sectional area with radius R runs a current I with a uniform current density distribution. How are the magnetic induction field lines $\vec{\mathcal{B}}$?
a. Calculate $\vec{\mathcal{B}}$ inside and outside the conductor.
b. Prepare a scheme of the profile $\mathcal{B}(r) \equiv |\vec{\mathcal{B}}(r)|$, where r be the distance from the symmetry axis of the conductor in a direction perpendicular to it.

Solution: *In Cartesian coordinates $\mathbf{j} = (0, 0, I/(\pi R^2))$. For symmetry reasons the $\vec{\mathcal{B}}$-field lines follow circles in the planes perpendicular to the conductor symmetry axis.*
a. We have $\nabla \times \vec{\mathcal{B}} = 4\pi\mathbf{j}/c$. We now integrate over a circular area S with radius r in a plane perpendicular to the symmetry axis of the conductor. The symmetry axis crosses the center of the area,

$$\int_{\mathcal{S}} (\nabla \times \vec{\mathcal{B}}) \cdot d\mathbf{S} = \frac{4\pi}{c} \int_{\mathcal{S}} \mathbf{j} \cdot d\mathbf{S}$$
$$= \frac{4\pi}{c} \frac{I}{\pi R^2} \begin{cases} \pi r^2 & ser \leq R \\ \pi R^2 & ser > R \end{cases} .$$

On the other hand, Stokes's law shows,

$$\int_{\mathcal{S}} (\nabla \times \vec{\mathcal{B}}) \cdot d\mathbf{S} = \int_{\partial\mathcal{S}} \vec{\mathcal{B}} \cdot d\mathbf{S} = 2\pi r B(r)$$

This gives,

$$\mathcal{B}(r) = \frac{2I}{c} \begin{cases} \frac{r}{R^2} & ser \leq R \\ \frac{1}{r} ser > R . \end{cases}$$

b. Is trivial.

15.2.4.10 Ex: Helmholtz and anti-Helmholtz coils

a. Show that the magnetic field of a round current loop conductor with radius R on the symmetry axis is given by,

$$\vec{\mathcal{B}}(z) = -\frac{\mu_0 I}{2}\frac{R^2}{\sqrt{R^2+z^2}^3}\hat{\mathbf{e}}_z \ .$$

b. Now consider two identical parallel loops placed on the symmetry axis with distance $d = R$. The loops are traversed by currents of equal amplitude. What is the behavior of the magnetic field on the symmetry axis for (i) equal directions of currents (ii) opposite directions? Choosing as the origin the center between the two coils, expands the magnetic field to second order in a Taylor series around the origin.

Solution: *a. The current density can be parametrized by* $\mathbf{j}(\mathbf{r}) = I\delta(\rho - R)\delta(z)\hat{\mathbf{e}}_\phi$. *The vector potential is,*

$$\mathbf{A}(\mathbf{r}) = \frac{\mu_0}{4\pi}\int \frac{\mathbf{j}(\mathbf{r}')}{|\mathbf{r}-\mathbf{r}'|}d^3r' \ .$$

Following the Biot-Savart law the magnetic field is,

$$\begin{aligned}
\vec{\mathcal{B}}(\mathbf{r}) &= \frac{\mu_0}{4\pi}\int \nabla\times\frac{\mathbf{j}(\mathbf{r}')}{|\mathbf{r}-\mathbf{r}'|}d^3r' = \frac{\mu_0}{4\pi}\int d^3\mathbf{r}'\frac{(\mathbf{r}-\mathbf{r}')\times\mathbf{j}(\mathbf{r}')}{|\mathbf{r}-\mathbf{r}'|^3} \\
&= \frac{\mu_0 I}{4\pi}\int \rho' d\rho' d\phi' dz' \frac{\delta(\rho'-R)\delta(z')(\mathbf{r}-\mathbf{r}')\times\hat{\mathbf{e}}_{\phi'}}{|\mathbf{r}-\mathbf{r}'|^3} \\
&= \frac{\mu_0 I}{4\pi}\int \rho' d\rho' d\phi' dz' \frac{\delta(\rho'-R)\delta(z')\begin{pmatrix}\rho\cos\phi-\rho'\cos\phi'\\ \rho\sin\phi-\rho'\sin\phi'\\ z-z'\end{pmatrix}\times\begin{pmatrix}-\sin\phi'\\ \cos\phi'\\ 0\end{pmatrix}}{\sqrt{(\rho\cos\phi-\rho'\cos\phi')^2+(\rho\sin\phi-\rho'\sin\phi')^2+(z-z')^2}^3} \\
&= \frac{\mu_0 I}{4\pi}\int Rd\phi' \frac{\begin{pmatrix}-z\cos\phi'\\ -z\sin\phi'\\ (\rho\cos\phi-R\cos\phi')\cos\phi'+(\rho\sin\phi-R\sin\phi')\sin\phi'\end{pmatrix}}{\sqrt{(\rho\cos\phi-R\cos\phi')^2+(\rho\sin\phi-R\sin\phi')^2+z^2}^3} \ .
\end{aligned}$$

Along the axis $\rho = 0$,

$$\begin{aligned}
\vec{\mathcal{B}}(z) &= \frac{\mu_0 I}{4\pi}\int Rd\phi' \frac{1}{\sqrt{R^2+z^2}^3}\begin{pmatrix}-z\cos\phi'\\ -z\sin\phi'\\ -R\end{pmatrix} = \frac{\mu_0 I}{4\pi}2\pi R\frac{1}{\sqrt{R^2+z^2}^3}\begin{pmatrix}0\\ 0\\ -R\end{pmatrix} \\
&= -\frac{\mu_0 I}{2}\frac{R^2}{\sqrt{R^2+z^2}^3}\hat{\mathbf{e}}_z = -\frac{\mu_0 I}{2}\frac{R^2}{\sqrt{R^2+z^2}^3}\hat{\mathbf{e}}_z \ .
\end{aligned}$$

b. For two conductive loops distant by $d = R$,

$$\vec{\mathcal{B}}_t(z) = \vec{\mathcal{B}}(z-R/2)\pm\vec{\mathcal{B}}(z+R/2) = -\frac{\mu_0 I}{2}\hat{\mathbf{e}}_z\left(\frac{R^2}{\sqrt{R^2+(z-R/2)^2}^3}\pm\frac{R^2}{\sqrt{R^2+(z+R/2)^2}^3}\right) \ .$$

A Taylor expansion for identical, respectively, opposite currents gives,

$$\vec{\mathcal{B}}_{t+}(z) = -\frac{8}{5\sqrt{5}}\frac{\mu_0 I\hat{\mathbf{e}}_z}{R}[1+O(z^3)]$$
$$\vec{\mathcal{B}}_{t-}(z) = -\frac{48}{25\sqrt{5}}\frac{\mu_0 I\hat{\mathbf{e}}_z}{R^2}[z+O(z^3)]\ .$$

Alternatively, the formula can be derived from the magnetic field of a current element,

$$d\vec{\mathcal{B}} = \frac{\mu_0 I}{4\pi}\frac{d\mathbf{l}\times(\mathbf{r}-\mathbf{r}')}{|\mathbf{r}-\mathbf{r}'|^3}$$
$$d\mathcal{B}_z = d\mathcal{B}\sin\alpha = d\mathcal{B}\frac{R}{\sqrt{R^2+z^2}}$$
$$\mathcal{B}_z = \frac{\mu_0 I}{4\pi}\oint\frac{\left|d\vec{l}\times(\mathbf{r}-\mathbf{r}')\right|}{|\mathbf{r}-\mathbf{r}'|^3}\frac{R}{\sqrt{R^2+z^2}} = \frac{\mu_0 I}{4\pi}2\pi R\frac{R}{\sqrt{R^2+z^2}^3} = \frac{\mu_0 I}{2}\frac{R^2}{\sqrt{R^2+z^2}^3}\ .$$

15.2.4.11 Ex: Helmholtz coils

Two identical circular coils of radius R and negligible thickness are mounted with their axes coinciding with the z-axis, as shown in the figure below. Their centers are separated by a distance d, with the midpoint P coinciding with the origin of the z-axis. The coils carry electric currents of the same intensity I, and both counterclockwise.
a. Use the Biot-Savart law to show that the magnetic field $\mathcal{B}(z)$ along the z-axis is,

$$\vec{\mathcal{B}}_{t+}(z) = -\frac{\mu_0 I}{2}\hat{\mathbf{e}}_z\left(\frac{R^2}{\sqrt{R^2+(z-R/2)^2}^3}\pm\frac{R^2}{\sqrt{R^2+(z+R/2)^2}^3}\right)\ .$$

b. Assuming that the spacing d is equal to the radius R of the coils, show that at point P the following equalities are valid: $d\mathcal{B}/dz = 0$ and $d^2\mathcal{B}/dz^2 = 0$.
c. Looking at the graphs below, which curve describes the magnetic field along the z-axis in the configuration of item (b)? Justify!
d. Assuming that the current in the upper coil is reversed, calculate the new value of the magnetic field at point P.

Solution: *a. The magnetic field generated at a position* $\mathbf{r}$ *by a current element* $d\mathbf{l}$ *located at position* $\mathbf{r}'$ *is,*

$$d\vec{\mathcal{B}}(\mathbf{r}) = \frac{\mu_0 I}{4\pi}\frac{d\vec{l}\times(\mathbf{r}-\mathbf{r}')}{|\mathbf{r}-\mathbf{r}'|^3}\ .$$

Considering a circular coil located in the xz*-plane and integrating with* $\mathbf{r} = (0,0,z)$ *and* $\mathbf{r}' = R(\cos\phi,\sin\phi,0)$ *and* $d\vec{\ell} = Rd\phi(\sin\phi,-\cos\phi,0)$*,*

$$\mathcal{B}_z = \frac{\mu_0 I}{4\pi}\oint\frac{(d\vec{l}\times(\mathbf{r}-\mathbf{r}'))_z}{|\mathbf{r}-\mathbf{r}'|^3} = \frac{\mu_0 I}{4\pi}\int_0^{2\pi}\frac{-R^2 d\phi}{|\mathbf{r}-\mathbf{r}'|^3} = \frac{\mu_0 I}{2}\frac{R^2}{\sqrt{R^2+z^2}^3}\ .$$

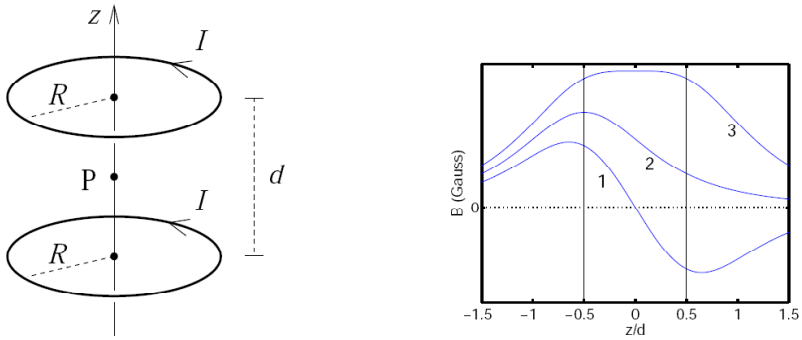

Figure 15.14: (code) Geometry and magnetic field amplitude of a pair of Helmholtz coils.

Now, for two coils distant by $d = R$,

$$\vec{\mathcal{B}}_t(z) = \vec{\mathcal{B}}(z-R/2) \pm \vec{\mathcal{B}}(z+R/2) = -\frac{\mu_0 I}{2}\hat{\mathbf{e}}_z \left(\frac{R^2}{\sqrt{R^2+(z-R/2)^2}^3} \pm \frac{R^2}{\sqrt{R^2+(z+R/2)^2}^3} \right) .$$

b. Taylor expansion for equal and opposite current directions,

$$\vec{\mathcal{B}}_{t+}(z) = -\frac{8}{5\sqrt{5}}\frac{\mu_0 I \hat{\mathbf{e}}_z}{R}[1+O(z^3)]$$
$$\vec{\mathcal{B}}_{t-}(z) = -\frac{48}{25\sqrt{5}}\frac{\mu_0 I \hat{\mathbf{e}}_z}{R^2}[z+O(z^3)] .$$

It is obvious that for equal directions the first and second derivatives of the field disappear.
c. Curve (3) corresponds to the Helmholtz configuration, since this curve satisfies $d\mathcal{B}/dz = 0 = d^2\mathcal{B}/dz^2$ in the center. Curve (1) describes the anti-Helmholtz configuration, since this curve is linear in the center.
d. The magnetic field at point P for anti-Helmholtz configuration is 0 according to the formula obtained in item (a) or in the Taylor expansion in item (b).

15.2.4.12 Ex: Helmholtz coils

A pair of identical coils, each with a radius of 30 cm, is separated by a distance equal to their radii. Called Helmholtz coils, they are coaxial and carry equal currents oriented such that their axial fields point into the same z-direction. A feature of Helmholtz coils is, that the resulting magnetic field in the region between the coils is quite uniform. Assume that the current in each one is 15 A and that there are 250 turns for each coil. Using a spreadsheet, calculate and plot the magnetic field along the z-axis for $-30\,\text{cm} < z < +30\,\text{cm}$. Within which z-range does the field vary by less than 20%?

Solution: *See the figure.*

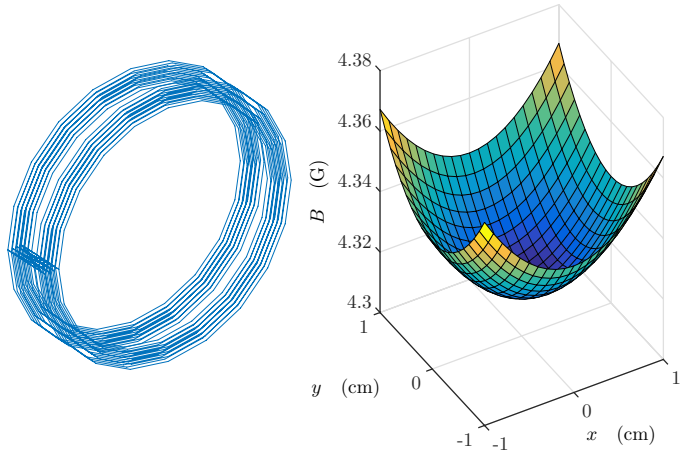

Figure 15.15: Numerical integration of the Biot-Savart law.

15.3 The magnetic vector potential

The fact that the divergence of the magnetic field vanishes, $\nabla \cdot \vec{\mathcal{B}} = 0$, allows us to introduce a vector field $\mathbf{A}$ called *vector potential* of which the magnetic field is the rotation,

$$\boxed{\vec{\mathcal{B}} = \nabla \times \mathbf{A}} \, . \tag{15.20}$$

15.3.1 The Laplace and Poisson equations

Ampère's law says,

$$\mu_0 \mathbf{j} = \nabla \times \vec{\mathcal{B}} = \nabla \times (\nabla \times \mathbf{A}) = \nabla(\nabla \cdot \mathbf{A}) - \nabla^2 \mathbf{A} \, . \tag{15.21}$$

Note that, just as we can add a constant to the electrostatic potential without changing the electric field, we have the freedom to add to the vector potential the *gradient of a scalar field*,

$$\nabla \times \mathbf{A} = \nabla \times (\mathbf{A} + \nabla \chi) \, , \tag{15.22}$$

since the rotation of a gradient always vanishes. This freedom allows us to impose other conditions on this scalar field $\chi(\mathbf{r})$. One of them is called the *Coulomb gauge*,

$$\boxed{\nabla \cdot \mathbf{A} \equiv 0} \, . \tag{15.23}$$

To show that it is always possible to choose a function χ such, that the potential vector $\mathbf{A} + \nabla\chi$ satisfies the condition (15.23) and at the same time produces the same magnetic field (15.22), we just insert this potential into Eq. (15.23) and find a formal solution of the following Poisson equation,

$$\nabla^2 \chi = -\nabla \cdot \mathbf{A} \, . \tag{15.24}$$

is simply the Coulomb potential [see (13.33)],

$$\chi(\mathbf{r}) = \frac{1}{4\pi}\int_{\mathcal{V}} \frac{\nabla_{r'}\cdot\mathbf{A}(\mathbf{r}')}{|\mathbf{r}-\mathbf{r}'|}dV' \ , \tag{15.25}$$

supposing that $\nabla\cdot\mathbf{A} \overset{r\to\infty}{\longrightarrow} 0$.

Within the Coulomb gauge the Eq. (15.21) also adopts the simple form of a Poisson equation,

$$\boxed{\nabla^2\mathbf{A} = -\mu_0\mathbf{j}} \ , \tag{15.26}$$

which we can solve,

$$\boxed{\mathbf{A}(\mathbf{r}) = \frac{\mu_0}{4\pi}\int \frac{\mathbf{j}(\mathbf{r}')}{|\mathbf{r}-\mathbf{r}'|}d^3\mathbf{r}'} \ . \tag{15.27}$$

This relationship is the equivalent of the electrostatic potential (13.35). We verify that we recover Biot-Savart's law (15.8) via,

$$\nabla_r\times\mathbf{A}(\mathbf{r}) = \frac{\mu_0}{4\pi}\int_{\mathcal{V}}\mathbf{j}(\mathbf{r}')\times\frac{|\mathbf{r}-\mathbf{r}'|}{|\mathbf{r}-\mathbf{r}'|^3}dV' \ . \tag{15.28}$$

Example 73 (*Vector potential of a one-dimensional current*): As an example we consider a one-dimensional current, $\mathbf{j}(\mathbf{r}') = I\delta^2(\mathbf{r}'-\mathbf{s}_\perp)\hat{\mathbf{e}}'_j$,

$$\mathbf{A}(\mathbf{r}) = \frac{\mu_0 I}{4\pi}\int_{\mathcal{C}}\frac{d\mathbf{s}'}{|\mathbf{r}-\mathbf{r}'|} \qquad \text{and} \qquad \vec{\mathcal{B}}(\mathbf{r}) = \frac{\mu_0 I}{4\pi}\int_{\mathcal{C}}\frac{d\mathbf{s}'\times|\mathbf{r}-\mathbf{r}'|}{|\mathbf{r}-\mathbf{r}'|^3} \ .$$

For a current element oriented along the z-axis,

$$\mathbf{A}(\mathbf{r}) = \frac{\mu_0 I}{4\pi}\int_0^a \frac{\hat{\mathbf{e}}_z dz'}{\sqrt{\rho^2+(z-z')^2}} = \frac{\mu_0 I}{4\pi}\hat{\mathbf{e}}_z \ln\frac{-(z-a)+\sqrt{r^2+(z-a)^2}}{-z+\sqrt{r^2+z^2}} \ .$$

The scheme 15.16 summarizes the fundamental laws of magnetostatics.

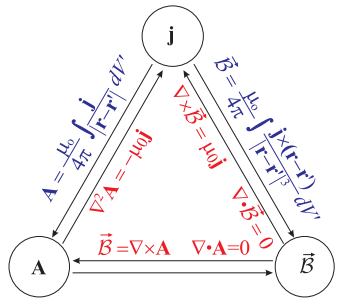

Figure 15.16: Organization chart for the fundamental laws of magnetostatics. Note, that there is no simple expression to calculate $\mathbf{A}$ from $\vec{\mathcal{B}}$.

15.3.2 Magnetostatic boundary conditions

In order to find the magnetostatic boundary conditions imposed by current-carrying interfaces, we proceed in the same way as in the electrostatic case. First, we consider a 'pill box', as schematized in Fig. 15.17. From

$$\oint \vec{\mathcal{B}} \cdot d\mathbf{S} = 0 \ , \tag{15.29}$$

we find for the component of the magnetic field perpendicular to the interface,

$$\mathcal{B}^{\perp}_{top} = \mathcal{B}^{\perp}_{down} \ . \tag{15.30}$$

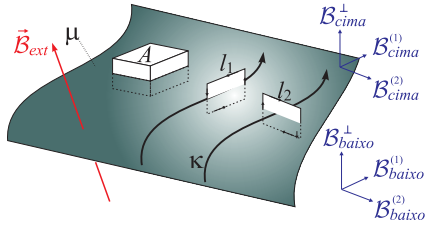

Figure 15.17: Illustration of the pillbox-shaped volume delimited by the surface A cutting through a small part of the interface. Also shown are paths on the interface being perpendicular (l_1) or parallel (l_2) to the surface current κ.

We now consider a closed loop in the plane defined by the magnetic field and perpendicular to the current. From

$$\oint \vec{\mathcal{B}} \cdot d\mathbf{l}_2 = (\mathcal{B}^{(2)}_{top} - \mathcal{B}^{(2)}_{bottom}) l_2 = \mu_0 I = \mu_0 \kappa l_2 \ , \tag{15.31}$$

where we defined $\kappa \equiv I/l_2$ as the surface current density, that is, the current dI flowing through a ribbon of width dl_2 sticking to the interface. We find,

$$\mathcal{B}^{(2)}_{top} - \mathcal{B}^{(2)}_{bottom} = \mu_0 \kappa \ . \tag{15.32}$$

Thus, the component of $\vec{\mathcal{B}}$ parallel to the surface but perpendicular to the current is discontinuous by a value $\mu_0 \kappa$.

Similarly, a closed loop in the direction parallel to the current shows that the parallel component of $\vec{\mathcal{B}}$ is continuous,

$$\oint \vec{\mathcal{B}} \cdot d\mathbf{l}_1 = (\mathcal{B}^{(1)}_{top} - \mathcal{B}^{(1)}_{bottom}) l_1 = 0 \ . \tag{15.33}$$

In summary,

$$\vec{\mathcal{B}}_{top} - \vec{\mathcal{B}}_{bottom} = \vec{\mathcal{B}}^{\parallel}_{top} - \vec{\mathcal{B}}^{\parallel}_{bottom} = \mu_0 \vec{\kappa} \times \hat{\mathbf{n}} \ . \tag{15.34}$$

In the same way as the scalar potential in electrostatics, the potential vector remains continuous through the interface,

$$\mathbf{A}_{top} = \mathbf{A}_{bottom} \ , \tag{15.35}$$

because $\nabla \cdot \mathbf{A} = 0$ ensures that the normal component is continuous and,

$$\oint \mathbf{A} \cdot d\mathbf{l} = \int \nabla \times \mathbf{A} \cdot d\mathbf{S} = \int \vec{\mathcal{B}} \cdot d\mathbf{S} = \Psi_M \ , \tag{15.36}$$

means that the tangential components are continuous (the flux through an Amperian loop of negligible thickness vanishes). On the other hand, the derivative of $\mathbf{A}$ inherits the discontinuity of $\vec{\mathcal{B}}$:

$$\frac{\partial \mathbf{A}_{top}}{\partial n} - \frac{\partial \mathbf{A}_{bottom}}{\partial n} = -\mu_0 \vec{\kappa} \ , \tag{15.37}$$

where n is the coordinate perpendicular to the surface.

Example 74 (*Proof of the discontinuity of the derivative of the vector potential*): To prove the statement (15.37) we consider a surface current in the direction $\vec{\kappa} = \kappa \hat{\mathbf{e}}_x$ within an interface located in the x-y-plane. So,

$$\vec{\mathcal{B}}_{top} - \vec{\mathcal{B}}_{bottom} = \begin{pmatrix} 0 \\ \mu_0 \kappa \\ 0 \end{pmatrix} = \begin{pmatrix} \partial_y A^{(z)}_{top} - \partial_z A^{(y)}_{top} \\ \partial_z A^{(x)}_{top} - \partial_x A^{(z)}_{top} \\ \partial_x A^{(y)}_{top} - \partial_y A^{(x)}_{top} \end{pmatrix} - \begin{pmatrix} \partial_y A^{(z)}_{bottom} - \partial_z A^{(y)}_{bottom} \\ \partial_z A^{(x)}_{bottom} - \partial_x A^{(z)}_{bottom} \\ \partial_x A^{(y)}_{bottom} - \partial_y A^{(x)}_{bottom} \end{pmatrix} \ .$$

Now,

$$0 = \partial_y A^{(z)}_{top} - \partial_y A^{(z)}_{bottom} = \partial_z A^{(y)}_{top} - \partial_z A^{(y)}_{bottom} = \partial_x A^{(y)}_{top} - \partial_x A^{(y)}_{bottom} = \partial_y A^{(x)}_{top} - \partial_y A^{(x)}_{bottom}$$
$$\mu_0 \kappa_x = \partial_z A^{(x)}_{top} - \partial_z A^{(x)}_{bottom} - \partial_x A^{(z)}_{top} + \partial_x A^{(z)}_{bottom} \ .$$

Assuming a uniform field, only the derivative in z can contribute, such that,

$$\mu_0 \kappa_x = \partial_z A^{(x)}_{top} - \partial_z A^{(x)}_{bottom} \ .$$

15.3.3 Exercises

15.3.3.1 Ex: Vector potential and electric field of a rotating charged sphere

On the surface of a hollow sphere with radius R be evenly distributed the charge Q. The sphere rotates at constant angular velocity $\vec{\omega}$ around one of its diameters.
a. Determine the current density generated by the motion $\mathbf{j}(\mathbf{r})$.
b. Derive the components of the potential vector $\mathbf{A}(\mathbf{r})$ and the magnetic field $\vec{\mathcal{B}}(\mathbf{r})$.

Solution: *a. The charge density is,*

$$\rho(\mathbf{r}) = \frac{Q}{4\pi R^2} \delta(r - R) \ ,$$

giving the current density,

$$\mathbf{j}(\mathbf{r}) = \rho(\mathbf{r}) \mathbf{v}(\mathbf{r}) = \rho(\mathbf{r}) [\vec{\omega} \times \mathbf{r}]$$

Now, we have at the surface,

$$\mathbf{r} = R\hat{\mathbf{e}}_r = R(\sin\theta\cos\phi, \sin\theta\sin\phi, \cos\theta) \ .$$

With $\vec{\omega} = \omega\hat{\mathbf{e}}_z = \omega(0,0,1)$ *we obtain,*

$$\hat{\mathbf{e}}_z \times \hat{\mathbf{e}}_r = (-\sin\theta\sin\phi, \sin\theta\cos\phi, 0) = \sin\theta(-\sin\phi, \cos\phi, 0) = \sin\theta\hat{\mathbf{e}}_\phi$$

and therefore the current density,

$$\mathbf{j}(\mathbf{r}) = \frac{Q\omega}{4\pi R}\sin\theta\delta(r-R)\hat{\mathbf{e}}_\phi$$

b. For the potential vector we have,

$$\mathbf{A}(\mathbf{r}) = \frac{\mu_0}{4\pi}\int \frac{\mathbf{j}(\mathbf{r}')}{|\mathbf{r}-\mathbf{r}'|}d^3r' = \frac{Q}{(4\pi)^2R^2}\vec{\omega}\times\int d^3\mathbf{r}\ '\delta(r'-R)\frac{\mathbf{r}'}{|\mathbf{r}-\mathbf{r}'|} \ .$$

For the integration we let $\mathbf{r}$ *go towards* z *(in this case, the direction of* $\vec{\omega}$ *is no longer the* z*-axis). Now we have,* $|\mathbf{r}-\mathbf{r}'| = \sqrt{r^2+r'^2-2rr'\cos\theta'}$ *and* $\mathbf{r}' = r'(\sin\theta'\cos\phi', \sin\theta'\sin\phi', \cos\theta'$ *A integration over* ϕ' *then gives for the* x *and* y *components the value 0. Denoting* $\cos'$ *by* u' *and replacing* $\hat{\mathbf{e}}_z$*, we get again, after integration for* $\hat{\mathbf{e}}_r$*,*

$$\begin{aligned}\mathbf{A}(\mathbf{r}) &= \frac{2\pi Q}{(4\pi)^2R^2}(\vec{\omega}\times\hat{\mathbf{e}}_r)\int r'^3\delta(r'-R)\int_{-1}^{+1}\frac{u'du'}{\sqrt{r^2+r'^2-2rr'u'}}dr' \\ &= \frac{\mu_0 QR}{8\pi}(\vec{\omega}\times\hat{\mathbf{e}}_r)\int_{-1}^{+1}\frac{u'du'}{\sqrt{r^2+R^2-2rRu'}} \ .\end{aligned}$$

The integral can be resolved by partial integration,

$$\begin{aligned}I &= \int_{-1}^{+1}\frac{u'du'}{\sqrt{r^2+R^2-2rRu'}} = -\frac{1}{rR}\left[u'\sqrt{r^2+R^2-2rRu'}\right]_{-1}^{+1} + \frac{1}{rR}\int_{-1}^{+1}\sqrt{r^2+R^2-2rRu'} \\ &= -\frac{1}{rR}(|r-R|+|r+R|) + \frac{1}{rR}\left[-\frac{2}{3}\frac{1}{2rR}(r^2+R^2-2rRu')^{3/2}\right]_{-1}^{+1} \\ &= -\frac{1}{rR}(|r-R|+|r+R|) - \frac{1}{3r^2R^2}(|r-R|^3-|r+R|^3) \ .\end{aligned}$$

For $r > R$ *we get from this* $I = \frac{2R}{3r^2}$*, while for* $r < R$ *we find* $I = \frac{2r}{3R^2}$*. With this we get for the potential vector,*

$$\mathbf{A}(\mathbf{r}) = \frac{\mu_0 QR}{12\pi}(\vec{\omega}\times\hat{\mathbf{e}}_r)\begin{cases}\frac{r}{R^2} & if \ \ r<R \\ \frac{R}{r^2} & se \ \ r>R\end{cases} = \frac{\mu_0 QR}{12\pi}\omega\sin\theta\hat{\mathbf{e}}_\phi\begin{cases}\frac{r}{R^2} & if \ \ r<R \\ \frac{R}{r^2} & se \ \ r>R\end{cases}$$

where we use again that $\vec{\omega} = \omega\hat{\mathbf{e}}_z$ *and* $\hat{\mathbf{e}}_z\times\hat{\mathbf{e}}_r = \sin\theta\hat{\mathbf{e}}_\phi$*. Obviously,* $\mathbf{A}$ *has only the component* ϕ*.*

b. Now the magnetic induction is $\vec{\mathcal{B}} = \nabla\times\mathbf{A}$*. Using the rotation in spherical coordinates (12.80), we get immediately,*

$$\vec{\mathcal{B}} = \hat{\mathbf{e}}_r\left[\frac{1}{r\sin\theta}\frac{\partial A_\phi\sin\theta}{\partial\theta}\right] - \hat{\mathbf{e}}_\theta\left[\frac{1}{r}A_\phi + \frac{\partial A_\phi}{\partial r}\right] = \frac{\mu_0 Q\omega}{6\pi R}\begin{cases}(\hat{\mathbf{e}}_r\cos\theta - \hat{\mathbf{e}}_\theta\sin\theta) & if \ \ r<R \\ \frac{R^3}{r^3}(\hat{\mathbf{e}}_r\cos\theta + \frac{1}{2}\hat{\mathbf{e}}_\theta\sin\theta) & if \ \ r>R\end{cases}$$

With $\hat{\mathbf{e}}_r\cos\theta - \hat{\mathbf{e}}_\theta\sin\theta = \hat{\mathbf{e}}_z$ *we find that, curiously, the magnetic field is homogeneous within the layer.*

15.3.3.2 Ex: Magnetic field of a rotating spherical layer with spherical harmonics

Calculate the vector potential, magnetic field and magnetization of a charged rotating spherical layer using spherical harmonics.

Solution: *We can express the current density in Cartesian coordinates,*

$$\begin{aligned} j_x &= -v_\phi \sin\phi = -\tfrac{e\omega}{4\pi r_e}\delta(r-r_e)\sin\theta\sin\phi \\ j_y &= +v_\phi \cos\phi = +\tfrac{e\omega}{4\pi r_e}\delta(r-r_e)\sin\theta\cos\phi \\ j_z &= 0 \ . \end{aligned}$$

Now we have,

$$\begin{aligned} Y_{1\pm1}(\theta,\phi) &= \mp\sqrt{\tfrac{3}{8\pi}}\sin\theta(\cos\phi \pm i\sin\phi) \\ Y_{11}+Y_{1-1} &= -2\imath\sqrt{\tfrac{3}{8\pi}}\sin\theta\sin\phi \\ Y_{11}-Y_{1-1} &= -2\sqrt{\tfrac{3}{8\pi}}\sin\theta\cos\phi \ , \end{aligned}$$

that is,

$$\begin{aligned} j_x &= \frac{e\omega}{4\pi r_e}\delta(r-r_e)\left(+\frac{1}{2i}\sqrt{\tfrac{8\pi}{3}}\right)(Y_{11}+Y_{1-1}) \\ j_y &= \frac{e\omega}{4\pi r_e}\delta(r-r_e)\left(-\frac{1}{2}\sqrt{\tfrac{8\pi}{3}}\right)(Y_{11}-Y_{1-1}) \ . \end{aligned}$$

Now we have,

$$\mathbf{A} = \frac{1}{c}\int d\tau' \frac{\mathbf{j}(\mathbf{r}')}{|\mathbf{r}-\mathbf{r}'|}$$

and also,

$$\frac{1}{|\mathbf{r}-\mathbf{r}'|} = \sum_{lm}\frac{4\pi}{2l+1}\frac{r_<^l}{r_>^{l+1}}{Y_{lm}}^*(\theta',\phi')Y_{lm}(\theta,\phi) \ .$$

The current density is limited to the surface of the sphere. For the calculation of the vector potential in outer space we obtain, $r_< = r'$ and $r_> = r$. With that we get,

$$\begin{aligned} \begin{pmatrix} A_x \\ A_y \end{pmatrix} &= \begin{pmatrix} \frac{1}{2i}\sqrt{\frac{8\pi}{3}} \\ -\frac{1}{2}\sqrt{\frac{8\pi}{3}} \end{pmatrix} \frac{e\omega}{4\pi r_e c}\sum_{lm}\frac{4\pi}{2l+1}Y_{lm}(\theta,\phi)\cdot\int\delta(r'-r_e){r'}^{l+2}Y_{lm}^*(\theta',\phi')\begin{pmatrix} Y_{11}+Y_{1-1} \\ Y_{11}-Y_{1-1} \end{pmatrix}dr'd\Omega' \\ &= \frac{e\omega}{3c}\left(\frac{r}{r_e}\right)^2 \begin{matrix} \frac{1}{2i}\sqrt{\frac{8\pi}{3}}(Y_{11}+Y_{1-1}) \\ -\frac{1}{2}\sqrt{\frac{8\pi}{3}}(Y_{11}-Y_{1-1}) \end{matrix} \ . \end{aligned}$$

So,

$$\begin{aligned} A_x &= -\frac{e\omega}{3c}\left(\frac{r_e}{r}\right)^2\sin\theta\sin\phi \\ A_y &= +\frac{e\omega}{3c}\left(\frac{r_e}{r}\right)^2\sin\theta\cos\phi \\ A_z &= 0 \end{aligned}$$

that is,

$$\mathbf{A} = A_\phi \hat{\mathbf{e}}_\phi \qquad with \qquad A_\phi = \frac{e\omega}{3c}\left(\frac{r_e}{r}\right)^2 \sin\theta \ .$$

Now we have $\vec{\mathcal{B}} = \nabla \times \mathbf{A}$. *We get immediately,*

$$\begin{aligned}
\mathcal{B}_r &= \frac{1}{r\sin\theta}\left[\frac{\partial}{\partial\theta}(\sin\theta A_\phi)\right] = \frac{e\omega r_e^2}{3cr^3} 2\cos\theta \\
\mathcal{B}_\theta &= -\frac{1}{r}\left[\frac{\partial}{\partial r}(r A_\phi)\right] = \frac{e\omega r_e^2}{3cr^3}\sin\theta \\
\mathcal{B}_\phi &= 0 \ .
\end{aligned}$$

Comparing with Exc. 15.4.2.19(d) we get,

$$\vec{\mathcal{M}} = \frac{e\omega r_e^2}{3c}\hat{\mathbf{e}}_z = \frac{e\omega r_e^2}{3c}\left(\cos\theta\hat{\mathbf{e}}_r - \sin\theta\hat{\mathbf{e}}_\phi\right) \ .$$

15.3.3.3 Ex: Conducting thin loops

Consider a circular conducting loop with radius R. The wire of the loop is infinitely thin (δ-function). Through the loop flows a continuous current I.
a. What is the expression for current density $\mathbf{j}(\mathbf{r})$? Express the result in spherical coordinates considering that the integral of the current over a surface perpendicular to the wire must give I.
b. Calculate the magnetic dipolar moment of this current loop,

$$\mathbf{m} = \frac{1}{2}\int [\mathbf{r}\times\mathbf{j}(\mathbf{r})] d^3r \ .$$

c. For large distances from a localized current distribution, the potential vector $\mathbf{A}$ is dominated by the dipolar contribution,

$$\mathbf{A}(\mathbf{r}) = \frac{\mathbf{m}\times\mathbf{r}}{r^3} \ .$$

What are, in this approximation, the values of the potential vector $\mathbf{A}$ and the magnetic field $\vec{\mathcal{B}}$ for the conducting loop?

Solution: *a. The useful parametrization is* $\mathbf{j}(\mathbf{r},t) = I\hat{\mathbf{e}}_z\delta(z)\delta(\rho - R)$.
b. We use the definition,

$$\mathbf{m} = \tfrac{1}{2}\int \mathbf{r}'\times\mathbf{j}(\mathbf{r}',t)d^3r' = \tfrac{1}{2}\int \mathbf{r}'\times I\hat{\mathbf{e}}_\phi\delta(z')\delta(\rho'-R)\rho' d\rho' dz' d\phi' = \tfrac{1}{2}I2\pi R\mathbf{R}\times\hat{\mathbf{e}}_\phi = I\pi R^2\hat{\mathbf{e}}_z \ .$$

c. Inserting into the expression for potential vector,

$$\mathbf{A}(\mathbf{r}) = \frac{I\pi R^2\hat{\mathbf{e}}_z\times\mathbf{r}}{r^3} = \frac{I\pi R^2}{r^2}\hat{\mathbf{e}}_\phi \ .$$

Using the relation with the magnetic field and the expression for the rotation in spherical coordinates (12.80),

$$\vec{\mathcal{E}}(\mathbf{r}) = \nabla \times \mathbf{A} = \hat{\mathbf{e}}_r \frac{1}{r\sin\theta}\frac{\partial}{\partial\theta}(\sin\theta A_\phi) - \hat{\mathbf{e}}_\theta \frac{1}{r}\frac{\partial}{\partial r}(rA_\phi)$$
$$= I\pi R^2 \left[\hat{\mathbf{e}}_r \frac{1}{r\sin\theta}\frac{1}{r^2}\frac{\partial \sin\theta}{\partial\theta} - \hat{\mathbf{e}}_\theta \frac{1}{r}\frac{\partial}{\partial r}\frac{1}{r}\right] = \frac{I\pi R^2}{r^3}(\hat{\mathbf{e}}_\theta - \hat{\mathbf{e}}_r \cot\theta) \ .$$

15.3.3.4 Ex: Conducting thin loops

Consider a system of N different conducting loops (use δ-functions) through which runs a current I_j $(j = 1, \ldots, N)$. The magnetic flux through the j-th loop is then given by,

$$\Phi_j = \sum_{m=1}^{N} \int_{F_j} \vec{\mathcal{B}}_m \cdot d\mathbf{S} \ ,$$

where the integral must be taken over the area enclosed by the current loops j and $\vec{\mathcal{B}}_m$ is the part of the magnetic field due to the j-th loop.
a. Show,

$$\Phi_j = c \sum_{m=1}^{N} L_{jm} I_m$$

with the induction coefficient,

$$L_{jm} = \frac{\frac{1}{c^2}\int_j \int_m d\mathbf{r}_j \cdot d\mathbf{r}_m}{|\mathbf{r}_j - \mathbf{r}_m|} \ ,$$

where the integrals are taken over the loops j and m.
b. Also show that the magnetic field energy of the loop system is given by,

$$W = \frac{1}{2}\sum_{j,m} L_{jm} I_j I_m \ .$$

Solution:

15.3.3.5 Ex: Conducting thin loops

A conducting loop made of two semicircles (see diagram) with radii $r_i = 0.3\,\mathrm{m}$ and $r_a = 0.5\,\mathrm{m}$ carries a current $I = 1.5\,\mathrm{A}$.
a. Calculate the magnetic moment $\vec{\mu}$ of the conducting loop.
b. The conducting loop is now traversed by a $\mathcal{B}$-field of amplitude $\mathcal{B} = 0.3\,\mathrm{T}$. Calculate the resulting torque $\mathbf{m}$ on the loop, when the $\mathcal{B}$-field is directed (i) toward z, (ii) toward x, and (iii) orthogonal to the plane of the scheme.

Solution:

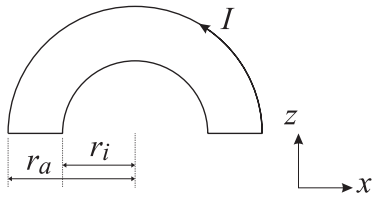

Figure 15.18: Loop.

15.3.3.6 Ex: Gauge transformation

Be given the potential vector,

$$\mathbf{A}(\mathbf{r}) = \frac{1}{y^2+z^2+a^2}\begin{pmatrix}0\\ z\\ -y\end{pmatrix} .$$

Discusses the corresponding magnetic field $\vec{\mathcal{B}} = \nabla \times \mathbf{A}$.
a. Show that the potential

$$\mathbf{A}'(\mathbf{r}) = \frac{1}{y^2+z^2+a^2}\begin{pmatrix}0\\ y+z\\ z-y\end{pmatrix}$$

gives the same magnetic field as the potential $\mathbf{A}(\mathbf{x})$.
b. Show:

$$\mathbf{A}'(\mathbf{r}) = \mathbf{A}(\mathbf{r}) - \nabla\alpha(\mathbf{r})$$

and determine $\alpha(\mathbf{r})$.

Solution: *It is easy to verify that,*

$$\vec{\mathcal{B}}(\mathbf{r}) = -\frac{2a^2}{(y^2+z^2+a^2)^2}\hat{\mathbf{e}}_z ,$$

for both potentials $\mathbf{A}(\mathbf{r})$ *and* $\mathbf{A}'(\mathbf{r})$. *The function* $\alpha(\mathbf{r})$ *is obtained by the relation:*

$$\mathbf{A}'(\mathbf{r}) - \mathbf{A}(\mathbf{x}) = \frac{1}{y^2+z^2+a^2}\begin{pmatrix}0\\ y\\ z\end{pmatrix} = \frac{1}{2}\nabla\ln(y^2+z^2+a^2) ,$$

and hence,

$$\alpha(\mathbf{r}) = -\frac{1}{2}\ln(y^2+z^2+a^2).$$

15.3.3.7 Ex: Coulomb gauge

Be given the vector potential,

$$\mathbf{A}(x,y,z) = \frac{(x+y)\hat{\mathbf{e}}_x + (-x+y)\hat{\mathbf{e}}_y}{\sqrt{x^2+y^2}} \ .$$

Find a gauge transformation $\alpha(x,y,z)$, where $\mathbf{A} \to \mathbf{A}' = \mathbf{A} - \nabla\alpha$, such that transformed vector potential satisfies the Coulomb gauge.
Help: The Laplace operator in cylindrical coordinates has the form,

$$\Delta = \frac{1}{\rho}\frac{\partial}{\partial\rho}\left(\rho\frac{\partial}{\partial\rho}\right) + \frac{\partial^2}{\partial z^2} + \frac{1}{\rho^2}\frac{\partial^2}{\partial\phi^2} \ .$$

where $\rho^2 = x^2 + y^2$.

Solution: *In the Coulomb gauge,* $\nabla \cdot \mathbf{A}' = 0$*; it implies* $\Delta\alpha = \nabla \cdot \mathbf{A}$*. From the given expression for the potential vector* $\mathbf{A}$ *we get,*

$$\nabla \cdot \mathbf{A} = \frac{2}{\sqrt{x^2+y^2}} \ .$$

The function α *is the solution to the differential equation.:*

$$\Delta\alpha(x,y,z) = \frac{2}{\sqrt{x^2+y^2}} \ .$$

The easiest is to solve this equation in cylindrical coordinates. With $\rho = \sqrt{x^2+y^2}$*, we have:*

$$\frac{\partial}{\partial\rho}\left(\rho\frac{\partial}{\partial\rho}\alpha\right) = 2 \ .$$

(We already used the fact that the function α *does not depend on* z, ϕ*). The solution is straightforward,* $\alpha = 2\rho$*; in Cartesian coordinates,* $\alpha = 2\sqrt{x^2+y^2}$*.*

15.3.3.8 Ex: Vector potential of a homogeneous field

We consider a homogeneous magnetic field in z-direction,

$$\vec{\mathcal{B}} = \mathcal{B}\hat{\mathbf{e}}_z \ .$$

Invent a potential vector $\mathbf{A}$, such that $\vec{\mathcal{B}} = \text{rot } \mathbf{A}$. How does the potential vector look like in the Coulomb gauge (that is, under the condition: div $\mathbf{A} = 0$).

Solution: *The potential vector,*

$$\mathbf{A} = \tfrac{1}{2}\vec{\mathcal{B}} \times \mathbf{r} = \tfrac{\mathcal{B}}{2}(-y\hat{\mathbf{e}}_x + x\hat{\mathbf{e}}_y)$$

gives the magnetic field,

$$\vec{\mathcal{B}} = \nabla \times \mathbf{A} = \tfrac{\mathcal{B}}{2}\nabla \times (-y\hat{\mathbf{e}}_x + x\hat{\mathbf{e}}_y) = \tfrac{\mathcal{B}}{2}\begin{pmatrix} \partial_y 0 - \partial_z x \\ \partial_z(-y) - \partial_x 0 \\ \partial_x x - \partial_y(-y) \end{pmatrix} = \mathcal{B}\hat{\mathbf{e}}_z \ .$$

15.4 Multipolar expansion

Using the expansion (13.91) we can expand the vector potential in the same way as we did with the electrostatic potential in formula (13.92),

$$\mathbf{A}(\mathbf{r}) = \frac{\mu_0 I}{4\pi} \oint \frac{1}{|\mathbf{r}-\mathbf{r}'|} d\mathbf{l}' = \frac{\mu_0 I}{4\pi} \sum_{\ell=0}^{\infty} \frac{1}{r^{\ell+1}} \oint r'^{\ell} P_\ell(\cos\theta') d\mathbf{l}' \ . \tag{15.38}$$

Explicitly,

$$\mathbf{A}(\mathbf{r}) = \frac{\mu_0 I}{4\pi} \left[\frac{1}{r} \oint d\mathbf{l}' + \frac{1}{r^2} \oint r' \cos\theta' d\mathbf{l}' + \frac{1}{r^3} \oint r'^2 (\tfrac{3}{2}\cos^2\theta' - \tfrac{1}{2}) d\mathbf{l}' + ... \right] \ . \tag{15.39}$$

15.4.1 Multipolar magnetic moments

Since there are no magnetic monopoles, the first term of the multipolar expansion will be $\oint d\mathbf{l}' = 0$. The next term is the dipole term,

$$\mathbf{A}_{dip} = \frac{\mu_0 I}{4\pi r^2} \oint \hat{\mathbf{r}} \cdot \mathbf{r}' d\mathbf{l}' \ . \tag{15.40}$$

Doing the calculation,

$$\begin{aligned} \mathbf{c} \cdot \oint \hat{\mathbf{r}} \cdot \mathbf{r}' d\mathbf{l}' = \oint \mathbf{c}(\hat{\mathbf{r}} \cdot \mathbf{r}') \cdot d\mathbf{l}' = \int \nabla_{r'} \times [\mathbf{c}(\hat{\mathbf{r}} \cdot \mathbf{r}')] \cdot d\mathbf{S}' \qquad (15.41) \\ = -\int [\mathbf{c} \times \nabla_{r'}(\hat{\mathbf{r}} \cdot \mathbf{r}')] \cdot d\mathbf{S}' = -(\mathbf{c} \times \hat{\mathbf{r}}) \cdot \int d\mathbf{S}' = -\mathbf{c} \cdot \left(\hat{\mathbf{r}} \times \int d\mathbf{S}' \right) \ , \end{aligned}$$

for arbitrary constants $\mathbf{c}$, we find,

$$\boxed{\mathbf{A}_{dip} = -\frac{\mu_0 I}{4\pi r^2} \hat{\mathbf{r}} \times \int d\mathbf{S}' = \frac{\mu_0}{4\pi} \frac{\mathbf{m} \times \hat{\mathbf{r}}}{r^2}} \quad \text{where} \quad \boxed{\mathbf{m} \equiv I \int d\mathbf{S}} \tag{15.42}$$

is the *magnetic dipole moment*.

> **Example 75 (*Magnetic moment of a current loop*):** The magnetic moment of a conductive coil of radius R lying in the x-y-plane and traversed by a current is calculated by,
>
> $$\mathbf{m} = I \int d\mathbf{S} = I\pi R^2 \hat{\mathbf{e}}_z \ .$$

We will show in Exc. 15.4.2.1 how the magnetic dipole moment of a current loop can also be calculated from a suitable parametrization via the definition,

$$\boxed{\mathbf{m} = \tfrac{1}{2} \int \mathbf{r}' \times \mathbf{j}(\mathbf{r}', t) d^3 r'} \ . \tag{15.43}$$

15.4.2 Exercises

15.4.2.1 Ex: Magnetic moment

Calculate the torque on a rectangular coil with N loops placed in a homogeneous magnetic field, as shown in the figure.

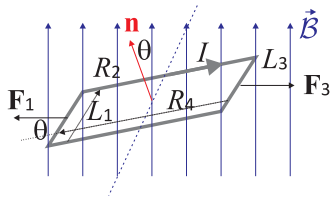

Figure 15.19: Magnetic moment.

Solution:

15.4.2.2 Ex: Magnetic moment

a. Determine the magnetic moment of a circular conducting loop with radius R carrying a current I_1. The loop is in the xy-plane.
b. Now two outer segments of the circle are deformed at a distance a at right angles to the direction $-\hat{\mathbf{e}}_z$. What is the magnetic moment of the new configuration.
c. Now consider an infinitely long current line I_2 at a distance d from the origin and oriented in z-direction. What is the torque acting on the configurations in (a) and (b).

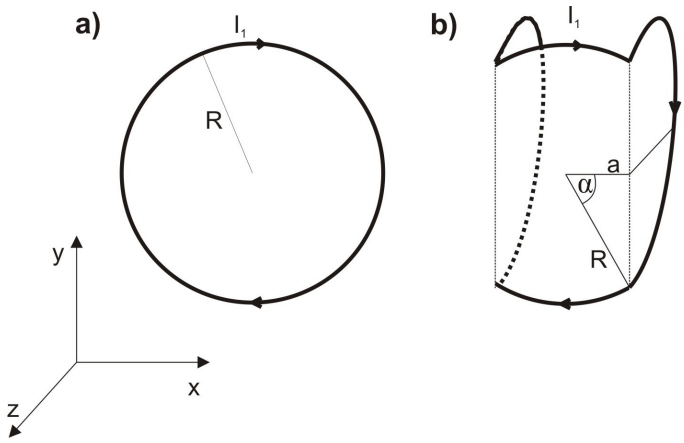

Figure 15.20: Magnetic moment.

Solution: *a.* $\mathbf{m}_1 = I_1\mathbf{F} = -\pi r^2 I_1 \hat{\mathbf{e}}_z$

b. The magnetic moment of the deformed segments is exactly opposite. Therefore, only the magnetic moment of the area in the plane x-y is relevant. The inner area has the value: $F = r^2(\pi - 2\alpha - \sin 2\alpha)$ *with* α *in rad. Hence,* $\mathbf{m}_2 = I_1\mathbf{F} = -r^2(\pi - 2\alpha - \sin 2\alpha)I_1\hat{\mathbf{e}}_z$.
c. The magnetic field of an infinitely long wire is given by:

$$\mathcal{B}(r) = \mu_0 I_2/2\pi r \Rightarrow \mathcal{B}(d) = \mu_0 I_2/2\pi d \ .$$

In the questions (a) and (b): $\mathbf{d}_{1,2} = \mathbf{m}_{1,2} \times \vec{\mathcal{B}}$.

15.4.2.3 Ex: Magnetic moment of a cube

A conductor carries the current $I = 6\,\mathrm{A}$ along the path shown in the figure, which runs through 8 of the 12 corners of the cube whose length is $L = 10\,\mathrm{cm}$.
a. Calculate dipole magnetic moment along the way.
b. Calculate the magnetic induction $\vec{\mathcal{B}}$ at the points $(x, y, z) = (0, 5\,\mathrm{m}, 0)$ and $(x, y, z) = (5\,\mathrm{m}, 0, 0)$.

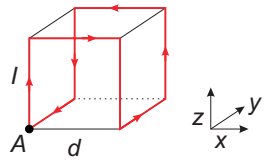

Figure 15.21: Magnetic moment.

Solution: *a. Explicitly the magnetic moment follows from the definition,*

$$\mathbf{m} = \tfrac{1}{2}\int \mathbf{r}' \times \mathbf{j}(\mathbf{r}')d^3\mathbf{r}' \ .$$

Hence,

$$
\begin{aligned}
\mathbf{m} &= \frac{1}{2}\int \mathbf{r}'\times\hat{\mathbf{e}}_z\delta(x')\delta(y')d^3\mathbf{r}' + \frac{1}{2}\int \mathbf{r}'\times\hat{\mathbf{e}}_x\delta(y')\delta(z'-L)d^3\mathbf{r}' - \frac{1}{2}\int \mathbf{r}'\times\hat{\mathbf{e}}_z\delta(x'-L)\delta(y')d^3\mathbf{r}' \\
&+ \frac{1}{2}\int \mathbf{r}'\times\hat{\mathbf{e}}_y\delta(x'-L)\delta(z')d^3\mathbf{r}' + \frac{1}{2}\int \mathbf{r}'\times\hat{\mathbf{e}}_z\delta(x'-L)\delta(y'-L)d^3\mathbf{r}' - \frac{1}{2}\int \mathbf{r}'\times\hat{\mathbf{e}}_x\delta(y'-L)\delta(z'-L)d^3\mathbf{r}' \\
&- \frac{1}{2}\int \mathbf{r}'\times\hat{\mathbf{e}}_z\delta(x')\delta(y'-L)d^3\mathbf{r}' - \frac{1}{2}\int \mathbf{r}'\times\hat{\mathbf{e}}_y\delta(x')\delta(z')d^3\mathbf{r}' \\
&= \frac{1}{2}\int_0^L \begin{pmatrix} y' \\ -x' \\ 0 \end{pmatrix}\delta(x')\delta(y')d^3\mathbf{r}' + \frac{1}{2}\int_0^L \begin{pmatrix} 0 \\ z' \\ -y' \end{pmatrix}\delta(y')\delta(z'-L)d^3\mathbf{r}' - \frac{1}{2}\int_0^L \begin{pmatrix} y' \\ -x' \\ 0 \end{pmatrix}\delta(x'-L)\delta(y')d^3\mathbf{r}' \\
&+ \frac{1}{2}\int \begin{pmatrix} -z' \\ 0 \\ x' \end{pmatrix}\delta(x'-L)\delta(z')d^3\mathbf{r}' + \frac{1}{2}\int \begin{pmatrix} y' \\ -x' \\ 0 \end{pmatrix}\delta(x'-L)\delta(y'-L)d^3\mathbf{r}' - \frac{1}{2}\int \begin{pmatrix} 0 \\ z' \\ -y' \end{pmatrix}\delta(y'-L)\delta(z'-L)d^3\mathbf{r}' \\
&- \frac{1}{2}\int \begin{pmatrix} y' \\ -x' \\ 0 \end{pmatrix}\delta(x')\delta(y'-L)d^3\mathbf{r}' - \frac{1}{2}\int \begin{pmatrix} -z' \\ 0 \\ x' \end{pmatrix}\delta(x')\delta(z')d^3\mathbf{r}' \\
&= \frac{1}{2}\int_0^L \begin{pmatrix} 0 \\ 0 \\ 0 \end{pmatrix}dz' + \frac{1}{2}\int_0^L \begin{pmatrix} 0 \\ L \\ 0 \end{pmatrix}dx' - \frac{1}{2}\int_0^L \begin{pmatrix} 0 \\ -L \\ 0 \end{pmatrix}dx' \\
&+ \frac{1}{2}\int_0^L \begin{pmatrix} 0 \\ 0 \\ L \end{pmatrix}dy' + \frac{1}{2}\int_0^L \begin{pmatrix} L \\ -L \\ 0 \end{pmatrix}dz' - \frac{1}{2}\int_0^L \begin{pmatrix} 0 \\ L \\ -L \end{pmatrix}dx' \\
&- \frac{1}{2}\int_0^L \begin{pmatrix} L \\ 0 \\ 0 \end{pmatrix}dz' - \frac{1}{2}\int_0^L \begin{pmatrix} 0 \\ 0 \\ 0 \end{pmatrix}dy' \\
&= \frac{L^2}{2}\left(\mathbf{0} + \hat{\mathbf{e}}_y + \hat{\mathbf{e}}_y + \hat{\mathbf{e}}_z + (\hat{\mathbf{e}}_x - \hat{\mathbf{e}}_y) - (\hat{\mathbf{e}}_y - \hat{\mathbf{e}}_z) - \hat{\mathbf{e}}_x - \vec{0}\right) = L^2\hat{\mathbf{e}}_z \ .
\end{aligned}
$$

Alternatively, the path can be decomposed into three flat loops. Their magnetic moments are additive,

$$\mathbf{m} = \mathbf{m}_{x=0,y,z} + \mathbf{m}_{x,y,z=L} + \mathbf{m}_{x=L,y,z} = -L^2\hat{\mathbf{e}}_x + L^2\hat{\mathbf{e}}_z + L^2\hat{\mathbf{e}}_x = L^2\hat{\mathbf{e}}_z \ .$$

15.4.2.4 Ex: Magnetic moment of thin circular disk

Consider a very thin disk with radius R, homogeneously charged with the charge Q, and spinning around the z-axis with angular velocity ω.
a. Parametrize the charge and current distributions.
b. Calculate the magnetic moment.

Solution: *a. The charge distribution is,*

$$\rho(\mathbf{r}) = \frac{Q}{\pi R^2}\delta(z) \qquad para \qquad r \le R \ .$$

The current distribution is,

$$\mathbf{j}(\mathbf{r}) = \rho(\mathbf{r})\vec{v}(\mathbf{r}) = \rho(\mathbf{r})\vec{\omega}\times\mathbf{r} = \frac{Q}{\pi R^2}\delta(z)\omega r\hat{\mathbf{e}}_\phi \qquad for \qquad r \le R \ .$$

b. With this we get the magnetic moment,

$$\vec{m} = \frac{1}{2}\int_V \mathbf{r}\times\mathbf{j}(\mathbf{r})\; d^3\mathbf{r} = \frac{1}{2}\frac{Q}{\pi R^2}\omega\int_V \delta(z) r^2 \hat{\mathbf{e}}_r \times \hat{\mathbf{e}}_\phi \; d^3\mathbf{r}$$
$$= \frac{1}{2}\frac{Q}{\pi R^2}\omega\hat{\mathbf{e}}_z \int_0^{2\pi}\int_0^R r^2 \; r dr d\phi = \frac{1}{2}\frac{Q}{\pi R^2}\omega\hat{\mathbf{e}}_z 2\pi\frac{R^4}{4} = \frac{1}{4}QR^2\omega\hat{\mathbf{e}}_z \; .$$

15.4.2.5 Ex: Magnetic compass

A topographer uses a magnetic compass while standing 6.1 m under a high voltage line on which flows a current of 100 A. The horizontal component of the Earth's magnetic field at this place is 20 μT. How large is the magnetic field due to the current at the position of the compass? Will the magnetic field disturb the compass noticeably?

Solution: *The magnetic field of the conductor at the distance r follows from* $\oint \vec{\mathcal{B}}\cdot d\vec{s} = \mu_0 I$*, giving,*

$$\mathcal{B}(r) = \frac{\mu_0 I}{2\pi r} \simeq 3.3\,\mu\mathrm{T} \; .$$

This is not negligible compared to the magnetic field of the Earth.

15.4.2.6 Ex: Torque of a magnetic needle

A magnetic needle has a dipolar magnetic moment $\mu = 10^{-2}\,\mathrm{Am}^2$. Calculate the torque on the needle due to the horizontal component of the Earth's magnetic field at the equator ($\mathcal{B}_H = 4\cdot 10^{-5}\,\mathrm{T}$), if the magnetic north pole of the needle points in northeastern direction.

Solution: *The torque of a magnetic needle is,*

$$\mathbf{d} = \mathbf{m}\times\vec{\mathcal{B}}_H = -m\sin\phi\cdot\mathcal{B}_H\hat{\mathbf{e}}_z = -10^{-2}\,\mathrm{Am}^2\cdot 0.71\cdot 4\cdot 10^{-5}\,\mathrm{T}\cdot\hat{\mathbf{e}}_z = 2.8\cdot 10^{-7}\,\mathrm{Nm}\cdot\hat{\mathbf{e}}_z \; .$$

15.4.2.7 Ex: Curved conductive circuit

A rectangular conducting loop is deformed in the middle of the edges (length a) to form a right angle. The conducting loop is traversed by a current I. Calculate the dipolar magnetic moment $\mathbf{m}$ of this configuration. Give the absolute value and orientation of $\mathbf{m}$.
Help: Use the overlapping principle and replace the above geometry with an overlap of two conductive loops.

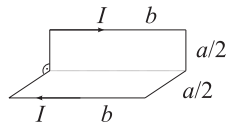

Figure 15.22: Curved conductive circuit.

Solution: *We consider two conductive loops, closed by the dashed line in the figure. For the loop in the xy-plane,*

$$\mathbf{m}_{xy} = \frac{Iab}{2}\hat{\mathbf{e}}_z \ .$$

For the loop in the xz-plane,

$$\mathbf{m}_{xz} = \frac{Iab}{2}\hat{\mathbf{e}}_x \ .$$

In total,

$$\mathbf{m} = \mathbf{m}_{xy} + \mathbf{m}_{xz} = \frac{Iab}{2}(\hat{\mathbf{e}}_z + \hat{\mathbf{e}}_x) \ .$$

The direction of the magnetic momentum is the diagonal in the xz-plane. The absolute value is,

$$m = \frac{Iab}{\sqrt{2}} \ .$$

15.4.2.8 Ex: Magnetic dipole

A magnetic dipole $\vec{\mu} = \mu\hat{\mathbf{e}}_z$ is at origin of the coordinate system and has the value $\mu = 1\,\mathrm{esu}\cdot\mathrm{cm}$. This dipole generates a magnetic field of the form,

$$\vec{\mathcal{B}}(\mathbf{r}) = \frac{3\mathbf{r}(\vec{\mu}\cdot\mathbf{r}) - r^2\vec{\mu}}{r^5} \ .$$

a. At what distance from the origin does the absolute value of $\vec{\mathcal{B}}$ take the value $1\,\mathrm{esu/cm}^2$ going (i) in z-direction, (ii) in x-direction, and (iii) in a diagonal direction with in the xz-plane?
b. Which direction does $\vec{\mathcal{B}}$ point in these three cases?

Solution: *The evaluation of the given formula immediately yields,*

$$\begin{aligned} r^3\mathcal{B}_x &= \mu 3\cos\theta\sin\theta\cos\phi \\ r^3\mathcal{B}_y &= \mu 3\cos\theta\sin\theta\sin\phi \\ r^3\mathcal{B}_z &= \mu(3\cos^2\theta - 1) \ . \end{aligned}$$

For $y = 0$ we obviously have $\phi = 0$ and hence $\sin\phi = 0$ and $\cos\phi = 1$.
a. Thus we get (for $y = 0$),

$$r^3|\vec{\mathcal{B}}| = \mu\sqrt{9\cos^2\theta\sin^2\theta + (3\cos^2\theta - 1)^2} \ .$$

In the direction of the z-axis [case (i)] we have $\theta = 0$, in the direction of the x-axis [case (ii)] we have $\theta = 90°$, and in the diagonal direction [case (iii)] we have $\theta = 45°$. Therefore,

$$(i) \quad r^3|\vec{\mathcal{B}}| = 2\mu \quad , \quad (ii) \quad r^3|\vec{\mathcal{B}}| = \mu \quad , \quad (iii) \quad r^3|\vec{\mathcal{B}}| = \tfrac{\sqrt{10}}{2}\mu \ .$$

For $\mu/|\vec{\mathcal{B}}| = 1\,\mathrm{cm}^3$, giving,

$$(i) \quad r = 2^{1/3}\,\mathrm{cm} \quad , \quad (ii) \quad r = 1\,\mathrm{cm} \quad , \quad (iii) \quad r = (\tfrac{\sqrt{10}}{2})^{1/3}\,\mathrm{cm} \ .$$

b. For the orientations of $\vec{\mathcal{B}}$ in all three cases follows,

$$(i) \quad +\hat{\mathbf{e}}_z \quad , \quad (ii) \quad -\hat{\mathbf{e}}_z \quad , \quad (iii) \quad \tfrac{3}{2}\hat{\mathbf{e}}_x + \tfrac{1}{2}\hat{\mathbf{e}}_z \ .$$

15.4.2.9 Ex: Fields of electric and magnetic point dipoles

a. Calculate the field of an electric dipole taking care to remove the divergence in the center of origin by calculating the field averaged over a sphere and comparing it with known results.
b. Repeat the procedure of (b) for a magnetic dipole.

Solution: *The scalar electrostatic potential and field of an electric dipole at the origin are given by,*

$$\begin{aligned}
\mathbf{\Phi}_{dip}(\mathbf{r}) &= \frac{1}{4\pi\varepsilon_0}\frac{p\cos\theta}{r^2} = \frac{1}{4\pi\varepsilon_0}\frac{\mathbf{p}\cdot\hat{\mathbf{e}}_r}{r^2} \\
\vec{\mathcal{E}}_{dip}(\mathbf{r}) &= -\nabla\Phi_{dip} = \frac{p}{4\pi\varepsilon_0 r^3}(2\hat{\mathbf{e}}_r\cos\theta + \hat{\mathbf{e}}_\theta\sin\theta) = \frac{1}{4\pi\varepsilon_0 r^3}[3(\mathbf{p}\cdot\hat{\mathbf{e}}_r)\hat{\mathbf{e}}_r - \mathbf{p}] \ ,
\end{aligned}$$

where $\mathbf{p}$ is the electric dipole moment. This term appears as the second term in the multipolar expansion of any electrostatic potential $\Phi(\mathbf{r})$. If the source of $\Phi(\mathbf{r})$ is a dipole, this term is the only term that does not go to zero in the multipolar expansion of $\Phi(\mathbf{r})$. The average field is, by symmetry, oriented in z-direction. Hence, using $\hat{\mathbf{e}}_z\cdot\hat{\mathbf{e}}_r = \cos\theta$ and $\hat{\mathbf{e}}_z\cdot\hat{\mathbf{e}}_\theta = -\sin\theta$,

$$\begin{aligned}
\bar{\vec{\mathcal{E}}} &= \frac{\int_0^R\int_0^\pi\int_0^{2\pi}(\vec{\mathcal{E}}_{dip}\cdot\hat{\mathbf{e}}_z)\hat{\mathbf{e}}_z r^2\sin\theta d\theta dr d\phi}{\int_0^R\int_0^\pi\int_0^{2\pi} r^2\sin\theta d\theta dr d\phi} \\
&= \frac{3\mu_0}{8\pi R^3}\hat{\mathbf{e}}_z\int_0^R\frac{1}{r}dr\int_0^\pi(2\cos^2\theta - \sin^2\theta)\sin\theta d\theta = \frac{3\mu_0}{8\pi R^3}\hat{\mathbf{e}}_z\ \infty\cdot 0 \ .
\end{aligned}$$

If we integrate over any lower limit $\epsilon > 0$ out to R, the problem goes away and the integral is a well-behaved zero, $0\cdot\int_\epsilon^R\frac{1}{r}dr = 0$. We know however that average field of a charge distribution within a sphere is,

$$\bar{\vec{\mathcal{E}}} = -\frac{\mathbf{p}}{4\pi\varepsilon_0 R^3} = \frac{-\frac{\mathbf{p}}{3\varepsilon_0}\int_{\mathbb{R}^3}\delta^3(\mathbf{r})d^3r}{\frac{4\pi}{3}R^3} \ .$$

We may thus write (although it is not really correct),

$$\boxed{\vec{\mathcal{E}}_{dip}(\mathbf{r}) = \frac{1}{4\pi\varepsilon_0 r^3}[3(\mathbf{p}\cdot\hat{\mathbf{e}}_r)\hat{\mathbf{e}}_r - \mathbf{p}] - \frac{\mathbf{p}}{3\varepsilon_0}\delta^3(\mathbf{r})} \ ,$$

understanding that the first term doesn't apply at $r = 0$.
b. The vector potential and field of a magnetic dipoles are given by,

$$\mathbf{A}_{dip}(\mathbf{r}) = \frac{\mu_0}{4\pi}\frac{m\sin\theta}{r^2}\hat{\mathbf{e}}_\theta = \frac{\mu_0}{4\pi}\frac{\mathbf{m}\times\hat{\mathbf{e}}_r}{r^2}$$
$$\vec{\mathcal{B}}_{dip}(\mathbf{r}) = \nabla\times\mathbf{A}_{dip} = \frac{\mu_0 m}{4\pi r^3}(2\hat{\mathbf{e}}_r\cos\theta + \hat{\mathbf{e}}_\theta\sin\theta) = \frac{\mu_0 m}{4\pi r^3}[3(\mathbf{m}\cdot\hat{\mathbf{e}}_r)\hat{\mathbf{e}}_r - \mathbf{m}] \ ,$$

where $\mathbf{r}$ is the vector between the position of the dipole to the position where the field is measured. It is exactly the field of a point-like dipole, just the dipolar term in the multipole expansion of an arbitrary field, and roughly the field of an arbitrary dipolar configuration at long distance. The average is, by symmetry, in the z-direction. Hence, using $\hat{\mathbf{e}}_z\cdot\hat{\mathbf{e}}_r = \cos\theta$ and $\hat{\mathbf{e}}_z\cdot\hat{\mathbf{e}}_\theta = -\sin\theta$,

$$\bar{\vec{\mathcal{B}}} = \frac{\int_0^R\int_0^\pi\int_0^{2\pi}(\vec{\mathcal{B}}_{dip}\cdot\hat{\mathbf{e}}_z)\hat{\mathbf{e}}_z r^2\sin\theta d\theta dr d\phi}{\int_0^R\int_0^\pi\int_0^{2\pi} r^2\sin\theta d\theta dr d\phi}$$
$$= \frac{3\mu_0}{8\pi R^3}\hat{\mathbf{e}}_z\int_0^R\frac{1}{r}dr\int_0^\pi(2\cos^2\theta - \sin^2\theta)\sin\theta d\theta = \frac{3\mu_0}{8\pi R^3}\hat{\mathbf{e}}_z\ \infty\cdot 0 \ .$$

If we integrate over any lower limit $\epsilon > 0$ out to R, the problem goes away and the integral is a well-behaved zero, $0\cdot\int_\epsilon^R\frac{1}{r}dr = 0$. We know however that average field of a charge distribution within a sphere is,

$$\bar{\vec{\mathcal{B}}} = \frac{2\mu_0\mathbf{m}}{4\pi R^3} = \frac{\frac{2}{3}\mu_0\mathbf{m}\int_{R^3}\delta^3(\mathbf{r})d^3r}{\frac{4\pi}{3}R^3} \ .$$

We may thus write (although it is not really correct),

$$\boxed{\vec{\mathcal{B}}_{dip}(\mathbf{r}) = \frac{\mu_0 m}{4\pi r^3}[3(\mathbf{m}\cdot\hat{\mathbf{e}}_r)\hat{\mathbf{e}}_r - \mathbf{m}] + \frac{2}{3}\mu_0\mathbf{m}\delta^3(\mathbf{r})} \ ,$$

understanding that the first term doesn't apply at $r = 0$.
In cylindrical coordinates the distant field of a magnetic dipole is given by,

$$\mathcal{B}(m, r, \lambda) = \frac{\mu_0}{4\pi}\frac{m}{r^3}\sqrt{1 + 3\sin^2\lambda} \ ,$$

where r is the distance from the center, λ is the magnetic latitude (equal to $0^\circ - \theta$, where θ is measured from the dipole axis. We convert to cylindrical coordinates using $r^2 = z^2 + \rho^2$ and $\lambda = \arcsin\frac{z}{\sqrt{z^2+\rho^2}}$, where ρ is the perpendicular distance from the z-axis. So,

$$\mathcal{B}(\rho, z) = \frac{\mu_0 m}{4\pi(z^2+\rho^2)^{3/2}}\sqrt{1 + \frac{3z^2}{z^2+\rho^2}} \ .$$

15.4.2.10 Ex: Magnetic dipole moment of a rectangular conducting loop

A (ideal) rectangular conducting loop with edge lengths a and b carries a current I.
a. Give the current density distribution $\mathbf{j}$.
b. Calculate the corresponding dipolar magnetic moment $\vec{\mathcal{M}}$.

Solution: *a. We place the conducting loop symmetrically around the origin within the xy-plane. The current density distribution is then,*

$$\mathbf{j}(\mathbf{r}) = I\delta(z)\left[(\delta(x-\tfrac{a}{2})-\delta(x+\tfrac{a}{2}))\Theta(\tfrac{b}{2}-|y|)\hat{\mathbf{e}}_y-(\delta(y-\tfrac{b}{2})-\delta(x+\tfrac{b}{2}))\Theta(\tfrac{a}{2}-|x|)\hat{\mathbf{e}}_x\right] .$$

b. We have,

$$\begin{aligned}\mathbf{r}\times\mathbf{j}(\mathbf{r}) = I\delta(z)\big[&(\delta(x-\tfrac{a}{2})-\delta(x+\tfrac{a}{2}))\Theta(\tfrac{b}{2}-|y|)x\hat{\mathbf{e}}_z+(\delta(y-\tfrac{b}{2})-\delta(y+\tfrac{b}{2}))\Theta(\tfrac{a}{2}-|x|)y\hat{\mathbf{e}}_z\\ &-(\delta(x-\tfrac{a}{2})-\delta(x+\tfrac{a}{2}))\Theta(\tfrac{b}{2}-|y|)z\hat{\mathbf{e}}_x-(\delta(y-\tfrac{b}{2})-\delta(y+\tfrac{b}{2}))\Theta(\tfrac{a}{2}-|x|)z\hat{\mathbf{e}}_y\big] .\end{aligned}$$

We use now that,

$$\int dy\Theta(\tfrac{b}{2}-|y|) = \int_{-b/2}^{+b/2} dy = b .$$

and we immediately get,

$$\vec{\mathcal{M}} = \frac{1}{2c}\int d^3\mathbf{r}'\ (\mathbf{r}'\times\mathbf{j}(\mathbf{r}')) = \frac{Iab}{c}\hat{\mathbf{e}}_z .$$

15.4.2.11 Ex: Dipolar magnetic moment of a rectangular loop

The rectangular conducting loop of Exc. 15.4.2.10 is deformed in the middle of the edges (length a) to form a right angle (see figure). It is traversed by a current I. Calculate the dipolar magnetic moment of this geometry.

Solution: *We first want to solve the exercise 'by hand'. For the current density distribution holds,*

$$\begin{aligned}\mathbf{j}(\mathbf{r}) = I\big\{&\delta(z)\delta(x-\tfrac{a}{2}\Theta(\tfrac{b}{2}-|y|)\hat{\mathbf{e}}_y-\delta(x)\delta(z-\tfrac{a}{2})\Theta(\tfrac{b}{2}-|y|)\hat{\mathbf{e}}_y\\ &-\delta(z)(\delta(y-\tfrac{b}{2})-\delta(y+\tfrac{b}{2}))\Theta(\tfrac{a}{2}-x)\Theta(x)\hat{\mathbf{e}}_x+\delta(x)(\delta(y-\tfrac{b}{2})-\delta(y+\tfrac{b}{2}))\Theta(\tfrac{a}{2}-z)\Theta(z)\hat{\mathbf{e}}_z\big\} .\end{aligned}$$

This gives,

$$\begin{aligned}\mathbf{r}\times\mathbf{j}(\mathbf{r}) = I\ \big\{&\delta(z)\delta(x-\frac{a}{2})\Theta(\tfrac{b}{2}-|y|)(x\hat{\mathbf{e}}_z-z\hat{\mathbf{e}}_x)-\delta(x)\delta(z-\tfrac{a}{2})\Theta(\tfrac{b}{2}-|y|)(x\hat{\mathbf{e}}_z-z\hat{\mathbf{e}}_x)\\ &\delta(z)(\delta(y-\tfrac{b}{2})-\delta(y+\tfrac{b}{2}))\Theta(\tfrac{a}{2}-x)\Theta(x)(z\hat{\mathbf{e}}_y-y\hat{\mathbf{e}}_z)\\ &+\delta(x)(\delta(y-\tfrac{b}{2})-\delta(y+\tfrac{b}{2}))\Theta(\tfrac{a}{2}-z)\Theta(z)(y\hat{\mathbf{e}}_x-x\hat{\mathbf{e}}_y)\big\} .\end{aligned}$$

Integration provides immediately,

$$\vec{\mathcal{M}} = \frac{I}{2c}\left(\frac{ba}{2}\hat{\mathbf{e}}_z\ +\ \frac{ba}{2}\hat{\mathbf{e}}_x+\frac{ba}{2}\hat{\mathbf{e}}_z\ +\ \frac{ba}{2}\hat{\mathbf{e}}_x\right) = \frac{Iab}{2c}(\hat{\mathbf{e}}_z+\hat{\mathbf{e}}_x) .$$

However, we can solve the exercise much more elegantly by letting the same current I run in the directions $+z$ and $-z$, as well. The total current then disappears. Now, we are considering two independent rectangular loops (edge lengths b and $a/2$). Exc. ?? then provides for the loop in the xy-plane,

$$\vec{\mathcal{M}}_{xy} = \frac{Iab}{2c}\hat{\mathbf{e}}_z \ .$$

and for the loop in the yz-plane,

$$\vec{\mathcal{M}}_{yz} = \frac{Iab}{2c}\hat{\mathbf{e}}_x \ .$$

therefore,

$$\vec{\mathcal{M}} = \vec{\mathcal{M}}_{xy} + \vec{\mathcal{M}}_{yz} = \frac{Iab}{2c}(\hat{\mathbf{e}}_z + \hat{\mathbf{e}}_x) \ .$$

15.4.2.12 Ex: Force on the walls of a hollow cylinder

Consider an infinitely long cylindrical shell of radius a in which flows a current. The magnetic force on this hollow cylinder is such that it tries to compress the cylinder. To counteract this force, we can fill the inside of the cylinder with a gas of pressure P. What is the pressure required to balance the magnetic force?

Solution: *We let the current flow in $+z$-direction and choose cylindrical coordinates. So,*

$$\mathbf{j} = \frac{I}{2\pi a}\delta(\rho - a)\hat{\mathbf{e}}_z \ .$$

With the Ampère's law we have,

$$\nabla \times \vec{\mathcal{B}} = \mu_0 \mathbf{j} = \mu_0 \frac{I}{2\pi a}\delta(\rho - a)\hat{\mathbf{e}}_z \ .$$

As the integration area we chose a circular area perpendicular to the symmetry axis of the cylinder with radius ρ and centered at the origin. Application of Stokes's law then gives for $\rho \geq a$,

$$2\pi\rho\mathcal{B}(\rho) = \mu_0 I \ .$$

that is,

$$\vec{\mathcal{B}} = \frac{\mu_0 I}{2\pi\rho}\hat{\mathbf{e}}_\phi \ ,$$

while inside the cylinder the magnetic field obviously zeroes. Now, we calculate the force acting on an infinitesimal area $\Delta S = \rho\Delta\phi\Delta z$ of the conductor by,

$$\begin{aligned}\mathbf{F} &= \int_{\Delta\mathcal{V}} \mathbf{j} \times \vec{\mathcal{B}} dV = \frac{I}{2\pi a}\frac{\mu_0 I}{2\pi}\int_{\Delta\mathcal{V}} \frac{\delta(\rho - a)}{\rho}\hat{\mathbf{e}}_z \times \hat{\mathbf{e}}_\phi \rho d\rho dz d\phi \\ &= \frac{\mu_0 I^2}{4\pi^2 a}\int_0^{\Delta z}\int_0^{\Delta\phi}(-\hat{\mathbf{e}}_\rho)dzd\phi = -\frac{\mu_0 I^2}{4\pi^2 a}\Delta z\Delta\phi\hat{\mathbf{e}}_\rho \ .\end{aligned}$$

Obviously, the direction of the force depends on where we choose the integration volume. To compensate for the force, we need gas exerting the opposite pressure,

$$P = \frac{F}{a\Delta\phi\Delta z} = \frac{\mu_0 I^2}{4\pi^2 a^2} \ .$$

15.4.2.13 Ex: Infinitely dense coil

A coil with N 'infinitely dense' windings carries a current I. It forms with respect to the z-axis a torus with rotational symmetry with an inner radius $b-a$ and an outer radius $b+a$. The figure shows the cross-sectional area of a cut in the plane perpendicular to the xy-plane.
a. Calculate by exploiting the symmetric geometry of this device in cylindrical coordinates (ρ, ϕ, z) a ϕ-component of the magnetic $\vec{\mathcal{B}}$-field in the xy-plane (that is, for $z = 0$) as a function of the distance ρ from the origin of the coordinate system. **Help:** Use Stokes' law.
b. What is the value of the ϕ-component of $\vec{\mathcal{B}}$ in the entire space *outside* of the torus (that is, also for $z \neq 0$).
c. Draw the profile of $\mathcal{B}_\phi(\rho)$ in the $z = 0$ plane as a function of ρ.
d. Let $a = 1$ cm. What should be the value of b in first approximation, so that $\mathcal{B}_\phi$ in the torus is constant within 1%? **Help:** $(1 \pm \epsilon)^{-1} \ \approx \ 1 \mp \epsilon$.

Solution: *a. Because of the symmetry of the device, $\vec{\mathcal{B}}$ is independent of the angle ϕ. We chose as integration area a circular area in the xy ($z = 0$) plane centered at the origin and having the radius ρ. Thus the area element is, $d\mathbf{S} \ \sim \ \hat{\mathbf{e}}_z$ and the border element is $d\mathbf{l} \ \sim \ \hat{\mathbf{e}}_\phi$. With Stokes' law we get for $\mathcal{B}_\phi(\rho)$ in the $z = 0$ plane,*

$$\int\limits_{\mathcal{S}(\rho)} (\nabla \times \vec{\mathcal{B}}) \cdot d\mathbf{S} = \int\limits_{\partial\mathcal{S}(\rho)} \vec{\mathcal{B}} \cdot d\mathbf{l} = 2\pi\rho\mathcal{B}_\phi(\rho) = \frac{4\pi}{c} \int\limits_{\mathcal{S}(\rho)} \mathbf{j} \cdot d\mathbf{l} \ .$$

With that we get,

$$\begin{aligned}
&\text{Für } 0 < \rho < b-a \ : \qquad 2\pi\rho\mathcal{B}_\phi(\rho) = 0 \\
&\text{Für } b-a \leq \rho < b+a \ : \qquad 2\pi\rho\mathcal{B}_\phi(\rho) = \frac{4\pi}{c} \ NI \\
&\text{Für } b+a \leq \rho < \infty \ : \qquad 2\pi\rho\mathcal{B}_\phi(\rho) = \frac{4\pi}{c} \ (NI - NI) = 0 \ .
\end{aligned}$$

b. Outside the torus $\mathcal{B}_\phi$ is zero everywhere, because each circular area symmetrically centered around the z-axis and parallel to the xy-plane with $\rho < b-a$ or $\rho > b+a$ is always traversed by the total current $\int_{\mathcal{S}(\rho)} \mathbf{j} \cdot d\mathbf{S} = 0$.
c. Following part (a) the field $\mathcal{B}_\phi(\rho)$ zeroes for $\rho < b-a$ and $\rho > b+a$. At $\rho = b-a$ it adopts the value $\frac{2NI}{c(b-a)}$ and then drops proportionally $(\frac{1}{\rho})$ down to the value $\frac{2NI}{c(b+a)}$ at $\rho = b+a$.
d. An approximately constant magnetic field in the toroid can be, based on part (c),

only obtained for the case $b \gg a$. We need,

$$\frac{1}{b-a} - \frac{1}{b+a} \approx \frac{1}{100(b+a)} \qquad \textit{resp.} \qquad \frac{1}{1-\frac{a}{b}} - \frac{1}{1+\frac{a}{b}} \approx \frac{1}{100(1+\frac{a}{b})} \ .$$

From this follows in first approximation,

$$1 + \frac{a}{b} - 1 + \frac{a}{b} \approx \frac{1}{100} \qquad \textit{hence} \qquad b \approx 200a \ .$$

For $a = 1\,\mathrm{cm}$, therefore we need $b = 2\,\mathrm{m}$.

15.4.2.14 Ex: Magnetic field in a cylindrical hollow space

Parallel to the axis of an infinitely long massive conducting cylinder of radius a at a distance d from it, there is a hollow cylindrical space of radius b ($d + b < a$). The current density within this perforated metal cylinder is homogeneous and oriented parallel to the symmetry axis. Using Ampère's law and the linear superposition principle, determine the absolute value and orientation of the magnetic field inside the hollow space.

Solution: *To start with we use the known solution for the solid cylinder, replacing the (constant) current density $I/(\pi a^2)$ with j and noting that $\vec{\mathcal{B}}$ only has the ϕ-component. In addition, we focus on the region $r < a$,*

$$\vec{\mathcal{B}}_a = B_a(r)\hat{\mathbf{e}}_\phi = \frac{2\pi j}{c} r\hat{\mathbf{e}}_\phi$$

Now we use $\hat{\mathbf{e}}_\phi = -\sin\phi\hat{\mathbf{e}}_x + \cos\phi\hat{\mathbf{e}}_y$ and $\theta = 90°$. with this,

$$\vec{\mathcal{B}}_a = \frac{2\pi j}{c}(-y\hat{\mathbf{e}}_x + x\hat{\mathbf{e}}_y)$$

In the same way we get for the field of a solid cylinder with radius b, whose center is, as indicated, displaced by d along the x-axis in its interior region,

$$\vec{\mathcal{B}}_b = \frac{2\pi j}{c}(-y\hat{\mathbf{e}}_x + (x-d)\hat{\mathbf{e}}_y)$$

For the field inside and outside the cavity we get simply by subtraction,

$$\vec{\mathcal{B}}_{int} = \frac{2\pi j}{c} d\hat{\mathbf{e}}_y$$

resp., letting the total current be $I = \pi(a^2 - b^2)j$,

$$\vec{\mathcal{B}}_{int} = \frac{2Id}{(a^2-b^2)c}\hat{\mathbf{e}}_y \ .$$

Inside the cavity the field is therefore constant and oriented toward y. It disappears for $d = 0$, i.e. when the empty space is centered.

15.4.2.15 Ex: Torque of a conducting cylinder

Determine the torque (per unit length) felt by a massive conducting cylinder of radius R that slowly rotates with constant angular velocity ω inside a homogeneous $\vec{\mathcal{B}}$-field around its symmetry axis. $\vec{\mathcal{B}}$ be oriented orthogonal to the axis of the cylinder.

Solution: *We place the axis of the cylinder (same as the rotation axis) in direction* 3 *and the $\vec{\mathcal{B}}$-field in direction* 2*. For the torque per unit length l we get,*

$$\frac{\vec{\tau}}{l} = \frac{1}{c} \int\limits_{V(l=1)} d^3\mathbf{r}\mathbf{r} \times (\mathbf{j} \times \vec{\mathcal{B}}) \ .$$

where $V(l=1)$ is the volume of the cylinder with unit length. Denoting the conductivity by σ, the current is given by,

$$\mathbf{j} = \sigma \vec{\mathcal{E}}' = \sigma \left(\frac{\vec{v}}{c} \times \vec{\mathcal{B}} \right) \ .$$

where $\vec{\mathcal{E}}'$ is the induced field in the coordinate system rotating together with the cylinder. Now we use $\mathbf{v} = \vec{\omega} \times \mathbf{r}$ and let $\mathbf{r}$ be within the xy-plane (because we want to determine the torque per unit length). We obtain,

$$\mathbf{j} = \frac{\sigma\omega\mathcal{B}}{c} \left[(\hat{\mathbf{e}}_3 \times \mathbf{r}) \times \hat{\mathbf{e}}_2 \right] = -\frac{\sigma\omega\mathcal{B}}{c} y\hat{\mathbf{e}}_3 \ .$$

Follows,

$$\mathbf{j} \times \vec{\mathcal{B}} = -\frac{\sigma\omega\mathcal{B}^2}{c} y\hat{\mathbf{e}}_3 \times \hat{\mathbf{e}}_2 = \frac{\sigma\omega\mathcal{B}^2}{c} y\hat{\mathbf{e}}_1 \ .$$

as well as,

$$\mathbf{r} \times (\mathbf{j} \times \vec{\mathcal{B}}) = \frac{\sigma\omega\mathcal{B}}{c} y(x\hat{\mathbf{e}}_1 + y\hat{\mathbf{e}}_2) \times \hat{\mathbf{e}}_1 = -\frac{\sigma\omega\mathcal{B}^2}{c} y^2\hat{\mathbf{e}}_3 \ .$$

In cylindrical coordinates we have $y^2 = r^2 \sin^2\phi$ and hence,

$$\frac{\vec{\tau}}{l} = -\frac{\sigma\omega\mathcal{B}^2}{c^2} \int\limits_0^R dr r^3 \int\limits_0^{2\pi} d\phi \sin^2\phi \hat{\mathbf{e}}_3 = -\frac{\pi\sigma\omega\mathcal{B}^2 a^4}{4c^2} \hat{\mathbf{e}}_3 \ .$$

15.4.2.16 Ex: Rotating rings

Consider two 'infinitely thin' concentric rings with radii a and b ($a < b$). The rings are in the xy-plane and their common center is at the origin. On the inner ring there is a homogeneously distributed charge $+q$ (that is, the linear charge density is constant), and the outer ring carries the homogeneously distributed charge $-q$.
a. Write down the charge density $\rho(\mathbf{r}) = \rho(r, \phi, z)$ in cylindrical coordinates.
b. Now the entire device rotates with constant angular velocity ω around the symmetry axis z. Determine the resulting current density $\mathbf{j}(\mathbf{r}) = \mathbf{j}(r, \phi, z)$ in cylindrical

coordinates, as well.
c. What are the Cartesian components of current density $\mathbf{j}$?
d. Calculate the magnetic dipole moment $\mathbf{m}$ of the rotating device.

Solution: *We do the following ansatz* $\rho(\mathbf{r}) = C\delta(z)\delta(r-a) - C\delta(z)\delta(r-b)$. *The normalization is* $q = \int \rho(\mathbf{r})dV$. *a. In cylindrical coordinates the current density is,*

$$\rho(r,\phi,z) = \frac{q}{2\pi}\delta(z)\left[\frac{1}{a}\delta(r-a) - \frac{1}{b}\delta(r-b)\right] \ .$$

b. $\mathbf{v}(r,\phi,z) = r\omega\hat{\mathbf{e}}_\phi$ *and therefore, (since* $Id\mathbf{l} = Qd\mathbf{v}$, *such that* $I = Qr\omega$*),*

$$\mathbf{j}(r,\phi,z) = \frac{q\omega}{2\pi}\delta(z)[\delta(r-a) - \delta(r-b)]\hat{\mathbf{e}}_\phi \ .$$

c. With this we get for the Cartesian coordinates,

$$\begin{aligned} j_x &= -\frac{q\omega}{2\pi}\delta(z)[\delta(r-a) - \delta(r-b)]\sin\phi \\ j_y &= +\frac{q\omega}{2\pi}\delta(z)[\delta(r-a) - \delta(r-b)]\cos\phi \\ j_z &= 0 \ . \end{aligned}$$

d. We have,

$$\mathbf{r}\times\mathbf{j} = \det\begin{pmatrix} \hat{\mathbf{e}}_x & \hat{\mathbf{e}}_y & \hat{\mathbf{e}}_z \\ x & y & z \\ j_x & j_y & 0 \end{pmatrix} = -zj_y\hat{\mathbf{e}}_x + zj_x\hat{\mathbf{e}}_y + (xj_y - yj_x)\hat{\mathbf{e}}_z \ .$$

Hence,

$$\mathbf{m} = \frac{1}{2}\frac{q\omega}{2\pi}\int_0^{2\pi}d\phi'\int_0^\infty dr'r'\int_{-\infty}^\infty dz'\delta(z')[\delta(r'-a)-\delta(r'-b)]\cdot \\ \cdot\left[-z'\cos\phi'\hat{\mathbf{e}}_x - z'\sin\phi'\hat{\mathbf{e}}_y + (r'\cos^2\phi' + r'\sin^2\phi')\hat{\mathbf{e}}_z\right] = \frac{q\omega}{2}[a^2-b^2]\hat{\mathbf{e}}_z \ .$$

d. Alternatively,

$$\mathbf{r}\times\mathbf{j} = (r\hat{\mathbf{e}}_r + z\hat{\mathbf{e}}_z)\times\mathbf{j} = \hat{\mathbf{e}}_z rj = \frac{q\omega}{2\pi}(a\delta(r-a) - b\delta(r-b))\delta(z) \ .$$

Hence,

$$\mathbf{m} = \frac{1}{2}\int_V \mathbf{r}'\times\mathbf{j}(\mathbf{r}')d^3\mathbf{r}' = \frac{1}{2}\frac{q\omega}{2\pi}2\pi\hat{\mathbf{e}}_z\left[\int a\delta(r-a)rdr - \int b\delta(r-b)rdr\right] = \frac{q\omega}{2}\hat{\mathbf{e}}_z(a^2-b^2) \ .$$

15.4.2.17 Ex: Magnetic field inside a current tube

A thin hollow conducting tube is traversed by a current along its symmetry axis. The current is homogeneously distributed. Calculate the magnetic field inside and outside
a. from Ampère's law,
b. from the Biot-Savart law.

Solution: *To find the parametrization for the current density* $\mathbf{j}(\mathbf{r}')$ *we consider the normalization condition,*

$$I = \int_S \mathbf{j}(\mathbf{r}') \cdot d\mathbf{S}' = \eta \int_S I\delta(\rho' - R)\hat{\mathbf{e}}_z \cdot d\mathbf{S}' = \eta I \int_S \delta(\rho' - R)\rho' d\rho' d\phi' = \eta I 2\pi R \ ,$$

giving $\eta = \frac{1}{2\pi R}$*, such that,*

$$\mathbf{j}(\mathbf{r}') = \frac{I}{2\pi R}\delta(\rho' - R)\hat{\mathbf{e}}_z \ .$$

The potential vector is now,

$$\begin{aligned}
\mathbf{A}(\mathbf{r}) &= \frac{\mu_0}{4\pi}\int \frac{\mathbf{j}(\mathbf{r}')dV'}{|\mathbf{r} - \mathbf{r}'|} = \frac{\mu_0}{4\pi}\frac{I}{2\pi R}\int \frac{\delta(\rho' - R)\hat{\mathbf{e}}_z}{|\mathbf{r} - \rho'\hat{\mathbf{e}}_{\rho'} - z'\hat{\mathbf{e}}_z|}\rho' d\rho' d\phi' dz' \\
&= \frac{\mu_0}{4\pi}\frac{I}{2\pi R}\int \frac{\delta(\rho' - R)\hat{\mathbf{e}}_z}{\sqrt{(\rho\cos\phi - \rho'\cos\phi')^2 + (\rho\sin\phi - \rho'\sin\phi')^2 + (z - z')^2}}\rho' d\rho' d\phi' dz' \\
&= \frac{\mu_0 I}{8\pi^2}\hat{\mathbf{e}}_z \int \frac{1}{\sqrt{\rho^2 + R^2 - 2R\rho\cos(\phi + \phi') + (z - z')^2}} d\phi' dz' \ ,
\end{aligned}$$

as the result cannot depend on z *nor on* ϕ*, we can set* $z = 0$ *and* $\phi = 0$*,*

$$\mathbf{A}(\mathbf{r}) = \frac{\mu_0 I}{8\pi^2}\hat{\mathbf{e}}_z \int_0^{2\pi}\int_{-\infty}^{\infty} \frac{1}{\sqrt{\rho^2 + R^2 - 2R\rho\cos\phi' + z'^2}} dz' d\phi' = ???$$

Maybe the magnetic field is easier to calculate,

$$\begin{aligned}
\vec{\mathcal{B}}(\mathbf{r}) &= \frac{\mu_0}{4\pi}\int \frac{\mathbf{j}(\mathbf{r}') \times (\mathbf{r} - \mathbf{r}')dV'}{|\mathbf{r} - \mathbf{r}'|^3} \\
&= \frac{\mu_0}{4\pi}\frac{I}{2\pi R}\int \frac{\delta(\rho' - R)\hat{\mathbf{e}}_z \times (\mathbf{r} - \mathbf{r}')}{\sqrt{(\rho\cos\phi - \rho'\cos\phi')^2 + (\rho\sin\phi - \rho'\sin\phi')^2 + (z - z')^2}^3}\rho' d\rho' d\phi' dz' \\
&= \frac{\mu_0 I}{8\pi^2}\int \frac{\rho\hat{\mathbf{e}}_\phi - \rho'\hat{\mathbf{e}}_{\phi'}}{\sqrt{\rho^2 + R^2 - 2R\rho\cos(\phi + \phi') + (z - z')^2}^3} d\phi' dz' \ .
\end{aligned}$$

Since the result cannot depend on z *nor on* ϕ*, we can set* $z = 0$ *and* $\phi = 0$*. For this choice the* x*-component vanishes,*

$$\mathcal{B}_x(\mathbf{r}) = \frac{\mu_0 I}{8\pi^2}\int_{-\infty}^{\infty}\int_0^{2\pi} \frac{R\sin\phi'}{\sqrt{\rho^2 + R^2 - 2R\rho\cos\phi' + z'^2}^3} d\phi' dz' = 0$$

and the y*-component*

$$\mathcal{B}_y(\mathbf{r}) = \frac{\mu_0 I}{8\pi^2}\int_{-\infty}^{\infty}\int_0^{2\pi} \frac{\rho - R\cos\phi'}{\sqrt{\rho^2 + R^2 - 2R\rho\cos\phi' + z'^2}^3} d\phi' dz' = ???$$

15.4.2.18 Ex: Magnetic induction in a hollow conductor

A conductor (ideal and infinitely thin) be on the z-axis and carries a current I flowing in $+z$-direction. This conductor is enclosed by a conductive hollow cylinder with radius R, within which a homogeneously distributed total current I runs in the opposite direction $-z$ (coaxial cable). Calculate the magnetic induction inside and outside this device.

Solution: *In cylindrical coordinates we have,*

$$\mathbf{j}(\mathbf{r}) = \left[\frac{I}{\rho}\delta(\rho)\delta(\phi) - \frac{I}{2\pi R}\delta(\rho - R)\right]\hat{\mathbf{e}}_z \ .$$

We now use for the integration a circular area with radius ρ in $+z$-direction. So, $d\vec{f} = \rho' d\rho' d\phi' \hat{\mathbf{e}}_z$ and hence,

$$\int\limits_{F(\rho)} (\nabla \times \vec{\mathcal{B}}) \cdot d\mathbf{f} = \frac{4\pi}{c} \int\limits_{F(\rho} \mathbf{j} \cdot d\mathbf{f} = \frac{4\pi}{c} I \begin{cases} 1 & for \rho < R \\ 0 & else \end{cases}$$
$$= \int\limits_{R(\rho} \vec{\mathcal{B}} \cdot d\vec{s} = 2\pi\rho\mathcal{B}(\rho)$$

With that we immediately get,

$$\vec{\mathcal{B}} = \frac{2I}{c\rho} \begin{cases} 1 & for \rho < R \\ 0 & else \end{cases} \ .$$

15.4.2.19 Ex: Current ring

A (ideal) current ring in the xy-plane with radius a and centered at the origin is traversed by a current I. In spherical coordinates the current density is given by,

$$\mathbf{j}(\mathbf{r}) = \mathbf{j}(r, \theta, \phi) = \frac{I}{a}\delta(\cos\theta)\delta(r - a)\hat{\mathbf{e}}_\phi \ .$$

For $|\mathbf{r}| \gg a$ the corresponding potential then has the form,

$$\mathbf{A}(\mathbf{r}) = \mathbf{A}(r, \theta, \phi) = \frac{I\pi a^2}{cr^2} \sin\theta \hat{\mathbf{e}}_\phi \ .$$

and for magnetic field holds,

$$\vec{\mathcal{B}}(\mathbf{r}) = \vec{\mathcal{B}}(r, \theta, \phi) = \frac{I\pi a^2}{cr^3} \left(2\cos\theta \hat{\mathbf{e}}_r + \sin\theta \hat{\mathbf{e}}_\theta\right) \ .$$

where $\hat{\mathbf{e}}_r$, $\hat{\mathbf{e}}_\theta$, and $\hat{\mathbf{e}}_\phi$ are the unit vectors in r, θ, and ϕ-direction.
a. Calculate the Cartesian components of $\mathbf{j}(\mathbf{r})$.

b. Calculate the Cartesian components of the dipolar magnetic moment $\vec{\mathcal{M}}$ using the formula,

$$\vec{\mathcal{M}} = \frac{1}{2c}\int d^3r'(\mathbf{r}' \times \mathbf{j}(\mathbf{r}')) \ .$$

c. What are the components of $\vec{\mathcal{M}}$ in r, θ, and ϕ-direction.
d. Show with the help of (c) that the magnetic field at a point $\mathbf{r}$ of the arbitrary surface can be written,

$$\vec{\mathcal{B}}(\mathbf{r}) = \frac{3\hat{\mathbf{e}}_r(\vec{\mathcal{M}}\cdot\hat{\mathbf{e}}_r) - \vec{\mathcal{M}}}{r^3} \ .$$

e. Calculate the Cartesian components of magnetic field and check, with the help of (b), that also in Cartesian coordinates holds,

$$\vec{\mathcal{B}}(\mathbf{r}) = \frac{3\mathbf{r}(\vec{\mathcal{M}}\cdot\mathbf{r}) - r^2\vec{\mathcal{M}}}{r^5} \ .$$

Solution: *a. We have,*

$$\begin{aligned}
\hat{\mathbf{e}}_r &= \sin\theta\cos\phi\hat{\mathbf{e}}_x + \sin\theta\sin\phi\hat{\mathbf{e}}_y + \cos\theta\hat{\mathbf{e}}_z \\
\hat{\mathbf{e}}_\theta &= \cos\theta\cos\phi\hat{\mathbf{e}}_x + \cos\theta\sin\phi\hat{\mathbf{e}}_y - \sin\theta\hat{\mathbf{e}}_z \\
\hat{\mathbf{e}}_\phi &= -\sin\phi\hat{\mathbf{e}}_x + \cos\phi\hat{\mathbf{e}}_y \ .
\end{aligned}$$

From this follows,

$$\mathbf{j}(\mathbf{r}) = j_x(r,\theta,\phi)\hat{\mathbf{e}}_x + j_y(r,\theta,\phi)\hat{\mathbf{e}}_y = \frac{I}{a}\delta(r-a)\delta(cos\theta)\begin{pmatrix} -\sin\phi \\ \cos\phi \\ 0 \end{pmatrix} \ .$$

b. With the result of (a) we get,

$$\mathbf{r}\times\mathbf{j}(\mathbf{r}) = \det\begin{pmatrix} \hat{\mathbf{e}}_x & \hat{\mathbf{e}}_y & \hat{\mathbf{e}}_z \\ x & y & z \\ j_x & j_y & 0 \end{pmatrix} = -zj_y\hat{\mathbf{e}}_x + zj_x\hat{\mathbf{e}}_y + (xj_y - yj_x)\hat{\mathbf{e}}_z \ .$$

Now,

$$x = r\sin\theta\cos\phi, \quad y = r\sin\theta\sin\phi \qquad \textit{and} \qquad z = r\cos\theta \ ,$$

and therefore we get,

$$\begin{aligned}
\mathbf{r}\times\mathbf{j}(\mathbf{r}) = -\frac{I}{a}\delta(r-a)\delta(\cos\theta)r[&\cos\theta\cos\phi\hat{\mathbf{e}}_x + \cos\theta\sin\phi\hat{\mathbf{e}}_y \\
&- (\sin\theta\cos^2\phi + \sin\theta\sin^2\phi)\hat{\mathbf{e}}_z] \ .
\end{aligned}$$

that is,

$$\mathbf{r}\times\mathbf{j}(\mathbf{r}) = -\frac{I}{a}\delta(r-a)\delta(\cos\theta)r[\cos\theta\cos\phi\hat{\mathbf{e}}_x + \cos\theta\sin\phi\hat{\mathbf{e}}_y - \sin\theta\hat{\mathbf{e}}_z] \ .$$

With that we get,

$$\begin{aligned}\vec{\mathcal{M}} &= \frac{1}{2c}\int d^3\mathbf{r}'\mathbf{r}'\times\mathbf{j}(\mathbf{r}') \\ &= -\frac{I}{2ac}\int dr'd(\cos\theta')d\phi' {r'}^3\delta(\cos\theta')\delta(r'-a)[\cos\theta'\cos\phi'\hat{\mathbf{e}}_x+\cos\theta'\sin\phi'\hat{\mathbf{e}}_y-\sin\theta'\hat{\mathbf{e}}_z]\ .\end{aligned}$$

Due to $\delta(\cos\theta')$ only the last term survives, and we get,

$$\vec{\mathcal{M}} = \frac{Ia^2\pi}{c}\hat{\mathbf{e}}_z\ .$$

c. Here we need to express Cartesian unit vectors by spherical coordinates. A simple calculation [see (a)] gives,

$$\begin{aligned}\hat{\mathbf{e}}_x &= \cos\phi\sin\theta\hat{\mathbf{e}}_r+\cos\phi\cos\theta\hat{\mathbf{e}}_\theta-\sin\phi\hat{\mathbf{e}}_\phi \\ \hat{\mathbf{e}}_y &= \sin\phi\sin\theta\hat{\mathbf{e}}_r+\sin\phi\cos\theta\hat{\mathbf{e}}_\theta+\cos\phi\hat{\mathbf{e}}_\phi \\ \hat{\mathbf{e}}_z &= \cos\theta\hat{\mathbf{e}}_r-\sin\theta\hat{\mathbf{e}}_\theta\ .\end{aligned}$$

With that we get immediately,

$$\mathcal{M}_r = \frac{Ia^2\pi}{c}\cos\theta \quad , \quad \mathcal{M}_\theta = -\frac{Ia^2\pi}{c}\sin\theta \quad , \quad \mathcal{M}_\phi = 0\ .$$

d. We obtain,

$$\frac{3\hat{\mathbf{e}}_r(\vec{\mathcal{M}}\cdot\hat{\mathbf{e}}_r)-\vec{\mathcal{M}}}{r^3} = \frac{Ia^2\pi}{cr^3}(3\cos\theta\hat{\mathbf{e}}_r-\cos\theta\hat{\mathbf{e}}_r+\sin\theta\hat{\mathbf{e}}_\theta) = \frac{Ia^2\pi}{cr^3}[2\cos\theta\hat{\mathbf{e}}_r+\sin\theta\hat{\mathbf{e}}_\theta] = \vec{\mathcal{B}}(\mathbf{r})\ .$$

e. With part (c) follows,

$$\begin{aligned}2\cos\theta\hat{\mathbf{e}}_r+\sin\theta\hat{\mathbf{e}}_\theta &= 2\cos\theta\sin\theta\cos\phi\hat{\mathbf{e}}_x+2\cos\theta\sin\theta\sin\phi\hat{\mathbf{e}}_y+2\cos^2\theta\hat{\mathbf{e}}_z \\ &\quad+\sin\theta\cos\theta\cos\phi\hat{\mathbf{e}}_x+\sin\theta\cos\theta\sin\phi\hat{\mathbf{e}}_y-\sin^2\theta\hat{\mathbf{e}}_z \\ &= 3\sin\theta\cos\theta\cos\phi\hat{\mathbf{e}}_x+3\sin\theta\cos\theta\sin\phi\hat{\mathbf{e}}_y+(3\cos^2\theta-1)\hat{\mathbf{e}}_z\ .\end{aligned}$$

Therefore, we get,

$$\vec{\mathcal{B}} = \frac{3Ia^2\pi}{cr^3}\begin{pmatrix}\cos\theta\sin\theta\cos\phi\\ \cos\theta\sin\theta\sin\phi\\ \cos^2\theta-\frac{1}{3}\end{pmatrix}\ .$$

With

$$\mathcal{M}_x = \mathcal{M}_y = 0 \quad , \quad \mathcal{M}_z = \frac{Ia^2\pi}{c}\ ,$$

follows immediately,

$$\begin{aligned}\frac{3\mathbf{r}(\vec{\mathcal{M}}\cdot\mathbf{r})}{r^5}-\frac{\vec{\mathcal{M}}}{r^3} &= \frac{Ia^2\pi}{cr^3}\left[\frac{3\mathbf{r}z}{r^2}-\hat{\mathbf{e}}_z\right] \\ &= \frac{Ia^2\pi}{cr^3}\left[\frac{3xz}{r^2}\hat{\mathbf{e}}_x+\frac{3yz}{r^2}\hat{\mathbf{e}}_y+\frac{3z^2}{r^2}\hat{\mathbf{e}}_z-\hat{\mathbf{e}}_z\right] \\ &= \frac{Ia^2\pi}{cr^3}\left[3\cos\theta\sin\theta\cos\phi\hat{\mathbf{e}}_x+3\cos\theta\sin\theta\sin\phi\hat{\mathbf{e}}_y+(3\cos^2\theta-1)\hat{\mathbf{e}}_z\right] = \vec{\mathcal{B}}(\mathbf{r})\ .\end{aligned}$$

15.4.2.20 Ex: Magnetic field of a long coil

Determine the magnetic $\vec{\mathcal{H}}$-field inside a very long current-carrying coil. The number of turns is n, the length of the coil l, its radius a, and the amplitude of the current I. How does the magnetic field change, if the coil has an iron core with the permeability μ?

Solution: *We place the symmetry axis of the coil on the x-axis and choose as integration path a rectangle in the xz-plane defined by the points.* $(0,0,0)$, $(s,0,0)$, $(s,0,b)$, *and (0,0,b). Here we choose $b > a$ so big that $\vec{\mathcal{H}}$ will vanish there. With that, we get immediately, by applying Stokes' law,*

$$\int_{\mathcal{S}} (\nabla \times \vec{\mathcal{H}}(\mathbf{r})) \cdot d\mathbf{S} = \int_{\partial\mathcal{S}} \vec{\mathcal{H}}(\mathbf{r}) \cdot d\mathbf{r} = \frac{4\pi}{c} \int_{\mathcal{S}} \mathbf{j}(\mathbf{r}) \cdot d\mathbf{S} = \mathcal{H}s = \frac{4\pi}{c} \frac{n}{l} sI \ .$$

Inserting the iron core into the coil changes the magnetic $\vec{\mathcal{B}}$-field, but not the $\vec{\mathcal{H}}$-field inside the coil. So we get for the interior,

$$\mathcal{H} = \frac{4\pi}{c} \frac{n}{l} I \qquad , \qquad \mathcal{B} = \mu \frac{4\pi}{c} \frac{n}{l} I \ .$$

15.4.2.21 Ex: Shielded dipolar field

The magnetic field of a dipole is shielded by a hollow sphere (inner radius a, outer radius b) made of a material with permeability μ. The dipole $\vec{\mathcal{P}}_M$ is in the center of the sphere and points towards z.
a. Show that the magnetic field $\vec{\mathcal{H}}$ in the entire space can be written as the negative gradient of a potential $\Phi_M(\mathbf{r})$.
b. Show that this magnetic potential satisfies the Laplace equation in whole space, $\triangle \Phi_M(\mathbf{r}) = 0$.
c. To solve this Laplace equation, do the following ansatz of variable separation,

$$\Phi_M^{(i)}(r, \theta\phi) = \sum_{l=0}^{\infty} \sum_{m=-l}^{+l} \frac{4\pi}{2l+1} \left[\beta_{lm}^{(i)} r^l + \gamma_{lm}^{(i)} \frac{1}{r^{l+1}} \right] Y_{lm}(\theta, \phi) \ .$$

where the $\beta_{lm}^{(i)}$ and $\gamma_{lm}^{(i)}$ be constant and $i = I, II, II$ denote the different regions $(I : 0 \leq r < a \ , II : a \leq r \leq b \ , III : b < r)$. What are the consequences for $\beta_{lm}^{(i)}$ and $\gamma_{lm}^{(i)}$ due to the fact that Φ_M
i. is, in the origin, the potential of a pure dipolar field $\vec{\mathcal{P}}_M$?
ii. is cylindrically symmetrical about the z-axis?
iii. disappears at infinity?
d. At the interfaces between the different regions the normal component of the magnetic $\vec{\mathcal{B}}$-field and the tangential component of the $\vec{\mathcal{H}}$-field are discontinuous. Use these conditions to establish a system of equations for the coefficients $\beta_{lm}^{(i)}$ and $\gamma_{lm}^{(i)}$, using

$\text{grad}_r \Phi_M = \frac{\partial \Phi_M}{\partial r}$, $\text{grad}_\theta \Phi_M = \frac{1}{r}\frac{\partial \Phi_M}{\partial \theta}$, $\frac{\partial Y_{10}}{\partial \theta} = \sqrt{\frac{2l+1}{4\pi}} P_l^1(\cos\theta)$, as well as the orthogonality relations $\int d\Omega Y_{l0}^*(\Omega) Y_{l'0}(\Omega) = \delta_{ll'}$ and $\int_{-1}^{+1} dx P_l^1(x) P_{l'}^1(x) = \delta_{ll'} \frac{2}{2l+1} \frac{(l+1)!}{(l-1)!}$.
e. Solve the equation system first for the case $l \neq 1$.
f. Solve the system of equations for $l = 1$.
g. What does the magnetic field look like outside the sphere for $\mu \gg 1$?

Solution: *a. For the current density holds in the entire space,*

$$\mathbf{j}(\mathbf{r}) = 0 \ .$$

From this immediately follows,

$$\nabla \times \vec{\mathcal{H}} = \frac{4\pi}{c}\mathbf{j} = 0 \ .$$

Therefore we have,

$$\vec{\mathcal{H}} = -\nabla \Phi_M(\mathbf{r}) \ .$$

b. Since

$$\nabla \cdot \vec{\mathcal{B}} = 0 \qquad \textit{and} \qquad \vec{\mathcal{B}} = \mu \vec{H} \ .$$

and with (a) we get in the entire space,

$$\nabla \cdot \vec{\mathcal{H}} = -\nabla \cdot \nabla \Phi_M = 0 \ .$$

hence the Laplace equation,

$$\triangle \Phi_M = 0 \ .$$

c. We separated the variables,

$$\Phi_M^{(i)} r, \theta\phi) = \sum_{l=0}^{\infty} \sum_{m=-l}^{+l} \frac{4\pi}{2l+1} \left[\beta_{lm}^{(i)} r^l + \gamma_{lm}^{(i)} \frac{1}{r^{l+1}} \right] Y_{lm}(\theta, \phi) \ .$$

(1) For $r \to 0$ we have a pure dipolar field towards z:

$$\Phi_{Dipol} = \frac{4\pi}{3} q_{10} \frac{Y_{10}}{r^2} = \sqrt{\frac{4\pi}{3}} P_M \frac{Y_{10}}{r^2} \ .$$

From this follows,

$$\gamma_{lm}^{(I)} = \sqrt{\frac{3}{4\pi}} P_M \delta_{l1} \delta_{m0} \ .$$

(2) Because of the cylindrical symmetry of the problem, Φ_M cannot depend on the angle ϕ. From this follows for all three regions ($i = I, II, III$),

$$\beta_{lm}^{(i)} = \beta_l^{(i)} \delta_{m0}$$
$$\gamma_{lm}^{(i)} = \gamma_l^{(i)} \delta_{m0} \ .$$

(3) $\vec{\mathcal{H}}$ must disappear in the infinite. So we normalize our potential in such a way that Φ_M disappears (becomes constant) at infinity. This means that for all l,

$$\beta_l^{(III)} = 0 \ .$$

d. Be $a_\pm \equiv a \pm \epsilon$ *and* $b_\pm \equiv b \pm \epsilon$. *The continuity of the normal component of* $\vec{\mathcal{B}}$ *provides the boundary conditions,*

$$\begin{aligned}(\nabla\Phi_M(a_-,\theta))_r &= \mu(\nabla\Phi_M(a_+,\theta))_r \\ \mu(\nabla\Phi_M(b_-,\theta))_r &= (\nabla\Phi_M(b_+,\theta))_r \ .\end{aligned}$$

the one of the tangential component of $\vec{\mathcal{H}}$ *provides,*

$$\begin{aligned}(\nabla\Phi_M(a_-,\theta))_\theta &= (\nabla\Phi_M(a_+,\theta))_\theta \\ (\nabla\Phi_M(b_-,\theta))_\theta &= (\nabla\Phi_M(b_+,\theta))_\theta \ .\end{aligned}$$

If we now use,

$$(\nabla\Phi_M)_r = \frac{\partial\Phi_M}{\partial r} \qquad \textit{and} \qquad (\nabla\Phi_M)_\theta = \frac{1}{r}\frac{\partial\Phi_M}{\partial\theta} \ .$$

as well as,

$$\frac{\partial Y_{10}}{\partial\theta} = \sqrt{\frac{2l+1}{4\pi}}P_l^1(\cos\theta) \ .$$

we get consecutively,

$$\begin{aligned}
\sum_l \frac{4\pi}{2l+1}Y_{l0}\left[\beta_l^{(I)}la^{l-1} - \gamma_l^{(I)}\frac{l+1}{a^{l+2}}\delta_{l1}\right] &= \mu\sum_l \frac{4\pi}{2l+1}Y_{l0}\left[\beta_l^{(II)}la^{l-1} - \gamma_l^{(II)}\frac{l+1}{a^{l+2}}\right] \\
\mu\sum_l \frac{4\pi}{2l+1}Y_{l0}\left[\beta_l^{(II)}lb^{l-1} - \gamma_l^{(II)}\frac{l+1}{b^{l+2}}\right] &= -\sum_l \frac{4\pi}{2l+1}Y_{l0}\gamma_l^{(III)}\frac{l+1}{b^{l+2}} \\
\sum_l \sqrt{\frac{4\pi}{2l+1}}P_l^1\left[\beta_l^{(I)}a^l + \frac{\gamma_l^{(I)}}{a^{l+1}}\delta_{l1}\right] &= \sum_l \sqrt{\frac{4\pi}{2l+1}}P_l^1\left[\beta_l^{(II)}a^l + \frac{\gamma_l^{(II)}}{a^{l+1}}\right] \\
\sum_l \sqrt{\frac{4\pi}{2l+1}}P_l^1\left[\beta_l^{(II)}b^l + \frac{\gamma_l^{(II)}}{b^{l+1}}\right] &= \sum_l \sqrt{\frac{4\pi}{2l+1}}P_l^1\frac{\gamma_l^{(III)}}{b^{l+1}} \ .
\end{aligned}$$

We now multiply the first two equations with Y_{l0}^* *(*l *is fixed) and integrate over* Ω*; we multiply the last two equations with* P_l^1 *and we integrate over* $x = \cos\theta$. *This gives, exploiting the given orthogonalaty relations, the following system of equations,*

$$\begin{pmatrix} la^{l-1} & -\mu la^{l-1} & \mu\frac{l+1}{a^{l+2}} & 0 \\ 0 & \mu lb^{l-1} & -\mu\frac{l+1}{b^{l+2}} & \frac{l+1}{b^{l+2}} \\ a^l & -a^l & -\frac{1}{a^{l+1}} & 0 \\ 0 & b^l & \frac{1}{b^{l+1}} & -\frac{1}{b^{l+1}} \end{pmatrix}\begin{pmatrix} \beta_l^{(I)} \\ \beta_l^{(II)} \\ \gamma_l^{(II)} \\ \gamma_l^{(III)} \end{pmatrix} = \begin{pmatrix} \gamma_l^{(I)}\frac{l+1}{a^{l+2}}\delta_{l1} \\ 0 \\ -\gamma_l^{(I)}\frac{1}{a^{l+1}}\delta_{l1} \\ 0 \end{pmatrix} \ .$$

e. For $l \neq 1$ the above system of equations is homogeneous. The determinant of the matrix of coefficients is,

$$
\begin{aligned}
\det A \equiv \det & \begin{pmatrix} la^{l-1} & -\mu l a^{l-1} & \mu\frac{l+1}{a^{l+2}}0 & \\ 0 & \mu l b^{l-1} & -\mu\frac{l+1}{b^{l+2}} & \frac{l+1}{b^{l+2}} \\ a^l & -a^l & -\frac{1}{a^{l+1}} & 0 \\ 0 & b^l & \frac{1}{b^{l+1}} & -\frac{1}{b^{l+1}} \end{pmatrix} \\
= \det & \begin{pmatrix} la^{l-1} & (1-\mu) l a^{l-1} & \mu\frac{l+1}{a^{l+2}}0 & \\ 0 & \mu l b^{l-1} & (1-\mu)\frac{l+1}{b^{l+2}} & \frac{l+1}{b^{l+2}} \\ a^l & 0 & -\frac{1}{a^{l+1}} & 0 \\ 0 & b^l & 0 & -\frac{1}{b^{l+1}} \end{pmatrix} \\
= la^{l-1} \det & \begin{pmatrix} \mu l b^{l-1} & (1-\mu)\frac{l+1}{b^{l+2}} & \frac{l+1}{b^{l+2}} \\ 0 & -\frac{1}{a^{l+1}} & 0 \\ b^l & 0 & -\frac{1}{b^{l+1}} \end{pmatrix} + a^l \det \begin{pmatrix} (1-\mu) l a^{l-1} & \mu\frac{l+1}{a^{l+2}} & 0 \\ \mu l b^{l-1} & (1-\mu)\frac{l+1}{b^{l+2}} & \frac{l+1}{b1 l+2} \\ b^l & 0 & -\frac{1}{b^{l+1}} \end{pmatrix} \\
= la^{l-1} & \left[\frac{\mu l b^{l-1}}{a^{l+1} b^{l+1}} + \frac{(l+1) b^l}{a^{l+1} b^{l+2}} \right] \\
& + a^l \left[-(1-\mu)^2 \frac{l(l+1) a^{l-1}}{b^{l+1} b^{l+2}} + \frac{\mu (l+1)^2 b^l}{a^{l+2} b^{l+2}} + \frac{\mu^2 l (l+1) b^{l-1}}{a^{l+2} b^{l+1}} \right] \\
= \frac{a^{2l-1}}{b^2} & \left[\frac{\mu l^2}{a^{2l+1}} + \frac{l(l+1)}{a^{2l+1}} - (1-\mu)^2 \frac{l(l+1)}{b^{2l+1}} + \frac{\mu (l+1)^2}{a^{2l+1}} + \frac{\mu^2 l (l+1)}{a^{2l+1}} \right] \\
= \frac{a^{2l-1}}{b^2} & \left[(1-\mu)^2 \left\{ \frac{1}{a^{2l+1}} - \frac{1}{b^{2l+1}} \right\} + \mu \frac{(2l+1)^2}{a^{2l+1}} \right] .
\end{aligned}
$$

where we have used that

$$l^2 + (l+1)^2 + 2l(l+1) = 4l^2 + 4l + 1 = (2l+1)^2 .$$

Now $0 < a < b$ and $\mu \geq 1$. So we always have,

$$\det A > 0 .$$

and therefore for $l \neq 1$ only exist trivial solutions,

$$\beta_l^{(I)} = \beta_l^{(II)} = \gamma_l^{(II)} = \gamma_l^{(III)} = 0 .$$

Since moreover for $l \neq 1$ we know,

$$\beta_l^{(III)} = \gamma_l^{(I)} = 0 .$$

we get as a result that the magnetic potential has only a $l = 1$ (dipolar) component.
f. For $l = 1$ we have the following system of equations (for simplicity, we suppress the

index $l = 1$ in the following),

$$\begin{aligned}
\beta^{(I)} - \mu\beta^{(II)} + \frac{2\mu}{a^3}\gamma^{(II)} &= \frac{2}{a^3}\gamma^{(I)} \\
\mu\beta^{(II)} - \frac{2\mu}{b^3}\gamma^{(II)} + \frac{2}{b^3}\gamma^{(III)} &= 0 \\
a\beta^{(I)} - a\beta^{(II)} - \frac{1}{a^2}\gamma^{(II)} &= -\frac{1}{a^2}\gamma^{(I)} \\
b\beta^{(II)} + \frac{1}{b^2}\gamma^{(II)} - \frac{1}{b^2}\gamma^{(III)} &= 0 \ .
\end{aligned}$$

We now multiply the last of these equations with $2/b$ and add it to the second, which gives,

$$(2+\mu)\beta^{(II)} - \frac{2(\mu-1)}{b^3}\gamma^{(II)} = 0 \ .$$

resp.

$$\gamma^{(II)} = \frac{b^3(\mu+2)}{2(\mu-1)}\beta^{(II)} \ .$$

We now divide the third equation by a and subtract it from the first, which gives,

$$-(\mu-1)\beta^{(II)} + \frac{1}{a^3}(2\mu+1)\gamma^{(II)} = \frac{3}{a^3}\gamma^{(I)} \ .$$

Hence,

$$-(\mu-1)\beta^{(II)} + \frac{1}{a^3}(2\mu+1)\frac{b^3(\mu+2)}{2(\mu-1)}\beta^{(II)} = \frac{3}{a^3}\gamma^{(I)} \ .$$

and therefore,

$$\beta^{(II)}\left(\frac{b^3(2\mu+1)(\mu+2) - 2a^3(\mu-1)^2}{2(\mu-1)}\right) = 3\gamma^{(I)} \ .$$

Therefore we get,

$$\begin{aligned}
\beta^{(II)} &= \frac{6(\mu-1)\gamma^{(I)}}{b^3(2\mu+1)(\mu+2) - 2a^3(\mu-1)^2} \\
\gamma^{(II)} &= \frac{3b^3(\mu+2)\gamma^{(I)}}{b^3(2\mu+1)(\mu+2) - 2a^3(\mu-1)^2} \\
\gamma^{(III)} &= \frac{9b^3\mu\gamma^{(I)}}{b^3(2\mu+1)(\mu+2) - 2a^3(\mu-1)^2} \\
\beta^{(I)} &= -\frac{2(\mu-1)(\mu+2)\left[\frac{b^3}{a^3} - 1\right]\gamma^{(I)}}{b^3(2\mu+1)(\mu+2) - 2a^3(\mu-1)^2} \ .
\end{aligned}$$

Moreover, we had,

$$\beta^{(III)} \equiv 0 \qquad \textit{and} \qquad \gamma^{(I)} = \sqrt{\frac{3}{4\pi}}P_M \ .$$

The result can be verified by letting $\mu = 1$. In this case,

$$\beta^{(I)} = \beta^{(II)} = \beta^{(III)} \qquad \text{and} \qquad \gamma^{(II)} = \gamma^{(III)} = \gamma^{(I)} = \sqrt{\frac{3}{4\pi}} P_M \ ,$$

giving the dipolar field in vacuum.
g. In region III we have,

$$\beta^{(III)} = 0 \qquad ; \qquad \gamma^{(III)} = \frac{9}{2}\gamma^{(I)} \frac{1}{\frac{(2\mu+1)(\mu+2)}{2\mu} - \frac{a^3}{b^3}\frac{(\mu-1)^2}{\mu}} \ .$$

Para $\mu \gg 1$ segue,

$$\gamma^{(III)} \sim \frac{9}{2}\gamma^{(I)} \frac{1}{1 - \frac{a^3}{b^3}} \frac{1}{\mu} \ .$$

15.5 Further reading

T. Bergeman et al., *Magnetostatic trapping fields for neutral atoms* [127]DOI

Chapter 16

Magnetic properties of matter

The most common manifestations of magnetism are certainly magnets, compass needles, and the Earth's magnetic field, and it is not obvious how they are related to the magnetic fields produced by currents, discussed in the previous chapter. Nevertheless, all magnetic phenomena are ultimately due to currents, even if they are microscopic, for example, electrons orbiting atomic nuclei or spinning around their own axis. From the macroscopic point of view we can treat these circular currents as magnetic dipoles. Generally, the dipoles of a medium have random orientations, such that the generated magnetic fields cancel out. However, when we apply a *external* magnetic field, the dipoles can realign and *magnetize* the medium.

16.1 Magnetization

There are several macroscopic manifestations of microscopic dipole moments known as para-, dia-, and ferromagnetism. We will discuss these in the following sections.

16.1.1 Energy of permanent dipoles and paramagnetism

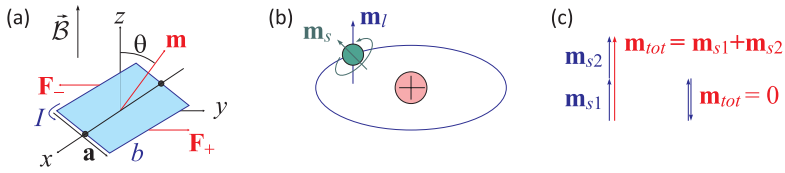

Figure 16.1: (a) Illustration of the torque exerted by a magnetic field on a magnetic dipole. (b) An electron spinning around a nucleus may have orbital and intrinsic angular momentum. (c) Dipole moments are added as vectors.

We consider current loops of rectangular shape [1]. In the case of the geometry shown in Fig. 16.1(a) the Lorentz forces acting on the wire sections a being parallel to the z-y-plane compensate each other, because the forces and the points on which they act are all on a straight line. On the other side, the forces acting on the wire sections b,

$$\mathbf{F}_{\pm} = \pm I\mathbf{b} \times \vec{\mathcal{B}} = \pm Ib\mathcal{B}\hat{\mathbf{e}}_y \ , \tag{16.1}$$

[1] Arbitrary shapes can be constructed by two-dimensional arrays of rectangular loops.

both contribute to create a torque,

$$\vec{\tau} = \tfrac{\mathbf{a}}{2} \times \mathbf{F}_+ + \tfrac{-\mathbf{a}}{2} - \times \mathbf{F}_- = I\mathcal{B}b\mathbf{a} \times \hat{\mathbf{e}}_y = Iab\mathcal{B}\hat{\mathbf{e}}_x \sin\theta \ , \tag{16.2}$$

With the definition of the magnetic moment (15.42) we find,

$$\boxed{\vec{\tau} = \mathbf{m} \times \vec{\mathcal{B}}} \ . \tag{16.3}$$

We can also calculate the energy of a dipole in a magnetic field by the work required to rotate it out of its equilibrium position,

$$H_{int} = \int_0^\theta \vec{\tau} \cdot d\theta = \int_0^\theta \mathbf{m} \times \vec{\mathcal{B}} d\theta = \int_0^\theta m\mathcal{B} \sin\theta d\theta = -m\mathcal{B}\cos\theta \ , \tag{16.4}$$

such that,

$$\boxed{H_{int} = -\mathbf{m} \cdot \vec{\mathcal{B}}} \ . \tag{16.5}$$

The formula (16.3) holds for homogeneous magnetic fields or, alternatively, for almost point-like dipoles in inhomogeneous fields. It represents the magnetic equivalent of the torque on electric dipoles (14.4). The torque is oriented so as to align the dipole moment to the direction of the magnetic field. This mechanism is used to explain the phenomenon of paramagnetism [see Fig. 16.3(a)].

In atomic physics we learn that electrons bound to atoms may have, besides an orbital angular momentum due to the planetary motion around the atomic nucleus, an *intrinsic angular momentum* called *spin* as if the electron were a small electrically charged sphere rotating about its own axis [see illustration of Fig. 16.1(b)]. The spins of the various electrons in the electron layer of an atom generally couple to form a total dipole moment, which then interacts with external magnetic fields. This is called *Zeeman effect*. The spins may pair and add up or compensate pairwise such as to zero the magnetic dipole moment of the atom [see illustration of Fig. 16.1(c)]. Note that a strong external magnetic field can break the angular momentum coupling and interact with the electron spins separately. This is called *Paschen-Back effect*.

The phenomenon of *paramagnetism* is observed in materials whose molecules have permanent magnetic dipole moments, that is, in chemical elements with unpaired valence electrons. It is not observed in noble gases, covalent crystals, etc..

Unlike the torque, the *force exerted by a homogeneous field* on a dipole vanishes,

$$\mathbf{F} = I \oint d\mathbf{l} \times \vec{\mathcal{B}} = I \left(\oint d\mathbf{l} \right) \times \vec{\mathcal{B}} = 0 \ . \tag{16.6}$$

For inhomogeneous fields we need to calculate the force from the energy gradient as,

$$\mathbf{F} = -\nabla H_{int} = \nabla(\mathbf{m} \cdot \vec{\mathcal{B}}) = \mathbf{m} \times (\nabla \times \vec{\mathcal{B}}) + (\mathbf{m} \cdot \nabla)\vec{\mathcal{B}} = (\mathbf{m} \cdot \nabla)\vec{\mathcal{B}} \ . \tag{16.7}$$

This formula can be obtained by Taylor expansion of the magnetic field (see Exc. 16.1.7.1).

16.1.2 Impact of magnetic fields on electronic orbits and diamagnetism

A magnetic field can have another effect on the motion of electrons. Let us consider an electron rotating on a circular orbit of radius R. If the motion of the electron is

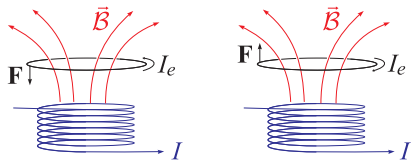

Figure 16.2: Illustration of the force exerted by an inhomogeneous magnetic field on a magnetic dipole: A dipole oriented in the same direction as the magnetic field will be drawn to the field maximum, if it is oriented anti-parallel, it is repelled from the field maximum.

fast, it will generate a current,

$$I = \frac{-e}{T} = \frac{-ev}{2\pi R} \ , \tag{16.8}$$

creating a dipole moment,

$$\mathbf{m} = I\mathbf{A} = \frac{-e}{T}\pi R^2 \hat{\mathbf{e}}_z = \frac{-e}{2} vR\hat{\mathbf{e}}_z \ . \tag{16.9}$$

Now, the orbit of the electron can be, for example, an atomic orbital or a trajectory of a free electron in a conductor. The magnetism of a free electron gas in a metal is treated by the theory of *Landau diamagnetism*. This theory considers the trajectories of electrons as being curved by the Lorentz force which, because of the rule of Lenz, generates a field contrary to the applied magnetic field. That is, the magnetic flux is expelled from the material. Hence, in inhomogeneous magnetic fields, diamagnetic materials are repelled from high field regions [2].

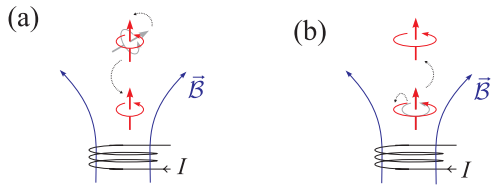

Figure 16.3: Classical interpretation of paramagnetism (a) and diamagnetism (b): In paramagnetic materials the permanent dipoles reorient in the direction of the external field. Exposed to inhomogeneous fields, the dipoles are thus attracted to field maxima. In diamagnetism, currents are forced into circular orbits, and the so-formed dipoles are oriented in a direction opposite the external external. Exposed to inhomogeneous fields, the dipoles are thus repelled from the field maxima.

The case of electronic orbitals in atoms is treated by the theory of *Langevin diamagnetism*. In this theory we consider Bohr orbitals of electrons bound to a nucleus by the Coulomb force. In the presence of an external magnetic field the dipole feels a torque, but in addition, the field has the effect of accelerating or decelerating the electron depending on its orientation. To estimate this effect we consider the equilibrium condition for an electronic orbit,

$$\mathbf{F}_C = \frac{1}{4\pi\varepsilon_0}\frac{e^2}{R^2} = m_e\frac{v^2}{R} = \mathbf{F}_{centrifugal} \ . \tag{16.10}$$

[2]Note that some metals may be weakly paramagnetic due to an effect called *Pauli paramagnetism*.

Adding a magnetic field oriented along the rotation axis [3],

$$\mathbf{F}_C + \mathbf{F}_L = \frac{1}{4\pi\varepsilon_0}\frac{e^2}{R^2} + ev'\Delta\mathcal{B} = m_e\frac{v'^2}{R} = \mathbf{F}_{centrifugal} \ . \tag{16.11}$$

Subtracting these equations,

$$ev'\Delta\mathcal{B} = \frac{m_e}{R}(v'^2 - v^2) = \frac{m_e}{R}(v' - v)(v' + v) \simeq \frac{2m_e}{R}v'\Delta v \ , \tag{16.12}$$

such that,

$$\Delta v = \frac{eR\Delta\mathcal{B}}{2m_e} \ . \tag{16.13}$$

The acceleration of the electron, when we switch on the magnetic field, increases the value of the dipole moment because, with the formula (16.9),

$$\Delta\mathbf{m} = \frac{-e}{2}\Delta v R\hat{\mathbf{e}}_z = -\frac{e^2R^2}{4m_e}\Delta\vec{\mathcal{B}} \ . \tag{16.14}$$

But the ***variation*** is *always contrary to the direction of the magnetic field*, even if the dipole moment was initially aligned to the field [see Fig. 16.3(b)] [4]. Therefore, the dipole is repelled by an inhomogeneous magnetic field. Note that changing the sign of the charge does not affect $\Delta\mathbf{m}$.

Diamagnetism is a property of all materials, but is often hidden by the presence of permanent magnetic moments. Therefore, to observe diamagnetism, one must choose materials with no permanent magnetic moment, such as atoms with completely filled electron shells. Many amorphous materials (such as wood, glass, rubber, etc.) and many metals as diamagnets.

It is worth mentioning that the magnetic behavior of a macroscopic body is not necessarily the same as the one of its elementary components. For example, metallic sodium is diamagnetic, while gaseous sodium is paramagnetic.

paramagnetism	diamagnetism
atoms with unpaired e^-	atoms with paired e^-
$\mathbf{m}$ robust and independent of $\vec{\mathcal{B}}$	$\mathbf{m}$ weak and $\mathbf{m} \propto \vec{\mathcal{B}}$
$\vec{\mathcal{M}} \parallel \vec{\mathcal{B}} \curvearrowright$ attractive force	$\vec{\mathcal{M}} \parallel -\vec{\mathcal{B}} \curvearrowright$ repulsive force
$\mu > 1 \curvearrowright \chi > 0$	$\mu < 1 \curvearrowright \chi < 0$

It is also important to note that essential aspects of *para- and atomic diamagnetism are quantum*. That is, quantitative theories must be formulated within quantum mechanics. A classical theory can only give an qualitative picture of the effect.

[3] In Exc. 16.1.7.2 we have shown, that the radius of the electronic orbit does not change under the influence of an external magnetic field.

[4] If the charge distribution is spherically symmetric, we can assume $\langle x^2\rangle = \langle y^2\rangle = \langle z^2\rangle = \frac{1}{3}\langle r^2\rangle$, where $\langle r^2\rangle$ is the average distance between the electron and the nucleus. Therefore, $\langle R^2\rangle = \langle x^2\rangle + \langle y^2\rangle = \frac{2}{3}\langle r^2\rangle$. If N is the number of atoms per unit volume, we have $\chi = \frac{\mu_0 Nm}{\mathcal{B}} = -\frac{\mu_0 NZe^2}{6m}\langle r^2\rangle$.

16.1.3 Macroscopic magnetization

In the presence of a magnetic field, matter becomes magnetized, that is, the atomic or molecular dipoles align in a particular direction. We have already discussed two possible mechanisms causing this reorientation, the para- and the diamagnetism. Regardless of the mechanism we measure the degree of alignment by the vector quantity,

$$\vec{\mathcal{M}} = \frac{N\mathbf{m}}{V} \tag{16.15}$$

called *magnetization*. It plays the same role as the polarization in electrostatics. In the following section we will calculate for a given magnetization $\vec{\mathcal{M}}$ the field that it produces.

In most materials diamagnetism and paramagnetism are very weak effects and can only be detected by sensitive measurements and strong magnetic fields. In *non-ferromagnetic* materials, the weakness of the magnetization allows us to neglect the magnetic field produced by magnetization. In contrast, in iron, nickel or cobalt the forces are between 10^4 and 10^5 greater.

16.1.4 Magnetostatic field of a magnetized material

We consider a sample of magnetic dipoles. According to the formula (15.42), the vector potential is given by,

$$\mathbf{A}(\mathbf{r}) = \frac{\mu_0}{4\pi}\sum_k \frac{\mathbf{m}\times(\mathbf{r}-\mathbf{r}')}{|\mathbf{r}-\mathbf{r}'|^3} \longrightarrow \frac{\mu_0}{4\pi}\int_{\mathcal{V}} dV' \frac{\vec{\mathcal{M}}\times(\mathbf{r}-\mathbf{r}')}{|\mathbf{r}-\mathbf{r}'|^3}\ , \tag{16.16}$$

where we introduced the dipole moment distribution $\vec{\mathcal{M}}(\mathbf{r}')$ via $\mathbf{m}_k \to \vec{\mathcal{M}}dV'$. As in the electrostatic case, we can rewrite the integral in the form,

$$\begin{aligned}\mathbf{A}(\mathbf{r}) &= \frac{\mu_0}{4\pi}\int_{\mathcal{V}} \vec{\mathcal{M}}(\mathbf{r}')\times\nabla'\frac{1}{|\mathbf{r}-\mathbf{r}'|}dV' \\ &= \frac{\mu_0}{4\pi}\left[-\int_{\mathcal{V}}\nabla'\times\frac{\vec{\mathcal{M}}(\mathbf{r}')}{|\mathbf{r}-\mathbf{r}'|}dV' + \int_{\mathcal{V}}\frac{1}{|\mathbf{r}-\mathbf{r}'|}\nabla'\times\vec{\mathcal{M}}(\mathbf{r}')dV'\right] \\ &= \frac{\mu_0}{4\pi}\oint_{\partial\mathcal{V}}\frac{\vec{\mathcal{M}}(\mathbf{r}')\times d\mathbf{S}'}{|\mathbf{r}-\mathbf{r}'|} + \frac{\mu_0}{4\pi}\int_{\mathcal{V}}\frac{1}{|\mathbf{r}-\mathbf{r}'|}\nabla'\times\vec{\mathcal{M}}(\mathbf{r}')dV'\ .\end{aligned} \tag{16.17}$$

Comparing these terms with the formula (15.27), we find that the first term looks like the potential of a surface current, while the second term looks like the potential of a volume current. Defining,

$$\boxed{\vec{\kappa}_b \equiv \vec{\mathcal{M}}\times\mathbf{n}_S} \quad \text{and} \quad \boxed{\mathbf{j}_b \equiv \nabla\times\vec{\mathcal{M}}}\ , \tag{16.18}$$

we obtain,

$$\mathbf{A}(\mathbf{r}) = \frac{\mu_0}{4\pi}\oint_{\partial\mathcal{V}}\frac{\vec{\kappa}_b}{|\mathbf{r}-\mathbf{r}'|}dS' + \frac{\mu_0}{4\pi}\int_{\mathcal{V}}\frac{\mathbf{j}_b}{|\mathbf{r}-\mathbf{r}'|}dV'\ . \tag{16.19}$$

The meaning of this result is that the potential (and therefore the field) of a magnetized object is the same as the one produced by a volume current distribution

$\mathbf{j}_b$ plus a surface current distribution $\vec{\kappa}_b$. Instead of integrating the contributions of all individual infinitesimal dipoles, as in Eq. (16.17), we can try to find these bound currents, and then calculate the fields they produce, as we did in the previous chapter.

16.1.5 The H-field

In the previous section we found that the phenomenon of magnetization of a body can be understood as being due to *localized currents* inside the material, $\mathbf{j}_b = \nabla \times \vec{\mathcal{M}}$, and on the surface of the body, $\vec{\kappa}_b = \vec{\mathcal{M}} \times \hat{n}_S$. The magnetization field is the magnetic field produced by these currents. In addition, there are obviously *free currents*, such as those generated by the motion of free electrons in a metal.

16.1.5.1 Ampère's law in magnetized materials

Ampère's law can now be generalized for arbitrary media,

$$\tfrac{1}{\mu_0} \nabla \times \vec{\mathcal{B}} = \mathbf{j} = \mathbf{j}_b + \mathbf{j}_f = \nabla \times \vec{\mathcal{M}} + \mathbf{j}_f \ , \tag{16.20}$$

where $\vec{\mathcal{B}}$ is the total magnetic field. Defining a new field $\vec{\mathcal{H}}$, sometimes called *magnetic excitation*,

$$\boxed{\vec{\mathcal{H}} \equiv \mu_0^{-1} \vec{\mathcal{B}} - \vec{\mathcal{M}}} \ , \tag{16.21}$$

we can now write,

$$\nabla \times \vec{\mathcal{H}} = \mathbf{j}_f \ . \tag{16.22}$$

The field $\vec{\mathcal{H}}$ is that part of the magnetic field, which comes only from free currents. We can also define the *magnetic susceptibility* χ_μ via [5],

$$\vec{\mathcal{M}} = \chi_\mu \vec{\mathcal{H}} \ , \tag{16.23}$$

or the *permeability* μ via,

$$\vec{\mathcal{B}} = \mu \vec{\mathcal{H}} = \mu_0 (1 + \chi_\mu) \vec{\mathcal{H}} \ . \tag{16.24}$$

Note, that the divergence of the *magnetization does not necessarily vanish*, since the susceptibility may depend on position, $\chi_\mu = \chi_\mu(\mathbf{r})$,

$$\nabla \cdot \vec{\mathcal{H}} = \mu_0^{-1} \nabla \cdot \vec{\mathcal{B}} - \nabla \cdot \vec{\mathcal{M}} = -\nabla \cdot (\chi_\mu \vec{\mathcal{H}}) \neq 0 \ . \tag{16.25}$$

Hence, $\vec{\mathcal{H}}$ generally can not be derived from a vector potential, and Biot-Savart's law is not valid for $\vec{\mathcal{H}}$. In anisotropic materials the susceptibility and the permeability must be understood as tensors.

[5] Note, that this definition is not symmetric with that of the electric susceptibility (14.20).

16.1.5.2 Boundary conditions involving magnetic materials

The integral version of Eq. (16.25), $\oint \vec{\mathcal{H}} \cdot d\mathbf{S} = -\oint \vec{\mathcal{M}} \cdot d\mathbf{S}$, allows us to determine the behavior of the magnetic excitation near interfaces,

$$H^{\perp}_{top} - H^{\perp}_{bottom} = -M^{\perp}_{top} + M^{\perp}_{bottom} \ . \tag{16.26}$$

On the other hand Ampère's law, $\nabla \times \vec{\mathcal{H}} = \mathbf{j}_f$, yields,

$$\vec{\mathcal{H}}^{\parallel}_{top} - \vec{\mathcal{H}}^{\parallel}_{bottom} = \vec{\kappa}_f \times \hat{\mathbf{n}} \ . \tag{16.27}$$

This is in contrast to the behavior of the magnetic $\vec{\mathcal{B}}$ field at interfaces described by Eqs. (15.30), (15.32), and (15.34). Do the Excs. 16.1.7.7 to 16.1.7.9.

16.1.6 Magnetic susceptibility and permeability

Materials respond to applied magnetic fields $\vec{\mathcal{H}}$ generating a magnetization $\vec{\mathcal{M}}$, such that the total magnetic field is $\vec{\mathcal{B}} = \mu_0 \vec{\mathcal{H}} + \mu_0 \vec{\mathcal{M}}$. The behavior of a material depends on the value of its susceptibility. In vacuum $\chi_\mu = 0$, for typical diamagnets $\chi_\mu \lesssim 0$, for superconductors $\chi_\mu = -1$, for paramagnets $\chi_\mu \gtrsim 0$, and for ferromagnets $\chi_\mu \gg 1$.

Typical values are listed in the following table:

material	$\chi_\mu[10^{-5}]$	type of magnetism
superconductor	-10^5	dia-
carbon	-2.1	Langevin dia-
copper	-1	Landau dia-
water	-0.9	Langevin dia-
hydrogen	-0.00022	Langevin dia-
oxygen (gas)	0.2	para-
sodium (metal)	0.7	Pauli para-
magnesium	1.2	Pauli para-
lithium	1.4	Pauli para-
cesium	5.1	Pauli para-
platinum	28	
oxygen(liquid)	390	
gadolinium	48000	ferro-
iron		ferro-

16.1.6.1 Linear media

In many materials, as long as the applied magnetic field is not too strong, the magnetization is proportional to the field, $\vec{\mathcal{M}} \propto \vec{\mathcal{B}}$, i.e. the magnetic susceptibility depends

on the material's microscopic properties and external factors, such as temperature, but not on the applied field, $\chi_\mu \neq \chi_\mu(\vec{\mathcal{B}})$. Hence, linear media can be characterized by a constant,

$$\mu_r \equiv \frac{\mu}{\mu_0} \ , \tag{16.28}$$

called *relative permeability*.

16.1.6.2 The role of temperature in paramagnetism

Experiments show, that in inhomogeneous magnetic fields, paramagnetic materials are attracted toward high field regions, but with a force that decreases with temperature. This is understood by the Zeeman effect: The dipole moment can only adopt a few possible (quantized) values corresponding to levels of well-defined positive or negative energy (called Zeeman sub-levels). At high temperature all Zeeman sub-levels are equally populated, such that the total force cancels. At low temperature the populations are distributed according to Boltzmann's law, $n_k/n_l = e^{-(E_k-E_l)/k_BT}$, that is, the lower levels (which are precisely the *high-field seekers*) dominate.

Example 76 (*Paramagnetism of hot samples*): As an example, we consider atoms with two possible orientations for the permanent magnetic moment, $\mathbf{m} \cdot \vec{\mathcal{B}} = \pm m\mathcal{B}$. The magnetization produced by $n = n_+ + n_-$ atoms is then $\vec{\mathcal{M}} = n_+\mathbf{m}_+ + n_-\mathbf{m}_-$. The two orientations are populated according to Boltzmann's law $n_+/n_- = e^{-2m\mathcal{B}/k_BT}$, such that,

$$\frac{\vec{\mathcal{M}}}{n} = \frac{e^{m\mathcal{B}/k_BT} - e^{-m\mathcal{B}/k_BT}}{e^{m\mathcal{B}/k_BT} + e^{-m\mathcal{B}/k_BT}}\mathbf{m} \simeq \frac{m\mathcal{B}}{k_BT}\mathbf{m} \ .$$

For weak fields, we obtain the *Curie law*,

$$\chi_\mu = \frac{M}{H} \simeq \frac{nm^2\mathcal{B}}{k_BTH} \simeq \frac{\mu_0 nm^2}{k_BT} \sim T^{-1} \ .$$

For strong fields, the magnetization saturates. Assuming $m \simeq \mu_B$ (see Exc. 16.1.7.4), we estimate for a metal with $n \approx 10^{22}\,\mathrm{cm}^{-3}$ at room temperature, $\chi_\mu \approx 2.6 \times 10^{-4}$ [6].

16.1.6.3 Ferromagnetism

In a linear medium the alignment of the magnetic dipoles is maintained by the application of an external field. There are, however, magnetic materials that do not depend on applied fields. This phenomenon of 'frozen' magnetization is called *ferromagnetism*. As in the case of paramagnetism, ferromagnets develop dipoles associated with the spins of unpaired electrons, but in addition, the dipoles strongly interact with

[6] In metals free electrons contribute to paramagnetism. In metals the Curie law does not apply, but χ is found to be almost constant. The reason is, that the Boltzmann distribution is inappropriate for electrons, so we need to use the Fermi-Dirac distribution. The energy distribution $\rho(\epsilon)n_{FD}(\epsilon)$ of the electrons depends on the orientation of their spin with respect to the applied magnetic field: electrons with (anti-)parallel spin see their energy increased (reduced). To maintain a uniform E_F, electrons with parallel spin will flip it to antiparallel spin, such that the entire system is slightly *high-field seeking*. This is called *Pauli paramagnetism*. This effect always competes with diamagnetism, which involves all electrons and has opposite sign.

each other and, for reasons that can only be understood within a quantum theory, like to orient themselves in parallel [7].

The correlation is so strong that within regions called *Weiss domains* almost 100% of the dipoles are aligned. On the other hand, a block of ferromagnetic material consists of many spatially separated domains, each domain having a magnetization pointing in a random direction, such that the block as a whole does not exhibit macroscopic magnetization. Inside a Weiss domain the magnetization is so strong that even a strong external magnetic field can not influence the alignment. On the other hand, at the boundaries between Weiss domains the alignment is not well defined, such that the external field can exert a torque $\tau = \mathbf{m} \times \vec{\mathcal{B}}$ shifting the boundaries in a way to favor those domains, which are already aligned. For a sufficiently strong field one domain will prevail and the ferromagnetic material saturate.

Experiments show that the alignment is not fully reversible, that is, not all Weiss domains return to their initial orientation (before the external magnetic field was applied). Consequently, the material remains permanently magnetized. This effect is called *remanescence*.

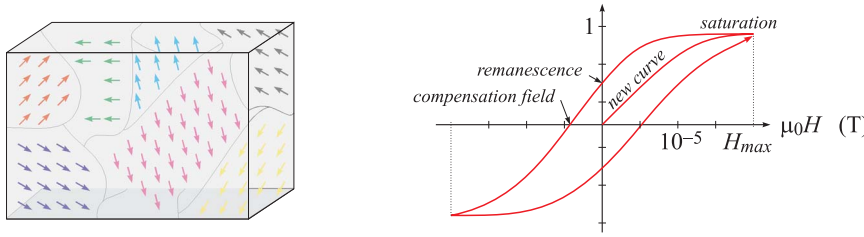

Figure 16.4: Hysteresis curve of magnetization. To allow for a comparison of the scales we plot in real units (Tesla) the applied field ($\vec{\mathcal{H}} \propto I$ in the case of a solenoid) versus the obtained field ($\vec{\mathcal{B}} \simeq \vec{\mathcal{M}}$).

To compensate for remanescence, it is necessary to apply a *compensation field* oriented in the opposite direction (see Fig. 16.4) [8] Beyond the compensation field we observe saturation in the opposite direction. Finally, returning to the initial situation, we draw a curve called *hysteresis curve*, which indicates that magnetization does not only depend on the applied magnetic field, but also on the 'history' of applied fields. Fig. 16.4 shows how an applied field can be dramatically amplified by ferromagnetism.

As already discussed, temperature tends to randomize the alignment of atomic dipoles. At low temperature the heat will not be sufficient to misalign the dipoles within the Weiss domains. But interestingly, beyond a well-defined temperature (the *Curie temperature* of iron is 770 C), the iron undergoes an abrupt phase transition to a paramagnetic state.

[7] The survival of domains in thermal reservoirs can not be understood by classical interactions between dipoles, but we need to contemplate band structure models. In particular, the $3d$ orbital bands provide electrons to the ferromagnetic elements Fe, Co, Ni. These bands are so close that the exchange interaction influences the orientation of spins in neighboring bands, which induces correlations between the spins of neighboring atoms.

[8] In practice, to demagnetize an iron block, we apply an alternating voltage gradually reducing its amplitude.

Note, that there are also antiferromagnetic materials (MnO_2), where neighboring atoms have antiparallel spins.

Example 77 (*Microscopic theory of induced dipoles*): The permittivity and relative permeability of a dense gas can be connected to the microscopic quantities through the *Clausius-Mossotti formula*,

$$\varepsilon_r = \frac{1+\frac{2}{3}\frac{N}{V}\alpha_{pol,e}}{1-\frac{1}{3}\frac{N}{V}\alpha_{pol,e}} \quad , \quad \mu_r = \frac{1+\frac{2}{3}\frac{N}{V}\alpha_{pol,m}}{1-\frac{1}{3}\frac{N}{V}\alpha_{pol,m}} \ , \tag{16.29}$$

that is, to the susceptibilities,

$$\chi_\varepsilon = \varepsilon_r - 1 = \frac{\frac{N}{V}\alpha_{pol,e}}{1-\frac{1}{3}\frac{N}{V}\alpha_{pol,e}} \quad , \quad \chi_\mu = \mu_r - 1 = \frac{\frac{N}{V}\alpha_{pol,m}}{1-\frac{1}{3}\frac{N}{V}\alpha_{pol,m}} \ , \tag{16.30}$$

where the induced electric and magnetic polarizabilities are,

$$\alpha_{pol,e} = \frac{2d_{fi}}{|\vec{\mathcal{E}}_p|}\rho_{if} \quad , \quad \alpha_{pol,m} = \frac{2m_{fi}}{|\vec{\mathcal{B}}_p|}\rho_{if} \ . \tag{16.31}$$

d_{fi} and m_{fi} are the dipole moments for electric and magnetic transitions and ρ_{if} the coherences excited in these transitions, which can be calculated from the Bloch equations. The relative strength between magnetic and electrical transitions is,

$$\frac{2\mu_B}{cea_B} = \alpha \ . \tag{16.32}$$

16.1.7 Exercises

16.1.7.1 Ex: Dipole in an inhomogeneous field

Derive the formula for the force on a dipole in an inhomogeneous field.

Solution: *An inhomogeneous magnetic field can be approximated by,*

$$\vec{\mathcal{B}}(\mathbf{r}) = \vec{\mathcal{B}}(\mathbf{r}') + [(\mathbf{r}-\mathbf{r}')\cdot\nabla']\vec{\mathcal{B}}(\mathbf{r}') \ .$$

We need to show,

$$\mathbf{F} = I\oint d\mathbf{l}\times[(\mathbf{r}\cdot\nabla')\vec{\mathcal{B}}(\mathbf{r}')] = ... = (\mathbf{m}\cdot\nabla)\vec{\mathcal{B}} \ .$$

We know,

$$\oint(\mathbf{c}\cdot\mathbf{r})d\mathbf{l} = \mathbf{S}\times\mathbf{c} \ ,$$

where

$$\mathbf{S} = \int_{\mathcal{S}} d\mathbf{S} = \frac{1}{2}\oint \mathbf{r}\times d\mathbf{l} \ .$$

Thereby,

$$(\mathbf{S}\times\mathbf{c})_k = \epsilon_{kgj}S_g c_j = \oint c_m r_m dl_k \ .$$

Now using

$$\epsilon_{ikn}\epsilon_{kgj} = \epsilon_{ikn}\epsilon_{jkg} = \delta_{ij}\delta_{ng} - \delta_{ig}\delta_{nj} \ ,$$

we calculate,

$$F_i = I\epsilon_{ikn}(\oint r_m dl_k)[\nabla'_m \mathcal{B}_n(\mathbf{r}')] = I\epsilon_{ikn}\epsilon_{kgj}S_g[\nabla'_j \mathcal{B}_n(\mathbf{r}')] = (\delta_{ij}\delta_{ng} - \delta_{ig}\delta_{nj})m_g[\nabla'_j \mathcal{B}_n(\mathbf{r}')]$$
$$= m_n[\nabla'_i \mathcal{B}_n(\mathbf{r}')] - m_i[\nabla'_n \mathcal{B}_n(\mathbf{r}')] = m_n[\nabla'_i \mathcal{B}_n(\mathbf{r}')] - m_i(\nabla' \cdot \vec{\mathcal{B}}) = m_n[\nabla'_i \mathcal{B}_n(\mathbf{r}')] \ .$$

16.1.7.2 Ex: Langevin diamagnetism

An electron circulates around its atomic nucleus on an orbit of radius R.
a. Calculate the magnetic dipole moment generated by this movement as a function of velocity.
b. Now a weak magnetic field $\vec{\mathcal{B}}$ is slowly turned on perpendicular to the orbital plane. Calculate the increase of the electron's velocity due to the electric field induced by turning on the magnetic field using Faraday's law.
c. Show that the increase in kinetic energy, ΔE_{kin}, corresponds to the interaction energy between the electronic dipole moment and the magnetic field.
d. Does the turning on of the magnetic field change the radius of the electronic orbit? Justify your answer!

Solution: *a. The current corresponding to the motion being $I = -e/T$, we obtain,*

$$\mathbf{m} = I\mathbf{S} = -\frac{ev}{2\pi R}\pi R^2 \hat{\mathbf{n}} = -\frac{e}{2}\mathbf{R} \times \mathbf{v} \ .$$

b. We assume that the magnetic field ranges from 0 to $\mathcal{B}$ within a period of time t. This variation produces a rotation of an electric field given by $\nabla \times \vec{\mathcal{E}} = \partial_t \vec{\mathcal{B}}$. With Stokes law,

$$\oint_{\partial \mathcal{S}} \vec{\mathcal{E}} \cdot d\mathbf{l} = \int_{\mathcal{S}} \nabla \times \vec{\mathcal{E}} \cdot d\mathbf{S} = -\frac{\partial}{\partial t}\int_{\mathcal{S}} \vec{\mathcal{B}} \cdot d\mathbf{S} \ ,$$

or $\mathcal{E} 2\pi R = \pi R^2 \dot{\mathcal{B}}$. Thus, the variation of the electron velocity is,

$$\Delta v = \int_0^t \frac{F}{m_e} dt = \int_0^t \frac{-e\mathcal{E}}{m_e} dt = \int_0^t \frac{-eR\dot{\mathcal{B}}}{2m_e} dt = \frac{-eR}{2m_e}\int_0^{\mathcal{B}} d\mathcal{B} = \frac{-eR}{2m_e}\mathcal{B} \ .$$

(This is the same formula derived from Langevin's discussion of diamagnetism under the premise that the radius of the orbit is constant.)
c. The increase in kinetic energy is,

$$\Delta E_{kin} = \frac{m_e}{2}(v+\Delta v)^2 - \frac{m_e}{2}v^2 \simeq m_e v \Delta v = m_e\left(-\frac{2|\mathbf{m}|}{eR}\right)\frac{-eR}{2m_e}\mathcal{B} = -\mathbf{m}\cdot\vec{\mathcal{B}} = \Delta E_{zee} \ .$$

d. The fact that all energy added goes to kinetic energy and nothing is left for the Coulomb energy shows, that the assumption of a fixed radius used in the discussion of Langevin's diamagnetism is justified.

16.1.7.3 Ex: Magnetic susceptibility

By molecular magnetism it is possible to lift any objects in a sufficiently strong magnetic field. Estimate the magnetic field $|\vec{\mathcal{B}}|$ and the field gradient $\nabla|\vec{\mathcal{B}}|^2$ (one may estimate $\nabla|\vec{\mathcal{B}}|^2 = 2|\vec{\mathcal{B}}|\nabla|\vec{\mathcal{B}}| \simeq |\vec{\mathcal{B}}|^2/l$ with $l \simeq 10\,\mathrm{cm}$ as the typical length for such strong magnetic fields), needed to lift a frog. Water is predominantly diamagnetic with $\chi_\mu \simeq -0.9 \cdot 10^{-5}$ is the magnetic susceptibility of water.

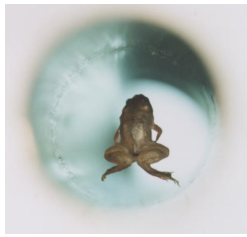

Figure 16.5: Magnetic susceptibility.

Solution: *The condition for frog levitation is,*

$$\mathbf{F}_{lev} = (\sum\nolimits_k \mathbf{m}_k \cdot \nabla)\vec{\mathcal{B}} > m_{frog} g = \mathbf{F}_{peso} \ ,$$

taking the sum over all diamagnetic moments of the frog,

$$\sum_k \mathbf{m}_k = \vec{\mathcal{M}} V = \chi_\mu \vec{\mathcal{H}} V = \frac{\chi_\mu}{\mu} \vec{\mathcal{B}} V \ .$$

For the vertical axis we get,

$$F_{lev} = \frac{\chi_\mu}{\mu} \mathcal{B} V \frac{d\mathcal{B}}{dz} > m_{frog} g = \rho_{water} V g \ ,$$

giving the necessary condition for diamagnetic levitation,

$$\mathcal{B}\frac{d\mathcal{B}}{dz} = \mu_0 \rho \frac{g}{\chi_m u} \ ,$$

Water levitates at $\mathcal{B}\frac{d\mathcal{B}}{dz} \approx 1370\,\mathrm{T}^2/\mathrm{m}$. *To levitate a frog, however, we need very strong magnetic fields of the order of* $\mathcal{B} = \sqrt{l\mu_0\rho\frac{g}{\chi_m u}} \approx 12\,\mathrm{T}$.

16.1.7.4 Ex: Larmor precession of a Bohr atom in a magnetic field

As a model of the Larmor precession, consider the Bohr's atom model: An electron flying on circular orbits around a proton. Only certain discrete orbits with the radii $r_n = n^2 a_B$, where $a_B = 4\pi\varepsilon_0 \frac{\hbar^2}{m_e e^2}$, are allowed. The movement of the electron on these orbits is not accompanied by radiative emission.
a. Calculate the velocity of the electron in its ground state $n = 1$ and compare the

result with the speed of light in vacuum c.
b. What is the orbital momentum $\mathbf{L}$ of the electron in a hydrogen atom in this state?
c. Relate the magnetic moment $\mathbf{m}_L$ due to the circular current generated by the electron to the orbital momentum $\mathbf{L}$.
d. Placed in a magnetic field of $\mathcal{B} = 1\,\mathrm{T}$ the atom suffers a torque, which creates a precession of the angular momentum vector $\mathbf{L}$ around the direction of the $\vec{\mathcal{B}}$-field. Determine the frequency of this Larmor precession from $\omega_L = \dot{L}/(L\sin\theta)$, where θ is the angle between $\mathbf{m}_L$ and $\vec{\mathcal{B}}$. ($\hbar = 1.034 \cdot 10^{-34}\,\mathrm{Js}$, $e = 1.602 \cdot 10^{-19}\,\mathrm{C}$, $\varepsilon_0 = 8.854 \cdot 10^{-8}\,\mathrm{As/Vm}$.

Solution: *a. In the ground state the equilibrium of the electron orbit is given by,*

$$F_C = \frac{1}{4\pi\varepsilon_0}\frac{e^2}{a_B^2} = m_e\frac{v^2}{a_B} = F_{centrifug}\ .$$

Therefore, the velocity is,

$$v = \sqrt{\frac{1}{4\pi\varepsilon_0}\frac{e^2}{m_e a_B}} = \frac{e^2}{4\pi\varepsilon_0\hbar} = 2.2\cdot 10^6\,\mathrm{m/s} = \alpha c\ .$$

b. The orbital momentum is,

$$\mathbf{L} = \mathbf{r}\times\mathbf{p} = m_e a_B v\hat{\mathbf{L}} = m_e 4\pi\varepsilon_0\frac{\hbar^2}{m_e e^2}\frac{e^2}{4\pi\varepsilon_0\hbar}\hat{\mathbf{L}} = \hbar\hat{\mathbf{L}}\ .$$

c. The rotation of the electron on its orbit produces a current, $I = -ev/2\pi R$, which produces a magnetic moment,

$$\mathbf{m}_L = I\mathbf{A} = \frac{-eva_B\hat{\mathbf{L}}}{2} = \frac{-e}{2m_e}\mathbf{L}\ .$$

d. We have, $dL = L\sin\theta\cdot\omega_L dt$. Thus, the frequency of Larmor is,

$$\omega_L = \frac{\dot{L}}{L\sin\theta} = \frac{\tau}{L\sin\theta} = \frac{m_L\mathcal{B}\sin\theta}{L\sin\theta} = \frac{m_L\mathcal{B}}{L} = \frac{-e}{2m_e}\mathcal{B}\ .$$

Note, that,

$$\mu_B = \frac{e\hbar}{2m_e}$$

It's called Bohr's magneton.

16.1.7.5 Ex: H-field of a cylindrical current wire

A cylindrical wire with radius a and permeability μ is traversed by a constant current density $\mathbf{j}$.
a. Calculate the absolute values and the directions of the $\vec{\mathcal{H}}$ and $\vec{\mathcal{B}}$-fields in- and outside the wire using Stokes law.
b. The electric field $\vec{\mathcal{E}}$ within the wire and the current $\mathbf{j}$ are connected by Ohm's law

$\mathbf{j} = \sigma\vec{\mathcal{E}}$, where σ is the electrical conductivity. What is the value and direction of the Poynting vector $\mathbf{s}$ on the wire surface?
c. Calculate the total energy flow across the surface of a piece of wire of length L. Show that the energy flow corresponds exactly to the power converted, in this piece of wire, to ohmic heat.
Help: The energy conservation law of electrodynamics is given by: $-\frac{\partial u}{\partial t} = \nabla\cdot\mathbf{s}+\mathbf{j}\cdot\vec{\mathcal{E}}$, where $u = \frac{1}{2}(\vec{\mathcal{E}}\cdot\vec{\mathcal{D}} + \vec{\mathcal{B}}\cdot\vec{\mathcal{H}})$ is the total energy density, $\mathbf{s} = \vec{\mathcal{E}}\times\vec{\mathcal{H}}$ the flow of energy, and $\mathbf{j}\cdot\vec{\mathcal{E}}$ the work done by the field on the electric current density.

Solution: *a. Assuming an isotropic wire medium we know $\vec{\mathcal{B}} = \mu\vec{\mathcal{H}}$ inside the wire and $\vec{\mathcal{B}} = \mu_0\vec{\mathcal{H}}$ outside, which means that both fields are parallel everywhere and that there is a magnetization inside the wire $\vec{\mathcal{M}} = (\mu_0^{-1} - \mu^{-1})\vec{\mathcal{B}}$. The wire of length L carries a current I generated by a voltage U. Hence, the electric field inside the wire is,*

$$\vec{\mathcal{E}} = \frac{U}{L}\hat{\mathbf{e}}_z \ .$$

Imagining an Ampèrian loop inside and outside the wire we find, using the Ampère-Maxwell equation,

$$\oint \mathcal{H}\cdot d\mathbf{r} = 2\pi r\mathcal{B}(r) = \int \nabla\times\vec{\mathcal{H}}\cdot d\mathbf{S} = \int \mathbf{j}\cdot d\mathbf{S} = \begin{cases} I\frac{r^3}{R^3} & for \ \ r < R \\ I & for \ \ r > R \end{cases} .$$

Hence,

$$\vec{\mathcal{H}}(\mathbf{r}) = \begin{cases} \frac{I}{2\pi}\frac{r^2}{R^3}\hat{\mathbf{e}}_\phi & for \ \ r < R \\ \frac{I}{2\pi}\frac{1}{r}\hat{\mathbf{e}}_\phi & for \ \ r > R \end{cases} ,$$

and we see that the parallel component of the $\vec{\mathcal{H}}$-field is continuous at the wire surface, but this cannot be the case for $\vec{\mathcal{B}}$, which will have a discontinuity corresponding to the magnetization.
b. The Poynting vector

$$\mathbf{s} = \vec{\mathcal{E}}\times\vec{\mathcal{H}} = \frac{U}{L}\hat{\mathbf{e}}_z \times \frac{\mu}{2\pi}I\frac{r^2}{R^3}\hat{\mathbf{e}}_\phi = \begin{cases} -\frac{U}{L}\frac{\mu I}{2\pi}\frac{r^2}{R^3}\hat{\mathbf{e}}_\rho & for \ \ r < R \\ -\frac{U}{L}\frac{\mu I}{2\pi}\frac{1}{r}\hat{\mathbf{e}}_\rho & for \ \ r > R \end{cases}$$

is perpendicular to the wire surface.
c. The total energy flow across the surface is,

$$\int \mathbf{s}\cdot d\mathbf{S} = s(2\pi aL) = UI = R_{heat} \ .$$

16.1.7.6 Ex: Ferromagnetism

a. Make a scheme of the dependence of the magnetization $\mathcal{M}$ of a ferromagnetic material on the magnetic 'excitation' $\mathcal{H}$ with the initial condition $\mathcal{M} = \mathcal{H} = 0$ and

letting $\mathcal{H}(t)$ cycle through $0 \to \mathcal{H}_{max} \to -\mathcal{H}_{max} \to \mathcal{H}_{max}$. Indicate the remaining magnetization in the scheme.
b. How does the magnetization of a ferromagnet change when we heat it up above the Curie temperature T_C? How does the magnetic susceptibility behave in this case χ_m?
c. It explains the order of the atomic magnetic moments in ferro-, antiferro- and ferrimagnets and its influence on their magnetization.

Solution: *a. The 'virgin curve' shows the magnetization of an initially non-magnetized ferromagnet, when it is exposed to an external magnetic excitation field rising from 0 to $\mathcal{H}_{max}$.*
b. When heat above T_C, the ferromagnetic order is lost, and the ferromagnet becomes a paramagnet. The magnetic susceptibility behaves at temperatures $T > T_C$ as $\chi_m \propto 1/(T - T_C)$.
c. Within ordered areas (Weiss domains) for ferromagnets all magnetic dipolar moments are equal and oriented in parallel. For antiferromagnets the magnetic dipole moments are also equal, but oriented antiparallel. For ferrimagnets the magnetic dipolar moments of neighboring atoms are different and antiparallel. The resulting magnetization is large for ferromagnets, lower for ferrimagnet and zero for antiferromagnet (see Fig. 16.4).

16.1.7.7 Ex: Rectangular toroidal coil

A circular coil is made of a core with rectangular cross-sectional area, $A = h(r_2 - r_1)$, on which two coils are densely wound on top of each other, one with the number of turns N_1 and the other with N_2. Establishes a relationship for the mutual inductance L of the two coils.
Help: To calculate the mutual inductance, invoke the flux equation for the case that the coil N_1 is traversed by the current I_1, that is, $\oint \mathcal{H} \cdot d\mathbf{s} = N_1 I_1$ and calculate the induced flux Φ.

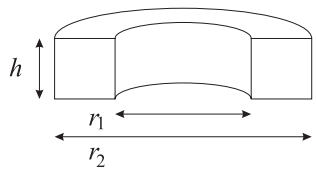

Figure 16.6: Rectangular toroidal coil.

Solution: *The first coil produces a magnetic flux,*

$$\Phi = \frac{L_1}{N_1} I_1 \ .$$

This flux produces in the second coil the current,

$$I_2 = \frac{N_2}{L_2}\Phi = \frac{N_2}{N_1}\frac{L_1}{L_2} I_1 \ .$$

16.1.7.8 Ex: Toroidal coil

Consider a toroidal coil with the average radius R, which consists of N turns carrying the current I. The coil is filled with an iron core of permeability μ.
a. Calculate the amplitude of the fields $\mathcal{H}$ and $\mathcal{B}$ inside the coil.
b. Now consider a core with an air gap d with $d \ll R$ interrupting the torus. Calculate once again the fields $\mathcal{H}$ and $\mathcal{B}$ within the slot.

Solution: *a. Let the coil be in the xy-plane. With the Ampère's law,*

$$\oint \vec{\mathcal{H}} \cdot d\mathbf{l} = 2\pi R\mathcal{H} = \int \mathbf{j} \cdot d\mathbf{S} = NI \ .$$

With this follows,

$$\mathcal{H} = \frac{NI}{2\pi R} \qquad \textit{and} \qquad \mathcal{B} = \mu\mu_0\mathcal{H} = \mu\mu_0\frac{NI}{2\pi R} \ .$$

b. At the transition between iron and air the normal component of $\vec{\mathcal{B}}$ and the parallel component of $\vec{\mathcal{H}}$ are continuous. Therefore, since in our geometry ($d \ll R$) the fields $\vec{\mathcal{B}}$ and $\vec{\mathcal{H}}$ are approximately uniform, we only have normal components, such that: $\mathcal{B}_{Fe} = \mathcal{B}_{ar}$ and $\mu\mathcal{H}_{Fe} = \mathcal{H}_{ar}$. Now, we have,

$$\oint \vec{\mathcal{H}} \cdot d\mathbf{l} = (2\pi R - d)\mathcal{H}_{Fe} + d\mathcal{H}_{ar} = (2\pi R - d)\frac{\mathcal{H}_{ar}}{\mu} + d\mathcal{H}_{ar} = \int \mathbf{j} \cdot d\mathbf{S} = NI \ .$$

Hence,

$$\mathcal{H}_{ar} = \frac{NI\mu}{2\pi R - d + \mu d} \ ,$$

and

$$\mathcal{B}_{ar} = \mu_0\mathcal{H}_{ar} = \frac{NI\mu\mu_0}{2\pi R + (\mu - 1)d} \ .$$

For a very narrow gap with $\mu \simeq 2000$ we get a big amplification of the field:

$$\mathcal{B}_{ar} \simeq \frac{NI\mu\mu_0}{2\pi R} \ .$$

16.1.7.9 Ex: Toroidal coil

A slotted steel ring has the dimensions: $b = 20\,\text{mm}$, $r = 80\,\text{mm}$, $a = 15\,\text{mm}$, and $d = 1\,\text{mm}$ (see the figure).
a. Calculate, first without air gap, for a magnetic flux density $\mathcal{B}$ the total magnetic flux Ψ_M and the corresponding $\mathcal{H}$ field. What is the amount of current I required generate this flux in a coil of N turns?

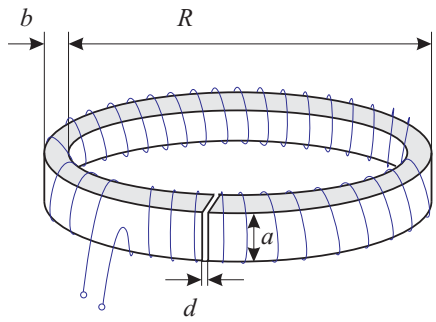

Figure 16.7: Toroidal coil.

b. How must $\mathcal{H}$ and I be modified, if the ring is interrupted by a 1 mm wide air gap, to reach the same flux? Use $\mathcal{B} = 1.2\,\mathrm{T}$, $N = 300$, $\mu_r = 650$.

Solution: *a. The magnetic field of a long coil is* $\mathcal{H} = \mathcal{B}/\mu_0\mu_r$ *and is related to the current by* $\mathcal{H} = NI/l$. *It follows for the current,*

$$I = \frac{l\mathcal{B}}{\mu_0\mu_r N} = \frac{2\pi r\mathcal{B}}{\mu_0\mu_r N} \simeq 1.5385\,\mathrm{A} \ .$$

The flux is,

$$\Phi = \int \vec{\mathcal{B}} \cdot d\mathbf{S} = \mathcal{B}S \simeq 3.6 \cdot 10^{-4}\,\mathrm{Vs} \ .$$

b. The magnetic fields in the core and the slot are,

$$\mathcal{H}_{fe} = \frac{\mathcal{B}}{\mu_0\mu_r} \simeq 1470 \qquad \textit{and} \qquad \mathcal{H}_{ar} = \frac{\mathcal{B}}{\mu_0} \simeq 955\ 000\,\mathrm{A/m} \ .$$

The current is,

$$I = \frac{1}{N}\int \vec{\mathcal{H}} \cdot d\mathbf{l} = \frac{\mathcal{H}_{fe}}{N}(2\pi r - \Delta s) + \frac{\mathcal{H}_{ar}}{N}\Delta s \simeq 4.72\,\mathrm{A} \ .$$

16.2 Induction of currents and inductance

We have already seen that the fundamental cause of current $\mathbf{j}$ is a motion of charges Q [see Eq. (14.38)]. To incite charges to move we need a force,

$$\boxed{\mathbf{j} = \varsigma\frac{\mathbf{F}}{Q}} \ , \tag{16.33}$$

where ς is a proportionality factor called *conductivity* and $\mathbf{F}$ is the Coulomb-Lorentz force, such that,

$$\boxed{\mathbf{j} = \varsigma(\vec{\mathcal{E}} + \mathbf{v} \times \vec{\mathcal{B}})} \ . \tag{16.34}$$

The first part, $\mathbf{j} = \varsigma\vec{\mathcal{E}}$, is Ohm's law already discussed in Sec. 14.3. Now, in addition to taking into account the Coulomb force acting on electrons traveling in conductors, let us also consider the Lorentz force.

16.2.1 The electromotive force

When we consider a closed electric circuit with a current source and a consumer, knowing the slow average velocity of the electrons carrying the current (see Exc. 14.3.3.3), it is not immediately obvious why the current starts to flow simultaneously in all parts of the circuit. The explanation is that if this were not the case, charges would accumulate in parts of the circuit creating local imbalances. The consequence of this would be the creation of electric fields working to eliminate the imbalances. These fields $\vec{\mathcal{E}}$ are superposed to the electromotive force $\mathbf{f}_0$ exerted by the current source. If the source has an internal resistance, as schematized in Fig. 16.8(a), part of the electromotive force $\mathbf{f}_i$ is spent on it,

$$\mathbf{f}_i = \mathbf{f}_0 + \vec{\mathcal{E}} \ . \tag{16.35}$$

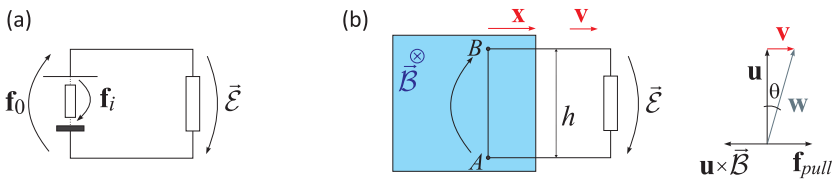

Figure 16.8: (a) Illustration of the electromotive force $\mathbf{f}_0$ exerted by an arbitrary voltage source, the force $\mathbf{f}_i$ spent on the internal resistance of the source, and the electrostatic force $\vec{\mathcal{E}}$ on the circuit. (b) Electromotive force $\mathbf{f}_0$ generated by the motion of a part of the circuit inside a magnetic field.

In the case of an ideal source, $\mathbf{f}_i = 0$, the path integral along the circuit,

$$\mathcal{E} \equiv \int_+^- \mathbf{f}_0 \cdot d\mathbf{l} = -\int_+^- \vec{\mathcal{E}} \cdot d\mathbf{l} = U \ , \tag{16.36}$$

yields exactly the voltage.

The electromotive force can be caused by batteries, photocells, generators, etc. In the case of a generator, the electromotive force is the Lorentz force acting on the free charges of a conductor moved within an applied magnetic field. Let us consider the setup schematized in Fig. 16.8(b). When the part of the conductor between the points A and B (length h) is moved to the right with velocity $\mathbf{v}$ within the magnetic field $\vec{\mathcal{B}}$, positive charges are accelerated upwards, as in the case of the Hall effect. We obtain an electromotive force,

$$\mathcal{E} \equiv \oint \mathbf{f}_L \cdot d\mathbf{l} = hv\mathcal{B} \ , \tag{16.37}$$

which acts as a source of voltage. Of course, it is not the magnetic field which does the work through the Lorentz force, but the person pushing the conductor: Calling

u the velocity along the conductor acquired by the accelerated charges, this velocity creates inside the magnetic field an electromotive force $\mathbf{u} \times \vec{\mathcal{B}}$ against the motion of the conductor exerting per unit of charge the work,

$$\int \mathbf{f}_{pull} \cdot d\mathbf{l}_w = -\int (\mathbf{u} \times \vec{\mathcal{B}}) \cdot d\mathbf{l}_w = \int u\mathcal{B}\hat{\mathbf{e}}_x \cdot d\mathbf{l}_w \tag{16.38}$$
$$= \int_0^h \frac{v}{\tan\theta} \mathcal{B}\cos(90^\circ - \theta)\frac{dh}{\cos\theta} = hv\mathcal{B} = \mathcal{E} \ .$$

We find that the work exerted per unit of charge exactly compensates the electromotive force.

Applying the definition of the magnetic flux (15.12), to the situation illustrated in Fig. 16.8(b),

$$\Psi_M = \int \vec{\mathcal{B}} \cdot d\mathbf{S} = \mathcal{B}hx \ , \tag{16.39}$$

we can reshape the Eq. (16.37),

$$h\mathcal{B}v = -h\mathcal{B}\dot{x} = \boxed{-\frac{d\Psi_M}{dt} = \mathcal{E}} \ . \tag{16.40}$$

Hence, the temporal variation of the magnetic flux induces a *counteracting* electromotive force. This is known as *Lenz's rule*.

16.2.2 The Faraday-Lenz law

In a series of experiments *Michael Faraday* demonstrated that the relationship (16.40) can be generalized to any geometry of the circuit immersed in a magnetic field, to any velocity of the motion, and even to time-varying geometries. The applications of this effect are innumerable, see Exc. 16.2.3.1 to 16.2.3.23. Relating the electromotive force on one side to the generation of a voltage (16.36), $\mathcal{E} = \oint \vec{\mathcal{E}} \cdot d\mathbf{l}$, and on the other side to the variation of the flux (16.40), $\mathcal{E} = -\frac{d\Psi_M}{dt}$, we can write,

$$\boxed{\oint \vec{\mathcal{E}} \cdot d\mathbf{l} = -\frac{\partial}{\partial t}\int \vec{\mathcal{B}} \cdot d\mathbf{S}} \ . \tag{16.41}$$

In the differential version we get,

$$\boxed{\nabla \times \vec{\mathcal{E}} = -\frac{\partial \vec{\mathcal{B}}}{\partial t}} \ . \tag{16.42}$$

Note that, without temporal variations of the magnetic field, we recover electrostatics, $\nabla \times \vec{\mathcal{E}} = 0$.

16.2.2.1 Mutual inductance

Here, we consider two loops of arbitrary shapes. The first loop carries the current I_1 and produces a magnetic field, which we can calculate, for example, by Biot-Savart's law,

$$\vec{\mathcal{B}}_1 = \frac{\mu_0 I_1}{4\pi} \oint \frac{d\mathbf{l}_1 \times (\mathbf{r} - \mathbf{r}')}{|\mathbf{r} - \mathbf{r}'|^3} \ . \tag{16.43}$$

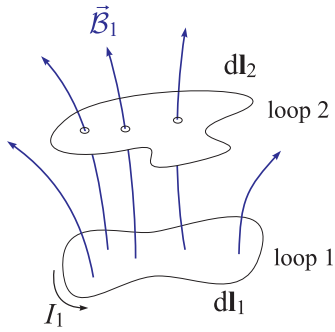

Figure 16.9: Indução.

The part of the magnetic flux passing through the second loop is,

$$\Psi_{M2} = \int \vec{\mathcal{B}}_1 \cdot d\mathbf{S}_2 \equiv M_{21} I_1 \ , \tag{16.44}$$

where M_{21} is a constant that depends only on the geometry of the two loops. It is called *mutual inductance* and can be expressed as,

$$\begin{aligned} M_{21} &= \frac{1}{I_1} \int \nabla \times \mathbf{A}_1 \cdot d\mathbf{S}_2 = \frac{1}{I_1} \oint \mathbf{A}_1 \cdot d\mathbf{l}_2 \\ &= \frac{1}{I_1} \oint \left(\frac{\mu_0 I_1}{4\pi} \oint \frac{d\mathbf{l}_1}{|\mathbf{r} - \mathbf{r}'|} \right) \cdot d\mathbf{l}_2 = \frac{\mu_0}{4\pi} \oint \oint \frac{d\mathbf{l}_1 \cdot d\mathbf{l}_2}{|\mathbf{r} - \mathbf{r}'|} \ . \end{aligned} \tag{16.45}$$

The symmetry of this formula suggests,

$$M_{21} = M_{12} = M \ . \tag{16.46}$$

We can drop the indices and call both constants M. The conclusion of this is that, regardless of the shapes and positions of the loops, the flux through loop 2 when we throw a current I into the loop 1 is identical to the flux through 1 when we throw the same current I into 2,

$$I_1 = I_2 = I \Longrightarrow \int \vec{\mathcal{B}}_1 \cdot d\mathbf{S}_2 = \int \vec{\mathcal{B}}_2 \cdot d\mathbf{S}_1 \ . \tag{16.47}$$

Example 78 (*Dynamo*): We consider a rotating coil set in motion by a crank inside a magnetic field, as shown in the figure. The voltage wasted by the resistor is,

$$U = \oint \vec{\mathcal{E}} \cdot d\mathbf{l} = -\frac{d}{dt} \Psi_M = -\frac{d}{dt} \int \vec{\mathcal{B}} \cdot d\mathbf{A} = -\frac{d}{dt} \mathcal{B} A \cos \omega t = \omega \mathcal{B} A \sin \omega t \ .$$

16.2.2.2 Self-inductance

The magnetic flux produced by the current in loop 1 not only traverses the second loop, but also the first loop itself. Therefore, any variation of the flux will also induce an electromotive force in this loop 1,

$$\Psi_{M1} = M_{11} I_1 \equiv L I_1 \ , \tag{16.48}$$

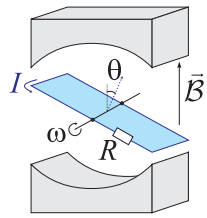

Figure 16.10: Schematic of a generator of alternating voltage (or dynamo).

where the constant L is called *self-inductance*. With the law of Lenz-Faraday,

$$\mathcal{E} = -\frac{d\Psi_M}{dt} = -L\dot{I} \ . \tag{16.49}$$

Example 79 (*Self-inductance of a solenoid*): Consider the solenoid shown in Fig. 16.11. With the formula of the example 72 we calculate the magnetic flux,

$$\Psi_M = \int \vec{\mathcal{B}} \cdot d\mathbf{A} = \mu I \frac{N}{l} \ N\pi R^2 \ .$$

Comparing with the formula (16.48), we find self-inductance,

$$L = \mu \frac{N^2}{l} \ \pi R^2$$

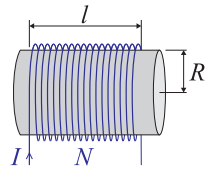

Figure 16.11: Scheme of a solenoid characterized by a self-inductance L.

16.2.3 Exercises

16.2.3.1 Ex: Application of the Faraday-Lenz law

The current in a coil characterized by the inductance $L = 1\,\text{mH}$ is linearly reduced in one second from 1 A to 0. Calculate the induced voltage.

Solution: *The induced voltage is,*

$$U_L = -L\dot{I} = 1\,\text{mV} \ .$$

16.2.3.2 Ex: Breathing charge distribution

A radially symmetric charge distribution varies over time as $\lambda(t)$ in a 'breathing oscillation',

$$\varrho(\mathbf{r},t) = \varrho_0\lambda(t)\frac{1}{r^2}e^{-a\lambda(t)r} \ ,$$

where $\varrho_0 = const.$ and $a = const.$
a. What is the value of the total charge?
b. Calculate the current density $\mathbf{j}(\mathbf{r},t)$, which corresponds to $\varrho(\mathbf{r},t)$ from the continuity equation.
c. Determine $\vec{\mathcal{E}}(\mathbf{r},t)$ from the ansatz $\vec{\mathcal{E}}(\mathbf{r},t) = \mathcal{E}(r,t)\frac{\mathbf{r}}{r}$ (radial symmetry).
d. Calculate the corresponding magnetic field $\vec{\mathcal{B}}$.
e. Show that the solutions for $\vec{\mathcal{E}}$ and $\vec{\mathcal{B}}$ satisfy Maxwell's equations.

Solution: *a. The total charge is,*

$$Q = \int_{\mathbf{V}} \varrho(\mathbf{r},t)dV = 4\pi\varrho_0\lambda(t)\int_0^\infty \frac{1}{r^2}e^{-a\lambda(t)r}r^2dr = 4\pi\varrho_0\lambda(t)\left[\frac{e^{-a\lambda(t)r}}{-a\lambda(t)}\right]_0^\infty = \frac{4\pi\varrho_0}{a} \ .$$

b. From the continuity equation we calculate,

$$\begin{aligned} 4\pi r^2 j_r &= \oint_{\partial\mathcal{V}} \mathbf{j}\cdot d\mathbf{S} = -\partial_t\int_{\mathcal{V}}\varrho dV = -4\pi\varrho_0\partial_t\lambda(t)\int_0^r e^{-a\lambda(t)r'}dr' \\ &= \frac{4\pi\varrho_0}{a}\partial_t[e^{-a\lambda(t)r}-1] = -4\pi\varrho_0 r\dot{\lambda}(t)e^{-a\lambda(t)r} \ , \end{aligned}$$

giving,

$$j_r = -\frac{\varrho_0\dot{\lambda}(t)}{r}e^{-a\lambda(t)r} \ .$$

c. From the Gauß law,

$$4\pi r^2\mathcal{E}_r = \oint_{\partial\mathcal{V}}\vec{\mathcal{E}}\cdot d\mathbf{S} = \int_{\mathcal{V}}\frac{\varrho}{\varepsilon_0}dV = \frac{1}{\varepsilon_0}4\pi\varrho_0\lambda(t)\left[\frac{e^{-a\lambda(t)r}}{-a\lambda(t)}\right]_0^r = \frac{4\pi\varrho_0}{\varepsilon_0 a}(1-e^{-a\lambda(t)r}) \ ,$$

giving,

$$\mathcal{E}_r = \frac{\varrho_0}{\varepsilon_0 a r^2}(1-e^{-a\lambda(t)r}) \ .$$

d. The magnetic field is zero, because by symmetry it could only be radial. However, the rotational radial field is zero, $\nabla\times\vec{\mathcal{B}} = 0$. As the divergent also zeroes, $\nabla\cdot\vec{\mathcal{B}} = 0$, we conclude $\vec{\mathcal{B}} = 0$.
e. Maxwell's first equation then gets,

$$\nabla\times\vec{\mathcal{B}} = \mu_0\mathbf{j} + \varepsilon_0\mu_0\partial_t\vec{\mathcal{E}} = 0 \ ,$$

what we verified with the results of (b) and (c).

16.2.3.3 Ex: Law of induction

a. Explain the concept of magnetic flux across an area F. How does magnetic flux depend on the choice of surface?
b. What is the form of Faraday's induction law? What are the experimental observations underlying this law?
c. What is the physical content of Lenz's law?
d. What is Maxwell's displacement current? Give a physical justification for this current.
e. Write down Maxwell's equations.
f. What is the motivation for introducing the electromagnetic potentials Φ and $\mathbf{A}$?
g. What is the allowed gauge transformation for electromagnetic potentials?
h. What is the meaning of the Lorentz gauge? What advantages does it offer?
i. Formulate the energy conservation law of electrodynamics.
j. What is the physical meaning of the Poynting vector?

Solution: *a. The magnetic flux is* $\Psi = \int_F \vec{\mathcal{B}} \cdot d\mathbf{S}$. *For a given field* $\vec{\mathcal{B}}$ *the flux across two different surfaces with the same edge is the same.*
b. $U_{ind} = \oint \vec{\mathcal{E}} \cdot d\mathbf{S} = -d\Psi/dt$. *Temporally varying magnetic fields induce voltages in conductive loops.*
c. The voltage induced by a variable magnetic field generates a current and therefore a magnetic field oriented opposite to the variation of the original magnetic field.
d. A temporal variation of the electric displacement field $\partial\vec{\mathcal{D}}/\partial t$ *can be interpreted via a displacement current. This is the only way current can be transported through a capacitor, once there is no charge flow possible between the plates.*
e. rot $\vec{\mathcal{H}} = \dot{\vec{\mathcal{D}}} + \mathbf{j}$, *rot* $\vec{\mathcal{E}} = -\dot{\vec{\mathcal{B}}}$, *div* $\vec{\mathcal{D}} = \rho$, *and div* $\vec{\mathcal{B}} = 0$.
f. The potentials are introduced by $\vec{\mathcal{B}} = \nabla \times \mathbf{A} = 0$ *and* $\vec{\mathcal{E}} = -\nabla\Phi - d\mathbf{A}/dt$.
g. Allowed is $\mathbf{A}' = \mathbf{A} + \nabla\Lambda$ *and* $\Phi' = \Phi - d\Lambda/dt$.
h. With $\nabla \cdot \mathbf{A}'/\mu_0 + \varepsilon_0 d\Phi/dt = 0$ *follows* $-\Delta\Phi + \mu_0\varepsilon_0\ddot{\Phi} = \rho/\varepsilon_0$ *and* $-\Delta\mathbf{A} + \mu_0\varepsilon_0\ddot{\mathbf{A}} = \mu_0\mathbf{j}$.
i. $du/dt = \nabla \cdot \mathbf{S} + \mathbf{j} \cdot \vec{\mathcal{E}}$ *with* $u = \frac{1}{2}(\vec{\mathcal{E}} \cdot \vec{\mathcal{D}} + \vec{\mathcal{B}} \cdot \vec{\mathcal{H}})$.
j. The Poynting vector describes the flow of energy: $\mathbf{S} = \vec{\mathcal{E}} \times \vec{\mathcal{H}}$.

16.2.3.4 Ex: Induction and Lorentz force

Two parallel metal rods are tilted by an angle φ with respect to the ground (see diagram). Between the rods a third movable rod of mass m and length L placed at right angles glides without friction. A homogeneous magnetic field $\vec{\mathcal{B}}$ crosses perpendicularly the plane defined by the three rods. The parallel rods are connected at the top end by a capacitor C, such that a closed current circuit is formed together with the transverse rod.
a. Set up the equation of motion for the transverse rod.
b. Determine the solution $x(t)$ of the equation of motion for the initial condition $x(0) = v(0) = 0$.

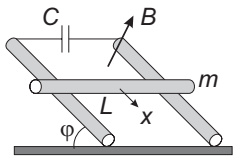

Figure 16.12: Induction.

Solution: *a. The equation of motion is,*

$$m\ddot{x} = mg\sin\varphi + BIL \ .$$

By definition,

$$I = -\frac{dq}{dt}$$

and

$$q = CU_{ind} = C(-\frac{d\Phi}{dt}) = -C\mathcal{B}\frac{dS}{dt} = -C\mathcal{B}L\frac{dx}{dt} \ .$$

Now we get,

$$m\ddot{x} = mg\sin\varphi + C\mathcal{B}^2L^2\ddot{x}$$

or

$$\ddot{x} = \frac{mg\sin\varphi}{m - C\mathcal{B}^2L^2} \ .$$

b. The trivial solution of the differential equation is,

$$x(t) = \frac{mg\sin\varphi}{m - C\mathcal{B}^2L^2}t^2 \ .$$

16.2.3.5 Ex: Magnetic flux and induction

Consider the conductive ring of radius l and negligible electrical resistance shown in the figure. Perpendicular to the plane of the ring there is a homogeneous magnetic field $\vec{\mathcal{B}}$. A rod 2 rotates with angular frequency ω. Calculate the current I across the resistance R of another resting rod 1.

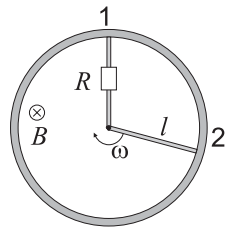

Figure 16.13: Induction.

Solution: *The voltage induced by the decrease of the left area is,*

$$U_{ind,e} = -\frac{d\Phi}{dt} = -\frac{\vec{\mathcal{B}} \cdot \Delta \mathbf{S}_e}{\Delta t} \ ,$$

where

$$\Delta S_e = \frac{l(ld\phi)}{2}\hat{\mathbf{e}}_z \ ,$$

with $d\phi$ the angle of variation of the rotary motion. Therefore, the induced voltage is,

$$U_{ind,e} = -\frac{\mathcal{B}l^2}{2}\frac{d\phi}{dt} = -\frac{-\mathcal{B}\omega l^2}{2} \ .$$

At the same time, the right area grows by an area,

$$\Delta S_d \hat{\mathbf{e}}_z = -\Delta S_e(-\hat{\mathbf{e}}_z) \ .$$

inducing a voltage,

$$U_{ind,d} = \frac{\mathcal{B}\omega l^2}{2} \ .$$

Hence, the two voltages produce a current going through the resistor,

$$I = -\frac{|U_{ind,e}|}{R} - \frac{|U_{ind,d}|}{R} = \frac{\omega \mathcal{B} l^2}{R} \ .$$

The directions of the currents must be the same, since following Lenz's law, I_e must generate a magnetic field supporting the diminishing flux in the area S_e and I_d must generate a field preventing the increasing flux in the area S_d. Alternatively we calculate:

$$\mathcal{E} = \int \vec{\mathcal{E}} \cdot d\mathbf{l} = \tfrac{1}{q}\int \mathbf{F} \cdot d\mathbf{l} = \int_0^l \mathbf{v}_{tot} \times \vec{\mathcal{B}} d\mathbf{l} = \int_0^l (-\omega l \hat{\mathbf{e}}_\phi - v_i \hat{\mathbf{e}}_\rho) \times \vec{\mathcal{B}} d\mathbf{l} = \frac{\omega l^2 B}{2} - v_i \mathcal{B} l \hat{\mathbf{e}}_\phi \ .$$

16.2.3.6 Ex: Induction

Consider the conductive loop at right angle shown in the figure. There is a homogeneous magnetic field given by,

$$\vec{\mathcal{B}}(\mathbf{r}) = \mathcal{B}_0 \hat{e}_y \ .$$

The conductive loop rotates around the bending axis (z-axis) with constant angular frequency.ω.
a. What is the voltage induced in the loop as a function of time?
b. Calculate the time average of the induced voltage.

Solution: *a. We calculate the flux Φ as a function of the rotation angle ϕ by separately considering the areas A_1 and A_2 defined by the two parts of the loop. The*

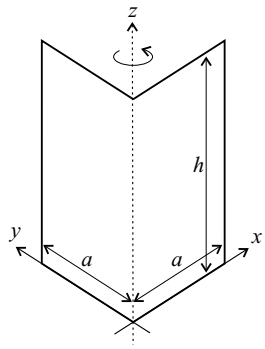

Figure 16.14: Induction.

flux through the area A_1 is $\Phi_1 = \mathcal{B}_0 \cdot h \cdot a \cdot \cos\phi$, and the flux through the area A_2 is $\Phi_2 = B_0 \cdot h \cdot a \cdot \sin\phi$. So the total flux is,

$$\Phi_{tot} = \Phi_1 + \Phi_2 \ .$$

The derivative of the total flux is,

$$\frac{d}{dt}(\mathcal{B}_0 ha(\cos\phi + \sin\phi)) = \mathcal{B}_0 ha(-\dot{\phi}\sin\phi + \dot{\phi}\cos\phi) \ ,$$

and with $\phi = \omega t$ resp. $\omega = \dot{\phi}$ follows,

$$\dot{\Phi}_{tot} = \mathcal{B}_0 ha\omega[\cos(\omega t) - \sin(\omega t)] = \mathcal{B}_0 ha\sqrt{2}\sin(\tfrac{\pi}{4} - \omega t) \ .$$

The induced voltage now follows via,

$$U_{ind} = -\dot{\Phi}_{tot} = -\omega\mathcal{B}_0 ha\sqrt{2}\cos(\tfrac{\pi}{4} - \omega t) \ .$$

b. Also,

$$\int_0^{2\pi/\omega} dt[\cos(\omega t) - \sin(\omega t)] = 0 \to \bar{U}_{ind} = 0 \ .$$

16.2.3.7 Ex: Induction

A circular ring with radius R rotates with constant angular velocity ω around a diameter. Perpendicular to the rotation axis there is a magnetic field $\vec{\mathcal{B}}$.
a. Calculate the voltage induced in the ring as a function of time.
b. The ring consists of a metallic wire with conductivity σ. What current $I(t)$ flows through the ring, assuming the current is evenly distributed across the cross section of the wire?

Solution: *We call $\hat{\mathbf{e}}_n$ the normal vector perpendicular to the area spanned by the*

wire. So the surface element is, $d\mathbf{S} = dS\hat{\mathbf{e}}_n$*, and for the angle* $\phi(t)$ *that the* $\vec{\mathcal{B}}$*-field forms with* $\hat{\mathbf{e}}_n$*, holds* $\phi(t) = \omega(t - t_0)$*.*
a. For the induced voltage,

$$U_{ind} = -\frac{\partial}{\partial t}\Phi(t) \ ,$$

and

$$\Phi(t) = \int\limits_{circular\ area} d\mathbf{F} \cdot \vec{\mathcal{B}} = \int\limits_{circular\ area} df\hat{\mathbf{e}}_n \cdot \vec{\mathcal{B}}$$
$$= \mathcal{B}\cos[\omega(t - t_0)] \int\limits_{circular\ area} df = \mathcal{B}\pi R^2 \cos[\omega(t - t_0)]$$

hence,

$$U_{ind} = \mathcal{B}\pi R^2 \omega \sin[\omega(t - t_0)] \ .$$

b. For the conductive ring holds,

$$U_{ind} = \int\limits_{circularborder} \vec{\mathcal{E}} \cdot d\mathbf{r} = \frac{1}{\sigma} \int\limits_{circular\ border} \mathbf{j} \cdot d\mathbf{r} = \frac{I}{\sigma A} \int\limits_{circular\ border} dr = \frac{2\pi R}{\sigma A} I \ .$$

From this, and using (a) follows immediately,

$$I(t) = \frac{1}{2}\sigma \mathcal{B} A R \omega \sin[\omega(t - t_0)] \ .$$

16.2.3.8 Ex: Induction

An equidistant triangle-shaped conductive loop (edge length S) in the xy-plane is 'immersed' with constant velocity $\mathbf{v} = v\hat{\mathbf{e}}_x$ starting at the tip into a homogeneous magnetic field $\vec{\mathcal{B}} = \mathcal{B}\hat{\mathbf{e}}_z$ ($\mathcal{B}$ is constant) (see diagram) until being completely inside the magnetic field.
a. Calculate the maximum voltage induced in the loop.
b. Make a scheme of the time evolution of the induced voltage.

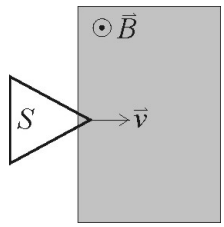

Figure 16.15: Induction.

Solution: *Calculation of the induced voltage,*

$$U_{ind} = \oint \vec{\mathcal{E}} \cdot d\mathbf{l} = \int (\nabla \times \vec{\mathcal{E}}) \cdot d\mathbf{S} = -\frac{d}{dt} \int \vec{\mathcal{B}} \cdot d\mathbf{S} = -\frac{d\Psi}{dt} \ .$$

Hence,

$$\Psi(t) = \int_A \vec{\mathcal{B}} \cdot d\mathbf{f} = \mathcal{B} \int_A df = \mathcal{B}A(t) \ ,$$

since $\vec{\mathcal{B}} \| d\mathbf{S}$ *and* $\mathcal{B} = const.$ *Now,*

$$A(t) = \frac{1}{2} s(t) v(t) = \frac{1}{\sqrt{3}} v^2 t^2$$

since $h^2 + \frac{s^2}{4} = s^2$ *resp.* $h(t) = \frac{\sqrt{3}}{2} s(t) = vt$. *With that we get for the flux and the induced voltage,*

$$\Psi(t) = \frac{1}{\sqrt{3}} \mathcal{B} v^2 t^2 \qquad \textit{and} \qquad U_{ind}(t) = -\frac{2}{\sqrt{3}} \mathcal{B} v^2 t \ .$$

The maximum voltage is finally,

$$U_{ind}^{\max} = U_{ind}(t = T)$$

with $T = \frac{H}{v} = \frac{\sqrt{3}}{2v} s$.

16.2.3.9 Ex: Induction

A rectangular conducting loop with height $2a$ and width $2b$ rotates with angular velocity ω around the z-axis. At time $t = 0$ the conducting loop is in the xz-plane. In addition, the loop is exposed to the inhomogeneous time-varying magnetic field $\vec{\mathcal{B}}(\mathbf{r}, t) = \mathcal{B}_0 t z^2 \hat{\mathbf{e}}_x$.
a. Show, $\nabla \cdot \vec{\mathcal{B}}(\mathbf{r}, t) = 0$.
b. Calculate the magnetic flux $\Psi(\mathbf{r}, t) = \int \vec{\mathcal{B}} \cdot d\mathbf{F}$ through the rotating loop as a function of time.
c. What is the value of the voltage $U_{ind}(t)$ induced in the loop as a function of time?

Solution: *a. Obvious.*
b. The normal vector of the area is time-dependent $d\mathbf{S} = \hat{\mathbf{e}}_x dS \sin\omega t + \hat{\mathbf{e}}_y dS \cos\omega t$. *Therefore, the magnetic flux is,*

$$\begin{aligned} \Phi(\mathbf{r}, t) &= \int \vec{\mathcal{B}} \cdot d\mathbf{S} = \int \mathcal{B}_0 t z^2 \hat{\mathbf{e}}_x \cdot (\hat{\mathbf{e}}_x dx \sin\omega t + \hat{\mathbf{e}}_y dy \cos\omega t) \ dz \\ &= \mathcal{B}_0 t \sin\omega t \int_{-a}^{a} \int_{-b}^{b} z^2 \ dxdz = \mathcal{B}_0 t \sin\omega t \, [x]_{-b}^{b} \left[\frac{z^3}{3}\right]_{-a}^{a} = \frac{4a^3 b}{3} \mathcal{B}_0 t \sin\omega t \ . \end{aligned}$$

c. The induced voltage is,

$$U_{ind}(t) = -\dot{\Psi}(t) = -\frac{4}{3} b a^3 \mathcal{B}_0 [\sin\omega t + \omega t \cos\omega t] \ .$$

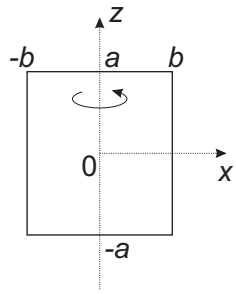

Figure 16.16: Induction.

16.2.3.10 Ex: Induction in a coil

Calculate the magnetic $\mathcal{B}$-field in the middle and at the end of a coil of length $L = 1\,\mathrm{m}$. The number of turns is $N = 2000$, the radius $r = 2\,\mathrm{cm}$, and the current through the coil $I = 5\,\mathrm{A}$. To do this first calculate, using the Biot-Savart law, the magnetic field $\mathcal{B}_1(0,0,z)$ of a single circular conductor with radius r located at a point z_1 of the coil's symmetry axis. Use the formula obtained for $\mathcal{B}_1$ to describe the magnetic field generated by a coil element dz.

Solution: *The magnetic field of a conductive loop about its symmetry axis has already been calculated,*

$$\vec{\mathcal{B}}_{loop}(z) = \frac{\mu_0 I}{2}\frac{r^2}{\sqrt{r^2+z^2}^3}\hat{\mathbf{e}}_z \ .$$

For the whole coil holds,

$$\begin{aligned}
\vec{\mathcal{B}}(z) &= \sum_{n=1}^{2000}\frac{\mu_0 I}{2}\frac{r^2}{\sqrt{r^2+(z-nL/N)^2}^3}\hat{\mathbf{e}}_z = \frac{\mu_0 NI}{L}\frac{r^2}{2}\hat{\mathbf{e}}_z\int_0^L\frac{1}{\sqrt{r^2+(z-z')^2}^3}dz' \\
&= \frac{\mu_0 NI}{L}\frac{r^2}{2}\hat{\mathbf{e}}_z\frac{\sqrt{r^2+z^2}(L-z)+z\sqrt{r^2+(z-L)^2}}{r^2\sqrt{r^2+z^2}\sqrt{r^2+(z-L)^2}} \\
&= \frac{\mu_0 NI}{2L}\hat{\mathbf{e}}_z\frac{\sqrt{r^2+z^2}(L-z)+z\sqrt{r^2+(z-L)^2}}{\sqrt{r^2+z^2}\sqrt{r^2+(z-L)^2}} \ .
\end{aligned}$$

At the given positions we have,

$$\begin{aligned}
\vec{\mathcal{B}}(L/2) &= \mu_0 NI\hat{\mathbf{e}}_z\frac{1}{\sqrt{4r^2+L^2}} \simeq \mu_0 NI\hat{\mathbf{e}}_z\frac{1}{L} \ , \\
\vec{\mathcal{B}}(0) &= \mu_0 NI\hat{\mathbf{e}}_z\frac{1}{2\sqrt{r^2+L^2}} \simeq \mu_0 NI\hat{\mathbf{e}}_z\frac{1}{2L} \ .
\end{aligned}$$

16.2.3.11 Ex: Induction in a rectangular mesh

A rectangular conducting loop has the length a and the width b. In the same plane defined by the loop, parallel to a distance d is a straight conductor traversed by a

current I, as shown in the figure.
a. Calculate the magnetic field produced by the current.
b. Calculate the flux through the loop.
c. Calculate the self-inductance imposed on the current circuit by the existence of the loop.
d. Linearize the expression of self-inductance for $b/d \ll 1$.

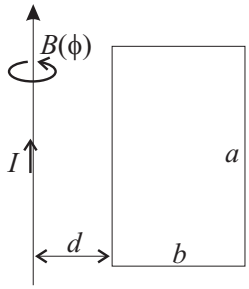

Figure 16.17: Induction.

Solution: *a. By the law of Ampère,* $2\pi\rho\mathcal{B}_\rho = \oint \vec{\mathcal{B}} \cdot \mathbf{l} = \mu_0 I$*, we find,*

$$\vec{\mathcal{B}} = \frac{\mu_0 I}{2\pi\rho}\hat{\mathbf{e}}_\phi \ .$$

b. The flux is,

$$\Psi_M = \int \vec{\mathcal{B}} \cdot d\mathbf{S} = \int_d^{d+b} \int_0^a \frac{\mu_0 I}{2\pi\rho}\hat{\mathbf{e}}_\phi \cdot \hat{\mathbf{e}}_\phi dz d\rho = \frac{\mu_0 I a}{2\pi} \ln\left(1 + \frac{b}{d}\right) \ .$$

c. The self-inductance L *is defined by,*

$$U_{ind} = -L\dot{I} \ .$$

On the other hand, the voltage induced in the loop, U_{ind}*, depends on the magnetic flux* Ψ_M *through Faraday's induction law,*

$$\dot{\Psi}_M = -U_{ind} \ .$$

The variable varying in time is the current $I \equiv I(t)$*, which leads to a temporal variation of the flux* $\Phi \equiv \Phi(t)$*. Comparing the two equations we get,*

$$L = \frac{\mu_0}{2\pi} a \ln\left(1 + \frac{b}{d}\right) \ .$$

d. With the linearization $\ln(1+x) \approx x$ *(truncation of the Taylor expansion for* $|x| \ll 1$ *very small) we get,*

$$L = \frac{\mu_0}{2\pi}\frac{ab}{d} \ .$$

16.2.3.12 Ex: Falling rod

A metal rod of $L = 1\,\mathrm{m}$ length falls in the gravitational field of the Earth. At time $t = 0$ the initial velocity is 0. The rod is oriented parallel to the ground. Perpendicular to the rod and parallel to the ground there is a magnetic field $\vec{\mathcal{B}}$ with the absolute value $2 \cdot 10^{-5}\,\mathrm{T}$.
a. What voltage is induced between the ends of the rod as a function of the distance traveled h?
b. What value is obtained for the voltage after a fall of 5 m?

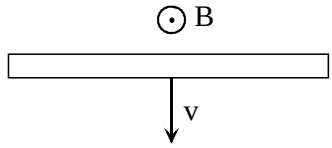

Figure 16.18: Induction.

Solution: *a. Following Faraday's law we have,*

$$U_{ind} = \oint_C \vec{\mathcal{E}} \cdot d\vec{\ell} = -\frac{d}{dt} \int \vec{\mathcal{B}} \cdot d\mathbf{S} = -\frac{d}{dt}[\mathcal{B}L(x_0 + \frac{g}{2}t^2)] = \mathcal{B}Lgt = \mathcal{B}L\sqrt{2gh}\ .$$

Alternatively, we consider the rod as a Hall probe. The condition for an equilibrium of charges,

$$F_C = q\mathcal{E} = q\frac{U_{ind}}{L} = qgt\mathcal{B} = qv\mathcal{B} = F_L\ .$$

Hence we get the same result.
b. Entering the distance of 5 m*, we get,*

$$U_{ind} = \mathcal{B}L\sqrt{2gh} \approx 1.98 \cdot 10^{-4}\,\mathrm{V}\ .$$

16.2.3.13 Ex: Sliding rod

We consider two parallel metal rails (distance $d = 10\,\mathrm{cm}$) inclined by an angle ϕ with respect to the ground. Between the rails slides a frictionless rod (mass $M = 100$ g). At a right angle to the plane defined by the rails there is a homogeneous magnetic field $\mathcal{B}$ (amplitude: $0.1\,\mathrm{T}$). We sent a current of $I = 9.8\,\mathrm{A}$ through the rails and through the rod. What is the maximum allowable value of ϕ necessary to let the rod move upward along the rails?

Solution: *With Ampère we know $d\mathbf{F} = Id\mathbf{l} \times \vec{\mathcal{B}}$. Therefore, the force on the moving rod is given by $F_I = Id\mathcal{B}$; it goes in the direction of the rails. It should point upward, but for this, either $\vec{\mathcal{B}}$ or I must be opposite.*
In z-direction downward acts the force of the weight $F_G = Mg$, which has a component $-Mg\sin\phi$ along the rails. In order for the transverse rod to slide up, we need

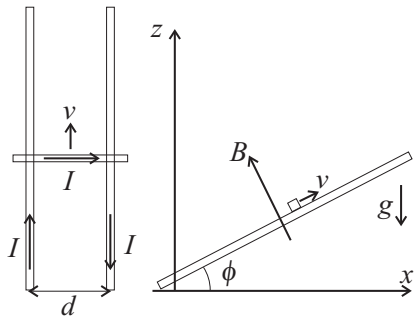

Figure 16.19: Sliding rod.

$Id\mathcal{B} > Mg\sin\phi$, that is, $\phi < \arcsin(Id\mathcal{B}/Mg) \approx 5.6°$.

16.2.3.14 Ex: Conductive ring in oscillating magnetic field

A circular conductive loop (inductance L, resistance R) is traversed by an oscillating magnetic flux, $\Psi = \Psi_0 e^{\imath\omega t}$.
a. Calculate the amplitude of the current in the conductor as well as its phase relative to Ψ.
b. What is the average power dissipated in the conductor? Also discuss the limiting cases $\omega \to 0$ and $\omega \to \infty$.
Help: Start setting up an equivalent circuit incorporating a voltage source, a resistance, and an inductance.

Solution: *a. The equivalent circuit consist of a voltage source U, a resistance R, and an inductance L in series. The induced voltage $U_{ind} = -\dot{\Psi} = -\imath\omega\Psi_0 e^{\imath\omega t}$ corresponds to the voltage source U. With this we have $U = (R + \imath\omega L)I$ or $I = \frac{U}{R+\imath\omega L} = \frac{-\imath\omega\Phi_0}{R+\imath\omega L} e^{\imath\omega t} = I_0 e^{\imath\omega t}$. Holds,*

$$I_0 = \frac{-\imath\omega}{R + \imath\omega L}\Psi_0 = \frac{-\imath\omega(R - \imath\omega L)}{R^2 + \omega^2 L^2}\Psi_0 = \frac{\omega^2 L - \imath\omega R}{R^2 + \omega^2 L^2}\Psi_0 \ ,$$

with the absolute value,

$$|I_0| = \sqrt{I_0 I_0^*} = \frac{-\imath\omega\Psi_0}{R + \imath\omega L} = \frac{\omega\Psi_0}{\sqrt{R^2 + \omega^2 L^2}}$$

and the phase,

$$\delta = \arctan\frac{-\omega R\Psi_0}{\omega^2 L\Psi_0} = \arctan\frac{-R}{\omega L} \ .$$

b. The power is,

$$P = UI^* = -\imath\omega\Phi_0\frac{\imath\omega\Psi_0}{R - \imath\omega L} = \frac{\omega^2\Psi_0^2 R + \imath\omega^3\Psi_0^2 L}{R^2 + \omega^2 L^2} = P_W + \imath P_B \ .$$

The average active power is,

$$\overline{P_W} = \frac{\Psi_0^2}{2}\frac{R\omega^2}{R^2+\omega^2 L^2} \ .$$

In the limiting case $\omega \to 0$ *we have* $\overline{P_W} \to 0$. *In the limiting case* $\omega \to \infty$ *we have* $\overline{P_W} \to \frac{\Psi_0^2}{2}\frac{R}{L^2}$.

16.2.3.15 Ex: Self-inductance of a current loop

Calculate the self-inductance of a current loop.

Solution: *The current density can be parametrized as* $\mathbf{j}(\mathbf{r}) = I\delta(\rho - R)\delta(z)\hat{\mathbf{e}}_\phi$. *The potential vector is,*

$$\mathbf{A}(\mathbf{r}) = \frac{\mu_0}{4\pi}\int \frac{\mathbf{j}(\mathbf{r}')}{|\mathbf{r}-\mathbf{r}'|}d^3\mathbf{r}' \ .$$

According to Biot-Savart law the magnetic field is,

$$\begin{aligned}
\vec{\mathcal{B}}(\mathbf{r}) &= \frac{\mu_0}{4\pi}\int \nabla \times \frac{\mathbf{j}(\mathbf{r}')}{|\mathbf{r}-\mathbf{r}'|}d^3\mathbf{r}' = \frac{\mu_0}{4\pi}\int d^3\mathbf{r}'\frac{(\mathbf{r}-\mathbf{r}')\times\mathbf{j}(\mathbf{r}')}{|\mathbf{r}-\mathbf{r}'|^3} \\
&= \frac{\mu_0 I}{4\pi}\int \rho' d\rho' d\phi' dz' \frac{\delta(\rho'-R)\delta(z')(\mathbf{r}-\mathbf{r}')\times\hat{\mathbf{e}}_{\phi'}}{|\mathbf{r}-\mathbf{r}'|^3} \\
&= \frac{\mu_0 I}{4\pi}\int \rho' d\rho' d\phi 1 dz' \frac{\delta(\rho'-R)\delta(z')\begin{pmatrix}\rho\cos\phi-\rho'\cos\phi'\\ \rho\sin\phi-\rho'\sin\phi'\\ z-z'\end{pmatrix}\times\begin{pmatrix}-\sin\phi'\\ \cos\phi'\\ 0\end{pmatrix}}{\sqrt{(\rho\cos\phi-\rho'\cos\phi')^2+(\rho\sin\phi-\rho'\sin\phi')^2+(z-z')^2}^3} \\
&= \frac{\mu_0 I}{4\pi}\int Rd\phi' \frac{\begin{pmatrix}-z\cos\phi'\\ -z\sin\phi'\\ (\rho\cos\phi-R\cos\phi')\cos\phi'+(\rho\sin\phi-R\sin\phi')\sin\phi'\end{pmatrix}}{\sqrt{(\rho\cos\phi-R\cos\phi')^2+(\rho\sin\phi-R\sin\phi')^2+z^2}^3} \ .
\end{aligned}$$

The field through $z = 0$ *plane is,*

$$\begin{aligned}
\mathcal{B}_z(x,y) &= \frac{\mu_0 IR}{4\pi}\int_0^{2\pi} d\phi' \frac{(\rho\cos\phi-R\cos\phi')\cos\phi'+(\rho\sin\phi-R\sin\phi')\sin\phi'}{\sqrt{(\rho\cos\phi-R\cos\phi')^2+(\rho\sin\phi-R\sin\phi')^2}^3} \\
&= \frac{\mu_0 IR}{4\pi}\int_0^{2\pi} d\phi' \frac{\rho\cos\phi\cos\phi'+\rho\sin\phi\sin\phi'-R}{\sqrt{\rho^2+R^2-2\rho R\cos\phi\cos\phi'-2\rho R\sin\phi\sin\phi'}^3} \\
&= \frac{\mu_0 IR}{4\pi}\int_0^{2\pi} d\phi' \frac{\rho\cos(\phi-\phi')-R}{\sqrt{\rho^2+R^2-2\rho R\cos(\phi-\phi')}^3} \\
&= \frac{\mu_0 IR}{4\pi}\int_0^{2\pi} d\alpha \frac{\rho\cos\alpha-R}{\sqrt{\rho^2+R^2-2\rho R\cos\alpha}^3} \ ,
\end{aligned}$$

and the flux through the $z = 0$ plane is,

$$\begin{aligned}
\Psi &= \int_A \mathcal{B}_z(x,y)dA = \frac{\mu_0 IR}{4\pi}\int_0^{2\pi} d\phi \int_0^R \rho d\rho \int_0^{2\pi} d\alpha \frac{\rho\cos\alpha - R}{\sqrt{\rho^2+R^2-2\rho R\cos\alpha}^3} \\
&= \frac{\mu_0 IR}{4\pi} 2\pi \int_0^R \rho d\rho \int_0^{2\pi} d\alpha \frac{\rho\cos\alpha - R}{\sqrt{\rho^2+R^2-2\rho R\cos\alpha}^3} = \frac{\mu_0 IR}{4\pi} 2\pi \int_0^{2\pi} d\alpha \int_0^1 \zeta d\zeta \frac{\zeta\cos\alpha - 1}{\sqrt{\zeta^2+1-2\zeta\cos\alpha}^3} \\
&= \frac{\mu_0 IR}{4\pi} 2\pi \int_0^{2\pi} d\alpha \frac{-2\cos\alpha + \left(\cos\alpha \ln(-\cos\alpha + 1 + \sqrt{2-2\cos\alpha})\right)\sqrt{2-2\cos\alpha} + 1 - (\cos\alpha \ln(-\cos\alpha +}{\sqrt{2-2\cos\alpha}} \\
&= \frac{\mu_0 IR}{4\pi} 2\pi \int_0^{2\pi} d\alpha \frac{-2\cos\alpha + \left(\cos\alpha \ln\left(-\cos\alpha + 1 + 2\sin\frac{\alpha}{2}\right)\right) 2\sin\frac{\alpha}{2} + 1 - (\cos\alpha \ln(-\cos\alpha + 1))2\sin\frac{\alpha}{2}}{2\sin\frac{\alpha}{2}} \\
&= \frac{\mu_0 IR}{4\pi} 2\pi 4 = 2\mu_0 IR \ .
\end{aligned}$$

Finally, self-inductivity becomes,

$$L = \frac{\Phi}{I} = 2\mu_0 R \ .$$

When there are N windings, we have,

$$L_N = N^2 L \ .$$

16.2.3.16 Ex: Potentials

Be given are scalar potential and vector potential:

$$\Phi(\mathbf{r},t) = b\frac{\mathbf{r}\hat{\mathbf{e}}_z}{r^3}e^{\imath\omega t} \qquad \text{and} \qquad A(\mathbf{r},t) = \imath k b \frac{e^{\imath kr}}{r^3} e^{\imath\omega t}\hat{\mathbf{e}}_z \ ,$$

where $\omega = ck$ and $r = |\mathbf{r}|$. Calculate the corresponding electric field $\vec{\mathcal{E}}(\mathbf{r},t)$ and the magnetic field $\vec{\mathcal{B}}(\mathbf{r},t)$.

Solution: *With the given potentials,*

$$\nabla\phi = be^{\imath\omega t}\nabla\frac{z}{r^3} = be^{\imath\omega t}\begin{pmatrix} \frac{d}{dx}\frac{z}{(x^2+y^2+z^2)^{3/2}} \\ \frac{d}{dy}\frac{z}{(x^2+y^2+z^2)^{3/2}} \\ \frac{d}{dz}\frac{z}{(x^2+y^2+z^2)^{3/2}} \end{pmatrix} = \frac{be^{\imath\omega t}}{r^5}\begin{pmatrix} -3xz \\ -3yz \\ r^2-3z^2 \end{pmatrix} \ ,$$

and

$$\frac{\partial}{\partial t}\mathbf{A} = \frac{\partial}{\partial t}\imath k b e^{\imath\omega t}\frac{e^{\imath kr}}{r}\hat{\mathbf{e}}_z = -k\omega b e^{\imath\omega t}\frac{e^{\imath kr}}{r}\hat{\mathbf{e}}_z \ .$$

With this the $\vec{\mathcal{E}}$-field becomes,

$$\vec{\mathcal{E}} = -\nabla\phi - \frac{\partial\mathbf{A}}{\partial t} = -\frac{be^{\imath\omega t}}{r^5}\begin{pmatrix} -3xz \\ -3yz \\ r^2-3z^2 \end{pmatrix} + k\omega b e^{\imath\omega t}\frac{e^{\imath kr}}{r}\hat{\mathbf{e}}_z = be^{\imath\omega t}\begin{pmatrix} \frac{3xz}{r^5} \\ \frac{3yz}{r^5} \\ \frac{3z^2-r^2}{r^5} + k\omega\frac{e^{\imath kr}}{r} \end{pmatrix} \ .$$

The $\vec{\mathcal{B}}$-field becomes,

$$\vec{\mathcal{B}} = \nabla \times \mathbf{A} = \nabla \times \begin{pmatrix} 0 \\ 0 \\ \imath k b \frac{e^{\imath kr}}{r^3} e^{\imath \omega t} \end{pmatrix} = e^{\imath \omega t} b k (kr + 3\imath) \frac{e^{\imath kr}}{r^5} \begin{pmatrix} -y \\ x \\ 0 \end{pmatrix} .$$

16.2.3.17 Ex: Motion-induced electromotive force

In the figure a conductive rod of mass m and negligible resistance is free to slide without friction along two parallel rails that have negligible resistances, are separated by a distance ℓ, and connected by a resistance R. The rails are attached to a long plane inclined by an angle θ from the horizontal. There is a magnetic field pointing upwards as shown.
a. Show that there is a retarding force directed upward on the inclined plane given by $F = (\mathcal{B}^2 \ell^2 v \cos^2\theta)/R$.
b. Show that the terminal velocity of the stick is $v_t = mgR \sin\theta/(\mathcal{B}^2 \ell^2 \cos^2\theta)$.

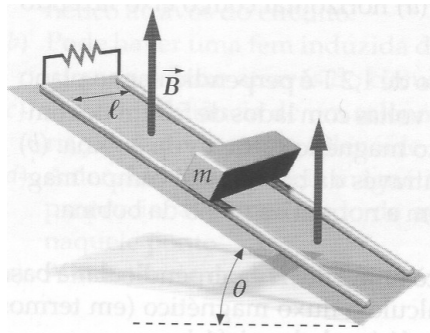

Figure 16.20: Motion-induced electromotive force.

Solution: *a. The induced voltage is,*

$$U_{ind} = -\dot{\Psi} = -\vec{\mathcal{B}} \cdot \dot{\mathbf{A}} = -\mathcal{B} \frac{d}{dt}(\ell v t \cos\theta) = -\mathcal{B} \ell v \cos\theta \ ,$$

creating a current,

$$I = \frac{U_{ind}}{R} \ ,$$

creating a Lorentz force,

$$F_L = I \ell \mathcal{B} = -\frac{\mathcal{B} \ell v \cos\theta}{R} \ell \mathcal{B} \ .$$

The projection of the force onto the plane of the rails is,

$$F_\theta = F_L \cos\theta = -\frac{\mathcal{B}^2 \ell^2 v \cos^2\theta}{R} \ .$$

b. This force is in equilibrium with the gravitational acceleration force, $F_g = mg\sin\theta$*, when,*

$$-\frac{\mathcal{B}^2\ell^2 v_t\cos^2\theta}{R} = mg\sin\theta \ ,$$

giving the final velocity,

$$v_t = \frac{mgR\sin\theta}{\mathcal{B}^2\ell^2\cos^2\theta} \ .$$

16.2.3.18 Ex: Induction

An insulated wire with resistance of $18.0\,\Omega/\mathrm{m}$ and length of $9.0\,\mathrm{m}$ will be used to build a resistor. First the wire is bent in half and doubled, and then the double wire is wound into a cylindrical shape (see figure) to create a $25\,\mathrm{cm}$ long, $2.0\,\mathrm{cm}$ diameter helix. Determine the resistance and inductance of this twisted wire resistor.

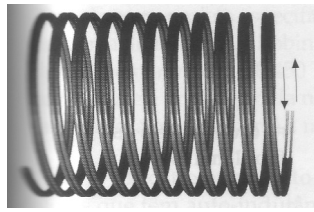

Figure 16.21: Induction.

Solution: $L = 0,\ R = 162\,\Omega.$

16.2.3.19 Ex: R-L-circuit

In the circuit shown in the figure the inductor has negligible internal resistance, and the switch S has been left open for a long time. Now, the switch is closed.
a. Determine the current in the battery, the current in the $100\,\Omega$ resistor, and the current in the inductance immediately after the switch has been closed.
b. Determine the current in the battery, the current in the $100\,\Omega$ resistor, and the current in the inductance a long time after the switch has been closed.
c. After being closed for a long time, the key is now opened again. Determine the current in the battery, the current in the $100\,\Omega$ resistor, and the current in the inductance immediately after the switch has been opened.
d. Determine the current in the battery, the current in the $100\,\Omega$ resistor, and the current in the inductance a long time after the key has been reopened.

Solution: *a. Immediately after the switch has been closed the inductor has an infinite resistance such that all current flows through the* $100\,\Omega$*,*

$$I_L = 0 \qquad \textit{and} \qquad I_R = \frac{U}{R_{100}+R_{10}} = \frac{10}{110}\,\mathrm{A} \ .$$

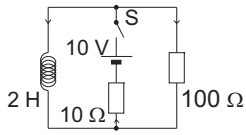

Figure 16.22: Circuit.

b. A long time after the key has been closed the inductor has zero resistance such that all current flows through the inductance,

$$I_R = 0 \qquad and \qquad I_L = \frac{U}{R_{10}} = 1\,\mathrm{A}\ .$$

c. Immediately after the switch has been opened the inductance produces an induced voltage trying to preserve the magnetic field, i.e. the current. This is only possible if the current is deviated to the $100\,\Omega$ *resistor,*

$$I_L = I_R = \frac{U}{R_{10}} = 1\,\mathrm{A}\ .$$

d. A long time after the switch has been reopened all magnetostatic energy stored in the inductance is spent in the resistor, and the current disappears,

$$I_R = 0 \qquad and \qquad I_L = 0\ .$$

16.2.3.20 Ex: Low pass filter

The circuit shown in the figure is an example of a *low-pass filter*. (Consider that the output is connected to a load that conducts negligible current.)
a. If the input voltage is given by $V_{in} = V_{in,pico}\cos\omega t$, shows that the output voltage is $V_{out} = V_L\cos(\omega t - \phi)$, where $V_L = V_{in,pico}/\sqrt{1+(\omega RC)^{-2}}$.
b. Discuss the trend in the limiting cases $\omega \to 0$ and $\omega \to \infty$.

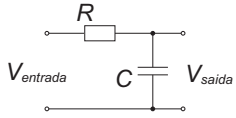

Figure 16.23: Low pass filter.

Solution: *a. We have,*

$$V_{out} = V_{in}\frac{\frac{1}{iC\omega}}{R+\frac{1}{iC\omega}}\ .$$

With this,

$$|V_{out}| = |V_{in}|\sqrt{\frac{1}{1+(\omega RC)^2}}\ .$$

b. For $\omega \to 0$ *we get,*

$$V_{out} = V_{in} \ ,$$

and for $\omega \to \infty$ *we get,*

$$V_{out} = 0 \ .$$

Gabartite: *b.* $V_L \overset{\to 0}{\longrightarrow} V_{in,pico}$ *and* $V_L \overset{\to \infty}{\longrightarrow} 0$.

16.2.3.21 Ex: Notch filter

The circuit shown in the figure is a *cutoff filter*. (Consider that the output is connected to a load carrying a negligible current.)
a. Show that the cutoff filter rejects signals in a frequency band centered in $\omega = 1/\sqrt{LC}$.
How does the width of the rejected frequency band depend on R?

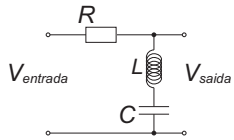

Figure 16.24: Notch filter.

Solution: *a. We have,*

$$V_{saida} = V_{ent} \frac{iL\omega + \frac{1}{iC\omega}}{R + iL\omega + \frac{1}{iC\omega}} \ .$$

With this,

$$|V_{saida}| = |V_{ent}| \frac{L\omega - \frac{1}{C\omega}}{\sqrt{R^2 + \left(L\omega - \frac{1}{C\omega}\right)^2}} \ .$$

b. $\Delta\omega = \frac{R}{L}$.

16.2.3.22 Ex: Effective power

Show that the expression $P_{med} = R\mathcal{E}_{rms}^2/Z^2$ provides the correct result for a circuit containing only one ideal *ac*-generator and
a. one resistor R,
b. one capacitor C and
c. one inductance L. In the given expression, P_{med} is the average power supplied by the generator, $\mathcal{E}_{rms}$ is the average quadratic value of the emf-generator.

Solution: *We have,*

$$P_{med} = \frac{1}{T} \int_0^T UIdt = \ .$$

16.2.3.23 Ex: *R*-*L*-*C*-circuit

In the circuit shown in the figure the ideal generator produces a voltage of 115 V when operated at 60 Hz. What is the *rms*-voltage between the points
a. A and B, b. B and C, c. C and D, d. A and C, and e. B and D?

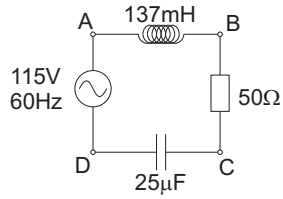

Figure 16.25: Circuit.

Solution: *a.* 80 V, *b.* 78 V, *c.* 170 V, *d.* 110 V, *e.* 180 V.

16.3 Magnetostatic energy

To calculate the magnetostatic energy stored in a magnetic field we will proceed as follows: We will look for a general expression guessed by analogy with the electrostatic energy, $W = \frac{1}{2}\int \varrho\Phi dV$, and show that, applied to a current-carrying loop, this expression gives the correct result. The analogous formula is,

$$W = \tfrac{1}{2}\int \mathbf{j}\cdot\mathbf{A}dV \ . \tag{16.50}$$

16.3.1 Energy density of a magnetostatic field

The energy of a current distribution can be rewritten using Ampere's law,

$$W = \tfrac{1}{2\mu_0}\int (\nabla\times\vec{\mathcal{B}})\cdot\mathbf{A}dV \ . \tag{16.51}$$

Integration by parts allows transferring the derivative from $\vec{\mathcal{B}}$ to $\mathbf{A}$,

$$W = \tfrac{1}{2\mu_0}\left[-\oint(\mathbf{A}\times\vec{\mathcal{B}})\cdot d\mathbf{S} + \int \vec{\mathcal{B}}\cdot(\nabla\times\mathbf{A})dV\right] \ . \tag{16.52}$$

The surface integral can be neglected because we can choose the integration volume $\mathcal{V}$ to be arbitrarily large. Expressing the rotation by the field,

$$W = \tfrac{1}{2\mu_0}\int \vec{\mathcal{B}}^2 dV = \tfrac{1}{2\mu_0}\int u dV \ , \tag{16.53}$$

and introducing the *energy density*,

$$\boxed{u \equiv \frac{1}{2\mu_0}\vec{\mathcal{B}}^2} \ . \tag{16.54}$$

It may seem strange, that we need energy to build up a magnetic field which in turn can not exert work. On the other hand, to create this magnetic field, we have to ramp it up from zero which, according to Faraday's law induces an electric field. This field, in turn, can work. Initially there is no $\vec{\mathcal{E}}$ and at the end of the process there is no $\vec{\mathcal{E}}$ neither; but in between, while $\vec{\mathcal{B}}$ is being constructed, there is. The work has to be exerted against the $\vec{\mathcal{E}}$-field.

16.3.2 Inductors and storage of magnetostatic energy

Using the magnetostatic energy formula,

$$W = \frac{1}{2}\int \mathbf{j}\cdot\mathbf{A}dV = \frac{1}{2}\oint \mathbf{I}\cdot\mathbf{A}dl = \frac{I}{2}\oint \mathbf{A}\cdot d\mathbf{l} = \frac{I}{2}\int (\nabla\times\mathbf{A})\cdot d\mathbf{S} = \frac{I}{2}\int \vec{\mathcal{B}}\cdot d\mathbf{S} = \frac{I}{2}\Psi_M \ . \tag{16.55}$$

Finally, considering a coil and using the formula (16.48),

$$\boxed{W = \frac{1}{2}LI^2} \ , \tag{16.56}$$

which corresponds to the power,

$$\frac{dW}{dt} = -\mathcal{E}I = LI\frac{dI}{dt} \ . \tag{16.57}$$

16.3.3 Exercises

16.3.3.1 Ex: Switching processes

Consider the RL-circuit show in the figure, where the ohmic resistor $R = R(t)$ varies over time. Let τ be the length of the switching-on process starting at time $t = 0$. The resistance be,

$$R(t) = \begin{cases} \infty & \text{for } t < 0 \\ R_0\tau/t & \text{for } 0 \le t \le \tau \\ R_0 \text{for } \tau \le t \end{cases} \ .$$

a. Set up for the time intervals $t \in [0, \tau]$ and $t \in [\tau, \infty]$ separate differential equations for the current $I(t)$.
b. Solve the differential equations (using a simple ansatz or a method of variable separation) and connect the solutions continuously at $t = \tau$. What is the condition for fast or slow switching?

Solution: *a. The differential equation to solve* $L\dot{I}(t) + R(t)I(t) = U$ *becomes for* $0 \le t \le \tau$

$$L\dot{I}_<(t) + \frac{R_0\tau}{t}I_<(t) = U \ .$$

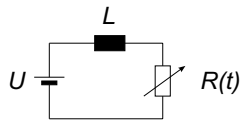

Figure 16.26: Circuit.

For $t \geq \tau$ the equation is,

$$L\dot{I}_>(t) + R_0 I_>(t) = U \ .$$

b. For $0 \leq t \leq \tau$ with the ansatz $I_<(t) = \alpha t$ we obtain $\alpha = \frac{U}{L+R_0\tau}$, hence,

$$I_<(t) = \frac{U}{L + R_0\tau} t \ .$$

For $t \geq \tau$ with the ansatz $I_>(t) = \beta e^{-\kappa t} + \gamma$ we obtain $-\kappa L\beta e^{-\kappa t} + R_0\left(\beta e^{-\kappa t} + \gamma\right) = U$, hence,

$$\gamma = \frac{U}{R_0} \qquad \text{and} \qquad \kappa = \frac{R_0}{L} \ ,$$

and finally,

$$I_>(t) = \beta e^{-\frac{R_0}{L}t} + \frac{U}{R_0} \ .$$

The continuity of the current requires $I_<(\tau) = I_>(\tau)$, which means,

$$\beta = -e^{\frac{R_0}{L}\tau}\left(\frac{U}{R_0} - \frac{U}{L + R_0\tau}\tau\right) \ .$$

With this,

$$I_>(t) = \frac{U}{R_0}\left(1 - \frac{L/R_0}{L/R_0 + \tau} e^{-\frac{R_0}{L}(t-\tau)}\right) \ .$$

The final value U/R_0 is reached exponentially. The temporal constant of the switching is L/R_0. For $\tau \ll L/R_0$ the switching is fast $I(\tau) \ll U/R_0$. For $\tau \gg L/R_0$ it is slow $I(\tau) \approx U/R_0$.

16.3.3.2 Ex: Current density of a rotating charge

The surface of a hollow sphere with radius R carries a uniformly distributed charge Q. The sphere rotates with the constant angular velocity ω around one of its diameters.
a. Determine the current density $\mathbf{j}(\mathbf{r})$ generated by this movement.
b. Calculate the magnetic moment produced by $\mathbf{j}$.
c. Derive the components of the potential vector $\mathbf{A}(\mathbf{r})$ and the magnetic field $\vec{\mathcal{B}}(\mathbf{r})$.

Solution: *The charge density is, $\rho(\mathbf{r}) = \frac{Q}{4\pi R^2}\delta(r - R)$. The current density is $\mathbf{j}(\mathbf{r}) = \rho(\mathbf{r})\mathbf{v}(\mathbf{r}) = \rho(\mathbf{r})(\vec{\omega} \times \mathbf{r})$. In the coordinate system defined by $\vec{\omega} = \omega\hat{\mathbf{e}}_z = \omega(0, 0, 1)$ the surface normal is given by $\mathbf{r} = R\hat{\mathbf{e}}_r = R(\sin\theta\cos\phi, \sin\theta\sin\phi, \cos\theta)$. With that we get, $\hat{\mathbf{e}}_z \times \hat{\mathbf{e}}_r = \sin\theta\hat{\mathbf{e}}_\phi$ and finally the current density,*

$$\mathbf{j}(\mathbf{r}) = \frac{Q\omega}{4\pi R}\sin\theta\delta(r - R)\hat{\mathbf{e}}_\phi \ .$$

16.3.3.3 Ex: Train track

The two iron rails of a toy train have a thickness of $d = 5\,\text{mm}$ and a reciprocal distance of $a = 50\,\text{mm}$ They are connected by a metal rod of mass $m = 0.5\,\text{g}$, which is movable without friction in a direction perpendicular to the rails. A current applied to the rails, which also runs through the metal rod, causes the rod to accelerate along the rails.
a. Calculate the magnetic field between the two rails, if through them runs the same current I but in inverse directions. Neglect inhomogeneities at the ends of the rails and the magnetic field generated by the current passing through the rod.
b. How strong is the force accelerating the rod along the rails?
c. What current would be needed to accelerate the rod over a distance of $l = 5\,\text{m}$, up to a speed of $10\,\text{m/s}$? Ignore all friction effects.

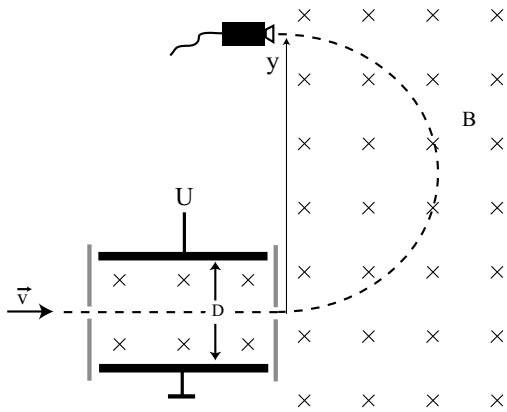

Figure 16.27: Circuit.

Solution:

16.3.3.4 Ex: Mass spectrometer

A mass spectrometer consists, as shown in the figure, of a plate capacitor with $D = 5\,\text{mm}$ distance between the electrodes, placed within a magnetic field $\mathcal{B} = 0.4\,\text{T}$ with homogeneous amplitude. A mixture of isotopes of carbon ion $^{12}C^{+}$ and $^{14}C^{+}$ penetrates the capacitor through a circular slot. After transit through the capacitor the ions move in the magnetic field on a semicircular path and are counted by a detector, whose distance y from the slot can be varied.
a. What voltage should be applied to the plates of the capacitor to ensure that only ions with the velocity $v = 10^5\,\text{m/s}$ can exit the capacitor through the second slot?
b. At what distances y can the two isotopes be detected respectively?

Solution:

16.3.3.5 Ex: Transformer

Consider two similar coils with number of turns N_1 and N_2 connected by an iron yoke. In the first coil we apply a time-varying voltage U_1. Therefore, in this coil (called primary) runs a current I_1, producing a magnetic flux Ψ, which is transmitted entirely through the iron yoke to the second (second) coil. Here, a voltage U_2 is induced.
a. Calculate the ratio U_2/U_1 as a function of the number of turns. What is the behavior of the phase between U_1 and U_2.
b. What are the phases of the currents I_1 and I_2 running through the coils with respect to phases of the voltages? What is the consequence for the average power in the coils?

Solution: *a. The voltage in the primary coil U_1 belongs to a flux through the coil induced by $U_1 = -N_1\dot{\Psi}_1$. Since the entire flux also flows through the second coil, we have $\Psi_2 = \Psi_1$. For the voltage in the second coil we have analogously: $U_2 = -N_2\dot{\Psi}_2$. Hence,*

$$U_2 = -N_2\dot{\Psi}_2 = -N_2\dot{\Psi}_1 = \frac{N_2}{N_1}U_1 \ .$$

The ratio between voltages, therefore, is equal to the ratio of the number of turns. Both voltages oscillate synchronously with the same phase.
b. The currents are proportional to the magnetic fields that, in turn, are proportional to the magnetic flux:

$$I_{1,2} \propto \mathcal{B}_{1,2} \propto \Psi_{1,2} = \Psi \ .$$

Due to,

$$\dot{\Psi} \propto U_{1,2} \propto \cos\omega t$$

we have after integration,

$$I_{1,2} \propto \Psi \propto \sin\omega t \ .$$

For the power $P = UI$ we get,

$$P \propto \sin\omega t \cos\omega t \ .$$

In the time average (integration of P over a period of oscillation) the oscillatory part cancels out in P, so we have $\bar{P} = 0$.
*b. **Presence of a consumer on the secondary side:** We have for the primary and the secondary mesh,*

$$\begin{aligned} U_{01}e^{i\omega t} &= L_1\dot{I}_1 + M\dot{I}_2 \\ -RI_2 &= L_2\dot{I}_2 + M\dot{I}_1 \ . \end{aligned}$$

Eliminating I_1 gives us a differential equation for I_2:

$$\dot{I}_2 + \frac{L_1 R}{L_1L_2 - M^2}I_2 = -\frac{MU_{01}e^{i\omega t}}{L_1L_2 - M^2} \ ,$$

that can be solved by the ansatz $I_2 = I_{02}e^{\imath\omega t+\imath\phi}$*, giving,*

$$\imath\omega I_{02}e^{\imath\phi} + \frac{L_1R}{L_1L_2 - M^2}I_{02}e^{\imath\phi} = -\frac{MU_{01}}{L_1L_2 - M^2} \ .$$

$$I_{02}e^{\imath\phi} = -\frac{MU_{01}}{(L_1L_2 - M^2)\left(\imath\omega + \frac{L_1R}{L_1L_2-M^2}\right)} \ .$$

The absolute value and phase of the current, therefore, are:

$$I_{02} = \left|-\frac{MU_{01}}{(L_1L_2 - M^2)\left(i\omega + \frac{L_1R}{L_1L_2-M^2}\right)}\right| = \frac{MU_{01}}{(L_1L_2 - M^2)}\sqrt{\omega^2 + \left(\frac{L_1R}{L_1L_2 - M^2}\right)^2}$$

$$\tan\phi = \frac{\mathfrak{Im}\ \left(\imath\omega + \frac{L_1R}{L_1L_2-M^2}\right)^{-1}}{\mathfrak{Re}\ \left(\imath\omega + \frac{L_1R}{L_1L_2-M^2}\right)^{-1}} = \frac{-\omega(L_1L_2 - M^2)}{L_1R} \ .$$

16.3.3.6 Ex: Resonant L-R-C-circuit

Consider an excited LRC serial circuit. The components of the oscillating circuit have the values $R = 5\,\Omega$, $C = 10\,\mu\text{F}$, $L = 1\,\text{H}$, and $U = 30\,\text{V}$.
a. At what excitation frequency ω_a does the amplitude of the current have its maximum value? Give the value of the current?
b. At what angular frequencies ω_{a1} and ω_{a2} does the amplitude of the current have exactly half the maximum value? What is therefore the FWHM width of the resonance curve for this oscillating circuit? Show that the width of the resonance curve is given by,

$$\frac{\omega_{a1} - \omega_{a2}}{\omega_a} = R\sqrt{\frac{3C}{L}} \ .$$

c. Make a scheme of some resonance curves for various values of R.

Solution: ***Error, because*** α ***also depends on*** ω***:*** *a. After transient oscillations the current is given by,*

$$I_s(t) = |A|e^{\imath(\omega t+\phi)}$$

with

$$A = -\frac{\alpha}{\omega^2 - \omega_0^2 - i2\beta\omega}$$

where

$$|A| = \frac{\alpha}{\sqrt{(\omega^2 - \omega_0^2)^2 + 4\beta^2\omega^2}} \qquad \textit{and} \qquad \tan\phi = \frac{\mathfrak{Im}\ A}{\mathfrak{Re}\ A} = \frac{2\beta\omega}{\omega^2 - \omega_0^2} \ .$$

Here, we have,

$$\omega_0^2 = \frac{1}{LC} \qquad \textit{and} \qquad 2\beta = \frac{R}{L} \qquad \textit{and} \qquad \alpha = \frac{U_0\omega}{L} \ .$$

The amplitude $|A|$ is maximum when,

$$0 = \frac{d|A|}{d\omega} = \frac{d}{d\omega}\frac{\alpha}{\sqrt{(\omega^2-\omega_0^2)^2+4\beta^2\omega^2}} = 2\alpha\omega\frac{-\omega^2+\omega_0^2-2\beta^2}{\sqrt{(\omega^2-\omega_0^2)^2+4\beta^2\omega^2}^3} \ ,$$

which means,

$$\omega_a = \sqrt{\omega_0^2-2\beta^2} = \sqrt{\frac{1}{LC}-\frac{R^2}{2L^2}} \ .$$

With the given values we get, $\omega_a = 2\pi\cdot 50.326\,\mathrm{Hz}$, during $\omega_0 = 2\pi\cdot 50.329\,\mathrm{Hz}$. The amplitude of the current here is,

$$|A| = \frac{\alpha}{\sqrt{4\beta^4+4\beta^2(\omega_0^2-2\beta^2)}} = \frac{\alpha}{2\beta\omega_0} = \frac{U_0\omega_a}{L}\frac{L}{R}\frac{1}{\omega_0} \simeq \frac{U_0}{R} \ .$$

With the given values we get, $|A| = 6\,\mathrm{A}$.
b. From $\frac{|A(\omega_a)|}{2} = |A(\omega_{a1})|$ we obtain,

$$\begin{aligned}\frac{1}{2\sqrt{4\beta^4+4\beta^2(\omega_0^2-2\beta^2)}} &= \frac{1}{\sqrt{(\omega_{a1}^2-\omega_0^2)^2+4\beta^2\omega_{a1}^2}} \\ &\Longrightarrow \omega_{a1}^4+(4\beta^2-2\omega_0^2)\omega_{a1}^2 = 16\beta^2\omega_0^2-16\beta^4-\omega_0^4 \\ &\Longrightarrow \omega_{a1}^2 = \omega_0^2-2\beta^2\pm 2\sqrt{3\beta^2(\omega_0^2-\beta^2)} \simeq \omega_0^2\pm 2\beta\omega_0\sqrt{3} \ .\end{aligned}$$

With the given values we get, $\omega_{a1} = 2\pi\cdot 51.41\,\mathrm{Hz}$ and $\omega_{a1} = 2\pi\cdot 49.22\,\mathrm{Hz}$. For $\omega_0 \gg \beta$ follows,

$$\begin{aligned}&\omega_{a1}^2 \simeq \omega_0^2 \pm 2\beta\omega_0\sqrt{3} \\ &\Longrightarrow \frac{\omega_{a1}-\omega_{a2}}{\omega_0} = \frac{1}{\omega_0}\frac{\omega_{a1}^2-\omega_{a2}^2}{\omega_{a1}+\omega_{a2}} \simeq \frac{4\beta\omega_0\sqrt{3}}{2\omega_0^2} = \frac{2\beta\sqrt{3}}{\omega_0} = \frac{R\sqrt{3CL}}{L} = R\sqrt{\frac{3C}{L}} \ .\end{aligned}$$

Correction:
a. After the transient process the current is given by,

$$I_s(t) = |A|e^{\imath(\omega t+\phi)}$$

which

$$A = -\frac{U_0}{L}\frac{\omega}{\omega^2-\omega_0^2-i2\beta\omega} \ ,$$

where

$$|A| = \frac{U_0}{L}\frac{\omega}{\sqrt{(\omega^2-\omega_0^2)^2+4\beta^2\omega^2}} \qquad \textit{and} \qquad \tan\phi = \frac{\mathfrak{Im}\ A}{\mathfrak{Re}\ A} = \frac{2\beta\omega}{\omega^2-\omega_0^2} \ .$$

Here, we have,

$$\omega_0^2 = \frac{1}{LC} \qquad \textit{and} \qquad 2\beta = \frac{R}{L} \qquad \textit{and} \qquad \alpha = \frac{U_0\omega}{L} \ .$$

The amplitude $|A|$ is maximum when,

$$0 = \frac{d|A|}{d\omega} = \frac{U_0}{L}\frac{d}{d\omega}\frac{\omega}{\sqrt{(\omega^2-\omega_0^2)^2+4\beta^2\omega^2}} = \frac{U_0}{L}\frac{-\omega^4+\omega_0^4}{\sqrt{(\omega^2-\omega_0^2)^2+4\beta^2\omega^2}^3} \ ,$$

which means,

$$\omega_a = \omega_0 = \sqrt{\frac{1}{LC}} \ .$$

With the given values we get, $\omega_a = 2\pi \cdot 50.326\,\mathrm{Hz}$. The amplitude of the current here is,

$$|A| = \frac{U_0}{L}\frac{\omega}{\sqrt{(\omega^2-\omega_0^2)^2+4\beta^2\omega^2}} = \frac{U_0}{L}\frac{1}{2\beta} = \frac{U_0}{L}\frac{L}{R} \simeq \frac{U_0}{R} \ .$$

With the given values we get, $|A| = 6\,\mathrm{A}$.
b. From $\frac{|A(\omega_a)|}{2} = |A(\omega_{a1})|$ we obtain for $\omega_0 \gg \beta$

$$\begin{aligned}\frac{\omega_a}{2\sqrt{(\omega_a^2-\omega_0^2)^2+4\beta^2\omega_a^2}} &= \frac{\omega_h}{\sqrt{(\omega_h^2-\omega_0^2)^2+4\beta^2\omega_h^2}} \\ &\Longrightarrow \sqrt{(\omega_h^2-\omega_0^2)^2+4\beta^2\omega_h^2} = 4\beta\omega_h \\ &\Longrightarrow \omega_h^2 = (\omega_0^2+6\beta^2) \pm \sqrt{(\omega_0^2+3\beta^2)12\beta^2} \simeq \omega_0^2 \pm \sqrt{12}\beta\omega_0 \ .\end{aligned}$$

With the given values we get, $\omega_{a1} = 2\pi \cdot 51.41\,\mathrm{Hz}$ and $\omega_{a1} = 2\pi \cdot 49.22\,\mathrm{Hz}$. Follows,

$$\frac{\omega_{a1}-\omega_{a2}}{\omega_0} = \frac{1}{\omega_0}\frac{\omega_{a1}^2-\omega_{a2}^2}{\omega_{a1}+\omega_{a2}} \simeq \frac{4\beta\omega_0\sqrt{3}}{2\omega_0^2} = \frac{2\beta\sqrt{3}}{\omega_0} = \frac{R\sqrt{3CL}}{L} = R\sqrt{\frac{3C}{L}} \ .$$

16.3.3.7 Ex: Inductive circuit

Consider the circuit shown in the figure, which consists of a coil L, a voltage source U, and an ohmic resistor $R = 100\,\Omega$. The coil is a long solenoid with 50 turns per cm and an inductance of 200 mH. For times $t < 0$ there is no current flow through the solenoid. At time $t = 0$, the voltage is suddenly increased from 0 to 10 V. How long does it take the magnetic field in the solenoid to reach the value $\pi \cdot 10^{-4}\,\mathrm{T}$?

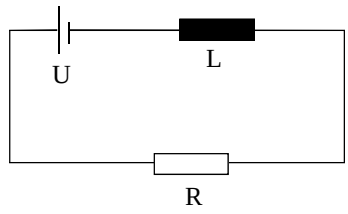

Figure 16.28: Circuit.

Solution: *By Kirchhoff laws,*

$$U(t) = L\dot{I} + RI \ .$$

The homogeneous differential equation is,

$$\frac{dI}{I} = -\frac{R}{L}dt$$

The general solution of the inhomogeneous differential equation is $I(t) = I_0 e^{-Rt/L} + I_{inh}$ *with* $I_{inh} = U_0/R$. *With the initial condition* $I(0) = 0$ *follows* $I_0 = -U_0/R$. *The induced voltage, therefore, is* $U_{ind}(t) = -L\dot{I} = U_0 e^{-Rt/L}$ *and the current after switching on is,*

$$I(t) = \frac{U_0}{R}(1 - e^{-Rt/L}) \ .$$

The magnetic field in the long coil is now,

$$\mathcal{B}_z(t) = \mu_0 \frac{N}{l} I(t) = \mu_0 \frac{N}{l}\frac{U_0}{R}\left(1 - e^{-Rt/L}\right) \ .$$

The given value for the field is reached after a time,

$$t = -\frac{L}{R}\ln\left(1 - \frac{lR\mathcal{B}_z}{\mu_0 N U_0}\right) \simeq 1.39\,\text{ms} \ .$$

16.3.3.8 Ex: Inductive circuit

Consider the circuit shown in the figure, which consists of a coil L, a voltage source $U_0 = 10\,\text{V}$, and three ohmic resistors $R = 100\,\Omega$. The coil is a long solenoid with 50 turns per cm and an inductance of 200 mH. Initially, the switch is open for a long time. Then at time $t = 0$, it is closed.
a. What is the initial value of the magnetic field in the solenoid while the switch is still open?
b. Using Kirchhoff's laws, derive the formula describing the temporal evolution of the field after the switch has been closed.
c. Determine the field for long times after the switch has been closed.

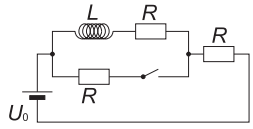

Figure 16.29: Circuit.

Solution: *a. While the switch is open, current only flows through the branch of the solenoid. We have by Kirchhoff's laws,*

$$U_0 = L\dot{I} + RI + RI = 2RI \ ,$$

because at long times, $\dot{I} = 0$. Therefore, the current is,

$$I = \frac{U_0}{2R} \ ,$$

giving $I = 50\,\mathrm{mA}$. The field of the solenoid is now,

$$\mathcal{B} = \mu_0 \frac{N}{\ell} I = \mu_0 \frac{N}{\ell} \frac{U_0}{2R} \ ,$$

giving $\mathcal{B} = 3.14 \cdot 10^{-4}\,\mathrm{T}$.
b. After the switch is closed, the current flows in both branches. We have by Kirchhoff's laws,

$$U_0 = L\dot{I}_L + RI_L + RI \quad , \quad U_0 = RI_R + RI \quad , \quad I = I_L + I_R \ .$$

Eliminating I

$$U_0 = L\dot{I}_L + RI_L + R(I_L + I_R) \quad , \quad U_0 = RI_R + R(I_L + I_R) \ ,$$

and eliminating I_R,

$$U_0 = L\dot{I}_L + RI_L + RI_L + \tfrac{1}{2}(U_0 - RI_L) = L\dot{I}_L + \tfrac{3}{2}RI_L + \tfrac{1}{2}U_0 = 2L\dot{I}_L + 3RI_L \ .$$

We get the differential equation,

$$\int_{I_0}^{I} \frac{dI_L}{I_L - U_0/3R} = -\frac{3R}{2L} \int_0^t dt \ ,$$

with the solution,

$$\ln\left(I_L - \frac{U_0}{3R}\right)\Big|_{I_0}^{I} = -\frac{3R}{2L}t \ .$$

Finally,

$$I_L(t) = \frac{2U_0}{3R} + \left(I_0 - \frac{2U_0}{3R}\right) e^{-3Rt/2L} = \frac{2U_0}{3R} - \frac{U_0}{6R} e^{-3Rt/2L} \ .$$

The magnetic field in the solenoid is now,

$$\mathcal{B}(t) = \mu_0 \frac{N}{\ell} I(t) = \mu_0 \frac{N}{\ell} \frac{U_0}{3R} \left(1 + \frac{1}{2}\right) e^{-3Rt/2L} \ .$$

c. For long times we get,

$$\mathcal{B}(t) = \mu_0 \frac{N}{\ell} \frac{U_0}{3R} \ ,$$

giving $\mathcal{B}(\infty) = 2.09 \cdot 10^{-4}\,\mathrm{V/m}$.

16.3.3.9 Ex: Conductive circular rings

Consider two infinitely thin conducting rings. They are concentric with radii a and b ($a < b$) and arranged in the xy-plane with a common center at the coordinate origin. The inner ring carries a homogeneously distributed charge $+q$ (that is, with linear constant charge density), the outer ring carries the homogeneously distributed charge $-q$.
a. First, write the charge density $\rho(\mathbf{r}) = \rho(r, \phi, z)$ in cylindrical coordinates. Now, let the inner ring rotate with the constant angular velocity ω about the symmetry axis (that is, the z-axis). Write the resulting current density also in cylindrical coordinates. **Help:** $\mathbf{j}(\mathbf{r}) = \rho(\mathbf{r}) \cdot \mathbf{v}(\mathbf{r})$ where $\mathbf{v}(\mathbf{r})$ is the velocity at the position $\mathbf{r}$. b. Determine by an explicit calculation the dipolar magnetic moment $\mathbf{m} = \frac{1}{2} \int d^3r \; \mathbf{r} \times \mathbf{j}(\mathbf{r})$ of the rotating ring.

Solution:

16.4 Alternating current

16.4.1 Electromagnetic oscillations

We have already met the plate capacitor as the most basic device for storing electrostatic energy in an (homogeneous) electric field. Similarly, the solenoid is the most basic device for storing magnetostatic energy in a (homogeneous) magnetic field. Placing a solenoid with inductance L and a capacitor with capacitance C in an electric circuit we find that electric energy can be converted into magnetic energy (and vice versa) in an analogous way as potential energy can be converted into kinetic energy (and vice versa) in a mass-spring system. This can generate (electromagnetic) oscillations.

Example 80 (*Oscillating circuits*): Let us first consider a circuit with a coil and a capacitor connected in series. Kirchhoff's law of meshes requires, $U_{ind} = U_C$, which gives,

$$-L\frac{dI}{dt} = \frac{Q}{C}$$

or

$$L\ddot{I} + C^{-1}I = 0 \; .$$

We now consider a circuit with a battery, a switch, a coil, and a resistor in series. Kirchhoff's law of meshes requires, $U_0 = -U_{ind} + U_R = L\dot{I} + RI$, which gives,

$$\frac{dI}{I - U_0/R} = -\frac{R}{L}dt$$

with the solution

$$I(t) = \frac{U_0}{R} + \left(I_0 - \frac{U_0}{R}\right) e^{-Rt/L} \; ,$$

where we choose the initial current $I_0 = 0$.

16.4.2 Alternating current circuits

To discuss alternating voltages, we consider the circuit shown in Fig. 16.30 fed by a voltage source, $U(t) = U_0 e^{\imath\omega t}$. To simplify the mathematical expressions we adopt a complex notation. The objective is to calculate the current for the various types of consumers Z that we already got to know. In the case of an ohmic resistance we have,

$$I = \frac{U_0}{R} e^{\imath\omega t} = \frac{U}{R} \ . \tag{16.58}$$

Hence,

$$Z = \frac{U}{I} = R \ . \tag{16.59}$$

In the case of a capacitance we have,

$$I = \dot{Q} = C U_0 \frac{d}{dt} e^{\imath\omega t} = \imath\omega C U \ . \tag{16.60}$$

Hence,

$$Z = \frac{U}{I} = \frac{1}{\imath\omega C} \ . \tag{16.61}$$

In the case of an inductance we have,

$$I = \int_0^t L U_0 e^{\imath\omega t} dt = \frac{U}{\imath\omega L} \ . \tag{16.62}$$

Hence,

$$Z = \frac{U}{I} = \imath\omega L \ . \tag{16.63}$$

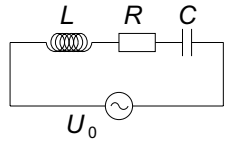

Figure 16.30: *L-R-C* circuit powered by an alternating voltage.

These results can be interpreted graphically (plotting Im U versus Re U) or analytically substituting $\imath = e^{\imath\pi/2}$. For the above three cases we obtain,

$$R = \frac{U_0 e^{\imath\omega t}}{I_0 e^{\imath\omega t + \pi/2}} \quad , \quad L\omega = \frac{U_0 e^{\imath\omega t}}{I_0 e^{\imath\omega t + \imath\pi/2}} \quad , \quad \frac{1}{C\omega} = \frac{U_0 e^{\imath\omega t}}{I_0 e^{\imath\omega t - \imath\pi/2}} \ . \tag{16.64}$$

This means that in the case of an inductance or capacitance, the voltage is not in phase with the current but has, respectively, an advance or a delay of 90°.

In cases of combinations of resistors and reactants the expression to calculate this phase shift becomes more complicated and may vary with the frequency imposed by the alternating source. Let us see how to calculate it at the example of the *L-R-C* circuit in series, writing in the same way as before,

$$Z = \frac{U}{I} = \imath L\omega + R + \frac{1}{\imath C\omega} = |Z| e^{\imath\phi} \ . \tag{16.65}$$

Hence,

$$|Z| = ZZ^* = \sqrt{R^2 + \left(L\omega - \frac{1}{\imath C\omega}\right)^2} \qquad \text{and} \qquad \tan\phi = \frac{\sin\phi}{\cos\phi} = \frac{L\omega - \frac{1}{C\omega}}{R} \ . \quad (16.66)$$

A resonance is met when $\omega = 1/\sqrt{LC}$. Other combinations of components are treated in the same way.

16.4.3 Exercises

16.4.3.1 Ex: High-pass filter

The circuits shown in the figure are called (a) first-order and (b) second-order high-pass filter. Calculate for both cases the ratio of output voltage U_a and input voltage U_e. Suppose that $U_e(t) = U_e \cos\omega t$ and $U_a(t) = U_a \cos(\omega t + \phi)$. Plot the result as a function of frequency on a logarithmic graph with the y-axis $\log(U_a/U_e)$ and the x-axis $\log\omega$. (This graph is called 'Bode diagram'.) What is the phase shift ϕ as a function of frequency?

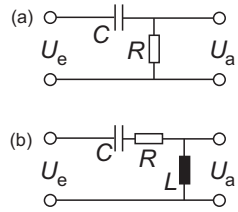

Figure 16.31: High pass.

Solution: *a. First order high-pass filter: We start with the (complex) impedance Z,*

$$Z = \frac{1}{\imath\omega C} + R \ .$$

With this we calculate the current I,

$$I(t) = \frac{U_e}{Z} = \frac{U_0 e^{\imath\omega t}}{1/\imath C\omega + R} \ .$$

The output voltage U_a equals the voltage drop at this impedance.,

$$U_a(t) = U_R = RI(t) = \frac{U_0 e^{\imath\omega t}}{1/\imath CR\omega + 1} = U_0 \frac{\frac{1}{\imath CR\omega} - 1}{\left(\frac{1}{\imath CR\omega}\right)^2 + 1} e^{\imath\omega t}$$
$$= U_0 \frac{\omega CR}{\sqrt{1 + (\omega CR)^2}} e^{\imath[\omega t + \arctan(\omega CR)]} = \tilde{U}_0(\omega) e^{\imath[\omega t + \phi]} \ .$$

b. Second order high-pass filter: Same procedure as above, the output voltage is measured in the coil,

$$Z = \frac{1}{\imath\omega C} + R + \imath L\omega \ .$$

Current,

$$I(t) = \frac{U_e}{Z} = \frac{U_0 e^{\imath\omega t}}{\frac{1}{\imath C\omega} + R + \imath\omega L}$$

Voltage,

$$\begin{aligned} U_a(t) = U_L = -L\dot{I}(t) = \frac{\imath\omega L U_0 e^{\imath\omega t}}{\frac{1}{\imath C\omega} + R + \imath\omega L} = U_0 \frac{1}{-\frac{1}{LC\omega^2} + \frac{R}{\imath\omega L} + 1} e^{\imath\omega t} \\ = U_0 \frac{1 - \frac{1}{LC\omega^2} - \frac{R}{\imath\omega L}}{\left(1 - \frac{1}{LC\omega^2}\right)^2 + \left(\frac{R}{\omega L}\right)^2} e^{\imath\omega t} = \frac{U_0 e^{\imath\left[\omega t + \arctan\left(\frac{R}{\omega L - 1/\omega C}\right)\right]}}{\sqrt{\left(1 - \frac{1}{LC\omega^2}\right)^2 + \left(\frac{R}{\omega L}\right)^2}} \ . \end{aligned}$$

16.4.3.2 Ex: Band and notch filter

The circuits shown in the figure are called (a) bandpass and (b) notch filter. Calculate

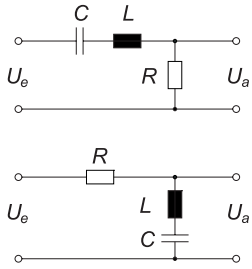

Figure 16.32: Filter.

for both cases the output voltage $U_a(t)$ under the condition that the input voltage is a sinusoidal oscillation, $U_e(t) = U_0 \cos\omega t$. Draw the amplitude of the output voltages as a function of frequency.
a. How do the amplitudes behave in the resonant case?
b. Discuss the limiting cases (i) $L \to 0$ resp., (ii) $C \to \infty$ based on transfer functions.

Solution: *a. For the bandpass filter we have the impedance, resistance, and phase shift,*

$$\begin{aligned} Z(\omega) &= \frac{U_a(\omega)}{U_e(\omega)} = \frac{R}{R + \imath L\omega + \frac{1}{\imath C\omega}} = \frac{R^2 - \imath\left(LR\omega - \frac{R}{C\omega}\right)}{R^2 + \left(L\omega - \frac{1}{C\omega}\right)^2} \\ |Z(\omega)|^2 &= \frac{R^2}{R^2 + \left(L\omega - \frac{1}{C\omega}\right)^2} \\ \phi(\omega) &= \arctan\frac{\mathfrak{Im}\ Z(\omega)}{\mathfrak{Re}\ Z(\omega)} = -\frac{1}{R}\left(L\omega - \frac{1}{C\omega}\right) \ . \end{aligned}$$

In resonance, $|U_a| = |U_e|$.
b. For the notch filter we have the impedance, resistance, and phase shift,

$$Z(\omega) = \frac{U_a(\omega)}{U_e(\omega)} = \frac{\imath L\omega + \frac{1}{\imath C\omega}}{R + \imath L\omega + \frac{1}{\imath C\omega}} = \frac{\left(L\omega - \frac{1}{C\omega}\right)^2 + \imath\left(LR\omega - \frac{R}{C\omega}\right)}{R^2 + \left(L\omega - \frac{1}{C\omega}\right)^2}$$

$$|Z(\omega)|^2 = \frac{\left(L\omega - \frac{1}{C\omega}\right)^2}{R^2 + \left(L\omega - \frac{1}{C\omega}\right)^2}$$

$$\phi(\omega) = \arctan \frac{\mathfrak{Im}\ Z(\omega)}{\mathfrak{Re}\ Z(\omega)} = \frac{R}{L\omega - \frac{1}{C\omega}} \ .$$

In resonance, $|U_a| = 0$.
c. Cases (a.i) and (b.ii) make high-pass filters, cases (a.ii) and (b.i) make low-pass filters.

16.4.3.3 Ex: Coaxial cable

A coaxial cable consists of a cylindrical conductor of radius a and a thin cylindrical waveguide of radius $b > a$. Between the conductors there is a voltage difference of U, and inside them flow currents in opposite directions I. Calculate the Poynting vector in the empty space and the power carried through the cable.
Help: Calculate the electric field between the conductors using Gauß' law and the magnetic field between the conductors using Ampere law.

Solution: *The z-axis is chosen as the rotational symmetry axis of the coaxial cable.*
Calculations of the $\vec{\mathcal{E}}$-field: *Over the inner cable is distributed the charge Q per length L. As always, because of symmetry reasons, the absolute value of the $\vec{\mathcal{E}}$ field only depends on the distance $\rho = \sqrt{x^2 + y^2}$ from the z-axis of the cylinder. Including the direction we have therefore,*

$$\vec{\mathcal{E}} = \mathcal{E}_\rho \hat{\mathbf{e}}_\rho(\mathbf{r})$$

for all $\mathbf{r} = (x, y, z) \in \mathbb{R}^3$ with $\rho \neq 0$. We now consider a cylindrical volume Z_ρ of length L and radius $a \leq \rho < b$, with the z-axis as the axis of rotational symmetry. Now with the law of Gauß and div $\vec{\mathcal{E}} = \rho/\varepsilon_0$, we get,

$$\frac{Q}{\varepsilon_0} = \int_{\partial Z_\rho} \vec{\mathcal{E}} \cdot d\mathbf{F} = 2\pi\rho L \mathcal{E}_\rho \ .$$

Hence, $\mathcal{E}_\rho = \frac{Q}{2\pi\varepsilon_0 L\rho}$ for all the $\rho \in [a, b[$. This leads to the potential,

$$\Phi(\mathbf{r}) \equiv \Phi(\rho) = -\frac{Q}{2\pi\varepsilon_0 L} \ln \rho \ ,$$

for all $\rho \in [a, b]$. (Note that the potential must be continuous, that is, it can be continued to the point $\rho = b$.) The voltage U between the inner and outer conductor is given by the potential difference,

$$U = \Phi(a) - \Phi(b) = \frac{Q}{2\pi\varepsilon_0 L} \ln(b/a) \ .$$

Follows,

$$Q = \frac{2\pi\varepsilon_0 LU}{\ln(b/a)} \ .$$

Inserting the last expression in the formula for $\mathcal{E}_\rho$*, we obtain,*

$$\mathcal{E}_\rho = \frac{U}{\ln(b/a)\rho} \ ,$$

for all $\rho \in [a, b]$*.*

Calculations of the* $\vec{\mathcal{B}}$*-field: *In the inner cable the direction of positive current is chosen to be the* z*-direction. For symmetry reasons the absolute value of the* B*-field only depends on the distance* $\rho = \sqrt{x^2 + y^2}$ *from the* z*-axis of the cylinder, that is,*

$$\vec{\mathcal{B}}(\mathbf{r}) = \mathcal{B}_\rho \hat{\mathbf{e}}_\phi(\mathbf{r})$$

for all $\mathbf{r} = (x, y, z) \in \mathbb{R}^3$ *without the* z*-axis. We consider the area of a disk* K_ρ *with radius* $\rho > 0$ *and the* z*-axis as the axis of symmetry. Then, using Ampere's law,*

$$2\pi\rho\mathcal{B}_\rho = \int_{\partial K_\rho} \vec{\mathcal{B}} \cdot d\mathbf{S} = \mu_0 I(K_\rho) = \mu_0 I$$

for $a \leq \rho < b$ *and* $2\pi\rho B_\rho = 0$ *else. Here,* $I(K_\rho)$ *means the entire current going through the disk* K_ρ*. Hence,*

$$\mathcal{B}_\rho = \frac{\mu_0 I}{2\pi\rho}$$

for $\rho \in [a, b[$*.*

Calculation of the Poynting vector = Energy flow: *We have* $\hat{\mathbf{e}}_\rho(\mathbf{r}) \times \hat{\mathbf{e}}_\phi(\mathbf{r}) = \hat{\mathbf{e}}_z$ *para cada ponto* $\mathbf{r} \in \mathbb{R}$ *except on the* z*-axis, where* $\hat{\mathbf{e}}_\rho$ *and* $\hat{\mathbf{e}}_\phi$ *are not defined. With that, the Poynting vector gets,*

$$\mathbf{S}(\mathbf{r}) = \frac{1}{\mu_0}\vec{\mathcal{E}}(\mathbf{r}) \times \vec{\mathcal{B}}(\mathbf{r}) = \frac{1}{\mu_0} E_\rho \mathcal{B}_\rho \hat{\mathbf{e}}_z = \hat{\mathbf{e}}_z \frac{IU}{2\pi \ln(b/a)\rho^2}$$

for $\rho \in [a, b[$ *and* $\mathbf{S} = 0$ *else, for each point of space* $\mathbf{r} \in \mathbb{R}^3$ *which is not on the* z*-axis. As a result, energy flow only occurs in the space between the inner conductor and the outer conductor, in the direction along the coaxial cable.*

16.4.3.4 Ex: *ac*-resistance

Calculate the work performed by an alternating current $I = I_0 \sin \omega t$ on a conductor with ohmic resistance R over a time period T. Make a scheme of the evolution in a diagram power versus time.

Solution:

16.4.3.5 Ex: *ac*-motor

An alternating voltage motor provides with an alternating voltage of $U = 220\,\mathrm{V}$ at $f = 50\,\mathrm{Hz}$ with the power $P = UI\cos\phi = 2.2\,\mathrm{kW}$. The power factor of the engine is $\cos\phi = 0.6$ and the efficiency $\eta = P_{out}/P_{in} = 0.89$.
a. What current does the motor receive?
b. Which capacitor must be connected in parallel to the terminals of the motor in order to increase the power factor to a value of $\cos\phi = 0.9$? Sketch the current pointer in the $U - I$-plane.

Solution:

16.4.3.6 Ex: Displacement current

a. Explain the significance of the continuity equation,

$$\oint \mathbf{j} \cdot d\mathbf{S} + \frac{d}{dt}\int \rho dV = 0\ .$$

b. Consider an enclosed area $S_1 + S_2$, because here the continuity equation has the form,

$$\oint \mathbf{j} \cdot d\mathbf{S} - \frac{d}{dt}\int \vec{\mathcal{D}} \cdot d\vec{\mathcal{D}}V = 0\ .$$

Show that holds,

$$\oint_C \vec{\mathcal{H}} \cdot d\mathbf{l} = \int_{S_2} \frac{d}{dt}\int \vec{\mathcal{D}} \cdot d\mathbf{S}\ .$$

Help: No field lines penetrate through the area S_1, and no current flows through the area S_2.

Solution:

16.4.3.7 Ex: Resonant *LC*-circuit

The capacitor of an undamped oscillating electromagnetic circuit has the capacity $C = 22$ nF. The eigenfrequency of the circuit is $f_0 = 5735\,\mathrm{Hz}$. At time $t = 0$ the capacitor has its maximum charge: $Q_0 = 0.33\,\mu\mathrm{C}$.
a. Derive for the undamped oscillating circuit the differential equation for $Q(t)$ from the energy conservation law and determine the solution. Write down the equation for eigenfrequency f.
b. Calculate inductance of the coil.
c. Set up equations for the energy content of the coil and and the capacitor as a function of time t.
d. Calculate the instant of time t_2, at which the energy content of the coil is, for the second time, half the energy content of the capacitor.

Solution: *a. The total energy is,* $E_G = E_C(t) + E_L(t) = \frac{1}{2}CU_C^2(t) + \frac{1}{2}LI_L^2(t)$. *With this follows,*

$$\begin{aligned} 0 = \frac{d}{dt}E_G &= CU_C(t)\dot{U}_C(t) + LI_L(t)\dot{I}_C(t) \\ 0 &= \frac{1}{C}Q(t)\dot{Q}(t) + L\dot{Q}(t)\ddot{Q}(t) \\ 0 &= \ddot{Q}(t) + LCQ(t) \ . \end{aligned}$$

The trial of a possible solution $Q(t) = Q_0 \sin(\omega t + \phi)$ *leads us, with* $Q(0) = Q_0$ *to* $\phi = \pi/2$ *and,*

$$f = \frac{1}{2\pi\sqrt{LC}} \ .$$

b. With this the inductance of the coil becomes,

$$L = \frac{1}{4\pi^2 C f} = 35\,\mathrm{mH} \ .$$

c. Energy of the capacitor,

$$E_C(t) = \frac{1}{2}\frac{Q^2}{C} = \frac{1}{2}\frac{Q_0^2\cos^2\omega t}{C} \ .$$

Energy of the coil,

$$E_L(t) = \frac{1}{2}LI^2(t) = \frac{1}{2}\omega^2 L Q_0^2 \sin^2\omega t \ .$$

d. From,

$$\begin{aligned} 2 = \frac{E_C(t)}{E_L(t)} &= \frac{\frac{1}{2}\frac{Q_0^2}{C}\cos^2\omega t}{\frac{1}{2}\omega^2 Q_0^2 \sin^2\omega t} = \frac{1}{\omega^2 C\tan^2\omega t} \\ t &= \frac{1}{\omega}\arctan\frac{1}{\sqrt{2C}\omega} \ . \end{aligned}$$

follows $\Delta t =$.

16.4.3.8 Ex: Resonant *LRC*-circuit

The oscillating *LRC*-circuit shown in 16.30 is excited by the alternating voltage source $U(t) = U_0 \cos\omega t$.
a. Calculate the total impedance Z as a function of ω and prepare graphs of the amplitude response $|Z(\omega)|$ and the phase response $\phi(\omega) = \arctan\frac{\Im\mathfrak{m}\ Z(\omega)}{\Re\mathfrak{e}\ Z(\omega)}$.
b. Establish the differential equation for the current. Start by solving the homogeneous differential equation and then the inhomogeneous one.

Solution: *a. Total impedance and square of absolute value are,*

$$\begin{aligned} Z(\omega) &= \imath\omega L + R + \frac{1}{\imath C\omega} \\ &= R + \imath\left(\omega L - \frac{1}{C\omega}\right) \\ |Z|^2 &= R^2 + (\omega L)^2 + \left(\frac{1}{\omega C}\right)^2 - \frac{2L}{C} \ . \end{aligned}$$

b. $U(T)$ defines a voltage. The coil, resistance and capacitor are opposite. The differential equation, therefore, is,

$$\begin{aligned} U_0 e^{\imath\Omega t} &= U_L + U_R + U_C \\ &= L\dot{I} + RI + \frac{Q}{C} \ . \end{aligned}$$

Drifting once again with $\dot{Q} = I$, we obtain,

$$\frac{U_0\imath\Omega}{L} e^{\imath\Omega t} = \ddot{I} + \frac{R}{L}\dot{I} + \frac{1}{CL} I \ .$$

With the respective definitions for the damping term and the eigenfrequency, the equation is equivalent to that of the harmonic, damped and forced pendulum:

$$\alpha e^{\imath\Omega t} = \ddot{I} + 2\beta\dot{I} + \omega_0^2 I \ .$$

With the trial solution for the homogeneous differential equation $I(t) = I_0 e^{\lambda t}$ we get the characteristic equation,

$$0 = \lambda^2 + 2\beta\lambda + \omega_0^2$$

hence, $\lambda_{1,2} = -\beta \pm \imath\sqrt{\omega_0^2 - \beta^2} \equiv -\beta \pm \imath\omega$. That is, the homogeneous general form is,

$$I_a(t) = e^{-\beta t}\left(B_1 e^{\imath\omega t} + B_2 e^{-\imath\omega t}\right) \ .$$

This solution decays exponentially with the damping constant $\beta = R/2L$. In the general solution, which represents the sum of this homogeneous solution and a particular solution, the homogeneous contribution may be neglected after a characteristic transient phase,

$$I(t) = I_a(t) + I_s(t)$$

with $I_a(t) \to 0$ for $t \gg \beta^{-1}$. We are now looking for another particular solution. The ansatz $I_s(t) = Ae^{\imath\Omega t}$ in the initial equation gives,

$$\alpha = A\left(-\Omega^2 + \imath 2\beta\Omega + \omega_0^2\right) \ .$$

Since A is complex the solution can also be written,

$$A = -\frac{\alpha}{\Omega^2 - \omega_0^2 - \imath 2\beta\Omega} = -\alpha\frac{\Omega^2 - \omega_0^2 + \imath 2\beta\Omega}{\left(\Omega^2 - \omega_0^2\right)^2 + 4\beta^2\Omega^2} = |A|e^{\imath\phi}$$

with

$$|A| = \frac{\alpha}{\sqrt{(\Omega^2 - \omega_0^2)^2 + 4\beta^2\Omega^2}} \qquad \textit{and} \qquad \tan\phi = \frac{\mathfrak{Im}\ A}{\mathfrak{Re}\ A} = \frac{2\beta\Omega}{\Omega^2 - \omega_0^2} \ .$$

Hence, we have the particular solution,

$$I_s(t) = |A|e^{\imath(\Omega t+\phi)} \ .$$

16.4.3.9 Ex: Resonant LRC-circuit

The components of an RLC-circuit (see 16.30) have the values $R = 5\ \Omega$, $C = 10\,\mu\text{F}$, $L = 1\,\text{H}$, and $U = 30\,\text{V}$.
a. At what angular frequency ω_a does the current amplitude have its maximum value? What is the corresponding current?
b. At what angular frequencies ω_{a1} and ω_{a2} does the amplitude of the current have half the maximum value? What is the relative half-width of the resonance curve for this resonant circuit?
c. Show with the help of the formulas of (b) that the relative half-width of each resonance curve is given by,

$$\frac{\Delta_a}{\omega} = R\sqrt{\frac{3C}{L}} \ ,$$

where Δ_a is the width of the resonance profile at half the maximum amplitude.
d. Prepare schemes of the resonance profile for various values of R. When is the current circuit predominantly capacitive and when inductive?
e. Show that the damping term $e^{-Rt/2L}$ (containing L but not C!) can be written in a more symmetrical form in L and C as follows,

$$e^{-\pi R\frac{t}{T}\sqrt{\frac{C}{L}}} \ .$$

Here, T is the period of oscillation when we neglect resistance. What is the SI-unit of the term $\sqrt{C/L}$?
f. Show, based on the result (e), that the condition for a smaller relative energy loss per oscillation cycle is: $R \ll \sqrt{L/C}$.

Solution:

16.4.3.10 Ex: Resonant LRC-circuit

Consider a dampened oscillating RLC-circuit. The charge $\bar{q}$ on the capacitor is described by the differential equation,

$$L\frac{d^2\bar{q}}{dt^2} + R\frac{d\bar{q}}{dt} + \frac{1}{C}\bar{q} = 0 \ .$$

a. Use the ansatz $\bar{q} = q_0 e^{\imath\omega t}$ and show that,

$$\omega_{1,2} = \imath\frac{R}{2L} \pm \omega' \qquad \text{where} \qquad \omega' = \omega_0\sqrt{1 - \frac{R^2C}{4L}}$$

with $\omega_0 = 1/\sqrt{LC}$ solves the differential equation.
b. Since this is a second order differential equation, we need two boundary conditions to determine the general solution of the form,

$$\bar{q}(t) = a\bar{q}_1(t) + b\bar{q}(t) \qquad \text{with} \qquad \bar{q}_{1,2} = \bar{q}_0 e^{-\frac{R}{2L}t} e^{\pm \imath\omega' t} \ .$$

Use the conditions $\bar{q}(0) = 0$ and $\dot{\bar{q}}(0) = I_0$ and determine the coefficients a and b. What is the solution for the charge $\bar{q}(t)$ in this case, and for the current $I(t) = \dot{\bar{q}}(t)$?
c. Sketch the evolution of the charge and the current on the capacitor for the following set of parameters and interpret the curves. What is the respective duration T of an oscillation period? Give for each of the following parameter sets the respective general solution before entering the values:
i. $I_0 = 1\,\text{mA}$, $R = 10\,\Omega$, $L = 1\,\text{mH}$, $C = 0.1\,\mu\text{F}$
ii. $I_0 = 1\,\text{mA}$, $R = 200\,\Omega$, $L = 1\,\text{mH}$, $C = 0.1\,\mu\text{F}$
iii. $I_0 = 1\,\text{mA}$, $R = 500\,\Omega$, $L = 1\,\text{mH}$, $C = 0.1\,\mu\text{F}$

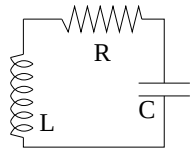

Figure 16.33: Resonant LRC-circuit.

Solution:

16.4.3.11 Ex: Magnetized sphere

We consider a sphere with radius R magnetized such that, inside the sphere, the magnetic field density is given by $\vec{\mathcal{B}} = \mathcal{B}_0 \hat{\mathbf{e}}_z$. The outer space is empty, that is, there are no currents, such that rot $\vec{\mathcal{B}} = 0$ and div $\vec{\mathcal{B}} = 0$. Therefore, we can let for the outer space,

$$\vec{\mathcal{B}} = -\text{grad}\Psi \quad \text{and} \quad \Psi(r, \vartheta, \varphi) = \sum_{l=0}^{\infty} \alpha_l \frac{P_l(\cos\vartheta)}{r^{l+1}} \ ,$$

with P_l the Legendre polynomials and r, ϑ and φ the usual spherical coordinates. Consider the boundary conditions for $\mathcal{B}_r$, $\mathcal{B}_\theta$ as well as for $\mathcal{H}_r$ and $\mathcal{H}_\theta$ at the transition between the inner and outer space of the sphere. Determine from this the expansion coefficients α_l as well as the magnetization $\vec{\mathcal{M}}$ inside the sphere. With this we finally get the magnetic field density $\vec{\mathcal{B}}$ magnetic $\vec{\mathcal{H}}$-field in the inner and outer space.

Solution:

16.4.3.12 Ex: Magnetic dipole moving through a conductive loop

What is the current signal produced by a ^{87}Rb Bose-Einstein condensate with its spin being polarized in the state $|F, m_F\rangle = |2, 2\rangle$ when it falls through a SQUID? Assume

that the SQUID has the diameter $2a = 3\,\mathrm{cm}$, the condensate consists of $N = 100000$ atoms and has a constant velocity of $v_z = 10\,\mathrm{cm/s}$.

Solution: *In the specified state each atom has a dipolar magnetic moment $\mu = \mu_B$. This moment creates, at the point $\mathbf{r} = (x, y, z)$, a magnetic field,*

$$\vec{\mathcal{B}} = \frac{\mu_0}{4\pi r^5} \begin{pmatrix} 3xz \\ 3yz \\ 3z^2 - r^2 \end{pmatrix} .$$

The magnetic flux through the SQUID enclosing an area $\mathbf{A} = \pi a^2 \mathbf{n}$ in the $x = y = 0$ plane then is,

$$\Psi = \int_A \vec{\mathcal{B}} \cdot \hat{\mathbf{e}}_n dF = \int_0^a 2\pi\rho \mathcal{B}_z d\rho = \frac{\mu_0}{2} \int_0^a \frac{3z^2 - r^2}{r^5} \rho d\rho = \frac{\mu_0}{2} \frac{a^2}{(a^2 + z^2)^{3/2}} .$$

For a point dipole we can suppose, $z = \dot{z}t$. The induced current in the SQUID is now,

$$U_{ind}(t) = -\dot{\Psi} = \frac{3a^2\mu_0}{2} \frac{z\dot{z}}{(a^2 + z^2)^{5/2}} .$$

With the specified numerical values we get voltages on the order of $10^{-17}\,\mathrm{V}$ and currents in the SQUID of the order of pA.

16.4.3.13 Ex: Electric current and magnetism

a. How are current and current density defined? What is a 'current line'?
b. What conditions should charge and current densities meet in magnetostatics?
c. How is the magnetic field $\vec{\mathcal{B}}$ defined empirically?
d. Writes the general form of Ampère's law. How is Ampère's law expressed in the case of two parallel conductors carrying currents I_1 and I_2?
e. What does the Ampère's law say?
f. What is the magnetic moment of an arbitrary, flat, closed current circuit?
g. What are the force and thye torque on a magnetic dipole in an external field $\vec{\mathcal{B}}(\mathbf{r})$.
h. Explain the term 'magnetization current density'.
i. What are the macroscopic equations of the magnetostatic field?
j. What is diamagnetism and paramagnetism? What differentiates these two phenomena? What is ferromagnetism?

Solution: *a. The current is defined by $I = \dot{Q}$; the current density is $\mathbf{j} = I/A$; a current wire is an idealization of current flow to 1 dimension.*
b. The current and current density must satisfy the continuity equation $\frac{\partial \rho}{\partial t} = \nabla \cdot \mathbf{j} = 0$.
c. Empirically the magnetic field $\vec{\mathcal{B}}$ is defined by Lorentz forces acting on currents. Currents are the cause of the field, but simultaneously subject to their action.
d. Ampère's law on forces is $d\mathbf{A} = Id\mathbf{l} \times \vec{\mathcal{B}}$. In the case of two parallel conductors with currents I_1 and I_2 the law predicts a force of mutual attraction.

e. Ampère's law on fluxes $\oint \vec{\mathcal{B}} \cdot d\mathbf{s} = \mu_0 I$ *says, that magnetic field lines are always closed (unlike electrostatic ones). Magnetic fields have no start or end points. Currents produce closed field lines around them. Here, the line integral over the magnetic field density on the edge of a surface is proportional to the total current crossing this surface.*
f. The magnetic moment of an arbitrary, flat and closed current circuit is, $\mathbf{m} = \frac{1}{2}\int \mathbf{r}' \times \mathbf{j}(\mathbf{r}')d^3r' = \frac{1}{2}\oint_{\partial\mathcal{S}} \mathbf{r}' \times d\mathbf{l} = I\int_F d\mathbf{A} = I\mathbf{A}$.
g. The force on a magnetic dipole in an external field is $\mathbf{F} = -\nabla U$ *with* $U = -\mathbf{m}\cdot\vec{\mathcal{B}}$. *The torque is,* $\vec{\mathcal{D}} = \mathbf{m} \times \vec{\mathcal{B}}$.
h. In matter with magnetization (density of magnetic dipoles) $\vec{\mathcal{M}}$ *the magnetization current density* $\mathbf{m} = \nabla \times \vec{\mathcal{M}}$ *adds to the macroscopic current density.*
i. The macroscopic field equations of magnetostatics are, $\text{rot}\,\vec{\mathcal{B}} = \mu_0\mathbf{j}$ *and* $\text{div}\,\vec{\mathcal{B}} = 0$ *respectively, with Stokes and Gauß laws,* $\int_s \vec{\mathcal{B}}\cdot d\mathbf{r} = \mu_0\int \mathbf{j}\cdot d\mathbf{A} = I$ *and* $\oint_f \vec{\mathcal{B}}\cdot d\mathbf{A} = 0$.
j. Diamagnetism is generated by induced dipoles. In the material, due to an applied magnetic field, an opposite magnetization is formed. Diamagnetic bodies are repelled by a permanent magnet in the direction opposite to the field gradient. Paramagnetism is generated by permanent dipoles located within the material. Paramagnetic bodies are attracted to a magnet. For diamagnetism, $\chi_m < 0$, *for paramagnetism,* $\chi_m > 0$. *In the case of ferromagnetism, the permanent dipole moments align within the so-called Weiß domains and therefore amplify.*

16.4.3.14 Ex: Electro-motor

Consider the electromotor of the scheme. Two pairs of Helmholtz coils aligned along the x- and y-axes are powered by alternating currents, $I_x(t) = I_0\cos\omega t$ and $I_y(t) = I_0\sin\omega t$, respectively. In the field there is a rotating rectangular coil traversed by a constant current I. The inertial moment of the coil is $\mathcal{I}$.
a. Show that the field in the center is given by $\mathcal{B}_x(0) = \frac{-8}{5\sqrt{5}}\frac{\mu_0 I_x \hat{\mathbf{e}}_x}{R}$.
b. Describes the temporal behavior of the magnetic field.
c. Relate the torque with the angular acceleration of the coil.
d. Calculate the instantaneous torque acting on the coil.
e. Suppose that the coil initially rotates with an angular velocity Ω such that, $\theta(t) = \theta_0 + \Omega t$. How you should choose Ω and the initial angle θ_0 to ensure an always positive torque? **Help:** $\sin\alpha\cos\beta + \cos\alpha\sin\beta = \sin(\alpha+\beta)$
f. Calculate the voltage induced in the coil. **Help:** $\sin\alpha\sin\beta + \cos\alpha\cos\beta = \cos(\alpha-\beta)$
g. Suppose the coil has an ohmic resistance ...

Solution: *a.*
b. The coils generate a rotating magnetic field, $\vec{\mathcal{B}}(t) = \mathcal{B}_0(\hat{\mathbf{e}}_x\cos\omega t + \hat{\mathbf{e}}_y\sin\omega t)$.
c. The torque is,

$$\vec{\tau} = \mathcal{I}\ddot{\theta}\ .$$

d. The Lorentz force is,

$$\mathbf{F}(t) = I\mathbf{l}\times\vec{\mathcal{B}}(t) = I\mathcal{B}_0(\mathbf{l}\times\hat{\mathbf{e}}_x\cos\omega t + \mathbf{l}\times\hat{\mathbf{e}}_y\sin\omega t) = Il\mathcal{B}_0(-\hat{\mathbf{e}}_y\cos\omega t + \hat{\mathbf{e}}_x\sin\omega t)\ .$$

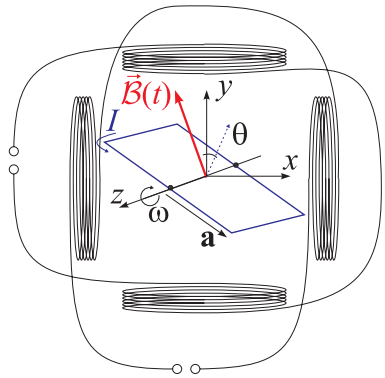

Figure 16.34: Electro-motor.

we write the vector, $\mathbf{a} = a[\hat{\mathbf{e}}_x \cos(\theta - 90^\circ) + \hat{\mathbf{e}}_y \sin(\theta - 90^\circ)] = a\hat{\mathbf{e}}_x \sin\theta - a\hat{\mathbf{e}}_y \cos\theta$. *With this the torque becomes,*

$$\begin{aligned}\vec{\tau} = \mathbf{a} \times \mathbf{F}(t) &= aIlB_0(\hat{\mathbf{e}}_x \sin\theta - \hat{\mathbf{e}}_y \cos\theta) \times (-\hat{\mathbf{e}}_y \cos\omega t + \hat{\mathbf{e}}_x \sin\omega t) \\ &= aIlB_0\hat{\mathbf{e}}_z(-\sin\theta\cos\omega t + \cos\theta\sin\omega t) = \sin(\omega t - \theta)\ .\end{aligned}$$

e. The initial angle should be,

$$\sin[\omega t - (\Omega t + \theta_0)] = -\sin\theta_0 > 0\ .$$

That is, we need $\Omega = \Omega$ *and* $\theta_0 \in [-180^\circ, 0]$.
f. Expressing the surface as $\mathbf{A} = la(-\hat{\mathbf{e}}_x \sin\theta + \hat{\mathbf{e}}_y \cos\theta)$, *the induced voltage is,*

$$\begin{aligned}U_{ind} = -\frac{d}{dt}\vec{\mathcal{B}} \cdot \mathbf{A} &= -la\mathcal{B}_0 \frac{d}{dt}(\hat{\mathbf{e}}_x \cos\omega t + \hat{\mathbf{e}}_y \sin\omega t) \cdot (-\hat{\mathbf{e}}_x \sin\theta + \hat{\mathbf{e}}_y \cos\theta) \\ &= -la\mathcal{B}_0(-\hat{\mathbf{e}}_x \sin\omega t + \hat{\mathbf{e}}_y \cos\omega t) \cdot (-\hat{\mathbf{e}}_x \sin\theta + \hat{\mathbf{e}}_y \cos\theta) \\ &= -la\mathcal{B}_0(\sin\omega t \sin\theta + \cos\omega t \cos\theta) \\ &= \cos(\omega t - \theta) = \cos\theta_0\ .\end{aligned}$$

g.

16.4.3.15 Ex: Magnetism

A given magnetic material is composed of N non-interacting atoms, whose magnetic moments μ can point in three possible directions, as shown in the figure, μx, μy, and $-\mu x$. The system is in thermal equilibrium at temperature T and subject to a uniform magnetic field oriented along the y-direction, $\vec{\mathcal{H}} = \mathcal{H}\hat{\mathbf{e}}_y$, so the energy levels corresponding to a single atom are $\varepsilon_0 = -\mu\mathcal{H}$, $\varepsilon_1 = 0$, and $\varepsilon_2 = 0$.
a. Get the canonical partition function z for one atom, the canonical partition function Z of the system, and the Helmholtz free energy f per atom.
b. Determine the mean energy $u \equiv \langle\varepsilon_n\rangle$ and the entropy s/k_B per atom.
c. Get magnetization per atom $\mathbf{m} \equiv \langle\vec{\mu}_n\rangle = m_x\hat{x} + m_y\hat{y}$.

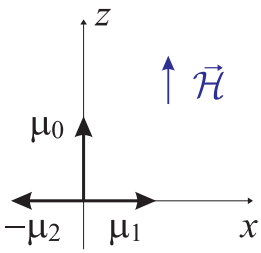

Figure 16.35:

d. Verify that the isothermal susceptibility $\chi_T \equiv (\partial m_y/\partial \mathcal{H})_T \propto 1/T$ at zero field obeys Curie's law of paramagnetism, $\chi_T(\mathcal{H} \to 0) \propto 1/T$.

Solution: *a. We have* $\varepsilon_0 = -\mu\mathcal{H}$ *and* $\varepsilon_1 = \varepsilon_2 = 0$. *Now,*

$$z = \sum_{n=0}^{2} e^{-\beta\varepsilon_n} = e^{\beta\mu\mathcal{H}} + 2$$
$$Z = \sum_{n} e^{-\beta E_n} = z^N = (e^{\beta\mu\mathcal{H}} + 2)^N$$
$$f = -\tfrac{1}{\beta}\ln z = -\frac{1}{\beta}\ln(e^{\beta\mu\mathcal{H}} + 2)\ .$$

b. Firstly,

$$u \equiv \langle\varepsilon_n\rangle = \sum_{n=0}^{2}\frac{\varepsilon_n e^{-\beta\varepsilon_n}}{z} = -\tfrac{1}{z}\sum_{n=0}^{2}\frac{\partial e^{-\beta\varepsilon_n}}{\partial\beta} = -\frac{1}{z}\frac{\partial z}{\partial\beta} = -\frac{\partial\ln z}{\partial\beta} = -\frac{\mu\mathcal{H}e^{\beta\mu\mathcal{H}}}{e^{\beta\mu\mathcal{H}}+2}\ .$$

From the definition $f = u - Ts$, *we get,*

$$\frac{s}{k_B} = \beta(u-f) = -\frac{\beta\mu\mathcal{H}e^{\beta\mu\mathcal{H}}}{e^{\beta\mu\mathcal{H}}-2} + \ln(e^{\beta\mu\mathcal{H}}+2)\ .$$

c. We have,

$$m = \langle\mu_n\rangle = \tfrac{1}{z}\sum_{n=0}^{2}\mu_n e^{-\beta\varepsilon_n} = \tfrac{1}{z}(\mu\hat{y}e^{\beta\mu\mathcal{H}} + \mu\hat{x} - \mu\hat{x}) = \frac{\mu\hat{y}e^{\beta\mu\mathcal{H}}}{e^{\beta\mu\mathcal{H}}+2}\ .$$

d. We already know $m_y = \mu/(1+2e^{-\beta\mu\mathcal{H}})$. *Thereby,*

$$\chi_T \equiv \left(\frac{\partial m_y}{\partial\mathcal{H}}\right)_T = \frac{2\beta\mu^2 e^{-\beta\mu\mathcal{H}}}{(1+2e^{-\beta\mu\mathcal{H}})^2}\ .$$

Thereby, $\chi_T(\mathcal{H}\to 0) = \frac{2}{9}\beta\nu^2 = \frac{2}{9}\mu^2/k_BT$.
Alternative solution:
Expanding

$$m_y = \tfrac{1}{3}\frac{\mu}{(1-\frac{2}{3}\beta\mu\mathcal{H})} + O(\beta\mu\mathcal{H})^2 = \tfrac{1}{3}(1+\tfrac{2}{3}\beta\mu\mathcal{H}) + O(\beta\mu\mathcal{H})^2\ .$$

Now,

$$\chi_T \equiv \left.\frac{\partial m_y}{\partial \mathcal{H}}\right|_T = \tfrac{2}{9}\beta\mu^2 + O(\beta\mu\mathcal{H}) \ ,$$

and

$$\chi_T(\mathcal{H} \to 0) = \tfrac{2}{9}\beta\mu^2 = \tfrac{2}{9}\mu^2 k_B T \ .$$

16.5 Further reading

D.J. Griffiths, *Introduction to Electrodynamics* [545]ISBN

D. Halliday, R. Resnick, and J. Walker, *Fundamentals of Physics* [577]ISBN

H.M. Nussenzveig, *Curso de Física Básica: Eletromagnetismo (Volume 3)* [963]ISBN

Chapter 17

Maxwell's equations

In the first part of the course, we derived the laws of electromagnetism from experimental observations related to the Coulomb force on electric charges and the Lorentz force on electric currents. We have found that these forces can be understood by introducing electric fields $\vec{\mathcal{E}}$ and magnetic fields $\vec{\mathcal{B}}$, to which the laws of electromagnetism apply. These laws were all known before Maxwell. These are,

$$\begin{aligned}
\nabla \times \vec{\mathcal{B}} &= \mu_0 \mathbf{j} && \textit{Ampère's law} \text{ leading to } \textit{Biot-Savart's law} \\
\nabla \times \vec{\mathcal{E}} &= -\partial_t \vec{\mathcal{B}} && \textit{Faraday's law} \\
\nabla \cdot \vec{\mathcal{E}} &= \varepsilon_0^{-1} \varrho && \textit{Gauß' law} \text{ leading to } \textit{Poisson's law} \text{ and } \textit{Coulomb's law} \\
\nabla \cdot \vec{\mathcal{B}} &= 0 && \text{absence of magnetic monopoles}
\end{aligned} \tag{17.1}$$

As we will show shortly, well-behaved vector fields are entirely defined by their divergences and rotations, so that we can expect that the set of laws (17.1) be complete, that is, it should be able to describe all electromagnetic phenomena.

However, by comparing the laws of Faraday and Ampère, we perceive an inconsistency: taking the divergences of the rotations, we expect them to zero:

$$\begin{aligned}
0 = \nabla \cdot (\nabla \times \vec{\mathcal{E}}) &= \nabla \cdot \left(-\frac{\partial \vec{\mathcal{B}}}{\partial t} \right) = -\frac{\partial}{\partial t} (\nabla \cdot \vec{\mathcal{B}}) \\
0 = \nabla \cdot (\nabla \times \vec{\mathcal{B}}) &= \mu_0 (\nabla \cdot \mathbf{j}) = -\mu_0 \frac{\partial \varrho}{\partial t} \neq 0 \ ,
\end{aligned} \tag{17.2}$$

where the last step makes use of the continuity equation (14.39). For temporal variations of the charge distribution the second equation can not be correct.

Maxwell's idea for solving the problem was to simply subtract from Ampère's law the term that prevents the second equation (17.2) from zeroing. With

$$\boxed{\nabla \times \vec{\mathcal{B}} = \mu_0 \mathbf{j} + \varepsilon_0 \mu_0 \frac{\partial \vec{\mathcal{E}}}{\partial t}} \ , \tag{17.3}$$

we verify,

$$\nabla \cdot (\nabla \times \vec{\mathcal{B}}) = \mu_0 \nabla \cdot \mathbf{j} + \varepsilon_0 \mu_0 \frac{\partial \nabla \cdot \vec{\mathcal{E}}}{\partial t} = \mu_0 \left(\nabla \cdot \mathbf{j} + \frac{\partial \varrho}{\partial t} \right) = 0 \ , \tag{17.4}$$

where, once more, we used the continuity equation. The Eq. (17.3) could be called *Maxwell's law* and the surface integral of the additional term,

$$\varepsilon_0 \frac{\partial}{\partial t} \oint_{\mathcal{S}} \vec{\mathcal{E}} \cdot d\mathbf{S} \equiv \oint_{\mathcal{S}} \mathbf{j}_d \cdot d\mathbf{S} = I_d \ . \tag{17.5}$$

is named *displacement current*. We will study consequences of this law in the Excs. 17.1.5.1 and 17.1.5.2.

Example 81 (*Necessity of a displacement current*): We consider the circuit shown in Fig. 17.1. On the one hand, the current passing through the Ampèrian loop must be independent of the shape of the enclosed area,

$$I = \int_{\mathcal{S}} \mathbf{j} \cdot d\mathbf{S} = \tfrac{1}{\mu_0} \oint_{\partial\mathcal{S}} \vec{\mathcal{B}} \cdot d\mathbf{l} \ .$$

On the other hand, we know that the current can not cross the capacitor and must accumulate on one of the electrodes.
The problem is solved by identifying the electric field, which is developing due to the accumulated charge,

$$\frac{\partial Q}{\partial t} = \varepsilon_0 \frac{\partial}{\partial t} \int_{\mathcal{V}} \nabla \cdot \vec{\mathcal{E}} dV = \varepsilon_0 \frac{\partial}{\partial t} \int_{\partial\mathcal{V}} \vec{\mathcal{E}} \cdot d\mathbf{S} \equiv I_d \ ,$$

with a *displacement current* I_d.

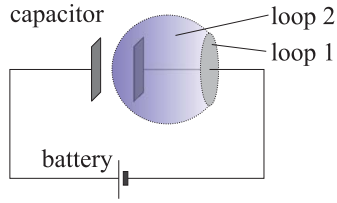

Figure 17.1: Necessity for a displacement current: The magnetic field at the edge of the loops 1 and 2 can not depend on the shape of the chosen surface.

17.1 The fundamental laws of electrodynamics

With these results we can finally summarize the *Maxwell equations* as,

$$\boxed{\begin{array}{lrcl} \text{(i)} & \nabla \times \vec{\mathcal{B}} - \varepsilon_0 \mu_0 \partial_t \vec{\mathcal{E}} & = & \mu_0 \mathbf{j} \\ \text{(ii)} & \nabla \times \vec{\mathcal{E}} + \partial_t \vec{\mathcal{B}} & = & 0 \\ \text{(iii)} & \nabla \cdot \vec{\mathcal{E}} & = & \varepsilon_0^{-1} \varrho \\ \text{(iv)} & \nabla \cdot \vec{\mathcal{B}} & = & 0 \end{array}} \ . \tag{17.6}$$

These equations form the complete basis of the electrodynamical theory initially motivated by the empirical observation of forces acting on features of matter identified

as *charges* and *currents*, that is, the electric (Coulomb) force and magnetic (Lorentz) force,

$$\mathbf{F}_{Lor} = Q(\vec{\mathcal{E}} + \mathbf{v} \times \vec{\mathcal{B}}) \ , \tag{17.7}$$

where $\vec{\mathcal{E}}$ is a *polar vector* ($\vec{\mathcal{E}} = -\vec{\mathcal{E}}_{mirrored}$) [1] and $\vec{\mathcal{B}}$ is an *axial vector* ($\vec{\mathcal{B}} = \vec{\mathcal{B}}_{mirrored}$). The electric field $\vec{\mathcal{E}}$ and the magnetic field $\vec{\mathcal{B}}$ and their field equations were 'invented' to explain the Coulomb-Lorentz force. They are only observable through their action on charged particles. According to the *Helmholtz theorem* discussed in the next section, arbitrary (but well-behaved) field vectors are fully defined by their divergence and rotation properties. That is exactly what Maxwell's equations do with the electric and magnetic fields.

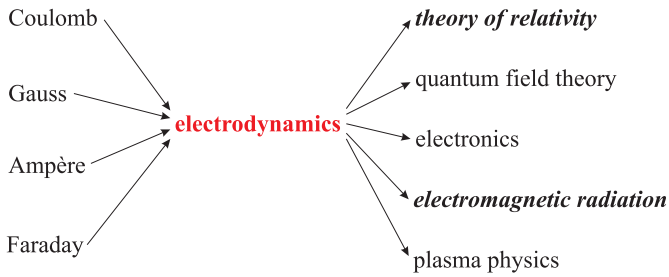

Figure 17.2: Construction and application of the theory of electrodynamics.

Once we know the fundamental laws of electromagnetism [2], we can reverse the reasoning by placing them as postulates and deriving the observable phenomena from them. This will be the procedure of this second part of the course of electromagnetism.

Example 82 (*Derivation of electro- and magnetostatics from Maxwell's equations*): For static systems we can let $\dot{\mathbf{E}} = \dot{\mathbf{B}} = 0$. In particular for the electrostatic case, we ignore currents, $\mathbf{j} = 0$, and for the magnetostatic case we ignore charges, $\varrho = 0$. Maxwell's equations then simplify considerably and can often be replaced by the Poisson equations,

$$-\nabla \cdot \vec{\mathcal{E}} = \nabla \cdot (\nabla\Phi) = \nabla^2\Phi = -\varepsilon_0^{-1}\varrho$$
$$-\nabla \times \vec{\mathcal{B}} = -\nabla \times (\nabla \times \mathbf{A}) = \nabla^2\mathbf{A} - \nabla(\cancelto{0}{\nabla \cdot \mathbf{A}}) = -\mathbf{j} \ ,$$

where the divergence of $\mathbf{A}$ is set to zero in the Coulomb gauge.

We will apply Maxwell's equations to solve the Excs. 17.1.5.3 to Excs. 17.1.5.5. In the Excs. 17.1.5.6, 17.1.5.7, and 17.1.5.8 we study implications of a supposed existence of *magnetic charges* or *magnetic monopoles*.

[1] Mirroring means inversion of the dynamic quantities $\mathbf{v} \to -\mathbf{v}$, $\mathbf{F}_{Lor} \to -\mathbf{F}_{Lor}$. Examples for polar vectors are $\mathbf{r}$, $\mathbf{p}$, $\vec{\mathcal{E}}$. Examples for axial vectors are $\mathbf{L}$, ω, $\vec{\mathcal{B}}$. We have for axial vectors $\mathbf{a}_i$ and polar vectors $\mathbf{p}_i$, the following relations,

$$\mathbf{a}_1 \times \mathbf{a}_2 = \mathbf{a}_3 \quad , \quad \mathbf{p}_1 \times \mathbf{p}_2 = \mathbf{a}_3 \quad , \quad \mathbf{p}_1 \times \mathbf{a}_2 = \mathbf{p}_3 \ .$$

[2] We note, that Maxwell's laws can be deduced from more fundamental principles, including the conservation laws for energy, momentum, angular momentum, and charge and the relativistic Lorentz transform.

17.1.1 Helmholtz's theorem

The *Helmholtz theorem* says that, knowing the divergence and the rotation of an unknown vector field $\mathbf{F}$, we can reconstruct this field under the condition that the divergence and the rotation disappear sufficiently fast in the infinity [3] and that $|\mathbf{F}|$ disappears at least as fast as $1/r^2$. That is, knowing the scalar field,

$$D(\mathbf{r}) \equiv \nabla \cdot \mathbf{F}(\mathbf{r}) \tag{17.8}$$

and the vectorial field,

$$\mathbf{C}(\mathbf{r}) \equiv \nabla \times \mathbf{F}(\mathbf{r}) \ , \tag{17.9}$$

the field $\mathbf{F}$ is completely defined. Note that obviously, $\nabla \cdot \mathbf{C} = 0$.

To prove this, we show that,

$$\mathbf{F} = -\nabla\Phi + \nabla \times \mathbf{A} \ , \tag{17.10}$$

where

$$\Phi(\mathbf{r}) \equiv \frac{1}{4\pi}\int_{\mathbb{R}^3} \frac{D(\mathbf{r}')}{|\mathbf{r}-\mathbf{r}'|}dV' \qquad \text{and} \qquad \mathbf{A}(\mathbf{r}) \equiv \frac{1}{4\pi}\int_{\mathbb{R}^3} \frac{\mathbf{C}(\mathbf{r}')}{|\mathbf{r}-\mathbf{r}'|}dV' \ , \tag{17.11}$$

meets the requirements (17.8) and (17.9). The divergence is,

$$\begin{aligned} \nabla_{\mathbf{r}} \cdot \mathbf{F} &= -\nabla^2_{\mathbf{r}}\Phi + \cancelto{0}{\nabla_{\mathbf{r}} \cdot \nabla_{\mathbf{r}} \times \mathbf{A}} \\ &= -\frac{1}{4\pi}\int D(\mathbf{r}')\nabla^2_{\mathbf{r}}\left(\frac{1}{|\mathbf{r}-\mathbf{r}'|}\right)dV' = \int D(\mathbf{r}')\delta^3(\mathbf{r}-\mathbf{r}')dV' = D(\mathbf{r}) \ . \end{aligned} \tag{17.12}$$

We verify,

$$\begin{aligned} 4\pi\nabla_{\mathbf{r}} \cdot \mathbf{A} &= \int \mathbf{C}(\mathbf{r}') \cdot \nabla_{\mathbf{r}} \frac{1}{|\mathbf{r}-\mathbf{r}'|}dV' = -\int \mathbf{C}(\mathbf{r}') \cdot \nabla_{\mathbf{r}'} \frac{1}{|\mathbf{r}-\mathbf{r}'|}dV' \\ &= -\int \frac{1}{|\mathbf{r}-\mathbf{r}'|} \cancelto{\nabla \cdot \nabla \times \mathbf{F} = 0}{\nabla_{\mathbf{r}'} \cdot \mathbf{C}(\mathbf{r}')}dV' - \oint \frac{1}{|\mathbf{r}-\mathbf{r}'|}\mathbf{C}(\mathbf{r}') \cdot d\mathbf{S}' \longrightarrow 0 \ , \end{aligned} \tag{17.13}$$

because the surface integral can be arbitrarily reduced by choosing very distant surfaces $\mathbf{r}' \to \infty$. Finally, the rotation is,

$$\begin{aligned} \nabla_{\mathbf{r}} \times \mathbf{F} &= \cancelto{0}{-\nabla_{\mathbf{r}} \times \nabla_{\mathbf{r}}\Phi} + \nabla_{\mathbf{r}} \times \nabla_{\mathbf{r}} \times \mathbf{A} = -\nabla^2_{\mathbf{r}}\mathbf{A} + \nabla_{\mathbf{r}}(\cancelto{0}{\nabla_{\mathbf{r}} \cdot \mathbf{A}}) \\ &= -\frac{1}{4\pi}\int \mathbf{C}(\mathbf{r}')\nabla^2_{\mathbf{r}}\left(\frac{1}{|\mathbf{r}-\mathbf{r}'|}\right)dV' = \int \mathbf{C}(\mathbf{r}')\delta^3(\mathbf{r}-\mathbf{r}')dV' = \mathbf{C}(\mathbf{r}) \ , \end{aligned} \tag{17.14}$$

using rules of vector analysis summarized in (21.111).

17.1.2 Potentials in electrodynamics

In electrodynamics, two fields are required to describe the Coulomb and Lorentz forces, the electric and the magnetic field. With Helmholtz's theorem we can now

[3] Faster than $1/r$ in order to guarantee that the integrals (17.8) and (17.9) converge.

declare that four equations are necessary and sufficient to completely characterize these fields through the following rotations and divergences,

$$\text{rot}\,\vec{\mathcal{B}} = \ldots \quad , \quad \text{rot}\,\vec{\mathcal{E}} = \ldots \quad , \quad \text{div}\,\vec{\mathcal{E}} = \ldots \quad , \quad \text{div}\,\vec{\mathcal{B}} = \ldots \,. \tag{17.15}$$

These equations are precisely those of Maxwell. In addition, the derivation of the preceding section showed that

> *each vector field which disappears fast enough at long distances can be expressed as the sum of the gradient of a scalar function and rotation of a vector function,*

since,

$$\mathbf{F} = -\nabla\Phi + \nabla\times\mathbf{A} = -\nabla\frac{1}{4\pi}\int_{\mathbb{R}^3}\frac{D(\mathbf{r}')}{|\mathbf{r}-\mathbf{r}'|}dV' + \nabla\times\frac{1}{4\pi}\int_{\mathbb{R}^3}\frac{\mathbf{C}(\mathbf{r}')}{|\mathbf{r}-\mathbf{r}'|}dV' \,. \tag{17.16}$$

The functions Φ and $\mathbf{A}$ are called *scalar potential* and *vector potential*, respectively.

Irrotational fields, that is, fields without vortices are conservative and can be expressed by the gradient of a scalar field,

$$\nabla\times\mathbf{F} = 0 \quad \Longleftrightarrow \quad \mathbf{A} = 0 \quad \Longleftrightarrow \quad \mathbf{F} = -\nabla\Phi \quad \Longleftrightarrow \quad \oint \mathbf{F}\cdot d\mathbf{l} = 0 \,. \tag{17.17}$$

Example 83 (*Potentials in electrostatics*): Electrostatics is an example for an irrotational field, since Maxwell's electrostatic equations are precisely, $\nabla\times\vec{\mathcal{E}} = 0$ and $\nabla\cdot\vec{\mathcal{E}} = D = \varrho/\varepsilon_0$. Therefore, there is an electric potential Φ, such that $-\nabla\Phi = \vec{\mathcal{E}}$.

Fields without divergences, that is, without sources or sinks, can be expressed by the rotation of a vector field,

$$\nabla\cdot\mathbf{F} = 0 \quad \Longleftrightarrow \quad \Phi = 0 \quad \Longleftrightarrow \quad \mathbf{F} = \nabla\times\mathbf{A} \quad \Longleftrightarrow \quad \oint \mathbf{F}\cdot d\mathbf{S} = 0 \,. \tag{17.18}$$

Example 84 (*Potentials in magnetostatics*): Magnetostatics is an example for a field without divergences, since Maxwell's magnetostatic equations are precisely, $\nabla\times\vec{\mathcal{B}} = \mathbf{C} = \mu_0\mathbf{j}$ and $\nabla\cdot\vec{\mathcal{B}} = 0$. Therefore, there is a vector potential $\mathbf{A}$, such that $\nabla\times\mathbf{A} = \vec{\mathcal{B}}$.

We will train the calculation with potentials in Excs. 17.1.5.9 and 17.1.5.10.

17.1.3 The macroscopic Maxwell equations

Electric and magnetic fields and electromagnetic waves survive in vacuum. Maxwell's equations (17.6) are formulated for this environment. On the other hand, we saw in the first part of the course, that charges (14.17) and currents (16.20) that are free or localized in a medium generate a polarization and a magnetization of the medium which can influence the fields.

In this section, we will repeat the derivation of the equations (14.18), respectively, (16.21) in a more stringent way from a microscopic model of matter. We suppose

matter to be made of molecules, each one being constructed from atoms composed of positively charged nuclei orbited by negatively charged electrons. On each of these elementary particles considered as point-like, the electromagnetic field diverges. But doing this statement, we are talking about microscopic electromagnetic fields, which can not be measured by macroscopic probes which, are composed of atoms themselves. We can not directly measure microscopic quantities with a macroscopic apparatus.

According to the model of matter already formulated by Democritus 300 years before Christ, we suppose the space between the elementary particles to be empty, such that we can assume the validity of Maxwell's equations for vacuum in a *microscopic environment*, that is, we believe in the equations (17.6) for the fields $\vec{\mathcal{E}}_{mic}$ and $\vec{\mathcal{B}}_{mic}$, where the subscript *mic* indicates the presence of localized or moving point-like charges. A macroscopic measurement apparatus will always deliver an effective mean value, averaged in space and time, of electromagnetic quantities. We will show in the following [659] how, via spatial averaging of Maxwell's microscopic equations, it is possible to deduce Maxwell's macroscopic equations taking account of polarization and magnetization (14.18), respectively, (16.21).

We obtain the spatial average by smearing out the microscopic quantities within a characteristic volume defined by a spherically symmetric function $f(r)$, chosen to cancel out exponentially at sufficiently large distances [4]. The reach of this function must be adapted to the resolution of the macroscopic device. For example, the resolution limit for devices based on optics will limit the reach of the function $f(r)$ to some 100 nm [5]. The spatial average of the electromagnetic quantities $\vec{\mathcal{E}}_{mic}(\mathbf{r},t)$, $\vec{\mathcal{B}}_{mic}(\mathbf{r},t)$, $\varrho_{mic}(\mathbf{r},t)$, and $\mathbf{j}_{mic}(\mathbf{r},t)$ is then,

$$\langle X_{mic}(\mathbf{r},t)\rangle \equiv \int_{\mathbb{R}^3} d^3\mathbf{r}' f(\mathbf{r}') X_{mic}(\mathbf{r}-\mathbf{r}',t)\ . \tag{17.19}$$

The macroscopic fields are defined as the averages of the respective microscopic fields:

$$\vec{\mathcal{E}}(\mathbf{r},t) \equiv \langle \vec{\mathcal{E}}_{mic}(\mathbf{r},t)\rangle \qquad \text{and} \qquad \vec{\mathcal{B}}(\mathbf{r},t) \equiv \langle \vec{\mathcal{B}}_{mic}(\mathbf{r},t)\rangle\ , \tag{17.20}$$

where macroscopic quantities do not have the subscript *mic*.

Now, taking the averages of the microscopic Maxwell equations, we obtain,

$$\begin{array}{lrcl}
\text{(i)} & \langle \nabla\times\vec{\mathcal{B}}_{mic}(\mathbf{r},t)\rangle - \varepsilon_0\mu_0\left\langle \frac{\partial\vec{\mathcal{E}}_{mic}(\mathbf{r},t)}{\partial t}\right\rangle &=& \mu_0\langle \mathbf{j}_{mic}(\mathbf{r},t)\rangle \\
\text{(ii)} & \langle \nabla\times\vec{\mathcal{E}}_{mic}(\mathbf{r},t)\rangle + \left\langle \frac{\partial\vec{\mathcal{B}}_{mic}(\mathbf{r},t)}{\partial t}\right\rangle &=& 0 \\
\text{(iii)} & \langle \nabla\cdot\vec{\mathcal{E}}_{mic}(\mathbf{r},t)\rangle &=& \frac{1}{\varepsilon_0}\langle \varrho_{mic}(\mathbf{r},t)\rangle \\
\text{(iv)} & \langle \nabla\cdot\vec{\mathcal{B}}_{mic}(\mathbf{r},t)\rangle &=& 0
\end{array}\ . \tag{17.21}$$

However,

$$\begin{aligned}
\langle \nabla\cdot\vec{\mathcal{E}}_{mic}(\mathbf{r},t)\rangle &= \nabla\cdot\langle\vec{\mathcal{E}}_{mic}(\mathbf{r},t)\rangle = \nabla\cdot\vec{\mathcal{E}}(\mathbf{r},t) \\
\langle \nabla\times\vec{\mathcal{E}}_{mic}(\mathbf{r},t)\rangle &= \nabla\times\langle\vec{\mathcal{E}}_{mic}(\mathbf{r},t)\rangle = \nabla\times\vec{\mathcal{E}}(\mathbf{r},t)\ ,
\end{aligned} \tag{17.22}$$

[4] An example for a normalized smoothing function is $f(\mathbf{r}') \equiv (a/\pi)^{3/2}e^{-ar'^2}$, as it satisfies $\int_{\mathbb{R}^3} f(\mathbf{r}')d^3r' = 1$.

[5] In contrast, X-rays with a resolution of about 10 nm allow for an analysis of the microscopic structure of matter.

and analogously for $\vec{\mathcal{B}}_{mic}$, since ∇ acts only on $\mathbf{r}$ and not on the integration variable $\mathbf{r}'$. On the other hand, the partial time-derivative also does not act on $\mathbf{r}$ nor on $\mathbf{r}'$,

$$\left\langle \frac{\partial \vec{\mathcal{E}}_{mic}(\mathbf{r},t)}{\partial t} \right\rangle = \frac{\partial}{\partial t}\langle \vec{\mathcal{E}}_{mic}(\mathbf{r},t)\rangle = \frac{\partial \vec{\mathcal{E}}(\mathbf{r},t)}{\partial t} \ , \tag{17.23}$$

and analogously for $\vec{\mathcal{B}}_{mic}$. Thus, we already deduced the two homogeneous macroscopic Maxwell equations (ii) and (iv), and the set of equations (17.21) simplifies to:

$$\begin{aligned}
&\text{(i)} && \nabla\times\vec{\mathcal{B}}(\mathbf{r},t) - \varepsilon_0\mu_0\partial_t\vec{\mathcal{E}}(\mathbf{r},t) &&= \mu\langle \mathbf{j}_{mic}(\mathbf{r},t)\rangle \\
&\text{(ii)} && \nabla\times\vec{\mathcal{E}}(\mathbf{r},t) + \partial_t\vec{\mathcal{B}}(\mathbf{r},t) &&= 0 \\
&\text{(iii)} && \nabla\cdot\vec{\mathcal{E}}(\mathbf{r},t) &&= \tfrac{1}{\varepsilon_0}\langle \varrho_{mic}(\mathbf{r},t)\rangle \\
&\text{(iv)} && \nabla\cdot\vec{\mathcal{B}}(\mathbf{r},t) &&= 0
\end{aligned} \ , \tag{17.24}$$

but we still need to calculate $\langle \varrho_{mic}(\mathbf{r},t)\rangle$ and $\langle \mathbf{j}_{mic}(\mathbf{r},t)\rangle$.

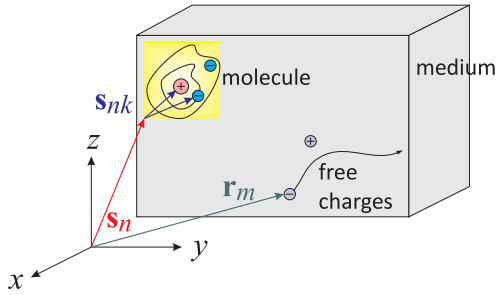

Figure 17.3: Charges localized in molecules and free charges.

To do so we imagine that, as illustrated in Fig. 17.3, there are N charges in each molecule of the material and, for simplicity, we also assume the material to be a pure substance, that is to say, composed of identical molecules. Be $\vec{\mathcal{S}}_n$ the position of the n-th molecule, measured from an arbitrary origin of the coordinate system. Thus, the k-th charge q_{kn} of the n-th molecule is at the point $\vec{\mathcal{S}}_{kn}$, with respect to the position vector of the molecule $\vec{\mathcal{S}}_n$. This means that, with respect to the origin of the coordinate system, the position of the charge q_{kn} is given by $\vec{\mathcal{S}}_{kn} + \vec{\mathcal{S}}_n$. We will also allow for free charges, q_m, at positions $\mathbf{r}_m$. As all the charges can move, all their positions $\mathbf{r}_m(t)$, $\vec{\mathcal{S}}_n(t)$, and $\vec{\mathcal{S}}_{kn}(t)$ must be considered as functions of time.

First, we will calculate the charge density,

$$\varrho_{mic}(\mathbf{r},t) = \sum_m q_m\delta^{(3)}(\mathbf{r}-\mathbf{r}_m) + \sum_{n,k} q_{kn}\delta^{(3)}(\mathbf{r}-\vec{\mathcal{S}}_{kn}-\vec{\mathcal{S}}_n) \ , \tag{17.25}$$

and using the definition of the spatial average (17.19),

$$\langle \varrho_{mic}(\mathbf{r},t)\rangle = \sum_m q_m f(\mathbf{r}-\mathbf{r}_m) \ (\to \varrho(\mathbf{r},t)) + \sum_{n,k} q_{kn} f(\mathbf{r}-\vec{\mathcal{S}}_{kn}-\vec{\mathcal{S}}_n) \ , \tag{17.26}$$

where we recall, that the first term represents the macroscopic density of free charges $\varrho(\mathbf{r},t)$. Typically, $|\vec{\mathcal{S}}_{kn}|$ is on the order of some Angströms only, and therefore the 'smoothing' function $f(\mathbf{r}-\vec{\mathcal{S}}_{kn}-\vec{\mathcal{S}}_n)$ does not appreciably differ from $f(\mathbf{r}-\vec{\mathcal{S}}_n)$, such that we can approximate:

$$f(\mathbf{r}-\vec{\mathcal{S}}_{kn}-\vec{\mathcal{S}}_n) \simeq f(\mathbf{r}-\vec{\mathcal{S}}_n) - \vec{\mathcal{S}}_{kn}\cdot\nabla f(\mathbf{r}-\vec{\mathcal{S}}_n) + \tfrac{1}{2}(\vec{\mathcal{S}}_{kn}\cdot\nabla)^2 f(\mathbf{r}-\vec{\mathcal{S}}_n)\ , \quad (17.27)$$

and, with this approximation, obtain,

$$\begin{aligned}\langle\varrho_{mic}(\mathbf{r},t)\rangle &\simeq \varrho(\mathbf{r},t) + \sum_{n,k} q_{kn} f(\mathbf{r}-\vec{\mathcal{S}}_n) - \sum_{n,k} q_{kn}\vec{\mathcal{S}}_{kn}\cdot\nabla f(\mathbf{r}-\vec{\mathcal{S}}_n) \\ &\quad + \sum_{n,k} q_{kn}\tfrac{1}{2}(\vec{\mathcal{S}}_{kn}\cdot\nabla)^2 f(\mathbf{r}-\vec{\mathcal{S}}_n) \\ &= \varrho(\mathbf{r},t) + \cancelto{0}{\sum_{n,k} q_{kn}} f(\mathbf{r}-\vec{\mathcal{S}}_n) - \nabla\cdot\sum_n\left(\sum_k q_{kn}\vec{\mathcal{S}}_{kn}\right) f(\mathbf{r}-\vec{\mathcal{S}}_n) \\ &\quad + \tfrac{1}{6}\sum_n \nabla\cdot\left[\left(3\cancelto{0}{\sum_k q_{kn}\vec{\mathcal{S}}_{kn}\vec{\mathcal{S}}_{kn}}\right)\cdot\nabla f(\mathbf{r}-\vec{\mathcal{S}}_n)\right] \\ &= \varrho(\mathbf{r},t) - \nabla\cdot\sum_n \mathbf{d}_n f(\mathbf{r}-\vec{\mathcal{S}}_n)\ .\end{aligned} \quad (17.28)$$

In the last line we assumed that each molecule is neutral,

$$\sum_k q_{kn} = 0\ , \quad (17.29)$$

we use the definition of the electric dipole moment of the n-th molecule,

$$\mathbf{d}_n = \sum_k q_{kn}\vec{\mathcal{S}}_{kn}\ , \quad (17.30)$$

and we suppose, to simplify our calculations below, that the electric quadrupole momentum of the n-th molecule,

$$\overleftrightarrow{Q}_n \equiv 3\sum_k q_{kn}\vec{\mathcal{S}}_{kn}\vec{\mathcal{S}}_{kn} \stackrel{!}{=} \overleftrightarrow{0}\ , \quad (17.31)$$

is zero, that is, that the molecules of the material have zero electric quadrupolar momentum. As shown in the discussion of the relationship (??), the polarization of a medium is the sum of the individual instantaneous dipole moments of each molecule,

$$\vec{\mathcal{P}}_{mic}(\mathbf{r},t) = \sum_n \mathbf{d}_n\delta^{(3)}(\mathbf{r}-\vec{\mathcal{S}}_n)\ , \quad (17.32)$$

With these observations, we conclude that,

$$\langle\vec{\mathcal{P}}_{mic}(\mathbf{r},t)\rangle = \sum_n \mathbf{d}_n f(\mathbf{r}-\vec{\mathcal{S}}_n)\ , \quad (17.33)$$

and, identifying this quantity in the expression (17.28), we get,

$$\langle \varrho_{mic}(\mathbf{r},t)\rangle \simeq \varrho(\mathbf{r},t) - \nabla\cdot\vec{\mathcal{P}}(\mathbf{r},t)\ , \tag{17.34}$$

where we introduced the abbreviation, $\vec{\mathcal{P}}(\mathbf{r},t) \equiv \langle \vec{\mathcal{P}}_{mic}(\mathbf{r},t)\rangle$, analogously to the electrostatic case. The macroscopic Gauß law (17.21)(iii) becomes then,

$$\nabla\cdot\vec{\mathcal{E}}(\mathbf{r},t) = \tfrac{1}{\varepsilon_0}[\varrho(\mathbf{r},t) - \nabla\cdot\vec{\mathcal{P}}(\mathbf{r},t)]\ , \tag{17.35}$$

that is,

$$\nabla\cdot\vec{\mathcal{D}}(\mathbf{r},t) = \varrho(\mathbf{r},t)\ , \tag{17.36}$$

where we defined the field of *electric displacement* as,

$$\boxed{\vec{\mathcal{D}}(\mathbf{r},t) \equiv \varepsilon_0\vec{\mathcal{E}}(\mathbf{r},t) + \vec{\mathcal{P}}(\mathbf{r},t)}\ . \tag{17.37}$$

Let us now calculate, $\langle \mathbf{j}_{mic}(\mathbf{r},t)\rangle$. From the very definition of the microscopic current we have,

$$\mathbf{j}_{mic}(\mathbf{r},t) \equiv \varrho_{mic}(\mathbf{r},t)\mathbf{v}_{mic}(\mathbf{r},t)\ , \tag{17.38}$$

where $\mathbf{v}_{mic}(\mathbf{r},t)$ is the velocity field of the charges of the material medium. By inserting the expression (17.25) for the charge density,

$$\begin{aligned}\mathbf{j}_{mic}(\mathbf{r},t) &= \sum_m q_m\delta^{(3)}(\mathbf{r}-\mathbf{r}_m)\mathbf{v}_{mic}(\mathbf{r},t) + \sum_{n,k} q_{kn}\delta^{(3)}(\mathbf{r}-\vec{\mathcal{S}}_{kn}-\vec{\mathcal{S}}_n)\mathbf{v}_{mic}(\mathbf{r},t) \\ &= \sum_m q_m\dot{\mathbf{r}}_m\delta^{(3)}(\mathbf{r}-\mathbf{r}_m) + \sum_{n,k} q_{kn}(\dot{\mathbf{s}}_{kn}+\dot{\mathbf{s}}_n)\delta^{(3)}(\mathbf{r}-\vec{\mathcal{S}}_{kn}-\vec{\mathcal{S}}_n)\ ,\end{aligned} \tag{17.39}$$

where the field of charge velocities calculated exactly at the location of the m-th charge gives the value of its velocity,

$$\delta^{(3)}(\mathbf{r}-\mathbf{x})\mathbf{v}_{mic}(\mathbf{r},t) = \delta^{(3)}(\mathbf{r}-\mathbf{x})\dot{\mathbf{x}}\ .$$

We can now evaluate the average (17.19),

$$\langle \mathbf{j}_{mic}(\mathbf{r},t)\rangle = \sum_m q_m\dot{\mathbf{r}}_m f(\mathbf{r}-\mathbf{r}_m) \longrightarrow \mathbf{j}(\mathbf{r},t) + \sum_{n,k} q_{kn}(\dot{\mathbf{s}}_{kn}+\dot{\mathbf{s}}_n)f(\mathbf{r}-\vec{\mathcal{S}}_{kn}-\vec{\mathcal{S}}_n)\ , \tag{17.40}$$

where we recall, that the first term represents the macroscopic density of free current $\mathbf{j}(\mathbf{r},t)$. Approximating again,

$$f(\mathbf{r}-\vec{\mathcal{S}}_{kn}-\vec{\mathcal{S}}_n) \simeq f(\mathbf{r}-\vec{\mathcal{S}}_n) - \vec{\mathcal{S}}_{kn}\cdot\nabla f(\mathbf{r}-\vec{\mathcal{S}}_n)\ , \tag{17.41}$$

and, with this approximation, we obtain,

$$\langle \mathbf{j}_{mic}(\mathbf{r},t)\rangle \simeq \mathbf{j}(\mathbf{r},t) + \sum_{n,k} q_{kn}(\dot{\mathbf{s}}_{kn}+\dot{\mathbf{s}}_n)f(\mathbf{r}-\vec{\mathcal{S}}_n) - \sum_{k,n} q_{kn}(\dot{\mathbf{s}}_{kn}+\dot{\mathbf{s}}_n)\vec{\mathcal{S}}_{kn}\cdot\nabla f(\mathbf{r}-\vec{\mathcal{S}}_n)\ . \tag{17.42}$$

As we are now working to obtain the macroscopic Ampère-Maxwell equation, we need to let appear in the above results the rotation of the magnetization, in addition to the time derivative of the polarization. Recalling that the magnetic dipole moment of the n-th molecule $\vec{\mu}_n$ is defined by equation (15.43) as,

$$\vec{\mu}_n \equiv \tfrac{1}{2}\sum_k q_{kn}\vec{\mathcal{S}}_{kn}\times\dot{\mathbf{s}}_{kn}\ , \tag{17.43}$$

based on the relationship (16.15), we can write magnetization as the sum of the instantaneous magnetic dipole moments of every molecule,

$$\vec{\mathcal{M}}_{mic}(\mathbf{r},t) = \sum_n \vec{\mu}_n \delta^{(3)}(\mathbf{r}-\vec{\mathcal{S}}_n)\ , \tag{17.44}$$

Thus, we want to identify, in the expression for $\langle \mathbf{j}_{mic}(\mathbf{r},t)\rangle$, the rotation of $\langle\vec{\mathcal{M}}_{mic}(\mathbf{r},t)\rangle$:

$$\begin{aligned}\nabla\times\langle\vec{\mathcal{M}}_{mic}(\mathbf{r},t)\rangle &= \nabla\times\sum_n\vec{\mu}_n f(\mathbf{r}-\vec{\mathcal{S}}_n) = -\sum_n\vec{\mu}_n\times\nabla f(\mathbf{r}-\vec{\mathcal{S}}_n) \\ &= -\tfrac{1}{2}\sum_{n,k} q_{kn}(\vec{\mathcal{S}}_{kn}\times\dot{\mathbf{s}}_{kn})\times\nabla f(\mathbf{r}-\vec{\mathcal{S}}_n) \\ &= -\tfrac{1}{2}\sum_{n,k} q_{kn}\dot{\mathbf{s}}_{kn}[\vec{\mathcal{S}}_{kn}\cdot\nabla f(\mathbf{r}-\vec{\mathcal{S}}_n)] + \tfrac{1}{2}\sum_{n,k} q_{kn}\vec{\mathcal{S}}_{kn}[\dot{\mathbf{s}}_{kn}\cdot\nabla f(\mathbf{r}-\vec{\mathcal{S}}_n)]\ ,\end{aligned} \tag{17.45}$$

using the BAC-CAB rule (21.110)(v), and continuing,

$$\begin{aligned}\nabla\times\langle\vec{\mathcal{M}}_{mic}(\mathbf{r},t)\rangle &= -\sum_{n,k} q_{kn}\dot{\mathbf{s}}_{kn}\vec{\mathcal{S}}_{kn}\cdot\nabla f(\mathbf{r}-\vec{\mathcal{S}}_n) + \tfrac{1}{2}\sum_n\left[\sum_k q_{kn}\frac{d}{dt}(\vec{\mathcal{S}}_{kn}\vec{\mathcal{S}}_{kn})\right]\cdot\nabla f(\mathbf{r}-\vec{\mathcal{S}}_n) \\ &= -\sum_{n,k} q_{kn}\dot{\mathbf{s}}_{kn}\vec{\mathcal{S}}_{kn}\cdot\nabla f(\mathbf{r}-\vec{\mathcal{S}}_n) + \tfrac{1}{6}\sum_n\left[\frac{d}{dt}\left(3\sum_k q_{kn}\vec{\mathcal{S}}_{kn}\vec{\mathcal{S}}_{kn}\right)^{0}\right]\cdot\nabla f(\mathbf{r}-\vec{\mathcal{S}}_n)\ .\end{aligned} \tag{17.46}$$

The second term is zero again because, as in (17.31), we are assuming that $\overleftrightarrow{Q}_n \overset{!}{=} \overleftrightarrow{0}$. Continuing the calculation (17.42),

$$\begin{aligned}\langle\mathbf{j}_{mic}(\mathbf{r},t)\rangle = \mathbf{j}(\mathbf{r},t) &+ \sum_{n,k} q_{kn}\dot{\mathbf{s}}_{kn} f(\mathbf{r}-\vec{\mathcal{S}}_n) + \sum_{n,k} q_{kn}^{\ 0}\dot{\mathbf{s}}_n f(\mathbf{r}-\vec{\mathcal{S}}_n) \\ &+ \nabla\times\langle\vec{\mathcal{M}}_{mic}(\mathbf{r},t)\rangle - \sum_{n,k} q_{kn}\dot{\mathbf{s}}_n\vec{\mathcal{S}}_{kn}\cdot\nabla f(\mathbf{r}-\vec{\mathcal{S}}_n)\ .\end{aligned} \tag{17.47}$$

The third term disappears, because again we are assuming that the total charge of every molecule is zero, $\sum_k q_{kn} = 0$. The partial temporal derivative of the polarization is given by the expression (17.33),

$$\begin{aligned}\frac{\partial\vec{\mathcal{P}}(\mathbf{r},t)}{\partial t} &= \frac{\partial}{\partial t}\sum_{n,k} q_{kn}\vec{\mathcal{S}}_{kn} f(\mathbf{r}-\vec{\mathcal{S}}_n) = \sum_{n,k} q_{kn}\frac{\partial\vec{\mathcal{S}}_{kn}}{\partial t} f(\mathbf{r}-\vec{\mathcal{S}}_n) + \sum_{n,k} q_{kn}\vec{\mathcal{S}}_{kn}\frac{\partial}{\partial t} f(\mathbf{r}-\vec{\mathcal{S}}_n) \\ &= \sum_{n,k} q_{kn}\dot{\mathbf{s}}_{kn} f(\mathbf{r}-\vec{\mathcal{S}}_n) - \sum_{n,k} q_{kn}\vec{\mathcal{S}}_{kn}\dot{\mathbf{s}}_n\cdot\nabla f(\mathbf{r}-\vec{\mathcal{S}}_n)\ .\end{aligned} \tag{17.48}$$

We can use this result to replace the second term in equation (17.47),

$$\langle \mathbf{j}_{mic}(\mathbf{r},t)\rangle \simeq \mathbf{j}(\mathbf{r},t) + \nabla\times\langle\vec{\mathcal{M}}_{mic}(\mathbf{r},t)\rangle + \frac{\partial\vec{\mathcal{P}}(\mathbf{r},t)}{\partial t} + \sum_{n,k} q_{kn}[\vec{\mathcal{S}}_{kn}\dot{\mathbf{s}}_n\cdot\nabla f(\mathbf{r}-\vec{\mathcal{S}}_n) - \dot{\mathbf{s}}_n\vec{\mathcal{S}}_{kn}\cdot\nabla f(\mathbf{r}-\vec{\mathcal{S}}_n)] \ . \tag{17.49}$$

Note, that the last term of this expression is identical to (17.45) with the difference, that the electronic velocities $\dot{\mathbf{s}}_{kn}$ of that expression or now replaced by the molecular velocities $\dot{\mathbf{s}}_n$.

Now let us suppose that the material itself is not in motion, so that the (averaged absolute) velocities of the molecules, $\dot{\mathbf{s}}_n$, are much smaller than the (averaged absolute) velocities of the charges in every molecule, $\dot{\mathbf{s}}_{kn}$. With this, we can neglect the last term of the above equation in comparison to the first,

$$\mu_0\langle \mathbf{j}_{mic}(\mathbf{r},t)\rangle \simeq \mu_0\mathbf{j}(\mathbf{r},t) + \mu_0\frac{\partial\vec{\mathcal{P}}(\mathbf{r},t)}{\partial t} + \mu_0\nabla\times\langle\vec{\mathcal{M}}_{mic}(\mathbf{r},t)\rangle \ . \tag{17.50}$$

The Ampère-Maxwell equation, then reads in its spatial average (17.21)(i),

$$\begin{aligned}\nabla\times\vec{\mathcal{B}}(\mathbf{r},t) &= \mu_0\langle\mathbf{j}_{mic}(\mathbf{r},t)\rangle + \varepsilon_0\mu_0\left\langle\frac{\partial\vec{\mathcal{E}}_{mic}(\mathbf{r},t)}{\partial t}\right\rangle \\ &= \mu_0\mathbf{j}(\mathbf{r},t) + \mu_0\frac{\partial\vec{\mathcal{P}}(\mathbf{r},t)}{\partial t} + \mu_0\nabla\times\langle\vec{\mathcal{M}}_{mic}(\mathbf{r},t)\rangle + \varepsilon_0\mu_0\frac{\partial\vec{\mathcal{E}}(\mathbf{r},t)}{\partial t} \ ,\end{aligned} \tag{17.51}$$

or,

$$\nabla\times[\vec{\mathcal{B}}(\mathbf{r},t) - \mu_0\nabla\times\langle\vec{\mathcal{M}}_{mic}(\mathbf{r},t)\rangle] = \mu_0\mathbf{j}(\mathbf{r},t) + \mu_0\frac{\partial}{\partial t}[\varepsilon\vec{\mathcal{E}}(\mathbf{r},t) + \vec{\mathcal{P}}(\mathbf{r},t)] \ , \tag{17.52}$$

Introducing the abbreviation,

$$\vec{\mathcal{M}}(\mathbf{r},t) \equiv \langle\vec{\mathcal{M}}_{mic}(\mathbf{r},t)\rangle \ , \tag{17.53}$$

defining *magnetic excitation* field,

$$\boxed{\vec{\mathcal{H}}(\mathbf{r},t) \equiv \tfrac{1}{\mu_0}\vec{\mathcal{B}}(\mathbf{r},t) - \vec{\mathcal{M}}(\mathbf{r},t)} \ , \tag{17.54}$$

and recognizing the electric displacement field, $\vec{\mathcal{D}}(\mathbf{r},t) = \varepsilon_0\vec{\mathcal{E}}(\mathbf{r},t) + \vec{\mathcal{P}}(\mathbf{r},t)$, we obtain,

$$\nabla\times\vec{\mathcal{H}}(\mathbf{r},t) = \frac{\partial\vec{\mathcal{D}}(\mathbf{r},t)}{\partial t} + \mathbf{j}(\mathbf{r},t) \ , \tag{17.55}$$

which is the macroscopic Ampère-Maxwell equation.

The above derivations show that $\vec{\mathcal{P}}$ and $\vec{\mathcal{M}}$ do not exist as exact physical quantities in the microscopic sense. They are artifacts of a process of smearing out the microscopic charges and currents over smooth macroscopic distributions, with the aim of facilitating the calculation with macroscopic quantities.

17.1.4 The fundamental laws in polarizable and magnetizable materials

The derivations made in the previous chapter led to Maxwell's macroscopic equations, which correspond to the Maxwell equations for vacuum complemented by material equations characterizing the medium. In short,

$$\boxed{\begin{array}{lrcl} \text{(i)} & \nabla \times \vec{\mathcal{H}} & = & \partial_t \vec{\mathcal{D}} + \mathbf{j} \\ \text{(ii)} & \nabla \times \vec{\mathcal{E}} & = & -\partial_t \vec{\mathcal{B}} \\ \text{(iii)} & \nabla \cdot \vec{\mathcal{D}} & = & \varrho \\ \text{(iv)} & \nabla \cdot \vec{\mathcal{B}} & = & 0 \end{array}} \; . \tag{17.56}$$

The fields are related by the macroscopic *polarization* and *magnetization*,

$$\vec{\mathcal{P}} = \vec{\mathcal{D}} - \varepsilon_0 \vec{\mathcal{E}} \quad \text{and} \quad \vec{\mathcal{M}} = \mu_0^{-1} \vec{\mathcal{B}} - \vec{\mathcal{H}} \; . \tag{17.57}$$

For a given free charge density distribution $\varrho(\mathbf{r}, t)$ and a free current density distribution $\mathbf{j}(\mathbf{r}, t)$, the above six equations (17.56) and (17.57) define the six components of the fields unambiguously. In vacuum $\varepsilon_0 \vec{\mathcal{E}} = \vec{\mathcal{D}}$ and $\mu_0^{-1} \vec{\mathcal{B}} = \vec{\mathcal{H}}$ Maxwell's equations simplify. In material media, however, the secondary quantities $\vec{\mathcal{D}}$ and $\vec{\mathcal{H}}$ are not equal to the fields.

Depending on its structure, a medium may have (or not) bound or free charges and currents, responding in a specific way to applied electric and magnetic fields and giving rise to a wide variety of features. For example, a medium is *non-conductive* when, even in the presence of electric fields applied to the medium, there is no flux of current. A medium is *linear* when the polarization and the magnetization depend linearly on the electric and magnetic fields, respectively. A medium is *homogeneous* when the susceptibilities do not vary across the medium. When the directions of induced polarization and magnetization are parallel, respectively, to the electric and magnetic fields, the medium is said to be *isotropic*, otherwise it is said to be *anisotropic*.

Depending on the type of material and its properties the equations do sometimes simplify. For example, we have for a

medium	condition
dielectric	$\vec{\mathcal{D}} = \varepsilon\vec{\mathcal{E}}$, $\vec{\mathcal{P}} = \chi_\varepsilon\varepsilon_0\vec{\mathcal{E}}$, $\varepsilon = 1 + \chi_\varepsilon$
non-linear dielectric	$\vec{\mathcal{D}} = \vec{\mathcal{D}}(\vec{\mathcal{E}}) \nsim \vec{\mathcal{E}}$
dia- and paramagnetic	$\vec{\mathcal{B}} = \mu\vec{\mathcal{H}}$, $\vec{\mathcal{M}} = \chi_\mu\vec{\mathcal{H}}$, $\mu = 1 + \chi_\mu$
non-linear magnetic	$\vec{\mathcal{B}} = \vec{\mathcal{B}}(\vec{\mathcal{H}}) \nsim \vec{\mathcal{B}}$
neutral	$\rho = 0$
isolating	$\mathbf{j} = 0$
ohmic	$\mathbf{j} = \sigma\vec{\mathcal{E}}$
non ohmic	$\mathbf{j} = \mathbf{j}(\vec{\mathcal{E}}) \nsim \vec{\mathcal{E}}$

The material equations define the material constants, that is, the *permittivity* ε, the *permeability* μ, and the *conductivity* σ. These quantities are scalar for isotropic media and tensors for anisotropic media. Resolve the Exc. 17.1.5.11.

17.1.5 Exercises

17.1.5.1 Ex: Displacement current

Consider a straight big conducting wire of radius a with a small transverse gap of width $w \ll a$ carrying a constant current I. Find the magnetic field in the gap for distances of the symmetry axis $r < a$ as a function of the current.

Solution: *The two surfaces on either side of the gap act as a plate capacitor as the charges build up on these surfaces. Consequently, the electric field between the plates increases, which generates a magnetic field. Neglecting boundary effects at the edges of the plates, the temporal variation of the electric field between the plates is,*

$$\frac{\partial\mathcal{E}}{\partial t} = \frac{\partial}{\partial t}\frac{\sigma}{\varepsilon_0} = \frac{\partial}{\partial t}\frac{Q}{\pi a^2\varepsilon_0} = \frac{I}{\pi a^2\varepsilon_0} \ .$$

Taking a circular path of radius r between the plates (there is no current here, so that $\mathbf{j} = 0$), we have,

$$2\pi r\mathcal{B} = \oint_{\partial\mathcal{S}} \vec{\mathcal{B}}\cdot d\mathbf{l} = \int_{\mathcal{S}} \nabla\times\vec{\mathcal{B}}\cdot d\mathbf{S} = \varepsilon_0\mu_0\int_{\mathcal{S}} \frac{\partial\vec{\mathcal{E}}}{\partial t}\cdot d\mathbf{S} = \varepsilon_0\mu_0\int_{\mathcal{S}} \frac{I}{\pi a^2\varepsilon_0}dS = \varepsilon_0\mu_0\frac{I}{\pi a^2\varepsilon_0}\pi r^2 \ .$$

Hence,

$$\vec{\mathcal{B}} = \mu_0\frac{Ir}{2\pi a^2}\hat{\mathbf{e}}_\phi \ ,$$

by symmetry and using the right hand rule, and taking the z-direction as showing from the positive plate towards the negative plate.

17.1.5.2 Ex: Plate capacitor

A disk-shaped plate capacitor with radius R, distance d, and $\varepsilon = 1$ is charged by a constant current I.
a. Calculate from the continuity equation, neglecting edge effects, the temporal variation of the charges on the plates $q(t)$, respectively, $-q(t)$.
b. Calculate the temporal variation of the electric field between the plates and Maxwell's displacement current density.
c. Calculate the magnetic field $\vec{\mathcal{B}}$ between the plates along a circular path Γ inside ($\rho < R$) and outside ($\rho > R$) the capacitor.
d. Show that the $\vec{\mathcal{B}}$-field between the plates is, for $\rho > R$, equal to the $\vec{\mathcal{B}}$-field produced by the charging current I around the conductors feeding the capacitor.

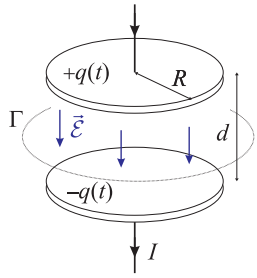

Figure 17.4: Plate capacitor.

Solution: *a. The surface integral over a closed area S surrounding the upper plate of the capacitor is,*

$$\oint \mathbf{j} \cdot d\mathbf{S} = -I \ .$$

With the law of Gauß and the continuity equation,

$$\oint \mathbf{j} \cdot d\mathbf{S} = \int_V \nabla \cdot \mathbf{j} dV = -\frac{\partial}{\partial t} \int \rho dV = -\frac{\partial}{\partial t} q(t) \ .$$

Follows,

$$q(t) = It + q(0) \ .$$

b. Maxwell's third equation,

$$\nabla \cdot \vec{\mathcal{D}} = \rho \ ,$$

where $\vec{\mathcal{D}} = \varepsilon_0 \vec{\mathcal{E}} \equiv -\varepsilon_0 \mathcal{E} \hat{\mathbf{e}}_z$ without dielectric. Thereby,

$$\oint \vec{\mathcal{D}} \cdot d\mathbf{S} = \mathcal{D} \pi R^2 = q \ .$$

Hence, $\varepsilon_0 \dot{\mathcal{E}} = \dot{\mathcal{D}} = \frac{\dot{q}(t)}{\pi R^2}$. According to (17.5) Maxwell's displacement current density is defined as,

$$\mathbf{j}_d \equiv \varepsilon_0 \frac{\partial \vec{\mathcal{E}}}{\partial t} = -\frac{\dot{q}}{\pi R^2} \hat{\mathbf{e}}_z = -\frac{I}{\pi R^2} \hat{\mathbf{e}}_z \ .$$

c. Between the plates we have no free charges, $\mathbf{j} = 0$. *The line integral along the circle* Γ *between the capacitor plates around the z-axis is,*

$$\oint_\Gamma \vec{\mathcal{B}} \cdot d\mathbf{l} = \mu_0 \int \mathbf{j}_d \cdot d\mathbf{S} \ .$$

For a radius of the circle less than the radius of the plates, $\rho < R$, *we have* $\mathcal{B}_\rho 2\pi\rho = \mu_0 \left(-\frac{I}{\pi R^2}\right) \hat{\mathbf{e}}_z \cdot \hat{\mathbf{e}}_z \pi\rho^2$. *Hence,*

$$\vec{\mathcal{B}}_\rho = -\frac{\mu_0 I}{2\pi R^2}\rho\hat{\mathbf{e}}_\phi \ .$$

For $\rho > R$, *we have* $\mathcal{B}_\rho 2\pi\rho = -\mu_0 \frac{I}{\pi R^2}\pi R^2$. *Hence,*

$$\vec{\mathcal{B}}_\rho = -\frac{\mu_0 I}{2\pi\rho}\hat{\mathbf{e}}_\phi \ .$$

d. Above the capacitor the field $\mathcal{B}_\rho$ *is, due to* $\mathbf{j}_{displ} = 0$,

$$\oint \vec{\mathcal{B}} \cdot d\mathbf{S} = \mu_0 \int \mathbf{j} \cdot d\mathbf{S}$$

Hence, $\mathcal{B}2\pi\rho = -\mu_0 I$, *that is,*

$$\vec{\mathcal{B}}_\rho = -\frac{\mu_0 I}{2\pi\rho}\hat{\mathbf{e}}_\phi \ .$$

17.1.5.3 Ex: Maxwell's equations for a particular charge and current density distribution

Determine the charge and current density distributions producing the fields,

$$\vec{\mathcal{E}}(\mathbf{r}, t) = -\frac{1}{4\pi\varepsilon_0}\frac{q}{r^2}\Theta(vt - r)\hat{\mathbf{e}}_r \qquad \text{and} \qquad \vec{\mathcal{B}}(\mathbf{r}, t) = 0 \ ,$$

where Θ is the Heavyside function and v is a constant. Show that the fields satisfy all Maxwell equations. Describe the physical situation producing these fields.

Solution: *It is easy to show,*

$$\nabla \cdot \vec{\mathcal{B}} = \nabla \times \vec{\mathcal{B}} = \nabla \times \vec{\mathcal{E}} = 0 \ ,$$

because the electric field is radial. The third Maxwell equation gives,

$$\begin{aligned}
\varrho &= \varepsilon_0 \nabla \cdot \vec{\mathcal{E}} = -\frac{q}{4\pi}\nabla \cdot \frac{\Theta(vt - r)\hat{\mathbf{e}}_r}{r^2} \\
&= -\frac{q}{4\pi}\left(\Theta(vt - r)\nabla \cdot \frac{\hat{\mathbf{e}}_r}{r^2} + \frac{\hat{\mathbf{e}}_r}{r^2} \cdot \nabla\Theta(vt - r)\right) \\
&= -\frac{q}{4\pi}\left(\Theta(vt - r)4\pi\delta^3(\mathbf{r}) + \frac{\hat{\mathbf{e}}_r}{r^2} \cdot [-\delta(vt - r)\hat{\mathbf{e}}_r]\right) \\
&= -\frac{q}{4\pi}\left(4\pi\delta^3(\mathbf{r}) + \frac{\hat{\mathbf{e}}_r}{r^2} \cdot [-\delta(vt - r)\hat{\mathbf{e}}_r]\right) = -q\delta^3(\mathbf{r}) + \frac{q}{4\pi r^2}\delta(vt - r) \ .
\end{aligned}$$

Also, we obtain from Maxwell's first equation,

$$\mathbf{j} = -\varepsilon_0 \frac{\partial \vec{\mathcal{E}}}{\partial t} = \frac{qv}{4\pi r^2}\delta(vt-r)\hat{\mathbf{e}}_r \ .$$

With the temporal variation of the charge density,

$$\frac{\partial \varrho}{\partial t} = \frac{q}{4\pi r^2}\frac{\partial \delta^3(ct-r)}{\partial t} \ ,$$

and the divergence of the current density,

$$\begin{aligned}\nabla\cdot\mathbf{j}(\mathbf{r},t) &= \frac{qv}{4\pi r^2}\delta(vt-r)\nabla\cdot\frac{\mathbf{r}}{r^3} + \frac{qv}{4\pi r^2}\nabla\delta(vt-r) \\ &= \frac{qv}{4\pi r^2}\cancelto{0}{\delta(vt-r)(-4\pi)\delta^3(\mathbf{r})} - \frac{qv}{4\pi r^2}\frac{\partial\delta^3(vt-r)}{\partial r} \ ,\end{aligned}$$

we see that the continuity equation is satisfied. The situation corresponds to a point charge $+q$ at the origin and a spherical shell charge distribution (with the total charge $-q$) expanding with velocity v). The electric field inside the shell is entirely due to the charge at the origin, and the field outside the sphere is zero, since the total enclosed charge is zero. Only the expanding sphere contributes to the current density.

17.1.5.4 Ex: Atomic diamagnetism

An electron (charge q) orbits a nucleus (charge Q) at a distance r, the centripetal acceleration being provided by the Coulomb attraction. Now, a small magnetic field $d\mathcal{B}$ is slowly ramped up, perpendicular to the plane of the orbit. Show that the increase of the kinetic energy, dT, transferred to the electron via the induced electric field, is exactly the one necessary to keep the circular motion on the original radius r. (This allows us, in the discussion of *diamagnetism*, to assume a fixed electron radius.)

Solution: *The atom is stable if,*

$$\frac{mv^2}{r} = \frac{Qq}{4\pi\varepsilon_0 r^2} \ .$$

In the presence of a magnetic field the force balance is modified by the Lorentz force,

$$\frac{mv_1^2}{r} = \frac{Qq}{4\pi\varepsilon_0 r^2} - qv_1 d\mathcal{B} \ .$$

That is, we observe a variation of the kinetic energy which, assuming that the radius stays unchanged, is given by,

$$dT = \tfrac{m}{2}v_1^2 - \tfrac{m}{2}v^2 = -\tfrac{1}{2}qrvd\mathcal{B} \ .$$

This may seem surprising knowing that magnetic fields do not work. The solution is that the increase of the kinetic energy must come from the electric field induced by the temporal variation of the magnetic field,

$$\pi r^2\frac{\partial\mathcal{B}}{\partial t} = \int\frac{\partial\vec{\mathcal{B}}}{\partial t}\cdot d\mathbf{S} = -\int_{\mathcal{S}}\nabla\times\vec{\mathcal{E}}d\mathbf{S} = -\oint_{\partial\mathcal{S}}\vec{\mathcal{E}}\cdot d\mathbf{l} = -2\pi r\mathcal{E} \ .$$

The force on the electron is now a Coulomb force,

$$\mathbf{F}_E = q\mathcal{E}\hat{\mathbf{e}}_\phi = -\frac{qr}{2}\frac{\partial \mathcal{B}}{\partial t}\hat{\mathbf{e}}_\phi \ .$$

Therefore, the kinetic energy varies by,

$$dT = F_E dl = -\frac{qr}{2}\frac{\partial \mathcal{B}}{\partial t}dl = -\frac{qr}{2}\frac{\partial \mathcal{B}}{\partial t}vdt = -\frac{qr}{2}vd\mathcal{B} \ ,$$

which corresponds to the value determined above by assuming an invariable radius [6].

17.1.5.5 Ex: Variable charge with constant current

Suppose that $\mathbf{j}(\mathbf{r})$ is constant over time, but not $\varrho(\mathbf{r}, t)$. Such conditions can prevail, for example, during the charging process of a capacitor.
a. Show that the charge density at any point is a linear function of time: $\varrho(\mathbf{r}, t) = \varrho(\mathbf{r}, 0) + \dot{\varrho}(\mathbf{r}, 0)t$.
b. Despite the fact that this configuration is not electrostatic or magnetostatic, both the Coulomb law and the Biot-Savart law remain valid, since they satisfy Maxwell's equations. Show in particular that,

$$\vec{\mathcal{B}}(\mathbf{r}) = \frac{\mu_0}{4\pi}\int \frac{\mathbf{j}(\mathbf{r}') \times \hat{\mathbf{e}}_R}{R^2} d^3r'$$

with $R \equiv |\mathbf{r} - \mathbf{r}'|$ obeys Ampère's law including Maxwell's displacement term.

Solution: *a. From the continuity equation,*

$$\dot{\varrho}(\mathbf{r}, t) = -\nabla \cdot \mathbf{j}(\mathbf{r}) = const = \dot{\varrho}(\mathbf{r}, 0)$$

we check,

$$\varrho(\mathbf{r}, t) - \varrho(\mathbf{r}, 0) = \dot{\varrho}(\mathbf{r}, 0)\int_0^t d\tau = \dot{\varrho}(\mathbf{r}, 0)t \ .$$

b. Inserting the given magnetic field into the first Maxwell equation we calculate, using the rule $\nabla \times (\mathbf{A} \times \mathbf{B}) = (\mathbf{B} \cdot \nabla)\mathbf{A} - (\mathbf{A} \cdot \nabla)\mathbf{B} + \mathbf{A}(\nabla \cdot \mathbf{B}) - \mathbf{B}(\nabla \cdot \mathbf{A})$,

$$\begin{aligned}\nabla \times \vec{\mathcal{B}}(\mathbf{r}) &= \frac{\mu_0}{4\pi}\int \nabla \times \frac{\mathbf{j}(\mathbf{r}') \times \hat{\mathbf{e}}_R}{R^2} d^3r' = \frac{\mu_0}{4\pi}\int \left(- [\mathbf{j}(\mathbf{r}') \cdot \nabla] \frac{\hat{\mathbf{e}}_R}{R^2} + \mathbf{j}(\mathbf{r}') \left[\nabla \cdot \frac{\hat{\mathbf{e}}_R}{R^2}\right]\right) d^3r' \\ &= -\frac{\mu_0}{4\pi}\int [\mathbf{j}(\mathbf{r}') \cdot \nabla'] \frac{\hat{\mathbf{e}}_R}{R^2} d^3r' + \frac{\mu_0}{4\pi}\int \mathbf{j}(\mathbf{r}') 4\pi\delta^3(\mathbf{r}) d^3r' \ ,\end{aligned}$$

[6] We note that in quantum mechanics, we also calculate the Zeeman effect assuming in first order, that the electronic orbitals $|n\rangle$ remain unchanged, $E^{(1)} = \langle n|\hat{H}^{(1)}|n\rangle$.

where in the second line we replaced ∇ with ∇'. Now, we consider the coordinate x,

$$\begin{aligned}\left[\nabla\times\vec{\mathcal{B}}(\mathbf{r})\right]_x &= -\frac{\mu_0}{4\pi}\int\left[\mathbf{j}(\mathbf{r}')\cdot\nabla'\right]\frac{x-x'}{R^3}d^3r' + \mu_0 j_x(\mathbf{r}) \\ &= -\frac{\mu_0}{4\pi}\int\left\{\nabla'\cdot\left[\mathbf{j}(\mathbf{r}')\frac{x-x'}{R^3}\right] - \frac{x-x'}{R^3}\nabla'\cdot\mathbf{j}(\mathbf{r}')\right\}d^3r' + \mu_0 j_x(\mathbf{r}) \\ &= -\frac{\mu_0}{4\pi}\oint\mathbf{j}(\mathbf{r}')\frac{x-x'}{R^3}\cdot d\mathbf{S}' + \frac{\mu_0}{4\pi}\int\frac{x-x'}{R^3}(-\dot{\varrho})d^3r' + \mu_0 j_x(\mathbf{r}) \\ &= -\frac{\mu_0}{4\pi}\frac{d}{dt}\int\frac{x-x'}{R^3}\varrho d^3r' + \mu_0 j_x(\mathbf{r}) = -\frac{\mu_0}{4\pi}\frac{d}{dt}4\pi\varepsilon_0\mathcal{E}_x + \mu_0 j_x(\mathbf{r})\ ,\end{aligned}$$

neglecting surface terms. Hence,

$$\begin{aligned}\nabla\times\vec{\mathcal{B}} &= \nabla\times\frac{\mu_0}{4\pi}\int\frac{\mathbf{j}(\mathbf{r}')\times\hat{\mathbf{e}}_R}{R^2}d^3r' \\ &= \mu_0\varepsilon_0\frac{d}{dt}\frac{1}{4\pi\varepsilon_0}\int\frac{\varrho(\mathbf{r}',t)\hat{\mathbf{e}}_R}{R^2}d^3r' + \mu_0\mathbf{j}(\mathbf{r}) = \mu_0\varepsilon_0\frac{d\vec{\mathcal{E}}}{dt} + \mu_0\mathbf{j}(\mathbf{r})\ .\end{aligned}$$

17.1.5.6 Ex: Force on magnetic monopoles

In free space Maxwell's equations are perfectly symmetric under the operation $\vec{\mathcal{E}}\to\vec{\mathcal{B}}\to-\varepsilon_0\mu_0\vec{\mathcal{E}}$. But the existence of charges and electric currents breaks this symmetry. The introduction of 'magnetic charges' and 'magnetic currents' would restore the symmetry, but they were never observed [7]. In this exercise we assume the existence of a 'Coulomb law' for 'magnetic charges' q_m,

$$\mathbf{F} = \frac{\mu_0}{4\pi}\frac{q_{m_1}q_{m_2}}{|\mathbf{r}-\mathbf{r}'|^3}(\mathbf{r}-\mathbf{r}')\ .$$

a. Find the force law for a magnetic charge moving with velocity $\mathbf{v}$ through electric and magnetic fields $\vec{\mathcal{E}}$ and $\vec{\mathcal{B}}$ [1097].
b. One of the methods used to search for magnetic monopoles in laboratory [227] consists of passing them through a wire loop with the self-inductance L. What current would be induced in the circuit by the passage of a magnetic monopole?

Solution: *a. It is sufficient to look at the symmetry of Maxwell's equations to find,*

$$\mathbf{F} = q_m\vec{\mathcal{B}} - \frac{q_m}{c^2}\mathbf{v}\times\vec{\mathcal{E}}\ .$$

b. One of the experiments trying to discover magnetic monopoles [227] consisted of a superconducting ring (i.e. without resistance) with a magnet aligned to attract the monopoles (if they exist) through the ring. Assuming that a single 'magnetic charge' q_m produces a Coulomb magnetic field,

$$\vec{\mathcal{B}} = \frac{\mu_0}{4\pi}\frac{q_m}{r^2}\hat{\mathbf{e}}_r\ ,$$

[7] Dirac showed that the existence of magnetic charges would explain the quantization of charge.

we can estimate the flux through the ring (radius b) upon passage of the monopole along the symmetry axis. Let v be the velocity of the monopole. We place the origin in the center of the ring and choose z as the axis of symmetry. We must integrate the magnetic field over the disk-shaped area enclosed by the ring to obtain the flux,

$$\Phi_m = \int_{disco} \vec{\mathcal{B}} \cdot d\mathbf{a} \ .$$

When the monopole is at position $d\hat{\mathbf{e}}_z$, the magnetic field observed at a point on the disk with distance ρ from the z-axis is,

$$\vec{\mathcal{B}} = \frac{\mu_0}{4\pi} \frac{q_m}{|\rho\hat{\mathbf{e}}_\rho - d\hat{\mathbf{e}}_z|^2} (\rho\hat{\mathbf{e}}_\rho - d\hat{\mathbf{e}}_z) \ .$$

The surface element is,

$$d\mathbf{a} = \hat{\mathbf{e}}_z \rho d\rho d\phi \ ,$$

such that the flux is,

$$\begin{aligned} \Phi_m &= \frac{\mu_0 q_m}{4\pi} \int_0^{2\pi} \int_0^b \frac{\rho\hat{\mathbf{e}}_\rho - d\hat{\mathbf{e}}_z}{d^2+\rho^2} \cdot \hat{\mathbf{e}}_z \rho d\rho d\phi \\ &= \frac{\mu_0 q_m d}{2} \int_0^b \frac{\rho d\rho}{\sqrt{d^2+\rho^2}^3} = \frac{\mu_0 q_m}{2} \left(1 - \frac{d}{\sqrt{d^2+b^2}}\right) \ . \end{aligned}$$

We take $t = 0$ as the time when the monopole crosses the plane of the ring, so that $d = -vt$ and $\vec{\mathcal{B}} \cdot d\mathbf{a} > 0$ for $t < 0$ and $d = +vt$ and $\vec{\mathcal{B}} \cdot d\mathbf{a} < 0$ for $t > 0$. Hence,

$$\Phi_m = \frac{\mu_0 q_m}{2} \left(1 - 2\Theta(t) + \frac{vt}{\sqrt{(vt)^2+b^2}}\right) \ .$$

Now, we consider the generalized Maxwell equation for magnetic monopoles,

$$\nabla \times \vec{\mathcal{E}} = -\frac{\partial \vec{\mathcal{B}}}{\partial t} - \mu_0 \mathbf{j}_m \ ,$$

where $\mathbf{j}_m$ is the density of 'magnetic current'. Applying Stokes' theorem, we integrate the electric field along the ring and the terms on the right-hand side over the area enclosed by the ring,

$$U \equiv \oint_{anel} \vec{\mathcal{E}} \cdot d\mathbf{l} = -\frac{\partial \Phi_m}{\partial t} - \mu_0 \int_{disco} \mathbf{j}_m \cdot d\mathbf{a} \equiv -\frac{\partial \Phi_m}{\partial t} - \mu_0 I_{m,enc} \ ,$$

where U is the retro-induced electromotive force, which can be written in terms of the self-inductance L of the ring:

$$U = -L\frac{dI(t)}{dt} \ ,$$

and $I_{m,enc}$ is the magnetic current flowing through the ring. Considering that we have only a single monopole to make the 'magnetic current', we write it as a δ-function:

$$I_{m,enc} = q_m \delta(t) \ .$$

That is, there is a current consisting of a single 'magnetic charge' passing through the area enclosed by the ring only at time $t = 0$. Since the δ-function is the derivative of the Heaviside Θ-function, we can integrate Faraday's law to obtain,

$$LI(t) = \int_{-\infty}^{t} \mu_0 I_{m,enc} dt' + \Phi_m(t) = \mu_0 q_m \Theta(t) + \Phi_m(t) \ .$$

With this,

$$I(t) = \frac{\mu_0 q_m}{L}\Theta(t) + \frac{\mu_0 q_m}{2L}\left(1 - 2\Theta(t) + \frac{vt}{\sqrt{(vt)^2 + b^2}}\right) = \frac{\mu_0 q_m}{2L}\left(1 + \frac{vt}{\sqrt{(vt)^2 + b^2}}\right) \ .$$

For $t \to -\infty$ we have $I \to 0$, while for $t \to \infty$ we have $I \to \mu_0 q_m / L$. This means, that when monopole is approaching but still distant, there is no induced current. The current increases, when the monopole is closer, but since the superconducting ring has no resistance, the generated current never dissipates and tends to a finite value when the monopole moves away on the other side of the ring.

17.1.5.7 Ex: Duality transform

a. In the case of existing magnetic charges and currents, Maxwell's equations would take the form,

$$\begin{aligned}
&\text{(i)} && \nabla \times \vec{\mathcal{B}} - \varepsilon_0 \mu_0 \partial_t \vec{\mathcal{E}} = \mu_0 \mathbf{j}_e \\
&\text{(ii)} && \nabla \times \vec{\mathcal{E}} + \partial_t \vec{\mathcal{B}} = -\mu_0 \mathbf{j}_m \\
&\text{(iii)} && \nabla \cdot \vec{\mathcal{E}} = \varepsilon_0^{-1} \varrho_e \\
&\text{(iv)} && \nabla \cdot \vec{\mathcal{B}} = \mu_0 \varrho_m \ .
\end{aligned}$$

Show that these equations are invariant under the *duality transform* given by,

$$\begin{pmatrix} \vec{\mathcal{E}}' \\ c\vec{\mathcal{B}}' \end{pmatrix} = \begin{pmatrix} \cos\alpha & \sin\alpha \\ -\sin\alpha & \cos\alpha \end{pmatrix} \begin{pmatrix} \vec{\mathcal{E}} \\ c\vec{\mathcal{B}} \end{pmatrix} \quad , \quad \begin{pmatrix} cq_e' \\ q_m' \end{pmatrix} = \begin{pmatrix} \cos\alpha & \sin\alpha \\ -\sin\alpha & \cos\alpha \end{pmatrix} \begin{pmatrix} cq_e \\ q_m \end{pmatrix} \ ,$$

where α is an arbitrary rotation angle in the $\mathcal{E}$-$\mathcal{B}$ space. Densities of charges and currents transform in the same way as q_e and q_m. This means, in particular, that if you would know the fields produced by an electric charge configuration, you could immediately (using $\alpha = 90°$) deduce the fields produced by a corresponding arrangement of the magnetic charge.

b. Show that the force law derived in Exc. 17.1.5.6,

$$\mathbf{F} = q_e(\vec{\mathcal{E}} + \mathbf{v} \times \vec{\mathcal{B}}) + q_m(\vec{\mathcal{B}} - \tfrac{1}{c^2}\mathbf{v} \times \vec{\mathcal{E}})$$

is also invariant under duality transformation.

Solution: *a. Inserting the transformation into the given extended Maxwell equations,*

$$\begin{aligned}
\nabla \times \left(\vec{\mathcal{B}}\cos\alpha - \tfrac{1}{c}\vec{\mathcal{E}}\sin\alpha\right) - \varepsilon_0\mu_0\frac{\partial\left(\vec{\mathcal{E}}\cos\alpha + c\vec{\mathcal{B}}\sin\alpha\right)}{\partial t} &= \mu_0\left(\mathbf{j}_e\cos\alpha + \tfrac{1}{c}\mathbf{j}_m\sin\alpha\right)\\
\nabla \times \left(\vec{\mathcal{E}}\cos\alpha + c\vec{\mathcal{B}}\sin\alpha\right) - \frac{\partial\left(\vec{\mathcal{B}}\cos\alpha - \frac{1}{c}\vec{\mathcal{E}}\sin\alpha\right)}{\partial t} &= -\mu_0\left(\mathbf{j}_m\cos\alpha - c\mathbf{j}_e\sin\alpha\right)\\
\nabla\cdot\left(\vec{\mathcal{E}}\cos\alpha + c\vec{\mathcal{B}}\sin\alpha\right) &= \frac{\varrho_e\cos\alpha + \frac{1}{c}\varrho_m\sin\alpha}{\varepsilon_0}\\
\nabla\cdot\left(\vec{\mathcal{B}}\cos\alpha - \tfrac{1}{c}\vec{\mathcal{E}}\sin\alpha\right) &= \mu_0\left(\varrho_m\cos\alpha - c\varrho_e\sin\alpha\right)\ .
\end{aligned}$$

Obviously, the terms in cos *and* sin *satisfy the Maxwell equations separately.*
b. Inserting the transformation into given expression for the Lorentz force,

$$\begin{aligned}
\mathbf{F} &= \left(q_e\cos\alpha + \tfrac{q_m}{c}\sin\alpha\right)\left[\vec{\mathcal{E}}\cos\alpha + c\vec{\mathcal{B}}\sin\alpha + \mathbf{v}\times\left(\vec{\mathcal{B}}\cos\alpha - \tfrac{1}{c}\vec{\mathcal{E}}\sin\alpha\right)\right]\\
&\quad + \left(q_m\cos\alpha - cq_e\sin\alpha\right)\left[\vec{\mathcal{B}}\cos\alpha - \tfrac{1}{c}\vec{\mathcal{E}}\sin\alpha - \tfrac{1}{c^2}\mathbf{v}\times\left(\vec{\mathcal{E}}\cos\alpha + c\vec{\mathcal{B}}\sin\alpha\right)\right]\\
&= q_e(\vec{\mathcal{E}} + \mathbf{v}\times\vec{\mathcal{B}})\cos^2\alpha + \left[q_e\left(c\vec{\mathcal{B}} - \tfrac{1}{c}\mathbf{v}\times\vec{\mathcal{E}}\right) + \tfrac{q_m}{c}\left(\vec{\mathcal{E}} + \mathbf{v}\times\vec{\mathcal{B}}\right)\right]\cos\alpha\sin\alpha\\
&\quad + q_m\left(\vec{\mathcal{B}} - \tfrac{1}{c^2}\mathbf{v}\times\vec{\mathcal{E}}\right)\sin^2\alpha + q_m\left(\vec{\mathcal{B}} - \tfrac{1}{c^2}\mathbf{v}\times\vec{\mathcal{E}}\right)\cos^2\alpha\\
&\quad + \left[-q_e\left(c\vec{\mathcal{B}} - \tfrac{1}{c}\mathbf{v}\times\vec{\mathcal{E}}\right) - \tfrac{q_m}{c}(\vec{\mathcal{E}} + \mathbf{v}\times\vec{\mathcal{B}})\right]\cos\alpha\sin\alpha\\
&\quad + q_e(\vec{\mathcal{E}} + \mathbf{v}\times\vec{\mathcal{B}})\sin^2\alpha\\
&= q_e(\vec{\mathcal{E}} + \mathbf{v}\times\vec{\mathcal{B}}) + q_m\left(\vec{\mathcal{B}} - \tfrac{1}{c^2}\mathbf{v}\times\vec{\mathcal{E}}\right)\ .
\end{aligned}$$

17.1.5.8 Ex: Quantization of magnetic monopoles

a. Show that the vector potential,

$$\mathbf{A} = \frac{g(1-\cos\theta)}{r\sin\theta}\hat{\mathbf{e}}_\phi$$

produces a Coulomb-type magnetic field [1053].
b. Calculate the magnetic flux across the solid angle delimited by the polar angle θ.
c. Calculate the vector potential $\mathbf{A}'$ obtained by a gauge transformation with the gauge field $\chi = 2g\phi$.
d. Now consider the vector potential defined by $\mathbf{A}'' \equiv \mathbf{A}$ for $\theta \leq \frac{\pi}{2}$ and $\mathbf{A}'' \equiv \mathbf{A}'$ for $\theta \geq \frac{\pi}{2}$. This potential has no more singularity. Derive, from the condition that the transformation $U_{cl} = e^{-\imath e\chi/\hbar}$ be unique, the value of the magnetic charge.

Solution: *a. With the rotation operator expressed in spherical coordinates we easily*

calculate,

$$\begin{aligned}\vec{\mathcal{B}}_{mon} &= \nabla\times\mathbf{A}\\ &= \frac{\hat{\mathbf{e}}_r}{r\sin\theta}\left[\frac{\partial}{\partial\theta}(\sin\theta a_\phi)-\frac{\partial}{\partial\phi}(a_\theta)\right]+\frac{\hat{\mathbf{e}}_\theta}{r\sin\theta}\left[\frac{\partial}{\partial\phi}(a_r)-\sin\theta\frac{\partial}{\partial r}(ra_\phi)\right]\\ &\quad+\frac{\hat{\mathbf{e}}_\phi}{r}\left[\frac{\partial}{\partial r}(ra_\theta)-\frac{\partial}{\partial\theta}(a_r)\right]=\frac{g}{r^2}\hat{\mathbf{e}}_r\ .\end{aligned}$$

b. The flux is,

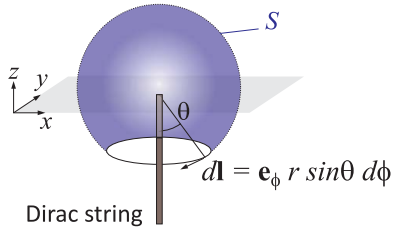

Figure 17.5: Magnetic monopole.

$$\begin{aligned}\Phi_m &= \int_0^{2\pi}\int_0^{\theta}\vec{\mathcal{B}}_{mon}\cdot d\mathbf{S}=\oint\mathbf{A}\cdot d\mathbf{l}=\oint\frac{g(1-\cos\theta)}{r\sin\theta}\hat{\mathbf{e}}_\phi\cdot d\mathbf{l}\\ &=\oint\frac{g(1-\cos\theta)}{r\sin\theta}r\sin\theta d\phi=2\pi g(1-\cos\theta)\ .\end{aligned}$$

However, we must look more carefully at this result, because for $\theta\to\pi$ we obtain $\Phi_m=4\pi g$. But that can not be right, since the integration path converges to 0. The singular line $4\pi g\Theta(-z)\delta(x)\delta(y)\hat{\mathbf{e}}_z$ is called the Dirac string. We can correct by subtracting the singularity,

$$\nabla\times\mathbf{A}_{Dir}=\nabla\times\mathbf{A}-4\pi g\Theta(-z)\delta(x)\delta(y)\hat{\mathbf{e}}_z=\frac{g}{r^2}\hat{\mathbf{e}}_r-4\pi g\Theta(-z)\delta(x)\delta(y)\hat{\mathbf{e}}_z\ ,$$

such that,

$$\Phi_m=\int\nabla\times\mathbf{A}_{Dir}\cdot d\mathbf{S}=\begin{cases}2\pi g(1-\cos\theta) & for\ \theta<\pi\\ 0 & for\ \theta=\pi\end{cases}\ .$$

c. The gradient in spherical coordinates is,

$$\nabla\chi=\hat{\mathbf{e}}_r\frac{\partial\chi}{\partial r}+\hat{\mathbf{e}}_\theta\frac{1}{r}\frac{\partial\chi}{\partial\theta}+\hat{\mathbf{e}}_\phi\frac{1}{r\sin\theta}\frac{\partial\chi}{\partial\phi}=\frac{2g}{r\sin\theta}\hat{\mathbf{e}}_\phi\ ,$$

such that the new vector potential is,

$$\mathbf{A}'=\mathbf{A}-\nabla\chi=-\frac{g(1+\cos\theta)}{r\sin\theta}\hat{\mathbf{e}}_\phi\ .$$

d. For the transformation to be unequivocal, we need,

$$e^{-\imath e\chi(\phi=0)/\hbar}=e^0=e^{-\imath e2g2\pi/\hbar}=e^{-\imath e\chi(\phi=2\pi)/\hbar}\ .$$

That is,

$$n = \frac{2eg}{\hbar} = 0, \pm 1, \pm 2, \ldots \ .$$

17.1.5.9 Ex: Green's identities

Be ϕ and ψ two continuously differentiable functions and V a volume with the border ∂V. Show with the help of Gauß' theorem,

a.

$$\int\limits_{\mathcal{V}} \left[\phi \nabla^2 \psi + (\nabla\phi)\cdot(\nabla\psi)\right] \ dV = \int\limits_{\partial\mathcal{V}} \phi(\nabla\psi) \ d\mathbf{S} \ ,$$

b.

$$\int\limits_{\mathcal{V}} \left[\phi \nabla^2 \psi - \psi \nabla^2 \phi\right] \ dV = \int\limits_{\partial\mathcal{V}} \left[\phi \nabla\psi - \psi\nabla\phi\right] \ d\mathbf{S} \ .$$

Solution: *a. Green's first identity is solved by Gauß' theorem and the chain rule:*

$$\int\limits_{\partial\mathcal{V}} \phi(\nabla\psi) \ d\mathbf{S} = \int\limits_{\mathcal{V}} \nabla\cdot\left[\phi(\nabla\psi)\right] \ dV = \int\limits_{\mathcal{V}} \left[\phi\nabla^2\psi + (\nabla\phi)\cdot(\nabla\psi)\right] \ dV \ .$$

b. Green's second identity follows from the first:

$$\int\limits_{\mathcal{V}} \left[\phi \nabla^2 \psi + (\nabla\phi)\cdot(\nabla\psi)\right] \ dV = \int\limits_{\partial\mathcal{V}} \phi(\nabla\psi) \ d\mathbf{S}$$

$$\int\limits_{\mathcal{V}} \left[\psi \nabla^2 \phi + (\nabla\psi)\cdot(\nabla\phi)\right] \ dV = \int\limits_{\partial\mathcal{V}} \psi(\nabla\phi) \ d\mathbf{S} \ .$$

Subtracting the second equation from the first, we obtain the second Green identity.

17.1.5.10 Ex: Decomposition of vector fields

Be $\mathbf{F}(\mathbf{r},t)$ an arbitrary vector field defined on $\mathbb{R}$, which tends (along with its derivatives) to zero in sufficiently high order, when $|\mathbf{r}| \to \infty$. This field can be decomposed into a sum of a longitudinal and a transverse component, $\mathbf{F} = \mathbf{F}_l + \mathbf{F}_t$ with $\nabla\times\mathbf{F}_l = 0$ and $\nabla\cdot\mathbf{F}_t = 0$.

a. Prove,

$$\mathbf{F}_l(\mathbf{r},t) = -\frac{1}{4\pi}\nabla\int\frac{\nabla'\cdot\mathbf{F}(\mathbf{r}',t)}{|\mathbf{r}-\mathbf{r}'|}d^3r' \quad \text{and} \quad \mathbf{F}_t(\mathbf{r},t) = +\frac{1}{4\pi}\nabla\times\nabla\times\int\frac{\mathbf{F}(\mathbf{r}',t)}{|\mathbf{r}-\mathbf{r}'|}d^3r' \ .$$

Help: Begin showing that,

$$\mathbf{F}(\mathbf{r},t) = -\frac{1}{4\pi}\triangle\int\frac{\mathbf{F}(\mathbf{r}',t)}{|\mathbf{r}-\mathbf{r}'|}d^3r'$$

and use the vector identity,

$$\nabla \times \nabla \times \mathbf{A} = \nabla(\nabla \cdot \mathbf{A}) - \triangle \mathbf{A} \ .$$

b. Show that the vector field $\mathbf{F}(\mathbf{r})$ is unequivocally given by its sources, $\nabla \cdot \mathbf{F}(\mathbf{r})$, and vertices, $\nabla \times \mathbf{F}(\mathbf{r})$.

Solution: *We have,*

$$\begin{aligned} \triangle_{\mathbf{r}} \int d^3\mathbf{r}' \frac{\mathbf{F}(\mathbf{r}',t)}{|\mathbf{r}-\mathbf{r}'|} &= \int d^3r' \mathbf{F}(\mathbf{r}',t) \triangle_{\mathbf{r}} \frac{1}{|\mathbf{r}-\mathbf{r}'|} \\ &= \int d^3r' \mathbf{F}(\mathbf{r}',t)[-4\pi\delta(\mathbf{r}-\mathbf{r}')] = -4\pi\mathbf{F}(\mathbf{r},t) \ , \end{aligned}$$

and hence,

$$\mathbf{F}(\mathbf{r},t) = -\frac{1}{4\pi} \triangle \int d^3r' \frac{\mathbf{F}(\mathbf{r}',t)}{|\mathbf{r}-\mathbf{r}'|} \qquad (*) \ .$$

Now, $\triangle \mathbf{A} = \nabla(\nabla \cdot \mathbf{A}) - \nabla \times \nabla \times \mathbf{A}$ *and hence,*

$$\triangle \int d^3\mathbf{r}' \frac{\mathbf{F}(\mathbf{r}',t)}{|\mathbf{r}-\mathbf{r}'|} = \nabla \left(\nabla \cdot \int d^3r' \frac{\mathbf{F}(\mathbf{r}',t)}{|\mathbf{r}-\mathbf{r}'|} \right) - \nabla \times \left(\nabla \times \int d^3r' \frac{\mathbf{F}(\mathbf{r}',t)}{|\mathbf{r}-\mathbf{r}'|} \right) \ .$$

For the first term we obtain by partial integration,

$$\begin{aligned} \nabla \cdot \int d^3r' \frac{\mathbf{F}(\mathbf{r}',t)}{|\mathbf{r}-\mathbf{r}'|} &= + \int d^3r' \mathbf{F}(\mathbf{r}',t) \cdot \nabla_{\mathbf{r}'} \frac{1}{|\mathbf{r}-\mathbf{r}'|} \\ &= - \int d^3r' \mathbf{F}(\mathbf{r}',t) \cdot \nabla_{\mathbf{r}'} \frac{1}{|\mathbf{r}-\mathbf{r}'|} \\ &= + \int d^3r' \frac{1}{|\mathbf{r}-\mathbf{r}'|} \nabla_{\mathbf{r}'} \cdot \mathbf{F}(\mathbf{r}',t) \ . \end{aligned}$$

With $(*)$ *follows,*

$$\mathbf{F}(\mathbf{r},t) = -\frac{1}{4\pi} \nabla_{\mathbf{r}} \left(\int d^3r' \frac{\nabla_{\mathbf{r}'} \cdot \mathbf{F}(\mathbf{r}',t)}{|\mathbf{r}-\mathbf{r}'|} \right) = +\frac{1}{4\pi} \nabla_{\mathbf{r}} \times \left(\nabla_{\mathbf{r}} \int d^3r' \frac{\mathbf{F}(\mathbf{r}',t)}{|\mathbf{r}-\mathbf{r}'|} \right) \ .$$

The rotation of a gradient disappears, as well as the divergent of a rotation. Therefore,

$$\begin{aligned} \mathbf{F}_l(\mathbf{r},t) &= -\frac{1}{4\pi} \nabla \int d^3r' \frac{\nabla' \cdot \mathbf{F}(\mathbf{r}',t)}{|\mathbf{r}-\mathbf{r}'|} \qquad \textit{with} \qquad \nabla \times \mathbf{F}_l = 0 \\ \mathbf{F}_t(\mathbf{r},t) &= +\frac{1}{4\pi} \nabla \times \nabla \int d^3r' \frac{\mathbf{F}(\mathbf{r}',t)}{|\mathbf{r}-\mathbf{r}'|} \qquad \textit{with} \qquad \nabla \cdot \mathbf{F}_t = 0 \ , \end{aligned}$$

and obviously holds,

$$\mathbf{F} = \mathbf{F}_l + \mathbf{F}_t \ .$$

17.1.5.11 Ex: Conductivity of seawater

Sea water has at the frequency $v = 4 \cdot 10^8\,\mathrm{Hz}$ the permittivity $\varepsilon = 81\varepsilon_0$, the permeability $\mu = \mu_0$, and the resistivity $\rho = 0.23\,\Omega\mathrm{m}$. What is the ratio between the conduction current and the displacement current? **Help:** Consider a parallel-plate capacitor immersed in seawater and driven by a voltage $V_0\cos(2\pi\nu t)$.

Solution: *The conduction current density is,*

$$j_{cond} = \frac{\mathcal{E}}{\rho} = \frac{dV_0\cos(2\pi\nu t)}{\rho}\ .$$

The displacement current density is,

$$j_{disp} = \frac{\partial D}{\partial t} = \frac{\partial \varepsilon d V_0\cos(2\pi\nu t)}{\partial t} = -2\pi\nu\varepsilon d V_0\sin(2\pi\nu t)\ .$$

The ratio of their amplitudes is,

$$\frac{j_{cond}}{j_{disp}} = -\frac{dV_0}{2\pi\nu\varepsilon d V_0\rho} = \frac{1}{2\pi\nu\varepsilon\rho} \approx 2.4\ .$$

17.2 Conservation laws in electromagnetism

The importance of *conservation laws* and *symmetries* lies in their universal validity and their independence of a particular theory (mechanics, electrodynamics, ..). They often allow the derivation of laws, which are specific for a theory and of equations of motion for particular systems. For example, in classical mechanics, we can derive Newtonian axioms from the conservation of linear momentum, and in electrodynamics, as we shall see later, we can derive Maxwell's equations from the principles of Lorentz invariance, gauge invariance, and electric charge conservation, as expressed by the continuity equation. The question which we will elucidate in the following sections will be that of the validity of other mechanical conservation laws in electrodynamics, that is, the laws of energy, linear momentum, and angular momentum conservation.

In the context of preparing the deductions, let us defined some important quanti-

ties [8],

$$\begin{array}{lll} \text{(i)} & u = \frac{1}{2}(\vec{\mathcal{E}}\cdot\vec{\mathcal{D}} + \vec{\mathcal{B}}\cdot\vec{\mathcal{H}}) & \textit{energy density} \\ \text{(ii)} & \vec{\mathcal{S}} = \vec{\mathcal{E}}\times\vec{\mathcal{H}} & \textit{energy flux} \text{ or } \textit{Poynting vector} \\ \text{(iii)} & \mathbf{f} = \varrho\vec{\mathcal{E}} + \mathbf{j}\times\vec{\mathcal{B}} & \textit{Lorentz force density} \\ \text{(iv)} & \vec{\wp}^A = \varepsilon_0\mu_0\vec{\mathcal{S}} = \frac{1}{c^2}\vec{\mathcal{E}}\times\vec{\mathcal{H}} & \textit{Abraham momentum density} \\ \text{(iv)} & \vec{\wp}^M = \vec{\mathcal{D}}\times\vec{\mathcal{B}} & \textit{Minkowski momentum density} \\ \text{(v)} & \vec{\ell} = \mathbf{r}\times\vec{\wp} & \textit{angular momentum density} \\ \text{(vi)} & \overleftrightarrow{\mathbf{T}} = \vec{\mathcal{D}}\otimes\vec{\mathcal{E}} + \vec{\mathcal{H}}\otimes\vec{\mathcal{B}} - \frac{1}{2}u\mathbb{I} & \textit{Maxwell stress tensor}\,. \end{array} \tag{17.58}$$

All fields are time-dependent. From Maxwell's equations we derive the *electrodynamical continuity equation*, the *Poynting theorem*, and the conservation of linear and angular momentum. Resolve the Exc. 17.2.5.1.

17.2.1 Charge conservation and continuity equation

Calculating the divergence of Maxwell's first equation and using the third,

$$\nabla\cdot(\nabla\times\vec{\mathcal{H}}) = \partial_t\nabla\cdot\vec{\mathcal{D}} + \nabla\cdot\mathbf{j} = \boxed{\partial_t\varrho + \nabla\cdot\mathbf{j} = 0}\,. \tag{17.59}$$

This law describes *charge conservation* in electrodynamics.

17.2.2 Energy conservation and Poynting's theorem

The time derivative of the energy density (17.58)(i) is,

$$\partial_t u = \tfrac{1}{2}(\vec{\mathcal{E}}\cdot\partial_t\vec{\mathcal{D}} + \vec{\mathcal{D}}\cdot\partial_t\vec{\mathcal{E}} + \vec{\mathcal{B}}\cdot\partial_t\vec{\mathcal{H}} + \vec{\mathcal{H}}\cdot\partial_t\vec{\mathcal{B}}) = \vec{\mathcal{E}}\cdot\partial_t\vec{\mathcal{D}} + \vec{\mathcal{H}}\cdot\partial_t\vec{\mathcal{B}}\,, \tag{17.60}$$

supposing $\vec{\mathcal{D}} = \varepsilon\vec{\mathcal{E}}$ and $\vec{\mathcal{H}} = \vec{\mathcal{B}}/\mu$ with time- and space-independent $\varepsilon, \mu = const.$ The divergence of the Poynting vector is,

$$\nabla\cdot\vec{\mathcal{S}} = \nabla\cdot(\vec{\mathcal{E}}\times\vec{\mathcal{H}}) = \vec{\mathcal{H}}\cdot(\nabla\times\vec{\mathcal{E}}) - \vec{\mathcal{E}}\cdot(\nabla\times\vec{\mathcal{H}}) = -\vec{\mathcal{H}}\cdot\partial_t\vec{\mathcal{B}} - \vec{\mathcal{E}}\cdot(\partial_t\vec{\mathcal{D}} + \mathbf{j})\,. \tag{17.61}$$

With this we immediately see,

$$\boxed{\partial_t u + \nabla\cdot\vec{\mathcal{S}} = -\mathbf{j}\cdot\vec{\mathcal{E}}}\,. \tag{17.62}$$

To better understand this theorem, we calculate the work exerted by the Coulomb-Lorentz force per unit time on a test charge q,

$$\frac{dW}{dt} = \frac{d}{dt}\int_{\mathcal{C}}\mathbf{F}\cdot d\mathbf{l} = \frac{d}{dt}\int q(\vec{\mathcal{E}} + \cancelto{0}{\mathbf{v}\times\vec{\mathcal{B}}})\cdot\mathbf{v}dt = q\mathbf{v}\cdot\vec{\mathcal{E}}\,. \tag{17.63}$$

[8] The question of the correct expression for the momentum density is difficult and will be dealt with later.

The current generated by the charge can be derived from the parametrization $\mathbf{j}(\mathbf{r}) = q\mathbf{v}\delta^3(\mathbf{r}-\mathbf{r}')$. Thus, we derive the *Poynting theorem*,

$$\frac{dW}{dt} = \int_{\mathcal{V}} \vec{\mathcal{E}}\cdot\mathbf{j}dV = -\frac{d}{dt}\int_{\mathcal{V}} udV - \int_{\mathcal{V}} \nabla\cdot\vec{\mathcal{S}}dV = -\frac{dU_{erg}}{dt} - \oint_{\partial\mathcal{V}} \vec{\mathcal{S}}\cdot d\mathbf{S}\ . \quad (17.64)$$

This theorem postulates *energy conservation*. That is, the electromagnetic energy U_{erg} within a volume $\mathcal{V}$ can only change 1. by diffusion out of the volume via a flux $\int \vec{\mathcal{S}}\cdot d\mathbf{S}$ of the Poynting vector, or 2. when mechanical work W is done on the volume or when the electromagnetic energy in the volume is dissipated into other forms of energy, for example heat. We apply the Poynting theorem to a current-carrying wire in Exc. 17.2.5.2.

Example 85 (*Derivation of Ohm's law by the Poynting vector*): The current flux through a wire exerts *work*, because the wire heats up. We calculate the energy transferred to the wire per unit time via the Poynting vector. The electric field (assumed to be uniform) along the wire (length L and radius a) is,

$$\mathcal{E} = \frac{U}{L}\ ,$$

where U is the voltage between the ends of the wire. The magnetic field at the surface of the wire is,

$$\mathcal{B} = \frac{\mu_0 I}{2\pi a}\ .$$

Therefore, the absolute value of the Poynting vector is,

$$s = \frac{1}{\mu_0}\mathcal{E}\mathcal{B} = \frac{UI}{2\pi aL}\ .$$

pointing into the wire, $\vec{\mathcal{S}} \propto -\hat{\mathbf{e}}_r$. The energy per unit of time passing through the surface of the wire is therefore,

$$\int \vec{\mathcal{S}}\cdot d\mathbf{S} = s(2\pi aL) = UI\ ,$$

confirming previously obtained results. As the fields are stationary, the electromagnetic energy does not vary with time, neither, $\partial_t U_{erg} = 0$.

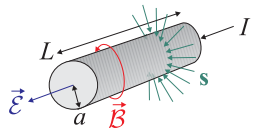

Figure 17.6: Energy flux into the wire causes heating.

17.2.3 Conservation of linear momentum and Maxwell's stress tensor

The interaction between two charges is described by the Coulomb-Lorentz force. However, when these charges accelerate each other mutually, they generate non-stationary

fields, so that the force laws of Coulomb and Biot-Savart do not apply. We will see later, how to generalize these laws.

Nevertheless, at first glance, the Coulomb force seems compatible with the third Newton law: *actio = reactio*, but not with the Lorentz force.

Example 86 (*Linear momentum of the electromagnetic field*): To see this, we consider two charged particles with trajectories,

$$\mathbf{l}_1(t) = vt\hat{\mathbf{e}}_y \quad , \quad \mathbf{l}_2(t) = vt\hat{\mathbf{e}}_x \ .$$

Charge 1 produces a field $\vec{\mathcal{B}}_1$ at the position of charge 2 and vice versa. At time $t = 0$, when they collide, the forces become orthogonal:

$$\mathbf{F}_{12} = q\mathbf{v}_2 \times \vec{\mathcal{B}}_1 \perp q\mathbf{v}_1 \times \vec{\mathcal{B}}_2 = \mathbf{F}_{21} \ .$$

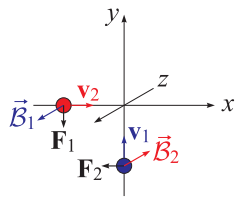

Figure 17.7: The Lorentz forces exerted by approaching charges are mutually orthogonal.

Obviously, in electrodynamics, the Lorentz force flagrantly violates Newton's third law in way to raise questions about the validity of momentum conservation. The solution is that in electrodynamics, *the electromagnetic field itself may lose or gain momentum* and should be included in the formulation of a law of momentum conservation. Moreover, the field does not move instantaneously, but propagates at the speed of light and is subject to retardation effects. The law *actio = reactio* postulates the existence of forces acting at a distance that, as we nowadays know, do not exist [9]. We shall return to this problem in the discussion of the relativistic Lorentz transformation.

17.2.3.1 Maxwell's tress tensor

We now consider the Lorentz force density, which we will try to express totally in terms of fields, eliminating the charge and current densities [898],

$$\mathbf{f} = \varrho\vec{\mathcal{E}} + \mathbf{j} \times \vec{\mathcal{B}} = \vec{\mathcal{E}}(\nabla \cdot \vec{\mathcal{D}}) + \left(\nabla \times \vec{\mathcal{H}} - \frac{\partial \vec{\mathcal{D}}}{\partial t}\right) \times \vec{\mathcal{B}} \ . \tag{17.65}$$

We reformulate the last term,

$$-\frac{\partial \vec{\mathcal{D}}}{\partial t} \times \vec{\mathcal{B}} = \vec{\mathcal{D}} \times \frac{\partial \vec{\mathcal{B}}}{\partial t} - \frac{\partial}{\partial t}(\vec{\mathcal{D}} \times \vec{\mathcal{B}}) = -\vec{\mathcal{D}} \times (\nabla \times \vec{\mathcal{E}}) - \frac{\partial}{\partial t}(\vec{\mathcal{D}} \times \vec{\mathcal{B}}) \ . \tag{17.66}$$

[9] One of the important changes of paradigm in the history of physics is from interaction at a distance to local interaction. Newton was a supporter of non-local interaction for gravity. Ironically he argued against waves in favor of particles for light. Today the opinion thinks the other way round: Particles are mediators of local interactions, while only waves can mediate non-local features.

Knowing $\vec{\mathcal{H}}(\nabla \cdot \vec{\mathcal{B}}) = 0$, we can add this term to the force without cost,

$$\mathbf{f} = \vec{\mathcal{E}}(\nabla \cdot \vec{\mathcal{D}}) - \vec{\mathcal{D}} \times (\nabla \times \vec{\mathcal{E}}) + \vec{\mathcal{H}}(\nabla \cdot \vec{\mathcal{B}}) - \vec{\mathcal{B}} \times (\nabla \times \vec{\mathcal{H}}) - \frac{\partial}{\partial t}(\vec{\mathcal{D}} \times \vec{\mathcal{B}}) \ . \tag{17.67}$$

We use the rule from vector analysis,

$$\begin{aligned} \nabla(\vec{\mathcal{E}} \cdot \vec{\mathcal{D}}) &= \vec{\mathcal{E}} \times (\nabla \times \vec{\mathcal{D}}) + \vec{\mathcal{D}} \times (\nabla \times \vec{\mathcal{E}}) + (\vec{\mathcal{E}} \cdot \nabla)\vec{\mathcal{D}} + (\vec{\mathcal{D}} \cdot \nabla)\vec{\mathcal{E}} \\ &= 2\vec{\mathcal{D}} \times (\nabla \times \vec{\mathcal{E}}) + 2(\vec{\mathcal{E}} \cdot \nabla)\vec{\mathcal{D}} \ , \end{aligned} \tag{17.68}$$

and analogously for $\vec{\mathcal{B}} \cdot \vec{\mathcal{H}}$. The second equation holds, because for $\vec{\mathcal{D}} = \varepsilon\vec{\mathcal{E}}$ with $\varepsilon = const$, we can arbitrarily exchange the order of products between $\vec{\mathcal{D}}$ and $\vec{\mathcal{E}}$. We also assume $\mu = const$, which allows us to exchange the order of products between $\vec{\mathcal{H}}$ and $\vec{\mathcal{B}}$. We use the rule (17.68) to replace the terms with vector products in equation (17.67),

$$\begin{aligned} \mathbf{f} &= \vec{\mathcal{E}}(\nabla \cdot \vec{\mathcal{D}}) - \tfrac{1}{2}\nabla(\vec{\mathcal{E}} \cdot \vec{\mathcal{D}}) + (\vec{\mathcal{E}} \cdot \nabla)\vec{\mathcal{D}} \\ &+ \vec{\mathcal{H}}(\nabla \cdot \vec{\mathcal{B}}) - \tfrac{1}{2}\nabla(\vec{\mathcal{H}} \cdot \vec{\mathcal{B}}) + (\vec{\mathcal{H}} \cdot \nabla)\vec{\mathcal{B}} - \partial_t \vec{\mathcal{D}} \times \vec{\mathcal{B}} \ . \end{aligned} \tag{17.69}$$

The last term is nothing more than the time derivative of the *Minkowski momentum density* of the electromagnetic field defined in (17.58), $\vec{\wp}^M \equiv \vec{\mathcal{D}} \times \vec{\mathcal{B}}$, which still awaits interpretation.

Now we introduce the *Maxwell stress tensor* (in Minkowski's form) by [10],

$$\boxed{T^M_{ij} \equiv \mathcal{D}_i\mathcal{E}_j + \mathcal{H}_i\mathcal{B}_j - \tfrac{\delta_{ij}}{2}(\vec{\mathcal{E}} \cdot \vec{\mathcal{D}} + \vec{\mathcal{H}} \cdot \vec{\mathcal{B}})} \ . \tag{17.70}$$

Defining the divergent of a matrix, we obtain using Einstein's sum convention,

$$\begin{aligned} (\nabla \cdot \overleftrightarrow{\mathbf{T}})_j \equiv (\partial_i T_{ij})_j &= \Big(\partial_i(\mathcal{D}_i\mathcal{E}_j) + \partial_i(\mathcal{H}_i\mathcal{B}_j) - \partial_i \tfrac{\delta_{ij}}{2}(\vec{\mathcal{E}} \cdot \vec{\mathcal{D}} + \vec{\mathcal{H}} \cdot \vec{\mathcal{B}})\Big)_j \\ &= \Big(\mathcal{E}_j\nabla \cdot \vec{\mathcal{D}} + \vec{\mathcal{D}} \cdot \nabla\mathcal{E}_j + \mathcal{B}_j\nabla \cdot \vec{\mathcal{H}} + \vec{\mathcal{H}} \cdot \nabla\mathcal{B}_j - \tfrac{1}{2}\partial_j(\vec{\mathcal{E}} \cdot \vec{\mathcal{D}} + \vec{\mathcal{H}} \cdot \vec{\mathcal{B}})\Big)_j \ . \end{aligned} \tag{17.71}$$

These terms coincide with those of the equation (17.69) except for the last one. Now, we can reshape the Lorentz force,

$$\boxed{-\partial_t\vec{\wp}^M + \nabla \cdot \overleftrightarrow{\mathbf{T}} = \mathbf{f}} \ . \tag{17.72}$$

The mechanical force acting on a volume $\mathcal{V}$,

$$\mathbf{F} = \oint_{\partial\mathcal{V}} \overleftrightarrow{\mathbf{T}} \cdot d\mathbf{S} - \frac{d}{dt}\int_{\mathcal{V}} \vec{\wp}^M dV \ , \tag{17.73}$$

can be expressed by a momentum flux escaping the volume plus a 'stress' acting on its surface in every direction. The diagonal components T_{ii} represent 'pressures' and the non-diagonal 'shear stresses'. In static situations only the stress results in forces.

[10] In matrix notation,

$$\nabla \cdot \overleftrightarrow{T} = \begin{pmatrix} \frac{d}{dx} & \frac{d}{dy} & \frac{d}{dz} \end{pmatrix} \begin{pmatrix} T_{xx} & T_{xy} & T_{xz} \\ T_{yx} & T_{yy} & T_{xz} \\ T_{zx} & T_{zy} & T_{zz} \end{pmatrix} \ .$$

Example 87 (*Force on a charged body*): As an example of application of the stress tensor we calculate the force exerted by a solid uniformly charged (charge Q) sphere of radius R on its own upper part. The volume of the upper hemisphere is enclosed by two surfaces: one hemispheric surface and a flat one. In Cartesian coordinates,

$$\hat{\mathbf{e}}_r = \hat{\mathbf{e}}_x \sin\theta\cos\phi + \hat{\mathbf{e}}_y \sin\theta\sin\phi + \hat{\mathbf{e}}_z \cos\theta \ ,$$

for the hemispherical surface, we write the electric field and the surface element as,

$$\vec{\mathcal{E}} = \frac{1}{4\pi\varepsilon_0}\frac{Q}{R^2}\hat{\mathbf{e}}_r \qquad \text{and} \qquad d\mathbf{a} = \hat{\mathbf{e}}_r R^2 \sin\theta d\theta d\phi \ .$$

We calculate the stress tensor,

$$\begin{aligned}\overleftrightarrow{\mathbf{T}} &= \varepsilon_0 \begin{pmatrix} \mathcal{E}_x^2 - \frac{1}{2}\mathcal{E}^2 & \mathcal{E}_x\mathcal{E}_y & \mathcal{E}_x\mathcal{E}_z \\ \mathcal{E}_x\mathcal{E}_y & \mathcal{E}_y^2 - \frac{1}{2}\mathcal{E}^2 & \mathcal{E}_y\mathcal{E}_z \\ \mathcal{E}_x\mathcal{E}_z & \mathcal{E}_y\mathcal{E}_z & \mathcal{E}_z^2 - \frac{1}{2}\mathcal{E}^2 \end{pmatrix} \\ &= \varepsilon_0 \left(\frac{1}{4\pi\varepsilon_0}\frac{Q}{R^2}\right)^2 \begin{pmatrix} \sin^2\theta\cos^2\phi - \frac{1}{2} & \sin^2\theta\cos\phi\sin\phi & \cos\theta\sin\theta\cos\phi \\ \sin^2\theta\cos\phi\sin\phi & \sin^2\theta\sin^2\phi - \frac{1}{2} & \cos\theta\sin\theta\sin\phi \\ \cos\theta\sin\theta\cos\phi & \cos\theta\sin\theta\sin\phi & \cos^2\theta - \frac{1}{2} \end{pmatrix} \ .\end{aligned}$$

The integral of the tensor over the surface can be evaluated by Maple,

$$\int \overleftrightarrow{\mathbf{T}} d\mathbf{a} = \int_0^{2\pi}\int_0^{\pi/2} \overleftrightarrow{\mathbf{T}}\hat{\mathbf{e}}_r R^2 \sin\theta d\theta d\phi = \frac{Q^2}{32\pi\varepsilon_0 R^2}\hat{\mathbf{e}}_z \ .$$

For the flat surface we write,

$$\vec{\mathcal{E}} = \frac{1}{4\pi\varepsilon_0}\frac{Q}{R^3} r\hat{\mathbf{e}}_r \qquad \text{and} \qquad d\mathbf{a} = -\hat{\mathbf{e}}_z r dr d\phi \ .$$

Now we calculate with $\theta = \pi/2$,

$$\overleftrightarrow{\mathbf{T}} = \varepsilon_0 \frac{1}{(4\pi\varepsilon_0)^2}\frac{Q^2}{R^6} \begin{pmatrix} r^2\cos^2\phi - \frac{1}{2} & r^2\cos\phi\sin\phi & 0 \\ r^2\cos\phi\sin\phi & r^2\sin^2\phi - \frac{1}{2} & 0 \\ 0 & 0 & -\frac{1}{2}r^2 \end{pmatrix} \ .$$

The integral over the surface gives,

$$\int \overleftrightarrow{\mathbf{T}} d\mathbf{a} = -\int_0^{2\pi}\int_0^{R} \overleftrightarrow{\mathbf{T}}\hat{\mathbf{e}}_z r dr d\phi = \frac{Q^2}{64\pi\varepsilon_0 R^2}\hat{\mathbf{e}}_z \ .$$

Combining the results we obtain the force by the equation (17.73),

$$\mathbf{F} = \oint_{\text{hemisphere}} \overleftrightarrow{\mathbf{T}} d\mathbf{a} = \frac{3Q^2}{64\pi\varepsilon_0 R^2}\hat{\mathbf{e}}_z \ .$$

The result of this example demonstrates, how we can reduce the calculation of a force acting on a volume to an integral over the surface enclosing the volume. We will calculate other examples in Excs. 17.2.5.3 to 17.2.5.6.

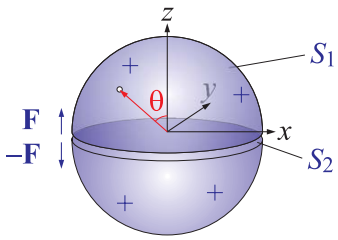

Figure 17.8: Electrostatic forces inside a charged sphere.

17.2.3.2 Conservation of linear momentum

According to Newton's second law, $\mathbf{F} = \partial_t \mathbf{p}_{mec}$ or $\mathbf{f} = \partial_t \vec{\wp}_{mec}$, the Lorentz force produces a variation of the *mechanical momentum*. In addition, there is a momentum $\mathbf{p}^M = \int_\mathcal{V} \vec{\wp}^M dV$, which must be attributed to the *electromagnetic field*, since it only exists in the presence of both electric and magnetic fields. $\mathbf{p}_{mec}$ and $\mathbf{p}^M$ can be interconverted, as in the example of the photonic recoil received by an atom upon an absorption process. But the sum of the mechanical momentum and the momentum of the field can only change through the term $\nabla \cdot \overleftrightarrow{\mathbf{T}}$. This is the law of *linear momentum conservation*. Evidently, $-\overleftrightarrow{\mathbf{T}}$ is the momentum flux density, playing a role similar to the one of the current density $\mathbf{j}$ in the continuity equation or of the energy flux density $\vec{\mathcal{S}}$ in Poynting's theorem. $-T_{ij}$ is the momentum per unit area and time in the direction i passing a surface oriented in j-direction.

We note two very different roles of the Poynting vector: In the energy conservation equation $\vec{\mathcal{S}}$ is the energy per unit area and time carried by electromagnetic fields, while in the momentum conservation equation, $\vec{\wp}^M = \varepsilon_0 \mu_0 \vec{\mathcal{S}}$ is the momentum per unit volume stored in these fields. Similarly, $\overleftrightarrow{\mathbf{T}}$ plays two roles: $\overleftrightarrow{\mathbf{T}}$ is the electromagnetic stress (i.e. a force per unit area or pressure) acting on a surface, while $-\overleftrightarrow{\mathbf{T}}$ describes the momentum flux (momentum current density) carried by these fields.

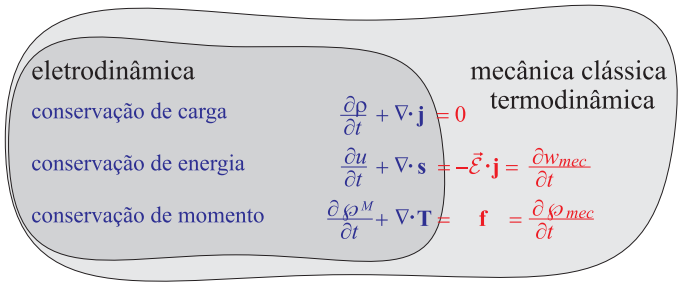

Figure 17.9: The laws of energy and momentum conservation connect the theories of electrodynamics with classical mechanics and thermodynamics.

Forces exerted by (non-radiating) fields on particles can be interpreted as being due to a scattering of 'virtual particles'. For example, the electrostatic force between charged particles and the magnetostatic force between magnetic dipoles are caused

by an exchange of virtual photons. These photons carry momentum that is transferred via recoil in a scattering event. Since the photon has no mass, the electric (respectively, magnetic) potential has infinite range.

The photonic concept can be extended to electromagnetic fields, as demonstrated by *Max Planck* in his discussion of the blackbody radiation. The spontaneous emission of a photon during the decay of an excited atom, postulated by *Albert Einstein*, is forbidden in 'classical' quantum mechanics, and requires quantization of the electromagnetic field for its explanation. The quantized energy packets, called (real) photons, also carry momentum, which can be transferred to bodies absorbing the radiation. The fact that light beams can exert forces is nowadays commonly exploited in techniques for cooling atomic gases. This process is called *radiation pressure* and will be discussed in the next chapter.

Example 88 (*The Abraham-Minkowski dilemma*): The expression $\vec{\wp}^A = \frac{1}{c^2}\vec{\mathcal{E}} \times \vec{\mathcal{H}}$ for the momentum flux in dielectric media was proposed by Abraham in 1909, but it is not obvious that this expression is correct. In fact, in the same year 1909 Minkowski proposed the expression $\vec{\wp}^M = \vec{\mathcal{D}} \times \vec{\mathcal{B}}$, and until today this *Abraham-Minkowski dilemma* is not satisfactorily solved [98, 1358]. See also (watch talk).

In an (over-)simplified way, we may illustrate the dilemma by the fact that even the correct expression for the photonic momentum within a dielectric is unknown. For, knowing that the phase velocity is reduced in a dielectric medium, $c \to c/n$, we could derive from the kinetic momentum in vacuum, $p = m\frac{c}{n}$, where the mass follows from Einstein's formula, $m = \frac{\hbar\omega}{c^2}$. That is, the photonic momentum within a dielectric medium should be,

$$p = \frac{\hbar\omega}{nc} \ .$$

This is Abraham's conclusion, which emphasizes the corpuscular aspect of the photon. On the other side, starting with de Broglie's expression, $p = \frac{\hbar}{\lambda}$, using the dispersion relation, $\lambda = \frac{c}{n\nu}$, we would conclude that the photonic momentum within a dielectric medium must be,

$$p = \frac{n\hbar\omega}{c} \ ,$$

which is Minkowski's result emphasizing the undulating features of the photon. In fact, the dilemma arises because, a priori, it is not clear whether the correct expression for the momentum carried by an electromagnetic wave is,

$$\vec{\wp}^A = \tfrac{1}{c^2}\mathbf{S} = \tfrac{1}{c^2}\vec{\mathcal{E}} \times \vec{\mathcal{H}} \qquad \text{or} \qquad \vec{\wp}^M = \vec{\mathcal{D}} \times \vec{\mathcal{B}} \ .$$

In vacuum there is no difference, but in the case of a plane wave inside a dielectric medium, $\vec{\mathcal{E}}(\mathbf{r},t) = \mathcal{E}_0\hat{\mathbf{e}}_x \cos\omega(t - \frac{n}{c}z)$ and $\vec{\mathcal{B}}(\mathbf{r},t) = \frac{n}{c}\hat{\mathbf{e}}_z \times \vec{\mathcal{E}}(\mathbf{r},t)$, we calculate,

$$\begin{aligned}
\wp^A &\equiv \tfrac{1}{c^2}\overline{\vec{\mathcal{E}} \times \vec{\mathcal{H}}} = \tfrac{1}{\mu_0 c^2}\overline{\vec{\mathcal{E}} \times \vec{\mathcal{B}}} = \tfrac{1}{\mu_0 c^2}\mathcal{E}_0^2\hat{\mathbf{e}}_z\tfrac{n}{c}\overline{\cos^2\omega(t - \tfrac{n}{c}z)} \\
&= \tfrac{1}{\mu_0 c^2}\mathcal{E}_0^2\hat{\mathbf{e}}_z\tfrac{n}{c}\tfrac{1}{2} = \tfrac{1}{\varepsilon_0\mu_0 c^2} - \hat{\mathbf{e}}_z\tfrac{u}{nc} = \hat{\mathbf{e}}_z\tfrac{u}{nc} \\
\wp^M &\equiv \overline{\vec{\mathcal{D}} \times \vec{\mathcal{B}}} = \varepsilon_0\overline{\vec{\mathcal{E}} \times \vec{\mathcal{B}}} = \varepsilon_0\mu_0 c^2\vec{\wp}^A = n^2\vec{\wp}^A \ .
\end{aligned}$$

17.2.4 Conservation of angular momentum of the electromagnetic field

The *angular momentum conservation* (17.58) is also ruled by Maxwell's equations. But its derivation is complicated [545, 659] and will not be reproduced here. In Exc. 17.2.5.7 we calculate the angular momentum stored in a static combination of electric and magnetic fields. In Exc. 17.2.5.8 we calculate the torque acting on charges due to a temporal variation of electromagnetic fields. Finally, in Exc. 17.2.5.9 we try classical discussion of the intrinsic angular momentum (spin) of the electron.

Example 89 (*Angular momentum of electromagnetic fields*): Imagine a very long solenoid with radius R, n windings per unit length, and carrying the current I. Coaxially to the solenoid there are two long cylindrical layers of length d. The first one, of radius a, lies inside the solenoid and carries a charge $+Q$ evenly distributed over the surface; the other one, of radius b, is outside the solenoid and carries the charge $-Q$, as shown in Fig. 17.10. We suppose $d \gg b$. When the current in the solenoid is gradually reduced, the cylinders begin to rotate. The question is, where does the angular momentum come from?

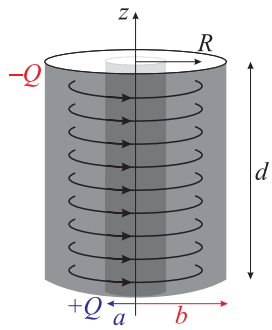

Figure 17.10: Device with a solenoid and charged cylinders illustrating the conservation of angular momentum.

Let us first calculate the angular momentum stored in the electric and magnetic field before we started to reduce the current. In the region between the cylinders, $a < \rho < b$, we had the electric field $\vec{\mathcal{E}} = \frac{Q}{2\pi\varepsilon_0 d}\frac{\hat{\mathbf{e}}_\rho}{\rho}$, and in the inner region of the solenoid, $\rho < R$, the magnetic field, $\vec{\mathcal{B}} = \mu_0 nI\hat{\mathbf{e}}_z$. Therefore, in the region $a < \rho < R$, the momentum density (17.58) was,

$$\vec{\wp} = \varepsilon_0 \vec{\mathcal{E}} \times \vec{\mathcal{B}} = -\frac{\mu_0 QnI}{2\pi\rho d}\hat{\mathbf{e}}_\phi$$

The angular momentum density,

$$\vec{\ell} = \mathbf{r} \times \vec{\wp} = -\frac{\mu_0 nIQ}{2\pi d}\hat{\mathbf{e}}_z \ ,$$

was constant, which facilitates the calculation of the total orbital angular momentum,

$$\mathbf{L} = \int \vec{\ell} dV = \vec{\ell}\pi(R^2 - a^2)d = -\tfrac{1}{2}\mu_0 nIQ(R^2 - a^2)\hat{\mathbf{e}}_z \ .$$

Apparently, the existence of an orbital angular momentum is conditioned to the presence of both, a charge and a current.
Now, when the current is turned off, the variation of the magnetic field induces a circumferential electric field, given by Faraday's law:

$$\vec{\mathcal{E}} = -\tfrac{1}{2}\mu_0 n \frac{dI}{dt}\hat{\mathbf{e}}_\phi \begin{cases} \rho & \text{for} \quad \rho < R \\ \frac{R^2}{\rho} & \text{for} \quad \rho > R \end{cases} .$$

The Coulomb force exerted by the electric field on the charged outer cylinder produces a torque on the cylinder,

$$\mathbf{N}_b = \mathbf{r} \times (-Q\vec{\mathcal{E}}) = \tfrac{1}{2}\mu_0 n Q R^2 \frac{dI}{dt}\hat{\mathbf{e}}_z ,$$

so that it receives the angular momentum,

$$\mathbf{L}_b = \int_0^\infty \mathbf{N}_b dt = \tfrac{1}{2}\mu_0 n Q R^2 \hat{\mathbf{e}}_z \int_I^0 \frac{dI}{dt} dt = -\tfrac{1}{2}\mu_0 n I Q R^2 \hat{\mathbf{e}}_z .$$

In the same way, we obtain for the inner cylinder,

$$\mathbf{N}_a = -\tfrac{1}{2}\mu_0 n Q a^2 \frac{dI}{dt}\hat{\mathbf{e}}_z \quad , \quad \mathbf{L}_a = \tfrac{1}{2}\mu_0 n I Q a^2 \hat{\mathbf{e}}_z .$$

Hence, we verify that $\mathbf{L} = \mathbf{L}_a + \mathbf{L}_b$. The angular momentum lost by the fields is precisely equal to the angular momentum acquired by the cylinders, that is, the total angular momentum is conserved.

17.2.5 Exercises

17.2.5.1 Ex: Poynting vector for free charges and currents

Write down the Poynting vector and the momentum density for the case, that there are only free *charges and currents*.

Solution: *We suppose,* $\varrho = \varrho_l$ *and* $\mathbf{j} = \mathbf{j}_l$. *We then deduce that the polarization is* $-\nabla \cdot \vec{\mathcal{P}} = \varrho_b = 0$ *and the magnetization* $\nabla \times \vec{\mathcal{M}} = \mathbf{j}_b$. *Hence,*

$$\vec{\mathcal{S}} = \vec{\mathcal{E}} \times \vec{\mathcal{H}} = \tfrac{1}{\mu_0}\vec{\mathcal{E}} \times \vec{\mathcal{B}} ,$$

and

$$\wp = \vec{\mathcal{D}} \times \vec{\mathcal{B}} = \varepsilon_0 \vec{\mathcal{E}} \times \vec{\mathcal{B}} .$$

17.2.5.2 Ex: Energy flux in a current-carrying wire

A cylindrical wire with radius a and permeability μ is traversed by a constant current density $\mathbf{j}$. The electric field $\vec{\mathcal{E}}$ inside the wire and the current density $\mathbf{j}$ are connected by Ohm's law $\mathbf{j} = \varsigma\vec{\mathcal{E}}$, where ς is the electrical conductivity.
a. What absolute value and which direction does the Poynting vector $\vec{\mathcal{S}}$ have in the wire and on the wire surface?
b. Calculate the total energy flux running through the surface of a piece of wire of

length l. Show that this flux of energy is precisely the power dissipated within this piece for the production of ohmic heat.
Help: The law of energy conservation in electrodynamics is given by $-\frac{du}{dt} = \nabla\vec{\mathcal{S}} + \mathbf{j}\cdot\vec{\mathcal{E}}$, where $u = \frac{1}{2}(\vec{\mathcal{E}}\cdot\vec{\mathcal{D}} + \vec{\mathcal{B}}\cdot\vec{\mathcal{H}})$ is the total energy density, $\vec{\mathcal{S}} = \vec{\mathcal{E}}\times\vec{\mathcal{H}}$ the energy flux and $\mathbf{j}\cdot\vec{\mathcal{E}}$ the work exerted on the electric current density.

Solution: *a. We calculate,*

$$2\pi\rho\mathcal{H} = \oint \vec{\mathcal{H}}\cdot d\mathbf{l} = I = j\pi\rho^2 = \int \mathbf{j}\cdot d\mathbf{S} \ .$$

We replace $\vec{\mathcal{E}} = \frac{1}{\varsigma}\mathbf{j}$ *and* $\vec{\mathcal{H}} = \frac{j}{2}\rho\hat{\mathbf{e}}_\phi$ *in the Poynting vector,*

$$\vec{\mathcal{S}} = \vec{\mathcal{E}}\times\vec{\mathcal{H}} = \tfrac{1}{\varsigma}\mathbf{j}\times\tfrac{j}{2}\rho\hat{\mathbf{e}}_\phi = -\tfrac{1}{2\varsigma}j^2\rho\hat{\mathbf{e}}_z\times\hat{\mathbf{e}}_\phi = -\tfrac{1}{2\varsigma}j^2\rho\hat{\mathbf{e}}_\rho \ .$$

$\vec{\mathcal{S}}$ points in radial direction towards the interior of the cylinder, energy flows from the outside into the cylinder. On the surface the Poynting vector is,

$$\vec{\mathcal{S}} = -\tfrac{1}{2\varsigma}j^2 a\hat{\mathbf{e}}_r \ .$$

b. The energy flow from outside to the inside of the wire is (note, that $\vec{\mathcal{S}}$ and $d\mathbf{S}$ have opposite signs),

$$\int_{cyl.surf} \vec{\mathcal{S}}\cdot d\mathbf{S} = -s\ 2\pi al = -\tfrac{1}{2\varsigma}j^2 a\ 2\pi al \ .$$

The ohmic power is,

$$\int \mathbf{j}\cdot\vec{\mathcal{E}}\ dV = \frac{j^2}{\varsigma}\pi a^2 l \ .$$

The time dependence of the energy density disappears, since $\vec{\mathcal{E}}$ and $\vec{\mathcal{H}}$ are constants,

$$\int_{wire.piece} \frac{du}{dt} dV = 0 \ .$$

Hence,

$$\int_{wire.piece} \nabla\cdot\vec{\mathcal{S}}\ dV = \int_{cyl.surf} \vec{\mathcal{S}}\cdot d\mathbf{S} = -\int_{wire.piece} \mathbf{j}\cdot\vec{\mathcal{E}}\ dV = 0 \ ,$$

as calculated above.

17.2.5.3 Ex: Intrinsic force in a rotating charged shell via Maxwell's tensor

Calculate the attractive magnetic force between the north and south hemispheres of a uniformly charged spherical shell (radius R and surface charge density Q) rotating with the angular velocity ω. Use the result of Exc. 15.3.3.1 (clicking on the title).

Solution: *We use the result of Exc. 15.3.3.1,*

$$\vec{\mathcal{B}} = \frac{\mu_0 Q\omega}{6\pi R}\begin{cases}\hat{\mathbf{e}}_z & for \;\; r<R \\ \frac{R^3}{r^3}(\hat{\mathbf{e}}_r\cos\theta + \frac{1}{2}\hat{\mathbf{e}}_\theta \sin\theta) & for \;\; r>R\end{cases} .$$

We chose an arbitrary volume enclosing the northern hemisphere. Choosing this very large volume, we only need to integrate the stress tensor in the equatorial plane ($\theta = \pi/2$, $\hat{\mathbf{e}}_\theta = -\hat{\mathbf{e}}_z$),

$$d\mathbf{a} = -\hat{\mathbf{e}}_z r dr d\phi \ ,$$

where the magnetic field is,

$$\vec{\mathcal{B}} = \frac{\mu_0 Q\omega}{6\pi R}\hat{\mathbf{e}}_z\begin{cases}1 & for \;\; r<R \\ -\frac{R^3}{2r^3} & for \;\; r>R\end{cases} .$$

We calculate the stress tensor by,

$$\overleftrightarrow{\mathbf{T}} = \frac{1}{\mu_0}\begin{pmatrix}\mathcal{B}_x^2 - \frac{1}{2}\mathcal{B}^2 & \mathcal{B}_x\mathcal{B}_y & \mathcal{B}_x\mathcal{B}_z \\ \mathcal{B}_x\mathcal{B}_y & \mathcal{B}_y^2 - \frac{1}{2}\mathcal{B}^2 & \mathcal{B}_y\mathcal{B}_z \\ \mathcal{B}_x\mathcal{B}_z & \mathcal{B}_y\mathcal{B}_z & \mathcal{B}_z^2 - \frac{1}{2}\mathcal{B}^2\end{pmatrix} = \frac{1}{2\mu_0}\mathcal{B}_z^2\begin{pmatrix}-1 & 0 & 0 \\ 0 & -1 & 0 \\ 0 & 0 & 1\end{pmatrix}$$

$$= \frac{1}{2\mu_0}\left(\frac{\mu_0 Q\omega}{6\pi R}\right)^2\begin{pmatrix}-1 & 0 & 0 \\ 0 & -1 & 0 \\ 0 & 0 & 1\end{pmatrix}\begin{cases}1 & for \;\; r<R \\ \frac{R^6}{4r^6} & for \;\; r>R\end{cases} .$$

The force on the upper equatorial plane is,

$$F_z = \int T_{zz}^{r<R}\hat{\mathbf{e}}_z\cdot\hat{\mathbf{e}}_z da + \int T_{zz}^{r>R}\hat{\mathbf{e}}_z\cdot\hat{\mathbf{e}}_z da$$
$$= \left(\frac{\mu_0 Q\omega}{6\pi R}\right)^2\frac{1}{2\mu_0}\int_0^R\int_0^{2\pi} r dr d\phi + \left(\frac{\mu_0 Q\omega}{6\pi R}\right)^2\frac{1}{2\mu_0}\int_R^\infty\int_0^{2\pi}\frac{R^6}{4r^6} r dr d\phi = \frac{\mu_0 Q^2\omega^2}{64\pi} .$$

17.2.5.4 Ex: Coulomb force via Maxwell's tensor

Consider two equal (or opposite) point charges q, separated by distance $2a$. Construct the plane which is equidistant from the two charges. Determine the mutual force between the charges.

Solution: *The electric field,*

$$\vec{\mathcal{E}} = \frac{1}{4\pi\varepsilon_0}\frac{Q}{|\mathbf{r}-\mathbf{a}|^3}(\mathbf{r}-\mathbf{a}) \pm \frac{1}{4\pi\varepsilon_0}\frac{Q}{|\mathbf{r}+\mathbf{a}|^3}(\mathbf{r}+\mathbf{a})$$

lies in the symmetry plane,

$$\vec{\mathcal{E}}_{plane} = \frac{1}{4\pi\varepsilon_0}\frac{Q}{\sqrt{\rho^2+a^2}^3}[(\mathbf{r}-\mathbf{a}) \pm (\mathbf{r}+\mathbf{a})] \ ,$$

with $\rho^2 \equiv x^2 + y^2$. *With this, Maxwell's stress tensor,*

$$\overleftrightarrow{\mathbf{T}}_{\pm,plane} = \varepsilon_0 \begin{pmatrix} -\frac{1}{2}\mathcal{E}_z^2 & 0 & 0 \\ 0 & -\frac{1}{2}\mathcal{E}_z^2 & 0 \\ 0 & 0 & \frac{1}{2}\mathcal{E}_z^2 \end{pmatrix}$$

lies in the plane in the case of equal (or opposite) charges,

$$\overleftrightarrow{\mathbf{T}}_{-,plane} = \frac{1}{32\pi^2\varepsilon_0}\frac{Q^2 4a^2}{(\rho^2+a^2)^3}\begin{pmatrix} -1 & 0 & 0 \\ 0 & -1 & 0 \\ 0 & 0 & 1 \end{pmatrix}$$

$$\textit{and} \quad \overleftrightarrow{\mathbf{T}}_{+,plane} = \frac{1}{32\pi^2\varepsilon_0}\frac{Q^2 4\rho^2}{(\rho^2+a^2)^3}\begin{pmatrix} -1 & 0 & 0 \\ 0 & -1 & 0 \\ 0 & 0 & 1 \end{pmatrix} \ .$$

With the surface element in the plane $d\mathbf{a} = \hat{\mathbf{e}}_z r dr d\phi$, *the force follows as the integral of the tensor,*

$$\int \overleftrightarrow{\mathbf{T}}_{\pm,plane} d\mathbf{a} = \int_0^{2\pi}\int_0^{\infty} \overleftrightarrow{\mathbf{T}}_{-,plane}\hat{\mathbf{e}}_z \rho d\rho d\phi$$

for the case of equal (or opposite) charges,

$$\int \overleftrightarrow{\mathbf{T}}_{-,plane} d\mathbf{a} = \int_0^{2\pi}\int_0^{\infty} \frac{1}{32\pi^2\varepsilon_0}\frac{Q^2 4a^2}{(\rho^2+a^2)^3}\hat{\mathbf{e}}_z \rho d\rho d\phi = \frac{1}{4\pi\varepsilon_0}\frac{Q^2}{(2a)^2}\hat{\mathbf{e}}_z$$

$$\int \overleftrightarrow{\mathbf{T}}_{+,plane} d\mathbf{a} = \int_0^{2\pi}\int_0^{\infty} \frac{1}{32\pi^2\varepsilon_0}\frac{Q^2 4\rho^2}{(\rho^2+a^2)^3}\hat{\mathbf{e}}_z \rho d\rho d\phi = \frac{1}{4\pi\varepsilon_0}\frac{Q^2}{(2a)^2}\hat{\mathbf{e}}_z \ .$$

17.2.5.5 Ex: Force on a current distribution in a magnetic field

The force felt by a current distribution $\mathbf{j}(\mathbf{r})$ in an external magnetic field is,

$$\mathbf{F} = \int_{\mathcal{V}} d^3r' \mathbf{j}(\mathbf{r}') \times \vec{\mathcal{B}}(\mathbf{r}') \ .$$

Show that this force can also be written as an integral over the surface $\mathcal{S} \equiv \partial\mathcal{V}$ enclosing the volume $\mathcal{V}$:

$$F_j = \oint_{\mathcal{S}} \sum_{i=1}^{3} dS_i \ T_{ij} \qquad \text{with} \qquad T_{ij} = \tfrac{1}{\mu_0}\left(\mathcal{B}_i\mathcal{B}_j - \tfrac{1}{2}\mathcal{B}^2\delta_{ij}\right) \ .$$

Solution: *We have,*

$$\mathbf{F} = \int\limits_{\mathcal{V}} d^3\mathbf{r}'\mathbf{j}(\mathbf{r}') \times \vec{\mathcal{B}}(\mathbf{r}') = \tfrac{1}{\mu_0}\int\limits_{\mathcal{V}} d^3\mathbf{r}'(\nabla\times\vec{\mathcal{B}})\times\vec{\mathcal{B}}\ .$$

and hence,

$$F_i = \tfrac{1}{\mu_0}\int\limits_{\mathcal{V}} d^3\mathbf{r}'\left\{(\nabla\times\vec{\mathcal{B}})\times\vec{\mathcal{B}}\right\}_i\ .$$

Now,

$$\begin{aligned}\left\{(\nabla\times\vec{\mathcal{B}})\times\vec{\mathcal{B}}\right\}_i &= \epsilon_{ijk}(\nabla\times\vec{\mathcal{B}})_j\mathcal{B}_k \\ &= \epsilon_{ijk}\epsilon_{jmn}(\partial_m\mathcal{B}_n)\mathcal{B}_k = -\epsilon_{ikj}\epsilon_{mnj}(\partial_m\mathcal{B}_n)\mathcal{B}_k \\ &= -(\delta_{im}\delta_{kn}-\delta_{in}\delta_{km})(\partial_m\mathcal{B}_n)\mathcal{B}_k \\ &= (\partial_k\mathcal{B}_i)\mathcal{B}_k - (\partial_i\mathcal{B}_k)\mathcal{B}_k\ .\end{aligned}$$

We now use,

$$\mathcal{B}_k(\partial_k\mathcal{B}_i) = \partial_k(\mathcal{B}_i\mathcal{B}_k) - \mathcal{B}_i(\partial_k\mathcal{B}_k) = \partial_k(\mathcal{B}_i\mathcal{B}_k)\ .$$

since $\nabla\cdot\vec{\mathcal{B}} = 0$*, as well as,*

$$\mathcal{B}_k(\partial_i\mathcal{B}_k) = \tfrac{1}{2}\partial_i(\mathcal{B}_k\mathcal{B}_k) = \tfrac{1}{2}\partial_i\mathcal{B}^2\ .$$

Hence,

$$\left\{(\nabla\times\vec{\mathcal{B}})\times\vec{\mathcal{B}}\right\}_i = \frac{\partial}{\partial x_k}\left(\mathcal{B}_i\mathcal{B}_k - \tfrac{1}{2}\delta_{ik}\mathcal{B}^2\right) = \mu_0\frac{\partial}{\partial x_k}T_{ki}\ .$$

This is the divergence of a vector field (k indexes). Applying Gauß' law immediately follows the statement.

17.2.5.6 Ex: Force on the plates of a capacitor

Consider an infinite parallel-plate capacitor, with the lower plate (at $z = -d/2$) carrying the charge density $-\sigma$ and the upper plate (at $z = +d/2$) carrying the charge density σ. Determine the stress tensor in the region between the plates.

Solution: *The electric field is,*

$$\mathcal{E}_z = \frac{\sigma}{\varepsilon_0}\ .$$

Therefore, the stress tensor is,

$$\overleftrightarrow{\mathbf{T}} = \varepsilon_0\begin{pmatrix}-\frac{1}{2}\mathcal{E}_z^2 & 0 & 0\\ 0 & -\frac{1}{2}\mathcal{E}_z^2 & 0\\ 0 & 0 & \frac{1}{2}\mathcal{E}_z^2\end{pmatrix} = \frac{\sigma^2}{2\varepsilon_0}\begin{pmatrix}-1 & 0 & 0\\ 0 & -1 & 0\\ 0 & 0 & 1\end{pmatrix}\ .$$

So the pressure is,

$$\mathbf{P} = \frac{\mathbf{F}}{A} = -T_{zz}\hat{\mathbf{e}}_z = -\frac{\sigma^2}{2\varepsilon_0}\hat{\mathbf{e}}_z \ .$$

This force corresponds to a momentum flux per unit area and per unit time, crossing the x-y-plane. On the plates this momentum is absorbed, and the plates recoil (unless there is some non-electric force holding them in position).

17.2.5.7 Ex: Angular momentum of an electromagnetic field

Assuming the existence of an electric charge q_e and a magnetic monopole q_m, calculate the total angular momentum stored in the fields,

$$\vec{\mathcal{E}} = \frac{q_e}{4\pi\varepsilon_0}\frac{\hat{\mathbf{e}}_r}{R^2} \qquad \text{and} \qquad \vec{\mathcal{B}} = \frac{\mu_0 q_m}{4\pi}\frac{\hat{\mathbf{e}}_r}{R^2} \ ,$$

when the two charges are separated by a distance d.

Solution: *We place the origin at the position of the electric charge, such that the magnetic charge is at the position* $\mathbf{d} = d\hat{\mathbf{e}}_z$*. Then,*

$$\begin{aligned}\mathbf{L} &= \int \varepsilon_0 \mathbf{r} \times (\vec{\mathcal{E}} \times \vec{\mathcal{B}}) d^3r = \int \varepsilon_0 \mathbf{r} \times \left(\frac{q_e}{4\pi\varepsilon_0}\frac{\mathbf{r}}{r^3} \times \frac{\mu_0 q_m}{4\pi}\frac{\mathbf{r} - d\hat{\mathbf{e}}_z}{|\mathbf{r} - d\hat{\mathbf{e}}_z|^3} \right) d^3r \\ &= \frac{\mu_0 q_e q_m}{(4\pi)^2} \int \frac{\mathbf{r} \times (\mathbf{r} \times d\hat{\mathbf{e}}_z)}{r^3 |\mathbf{r} - d\hat{\mathbf{e}}_z|^3} d^3r \ .\end{aligned}$$

Using,

$$\begin{aligned}\mathbf{r} \times (\mathbf{r} \times d\hat{\mathbf{e}}_z) &= \mathbf{r}(\mathbf{r} \cdot d\hat{\mathbf{e}}_z) - d\hat{\mathbf{e}}_z(\mathbf{r} \cdot \mathbf{r}) \\ &= dr^2(\hat{\mathbf{e}}_r \cos\theta - \hat{\mathbf{e}}_z) \\ &= dr^2(\sin\theta\cos\theta\cos\phi\hat{\mathbf{e}}_x + \sin\theta\cos\theta\sin\phi\hat{\mathbf{e}}_y + \cos^2\theta\hat{\mathbf{e}}_z - \hat{\mathbf{e}}_z) \\ &= dr(\sin\theta\cos\theta\cos\phi\hat{\mathbf{e}}_x + \sin\theta\cos\theta\sin\phi\hat{\mathbf{e}}_y - \sin^2\theta\hat{\mathbf{e}}_z) \ ,\end{aligned}$$

we conclude the calculation,

$$\begin{aligned}\mathbf{L} &= \frac{\mu_0 q_e q_m}{(4\pi)^2} \int \frac{dr^2(\cancelto{0}{\sin\theta\cos\theta\cos\phi\hat{\mathbf{e}}_x} + \cancelto{0}{\sin\theta\cos\theta\sin\phi\hat{\mathbf{e}}_y} - \sin^2\theta\hat{\mathbf{e}}_z)}{r^3|\mathbf{r} - d\hat{\mathbf{e}}_z|^3} r^2\sin\theta d\theta d\phi dr \\ &= -\frac{\mu_0 q_e q_m}{(4\pi)^2} 2\pi d\hat{\mathbf{e}}_z \int_0^\pi \int_0^\infty \frac{r\sin^3\theta}{\sqrt{r^2 + d^2 - 2rd\cos\theta}^3} dr d\theta \\ &= -\frac{\mu_0 q_e q_m}{(4\pi)^2} 2\pi d\hat{\mathbf{e}}_z \left(\frac{2}{d}\right) = -\frac{\mu_0 q_e q_m}{4\pi}\hat{\mathbf{e}}_z \ .\end{aligned}$$

17.2.5.8 Ex: Torque on a demagnetized or discharged iron sphere

We imagine an iron sphere of radius R carrying a charge Q and a uniform magnetization $\vec{\mathcal{M}} = \mathcal{M}\hat{\mathbf{e}}_z$. The sphere is initially at rest.
a. Calculate the angular momentum stored in the electromagnetic fields.
b. Suppose the sphere is gradually (and uniformly) demagnetized (perhaps by heating it beyond the Curie point). Use Faraday's law to determine the induced electric field and find the torque that this field exerts on the sphere. Calculate the total angular momentum transferred to the sphere during demagnetization.
c. Suppose that, instead of demagnetizing the sphere, we discharge it by connecting the north pole of the sphere via a wire to Earth. Suppose that the current flows on the surface in such a way, that the charge density remains uniform. Use the Lorentz force law to determine the torque on the sphere and calculate the total angular momentum given to the sphere during the discharge. (The magnetic field is discontinuous on the surface ... does this matter?)

Solution: *a. We start from the known magnetic field of a uniformly magnetized iron sphere,*

$$\vec{\mathcal{B}} = \begin{cases} \frac{2}{3}\mu_0\mathcal{M}\hat{\mathbf{e}}_z = \frac{2}{3}\mu_0\mathcal{M}(\hat{\mathbf{e}}_r\cos\theta - \hat{\mathbf{e}}_\theta\sin\theta) & for \;\; r < R \\ \frac{\mu_0\mathcal{M}R^3}{3r^3}(2\hat{\mathbf{e}}_r\cos\theta + \hat{\mathbf{e}}_\theta\sin\theta) & for \;\; r > R \end{cases} .$$

The electric field is,

$$\vec{\mathcal{E}} = \begin{cases} 0 & for \;\; r < R \\ \frac{Q}{4\pi\varepsilon_0 r^2} & for \;\; r > R \end{cases} .$$

The linear momentum density is then,

$$\vec{\wp} = \varepsilon_0\vec{\mathcal{E}}\times\vec{\mathcal{B}} = \frac{\mu_0\mathcal{M}QR^3}{12\pi r^5}\hat{\mathbf{e}}_\phi\sin\theta \;,$$

for $r > R$, such that the angular momentum density is,

$$\ell = \mathbf{r}\times\vec{\wp} = -\frac{\mu_0\mathcal{M}QR^3}{12\pi r^4}\hat{\mathbf{e}}_\theta\sin\theta \;.$$

The total angular momentum is,

$$\mathbf{L} = -\frac{\mu_0\mathcal{M}QR^3}{12\pi}\int_R^\infty\int_0^\pi\int_0^{2\pi}\hat{\mathbf{e}}_\theta\frac{\sin\theta}{r^4}r^2 dr\sin\theta d\theta d\phi \;.$$

Since the unit vector $\hat{\mathbf{e}}_\theta$ varies in space, we must express it in spherical coordinates,

$$\hat{\mathbf{e}}_\theta = \hat{\mathbf{e}}_x\cos\theta\cos\phi + \cos\theta\sin\phi - \hat{\mathbf{e}}_z\sin\theta \;.$$

The integrals over ϕ vanish, such that,

$$\mathbf{L} = -\frac{\mu_0\mathcal{M}QR^3}{12\pi}2\pi\hat{\mathbf{e}}_z\int_R^\infty\hat{\mathbf{e}}_\theta\frac{dr}{r^2}\int_0^\pi\sin^3\theta d\theta = \tfrac{2}{9}\mu_0\mathcal{M}QR^2\hat{\mathbf{e}}_z \;.$$

b. Now the magnetic field is turned off, which, according to Faraday's law, generates a rotational electric field,

$$\oint \vec{\mathcal{E}} \cdot \mathbf{l} = -\frac{d\Phi}{dt} = \int \frac{\partial \vec{\mathcal{B}}}{\partial t} \cdot d\mathbf{a} \ .$$

Choosing as the integration path a circle on the surface of the sphere perpendicular to the symmetry axis, we get the radius $R \in \theta$ for the circle as a function of z. Then the last relation gives,

$$\mathcal{E} 2\pi R \sin\theta = -\pi (R \sin\theta) \frac{\partial \mathcal{B}}{\partial t} \ ,$$

that is,

$$\vec{\mathcal{E}} = -\frac{R \sin\theta}{2} \frac{\partial B}{\partial t} \hat{\mathbf{e}}_\phi \ .$$

Now, we imagine the circle as a circular ribbon with circumference $2\pi R \sin\theta$ and width $Rd\theta$. With the surface charge density $\sigma = Q/4\pi R^2$ we find the charge on this ribbon,

$$dq = \frac{Q}{4\pi R^2} (2\pi R \sin\theta) R d\theta = \tfrac{1}{2} Q \sin\theta d\theta \ .$$

The force on this ribbon is,

$$d\mathbf{F} = \vec{\mathcal{E}} dq = -\frac{1}{4} RQ \sin^2\theta d\theta \frac{\partial \mathcal{B}}{\partial t} \hat{\mathbf{e}}_\phi \ ,$$

and the torque,

$$d\mathbf{N} = \mathbf{r} \times d\mathbf{F} = -(R \sin\theta) \frac{1}{4} RQ \sin^2\theta d\theta \frac{\partial \mathcal{B}}{\partial t} \hat{\mathbf{e}}_z = -\frac{R^2 Q \sin^3\theta)}{4} d\theta \frac{\partial \mathcal{B}}{\partial t} \hat{\mathbf{e}}_z \ .$$

The total torque on the sphere is,

$$\mathbf{N} = \int_0^\pi d\mathbf{N}(\theta) = -\frac{QR^2}{3} \frac{\partial \mathcal{B}}{\partial t} \hat{\mathbf{e}}_z \ .$$

We obtain the final angular momentum by integrating the torque over time,

$$\mathbf{L} = -\frac{QR^2}{3} \hat{\mathbf{e}}_z \int_0^\infty \frac{\partial \mathcal{B}}{\partial t} dt = \tfrac{2}{9} \mu_0 \mathcal{M} Q R^2 \hat{\mathbf{e}}_z \ ,$$

which agrees with the angular momentum initially stored in the fields.
c. Now the charge is removed in a way as to let the charge density be always uniform. The drainage current inside the field of the magnetization will generate a force. To calculate the current we consider the same ribbon of item (b). The current $I(\theta)$ passing through a ribbon located at the position θ should be composed of the drainage current passing through the lower ribbon $I(\theta + d\theta)$ and the draining of the ribbon itself,

$$I(\theta) = I(\theta + d\theta) + \frac{\partial \sigma}{\partial t} (2\pi R \sin\theta)(R d\theta) \ ,$$

that is,

$$\frac{dI}{d\theta} = -\frac{\partial \sigma}{\partial t} 2\pi R^2 \sin\theta \ ,$$

with the solution,

$$I(\theta) = \frac{\partial\sigma}{\partial t} 2\pi R^2 \cos\theta + \alpha \ .$$

The integration constant α can be determined by the boundary condition, $I(\pi) = 0$,

$$I(\theta) = \frac{\partial\sigma}{\partial t} 2\pi R^2 (1 + \cos\theta) \ .$$

For the discharging process we can make a capacitor model,

$$\sigma(t) = \sigma(0) e^{-t/\tau} = \frac{Q}{4\pi R^2} e^{-t/\tau} \ .$$

Now we can calculate the Lorentz force on a ribbon,

$$\begin{aligned} d\mathbf{F} &= I(\theta)(Rd\theta)\hat{\mathbf{e}}_\theta \times \vec{\mathcal{B}} = \frac{\partial\sigma}{\partial t} 2\pi R^2 (1+\cos\theta)(Rd\theta)\hat{\mathbf{e}}_\theta \times \tfrac{2}{3}\mu_0 \mathcal{M}(\hat{\mathbf{e}}_r \cos\theta - \hat{\mathbf{e}}_\theta \sin\theta) \\ &= -\frac{1}{\tau}\frac{Q}{4\pi R^2} e^{-t/\tau} 2\pi R^2 (1+\cos\theta)(Rd\theta)\tfrac{2}{3}\mu_0 \mathcal{M}\cos\theta(-\hat{\mathbf{e}}_\phi) \ . \end{aligned}$$

The torque on the ribbon is,

$$d\mathbf{N} = \mathbf{r} \times d\mathbf{F} = \frac{\mu_0 \mathcal{M} Q R^2}{3\tau} e^{-t/\tau} \hat{\mathbf{e}}_z \sin\theta\cos\theta(1+\cos\theta) \ .$$

The total torque, therefore, is,

$$\mathbf{N} = \int_0^\pi d\mathbf{F} = \frac{2\mu_0 \mathcal{M} Q R^2}{9\tau} e^{-t/\tau} \hat{\mathbf{e}}_z \ .$$

Finally, we integrate over time,

$$\mathbf{L} = \int_0^\infty \mathbf{N} = \tfrac{2}{9}\mu_0 \mathcal{M} Q R^2 \hat{\mathbf{e}}_z \ .$$

The discontinuity of the magnetic field does not matter, since the angular momentum is stored in the zone outside the sphere, where the fields superpose.

17.2.5.9 Ex: Magnetic moment of the electron

In relativistic quantum mechanics the magnetic moment of the electron has the value,

$$\mu = g\mu_B \frac{1}{2} = \frac{e\hbar}{2mc} = 9.28 \cdot 10^{-25} \text{ T m}^3 \ .$$

This exercise aims to show that the classical interpretation of this magnetic moment, as being due to a rotating charge distribution, leads to intrinsic contradictions. Let us regard the electron as a sphere of mass m_e with radius r_e carrying the charge e homogeneously distributed over its surface. It rotates around its z-axis with the angular velocity ω. Classically, the movement of the surface charge causes a magnetic moment.
a. Calculate the total energy contained in the electromagnetic fields.

b. Calculate the total angular momentum contained in the fields.
c. According to Einstein's formula, $W_{ED} = m_e c^2$, the energy in the fields must contribute to the mass of the electron. Lorentz and other scientists have speculated that the entire mass of the electron could be understood in this way. Suppose, furthermore, that the rotational angular momentum (spin) of the electron is entirely attributable to the electromagnetic fields: $L_{ED} = \hbar/2$. From these two premisses, determine the radius and the angular velocity of the electron, as well as the product ωr_e. Does this classical model make sense?
d. Determine the magnetic moment of the rotating electron.

Solution: *a. The electric field produced by a spherical surface charge density,*

$$\rho(\mathbf{r}) = \frac{e}{4\pi r_e^2}\delta(r - r_e) \ ,$$

has already been calculated in other exercises, e.g. 13.2.4.4,

$$\vec{\mathcal{E}}(r) = \begin{cases} 0 \quad for \quad r < r_e \\ \frac{e}{4\pi\varepsilon_0 r^2}\hat{\mathbf{e}}_r \quad for \quad r > r_e \end{cases} \ .$$

For the electrostatic energy we obtain, then,

$$W_e = \frac{\varepsilon_0}{2}\int \mathcal{E}^2 dV = \frac{e^2}{32\pi^2\varepsilon_0^2}4\pi\int_{r>r_e} dr\frac{1}{r^2} = \frac{e^2}{8\pi\varepsilon_0 r_e} \ .$$

The magnetic field produced by a surface current distribution,

$$\mathbf{j}(\mathbf{r}) = j_\phi\hat{\mathbf{e}}_\phi = \rho(\mathbf{r})v_\phi\hat{\mathbf{e}}_\phi = \frac{e}{4\pi r_e}\delta(r - r_e)\omega\sin\theta\hat{\mathbf{e}}_\phi \ ,$$

was also calculated in other exercises, e.g. 15.3.3.1,

$$\vec{\mathcal{B}}(r) = \frac{\mu_0 e\omega}{6\pi r_e}\begin{cases} \hat{\mathbf{e}}_z \quad for \quad r < r_e \\ \frac{r_e^2}{r^3}(\hat{\mathbf{e}}_r\cos\theta + \frac{1}{2}\hat{\mathbf{e}}_\theta\sin\theta) \quad for \quad r > r_e \end{cases} \ .$$

For the magnetostatic energy we obtain, then,

$$\begin{aligned} W_m &= \frac{1}{2\mu_0}\int \mathcal{B}^2 dV \\ &= \frac{1}{2\mu_0}\left[\int_{r<r_e}\left(\frac{\mu_0 e\omega}{6\pi R}\right)^2 d^3r + \int_{r>r_e}\left(\frac{1}{4\pi\varepsilon_0}\right)^2\left(\frac{e\omega r_e^2}{3cr^3}\right)^2(4\cos^2 y + \sin^2 y)\sin y dy d\phi\right] \\ &= \frac{1}{2\mu_0}\frac{4\pi R^3}{3}\left(\frac{\mu_0 e\omega}{6\pi R}\right)^2 + \left(\frac{1}{4\pi\varepsilon_0}\right)^2\frac{1}{2\mu_0}\left(\frac{e\omega r_e^2}{3c}\right)^2\int_a^\infty \frac{1}{r^6}r^2 dr\int_0^{2\pi} d\phi\int_0^\pi(4\cos^2 y + \sin^2 y)\sin y dy \\ &= \frac{\mu_0 e^2\omega^2 r_e c^2}{54\pi} + \frac{1}{2\mu_0}\left(\frac{e\omega r_e^2}{3c}\right)^2\frac{1}{3r_e^3}2\pi 4\left(\frac{1}{4\pi\varepsilon_0}\right)^2 = \frac{\mu_0 e^2\omega^2 r_e c^2}{36\pi} \ . \end{aligned}$$

b. Only in the outer region the momentum density does not vanish ,

$$\vec{\wp} = \varepsilon_0\vec{\mathcal{E}}\times\vec{\mathcal{B}} = \varepsilon_0\frac{e}{4\pi\varepsilon_0 r^2}\hat{\mathbf{e}}_r \times \frac{\mu_0 e\omega}{6\pi r_e}\frac{r_e^2}{r^3}\frac{\hat{\mathbf{e}}_\theta}{2}\sin\theta = \frac{\mu_0 e^2\omega r_e^2}{48\pi^2}\frac{\sin\theta}{r^5}\hat{\mathbf{e}}_\phi \ ,$$

and the angular momentum density,

$$\vec{\ell} = \mathbf{r} \times \vec{\wp} = -\frac{\mu_0 e^2 \omega r_e}{48\pi^2} \frac{\sin\theta}{r^4} \hat{\mathbf{e}}_\theta \ .$$

The total angular momentum of the field is obtained by inserting $\hat{\mathbf{e}}_\theta = \hat{\mathbf{e}}_x \cos\theta\cos\phi + \hat{\mathbf{e}}_y \cos\theta \sin\phi - \hat{\mathbf{e}}_z \sin\theta$,

$$\mathbf{L}_{ED} = -\frac{\mu_0 e^2 \omega r_e^2}{48\pi^2} \int_{r>r_e} \frac{\sin\theta}{r^4} \hat{\mathbf{e}}_\theta d^3 r = \frac{\mu_0 e^2 \omega r_e^2}{24\pi} \hat{\mathbf{e}}_z \int_{r_e}^{\infty} \int_0^\pi \frac{\sin^3\theta}{r^2} d\theta dr = \frac{\mu_0 e^2 \omega r_e}{18\pi} \hat{\mathbf{e}}_z \ .$$

c. Equalizing the energy of the electromagnetic field with the rest mass of the electron, $m_e c^2$, *and the angular momentum with* $\frac{1}{2}\hbar$, *we obtain,*

$$\frac{e^2}{8\pi\varepsilon_0 r_e} + \frac{\mu_0 e^2 \omega^2 r_e c^2}{36\pi} = m_e c^2 \qquad , \qquad \frac{\mu_0 e^2 \omega r_e}{18\pi} = \frac{\hbar}{2} \ .$$

Resolving by r_e *and* ω,

$$r_e = \frac{1}{8} \frac{18\hbar^2\pi^2\varepsilon_0 + e^4\mu_0}{m_e \pi e^2} = \frac{9\pi\varepsilon_0\hbar^2}{4me^2} + \frac{e^2}{8\pi\varepsilon_0 m_e c^2} \approx 2.98 \cdot 10^{-11}\,\mathrm{m} + 1.41 \cdot 10^{-15}\,\mathrm{m} \ ,$$

and

$$\omega = 72 \frac{\hbar\pi^2 m_e c^2 \varepsilon_0}{18\hbar^2\pi^2\varepsilon_0 + e^4\mu_0} \approx 3.105 \cdot 10^{21}\,\mathrm{s}^{-1} \ .$$

This gives a ridiculously high orbital velocity in the equatorial plane,

$$\omega r_e = 9.246 \cdot 10^{10}\,\mathrm{m/s} \ .$$

d. Using $-\hat{\mathbf{e}}_r \times \hat{\mathbf{e}}_\phi = \hat{\mathbf{e}}_\theta = \hat{\mathbf{e}}_x \cos\theta\cos\phi + \hat{\mathbf{e}}_y \cos\theta\sin\phi - \hat{\mathbf{e}}_z \sin\theta$ *we calculate,*

$$\begin{aligned}
\vec{\mathcal{M}}_e &= \tfrac{1}{2} \int \mathbf{r}' \times \mathbf{j}(\mathbf{r}', t) d^3 r' = \frac{1}{2} \int \mathbf{r}' \times \frac{e\omega}{4\pi\varepsilon_0} \delta(r' - r_e) \sin\theta' \hat{\mathbf{e}}'_\phi d^3 r' \\
&= \frac{1}{2} \frac{e\omega}{4\pi\varepsilon_0} \int_0^{2\pi} \int_0^\pi \int_0^\infty \delta(r' - r_e) \sin\theta' \hat{\mathbf{e}}_{r'} \times \hat{\mathbf{e}}_{\phi'} r'^3 \sin\theta' d\theta' dr' d\phi' \\
&= -\frac{1}{2} \frac{e\omega}{4\pi\varepsilon_0} \int_0^{2\pi} \int_0^\pi \int_0^\infty \delta(r' - r_e) \sin\theta' (\hat{\mathbf{e}}_x \cos\theta' \cos\phi' + \hat{\mathbf{e}}_y \cos\theta' \sin\phi' - \hat{\mathbf{e}}_z \sin\theta') r'^3 \sin\theta' d\theta' dr' d\phi' \\
&= \frac{\hat{\mathbf{e}}_z}{2} \frac{e\omega}{4\pi\varepsilon_0} \frac{r_e^4}{4} \int_0^\pi \sin^3\theta' d\theta' = \frac{e\omega r_e^4}{24\pi\varepsilon_0} \hat{\mathbf{e}}_z \approx 3.7 \cdot 10^{-12}\,\mathrm{T\ m^3} \ .
\end{aligned}$$

We note, that the classical electron radius is defined by,

$$r_{cl} = \frac{e^2}{4\pi\varepsilon_0 m_e c^2} \ .$$

17.3 Potential formulation of electrodynamics

17.3.1 The vector and the scalar potential

All quantities involved in Maxwell's equations for vacuum, the fields $\vec{\mathcal{E}}(\mathbf{r},t)$ and $\vec{\mathcal{B}}(\mathbf{r},t)$ as well as charge ($\rho(\mathbf{r},t)$) and current ($\mathbf{j}(\mathbf{r},t)$) distributions they depend on space and time. Knowing that the divergence of a field is zero everywhere, $\nabla\cdot\vec{\mathcal{B}}=0$, we conclude that this field must be the rotation of another field. That is, there is a vector field $\mathbf{A}(\mathbf{r},t)$, such that,

$$\vec{\mathcal{B}}(\mathbf{r},t)=\nabla\times\mathbf{A}(\mathbf{r},t)\ . \tag{17.74}$$

Substituting the so-called *vector potential* $\mathbf{A}(\mathbf{r},t)$ in Faraday's law, $\nabla\times\vec{\mathcal{E}}=-\frac{\partial\vec{\mathcal{B}}}{\partial t}$, we obtain,

$$\nabla\times\vec{\mathcal{E}}=-\frac{\partial}{\partial t}(\nabla\times\mathbf{A})=-\nabla\times\frac{\partial\mathbf{A}}{\partial t}\ . \tag{17.75}$$

Hence,

$$\nabla\times\left(\vec{\mathcal{E}}+\frac{\partial\mathbf{A}}{\partial t}\right)=0\ . \tag{17.76}$$

Now, since the rotational field within the parentheses is null everywhere, it follows that there exists a scalar field $\Phi(\mathbf{r},t)$, called *scalar potential*, such that,

$$\vec{\mathcal{E}}+\frac{\partial\mathbf{A}}{\partial t}=-\nabla\Phi\ . \tag{17.77}$$

The minus sign in front of the gradient of $\Phi(\mathbf{r},t)$, is introduced to recover the electrostatic case when $\mathbf{A}(\mathbf{r},t)$ does not depend on time. In summary, if we know the vector and scalar potentials, we can calculate the fields $\vec{\mathcal{E}}(\mathbf{r},t)$ and $\vec{\mathcal{B}}(\mathbf{r},t)$ following the prescription expressed by the equations:

$$\boxed{\vec{\mathcal{E}}(\mathbf{r},t)=-\nabla\Phi(\mathbf{r},t)-\frac{\partial\mathbf{A}(\mathbf{r},t)}{\partial t}\qquad\text{and}\qquad\vec{\mathcal{B}}(\mathbf{r},t)=\nabla\times\mathbf{A}(\mathbf{r},t)}\ . \tag{17.78}$$

17.3.2 Gauge transformation

Substituting the expression for the electric field by the vector and scalar potentials in Gauß' law, $\nabla\cdot\vec{\mathcal{E}}=\frac{\varrho}{\varepsilon_0}$,

$$\frac{\varrho}{\varepsilon_0}=\nabla\cdot\left(-\nabla\Phi-\frac{\partial\mathbf{A}}{\partial t}\right)=-\nabla^2\Phi-\frac{\partial\nabla\cdot\mathbf{A}}{\partial t}\ . \tag{17.79}$$

Replacing the fields $\vec{\mathcal{E}}(\mathbf{r},t)$ and $\vec{\mathcal{B}}(\mathbf{r},t)$ by the potentials defined in (17.78), within the law of Ampère-Maxwell, $\nabla\times\vec{\mathcal{B}}=\mu_0\mathbf{j}+\varepsilon_0\mu_0\frac{\partial\vec{\mathcal{E}}}{\partial t}$, we obtain,

$$\nabla\times(\nabla\times\mathbf{A})=\nabla(\nabla\cdot\mathbf{A})-\nabla^2\mathbf{A}=\mu_0\mathbf{j}-\frac{1}{c^2}\frac{\partial}{\partial t}\left(-\nabla\Phi-\frac{\partial\mathbf{A}}{\partial t}\right)\ . \tag{17.80}$$

that is,

$$\nabla^2\mathbf{A}-\frac{1}{c^2}\frac{\partial\mathbf{A}^2}{\partial t^2}-\nabla\left(\nabla\cdot\mathbf{A}+\frac{1}{c^2}\frac{\partial\Phi}{\partial t}\right)=-\mu_0\mathbf{j}\ . \tag{17.81}$$

The coupled differential equations (17.79) and (17.81) allow us, in principle, to derive a set of potentials Φ and $\mathbf{A}$, generated by a charge and current distribution ϱ and $\mathbf{j}$, from which the fields $\vec{\mathcal{E}}$ and $\vec{\mathcal{B}}$ can be calculated. However, these *potentials are not unique*. To see this, let us suppose new potentials,

$$\Phi_1 \equiv \Phi - \frac{\partial \chi}{\partial t} \qquad \text{and} \qquad \mathbf{A}_1 \equiv \mathbf{A} + \nabla\chi \; . \tag{17.82}$$

Obviously, these potentials produce the same fields, since,

$$\vec{\mathcal{B}}_1 = \nabla \times (\mathbf{A} + \nabla\chi) = \vec{\mathcal{B}} \; , \tag{17.83}$$

using the expressions (17.78) and,

$$\vec{\mathcal{E}}_1 = -\nabla\left(\Phi - \frac{\partial\chi}{\partial t}\right) - \frac{\partial}{\partial t}(\mathbf{A} + \nabla\chi) = -\nabla\Phi - \frac{\partial}{\partial t}\mathbf{A} = \vec{\mathcal{E}} \; . \tag{17.84}$$

Thus, it is clear that the fields are the same for an infinite number of different potentials, provided they follow from each other by a so-called *gauge transform*,

$$\boxed{\mathbf{A} \longrightarrow \mathbf{A} + \nabla\chi \qquad \text{and} \qquad \Phi \longrightarrow \Phi - \partial_t\chi} \; . \tag{17.85}$$

This *gauge invariance* leaves the observable fields $\vec{\mathcal{E}}$ and $\vec{\mathcal{B}}$ invariant.

The freedom of choosing an appropriate gauge field can be employed to simplify the set of equations (17.79) and (17.81) for particular problems, as we will discuss in the following sections.

17.3.2.1 Lorentz gauge

We note that if the expression within the brackets of Eq. (17.81) were zero,

$$\boxed{\nabla \cdot \mathbf{A} + \frac{1}{c^2}\frac{\partial\Phi}{\partial t} \stackrel{!}{=} 0} \tag{17.86}$$

we would have from the equations (17.79) and (17.81) 'wave' type equations for the potentials,

$$\nabla^2\Phi - \frac{1}{c^2}\frac{\partial^2\Phi}{\partial t^2} = -\frac{\varrho}{\varepsilon_0} \qquad \text{and} \qquad \nabla^2\mathbf{A} - \frac{1}{c^2}\frac{\partial^2\mathbf{A}}{\partial t^2} = -\mu_0\mathbf{j} \; . \tag{17.87}$$

To analyze the viability of the expression (17.86), we apply a gauge transformation,

$$\nabla \cdot (\mathbf{A} + \nabla\chi) + \frac{1}{c^2}\frac{\partial(\Phi - \partial_t\chi)}{\partial t} = \nabla^2\chi - \frac{1}{c^2}\frac{\partial^2\chi}{\partial t^2} = 0 \; . \tag{17.88}$$

Hence, imposing the additional condition (17.86) is legal, because it can always be satisfied by a simple gauge transformation with a field χ satisfying the wave equation (17.88).

The equation (17.86) is known as the *Lorentz gauge*. We emphasize that *it is not necessary to postulate the equation*, but it is always possible to find a scalar function χ,

which allows the use of new potentials, giving the same $\vec{\mathcal{E}}$ and $\vec{\mathcal{B}}$ fields and satisfying this equation [11].

Introducing the notation of the *d'Alembert operator*,

$$\Box \equiv \nabla^2 - \varepsilon_0\mu_0 \frac{\partial^2}{\partial t^2} \ , \tag{17.89}$$

the wave equations (17.87) become,

$$\Box\Phi = -\varepsilon_0^{-1}\varrho \qquad \text{and} \qquad \Box\mathbf{A} = -\mu_0\mathbf{j} \ . \tag{17.90}$$

They generalize the electro- and magnetostatic equations (17.6) to include temporal variations simply by replacing the Laplacian with a d'Alembertian. The democratic treatment of Φ and $\mathbf{A}$ by a Poisson-like equation in four space-time dimensions is particularly interesting in the context of special relativity. We study examples of the Lorentz gauge in Excs. 15.3.3.6 to 15.3.3.8 and 17.3.8.1 to 17.3.8.7.

17.3.2.2 Coulomb gauge, transverse and longitudinal currents

Another condition that can be applied to the potentials in order to simplify the differential equations (17.86) and (17.88) consists in setting,

$$\boxed{\nabla\cdot\mathbf{A} \stackrel{!}{=} 0} \ . \tag{17.91}$$

This is called the *Coulomb gauge*. With this condition we obtain from (17.79) the *Poisson equation* as well as an equation for the vector potential,

$$\begin{aligned} -\nabla^2\Phi &= \frac{\varrho}{\varepsilon_0} \\ -\nabla^2\mathbf{A} + \frac{1}{c^2}\left(\frac{\partial^2\mathbf{A}}{\partial t^2} + \frac{\partial}{\partial t}\nabla\Phi\right) &= \mu_0\mathbf{j} \ . \end{aligned} \tag{17.92}$$

These two equations determine the vector and scalar potentials if the current and charge density distributions are specified [12]. The first Eq. (17.92) is solved by *Coulomb's law*, letting $\Phi(\infty) = 0$,

$$\Phi(\mathbf{r},t) = \frac{1}{4\pi\varepsilon_0}\int \frac{\varrho(\mathbf{r}',t)}{|\mathbf{r}-\mathbf{r}'|}d^3r' \ . \tag{17.93}$$

It is important to be aware that, unlike in electrostatics, we need to know also $\mathbf{A}(\mathbf{r},t)$ to be able to calculate the field $\vec{\mathcal{E}}(\mathbf{r},t)$ through the formula (17.78).

It may seem strange that the scalar potential in Coulomb's gauge is determined by the instantaneous charge distribution: Moving an electron at a point $\mathbf{r}'$, the potential at a distant point, $\Phi(\mathbf{r})$, immediately captures this change, not being limited by the speed limit for the transmission of information postulated by special relativity. The explanation is, that Φ is not an observable physical quantity. To infer a change of ϱ, we must measure $\vec{\mathcal{E}}$, which depends on $\mathbf{A}$ as well. Somehow it is encoded into the

[11] E.g. choosing χ such that $\nabla\chi = -\mathbf{A}$ and $c^{-1}\partial_t\chi = \phi$.

[12] The determination still leaves the freedom to add fields satisfying $\nabla^2\Theta = 0$.

Coulomb gauge that, while $\Phi(\mathbf{r})$ instantly reflects all variations of $\varrho(\mathbf{r}')$, the vector potential depends in a much more complicated way on these variations, such that the combination $-\nabla\Phi - \partial\mathbf{A}/\partial t$ only responds to the variations after a long enough time for information to arrive.

The advantage of the Coulomb gauge is that the scalar potential is simple to calculate. The disadvantage is that, in addition to the non-causal appearance of Φ, it is particularly difficult to calculate $\mathbf{A}$: The differential equation for $\mathbf{A}$ in the Coulomb gauge is (17.81).

In order to obtain an equation involving only the vector field and the current density, we use Helmholtz's theorem to write the current density as the sum of *transverse* and *longitudinal* components,

$$\mathbf{j} = \mathbf{j}_T + \mathbf{j}_L \ , \tag{17.94}$$

where the terms 'transverse' and 'longitudinal' are defined by the following two conditions,

$$\boxed{\nabla \cdot \mathbf{j}_T = 0 \qquad \text{and} \qquad \nabla \times \mathbf{j}_L = 0} \ . \tag{17.95}$$

Calculating the rotation of the second equation (17.92) we see that the term containing the gradient of the scalar potential vanishes. Hence,

$$-\nabla^2\mathbf{A} + \frac{1}{c^2}\frac{\partial^2\mathbf{A}}{\partial t^2} = \mu_0\mathbf{j}_T \ , \tag{17.96}$$

which shows that the transverse component of $\mathbf{j}$ is fully associated only with the vector potential. Now, substituting this result into the second equation (17.92) we are left with,

$$\varepsilon_0\frac{\partial}{\partial t}\nabla\Phi = \mathbf{j}_L \ . \tag{17.97}$$

That is, the longitudinal component of $\mathbf{j}$ is fully associated to the scalar potential. The solution of Eq. (17.96) requires some preparation and will be given in the following sections.

17.3.3 Green's function

A useful tool for solving Laplace equations, such as derived in Eq. (17.87) or (17.96), is the *Green's function*. The dynamics of physical systems are often described by differential equations of the type,

$$\mathcal{L}u(\mathbf{r}) = \varrho(\mathbf{r}) \ , \tag{17.98}$$

where $\mathcal{L} = \mathcal{L}(\mathbf{r})$ is a linear *differential operator*. While this operator has a very generic form, the behavior of a particular system depends on the choice of the function ϱ. The Laplace equation, where $\mathcal{L}(\mathbf{r}) \equiv \nabla^2$ and ϱ is a particular charge distribution is an example.

One method of solving this differential equation is to first solve the following equation,

$$\mathcal{L}\mathcal{G}(\mathbf{r}, \mathbf{x}) = \delta^3(\mathbf{r} - \mathbf{x}) \ , \tag{17.99}$$

where $\mathcal{G}(\mathbf{r}, \mathbf{x})$ is called the Green function of the operator. In general, the Green function is not unique. However, in practice, some combination of symmetry, boundary conditions and/or other externally imposed criteria can make the Green function unique.

Green functions are useful tools for solving wave and diffusion equations. In quantum mechanics, the Green function of the Hamiltonian is intrinsically connected to the concept of density of states. If the operator is invariant under translations, that is, if $\mathcal{L}$ has constant coefficients with respect to $\mathbf{r}$, then the Green function can be taken as the convolution [13],

$$\mathcal{G}(\mathbf{r}, \mathbf{x}) = \mathcal{G}(\mathbf{r} - \mathbf{x}) \ . \tag{17.100}$$

If such a function $\mathcal{G}$ can be found for the operator $\mathcal{L}$, then multiplying Eq. (17.99) for the Green function by $\varrho(\mathbf{x})$, and then integrating by the variable $\mathbf{x}$, we obtain:

$$\int \mathcal{L}\mathcal{G}(\mathbf{r}, \mathbf{x})\varrho(\mathbf{x})d^3x = \int \delta^3(\mathbf{r} - \mathbf{x})\varrho(\mathbf{x})d^3x = \varrho(\mathbf{r}) = \mathcal{L}u(\mathbf{r}) \ , \tag{17.101}$$

comparing the result with the Eq. (17.98). As we assume, that the operator $\mathcal{L} = \mathcal{L}(\mathbf{r})$ is linear and acts only on the variable $\mathbf{r}$ (and not on the integration variable $\mathbf{x}$), we can put $\mathcal{L}$ out of the integral on the right side. We conclude,

$$u(\mathbf{r}) = \int \mathcal{G}(\mathbf{r}, \mathbf{x})\varrho(\mathbf{x})d^3x \ . \tag{17.102}$$

Hence, we can obtain the function $u(\mathbf{r})$ from the Green function $\mathcal{G}(\mathbf{r}, \mathbf{x})$, determined by Eq. (17.99), and the source term $\varrho(\mathbf{x})$.

The Green function, also called the fundamental solution associated with the operator $\mathcal{L}$, can be considered as the inversion of $\mathcal{L} \equiv \mathcal{G}^{-1}$. Not every operator $\mathcal{L}$ admits a Green function. In practice, not only calculating the Green function can be difficult for a particular operator, but also evaluating the integral in Eq. (17.102). In Exc. 17.3.8.8 we will get to know a Green function of the wave equation.

Example 90 (*Solving the Laplace equation by Green's method*): The Laplace equation is,

$$\nabla^2\Phi(\mathbf{r}) = -\varepsilon_0^{-1}\varrho(\mathbf{r}) \ .$$

The Green function,

$$\mathcal{G}(\mathbf{r}, \mathbf{r}') = \mathcal{G}(\mathbf{r} - \mathbf{r}') = -\frac{1}{4\pi|\mathbf{r} - \mathbf{r}'|} \ ,$$

resolves the Poisson equation,

$$\nabla^2\mathcal{G}(\mathbf{r} - \mathbf{r}') = \delta^3(\mathbf{r} - \mathbf{r}') \ .$$

Therefore, the solution of the Laplace equation is,

$$\Phi(\mathbf{r}) = \frac{1}{4\pi\varepsilon_0}\int \frac{\varrho(\mathbf{r}')d^3r'}{|\mathbf{r} - \mathbf{r}'|} \ .$$

To solve the wave equations (17.90), we need to find the Green function for a spatio-temporal differential operator $\mathcal{L}(\mathbf{r}, t) = \Box$. We will do this in the example 91, but for now, in the following section, we will adopt more empirical arguments.

[13] In this case, the Green function is the same as the *pulse response* in the theory of time-independent linear systems.

17.3.4 Retarded potentials of continuous charge distributions

In the Lorentz gauge Φ and $\mathbf{A}$ satisfy the inhomogeneous wave equations (17.90) incorporating a 'source' term. We will use in the following exclusively the Lorentz gauge within which the entire electrodynamics comes down to solving (17.90).

But before that, let us take a look at the static situation, where the equations (17.90) reduce to Poisson equations,

$$\nabla^2\Phi = -\varepsilon_0^{-1}\varrho \qquad \text{and} \qquad \nabla^2\mathbf{A} = -\mu_0\mathbf{j}\ , \tag{17.103}$$

with the known solutions,

$$\Phi(\mathbf{r}) = \frac{1}{4\pi\varepsilon_0}\int \frac{\varrho(\mathbf{r}')}{|\mathbf{r}-\mathbf{r}'|}d^3r' \qquad \text{and} \qquad \mathbf{A}(\mathbf{r}) = \frac{\mu_0}{4\pi}\int \frac{\mathbf{j}(\mathbf{r}')}{|\mathbf{r}-\mathbf{r}'|}d^3r'\ . \tag{17.104}$$

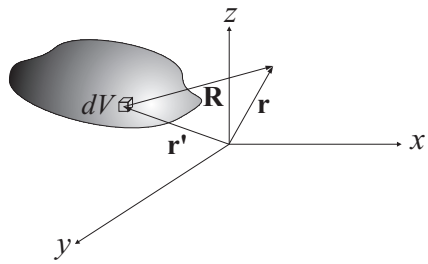

Figure 17.11: Geometry of source and the observation point.

In the dynamic case, the charge confined in the volume dV' (see Fig. 17.11) can move, but for the information on this movement to reach the point of observation $\mathbf{r}$ it takes a time determined by the propagation velocity of the light: $|\mathbf{r}-\mathbf{r}'|/c$. Introducing the distance R between the position of the charge and the observation point and the time retardation t_r by,

$$\mathbf{R} \equiv \mathbf{r}-\mathbf{r}' \qquad \text{and} \qquad t_r \equiv t - \tfrac{R}{c}\ , \tag{17.105}$$

we expect the following generalization of the equation (17.104),

$$\boxed{\Phi(\mathbf{r},t) = \frac{1}{4\pi\varepsilon_0}\int \frac{\varrho(\mathbf{r}',t_r)}{R}d^3r' \qquad \text{and} \qquad \mathbf{A}(\mathbf{r}) = \frac{\mu_0}{4\pi}\int \frac{\mathbf{j}(\mathbf{r}',t_r)}{R}d^3r'}\ , \tag{17.106}$$

called *retarded potential*.

The argument given above seems reasonable, but does not represent a stringent derivation, which will be given in the following. In fact, the same argument applied to the fields $\vec{\mathcal{E}}$ and $\vec{\mathcal{B}}$ would give false results, as we shall see later.

To verify the correctness of the assertion (17.106) we can simply show that it satisfies the wave equation (17.90) and the Lorentz gauge (17.89). However, this is not trivial, since the integral expressions depend on $\mathbf{r}$ explicitly (via the distance R

in the denominator) and implicitly (via the retarded time t_d). Here, we present the calculation for the scalar potential,

$$\begin{aligned}\nabla_r\Phi(\mathbf{r}) &= \frac{1}{4\pi\varepsilon_0}\int \nabla_r \frac{\varrho(\mathbf{r}', t-\frac{|\mathbf{r}-\mathbf{r}'|}{c})}{|\mathbf{r}-\mathbf{r}'|} d^3r' \qquad (17.107)\\ &= \frac{1}{4\pi\varepsilon_0}\int \left[\frac{1}{R}\nabla_r\varrho + \varrho\nabla_r\frac{1}{R}\right] d^3r' = \frac{1}{4\pi\varepsilon_0}\int \left[\frac{1}{R}\frac{-\dot\varrho}{c}\frac{\mathbf{R}}{R} + \varrho\frac{-\mathbf{R}}{R^3}\right] d^3r' \ .\end{aligned}$$

The divergence of the gradient,

$$\begin{aligned}\nabla_r^2\Phi(\mathbf{r}) &= \frac{1}{4\pi\varepsilon_0}\int \left[\frac{-\dot\varrho}{c}\left(\nabla_r\cdot\frac{\mathbf{R}}{R^2}\right) - \frac{\mathbf{R}}{R^2}\cdot\left(\frac{\nabla_r\dot\varrho}{c}\right) - (\nabla_r\varrho)\cdot\frac{\mathbf{R}}{R^3} - \varrho\left(\nabla_r\cdot\frac{\mathbf{R}}{R^3}\right)\right] d^3r'\\ &= \frac{1}{4\pi\varepsilon_0}\int \left[\cancel{\frac{-\dot\varrho}{c}\frac{1}{R^2}} - \frac{\mathbf{R}}{R^2}\cdot\left(\frac{-\ddot\varrho\mathbf{R}}{c^2R}\right) - \cancel{\left(\frac{-\dot\varrho\mathbf{R}}{cR}\right)\cdot\frac{\mathbf{R}}{R^3}} - \varrho 4\pi\delta^3(\mathbf{R})\right] d^3r'\\ &= \frac{1}{4\pi\varepsilon_0}\int \left[\frac{\ddot\varrho}{c^2R} - 4\pi\varrho\delta^3(\mathbf{R})\right] d^3r' = \frac{1}{c^2}\frac{\partial^2\Phi}{\partial t^2} - \frac{\varrho(\mathbf{r},t)}{\varepsilon_0}\ , \qquad (17.108)\end{aligned}$$

where we replaced in the last line the integral of $\ddot\varrho/c^2R$ by the expression (17.106), reproduces the wave equation. In Exc. 17.3.8.9 we verify that the retarded potentials (17.106) satisfy the Lorentz gauge.

It is interesting to note that the same calculation can be made for advanced times, where the potential would be affected by a *future* movement of the charge, $t_a = t + \frac{R}{c}$. But this would violate causality.

Example 91 (*Resolution of the wave equation by the Greens function*): We showed in the previous section that in the Lorentz gauge, given the sources ϱ and $\mathbf{j}$, all we have to do to find the scalar and vector potentials is to solve wave type differential equations (17.87),

$$\nabla^2\psi(\mathbf{r},t) - \frac{1}{c^2}\frac{\partial^2\psi(\mathbf{r},t)}{\partial t^2} = f(\mathbf{r},t)\ ,$$

where ψ is a variable to denote the fields Φ or $\mathbf{A}$ and f to denote the sources ϱ or $\mathbf{j}$. First, we want to find a particular solution of this equation. To this end, we use the Green function $\mathcal{G}(\mathbf{r},t,\mathbf{r}',t')$, which by definition satisfies,

$$\boxed{\nabla^2\mathcal{G}(\mathbf{r},t,\mathbf{r}',t') - \frac{1}{c^2}\frac{\partial^2}{\partial t^2}\mathcal{G}(\mathbf{r},t,\mathbf{r}',t') = \delta^{(3)}(\mathbf{r}-\mathbf{r}')\delta(t-t')}\ .$$

We can perform the Fourier transform with respect to the variable t and obtain,

$$\nabla^2 g(\mathbf{r},\omega,\mathbf{r}',t') + \frac{\omega^2}{c^2}g(\mathbf{r},\omega,\mathbf{r}',t') = \delta^{(3)}(\mathbf{r}-\mathbf{r}')\frac{e^{\imath\omega t'}}{2\pi}\ ,$$

where we used the integral representation of the Dirac delta function, i.e.,

$$\delta(t-t') = \frac{1}{2\pi}\int_{-\infty}^{\infty} e^{-\imath\omega(t-t')}d\omega$$

and we defined,

$$\mathcal{G}(\mathbf{r},t,\mathbf{r}',t') \equiv \int_{-\infty}^{\infty} e^{-\imath\omega t} g(\mathbf{r},\omega,\mathbf{r}',t')d\omega\ .$$

As we will explain later, instead of solving the above differential equation, we will modify it:

$$\nabla^2 g_\eta(\mathbf{r},\omega,\mathbf{r}',t') + (k_0+\imath\eta)^2 g_\eta(\mathbf{r},\omega,\mathbf{r}',t') = \delta^{(3)}(\mathbf{r}-\mathbf{r}')\frac{e^{\imath\omega t'}}{2\pi} \ ,$$

with $k_0 \equiv \omega/c$ assuming positive and negative values for ω: We can now take the Fourier transform with respect to the variable $\mathbf{r}$ and obtain,

$$-k^2 \bar{g}_\eta(\mathbf{k},\omega,\mathbf{r}',t') + (k_0+\imath\eta)^2 \bar{g}_\eta(\mathbf{k},\omega,\mathbf{r}',t') = \frac{e^{-\imath\mathbf{k}\cdot\mathbf{r}'+\imath\omega t'}}{(2\pi)^4} \ ,$$

where we used,

$$\delta^{(3)}(\mathbf{r}-\mathbf{r}') = \frac{1}{(2\pi)^3}\int_{\mathbb{R}^3} e^{\imath\mathbf{k}\cdot(\mathbf{r}-\mathbf{r}')} d^3k \ ,$$

and defined,

$$g_\eta(\mathbf{r},\omega,\mathbf{r}',t') \equiv \int e^{\imath\mathbf{k}\cdot\mathbf{r}} \bar{g}_\eta(\mathbf{k},\omega,\mathbf{r}',t') d^3k \ .$$

Hence,

$$\bar{g}_\eta(\mathbf{k},\omega,\mathbf{r}',t') = \frac{e^{-\imath\mathbf{k}\cdot\mathbf{r}'+\imath\omega t'}}{(2\pi)^4[-k^2+(k_0+\imath\eta)^2]} \ ,$$

and therefore,

$$g_\eta(\mathbf{r},\omega,\mathbf{r}',t') = \int \frac{e^{-\imath\mathbf{k}\cdot(\mathbf{r}-\mathbf{r}')+\imath\omega t'}}{(2\pi)^4[-k^2+(k_0+\imath\eta)^2]} d^3k \ .$$

Note that, if we had not modified the original equation (i.e. set $\eta = 0$), the integral above would not converge, and we could not find a Green function by the present method. Now, however, the Green function is,

$$\mathcal{G}_\eta(\mathbf{r}-\mathbf{r}',t-t') = \int_{-\infty}^{\infty} e^{-\imath\omega t} g_\eta(\mathbf{r},\omega,\mathbf{r}',t') d\omega = \int d^3k \int_{-\infty}^{\infty} d\omega \frac{e^{\imath\mathbf{k}\cdot(\mathbf{r}-\mathbf{r}')-\imath\omega(t-t')}}{(2\pi)^4[-k^2+(k_0+\imath\eta)^2]} \ ,$$

or yet,

$$\mathcal{G}_\eta(\mathbf{r},t) = \int d^3k \int_{-\infty}^{\infty} \frac{d\omega\ e^{\imath\mathbf{k}\cdot\mathbf{r}-\imath\omega t}}{(2\pi)^4[-k^2+(k_0+\imath\eta)^2]} = \frac{1}{(2\pi)^4}\int_{-\infty}^{\infty} d\omega e^{-\imath\omega t} \int \frac{d^3k\ e^{\imath\mathbf{k}\cdot\mathbf{r}}}{[k^2-(k_0+\imath\eta)^2]} \ .$$

In polar coordinates, choosing the orientation of the $\mathbf{k}$-vector space such that k_z is parallel to the vector $\mathbf{r}$,

$$\begin{aligned}
\int d^3k \frac{e^{\imath\mathbf{k}\cdot\mathbf{r}}}{[k^2-(k_0+\imath\eta)^2]} &= \int_0^\infty k^2 dk \frac{1}{[k^2-(k_0+\imath\eta)^2]} \int_0^{2\pi} d\phi_k \int_0^\pi d\theta_k \sin\theta_k e^{\imath\mathbf{k}\cdot\mathbf{r}} \\
&= \int_0^\infty dk \frac{k^2}{[k^2-(k_0+\imath\eta)^2]} \int_0^{2\pi} d\phi_k \int_0^\pi d\theta_k \sin\theta_k e^{\imath kr\cos\theta_k} \\
&= \int_0^\infty dk \frac{2\pi k^2}{[k^2-(k_0+\imath\eta)^2]} \int_{-1}^1 du e^{\imath kru} \\
&= \frac{2\pi}{\imath r}\int_0^\infty dk \frac{k}{[k^2-(k_0+\imath\eta)^2]}(e^{\imath kr}-e^{-\imath kr}) \ ,
\end{aligned}$$

where we used the substitution $u \equiv \cos\theta_k$. Since,

$$\int_0^\infty dk \frac{ke^{-\imath kr}}{[k^2-(k_0+\imath\eta)^2]} = -\int_{-\infty}^0 dk \frac{ke^{\imath kr}}{[k^2-(k_0+\imath\eta)^2]} \ ,$$

we can write,

$$\int d^3k \frac{e^{\imath \mathbf{k}\cdot\mathbf{r}}}{[k^2-(k_0+\imath\eta)^2]} = \frac{2\pi}{\imath r}\int_{-\infty}^{\infty} dk \frac{ke^{\imath kr}}{[k^2-(k_0+\imath\eta)^2]} \ .$$

The poles of this integral are given by,

$$Z_\pm = \pm(k_0+\imath\eta) \ .$$

We consider the integral in the complex plane:

$$\oint_C \frac{Ze^{\imath rZ}}{(Z-Z_+)(Z-Z_-)}dZ \ ,$$

where the contour is closed over the upper complex half-plane. When $\eta \to 0^+$ [see Fig. 17.12(a)], we get,

$$\oint_C \frac{Ze^{\imath rZ}}{(Z-Z_+)(Z-Z_-)}dZ = 2\pi\imath\frac{Z_+e^{\imath rZ_+}}{Z-Z_+} = \imath\pi e^{\imath k_0 r} \ .$$

When $\eta \to 0^-$ [see Fig. 17.12(b)], we get,

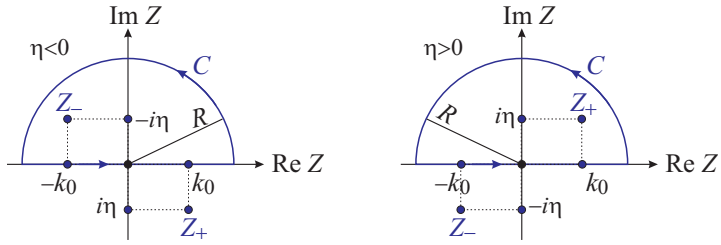

Figure 17.12: Illustration of the integration path.

$$\oint_C \frac{Ze^{\imath rZ}}{(Z-Z_+)(Z-Z_-)}dZ = \imath\pi e^{-\imath k_0 r} \ .$$

But, with the closed contour over the upper complex half-plane,

$$\int_{-\infty}^{\infty} dk \frac{ke^{\imath kr}}{[k^2-(k_0+\imath\eta)^2]} = \oint_C \frac{Ze^{\imath rZ}}{(Z-Z_+)(Z-Z_-)}dZ = \imath\pi e^{\pm\imath k_0 r} \ .$$

With these results, we can conclude that,

$$\int d^3k \frac{e^{\imath \mathbf{k}\cdot\mathbf{r}}}{[k^2-(k_0+\imath\eta)^2]} = \frac{2\pi^2}{r}e^{\pm\imath k_0 r} \ ,$$

and hence,

$$\mathcal{G}_\pm(\mathbf{r},t) = -\frac{1}{(2\pi)^4}\int_{-\infty}^{\infty} d\omega e^{-\imath\omega t}\frac{2\pi^2}{r}e^{\pm\imath k_0 r} = -\frac{1}{8\pi^2 r}\int_{-\infty}^{\infty} d\omega e^{-\imath\omega(t\mp\frac{r}{c})} = -\frac{1}{4\pi r}\delta(t\mp\tfrac{r}{c}) \ .$$

Thus, we also have,

$$\mathcal{G}_\pm(\mathbf{r}-\mathbf{r}',t-t') = -\frac{1}{4\pi}\frac{1}{|\mathbf{r}-\mathbf{r}'|}\delta(t-t'\mp\tfrac{|\mathbf{r}-\mathbf{r}'|}{c}) \ .$$

There are, therefore, two possible solutions to the problem:

$$\psi(\mathbf{r},t) = \int d^3r' \int_{-\infty}^{\infty} dt' \mathcal{G}_{\pm}(\mathbf{r}-\mathbf{r}', t-t') f(\mathbf{r}', t')$$
$$= -\frac{1}{4\pi} \int \frac{d^3r'}{|\mathbf{r}-\mathbf{r}'|} \int_{-\infty}^{\infty} dt' \delta(t' - t \pm \tfrac{|\mathbf{r}-\mathbf{r}'|}{c}) f(\mathbf{r}', t') = -\frac{1}{4\pi} \int d^3r' \frac{f(\mathbf{r}', t \mp \frac{|\mathbf{r}-\mathbf{r}'|}{c})}{|\mathbf{r}-\mathbf{r}'|} \,.$$

In this case, we will use retarded rather than advanced solutions, i.e.,

$$\Phi(\mathbf{r},t) = \frac{1}{4\pi\varepsilon_0} \int \frac{\varrho(\mathbf{r}', t - \frac{|\mathbf{r}-\mathbf{r}'|}{c})}{|\mathbf{r}-\mathbf{r}'|} d^3\mathbf{r}' \quad \text{and} \quad \mathbf{A}(\mathbf{r},t) = \frac{\mu_0}{4\pi} \int \frac{\mathbf{j}(\mathbf{r}', t - \frac{|\mathbf{r}-\mathbf{r}'|}{c})}{|\mathbf{r}-\mathbf{r}'|} d^3\mathbf{r}' \,.$$

17.3.5 Retarded fields in electrodynamics and Jefimenko's equations

From the retarded potentials (17.106) we can determine the fields through equations (17.78),

$$\vec{\mathcal{E}}(\mathbf{r},t) = -\nabla_r \Phi - \frac{\partial \mathbf{A}}{\partial t} = -\frac{1}{4\pi\varepsilon_0} \int \left[\frac{1}{R} \frac{-\dot{\varrho}}{c} \frac{\mathbf{R}}{R} + \varrho \frac{-\mathbf{R}}{R^3} \right] d^3r' - \frac{\mu_0}{4\pi} \int \frac{\dot{\mathbf{j}}(\mathbf{r}', t_r)}{R} d^3r' \,,$$

using the result (17.107). With $c^2 = 1/\varepsilon_0\mu_0$ we obtain the time-dependent generalization of Coulomb's law,

$$\boxed{\vec{\mathcal{E}}(\mathbf{r},t) = \frac{1}{4\pi\varepsilon_0} \int \left[\frac{\varrho(\mathbf{r}', t_r)}{R^2} \hat{\mathbf{e}}_R + \frac{\dot{\varrho}(\mathbf{r}', t_r)}{cR} \hat{\mathbf{e}}_R - \frac{\dot{\mathbf{j}}(\mathbf{r}', t_r)}{c^2 R} \right] d^3r'} \,. \tag{17.109}$$

In static situations the second and third term cancel, $\varrho(\mathbf{r}', t') = \varrho(\mathbf{r}')$ becomes independent of time, and we recover the electrostatic Coulomb law.

We now calculate the magnetic field via the rotation,

$$\vec{\mathcal{B}}(\mathbf{r},t) = \nabla_r \times \mathbf{A} = \frac{\mu_0}{4\pi} \int \left[\frac{1}{R} (\nabla_r \times \mathbf{j}) - \mathbf{j} \times \nabla_r \left(\frac{1}{R} \right) \right] d^3r' \,. \tag{17.110}$$

With,

$$[\nabla_r \times \mathbf{j}(\mathbf{r}', t - \tfrac{R}{c})]_x = \frac{\partial j_z}{\partial y} - \frac{\partial j_y}{\partial z} = \dot{j}_z \frac{\partial t_r}{\partial y} - \dot{j}_y \frac{\partial t_r}{\partial z} \tag{17.111}$$
$$= -\frac{1}{c} \left(\dot{j}_z \frac{\partial R}{\partial y} - \dot{j}_y \frac{\partial R}{\partial z} \right) = \left[\frac{1}{c} \dot{\mathbf{j}} \times \nabla_r R \right]_x = \left[\frac{1}{c} \dot{\mathbf{j}} \times \frac{\mathbf{R}}{R} \right]_x \,.$$

Thus, the time-dependent generalization of the Biot-Savart law is,

$$\boxed{\vec{\mathcal{B}}(\mathbf{r},t) = \frac{\mu_0}{4\pi} \int \left[\frac{\mathbf{j}(\mathbf{r}', t_r)}{R^2} + \frac{\dot{\mathbf{j}}(\mathbf{r}', t_r)}{cR} \right] \times \frac{\mathbf{R}}{R} d^3r'} \,. \tag{17.112}$$

The equations (17.109) and (17.112) are the (causal) solutions of Maxwell's equations published by *Jefimenko* in 1966. In practice, these equations are of limited

utility, since it is usually easier to calculate the retarded potentials, instead of going directly to the fields. However, they provide the satisfying sensation of a closed theory. We note that the simple replacement of the times t by t_r made for the potentials in (17.106) does not apply to the fields, as it would only produce the first terms of Jefimenko's expressions.

In the Excs. 17.3.8.10 and 17.3.8.11 we evaluate the fields for slow current variations.

17.3.6 The Liénard-Wiechert potentials

The goal now is to calculate the retarded electromagnetic potentials produced by a moving point charge q along a predefined path $\mathbf{w}(t)$. The presence of the charge at a time t_r at a point $\mathbf{w}(t_r)$, called the *retarded position* of this trajectory, has an impact on an arbitrary point of space $\mathbf{r}$ at a time t given by,

$$t = t_r + \frac{|\mathbf{r}-\mathbf{w}(t_r)|}{c} \ . \tag{17.113}$$

At a given instant of time t, the potentials $\Phi(\mathbf{r},t)$ and $\mathbf{A}(\mathbf{r},t)$ evaluated at the point

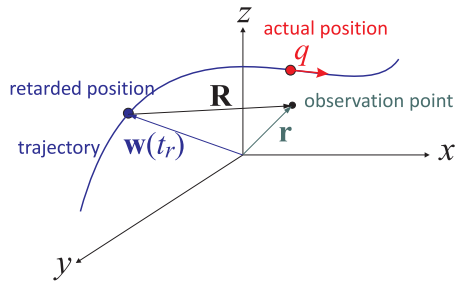

Figure 17.13: Retardation of potentials.

$\mathbf{r}$ *depend only on a single point* of the trajectory $\mathbf{w}(t_r)$ occupied by the charge in the past. The equation (17.106) now allows you to calculate the potentials. For a given trajectory $\mathbf{w}(t')$ the charge and current densities are parametrized by,

$$\boxed{\varrho(\mathbf{r}',t') = q\delta^3(\mathbf{r}'-\mathbf{w}(t')) \qquad \text{and} \qquad \mathbf{j}(\mathbf{r}',t') = \mathbf{v}\varrho(\mathbf{r}',t')} \ . \tag{17.114}$$

However, we need the density at the retarded time t_r [14],

$$\varrho(\mathbf{r}',t_r) = q\int \delta^3(\mathbf{r}'-\mathbf{w}(t'))\delta(t'-t_r)dt' \ . \tag{17.115}$$

We obtain,

$$\begin{aligned}\Phi(\mathbf{r},t) = \frac{q}{4\pi\varepsilon_0}\int\frac{\varrho(\mathbf{r}',t_r)}{|\mathbf{r}-\mathbf{r}'|}d^3r' &= \frac{q}{4\pi\varepsilon_0}\int\int\frac{\delta^3(\mathbf{r}'-\mathbf{w}(t'))}{|\mathbf{r}-\mathbf{r}'|}\delta(t'-t_r)d^3r'dt' \\ &= \frac{q}{4\pi\varepsilon_0}\int\frac{1}{|\mathbf{r}-\mathbf{w}(t')|}\delta(t'-(t-\tfrac{|\mathbf{r}-\mathbf{w}(t')|}{c}))dt' \ ,\end{aligned} \tag{17.116}$$

[14] Can not simply replace $t' \to t_r$ in the argument of $\mathbf{w}(t')$, because t_r implicitly depends on $\mathbf{w}(t')$ via the expression (17.113).

where spatial integration replaced $\mathbf{r}' = \mathbf{w}(t')$.

To evaluate a function $\delta(g(x))$ which depends on another function $g(x)$, we make the substitution,

$$u \equiv g(x) \qquad \text{with} \qquad du = \tfrac{dg}{dx} dx \ , \tag{17.117}$$

such that,

$$\int \delta(g(x))dx = \int \frac{\delta(u)}{|dg/dx|} du = \frac{1}{\left|\frac{dg(x_0)}{dx}\right|} \ , \tag{17.118}$$

where x_0 is defined by $u = g(x_0) = 0$. Applied to our problem, we identify,

$$u = g(t') = t' - \left(t - \tfrac{|\mathbf{r}-\mathbf{w}(t')|}{c}\right) = t' - t_r \ . \tag{17.119}$$

That is, the time when $u = g(t') = 0$ is simply $t' = t_r$. Now, the time derivative is,

$$\frac{dg}{dt'} = 1 + \frac{1}{c}\frac{d}{dt'}|\mathbf{r} - \mathbf{w}(t')| = 1 - \frac{\mathbf{v}(t')}{c} \cdot \frac{\mathbf{r} - \mathbf{w}(t')}{|\mathbf{r} - \mathbf{w}(t')|} \ , \tag{17.120}$$

with $\mathbf{v} \equiv \dot{\mathbf{w}}$. With this, the expression (17.116) becomes,

$$\Phi = \frac{q}{4\pi\varepsilon_0} \int \frac{1}{|\mathbf{r} - \mathbf{w}(t')|} \frac{\delta(u)}{\left|\frac{dg}{dt'}\right|} du = \frac{q}{4\pi\varepsilon_0} \frac{1}{|\mathbf{r} - \mathbf{w}(t_r)|} \frac{1}{|1 - \frac{\mathbf{v}(t_r)}{c} \cdot \frac{\mathbf{r}-\mathbf{w}(t_r)}{|\mathbf{r}-\mathbf{w}(t_r)|}|} \ , \tag{17.121}$$

where the application of the $\delta(u)$ function comes down to replacing t' by t_r. Finally, recalling the abbreviation $\mathbf{R} \equiv \mathbf{r} - \mathbf{w}(t_r)$,

$$\boxed{\Phi(\mathbf{r},t) = \frac{1}{4\pi\varepsilon_0} \frac{qc}{Rc - \mathbf{R}\cdot\mathbf{v}}} \qquad \text{and} \qquad \boxed{\mathbf{A}(\mathbf{r},t) = \frac{\mu_0}{4\pi} \frac{qc\mathbf{v}}{Rc - \mathbf{R}\cdot\mathbf{v}} = \frac{\mathbf{v}}{c^2}\Phi(\mathbf{r},t)} \ , \tag{17.122}$$

where the vector potential is obtained in an analogous way. These are the so-called *Liénard-Wiechert potentials* [15]. In Exc. 17.3.8.12 we calculate the potentials of a point charge in uniform motion.

17.3.7 The fields of a moving point charge

Fields produced by a moving point charge are calculated from the potentials (17.122) using (17.78). The calculation is complicated, because we must evaluate both, distance and speed,

$$\mathbf{R} = \mathbf{r} - \mathbf{w}(t_r) \qquad \text{and} \qquad \mathbf{v} = \dot{\mathbf{w}}(t_r) \tag{17.123}$$

at the retarded time, which is implicitly defined by the equation,

$$R = |\mathbf{r} - \mathbf{w}(t_r)| = c(t - t_r) \ . \tag{17.124}$$

We start with the gradient of the scalar potential (17.122),

$$\nabla\Phi = \frac{qc}{4\pi\varepsilon_0} \frac{-1}{(Rc - \mathbf{R}\cdot\mathbf{v})^2} \nabla(Rc - \mathbf{R}\cdot\mathbf{v}) \ , \tag{17.125}$$

[15] We get the same result from the argument, that light needs a finite time to cross the volume of the charge distribution $d^3r' = dV'$, such that the volume appears stretched at the time instant t_r, $dV' \longrightarrow \frac{dV'}{1-\hat{\mathbf{e}}_r\cdot\mathbf{v}/c}$.

and evaluate both terms separately. Using (17.124) we find,

$$\nabla(Rc) = -c^2 \nabla t_r \ , \tag{17.126}$$

where we leave the calculation of the gradient of retarded time for later. Also, using the rule (21.111)(ix), we find,

$$\nabla(\mathbf{R}\cdot\mathbf{v}) = (\mathbf{R}\cdot\nabla)\mathbf{v} + (\mathbf{v}\cdot\nabla)\mathbf{R} + \mathbf{R}\times(\nabla\times\mathbf{v}) + \mathbf{v}\times(\nabla\times\mathbf{R}) \ . \tag{17.127}$$

The first term of this expression gives,

$$(\mathbf{R}\cdot\nabla)\mathbf{v}(t_r) = R_x\frac{\partial t_r}{\partial x}\frac{d\mathbf{v}}{dt_r} + R_y\frac{\partial t_r}{\partial y}\frac{d\mathbf{v}}{dt_r} + R_z\frac{\partial t_r}{\partial z}\frac{d\mathbf{v}}{dt_r} = \mathbf{a}(\mathbf{R}\cdot\nabla t_r) \ , \tag{17.128}$$

where $\mathbf{a} \equiv \dot{\mathbf{v}}$ is the acceleration at the retarded time. The second term is,

$$(\mathbf{v}\cdot\nabla)\mathbf{R} = (\mathbf{v}\cdot\nabla)\mathbf{r} - (\mathbf{v}\cdot\nabla)\mathbf{w} = \mathbf{v} - \mathbf{v}(\mathbf{v}\cdot\nabla t_r) \ . \tag{17.129}$$

Now, using,

$$\nabla\times\mathbf{v} = \left(\frac{\partial t_r}{\partial y}\frac{dv_z}{dt_r} - \frac{\partial t_r}{\partial z}\frac{dv_y}{dt_r}\right)\hat{\mathbf{e}}_x + ... = -\mathbf{a}\times\nabla t_r \ , \tag{17.130}$$

the third term becomes,

$$\mathbf{R}\times(\nabla\times\mathbf{v}) = -\mathbf{R}\times(\mathbf{a}\times\nabla t_r) \ . \tag{17.131}$$

Finally, using,

$$\nabla\times\mathbf{R} = \cancelto{0}{\nabla\times\mathbf{r}} - \nabla\times\mathbf{w} = \mathbf{v}\times\nabla t_r \ , \tag{17.132}$$

the fourth term is,

$$\mathbf{v}\times(\nabla\times\mathbf{R}) = \mathbf{v}\times(\mathbf{v}\times\nabla t_r) \ . \tag{17.133}$$

With these results the expression (17.127) becomes,

$$\begin{aligned}\nabla(\mathbf{R}\cdot\mathbf{v}) &= \mathbf{a}(\mathbf{R}\cdot\nabla t_r) + \mathbf{v} - \mathbf{v}(\mathbf{v}\cdot\nabla t_r) - \mathbf{R}\times(\mathbf{a}\times\nabla t_r) + \mathbf{v}\times(\mathbf{v}\times\nabla t_r) \\ &= \mathbf{v} + (\mathbf{R}\cdot\mathbf{a} - v^2)\nabla t_r \ ,\end{aligned} \tag{17.134}$$

using in the last step the rule $\mathbf{A}\times(\mathbf{B}\times\mathbf{C}) = \mathbf{B}(\mathbf{A}\cdot\mathbf{C}) - \mathbf{C}(\mathbf{A}\cdot\mathbf{B})$. Now, we calculate ∇t_r,

$$\begin{aligned}\nabla t_r &= -\tfrac{1}{c}\nabla R = -\tfrac{1}{c}\nabla\sqrt{\mathbf{R}\cdot\mathbf{R}} = -\frac{1}{2c\sqrt{\mathbf{R}\cdot\mathbf{R}}}\nabla(\mathbf{R}\cdot\mathbf{R}) \\ &= -\frac{1}{cR}[(\mathbf{R}\cdot\nabla)\mathbf{R} \ + \ \mathbf{R}\times(\nabla\times\mathbf{R})] \\ &= -\frac{1}{cR}[(\mathbf{R}\cdot\nabla)\mathbf{r} - (\mathbf{R}\cdot\nabla)\mathbf{w} \ + \ \mathbf{R}\times(\nabla\times\mathbf{R})] \\ &= -\frac{1}{cR}[\mathbf{R} - \mathbf{v}(\mathbf{R}\cdot\nabla t_r) \ + \ \mathbf{R}\times(\mathbf{v}\times\nabla t_r)] = -\frac{1}{cR}[\mathbf{R} - (\mathbf{R}\cdot\mathbf{v})\nabla t_r)] \ .\end{aligned} \tag{17.135}$$

To get $(\mathbf{R}\cdot\nabla)\mathbf{w}$ we did a calculation similar to (17.128) and $\nabla\times\mathbf{R}$ was already calculated in (17.132). Solving the result (17.135) by ∇t_r,

$$\nabla t_r = -\frac{\mathbf{R}}{cR - \mathbf{R}\cdot\mathbf{v}} \ . \tag{17.136}$$

Finally, the gradient of the scalar potential (17.125) is,

$$\nabla\Phi = \frac{1}{4\pi\varepsilon_0}\frac{qc}{(cR-\mathbf{R}\cdot\mathbf{v})^3}\left[(cR-\mathbf{R}\cdot\mathbf{v})\mathbf{v}-(c^2-v^2+\mathbf{R}\cdot\mathbf{a})\mathbf{R}\right] . \tag{17.137}$$

A similar calculation for the temporal derivative of the vector potential gives the result,

$$\frac{\partial\mathbf{A}}{\partial t} = \frac{1}{4\pi\varepsilon_0}\frac{qc}{(cR-\mathbf{R}\cdot\mathbf{v})^3}\left[(cR-\mathbf{R}\cdot\mathbf{v})(-\mathbf{v}+\frac{R}{c}\mathbf{a})+\frac{R}{c}(c^2-v^2+\mathbf{R}\cdot\mathbf{a})\mathbf{v}\right] . \tag{17.138}$$

The rotation of the vector potential yields,

$$\begin{aligned}\nabla\times\mathbf{A} &= \frac{1}{c^2}\nabla\times(\Phi\mathbf{v}) = \frac{1}{c^2}[\Phi(\nabla\times\mathbf{v})-\mathbf{v}(\nabla\Phi)] \\ &= -\frac{1}{c}\frac{q}{4\pi\varepsilon_0}\frac{1}{(\mathbf{R}\cdot\mathbf{u})^3}\mathbf{R}\times[(c^2-v^2)\mathbf{v}+(\mathbf{R}\cdot\mathbf{a})\mathbf{v}+(\mathbf{R}\cdot\mathbf{u})\mathbf{a}] ,\end{aligned} \tag{17.139}$$

using the expressions (17.130) and (17.137) and introducing the abbreviation $\mathbf{u} \equiv c\hat{\mathbf{e}}_R - \mathbf{v}$.

Combining these results with equations (17.78), we find the fields,

$$\boxed{\vec{\mathcal{E}}(\mathbf{r},t) = \frac{q}{4\pi\varepsilon_0}\frac{R}{(\mathbf{R}\cdot\mathbf{u})^3}[(c^2-v^2)\mathbf{u}+\mathbf{R}\times(\mathbf{u}\times\mathbf{a})]} , \tag{17.140}$$

and,

$$\boxed{\vec{\mathcal{B}}(\mathbf{r},t) = \tfrac{1}{c}\hat{\mathbf{e}}_R\times\vec{\mathcal{E}}(\mathbf{r},t)} . \tag{17.141}$$

Obviously, the magnetic field of a point charge is always perpendicular to the electric field and to the vector of the retarded point. The first term in $\vec{\mathcal{E}}$ (involving $(c^2-v^2)\cdot\mathbf{u}$) falls off like $1/R^2$. If the velocity $\mathbf{v}$ and the acceleration $\mathbf{a}$ were zero, this term survives and reduces to the old electrostatic result (13.3). For this reason, this term is called the generalized Coulomb field. The second term (involving $\mathbf{R}\times(\mathbf{u}\times\mathbf{a})$) falls off like $1/R$ and thus becomes dominant at large distances. As we will see in Sec. 19.4, this is the term responsible for electromagnetic radiation.

Knowing the fields generated by the moving charge q we can, by the laws of the *Coulomb force* and the *Lorentz force*, determine the force acting on a test particle Q located at $\mathbf{r}$ and moving with velocity $\mathbf{V}$,

$$\begin{aligned}\mathbf{F}(\mathbf{r},t) = \frac{qQ}{4\pi\varepsilon_0}\frac{R}{(\mathbf{R}\cdot\mathbf{u})^3}\Big\{&[(c^2-v^2)\mathbf{u}+\mathbf{R}\times(\mathbf{u}\times\mathbf{a})] \\ &+\frac{\mathbf{V}}{c}\times\left[\hat{\mathbf{e}}_R\times[(c^2-v^2)\mathbf{u}+\mathbf{R}\times(\mathbf{u}\times\mathbf{a})]\right]\Big\} ,\end{aligned} \tag{17.142}$$

where $\mathbf{r}$, $\mathbf{u}$, $\mathbf{v}$, and $\mathbf{a}$ are all evaluated at the retarded time. The entire classical electrodynamics is contained in this equation because, since the charge is quantized, we can apply the superposition principle and calculate the impact of any charge distribution on a test particle Q. However, in view of the complexity of (17.142), the necessary effort seems huge. The scheme 17.14 summarizes the fundamental laws of electrodynamics.

Resolve the Excs. 17.3.8.13 to 17.3.8.16.

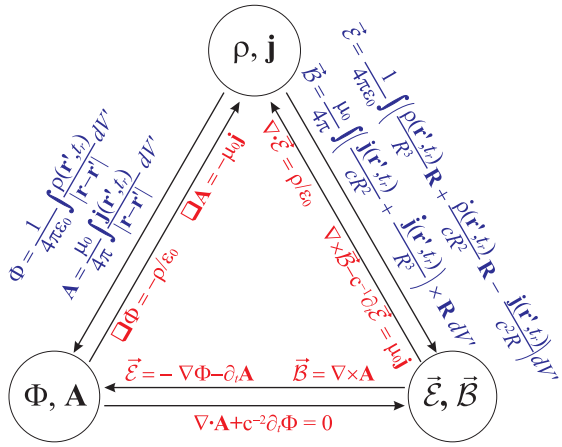

Figure 17.14: Organization chart of the fundamental laws of electrodynamics. Compare with the corresponding charts in electrostatics Fig. 13.11 and magnetostatics Fig. 15.16.

Example 92 (*Electric and magnetic fields generated by a uniformly moving charge*): Letting $\mathbf{a} = 0$ in (17.140),

$$\vec{\mathcal{E}}(\mathbf{r},t) = \frac{q}{4\pi\varepsilon_0}\frac{R}{(\mathbf{R}\cdot\mathbf{u})^3}(c^2-v^2)\mathbf{u}\ ,$$

we can express the position of the charge at the retarded time by its constant velocity, $\dot{\mathbf{w}} = \mathbf{v}$. We calculate using the definition of $\mathbf{u}$,

$$R\mathbf{u} = c\mathbf{R} - R\mathbf{v} = c\mathbf{R} - R\dot{\mathbf{w}} = c(\mathbf{r}-\mathbf{v}t_r) - c(t-t_r)\mathbf{v} = c(\mathbf{r}-\mathbf{v}t)\ .$$

The square of the relationship $|\mathbf{r}-\mathbf{v}t_r| = c(t-t_r)$ resolved by t_r gives,

$$t_r = \frac{(c^2t - \mathbf{r}\cdot\mathbf{v}) \pm \sqrt{(c^2t-\mathbf{r}\cdot\mathbf{v})^2 + (c^2-v^2)(r^2-c^2t^2)}}{c^2-v^2}\ ,$$

where we only consider the sign $-$. With this we calculate,

$$\begin{aligned}\mathbf{R}\cdot\mathbf{u} &= Rc - \mathbf{R}\cdot\mathbf{v} = c^2(t-t_r) - (\mathbf{r}-\mathbf{v}t_r)\cdot\mathbf{v} = c^2t - \mathbf{r}\cdot\mathbf{v} - (c^2-v^2)t_r\\ &= \sqrt{(c^2t-\mathbf{r}\cdot\mathbf{v})^2 + (c^2-v^2)(r^2-c^2t^2)}\\ &= \sqrt{(c^2-v^2)(\mathbf{r}-\mathbf{v}t)^2 + [(\mathbf{r}-\mathbf{v}t)\cdot\mathbf{v}]^2}\\ &= \sqrt{(c^2-v^2)d^2 + (\mathbf{d}\cdot\mathbf{v})^2} = d\sqrt{c^2-v^2+v^2\cos^2\theta} = dc\sqrt{1-\tfrac{v^2}{c^2}\sin^2\theta}\ ,\end{aligned}$$

where the abbreviation $\mathbf{d} \equiv \mathbf{r} - \mathbf{v}t$ is the vector between $\mathbf{r}$ and the *actual position* of the particle and θ is the angle between $\mathbf{d}$ and $\mathbf{v}$. Then,

$$\vec{\mathcal{E}}(\mathbf{r},t) = \frac{q}{4\pi\varepsilon_0}\frac{1-v^2/c^2}{(1-\frac{v^2}{c^2}\sin^2\theta)^{3/2}}\frac{\hat{\mathbf{e}}_d}{d^2}\ .$$

Note that $\vec{\mathcal{E}}$ points along the distance $\mathbf{d}$. This is an extraordinary coincidence; after all, the 'message' came from the retarded position. Because of the $\sin^2\theta$ in the denominator, the field of a charge moving fast is flattened like a pancake

in the direction perpendicular to the motion (see Fig. 17.15). In the forward and backward directions $\vec{\mathcal{E}}$ is reduced by a factor $(1-v^2/c^2)$ with respect to the field of a charge at rest; in the perpendicular direction is amplified by a factor $1/\sqrt{1-v^2/c^2}$.
To get $\vec{\mathcal{B}}$ we calculate,

$$\hat{\mathbf{e}}_R = \frac{\mathbf{r}-\mathbf{v}t_r}{R} = \frac{(\mathbf{r}-\mathbf{v}t)+(t-t_r)\mathbf{v}}{R} = \frac{\mathbf{d}}{R}+\frac{\mathbf{v}}{c}\ ,$$

and hence,

$$\vec{\mathcal{B}} = \tfrac{1}{c}(\hat{\mathbf{e}}_R \times \vec{\mathcal{E}}) = \tfrac{1}{c^2}(\mathbf{v}\times\vec{\mathcal{E}})\ .$$

The $\vec{\mathcal{B}}$-field lines form circles around the charge, as shown in Fig. 17.15. At low velocities, $v \ll c$,

$$\vec{\mathcal{E}}(\mathbf{r},t) = \frac{q}{4\pi\varepsilon_0}\frac{\mathbf{d}}{d^2} \quad , \quad \vec{\mathcal{B}} = \frac{\mu_0 q}{4\pi}\frac{\mathbf{v}\times\hat{\mathbf{e}}_d}{d^2}\ .$$

we recover the laws of Coulomb and Biot-Savart for point charges.

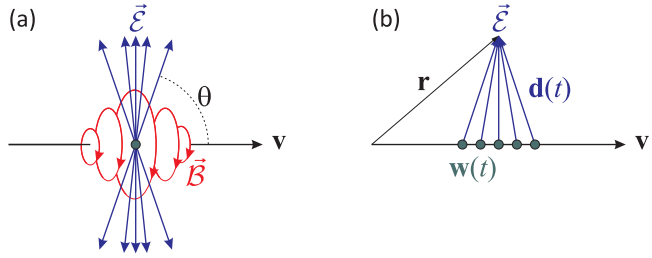

Figure 17.15: (a) Electric and magnetic field generated by of a point charge in uniform motion. (b) Electric field seen from an observation point $\mathbf{r}$ fixed in space.

17.3.8 Exercises

17.3.8.1 Ex: Potentials, fields and the Lorentz gauge

Consider a scalar field and a vector field of the form,

$$\Phi(\mathbf{r},t) = cd\frac{\mathbf{r}\cdot\hat{\mathbf{e}}_z}{r^3}e^{\imath\omega t} \quad \text{and} \quad \mathbf{A}(\mathbf{r},t) = \imath kd\frac{e^{\imath kr}}{r}e^{\imath\omega t}\,\hat{\mathbf{e}}_z\ .$$

where $k=\omega/c$.
a. Calculate the corresponding fields $\vec{\mathcal{B}}$ and $\vec{\mathcal{E}}$.
b. Show that for small r the given potentials satisfy the Lorentz gauge.

Solution: *a. We have for the $\vec{\mathcal{B}}$-field,*

$$\vec{\mathcal{B}} = \nabla\times\mathbf{A} = \begin{pmatrix} \partial_y A_z \\ -\partial_x A_z \\ 0 \end{pmatrix}\ .$$

Now,

$$\partial_i\left(\frac{e^{\imath kr}}{r}\right)=\frac{\imath kre^{\imath kr}\partial_i r-e^{\imath kr}\partial_i r}{r^2}=\frac{e^{\imath kr}}{r}\left(\imath k\frac{x_i}{r}-\frac{x_i}{r^2}\right)\ .$$

Hence,

$$\vec{\mathcal{B}}=\imath kd\frac{e^{\imath kr}}{r}\left(\imath k-\frac{1}{r}\right)e^{\imath\omega t}\begin{pmatrix}y/r\\-x/r\\0\end{pmatrix}=-k^2de^{\imath\omega t}\frac{e^{\imath kr}}{r}\left(1-\frac{1}{\imath kr}\right)(\hat{\mathbf{e}}_r\times\hat{\mathbf{e}}_z)\ .$$

For the $\vec{\mathcal{E}}$-field we have,

$$\vec{\mathcal{E}}=-\nabla\Phi-\frac{1}{c}\frac{\partial\mathbf{A}}{\partial t}=-\nabla\Phi-k^2d\frac{e^{\imath kr}}{r}e^{\imath\omega t}\hat{\mathbf{e}}_z\ .$$

Now,

$$\partial_i\left(\frac{z}{r^3}\right)=\frac{\delta_{iz}}{r^3}-\frac{3zx_i}{r^5}\ .$$

Hence,

$$-\nabla\Phi=-cde^{\imath\omega t}\nabla\frac{z}{r^3}=cde^{\imath\omega t}\frac{3\mathbf{r}(\mathbf{r}\cdot\hat{\mathbf{e}}_z)-r^2\hat{\mathbf{e}}_z}{r^5}\ .$$

and so,

$$\vec{\mathcal{E}}=de^{\imath\omega t}\left[c\frac{3(\mathbf{r}\cdot\hat{\mathbf{e}}_z)\mathbf{r}}{r^5}-\hat{\mathbf{e}}_z\left(c\frac{1}{r^3}-k^2\frac{e^{\imath kr}}{r}\right)\right]\ .$$

b. We have,

$$\nabla\cdot\mathbf{A}=\partial_zA_z=\imath kde^{\imath\omega t}\partial_z\frac{e^{\imath kr}}{r}=-k^2de^{\imath\omega t}\frac{e^{\imath kr}}{r}\left(1-\frac{1}{\imath kr}\right)\frac{z}{r}\ .$$

and

$$\frac{1}{c^2}\frac{\partial\Phi}{\partial t}=\frac{d}{c}\frac{\mathbf{r}\cdot\hat{\mathbf{e}}_z}{r^3}\imath\omega e^{\imath\omega t}=\imath kde^{\imath\omega t}\ \frac{z}{r^3}\ .$$

For small r now holds $e^{\imath kr}\simeq 1$ and the term $1/r^3$ dominates. For this case,

$$\nabla\cdot\mathbf{A}=-\imath kde^{\imath\omega t}\frac{z}{r^3}\ .$$

With this, the Lorentz gauge is satisfied.

17.3.8.2 Ex: Fields, potentials, and the gauge transformation

Find the charge and current distributions producing the following potential,

$$\Phi(\mathbf{r},t)=0\qquad\text{and}\qquad\mathbf{A}(\mathbf{r},t)=\frac{\mu_0k}{4c}(ct-|x|)^2\hat{\mathbf{e}}_z\ \Theta(|x|-ct)\ ,$$

where $k = const.$

Solution: *We calculate the fields,*

$$\vec{\mathcal{E}} = -\nabla\Phi - \frac{\partial \mathbf{A}}{\partial t} = -\frac{\mu_0 k}{2}(ct - |x|)\hat{\mathbf{e}}_z\Theta(ct - |x|) \ ,$$

and

$$\vec{\mathcal{B}} = \nabla \times \mathbf{A} = \frac{\mu_0 k}{4c}\Theta(ct-|x|)\hat{\mathbf{e}}_y\frac{\partial}{\partial x}(ct-|x|)^2 = \frac{\mu_0 k}{4c}\Theta(ct-|x|)\vec{\mathcal{E}}_y 2(ct-|x|)[1-2\Theta(x)] \ .$$

With this we calculate the charge densities,

$$\varrho = \varepsilon_0 \nabla \cdot \vec{\mathcal{E}} = -\varepsilon_0 \frac{\mu_0 k}{2}\Theta(ct - |x|)\frac{\partial}{\partial z}(ct - |x|) = 0 \ ,$$

and the current densities,

$$\begin{aligned}
\mathbf{j} &= \tfrac{1}{\mu_0}\nabla \times \vec{\mathcal{B}} - \varepsilon_0 \frac{\partial \vec{\mathcal{E}}}{\partial t} \\
&= \frac{1}{\mu_0}\frac{\mu_0 k}{4c} 2\Theta(ct - |x|)[1 - 2\Theta(x)]\hat{\mathbf{e}}_z \frac{\partial}{\partial x}(ct - |x|) + \frac{\varepsilon_0\mu_0 ck}{2}\hat{\mathbf{e}}_z\Theta(ct - |x|) \\
&= -\frac{1}{\mu_0}\hat{\mathbf{e}}_z\frac{\mu_0 k}{2c}\Theta(ct - |x|)[1 - 2\Theta(x)]^2 + \frac{\varepsilon_0\mu_0 ck}{2}\hat{\mathbf{e}}_z\Theta(ct - |x|) = 0 \ .
\end{aligned}$$

Of course, here we have a uniform surface current flowing in z-direction on the $x = 0$-plane. It starts at $t = 0$ and increases proportionally with t. Notice that the perturbation travels (in both directions) at the speed of light: for points $|x| > ct$ the perturbation (the notice that the current is now flowing) has not yet arrived, hence, the fields must be zero.

17.3.8.3 Ex: Fields derived from potentials

Show that the differential equations for Φ and $\mathbf{A}$ can be written in a more symmetric form as,

$$\Box\Phi + \frac{\partial L}{\partial t} = -\frac{\varrho}{\varepsilon_0} \qquad \text{and} \qquad \Box\mathbf{A} - \nabla L = -\mu_0\mathbf{j} \ ,$$

where $L \equiv \nabla \cdot \mathbf{A} + \varepsilon_0\mu_0\frac{\partial\Phi}{\partial t}$.

Solution: *We calculate,*

$$\begin{aligned}
\Box\Phi + \frac{\partial L}{\partial t} &= \nabla^2\Phi - \varepsilon_0\mu_0\frac{\partial^2\Phi}{\partial t^2} + \frac{\partial}{\partial t}\left(\nabla \cdot \mathbf{A} + \varepsilon_0\mu_0\frac{\partial\Phi}{\partial t}\right) \\
&= \nabla^2\Phi + \frac{\partial}{\partial t}\nabla \cdot \mathbf{A} = \nabla \cdot \left(\nabla\Phi + \frac{\partial \mathbf{A}}{\partial t}\right) = -\nabla \cdot \vec{\mathcal{E}} = -\frac{\varrho}{\varepsilon_0} \ ,
\end{aligned}$$

and,

$$\begin{aligned}\Box\mathbf{A} - \nabla L &= \nabla^2\mathbf{A} - \varepsilon_0\mu_0\frac{\partial^2\mathbf{A}}{\partial t^2} - \nabla\left(\nabla\cdot\mathbf{A} + \varepsilon_0\mu_0\frac{\partial\Phi}{\partial t}\right)\\ &= \nabla^2\mathbf{A} - \nabla(\nabla\cdot\mathbf{A}) - \varepsilon_0\mu_0\frac{\partial^2\mathbf{A}}{\partial t^2} - \varepsilon_0\mu_0\frac{\partial\nabla\Phi}{\partial t}\\ &= -\nabla\times(\nabla\times\mathbf{A}) - \varepsilon_0\mu_0\frac{\partial^2\mathbf{A}}{\partial t^2} - \varepsilon_0\mu_0\frac{\partial\nabla\Phi}{\partial t} = -\nabla\times\vec{\mathcal{B}} + \varepsilon_0\mu_0\frac{\partial\vec{\mathcal{E}}}{\partial t} = -\mu_0\mathbf{j}\ .\end{aligned}$$

17.3.8.4 Ex: Fields derived from potentials

a. Find the fields and the charge and current distributions corresponding to,

$$\Phi(\mathbf{r},t) = 0 \qquad \text{and} \qquad \mathbf{A}(\mathbf{r},t) = -\frac{1}{4\pi\varepsilon_0}\frac{qt}{r^2}\hat{\mathbf{e}}_r\ .$$

b. Use the gauge function $\chi = -\frac{1}{4\pi\varepsilon_0}\frac{qt}{r}$ to transform the potentials in (a), and comment the result.
c. Check whether the potentials are in the Lorentz or in the Coulomb gauge.

Solution: *a. We find with the relationships (17.78),*

$$\vec{\mathcal{E}} = -\nabla\Phi - \frac{\partial\mathbf{A}}{\partial t} = \frac{1}{4\pi\varepsilon_0}\frac{q}{r^2}\hat{\mathbf{e}}_r\ ,$$

and,

$$\vec{\mathcal{B}} = \nabla\times\mathbf{A} = 0\ .$$

b. The transformed potentials are,

$$\begin{aligned}\Phi' &= \Phi - \frac{\partial\chi}{\partial t} = 0 + \frac{\partial}{\partial t}\frac{qt}{4\pi\varepsilon_0 r} = \frac{q}{4\pi\varepsilon_0 r}\\ \mathbf{A}' &= \mathbf{A} + \nabla\chi = -\frac{qt}{4\pi\varepsilon_0 r^2}\hat{\mathbf{e}}_r - \nabla\frac{qt}{4\pi\varepsilon_0 r} = -\frac{qt}{4\pi\varepsilon_0 r^2}\hat{\mathbf{e}}_r - \frac{qt}{4\pi\varepsilon_0}\frac{-\mathbf{r}}{r^3} = 0\ .\end{aligned}$$

Thus, we see that this is a Colombian potential.
c. For the original potentials we find,

$$\frac{\partial\Phi}{\partial t} = \frac{\partial}{\partial t}0 = 0 \qquad \textit{and} \qquad \nabla\cdot\mathbf{A} = -\nabla\cdot\left(\frac{1}{4\pi\varepsilon_0}\frac{qt}{r^2}\hat{\mathbf{e}}_r\right) = -\frac{qt}{\varepsilon_0}\delta^{(3)}\mathbf{r}\ ,$$

such that they are neither in the Lorentz nor in the Coulomb gauge. For the transformed potentials we find,

$$\frac{\partial\Phi'}{\partial t} = \frac{\partial}{\partial t}\frac{q}{4\pi\varepsilon_0 r} = 0 \qquad \textit{and} \qquad \nabla\cdot\mathbf{A}' = \nabla\cdot\mathbf{0} = 0\ ,$$

such that they satisfy simultaneously both gauges.

17.3.8.5 Ex: Fields derived from potentials

a. Suppose $\Phi = 0$ and $\mathbf{A} = A_0 \sin(kx - \omega t)\hat{\mathbf{e}}_y$, where A_0, ω, and k are constants. Find $\vec{\mathcal{E}}$ and $\vec{\mathcal{B}}$, and verify, that they satisfy Maxwell's equations in vacuum. What conditions should be imposed to ω and k?
b. Check whether the potentials are in the Lorentz or in the Coulomb gauge.

Solution: *We find with the relationships (17.78),*

$$\vec{\mathcal{E}} = -\nabla\Phi - \frac{\partial \mathbf{A}}{\partial t} = \omega A_0 \cos(kx - \omega t)\hat{\mathbf{e}}_y \ ,$$

and,

$$\vec{\mathcal{B}} = \nabla \times \mathbf{A} = kA_0 \cos(kx - \omega t)\hat{\mathbf{e}}_z \ .$$

We calculate,

$$\nabla \times \vec{\mathcal{E}} = -\omega k A_0 \sin(kx - \omega t)\hat{\mathbf{e}}_z = -\frac{\partial \vec{\mathcal{B}}}{\partial t}$$
$$\nabla \times \vec{\mathcal{B}} = k^2 A_0 \sin(kx - \omega t)\hat{\mathbf{e}}_y = \frac{k^2}{\omega^2}\frac{\partial \vec{\mathcal{E}}}{\partial t}$$
$$\nabla \cdot \vec{\mathcal{E}} = 0 = \nabla \cdot \vec{\mathcal{B}} \ .$$

The condition to satisfy Maxwell's law (second equation) is,

$$\frac{k^2}{\omega^2} = \varepsilon_0 \mu_0 = \frac{1}{c^2} \ .$$

b. For the potentials we find,

$$\frac{\partial \Phi}{\partial t} = \frac{\partial}{\partial t} 0 = 0 \qquad \textit{and} \qquad \nabla \cdot \mathbf{A} = \nabla \cdot A_0 \sin(kx - \omega t)\hat{\mathbf{e}}_y = 0 \ ,$$

such that they satisfy simultaneously both gauges.

17.3.8.6 Ex: Other gauges

Check the viability of a gauge defined by $\Phi \equiv 0$ and a gauge defined by $\mathbf{A} \equiv 0$.

Solution: *Allowed gauges χ transform the potentials as,*

$$\mathbf{A}' = \mathbf{A} + \nabla\chi \qquad \textit{and} \qquad \Phi' = \Phi - c^{-1}\partial_t \chi \ .$$

Choosing $\partial_t \chi = c\Phi$ we can design a scalar potential $\Phi' = 0$ yielding the electric and magnetic fields,

$$\vec{\mathcal{E}} = -\frac{\partial \mathbf{A}'}{\partial t} - \cancelto{0}{\nabla\Phi'} = -\frac{\partial(\mathbf{A} + \nabla\chi)}{\partial t} = -\frac{\partial \mathbf{A}}{\partial t} - c\Phi$$
$$\vec{\mathcal{B}} = \nabla \times \mathbf{A}' = \nabla \times (\mathbf{A} + \cancelto{0}{\nabla\chi}) = \nabla \times \mathbf{A} \ .$$

On the other hand, the choice $\mathbf{A} = -\nabla\chi$ does not produce a magnetic field because $\vec{\mathcal{B}} = -\nabla \times (\nabla\chi) = 0$.

17.3.8.7 Ex: Coulomb gauge

a. Show that the vector potential can be expressed by the magnetic field as,

$$\mathbf{A}(\mathbf{r},t) = \nabla \times \int \frac{\vec{\mathcal{B}}(\mathbf{r}',t)}{4\pi|\mathbf{r}-\mathbf{r}'|} d^3r' \ .$$

Show that, given by this expression, the potential vector satisfies the Coulomb gauge.
b. Show that for uniform and constant magnetic fields,

$$\mathbf{A}(\mathbf{r},t) = -\tfrac{1}{2}\mathbf{r} \times \vec{\mathcal{B}} \ .$$

Why can't you use the formula in (a) to solve the problem?

Solution: *a. The ∇ operator does not act on the integration coordinate $\mathbf{r}'$. Therefore, the vector potential can be written,*

$$\mathbf{A}(\mathbf{r},t) = \nabla \times \int \frac{\vec{\mathcal{B}}(\mathbf{r}',t)}{4\pi R} d^3r' = \int \left(\nabla \frac{1}{4\pi R}\right) \times \vec{\mathcal{B}}(\mathbf{r}',t) d^3r' = -\int \frac{\mathbf{r}}{4\pi R^3} \times \vec{\mathcal{B}}(\mathbf{r}',t) d^3r' \ .$$

With this, the rotation becomes,

$$\begin{aligned}
\nabla \times \mathbf{A}(\mathbf{r},t) &= -\int \nabla \times \left[\frac{\mathbf{r}}{4\pi R^3} \times \vec{\mathcal{B}}(\mathbf{r}',t)\right] d^3r' \\
&= \frac{1}{4\pi} \int \left[\vec{\mathcal{B}}(\mathbf{r}',t)\left(\nabla \cdot \frac{\mathbf{r}}{R^3}\right) - \left(\vec{\mathcal{B}}(\mathbf{r}',t) \cdot \nabla\right) \frac{\mathbf{r}}{R^3}\right] d^3r' \\
&= \frac{1}{4\pi} \int \vec{\mathcal{B}}(\mathbf{r}',t) 4\pi\delta(\mathbf{r}) d^3r' + \frac{1}{4\pi} \int \left[\nabla\left(\frac{\mathbf{r}}{R^3} \cdot \vec{\mathcal{B}}(\mathbf{r}',t)\right) - \vec{\mathcal{B}}(\mathbf{r}',t) \times \cancelto{0}{\left(\nabla \times \frac{\mathbf{r}}{R^3}\right)}\right] d^3r' \\
&= \vec{\mathcal{B}}(\mathbf{r},t) + \frac{1}{4\pi} \oint \frac{\mathbf{r}}{R^3} \cdot \vec{\mathcal{B}}(\mathbf{r}',t) d\mathbf{S}' = \vec{\mathcal{B}}(\mathbf{r},t) \ .
\end{aligned}$$

The vector potential satisfies the Coulomb gauge, since its divergence is,

$$\nabla \cdot \mathbf{A}(\mathbf{r},t) = \cancelto{0}{\nabla \cdot \nabla \times} \int \frac{\vec{\mathcal{B}}(\mathbf{r}',t)}{4\pi R} d^3r' = 0 \ .$$

b. For uniform magnetic fields,

$$\nabla \times \mathbf{A}(\mathbf{r},t) = \nabla \times \left(-\tfrac{1}{2}\mathbf{r} \times \vec{\mathcal{B}}\right) = -\tfrac{1}{2}\left(\vec{\mathcal{B}} \cdot \nabla\right)\mathbf{r} + \tfrac{1}{2}\vec{\mathcal{B}}(\nabla \cdot \mathbf{r}) = -\tfrac{1}{2}\vec{\mathcal{B}} + \tfrac{3}{2}\vec{\mathcal{B}} = \vec{\mathcal{B}} \ .$$

The vector potential satisfies the Coulomb gauge, since,

$$\nabla \cdot \mathbf{A}(\mathbf{r},t) = -\nabla \cdot \tfrac{1}{2}(\mathbf{r} \times \vec{\mathcal{B}}) = -\tfrac{1}{2}(\nabla \times \mathbf{r}) \cdot \vec{\mathcal{B}} + \tfrac{1}{2}\mathbf{r} \cdot (\nabla \times \vec{\mathcal{B}}) = 0 \ .$$

To solve the problem, we also could try to use formula in (a) inserting $\vec{\mathcal{B}}(\mathbf{r}',t) = \vec{\mathcal{B}}$. However, the integral diverges at $\mathbf{r}' = \mathbf{r}$.

17.3.8.8 Ex: Green function

Show that $G(\mathbf{r},\mathbf{r}') = \frac{e^{\imath k|\mathbf{r}-\mathbf{r}'|}}{4\pi|\mathbf{r}-\mathbf{r}'|}$ is the Green function of the operator $\mathcal{L} = \nabla^2 + k^2$.

Solution: *We calculate,*

$$\nabla_r^2 \frac{e^{\imath k|\mathbf{r}-\mathbf{r}'|}}{4\pi|\mathbf{r}-\mathbf{r}'|} = \nabla_R^2 \frac{e^{\imath kR}}{4\pi R} = \frac{1}{R^2}\frac{\partial}{\partial R}\left(R^2 \frac{\partial}{\partial R}\frac{e^{\imath kR}}{4\pi R}\right) = -k^2\frac{e^{\imath kR}}{4\pi R} = -k^2\frac{e^{\imath k|\mathbf{r}-\mathbf{r}'|}}{4\pi|\mathbf{r}-\mathbf{r}'|}$$

.

17.3.8.9 Ex: Gauge of retarded potentials

Confirm, that retarded potentials (17.106) are in the Lorentz gauge.

Solution: *From the retarded potentials,*

$$\Phi(\mathbf{r},t) = \frac{1}{4\pi\varepsilon_0}\int \frac{\varrho(\mathbf{r}',t_r)}{R}d^3r' \qquad \textit{and} \qquad \mathbf{A}(\mathbf{r},t) = \frac{\mu_0}{4\pi}\int \frac{\mathbf{j}(\mathbf{r}',t_r)}{R}d^3r'$$

we calculate the derivatives,

$$\frac{d}{dt}\Phi(\mathbf{r},t) = \frac{1}{4\pi\varepsilon_0}\int \frac{\dot{\varrho}(\mathbf{r}',t_r)}{R}d^3r' \qquad \textit{and} \qquad \nabla\cdot\mathbf{A}(\mathbf{r},t) = \frac{\mu_0}{4\pi}\int \nabla\cdot\frac{\mathbf{j}(\mathbf{r}',t_r)}{R}d^3r' \ .$$

To evaluate the divergence of the vector potential we first calculate,

$$\nabla\cdot\frac{\mathbf{j}}{R} - \frac{1}{R}\nabla\cdot\mathbf{j} = \mathbf{j}\cdot\nabla\frac{1}{R} = -\mathbf{j}\cdot\nabla'\frac{1}{R} = -\nabla'\cdot\frac{\mathbf{j}(\mathbf{r}',t-R/c)}{R} + \frac{1}{R}\nabla'\cdot\mathbf{j} \ .$$

We now calculate the divergence of the current,

$$\nabla'\cdot\mathbf{j}(\mathbf{r}',t-R/c) = \frac{\partial\mathbf{j}}{\partial\mathbf{r}'} + \frac{\partial\mathbf{j}}{\partial t_r}\cdot\nabla' t_r = \frac{\partial\mathbf{j}}{\partial\mathbf{r}'} - \frac{\partial\mathbf{j}}{\partial t_r}\cdot\nabla t_r = \frac{\partial\mathbf{j}}{\partial\mathbf{r}'} - \nabla\cdot\mathbf{j}(\mathbf{r}',t-R/c) \ ,$$

where we defined the explicit spatial derivative, $\frac{\partial\mathbf{j}}{\partial\mathbf{r}'}$. *We conclude,*

$$\begin{aligned}
\nabla\cdot\mathbf{A}(\mathbf{r},t) &= \frac{\mu_0}{4\pi}\int \nabla\cdot\frac{\mathbf{j}(\mathbf{r}',t_r)}{R}d^3r' \\
&= \frac{\mu_0}{4\pi}\int\left[-\nabla'\cdot\frac{\mathbf{j}(\mathbf{r}',t-R/c)}{R} + \frac{1}{R}\nabla'\cdot\mathbf{j} + \frac{1}{R}\nabla\cdot\mathbf{j}\right]d^3r' \\
&= \frac{\mu_0}{4\pi}\cancelto{0}{\oint\frac{\mathbf{j}(\mathbf{r}',t-R/c)}{R}\cdot d\mathbf{S}} + \frac{\mu_0}{4\pi}\int\frac{1}{R}\cancelto{-\dot{\varrho}}{\frac{\partial\mathbf{j}}{\partial\mathbf{r}'}}d^3r' = -\varepsilon_0\mu_0\frac{d}{dt}\Phi(\mathbf{r},t) \ .
\end{aligned}$$

17.3.8.10 Ex: Jefimenko with constant current

Suppose that $\mathbf{j}(\mathbf{r})$ is constant in time, such that $\varrho(\mathbf{r},t) = \varrho(\mathbf{r},0) + \dot{\varrho}(\mathbf{r},0)t$. Demonstrate the validity of Coulomb's law with the charge density evaluated at the *non-retarded* time.

Solution: *Jefimenko's expression for the electric field is,*

$$\begin{aligned}\vec{\mathcal{E}}(\mathbf{r},t) &= \frac{1}{4\pi\varepsilon_0}\int\left[\frac{\varrho(\mathbf{r}',t_r)}{R^2}\hat{\mathbf{e}}_r + \frac{\dot{\varrho}(\mathbf{r}',t_r)}{cR}\hat{\mathbf{e}}_r - \frac{\cancelto{0}{\dot{\mathbf{j}}(\mathbf{r}',t_r)}}{c^2R}\right]d^3r' \\ &= \frac{1}{4\pi\varepsilon_0}\int\frac{\varrho(\mathbf{r}',t_r) + \frac{R}{c}\dot{\varrho}(\mathbf{r}',t_r)}{R^2}\hat{\mathbf{e}}_r d^3r' \ .\end{aligned}$$

Now,

$$\varrho(\mathbf{r}',t_r) + \tfrac{R}{c}\dot{\varrho}(\mathbf{r}',t_r) = \left[\varrho(\mathbf{r}',0) + \dot{\varrho}(\mathbf{r}',0)(t - \tfrac{R}{c})\right] + \tfrac{R}{c}\dot{\varrho}(\mathbf{r}',0) = \varrho(\mathbf{r}',t) \ .$$

17.3.8.11 Ex: Jefimenko with slowly varying current

Suppose a current density varying sufficiently slowly so that we can ignore all higher derivatives of the Taylor expansion $\mathbf{j}(\mathbf{r},t_r) = \mathbf{j}(\mathbf{r},t) + (t_r - t)\dot{\mathbf{j}}(\mathbf{r},t_r) + ...$ Demonstrate the validity of the Biot-Savart law with the charge density evaluated at the *non-retarded* time. This means that the quasi-static approximation is much better than could have expected.

Solution: *Jefimenko's expression for the magnetic field is,*

$$\vec{\mathcal{B}}(\mathbf{r},t) = \frac{\mu_0}{4\pi}\int\left[\frac{\mathbf{j}(\mathbf{r}',t_r)}{R^2} + \frac{\dot{\mathbf{j}}(\mathbf{r}',t_r)}{cR}\right]\times\hat{\mathbf{e}}_r d^3r' = \frac{\mu_0}{4\pi}\int\frac{\mathbf{j}(\mathbf{r}',t_r) + \frac{R}{c}\dot{\mathbf{j}}(\mathbf{r}',t_r)}{R^2}\times\hat{\mathbf{e}}_r d^3r' \ .$$

Now,

$$\mathbf{j}(\mathbf{r}',t_r) + \tfrac{R}{c}\dot{\mathbf{j}}(\mathbf{r}',t_r) = \mathbf{j}(\mathbf{r}',t) \ .$$

This looks like an adiabaticity condition: either *the variation is slow,* or *nearby.*

17.3.8.12 Ex: Potentials of a point charge in uniform motion

a. Calculate the potentials (17.122) produced by the uniform motion, $w(t) = \mathbf{v}t$, of a charge q.
b. Verify that these potentials satisfy the Lorentz gauge.

Solution: *a. For this, we need to express the retarded time given by* $|\mathbf{r} - \mathbf{v}t_r| = c(t - t_r)$*, that is,*

$$r^2 - 2\mathbf{r}\cdot\mathbf{v}t_r + v^2t_r^2 = c^2(t^2 - 2tt_r + t_r^2) \ .$$

Resolving by t_r,

$$t_r = \frac{c^2t - \mathbf{r}\cdot\mathbf{v} \pm \sqrt{(c^2t-\mathbf{r}\cdot\mathbf{v})^2 + (c^2-v^2)(r^2-c^2t^2)}}{c^2-v^2} \ .$$

As this formula, for the case $\mathbf{v}=0$, simplifies to $t_r = t \pm \frac{r}{c}$, we can eliminate the positive sign. Now we calculate,

$$\begin{aligned}\mathcal{D} \equiv Rc - \mathbf{R}\cdot\mathbf{v} &= c(t-t_r)c - (\mathbf{r}-\mathbf{v}t_r)\cdot\mathbf{v} \\ &= c^2t - \mathbf{r}\cdot\mathbf{v} - (c^2-v^2)t_r = \sqrt{(c^2t-\mathbf{r}\cdot\mathbf{v})^2 + (c^2-v^2)(r^2-c^2t^2)} \ ,\end{aligned}$$

where we replaced t_r in the last step. Therefore,

$$\boxed{\Phi(\mathbf{r},t) = \frac{1}{4\pi\varepsilon_0}\frac{qc}{\mathcal{D}} \qquad \textit{and} \qquad \mathbf{A}(\mathbf{r},t) = \frac{\mu_0}{4\pi}\frac{qc\mathbf{v}}{\mathcal{D}}} \ .$$

Using the substitution $\mathbf{r} = \mathbf{r} - \mathbf{v}t$ and the angle θ between $\mathbf{r}$ and $\mathbf{v}$ we can simplify the expressions. We calculate $\mathbf{r}\cdot\mathbf{v} = v^2t + Rv\cos\theta$ and $r^2 = R^2 + v^2t^2 + 2Rvt\cos\theta$. Thereby,

$$\begin{aligned}\mathcal{D} &= \sqrt{(c^2t-\mathbf{r}\cdot\mathbf{v})^2 + (c^2-v^2)(r^2-c^2t^2)} \\ &= \sqrt{(c^2t - v^2t - Rv\cos\theta)^2 + (c^2-v^2)(R^2+v^2t^2+2Rvt\cos\theta - c^2t^2)} \\ &= R\sqrt{1 - v^2\sin^2\theta/c^2} \ .\end{aligned}$$

Finally,

$$\boxed{\Phi(\mathbf{r},t) = \frac{1}{4\pi\varepsilon_0}\frac{q}{R\sqrt{1-\beta^2\sin^2\theta}} \qquad \textit{and} \qquad \mathbf{A}(\mathbf{r},t) = \frac{\mu_0}{4\pi}\frac{q\mathbf{v}}{R\sqrt{1-\beta^2\sin^2\theta}}} \ .$$

Of course, for low velocities, we recover the laws of Coulomb and Biot-Savart.
b. The potentials of a point charge passing through the origin at time $t=0$ are,

$$\Phi(\mathbf{r},t) = \frac{1}{4\pi\varepsilon_0}\frac{qc}{\sqrt{(c^2t-\mathbf{r}\cdot\mathbf{v})^2 + (c^2-v^2)(r^2-c^2t^2)}} \qquad , \qquad \mathbf{A}(\mathbf{r},t) = \varepsilon_0\mu_0\mathbf{v}\Phi(\mathbf{r},t) \ .$$

We calculate the time derivative of the scalar potential,

$$\begin{aligned}\frac{\partial\mathbf{\Phi}}{\partial t} &= \frac{qc}{4\pi\varepsilon_0}\frac{-1}{2\sqrt{(c^2t-\mathbf{r}\cdot\mathbf{v})^2 + (c^2-v^2)(r^2-c^2t^2)}^3}\frac{d}{dt}\left[(c^2t-\mathbf{r}\cdot\mathbf{v})^2 + (c^2-v^2)(r^2-c^2t^2)\right] \\ &= \frac{qc^3}{4\pi\varepsilon_0}\frac{\mathbf{r}\cdot\mathbf{v} - tv^2}{\sqrt{(c^2t-\mathbf{r}\cdot\mathbf{v})^2 + (c^2-v^2)(r^2-c^2t^2)}^3} \ ,\end{aligned}$$

and the divergence of the vector potential,

$$\begin{aligned}\nabla\cdot\mathbf{A} &= \frac{\mu_0qc}{4\pi}\mathbf{v}\cdot\nabla\frac{1}{\sqrt{(c^2t-\mathbf{r}\cdot\mathbf{v})^2 + (c^2-v^2)(r^2-c^2t^2)}} \\ &= -\frac{\mu_0qc}{4\pi}v_x\frac{-v_x(c^2t-\mathbf{r}\cdot\mathbf{v}) + (c^2-v^2)x}{\sqrt{(c^2t - xv_x - yv_y - zv_z)^2 + (c^2-v^2)(x^2+y^2+z^2-c^2t^2)}^3} + \ldots \\ &= -\frac{\mu_0qc^3}{4\pi}\frac{-v^2t + \mathbf{r}\cdot\mathbf{v}}{\sqrt{(c^2t-\mathbf{r}\cdot\mathbf{v})^2 + (c^2-v^2)(r^2-c^2t^2)}^3} \ .\end{aligned}$$

17.3.8.13 Ex: Liénard-Wiechert potentials for a rotating charge

A particle of charge q moves circularly with constant angular velocity ω in the center of the x-y-plane. At time $t = 0$ the charge is at the position $(a, 0)$. Find the Liénard-Wiechert potentials for the points of the z-axis.

Solution: *We parametrize the position and the velocity of the motion by,*

$$\mathbf{w}(t) = a\hat{\mathbf{e}}_x \cos\omega t + a\hat{\mathbf{e}}_y \sin\omega t \qquad \textit{and} \qquad \mathbf{v}(t) = \dot{\mathbf{w}} = -a\omega\hat{\mathbf{e}}_x \sin\omega t + a\omega\hat{\mathbf{e}}_y \cos\omega t \ .$$

For the observation point $\mathbf{r} = z\hat{\mathbf{e}}_z$ *the retarded time,*

$$t_r = t - \frac{|\mathbf{r} - \mathbf{w}(t)|}{c} = t - \frac{\sqrt{z^2 + a^2}}{c}$$

is independent of the position of the charge. Thus, the potentials are,

$$\Phi(\mathbf{r}, t) = \frac{1}{4\pi\varepsilon_0} \frac{qc}{Rc - \cancelto{0}{\mathbf{R}\cdot\mathbf{v}}} = \frac{1}{4\pi\varepsilon_0} \frac{q}{\sqrt{z^2 + a^2}} \qquad \textit{and} \qquad \mathbf{A}(\mathbf{r}, t) = \frac{\mathbf{v}}{c^2}\Phi(\mathbf{r}, t) \ .$$

17.3.8.14 Ex: Point charge moving on a straight line

Assume that a point charge q is constrained to move along the x-axis. Calculate the fields at points on the axis in front of and behind the charge.

Solution: *The fields generated by a fast moving charge are given by,*

$$\vec{\mathcal{E}}(\mathbf{r}, t) = \frac{q}{4\pi\varepsilon_0} \frac{R}{(\mathbf{r}\cdot\mathbf{u})^3}[(c^2 - v^2)\mathbf{u} + \mathbf{r} \times (\mathbf{u} \times \mathbf{a})] \qquad \textit{and} \qquad \vec{\mathcal{B}}(\mathbf{r}, t) = \frac{1}{c}\mathbf{r} \times \vec{\mathcal{E}}(\mathbf{r}, t) \ .$$

The confinement of the charge on the x-axis results in,

$$\mathbf{w}(t_r) = w(t_r)\hat{\mathbf{e}}_x \quad , \quad \mathbf{v}(t_r) = v(t_r)\hat{\mathbf{e}}_x \quad , \quad \mathbf{a}(t_r) = a(t_r)\hat{\mathbf{e}}_x \quad , \quad \mathbf{u}(t_r) \equiv c\hat{\mathbf{e}}_r - \mathbf{v} = c\hat{\mathbf{e}}_r - v\hat{\mathbf{e}}_x \ .$$

The observer be also on the x-axis, $\mathbf{r} = r\hat{\mathbf{e}}_x$*, in front of the charge,*

$$\mathbf{R} = \mathbf{r} - \mathbf{w}(t_r) = (r - w)\hat{\mathbf{e}}_x = R\hat{\mathbf{e}}_x \qquad \textit{with} \qquad r > w \ .$$

With this, we deduce,

$$\hat{\mathbf{e}}_r = \hat{\mathbf{e}}_x \qquad , \qquad \mathbf{u}(t_r) = (c - v)\hat{\mathbf{e}}_x \qquad , \qquad \mathbf{u} \times \mathbf{a} = 0 \ .$$

Under these conditions, the fields simplify to,

$$\vec{\mathcal{E}}(\mathbf{r}, t) = \frac{q}{4\pi\varepsilon_0} \frac{R}{(\mathbf{r}\cdot\mathbf{u})^3}(c^2 - v^2)\mathbf{u} = \frac{q}{4\pi\varepsilon_0} \frac{c + v}{c - v} \frac{\hat{\mathbf{e}}_x}{R^2} \qquad \textit{and} \qquad \vec{\mathcal{B}}(\mathbf{r}, t) = \frac{1}{c}\mathbf{r} \times \vec{\mathcal{E}}(\mathbf{r}, t) = 0 \ .$$

When is the charge behind, $r < w$, we must replace $v \to -v$ in the equations. Alternatively, we may use the Liénard-Wiechert potentials (17.122),

$$\Phi = \frac{1}{4\pi\varepsilon_0} \frac{qc}{Rc - \mathbf{R}\cdot\mathbf{v}} \qquad , \qquad \mathbf{A} = \frac{\mathbf{v}}{c^2}\Phi \ .$$

For a motion on a straight line, $\mathbf{r} = r\hat{\mathbf{e}}_x$, $\mathbf{v} = v\hat{\mathbf{e}}_x$, $\mathbf{R} = R\hat{\mathbf{e}}_x$, *we simplify,*

$$\Phi = \frac{1}{4\pi\varepsilon_0}\frac{qc}{R(c-v)} \quad , \quad \mathbf{A} = \frac{1}{4\pi\varepsilon_0}\frac{qv\hat{\mathbf{e}}_x}{cR(c-v)} \ .$$

Using (17.136), we calculate the derivatives of R,

$$\nabla R = -c\nabla t_r = -c\frac{-\mathbf{R}}{cR - \mathbf{R}\cdot\mathbf{v}} = \frac{c}{c-v}\hat{\mathbf{e}}_x$$
$$\frac{\partial R}{\partial t} = \frac{\partial(r - vt_r)}{\partial t} = -v\frac{\partial t_r}{\partial t} = -v\frac{\partial(t - \frac{R}{c})}{\partial t} = -v\left(1 - \frac{\partial R}{\partial ct}\right) = \frac{-v}{1-\frac{v}{c}} \ ,$$

using $R = r - vt_r$ *and* $t_r = t - \frac{R}{c}$. *This yields the derivatives of the potentials,*

$$\nabla\Phi = \frac{qc}{4\pi\varepsilon_0(c-v)}\nabla\frac{1}{R} = \frac{qc}{4\pi\varepsilon_0(c-v)}\frac{-1}{R^2}\nabla R = \frac{-qc^2}{4\pi\varepsilon_0 R^2(c-v)^2}\hat{\mathbf{e}}_x \ ,$$

using,

$$\frac{\partial\mathbf{A}}{\partial t} = \frac{1}{4\pi\varepsilon_0}\frac{qv\hat{\mathbf{e}}_x}{c(c-v)}\frac{\partial}{\partial t}\frac{1}{R} = \frac{1}{4\pi\varepsilon_0}\frac{qv\hat{\mathbf{e}}_x}{c(c-v)}\frac{-1}{R^2}\frac{\partial}{\partial t}R = \frac{1}{4\pi\varepsilon_0}\frac{qv^2}{R^2(c-v)^2}\hat{\mathbf{e}}_x \ .$$

Finally,

$$\vec{\mathcal{E}} = -\nabla\Phi - \frac{\partial\mathbf{A}}{\partial t} = \frac{q(c+v)\hat{\mathbf{e}}_x}{4\pi\varepsilon_0 R^2(c-v)} \ .$$

17.3.8.15 Ex: Charge on a hyperbolic motion

Determine the Liénard-Wiechert potentials for a charge on a hyperbolic motion, i.e. $\mathbf{w}(t) = \hat{\mathbf{e}}_x\sqrt{b^2 + c^2t^2}$.

Solution: *The motion corresponds to a reflection of a charge coming from and going back to* $+\infty$ *with the velocity,*

$$\mathbf{v}(t) = \frac{d\mathbf{w}}{dt} = \frac{c^2t\hat{\mathbf{e}}_x}{\sqrt{b^2 + c^2t^2}} \ .$$

We derive the retarded time from,

$$|\mathbf{r} - \mathbf{w}(t_r)| = c(t - t_r) \ .$$

We are only considering observation points on the axis $\mathbf{r} = x\hat{\mathbf{e}}_x$ *to the right side of the charge, that is for* $x > w$. *Then,*

$$x - \sqrt{b^2 + c^2t_r^2} = c(t - t_r) \ ,$$

that is,

$$t_r = \frac{b^2 - (x - ct)^2}{2c(x - ct)} \ .$$

Note that for $t = 0$ and when $x \to \infty$ we have $t_r \to \infty$, which makes sense, since further on the x-axis we place the observer, further we must go to the past to get a signal of the charge. We can substitute this in the trajectory of the charge,

$$\mathbf{w}(t_r) = \hat{\mathbf{e}}_x\sqrt{b^2 + c^2t_r^2} = \hat{\mathbf{e}}_x\sqrt{\frac{1}{4}\frac{(x^2 - 2xct + c^2t^2 + b^2)^2}{(ct - x)^2}} = \pm\hat{\mathbf{e}}_x\frac{(x - ct)^2 + b^2}{2(ct - x)} \ .$$

To determine the correct signal, we consider the point $t = 0$, where $\mathbf{w}(t_r)$ must be positive. We see that we should choose the negative sign,

$$\mathbf{r} = \mathbf{r} - \mathbf{w}(t_r) = \hat{\mathbf{e}}_x(x - \frac{(x - ct)^2 + b^2}{2(x - ct)}) = \frac{\hat{\mathbf{e}}_x}{2}\frac{x^2 - c^2t^2 - b^2}{x - ct} \ .$$

The velocity at the retarded time is,

$$\mathbf{v}(t_r) = \frac{c^2t_r\hat{\mathbf{e}}_x}{\sqrt{b^2 + c^2t_r^2}} = \frac{c^2}{\sqrt{b^2 + c^2\left(\frac{b^2-(x-ct)^2}{2c(x-ct)}\right)^2}}\left(\frac{b^2 - (x - ct)^2}{2c(x - ct)}\right)\hat{\mathbf{e}}_x = \pm c\frac{b^2 - (x - ct)^2}{(x - ct)^2 + b^2}\hat{\mathbf{e}}_x \ .$$

To determine the correct sign, we consider the point $t = 0$. For large x, the signal from the charge comes at a distant past, while it was moving toward the origin. Then we must have a negative velocity using the negative sign. Finally, we were able to calculate the potential,

$$\begin{aligned}\Phi(\mathbf{r}, t) &= \frac{1}{4\pi\varepsilon_0}\frac{qc}{Rc - \mathbf{r}\cdot\mathbf{v}} = \frac{1}{4\pi\varepsilon_0}\frac{qc}{\frac{c}{2}\frac{x^2-c^2t^2-b^2}{x-ct} - \frac{x^2-c^2t^2-b^2}{2(x-ct)}c\frac{b^2-(x-ct)^2}{(x-ct)^2+b^2}} \\ &= \frac{q}{4\pi\varepsilon_0}\frac{(x - ct)^2 + b^2}{(x - ct)(x^2 - c^2t^2 - b^2)} \ .\end{aligned}$$

17.3.8.16 Ex: Actio=reactio with the Lorentz force

Suppose that two charges in uniform motion, the first one along the x-axis and the second along the y-axis, are at the origin at time $t = 0$. Calculate the reciprocal Coulomb-Lorentz forces.

Solution: *The force exerted by a charge q in accelerated motion on another test charge Q with instantaneous velocity $\mathbf{V}$ has been derived in (17.142) and in example 92. If the source charge q is not accelerated, the expression simplifies to,*

$$\begin{aligned}\mathbf{F}(\mathbf{r}, t) &= \frac{qQ}{4\pi\varepsilon_0}\frac{(c^2 - v^2)R}{(\mathbf{R}\cdot\mathbf{u})^3}\left\{\mathbf{u} + \frac{\mathbf{V}}{c}\times(\hat{\mathbf{e}}_R\times\mathbf{u})\right\} \\ &= \frac{qQ}{4\pi\varepsilon_0}\frac{1 - \beta^2}{d^2\sqrt{1 - \beta^2\sin^2\theta}^3}\left\{\hat{\mathbf{e}}_d + \frac{\mathbf{V}}{c}\times\left(\frac{\mathbf{v}}{c}\times\hat{\mathbf{e}}_d\right)\right\} \ ,\end{aligned}$$

with the abbreviations $\mathbf{u} \equiv c\hat{\mathbf{e}}_R - \mathbf{v}$, the distance between the position of the test charge and the retarded *position of the source charge, $\mathbf{R} \equiv \mathbf{r} - \mathbf{w}(t_r)$, and the distance*

between the position of the test charge and the actual *position of the source charge,* $\mathbf{d} \equiv \mathbf{r} - \mathbf{w}(t)$.
Now consider the following situation: The test charge Q, located at position $\mathbf{r}$ where the fields and the Coulomb-Lorentz force have to be evaluated, moves along the x-axis, such that $\mathbf{r} = Vt\hat{\mathbf{e}}_x$ and $\mathbf{V} = V\hat{\mathbf{e}}_x$. The charge q producing the field moves uniformly along the y-axis, such that $\mathbf{a} = 0$ and $\mathbf{v} = v\hat{\mathbf{e}}_y$ and $\mathbf{w}(t) = vt\hat{\mathbf{e}}_y$. Then,

$$\mathbf{d} = Vt\hat{\mathbf{e}}_x - vt\hat{\mathbf{e}}_y \qquad \text{and} \qquad \hat{\mathbf{e}}_d = \frac{Vt\hat{\mathbf{e}}_x - vt\hat{\mathbf{e}}_y}{|Vt\hat{\mathbf{e}}_x - vt\hat{\mathbf{e}}_y|} = \frac{V\hat{\mathbf{e}}_x - v\hat{\mathbf{e}}_y}{\sqrt{V^2+v^2}} \ .$$

With that, the force is,

$$\begin{aligned}\mathbf{F}(x,t) &= \frac{qQ}{4\pi\varepsilon_0}\frac{1-\beta^2}{d^2\sqrt{1-\beta^2\sin^2\theta}^3}\left\{\frac{V\hat{\mathbf{e}}_x - v\hat{\mathbf{e}}_y}{\sqrt{V^2+v^2}} + \frac{V\hat{\mathbf{e}}_x}{c}\times\left(\frac{v\hat{\mathbf{e}}_y}{c}\times\frac{V\hat{\mathbf{e}}_x - v\hat{\mathbf{e}}_y}{\sqrt{V^2+v^2}}\right)\right\} \\ &= \frac{qQ}{4\pi\varepsilon_0}\frac{1-\beta^2}{t^2\sqrt{1-\beta^2\sin^2\theta}^3\sqrt{V^2+v^2}^3}\left\{V\hat{\mathbf{e}}_x - v\hat{\mathbf{e}}_y + \frac{vV^2}{c^2}\hat{\mathbf{e}}_y\right\} \ .\end{aligned}$$

Assuming equal velocities, $v = V$,

$$\mathbf{F}(x,t) = \frac{qQ}{4\pi\varepsilon_0}\frac{1-\beta^2}{t^2\sqrt{1-\beta^2\sin^2\theta}^3\sqrt{2}^3}\{\hat{\mathbf{e}}_x - (1-\beta^2)\hat{\mathbf{e}}_y\} \ .$$

Assuming low velocities,

$$\mathbf{F}(x,t) = \frac{qQ}{4\pi\varepsilon_0}\frac{1}{t^2\sqrt{V^2+v^2}^3}\{V\hat{\mathbf{e}}_x - v\hat{\mathbf{e}}_y\} \ .$$

17.4 Further reading

J.D. Jackson, *Classical Electrodynamics* [659]ISBN

D.J. Griffiths, *Introduction to Electrodynamics* [545]ISBN

Chapter 18

Electromagnetic waves

The phenomenon of waves is usually introduced in undergraduate Physics courses. We already discussed that, unlike classical longitudinal or transverse waves, *electromagnetic waves* do not require a propagation medium, but move through the vacuum with the speed of light. And we showed that the wave equation is form-invariant to the Lorentz, but not to the Galilei transform [1].

The electromagnetic waves are generated when charges change their positions. Therefore, the theory of electromagnetic waves is also a consequence of electrodynamic theory, which is summarized in the *Maxwell equations*. In this chapter we will consider these equations as given and deduce from them the properties of electromagnetic waves.

18.1 Wave propagation

By *wave* we mean the propagation of a perturbation $f(\mathbf{r},t)$, which can be a scalar or vector quantity. When it propagates in one dimension, the wave is described by the *wave equation*,

$$\frac{\partial^2 f}{\partial z^2} = \frac{1}{v^2}\frac{\partial^2 f}{\partial t^2} \ , \tag{18.1}$$

where v is the propagation velocity of the wave. The most common waveform is the sine wave,

$$f(z,t) = A\cos(kz-\omega t+\delta) = \mathfrak{Re}\ [\tilde{A}e^{\imath(kz-\omega t)}] = \mathfrak{Re}\ \tilde{f}(z,t) \ , \tag{18.2}$$

in complex notation (often ornamented by a tilde) introducing the complex amplitude $\tilde{A} \equiv Ae^{\imath\delta}$. The wave equation satisfies the superposition principle allowing for the expansion of any wave type according to,

$$\tilde{f}(z,t) = \int_{-\infty}^{\infty} \tilde{A}(k)e^{\imath(kz-\omega t)}dk \ . \tag{18.3}$$

We will show in Exc. 18.1.8.1, that all functions satisfying $f(z,t) = g(z \pm vt)$ automatically obey the wave equation. The most general solution of the wave equation is given by,

$$f(z,t) = g_1(z-vt) + g_2(z+vt) \ . \tag{18.4}$$

We show this in the following example directly generalizing to three dimensions.

[1] See script on *Vibrations and waves* (2020), Sec. 2.2.3.

Example 93 (*General solution of the wave equation*): The three-dimensional wave equation is,

$$\frac{1}{c^2}\frac{\partial^2 f}{\partial t^2} - \nabla^2 f = 0 \ .$$

Using for the Dirac function the representation, $\delta^{(3)}(\mathbf{r}-\mathbf{r}') = \frac{1}{(2\pi)^3}\int d^3k e^{\imath \mathbf{k}\cdot(\mathbf{r}-\mathbf{r}')}$, we can write,

$$\begin{aligned} f(\mathbf{r},t) &= \int_{V_\infty} d^3r' \delta^{(3)}(\mathbf{r}-\mathbf{r}') f(\mathbf{r}',t) \\ &= \int d^3k e^{\imath \mathbf{k}\cdot\mathbf{r}} \int_{V_\infty} d^3r' \tfrac{e^{-\imath \mathbf{k}\cdot\mathbf{r}'}}{(2\pi)^3} f(\mathbf{r}',t) = \int d^3k e^{\imath \mathbf{k}\cdot\mathbf{r}} A(\mathbf{k},t) \ , \end{aligned}$$

where $A(\mathbf{k},t) \equiv \int_{V_\infty} d^3r' \frac{1}{(2\pi)^3} e^{-\imath \mathbf{k}\cdot\mathbf{r}'} f(\mathbf{r}',t)$ is the Fourier transform of f. Applying the operator $\nabla^2 - \frac{1}{c^2}\frac{\partial^2}{\partial t^2}$ to the expression for f gives,

$$\begin{aligned} 0 = \frac{1}{c^2}\frac{\partial^2 f}{\partial t^2} - \nabla^2 f &= \frac{1}{c^2}\int d^3k e^{\imath \mathbf{k}\cdot\mathbf{r}} \frac{\partial^2 A(\mathbf{k},t)}{\partial t^2} - \int d^3k A(\mathbf{k},t) \nabla^2 e^{\imath \mathbf{k}\cdot\mathbf{r}} \\ &= \int d^3k e^{\imath \mathbf{k}\cdot\mathbf{r}} \left[\frac{1}{c^2}\frac{\partial^2 A(\mathbf{k},t)}{\partial t^2} + k^2 A(\mathbf{k},t) \right] \ . \end{aligned}$$

Hence,

$$\frac{1}{c^2}\frac{\partial^2 A(\mathbf{k},t)}{\partial t^2} + k^2 A(\mathbf{k},t) = 0 \ .$$

The general solution of this equation can be written as,

$$A(\mathbf{k},t) = a(\mathbf{k}) e^{\imath kct} + b(\mathbf{k}) e^{-\imath kct} \ ,$$

where $a(\mathbf{k})$ and $b(\mathbf{k})$ are arbitrary functions of $\mathbf{k}$. Thus, the general solution for f is given by,

$$f(\mathbf{r},t) = \int a(\mathbf{k}) e^{\imath \mathbf{k}\cdot\mathbf{r} + \imath kct} d^3k + \int b(\mathbf{k}) e^{\imath \mathbf{k}\cdot\mathbf{r} - \imath kct} d^3k \ .$$

Since f is a real quantity, $f(\mathbf{r},t)^* = f(\mathbf{r},t)$, we must have,

$$a(-\mathbf{k})^* = b(\mathbf{k}) \ ,$$

and,

$$f(\mathbf{r},t) = \mathfrak{Re} \left[\int 2b(\mathbf{k}) e^{\imath \mathbf{k}\cdot\mathbf{r} - \imath kct} d^3k \right] \ .$$

The scalar functions $e^{\imath \mathbf{k}\cdot\mathbf{r} - \imath kct}$ satisfy the wave equation for all $\mathbf{k}$.

Waves of vector quantities must be characterized by a *polarization vector* $\hat{\epsilon} \equiv \mathbf{b}/b$. Therefore, we define,

$$\vec{\mathcal{E}} = \mathfrak{Re}\ \vec{\tilde{\mathcal{E}}} \qquad \text{with} \qquad \vec{\tilde{\mathcal{E}}}(\mathbf{r},t) = \hat{\epsilon}\mathcal{E}_0 e^{\imath \mathbf{k}\cdot\mathbf{r} - \imath kct} \ , \tag{18.5}$$

where $\mathcal{E}_0$ is real and $\omega \equiv kc$, as the vector functions forming the functional basis for the fields. These functions represent plane waves, because on a wavefront, the value of $\vec{\tilde{\mathcal{E}}}(\mathbf{r},t)$ is fixed, and this occurs only when $e^{\imath \mathbf{k}\cdot\mathbf{r} - \imath kct}$ is constant [2].

[2] We shall see later that, when a wave passes through zones with different propagation velocities v, the amplitude $\mathbf{A}$ and the polarization $\hat{\epsilon}$ may change. However, any change must be such that $\tilde{\mathbf{F}}(z_0,t)$ and the derivative $\tilde{\mathbf{F}}'(z_0,t)$ are continuous at the transition point z_0.

To calculate the magnetic field from the complex representation of the electric field, we write first,

$$\vec{\mathcal{B}} = \mathfrak{Re}\ \vec{\tilde{\mathcal{B}}} \qquad \text{with} \qquad \vec{\tilde{\mathcal{B}}}(\mathbf{r},t) = \hat{\epsilon}'\mathcal{B}_0 e^{\imath\mathbf{k}'\cdot\mathbf{r}-\imath k' ct}\ , \tag{18.6}$$

where $\vec{\tilde{\mathcal{B}}}$ is the magnetic plane wave, since both $\vec{\tilde{\mathcal{E}}}$ as well as $\vec{\tilde{\mathcal{B}}}$ satisfy the same wave equation. With Maxwell's equations in the absence of sources, it is obvious that,

$$\mathbf{k} = \mathbf{k}'\ , \tag{18.7}$$

because the equations that couple $\vec{\tilde{\mathcal{E}}}$ and $\vec{\tilde{\mathcal{B}}}$ must be satisfied at every point of space and at every instant of time.

18.1.1 Helmholtz's equation

Electromagnetic waves differ from classical longitudinal or transverse waves in several aspects. For example, they do not require a propagation medium, but move through the vacuum at extremely high speed. Being exactly $c = 299792458$ m/s the speed of light is so high, that the laws of classical mechanics are no longer valid. And because there is no propagation medium, in vacuum all inertial systems are equivalent, and this will have important consequences for the Doppler effect. We will show that the electromagnetic wave equation almost comes out as a corollary of the theory of special relativity.

We have shown in Sec. 5.1 how the periodic conversion between kinetic and potential energy in a pendulum can propagate in space, when the pendulum is coupled to other pendulums hung in an array, and that this model explains the propagation of a pulse along a string. We also discussed, how electric and magnetic energy can be interconverted in an electronic *L-C* circuit constiting of a capacitor (storing electrical energy) and an inductance (a coil storing magnetic energy). The law of electrodynamics describing the transformation of electric field variations into magnetic energy is *Ampère's law*, and the law describing the transformation of magnetic field variations into electric energy is *Faraday's law*,

$$\frac{\partial\vec{\mathcal{E}}}{\partial t} \curvearrowright \vec{\mathcal{B}}(t) \qquad , \qquad \frac{\partial\vec{\mathcal{B}}}{\partial t} \curvearrowright -\vec{\mathcal{E}}(t)\ . \tag{18.8}$$

Extending the *L-C* circuit to an array, it is possible to show that the electromagnetic oscillation propagates along the array. This model describes well the propagation of electromagnetic energy along a coaxial cable or the propagation of light in free space.

The *electrical energy* stored in the capacitor and the *magnetic energy* stored in the coil are given by,

$$E_{ele} = \tfrac{\varepsilon_0}{2}|\vec{\mathcal{E}}|^2 \qquad , \qquad E_{mag} = \tfrac{1}{2\mu_0}|\vec{\mathcal{B}}|^2\ , \tag{18.9}$$

where the constants $\varepsilon_0 = 8.854\cdot 10^{-12}$ As/Vm and $\mu_0 = 4\pi\cdot 10^{-7}$ Vs/Am are called *vacuum permittivity* and *vacuum permeability*. The constant $Z_0 \equiv \sqrt{\mu_0/\varepsilon_0}$ is called *vacuum impedance*.

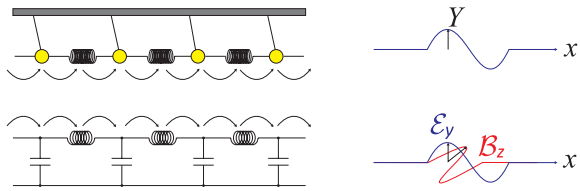

Figure 18.1: Analogy between propagation of mechanical waves (above) and electromagnetic waves (below).

From Maxwell's equations in free space,

$$\nabla \times \vec{\mathcal{B}} - \varepsilon_0 \mu_0 \partial_t \vec{\mathcal{E}} = 0 \qquad \text{and} \qquad \nabla \times \vec{\mathcal{E}} + \partial_t \vec{\mathcal{B}} = 0 \ , \tag{18.10}$$

deriving the first and inserting this into the second, and using the fact that the divergences vanish,

$$\frac{1}{c^2}\frac{\partial^2 \vec{\mathcal{E}}}{\partial t^2} = \frac{1}{\varepsilon_0 \mu_0 c^2}\frac{\partial}{\partial t}\nabla \times \vec{\mathcal{B}} = -\nabla \times (\nabla \times \vec{\mathcal{E}}) = -\nabla(\nabla \cdot \vec{\mathcal{E}}) + \nabla^2 \vec{\mathcal{E}} = \nabla^2 \vec{\mathcal{E}} \tag{18.11}$$

$$\frac{1}{c^2}\frac{\partial^2 \vec{\mathcal{B}}}{\partial t^2} = -\frac{1}{c^2}\frac{\partial}{\partial t}\nabla \times \vec{\mathcal{E}} = -\frac{1}{\varepsilon_0 \mu_0 c^2}\nabla \times (\nabla \times \vec{\mathcal{B}}) = -\nabla(\nabla \cdot \vec{\mathcal{B}}) + \nabla^2 \vec{\mathcal{B}} = \nabla^2 \vec{\mathcal{B}} \ .$$

These are the homogeneous *Helmholtz equations*. We will check in Exc. 18.1.8.2, that

- electromagnetic waves (in free space) are transverse;
- the amplitude of the electric field, the magnetic field, and the direction of propagation are orthogonal;
- the propagation velocity is the speed of light, because $c^2 = 1/\varepsilon_0 \mu_0$.

18.1.2 The polarization of light

A consequence of the requirement, $\nabla \cdot \vec{\mathcal{E}} = 0 = \nabla \cdot \vec{\mathcal{B}}$, following from Maxwell's equations in vacuum is, that the electromagnetic waves are transverse with orthogonal electric and magnetic fields. This is easy to see in the case of plane wave:

$$0 = \nabla \cdot \vec{\mathcal{E}} = \vec{\mathcal{E}}_0 \cdot \nabla e^{\imath(\mathbf{k}\cdot\mathbf{r}-\omega t)} = \imath \vec{\mathcal{E}}_0 \cdot \mathbf{k} e^{\imath(\mathbf{k}\cdot\mathbf{r}-\omega t)} \ , \tag{18.12}$$

and analogously for $\vec{\mathcal{B}}$. We conclude,

$$\boxed{\mathbf{k} \cdot \vec{\mathcal{E}} = 0 = \mathbf{k} \cdot \vec{\mathcal{B}}} \ . \tag{18.13}$$

In addition, from Faraday's law,

$$\vec{\mathcal{B}}_0 \ \imath\omega e^{\imath(\mathbf{k}\cdot\mathbf{r}-\omega t)} = -\frac{\partial \vec{\mathcal{B}}}{\partial t} = \nabla \times \vec{\mathcal{E}} = -\vec{\mathcal{E}}_0 \times \nabla e^{\imath(\mathbf{k}\cdot\mathbf{r}-\omega t)} = -\vec{\mathcal{E}}_0 \times \imath \mathbf{k} e^{\imath(\mathbf{k}\cdot\mathbf{r}-\omega t)} \ . \tag{18.14}$$

together with an analogous result obtained from Ampère-Maxwell's law, we can summarize,

$$\boxed{\vec{\mathcal{B}} = \tfrac{\mathbf{k}}{\omega} \times \vec{\mathcal{E}} \qquad \text{and} \qquad \vec{\mathcal{E}} = -\tfrac{c^2 \mathbf{k}}{\omega} \times \vec{\mathcal{B}}} \ . \tag{18.15}$$

We conclude that the fields $\vec{\mathcal{E}}$ and $\vec{\mathcal{B}}$ and the propagation wavevector are all mutually orthogonal for waves in free space. In the Excs. 18.1.8.3 and 18.1.8.4 we study the polarization of light.

Example 94 (*Circular polarization*): Let us study the example of polarized light,

$$\vec{\tilde{\mathcal{E}}} = (\mathcal{E}_x \hat{\mathbf{e}}_x + \imath \mathcal{E}_y \hat{\mathbf{e}}_y) e^{\imath k_z z - \imath \omega t} \ .$$

If $\mathcal{E}_x = \mathcal{E}_y$, we have circular polarization. If $\mathcal{E}_x \neq \mathcal{E}_y$, the polarization is said to be elliptical. The reason is easily seen by taking the real part of the plane wave:

$$\vec{\mathcal{E}} = \mathfrak{Re}\ \vec{\tilde{\mathcal{E}}} = \mathcal{E}_x \hat{\mathbf{e}}_x \cos(k_z z - \omega t) - \mathcal{E}_y \hat{\mathbf{e}}_y \sin(k_z z - \omega t) \ .$$

In the plane defined by $z = z_0$, with z_0 constant, the electric field vector describes an ellipse as time passes; the ellipse is a circle if $\mathcal{E}_x = \mathcal{E}_y$.
Other polarizations are possible in free space although sometimes a bit more difficult to realize in practice, for example, radial polarization,

$$\vec{\tilde{\mathcal{E}}} = \mathcal{E}_0 \hat{\mathbf{e}}_r e^{\imath k_z z - \imath \omega t} \qquad \text{and} \qquad \vec{\tilde{\mathcal{B}}} = \mathcal{B}_0 \hat{\mathbf{e}}_\theta e^{\imath k_z z - \imath \omega t} \ .$$

18.1.2.1 Polarization optics

A laser generally has a well-defined polarization, for example, linear or circular. The polarizations can be transformed into each other through *birefringent optical elements*, such as birefringent waveplates, Fresnel rhombs, or electro-optical modulators. Superpositions of different polarizations can be separated with polarizing *beam splitters*.

It is important to distinguish between the *polarization*, which is always specified in relation to a fixed coordinate system, and *helicity*, i.e. the rotation direction of the polarization vector with respect to the propagation direction of the light beam. The polarization of a beam propagating in z-direction can easily be expressed by a vector of complex amplitude,

$$\vec{\mathcal{E}}(\mathbf{r}, t) = \begin{pmatrix} a \\ b \\ 0 \end{pmatrix} e^{\imath \mathbf{k}\cdot\mathbf{r} - \imath\omega t} = \begin{pmatrix} 1 \\ e^{-\imath\phi}|b|/|a| \\ 0 \end{pmatrix} |a| e^{\imath \mathbf{k}\cdot\mathbf{r} - \imath\omega t} \ . \tag{18.16}$$

The angle $\phi = \arctan \frac{\mathfrak{Im}\ ab^*}{\mathfrak{Re}\ ab^*}$ determines the polarization of the light beam. The polarization is linear for $\phi = 0$ and circular for $\phi = \pi/2$. $|b|/|a|$ then gives the degree of ellipticity. A device rotating the (linear) polarization of a light beam (e.g. a sugar solution) is described by the so-called *Jones matrix* (we restrict ourselves to the xy-plane orthogonal to the propagation direction),

$$M_{rotator}(\phi) = \begin{pmatrix} \cos\phi & \sin\phi \\ -\sin\phi & \cos\phi \end{pmatrix} \ , \tag{18.17}$$

where ϕ is the angle of rotation. For birefringent half-waveplates the rotation angle is independent on the propagation direction. In devices called *Faraday rotators*, in

contrast, the sign of the rotation angle depends on the propagation direction of the laser beam,

$$M_{Faraday}(\phi) = \begin{pmatrix} \cos\phi & \mathbf{k}\cdot\hat{\mathbf{e}}_z \sin\phi \\ -\mathbf{k}\cdot\hat{\mathbf{e}}_z \sin\phi & \cos\phi \end{pmatrix} , \tag{18.18}$$

A *polarizer* projects the polarization to a specific axis. In case of a polarizer aligned to the x-axis the Jones matrix is,

$$M_{polarizer} = \begin{pmatrix} 1 & 0 \\ 0 & 0 \end{pmatrix} , \tag{18.19}$$

while for an arbitrary axis given by the angle ϕ, it is,

$$M_{polarizer}(\phi) = \begin{pmatrix} \cos\phi & \sin\phi \\ -\sin\phi & \cos\phi \end{pmatrix} \begin{pmatrix} 1 & 0 \\ 0 & 0 \end{pmatrix} \begin{pmatrix} \cos\phi & \sin\phi \\ -\sin\phi & \cos\phi \end{pmatrix}^{-1} . \tag{18.20}$$

A birefringent crystal acts only on one of the two optical axes. Assuming that only the y-axis is optically active, its Jones's matrix is,

$$M_{\theta\text{-waveplate}} = \begin{pmatrix} 1 & 0 \\ 0 & e^{\imath\theta} \end{pmatrix} . \tag{18.21}$$

For $\theta = 2\pi/n$ we obtain a so-called λ/n-*waveplate*. When we rotate the waveplate (and therefore the optically active about the inactive axis) by an angle ϕ, the Jones matrix becomes [3],

$$\begin{aligned} M_{\theta\text{-waveplate}}(\phi) &= \begin{pmatrix} \cos\phi & \sin\phi \\ -\sin\phi & \cos\phi \end{pmatrix} \begin{pmatrix} 1 & 0 \\ 0 & e^{\imath\theta} \end{pmatrix} \begin{pmatrix} \cos\phi & \sin\phi \\ -\sin\phi & \cos\phi \end{pmatrix}^{-1} \\ &= \begin{pmatrix} \cos^2\phi + e^{\imath\theta}\sin^2\phi & -\sin\phi\cos\phi + e^{\imath\theta}\sin\phi\cos\phi \\ -\sin\phi\cos\phi + e^{\imath\theta}\sin\phi\cos\phi & \sin^2\phi + e^{\imath\theta}\cos^2\phi \end{pmatrix} . \end{aligned} \tag{18.22}$$

We use in most cases $\lambda/4$-waveplates,

$$M_{\lambda/4}(\phi) = \begin{pmatrix} \cos^2\phi + \imath\sin^2\phi & (-1+\imath)\sin\phi\cos\phi \\ (-1+\imath)\sin\phi\cos\phi & \sin^2\phi + \imath\cos^2\phi \end{pmatrix} \tag{18.23}$$

or $\lambda/2$-waveplates,

$$M_{\lambda/2}(\phi) = \begin{pmatrix} \cos 2\phi & -\sin 2\phi \\ -\sin 2\phi & -\cos 2\phi \end{pmatrix} . \tag{18.24}$$

Note that interestingly $M_{\lambda/2}(\phi)^2 = \mathbb{I}$.

[3] See script on *Optical spectroscopy* (2020), Sec. 2.3.1.

Example 95 (*Generating circular polarization*): We can use $\lambda/4$-waveplates to create, from linearly polarized light, circularly polarized light. Choosing an angle $\theta = 45^\circ$ we get from (18.23),

$$M_{\lambda/4}(\pm\pi/4)\begin{pmatrix}1\\0\end{pmatrix} = \begin{pmatrix}\frac{1}{2}+\frac{1}{2}\imath & \mp\frac{1}{2}\pm\frac{1}{2}\imath\\ \mp\frac{1}{2}\pm\frac{1}{2}\imath & \frac{1}{2}+\frac{1}{2}\imath\end{pmatrix}\begin{pmatrix}1\\0\end{pmatrix} = \frac{e^{\imath\pi/4}}{\sqrt{2}}\begin{pmatrix}1\\\pm\imath\end{pmatrix} .$$

Example 96 (*Polarization behavior of upon reflection from a mirror*): A light beam reflected from a mirror under normal incidence does not changes its polarization vector, but only its wavevector. This can be interpreted as conservation of the angular momentum of light upon reflection. One consequence of this is, that $\sigma^\pm$ light turns into $\sigma^\pm$ light upon reflection.

Example 97 (*Action of birefringent waveplates as a function of propagation direction*): The Jones matrices for λ/n-waveplates *do not depend* on the propagation direction, simply because the wavevector does not appear in the expressions. That is, the polarization $\hat{\epsilon} = \hat{\mathbf{e}}_x$ of a beam propagating towards $\pm k\hat{\mathbf{e}}_z$ is transformed by a $M_{\lambda/4}(\pi/4)$ waveplate into σ^+-polarized light regardless of the propagation direction. A consequence of this is that a beam traversing the waveplate $M_{\lambda/4}(\pi/4)$ twice in the round-trip (e.g. being reflected by a mirror) will undergo a rotation of amplitude by 90°,

$$M_{\lambda/4}(\tfrac{\pi}{2})\begin{pmatrix}1\\0\end{pmatrix} = \begin{pmatrix}\imath\\0\end{pmatrix}$$
$$M_{\lambda/4}(\tfrac{\pi}{4})M_{\lambda/4}(\tfrac{\pi}{4}) = \begin{pmatrix}0 & -1\\-1 & 0\end{pmatrix} .$$

This feature is often used to separate counterpropagating light fields via a polarizing beamsplitter.
On the other hand, for $\lambda/2$-waveplates, it is easy to check the following results,

$$M_{\lambda/2}(\tfrac{\pi}{4})\begin{pmatrix}1\\0\end{pmatrix} = \begin{pmatrix}0\\-1\end{pmatrix}$$
$$M_{\lambda/2}(\tfrac{\pi}{8})\begin{pmatrix}1\\0\end{pmatrix} = \tfrac{1}{\sqrt{2}}\begin{pmatrix}1\\-1\end{pmatrix} .$$

In addition, for any ϕ,

$$M_{\lambda/2}(\phi)M_{\lambda/2}(\phi) = \begin{pmatrix}1 & 0\\0 & 1\end{pmatrix} .$$

Thus, the double passage through a $\lambda/2$-waveplate cancels its effect.

18.1.3 The energy density and flow in plane waves

The energy densities stored in the electric field and the magnetic field are given by,

$$u_{ele} = \tfrac{\varepsilon_0}{2}|\vec{\mathcal{E}}|^2 \quad , \quad u_{mag} = \tfrac{1}{2\mu_0}|\vec{\mathcal{B}}|^2 \ . \tag{18.25}$$

In the case of a monochromatic wave parametrized by $\vec{\mathcal{E}}(\mathbf{r},t) = \vec{\mathcal{E}}_0\cos(\mathbf{k}\cdot\mathbf{r}-\omega t)$ the calculus (18.15) shows that $|\vec{\mathcal{B}}| = \frac{k}{\omega}|\vec{\mathcal{E}}| = \frac{1}{c}|\vec{\mathcal{E}}|$, such that the average energy density is,

$$\langle u(\mathbf{r})\rangle = \left\langle |\varepsilon_0\vec{\mathcal{E}}_0\cos(\mathbf{k}\cdot\mathbf{r}-\omega t)|^2 \right\rangle = \tfrac{1}{2}\varepsilon_0|\vec{\mathcal{E}}_0|^2 = \tfrac{1}{2\mu_0}|\vec{\mathcal{B}}_0|^2 \ , \tag{18.26}$$

consistent with the expressions (17.58). When the wave propagates, it carries with it this amount of energy. The energy flux density is calculated by the *Poynting vector*,

$$\langle\vec{\mathcal{S}}(\mathbf{r})\rangle = \tfrac{1}{\mu_0}\left\langle \vec{\mathcal{E}}(\mathbf{r},t)\times\vec{\mathcal{B}}(\mathbf{r},t)\right\rangle = \tfrac{1}{2}c\varepsilon_0|\vec{\mathcal{E}}_0|^2\hat{\mathbf{e}}_k \ . \tag{18.27}$$

The absolute value is the *intensity* of the light field,

$$\langle I(\mathbf{r},t)\rangle = \langle|\vec{\mathcal{S}}(\mathbf{r},t)|\rangle \ . \tag{18.28}$$

In addition, a radiation field can have linear momentum. In vacuum, the momentum is connected to the Poynting vector,

$$\langle\wp\rangle = \left\langle c\varepsilon_0|\vec{\mathcal{E}}(\mathbf{r},t)|^2\hat{\mathbf{e}}_k\right\rangle = c\varepsilon_0|\vec{\mathcal{E}}_0|^2\hat{\mathbf{e}}_k \ . \tag{18.29}$$

but in dielectric media things are different, as we will see later. The *momentum density* is responsible for the *radiation pressure*. When light hits the surface A of a perfect absorber, it transfers, during the time interval Δt, the momentum $\Delta\mathbf{p} = \langle\wp\rangle Ac\Delta t$ to the body. Thus, the pressure is,

$$P = \frac{1}{A}\frac{\Delta p}{\Delta t} = \frac{\varepsilon_0\mathcal{E}_0^2}{2} = \frac{I}{c} \ . \tag{18.30}$$

Note that for a perfect reflector the pressure is doubled.

In Exc. 18.1.8.5 we show a trick how to quickly calculate the temporal average of expressions containing products of oscillating field. We solve problems about the radiative pressure in Excs. 18.1.8.6 to 18.1.8.8. In the Excs. 18.1.8.10 to 18.1.8.12 we calculate u and $\vec{\mathcal{S}}$ for various types of waves.

18.1.3.1 Spherical waves

Other wave geometries are possible (see Exc. 18.1.8.13). For example, it is easy to show that spherical scalar fields of the type $\Phi(\mathbf{r},t) = \Phi_0\frac{e^{\imath(kr-\omega t)}}{r}$ and spherical vector fields of the type $\mathbf{A}(\mathbf{r},t) = \mathbf{A}_0\frac{e^{\imath(kr-\omega t)}}{r}$ satisfy the wave equation,

$$\begin{aligned} 0 &= \nabla^2\Phi - \frac{1}{c^2}\frac{\partial^2\Phi}{\partial t^2} \\ &= \frac{1}{r^2}\frac{\partial}{\partial r}\left(r^2\frac{\partial\Phi}{\partial r}\right) + \cancel{\frac{1}{r^2\sin\theta}\frac{\partial}{\partial\theta}\left(\sin\theta\frac{\partial\Phi}{\partial\theta}\right)}^{0} + \cancel{\frac{1}{r^2\sin^2\theta}\frac{\partial^2\Phi}{\partial\phi^2}}^{0} - \frac{1}{c^2}\frac{\partial^2\Phi}{\partial t^2} \\ &= -k^2\Phi + \frac{\omega^2}{c^2}\Phi \ . \end{aligned} \tag{18.31}$$

This also applies to electric and magnetic fields,

$$\vec{\mathcal{E}}(\mathbf{r},t) \stackrel{?}{=} \vec{\mathcal{E}}_0 \frac{e^{\imath(kr-\omega t)}}{r} \qquad \text{and} \qquad \vec{\mathcal{B}}(\mathbf{r},t) \stackrel{?}{=} \vec{\mathcal{B}}_0 \frac{e^{\imath(kr-\omega t)}}{r} \ . \tag{18.32}$$

But it does not mean that these fields obey Maxwell's equations. In fact, the simplest possible spherical wave corresponds a the dipole radiation, which will be discussed in the next chapter. We will find in Exc. 19.1.6.3 that the expressions for electric dipole radiation satisfy Maxwell's equations and in Exc. 18.1.8.14, that the expressions (18.32) do not satisfy them. In Excs. 18.1.8.15 and 18.1.8.16 we will deepen this discussion.

18.1.4 Slowly varying envelope approximation

The slowly varying envelope approximation [42] (SVEA) is the assumption that the envelope of a forward-traveling wave pulse varies slowly in time and space compared to a period or wavelength. This requires the spectrum of the signal to be narrow-banded. The SVEA is often used because the resulting equations are in many cases easier to solve than the original equations, reducing the order of all (or some) of the highest-order partial derivatives. But the validity of the assumptions which are made need to be justified.

For example, consider the electromagnetic wave equation:

$$\nabla^2 \mathcal{E} - \mu_0 \varepsilon_0 \frac{\partial^2 \mathcal{E}}{\partial t^2} = 0 \ . \tag{18.33}$$

If k_0 and ω_0 are the wave number and angular frequency of the (characteristic) carrier wave for the signal $\mathcal{E}(\mathbf{r},t)$, the following representation is useful:

$$\mathcal{E}(\mathbf{r},t) = \mathfrak{Re}\left[\mathcal{E}_0(\mathbf{r},t) e^{\imath(\mathbf{k}_0\cdot\mathbf{r}-\omega_0 t)}\right] \ . \tag{18.34}$$

In the SVEA it is assumed that the complex amplitude $\mathcal{E}_0(\mathbf{r},t)$ only varies slowly with $\mathbf{r}$ and t. This inherently implies that $\mathcal{E}_0(\mathbf{r},t)$ represents waves propagating forward, predominantly in the $\mathbf{k}_0$ direction. As a result of the slow variation of $\mathcal{E}_0(\mathbf{r},t)$, when taking derivatives, the highest-order derivatives may be neglected [220]:

$$|\nabla^2 \mathcal{E}_0| \ll |\mathbf{k}_0 \cdot \nabla \mathcal{E}_0| \qquad \text{and} \qquad \left|\frac{\partial^2 \mathcal{E}_0}{\partial t^2}\right| \ll \left|\omega_0 \frac{\partial \mathcal{E}_0}{\partial t}\right| \ . \tag{18.35}$$

Consequently, the wave equation is approximated in the SVEA as,

$$2\imath \mathbf{k}_0 \cdot \nabla \mathcal{E}_0 + 2\imath \omega_0 \mu_0 \varepsilon_0 \frac{\partial \mathcal{E}_0}{\partial t} - (k_0^2 - \omega_0^2 \mu_0 \varepsilon_0)\mathcal{E}_0 = 0 \ . \tag{18.36}$$

It is convenient to choose k_0 and ω_0 such that they satisfy the dispersion relation, $k_0^2 - \omega_0^2 \mu_0 \varepsilon_0 = 0$. This gives the following approximation to the wave equation,

$$\mathbf{k}_0 \cdot \nabla \mathcal{E}_0 + \omega_0 \mu_0 \varepsilon_0 \frac{\partial \mathcal{E}_0}{\partial t} = 0 \ . \tag{18.37}$$

This is a hyperbolic partial differential equation, like the original wave equation, but now of first-order instead of second-order. It is valid for coherent forward-propagating

waves in directions near the k_0-direction. The space and time scales over which $\mathcal{E}_0$ varies are generally much longer than the spatial wavelength and temporal period of the carrier wave. A numerical solution of the envelope equation thus can use much larger space and time steps, resulting in significantly less computational effort.

Example 98 (*Parabolic SVEA approximation*): Assuming that the wave propagation is dominantly in z-direction, and k_0 is taken in this direction. The SVEA is only applied to the second-order spatial derivatives in the z-direction and time. If $\nabla_\perp = \hat{\mathbf{e}}_x\partial/\partial x + \hat{\mathbf{e}}_y\partial/\partial y$ is the gradient in the x-y plane, the result is [1281],

$$k_0\frac{\partial\mathcal{E}_0}{\partial z} + \omega_0\mu_0\varepsilon_0\frac{\partial\mathcal{E}_0}{\partial t} - \tfrac{1}{2}\imath\nabla_\perp^2\mathcal{E}_0 = 0\ .$$

This is a parabolic partial differential equation. This equation has enhanced validity as compared to the full SVEA: it represents waves propagating in directions significantly different from the z-direction. It is the starting point of the theory of Gaussian beams, which will be studied in Sec. 18.4.1.

18.1.5 Plane waves in linear dielectrics and the refractive index

In dielectric (non-conducting) media we have $\varrho = 0$ and $\mathbf{j} = 0$ but $\dot{\vec{\mathcal{E}}}, \dot{\vec{\mathcal{B}}} \neq 0$. If the medium is linear and homogeneous, the permittivity ε and the permeability μ are constant, and we can substitute $\vec{\mathcal{D}} = \varepsilon\vec{\mathcal{E}}$ and $\vec{\mathcal{H}} = \mu^{-1}\vec{\mathcal{B}}$. Thus, Maxwell's equations (17.56) become equal to those holding for vacuum (17.6) but with the generalizations $\varepsilon_0 \to \varepsilon$ and $\mu_0 \to \mu$. Therefore, the wave equations remain valid,

$$\left(\frac{1}{c_n^2}\frac{\partial^2}{\partial t^2} - \nabla^2\right)\vec{\mathcal{E}} = 0 = \left(\frac{1}{c_n^2}\frac{\partial^2}{\partial t^2} - \nabla^2\right)\vec{\mathcal{B}}\ , \tag{18.38}$$

with the propagation velocity now reading,

$$c_n = \frac{1}{\sqrt{\varepsilon\mu}} = \frac{c}{n}\ , \tag{18.39}$$

where we defined the index of refraction,

$$n \equiv \sqrt{\frac{\varepsilon\mu}{\varepsilon_0\mu_0}}\ . \tag{18.40}$$

In dielectric media, we must use the original definitions for the energy and momentum densities and flows (17.58). The polarization and magnetization of the medium may cause new phenomena. For example, in anisotropic optical media the Poynting vector is not necessarily parallel to the wave vector. Resolve the Excs. 18.1.8.17 to 18.1.8.22.

18.1.6 Reflection and transmission by interfaces and Fresnel's formulas

So far we have considered homogenous media. An interesting question is, what happens when a field traverses regions characterized by different ε and μ. The boundary

conditions can be discussed from the integral form of the Maxwell equations, which follow immediately from the differential form via the theorems of Gauss and Stokes:

$$\begin{array}{lrcl} \text{(i)} & \oint_{\partial\mathcal{S}} \vec{\mathcal{H}} \cdot d\mathbf{l} & = & \frac{d}{dt}\int_{\mathcal{S}} \vec{\mathcal{D}} \cdot d\mathbf{S} + I_{enc} \\ \text{(ii)} & \oint_{\partial\mathcal{S}} \vec{\mathcal{E}} \cdot d\mathbf{l} & = & -\frac{d}{dt}\int_{\mathcal{S}} \vec{\mathcal{B}} \cdot d\mathbf{S} \\ \text{(iii)} & \oint_{\partial\mathcal{V}} \vec{\mathcal{D}} \cdot d\mathbf{S} & = & Q_{enc} \\ \text{(iv)} & \oint_{\partial\mathcal{V}} \vec{\mathcal{B}} \cdot d\mathbf{S} & = & 0 \end{array} \quad . \tag{18.41}$$

Let us consider two media with different permittivities $\varepsilon_{1,2}$ and permeabilities $\mu_{1,2}$ joined together at an interface. The closed path $\partial\mathcal{S}$ around a surface $\mathcal{S}$ and the closed surface $\partial\mathcal{V}$ around a volume $\mathcal{V}$ are chosen such as to cross the interface, as illustrated in Figs. 13.12 and 15.17. The surface integrals in equations (i) and (ii) vanish in the limit, where we choose the path $\partial\mathcal{S}$ very close to the interface.

From these equations, and as already shown in the derivations of the static equations (13.37), (13.39), (15.30), and (15.32), we have for linear media and in the absence of free surface charges σ_f and free surface currents $\mathbf{k}_f$,

$$\begin{array}{lrcl} \text{(i)} & \frac{1}{\mu_1}\vec{\mathcal{B}}_1^{\parallel} - \frac{1}{\mu_2}\vec{\mathcal{B}}_2^{\parallel} & = & |\mathbf{k}_f \times \hat{\mathbf{e}}_n| \longrightarrow 0 \\ \text{(ii)} & \vec{\mathcal{E}}_1^{\parallel} - \vec{\mathcal{E}}_2^{\parallel} & = & 0 \\ \text{(iii)} & \varepsilon_1\vec{\mathcal{E}}_1^{\perp} - \varepsilon_2\vec{\mathcal{E}}_2^{\perp} & = & \sigma_f \longrightarrow 0 \\ \text{(iv)} & \vec{\mathcal{B}}_1^{\perp} - \vec{\mathcal{B}}_2^{\perp} & = & 0 \end{array} \quad . \tag{18.42}$$

We will use these equations to establish the theory of reflection and refraction.

18.1.6.1 Normal incidence

Electromagnetic waves can be guided by interfaces (waveguides). From Maxwell's equations we can deduce useful rules for the behavior of waves near interfaces. First, we consider a plane wave propagating in the direction z within a dielectric medium characterized by the refraction index n_1,

$$\vec{\mathcal{E}}_i(z,t) = \hat{\mathbf{e}}_x \mathcal{E}_i e^{\imath(k_{z1}z - \omega t)} \quad , \quad \vec{\mathcal{B}}_i(z,t) = \hat{\mathbf{e}}_y \frac{n_1 \mathcal{E}_i}{c} e^{\imath(k_{z1}z - \omega t)} \; . \tag{18.43}$$

At position $z = 0$ there be a partially reflecting interface, as shown in Fig. 18.2(a). The reflected part is,

$$\vec{\mathcal{E}}_r(z,t) = \hat{\mathbf{e}}_x \mathcal{E}_r e^{\imath(-k_{z1}z - \omega t)} \quad , \quad \vec{\mathcal{B}}_r(z,t) = -\hat{\mathbf{e}}_y \frac{n_1 \mathcal{E}_r}{c} e^{\imath(-k_{z1}z - \omega t)} \; . \tag{18.44}$$

The negative sign comes from the relation $\vec{\mathcal{B}}(\mathbf{r},t) = \frac{1}{c}\mathbf{k} \times \vec{\mathcal{E}}(\mathbf{r},t)$. The transmitted part is,

$$\vec{\mathcal{E}}_t(z,t) = \hat{\mathbf{e}}_x \mathcal{E}_t e^{\imath(k_{z2}z - \omega t)} \quad , \quad \vec{\mathcal{B}}_r(z,t) = \hat{\mathbf{e}}_y \frac{n_2 \mathcal{E}_t}{c} e^{\imath(k_{z2}z - \omega t)} \; . \tag{18.45}$$

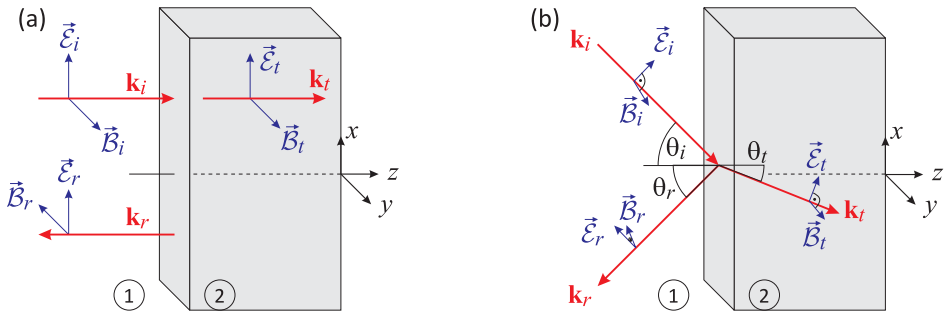

Figure 18.2: Electric and magnetic fields reflected and transmitted at an interface under (a) normal and (b) inclined incidence.

At the position $z = 0$ the total radiation must satisfy the boundary conditions. Since under normal incidence, there are only parallel components,

$$\vec{\mathcal{E}}_i(0,t) + \vec{\mathcal{E}}_r(0,t) = \vec{\mathcal{E}}_t(0,t) \quad , \quad \tfrac{1}{\mu_1}[\vec{\mathcal{B}}_i(0,t) + \vec{\mathcal{B}}_r(0,t)] = \tfrac{1}{\mu_2}\vec{\mathcal{B}}_t(0,t) \ . \tag{18.46}$$

Dividing all terms by $e^{-\imath\omega t}$,

$$\mathcal{E}_i + \mathcal{E}_r = \mathcal{E}_t \quad , \quad \tfrac{n_1}{\mu_1 c}[\mathcal{E}_i - \mathcal{E}_r] = \tfrac{n_2}{\mu_2 c}\mathcal{E}_t \ . \tag{18.47}$$

Solving the system of equations,

$$\boxed{\frac{\mathcal{E}_r}{\mathcal{E}_i} = \frac{1-\beta}{1+\beta} \quad , \quad \frac{\mathcal{E}_t}{\mathcal{E}_i} = \frac{2}{1+\beta}} \ , \tag{18.48}$$

defining

$$\beta \equiv \frac{\mu_1 n_2}{\mu_2 n_1} \ . \tag{18.49}$$

Example 99 (*Reflection on an air-glass interface*): We consider an air-glass interface, $n_1 = 1$ and $n_2 = 1.5$. Taking $\mu_1 = \mu_2 = \mu_0$ we have $\beta = 1.5$, and we calculate that the interface reflects the energy,

$$R \equiv \frac{I_r}{I_i} = \frac{\varepsilon_1 c_1 |\vec{\mathcal{E}}_r|^2}{\varepsilon_1 c_1 |\vec{\mathcal{E}}_i|^2} = \left(\frac{1-\beta}{1+\beta}\right)^2 = 0.04 \ ,$$

and transmits the energy,

$$T \equiv \frac{I_t}{I_i} = \frac{\varepsilon_2 c_2 |\vec{\mathcal{E}}_t|^2}{\varepsilon_1 c_1 |\vec{\mathcal{E}}_i|^2} = \frac{\varepsilon_2 c_2}{\varepsilon_1 c_1}\left(\frac{2}{1+\beta}\right)^2 = 0.96 \ .$$

We check $R + T = 1$.

18.1.6.2 Inclined incidence and geometric optics

When the wave strikes perpendicular to the interface, the polarization of the light is irrelevant. This is no longer true for inclined incidence, as shown in Fig. 18.2(b). In this case the Eqs. (18.43)-(18.45) must be generalized,

$$\vec{\mathcal{E}}_m(\mathbf{r},t) = \vec{\mathcal{E}}_{0m} e^{\imath(\mathbf{k}_m \cdot \mathbf{r} - \omega t)} \quad , \quad \vec{\mathcal{B}}_m(\mathbf{r},t) = \frac{n_m}{c}\hat{\mathbf{k}}_m \times \vec{\mathcal{E}}_m(\mathbf{r},t) \ , \tag{18.50}$$

for $m = i, r, t$. Obviously the frequency is the same for all waves, such that by inserting each wave into the wave equation we find,

$$k_i c_i = k_r c_r = k_t c_t = \omega \ , \tag{18.51}$$

with $c_m \equiv c/n_m$ and $c_i = c_r \equiv c_1$ and $c_t \equiv c_2$. We now need to join the fields $\vec{\mathcal{E}}_i + \vec{\mathcal{E}}_r$ and $\vec{\mathcal{B}}_i + \vec{\mathcal{B}}_r$ of one side of the interface with the fields $\vec{\mathcal{E}}_t$ and $\vec{\mathcal{B}}_t$ of the other side at the plane $z = 0$, respecting the boundary conditions (18.42). We get generic expressions,

$$(\cdot) e^{\imath(\mathbf{k}_i \cdot \mathbf{r} - \omega t)} + (\cdot) e^{\imath(\mathbf{k}_r \cdot \mathbf{r} - \omega t)} = (\cdot) e^{\imath(\mathbf{k}_t \cdot \mathbf{r} - \omega t)} \qquad \text{at} \qquad z = 0 \tag{18.52}$$

at all times t, where $(\cdot) \equiv \varepsilon_m \vec{\mathcal{E}}_m^{\perp}, \vec{\mathcal{E}}_m^{\parallel}, \vec{\mathcal{B}}_m^{\perp}, \frac{1}{\mu_m} \vec{\mathcal{B}}_m^{\parallel}$. Since the equation (18.52) must be valid at any point (x, y) of the plane $z = 0$, the exponential factors must be equal,

$$e^{\imath \mathbf{k}_i \cdot \mathbf{r}} = e^{\imath \mathbf{k}_r \cdot \mathbf{r}} = e^{\imath \mathbf{k}_t \cdot \mathbf{r}} \ , \tag{18.53}$$

that is,

$$\boxed{\mathbf{k}_i \cdot \hat{\mathbf{e}}_x = \mathbf{k}_r \cdot \hat{\mathbf{e}}_x = \mathbf{k}_t \cdot \hat{\mathbf{e}}_x \qquad \text{and} \qquad \mathbf{k}_i \cdot \hat{\mathbf{e}}_y = \mathbf{k}_r \cdot \hat{\mathbf{e}}_y = \mathbf{k}_t \cdot \hat{\mathbf{e}}_y} \ , \tag{18.54}$$

that is, the wavevectors $\mathbf{k}_i$, $\mathbf{k}_r$, $\mathbf{k}_t$ and the normal vector $\hat{\mathbf{e}}_z$ of the interface are in the same plane. We can orient the coordinate system such that $\mathbf{k}_i \cdot \hat{\mathbf{e}}_y \equiv 0$ (see Fig. 18.2). Defining the angles of incidence, reflection and refraction, we find,

$$\mathbf{k}_m \cdot \hat{\mathbf{e}}_x = k_i \sin\theta_i = k_r \sin\theta_r = k_t \sin\theta_t \ . \tag{18.55}$$

With (18.51) we deduce the *law of reflection*:

$$\boxed{\theta_i = \theta_r} \ , \tag{18.56}$$

and the *law of refraction* or *Snell's law*:

$$\boxed{\frac{\sin\theta_t}{\sin\theta_i} = \frac{n_1}{n_2}} \ . \tag{18.57}$$

The equations (18.54), (18.56), and (18.57) form the basis of geometric optics.

18.1.6.3 Polarization behavior and Fresnel's formulas

Going back to the condition (18.52) and eliminating the exponentials, we get,

$$\begin{aligned}
\text{for } \vec{\mathcal{B}}_m^{\parallel} \ : \quad & \tfrac{1}{\mu_1} \vec{\mathcal{B}}_i \cdot \hat{\mathbf{e}}_{x,y} + \tfrac{1}{\mu_1} \vec{\mathcal{B}}_r \cdot \hat{\mathbf{e}}_{x,y} &&= \tfrac{1}{\mu_2} \vec{\mathcal{B}}_t \cdot \hat{\mathbf{e}}_{x,y} \\
\text{for } \vec{\mathcal{E}}_m^{\parallel} \ : \quad & \vec{\mathcal{E}}_i \cdot \hat{\mathbf{e}}_{x,y} + \vec{\mathcal{E}}_r \cdot \hat{\mathbf{e}}_{x,y} &&= \vec{\mathcal{E}}_t \cdot \hat{\mathbf{e}}_{x,y} \\
\text{for } \vec{\mathcal{E}}_m^{\perp} \ : \quad & \varepsilon_1 \vec{\mathcal{E}}_i \cdot \hat{\mathbf{e}}_z + \varepsilon_1 \vec{\mathcal{E}}_r \cdot \hat{\mathbf{e}}_z &&= \varepsilon_2 \vec{\mathcal{E}}_t \cdot \hat{\mathbf{e}}_z \\
\text{for } \vec{\mathcal{B}}_m^{\perp} \ : \quad & \vec{\mathcal{B}}_i \cdot \hat{\mathbf{e}}_z + \vec{\mathcal{B}}_r \cdot \hat{\mathbf{e}}_z &&= \vec{\mathcal{B}}_t \cdot \hat{\mathbf{e}}_z \ .
\end{aligned} \tag{18.58}$$

We again orient the coordinate system such that $\mathbf{k}_i \cdot \hat{\mathbf{e}}_y \equiv 0$. We first assume, that the polarization of the incident field is within the plane of incidence (that is, the

plane spanned by the vectors $\mathbf{k}_i$ and $\mathbf{k}_r$), that is, $\vec{\mathcal{E}}_i \cdot \hat{\mathbf{e}}_y = 0 = \vec{\mathcal{B}}_i \cdot \hat{\mathbf{e}}_x$. This is called *p-polarization*. In this case, the conditions (18.58) become,

$$\begin{aligned}
\tfrac{1}{\mu_1}\vec{\mathcal{B}}_i \cdot \hat{\mathbf{e}}_y + \tfrac{1}{\mu_1}\vec{\mathcal{B}}_r \cdot \hat{\mathbf{e}}_y = \tfrac{1}{\mu_1}\mathcal{B}_i + \tfrac{1}{\mu_1}\mathcal{B}_r = \tfrac{1}{\mu_1 c_1}(\mathcal{E}_i - \mathcal{E}_r) &\stackrel{!}{=} \tfrac{1}{\mu_2 c_2}\mathcal{E}_t = \tfrac{1}{\mu_2}\mathcal{B}_t = \tfrac{1}{\mu_2}\vec{\mathcal{B}}_t \cdot \hat{\mathbf{e}}_y \\
\vec{\mathcal{E}}_i \cdot \hat{\mathbf{e}}_x + \vec{\mathcal{E}}_r \cdot \hat{\mathbf{e}}_x = \mathcal{E}_i \cos\theta_i + \mathcal{E}_r \cos\theta_r = (\mathcal{E}_i + \mathcal{E}_r)\cos\theta_r &\stackrel{!}{=} \mathcal{E}_t \cos\theta_t = \vec{\mathcal{E}}_t \cdot \hat{\mathbf{e}}_x \\
\varepsilon_1 \mathcal{E}_i \sin\theta_i + \varepsilon_1 \mathcal{E}_r \sin\theta_r = \varepsilon_1(\mathcal{E}_i - \mathcal{E}_r)\sin\theta_i &\stackrel{!}{=} \varepsilon_2 \mathcal{E}_t \sin\theta_t \\
0 &\stackrel{!}{=} 0 \ .
\end{aligned} \tag{18.59}$$

Using the abbreviation (18.49) and introducing another abbreviation,

$$\alpha \equiv \frac{\cos\theta_t}{\cos\theta_i} = \frac{\sqrt{1 - (n_1/n_2)^2 \sin^2\theta_i}}{\cos\theta_i} \ , \tag{18.60}$$

and solving the system of equations (18.59), we find *Fresnel's formula* for p-polarization [4],

$$\boxed{r_p \equiv \left.\frac{\mathcal{E}_r}{\mathcal{E}_i}\right|_p = \frac{\alpha - \beta}{\alpha + \beta} = \frac{n_1 \cos\theta_t - n_2 \cos\theta_i}{n_1 \cos\theta_t + n_2 \cos\theta_i} \quad \text{and} \quad t_p \equiv \left.\frac{\mathcal{E}_t}{\mathcal{E}_i}\right|_p = \frac{2}{\alpha + \beta}} \ . \tag{18.61}$$

We now assume that the polarization of the incident field is perpendicular to the plane of incidence, $\vec{\mathcal{E}}_i \cdot \hat{\mathbf{e}}_x = 0 = \vec{\mathcal{B}}_i \cdot \hat{\mathbf{e}}_y$. This is called *s-polarization*. In this case the equations (18.58) yield,

$$\begin{aligned}
\tfrac{1}{\mu_1}\vec{\mathcal{B}}_i \cdot \hat{\mathbf{e}}_x + \tfrac{1}{\mu_1}\vec{\mathcal{B}}_r \cdot \hat{\mathbf{e}}_x = \tfrac{1}{\mu_1 c_1}(\mathcal{E}_i \cos\theta_i - \mathcal{E}_r \cos\theta_r) &\stackrel{!}{=} \tfrac{1}{\mu_2 c_2}\mathcal{E}_t \cos\theta_t = \tfrac{1}{\mu_2}\vec{\mathcal{B}}_t \cdot \hat{\mathbf{e}}_x \\
\vec{\mathcal{E}}_i \cdot \hat{\mathbf{e}}_y + \vec{\mathcal{E}}_r \cdot \hat{\mathbf{e}}_y = \mathcal{E}_i + \mathcal{E}_r &\stackrel{!}{=} \mathcal{E}_t = \vec{\mathcal{E}}_t \cdot \hat{\mathbf{e}}_y \\
0 &\stackrel{!}{=} 0 \\
\mathcal{B}_i \sin\theta_i + \mathcal{B}_r \sin\theta_r = \tfrac{1}{c_1}(\mathcal{E}_i - \mathcal{E}_r)\sin\theta_i &\stackrel{!}{=} \tfrac{1}{c_2}\mathcal{E}_t \sin\theta_t = \mathcal{B}_t \sin\theta_t \ .
\end{aligned} \tag{18.62}$$

Similar to the case of p-polarization we obtain the Fresnel formulas for s-polarization,

$$\boxed{r_s \equiv \left.\frac{\mathcal{E}_r}{\mathcal{E}_i}\right|_s = -\frac{1 - \alpha\beta}{1 + \alpha\beta} = -\frac{n_1 \cos\theta_i - n_2 \cos\theta_t}{n_1 \cos\theta_i + n_2 \cos\theta_t} \quad \text{and} \quad t_s \equiv \left.\frac{\mathcal{E}_t}{\mathcal{E}_i}\right|_s = \frac{\sqrt{\alpha\beta}}{1 + \alpha\beta}} \ . \tag{18.63}$$

See also Exc. 18.1.8.23.

The power flux density incident on the interface is the projection of the intensity, $\vec{\mathcal{S}} \cdot \hat{\mathbf{e}}_z$. Therefore the intensities are,

$$I_m = \tfrac{1}{2}\varepsilon_1 c_m \mathcal{E}_m^2 \cos\theta_m \ , \tag{18.64}$$

[4] Using Snell's law (18.57) the Fresnel formulas can also be written as,

$$\begin{aligned}
r_p^2 &= \frac{\tan^2(\theta_i - \theta_t)}{\tan^2(\theta_i \theta_t)} \quad \text{and} \quad r_s^2 = \frac{\sin^2(\theta_i - \theta_t)}{\sin^2(\theta_i + \theta_t)} \\
t_p^2 &= \frac{\sin 2\theta_i \sin 2\theta_t}{\sin^2(\theta_i + \theta_t)\cos^2(\theta_i - \theta_t)} \quad \text{and} \quad t_s^2 = \frac{\sin 2\theta_i \sin 2\theta_t}{\sin^2(\theta_i + \theta_t)} \ .
\end{aligned}$$

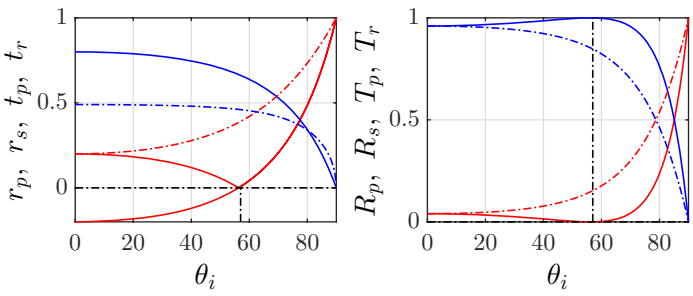

Figure 18.3: (code) Fresnel formulas for the transmitted (blue) and reflected (red) amplitude (left) and intensity (right). The dotted curve holds for s-polarization and the solid curve for p-polarization.

with $m = i, r, t$. Thus the reflection and the transmission are for p-polarization,

$$R_p = \left(\frac{\mathcal{E}_r}{\mathcal{E}_i}\right)_p^2 = \left(\frac{\alpha-\beta}{\alpha+\beta}\right)^2 \qquad \text{and} \qquad T_p = \frac{\varepsilon_2 c_2}{\varepsilon_1 c_1}\frac{\cos\theta_t}{\cos\theta_i}\left(\frac{\mathcal{E}_t}{\mathcal{E}_i}\right)_p^2 = \alpha\beta\left(\frac{2}{\alpha+\beta}\right)^2 = 1 - R_p \ . \tag{18.65}$$

For s-polarization we have,

$$R_s = \left(\frac{\mathcal{E}_r}{\mathcal{E}_i}\right)_s^2 = \left(\frac{1-\alpha\beta}{1+\alpha\beta}\right)^2 \qquad \text{and} \qquad T_s = \frac{\varepsilon_2 c_2}{\varepsilon_1 c_1}\frac{\cos\theta_t}{\cos\theta_i}\left(\frac{\mathcal{E}_t}{\mathcal{E}_i}\right)_s^2 = \alpha\beta\left(\frac{2}{1+\alpha\beta}\right)^2 = 1 - R_s \ . \tag{18.66}$$

18.1.6.4 The Brewster angle

For an angle of incidence of $\theta_i = 0°$ ($\alpha = 1$) we recover the expressions (18.48). For $\theta_i = 90°$ ($\alpha \to \infty$), all light is reflected. Looking at the formula (18.61) it is interesting to note the existence of an angle, where the reflection vanishes for the case of the s-polarization. It is given by $\alpha = \beta$, that is,

$$\sin^2\theta_{i,B} \equiv \sin^2\theta_i = \frac{1-\beta^2}{(n_1/n_2)^2 - \beta^2} \ . \tag{18.67}$$

θ_B is the *Brewster angle*. When $\mu_1 \simeq \mu_2$ we can simplify to,

$$\boxed{\theta_{i,B} = \arcsin\frac{1-\beta^2}{(n_1/n_2)^2-\beta^2} \simeq \arctan\frac{n_2}{n_1}} \ . \tag{18.68}$$

That is, a p-polarized beam of light traveling in a vacuum and encountering a dielectric with refractive index $n_2 = 1.5$ under the angle of $\theta_{i,B} \approx 56.3°$ is fully transmitted. This is seen in Fig. 18.3(right), where the reflected intensity I_r/I_0 of p-polarized light vanishes at a specific angle, and illustrated in Fig. 18.4(a).

18.1.6.5 Internal total reflection and the Goos-Hänchen shift

We now consider a light beam traveling in a dielectric with refractive index n_1 and encountering an interface to an optically less dense medium, $n_2 < n_1$, as illustrated

in Fig. 18.4(b). Increasing the angle of incidence θ_i, according to Snell's law (18.57) we will come to a point, where the outgoing angle reaches $\theta_t = 90°$. Snell's law gives the critical angle for this to happen,

$$\boxed{\theta_{i,tot} = \arcsin \frac{n_2}{n_1}} \ . \tag{18.69}$$

For an index of refraction $n_1 = 1.5$ this angle is $\theta_{i,tot} \approx 41.8°$. Above this angle, $\theta_i > \theta_{i,tot}$, all energy is reflected by the optically denser medium. This phenomenon of *total internal reflection* is used e.g. to guide light in optical fibers. Nevertheless, the fields do not completely disappear in the medium 2 but form, a so-called *evanescent wave*, which is exponentially attenuated and does not carry energy into the medium 2. A quick way to construct the evanescent wave consists in simply extending to the complex domain the formulas obtained for inclined incidence of light on interfaces. For $\theta_i > \theta_{i,tot}$,

$$\sin\theta_t = \frac{n_1}{n_2}\sin\theta_i > \frac{n_1}{n_2}\sin\theta_{i,tot} = \sin\theta_{t,tot} = 1 \ , \tag{18.70}$$

Obviously θ_t can no longer be interpreted as an angle! We will show in Exc. 18.1.8.24 that, for the geometry illustrated in Fig. 18.4(b), the electric field generated in region 2 is given by,

$$\vec{\mathcal{E}}_t(\mathbf{r},t) = \vec{\mathcal{E}}_0 e^{-\kappa z} e^{\imath(kx-\omega t)} \ , \tag{18.71}$$

where

$$\kappa \equiv \tfrac{\omega}{c}\sqrt{(n_1\sin\theta_i)^2 - n_2^2} \qquad \text{and} \qquad k \equiv \tfrac{\omega n_1}{c}\sin\theta_i \ . \tag{18.72}$$

(18.71) is a wave propagating in x-direction, parallel to the interface, and being

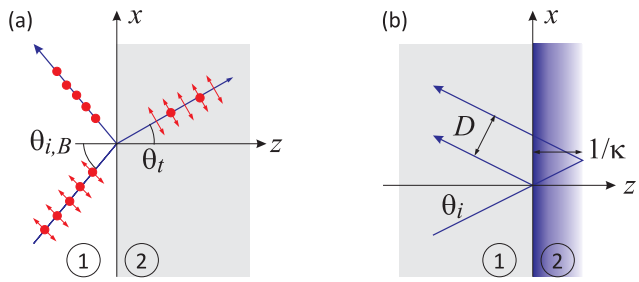

Figure 18.4: (a) Illustration of the effect of the Brewster angle on the polarization of light. (b) Illustration of the Goos-Hänchen shift.

attenuated in z-direction. The penetration depth of is κ^{-1}. Also in Exc. 18.1.8.24 we will show that for both polarizations p and s the reflection coefficient is 1, which confirms that there is no energy transported into the medium 2.

Example 100 (*The Goos-Hänchen shift*): The fact that the light wave penetrates region 2 up to a depth of κ^{-1} causes a transverse displacement of the wave known as *Goos-Hänchen shift* named after *Gustav Goos* and *Hilda Hänchen*. From Fig. 18.4 it is easy to verify that this displacement is of the order of magnitude $D \simeq \frac{2}{\kappa}\sin\theta_i$. It can be measured taking a beam of light with finite radial extent.

18.1.7 Transfer matrix formalism

For a propagating wave the amplitude of the field at a point $z = 0$ can be related to another point z via $\vec{\mathcal{E}}_z = M\vec{\mathcal{E}}_0$, where M is a phase factor of the type $e^{\imath kz}$. A counter-propagating wave (e.g. generated by partial reflection at an interface) suffers, over the same distance, a phase shift of $e^{-\imath kz}$. Since both waves interfere, it is useful to set up a model describing in a compact manner the amplitude and phase variations of the two counterpropagating waves along the optical axis. The *transfer matrix formalism* represents such a model.

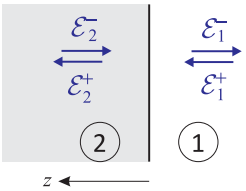

Figure 18.5: Illustration of the transfer matrix formalism.

18.1.7.1 The $\mathcal{T}$-matrix

Let us consider a beam of light propagating along the z-axis toward $+\infty$ through an inhomogeneous dielectric medium described by the refractive index $n(z)$. Each interface where the refractive index varies causes a partial reflection of the beam into the opposite direction. The fields reflected at different positions z interfere constructively or destructively depending on the accumulated phase. To address the problem mathematically, we divide the medium into layers treated as homogeneous and delimited by interfaces located at positions z, as shown in Fig. 18.5. We define the complex transfer matrix $\mathcal{T}_{12}$ describing the transition between from medium 1 to medium 2 by,

$$\boxed{\begin{pmatrix}\mathcal{E}_2^+\\ \mathcal{E}_2^-\end{pmatrix} = \mathcal{T}_{12}\begin{pmatrix}\mathcal{E}_1^+\\ \mathcal{E}_1^-\end{pmatrix}}\,. \tag{18.73}$$

Here, the fields $\mathcal{E}^\pm$ propagate toward $\pm\infty$. That is, the fields $\mathcal{E}_1^+$ and $\mathcal{E}_2^-$ move toward the interface and the fields $\mathcal{E}_1^-$ and $\mathcal{E}_2^+$ move away from the interface. In (18.48) we showed that the reflectivity and the transmissivity of the interface for a transition from region 1 to region 2 are given by,

$$r_{12} = \frac{n_1 - n_2}{n_1 + n_2} \qquad \text{and} \qquad t_{12} = \frac{2n_1}{n_1 + n_2}\,. \tag{18.74}$$

Obviously, we have $r_{21} = -r_{12}$ and $t_{21} = \frac{n_2}{n_1}t_{12}$. Therefore,

$$\mathcal{E}_2^+ = t_{12}\mathcal{E}_1^+ + r_{21}\mathcal{E}_2^- \qquad \text{and} \qquad \mathcal{E}_1^- = t_{21}\mathcal{E}_2^- + r_{12}\mathcal{E}_1^+\,, \tag{18.75}$$

that is,

$$\mathcal{E}_2^+ = \left(t_{12} - \tfrac{r_{12}r_{21}}{t_{21}}\right)\mathcal{E}_1^+ + \tfrac{r_{21}}{t_{21}}\mathcal{E}_1^- \qquad \text{and} \qquad \mathcal{E}_2^- = -\tfrac{r_{12}}{t_{21}}\mathcal{E}_1^+ + \tfrac{1}{t_{21}}\mathcal{E}_1^-\,. \tag{18.76}$$

The matrix, therefore, is,

$$\boxed{\mathcal{T}_{12} = \begin{pmatrix} t_{12} - \frac{r_{12}r_{21}}{t_{21}} & \frac{r_{21}}{t_{21}} \\ -\frac{r_{12}}{t_{21}} & \frac{1}{t_{21}} \end{pmatrix} = \frac{1}{2n_2}\begin{pmatrix} n_2+n_1 & n_2-n_1 \\ n_2-n_1 & n_2+n_1 \end{pmatrix}} \,. \tag{18.77}$$

The determinant is $\det \mathcal{T} = \frac{t_{12}}{t_{21}} = \frac{n_1}{n_2}$.

The simple propagation over a distance Δz through a homogeneous medium simply causes a phase shift, since $\mathcal{E}_z^+ = e^{\imath kz}\mathcal{E}_0^+$ and $\mathcal{E}_0^- = e^{\imath kz}\mathcal{E}_z^-$. The corresponding transfer matrix is,

$$\boxed{\mathcal{T}_{\Delta z} = \begin{pmatrix} e^{\imath k\Delta z} & 0 \\ 0 & e^{-\imath k\Delta z} \end{pmatrix}} \,. \tag{18.78}$$

Absorption losses can attenuate the beam. This can be taken into account via an absorption coefficient α in the matrix,

$$\boxed{\mathcal{T}_{abs} = \begin{pmatrix} e^{-\alpha} & 0 \\ 0 & e^{\alpha} \end{pmatrix}} \,. \tag{18.79}$$

satisfying $\det \mathcal{T} = 1$.

18.1.7.2 AR and HR coating

Concatenating the matrices (18.77) and (18.78), $\mathcal{M} = \mathcal{T}_{\Delta z}\mathcal{T}_{12}\mathcal{T}_{abs}$, we can now describe the transmission of a light beam through a dielectric layer with refractive index n_2 and thickness Δz.

Example 101 (*Anti-reflection coating*): Here we consider the transition between a medium n_0 through a thin layer n_1 of thickness $\lambda/4$ to a medium n_2. The transition is described by the concatenation of three matrices,

$$\begin{pmatrix} \mathcal{E}_2^+ \\ 0 \end{pmatrix} = \mathcal{T}_{12}\mathcal{T}_{\lambda/4}\mathcal{T}_{01}\begin{pmatrix} \mathcal{E}_0^+ \\ \mathcal{E}_0^- \end{pmatrix} = \begin{pmatrix} M_{11} & M_{12} \\ M_{21} & M_{22} \end{pmatrix}\begin{pmatrix} \mathcal{E}_0^+ \\ \mathcal{E}_0^- \end{pmatrix} = \begin{pmatrix} M_{11} - \frac{M_{12}M_{21}}{M_{22}} \\ 0 \end{pmatrix}\mathcal{E}_0^+ \,.$$

The total matrix is,

$$\begin{aligned} \mathcal{M} &= \frac{1}{2n_2}\begin{pmatrix} n_2+n_1 & n_2-n_1 \\ n_2-n_1 & n_2+n_1 \end{pmatrix}\begin{pmatrix} e^{\imath\pi/2} & 0 \\ 0 & e^{-\imath\pi/2} \end{pmatrix}\frac{1}{2n_1}\begin{pmatrix} n_1+n_0 & n_1-n_0 \\ n_1-n_0 & n_1+n_0 \end{pmatrix} \\ &= \frac{\imath}{2n_1n_2}\begin{pmatrix} n_1^2+n_0n_2 & n_1^2-n_0n_2 \\ -n_1^2+n_0n_2 & -n_1^2-n_0n_2 \end{pmatrix} \,. \end{aligned}$$

Finally, we obtain the fields,

$$\begin{aligned} \mathcal{E}_2^+ &= M_{11} - \frac{M_{12}M_{21}}{M_{22}}\mathcal{E}_0^+ = \frac{2in_0n_1}{n_1^2+n_0n_2}\mathcal{E}_0^+ \overset{n_1^2\equiv n_0n_2}{\longrightarrow} \frac{in_0}{n_1}\mathcal{E}_0^+ \\ \mathcal{E}_0^- &= -\frac{M_{21}}{M_{22}}\mathcal{E}_0^+ = \frac{n_1^2-n_0n_2}{n_1^2+n_0n_2}\mathcal{E}_0^+ \overset{n_1^2\equiv n_0n_2}{\longrightarrow} 0 \,. \end{aligned}$$

Choosing $n_1^2 \equiv n_0 n_2$ we can cancel out the reflection and maximize the transmission. We check,

$$T = \frac{I_t}{I_i} = \frac{\varepsilon_2 c_2 |\mathcal{E}_2^+|^2}{\varepsilon_0 c_0 |\mathcal{E}_0^+|^2} = \frac{\frac{n_2^2}{c^2}\frac{c}{n_2}\left|\frac{2\imath n_0 n_1}{n_1^2+n_0 n_2}\right|^2}{\frac{n_0^2}{c^2}\frac{c}{n_0}} = \frac{4 n_0 n_1^2 n_2}{(n_1^2+n_0 n_2)^2}$$

$$R = \frac{I_r}{I_i} = \frac{\varepsilon_0 c_0 |\mathcal{E}_0^-|^2}{\varepsilon_0 c_0 |\mathcal{E}_0^+|^2} = \left|\frac{n_1^2 - n_0 n_2}{n_1^2 + n_0 n_2}\right|^2 = 1 - T \ .$$

Fig. 18.6 shows the transmission through a stack of dielectric layers. The transfer matrix is,

$$\mathcal{M} = (\mathcal{T}_{21}\mathcal{T}_{\Delta z_2}\mathcal{T}_{abs}\mathcal{T}_{12}\mathcal{T}_{\Delta z_1}\mathcal{T}_{abs})^N \mathcal{T}_{01} \ . \tag{18.80}$$

We observe a large reflection band (600..660 nm) called one-dimensional *photonic band gap*. Dielectric mirrors can, nowadays, achieve reflections up to $R = 99.9995\%$, while the reflectivity of metal mirrors is always limited by losses.

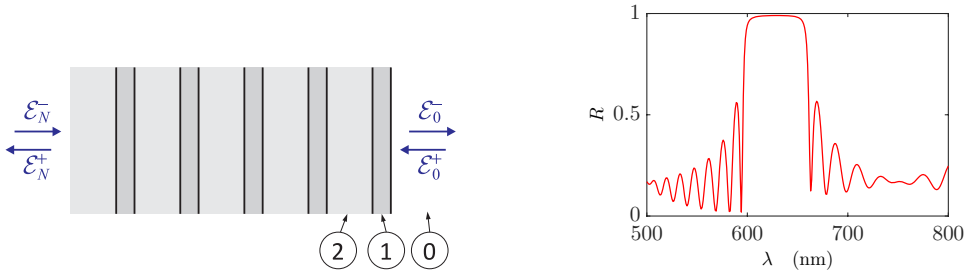

Figure 18.6: (code) Reflection by a high reflecting mirror made of 10 layers with $n_1 = 2.4$ and $\Delta z_1 = 80$ nm alternating with 10 layers with $n_2 = 1.5$ and $\Delta z_2 = 500$ nm. The absorption coefficient for each layer is supposed to be $\alpha = 0.2\%$. The beam impinges from vacuum, $n_0 = 1$.

Example 102 (*Use of transfer matrices in cavities*): The transfer matrix formalism can be used for *impedance matching* the reflection of optical cavities [5]. In order to deserve the label *mode*, a geometric configuration of a cavity must be self-consistent, that is, any field $\mathcal{E}^{\pm}(z)$ wanting to fill the mode must be the same after a round-trip around the cavity.
We proceed to calculating the real and imaginary parts of the transfer matrices,

$$\begin{pmatrix} \mathcal{E}_z^+ + \mathcal{E}_z^- \\ \mathcal{E}_z^+ - \mathcal{E}_z^- \end{pmatrix} = \mathcal{M} \begin{pmatrix} \mathcal{E}_0^+ + \mathcal{E}_0^- \\ \mathcal{E}_0^+ - \mathcal{E}_0^- \end{pmatrix} \ .$$

For example, the phase shift due to free space propagation is described by the matrix,

$$\mathcal{M}_{phase} = \begin{pmatrix} \cos kz & \imath \sin kz \\ \imath \sin kz & \cos kz \end{pmatrix} \ .$$

[5] Not to be confused with *phase matching* of optical cavities, which is an important requirement for coupling light efficiently into a cavity, but must be treated within the theory of Gaussian optics.

Reflection and transmission from a classical object with can be written as, $\vec{\mathcal{E}}_z^+ = t_a\mathcal{E}_0^+ + r_a\vec{\mathcal{E}}_z^-$ and $\mathcal{E}_0^- = t_a\vec{\mathcal{E}}_z^- - r_a\mathcal{E}_0^+$, where $r_a^2 + t_a^2 = 1$. Transforming to the basis $\mathcal{E}_j^+ \pm \mathcal{E}_j^-$, we obtain,

$$\mathcal{M}_{pump} = \begin{pmatrix} \frac{1+r_a}{t_a} & 0 \\ 0 & \frac{1-r_a}{t_a} \end{pmatrix} .$$

Let us assume that the cavity is pumped from one side by the field $\mathcal{E}_{in}$. We get after a round-trip,

$$\begin{pmatrix} \mathcal{E}^+ + \mathcal{E}^- \\ \mathcal{E}^+ - \mathcal{E}^- \end{pmatrix} = \mathcal{M} \begin{pmatrix} \mathcal{E}^+ + \mathcal{E}^- \\ \mathcal{E}^+ - \mathcal{E}^- \end{pmatrix} + t_{in} \begin{pmatrix} \mathcal{E}_{in}^+ + \mathcal{E}_{in}^- \\ \mathcal{E}_{in}^+ - \mathcal{E}_{in}^- \end{pmatrix} = t_{in}(1-\mathcal{M})^{-1} \begin{pmatrix} \mathcal{E}_{in}^+ + \mathcal{E}_{in}^- \\ \mathcal{E}_{in}^+ - \mathcal{E}_{in}^- \end{pmatrix} .$$

The phase minimum of the determinant $\det(1-\mathcal{M})$ determines the eigenvalues of the cavity. For a round-trip with losses in the mirrors the determinant is $\det(1 - \mathcal{M}_{phase}\mathcal{M}_{loss}) = 2 - (t_c + t_c^{-1})\cos\phi$, where t_c is the total transmission coefficient of the cavity. Phase minima always occur when $\phi = 2\pi n$. The amplification of the intensity at theses phases is given by,

$$\frac{I_{cav}}{I_{in}} = \frac{|\mathcal{E}^+ + \mathcal{E}^-|^2}{|\mathcal{E}_{in}^+ + \mathcal{E}_{in}^-|^2} = \frac{t_{in}^2}{(1-t_c)^2} .$$

Exc. 18.1.8.25 can be solved using transfer matrices.

The transfer matrix formalism can also be applied to modeling the passage of a laser beam through a gas of two levels atoms periodically organized in one dimension like a stack of pancakes [1220, 1158]. One only has to consider that the variation of the density of the gas along the optical axis generates a spatial modulation of the refractive index [6].

18.1.8 Exercises

18.1.8.1 Ex: Wave equation and Galilei transform

Show that any function of the form $y(x,t) = f(x-vt)$ or $y(x,t) = g(x+vt)$ satisfies the wave equation.

Solution: *We have,*

$$\frac{1}{v^2}\frac{\partial^2 y}{\partial t^2} + \frac{\partial^2 y}{\partial x^2} = \frac{1}{v^2}\frac{\partial^2 f(x-vt)}{\partial t^2} + \frac{\partial^2 f(x-vt)}{\partial x^2} = \frac{1}{v^2}\frac{\partial}{\partial t}(-v)f' + \frac{\partial}{\partial x}f' = \frac{1}{v^2}(-v)^2 f'' + f'' = 0 .$$

[6] We will discuss this system in Sec. 39.4.2 .

18.1.8.2 Ex: Plane waves

Consider a set of solutions for plane electromagnetic waves in vacuum, whose fields (electric or magnetic) are described by the real part of the functions $\mathbf{u}(\mathbf{r},t) = \mathbf{A}e^{\imath(\mathbf{k}\cdot\mathbf{r}-\omega t)}$, with constant phase $(\mathbf{k}\cdot\mathbf{r}-\omega t)$. In these expressions, $\mathbf{k}$ is the wavevector (determining the propagation direction of the wave) and $\omega = vk$ is the angular frequency, where $v = 1/\sqrt{\varepsilon\mu}$ is the propagation velocity of the waves.
a. Show that the divergent $\mathbf{u}(x,t)$ satisfies: $\nabla\cdot\mathbf{u} = \imath\mathbf{k}\cdot\mathbf{u}$;
b. Show that the rotation $\mathbf{u}(x,t)$ satisfies: $\nabla\times\mathbf{u} = \imath\mathbf{k}\times\mathbf{u}$;
c. Show that the waves are transverse and that the vectors $\vec{\mathcal{E}}$, $\vec{\mathcal{B}}$, and $\mathbf{k}$ are mutually perpendicular.

Solution: *a. First, we note that* $\mathbf{u}(\mathbf{r},t) = \mathbf{A}e^{\imath(k_x x+k_y y+k_z z-\omega t)}$. *Hence,*

$$\begin{aligned}\frac{\partial}{\partial x}\mathbf{u}(\mathbf{r},t) &= \imath k_x\mathbf{A}e^{\imath(k_x x+k_y y+k_z z-\omega t)}\\ \frac{\partial}{\partial y}\mathbf{u}(\mathbf{r},t) &= \imath k_y\mathbf{A}e^{\imath(k_x x+k_y y+k_z z-\omega t)}\\ \frac{\partial}{\partial z}\mathbf{u}(\mathbf{r},t) &= \imath k_z\mathbf{A}e^{\imath(k_x x+k_y y+k_z z-\omega t)}\ ,\end{aligned}$$

which can be generalized in the form:

$$\frac{\partial}{\partial x_j}\mathbf{u}(\mathbf{r},t) = \imath k_j\mathbf{A}e^{\imath(\sum_j k_j x_j-\omega t)}\ .$$

thus, the divergent is:

$$\nabla\cdot\mathbf{u} = \sum_j \frac{\partial}{\partial x_j}u_j(\mathbf{r},t) = \imath k_x A_x e^{\imath(\mathbf{k}\cdot\mathbf{r}-\omega t)} + \imath k_y A_y e^{\imath(\mathbf{k}\cdot\mathbf{r}-\omega t)} + \imath k_z A_z e^{\imath(\mathbf{k}\cdot\mathbf{r}-\omega t)} = \imath\mathbf{k}\cdot\mathbf{u}\ .$$

Therefore,

$$\nabla\cdot\mathbf{u} = \imath\mathbf{k}\cdot\mathbf{u}\ .$$

b. This can be proved analogously by calculating the determinant or the properties of the Levi-Civita tensor:

$$(\nabla\times\mathbf{u})_i = \epsilon_{ijk}\frac{\partial}{\partial x_j}u_k = \epsilon_{ijk}\frac{\partial}{\partial x_j}A_k e^{\imath(\mathbf{k}\cdot\mathbf{r}-\omega t)} = \epsilon_{ijk}(\imath k_j)A_k e^{\imath(\mathbf{k}\cdot\mathbf{r}-\omega t)} = \imath\epsilon_{ijk}k_j u_k = \imath(\mathbf{k}\times\mathbf{u})_i\ .$$

If it holds for the component i, it holds for every component:

$$\nabla\times\mathbf{u} = \imath\mathbf{k}\times\mathbf{u}\ .$$

c. Since $\vec{\mathcal{E}}(\mathbf{r},t)$ *and* $\vec{\mathcal{B}}(\mathbf{r},t)$ *are described by the real part of* $\mathbf{u}(\mathbf{r},t)$, *we get,*

$$\begin{aligned}\vec{\mathcal{E}}(\mathbf{r},t) &= \mathfrak{Re}\ [\hat{\mathbf{e}}_0 e^{\imath(\mathbf{k}\cdot x-\omega t)}]\\ \vec{\mathcal{B}}(\mathbf{r},t) &= \mathfrak{Re}\ [\vec{\mathcal{B}}_0 e^{\imath(\mathbf{k}\cdot x-\omega t)}]\ .\end{aligned}$$

Thus, using the result of item (a) and the divergence equations, we have:

$$\nabla \cdot \vec{\mathcal{E}}(\mathbf{r},t) = 0 \implies \mathbf{k} \cdot \vec{\mathcal{E}} = 0$$
$$\nabla \cdot \vec{\mathcal{B}}(\mathbf{r},t) = 0 \implies \mathbf{k} \cdot \vec{\mathcal{B}} = 0 \ .$$

from what we conclude, that the waves are transverse, that is, $\vec{\mathcal{E}}$ and $\vec{\mathcal{B}}$ are perpendicular to $\mathbf{k}$. We also verify that the time derivative of $\mathbf{u}(\mathbf{r},t)$ satisfies:

$$\frac{\partial}{\partial t}\mathbf{u}(\mathbf{r},t) = -\imath\omega\mathbf{A}e^{\imath(k_x x + k_y y + k_z z - \omega t)} = -\imath\omega\mathbf{u}(\mathbf{r},t) \ .$$

(Just do one of the following options:)
And, similarly, using the result of item (b) and Ampère's equation, we have:

$$\nabla \times \vec{\mathcal{B}}(\mathbf{r},t) = \mu\varepsilon\frac{\partial}{\partial t}\vec{\mathcal{E}}(\mathbf{r},t) \implies \imath\mathbf{k} \times \vec{\mathcal{B}} = -\imath\omega\mu\varepsilon\vec{\mathcal{E}} \implies \vec{\mathcal{E}} = -\frac{\mathbf{k} \times \vec{\mathcal{B}}}{k\sqrt{\mu\varepsilon}} \ .$$

And, similarly, using the result of item (b) and Faraday's equation, we have:

$$\nabla \times \vec{\mathcal{E}}(\mathbf{r},t) = -\frac{\partial}{\partial t}\vec{\mathcal{B}}(\mathbf{r},t) \implies \imath\mathbf{k} \times \vec{\mathcal{E}} = \imath\omega\vec{\mathcal{B}} \implies \vec{\mathcal{B}} = \frac{\mathbf{k} \times \vec{\mathcal{E}}}{k/\sqrt{\mu\varepsilon}} \ .$$

which demonstrates that the vectors $\vec{\mathcal{E}}$, $\vec{\mathcal{B}}$, and $\mathbf{k}$ are mutually perpendicular.

18.1.8.3 Ex: Polarization of a wave in vacuum

A transverse electromagnetic wave propagates through an isotropic, non-conducting medium without charges (vacuum) in positive z-direction. The projection of the vector of the electric field on the plane x-y has the form,

$$\vec{\mathcal{E}} = \vec{\mathcal{E}}_0 \sin(kz - \omega t) = (\mathcal{E}_{0x}, \mathcal{E}_{0y}, 0)\sin(kz - \omega t) \ .$$

a. Illustrate the motion of the electric field vector by a scheme. How is the wave polarized?
b. Show from Maxwell's equations, that the magnetic field vector can be written as,

$$\vec{\mathcal{B}}(\mathbf{r},t) = \frac{1}{\omega}(\mathbf{k} \times \vec{\mathcal{E}})$$

with the wavevector $\mathbf{k} = k\hat{\mathbf{e}}_z$.
c. Calculate the energy flux of the wave (Poynting vector) $\vec{\mathcal{S}}(\mathbf{r},t)$ as a function of the (phase) velocity of the wave c_0. How does the phase change in other media ($\mu \neq \mu_0$ and $\varepsilon \neq \varepsilon_0$)? What does this mean for $\vec{\mathcal{S}}(\mathbf{r},t)$.

Solution: *a. The wave is linearly polarized in the plane $\vec{\mathcal{E}}_0 = \vec{\mathcal{E}}_{0x}\hat{\mathbf{e}}_x + \vec{\mathcal{E}}_{0y}\hat{\mathbf{e}}_y$.*
b. We insert the electric field into Maxwell's second law,

$$\nabla \times \vec{\mathcal{E}} = \begin{pmatrix} -\partial_z\vec{\mathcal{E}}_y \\ \partial_z\vec{\mathcal{E}}_x \\ 0 \end{pmatrix} = \begin{pmatrix} -k\vec{\mathcal{E}}_{0y} \\ k\vec{\mathcal{E}}_{0x} \\ 0 \end{pmatrix} \cos(kz - \omega t) = k\hat{\mathbf{e}}_z \times \vec{\mathcal{E}}_0 \cos(kz - \omega t) \ .$$

Integrated in time we obtain the magnetic field,

$$\vec{\mathcal{B}} = -\int_0^t \nabla\times\vec{\mathcal{E}}dt' = -k\hat{\mathbf{e}}_z\times\vec{\mathcal{E}}_0\int_0^t \cos(kz-\omega t)dt' = \frac{k}{\omega}\hat{\mathbf{e}}_z\times\vec{\mathcal{E}}_0\sin(kz-\omega t) = \frac{k}{\omega}\hat{\mathbf{e}}_z\times\vec{\mathcal{E}}\ .$$

c. The Poynting vector then becomes,

$$\vec{\mathcal{S}} = \frac{1}{\mu}\vec{\mathcal{E}}\times\vec{\mathcal{B}} = \frac{1}{\mu}\vec{\mathcal{E}}\times\frac{1}{c}(\hat{\mathbf{e}}_z\times\vec{\mathcal{E}}) = \sqrt{\frac{\varepsilon}{\mu}}\vec{\mathcal{E}}^2\hat{\mathbf{e}}_k\ .$$

The intensity is,

$$I = |\vec{\mathcal{S}}| = \sqrt{\frac{\varepsilon\mu_0}{\varepsilon_0\mu}}I_{vac}\ .$$

Apparently, part of the energy transported by an electromagnetic wave through a dielectric is due to a polarization wave $\vec{\mathcal{P}}(\mathbf{r},t)$.

18.1.8.4 Ex: Jones matrices for a three-beam MOT

A three-beam magneto-optical trap (MOT) is characterized by the fact that each of three linearly polarized laser beams passes through a $\lambda/4$-waveplate rotated in a way to leave them circularly polarized. Then the beam traverses the MOT a first time, behind the MOT it passes through a second waveplate, and being finally reflected by a mirror, it makes all the way back, as shown in the figure. Show that the polarization of the laser beam at the position of the mirror is always *linear* independently of the rotation angle of the second waveplate.

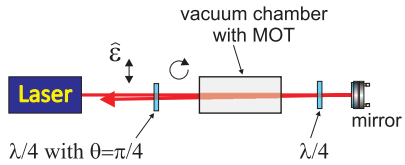

Figure 18.7: One of three retroreflected beams of a MOT.

Solution: *We use the Jones matrices for the $\lambda/4$ and $\lambda/2$-waveplates. To obtain the polarizations $\sigma^{\mp}$, the $\lambda/4$-waveplate must be rotated by $\pm 45°$:*

$$M_{\lambda/4}(\pm\tfrac{\pi}{4})\begin{pmatrix}1\\0\end{pmatrix} = \frac{e^{\imath\pi/4}}{\sqrt{2}}\begin{pmatrix}1\\ e^{\mp\imath\pi/2}\end{pmatrix} \propto \begin{pmatrix}1\\ \mp\imath\end{pmatrix}\ .$$

Now, passing through two $\lambda/4$-waveplates, we get,

$$M_{\lambda/4}(\phi)M_{\lambda/4}(\tfrac{\pi}{4})\begin{pmatrix}1\\0\end{pmatrix} = \begin{pmatrix}-\frac{1}{2}+\frac{\imath}{2}+\cos^2\phi-\imath\sin\phi\cos\phi\\ -\imath\left(-\frac{1}{2}-\frac{\imath}{2}+\cos^2\phi-\imath\sin\phi\cos\phi\right)\end{pmatrix} = -\tfrac{1}{2}(\imath+e^{-2\imath\phi})\begin{pmatrix}1\\ \frac{1+\sin 2\phi}{\cos 2\phi}\end{pmatrix}\ .$$

That is, the light is linearly polarized independently on the rotation angle ϕ. After the second passage through the second $\lambda/4$-waveplate, we get,

$$M_{\lambda/4}(\phi)^2 M_{\lambda/4}(\tfrac{\pi}{4}) \begin{pmatrix} 1 \\ 0 \end{pmatrix} = \begin{pmatrix} (\frac{1}{2}+\frac{\imath}{2})\cos 2\phi + (\frac{1}{2}-\frac{\imath}{2})\sin 2\phi \\ (\frac{1}{2}-\frac{\imath}{2})\cos 2\phi - (\frac{1}{2}+\frac{\imath}{2})\sin 2\phi \end{pmatrix} = \tfrac{1}{\sqrt{2}}(e^{\imath\pi/4}\cos 2\phi + e^{-\imath\pi/4}\sin 2\phi) \begin{pmatrix} 1 \\ -\imath \end{pmatrix} .$$

That is, the light is circularly polarized independently on the rotation angle ϕ. Finally, after the second passage through the first $\lambda/4$-waveplate, we get,

$$M_{\lambda/4}(\tfrac{\pi}{4}) M_{\lambda/4}(\phi) M_{\lambda/4}(\phi) M_{\lambda/4}\left(\tfrac{\pi}{4}\right) \begin{pmatrix} 1 \\ 0 \end{pmatrix} = \begin{pmatrix} \imath e^{-2\imath\phi} \\ 0 \end{pmatrix} .$$

Hence, after the fourth transmission, we always have linearly polarized light with the same polarization as the incident beam, and we see that the norm is preserved.

18.1.8.5 Ex: Temporal average of waves in complex notation

In complex notation there is a practical recipe for finding the temporal average of a product of waves. Consider $f(\mathbf{r},t) = \cos(\mathbf{k}\cdot\mathbf{r} - \omega t + \delta_a)$ and $g(\mathbf{r},t) = \cos(\mathbf{k}\cdot\mathbf{r} - \omega t + \delta_b)$. Show $\overline{fg} = \frac{1}{2}\mathfrak{Re}\,(\tilde{f}\tilde{g}^*)$. Note, that this only works, when the two waves have the same wavevector $\mathbf{k}$ and the same frequency ω, but they may have arbitrary amplitudes and phases. For example,

$$\langle u \rangle = \tfrac{1}{4}\mathfrak{Re}\,(\varepsilon_0 \vec{\tilde{\mathcal{E}}}\cdot\vec{\tilde{\mathcal{E}}}^* + \tfrac{1}{\mu_0}\vec{\tilde{\mathcal{B}}}\cdot\vec{\tilde{\mathcal{B}}}^*) \qquad \text{and} \qquad \langle \vec{\mathcal{S}} \rangle = \tfrac{1}{2\mu_0}\mathfrak{Re}\,(\vec{\tilde{\mathcal{E}}}\times\vec{\tilde{\mathcal{B}}}^*) .$$

Solution: *In complex notation,*

$$\tilde{f}(\mathbf{r},t) = e^{\imath(\mathbf{k}\cdot\mathbf{r}-\omega t+\delta_a)} \qquad \textit{and} \qquad \tilde{g}(\mathbf{r},t) = e^{\imath(\mathbf{k}\cdot\mathbf{r}-\omega t+\delta_b)} ,$$

we calculate on one hand,

$$\begin{aligned} \overline{fg} &= \frac{\omega}{2\pi}\int_0^{2\pi/\omega} \cos(\mathbf{k}\cdot\mathbf{r}-\omega t+\delta_a)\cos(\mathbf{k}\cdot\mathbf{r}-\omega t+\delta_b)dt \\ &= \frac{\omega}{2\pi}\int_0^{2\pi/\omega} \left[\tfrac{1}{2}\cos(\delta_a-\delta_b) + \tfrac{1}{2}\cos(2\mathbf{k}\cdot\mathbf{r}-2\omega t+\delta_a+\delta_b)\right] dt = \tfrac{1}{2}\cos(\delta_a-\delta_b) . \end{aligned}$$

On the other hand, we have,

$$\tfrac{1}{2}\mathfrak{Re}\,(\tilde{f}\tilde{g}^*) = \tfrac{1}{2}\mathfrak{Re}\,\left[e^{\imath(\mathbf{k}\cdot\mathbf{r}-\omega t+\delta_a)}e^{-\imath(\mathbf{k}\cdot\mathbf{r}-\omega t+\delta_b)}\right] = \tfrac{1}{2}\mathfrak{Re}\; e^{\imath(\delta_a-\delta_b)} = \tfrac{1}{2}\cos(\delta_a-\delta_b) .$$

18.1.8.6 Ex: Radiation pressure of a plane wave

A plane electromagnetic wave impinges vertically on a plane.
a. Show that the radiation pressure exerted on a surface is equal to the energy density in the incident beam. Does this ratio depend on the reflected part of the radiation?
b. Now consider a beam of small massive balls of mass m incident on a plane. What is the relationship between the mean pressure on the surface and the kinetic energy in this case?

Solution: *a. We calculate the radiative pressure as,*

$$P = \frac{1}{A}\frac{\Delta p}{\Delta t} = \frac{\varepsilon_0}{2}\mathcal{E}_0^2 = \frac{I}{c} = u \ ,$$

when light is fully absorbed.
b. Let N be the number of balls beating the plane per unit time. In the case of inelastic collisions,

$$P = \frac{Nmv}{A} = \frac{Nm}{A}\sqrt{\frac{2}{m}E_{kin}} = \frac{N}{A}\sqrt{2mE_{kin}} \ .$$

For elastically reflected collisions, the pressure will double. Unlike the radiative pressure of light, the pressure exerted by the balls goes with the root of the energy of the beam. This is due to the different dispersion relations for photons and massive particles.

18.1.8.7 Ex: Radiation pressure of solar light

Estimate the radiation pressure force exerted by the Sun on the Earth, and compare this force to the gravitational force on Earth and at the atmospheric pressure. (The intensity of sunlight at the Earth's orbit is $I = 1.37\,\mathrm{kW/m^2}$).
b. Repeat part (a) for Mars, which has an average distance of $2.28 \cdot 10^8\,\mathrm{km}$ from the Sun and has a radius of 3400 km.
c. What is the exerted radiation pressure when light strikes a perfect absorber (reflector)?

Solution: *a. The radiation pressure of the sun on the Earth is,*

$$\tfrac{I_{earth}}{c} = 4.5 \cdot 10^{-6}\,\mathrm{Pa} \ ,$$

which is small compared to the atmospheric pressure of $10^{13}\,\mathrm{hPa}$. The total force of the solar radiation on the Earth is,

$$F_{rad,earth} = \int_{earth} \tfrac{I}{c} \cdot d\mathbf{a} = \tfrac{I}{c}\pi r_{earth}^2 = 5.83 \cdot 10^8\,\mathrm{N} \ .$$

In comparison, $F_{g,earth} = 1.65 \cdot 10^{-14} F_{rad,earth}$.
b. The intensity decreases with the square of the distance of the source, such that,

$$\frac{I_{mars}}{c} \propto \frac{d_{sun-earth}^2}{d_{sol-mars}^2}\frac{I_{earth}}{c} = \left(\frac{149\ 600\ 000}{249\ 200\ 000}\right)^2 \tfrac{I_{earth}}{c} \ ,$$

which is still small compared to the atmospheric pressure on Mars, which is $0.6\% \cdot 10^{13}\,\mathrm{hPa}$. *Also,*

$$\frac{F_{rad,mars}}{F_{rad,earth}} = \frac{d_{sun-earth}^2 r_{mars}^2}{d_{sun-mars}^2 r_{earth}^2} \ .$$

c. The radiative pressure hitting a perfect reflector is twice the pressure when hitting a perfect absorber of the same size.
Gabarite: $F_{rad,mars} = 7.18 \cdot 10^7\,\mathrm{N}$, $F_{g,mars} = 4.27 \cdot 10^{-14}\,\mathrm{F_{rad,mars}}$.

18.1.8.8 Ex: Radiation pressure of a point-like emitter onto a plane

A punctual and intense source of light isotropically radiates 1.0 MW. The source is located 1.0 m above an infinite and perfectly reflecting plane. Determine the force that the radiation pressure exerts on the plane.

Solution: *The force is*

$$F = \int \mathbf{p} \cdot d\mathbf{A} = \int_0^\infty \int_0^{2\pi} \frac{I(\sqrt{a^2+r^2})}{c} \cos\theta r dr d\phi = \int_0^\infty \int_0^{2\pi} \frac{P}{c4\pi(a^2+r^2)} \frac{a}{\sqrt{r^2+a^2}} r dr d\phi$$
$$= \frac{aP}{2c} \int_0^\infty \frac{r dr}{(a^2+r^2)^{3/2}} = \frac{aP}{2c} \left. \frac{-1}{\sqrt{a^2+r^2}} \right|_0^\infty = \frac{P}{2c} = 3.3\,\mathrm{mN} \ .$$

18.1.8.9 Ex: Maxwell's tensor for a plane wave

Find all the elements of Maxwell's stress tensor for a monochromatic plane wave traveling in z-direction and being linearly polarized in y-direction. Interpret the result remembering that $\overleftrightarrow{T}$ represents a momentum flux density. How is $\overleftrightarrow{T}$ related to the energy density in this case?

Solution: *With the electric field,*

$$\vec{\mathcal{E}} = \mathcal{E}_0 \hat{\mathbf{e}}_x \sin(kz - \omega t) \ ,$$

the magnetic field is,

$$\vec{\mathcal{B}} = \tfrac{1}{c} \mathcal{E}_0 \hat{\mathbf{e}}_y \sin(kz - \omega t) \ .$$

For the tensor we calculate,

$$\begin{aligned} T_{ij} &= \varepsilon_0 (\mathcal{E}_i \mathcal{E}_j - \tfrac{1}{2}\delta_{ij}\mathcal{E}^2) + \tfrac{1}{\mu_0}(\mathcal{B}_i \mathcal{B}_j - \tfrac{1}{2}\delta_{ij}\mathcal{B}^2) \\ &= \tfrac{\varepsilon_0}{2}(\mathcal{E}^2\delta_{ix} - \mathcal{E}^2\delta_{iy} - \mathcal{E}^2\delta_{iz})\delta_{ij} + \tfrac{1}{\mu_0 c^2}(-\mathcal{E}^2\delta_{ix} + \mathcal{E}^2\delta_{iy} - \mathcal{E}^2\delta_{iz}) \\ &= -\varepsilon_0 \mathcal{E}^2 \delta_{iz}\delta_{jz} = -u\delta_{iz}\delta_{jz} \ . \end{aligned}$$

For the Poynting vector we calculate,

$$\vec{\mathcal{S}} = \tfrac{1}{\mu_0} \vec{\mathcal{E}} \times \vec{\mathcal{B}} = \varepsilon_0 \mathcal{E}^2 \hat{\mathbf{e}}_z \ ,$$

concluding that $s = T_{zz}$.

18.1.8.10 Ex: Superposition of waves

Suppose $Ae^{\imath ax} + Be^{\imath bx} = Ce^{\imath cx}\ \forall x$. Prove that $a = b = c$ and $A + B = C$.

Solution: *Obviously, the relation must also be valid at $x = 0$, which proves immediately,*

$$A + B = C \ .$$

Evaluating the derivative of the equation, $\imath aAe^{\imath ax} + \imath bBe^{\imath bx} = \imath c(A + B)e^{\imath cx}$, also at the point $x = 0$, we conclude,

$$aA + bB = c(A + B) \ ,$$

and evaluating the second derivative, $-a^2Ae^{\imath ax} - b^2Be^{\imath bx} = -c^2(A + B)e^{\imath cx}$, also at the point $x = 0$, we conclude,

$$a^2A + b^2B = c^2(A + B) \ .$$

Solving the second relation by c and substituting into the third,

$$a^2A + b^2B = \left(\frac{aA + bB}{A + B}\right)^2 (A + B) \ ,$$

which simplifies to,

$$a^2 + b^2 = 2ab \ ,$$

which requires $a = b$. Then $a = c$ is obvious.

18.1.8.11 Ex: Poynting vector of a superposition of two waves

The electric fields of two harmonic electromagnetic waves of angular frequencies ω_1 and ω_2 are given by $\vec{\mathcal{E}}_1 = \mathcal{E}_{10}\cos(k_1x - \omega_1t)\hat{\mathbf{e}}_y$ and by $\vec{\mathcal{E}}_2 = \mathcal{E}_{20}\cos(k_2x - \omega_2t + \delta)\hat{\mathbf{e}}_y$. For the superposition of these two waves, determine
a. the instantaneous Poynting vector and
b. the temporal average of the Poynting vector.
c. Repeat parts (a) and (b) for an inverted propagation direction of the second wave, i.e. $\vec{\mathcal{E}}_2 = \mathcal{E}_{20}\cos(k_2x + \omega_2t + \delta)\hat{\mathbf{e}}_y$.

Solution: *a. The instantaneous Poynting vector is,*

$$\begin{aligned}\vec{\mathcal{S}} &= \tfrac{1}{\mu_0}\vec{\mathcal{E}} \times \vec{\mathcal{B}} = \tfrac{1}{\mu_0}(\vec{\mathcal{E}}_1 + \vec{\mathcal{E}}_2) \times (\vec{\mathcal{B}}_1 + \vec{\mathcal{B}}_2) \\ &= \tfrac{1}{\mu_0}\hat{\mathbf{e}}_x[\mathcal{E}_{10}\mathcal{B}_{10}\cos^2(k_1x - \omega_1t) \\ &+ \mathcal{E}_{20}\mathcal{B}_{20}\cos^2(k_2x - \omega_2t + \delta) + (\mathcal{E}_{10}\mathcal{B}_{20} + \mathcal{E}_{20}\mathcal{B}_{10})\cos(k_1x - \omega_1t)\cos(k_2x - \omega_2t + \delta)] \ .\end{aligned}$$

b. Using the trigonometric formula $\cos a \cos b = \frac{1}{2}[\cos(a-b) + \cos(a+b)]$, we calculate the temporal average of the Poynting vector,

$$\begin{aligned}\langle\vec{\mathcal{S}}\rangle &= \tfrac{1}{\mu_0}\hat{\mathbf{e}}_x\left\langle\mathcal{E}_{10}\mathcal{B}_{10}\cos^2(k_1x - \omega_1t) + \mathcal{E}_{20}\mathcal{B}_{20}\cos^2(k_2x - \omega_2t + \delta)\right. \\ &\quad \left. + \tfrac{\mathcal{E}_{10}B_{20} + \mathcal{E}_{20}\mathcal{B}_{10}}{2}[\cos(\Delta kx - \Delta\omega t - \delta) + \cos(Kx - \Omega t + \delta)]\right\rangle \\ &= \tfrac{1}{\mu_0}\hat{\mathbf{e}}_x\left[\tfrac{\mathcal{E}_{10}\mathcal{B}_{10} + \mathcal{E}_{20}\mathcal{B}_{20}}{2} + \tfrac{\mathcal{E}_{10}\mathcal{B}_{20} + \mathcal{E}_{20}\mathcal{B}_{10}}{2}\langle\cos(\Delta kx - \Delta\omega t - \delta)\rangle\right] \\ &\overset{T\to\infty}{\longrightarrow} \tfrac{1}{\mu_0}\hat{\mathbf{e}}_x\left[\tfrac{\mathcal{E}_{10}\mathcal{B}_{10} + \mathcal{E}_{20}\mathcal{B}_{20}}{2} + \tfrac{\mathcal{E}_{10}\mathcal{B}_{20} + \mathcal{E}_{20}\mathcal{B}_{10}}{2}\cos\delta\ \delta_{k_1\neq k_2}\right] \ .\end{aligned}$$

c. In the case of counterpropagating beams,

$$\vec{\mathcal{S}} = \tfrac{1}{\mu_0}\hat{\mathbf{e}}_x[\mathcal{E}_{10}^2\cos^2(k_1x-\omega_1t) - \mathcal{E}_{20}^2\cos^2(k_2x+\omega_2t+\delta)] \ ,$$

and

$$\langle\vec{\mathcal{S}}\rangle = \tfrac{1}{2\mu_0}\hat{\mathbf{e}}_x\tfrac{\mathcal{E}_{10}^2+\mathcal{E}_{20}^2}{2} \ .$$

18.1.8.12 Ex: Poynting vector of a standing wave

The electric field $\vec{\mathcal{E}}(\mathbf{r},t)$ of a standing electromagnetic wave in vacuum be given by,

$$\vec{\mathcal{E}}(\mathbf{r},t) = \mathfrak{Re}\ \left(\mathcal{E}_0\hat{\mathbf{e}}_x e^{\imath(kz-\omega t)} - \mathcal{E}_0\hat{\mathbf{e}}_x e^{\imath(-kz-\omega t)}\right) = 2\mathcal{E}_0\sin kz\sin\omega t\hat{\mathbf{e}}_x$$

with $\mathcal{E}_0 \in \mathbb{R}$.
a. Determine the corresponding magnetic field $\vec{\mathcal{B}}(\mathbf{r},t)$.
b. Calculate the Poynting vector $\vec{\mathcal{S}}(\mathbf{r},t)$. What follows for the energy flow $\bar{s}$ of the standing electromagnetic wave in the temporal average, that is, calculate

$$\bar{s} = \frac{\int dt\ s}{\int dt} \ ,$$

where both integrals should be evaluated between $t=0$ and $t=2\pi/\omega$.

Solution: *a. With* $\nabla\times\vec{\mathcal{E}} = -\frac{\partial}{\partial t}\vec{\mathcal{B}}$ *follows,*

$$\hat{\mathbf{e}}_y\frac{\partial}{\partial z}\vec{\mathcal{E}}_x = -\frac{\partial}{\partial t}\vec{\mathcal{B}}_y\hat{\mathbf{e}}_y \ .$$

With $-2\mathcal{E}_0k\cos kz\sin\omega t = \frac{\partial}{\partial t}\vec{\mathcal{B}}_y$ *we obtain,*

$$\vec{\mathcal{B}} = \hat{\mathbf{e}}_y\mathcal{B}_0\cos kz\cos\omega t$$

with $\mathcal{B}_0 = \frac{2\mathcal{E}_0k}{\omega} = \frac{2\mathcal{E}_0}{c}$.
b. The Poynting vector is,

$$\begin{aligned}\vec{\mathcal{S}} &= \vec{\mathcal{E}}\times\vec{\mathcal{H}} = \varepsilon_0c^2\vec{\mathcal{E}}\times\vec{\mathcal{B}} = \varepsilon_0c\hat{\mathbf{e}}_z4\mathcal{E}_0^2\sin kz\cos kz\sin\omega t\cos\omega t \\ &= \varepsilon_0c\hat{\mathbf{e}}_z\mathcal{E}_0^2\sin 2kz\sin 2\omega t \ .\end{aligned}$$

In the temporal average,

$$\int_0^{2\pi/\omega}\sin 2\omega t\ dt = -\frac{1}{2\omega}\cos 2\omega t\Big|_0^{2\pi/\omega} = -\frac{1}{2\omega}[\cos 4\pi - \cos 0] = 0 \ .$$

Hence, $\bar{s}=0$.

18.1.8.13 Ex: Phase fronts of planar and spherical waves

Describes the phase front for (a) a plane wave and (b) a spherical wave.

Solution: *a. A plane wave is defined by,*

$$\psi(\mathbf{r},t) = A_0 e^{\imath(\mathbf{k}\cdot\mathbf{r}-\omega t)} \ .$$

Inserting into the wave equation (18.1) yields $|\mathbf{k}| = \omega/c$ *when* A_0 *is constant. The phase front is given by,*

$$\mathbf{k}\cdot\mathbf{r} - \omega t = const.$$

That is, for a given time t*, all points* $\mathbf{r}$ *satisfying the above equation form a surface perpendicular to* $\mathbf{k}$*. Since* $\phi = \mathbf{k}\cdot\mathbf{r}$*, we have* $\nabla\phi = \mathbf{k}$ *and the phase velocity is* $c \equiv \omega/|\nabla\phi|$*. Along the direction* $\mathbf{k}$*, the wave is periodic in space. The periodicity, called wavelength* λ*, is given by* $|\mathbf{k}| = 2\pi/\lambda$*.*
b. A spherical wave is defined by,

$$\psi(\mathbf{r},t) = \frac{A_0}{r} e^{\imath(kr-\omega t)} \ .$$

We notice that the expression is in spherical coordinates, and $\phi = kr$ *is not a scalar product of two vectors, but a product of two scalar quantities. Once again,* $k = \omega/c = 2\pi/\lambda$*, but* $\nabla\phi = k\hat{r}$*. The inverse dependence of the amplitude of* r *is a result of energy conservation.*

18.1.8.14 Ex: Fake spherical wave

We verified in class, that spherical waves of the form

$$\vec{\mathcal{E}}_\pm(\mathbf{r},t) = \vec{\mathcal{E}}_0 \frac{1}{r} e^{\imath(kr\pm\omega t)} \qquad \text{and} \qquad \vec{\mathcal{B}}_\pm(\mathbf{r},t) = \vec{\mathcal{B}}_0 \frac{1}{r} e^{\imath(kr\pm\omega t)}$$

with $\omega = ck$, $c^2 = 1/(\varepsilon_0\mu_0)$ satisfy the Helmholtz equation. Argue, why nevertheless, they can not be electromagnetic waves. Check whether such waves satisfy the homogeneous Maxwell equations.

Solution: *A spherical wave can not have homogeneous polarization.*
To verify Maxwell's equations in vacuum, we first calculate the gradient,

$$\nabla \frac{e^{\imath(kr\pm\omega t)}}{r} = \frac{e^{\imath(kr\pm\omega t)}}{r^3}(-1+\imath kr)\mathbf{r} \ .$$

With this the third equation gives the result,

$$0 = \nabla\cdot\vec{\mathcal{E}}_\pm = \vec{\mathcal{E}}_0\cdot\mathbf{r}\frac{e^{\imath(kr\pm\omega t)}}{r^3}(-1+\imath kr) = \vec{\mathcal{E}}_0\cdot\mathbf{r}\frac{e^{\imath(kr\pm\omega t)}}{r^3}(-1+\imath kr) = \frac{-1+\imath kr}{r^2}\vec{\mathcal{E}}_\pm\cdot\mathbf{r} \ ,$$

and the forth,

$$0 = \nabla\cdot\vec{\mathcal{B}}_\pm = \frac{-1+\imath kr}{r^2}\vec{\mathcal{B}}_\pm\cdot\mathbf{r} \ .$$

Thus, the equations for the divergences confirm that the polarizations of the fields must be perpendicular to the radial propagation direction. But this contradicts the fixed polarization assumed in the ansatz. Now, we check the first homogeneous Maxwell equation:

$$0 = \nabla \times \vec{\mathcal{B}}_\pm - \frac{\partial \vec{\mathcal{E}}_\pm}{c^2 \partial t} = \frac{e^{\imath(kr \pm \omega t)}}{r} \nabla \times \vec{\mathcal{B}}_0 + \left(\nabla \frac{e^{\imath(kr \pm \omega t)}}{r} \right) \times \vec{\mathcal{B}}_0 - \frac{\partial}{\partial t} \frac{e^{\imath(kr \pm \omega t)}}{c^2 r} \vec{\mathcal{E}}_0$$
$$= \frac{e^{\imath(kr \pm \omega t)}}{r^3} (-1 + \imath kr) \mathbf{r} \times \vec{\mathcal{B}}_0 \mp \frac{\imath\omega}{c^2} \frac{e^{\imath(kr \pm \omega t)}}{r} \vec{\mathcal{E}}_0 = \frac{-1 + \imath kr}{r} \hat{\mathbf{e}}_r \times \vec{\mathcal{B}} \mp \frac{\imath\omega}{c^2} \vec{\mathcal{E}} \ .$$

The second one gives,

$$0 = \nabla \times \vec{\mathcal{E}}_\pm + \frac{\partial \vec{\mathcal{B}}_\pm}{\partial t} = \frac{-1 + \imath kr}{r} \hat{\mathbf{e}}_r \times \vec{\mathcal{E}} \pm \imath\omega \vec{\mathcal{B}} \ ,$$

which must be satisfied for all r. Thus, the equations for the rotations also violate Maxwell's equations.

18.1.8.15 Ex: Spherical wave

Consider a spherical electromagnetic wave,

$$\vec{\mathcal{E}}(\mathbf{r}, t) = \vec{\mathcal{E}}_0(r, \theta) e^{\imath(kr - \omega t)} \qquad \text{and} \qquad \vec{\mathcal{B}}(\mathbf{r}, t) = \vec{\mathcal{B}}_0(r, \theta) e^{\imath(kr - \omega t)} \ .$$

Show that the validity of Maxwell's equations for $\nabla \cdot \vec{\mathcal{E}} = 0 = \nabla \cdot \vec{\mathcal{B}}$ for the case of vanishing charge and current densities implies that $\vec{\mathcal{E}}$, $\vec{\mathcal{B}}$, and $\hat{\mathbf{e}}_r$ are mutually orthogonal (transversality).

Solution: *Inserting the electric field into Maxwell's equations,*

$$\nabla \cdot \vec{\mathcal{E}}(\mathbf{r}, t) = e^{\imath(kr - \omega t)} [\nabla \cdot \vec{\mathcal{E}}_0(r, \theta) + \imath k \hat{\mathbf{e}}_r \cdot \vec{\mathcal{E}}_0(r, \theta)] = 0$$
$$\nabla \times \vec{\mathcal{E}}(\mathbf{r}, t) = e^{\imath(kr - \omega t)} [\nabla \times \vec{\mathcal{E}}_0(r, \theta) + \imath k \hat{\mathbf{e}}_r \times \vec{\mathcal{E}}_0(r, \theta)] = \imath\omega \vec{\mathcal{B}}_0(r, \theta) e^{\imath(kr - \omega t)} = -\frac{\partial \vec{\mathcal{B}}}{\partial t} \ .$$

Now, we divide by $e^{\imath(kr - \omega t)}$ and separate the real and imaginary parts,

$$\begin{aligned}
\nabla \cdot \vec{\mathcal{E}}_0(r, \theta) = 0 \qquad & \textit{and} \qquad \hat{\mathbf{e}}_r \cdot \vec{\mathcal{E}}_0(r, \theta) = 0 \\
\nabla \times \vec{\mathcal{E}}_0(r, \theta) = 0 \qquad & \textit{and} \qquad k \hat{\mathbf{e}}_r \times \vec{\mathcal{E}}_0(r, \theta) = \omega \vec{\mathcal{B}}_0(r, \theta) \\
\nabla \cdot \vec{\mathcal{B}}_0(r, \theta) = 0 \qquad & \textit{and} \qquad \hat{\mathbf{e}}_r \cdot \vec{\mathcal{B}}_0(r, \theta) = 0 \\
\nabla \times \vec{\mathcal{B}}_0(r, \theta) = 0 \qquad & \textit{and} \qquad k \hat{\mathbf{e}}_r \times \vec{\mathcal{B}}_0(r, \theta) = -\tfrac{\omega}{c^2} \vec{\mathcal{E}}_0(r, \theta) \ .
\end{aligned}$$

where we included the results of similar calculations for the magnetic field. We conclude that $\vec{\mathcal{E}}$, $\vec{\mathcal{B}}$, and $\hat{\mathbf{e}}_r$ are mutually orthogonal.

18.1.8.16 Ex: Spherical wave in a neutral dielectric medium

a. Show that spherical waves $\vec{\mathcal{E}}(\mathbf{r},t) = \frac{\vec{\mathcal{E}}_0}{r} e^{\imath(kr-\omega t)}$ solve the wave equation in a vacuum, when $\omega = ck$. The Laplace operator in spherical coordinates is,

$$\nabla^2 = \frac{1}{r^2}\frac{\partial}{\partial r}\left(r^2\frac{\partial}{\partial r}\right) + \frac{1}{r^2}\Delta_{\theta,\phi} \ .$$

The second term only acts on the parts that depend on the angles. Verify that $\Delta_{\theta,\phi}\vec{\mathcal{E}} \equiv 0$.
b. Show that the wave equations have the form,

$$\nabla^2\vec{\mathcal{E}} - \frac{1}{c^2}\frac{\partial^2\vec{\mathcal{E}}}{\partial t^2} = \frac{1}{\varepsilon_0 c^2}\frac{\partial^2\vec{\mathcal{P}}}{\partial t^2} \ ,$$

when the wave does not propagate in a vacuum, but in a neutral dielectric medium (i.e. without free charges). Assume the simple case that the dielectric displacement $\vec{\mathcal{D}} = \varepsilon_0\vec{\mathcal{E}} + \vec{\mathcal{P}}$ has the form,

$$\vec{\mathcal{P}} = \varepsilon_0\chi\vec{\mathcal{E}} \ .$$

What is the form of the wave equations in this case? How do you change the phase velocity c of the wave? You can identify the meaning of the quantity $n \equiv \sqrt{1+\chi}$?

Solution: *a. Inserting the ansatz for the spherical wave into the differential equation,*

$$\frac{1}{r^2}\frac{\partial}{\partial r}\left(r^2\frac{\partial\vec{\mathcal{E}}}{\partial r}\right) - \frac{1}{c^2}\frac{\partial^2\vec{\mathcal{E}}}{\partial t^2} = 0 \ ,$$

we find,

$$\omega = ck \ .$$

b. From the Maxwell equations for a dielectric ($\varrho = 0$, $\mathbf{j} = 0$, $\varepsilon \neq \varepsilon_0$, $\mu = \mu_0$),

$$\begin{aligned} \nabla\times\vec{\mathcal{B}} = \varepsilon_0\mu_0\partial_t\vec{\mathcal{E}} + \mu_0\partial_t\vec{\mathcal{P}} \quad &, \quad \nabla\cdot\vec{\mathcal{B}} = 0 \\ \nabla\times\vec{\mathcal{E}} = -\partial_t\vec{\mathcal{B}} \quad &, \quad \nabla\cdot\vec{\mathcal{E}} = -\tfrac{1}{\varepsilon_0}\nabla\cdot\vec{\mathcal{P}} \ . \end{aligned}$$

Hence,

$$\begin{aligned} \nabla^2\vec{\mathcal{E}} &= \nabla^2\vec{\mathcal{E}} + \tfrac{1}{\varepsilon_0}\nabla(-\nabla\cdot\vec{\mathcal{D}} + \nabla\cdot\vec{\mathcal{P}}) = \nabla^2\vec{\mathcal{E}} - \nabla(\nabla\cdot\vec{\mathcal{E}}) = -\nabla\times(\nabla\times\vec{\mathcal{E}}) \\ &= \nabla\times\partial_t\vec{\mathcal{B}} = \partial_t(\varepsilon_0\mu_0\partial_t\vec{\mathcal{E}} + \mu_0\partial_t\vec{\mathcal{P}}) \ . \end{aligned}$$

This is only valid when $\vec{\mathcal{P}} \propto \vec{\mathcal{E}}$, such that we can use $\nabla\cdot\vec{\mathcal{P}} = 0$. (We note, that generally $\vec{\mathcal{P}}(\mathbf{r},t) = \chi^{(1)}\vec{\mathcal{E}}(\mathbf{r},t) + \vec{\mathcal{P}}_{nl}(\mathbf{r},t)$.) Now inserting the ansatz, $\vec{\mathcal{E}}(\mathbf{r},t) = \vec{\mathcal{E}}_0 e^{\imath(\mathbf{k}\cdot\mathbf{r}-\omega t)} + c.c.$, and separating the susceptibility into a real part and an imaginary part, $\chi^{(1)} = \mathfrak{Re}\ \chi^{(1)} + \imath\mathfrak{Im}\ \chi^{(1)}$, we obtain,

$$\frac{\partial^2\vec{\mathcal{E}}(z,t)}{\partial z^2} + k^2(1+\mathfrak{Re}\ \chi^{(1)})\vec{\mathcal{E}}(z,t) + \imath k^2\mathfrak{Im}\ \chi^{(1)}\vec{\mathcal{E}}(z,t) = 0 \ .$$

Thus, we find that $n = \sqrt{1+\mathfrak{Re}\ \chi^{(1)}}$ is the refractive index. With this, the wave is,

$$\vec{\mathcal{E}}(z,t) = \vec{\mathcal{E}}_0 e^{-(k/2)\mathfrak{Im}\ \chi^{(1)}z} e^{\imath(knz-\omega t)}\hat{\mathbf{e}}(\theta,\varepsilon) + c.c. \ .$$

18.1.8.17 Ex: Refraction in a bath of water

An observer stands at the edge of a basin filled with water down to a depth of $h = 2.81$ m. He looks at an object lying on the bottom. At what depth h' appears the image of the object, if the direction of observation in which the observer perceives the image forms with the normal direction to the water surface an angle of $\alpha = 60°$? Prepare a scheme.

Solution: *According to the scheme we have,*

$$h' \tan\alpha = h \tan\beta \ .$$

Thus, using Snell's law, $n_{water} = \frac{\sin\alpha}{\sin\beta} = 1.3325$,

$$h' = h\frac{\tan\beta}{\tan\alpha} = h\frac{\cos\alpha\sin\beta}{\sin\alpha\sqrt{1-\sin^2\beta}} = h\frac{\cos\alpha}{\sqrt{n_{water}^2 - \sin^2\alpha}} \approx 0.49h \ .$$

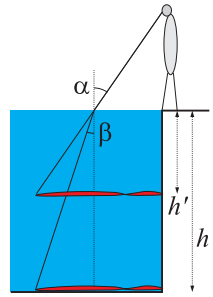

Figure 18.8: Refraction in a bath of water.

18.1.8.18 Ex: Poynting vector of a partially reflected wave

A plane wave $\vec{\mathcal{E}}_{in}(z,t)$ which is linearly polarized in x-direction runs along the z-axis from $-\infty$ towards an interface ($z = 0$-plane). At the interface, a part r of the wave is reflected without phase shift.
a. Give the amplitudes of the electric and the magnetic field in the half-space $z < 0$ in real numbers.
b. Give the Poynting vector $\vec{\mathcal{S}}(z,t)$ and its time average.

Solution: *a. The total amplitude of the electric field follows as a superposition,*

$$\begin{aligned}\vec{\mathcal{E}}(z,t) &= \vec{\mathcal{E}}_{in}(z,t) + r\vec{\mathcal{E}}_{in}(-z,t) = \mathcal{E}_0\hat{\mathbf{e}}_x e^{\imath(\omega t - kz)} + r\mathcal{E}_0\hat{\mathbf{e}}_x e^{\imath(\omega t + kz)} \\ &= \mathcal{E}_0\hat{\mathbf{e}}_x e^{\imath\omega t}[(1-r)e^{-\imath kz} + 2r\cos kz] \ .\end{aligned}$$

Magnetic field follows from $\nabla \times \vec{\mathcal{E}} = -\partial_t \vec{\mathcal{B}}$ *and is,*

$$\vec{\mathcal{B}}_{in}(z,t) = -\int dt\ \nabla \times \mathcal{E}_0 \hat{\mathbf{e}}_x e^{\imath(\omega t - kz)} = -\mathcal{E}_0 \int dt\ \nabla \times \hat{\mathbf{e}}_x e^{\imath(\omega t - kz)} = \mathcal{E}_0 \int dt\ \imath k e^{\imath(\omega t - kz)} \hat{\mathbf{e}}_y$$
$$= \mathcal{E}_0 \imath k \frac{1}{\imath\omega} e^{\imath(\omega t - kz)} \hat{\mathbf{e}}_y = \frac{1}{c} \mathcal{E}_0 \hat{\mathbf{e}}_y e^{\imath(\omega t - kz)}$$

hence,

$$\vec{\mathcal{B}}(z,t) = \vec{\mathcal{B}}_{in}(z,t) + r\vec{\mathcal{B}}_{in}(-z,t) = \frac{1}{c}\mathcal{E}_0 \hat{\mathbf{e}}_y e^{\imath(\omega t - kz)} - \frac{1}{c} r \mathcal{E}_0 \hat{\mathbf{e}}_y e^{\imath(\omega t + kz)}$$
$$= \frac{1}{c}\mathcal{E}_0 \hat{\mathbf{e}}_y e^{\imath\omega t}[(1-r)e^{-\imath kz} - 2\imath r \sin kz] \ .$$

b. The Poynting vector is now,

$$\vec{\mathcal{S}}(z,t) = \varepsilon_0 c^2 (\mathfrak{Re}\ \vec{\mathcal{E}} \times \mathfrak{Re}\ \vec{\mathcal{B}})$$
$$= \varepsilon_0 c^2 \left([\mathcal{E}_0 \hat{\mathbf{e}}_x \cos(\omega t - kz) + r\mathcal{E}_0 \hat{\mathbf{e}}_x \cos(\omega t + kz)] \times \right.$$
$$\left. \times \left[\tfrac{1}{c}\mathcal{E}_0 \hat{\mathbf{e}}_y \cos(\omega t - kz) - \tfrac{1}{c} r \mathcal{E}_0 \hat{\mathbf{e}}_y \cos(\omega t + kz) \right] \right)$$
$$= \varepsilon_0 c 2 \mathcal{E}_0^2 \hat{\mathbf{e}}_z [\cos(\omega t - kz) + r\cos(\omega t + kz)][\cos(\omega t - kz) - r\cos(\omega t + kz)]$$
$$= \varepsilon_0 c^2 \tfrac{1}{c} \mathcal{E}_0^2 \hat{\mathbf{e}}_z [\cos^2(\omega t - kz) - r^2 \cos^2(\omega t + kz)] \ .$$

The temporal average of the Poynting vector is,

$$\mathbf{I}(z) = \frac{\omega}{2\pi} \int_0^{2\pi/\omega} \vec{\mathcal{S}}(z,t) dt = \varepsilon_0 c \mathcal{E}_0^2 \hat{\mathbf{e}}_z \frac{\omega}{2\pi} \int_0^{2\pi/\omega} [\cos^2(\omega t - kz) - r^2 \cos^2(\omega t + kz)] dt$$
$$= \varepsilon_0 c \mathcal{E}_0^2 \hat{\mathbf{e}}_z \frac{\omega}{2\pi} \left[\frac{\pi}{\omega} - r^2 \frac{\pi}{\omega} \right] = \frac{1}{2} \varepsilon_0 c \mathcal{E}_0^2 \hat{\mathbf{e}}_z (1 - r^2) \ .$$

18.1.8.19 Ex: Energy flow upon refraction

Two infinitely extended media with relative dielectric constants ϵ_1 and ϵ_2 and permeabilities $\mu_1 = \mu_2 = \mu_0$, that is, with refraction indices $n_1 = \sqrt{\epsilon_1}$ and $n_2 = \sqrt{\epsilon_2}$, be separated by the $z = 0$-plane. Coming from the medium n_1 traveling in x-direction a linearly polarized plane wave with frequency ω and wavenumber k_1 hits the interface perpendicularly. The amplitude is $\mathcal{E}_0$.
a. Use the continuity of the normal components of $\vec{\mathcal{D}}$ and $\vec{\mathcal{B}}$, as well as of the tangential components of $\vec{\mathcal{E}}$ and $\vec{\mathcal{H}}$, at the interface to calculate the amplitudes of refracted part and the reflected part of the incident wave.
b. The energy flux is defined by the temporal average of the real part of the Poynting vector $\vec{\mathcal{S}}$: $\vec{\varphi} \equiv \mathfrak{Re}\ [\vec{\mathcal{E}} \times \vec{\mathcal{H}}^*]$. Calculate the incident, reflected, and refracted energy fluxes. What is the total flux in front and behind of the interface?
c. Determine the reflection coefficient r (the ratio between the absolute values of the reflected and incident fluxes) and the transmission coefficient t (the ratio between the absolute values of the transmitted and incident fluxes).

Solution: *a. Because of* $\mu_1 = \mu_2 = \mu_0$ *we have* $\vec{\mathcal{B}}_i = \mu_0 \vec{\mathcal{H}}_i$ *and* $n_i = \sqrt{\epsilon_i}$ *for* $i = 1, 2$. *Therefore, in front of the interface,*

$$\vec{\mathcal{E}}_1 = \hat{\mathbf{e}}_x \mathcal{E}_0 e^{-\imath\omega t} \left[e^{\imath k_1 z} + c_1 e^{-\imath k_1 z} \right]$$
$$\vec{\mathcal{B}}_1 = \hat{\mathbf{e}}_y \tfrac{\mathcal{E}_0}{c} e^{-\imath\omega t} n_1 \left[e^{\imath k_1 z} - c_1 e^{-\imath k_1 z} \right] \ ,$$

where the terms proportional to $e^{\imath k_1 z}$ *represent the incident part of the wave and the terms* $e^{-\imath k_1 z}$ *the reflected part. Behind the interface there is only a transmitted part, which is given by,*

$$\vec{\mathcal{E}}_2 = \hat{\mathbf{e}}_x \mathcal{E}_0 e^{-\imath\omega t} c_2 e^{\imath k_2 z}$$
$$\vec{\mathcal{B}}_2 = \hat{\mathbf{e}}_y \tfrac{\mathcal{E}_0}{c} e^{-\imath\omega t} n_2 c_2 e^{\imath k_2 z} \ .$$

Now, in the interface (that is, at $z = 0$*) the tangential component of* $\vec{\mathcal{E}}$ *(and hence, because of the linear polarization* $\vec{\mathcal{E}}$ *as well) and the tangential component of* $\vec{\mathcal{H}}$ *(and hence* $\vec{\mathcal{B}}$ *as well) are continuous. From this follows,*

$$1 + c_1 = c_2 \qquad \textit{continuity of } \vec{\mathcal{E}}_t$$
$$n_1(1 - c_1) = n_2 c_2 \qquad \textit{continuity of } \vec{\mathcal{H}}_t \ .$$

We obtain thus,

$$n_1(1 - c_1) = n_2 c_2 = n_2(1 + c_1)$$

and hence,

$$c_1 = \frac{n_1 - n_2}{n_1 + n_2} \qquad \textit{and} \qquad c_2 = \frac{2n_1}{n_1 + n_2} \ .$$

For the amplitudes of the reflected ($\mathcal{E}_{0r}$) *and refracted* ($\mathcal{E}_{0g}$) *parts we obtain thus,*

$$\mathcal{E}_{0r} = \frac{n_1 - n_2}{n_1 + n_2} \mathcal{E}_0 \qquad \textit{and} \qquad \mathcal{E}_{0g} = \frac{2n_1}{n_1 + n_2} \mathcal{E}_0 \ .$$

Upon reflection from an optically denser medium ($n_2 > n_1$) *the wave exhibits a phase jump with respect to the incident wave* ($n_1 - n_2 < 0$). *This is not the case for reflection by a less dense medium* ($n_2 < n_1$).
b. We get,

$$\vec{\varphi}_e = \mathfrak{Re}\ \vec{\mathcal{S}}_e = \tfrac{1}{\mu_0} \mathfrak{Re}\ (\vec{\mathcal{E}}_e \times \vec{\mathcal{B}}_e^*) = \tfrac{1}{\mu_0} \mathcal{E}_0^2 n_1 \hat{\mathbf{e}}_z$$
$$\vec{\varphi}_g = \mathfrak{Re}\ \vec{\mathcal{S}}_g = \tfrac{1}{\mu_0} \mathfrak{Re}\ (\vec{\mathcal{E}}_g \times \vec{\mathcal{B}}_g^*) = \tfrac{1}{\mu_0} \mathcal{E}_0^2 n_2 \left(\frac{2n_1}{n_1 + n_2} \right)^2 \hat{\mathbf{e}}_z$$
$$\vec{\varphi}_r = \mathfrak{Re}\ \vec{\mathcal{S}}_r = \tfrac{1}{\mu_0} \mathfrak{Re}\ (\vec{\mathcal{E}}_r \times \vec{\mathcal{B}}_r^*) = \tfrac{1}{\mu_0} \mathcal{E}_0^2 n_1 \left(\frac{n_1 - n_2}{n_1 + n_2} \right)^2 \hat{\mathbf{e}}_z \ .$$

For the total flux in front of the interface we have,

$$\vec{\varphi}_1 = \tfrac{1}{\mu_0} \mathfrak{Re}\ (\vec{\mathcal{E}}_1 \times \vec{\mathcal{B}}_1^*) = \tfrac{1}{\mu_0} \mathfrak{Re}\ \left((\vec{\mathcal{E}}_e + \vec{\mathcal{E}}_r) \times (\vec{\mathcal{B}}_e + \vec{\mathcal{B}}_r)^* \right)$$
$$= \tfrac{1}{\mu_0} \mathfrak{Re}\ \left((\vec{\mathcal{E}}_e \times \vec{\mathcal{B}}_e^*) + (\vec{\mathcal{E}}_r \times \vec{\mathcal{B}}_r^*) + (\vec{\mathcal{E}}_r \times \vec{\mathcal{B}}_e^* + \vec{\mathcal{E}}_e \times \vec{\mathcal{B}}_r^*) \right)$$
$$= \vec{\varphi}_e + \vec{\varphi}_r + \tfrac{1}{\mu_0} \mathcal{E}_0^2 n_1 \frac{n_1 - n_2}{n_1 + n_2} \mathfrak{Re}\ \left[e^{-\imath 2 k_1 z} - e^{\imath 2 k_1 z} \right] = \vec{\varphi}_e + \vec{\varphi}_r \ .$$

Behind the interface, obviously, we get,

$$\vec{\varphi}_2 = \vec{\varphi}_g \ .$$

Now,

$$\begin{aligned}\vec{\varphi}_e + \vec{\varphi}_r &= \tfrac{1}{\mu_0}\mathcal{E}_0^2 n_1 \left[1 - \left(\frac{n_1 - n_2}{n_1 + n_2}\right)^2\right] \hat{\mathbf{e}}_z \\ &= \tfrac{1}{\mu_0}\mathcal{E}_0^2 n_1 \frac{n_1^2 + n_2^2 + 2n_1 n_2 - n_1^2 - n_2^2 + 2n_1 n_2}{(n_1 + n_2)^2}\hat{\mathbf{e}}_z = \tfrac{1}{\mu_0}\mathcal{E}_0^2 n_2 \left(\frac{2n_1}{n_1 + n_2}\right)^2 \hat{\mathbf{e}}_z = \vec{\varphi}_g \ .\end{aligned}$$

Therefore, the flow of energy is continuous,

$$\vec{\varphi}_1 = \vec{\varphi}_e + \vec{\varphi}_r = \vec{\varphi}_g = \vec{\varphi}_2 \ .$$

c. The coefficients for reflection and transmissions are,

$$R \equiv \frac{|\vec{\varphi}_r|}{|\vec{\varphi}_e|} = \left(\frac{n_1 - n_2}{n_1 + n_2}\right)^2 \qquad \textit{and} \qquad T \equiv \frac{|\vec{\varphi}_g|}{|\vec{\varphi}_e|} = \frac{n_2}{n_1}\left(\frac{2n_1}{n_1 + n_2}\right)^2 \ .$$

It is easy to check,

$$R + T = 1 \ .$$

18.1.8.20 Ex: Birefringent crystal

An optically anisotropic crystal has in the x-direction the dielectric constant ε_1 (that is, the refractive index $n_1 = c\sqrt{\varepsilon_1 \mu_1}$) and in the y-direction ε_2, respectively, n_2. A linearly polarized plane wave with frequency ω propagating in z-direction impinges, coming from the vacuum, at normal incidence on a disc of thickness d of this material in such a way, that the plane of the polarization forms with the x and y-axes an angle of 45°. What is the polarization of the plane wave after the transition through the disk? How should we choose d, so that the wave is circularly polarized? Express this thickness in terms of the vacuum wavelength.

Solution: *For the incident wave we have,*

$$\vec{\mathcal{E}} = \mathcal{E}_0 e^{\imath(kz - \omega t)}(\hat{\mathbf{e}}_x + \hat{\mathbf{e}}_y) \ .$$

Furthermore, we have for the wavevector in transmission through the medium,

$$k = \frac{\omega}{v} = \omega\sqrt{\varepsilon\mu} = n\frac{\omega}{c} = \frac{2\pi}{\lambda} \ .$$

After the transmission through the disc, we obtain,

$$\begin{aligned}\vec{\mathcal{E}}_x &= \mathcal{E}_0 e^{\imath(kz + k_1 d - \omega t)} \qquad \textit{with} \qquad k_1 = n_1\frac{\omega}{c} \\ \vec{\mathcal{E}}_y &= \mathcal{E}_0 e^{\imath(kz + k_2 d - \omega t)} \qquad \textit{with} \qquad k_2 = n_2\frac{\omega}{c} \\ &= e^{\imath(k_2 d - k_1 d)}\vec{\mathcal{E}}_x \ .\end{aligned}$$

The components, therefore, have a phase difference of $k_2 d - k_1 d$ after transmission through the disk. In general, the wave is elliptically polarized. For circular polarization, the phase difference must be $\pi/2$ (depending on whether we want the light to be circularly polarized to the left or to the right). With this follows,

$$d = \pm\frac{\pi}{2}\,\frac{1}{k_2 - k_1} = \pm\frac{\pi}{2}\frac{c}{\omega}\,\frac{1}{n_2 - n_1}\ .$$

or with the wavelength in vacuum $\lambda = 2\pi c/\omega$

$$d(n_2 - n_1) = \pm\frac{\lambda}{4}\ ,$$

where the left-hand side gives the optical path difference. Therefore, we also speak of $\lambda/4$-waveplates.

18.1.8.21 Ex: Glass cube

At the center of a glass cube of length $d = 10\,\mathrm{mm}$ with the refractive index $n = 1.5$ there is a small spot. Which parts should the surfaces be covered so that the spot is invisible from outside the cube regardless of the direction of vision? Neglect the light refracted out of the cube after a first reflection inside the cube.

Solution: *The total internal reflection angle is $\theta_{i,tot} = \arcsin 1/n = 41.8°$. Thus, covering a centered area of,*

$$A = \pi\left(\tfrac{d}{2}\sin\theta_{i,tot}\right)^2 = \pi\left(\tfrac{d}{2n}\right)^2 \approx 0.35\,\mathrm{cm}^2\ .$$

18.1.8.22 Ex: Total internal reflection

a. We consider the transition of a beam of light from an optically dense medium (1) to a more dilute medium (2). Extending the theory of light refraction at interfaces beyond the angle of total internal reflection (18.70), derive the expression for the electric field in the medium (2).
b. Noting that α [from Eq. (18.60)] is now imaginary, use the equation (18.61) to calculate the reflection coefficient for the polarization parallel to the plane of incidence [7].
c. Do the same for polarization that is perpendicular to the plane of incidence.
d. In case of perpendicular polarization, show that the (real) evanescent fields are,

$$\vec{\mathcal{E}}(\mathbf{r},t) = \mathcal{E}_0 e^{-\kappa z}\cos(kx-\omega t)\hat{\mathbf{e}}_y \quad , \quad \vec{\mathcal{B}}(\mathbf{r},t) = \mathcal{E}_0 e^{-\kappa z}[\kappa\sin(kx-\omega t)\hat{\mathbf{e}}_x + k\cos(kx-\omega t)\hat{\mathbf{e}}_z]\ .$$

e. Verify that the fields in (d) satisfy all Maxwell equations without sources.
f. For the fields in (d), construct the Poynting vector and show that, on average, no energy is transmitted in z-direction.

[7] We observe 100% reflection, which is better than on a conductive surface.

Solution: *a. We choose the geometry such that the interface is in the $z = 0$ plane and all the beams lie within the $y = 0$ plane, that is,*

$$\mathbf{k}_t = k_t(\hat{\mathbf{e}}_x \sin\theta_t + \hat{\mathbf{e}}_z \cos\theta_t) \qquad with \qquad k_t = \omega n_2/c \ .$$

We now assume that $\theta_i > \theta_{i,total}$. In this case,

$$\cos\theta_t = \sqrt{1-\sin^2\theta_t} = \imath\sqrt{\sin^2\theta_t - 1} = \imath\sqrt{\tfrac{n_1^2}{n_2^2}\sin^2\theta_i - 1} \ ,$$

applying Snell's law. Inserting this into the equation for $\mathbf{k}_t$,

$$\mathbf{k}_t = k_t\left(\frac{n_1}{n_2}\hat{\mathbf{e}}_x \sin\theta_i + \imath\hat{\mathbf{e}}_z\sqrt{\frac{n_1^2}{n_2^2}\sin^2\theta_i - 1}\right) \equiv k\hat{\mathbf{e}}_x + \imath\kappa\hat{\mathbf{e}}_z \ ,$$

where

$$k \equiv \frac{\omega n_1}{c}\sin\theta_i \qquad and \qquad \kappa = \frac{\omega}{c}\sqrt{n_1^2\sin^2\theta_i - n_2^2} \ .$$

That is, we venture into the realm of complex variables, where θ_t can no longer be interpreted as a geometric angle. Nevertheless, we will continue with the analysis and see what happens. First, we look at the electric field, which has the general form,

$$\vec{\tilde{\mathcal{E}}}_t(\mathbf{r},t) = \vec{\tilde{\mathcal{E}}}_{0t}e^{\imath(\mathbf{k}_t\cdot\mathbf{r}-\omega t)} \ .$$

Replacing the wavevector, we obtain,

$$\vec{\tilde{\mathcal{E}}}_t(\mathbf{r},t) = \vec{\tilde{\mathcal{E}}}_{0t}e^{-\kappa z}e^{\imath(kx-\omega t)} \ .$$

That is, the transmitted wave propagates in x-direction (parallel to the interface) and is attenuated in z-direction.
b. How much of the wave is reflected in this case? For a wave polarized parallel to the incident plane (i.e. $\vec{\mathcal{E}}$ has only a x-component), we previously found that the reflected amplitude is,

$$\mathcal{E}_r = \frac{\alpha-\beta}{\alpha+\beta}\mathcal{E}_i \ ,$$

where,

$$\alpha \equiv \frac{\cos\theta_t}{\cos\theta_i} \qquad , \qquad \beta \equiv \frac{\mu_1\nu_1}{\mu_2\nu_2} = \frac{\mu_1 n_2}{\mu_2 n_1} \ .$$

In this case, α is purely imaginary and β is real, so the reflection coefficient is,

$$R = \left|\frac{\mathcal{E}_r}{\mathcal{E}_i}\right|^2 = \left|\frac{\alpha-\beta}{\alpha+\beta}\right|^2 = 1 \ ,$$

since,

$$|\alpha-\beta|^2 = |\alpha|^2 + \beta^2 = |\alpha+\beta|^2 \ .$$

c. For perpendicular polarization, we have,

$$\mathcal{E}_r = \frac{1-\alpha\beta}{1+\alpha\beta}\mathcal{E}_i \ ,$$

and once again, since 1 is real and $\alpha\beta$ is purely imaginary,

$$R = \left|\frac{1-\alpha\beta}{1+\alpha\beta}\right|^2 = 1 \ .$$

Thus, the reflection is, in fact, total for both polarizations.
d. Still with perpendicular polarization, the electric field lies entirely in y-direction, so,

$$\vec{\tilde{\mathcal{E}}}_t = \vec{\tilde{\mathcal{E}}}_0 e^{-\kappa z} e^{\imath(kx-\omega t)} \hat{\mathbf{e}}_y \ .$$

The magnetic field is (replacing the wavevector and with $\mathbf{k}_t = \frac{\omega n_2}{c}\hat{\mathbf{e}}_{k_t}$ and $\nu_2 = c/n_2$),

$$\vec{\tilde{\mathcal{B}}}_t = \frac{1}{\nu_2}\mathbf{k}_t \times \vec{\tilde{\mathcal{E}}}_t = \frac{1}{\nu_2}\frac{c}{\omega n_2}\tilde{\mathcal{E}}_0 e^{-\kappa z} e^{\imath(kx-\omega t)}(k\hat{\mathbf{e}}_z - \imath\kappa\hat{\mathbf{e}}_x) = \frac{\tilde{\mathcal{E}}_0}{\omega} e^{-\kappa z} e^{\imath(kx-\omega t)}(k\hat{\mathbf{e}}_z - \imath\kappa\hat{\mathbf{e}}_x) \ .$$

Taking the real parts to get the real fields, we have,

$$\vec{\mathcal{E}}_t = \mathcal{E}_0 e^{-\kappa z}\cos(kx-\omega t)\hat{\mathbf{e}}_y \quad , \quad \vec{\mathcal{B}}_t = \frac{\mathcal{E}_0}{\omega} e^{-\kappa z}[k\cos(kx-\omega t)\hat{\mathbf{e}}_z + \kappa\sin(kx-\omega t)\hat{\mathbf{e}}_x] \ .$$

e. To verify whether these fields satisfy the Maxwell equations, we first calculate the divergences,

$$\nabla\cdot\vec{\mathcal{E}}_t = 0 = \nabla\cdot\vec{\mathcal{B}}_t \ .$$

The rotations yield,

$$\nabla\times\vec{\mathcal{E}}_t = \mathcal{E}_0 e^{-\kappa z}[-k\sin(kx-\omega t)\hat{\mathbf{e}}_z + \kappa\cos(kx-\omega t)\hat{\mathbf{e}}_x = -\frac{\partial\vec{\mathcal{B}}_t}{\partial t}$$

$$\nabla\times\vec{\mathcal{B}}_t = \frac{\mathcal{E}_0}{\omega}e^{-\kappa z}\sin(kx-\omega t)\hat{\mathbf{e}}_y(k^2-\kappa^2) = \frac{n_2^2}{c^2}\omega\mathcal{E}_0 e^{-\kappa z}\sin(kx-\omega t)\hat{\mathbf{e}}_y = \frac{1}{\nu_2^2}\frac{\partial\vec{\mathcal{E}}_t}{\partial t} \ .$$

Thus, all four Maxwell equations are satisfied.
f. The Poynting vector is,

$$\vec{\mathcal{S}} = \tfrac{1}{\mu_0}\vec{\mathcal{E}}_t\times\vec{\mathcal{B}}_t = \frac{\mathcal{E}_0^2 e^{-2\kappa z}}{\mu_0\omega}[k\cos^2(kx-\omega t)\hat{\mathbf{e}}_x - \kappa\sin(kx-\omega t)\cos(kx-\omega t)\hat{\mathbf{e}}_z] \ .$$

Integrating this over a cycle ($t = 0$ to $2\pi/\omega$) Gives zero for the component z, so no energy is transmitted perpendicular to the interface, and all energy flows in x-direction, parallel to the interface.

18.1.8.23 Ex: Fresnel formulae

Rewrite the Fresnel formulae (18.61) and (18.63) in terms of the wavevectors of the incident, reflected and transmitted waves.

Solution: *Exploiting,*

$$\frac{k_2}{k_1} = \frac{c_1}{c_2} = \frac{n_2}{n_1} = \sqrt{\frac{\varepsilon_2\mu_2}{\varepsilon_1\mu_1}}$$

and with $k_{zm} = k_m \cos\theta_m$ for $m = i, r, t$, Eq. (18.61) for p-polarization can be rewritten as,

$$r^p = \frac{\varepsilon_1\mu_1 k_{zt} - \varepsilon_2\mu_2 k_{zi}}{\varepsilon_1\mu_1 k_{zt} + \varepsilon_2\mu_2 k_{zi}} \ ,$$

and Eq. (18.63) for s-polarization as,

$$r^s = \frac{k_{zt} - k_{zi}}{k_{zi} + k_{zt}} \ .$$

18.1.8.24 Ex: The Goos-Hänchen effect

The Goos-Hänchen shift is an optical phenomenon in which a linearly polarized light beam with finite transverse extension suffers, under total internal reflection from a plane interface, a small lateral displacement within the plane of incidence. The effect is due to an interference of the partial waves composing the finite-sized beam, hitting the interface under different angles and thus undergoing different phase shifts upon reflection. The sum of the reflected waves with different phase shifts form an interference pattern transverse to the mean propagation direction leading to a lateral displacement of the beam. Thus, the Goos-Hänchen effect is a coherence phenomenon [522, 523, 659].

To describe this phenomenon quantitatively, we consider a linearly polarized light beam of wavelength λ, with finite transverse size. This beam is fully internally reflected at the interface between two non-permeable media with refractive indices n_1 and $n_2 < n_1$. The relationship between the reflected and incident amplitudes is a complex number, which can be expressed by $\mathcal{E}_0''/\mathcal{E}_0 = e^{\imath\phi(\theta_i,\theta_{i,total})}$ for the angle of incidence $\theta_i > \theta_{i,total}$, where $\sin\theta_{i,total} = \frac{n_2}{n_1}$.

a. Show that for a beam of 'monochromatic' radiation in z-direction with an electric field amplitude of $\mathcal{E}(x)e^{\imath kz - \imath\omega t}$, where $\mathcal{E}(x)$ is smooth and finite in transverse direction (albeit extending over many wavelengths), the first approximation in terms of plane waves is,

$$\vec{\mathcal{E}}(x,z,t) = \hat{\epsilon}\int A(\kappa)e^{\imath\kappa x + \imath kz - \imath\omega t}d\kappa \ ,$$

where $\hat{\epsilon}$ is a polarization vector and $A(\kappa)$ is the Fourier transform of $\mathcal{E}(x)$ with respect to κ around $\kappa = 0$ small compared to k. The finite-sized beam consists of plane waves with a small range of angles of incidence centered around the valor predicted by geometric optics.

b. Consider the reflected beam and show that for $\theta_i > \theta_{i,total}$ the electric field can be expressed approximately as,

$$\vec{\mathcal{E}}_r(x,z,t) = \hat{\epsilon}_r\mathcal{E}(\xi - \delta\xi)e^{\imath\mathbf{k}_r\cdot\mathbf{r} - \imath\omega t + \imath\phi(\theta_i)} \ ,$$

where $\hat{\epsilon}_r$ is a polarization vector, ξ is the coordinate perpendicular to $\mathbf{k}_r$, which is the reflected wavevector and $\delta\xi = -\frac{1}{k}\frac{d\phi(\theta_i)}{d\theta_i}$.

c. With the Fresnel expressions for the phases $\phi(\theta_i)$ and for the two polarization states

of the plane, show that the lateral displacements of the beams with respect to the position predicted by geometric optics are,

$$\mathcal{D}_s = \frac{\lambda}{\pi}\frac{\sin\theta_i}{\sqrt{\sin^2\theta_i - \sin^2\theta_{i,total}}} \qquad \text{and} \qquad \mathcal{D}_p = \mathcal{D}_s \frac{\sin^2\theta_{i,total}}{\sin^2\theta_i - \cos^2\theta_i \sin^2\theta_{i,total}} \ .$$

Solution: *a. The purpose of this part is to show that, when a light beam has a finite diameter, it can be expanded into a superposition of partial planes wave of infinite radial extent. We therefore write the finite beam as,* $\vec{\mathcal{E}}(x,z,t) = \hat{\epsilon}E(x)e^{\imath kz-\imath\omega t}$ *with* $k = \frac{\omega}{c}n_1$*, and we insert this ansatz into the wavefunction,*

$$-\frac{\omega^2}{c^2}\vec{\mathcal{E}} = \frac{1}{c^2}\frac{\partial^2\vec{\mathcal{E}}}{\partial t^2} = \nabla^2\vec{\mathcal{E}} = -k^2\hat{\epsilon}\mathcal{E}(x)e^{\imath kz-\imath\omega t} + \hat{\epsilon}\frac{d^2\mathcal{E}(x)}{dx^2}e^{\imath kz-\imath\omega t}$$
$$= \hat{\epsilon}e^{\imath kz-\imath\omega t}\left(-k^2\mathcal{E}(x) + \frac{d^2\mathcal{E}(x)}{dx^2}\right) \ .$$

Now, we express $\mathcal{E}(x)$ *by its Fourier transform,* $A(\kappa) = \frac{1}{2\pi}\int \mathcal{E}(x)e^{-\imath\kappa x}dx$*. Thus* [8]*,*

$$-\frac{\omega^2}{c^2}\vec{\mathcal{E}} = \hat{\epsilon}e^{\imath kz-\imath\omega t}\mathcal{F}\left[-k^2\widetilde{\mathcal{E}(x)} + \widetilde{\frac{d^2\mathcal{E}(x)}{dx^2}}\right] = \hat{\epsilon}e^{\imath kz-\imath\omega t}\mathcal{F}\left[-k^2A(\kappa) + (\imath\kappa)^nA(\kappa)\right]$$
$$= \hat{\epsilon}e^{\imath kz-\imath\omega t}\int(-k^2-\kappa^2)A(\kappa)e^{\imath\kappa x}d\kappa$$
$$= \hat{\epsilon}\nabla^2\int A(\kappa)e^{\imath\kappa x+\imath kz-\imath\omega t}d\kappa = \hat{\epsilon}\nabla^2\left[\mathcal{E}(x)e^{\imath kz-\imath\omega t}\right] = \nabla^2\vec{\mathcal{E}} \ .$$

That is, the wave equation is satisfied under the condition $\mathcal{E}(x) = \int A(\kappa)e^{\imath\kappa x}dx$*, that is,* $\mathcal{E}(x)$ *can be understood as a distribution of partial wave amplitudes with wavevectors* κ*.*

b. Taking into account the angular distribution of the partial waves composing the light beam, the incident wave can be written as,

$$\vec{\mathcal{E}}_i(x,z,t) = \hat{\epsilon}\int A(\kappa)e^{\imath(\mathbf{k}_i+\vec{\kappa}_i)\cdot\mathbf{r}-\imath\omega t}d\kappa \qquad \textit{with} \qquad \begin{cases}\mathbf{k}_i = k(\hat{\mathbf{e}}_x\sin\theta_i + \hat{\mathbf{e}}_z\cos\theta_i)\\ \vec{\kappa}_i = \kappa(\hat{\mathbf{e}}_x\cos\theta_i - \hat{\mathbf{e}}_z\sin\theta_i)\end{cases}$$
$$= \hat{\epsilon}\int A(\kappa)e^{\imath k\zeta+\imath\kappa\xi-\imath\omega t}d\kappa \qquad \textit{with} \qquad \begin{cases}\zeta = x\sin\theta_i + z\cos\theta_i\\ \xi = x\cos\theta_i - z\sin\theta_i\end{cases} \ .$$

For a narrow distribution of partial waves we can approximate $\kappa \simeq k\delta\theta$*. Consequently, taking account of a phase shift* $\phi_i \equiv \phi(\theta_i+\delta\theta)$*, which depends on the angle of incidence,*

[8] A property of the Fourier transform defined by $\tilde{f}(\kappa) = \frac{1}{\sqrt{2\pi}}\int f(x)e^{-\imath\kappa x}dx$ is,

$$\left[\widetilde{\frac{d^nf}{dx^n}}\right](\kappa) = \frac{1}{\sqrt{2\pi}}\int\frac{d^nf(x)}{dx^n}e^{-\imath\kappa x}dx = \frac{(\imath\kappa)^n}{\sqrt{2\pi}}\int f(x)e^{-\imath\kappa x}dx = (\imath\kappa)^n\tilde{f}(\kappa) \ .$$

the reflected wave can be written as,

$$\begin{aligned}
\vec{\mathcal{E}}_r(x,z,t) &= \hat{\epsilon}\int A(\kappa)e^{\imath(\mathbf{k}_r+\vec{\kappa}_r)\cdot\mathbf{r}-\imath\omega t+\imath\phi_i}d\kappa \qquad with \qquad \begin{cases}\mathbf{k}_r = k(\hat{\mathbf{e}}_x\sin\theta_i - \hat{\mathbf{e}}_z\cos\theta_i)\\ \vec{\kappa}_r = \kappa(\hat{\mathbf{e}}_x\cos\theta_i + \hat{\mathbf{e}}_z\sin\theta_i)\end{cases}\\
&= \hat{\epsilon}\int A(\kappa)e^{\imath\kappa\xi+\imath k\zeta-\imath\omega t+\imath\phi_i}d\kappa \qquad with \qquad \begin{cases}\zeta = x\sin\theta_i - z\cos\theta_i\\ \xi = x\cos\theta_i + z\sin\theta_i\end{cases}\\
&= \hat{\epsilon}e^{\imath k(x\sin\theta_i - z\cos\theta_i)-\imath\omega t+\imath\phi_i}\int A(\kappa)e^{\imath\kappa(x\cos\theta_i+z\sin\theta_i)}d\kappa\\
&= \hat{\epsilon}e^{\imath k\zeta-\imath\omega t}\int A(\kappa)e^{\imath\kappa\xi+\imath\phi_i}d\kappa\ .
\end{aligned}$$

We expand the phase shift [9]*,*

$$\phi_i = \phi(\theta_i+\delta\theta) = \phi(\theta_i) + \delta\theta\frac{d\phi(\theta_i)}{d\theta_i} = \phi(\theta_i) - \kappa\delta\xi \qquad with \qquad \delta\xi \equiv -\frac{1}{k}\frac{d\phi(\theta_i)}{d\theta_i}\ ,$$

and insert it into the expression for the reflected field,

$$\vec{\mathcal{E}}_r(x,z,t) = \hat{\epsilon}e^{\imath k\zeta-\imath\omega t+\phi(\theta_i)}\int A(\kappa)e^{\imath\kappa\xi-\imath\kappa\delta\xi}d\kappa = \hat{\epsilon}e^{\imath k\zeta-\imath\omega t}\mathcal{E}(\xi-\delta\xi)\ .$$

c. Now we just need to calculate the transverse displacements,

$$\mathcal{D}_{s,p} \equiv d\xi_{s,p} = -\frac{1}{k}\frac{d\phi_{s,p}(\theta_i)}{d\theta_i}\ .$$

To do this, using the definitions,

$$\alpha \equiv \frac{\cos\theta_t}{\cos\theta_i} \qquad with \qquad \cos\theta_t = \imath\sqrt{\frac{n_1^2}{n_2^2}\sin^2\theta_i - 1} \qquad and \qquad \beta \equiv \frac{n_2}{n_1}\ ,$$

we first calculate the reflection coefficient for s-polarization,

$$r_s = \frac{1-\alpha\beta}{1-\alpha\beta} = \frac{1-\frac{\imath\sin\theta_{i,total}}{\cos\theta_i}\sqrt{\frac{n_1^2}{n_2^2}\sin^2\theta_i-1}}{1+\frac{\imath\sin\theta_{i,total}}{\cos\theta_i}\sqrt{\frac{n_1^2}{n_2^2}\sin^2\theta_i-1}} = \frac{\cos\theta_i - \imath\sqrt{\sin^2\theta_i-\sin^2\theta_{i,total}}}{\cos\theta_i+\imath\sqrt{\sin^2\theta_i-\sin^2\theta_{i,total}}}\ .$$

The imaginary and real parts are,

$$\mathfrak{Im}\ r_s = \frac{-2\cos\theta_i\sqrt{\sin^2\theta_i-\sin^2\theta_{i,total}}}{1-\sin^2\theta_{i,total}} \quad , \quad \mathfrak{Re}\ r_p = \frac{\cos^2\theta_i - \sin^2\theta_i + \sin^2\theta_{i,total}}{1-\sin^2\theta_{i,total}}\ ,$$

[9] Other properties of the Fourier transform are,

$$\widetilde{[fg]}(\kappa) = \frac{1}{\sqrt{2\pi}}\int f(x)g(x)e^{-\imath\kappa x}dx = \frac{1}{2\pi}\int\int\int f(x')e^{-\imath\kappa' x'}g(x)e^{-\imath(\kappa-\kappa')x}d\kappa' dx dx' = \frac{1}{\sqrt{2\pi}}[\tilde{f}\star\tilde{g}](\kappa)$$

$$\widetilde{[e^{iqx}]}(\kappa) = \frac{1}{\sqrt{2\pi}}\int e^{iqx}e^{-\imath\kappa x}dx = \sqrt{2\pi}\delta(q-\kappa)$$

$$\widetilde{[fe^{iqx}]}(\kappa) = \frac{1}{\sqrt{2\pi}}\int f(x)e^{iqx}e^{-\imath\kappa x}dx = \frac{1}{\sqrt{2\pi}}\int f(x)e^{\imath(q-\kappa)x}dx = f(q-\kappa)\ .$$

and the phase shift,

$$\phi_s = \arctan \frac{\mathfrak{Im}\ r_s}{\mathfrak{Re}\ r_s} = \arctan \frac{-2\cos\theta_i \sqrt{\sin^2\theta_i - \sin^2\theta_{i,total}}}{\cos^2\theta_i - \sin^2\theta_i + \sin^2\theta_{i,total}} \ .$$

Finally, the transverse displacement is,

$$\mathcal{D}_s = -\frac{1}{k}\frac{d\phi_s}{d\theta_i} = \frac{2}{k}\frac{\sin\theta}{\sqrt{\sin^2\theta - \sin^2\theta_{i,total}}} \ .$$

An analogous calculation for p-polarization gives the reflection coefficient,

$$r_p = \frac{\alpha - \beta}{\alpha + \beta} = \frac{\frac{\cos\theta_t}{\cos\theta_i} - \frac{n_2}{n_1}}{\frac{\cos\theta_t}{\cos\theta_i} + \frac{n_2}{n_1}} = \frac{\imath\sqrt{\sin^2\theta_i - \sin^2\theta_{i,total}} - \cos\theta_i \sin^2\theta_{i,total}}{\imath\sqrt{\sin^2\theta_i - \sin^2\theta_{i,total}} + \cos\theta_i \sin^2\theta_{i,total}} \ .$$

The imaginary and real parts are,

$$\mathfrak{Im}\ r_p = \frac{2\cos\theta_i \sin^2\theta_{i,total}\sqrt{\sin^2\theta_i - \sin^2\theta_{i,total}}}{\sin^2\theta_i - \sin^2\theta_{i,total} + \cos^2\theta_i \sin^4\theta_{i,total}} \ ,$$

$$\mathfrak{Re}\ r_p = \frac{\sin^2\theta_i - \sin^2\theta_{i,total} - \cos^2\theta_i \sin^4\theta_{i,total}}{\sin^2\theta_i - \sin^2\theta_{i,total} + \cos^2\theta_i \sin^4\theta_{i,total}} \ ,$$

and the phase shift,

$$\phi_p = \arctan \frac{\mathfrak{Im}\ r_p}{\mathfrak{Re}\ r_p} = \arctan \frac{2\cos\theta_i \sin^2\theta_{i,total}\sqrt{\sin^2\theta_i - \sin^2\theta_{i,total}}}{\sin^2\theta_i - \sin^2\theta_{i,total} - \cos^2\theta_i \sin^4\theta_{i,total}} \ .$$

Finally, the transverse displacement is,

$$\begin{aligned}\mathcal{D}_p = -\frac{1}{k}\frac{d\phi_p}{d\theta_i} &= -\frac{1}{k}\frac{2\sin\theta\sin^2\theta_{i,total}}{\left(\cos^2\theta\sin^2\theta_{i,total} - \sin^2\theta\right)\sqrt{\sin^2\theta - \sin^2\theta_{i,total}}} \\ &= \frac{\mathcal{D}_s \sin^2\theta_{i,total}}{\sin^2\theta - \cos^2\theta\sin^2\theta_{i,total}} \ .\end{aligned}$$

18.1.8.25 Ex: Interfaces

A light field of angular frequency ω passes from a medium (1), through a slab of thickness d representing a medium (2), to a medium (3). All three media are linear and homogeneous. Calculate the transmission coefficient between the media 1 and 3 for normal incidence.

Solution: *The transfer of the electric field through a system characterized by a matrix* $\mathcal{M}_{13}$ *is given by,*

$$\begin{pmatrix} \mathcal{E}_3^+ \\ 0 \end{pmatrix} = M_{13} \begin{pmatrix} \mathcal{E}_1^+ \\ \mathcal{E}_1^- \end{pmatrix} = M_{23} M_d M_{12} \begin{pmatrix} \mathcal{E}_1^+ \\ \mathcal{E}_1^- \end{pmatrix} ,$$

or equivalently,

$$\begin{pmatrix} \mathcal{E}_1^+ \\ \mathcal{E}_1^- \end{pmatrix} = M_{13}^{-1} \begin{pmatrix} \mathcal{E}_3^+ \\ 0 \end{pmatrix} = M_{12}^{-1} M_d^{-1} M_{23}^{-1} \begin{pmatrix} \mathcal{E}_3^+ \\ 0 \end{pmatrix} = M_{21} M_d M_{32} \begin{pmatrix} \mathcal{E}_3^+ \\ 0 \end{pmatrix} ,$$

exploiting the simple fact that $M_{12}^{-1} = M_{21}$*. Now, we find,*

$$\begin{aligned} \begin{pmatrix} \mathcal{E}_1^+ \\ \mathcal{E}_1^- \end{pmatrix} &= \frac{1}{2n_1} \begin{pmatrix} n_1+n_2 & n_1-n_2 \\ n_1-n_2 & n_1+n_2 \end{pmatrix} \begin{pmatrix} e^{-\imath k_2 d} & 0 \\ 0 & e^{\imath k_2 d} \end{pmatrix} \frac{1}{2n_2} \begin{pmatrix} n_2+n_3 & n_2-n_3 \\ n_2-n_3 & n_2+n_3 \end{pmatrix} \begin{pmatrix} \mathcal{E}_3^+ \\ 0 \end{pmatrix} \\ &= \frac{1}{4n_2 n_1} \begin{pmatrix} (n_2+n_1)e^{-\imath k_2 d}(n_2+n_3) + (n_1-n_2)e^{\imath k_2 d}(n_2-n_3) \\ (n_1-n_2)e^{-\imath k_2 d}(n_2+n_3) + (n_2+n_1)e^{\imath k_2 d}(n_2-n_3) \end{pmatrix} \mathcal{E}_3^+ , \end{aligned}$$

such that the transmission becomes,

$$\begin{aligned} T = \frac{I_3}{I_1} &= \frac{\varepsilon_3 c_3 |\mathcal{E}_3^+|^2}{\varepsilon_1 c_1 |\mathcal{E}_1^+|^2} = \frac{n_3}{n_1} \frac{|\mathcal{E}_3^+|^2}{|\mathcal{E}_1^+|^2} \\ &= \frac{n_3}{n_1} \frac{(4n_2 n_1)^2}{\left|(n_2+n_1)e^{-\imath k_2 d}(n_2+n_3) + (n_1-n_2)e^{\imath k_2 d}(n_2-n_3)\right|^2} \\ &= \frac{4n_1 n_2^2 n_3}{n_2^2(n_1+n_3)^2 + (n_1^2-n_2^2)(n_3^2-n_2^2)\sin^2 k_2 d} . \end{aligned}$$

18.2 Optical dispersion in material media

18.2.1 Plane waves in conductive media

When there are free charges in the propagation medium, we can not neglect neither ϱ_f nor $\mathbf{j}_f$ in the Maxwell equations used to describe the wave propagation, because the electric field of the wave will itself generate a current $\mathbf{j}_f = \varsigma \vec{\mathcal{E}}$, where ς is the conductivity introduced in Eq. (14.42). Thus, for linear media we must use the complete equations (17.6).

For a homogeneous and linear medium, the continuity equation gives,

$$\frac{\partial \varrho_f}{\partial t} = -\nabla \cdot \mathbf{j}_f = -\varsigma \nabla \cdot \vec{\mathcal{E}} = -\frac{\varsigma}{\varepsilon} \varrho_f , \tag{18.81}$$

with the solution

$$\varrho_f(t) = e^{-(\varsigma/\varepsilon)t} \varrho_f(0) . \tag{18.82}$$

Therefore, every initial free charge density $\varrho_f(0)$ diffuses within a characteristic time $\tau = \varepsilon/\varsigma$. This reflects the familiar fact that free charges in a conductor migrate to its edges with a speed that depends on the conductivity ς. For a good conductor, the relaxation time is much shorter than other characteristic times of the system, e.g. for oscillatory systems $\tau \ll \omega^{-1}$. In stationary situations we can assume, $\varrho = 0$, such that the relevant Maxwell equations,

$$\begin{array}{lrcl} \text{(i)} & \nabla \times \vec{\mathcal{B}} - \varepsilon\mu\partial_t\vec{\mathcal{E}} &=& \mu\varsigma\vec{\mathcal{E}} \\ \text{(ii)} & \nabla \times \vec{\mathcal{E}} + \partial_t\vec{\mathcal{B}} &=& 0 \\ \text{(iii)} & \nabla \cdot \vec{\mathcal{E}} &=& 0 \\ \text{(iv)} & \nabla \cdot \vec{\mathcal{B}} &=& 0 \end{array} \quad , \tag{18.83}$$

only differ from the Maxwell equations for dielectric media by the existence of the term $\mu\varsigma\vec{\mathcal{E}}$.

Letting the rotation operator act on equations (i) and (ii) and exploiting the disappearance of the field divergences we obtain generalized wave equations,

$$\nabla^2\vec{\mathcal{E}} = \varepsilon\mu\frac{\partial^2\vec{\mathcal{E}}}{\partial t^2} + \varsigma\mu\frac{\partial\vec{\mathcal{E}}}{\partial t} \qquad \text{and} \qquad \nabla^2\vec{\mathcal{B}} = \varepsilon\mu\frac{\partial^2\vec{\mathcal{B}}}{\partial t^2} + \varsigma\mu\frac{\partial\vec{\mathcal{B}}}{\partial t} \ . \tag{18.84}$$

These equations still accept plane wave solutions,

$$\vec{\mathcal{E}}(z,t) = \vec{\mathcal{E}}_0 e^{\imath(\tilde{k}z-\omega t)} \qquad \text{and} \qquad \vec{\mathcal{B}}(z,t) = \vec{\mathcal{B}}_0 e^{\imath(\tilde{k}z-\omega t)} \ , \tag{18.85}$$

but this time the wavevector is complex,

$$\tilde{k}^2 = \varepsilon\mu\omega^2 + \imath\varsigma\mu\omega \ , \tag{18.86}$$

which can easily be verified by inserting a plane wave into the wave equations (18.84). The root of this expression gives,

$$\boxed{\begin{array}{lllll} \tilde{k} = k + \imath\kappa & \text{with} & k & \equiv \omega\sqrt{\frac{\varepsilon\mu}{2}}\left(\sqrt{1+\left(\frac{\varsigma}{\varepsilon\omega}\right)^2}+1\right)^{1/2} \\ & \text{and} & \kappa & \equiv \omega\sqrt{\frac{\varepsilon\mu}{2}}\left(\sqrt{1+\left(\frac{\varsigma}{\varepsilon\omega}\right)^2}-1\right)^{1/2} \end{array}} \ . \tag{18.87}$$

The imaginary part results in an attenuation of the wave in z-direction:

$$\vec{\tilde{\mathcal{E}}}(z,t) = \vec{\tilde{\mathcal{E}}}_0 e^{-\kappa z} e^{\imath(kz-\omega t)} \qquad \text{and} \qquad \vec{\tilde{\mathcal{B}}}(z,t) = \vec{\tilde{\mathcal{B}}}_0 e^{-\kappa z} e^{\imath(kz-\omega t)} \ . \tag{18.88}$$

The typical attenuation distance, κ^{-1}, called *skin depth*, measures the penetration depth of the wave in a conductor, while the real part k determines the propagation of the wave. As before, the equations (18.83)(iii) and (iv) exclude components perpendicular to the interface. The wave only has transverse components, that is, parallel to the interface, so that we can let the electric field be along $\hat{\mathbf{e}}_x$,

$$\vec{\tilde{\mathcal{E}}}(z,t) = \tilde{\mathcal{E}}_0\hat{\mathbf{e}}_x e^{-\kappa z} e^{\imath(kz-\omega t)} \qquad \text{and} \qquad \vec{\tilde{\mathcal{B}}}(z,t) = \tilde{\mathcal{B}}_0\hat{\mathbf{e}}_y e^{-\kappa z} e^{\imath(kz-\omega t)} \ . \tag{18.89}$$

By the equation (18.83)(ii) we verify,

$$\tilde{\mathcal{B}}_0 = \frac{\tilde{k}}{\omega}\tilde{\mathcal{E}}_0 \ . \tag{18.90}$$

Expressing the wavevector and the complex amplitudes by phase factors,

$$\tilde{k} = Ke^{\imath\phi} \quad , \quad \tilde{\mathcal{E}}_0 = \mathcal{E}_0 e^{\imath\delta_E} \quad , \quad \tilde{\mathcal{B}}_0 = \mathcal{B}_0 e^{\imath\delta_B} \ , \tag{18.91}$$

with $K, \mathcal{E}_0, \mathcal{B}_0 \in \mathbb{R}$, we finally find,

$$\mathcal{B}_0 e^{\imath\delta_B} = \frac{Ke^{\imath\phi}}{\omega}\mathcal{E}_0 e^{\imath\delta_E} \ , \tag{18.92}$$

that is,

$$\frac{\mathcal{B}_0}{\mathcal{E}_0} = \frac{K}{\omega} = \frac{\sqrt{k^2+\kappa^2}}{\omega} = \sqrt{\varepsilon\mu\sqrt{1+\left(\frac{\varsigma}{\varepsilon\omega}\right)^2}} \tag{18.93}$$

and

$$\begin{aligned} \vec{\mathcal{E}}(z,t) &= \mathcal{E}_0\hat{\mathbf{e}}_x e^{-\kappa z}\cos(kz-\omega t+\delta_E) \\ \vec{\mathcal{B}}(z,t) &= \mathcal{B}_0\hat{\mathbf{e}}_y e^{-\kappa z}\cos(kz-\omega t+\delta_E+\phi) \ , \end{aligned} \tag{18.94}$$

as illustrated in Fig. 18.9. Such a wave is called *evanescent wave*. From Eqs. (18.93) and (18.87) we immediately deduce,

$$\begin{aligned} K &\overset{\varsigma\to 0}{\longrightarrow} \frac{\omega}{c_n} \quad \text{and} \quad \phi = \arctan\frac{\kappa}{k} \overset{\varsigma\to 0}{\longrightarrow} 0 \\ K &\overset{\varsigma\to\infty}{\longrightarrow} \infty \quad \text{and} \quad \phi \overset{\varsigma\to\infty}{\longrightarrow} \tfrac{\pi}{4} \ . \end{aligned} \tag{18.95}$$

Do the Exc. 18.2.7.1 and 18.2.7.2.

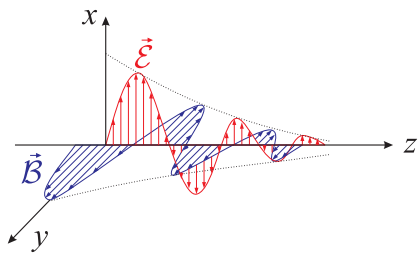

Figure 18.9: Attenuation of a wave by a conducting medium.

18.2.1.1 Reflection by a conductive surface

In the presence of free charges and currents the boundary conditions derived in (18.42) must be generalized,

$$\begin{array}{lrcl} \text{(i)} & \frac{1}{\mu_1}\vec{\mathcal{B}}_1^{\parallel} - \frac{1}{\mu_2}\vec{\mathcal{B}}_2^{\parallel} &=& \mathbf{k}_f \times \hat{\mathbf{e}}_n \\ \text{(ii)} & \vec{\mathcal{E}}_1^{\parallel} - \vec{\mathcal{E}}_2^{\parallel} &=& 0 \\ \text{(iii)} & \varepsilon_1\vec{\mathcal{E}}_1^{\perp} - \varepsilon_2\vec{\mathcal{E}}_2^{\perp} &=& \sigma_f \\ \text{(iv)} & \vec{\mathcal{B}}_1^{\perp} - \vec{\mathcal{B}}_1^{\perp} &=& 0 \end{array} \quad , \tag{18.96}$$

where σ_f is the density of free surface charges, $\mathbf{k}_f$ is the density of free surface currents, and $\hat{\mathbf{e}}_n$ the normal vector of the surface pointing into the direction of medium 1 (compare with Fig. 15.17).

We now assume that the interface at $z = 0$ separates the dielectric medium 1 from the conductive medium 2. A monochromatic plane wave is partially reflected and transmitted, as discussed above,

$$\begin{array}{lcl} \vec{\tilde{\mathcal{E}}}_i(z,t) = \tilde{\mathcal{E}}_{0i}\hat{\mathbf{e}}_x e^{\imath(k_1 z - \omega t)} & , & \vec{\tilde{\mathcal{B}}}_i(z,t) = -\frac{1}{c_1}\tilde{\mathcal{E}}_{0i}\hat{\mathbf{e}}_y e^{\imath(k_1 z - \omega t)} \\ \vec{\tilde{\mathcal{E}}}_r(z,t) = \tilde{\mathcal{E}}_{0r}\hat{\mathbf{e}}_x e^{\imath(-k_1 z - \omega t)} & , & \vec{\tilde{\mathcal{B}}}_r(z,t) = \frac{1}{c_1}\tilde{\mathcal{E}}_{0r}\hat{\mathbf{e}}_y e^{\imath(k_1 z - \omega t)} \\ \vec{\tilde{\mathcal{E}}}_t(z,t) = \tilde{\mathcal{E}}_{0t}\hat{\mathbf{e}}_x e^{\imath(\tilde{k}_2 z - \omega t)} & , & \vec{\tilde{\mathcal{B}}}_t(z,t) = \frac{\tilde{k}_2}{\omega}\tilde{\mathcal{E}}_{0t}\hat{\mathbf{e}}_y e^{\imath(\tilde{k}_2 z - \omega t)} \end{array} \quad , \tag{18.97}$$

Obviously, the transmitted wave penetrating the conductive medium is attenuated.

The boundary conditions at $z = 0$ become, for the considered case ($\vec{\mathcal{E}}^{\perp} = 0 = \vec{\mathcal{B}}^{\perp}$) and with $\mathbf{k}_f = 0$,

$$\begin{array}{lrcl} \text{(i)} & \frac{1}{\mu_1 c_1}(\mathcal{E}_{0i} - \mathcal{E}_{0r}) &=& \frac{\tilde{k}_2}{\mu_2\omega}\mathcal{E}_{0t} \\ \text{(ii)} & \tilde{\mathcal{E}}_{0i} + \tilde{\mathcal{E}}_{0r} &=& \tilde{\mathcal{E}}_{0t} \\ \text{(iii)} & 0 &=& \sigma_f \\ \text{(iv)} & 0 &=& 0\ . \end{array} \quad , \tag{18.98}$$

Defining,

$$\tilde{\beta} \equiv \frac{\mu_1\tilde{k}_2}{\mu_2 k_1}\ , \tag{18.99}$$

we derive,

$$\frac{\tilde{\mathcal{E}}_{0r}}{\tilde{\mathcal{E}}_{0i}} = \frac{1-\tilde{\beta}}{1+\tilde{\beta}} \quad \text{and} \quad \frac{\tilde{\mathcal{E}}_{0t}}{\tilde{\mathcal{E}}_{0i}} = \frac{2}{1+\tilde{\beta}}\ . \tag{18.100}$$

The formulas are formally similar to (18.48), but they are complex. For a bad conductor ($\varsigma = 0 \quad \rightarrow \quad \kappa = 0$) we recover the equation (18.48). For a perfect conductor ($\varsigma = \infty \quad \rightarrow \quad \kappa = \infty \quad \rightarrow \quad \tilde{\beta} = \imath\infty$) we find $\tilde{\mathcal{E}}_{0r} = -\tilde{\mathcal{E}}_{0i}$ and $\tilde{\mathcal{E}}_{0t} = 0$. That is, the wave is fully reflected with a phase change of 180° [10].

[10] The 'skin depth' in silver (for optical frequencies) is in the order of 10 nm. For this reason, thin layers of good conductors already represent good mirrors.

18.2.2 Linear and quadratic dispersion

The refractive index may depend on the wavelength. Even the *refractive index of air* exhibits dispersion, as shown in Fig. 18.10 [11].

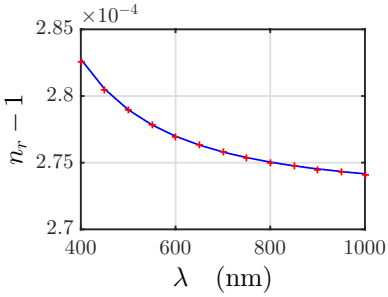

Figure 18.10: (code) Refractive index of air. The crosses were calculated by the Cauchy formula (18.146), with $A = 0.0002725$ and $B = 0.0059$.

We consider a superposition of two waves,

$$\begin{aligned} Y_1(x,t) + Y_2(x,t) &= a\cos(k_1 x - \omega_1 t) + a\cos(k_2 x - \omega_2 t) \\ &= 2a\cos\left[\tfrac{(k_1-k_2)x}{2} - \tfrac{(\omega_1-\omega_2)t}{2}\right]\cos\left[\tfrac{(k_1+k_2)x}{2} - \tfrac{(\omega_1+\omega_2)t}{2}\right] . \end{aligned} \tag{18.101}$$

The resulting wave can be seen as a wave of frequency $\frac{1}{2}(\omega_1+\omega_2)t$ and wavelength $\frac{1}{2}(k_1+k_2)$ whose amplitude is modulated by an envelope of frequency $\frac{1}{2}(\omega_1-\omega_2)t$ and wavelength $\frac{1}{2}(k_1-k_2)x$.

In the absence of dispersion the *phase velocities* of the two waves and the propagation velocity of the envelope, called *group velocity*, are equal,

$$c = \frac{\omega_1}{k_1} = \frac{\omega_2}{k_2} = \frac{\omega_1-\omega_2}{k_1-k_2} = \frac{\Delta\omega}{\Delta k} = v_g \ . \tag{18.102}$$

But the phase velocities of the two harmonic waves may be different, $c = c(k)$, such that the frequency depends on the wavelength, $\omega = \omega(k)$. In this case, the group velocity also varies with the wavelength,

$$v_g = \frac{d\omega}{dk} = \frac{d}{dk}(kc) = c + k\frac{dc}{dk} \ . \tag{18.103}$$

Often, this variation is not very strong, such that it is possible to expand around an average value ω_0 of the spectral region of interest,

$$\boxed{\begin{aligned} \omega(k) &= \omega_0 + \left.\frac{d\omega}{dk}\right|_{k_0}\cdot(k-k_0) + \frac{1}{2}\left.\frac{d^2\omega}{dk^2}\right|_{k_0}\cdot(k-k_0)^2 \\ &\equiv \omega_0 + v_g(k-k_0) + \beta(k-k_0)^2 \end{aligned}} \ . \tag{18.104}$$

[11] The refractive index of air can be calculated by the formula $n = 1 + (n_s - 1)\frac{0.00185097\ P}{1+0.003661\ T}$ with $n_s = \sqrt{1 + \frac{4.334446\cdot10^{-4}\lambda^2}{\lambda^2 - 3.470339\cdot10^{-3}} + \frac{1.118728\cdot10^{-4}\lambda^2}{\lambda^2 - 1.394001\cdot10^{-2}}}$, where T is the temperature in Celsius and P the atmospheric pressure in mbar.

Generally, $v_g < c$, in which situation we speak of *normal dispersion*. But there are situations of *anomalous dispersion*, where $v_g > c$, e.g. close to resonances or when the wave under study is a *matter wave* characterized by quadratic dispersion [12], $\hbar\omega = (\hbar k)^2/2m$.

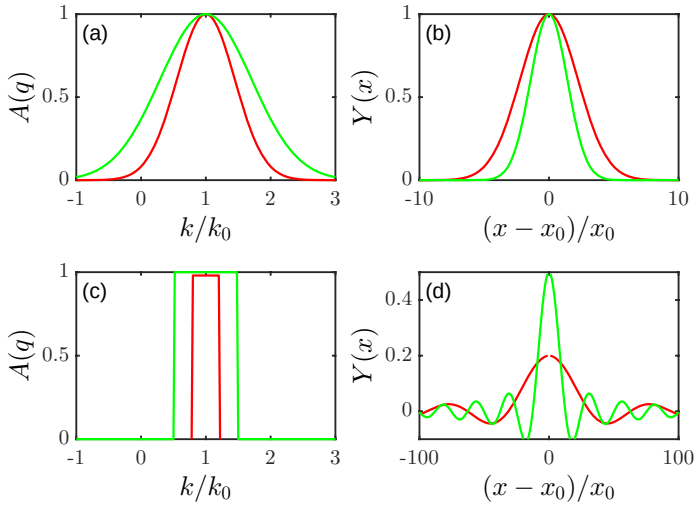

Figure 18.11: (code) Gaussian amplitude distribution (a,b) and rectangular distribution (c,d) in momentum space (a,c) and in position space (b,d).

Example 103 (*Rectangular wave packet with linear dispersion*): As an example we determine the shape of the wavepacket for a rectangular amplitude distribution, $A(k) = A_0\chi_{[k_0-\Delta k/2, k_0+\Delta k/2]}$, subject to linear dispersion (expansion up to the linear term in Eq. (18.104)). Via the Fourier theorem,

$$
\begin{aligned}
Y(x,t) &= \int_{-\infty}^{\infty} A(k) e^{\imath(kx-\omega t)} dk = A_0 \int_{k_0-\Delta k/2}^{k_0+\Delta k/2} e^{\imath(kx-\omega_0 t + v_g(k-k_0)t)} dk \\
&= A_0 e^{\imath(k_0 x-\omega_0 t)} \int_{k_0-\Delta k/2}^{k_0+\Delta k/2} e^{\imath(k-k_0)(x-v_g t)} dk \\
&= A_0 e^{\imath(k_0 x-\omega_0 t)} \int_{-\Delta k/2}^{\Delta k/2} e^{\imath k(\cancel{x - v_g t}^{\,u})} dk \\
&= A_0 \frac{e^{\imath u \Delta k/2} - e^{-\imath u \Delta k/2}}{\imath u} e^{\imath(k_0 x-\omega_0 t)} = 2A_0 \frac{\sin\frac{u\Delta k}{2}}{u} e^{\imath(k_0 x-\omega_0 t)} \equiv A(x,t) e^{\imath(k_0 x-\omega_0 t)} \,.
\end{aligned}
$$

The envelope $A(x,t)$ has the shape of a 'sinc' function, such that the wave intensity is,

$$|Y(x,t)|^2 = A_0^2 \Delta k^2 \ \mathrm{sinc}^2\left[\tfrac{\Delta k}{2}(x - v_g t)\right] \,.$$

Obviously, the *wave packet* is at any time t localized in space, as illustrated by the lower graphs of Figs. 18.11. It *moves with group velocity*, v_g, but it does not spread.

[12] Since $c = \frac{\omega}{c} = \frac{\hbar k}{2m} < \frac{\hbar k}{m} = v_g$.

The last example showed, that linear dispersion does not lead to spreading (or diffusion) of a wavepacket, as opposed to quadratic dispersion, which we will show in the following example.

Example 104 (*Dispersion of a Gaussian wavepacket subject to quadratic dispersion*): Quadratic dispersion causes spreading of wavepackets. We show this at the example of the Gaussian wavepacket, $A(k) = A_0 e^{-\alpha(k-k_0)^2}$, expanding the dispersion relation (18.104) up to the quadratic term. Via the Fourier theorem,

$$\begin{aligned} Y(x,t) &= \int_{-\infty}^{\infty} A(k) e^{\imath(kx-\omega t)} dk = A_0 e^{\imath(k_0 x - \omega_0 t)} \int_{-\infty}^{\infty} e^{\imath(k-k_0)(x-v_g t) - (\alpha + \imath\beta t)(k-k_0)^2} dk \\ &= A_0 e^{\imath(k_0 x - \omega_0 t)} \int_{-\infty}^{\infty} e^{\imath k(\cancel{x - v_g t}^{\,u}) - (\cancel{\alpha + \imath\beta t}^{\,v})k^2} dk \\ &\equiv A_0 e^{\imath(k_0 x - \omega_0 t)} \int_{-\infty}^{\infty} e^{\imath k u - v k^2} dk = A_0 \sqrt{\frac{\pi}{v}} e^{\imath(k_0 x - \omega_0 t)} e^{-u^2/4v} \ . \end{aligned}$$

The absolute square of the solution describes the spatial energy distribution of the packet,

$$|Y(x,t)|^2 = A_0^2 \frac{\pi}{\sqrt{v v^*}} e^{-u^2/4v - u^2/4v^*} = A_0^2 \frac{\pi}{x_0 \sqrt{\alpha/2}} e^{-(x-v_g t)^2/x_0^2} \ ,$$

with $x_0 \equiv \sqrt{2\alpha}\sqrt{1 + \frac{\beta^2}{\alpha^2} t^2}$. Obviously, for long times the pulse spreads with constant velocity. Since the constant α gives the initial width of the pulse, we realize that an initially compressed pulse spreads faster. Therefore, the angular coefficient of the dispersion relation determines the group velocity, while the curvature determines the spreading velocity. See upper graphs of Figs. 18.11.

Resolve the Excs. 18.2.7.3 to 18.2.7.5.

18.2.3 Microscopic dispersion and the Lorentz model

Obviously, the structure that we assume for the matter also influences its reaction to electromagnetic waves, which interact differently with the charged components of the matter. The planetary model proposed by *E. Rutherford* considers matter to be made of atoms, which in turn are composed of *bound electrons* orbiting small positively charged nuclei. On the other side, metals have free electrons. The inertia of the charged particles (free or bound electrons, ions) being accelerated by incident electromagnetic waves is the reason for the dispersion phenomena that we will treat in the following sections.

Thomson scattering is the elastic scattering of light (photons) by free or quasi-free electrically charged particles (that is, weakly bound as compared to photon energies). A charged particle is prompted by the field of an electromagnetic wave to perform harmonic oscillations within the plane spanned by the electric and the magnetic field vectors. As the oscillation is an accelerated motion, the particle simultaneously re-emits energy in the form of an electromagnetic wave with the same frequency (dipole radiation). Thomson scattering does not consider photonic recoil, that is, there is no transfer of momentum from the photon to the electron, which is only a good assumption when the energy of the incident photons is small enough, that is, $\hbar\omega \ll$

$m_e c^2$, so that the wavelength of the electromagnetic radiation is much longer than the Compton wavelength $\lambda \gg \lambda_C = h/mc \simeq 2.4\,\text{pm}$ of the electron (which is the case for optical wavelengths). For higher energies, it is necessary to take the recoil of the electron into consideration (as done in the case of Compton scattering) [13].

18.2.3.1 Lorentz model

In classical physics the scattering of light by charges is described by the *Lorentz model* [547]. Assuming a harmonic electric field, $\vec{\mathcal{E}}(t) = \vec{\mathcal{E}}_0 e^{-\imath\omega t}$, we derive a force acting on an electron harmonically bound to a potential [14],

$$\mathbf{F} = -e\vec{\mathcal{E}}(t) \tag{18.105}$$

with e the elementary charge. The equation of motion is that of a damped harmonic oscillator:

$$m_e\ddot{\mathbf{r}} + m_e\gamma_\omega\dot{\mathbf{r}} + m_e\omega_0^2\mathbf{r} = -e\vec{\mathcal{E}}(t) \tag{18.106}$$

with the mass m_e of the electron, the damping γ_ω (by collisions, radiative losses, etc.), and a resonance frequency ω_0. We note, that the damping may depend on the excitation frequency.

After some time, when the transient processes are damped out, the electrons oscillate with the angular frequency ω of the external field. For this inhomogeneous solution we make the ansatz:

$$\mathbf{r}(t) = \mathbf{r}_e e^{-\imath\omega t} \tag{18.107}$$

with the constant complex amplitude $\mathbf{r}_e$. Inserting this into the equation of motion, we obtain for the atomic dipole moment induced by the electromagnetic field [15]:

$$\boxed{\mathbf{d}(t) \equiv -e\mathbf{r}(t) = \frac{e^2/m_e}{\omega_0^2 - \omega^2 - \imath\gamma_\omega\omega}\vec{\mathcal{E}}(t) \equiv \alpha_{pol}(\omega)\vec{\mathcal{E}}(t)}\,, \tag{18.108}$$

where we used the *electric polarizability* α_{pol} introduced in (14.6) and relating the amplitudes of the field and the dipole moment. The imaginary term in the denominator means that the oscillation of $\mathbf{d}$ is out of phase with $\vec{\mathcal{E}}$ being delayed by an angle

$$\varphi = \arctan\frac{\gamma_\omega\omega}{\omega_0^2 - \omega^2}\,, \tag{18.109}$$

which is very small when $\omega \ll \omega_0$ and approaches π when $\omega \gg \omega_0$ [1219]. This is illustrated in Fig. 18.14(left).

[13] Thomson scattering can be considered the limiting case of *Compton scattering* for small photon energies. The Thomson model holds for free electrons in a metal, whose resonant frequency tends, due to the absence of restoring forces, to zero. Scattering by bound electrons is called *Rayleigh scattering*.
In practice, Thomson scattering is used to determine the electron density through the intensity and temperature of the spectral distribution of scattered radiation assuming a Maxwell distribution for the electron velocities.

[14] Let us imagine for the sake of illustration that the displacement of the electron from its equilibrium position generates (to first order) an elastic restoring force with resonances at certain frequencies.

[15] See Sec. 4.3.

The temporal average of the dipole moment is,

$$\sqrt{\overline{d^2}} = \alpha_{pol}\mathcal{E}_0\sqrt{\tfrac{1}{T}\int_0^T \cos^2\omega t dt} = \alpha_{pol}\mathcal{E}_0\sqrt{\tfrac{1}{2}} \equiv d_0\sqrt{\tfrac{1}{2}} \ . \tag{18.110}$$

To calculate the emitted radiation we must borrow a result from future lessons: From the electromagnetic fields (19.40) of an oscillating dipole we will derive the expression for the Poynting vector (19.44),

$$\langle\vec{\mathcal{S}}\rangle = \tfrac{1}{\mu_0}\langle\vec{\mathcal{E}}\times\vec{\mathcal{B}}\rangle = \frac{\mu_0 d_0^2\omega^4}{16\pi^2 c}\frac{\sin^2\theta}{r^2}\hat{\mathbf{e}}_r = \frac{d_0^2\omega^4}{32\pi^2\varepsilon_0 c^3}\frac{\sin^2\theta}{r^2}\hat{\mathbf{e}}_r \ . \tag{18.111}$$

Obviously, the radiation is not isotropic, but concentrated in directions perpendicular to the dipole moment. In fact, the spherical harmonic function ($\sin\theta$), responsible for this toroidal angular distribution, is precisely the p-wave [16]. The total power radiated by the dipole can be derived from the Poynting vector,

$$\boxed{P = \int_0^{2\pi}\int_0^{\pi}\langle\vec{\mathcal{S}}\rangle\cdot\hat{\mathbf{e}}_r r^2\sin\theta d\theta d\phi = \frac{\mu_0 d_0^2\omega^4}{32\pi^2 c}\ 2\pi\int_0^{\pi}\sin^3\theta d\theta = \frac{\mu_0\omega^4 d_0^2}{12\pi c}} \ , \tag{18.112}$$

knowing $\int_0^{\pi}\sin^3 x dx = \frac{4}{3}$. This result is known as the *Larmor formula*.

18.2.3.2 Thompson and Rayleigh scattering

We now imagine that the dipole is excited by an incident wave of intensity,

$$I = \tfrac{1}{2}\varepsilon_0 c\vec{\mathcal{E}}_0^2 \ , \tag{18.113}$$

and scatters the radiation to a solid angle $d\Omega$, such that the angular distribution of scattered power is,

$$\frac{dP}{d\Omega} = |\langle\vec{\mathcal{S}}\rangle| r^2 \ . \tag{18.114}$$

We can now calculate the differential *scattering cross section* inserting the polarizability (18.108),

$$\begin{aligned}\frac{d\sigma}{d\Omega} = \frac{dP/d\Omega}{I} &= \frac{d_0^2\omega^4\sin^2\theta}{32\pi^2\varepsilon_0 c^3 r^2}r^2\frac{1}{\frac{1}{2}\varepsilon_0 c\mathcal{E}_0^2} = \frac{|\alpha_{pol}|^2\mathcal{E}_0^2\omega^4\sin^2\theta}{16\pi^2\varepsilon_0^2 c^4\mathcal{E}_0^2} \\ &= \left|\frac{e^2/m_e}{\omega_0^2-\omega^2-\imath\gamma_\omega\omega}\right|^2\frac{\omega^4\sin^2\theta}{16\pi^2\varepsilon_0^2 c^4} = \frac{r_e^2\omega^4\sin^2\theta}{(\omega_0^2-\omega^2)^2+\gamma_\omega^2\omega^2} \ ,\end{aligned} \tag{18.115}$$

where we defined the abbreviation,

$$r_e \equiv \frac{1}{4\pi\varepsilon_0}\frac{e^2}{m_e c^2} \approx 2.8\cdot 10^{-15}\,\mathrm{m} \tag{18.116}$$

being the *classical electron radius*. The total cross section,

$$\boxed{\sigma(\omega) = \int_{\mathbb{R}^2}\frac{d\sigma}{d\Omega}d\Omega = \frac{8\pi}{3}r_e^2\frac{\omega^4}{(\omega_0^2-\omega^2)^2+\gamma_\omega^2\omega^2}} \ , \tag{18.117}$$

describes a resonance of Lorentzian profile.

We have the following limiting cases:

[16] $Y_1^{\pm 1}(\theta,\phi) = \mp\frac{1}{2}\sqrt{\frac{3}{2\pi}}e^{\pm\imath\phi}\sin\theta$.

- $\omega \gg \omega_0$ Thomson scattering ,
- $\omega = \omega_0$ resonance fluorescence ,
- $\omega \ll \omega_0$ Rayleigh scattering .

A *Thomson cross section* follows in the limit of high energies in comparison with the eigenfrequency, $\omega \gg \omega_0 \gg \gamma_\omega$ from the Lorentz model [17],

$$\sigma_{Thom} = \frac{8\pi}{3} r_e^2 \approx 6.65 \cdot 10^{-29}\,\mathrm{m}^2 \quad . \tag{18.118}$$

Example 105 (*Rayleigh scattering and the blue sky*): We consider the scattering cross section (18.117). For $\omega \to \omega_0$ we obtain a resonant amplification of the cross session of ω^2/γ_ω^2. The resonances of the particles in the atmosphere are in the blue region of the electromagnetic spectrum. Therefore, the visible frequencies are $\omega \ll \omega_0$, and the cross session is $\propto \omega^4$. For this reason, the blue region dominates. The sky just does not look violet, because the eyes are not sensitive for these colors.
The dependence on the observation angle $\propto \sin^2\theta$, where $\theta = \angle(\hat{\epsilon}, \mathbf{k}_s)$ is only valid for polarized light. For non-polarized light, which can be understood as a superposition of two waves with orthogonal polarization, the dependence is $\propto 1 + \cos^2\vartheta$, where $\vartheta = \angle(\mathbf{k}, \mathbf{k}_s)$.

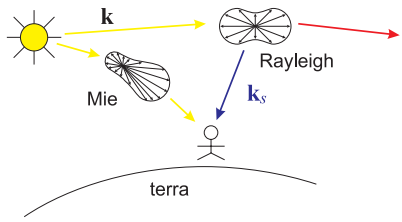

Figure 18.12: Dependence of the Rayleigh and Mie scattering on the observation angle.

Rayleigh scattering dominates for molecules and small scattering objects, $< \lambda/10$. *Mie scattering* is more important for $> \lambda/10$, e.g. water drops. This type of scattering is governed by boundary conditions defined by the surfaces of objects. The angular distributions are strongly oriented in forward direction, particularly when the objects are large. Therefore, this type of scattering only dominates at small angles with respect to the sun, where we observe a bleaching of the blue color of the sky).

18.2.3.3 Atomic polarizability

In atoms, the damping rate γ_ω is due to the radiative energy loss (given by Larmor's formula). It is calculated as the ratio between the classically radiated power and the

[17] A better approximation for small energies is obtained by expansion of the Klein-Nishina formula,

$$\sigma(\nu) = \sigma_{Thom}\left(1 - 2\alpha + \tfrac{56}{5}\alpha^2 + \dots\right)$$

with the factor $\alpha = \frac{h\nu}{m_e c^2}$.

kinetic energy of the electron orbiting the nucleus,

$$\gamma_\omega = \frac{P}{E_{kin}} = \frac{\mu_0 e^2 a^2/12\pi c}{m_e \omega^2 r^2/2} \ , \tag{18.119}$$

where $a = \omega^2 r$ is the acceleration of the electron. We get [547] [18],

$$\boxed{\gamma_\omega = \frac{e^2\omega^2}{6\pi\varepsilon_0 m_e c^3}} \ . \tag{18.120}$$

Defining $\Gamma \equiv \gamma_{\omega_0}$ and inserting into equation (18.108), we can calculate the polarizability within the Lorentz model,

$$\alpha_{pol} = 6\pi\varepsilon_0 c^3 \frac{\Gamma/\omega_0^2}{\omega_0^2 - \omega^2 - \imath(\omega^3/\omega_0^2)\Gamma} \ . \tag{18.121}$$

Close to narrow resonances we can approximate $(\omega_0 + \omega) \to 2\omega_0$ and $(\omega^3/\omega_0^2)\Gamma \to \omega_0\Gamma$ in the denominator of the formula (18.121). Hence, the *polarizability* simplifies to,

$$\boxed{\frac{\alpha_{pol}}{\varepsilon_0} \simeq \frac{6\pi}{k_0^3} \frac{-1}{\imath + 2\Delta/\Gamma}} \ , \tag{18.122}$$

defining the detuning $\Delta \equiv \omega - \omega_0$. Resolve the Excs. 18.2.7.6 to 18.2.7.9.

18.2.4 Classical theory of radiative forces

The Lorentz model permits a classical calculation of the forces exerted by a radiation wave on an electric dipole moment oscillating with the excitation frequency ω [659, 547] [19]. With the dipole moment given by equation (18.108) and the polarizability given by equation (18.121) we can write the dipolar interaction potential as the time-average,

$$\boxed{U_{dip}(\mathbf{r}) = -\frac{1}{2}\overline{\mathbf{d}\cdot\vec{\mathcal{E}}} = -\frac{1}{2\varepsilon_0 c} I(\mathbf{r}) \mathfrak{Re}\ \alpha_{pol}} \ , \tag{18.123}$$

with the field intensity $I = 2\varepsilon_0 c|\vec{\mathcal{E}}|^2$. The factor $\frac{1}{2}$ takes into account the fact, that the dipole moment is induced rather than permanent, as shown in equation (14.10).

Therefore, the potential energy of the atom in the field is proportional to the intensity $I(\mathbf{r})$ and the real part of the polarizability, which describes the *in-phase* component of the dipolar oscillation, being responsible for the dispersive properties of the interaction. The dipole force comes from the gradient of the interaction potential,

$$\mathbf{F}_{dip}(\mathbf{r}) = -\nabla U_{dip}(\mathbf{r}) = \frac{1}{\varepsilon_0 c} \nabla I(\mathbf{r}) \mathfrak{Re}\ \alpha_{pol} \ . \tag{18.124}$$

[18] In quantum mechanics we learn, that the rate for spontaneous emission is, $\Gamma = d^2k^3/3\pi\varepsilon_0\hbar$. This rate coincides with Eq. (18.120) when we assume an amplitude for the electron's oscillation equal to the size of the ground state of a harmonic oscillator,

$$d_0 = er = e\sqrt{\frac{\hbar}{m_e\omega}} = \overline{d^2}\sqrt{2} \ .$$

[19] In principle, we could also use Maxwell's stress tensor.

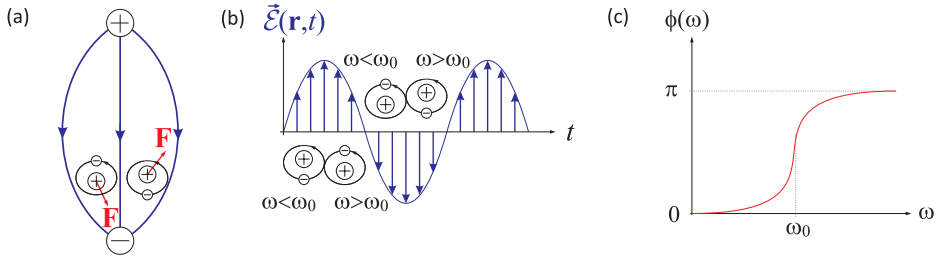

Figure 18.13: (a) Lorentz force on electric dipoles in an electrostatic field gradient. (b) Orientation of induced dipoles in an electromagnetic field. (c) Phase-shift of a harmonic oscillator with a resonance frequency at ω_0 driven at frequency ω.

It is a conservative force proportional to the intensity gradient of the light field. As illustrated in Fig. 18.13, below resonance ($\omega < \omega_0$) the induced electric dipole will be oriented parallel to the electric field such as to minimize its energy by seeking strong field regions. Above resonance ($\omega > \omega_0$) the orientation is reversed so that the dipole can minimize its energy by seeking low field regions.

The power of the field absorbed by the dipolar oscillator (and reemitted as dipolar radiation) is given by,

$$P_{abs} = \overline{\dot{\mathbf{d}} \cdot \vec{\mathcal{E}}} = 2\omega \mathfrak{Im}\ \tilde{\mathbf{d}} \cdot \vec{\tilde{\mathcal{E}}} = -\frac{\omega}{\varepsilon_0 c} I(\mathbf{r}) \mathfrak{Im}\ \alpha_{pol}\ . \tag{18.125}$$

The absorption results from the imaginary part of the polarizability, which describes the *out of phase* component of the dipolar oscillation. Considering the light as a stream of photons with energy $\hbar\omega$, the absorptive part can be interpreted in terms of photon absorption processes followed by spontaneous reemission. The corresponding scattering rate is,

$$\boxed{\Gamma_{sct}(\mathbf{r}) = \frac{P_{abs}}{\hbar\omega} = \frac{1}{\hbar\varepsilon_0 c} I(\mathbf{r}) \mathfrak{Im}\ \alpha_{pol}}\ . \tag{18.126}$$

We emphasize that these expressions are valid for any polarizable neutral particle exposed to an oscillating electric field, provided that saturation effects can be neglected. That it, the expressions hold for atoms and molecules excited near or far from resonances, as well as for a classical antenna [20].

Inserting the polarizability (18.121) in the expressions (18.123) for the dipolar potential and (18.126) for the (Rayleigh) scattering rate we obtain, for the case of large detunings in comparison to the transition linewidth, $\Delta \gg \Gamma$, and negligible saturation,

$$\begin{aligned} U_{dip}(\mathbf{r}) &= -\frac{1}{2\varepsilon_0 c} I(r) \mathfrak{Re}\ \frac{6\pi\varepsilon_0 c^3 \Gamma/\omega_0^2}{\omega_0^2 - \omega^2 - \imath(\omega^3/\omega_0^2)\Gamma} \\ &\simeq -\frac{3\pi c^2}{\omega_0^2} I(\mathbf{r}) \frac{\Gamma}{\omega_0^2 - \omega^2} = -\frac{3\pi c^2}{2\omega_0^3} I(\mathbf{r}) \left(\frac{\Gamma}{\omega_0 - \omega} + \frac{\Gamma}{\omega_0 + \omega} \right)\ , \end{aligned} \tag{18.127}$$

[20] An important difference between quantum and classical oscillators is the possible occurrence of saturation. When the intensity of the driving field is too high, the excited state becomes strongly populated and the derived results are no longer valid. However, for large detunings we are far below the saturation, such that the expressions can be used even for quantum oscillators.

and

$$\hbar\Gamma_{sct}(\mathbf{r}) = \frac{1}{\varepsilon_0 c} I(\mathbf{r}) \Im\mathfrak{m} \, \frac{6\pi\varepsilon_0 c^3 \Gamma/\omega_0^2}{\omega_0^2 - \omega^2 - \imath(\omega^3/\omega_0^2)\Gamma} \tag{18.128}$$
$$\simeq \frac{-6\pi c^2 \Gamma^2 \omega^3}{\omega_0^4} I(\mathbf{r}) \frac{1}{(\omega_0^2 - \omega^2)^2} = \frac{-3\pi c^2}{2\omega_0^3} \left(\frac{\omega}{\omega_0}\right)^3 I(\mathbf{r}) \left(\frac{\Gamma}{\omega_0 - \omega} + \frac{\Gamma}{\omega_0 + \omega}\right)^2 .$$

These expressions exhibit two resonant contributions: In addition to the usual resonance at $\omega = \omega_0$, there is a so-called *counter-rotating* term resonant at $\omega = -\omega_0$. In most applications the radiation source is tuned relatively close to the resonance at ω_0, such that the counter-rotating term can be neglected, which simplifies the expressions to,

$$\boxed{U_{dip}(\mathbf{r}) = \frac{3\pi c^2}{2\omega_0^3} \frac{\Gamma}{\Delta} I(\mathbf{r}) \qquad \text{and} \qquad \hbar\Gamma_{sct}(\mathbf{r}) = \frac{3\pi c^2}{2\omega_0^3} \frac{\Gamma^2}{\Delta^2} I(\mathbf{r})} \, . \tag{18.129}$$

The obvious relationship between the scattering rate and the dipolar potential,

$$\hbar\Gamma_{sct} = \frac{\Gamma}{\Delta} U_{dip} \, , \tag{18.130}$$

is a direct consequence of the profound relationship between the absorptive and dispersive responses of the oscillator. We furthermore emphasize the following relevant points:

- The sign of the detuning: Below an atomic resonance ('red detuning', $\Delta < 0$) the dipolar potential is negative and the interaction attracts the atom to regions of high intensity, e.g. toward the optical axis of a Gaussian light beam or towards the anti-nodes of a standing light wave. Above the atomic resonance ('blue detuning', $\Delta > 0$) is the opposite; the atom is repelled out of high-intensity regions.
- Intensity and detuning-dependence: The dipolar potential is $\propto I/\Delta$, while the scattering rate is $\propto I/\Delta^2$. Therefore, dipolar optical traps are generally realized at large detunings and high intensities in order to reduce the scattering rate while maintaining the potential depth.

18.2.4.1 Microscopic model of the susceptibility, anomalous dispersion

Until now we considered a single valence electron bound to a nucleus. If there are several electrons, the relationship (18.108) must be generalized. Electrons located at different orbitals of a molecule feel different spring constants f_j, natural frequencies ω_j, and damping coefficients γ_j. In the presence of several electrons per molecule and N molecules per volume unit, the polarization $\vec{\mathcal{P}}$ is given by the real part of (14.12),

$$\vec{\tilde{\mathcal{P}}} = \frac{Nq^2}{m} \left(\sum_j \frac{f_j}{\omega_j^2 - \omega^2 - \imath\gamma_j\omega} \right) \vec{\tilde{\mathcal{E}}} \, . \tag{18.131}$$

In equation (14.20) we defined the electric susceptibility χ_ε as proportionality constant between the electric field and the polarization. In the case considered here, $\vec{\mathcal{P}}$ *is not*

proportional to $\vec{\mathcal{E}}$ (strictly speaking, it is not a linear medium), because there is a phase shift between $\vec{\mathcal{P}}$ and $\vec{\mathcal{E}}$. But at least the *complex* polarization $\tilde{\vec{\mathcal{P}}}$ *is proportional to the complex field* $\tilde{\vec{\mathcal{E}}}$, which suggests the introduction of a *complex susceptibility* $\tilde{\chi}_\varepsilon$,

$$\tilde{\vec{\mathcal{P}}} = \varepsilon_0 \tilde{\chi}_\varepsilon \tilde{\vec{\mathcal{E}}} \ . \tag{18.132}$$

All manipulations made so far remain valid, if we assume that the physical polarization is the real part of $\tilde{\vec{\mathcal{P}}}$, in the same way as the physical field is the real part of $\tilde{\vec{\mathcal{E}}}$. In particular, the proportionality between $\tilde{\vec{\mathcal{D}}}$ and $\tilde{\vec{\mathcal{E}}}$ is the complex permittivity $\tilde{\varepsilon} = \varepsilon_0(1+\tilde{\chi}_\varepsilon)$, and the complex dielectric constant (in this model) is,

$$\tilde{\epsilon} \equiv \frac{\tilde{\varepsilon}}{\varepsilon_0} = 1 + \frac{Nq^2}{m\varepsilon_0} \sum_j \frac{f_j}{\omega_j^2 - \omega^2 - \imath\gamma_j\omega} \ . \tag{18.133}$$

Generally, the imaginary part is despicable; however, when ω is very close to one of the resonant frequencies ω_j, it will play a crucial role, as we shall see later.

In a dispersive medium the wave equation for a given frequency is,

$$\nabla^2 \tilde{\vec{\mathcal{E}}} = \tilde{\varepsilon}\mu_0 \frac{\partial^2 \tilde{\vec{\mathcal{E}}}}{\partial t^2} \ . \tag{18.134}$$

It admits plane wave solutions as before,

$$\tilde{\vec{\mathcal{E}}}(z,t) = \tilde{\vec{\mathcal{E}}}_0 e^{\imath(\tilde{k}z - \omega t)} \ , \tag{18.135}$$

with the complex wavenumber,

$$\tilde{k} = \omega\sqrt{\tilde{\varepsilon}\mu_0} = \tfrac{\omega}{c}\sqrt{\tilde{\epsilon}} \ . \tag{18.136}$$

Writing $\tilde{k}$ in terms of its real and imaginary parts, $\tilde{k} = k + \imath\kappa$, the plane wave becomes,

$$\tilde{\vec{\mathcal{E}}}(z,t) = \tilde{\vec{\mathcal{E}}}_0 e^{-\kappa z} e^{\imath(kz - \omega t)} \ . \tag{18.137}$$

Obviously, the wave is attenuated (this is not surprising, since the damping absorbs energy). Since the intensity is proportional to $\vec{\mathcal{E}}^2$ (and consequently to $e^{-2\kappa z}$), the quantity,

$$\alpha \equiv 2\kappa \tag{18.138}$$

is called *absorption coefficient*. The relationship,

$$I \propto e^{-\alpha z} \tag{18.139}$$

is called the *Lambert-Beer law*. However, the velocity of the wave is ω/k, and the *refraction index* is,

$$n = \frac{ck}{\omega} \ . \tag{18.140}$$

In the present case k and κ have nothing to do with conductivity, as in the case of Eq. (18.87); but they are determined by the parameters of our damped harmonic

oscillator. For gases, the second term in (18.133) is small, and we can approximate the square root (18.136) by the first term of the binomial expansion $\sqrt{1+\tilde{\chi}_\varepsilon} \simeq 1 + \frac{1}{2}\tilde{\chi}_\varepsilon$. Hence,

$$\tilde{k} = \frac{\omega}{c}\sqrt{\tilde{\epsilon}} \simeq \frac{\omega}{c}\left(1+\frac{\tilde{\chi}_\varepsilon}{2}\right) = \frac{\omega}{c}\left(1+\frac{Nq^2}{2m\varepsilon_0}\sum_j \frac{f_j}{\omega_j^2-\omega^2-\imath\gamma_j\omega}\right) . \tag{18.141}$$

therefore,

$$\boxed{\begin{array}{rcccl} n & = & \mathfrak{Re}\,\sqrt{\epsilon} & \simeq & 1+\dfrac{Nq^2}{2m\varepsilon_0}\displaystyle\sum_j \frac{f_j(\omega_j^2-\omega^2)}{(\omega_j^2-\omega^2)^2+\gamma_j^2\omega^2} \\ \alpha & = & \dfrac{2\omega}{c}\mathfrak{Im}\,\sqrt{\epsilon} & \simeq & \dfrac{Nq^2\omega^2}{m\varepsilon_0 c}\displaystyle\sum_j \frac{f_j\gamma_j}{(\omega_j^2-\omega^2)^2+\gamma_j^2\omega^2} \end{array}} . \tag{18.142}$$

In Fig. 18.14 we plot the refractive index and the absorption coefficient in the neighborhood of one of the resonances $\omega_0 = \omega_j$. In most cases the refractive index gradually increases with frequency, which is consistent with our experience in optics (Fig. 18.10). However, near a resonance the refraction index drops abruptly. Being atypical, this behavior is called *anomalous dispersion*. We observe that the region of anomalous dispersion ($\omega_1 < \omega < \omega_2$ in the figure) coincides with the region of maximum absorption. In fact, the material can be almost opaque in this spectral region. The reason is, we now excite the electrons on their 'preferred' frequency; the amplitude of their oscillation is relatively large, and therefore much energy is dissipated by the damping mechanism.

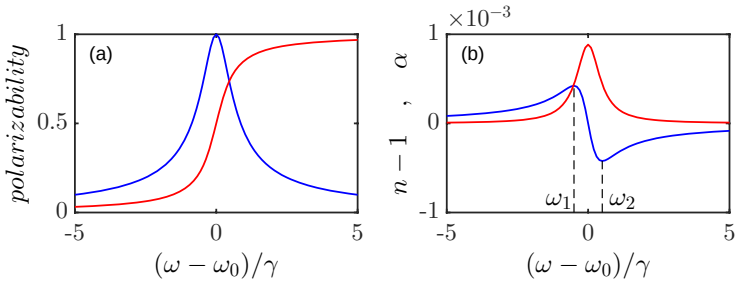

Figure 18.14: (code) (a) Profile of the polarizability $|\alpha_{pol}|$ (blue curve) and of the phase shift $\arctan \frac{\mathfrak{Im}\ \alpha_{pol}}{\pi \mathfrak{Re}\ \alpha_{pol}}$ (red curve). (b) Refractive index (blue curve) and the absorption (red curve). In the spectral region between ω_1 and ω_2 we have anomalous dispersion.

The refractive index n plotted in Fig. 18.14 may be below 1 above the resonance, suggesting that the *velocity of the wave exceeds* c. But we must remember that energy propagates at the group velocity, which is always below c. The graph does not include the contributions of other terms in the sum, because they are negligible when the resonances are narrow or distant from each other. Out of the resonances, the damping can be ignored, and the formula for the refractive index simplifies:

$$n = 1 + \frac{Nq^2}{2m\varepsilon_0}\sum_j \frac{f_j}{\omega_j^2-\omega^2} . \tag{18.143}$$

For most substances the natural frequencies ω_j are distributed across the spectrum in a chaotic way. In transparent materials, the resonances are in the ultraviolet regime, such that the visible frequencies ω are far below the resonances, $\omega \ll \omega_j$. In this case,

$$\frac{1}{\omega_j^2 - \omega^2} \simeq \frac{1}{\omega_j^2}\left(1 + \frac{\omega^2}{\omega_j^2}\right) . \tag{18.144}$$

and (18.143) adopts the form,

$$n = 1 + \frac{Nq^2}{2m\varepsilon_0}\sum_j \frac{f_j}{\omega_j^2} + \omega^2 \frac{Nq^2}{2m\varepsilon_0}\sum_j \frac{f_j}{\omega_j^4} . \tag{18.145}$$

Or, in terms of vacuum wavelengths ($\lambda = 2\pi c/\omega$):

$$\boxed{n = 1 + A\left(1 + \frac{B}{\lambda^2}\right)} . \tag{18.146}$$

This is the *Cauchy formula*; the constant A is called the *refraction coefficient* and B is called *dispersion coefficient*. The Cauchy equation applies reasonably well to most gases in the optical regime. Fig. 18.10 shows the example of the refractive index of air.

The Lorentz model certainly does not account for all dispersion phenomena in non-conductive media. But at least, it indicates how the damped harmonic motion of electrons can generate a dispersive refractive index, and it also explains why n is usually a slowly increasing function of ω with occasional 'anomalous' regions.

Example 106 (*Energy density and Poynting vector in a dielectric medium*): The energy density in vacuum, $\bar{u} = \frac{\varepsilon_0}{4}|\vec{\mathcal{E}}|^2 + \frac{1}{4\mu_0}|\vec{\mathcal{B}}|^2$, becomes in a dielectric medium,

$$\begin{aligned}\bar{u}^{(\chi)} &= \frac{1}{4}\mathfrak{Re}\,(\varepsilon\vec{\mathcal{E}}\cdot\vec{\mathcal{E}}^* + \frac{1}{\mu_0}\vec{\mathcal{B}}\cdot\vec{\mathcal{B}}^*) = \frac{\mathfrak{Re}\,\varepsilon}{4}|\vec{\mathcal{E}}|^2 + \frac{1}{4\mu_0}\left|\frac{k+\imath\kappa}{\omega}\vec{\mathcal{E}}\right|^2 \\ &= \frac{\varepsilon_0}{4}(1+\chi_e')\mathcal{E}_0^2 + \frac{\varepsilon_0}{4\omega^2}|k+\imath\kappa|^2\mathcal{E}_0^2 = (k^2-\kappa^2+k^2+\kappa^2)\frac{\varepsilon_0}{4}\mathcal{E}_0^2 = \frac{\varepsilon_0}{2}\frac{k^2}{\omega^2}\mathcal{E}_0^2 ,\end{aligned}$$

where we only consider the real part of the susceptibility χ_ε. On the other hand, the Poynting vector is,

$$\bar{I} = \frac{1}{2\mu_0}\mathfrak{Re}\,[\vec{\mathcal{E}}\times\vec{\mathcal{B}}^*] = \frac{\varepsilon_0 c^2}{2}\mathcal{E}_0^2\left[e^{-2\omega\kappa z/c}\mathfrak{Re}\,\frac{k+\imath\kappa}{\omega}\right] = \frac{\varepsilon_0 c^2}{2}\frac{k}{\omega}\mathcal{E}_0^2 e^{-2\omega\kappa z/c} .$$

18.2.4.2 The Fresnel-Fizeau effect

Naively, the index of refraction is due to a finite time lag between photon absorption and emission. The time spend in an excited state slows down the light propagation velocity. If during this time the atom travels, the atomic velocity adds to (or reduces) the light propagation velocity. This effect which is known as *Fresnel-Fizeau effect* is an internal degrees of freedom effect. Consider a medium with the index of refraction n

(measured in the moving frame) which is moving with velocity v. The copropagation velocity of light is for $v \ll c$,

$$c_v = \frac{c}{n_{rf}} \frac{c + n_{rf} v}{c + v/n_{rf}} \approx \frac{c}{n_{rf}} + v \left(1 - \frac{1}{n_{rf}^2}\right) . \tag{18.147}$$

This is the Fresnel 'drag' coefficient. In particular, it is easy to show that,

$$c_{-v} < c/n_{rf} < c_v < c . \tag{18.148}$$

Expressing the refraction index by the susceptibility, $n_{rf} = \sqrt{1 + \chi_\varepsilon} \approx 1 + \frac{1}{2}\chi_\varepsilon$, we get,

$$\frac{c_v - c_{-v}}{2v} = 1 - \frac{1}{n_{rf}^2} = \frac{\chi_\varepsilon}{1 + \chi_\varepsilon} . \tag{18.149}$$

Knowing that,

$$\chi_\varepsilon = \frac{2nd^2}{3\varepsilon_0 \hbar} \frac{\Delta + \imath\Gamma}{4\Delta^2 + 2\Omega^2 + \Gamma^2} \qquad \text{and} \qquad d = \sqrt{\frac{3\pi\varepsilon_0 \hbar \Gamma}{k^3}} \tag{18.150}$$

$$\mathfrak{Re}\ \chi_\varepsilon = \frac{2\pi\Gamma n}{k^3} \frac{\Delta}{4\Delta^2 + 2\Omega^2 + \Gamma^2}$$

it follows,

$$\frac{c_v - c_{-v}}{2v} = \frac{1}{1 + \left(\frac{2\pi\Gamma n}{k^3} \frac{\Delta}{4\Delta^2 + 2\Omega^2 + \Gamma^2}\right)^{-1}} . \tag{18.151}$$

For small detunings within the natural linewidth,

$$\frac{c_v - c_{-v}}{2v} \approx \frac{1}{1 + \frac{k^3}{2\pi n} \frac{\Gamma}{\Delta}} , \tag{18.152}$$

a long excited state lifetime is advantageous. For very large detunings and $\Omega \to 0$,

$$\frac{c_v - c_{-v}}{2v} \approx \frac{1}{1 + \frac{2k^3}{\pi n} \frac{\Delta}{\Gamma}} . \tag{18.153}$$

This shows that (far from resonance) the effect increases for large densities, broad linewidths and smaller detunings. For example, the *Rb* D_1 line for typical conditions the coefficient is $\frac{2k^3}{\pi n} \approx 1000$ [21].

18.2.5 Light interaction with metals and the Drude model

The *Drude model* is based on a classical kinetic theory of non-interacting electrons in a metal. Since the conduction electrons are considered to be free, the Drude oscillator is

[21] For the high-finesse ring-cavity CARL experiment this means that the Fresnel-Fizeau effect is negligible. Far from resonance the atoms do not spend time in the excited state. The adiabatic elimination of the internal degrees of freedom removes the effect from the theoretical model. It also means that the counter-propagating modes of the ring-cavity do not split because of the atomic velocity, $n_{rf+} = n_{rf-}$. The calculation shows that the back-scattered light is not perfectly resonant, but that this shift is negligibly small.

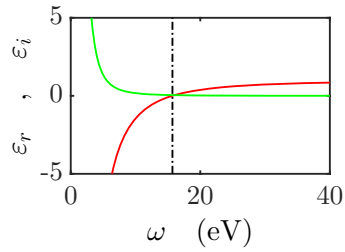

Figure 18.15: (code) Real (red) and imaginary (green) parts of the dielectric function as a function of the excitation frequency.

an extension of the Lorentz model of a single oscillator to the case, when the restoring force and the atomic resonance frequency are zero, $\Gamma_0 = \omega_0 = 0$. The equation of motion is,

$$m\frac{d\mathbf{v}}{dt} + m\Gamma_d\mathbf{v} = -e\vec{\mathcal{E}}\ , \tag{18.154}$$

where $m\frac{d\mathbf{v}}{dt}$ is the force accelerating the electron, $m\Gamma_d\mathbf{v}$ is the friction due to collisions with ions of the crystalline lattice and $-e\vec{\mathcal{E}} = -e\vec{\mathcal{E}}_0 e^{\imath\omega t}$ is the Coulomb force exerted by the oscillating field. We find,

$$\mathbf{v} = \mathbf{v}_0 e^{\imath\omega t} = -\frac{e}{m}\frac{\vec{\mathcal{E}}_0}{\imath\omega + \Gamma_d}e^{\imath\omega t}\ . \tag{18.155}$$

The current density corresponding to the motion of n electrons per unit volume is,

$$\mathbf{j}_c(\omega) = -ne\mathbf{v} = \frac{ne^2}{m(\Gamma_d + \imath\omega)}\vec{\mathcal{E}}\ . \tag{18.156}$$

In addition we have the current that corresponds to the electric displacement in vacuum,

$$\mathbf{j}_d(\omega) = \frac{\partial\vec{\mathcal{D}}}{\partial t} = \imath\omega\varepsilon_0\vec{\mathcal{E}}\ , \tag{18.157}$$

where $\vec{\mathcal{D}} = \varepsilon_0\vec{\mathcal{E}}$. The total current density is given by,

$$\mathbf{j}(\omega) = \mathbf{j}_c(\omega) + \mathbf{j}_d(\omega) = \left[\frac{ne^2}{m(\Gamma_d + \imath\omega)} + \imath\omega\varepsilon_0\right]\vec{\mathcal{E}}\ . \tag{18.158}$$

Assuming the total current as being created by a total electric displacement, $\vec{\mathcal{D}}_{tot} = \tilde{\varepsilon}\vec{\mathcal{E}}$, where again the electric field and the displacement are related by a complex permittivity, we find,

$$\mathbf{j}(\omega) = \frac{\partial\vec{\mathcal{D}}_{tot}}{\partial t} = \imath\omega\tilde{\varepsilon}\vec{\mathcal{E}}\ , \tag{18.159}$$

and comparing the last two expressions,

$$\left[\frac{ne^2}{m(\Gamma_d + \imath\omega)} + \imath\omega\varepsilon_0\right]\vec{\mathcal{E}} = \imath\omega\tilde{\varepsilon}(\omega)\vec{\mathcal{E}}\ . \tag{18.160}$$

Resolving by $\tilde{\varepsilon}$,

$$\boxed{\tilde{\epsilon}(\omega) = 1 - \frac{\omega_p^2}{i\omega\Gamma_d - \omega^2}} \ , \tag{18.161}$$

where

$$\omega_p \equiv \sqrt{\frac{ne^2}{m\varepsilon_0}} \tag{18.162}$$

is called the *plasma frequency*, which corresponds to the energy, where $\epsilon(\omega_p) \simeq 0$. Separated into real and imaginary parts,

$$\epsilon'(\omega) = 1 - \frac{\omega_p^2}{\Gamma_d^2 + \omega^2} \quad , \quad \epsilon''(\omega) = \frac{\omega_p^2 \Gamma_d}{\omega(\Gamma_d^2 + \omega^2)} \tag{18.163}$$

For $\omega < \omega_p$ and small Γ_d, the real part ϵ' is negative. No electric field can penetrate the metal, which therefore becomes fully reflecting.
For $\omega = \omega_p$, the real part ϵ' is zero. That is, the electrons oscillate in phase with the field along the propagation distance in the metal.
For $\omega \gg \omega_p$, the imaginary (absorptive) part ε'' disappears at high frequencies.

For metals, usually we have $\omega_p = (2\pi)\ 1000...4000\,\mathrm{THz}$ and $\Gamma_d \approx 100\,\mathrm{s}^{-1}$. Note that the model can not describe semiconductors.

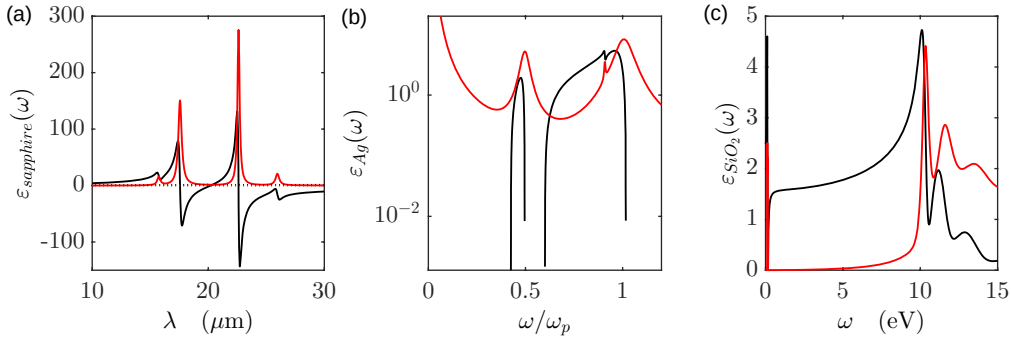

Figure 18.16: (code) Examples of frequency-dependent permittivities for (a) sapphire [444, **?**], (b) silver [1070], and (c) amorphous glas [375].

18.2.6 Causality connecting $\vec{\mathcal{D}}$ with $\vec{\mathcal{E}}$ and the Kramers-Kronig relations

A consequence of the dispersion of $\varepsilon(\omega)$ is the temporarily nonlocal connection between the displacement $\vec{\mathcal{D}}$ and the electric field $\vec{\mathcal{E}}$. Calculating the Fourier transform of,

$$\vec{\mathcal{D}}(\mathbf{r},\omega) = \varepsilon(\omega)\vec{\mathcal{E}}(\mathbf{r},\omega) = \varepsilon_0[1 + \chi_\varepsilon(\omega)]\vec{\mathcal{E}}(\mathbf{r},\omega) \ , \tag{18.164}$$

we obtain, using the convolution theorem,

$$\begin{aligned}\vec{\mathcal{D}}(\mathbf{r},t) &= \frac{1}{\sqrt{2\pi}}\int_{-\infty}^{\infty}\varepsilon(\omega)\vec{\mathcal{E}}(\mathbf{r},\omega)e^{-\imath\omega t}d\omega \\ &= \varepsilon_0\vec{\mathcal{E}}(\mathbf{r},t) + \frac{\varepsilon_0}{\sqrt{2\pi}}\int_{-\infty}^{\infty}\chi_\varepsilon(\omega)\vec{\mathcal{E}}(\mathbf{r},\omega)e^{-\imath\omega t}d\omega \\ &= \varepsilon_0\vec{\mathcal{E}}(\mathbf{r},t) + \frac{\varepsilon_0}{\sqrt{2\pi}}\int_{-\infty}^{\infty}\chi_\varepsilon(\tau)\vec{\mathcal{E}}(\mathbf{r},t-\tau)d\tau\ ,\end{aligned} \tag{18.165}$$

where $\chi_\varepsilon(\tau)$ is the Fourier transform of the electric susceptibility. This results shows that the displacement field $\vec{\mathcal{D}}$ depends on all values the incident electric field $\vec{\mathcal{E}}$ had at all times. Only if $\chi_\varepsilon(\omega)$ were independent of ω would we have $\chi_\varepsilon(\tau) \propto \delta(\tau)$.

Example 107 (*Simple model of the susceptibility*): To illustrate the implications of equation (18.165) we consider a permittivity of the following form,

$$\frac{\varepsilon(\omega)}{\varepsilon_0} = \frac{\omega_p}{\omega_0^2 - \omega^2 - \imath\gamma\omega}\ . \tag{18.166}$$

The kernel related to the susceptibility,

$$\chi_\varepsilon(\tau) = \frac{\omega_p^2}{2\pi}\int_{-\infty}^{\infty}\frac{e^{-\imath\omega\tau}d\tau}{\omega_0^2 - \omega^2 - \imath\gamma\omega}\ , \tag{18.167}$$

can be evaluated by contour integration, the result being,

$$\chi_\varepsilon(\tau) = \omega_p^2 e^{-\gamma\tau/2}\frac{\sin\tau\sqrt{\omega_0^2 - (\gamma/2)^2}}{\sqrt{\omega_0^2 - (\gamma/2)^2}}\Theta(\tau)\ , \tag{18.168}$$

where $\Theta(\tau)$ is the Heaviside function.

This example shows that the displacement field $\vec{\mathcal{D}}$ only depends on the electric field at *past times*, which is fortunate as it allows causality to be respected.

18.2.6.1 The Kramers-Kronig relations

The *Kramers-Kronig relations* are bidirectional mathematical relations, connecting the real and imaginary parts of any complex function that is an *analytic function* on the upper half-plane [22]. These relationships are often used to calculate the real part of response functions in physical systems from the imaginary part (or vice versa). This works because, in stable physical systems, *causality and analyticity* are equivalent conditions. Be $\chi(\omega)$ a complex function of the complex variable ω. We assume this function to be analytic in the upper closed half-plane of ω and to disappear as $1/|\omega|$ or faster for $|\omega| \to \infty$. The Kramers-Kronig relations are given by,

$$\boxed{\mathfrak{Re}\ \chi(\omega) = \frac{1}{\pi}\mathcal{P}\int_{-\infty}^{\infty}\frac{\mathfrak{Im}\ \chi(\omega')}{\omega'-\omega}d\omega' \quad \text{and} \quad \mathfrak{Im}\ \chi(\omega) = -\frac{1}{\pi}\mathcal{P}\int_{-\infty}^{\infty}\frac{\mathfrak{Re}\ \chi(\omega')}{\omega'-\omega}d\omega'}\ , \tag{18.169}$$

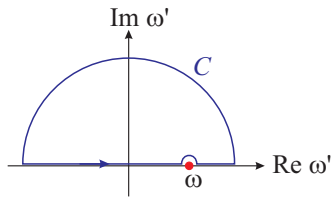

Figure 18.17: Path of the contour integral illustrating Cauchy's theorem.

where $\mathcal{P}$ denotes the *Cauchy principal value*. Thus, the real and imaginary parts of such a function are not independent, and the complete function can be reconstructed from only one of its parts.

For any analytic function χ defined on the upper closed half-plane, the function $\omega' \to \chi(\omega')/(\omega' - \omega)$ where $\omega \in \mathbb{R}$, will also be analytic in the upper half-plane. The *Cauchy's residue theorem* for integration consequently says, that

$$\oint \frac{\chi(\omega')}{\omega' - \omega} d\omega' = 0 \ . \tag{18.170}$$

We chose the contour to follow the real axis, making a loop around the pole at $\omega' = \omega$, and a large semicircle in the upper half-plane, as shown in Fig. 18.17. We now decompose the integral into its contributions along each one of these three paths and then evaluate the limits. The length of the semicircular path increases proportionally to $|\omega'|$, but the integral along it disappears in this limit, since $\chi(\omega')$ disappears at least as fast as $1/|\omega'|$. Letting the size of the semicircle go to zero we get,

$$0 = \oint \frac{\chi(\omega')}{\omega' - \omega} d\omega' = \mathcal{P} \int_{-\infty}^{\infty} \frac{\chi(\omega')}{\omega' - \omega} d\omega' - \imath\pi\chi(\omega) \ . \tag{18.171}$$

The second term in the last expression is obtained using the Sokhotski-Plemelj theorem of residues. After rearrangement we arrive at the compact form of the Kramers-Kronig relations,

$$\chi(\omega) = \frac{1}{\imath\pi} \mathcal{P} \int_{-\infty}^{\infty} \frac{\chi(\omega')}{\omega' - \omega} d\omega' \ . \tag{18.172}$$

The imaginary unit in the denominator makes the connection between the real and the imaginary components. Finally, we separate $\chi(\omega)$ and the equation (18.172) into their real and imaginary parts, and we get the expressions from above (18.169).

18.2.6.2 Physical interpretation in terms of causality

We can apply the Kramers-Kronig formalism to response functions. In certain linear and time-invariant physical systems or signal processing applications, the response function $h(t)$ describes, how some time-dependent property of the system, responds to a force $F(t')$ pulsed during a time t'. For example, the property of the system can be the angle of a pendulum and the force applied by a motor kicking the pendulum.

[22] A function is analytic if and only if its Taylor series about a point $\mathbf{r}_0$ converges to the function in some neighborhood for every $\mathbf{r}_0$ in its domain. Hence, analytic functions must be infinitely differentiable.

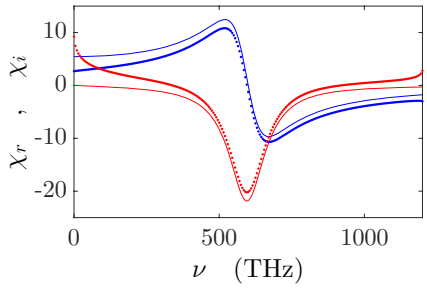

Figure 18.18: (code) Real (blue) and imaginary (red) parts of the susceptibility. The dashed curves are calculated by the Kramers-Kronig formulas.

The response function must be zero for $t < 0$, since the system can not respond to the force before it has been applied. It can be shown that this request for causality *in time domain* implies *in frequency domain*, that the Fourier transform $\chi(\omega)$ of $h(t)$ is analytical inside the upper half-plane. Furthermore, if we subject the system to an oscillating force with a frequency much higher than its highest resonance frequency, there will be almost no time for the system to respond before the forcing has alternated the direction, and hence the frequency response $\chi(\omega)$ converges to zero, when ω becomes very large. From these physical considerations, we see that $\chi(\omega)$ will normally satisfy the conditions necessary for the Kramers-Kronig relations to apply.

The frequency response of a system forced to generate an impulse response $h(t)$ is given by the Fourier-transform,

$$\chi(\omega) = \tfrac{1}{\sqrt{2\pi}} \int_{-\infty}^{\infty} h(t) e^{-\imath\omega t} dt = \mathcal{F}[h(t)] \ , \tag{18.173}$$

which for an electrical system corresponds to its impedance. Now, the boundary condition of causality can be implemented with the use of the Heaviside step function $\Theta(t)$,

$$\chi(\omega) = \tfrac{1}{\sqrt{2\pi}} \int_{-\infty}^{\infty} h(t)\Theta(t) e^{-\imath\omega t} dt = \mathcal{F}[h(t)\Theta(t)] = \mathcal{F}[h(t)\Theta(t)\Theta(t)] \ . \tag{18.174}$$

Note that the implementation of causality via the Heaviside step function is directly implemented when replacing the Fourier transform by the *Laplace transform*. Applying the convolution theorem to the Fourier transform and using the Fourier transform of the Heaviside function we get [23],

$$\boxed{\chi(\omega) = \mathcal{F}[h(t)\Theta(t)] \star \mathcal{F}[\Theta(t)] = \chi(\omega) \star (\mathcal{F}\Theta)(\omega) = \chi(\omega) \star \left(\tfrac{1}{2\pi\imath\omega} + \tfrac{1}{2}\delta(\omega)\right)} \ . \tag{18.175}$$

This equality can be considered an early or raw form of the Kramers-Kronig relations and will turn out to be equivalent to them. To see this, we carry out the convolution explicitly,

$$\chi(\omega) = \frac{1}{2\pi} \int_{-\infty}^{\infty} \frac{\chi(\omega')d\omega'}{\imath(\omega - \omega')} + \frac{1}{2}\chi(\omega) \ , \tag{18.176}$$

[23] $\mathcal{F}[\Theta(t)] = \frac{1}{\imath\sqrt{2\pi}\omega} + \sqrt{\frac{\pi}{2}}\delta(\omega)$

or isolating $\chi(\omega)$,

$$\chi(\omega) = \frac{1}{\pi}\int_{-\infty}^{\infty} \frac{\chi(\omega')d\omega'}{\imath(\omega-\omega')} \ . \tag{18.177}$$

This is the frequency response of causal systems being invariant under a Hilbert-transform. It is equivalent to the Kramers-Kronig relations (18.169). Rewriting it for only positive integration limits, the integral splits up like,

$$\chi(\omega) = \frac{1}{\pi}\int_{0}^{\infty} \frac{\chi(\omega')d\omega'}{\imath(\omega-\omega')} + \frac{1}{\pi}\int_{0}^{\infty} \frac{\chi(-\omega')d\omega'}{\imath(\omega+\omega')} \ . \tag{18.178}$$

From the definition of the Fourier integral of the real quantity $h(t)$ follows directly $\chi(-\omega) = \chi^*(\omega)$, that is, the positive frequency response determines the negative frequency response. Therefore,

$$\begin{aligned}\chi(\omega) &= \frac{1}{\pi}\int_{0}^{\infty} \frac{\chi(\omega')(\omega+\omega') + \chi^*(\omega')(\omega-\omega')}{\imath(\omega^2-\omega'^2)}d\omega' \\ &= \frac{1}{\pi}\int_{0}^{\infty} \frac{\omega'\mathfrak{Im}\ \chi(\omega') - \imath\omega\mathfrak{Re}\ \chi^*(\omega')}{\omega^2-\omega'^2}d\omega' \ .\end{aligned} \tag{18.179}$$

from which we obtain the Kramers-Kronig relations for the real and imaginary parts in a format, where they are useful for physically realistic response functions,

$$\boxed{\mathfrak{Re}\ \chi(\omega) = \frac{2}{\pi}\int_{0}^{\infty} \frac{\omega'\mathfrak{Im}\ \chi(\omega')}{\omega^2-\omega'^2}d\omega' \quad \text{and} \quad \mathfrak{Im}\ \chi(\omega) = \frac{-2}{\pi}\int_{0}^{\infty} \frac{\omega\mathfrak{Re}\ \chi(\omega')}{\omega^2-\omega'^2}d\omega'} \ . \tag{18.180}$$

The imaginary part of a response function describes, being *out of phase* with the driving force, how a system dissipates energy. The Kramers-Kronig relations imply that observing the *dissipative* response of a system is sufficient to determine its (reactive) *in-phase* response, and vice versa.

18.2.7 Exercises

18.2.7.1 Ex: Skin depth

a. Consider a piece of glass containing some free charges. How long does it take for the charges to migrate to the surface?
b. Suppose you were designing a microwave experiment at a frequency of 10^{10} Hz. How thick would you make a silver coating?
c. Find the wavelength and propagation velocity in copper for radio waves at 1 MHz. Compare with the corresponding values in air (or vacuum).

Solution: *a. The continuity equation tells us that in a conductor,*

$$\frac{\partial \varrho_f}{\partial t} = -\nabla\cdot\mathbf{j}_f = -\nabla\cdot\sigma\vec{\mathcal{E}} = -\sigma\frac{\varrho_f}{\varepsilon_0} \ .$$

The solution of the differential equation is,

$$\varrho_f(t) = \varrho_f(0)e^{-\sigma t/\varepsilon_0} \ .$$

With a conductivity of glass of $\sigma = 10^{-11}\,\mathrm{Sm}^{-1}$ *and a permittivity of* $\varepsilon = 4.7\varepsilon_0$ *we find a time constant for the drift of* $\tau \approx 4.16\,\mathrm{s}$.
b. Skin depth was derived in class,

$$d = \frac{1}{\kappa} = \frac{1}{\omega}\left[\frac{\mu\varepsilon}{2}\sqrt{1+\left(\frac{\sigma}{\varepsilon\omega}\right)^2}\right]^{-1/2} .$$

The conductivity of silver is $\sigma \approx 6.30\cdot 10^7\,\mathrm{Sm}^{-1}$. *Since it represents an excellent conductor,* $\varepsilon \simeq \varepsilon_0$. *Also, we have* $\mu \simeq \mu_0$. *Thus, at the given microwave frequency,*

$$d \simeq \sqrt{\frac{2}{\omega\mu_0\sigma}} \approx 634\,\mathrm{nm} .$$

c. For copper ($\sigma \approx 5.96\cdot 10^7\,\mathrm{Sm}^{-1}$*) we evaluate, at the given radiofrequency, the wavelength from the real part of* $\tilde{k}$,

$$\lambda = 2\pi/k \simeq 2\pi\sqrt{\frac{2}{\omega\mu_0\sigma}} \approx 4.1\cdot 10^{-4}\,\mathrm{m} ,$$

which is much shorter than radiofrequency wavelengths in free space. The propagation velocity,

$$v = \omega/k = \frac{\omega\lambda}{2\pi} \approx 410\,\mathrm{m/s}$$

and obviously much slower than the speed of light in free space, which points to large refraction index, $n = ck/\omega$.

18.2.7.2 Ex: Complex refractive index

A light wave described by the electric field $\mathcal{E}_i = \mathcal{E}_0 e^{\imath k_0 z}$ comes from the vacuum and impinges on a metal surface characterized by the complex refractive index $n = n' + \imath n''$. Determine from the relation $n = \sqrt{\epsilon}$ the relative dielectric constant ϵ.
a. At what depth the field falls to e^{-1}, if $\mathcal{E}_{met} \simeq 0.05\mathcal{E}_0$ and $k_{met} = nk_0$.
b. Now despise the penetrating field, $|\mathcal{E}_{met}| \simeq 0$, and consider the reflected field $\mathcal{E}_r = \mathcal{E}_0 e^{-\imath kx + \imath\Delta\phi}$. Calculate the intensity resulting from the superposition of $\mathcal{E}_i$ and $\mathcal{E}_r$.

Solution: *a. The wavefunction on the metal is,*

$$\mathcal{E}_{met} e^{\imath n k_0 x} = \mathcal{E}_{met} e^{-n'' k_0 x} e^{\imath n' k_0 x} .$$

Hence, $l_{1/2} = 1/(n'' k_0)$.
b. Factorizing $e^{\imath\Delta\phi/2}$ *we obtain,*

$$\begin{aligned} I &= \varepsilon_0 c|\mathcal{E}_i + \mathcal{E}_r|^2 = \varepsilon_0 c|\mathcal{E}_0 e^{\imath k_0 x} + \mathcal{E}_0 e^{\imath k_0 x + \imath\Delta\phi}|^2 \\ &= \varepsilon_0 c|e^{\imath\Delta\phi/2}|\cdot|\mathcal{E}_0 e^{\imath k_0 x - \imath\Delta\phi/2} + \mathcal{E}_0 e^{\imath k_0 x + \imath\Delta\phi/2}|^2 = \cos^2(kx - \Delta/2) . \end{aligned}$$

18.2.7.3 Ex: Fourier expansion

The Fourier inversion theorem says that,

$$f(z) = \int_{-\infty}^{\infty} A(k) e^{\imath kz} dk \qquad \Longleftrightarrow \qquad A(k) = \tfrac{1}{2\pi} \int_{-\infty}^{\infty} f(z) e^{-\imath kz} dz \ .$$

Use the theorem to determine $A(k)$ for the wavepacket given by $f(z,t) = \int_{-\infty}^{\infty} A(k) e^{\imath[kz - \omega(k)t]} dk$ as a function of the real parts $\mathfrak{Re}\ f(z,0)$ and $\mathfrak{Re}\ \dot{f}(z,0)$.

Solution: *The time derivative of the packet is,*

$$\dot{f}(z,t) = -\imath \int_{-\infty}^{\infty} \omega A(k) e^{\imath(kz - \omega t)} dk \ .$$

With this we calculate,

$$f(z,0) = \int_{-\infty}^{\infty} A(k) e^{\imath kz} dk \qquad \textit{and} \qquad \dot{f}(z,0) = -\imath \int_{-\infty}^{\infty} \omega A(k) e^{\imath kz} dk \ ,$$

that is,

$$A(k) = \tfrac{1}{2\pi} \int_{-\infty}^{\infty} f(z,0) e^{-\imath kz} dz \qquad \textit{and} \qquad -\imath\omega A(k) = \tfrac{1}{2\pi} \int_{-\infty}^{\infty} \dot{f}(z,0) e^{-\imath kz} dz \ .$$

Now, we decompose, $f = f_r + \imath f_i$, to get,

$$A(k) = \tfrac{1}{2\pi} \int_{-\infty}^{\infty} f(z,0) e^{-\imath kz} dz = \frac{1}{2\pi} \int_{-\infty}^{\infty} (f_r + \imath f_i) e^{-\imath kz} dz \stackrel{!}{=} \tfrac{1}{2\pi} \int_{-\infty}^{\infty} \frac{\dot{f}_r + \imath \dot{f}_i}{-\imath\omega} e^{-\imath kz} dz \ .$$

Since obviously $f_r = -\dot{f}_i/\omega$ and $f_i = \dot{f}_r/\omega$, we obtain,

$$A(k) = \tfrac{1}{2\pi} \int_{-\infty}^{\infty} \left[f_r(z,0) + \tfrac{\imath \dot{f}_r(z,0)}{\omega} \right] e^{-\imath kz} dz \ .$$

18.2.7.4 Ex: Electromagnetic wave

In a dispersionless medium ($\varepsilon = \varepsilon_0$ and $\mu = \mu_0$) we have for a component $u(x,t)$ of an electromagnetic wave (here without dimension),

$$u(x,t) = \frac{1}{\sqrt{2\pi}} \int_{-\infty}^{\infty} dk A(k) e^{\imath kx - \imath\omega(k)t} \qquad \text{with} \qquad \omega(k) = ck \ ,$$

and

$$A(k) = \frac{1}{\sqrt{2\pi}} \int_{-\infty}^{\infty} dx u(x,0) e^{-\imath kx} \ .$$

a. Show that $u(x,t)$ satisfies the one-dimensional wave equation for vacuum.
b. Calculate the spectral distribution $A(k)$ for $u(x,t) = e^{\imath k_0 x - \imath\omega_0 t}$.
c. Calculate the spectral distribution $A(k)$ for $\{u(x,t) = e^{\imath k_0 x - \imath\omega_0 t}$ for $-L < x - (\omega_0/k_0)t < L$ and 0 else$\}$.
d. Calculate $u(x,t)$, when $u(x,0) = \int_{-a}^{+a} \delta(x-a)da$.
e. Try to understand in an elementary way the relation of part (c) between the bandwidth and the length of the wavepacket. Perform the transition to the limit $L \to \infty$ explicitly. For the case (d) discuss the propagation of the wavepacket in space.
Formulas:

$$\delta(k_0 - k) = \frac{1}{2\pi} \int_{-\infty}^{\infty} dx e^{\imath(k_0-k)x} = \frac{1}{\pi} \lim_{L\to\infty} \frac{\sin(k_0-k)}{k_0-k}$$

$$\Theta(a) = \frac{1}{2\pi\imath} \int_{-\infty}^{\infty} dk \frac{e^{\imath k a}}{k} = \begin{cases} 1 & \text{for } a > 0 \\ 0 & \text{else} \end{cases} .$$

Solution: *a. Integration and differentiation are interchangeable.* $u(x,t)$ *therefore satisfies the one-dimensional wave equation,*

$$\left(\frac{\partial^2}{\partial x^2} - \frac{1}{c^2} \frac{\partial^2}{\partial t^2} \right) u(x,t) = 0$$

provided, as requested in the problem, $\omega(k) = ck$.
b. With the given formula we find,

$$A(k) = \frac{1}{\sqrt{2\pi}} \int_{-\infty}^{\infty} dx\ e^{\imath(k_0-k)x} = \sqrt{2\pi}\delta(k_0 - k) .$$

c. We obtain,

$$A(k) = \frac{1}{\sqrt{2\pi}} \int_{-L}^{+L} dx\ e^{\imath(k_0-k)x} = \frac{1}{\sqrt{2\pi}} \frac{1}{\imath(k_0-k)} [e^{\imath(k_0-k)L} - e^{-\imath(k_0-k)L}]$$
$$= \frac{2L}{\sqrt{2\pi}} \frac{\sin([k_0-k]L)}{[k_0-k]L} .$$

d. We derive,

$$A(k) = \frac{1}{\sqrt{2\pi}} \int_{-\infty}^{\infty} dx \int_{-a}^{+a} da\ \delta(x-a) e^{-\imath k x} = \frac{1}{\sqrt{2\pi}} \int_{-a}^{+a} dx\ e^{-\imath k x}$$
$$= \frac{1}{\sqrt{2\pi}} \frac{1}{\imath k} [e^{\imath k a} - e^{-\imath k x}] = \frac{2}{\sqrt{2\pi}} \frac{\sin ka}{k} ,$$

and hence,

$$u(x,t) = \frac{1}{2\pi\imath}\int_{-\infty}^{+\infty} dk\ \frac{e^{\imath ka} - e^{-\imath ka}}{k} e^{\imath k(x-ct)}$$
$$= \frac{1}{2\pi\imath}\int_{-\infty}^{+\infty} dk\ \frac{1}{k}(e^{\imath k(a+x)} - e^{\imath k(x-a)})e^{-\imath kct}$$
$$= \frac{1}{2\pi\imath}\int_{-\infty}^{+\infty} dk\ \left(\frac{e^{\imath k(x+a-ct)}}{k} - \frac{e^{\imath k(x-a-ct)}}{k}\right) = \Theta(x+a-ct) - \Theta(x-a-ct)\ .$$

From this follows that $u(x,t) = 1$ within the range $ct - a < x < ct + a$ and $u(x,t) = 0$ outside.
e. We had in part (c),

$$A(k) = \frac{2L}{\sqrt{2\pi}} \frac{\sin([k_0 - k]L)}{[k_0 - k]L}\ .$$

The main maximum is in $k = k_0$. Here, $A(k_0) = 2L/\sqrt{2\pi}$. It follows immediately,

$$\|A\left(k_0 \pm \tfrac{2n\pi}{L} \pm \tfrac{\pi}{2L}\right)\| = \frac{2L}{\sqrt{2\pi}(2n\pi \pm \pi/2)}$$

The bandwidth of the spectral distribution is twice the distance between two consecutive maxima, i.e. here, $\Delta k = 2\pi/L$. The spatial extent of the wavepacket is $\Delta x = 2L$. From this immediately follows a kind of 'uncertainty relationship' $\Delta k \Delta x = 4\pi > 1$. In the limit $L \to \infty$ follows immediately,

$$\lim_{L\to\infty} A(k) = \sqrt{2\pi}\frac{1}{\pi}\lim_{L\to\infty} \frac{\sin([k_0 - k)]L}{[k_0 - k]L} = \sqrt{2\pi}\delta(k_0 - k)$$

18.2.7.5 Ex: Phase and group velocity

Let us study the one-dimensional motion of a wavepacket in x-direction, which spreads in infinite space. The law of dispersion is given by $\omega = \omega(k)$. The motion of a wavepacket is then described by,

$$u(x,t) = \frac{1}{\sqrt{2\pi}}\int_{-\infty}^{\infty} dk A(k) e^{\imath kx - \imath\omega(k)t}\ ,$$

where the spectral distribution $A(k)$ is given by shape of the wavepacket at time $t = 0$:

$$A(k) = \frac{1}{\sqrt{2\pi}}\int_{-\infty}^{\infty} dx u(x,0) e^{-\imath kx}\ .$$

The maximum of $A(k)$ be at $k = k_0$. We call $v_{ph} = \omega(k)/k$ the *phase velocity* and $v_{gr} = [d\omega(k)/dk]_{k_0}$ the *group velocity*, because in specific idealized situations a

wavepacket propagates precisely at this speed. In the following we consider a propagation of the wavepacket given by,

$$u(x,0) = c\exp\left\{-\frac{x^2}{2a^2} + \imath k_0 x\right\}$$

for a medium characterized by the dispersion relation $\omega(k) = b^2k^2$ (for a de Broglie matter wave).
a. Plot the shape of the wavepacket at time $t = 0$ via the intensity distribution $|u(x,0)|^2$. The 'width' of a Gaussian profile is given by the points, where the profile fell to $(1/e)$ of the maximum value. Calculate the width $\triangle x(t=0)$ of the intensity distribution.
b. Calculate the spectral distribution $A(k)$ and the width $\triangle k$ of the corresponding intensity distribution $|A(k)|^2$.
c. Now calculate $u(x,t)$ at a later time t. Express $u(x,t)$ in the form
$u(x,t) = \alpha e^{-(x-\beta t)^2/\gamma} e^{\imath(k_0 x - \omega(k_0)t)} e^{\imath\phi}$, where α, β, γ, and ϕ are real quantities which, nevertheless, may depend on t and x.
d. Calculate the intensity distribution $|u(x,t)|^2$ at time t. At what speed does the maximum move? Calculate the width $\triangle x(t)$ of the intensity distribution. What is the temporal evolution of $\triangle x(t)\triangle k$?
e. Compare $|u(x,t)|^2$ width $|u(x,0)|^2$.
Help:

$$\int_{-\infty}^{+\infty} dx\ e^{-ax^2+bx+c} = \sqrt{\tfrac{\pi}{a}}\exp\left[\tfrac{b^2+4ac}{4a}\right]\ .$$

Solution: *a. We have,*

$$u(x,0) = e^{-x^2/2a^2}e^{\imath k_0 x} \qquad \textit{and hence} \qquad |u(x,0)|^2 = c^2 e^{-x^2/a^2}\ .$$

The intensity distribution reaches the fraction $(1/e)$ of the maximum value (at $x=0$), when $x^2/a^2 = 1$, that is, $x = \pm a$. Therefore, its width is precisely given by $\Delta x(t=0) = 2a$. It describes the spatial extent of the wavepacket at time $t = 0$.
b. With the help of the given formula we obtain immediately,

$$\begin{aligned} A(k) &= \frac{1}{\sqrt{2\pi}}\int_{-\infty}^{+\infty} dx u(x,0)\exp[-\imath kx] = \frac{c}{\sqrt{2\pi}}\int_{-\infty}^{+\infty} dx\exp\left\{-\frac{x^2}{2a^2} + \imath(k_0-k)x\right\} \\ &= \frac{c}{\sqrt{2\pi}}\sqrt{2\pi a^2}\exp\left\{-\frac{a^2}{2}(k_0-k)^2\right\} = ac\exp\left\{-\frac{a^2}{2}(k_0-k)^2\right\}\ . \end{aligned}$$

With this, we obtain for the corresponding intensity distribution,

$$|A(k)|^2 = a^2c^2e^{-a^2(k_0-k)^2}\ .$$

It is independent of time, has its maximum value at $k = k_0$ and reaches at $k_0 - k = \pm 1/a$ the fraction $(1/e)$ of this value. Its width, therefore, is $\Delta k(t=0) = 2/a$. The larger the spatial extent, the narrower the momentum distribution, and vice versa.
c. We have,

$$u(x,t) = \frac{1}{\sqrt{2\pi}}\int_{-\infty}^{+\infty} dk A(k) e^{\imath kx - \imath\omega(k)t}\ .$$

With $A(k)$ of part (b) and $\omega(k) = b^2k^2$ we consecutively get,

$$\begin{aligned}
u(x,t) &= \frac{ac}{\sqrt{2\pi}} \int_{-\infty}^{+\infty} dk \exp\left\{ -\left[\frac{a^2}{2} + \imath b^2 t\right] k^2 + [a^2 k_0 + \imath x]k - \frac{a^2}{2}k_0^2 \right\} \\
&= \frac{ac}{\sqrt{2\pi}} \frac{\sqrt{\pi}}{\sqrt{\frac{a^2}{2} + \imath b^2 t}} \exp\left\{ \frac{a^4 k_0^2 + \imath 2a^2 k_0 x - x^2 - a^2 k_0^2 (a^2 + 2\imath b^2 t)}{2a^2 + 4\imath b^2 t} \right\} \\
&= \frac{c}{\sqrt{1 + \imath 2\frac{b^2}{a^2}t}} \exp\left\{ \frac{\imath 2a^2 k_0 x - \imath 2a^2 b^2 k_0^2 t - x^2}{2a^2\left(1 + \imath 2\frac{b^2}{a^2}t\right)} \right\} \\
&= \frac{c}{\sqrt{1 + \imath 2\frac{b^2}{a^2}t}} \exp\left\{ -\frac{(x^2 - \imath 2a^2[k_0 x - b^2 k_0^2 t])\left(1 - \imath 2\frac{b^2}{a^2}t\right)}{2a^2\left(1 + \left(2\frac{b^2}{a^2}t\right)^2\right)} \right\} \\
&= \frac{c}{\sqrt{1 + \imath 2\frac{b^2}{a^2}t}} \exp\left\{ -\frac{x^2 - 4b^2 t[k_0 x - b^2 k_0^2 t] - 2a^2 \imath[k_0 x - b^2 k_0^2 t] - \imath 2\frac{b^2}{a^2} t x^2}{2a^2\left(1 + \left(2\frac{b^2}{a^2}t\right)^2\right)} \right\} .
\end{aligned}$$

Regrouping provides,

$$u(x,t) = \frac{c}{\sqrt{1 + \imath 2\frac{b^2}{a^2}t}} \exp\left\{ -\frac{(x - 2b^2 k_0 t)^2}{2a^2\left(1 + \left(2\frac{b^2}{a^2}t\right)^2\right)} \right\} \cdot$$

$$\cdot \exp\left\{ \imath \frac{2a^2[k_0 x - b^2 k_0^2 t] + 2\frac{b^2}{a^2}t + 2a^2\left(2\frac{b^2}{a^2}t\right)^2 [k_0 x - b^2 k_0^2 t] - 2a^2\left(2\frac{b^2}{a^2}t\right)^2 [k_0 x - b^2 k_0^2 t]}{2a^2\left(1 + \left(2\frac{b^2}{a^2}t\right)^2\right)} \right\}$$

$$= \frac{c}{\sqrt{1 + \imath 2\frac{b^2}{a^2}t}} \exp\left\{ -\frac{(x - 2b^2 k_0 t)^2}{2a^2\left(1 + \left(2\frac{b^2}{a^2}t\right)^2\right)} \right\} e^{\imath(k_0 x - b^2 k_0^2 t)} \cdot \exp\left\{ \imath \frac{2\frac{b^2}{a^2}t(x^2 - 4b^2 k_0 x t + 4b^4 k_0^2 t^2)}{2a^2\left(1 + \left(2\frac{b^2}{a^2}t\right)^2\right)} \right\}$$

$$= \frac{c}{\sqrt{1 + \imath 2\frac{b^2}{a^2}t}} \exp\left\{ -\frac{(x - 2b^2 k_0 t)^2}{2a^2\left(1 + \left(2\frac{b^2}{a^2}t\right)^2\right)} \right\} e^{\imath(k_0 x - b^2 k_0^2 t)} \cdot \exp\left\{ \imath \frac{2\frac{b^2}{a^2}t(x - 2b^2 k_0^t)^2}{2a^2\left(1 + \left(2\frac{b^2}{a^2}t\right)^2\right)} \right\} .$$

Now,

$$1 + \imath 2\frac{b^2}{a^2}t = \sqrt{1 + \left(2\frac{b^2}{a^2}t\right)^2} \exp\left\{ \imath \text{arctg}\left[\frac{2b^2}{a^2}t\right] \right\} ,$$

and hence,

$$u(x,t) = \frac{c}{\left[1 + \left(2\frac{b^2}{a^2}t\right)^2\right]^{-1/4}} \exp\left\{ -\frac{(x - 2b^2 k_0 t)^2}{2a^2\left(1 + \left(2\frac{b^2}{a^2}t\right)^2\right)} \right\} \exp\left\{\imath[k_0 x - b^2 k_0^2 t]\right\} \cdot$$

$$\cdot \exp\left\{ \imath \left[\frac{2\frac{b^2}{a^2}t(x - 2b^2 k_0 t)^2}{2a^2\left(1 + \left(2\frac{b^2}{a^2}t\right)^2\right)} - \frac{1}{2}\text{arcctg}\left(\frac{2b^2}{a^2}t\right) + n\pi \right] \right\} .$$

where the additional phase $\imath n\pi$ was introduced to remove the phase ambiguity of the arctan.
d. With part (c) immediately follows,

$$|u(x,t)|^2 = \frac{c^2}{\sqrt{1+\left(2\frac{b^2}{a^2}t\right)^2}} \exp\left\{-\frac{(x-2b^2k_0t)^2}{a^2\left(1+\left(2\frac{b^2}{a^2}t\right)^2\right)}\right\} .$$

The spatial intensity distribution has its maximum at,

$$x_m(t) = 2b^2k_0t .$$

This maximum propagates with the speed,

$$2b^2k_0 = \left[\frac{d\omega(k)}{dk}\right]_{k_0} \equiv v_{gr} .$$

The decay to $(1/e)$ happens, when

$$(x-v_{gr}t)^2 = a^2\left(1+\left(2\frac{b^2}{a^2}t\right)^2\right) .$$

This follows the width (spatial extent) at time t,

$$\Delta x(t) = 2a\sqrt{1+\left(2\frac{b^2}{a^2}t\right)^2} .$$

Since, on the other hand, $\Delta k = \frac{2}{a}$ is independent of time, we get an 'uncertainty relation' of the form,

$$\Delta x(t)\Delta k = 4\sqrt{1+\left(2\frac{b^2}{a^2}t\right)^2} \geq 4 .$$

e. The maximum of the spatial intensity distribution moves at group velocity, the width increases in the manner calculated in (d). The wave packet 'spreads'. For long t we obtain,

$$\Delta x(t) \to \frac{4b^2}{a}t \sim t .$$

Width increases linearly over time.

18.2.7.6 Ex: Radiation force acting on a small dielectric particle

The polarizability of a small ($a \ll \lambda$) dielectric particle with complex refraction index $n_p = \mathfrak{Re}\ n_p - \imath\frac{\alpha\lambda}{4\pi}$ immersed in a medium of refraction index n_m is given by,

$$\alpha_{rad} = \frac{4\pi a^3 \frac{n_p^2-n_m^2}{n_p^2+2n_m^2} n_m^2\varepsilon_0}{1-\frac{n_p^2-n_m^2}{n_p^2+2n_m^2}\left[\left(\frac{n_m\omega_0}{c}a\right)^2 - \frac{2}{3}\imath\left(\frac{n_m\omega_0}{c}a\right)^3\right]} .$$

Calculate the total force acting on it when subject to an electromagnetic field.

Solution: *Let us assume the particle to be in the Rayleigh regime of dipolar approximation, $a \ll \lambda$, where a small dielectric particle behaves like an induced electric dipole,*

$$\vec{\mathcal{P}}(\mathbf{r},t) = \alpha_{rad}\vec{\mathcal{E}}(\mathbf{r},t) \ .$$

The Lorentz force is,

$$\begin{aligned}\mathbf{F}(\mathbf{r}) &= [\vec{\mathcal{P}}(\mathbf{r})\cdot\nabla]\vec{\mathcal{E}}(\mathbf{r}) + \imath\frac{n_m\omega_0}{c}\vec{\mathcal{P}}(\mathbf{r})\times\vec{\mathcal{B}}(\mathbf{r}) \\ &= \alpha_{rad}\left\{[\vec{\mathcal{E}}(\mathbf{r})\cdot\nabla]\vec{\mathcal{E}}(\mathbf{r}) + \vec{\mathcal{E}}(\mathbf{r})\times[\nabla\times\vec{\mathcal{E}}(\mathbf{r})]\right\} = \tfrac{1}{2}\alpha_{rad}\nabla\vec{\mathcal{E}}^2(\mathbf{r}) \ .\end{aligned}$$

Time-averaged,

$$\begin{aligned}\langle\mathbf{F}(\mathbf{r})\rangle &= \tfrac{1}{2}\mathfrak{Re}\ \left[\alpha_{rad}\left\{[\vec{\mathcal{E}}(\mathbf{r})\cdot\nabla]\vec{\mathcal{E}}^*(\mathbf{r}) + \vec{\mathcal{E}}(\mathbf{r})\times\left[\nabla\times\vec{\mathcal{E}}^*(\mathbf{r})\right]\right\}\right] \\ \langle\mathbf{F}^i\rangle &= \tfrac{1}{2}\mathfrak{Re}\ \left[\alpha_{rad}E_j\partial^i(E^j)^*\right] \ .\end{aligned}$$

18.2.7.7 Ex: Lorentz model

Based on the Lorentz model, derive the differential equation for the oscillation amplitude of the electrons and calculate the response of the matter reacting via a polarization $P = Nex$, where N is the number of electrons and x their oscillation amplitude. Calculate the absorptive part $\mathfrak{Im}\ \chi$ and the dispersive part $\mathfrak{Re}\ \chi$ of the susceptibility $\chi \equiv P/\varepsilon_0\mathcal{E}$.
With this calculate the index of refraction n and the coefficient of absorption α in the Lorentz model.

Solution: *Differently from the Thomson model, the Lorentz model considers electrons bound to an atom. Of course, this bond influences the electronic motion. Let the light wave be $\mathcal{E} = \mathcal{E}_0 e^{\imath\omega t}$. The differential equation is,*

$$\ddot{x} + \gamma_\omega\dot{x} + \omega_0^2 = \frac{e}{m_e}\mathcal{E}_0 e^{\imath\omega t} \ .$$

The ansatz $x \equiv x_0 e^{\imath\omega t}$ leads to the oscillation amplitude,

$$x_0 = \frac{e\mathcal{E}_0}{m_e}\frac{1}{\omega_0^2 - \omega^2 - \imath\gamma_\omega\omega} \ .$$

For small detunings $\Delta = \omega - \omega_0 \ll \omega$ we get,

$$x_0 \simeq \frac{1}{2\omega}\frac{-\Delta + \imath\gamma_\omega/2}{\Delta^2 + (\gamma_\omega/2)^2} \ .$$

Hence,

$$\chi = \frac{Ne^2}{\varepsilon_0 m_e 2\omega}\frac{-\Delta + \imath\gamma_\omega/2}{\Delta^2 + (\gamma_\omega/2)^2} \ .$$

Writing the intensity as $I = I_0 e^{\imath\alpha z}$, we find the refraction index and the absorption coefficient,

$$n = 1 + \mathfrak{Im}\ \chi \qquad \text{and} \qquad \alpha = \mathfrak{Re}\ \chi\ .$$

We also have,

$$\phi(\omega) = \frac{\mathfrak{Im}\ \alpha}{\mathfrak{Re}\ \alpha} = \frac{-\gamma_\omega \omega^2}{\omega^2 - \omega_0^2} \overset{\omega\to\omega_0}{\to} \frac{\gamma_\omega}{2\Delta}\ .$$

18.2.7.8 Ex: Lorentz force on a single atomic dipole

Calculate the Lorentz force on a single atom within the dipole approximation from the expression [619],

$$\mathbf{F} = \int d^3r [\varrho(\mathbf{r})\vec{\mathcal{E}}(\mathbf{r}) + \mathbf{j}(\mathbf{r}) \times \vec{\mathcal{B}}(\mathbf{r})]\ .$$

Solution: *With the given formula, understanding the atom as a permanent dipole, $\mathbf{d} = -e(\mathbf{r}_1 - \mathbf{r}_2)$, we find the parametrization,*

$$\varrho(\mathbf{r}) \equiv -e\delta(\mathbf{r} - \mathbf{r}_1) + e\delta\mathbf{r} - \mathbf{r}_2) \qquad \text{and} \qquad \mathbf{j}(\mathbf{r}) \equiv -e\dot{\mathbf{r}}\delta(\mathbf{r} - \mathbf{r}_1) + e\dot{\mathbf{r}}\delta(\mathbf{r} - \mathbf{r}_2)\ .$$

The force then becomes,

$$\begin{aligned}
\mathbf{F} &= -e\vec{\mathcal{E}}(\mathbf{r}_1) + e\vec{\mathcal{E}}(\mathbf{r}_2) - e\dot{\mathbf{r}}_1 \times \vec{\mathcal{B}}(\mathbf{r}_1) + e\dot{\mathbf{r}}_2 \times \vec{\mathcal{B}}(\mathbf{r}_2) \\
&= (\mathbf{d}\cdot\nabla)\vec{\mathcal{E}} + \dot{\mathbf{d}} \times \vec{\mathcal{B}} \\
&= (\mathbf{d}\cdot\nabla)\vec{\mathcal{E}} + \frac{d}{dt}(\mathbf{d} \times \vec{\mathcal{B}}) - \mathbf{d} \times \dot{\vec{\mathcal{B}}} \\
&= (\mathbf{d}\cdot\nabla)\vec{\mathcal{E}} + \frac{d}{dt}(\mathbf{d} \times \vec{\mathcal{B}}) + \mathbf{d} \times (\nabla \times \tilde{\mathcal{E}})\ .
\end{aligned}$$

Use a plane wave $\vec{\mathcal{E}}(\mathbf{r}, t) = \mathcal{E}(kz - \omega t)\cos(kz - \omega t)\hat{\mathbf{e}}$. Then, $\nabla \times \vec{\mathcal{E}} = 0$.

18.2.7.9 Ex: The Faraday effect

Derive the *Faraday effect* from the Lorentz model using the following procedure:
a. Formulate the equation of motion for the position $\mathbf{s}$ of a bound electron according to (18.106) in the presence of a homogeneous magnetic field $\vec{\mathcal{B}} = \mathcal{B}\hat{\mathbf{e}}_z$ and an electromagnetic wave characterized by $\vec{\mathcal{E}}(z,t) = \mathcal{E}(z)\hat{\epsilon}e^{-\imath\omega t}$ and assumed to be initially linearly polarized in x-direction.
b. Express the motion of the electron in the xy-plane in a new basis given by $\hat{\mathbf{e}}_\pm = \frac{1}{\sqrt{2}}(\hat{\mathbf{e}}_x \pm \imath\hat{\mathbf{e}}_y)$.
c. Solve the equations of motion for the decoupled components $s_\pm(z,t) \equiv s_x \mp \imath s_y$ and determine the susceptibility.
d. Calculate the electric field and the angle by which the linear polarization vector is

rotated as a function of z.

Solution: *a. We write the equations for an electron at position* $\mathbf{s}$ *bound to a molecule in a dielectric medium subject to an electric and a magnetic field as,*

$$m_e\ddot{\mathbf{s}} + m_e\gamma_\omega\dot{\mathbf{s}} + m_e\omega_0^2\vec{\mathcal{S}} = -e(\vec{\mathcal{E}} + \dot{\mathbf{s}} \times \vec{\mathcal{B}}) \ . \tag{18.181}$$

Now, we describe the electric field as a plane wave propagating in z*-direction and being, at* $z = 0$*, linearly polarized in* x*-direction,* $\vec{\mathcal{E}}(0,t) = \mathcal{E}(0)\hat{\mathbf{e}}_x e^{-\imath\omega t}$*. In the internal region of the dielectric, the electric field will acquire components along* $\hat{\mathbf{e}}_x$ *and* $\hat{\mathbf{e}}_y$*. Thus we have to allow for a general ansatz,*

$$\vec{\mathcal{E}}(z,t) = \mathcal{E}_x(z)\hat{\mathbf{e}}_x + \mathcal{E}_y(z)\hat{\mathbf{e}}_y \ . \tag{18.182}$$

In the equation of motion (18.181), due to the construction of the plane wave, the force applied to the electron is contained in the xy*-plane, thus leading to a harmonic motion confined to this plane. Thus, the evolution of the components* $\mathcal{E}_{x,y}$ *under the action of the fields* $\vec{\mathcal{E}}$ *and* $\vec{\mathcal{B}}$ *must be determined.*

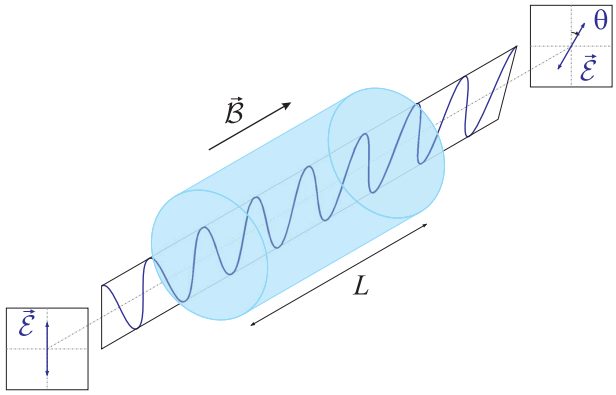

Figure 18.19: Scheme of the Faraday effect.

b. The position of the electron $\mathbf{s}$ *is obtained as the response of the medium to the action of the wave's electric field. That is, the wave induces a movement of the electron, so we can write* $\mathbf{s}(z,t) = s_x(z,t)\hat{\mathbf{e}}_x + s_y(z,t)\hat{\mathbf{e}}_y$*. Replacing* $\mathbf{s}(z,t)$*,* $\vec{\mathcal{E}}(z,t)$*, and* $\vec{\mathcal{B}}$ *in Eq. (18.181) we obtain,*

$$\begin{aligned} &m_e(\ddot{s}_x\hat{\mathbf{e}}_x + \ddot{s}_y\hat{\mathbf{e}}_y) + m_e\gamma_\omega(\dot{s}_x\hat{\mathbf{e}}_x + \dot{s}_y\hat{\mathbf{e}}_y) + m_e\omega_0^2(s_x\hat{\mathbf{e}}_x + s_y\hat{\mathbf{e}}_y) \\ &\quad = -e(\mathcal{E}_x\hat{\mathbf{e}}_x + \mathcal{E}_y\hat{\mathbf{e}}_y) + e(\dot{s}_x\mathcal{B}\hat{\mathbf{e}}_y - \dot{s}_y\mathcal{B}\hat{\mathbf{e}}_x) \ . \end{aligned} \tag{18.183}$$

Eq. (18.182) represents a system of coupled equations. We now replace the base formed by $\hat{\mathbf{e}}_x$ *and* $\hat{\mathbf{e}}_y$ *with the base formed by the circular polarization vectors* $\hat{\mathbf{e}}_\pm = \frac{1}{\sqrt{2}}(\hat{\mathbf{e}}_x \pm \imath\hat{\mathbf{e}}_y)$*. Separating the terms of this equation by components we get,*

$$\begin{aligned} &(\ddot{s}_x + \imath\ddot{s}_y) + (\gamma_\omega - \imath\Omega)(\dot{s}_x + \imath\dot{s}_y) + \omega_0^2(s_x + \imath s_y) = -\tfrac{e}{m_e}(\mathcal{E}_x + \imath\mathcal{E}_y) \\ &(\ddot{s}_x - \imath\ddot{s}_y) + (\gamma_\omega + \imath\Omega)(\dot{s}_x - \imath\dot{s}_y) + \omega_0^2(s_x - \imath s_y) = -\tfrac{e}{m_e}(\mathcal{E}_x - \imath\mathcal{E}_y) \ , \end{aligned} \tag{18.184}$$

where $\Omega = e\mathcal{B}/m_e$ is the cyclotron frequency. Defining new variables,

$$s_\pm(z,t) \equiv s_x(z,t) \mp \imath s_y(z,t) \quad , \quad \mathcal{E}_\pm(z,t) = [\mathcal{E}_x(z) \mp \imath \mathcal{E}_y(z)]e^{-\imath\omega t} = \mathcal{E}_0 e^{\imath(k_\pm z - \omega t)} \ , \tag{18.185}$$

a new system of equations is obtained from (18.184),

$$\begin{aligned} \ddot{s}_+ + (\gamma_\omega + \imath\Omega)\dot{s}_+ + \omega_0^2 s_+ &= -\tfrac{e}{m_e}\mathcal{E}_0 e^{\imath(k_+ z - \omega t)} \\ \ddot{s}_- + (\gamma_\omega - \imath\Omega)\dot{s}_- + \omega_0^2 s_- &= -\tfrac{e}{m_e}\mathcal{E}_0 e^{\imath(k_- z - \omega t)} \ . \end{aligned} \tag{18.186}$$

In doing so, we allowed for the possibility that the two circularly polarized plane waves may have different propagation velocities and thus phase shifts.
c. Neglecting γ_ω the solutions for $s_\pm$ are as follows:

$$s_\pm(z,t) = \frac{-e\mathcal{E}_0}{m_e(\omega_0^2 - \omega^2 \pm \omega\Omega)} e^{\imath(k_\pm z - \omega t)} = \frac{-e\mathcal{E}_\pm(z,t)}{m_e(\omega_0^2 - \omega^2 \pm \omega\Omega)} \ . \tag{18.187}$$

With these equations, the components of the electric dipole moment, $d_\pm(z,t) = -es_\pm(z,t)$ and the total polarization vector, $\mathcal{P}_\pm(z,t) = Nd_\pm(z,t)$ are, in the case of a linear dielectric,

$$\mathcal{P}_\pm(z,t) = \varepsilon_0 \chi_\varepsilon \mathcal{E}_\pm(z,t) = \frac{-Ne^2\mathcal{E}_\pm(z,t)}{m_e(\omega_0^2 - \omega^2 \pm \omega\Omega)} \ . \tag{18.188}$$

Thus the susceptibility in the circular basis is,

$$\chi_{\varepsilon\pm} = \frac{Ne^2}{m_e\varepsilon_0(\omega_0^2 - \omega^2 \pm \omega\Omega)} \tag{18.189}$$

d. Physically, this result represents the difference between the refraction indices n_+ and n_- obtained through the application of the magnetic field. The electric field (18.185) at a position z inside the dielectric becomes in the Cartesian basis, making the substitutions $k_\pm = n_\pm k_0$, $\bar{n} = (n_+ + n_-)/2$, and $\delta n = n_+ - n_-$,

$$\vec{\mathcal{E}}(z,t) = \mathcal{E}_0 e^{\imath(\bar{n}k_0 z - \omega t)}[\hat{\mathbf{e}}_x \cos\tfrac{\delta n\ k_0 z}{2} - \hat{\mathbf{e}}_y \sin\tfrac{\delta n\ k_0 z}{2}] \ . \tag{18.190}$$

The angular rotation of the polarization is,

$$\phi(z) = -\tfrac{1}{2}\delta n\ k_0 z \ . \tag{18.191}$$

Since $n_\pm^2 = 1 + \chi_{\varepsilon\pm}$ for a linear dielectric, expanding in Ω up to first order, we obtain,

$$\delta n = -\frac{Ne^2\omega\Omega}{m_e\varepsilon_0(\omega_0^2 - \omega^2)} \qquad \text{and} \qquad \bar{n} = \sqrt{1 + \frac{Ne^2}{m_e\varepsilon_0(\omega_0^2 - \omega^2)}} \ . \tag{18.192}$$

Substituting $k_0 = \omega/c$,

$$\boxed{\phi(z) = -\frac{Ne^3\omega^2}{m_e^2\varepsilon_0 2c(\omega_0^2 - \omega^2)^2}\mathcal{B}z \equiv V\mathcal{B}z} \ . \tag{18.193}$$

V it is called Verdet constant and is characteristic for the medium and also depends on the wavelength on the incident light [132, 767].

18.2.7.10 Ex: Complex refraction index and extinction coefficient

a. Derive the relations $n'^2 - n''^2 = 1 + \chi'_\varepsilon$ and $2n'n'' = \chi_\varepsilon$. **Note:** In a transparent dielectric medium there is no absorption, such that, $n'^2 = 1 + \chi'_\varepsilon = \frac{\varepsilon}{\varepsilon_0}$.
b. Calculate the *absorption coefficient* for a light field traversing a dielectric medium.

Solution: *a. From,*

$$n' = \mathfrak{Re}\ \sqrt{\epsilon} = \mathfrak{Re}\ \sqrt{1+\tilde{\chi}_\varepsilon} = \mathfrak{Re}\ \sqrt{1+\chi'_\varepsilon+\imath\chi''_\varepsilon} = \sqrt{\tfrac{1}{2}}\sqrt{\sqrt{(1+\chi'_\varepsilon)^2+\chi''^2_\varepsilon}+(1+\chi'_\varepsilon)}$$
$$n'' = \mathfrak{Im}\ \sqrt{\epsilon} = \mathfrak{Im}\ \sqrt{1+\tilde{\chi}_\varepsilon} = \mathfrak{Im}\ \sqrt{1+\chi'_\varepsilon+\imath\chi''_\varepsilon} = \sqrt{\tfrac{1}{2}}\sqrt{\sqrt{(1+\chi'_\varepsilon)^2+\chi''^2_\varepsilon}-(1+\chi'_\varepsilon)}\ ,$$

we calculate,

$$n'^2 - n''^2 = \left(\mathfrak{Re}\ \sqrt{1+\chi'_\varepsilon+\imath\chi''_\varepsilon}\right)^2 - \left(\mathfrak{Im}\ \sqrt{1+\chi'_\varepsilon+\imath\chi''_\varepsilon}\right)^2 = 1+\chi'_\varepsilon$$
$$2n'n'' = 2\mathfrak{Re}\ \sqrt{1+\chi'_\varepsilon+\imath\chi''_\varepsilon}\mathfrak{Im}\ \sqrt{1+\chi'_\varepsilon+\imath\chi''_\varepsilon} = \chi''_\varepsilon\ .$$

b. Within a dielectric medium, we obtain the propagating wave solutions of Maxwell's equations by substituting k with $\tilde{k}$,

$$\vec{\mathcal{E}} = \vec{\mathcal{E}}_0 e^{\imath\omega(\frac{n'z}{c}-t)-\omega\frac{n''}{c}z}\ .$$

The relationship between the amplitudes of the electric and magnetic fields is [24],

$$\mathcal{B}_0^{(\chi)} = \sqrt{\varepsilon\mu}\mathcal{E}_0 = \sqrt{\varepsilon_0\mu_0}\sqrt{1+\tilde{\chi}_\varepsilon}\ \mathcal{E}_0 = \frac{1}{c}(n'+\imath n'')\mathcal{E}_0 = (n'+\imath n'')\mathcal{B}_0\ .$$

We use the subscript (χ) to mark quantities within the dielectric medium. The average energy density is,

$$\bar{u}^{(\chi)} = \tfrac{1}{2}\varepsilon_0 n'^2|\vec{\mathcal{E}}|^2 = n'^2\bar{u}\ .$$

Now, the intensity of the light beam in a dielectric medium is attenuated,

$$\bar{I}^{(\chi)} = \tfrac{1}{\mu_0}|\vec{\mathcal{E}}\times\vec{\mathcal{B}}| = \tfrac{1}{2}\varepsilon_0 cn'|\vec{\mathcal{E}}|^2 = \tfrac{1}{2}\varepsilon_0 cn'\vec{\mathcal{E}}_0^2 e^{-2\omega n''z/c} = \bar{I}_0^{(\chi)}e^{-Kz}\ ,$$

where

$$\bar{I}_0^{(\chi)} = \tfrac{1}{2}\varepsilon_0 cn'\vec{\mathcal{E}}_0^2$$

is the intensity at the point, where the light enters the medium, and

$$K = 2\frac{\omega n''}{c} = \frac{\omega}{n'c}\chi''_\varepsilon$$

is called absorption coefficient. Note, that the energy flow $\bar{I}^{(\chi)}$ in the dielectric medium is always the product of energy density and propagation velocity c/n'. Note also, since the frequency ω of the light propagating through the dielectric remains the same, the wavelength shrinks like $\lambda = \frac{c/n'}{\nu}$ [816].

[24] In a dielectric medium, $\mu \simeq \mu_0$.

18.3 Plasmons, waveguides and resonant cavities

18.3.1 Green's tensor for wave propagation in dielectric media

The electromagnetic field in the presence of macroscopic dielectrics is governed by an inhomogeneous vector Helmholtz equation. Defining the permittivity and the permeability as tensor fields $\vec{\mathcal{D}}(\mathbf{r},\omega) = \epsilon(\mathbf{r},\omega)\varepsilon_0\vec{\mathcal{E}}(\mathbf{r},\omega)$ and $\vec{\mathcal{B}}(\mathbf{r},\omega) = \mu(\mathbf{r},\omega)\mu_0\vec{\mathcal{H}}(\mathbf{r},\omega)$ the Maxwell equations (17.6), become after a temporal Fourier transform,

$$\begin{aligned} \nabla\times\vec{\mathcal{H}} &= -\imath\omega\epsilon\varepsilon_0\vec{\mathcal{E}} + \mathbf{j} \\ \nabla\times\vec{\mathcal{E}} &= \imath\omega\mu\mu_0\vec{\mathcal{H}} \\ \nabla\cdot\epsilon\varepsilon_0\vec{\mathcal{E}} &= \varrho \\ \nabla\cdot\mu\mu_0\vec{\mathcal{H}} &= 0\ . \end{aligned} \tag{18.194}$$

It is easy to see, that the *inhomogeneous Helmholtz equation* [786, 946, 210],

$$\boxed{\left[\nabla\times\frac{1}{\mu(\mathbf{r},\omega)}\nabla\times - \frac{\omega^2}{c^2}\epsilon(\mathbf{r},\omega)\right]\vec{\mathcal{E}}(\mathbf{r},\omega) = \imath\omega\mu_0\mathbf{j}(\mathbf{r},\omega)} \tag{18.195}$$

satisfies the above Maxwell equations with $\vec{\mathcal{E}}(\mathbf{r},\omega)\to 0$ for $r\to\infty$. Using the Green's function formalism, the solution to the Helmholtz equation can be given by,

$$\vec{\mathcal{E}}(\mathbf{r},\omega) = \imath\omega\mu_0\int_V d^3r'\mathcal{G}(\mathbf{r},\mathbf{r}',\omega)\cdot\mathbf{j}(\mathbf{r}',\omega)\ , \tag{18.196}$$

where the *Green's tensor* is the solution to

$$\boxed{\left[\nabla_{\mathbf{r}}\times\frac{1}{\mu(\mathbf{r},\omega)}\nabla_{\mathbf{r}}\times - \frac{\omega^2}{c^2}\epsilon(\mathbf{r},\omega)\right]\mathcal{G}(\mathbf{r},\mathbf{r}',\omega) = \delta^{(3)}(\mathbf{r}-\mathbf{r}')\mathbb{I}} \tag{18.197}$$

together with the boundary condition $\mathcal{G}(\mathbf{r},\mathbf{r}',\omega)\to 0$ for $|\mathbf{r}-\mathbf{r}'|\to\infty$. The volume of integration V is a small volume surrounding the point $\mathbf{r}=\mathbf{r}'$ in order to avoid the singularity.

The Green's tensor represents the electric field radiated at position $\mathbf{r}$ by three orthogonal dipoles located at $\mathbf{r}'$.

18.3.1.1 Bulk medium

Let us now consider the simplest case of a bulk medium, i.e. an infinitely extended, homogeneous dielectric independent of $\mathbf{r}$, that is, $\epsilon(\mathbf{r},\omega)=\epsilon(\omega)$ and $\mu(\mathbf{r},\omega)=\mu(\omega)$. In this case, the Helmholtz equation further simplifies to,

$$[\nabla_{\mathbf{r}}\times\nabla_{\mathbf{r}}\times -k(\omega)^2]\vec{\mathcal{E}}_b(\mathbf{r},\omega) = \imath\omega\mu_0\mathbf{j}(\mathbf{r},\omega) \tag{18.198}$$

with $k(\omega)^2 = \frac{\omega^2}{c^2}\mu(\omega)\epsilon(\omega)$ defined at $\mathbf{r}$. The Green tensor is then the solution to,

$$\nabla_{\mathbf{r}}\times\nabla_{\mathbf{r}}\times\mathcal{G}_b(\mathbf{r},\mathbf{r}',\omega) - k^2\mathcal{G}_b(\mathbf{r},\mathbf{r}',\omega) = \delta^{(3)}(\mathbf{r}-\mathbf{r}')\mathbb{I}\ . \tag{18.199}$$

18.3.1.2 The scalar Helmholtz equation

The bulk medium vector Helmholtz equation (18.199) can be reduced to a scalar Helmholtz equation. To that end, we take its divergence and find,

$$\nabla \cdot \mathcal{G}_b(\mathbf{r},\mathbf{r}',\omega) = -\tfrac{1}{k^2}\nabla\delta^{(3)}(\mathbf{r}-\mathbf{r}') \ . \tag{18.200}$$

Using this identity and expanding,

$$\nabla_{\mathbf{r}}\times\nabla_{\mathbf{r}}\times\mathcal{G}_b = \begin{pmatrix} \partial_x^2-\triangle & \partial_x\partial_y & \partial_x\partial_z \\ \partial_x\partial_y & \partial_y^2-\triangle & \partial_y\partial_z \\ \partial_x\partial_z & \partial_y\partial_z & \partial_z^2-\triangle \end{pmatrix} \begin{pmatrix} G_{xx} & G_{xy} & G_{xz} \\ G_{yx} & G_{yy} & G_{yz} \\ G_{zx} & G_{zy} & G_{zz} \end{pmatrix} = (\nabla\otimes\nabla - \mathbb{I}\triangle)\,\mathcal{G}_b \ , \tag{18.201}$$

we may write,

$$\begin{aligned} [\Delta + k^2]\mathcal{G}_b(\mathbf{r},\mathbf{r}',\omega) &= \nabla\nabla\cdot\mathcal{G}_b(\mathbf{r},\mathbf{r}',\omega) - \nabla\times\nabla\times\mathcal{G}_b(\mathbf{r},\mathbf{r}',\omega) + k^2\mathcal{G}_b(\mathbf{r},\mathbf{r}',\omega) \\ &= \nabla\nabla\cdot\mathcal{G}_b(\mathbf{r},\mathbf{r}',\omega) - \delta^{(3)}(\mathbf{r}-\mathbf{r}')\mathbb{I} \\ &= -\tfrac{1}{k^2}\nabla\nabla\delta^{(3)}(\mathbf{r}-\mathbf{r}') - \delta^{(3)}(\mathbf{r}-\mathbf{r}')\mathbb{I} = -\left[\mathbb{I} + \tfrac{1}{k^2}\nabla\nabla\right]\delta^{(3)}(\mathbf{r}-\mathbf{r}') \ . \end{aligned} \tag{18.202}$$

The vector Helmholtz equation can hence be solved by writing,

$$\mathcal{G}_b(\mathbf{r},\mathbf{r}',\omega) = \left[\mathbb{I} + \tfrac{1}{k^2}\nabla\nabla\right] g(\mathbf{r},\mathbf{r}',\omega) \ , \tag{18.203}$$

where the scalar Green function g obeys the scalar Helmholtz equation,

$$\boxed{[\triangle + k^2]g(\mathbf{r},\mathbf{r}',\omega) = -\delta^{(3)}(\mathbf{r}-\mathbf{r}')} \ , \tag{18.204}$$

the solution of which is simply,

$$g(\mathbf{r},\mathbf{r}',\omega) = \frac{e^{\imath k|\mathbf{r}-\mathbf{r}'|}}{4\pi|\mathbf{r}-\mathbf{r}'|} \ , \tag{18.205}$$

where the boundary condition at infinity implies that k must have a positive imaginary part, $k = \sqrt{\varepsilon(\omega)}\frac{\omega}{c}$ with $\mathfrak{Im}\ k > 0$. Combining these results, we obtain the Green tensor of a bulk medium [994, 210],

$$\begin{aligned} \mathcal{G}_b(\mathbf{r},\mathbf{r}',\omega) &= \left[\mathbb{I} + \tfrac{1}{k^2}\nabla\nabla\right]\frac{e^{\imath k|\mathbf{r}-\mathbf{r}'|}}{4\pi|\mathbf{r}-\mathbf{r}'|} \\ &= \frac{\delta^{(3)}(\mathbf{R})\mathbb{I}}{3k^2} - \frac{e^{\imath kR}}{4\pi k^2R^3}\left\{[1-\imath kR-(kR)^2]\mathbb{I} - [3-3\imath kR-(kR)^2]\hat{\mathbf{e}}_R\otimes\hat{\mathbf{e}}_R\right\} \ , \end{aligned} \tag{18.206}$$

with $\mathbf{R} \equiv \mathbf{r}-\mathbf{r}'$, as will be shown in Exc. 18.3.7.1. The real and imaginary part are (for $\mathbf{R}\neq 0$),

$$\begin{aligned} \tfrac{4\pi}{k}\mathfrak{Re}\ \mathcal{G}_b(\mathbf{r},\mathbf{r}',\omega_0) &= (\mathbb{I}-\hat{\mathbf{e}}_R\otimes\hat{\mathbf{e}}_R)\frac{\cos kR}{kR} - (\mathbb{I}-3\hat{\mathbf{e}}_R\otimes\hat{\mathbf{e}}_R)\left(\frac{\sin kR}{k^2R^2} - \frac{\cos kR}{k^3R^3}\right) \\ \tfrac{4\pi}{k}\mathfrak{Im}\ \mathcal{G}_b(\mathbf{r},\mathbf{r}',\omega_0) &= (\mathbb{I}-\hat{\mathbf{e}}_R\otimes\hat{\mathbf{e}}_R)\frac{\sin kR}{kR} + (\mathbb{I}-3\hat{\mathbf{e}}_R\otimes\hat{\mathbf{e}}_R)\left(\frac{\cos kR}{k^2R^2} - \frac{\sin kR}{k^3R^3}\right) \ . \end{aligned} \tag{18.207}$$

Furthermore is is possible to show [210],

$$\mathfrak{Re}\ \mathcal{G}_b(\mathbf{r},\mathbf{r},\omega)=0 \qquad \text{and} \qquad \mathfrak{Im}\ \mathcal{G}_b(\mathbf{r},\mathbf{r},\omega)=\frac{k}{6\pi}\mathbb{I}\ . \tag{18.208}$$

Example 108 (*Electric field of a point dipole in an inhomogeneous dielectric*): Parametrizing the current generated by a point dipole located at $\mathbf{r}=\mathbf{r}_s$ by

$$\mathbf{j}(\mathbf{r},\omega)=-\imath\omega\mathbf{d}_s\delta^{(3)}(\mathbf{r}-\mathbf{r}_s)\ , \tag{18.209}$$

the generated electric field in an environment characterized by the Green function $\mathcal{G}(\mathbf{r},\mathbf{r}_s,\omega)$ can be evaluated from Eq. (18.196),

$$\vec{\mathcal{E}}(\mathbf{r},\mathbf{r}_s,\omega)=\omega^2\mu_0\mathcal{G}(\mathbf{r},\mathbf{r}_s)\cdot\mathbf{d}_s\ . \tag{18.210}$$

Using the solution (18.206) for bulk media we find,

$$\vec{\mathcal{E}}_b(\mathbf{r},\mathbf{r}_s,\omega)=\omega^2\mu_0\left[-\frac{e^{\imath kR}}{4\pi k^2R^3}\left\{[1-\imath kR-(kR)^2]\mathbb{I}-[3-3\imath kR-(kR)^2]\hat{\mathbf{e}}_R\otimes\hat{\mathbf{e}}_R\right\}\right]\cdot\mathbf{d}_s\ . \tag{18.211}$$

with $k=k(\omega)$.

18.3.1.3 Bulk medium Green tensor projected on particular orientations

The Green tensor can be used to relate two dipoles $\hat{\mathbf{e}}_d$ and $\hat{\mathbf{e}}'_d$ respectively located at $\mathbf{r}$ and $\mathbf{r}'$. Using the identity,

$$R^2\hat{\mathbf{e}}'^*_d(\hat{\mathbf{e}}_R\otimes\hat{\mathbf{e}}_R)\hat{\mathbf{e}}_d=\begin{pmatrix}d'_x & d'_y & d'_z\end{pmatrix}\begin{pmatrix}x^2 & xy & xz\\ xy & y^2 & yz\\ xz & yz & z^2\end{pmatrix}\begin{pmatrix}d_x\\ d_y\\ d_z\end{pmatrix}=(\hat{\mathbf{e}}'_d\cdot\hat{\mathbf{e}}_R)(\hat{\mathbf{e}}_d\cdot\hat{\mathbf{e}}_R)\ , \tag{18.212}$$

we calculate from (18.207),

$$\begin{aligned}&\tfrac{4\pi}{k}\hat{\mathbf{e}}'^*_d\ \mathfrak{Re}\ \mathcal{G}_b(\mathbf{r},\mathbf{r}',\omega)\ \hat{\mathbf{e}}_d \qquad (18.213)\\ &=[\hat{\mathbf{e}}'_d\cdot\hat{\mathbf{e}}_d-(\hat{\mathbf{e}}'_d\cdot\hat{\mathbf{e}}_R)(\hat{\mathbf{e}}_R\cdot\hat{\mathbf{e}}_d)]\frac{\cos kR}{kR}-[\hat{\mathbf{e}}'_d\cdot\hat{\mathbf{e}}_d-3(\hat{\mathbf{e}}'_d\cdot\hat{\mathbf{e}}_R)(\hat{\mathbf{e}}_R\cdot\hat{\mathbf{e}}_d)]\left(\frac{\sin kR}{k^2R^2}-\frac{\cos kR}{k^3R^3}\right)\\ &\tfrac{4\pi}{k}\hat{\mathbf{e}}'^*_d\ \mathfrak{Im}\ \mathcal{G}_b(\mathbf{r},\mathbf{r}',\omega)\ \hat{\mathbf{e}}_d\\ &=[\hat{\mathbf{e}}'_d\cdot\hat{\mathbf{e}}_d-(\hat{\mathbf{e}}'_d\cdot\hat{\mathbf{e}}_R)(\hat{\mathbf{e}}_R\cdot\hat{\mathbf{e}}_d)]\frac{\sin kR}{kR}+[\hat{\mathbf{e}}'_d\cdot\hat{\mathbf{e}}_d-3(\hat{\mathbf{e}}'_d\cdot\hat{\mathbf{e}}_R)(\hat{\mathbf{e}}_R\cdot\hat{\mathbf{e}}_d)]\left(\frac{\cos kR}{k^2R^2}-\frac{\sin kR}{k^3R^3}\right)\ .\end{aligned}$$

Note that dipole moment is complex in the case of circular polarization. The formula (18.213) simplifies when the dipoles are parallel,

$$\begin{aligned}&\tfrac{4\pi}{k}\hat{\mathbf{e}}^*_d\ \mathfrak{Re}\ \mathcal{G}_b(\mathbf{r},\mathbf{r}',\omega)\ \hat{\mathbf{e}}_d=[1-(\hat{\mathbf{e}}_d\cdot\hat{\mathbf{e}}_R)^2]\frac{\cos kR}{kR}-[1-3(\hat{\mathbf{e}}_d\cdot\hat{\mathbf{e}}_R)^2]\left(\frac{\sin kR}{k^2R^2}+\frac{\cos kR}{k^3R^3}\right)\\ &\tfrac{4\pi}{k}\hat{\mathbf{e}}^*_d\ \mathfrak{Im}\ \mathcal{G}_b(\mathbf{r},\mathbf{r}',\omega)\ \hat{\mathbf{e}}_d=[1-(\hat{\mathbf{e}}_d\cdot\hat{\mathbf{e}}_R)^2]\frac{\sin kR}{kR}+[1-3(\hat{\mathbf{e}}_d\cdot\hat{\mathbf{e}}_R)^2]\left(\frac{\cos kR}{k^2R^2}-\frac{\sin kR}{k^3R^3}\right)\ .\end{aligned} \tag{18.214}$$

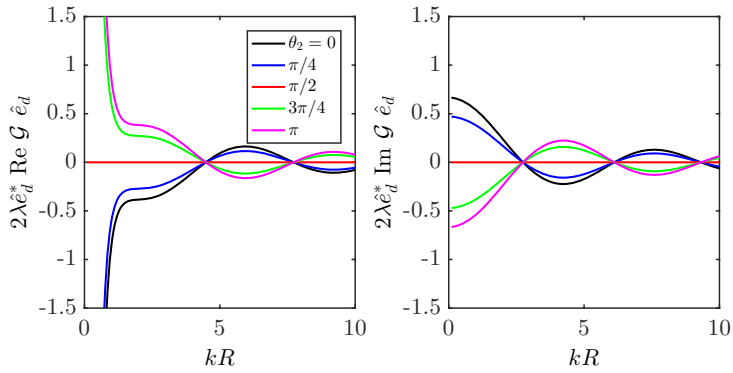

Figure 18.20: (code) Real and imaginary part of the bulk Green tensor for various orientations of the dipoles: $\hat{\mathbf{e}}_d'^* = \hat{\mathbf{e}}_x$ and $\hat{\mathbf{e}}_d$ as indicated in the legend.

18.3.1.4 Dispersion relation in anisotropic media

A homogeneous medium can still be anisotropic if,

$$\epsilon(\mathbf{r},\omega) = \epsilon(\omega) \qquad \text{although} \qquad \epsilon(\omega)\cdot\hat{\mathbf{e}}_r \neq const\ . \tag{18.215}$$

Then, $\epsilon(\omega)$ and $\mu(\omega)$ still need to be represented by tensors, which however do not depend on coordinates. The Helmholtz equation then simplifies to,

$$\left[\nabla_{\mathbf{r}} \times \nabla_{\mathbf{r}} \times -\frac{\omega^2}{c^2}\mu(\omega)\epsilon(\omega)\right] \vec{\mathcal{E}}_b(\mathbf{r},\omega) = \imath\omega\mu_0 \mathbf{j}(\mathbf{r},\omega)\ , \tag{18.216}$$

in analogy to (18.198). Assuming no currents, $\mathbf{j}(\mathbf{r},\omega) = 0$, and plane electromagnetic waves, $\vec{\mathcal{E}}_b(\mathbf{r},\omega) = \vec{\mathcal{E}}_0(\omega) e^{\imath\mathbf{k}\cdot(\mathbf{r}-\mathbf{r}')}$, we obtain with the identity (18.201),

$$\begin{aligned} 0 &= \left[\nabla_{\mathbf{r}} \otimes \nabla_{\mathbf{r}} - \mathbb{I}\triangle - \frac{\omega^2}{c^2}\mu\epsilon\right] \vec{\mathcal{E}}_0 e^{\imath\mathbf{k}\cdot(\mathbf{r}-\mathbf{r}')} \\ &= \left[-\mathbf{k}\otimes\mathbf{k} + k^2 - \frac{\omega^2}{c^2}\mu\epsilon\right] \vec{\mathcal{E}}_0 e^{\imath\mathbf{k}\cdot(\mathbf{r}-\mathbf{r}')}\ , \end{aligned} \tag{18.217}$$

where $\mu\epsilon$ is to be understood as a product between two matrices. From this we derive the dispersion relation,

$$0 = \left| -k_i k_j + k^2\delta_{ij} - \frac{\omega^2}{c^2}(\mu)_{il}(\epsilon)_{lj} \right|\ , \tag{18.218}$$

for $i,j = x,y,z$.

We will discuss anisotropic homogeneous media in the context of hyperbolic metamaterials in Sec. 18.3.3.

18.3.1.5 Interaction between dipoles near dielectric media

The vector Green tensor describes the interaction between two points in space via an electromagnetic field. It can be used to solve a variety of problems, for example,

- the interaction between dipoles in free space;
- the modification of a dipole due to the presence of a dielectric boundary (Purcell effect);
- the modification of the interaction between dipoles due to the presence of a dielectric boundary.

The linearity of Maxwell's equations allows us to exploit the superposition principle applying it to the Green tensor. For example, we can express the interaction between two point dipoles $\mathbf{r}_1$ and $\mathbf{r}_2$ near a dielectric boundary by simply adding to the bulk tensor for their interaction in free space $\mathcal{G}_b(\mathbf{r}_1, \mathbf{r}_2, \omega)$ a tensor $\mathcal{G}_d(\mathbf{r}_1, \mathbf{r}_2, \omega)$ accounting for the presence of the dielectric,

$$\boxed{\mathcal{G} = \mathcal{G}_b + \mathcal{G}_d} \,. \tag{18.219}$$

18.3.2 Plasmons at metal-dielectric interfaces

A *surface plasmon polariton* (SPP) or simply *plasmon* is an electromagnetic wave in the infrared or visible spectral regime, which propagates along a metal-dielectric or metal-air interface. The term SPP explains that the wave involves both, the motion of charges in the metal and electromagnetic waves in the air or the dielectric.

SPPs are a type surface waves, guided along the interface in a similar way as light can be guided by an optical fiber. The wavelengths of SPPs are shorter than that of the incident light, which created them. Thus, they can be more localized and more intense. Perpendicularly to the interface, they are confined to the scale of a wavelength. The propagation of SPPs along the interface is limited by absorption losses in the metal or by photon scattering into other directions, e.g. into free space.

SPPs can be excited by electronic or photonic bombardment. For a photon to excite an SPP, both must have the same frequency and the same momentum. However, at a given frequency, a free space photon has less momentum than an SPP because the two have different dispersion relations (see below). Therefore, a photon coming from free space can not directly couple to an SPP. For the same reason, an SPP (on a perfectly smooth metal surface) can not emit photons into free space (assumed uniform). This incompatibility is analogous to the absence of transmission at total internal reflection.

However, the coupling of photons to SPPs can be achieved using a coupling medium, such as a dielectric or a grating, designed to match the wavevectors of photons and SPPs, until their momenta coincide. For example, a glass prism may be positioned against a thin metal film in Kretschmann configuration, as shown in Fig. 18.21(a). Single insulated surface defects, such as isolated or periodic grooves, slits or elevations, provide a mechanism coupling free space radiation and SPPs, which then can exchange energy.

18.3.2.1 Fields and plasmonic dispersion relation

The properties of a SPP can be derived from Maxwell's equations. Let $z > 0$ be the space occupied by the dielectric and $z < 0$ the space occupied by the metal. The electric and magnetic fields must obey Maxwell's equations and, in particular, the

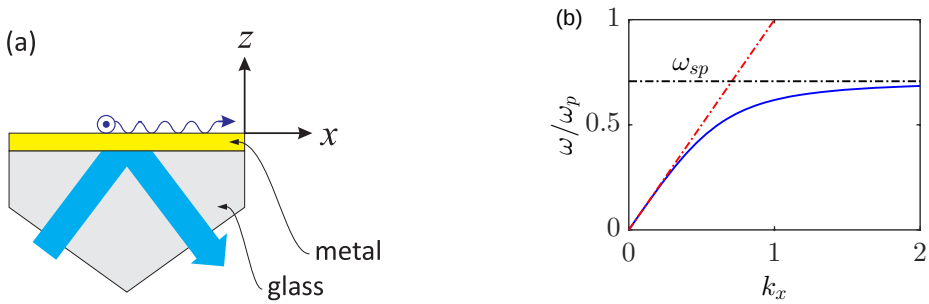

Figure 18.21: (code) (a) Kretschmann configuration of attenuated total reflection for the coupling of surface plasmons. The component of the scattered wavevector parallel to the surface forms SPPs, which then propagate along the metal-dielectric interface. (b) Dispersion curve for a SPP (blue). At low k_x it approaches the photonic dispersion curve (red).

boundary conditions (18.42)(i-iv) at the interface. We will show in Exc. 18.3.7.2, that the fields must have the following form:

$$\vec{\mathcal{H}}_n(\mathbf{r},t) = \begin{pmatrix} 0 \\ 1 \\ 0 \end{pmatrix} \mathcal{H}_0 e^{\imath k_x x + \imath k_{z,n}|z| - \imath\omega t} \quad , \quad \vec{\mathcal{E}}_n(\mathbf{r},t) = \begin{pmatrix} \pm k_{z,n} \\ 0 \\ -k_x \end{pmatrix} \frac{\mathcal{H}_0}{\omega\varepsilon_n} e^{\imath k_x x + \imath k_{z,n}|z| - \imath\omega t} \,, \tag{18.220}$$

under the condition that,

$$\frac{k_{z,\mathrm{m}}}{\varepsilon_\mathrm{m}} = -\frac{k_{z,\mathrm{d}}}{\varepsilon_\mathrm{d}} \,, \tag{18.221}$$

where n indicates the material ($n = \mathrm{m}$ for the metal and $n = \mathrm{d}$ for the dielectric). This condition guarantees the continuity of the electric field parallel to the boundary. Upper signs apply to the dielectric region ($z > 0$) and lower signs to the metallic region ($z < 0$). That is, SPPs are always transverse magnetic waves (TM). The wavevector $\mathbf{k}$ is complex. In case of a lossless SPP, the k_x component is real and the k_z component imaginary,

$$k_{z,m} = \imath\kappa_{z,\mathrm{m}} \,, \tag{18.222}$$

such that the wave propagates along the x-direction and decays exponentially toward $\pm z$. While k_x is always the same in both materials, $k_{z,\mathrm{m}}$ is generally different from $k_{z,\mathrm{d}}$. Entering the fields (18.220) in the wave equation,

$$\nabla^2\vec{\mathcal{H}}_n = \varepsilon_n\mu_n\frac{\partial^2\vec{\mathcal{H}}_n}{\partial t^2} \,, \tag{18.223}$$

we easily verify that,

$$k_x^2 + k_{z,n}^2 = \omega^2\varepsilon_n\mu_n = \epsilon_n\left(\frac{\omega}{c}\right)^2 \,, \tag{18.224}$$

where we assume $\mu_n = \mu_0$ and $\varepsilon_n = \varepsilon_0\epsilon_n$, where the 'breve' denotes relative permittivities. Solving the two equations (18.224) for $n = \mathrm{m}, \mathrm{d}$ together with the relationship

(18.221), we obtain the dispersion relation for a plasmon wave propagating on the surface,

$$\boxed{k_x = \frac{\omega}{c}\sqrt{\frac{\epsilon_\mathrm{d}\epsilon_\mathrm{m}}{\epsilon_\mathrm{d}+\epsilon_\mathrm{m}}}} \,. \tag{18.225}$$

To apply this relation in practice, we must specify the two permittivities ϵ_n. For simplicity, we assume $\epsilon_\mathrm{d} = 1$, and for ϵ_m we resort to the *Drude model* using (18.161), where for now we despise the attenuation $\Gamma_d = 0$,

$$\epsilon_m(\omega) = 1 - \frac{\omega_p^2}{\omega^2} \,, \tag{18.226}$$

where ω_p is the plasma frequency (18.162). Joining the expressions (18.225) and (18.226) we obtain,

$$ck_x = \sqrt{\frac{\omega^2-\omega_p^2}{2\omega^2-\omega_p^2}} \,. \tag{18.227}$$

This relationship is plotted in Fig. 18.21(b).

At low k_x, the SPP behaves like a photon, but as k_x increases, the dispersion relation becomes flatter and reaches an asymptotic limit ω_{sp} called 'surface plasma frequency'. If $\omega < \omega_{sp}$, the SPP has a shorter wavelength than the radiation in the free space, such that the components $k_{z,\mathrm{m}}$ are purely imaginary and exhibit evanescent decay. The plasma frequency at the surface ($\epsilon_\mathrm{d} = 1$) is,

$$\omega_{sp} = \lim_{k_x\to\infty} \omega = \frac{\omega_p}{\sqrt{2}} \,. \tag{18.228}$$

18.3.2.2 Absorption of plasmons

The formula (18.226) predicts $\varepsilon_\mathrm{m} < 0$ below the plasmon frequency. Electromagnetic waves propagating in metals suffer damping due to ohmic losses and interactions between the electrons and the atoms of the metallic lattice. These effects appear as an imaginary component of the dielectric function. To take this into account, we express the dielectric function of a metal in the complex plane,

$$\epsilon_\mathrm{m} = \epsilon'_\mathrm{m} + \imath\epsilon''_\mathrm{m} \,. \tag{18.229}$$

Generally, we have, $|\epsilon'_\mathrm{m}| \gg \epsilon''_\mathrm{m}$, such that the wavevector can be expressed in terms of its real and imaginary components as (see Exc. 18.3.7.3),

$$k_x = k'_x + \imath k''_x = \frac{\omega}{c}\sqrt{\frac{\epsilon_d\epsilon'_\mathrm{m}}{\epsilon_\mathrm{d}+\epsilon'_\mathrm{m}}} + \imath\frac{\omega}{c}\sqrt{\frac{\epsilon_d\epsilon'_\mathrm{m}}{\epsilon_\mathrm{d}+\epsilon'_\mathrm{m}}}^3 \frac{\epsilon''_\mathrm{m}}{2(\epsilon'_\mathrm{m})^2} \,. \tag{18.230}$$

The wavevector gives us insight into the physically significant properties of the electromagnetic wave, such as its spatial extent and mode matching conditions.

18.3.2.3 Distance of propagation and depth of penetration

As an SPP propagates along the surface, it loses energy to the metal due to absorption. The intensity of the surface plasmon decays with the square of the electric field, therefore, over a distance x, the intensity decreases by a factor of $e^{-2k_x x}$. The propagation length is defined as the distance, where the SPP intensity has decreased by a factor of $1/e$. This condition is satisfied at a length $L = \frac{1}{2k''_x}$.

Likewise, the electric field decays perpendicular to the surface of the metal. At low frequencies, the penetration depth of the SPP into the metal is commonly approximated using the skin depth formula. In a dielectric, the field will decay much more slowly. The decay depth in the metal and the dielectric medium can be expressed as

$$z_n = \frac{\lambda}{2\pi}\left(\frac{|\epsilon'_{\rm m}| + \epsilon_{\rm d}}{\epsilon_n^2}\right)^{1/2} , \tag{18.231}$$

where n indicates the propagation medium. SPPs are very sensitive to small perturbations within the skin depth and, therefore, are often used to probe surface inhomogeneities. Resolve the Exc. 18.3.7.4.

18.3.3 Negative refraction and metamaterials

The general dispersion relation for anisotropic media has been derived in (18.218),

$$\boxed{\left|\tfrac{\omega^2}{c^2}\epsilon_{il}\mu_{lj} - k^2\delta_{ij} + k_i k_j\right| = 0} , \tag{18.232}$$

which, for isotropic media simplifies to $\frac{\omega^2}{c^2}n^2 = k^2$, where $n^2 = \epsilon\mu$. Apparently, inverting the signs of both, the permittivity and the permeability, $\varepsilon, \mu < 0$ has no effect on the equations. However, one can show [1335], that inserting into the first and second Maxwell equations,

$$\begin{aligned} \nabla\times\vec{\mathcal{H}} = \partial_t\vec{\mathcal{D}} \quad &, \quad \nabla\times\vec{\mathcal{E}} = -\partial_t\vec{\mathcal{B}} \\ \text{with} \quad \vec{\mathcal{D}} = \varepsilon\vec{\mathcal{E}} \quad &, \quad \vec{\mathcal{B}} = \mu\vec{\mathcal{H}} \end{aligned} \tag{18.233}$$

a plane wave, $\vec{\mathcal{E}}, \vec{\mathcal{D}}, \vec{\mathcal{B}}, \vec{\mathcal{H}} \propto e^{\imath(\mathbf{k}\cdot\mathbf{r}-\omega t)}$,

$$\mathbf{k}\times\vec{\mathcal{H}}_0 = -\omega\varepsilon\vec{\mathcal{E}}_0 \quad , \quad \mathbf{k}\times\vec{\mathcal{E}}_0 = \omega\mu\vec{\mathcal{H}}_0 , \tag{18.234}$$

one obtains for $\varepsilon, \mu > 0$, a right-handed triplet of vectors $\mathbf{k}$, $\vec{\mathcal{E}}$, $\vec{\mathcal{H}}$, whereas for $\varepsilon, \mu < 0$ one obtains a left-handed triplet. Defining the handedness via,

$$p \equiv \frac{(\mathbf{k}\times\vec{\mathcal{E}})\cdot\vec{\mathcal{H}}}{|(\mathbf{k}\times\vec{\mathcal{E}})\cdot\vec{\mathcal{H}}|} , \tag{18.235}$$

if $p = \pm 1$, we call the material is right(left)-handed. The energy flux,

$$\vec{\mathcal{S}} = \vec{\mathcal{E}}\times\vec{\mathcal{H}} \tag{18.236}$$

is parallel to $\mathbf{k}$ for right-handed materials and anti-parallel for left-handed, which means that phase and group velocities are reversed. Also, in left-handed materials we expect a reversed Doppler effect.

At the interface between two materials with different handednesses, $\varepsilon_1, \mu_1 > 0$ and $\varepsilon_2, \mu_2 < 0$, the equations (18.42) must still hold,

$$\begin{array}{ll} \text{(i)} & \vec{\mathcal{H}}_1^{\parallel} = \vec{\mathcal{H}}_2^{\parallel} \\ \text{(ii)} & \vec{\mathcal{E}}_1^{\parallel} = \vec{\mathcal{E}}_2^{\parallel} \\ \text{(iii)} & \varepsilon_1 \vec{\mathcal{E}}_1^{\perp} = \varepsilon_2 \vec{\mathcal{E}}_2^{\perp} \\ \text{(iv)} & \mu_1 \vec{\mathcal{H}}_1^{\perp} = \mu_2 \vec{\mathcal{H}}_2^{\perp} \end{array} \quad . \tag{18.237}$$

but now, the signs of $\mathcal{E}_2^{\perp}$ and $\mathcal{H}_2^{\perp}$ are inverted. We calculate,

$$\vec{\mathcal{E}}_0 \times \vec{\mathcal{H}}_0 = \frac{1}{\omega\mu} \vec{\mathcal{E}}_0 \times (\mathbf{k} \times \vec{\mathcal{E}}_0) = \frac{1}{\omega\mu} [\mathbf{k}(\vec{\mathcal{E}}_0 \cdot \vec{\mathcal{E}}_0) - \vec{\mathcal{E}}_0(\mathbf{k} \cdot \vec{\mathcal{E}}_0)] = \frac{\mathcal{E}_0^2}{\omega\mu} \mathbf{k} \uparrow\uparrow -\vec{\mathcal{S}} \; . \tag{18.238}$$

As a consequence Snell's law (18.57) must be corrected,

$$\frac{\sin\theta_t}{\sin\theta_i} = \frac{n_1}{n_2} = \frac{p_2}{p_1} \left| \sqrt{\frac{\varepsilon_2 \mu_2}{\varepsilon_1 \mu_1}} \right| \; . \tag{18.239}$$

The *complex refractive index*,

$$n = n' + \imath n'' = c\sqrt{\varepsilon\mu} = c\sqrt{(\varepsilon' + \imath\varepsilon'')(\mu' + \imath\mu'')} = c\sqrt{|\varepsilon\mu|} e^{\imath\phi/2} \tag{18.240}$$

can have negative real part, $\mathfrak{Re}\; n < 0$, if the angle is $\phi > \pi$, that is, if,

$$\sin\phi = \frac{\mathfrak{Im}\; \varepsilon\mu}{|\varepsilon\mu|} = \frac{\varepsilon''\mu' + \varepsilon'\mu''}{|\varepsilon\mu|} < 0 \; . \tag{18.241}$$

Since the absorption is necessarily $\varepsilon'', \mu'' > 0$, the condition (18.241) is satisfied if $\varepsilon', \mu' < 0$. More generally, a sufficient but not necessary condition for *negative refraction* is,

$$\varepsilon'|\mu' + \imath\mu''| + \mu'|\varepsilon' + \imath\varepsilon''| < 0 \; . \tag{18.242}$$

The direction of the phase velocity is $\mathbf{k}$, while the energy flows along $\vec{\mathcal{S}} = \vec{\mathcal{E}} \times \vec{\mathcal{H}}$. For $n' > 0$ the dispersive medium is called *right-handed*, because $\mathbf{k}$, $\vec{\mathcal{E}}$ and $\vec{\mathcal{H}}$ form a tripod. For $n' < 0$ the medium is called *left-handed*, because $-\mathbf{k}$, $\vec{\mathcal{E}}$ and $\vec{\mathcal{H}}$ form a tripod, that is, $\mathbf{k}$ and $\vec{\mathcal{S}}$ are contrary. We will check this in Exc. 18.3.7.5. Such media are always very dispersive.

Left-handed media have attracted much attention, because of the theoretical possibility of performing *perfect lenses* with a focusing power not being limited by diffraction. Left-handed media are studied in non-homogeneous and non-isotropic *metamaterials* [25], but there are also ideas on how to design them in homogeneous and isotropic atomic gases [26]

[25] See [1010, 1011, 1193, 824, 825, 827, 826, 1013, 62, 1291, 252, 211, 820, 1187, 790].
[26] See Sec. 34.7 and Excs. 34.8.4.11 and 34.8.4.12 .

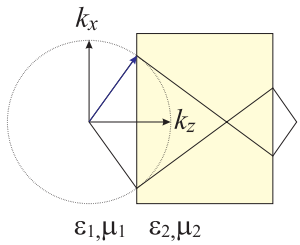

Figure 18.22: Refraction at the interface between 'right-handed' and 'left-handed' media.

18.3.3.1 Hyperbolic metamaterials

Hyperbolic metamaterials (HMM) are artificial media with sub-optical-wavelength nano-structuring, which exhibit unusual optical properties. In particular, they are characterized by extreme anisotropy, behaving like dielectrics when illuminated from one side and like metals when illuminated from another. As already mentioned in Sec. 18.3.1, in a hyperbolic metamaterial the dispersion relation is anisotropic, corresponding to permittivity and permeability tensors of the form,

$$\varepsilon = \begin{pmatrix} \varepsilon_\perp & & \\ & \varepsilon_\perp & \\ & & \varepsilon_{\shortparallel} \end{pmatrix} \quad \text{and} \quad \mu = \begin{pmatrix} \mu_\perp & & \\ & \mu_\perp & \\ & & \mu_{\shortparallel} \end{pmatrix} . \tag{18.243}$$

In the case $\varepsilon_\perp \varepsilon_{\shortparallel} < 0$ or $\mu_\perp \mu_{\shortparallel} < 0$ the dispersion relation,

$$\frac{k_x^2 + k_y^2}{\varepsilon_{\shortparallel}} + \frac{k_z^2}{\varepsilon_\perp} = \frac{(\omega/c)^2}{\varepsilon_0} , \tag{18.244}$$

becomes hyperbolic [27]. In Exc. 18.3.7.7 we derive from the Maxwell equations, allowing for an anisotropic (but homogeneous) permittivity tensor, the hyperbolic dispersion relation.

> **Example 109 (*Interest of hyperbolic metamaterials*):** Hyperbolic metamaterials are investigated for their potential interest in engineering the decay routes of quantum emitters by manipulating the local density-of-states. The reason is, that HMMs allow for the propagation of modes with wavevectors (known as high-k modes) much higher than the free-space wavevector. Thus, the evanescent waves (also with high-k) of an emitter couple more easily to a sufficiently close HMM, and thus emitting their photons faster.
> The elementary cells of a metamaterial are often complicated, and a stratification is helpful to describe its response to incident light. For example, many features of an HMM can be grasped by frequency-dependent effective permittivity and permeability tensors.

[27] Note that a more correct treatment would need to account for the polarizations of the electric and magnetic fields. We leave this to an upcoming version of the script.

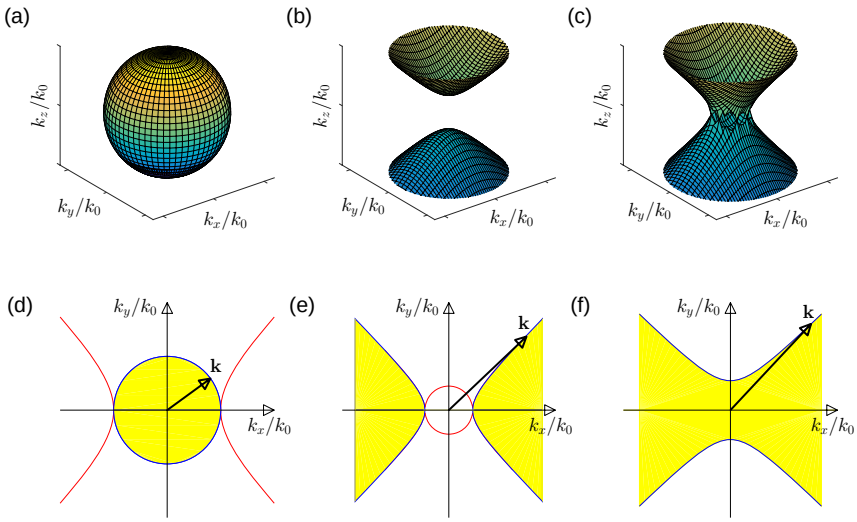

Figure 18.23: Isofrequency surfaces of hyperbolic dispersion relations. (a) Isotropic dielectric ($\varepsilon_\perp = \varepsilon_{\shortparallel}$); (b) two-sheeted hyperboloid ($\varepsilon_\perp < 0$ and $\varepsilon_{\shortparallel} > 0$); (c) one-sheeted hyperboloid ($\varepsilon_\perp > 0$ and $\varepsilon_{\shortparallel} < 0$). (d-f) Projection of the two-dimensional isofrequency surfaces shown in (a-c) on the $k_y = 0$ plane. The yellow-shaded areas correspond to lossy regions (real parts).

In Exc. 18.3.7.8 we show, that the effective permittivity of a nanostructure having the shape of a stack of alternating intrinsically homogeneous layers with permittivities ε_d and ε_m and thicknesses $d_\mathrm{d}, d_\mathrm{m} \ll \lambda$ [see Fig. 18.24(b)] is given by [1123],

$$\varepsilon_{\shortparallel} = \frac{\varepsilon_\mathrm{d} d_\mathrm{d} + \varepsilon_\mathrm{m} d_\mathrm{m}}{d_\mathrm{d} + d_\mathrm{m}} \qquad \text{and} \qquad \frac{1}{\varepsilon_\perp} = \frac{d_\mathrm{d}/\varepsilon_\mathrm{d} + d_\mathrm{m}/\varepsilon_\mathrm{m}}{d_\mathrm{d} + d_\mathrm{m}} \ . \tag{18.245}$$

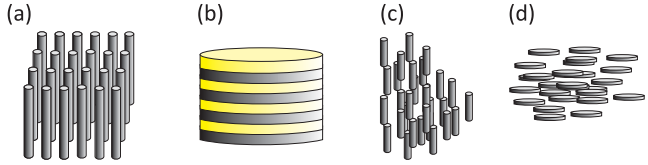

Figure 18.24: Hyperbolic dispersion materials. In order to achieve a negative permittivity in a given direction, the electrons must move freely along it, like in a metal.

Example 110 (*Anisotropy of a metamaterial*): For example, choosing $d_\mathrm{m} = d_\mathrm{d}$, $\varepsilon_\mathrm{d} = 1$ and $\varepsilon_\mathrm{m} = -2$, we obtain $\varepsilon_{\shortparallel} = \frac{1}{4}$ and $\varepsilon_\perp = -\frac{1}{2}$.

In Exc. 18.3.7.9 we discuss, whether it is possible to realize a hyperbolic dispersion relation in an atomic gas.

18.3.4 Wave guides

The presence of conductive interfaces influences the propagation of electromagnetic waves. Interfaces, which influence the propagation direction of electromagnetic waves are called *waveguides*. Let us consider a waveguide such as the one illustrated in Figs. 18.25. In the volume enclosed by the waveguide, supposedly perfectly conductive ($\vec{\mathcal{E}} = 0 = \vec{\mathcal{B}}$ inside the wave guide material), every electromagnetic field must satisfy the boundary conditions (18.42), that is, we have,

$$\boxed{\vec{\mathcal{E}}^{\parallel} = 0 \qquad \text{and} \qquad \vec{\mathcal{B}}^{\perp} = 0} \tag{18.246}$$

on all interior surfaces of the waveguide. Free surface charges and currents will automatically be generated in such a way as to endorse these conditions, and all conclusions derived in the following sections are basically corollaries of these boundary conditions.

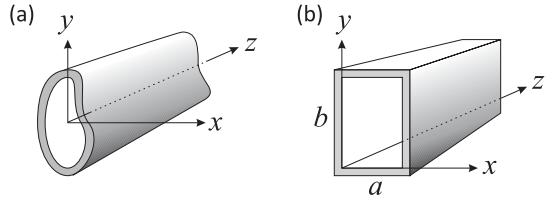

Figure 18.25: Waveguides of arbitrarily (i) and rectangular (ii) shape.

Let us now consider monochromatic waves propagating along a tube oriented in z-direction,

$$\vec{\mathcal{E}}(x,y,z,t) = \vec{\mathcal{E}}(x,y)e^{\imath(k_z z-\omega t)} \qquad \text{and} \qquad \vec{\mathcal{B}}(x,y,z,t) = \vec{\mathcal{B}}(x,y)e^{\imath(k_z z-\omega t)} \,. \tag{18.247}$$

Obviously, the $\vec{\mathcal{E}}$ and $\vec{\mathcal{B}}$ fields must simultaneously satisfy the vacuum Maxwell equations (17.6) inside the guide and the boundary conditions (18.246). To implement these conditions, we reformulate Maxwell's equations. We insert (18.247) and the expansions $\vec{\mathcal{E}}(x,y) = \sum_{k=x,y,z} \mathcal{E}_k(x,y)\hat{\mathbf{e}}_k$ and $\vec{\mathcal{B}}(x,y) = \sum_{k=x,y,z} \mathcal{B}_k(x,y)\hat{\mathbf{e}}_k$ in the Maxwell equations (17.6)(i) and (ii) and obtain,

$$\begin{aligned}
&\text{(i)} \quad \partial_y\mathcal{E}_z - \imath k_z\mathcal{E}_y = \imath\omega\mathcal{B}_x && \text{(ii)} \quad \partial_y\mathcal{B}_z - \imath k_z\mathcal{B}_y = -\imath\tfrac{\omega}{c^2}\mathcal{E}_x \\
&\text{(iii)} \quad \imath k_z\mathcal{E}_x - \partial_x\mathcal{E}_z = \imath\omega\mathcal{B}_y && \text{(iv)} \quad \imath k_z\mathcal{B}_x - \partial_x\mathcal{B}_z = -\imath\tfrac{\omega}{c^2}\mathcal{E}_y \\
&\text{(v)} \quad \partial_x\mathcal{E}_y - \partial_y\mathcal{E}_x = \imath\omega\mathcal{B}_z && \text{(vi)} \quad \partial_x\mathcal{B}_y - \partial_y\mathcal{B}_x = -\imath\tfrac{\omega}{c^2}\mathcal{E}_z \,.
\end{aligned} \tag{18.248}$$

Inserting the component $\mathcal{B}_y$ of the third into the second equation, the $\mathcal{B}_x$ of the first into the fourth equation, the $\mathcal{E}_y$ of the fourth into the first equation, and the $\mathcal{E}_x$ of the second in the third equation, we arrive at,

$$\begin{aligned}
&\text{(i)} \quad \mathcal{E}_x = \tfrac{\imath}{(\omega/c)^2-k_z^2}(k_z\partial_x\mathcal{E}_z + \omega\partial_y\mathcal{B}_z) \\
&\text{(ii)} \quad \mathcal{E}_y = \tfrac{\imath}{(\omega/c)^2-k_z^2}(k_z\partial_y\mathcal{E}_z - \omega\partial_x\mathcal{B}_z) \\
&\text{(iii)} \quad \mathcal{B}_x = \tfrac{\imath}{(\omega/c)^2-k_z^2}(k_z\partial_x\mathcal{B}_z - \tfrac{\omega}{c^2}\partial_y\mathcal{E}_z) \\
&\text{(iv)} \quad \mathcal{B}_y = \tfrac{\imath}{(\omega/c)^2-k_z^2}(k_z\partial_y\mathcal{B}_z + \tfrac{\omega}{c^2}\partial_x\mathcal{E}_z) \,.
\end{aligned} \tag{18.249}$$

And inserting these equations into Maxwell's equations (iii) and (iv), we arrive at,

$$\left[\frac{\partial^2}{\partial x^2}+\frac{\partial^2}{\partial y^2}+(\omega/c)^2-k_z^2\right]\mathcal{E}_z=0=\left[\frac{\partial^2}{\partial x^2}+\frac{\partial^2}{\partial y^2}+(\omega/c)^2-k_z^2\right]\mathcal{B}_z\ . \tag{18.250}$$

Hence, we can solve the waveguide problem by first solving the wave equations for the components $\mathcal{E}_z$ and $\mathcal{B}_z$ and then inserting the solutions into Eqs. (18.249) in order to obtain the other field components.

When $\mathcal{E}_z = 0$ we call these waves *transverse electric waves* (TE), when $\mathcal{B}_z = 0$ we call them *transverse magnetic waves* (TM), and when $\mathcal{E}_z = 0 = \mathcal{B}_z$ we call them *transverse electro-magnetic waves* (TEM). TEM waves can not exist in a hollow waveguide, as we will show in Exc. 18.3.7.10.

18.3.4.1 Waveguide with constant rectangular cross section

Here, we consider the transmission of TE waves through a waveguide of constant rectangular cross-section, as shown in Fig. 18.25(ii). Similarly to the procedure for solving the Laplace equation in electrostatics, we make a separation ansatz for the variables in a way suggested by the symmetry of the problem, that is, we assume the existence of two functions X and Y, such that inserting the ansatz

$$\mathcal{E}_z=0 \qquad \text{and} \qquad \mathcal{B}_z=X(x)Y(y)\ , \tag{18.251}$$

in the wave equation,

$$Y\frac{d^2X}{dx^2}+X\frac{d^2Y}{dy^2}+[(\omega/c)^2-k_z^2]=0\ , \tag{18.252}$$

leaves us with,

$$\frac{1}{X}\frac{d^2X}{dx^2}=-k_x^2 \quad \text{and} \quad \frac{1}{Y}\frac{d^2Y}{dy^2}=-k_y^2 \quad \text{with} \quad -k_x^2-k_y^2+(\omega/c)^2-k_z^2=0\ . \tag{18.253}$$

$\mathcal{B}_x$ must vanish on the surfaces at $x = 0, a$ and, because of (18.249)(iii) $\partial_x\mathcal{B}_z$ as well, such that $dX/dx = 0$, that is, X is a cosine. In the same way, $\mathcal{B}_y$ must vanish on the surfaces at $y = 0, b$, such that Y is a cosine. Therefore, the solution is,

$$\mathcal{B}_z=\mathcal{B}_0\cos k_x x\cos k_y y \qquad \text{with} \qquad k_x=\tfrac{m\pi}{a} \qquad \text{and} \qquad k_y=\tfrac{n\pi}{b}\ . \tag{18.254}$$

With this, the wavevector becomes,

$$k_z=\sqrt{(\omega/c)^2-\pi^2[(m/a)^2+(n/b)^2]}\ . \tag{18.255}$$

Consequently, the frequency must be higher than,

$$\omega>c\pi\sqrt{(m/a)^2+(n/b)^2}\equiv\omega_{mn}\ , \tag{18.256}$$

to avoid exponentially attenuated fields. The frequency ω_{mn} is called *cut-off frequency*. The components $\mathcal{B}_x$ and $\mathcal{B}_y$ can be determined from (18.249)(iii) and (iv),

$$\boxed{\begin{aligned}\vec{\mathcal{E}} &= \mathcal{E}_0 \begin{pmatrix} \frac{\imath\omega k_y}{k_x^2+k_y^2}\cos k_x x \sin k_y y \\ \frac{-\imath\omega k_x}{k_x^2+k_y^2}\sin k_x x \cos k_y y \\ 0 \end{pmatrix} e^{\imath(k_z z-\omega t)} \\ \vec{\mathcal{B}} &= \mathcal{B}_0 \begin{pmatrix} \frac{\imath k_z k_x}{k_x^2+k_y^2}\sin k_x x \cos k_y y \\ \frac{\imath k_z k_y}{k_x^2+k_y^2}\cos k_x x \sin k_y y \\ \cos k_x x \cos k_y y \end{pmatrix} e^{\imath(k_z z-\omega t)} \end{aligned}} \quad . \tag{18.257}$$

Inserting ω_{mn} in the dispersion relation (18.255), we notice that the formula for the phase propagation velocity,

$$c = \frac{\omega}{k_z} = \frac{c}{\sqrt{1-(\omega_{mn}/\omega)^2}} > c \ , \tag{18.258}$$

predicts a velocity above the speed of light. However, the group velocity,

$$v_g = \frac{1}{dk_z/d\omega} = c\sqrt{1-(\omega_{mn}/\omega)^2} < c \ , \tag{18.259}$$

is slower. Resolve Exc. 18.3.7.11 and 18.3.7.12 [28].

18.3.5 The coaxial line

We have already mentioned the possibility of TEM waves in a *coaxial waveguide*, as shown in Fig. 18.26. Inserting $\mathcal{E}_z = 0 = \mathcal{B}_z$ in the equations (18.248) we obtain,

$$\begin{aligned} c\mathcal{B}_y = \mathcal{E}_x \qquad & \text{and} \qquad c\mathcal{B}_x = -\mathcal{E}_y \\ \partial_x\mathcal{E}_y - \partial_y\mathcal{E}_x = 0 \quad & = \partial_x\mathcal{B}_y - \partial_y\mathcal{B}_x \\ \partial_x\mathcal{E}_x + \partial_y\mathcal{E}_y = 0 \quad & = \partial_x\mathcal{B}_x + \partial_y\mathcal{B}_y \end{aligned} \ , \tag{18.260}$$

where we join the Maxwell equations (iii) and (iv) in the last line. In Exc. 18.3.7.13 we will show that,

$$\vec{\mathcal{E}}(\rho,\phi,z,t) = \frac{A\cos(k_z z-\omega t)}{\rho}\hat{\mathbf{e}}_\rho \qquad \text{and} \qquad \vec{\mathcal{B}}(\rho,\phi,z,t) = \frac{A\cos(k_z z-\omega t)}{c\rho}\hat{\mathbf{e}}_\phi \ , \tag{18.261}$$

satisfies Maxwell's equations. Solve Exc. 18.3.7.14.

[28] Rectangular waveguides are used, for example, in radio detection and ranging (RADAR) systems to guide microwave signals from a synthesizer to an antenna.

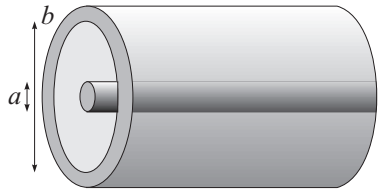

Figure 18.26: Guia de onda coaxial.

18.3.6 Cavities

An *optical resonator* consists of an arrangement of mirrors reflecting light beams in such a way as to form a closed path. Light which entered the cavity carries out many round-trips before it is transmitted again through a (partially reflecting) mirror, scattered out of the cavity mode or absorbed by impurities in the mirrors. Thus, the light power is considerably increased. That is, cavities can store light. Do Exc. 18.3.7.15 to 18.3.7.17.

In order to resonate in a cavity, a light beam must satisfy the boundary condition, that the mirror surfaces coincide with nodes of the standing light wave formed by the beam and its reflections at the mirrors. Therefore, in a cavity of length L, only a discrete spectrum of wavelengths $N\lambda/2 = L$ can be resonantly amplified, where N is a natural number. Because of this property, cavities are often used as frequency filters or optical spectrum analyzers: Only frequencies close to $\nu = N\delta_{fsr}$ are transmitted, where $\delta_{fsr} = c/2L$ is the called the *free spectral range* of the cavity.

A cavity is characterized on one hand by its geometry, that is, the curvature and the distance of its mirrors, and on the other hand by its finesse, which is given by the reflectivity of its mirrors. Let us first study the finesse and postpone the discussion of its geometry to Sec. 18.4.1. Treating the cavity as a multiple path interferometer (or *Fabry-Perot cavity*), we can derive an expression for the reflected and transmitted intensity as a function of frequency,

$$(k + \Delta k)L = \frac{(\omega_c + \Delta)L}{c} = \frac{\omega_c + \Delta}{2\delta_{fsr}} = \pi N + \frac{\Delta}{2\delta_{fsr}} . \tag{18.262}$$

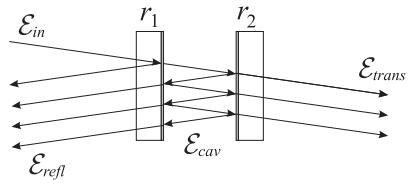

Figure 18.27: Multiple interference in an optical cavity of two mirrors characterized by reflectivities $r_{1,2}$.

The so-called *Airy formulas* for reflection and transmission are,

$$\boxed{\begin{aligned} I_{refl} &= I_{in}\frac{(2F/\pi)^2\sin^2(\Delta/2\delta_{fsr})}{1+(2F/\pi)^2\sin^2(\Delta/2\delta_{fsr})} \\ I_{trns} &= I_{in}\frac{1}{1+(2F/\pi)^2\sin^2(\Delta/2\delta_{fsr})} \end{aligned}}\ , \tag{18.263}$$

where $R=|r|^2$ is the reflectivity of a mirror and Δ the detuning between the laser and the cavity (in radians/s). We will derive the formulas in Exc. 18.3.7.18. The transmission curve of the cavity has a finite bandwidth κ_{int}, which depends on the reflectivity of the mirrors. The *finesse* of the cavity is defined by,

$$F \equiv \frac{2\pi\delta_{fsr}}{\kappa_{int}} = \frac{\pi\sqrt{R}}{1-R}\ . \tag{18.264}$$

Note that δ_{fsr} is given in terms of a real frequency, while κ_{int} is a radiant [29].

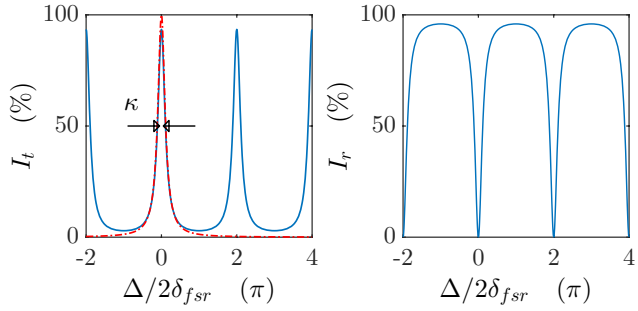

Figure 18.28: (code) Transmission and reflection of a resonator. The chosen mirror reflectivities are $R=70\%$, the absorption losses $S=1\%$. The red dash-dotted line is the Lorentzian approximation. Apparently, it fails off resonance.

The Airy formula was derived under the assumption of plane waves, but this assumption is not always realistic. Indeed, as we will show in Sec. 18.4.1, light propagates in transversely delimited modes and is subject to diffraction. We will see, that the resonance of a cavity not only depends on the order number N of the *longitudinal mode*, but also on the order of the *transverse mode*. The free space modes are TEM-modes.

18.3.6.1 Damping of the cavity

The decay time τ of the cavity is defined by the number of 'round-trips' with reflections at both mirrors R_1 and R_2, that a light beam can do before its intensity falls to e^{-1} of its original value [1407](p.148):

$$I(\tau) = I_0\sqrt{R_1R_2}^{c\tau/2L} \stackrel{!}{=} e^{-1}I_0\ . \tag{18.265}$$

[29] Note, that κ_{int} is defined as the FWHM of the intensity transmission curve.

Letting $R_1 = R_2 = 1 - T$, this yields,

$$\begin{aligned}\tau &= \frac{2L}{c}\frac{\ln e^{-1}}{\ln R_1 R_2} = \frac{1}{\delta_{fsr}}\frac{-1}{\ln(1-T)^2} \simeq \frac{1}{\delta_{fsr}}\frac{1}{2T} \\ &= \frac{1}{2\delta_{fsr}}\frac{1}{1-\sqrt{R_1 R_2}} \simeq \frac{F}{2\pi\delta_{fsr}} = \frac{1}{\kappa_{int}}\ ,\end{aligned} \tag{18.266}$$

approximating $\sqrt{R} \simeq 1$. Hence, κ_{int} has also the meaning of a intensity decay constant [30].

18.3.7 Exercises

18.3.7.1 Ex: Green function for vector Helmholtz equation

Derive the expression (18.206) in Cartesian coordinates.

Solution: *To evaluate,*

$$\left[\mathbb{I} + \tfrac{1}{k^2}\nabla\nabla^{\intercal}\right]\frac{e^{\imath kR}}{4\pi kR}\ ,$$

we first calculate the first and second derivatives in Cartesian coordinates,

$$\begin{aligned}\frac{\partial}{\partial x}\frac{e^{\imath kR}}{4\pi kR} &= (-1+\imath kR)x\frac{e^{\imath kR}}{4\pi kR^3} \\ \frac{\partial}{\partial x}\left((-1+\imath kR)x\frac{e^{\imath kR}}{4\pi kR^3}\right) &= [(-3+\imath kR)x^2 + R^2](-1+\imath kR)\frac{e^{\imath kR}}{4\pi kR^5} \\ \frac{\partial}{\partial y}\left((-1+\imath kR)x\frac{e^{\imath kR}}{4\pi kR^3}\right) &= (-3+\imath kR)xy(-1+\imath kR)\frac{e^{\imath kR}}{4\pi kR^5}\ .\end{aligned}$$

With this,

$$\left[\mathbb{I} + \frac{1}{k^2}\nabla\nabla\right]\frac{e^{\imath kR}}{4\pi kR} = \begin{pmatrix}1&0&0\\0&1&0\\0&0&1\end{pmatrix}\frac{e^{\imath kR}}{4\pi kR} + \begin{pmatrix}\partial_x^2 & \partial_x\partial_y & \partial_x\partial_z \\ \partial_y\partial_x & \partial_y^2 & \partial_y\partial_z \\ \partial_z\partial_x & \partial_z\partial_y & \partial_z^2\end{pmatrix}\frac{(-1+\imath kR)e^{\imath kR}}{4\pi k^3R^5}$$

$$= \frac{e^{\imath kR}\mathbb{I}}{4\pi kR} + \begin{pmatrix}(-3+\imath kR)x^2+R^2 & (-3+\imath kR)xy & (-3+\imath kR)xz \\ (-3+\imath kR)xy & (-3+\imath kR)y^2+R^2 & (-3+\imath kR)yz \\ (-3+\imath kR)xz & (-3+\imath kR)yz & (-3+\imath kR)z^2+R^2\end{pmatrix}\frac{(-1+\imath kR)e^{\imath kR}}{4\pi k^3R^5}$$

$$= -\frac{e^{\imath kR}}{4\pi k^3R^3}\left\{[1-\imath kR-(kR)^2]\mathbb{I} + (3-4\imath kR-(kR)^2)\hat{\mathbf{e}}_R\otimes\hat{\mathbf{e}}_R\right\}\ .$$

See also [210].

[30] It should not be confused with the electric field *amplitude* decay rate defined as $\kappa = \kappa_{int}/2$.

18.3.7.2 Ex: The fields of a plasmon

From the ansatz,

$$\vec{\mathcal{H}}_n(\mathbf{r},t) = \begin{pmatrix} 0 \\ \mathcal{H}_{y,n} \\ 0 \end{pmatrix} e^{\imath k_x x + \imath k_{z,n}|z| - \imath\omega t}$$

for a plasmonic wave, with $n = \mathrm{m}$ in the metallic region ($z < 0$) and $n = \mathrm{d}$ in the dielectric region ($z > 0$), construct the electric and magnetic fields on both sides of a metal-dielectric interface.

Solution: *From Maxwell's first equation we know, $\vec{\mathcal{E}}_n \propto \nabla \times \vec{\mathcal{H}}_n$, such that the fields have the generic form,*

$$\vec{\mathcal{H}}_n(\mathbf{r},t) = \begin{pmatrix} 0 \\ \mathcal{H}_{y,n} \\ 0 \end{pmatrix} e^{\imath k_x x + \imath k_{z,n}|z| - \imath\omega t} \quad , \quad \vec{\mathcal{E}}_n(\mathbf{r},t) = \begin{pmatrix} \mathcal{E}_{x,n} \\ 0 \\ \mathcal{E}_{z,n} \end{pmatrix} e^{\imath k_x x + \imath k_{z,n}|z| - \imath\omega t} \ .$$

In the interface, the fields must meet the conditions (18.98)(i-iv), giving,

$$\mathcal{H}_{y,m} = \mathcal{H}_{y,d} \equiv \mathcal{H}_0 \quad , \quad \mathcal{E}_{x,m} = \mathcal{E}_{x,d} \equiv \mathcal{E}_0 \quad , \quad \varepsilon_m \mathcal{E}_{z,m} = \varepsilon_d \mathcal{E}_{z,d} \ .$$

Inserting $\vec{\mathcal{H}}_n(\mathbf{r},t)$ in Maxwell's first equation,

$$\nabla \times \vec{\mathcal{H}}_n = \begin{pmatrix} -\partial_z \mathcal{H}_0 \\ 0 \\ \partial_x \mathcal{H}_0 \end{pmatrix} = \begin{pmatrix} \mp \imath k_{z,n} \\ 0 \\ \imath k_x \end{pmatrix} \mathcal{H}_0 e^{\imath k_x x + \imath k_{z,n}|z| - \imath\omega t}$$

$$= \varepsilon_n \begin{pmatrix} \mathcal{E}_0 \\ 0 \\ \mathcal{E}_{z,n} \end{pmatrix} \partial_t e^{\imath k_x x + \imath k_{z,n}|z| - \imath\omega t} = \partial_t \varepsilon_n \vec{\mathcal{E}}_n \ ,$$

where the upper signs hold for the dielectric region ($z > 0$), we can determine,

$$\mp \imath k_{z,n} \mathcal{H}_0 = -\imath\omega\varepsilon_n \mathcal{E}_0 \quad \textit{and} \quad \imath k_x \mathcal{H}_0 = -\imath\omega\varepsilon_n \mathcal{E}_{z,n} \ ,$$

such that,

$$\vec{\mathcal{H}}_n(\mathbf{r},t) = \begin{pmatrix} 0 \\ 1 \\ 0 \end{pmatrix} \mathcal{H}_0 e^{\imath k_x x + \imath k_{z,n}|z| - \imath\omega t} \quad , \quad \vec{\mathcal{E}}_n(\mathbf{r},t) = \begin{pmatrix} \pm k_{z,n} \\ 0 \\ -k_x \end{pmatrix} \frac{\mathcal{H}_0}{\omega\varepsilon_n} e^{\imath k_x x + \imath k_{z,n}|z| - \imath\omega t} \ ,$$

under the condition that,

$$\frac{k_{z,m}}{\varepsilon_m} = -\frac{k_{z,d}}{\varepsilon_d} \ .$$

For metals, as we know from Eqs. (18.87) and (18.161), the wavevector and the permittivity can be complex. For lossless plasmons, according to (18.222) the wavevector in z-direction is purely imaginary, such that fields stick to the surface and propagate along it.

18.3.7.3 Ex: Absorption of plasmons

Derive the expression (18.230).

Solution: *The complex dispersion relation is,*

$$ck_x = c(k'_x + \imath k''_x) = \omega\sqrt{\frac{\hat{\varepsilon}_d(\hat{\varepsilon}'_m + \imath\hat{\varepsilon}''_m)}{\hat{\varepsilon}_d + \hat{\varepsilon}'_m + \imath\hat{\varepsilon}''_m}}$$
$$= \omega\sqrt{\hat{\varepsilon}_d}\sqrt{\frac{\hat{\varepsilon}'_m(\hat{\varepsilon}_d + \hat{\varepsilon}'_m) + (\hat{\varepsilon}''_m)^2}{(\hat{\varepsilon}_d + \hat{\varepsilon}'_m)^2 + (\hat{\varepsilon}''_m)^2} + \imath\frac{\hat{\varepsilon}''_m(\hat{\varepsilon}_d + \hat{\varepsilon}'_m) - (\hat{\varepsilon}''_m)^2}{(\hat{\varepsilon}_d + \hat{\varepsilon}'_m)^2 + (\hat{\varepsilon}''_m)^2}} \ .$$

neglecting quadratic terms and expanding for small $\hat{\varepsilon}''_m$,

$$ck_x \simeq \omega\sqrt{\frac{\hat{\varepsilon}_d}{\hat{\varepsilon}_d + \hat{\varepsilon}'_m}}\sqrt{\hat{\varepsilon}'_m + \imath\hat{\varepsilon}''_m} = \omega\sqrt{\frac{\hat{\varepsilon}_d\hat{\varepsilon}'_m}{\hat{\varepsilon}_d + \hat{\varepsilon}'_m}}\left(1 + \frac{\imath\hat{\varepsilon}''_m}{2\hat{\varepsilon}'_m} + ..\right) = ck_x\left(1 + \frac{\imath\hat{\varepsilon}''_m}{2\hat{\varepsilon}'_m} + ..\right) \ .$$

18.3.7.4 Ex: Poynting vector of plasmons

At the interface between the vacuum and a metal surface there live solutions of the Maxwell equations, which decay exponentially in z-direction. We consider in this exercise only those parts of the waves, which live on the vacuum side $z > 0$, as illustrated in Fig. 18.21(a). The magnetic field, in this scheme, takes the following form:

$$\vec{\mathcal{H}}(\mathbf{r}, t) = \begin{pmatrix} 0 \\ \mathcal{H}_0 \\ 0 \end{pmatrix} \cos(kx - \omega t)e^{-\kappa z} \ (z > 0) \ .$$

a. Derive with the help of Maxwell's equation $\nabla \times \vec{\mathcal{H}} - \frac{\partial\vec{\mathcal{D}}}{\partial t} = \mathbf{j}$ the corresponding electric field $\vec{\mathcal{E}}(\mathbf{r}, t)$ in the half-space $z > 0$.
b. Calculate the Poynting vector $\vec{\mathcal{S}}(\mathbf{r}, t)$ in the half-space $z > 0$.
c. Calculate the total energy flow in x-direction. To do this, calculate the average over an oscillation period and integrate over the half-space $z > 0$.

Solution: *a. The electric field follows with $\mathbf{j} = 0$ and $\vec{\mathcal{D}} = \varepsilon_0\vec{\mathcal{E}}$ from,*

$$\nabla \times \vec{\mathcal{H}} = \begin{pmatrix} -\partial_z\mathcal{H}_y \\ 0 \\ \partial_x\mathcal{H}_y \end{pmatrix} = \begin{pmatrix} \mathcal{H}_0\kappa\cos(kx - \omega t)e^{-\kappa z} \\ 0 \\ -\mathcal{H}_0 k\sin(kx - \omega t)e^{-\kappa z} \end{pmatrix} = \partial_t\varepsilon_0\mathcal{E} \ .$$

We now integrate the result by t:

$$\int dt \begin{pmatrix} \mathcal{H}_0\kappa\cos(kx-\omega t)e^{-\kappa z} \\ 0 \\ -\mathcal{H}_0 k\sin(kx-\omega t)e^{-\kappa z}\end{pmatrix} = \begin{pmatrix} \frac{-\mathcal{H}_0\kappa}{\omega}\sin(kx-\omega t)e^{-\kappa z} \\ 0 \\ \frac{-\mathcal{H}_0 k}{\omega}\cos(kx-\omega t)e^{-\kappa z}\end{pmatrix} .$$

With this, we obtain:

$$\vec{\mathcal{E}} = \frac{-\mathcal{H}_0}{\omega\varepsilon_0}e^{-\kappa z}\begin{pmatrix} \kappa\sin(kx-\omega t) \\ 0 \\ k\cos(kx-\omega t)\end{pmatrix} .$$

b. The Poynting vector is,

$$\begin{aligned}\vec{\mathcal{S}} = \vec{\mathcal{E}}\times\vec{\mathcal{H}} &= -\frac{\mathcal{H}_0^2}{\omega\varepsilon_0}e^{-2\kappa z}\begin{pmatrix} \kappa\sin(kx-\omega t) \\ 0 \\ k\cos(kx-\omega t)\end{pmatrix}\times\begin{pmatrix} 0 \\ \cos(kx-\omega t) \\ 0\end{pmatrix} \\ &= -\frac{\mathcal{H}_0^2}{\omega\varepsilon_0}e^{-2\kappa z}\begin{pmatrix} -k\cos^2(kx-\omega t) \\ 0 \\ \kappa\sin(kx-\omega t)\cos(kx-\omega t)\end{pmatrix} .\end{aligned}$$

c. In x-direction we must take the time average of $\cos^2$, which gives the factor $1/2$. The integral over z gives:

$$\int_0^\infty dz e^{-2\kappa z} = \frac{1}{2\kappa}e^{-2\kappa z}\Big|_0^\infty = \frac{1}{2\kappa} .$$

Therefore, the total energy flux is,

$$\bar{s}_1^{tot} = \frac{\mathcal{H}_0^2 k}{4\omega\varepsilon_0\kappa} .$$

18.3.7.5 Ex: Negative refraction

Show that a medium with negative refractive index is left-handed and allows for perfect focusing.

Solution: *Let us look more closely at the reasons for limitation in performance [1011]. Consider an infinitesimal dipole of frequency ω in front of a lens. The electric component of the field will be given by some 2D Fourier expansion,*

$$\mathcal{E}(\mathbf{r},t) = \sum_{\sigma,k_x,k_y}\mathcal{E}_\sigma(k_x,k_y)e^{\imath k_z+\imath k_x+\imath k_y-\imath\omega t} ,$$

where we choose the axis of the lens to be the z axis. Maxwell's equations tell us that,

$$k_z = \sqrt{\omega^2/c^2 - k_x^2 - k_y^2}$$

the lens is to apply a phase correction to each of the Fourier components, so that at some distance beyond the lens the fields reassemble to a focus, and an image of the dipole source appears. However, for larger values of the transverse wave vector, $\omega^2/c^2 < k_x^2 + k_y^2$, k_z turns imaginary. These evanescent waves decay exponentially with z and no phase correction will restore them to their proper amplitude. They are effectively removed from the image, which generally comprises only the propagating waves. Since the propagating waves are limited to,

$$\omega^2/c^2 > k_x^2 + k_y^2$$

the maximum resolution in the image can never be greater than

$$res = \frac{2\pi}{k_{max}} = \frac{2\pi c}{\omega} = \lambda \ ,$$

and this is true however perfect the lens and however large the aperture.
There is an unconventional alternative to a lens. Material with negative refractive index ($\varepsilon, \mu < 0$) will focus light even when the lens consists of a parallel-sided dielectric slab. Fig. 18.22 sketches the focusing of such a slab, assuming that the refractive index is $n = -1$. Still the propagation of light at the interfaces obeys Snell's laws of refraction, as light inside the medium makes a negative angle with the surface normal. The other characteristic of the system is the double focusing effect revealed by a simple ray diagram. Light transmitted through a slab of thickness d_2 located a distance d_1 from the source comes to a second focus when, $z = d_2 - d_1$.

18.3.7.6 Ex: Negative refraction in chiral media

In a *chiral medium* the electric polarization $\vec{\mathcal{P}}$ couples to the magnetic field $\vec{\mathcal{H}}$ of an electromagnetic wave and the magnetization $\vec{\mathcal{M}}$ couples to the electric field $\vec{\mathcal{E}}$ like,

$$\vec{\mathcal{P}} = \varepsilon_0 \chi_\varepsilon \vec{\mathcal{E}} + \tfrac{1}{c}\xi_{EH}\vec{\mathcal{H}} \qquad \text{and} \qquad \vec{\mathcal{M}} = \tfrac{1}{c}\xi_{HE}\vec{\mathcal{E}} + \chi_m \vec{\mathcal{H}} \ ,$$

where ξ_{EH} and ξ_{HE} are the complex chirality coefficients. Show that a chiral medium allows for a negative refraction coefficient.

Solution: *The chirality coefficients lead to additional contributions to the refractive index for one circular polarization,*

$$n = \sqrt{\varepsilon\mu - \tfrac{1}{4}(\xi_{EH} + \xi_{HE})^2} + \tfrac{\imath}{2}(\xi_{EH} - \xi_{HE}) \ .$$

Such a chiral medium allows $n < 0$ without requiring $\mu < 0$ if there is a positive imaginary part of $\xi_{EH} - \xi_{HE}$ of sufficiently large magnitude. For example, choosing the phases of the complex chirality coefficients such that $\xi_{EH} = -\xi_{HE} = \imath\xi$, with $\xi, \varepsilon, \mu > 0$, the index of refraction becomes $n = \sqrt{\varepsilon\mu} - \xi$, and $n < 0$ when $\xi > \sqrt{\varepsilon\mu}$ [1012].

18.3.7.7 Ex: Hyperbolic metamaterials

Hyperbolic metamaterials are artificial media with sub-wavelength nanostructuring below exhibiting uncommon optical properties, such as an extreme anisotropy giving rise to permittivity and permeability tensors of the form,

$$\epsilon = \begin{pmatrix} \varepsilon_\perp & & \\ & \varepsilon_\perp & \\ & & \varepsilon_{\shortparallel} \end{pmatrix} \quad \text{and} \quad \mu = \begin{pmatrix} \mu_\perp & & \\ & \mu_\perp & \\ & & \mu_{\shortparallel} \end{pmatrix} .$$

In the case $\varepsilon_\perp \varepsilon_{\shortparallel} < 0$ or $\mu_\perp \mu_{\shortparallel} < 0$ the dispersion relation,

$$\frac{k_x^2 + k_y^2}{\varepsilon_{\shortparallel}} + \frac{k_z^2}{\varepsilon_\perp} = \frac{(\omega/c)^2}{\varepsilon_0} ,$$

becomes hyperbolic.
Derive from the Maxwell equations, allowing for an anisotropic (but homogeneous) permittivity tensor, the hyperbolic dispersion relation.

Solution: *Inserting the first into the second Maxwell equation, we derive, accounting for the anisotropy of the permittivity tensor, the equation,*

$$\frac{\partial^2 \epsilon \vec{\mathcal{E}}}{\partial t^2} = \frac{\partial^2 \vec{\mathcal{D}}}{\partial t^2} = \frac{\partial}{\partial t} \nabla \times \vec{\mathcal{H}} = \nabla \times \frac{\partial}{\partial t} \frac{\vec{\mathcal{B}}}{\mu} = -\frac{1}{\mu} \nabla \times (\nabla \times \vec{\mathcal{E}}) = -\frac{1}{\mu} [\nabla (\nabla \cdot \vec{\mathcal{E}}) - \nabla^2 \vec{\mathcal{E}}] .$$

Inserting plane waves, $\vec{\mathcal{E}} = \vec{\mathcal{E}}_0 e^{\imath(\mathbf{k}\cdot\mathbf{r} - \omega t)}$, we calculate,

$$-\omega^2 \begin{pmatrix} \varepsilon_\perp \mathcal{E}_{0x} \\ \varepsilon_\perp \mathcal{E}_{0y} \\ \varepsilon_{\shortparallel} \mathcal{E}_{0z} \end{pmatrix} e^{\imath(\mathbf{k}\cdot\mathbf{r} - \omega t)} = -\frac{1}{\mu} \nabla (\imath k_x \mathcal{E}_{0x} + \imath k_y \mathcal{E}_{0y} + \imath k_z \mathcal{E}_{0z} e^{\imath(\mathbf{k}\cdot\mathbf{r} - \omega t)} + \frac{1}{\mu} \mathbf{k}^2 \begin{pmatrix} \mathcal{E}_{0x} \\ \mathcal{E}_{0y} \\ \mathcal{E}_{0z} \end{pmatrix} e^{\imath(\mathbf{k}\cdot\mathbf{r} - \omega t)}$$

$$= -\frac{1}{\mu} \begin{pmatrix} -k_x^2 \mathcal{E}_{0x} - k_x k_y \mathcal{E}_{0y} - k_x k_z \mathcal{E}_{0z} \\ -k_x k_y \mathcal{E}_{0x} - k_y^2 \mathcal{E}_{0y} - k_y k_z \mathcal{E}_{0z} \\ -k_x k_z \mathcal{E}_{0x} - k_y k_z \mathcal{E}_{0y} - k_z^2 \mathcal{E}_{0z} \end{pmatrix} e^{\imath(\mathbf{k}\cdot\mathbf{r} - \omega t)} + \frac{1}{\mu} \mathbf{k}^2 \begin{pmatrix} \mathcal{E}_{0x} \\ \mathcal{E}_{0y} \\ \mathcal{E}_{0z} \end{pmatrix} e^{\imath(\mathbf{k}\cdot\mathbf{r} - \omega t)} .$$

That is,

$$0 = \begin{pmatrix} \omega^2 \mu \varepsilon_\perp - k_y^2 - k_z^2 & k_x k_y & k_x k_z \\ k_x k_y & \omega^2 \mu \varepsilon_\perp - k_z^2 - k_x^2 & k_y k_z \\ k_x k_z & k_y k_z & \omega^2 \mu \varepsilon_{\shortparallel} - k_x^2 - k_y^2 \end{pmatrix} \begin{pmatrix} \mathcal{E}_{0x} \\ \mathcal{E}_{0y} \\ \mathcal{E}_{0z} \end{pmatrix} .$$

The determinant must vanish in order to obtain non-trivial solutions,

$$\begin{aligned} 0 = {} & \mu^3 \varepsilon_\perp^2 \varepsilon_{\shortparallel} \omega^6 - \mu^2 \varepsilon_\perp \varepsilon_{\shortparallel} k_x^2 \omega^4 - \mu^2 \varepsilon_\perp \varepsilon_{\shortparallel} k_y^2 \omega^4 - 2\mu^2 \varepsilon_\perp \varepsilon_{\shortparallel} k_z^2 \omega^4 - \mu^2 \varepsilon_\perp^2 k_x^2 \omega^4 - \mu^2 \varepsilon_\perp^2 k_y^2 \omega^4 \\ & + \mu \varepsilon_\perp k_x^4 \omega^2 + \mu \varepsilon_\perp k_y^4 \omega^2 + \mu \varepsilon_{\shortparallel} k_z^4 \omega^2 + \mu \varepsilon_\perp k_x^2 k_z^2 \omega^2 + \mu \varepsilon_\perp k_y^2 k_z^2 \omega^2 + 2\mu \varepsilon_\perp k_x^2 k_y^2 \omega^2 \\ & + \mu \varepsilon_{\shortparallel} k_x^2 k_z^2 \omega^2 + \mu \varepsilon_{\shortparallel} k_y^2 k_z^2 \omega^2 . \end{aligned}$$

Apart from the trivial solution $\omega = 0$, we get,

$$0 = \omega^4 - \left(\frac{k_x^2}{\varepsilon_{\shortparallel}} + \frac{k_y^2}{\varepsilon_{\shortparallel}} + \frac{k_z^2}{\varepsilon_{\perp}} + \frac{k^2}{\varepsilon_{\perp}} \right) \frac{\omega^2}{\mu} + \frac{k^2}{\mu^2 \varepsilon_{\perp}} \left(\frac{k_x^2}{\varepsilon_{\shortparallel}} + \frac{k_y^2}{\varepsilon_{\shortparallel}} + \frac{k_z^2}{\varepsilon_{\perp}} \right) \ .$$

Which is satisfied provided the dispersion relation is, $c^2 = \frac{1}{\varepsilon_0 \mu}$.

18.3.7.8 Ex: Stacked layer metamaterial

Show that the effective permittivity of a nanostructure having the shape of an alternating stack of two different but intrinsically homogenous layers with the permittivity ε_d and ε_m and thicknesses $d_d, d_m \ll \lambda$ is given by,

$$\varepsilon_{\perp} = \frac{\varepsilon_d d_d + \varepsilon_m d_m}{d_d + d_m} \qquad \text{and} \qquad \varepsilon_{\shortparallel} = \frac{d_d/\varepsilon_d + d_m/\varepsilon_m}{d_d + d_m} \ .$$

Solution: *Apply the Fresnel equations and calculate the $\mathcal{T}$-matrix of an infinite stack as done in [1123].*

18.3.7.9 Ex: Hyperbolic dispersion relation in gases

Discuss, whether it is possible to realize a hyperbolic dispersion relation in an atomic gas.

Solution: *How to induce anisotropy on the atomic level? Via electric or magnetic fields? Dispersion relation of a gas which can only do π transitions along a predefined axis?*
For hyperbolic, we need negative ε, i.e. EIT.
What are the signatures of negative ε.

18.3.7.10 Ex: TEM waves in a hollow wave guide

Verify that TEM waves can not occur in hollow waveguides. Do not use the already derived results (18.249).

Solution: *We define the TEM wave with respect to the z-axis, such that $\vec{\mathcal{E}}_z = 0$ and $\vec{\mathcal{E}} = \vec{\mathcal{E}}_x(x,y)\hat{\mathbf{e}}_x + \vec{\mathcal{E}}_y(x,y)\hat{\mathbf{e}}_y$ and analogously for $\vec{\mathcal{B}}$. The third and second Maxwell equations then require,*

$$\frac{\partial \vec{\mathcal{E}}_x}{\partial x} + \frac{\partial \vec{\mathcal{E}}_y}{\partial y} = 0 = \frac{\partial \vec{\mathcal{E}}_y}{\partial x} - \frac{\partial \vec{\mathcal{E}}_x}{\partial y} \ ,$$

that is, $\nabla \cdot \vec{\mathcal{E}} = 0 = \nabla \times \vec{\mathcal{E}}$. Since the rotation is zero, there exists a gradient, such that $\vec{\mathcal{E}} = -\nabla\Phi$, e

$$0 = \nabla \cdot \vec{\mathcal{E}} = -\nabla \cdot (\nabla\Phi) = -\nabla^2\Phi \ .$$

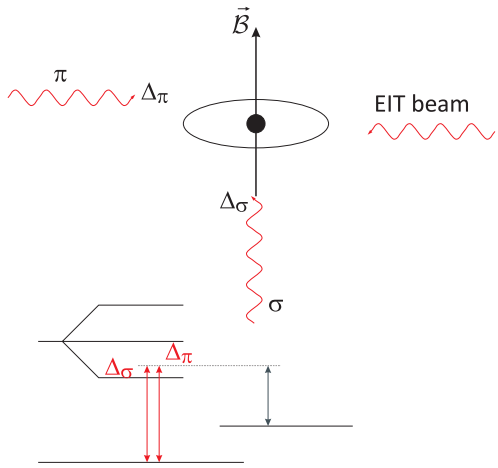

Figure 18.29: Hyperbolic dispersion materials.

The boundary condition of a waveguide is an equipotential surface, but since the Laplace equation does not admit local maximums or minimums, the potential has to be $\Phi = const$, that is $\vec{\mathcal{E}} = 0$.
Note that this argument only applies to a completely empty waveguide. Placing another conductor in the middle of the guide, the potential on its inner surface does not have to be the same as on the outer surface, and therefore a non-trivial potential is possible.

18.3.7.11 Ex: The TE_{00} mode in the rectangular waveguide

Show that the TE_{00} mode can not occur in a rectangular waveguide.

Solution: *For a hollow waveguide the dispersion relation simplifies to $\omega/c = k$. For TE_{00} modes we have $\mathcal{E}_z = 0$. Maxwell's equations then yield,*

$$\begin{aligned} \partial_x\mathcal{E}_y - \partial_y\mathcal{E}_x = \imath\omega\mathcal{B}_z \qquad & and \qquad \partial_x\mathcal{B}_y - \partial_y\mathcal{B}_x = 0 \\ -\imath k\mathcal{E}_y = \imath\omega\mathcal{B}_x \qquad & and \qquad \partial_y\mathcal{B}_z - \imath k\mathcal{B}_y = -\tfrac{\imath\omega}{c^2}\mathcal{E}_x \\ \imath k\mathcal{E}_x = \imath\omega\mathcal{B}_y \qquad & and \qquad \imath k\mathcal{B}_x - \partial_x\mathcal{B}_z = -\tfrac{\imath\omega}{c^2}\mathcal{E}_y \ . \end{aligned}$$

Solving the third equation by $\mathcal{E}_y$ and substituting it into the last equation,

$$\imath k\mathcal{B}_x - \partial_x\mathcal{B}_z = -\tfrac{\imath\omega}{c^2}\tfrac{-\omega}{k}\mathcal{B}_x \ ,$$

we find $\partial_x\mathcal{B}_z = 0$. Solving the fifth equation by $\mathcal{E}_x$ and substituting it into the fourth equation,

$$\partial_y\mathcal{B}_z - \imath k\mathcal{B}_y = -\tfrac{\imath\omega}{c^2}\tfrac{\omega}{k}\mathcal{B}_y \ ,$$

we find $\partial_y\mathcal{B}_z = 0$, that is, the field $\mathcal{B}_z(x,y) = \mathcal{B}_0$ is constant, that is,

$$\vec{\mathcal{B}} = \vec{\mathcal{B}}_0 e^{\imath(kz-\omega t)} \qquad and \qquad \frac{\partial\vec{\mathcal{B}}}{\partial t} = -\imath\omega\vec{\mathcal{B}}_0 e^{\imath(kz-\omega t)} \ .$$

Applying Faraday's law in the integral form to the cross-section of the waveguide ($S = ab$),

$$\oint \vec{\mathcal{E}}^{\parallel} dl = \oint \vec{\mathcal{E}} \cdot d\mathbf{l} = -\int \frac{\partial \vec{\mathcal{B}}}{\partial t} \cdot d\mathbf{S} = \int \imath\omega \vec{\mathcal{B}}_0 e^{\imath(kz-\omega t)} \cdot d\mathbf{S} = \imath\omega \mathcal{B}_0 e^{\imath(kz-\omega t)} ab \ .$$

The integration path follows the inner edges of the waveguide, where $\mathcal{E}^{\parallel} = 0$,

$$\oint \vec{\mathcal{E}} \cdot d\mathbf{l} = \oint \vec{\mathcal{E}}^{\parallel} dl = 0 \ .$$

such that $\mathcal{B}_0 = 0$. Then it would be a TEM_{00} mode, for which we already have shown in class that it does not exist in a hollow waveguide.

18.3.7.12 Ex: Cut-off frequency

Calculate the radial size of a hollow rectangular wave guide capable of guiding a (i) 60 Hz signal, (ii) a 10 MHz signal, and (iii) a 9.1 GHz signal.

Solution: *The frequency of the guided signal must be higher than the cut-off frequency. For a TE_{10} mode we get from Eq. (18.256) the condition $\omega > c\pi/a$, or $a > \lambda/2$. Hence, $\lambda_i = 2.5km$, $\lambda_{ii} = 15m$, and $\lambda_{iii} = 1.65cm$.*

18.3.7.13 Ex: Cylindrical waveguide

Show that the fields (18.261) satisfy the Maxwell equations with the boundary conditions (18.246) [545](p.411).

Solution: *The fields are,*

$$\vec{\mathcal{E}} = \frac{A\cos(kz-\omega t)}{\rho}\hat{\mathbf{e}}_\rho \equiv A_\rho \hat{\mathbf{e}}_\rho \qquad \text{and} \qquad \vec{\mathcal{B}} = \frac{A\cos(kz-\omega t)}{c\rho}\hat{\mathbf{e}}_\phi \equiv A_\phi \hat{\mathbf{e}}_\phi \ .$$

Obviously they satisfy the boundary conditions on the surface of the waveguide,

$$\vec{\mathcal{E}}^{\parallel} = 0 \qquad \text{and} \qquad \vec{\mathcal{B}}^{\perp} = 0 \ .$$

By inserting them into the second Maxwell equation with the rotational written in cylindrical coordinates (12.72),

$$\begin{aligned}\nabla \times \vec{\mathcal{E}} + \frac{\partial \vec{\mathcal{B}}}{\partial t} &= \hat{\mathbf{e}}_\phi \frac{\partial}{\partial z} A_\rho - \hat{\mathbf{e}}_z \frac{1}{\rho}\frac{\partial}{\partial \phi} A_\rho + \hat{\mathbf{e}}_\rho \frac{\partial}{\partial t} A_\rho \\ &= \hat{\mathbf{e}}_\phi \frac{\partial}{\partial z}\frac{A\cos(kz-\omega t)}{\rho} + \hat{\mathbf{e}}_\phi \frac{\partial}{\partial t}\frac{A\cos(kz-\omega t)}{c\rho} = \hat{\mathbf{e}}_\phi \frac{A\sin(kz-\omega t)}{\rho}\left(-k + \frac{\omega}{c}\right) = 0 \ .\end{aligned}$$

The third Maxwell equation with the divergence written in cylindrical coordinates (12.71) gives,

$$\nabla \cdot \vec{\mathcal{E}} = \frac{1}{\rho}\frac{\partial}{\partial \rho}(\rho A_\rho) + \frac{1}{\rho}\frac{\partial}{\partial \rho} A_\phi + \frac{\partial}{\partial z} A_z = \frac{1}{\rho}\frac{\partial}{\partial \rho}(\rho A_\rho) = \frac{1}{\rho} A \frac{\partial}{\partial \rho}\cos(kz-\omega t) = 0 \ .$$

The calculations for Maxwell's first and fourth equations are analogous.

18.3.7.14 Ex: Propagation of a TEM mode along a coaxial cable

A transmission line made of two concentric circular metallic cylinders with conductivity ρ and skin depth δ is filled with a lossless uniform dielectric (ε, μ). A TEM mode propagates along this line.
a. Show that the time averaged energy flux along the line is,

$$P = \sqrt{\frac{\mu}{\varepsilon}} \pi a^2 |\mathcal{H}_0|^2 \ln \frac{b}{a} \ ,$$

where H_0 is the maximum value of the azimuthal magnetic field on the surface of the inner conductor.
b. Show that the transmitted power is attenuated along the line like,

$$P(z) = P_0 e^{-2\gamma z} \ ,$$

where,

$$\gamma = \frac{1}{2\sigma\delta} \sqrt{\frac{\varepsilon}{\mu}} \frac{a^{-1} + b^{-1}}{ln(b/a)} \ .$$

c. The characteristic impedance Z_0 of the line is defined as the ratio between the voltage between the cylinders and the current flowing in axial direction inside one of the cylinders at any position z. Show that for this line,

$$Z_0 = \frac{1}{2\pi} \sqrt{\frac{\mu}{\varepsilon}} \ln \frac{b}{a} \ .$$

d. Show that the resistance and the serial inductance per unit length of the line are,

$$R = \frac{1}{2\pi\sigma\delta} \left(\frac{1}{a} + \frac{1}{b} \right) \quad , \quad L = \frac{\mu}{2\pi} \ln \frac{b}{a} + \frac{\mu_c \delta}{4\pi} \left(\frac{1}{a} + \frac{1}{b} \right) \ ,$$

where μ_c is the permeability of the conductor. The correction for the inductance comes from the penetration of the flux into the conductors by the distance of the order δ.

Solution:

18.3.7.15 Ex: Resonant cavity

Consider a perfectly conducting resonant cavity having the shape of a 3D rectangular box with the volume defined by $x \in [0, L_x]$, $y \in [0, L_y]$, and $z \in [0, L_z]$. Show that the resonant frequencies for both the TE and TM modes are given by $\omega_{n_x,n_y,n_z} = c\pi\sqrt{(n_x/L_x)^2 + (n_y/L_y)^2 + (n_z/L_z)^2}$ for integers n_i. Find the associated electric and magnetic fields.

Solution: *The rectangular symmetry of the problem allows us to separate the Cartesian variables, as shown in equation (13.76). For every component of the vector* $\vec{\mathcal{E}}$,

e.g. the $\mathcal{E}_x$ component, we can make an ansatz $\mathcal{E}_x = X_x(x)Y_x(y)Z_x(z)$ which, inserted in the wave equation gives,

$$\begin{aligned} X_x(x) &= A_{xx}\sin k_{xx}x + C_{xx}\cos k_{xx}x \\ Y_x(y) &= A_{xy}\sin k_{xy}y + C_{xy}\cos k_{xy}y \\ Z_x(z) &= A_{xz}\sin k_{xz}z + C_{xz}\cos k_{xz}z \ , \end{aligned}$$

and similarly for the components $\mathcal{E}_y$ and $\mathcal{E}_z$. The lengths being fixed by the boundary conditions,

$$\vec{\mathcal{E}}^{\parallel} = 0 \qquad \textit{and} \qquad \vec{\mathcal{B}}^{\perp} = 0 \ ,$$

for the $\mathcal{E}_x$ component we get on the surfaces $y = 0, L_y$ and $z = 0, L_z$,

$$C_{xy} = C_{xz} = 0 \qquad \textit{and} \qquad k_{xy} = \pi\tfrac{n_y}{L_y} \qquad , \qquad k_{xz} = \pi\tfrac{n_z}{L_z} \ .$$

We let $A_{xy} = 1 = A_{xz}$ and obtain, extending the procedure to the other components,

$$\begin{aligned} \mathcal{E}_x &= (A_{xx}\sin k_{xx}x + C_{xx}\cos k_{xx}x)\sin\tfrac{\pi n_y y}{L_y}\sin\tfrac{\pi n_z z}{L_z} \\ \mathcal{E}_y &= (A_{yy}\sin k_{yy}y + C_{yy}\cos k_{yy}y)\sin\tfrac{\pi n_x y}{L_x}\sin\tfrac{\pi n_z z}{L_z} \\ \mathcal{E}_z &= (A_{zz}\sin k_{zz}z + C_{zz}\cos k_{zz}z)\sin\tfrac{\pi n_x y}{L_x}\sin\tfrac{\pi n_y y}{L_y} \ . \end{aligned}$$

Now, we invoke Gauss's law,

$$\begin{aligned} 0 = \nabla\cdot\vec{\mathcal{E}} = {} & k_{xx}(A_{xx}\cos k_{xx}x - C_{xx}\sin k_{xx}x)\sin\tfrac{\pi n_y y}{L_y}\sin\tfrac{\pi n_z z}{L_z} \\ & + k_{yy}(A_{yy}\cos k_{yy}y - C_{yy}\sin k_{yy}y)\sin\tfrac{\pi n_x y}{L_x}\sin\tfrac{\pi n_z z}{L_z} \\ & + k_{zz}(A_{zz}\cos k_{zz}z - C_{zz}\sin k_{zz}z)\sin\tfrac{\pi n_x y}{L_x}\sin\tfrac{\pi n_y y}{L_y} \ . \end{aligned}$$

This equation must be valid in every point (x, y, z), hence also at $x = 0$, which is only possible when $A_{xx} = 0$. By symmetry, we must also set $A_{yy} = 0 = A_{zz}$, yielding,

$$\begin{aligned} 0 = \nabla\cdot\vec{\mathcal{E}} = {} & - k_{xx}C_{xx}\sin k_{xx}x\sin\tfrac{\pi n_y y}{L_y}\sin\tfrac{\pi n_z z}{L_z} \\ & - k_{yy}C_{yy}\sin k_{yy}y\sin\tfrac{\pi n_x y}{L_x}\sin\tfrac{\pi n_z z}{L_z} \\ & - k_{zz}C_{zz}\sin k_{zz}z\sin\tfrac{\pi n_x y}{L_x}\sin\tfrac{\pi n_y y}{L_y} \ . \end{aligned}$$

Finally, introducing the abbreviations $k_j = \pi n_j/L_j$, we get the electric field,

$$\begin{aligned} \vec{\tilde{\mathcal{E}}} = {} & C_{xx}e^{-\imath\omega t}\hat{\mathbf{e}}_x\cos k_x x\sin k_y y\sin k_z z \\ & + C_{yy}e^{-\imath\omega t}\hat{\mathbf{e}}_y\sin k_x x\cos k_y y\sin k_z z \\ & + C_{zz}e^{-\imath\omega t}\hat{\mathbf{e}}_z\sin k_x x\sin k_y y\cos k_z z \ . \end{aligned}$$

The magnetic field is obtained by Maxwell's equation,

$$\begin{aligned} -\imath\omega\vec{\tilde{\mathcal{B}}} = \frac{\partial\vec{\tilde{\mathcal{B}}}}{\partial t} = -\nabla\times\vec{\tilde{\mathcal{E}}} = {} & -(C_{zz}k_y - C_{yy}k_z)e^{-\imath\omega t}\hat{\mathbf{e}}_x\sin k_x x\cos k_y y\cos k_z z \\ & -(C_{xx}k_z - C_{zz}k_x)e^{-\imath\omega t}\hat{\mathbf{e}}_y\cos k_x x\sin k_y y\cos k_z z \\ & -(C_{yy}k_x - C_{xx}k_y)e^{-\imath\omega t}\hat{\mathbf{e}}_z\cos k_x x\cos k_y y\sin k_z z \ . \end{aligned}$$

The resonant frequency for the mode (n_x, n_y, n_z) *is,*

$$\omega_{n_x,n_y,n_z} = c\pi\sqrt{k_x^2 + k_y^2 + k_z^2} \ .$$

18.3.7.16 Ex: Spherical holes in conductors such as cavities

A spherical hole of radius a in a conductive medium may serve as an electromagnetic resonant cavity.
a. Assuming infinite conductivity, determine the transcendental equations for the characteristic frequencies $\omega_{\ell m}$ of the cavity for TE and TM modes.
b. Calculate numerical values for the wavelength $\lambda_{\ell m}$ in units of the radius a for the four lowest modes for TE and TM waves.
c. Explicitly calculate the electric and magnetic fields inside the cavity for the lowest TE mode and the lowest TM mode.

Solution:

18.3.7.17 Ex: Schumann resonances

A resonant cavity consists of the void space between two perfectly conducting and concentric spherical layers. The smaller one has the external radius a, the larger one the internal radius b. The azimuthal magnetic field has a radial dependence given by spherical Bessel functions, $j_\ell(kr)$ and $n_\ell(kr)$, where $k = \omega/c$.
a. Write the transcendental equation for the characteristic frequencies of the cavity for arbitrary ℓ.
b. For $\ell = 1$ use the explicit forms of the spherical Bessel functions to show that the characteristic frequencies are given by,

$$\frac{\tan kh}{kh} = \frac{k^2 + (ab)^{-1}}{k^2 + ab(k^2 - a^{-2})(k^2 - b^{-2})} \ ,$$

where $h = b - a$.
c. For $h/a \ll 1$, verify that the result of part (b) reproduces the frequency found in [659], Sec. 8.9, and determine the first-order corrections in h/a.
Now, we apply this cavity as a model for the atmosphere enclosed by the Earth's surface and its ionosphere.
d. For the Schumann resonances of Sec. 8.9 calculate the values Q under the assumption that the Earth has the conductivity σ_e and the ionosphere the conductivity σ_i with corresponding skin depths δ_e and δ_i. Show that in the lowest order in h/a the value Q is given by $Q = Nh/(\delta_e + \delta_i)$ and determine the numerical factor N for all ℓ.
e. For the lowest Schumann resonance evaluate the value Q assuming $\sigma_e = 0.1\ (\Omega m)^{-1}$, $\sigma_e = 10^{-5}\ (\Omega m)^{-1}$, $h = 100$ km.
f. Discuss the validity of the approximations used in part (a) for the parameter regime used in part (b).

Solution:

18.3.7.18 Ex: Airy formula

To derive the *Airy formulas*, consider a light field described by $\mathcal{E}_{in}$ incident on a Fabry-Pérot cavity of length L. The cavity mirrors are glass substrates having a surface with dielectric coating. The surfaces of the two mirrors are characterized by the transmission rates t_1, t_2 and reflection rates r_1, r_2. Note, that the reflected wave suffers a phase shift of π, when the reflection occurs at a denser medium $n > 1$. Disregard energy losses by absorption.

Solution: *The wave is reflected several times. For the field inside the cavity we find,*

$$\begin{aligned}\mathcal{E}_{cav}(z) &= \mathcal{E}_{in}t_1 \sum_n \left[(r_1r_2)^n e^{\imath k[2nL+z]} - r_2(r_1r_2)^n e^{\imath k[(2n+2)L-z]}\right] \\ &= \mathcal{E}_{in}t_1 \frac{e^{\imath kz} - r_2 e^{\imath k(2L-z)}}{1 - r_1r_2e^{\imath k2L}} \ ,\end{aligned} \tag{18.267}$$

using the Fourier expansion of $(1-s)^{-1} = \sum_n s^n$. *The reflected and transmitted fields are,*

$$\begin{aligned}\mathcal{E}_{rfl} &= r_1\mathcal{E}_{in} + \mathcal{E}_{in}\sum_{n=0}^{\infty} t_1(-r_2)(r_1r_2)^n t_1 e^{\imath k2(n+1)L} = \mathcal{E}_{in}\left(r_1 - \frac{e^{\imath k2L}t_1^2 r_2}{1 - r_1r_2e^{2\imath kL}}\right) \\ \mathcal{E}_{trns} &= \mathcal{E}_{in}\sum_{n=0}^{\infty} t_1(r_1r_2)^n t_2 e^{\imath k(2n+1)L} = \mathcal{E}_{in}\frac{t_1t_2e^{\imath kL}}{1 - r_1r_2e^{2\imath kL}} \ .\end{aligned} \tag{18.268}$$

Assuming $r_1 = r_2$, $t_1 = t_2$ *and* $T + R = 1$, *the formulas simplify to,*

$$\begin{aligned}\frac{\mathcal{E}_{cav}(z)}{\mathcal{E}_{in}} &= t_1\frac{e^{\imath kz} - r_2e^{\imath k(2L-z)}}{1 - r_1r_2e^{\imath k2L}} \\ \frac{\mathcal{E}_{rfl}}{\mathcal{E}_{in}} &= \sqrt{R}\frac{1 - e^{\imath k2L}}{1 - Re^{2\imath kL}} \\ \frac{\mathcal{E}_{trns}}{\mathcal{E}_{in}} &= \frac{(1-R)e^{\imath kL}}{1 - Re^{2\imath kL}} \ ,\end{aligned} \tag{18.269}$$

The intensities are,

$$\begin{aligned}I_{cav} &= I_{in}(1-R)\frac{(1-\sqrt{R})^2 + 4\sqrt{R}\sin^2 k(L-z)}{(1-R)^2 + 4R\sin^2 kL} \\ I_{refl} &= I_{in}R\frac{4\sin^2 kL}{(1-R)^2 + 4R\sin^2 kL} \\ I_{trns} &= I_{in}\frac{(1-R)^2}{(1-R)^2 + 4R\sin^2 kL} = 1 - I_{refl} \ .\end{aligned} \tag{18.270}$$

These are the Airy formulas. Using the free spectral range, we can write,

$$\omega = N2\pi\delta_{fsr} + \Delta \tag{18.271}$$
$$kL = kc/2\delta_{fsr} = \omega/2\delta_{fsr} = \pi N + \frac{\Delta}{2\delta_{fsr}} \ ,$$

and we obtain the form (18.263). Note that the free spectral range δ_{fsr} is given in terms of real frequencies.
Let us investigate the transmission spectrum close to resonance, that is $kL = N\pi$ or $|\Delta| \ll 2\pi\delta_{fsr}$. We can expand the sine,

$$I_{trns} = I_{in}\frac{(1-R)^2}{(1-R)^2 + 4R\sin^2\frac{\Delta}{2\delta_{fsr}}} = I_{in}\frac{(1-R)^2}{(1-R)^2 + 4R\left(\frac{\Delta}{2\delta_{fsr}}\right)^2 + ...} \tag{18.272}$$
$$\simeq I_{in}\frac{\delta_{fsr}^2\frac{(1-R)^2}{R}}{\delta_{fsr}^2\frac{(1-R)^2}{R} + \Delta^2} \equiv I_{in}\frac{\left(\frac{\kappa_{int}}{2}\right)^2}{\left(\frac{\kappa_{int}}{2}\right)^2 + \Delta^2} \ ,$$

utilizing

$$F = \frac{2\pi\delta_{fsr}}{\kappa_{int}} = \frac{\pi\sqrt{R}}{1-R} \simeq \frac{\pi}{1-R} \ . \tag{18.273}$$

We obtain a Lorentzian function.
Repeating the procedure for the intracavity field at the location of an antinode, $z = \lambda/4$,

$$\frac{I_{cav}}{I_{in}} = (1-R)\frac{(1-\sqrt{R})^2 + 4\sqrt{R}\sin^2\left(\frac{\Delta}{2\delta_{fsr}} - \frac{\pi}{2}\right)}{(1-R)^2 + 4R\sin^2\frac{\Delta}{2\delta_{fsr}}} = \frac{\frac{(1+\sqrt{R})^2}{1-R} - \frac{4\sqrt{R}}{1-R}\sin^2\frac{\Delta}{2\delta_{fsr}}}{1 + \left(\frac{2\sqrt{R}}{1-R}\right)^2\sin^2\frac{\Delta}{2\delta_{fsr}}} \ . \tag{18.274}$$

For large finesse, $1 + \sqrt{R} \simeq 2\sqrt{R}$, we find,

$$\frac{I_{cav}}{I_{in}} \simeq \frac{4F}{\pi}\frac{\cos^2\frac{\Delta}{2\delta_{fsr}}}{1 + \left(\frac{2F}{\pi}\right)^2\sin^2\frac{\Delta}{2\delta_{fsr}}} < \frac{4F}{\pi} \ . \tag{18.275}$$

Expanding the trigonometric functions,

$$\frac{I_{cav}}{I_{in}} \simeq \frac{4F}{\pi}\frac{1}{1 + (\Delta/\kappa)^2} < \frac{4F}{\pi} \ . \tag{18.276}$$

Alternatively, we can derive the Airy formulas from a self-consistency condition. The field at position x is,

$$\mathcal{E}_{cav}(x) = e^{\imath kx}t_1\mathcal{E}_{in} + e^{\imath k(L-x)}(-r_2)e^{\imath kL}t_1\mathcal{E}_{in} + r_1r_2e^{2\imath kL}\mathcal{E}_{cav}(x) \tag{18.277}$$
$$= \mathcal{E}_{in}t_1\frac{e^{\imath kx} - r_2e^{\imath k(2L-x)}}{1 - r_1r_2e^{2\imath kL}} \ ,$$

giving the same result as in (18.267).
Repeating the procedure for the intracavity field, but now averaging over the cavity

mode volume, $\frac{1}{2\pi}\int_0^{2\pi}\sin^2 x dx = \frac{1}{2}$*, the intracavity intensity from Eq. (18.270) yields,*

$$\frac{I_{cav}}{I_{in}} \to \frac{\frac{1+R}{1-R}}{1+\frac{4R}{(1-R)^2}\sin^2\frac{\Delta}{2\delta_{fsr}}} = \frac{\sqrt{1+\left(\frac{2F}{\pi}\right)^2}}{1+\left(\frac{2F}{\pi}\right)^2\sin^2\frac{\Delta}{2\delta_{fsr}}} \tag{18.278}$$
$$\simeq \frac{\sqrt{1+\left(\frac{2F}{\pi}\right)^2}}{1+(\Delta/\kappa)^2} \simeq \frac{2F}{\pi}\frac{1}{1+(\Delta/\kappa)^2} < \frac{2F}{\pi} .$$

The result can be generalized to cavities with more than two mirrors having the reflection coefficients $R_i = r_i^2$*, the transmission coefficients* $T_i = t_i^2$*, and the absorption coefficients* $S_i = 1 - R_i - T_i$*. In resonance we expect:*

$$I_{cav}(\delta = 0) = I_{in}\frac{4t_1\left(1 - S_{in} - \sum_i (S_i + T_i)\right)}{\left(t_1 + S_{in} + \sum_i (S_i + T_i)\right)^2} , \tag{18.279}$$

giving the factor of power amplification *of the cavity. The optimization of* I_{cav} *as a function of* R *is called impedance matching.*

18.4 Beam and wave optics

While the propagation of high wavelength radiation is dominated by diffraction effects, we observe that visible light tends to form bundles that apparently propagate (in homogeneous media) in a straight line. With the invention of the laser, the optical regime has become the preferred spectral regime for many spectroscopic applications. Therefore, we will dedicate the following section to the propagation of laser beams, which is understood within the theory of Gaussian optics.

18.4.1 Gaussian optics

At first glance, one might think that the propagation of laser light is well described by the laws of geometrical optics. Closer inspection, however, shows that a laser beam in many ways behaves more like a wave, although its energy is concentrated near an optical axis. The fields satisfy the wave equation. By inserting the propagating wave $u = \psi_z(x, y)e^{\imath(kz-\omega t)}$, we obtain an equation similar to the Schrödinger equation [734],

$$0 = \left[\frac{1}{c^2}\frac{\partial^2}{\partial t^2} - \nabla^2\right]\psi e^{\imath(kz-\omega t)} = e^{\imath(kz-\omega t)}\left(2\imath k\frac{\partial\psi}{\partial z} - \nabla^2\psi\right) . \tag{18.280}$$

Neglecting the second derivative for z, we obtain,

$$\left[2\imath k\frac{\partial}{\partial z} - \left(\frac{\partial^2}{\partial x^2} + \frac{\partial^2}{\partial y^2}\right)\right]\psi = 0 . \tag{18.281}$$

To describe a Gaussian beam, we choose an exponential ansatz and introduce two parameters that may vary along the propagation axis z: $\varphi(z)$ is a complex phase shift

and $q(z)$ a complex parameter, whose imaginary part describes the diameter of the beam. Inserting the ansatz

$$\psi = e^{-\imath\left[\varphi(z)+k(x^2+y^2)/2q(z)\right]} \tag{18.282}$$

into the Schrödinger equation, we obtain,

$$\begin{aligned} 0 = {} & 2\imath k e^{-\imath[\varphi+k(x^2+y^2)/2q]}\left(-\imath\frac{\partial\varphi}{\partial z}+\frac{\imath k(x^2+y^2)}{2q^2}\frac{\partial q}{\partial z}\right) - 2e^{-\imath[\varphi+k(x^2+y^2)/2q]}\frac{-\imath k}{q} \\ & - e^{-\imath[\varphi+k(x^2+y^2)/2q]}\left(\frac{-\imath kx}{q}\right)^2 - e^{-\imath[\varphi+k(x^2+y^2)/2q]}\left(\frac{-\imath ky}{q}\right)^2 . \end{aligned} \tag{18.283}$$

This leads directly to the equation,

$$0 = (q'-1)\frac{\imath k(x^2+y^2)}{q^2} - 2\imath\varphi' + \frac{2}{q} . \tag{18.284}$$

For Eq. (18.284) to be valid at all x and y, we need $q' = 1$ and $\varphi' = \frac{-\imath}{q}$. Integrating q', we find,

$$q(z) = q_0 + z . \tag{18.285}$$

It is practical to introduce real beam parameters

$$\boxed{\frac{1}{q} \equiv \frac{1}{R} - \imath\frac{\lambda}{\pi w^2}} . \tag{18.286}$$

Inserting this into the ansatz (18.282),

$$\psi = e^{-\imath\varphi - \imath\frac{k(x^2+y^2)}{2R^2} - \frac{(x^2+y^2)}{w^2}} , \tag{18.287}$$

it becomes clear that $R(z)$ is the radius of curvature and $w(z)$ is the diameter of the beam. Evaluating q_0 at the position of the focus (beam waist), where $R = \infty$, we get from (18.285) along with the definition (18.286),

$$\frac{1}{\frac{1}{R_z} - \imath\frac{\lambda}{\pi w_z^2}} = q(z) = q_0 + z = \frac{1}{\frac{1}{\infty} - \imath\frac{\lambda}{\pi w_0^2}} + z = \imath\frac{\pi w_0^2}{\lambda} + z , \tag{18.288}$$

The separation of this result into a real part and an imaginary part gives,

$$\frac{z}{R} + \frac{w_0^2}{w^2} = 1 \qquad \text{and} \qquad \frac{\pi w^2}{\lambda R} = \frac{\lambda z}{\pi w_0^2} . \tag{18.289}$$

Solving the second equation for $1/R$ and replacing this in the first equation gives an equation for w,

$$\boxed{w^2 = w_0^2\left[1 + \left(\frac{\lambda z}{\pi w_0^2}\right)^2\right]} . \tag{18.290}$$

This expression can now be replaced in the second equation,

$$\boxed{R = z\left[1 + \left(\frac{\pi w_0^2}{\lambda z}\right)^2\right]} . \tag{18.291}$$

We call $z_R \equiv q_0$ the *Rayleigh length*. Now we integrate φ',

$$\varphi = \int_0^z \frac{-\imath}{q} dz = \int_0^z \frac{-\imath dz}{\imath z_R + z} = -\imath \int_0^z \frac{z dz}{z_R^2 + z^2} - \int_0^z \frac{z_R dz}{z_R^2 + z^2} \tag{18.292}$$
$$= -\frac{\imath}{2} \ln \frac{z_R^2 + z^2}{z_R^2} - \arctan \frac{z}{z_R} = -\imath \ln \frac{w}{w_0} - \arctan \frac{\lambda z}{\pi w_0^2} \, .$$

Hence,

$$\boxed{\psi(\mathbf{r}) = \frac{w_0}{w} e^{\imath \arctan(-z/q_0) - \imath k(x^2+y^2)/2q}} \, . \tag{18.293}$$

We note that the function $|\psi|^2$ is normalized by the radial integral,

$$\int |\psi|^2 dx dy = \frac{w_0^2}{w^2} \int |e^{-k(x^2+y^2)/2q(z)}|^2 dx dy \tag{18.294}$$
$$= \frac{w^2}{w_0^2} \left(\int_{-\infty}^{\infty} e^{-2x^2/w^2} dx \right)^2 = \frac{\pi w_0^2}{2} \, ,$$

which is independent of z and thus ensures conservation of energy along the beam. The intensity profile of a Gaussian beam is proportional to $|\psi|^2$ and normalized to the total power P, that is,

$$\boxed{I(\mathbf{r}) = \frac{2P}{\pi w_0^2} |\psi(\mathbf{r})|^2 = \frac{2P}{\pi w(z)^2} e^{-2(x^2+y^2)/w(z)^2}} \, . \tag{18.295}$$

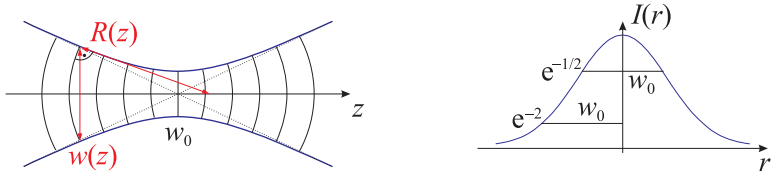

Figure 18.30: (Left) Propagation of the beam along the optical axis. (Right) Cross section of the Gaussian beam.

The above treatment shows that modes do not only exist in cavities but also in free space. In Excs. 18.4.4.1 and 18.4.4.2 we are dealing with modes of Gaussian light beams that are often used in laser beam optics.

Example 111 (*Gaussian optics*): The expansion of the Gaussian beam $\mathcal{E}(\mathbf{r}) = \mathcal{E}_0 e^{-(x^2+y^2)/w(z)^2 - z^2/z_R^2}$ into plane waves simply is,

$$\mathcal{E}(\mathbf{k}) = \int \mathcal{E}(\mathbf{r}) e^{\imath \mathbf{k}\cdot\mathbf{r}} d^3 r = \mathcal{E}_0 e^{-(k_x^2+k_y^2)w(z)^2 - k_z^2 z_R^2} \, .$$

18.4.1.1 Optical components

In *geometrical optics* (or ray optics) we work a lot with *transfer matrices* $\mathcal{M}$ defined by their feature of transforming the two-component vector, which consists of the distance of a ray from the optical axis $y(z)$ and its divergence $y'(z)$ [31]:

$$\begin{pmatrix} y(z) \\ y'(z) \end{pmatrix} = \mathcal{M} \begin{pmatrix} y(0) \\ y'(0) \end{pmatrix} . \tag{18.296}$$

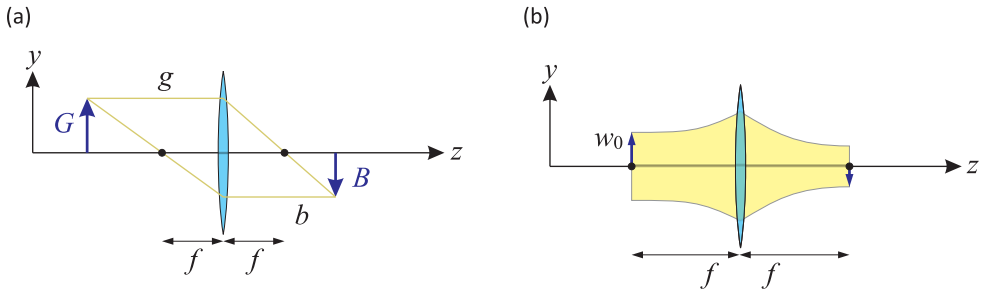

Figure 18.31: (a) Image formation through a lens with ray optics. (b) Focusing a laser beam with Gaussian optics.

Now, it is possible to show that the same matrix $\mathcal{M}$ can describe the transformation of a Gaussian beam through optical components along the optical axis, provided that we apply the transformation to the beam parameter q in the following way:

$$\boxed{q(z) = \frac{M_{11}q(0) + M_{12}}{M_{21}q(0) + M_{22}}} . \tag{18.297}$$

Hence, the transfer matrices allow us to calculate, how the parameters R and w transform along the optical axis through optical elements or in free propagation. The most common optical elements are lenses, crystals, prisms, mirrors, and cavities. For example, the matrix for free propagation of a beam over a distance d is,

$$\mathcal{M}_{dist} = \begin{pmatrix} 1 & d \\ 0 & 1 \end{pmatrix} , \tag{18.298}$$

and the matrix describing the passage through a thin lens with focal length f,

$$\mathcal{M}_{lens} = \begin{pmatrix} 1 & 0 \\ -1/f & 1 \end{pmatrix} . \tag{18.299}$$

In Exc. 18.4.4.3 we use these matrices to derive the lens equations in ray optics and Gaussian optics.

[31] Note that these matrices have nothing to do with the matrices describing the transmission and reflection of electric and magnetic fields by interfaces.

18.4.1.2 Modes of a linear cavity

We will now apply the formalism of the transfer matrices to calculate the modal structure of a linear cavity. Let $\mathcal{M}$ be the matrix describing the round-trip of a beam of light in the cavity. For the cavity to be stable, the fields must be stationary. This is only possible if the mode geometry is self-consistent. That is, at any position z, the beam parameter $q(z) = q_z$ must satisfy [734],

$$q_z = \frac{M_{11}q_z + M_{12}}{M_{21}q_z + M_{22}} \ . \tag{18.300}$$

Using, $M_{11}M_{22} - M_{12}M_{21} = 1$, the condition (18.300) can be solved by,

$$\frac{1}{q_z} = \frac{M_{22} - M_{11}}{2M_{12}} \pm \frac{\imath}{2M_{12}}\sqrt{4 - (M_{11} + M_{22})^2} \ , \tag{18.301}$$

or separating the real part from the imaginary part according to the definition (18.286) of the beam parameter,

$$w_z^2 = \frac{2\lambda M_{12}}{\pi\sqrt{4 - (M_{11} + M_{22})^2}} \qquad \text{and} \qquad R_z = \frac{2M_{12}}{M_{22} - M_{11}} \ . \tag{18.302}$$

Figure 18.32: (code) (Left) Scheme of a linear cavity. (Right) Radial profiles of the lowest order transverse Hermite-Gaussian modes TEM_{mn} of a linear cavity.

We now consider the cavity of length L schematized in Fig. 18.32. It consists of two mirrors with radii of curvature ρ_a and ρ_b. The transfer matrix for a round-trip beginning and ending at the position of mirror 'a' is,

$$\begin{aligned}\mathcal{M} &= \begin{pmatrix} 1 & 0 \\ -1/f_a & 1 \end{pmatrix}\begin{pmatrix} 1 & L \\ 0 & 1 \end{pmatrix}\begin{pmatrix} 1 & 0 \\ -1/f_b & 1 \end{pmatrix}\begin{pmatrix} 1 & L \\ 0 & 1 \end{pmatrix} \\ &= \frac{1}{f_a f_b}\begin{pmatrix} f_a(f_b - L) & f_a L(2f_b - L) \\ L - f_b - f_a & L(L - 2f_b) + f_a(f_b - L) \end{pmatrix} \ ,\end{aligned} \tag{18.303}$$

where $f_k = -\rho_k/2$ are the focal lengths of the mirrors. With (18.302) we obtain the diameter w_a and the radius of curvature R_a of the beam at the position of the mirror 'a',

$$w_a^2 = \frac{2\lambda f_a L(2f_b - L)}{\pi\sqrt{4f_a^2 f_b^2 - (L^2 - 2f_a L - 2f_b L + 2f_a f_b)^2}} \qquad \text{and} \qquad R_a = -2f_a \ . \tag{18.304}$$

Applying the second equation (18.289), we find,

$$\frac{\lambda a}{\pi w_0^2} = \frac{\pi w_a^2}{\lambda R_a} = \frac{L(2f_b - L)}{\sqrt{4f_a^2 f_b^2 - (L^2 - 2f_a L - 2f_b L + 2f_a f_b)^2}} \,, \tag{18.305}$$

and analogously for $\lambda b/\pi w_0^2$. We replace $f_k = \rho_k/2$ and introduce the abbreviation,

$$x_a \equiv \frac{\pi w_a^2}{\lambda R_a} = \frac{\frac{2L}{\rho_a}\left(1 - \frac{L}{\rho_b}\right)}{\sqrt{1 - \left(1 - \frac{2L}{\rho_a} - \frac{2L}{\rho_b} + \frac{2L^2}{\rho_a \rho_b}\right)^2}} \,, \tag{18.306}$$

and analogously for x_b. With the help of MAPLE we calculate,

$$\frac{x_a x_b - 1}{\sqrt{(1 + x_a^2)(1 + x_b^2)}} = \sqrt{1 - \frac{L}{\rho_a}}\sqrt{1 - \frac{L}{\rho_b}} \,. \tag{18.307}$$

The phase shift between the waist of the beam and mirror 'a' is given by the real part of the formula (18.292). The phase shift accumulated between the mirrors 'a' and 'b' is,

$$\begin{aligned} \varphi &= \varphi_a + \varphi_b = \arctan x_a + \arctan x_b \\ &= \pi - \arccos \frac{x_a x_b - 1}{\sqrt{1 + x_a^2}\sqrt{1 + x_b^2}} = \pi - \arccos \sqrt{1 - \frac{L}{\rho_a}}\sqrt{1 - \frac{L}{\rho_b}} \,, \end{aligned} \tag{18.308}$$

where we used tabulated trigonometric relationships to convert the arctan into a arccos.

The spectrum of transverse modes follows from the condition, that the total phase is a multiple of π, i.e.,

$$N = \frac{kL + \varphi}{\pi} = \frac{2L\nu}{c} + \frac{\varphi}{\pi} \,, \tag{18.309}$$

that is,

$$\boxed{\frac{\nu}{\delta_{fsr}} = N - 1 + \frac{1}{\pi} \arccos \sqrt{\left(1 - \frac{L}{\rho_a}\right)\left(1 - \frac{L}{\rho_b}\right)}} \,, \tag{18.310}$$

where we used the *free spectral range* $\delta_{fsr} \equiv c/2L$. This formula represents a generalization of the previously derived formula (18.262), which only holds in the limit of plane waves, $\rho_k \to \infty$.

The diameter of the beam waist in the cavity is,

$$w_0 = \sqrt[4]{\left(\frac{\lambda}{\pi}\right)^2 \frac{L(\rho_a - L)(\rho_b - L)(\rho_a + \rho_b - L)}{(\rho_a + \rho_b - 2L)^2}} \,. \tag{18.311}$$

For optimum coupling, the geometries of the Gaussian light beam and of the cavity must be matched, i.e. the diameter and divergence of the laser beam must be adjusted to the cavity mode, e.g. using a suitable arrangement of lenses. In Exc. 18.4.4.4, we will extend the calculation to ring cavities.

18.4.1.3 Hermite-Gaussian transverse modes

We can generalize the ansatz (18.282) to allow for more complicated radial intensity distributions described by the functions g and h,

$$\psi = g\left(\frac{x}{w}\right) h\left(\frac{y}{w}\right) e^{-\imath\left[\varphi(z)+k(x^2+y^2)/2q(z)\right]} \,. \tag{18.312}$$

Inserting the ansatz into the equation (18.281), we will show in Exc. 18.4.4.5, that the solution is given by,

$$\psi(x,y,z) = \frac{w_0}{w} H_m\left(\frac{\sqrt{2}x}{w}\right) H_n\left(\frac{\sqrt{2}y}{w}\right) e^{\imath(m+n+1)\arctan\frac{2z}{kw_0^2} - r^2\left(\frac{1}{w^2}+\frac{\imath k}{2R}\right)} \,. \tag{18.313}$$

Fig. 18.32(right) shows radial profiles of the lowest order transverse Hermite-Gaussian modes TEM_{mn} of a linear cavity.

In the presence of higher-order transverse modes TEM_{mn} the cavity spectrum becomes,

$$\boxed{\frac{\nu}{\delta_{fsr}} = N - 1 + \frac{m+n+1}{\pi} \arccos\sqrt{\left(1-\frac{L}{\rho_a}\right)\left(1-\frac{L}{\rho_b}\right)}} \,. \tag{18.314}$$

This formula can be derived using the self-consistency requirement for the light beam circulating inside the cavity. It represents yet another generalization of the formula (18.262) and lifts the degeneracy of the longitudinal modes described by the Airy formula and exhibited in Fig. 18.28. On the other hand, a *confocal cavity* with degenerate transverse modes, $\rho_a = \rho_b = L$, is particularly suited to work as a spectrum analyzer, as we will show in Exc. 53.1.10.8.

18.4.1.4 Splitting of TEM_{mn} modes having the same $m+n$

In a cylindrically symmetric mode, all modes TEM_{mn} with the same $m+n$ are degenerate. If however cylindrical symmetry is broken, e.g. due to alignment imperfection or in the case of a ring cavity, the degeneracy is lifted [1203]. If the problem of tilted incidence of the beams onto a mirror surface can be boiled down to assuming elliptically shaped mirrors, i.e. mirrors having different radii of curvatures in two orthogonal axis, the different phase shifts for the two axis can be calculated, as discussed in Exc. 18.4.4.4 and in Ref. [430]:

$$\nu/\delta_{fsr} = (q+1) + 2\frac{2m+1}{2\pi}\phi_h + 2\frac{2n+1}{2\pi}\phi_v \,. \tag{18.315}$$

where $\phi_k = \arccos\sqrt{\left(1-\frac{2a}{\rho_k}\right)\left(1-\frac{b}{\rho_k}\right)}$ for $k = h, v$. The splitting between the TEM_{01} and TEM_{10} modes is,

$$\tfrac{2}{\pi}\arccos\sqrt{\left(1-\tfrac{2a}{\rho_h}\right)\left(1-\tfrac{b}{\rho_h}\right)} - \tfrac{2}{\pi}\arccos\sqrt{\left(1-\tfrac{2a}{\rho_v}\right)\left(1-\tfrac{b}{\rho_v}\right)} \,. \tag{18.316}$$

The splitting observed for ring cavities is on the same order as the free spectra range.

Furthermore, different phase shifts in the dielectric surfaces lead to different resonance conditions [800]. Since, according to Fresnel's formulas, s and p-polarized light fields have different reflectivities under inclined incidence on mirrors, they also suffer different phase shifts and, hence, exhibit different eigenfrequencies of the cavity. In high-finesse ring cavities this leads to a dramatic splitting of s and p-polarized modes, which can be on the order of the free spectral range itself.

18.4.2 Non-Gaussian beams

The Hermite-Gaussian ansatz (18.312) to solve the wave equation represents only one possibility. But we nowadays know a large variety of beams with different transverse distributions of intensity, polarization and angular momentum. Examples are transverse Gaussian modes with Cartesian or circular symmetry, Bessel modes, Laguerre-Gaussian modes with angular momentum, and modes with radial or azimuthal polarization.

18.4.2.1 Bessel beams

Ideally, a *Bessel beam* (BB) is a non-diffracting monochromatic solution to the scalar wave equation in cylindrical coordinates carrying an infinite amount of energy [401, 863]. Inserting into the wave equation,

$$\left(\frac{1}{c^2}\frac{\partial^2}{\partial t^2} - \nabla^2\right)\psi(\mathbf{r},t) = 0 \tag{18.317}$$

the ansatz,

$$\psi(\mathbf{r},t) = e^{\imath(\beta z-\omega t)}\int_0^{2\pi} A(\phi)e^{\imath\alpha(x\cos\phi+y\sin\phi)}d\phi \ , \tag{18.318}$$

we get the dispersion relation,

$$\alpha^2+\beta^2 = \frac{\omega^2}{c^2} \ . \tag{18.319}$$

For β real the intensity profile does not vary along the z-axis,

$$|\psi(\mathbf{r},t)|^2 = \left|\int_0^{2\pi} A(\phi)e^{\imath\alpha(x\cos\phi+y\sin\phi)}d\phi\right|^2 = |\psi(x,y,z=0,t)|^2 \ . \tag{18.320}$$

For axial symmetry $A(\phi)=A$, we get what is called the 2^{st} type 0-order Bessel beam,

$$\psi(\mathbf{r},t) = Ae^{\imath(\beta z-\omega t)}\int_0^{2\pi} e^{\imath\alpha(x\cos\phi+y\sin\phi)}d\phi = Ae^{\imath(\beta z-\omega t)}J_0(\alpha\rho) \ . \tag{18.321}$$

For $0<\alpha\leq\omega/c$ we get a non-trivial solution decaying like $(\alpha\rho)^{-1}$.

In its simplest form, the electric field of an arbitrary ν-th order BB with wavelength λ can be written as,

$$\mathcal{E}(\rho,\phi,z) = A_0\exp(\imath k_z z)J_\nu(k_\rho\rho)\exp(\imath\nu\phi) \ , \tag{18.322}$$

where A_0 is the electric field strength and J_ν is the ν-th order Bessel function of the first kind. In Eq. (18.322), k_z and k_ρ are the longitudinal and transverse wave numbers satisfying the dispersion relation $k^2 = k_z^2 + k_\rho^2 = (2\pi/\lambda)^2$, such that $k_z = k\cos\theta$ and $k_\rho = k\sin\theta$, being θ the axicon angle associated to the tilted plane of waves propagating along the surface of a cone of half-angle θ in the angular spectrum decomposition. Cylindrical coordinates (ρ, ϕ, z) have been adopted, and a time harmonic factor $e^{\imath\omega t}$ has been omitted for brevity. For our purposes, the Rayleigh range is an essential parameter to be considered since the non-diffracting beam must propagate through a 20 cm long differential vacuum tube to minimize losses of atoms during their guidance to the science chamber. The maximum propagation distance up to which a BB can overcome diffraction is given by $Z_{max} = 2\pi R\bar{r}/\lambda$, where R is the aperture radius and $\bar{r}$ is the beam radius [401]. It should be noticed that, in general, Z_{max} is much greater than the Rayleigh range of a Gaussian beam with an equivalent beam waist radius $w_g = \bar{r}$.

Example 112 (*Frozen Bessel beams*): Certain superposition of these non-diffracting Bessel beams have interesting properties,

$$\psi(\mathbf{r}, t) = e^{-\imath\omega t} \sum_{n=-N}^{N} A_n J_0(k_{\rho n}\rho) e^{\imath\beta_n z} \ . \tag{18.323}$$

A *frozen Bessel beam* can be constructed by a continuous superposition of 0^{th}-order scalar BBs over the longitudinal wavenumber k_z, as given by the following integral solution of the scalar Helmholtz equation with azimuthal symmetry,

$$\Psi_0(\rho, z, t) = e^{-\imath\omega t} \int_{-k}^{k} S(k_z) J_0(\rho\sqrt{k^2 - k_z^2}) e^{-\imath k_z z} dk_z \ , \tag{18.324}$$

where $k \equiv \omega/c$ and $k_\rho^2 \equiv \omega^2/c^2 - k_z$ is the transverse wave number. The quantity k_ρ^2 must be positive since evanescent waves do come into play.
Higher-order Bessel beams can be constructed via [1422, 1421],

$$\Psi_1(\rho, \phi, z) = \mathcal{U}\Psi_0(\rho, z) \qquad \text{with} \qquad \mathcal{U} \equiv e^{\imath\phi}\left(\frac{\partial}{\partial\rho} + \frac{\imath}{\rho}\frac{\partial}{\partial\phi}\right) \ , \tag{18.325}$$

Apparently, they can carry angular orbital momentum.

18.4.3 Fourier optics

We have derived in Sec. 5.3.5 the Fresnel integral for the description of the propagation of phase fronts. In the following sections we will show that the expression can also be derived from the more general Huygens principle, and how they can be used for numerical calculations of phase front propagation. We will also show how it can be used for numerical calculations of phase front propagation.

18.4.3.1 Rayleigh-Sommerfeld solution

We consider the propagation of monochromatic light from a 2D planar source of area Σ indicated by the coordinates ξ and η, as illustrated in Fig. 18.33. The field distribution in the source plane is given by $\psi_0(\xi, \eta)$, and the field $\psi_z(x, y)$ in a distant

observation plane can be predicted using the first Rayleigh-Sommerfeld diffraction solution [521, 1338],

$$\boxed{\psi_z(x,y) = \frac{1}{\imath\lambda}\iint_\Sigma \frac{z}{r_{12}}\frac{e^{\imath k r_{12}}}{r_{12}}\psi_0(\xi,\eta)d\xi d\eta} \ . \tag{18.326}$$

The formula will be derived from the wave equation in Exc. 18.4.4.6. Here, z is the distance between the centers of the source and observation coordinate systems and

$$r_{12} = \sqrt{z^2 + (x-\xi)^2 + (y-\eta)^2} \tag{18.327}$$

is the distance between a position on the source plane and a position in the observation plane, with the planes assumed to be parallel.

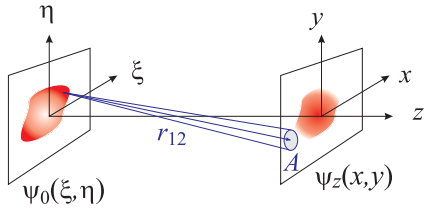

Figure 18.33: Propagation geometry for parallel source and observation planes. Every point of the source plane generates a spherical wave $\propto e^{\imath k r_{12}}/r_{12}$. The projection of the field within a solid angle element onto the xy-plane, which is proportional to z/r_{12} generates a new spherical wave propagating further along the z optical axis.

Expression (18.326) is a statement of the *Huygens-Fresnel principle*, which supposes that the source acts as an infinite collection of fictitious point sources located at (ξ,η), each one producing a spherical wave. The interference of the spherical waves at any observation position (x,y), expressed by the projection onto the propagation axis z in (18.326), can be written as a two-dimensional convolution integral,

$$\psi_z(x,y) = \iint_\Sigma h_z(x-\xi, y-\eta)\psi_0(\xi,\eta)d\xi d\eta = (h_z * \psi_0)(x,y) \ , \tag{18.328}$$

where the general form of the *Rayleigh-Sommerfeld impulse response*,

$$h_z(x,y) = \frac{z}{\imath\lambda}\frac{e^{\imath k r}}{r^2} \ , \tag{18.329}$$

where $r = \sqrt{z^2+x^2+y^2}$ is simply the field distribution $\psi_z(x,y)$ observed in case of a point-like source $\psi_0(\xi,\eta) = \delta(\xi)\delta(\eta)$.

The Fourier convolution theorem allows to write Eq. (18.328) as,

$$\psi_z(x,y) = \mathcal{F}^{-1}\{\mathcal{F}[h_z * \psi_0](x,y)\} = \mathcal{F}^{-1}\{\mathcal{F}[h_z(x,y)]\mathcal{F}[\psi_0(x,y)]\} \ , \tag{18.330}$$

where $\mathcal{F}$ denotes the two-dimensional Fourier transform. Introducing the *Rayleigh-Sommerfeld transfer function* H_z, we may also write,

$$\boxed{\begin{array}{rcl} \psi_z(x,y) & = & \mathcal{F}^{-1}\{H_z(f_x,f_y)\cdot\mathcal{F}[\psi_0(x,y)]\} \\ \text{where} \quad H_z(f_x,f_y) & = & e^{\imath k z\sqrt{1-(\lambda f_x)^2-(\lambda f_y)^2}} \end{array}} \ . \tag{18.331}$$

Strictly speaking, $\sqrt{f_x^2 + f_y^2} < \lambda^{-1}$ must be satisfied for propagating field components. The Rayleigh-Sommerfeld expression is the most accurate diffraction solution as, other than the assumption of scalar diffraction, this solution only requires that $r \gg \lambda$, the distance between the source and the observation position, be much greater than a wavelength.

18.4.3.2 Fresnel approximation

Let us simplify the transfer function by expanding the distance (18.327),

$$r_{12} \simeq z + \tfrac{1}{2}\tfrac{(x-\xi)^2}{z} + \tfrac{1}{2}\tfrac{(y-\eta)^2}{z} \ , \tag{18.332}$$

which amounts to assuming a parabolic radiation wave rather than a spherical wave for the fictitious point sources. Furthermore, we use the approximation $r_{12} \simeq z$ in the denominator of Eq. (18.326) to arrive at the Fresnel diffraction expression:

$$\boxed{\psi_z(x,y) = \frac{e^{\imath kz}}{\imath\lambda z} \iint\limits_{\Sigma} e^{\imath k[(x-\xi)^2+(y-\eta)^2]/2z} \psi_0(\xi,\eta) d\xi d\eta} \ . \tag{18.333}$$

This expression is also a convolution of the form in Eq. (18.328), where the impulse response is,

$$h_z(x,y) = \frac{e^{\imath kz}}{\imath\lambda z} e^{\imath k\rho^2/2z} \ , \tag{18.334}$$

and the transfer function is,

$$H_z(f_x, f_y) = e^{\imath kz} e^{-\imath\pi z\lambda(f_x^2+f_y^2)} \ . \tag{18.335}$$

The expressions in Eqs. (18.331) are again applicable in this case for computing diffraction results.

Another useful form of the Fresnel diffraction expression is obtained by moving the quadratic phase term in x and y outside the integrals:

$$\psi_z(x,y) = \frac{e^{\imath kz}}{\imath\lambda z} e^{\imath k(x^2+y^2)/2z} \iint\limits_{\Sigma} e^{\imath k(\xi^2+\eta^2)/2z} e^{-\imath k(x\xi+y\eta)/z} \psi_0(\xi,\eta) d\xi d\eta \ . \tag{18.336}$$

18.4.3.3 Fraunhofer approximation

Fraunhofer diffraction, which refers to diffraction patterns in a regime that is commonly known as the 'far field', is arrived at by approximating the chirp term multiplying the initial field within the integrals of Eq. (18.336) as unity. The assumption involved is,

$$z \gg \max[\tfrac{k}{2}(\xi^2 + \eta^2)] \tag{18.337}$$

and results in the Fraunhofer diffraction expression:

$$\boxed{\begin{aligned} \psi_z(x,y) &= \frac{e^{\imath kz}}{\imath\lambda z} e^{\imath k\rho^2/2z} \iint\limits_{\Sigma} e^{-\imath k(x\xi+y\eta)/z} \psi_0(\xi,\eta) d\xi d\eta \\ &= \frac{e^{\imath kz}}{\imath\lambda z} e^{\imath\frac{k}{2z}\rho^2} (\mathcal{F}\psi_0)(\tfrac{kx}{z}, \tfrac{ky}{z}) \end{aligned}} \ . \tag{18.338}$$

Along with multiplicative factors out front, the Fraunhofer expression can be recognized simply as a Fourier transform of the source field. The condition of Eq. (18.337), typically, requires very long propagation distances relative to the source support size. However, a form of the Fraunhofer pattern also appears in the propagation analysis involving lenses. The Fraunhofer diffraction expression is a powerful tool and finds use in many applications such as laser beam propagation, image analysis, and spectroscopy.

The Fraunhofer expression cannot be written as a convolution integral, so there is no impulse response or transfer function. But, since it is a scaled version of the Fourier transform of the initial field, it can be relatively easy to calculate, and as with the Fresnel expression, the Fraunhofer approximation is often used with success in situations where Eq. (18.337) is not satisfied. For simple source structures such as a plane-wave illuminated aperture, the Fraunhofer result can be useful even when Eq. (18.337) is violated by more than a factor of 10, particularly if the main quantity of interest is the irradiance pattern at the receiving plane. Using the *Fresnel number* defined as,

$$N_F = \frac{\max(\xi^2 + \eta^2)}{z\lambda} \ , \tag{18.339}$$

the commonly accepted requirement for the Fraunhofer region is $N_F \ll 1$.

18.4.3.4 Propagation of phase fronts across optical elements

To propagate an optical phase front located at z_0, we conveniently start from a Gaussian laser beam,

$$\psi_{Gauss}(\rho) = e^{-\rho^2/w_0^2} \ . \tag{18.340}$$

with $\rho = \sqrt{x^2 + y^2}$ the distance from the optical axis. For a given total power the electric field is obtained via normalization,

$$\mathcal{E}_0 = \sqrt{\frac{P}{\frac{1}{2}\varepsilon_0 c \int |u|^2 d^2\rho}} \ , \tag{18.341}$$

where $\eta \equiv \sqrt{\mu_0/\varepsilon_0} = 1/(\varepsilon_0 c)$ is the vacuum impedance.

Optical elements can shape the phase front of a light beam by phase shift or absorption. If the element can be assumed to be thin we may neglect the axial displacement, $\Delta z \simeq 0$, and simply multiply the phase front with an xy-matrix,

$$\boxed{\psi'_z(x,y) = e^{-\alpha_{component}(x,y)}\psi_z(x,y)} \ , \tag{18.342}$$

where $\alpha(x,y) = \sigma(x,y) + \imath\delta(x,y)$. For instance, a *pinhole* with radius R will transform a phase front like,

$$\alpha_{pinhole}(\rho) = \infty\Theta(\rho - R) \ , \tag{18.343}$$

where Θ is the Heavyside function. A *thin lens* with focal distance f will transform a phase front like,

$$\alpha_{lens}(\rho) = \imath\tfrac{k}{R}\rho^2 = \imath\tfrac{k}{2f}\rho^2 \ , \tag{18.344}$$

where R is the radius of the spherical lens. For an *axicon* of base angle α made of material with refractive index n_{refr},

$$\alpha_{axicon}(\rho) = \imath k(n_{refr} - 1)\rho \tan\alpha \ . \tag{18.345}$$

In Exc. 18.4.4.9 we will derive the phase front transformation matrices for other interesting optical components. We will do a numerical simulation in 18.4.4.10.

18.4.4 Exercises

18.4.4.1 Ex: Gaussian light mode

The light of a laser propagates in light modes called Gaussian. A beam propagating along $\hat{\mathbf{e}}_z$ and linearly polarized along $\hat{\mathbf{e}}_x$ is described by the potential vector, $\mathbf{A}(\mathbf{r},t) = \hat{\mathbf{e}}_x u(\mathbf{r}) e^{\imath(\omega t - kz)}$, where $u(\mathbf{r}) = \frac{u_0}{w(z)} e^{-(x^2+y^2)/w(z)^2}$ is the energy density and $w(z) = w_0\sqrt{1 + (\lambda z/\pi w_0^2)^2}$ the diameter of the beam at the position z. Calculate the Poynting vector in the Lorentz gauge, $\Phi = -\frac{c^2}{\imath\omega}\nabla\cdot\mathbf{A}$.

Solution: *First, we define as an abbreviation the Rayleigh length, $z_R \equiv \pi w_0^2/\lambda$. With this, we calculate the derivative of the waist $w = w(z)$,*

$$\frac{\partial w}{\partial z} = w_0 \frac{\partial}{\partial z}\sqrt{1 + (z/z_R)^2} = \frac{w_0}{\sqrt{1 + (z/z_R)^2}} \frac{z}{z_R^2} = \frac{w_0^2 z}{w z_R^2} = \frac{2z}{k w z_R} \equiv \mathcal{D} \ .$$

The gradient of the mode $u = u(x,y,z)$ now is,

$$\nabla u = \begin{pmatrix} \partial_x \\ \partial_y \\ \partial_z \end{pmatrix} \frac{u_0}{w} e^{-(x^2+y^2)/w^2} = \begin{pmatrix} \frac{-2x}{w^2}\frac{u_0}{w} e^{-\rho^2/w^2} \\ \frac{-2y}{w^2}\frac{u_0}{w} e^{-\rho^2/w^2} \\ u_0 e^{-\rho^2/w^2}\frac{-1}{w^2}\mathcal{D} + \frac{u_0}{w} e^{-\rho^2/w^2}\rho^2\frac{2}{w^3}\mathcal{D} \end{pmatrix} = -\begin{pmatrix} 2\tilde{x}\tilde{u} \\ 2\tilde{y}\tilde{u} \\ \mathcal{D}(1 - 2\tilde{\rho}^2)\tilde{u} \end{pmatrix} ,$$

where we defined normalized coordinates $\tilde{\rho} \equiv \rho/w$, $\tilde{u} \equiv u/w$ and $\tilde{z} \equiv z/z_R$. Within the Lorentz gauge we can calculate the scalar potential,

$$\Phi = -\frac{c^2}{\imath\omega}\nabla\cdot\mathbf{A} = -\frac{c^2}{\imath\omega}\nabla\cdot[\hat{\mathbf{e}}_x u e^{\imath(\omega t - kz)}] = -\frac{c^2}{\imath\omega} e^{\imath(\omega t - kz)}\frac{\partial u}{\partial x} = \frac{c^2}{\imath\omega} 2\tilde{x}\tilde{u} e^{\imath(\omega t - kz)} \ .$$

The magnetic field is,

$$\vec{\mathcal{B}} = \nabla\times\mathbf{A} = \begin{pmatrix} 0 \\ \frac{\partial}{\partial z}[u e^{\imath(\omega t - kz)}] \\ -\frac{\partial}{\partial y}[u e^{\imath(\omega t - kz)}] \end{pmatrix} = \begin{pmatrix} 0 \\ -\imath k w - \mathcal{D}(1 - 2\tilde{\rho}^2) \\ 2\tilde{y} \end{pmatrix} \tilde{u} e^{\imath(\omega t - kz)} \ .$$

The electric field is,

$$\begin{aligned}\vec{\mathcal{E}} &= -\nabla\Phi = -\frac{c^2}{\imath\omega}\begin{pmatrix}\partial_x\\ \partial_y\\ \partial_z\end{pmatrix}\frac{2xu}{w^2}e^{\imath(\omega t-kz)}\\ &= -\frac{c^2}{\imath\omega}\begin{pmatrix}\frac{e^{\imath(\omega t-kz)}}{w^2}\left(2u+2x\frac{\partial u}{\partial x}\right)\\ \frac{e^{\imath(\omega t-kz)}}{w^2}2x\frac{\partial u}{\partial y}\\ 2x\left(\frac{1}{w^2}u\frac{\partial}{\partial z}e^{\imath(\omega t-kz)}+\frac{e^{\imath(\omega t-kz)}}{w^2}\frac{\partial u}{\partial z}+ue^{\imath(\omega t-kz)}\frac{\partial}{\partial z}\frac{1}{w^2}\right)\end{pmatrix}\\ &= -\frac{c^2}{\imath\omega}\frac{2\tilde{u}e^{\imath(\omega t-kz)}}{w}\begin{pmatrix}1-2\tilde{x}^2\\ -2\tilde{x}\tilde{y}\\ -\imath kx-\tilde{x}(3-2\tilde{\rho}^2)\mathcal{D}\end{pmatrix}.\end{aligned}$$

Finally, we can derive the vector of Poynting,

$$\vec{\mathcal{S}} = \tfrac{1}{\mu_0}\vec{\mathcal{E}}\times\vec{\mathcal{B}}^* = -\frac{1}{\mu_0}\frac{c^2}{\imath\omega}2\tilde{u}^2\begin{pmatrix}-4xy^2-[-\imath kx-x(3-2\rho^2)\mathcal{D}][-\imath kw-\mathcal{D}(1-2\rho^2)]\\ -2(1-2x^2)y\\ (1-2x^2)[-\imath kw-\mathcal{D}(1-2\rho^2)]\end{pmatrix}.$$

On the optical axis,

$$\vec{\mathcal{S}} = -\hat{\mathbf{e}}_z\frac{1}{\mu_0}\frac{c^2}{\imath\omega}2\tilde{u}^2\imath kw \xrightarrow{z=0} -\hat{\mathbf{e}}_z\frac{c}{\mu_0}2\tilde{u}^2w\ .$$

In the focal plane,

$$\vec{\mathcal{S}} = -\frac{1}{\mu_0}\frac{c^2}{\imath\omega}2\tilde{u}^2\begin{pmatrix}-4xy^2+k^2xw\\ -2(1-2x^2)y\\ (1-2x^2)(-\imath kw)\end{pmatrix}.$$

We integrate radially,

$$P = \int_{\mathbb{R}^2}\vec{\mathcal{S}}\cdot d\mathbf{A} = xxx\ .$$

18.4.4.2 Ex: Volume and power of a Gaussian beam mode

a. Derive the expression for the mode volume V_m of a Gaussian beam of length L from the definition $I(0)V_m = \int I(\mathbf{r})dV$.
b. In quantum mechanics we learn, that the zero point energy of the harmonic oscillator is $\hbar\omega/2$. Use this notion to calculate the maximum electric field amplitude $\mathcal{E}_1(0)$ created by a single photon in terms of the mode volume.
c. A linear cavity of length L has the free spectral range $\delta_{fsr} = c/2L$. Express the

power of the beam in terms of the number of photons contained in the cavity.

Solution: *a. The intensity distribution in a Gaussian mode is,*

$$I(\mathbf{r}) = \frac{2P}{\pi w^2(z)} e^{-2\rho^2/w^2(z)} \qquad with \qquad w(z) = w_0 \sqrt{1 + \left(\frac{\lambda z}{\pi w_0^2}\right)^2} \ .$$

With this, we calculate,

$$V_m = \frac{1}{I(0)} \int I(r) dV = \int_0^L \int_0^\infty \frac{w_0^2}{w^2(z)} e^{-2\rho^2/w^2(z)} 2\pi\rho d\rho dz = \frac{\pi}{2} L w_0^2 \ .$$

b. The intensity is related to the electric field $\vec{\mathcal{E}}_1$ generated by a single photon and to the number of photons n by,

$$I(\mathbf{r}) = n\varepsilon_0 c \vec{\mathcal{E}}_1^2(\mathbf{r}) \ .$$

With this, we calculate the zero point energy,

$$\frac{\hbar\omega}{2} = \int u_1(\mathbf{r}) dV = \int \frac{I_1(\mathbf{r})}{c} dV = \frac{1}{c} I_1(0) V_m \ .$$

Hence,

$$\mathcal{E}_1(0) = \sqrt{\frac{I_1(0)}{\varepsilon_0 c}} = \sqrt{\frac{1}{\varepsilon_0 c} \frac{\hbar\omega}{2} \frac{c}{V_m}} = \sqrt{\frac{\hbar\omega}{2\varepsilon_0 V_m}} \ .$$

c. We get,

$$P = \frac{\pi w_0^2 I(0)}{2} = \frac{\pi w_0^2}{2} n\varepsilon_0 c \mathcal{E}_1(0)^2 = \frac{\pi w_0^2}{2} n\varepsilon_0 c \frac{\hbar\omega}{2\varepsilon_0 V_m} = \frac{\pi w_0^2}{2} n\varepsilon_0 c \frac{\hbar\omega}{2\varepsilon_0} \frac{2}{L\pi w_0^2} = n\hbar\omega\delta_{fsr} \ .$$

18.4.4.3 Ex: The lens in ray and wave optics

a. Use the transfer matrices (18.298) and (18.299) to derive the lens equations of geometric optics from the relation (18.296).
b. Now, use the transfer matrices (18.298) and (18.299) to derive, from the relation (18.296), the transformation of a Gaussian beam. How do the waists behave upon transformation?
c. You have a laser of $\lambda = 632\,\text{nm}$ wavelength producing a Gaussian beam of diameter $w_1 = 1\,\text{mm}$ in its waist. Now, you want to match the beam into a cavity, whose mode (defined by the radii of curvature of the mirrors) has a waist of diameter $w_2 = 100\,\mu\text{m}$. To do this, you have at your disposal a lens of $f = 500\,\text{mm}$ focal distance. Using the formulas derived in (b), determine, how the distances d_1 (between the location of the waist of the laser beam and the lens) and d_2 (between the lens and the location of the waist of the cavity) must be chosen.

Solution: *a. We concatenate the matrices for free propagation by a distance d_1,*

for the transformation of the beam by a lens with focal distance f, and another free propagation by a distance d_2,

$$\mathcal{M} = \begin{pmatrix} 1 & d_2 \\ 0 & 1 \end{pmatrix} \begin{pmatrix} 1 & 0 \\ -1/f & 1 \end{pmatrix} \begin{pmatrix} 1 & d_1 \\ 0 & 1 \end{pmatrix} = \begin{pmatrix} 1 - d_2/f & d_1 + d_2 - d_1 d_2/f \\ -1/f & 1 - d_1/f \end{pmatrix} .$$

An image forms when the element M_{12} vanishes,

$$\mathcal{M} = \begin{pmatrix} -d_2/d_1 & 0 \\ -1/f & -d_1/d_2 \end{pmatrix} ,$$

implying,

$$\boxed{\frac{1}{f} = \frac{1}{d_1} + \frac{1}{d_2} \qquad \textit{and} \qquad \frac{y_2}{y_1} = -\frac{d_2}{d_1}} .$$

b. We concatenate the same matrices as in (a), but now we consider the beam parameter, which transforms like,

$$q_2 = \frac{M_{11} q_1 + M_{12}}{M_{21} q_1 + M_{22}} = \frac{(1 - d_2/f) q_1 + d_1 + d_2 - d_1 d_2/f}{-q_1/f + 1 - d_1/f} .$$

We assume that at the positions $d_{1,2}$ the beam has waists, such that $R_{1,2} = \infty$,

$$q_{1,2} = \frac{\imath \pi w_{1,2}^2}{\lambda} .$$

With this we obtain the condition,

$$\frac{\imath \pi w_2^2}{\lambda} \left(-\frac{\imath \pi w_1^2}{\lambda f} + 1 - \frac{d_1}{f} \right) = \left(1 - \frac{d_2}{f} \right) \frac{\imath \pi w_1^2}{\lambda} + d_1 + d_2 - \frac{d_1 d_2}{f} ,$$

or separating the real and imaginary parts,

$$\boxed{\frac{k^2 w_1^2 w_2^2}{4 f d_1 d_2} = \frac{1}{d_1} + \frac{1}{d_2} - \frac{1}{f} \qquad \textit{and} \qquad \frac{w_2^2}{w_1^2} = \frac{d_2 - f}{d_1 - f}} .$$

c. Solving the two formulas derived in (b) by d_2,

$$d_2 = \frac{k^2 w_1^2 w_2^2 - 4 f d_1}{4 f - 4 d_1} \qquad \textit{and} \qquad d_2 = f + (d_1 - f) \frac{w_2^2}{w_1^2} .$$

Solving the difference between the two formulas by d_1 and inserting this in the first formula,

$$(d_1 - f)^2 \frac{w_2^2}{w_1^2} = f^2 - \frac{k^2 w_1^2 w_2^2}{4} = (d_2 - f)^2 \frac{w_1^2}{w_2^2} .$$

For the given values we calculate,

$$d_1 = 1039\,\mathrm{mm} \qquad \textit{and} \qquad d_2 = 505\,\mathrm{mm} .$$

18.4.4.4 Ex: Transverse modes of a ring cavity

In this exercise we consider a ring cavity made of a plane input coupler and two identical curved high-reflectors (radius of curvature $\rho = 2f$) forming an isosceles triangle. Let $a = L/(2+\sqrt{2})$ be the two short distances and $b = L/(1+\sqrt{2})$ the long one, so that $L = 2a + b$.
a. How many waists does the cavity modes have, and where are they located?
b. Derive the round-trip matrix starting from the location of any one of the waists.
c. Calculate the waists.
d. Calculate the transverse mode spectrum, and prepare a plot for $\rho = 30\,\mathrm{cm}$ and $L = 8.7\,\mathrm{cm}$.
e. The above results presume cylindrical symmetry. However, incidence on curved mirrors under a tilted angle θ produces astigmatism. This can be accounted for by assuming different radii of curvature for the horizontal and vertical axis:

$$R_h = R\cos\theta \qquad \text{and} \qquad R_v = R/\cos\theta\ . \tag{18.346}$$

Calculate the impact waist sizes in the horizontal and vertical axis.

Solution: *a. The cavity has two waists, one at the input coupler, w_a, the other in free space, w_b.*
b. When we start from the input coupler, the round-trip matrix is,

$$\begin{pmatrix} 1 & a \\ 0 & 1 \end{pmatrix} \begin{pmatrix} 1 & 0 \\ -1/f & 1 \end{pmatrix} \begin{pmatrix} 1 & b \\ 0 & 1 \end{pmatrix} \begin{pmatrix} 1 & 0 \\ -1/f & 1 \end{pmatrix} \begin{pmatrix} 1 & a \\ 0 & 1 \end{pmatrix}\ . \tag{18.347}$$

From it we determine the beam radius and the radius of curvature at the input coupler,

$$w_a^2 = \frac{2\lambda B}{\pi\sqrt{4-(A+D)^2}} = \frac{\lambda(2af^2-2abf-2a^2f+ba^2+bf^2)}{\pi\sqrt{f^4-(f^2-bf-2af+ba)^2}} \quad \textit{and} \quad R = \frac{2B}{D-A} = \infty\ . \tag{18.348}$$

One the other hand, when we start from the free space waist, the round-trip matrix is

$$\begin{pmatrix} 1 & b/2 \\ 0 & 1 \end{pmatrix} \begin{pmatrix} 1 & 0 \\ -1/f & 1 \end{pmatrix} \begin{pmatrix} 1 & 2a \\ 0 & 1 \end{pmatrix} \begin{pmatrix} 1 & 0 \\ -1/f & 1 \end{pmatrix} \begin{pmatrix} 1 & b/2 \\ 0 & 1 \end{pmatrix}\ . \tag{18.349}$$

c. The beam radius and the radius of curvature in free space is given by

$$w_b^2 = \frac{2\lambda B}{\pi\sqrt{4-(A+D)^2}} = \frac{\lambda(2bf^2-b^2f-4abf+b^2a+4af^2)}{2\pi\sqrt{f^4-(f^2-bf-2af+ba)^2}} \quad \textit{and} \quad R = \frac{2B}{D-A} = \infty\ . \tag{18.350}$$

d. The round-trip phase shift is given by twice the phase shift between the input coupler and the free space waist,

$$\begin{aligned} \nu/\delta_{fsr} &= (q+1) + 2\phi_{mn}(a)/\pi + 2\phi_{mn}(b)/\pi \\ &= (q+1) + \frac{m+n+1}{\pi}\left(2\arctan\frac{\lambda a}{\pi w_a^2} + 2\arctan\frac{\lambda b/2}{\pi w_b^2}\right)\ , \end{aligned} \tag{18.351}$$

Using the identity

$$\arctan x + \arctan y = \arccos \frac{1 - xy}{\sqrt{(1+x^2)(1+y^2)}} \ , \tag{18.352}$$

after some algebraic manipulations aided by MAPLE be arrive at

$$\nu/\delta_{fsr} = (q+1) + 2\frac{m+n+1}{\pi} \arccos \sqrt{\left(1 - \frac{2a}{R}\right)\left(1 - \frac{b}{R}\right)} \ . \tag{18.353}$$

For $R = 30\,\mathrm{cm}$ and $L = 8.7\,\mathrm{cm}$ the transverse mode splitting in terms of the free

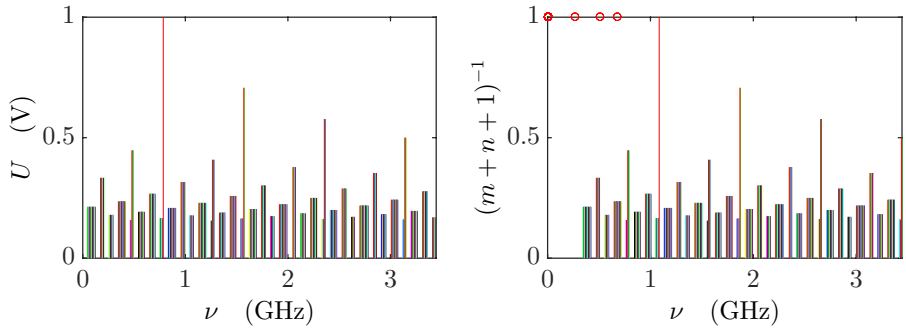

Figure 18.34: Transverse modes of a ring cavity. Top: high finesse, bottom: low finesse. The lifting of the $m+n$ degeneracy is indicated by a small (underestimated splitting).

spectral range is

$$\frac{2}{\pi} \arccos \sqrt{\left(1 - \frac{2a}{R}\right)\left(1 - \frac{b}{R}\right)} = 0.34 \ . \tag{18.354}$$

e.

18.4.4.5 Ex: Transverse Hermite-Gauss modes

Derive the spectrum of Hermite-Gauss transverse modes.

Solution: *We choose the ansatz,*

$$\psi = g\left(\frac{x}{w(z)}\right) h\left(\frac{y}{w(z)}\right) e^{-\imath[\varphi(z) + k(x^2+y^2)/2q(z)]} \ .$$

First, we note that the solution should work for $g = h = 1$, a case which has already been studied. The obtained results,

$$q' = 1 \qquad \textit{and} \qquad \varphi' = \frac{-\imath}{q} \ ,$$

can not depend on the choice of g and h and therefore can be used in the following. Inserting the ansatz into the equation (18.281) we calculate the derivatives,

$$\begin{aligned}
2\imath k\frac{\partial\psi}{\partial z} &= \left[2\imath k\left(-x\frac{g'}{g}-y\frac{h'}{h}\right)\frac{w'}{w^2}-\frac{2\imath k}{q}-\frac{k^2(x^2+y^2)}{q^2}\right]ghe^{-\imath[.]}\\
\frac{\partial}{\partial x}\psi &= \left(\frac{1}{w}g'-\frac{\imath kx}{q}g\right)he^{-\imath[.]}\\
\frac{\partial^2}{\partial x^2}\psi &= \left[\frac{1}{w^2}\frac{g''}{g}-\frac{2\imath kx}{qw}\frac{g'}{g}-\frac{k^2x^2}{q^2}-\frac{\imath k}{q}\right]ghe^{-\imath[.]}\ .
\end{aligned}$$

Now,

$$\begin{aligned}
0 &= 2\imath k\frac{\partial\psi}{\partial z}-\frac{\partial^2}{\partial x^2}\psi-\frac{\partial^2}{\partial y^2}\psi\\
&= \left[2\imath k\left(-x\frac{g'}{g}-y\frac{h'}{h}\right)\frac{w'}{w^2}-\frac{2\imath k}{q}-\frac{k^2(x^2+y^2)}{q^2}\right]-\left[\frac{1}{w^2}\frac{g''}{g}-\frac{2\imath kx}{qw}\frac{g'}{g}-\frac{k^2x^2}{q^2}-\frac{\imath k}{q}\right]-[...]\\
&= -\frac{1}{w^2}\frac{g''}{g}+\frac{2\imath kx}{w}\left(\frac{1}{q}-\frac{w'}{w}\right)\frac{g'}{g}-[...]\ .
\end{aligned}$$

hence we stay with,

$$C=-\frac{1}{w^2}\frac{g''}{g}+\frac{2\imath kx}{w}\left(\frac{1}{q}-\frac{w'}{w}\right)\frac{g'}{g}=-\frac{dg}{gdx}+2\imath kx\left(\frac{1}{q}-\frac{w'}{w}\right)\frac{dg}{gdx}\ ,$$

which must be valid for $z=0$, where $w=w_0$ and $w'=0$,

$$\frac{d^2g}{dx^2}-\frac{\imath k}{q_0}2x\frac{dg}{dx}+gC=\frac{d^2g}{dx^2}-\frac{2}{w_0^2}2x\frac{dg}{dx}+Cg=0\ .$$

This is already (almost) the differential equation of the Hermite polynomials,

$$\frac{d^2H_m(u)}{du^2}-2u\frac{dH_m(u)}{du}+2mH_m(u)=0\ ,$$

with $gh=H_m(\sqrt{2}x/w)H_m(\sqrt{2}y/w)$.

18.4.4.6 Ex: Derivation of the Rayleigh-Sommerfeld formula

Derive the Rayleigh-Sommerfeld formula (18.326).

Solution: *For any point $\mathbf{r}$ of an aperture we know that the function $\psi(\mathbf{r})$ satisfies the Helmholtz equation,*

$$(\nabla^2+k^2)\psi(\mathbf{r})=0\ .$$

There will also be a Green function that in a region $V=\{(x,y,z)|z>0\}$ which satisfies the equation:

$$(\nabla^2+k^2)G(\mathbf{r}-\mathbf{r}')=\delta^3(\mathbf{r}-\mathbf{r}')\ ,$$

where $\mathbf{r}'$ is an observation point in V. The solution of the latter equation is given by,

$$G(\mathbf{r}-\mathbf{r}') = -\frac{1}{4\pi}\frac{e^{\imath k|\mathbf{r}-\mathbf{r}'|}}{|\mathbf{r}-\mathbf{r}'|} \ . \tag{18.355}$$

Know we can write,

$$\psi(\mathbf{r}') = \int_V \psi(\mathbf{r})\delta^3(\mathbf{r}-\mathbf{r}')d^3r = \int_V \psi(\mathbf{r})(\nabla^2+k^2)G(\mathbf{r}-\mathbf{r}')d^3r \ .$$

We integrate the first term of the sum by parts,

$$\begin{aligned}\int_V \psi(\mathbf{r})\nabla^2 G d^3r &= \int_{\partial V}\psi(\mathbf{r})\nabla G\cdot d\mathbf{S} - \int_V \nabla\psi(\mathbf{r})\cdot\nabla G d^3r \\ &= \int_{\partial V}\psi(\mathbf{r})\nabla G\cdot d\mathbf{S} - \left[\int_{\partial V}\nabla\psi(\mathbf{r})\cdot G d\mathbf{S} - \int_V \nabla^2\psi(\mathbf{r})G d^3r\right] \ .\end{aligned}$$

Substituting this integral in the previous equation, we are left with,

$$\psi(\mathbf{r}') = \int_{\partial V}[\psi(\mathbf{r})\nabla G - \nabla\psi(\mathbf{r})]\cdot d\mathbf{S} + \cancelto{0}{\int_V(\nabla^2+k^2)\psi(\mathbf{r})G d^3r} \ .$$

Since $\nabla\psi$ is unknown and the integral is not null except at $z=0$, we look out for a Green function that is zero for $z\neq 0$, so that there is no need to worry about $\nabla\psi$, and the second term in the above equation vanishes. Defining a vector $\tilde{\mathbf{r}}' = (x', y', -z')$ outside the region V, we can write $G(\mathbf{r}-\mathbf{r}')$:

$$G(\mathbf{r}-\mathbf{r}') = -\frac{1}{4\pi}\frac{e^{\imath k|\mathbf{r}-\mathbf{r}'|}}{|\mathbf{r}-\mathbf{r}'|} + \frac{1}{4\pi}\frac{e^{\imath k|\mathbf{r}-\tilde{\mathbf{r}}'|}}{|\mathbf{r}-\tilde{\mathbf{r}}'|} \ .$$

Which is also a solution of the Eq. (18.355). Hence, at $z=0$, we get $|\mathbf{r}-\mathbf{r}'| = |\mathbf{r}-\tilde{\mathbf{r}}'|$, and therefore $G=0$ at $z=0$. The integral at the aperture Σ at $z=0$ becomes,

$$\psi(\mathbf{r}') = \int_\Sigma \psi(\mathbf{r})\partial_z G dS \ .$$

Knowing that the derivative is given by,

$$\frac{\partial G}{\partial z} = -\frac{1}{2\pi}\left(\imath k - \frac{1}{R}\right)\left(\frac{z}{R}\right)\frac{e^{\imath kR}}{R} \ .$$

We finally find the wave $\psi(\mathbf{r}')$,

$$\psi(\mathbf{r}') = -\frac{\imath k}{2\pi}\int_\Sigma \psi_{z=0}\left(\imath k - \frac{1}{R}\right)\frac{z}{R}\frac{e^{\imath kR}}{R}dS \ .$$

Using the approximation that $R \gg k$,

$$\psi(\mathbf{r}') \simeq -\frac{\imath k}{2\pi}\int_\Sigma \psi_0\frac{z}{R}\frac{e^{\imath kR}}{R}dS \ ,$$

and so we managed to propagate the beam given the initial beam for the entire V region.

18.4.4.7 Ex: Phasefront distorsion by an axicon and a thin lens

Calculate the phasefront distorsion suffered by a plane wave upon traversing (a) an axicon with base angle α and (b) a thin lens with focal length f.

Solution: *a. We consider an axicon with base angle α made of glas with refraction index n_{rfr} illuminated by a phase front of light with wavelength λ. The width w of the axicon depends on the distance r from the symmetry axis as,*

$$w = w_{max} - r\tan\alpha \ .$$

In a given time interval Δt the phase front travels by a distance depending on where

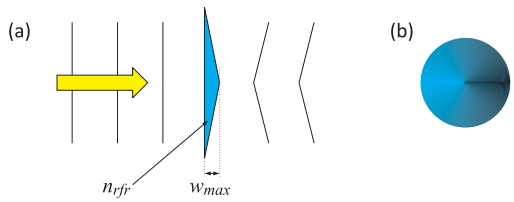

Figure 18.35: (a) Phase shift of a phase front passing through an axicon. (b) Top view of an axicon lens.

the beam hits the lens surface,

$$\Delta z = c\Delta t_1 + c_n(\Delta t - \Delta t_1) \ ,$$

with $\Delta t_1 \equiv w/c_n$. Choosing the time long enough for the phase front to cross the lens, $\Delta t = w_{max}/c_n$, the phase shift is,

$$\Delta\phi(r) = \frac{2\pi\Delta z}{\lambda} = 2\pi\frac{(n_{rfr}-1)w + w_{max}}{\lambda} \ .$$

That is,

$$\boxed{\Delta\phi(r) = -(n_{rfr}-1)kr\tan\alpha = -2\pi\frac{r}{r_{2\pi}}} \ ,$$

where $r_{2\pi}$ is the distance from the optical axis, where the phase shift is just 2π.
b. Thin lenses with focal length f have spherical surfaces with radius of curvature,

$$R = \frac{f}{2} \ .$$

The width Δw of a spherical segment depends on the distance r from the symmetry axis as,

$$\Delta w = R - \sqrt{R^2 - r^2} \ .$$

Hence, the width of the lens is,

$$w = w_{max} - \left(R - \sqrt{R^2 - r^2}\right) \simeq w_{\max} - \frac{r^2}{2R} \ .$$

In a given time interval Δt the phase front travels by a distance depending on where the beam hits the lens surface,

$$\Delta z = c\Delta t_1 + c_n(\Delta t - \Delta t_1) \ ,$$

with $\Delta t_1 = w/c_n$. Choosing the time long enough for the phase front to cross the lens, $\Delta t = w_{\max}/c_n$, the phase shift is,

$$\Delta\phi(r) = 2\pi\frac{\Delta z}{\lambda} = 2\pi\frac{(n_{rfr}-1)w + w_{max}}{\lambda} \ .$$

That is,

$$\boxed{\Delta\phi(r) = -(n_{rfr}-1)k\frac{r^2}{f} = -2\pi\frac{r^2}{r_{2\pi}^2}} \ ,$$

where $r_{2\pi}$ is the distance from the optical axis, where the phase shift is just 2π.

18.4.4.8 Ex: Transmission through a pinhole

Calculate the light field distribution after a circular pinhole of radius a.

Solution: *We now calculate the light field distribution after a pinhole. Conveniently switching to polar coordinates,*

$$\begin{aligned} k_x = k\cos\theta \quad &, \quad k_y = k\sin\theta \\ x = r\cos\phi \quad &, \quad y = r\sin\phi \\ k_x x + k_y y &= kr(\cos\phi\cos\theta + \sin\phi\sin\theta) = kr\cos(\phi-\theta) \\ 1-(\lambda k_x)^2 - (\lambda k_y)^2 &= 1-\lambda^2k^2 \ , \end{aligned}$$

we expect

$$\begin{aligned} u_{prop} &= \mathcal{F}^{-1}\{H\cdot\mathcal{F}\{[\min(a,\sqrt{x^2+y^2})]\} \\ &= \int dk_x dk_y e^{-\imath k_x x - \imath k_y y}\left(e^{\imath kz\sqrt{1-(\lambda k_x)^2-(\lambda k_y)^2}}\int dxdy e^{\imath k_x x+\imath k_y y}\min(a,\sqrt{x^2+y^2})\right) \\ &= \int\left(e^{-\imath kr\cos(\phi-\theta)}e^{\imath kz\sqrt{1-\lambda^2k^2}}\int_0^a\int_0^{2\pi} r' e^{\imath kr'\cos(\phi'-\theta)}d\phi' dr'\right)kdkd\theta \ . \end{aligned}$$

Introducing the Bessel function via $J_n(z) = \frac{1}{2\pi}\int_{-\pi}^{\pi} e^{\imath(z\sin\tau - n\tau)}d\tau$, it is possible to show that,

$$\frac{I(\theta)}{I_0} = \left(\frac{2J_1(ka\sin\theta)}{ka\sin\theta}\right)^2 \ .$$

The first ring of destructive interference is expected for $J_1(ka\sin\theta) = 0 = J_1(3.83205..)$,

$$\theta_0 \simeq \boxed{\sin\theta_0 = 1.22\frac{\lambda}{2a}} \simeq 3.83\frac{\lambda}{2\pi a} \ .$$

The angle under which the intensity is reduced to its rms*-value,*

$$\frac{I(\theta_e)}{I_0} = \frac{1}{\sqrt{e}} = 0.6065..$$

is given by $J_1(ka\sin\theta_e) = 0.6065 = J_1(1.3845..)$ *and has the value,*

$$\theta_e \simeq \sin\theta_e = 1.3845\frac{\lambda}{2\pi a} \ .$$

This is similar to a Gaussian beam with waist w_0*, since according to formula (18.290) we have,*

$$\frac{w^2 - w_0^2}{z^2} = \frac{w_0^2}{z_R^2} \ ,$$

hence, for large distances from the pinhole,

$$\theta \simeq \frac{w}{z} \simeq \frac{w_0}{z_R} = \frac{\lambda}{\pi w_0} \ .$$

This means, that the beam transmitted through a pinhole approximately behaves like a Gaussian beam with waist $w_0 = 2a/1.3845$*.*

18.4.4.9 Ex: Transmission through a various optical components

Calculate the phase front transformation matrix
a. for a Fresnel zone plate
b. for a Laguerre-Gauss zone plate.

Solution: *a. For a Fresnel zone plate we have,*

$$\alpha_{Fresnel} = \cos\left(\frac{\pi}{2} + \frac{k\rho^2 z_1}{2z_R^2}\right) \ .$$

where z_R *is the Rayleigh lens.*
b. For a Laguerre-Gauss zone plate we have,

$$\beta_{LG} \equiv \alpha_{Fresnel} - l\arctan\frac{Y}{X+\varepsilon} \quad , \quad \beta_{LG} = sign[\beta_{LG}(X<0) + (-1)^l\beta_{LG}(X<0)] \ .$$

18.4.4.10 Ex: Numerical phasefront propagation

Numerical phasefront propagation through a thin lens.

Solution: *The result of the simulation is exhibited in the figure.*

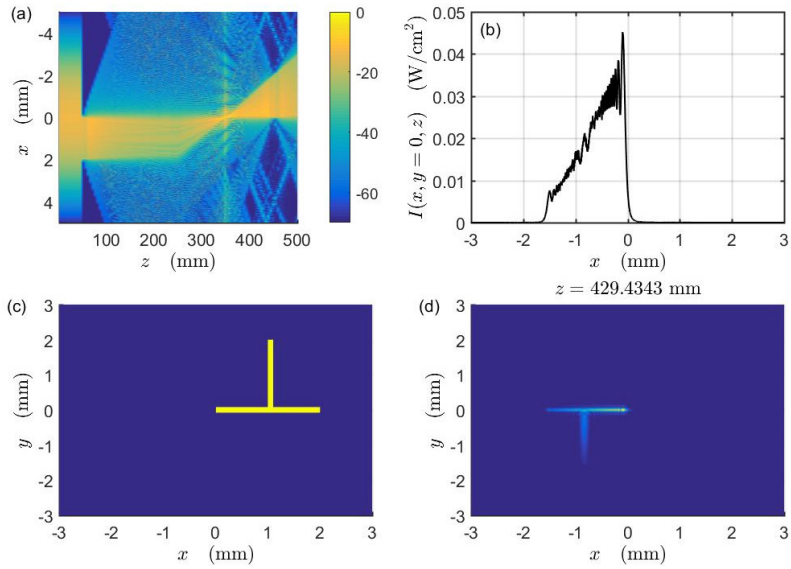

Figure 18.36: (code) Numerical phasefront propagation.

18.5 Further reading

18.5.1 on optics

H. Kogelnik et al., *Laser Beams and Resonators* [734]DOI

D.G. Voelz, *Computational Fourier Optics: a MATLAB tutorial* [1338]ISBN

P.R. Berman, *Optical Faraday rotation* [132]DOI

G. Labeyrie et al., *Large Faraday rotation of resonant light in a cold atomic cloud* [767]DOI

W.J. Wild et al., *Goos-Haenchen shifts from absorbing media* [1376]DOI

18.5.2 on metamaterials

J. Sinova et al., *Spin Hall effects* [1212]DOI

J.B. Pendry, *Negative refraction makes a perfect lens* [1011]DOI

J.B. Pendry, *A chiral route to negative refraction* [1012]DOI

S.M. Rytov, *Electromagnetic properties of a finely stratified medium* [1123]DOI

P. Szarek, *Electric permittivity in individual atomic and molecular systems through direct associations with electric dipole polarizability and chemical hardness* [1287]DOI

V.G. Veselago, *The electrodynamics of substances with simultaneously negative values of E and M* [1335]DOI

A. Poddubny et al., *Hyperbolic metamaterials* [1040]$_{\text{DOI}}$

P. Shekhar et al., *Strong Coupling in Hyperbolic Metamaterials* [1192]$_{\text{DOI}}$

H.N.S. Krishnamoorthy et al., *Topological transitions in metamaterials* [753]$_{\text{DOI}}$

Chapter 19

Radiation

In the previous sections we discussed the propagation of electromagnetic waves, but we do not say how these waves were produced in the first place. For now, we only know, that it need's accelerated charges or varying currents. Now, we will show how such 'sources' can emit energy by 'radiating' electromagnetic waves.

To begin with, let us consider sources located near the origin and confined within a sphere of radius r. The total power crossing the sphere's surface is the integral of the Poynting vector,

$$P(r) = \oint \vec{\mathcal{S}} \cdot d\mathbf{a} = \tfrac{1}{\mu_0} \oint (\vec{\mathcal{E}} \times \vec{\mathcal{B}}) \cdot d\mathbf{a} \ . \tag{19.1}$$

The radiated power is then the energy per unit area transported to infinity without ever returning,

$$P_{rad} = \lim_{r\to\infty} P(r) \ . \tag{19.2}$$

Now, the area of the sphere's surface is $4\pi r^2$ such that, in order to have non-vanishing radiation, the Poynting vector must decrease (for large r) no faster than as $1/r^2$. Following the Coulomb law, electrostatic fields decrease like $1/r^2$ or faster, when the total enclosed charge is zero. And Biot-Savart's law states that magnetostatic fields decrease at least as fast as $1/r^2$, such that $|\vec{\mathcal{S}}| \propto 1/r^4$, for static configurations. Hence, static sources do not radiate. On the other hand, Jefimenko's equations (17.109) and (17.112) indicate the existence of time-dependent terms (involving $\dot{\varrho}$ and $\dot{\mathbf{j}}$), which are proportional to $1/r$. These are the terms responsible for electromagnetic radiation. To study the radiation we choose the parts of $\vec{\mathcal{E}}$ and $\vec{\mathcal{B}}$ going as $1/r$ at large distances from the source, combine them to terms going as $1/r^2$ in the Poynting vector $\vec{\mathcal{S}}$, and integrate $\vec{\mathcal{S}}$ on a large spherical surface taking the limit $r \to \infty$.

19.1 Multipolar expansion of the radiation

19.1.1 The radiation of an arbitrary charge distribution

In this section we will calculate the radiation emitted by arbitrary time-dependent variations of charge and current distributions, but which are confined within a small volume near the origin. The retarded scalar potential is according to (17.106),

$$\Phi(\mathbf{r}, t) = \frac{1}{4\pi\varepsilon_0} \int \frac{\varrho(\mathbf{r}', t - R/c)}{R} d^3r' \ , \tag{19.3}$$

where $R = \sqrt{r^2 + r'^2 - 2\mathbf{r}\cdot\mathbf{r}'}$, as illustrated in Fig. 17.11. Within the small source approximation, $r' \ll r$, we have,

$$R \simeq r\left(1 - \frac{\mathbf{r}\cdot\mathbf{r}'}{r^2}\right) \qquad \text{and} \qquad \frac{1}{R} \simeq \frac{1}{r}\left(1 + \frac{\mathbf{r}\cdot\mathbf{r}'}{r^2}\right) , \tag{19.4}$$

such that, defining,

$$t_0 \equiv t - \tfrac{r}{c} , \tag{19.5}$$

we obtain,

$$\varrho(\mathbf{r}', t - R/c) \simeq \varrho(\mathbf{r}', t - \tfrac{r}{c} + \tfrac{\hat{\mathbf{e}}_r\cdot\mathbf{r}'}{c}) \equiv \varrho(\mathbf{r}', t_0 + \tfrac{\hat{\mathbf{e}}_r\cdot\mathbf{r}'}{c}) . \tag{19.6}$$

Expanding ϱ in a Taylor series around the retarded time at the origin t_0, we get,

$$\varrho(\mathbf{r}', t - R/c) \simeq \varrho(\mathbf{r}', t_0) + \dot{\varrho}(\mathbf{r}', t_0)\tfrac{\hat{\mathbf{e}}_r\cdot\mathbf{r}'}{c} + ... \tag{19.7}$$

Substituting the numerator and denominator in the formula (19.3) by the expansions (19.4) and (19.7) we get up to the first order,

$$\Phi(\mathbf{r}, t) = \frac{1}{4\pi\varepsilon_0 r}\left[\int \varrho(\mathbf{r}', t_0)d^3r' + \frac{\hat{\mathbf{e}}_r}{r}\cdot\int \mathbf{r}'\varrho(\mathbf{r}', t_0)d^3r' + \frac{\hat{\mathbf{e}}_r}{c}\cdot\frac{d}{dt}\int \mathbf{r}'\varrho(\mathbf{r}', t_0)d^3r'\right] . \tag{19.8}$$

The first integral is simply the charge [1], the other two represent the electric dipole at time t_0,

$$\Phi(\mathbf{r}, t) = \frac{1}{4\pi\varepsilon_0}\left[\frac{Q}{r} + \frac{\hat{\mathbf{e}}_r\cdot\mathbf{d}(t_0)}{r^2} + \frac{\hat{\mathbf{e}}_r\cdot\dot{\mathbf{d}}(t_0)}{cr}\right] . \tag{19.9}$$

In the static case, the first two terms are the contributions of the monopole and dipole to the multipolar expansion of Φ, the third term would not be present.

The vector potential,

$$\mathbf{A}(\mathbf{r}, t) = \frac{\mu_0}{4\pi}\int \frac{\mathbf{j}(\mathbf{r}', t - R/c)}{R}d^3r' , \tag{19.10}$$

is easily expanded up to first order by,

$$\mathbf{A}(\mathbf{r}, t) \simeq \frac{\mu_0}{4\pi r}\int \mathbf{j}(\mathbf{r}', t_0)d^3r' , \tag{19.11}$$

since, as we will show in Exc. 19.1.6.1,

$$\boxed{\mathbf{A}(\mathbf{r}, t) \simeq \frac{\mu_0}{4\pi}\frac{\dot{\mathbf{d}}(t_0)}{r}} , \tag{19.12}$$

that is, $\mathbf{d} \sim \mathbf{r}'$ is already of first order in $\mathbf{r}'$.

Now we must calculate the fields. Again, we are interested in the radiation zone (that is, in fields surviving great distances from the source), discarding all terms in $\vec{\mathcal{E}}$ and $\vec{\mathcal{B}}$ which decrease like $1/r^2$ or faster, which will not be the case for the first term

[1] The charge is evaluated at time t_0, but since it is conserved, it stays the same at all times.

(Coulomb) and the second term in (19.9). Therefore, considering the abbreviation (19.5), we obtain,

$$\nabla\Phi \simeq \frac{1}{4\pi\varepsilon_0}\nabla\frac{\hat{\mathbf{e}}_r\cdot\dot{\mathbf{d}}(t_0)}{rc} = \frac{1}{4\pi\varepsilon_0}\left[\cancelto{0}{\frac{\dot{\mathbf{d}}(t_0)}{cr^2}} + \frac{\hat{\mathbf{e}}_r\cdot\ddot{\mathbf{d}}(t_0)}{cr}\nabla t_0 - \cancelto{0}{\frac{2\hat{\mathbf{e}}_r\cdot\dot{\mathbf{d}}(t_0)}{cr^2}\hat{\mathbf{e}}_r}\right]$$
$$\simeq \frac{1}{4\pi\varepsilon_0}\frac{\hat{\mathbf{e}}_r\cdot\ddot{\mathbf{d}}(t_0)}{cr}\left(-\frac{\hat{\mathbf{e}}_r}{c}\right) . \tag{19.13}$$

Similarly,

$$\nabla\times\mathbf{A} = \nabla\times\frac{\mu_0}{4\pi}\frac{\dot{\mathbf{d}}(t_0)}{r} = \frac{\mu_0}{4\pi}\left[\frac{1}{r}\nabla\times\dot{\mathbf{d}}(t_0) + \left(\nabla\frac{1}{r}\right)\times\dot{\mathbf{d}}(t_0)\right] \tag{19.14}$$
$$= \frac{\mu_0}{4\pi}\left[-\frac{\ddot{\mathbf{d}}(t_0)}{r}\times\nabla t_0 - \cancelto{0}{\frac{\hat{\mathbf{e}}_r\times\dot{\mathbf{d}}(t_0)}{r^2}}\right] = -\frac{\mu_0}{4\pi}\frac{\ddot{\mathbf{d}}(t_0)}{r}\times\left(\frac{-\hat{\mathbf{e}}_r}{c}\right) = -\frac{\mu_0}{4\pi}\frac{\hat{\mathbf{e}}_r\times\ddot{\mathbf{d}}(t_0)}{cr} .$$

and,

$$\frac{\partial\mathbf{A}}{\partial t} \simeq \frac{\mu_0}{4\pi}\frac{\ddot{\mathbf{d}}(t_0)}{r} . \tag{19.15}$$

Hence, the Eqs. (17.78) tell us,

$$\vec{\mathcal{E}}(\mathbf{r},t) \simeq \frac{\mu_0}{4\pi r}[(\hat{\mathbf{e}}_r\cdot\ddot{\mathbf{d}}(t_0))\hat{\mathbf{e}}_r - \ddot{\mathbf{d}}(t_0)] = \frac{\mu_0}{4\pi r}[\hat{\mathbf{e}}_r\times(\hat{\mathbf{e}}_r\times\ddot{\mathbf{d}}(t_0)] \tag{19.16}$$
$$\vec{\mathcal{B}}(\mathbf{r},t) \simeq -\frac{\mu_0}{4\pi cr}[\hat{\mathbf{e}}_r\times\ddot{\mathbf{d}}(t_0)] .$$

In spherical coordinates,

$$\vec{\mathcal{E}}(r,\theta,\phi,t) \simeq \frac{\mu_0\ddot{d}(t_0)}{4\pi}\frac{\sin\theta}{r}\hat{\mathbf{e}}_\theta \quad \text{and} \quad \vec{\mathcal{B}}(r,\theta,\phi,t) \simeq \frac{\mu_0\ddot{d}(t_0)}{4\pi c}\frac{\sin\theta}{r}\hat{\mathbf{e}}_\phi . \tag{19.17}$$

The Poynting vector is,

$$\boxed{\vec{\mathcal{S}} \simeq \tfrac{1}{\mu_0}\vec{\mathcal{E}}\times\vec{\mathcal{B}} = \frac{\mu_0\ddot{d}(t_0)^2}{16\pi^2 c}\frac{\sin^2\theta}{r^2}\hat{\mathbf{e}}_r} , \tag{19.18}$$

which is a result that we already used in (18.111). And for total radiated power we get the *Larmor formula*,

$$P \simeq \oint\vec{\mathcal{S}}\cdot d\mathbf{a} = \frac{\mu_0\ddot{d}(t_0)}{6\pi c} . \tag{19.19}$$

The calculation is equivalent to a multipolar expansion of the retarded potentials up to the lowest order in r' which can still radiate, and which turns out to be an electric dipole radiation. Multipolar orders of radiation usually only come into play, when for some reason (e.g. a selection rule) the electric dipole radiation cancels. The next multipolar order will be, as we will soon see, a combination of magnetic dipole and quadrupolar electric radiation.

19.1.2 Multipolar expansion of retarded potentials

In order to simplify the multipolar treatment, we use the superposition principle, allowing us to decompose any temporal oscillation of a charge distribution into harmonic oscillations,

$$\varrho(\mathbf{r},t_r)=\varrho(\mathbf{r})e^{-\imath\omega t_r} \qquad \text{and} \qquad \mathbf{j}(\mathbf{r},t_r)=\mathbf{j}(\mathbf{r})e^{-\imath\omega t_r}\ . \tag{19.20}$$

By inserting these dependencies into the *retarded potentials* (17.106), we obtain with $t_r = t - |\mathbf{r}-\mathbf{r}'|/c$,

$$\Phi(\mathbf{r})=\frac{1}{4\pi\varepsilon_0}\int \varrho(\mathbf{r}_r)\frac{e^{\imath k|\mathbf{r}-\mathbf{r}'|}}{|\mathbf{r}-\mathbf{r}'|}d^3r' \qquad \text{and} \qquad \mathbf{A}(\mathbf{r})=\frac{\mu_0}{4\pi}\int \mathbf{j}(\mathbf{r}')\frac{e^{\imath k|\mathbf{r}-\mathbf{r}'|}}{|\mathbf{r}-\mathbf{r}'|}d^3r'\ , \tag{19.21}$$

with $k=\omega/c$ and implying $\Phi(\mathbf{r},t)=\Phi(\mathbf{r})e^{-\imath\omega t}$ and $\mathbf{A}(\mathbf{r},t)=\mathbf{A}(\mathbf{r})e^{-\imath\omega t}$.

From these expressions we can, knowing the sources (19.20), calculate the fields via the expressions (17.78) or alternatively (based only on the vector potential) via,

$$\vec{\mathcal{B}}=\nabla\times\mathbf{A} \qquad \text{and} \qquad \vec{\mathcal{E}}=\tfrac{\imath c^2}{\omega}\nabla\times\vec{\mathcal{B}} \qquad \text{and} \qquad \vec{\mathcal{B}}=\tfrac{-\imath}{\omega}\nabla\times\vec{\mathcal{E}}\ , \tag{19.22}$$

where $\vec{\mathcal{E}}$ is evaluated outside the source. We will consider sources which are small (size d) compared to the wavelength λ and distinguish three regions characterized by fields with very different properties:

• near-field (or static) zone	$r' < d \ll r \ll \lambda$
• intermediate (or inductive) zone	$r' < d \ll r \sim \lambda$
• far-field (or radiative) zone	$r' < d \ll \lambda \ll r$

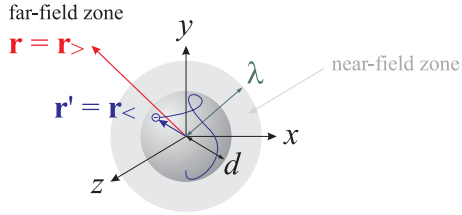

Figure 19.1: Geometry of source ($r' < d$) and observer ($r > d$) coordinates.

To handle the expression (19.21) we expand the Green function into spherical harmonics,

$$\frac{e^{\imath k|\mathbf{r}-\mathbf{r}'|}}{4\pi|\mathbf{r}-\mathbf{r}'|}=\imath k\sum_{\ell=0}^{\infty}h_\ell^{(1)}(kr_>)j_\ell(kr_<)\sum_{m=-\ell}^{\ell}Y^*_{\ell m}(\theta',\phi')Y_{\ell m}(\theta,\phi)\ , \tag{19.23}$$

where (placing the observer out of the source region) $r_< \equiv \min(r,r') = r'$ and $r_> \equiv \max(r,r') = r$. j_ℓ and $h_\ell^{(1)}$ are the *Bessel functions* and *Hankel functions* of the first type. This formula can be simplified by the sum rule,

$$\sum_{m=-\ell}^{\ell}Y^*_{\ell m}(\hat{\mathbf{e}}_{r'})Y_{\ell m}(\hat{\mathbf{e}}_r)=\frac{2\ell+1}{4\pi}P_\ell(\hat{\mathbf{e}}_{r'}\cdot\hat{\mathbf{e}}_r)\ , \tag{19.24}$$

where P_ℓ are *Legendre polynomials*. We write,

$$\frac{e^{\imath k|\mathbf{r}-\mathbf{r}'|}}{|\mathbf{r}-\mathbf{r}'|} = \imath k \sum_{\ell=0}^{\infty} (2\ell+1) h_\ell^{(1)}(kr) j_\ell(kr') P_\ell(\hat{\mathbf{e}}_{r'} \cdot \hat{\mathbf{e}}_r) \ . \tag{19.25}$$

For observation points $\mathbf{r}$ out of the source (which is certainly satisfied in the limit $r' \ll r$) the Eq. (19.21) becomes,

$$\mathbf{A}(\mathbf{r}) = \frac{\mu_0}{4\pi} (2\ell+1) \imath k \sum_{\ell=0}^{\infty} h_\ell^{(1)}(kr) \int \mathbf{j}(\mathbf{r}') j_\ell(kr') P_\ell(\hat{\mathbf{e}}_{r'} \cdot \hat{\mathbf{e}}_r) d^3r' \ . \tag{19.26}$$

Since we will always be considering the limit $kr' \ll 1$, we can expand the Bessel function for small arguments,

$$j_\ell(x) \overset{x\to 0}{\longrightarrow} \frac{x^\ell}{(2\ell+1)!!} \left(1 - \frac{x^2}{2(2\ell+3)} + ... \right) \ . \tag{19.27}$$

We obtain for the vector potential,

$$\boxed{\mathbf{A}(\mathbf{r}) \simeq \frac{\mu_0}{4\pi} \imath k \sum_{\ell=0}^{\infty} \frac{1}{(2\ell-1)!!} h_\ell^{(1)}(kr) \int \mathbf{j}(\mathbf{r}') (kr')^\ell P_\ell(\hat{\mathbf{e}}_{r'} \cdot \hat{\mathbf{e}}_r) d^3r'} \ . \tag{19.28}$$

Now, let us discuss the limiting cases by comparing the observation distance r with the wavelength. In the *near-field zone*, where $kr \ll 1$, we can also expand the Bessel function for small arguments,

$$n_\ell(x) \overset{x\to 0}{\longrightarrow} -\frac{(2\ell-1)!!}{x^{\ell+1}} \left(1 - \frac{x^2}{2(1-2\ell)} + ... \right) \tag{19.29}$$

$$\text{and} \qquad h_\ell^{(1)}(x) = j_\ell(x) + \imath n_\ell(x) \overset{x\to 0}{\longrightarrow} \imath n_\ell(x) \ ,$$

resulting in the vector potential,

$$\boxed{\mathbf{A}(\mathbf{r}) \overset{kr\to 0}{\longrightarrow} \frac{\mu_0}{4\pi} k \sum_{\ell=0}^{\infty} \frac{1}{(kr)^{\ell+1}} \int \mathbf{j}(\mathbf{r}') (kr')^\ell P_\ell(\hat{\mathbf{e}}_{r'} \cdot \hat{\mathbf{e}}_r) d^3r'} \ . \tag{19.30}$$

This formula could already have been derived by approximating the exponential of the formula (19.21) by $e^{\imath k|\mathbf{r}-\mathbf{r}'|} \simeq 1$ and expanding the following Green function into spherical harmonics [2],

$$\frac{1}{4\pi|\mathbf{r}-\mathbf{r}'|} = \sum_{\ell=0}^{\infty} \sum_{m=-\ell}^{\ell} \frac{1}{2\ell+1} \frac{r_<^\ell}{r_>^{\ell+1}} Y_{\ell m}^*(\theta', \phi') Y_{\ell m}(\theta, \phi) \ . \tag{19.31}$$

[2] This expansion is obtained by expanding the Legendre polynomials in the expansion (13.91),

$$\frac{1}{|\mathbf{r}-\mathbf{r}'|} = \frac{1}{r} \sum_{\ell=0}^{\infty} \frac{r_<^\ell}{r_>^{\ell+1}} P_\ell(\cos\theta') \qquad \text{with} \qquad P_\ell(\cos\theta') = \frac{4\pi}{2\ell+1} \sum_{m=\ell}^{\ell} Y_{\ell m}^*(\theta', \phi') Y_{\ell m}(\theta, \phi) \ ,$$

.

The absence of propagating terms in the expression (19.30) (the wave vector k can be eliminated from the expression (19.30)) demonstrates the *quasi-static* character of the fields within the near zone, that is, apart from a uniform and harmonic oscillation described by $e^{-\imath\omega t}$. The radial components depend on the details of the source's geometry. The scalar and vector potentials are of the form already derived in electrostatics (13.92) and magnetostatics (15.39).

On the other hand, in *far-field zone*, where $kr \gg 1$, the exponential in (19.21) oscillates rapidly and determines the behavior of vector potential. Here, we must resort to the complete expression (19.28), but we can expand the Hankel functions like,

$$h_\ell^{(1)}(x) = (-\imath)^{\ell+1}\frac{e^{\imath x}}{x}\sum_{m=0}^{\ell}\frac{\imath^m}{m!(2x)^m}\frac{(\ell+m)!}{(\ell-m)!} \ . \tag{19.32}$$

Knowing,

$$\begin{aligned} h_0^{(1)}(x) &= -\imath\tfrac{e^{\imath x}}{x} \quad , \quad P_0(x) = 1 \\ h_1^{(1)}(x) &= -\tfrac{e^{\imath x}}{x}\left(1-\tfrac{1}{\imath x}\right) \quad , \quad P_1(x) = x \ . \end{aligned} \tag{19.33}$$

we calculate the potentials,

$$\begin{aligned} \mathbf{A}_{\ell=0}(\mathbf{r}) &\simeq \frac{\mu_0}{4\pi}\frac{e^{\imath kr}}{r}\int \mathbf{j}(\mathbf{r}')d^3r' \\ \mathbf{A}_{\ell=1}(\mathbf{r}) &\simeq -\frac{\mu_0}{4\pi}\imath k\frac{e^{\imath kr}}{r}\left(1-\frac{1}{\imath kr}\right)\int \mathbf{j}(\mathbf{r}')\mathbf{r}'\cdot\hat{\mathbf{e}}_r d^3r' \ , \end{aligned} \tag{19.34}$$

We will see in the following sections that $\mathbf{A}_{\ell=0}$ is the potential for electric dipole radiation and $\mathbf{A}_{\ell=1}$ the potential for magnetic dipole radiation and electric quadrupolar radiation.

Example 113 (*The far-field limit*): Assuming that the spatial extent of the radiation source is small, $r' \lesssim d \ll r$, it is sufficient to approximate directly in the expression (19.21),

$$|\mathbf{r}-\mathbf{r}'| \simeq r - \hat{\mathbf{e}}_r\cdot\mathbf{r}' \ .$$

Moreover, if only the principal term in kr is desired [3], the inverse distance in (19.21) can be replaced by r. Then, the vector potential is,

$$\lim_{kr\to\infty}\mathbf{A}(\mathbf{r}) = \frac{\mu_0}{4\pi}\frac{e^{\imath kr}}{r}\int \mathbf{j}(\mathbf{r}')e^{-\imath k\hat{\mathbf{e}}_r\cdot\mathbf{r}'}d^3r' \ .$$

This shows that, in the far-field zone, the vector potential behaves like a spherically expanding wave modulated by an angular coefficient. It is easy to show, that the fields calculated from (19.22) are transverse to the radius vector and fall off as $1/r$. They correspond thus to the radiation fields. If the size of the source

[3] The expansion by $\frac{1}{kr}$ gives,

$$\frac{e^{-\imath k\hat{\mathbf{e}}_r\cdot r'}}{kr-k\hat{\mathbf{e}}_r\cdot r'} = \frac{e^{-\imath k\hat{\mathbf{e}}_r\cdot r'}}{kr}\left[\frac{\hat{\mathbf{e}}_r\cdot r'}{r}+\left(\frac{\hat{\mathbf{e}}_r\cdot r'}{r}\right)^2+\ldots\right] \simeq \frac{e^{-\imath k\hat{\mathbf{e}}_r\cdot r'}}{kr} \ .$$

is small compared to a wavelength, it is appropriate to expand the exponential in the integral in (19.25) in powers of k,

$$\lim_{kr\to\infty}\mathbf{A}(\mathbf{r})=\frac{\mu_0 k}{4\pi}\sum_n\frac{(-\imath)^n}{n!}\frac{e^{\imath kr}}{kr}\int\mathbf{j}(\mathbf{r}')(\hat{\mathbf{e}}_r\cdot k\mathbf{r}')^n d^3r' \ .$$

The magnitude of the n-th term is given by $\frac{1}{n!}\int\mathbf{j}(\mathbf{r}')(\hat{\mathbf{e}}_r\cdot k\mathbf{r}')^n d^3r'$. Since the order of magnitude of $\mathbf{r}'$ is d, and since we assumed $kr'\ll 1$, consecutive terms decrease rapidly with n. Consequently, the radiation emitted from the source comes mainly from the first terms of the expansion (19.26).

19.1.2.1 The electric monopole

We notice that the lowest order radiation found in the expansion of $\mathbf{A}$ is dipolar. How about monopolar fields? Let us examine the issue of electric monopole fields, when the sources vary in time. The contribution of the electric monopole is obtained by substituting $|\mathbf{r}-\mathbf{r}'|\to|\mathbf{r}|=r$ in the integral (19.21) for the potential Φ. The result is,

$$\Phi_{monopole}(\mathbf{r},t)=\frac{1}{4\pi\varepsilon_0}\frac{e^{\imath kr}}{r}\int\rho(\mathbf{r}')d^3r'=\frac{Q}{4\pi\varepsilon_0}\frac{e^{\imath kr}}{r} \ . \tag{19.35}$$

where $q(t)$ is the total charge of the source. Since the charge is localized in the source (and therefore conserved), the total charge q is independent of time. Thus, the electrical monopole part of the potential of a localized source is necessarily static. Radiation with harmonic temporal dependence, $e^{-\imath\omega t}$, does not have monopolar terms in the fields.

Now let us go back to multipolar fields. Since these fields can be calculated from the vector potential via (19.23), we omit explicit references to the scalar potential in the following.

19.1.3 Radiation of an oscillating electric dipole

Keeping only the first term in (19.30) we get the potential vector (19.33),

$$\mathbf{A}(\mathbf{r})=\frac{\mu_0}{4\pi}\frac{e^{\imath kr}}{r}\int\mathbf{j}(\mathbf{r}')d^3r' \ . \tag{19.36}$$

which is valid everywhere outside the source. Using the continuity equation we can rewrite it, using a result from Exc. 19.1.6.1,

$$\mathbf{A}(\mathbf{r})=-\frac{\mu_0}{4\pi}\frac{e^{\imath kr}}{r}\int\mathbf{r}'(\nabla'\cdot\mathbf{j})d^3r'=-\frac{\mu_0}{4\pi}\frac{e^{\imath kr}}{r}\imath\omega\int\mathbf{r}'\varrho(\mathbf{r}')d^3r' \ . \tag{19.37}$$

With the *electric dipole moment*,

$$\mathbf{d}\equiv\int\mathbf{r}'\varrho(\mathbf{r}')d^3r' \ , \tag{19.38}$$

defined in electrostatics we write,

$$\boxed{\mathbf{A}(\mathbf{r})=-\frac{\mu_0}{4\pi}\frac{e^{\imath kr}}{r}\imath\omega\mathbf{d}} \ . \tag{19.39}$$

We obtain the fields via the equations (19.22),

$$\boxed{\begin{aligned}\vec{\mathcal{B}} &= -\frac{ck^3\mu_0}{4\pi}(\hat{\mathbf{e}}_r \times \mathbf{d})\frac{e^{\imath kr}}{kr}\left(1-\frac{1}{\imath kr}\right)\\ \vec{\mathcal{E}} &= \frac{k^3}{4\pi\varepsilon_0}\left\{(\hat{\mathbf{e}}_r \times \mathbf{d})\times\hat{\mathbf{e}}_r\frac{e^{\imath kr}}{kr} + [3\hat{\mathbf{e}}_r(\hat{\mathbf{e}}_r\cdot\mathbf{d})-\mathbf{d}]\left(\frac{1}{(kr)^3}-\frac{\imath}{(kr)^2}\right)e^{\imath kr}\right\}\end{aligned}} \; . \tag{19.40}$$

We observe that the magnetic field is transverse to the radius vector $\hat{\mathbf{e}}_r$ at all distances, but that the electric field has components parallel and perpendicular to $\hat{\mathbf{e}}_r$. In Exc. 19.1.6.2 we will derive the fields (19.40) directly from the potentials.

In the radiation zone $kr \gg 1$ the fields adopt the typical behavior,

$$\vec{\mathcal{B}} = -\frac{ck^3\mu_0}{4\pi}(\hat{\mathbf{e}}_r \times \mathbf{d})\frac{e^{\imath kr}}{kr} \quad \text{and} \quad \vec{\mathcal{E}} = \frac{k^3}{4\pi\varepsilon_0}(\hat{\mathbf{e}}_r \times \mathbf{d})\times\hat{\mathbf{e}}_r\frac{e^{\imath kr}}{kr} \; . \tag{19.41}$$

In the near-field zone $kr \ll 1$,

$$\vec{\mathcal{B}} = \frac{\imath\omega\mu_0}{4\pi}(\hat{\mathbf{e}}_r \times \mathbf{d})\frac{1}{r^2} \quad \text{and} \quad \vec{\mathcal{E}} = \frac{1}{4\pi\varepsilon_0}[3\hat{\mathbf{e}}_r(\hat{\mathbf{e}}_r\cdot\mathbf{d})-\mathbf{d}]\frac{1}{r^3} \; , \tag{19.42}$$

does not have the propagation term $e^{\imath kr}$. The electric field, apart from its temporal oscillations, is just a static electric dipole. The magnetic field is, apart from a constant $Z_0 \equiv \sqrt{\mu_0/\varepsilon_0}$ called *vacuum impedance*, smaller by a factor kr than the electric field in the region where $kr \ll 1$. Thus, the fields in the near-field zone are of predominantly electrical nature. The magnetic field disappears, obviously, in the static limit $k \to 0$. In this case, the near-field zone extends to infinity.

The Poynting vector in the far-field due to the oscillation of the dipole moment $\mathbf{d}$ is, inserting (19.41),

$$\begin{aligned}\vec{\mathcal{S}} &= \frac{1}{2\mu_0}\vec{\mathcal{E}}\times\vec{\mathcal{B}}^* = -\frac{ck^4}{32\pi^2\varepsilon_0 r^2}\{[\hat{\mathbf{e}}_r \times \mathbf{d})\times\hat{\mathbf{e}}_r]\times(\hat{\mathbf{e}}_r \times \mathbf{d})\} \qquad (19.43)\\ &= -\frac{ck^4}{32\pi^2\varepsilon_0 r^2}(d^2-d_r^2)\hat{\mathbf{e}}_r = -\frac{ck^4}{32\pi^2\varepsilon_0 r^2}\hat{\mathbf{e}}_r d^2\sin^2\theta \; .\end{aligned}$$

The radiated power is given by the absolute value of (19.43) per solid angle element [4]. If the components of $\mathbf{d}$ all have the same phase, the angular distribution is a typical dipole pattern,

$$\frac{dP}{d\Omega} = \frac{c}{32\pi^2\varepsilon_0}k^4|\mathbf{d}|^2\sin^2\theta \; . \tag{19.44}$$

where the angle θ is measured from the direction of $\mathbf{d}$. The total radiated power, regardless of the relative phases of the components of $\mathbf{d}$, is,

$$P = \frac{cZ_0}{12\pi\varepsilon_0}|\mathbf{d}|^2 = \frac{\mu_0}{12\pi c}|\mathbf{d}|^2 \; , \tag{19.45}$$

[4] When writing angular distributions of radiation, we will always exhibit the polarization explicitly by writing the absolute square of a vector that is proportional to the electric field. If the angular distribution of a particular polarization is desired, it can then be obtained by taking the scalar product of the vector with the appropriate polarization vector before the square.

which is half of the value calculated in the derivation of the Larmor formula (19.19), because in (19.43) we choose to calculate directly the temporal average of the Poynting vector.

Resolve the 19.1.6.3. In Exc. 19.1.6.4 we will verify the gauge of the dipolar potential and in Exc. 19.1.6.5 we calculate the fields of a linear antenna.

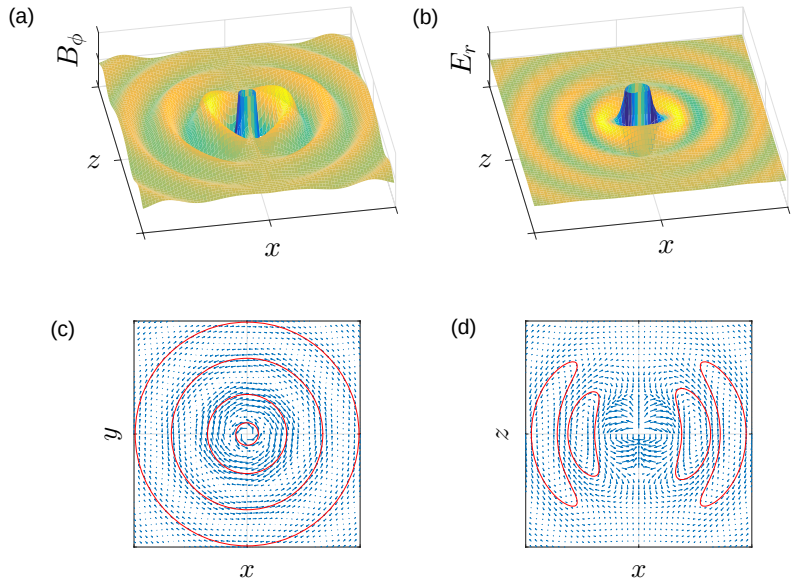

Figure 19.2: (code) Electric dipole radiation patterns. (a) Cut through $\vec{\mathcal{B}}_\phi$, (b) cut through $\vec{\mathcal{E}}_r$, (c) field lines of $\vec{\mathcal{B}}$ in the xy-plane, and (d) field lines of $\vec{\mathcal{E}}$ in the xz-plane. A movie can be seen at (watch movie).

Example 114 (*Linear antenna*): As an example, we calculate the power radiated by an oscillating charge $\varrho(\mathbf{r},t) = Q\delta(x)\delta(y)\delta(z - z_0 e^{-\imath\omega t})$. The dipole moment is,

$$\mathbf{d} = \int \mathbf{r}'\varrho(\mathbf{r}',t)dV' = Q\hat{\mathbf{e}}_z z_0 e^{-\imath\omega t} \ .$$

Inserted into the formula (19.45),

$$P = \frac{cZ_0 Q^2 z_0^2}{12\pi\varepsilon_0} \ .$$

Example 115 (*Linear antenna*): As another example we calculate the power radiated by a simple linear antenna, characterized by a current distribution $\mathbf{j}(\mathbf{r},t) = I_0\hat{\mathbf{e}}_z\delta(x)\delta(y)(1 - 2|z|/a)e^{-\imath\omega t}$. The dipole moment is,

$$\mathbf{d} = \frac{\imath}{\omega}\int \mathbf{j}dV' = \frac{\imath}{\omega} I_0\hat{\mathbf{e}}_z e^{-\imath\omega t}\int_{-a/2}^{a/2}\mathbf{j}dV'\left(1 - \frac{2|z'|}{a}\right)dz' = \frac{\imath I_0 a}{2\omega}\hat{\mathbf{e}}_z e^{-\imath\omega t} \ .$$

Inserted into the formula (19.45),

$$P = \frac{Z_0 I_0^2 (ka)^2}{48\pi} \ .$$

19.1.4 Magnetic dipole and electric quadrupole radiation

The term $\ell = 1$ in the expansion (19.28) leads to the second vector potential (19.34),

$$\mathbf{A}(\mathbf{r}) = -\imath\frac{\mu_0}{4\pi}\imath k h_1^{(1)} \int \mathbf{j}(\mathbf{r}')(\hat{\mathbf{e}}_r \cdot \mathbf{r}')d^3r' = \frac{\mu_0}{4\pi}\frac{e^{\imath kr}}{r}\left(\frac{1}{r} - \imath k\right)\int \mathbf{j}(\mathbf{r}')(\hat{\mathbf{e}}_r \cdot \mathbf{r}')d^3r' \ . \tag{19.46}$$

This vector potential can be written as the sum of two terms: one gives a transverse magnetic field and the other gives a transverse electric field. These physically distinct contributions can be separated by rewriting the integrand in (19.46) as the sum of a part, which is symmetric about an exchange of $\mathbf{j}$ and $\mathbf{r}'$, and an antisymmetric part. Therefore,

$$(\hat{\mathbf{e}}_r \cdot \mathbf{r}')\mathbf{j} = \tfrac{1}{2}[(\hat{\mathbf{e}}_r \cdot \mathbf{r}')\mathbf{j} + (\hat{\mathbf{e}}_r \cdot \mathbf{j})\mathbf{r}'] - \hat{\mathbf{e}}_r \times \tfrac{1}{2}(\mathbf{r}' \times \mathbf{j}) \ , \tag{19.47}$$

using the rule $B(AC) - C(AB)$. The second (antisymmetric) part is recognizable as the magnetization due to the current $\mathbf{j}$:

$$\vec{\mathcal{M}} = \tfrac{1}{2}(\mathbf{r}' \times \mathbf{j}) \ . \tag{19.48}$$

We will see, that the first (symmetric) term is related to the electric quadrupole moment density.

19.1.4.1 Magnetic dipole radiation

Considering, for the moment, only the magnetization term, we get the vector potential,

$$\boxed{\mathbf{A}(\mathbf{r}) = \frac{\imath k\mu_0}{4\pi}(\hat{\mathbf{e}}_r \times \mathbf{m})\frac{e^{\imath kr}}{r}\left(1 - \frac{1}{\imath kr}\right)} \ , \tag{19.49}$$

where $\mathbf{m}$ is the *magnetic dipole moment*,

$$\mathbf{m} = \int \vec{\mathcal{M}} d^3r = \tfrac{1}{2}\int (\mathbf{r} \times \mathbf{j})d^3r \ . \tag{19.50}$$

The fields can be determined by observing that the vector potential (19.49) is proportional to the magnetic field (19.40) of an electric dipole (except that we have to exchange the electric by the magnetic dipole moment). Thus, we can use the calculations we already made and transfer the results to the fields of a magnetic dipole via Eqs. (19.22):

$$\boxed{\begin{aligned} \vec{\mathcal{B}} &= \frac{k^3\mu_0}{4\pi}\left\{(\hat{\mathbf{e}}_r \times \mathbf{m}) \times \hat{\mathbf{e}}_r \frac{e^{\imath kr}}{kr} + [3\hat{\mathbf{e}}_r(\hat{\mathbf{e}}_r \cdot \mathbf{m}) - \mathbf{m}]\left(\frac{1}{(kr)^3} - \frac{\imath}{(kr)^2}\right)e^{\imath kr}\right\} \\ \vec{\mathcal{E}} &= -\frac{ck^3\mu_0}{4\pi}(\hat{\mathbf{e}}_r \times \mathbf{m})\frac{e^{\imath kr}}{kr}\left(1 - \frac{1}{\imath kr}\right) \end{aligned}} \ . \tag{19.51}$$

In Exc. 19.1.6.6 we will derive the fields (19.51) directly from the potentials.

All arguments concerning the behavior of the fields in the near-field and far-field regions are the same as those proposed for the electric dipole radiation with the modifications,

$$\begin{aligned} \vec{\mathcal{E}}^{(M1)} &\overset{\mathbf{m}\leftrightarrow c\mathbf{d}}{\longleftrightarrow} c\vec{\mathcal{B}}^{(E1)} \\ c\vec{\mathcal{B}}^{(M1)} &\overset{\mathbf{m}\leftrightarrow c\mathbf{d}}{\longleftrightarrow} \vec{\mathcal{E}}^{(E1)} \ . \end{aligned} \tag{19.52}$$

Likewise, the radiation pattern and the total radiated power are the same for the two types of dipole. The only difference in the radiation fields are their polarizations. For an electric dipole, the electric field vector lies in the plane defined by $\hat{\mathbf{e}}_r$ and $\mathbf{d}$, whereas for a magnetic dipole, it is perpendicular to the plane defined by $\hat{\mathbf{e}}_r$ and $\mathbf{m}$.

19.1.4.2 Electric quadrupole radiation

The integral of the symmetric term in (19.47) can be transformed using the continuity equation and integrating by parts:

$$\tfrac{1}{2}\int[(\hat{\mathbf{e}}_r\cdot\mathbf{r}')\mathbf{j}+(\hat{\mathbf{e}}_r\cdot\mathbf{j})\mathbf{r}']d^3r' = -\tfrac{\imath\omega}{2}\int\mathbf{r}'(\hat{\mathbf{e}}_r\cdot\mathbf{r}')\varrho(\mathbf{r}')d^3r' \ . \tag{19.53}$$

This will be demonstrated in Exc. 19.1.6.1. Since this integral involves the second moments of charge density, it corresponds to a quadrupolar electric radiation source. The potential vector is,

$$\boxed{\mathbf{A}(\mathbf{r}) = -\frac{\mu_0 ck^2}{8\pi}\frac{e^{\imath kr}}{r}\left(1-\frac{1}{\imath kr}\right)\int\mathbf{r}'(\hat{\mathbf{e}}_r\cdot\mathbf{r}')\varrho(\mathbf{r}')d^3r'} \ . \tag{19.54}$$

The expressions for the fields are a bit complicated, such that we focus on the radiation zone, where it is easy to verify that,

$$\vec{\mathcal{B}} = \nabla\times\mathbf{A} = \imath k\hat{\mathbf{e}}_r\times\mathbf{A} \quad , \quad \vec{\mathcal{E}} = \imath ck(\hat{\mathbf{e}}_r\times\mathbf{A})\times\hat{\mathbf{e}}_r \ . \tag{19.55}$$

Consequently, the magnetic field is,

$$\vec{\mathcal{B}} = -\frac{\imath ck^3\mu_0}{8\pi}\frac{e^{\imath kr}}{r}\int(\hat{\mathbf{e}}_r\times\mathbf{r}')(\hat{\mathbf{e}}_r\cdot\mathbf{r}')\varrho(\mathbf{r}')d^3re' \ . \tag{19.56}$$

With the definition of the tensor of the quadrupolar moment,

$$Q_{\alpha\beta} \equiv \int(3x_\alpha x_\beta - r^2\delta_{\alpha\beta})\varrho(\mathbf{r}')d^3r' \ , \tag{19.57}$$

the integral (19.56) can be written as,

$$\hat{\mathbf{e}}_r\times\int\mathbf{r}'(\hat{\mathbf{e}}_r\cdot\mathbf{r}')\varrho(\mathbf{r}')d^3\mathbf{r}' = \tfrac{1}{3}\hat{\mathbf{e}}_r\times\mathbf{Q}(\hat{\mathbf{e}}_r) \ , \tag{19.58}$$

where the vector $\mathbf{Q}(\hat{\mathbf{e}}_r)$ is defined via its components,

$$Q_\alpha = \sum_{\alpha\beta} Q_{\alpha\beta}\hat{\mathbf{e}}_\beta \ . \tag{19.59}$$

We note that its magnitude and direction depend on the direction of observation as well as on the properties of the source. With these definitions, we get the magnetic field,

$$\vec{\mathcal{B}} = -\frac{\imath c k^3 \mu_0}{24\pi} \frac{e^{\imath kr}}{r} \hat{\mathbf{e}}_r \times \mathbf{Q}(\hat{\mathbf{e}}_r) \ , \tag{19.60}$$

and the time-averaged power radiated into a solid angle,

$$\frac{dP}{d\Omega} = \frac{c^2 Z_0}{1152\pi^2} k^6 |[\hat{\mathbf{e}}_r \times \mathbf{Q}(\hat{\mathbf{e}}_r)] \times \hat{\mathbf{e}}_r|^2 \ . \tag{19.61}$$

The final expressions are complicated [659], but for the example of a ellipsoidal charge distribution periodically changing its 'aspect ratio', it is possible to show that the angular distribution of the radiation pattern exhibits four lobes,

$$\frac{dP}{d\Omega} = \frac{c^2 Z_0 k^6}{512\pi^2} Q_0^2 \sin^2\theta \cos^2\theta \ , \tag{19.62}$$

and the total radiated power is,

$$P = \frac{c^2 Z_0 k^6}{960\pi} Q_0^2 \ . \tag{19.63}$$

For multipoles of higher order the formulas become more and more complicated. Other techniques based on the multipolar expansion of the wave equation, rather than deriving the radiation patterns directly from the retarded potentials, are more suitable. Resolve the Exc. 19.1.6.7.

19.1.5 Multipolar expansion of the wave equation

The radiation from sources which are small in comparison with the observation distance exhibits a symmetry suggesting a reformulation of the wave equation in spherical coordinates, as we have already done in Sec. 13.6.3. In short, we consider a scalar field $\psi(\mathbf{r}, t)$ satisfying the wave equation,

$$\nabla^2 \psi - \frac{1}{c^2} \frac{\partial^2 \psi}{\partial t^2} = 0 \ . \tag{19.64}$$

The temporal dependency is separated by a Fourier transform,

$$\psi(\mathbf{r}, t) = \int_{-\infty}^{\infty} \phi(\mathbf{r}, \omega) e^{-\imath\omega t} d\omega \ , \tag{19.65}$$

yielding a distribution of the amplitudes which satisfying the Poisson equation,

$$(\nabla^2 + k^2)\phi(\mathbf{r}, \omega) = 0 \ , \tag{19.66}$$

with $\omega^2 = c^2 k^2$. Expanding into spherical harmonics by the ansatz,

$$\phi(\mathbf{r}, \omega) = \sum_{\ell, m} f_\ell(r) Y_{\ell,m}(\theta, \phi) \ , \tag{19.67}$$

we transform (19.66), where the Laplacian is expressed in spherical coordinates, into a differential equation which is independent of m,

$$\left[\frac{d^2}{dr^2} + \frac{2}{r}\frac{d}{dr} + k^2 - \frac{\ell(\ell+1)}{r^2}\right] f_\ell(r) = 0 \ . \tag{19.68}$$

This equation is precisely the spherical Bessel equation, whose solutions are linear combinations of spherical Bessel and von Neumann functions,

$$A_\ell j_\ell(kr) + B_\ell n_\ell(kr) \ . \tag{19.69}$$

With respect to the spherical part, we note that the spherical harmonics are the eigenfunctions of the square of an angular momentum operator $\hat{\mathbf{L}}$, which can be identified with the angular part of the Laplacian in spherical coordinates,

$$\hat{\mathbf{L}}^2 = -\left[\frac{1}{\sin\theta}\frac{\partial}{\partial \sin\theta}\left(\sin\theta\frac{\partial}{\partial \sin\theta}\right) + \frac{1}{\sin^2\theta}\frac{\partial}{\partial\phi}\right] \ , \tag{19.70}$$

and has as eigenvalues the integer numbers $\ell(\ell+1)$,

$$\hat{\mathbf{L}}^2 Y_{\ell m} = \ell(\ell+1) Y_{\ell m} \ . \tag{19.71}$$

The Lie algebra ruling the calculation with angular momentum operators will not be reproduced here [5].

Clearly, the simplicity of the multipolar expansion of the wave equation (19.64) into spherical coordinates is due to its scalar nature, and a similar procedure is used to solve the scalar Schrödinger equation for the hydrogen atom. Electromagnetic fields, however, are vectorial which complicates the calculus, as we will see in the following.

19.1.5.1 Multipolar expansion of the fields

Assuming a time dependence as $e^{-\imath\omega t}$ and combining the Maxwell equations for the field rotations to derive the Helmholtz equation, we obtain a set of equations, which is equivalent to the Maxwell equations,

$$(\nabla^2 + k^2)\vec{\mathcal{B}} = 0 \qquad \text{and} \qquad \nabla\cdot\vec{\mathcal{B}} = 0 \qquad \text{with} \qquad \vec{\mathcal{E}} = \imath\frac{c}{k}\nabla\times\vec{\mathcal{B}} \ , \tag{19.72}$$

or alternatively,

$$(\nabla^2 + k^2)\vec{\mathcal{E}} = 0 \qquad \text{and} \qquad \nabla\cdot\vec{\mathcal{E}} = 0 \qquad \text{with} \qquad \vec{\mathcal{B}} = \imath\frac{1}{ck}\nabla\times\vec{\mathcal{E}} \ . \tag{19.73}$$

Now, we have for any well-behaved vector field $\mathbf{X}$,

$$\nabla^2(\mathbf{r}\cdot\mathbf{X}) = \mathbf{r}\cdot(\nabla^2\mathbf{X}) + 2\nabla\cdot\mathbf{X} \ . \tag{19.74}$$

Applying this relation to the electromagnetic fields, we find,

$$\boxed{(\nabla^2 + k^2)(\mathbf{r}\cdot\vec{\mathcal{B}}) = 0 \qquad \text{and} \qquad (\nabla^2 + k^2)(\mathbf{r}\cdot\vec{\mathcal{E}}) = 0} \ . \tag{19.75}$$

[5] See the treatment of spherical potentials in Sec. 23.3.1 .

The *transverse magnetic field* and the *transverse electric field* can be rewritten by the rotation of the equations (19.72) respectively (19.73),

$$\begin{aligned} \mathbf{r}\cdot\vec{\mathcal{B}} &= \tfrac{\imath}{ck}\mathbf{r}\cdot(\nabla\times\vec{\mathcal{E}}) = \tfrac{\imath}{ck}(\mathbf{r}\times\nabla)\cdot\vec{\mathcal{E}} \equiv \tfrac{1}{ck}\mathbf{L}\cdot\vec{\mathcal{E}} \\ \mathbf{r}\cdot\vec{\mathcal{E}} &= \tfrac{\imath c}{k}\mathbf{r}\cdot(\nabla\times\vec{\mathcal{B}}) = \tfrac{\imath c}{k}(\mathbf{r}\times\nabla)\cdot\vec{\mathcal{B}} \equiv \tfrac{c}{k}\mathbf{L}\cdot\vec{\mathcal{B}} \end{aligned} \quad , \tag{19.76}$$

defining in this way the operator for the orbital angular momentum $\mathbf{L}$.

These scalar fields can now be expanded as demonstrated in (19.67) and (19.69). That is, we can expand the transverse parts of electric and magnetic fields into magnetic (electric) multipoles as,

$$\begin{aligned} \mathbf{r}\cdot\vec{\mathcal{B}}^{(M)}_{\ell m} &= \tfrac{\ell(\ell+1)}{k} g_\ell(kr) Y_{\ell m}(\theta,\phi) = \tfrac{1}{ck}\mathbf{L}\cdot\vec{\mathcal{E}}^{(M)}_{\ell m} \quad \text{and} \quad \mathbf{r}\cdot\vec{\mathcal{E}}^{(M)}_{\ell m} = 0 \\ \mathbf{r}\cdot\vec{\mathcal{E}}^{(E)}_{\ell m} &= -Z_0\tfrac{\ell(\ell+1)}{k} f_\ell(kr) Y_{\ell m}(\theta,\phi) = \tfrac{c}{k}\mathbf{L}\cdot\vec{\mathcal{B}}^{(E)}_{\ell m} \quad \text{and} \quad \mathbf{r}\cdot\vec{\mathcal{B}}^{(E)}_{\ell m} = 0 \end{aligned} \quad . \tag{19.77}$$

where g_ℓ is a linear combination of Bessel and Hankel functions and $\ell(\ell+1)/k$ a convenient normalization factor.

We can see (by simplifying the argument a bit) that, by comparing (19.77) with the equation (19.71) the field $\vec{\mathcal{E}}^{(M)}$ must contain the operator $\mathbf{L}$,

$$\boxed{\begin{aligned} \vec{\mathcal{E}}^{(M)} &= c g_\ell(kr)\mathbf{L}Y_{\ell m}(\theta,\phi) \quad \text{with} \quad \vec{\mathcal{B}}^{(M)} = -\tfrac{\imath}{ck}\nabla\times\vec{\mathcal{E}}^{(M)}_{\ell m} \\ \vec{\mathcal{B}}^{(E)} &= \mu_0 g_\ell(kr)\mathbf{L}Y_{\ell m}(\theta,\phi) \quad \text{with} \quad \vec{\mathcal{E}}^{(E)} = -\tfrac{\imath c}{k}\nabla\times\vec{\mathcal{B}}^{(E)}_{\ell m} \end{aligned}} \quad . \tag{19.78}$$

The functions,

$$\mathbf{X}_{\ell m}(\theta,\phi) = \frac{1}{\sqrt{\ell(\ell+1)}}\mathbf{L}Y_{\ell m}(\theta,\phi) \ , \tag{19.79}$$

are known as *vector spherical harmonics*. Combining the expansions into electric and magnetic multipoles we obtain,

$$\begin{aligned} \vec{\mathcal{B}} &= \sum_{\ell m}\left[a^{(E)}_{\ell,m} f_\ell(kr)\mathbf{X}_{\ell,m} - \tfrac{\imath}{k}a^{(M)}_{\ell,m}\nabla\times g_\ell(kr)\mathbf{X}_{\ell m}\right] \\ \vec{\mathcal{E}} &= \sum_{\ell m}\left[\tfrac{\imath}{k}a^{(E)}_{\ell,m}\nabla\times f_\ell(kr)\mathbf{X}_{\ell,m} - a^{(M)}_{\ell,m} g_\ell(kr)\mathbf{X}_{\ell m}\right] \ . \end{aligned} \tag{19.80}$$

The coefficients can be determined from the radial projections of the fields.

19.1.5.2 Vector spherical harmonics

The *vector spherical harmonics* defined above are a particular case of those defined for the coupling of two spins $\mathbf{L}$ and $\mathbf{S}$ with $S=1$ in the following sense,

$$\boxed{\mathbf{Y}_{j\ell m} = \sum_q \begin{pmatrix} J & 1 & L \\ -m & q & m-q \end{pmatrix} Y^{(\ell)}_{m-q}\hat{\mathbf{e}}_q} \ , \tag{19.81}$$

where the basis is in Cartesian coordinates,

$$\hat{\mathbf{e}}_0 = \hat{\mathbf{e}}_z \qquad \text{and} \qquad \hat{\mathbf{e}}_\pm = -\tfrac{1}{\sqrt{2}}(\hat{\mathbf{e}}_x \pm \imath\hat{\mathbf{e}}_y) \ . \tag{19.82}$$

These functions are tensor operators of rank $(1,\ell)$, since $\mathbf{Y}_{j\ell m} = (Y^{(\ell)} \otimes \hat{\mathbf{e}}^{(1)})^{(j)}_m$. This means they have vectorial properties via $\hat{\mathbf{e}}^{(1)}_q$ and, at the same time, are tensor operators just like the spherical harmonics $Y^{(\ell)}_m$. It is possible to check the following expressions,

$$\begin{aligned}
\mathbf{J}^2\mathbf{Y}_{j\ell m} &= j(j+1)\mathbf{Y}_{j\ell m} \\
\mathbf{L}^2\mathbf{Y}_{j\ell m} &= \ell(\ell+1)\mathbf{Y}_{j\ell m} \\
\mathbf{S}^2\mathbf{Y}_{j\ell m} &= 2\mathbf{Y}_{j\ell m} \\
\mathbf{J}_z\mathbf{Y}_{j\ell m} &= m\mathbf{Y}_{j\ell m} \ .
\end{aligned} \tag{19.83}$$

Furthermore, comparing (19.83) and (19.79),

$$\begin{aligned}
\frac{\mathbf{L}}{\sqrt{\ell(\ell+1)}}Y^{(\ell)}_m = -\imath\mathbf{Y}_{\ell\ell m} &= \mathbf{X}_{\ell m} \\
\frac{\mathbf{r}}{r}Y^{(\ell)}_m = \imath\sqrt{\frac{\ell+1}{2\ell+1}}\mathbf{Y}_{\ell\ \ell+1\ m} &- \imath\sqrt{\frac{l}{2\ell+1}}\mathbf{Y}_{\ell\ \ell-1\ m} \\
0 = \mathbf{r}\cdot\mathbf{Y}_{\ell\ell m} &= \mathbf{p}\cdot\mathbf{Y}_{\ell\ell m} \ .
\end{aligned} \tag{19.84}$$

In 19.1.6.8 we calculate the following examples, $\mathbf{Y}_{000} = 0$ and,

$$r\mathbf{Y}_{110} = \sqrt{\tfrac{3}{16\pi}}\begin{pmatrix} -\imath y \\ \imath x \\ 0 \end{pmatrix} \quad , \quad r\mathbf{Y}_{11\pm1} = \sqrt{\tfrac{3}{16\pi}}\begin{pmatrix} z \\ \pm\imath \\ -(x\pm\imath y) \end{pmatrix} \quad , \quad r\mathbf{Y}_{10\pm1} = -\sqrt{\tfrac{1}{24\pi}}\begin{pmatrix} x \\ \pm\imath y \\ 0 \end{pmatrix} \ . \tag{19.85}$$

Also,

$$\mathbf{Y}^2_{\kappa\kappa m} = [\kappa(\kappa+1)-m(m+1)]|Y_{\kappa\ m+1}|^2+2m^2|Y_{\kappa\ m}|^2+[\kappa(\kappa+1)-m(m-1)]|Y_{\kappa\ m-1}|^2 \ . \tag{19.86}$$

Applying the formulas [1368](Chp. 10.1) to scalar and vector products of vector spherical harmonics, it is possible to derive the energy density $\frac{\varepsilon_0}{2}\vec{\mathcal{E}}^2_{jm\tau} + \frac{1}{2\mu_0}\vec{\mathcal{B}}^2_{jm\tau}$ and the Poynting vector $\varepsilon_0|\vec{\mathcal{E}}_{jm\tau}\times\vec{\mathcal{B}}_{jm\tau}|$. The calculation is complicated, because we must calculate $(3j)$, $\{6j\}$, and $\{9j\}$ coefficients. Considering that the angular distribution is the same for electric and magnetic multipolar radiation, we obtain,

$$u_{jm\tau}(\mathbf{r}) = \frac{1}{2\mu_0}\vec{\mathcal{B}}^2_{jm\tau}(\mathbf{r}) = -\frac{\hbar\omega}{4V}\left(\frac{j+1}{2j+1}\right)^2\frac{(kr)^{2j}}{(2j+1)!!^2}\mathbf{Y}^2_{jjm} \ , \tag{19.87}$$

The question now is, with what polarization ε and under what angle of incidence $\mathbf{k}$ can we excite a particular multipolar transition. The transition can only be excited by a mode, to which it couples and, therefore, into which it can radiate light. Therefore, it is sufficient to analyze the angular distribution and the polarization of spontaneously

emitted radiation. In the far-field of a point source the electric and magnetic fields satisfy the Helmholtz equation [1368],

$$(\triangle + \mathbf{k}^2)\vec{\mathcal{E}}(\mathbf{r},t) = 0 \ , \tag{19.88}$$

and similarly for the magnetic field $\vec{\mathcal{B}}(\mathbf{r},t)$. An atomic transition $|J,m_J\rangle \leftrightarrow |J+\kappa, m_J+m\rangle$ interacts with the electric or magnetic multipolar part κ of the radiation field. The general solution of the Helmholtz equation, therefore, is expanded into spherical harmonics $Y_{\kappa m}(\theta,\phi)$:

$$\vec{\mathcal{E}} = \sum_{\kappa=0}^{\infty}\sum_{m=-\kappa}^{\kappa}\left(\vec{\mathcal{E}}_m^{(E\kappa)} + \vec{\mathcal{E}}_m^{(M\kappa)}\right) \tag{19.89}$$

and similarly for the magnetic field. The angular distributions of the multipolar electric field components are calculated by,

$$\vec{\mathcal{E}}_m^{(E\kappa)} = -\imath k^{-1}\nabla\times\vec{\mathcal{B}}_m^{(E\kappa)} \tag{19.90}$$

$$\vec{\mathcal{B}}_m^{(E\kappa)} = -\imath\left(\mathbf{k}\times\nabla\right)Y_{\kappa m}(\theta,\phi) \equiv \sqrt{\kappa(\kappa+1)}\mathbf{Y}_{\kappa\kappa m}(\theta,\phi) \ , \tag{19.91}$$

and similarly for the magnetic field. The field components can be expressed by the vector spherical harmonics $\mathbf{Y}_{\kappa\kappa m}$. The angular distribution of the radiated intensity follows from the absolute value of the Poynting vector,

$$I_m^{(E\kappa)}(\mathbf{r}) = \mu_0^{-1}\left|\vec{\mathcal{E}}_m^{(E\kappa)}(\mathbf{r})\times\vec{\mathcal{B}}_m^{(E\kappa)}(\mathbf{r})\right| = \mu_0^{-1}\left|\vec{\mathcal{B}}_m^{(E\kappa)}(\mathbf{r})\right|^2 \propto \mathbf{Y}_{\kappa\kappa m}(\theta,\phi)^2 \ . \tag{19.92}$$

The multipolar order of a radiation can, in principle, be determined by measuring its angular distribution. The above distribution integrate over all possible polarizations. If polarized light is used, in order to excite transitions between selected Zeeman levels, the angular intensity distribution of *polarized radiation* must be calculated. The transition rate between two levels $|a\rangle$ and $|b\rangle$ for light incident from a given direction $\mathbf{r}$ with a given polarization $\hat{\varepsilon}$ is, $|\langle b|\hat{\varepsilon}\vec{\mathcal{E}}_m^{(E\kappa)}(\mathbf{r})|a\rangle|^2$, where $\vec{\mathcal{E}}_m^{(E\kappa)}(\mathbf{r}) = -\imath k^{-1}\nabla\times\vec{\mathcal{B}}_m^{(E\kappa)}(\mathbf{r})$. The cases of linear polar polarization (respectively axial) of the light field in relation to the quantization axis are expressed by the fractions $\hat{\varepsilon}_{polar}\cdot\mathbf{Y}_{\kappa\kappa m}$, respectively, $\hat{\varepsilon}_{axial}\cdot\mathbf{Y}_{\kappa\kappa m}$, the absolute square values of which add up to the angular intensity distribution,

$$\begin{aligned}
u_{10} &\sim 4|Y_1^{(1)}|^2 &&= \tfrac{3}{4\pi}2\sin^2\theta \\
u_{1\pm1} &\sim 2|Y_1^{(1)}|^2 + 2|Y_0^{(1)}|^2 &&= \tfrac{3}{4\pi}(1+\cos^2) \\
u_{20} &\sim 12|Y_1^{(2)}|^2 &&= \tfrac{5}{4\pi}18\sin^2\cos^2 \\
u_{2\pm1} &\sim 4|Y_2^{(2)}|^2 + 2|Y_1^{(2)}|^2 + 6|Y_0^{(2)}|^2 &&= \tfrac{5}{4\pi}3(4\cos^2 -3\cos^2 +1) \\
u_{2\pm2} &\sim 8|Y_2^{(2)}|^2 + 4|Y_1^{(2)}|^2 &&= \tfrac{5}{4\pi}3\sin^2(1+\cos^2) \\
u_{30} &\sim 24|Y_1^{(3)}|^2 &&= \tfrac{7}{4\pi}\tfrac{9}{2}\sin^2(5\cos^2 -1)^2 \\
u_{3\pm1} &\sim 10|Y_2^{(3)}|^2 + 2|Y_1^{(3)}|^2 + 12|Y_0^{(3)}|^2 &&= \tfrac{7}{4\pi}\tfrac{3}{8}(225\cos^6 -305\cos^4 +111\cos^2 +1) \\
u_{3\pm2} &\sim 6|Y_3^{(3)}|^2 + 8|Y_2^{(3)}|^2 + 10|Y_1^{(3)}|^2 &&= \tfrac{7}{4\pi}\tfrac{15}{4}\sin^2(9\cos^4 -2\cos^2 +1) \\
u_{3\pm3} &\sim 18|Y_3^{(3)}|^2 + 6|Y_2^{(3)}|^2 &&= \tfrac{7}{4\pi}\tfrac{45}{8}\sin^4(1+\cos^2) \ .
\end{aligned} \tag{19.93}$$

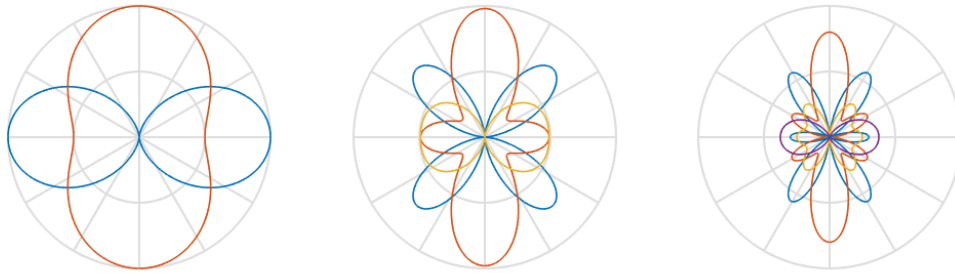

Figure 19.3: (code) Angular dependence of dipolar radiation u_{1m} (left), quadrupolar u_{2m} (center) and u_{3m} octupolar (right) with their respective contributions $m = 0$ (blue), $m = \pm 1$ (red), $m = \pm 2$ (yellow) and $m = \pm 3$ (magenta).

In the equatorial plane, only the parts $u_{j\pm 1}$ contribute; but these disappear in polar direction. All other components lie in the equatorial plane. For non-polarized radiation the angular distribution is uniform,

$$\sum_{m=-j}^{j} u_{jm} \sim \tfrac{2j+1}{4\pi} 2(j+1)! \; . \tag{19.94}$$

19.1.5.3 Distribution of the polarization of multipolar radiation

The axial and polar components of the vector spherical harmonics $\mathbf{Y}_{j\ell m}(\theta, \phi)$ at the observation point $\mathbf{r}$ can be determined as follows: First, we orient the coordinate system via the application of two rotation matrices $M_z(\phi)$ and $M_y(\theta)$ such that the observation point lies on top of the x axis. Then, we project the vector spherical harmonic via the application of a projection matrix $M_p(\lambda)$ on a straight line, which is perpendicular to the x-axis and forms with the y-axis an angle λ, as illustrated in Fig. 19.4. Finally, the coordinate system is rotated back to the original position:

$$\mathbf{Y}^{\lambda}_{jlm}(\theta, \phi) = M_z(\phi)^{-1} M_y(\theta)^{-1} M_p(\lambda) M_y(\theta) M_z(\phi) \mathbf{Y}_{jlm}(\theta, \phi) \tag{19.95}$$

with

$$M_p(\lambda) = \begin{pmatrix} 1 & 0 & 0 \\ 0 & \sin\lambda & 0 \\ 0 & 0 & \cos\lambda \end{pmatrix} \quad , \quad M_y(\theta) = \begin{pmatrix} \cos\theta & 0 & -\sin\theta \\ 0 & 1 & 0 \\ \sin\theta & 0 & \cos\theta \end{pmatrix} \quad , \tag{19.96}$$

$$M_z(\phi) = \begin{pmatrix} \cos\phi & -\sin\phi & 0 \\ \sin\phi & \cos\phi & 0 \\ 0 & 0 & 1 \end{pmatrix} \; . \tag{19.97}$$

The projection of the vector spherical harmonics $\mathbf{Y}_{jlm}(\theta, \phi)$ onto the vector field $\mathbf{Y}^{\lambda}_{j\ell m}(\theta, \phi)$ describes, how the light emitted by the multipolar transition is modified by transmission through a polarizer, whose main axis is rotated about the quantization axis by an angle λ.

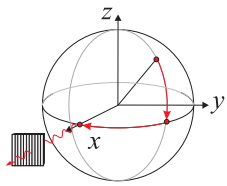

Figure 19.4: Illustration of the measurement of $\mathbf{Y}_{j\ell m}(\vartheta,\varphi)$.

19.1.5.4 Coupling of multipolar fields to radiation sources

We consider distributions of charges, currents, and *intrinsic magnetization*, e.g. the electron spin.

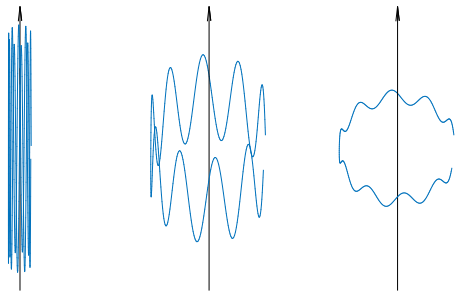

Figure 19.5: Classical picture of the electronic motion excited by (a) π-light, (c) $\sigma^{\pm}$-light, and (b) both.

19.1.5.5 Atomic multipoles

Here, we consider the electric charges and currents of an atom interacting with electromagnetic fields. We borrow the parametrization of the charges (17.25) and currents (17.39) in the atomic layer from the microscopic model of Maxwell's equations,

$$\varrho_{mic}(\mathbf{r}) = Ze\delta(\mathbf{r}) - \sum_j e\delta(\mathbf{r}-\mathbf{r}_j) \quad , \quad \mathbf{j}_{mic}(\mathbf{r}) = \sum_j e\dot{\mathbf{r}}_j\delta(\mathbf{r}-\mathbf{r}_j) \ . \tag{19.98}$$

We derive a polarization (17.34) and a magnetization (17.50) which, in the absence of free charges and currents, are given by,

$$\varrho_{mic}(\mathbf{r}) = -\nabla\cdot\vec{\mathcal{P}}(\mathbf{r}) \quad , \quad \mathbf{j}_{mic}(\mathbf{r}) = \dot{\mathbf{P}}(\mathbf{r}) + \nabla\times\vec{\mathcal{M}}(\mathbf{r}) \ . \tag{19.99}$$

Interacting with radiation fields $\vec{\mathcal{E}}$ and $\vec{\mathcal{B}}$, the interaction energy is,

$$W = -\int \vec{\mathcal{E}}(\mathbf{r})\cdot\vec{\mathcal{P}}(\mathbf{r})\ d^3r - \int \vec{\mathcal{M}}(\mathbf{r})\cdot\vec{\mathcal{B}}(\mathbf{r})\ d^3r \ . \tag{19.100}$$

The multipolar expansion using the above five equations gives,

$$\begin{aligned} W = e\sum\nolimits_j \left[1 + \tfrac{1}{2!}(\mathbf{r}_j\cdot\nabla) + \tfrac{1}{3!}(\mathbf{r}_j\cdot\nabla)^2 + ..\right]\mathbf{r}_j\cdot\vec{\mathcal{E}}(0) + \\ + \tfrac{e}{m}\sum\nolimits_j \left[\tfrac{1}{2!} + \tfrac{2}{3!}(\mathbf{r}_j\cdot\nabla) + \tfrac{3}{4!}(\mathbf{r}_j\cdot\nabla)^2 + ..\right]\mathbf{l}_j\cdot\vec{\mathcal{B}}(0) \ , \end{aligned} \tag{19.101}$$

where $\mathbf{l}_j \equiv m\mathbf{r}_j \times \dot{\mathbf{r}}_j$. Introducing dipole, quadrupole, and octupolar electric and magnetic moments,

$$\begin{array}{ll} \mathbf{d}_E = \sum_j \mathbf{r}_j & \mathbf{d}_M = \frac{1}{2!}\frac{1}{cm}\sum_j \mathbf{l}_j \\ \mathbf{q}_E = \frac{1}{2!}\sum_j \mathbf{r}_j \otimes \mathbf{r}_j & \mathbf{q}_M = \frac{2}{3!}\frac{1}{cm}\sum_j \mathbf{l}_j \otimes \mathbf{r}_j \\ \mathbf{o}_E = \frac{1}{2!}\sum_j \mathbf{r}_j \otimes \mathbf{r}_j \otimes \mathbf{r}_j & \mathbf{o}_M = \frac{3}{4!}\frac{1}{cm}\sum_j \mathbf{l}_j \otimes \mathbf{r}_j \otimes \mathbf{r}_j \end{array} \tag{19.102}$$

and making the ansatz for the fields $\vec{\mathcal{E}}(\mathbf{r}) = \hat{\epsilon}\vec{\mathcal{E}}_0 e^{\imath \mathbf{k}\cdot\mathbf{r}}$ and $\vec{\mathcal{B}}(\mathbf{r}) = (\mathbf{k}\times\hat{\epsilon})\vec{\mathcal{B}}_0 e^{\imath\mathbf{k}\cdot\mathbf{r}}$, where $\vec{\mathcal{B}}_0 = \vec{\mathcal{E}}_0/c$ we obtain,

$$\begin{aligned} W = {} & e\vec{\mathcal{E}}_0\hat{\varepsilon}[\mathbf{d}_E + \mathbf{q}_E\nabla + \mathbf{o}_E(\nabla\otimes\nabla) + ..]\; e^{\imath\mathbf{k}\cdot\mathbf{r}}\big|_{\mathbf{r}=0} \\ & + e\vec{\mathcal{E}}_0(\mathbf{k}\times\hat{\varepsilon})[\mathbf{d}_M + \mathbf{q}_M\nabla + \mathbf{o}_M(\nabla\otimes\nabla) + ..]\; e^{\imath\mathbf{k}\cdot\mathbf{r}}\big|_{\mathbf{r}=0}\ . \end{aligned} \tag{19.103}$$

The gradient only acts on the coordinate $\mathbf{r}$,

$$W = e\vec{\mathcal{E}}_0\hat{\varepsilon}[\mathbf{d}_E + \mathbf{q}_E\imath\mathbf{k} - \mathbf{o}_E(\mathbf{k}\otimes\mathbf{k}) + ..] + e\vec{\mathcal{E}}_0(\hat{\mathbf{k}}\times\hat{\varepsilon})[\mathbf{d}_M + \mathbf{q}_M\imath\mathbf{k} - \mathbf{o}_M(\mathbf{k}\otimes\mathbf{k}) + ..]\ . \tag{19.104}$$

To render irreducible multipolar component we replace,

$$\mathbf{q}_E \to \mathbf{q}_E - \tfrac{1}{3}\vec{\mathcal{E}}_3 \mathrm{Tr}\ \mathbf{q}_E = \tfrac{1}{2!}\left(\mathbf{r}\otimes\mathbf{r} - \tfrac{1}{3}\vec{\mathcal{E}}_3 r^2\right)\ . \tag{19.105}$$

19.1.5.6 Multipolar expansion of the vector potential

When the radiation has a small wavelength, or when dipolar transitions are prohibited by selection rules, higher multipolar orders can enter the game [718]. Then we expand the plane waves into spherical waves,

$$e^{\imath\mathbf{k}\cdot\mathbf{r}} = 4\pi\sum_{\ell=0}^{\infty}\sum_{m=-\ell}^{\ell}\imath^\ell j_\ell(kr)Y_\ell^m(\hat{\mathbf{e}}_k)Y_\ell^{m*}(\hat{\mathbf{e}}_r) = \sum_{\ell=0}^{\infty}(2\ell+1)\imath^\ell j_\ell(kr)P_\ell(\hat{\mathbf{e}}_k\cdot\hat{\mathbf{e}}_r)\ . \tag{19.106}$$

The quantum operator for the vector potential is,

$$\boxed{\begin{array}{lll} \hat{\mathbf{A}}^-(\mathbf{r}) = \sqrt{\frac{\hbar\omega}{2\varepsilon_0 V}}\hat{\epsilon}e^{\imath\mathbf{k}\cdot\mathbf{r}}\hat{a} & = \sum_{j=0}^{\infty}\sum_{m=-j}^{j}\sum_{\tau=\pm(-1)^j}\hat{\mathbf{A}}^-_{jm\tau}(\mathbf{r}) & \\ \quad \text{onde} \quad \hat{\mathbf{A}}^-_{jm(-1)^j}(\mathbf{r}) & = \sqrt{\frac{\hbar\omega}{2\varepsilon_0 V}}\frac{1}{\sqrt{j(j+1)}}\frac{-\imath}{k}\nabla\times(\nabla\times\mathbf{r})Y_{jm}(\theta,\phi)j_j(kr)\hat{a}_{jm\tau} & . \\ \quad \text{and} \quad \hat{\mathbf{A}}^-_{jm(-1)^{j+1}}(\mathbf{r}) & = \sqrt{\frac{\hbar\omega}{2\varepsilon_0 V}}\frac{1}{\sqrt{j(j+1)}}\nabla\times\mathbf{r}Y_{jm}(\theta,\phi)j_j(kr)\hat{a}_{jm\tau} & \end{array}} \tag{19.107}$$

Multipolar electric radiation has the parity $\tau = (-1)^j$ and magnetic radiation the parity $\tau = -(-1)^j$,

$$\Pi\hat{\mathbf{A}}_{jm\tau}(\mathbf{r}) = -\hat{\mathbf{A}}_{jm\tau}(-\mathbf{r}) = \tau\hat{\mathbf{A}}_{jm\tau}(\mathbf{r})\ . \tag{19.108}$$

The partial fields $\hat{\mathbf{A}}_{jm\tau}$ are irreducible tensor fields of order j:

$$U_R \hat{\mathbf{A}}_{jm\tau}(\mathbf{r}) U_R^* = \hat{\mathbf{A}}_{jm\tau}(R^{-1}\mathbf{r}) = \sum_{m'} \hat{\mathbf{A}}_{jm'\tau}(\mathbf{r}) D^j_{mm'} \ . \tag{19.109}$$

As a result, the elements of the transition matrix are,

$$\langle j_f m_f \tau_f | \imath \hat{\mathbf{A}}_{jm\tau}(\mathbf{r}) \hat{p} | j_i m_i \tau_i \rangle \ . \tag{19.110}$$

19.1.5.7 Representation in terms of vector spherical harmonics

The electric vector potential can be written as,

$$\begin{aligned}
\hat{\mathbf{A}}^{(E)}_{jm\tau}(\mathbf{r}) &= \sqrt{\frac{\hbar}{2\varepsilon_0 V\omega}} \frac{1}{\sqrt{j(j+1)}} \frac{-\imath}{k} \nabla \times \mathbf{j} Y^{(j)}_m(\Omega) j_j(kr) \qquad (19.111)\\
&= \sqrt{\frac{\hbar}{2\varepsilon_0 V\omega}} \frac{-\imath}{k} \nabla \times Y_{jjm}(\Omega) j_j(kr) \\
&= \sqrt{\frac{\hbar}{2\varepsilon_0 V\omega}} \left[-\sqrt{j} 2j+1 \cancelto{0}{j_{j+1}(kr)} Y_{jj+1m}(\Omega) + \sqrt{\frac{j+1}{2j+1}} j_{j-1}(kr) Y_{jj-1m}(\Omega) \right] \ ,
\end{aligned}$$

because for a small source sizes we can approximate, $j_j(kr) \simeq (kr)^j/(2j+1)!!$. We obtain,

$$\boxed{\begin{aligned}
\hat{\mathbf{A}}^{(E)}_{jm\tau}(\mathbf{r}) &= \sqrt{\tfrac{\hbar}{2\varepsilon_0 V\omega}} \sqrt{\tfrac{j+1}{2j+1}} \tfrac{(kr)^{j-1}}{(2j-1)!!} Y_{jj-1m} \\
\hat{\vec{\mathcal{E}}}^{(E)}_{jm\tau}(\mathbf{r}) &= -\tfrac{\partial \hat{\mathbf{A}}^{(E)}_{jm\tau}}{\partial t} = \imath \sqrt{\tfrac{\hbar\omega}{2\varepsilon_0 V}} \sqrt{\tfrac{j+1}{2j+1}} \tfrac{(kr)^{j-1}}{(2j-1)!!} Y_{jj-1m} \\
\hat{\vec{\mathcal{B}}}^{(E)}_{jm\tau}(\mathbf{r}) &= \nabla \times \hat{\mathbf{A}}^{(E)}_{jm\tau} = -\imath \sqrt{\tfrac{\mu_0 \hbar\omega}{2V}} \tfrac{j+1}{2j+1} \tfrac{(kr)^j}{(2j+1)!!} Y_{jjm} \ .
\end{aligned}} \tag{19.112}$$

Similarly we obtain for the magnetic vector potential,

$$\hat{\mathbf{A}}^{(M)}_{jm\tau}(\mathbf{r}) = -\imath \sqrt{\frac{\hbar}{2\varepsilon_0 V\omega}} \frac{1}{\sqrt{j(j+1)}} \mathbf{j} Y^{(j)}_m(\Omega) j_j(kr) = -\imath \sqrt{\frac{\hbar}{2\varepsilon_0 V\omega}} j_j(kr) Y_{jjm}(\Omega) \ , \tag{19.113}$$

and for a small source sizes,

$$\boxed{\begin{aligned}
\hat{\mathbf{A}}^{(M)}_{jm\tau}(\mathbf{r}) &= -\imath \sqrt{\tfrac{\hbar}{2\varepsilon_0 V\omega}} \tfrac{(kr)^j}{(2j+1)!!} Y_{jjm} \\
\hat{\vec{\mathcal{E}}}^{(M)}_{jm\tau}(\mathbf{r}) &= \sqrt{\tfrac{\hbar\omega}{2\varepsilon_0 V}} \tfrac{(kr)^j}{(2j+1)!!} Y_{jjm} \\
\hat{\vec{\mathcal{B}}}^{(M)}_{jm\tau}(\mathbf{r}) &= \sqrt{\tfrac{\mu_0 \hbar\omega}{2V}} \sqrt{\tfrac{j+1}{2j+1}} \tfrac{(kr)^{j-1}}{(2j-1)!!} Y_{jj-1m} \ .
\end{aligned}} \tag{19.114}$$

19.1.5.8 Interaction with light fields

The interaction energy is expressed by insertion of the field operators for $\vec{\mathcal{E}}$ and $\vec{\mathcal{B}}$,

$$\hat{\vec{\mathcal{E}}}(\mathbf{r})^- = \hat{\vec{\mathcal{E}}}_0^- \hat{\epsilon} e^{\imath \mathbf{k}\cdot\mathbf{r}} \quad \text{and} \quad \hat{\vec{\mathcal{B}}}(\mathbf{r})^- = \hat{\vec{\mathcal{E}}}_0^- \tfrac{1}{\omega} \mathbf{k} \times \hat{\epsilon} e^{\imath \mathbf{k}\cdot\mathbf{r}} \quad \text{with} \quad \hat{\vec{\mathcal{E}}}_0^- \equiv \imath \sqrt{\frac{\hbar\omega}{2\varepsilon_0 V}} \hat{a} \ . \tag{19.115}$$

Here, $\hat{\vec{\mathcal{E}}}_0^+$ creates a photon, while $\hat{\vec{\mathcal{E}}}_0^-$ annihilates a photon. Considering first order processes (RWA), we obtain for the matrix element $\langle f|\hat{H}_{ww}|i\rangle$ for the emission of a photon (and similarly for absorption),

$$\langle g, n+1|\hat{H}_{ww}|e, n\rangle = -ie\sqrt{\frac{\hbar\omega}{2\varepsilon_0 V}}\langle n+1|\hat{a}^\dagger|n\rangle\left[\hat{\epsilon}\langle g|\mathbf{d}_E + ...|e\rangle + (\hat{\mathbf{e}}_k \times \hat{\epsilon})\langle g|\mathbf{d}_M + ...|e\rangle)\right] . \tag{19.116}$$

Finally, the matrix elements for the first three multipolar orders are,

$$\begin{aligned}\langle f|\hat{H}_{ww}|i\rangle = -ie\sqrt{\frac{\hbar\omega}{2\varepsilon_0 V}}\sqrt{\cdot}\,[\hat{\epsilon}(\langle g|\mathbf{d}_E|e\rangle + \imath\langle g|\mathbf{q}_E|e\rangle\mathbf{k} - \langle g|\mathbf{o}_E|e\rangle\mathbf{k}\times\mathbf{k} + ...) \\ +(\hat{\mathbf{e}}_k \times \hat{\epsilon})(\langle g|\mathbf{d}_M|e\rangle + \imath\langle g|\mathbf{q}_M|e\rangle\mathbf{k} - \langle g|\mathbf{o}_M|e\rangle\mathbf{k}\times\mathbf{k} + ...)] .\end{aligned} \tag{19.117}$$

For $\sqrt{\cdot} = \sqrt{n+1}$ this formula describes induced and spontaneous emission and for $\sqrt{\cdot} = \sqrt{n}$ absorption.

19.1.5.9 Matrix element for electromagnetic transitions

The matrix element is a tensor product between the vector operator $\hat{\mathbf{p}}$ and a vector spherical harmonic $\mathbf{Y}_{j\ell m}$. Therefore,

$$\begin{aligned}\hat{\mathbf{A}}^{(E)}_{jm\tau}(\mathbf{r})\cdot\hat{\mathbf{p}} &= \imath\sqrt{\frac{\hbar}{2\varepsilon_0 V\omega}}\frac{\sqrt{j+1}}{(2j+1)!!}\langle j||p^{(1)}||j-1\rangle(kr)^{j-1}Y^{(j)}_m \\ \hat{\mathbf{A}}^{(M)}_{jm\tau}(\mathbf{r})\cdot\hat{\mathbf{p}} &= -\imath\sqrt{\frac{\hbar}{2\varepsilon_0 V\omega}}\frac{1}{\sqrt{j+1}(2j+1)!!}\langle j||p^{(1)}||j\rangle(kr)^{j}Y^{(j)}_m .\end{aligned} \tag{19.118}$$

In addition, we have $Y^{(j)}_m = \imath^{-j}\langle\Omega|jm\rangle$, and therefore,

$$\langle j_f m_f|Y^{(j)}_m|j_i m_i\rangle = \imath^{j_j - j_i}\frac{\sqrt{2j+1}\sqrt{2j_i+1}}{\sqrt{4\pi}\sqrt{2j_f+1}}\left(\begin{array}{c|ccc} j_f & j & j_i \\ m_f & m & m_i\end{array}\right)\left(\begin{array}{c|ccc} j_f & j & j_i \\ 0 & 0 & 0\end{array}\right) . \tag{19.119}$$

This relation contains the selection rules for the matrix element $\langle j_j m_j \tau_f|\hat{\mathbf{A}}_{jm\tau}(\mathbf{r})\cdot\hat{\mathbf{p}}|j_i m_i \tau_i\rangle$, i.e. the conservation laws for angular momentum and parity:

$$|j_f - j_i| \le j \le j_f + j_i \qquad \text{and} \qquad (-)^{j_j+j_i} = \tau . \tag{19.120}$$

19.1.5.10 Matrix element without hyperfine and fine structure

This matrix element relates the initial state to the final state by,

$$\langle\alpha L m|\hat{\mathbf{T}}^{(k)}_q|\alpha' L' m'\rangle . \tag{19.121}$$

The angular momentum of the electronic layer is not split any more. Following the Wigner-Eckart theorem we have,

$$\langle Lm|\hat{\mathbf{T}}^{(k)}_q|L'm'\rangle = (-)^{L-m_L}\begin{pmatrix} L' & k & L \\ m'_L & q & -m_L\end{pmatrix}\langle L||\hat{\mathbf{T}}^{(k)}_q||L'\rangle . \tag{19.122}$$

With the $(3j)$-symbol being $(3j) \sim \delta(L'kL)\delta_{m'_L+q,m_L}$ the following selection rules apply,

$$|L - L'| \leq k \leq L + L \qquad \text{and} \qquad m'_L + q = m_L \ . \tag{19.123}$$

The Zeeman splitting is normalized by,

$$\sum_{m_L, m'_L} |\langle Lm|\hat{\mathbf{T}}^{(k)}_q|L'm'\rangle|^2 = |\langle L||\hat{\mathbf{T}}^{(k)}_q||L'\rangle|^2 \ . \tag{19.124}$$

With this, we obtain for the relative oscillator strengths,

$$\left| \frac{\langle Lm|\hat{\mathbf{T}}^{(k)}_q|L'm'\rangle}{\langle L||\hat{\mathbf{T}}^{(k)}_q||L'\rangle} \right|^2 = \begin{pmatrix} L' & k & L \\ m'_L & q & -m_L \end{pmatrix}^2 \ . \tag{19.125}$$

However, electric multipole radiation does not act on $\mathbf{L}$, but on $\mathbf{J}$. For example, in the ion Yb^+ the transition ${}^2D_{5/2} - {}^2P_{1/2}$ is dipolarly prohibited, but not ${}^2D_{3/2} - {}^2P_{1/2}$.

19.1.5.11 Fermi's golden rule

A *Fermi's Golden rule* (first perturbative order) allows us to make a gross estimation of the transition rate,

$$\frac{1}{\tau} = \frac{2\pi}{\hbar^2}|\langle f|\hat{H}_{ww}|i\rangle|^2\delta(\omega - \omega_0) \ . \tag{19.126}$$

For spontaneous emission we have,

$$\frac{1}{\tau} = \frac{2\pi}{\hbar^2}\frac{e^2}{m^2}\frac{\hbar}{\omega 2\varepsilon_0 V}|\langle g|e^{\imath\mathbf{k}\cdot\mathbf{r}}\hat{H}_{ww}|i\rangle|^2 \ . \tag{19.127}$$

Approximating $p/m \simeq c$ and $V \simeq \lambda^3$ and using $\alpha \equiv e^2/(4\pi\varepsilon_0\hbar c)$ and $r \simeq a_B$, we obtain,

$$\frac{1}{\tau} = \frac{\alpha}{2\pi}\omega^2|\langle e^{\imath k a_B}\rangle|^2\delta(\omega) \ . \tag{19.128}$$

Now, expanding the exponential function into plane waves (19.106) and using the limit $kr \ll \ell$, where the Bessel function is well approximated by (19.27), we obtain,

$$\frac{1}{\tau} = \frac{2\pi\alpha}{(2\ell+1)!!^2}(ka_B)^{2\ell}\omega|\langle||\rangle|^2 \ . \tag{19.129}$$

19.1.6 Exercises

19.1.6.1 Ex: Relationship between current density and electric dipole moment

a. For a charge and current configuration contained in a volume $\mathcal{V}$ show that, $\int_{\mathcal{V}} \mathbf{j} dV = \frac{d\mathbf{d}}{dt}$, where $\mathbf{d}$ is the total dipolar moment.
b. Demonstrate the relationship, $\int \mathbf{r}'(\hat{\mathbf{e}}_r\cdot\mathbf{r}')\dot{\varrho}(\mathbf{r}')d^3r' = \int \{\mathbf{j}(\mathbf{r}')(\hat{\mathbf{e}}_r\cdot\mathbf{r}') + \mathbf{r}'[\hat{\mathbf{e}}_r\cdot\mathbf{j}(\mathbf{r}')]\}\, d^3r'$.

Solution: *a. We first calculate,*

$$0 = \oint_{\partial\mathcal{V}} x\mathbf{j}\cdot d\mathbf{S} = \int_{\mathcal{V}} \nabla\cdot(x\mathbf{j})dV = \int_{\mathcal{V}} (\nabla x\cdot\mathbf{j} + x\nabla\cdot\mathbf{j})dV$$
$$= \int_{\mathcal{V}} (j_x + x\nabla\cdot\mathbf{j})dV = \int_{\mathcal{V}} \left(j_x - x\frac{\partial\varrho}{\partial t}\right) dV \ ,$$

where we used the continuity equation. By choosing the volume large enough, the surface integral vanishes. Generalizing to 3D, we get,

$$\int_{\mathcal{V}} \mathbf{j}dV = \int_{\mathcal{V}} \mathbf{r}\frac{\partial\varrho}{\partial t}dV \equiv \frac{d\mathbf{d}}{dt} \ ,$$

which is the definition of the dipole moment.
b. The continuity equation allows us to replace $\imath\omega\varrho(\mathbf{r}')$ *by* $\nabla\cdot\mathbf{j}(\mathbf{r}')$*,*

$$-\tfrac{\imath\omega}{2}\int \mathbf{r}'(\hat{\mathbf{e}}_r\cdot\mathbf{r}')\varrho(\mathbf{r}')d^3r' = -\tfrac{1}{2}\int \mathbf{r}'(\hat{\mathbf{e}}_r\cdot\mathbf{r}')\nabla\cdot\mathbf{j}(\mathbf{r}')d^3r' \ .$$

Considering only one coordinate, we can apply the rule of integration by parts,

$$0 = \oint (\psi\mathbf{j})\cdot d\mathbf{S} = \int \nabla(\psi\mathbf{j})d^3r' = \int (\mathbf{j}\cdot\nabla\psi + \psi\nabla\cdot\mathbf{j})d^3r' \ .$$

In the following way,

$$-\int x'(\hat{\mathbf{e}}_r\cdot\mathbf{r}')\nabla\cdot\mathbf{j}(\mathbf{r}')d^3r' = \int \mathbf{j}(\mathbf{r}')\cdot\nabla[x'(\hat{\mathbf{e}}_r\cdot\mathbf{r}')]d^3r'$$
$$= \int \mathbf{j}(\mathbf{r}')\cdot[(\hat{\mathbf{e}}_r\cdot\mathbf{r}')\nabla x' + x'\nabla(\hat{\mathbf{e}}_r\cdot\mathbf{r}')]d^3r'$$
$$= \int \mathbf{j}(\mathbf{r}')\cdot[(\hat{\mathbf{e}}_r\cdot\mathbf{r}')\hat{\mathbf{e}}_x + x'\hat{\mathbf{e}}_r]d^3r' = \int \{j_x(\mathbf{r}')(\hat{\mathbf{e}}_r\cdot\mathbf{r}') + x'[\hat{\mathbf{e}}_r\cdot\mathbf{j}(\mathbf{r}')]\}\, d^3r' \ .$$

Such that finally,

$$-\tfrac{\imath\omega}{2}\int \mathbf{r}'(\hat{\mathbf{e}}_r\cdot\mathbf{r}')\varrho(\mathbf{r}')d^3r' = \int \{\mathbf{j}(\mathbf{r}')(\hat{\mathbf{e}}_r\cdot\mathbf{r}') + \mathbf{r}'[\hat{\mathbf{e}}_r\cdot\mathbf{j}(\mathbf{r}')]\}\, d^3r' \ .$$

19.1.6.2 Ex: Hertz dipole

A Hertz dipole with vertical orientation is in the focus of a parabolic antenna PA1 and emits electromagnetic radiation with a frequency of 3 GHz. The shape of the antenna is such that the electromagnetic radiation is reflected forming a 'parallel' beam with diameter $d = 3\,\mathrm{m}$. The electric field within the beam can be roughly described by the following formula:

$$\vec{\mathcal{E}}_1(\mathbf{r},t) = \vec{\mathcal{E}}_0\cos(\mathbf{k}_1\cdot\mathbf{r} - \omega t)\ \hat{\mathbf{e}}_z \qquad \text{where} \qquad \mathbf{k}_1 = -k\hat{\mathbf{e}}_x\sin\alpha + k\hat{\mathbf{e}}_y\cos\alpha \ .$$

a. Determine the parameter k using the wave equation.
b. What is the amplitude $\vec{\mathcal{E}}_0$ of the electric field assuming that the parabolic antenna emits a power of 5 W?
c. There is a second Hertz dipole, acting as a detector, oriented orthogonal to $\mathbf{k}_1$. The maximum amplitude of the electric field detected by D2 is around 0.1 V/m. Estimate the angle of the orientation of the dipole with respect to the vertical axis (without calculation, but with a short justification).
d. Now, the emitter dipole D1 is also rotated in such a way that, regardless of the orientation of the dipole D2, it does not receive signals. What is the orientation of the dipole emitter? Give a short justification.
e. The dipole emitter is again oriented vertically. Another parabolic antenna PA2, identical to PA1, is now integrated into the experiment, as shown in the figure. Calculate the power density S on the axis x in the time average. ($\alpha = 5°$)
Help: Addition theorems:

$$\cos(\alpha \pm \beta) = \cos\alpha\cos\beta \mp \sin\alpha\sin\beta \qquad \text{and} \qquad \cos 2\alpha = \cos^2\alpha - \sin^2\alpha$$

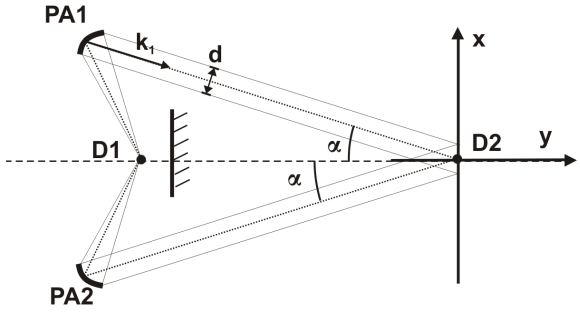

Figure 19.6: Hertz dipole.

Solution: *a. The wave equation gives,*

$$0 = \frac{1}{c^2}\frac{\partial^2\vec{\mathcal{E}}_1}{\partial t^2} - \nabla^2\vec{\mathcal{E}}_1 = \frac{-\omega^2}{c^2}\vec{\mathcal{E}}_1 - \frac{\partial^2}{\partial x^2}\vec{\mathcal{E}}_1 - \frac{\partial^2}{\partial y^2}\vec{\mathcal{E}}_1 - \cancelto{0}{\frac{\partial^2}{\partial z^2}\vec{\mathcal{E}}_1}$$
$$= \frac{-\omega^2}{c^2}\vec{\mathcal{E}}_1 + k^2\vec{\mathcal{E}}_1\sin^2\alpha + k^2\vec{\mathcal{E}}_1\cos^2\alpha = \frac{-\omega^2}{c^2}\vec{\mathcal{E}}_1 + k^2\vec{\mathcal{E}}_1 \ ,$$

such that, $k = \omega/c$.
b. The power being,

$$P = I\pi\frac{d^2}{4} = c\varepsilon_0\vec{\mathcal{E}}_0^2\pi\frac{d^2}{4} = 5\,\mathrm{W} \ ,$$

we calculate $\vec{\mathcal{E}}_0 \approx 23\,\mathrm{V/m}$. c. The dipole D2 is oriented in the direction ???
d. The dipole D2 is oriented such as to oscillate along the line D1-PA1.
e.

19.1.6.3 Ex: Dipolar spherical waves

We derived in class, starting from the relations $\vec{\mathcal{B}} = \nabla \times \mathbf{A}$ and $\vec{\mathcal{E}} = \frac{\imath c}{k}\nabla \times \vec{\mathcal{B}}$, the expressions (19.40) for the magnetic and electric fields of a electric dipole radiation produced by the dipole moment $\mathbf{d} = d\hat{\mathbf{e}}_z$.
a. Show that the magnetic field can be expressed in the form $\vec{\mathcal{B}} = \vec{\mathcal{B}}_\phi(r,\theta)\hat{\mathbf{e}}_\phi$.
b. Show that the electric field can be expressed in the form $\vec{\mathcal{E}} = \vec{\mathcal{E}}_r(r,\theta)\hat{\mathbf{e}}_r + \vec{\mathcal{E}}_\theta(r,\theta)\hat{\mathbf{e}}_\theta$.
c. The purpose of this exercise is to check in spherical coordinates, where the divergence and rotation are given by (12.79) and (12.80), that these fields satisfy Maxwell's equations.

Solution: *a. We calculate,*

$$\begin{aligned}\vec{\mathcal{B}} = \frac{ck^3\mu_0}{4\pi}\mathfrak{Re}\left[\hat{\mathbf{e}}_r \times \mathbf{d}\frac{e^{\imath(kr-\omega t)}}{kr}\left(1-\frac{1}{\imath kr}\right)\right] &= -\frac{ck^3 d\mu_0}{4\pi}\sin\theta\hat{\mathbf{e}}_\phi Re\left[\frac{e^{\imath u}}{kr}\left(1-\frac{1}{\imath kr}\right)\right] \\ &= -\frac{ck^3 d\mu_0}{4\pi}\sin\theta\left[\frac{\cos u}{kr}-\frac{\sin u}{(kr)^2}\right]\hat{\mathbf{e}}_\phi \\ &\equiv \vec{\mathcal{B}}_\phi\hat{\mathbf{e}}_\phi \ ,\end{aligned}$$

where we introduced the abbreviation $u \equiv kr - \omega t$ and used $\hat{\mathbf{e}}_r \times \hat{\mathbf{e}}_z = -\hat{\mathbf{e}}_\phi$.
b. We calculate,

$$\begin{aligned}\vec{\mathcal{E}} &= \frac{k^3}{4\pi\varepsilon_0}\mathfrak{Re}\left[(\hat{\mathbf{e}}_r\times\mathbf{d})\times\hat{\mathbf{e}}_r\frac{e^{\imath(kr-\omega t)}}{kr} + [3\hat{\mathbf{e}}_r(\hat{\mathbf{e}}_r\cdot\mathbf{d})-\mathbf{d}]\left(\frac{1}{(kr)^2}+\frac{1}{\imath kr}\right)\frac{e^{\imath(kr-\omega t)}}{kr}\right] \\ &= \frac{k^3 d}{4\pi\varepsilon_0}\mathfrak{Re}\left[-\sin\theta\hat{\mathbf{e}}_\theta\frac{e^{\imath(kr-\omega t)}}{kr} + [2\cos\theta\hat{\mathbf{e}}_r+\sin\theta\hat{\mathbf{e}}_\theta]\left(\frac{1}{(kr)^2}+\frac{1}{\imath kr}\right)\frac{e^{\imath(kr-\omega t)}}{kr}\right] \\ &= \frac{k^3 d}{4\pi\varepsilon_0}Re\left[2\cos\theta\left(\frac{1}{(kr)^2}+\frac{1}{\imath kr}\right)\frac{e^{\imath u}}{kr}\hat{\mathbf{e}}_r + \sin\theta\left(\frac{1}{(kr)^2}+\frac{1}{\imath kr}-1\right)\frac{e^{\imath u}}{kr}\hat{\mathbf{e}}_\theta\right] \\ &= \frac{k^3 d}{4\pi\varepsilon_0}\left[2\cos\theta\left(\frac{\cos u}{(kr)^2}+\frac{\sin u}{kr}\right)\frac{1}{kr}\hat{\mathbf{e}}_r + \sin\theta\left(\frac{\cos u}{(kr)^2}+\frac{\sin u}{kr}-\cos u\right)\frac{1}{kr}\hat{\mathbf{e}}_\theta\right] \\ &\equiv \vec{\mathcal{E}}_r\hat{\mathbf{e}}_r + \vec{\mathcal{E}}_\theta\hat{\mathbf{e}}_\theta \ ,\end{aligned}$$

where we used $\hat{\mathbf{e}}_\phi \times \hat{\mathbf{e}}_r = \hat{\mathbf{e}}_\theta$ and $\hat{\mathbf{e}}_z = \hat{\mathbf{e}}_r\cos\theta - \hat{\mathbf{e}}_\theta\sin\theta$.
c. Maxwell's fourth equation is obvious,

$$\nabla\cdot\vec{\mathcal{B}} = \frac{1}{r\sin\theta}\frac{\partial}{\partial\phi}[\vec{\mathcal{B}}_\phi] = 0 \ .$$

The third gives,

$$\begin{aligned}\nabla\cdot\vec{\mathcal{E}} &= \frac{1}{r^2}\frac{\partial}{\partial r}[r^2\vec{\mathcal{E}}_r] + \frac{1}{r\sin\theta}\frac{\partial}{\partial\theta}(\sin\theta\vec{\mathcal{E}}_\theta) \\ &= \frac{k^3 d}{4\pi\varepsilon_0}2\cos\theta\frac{1}{(kr)^2}\frac{\partial}{\partial r}\left[\left(\frac{1}{kr}+\frac{1}{\imath}\right)e^{iu}\right] + \frac{k^3 d}{4\pi\varepsilon_0}\left(\frac{1}{(kr)^2}+\frac{1}{\imath kr}-1\right)\frac{e^{\imath u}}{kr}\frac{1}{r\sin\theta}\frac{\partial}{\partial\theta}\sin^2\theta \\ &= 0 \ .\end{aligned}$$

The second gives,

$$\begin{aligned}
\nabla\times\vec{\mathcal{E}} &= \frac{k^3 d}{4\pi\varepsilon_0}\frac{1}{r}\left[\frac{\partial}{\partial r}(r\vec{\mathcal{E}}_\theta)-\frac{\partial}{\partial\theta}(\vec{\mathcal{E}}_r)\right]\hat{\mathbf{e}}_\phi \\
&= \frac{k^3 d}{4\pi\varepsilon_0}\frac{1}{r}\left[\frac{1}{k}\sin\theta\frac{\partial}{\partial r}\left\{\left(\frac{1}{(kr)^2}+\frac{1}{\imath kr}-1\right)e^{\imath u}\right\}-\left(\frac{1}{(kr)^3}+\frac{1}{\imath(kr)^2}\right)e^{\imath u}\frac{\partial}{\partial\theta}2\cos\theta\right]\hat{\mathbf{e}}_\phi \\
&= -\imath\omega\frac{ck^3 d\mu_0}{4\pi}\sin\theta\left[\left(1-\frac{1}{\imath kr}\right)\frac{e^{\imath u}}{kr}\right]\hat{\mathbf{e}}_\phi = \frac{ck^3 p\mu_0}{4\pi}\frac{\partial}{\partial t}\sin\theta\left[\left(1-\frac{1}{\imath kr}\right)\frac{e^{\imath u}}{kr}\right]\hat{\mathbf{e}}_\phi \\
&= -\frac{\partial\vec{\mathcal{B}}}{\partial t}\ .
\end{aligned}$$

Finally, the first one gives,

$$\begin{aligned}
\nabla\times\vec{\mathcal{B}} &= \hat{\mathbf{e}}_r\frac{1}{r\sin\theta}\left[\frac{\partial}{\partial\theta}(\vec{\mathcal{B}}_\phi\sin\theta)\right]+\hat{\mathbf{e}}_\theta\frac{1}{r\sin\theta}\left[-\sin\theta\frac{\partial}{\partial r}(r\vec{\mathcal{B}}_\phi)\right] \\
&= -\frac{ck^3 d\mu_0}{4\pi}\left[\frac{1}{r\sin\theta}\left(\frac{1}{kr}-\frac{1}{\imath(kr)^2}\right)e^{\imath u}\frac{\partial}{\partial\theta}\sin^2\theta\hat{\mathbf{e}}_r-\frac{\sin\theta}{kr}\frac{\partial}{\partial r}\left(1-\frac{1}{\imath kr}\right)e^{\imath u}\hat{\mathbf{e}}_\theta\right] \\
&= -\imath\omega\frac{k^3 d\mu_0}{4\pi}\left[2\cos\theta\left(\frac{1}{(kr)^2}+\frac{1}{\imath kr}\right)\frac{e^{\imath u}}{kr}\hat{\mathbf{e}}_r+\sin\theta\left(\frac{1}{(kr)^2}+\frac{1}{\imath kr}-1\right)\frac{e^{\imath u}}{kr}\hat{\mathbf{e}}_\theta\right] \\
&= \frac{k^3 d}{4\pi\varepsilon_0}\frac{\partial}{c^2\partial t}\left[2\cos\theta\left(\frac{1}{(kr)^2}+\frac{1}{\imath kr}\right)\frac{e^{\imath u}}{kr}\hat{\mathbf{e}}_r+\sin\theta\left(\frac{1}{(kr)^2}+\frac{1}{\imath kr}-1\right)\frac{e^{\imath u}}{kr}\hat{\mathbf{e}}_\theta\right] \\
&= \frac{\partial\vec{\mathcal{E}}}{c^2\partial t}\ .
\end{aligned}$$

For an illustration see Fig. 19.2.

19.1.6.4 Ex: Gauges of dipolar potentials

Verify that the retarded potentials of an oscillating dipole,

$$\begin{aligned}
\Phi(r,\theta,t) &= \frac{p_0\cos\theta}{4\pi\varepsilon_0 r}\left\{-\frac{\omega}{c}\sin[\omega(t-r/c)]+\frac{1}{r}\cos[\omega(t-r/c)]\right\} \\
\mathbf{A}(r,\theta,t) &= -\frac{\mu_0 p_0\omega}{4\pi r}\sin[\omega(t-r/c)]\hat{\mathbf{e}}_z\ ,
\end{aligned}$$

satisfy the Lorentz gauge.

Solution: *With* $\hat{\mathbf{e}}_z = \cos\theta\hat{\mathbf{e}}_r - \sin\theta\hat{\mathbf{e}}_\theta$, *we calculate,*

$$\begin{aligned}
\nabla\cdot\mathbf{A} &= \frac{1}{r^2}\frac{\partial}{\partial r}[r^2 A_r] + \frac{1}{r\sin\theta}\frac{\partial}{\partial\theta}[\sin\theta A_\theta] + \frac{1}{r\sin\theta}\frac{\partial}{\partial\phi}[A_\phi] \\
&= -\frac{\mu_0 p_0\omega}{4\pi}\left\{\frac{1}{r^2}\frac{\partial}{\partial r}\frac{r^2\cos\theta\sin(\omega t-\omega r/c)}{r} + \frac{1}{r\sin\theta}\frac{\partial}{\partial\theta}\frac{-\sin^2\theta\sin(\omega t-\omega r/c)}{r}\right\} \\
&= -\frac{\mu_0 p_0\omega}{4\pi}\left\{-\cos\theta\frac{-c\sin(\omega t-\omega r/c)+r\omega\cos(\omega t-\omega r/c)}{cr^2} - \frac{2\cos\theta\sin(\omega t-\omega r/c)}{r^2}\right\} \\
&= -\frac{\mu_0 p_0\omega\cos\theta}{4\pi r}\left\{-\frac{\omega\cos[\omega(t-r/c)]}{c} - \frac{\sin[\omega(t-r/c)]}{r}\right\} \\
&= -\frac{1}{c^2}\frac{p_0\cos\theta}{4\pi\varepsilon_0 r}\frac{\partial}{\partial t}\left\{-\frac{\omega}{c}\sin[\omega(t-r/c)] + \frac{1}{r}\cos[\omega(t-r/c)]\right\} = -\frac{\partial\Phi}{c^2\partial t}\ .
\end{aligned}$$

19.1.6.5 Ex: Electric and magnetic fields of an oscillating electric dipole

Calculate the electric and magnetic fields of an oscillating electric dipole in the dipolar approximation ($kr' \ll 1$) but for arbitrary distances ($kr \lesseqgtr 1$) directly from the retarded potentials in spherical coordinates. Find the Poynting vector and show that the radiation intensity is exactly the same, as the one derived within the far-field approximation ($kr \gg 1$).

Solution: *To create an electric dipole, we imagine a charge oscillating between the two ends of a linear antenna of length* b, *such that* $Q(t) = Q_0\cos\omega t$. *The electric dipole moment is,*

$$\mathbf{d} = Q\mathbf{b} = Q_0 b\hat{\mathbf{e}}_z\cos\omega t\ ,$$

the oscillating charge distribution can be parametrized by [6],

$$\varrho(\mathbf{r}', t_r) = Q_0\cos\omega t_r\left[\delta^{(3)}(z'-b) - \delta^{(3)}(z'+b)\right]\ .$$

The retarded scalar potential is,

$$\Phi(\mathbf{r},t) = \frac{1}{4\pi\varepsilon_0}\int\frac{\varrho(\mathbf{r}',t_r)}{R}d^3r' = \frac{1}{4\pi\varepsilon_0}\left(\frac{Q_0\cos\omega t}{R_+} - \frac{Q_0\cos\omega t}{R_-}\right)\ ,$$

with $t_r = t - R/c$. *We parametrize the extremities by* $\mathbf{b} = b\hat{\mathbf{e}}_z$ *and concentrate on a point in the* $y = 0$ *plane, such that* $\mathbf{r} = r\hat{\mathbf{e}}_x\sin\theta + r\hat{\mathbf{e}}_z\cos\theta$. *Then the distances are,*

$$R_\pm = \sqrt{(\mathbf{r}-\mathbf{b})^2} = \sqrt{r^2 + (b/2)^2 \mp 2rb\cos\theta}\ .$$

For a perfect dipole we require a small antenna size, $b \ll r$. *This allows us to approximate, to first order in* b,

$$R_\pm \simeq r\left(1 \mp \frac{b}{2r}\cos\theta\right) \qquad \textit{and} \qquad \frac{1}{R_\pm} \simeq \left(1 \pm \frac{b}{2r}\cos\theta\right)\ , \tag{19.130}$$

[6] Note that these oscillations do not presuppose the existence of a current. We could also have assumed an oscillating current parametrized by $\varrho(\mathbf{r}', t_r) = Q_0\delta^{(3)}(kz' - b\cos\omega t_r)$.

such that,

$$\begin{aligned}\cos[\omega(t-\tfrac{R_\pm}{c})] &\simeq \cos\left[\omega(t-\tfrac{r}{c}) \pm \tfrac{\omega b}{2c}\cos\theta\right] \\ &= \cos[\omega(t-\tfrac{r}{c})]\cos\left(\tfrac{\omega b}{2c}\cos\theta\right) \mp \sin[\omega(t-\tfrac{r}{c})]\sin\left(\tfrac{\omega b}{2c}\cos\theta\right) \ .\end{aligned}$$

In the dipolar approximation we assume, $b \ll c/\omega$, such that,

$$\cos[\omega(t-\tfrac{R}{c})] \simeq \cos[\omega(t-\tfrac{r}{c})] \mp \tfrac{\omega b}{2c}\cos\theta\sin[\omega(t-\tfrac{r}{c})] \ . \tag{19.131}$$

Inserting the approximations (19.130) and (19.131) in the expression for the vector potential and introducing the abbreviation $X \equiv \omega(t-\frac{r}{c})$, we obtain,

$$\boxed{\Phi(\mathbf{r},t) = \frac{p_0 b}{4\pi\varepsilon_0}\cos\theta\left(\frac{\cos X}{r^2} - \frac{\omega\sin X}{cr}\right)} \ .$$

The oscillation of the charges is necessarily due to a current, $I(t)\hat{\mathbf{e}}_z = \dot{Q}(t)\hat{\mathbf{e}}_z = -Q_0\omega\hat{\mathbf{e}}_z\sin\omega t$,

$$\mathbf{A}(\mathbf{r},t) = \frac{\mu_0}{4\pi}\int\frac{\mathbf{j}(\mathbf{r}',t_r)}{R}d^3r' = \frac{\mu_0}{4\pi}\int_{antenna}\frac{-Q_0\omega\hat{\mathbf{e}}_z\sin\omega t}{R}d\vec{\mathcal{S}}' \ ,$$

such that,

$$\boxed{\mathbf{A}(\mathbf{r},t) = -\frac{\mu_0 p_0\omega}{4\pi r}\hat{\mathbf{e}}_z\sin X} \ .$$

The derivatives are,

$$\begin{aligned}\nabla\Phi &= \hat{\mathbf{e}}_r\frac{\partial\Phi}{\partial t} + \hat{\mathbf{e}}_\theta\frac{1}{r}\frac{\partial\Phi}{\partial\theta} = \frac{p_0\omega}{4\pi\varepsilon_0 c}\hat{\mathbf{e}}_r\cos\theta\left(\frac{\omega\cos X}{cr} + \frac{\sin X}{r^2}\right) + \frac{p_0\omega}{4\pi\varepsilon_0 c}\hat{\mathbf{e}}_\theta\sin\theta\frac{\sin X}{r^2} \\ \frac{\partial\mathbf{A}}{\partial t} &= -\frac{p_0\omega^2}{4\pi\varepsilon_0 c^2}(\hat{\mathbf{e}}_r\cos\theta - \hat{\mathbf{e}}_\theta\sin\theta)\frac{\cos X}{r} \\ \nabla\times\mathbf{A} &= \frac{1}{r}\frac{\partial(rA_\theta)}{\partial r} - \frac{1}{r}\frac{\partial A_r}{\partial\theta} = -\frac{\mu_0 p_0\omega}{4\pi}\hat{\mathbf{e}}_\phi\sin\theta\left(\frac{\omega\cos X}{cr} + \frac{\sin X}{r^2}\right) \ .\end{aligned}$$

With this, the fields are,

$$\begin{aligned}\vec{\mathcal{E}} &= -\nabla\Phi - \frac{\partial\mathbf{A}}{\partial t} = -\frac{p_0\omega}{4\pi\varepsilon_0 c}\hat{\mathbf{e}}_r\cos\theta\frac{\sin X}{r^2} - \frac{p_0\omega}{4\pi\varepsilon_0 c}\hat{\mathbf{e}}_\theta\sin\theta\left(\frac{\omega\cos X}{cr} + \frac{\sin X}{r^2}\right) \\ \vec{\mathcal{B}} &= \nabla\times\mathbf{A} = -\frac{\mu_0 p_0\omega}{4\pi}\hat{\mathbf{e}}_\phi\sin\theta\left(\frac{\omega\cos X}{cr} + \frac{\sin X}{r^2}\right) \ .\end{aligned}$$

The Poynting vector is ...

19.1.6.6 Ex: Electric and magnetic fields of an oscillating magnetic dipole

Calculate the electric and magnetic fields of an oscillating magnetic dipole in the dipolar approximation ($kr' \ll 1$), but for arbitrary distances ($kr \lesseqgtr 1$) directly from the

retarded potentials in spherical coordinates. Compare with the fields of an oscillating electric dipole. Find the Poynting vector and show that the intensity of the radiation is exactly the same, as the one derived within the far-field approximation ($kr \gg 1$).

Solution: *To create a magnetic dipole, we imagine a circular loop of radius b traversed by a current $I(t) = I_0 \cos\omega t$. The magnetic dipole moment is,*

$$\mathbf{m} = I\mathbf{a} = \pi b^2 I_0 \hat{\mathbf{e}}_z \cos\omega t \ .$$

If the loop is electrically neutral, the retarded potentials are,

$$\Phi = 0 \qquad \textit{and}$$

$$\mathbf{A}(\mathbf{r},t) = \frac{\mu_0}{4\pi}\int \frac{\mathbf{j}(\mathbf{r}',t_r)}{R} d^3r' = \frac{\mu_0}{4\pi}\int_{loop} \frac{I_0\cos\omega t_r}{R} d\vec{\mathcal{S}}' = \frac{\mu_0 I_0 b}{4\pi}\hat{\mathbf{e}}_y \int_0^{2\pi} \frac{\cos\omega t_r}{R}\cos\phi' d\phi' \ ,$$

with $t_r = t - R/c$. To evaluate the integral we parametrize any point of the loop as $\mathbf{b} = b\hat{\mathbf{e}}_x\cos\phi' + b\hat{\mathbf{e}}_y \sin\phi'$ and concentrate on a point in the $y = 0$ plane, such that $\mathbf{r} = r\hat{\mathbf{e}}_x \sin\theta + r\hat{\mathbf{e}}_z\cos\theta$,

$$R = \sqrt{(\mathbf{r}-\mathbf{b})^2} = \sqrt{r^2 + b^2 - 2rb\sin\theta\cos\phi'} \ .$$

For a perfect dipole we require a small size of the loop, $b \ll r$. This allows us to approximate, to first order in b,

$$R \simeq r\left(1 - \frac{b}{r}\sin\theta\cos\phi'\right) \qquad \textit{and} \qquad \frac{1}{R} \simeq \left(1 + \frac{b}{r}\sin\theta\cos\phi'\right) \ , \tag{19.132}$$

such that,

$$\begin{aligned}\cos[\omega(t - \tfrac{R}{c})] &\simeq \cos\left[\omega(t-\tfrac{r}{c}) + \tfrac{\omega b}{c}\sin\theta\cos\phi'\right] \\ &= \cos[\omega(t-\tfrac{r}{c})]\cos\left(\tfrac{\omega b}{c}\sin\theta\cos\phi'\right) - \sin[\omega(t-\tfrac{r}{c})]\sin\left(\tfrac{\omega b}{c}\sin\theta\cos\phi'\right) \ .\end{aligned}$$

In the dipolar approximation we assume, $b \ll c/\omega$, such that,

$$\cos[\omega(t - \tfrac{R}{c})] \simeq \cos[\omega(t-\tfrac{r}{c})] - \tfrac{\omega b}{c}\sin\theta\cos\phi'\sin[\omega(t-\tfrac{r}{c})] \ . \tag{19.133}$$

Inserting the approximations (19.132) and (19.133) in the expression for the vector potential and introducing the abbreviation $X \equiv \omega(t - \frac{r}{c})$, we obtain,

$$\mathbf{A}(\mathbf{r},t) = \frac{\mu_0 I_0 b}{4\pi r}\hat{\mathbf{e}}_y \int_0^{2\pi}\left\{\cos X + b\sin\theta\cos\phi'\left(\frac{\cos X}{r} - \frac{\omega\sin X}{c}\right)\right\}\cos\phi' d\phi' \ .$$

The first term gives zero because $\int_0^{2\pi}\cos\phi' d\phi' = 0$. For the second we use $\int_0^{2\pi}\cos^2\phi' d\phi' = \pi$, such that,

$$\boxed{\mathbf{A}(\mathbf{r},t) = \frac{\mu_0 m_0}{4\pi}\hat{\mathbf{e}}_\phi \sin\theta\left(\frac{\cos X}{r^2} - \frac{\omega\sin X}{cr}\right)} \ ,$$

with $m_0 \equiv \pi b^2 I_0$. Here, we relax the specialization on the y-axis by replacing e_y by $\hat{\mathbf{e}}_\phi$. The derivatives are,

$$\nabla\times\mathbf{A} = \hat{\mathbf{e}}_r \frac{1}{r\sin\theta}\frac{\partial}{\partial\theta}(A_\phi\sin\theta) - \hat{\mathbf{e}}_\theta\frac{1}{r}\frac{\partial}{\partial r}(rA_\phi) \ .$$

The fields are,

$$\vec{\mathcal{E}} = -\frac{\partial \mathbf{A}}{\partial t} = \frac{\mu_0 m_0 \omega}{4\pi} \hat{\mathbf{e}}_\phi \sin\theta \left(\frac{\omega \cos X}{cr} + \frac{\sin X}{r^2} \right)$$

$$\vec{\mathcal{B}} = \nabla \times \mathbf{A}$$

$$= \frac{\mu_0 m_0}{2\pi} \hat{\mathbf{e}}_r \cos\theta \left(\frac{\cos X}{r^3} - \frac{\omega \sin X}{cr^2} \right) + \frac{\mu_0 m_0}{4\pi} \hat{\mathbf{e}}_\theta \sin\theta \left[\left(\frac{1}{r^3} - \frac{\omega^2}{c^2 r} \right) \cos X - \frac{\omega \sin X}{cr^2} \right] .$$

The Poynting vector is,

$$\vec{\mathcal{S}} = \tfrac{1}{\mu_0} \vec{\mathcal{E}} \times \vec{\mathcal{B}} = ...$$

The time average is,

$$\overline{\vec{\mathcal{S}}} = \frac{\mu_0 m_0^2 \omega^4 \sin^2\theta}{32\pi^2 c^3 r^2} .$$

19.1.6.7 Ex: Spherical harmonics

The spherical harmonic function for $\ell = 2$ and $m = 1$ has the form,

$$Y_{21}(\vartheta, \varphi) = \sqrt{\tfrac{15}{8\pi}} \sin\vartheta \cos\vartheta (\cos\varphi + \imath \sin\varphi) .$$

Express the quadrupolar momentum q_{21} as a linear combination in Cartesian coordinates,

$$Q_{ij} = \int \rho(\mathbf{r})(3x_i x_j - \delta_{ij} r^2)\, dr^3 .$$

Solution:

19.1.6.8 Ex: Vector spherical harmonics

Calculate the angular distribution of $E1$ and $M1$ radiation.Derive Eq. (19.85).

Solution: *The general formula is given by (19.129),*

$$\mathbf{Y}_{jlm} = \sum_q \begin{pmatrix} J & 1 & L \\ -m & q & m-q \end{pmatrix} Y^{(\ell)}_{m-q} \hat{\mathbf{e}}_q ,$$

where $\hat{\mathbf{e}}_q$ is given by $\hat{\mathbf{e}}_\pm \equiv -\frac{1}{\sqrt{2}}(\hat{\mathbf{e}}_x \pm \imath \hat{\mathbf{e}}_y)$ and $\hat{\mathbf{e}}_0 = \hat{\mathbf{e}}_z$. For $E1$ and $M1$ radiation we have to calculate the vector spherical harmonics $\mathbf{Y}_{11m}$ and $\mathbf{Y}_{10m}$. Using the tabulated spherical harmonics, we find,

$$r\mathbf{Y}_{100} = \begin{pmatrix} 1 & 1 & 0 \\ 0 & 0 & 0 \end{pmatrix} Y^{(0)}_m \hat{\mathbf{e}}_0 = \sqrt{\tfrac{1}{3}} \sqrt{\tfrac{1}{4\pi}} r \hat{\mathbf{e}}_0 = -\sqrt{\tfrac{1}{12\pi}} \begin{pmatrix} 0 \\ 0 \\ r \end{pmatrix} ,$$

and

$$r\mathbf{Y}_{10\pm1} = \begin{pmatrix} 1 & 1 & 0 \\ \mp 1 & 1 & 0 \end{pmatrix} rY_0^{(0)}\hat{\mathbf{e}}_1 + \begin{pmatrix} 1 & 1 & 0 \\ \mp 1 & -1 & 0 \end{pmatrix} rY_0^{(0)}\hat{\mathbf{e}}_{-1} \quad = \sqrt{\tfrac{1}{3}}\sqrt{\tfrac{1}{4\pi}}r\hat{\mathbf{e}}_{\pm1} = -\sqrt{\tfrac{1}{24\pi}}\begin{pmatrix} x \\ \pm\imath y \\ 0 \end{pmatrix} ,$$

and

$$\begin{aligned} r\mathbf{Y}_{110} &= \begin{pmatrix} 1 & 1 & 1 \\ 0 & 1 & -1 \end{pmatrix} rY_{-1}^{(1)}\hat{\mathbf{e}}_1 + \begin{pmatrix} 1 & 1 & 1 \\ 0 & 0 & 0 \end{pmatrix} rY_0^{(1)}\hat{\mathbf{e}}_0 + \begin{pmatrix} 1 & 1 & 1 \\ 0 & -1 & 1 \end{pmatrix} rY_1^{(1)}\hat{\mathbf{e}}_{-1} \\ &= -\sqrt{\tfrac{1}{2}}\left(rY_{-1}^{(1)}\hat{\mathbf{e}}_1 + rY_1^{(1)}\hat{\mathbf{e}}_{-1}\right) = \frac{1}{2}r\begin{pmatrix} Y_{-1}^{(1)} + Y_1^{(1)} \\ \imath(Y_{-1}^{(1)} - iY_1^{(1)}) \\ 0 \end{pmatrix} \\ &= \tfrac{1}{2}\imath\sqrt{\tfrac{3}{2\pi}}\begin{pmatrix} -\sin\theta\sin\phi \\ \sin\theta\cos\phi \\ 0 \end{pmatrix} = \tfrac{1}{2}\imath\sqrt{\tfrac{3}{2\pi}}\begin{pmatrix} -y \\ x \\ 0 \end{pmatrix} , \end{aligned}$$

and

$$\begin{aligned} r\mathbf{Y}_{11\pm1} &= \begin{pmatrix} 1 & 1 & 1 \\ \mp 1 & 1 & \pm 1 - 1 \end{pmatrix} rY_{\pm1-1}^{(1)}\hat{\mathbf{e}}_1 + \begin{pmatrix} 1 & 1 & 1 \\ \mp 1 & 0 & \pm 1 - 0 \end{pmatrix} rY_{\pm1-0}^{(1)}\hat{\mathbf{e}}_0 + \begin{pmatrix} 1 & 1 & 1 \\ \mp 1 & -1 & \pm 1 + 1 \end{pmatrix} rY_{\pm1+1}^{(1)}\hat{\mathbf{e}}_{-1} \\ &= \sqrt{\tfrac{1}{2}}\left(rY_0^{(1)}\hat{\mathbf{e}}_1 + rY_{\pm1}^{(1)}\hat{\mathbf{e}}_0 + rY_0^{(1)}\hat{\mathbf{e}}_{-1}\right) = \tfrac{1}{2}r\begin{pmatrix} Y_0^{(1)} \\ \pm iY_0^{(1)} \\ \pm\sqrt{2}Y_{\pm1}^{(1)} \end{pmatrix} \\ &= \tfrac{1}{4}\sqrt{\tfrac{3}{\pi}}r\begin{pmatrix} \cos\theta \\ \pm\imath\cos\theta \\ \sin\theta e^{\pm\imath\phi} \end{pmatrix} = \tfrac{1}{4}\sqrt{\tfrac{3}{\pi}}\begin{pmatrix} z \\ \pm iz \\ -(x \pm \imath y) \end{pmatrix} . \end{aligned}$$

19.2 Radiation of point charges

The fundamental structure of matter is based on electromagnetic forces: Electrons are bound to nuclei by the Coulomb-Lorentz force, the orbital motion of the electrons produces magnetic fields, which can interact with the intrinsic spins of electrons and nuclei, external electromagnetic fields can influence the motion of electrons. Therefore, it is of primary interest to understand the radiation emitted by accelerated point-like electric charges.

19.2.1 Power radiated by an accelerated point charge

We derived in an earlier chapter the fields (17.140) and (17.141) produced by an arbitrary moving charge,

$$\begin{aligned} \vec{\mathcal{E}}(\mathbf{r},t) &= \frac{q}{4\pi\varepsilon_0}\frac{R}{(\mathbf{R}\cdot\mathbf{u})^3}[(c^2-v^2)\mathbf{u} + \mathbf{R}\times(\mathbf{u}\times\mathbf{a})] \\ \vec{\mathcal{B}}(\mathbf{r},t) &= \tfrac{1}{c}\mathbf{R}\times\vec{\mathcal{E}}(\mathbf{r},t) , \end{aligned} \tag{19.134}$$

with $\mathbf{u} = c\hat{\mathbf{e}}_r - \mathbf{v}$. We call the first term in (19.134) *velocity field* and the second *acceleration field*. The Poynting vector is,

$$\vec{\mathcal{S}} = \tfrac{1}{\mu_0}(\vec{\mathcal{E}} \times \vec{\mathcal{B}}) = \tfrac{1}{\mu_0 c}[\vec{\mathcal{E}} \times (\mathbf{R} \times \vec{\mathcal{E}})] = \tfrac{1}{\mu_0 c}[\mathcal{E}^2 \hat{\mathbf{e}}_r - (\hat{\mathbf{e}}_r \cdot \vec{\mathcal{E}})\vec{\mathcal{E}}] \ . \tag{19.135}$$

However, not all of this energy flow constitutes radiation; part of it is field energy *transported* by the particle as it moves. The *radiated* energy is the part that separates from the charge and propagates to infinity. To calculate the total power radiated by the particle at time t_r we draw a large sphere of radius R, centered on the position of the particle at time t_r, we wait for the appropriate interval,

$$t - t_r \equiv \frac{R}{c} \ , \tag{19.136}$$

for the radiation to reach the sphere and, at that moment, we integrate the Poynting vector on the surface. The notation t_r points to the fact, that this is the retarded time for all points on the sphere at time t. Now, the area of the sphere is proportional to R^2, hence any term in $\vec{\mathcal{S}}$ that goes like $1/R^2$ will produce a finite response, but terms like $1/R^3$ or $1/R^4$ will not contribute in the limit $R \to \infty$. For this reason, only the acceleration field truly radiates:

$$\vec{\mathcal{E}}_{rad} = \frac{q}{4\pi\varepsilon_0} \frac{R}{(\mathbf{R} \cdot \mathbf{u})^3} [\mathbf{R} \times (\mathbf{u} \times \mathbf{a})] \ . \tag{19.137}$$

Since $\vec{\mathcal{E}}_{rad} \perp \mathbf{R}$, the second term in Eq. (19.135) disappears:

$$\vec{\mathcal{S}}_{rad} = \frac{1}{\mu_0 c} \vec{\mathcal{E}}^2_{rad} \hat{\mathbf{e}}_r \ . \tag{19.138}$$

Example 116 (*Radiation at the turning point*): If at time t_r the charge is instantaneously at rest, $\mathbf{v}(t_r) = 0$, for example at the turning points of a harmonic oscillation, then $\mathbf{u} = c\hat{\mathbf{e}}_r$, and,

$$\vec{\mathcal{E}}_{rad} = \frac{q}{4\pi\varepsilon_0 c^2 R} [\hat{\mathbf{e}}_r \times (\hat{\mathbf{e}}_r \times \mathbf{a})] = \frac{\mu_0 q}{4\pi R} [(\hat{\mathbf{e}}_r \cdot \mathbf{a})\hat{\mathbf{e}}_r - \mathbf{a}] \ . \tag{19.139}$$

In this case,

$$\vec{\mathcal{S}}_{rad} = \frac{1}{\mu_0 c} \left(\frac{\mu_0 q}{4\pi R} \right)^2 [a^2 - (\hat{\mathbf{e}}_r \cdot \mathbf{a})^2] \hat{\mathbf{e}}_r = \frac{\mu_0 q^2 a^2}{16\pi^2 c} \frac{\sin^2\theta}{R^2} \ , \tag{19.140}$$

where θ is the angle between $\hat{\mathbf{e}}_r$ and $\mathbf{a}$. No power is radiated in forward or backward directions. Instead, it is emitted in a torus around the instantaneous acceleration, as shown in Fig. 19.7(a).
The total radiated power is evidently,

$$P = \oint \vec{\mathcal{S}}_{rad} \cdot d\mathbf{S} = \frac{\mu_0 q^2 a^2}{16\pi^2 c} \int \frac{\sin^2\theta}{R^2} R^2 \sin\theta d\theta d\phi = \frac{\mu_0 q^2 a^2}{6\pi c} \ . \tag{19.141}$$

This, again, is the *Larmor formula*, which we previously obtained via another route (19.19). Although derived under the assumption that $v = 0$, the equations (19.140) and (19.141) represent a good approximation, since $v \ll c$.

An exact treatment of the case $v \neq 0$ is more difficult for two reasons. The first obvious reason is, that $\vec{\mathcal{E}}_{rad}$ is more complicated, and the second more subtle reason is that $\vec{\mathcal{S}}_{rad}$, which is the rate at which energy passes through the sphere, is not equal to the rate at which the energy separated from the particle. Suppose someone is throwing a stream of bullets through the window of a moving car. The rate N_t at which the bullets hit a stationary target is not the same as the rate N_g at which they left the weapon, because of the movement of the car. In fact, we can easily verify that $N_g = (1 - v/c)N_t$, if the car is moving toward the target, and,

$$N_g = \left(1 - \tfrac{\hat{\mathbf{e}}_r \cdot \mathbf{v}}{c}\right) N_t \tag{19.142}$$

for arbitrary directions (here v is the speed of the car, c is the velocity of the bullets, and $\mathbf{R}$ is a unit vector pointing from the car towards the target). In our case, if dW/dt is the rate at which energy passes through the sphere of radius R, then the rate at which the energy separated from the charge was,

$$\frac{dW}{dt_r} = \frac{dW/dt}{\partial t_r/\partial t} \ . \tag{19.143}$$

We calculate the denominator from the relation (19.136),

$$\begin{aligned} \frac{\partial t_r}{\partial t} = 1 - \frac{\partial\sqrt{[\mathbf{r} - \mathbf{w}(t_r)]^2}}{c\partial t} &= 1 - \frac{-2[\mathbf{r} - \mathbf{w}(t_r)]}{2c\sqrt{[\mathbf{r} - \mathbf{w}(t_r)]^2}} \cdot \frac{\partial \mathbf{w}(t_r)}{\partial t_r}\frac{\partial t_r}{\partial t} \\ &= 1 + \frac{\mathbf{R}}{cR} \cdot \mathbf{v}\frac{\partial t_r}{\partial t} = \frac{1}{1 - \hat{\mathbf{e}}_R \cdot \mathbf{v}/c} = \frac{cR}{\mathbf{R} \cdot \mathbf{u}} \ . \end{aligned} \tag{19.144}$$

This factor is precisely that of the relation (19.142) between N_g and N_t; is a purely geometric factor (the same as in the Doppler effect).

Therefore, the power radiated by the particle into an area element, $R^2 \sin\theta d\theta d\phi = R^2 d\Omega$ of the sphere is, using the Poynting vector (19.138) and the radiated field (19.137), given by,

$$\frac{dP}{d\Omega} = \frac{\vec{\mathcal{S}}_{rad}}{\partial t_r/\partial t} = \frac{\mathbf{R} \cdot \mathbf{u}}{Rc}\frac{1}{\mu_0 c}\vec{\mathcal{E}}^2_{rad}R^2 = \frac{q^2}{16\pi^2\varepsilon_0}\frac{|\hat{\mathbf{e}}_r \times (\mathbf{u} \times \mathbf{a})|^2}{(\hat{\mathbf{e}}_r \cdot \mathbf{u})^5} \ , \tag{19.145}$$

where $d\Omega = \sin\theta d\theta d\phi$ is the solid angle at which this energy is radiated. Integrating over θ and ϕ to obtain the total radiated power is not easy, such that we simply quote the answer:

$$\boxed{P = \frac{\mu_0 q^2 \gamma^6}{6\pi c}\left(a^2 - \left|\frac{\mathbf{v} \times \mathbf{a}}{c}\right|^2\right)} \ , \tag{19.146}$$

where $\gamma \equiv 1/\sqrt{1 - v^2/c^2}$. This is *Liénard's generalization* of Larmor's formula, to which it reduces when $v \ll c$. The factor γ^6 means that the radiated power increases enormously as the velocity of the particle approaches the speed of light.

Resolve the Excs. 19.2.3.1 to 19.2.3.5.

19.2.1.1 Bremstrahlung

Suppose that $\mathbf{v}$ and $\mathbf{a}$ be instantaneously collinear (at time t_r), such as for a motion on a straight line. In this case $\mathbf{u} \times \mathbf{a} = (c\hat{\mathbf{e}}_r - \boldsymbol{\mathcal{V}}^0) \times \mathbf{a}$, then the angular distribution of radiation (19.145) gives,

$$\frac{dP}{d\Omega} = \frac{q^2 c^2}{16\pi^2 \varepsilon_0} \frac{|\hat{\mathbf{e}}_r \times (\hat{\mathbf{e}}_r \times \mathbf{a})|^2}{(c - \hat{\mathbf{e}}_r \cdot \mathbf{v})^5} \ . \tag{19.147}$$

Now with $|\hat{\mathbf{e}}_r \times (\hat{\mathbf{e}}_r \times \mathbf{a})| = a \sin\theta$ and letting $\mathbf{v} \equiv v\hat{\mathbf{e}}_z$,

$$\frac{dP}{d\Omega} = \frac{\mu_0 q^2 a^2}{16\pi^2 c} \frac{\sin^2\theta}{(1 - \beta\cos\theta)^5} \ , \tag{19.148}$$

where $\beta \equiv v/c$. This is consistent with the result (19.140), in the case $v = 0$. However, for very large v ($\beta \approx 1$), the torus of the radiation illustrated in Fig. 19.7(a) is stretched and pushed forward by a factor $(1-\beta\cos\theta)^{-5}$, as indicated in Fig. 19.7(b). Although there is still no radiation in the exact forward direction, most of the radiation is concentrated in an increasingly narrow cone around the forward direction.

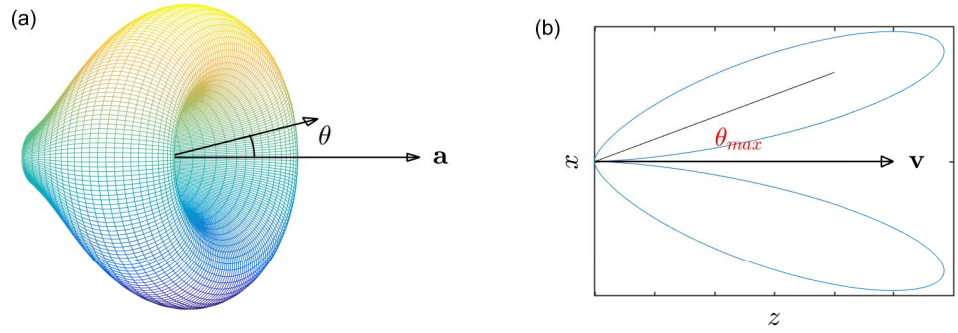

Figure 19.7: (code) (a) Radiation pattern of an accelerated charge. (b) Angular distribution of the bremsstrahlung.

The total emitted power is found by integrating equation (19.149) over all angles:

$$\begin{aligned} P &= \int \frac{dP}{d\Omega} d\Omega = \frac{\mu_0 q^2 a^2}{16\pi^2 c} \int \frac{\sin^2\theta}{(1-\beta\cos\theta)^5} \sin\theta d\theta d\phi \\ &= \frac{\mu_0 q^2 a^2}{8\pi c} \int_{-1}^{+1} \frac{1-x^2}{(1-\beta x)^5} dx = \frac{\mu_0 q^2 a^2}{8\pi c} \tfrac{4}{3}(1-\beta^2)^{-3} = \frac{\mu_0 q^2 a^2 \gamma^6}{6\pi c} \ . \end{aligned} \tag{19.149}$$

This result is consistent with the Liénard's formula (19.146), for the case when $\mathbf{v}$ and $\mathbf{a}$ are collinear. Note that the angular distribution of radiation is the same, whether the particle is accelerating or decelerating; it does not depend on $\mathbf{a}$, but only on velocity being concentrated in forward direction (with respect to the velocity) in both cases. When a high-speed electron hits a metal target, it decelerates rapidly, releasing what is called bremsstrahlung. This example is essentially the classical theory of *bremsstrahlung*.

We will calculate the *synchrotron radiation* in Exc. 19.2.3.6 and the *Cherenkov radiation* in Exc. 19.2.3.7. A movie illustrating the Cherenkov radiation emission can be viewed at (watch movie).

Example 117 (*Bremsstrahlung of thermal electrons*): The power lost by bremsstrahlung for not extremely relativistic velocities is,

$$P = \frac{\mu_0 q^2 a^2 \gamma^2}{6\pi c} \simeq \frac{\mu_0 q^2 a^2}{6\pi c} \ ,$$

such that,

$$\vec{\mathcal{E}}_{rad} = \int_0^t P dt = \frac{\mu_0 q^2 a^2}{6\pi c} \int_{v_0}^0 \frac{dv}{\dot{v}} = \frac{\mu_0 q^2 a}{6\pi c} \int_{v_0}^0 dv = \frac{\mu_0 q^2 a}{6\pi c} v_0 \ .$$

For an electron in a metal with a free path of $d \approx 3$ nm and a thermal velocity $v_0 = 100000$ m/s the deceleration $a = \frac{v_0^2}{2d}$ leads to a negligible radiated fraction,

$$\frac{\vec{\mathcal{E}}_{rad}}{E_{kin}} = \frac{\frac{\mu_0 q^2 a}{6\pi c} v_0}{\frac{m}{2} v_0^2} = \frac{\mu_0 q^2 a}{3\pi c m v_0} = \frac{\mu_0 q^2}{3\pi c m} \frac{v_0}{2d} \approx 2 \cdot 10^{-10} \ .$$

19.2.2 Radiation reaction

According to the laws of classical electrodynamics, an accelerated charge radiates. This radiation takes energy, which must come at the expense of the particle's kinetic energy. Under the influence of a given force, therefore, a charged particle accelerates less than a neutral particle of the same mass. The radiation evidently exerts a reactive force $\mathbf{F}_{rad}$ corresponding to a recoil. We will now derive the *radiation reaction* force from energy conservation.

For a non-relativistic particle ($v \ll c$), the total radiated power P is given by the *Larmor formula* (19.141). The conservation of energy suggests that this is also the rate at which the particle loses energy, under the influence of the radiative reaction force $\mathbf{F}_{rad}$:

$$\mathbf{F}_{rad} \cdot \mathbf{v} \stackrel{?}{=} -\frac{\mu_0 q^2 a^2}{6\pi c} = -P \ . \tag{19.150}$$

However, this equation is really wrong. For, to derive Larmor's formula, we calculated the radiated power by integrating the Poynting vector on a sphere of 'infinite' radius; in this calculation the velocity fields *did not contribute*, since they fall off very rapidly as a function of R. However, the velocity fields *carry* energy; they simply do not carry it to infinity. As the particle accelerates and decelerates, it exchanges energy with the velocity fields, while another part of the energy is irremediably radiated away by the acceleration fields. The equation (19.150) only takes into account this lost energy, but if we want to know the recoil force exerted by the fields on the charge, we must consider the power lost at each instant of time, not only the radiatively escaping power. (In this sense the term 'radiation reaction' is misleading and should be replaced by 'field reaction'.) In fact, we shall see shortly that F_{rad} is determined by the time derivative of the acceleration and can be nonzero, even if the acceleration is instantaneously zero, such that the particle does not radiate.

The energy lost by the particle during a given time interval, therefore, must equal the energy carried away by radiation plus the extra energy that has been pumped into the velocity fields. However, if we agree to consider only time intervals $[t_1, t_2]$ over which the *system returns to its initial state*, then the energy in the velocity fields is the same at both times, and the only loss is through radiation. Thus, equation (19.150), while instantly incorrect, is valid on average:

$$\int_{t_1}^{t_2} \mathbf{F}_{rad} \cdot \mathbf{v} dt = -\frac{\mu_0 q^2}{6\pi c} \int_{t_1}^{t_2} a^2 dt \ , \tag{19.151}$$

with the stipulation that the state of the system is identical at times t_1 and t_2. In the case of periodic movements, for example, we must integrate over a total number of complete cycles. Now, the right-hand side of the equation (19.151) can be integrated by parts:

$$\int_{t_1}^{t_2} \mathbf{a}^2 dt = \mathbf{v} \cdot \frac{d\mathbf{v}}{dt}\bigg|_{t_1}^{t_2} - \int_{t_1}^{t_2} \frac{d^2\mathbf{v}}{dt^2} \cdot \mathbf{v} dt \ . \tag{19.152}$$

The boundary term cancels, since the velocities and accelerations are identical at t_1 and t_2, then the equation (19.151) can be written in an equivalent way as,

$$\int_{t_1}^{t_2} \left(\mathbf{F}_{rad} - \frac{\mu_0 q^2}{6\pi c} \dot{\mathbf{a}} \right) \cdot \mathbf{v} dt = 0 \ . \tag{19.153}$$

This equation will certainly be satisfied if,

$$\boxed{\mathbf{F}_{rad} = \frac{\mu_0 q^2}{6\pi c} \dot{\mathbf{a}}} \ . \tag{19.154}$$

This is the *Abraham-Lorentz formula* for the radiation reaction force. Obviously, the equation (19.153) does not prove (19.154), because it does not say anything about the component of $\mathbf{F}_{rad}$ perpendicular to $\mathbf{v}$; and only informs us on the time-average of the parallel component for, moreover, very special time intervals.

The Abraham-Lorentz formula has disturbing implications, which are not fully understood nearly a century after the law was first proposed. Let us assume that a particle is not subject to external forces; then Newton's second law tells us,

$$F_{rad} = \frac{\mu_0 q^2}{6\pi c} \dot{a} = ma \ , \tag{19.155}$$

yielding,

$$a(t) = a_0 e^{t/\tau} \qquad \text{with} \qquad \tau = \frac{\mu_0 q^2}{6\pi mc} \ . \tag{19.156}$$

In the case of an electron, $\tau = 6 \cdot 10^{-24}$ s. The acceleration increases spontaneously exponentially with time! This absurd conclusion can be avoided, if we insist that $a_0 = 0$. But it turns out, that the systematic exclusion of such catastrophic solutions has an even more unpleasant consequence: if we now *switch on* an external force, the particle begins to respond to it *before it actually has been switch on* (see Exc. 19.2.3.8 and 19.2.3.9).

Example 118 (*Radiative damping*): Here, we calculate the radiative damping rate τ of a charged particle fixed to a spring by solving the equation of motion,

$$m\ddot{x} = F_{sprng} + F_{rad} + F_{excit} = -m\omega_0^2 x + m\tau\dddot{x} + F_{excit} \ .$$

With the oscillating system, $x(t) = x_0\cos(\omega t + \delta)$, we have,

$$\dddot{x} = -\omega^2\dot{x} \ .$$

Therefore,

$$m\ddot{x} + m\omega^2\tau\dot{x} + m\omega_0^2 x = F_{excit} \ ,$$

and the damping factor is given by $\omega^2\tau$.

Example 119 (*Radiation reaction*): In previous chapters, the problems of electrodynamics were divided into two classes: one class in which the charge and current sources are specified and the resulting electromagnetic fields are calculated, and the other class in which external electromagnetic fields are specified and the motion of charged particles of currents are calculated. Occasionally, as in the discussion of the bremsstrahlung, the two problems are combined. But the treatment is recursive: first, the motion of a charged particle in an external field is determined neglecting the radiation it emits; then the radiation of the particle is calculated from its (accelerated) trajectory treating the particle as a source of charge and current.
Obviously, this way of dealing with electrodynamical problems can only be approximate. The (accelerated) motion of charged particles within force fields necessarily involves the emission of radiation, removing energy, angular momentum, and momentum from the particles and thus influencing their subsequent motion. Consequently, the motion of radiation sources is (partially) determined by the emission of radiation, and a correct treatment must take account of the reaction of the radiation onto the motion of the sources. Fortunately, for many problems of electrodynamics the radiative reaction is negligibly small. On the other hand, there exists no completely satisfactory classical treatment. The difficulties presented by this problem touch upon fundamental aspects of physics, such as the nature of elementary particles. Nevertheless, there are viable partial solutions with limited regimes of validity. In quantum mechanics, the introduction of renormalization techniques was able to solve the divergences within the theory of *quantum electrodynamics* (QED).
In order to give a gross idea of 'radiative reaction', let us consider a charge q of a point particle distributed in space. For simplicity we choose 'sub-charges' $\frac{q}{2}$ located at two positions $\mathbf{d}_{1,2} = \pm\frac{d}{2}\hat{\mathbf{e}}_y$ and moving in an accelerated way in x-direction, that is, $\mathbf{a} = a\hat{\mathbf{e}}_x$. Only after the calculations will we go to the limit $d \to 0$. So with (17.140) we obtain for the electric field generated by the charge 2 at the place of the charge 1,

$$\begin{aligned}\vec{\mathcal{E}}_1(\mathbf{r},t) &= \frac{q/2}{4\pi\varepsilon_0}\frac{R}{(\mathbf{R}\cdot\mathbf{u})^3}[(c^2-v^2)\mathbf{u} + \mathbf{R}\times(\mathbf{u}\times\mathbf{a})] \\ &= \frac{q/2}{4\pi\varepsilon_0}\frac{R}{(\mathbf{R}\cdot\mathbf{u})^3}[(c^2-v^2+\mathbf{R}\cdot\mathbf{a})\mathbf{u} - \mathbf{a}(\mathbf{R}\cdot\mathbf{u})] \ .\end{aligned}$$

Now, we assume that the charge be instantly at rest, $\mathbf{v} = 0$, that is, $\mathbf{u} \equiv c\hat{\mathbf{e}}_r - \mathbf{v} = c\hat{\mathbf{e}}_r$. In Cartesian coordinates, $\mathbf{R} \equiv l\hat{\mathbf{e}}_x + d\hat{\mathbf{e}}_y$, where $l \equiv x(t) - x(t_r)$

is the distance between the actual position and the retarded position, we can write the x-component of the electric field as,

$$\vec{\mathcal{E}}_{x,1} = \frac{q/2}{4\pi\varepsilon_0}\frac{R}{c^3R^3}[(c^2 + \mathbf{R}\cdot\mathbf{a})u_x - (\mathbf{R}\cdot\mathbf{u})a_x] = \frac{q}{8\pi\varepsilon_0 c^2}\frac{c^2 l - d^2 a}{\sqrt{l^2+d^2}^3} \ .$$

By symmetry, $\vec{\mathcal{E}}_{x,1} = \vec{\mathcal{E}}_{x,2}$, such that the force on the dumbbell is,

$$\mathbf{F}_{self} = \frac{q}{2}(\vec{\mathcal{E}}_1 + \vec{\mathcal{E}}_2) = \frac{q}{8\pi\varepsilon_0 c^2}\frac{c^2 l - d^2 a}{\sqrt{l^2+d^2}^3}\hat{\mathbf{e}}_x \ .$$

Now, we expand l in terms of the retarded time,

$$l = x(t_r + T) - x(t_r) = \cancelto{0}{v\mathcal{T}} + \tfrac{1}{2}aT^2 + \tfrac{1}{6}\dot{a}T^3 + \dots \ ,$$

such that,

$$d = \sqrt{(cT)^2 - l^2} = cT\sqrt{1 - \left(\tfrac{aT}{2c} + \tfrac{\dot{a}T^2}{6c} + \dots\right)^2} = cT - \frac{a^2}{8c}T^3 + \dots \simeq cT - \frac{a^2}{8c}\left(\frac{d}{c}\right)^3 + \dots \ ,$$

where we replaced, in the last step, the first order solution in the expansion, $T \simeq d/c$, for the third order. Resolving by T,

$$T \simeq \frac{d}{c} + \frac{a^2 d^3}{8c^5} \ .$$

and inserting into the expansion of l,

$$l \simeq \frac{1}{2}a\left(\frac{d}{c} + \frac{a^2d^3}{8c^5}\right)^2 + \frac{1}{6}\dot{a}\left(\frac{d}{c} + \frac{a^2d^3}{8c^5}\right)^3 + \dots \simeq \frac{1}{2}a\left(\frac{d}{c}\right)^2 + \frac{1}{6}\dot{a}\left(\frac{d}{c}\right)^3 \ .$$

With this we obtain for reaction force,

$$\begin{aligned}\mathbf{F}_{self} \simeq \frac{q}{8\pi\varepsilon_0 c^2}\frac{c^2 l - d^2 a}{\sqrt{l^2+d^2}^3}\hat{\mathbf{e}}_x &\simeq \frac{q}{8\pi\varepsilon_0 c^2}\frac{c^2\left(\frac{1}{2}a\left(\frac{d}{c}\right)^2 + \frac{1}{6}\dot{a}\left(\frac{d}{c}\right)^3\right) - d^2 a}{\sqrt{(..)d^4 + d^2}^3}\hat{\mathbf{e}}_x \\ &\simeq \frac{q}{4\pi\varepsilon_0 c^2}\left(-\frac{a}{4d} + \frac{\dot{a}}{12c}\right)\hat{\mathbf{e}}_x \ ,\end{aligned}$$

considering that d is small. The acceleration is still expressed in terms of the retarded time, but this is easily remedied by,

$$a(t_r) = a(t) + \dot{a}(t)(t - t_r) = a(t) - \dot{a}(t)\frac{d}{c} \ .$$

Inserting into the force,

$$\begin{aligned}\mathbf{F}_{self} \simeq \frac{q}{4\pi\varepsilon_0 c^2}\left(-\frac{a}{4d} + \frac{\dot{a}}{12c}\right)\hat{\mathbf{e}}_x &= \frac{q}{4\pi\varepsilon_0}\left(-\frac{a(t)}{4c^2 d} - \frac{-\dot{a}(t)}{4c^3} + \frac{\dot{a}(t)}{12c^3}\right)\hat{\mathbf{e}}_x \\ &= \frac{q}{4\pi\varepsilon_0}\left(\frac{a(t)}{4c^2 d} + \frac{\dot{a}(t)}{3c^3}\right)\hat{\mathbf{e}}_x \ .\end{aligned}$$

Finally,

$$\mathbf{F} = m_{tot}a + \mathbf{F}_{rad} = \left(m_0 + \frac{1}{4\pi\varepsilon_0}\frac{q^2}{4dc^2}\right)\mathbf{a} + \frac{\mu_0 q^2 \dot{\mathbf{a}}}{12\pi c} \ ,$$

where m_0 is the sum of the two partial masses. We retrieve the Abraham-Lorentz formula by the second term. The missing factor of 2, when compared to (19.155), comes from the fact that we only consider the mutual reactions of partial charges. The expression in the parentheses corresponds to a correction of the inertial mass of the particle due to the Coulombian repulsion between the charges.

19.2.2.1 Radiation of a charge exposed to a gravitational field

Generalize Larmor's formula. Needs relative movement of charge and field [552].

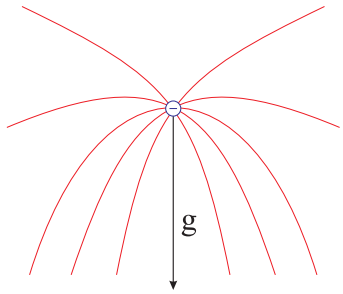

Figure 19.8: Illustration of the radiation field of a charge suspended in the Earth's gravitational field.

19.2.3 Exercises

19.2.3.1 Ex: Radiation emitted by a rotating electron

A particle with charge q moves with constant angular velocity ω in a circular orbit with radius R around the origin in the plane x-y. Its trajectory therefore is,

$$\mathbf{R}'(t) = R(\hat{\mathbf{e}}'_x \cos\omega t + \hat{\mathbf{e}}'_y \sin\omega t) \ .$$

a. Calculate the associated (temporary) charge density $\varrho(\mathbf{r}', t)$ and the dipole moment using the general rule,

$$\mathbf{d}(t) = \int \mathbf{r}' \varrho(\mathbf{r}', t) d^3\mathbf{r}' \ .$$

b. The rotating particle can be seen as a source of radiation. At a point $\mathbf{r}$ far from this source, in the dipole approximation, the associated electromagnetic fields are given by,

$$\vec{\mathcal{B}} = \tfrac{\mu_0}{4\pi c r} \hat{\mathbf{e}}_r \times \ddot{\mathbf{d}} \qquad \text{respectively} \qquad \vec{\mathcal{E}} = c\vec{\mathcal{B}} \times \hat{\mathbf{e}}_r \ .$$

Calculate the Poynting vector,

$$\vec{\mathcal{S}} = \tfrac{1}{\mu_0} \vec{\mathcal{E}} \times \vec{\mathcal{B}}$$

as well as its component $\mathcal{S}_n \equiv \hat{\mathbf{e}}_r \cdot \vec{\mathcal{S}}$ in the direction of the point $\mathbf{r}$. **Help:** Use the formula $\mathbf{a} \times \mathbf{b} \times \mathbf{c} = \mathbf{b}(\mathbf{a} \cdot \mathbf{c}) - \mathbf{c}(\mathbf{a} \cdot \mathbf{b})$.
c. Now calculate the time average of $\mathcal{S}_n$ over an orbit of the particle, that is, calculate $\bar{\mathcal{S}}_n = \int dt \mathcal{S}_n \ / \ \int dt$ with the two integrals taken between $t = 0$ and $t = 2\pi/\omega$. Express the result in spherical coordinates, so that $r^2 \bar{\mathcal{S}}_n$ is precisely the average power radiated to the solid angle element $d\Omega$ in the direction $\mathbf{r}$. Now integrate over the entire solid angle and evaluate the total emitted power P.

Solution: *a. The time-dependent charge density is in Cartesian coordinates,*

$$\varrho(\mathbf{r}', t) = q\delta(x' - R\cos\omega t)\delta(y' - R\sin\omega t)\delta(z') \ .$$

It is easy check that the volume integral over this charge density is, at all times, equal to the total existing charge. The electric dipole moment of our charge distribution is now,

$$\begin{aligned}\mathbf{d}(t) &= \int_{-\infty}^{\infty} dx' \int_{-\infty}^{\infty} dy' \int_{-\infty}^{\infty} dz' [x'\hat{\mathbf{e}}_x + y'\hat{\mathbf{e}}_y + z'\hat{\mathbf{e}}_z]\varrho(x', y', z', t) \\ &= qR(\hat{\mathbf{e}}_x \cos\omega t + \hat{\mathbf{e}}_y \sin\omega t) = q\mathbf{R}(t) \ .\end{aligned}$$

b. Using the result of part (a),

$$\ddot{\mathbf{d}} = -\omega^2 \mathbf{d} \ .$$

Thus, at a point $\mathbf{r}$ *very far from the radiation source, oscillating here at a frequency* ω*, the electromagnetic fields are given in the dipolar approximation by,*

$$\vec{\mathcal{B}} = -\frac{\mu_0\omega^2}{4\pi cr}[\hat{\mathbf{e}}_r \times \mathbf{d}] \qquad \textit{as well as} \qquad \vec{\mathcal{E}} = -\frac{\mu_0\omega^2}{4\pi r}\hat{\mathbf{e}}_r \times [\hat{\mathbf{e}}_r \times \mathbf{d}] \ .$$

With the given formulas the electric field can also be written,

$$\vec{\mathcal{E}} = \frac{\mu_0\omega^2}{4\pi r}[\mathbf{d} - \hat{\mathbf{e}}_r(\hat{\mathbf{e}}_r \cdot \mathbf{d})] \ .$$

For the Poynting vector we get in this way [7]*,*

$$\begin{aligned}\vec{\mathcal{S}} &= \frac{\mu_0}{c}\left(\frac{\omega^2}{4\pi r}\right)^2 [\mathbf{d} - \hat{\mathbf{e}}_r(\hat{\mathbf{e}}_r \cdot \mathbf{d})] \times [\hat{\mathbf{e}}_r \times \mathbf{d}] \\ &= \frac{\mu_0}{c}\left(\frac{\omega^2}{4\pi r}\right)^2 [\mathbf{d} \times [\hat{\mathbf{e}}_r \times \mathbf{d}] - (\hat{\mathbf{e}}_r \cdot \mathbf{d})\hat{\mathbf{e}}_r \times [\hat{\mathbf{e}}_r \times \mathbf{d}]] \\ &= \frac{\mu_0}{c}\left(\frac{\omega^2}{4\pi r}\right)^2 [\hat{\mathbf{e}}_r(\mathbf{d} \cdot \mathbf{d}) - \mathbf{d}(\hat{\mathbf{e}}_r \cdot \mathbf{d}) - (\hat{\mathbf{e}}_r \cdot \mathbf{d})^2\hat{\mathbf{e}}_r + \mathbf{d}(\hat{\mathbf{e}}_r \cdot \mathbf{d})] \\ &= \frac{\mu_0}{c}\left(\frac{\omega^2}{4\pi r}\right)^2 \hat{\mathbf{e}}_r[(\mathbf{d} \cdot \mathbf{d}) - (\hat{\mathbf{e}}_r \cdot \mathbf{d})^2] \ .\end{aligned}$$

[7] For time-dependent sinusoidal electromagnetic fields, the average power flux per unit time is often more useful. It can be found by using the analytical representation of the electric and magnetic fields as follows,

$$\begin{aligned}\vec{\mathcal{S}} &= \vec{\mathcal{E}} \times \vec{\mathcal{H}} = \mathfrak{Re}\ (\vec{\mathcal{E}}_0 e^{\imath\omega t}) \times \mathfrak{Re}\ (\vec{\mathcal{H}}_0 e^{\imath\omega t}) = \tfrac{1}{2}(\vec{\mathcal{E}}_0 e^{\imath\omega t} + \vec{\mathcal{E}}_0^* e^{-\imath\omega t}) \times \tfrac{1}{2}(\mathcal{H}_0 e^{\imath\omega t} + \vec{\mathcal{H}}_0^* e^{-\imath\omega t}) \\ &= \tfrac{1}{4}(\vec{\mathcal{E}}_0 \times \vec{\mathcal{H}}_0^* + \vec{\mathcal{E}}_0^* \times \vec{\mathcal{H}}_0 + \vec{\mathcal{E}}_0 \times \vec{\mathcal{H}}_0 e^{2\imath\omega t} + \mathcal{E}_0^* \times \vec{\mathcal{H}}_0^* e^{-2\imath\omega t}) \\ &= \tfrac{1}{4}[\vec{\mathcal{E}}_0 \times \vec{\mathcal{H}}_0^* + (\vec{\mathcal{E}}_0 \times \vec{\mathcal{H}}_0^*)^* + \vec{\mathcal{E}}_0 \times \vec{\mathcal{H}}_0 e^{2\imath\omega t} + (\vec{\mathcal{E}}_0 \times \vec{\mathcal{H}}_0^* e^{2\imath\omega t})^*] \\ &= \tfrac{1}{2}\mathfrak{Re}\ (\vec{\mathcal{E}}_0 \times \vec{\mathcal{H}}_0^*) + \tfrac{1}{2}\mathfrak{Re}\ (\vec{\mathcal{E}}_0 \times \vec{\mathcal{H}}_0 e^{2\imath\omega t}) \ .\end{aligned}$$

The temporal average is given by,

$$\langle\vec{\mathcal{S}}\rangle = \frac{1}{T}\int_0^T \vec{\mathcal{S}}(t)dt = \frac{1}{T}\int_0^T [\tfrac{1}{2}\mathfrak{Re}\ (\vec{\mathcal{E}}_0 \times \vec{\mathcal{H}}_0^*) + \tfrac{1}{2}\mathfrak{Re}\ (\vec{\mathcal{E}}_0 \times \vec{\mathcal{H}}_0^* e^{2\imath\omega t})]dt \ .$$

The second term is a sinusoidal curve, $\mathfrak{Re}\ e^{2\imath\omega t} = \cos 2\omega t$, and its average is zero, giving

$$\langle\vec{\mathcal{S}}\rangle = \frac{1}{2}\mathfrak{Re}\ (\vec{\mathcal{E}}_0 \times \vec{\mathcal{H}}_0^*) = \tfrac{1}{2}\mathfrak{Re}\ (\vec{\mathcal{E}}_0 e^{\imath\omega t} \times \vec{\mathcal{H}}_0^* e^{-\imath\omega t}) \ .$$

The component of Poynting vector in $\mathbf{r}$*-direction is, hence,*

$$\mathcal{S}_n = \hat{\mathbf{e}}_r \cdot \vec{\mathcal{S}} = \frac{\mu_0}{c}\left(\frac{\omega^2}{4\pi r}\right)^2 [(\mathbf{d}\cdot\mathbf{d}) - (\hat{\mathbf{e}}_r\cdot\mathbf{d})^2] \ .$$

For our example we obtain,

$$\begin{aligned}\mathcal{S}_n &= \frac{\mu_0}{c}\left(\frac{\omega^2 q}{4\pi r}\right)^2 (R^2 - [x\cos\omega t + y\sin\omega t]^2) \\ &= \frac{\mu_0}{c}\left(\frac{\omega^2 q}{4\pi r}\right)^2 (R^2 - x^2\cos^2\omega t - y^2\sin^2\omega t - 2xy\sin\omega t\cos\omega t) \ .\end{aligned}$$

c. The temporal average of $\mathcal{S}_n$ *over the period of an orbit gives, using*

$$\frac{\omega}{2\pi}\int_0^{2\pi/\omega} dt\cos^2\omega t = \frac{\omega}{2\pi}\int_0^{2\pi/\omega} dt\sin^2\omega t = \frac{1}{2}$$

and

$$\frac{\omega}{2\pi}\int_0^{2\pi/\omega} dt\cos\omega t\sin\omega t = 0$$

the result,

$$\bar{\mathcal{S}}_n = \frac{\mu_0}{c}\left(\frac{\omega^2 qR}{4\pi r}\right)^2 [R^2 - \frac{1}{2}(x^2+y^2)] = \frac{\mu_0}{2c}\left(\frac{\omega^2 q}{4\pi r}\right)^2 (1+\cos^2\theta) \ ,$$

where we moved in the last line to spherical coordinates. For the solid angle element $d\Omega$ *pointing in* $\mathbf{r}$*-direction we obtain the power radiated by the source,*

$$\frac{dP_n}{d\Omega} = r^2\bar{\mathcal{S}}_n = \frac{\mu_0}{2c}\left(\frac{\omega^2 q}{4\pi}\right)^2 (1+\cos^2\theta) \ .$$

Integration over $d\Omega = d\phi\sin\theta d\theta$ *gives the total radiated power,*

$$P = \frac{\mu_0}{2c}\left(\frac{\omega^2 q}{4\pi}\right)^2 \int_{-1}^{+1} dx(1+x^2) = \frac{\mu_0\omega^4 q^2 R^2}{6\pi c} \ .$$

19.2.3.2 Ex: Rutherford's atom model

In Rutherford's 'classical' atom model a hydrogen atom is described by an electron (charge $-e$) orbiting a nucleus (charge $+e$) in a circular trajectory with constant angular velocity ω. The equilibrium condition is chosen so that the Coulomb force and the centrifugal force compensate each other. However, according to the Exc. 19.2.3.1, such an electron represents a source of radiation. The radiated power decreased the energy of the electron [$dE/dt = -P$ with P taken from Exc. 19.2.3.1(c)]. Derive a differential equation for the temporal variation of the radius $R(t)$ of the electronic orbit, and integrate it with the boundary conditions $t_0 = 0$ and $R(t_0) = a_B$, where

$a_B = 0.53 \times 10^{-8}$ cm is the Bohr radius. After what time T do we get $R(T) = 0$?

Solution: *The equilibrium condition requires,*

$$m\omega^2 R = \frac{e^2}{R^2} \ .$$

The kinetic energy of the electron is then,

$$E_{kin} = \frac{1}{2}mv^2 = \frac{1}{2}m\omega^2 R^2 = \frac{1}{2}\frac{e^2}{R} \ ,$$

and its potential energy,

$$E_{pot} = -\frac{e^2}{R} \ .$$

Hence,

$$E = E_{kin} + E_{pot} = -\frac{1}{2}\frac{e^2}{R} \ .$$

The energy loss is, according to the Exc. 19.2.3.1,

$$\frac{dE}{dt} = -P = -\frac{2\omega^4 e^2 R^2}{3c^3} \ .$$

Now, understanding R as a function of time t, we obtain,

$$\frac{dE}{dt} = \frac{d}{dt}\left(-\frac{1}{2}\frac{e^2}{R}\right) = \frac{e^2}{R^2}\frac{dR}{dt} = -\frac{2\omega^4 e^2 R^2}{3c^3} \ ,$$

and with this, once again using the equilibrium condition, the differential equation,

$$\frac{dR}{dt} = -\frac{4}{3}\frac{e^4}{c^3 m^2}\frac{1}{R^2} \ .$$

Integration of this equation gives,

$$t - t_0 = -\frac{1}{4}\frac{c^3 m^2}{e^4}(R^3 - R^3(t_0)) \ .$$

Inserting $t_0 = 0$ and for $R(t_0) = a_B$ the Bohr radius, we obtain,

$$t = (a_B^3 - R^3)\frac{m^2 c^3}{4e^4} \ .$$

The time T when, due to the loss of energy, the radius of the electron's orbit becomes $R = 0$, is therefore,

$$T = \frac{m^2 c^3 a_B^3}{4e^4} \ .$$

Insertion of given values yields,

$$T \sim 1.6 \times 10^{-11}\,\mathrm{s} \ .$$

This is the radiation catastrophe of the classical model of the hydrogen atom.

19.2.3.3 Ex: Dynamics of charged point particles

Consider a point particle with charge q and mass m and general electromagnetic fields in vacuum, $\vec{\mathcal{E}}(\mathbf{r},t)$ and $\vec{\mathcal{B}}(\mathbf{r},t)$, which are not perturbed neither by the charge nor the current resulting from the particle's motion. On the particle acts the Coulomb-Lorentz force.
a. What are the equations of motion for the particle? What is the temporal variation of its total kinetic energy? What condition must be satisfied to ensure that the kinetic energy of the particle is temporally constant?
b. We now consider homogeneous fields $\vec{\mathcal{E}}(\mathbf{r},t) = \mathcal{E}_0\hat{\mathbf{e}}_z$ and $\vec{\mathcal{B}}(\mathbf{r},t) = \mathcal{B}_0\hat{\mathbf{e}}_z$. What are the equations of motion now?
c. The particle is at time $t = 0$ at the origin of the coordinate system and has the velocity $\mathbf{v}_0$. Solve the equations of motion. **Help:** Use the complex variable $\eta = x + \imath y$ and add the equations of motion to obtain a complex equation motion for η of the type $\ddot{\eta} = -\imath\omega\dot{\eta}$ with $\omega = q\vec{\mathcal{B}}_0/(mc)$.
d. How does the kinetic energy of the particle vary over time?

Solution: *a. From the specified force we derive, for the charged particle, Newton's equation of motion:*

$$m\ddot{\mathbf{r}} = \mathbf{F} = q(\vec{\mathcal{E}} + \mathbf{v}\times\vec{\mathcal{B}}) \ .$$

The temporal variation of the kinetic energy is given by,

$$\dot{W} \equiv \frac{d}{dt}\left(\frac{m}{2}\mathbf{v}^2\right) = m\mathbf{v}\cdot\dot{\mathbf{v}} = \mathbf{v}\cdot\mathbf{F} = q\mathbf{v}\cdot\vec{\mathcal{E}} \ .$$

For energy to remain constant, we need to guarantee,

$$\dot{W} = q\mathbf{v}\cdot\vec{\mathcal{E}} = 0 = q\dot{\mathbf{r}}\cdot\vec{\mathcal{E}} \ .$$

b. For time-independent and homogeneous fields, $\vec{\mathcal{E}}(\mathbf{r},t) = \vec{\mathcal{E}}_0\hat{\mathbf{e}}_z$ and $\vec{\mathcal{B}}(\mathbf{r},t) = \vec{\mathcal{B}}_0\hat{\mathbf{e}}_z$, we calculate for the force,

$$\mathbf{F} = q\vec{\mathcal{E}}_0\hat{\mathbf{e}}_z + \vec{\mathcal{B}}_0(v_x\hat{\mathbf{e}}_x + v_y\hat{\mathbf{e}}_y + v_z\hat{\mathbf{e}}_z)\times\hat{\mathbf{e}}_z = q\vec{\mathcal{E}}_0\hat{\mathbf{e}}_z + q\vec{\mathcal{B}}_0(-v_x\hat{\mathbf{e}}_y + v_y\hat{\mathbf{e}}_x) \ ,$$

and therefore for the equations of motion by components,

$$\ddot{x} = \frac{q\vec{\mathcal{B}}_0}{m}\dot{y} \quad , \quad \ddot{y} = -\frac{q\vec{\mathcal{B}}_0}{m}\dot{x} \quad , \quad \ddot{z} = \frac{q\vec{\mathcal{E}}_0}{m} \ .$$

c. The third equation can be integrated immediately. With the boundary conditions $z(0) = 0$ and $\dot{z}(0) = v_{0z}$ follows the 'free fall',

$$z(t) = \frac{q\vec{\mathcal{E}}_0}{2m}t^2 + v_{0z}t \ .$$

For the other two (coupled) equations we use a standard trick: we add $\imath$ times the second equation to the first one, and get,

$$\ddot{x} + \imath\ddot{y} = -\imath\frac{q\vec{\mathcal{B}}_0}{mc}\ (\dot{x} + \imath\dot{y}) \ .$$

that is, with the abbreviations $\eta = x + \imath y$ *and* $\omega = q\vec{\mathcal{B}}_0/(mc)$

$$\ddot{\eta} = -\imath\omega\dot{\eta} \ ,$$

we use that $\dot{\eta}(0) = v_{0x} + \imath v_{0y}$. *From this follows immediately,*

$$\dot{\eta}(t) = \dot{x} + \imath\dot{y} = (v_{0x} + \imath v_{0y})e^{-\imath\omega t} \ .$$

This equation can also be directly integrated,

$$\begin{aligned}\eta(t) = x + \imath y &= \frac{\imath}{\omega}e^{-\imath\omega t} + c \\ &= \left(\frac{v_{0x}}{\omega}\sin\omega t - \frac{v_{0y}}{\omega}\cos\omega t + \mathfrak{Re}\ c\right) + \imath\left(\frac{v_{0x}}{\omega}\cos\omega t + \frac{v_{0y}}{\omega}\sin\omega t + \mathfrak{Im}\ c\right) \ .\end{aligned}$$

Inserting the initial conditions,

$$\begin{aligned}x(t) &= \frac{v_{0x}}{\omega}\sin\omega t - \frac{v_{0y}}{\omega}(\cos\omega t - 1) \\ y(t) &= \frac{v_{0x}}{\omega}(\cos\omega t - 1) + \frac{v_{0y}}{\omega}\sin\omega t \ .\end{aligned}$$

d. From (c) follows,

$$\dot{x}^2 + \dot{y}^2 = v_{0x}^2 + v_{0y}^2 = constant \ .$$

Calling T_0 *the kinetic energy at time* $t = 0$ *we get,*

$$T(t) = \tfrac{m}{2}(\dot{x}^2 + \dot{y}^2 + \dot{z}^2) = T_0 + \tfrac{m}{2}q\vec{\mathcal{E}}_0 t(q\vec{\mathcal{E}}_0 t + 2v_{0z}) \ .$$

19.2.3.4 Ex: Excitation of an electron by circularly polarized light

Derive the expression for the dipole radiation from the Maxwell equations proceeding in the following way:
a. Derive the equation of motion of a point particle of charge q and mass m in an electromagnetic field $(\vec{\mathcal{E}},\ \vec{\mathcal{B}})$ neglecting the emission of radiation by the moving charge. Determine the temporal variation of the particle's energy W inside the external field.
b. A circularly polarized monochromatic wave in vacuum is described by the electric field, $\vec{\mathcal{E}}(\mathbf{r},t) = \mathcal{E}[\cos(kz - \omega t)\hat{\mathbf{e}}_x + \sin(kz - \omega t)\hat{\mathbf{e}}_y]$. Calculate the corresponding magnetic field $\vec{\mathcal{B}}(\mathbf{r},t)$.
c. Calculate the Poynting vector $\vec{\mathcal{S}}(\mathbf{r},t)$.
d. For an energy flux of the electromagnetic wave of $10\,\mathrm{W/m^2}$ calculate the amplitudes of the electric and the magnetic field.
e. For the particle of part (a) moving in the fields of part (b) establish the equation of motion.
f. Initially $(t = 0)$ the particle is at the origin of the coordinate system. How should the initial condition for the velocity be chosen in order to obtain a constant energy for the particle?
g. Determine the momentum $\mathbf{p}$ of the particle and verify that $\mathbf{p}_\perp = p_x\hat{\mathbf{e}}_x + p_y\hat{\mathbf{e}}_y$

coincides at every instant of time with the direction of $\vec{\mathcal{B}}$.
h. Solve the equation of motion with the initial conditions of part (d).
i. What is the form of the particle's trajectory in the x-y plane?

Solution: *a. The Lorentz force is,*

$$\mathbf{F} = q\vec{\mathcal{E}} + q(\mathbf{v} \times \vec{\mathcal{B}}) \ .$$

With Newton immediately follows the equation of motion,

$$\ddot{\mathbf{r}} = \tfrac{q}{m}\vec{\mathcal{E}} + \tfrac{q}{m}(\dot{\mathbf{r}} \times \vec{\mathcal{B}}) \ .$$

For the temporal variation of the particle's energy we obtain,

$$\dot{W} = \mathbf{v} \cdot \mathbf{F} = q\mathbf{v} \cdot \vec{\mathcal{E}} \ .$$

b. We have

$$\vec{\mathcal{B}} = \tfrac{1}{\omega}(\mathbf{k} \times \vec{\mathcal{E}}) \ ,$$

with $\mathbf{k} = k\hat{\mathbf{e}}_z$.
c. The Poynting vector is,

$$\vec{\mathcal{S}}(\mathbf{r}, t) = \varepsilon_0 c^2 (\vec{\mathcal{E}} \times \vec{\mathcal{B}}) = \varepsilon_0 c^2 \frac{\vec{\mathcal{E}}_0^2}{c} \left[\hat{\mathbf{e}}_z \sin^2(kz - \omega t) + \hat{\mathbf{e}}_z \cos^2(kz - \omega t)\right] = \varepsilon_0 c \vec{\mathcal{E}}_0^2 \hat{\mathbf{e}}_z \ ,$$

that is, we have a constant flow in the direction of the k vector.
d. The amplitudes are $\mathcal{E}_0 = \sqrt{s/\varepsilon_0 c} \approx 61\,\mathrm{V/m}$ *and* $\mathcal{B}_0 = \mathcal{E}_0/c \approx 2.1 \cdot 10^{-7}\,\mathrm{T}$.
e. Inserting the derived magnetic field into the equation of motion,

$$\ddot{\mathbf{r}} = \tfrac{q}{m}\vec{\mathcal{E}} + \tfrac{q}{m\omega}\mathbf{v} \times (\mathbf{k} \times \vec{\mathcal{E}}) = \tfrac{q}{m}\vec{\mathcal{E}} + \tfrac{q}{m\omega}(\mathbf{k}(\mathbf{v} \cdot \vec{\mathcal{E}}) - \vec{\mathcal{E}}(\mathbf{v} \cdot \mathbf{k})) \ .$$

Using one more time $\mathbf{k} = k\hat{\mathbf{e}}_z$ *and* $\omega = ck$, *we obtain by components,*

$$\begin{aligned}
\ddot{x} &= \frac{q}{m}\mathcal{E}_x \left(1 - \frac{\dot{z}}{c}\right) = \frac{q}{m}\mathcal{E} \left(1 - \frac{\dot{z}}{c}\right) \cos(kz - \omega t) \\
\ddot{y} &= \frac{q}{m}\mathcal{E}_y \left(1 - \frac{\dot{z}}{c}\right) = \frac{q}{m}\mathcal{E} \left(1 - \frac{\dot{z}}{c}\right) \sin(kz - \omega t) \\
\ddot{z} &= \frac{q}{mc}(\dot{\mathbf{r}} \cdot \vec{\mathcal{E}}) \ .
\end{aligned}$$

f. If we want $\dot{W} = 0$ *at all times, from (a) we get immediately that* $\dot{\mathbf{r}} \cdot \vec{\mathcal{E}} = 0$ *must always be satisfied. With the last equation of part (e) this implies* $\ddot{z} = 0$, *that is* $\dot{z} = \mathrm{const} = v_0$. *Insertion in the other two equations of motion provides,*

$$\begin{aligned}
\ddot{x} &= \frac{q\mathcal{E}}{m} \left(1 - \frac{v_0}{c}\right) \cos(kz - \omega t) \\
\ddot{y} &= \frac{q\mathcal{E}}{m} \left(1 - \frac{v_0}{c}\right) \sin(kz - \omega t) \ .
\end{aligned}$$

Integration gives,

$$\begin{aligned}
\dot{x} &= -\frac{q\mathcal{E}}{m\omega} \left(1 - \frac{v_0}{c}\right) \sin(kz - \omega t) + \dot{x}_0 \\
\dot{y} &= \frac{q\mathcal{E}}{m\omega} \left(1 - \frac{v_0}{c}\right) \cos(kz - \omega t) + \dot{y}_0 \ .
\end{aligned}$$

With this follows,

$$\begin{aligned} 0 = \dot{\mathbf{r}} \cdot \vec{\mathcal{E}} &= \left[-\frac{q\mathcal{E}}{m\omega} \left(1 - \frac{v_0}{c}\right) \sin(kz - \omega t) + \dot{x}_0 \right] \mathcal{E} \cos(kz - \omega t) \\ &+ \left[\frac{q\mathcal{E}}{m\omega} \left(1 - \frac{v_0}{c}\right) \cos(kz - \omega t) + \dot{y}_0 \right] \mathcal{E} \sin(kz - \omega t) \\ &= \dot{x}_0 \mathcal{E} \cos(kz - \omega t) + \dot{y}_0 \mathcal{E} \sin(kz - \omega t) \dot{\mathbf{r}}_0 \cdot \vec{\mathcal{E}} = \mathcal{E}_x \dot{x}_0 + \mathcal{E}_y \dot{y}_0 \ . \end{aligned}$$

For this expression to be zero at all times, we need $\dot{x}_0 = \dot{y}_0 = 0$. *Since* $z(t = 0) = 0$, *we obtain for the initial conditions we were looking for,*

$$\mathbf{v}(t = 0) = \begin{pmatrix} 0 & \frac{q\mathcal{E}}{m\omega} \left(1 - \frac{v_0}{c}\right) & 0 \end{pmatrix} \qquad \textit{with} \qquad v_0 \quad \textit{arbitrary} \ .$$

g. For the momentum we get,

$$\mathbf{p} = \begin{pmatrix} -\frac{q\mathcal{E}}{\omega} \left(1 - \frac{v_0}{c}\right) \sin(kz - \omega t) \\ \frac{q\mathcal{E}}{\omega} \left(1 - \frac{v_0}{c}\right) \cos(kz - \omega t) \\ m v_0 \end{pmatrix} \ .$$

A comparison with the magnetic field $\vec{\mathcal{E}}(\mathbf{r}, t) = \frac{\mathcal{E}}{c}[-\sin(kz - \omega t)\hat{\mathbf{e}}_x + \cos(kz - \omega t)\hat{\mathbf{e}}_y]$ *calculated in (b) shows that,*

$$\mathbf{p}_\perp = \frac{q}{ck} \left(1 - \frac{v_0}{c}\right) \vec{\mathcal{B}} \ .$$

h. Integration

$$\begin{aligned} x &= -\frac{q\mathcal{E}}{m\omega^2} \left(1 - \frac{v_0}{c}\right) \cos(kz - \omega t) \ + \ x_0 \\ y &= -\frac{q\mathcal{E}}{m\omega^2} \left(1 - \frac{v_0}{c}\right) \sin(kz - \omega t) \ + \ y_0 \\ z &= v_0 t \ + \ z_0 \ . \end{aligned}$$

With $x(t = 0) = y(t = 0) = z(t = 0) = 0$ *follows the solution,*

$$\begin{aligned} x(t) &= \frac{q\mathcal{E}}{m\omega^2} \left(1 - \frac{v_0}{c}\right) [1 - \cos(kz - \omega t)] \\ y(t) &= -\frac{q\mathcal{E}}{m\omega^2} \left(1 - \frac{v_0}{c}\right) \sin(kz - \omega t) \\ z(t) &= v_0 t \ . \end{aligned}$$

i. We define,

$$R \equiv \frac{q\mathcal{E}}{m\omega^2} \left(1 - \frac{v_0}{c}\right) \ .$$

We see immediately with part (f), that,

$$(x(t) - R)^2 + y^2(t) = R^2 \ .$$

Therefore, the trajectory is a circle with the radius R *and the center* $(R, 0)$.

19.2.3.5 Ex: Charge and current densities for radiative atomic transitions

The charge and current densities for radiative atomic transitions from the state $m = 0$, $2p$ of hydrogen to the ground state $1s$, are (neglecting the spin),

$$\varrho(r,\theta,\phi,t) = \frac{2e}{\sqrt{6}a_B^4} r e^{-3r/2a_B} Y_{00} Y_{10} e^{-\imath\omega_0 t} \quad , \quad \mathbf{j}(r,\theta,\phi,t) = -\imath v_0 \left(\frac{\hat{\mathbf{e}}_r}{2} + \frac{a_B}{z}\hat{\mathbf{e}}_z \right) \varrho(r,\theta,\phi,t) \ ,$$

where $v_0 = \alpha c$ is the orbital velocity of the electron, a_B the Bohr radius, and α the Sommerfeld constant.
a. Show that the effective transitional orbital 'magnetization' is,

$$\vec{\mathcal{M}}_{ef}(r,\theta,\phi,t) = -\imath \frac{\alpha c a_B}{2} \tan\theta (\hat{\mathbf{e}}_x \sin\phi - \hat{\mathbf{e}}_y \cos\phi) \varrho(r,\theta,\phi,t) \ .$$

Calculate $\nabla \cdot \vec{\mathcal{M}}_{ef}$ and evaluate the electric and magnetic dipole moments.
b. In the electric dipole approximation, calculate the temporal average of the total radiated power. Express your response in units of $(\hbar\omega_0)(\alpha^4 c/a_B)$.
c. Interpreting the classically calculated power as the energy of a photon ($\hbar\omega_0$) times the transition probability, numerically evaluate the transition probability in units of reciprocal seconds.
d. If, instead of the semiclassic charge density used above, the electron in the $2p$ state is described by a circular Bohr orbit of radius $2a_B$, rotating with the transition frequency ω_0, what would be the radiated power? Express your answer in the same units as in part (b), and evaluate the ratio of the two powers numerically.

Solution: *a. The magnetization is,*

$$\begin{aligned}
\vec{\mathcal{M}} = \tfrac{1}{2}\mathbf{r}\times\mathbf{j} &= \tfrac{1}{2}\mathbf{r}\times\left[-iv_0\left(\cancelto{0}{\frac{\hat{\mathbf{e}}_z}{2}} + \frac{a_B}{z}\hat{\mathbf{e}}_z\right)\varrho\right] = -\imath v_0 a_B \tfrac{1}{2}\hat{\mathbf{e}}_r \times \hat{\mathbf{e}}_z \tfrac{r}{z}\varrho \\
&= -\imath v_0 a_B \tfrac{1}{2}(-\hat{\mathbf{e}}_y \sin\theta\cos\phi + \hat{\mathbf{e}}_x \sin\theta \sin\phi)\tfrac{r}{z}\varrho \\
&= -\imath c\alpha a_B \tfrac{1}{2}\tan\theta(\hat{\mathbf{e}}_x \sin\phi - \hat{\mathbf{e}}_y\cos\phi)\varrho \equiv \mathbf{X}\varrho \ ,
\end{aligned}$$

defining $\mathbf{X} = -\imath c\alpha a_B \frac{1}{2}\left(\hat{\mathbf{e}}_x \frac{y}{r} - \hat{\mathbf{e}}_y \frac{x}{r}\right)\frac{r}{z}$. *We find* $Y_{00} = \sqrt{1/(4\pi)}$ *and* $Y_{10} = \sqrt{3/(4\pi)}z$ *in tables of mathematical formulas and introduce the abbreviation* $\kappa \equiv \frac{2q}{\sqrt{6}a_B^4}\frac{1}{\sqrt{4\pi}}\sqrt{\frac{3}{4\pi}}$. *With this the charge density becomes,*

$$\varrho = \kappa z e^{-3r/a_B} \ .$$

The divergence of magnetization is,

$$\begin{aligned}
\nabla\cdot\vec{\mathcal{M}} &= \varrho\nabla\cdot\mathbf{X} + \mathbf{X}\cdot\nabla\varrho = \varrho\cancelto{0}{\nabla\cdot\mathbf{X}} + \kappa\mathbf{X}\cdot\nabla z e^{-3r/2a_B} \\
&= \mathbf{X}\cdot\left\{ z e^{-3r/2a_B}\left[\frac{-3x}{2a_B r}\hat{\mathbf{e}}_x + \frac{-3y}{2a_B r}\hat{\mathbf{e}}_y + \left(\frac{1}{z} - \frac{3z}{2a_B r}\right)\hat{\mathbf{e}}_z\right]\right\} = 0 \ .
\end{aligned}$$

We can write the electric dipole moment as,

$$\mathbf{d} = \int (x\hat{\mathbf{e}}_x + y\hat{\mathbf{e}}_y + z\hat{\mathbf{e}}_z)\varrho(\mathbf{r})d^3r = \int (\cancelto{0}{x\hat{\mathbf{e}}_x + y\hat{\mathbf{e}}_y} + z\hat{\mathbf{e}}_z)\kappa z e^{\frac{-3}{2a_B}\sqrt{x^2+y^2+z^2}}\varrho(\mathbf{r})d^3r \ ,$$

because integrals of odd functions vanish. Now,

$$\mathbf{d} = \kappa\hat{\mathbf{e}}_z \int z^2 e^{\frac{-3}{2a_B}\sqrt{x^2+y^2+z^2}} \varrho(\mathbf{r}) d^3r = 2\pi\kappa\hat{\mathbf{e}}_z \left(\int_0^\infty r^4 e^{-3r/2a_B} dr\right)\left(\int_{-1}^1 \cos^2\theta d(\cos\theta)\right) .$$

Using $\int_0^\infty r^n e^{-\beta r} dr = \frac{n!}{\beta^{n+1}}$ *we finally get,*

$$\mathbf{d} = 2\pi\kappa\hat{\mathbf{e}}_z \left(\frac{4!}{(3/2a_B)^5}\right)\left(\frac{2}{3}\right)\mathbf{d} = \pi\kappa\hat{\mathbf{e}}_z \left(\frac{4a_B}{3}\right)^5 = \frac{2^9}{\sqrt{2}3^5} e a_B \approx 1.49 e a_B \hat{\mathbf{e}}_z .$$

Now we calculate the magnetic dipole moment,

$$\mathbf{m} = \int \vec{\mathcal{M}} d^3r = -\frac{-\imath a_B v_0}{2} \int \left(\frac{y}{z}\hat{\mathbf{e}}_x - \frac{x}{z}\hat{\mathbf{e}}_y\right) \varrho d^3r = 0 ,$$

because integrals of odd functions vanish, ϱ *being even in* x *and* y*.*
b. The time-averaged total radiated power is given by,

$$P_{Jackson} = \frac{\mu_0 c^3 k^4}{12\pi} \bar{p}^2 \approx 0.039\ (\hbar\omega_0)\left(\frac{\alpha^4 c}{a_B}\right) .$$

c. We obtain,

$$\Gamma = \frac{P}{\hbar\omega} \approx 6.3 \cdot 10^8\,\mathrm{s}^{-1} \approx (2\pi)\ 100\,\mathrm{MHz} .$$

d. For a Bohr transition from the state $2p$ *having the radius* $r = 2a_B$ *to the state* $2s$ *having the radius* aB*,*

$$\mathbf{d} = q(2a_B - a_B)\hat{\mathbf{e}}_z e^{-\imath\omega t} = q a_B e^{-\imath\omega t}\hat{\mathbf{e}}_z ,$$

gives an emitted power of,

$$P_{Bohr} = 0.018\ (\hbar\omega_0)\left(\frac{\alpha^4 c}{a_B}\right) \approx 0.45\ P_{Jackson} .$$

19.2.3.6 Ex: Synchrotron radiation

In the discussion of the Bremsstrahlung in class we assumed that the velocity and the acceleration were (at least instantaneously) *collinear*. Do the same analysis for the case, that they are *perpendicular*. Choose your axes so that v is along the z-axis and a along the x-axis (see Fig. 19.7), such that $\mathbf{v} = v\hat{\mathbf{e}}_z$, $\mathbf{a} = \hat{\mathbf{e}}_x$ and $\mathbf{R} = \sin\theta\cos\phi\hat{\mathbf{e}}_x + \sin\theta\sin\phi\hat{\mathbf{e}}_y + \cos\theta\hat{\mathbf{e}}_z$. Verify whether P is consistent with the Liénard formula.

Solution: *We start from the Liénard's generalization of Larmor's formula (19.146),*

$$\frac{dP}{d\Omega} = \frac{q}{16\pi\varepsilon_0} \frac{|\hat{\mathbf{e}}_r \times (\mathbf{u}\times\mathbf{a})|^2}{(c - \hat{\mathbf{e}}_r\cdot\mathbf{v})^5} ,$$

inserting boundary conditions, which are specific to the problem,

$$\mathbf{v} = v\hat{\mathbf{e}}_z \qquad \textit{and} \qquad \mathbf{a} = a\hat{\mathbf{e}}_x \qquad \textit{such that} \qquad \mathbf{u} = c\hat{\mathbf{e}}_r - \mathbf{v} = c\hat{\mathbf{e}}_r - v\hat{\mathbf{e}}_z \ .$$

Using $\hat{\mathbf{e}}_r = \hat{\mathbf{e}}_x \sin\theta\cos\phi + \hat{\mathbf{e}}_y \sin\theta\sin\phi + \hat{\mathbf{e}}_z\cos\theta$ *to calculate,*

$$\begin{aligned}
\frac{dP}{d\Omega} &= \frac{q^2}{16\pi\varepsilon_0}\frac{|\hat{\mathbf{e}}_r \times [(c\hat{\mathbf{e}}_r - v\hat{\mathbf{e}}_z)\times a\hat{\mathbf{e}}_x]|^2}{(c-\hat{\mathbf{e}}_r\cdot v\hat{\mathbf{e}}_z)^5} = \frac{q^2a^2}{16\pi\varepsilon_0 c^3}\frac{|\hat{\mathbf{e}}_r\times(\hat{\mathbf{e}}_r\times\hat{\mathbf{e}}_x) - \beta\hat{\mathbf{e}}_r\times(\hat{\mathbf{e}}_z\times\hat{\mathbf{e}}_x)|^2}{(1-\beta\hat{\mathbf{e}}_r\cdot\hat{\mathbf{e}}_z)^5} \\
&= \frac{q^2a^2}{16\pi\varepsilon_0 c^3}\frac{|\hat{\mathbf{e}}_r(\hat{\mathbf{e}}_r\cdot\hat{\mathbf{e}}_x) - \hat{\mathbf{e}}_x(\hat{\mathbf{e}}_r\cdot\hat{\mathbf{e}}_r) - \beta\hat{\mathbf{e}}_z(\hat{\mathbf{e}}_r\cdot\hat{\mathbf{e}}_x) + \beta\hat{\mathbf{e}}_x(\hat{\mathbf{e}}_r\cdot\hat{\mathbf{e}}_z)|^2}{(1-\beta\hat{\mathbf{e}}_r\cdot\hat{\mathbf{e}}_z)^5} \\
&= \frac{\mu_0 q^2a^2}{16\pi c}\frac{(\hat{\mathbf{e}}_r\sin\theta\cos\phi - \hat{\mathbf{e}}_x - \beta\hat{\mathbf{e}}_z\sin\theta\cos\phi + \beta\hat{\mathbf{e}}_x\cos\theta)^2}{(1-\beta\cos\theta)^5} \\
&= \frac{\mu_0 q^2a^2}{16\pi c}\frac{(\hat{\mathbf{e}}_r - \beta\hat{\mathbf{e}}_z)^2\sin^2\theta\cos^2\phi + (1-\beta\cos\theta)^2 - 2(\hat{\mathbf{e}}_r - \beta\hat{\mathbf{e}}_z)\cdot\hat{\mathbf{e}}_x\sin\theta\cos\phi(1-\beta\cos\theta)}{(1-\beta\cos\theta)^5} \\
&= \frac{\mu_0 q^2a^2}{16\pi c}\frac{(1+\beta^2-2\beta\cos\theta)\sin^2\theta\cos^2\phi + (1-\beta\cos\theta)^2 - 2\sin\theta\cos\phi(1-\beta\cos\theta)}{(1-\beta\cos\theta)^5} \\
&= \frac{\mu_0 q^2a^2}{16\pi c}\frac{(1-\beta\cos\theta)^2 - (1-\beta)^2\sin^2\theta\cos^2\phi}{(1-\beta\cos\theta)^5} \ .
\end{aligned}$$

The integral is,

$$\begin{aligned}
P &= \int\frac{dP}{d\Omega}d\Omega = \frac{\mu_0 q^2a^2}{16\pi c}\int_0^\pi\int_0^{2\pi}\frac{(1-\beta\cos\theta)^2 - (1-\beta)^2\sin^2\theta\cos^2\phi}{(1-\beta\cos\theta)^5}\sin\theta d\phi d\theta \\
&= \frac{\mu_0 q^2a^2}{16\pi^2 c}\frac{8}{3}\frac{\pi}{(1-\beta^2)^2} = \frac{\mu_0 q^2a^2\gamma^4}{6\pi c} \ .
\end{aligned}$$

For the relativistic velocities ($\simeq c$), the radiation is again accentuated in forward direction. The most important application of these formulas is the case of a circular movement. In this case the radiation is called synchrotron radiation. For a relativistic electron, the radiation sweeps like a locomotive beacon, as the particle moves.

19.2.3.7 Ex: Cherenkov radiation

Cherenkov radiation is observed, when a charge moves with relativistic velocity within a dielectric medium, which reduces the speed of light below the velocity of the particle. A blue superluminal shock wave is then formed.
a. Calculate the angle θ_c between the propagation direction of the charge and the propagation direction of the shock wavefront.
b. We now imagine the deceleration process of the charge inside the dielectric as being due to a collision with a heavy molecule of the dielectric material. The collision creates a photon emitted under the angle θ_c and the momentum of charge is deflected. We despise the recoil of the molecule. Based on relativistic energy and momentum conservation, calculate the angle θ_c in terms of the momenta of charge before and after the collision and of the radiated frequency.
c. Comparing the results obtained in (a) and (b), calculate the rest mass of the charge.
d. Calculate the retarded Liénard-Wiechert potentials inside and outside of the cone.

Solution: *a. From the diagram we can easily see,*

$$\cos\theta_c = \frac{1}{\beta_n} \qquad with \qquad \beta_n = \frac{nv}{c} \ .$$

b. Relativistic momentum and energy conservation,

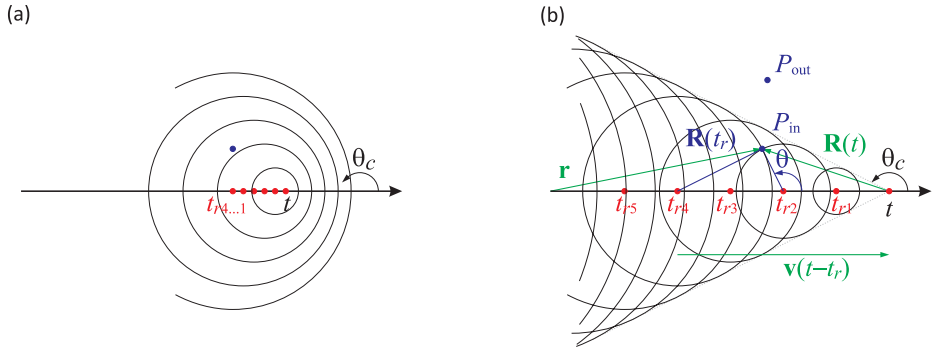

Figure 19.9: Scheme for Cherenkov radiation. (a) Charge moving at subluminal velocity, (b) at superluminal velocity.

$$\begin{pmatrix} \sqrt{c^2 p_{befor}^2 + m^2 c^4} \\ \mathbf{p}_{befor} \end{pmatrix} = \begin{pmatrix} \sqrt{c^2 p_{aftr}^2 + m^2 c^4} + \hbar\omega \\ \mathbf{p}_{aftr} + n\hbar\mathbf{k} \end{pmatrix} \ .$$

Momentum conservation,

$$p_{aftr}^2 = p_{befor}^2 + (n\hbar k)^2 - 2n\hbar k p_{antes})\cos\theta_c \qquad \Longrightarrow \qquad \cos\theta_c = \frac{p_{aftr}^2 - p_{befor}^2 + (n\hbar k)^2}{-2n\hbar k p_{befor}} \ .$$

Resolving the momentum conservation by p_{after}*,*

$$c^2 p_{aftr}^2 = \left(\sqrt{c^2 p_{antes}^2 + m^2 c^4} - \hbar\omega\right)^2 - m^2 c^4 = c^2 p_{befor}^2 + \hbar^2\omega^2 - 2\hbar\omega\sqrt{c^2 p_{before}^2 + m^2 c^4} \ ,$$

and replacing this in the formula for $\cos\theta_c$*,*

$$\begin{aligned} \cos\theta_c &= \frac{p_{before}^2 + \frac{\hbar^2\omega^2}{c^2} - \frac{2\hbar\omega}{c^2}\sqrt{c^2 p_{befor}^2 + m^2 c^4} - p_{befor}^2 + (n\hbar k)^2}{-2n\hbar k p_{befor}} \\ &= \frac{2\sqrt{c^2 p_{before}^2 + m^2 c^4} + (n^2 - 1)c\hbar k}{2cnp_{befor}} \ . \end{aligned}$$

c. Substituting $\cos\theta_c$ *by* $\frac{1}{\beta_n}$*,*

$$v = \frac{c^2 p_{befor}}{\sqrt{c^2 p_{befor}^2 + m^2 c^4} + (n^2 - 1)c\hbar k} \ .$$

d. From Fig. 19.9 we read,

$$\Delta t = t - t_r = \frac{|\mathbf{r} - \mathbf{w}(t_r)|}{c_n} \quad , \quad \mathbf{r} - \mathbf{w}(t_r) = \mathbf{R}(t_r) \quad , \quad \mathbf{v}\Delta t = \mathbf{R}(t_r) - \mathbf{R}(t) \quad , \quad \mathbf{w}(t) = \mathbf{r} - \mathbf{R}(t)$$

which allows us to calculate,

$$c_n \Delta t = R(t_r) = |\mathbf{v}\Delta t + \mathbf{R}(t)| = \sqrt{v^2\Delta t^2 + R^2(t) + 2v\Delta t R(t)\cos\theta} \ ,$$

which has two solution for Δt,

$$\Delta t = \frac{R(t)}{c_n^2 - v^2}\left(v\cos\theta \pm \sqrt{c_n^2 - v^2\sin^2\theta}\right) \ .$$

Since, only real solutions are possible, we get a condition for θ,

$$|\sin\theta| < \frac{c_n}{v} \equiv \sin\theta_C \ ,$$

where θ_C is the Cherenkov angle.
The Liénard-Wiechert potentials are now, using the Heaviside function,

$$\Phi(\mathbf{r},t) = \frac{1}{4\pi\varepsilon_0}\frac{qc_n}{R(t_r)c_n - \mathbf{R}(t_r)\cdot\mathbf{v}}\Theta(\cos\theta_C - \cos\theta) \qquad \textit{and} \qquad \mathbf{A}(\mathbf{r},t) = \frac{\mathbf{v}}{c_n^2}\Phi(\mathbf{r},t) \ .$$

The denominator of the potentials is,

$$\begin{aligned} R(t_r)c_n - \mathbf{R}(t_r)\cdot\mathbf{v} &= c_n^2\Delta t - [\mathbf{v}\Delta t + \mathbf{R}(t)]\cdot\mathbf{v} \\ &= (c_n^2 - v^2)\Delta t - vR(t)\cos\theta = \pm R(t)\sqrt{c_n^2 - v^2\sin^2\theta} \ , \end{aligned}$$

such that,

$$\Phi(\mathbf{r},t) = \pm\frac{q}{4\pi\varepsilon_0}\frac{\Theta(\cos\theta_C - \cos\theta)}{R(t)\sqrt{1 - \frac{v^2}{c_n^2}\sin^2\theta}} \ .$$

19.2.3.8 Ex: Electron subject to gravity

An electron is released from rest and falls under the influence of gravity. Within the first centimeter, what fraction of the lost potential energy is radiated?

Solution: *Accelerates by gravity the charge radiates. This means that not all lost potential energy is converted into kinetic energy, but also into radiation. Therefore, a charged object falls more slowly than an electrically neutral object. The dipole moment of the electron will be,*

$$\mathbf{p} = ez\hat{\mathbf{e}}_z \ .$$

The radiated power was derived in class,

$$P \simeq \frac{\mu_0\ddot{p}}{6\pi c} = \frac{\mu_0 eg}{6\pi c} \approx 5.7\cdot 10^{-52}\,\mathrm{Js}^{-1} \ .$$

To find out how much energy is radiated during the fall of the electron, we need to know, how long it takes the electron to drop by 1 cm. *If all lost potential energy were transformed into kinetic energy, we would have,* $v = gt$ *and* $d = \frac{1}{2}gt^2$. *Since the radiated power is very small, we can safely assume the validity of these expressions and verify that the response is consistent,*

$$t = \sqrt{\frac{2d}{g}} \approx 0.045\,\mathrm{s} \ ,$$

such that the radiated energy is,

$$Pt = 2.46 \cdot 10^{-53}\,\mathrm{J} \ .$$

The lost potential energy is,

$$V = mgh \approx 8.92 \cdot 10^{-32}\,\mathrm{J} \ ,$$

such as the fraction of potential energy lost by radiation is xxx.

19.2.3.9 Ex: Radiation reaction

Including the radiative reaction force (19.154), Newton's second law for a charged particle becomes,

$$a = \tau \dot{a} + \frac{F}{m} \ ,$$

where F is an external force acting on the particle.
a. In contrast to the case of an uncharged particle ($a = F/m$), the acceleration (in the same way as position and velocity) must be a continuous function of time, even when the force changes abruptly. (Physically, the radiative reaction dampens out any rapid variation in a.) Show that a is continuous at any time t by integrating the given equation of motion between $(t - \epsilon)$ and $(t + \epsilon)$ and evaluating the limit $\epsilon \to 0$.
b. A particle be subjected to a constant force F, beginning at time $t = 0$ and remaining until the time T. Find the most general solution $a(t)$ of the equation of motion in each of the three stages: (i) $t < 0$; (ii) $0 < t < T$; and (iii) $t > T$.
c. Impose the continuity condition (a) at times $t = 0$ and $t = T$. Show, that it is possible to *either* eliminate 'runaway-acceleration' in region (iii) *or* avoid 'pre-acceleration' in region (i), but not both.
d. Choosing to eliminate the runaway-acceleration, what will be the acceleration, as a function of time, in each stage (i-iii)? How will the velocity behave, which obviously must be continuous at $t = 0$ and $t = T$. Assume, that the particle was initially at rest: $v(-\infty) = 0$. Prepare schemes of $a(t)$ and $v(t)$ and compare with the behavior of a neutral particle.
e. Repeat (d) choosing the option to eliminate pre-acceleration.

Solution: *a. Including the radiative reaction force, Newton's second law for a charged particle becomes,*

$$a = \tau \dot{a} + \frac{F}{m} \qquad \textit{with} \qquad \tau \equiv \frac{\mu_0 Q^2}{6\pi c}\dot{a} \ .$$

For an electrically neutral particle, the reaction term disappears, which means that if F is discontinuous (as in the case of a suddenly applied force), then a also is. However, it turns out that adding the term $\tau\dot{a}$ guarantees that the acceleration is always continuous, even if the force is not. Suppose that we integrate this equation in a small time interval between $t-\epsilon$ and $t+\epsilon$,

$$\int_{t-\epsilon}^{t+\epsilon} a dt' = \int_{t-\epsilon}^{t+\epsilon} \left(\tau\dot{a} + \frac{F}{m}\right) dt' = \tau a(t+\epsilon) - \tau a(t-\epsilon) + \frac{1}{m}\int_{t-\epsilon}^{t+\epsilon} F dt' \ .$$

Given that both a and F are finite over the time interval (there are no divergences, such as delta functions), then both integrals, the one of the acceleration and the one of the force, should tend to zero as $\epsilon \to 0$. This is true, even F being discontinuous. The consequence is,

$$\lim_{\epsilon\to 0}[(a(t+\epsilon) - a(t-\epsilon)] = 0 \ ,$$

that is, a is continuous. In the case of the neutral particle, $Q=0$ and therefore $\tau = 0$ as well, such that $a(t+\epsilon) - a(t-\epsilon)$ vanishes in any case, and the argument fails.
b. Now, we consider the following example:

$$a(t) = \begin{cases} \tau\dot{a} & for \ \ t<0 \\ \tau\dot{a} + F/m & for \ \ 0<t<T \\ \tau\dot{a} & for \ \ T<t \end{cases} \ .$$

The partial solutions are,

$$a(t) = \begin{cases} a_0 e^{t/\tau} & for \ \ t<0 \\ a_1 e^{t/\tau} + F/m & for \ \ 0<t<T \\ a_2 e^{t/\tau} & for \ \ T<t \end{cases} \ .$$

c. The continuity of the acceleration at the times $t=0$ and $t=T$ requires,

$$a_0 = a_1 + F/m \qquad and \qquad a_1 e^{T/\tau} + F/m = a_2 e^{T/\tau} \ .$$

Eliminating t_1,

$$a_2 = \tfrac{F}{m}(e^{-T/\tau} - 1) + a_0 \ .$$

Since there were no forces before $t=0$, we let $a_0 = 0$. But this means, that we accept a constant (and negative, for $a_2 < 0$) acceleration in the third period without external force. Alternatively, we can let $a_2 = 0$, but that means that we accept a pre-acceleration in the first period, when the force has not yet come into action.
d. Accepting the condition $a_2 = 0$, we obtain the solutions,

$$a(t) = \begin{cases} \frac{F}{m}(1 - e^{-T/\tau})e^{t/\tau} & for \ \ t<0 \\ \frac{F}{m}(1 - e^{(t-T)/\tau}) & for \ \ 0<t<T \\ 0 & for \ \ T<t \end{cases} \ .$$

and

$$v(t) = \begin{cases} \frac{F\tau}{m}(1 - e^{-T/\tau})e^{t/\tau} & for \ \ t<0 \\ \frac{F}{m}(t - \tau e^{(t-T)/\tau}) + \frac{F\tau}{m} & for \ \ 0<t<T \\ \frac{FT}{m} & for \ \ T<t \end{cases} \ .$$

e. Accepting the condition $a_0 = 0$, we obtain the solutions,

$$a(t) = \begin{cases} 0 & \text{for } t < 0 \\ \frac{F}{m}(1 - e^{t/\tau}) & \text{for } 0 < t < T \\ \frac{F}{m}(e^{-T/\tau} - 1)e^{t/\tau} & \text{for } T < t \end{cases} .$$

and

$$v(t) = \begin{cases} 0 & \text{for } t < 0 \\ \frac{F}{m}(t - \tau e^{t/\tau}) + \frac{F\tau}{m} & \text{for } 0 < t < T \\ \frac{F\tau}{m}(e^{-T/\tau} - 1)e^{t/\tau} + \frac{FT}{m} & \text{for } T < t \end{cases} .$$

It is interesting to note that, changing the sign of $\tau \to -\tau$, behavior makes sense.

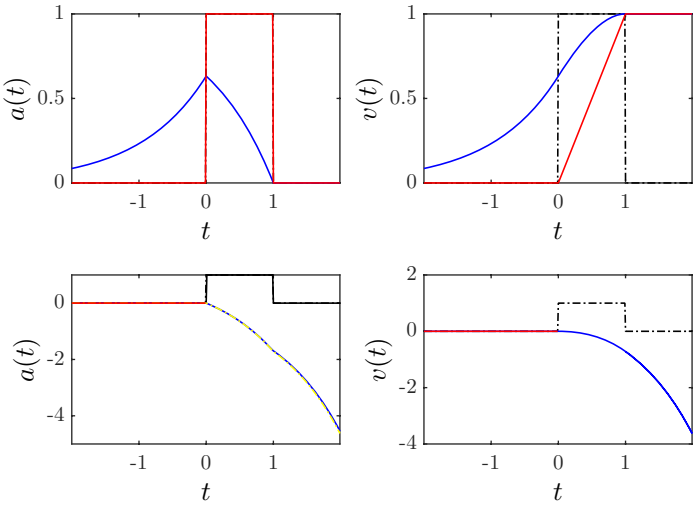

Figure 19.10: (code) Radiation reaction.

19.3 Diffraction and scattering

Radiation (let us call it 'light' for simplicity) incident on a target (e.g. a charge and current distribution, a dielectric body, an atomic cloud, or anything else) will be absorbed, diffracted or scattered. In the absence of absorption, the entire incident energy must be re-emitted. Whether the re-emission process is best described by *diffraction* or *scattering* models depends on the wavelength λ of light in relation to the size of the target and its structure. When the target is small, we can treat the problem in the lowest (usually dipolar) multipolar order; for a target of comparable size with λ, a complete multipolar treatment is required, and in the limit of a large target, we can resort to semi-geometrical methods to explain deviations from geometric optics caused by diffraction.

The topic of diffraction and scattering is well covered in the literature [659]. Rather than reproducing these theories here, we will give in this course a brief introduction

to the *coupled-dipoles model*. This model, which has received much attention in recent years, has proven capable, albeit renouncing of notions such as the refraction index, to give a microscopic view of many macroscopic scattering and diffraction phenomena.

19.3.1 Coupled dipoles model

The electrodynamics contained in Maxwell's macroscopic equations describes the interaction of light with matter characterized by a refractive index $n(\mathbf{r})$. The refractive index is understood as a continuous field, which fully describes the reaction of the target to incident light. On the other hand, we know how the microscopic constituents, that is, the atoms and molecules of the target material, react individually to incident light. In the simplest case, a two-level atom will absorb a photon carrying an electron to a higher orbit, and when the electron returns to the original state, it will emit a photon into an arbitrary direction, that is, isotropically in the time average.

The difficulty now resides in the linking of the macro- and microscopic images, illustrated in Fig. 19.11, to a complete theory. Indeed, all atoms or molecules in the crystal must *cooperate* in some way to generate a refractive index and macroscopic scattering phenomena described by the laws of Snellius, Lambert-Beer, or Ewald-Oseen [180]. The details of how this cooperation works are being studied in several laboratories around the world [1180, 1182, 298].

Figure 19.11: (Left) Macroscopic refraction and (right) microscopic scattering. See also (watch talk).

From a microscopic point of view, the refractive index is an artifact; it does not exist like an atom exists! Since Democritus' reflections on the nature of matter 350 years before Christ, we know that what does exist are 'atoms and empty space, the remainder is mere opinion'. The index of refraction can help us to simplify the description of how light interacts with macroscopic objects. But this does not always work, and in some circumstances even leads to paradoxical results, that are difficult to resolve within Maxwell's theory of electromagnetism. This is, for example, the case of the famous Abraham and Minkowski dilemma, which since 1909, when these two physicists proposed different calculations for the photonic momentum inside a dielectric medium leading to different results, still gives rise to debates. But there are also other situations, where microscopic theory is able to describe phenomena beyond the macroscopic approximation of continuous media. These are phenomena due to disorder, such as Anderson's localization of light or the spontaneous synchronization of atomic dipoles in superradiance.

In the simplest version of the coupled-dipoles model we imagine the target as a (more or less dense) sample of point-like two-level atoms, so that the radiation of the atoms can be described in the dipolar limit, $a_B \ll \lambda$, where the Bohr radius gives a

typical scale for the extension of the radiation source. We will not reproduce integrally the derivation of the coupled-dipoles model here, which borrows from the theory of quantum mechanics. Instead, we will superficially trace the line of argumentation and justify the results by showing that, in the limit of a smooth distribution of the atomic scatterers, we recover the classical laws of Maxwell's theory.

19.3.1.1 Rayleigh scattering

To describe the Rayleigh scattering from an atom, we need to understand the phenomenon of spontaneous emission. This is usually achieved by the *Weisskopf-Wigner theory* starting from the Hamiltonian describing the interaction of a single two-level atom of the sample (labeled j) interacting with an incident laser,

$$\hat{H}_j = \hbar g_{\mathbf{k}_0}\left(\hat{\sigma}_j e^{-\imath\omega_a t} + \hat{\sigma}_j^\dagger e^{\imath\omega_a t}\right)\left(\hat{a}_{\mathbf{k}_0}^\dagger e^{\imath\omega_0 t - \imath\mathbf{k}_0\cdot\mathbf{r}_j} + \hat{a}_{\mathbf{k}_0} e^{-\imath\omega_0 t + \imath\mathbf{k}_0\cdot\mathbf{r}_j}\right) + \sum_{\mathbf{k}} \hbar g_{\mathbf{k}}\left(\hat{\sigma}_j e^{-\imath\omega_a t} + \hat{\sigma}_j^\dagger e^{\imath\omega_a t}\right)\left(\hat{a}_{\mathbf{k}}^\dagger e^{\imath\omega_k t - \imath\mathbf{k}\cdot\mathbf{r}_j} + \hat{a}_{\mathbf{k}} e^{-\imath\omega_k t + \imath\mathbf{k}\cdot\mathbf{r}_j}\right) . \tag{19.157}$$

Here, ω_0, ω_a, and ω_k are, respectively, the frequencies of the incident laser, the atomic resonance and the scattered light [8]. $g_{\mathbf{k}_0}$ is the coupling strength between the atom and the incident light mode and $g_k = d\sqrt{\omega/(\hbar\varepsilon_0 V)}$ describes the coupling between the atom and a vacuum mode with the volume V. $\hat{\sigma}_j = |g\rangle\langle e|$ is the lowering operator of the atomic excitation, that is, it describes the transition of the j^{th} atom from the excited state $|e\rangle$ to the ground state $|g\rangle$. $\hat{a}_{\mathbf{k}}$ is the annihilation operator of a photon in the mode $\mathbf{k}$.

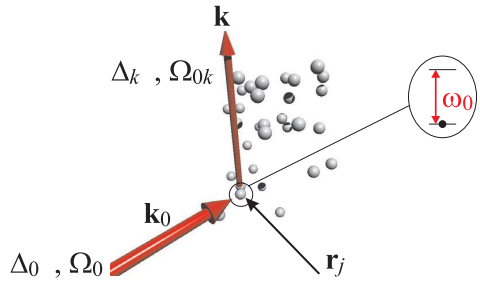

Figure 19.12: Scheme of the interaction of a light beam with a sample of atoms.

Now, considering an incident light mode (e.g. a laser beam) with high power,

$$\hat{a}_{\mathbf{k}_0}|n_0\rangle_{\mathbf{k}_0} = \sqrt{n_0}|n_0 - 1\rangle_{\mathbf{k}_0} \simeq \alpha_0|n_0\rangle_{\mathbf{k}_0} , \tag{19.158}$$

$\hat{a}_{\mathbf{k}_0}$ is approximately an observable, whose amplitude is proportional to the root of the intensity. As $[\hat{a}_{\mathbf{k}_0}, \hat{a}_{\mathbf{k}_0}^\dagger] \simeq 0$, we can disregard the quantum nature and treat the incident light as a classical field by replacing $\Omega_0 \equiv 2\alpha_0 g_{k_0}$, where Ω_0 is the Rabi frequency. The *rotating wave approximation* (RWA) allows us to neglect those terms

[8] We are only considering fixed atoms in space, that is, we do not allow acceleration by photonic recoil.

of the Hamiltonian, which (in the first perturbative order) do not conserve energy, that is, terms proportional to $\hat{\sigma}_j^- \hat{a}$ and $\hat{\sigma}_j^+ \hat{a}^\dagger$. Introducing the abbreviations,

$$\Delta_0 \equiv \omega_0 - \omega_a \qquad \text{and} \qquad \Delta_k \equiv \omega_k - \omega_a \ . \tag{19.159}$$

the Hamiltonian becomes,

$$\hat{H} = \tfrac{\hbar}{2}\Omega_0 \left(\hat{\sigma} \hat{a}_{\mathbf{k}_0}^\dagger e^{\imath \Delta_0 t} + h.c. \right) + \hbar \sum_{\mathbf{k}} \left(g_k \hat{\sigma} \hat{a}_{\mathbf{k}}^\dagger e^{\imath \Delta_k t} + h.c. \right) \ . \tag{19.160}$$

The system can be found in three states,

$$|\Psi(t)\rangle = \alpha(t)|0\rangle_a|0\rangle_{\mathbf{k}} + \beta(t)|1\rangle_a|0\rangle_{\mathbf{k}} + \sum_{\mathbf{k}} \gamma_{\mathbf{k}}(t)|0\rangle_a|1\rangle_{\mathbf{k}} \ . \tag{19.161}$$

Before the scattering the system is, with the probability amplitude α, in the state $|0\rangle_a|0\rangle_{\mathbf{k}}$. After the absorption of a photon, with the probability amplitude β, the atom is excited $|1\rangle_a|0\rangle_{\mathbf{k}}$. Finally, after the reemission of the photon to a mode $\mathbf{k}$, with the probability amplitude $\gamma_{\mathbf{k}}$, the state of the system is $|0\rangle_a|1\rangle_{\mathbf{k}}$. The temporal evolution of the probability amplitudes is obtained by inserting the Hamiltonian (19.160) and the ansatz (19.161) into the Schrödinger equation,

$$\frac{d}{dt}|\Psi(t)\rangle = -\frac{\imath}{\hbar}\hat{H}|\Psi(t)\rangle \ . \tag{19.162}$$

We get, after a calculation which is not reproduced here [9] and which makes use of the so-called *Markov approximation* postulating that the variation of the amplitudes $\beta_j(t)$ is slower than the evolution of the system given by $e^{\imath(\omega_k - \omega_0)t}$, the following equation of motion for the amplitudes β_j,

$$\boxed{\dot{\beta}_j = \left(\imath\Delta_0 - \frac{\Gamma}{2} \right) \beta_j - \frac{\imath\Omega_0}{2} e^{\imath \mathbf{k}_0 \cdot \mathbf{r}_j}} \ . \tag{19.163}$$

This equation correctly describes the dynamics of the probability amplitude of finding an atom exposed to a laser beam and subject to spontaneous emission of its excited state.

19.3.1.2 Collective scattering

In the presence of several atoms, the full Hamiltonian for the atomic cloud is simply obtained by summing over the N atoms [10],

$$\hat{H} = \sum_{j=1}^{N} \hat{H}_j \ . \tag{19.164}$$

Following the same scheme as in the last section, the Schrödinger equation with the Hamiltonian (19.164) where (19.157) can be resolved to the limit of weak excitation:

[9] See Sec. 39.1.2 .

[10] We do not consider in this Hamiltonian collisional interactions between the atoms, for example, of the van der Waals type, which can have a great impact at high densities $n \gg \lambda^{-3}$.

Let us restrict to the situation in which at most a single photon or a single atomic excitation can be in the system. This assumption is realistic, when the time for reemitting a photon is short. The state created by the passage of a single photon is a collective state, because the atomic sample can either be entirely in the ground state before a scattering event, $|g_1,..,g_N\rangle|0\rangle_{\mathbf{k}}$, or after a scattering event, $|g_1,..,g_N\rangle|1\rangle_{\mathbf{k}}$, or else any one of the atoms j can be excited, $|g_1,..,e_j,..,g_N\rangle|0\rangle_{\mathbf{k}}$, during the scattering event. All information on the system is coded in the temporal dependencies of the probability amplitudes for these states, which we obtain through the insertion of the wavefunction [11],

$$|\Psi\rangle = \alpha(t)|g_1\dots g_N\rangle|0\rangle_{\mathbf{k}} + e^{-\imath\Delta_0 t}\sum_{j=1}^{N}\beta_j(t)|g_1\dots e_j\dots g_N\rangle|0\rangle_{\mathbf{k}} \tag{19.165}$$
$$+\sum_{\mathbf{k}}\gamma_{\mathbf{k}}(t)|g_1\dots g_N\rangle|1\rangle_{\mathbf{k}} + \sum_{m,n=1}^{N}\epsilon_{m<n,\mathbf{k}}(t)|g_1\dots e_m\dots e_n\dots g_N\rangle|1\rangle_{\mathbf{k}}\ .$$

within the Schrödinger equation. What we get is a set of integro-differential equations for the amplitudes α, β, and $\gamma_{\mathbf{k}}$, which can be solved within the Markov approximation,

$$\boxed{\dot{\beta}_j = \left(\imath\Delta_0 - \frac{\Gamma}{2}\right)\beta_j - \frac{\imath\Omega_0}{2}e^{\imath\mathbf{k}_0\cdot\mathbf{r}_j} - \frac{\Gamma}{2}\sum_{m\neq j}\frac{e^{\imath k_0|\mathbf{r}_j-\mathbf{r}_m|}}{\imath k_0|\mathbf{r}_j-\mathbf{r}_m|}\beta_m}\ . \tag{19.166}$$

We note, that the first two terms of this equation correspond to the equation describing the dynamics of a single atom (19.163). The third term corresponds to processes, where photons scattered at an atom are reabsorbed by another atom.

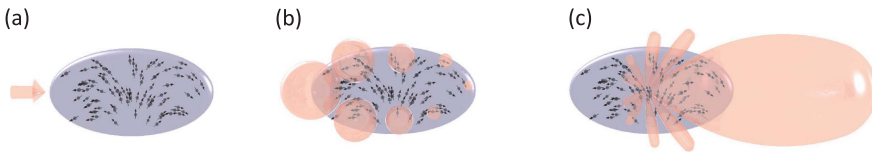

Figure 19.13: Illustration of cooperative scattering: From (a) to (c) a photon traversing an atomic cloud first excites the upstream dipoles, which immediately begin to radiate. The downstream dipoles are excited later on. The phase lag of the reemission processes leads to a radiative emission pattern being strongly peaked into forward direction.

The claim is now that equation (19.166) (or at least its generalization to level systems allowing to take account of the vectorial nature of light) is capable of reproducing all phenomena of macroscopic scattering, usually described by Maxwell's theory, for example, refraction, diffraction, Mie and Bragg scattering, etc. In addition, it correctly describes microscopic scattering phenomena, such as cooperative Rayleigh scattering, Anderson location, photonic band gaps, etc.

[11] The fourth term corresponds to the presence of two simultaneously excited atoms plus a (virtual) photon with 'negative' energy. These states need to be taken into account, if we do not want to make use ofthe RWA approximation.

19.3.2 The limit of the Mie scattering and the role of the refractive index

In practice, the exploitation of the N coupled equations (19.166) (one for each atom), which needs to be done numerically, is limited by computer capacity to some 100 000 atoms. On the other hand, at least, in the limit of high densities, we may hope, that the atomic cloud be well described by a continuous density distribution,

$$\sum_j \beta_j \to \int \beta(\mathbf{r}')\rho(\mathbf{r}')dV' \ . \tag{19.167}$$

Considering the stationary case, $\dot{\beta}_j = 0$, we arrive at,

$$\frac{\Omega_0}{2} e^{\imath \mathbf{k}_0 \cdot \mathbf{r}} = (\Delta_0 + \imath\Gamma)\beta(\mathbf{r}) + \frac{\Gamma}{2}\int \frac{e^{\imath k_0|\mathbf{r}-\mathbf{r}'|}}{k_0|\mathbf{r}-\mathbf{r}'|}\beta(\mathbf{r}')\rho(\mathbf{r}')dV' \ . \tag{19.168}$$

We note that the kernel of the above equation is the Green function of the Helmholtz equation, since,

$$[\nabla^2 + k_0^2]\frac{e^{\imath k_0|\mathbf{r}-\mathbf{r}'|}}{4\pi|\mathbf{r}-\mathbf{r}'|} = -\delta^{(3)}(\mathbf{r}-\mathbf{r}') \ . \tag{19.169}$$

Now, by applying the operator $[\nabla^2 + k_0^2]$ to both sides of equation (19.168), we arrive at,

$$0 = (\Delta_0 + \imath\Gamma)[\nabla^2 + k_0^2]\beta(\mathbf{r}) - 2\pi\Gamma\frac{\beta(\mathbf{r})\rho(\mathbf{r})}{k_0} \ , \tag{19.170}$$

that is [458, 66, 67],

$$\boxed{[\nabla^2 + k_0^2 n(\mathbf{r})^2]\beta(\mathbf{r}) = 0 \qquad \text{defining} \qquad n^2(\mathbf{r}) \equiv 1 - \frac{4\pi\rho(\mathbf{r})}{k_0^3(2\Delta_0/\Gamma + \imath)}} \ . \tag{19.171}$$

This is the *Helmholtz equation* of Maxwell's theory. The reappearance of the refractive index $n(\mathbf{r})$ is the price to pay for smoothing the density distribution, and with it we lose all effects related to discretization and cloud disorder. In Exc. 19.3.3.1 we compare the result of the smoothed coupled-dipole model (19.171) to the macroscopic susceptibility derived from the Lorentz model (18.142), and to the Clausius-Mossotti formula (14.28).

Example 120 (*Bragg scattering by partially disordered clouds*): Fig. 19.14 shows the example of Bragg scattering by an atomic cloud. Without disorder we would expect an incident laser beam to be partially reflected and partially transmitted. The simulation of the stationary version of equation (19.166) for the scattering of the cloud illustrated in (a) shows, in addition to transmission and reflection, a random pattern of specular scattering in all directions, which can be attributed to disorder.

Example 121 (*Collective radiative pressure*): The internal and the global structure of an atomic cloud both dramatically influence the radiative pressure force exerted on its center of mass. We compare two limiting cases [298]: (a) For

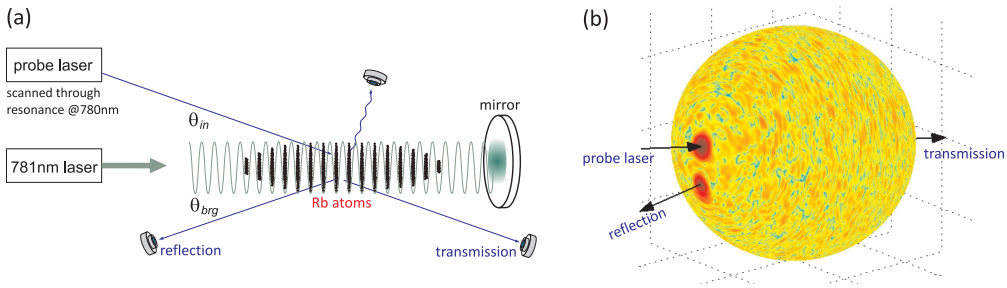

Figure 19.14: (a) Experimental scheme for Bragg reflection by an ordered atomic cloud in a periodic pile of pancakes. (b) Simulation of the stationary cloud scattering equation schematized in (a).

large dilute clouds, scattering by intrinsic disorder prevails. The more atoms are in the cloud, the more pronounced is the forward scattering of the light. Therefore, the radiative pressure force *per atom* exerted by the incident light decreases with N. (b) For small dense clouds, the scattering is rather governed by the global inhomogeneous shape of the cloud. The more atoms are in the cloud, the greater the variation of the refractive index and the greater the refractive deflection of photons off the optical axis [120]. Therefore, the radiation pressure force per atom exerted by the incident light increases with N, as shown in Fig. 19.15(c).

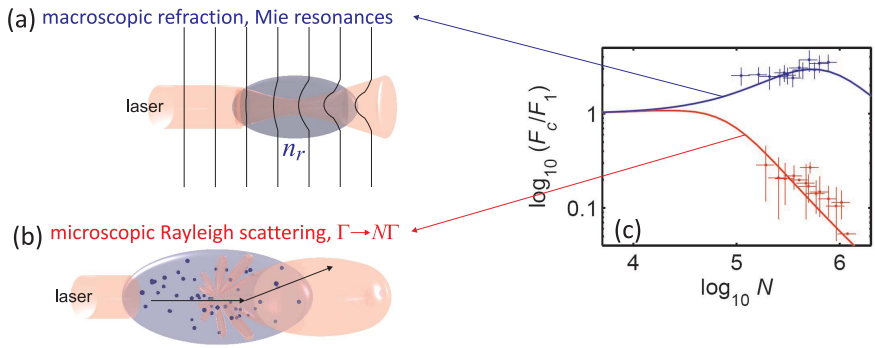

Figure 19.15: (a) Rayleigh scattering by a disordered cloud. (b) Mie scattering via wavefront deformation by the refractive index of an optically dense cloud. (c) Dependence of the radiation pressure force on the number of atoms for the two cases (a) and (b).

Microscopic collective scattering depends on one hand on the internal spatial distribution of the scatterers, that is, the intrinsic disorder, and on the other hand on the global distribution, i.e. the shape and the size of the cloud and its density distribution near the edges, which may be smooth or abrupt. In the limit of despicable disorder,

we have seen that the theory of collective scattering is equivalent to Maxwell's macroscopic theory. In this limit, we can describe the cloud of scatterers as a (locally) homogeneous sphere characterized by a refractive index $n(\mathbf{r})$, which varies spatially with the density of the scatterers. Let us assume, for simplicity, a spherical cloud with a homogeneous refraction index $n(\mathbf{r}) = n_0$ inside the cloud and $n(\mathbf{r}) = 1$ outside. The scattering of a plane wave of radiation by a dielectric sphere is known as *Mie scattering* . In Mie's theory we expand the incident plane wave into partial spherical waves,

$$e^{\imath \mathbf{k}\cdot\mathbf{r}} = \sqrt{4\pi} \sum_{\ell=0}^{\infty} \sqrt{2\ell+1}\imath^{\ell} j_{\ell}(kr) Y_{\ell 0}(\hat{\mathbf{e}}_r) \ , \tag{19.172}$$

which must satisfy the boundary condition for electromagnetic waves at the outer edge of the sphere. This is illustrated in Fig. 19.16. Theoretically it should be possible to observe Mie resonances with atomic clouds, albeit strictly speaking, they do not have a surface which could act like an abrupt boundary condition.

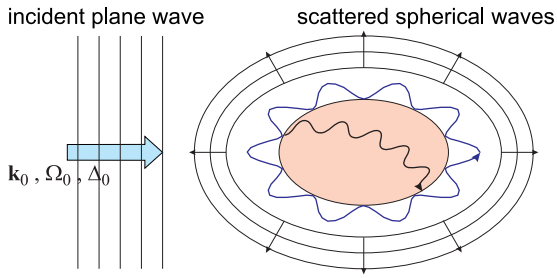

Figure 19.16: Two types of Mie resonances are possible: (i) Waves propagating in the interior of the body and form a stationary wave bounded by the surface and (ii) evanescent waves that propagate on the surface of the body (whispering gallery modes). The resonances of type (ii) require abrupt boundary conditions.

19.3.3 Exercises

19.3.3.1 Ex: Coupled dipoles versus Clausius-Mossotti

Compare the result of the smoothed coupled-dipole model (19.171) to the macroscopic susceptibility derived from the Lorentz model (18.142), and to the Clausius-Mossotti formula (14.28).

Solution:

19.4 Further reading

M.J. Berg et al., *A new explanation of the extinction paradox* [126]DOI

V.C. Ballenegger, *The Ewald-Oseen extinction theorem and extinction lengths* [79]DOI

Chapter 20

Theory of special relativity

Until the end of the nineteenth century people believed in the existence of an 'ether', that is, a medium capable of carrying oscillations of the electromagnetic field in a similar way as water transports surface waves or the air propagates the sound. The propagation velocity of the light must then have a certain value c in this ether. But when measured in another inertial system, according to the Galilei transformation, propagation velocity should be the sum of c and the velocity v of the inertial system through the ether. This ether would be fixed to the universe, and the earth would have a velocity v with respect to this ether.

With the objective of measuring the relative velocity between a fixed laboratory and the ether, *Michelson* and *Morley* did an experiment known as *Michelson-Morley experiment*, and which now represents one of the foundations of the theory of special relativity. It consists of a *Michelson interferometer*, which can be rotated in space. If an 'ether' existed, which is not fixed to the Earth, the speed of light must be anisotropic and the interference fringes observed in the interferometer must move when the interferometer is rotated. This was not observed.

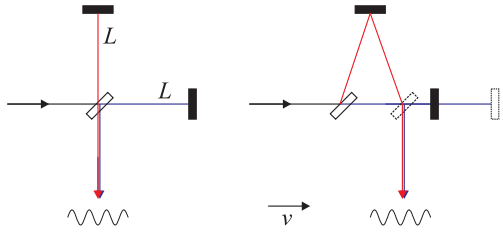

Figure 20.1: Scheme of the Michelson-Morley experiment.

Within the resting system (the ether) the times required for light to travel through each of the interferometer arms are,

$$t_{1,2} = \frac{2L}{c} \ . \tag{20.1}$$

In a frame moving in the direction of one of the arms these times would be,

$$t_1 = \frac{2L}{c}\frac{1}{\sqrt{1-\beta^2}} \qquad \text{and} \qquad t_2 = \frac{L}{c+v} + \frac{L}{c-v} = \frac{2L}{c}\frac{1}{1-\beta^2} \ . \tag{20.2}$$

The experiment confirms the result (20.1) *regardless of the rotation of the interferometer.*

Guided by Michelson's observation it was *Poincaré*, who first proposed the absence of an ether, which motivated *Einstein* to formulate the following postulates:

Law A: *The laws of physics do not depend on a translatory motion of the system as a whole. There is no particular system, in which the 'ether' would be at rest.*

Law B: *The speed of light is constant in all inertial systems and regardless of the speed of the emitting source.*

These postulates revolutionized classical mechanics. The new theory, called the theory of *special relativity*, still contains classical mechanics in the limit of slow velocities, but extends its validity to the limit of velocities approaching the speed of light. Moreover, special relativity reconciles mechanics with electrodynamics in a natural way, as we will show in the following sections.

20.1 Relativistic metric and Lorentz transform

In the theory of relativity, the space represented by the vector $\mathbf{r}$ and the time represented by the scalar ct (where we multiply the universal speed of light for dimensionality reasons) are treated on equal footing. There are other combinations of scalar and vectorial physical quantities such as energy E/c and linear momentum $\mathbf{p}$ which, when combined to a four-dimensional entity, allow for a more symmetrical representation of the fundamental laws of physics. Let us, in the following, set the foundations of this new formalism developed by Poincaré, Lorentz, Einstein, and Minkowski.

20.1.1 Ricci's calculus, Minkowski's metric, and space-time tensors

In the notation of 4-dimensional space-time vectors the physical quantities are described (or combined) by tensors of rank k, e.g. scalars A, vectors A^μ, matrices $A^{\mu\nu}$, and tensors of higher ranks $A^{\mu\nu\lambda\cdots}$. Tensors can be *contravariant*, A^μ, or *covariant*, A_μ, with respect to an index, depending on their behavior regarding the Lorentz transform (as we shall see shortly). Co- (or contra-) variant scalars are independent of the inertial system and, therefore, called *Lorentz invariants*. The contra- and covariant tensors are related by the *Minkowski metric* defined by (see also Sec. 12.4),

$$\boxed{(g^{\mu\nu}) \equiv \begin{pmatrix} 1 & 0 & 0 & 0 \\ 0 & -1 & 0 & 0 \\ 0 & 0 & -1 & 0 \\ 0 & 0 & 0 & -1 \end{pmatrix}} \,, \tag{20.3}$$

using the *sum rule of Einstein*, which consists in summing over all pairs of co- and contravariant indices,

$$a^\mu a_\mu \equiv \sum\nolimits_\mu a^\mu a_\mu \,, \tag{20.4}$$

via

$$a^\mu = g^{\mu\nu} a_\nu \,. \tag{20.5}$$

We note that the first index in a matrix counts the columns and the second index the rows. For flat space-time (that is, without curvature),

$$g_{\mu}{}^{\nu} = g_{\mu\alpha}g^{\alpha\nu} = \delta_{\mu}^{\nu} \quad , \quad g_{\mu\nu} = g^{\mu\nu} \quad \text{that is} \quad \check{g}^{-1} = \check{g} = \check{g}^{\intercal} \ , \tag{20.6}$$

where δ_{μ}^{ν} is the *Kronecker symbol* and the decoration '$\vee$' denotes a matrix, $\check{a} \equiv (a_{\mu\nu})$. Thus, the identity and the metric are the two faces of the same tensor, $\check{\delta} = \check{g}$. The norm is defined by,

$$\|(a^{\mu})\| \equiv \sqrt{a_{\mu}a^{\mu}} = \sqrt{a^{\mu}g_{\mu\nu}a^{\nu}} \ . \tag{20.7}$$

The product between two contravariant vectors is given by,

$$a^{\mu}b^{\mu} \equiv a^{\mu}g_{\mu\nu}b^{\nu} \ . \tag{20.8}$$

The tensors are represented by scalars, vectors and matrices. The vector symbol is used for the contravariant column vector,

$$\vec{a} \equiv (a^{\mu}) = \begin{pmatrix} a^0 \\ \mathbf{a} \end{pmatrix} \quad , \quad \check{a} \equiv (a^{\mu\nu}) = \begin{pmatrix} a^0 & (a^{m0}) \\ (a^{0n}) & (a^{mn}) \end{pmatrix} \ . \tag{20.9}$$

The covariant vector is also represented by a column,

$$\check{g}\vec{a} = (a_{\mu}) = (g_{\mu\nu}a^{\nu}) = \begin{pmatrix} a^0 \\ -\mathbf{a} \end{pmatrix} \ . \tag{20.10}$$

Often, Greek letters are used as indices for space-time tensors, while Roman letters are used as indices for spatial components. In order to work with vectors within Minkowski's formalism, we must interpret them as two-dimensional 1×4 matrices,

$$\vec{a} \equiv (a^{\mu 1}) \ , \tag{20.11}$$

where the '1' indicates the number of columns of the matrix. Introducing the *transposition*, denoted by the symbol '$\intercal$', as an exchange of the indices labeling rows and columns,

$$F_{\mu\nu} = (F^{\intercal})_{\nu\mu} \ , \tag{20.12}$$

we can represent the transposition of a vector by a 4×1 matrix,

$$\vec{a}^{\intercal} = (a^{\mu 1})^{\intercal} = (a^{1\mu}) = \begin{pmatrix} a^0 & \mathbf{a} \end{pmatrix} \ , \tag{20.13}$$

and define the scalar product between vectors in terms of the product between matrices as,

$$\begin{aligned} \vec{a} \cdot \vec{b} \equiv (a^{\mu 1}b_{\mu 1}) = (a^{\intercal})^{1\mu}(b_{\mu 1}) = (a^{\intercal})^{1\mu}g_{\mu\nu}(b^{\nu 1}) = \check{a}^{\intercal}\check{g}\check{b} \\ = \begin{pmatrix} a^0 & (a^m) \end{pmatrix} \begin{pmatrix} 1 & 0 \\ 0 & (-\delta^{mn}) \end{pmatrix} \begin{pmatrix} a^0 \\ (a^n) \end{pmatrix} \ . \end{aligned} \tag{20.14}$$

We conclude emphasizing that, to be able to multiply tensores as matrices, the indices to be contracted must be adjacent. If necessary, the tensors must be transposed,

$$A^{\mu\alpha}B^{\nu}{}_{\alpha} = A^{\mu\alpha}(B^{\intercal})_{\alpha}{}^{\nu} \ . \tag{20.15}$$

One has to be very careful, because in general $A^{\mu\alpha} \neq A^{\alpha\mu} \neq A_{\alpha\mu} \neq A_{\mu\alpha} \neq A_{\alpha}{}^{\mu} \neq A_{\mu}{}^{\alpha} \neq A^{\mu}{}_{\alpha} \neq A^{\alpha}{}_{\mu}$.

20.1.2 Lorentz transform

We are now in the shape to officially introduce our first explicit space-time vector by combining the physical quantities time and position,

$$\boxed{(r^\mu) \equiv \begin{pmatrix} ct \\ \mathbf{r} \end{pmatrix}} \,. \tag{20.16}$$

In classical mechanics the transformation to a system moving at velocity $\beta = v/c$ is described by the *Galilei transform* given by,

$$(G^\mu{}_\nu) \equiv \begin{pmatrix} 1 & 0 & 0 & 0 \\ 0 & 1 & 0 & 0 \\ 0 & 0 & 1 & 0 \\ -\beta & 0 & 0 & 1 \end{pmatrix} \quad , \quad (G^\mu{}_\nu)^{-1} = \begin{pmatrix} 1 & 0 & 0 & 0 \\ 0 & 1 & 0 & 0 \\ 0 & 0 & 1 & 0 \\ \beta & 0 & 0 & 1 \end{pmatrix} \,. \tag{20.17}$$

Example 122 (*Galilei transform*): Let us try out the Galilei transform on the space-time vector (20.16):

$$\begin{pmatrix} ct' \\ x' \\ y' \\ z' \end{pmatrix} = (r'^\mu) = (G^\mu{}_\nu)(r_\nu) = \begin{pmatrix} 1 & 0 & 0 & 0 \\ 0 & 1 & 0 & 0 \\ 0 & 0 & 1 & 0 \\ -\beta & 0 & 0 & 1 \end{pmatrix} \begin{pmatrix} ct \\ x \\ y \\ z \end{pmatrix} = \begin{pmatrix} ct \\ x \\ y \\ z - vt \end{pmatrix} \,.$$

In classical mechanics wave propagation is conditioned to the existence of a medium. Consequently, different inertial systems are not equivalent and, as will be shown in a later section, the wave equation *is not invariant* to the Galilei transform. Let us therefore look for another transformation, which preserves the shape of the wave equation. We may, for example, request the transformation to ensure that the propagation of the phase fronts of a spherical wave is independent of the inertial system: $c^2 t'^2 - \mathbf{r}'^2 = c^2 t^2 - \mathbf{r}^2$.

The story of the *Lorentz transform* begins with Poincaré, who introduced the idea of local time: According to him, simultaneity depends on the reference system. Voigt attempted in 1897 for the first time to find a transformation that would conserve the value of c, but it was Lorentz who found a transformation leaving Maxwell's equations invariant and, consequently, Helmholtz's wave equation as well. The Lorentz transform is linear with respect to the preservation of space-time intervals in Minkowski space and, as we will see shortly, it removes the contradictions between classical mechanics and electrodynamics.

Consider a system S' moving through our lab S at a velocity $\mathbf{v} = v\hat{\mathbf{e}}_z$. We define,

$$\beta = \frac{v}{c} \qquad \text{and} \qquad \gamma = \frac{1}{\sqrt{1-\beta^2}} \,. \tag{20.18}$$

The matrix describing the Lorentz transform from system S to system S' is,

$$\boxed{\check{\Lambda} = (\Lambda^{\mu}{}_{\nu}) \equiv \begin{pmatrix} \gamma & 0 & 0 & -\gamma\beta \\ 0 & 1 & 0 & 0 \\ 0 & 0 & 1 & 0 \\ -\gamma\beta & 0 & 0 & \gamma \end{pmatrix}} \quad , \quad \check{\Lambda}^{-1} = (\Lambda^{\mu}{}_{\nu})^{-1} = \begin{pmatrix} \gamma & 0 & 0 & \gamma\beta \\ 0 & 1 & 0 & 0 \\ 0 & 0 & 1 & 0 \\ \gamma\beta & 0 & 0 & \gamma \end{pmatrix} \tag{20.19}$$

that is, the inverse of the transformation matrix is obtained by changing the sign of the velocity, $v \to -v$. For the Lorentz transform tensor we can show,

$$\begin{aligned} (\Lambda^{\mu}{}_{\nu})^{-1} = g_{\mu\omega}\Lambda^{\omega}{}_{\kappa}g^{\kappa\nu} = \Lambda_{\mu}{}^{\nu} \qquad \text{that is} \qquad \check{\Lambda}^{-1} = \check{g}\check{\Lambda}\check{g} \\ \text{and} \qquad \Lambda^{\omega}{}_{\mu}g_{\omega\kappa}\Lambda^{\kappa}{}_{\nu} = g_{\mu\nu} \qquad \text{that is} \qquad \check{\Lambda}^{\intercal}\check{g}\check{\Lambda} = \check{g} \ . \end{aligned} \tag{20.20}$$

The transformation from a laboratory reference frame S into a rest frame S' is done by,

$$A'^{\mu} = \Lambda^{\mu}{}_{\nu}A^{\nu} \ . \tag{20.21}$$

Time-space scalars are always Lorentz invariant. We consider, for example,

$$x'_{\mu}x'^{\mu} = \Lambda_{\mu}{}^{\nu}x_{\nu}\Lambda^{\mu}{}_{\omega}x^{\omega} = (\check{\Lambda}^{-1}\check{\Lambda})^{\nu}{}_{\omega}x_{\nu}x^{\omega} = \mathbb{I}\ x^{\omega}x_{\omega} \ . \tag{20.22}$$

For space-time differentials, since,

$$dx'^{\mu} = \frac{\partial x'^{\mu}}{\partial x^{\nu}}dx^{\nu} \ , \tag{20.23}$$

comparing with the relationship (20.21), we can identify,

$$\Lambda^{\mu}{}_{\nu} = \frac{\partial x'^{\mu}}{\partial x^{\nu}} \ . \tag{20.24}$$

Contra- and covariant tensors are defined by their different behavior under arbitrary coordinate transformation. For example, in the case of Lorentz transforms,

$$A'_{\mu} = \frac{\partial x^{\nu}}{\partial x'^{\mu}}A_{\nu} \quad , \quad A'^{\mu} = \frac{\partial x'^{\mu}}{\partial x^{\nu}}A^{\nu} \ . \tag{20.25}$$

Similarly, tensors or higher rank satisfy,

$$A'_{\mu\nu} = \frac{\partial x^{\mu}}{\partial x'^{\nu}}\frac{\partial x^{\nu}}{\partial x'^{\beta}}A_{\nu\beta} \quad , \quad A'^{\mu\nu} = \frac{\partial x'^{\mu}}{\partial x^{\nu}}\frac{\partial x'^{\nu}}{\partial x^{\beta}}A^{\nu\beta} \ , \tag{20.26}$$

and also,

$$A'^{\mu_1..\mu_n}{}_{\nu_1..\nu_m} = \Lambda^{\mu_1}{}_{\omega_1}..\Lambda^{\mu_n}{}_{\omega_n}\Lambda_{\nu_1}{}^{\kappa_1}..\Lambda_{\nu_n}{}^{\kappa_n}A^{\omega_1..\omega_n}{}_{\kappa_1..\kappa_m} \ . \tag{20.27}$$

In Exc. 20.1.7.1 we show that the derivative by a covariant coordinate is contravariant.

Example 123 (*Lorentz transform*): In the limit of slow velocities, $v \ll c$, the Lorentz transform converges to the Galilei transform. This can be seen rewriting the Lorentz transform as,

$$\begin{pmatrix} t' \\ z' \end{pmatrix} = \begin{pmatrix} \gamma & -\frac{\gamma\beta}{c} \\ -\gamma\beta & \gamma \end{pmatrix} \begin{pmatrix} t \\ z \end{pmatrix} \simeq \begin{pmatrix} 1 & 0 \\ -\beta & 1 \end{pmatrix} \begin{pmatrix} t \\ z \end{pmatrix} \ .$$

Example 124 (*Lorentz transform*): We have,

$$\Lambda^{\mu}{}_{\nu} = \frac{\partial x'^{\mu}}{\partial x^{\nu}} = \left(\frac{\partial x'_{\mu}}{\partial x_{\nu}}\right)^{-1} = \left(\frac{\partial x^{\nu}}{\partial x'^{\mu}}\right)^{-1} = (\Lambda_{\mu}{}^{\nu})^{-1} \ .$$

20.1.3 Contraction of space

Einstein's theory has important consequences, such as the *contraction of space* and the *dilatation of time*. Let us consider a rod moving through the lab S with velocity v. The rod delimits two points $j = 1, 2$ in space-time for which we measure in the lab (at time $t = t_1 = t_2$) the distance $z_2 - z_1$. The spatio-temporal points are Lorentz-transformed to the system S', in which the rod is at rest (neglecting transverse spatial dimensions), by,

$$\begin{pmatrix} ct'_j \\ z'_j \end{pmatrix} = (\Lambda^{\mu}{}_{\nu}) \begin{pmatrix} ct \\ z_j \end{pmatrix} = \begin{pmatrix} \gamma ct - \gamma\beta z_j \\ -\gamma\beta ct + \gamma z_j \end{pmatrix} \ . \tag{20.28}$$

Hence,

$$z'_2 - z'_1 = -\gamma\beta ct + \gamma z_2 + \gamma\beta ct - \gamma z_1 = \gamma(z_2 - z_1) \ . \tag{20.29}$$

Consequently, in the lab the distance seems smaller than in the rest frame [1].

20.1.4 Dilatation of time

We consider a clock flying through the lab S at a velocity v. The clock produces regular time intervals, for which we measure in the lab the duration $t_2 - t_1$. The spatio-temporal points are Lorentz-transformed to the system S' in which the clock is at rest ($z' = z'_1 = z'_2$) via,

$$\begin{pmatrix} ct'_j \\ z' \end{pmatrix} = (\Lambda^{\mu}{}_{\nu}) \begin{pmatrix} ct_j \\ z_j \end{pmatrix} = \begin{pmatrix} \gamma ct_j - \gamma\beta z_j \\ -\gamma\beta ct_j + \gamma z_j \end{pmatrix} \ . \tag{20.30}$$

Hence,

$$\begin{aligned} t'_2 - t'_1 &= \gamma t_2 - \gamma\beta\frac{z_2}{c} - \gamma t_1 + \gamma\beta\frac{z_1}{c} \\ &= \gamma t_2 - \beta\left(\frac{z'}{c} + \gamma\beta t_2\right) - \gamma t_1 + \beta\left(\frac{z'}{c} + \gamma\beta t_1\right) = \gamma^{-1}(t_2 - t_1) \ . \end{aligned} \tag{20.31}$$

Consequently, in the lab the time interval seems longer than in the rest frame.

A good illustration of the effect of time dilatation is the *twin paradox*. A twin begins an interstellar voyage aboard a space ship traveling at a constant velocity. Twin B, who remained on Earth calculates, that the time elapsed for his twin A is smaller than his own time. Twin B calculates that the elapsed time for his twin A is shorter. Who's right? Twin A is wrong, because his system must be accelerated when taking off from Earth. Note that only special relativity is required to understand

[1] Alternatively, we can measure the instants of time t_j when the ends of the rod pass by a certain point z of the lab, such that $l = v(t_2 - t_1)$.

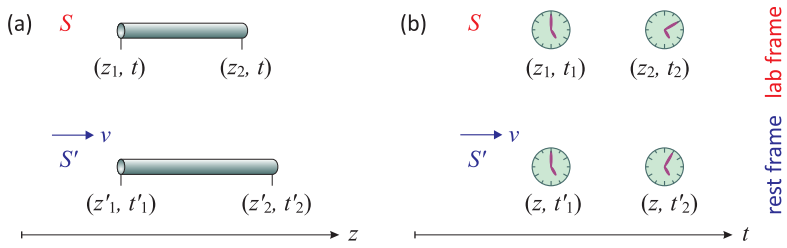

Figure 20.2: Illustration of (a) contraction of space and (b) dilatation of time.

the effect [2]: Take for example, a third person traveling back to Earth after having synchronized its clock with twin A. We calculate in Excs. 20.1.7.2 to 20.1.7.5 examples of temporal dilatation.

20.1.5 Transformational behavior of the wave equation

In the previous section we have seen that the relativistic metric is based on the covariant formulation of mechanics with the definition of relativistic space-time vectors. We introduced the *quadri-vectors* of the displacement Δr^μ, of the position (r^μ), and of the gradient (∂^μ),

$$\boxed{(\Delta r^\mu) \equiv \begin{pmatrix} c\Delta t \\ \Delta \mathbf{r} \end{pmatrix} \quad , \quad (r^\mu) \equiv \begin{pmatrix} ct \\ \mathbf{r} \end{pmatrix} \quad , \quad (\partial^\mu) \equiv \begin{pmatrix} \frac{1}{c}\frac{\partial}{\partial t} \\ -\nabla \end{pmatrix}} \; . \tag{20.32}$$

The contraction of quadri-vectors produces Lorentz invariants, such as the *quadri-scalars* of space-time intervals Δs^2, of proper time $\Delta\tau$, of proper distance $|\Delta\vec{\mathcal{S}}|$, or of the d'Alembertian $\Box$, given by,

$$\begin{aligned} \Delta s^2 &\equiv \Delta r_\mu \Delta r^\mu = c^2\Delta t^2 - \Delta \mathbf{r}^2 \; , \\ \Delta\tau &\equiv \sqrt{\tfrac{\Delta s^2}{c^2}} \qquad \text{for 'time'-like intervals} \qquad \Delta s^2 > 0 \; , \\ |\Delta \mathbf{s}| &\equiv \sqrt{-\Delta s^2} \qquad \text{for 'space'-like intervals} \qquad \Delta s^2 < 0 \; , \\ \Box &\equiv \partial_\mu \partial^\mu = \tfrac{1}{c^2}\tfrac{\partial^2}{\partial t^2} - \nabla^2 \; . \end{aligned} \tag{20.33}$$

With these definitions we can write the wave equation in the absence of sources,

$$\boxed{\Box\psi = \partial^\mu \partial_\mu \psi = 0} \; . \tag{20.34}$$

The covariant form of the wave equation already shows its compatibility with the Lorentz transform. Nevertheless, we will discuss the transformation properties in the following. These are fundamental, since the propagation of light, whose invariant velocity triggered the theory of relativity, is an undulatory phenomenon.

[2] [http://de.wikipedia.org/wiki/Zwillingsparadox]

20.1.5.1 Wave equation under Galilei transformation

The Galilei transformation claims that we obtain the coordinates of an object in a system S' simply by substituting $z \to z'$ and $t \to t'$ with [3],

$$\begin{aligned} t' \equiv t \quad & \text{and} \quad z' \equiv z - v_0 t \quad \text{or} \\ t \equiv t' \quad & \text{and} \quad z \equiv z' + v_0 t \ , \end{aligned} \tag{20.35}$$

which implies

$$v' = \frac{\partial z'}{\partial t'} = \frac{\partial z}{\partial t} - v_0 = v - v_0 \ . \tag{20.36}$$

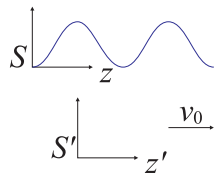

Figure 20.3: Wave in the inertial system S as seen by an observer in the system S' moving at a velocity u.

Newton's classical mechanics is *Galilei invariant*, which means that the fundamental equations of the type,

$$m\dot{v}_i = -\nabla_{x_i} \sum_j V_{ij}(|x_i - x_j|) \ , \tag{20.37}$$

do not change their shape under the *Galilei transform*. In contrast, the wave equation is *not* Galilei invariant. To see this, we consider a wave in the inertial system S, which is resting with respect to the propagation medium, being described by $Y(z,t)$ and satisfying the wave equation,

$$\frac{\partial^2 Y(z,t)}{\partial t^2} = c^2 \frac{\partial^2 Y(z,t)}{\partial z^2} \ . \tag{20.38}$$

An observer sits in the inertial system S' moving with respect to S with the speed v_0, such that $z' = z - v_0 t$. The question now is, what is the equation of motion for this wave described by $Y'(z',t')$, that is, we want to check the validity of

$$\frac{\partial^2 Y'(z',t')}{\partial t'^2} \stackrel{?}{=} c^2 \frac{\partial^2 Y'(z',t')}{\partial z'^2} \ . \tag{20.39}$$

For example, the wave $Y(z,t) = \sin k(z - ct)$ traveling to the right is perceived in the system S', which is also traveling to the right, as $Y'(z',t') = \sin k[z' - (c - v_0)t'] = Y(z,t)$ applying the Galilei transform. Therefore,

$$Y'(z',t') = Y(z,t) \ , \tag{20.40}$$

[3]Note that the Galilei transform (20.17) is unitary because $\det G = 1$.

that is, we expect that the laws valid in S are also valid in S'. We calculate the partial derivatives,

$$\frac{\partial Y'(z',t')}{\partial t'} = \frac{\partial Y(z,t)}{\partial t'} = \frac{\partial t}{\partial t'}\frac{\partial Y(z,t)}{\partial t}\bigg|_{z=const} + \frac{\partial z}{\partial t'}\frac{\partial Y(z,t)}{\partial z}\bigg|_{t=const} = \frac{\partial Y(z,t)}{\partial t} + v_0\frac{\partial Y(z,t)}{\partial z}$$
$$\frac{\partial Y'(z',t')}{\partial z'} = \frac{\partial Y(z,t)}{\partial z'} = \frac{\partial t}{\partial z'}\frac{\partial Y(z,t)}{\partial t}\bigg|_{z=const} + \frac{\partial z}{\partial z'}\frac{\partial Y(z,t)}{\partial z}\bigg|_{t=const} = \frac{\partial Y(z,t)}{\partial z} \ . \quad (20.41)$$

Therefore, we conclude that the wave equation in the propagating system is modified:

$$\begin{aligned}\frac{\partial^2 Y'(z',t')}{\partial t'^2} &\overset{\rightarrow}{=} \frac{\partial^2 Y(z,t)}{\partial t^2} + v_0^2\frac{\partial^2 Y(z,t)}{\partial z^2} + 2v_0\frac{\partial^2 Y(z,t)}{\partial t\partial z} \\ &\overset{\text{eq.onda}}{=} c^2\frac{\partial^2 Y(z,t)}{\partial z^2} + v_0^2\frac{\partial^2 Y(z,t)}{\partial z^2} + 2v_0\frac{\partial^2 Y(z,t)}{\partial t\partial z} \\ &\overset{\leftarrow}{=} (c^2 - v_0^2)\frac{\partial^2 Y'(z',t')}{\partial z'^2} + 2v_0\frac{\partial^2 Y'(z',t')}{\partial t'\partial z'} \ .\end{aligned} \quad (20.42)$$

Only in cases where the wave function can be written as $Y(z,t) = f(z-ct) = f(z'-(c-v_0)t') = f'(z'-ct') = Y'(z',t')$, will we obtain a similar wave equation to that of the system S, but with a modified propagation velocity. We calculate,

$$\frac{\partial f'(z'-ct')}{\partial t'} = \frac{\partial f(z'-(c-v_0)t')}{\partial t'} = (v_0-c)\frac{\partial f(z'-(c-v_0)t')}{\partial z'} = (v_0-c)\frac{\partial f'(z'-ct')}{\partial z'} \ , \quad (20.43)$$

and the second derivative,

$$\frac{\partial^2 f'(z'-ct')}{\partial t'^2} = (c-v_0)^2\frac{\partial^2 f'(z'-ct')}{\partial z'^2} \ . \quad (20.44)$$

The observation that the wave equation is not Galilei invariant expresses the fact, that there is a preferential system for the wave to propagate, which is simply the system in which the propagation medium is at rest. Only in this inertial system will a spherical wave propagate isotropically.

Example 125 (*Wave equation under Galilei transformation*): Let us now verify the correctness of the wave equation in the propagating system S' using the example of a sine wave,

$$\begin{aligned}&(c^2 - v_0^2)\frac{\partial^2 \sin k[z'-(c-v_0)t']}{\partial z'^2} + 2v_0\frac{\partial^2 \sin k[z'-(c-v_0)t']}{\partial z'\partial t'} \\ &= -k^2(c^2-v_0^2)\sin k[z'-(c-v_0)t'] + 2uk^2(c-v_0)\sin k[z'-(c-v_0)t'] \\ &= -k^2(c-v_0)^2\sin k[z'-(c-v_0)t'] = \frac{\partial^2 \sin k[z'-(c-v_0)t']}{\partial t'^2} \ .\end{aligned}$$

20.1.5.2 Wave equation under Lorentz transformation

The question now is, how to deal with electromagnetic waves which are lacking a propagation medium, as we have already noted and as has been verified by Michelson's famous experiment. If there is no propagation medium, all inertial systems should be equivalent, and the wave equation should be the same in all systems, and so should

be the propagation velocity, i.e. the speed of light. These were the consideration of *Henry Poincaré*. To solve the problem we need another transformation than that of *Galileo Galilei*. It was *Hendrik Antoon Lorentz* who found the solution, but the biggest intellectual challenge was to accept all consequences of this new transformation. *Albert Einstein* accepted the challenge and created a new mechanics, which he called *relativistic mechanics*. The wave equation for electromagnetic waves, called the *Helmholtz equation*, being a direct consequence of Maxwell's theory, it is not surprising that the relativistic theory proved not only compatible with electrodynamic theory, but provides a much deeper understanding of the latter.

We begin with the ansatz of a general transformation connecting temporal and spatial coordinates via four unknown parameters, γ, $\tilde{\gamma}$, β, and $\tilde{\beta}$,

$$ct = \gamma(ct' + \beta z') \qquad \text{and} \qquad z = \tilde{\gamma}(z' + \tilde{\beta}ct') \; . \tag{20.45}$$

A similar calculation as the one made for the Galilei transformation now gives the first derivatives,

$$\frac{\partial Y'(z',t')}{c\partial t'} = \frac{\partial Y(z,t)}{c\partial t'} = \frac{\partial t}{\partial t'}\,\frac{\partial Y(z,t)}{c\partial t}\bigg|_{z=const} + \frac{\partial z}{c\partial t'}\,\frac{\partial Y(z,t)}{\partial z}\bigg|_{t=const} = \gamma\frac{\partial Y(z,t)}{c\partial t} + \tilde{\gamma}\tilde{\beta}\frac{\partial Y(z,t)}{\partial z} \tag{20.46}$$

$$\frac{\partial Y'(z',t')}{\partial z'} = \frac{\partial Y(z,t)}{\partial z'} = \frac{c\partial t}{\partial z'}\,\frac{\partial Y(z,t)}{c\partial t}\bigg|_{z=const} + \frac{\partial z}{\partial z'}\,\frac{\partial Y(z,t)}{\partial z}\bigg|_{t=const} = \gamma\beta\frac{\partial Y(z,t)}{c\partial t} + \tilde{\gamma}\frac{\partial Y(z,t)}{\partial z} \; .$$

The second derivatives and the application of the wave equation in the system S give,

$$\begin{aligned}
\frac{\partial^2 Y'(z',t')}{c^2\partial t'^2} &\overset{\rightarrow}{=} \gamma^2\frac{\partial^2 Y(z,t)}{c^2\partial t^2} + 2\gamma\tilde{\gamma}\tilde{\beta}\frac{\partial^2 Y(z,t)}{c\partial t\partial z} + (\tilde{\gamma}\tilde{\beta})^2\frac{\partial^2 Y(z,t)}{\partial z^2} \\
&\overset{\text{wave eq.}}{=} \gamma^2\frac{\partial^2 Y(z,t)}{\partial z^2} + 2\gamma\tilde{\gamma}\tilde{\beta}\frac{\partial^2 Y(z,t)}{c\partial t\partial z} + (\tilde{\gamma}\tilde{\beta})^2\frac{\partial^2 Y(z,t)}{c^2\partial t^2} \\
&\overset{!}{=} (\gamma\beta)^2\frac{\partial^2 Y(z,t)}{c^2\partial t^2} + 2\gamma\tilde{\gamma}\beta\frac{\partial^2 Y(z,t)}{c\partial t\partial z} + \tilde{\gamma}^2\frac{\partial^2 Y(z,t)}{\partial z^2} \overset{\leftarrow}{=} \frac{\partial^2 Y'(z',t')}{\partial z'^2} \; .
\end{aligned} \tag{20.47}$$

That is, the wave equation in the system S' has the same form [4], under the condition that,

$$\gamma = \tilde{\gamma} \qquad \text{and} \qquad (\gamma\beta)^2 = (\tilde{\gamma}\tilde{\beta})^2 \qquad \text{and} \qquad \beta = \tilde{\beta} \; . \tag{20.48}$$

In addition, the transformation

$$\begin{pmatrix} ct' \\ z' \end{pmatrix} = \Lambda \begin{pmatrix} ct \\ z \end{pmatrix} \qquad \text{with} \qquad \Lambda \equiv \begin{pmatrix} \gamma & \gamma\beta \\ \gamma\beta & \gamma \end{pmatrix} \tag{20.49}$$

has to be unitary, that is,

$$1 = \det\Lambda = \gamma\tilde{\gamma} - \gamma\tilde{\gamma}\beta\tilde{\beta} = \gamma^2(1-\beta^2) \; , \tag{20.50}$$

which allows to relate the parameters γ and β by,

$$\gamma = \frac{1}{\sqrt{1-\beta^2}} \; . \tag{20.51}$$

[4] Note that the computation is dramatically simplified in the covariant formalism of 4-dimensional *space-time vectors* introduced by *Hermann Minkowski* and *Gregory Ricci-Curbastro*.

Finally and obviously, we expect to recover the Galilei transformation at low velocities,

$$ct = \gamma(ct' + \beta z') \to ct' \qquad \text{and} \qquad z = \gamma(z' + \beta ct') \to z' + v_0 t' \ . \tag{20.52}$$

That is, the limit is obtained by $\gamma \to 1$ and $\gamma\beta c \to v_0$, such that,

$$\beta = \frac{v_0}{c} \ . \tag{20.53}$$

The *Lorentz transform* from an inertial system S to another S' is,

$$\begin{aligned} t' &= \gamma\left(t - \tfrac{v_0}{c^2} z\right) \qquad \text{and} \qquad z' = \gamma(z - v_0 t) \qquad \text{or} \\ t &= \gamma\left(t' + \tfrac{v_0}{c^2} z'\right) \qquad \text{and} \qquad z = \gamma(z' + v_0 t') \ . \end{aligned} \tag{20.54}$$

20.1.6 The Lorentz boost

In this section we will construct the Lorentz transform from *infinitesimal generators* [659]. To begin with we introduce 6 fundamental matrices. The matrices,

$$K_k \equiv \begin{pmatrix} 0 & \hat{\mathbf{e}}_k \\ \hat{\mathbf{e}}_k & \mathbf{0}_3 \end{pmatrix} \ , \tag{20.55}$$

with the unit vectors $\hat{\mathbf{e}}_k = \hat{\mathbf{e}}_x, \hat{\mathbf{e}}_y, \hat{\mathbf{e}}_z$ generate linear boosts and the matrices,

$$S_k \equiv \begin{pmatrix} 0 & \mathbf{0} \\ \mathbf{0} & \mathbf{S}_k \end{pmatrix} \quad \text{with} \quad \mathbf{S}_x \equiv \hat{\mathbf{e}}_z\hat{\mathbf{e}}_y^\dagger - \hat{\mathbf{e}}_y\hat{\mathbf{e}}_z^\dagger \ , \ \mathbf{S}_y \equiv \hat{\mathbf{e}}_x\hat{\mathbf{e}}_z^\dagger - \hat{\mathbf{e}}_z\hat{\mathbf{e}}_x^\dagger \ , \ \mathbf{S}_z \equiv \hat{\mathbf{e}}_y\hat{\mathbf{e}}_x^\dagger - \hat{\mathbf{e}}_x\hat{\mathbf{e}}_y^\dagger \ , \tag{20.56}$$

generate spatial rotations around the 3 Cartesian axes. We note that the squares of all matrices S_k and K_k are diagonal and that,

$$[S_i, S_j] = \epsilon_{ijk} S_k \qquad , \qquad [S_i, K_j] = \epsilon_{ijk} K_k \qquad , \qquad [K_i, K_j] = -\epsilon_{ijk} S_k \ . \tag{20.57}$$

Example 126 (*Actions of the matrices K_k and S_k*): For example, the operation

$$(x'^\mu) = (\mathbb{I}_4 + K_z)^\mu{}_\nu (x^\nu) = \begin{pmatrix} 1 & \hat{\mathbf{e}}_z \\ \hat{\mathbf{e}}_z & \mathbb{I}_3 \end{pmatrix} \begin{pmatrix} ct \\ \mathbf{r} \end{pmatrix}$$

transports a space-time point $(ct, \mathbf{r})$ with light velocity along the z-axis to another point, $(ct', \mathbf{r}') = (ct + z, \mathbf{r} + ct\hat{\mathbf{e}}_z)$. And the operation

$$(x'^\mu) = (\mathbb{I}_4 + S_z)^\mu{}_\nu (x^\nu) = \begin{pmatrix} 1 & \mathbf{0} \\ \mathbf{0} & \mathbb{I}_3 + S_z \end{pmatrix} \begin{pmatrix} ct \\ \mathbf{r} \end{pmatrix} = \begin{pmatrix} ct \\ \begin{pmatrix} 1 & -1 & 0 \\ 1 & 1 & 0 \\ 0 & 0 & 1 \end{pmatrix} \mathbf{r} \end{pmatrix} = \begin{pmatrix} ct \\ x - y \\ y + x \\ z \end{pmatrix}$$

transports a space-time point $(ct, \mathbf{r})$ around the z-axis to another point, $(ct', \mathbf{r}') = (ct, x - y, y + x, z)$.

The *Lorentz boost* can now be written as,

$$\boxed{\begin{array}{llll} \Lambda = e^{L} & \text{with} & L & = -\vec{\omega}\cdot\mathbf{S} - \vec{\zeta}\cdot\mathbf{K} \\ & \text{where} & \mathbf{S} & \equiv \begin{pmatrix} S_x & S_y & S_z \end{pmatrix} \\ & \text{and} & \mathbf{K} & \equiv \begin{pmatrix} K_x & K_y & K_z \end{pmatrix} \end{array}} \quad . \tag{20.58}$$

We verify that,

$$\det \Lambda = \det e^{L} = e^{\mathrm{Tr}\ L} = \pm 1 \ . \tag{20.59}$$

Example 127 (*Lorentz-boost without rotation*): For a Lorentz-boost without rotation,

$$\Lambda = e^{-\vec{\zeta}\cdot\mathbf{K}} \qquad \text{with} \qquad \vec{\zeta} = \hat{\mathbf{e}}_\beta \ \tanh^{-1}\beta \ ,$$

we get,

$$\Lambda = \begin{pmatrix} \gamma & -\gamma\beta_x & -\gamma\beta_y & -\gamma\beta_z \\ -\gamma\beta_x & 1+\frac{(\gamma-1)\beta_x^2}{\beta^2} & \frac{(\gamma-1)\beta_x\beta_y}{\beta^2} & \frac{(\gamma-1)\beta_x\beta_z}{\beta^2} \\ -\gamma\beta_y & \frac{(\gamma-1)\beta_x\beta_y}{\beta^2} & 1+\frac{(\gamma-1)\beta_y^2}{\beta^2} & \frac{(\gamma-1)\beta_y\beta_z}{\beta^2} \\ -\gamma\beta_z & \frac{(\gamma-1)\beta_x\beta_z}{\beta^2} & \frac{(\gamma-1)\beta_y\beta_z}{\beta^2} & 1+\frac{(\gamma-1)\beta_z^2}{\beta^2} \end{pmatrix} = \begin{pmatrix} \gamma & -\gamma\vec{\beta} \\ -\gamma\vec{\beta} & \mathbb{I}_3 + (\gamma-1)\hat{\beta}_i\hat{\beta}_j \end{pmatrix} , \tag{20.60}$$

as will be shown in Exc. 20.1.7.6. The Lorentz transform (20.19) into a system moving along the z-axis follows immediately with $\beta_x = \beta_y = 0$.

20.1.6.1 The Thomas precession

We consider the circular motion of an electron around a nucleus about the z-axis subject to a centripetal (Coulombian) force. The nucleus is fixed in the lab frame S, the electron's rest frame S' moves with respect to the lab frame at the instantaneous velocity $\mathbf{v}(t) = c\vec{\beta}(t)$, as illustrated in Fig. 20.4.

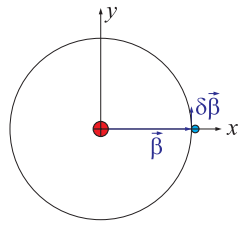

Figure 20.4: Circular motion of an electron around a nucleus.

At time t, when the electron's velocity is $\vec{\beta}(t)$, the Lorentz transform from S to S' is described by [659],

$$x'(t) = \Lambda_{boost}(\vec{\beta})x \ , \tag{20.61}$$

Note, that the nucleus' position does not change in the frame S, $x(t+\delta t) = x(t) = x$. At a later time $t+\delta t$, when the electron's velocity is $\vec{\beta}(t+\delta t) = \vec{\beta}(t) + \delta\vec{\beta}(t)$, the

Lorentz transform,

$$x'(t+\delta t) = \Lambda_{boost}(\vec{\beta}+\delta\vec{\beta})x = \Lambda_{boost}(\vec{\beta}+\delta\vec{\beta})\Lambda^{-1}_{boost}(\vec{\beta})x'(t) \tag{20.62}$$

can be expressed as a Lorentz transform from the electron's system S' at time t to the same S' at time $t+\delta t$. From the expression (20.60) for a Lorentz-boost without rotation, setting $\beta_z = 0$, we get for Lorentz-boost in the xy-plane,

$$\Lambda^{\pm 1}_{boost}(\beta_x\hat{\mathbf{e}}_x + \beta_y\hat{\mathbf{e}}_y) = \begin{pmatrix} \gamma & \mp\gamma\beta_x & \mp\gamma\beta_y & 0 \\ \mp\gamma\beta_x & 1+\frac{(\gamma-1)\beta_x^2}{\beta^2} & \frac{(\gamma-1)\beta_x\beta_y}{\beta^2} & 0 \\ \mp\gamma\beta_y & \frac{(\gamma-1)\beta_x\beta_y}{\beta^2} & 1+\frac{(\gamma-1)\beta_y^2}{\beta^2} & 0 \\ 0 & 0 & 0 & 1 \end{pmatrix} . \tag{20.63}$$

Now, setting the initial position of the electron along the direction $\vec{\beta}(t) = \beta\hat{\mathbf{e}}_x$, as shown in Fig. 20.4, we get,

$$\Lambda^{-1}_{boost}(\vec{\beta}) = \begin{pmatrix} \gamma & \gamma\beta & 0 & 0 \\ \gamma\beta & \gamma & 0 & 0 \\ 0 & 0 & 1 & 0 \\ 0 & 0 & 0 & 1 \end{pmatrix} , \tag{20.64}$$

and, expanding γ for small velocity changes like,

$$\gamma + \delta\gamma = \frac{1}{\sqrt{1-(\beta+\delta\beta)^2}} \simeq \gamma + \gamma^3\beta\delta\beta , \tag{20.65}$$

we find,

$$\begin{aligned} \Lambda_{boost}(\vec{\beta}+\delta\vec{\beta}) &= \begin{pmatrix} \gamma+\delta\gamma & -(\gamma+\delta\gamma)(\beta+\delta\beta_x) & -(\gamma+\delta\gamma)\delta\beta_y & 0 \\ -(\gamma+\delta\gamma)(\beta+\delta\beta_x) & 1+\frac{(\gamma+\delta\gamma-1)(\beta+\delta\beta_x)^2}{(\beta+\delta\beta_x)^2} & \frac{(\gamma+\delta\gamma-1)(\beta+\delta\beta_x)\delta\beta_y}{(\beta+\delta\beta_x)^2} & 0 \\ -(\gamma+\delta\gamma)\delta\beta_y & \frac{(\gamma+\delta\gamma-1)(\beta+\delta\beta_x)\delta\beta_y}{(\beta+\delta\beta_x)^2} & 1+\frac{(\gamma+\delta\gamma-1)(\delta\beta_y)^2}{(\beta+\delta\beta_x)^2} & 0 \\ 0 & 0 & 0 & 1 \end{pmatrix} \\ &\simeq \begin{pmatrix} \gamma+\gamma^3\beta\delta\beta_x & -\gamma\beta-\gamma^3\delta\beta_x & -\gamma\delta\beta_y & 0 \\ -\gamma\beta-\gamma^3\delta\beta_x & \gamma+\gamma^3\beta\delta\beta_x & \frac{\gamma-1}{\beta}\delta\beta_y & 0 \\ -\gamma\delta\beta_y & \frac{\gamma-1}{\beta}\delta\beta_y & 1 & 0 \\ 0 & 0 & 0 & 1 \end{pmatrix} . \end{aligned} \tag{20.66}$$

Multiplying the matrices (20.65) and (20.66) we get,

$$\Lambda_{Th}(\vec{\beta}+\delta\vec{\beta}) = \Lambda_{boost}(\vec{\beta}+\delta\vec{\beta})\Lambda^{-1}_{boost}(\vec{\beta}) \simeq \begin{pmatrix} 1 & -\gamma^2\delta\beta_x & -\gamma\delta\beta_y & 0 \\ -\gamma^2\delta\beta_x & 1 & \frac{\gamma-1}{\beta}\delta\beta_y & 0 \\ -\gamma\delta\beta_y & -\frac{\gamma-1}{\beta}\delta\beta_y & 1 & 0 \\ 0 & 0 & 0 & 1 \end{pmatrix} . \tag{20.67}$$

This represents an infinitesimal Lorentz transformation that, expressing the components of $\delta\vec{\beta}$ parallel and perpendicular to β by,

$$\delta\vec{\beta}_{\|} = \tfrac{\delta\vec{\beta}\cdot\vec{\beta}}{\beta^2}\vec{\beta} \qquad \text{and} \qquad \delta\vec{\beta}_{\perp} = \delta\vec{\beta} - \tfrac{\delta\vec{\beta}\cdot\vec{\beta}}{\beta^2}\vec{\beta} \tag{20.68}$$

can be written in terms of the matrices $\mathbf{S}$ and $\mathbf{K}$ as [5],

$$\boxed{\begin{aligned}\Lambda_{Th}(\vec{\beta}+\delta\vec{\beta}) &= \mathbb{I} - \tfrac{\gamma-1}{\beta^2}(\vec{\beta}\times\delta\vec{\beta})\cdot\mathbf{S} - (\gamma^2\delta\vec{\beta}_{\|} + \gamma\delta\vec{\beta}_{\perp})\cdot\mathbf{K} \\ &\simeq R(\Delta\vec{\Omega})\ \Lambda_{boost}(\Delta\vec{\beta})\end{aligned}} \ . \tag{20.69}$$

Here, we defined the *commuting* infinitesimal boosts and rotations called *Wigner rotations*,

$$\Lambda_{boost}(\Delta\vec{\beta}) \equiv \mathbb{I} - \Delta\vec{\beta}\cdot\mathbf{K} \qquad \text{and} \qquad R(\Delta\vec{\Omega}) \equiv \mathbb{I} - \Delta\vec{\Omega}\cdot\mathbf{S} \tag{20.70}$$

in terms of velocity and rotation angle,

$$\Delta\vec{\beta} \equiv \gamma^2\delta\vec{\beta}_{\|} + \gamma\delta\vec{\beta}_{\perp} \qquad \text{and} \qquad \Delta\vec{\Omega} \equiv \frac{\gamma-1}{\beta^2}\vec{\beta}\times\delta\vec{\beta}\ . \tag{20.71}$$

Clearly, the second line of (20.69) holds to first order in $\delta\vec{\beta}$. Thus, the pure Lorentz boost (20.62) to the frame with velocity $c(\vec{\beta}+\delta\vec{\beta})$ is equivalent to a boost (20.61) to a frame moving with velocity $c\vec{\beta}$, followed by an infinitesimal Lorentz transformation consisting of a boost with velocity $c\vec{\Delta}\beta$ and a rotation $\Delta\vec{\Omega}$.

In summary, we got,

$$\begin{aligned} x'(t+\delta t) &= \Lambda_{boost}(\vec{\beta}+\delta\vec{\beta})x = \Lambda_{boost}(\vec{\beta}+\delta\vec{\beta})\Lambda^{-1}_{boost}(\vec{\beta})x'(t) \\ &= \Lambda_{Th}(\vec{\beta}+\delta\vec{\beta})x'(t) = R(\Delta\Omega)\Lambda_{boost}(\Delta\vec{\beta})x'(t)\ . \end{aligned} \tag{20.72}$$

In terms of the interpretation of the moving frames as successive rest frames of the electron we do not want rotations as well as boosts. Non-relativistic equations of motion can be expected to hold provided the evolution of the rest frame is described by infinitesimal boosts without rotations. We are thus led to consider the rest-frame coordinates at time $t+\delta t$ that are given from those at time t by the boost $\Lambda_{boost}(\Delta\vec{\beta})$ instead of Λ_{Th}. Denoting these coordinates by $\tilde{x}'$ we have,

$$\begin{aligned} \tilde{x}'(t+\delta t) &= \Lambda_{boost}(\Delta\vec{\beta})x'(t) \\ &= R(-\Delta\vec{\Omega})x'(t+\delta t) = R(-\Delta\vec{\Omega})\Lambda_{boost}(\vec{\beta}+\delta\vec{\beta})x\ . \end{aligned} \tag{20.73}$$

The rest system of coordinates defined by $\tilde{x}'$ is rotated by $R(-\Delta\vec{\Omega})$ relative to the boosted laboratory axes x'. If a physical vector $\mathbf{G}$ has a (proper) time rate of change $(d\mathbf{G}/d\tau)$ in the rest frame, the precession of the rest-frame axes with respect to the

[5] We note that, for the case $\vec{\beta}(t) = \beta\hat{\mathbf{e}}_x$ Eq. (20.69) can be written as,

$$\Lambda_{Th} = \mathbb{I} - \frac{\gamma-1}{\beta}S_z\delta\beta_y - \gamma^2 K_x\delta\beta_x - \gamma K_y\delta\beta_y\ ,$$

which reproduces exactly Eq. (20.67).

laboratory makes the vector have a total time rate of change with respect to the laboratory axes of,

$$\left(\frac{d\mathbf{G}}{dt}\right)_{non-rot} = \left(\frac{d\mathbf{G}}{dt}\right)_{rest} + \vec{\omega}_{Th} \times \mathbf{G} \ . \tag{20.74}$$

with

$$\vec{\omega}_{Th} = -\lim_{\delta t \to 0} \frac{\Delta\Omega}{\delta t} = \frac{\gamma^2}{\gamma+1}\frac{\mathbf{a}\times\mathbf{v}}{c^2} \ , \tag{20.75}$$

where $\mathbf{a}$ is the acceleration in the laboratory frame and, to be precise,

$$\left(\frac{d\mathbf{G}}{dt}\right)_{rest} = \gamma^{-1}\left(\frac{d\mathbf{G}}{d\tau}\right)_{rest} \ . \tag{20.76}$$

The *Thomas precession* is purely kinematical in origin. If a component of acceleration exists perpendicular to $\mathbf{v}$, for whatever reason, then there is a Thomas precession, independent of other effects such as precession of the magnetic moment in a magnetic field.

Example 128 (*Circular motion*): Assuming a constant circular motion about the z-axis, as parametrized by $\mathbf{v} = r\dot{\theta}\hat{\mathbf{e}}_\theta$ and $\mathbf{a} = -r\dot{\theta}^2\hat{\mathbf{e}}_r = -\dot{\theta}v\hat{\mathbf{e}}_r$ with $\dot{\theta} = const$, we find,

$$\vec{\omega}_{Th} = \frac{\gamma^2}{\gamma+1}\frac{\mathbf{a}\times\mathbf{v}}{c^2} = \frac{\gamma^2}{\gamma+1}\frac{-\dot{\theta}v^2}{c^2}\hat{\mathbf{e}}_z = -\frac{\gamma^2\beta^2}{\gamma+1}\dot{\theta}\hat{\mathbf{e}}_z = -(\gamma-1)\dot{\theta}\hat{\mathbf{e}}_z \ .$$

20.1.6.2 Spin-Orbit coupling

For electrons in atoms the acceleration is caused by the screened Coulomb field. Thus the Thomas angular velocity is,

$$\vec{\omega}_{Th} \simeq -\frac{1}{2c^2}\frac{\mathbf{r}\times\mathbf{v}}{m}\frac{1}{r}\frac{dV}{dr} = -\frac{1}{2m^2c^2}\mathbf{L}\frac{1}{r}\frac{dV}{dr} \ . \tag{20.77}$$

It is evident that the extra contribution to the energy from the Thomas precession reduces the spin-orbit coupling, yielding,

$$U = \frac{-ge}{2mc}\vec{\mathcal{S}}\cdot\vec{\mathcal{B}} + \frac{(g-1)}{2m^2c^2}\vec{\mathcal{S}}\cdot\mathbf{L}\frac{1}{r}\frac{dV}{dr} \ . \tag{20.78}$$

20.1.7 Exercises

20.1.7.1 Ex: Contravariant partial derivation

Show that the partial derivative by the contravariant coordinate x^μ is covariant.

Solution: *Contravariance of x^μ means,*

$$x'^\mu = \Lambda^\mu{}_\nu x^\nu = \frac{\partial x'^\mu}{\partial x^\nu}x^\nu \ .$$

With this, we obtain the covariant transformation,

$$\partial'_\mu \equiv \frac{\partial}{\partial x'^\mu} = \frac{\partial x^\nu}{\partial x'^\mu}\frac{\partial}{\partial x^\nu} = (\Lambda^{-1})^\nu{}_\mu \partial_\nu = \Lambda_\mu{}^\nu \partial_\nu \ .$$

20.1.7.2 Ex: Time dilatation

Proxima Centauri, which is the closest star to our solar system with a distance of 4.22 light-years from Earth, is a so-called Red Dwarf of class M. At its 34th anniversary, Peter embarks on a journey from Earth to this star. His spaceship flies with a speed of 250000 km/s. How old is Peter when he arrives? What is the age of Peter's twin brother, who remained on Earth at this time?

Solution: *The elapsed time seen from the Earth is,*

$$T = \frac{s}{t} \Longleftrightarrow t = \frac{s}{v} = \frac{4.22\ Lj}{250000\,\mathrm{km/s}} = 5.064\,\mathrm{a} \ .$$

The time elapsed for the astronaut is, due to the smaller time dilatation:

$$T' = \frac{t}{\gamma(v)} = \frac{5.064\ a}{\sqrt{1-\frac{(250000\,\mathrm{km/s})^2}{(300000\,\mathrm{km/s})^2}}} \approx 2.8\,\mathrm{a} \ .$$

Therefore, Peter arrives at Proxima Centauri at the age of 36.8, while his twin brother is 39.1 years old.

20.1.7.3 Ex: The twin paradox

Explain the twin paradox by applying the Lorentz transform to the twin traveling on a round-trip to α-Centauri assuming a fixed distance between Earth and α-Centauri.

Solution: *Let us denote by (t_0, z_0) the coordinates of the Earth S at the instant when the twin takes off with a space ship S' and by (t_1, z_1) the position of α-Centauri and the arrival time as indicated by the Earth-bound clock. The flying twin calculates his own coordinates via,*

$$\begin{pmatrix} ct'_j \\ z'_j \end{pmatrix} = \begin{pmatrix} \gamma c t_j - \gamma\beta z_j \\ -\gamma\beta c t_j + \gamma z_j \end{pmatrix} \qquad with \qquad j = 0, 1 \ .$$

Inserting the take-off and arrival time coordinates the Earth-bound team gets,

$$t_1 - t_0 = \frac{1}{\gamma\beta c}(\gamma z_1 - z'_1) - \frac{1}{\gamma\beta c}(\gamma z_0 - z'_0) = \frac{1}{v}(z_1 - z_0) \ ,$$

while the twin located in his space ship at $z'_1 = z'_0$ reads on his clock,

$$\begin{aligned} t'_1 - t'_0 &= \left(\gamma t_1 - \frac{\gamma\beta}{c} z_1\right) - \left(\gamma t_0 - \frac{\gamma\beta}{c} z_0\right) \\ &= \gamma t_1 - \frac{\beta}{c}(z'_1 + \gamma\beta c t_1) - \gamma t_0 + \frac{\beta}{c}(z'_0 + \gamma\beta c t_0) = \frac{1}{\gamma}(t_1 - t_0) \ . \end{aligned}$$

On α-Centauri the traveling twin encounters another space ship S'' flying in opposite direction $v \to -v$. The crews of both ships quickly synchronize their clocks before continuing their trip through space. Space ship S'' calculates for its coordinates with respect to the Terrestrian coordinates,

$$\begin{pmatrix} ct_j'' \\ z_j'' \end{pmatrix} = \begin{pmatrix} \gamma ct_j + \gamma\beta z_j \\ \gamma\beta ct_j + \gamma z_j \end{pmatrix} \qquad \text{with} \qquad j = 1, 2 \ .$$

After a long voyage S'' arrives on Earth at the coordinates $(t_2, z_2 = z_0)$ according to the Earth-bound clock. Inserting the encounter and arrival time coordinates and knowing $z_2'' = z_1''$,

$$t_2 - t_1 = \frac{1}{v}(z_1 - z_2) \qquad \text{and} \qquad t_2'' - t_1'' = \frac{1}{\gamma}(t_2 - t_1) \ ,$$

in the same way as on the outbound flight. Hence, $t_2'' - t_0'' = \frac{2}{\gamma}(t_2 - t_0)$.

20.1.7.4 Ex: Muons

In the upper layers of the atmosphere (at 20 km altitude) about 250 muons are generated per square meter and second. After that they move with 99.98% of the speed of light towards the surface of the Earth. Muons at rest have a lifetime of 1.52 µs.
a. Assuming that there were no time dilatation, how many muons would arrive per square meter and second at the surface of the Earth?
b. How many muons actually reach the surface of the Earth?

Solution: *a. The number is,*

$$N = N_0 \cdot 0.5^{t/T_H} = N_0 \cdot 0.5^{s/(vT_H)} = 250 \cdot 0.5^{20\,\mathrm{km}\,/(0.9998 \cdot 300000\,\mathrm{km/s} \cdot 1.52 \cdot 10^{-6}\,\mathrm{s})} \approx 1.6 \cdot 10^{-11} \ .$$

Therefore, to observe on average a single muon, we would need to wait around 2000 years.
b. In fact, because of their high velocity, they decay much slower. At a speed of 99.98% of the speed of light the time dilatation factor is γ close to 50. Hence the lifetime increases to 76 µs.

$$N = N_0 \cdot 0.5^{t/T_H} = N_0 \cdot 0.5^{s/(vT_H)} = 250 \cdot 0.5^{20\,\mathrm{km}\,/(0.9998 \cdot 300000\,\mathrm{km/s} \cdot 50 \cdot 1.52 \cdot 10^{-6}\,\mathrm{s})} \approx 136 \ .$$

Consequently, we expect around 136 muons.

20.1.7.5 Ex: Atomic clocks

In 1971 atomic clocks were taken by a high-speed aircraft to measure time dilatation directly. How long must an aircraft fly at a speed of 3000 km/h, so that the airplane's clock and a clock fixed on Earth show, due to time dilatation, a difference of one second?

Solution: *We have,*

$$t - \frac{t}{\gamma} = \Delta t \Longrightarrow t = \frac{\Delta t}{1 - \frac{1}{\gamma}} = \frac{1\,\mathrm{s}}{1 - \sqrt{1 - \frac{3000:3.6}{3\cdot 10^8}}} \approx 8200\,\mathrm{a} \ .$$

20.1.7.6 Ex: Lorentz-boost without rotation

Derive the matrix (20.60) for the Lorentz-boost without rotation to a system moving in arbitrary direction.

Solution: *To find the Lorentz-boost to an arbitrary direction $\vec{\beta}$ we proceed as follows. We first rotate the vector $\vec{\beta}$ about the z-axis until its y-components vanishes,*

$$U_z = \begin{pmatrix} \cos\phi & \sin\phi & 0 \\ -\sin\phi & \cos\phi & 0 \\ 0 & 0 & 1 \end{pmatrix} = \frac{1}{\beta_\rho} \begin{pmatrix} \beta_x & \beta_y & 0 \\ -\beta_y & \beta_x & 0 \\ 0 & 0 & \beta_\rho \end{pmatrix} \ ,$$

where $\beta_\rho = \sqrt{\beta_x^2 + \beta_y^2}$. Then we rotate the resulting vector about the y-axis until it lies on the z-axis,

$$U_y = \begin{pmatrix} \cos\theta & 0 & \sin\theta \\ 0 & 1 & 0 \\ -\sin\theta & 0 & \cos\theta \end{pmatrix} = \frac{1}{\beta} \begin{pmatrix} \beta_z & 0 & -\beta_\rho \\ 0 & \beta & 0 \\ \beta_\rho & 0 & \beta_z \end{pmatrix} \ .$$

It is easy to verify,

$$U_y U_z \vec{\beta} = \beta \hat{\mathbf{e}}_z \ .$$

Now, we extend the total rotation matrix into space-time,

$$U = \frac{1}{\beta_\rho \beta} \begin{pmatrix} 1 & 0 & 0 & 0 \\ 0 & \beta_x\beta_z & \beta_y\beta_z & -\beta_\rho^2 \\ 0 & -\beta_y\beta & \beta_x\beta & 0 \\ 0 & \beta_x\beta_\rho & \beta_y\beta_\rho & \beta_z\beta_\rho \end{pmatrix} \ ,$$

apply the Lorentz-boost along the z-axis according to (20.19) and finally rotate back. The result is,

$$\Lambda_{\vec{\beta}} = U^{-1}\Lambda_z U = \begin{pmatrix} \gamma & -\gamma\beta_x & -\gamma\beta_y & -\gamma\beta_z \\ -\gamma\beta_x & 1 + \frac{(\gamma-1)\beta_x^2}{\beta^2} & \frac{(\gamma-1)\beta_x\beta_y}{\beta^2} & \frac{(\gamma-1)\beta_x\beta_z}{\beta^2} \\ -\gamma\beta_y & \frac{(\gamma-1)\beta_x\beta_y}{\beta^2} & 1 + \frac{(\gamma-1)\beta_y^2}{\beta^2} & \frac{\gamma-1}{\beta^2}\beta_y\beta_z \\ -\gamma\beta_z & \frac{(\gamma-1)\beta_x\beta_z}{\beta^2} & \frac{(\gamma-1)\beta_y\beta_z}{\beta^2} & 1 + \frac{(\gamma-1)\beta_z^2}{\beta^2} \end{pmatrix} \ ,$$

which is just the wanted formula (20.60).

20.2 Relativistic mechanics

20.2.1 The inherent time of an inertial system

The key to constructing relativistic theories is to find the quantities behaving well under Lorentz transformations. We have already defined some quantities in (20.32) and (20.33). But we need more to establish a *relativistic mechanics*. In the following sections we will analyze how other kinematic variables (velocity, momentum, and acceleration) fit into four-vectors. Since these variables are defined through time derivatives, an accurate characterization of the notion of *time intervals* is necessary.

We consider an object following a space-time trajectory. As the evaluation of traveled distances and elapsed time intervals depends on the observer's inertial system, there is no universal parametrization. But there is at least one 'natural' parametrization that all observers can agree on, which is the proper time τ, which is the duration of time felt by the object itself. Due to time dilatation, an observer sitting in some inertial system and measuring the motion of the object with the old-fashioned Newtonian tri-velocity $\mathbf{v}(t)$ infers, that the relation between his own time t and the proper time τ of the particle is given by,

$$\boxed{\frac{dt}{d\tau} = \gamma_v \equiv \frac{1}{\sqrt{1 - v^2/c^2}} > 1} \,. \tag{20.79}$$

Example 129 (*Common velocity under Lorentz transformation*): We could define the *common velocity* of a body via the distance $\mathbf{r}$ covered in a time interval t measured in the laboratory system (in relation to which the body travels with this velocity),

$$(v^\mu) \equiv \frac{d(r^\mu)}{dt} = \begin{pmatrix} c \\ \mathbf{v} \end{pmatrix}$$

However, the contraction of this 4-vector is not a Lorentz invariant because,

$$v_\mu v^\mu = c^2 - v^2 \neq c^2 - v'^2 = v'_\mu v'^\mu \,.$$

On the other hand, the notion of *proper time* allows us to define a true quadri-velocity. We assume that in some inertial system, the body follows the trajectory $r^\mu(\tau)$. Then the quantity,

$$\boxed{u^\mu \equiv \gamma_v v^\mu = \gamma_v \frac{dr^\mu}{dt} = \gamma_v \frac{d\tau}{dt}\frac{dr^\mu}{d\tau} = \frac{dr^\mu}{d\tau} \qquad \text{that is} \qquad (u^\mu) = \begin{pmatrix} \gamma_v c \\ \gamma_v \mathbf{v} \end{pmatrix}} \,, \tag{20.80}$$

called *proper velocity* is a Lorentz invariant, since,

$$u_\mu u^\mu = c^2 \,. \tag{20.81}$$

A useful illustration of the relation between space and time, as proposed by Minkowski, is exhibited in Fig. 20.5. The inner region of the cone represents the space-time points in a lab frame that a moving body can reach within a given time interval. The cone's surface are the points that can be reaches traveling at light speed, and the outer region remains inaccessible.

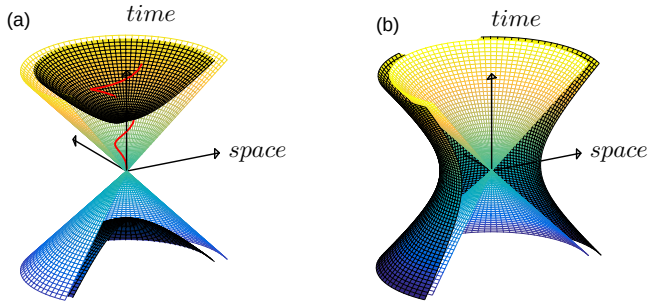

Figure 20.5: Two-dimensional illustration of Minkowski space-time. The cones delimits accessible (inside) from inaccessible (outside) regions. The red curve in (a) represents a possible trajectory for a moving body. The hyperboloid in (a) represents the hyperspace where a system S' with its *proper velocity* v is found after a time τ elapsed in the system S'. The hyperboloid in (b) represents the hyperspace of 'space'-like intervals according to (20.33).

20.2.2 Adding velocities

The Lorentz transformation from system S' moving with respect to another system S with the relative velocity v_0 must be applied to the proper velocity,

$$\begin{pmatrix} \gamma_{v'}c \\ \gamma_{v'}v' \end{pmatrix} = (\Lambda^{\mu}_{\ \nu}) \begin{pmatrix} \gamma_v c \\ \gamma_v v \end{pmatrix} = \begin{pmatrix} \gamma & -\gamma\beta \\ -\gamma\beta & \gamma \end{pmatrix} \begin{pmatrix} \gamma_v c \\ \gamma_v v \end{pmatrix} = \gamma_v\gamma \begin{pmatrix} c-\beta v \\ -\beta c + v \end{pmatrix} , \quad (20.82)$$

where we denote $\gamma \equiv \gamma_{v_0}$. Eliminating $\gamma_{v'}$ and resolving by v' we get,

$$\boxed{v' = \frac{v - v_0}{1 - v_0 v/c^2}} . \quad (20.83)$$

Obviously, the speed of light can not be exceeded. The velocity in the system S' is limited to $-c \leq v' \leq c$, even if $v = c$. Similar calculations can be made for the two transverse directions, and we obtain the general formula reproduced here without proof,

$$\mathbf{v} = \frac{\mathbf{v}' + \mathbf{v}_0 \left[\gamma(1 + \mathbf{v_0}\cdot\mathbf{v}'/v_0^2) - \mathbf{v}_0\cdot\mathbf{v}'/v_0^2\right]}{\gamma(1 + \mathbf{v}_0\cdot\mathbf{v}'/c^2)} . \quad (20.84)$$

We calculate in Exc. 20.2.6.1 an example of relativistic addition of velocities.

20.2.3 Relativistic momentum and rest energy

The *relativistic linear momentum* is given by,

$$\boxed{p^\mu \equiv mu^\mu = m\gamma_v v^\mu \qquad \text{or} \qquad (p^\mu) = \begin{pmatrix} E/c \\ \mathbf{p} \end{pmatrix}} \ . \tag{20.85}$$

We will show in Exc. 20.2.6.2 that an identification of the momentum p^μ with mv^μ would be inconsistent with the principle of momentum conservation and the principle of relativity. For zero velocity of the particle, $\mathbf{v} = 0$, the first line of the expression (20.85) is the famous Einstein equation on the equivalence of mass and energy,

$$E = mc^2 \ . \tag{20.86}$$

Thus, the mass is nothing more than the energy of the particle in its rest frame.

Transforming into the rest frame, we have:

$$p'_\mu p'^\mu = \left\| \begin{pmatrix} E/c \\ \mathbf{p} \end{pmatrix} \right\|^2 = \left\| \begin{pmatrix} mc \\ \mathbf{0} \end{pmatrix} \right\|^2 = p_\mu p^\mu \ , \tag{20.87}$$

yielding,

$$E = \sqrt{m^2c^4 + c^2\mathbf{p}^2} = mc^2\sqrt{1 + \gamma_v^2 \frac{\mathbf{v}^2}{c^2}} = \gamma_v mc^2 \ . \tag{20.88}$$

The kinetic energy in the non-relativistic limit follows from a Taylor expansion of the expression (20.88) for low velocities,

$$E_{kin} \equiv E - mc^2 = mc^2(\gamma_v - 1) \simeq \frac{p^2}{2m} - \frac{p^4}{8m^3c^2} \ . \tag{20.89}$$

Example 130 (*Compton scattering*): Here we consider the interaction of a photon with an electron. The electron has the rest mass m_e. Thus, transforming to the rest frame, we find its energy via, $(p_e)_\mu (p_e)^\mu = E_e^2/c^2 - \mathbf{p}^2 = m_e^2 c^4$. The photon has no rest mass. Thus, transforming to the rest frame, we find its energy via, $(p_\gamma)_\mu (p_\gamma)^\mu = (\hbar k)^2 = (\hbar\omega)^2/c^2$.

Now we let the photon with energy $\hbar\omega_i$ bounce off an electron initially at rest. After the collision the photon and the electron move away under angles of $\sin\theta_\gamma$, respectively, $\sin\theta_e$, with respect to the collision axis. As shown in Fig. 20.6, we can choose the collision axis along the z-axis and within the xy-plane. The photon has changed its energy to $\hbar\omega_f$ and its momentum to $\hbar k_f$, the

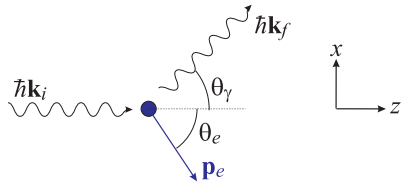

Figure 20.6: Scattering of a photon from an electron.

electron now has the momentum $\mathbf{p}_f$. For an elastic collision, energy and linear momentum conservation request,

$$p_i^\mu \equiv \begin{pmatrix} E_i/c \\ p_i^x \\ p_i^y \\ p_i^z \end{pmatrix} = \begin{pmatrix} \hbar\omega_i/c + m_e c \\ 0 \\ 0 \\ \hbar k_i \end{pmatrix} \stackrel{!}{=} \begin{pmatrix} \hbar\omega_f/c + \sqrt{m_e^2 c^2 + p_f^2} \\ -\hbar k_f \sin\theta_\gamma + p_f \sin\theta_e \\ 0 \\ \hbar k_f \cos\theta_\gamma + p_f \cos\theta_e \end{pmatrix} = \begin{pmatrix} E_f/c \\ p_f^x \\ p_f^y \\ p_f^z \end{pmatrix} \equiv p_f^\mu \ .$$

Solving the second line by θ_e and substituting into the fourth,

$$\begin{aligned} \frac{\hbar\omega_i}{c} = \hbar k_i &= p_f \cos\theta_e + \hbar k_f \cos\theta_\gamma = p_f \sqrt{1 - \sin^2\theta_e} + \hbar k_f \cos\theta_\gamma \\ &= p_f \sqrt{1 - \left(\frac{\hbar k_f}{p_f}\right)^2 \sin^2\theta_\gamma} + \hbar k_f \cos\theta_\gamma \ . \end{aligned}$$

Solving this by p_f,

$$\begin{aligned} c^2 p_f^2 &= (\hbar\omega_i - c\hbar k_f \cos\theta_\gamma)^2 - (c\hbar k_f)^2 \sin^2\theta_\gamma = (\hbar\omega_i)^2 - 2\hbar\omega_i c\hbar k_f \cos\theta_\gamma + (c\hbar k_f)^2 \\ &= (\hbar\omega_i)^2 - 2\hbar\omega_i \hbar\omega_f \cos\theta_\gamma + (\hbar\omega_f)^2 \ . \end{aligned}$$

Inserting this result into energy conservation,

$$\hbar\omega_i + m_e c^2 = \hbar\omega_f + \sqrt{m_e^2 c^4 + c^2 p_f^2} = \hbar\omega_f + \sqrt{m_e^2 c^4 + (\hbar\omega_i)^2 - 2\hbar\omega_i \hbar\omega_f \cos\theta_\gamma + (\hbar\omega_f)^2} \ .$$

Solving this by ω_f,

$$\frac{hc}{\lambda_f} = \hbar\omega_f = \frac{1}{(1 - \cos\theta_\gamma)/m_e c^2 + 1/\hbar\omega_i} \ ,$$

or defining the *Compton wavelength* of the electron,

$$\lambda_C \equiv \frac{h}{m_e c}$$

we find for the wavelength of the scattered photon,

$$\lambda_f = \lambda_i + \lambda_C (1 - \cos\theta_\gamma) \ .$$

Other examples of relativistic collisions will be studied in Excs. 20.2.6.3 to 20.2.6.5.

20.2.4 Relativistic Doppler effect

We have seen at the example of sonic waves, that the magnitude of the Doppler effect depends on who moves with respect to the *medium*: the source or the receiver. Electromagnetic waves, however, propagate in empty space, that is, there is no material medium, ether, or wind. According to Einstein's theory of relativity, there is no absolute motion and the propagation velocity of light is the same for all inertial systems. Therefore, the classical theory of the Doppler effect can not apply to electromagnetic waves.

By the fact that the vector k_μ given by,

$$\boxed{k^\mu \equiv \frac{p^\mu}{\hbar} \qquad \text{that is} \qquad (k^\mu) = \begin{pmatrix} \omega/c \\ \mathbf{k} \end{pmatrix}} \tag{20.90}$$

is a space-time vector,

$$k_\mu k^\mu = \omega^2/c^2 - k^2 = 0 \ , \tag{20.91}$$

we know that this vector transforms like,

$$\begin{aligned} \begin{pmatrix} \omega/c \\ k \end{pmatrix} = (\Lambda_{\mu\nu})^{-1} \begin{pmatrix} \omega'/c \\ k' \end{pmatrix} = \begin{pmatrix} \gamma & \gamma\beta \\ \gamma\beta & \gamma \end{pmatrix} \begin{pmatrix} \omega'/c \\ k' \end{pmatrix} \\ = \begin{pmatrix} \gamma\frac{\omega'}{c} + \gamma\beta k' \\ \gamma\beta\frac{\omega'}{c} + \gamma k' \end{pmatrix} = \frac{\omega'}{c}\gamma(1+\beta)\begin{pmatrix} 1 \\ 1 \end{pmatrix} \ , \end{aligned} \tag{20.92}$$

such that,

$$\boxed{\omega = ck = \omega'\sqrt{\frac{1+\beta}{1-\beta}} = \gamma\omega'(1+\beta)} \ . \tag{20.93}$$

Including the transverse motion, we obtain

$$\omega = \gamma\omega'\left(1 + \frac{\mathbf{v}_0 \cdot \mathbf{v}}{vc}\right) \ , \tag{20.94}$$

where $\mathbf{v}_0$ is the speed of the source. It is interesting to note that, even in case of a purely transverse motion $\mathbf{v}_0 \cdot \mathbf{v} = 0$, we observe a Doppler shift.

Example 131 (*Doppler effect on a moving laser*): We now consider a light source flying through the lab S, for example, a laser operating at a frequency ω', which is well-defined by an atomic transition of the active medium. A spectrometer installed in the same rest frame S' as the laser will measure just this frequency. We now ask, what frequency would be measured by a spectrometer installed in the lab frame. The classical response has already been derived for a moving sound source,

$$\omega' = \omega - kv = \omega - \frac{\omega}{c}v = \frac{\omega}{1+\frac{v}{c}} \ ,$$

with $k = \omega/c$. Because of time dilatation, we need to multiply by γ,

$$\omega' = \frac{\gamma^{-1}\omega}{1+\frac{v}{c}} = \omega\sqrt{\frac{1-\beta}{1+\beta}} \simeq \omega\left(1 \pm \frac{v}{c} + \frac{v^2}{2c^2}\right) \ .$$

The above example shows that, for non-relativistic velocities, one can distinguish the *first-order Doppler effect* from the *relativistic Doppler effect* due to time dilatation,

$$\boxed{\omega' \simeq \omega \pm kv + \tfrac{1}{2}\omega\beta^2} \ . \tag{20.95}$$

We will study the Doppler effect for the case of ultracold atoms in Excs. 20.2.6.6 to 20.2.6.8.

20.2.5 Relativistic Newton's law

The relativistic form of *Newton's law*,

$$\mathbf{F} = \frac{d\mathbf{p}}{dt} \ , \tag{20.96}$$

with the momentum given by (20.85) defines the *common* relativistic force. However, because it is derived from the momentum with respect to common time, the common force $\mathbf{F}$ *can not* be extended to a Lorentz invariant of the type F^μ. In contrast, *Minkowski force* defined as,

$$\boxed{K_\mu = \frac{dp_\mu}{d\tau} = \frac{\gamma_v dp_\mu}{dt} \qquad \text{that is} \qquad (K^\mu) = \begin{pmatrix} \gamma_v P/c \\ \gamma_v \mathbf{F} \end{pmatrix}} \ , \tag{20.97}$$

is covariant. Nevertheless, we will often be interested in the common force $\mathbf{F}$ acting on moving bodies as measured in a laboratory frame.

The work exerted on a particle increases its kinetic energy, such that,

$$\begin{aligned} W \equiv \int \mathbf{F}\cdot d\mathbf{l} &= \int \frac{d\mathbf{p}}{dt}\cdot d\mathbf{l} = \int \frac{d\mathbf{p}}{dt}\cdot \mathbf{v}\ dt = \int \frac{d}{dt}(\gamma_v m\mathbf{v})\cdot \mathbf{v}\ dt \\ &= \int (\gamma_v^3 m\dot{\mathbf{v}})\cdot \mathbf{v}\ dt = \int mc^2 \frac{d\gamma_v}{dt} dt = \int \frac{dE}{dt} dt = E_{final} - E_{initial} \ . \end{aligned} \tag{20.98}$$

Unlike the first two Newton laws, the third one (actio = reactio) does *not* apply in the relativistic regime. Indeed, the simultaneity of 'actions' and reactions' in the forces that two distant bodies A and B exert on each other depends on the velocity of the observer.

20.2.6 Exercises

20.2.6.1 Ex: Adding velocities

Imagine an array of flash lamps at rest in the system S. The lamps are aligned at distances of $\Delta s = 10\,\text{m}$ from each other. The array extends over a distance of many light-years. Now, the lamps are flashed successively (from left to right), so that the light seems to move to the right.
a. At what time interval Δt two adjacent lamps need to flash in order to generate an apparent velocity of $v_1 = 1.2c$?
b. An inertial system S' moves relative to S with velocity $v_2 = -0.56c$ in opposite direction to that of the motion of the flashes. At what velocity the flashes seem to be moving in the system S'?

Solution: *a. We have*

$$\Delta t = \frac{\Delta s}{v} = \frac{10\,\text{m}}{1.2c} = 2.78\cdot 10^{-8}\,\text{s} \ .$$

b. We consider the array of lamps at the instant in which the first lamp flashes, and we call this instant $t = 0$. In system S the distance of the lamps is $\Delta s = 10$ m. In

S' the situation is obviously different: the distance of the lamps is shortened and the clocks (fixed to the lamps) go more slowly and not in a synchronized way. We label the flash-lamps with an integer number j and parametrize the 'flashes' in the system S by,

$$z_j = j\Delta s = j \cdot 10\,\mathrm{m}$$
$$t_j = j\Delta t = j\frac{\Delta s}{v_1} = j\frac{10\,\mathrm{m}}{1.2c} \approx 2.89 \cdot 10^{-8}\,\mathrm{s}\ ,$$

and we transform to the system S',

$$z'_j = \gamma z_j - \gamma v_2 t_j = \gamma j\Delta s - \gamma v_2 j\frac{\Delta s}{v_1} = \left(1 - \frac{v_2}{v_1}\right)\gamma j\Delta s$$
$$t'_j = \gamma t_j - \gamma\frac{v_2}{c^2}z_j = \gamma j\frac{\Delta s}{v_1} - \gamma\frac{v_2}{c^2}j\Delta s = \left(\frac{1}{v_1} - \frac{v_2}{c^2}\right)\gamma j\Delta s\ .$$

Now, we can calculate the apparent velocity in the system S':

$$v'_2 = \frac{z'_j - z'_{j-1}}{t'_j - t'_{j-1}} = \frac{1 - \frac{v_2}{v_1}}{\frac{1}{v_1} - \frac{v_2}{c^2}} = \frac{v_1 - v_2}{1 - v_1 v_2/c^2} = \frac{1.2c + 0.56c}{1 + 1.2 \cdot 0.56} \approx 1.053c\ .$$

Surprisingly, the apparent velocity gets smaller, although we move in the direction opposite to the motion. We find the same value, when we simply apply Einstein's formula for the addition of velocities.
The term 'apparent velocity' means that, seen from far, the array looks like a single flashing light propagating in space. Traveling at a certain speed v_1 we would be at the position of every lamp of the array exactly when it flashes. If $v_1 > c$ this is of course not possible to realize. Note that there is no contradiction of relativity, because no information is transmitted through the flashing array. The flash lamps are assumed to have been programmed a long time ago and brought into their position afterward. Relativity does not impede events to occur at positions so distant that they cannot influence each other even by messengers traveling at the speed of light.

20.2.6.2 Ex: Covariant momentum

Show that an identification of the momentum p^μ with mv^μ would be inconsistent with the principle of momentum conservation and the principle of relativity.

Solution:

20.2.6.3 Ex: Inelastic collision

A particle of mass m whose total energy is twice its rest energy collides with an identical particle at rest. If they stick together, what is the mass of the resulting particle compound? What is its velocity?

Solution: *Conservation of energy and momentum requires,*

$$(p^{\mu}_{before}) = \begin{pmatrix} E_{before}/c \\ p^{z}_{before} \end{pmatrix} = \begin{pmatrix} 2mc + mc \\ \sqrt{3}mc \end{pmatrix} \stackrel{!}{=} \begin{pmatrix} \sqrt{m_{12}^2c^2 + p_{12}^2} \\ p_{12} \end{pmatrix} = (p^{\mu}_{after}) \ .$$

This gives,

$$2mc + mc = \sqrt{m_{12}^2c^2 + 3m^2c^2} \ .$$

Solving by m_{12},

$$m_{12} = \sqrt{6}m \ .$$

The time dilatation factor is,

$$\gamma = \frac{\gamma m}{m} = \frac{E/c^2}{m} = \frac{2m}{m} = 2 \ .$$

With this, the velocity in the lab frame is before the collision,

$$v = \frac{u}{\gamma} = \frac{p}{\gamma m} = \frac{\sqrt{3}mc}{\gamma m} = \sqrt{\frac{3}{4}}c \ ,$$

and after the collision,

$$v_{12} = \frac{u_{12}}{\gamma} = \frac{p_{12}}{\gamma m_{12}} = \frac{\sqrt{3}mc}{2m_{12}} = \frac{\sqrt{3}mc}{2\sqrt{6}m} = \sqrt{\frac{1}{8}}c = \sqrt{\frac{1}{6}}v \ .$$

20.2.6.4 Ex: Relativistic collision

Consider a relativistic completely inelastic frontal collision of two particles moving along the x-axis. Both particles have mass m. Before the collision, an observer A sitting in an inertial frame, notices that the masses move with the same constant velocities but in the opposite direction, that is, the particle 1 moves with velocity v and the particle 2 moves with velocity $-v$. According to another observer B, however, particle 1 is initially at rest.
a. Determine the velocity v'_x of particle 2 measured by observer B before collision.
b. Find the velocities v_A and v'_B of the particle resulting from the collision, measured, respectively, by the observers A and B.
c. Use the relativistic mass-energy conservation and calculate the mass M of the particle resulting from the collision.

Solution: *a. We can conclude that the observer B has the same velocity as the particle 1. Therefore, $v_B = v$, where v_B is the velocity of the observer B. The observer A, at rest, measures for the particle 2 the velocity $u_2 = -v$. From the Lorentz transformations, we see that particle 2 has the following velocity*

$$u'_2 = \frac{u_2 - v_B}{1 - \frac{u_2 v_B}{c^2}} \ .$$

Therefore, the velocity of the particle measured by the observer B is,

$$u_2' = \frac{-v - v}{1 - \frac{(-v)v}{c^2}} = \frac{-2v}{1 + v^2/c^2} \ .$$

b. After the collision, the observer A verifies that the final velocity is zero, $u_A = 0$. Considering again the Lorentz transform, the moving observer detects the following velocity for the particle resulting from the collision,

$$u_B' = \frac{u_A - v_B}{1 - \frac{u_A v_B}{c^2}} = -v \ .$$

c. The total energy of the system is equal to the sum of the energies of the particles,

$$\begin{aligned} E_{before} = E_1 + E_2 &= \frac{mc^2}{\sqrt{1 - u_1^2/c^2}} + \frac{mc^2}{\sqrt{1 - u_2^2/c^2}} \\ &= \frac{mc^2}{\sqrt{1 - v^2/c^2}} + \frac{mc^2}{\sqrt{1 - (-v)^2/c^2}} = \frac{2mc^2}{\sqrt{1 - u_1^2/c^2}} \ . \end{aligned}$$

Let's call M the mass of the compound after the collision and keep in mind that M is not necessarily $2m$:

$$E_{after} = \frac{Mc^2}{\sqrt{1 - u_A^2/c^2}} \ .$$

Since $u_A = 0$, it results $E_{after} = Mc^2$. In order to satisfy mass-energy conservation, we have $E_{before} = E_{after}$, that is,

$$\frac{2mc^2}{\sqrt{1 - v^2/c^2}} = Mc^2 \ .$$

Hence,

$$M = \frac{2m}{\sqrt{1 - v^2/c^2}} \ .$$

This is the mass of the resulting particle.

20.2.6.5 Ex: γ-rays

γ-rays produced by paired annihilation exhibit considerable Compton scattering. Consider a photon produced with the energy m_0c^2 by the annihilation of an electron and a positron, where m_0 is the rest mass of the electron. Suppose that this photon be scattered by a free electron and that the scattering angle is θ_γ, as shown in Fig. 20.6.

a. Find the maximum possible kinetic energy for the recoiling electron.

b. If the scattering angle were $\theta_\gamma = 120°$, determine the photon energy and the kinetic energy of the electron after the scattering.

c. If $\theta_\gamma = 120°$, what is the direction of motion of the electron after the scattering with respect to the direction of the incident photon?

Solution: *a. Given the expression for Compton scattering, where the apostrophe indicates the scattered photon,*

$$\lambda' - \lambda = \frac{h}{m_0 c}(1 - \cos\theta_\gamma) \ .$$

Multiplying it with $1/hc$*, we have,*

$$\frac{\lambda'}{hc} - \frac{\lambda}{hc} = \frac{1}{mc^2}(1 - \cos\theta_\gamma) \ .$$

But $E = hc/\lambda$*, and the initial photon energy is* $m_0 c^2$*, hence,*

$$\frac{1}{E'} - \frac{1}{m_0 c^2} = \frac{1}{m_0 c^2}(1 - \cos\theta_\gamma) \ .$$

The maximum momentum transfer to the electron occurs at,

$$\theta_\gamma = 180^\circ \ ,$$

then we can obtain the energy of the scattered photon,

$$E' = \frac{m_0 c^2}{3} \ .$$

By energy conservation, we have that the maximum kinetic energy is,

$$E_c^{max} = \frac{2m_0 c^2}{3} \ .$$

b. From the second expression, considering that $\cos 120^\circ = -\cos 60^\circ = -1/2$*, we have that,*

$$E' = \frac{2m_0 c^2}{5}$$

By energy conservation,

$$E_c = \frac{3m_0 c^2}{5} \ .$$

c. Because of momentum conservation, we have the following components (θ_e *is the angle of the electron with respect to the direction of the incident photon).*
In vertical direction (y), we have $p_e \sin\theta_e = p' \sin\theta_\gamma$*.*
In horizontal direction (x), we have $p_e \cos\theta_e = p - p' \cos\theta_\gamma$*.*
By dividing one expression by the other, we eliminate the variable p_e *and get,*

$$\tan\theta_e = \frac{p' \sin\theta_\gamma}{p - p' \cos\theta_\gamma} \ .$$

But for the photon, $E = pc$*, hence:* $\tan\theta_e = \frac{E' \sin\theta_\gamma}{E - E' \cos\theta_\gamma}$*, but since* $\cos 120^\circ = -\cos 60^\circ = -1/2$ *and* $\sin 120^\circ = \cos 30^\circ = \sqrt{3}/2$ *and given the values of* E *and* E'*, we arrive at,*

$$\tan\theta_e = \frac{\sqrt{3}}{6} \ .$$

20.2.6.6 Ex: Second order Doppler shift

The *second order Doppler shift* comes from the relativistic dilation of time. Periodic events occurring in a moving inertial system appear dilated to an observer in another system. Consider a strontium atom, which has a resonance at the wavelength $\lambda = 461\,\text{nm}$, located inside a resonant laser beam from which it absorbs and reemits photons.
a. Assume the atom initially at rest. What will be it's velocity after having absorbed a single photon?
b. Calculate the first and second order Doppler shift for the remitted photon as a function of the emission direction.

Solution: *a. The atomic mass of strontium is* $88u$. *The atomic velocity due to photonic recoil is,*

$$v = \frac{p}{m} = \frac{\hbar k}{m} = \frac{h}{m\lambda} = 9.9\,\text{mm/s} \ .$$

b. The first order Doppler shift is,

$$\mathbf{k}\cdot\mathbf{v} = kv\cos\theta = \frac{2\pi}{\lambda}\frac{h}{m\lambda}\cos\theta = (2\pi)\ 21259\,\text{Hz}\ \ \cos\theta \ ,$$

and the second order Doppler shift is,

$$\Delta\omega = \frac{\omega\beta^2}{2} = \frac{\pi v^2}{\lambda c} = (2\pi)\ 3.5\cdot 10^{-7}\,\text{Hz} \ .$$

20.2.6.7 Ex: Recoil- and Doppler-shift upon photon absorption

Derive the expressions for the recoil- and Doppler-shift upon the absorption of a photon of frequency ω_i by an atom with the initial velocity $\mathbf{v}_i$ using relativistic mechanics.

Solution: *Conservation of energy and linear momentum require that the photon absorption process* $i \to a$ *satisfies,*

$$p_i^\mu = \begin{pmatrix} \hbar\omega_i/c + E_i/c \\ \hbar\mathbf{k}_i + \mathbf{p}_i \end{pmatrix} = \begin{pmatrix} E_a/c + E^*/c \\ \mathbf{p}_a \end{pmatrix} = p_a^\mu \ .$$

The resonance frequency for the absorption of a photon of frequency $\omega = ck$ *by an atom traveling at velocity* $\mathbf{v} = \mathbf{p}/m$ *must be calculated relativistically,*

$$\begin{aligned} E^* - \hbar\omega_i = E_i - E_a &= \sqrt{m^2c^4 + c^2p_i^2} - \sqrt{m^2c^4 + c^2p_a^2} \\ &\simeq mc^2\left(1 + \frac{p_i^2}{2m^2c^2}\right) - mc^2\left(1 + \frac{(\hbar\mathbf{k}_i + \mathbf{p}_i)^2}{2m^2c^2}\right) \\ &\simeq -\frac{\hbar^2k_i^2}{2m} - \frac{\hbar\mathbf{k}_i\cdot\mathbf{p}_i}{m} = -\frac{\hbar^2\omega_i^2}{2mc^2} - \hbar\mathbf{k}_i\cdot\mathbf{v}_i \ . \end{aligned}$$

The first correction term accounts for photonic recoil, the second describes the linear Doppler effect.

20.2.6.8 Ex: Recoil- and Doppler-shift upon photon scattering in relativistic mechanics

Derive the expression for the recoil- and Doppler-shift upon the absorption and reemission of a photon of frequency ω_i by an atom with the initial velocity $\mathbf{v}_i$ using relativistic mechanics. Discuss the particular case, $\mathbf{v}_i = 0$.

Solution: *Conservation of energy and linear momentum require that the photon absorption process $i \to a$ and the reemission process $a \to f$ satisfy,*

$$p_i^\mu = \begin{pmatrix} \hbar\omega_i/c + E_i/c \\ \hbar\mathbf{k}_i + \mathbf{p}_i \end{pmatrix} = p_a^\mu = \begin{pmatrix} E_a/c + E^*/c \\ \mathbf{p}_a \end{pmatrix} = p_f^\mu = \begin{pmatrix} \hbar\omega_f/c + E_f/c \\ \hbar\mathbf{k}_f + \mathbf{p}_f \end{pmatrix} ,$$

where E^* is the excitation energy of the atom and,

$$m^2c^2 = (E_i/c)^2 - \mathbf{p}_i^2 = (E_a/c)^2 - \mathbf{p}_a^2 = (E_f/c)^2 - \mathbf{p}_f^2 ,$$

the atom's energy in its rest system. Hence,

$$\hbar\omega_i + \sqrt{m^2c^4 + c^2p_i^2} = \hbar\omega_f + \sqrt{m^2c^4 + c^2p_f^2}$$
$$\hbar\mathbf{k}_i + \mathbf{p}_i = \hbar\mathbf{k}_f + \mathbf{p}_f$$

from which we now aim at calculating the emission frequency ω_f as a function of the scattering angle $\vartheta \equiv \sphericalangle(\mathbf{k}_i, \mathbf{k}_f)$ and the initial atomic momentum $\mathbf{p}_i$in a similar way as we did in Sec. 38.3.1. Defining $\Delta\omega \equiv \omega_f - \omega_i$ and $\Delta\mathbf{k} \equiv \mathbf{k}_f - \mathbf{k}_i$, we get,

$$\hbar\Delta\omega = \sqrt{m^2c^4 + c^2p_i^2} - \sqrt{m^2c^4 + c^2(\mathbf{p}_i - \hbar\Delta\mathbf{k})^2} .$$

Let us consider the particular cases when $p_i = 0$ and introduce the recoil-frequency,

$$\omega_{rec} = \frac{\hbar\omega_i^2}{2mc^2} \simeq \frac{\hbar\omega_f^2}{2mc^2} ,$$

we recover the non-relativistic result (38.40) in first order,

$$\hbar\Delta\omega = mc^2 - \sqrt{m^2c^4 + \hbar^2c^2\Delta\mathbf{k}^2} \simeq -\frac{\hbar^2(\omega_f^2 + \omega_i^2 - 2\omega_f\omega_i\cos\vartheta)}{2mc^2} \simeq 2\omega_{rec}(-1+\cos\vartheta) .$$

20.3 Relativistic electrodynamics

20.3.1 Relativistic current and magnetism

To begin with, we introduce the space-time current density by,

$$\boxed{(j^\mu) \equiv \begin{pmatrix} c\varrho \\ \mathbf{j} \end{pmatrix}} \,. \tag{20.99}$$

This notation allows us to formulate the continuity equation as,

$$\boxed{\partial_\mu j^\mu = 0} \,. \tag{20.100}$$

Example 132 (*Electric charge under Lorentz transformation*): In order to convince ourselves that it makes sense to combine charge density and current as quadri-vectors, we consider a situation in which there are only static charges with density ϱ_0 and has no current: $j_\mu = (c\varrho_0 \; \mathbf{0})$. Now, in an inertial system moving at velocity $\mathbf{v}$, the charge density will appear as a current,

$$(j'^\mu) = (\Lambda^\mu{}_\nu j^\nu) = \begin{pmatrix} \gamma c\varrho_0 \\ -c\gamma\beta\varrho_0 \hat{\mathbf{e}}_z \end{pmatrix} = \begin{pmatrix} \gamma\varrho \\ -\gamma\varrho\mathbf{v} \end{pmatrix} \,.$$

That is, different observers observe different charge densities. The current $-\gamma\varrho\mathbf{v}$ appears due to the motion of the charge being contrary to the motion of the observer. Moreover, as the charge density is defined per unit volume and the volume is compressed due to Lorentz contraction, the observed charge density $\gamma\varrho_0$ appears to be increased.

The observation that a moving charge gives rise to a current is not new. But the fact that we can transform charge into current through a Lorentz transform already points to the close connection between the phenomena of electricity and magnetism in the theory of relativity: moving electric fields must generate magnetic fields. We will study the details of how this happens shortly. But first, let us have a look at a simple example, where we re-derive the magnetic force purely from the Coulomb force and a Lorentz contraction.

Example 133 (*Electric current under Lorentz transform*): We consider a sample of positive charges $+q$ moving along a conducting wire with velocity $+v$ and a sample of negative charges $-q$ moving in opposite direction with velocity $-v$, as shown Fig. 20.7. If the densities n of positive and negative charges is equal, the total charge density vanishes, while the currents add up to $I = 2nAqv$, where A is the cross section of the wire. We now consider a test particle, also carrying a charge q, which moves parallel to the wire at some velocity v_0. This charge does not feel any electrical force, because the wire is neutral, but we know that it experiences a magnetic force. We will now show, how to find an expression for this force without ever invoking the phenomenon of magnetism. The trick is to go to the inertial system S' of the test particle, which means that we have to transform to a velocity v_0. The formula for summing relativistic velocities tells us, that the velocities of the positive and negative charges are now different,

$$v_\pm = \frac{v \mp v_0}{1 \mp v_0 v/c^2} \,.$$

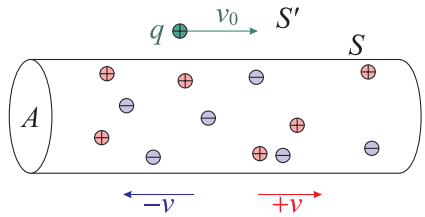

Figure 20.7: Illustration of the relativistic origin of the Lorentz force.

But with this transformation comes a Lorentz contraction modifying the density of the charges. In addition, the different velocities of the positive and negative charges cause that, seen from the system S' (rest frame of the test particle), the wire is no longer neutral. Let us see how this works: First, we introduce the density of positively (negatively) charged particles n_0 in the system S_+ (S_-) in which they are at rest. With this, the charge densities in the lab system S (rest frame of the wire) are,

$$\varrho_\pm = q n_\pm = \gamma_v q n_0 \ .$$

In the system S, the wire is neutral because the positive and negative charges travel at the same velocity, albeit in opposite directions, $\varrho_+ + \varrho_- = 0$. Now, in the system S', the charge densities are,

$$\begin{aligned}\varrho'_\pm = q\gamma_{v_\pm} n_0 &= \frac{1}{\sqrt{1-\left(\frac{v\mp v_0}{c\mp v v_0/c}\right)^2}} q n_0 \\ &= \frac{-c^2 \pm v v_0}{\sqrt{(c^2-v^2)(c^2-v_0^2)}} q n_0 = \left(1 \mp \frac{v_0 v}{c^2}\right)\gamma_{v_0}\gamma_v q n_0 \ ,\end{aligned}$$

Since $v_- > v_+$, we have $n'_- > n'_+$, and the wire carries negative charge. That is, the total charge density in the new system is,

$$\varrho' = q(n'_+ - n'_-) = -\frac{2 v_0 v}{c^2}\gamma_{v_0} q n_\pm \ .$$

But we know that a line of electric charges creates an electric field (using Gauß' law) of,

$$\vec{\mathcal{E}}'(r) = \frac{\varrho' A}{2\pi\varepsilon_0 r}\hat{\mathbf{e}}_r = -\frac{2 v_0 v}{c^2}\gamma_{v_0} q n_\pm \frac{A}{2\pi\varepsilon_0 r}\hat{\mathbf{e}}_r \ ,$$

where r is the radial direction perpendicular to the wire. This means that in its rest frame, the particle experiences a force,

$$F' = q\mathcal{E}'(r) = -v_0\gamma_{v_0}\frac{n_\pm A q^2 v}{\pi\varepsilon_0 c^2 r} \ ,$$

where the negative sign tells us, that the force is in radial direction toward the center of the wire for $v_0 > 0$. But if there is a force in one system, there must also be a force in the other one. Transforming back to the lab system S, we conclude that even when the wire is neutral, there will be a force,

$$F = \frac{F'}{\gamma_{v_0}} = -v_0\frac{n_\pm A q^2 v}{\pi\varepsilon_0 c^2 r} = -v_0 q\frac{\mu_0 I}{2\pi r} \ .$$

But this agrees precisely with the Lorentz force attracting or repelling two neutral current-carrying wires.

This analysis provides an explicit demonstration of how an electric force in one reference system is interpreted as a magnetic force in another. Another surprising observation is the following. We are accustomed to think of Lorentz contraction as an exotic result, which is only important, when we approach the speed of light. However, the electrons traveling on a wire are very slow, taking about an hour to travel a meter! Nevertheless, we can easily detect the magnetic force between two wires which, as we have seen above, can be directly attributed to the length contraction of the electronic density [6].

20.3.2 Electromagnetic potential and tensor

The shape of the *scalar and vector relativistic potentials* (17.104), as expressed by the laws of Coulomb and Biot-Savart, suggests their combination to a quadri-vector,

$$\boxed{(A^\mu) \equiv \begin{pmatrix} \frac{1}{c}\Phi \\ \mathbf{A} \end{pmatrix}} \,. \tag{20.101}$$

with this the *gauge transform* defined in (17.85) adopts the form,

$$\boxed{A^\mu \to A^\mu - \partial^\mu \chi} \,. \tag{20.102}$$

In particular, the *Lorentz gauge* (17.86) becomes,

$$\boxed{\partial_\mu A^\mu = 0} \,. \tag{20.103}$$

Now, let us have a look at the following antisymmetric construction,

$$\boxed{F^{\mu\nu} \equiv \partial^\mu A^\nu - \partial^\nu A^\mu} \,. \tag{20.104}$$

Obviously, this tensor is invariant under gauge transformation, since,

$$F^{\mu\nu} \to \partial^\mu (A^\nu - \partial^\nu \chi) - \partial^\nu (A^\mu - \partial^\mu \chi) = F^{\mu\nu} - \partial^\mu \partial^\nu \chi + \partial^\nu \partial^\mu \chi \,. \tag{20.105}$$

which already suggests, that the components of $F^{\mu\nu}$ have something to do with electromagnetic fields.

In fact, analyzing each component of (20.104) in the light of the equations (17.78), we find the so-called *electromagnetic field tensor*,

$$\check{F} = (F^{\mu\nu}) = \begin{pmatrix} 0 & -\frac{1}{c}\mathcal{E}_x & -\frac{1}{c}\mathcal{E}_y & -\frac{1}{c}\mathcal{E}_z \\ \frac{1}{c}\mathcal{E}_x & 0 & -\mathcal{B}_z & \mathcal{B}_y \\ \frac{1}{c}\mathcal{E}_y & \mathcal{B}_z & 0 & -\mathcal{B}_x \\ \frac{1}{c}\mathcal{E}_z & -\mathcal{B}_y & \mathcal{B}_x & 0 \end{pmatrix} = \begin{pmatrix} 0 & -\frac{1}{c}\vec{\mathcal{E}} \\ \frac{1}{c}\vec{\mathcal{E}} & (-\epsilon_{mnk}\mathcal{B}_k) \end{pmatrix} \,. \tag{20.106}$$

where ϵ_{mnk} it is the Levi-Civita tensor.

[6] The above discussion needs a small adjustment for real wires. In the rest frame of the wire the positive charges, which are ions, are fixed while the electrons move. According to the above explanation, we might think that this will lead to an imbalance of the charge densities. But this is not correct. The current is due to electrons injected by the battery into one end of the battery and drained at the other end in such a way, that the wire remains neutral in the rest frame, with the electron density accurately compensating the ionic density. In contrast, if we moved to a system in which ions and electrons had equal and opposite speeds, the wire would appear charged.

20.3.2.1 Maxwell's equations

The dual tensor is,

$$\check{\mathcal{F}} = (\mathcal{F}^{\mu\nu}) = (\tfrac{1}{2}\epsilon^{\mu\nu\alpha\beta}F_{\alpha\beta}) = \begin{pmatrix} 0 & -\mathcal{B}_x & -\mathcal{B}_y & -\mathcal{B}_z \\ \mathcal{B}_x & 0 & \frac{1}{c}\mathcal{E}_z & -\frac{1}{c}\mathcal{E}_y \\ \mathcal{B}_y & -\frac{1}{c}\mathcal{E}_z & 0 & \frac{1}{c}\mathcal{E}_x \\ \mathcal{B}_z & \frac{1}{c}\mathcal{E}_y & -\frac{1}{c}\mathcal{E}_x & 0 \end{pmatrix} = \begin{pmatrix} 0 & -\vec{\mathcal{B}} \\ \vec{\mathcal{B}} & (\frac{1}{c}\epsilon_{mnk}\mathcal{E}_k) \end{pmatrix} . \tag{20.107}$$

The spatio-temporal *Maxwell equations* are written,

$$\boxed{\partial_\mu F^{\mu\nu} = \mu_0 j^\nu \quad , \quad \partial_\mu \mathcal{F}^{\mu\nu} = 0} \, . \tag{20.108}$$

The first space-time Maxwell equation incorporates the familiar form of Maxwell's first and third equations,

$$\begin{aligned} (\partial_\mu F^{\mu\nu}) &= \begin{pmatrix} \frac{\partial}{c\partial t} & \nabla \end{pmatrix} \begin{pmatrix} 0 & -\frac{1}{c}\vec{\mathcal{E}} \\ \frac{1}{c}\vec{\mathcal{E}} & (-\epsilon_{mnk}\mathcal{B}_k) \end{pmatrix} = \begin{pmatrix} \frac{1}{c}\nabla\cdot\vec{\mathcal{E}} \\ -\frac{1}{c^2}\frac{\partial}{\partial t}\vec{\mathcal{E}} - \nabla\cdot(\epsilon_{mnk}B_k) \end{pmatrix}^\intercal \\ &= \begin{pmatrix} \frac{1}{c}\nabla\cdot\vec{\mathcal{E}} \\ -\frac{1}{c^2}\frac{\partial}{\partial t}\vec{\mathcal{E}} + \left(\epsilon_{mkn}\frac{\partial}{\partial x^m}\mathcal{B}_k\right) \end{pmatrix}^\intercal = \begin{pmatrix} \frac{1}{c}\nabla\cdot\vec{\mathcal{E}} \\ -\frac{1}{c^2}\frac{\partial}{\partial t}\vec{\mathcal{E}} + \nabla\times\vec{\mathcal{B}} \end{pmatrix}^\intercal = \mu_0 \begin{pmatrix} c\rho \\ \mathbf{j} \end{pmatrix}^\intercal = (\mu_0 j^\nu) \, , \end{aligned} \tag{20.109}$$

using the definition of the vector product,

$$(\mathbf{a}\times\mathbf{b})_k = \epsilon_{mnk}a_m b_n \, . \tag{20.110}$$

The second space-time Maxwell equation incorporates Maxwell's second and fourth equations. With the definition of the Levi-Civita tensor, we can rewrite the equation as,

$$\epsilon^{\mu\nu\kappa\lambda}\partial_\kappa F_{\mu\nu} = \partial_\kappa F_{\mu\nu} + \partial_\mu F_{\nu\kappa} + \partial_\nu F_{\kappa\mu} = 0 \, . \tag{20.111}$$

This form satisfies the requirement of cyclical permutability and also takes into account the fact, that all indexes must be different. If two indexes are equal, for example, $\mu = \kappa$, we would have $\partial_\kappa F_{\mu\mu} + \partial_\mu F_{\mu\kappa} + \partial_\mu F_{\kappa\mu}$. This expression is certainly zero because the field tensor is antisymmetric, $F^{\mu\nu} = -F^{\nu\mu}$.

20.3.3 Lorentz transformation of electromagnetic fields

The rapid motion of the electron within the electrostatic field $\vec{\mathcal{E}}$ of the nucleus produces, according to the theory of relativity, a magnetic field $\vec{\mathcal{B}}'$ in the reference frame of the electron. In atomic physics [7] we learn that this field can interact with the spin of the electron, thus giving rise to a considerable energy shift called the fine structure of the atomic spectrum. We calculate the interaction energy in the following.

[7] See script on *Quantum mechanics* (2023).

In the relativistic mechanics defined by the metric (20.3) and the Lorentz transform (20.19) the Maxwell field tensor is given by (20.106). With this we can calculate the field transformed into an inertial system propagating along the z-axis,

$$F'^{\mu\nu} = \Lambda^{\mu}{}_{\alpha} F^{\alpha\beta} \Lambda_{\beta}{}^{\nu} = \begin{pmatrix} 0 & -\frac{\gamma}{c}\mathcal{E}_x + \gamma\beta\mathcal{B}_y & -\frac{\gamma}{c}\mathcal{E}_y - \gamma\beta\mathcal{B}_x & -\frac{1}{c}\mathcal{E}_z \\ \frac{\gamma}{c}\mathcal{E}_x - \gamma\beta\mathcal{B}_y & 0 & -\mathcal{B}_z & -\gamma\frac{\beta}{c}\mathcal{E}_x + \gamma\mathcal{B}_y \\ \frac{\gamma}{c}\mathcal{E}_y + \gamma\beta\mathcal{B}_x & \mathcal{B}_z & 0 & -\gamma\frac{\beta}{c}\mathcal{E}_y - \gamma\mathcal{B}_x \\ \frac{1}{c}\mathcal{E}_z & \gamma\frac{\beta}{c}\mathcal{E}_x - \gamma B_y & \gamma\frac{\beta}{c}\mathcal{E}_y + \gamma B_x & 0 \end{pmatrix} . \tag{20.112}$$

Using $\mathbf{v} = v_z \hat{\mathbf{e}}_z$, that is $\beta_x = 0 = \beta_y$ and $\beta_z = \beta$, we find,

$$\vec{\mathcal{E}}' = \begin{pmatrix} \mathcal{E}'_x \\ \mathcal{E}'_y \\ \mathcal{E}'_z \end{pmatrix} = \begin{pmatrix} \gamma\mathcal{E}_x - \beta_z c\gamma\mathcal{B}_y \\ \gamma\mathcal{E}_y + \beta_z c\gamma\mathcal{B}_x \\ \mathcal{E}_z \end{pmatrix} = \begin{pmatrix} \gamma\mathcal{E}_x + \gamma c\beta_y\mathcal{B}_z - \gamma c\beta_z\mathcal{B}_y - \frac{\gamma^2}{\gamma+1}\beta_x\vec{\beta}\cdot\mathcal{E} \\ \gamma\mathcal{E}_y + \gamma c\beta_z\mathcal{B}_x - \gamma c\beta_x\mathcal{B}_z - \frac{\gamma^2}{\gamma+1}\beta_y\vec{\beta}\cdot\mathcal{E} \\ \gamma\mathcal{E}_z + \gamma c\beta_x\mathcal{B}_y - \gamma c\beta_y\mathcal{B}_x - \frac{\gamma^2}{\gamma+1}\beta_z\vec{\beta}\cdot\mathcal{E} \end{pmatrix} \tag{20.113}$$

$$\vec{\mathcal{B}}' = \begin{pmatrix} \mathcal{B}'_x \\ \mathcal{B}'_y \\ \mathcal{B}'_z \end{pmatrix} = \begin{pmatrix} \gamma\mathcal{B}_x + \frac{\beta_z}{c}\gamma\mathcal{E}_y \\ \gamma\mathcal{B}_y - \frac{\beta_z}{c}\gamma\mathcal{E}_x \\ \mathcal{B}_z \end{pmatrix} = \begin{pmatrix} \gamma\mathcal{B}_x - \gamma\frac{\beta_y}{c}\mathcal{E}_z + \gamma\frac{\beta_z}{c}\mathcal{E}_y - \frac{\gamma^2}{\gamma+1}\beta_x\vec{\beta}\cdot\mathcal{B} \\ \gamma\mathcal{B}_y - \gamma\frac{\beta_z}{c}\mathcal{E}_x + \gamma\frac{\beta_x}{c}\mathcal{E}_z - \frac{\gamma^2}{\gamma+1}\beta_y\vec{\beta}\cdot\mathcal{B} \\ \gamma\mathcal{B}_z - \gamma\frac{\beta_x}{c}\mathcal{E}_y + \gamma\frac{\beta_y}{c}\mathcal{E}_x - \frac{\gamma^2}{\gamma+1}\beta_z\vec{\beta}\cdot\mathcal{B} \end{pmatrix} .$$

yielding,

$$\boxed{\begin{aligned} \vec{\mathcal{E}}' &= \gamma(\vec{\mathcal{E}} + c\vec{\beta}\times\vec{\mathcal{B}}) - \frac{\gamma^2}{\gamma+1}\vec{\beta}(\vec{\beta}\cdot\vec{\mathcal{E}}) \\ \vec{\mathcal{B}}' &= \gamma(\vec{\mathcal{B}} - \tfrac{1}{c}\vec{\beta}\times\vec{\mathcal{E}}) - \frac{\gamma^2}{\gamma+1}\vec{\beta}(\vec{\beta}\cdot\vec{\mathcal{B}}) \end{aligned}} . \tag{20.114}$$

Although having been derived for the special case $\vec{\beta} = \beta\hat{\mathbf{e}}_z$, this result holds for arbitrary velocities, $\gamma \to 1$, in any direction $\vec{\beta}$. At lower velocities the result simplifies to,

$$\vec{\mathcal{E}}' \simeq \vec{\mathcal{E}} + c\vec{\beta}\times\vec{\mathcal{B}} \qquad \text{and} \qquad \vec{\mathcal{B}}' = \vec{\mathcal{B}} - \tfrac{1}{c}\vec{\beta}\times\vec{\mathcal{E}} . \tag{20.115}$$

The first of these equations is the Coulomb-Lorentz force: In the charge's rest frame the Lorentz part of the force has to disappear. The second equation becomes important only for relativistic velocities. Let us consider, for example, the orbital motion of an electron within the Colombian field generated by a proton. From the point of view of the proton, the motion of the electron corresponds to a circular current producing a magnetic field in the place of the proton, which can be approximated to first order in v/c by [8],

$$\vec{\mathcal{B}}' \simeq -\frac{\mathbf{v}}{c^2}\times\vec{\mathcal{E}} . \tag{20.116}$$

We conclude that magnetism can be seen as a relativistic electrical phenomenon. Do the Exc. 20.3.6.2.

[8] Note, however, that this derivation does not account for the rotation of electrons reference system giving rise to the so-called Thomas precession.

20.3.3.1 Lorentz force

The spatio-temporal *Lorentz force* is,

$$\boxed{K^\mu = \frac{dp^\mu}{d\tau} = qF^{\mu\nu}u_\nu} \,, \tag{20.117}$$

using the definition of the proper velocity (20.80) and of the proper momentum (20.85). Being covariant it is a Minkowski force of the type (20.97). Extracting the spatial components,

$$\mathbf{F} = \frac{d\mathbf{p}}{dt} = \frac{d\mathbf{p}}{\gamma d\tau} = q(\vec{\mathcal{E}} + \mathbf{v} \times \vec{\mathcal{B}}) \,, \tag{20.118}$$

Remembering that $\mathbf{p} = m\gamma\mathbf{v}$ is the relativistic momentum.

The temporal component of the Lorentz force,

$$\frac{dE/c}{dt} = \frac{dE/c}{\gamma d\tau} = \frac{q}{c}\vec{\mathcal{E}} \cdot \mathbf{v} \,, \tag{20.119}$$

simply informs us, that the kinetic energy $m\gamma c^2 - mc^2$ increases under the action of work.

The spatio-temporal *Lorentz force density* is,

$$\boxed{f^u = F^{\mu\nu}j_\nu} \,. \tag{20.120}$$

From this we obtain the equations,

$$\begin{aligned} f^u = F^{\mu\nu}j_\nu &= \begin{pmatrix} 0 & -\frac{1}{c}\vec{\mathcal{E}} \\ \frac{1}{c}\vec{\mathcal{E}} & (-\epsilon_{mnk}\mathcal{B}_k) \end{pmatrix} \begin{pmatrix} c\varrho \\ \mathbf{j} \end{pmatrix} = \begin{pmatrix} -\frac{1}{c}\vec{\mathcal{E}} \cdot \mathbf{j} \\ \varrho\vec{\mathcal{E}} - (\epsilon_{mnk}j_m\mathcal{B}_k) \end{pmatrix} \\ &= \begin{pmatrix} -\frac{1}{c}\vec{\mathcal{E}} \cdot \mathbf{j} \\ \varrho\vec{\mathcal{E}} + \mathbf{j} \times \vec{\mathcal{B}} \end{pmatrix} = \begin{pmatrix} \frac{1}{c}P \\ \mathbf{f} \end{pmatrix} \,. \end{aligned} \tag{20.121}$$

20.3.4 Energy and momentum tensor

The meaning of the 4-dimensional energy-momentum tensor is illustrated with the following matrix,

$$T^{\alpha\beta} = \begin{pmatrix} density & flux & flux & flux \\ flux & pressure & shear & shear \\ fluxo & shear & pressure & shear \\ flux & shear & shear & pressure \end{pmatrix} \,. \tag{20.122}$$

The *Maxwell stress tensor* for an electromagnetic field in the absence of sources is defined by,

$$T^{\mu\nu} = \frac{1}{\mu_0}\left(F^\mu_{\ \alpha}F^{\alpha\nu} + \frac{1}{4}F_{\alpha\beta}F^{\alpha\beta}g^{\mu\nu}\right) \,. \tag{20.123}$$

In matrix notation this gives,

$$(T^{\mu\nu}) = \tfrac{1}{\mu_0}\left(F^{\mu\gamma}g_{\gamma\alpha}F^{\alpha\nu} + \tfrac{1}{4}g_{\alpha\gamma}F^{\gamma\delta}g_{\delta\beta}F^{\alpha\beta}g^{\mu\nu}\right) = \tfrac{1}{\mu_0}\check{F}\check{g}\check{F} + \tfrac{1}{4\mu_0}\left\|\check{F}(\check{g}\check{F}\check{g})\right\|\check{g} \tag{20.124}$$

$$= \begin{pmatrix} u & \frac{1}{c}\vec{\mathcal{S}} \\ \frac{1}{c}\vec{\mathcal{S}} & -(T_{mn}) \end{pmatrix}$$

$$= \begin{pmatrix} \varepsilon_0\mathcal{E}^2 & \frac{1}{c}\mathcal{S}_x & \frac{1}{c}\mathcal{S}_y & \frac{1}{c}\mathcal{S}_z \\ \frac{1}{c}\mathcal{S}_x & -\varepsilon_0\mathcal{E}_x^2 - \frac{1}{\mu_0}\mathcal{B}_x^2 + \frac{1}{\mu_0}\mathcal{B}^2 & -\varepsilon_0\mathcal{E}_x\mathcal{E}_y - \frac{1}{\mu_0}\mathcal{B}_y\mathcal{B}_x & -\varepsilon_0\mathcal{E}_x\mathcal{E}_z - \frac{1}{\mu_0}\mathcal{B}_z\mathcal{B}_x \\ \frac{1}{c}\mathcal{S}_y & -\varepsilon_0\mathcal{E}_x\mathcal{E}_y - \frac{1}{\mu_0}\mathcal{B}_y\mathcal{B}_x & -\varepsilon_0\mathcal{E}_y^2 - \frac{1}{\mu_0}\mathcal{B}_y^2 + \frac{1}{\mu_0}\mathcal{B}^2 & -\varepsilon_0\mathcal{E}_y\mathcal{E}_z - \frac{1}{\mu_0}\mathcal{B}_z\mathcal{B}_y \\ \frac{1}{c}\mathcal{S}_z & -\varepsilon_0\mathcal{E}_x\mathcal{E}_z - \frac{1}{\mu_0}\mathcal{B}_z\mathcal{B}_x & -\varepsilon_0\mathcal{E}_y\mathcal{E}_z - \frac{1}{\mu_0}\mathcal{B}_z\mathcal{B}_y & -\varepsilon_0\mathcal{E}_z^2 - \frac{1}{\mu_0}\mathcal{B}_z^2 + \frac{1}{\mu_0}\mathcal{B}^2 \end{pmatrix}$$
$$+ \left(\tfrac{\varepsilon_0}{2}\mathcal{E}^2 - \tfrac{1}{2\mu_0}\mathcal{B}^2\right)(g^{\mu\nu}) \ ,$$

with the energy density $u = \frac{\varepsilon_0}{2}\mathcal{E}^2 + \frac{1}{2\mu_0}\mathcal{B}^2$, the Poynting vector $\vec{\mathcal{S}} = \frac{1}{\mu_0}\vec{\mathcal{E}} \times \vec{\mathcal{B}}$, the Maxwell stress tensor $\overleftrightarrow{\mathbf{T}} = \varepsilon_0\mathcal{E}_m\mathcal{E}_n + \frac{1}{\mu_0}\mathcal{B}_m\mathcal{B}_n - u\delta_{mn}$.

20.3.4.1 Energy and momentum conservation

Using the space-time formalism the energy and momentum conservation laws can be summarized by,

$$f^\mu + \partial_\nu T^{\mu\nu} = 0 \qquad \text{and} \qquad T^{\mu\nu} = T^{\nu\mu} \ . \tag{20.125}$$

This can be seen by applying Maxwell's equations,

$$F^{\mu\nu}j_v + \tfrac{1}{\mu_0}\partial_\nu\left(F^\mu{}_\alpha F^{\alpha\nu} + \tfrac{1}{4}F_{\alpha\beta}F^{\alpha\beta}g^{\mu\nu}\right) = 0 \ . \tag{20.126}$$

In matrix notation we obtain,

$$\begin{pmatrix} 0 & -\frac{1}{c}\vec{\mathcal{E}} \\ \frac{1}{c}\vec{\mathcal{E}} & -(\epsilon_{mnk}\mathcal{B}_k) \end{pmatrix} + \begin{pmatrix} \frac{\partial}{c\partial t}u + \frac{1}{c}\nabla\cdot\vec{\mathcal{S}} \\ \varepsilon_0\mu_0\frac{\partial}{\partial t}\vec{\mathcal{S}} - \nabla(T_{mn}) \end{pmatrix} = 0 \ , \tag{20.127}$$

and therefore,

$$\left(P/c \quad \mathbf{f}\right) + \left(\tfrac{\partial}{c\partial t} \quad \nabla\right)\begin{pmatrix} u & \frac{1}{c}\vec{\mathcal{S}} \\ \frac{1}{c}\vec{\mathcal{S}} & -(T_{mn}) \end{pmatrix} = \begin{pmatrix} \frac{P}{c} + \frac{\partial}{c\partial t}u + \frac{1}{c}\nabla\cdot\vec{\mathcal{S}} \\ \mathbf{f} + \frac{1}{c}\frac{\partial}{c\partial t}\vec{\mathcal{S}} - \nabla(T_{mn}) \end{pmatrix}^{\mathsf{T}} \tag{20.128}$$

$$= \begin{pmatrix} -\frac{1}{c}\mathbf{j}\cdot\vec{\mathcal{E}} + \frac{\partial}{c\partial t}u + \frac{1}{c}\nabla\cdot\vec{\mathcal{S}} \\ \rho\vec{\mathcal{E}} + \mathbf{j}\times\vec{\mathcal{B}} + \varepsilon_0\mu_0\frac{\partial}{\partial t}\vec{\mathcal{S}} - \nabla(T_{mn}) \end{pmatrix}^{\mathsf{T}} = 0 \ .$$

20.3.4.2 Properties of the energy and momentum tensor

Note however, that in a dielectric medium, the matrix elements can be decomposed into separate contributions of the radiation field and the medium. Taken by parts the contributions do not necessarily satisfy the symmetry requirements [9].

[9] See the Abraham-Minkowski controversy.

Defining the angular momentum density of the shear via,

$$M^{\mu\nu g} = T^{\mu\nu}x^g - T^{\mu g}x^\nu \ . \tag{20.129}$$

Conservation of angular momentum means,

$$\partial_\mu M^{\mu\nu g} = 0 \ . \tag{20.130}$$

20.3.5 Solution of the covariant wave equation

Inserting into Maxwell's equations (20.108) the representation of the fields in terms of potentials (20.104), we calculate,

$$\mu_0 j^\mu = \partial_\mu F^{\mu\nu} = \partial_\mu(\partial^\mu A^\nu - \partial^\nu A^\mu) = \Box A^\nu + \partial^\nu \underbrace{(\partial_\mu A^\mu)}_{\to 0} \ . \tag{20.131}$$

The second term disappears in the Lorentz gauge (20.103). Then, the inhomogeneous wave equation is,

$$\boxed{\Box A^\mu = \mu_0 j^\mu} \ . \tag{20.132}$$

Analogously to the three-dimensional Green function (17.99) we can define a four-dimensional one,

$$\Box D(x) \equiv \delta^{(4)}(x) \tag{20.133}$$

with $x = r - r'$. With the representation of the Dirac function,

$$\delta^{(4)}(x) = \tfrac{1}{(2\pi)^4} \int d^4k e^{-\imath k\cdot x} \ , \tag{20.134}$$

where $k \cdot x = k^\mu x_\mu = \omega t - \mathbf{k}\cdot\mathbf{r}$, and the Fourier transform of the Green function,

$$D(x) = \tfrac{1}{(2\pi)^4} \int d^4k \tilde{D}(k) e^{-\imath k\cdot x} \ , \tag{20.135}$$

the equation (20.132) becomes,

$$\begin{aligned}\left[\frac{1}{c^2}\frac{\partial^2}{\partial t^2} - \nabla^2\right] \frac{1}{(2\pi)^4} \int d^4k \tilde{D}(k) e^{-\imath k\cdot x} &= \frac{1}{(2\pi)^4} \int d^4k \tilde{D}(k) \left(-\frac{\omega^2}{c^2} + \mathbf{k}^2\right) e^{-\imath k\cdot x} \\ &= \frac{1}{(2\pi)^4} \int d^4k e^{-\imath k\cdot x} = \delta^{(4)}(x) \ , \end{aligned} \tag{20.136}$$

that is,

$$\tilde{D}(k) = -\frac{1}{k\cdot k} \ . \tag{20.137}$$

With this, the Green function becomes,

$$D(x) = \tfrac{-1}{(2\pi)^4} \int d^4k \frac{e^{-\imath k\cdot x}}{k\cdot k} \ . \tag{20.138}$$

The integral can be solved by contour integration [659], yielding,

$$D_{r,a}(r - r') = \tfrac{1}{2\pi}\theta(\pm ct \mp ct')\delta[(r - r')^2] \ , \tag{20.139}$$

where the index 'r' refers to *retarded* and 'a' to *advanced*. Finally the solution of inhomogeneous wave equation is,

$$\boxed{A^\mu(r) = A^\mu_{r,a}(r) + \mu_0 \int d^4r' D_{r,a}(r-r') j^\mu(r')} \ , \tag{20.140}$$

where $A^\mu_{r,a}(r)$ are the solutions of the homogeneous wave equation for an incoming, respectively, outgoing wave.

The radiation fields are defined by the difference of the incident and outgoing fields. Thus, the vector potential of the radiation is,

$$A^\mu_{rad}(r) = A^\mu_{out}(r) - A^\mu_{in}(r) = \mu_0 \int d^4r' D(r-r') j^\mu(r') \ , \tag{20.141}$$

with $D(x) \equiv D_r(x) - D_a(x)$.

We can generalize the parametrization of 4-current by,

$$j^\mu(r) = ec \int d\tau u^\mu(\tau) \delta^{(4)}[r - r'(\tau)] \ . \tag{20.142}$$

By inserting this current into (20.140) we obtain the Liénard-Wiechert potentials.

20.3.6 Exercises

20.3.6.1 Ex: Motion in constant fields

In the Newtonian world, electric fields accelerate particles on straight lines and magnetic fields make the particles move in circles. Here, we will re-analyze the Coulomb-Lorentz force in the relativistic framework. The force remains the same, but the momentum is now $\mathbf{p} = m\gamma\mathbf{u}$.
a. Consider a constant electric field $\vec{\mathcal{E}} = \mathcal{E}\hat{\mathbf{e}}_x$ without magnetic field.
b. Consider a constant magnetic field $\vec{\mathcal{B}} = \mathcal{B}\hat{\mathbf{e}}_z$ without electric field.

Solution: *a. The equation of motion for a charged particle with velocity* $\mathbf{u} = (u, 0, 0)$ *is,*

$$m\frac{d(\gamma u)}{dt} = q\mathcal{E} \qquad \Longrightarrow \qquad m\gamma u = q\mathcal{E}t \ ,$$

where we assume implicitly, that the particle starts at rest at $t = 0$*. Reorganizing, we get,*

$$u = \frac{dx}{dt} = \frac{q\mathcal{E}t}{\sqrt{m^2 + q^2\mathcal{E}^2t^2/c^2}} \overset{t\to\infty}{\longrightarrow} c \ .$$

If the particle starts at the origin, we have,

$$x = \frac{mc^2}{eQ}\left(\sqrt{1 + \frac{q^2\mathcal{E}^2t^2}{m^2c^2}} - 1\right) \ .$$

At the beginning, when the velocities are not very high, yet, this reduces to,

$$mx \simeq \tfrac{1}{2}q\mathcal{E}t^2 + \ldots \ ,$$

which is the usual non-relativistic result for particles undergoing a constant acceleration on a straight line.
b. Now, let's turn off the electric field and look at the case of the constant magnetic field $\vec{\mathcal{B}} = \mathcal{B}\hat{\mathbf{e}}_z$. *In the non-relativistic world we know that the particles rotate with the cyclotron frequency* $\omega = q\mathcal{B}/m$. *Looking at the temporal component of the force equation, we find, in the absence of an electric field,*

$$\frac{dP^0}{d\tau} = 0 \ .$$

This tells us that, as in the classical world, magnetic fields do not do work *in relativistic situations. We conclude, then, that the energy* $E = m\gamma c^2$, *is constant. Consequently, the (magnitude) of the velocity remains constant. In other words, the velocity, and therefore the position, continue to rotate in circles. The equation of motion is now,*

$$m\frac{d(\gamma\mathbf{u})}{dt} = q\mathbf{u} \times \vec{\mathcal{B}} \ .$$

Since γ *is constant, the equation adopts the same form as in the non-relativistic case and the solutions are circles. The only difference is, that the frequency with which the particle moves on a circle, now depends on how fast the particle is moving,*

$$\omega = \frac{q\mathcal{B}}{m\gamma} \ .$$

We can interpret this as being due to the relativistic increase of the mass of the moving particle.
So far, we have analyzed situations, where $\vec{\mathcal{E}} = 0$ *or* $\vec{\mathcal{B}} = 0$. *On the other hand, we have already seen that* $\vec{\mathcal{E}}\cdot\vec{\mathcal{B}} = 0$ *and* $\vec{\mathcal{E}}^2 - \vec{\mathcal{B}}^2$ *are two Lorentz-invariant quantities. This means that the solutions described above can be generalized to apply to any situation, where* $\vec{\mathcal{E}}\cdot\vec{\mathcal{B}} = 0$ *and* $\vec{\mathcal{E}}^2 - \vec{\mathcal{B}}^2$ *is* > 0 *or* < 0.

20.3.6.2 Ex: Electric and magnetic dipole moment of moving dipoles

The electric dipole moment $\mathbf{d}$ and the magnetic dipole moment $\vec{\mu}$ of a particle in its rest frame will appear in a lab frame through which the particle is moving with velocity $\mathbf{v}$ as,

$$\boxed{\mathbf{d}' = \mathbf{d} + \tfrac{1}{c^2}\mathbf{v}\times\vec{\mu} \qquad \text{and} \qquad \vec{\mu}' = \vec{\mu} - \tfrac{1}{2}\mathbf{v}\times\mathbf{d}} \ .$$

Verify this for a particle with a purely magnetic dipole moment via a Lorentz transform using by the following procedure:
a. Derive the Lorentz transform from a rest frame S, flying through the lab frame S' into arbitrary direction $\vec{\beta}$, back into the lab frame for (i) the charge-current density quadrivector, (ii) the time-position quadrivector, and (iii) a volume element using the generalized Lorentz boost (20.60).
b. Parametrize the electric and magnetic dipole moment by appropriate charge and current densities, e.g. assuming two equal charges dislocated in opposite directions of the z-axis, respectively, a circular current in the xy-plane.
c. Apply the Lorentz transform to the electric dipole moment by transforming all

quantities of the defining formula. (It is convenient to choose $\beta_y = 0$.)

Solution: *a. The Lorentz transform of the charge-current density quadrivector into a frame moving S' into arbitrary direction $\vec{\beta}$ is given by [448],*

$$\begin{pmatrix} c\varrho' \\ \mathbf{j}' \end{pmatrix} = (\Lambda^\mu_\nu)^{-1} \begin{pmatrix} c\varrho \\ \mathbf{j} \end{pmatrix} = \begin{pmatrix} \gamma & \gamma\vec{\beta} \\ \gamma\vec{\beta} & \mathbb{I}_3 + (\gamma-1)\hat{\beta}_i\hat{\beta}_j \end{pmatrix} \begin{pmatrix} c\varrho \\ \mathbf{j} \end{pmatrix}$$
$$= \begin{pmatrix} \gamma c\varrho + \gamma\vec{\beta}\cdot\mathbf{j} \\ \gamma c\vec{\beta}\varrho + \left(\mathbf{j} + \frac{\gamma-1}{\beta^2}\beta_i\beta_j\right) j_j \end{pmatrix} = \begin{pmatrix} \gamma c\varrho + \gamma\vec{\beta}\cdot\mathbf{j} \\ \mathbf{j} + \left(\gamma c\varrho + \frac{\gamma-1}{\beta^2}\vec{\beta}\cdot\mathbf{j}\right)\vec{\beta} \end{pmatrix} .$$

The same transformation of the position vector yields,

$$\begin{pmatrix} ct' \\ \mathbf{r}' \end{pmatrix} = (\Lambda^\mu_\nu)^{-1} \begin{pmatrix} ct \\ \mathbf{r} \end{pmatrix} = \begin{pmatrix} \gamma ct + \gamma\vec{\beta}\cdot\mathbf{r} \\ \mathbf{r} + \left(\gamma ct + \frac{\gamma-1}{\beta^2}\vec{\beta}\cdot\mathbf{r}\right)\vec{\beta} \end{pmatrix} .$$

Evaluating in the lab frame at $t' = 0$,

$$\mathbf{r}' = \mathbf{r} + \left(\gamma ct + \frac{\gamma-1}{\beta^2}\vec{\beta}\cdot\mathbf{r}\right)\vec{\beta} = \mathbf{r} + \left(-\gamma\vec{\beta}\cdot\mathbf{r} + \frac{\gamma-1}{\beta^2}\vec{\beta}\cdot\mathbf{r}\right)\vec{\beta} = \mathbf{r} - \frac{\gamma}{\gamma+1}\vec{\beta}\cdot\mathbf{r}\vec{\beta} .$$

And a volume element will always be contracted by,

$$d^3r' = \frac{1}{\gamma}d^3r .$$

b. For convenience, we assume that the electric dipole moment $\mathbf{d}$ is generated by two point charges displaced from the center along the z-axis by an amount b, and the magnetic dipole moment $\vec{\mu}$ is generated by a current line in the xy-plane at a distance R from the center,

$$\varrho(\mathbf{r}) = q\delta^3(\mathbf{r}) + \frac{d}{2b}[\delta^3(\mathbf{r}-b\hat{\mathbf{e}}_z) - \delta^3(\mathbf{r}+b\hat{\mathbf{e}}_z)] \quad \textit{and} \quad \mathbf{j}(\mathbf{r}) = \frac{1}{\pi R^4}\vec{\mu}\times\mathbf{r}\,\delta(\theta-\tfrac{\pi}{2})\delta(r-R) .$$

With this it is easy to verify the electric and magnetic dipole moments,

$$\mathbf{d} \equiv \int \mathbf{r}\varrho(\mathbf{r})d^3r \qquad \textit{and} \qquad \vec{\mu} \equiv \tfrac{1}{2}\int \mathbf{r}\times\mathbf{j}(\mathbf{r})d^3r ,$$

as can easily be verified.
c. The transformed dipole moment now reads, assuming $\varrho = 0$,

$$\mathbf{d}' = \int \mathbf{r}'\varrho' d^3r' = \int \left[\mathbf{r} - \frac{\gamma}{\gamma+1}(\vec{\beta}\cdot\mathbf{r})\vec{\beta}\right]\left[\gamma\vec{\beta}\cdot\mathbf{j}\right]\frac{1}{\gamma}d^3r$$
$$= \frac{1}{\pi R^4}\int \left[\mathbf{r} - \frac{\gamma}{\gamma+1}(\vec{\beta}\cdot\mathbf{r})\vec{\beta}\right]\left[\gamma\vec{\beta}\cdot(\vec{\mu}\times\mathbf{r})\delta(\theta-\tfrac{\pi}{2})\delta(r-R)\right]\frac{1}{\gamma}r^2\sin\theta dr d\theta d\phi ,$$

after inserting the current density parametrization. With,

$$\vec{\beta} = \beta_x\hat{\mathbf{e}}_x + \beta_z\hat{\mathbf{e}}_z \quad , \quad \vec{\mu} = \mu\hat{\mathbf{e}}_z \quad , \quad \mathbf{r} = r\hat{\mathbf{e}}_r \quad , \quad \mathbf{R} = R\hat{\mathbf{e}}_x\cos\phi + R\hat{\mathbf{e}}_z\sin\phi ,$$

we calculate,

$$\mathbf{d}' = \frac{-\beta_x \mu}{\pi R^4} \int \begin{pmatrix} \sin\theta\cos\phi - \frac{\gamma\beta_x}{\gamma+1}\left(\beta_x \sin\theta\cos\phi + \beta_z\cos\theta\right) \\ \sin\theta\sin\phi \\ \cos\theta - \frac{\gamma\beta_z}{\gamma+1}\left(\beta_x \sin\theta\cos\phi + \beta_z\cos\theta\right) \end{pmatrix} \sin\phi\delta(\theta - \tfrac{\pi}{2})\delta(r-R) r^4 \sin\theta dr d\theta d\phi$$

$$= \frac{-\beta_x \mu}{\pi} \int \begin{pmatrix} \sin\phi\cos\phi - \frac{\gamma}{\gamma+1}\beta_x^2 \sin\phi\cos\phi \\ \sin^2\phi \\ -\frac{\gamma}{\gamma+1}\beta_x\beta_z \sin\phi\cos\phi \end{pmatrix} d\phi = -\beta_x \mu \hat{\mathbf{e}}_y = \tfrac{1}{c}\vec{\beta} \times \vec{\mu} \ .$$

20.4 Lagrangian formulation of electrodynamics

20.4.1 Relation with quantum mechanics

In classical and relativistic mechanics we learn to deal with *masses* and in electrodynamics with *charges* and with fields and electromagnetic waves. We will show in Sec. 20.4.2.1 how electrodynamics can be integrated into the classical and relativistic mechanics by the prescription of *minimal coupling*,

$$\boxed{p^\mu \to p^\mu - qA^\mu} \ . \tag{20.143}$$

Revolutionary discoveries in the early twentieth century culminated in the development of quantum mechanics, where we learned to accept that the microscopic world works differently. On one hand, massive particles have undulating properties; they can diffract and interfere. On the other side, light has corpuscular properties; it consists of indivisible energy packets called *photons*. Fortunately, classical theories can be incorporated into quantum mechanics by canonical procedures called first and second quantization.

20.4.1.1 Treatment of massive particles in quantum mechanics

In quantum mechanics we learn [10] that matter propagates like a scalar wave (in contrast to electromagnetic waves, which are vectorial). Consequently, in quantum mechanics, massive particles are described by wavefunctions obeying wave equations. Slow particles obey the Schrödinger equation, whereas bosonic relativistic particles obey a wave equation called *Klein-Gordon equation* and fermions obey the *Dirac equation*. The Schrödinger and Klein-Gordon equations are obtained from a simple prescription for canonical quantization:

$$\boxed{p^\mu \to \imath\hbar\partial^\mu} \ . \tag{20.144}$$

Obtaining the Dirac equation is a bit more involved.

[10] See script on *Quantum mechanics* (2023).

20.4.1.2 Quantization of the electromagnetic field

We also learn in quantum mechanics [11] that light consists of indivisible energy packets. This fact is taken into account, by dividing space into modes that can be filled with discrete numbers of photons. Each mode is treated as a harmonic oscillator. Quantum field theories explain, how we must quantize non-radiative electric and magnetic fields.

These topics will not be covered in this course.

20.4.2 Classical mechanics of a point particle in a field

For a system with m degrees of freedom specified by generalized coordinates $q_1, .., q_m$ and the generalized velocities $\dot{q}_1, .., \dot{q}_m$ the classical action is determined by the *Lagrangian* $\mathcal{L}(q_i, \dot{q}_i)$ via,

$$\mathcal{S}[q_i, \dot{q}_i] = \int dt \mathcal{L}(q_i, \dot{q}_i, t) \ . \tag{20.145}$$

Thus, the action is a functional of the generalized coordinates. According to Hamilton's *least action principle*, the dynamics of a classical system is described by equations that minimize the action, $\delta\mathcal{S} = 0$. These equations of motion can be expressed by the Lagrangian in the form of *Euler-Lagrange equations*,

$$\frac{d}{dt}\frac{\partial \mathcal{L}}{\partial \dot{q}_i} - \frac{\partial \mathcal{L}}{\partial q_i} = 0 \ . \tag{20.146}$$

The *canonical momentum* is given by equation,

$$p_i(q_i, \dot{q}_i, t) = \frac{\partial \mathcal{L}}{\partial \dot{q}_i} \ , \tag{20.147}$$

and the Hamiltonian is defined by the *Legendre transform*,

$$\mathcal{H}(q_i, p_i) = \dot{q}_i \frac{\partial \mathcal{L}}{\partial \dot{q}_i} - \mathcal{L} = p_i \dot{q}_i - \mathcal{L}(q_i, \dot{q}_i) \ . \tag{20.148}$$

using Einstein's summing convention. Comparing the differential of both sides of this equation,

$$\left[\frac{\partial \mathcal{H}}{\partial q_i} dq_i + \frac{\partial \mathcal{H}}{\partial p_i} dp_i\right] + \frac{\partial \mathcal{H}}{\partial t} = d\mathcal{H} = \left[\dot{q}_i dp_i + p_i d\dot{q}_i - \frac{\partial \mathcal{L}}{\partial q_i} dq_i - \frac{\partial \mathcal{H}}{\partial \dot{q}_i} d\dot{q}_i\right] - \frac{\partial \mathcal{L}}{\partial t} \ , \tag{20.149}$$

we obtain Hamilton's equations of motion,

$$\dot{q}_i = \frac{\partial \mathcal{H}}{\partial p_i} \quad , \quad \dot{p}_i = -\frac{\partial \mathcal{H}}{\partial q_i} \quad , \quad \frac{\partial \mathcal{H}}{\partial t} = -\frac{\partial \mathcal{L}}{\partial t} \ . \tag{20.150}$$

From these equations it follows, that if the Hamiltonian is independent of a particular coordinate q_i, the corresponding moment p_i is constant. For conservative forces, the Lagrangian and the Hamiltonian can be written as $\mathcal{L} = T - V$ and $\mathcal{H} = T + V$, with T the kinetic energy and V the potential energy [12].

[11] See script on *Quantum mechanics* (2023).

[12] Thus, a particle chooses its trajectory in a way to minimize the conversion between kinetic and potential energy.

20.4.2.1 Electrodynamic Lagrangian

So far we have focused on free particles or particles confined by scalar potentials. In what follows, we will address the influence of a magnetic field on a charged particle. Classically, the force on a charged particle in electric and magnetic fields is given by the Lorentz force law and the exerted work by Ohm's law:

$$\frac{dW}{dt} = e\mathbf{v} \times \vec{\mathcal{E}} \qquad \text{and} \qquad \mathbf{F} = q(\vec{\mathcal{E}} + \mathbf{v} \times \vec{\mathcal{B}}) \ , \tag{20.151}$$

where q denotes the charge and v the velocity. In this case, the generalized coordinates $q_i \equiv r_i \equiv (r_1, r_2, r_3)$ are precisely the Cartesian coordinates specifying the position, and $\dot{q}_i = \dot{r}_i = (\dot{r}_1, \dot{r}_2, \dot{r}_3)$ the velocity of the particles. These equations of motion are sufficient to describe the dynamics of a system. The force which depends on the velocity and is associated with the magnetic field is quite different from the conservative forces associated with scalar potentials. Let us now study, how the Lorentz force appears in the Lagrange formulation of classical mechanics.

With revised these foundations, we will return to the problem of the influence of an electromagnetic field on the dynamics of a charged particle. Since the Lorentz force depends on velocity, it can not simply be expressed as a gradient of some potential. However, the classical trajectory of the particle is still specific to the least action principle.

The electric and magnetic fields can be expressed in terms of a scalar and a vector potential as,

$$\vec{\mathcal{E}} = -\nabla\Phi - \partial_t \mathbf{A} \qquad \text{and} \qquad \vec{\mathcal{B}} = \nabla \times \mathbf{A} \ . \tag{20.152}$$

The Lorentz force is,

$$\mathbf{F} = q\left[-\nabla\Phi - \frac{\partial \mathbf{A}}{\partial t} + \mathbf{v} \times (\nabla \times \mathbf{A})\right] \ . \tag{20.153}$$

We now analyze the x-component,

$$\begin{aligned} F_x &= q\left[-\frac{\partial\Phi}{\partial x} - \frac{\partial A_x}{\partial t} + v_y\left(\frac{\partial A_y}{\partial x} - \frac{\partial A_x}{\partial y}\right) - v_z\left(\frac{\partial A_x}{\partial z} - \frac{\partial A_z}{\partial x}\right) + v_x\frac{\partial A_x}{\partial x} - v_x\frac{\partial A_x}{\partial x}\right] \\ &= q\left[-\frac{\partial\Phi}{\partial x} + \mathbf{v}\cdot\frac{\partial \mathbf{A}}{\partial x} - \frac{dA_x}{dt}\right] \ , \end{aligned} \tag{20.154}$$

where we used,

$$\frac{d}{dt} = \frac{\partial}{\partial t} + v_i\frac{\partial}{\partial x_i} \ . \tag{20.155}$$

Since the potentials do not depend on the velocity, we can also write,

$$F_x = q\left[-\frac{\partial\Phi}{\partial x} + \frac{\partial \mathbf{v}\cdot\mathbf{A}}{\partial x} - \frac{d}{dt}\frac{\partial \mathbf{v}\cdot\mathbf{A}}{\partial v_x}\right] = -\frac{\partial U}{\partial x} + \frac{d}{dt}\frac{\partial U}{\partial v_x} \ , \tag{20.156}$$

introducing the generalized potential,

$$U \equiv q\Phi - q\mathbf{A}\cdot\mathbf{v} \ . \tag{20.157}$$

The corresponding Lagrangian takes the form:

$$\boxed{\mathcal{L}(r_i,\dot{r}_i) = \tfrac{m}{2}\dot{\mathbf{r}}^2 - q\Phi + q\dot{\mathbf{r}}\cdot\mathbf{A} = \tfrac{m}{2}\dot{r}_i\dot{r}_i - q\Phi + q\dot{r}_iA_i} \,. \tag{20.158}$$

The important point is that the *canonical momentum*

$$\boxed{p_i = \frac{\partial\mathcal{L}}{\partial\dot{r}_i} = m\dot{r}_i + qA_i} \tag{20.159}$$

is no longer equal to velocity times the mass, $mv_i \neq p_i$, because there is an extra term!

Using the definition of the corresponding Hamiltonian,

$$\begin{aligned}\mathcal{H}(r_i,p_i) &= (m\dot{r}_i + qA_i)\dot{r}_i - \tfrac{m}{2}\dot{r}_i\dot{r}_i + q\Phi - q\sum_i \dot{r}_iA_i \\ &= \left(\tfrac{m}{2}\dot{r}_i + qA_i\right)\dot{r}_i + q\Phi = \tfrac{m}{2}\mathbf{v}^2 + q\Phi \,.\end{aligned} \tag{20.160}$$

Obviously, the Hamiltonian has just the familiar form of the sum of kinetic and potential energies. However, to obtain Hamilton's equations of motion, the Hamiltonian must be expressed only in terms of the coordinates and the canonical momenta, that is,

$$\boxed{\mathcal{H}(r_i,p_i) = \frac{1}{2m}(\mathbf{p} - q\mathbf{A})^2 + q\Phi = qv_j\frac{\partial A_j}{\partial r_i} - q\frac{\partial\Phi}{\partial r_i}} \,. \tag{20.161}$$

Let us now consider Hamilton's equations of motion,

$$\begin{aligned}\dot{r}_i &= \frac{\partial\mathcal{H}}{\partial p_i} = \frac{1}{m}(p_i - qA_i) \\ \dot{p}_i &= -\frac{\partial\mathcal{H}}{\partial r_i} = -\frac{1}{2m}\frac{\partial}{\partial r_i}(p_j - qA_j)^2 - q\frac{\partial\Phi}{\partial r_i} \,.\end{aligned} \tag{20.162}$$

The first equation reproduces the canonical momentum (20.158), while the second gives the Lorentz force. To understand how, we need to remember that dp/dt *is not the acceleration*: The term dependent on $\mathbf{A}$ also varies over time in a rather complicated way, since it is the field seen by the moving particle.

Example 134 (*Lorentz force from the Lagrangian*): Obviously, we can recover the Lorentz force from the Hamiltonian: Differentiating the canonical momentum (20.158),

$$\begin{aligned}m\ddot{r}_i &= -q\dot{A}_i + \dot{p}_i = -q\dot{A}_i - \frac{\partial\mathcal{H}}{\partial r_i} \\ &= -q\dot{A}_i - \frac{\partial}{\partial r_i}q\left(\sum_j v_j\frac{\partial A_j}{\partial r_i} - \frac{\partial\Phi}{\partial r_i}\right) = -q\dot{A}_i + q\nabla_i(\mathbf{A}\cdot\mathbf{v}) - q\nabla_i\Phi \,.\end{aligned}$$

that is,

$$\begin{aligned}m\ddot{\mathbf{r}} &= -q\nabla\Phi + q\mathbf{v}\times(\nabla\times\mathbf{A}) + q(\mathbf{v}\cdot\nabla)\mathbf{A} - q\frac{d\mathbf{A}}{dt} \\ &= -q\nabla\Phi + q\mathbf{v}\times(\nabla\times\mathbf{A}) - q\frac{\partial\mathbf{A}}{\partial t} = q\vec{\mathcal{E}} + q\mathbf{v}\times\vec{\mathcal{B}}\end{aligned}$$

using the rules (20.155) and $\mathbf{v}\times(\nabla\times\mathbf{A}) = \nabla(\mathbf{A}\cdot\mathbf{v}) - (\nabla\cdot\mathbf{v})\mathbf{A}$.

Using the Coulomb gauge $\nabla \cdot \mathbf{A} = 0$ the Coulomb-Lorentz force can be derived from the Lagrangian via the equation (20.158) or from the Hamiltonian via the second equation (20.162).

20.4.3 Generalization to relativistic mechanics

We now want to generalize the Lagrangian treatment of a particle to relativistic mechanics. Not all forces known in classical mechanics can be put into a covariant form. One example is the Newtonian gravitational force, understood as a force acting at a distance, which is incompatible with the theory of relativity. On the other side, electrodynamics is automatically Lorentz-invariant. Therefore, let us discuss the Lagrangian only for two examples: 1. a totally free particle and 2. a particle under the influence of electromagnetic forces.

Analogously to the classical case, we want to derive, from the principle of minimum action (20.145) Euler-Lagrange type equations (20.146). To put the action into a Lorentz-invariant form, we go to the particle's rest frame via $t = \gamma\tau$,

$$\mathcal{S}[r^\mu, u^\mu] = \int \gamma \mathcal{L}(q^\mu, u^\mu, \tau) d\tau \ . \tag{20.163}$$

We note, however, that we must now distinguish co- and contravariant indices to take account of non-Euclidean metrics. Since $\mathcal{S}$ is an invariant scalar, $\gamma\mathcal{L}$ must be an invariant scalar as well. The Euler-Lagrange equations are now,

$$\frac{d}{d\tau}\frac{\partial \mathcal{L}}{\partial u_\mu} - \frac{\partial \mathcal{L}}{\partial x_\mu} = 0 \ . \tag{20.164}$$

The ansatz for the Lagrangian,

$$\mathcal{L} \equiv \tfrac{m}{2} u_\mu u^\mu \tag{20.165}$$

inserted into the Euler-Lagrange equation gives,

$$\frac{d}{d\tau} m u^\mu - 0 = \frac{d}{d\tau} p^\mu = 0 \ , \tag{20.166}$$

which makes sense in the absence of external forces [13].

20.4.3.1 Lagrangian relativistic electrodynamics

We now consider a charged particle interacting with an external electromagnetic field [659]. In relativistic notation the Lorentz force and the Ohm's law (20.145) become [compare (20.117)],

$$\frac{m du^\mu}{d\tau} = q F^{\mu\nu} u_\nu \ , \tag{20.167}$$

where m is the resting mass, τ the proper time in the particle's system, and $(u^\mu) = (\gamma c, \gamma \mathbf{u}) = (p^\mu/m)$ its 4-velocity. Following the classical model (20.157) we can make for the Lagrangian the covariant ansatz [519],

$$\boxed{\mathcal{L} = \mathcal{L}_{free} + \mathcal{L}_{int} = \tfrac{m}{2} u_\mu u^\mu + q u_\mu A^\mu} \ . \tag{20.168}$$

[13] We note, that any ansatz $\mathcal{L}(z) \equiv \mathcal{L}(u_\mu u^\mu)$ satisfying $\partial_z \mathcal{L} = \frac{m}{2}$ is possible. We will show this in Exc. 20.4.5.1.

The canonical momenta are,

$$p_\mu = \frac{\partial \mathcal{L}}{\partial u^\mu} = m u_\mu + q A_\mu \ , \tag{20.169}$$

such that the Euler-Lagrange equations (20.164) result in,

$$\frac{d}{d\tau}(m u_\mu + q A_\mu) - \frac{\partial}{\partial x_\mu}(q u_\nu A^\nu) = 0 \ . \tag{20.170}$$

That is,

$$K_\mu = \frac{d}{d\tau} m u_\mu = \frac{\partial}{\partial x_\mu}(q u_\nu A^\nu) - \frac{d}{d\tau}(q A_\mu) \ , \tag{20.171}$$

which is precisely the Minkowski type Lorentz force.

The total energy is,

$$E_{tot} = c p^0 = c(E + q\Phi) \ , \tag{20.172}$$

where E is the kinetic energy including the rest mass (20.88). We calculate,

$$m^2 u_\mu u^\mu = m^2 c^2 = (p_\mu - q A_\mu)(p^\mu - q A^\mu) = m^2 u_0 u^0 - (\mathbf{p} - q\mathbf{A})^2 = E^2/c^2 - (\mathbf{p} - q\mathbf{A})^2 \ . \tag{20.173}$$

That is,

$$E^2 = (\mathbf{p} - q\mathbf{A})^2 - m^2 c^2 \ . \tag{20.174}$$

In Exc. 20.4.5.3 we show an example for the application of the relativistic electrodynamic Lagrangian.

20.4.3.2 Charges and currents interacting with an electromagnetic field

In the case of continuous variables we use Lagrangian densities,

$$\mathcal{L} = \sum_i \mathcal{L}_i(q_i, \dot{q}_i) \longrightarrow \int \mathcal{L}(\phi_k, \partial^\alpha \phi_k) d^3x \ . \tag{20.175}$$

For example, the Lagrangian of the electromagnetic field is [520],

$$\mathcal{L} = T - V = \mathcal{L}_{field} + \mathcal{L}_{int} = -\tfrac{1}{4\mu_0} F^{\mu\nu} F_{\mu\nu} - A_\mu j^\mu \ , \tag{20.176}$$

but we will not deepen this here.

20.4.4 Symmetries and conservation laws

> *Symmetry* is a feature of a system conserving specific properties under some transformation.

For example, the geometry of a system does not change, when we apply a reflection and the interaction energy between two charges does not change when we switch their coordinates.

In the Lagrangian formalism we call a quantity (or generalized momentum) *conserved*, when the Lagrangian does not depend on the associated coordinate,

$$\mathcal{L} \neq \mathcal{L}(q_k) \qquad \Longrightarrow \qquad p_k \ \text{ is conserved} \ . \tag{20.177}$$

We can see this by the Euler-Lagrange equation,

$$\frac{dp_k}{dt} = \frac{d}{dt}\frac{\partial \mathcal{L}}{\partial \dot{q}_k} = \frac{\partial \mathcal{L}}{\partial q_k} = 0 \ . \tag{20.178}$$

Emmy Noether formulated the theorem, that a *symmetry transformation*, that is, a transformation that does not change the action,

$$t \to t + \delta t \qquad \text{and} \qquad \mathbf{q} \to \mathbf{q} + \delta \mathbf{q} \ , \tag{20.179}$$

conserves the following quantities:

$$\boxed{\left(\dot{\mathbf{q}} \cdot \frac{\partial \mathcal{L}}{\partial \dot{\mathbf{q}}} - \mathcal{L}\right) \delta t - \frac{\partial \mathcal{L}}{\partial \dot{\mathbf{q}}} \cdot \delta \mathbf{q}} \ . \tag{20.180}$$

For example, a *temporal translation*, $\delta t \neq 0$ without another transformed coordinate $\delta q_\alpha = 0 \ , \ \forall \alpha$, leaves the *total energy*,

$$\dot{\mathbf{q}} \frac{\partial \mathcal{L}}{\partial \dot{\mathbf{q}}} - \mathcal{L} = \mathcal{H} \ , \tag{20.181}$$

(known by the Legendre transform) unchanged. The *spatial translation*, $\delta q_\alpha = 0$ but $\delta t \neq 0$, leave the *linear momentum*,

$$\frac{\partial \mathcal{L}}{\partial \dot{q}_\alpha} = p_\alpha \ , \tag{20.182}$$

unchanged. We note that in relativistic theory, these two conservation laws are related. *Spatial rotation* around an axis $\hat{\mathbf{e}}_n$, defined in Cartesian coordinates by,

$$\mathbf{r} \to \mathbf{r} + \delta \vec{\theta} = \mathbf{r} + \delta(\hat{\mathbf{e}}_n \times \mathbf{r}) \ , \tag{20.183}$$

with $\delta t \neq 0$, leaves the angular momentum,

$$\frac{\partial \mathcal{L}}{\partial \dot{\mathbf{q}}} \cdot \delta(\hat{\mathbf{e}}_n \times \mathbf{r}) = \mathbf{p} \cdot (\hat{\mathbf{e}}_n \times \mathbf{r}) = \hat{\mathbf{e}}_n \cdot (\mathbf{r} \times \mathbf{p}) = \hat{\mathbf{e}}_n \cdot \mathbf{L} = 0 \ , \tag{20.184}$$

unchanged.

symmetry class	symmetry	invariance	conserved quantity
Lorentz	homogeneity of time	translation in time	energy
	homogeneity of space	translation in space	linear momentum
	isotropy of space	rotation in space	angular momentum
discrete	T (isotropy of time)	time reversal	temporal parity
	P	coordinate inversion	spatial parity
	C	charge conjugation	charge parity
internal	U(1)	gauge transformation	electric charge

20.4.5 Exercises

20.4.5.1 Ex: Lagrangian relativistic of a free particle

Show that the Lagrangian $\mathcal{L}(z) = \mathcal{L}(u_\mu u^\mu)$ with $\mathcal{L}' = \frac{m}{2}$ satisfies the Euler-Lagrange equation.

Solution: *We calculate,*

$$\frac{d}{d\tau}\frac{\partial \mathcal{L}}{\partial u_\mu} - \frac{\partial \mathcal{L}}{\partial x_\mu} = \frac{d}{d\tau} 2u_\mu \frac{\partial \mathcal{L}}{\partial z} = \frac{d}{d\tau} m u_\mu = 0 \ .$$

20.4.5.2 Ex: Motion of charged particles in a magnetic field

A non-relativistic particle with mass m and charge q be in a static magnetic field,

$$\vec{\mathcal{B}}(\mathbf{r}) = \mathcal{B}_x(x,y,z)\hat{\mathbf{e}}_x + \mathcal{B}_y(x,y,z)\hat{\mathbf{e}}_y + \mathcal{B}_z(x,y,z)\hat{\mathbf{e}}_z \ .$$

Its Lagrange function is then,

$$\mathcal{L} = \frac{1}{2}m\mathbf{v}^2 + \frac{q}{c}\mathbf{v}\cdot\mathbf{A} \ ,$$

where $\mathbf{v}$ is the velocity of the particle and $\mathbf{A}$ the vector potential corresponding to the magnetic field $\vec{\mathcal{B}}$.
a. If $\mathbf{A} = A_x(x,y,z)\hat{\mathbf{e}}_x + A_y(x,y,z)\hat{\mathbf{e}}_y + A_z(x,y,z)\hat{\mathbf{e}}_z$ is given, what are the Cartesian components of $\vec{\mathcal{B}}$?
b. Using the formula $\frac{d}{dt}\frac{\partial L}{\partial \dot{q}} = \frac{\partial L}{\partial q}$ derive the equations of motion for the Cartesian components of $\mathbf{v}$.
c. What is the condition for $\mathcal{B}_x = \mathcal{B}_y = 0$ and $\mathcal{B}_z = \mathcal{B}_0$ to be constant?
d. Now, consider $A_x = A_y = 0$ and $A_y = \mathcal{B}_0 x$. What equations of motion for v_x, v_y, and v_z follow from this?
e. Calculate $v_x(t)$, $v_y(t)$, and $v_z(t)$. Contour conditions be given by $v_z(t=0) = v_0^{(\|)}$, $v_y(t=0) = 0$ and $v_x(t=0) = v_0^{(\perp)}$. Use the abbreviation $\omega_0 = \frac{q\mathcal{B}_0}{mc}$.
f. Calculate $x(t)$, $y(t)$, and $z(t)$ choosing $x(t=0) = y(t=0) = z(t=0) = 0$. What is the form of the trajectory that corresponds to this motion?
g. Suppose now that $A_x = A_y = 0$ and $A_y = \mathcal{B}(z)x$. What is the consequence of this for $\mathcal{B}_x$, $\mathcal{B}_y$, and $\mathcal{B}_z$? What are the corresponding equations of motion for v_x, v_y, and v_z ?
h. Now, let $\frac{\partial \mathcal{B}(z)}{\partial z} = \mathcal{B}' =$constant. Discuss the motion equation for v_z, inserting as an approximation for $v_y(t)$ and $x(t)$ the solutions of parts (e) and (f). What, under this circumstance, is the consequence for $v_z(t)$?

Solution: *a. We have* $\vec{\mathcal{B}} = \nabla \times \mathbf{A}$ *and hence,*

$$\mathcal{B}_x = \frac{\partial A_z}{\partial y} - \frac{\partial A_y}{\partial z} \quad , \quad \mathcal{B}_y = \frac{\partial A_x}{\partial z} - \frac{\partial A_z}{\partial x} \quad , \quad \mathcal{B}_z = \frac{\partial A_y}{\partial x} - \frac{\partial A_x}{\partial y} \ .$$

b. The Lagrange function is,

$$\mathcal{L} = \tfrac{m}{2}(v_x^2 + v_y^2 + v_z^2) + \tfrac{q}{c}(v_x A_x + v_y A_y + v_z A_z) \ .$$

Therefore we get for $k = (x, y, z)$,

$$\frac{\partial \mathcal{L}}{\partial v_k} = m v_k + \frac{q}{c} A_k \qquad \textit{and} \qquad \frac{\partial \mathcal{L}}{\partial x_k} = \frac{q}{c}\left(v_x \frac{\partial A_x}{\partial x_k} + v_y \frac{\partial A_y}{\partial x_k} + v_z \frac{\partial A_z}{\partial x_k} \right) \ .$$

The Lagrange equations,

$$\frac{d}{dt}\frac{\partial \mathcal{L}}{\partial v_k} = \frac{\partial \mathcal{L}}{\partial x_k} \ ,$$

therefore, give for the x*-component of the velocity,*

$$m\frac{dv_x}{dt} + \frac{q}{c}\left(v_x \frac{\partial A_x}{\partial x} + v_y \frac{\partial A_x}{\partial y} + v_z \frac{\partial A_x}{\partial z} \right) = \frac{q}{c}\left(v_x \frac{\partial A_x}{\partial x} + v_y \frac{\partial A_y}{\partial x} + v_z \frac{\partial A_z}{\partial x} \right) \ .$$

resp.

$$\begin{aligned} \frac{dv_x}{dt} &= \frac{q}{mc}\left(v_y \left[\frac{\partial A_y}{\partial x} - \frac{\partial A_x}{\partial y} \right] - v_z \left[\frac{\partial A_x}{\partial z} - \frac{\partial A_z}{\partial x} \right] \right) = \frac{q}{mc}(v_y \mathcal{B}_z - v_z \mathcal{B}_y) \\ &= \frac{q}{mc}(\mathbf{v} \times \vec{\mathcal{B}})_x \ . \end{aligned}$$

In the same way,

$$\frac{dv_y}{dt} = \frac{q}{mc}(\mathbf{v} \times \vec{\mathcal{B}})_y \ .$$

and

$$\frac{dv_z}{dt} = \frac{q}{mc}(\mathbf{v} \times \vec{\mathcal{B}})_z \ .$$

Finally,

$$\frac{d\mathbf{v}}{dt} = \frac{q}{mc}\mathbf{v} \times \vec{\mathcal{B}} \ .$$

are the expected equations of motion for a particle under the influence of the Lorentz force.

c. For $\mathcal{B}_x = \mathcal{B}_y = 0$ *we have everywhere,*

$$\frac{\partial A_z}{\partial y} = \frac{\partial A_y}{\partial z} \qquad \textit{and} \qquad \frac{\partial A_z}{\partial x} = \frac{\partial A_x}{\partial z} \ .$$

Since $\mathcal{B}_z = \textit{constant} = \mathcal{B}_0$ *we also have everywhere,*

$$\mathcal{B}_0 = \frac{\partial A_y}{\partial x} - \frac{\partial A_x}{\partial y} \ .$$

We make the ansatz,

$$A_y = c_1 x + c_1' \qquad \textit{and} \qquad A_x = c_2 y + c_2' \ .$$

From this immediately follows,

$$\mathcal{B}_0 = c_1 - c_2 \ .$$

d. We can now, without restricting the generality of the result, choose,

$$A_x = A_z = 0 \qquad \textit{and} \qquad A_y = B_0 x \ .$$

Hence,

$$\mathcal{B}_x = \mathcal{B}_y = 0 \qquad \textit{and} \qquad \mathcal{B}_z = \mathcal{B}_0 \ ,$$

and therefore,

$$\frac{dv_x}{dt} = \frac{q\mathcal{B}_0}{mc} v_y \qquad \textit{and} \qquad \frac{dv_y}{dt} = -\frac{q\mathcal{B}_0}{mc} v_x \qquad \textit{and} \qquad \frac{dv_z}{dt} = 0 \ .$$

e. Because of,

$$\frac{dv_z}{dt} = 0 \qquad \textit{follows} \qquad v_z = \text{constant} \equiv v_0^{(\|)} \ .$$

We also have,

$$\frac{d^2 v_x}{dt^2} = \frac{q\mathcal{B}_0}{mc}\frac{dv_y}{dt} = -\left(\frac{q\mathcal{B}_0}{mc}\right)^2 v_x \ .$$

resp.

$$\frac{d^2 v_x}{dt^2} = -\omega_0^2 v_x \ .$$

From this immediately follows,

$$\begin{aligned} v_x &= +v_0^{(\perp)}(\cos\omega_0 t + \alpha \sin\omega_0 t) \\ v_y &= -v_0^{(\perp)}(\sin\omega_0 t - \alpha \cos\omega_0 t) \\ v_z &= \text{constant} = v_0^{(\|)} \ . \end{aligned}$$

Considering also the boundary condition $v_y(t=0) = 0$, necessarily, $\alpha = 0$ and, hence,

$$v_x = v_0^{(\perp)} \cos\omega_0 t \qquad , \qquad v_y = -v_0^{(\perp)} \sin\omega_0 t \qquad , \qquad v_z = v_0^{(\|)} \ .$$

With this, we see,

$$v^2 = (v_0^{(\|)})^2 + (v_0^{(\perp)})^2 = \text{constant} \ .$$

f. We obtain successively,

$$\frac{dz}{dt} = v_0^{(\|)} \qquad \textit{hence} \qquad z(t) = v_0^{(\|)} t + z_0 \ .$$

$$\frac{dx}{dt} = v_0^{(\perp)} \cos\omega_0 t \qquad \textit{hence} \qquad x(t) = \frac{v_0^{(\perp)}}{\omega_0} \sin\omega_0 t + x_0 \ .$$

$$\frac{dy}{dt} = -v_0^{(\perp)} \sin\omega_0 t \qquad \textit{hence} \qquad y(t) = \frac{v_0^{(\perp)}}{\omega_0} \cos\omega_0 t + y_0 \ .$$

With $x(t=0) = y(t=0) = z(t=0) = 0$ now we get, $x_0 = z_0 = 0$ and $y_0 = -v_0^{(\perp)}/\omega_0$. Hence, we obtain,

$$x(t) = \frac{v_0^{(\perp)}}{\omega_0} \sin\omega_0 t \qquad , \qquad y(t) = \frac{v_0^{(\perp)}}{\omega_0} \cos\omega_0 t - \frac{v_0^{(\perp)}}{\omega_0} \qquad , \qquad z(t) = v_0^{(\|)} t \ .$$

Therefore, the trajectory is a spiral around the z-axis.
g. Let now be $A_x = A_z = 0$ as above, but $A_y = \mathcal{B}(z)x$. In this case, we have,

$$\mathcal{B}_z = \mathcal{B}(z) \quad , \quad \mathcal{B}_y = 0 \quad , \quad \mathcal{B}_x = -x\frac{\partial \mathcal{B}(z)}{\partial z} \ .$$

respectively. For the equation of motion (let $\omega_0 = q\mathcal{B}_0/mc$ again),

$$\begin{aligned}
\frac{dv_x}{dt} &= +\omega_0 v_y \frac{\mathcal{B}(z)}{\mathcal{B}_0} \\
\frac{dv_y}{dt} &= -\omega_0 \left(v_x \frac{\mathcal{B}(z)}{\mathcal{B}_0} + x v_z \frac{1}{\mathcal{B}_0}\frac{\partial \mathcal{B}(z)}{\partial z} \right) \\
\frac{dv_z}{dt} &= +\omega_0 x v_y \frac{1}{\mathcal{B}_0}\frac{\partial \mathcal{B}(z)}{\partial z} \ .
\end{aligned}$$

h. From (e) and (f) follows:

$$v_y x = -\frac{(v_0^{(\perp)})^2}{\omega_0}\sin^2\omega_0 t \ .$$

and hence,

$$\frac{dv_z}{dt} \approx -(v_0^{(\perp)})^2 \sin^2\omega_0 t \frac{1}{\mathcal{B}_0}\frac{\partial \mathcal{B}(z)}{\partial z} \ .$$

If the derivative of $\mathcal{B}(z)$ by z is constant ($= B'$), we obtain,

$$v_z(t) \approx \frac{1}{2}(v_0^{(\perp)})^2 \left\{ \sin\omega_0 t \cos\omega_0 t - \omega_0 t \right\} \frac{\mathcal{B}'}{\mathcal{B}_0} + v_0^{(\parallel)} \ .$$

Hence, for large $\mathcal{B}'$ and t large v_z can change sign.

20.4.5.3 Ex: Connection between kinetic and canonical momentum and the Abraham-Minkowski debate

The nonrelativistic Lagrangian that governs the interaction of a particle with electric and magnetic dipole moment with external electromagnetic fields can be written,

$$\mathcal{L} = \tfrac{m}{2}v^2 + \vec{\mathcal{E}} \cdot \mathbf{d} + \vec{\mathcal{B}} \cdot \vec{\mu} \ .$$

a. Based on the results of Exc. 20.3.6.2 calculate the kinetic and canonical momenta of a particle with flying at velocity $\mathbf{v}$ through a lab.
b. Now, average over a macroscopic number of particles introducing the polarization $\vec{\mathcal{P}} = \langle \sum_n \mathbf{d}_n \delta^3(\mathbf{r} - \vec{\mathcal{S}}_n)\rangle$ and the magnetization $\vec{\mathcal{M}} = \frac{1}{2}\langle \sum_n \vec{\mu}_n \delta^3(\mathbf{r} - \vec{\mathcal{S}}_n)\rangle$, and compare the kinetic and canonical momenta with the Abraham and Minkowski expressions for the linear momentum density.

Solution: *a. The kinetic momentum is simply [1132],*

$$\mathbf{p}^{kin} = m\mathbf{v} \ .$$

Inserting the electric and magnetic dipole moments, as they appear in the lab frame, the Lagrangian becomes,

$$\mathcal{L} = \tfrac{m}{2}v^2 + \vec{\mathcal{E}}\cdot(\mathbf{d} + \tfrac{1}{c^2}\mathbf{v}\times\vec{\mu}) + \vec{\mathcal{B}}\cdot(\vec{\mu} - \tfrac{1}{2}\mathbf{v}\times\mathbf{d}) \ ,$$

and its derivative,

$$\begin{aligned} p_i^{can} = \frac{\partial L}{\partial v_i} &= mv_i + \frac{1}{c^2}\frac{\partial}{\partial v_i}\mathcal{E}_j\epsilon_{jmn}v_m\mu_n - \frac{c}{2}\frac{\partial}{\partial v_i}\mathcal{B}_j\epsilon_{jmn}v_m d_n \\ &= mv_i + \tfrac{1}{c^2}\epsilon_{inj}\mu_n\mathcal{E}_j - \tfrac{1}{2}\epsilon_{inj}d_n\mathcal{B}_j \ , \end{aligned}$$

or

$$\mathbf{p}^{can} - \mathbf{p}^{kin} = \tfrac{1}{c^2}\vec{\mu}\times\vec{\mathcal{E}} - \tfrac{1}{2}\mathbf{d}\times\vec{\mathcal{B}} \ .$$

b. We get for the macroscopic kinetic and canonical momenta,

$$\mathbf{p}^{can} - \mathbf{p}^{kin} = \tfrac{1}{c^2}\vec{\mathcal{M}}\times\vec{\mathcal{E}} - \vec{\mathcal{P}}\times\vec{\mathcal{B}} \ ,$$

and for the Abraham and Minkowski expressions linear momentum densities,

$$\vec{\wp}^A = \tfrac{1}{c^2}\vec{\mathcal{E}}\times\vec{\mathcal{H}} = \tfrac{1}{c^2}\vec{\mathcal{E}}\times\left(\tfrac{1}{\mu_0}\vec{\mathcal{B}} - \vec{\mathcal{M}}\right) \quad \textit{and} \quad \vec{\wp}^M = \vec{\mathcal{D}}\times\vec{\mathcal{B}} = (\varepsilon_0\vec{\mathcal{E}} + \vec{\mathcal{P}})\times\vec{\mathcal{B}} \ .$$

Hence,

$$\vec{\wp}^A - \vec{\wp}^M = \tfrac{1}{c^2}\vec{\mathcal{M}}\times\vec{\mathcal{E}} - \vec{\mathcal{P}}\times\vec{\mathcal{B}} = \mathbf{p}^{can} - \mathbf{p}^{kin} \ .$$

20.5 Relativistic gravity

The starting point of Einstein's theory on *general relativity* is the famous *equivalence principle* stating that there is no difference in heavy mass and inert mass, that is, gravity and acceleration are fundamentally the same. Taking this axiom seriously, we must accept a series of astonishing corollaries, such as the fact that space-time is neither Euclidian, nor Minkowskian, but distorted by the presence of mass. Time and space coordinates are intertwined (see also Secs. 6.4 and 36.5.2).

In the following, we briefly recapitulate Minkowskian metrics in Cartesian and spherical coordinates before introducing Schwarzschild metrics as a special case.

20.5.1 Metric and geodesic equation in curved space-time

Minkowskian metrics in Cartesian coordinates has been introduced in Sec. 20.1.1. In the following sections, we will briefly recapitulate it and extend it to spherical coordinates before generalizing the metrics to curved space-time.

20.5.1.1 Minkowski metrics

In Cartesian coordinates the line element and tetrad are given by,

$$\begin{aligned} ds^2 &= c^2t^2 - dx^2 - dy^2 - dz^2 \\ \mathbf{e}_t &= \frac{1}{c}\partial_t \quad , \quad \mathbf{e}_x = \partial_x \quad , \quad \mathbf{e}_y = \partial_y \quad , \quad \mathbf{e}_z = \partial_z \\ \mathbf{e}^t &= cdt \quad , \quad \mathbf{e}^x = dx \quad , \quad \mathbf{e}^y = dy \quad , \quad \mathbf{e}^z = dz \ , \end{aligned} \tag{20.185}$$

and the metric tensor by,

$$g_{\mu\nu} = \frac{\partial x_\alpha}{\partial \xi^\mu}\frac{\partial x^\alpha}{\partial \xi^\nu} = \begin{pmatrix} 1 & 0 & 0 & 0 \\ 0 & -1 & 0 & 0 \\ 0 & 0 & -1 & 0 \\ 0 & 0 & 0 & -1 \end{pmatrix} . \tag{20.186}$$

Note that the matrix representation of the metric is defined via,

$$\boxed{ds^2 = g^{\mu\nu}dx_\mu dx_\nu} \, . \tag{20.187}$$

In spherical coordinates,

$$\begin{pmatrix} t \\ x \\ y \\ z \end{pmatrix} = \begin{pmatrix} t \\ r\sin\theta\cos\phi \\ r\sin\theta\sin\phi \\ r\cos\theta \end{pmatrix} , \tag{20.188}$$

the line element and tetrad are given by,

$$\begin{aligned} ds^2 &= c^2t^2 - dr^2 - r^2d\theta^2 - r^2\sin^2\theta d\phi^2 \\ \mathbf{e}_t &= \frac{1}{c}\partial_t \quad , \quad \mathbf{e}_r = \partial_r \quad , \quad \mathbf{e}_\theta = \frac{1}{r}\partial_\theta \quad , \quad \mathbf{e}_\phi = \frac{1}{r\sin\theta}\partial_\phi \ , \end{aligned} \tag{20.189}$$

and the metric tensor,

$$g_{\mu\nu} = \frac{\partial x_\alpha}{\partial \xi^\mu}\frac{\partial x^\alpha}{\partial \xi^\nu} = \begin{pmatrix} 1 & 0 & 0 & 0 \\ 0 & -1 & 0 & 0 \\ 0 & 0 & -r^2 & 0 \\ 0 & 0 & 0 & -r^2\sin^2\theta \end{pmatrix} , \tag{20.190}$$

with $\xi^\mu, \xi^\nu = t, r, \theta, \phi$ and $x_\alpha = t, x, y, z$. The Minkowski metrics is a generalization of Euclidian metric to four-dimensional space-time.

20.5.2 Schwarzschild metric

General relativity breaks with the concept of Euclidian space allowing for space-time to be distorted. The simplest example is the *Schwarzschild metric* which assumes a distortion of time and space as a function of the distance from a heavy mass. Schwarzschild's solution was the first exact solution of Einstein's field equations. It holds on the outside of non-charged non-rotating masses.

Metric and tetrad of Schwarzschild coordinates (t, r, θ, ϕ) are given by,

$$c^2 d\tau^2 = \left(1 - \tfrac{r_s}{r}\right) c^2 dt^2 - \left(1 - \tfrac{r_s}{r}\right)^{-1} dr^2 - r^2 d\theta^2 - r^2 \sin^2\theta d\phi^2 \tag{20.191}$$

$$\mathbf{e}_t = \frac{1}{c\sqrt{1 - r_s/r}}\partial_t \quad , \quad \mathbf{r} = \sqrt{1 - \frac{r_s}{r}}\partial_r \quad , \quad \mathbf{e}_\theta = \frac{1}{r}\partial_\theta \quad , \quad \mathbf{e}_r = \frac{1}{r\sin\theta}\partial_\phi \ ,$$

where,

$$r_s \equiv \frac{2\gamma_N M}{c^2} \ , \tag{20.192}$$

is called the *Schwarzschild radius*. The metric tensor in free (massless) space is,

$$g_{\mu\nu} = \frac{\partial x_\alpha}{\partial \xi^\mu}\frac{\partial x^\alpha}{\partial \xi^\nu} = \begin{pmatrix} 1 - \frac{r_s}{r} & 0 & 0 & 0 \\ 0 & -(1 - \frac{r_s}{r})^{-1} & 0 & 0 \\ 0 & 0 & -r^2 & 0 \\ 0 & 0 & 0 & -r^2\sin^2\theta \end{pmatrix} . \tag{20.193}$$

For $r \gg r_s$ this reduces to the Minkowski metric.

20.5.3 Christoffel symbols for relativistic space-time and geodesic equation

The Christoffel symbols are defined by,

$$\Gamma^\mu_{\ \alpha\beta} \equiv \frac{\partial \mathbf{e}_\alpha}{\partial x^\beta} \cdot \mathbf{e}^\mu = \frac{\partial^2 \xi^\gamma}{\partial x^\alpha \partial x^\beta}\frac{\partial x^\mu}{\partial \xi^\gamma} \ . \tag{20.194}$$

They yields for spherical coordinates,

$$\Gamma^a_{\ it} = \begin{pmatrix} 0 & 0 & 0 & 0 \\ 0 & 0 & 0 & 0 \\ 0 & 0 & 0 & 0 \\ 0 & 0 & 0 & 0 \end{pmatrix} \quad , \quad \Gamma^a_{\ ir} = \begin{pmatrix} 0 & 0 & -r & 0 \\ 0 & 0 & 0 & 0 \\ 0 & 0 & 0 & 0 \\ 0 & 0 & 0 & 0 \end{pmatrix} \tag{20.195}$$

$$\Gamma^a_{\ i\theta} = \begin{pmatrix} 0 & 0 & -r & 0 \\ 0 & 0 & 0 & 0 \\ 0 & 0 & 0 & 0 \\ 0 & 0 & 0 & 0 \end{pmatrix} \quad , \quad \Gamma^a_{\ i\phi} = \begin{pmatrix} 0 & 0 & 0 & 0 \\ 0 & 0 & 0 & 0 \\ 0 & 0 & 0 & 0 \\ 0 & 0 & 0 & 0 \end{pmatrix} \ .$$

In relativistic space-time the *geodesic equation* is a curve representing in some sense the shortest path between two points in a surface. The geodesic line is obtained by solving the differential equation,

$$\boxed{\frac{d^2x^\mu}{d\tau^2} + \Gamma^\mu{}_{\alpha\beta}\frac{dx^\alpha}{d\tau}\frac{dx^\beta}{d\tau} = 0} \ . \tag{20.196}$$

Define *Einstein tensor*, *Ricci tensor* (see 12.4.3).

20.5.4 Exercises

20.5.4.1 Ex: Space-time metric in spherical coordinates

Write down the space-time metric for Earth in spherical coordinates.

Solution: *From Sec. 12.3.6 we derive,*

$$ds^2 = c^2dt^2 - dr^2 - r^2d\theta^2 - r^2\sin^2\theta d\phi^2 \ .$$

It is obtained from the Schwarzschild metric setting the Schwarzschild radius $r_s \simeq 0$. *For Earth* $r_s \approx 8.8\,\mathrm{mm}$.

20.6 Further reading

J.D. Jackson, *Classical Electrodynamics* [659]ISBN

D.J. Griffiths, *Introduction to Electrodynamics* [545]ISBN

Chapter 21

Appendices to 'Electrodynamics'

21.1 Special topic: Goos-Hänchen shift with light and matter waves

Newton's corpuscular light model predicts a lateral shift of a light beam when totally reflected from an interface to an optically thin medium. Photons leaving the optically dense medium are reattracted to it by gravitation. The lateral distance covered during their ballistic flight corresponds to the shift, called *Goos-Hänchen shift* (GHS). It seems as if the light beam was reflected at a plane lying behind the boundary within the region of the evanescent wave (EW). Although the underlying model is incorrect (although De Broglie himself conjectured that the effect could point towards a finite photon mass), newer model based on the Maxwell theory also predict an energy flux within the EW forming within the thin medium. Many unsuccessful attempts have been undertaken to observe this flux, and it has still not been directly observed nowadays. The problem is that any probe brought into the EW undermines it and vanishes the GHS. Goos and Hänchen circumvented the problem by measuring only the lateral shift in the optically dense medium [522, 523, 195]. The agreement of their observations with Maxwell theory gives confidence in the existence of the flux.

21.1.1 Evanescent wave potentials

A light field reflected at an angle θ ($= 52°$ for Landragin's dielectric prism) on a boundary to an optically thin medium is described by

$$\mathcal{E}(\mathbf{r}) = \mathcal{E}_0 e^{\imath q x - \kappa z} \ , \tag{21.1}$$

where $q = kn \sin\theta$ and $\kappa = k\sqrt{n^2 \sin^2\theta - 1}$. Introducing the Rabi frequency

$$\Omega(\mathbf{r}) = \sqrt{\frac{\sigma_0 \Gamma}{\hbar\omega} I(\mathbf{r})} = \sqrt{\frac{\epsilon_0 c^2 \sigma_0 \Gamma}{\hbar\omega}} \mathcal{E}_0 e^{-\kappa z} \ , \tag{21.2}$$

the interaction energy reads $\mathbf{d} \cdot \vec{\mathcal{E}} = \Omega(\mathbf{r}) e^{\imath q x}$. The force $\mathbf{F} = -\nabla \mathbf{d} \cdot \vec{\mathcal{E}}$ is made of two contributions. Using the optical Bloch equations, we find the stationary solutions for

the dipole and the dissipative forces [20]

$$\mathbf{F}_{dip} = -\frac{\hbar\Delta\Omega}{4\Delta^2 + 2\Omega(\mathbf{r})^2 + \Gamma^2}\nabla\Omega(\mathbf{r}) \ , \tag{21.3}$$
$$\mathbf{F}_{diss} = \frac{\hbar\Gamma\Omega^2}{4\Delta^2 + 2\Omega(\mathbf{r})^2 + \Gamma^2}\nabla\theta(\mathbf{r}) \ .$$

Treating the mechanical effects of light analogously to the Laguerre-Gaussian modes. For LGM the phase gradient is almost parallel with the Poynting vector except for higher order corrections for the axial component.

The dipole force can be derived from a conservative evanescent potential

$$V(z) = \frac{\Omega^2}{\Delta}e^{-2\kappa z} = \frac{\pi c^2\Gamma}{2\omega^3} \ I \ \left(\frac{1}{\Delta_{D1}} + \frac{2}{\Delta_{D2}}\right)e^{-2\kappa z} \ .$$

Apparently, radiation pressure accelerates the atoms not in the direction of the wavevector, but of the phase gradient [22]. Is this the same as the Poynting vector? This may lead to observable effects in evanescent waves. Hence, the observation of a transverse radiation pressure would already prove a Goos-Hänchen shift.

21.1.2 Energy flux in the evanescent wave

An incoming laser beam be expanded after phases

$$\mathcal{E}_i(x) = \mathcal{E}_{ip}\int f(\theta)e^{-\imath x k_{ix_0}\theta}d\theta \ . \tag{21.4}$$

The reflected beam then reads

$$\mathcal{E}_r(x) = \mathcal{E}_{ip}\int r(\theta)f(\theta)e^{-\imath x k_{ix_0}\theta}d\theta \ , \tag{21.5}$$

where $r(\theta) = \frac{a-\imath b}{a+\imath b}$ according to the Fresnel equations or $r = e^{i\varphi}$. We assume that we can linearize the phase $\varphi(\theta) = \varphi(\theta_0) + (\theta-\theta_0)\partial_\theta\varphi(\theta_0) \equiv \chi + \theta\partial_\theta\varphi(\theta_0)$. Then equation (21.5) can be written

$$\mathcal{E}_r(x) = \mathcal{E}_{ip}e^{-\imath\chi}\int f(\theta)e^{-\imath(x-\Delta x_{GH})k_{ix_0}\theta}d\theta = \mathcal{E}_i(x-\Delta x_{GH})e^{-\imath\chi} \ , \tag{21.6}$$

where $\Delta x_{GH} = \frac{2\cos\theta_0}{k_{ix_0}}\partial_\theta\varphi(\theta_0) = \frac{2}{k_i}\partial_\theta\varphi(\theta_0)$. The reflected laser beam is parallel shifted.

Calculations show [1091, 815] that the energy flux penetrates the thin medium only where the transverse profile of the beam shows a gradient. In the regions of constant intensity the flux is inside the plane of incidence and parallel to the surface. Hence, the Goos-Hänchen shift is only observable with spatially inhomogeneous beams.

21.1.2.1 Expression for the shift

Let us now estimate the GHS for a prism $n_1 = 1.5$, the Rb D_2-line for which $\lambda = 2\pi/k = 780$ nm. The EW penetration depth ζ is given by $k\zeta = \sqrt{n_1^2\sin^2\theta - n_2^2}^{-1}$

$$\frac{\Delta_{GH}}{2\zeta} = \frac{n_1^2n_2^2\sin\theta\cos^2\theta}{n_1^4\sin^2\theta + n_2^4\cos^2\theta - n_1^2n_2^2} \ . \tag{21.7}$$

We assume that the angle of incidence is close to the critical angle $\theta = \theta_c + \xi = \arcsin n_1^{-1} + \xi$. Near the critical angle the GHS diverges as does the penetration depth. Hence, the GHS should be measured very close to the critical angle. The expansion in ξ yields

$$\frac{\Delta_{GH}}{2\zeta} = \frac{n_1}{n_2}\left(1 + \xi\frac{n_2^2 n_1^2 - n_2^4 - 2n_1^4}{n_2^3\sqrt{n_1^2 - n_2^2}}\right) . \tag{21.8}$$

The Goos-Hänchen shift is proportional to the penetration depth of the evanescent wave. It has been measured by [195].

21.1.2.2 Goos-Hänchen shift with resonant absorbers

Resonant absorbers have an impact on the evanescent wave and hence on the Goos-Hänchen shift as has been measured by [1028]. Hence, we now consider the presence of an resonant gas with a small index of refraction, $n_2 = 1 + \bar{n}$, so that

$$\frac{k\Delta_{GH}}{2} = \frac{1}{\sqrt{n_1^2\sin^2\theta - (1+\bar{n})^2}}\frac{n_1^2(1+\bar{n})^2\sin\theta\cos^2\theta}{n_1^4\sin^2\theta + (1+\bar{n})^4\cos^2\theta - n_1^2(1+\bar{n})^2} . \tag{21.9}$$

To first order in $\bar{n}$ and ξ

$$\Delta_{GH}(\bar{n},\xi) \approx \frac{A\bar{n}}{\sqrt{\xi}\,(B\xi - \bar{n})} + \Delta_{GH}(\bar{n}=0,\xi) . \tag{21.10}$$

According to [953] (Eq. 4.6),

$$\begin{aligned} T &= -\frac{N|d\epsilon_1|^2}{\eta\varepsilon_0\hbar|\epsilon_1|^2}\int d\mathbf{v}W(\mathbf{v})\theta(v_z)\frac{1}{\Gamma + \eta k v_z - \imath\,(\Delta - \alpha k v_x)} \qquad (21.11)\\ &= -\frac{N|d|^2}{\eta\varepsilon_0\hbar}\left(\frac{3}{2\pi v_0^2}\right)^{3/2}\int_0^\infty dv_z e^{-3v_z^2/2v_0^2}\int_{-\infty}^\infty dv_y e^{-3v_y^2/2v_0^2}\int_{-\infty}^\infty dv_x e^{-3v_x^2/2v_0^2}\frac{1}{\Gamma - \imath\Delta}\\ &= -\frac{N|d|^2}{\eta\varepsilon_0\hbar}\frac{1}{\sqrt{2}}\frac{1}{\Gamma - \imath\Delta} . \end{aligned}$$

An effective refractive index variation may be define [953] (Eq. 3.16) with $\beta = i\eta$,

$$\delta n = -\beta T = \beta\frac{N|d|^2}{\sqrt{2}\eta\varepsilon_0\hbar}\frac{1}{\Gamma - \imath\Delta} = \imath\frac{N|d|^2}{\sqrt{2}\varepsilon_0\hbar}\frac{\Gamma + \imath\Delta}{\Gamma^2 + \Delta^2} . \tag{21.12}$$

The interesting question is, whether the energy flux in the evanescent wave is directly observable. The existence of an EW is not questionable. On the contrary it has become an important in quantum optics, where near-resonant EWs are used for *selective reflection spectroscopy*. In cold atom optics, far-off resonant EWs are used to repel ultracold atoms from surfaces. Does the energy flux related to the GHS leave any footprints in the atomic cloud (possibly a BEC)? Certainly, one has to stay at a detuning, where the flux in the evanescent wave satisfies $\mathfrak{Im}\,\mathbf{k} \perp \mathfrak{Re}\,\mathbf{k}$, so that there is no energy transfer. Think about phase shift of the de Broglie wave underneath a fixed envelope, analogy to geometric phases or the Aharonov-Bohm effect.

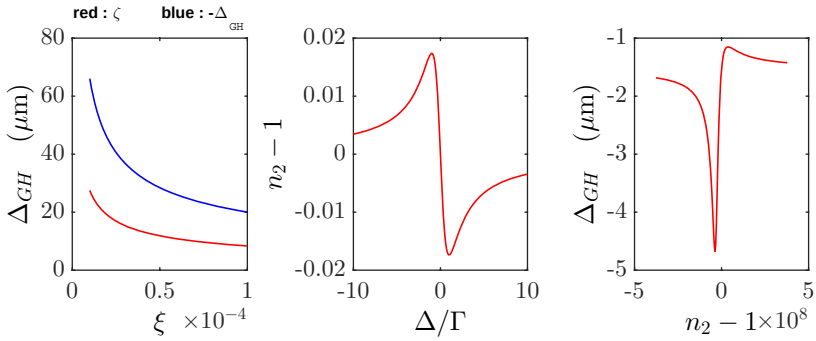

Figure 21.1: (code) Selective reflection Goos.

21.1.3 Imbert-Fedorov shift

A transverse shift should be expected for circularly polarized light or Laguerre-Gaussian modes. This shift called Imbert-Fedorov shift can be described with the flux method. The effect should be small, $\Delta x_{IF} \approx 0.1\ \Delta x_{GH}$. It has been observed with microwaves [307] and light [1034].

For this case it is interesting that the wavevector $\mathbf{k}$ and the flux $\mathbf{S}$ are both parallel to the surface, but orthogonal on each other. The flux is perpendicular to the plane of incidence.

The symmetry breaking (upward or downward flux) is inherent in the circularly polarized laser beam [23, 478, 975]. Here the Poynting vector describes a helix about the optical axis.

For matter waves the index of refraction can be tuned via the particle energy, which is not possible with light. E.g. if $E = V_2 > V_1$, the critical angle for total reflection is $\alpha = 0$. Do we expect a Imbert-Fedorov shift for spinor condensates? Is the plane wave approximation good or should be use real BEC wavefronts?

The total reflection of Laguerre-Gaussian beams has also been studied [969].

21.1.4 Matter wave Goos-Hänchen shift at a potential step

The phase of a BEC could be a sensitive probe for the Goos-Hänchen shift. Here, it is important that the de Broglie wavelength be longer than the edge of the potential. Otherwise, the effect is trivial even in the classical particle picture.

Matter waves behave analogously to optical waves, except that the Schrödinger equation must be used. Consider the situation of a particle moving towards a potential step at an angle α as shown in Fig. 21.2. The energy of the particle is $E > V_2 > V_1$. The incidence region V_1 corresponds to the atom optically thick medium (the de Broglie wavelength is shorter, the propagation velocity fast, $\hbar k_1 = \sqrt{2m(E - V_1)}$. V_2 is the atom optically thin medium.

Consequently we expect a critical angle α_c beyond which the matter wave is totally reflected,

$$\sin \alpha_c = \sqrt{\frac{E - V_2}{E - V_1}}\ . \tag{21.13}$$

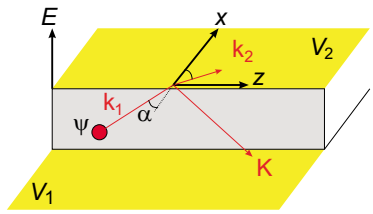

Figure 21.2: Matter wave refraction at a potential step.

For partial reflection, if the incident wave is described by [1091] $\psi_0 = e^{\imath x k_{x1} + \imath y k_{y1}}$, the reflected and refracted wave are

$$\psi_1 = \frac{\cos\alpha - \sqrt{\sin^2\alpha_c - \sin^2\alpha}}{\cos\alpha + \sqrt{\sin^2\alpha_c - \sin^2\alpha}} e^{-\imath x k_{x1} + \imath y k_{y1}} \tag{21.14}$$
$$\psi_2 = \frac{2\cos\alpha}{\cos\alpha + \sqrt{\sin^2\alpha_c - \sin^2\alpha}} e^{-\imath x \sqrt{k_2^2 - k_{y1}^2} + \imath y k_{y1}} \ .$$

For total reflection,

$$\psi_1 = \exp\left(-\imath 2 \arctan\sqrt{\frac{\sin^2\alpha - \sin^2\alpha_c}{1 - \sin^2\alpha}}\right) e^{-\imath x k_{x1} + \imath y k_{y1}} \tag{21.15}$$
$$\psi_2 = \frac{2\cos\alpha}{\cos\alpha + \imath\sqrt{\sin^2\alpha - \sin^2\alpha_c}} e^{-x\sqrt{k_{1y}^2 - k_2^2} + \imath y k_{y1}} \ .$$

The matter wave Goos-Hänchen shift Δ_{GH} can be estimated by comparing the matter wave flux $\mathbf{J} = -i\frac{\hbar}{2m}(\psi^*\nabla\psi - \psi\nabla\psi^*)$ in the evanescent wave with the flux in a Δ_{GH} wide strip of the reflected beam. The result [1091] is

$$\frac{\Delta_{GH}}{2} = \frac{\sin\alpha\cos^2\alpha}{k\cos^2\alpha_c\sqrt{\sin^2\alpha - \sin^2\alpha_c}} \ . \tag{21.16}$$

See [1091, 611].

The difficult question is now what the matter wave analogue of the Imbert-Fedorov shift would be. It is known for relativistic electrons that momentum and velocity must not necessarily be collinear [334]. How about particles with a real angular orbital momentum, e.g. the reflection of vortices?

21.2 Special topic: The dilemma of Abraham and Minkowski

If Minkowski is correct, then as a photon enters an atomic cloud with $n > 1$, then the cloud receives a collective momentum in the direction opposite to the photon propagation [230]. 'Momentum conservation requires then that the medium also has a mechanical momentum. When a pulse of light enters the medium, the particles in

the medium are accelerated by the leading edge of the pulse and decelerated by the trailing edge.' However, near resonance the refraction index is dispersive. I.e. for blue-detuning we should expect $n < 1$ and hence a collective momentum in the direction of photon propagation.

A picturesque interpretation would be, that the acceleration of the atoms by the leading or trailing edge of the light pulse is due to the dipole force (real part of susceptibility). For red (blue) detuning, the atoms are accelerated backwards (forwards) by the leading edge of the pulse and forwards (backwards) by the trailing edge. In case, that the cloud absorbs or diffracts photons, a net momentum should remain in the cloud: [817] "The propagation of an optical pulse through a transparent dielectric causes no transfer of momentum to the material, as a positive Lorentz force in the leading part of the pulse is exactly balanced by a negative Lorentz force in its trailing part. However, this balance is removed in the present problem because of the attenuation of the light by its interaction with the charge carriers. This causes the leading part of the pulse at a given time to be weaker than the trailing part and produces a net negative transfer of momentum to the bulk semiconductor."

Out side the medium, we know that the photon momentum is,

$$p_{out} = mc \ , \tag{21.17}$$

with $m = \hbar\omega/c^2$. Inside the medium, it is

$$p_{in} = m\frac{c}{\eta} = \frac{\hbar\omega}{\eta c} \ . \tag{21.18}$$

According to Minkowski, we must use $m = \hbar\omega/(c/\eta)^2$.

21.2.1 Calculation of the momentum of light in a dielectric medium

Let us consider [898] a plane light wave within a dielectric medium given by $\varepsilon = \eta^2\varepsilon_0$ and $\mu = \mu_0$,

$$\vec{\mathcal{E}}(\mathbf{r},t) = \hat{\mathbf{e}}_x\mathcal{E}_0\cos\omega\,(t - z/c) \qquad \text{and} \qquad \vec{\mathcal{H}}(\mathbf{r},t) = \hat{\mathbf{e}}_y\sqrt{\frac{\varepsilon}{\mu_0}}\mathcal{E}_0\cos\omega(t - z/c) \ , \tag{21.19}$$

The energy densities and the energy flows, called 'Poynting vector', are (taking the temporal average),

$$u = \frac{1}{2}(\vec{\mathcal{E}}\cdot\vec{\mathcal{D}} + \vec{\mathcal{B}}\cdot\vec{\mathcal{H}}) = \tfrac{1}{2}\varepsilon\mathcal{E}_0^2 \qquad \text{and} \qquad \mathbf{S} = \vec{\mathcal{E}}\times\vec{\mathcal{H}} = \tfrac{1}{2}\sqrt{\frac{\varepsilon}{\mu_0}}\mathcal{E}_0^2\hat{\mathbf{e}}_z = \frac{c}{\eta}u\hat{\mathbf{e}}_z \ . \tag{21.20}$$

Therefore, the intensity of a light field, $I = |\mathbf{S}|$, is increased by the dielectric. Rewriting this in terms of the average number of photons q in a volume V, we obtain for the energy,

$$\int u d^3r = \tfrac{1}{2}\varepsilon\mathcal{E}_0^2 V = N\hbar\omega \ . \tag{21.21}$$

The energy flow of a field of light is equal to the momentum carried by the photons. For a single photon, we have,

$$\mathbf{p}_{Abr} \equiv \frac{1}{N}\frac{1}{c^2}\int \mathbf{S}d^3r = \frac{\hbar\mathbf{k}_0}{\eta} \ . \tag{21.22}$$

However, Minkowski's point of view was,

$$\mathbf{p}_{Min} = \frac{1}{N}\int dV\vec{\mathcal{D}}\times\vec{\mathcal{B}} = \eta\hbar\mathbf{k}_0 \ . \tag{21.23}$$

The recoil frequency is modified from $\hbar\omega_{rec} = \frac{\hbar^2k^2}{2m}$ to $\hbar\omega_{rec}^{\eta} = \eta^2\omega_{rec}$ [230].

21.2.1.1 Kinetic versus canonical momentum

In reality, what is propagating in the medium is NOT a photon, but a photon interacting with atoms of the medium (otherwise we wouldn't need a refractive index to describe the propagation of light). The total momentum must, obviously, be conserved. Upon entering a medium, part of the radiation momentum is transferred to the medium [1132]:

$$\mathbf{p}^{tot} = \mathbf{p}^{med} + \mathbf{p}^{rad} \ . \tag{21.24}$$

But how this repartition is done is, as long as we do not attempt to measure one or the other component, arbitrary. We could chose $(\mathbf{p}^{med}, \mathbf{p}^{rad}) \rightarrow (\mathbf{p}^{med}_{kin}, \mathbf{p}^{rad}_{kin})$, and calling $\mathbf{p}_{Abr} \equiv \mathbf{p}^{rad}_{kin} = \frac{\varepsilon_0\mu_0}{N}\int\vec{\mathcal{E}}\times\vec{\mathcal{H}}dV$ the Abraham momentum, write,

$$\mathbf{p}^{tot} = \mathbf{p}^{med}_{kin} + \mathbf{p}_{Abr} \ . \tag{21.25}$$

We could also chose $(\mathbf{p}^{med}, \mathbf{p}^{rad}) \rightarrow (\mathbf{p}^{med}_{can}, \mathbf{p}^{rad}_{can})$, and calling $\mathbf{p}_{Min} \equiv \mathbf{p}^{rad}_{can} = \frac{1}{N}\int\vec{\mathcal{D}}\times\vec{\mathcal{B}}dV$ the Minkowski momentum, write,

$$\mathbf{p}^{tot} = \mathbf{p}^{med}_{can} + \mathbf{p}_{Min} \ . \tag{21.26}$$

We could also chose $(\mathbf{p}^{med}, \mathbf{p}^{rad}) \rightarrow (\mathbf{p}^{med}_{rel}, \mathbf{p}^{rad}_{rel})$, and calling $\mathbf{p}_{em} \equiv \mathbf{p}^{rad}_{rel} = \frac{\varepsilon_0}{N}\int\vec{\mathcal{E}}\times\vec{\mathcal{B}}dV$ the vacuum electromagnetic momentum, write,

$$\mathbf{p}^{tot} = \mathbf{p}^{med}_{rel} + \mathbf{p}_{em} \ . \tag{21.27}$$

$$\mathbf{p}_{rel} = \mathbf{p}_{kin} - \vec{\mathcal{E}}\times\tfrac{1}{c^2}\mathbf{m} \quad , \quad \mathbf{p}_{kin} = m\mathbf{v} \ . \tag{21.28}$$

21.2.1.2 Tentative explanations

People seem to agree on the interpretation that, as long as the propagation of the energy in a medium is concerned, the Abraham interpretation is valid. The kinetic momentum of a laser beam is given by the Abraham value p_{Abr}. But as soon as photons are localized by atoms, it is Minkowski? The scattering of a photon by an individual atom tears away the atoms from its neighbors. The difference p_{med} in the momentum p_{Min} imparted to the individual atom and the momentum carried by the photon p_{Abr} is imparted to neighboring atoms.

The total momentum transfer to bulk material, free of any boundary or surface effects, has the Abraham value of $\hbar\omega_0/\eta_g c$ but that the transfer to an attenuating subsystem within the bulk material has the Minkowski value of $\eta_p\hbar\omega_0/c$ [817].

The field carries a momentum p_{Abr} per photon, but that there is also a momentum p_{med} imparted by the field to the medium. An atom that absorbs or emits a photon of frequency ω in the medium therefore recoils with the momentum $p_{Abr} + p_{med} = p_{Min}$, as if the photon momentum were the Minkowski photon momentum p_{Min} [898].

A slide show about this topic can be visualized at (watch talk).

21.2.1.3 Energy and momentum tensor in a dielectric

In a dielectric,

$$T^{\alpha\beta} = \begin{pmatrix} g^0 & c\tilde{\mathbf{g}}^j_{rad} + c\tilde{\mathbf{g}}^j_{mat} \\ c\mathbf{g}^i_{rad} + c\mathbf{g}^i_{mat} & -\mathbf{T}^{ij}_{rad} - \mathbf{T}^{ij}_{mat} \end{pmatrix} . \tag{21.29}$$

We need $\mathbf{g}^i_{rad} + \mathbf{g}^i_{mat} = \tilde{\mathbf{g}}^i_{rad} + \tilde{\mathbf{g}}^i_{mat}$, but this does not necessarily imply, $\mathbf{g}^i_{rad} = \tilde{\mathbf{g}}^i_{rad}$. The Abraham form of the energy-momentum tensor is,

$$T^{\alpha\beta}_{Abr} = \begin{pmatrix} g^0 & c\mathbf{g}^j_{rad} + c\tilde{\mathbf{g}}^j_{mat} \\ c\mathbf{g}^i_{rad} + c\mathbf{g}^i_{mat} & -\mathbf{T}^{ij}_{rad} - \mathbf{T}^{ij}_{mat} \end{pmatrix} . \tag{21.30}$$

Obviously, the radiation term is symmetric. From the Minkowski form,

$$T^{\alpha\beta}_{Mkw} = \begin{pmatrix} g^0 & c^{-1}\vec{\mathcal{E}} \times \vec{\mathcal{H}} + c\tilde{\mathbf{g}}^j_{mat} \\ c\mathbf{D} \times \mathbf{B} + c\mathbf{g}^i_{mat} & -\mathbf{T}^{ij}_{rad} - \mathbf{T}^{ij}_{mat} \end{pmatrix} , \tag{21.31}$$

the radiation term is not symmetric. 'Every experiment is only sensitive to specific terms of the complete energy-momentum tensor. Every experiment involving only angular momentum will be insensitive to independently symmetric terms, and experiments involving only linear momentum will be insensitive to terms, which are divergence-free. ' [1027].

The total electromagnetic stress tensor contains the following components,

$$\begin{aligned} T^{\alpha\beta}_{(m)} &= \rho_0(c^2 + \epsilon_i)u^\alpha u^\beta + \phi\left(u^\alpha u^\beta + \delta^{\mu\nu}\right) \\ T^{\alpha\beta}_{(f)} &= \varepsilon_0 c^2\left(F^{\mu\gamma}F^{\nu}_{\ \gamma} - \tfrac{1}{4}F^2_{\gamma\delta}\delta^{\mu\nu}\right) \\ T^{\alpha\beta}_{(P)} &= \tfrac{1}{\varepsilon-\varepsilon_0}\left(P^{\mu\gamma}P^{\nu}_{\ \gamma} - \tfrac{1}{4}P^2_{\gamma\delta}\delta^{\mu\nu}\right) \\ T^{\alpha\beta}_{(M)} &= \tfrac{1}{\mu^{-1}-\mu_0^{-1}}\left(M^{\mu\gamma}M^{\nu}_{\ \gamma} - \tfrac{1}{4}M^2_{\gamma\delta}\delta^{\mu\nu}\right) - F^{*\mu\gamma}M^{\nu}_{\ \gamma} - F^{\mu\gamma}M^{*\nu}_{\ \ \gamma} , \end{aligned} \tag{21.32}$$

with

$$u^\beta = \begin{pmatrix} c \\ \mathbf{u} \end{pmatrix} \quad , \tag{21.33}$$

$$P^{\mu\nu} = \begin{pmatrix} 0 & \vec{\mathcal{P}} \\ \vec{\mathcal{P}} & \frac{1}{c}(v^a P^b - v^b P^a) \end{pmatrix} \quad , \quad M^{\mu\nu} = \begin{pmatrix} 0 & \vec{\mathcal{M}} \\ \vec{\mathcal{M}} & \frac{1}{c}(v^a M^b - v^b M^a) \end{pmatrix}$$

$$\vec{\mathcal{D}} = \varepsilon\vec{\mathcal{E}} = \varepsilon_0\vec{\mathcal{E}} + \vec{\mathcal{P}} + \tfrac{1}{c}\left(\tfrac{\mathbf{v}}{c} \times \vec{\mathcal{M}}\right) \quad , \quad \vec{\mathcal{H}} = \tfrac{1}{\mu}\vec{\mathcal{B}} = \tfrac{1}{\mu_0}\vec{\mathcal{B}} - \vec{\mathcal{M}} + c\left(\tfrac{\mathbf{v}}{c} \times \vec{\mathcal{P}}\right) .$$

Hence,

$$\begin{aligned} M^{\mu\nu\eta} &= T^{\mu\nu}x^\eta - T^{\mu\eta}x^\nu \\ 0 = \partial_\eta M^{\mu\nu\eta} &= T^{\mu\nu}\partial_\eta x^\eta - \partial_\eta T^{\mu\eta}x^\nu = 3T^{\mu\nu} . \end{aligned} \tag{21.34}$$

21.2.1.4 Discussion in the framework of cooperative scattering

- It seems to me that the problem does not even arise in our cooperative scattering theory, at least as long as we don't do the smooth density approximation. Cooperative scattering from a coarse-grained cloud's does not require the notion of a refractive index. The notion of refractive index is an artifact coming from the smooth density approximation. It is not surprising if its application to coarse-grained atomic clouds can lead to apparently paradox effects. The paradox disappears within a correct microscopic theory of cooperative scattering.

  On the other hand, the collective scattering theory may give some hints on sheer forces within the cloud. Coarse-grained atomic clouds do not have sharp boundaries. Thus, it is not essential, when the pulse enters the cloud, but when a photon is scattered by an individual atom. The Abraham momentum has never been measured really. If we measure p_m and p_{med} we could infer p_A from the difference.

- Timed Dicke state gives wrong results for photon momentum inside cloud...! Can we test this by manipulating the dispersive part of n?

- We can calculate the radiation pressure force. Can we also calculate the Poynting vector?

- Is the small displacement of the momentum halo ring into $-\hbar k_0$ direction real? They all assume that the bulk of the recoil is absorbed by a single atom, but that the other atoms also feel something. Perhaps, this holds for Bragg scattering, where the high cooperativity leave the atoms only with two choices: Be diffracted or stay in the cloud. In disordered clouds the situation may be not so clear.

21.2.1.5 Test using sub-recoil resolving cavities

Advantage: Due to high cavity cooperativity we can enforce backscattering, which facilitates the situation. If a single atom is backscattered from an atom inside the atomic cloud, the recoil imparted to rest of the atomic cloud should be $P = 2(\eta - 1)\hbar k_0$, or $p = P/N$ per atom. If many photons are scattered this should lead to an appreciable acceleration. The use of a sub-recoil resolving cavity could allow detecting the acceleration spectroscopically. Problem: How to distinguish this effect from the shift of the cavity eigenfrequencies due to η?

A cavity immersed in a dielectric medium with n changes its resonances to $\nu_0 = c/\eta\lambda$. This shows that the wavelength is altered in the medium. I.e. forward scattering with $\eta > 1$ shifts a cavity resonance to the red. What does it do to the atomic resonance? Is this the collective Lamb shift?

A microscopic quantum mechanical description, e.g. based on the coupled dipoles model detailed in Sec. 19.3.1 may lead to a deeper understanding of the interplay of radiation and matter in a dielectric medium [1027, 587, 495, 817, 506, 230].

21.2.1.6 Shared recoil?

Assume a BEC irradiated by two intersecting laser beams in Raman configuration tuned in a way as to generate Bragg diffraction. Applying a $\pi/2$ pulse, we observe

matter wave interference. What is the resulting N-body state [1]?

$$|\Psi\rangle = |\Psi_P\rangle \pm |-\Psi_P\rangle = |P, P, P...\rangle \pm |-P, -P, -P, ...\rangle \tag{21.35}$$

$$|\Phi\rangle = (|\psi_{1P}\rangle \pm |-\psi_{1P}\rangle)(|\psi_{2P}\rangle \pm |-\psi_{2P}\rangle)... \tag{21.36}$$

We know the answer: The second case is correct, and we do not create Schrödinger cat states. For every atom, the final state is completely independent of the presence of the other atoms, i.e. the scattering is NOT collective in the sense that the recoil momentum is distributed over several atoms.

Here are some question:

- Why does collective scattering seem to be negligible for Bragg diffraction? We believe that the state generated by a Bragg pulse is a product state (or Schrödinger kitten state): During the scattering process, every atom evolves by itself into a superposition of momentum states, which is shaped the the mean-field of other atoms.

- What does this mean for collective scattering? Is the final atomic state some intermediate situation between $|\Psi\rangle$ and $|\Phi\rangle$? Then there should be entanglement.

- How can we break down the N-body matter wave function we found for collective halos into the individual atoms?

- What is the correct ansatz for the state generated by a pump beam inside an atomic cloud: The timed Dicke ansatz or the product state? They are identical in the single-excited atom case, but different for higher excitations. Must the experiment decide?

  The $p = mc$ argument leads to Abraham, the $p = h/\lambda$ argument to Minkowski!

- 'Hidden' momentum discussion by Saldanha. Consider Amperian current loop in a uniform electric field: $S_{mat} = -I\mathcal{E}baN\hat{y} = \vec{\mathcal{M}} \times \vec{\mathcal{E}}$ There is a net material momentum up canceled by an el.mg. momentum down.

- No interfaces no surfaces in atomic clouds.

- To what might correspond the division into an el.mg. and a medium part in collective scattering?

21.2.2 Exercises

21.2.2.1 Ex: Einstein box Gedankenexperiment with a BEC

Estimate whether the Einstein box experiment is feasible with a BEC using EIT to cancel absorption?

[1] Same idea, assume a BEC in one of two possible hyperfine states. Apply a microwave $\pi/2$-pulse. Look at the internal degrees of freedom.

Solution: *Consider a transparent slab of thickness D and mass M traversed by a radiation pulse of wavevector $\hbar k_0$. The traversal time is,*

$$\tau = \frac{D + \Delta z}{c/\eta} \ , \tag{21.37}$$

where Δz is the displacement of the slab during the transit time. After the pulse entered the slab, the slab a velocity,

$$v_m = \frac{\hbar k_0 - \hbar k_M}{M} \ , \tag{21.38}$$

so that the displacement after the pulse left the slab is

$$\Delta z = v_m \tau = \frac{\hbar(k_0 - k_M)}{M} \frac{D + \Delta z}{c/\eta} \ , \tag{21.39}$$

or

$$Mc^2 = \hbar c(k_0 - k_M)\eta(D + \Delta z) = \hbar\omega(\eta - \eta\frac{k_M}{k_0})(D + \Delta z) \ . \tag{21.40}$$

Relativistic energy must be conserved, because the system is closed, i.e.

$$p_\mu p^\mu = E^2/c^2 - \mathbf{p} \cdot \mathbf{p} = Mc^2 \ . \tag{21.41}$$

Would such an experiment be able to yield one (or both) momenta: Abraham and Minkowski?

21.3 Special topic: Advanced Gaussian optics

The most common mode is a Gaussian laser beam, which is the lowest order Hermite-Gaussian mode. But other modes are possible.

21.3.1 Laguerre-Gaussian beams

Since several years, attention has been drawn on an unusual feature of light: The fact that it carries angular momentum when it is in special modes called a *Laguerre-Gaussian mode* [1208]. Furthermore, while it is well-known that the light polarization couples to the internal degrees of freedom of atoms, the light angular momentum has been predicted to couple to external degrees of freedom, i.e. light should be able to exert a torque to the atomic motion [21, 65, 22, 20, 23, 973]. The torque has been observed on macroscopic particles [1208]. For a hot atomic gas, the Doppler-effect precludes the direct observation of torsional effect. Recently, phase-conjugation by Non-Degenerate Four-Wave Mixing (ND4WM) in a Magneto-Optical Trap (MOT) has been used to indirectly proof that the atoms acquired angular momentum from light [1289]. Also, magneto-optical trap have been constructed based on laser beams [757, 1223]. Those experiments exploited the doonat-shaped intensity distribution of the LG modes, but did not demonstrate the effect of the torque. And frequency shift [302]. Most traps for neutral atoms are based on light forces, for example the MOT works with radiation pressure. Deliberate misalignement of the optical beams within a plane can give rise to vortex forces and set up a racetrack for the atoms [1351, 71].

Laguerre-Gaussian modes can be generated using a *Fresnel zone plate*.

21.3.1.1 Energy density in Laguerre-Gaussian modes

Besides plane and spherical waves, Gaussian beams and many other functions, the Laguerre-Gaussian modes (LGM) are a solution of Maxwell's equations, i.e. they satisfy $\nabla^2 u + k^2 u = 0$, where u is the scalar mode function of the beam [734]. The vector potential in the Lorentz gauge, $\Phi = -\frac{1}{\imath k}\nabla \cdot \mathbf{A}$, of those modes in the paraxial approximation [777] is given by [21],

$$\boxed{\begin{aligned} \mathbf{A}_{nm}(\mathbf{r}) &= \hat{\mathbf{e}}_x u_{nm}(\mathbf{r}) e^{-\imath kz} \\ u_{nm}(\mathbf{r}) &= u_{00}(\mathbf{r}) \left(\tfrac{r\sqrt{2}}{w(z)}\right)^{|l|} L_p^{|l|}\left(\tfrac{2r^2}{w(z)^2}\right) e^{-\imath l\phi}\, e^{\imath(2p+|l|)\arctan\frac{z}{z_R}} \\ u_{00}(\mathbf{r}) &= \tfrac{u_0}{\sqrt{z^2+z_R^2}}\, e^{-\frac{r^2}{w(z)^2}}\, e^{-\frac{\imath k r^2 z}{2(z^2+z_R^2)}}\, e^{\imath \arctan\frac{z}{z_R}} \end{aligned}} \quad , \tag{21.42}$$

where $l = n - m$ and $p = \min(n, m)$. In the following we will use the convenient cylindrical coordinate system defined in (12.43). Note that, for $l = p = 0$ we recover a Gaussian beam, as will be shown in Exc. 21.3.2.3.

21.3.1.2 Poynting vector in Laguerre-Gaussian modes

The energy flux is given by the Poynting vector $\vec{\mathcal{S}} = \mu_0^{-1}\vec{\mathcal{E}} \times \vec{\mathcal{B}} = c^2\mathbf{p}$. $|\vec{\mathcal{S}}|$ is the beam intensity. The energy density is $u = \frac{1}{2}(\varepsilon_0|\vec{\mathcal{E}}|^2 + \mu_0^{-1}|\vec{\mathcal{B}}|^2)$. The linear momentum and angular momentum densities and total momenta are defined as,

$$\begin{aligned} \mathbf{p} &= \int \vec{\wp} d^3r \qquad \text{with} \quad \vec{\wp} = \varepsilon_0 \vec{\mathcal{E}} \times \vec{\mathcal{B}} \\ \mathbf{L} &= \int \vec{\ell} d^3r \qquad \text{with} \quad \vec{\ell} = \mathbf{r} \times \vec{\wp} \end{aligned} \quad . \tag{21.43}$$

The cycle-average of the real part of the linear momentum density can in the paraxial approximation be traced back to the mode function u, respectively, the scalar potential Φ and the vector potential $\mathbf{A}$ using (17.78),

$$\begin{aligned} \langle \vec{\wp} \rangle &= \frac{\varepsilon_0}{2}(\vec{\mathcal{E}}^* \times \vec{\mathcal{B}} + \vec{\mathcal{E}} \times \vec{\mathcal{B}}^*) \\ &= \imath\omega\frac{\varepsilon_0}{2}(u^*\nabla u - u\nabla u^*) + \omega k \varepsilon_0 |u|^2 \hat{\mathbf{e}}_z + \omega\sigma\frac{\varepsilon_0}{2}\frac{\partial |u|^2}{\partial r}\hat{\mathbf{e}}_\phi \; . \end{aligned} \tag{21.44}$$

The components of the linear momentum density are [23],

$$\vec{\wp} = \varepsilon_0 \omega k |u|^2 \left[\hat{\mathbf{e}}_z + \frac{rz}{z^2 + z_r^2}\hat{\mathbf{e}}_r + \left(\frac{l}{kr} - \frac{\sigma}{2|u|^2}\frac{\partial |u|^2}{k\partial r}\right)\hat{\mathbf{e}}_\phi\right] \; . \tag{21.45}$$

The Poynting vector is in general not parallel to the wavevector $\mathbf{k}$, but spirals about the optical axis.

21.3.1.3 Poynting vector in Hermite-Gaussian modes

This holds even for Hermite-Gaussian beams, as we will show in the following. We start from the energy density of a LGM in Eq. (21.42). For a Gaussian mode $l = p = 0$,

$$|u_{00}(\mathbf{r})| = \frac{u_0 e^{-r^2/w(z)^2}}{w(z)} \ . \tag{21.46}$$

we find, as will be shown in Exc. 21.3.2.3,

$$\vec{\wp} = \varepsilon_0 \omega k |u|^2 \left[\hat{\mathbf{e}}_z + \frac{rz}{z^2 + z_r^2} \hat{\mathbf{e}}_r + \sigma \frac{r z_R}{z^2 + z_R^2} \hat{\mathbf{e}}_\phi \right] \ . \tag{21.47}$$

i.e. the radial component vanishes for small beam divergence, the azimuthal component is on the order $w_0/z_R \approx 500$ times smaller.

Inserting the full expression of the energy density of a LGM, one finds one term containing σ and hence predicting spin-orbit coupling. It can be shown that it results in a dissipative force proportional to $l\sigma$ [20].

21.3.1.4 Mechanical forces exerted by Laguerre-Gaussian modes

The Laguerre-Gaussian modes are labeled by n and m, where $l = n - m$ and $p = \min(n, m)$, such that $2p + |l| = m + n$. We should recover the Gaussian field for $l = 0$. The electric field $\mathcal{E}_{lp}(\mathbf{r}) = \varepsilon_{lp}(\mathbf{r}) e^{i\theta_{lp}(\mathbf{r})}$ is,

$$\begin{aligned} \varepsilon_{lp}(\mathbf{r}) &= \varepsilon_{00} \sqrt{\frac{p!}{(|l|+p)!}} \ \frac{e^{-r^2/w(z)^2}}{\sqrt{1 + z^2/z_R^2}} \ \left(\frac{r\sqrt{2}}{w(z)} \right)^{|l|} \ L_p^{|l|} \left(\tfrac{2r^2}{w(z)^2} \right) \ , \\ \theta_{lp}(\mathbf{r}) &= \frac{kr^2 z}{2\,(z^2 + z_R^2)} + l\phi + (2p + l + 1) \arctan \frac{z}{z_R} + kz \ . \end{aligned} \tag{21.48}$$

With the Rabi frequency defined through,

$$\Omega_{lp}(\mathbf{r}) = \Omega_0 \frac{w_0}{w(z)} \ e^{-r^2/w(z)^2} \ \left(\frac{r\sqrt{2}}{w(z)} \right)^{|n-m|} \ L_{\min(n,m)}^{|n-m|} \left(\tfrac{2r^2}{w(z)^2} \right) \ , \tag{21.49}$$

Using the optical Bloch equations, we find the stationary solutions for the dipole and the dissipative forces [20],

$$\begin{aligned} \mathbf{F}_{dip} &= -2\hbar \Omega_{lp}(\mathbf{r}) \ \frac{\Delta}{4\Delta^2 + 2\Omega_{lp}(\mathbf{r})^2 + \Gamma^2} \nabla \Omega_{lp}(\mathbf{r}) \ , \\ \mathbf{F}_{diss} &= 2\hbar \Omega_{lp}^2(\mathbf{r}) \ \frac{\Gamma}{4\Delta^2 + 2\Omega_{lp}(\mathbf{r})^2 + \Gamma^2} \nabla \theta_{lp}(\mathbf{r}) \ . \end{aligned} \tag{21.50}$$

where the gradients are,

$$\nabla \Omega_{lp}(\mathbf{r}) = ... \tag{21.51}$$

and,

$$\begin{aligned} \nabla \theta_{lp}(\mathbf{r}) &= -\nabla \left[-kz - l\phi - \frac{kr^2 z}{2(z^2 + z_R^2)} - (n + m + 1) \tan^{-1} \frac{z}{z_R} \right] \\ &= \left(k + \frac{kr^2}{2(z^2 + z_R^2)} \left(1 - \frac{2z^2}{z^2 + z_R^2} \right) + \frac{(n + m + 1) z_R}{z^2 + z_R^2} \right) \hat{\mathbf{e}}_z + \frac{krz}{z^2 + z_R^2} \hat{\mathbf{e}}_r + \frac{l}{r} \hat{\mathbf{e}}_\phi \ . \end{aligned} \tag{21.52}$$

Here we assume the velocity cold enough not to influence the detuning. Otherwise, we must substitute $\Delta \to \Delta - \mathbf{v}\nabla\theta$. At the waist $z = 0$ and for typical experimental conditions $r, k^{-1} \ll z_R$,

$$\nabla\theta_{lp}(\mathbf{r}) \approx k\hat{\mathbf{e}}_z + \frac{l}{r}\hat{\mathbf{e}}_\phi \ . \tag{21.53}$$

We can now write the azimuthal force and the torque in analogy to the radiation pressure,

$$\mathbf{F}_{az} = \hbar\frac{\mathbf{l}}{r}\ \frac{I}{\hbar\omega}\ \sigma(\Delta) \tag{21.54}$$

and,

$$\mathbf{T} = \hbar\frac{\mathbf{r}\times\mathbf{l}}{r}\ \frac{I}{\hbar\omega}\ \sigma(\Delta) \ . \tag{21.55}$$

If we further concentrate on the first Laguerre-Gaussian mode given by $l = 1$ and $p = 0$ or $n = 1$ and $m = 0$, and assume low saturation $\Omega \ll \Gamma$, we find the force,

$$\mathbf{F}_{diss} = -\hbar\Gamma\left[k\hat{\mathbf{e}}_z + \frac{\hat{\mathbf{e}}_\phi}{r}\right]\ e^{-2r^2/w_0^2}\ \frac{2r^2}{w_0^2}\ \frac{\Omega_0^2}{4\Delta^2+\Gamma^2} \ . \tag{21.56}$$

It consists of a rotational torque and a component in $\mathbf{k}$ direction. For a normal Gaussian field, $l = 0$. The LG modes have a ring-shaped intensity distribution $I^{(Lag)}(x, y)$. Therefore, the rotational force depends on the distance from the axis and has a maximum at the radius $r = w_0/2$. The dipole force contribution may be neglected close to resonance, and higher-order contributions from the LG mode as well.

21.3.1.5 Laguerre-Gaussian standing wave

Many experiments are performed within the Rayleigh range, $z \ll z_R$, where,

$$\begin{aligned} \mathcal{E}_{pl}(r,\phi) &= \mathcal{E}_0 f_{pl}(r)\ e^{-il\phi}e^{\imath(\omega t-kz)} \ , \\ f_{pl}(r) &= \frac{\Omega_{pl}(r)}{\Omega_0} = \frac{e^{-r_w^2/2}}{z_R}\ r_w^{|l|}\ L_p^{|l|}(r_w^2) \ . \end{aligned} \tag{21.57}$$

where we introduced the normalized paraxial distance $r_w \equiv r\sqrt{2}/w_0$. When such a Laguerre-Gaussian beam is reflected form a mirror reflected from a mirror it changes the signs of $k \longrightarrow -k$ but not $l \to l$. We obtain a standing wave, made of ring-shaped potentials,

$$\left|f_{pl}(r)\ e^{-\imath l\phi}e^{\imath(\omega t-kz)} + f_{pl}(r)\ e^{-\imath l\phi}e^{\imath(\omega t+kz)}\right|^2 = 4f_{pl}^2(r)\cos^2 kz \ . \tag{21.58}$$

At $z = 0$ the potential reads

$$U_{pl} = \frac{\Omega^2}{4\Delta} = \frac{\sigma_0\Gamma I(x,y)}{\hbar\omega 4\Delta} = \frac{\Omega_0^2}{4\Delta}4f_{pl}^2(r) \ , \tag{21.59}$$

If in contrast the counterpropagating beam has an inverse angular momentum,

$$\left|f_{pl}(r)\ e^{-\imath l\phi}e^{i(\omega t-kz)} + f_{pl}(r)\ e^{\imath l\phi}e^{\imath(\omega t+kz)}\right|^2 = 4f_{pl}^2(r)\cos^2(kz-l\phi) \ , \tag{21.60}$$

the superposition of a Laguerre-Gaussian beam with a reflected beam gives an azimuthally periodic modulation like a circular $1D$ lattice, which is twisted along the $\hat{z}$-axis. However there is no axial confinement. The intensity resembles a knot of l worms winding about the $\hat{z}$-axis at constant distance like helices. Axial modulation has to be obtained by an additional plane wave [27].

Let us calculate the dipole force via $\mathbf{F} = -\nabla U$,

$$\begin{aligned} \frac{\partial f_{pl}^2(r)}{\partial x} &= 2 f_{pl}(r) \frac{\partial r}{\partial x} \frac{\partial}{\partial r} \frac{e^{-r_w^2/2}}{z_R} \; r_w^{|l|} \; L_p^{|l|}(r_w^2) \\ &= f_{pl}(r)^2 \frac{8x}{w_0^2} \left[\frac{|l|}{2r_w^2} - \frac{1}{2} - \frac{L_{p-1}^{|l|+1}(r_w^2)}{L_p^{|l|}(r_w^2)} \right] \end{aligned} \tag{21.61}$$

using $\frac{d}{dx} L_n^{(m)}(x) = -L_{n-1}^{(m+1)}(x)$.

21.3.1.6 Creation of Laguerre-Gaussian modes

The polarization of light couples to the internal degrees of freedom of the atoms. But special light modes, i.e. the higher-order Laguerre-Gaussian (LG) modes, may carry orbital angular momentum. This angular momentum couples to the external degrees of freedom of the atoms [21, 65, 22, 20], i.e. the light exerts a torque onto the atoms. This light force is, however, very weak and in a gas cell with hot atoms, the Doppler-effect smears out the motional effect. Nevertheless, the torque has been observed with macroscopic particles [1208]. And in a Magneto-Optical Trap (MOT), phase-conjugation by nondegenerate four-wave mixing has been used to indirectly prove the transfer of angular momentum to the atoms [1289]. Finally, MOTs using Laguerre-Gaussian laser beams been constructed, however without demonstrating the effect of the torque [757, 1223].

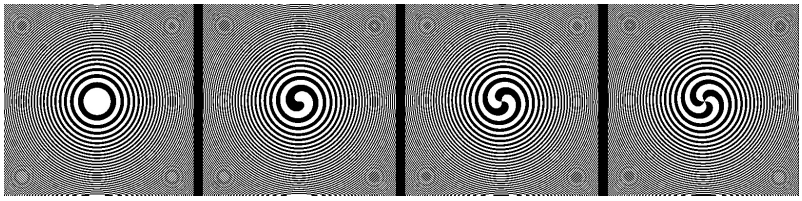

Figure 21.3: Masks for generating Laguerre-Gaussian beams.

The interference of such a mode with a plane wave v yields interference patterns proportional to,

$$u_{nm}(\mathbf{r}) e^{-ikz} + v_{nm}(\mathbf{r}) e^{-ikz} \propto \cos\left(-l\phi - \frac{kr^2 z}{2z_R^2} - (m+n+1) \arctan \frac{z}{z_R} \right) . \tag{21.62}$$

At some distance $z \neq 0$ and for $l \neq 0$ the patterns have Yin-Yang spiral shape. Inversely, like in holography, plane waves are *diffracted* at the spiral patterns in such a way that they generated a Laguerre-Gaussian mode. This is not an image. Images are also formed with undiffracted parts of the plane wave. The patterns form a fundamental focus at a distance f and subfoci at distances $f/2$, $f/3$, ... The fundamental

beam is separated from the undiffracted and higher-order Fresnel modes by a short focal length lens placed in the fundamental focus. A spiral mask can be generated by setting $z = z_R$ in Eq. (21.62) and filling black the region where r and ϕ satisfy [593],

$$\cos\left(-l\phi - \frac{kr^2}{2z_R} - \pi(n + 1/2)\right) > 0 \ . \tag{21.63}$$

A special case is defined by $l = 0$ which reproduces the *Fresnel zone plate*. The orbital momentum may be transferred to the atomic motion. Perhaps this also has an effect on the internal degrees of freedom: The higher-order orbital angular momentum may couple to higher multipole moments. At reflection on a mirror, the symmetry of the LG mode is inverted. Therefore, we can build a standing wave LG beam with no axial force (if the intensities are balanced and the waists matched) and twice the torque. LG modes can also be created from normal Gaussian modes with an arrangement of cylindrical lenses.

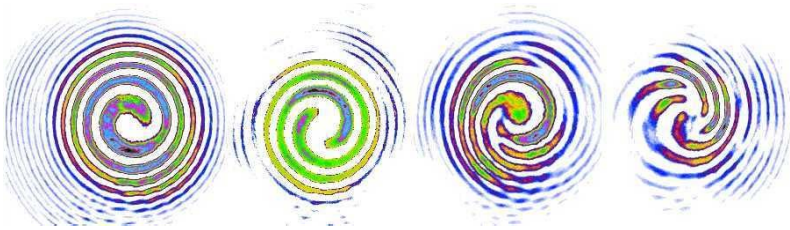

Figure 21.4: Laguerre-Gaussian beams with various charges.

21.3.1.7 Optical signatures

The interference of a Laguerre-Gaussian mode (LGM) with a phase-matched plane wave Gaussian beam yields interference patterns shown in the above figure. In the far-field, the laser beam forms a ring-shaped LGM. Higher-order topological charges are easily detected in the interference patterns through the occurrence of bifurcations or by the number of arms spiraling into the center.

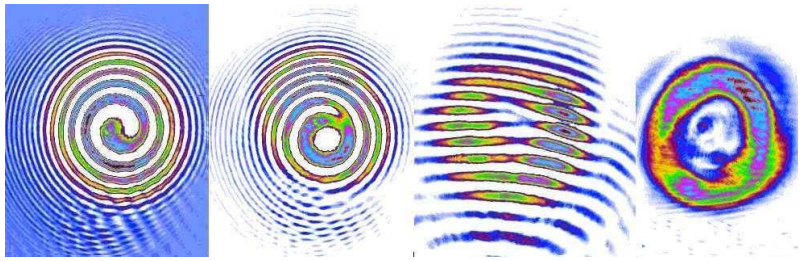

Figure 21.5: Bifurcations in a Laguerre-Gaussian beam.

21.3.1.8 Detection of photon torque in ion traps

The general force of a light beam on an atom consists of the dipole force which depends on the intensity gradient in the light beam and the radiation pressure which is proportional to the phase gradient. The dipole force has a neglegible contribution to the torque, so that we will concentrate on the radiation pressure.

The torque eventually accelerates a rotational motion of the irradiated atoms that may be directly detected by suitable velocimetric schemes (i.e. heterodyne beating [1371]). The methods are based either on the Doppler effect shifting the atomic resonance lines or on the spatial resolution of the coordinate ot momentum distribution of the atoms. We will discuss four possibilities: A. fluorescence spectra, B. excitation spectra, C. fluorescence imaging, D. absorption imaging.

For detection of the pure effect, one might consider either free atoms, optical molasses, atoms trapped in a MOT or ions confined in Penning or Paul traps. Ion traps are better suited for detecting the Doppler shift [1048]. The ion traps are very deep (several eV) so that they can stay trapped even when heated by laser beams. MOTs or molasses or cold atoms in free expansion might allow to detect the effect of redistribution of the atoms by the azimuthal force.

Hot gases have inhomogeneously Doppler broadened fluorescence spectra. For a Maxwell-Boltzmann velocity distribution, the line profile will be Gaussian. On the other hand, if the atoms are cold $k\bar{v} < \Gamma$, the inhomogeneous broadening disappears and the linewidth is given by the spontaneous decay of the upper level (Lamb-Dicke regime). If cold atoms are subject to a torque, the velocity distribution will exhibit a significant deviation from the Gaussian shape. The shape of the fluorescence spectrum also should strongly depend on the observation axis. In the simplest case of atoms rotating with a constant velocity of 12 m/s around the z-axis, watching perpendicularly to the z-axis the fluorescence spectrum should exhibit shoulders. Could also take stroboscopic TOF pictures. For sodium $\Gamma = 2\pi \times 10\,\mathrm{MHz}$ this corresponds to 6 m/s velocity or 40 μK temperature.

The excitation spectrum of a single oscillating two-level atom is easy to predict. For a sodium atom $\lambda = 589\,\mathrm{nm}$, rotating with $\omega_{rot} = 2\pi \times 10\,\mathrm{kHz}$ on an orbit with $r = 1\,\mathrm{mm}$, radius the excitation spectrum can be described by a convolution (figure). For multi-level systems, we have to solve the Bloch equations with an oscillating term using the method of infinite fractions. For sodium, the characteristics cannot be resolved because of the hyperfine splitting being smaller than $kv_{\max} \approx 2\pi \times 100\,\mathrm{MHz}$. Cesium might be better.

Experimentally, one could either analyze the *fluorescence spectrum* with homodyne beating or deduce the velocity distribution from the dependence of the optical cross section of the Doppler-induced detuning, i.e. by recording *excitation spectra* [2].

21.3.1.9 Detection of photon torque in atomic gases

Let us consider a cloud of 10^9 sodium atoms at densities around $10^9\,\mathrm{cm}^{-3}$ and temperatures around 300 μK. Then the magnetic field is suddenly switched off and the laser beams are detuned further from resonance and attenuated. This configuration consists a friction force for the atoms, but there is no restoring force. The atoms move

[2] An interesting question is whether there is coupling to higher multipole moments of internal transitions.

in this so-called *optical molasses* for 5 ms before the laser beams are switched off, too. After 15 ms, a time-of-flight image tells us the velocity distribution at the switch-off time. During the molasses period, we can irradiate two counterpropagating LG laser beams along the symmetry axis of the trap. This light is resonant to the $F = 2$ to $F' = 3$ transition of the $D2$ line.

Being released from the MOT, the atoms are initially inhomogeneously distributed in space as well as in velocity space. Then molasses, then atoms feel different $\Omega(\mathbf{r}, \Delta)$. Effects of optical pumping and repumping in a multi-level system? Problems with imbalanced z component in the standing wave LG beam? Consider collisions? Atoms get out of resonance when $kv \gg \Gamma, \Omega$.

Comparing the equations for radiation pressure and for the azimuthal force, we see that the relative strength of the forces is like k and r^{-1} which is on the order of 1:10000 for typical experimental conditions, and the wanted effect is rather small. The longitudinal radiation pressure can be compensated by taking two counterpropagating beams. Upon reflection on a mirror, the symmetry of the LG mode is inverted, so that it is easy to build a standing wave LG beam with no axial force (if the intensities are balanced and the waists matched) and twice the torque [3].

21.3.1.10 Monte-Carlo simulations

Numerical Monte-Carlo simulations of the motion of the atoms in a Laguerre-Gaussian beam can be performed by solving the deterministic Newton equations and adiabatically updating the initial conditions. This procedure disregards the stochastic recoil induced by spontaneous emission and therefore does not reproduce the random walk of the atoms. We start by generating a numeric atomic cloud trapped in a MOT with randomly distributed initial conditions in position and velocity space. The velocity distribution is chosen according to a temperature of 300 μK, the position distribution according to reproduce the experimentally observed size of the MOT, i.e. typically 3 mm. We sometimes arbitrarily distort the position distribution to make the influence of the torque more visible.

It is important to consider the cross saturation of both the molasses and the Laguerre beams $j = ML, LG$:

$$\sigma_{m=x,y,z}(\Delta^{(j)}) = \frac{\Gamma^2}{4(\Delta^{(j)} - k\hat{\mathbf{e}}_m\mathbf{v} - \mu_B/\hbar \cdot (\mathbf{r}\cdot\nabla)B)^2 + 2\sum_j \sum_{n=x,y,z} 2\Omega_n^{(j)}(\mathbf{r})^2 + \Gamma^2} , \tag{21.64}$$

where

$$\Omega^{(ML)}_{m=x,y,z}(\mathbf{r}) = \Omega^{(ML)} e^{-|\hat{\mathbf{e}}_m \times \mathbf{r}|^2/w^2_{mot}} \tag{21.65}$$

and

$$\Omega^{(LG)}_{m=x,y}(\mathbf{r}) = \Omega^{(LG)} e^{-|\hat{\mathbf{e}}_m \times \mathbf{r}|^2/w^2_{LG}} \sqrt{2}\frac{|\hat{\mathbf{e}}_m \times \mathbf{r}|}{w_{LG}} . \tag{21.66}$$

[3] An interesting question is whether LG beams can be coupled into linear cavities. If so, we expect ring-shaped intensity profiles, with axial standing wave modulation, having a constant angular momentum along axial direction. This would represent an ideal system to study torque, since the axial component is balanced *exactly*.

The forces of the molasses beams and the Laguerre-Gaussian beam are calculated in two dimensions by,

$$\mathbf{F} = \sum_{m=\pm x,\pm y,\pm z} \hat{\mathbf{e}}_m \hbar k \cdot \frac{\Omega_m^{(ML)}(\mathbf{r})}{\Gamma}^2 \cdot \frac{\sigma_m(\Delta^{(ML)})}{\sigma_0} + \sum_{m=\pm x,\pm y} \hat{\mathbf{e}}_\vartheta \hbar/r \cdot \frac{\Omega_m^{(LG)}(\mathbf{r})^2}{\Gamma} \cdot \frac{\sigma_m(\Delta^{(LG)})}{\sigma_0} \ . \tag{21.67}$$

Employing the Verlet algorithm for the Monte-Carlo iteration of the position and velocity of the atoms after each time step dt

$$\begin{aligned} \mathbf{r} &= \mathbf{r}_0 + \mathbf{v}_0 dt + \tfrac{1}{2m}\mathbf{F}_0 dt^2 \\ \mathbf{v} &= \mathbf{v}_0 + \tfrac{1}{2m}(\mathbf{F} + \mathbf{F}_0) dt \\ t &= t + dt \ . \end{aligned} \tag{21.68}$$

Here, Δ_{mot}, Ω_{mot}, and w_{mot} denote the detuning, Rabi frequency and waist of the molasses (and MOT) beams.

A more sophisticated method would simulate the random walk by including spontaneous emission either simultaneously doing Monte-Carlo wavefunction simulations of the optical Bloch equations or by simulating a random waiting time to the next absorption process.

The most obvious impact of the Laguerre-Gaussian beam on the atomic motion was seen when 1) a non-uniform spatial MOT distribution was generated, 2) the LG beam was strongly saturating and irradiated for several ms during the molasses period (that way, the velocity distribution was modified by the torque, but the viscous friction did not allow a radial acceleration), 3) the atoms were allowed to ballistically expand. This converted the velocity distribution into a position distribution and gave rise to a characteristic shape of the atomic cloud [478].

21.3.2 Exercises

21.3.2.1 Ex: Gaussian and Laguerre-Gaussian beams

Convince yourself that the Laguerre-Gaussian beam parametrized in (21.42) corresponds to the Gaussian beam of (18.293).

Solution: *The Gaussian beam is,*

$$\psi(\mathbf{r}) = \frac{w_0}{w} e^{\imath \arctan(-z/q_0) - \imath k(x^2+y^2)/2q} = \frac{w_0}{w} e^{-kr^2 z_R/2(z^2+z_R^2)} e^{\imath \arctan(-z/q_0) - \imath k r^2 z/2(z^2+z_R^2)} \ ,$$

using (18.288). On the other hand, the zero-order Laguerre-Gaussian beam is,

$$\begin{aligned} u_{00}(\mathbf{r}) &= \frac{u_0}{\sqrt{z^2+z_R^2}} e^{-kr^2 z_R/2(z^2+z_R^2)} e^{\imath \arctan(-z/q_0) - \imath k r^2 z/2(z^2+z_R^2} \\ &= \frac{u_0}{z_R}\frac{w_0}{w} e^{-kr^2 z_R/2(z^2+z_R^2)} e^{\imath \arctan(-z/q_0) - \imath k r^2 z/2(z^2+z_R^2)} = \frac{u_0}{z_R}\psi(\mathbf{r}) \ , \end{aligned}$$

using $L_0^0(x) = 1$.

21.3.2.2 Ex: Motion of atoms in Laguerre-Gaussian beams

Programs on the motion of atoms in Laguerre-Gaussian beams.

Solution: *LaguerreGaussian1*
LaguerreGaussian2 intensity and phase profile and force fields.
LaguerreGaussian3 beating with a plane wave.
LaguerreGaussian4 superposition with a reflected wave.
LaguerreExpansion Motion of a free atom in a MOT with Laguerre-Gaussian laser beam. Calculated trajectories and endpoints for several atoms, the force stops when Doppler shift ¿ linewidth.
LaguerreExpansion1 Only endpositions calculated.
LaguerreExpansion2 Makes a movie.
LaguerreExpansion3 Makes a movie, specializes on first order Laguerre beam.
LaguerreExpansion4 Nonlinearized molasses forces without random walk by spontaneous emission.
LaguerreExpansion5 Atomic motion in a ring built by counterpropagating LG beams with dipole force.

21.3.2.3 Ex: Linear momentum density for Hermite-Gaussian modes

Compare the linear momentum density for Hermite-Gaussian (18.293) and Laguerre-Gaussian (21.42) modes.

Solution: *Using (18.290) ...*

21.4 Special topic: Superconductivity

At low temperatures some metals completely give up electric resistance. This effect found by Kammerlingh-Onnes is called *superconductivity* and has been explained through Bose-Einstein condensation of electron pairs [290]. But before we outline this theory let us try a classical approach based on electrodynamics as proposed by Fritz and Heinz London.

21.4.1 London model of superconductivity and the Meissner effect

We learned in Sec. 14.3.2 that *Ohm's law* is explained within the Drude model by the fact that the accelerating Coulomb force of the electric field, $m\dot{\mathbf{v}} = q\vec{\mathcal{E}}$, is spoiled by collisions,

$$\mathbf{j} = \varsigma\vec{\mathcal{E}} \,. \tag{21.69}$$

Let us now suppose a perfect conductor, where collisions are absent. Then, if we want the current density $\mathbf{j} = \varrho\mathbf{v}$ to be constant,

$$0 = \dot{\mathbf{j}} = \varrho\dot{\mathbf{v}} = -\frac{q^2 n_e}{m}\vec{\mathcal{E}} \,, \tag{21.70}$$

where $\varrho = -en_e$ is the free electron charge density.

Let us now study the behavior of the magnetic field in a conductor with $\mu_0 = 0$. Maxwell's equations require,

$$\nabla \times \vec{\mathcal{E}} = -\dot{\vec{\mathcal{B}}} \quad \text{and} \quad \nabla \times \vec{\mathcal{B}} = \mu_0 \mathbf{j} + \dot{\vec{\mathcal{D}}} \,. \tag{21.71}$$

Assuming $\dot{\vec{\mathcal{D}}} = 0$ the above equations can easily be solved, yielding,

$$\boxed{\nabla^2 \dot{\vec{\mathcal{B}}} = \frac{\mu_0 n_e q^2}{m} \dot{\vec{\mathcal{B}}}} \,. \tag{21.72}$$

This equation describes the behavior of a magnetic field in and around a perfect conductor.

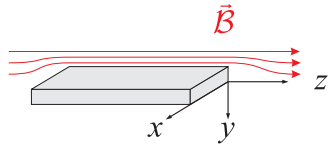

Figure 21.6: Scheme of the Meissner effect.

As we will see in Exc. 21.4.5.1, the solution of Eq. (21.72) predicts an expulsion of the magnetic field out of the conductor, as illustrated in Fig. 21.6. This effect is termed the *Meissner-Ochsenfeld effect*. That is, in the absence of resistivity, a conductor acts like a perfect diamagnetic (magnetic susceptibility $\chi_m = 1$). According to the Lenz rule, the electrons try to compensate any $\mathcal{B}$-field change by collectively rotating such as to counteract the change. The electrons rotate in such a way that the $\mathcal{B}$-field disappears inside the conductor, which leads to an amplification of the field near the surfaces. As a consequence, permanent magnets are repelled from superconducting surfaces.

The problem is that the discontinuity of the magnetic field at the periphery of the superconductor should violate the continuity equation. And in fact, it is experimentally observed, that the magnetic field is not completely expelled from thin superconducting films, because the magnetic field penetrates somewhat into the superconductor with the penetration depth λ_L. In order to understand this, it is necessary to replace the classical *Ohm's law* for the current density $\mathbf{j}$ and the electric field $\vec{\mathcal{E}}$, $\mathbf{j} = \varsigma \vec{\mathcal{E}}$, by the *London equation*.

The London brothers postulates that the magnetic field inside a superconductor would not only be constant, as predicted by Eq. (21.72) by vanish altogether,

$$\boxed{\nabla^2 \vec{\mathcal{B}} = \frac{\mu_0 n_e q^2}{m} \vec{\mathcal{B}}} \,. \tag{21.73}$$

We will study consequences of this equation in Exc. 21.4.5.2.

21.4.1.1 Derivation of the London equation

The London equation can be derived in the framework of quantum mechanics, considering the superconducting state as a macroscopically extended quantum state de-

scribed by the following wavefunction,

$$\psi(\mathbf{r}) = \psi_0 e^{\imath S(\mathbf{r})} \ , \tag{21.74}$$

where $S = S(\mathbf{r})$ is the phase of the macroscopic wavefunction. $\psi_0^2 = n_e$ corresponds to the density of the number of Cooper pairs in the superconductor. The implicit assumption of a homogeneous density of the Cooper pairs is reasonable, since the pairs are negatively charged and repel each other. Any imbalance of the density of pairs would therefore generate an electric field, which would be compensated immediately. The kinetic momentum operator in the presence of a magnetic field, $\mathbf{p} = -\imath\hbar\nabla - q\mathbf{A}$, where $\mathbf{A} = \mathbf{A}(\mathbf{r}, t)$ is the vector potential of the magnetic field, applied to the wavefunction ψ gives,

$$m\mathbf{v}\psi = \mathbf{p}\psi = (\hbar\nabla S - q\mathbf{A})\psi \ . \tag{21.75}$$

That is,

$$\mathbf{v} = \frac{\hbar}{m}\nabla S - \frac{q}{m}\mathbf{A} \ . \tag{21.76}$$

With $\mathbf{j} = qn_e\mathbf{v}$ follows immediately,

$$\boxed{\mathbf{j} = \frac{n_e q\hbar}{m}\nabla S - \frac{n_e q^2}{m}\mathbf{A}} \ . \tag{21.77}$$

This is the London equation.

There are two useful forms of this equation, sometimes referred to as the 1^{st} and the 2^{nd} London equation,

$$\partial_t \mathbf{j} = \frac{n_e q^2}{m}\vec{\mathcal{E}} \ , \tag{21.78}$$

and

$$\nabla \times \mathbf{j} = -\frac{n_e q^2}{m}\vec{\mathcal{B}} \ . \tag{21.79}$$

The phase S does not contribute to these two equations. It does not contribute to the first equation, because the phase is only dependent on the position and therefore constant in time, and it does not contribute to the second equation, because $\nabla \times \nabla S = 0$ [4]

21.4.2 BCS theory

Many-body effects like superconductivity are not explained by the free electron or the Bloch model. Superconductivity is characterized by two main features: The disappearance of electrical resistance in some metals at temperatures below roughly $T \simeq 10\,\mathrm{K}$, and the expulsion of magnetic flux lines out of the metals, known as Meissner-Ochsenfeld effect.

According to Bardeen-Cooper-Schrieffer near the edge of the Fermi surface induced by weak attractive interactions strong correlations in momentum space may build up.

[4] Note that, although the phase does not contribute to the last two formulas, it should not be neglected! If the phase component were not included, it would mean that the current density without magnetic field would have to be zero. In reality, however, the phase gradient can also contribute to the current density, which therefore need not necessarily be zero, i.e. the current density is not zero, although no magnetic field is applied.

Such interations can be mediated by local polarization traces, i.e. deformations of the lattice or phonons, imprinted by a moving electron into the metallic lattice and sensed by a second electron following at a reasonable distance [207, 244]. Thus Fermi gases are unstable with respect to formation of bound fermion pairs. However, fermion pairs are not bound in the ordinary sense, and the presence of a filled Fermi sea is essential. Rather, we have a many-body state. Hence, the interpretation as a Bose-condensate of Cooper pairs explains some characteristics like the existence of a delocalized macroscopic wavefunction and the superfluid-like behavior suppressing the electrical resistance. But it oversimplifies and does not account for the important role of fermionic statistics in the many-body state.

The requirements for Cooper pairing are 1. low temperature to rule out thermal phonons, 2. strong electron-lattice interaction, 3. many electrons just below E_F, 4. anti-parallel spins, and 5. antiparallel momentum of the electrons.

Below T_c the motions of the electrons and the ions in the lattice are highly correlated. Cooper pairs are weakly bound, in thermal equilibrium with unpaired electrons, and have a vanishing total momentum. The typical distance of the electrons in a pair is roughly 100 nm. Although the fraction of paired electrons is only 10^{-4}, their number within the volume occupied by a single pair is 10^6.

Cooper-pairs form through scattering processes. Since all states below the Fermi surface are occupied, the final momenta must be above k_F. In other words, the two electrons are excited from slightly below $E = E_F$ to slightly above $E + E_g/2 = E_F$, where they profit from the large amount of available empty states allowing for their high mobility and letting them transit into the strongly correlated pairing state. The pairs then have the binding energy E_g, because the increase in kinetic energy must be overcompensated by the potential energy. Such processes smooth out the Fermi edge even at $T = 0$, as if the temperature really were at $T \simeq T_c$.

An energy gap forms which has just the width E_g. Its origin is understood as follows: If an electron could slightly change its energy, the pair correlation would immediately break up and the binding energy E_g liberated. But this energy cannot be dissipated. Since the binding energy for Cooper pairs is roughly $E_g \simeq 3k_BT_c$, a thermal noise source must at least provide the energy $3k_BT_c$, which is not possible if $T < T_c$. At higher temperatures, the pairing gap narrows and vanishes at $T = T_c$. The gap can be spectroscopically probed with IR radiation.

Higher $\mathcal{B}$ fields require lower critical temperatures. The critical temperature drops with rising mass of the ions, $T_c m^{1/2} = const.$ This indicates that the vibration of the lattice ions is crucial for superconductivity.

Magnetic fields trying to penetrate superconducting wires perturb the superconductivity. This problem can be reduced in type II superconductors, where the size of the Cooper pairs are reduced and employing superconducting wires containing normal conducting channels.

The quantitative treatment starts with the two-body Schrödinger equation,

$$\left[-\frac{\hbar^2}{2m}(\nabla_1^2 + \nabla_2^2) + V(r_1 - r_2)\right] \Psi(r_1, r_2) = (E + 2E_F)\Psi(r_1, r_2) \ . \tag{21.80}$$

Here we assume singlet pairing s-wave collisions. Center-of-mass and relative coordinates are now separated, giving,

$$\left[-2\frac{\hbar^2}{2m}\nabla_r^2 + V(r)\right]\psi(r) = \left(E + 2E_F - \frac{\hbar^2 K^2}{4m}\right)\Psi(r) \ . \tag{21.81}$$

Transforming into momentum space, assuming that the Fourier transform $V(p,p') = V^{-1}\int e^{-\imath(p-p')r}V(r)d^3r$ is only nonzero, $= V_0$, inside an energy interval smaller than the Debye frequency $\hbar\omega_D$ close to the Fermi surface, we finally arrive at the binding energy of the Cooper-pair,

$$E = -\frac{2\hbar\omega_D}{e^{2/V_o D(E_F)} - 1} \ , \tag{21.82}$$

where $D(E_F) \propto k_F$ is the density of states at the Fermi surface. Estimating $V(r) \approx \hbar^2/ma^2$ the Fourier transform goes like $V_0 \propto a$, so that $k_B T_{BCS} \propto -e^{-\pi/2k_F|a_s|}$(see Sec. 49.4).

A full quantum treatment reveals the presence of a gap. This gap can also be understood in the following way. In the normal state the energy spectrum is twofold degenerate. A state with a hole in the Fermi surface has the same energy as a state with an electron above the Fermi surface. Cooper-pairing couples those states, which leads to energy splitting and introduces a *pairing gap*,

$$|u_k|^2 = \frac{1}{2}\left[1 + \frac{\epsilon_k - E_F}{\sqrt{\Delta_0^2 + (\epsilon_k - E_F)^2}}\right] = 1 - |v_k|^2 \tag{21.83}$$
$$\Delta = -\sum_k u_k v_k \ .$$

The product $u_k v_k$ only contributes near the Fermi surface. We get a density of states,

$$D_s(E) = D_n \frac{|E - E_F|}{\sqrt{-\Delta_0^2 + (\epsilon_k - E_F)^2}} \ , \tag{21.84}$$

which has a gap. The states are redistributed toward the edges of the gap.

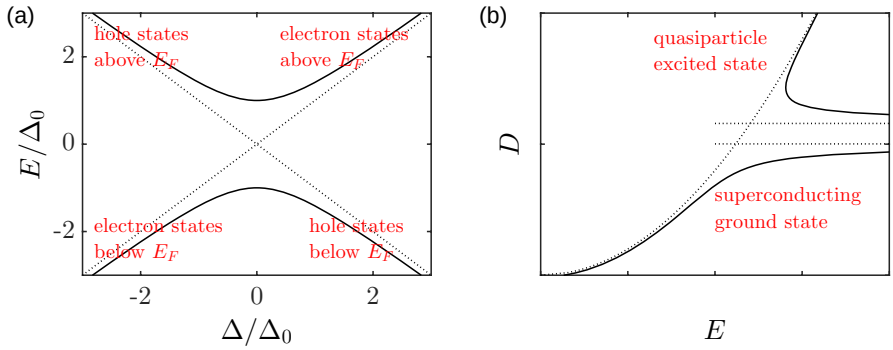

Figure 21.7: Pairing gap in the energy spectrum and the density of states.

21.4.3 Josephson junctions

Two superconductors that are joined by a nm thin isolating oxide layer build a *Josephson junction* (JJ) [685]. Cooper pairs may tunnel through the junction producing a current flow i_J. The basic JJ is described by,

$$i_J = I_c \sin\varphi \qquad \text{and} \qquad v = \frac{\Phi_0}{2\pi}\frac{d\varphi}{dt} \ , \tag{21.85}$$

where

$$\Phi_0 = \frac{h}{2e} \ . \tag{21.86}$$

I_c is the critical supercurrent of the junction, and v is the voltage at the JJ. φ is a dynamical variable describing the phase difference between the macroscopic wave functions on both sides of the junction. Note that for small φ we have $u \propto i$ similar to the situation in a magnetic coil. The *ac*-Josephson effect consists in applying a constant voltage. Then φ increases linearly in time and the Josephson-current oscillates at a given (microwave) frequency [505],

$$f_J = \frac{v}{\Phi_0} \ . \tag{21.87}$$

This allows a very precise measurement of h/e.

21.4.4 Synchronization of coupled Josephson junctions

The superconducting flux is quantized. A *superconducting quantum interference device* consist of two JJs connected in parallel. In that way the *supercurrent* is split and recombined.

21.4.4.1 Resistively shunted junctions

In a widely accepted model of nonideal *resistively shunted junctions* (RSJ) [1031] the junction current consists of three components: A superconducting current $i_J = I_c \sin\varphi$, a resistive current $i_R = v/R$, and a capacitance current $\dot{v}C$ (see Fig. 21.8). From Kirchhoff's laws using (21.85),

$$C\frac{\Phi_0}{2\pi}\frac{d^2\varphi}{dt^2} + \frac{1}{R}\frac{\Phi_0}{2\pi}\frac{d\varphi}{dt} + I_c \sin\varphi = i \ , \tag{21.88}$$

if the resistance is assumed independent of the applied voltage. Located in front of the term $\dot{\varphi}$ the resistivity is inversely proportional to the dissipation. The reason for this is that dissipation occurs via *single-particle tunneling*. Note that the equation is identical to that of an overdamped rotator or of a phase-locked loop.

Neglecting the resistance, the equation of motion can be derived from the Hamiltonian,

$$\hat{H} = \frac{p_\varphi^2}{2C\Phi_0/2\pi} - i\varphi - I_c \cos\varphi \ , \tag{21.89}$$

via $\dot{\varphi} = \frac{\partial H}{\partial p_\varphi}$ and $\dot{p}_\varphi = -\frac{\partial H}{\partial \varphi}$. The φ and p_φ are conjugate variables,

$$[\varphi, p_\varphi] = \imath \ . \tag{21.90}$$

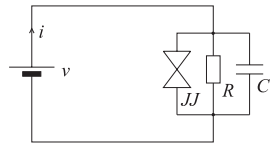

Figure 21.8: Resistively shunted Josephson junction.

Let us go to scaled variables via $\tilde{H} \equiv H/(C\Phi_0/2\pi)$, $\tilde{p_\varphi} \equiv p_\varphi/(C\Phi_0/2\pi)$, $K \equiv I_c/(C\Phi_0/2\pi)$, and $\lambda \equiv i/(C\Phi_0/2\pi)$,

$$\tilde{H} = \frac{\tilde{p}_\varphi^2}{2} - \lambda\varphi - K\cos\varphi \ , \tag{21.91}$$

In these units,

$$[\varphi, \tilde{p}_\varphi] = \imath\frac{e}{\hbar C} \ . \tag{21.92}$$

21.4.4.2 Response to *ac* driving sources

Let the applied voltage be $v(t) = V_0 + V_s\cos\omega_s t$. We may substitute the voltage in (21.85) and integrate,

$$\varphi = \varphi(0) + \frac{2\pi}{\Phi_0}V_0 t + \frac{2\pi}{\Phi_0}\frac{V_s}{\omega_s}\sin\omega_s t \ . \tag{21.93}$$

The resistive current is then,

$$i_R = \frac{V_0}{R} + \frac{V_s}{R}\cos\omega_s t \ , \tag{21.94}$$

and plugging (21.93) this into the Josephson current (21.85),

$$\begin{aligned} i_J &= I_c\sin\left(\varphi(0) + \frac{2\pi}{\Phi_0}V_0 t + \frac{2\pi V_s}{\Phi_0\omega_s}\sin\omega_s t\right) \\ &= I_c\sum_n (-1)^n J_n\left(\frac{2\pi V_s}{\Phi_0\omega_s}\right)\sin\left[(f_J - n\omega_s)t + \varphi(0)\right] \ , \end{aligned} \tag{21.95}$$

where we expanded the double sine into Bessel-functions. The time-averaged Josephson current disappears unless $f_J = n\omega_s$,

$$\bar{i}_J = I_c\sum_n (-1)^n J_n\left(\frac{2\pi V_s}{\Phi_0\omega_s}\right)\sin\left[\varphi(0)\right]\ \delta(f_J - n\omega_s) \ . \tag{21.96}$$

The averaged total current $\bar{i} = \bar{i}_R + \bar{i}_J$ as a function of the applied voltage v thus obtains a washboard-type characteristics,

$$\bar{i} = \frac{V_0}{R} + I_c\sum_n (-1)^n J_n\left(\frac{2\pi V_s}{\Phi_0\omega_s}\right)\sin\left[\varphi(0)\right]\ \delta(v - n\omega_s\Phi_0) \ . \tag{21.97}$$

The plateaus in the i-v characteristics are called *Shapiro steps*. They appear at voltages $n\hbar\omega_s/4\pi e$. In the case of arrays of m JJs, steps are also observed at voltages corresponding to rational fractions of frequencies $m\omega_j = n\omega_s$, provided the JJs are locked [249].

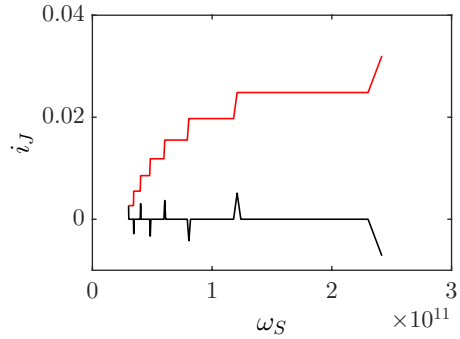

Figure 21.9: (code) Shapiro steps and their derivative.

21.4.4.3 Locking

To study the locking phenomenon we simplify the JJ equation by neglecting dissipation, $C = 0$,

$$\frac{\Phi_0}{2\pi}\frac{d\varphi}{dt} = Ri + RI_c \sin\varphi \ . \tag{21.98}$$

This is the so-called *Adler equation*,

$$\frac{d\psi}{dt} = -\nu + \varepsilon \sin\psi \ , \tag{21.99}$$

whose formal solution is [1031],

$$t = \int \frac{d\psi}{\varepsilon \sin\psi - \nu} \ . \tag{21.100}$$

The beat frequency is,

$$\Omega_\psi = 2\pi \left| \int \frac{d\psi}{\varepsilon\left(1 - \frac{\psi^2}{2}\right) - \nu} \right|^{-1} \ , \tag{21.101}$$

expanding around the maximum at $\psi = \pi/2$,

$$\Omega_\psi \simeq \pi\varepsilon \left| \int \frac{d\psi}{-\psi^2 - 2\frac{\nu}{\varepsilon} + 2} \right|^{-1} = \pi\sqrt{2\varepsilon}\sqrt{\varepsilon - \nu} \left| \int \frac{d\tilde{\psi}}{1 - \tilde{\psi}^2} \right|^{-1} \simeq \pi\sqrt{2\varepsilon}\sqrt{\nu - \varepsilon} \ . \tag{21.102}$$

This is due to a locking of the drive frequency and the frequency of the oscillators.

21.4.4.4 Devil's staircase

Locking can also happen between higher harmonics. To see this we chose an alternative treatment goes as follows. The equation of motion with a pure ac driving voltage without resistance is,

$$C\frac{\Phi_0}{2\pi}\frac{d^2\varphi}{dt^2} + I_c \sin\left(\varphi(0) + \frac{2\pi V_0}{\Phi_0}t + \frac{2\pi V_s}{\Phi_0\omega_s}\sin\omega_s t\right) = 0 \ . \tag{21.103}$$

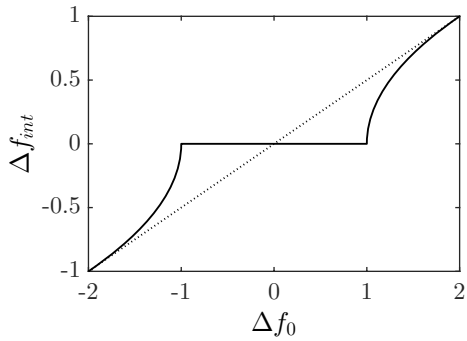

Figure 21.10: (code) Arnold tongue.

It can be derived from the Hamiltonian,

$$\hat{H} = \frac{p_\varphi^2}{2C\Phi_0/2\pi} - I_c \cos\left(\varphi(0) + \frac{2\pi V_0}{\Phi_0}t + \frac{2\pi V_s}{\Phi_0\omega_s}\sin\omega_s t\right) \ . \tag{21.104}$$

Substituting $\tilde{H} \equiv H/(C\Phi_0/2\pi)$, $\tilde{p_\varphi} \equiv p_\varphi/(C\Phi_0/2\pi)$, $K \equiv I_c/(\omega_s C\Phi_0/2\pi)$, and $\lambda \equiv \imath/(\omega_s C\Phi_0/2\pi)$, ...

We now go to the annulus map describing the Josephson junction. The JJ map can be interpreted as a δ-kicked rotor. The dissipative map [1431] predicts the occurrences of locking regions, known as Shapiro steps observed at all simple rational numbers m/n. They are equivalent to those of a *devil's staircase*.

21.4.4.5 Quantized JJ

The quantized energy levels of the JJ $\cos\psi$ potential result in a phase quantization. As a consequence, the energy exchange between an oscillating driving pump, ω_s, and the JJ, only occurs in multiples of ω_J.

To visualize quantum effects, one has to go to the quantum map $|\psi_{n+1}\rangle = \hat{U}\psi_n$.

21.4.5 Exercises

21.4.5.1 Ex: Perfect conductor

Calculate the magnetic field near a perfect conductor by solving equation (21.72).

Solution:

21.4.5.2 Ex: Perfect conductor

Quantify the Meissner effect for a thin layer by solving equation (21.73).

Solution:

21.4.5.3 Ex: Meissner-Ochsenfeld effect

Calculate the magnetic field inside a thin superconducting layer as a function of layer thickness and temperature.

Solution: *See Lucca 7300035/2020-2.*

21.5 Quantities and formulas in electromagnetism

21.5.1 Electromagnetic quantities

charge	Q	basic SI unit [C]
electric field (Coulomb law)	$\vec{\mathcal{E}}$	$d\vec{\mathcal{E}}(\mathbf{r}) = \frac{1}{4\pi\epsilon_0}\frac{dQ(\mathbf{r}-\mathbf{r}')}{\lvert\mathbf{r}-\mathbf{r}'\rvert^3}$
Coulomb law		$\vec{\mathcal{E}}(\mathbf{r}) = \frac{1}{4\pi\epsilon_0}\int_{\mathcal{V}}\frac{\rho(\mathbf{r}')(\mathbf{r}-\mathbf{r}')}{\lvert\mathbf{r}-\mathbf{r}'\rvert^3}d^3r'$
superposition principle		$\mathbf{F} = \mathbf{F}_1 + \mathbf{F}_2$
Coulomb force	$\mathbf{F}_C$	$\mathbf{F}_C = q\vec{\mathcal{E}}$
electric dipole moment	$\mathbf{p}$	$\mathbf{p} \equiv q\mathbf{r}$
electric torque	$\vec{\tau}$	$\tau = \mathbf{p} \times \vec{\mathcal{E}}$
potential energy of electric dipoles	U_e	$U_e = -\mathbf{p}\cdot\vec{\mathcal{E}}$
electric flux	Ψ_e	$\Psi_e \equiv \int_{\mathcal{S}}\vec{\mathcal{E}}\cdot d\mathbf{S}$
electric Gauß law		$\oint_{\mathcal{S}}\vec{\mathcal{E}}\cdot d\mathbf{S} = \frac{Q_{dentro}}{\epsilon_0} = \frac{1}{\epsilon_0}\int_{\mathcal{V}}\rho(\mathbf{r}')d^3r'$
gradient	∇	$\nabla \equiv \sum_k \hat{\mathbf{e}}_k\frac{\partial}{\partial x_k}$
potential	V	$V \equiv -\int_\gamma \vec{\mathcal{E}}\cdot d\mathbf{r}$
voltage	U	$U_{12} \equiv V_2 - V_1$
capacity	C	$C \equiv \frac{Q}{U}$
plate capacitor		$C = \frac{\epsilon_0 A}{d}$
resistance (Ohm's law)	R	$R \equiv \frac{U}{I}$
lei 1. de Kirchhoff		$\sum_k U_k = 0$ in every mesh
lei 2. de Kirchhoff		$\sum_k I_k = 0$ in every node
magnetic field (Biot-Savart law)	$\vec{\mathcal{B}}$	$d\vec{\mathcal{B}}(\mathbf{r}) = \frac{\mu_0}{4\pi}\int_{\mathcal{C}}\frac{Id\vec{\ell}\times(\mathbf{r}-\mathbf{r}')}{\lvert\mathbf{r}-\mathbf{r}'\rvert^3}$
Biot-Savart law		$\vec{\mathcal{B}}(\mathbf{r}) = \frac{\mu_0}{4\pi}\int_{\mathcal{V}}\frac{(\mathbf{r}-\mathbf{r}')\times\mathbf{j}(r')}{\lvert\mathbf{r}-\mathbf{r}'\rvert^3}d^3r'$
Lorentz force	$\mathbf{F}_L$	$\mathbf{F}_L = q\mathbf{v}\times\vec{\mathcal{B}}$
magnetic dipole moment	$\vec{\mu}$	$\vec{\mu} \equiv I\mathbf{A}$
magnetic torque	$\vec{\tau}$	$\vec{\tau} = \vec{\mu}\times\vec{\mathcal{B}}$
potential energy of magnetic dipoles	U_m	$U_m = -\vec{\mu}\cdot\vec{\mathcal{B}}$
magnetic flux	Ψ_m	$\Psi_m \equiv \int_{\mathcal{S}}\vec{\mathcal{B}}\cdot d\mathbf{S}$
magnetic Gauß law		$\oint_{\mathcal{S}}\vec{\mathcal{B}}\cdot d\mathbf{S} = 0$
Ampère's law		$\oint_{\mathcal{C}}\vec{\mathcal{B}}\cdot d\vec{\ell} = \mu_0 I_{dentro} = \mu_0\int_{\mathcal{S}} j(\mathbf{r}')d^2r'$
Faraday law		$U_{ind} = -\frac{d\Phi_m}{dt}$
inductance	L	$L \equiv -\frac{U_{ind}}{dI/dt}$
self-inductance of a coil		$L = \mu_0\frac{N^2\pi r^2}{\ell}$
Poynting vector	$\vec{\mathcal{S}}$	$\mathbf{S} \equiv \vec{\mathcal{E}}\times\vec{\mathcal{H}}$

electric displacement	$\vec{\mathcal{D}}$	$\vec{\mathcal{D}} = \varepsilon\vec{\mathcal{E}}$
polarization	$\vec{\mathcal{P}}$	$\vec{\mathcal{P}} = \vec{\mathcal{D}} - \varepsilon_0\vec{\mathcal{E}}$
magnetic excitation	$\vec{\mathcal{H}}$	$\vec{\mathcal{H}} = \mu^{-1}\vec{\mathcal{B}}$
magnetization	$\vec{\mathcal{M}}$	$\vec{\mathcal{M}} = \mu_0^{-1}\vec{\mathcal{B}} - \vec{\mathcal{H}}$

21.5.2 Formulas of special relativity

metric	Kronecker symbol	$(\delta_{\mu\nu})$
	Lévi-Civita symbol	$(\epsilon_{\mu\nu\omega\kappa})$
	Minkowski metric	$(\eta_{\mu\nu})$
	Lorentz transform	$(\Lambda_{\mu\nu})$
	position	$(r^\mu) \equiv \binom{ct}{\mathbf{r}}$
	displacement	$(\Delta r^\mu) \equiv \binom{c\Delta t}{\Delta \mathbf{r}}$
	space-time interval	$\Delta s^2 \equiv \Delta r_\mu \Delta r^\mu = c^2\Delta t^2 - \Delta\mathbf{r}^2$
	proper time	$\Delta\tau \equiv \sqrt{\frac{\Delta s^2}{c^2}}$ for 'time-like' intervals $\Delta s^2 > 0$
	proper distance	$\lvert\Delta\vec{\mathcal{S}}\rvert \equiv \sqrt{-\Delta s^2}$ for 'space-like' intervals $\Delta s^2 < 0$
	gradient	$(\partial^\mu) \equiv \binom{c^{-1}\partial_t}{-\nabla}$
	d'Alembertian	$\Box \equiv \partial_\mu\partial^\mu = \frac{1}{c^2}\frac{\partial^2}{\partial t^2} - \nabla^2$
mechanics	proper velocity	$(u^\mu) \equiv (\frac{\partial r^\mu}{\partial\tau}) = \binom{\gamma_u c}{\gamma_u \mathbf{u}}$
	momentum	$(p^\mu) \equiv (\frac{\partial u^\mu}{\partial\tau}) = \binom{E/c}{\mathbf{p}}$
	rest mass	$mc^2 = p_\mu p^\mu = \frac{E^2}{c^2} - \mathbf{p}^2$
	wave vector	$(k^\mu) \equiv \binom{\omega/c}{\mathbf{k}}$
	force	$(K^\mu) \equiv \binom{\gamma P/c}{\gamma\mathbf{F}}$
e-dynamics	current density	$(j^\mu) \equiv (\varrho_0 U^\mu) = \binom{c\varrho}{\mathbf{j}}$ with $\partial_\mu j^\mu = 0$
	el.-mag. potential	$(A^\mu) \equiv \binom{c^{-1}\phi}{\mathbf{A}}$ with $F^{\mu\nu} = \partial^\mu A^\nu - \partial^\nu A^\mu$
	Stokes theorem	$F\int F_{\mu\nu} ds^{\mu\nu} = \int A_\mu dx^\mu$
	el.-mag. flux	$(S^\mu) \equiv \binom{cu}{\mathbf{S}}$
	el.-mag. field tensor	$(F_{\mu\nu}) \equiv \begin{pmatrix} 0 & -\frac{1}{c}\vec{\mathcal{E}} \\ \frac{1}{c}\vec{\mathcal{E}} & (-\epsilon_{mnk}\mathcal{B}_k) \end{pmatrix}$
	dual tensor	$(\mathcal{F}_{\mu\nu}) \equiv \frac{1}{2}\epsilon^{\mu\nu\alpha\beta}F_{\alpha\beta} = \begin{pmatrix} 0 & -\vec{\mathcal{B}} \\ \vec{\mathcal{B}} & (\frac{1}{c}\epsilon_{mnk}\mathcal{E}_k) \end{pmatrix}$
	Lorentz force density	$f^\mu = F^{\mu\nu} j_\nu$
	Lagrangian	$\frac{1}{2\mu_0}F_{\mu\nu}F^{\mu\nu} = \frac{1}{\mu_0}\mathcal{B}^2 - \varepsilon_0\mathcal{E}^2$
		$\mathcal{F}_{\omega\kappa}F^{\omega\kappa} = \frac{1}{2}\epsilon_{\mu\nu\omega\kappa}F^{\mu\nu}F^{\omega\kappa} = -\frac{4}{c}\vec{\mathcal{B}}\cdot\vec{\mathcal{E}}$

21.5.3 CGS units

Often used in electrodynamics are *CGS units*, also called *Gaussian units*. In this script we will use exclusively *SI units* of the *Système International d'Unités*. To do

the conversion between the unit systems, it is enough let,

$$\begin{aligned} e \to e_{CGS}\sqrt{4\pi\varepsilon_0} \quad &, \quad \mathbf{j} \to \mathbf{j}_{CGS}\sqrt{4\pi\varepsilon_0} \\ \vec{\mathcal{E}} \to \vec{\mathcal{E}}_{CGS}\sqrt{\tfrac{1}{4\pi\varepsilon_0}} \quad &, \quad \vec{\mathcal{B}} \to \vec{\mathcal{B}}_{CGS}\sqrt{\tfrac{\mu_0}{4\pi}} \\ \vec{\mathcal{D}} \to \vec{\mathcal{D}}_{CGS}\sqrt{\tfrac{\varepsilon_0}{4\pi}} \quad &, \quad \vec{\mathcal{H}} \to \vec{\mathcal{H}}_{CGS}\sqrt{\tfrac{1}{4\pi\mu_0}} \\ \vec{\mathcal{P}} \to \vec{\mathcal{P}}_{CGS}\sqrt{4\pi\varepsilon_0} \quad &, \quad \vec{\mathcal{M}} \to \vec{\mathcal{M}}_{CGS}\sqrt{\tfrac{4\pi}{\mu_0}} \ . \end{aligned} \tag{21.105}$$

Maxwell's equations in the irrational Gaussian system are,

$$\text{rot}\ \vec{\mathcal{H}} = \tfrac{1}{c}\partial_t\vec{\mathcal{D}} + \tfrac{4\pi}{c}\mathbf{j} \quad , \quad \text{div}\ \vec{\mathcal{D}} = 4\pi\varrho \ . \tag{21.106}$$

Moreover,

$$u = \tfrac{1}{8\pi}(\vec{\mathcal{E}}^2 + \vec{\mathcal{B}}^2) \quad , \quad \mathbf{S} = \tfrac{c}{4\pi}(\vec{\mathcal{E}} \times \vec{\mathcal{B}}) \ . \tag{21.107}$$

The material equations for dielectric media are,

$$\vec{\mathcal{D}} = \varepsilon\vec{\mathcal{E}} \quad , \quad \vec{\mathcal{P}} = \chi_\varepsilon\vec{\mathcal{E}} \quad , \quad \varepsilon = 1 + 4\pi\chi_\varepsilon \ , \tag{21.108}$$

and for dia- and paramagnetic media,

$$\vec{\mathcal{B}} = \mu\vec{\mathcal{H}} \quad , \quad \vec{\mathcal{M}} = \chi_\mu\vec{\mathcal{H}} \quad , \quad \mu = 1 + 4\pi\chi_\mu \ . \tag{21.109}$$

21.6 Rules of vector analysis

21.6.1 Basic rules

(i) $\mathbf{A}\cdot\mathbf{B} = \mathbf{B}\cdot\mathbf{A}$ but $\mathbf{A}\cdot\nabla \neq \nabla\cdot\mathbf{A}$, (21.110)

(ii) $\phi\mathbf{B} = \mathbf{B}\phi$ but $\phi\nabla \neq \nabla\phi$,

(iii) $\mathbf{A}\times\mathbf{B} = -\mathbf{B}\times\mathbf{A}$ but $\mathbf{A}\times\nabla \neq -\nabla\times\mathbf{A}$,

(iv) $\mathbf{A}\cdot(\mathbf{B}\times\mathbf{C}) = \mathbf{B}\cdot(\mathbf{C}\times\mathbf{A})$,

(v) $\mathbf{A}\times(\mathbf{B}\times\mathbf{C}) = \mathbf{B}(\mathbf{A}\cdot\mathbf{C}) - \mathbf{C}(\mathbf{A}\cdot\mathbf{B})$,

(vi) $\nabla f(\phi(\mathbf{r})) = \dfrac{\partial f}{\partial\phi}\nabla\phi(\mathbf{r})$ chain rule ,

(vii) $\nabla(\mathbf{A}\cdot\mathbf{B}) = \nabla(A\mathbf{B}) + \nabla(\mathbf{A}B)$ product rule for scalars and vectors .

21.6.2 Deduced rules

$$
\begin{aligned}
&\text{(i)} && \nabla(\phi+\psi) = \nabla\phi + \nabla\psi \ , && (21.111)\\
&\text{(ii)} && \nabla(\phi\psi) = \phi\nabla\psi + \psi\nabla\phi \ , \\
&\text{(iii)} && \nabla\cdot(\mathbf{A}+\mathbf{B}) = \nabla\cdot\mathbf{A} + \nabla\cdot\mathbf{B} \ , \\
&\text{(iv)} && \nabla\times(\mathbf{A}+\mathbf{B}) = \nabla\times\mathbf{A} + \nabla\times\mathbf{B} \ , \\
&\text{(v)} && \nabla\cdot(\phi\mathbf{A}) = \phi(\nabla\cdot\mathbf{A}) + (\nabla\phi)\cdot\mathbf{A} \ , \\
&\text{(vi)} && \nabla\times(\phi\mathbf{A}) = \phi(\nabla\times\mathbf{A}) + (\nabla\phi)\times\mathbf{A} \ , \\
&\text{(vii)} && \nabla\cdot(\mathbf{A}\times\mathbf{B}) = (\nabla\times\mathbf{A})\cdot\mathbf{B} - \mathbf{A}\cdot(\nabla\times\mathbf{B}) \ , \\
&\text{(viii)} && \nabla\times(\mathbf{A}\times\mathbf{B}) = (\mathbf{B}\cdot\nabla)\mathbf{A} - (\mathbf{A}\cdot\nabla)\mathbf{B} + \mathbf{A}(\nabla\cdot\mathbf{B}) - \mathbf{B}(\nabla\cdot\mathbf{A}) \ , \\
&\text{(ix)} && \nabla(\mathbf{A}\cdot\mathbf{B}) = \mathbf{A}\times(\nabla\times\mathbf{B}) + \mathbf{B}\times(\nabla\times\mathbf{A}) + (\mathbf{A}\cdot\nabla)\mathbf{B} + (\mathbf{B}\cdot\nabla)\mathbf{A} \ , \\
&\text{(x)} && \nabla\times(\nabla\phi) = 0 = \nabla\cdot(\nabla\times\mathbf{A}) \ , \\
&\text{(xi)} && \nabla\times(\nabla\times\mathbf{A}) = \nabla(\nabla\cdot\mathbf{A}) - \triangle\mathbf{A} \ , \\
&\text{(xii)} && \nabla\cdot(\nabla\phi) = \triangle\phi \ , \\
&\text{(xiii)} && \mathbf{A}\cdot(\nabla\phi) = (\mathbf{A}\cdot\nabla)\phi \ , \\
&\text{(xiv)} && \mathbf{A}\times(\nabla\phi) = (\mathbf{A}\times\nabla)\phi \ , \\
&\text{(xv)} && \nabla\phi = \frac{d\phi}{dr}\nabla r \qquad \text{chain rule} \ , \\
&\text{(xvi)} && \nabla\phi(\psi) = \frac{d\phi(\psi)}{d\psi}\nabla\psi \ , \\
&\text{(xvii)} && \nabla\cdot\mathbf{A}(\psi) = \frac{d\mathbf{A}(\psi)}{d\psi}\cdot\nabla\psi \ , \\
&\text{(xviii)} && \nabla\times\mathbf{A}(\psi) = -\frac{d\mathbf{A}(\psi)}{d\psi}\times\nabla\psi \ .
\end{aligned}
$$

21.6.3 Integral rules

(i) $$\int_{\mathcal{V}} \nabla\phi dV = \int_{\mathcal{S}} \phi d\mathbf{S}, \tag{21.112}$$

(ii) $$\int_{\mathcal{V}} \nabla\cdot\vec{\mathcal{E}} dV = \oint_{\partial\mathcal{V}} \vec{\mathcal{E}}\cdot d\mathbf{S} \qquad \text{Gauß' rule ,}$$

(iii) $$\int_{\mathbf{A}} \nabla\times\vec{\mathcal{E}}\cdot d\mathbf{S} = \oint_{\partial\mathcal{C}} \vec{\mathcal{E}}\cdot d\mathbf{l} \qquad \text{Stokes' rule ,}$$

(iv) $$\int_{\mathcal{V}} \phi(\nabla\psi) dV = \int_{\partial\mathcal{V}} \phi\psi d\mathbf{S} - \int_{\mathcal{V}} (\nabla\phi)\psi dV \qquad \text{Green's rule ,}$$

(v) $$\int_{\mathcal{V}} \left[\phi(\triangle\psi) - (\triangle\phi)\psi\right] dV = \int_{\partial V} \left[\phi(\nabla\psi) - (\nabla\phi)\psi\right]\cdot d\mathbf{S}$$

(vi) $$\int_{\mathcal{V}} \phi(\triangle\psi) dV = \int_{\mathcal{V}} (\triangle\phi)\psi dV \tag{21.113}$$

where $\triangle$ is hermitian, when $\lim_{r\to\infty} r\phi(r) = 0 = \lim_{r\to\infty} r\psi(r)$,

(vii) $$\frac{d}{dt}\int_{a(t)}^{b(t)} f(x,t)dx = \int_{a(t)}^{b(t)} \frac{\partial f}{\partial\tau}(x,t)dx + \frac{db(t)}{dt} f(b,t)dx - \frac{da(t)}{dt} f(a,t)dx \ .$$

Notation,

$$\nabla\phi\cdot d\mathbf{S} = \nabla\phi\cdot\mathbf{n}\ dS = \frac{\partial\phi}{\partial\mathbf{n}}\ dS \ . \tag{21.114}$$

21.7 Rules for Laplace and Fourier transforms

21.7.1 Laplace transform

Formulas for the *Laplace transform*:

(definition) $$(\mathcal{L}f)(p) = \int_0^\infty f(t)e^{-pt}dt \tag{21.115}$$

(inversion) $$\mathcal{L}^{-1}\mathcal{L}f = f \quad \text{where} \quad (\mathcal{L}^{-1}\mathcal{L}f)(t) = \int_{\varepsilon-\imath\omega}^{\varepsilon+\imath\omega} \mathcal{L}f(p)e^{pt}\frac{dp}{2\pi\imath}$$

(linearity) $$\mathcal{L}(af+bg) = a\mathcal{L}(f) + b\mathcal{L}(g)$$

(similarity) $$\mathcal{L}[f(at)] = a^{-1}\mathcal{L}f(a^{-1}p)$$

(translation) $$\mathcal{L}\mathcal{T}f = \mathcal{L}f \cdot e^{-pT} \quad \text{where} \quad \mathcal{T}f(t) = f(t-T)$$

$$\mathcal{L}\left(fe^{qt}\right) = \mathcal{T}\mathcal{L}f$$

(differentiation) $$\mathcal{L}\partial_t f = p\mathcal{L}f - f(0)$$

$$\mathcal{L}(-tf) = \partial_p\mathcal{L}f$$

(pulse response) $$\mathcal{L}\delta = 1 \quad \text{where} \quad \delta(t) = \mathcal{L}^{-1}1$$

(step response) $$\mathcal{L}\delta' = p^{-1}$$

(integration) $$\mathcal{L}\int_0^t dt\ f = p^{-1}\mathcal{L}f$$

$$\mathcal{L}(t^{-1}f) = \int_p^\infty dp\ \mathcal{L}f$$

(convolution) $$\mathcal{L}(f\star g) = \mathcal{L}f \cdot \mathcal{L}g$$

(periodic functions) $$\mathcal{L}(f = \mathcal{T}f) = \int_0^{-T} dt\ \frac{e^{-pt}f(t)}{1-e^{pT}}$$

(eigenfunctions) $$f\star e^{pt} = \mathcal{L}f \cdot e^{pt}\ .$$

21.7.2 Correlation

Formulas for the *correlation*:

(definition) $$(f\diamond g)(t) = \int_{-\infty}^\infty f(\tau)g(t+\tau)d\tau \tag{21.116}$$

(non-commutativity) $$(f\diamond g)(t) = (g\diamond f)^s$$

(complex autocorrelation) $$|f\diamond g^*| \le f\diamond g^*(0)\ .$$

21.7.3 Fourier transform

Formulas for the *Fourier transform*:

(definition) $$(\mathcal{F}f)(\omega) = \int_{-\infty}^{\infty} f(t)e^{-\imath\omega t}dt \tag{21.117}$$

(inversion) $$\mathcal{F}^{-1}\mathcal{F}f = f \quad \text{where} \quad (\mathcal{F}^{-1}\mathcal{F}f)(t) = \int_{-\infty}^{\infty} \mathcal{F}f(\omega)e^{\imath\omega t}d\omega$$

(linearity) $$\mathcal{F}(af + bg) = a\mathcal{F}(f) + b\mathcal{F}(g)$$

(similarity) $$?$$

(translation) $$\mathcal{F}\mathcal{T}f = \mathcal{F}f \cdot e^{-\imath\omega T} \quad \text{where} \quad \mathcal{T}f(t) = f(t-T)$$

$$\mathcal{F}\left(fe^{\imath\omega t}\right) = \mathcal{T}\mathcal{F}f$$

(differentiation) $$\mathcal{F}[tf(t)] = \imath\partial_\omega(Ff)(\omega)$$

$$\mathcal{F}[f'(t)] = \imath\omega(Ff)(\omega)$$

(pulse response) $$\mathcal{F}\delta = 1 \quad \text{where} \quad \delta(t) = \mathcal{F}^{-1}1$$

(step response) $$\mathcal{F}\delta' = ?$$

(duality) $$\mathcal{F}\mathcal{F}\ f = f^s \quad \text{where} \quad f^s(t) = f(-t)$$

$$\mathcal{F}\ f^* = (\mathcal{F}\ f)^{*s} \quad \text{where} \quad f^s(t) = f(-t)$$

(symmetry) $$f = f^s = f^* \quad \Leftrightarrow \quad \mathcal{F}\ f = (\mathcal{F}\ f)^s$$

$$f = -f^s = f^* \quad \Leftrightarrow \quad \mathcal{F}\ f = -(\mathcal{F}\ f)^*$$

$$f = f^* \quad \Leftrightarrow \quad \mathcal{F}\ f = (\mathcal{F}\ f)^{*s}$$

(convolution) $$\mathcal{F}(f \star g) = \mathcal{F}f \cdot \mathcal{F}g$$

$$\mathcal{F}(f \cdot g) = \mathcal{F}f \star \mathcal{F}g$$

(eigenfunctions) $$f \star e^{\imath\omega t} = \mathcal{F}f \cdot e^{\imath\omega t}\ .$$

21.7.3.1 Fast Fourier transform

The *discrete Fourier transform* is defined by,

$$\begin{aligned} H_n &= \sum_{k=0}^{N-1} e^{-2\pi\imath nk/N} h_k \\ &= \sum_{k=0}^{N-1} e^{-2\pi\imath nk/(N/2)} h_{2k} + e^{-2\pi\imath k/N} \sum_{k=0}^{N/2-1} e^{-2\pi\imath nk/(N/2)} h_{2k+1} \\ &= even + odd\ . \end{aligned} \tag{21.118}$$

The inverse transform is,

$$h_k = \frac{1}{N}\sum_{k=0}^{N-1} e^{2\pi\imath nk/N} H_n\ . \tag{21.119}$$

The sine transform of a real vector s_k is,

$$S_n = \frac{2}{N}\sum_{k=1}^{N-1} s_k \sin \pi nk/N\ . \tag{21.120}$$

In MATLAB the fast Fourier transform is defined by:

$$F(k+1) = \sum_{n=0}^{N-1} f(n+1) e^{-2\pi\imath/N \cdot kn} \ . \tag{21.121}$$

inversion:

$$f(n+1) = \frac{1}{N} \sum_{k=0}^{N-1} F(k+1) e^{2\pi\imath/N \cdot kn} \ . \tag{21.122}$$

symmetry,

$$\begin{aligned} & f(n+1) = f^*(n+1) \qquad (21.123) \\ & \Longrightarrow K(k+1) = \sum_{n=0}^{N-1} f^*(n+1) e^{-2\pi\imath/N \cdot kn} e^{-2\pi\imath/N \cdot Nn} = F^*(N-k+1) \ . \end{aligned}$$

and,

$$\begin{aligned} & f(N-n) = f(n+1) = f^*(n+1) \qquad (21.124) \\ & \Longrightarrow F(k+1) = \sum_{n=0}^{N-1} f^*(N-n) e^{-2\pi\imath/N \cdot kn} \\ & \qquad = \sum_{n=0}^{N-1} f^*(n'+1) e^{2\pi\imath/N \cdot kn'} e^{-2\pi\imath/N \cdot (N-1)} = F^*(k+1) e^{2\pi\imath/N} \ . \end{aligned}$$

and,

$$\begin{aligned} & -f(N-n) = f(n+1) = f^*(n+1) \qquad (21.125) \\ & \Longrightarrow F(k+1) = \sum_{n=0}^{N-1} -f^*(N-n) e^{-2\pi\imath/N \cdot kn} \\ & \qquad = \sum_{n=0}^{N-1} -f^*(n'+1) e^{2\pi\imath/N \cdot kn'} e^{-2\pi\imath/N \cdot (N-1)} = -F^*(k+1) e^{2\pi\imath/N} \ . \end{aligned}$$

Hence, we choose, $\mathcal{F} f(n+1) = F(k+1) e^{-\pi\imath/N}$.

21.7.3.2 Fourier expansion

The complex *Fourier expansion* is defined by,

$$\boxed{f_N(x) = \sum_{n=-N}^{N} c_n e^{\imath n x}} \ , \tag{21.126}$$

where

$$c_n \equiv \frac{1}{2\pi} \int_{2\pi} s(x) e^{-\imath n x} dx \ . \tag{21.127}$$

21.7.4 Convolution

Formulas for the *convolution*:

$$
\begin{aligned}
&\text{(definition)} && (f\star g)(t) = \int_{-\infty}^{\infty} f(\tau)g(t-\tau)d\tau && (21.128)\\
&\text{(neutral element)} && f\star\delta^{(n)} = f^{(n)}\\
&\text{(distributivity)} && (f+g)\star h = f\star h + g\star h\\
& && af\star g = f\star ag\\
&\text{(commutativity)} && f\star g = g\star f\\
&\text{(associativity)} && (f\star g)\star h = f\star(g\star h)\\
&\text{(translational invariance)} && \mathcal{T}(f\star g) = \mathcal{T}f\star g = f\star\mathcal{T}\\
&\text{(differentiation)} && \partial_x(f\star g) = \partial_x f\star g = f\star\partial_x g\\
&\text{(integration)} && \int_x (f\star g) = \int_x f\int_x g\\
&\text{(complexity)} && f = f_r + \imath f_i\\
&\text{(Dirac function)} && \mathcal{T}f = f\star\mathcal{T}\delta\\
& && f(T) = f\cdot\mathcal{T}\delta\ .
\end{aligned}
$$

Example 135 (*Convolution of two Lorentzians*): The convolution of two *Lorentzians*,

$$\mathcal{L}_a(x) \equiv \frac{a}{\pi}\frac{1}{x^2+a^2} \qquad \text{with} \qquad \int_{-\infty}^{\infty}\mathcal{L}_a(x)dx = 1\ ,$$

is simply another Lorentzian with the linewidth $a+b$,

$$\boxed{(\mathcal{L}_a\star\mathcal{L}_b)(x) = \mathcal{L}_{a+b}(x)}\ .$$

In order to demonstrate this, we first we apply the method of partial fractions to the expression,

$$
\begin{aligned}
&\frac{1}{y^2+a^2}\frac{1}{(x-y)^2+b^2} = \frac{A}{y^2+a^2} + \frac{B}{(x-y)^2+b^2}\\
&\text{with}\quad A = \frac{2xy+(x^2-a^2+b^2)}{(x^2+a^2+b^2)^2-4a^2b^2}\quad,\quad B = \frac{-2x(y-x)+(x^2+a^2-b^2)}{(x^2+a^2+b^2)^2-4a^2b^2}\ .
\end{aligned}
$$

Now, we calculate the convolution,

$$
\begin{aligned}
&(\mathcal{L}_a\star\mathcal{L}_b)(x) = \frac{ab}{\pi^2}\int_{-\infty}^{\infty}\frac{1}{y^2+a^2}\frac{1}{(x-y)^2+b^2}dy\\
&= \frac{ab}{\pi^2}\frac{1}{(x^2+a^2+b^2)^2-4a^2b^2}\left(\int_{-\infty}^{\infty}\frac{2xy+(x^2-a^2+b^2)}{y^2+a^2}dy + \int_{-\infty}^{\infty}\frac{-2x(y-x)+(x^2+a^2-b^2)}{(x-y)^2+b^2}dy\right)\\
&= \frac{ab}{\pi^2}\frac{1}{(x^2+a^2+b^2)^2-4a^2b^2}\left((x^2-a^2+b^2)\int_{-\infty}^{\infty}\frac{1}{y^2+a^2}dy + (x^2+a^2-b^2)\int_{-\infty}^{\infty}\frac{1}{(x-y)^2+b^2}dy\right)\\
&= \frac{ab}{\pi^2}\frac{(x^2-a^2+b^2)\frac{\pi}{a}+(x^2+a^2-b^2)\frac{\pi}{b}}{(x^2+a^2+b^2)^2-4a^2b^2} = \frac{a+b}{\pi}\frac{1}{x^2+(a+b)^2} = \mathcal{L}_{a+b}(x)\ .
\end{aligned}
$$

Example 136 (*Convolution of two Gaussians*): The convolution of two *Gaussians*,

$$\mathcal{G}_a(x) \equiv \sqrt{\frac{1}{\pi}}\frac{1}{a}e^{-x^2/a^2} \qquad \text{with} \qquad \int_{-\infty}^{\infty}\mathcal{G}_a(x)dx = 1 \ ,$$

is simply another Gaussian with the linewidth $\sqrt{a^2+b^2}$,

$$\boxed{(\mathcal{G}_a \star \mathcal{G}_b)(x) = \mathcal{G}_{\sqrt{a^2+b^2}}(x)} \ .$$

We demonstrate this by calculating,

$$\begin{aligned}
(\mathcal{G}_a \star \mathcal{G}_b)(x) &= \frac{1}{\pi ab}\int_{-\infty}^{\infty} e^{-y^2/a^2}e^{-(x-y)^2/b^2}dy = \frac{\sqrt{ab}}{\pi}\int_{-\infty}^{\infty} e^{-(a^{-2}+b^{-2})y^2+2b^{-2}xy-b^{-2}x^2}dy \\
&= \frac{1}{\pi ab\sqrt{(a^{-2}+b^{-2})}}\int_{-\infty}^{\infty} e^{-\tilde{y}^2+\frac{2x}{b^2\sqrt{a^{-2}+b^{-2}}}\tilde{y}-b^{-2}x^2}d\tilde{y} \\
&= \frac{1}{\pi\sqrt{a^2+b^2}}\int_{-\infty}^{\infty} e^{-\left(\tilde{y}-\frac{x}{\sqrt{b^4/a^2+b^2}}\right)^2-\frac{x^2}{a^2+b^2}}d\tilde{y} \\
&= \frac{1}{\pi\sqrt{a^2+b^2}}e^{-\frac{x^2}{a^2+b^2}}\int_{-\infty}^{\infty} e^{-\tilde{y}^2}d\tilde{y} = \frac{1}{\sqrt{\pi}\sqrt{a^2+b^2}}e^{-\frac{x^2}{a^2+b^2}} = \mathcal{G}_{\sqrt{a^2+b^2}}(x) \ .
\end{aligned}$$

21.7.5 Green's functions

If a differential operator $\mathcal{L}_x$ acting on a variable x admits a *Green's function* $\mathcal{G}$ such that,

$$\boxed{\mathcal{L}_x\mathcal{G}(x,x') = \delta(x-x')} \ , \tag{21.129}$$

The Green function can be used to solve any equation,

$$\mathcal{L}_x f(x) = \varrho(x) \tag{21.130}$$

by calculating,

$$f(x) = \int \mathcal{G}(x,x')\varrho)(x)dx \ . \tag{21.131}$$

21.7.5.1 List of Green functions

The following table provides a list of useful Green functions.

differential operator $\mathcal{L}$	Green function $\mathcal{G}$
∂_t^n	$\frac{t^{n-1}}{(n-1)!}\Theta(t)$
$\partial_t + \gamma$	$\Theta(t)e^{-\gamma t}$
$\triangle$	$-\frac{1}{4\pi r}$
$\nabla\cdot$	$-\frac{\mathbf{r}-\mathbf{r}'}{4\pi R^3}$
$\nabla\times$	$-\frac{(\mathbf{r}-\mathbf{r}')\times(\mathbf{r}-\mathbf{r}')}{4\pi R^3}$
$\Box$	$-\frac{1}{4\pi r}\delta(t \mp \frac{1}{c}r)$
$\triangle + k^2$	$-\frac{e^{ikr}}{4\pi r}$
$-\nabla\times\nabla\times + k^2$	see Sec. 18.3.1

Example 137 (*Green function for time derivation*): To solve the differential equation,

$$(\partial_t + \gamma) f(t) = c \ ,$$

we search the Green function for the equation,

$$(\partial_t + \gamma)\mathcal{G}(t,t') = \delta(t-t') \ .$$

From the above table, we get,

$$f(t) = \int_{-\infty}^{\infty} \mathcal{G}(t,t') \ c \ dt' = c\int_{-\infty}^{\infty} \Theta(t-t')e^{-\gamma(t-t')}dt' = \frac{c}{\gamma}e^{-\gamma t} \ .$$

21.8 Further reading

R. Grimm et al., *Optical dipole traps for neutral atoms* [547]DOI

S. Varró et al., *Spontaneous emission of radiation by metallic electrons in the presence of electromagnetic fields of surface plasmon oscillations* [1330]DOI

B. Cabrera, *First Results from a Superconductive Detector for Moving Magnetic Monopoles* [227]DOI

R. Bachelard et al., *Resonances in Mie scattering by an inhomogeneous atomic cloud* [66]DOI

P.L. Saldanha et al., *Interaction between light and matter: a photon wave function approach* [1134]DOI

21.8.1 on the Abraham-Minkowski dilemma

G.K. Campbell et al., *Photon Recoil Momentum in Dispersive Media* [230]DOI

S.M. Barnett, *Resolution of the Abraham-Minkowski Dilemma* [98]DOI

I. Brevik et al., *Possibility of measuring the Abraham force using whispering gallery modes* [196]DOI

M. Mansuripur, *Resolution of the Abraham-Minkowski controversy* [841]DOI

P.W. Milonni et al., *Momentum of Light in a Dielectric Medium* [898]DOI

J.C. Garrison et al., *Canonical and kinetic forms of the electromagnetic momentum in an ad hoc quantization scheme for a dispersive dielectric* [495]DOI

N.I. Balazs, *The Energy-Momentum Tensor of the Electromagnetic Field inside Matter* [78]DOI

U. Leonhardt, *Energy-momentum balance in quantum dielectrics* [790]DOI

R. Loudon et al., *Radiation pressure and momentum transfer in dielectrics: The photon drag effect* [817]DOI

G.P. Fisher et al., *The Electric Dipole Moment of a Moving Magnetic Dipole* [448]DOI

Wen-Zhuo Zhang et al., *Testing the equivalence between the canonical and Minkowski momentum of light with ultracold atoms* [1428]DOI

Weilong She et al., *Observation of a Push Force on the End Face of a Nanometer Silica Filament Exerted by Outgoing Light* [1191]DOI

R.N.C. Pfeifer et al., *Colloquium: Momentum of an electromagnetic wave in dielectric media* [1027]DOI

C. Baxter et al., *Radiation pressure and the photon momentum in dielectrics* [107]DOI

C. Baxter et al., *Canonical approach to photon pressure* [106]DOI

F. Ravndal, *Symmetric and conserved energy-momentum tensors in moving media* [1075]DOI

E.A. Hinds et al., *Momentum Exchange between Light and a Single Atom: Abraham or Minkowski?* [619]DOI

M.P. Haugan et al., *Spectroscopy of atoms and molecules in gases: Corrections to the Doppler-recoil shift* [587]DOI

J.P. Gordon et al., *Radiation Forces and Momenta in Dielectric Media* [525]DOI

F. Goos et al., *Ein neuer und fundamentaler Versuch zur Totalreflektion* [522]DOI

Changbiao Wang et al., *Can the Abraham Light Momentum and Energy in a Medium Constitute a Lorentz Four-Vector?* [1358]DOI

P.L. Saldanha, *Division of the energy and of the momentum of electromagnetic waves in linear media into electromagnetic and material parts* [1130]DOI

P.L. Saldanha et al., *Hidden momentum and the Abraham-Minkowski debate* [1132]DOI

A.F. Gibson et al., *Photon drag in germanium* [506]DOI

Li Zhang et al., *Experimental evidence for Abraham pressure of light* [**?**]DOI

Part III

Quantum Mechanics

The courses in Quantum Mechanics A (QM/SFI5774), of Quantum Mechanics B (QO/SFI5708), of Atomic and Molecular Physics (AM/SFI5814), of Light Matter Interaction (LM/SFI5877), and of Atom Optics (OA/SFI5887) may have the following contents:

	Sections	QM	QO	AM	LM	AO
Antecedents	23.1.1-23.2.9			x		
Repetition of basic notions of quantum mechanics	24.1.1-24.5.4	x	x	x		
Motion in separable potentials & numerical approaches	25.1.1-25.4.2	x				
The harmonic oscillator	25.5.1-25.6.5	x	x			
Rotations, central potentials and spin coupling	26.1.1-26.4.4	x		x		
Periodic systems	27.1.1-27.3.1	x				
Stationary perturbation, variational method, WKB	28.1.1-28.2.2	x		x		
Time-dependent perturbation theory	28.4.1-28.4.5	x	x	x	x	
Spin of the electron & (hyper-)fine structure	30.1.1-30.4.4	x		x		
Charged particles in electromagnetic fields	31.1.1-31.1.2	x	x	x		
Atoms in stationary and electromagnetic fields	31.2.1-31.3.1	x		x		
Atoms with multiple electrons	32.1.1-32.4.3			x		
Dimeric molecules	33.1.1-33.3.4			x		
Collisions	34.1.1-34.5.5			x		
Absorption and emission of radiation and spectral lines	35.1.1-35.2.5			x	x	
Density operator & Bloch equations & NMR	35.3.1-35.4.5		x		x	
Spontaneous emission & saturation & line broadening	35.5.1-35.6.5		x		x	
Multilevel systems	35.7.1-35.7.5		x		x	
Quantization of radiation and dressed states	36.1.1-36.1.3		x		x	x
Probability distributions & squeezed states	36.2.1-36.3.3		x			
Jaynes-Cummings model and quantum correlations	36.2.1-36.2.3		x		x	
Spontaneous emission & resonance fluorescence	36.3.1-36.3.4		x			
Light scattering from multilevel atoms	36.4.4-36.4.2		x			
Beam splitting and quantum amplification	36.5.1-36.5.7				x	
Photon counting statistics	36.6.1-36.6.3				x	
Quantum measurement	37.1.1-37.6.2	x	x			
Nonlinear optics	38.1.1-38.2.6					
Forces exerted by electromagnetic fields	39.1.1-39.1.3	x	x		x	x
Optical forces & recoil	39.2.1-39.3.4		x		x	x
The structure factor & coupled dipoles model	40.1.1-40.1.7		x			
Mie scattering & scattering from disordered clouds	40.2.1-41.3.3		x			
Bragg scattering and photonic band gaps	40.4.1-40.4.3		x			
Interaction of atoms with cavities	41.1.1-41.3.6				x	
Interaction of atoms with surfaces	41.4.1-41.4.2				x	
Dicke model & super-/subradiance	42.1.1-42.2.2		x			
Interacting atoms	42.3.1-42.3.3		x			
Entanglement & quantum gates	42.4.1-42.6.4		x			
CARL & consorts in the classical and quantum regime	43.1.1-43.5.6		x			
Statistical models of CARL	43.6.1-43.8.2		x			
Manipulation of atomic gases	44.1.1-44.6.5					x
Thermodynamics of degenerate gases	45.1.1-45.2.10					x
Bose-Einstein condensation	46.1.1-46.8.3					x
Superfluid & coherent properties of condensed gases	47.1.1-47.4.3					x
Theories on the interaction of light and BECs	48.1.1-48.2.4					x
BEC Bragg diffraction and matter wave superradiance	48.3.1-48.4.3					x
BECs in superpositions of states coupled by light	48.4.1-48.4.2					x
Interaction of BECs with optical cavities	48.5.1-48.5.4					x
Condensates in reduced dimensions and other topics	49.1.1-50.8.8					x
Instrumentation of a quantum optics lab	51.1.1-56.4.3					x

Chapter 22

Antecedents of quantum mechanics

Developed at the beginning of the 20^{th} century, quantum mechanics is today the most fundamental and far-reaching theory in physics. It shaped our World more than any other science, as technologies based on quantum mechanical effects are the key to an industry representing today one third of the World's global domestic product. Boosted by the invention of the transistor and the laser, the industry today branches out in many areas including energy generation, electronics, optics, and photonics. Nevertheless and despite its long history and its incomparable success, quantum mechanics is far from being exhausted. The invention of novel techniques for quantum state manipulation and entanglement generation, awarded with various Nobel prizes in the past, and advances in information science during the past 25 years prepared the ground for a second wave of quantum-based technologies called Quantum Revolution 2.0. In terms of economic, military, and social advantages the stakes of this revolution are so important that they triggered a fierce international race for technological domination. This chapter traces briefly the historical conditions and the discoveries that led to the invention of quantum mechanics.

The fundamental idea of quantum mechanics is the assumption that there are entities which can not be subdivided beyond a certain limit. Examples are the mass of a body, the speed of an electron orbiting an atom, or the intensity of a beam of light. This idea was first uttered by *Leucippus* 500 years a.c. and his student *Democritus*, who imagined matter being made of smallest particles which they called *atoms*. These atoms move freely, collide, combine, and separate: 'There is nothing else than atoms and free space' they claimed. The microscopic atoms would have the same characteristics as the macroscopic objects they form when they combine, for example, color and shape. The idea of the atom resurfaced and was refined in the course of the 18^{th} century (see Tab. 1.1 below). Today, we know that the basic idea was good, but reality is a little more complicated.

Still, at the end of the 19^{th} century, the physical world seemed rather simple: matter and light was all that existed. Matter was made up of atoms and light was a wave. Therefore, to describe a real system, it was enough to calculate the trajectories of its elementary particles and the propagation of light between them. The way that light interacts with polarizable and magnetizable matter via electric and magnetic fields had been perfectly explained by laws discovered by Coulomb, Ampère, Faraday, and Maxwell.

Table 22.1: *Historical time line of the quantization of matter.*

500 a.c.	Democritus	invention of the atom
1800	Avogadro, Dalton	reinvention of the atom
1897	Thomson	charge transport, raisin-in-a-cake model
1909	Rutherford, Geiger, Marsden	α-scattering, charge localized in nuclei
1911	Rutherford	planetary model
1900	Bohr	quantized orbitals
1923	de Broglie	matter has characteristics of waves
1927	Davisson, Germer, Stern	electron and atoms diffraction

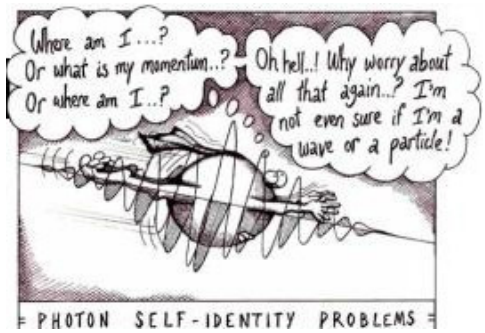

Figure 22.1: Particle-wave duality.

However, new experimental observations, such as the ultraviolet divergence of black-body radiation, that appeared in the late 19^{th} century, were incompatible with these traditional concepts. New ideas were pioneered by *Max Planck* who, in 1905, with a little help from Einstein quantized the electromagnetic field, and therefore the light, into small harmonic oscillators. This was the starting point for the development of a new theory called 'quantum mechanics'. Soon, this theory was applied to explain the photoelectric effect. The second important step was initialized by *Niels Bohr*, who quantized the hydrogen atom in 1913 into discrete excitation levels.

Table 22.2: *Historical time line of the quantization of light.*

1801	Young	light is diffracted like a wave
1860	Maxwell	unified theory of electrodynamics including light
1888	Hertz	detection of radio waves
$\sim$ 1890		accurate measurements of black-body radiation spectra
1900	Planck	quantum hypothesis: $E = h\nu$
1905	Einstein	photoelectric effect, light behaves like a particle

Nowadays we know that our universe is not as simple as classical mechanics sug-

gested, and that atoms are also waves and light also behaves like particles. This *duality principle* is one of the fundamental ideas of quantum mechanics. The appearance of an object as a wave or as a particle depends on the situation in which it is observed. While the wave nature of light was well established in classical physics since a long time, Louis de Broglie was the first in 1924 to apply the duality principle also to massive particles and to predict that particles, under certain conditions, behave like waves the wavelengths of which increase as their velocity decreases. Each particle (or body) is delocalized along a distance corresponding to this 'de Broglie wavelength'. This feature of matter was soon discovered experimentally in electron beams and is still used today in commercial devices, for example in electron microscopes.

22.1 The discovery of the atom

22.1.1 Democrit's model

'The principles of reality are atoms and emptiness while other things are mere opinions.' This is a quotation from the Greek philosopher *Democritus* 400 years before Christ and before Socrates. Together with his teacher Leucippus, he formed the first idea of indivisible particles: atoms.

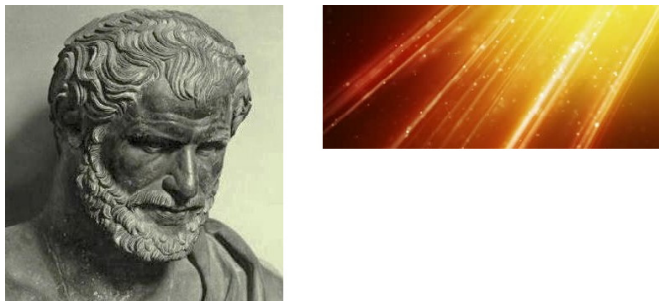

Figure 22.2: Democritus and dust in a sun ray.

Democritus' work only survived as second-hand accounts, the major part of it having been written down by *Aristotle*, who also, defending the idea of the continuum, was the greatest critic of Democritus' theory. Aristotle said that the reasoning that guided Democritus to affirm the existence of atoms was as follows. For a body to change its shape, it is necessary that its parts can move. This presupposes an emptiness (or vacuum) in which the matter moves. But if matter were divided infinitely into ever smaller parts, it would loose its consistency. Nothing could be formed because nothing could arise from the ever more infinitely deep dilution of matter into emptiness. Hence, he concluded that the division of matter can not be infinite, that is, there is an indivisible limit: the atom. 'There is only atoms and emptiness', he said.

Observing dust particles in a whirling motion within a ray of sunlight, Democritus was led to the idea that atoms would behave in the same way, randomly colliding, some crowding, others dispersing, others never yet joining with another atom.

The consistency of clusters of atoms, which makes something look solid, liquid, gaseous, or animated (which is the state of the soul) would then be determined by the shape of the atoms involved and their spatial arrangement. In this sense, water atoms are smooth and slippery; the atoms of steel have shapes with sharp edges that hold them solidly together; the atoms of salt, as their taste shows, are harsh and pointed; the atoms of air are small and little connected, penetrating all other materials; and the atoms of soul and fire are spherical and very delicate.

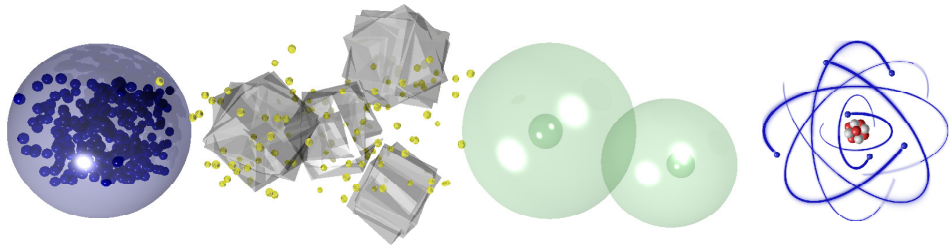

Figure 22.3: Atoms of steel and air, atoms of the soul, and Bohr's atom model.

We know nowadays that Democritus' first theory of the structure of matter was very close to the truth: There really are indivisible particles called atoms composed of a nucleus and an electronic shell, and the space between the atomic nuclei is, in fact, quite empty.

The atomic hypothesis came to be reborn in the modern age with the scientists Boyle, Clausius, Maxwell, and Boltzmann due to their successful explanations of the properties of gases based on the so-called kinetic theory, where they assumed a gas being constituted of identical molecules that collided elastically with each other and with the walls of the recipient containing them. The discovery of the atom through the *laws of proportions* in chemistry and the establishment of Avogadro's number considerably strengthened the atomic hypothesis. The hypothesis was definitely consecrated with the various experiments that established the charge of the electron and the mass ratio between electrons and protons.

By the beginning of the 19^{th} century the atomic nature of matter had definitely been established, and the basic composition of the atoms was already relatively well known. It was known, through experiments, that electrons could be removed from neutral atoms thus creating positively charged ions and that only a certain number of electrons could be removed from each atom. This number proved to be dependent on the atomic species and was called the atomic number Z. This information was fundamental for establishing the basic composition of atoms. The question that arose at this point concerned the dimensions and configurations of the atomic system. How would loads and masses be distributed in this entity?

22.1.2 Thomson's model and Rutherford's experiment

The internal structure of a body can be studied by throwing beams of small particles against it. The detection of the angular distribution of the scattered particles gives access to the structure factor of the body. In crystallography we throw X-rays

into super-complicated molecules to learn the architecture e.g. of proteins. And in medicine, X-rays reveal the internal structure of the human body. Obviously, the scattering technique is an extremely powerful tool, used in many areas of modern physics.

In a series of experiments done before 1911, *Ernest Rutherford* analyzed the internal structure of gold atoms using α-particles, i.e., He^{2+} atoms. The experiments carried out by Geiger, Marsden, and Rutherford consisted of observing the deflection of particles from a collimated beam when scattered by a thin metallic sheet (gold of thickness $\sim 1\,\mu m$) carefully obtained by electroplating [see Fig. 22.4(cd)].

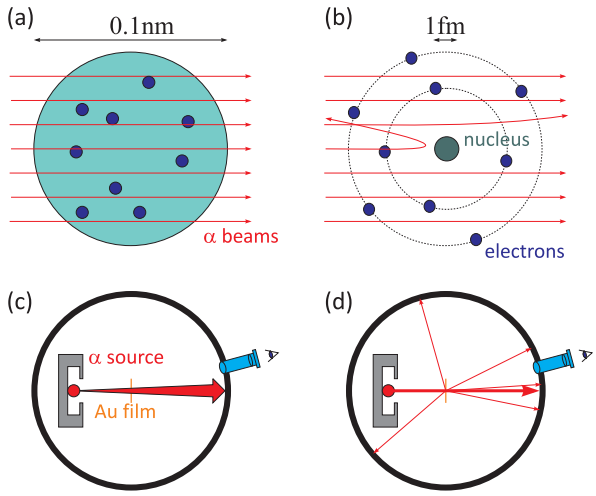

Figure 22.4: Comparison of Rutherford scattering by free electrons and electrons strongly bound to small nuclei. (a) Thomson's 'raisin-in-a-pudding' type atom; (b) Rutherford's 'planetary' atom. (c) Rutherford scattering by a raisin pudding atom and (d) by a planetary atom.

The atomic model proposed by *Joseph John Thomson* suggests a structure resembling a *pudding with raisins*: the electrons would be homogeneously distributed within an extended nucleus (size 0.1 nm) of positive charge thus compensating for the negative charge of the electrons. The α-particles would penetrate the gold nucleus, perceived as almost homogeneous, but would suffer multiple deflections due to collisions with the disordered electrons within the nucleus. Since electrons are very light, the angle of deflection θ would be small, even after many collisions. For this model we expect a Gaussian dependence of the particles' deflection angle given by the *scattering cross section* [see Fig. 22.4(a-b)],

$$\frac{d\sigma}{d\Omega} \propto e^{-\theta^2/\theta_0^2} \,, \tag{22.1}$$

where θ_0 is a small angle.

However, the measurements performed on this *Rutherford scattering* showed different results:

- For a fixed scattering angle, the amount of particles scattered into a solid angle element $d\Omega$ is proportional to the thickness of the metal foil.

- For a given fixed angle and a given metal sheet the amount of scattered particles in $d\Omega$ varies inversely with E_{kin}^2, where E_{kin} is the kinetic energy of the α-particles.
- For a given energy and a given metal sheet, the number of particles scattered into $d\Omega$ is proportional to $(\sin\frac{\theta}{2})^{-4}$.
- For a given energy and sheet thickness, the number of particles scattered into $d\Omega$ in a given direction is proportional to Z_{tg}^2, where Z_{tg} is the atomic number of the element that constitutes the sheet.

The extremely rare deflection of α-particles and their angular distribution can be understood by the assumption that the positive charge is concentrated in a very small volume (~ 1 fm, that is 10000 times less than the size of the atom itself). This volume is called the atomic nucleus, hence the denomination of *nuclear model*. Since most of the particles pass through the gold sheet without hindrance, there must be a large gap between the nuclei. The electrons, which move within a large (in comparison with the diameter of the nucleus) empty space (the vacuum) around the nucleus, shield the positive nuclear charge, so that the atom appears outwardly neutral.

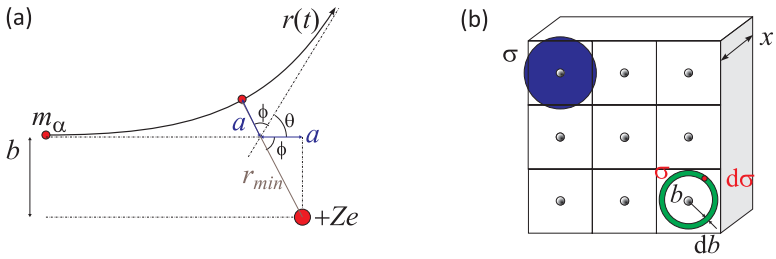

Figure 22.5: (a) Trajectory of an α-particle. (b) Illustration of the scattering cross section.

We now derive Rutherford's scattering formula from the hypothesis of a point-like nucleus. Due to the repulsive action of the Coulomb force,

$$F = \frac{Z_\alpha Z_{tg} e^2}{4\pi\varepsilon_0 r^2} \ , \tag{22.2}$$

we have for the trajectory of the α-particle ($Z_\alpha = 2$) a hyperbola [see Fig. 22.5(a)]. The large half-axis of the hyperbola can be determined from the following ansatz,

$$E_{\rm kin} = \frac{Z_\alpha Z_{tg} e^2}{4\pi\varepsilon_0}\frac{1}{2a} \ , \tag{22.3}$$

where $2a$ is the minimum distance of the particle α, when it collides with the nucleus in a central collision [1]. The distance a depends on the kinetic energy and can also be used for non-central collisions. The collision parameter b is the minimum distance of the α-particle to the nucleus, if it continued to fly in a straight line. In fact the

[1] In a central collision, when the α-particle reaches the minimum distance $2a$, its initial kinetic energy, $E_{\rm kin}$ is fully converted into potential energy.

α-particle will be deflected by an angle θ. From the geometry of the hyperbola, as $2\phi + \theta = 180°$, we obtain the following equation:

$$\tan\phi = \tfrac{b}{a} = \tan\left(90° - \tfrac{\theta}{2}\right) = \cot\tfrac{\theta}{2} \ , \tag{22.4}$$

and therefore

$$\cot\tfrac{\theta}{2} = \frac{b}{a} = \frac{8\pi\varepsilon_0 E_{\text{kin}}}{Z_\alpha Z_{tg} e^2} b \ , \tag{22.5}$$

replacing a with the formula (22.3). Taking the derivative of this latter formula, we obtain a relation between the width db of the hollow cone and the pertinent width $d\theta$ of the deflection angle θ,

$$-\frac{1}{2\sin^2\frac{\theta}{2}} d\theta = \frac{8\pi\varepsilon_0 E_{\text{kin}}}{Z_\alpha Z_{tg} e^2} db \ . \tag{22.6}$$

Let $n_{tg} = \frac{N_{tg}}{V}$ be the density of the particles in the target (N_{tg} atoms per volume V) and x the film thickness. Then $\sigma = \frac{A}{N_{tg}} = \frac{V/x}{N_{tg}} = \frac{1}{n_{tg}x}$ is the average cross-section per atom sensed by the α-particle on its way through the film. The probability $P(\theta)d\theta$ for the α-particle of being within a ring at distance b from the nucleus (whose area is $2\pi bdb$) and being scattered into the angle θ is then given by,

$$P(\theta)d\theta = \frac{2\pi bdb}{\sigma} = n_{tg} x 2\pi bdb \ . \tag{22.7}$$

These particles, i.e., dN of the N particles, are deflected into the hollow cone with the probability,

$$\begin{aligned} \frac{dN}{N} = P(\theta)d\theta &= n_{tg} x 2\pi \frac{Z_\alpha Z_{tg} e^2}{8\pi\varepsilon_0 E_{\text{kin}}} \cot\frac{\theta}{2} \cdot \frac{Z_\alpha Z_{tg} e^2}{8\pi\varepsilon_0 E_{\text{kin}}} \cdot \frac{1}{2\sin^2\frac{\theta}{2}} d\theta \\ &= n_{tg} x \frac{Z_\alpha^2 Z_{tg}^2 e^4}{64\pi\varepsilon_0^2 E_{\text{kin}}^2} \cdot \frac{\cos\frac{\theta}{2}}{\sin^3\frac{\theta}{2}} d\theta \ , \end{aligned} \tag{22.8}$$

where we replaced the parameters b and db with the expressions (22.5) and (22.6). The solid angle of the cone can be expressed by,

$$d\Omega = 2\pi \sin\theta d\theta = 4\pi \sin\tfrac{\theta}{2} \cos\tfrac{\theta}{2} d\theta \ . \tag{22.9}$$

Thus, the number dN of particles scattered to the solid angle $d\Omega$ remains,

$$\boxed{\frac{dN}{N} = n_{tg} x \frac{Z_\alpha^2 Z_{tg}^2 e^4}{256\pi^2\varepsilon_0^2 E_{\text{kin}}^2} \cdot \frac{1}{\sin^4\frac{\theta}{2}} d\Omega} \ . \tag{22.10}$$

That is Rutherford's scattering formula. Often, the formula is expressed with the *differential* cross section $\frac{d\sigma}{d\Omega}$. We get,

$$\frac{dN}{N} = \frac{d\sigma}{\sigma} = n_{tg} x d\sigma \ , \tag{22.11}$$

and therefore

$$\frac{d\sigma}{d\Omega} = \frac{dN}{N n_{tg} x d\Omega} = \left(\frac{Z_\alpha Z_{tg} e^2}{4\pi\varepsilon_0 \cdot 4E_{\text{kin}}}\right)^2 \frac{1}{\sin^4\frac{\theta}{2}} \ . \tag{22.12}$$

Here, we have to make some comments:

- The angle $\theta = 0$ is not defined, since there exists a minimum deflection angle $\theta_{\min}$. This angle is reached, when the α-particle moves at the distance $b = b_{\max}$ from the atom, that is, at the edge of the circular area of the cross section. For a greater collision parameter b, the α-particle traverses the field of the next neighboring atom, and the deflection angle increases again. We have:

$$\sigma = \frac{A}{N_{tg}} = \pi b_{\max}^2 \qquad \text{and} \qquad \frac{\theta_{\min}}{2} \simeq \tan\frac{\theta_{\min}}{2} = \frac{Z_\alpha Z_{tg} e^2}{8\pi\varepsilon_0 E_{\text{kin}} \cdot b_{\max}} \ , \tag{22.13}$$

  simply by inverting the formula (22.5). For very large impact parameters, that is, when the α-particle passes the atom outside its electronic layer, the electrons of the atom shield the charge of the nucleus, an effect called *screening*.

- For very high energies, the distribution of the nuclear charge over a finite volume influences the scattering, calling for corrections in the Rutherford formula. Moreover, at short internuclear distances, nuclear forces appear additionally to the electromagnetic interaction.

- The integral over the probability distribution $P(\theta)d\theta$ is normalized,

$$\int_{\theta_{\min}}^{\pi} P(\theta)d\theta = 1 \ . \tag{22.14}$$

  Similarly, we have for the surface integrals,

$$\int_{\theta \geqslant \theta_{\min}} \frac{d\sigma}{d\Omega} d\Omega = \sigma \ . \tag{22.15}$$

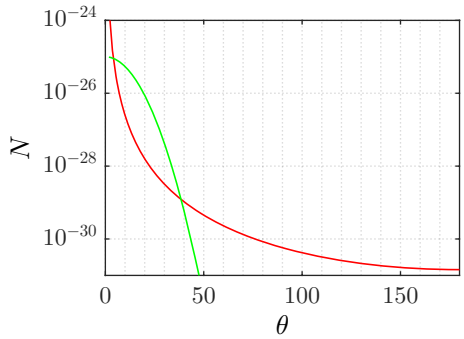

Figure 22.6: (code) Angular dependence of the cross-section corresponding to Thomson's (green) and Rutherford's (red) models.

Rutherford derived the formula (22.12) describing the scattering of α-particles within classical physics. A derivation from the laws governing quantum mechanics using the *Born approximation* shows that Rutherford's formula describes scattering correctly in first order, and that purely quantum effects present only minor corrections. We will review the Rutherford scattering in Excs. 22.1.6.1 and 22.1.6.2 and discuss the screening effect in Exc. 22.1.6.3.

22.1.3 Emission of radiation in the planetary model

The *planetary model* proposed by Rutherford suggests electrons spinning around a positively charged nucleus in circular orbits [2]. This motion of electrons should obey the laws of Maxwell's electrodynamic theory. Let us now calculate some consequences of this picture.

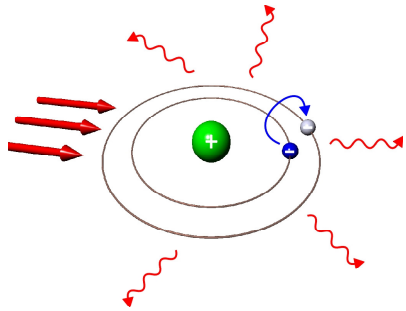

Figure 22.7: Light-induced transitions between orbits in the planetary model.

We now treat the atom as a rotor where the negative particle, the electron, orbits the positive particle. The dipole moment is,

$$p_0 = -er \ . \tag{22.16}$$

We calculate in the Exc. 22.1.6.4 the power emitted by the acceleration $a = \omega^2 r$ of the electron on its circular trajectory,

$$P = \frac{\mu_0 \omega^4 p_0^2}{12\pi c} \ . \tag{22.17}$$

The initial energy of the electron spinning around the nucleus (for a hydrogen atom $Z = 1$),

$$E = \frac{p^2}{2m_e} - \frac{e^2}{4\pi\varepsilon_0 r} = \frac{m_e \omega^2 r^2}{2} - \frac{e^2}{4\pi\varepsilon_0 r} \ , \tag{22.18}$$

is dissipated by radiation of the power (22.17), i.e.,

$$-P = \frac{dE}{dt} = m_e \omega^2 r \frac{dr}{dt} + \frac{e^2}{4\pi\varepsilon_0 r^2}\frac{dr}{dt} = 2m_e \omega^2 r \frac{dr}{dt} \ . \tag{22.19}$$

The latter equation supposes an equilibrium between the centrifugal force and the Coulomb force,

$$m_e \omega^2 r = \frac{e^2}{4\pi\varepsilon_0 r^2} \ , \tag{22.20}$$

allowing to link the revolution frequency ω to the instantaneous radius of the orbit $r(t)$. Resolving the Eq. (22.19) by $\dot{r}$ and replacing the power by the relation (22.17)

[2] This type of model had already been proposed by Jean Perrin in 1901 and by Hantaro Nagaoka in 1903, around the same time when Thompson developed his model. The planetary model was later on rescued by John William Nicholson in 1911.

and the frequency ω by the relation (22.20), we obtain,

$$\frac{dr}{dt} = -\frac{P}{2m_e\omega^2 r} = -\frac{\mu_0\omega^2 e^2}{24\pi m_e c} r = -\frac{e^4}{96\pi^2\varepsilon_0^2 m_e^2 c^3}\frac{1}{r^2} \ . \tag{22.21}$$

Integration of this equation gives,

$$t - t_0 = -\frac{32\pi^2\varepsilon_0^2 m_e^2 c^3}{e^4}[r^3 - r^3(t_0)] \ . \tag{22.22}$$

Now inserting $t_0 = 0$ and assuming $r(t_0) = a_B$, the time τ within which the loss of energy due to radiation emission decreases the radius of the electronic orbit to $r = 0$, is,

$$t = \tau = \frac{32\pi^2\varepsilon_0^2 m_e^2 c^3 a_B^3}{e^4} \ . \tag{22.23}$$

Insertion of the numerical values gives the decay time $\tau \sim 10^{-10}$ s. This is the effect called *radiation collapse* of the classical atomic model.

22.1.4 Zeeman effect in the planetary model

The orbital motion of the electron generates a ring current $I = e/T = e\omega/2\pi$, which produces an *orbital magnetic moment* which, as shown in Exc. 22.1.6.5, can be calculated following the laws of electromagnetism,

$$\vec{\mu}_\ell = IA\hat{\mathbf{n}} = \frac{e\omega}{2\pi}\pi r^2\hat{\mathbf{n}} \ , \tag{22.24}$$

where $A = \pi r^2$ is the area of the trajectory. Introducing the angular momentum $\mathbf{L} = m_e\omega r^2\hat{\mathbf{n}}$ we get in vector notation,

$$\vec{\mu}_\ell = \frac{e}{2m_e}\mathbf{L} \ . \tag{22.25}$$

We now imagine this atom in the presence of a magnetic field $\vec{\mathcal{B}}$ oriented in the direction that we will call z. This results in a precession of the magnetic moment around the field (similar to the precession of a spinning top in the presence of a gravitational field) governed by the equation,

$$\frac{d\mathbf{L}}{dt} = \vec{\mu}_\ell \times \vec{\mathcal{B}} = \frac{e}{2m_e}\mathbf{L} \times \vec{\mathcal{B}} = -\mathbf{\Omega}_L \times \mathbf{L} \ ,$$

with $\mathbf{\Omega}_L = \frac{e}{2m_e}\vec{\mathcal{B}}$ representing the precession frequency and being called *Larmor frequency*. It is evident that the presence of the magnetic field considerably alters the state of the atom, even producing profound modifications in the frequency of the orbit of the electron ω_0 and therefore in the energetic state of the atom. This change is called *Zeeman effect*.

The Zeeman effect can be calculated by imagining that the field has an arbitrary direction with respect to $\mathbf{L}$. In this case, the equation describing the electronic motion as resulting from an equilibrium between the centrifugal force and the Coulomb force needs to be complemented by a Lorentz force,

$$m_e\ddot{\mathbf{r}} + m_e\omega_0^2\mathbf{r} = \mathbf{F}_L = -e\mathbf{v} \times \vec{\mathcal{B}} \ . \tag{22.26}$$

where $m\ddot{\mathbf{r}}$ is the centrifugal force due to the circular motion of the electron and $m_e\omega_0^2\mathbf{r}$ the centripetal force due to the Coulomb attraction exerted by the nucleus. Assuming the direction of the magnetic field given by $\vec{\mathcal{B}} = \mathcal{B}\hat{\mathbf{e}}_z$ with $\mathcal{B} = 2m_e\Omega_L/e$, the equations of motion can be decomposed into,

$$\begin{aligned} \ddot{x} + \omega_0^2 x + 2\Omega_L \dot{y} &= 0 \\ \ddot{y} + \omega_0^2 y - 2\Omega_L \dot{x} &= 0 \\ \ddot{z} + \omega_0^2 z &= 0 \ . \end{aligned} \tag{22.27}$$

The z-direction is not influenced. With the ansatz $x = ae^{\imath\omega t}$ and $y = be^{\imath\omega t}$ we obtain the system of equations,

$$\begin{aligned} a(\omega_0^2 - \omega^2) + 2\imath\Omega_L\omega b &= 0 \\ b(\omega_0^2 - \omega^2) - 2\imath\Omega_L\omega a &= 0 \ , \end{aligned} \tag{22.28}$$

which has a non-trivial solution for a and b only when the determinant of the coefficients of a and b vanishes:

$$0 = \begin{vmatrix} \omega_0^2 - \omega^2 & 2\imath\Omega_L\omega \\ -2\imath\Omega_L\omega & \omega_0^2 - \omega^2 \end{vmatrix} = \omega^4 - (2\omega_0^2 + 4\Omega_L^2)\omega^2 + \omega_0^4 \ . \tag{22.29}$$

We get,

$$\omega = \omega_{1,2} = \sqrt{\omega_0^2 + 2\Omega_L^2 \pm 2\Omega_L\sqrt{\omega_0^2 + \Omega_L^2}} = \omega_0 \pm \Omega_L + \frac{1}{2}\frac{\Omega_L^2}{\omega_0} + \ldots \ , \tag{22.30}$$

or, as $\Omega_L \ll \omega$, we get $\omega_{1,2} = \omega_0 \mp \Omega_L$. The result is a splitting of the energy levels proportional to the magnetic field,

$$\Delta E = 2\hbar\Omega_L = \frac{\hbar e}{m_e}\mathcal{B} = 2\mu_B\mathcal{B} \ , \tag{22.31}$$

where the abbreviation $\mu_B = e\hbar/2m_e \simeq 9.27\cdot 10^{-24}\,\mathrm{JT}^{-1}$ is called the *magneton Bohr*.

Although the classical derivation shows quantitative deviations from experimental observations, it is quite interesting, as it illustrates several aspects which have a quantum mechanical equivalence.

Example 138 (*Stern-Gerlach experiment*): Among several historical experiments carried out to unravel the atomic structure, one of the most important is the experiment carried out by *Otto Stern* and *Walther Gerlach* in 1922 to measure the magnetic moment of atoms. The results of this experiment once again demonstrated the need for new concepts to explain the observations.
Using Bohr's quantization rule, $L = n\hbar$, within the formula (22.25) we get,

$$\vec{\mu} = -\mu_B\frac{\mathbf{L}}{\hbar} \ .$$

In the presence of a magnetic field the dipole undergoes an interaction $W = -\vec{\mu}\cdot\vec{\mathcal{B}}$, and therefore a feels a force,

$$\mathbf{F} = -\vec{\mu}\cdot\nabla\vec{\mathcal{B}} \ .$$

By subjecting beams of atoms to the gradient of a magnetic field and detecting this force, Stern and Gerlach were able to measure the magnetic moment produced by the rotation of the electrons around the atomic nuclei.

22.1.5 Bohr's theory and its limitations

The classical model of the planetary atom provides a mechanical illustration of the microscopic world but fails to quantitatively explain experimental observations such as the discrete nature of atomic spectra.

The radiation emitted by hydrogen atoms is characterized by discrete, spectrally very thin lines. The observed lines are grouped in series named after Lyman, Ballmer and others,

$$\frac{1}{\lambda} = R_H \frac{\mu}{m_e} \left(\frac{1}{m^2} - \frac{1}{n^2} \right) , \tag{22.32}$$

where m and n are integers. $R_H = (1/4\pi\epsilon)^2(m_e e^4/4\pi\hbar^3 c)$ is the Rydberg constant and $\mu = m_e m_{at}/(m_e + m_{at})$ the reduced mass.

The discrete nature of spectral lines and the problem of the radiation collapse led *Niels Bohr* to formulate the following *postulates*:

1. There are specific stationary orbits, where electrons do not emit energy.

2. Each emission or absorption of radiation energy by electrons comes with a transition between stationary orbits. The radiation emitted during this transition is homogeneous.

3. The laws of mechanics can describe the dynamic equilibrium of electrons in stationary states, but fails to describe the transition of electrons *between* stationary orbits.

Thus, Bohr's model predicts the quantization of energy levels, known as *first quantization* of quantum mechanics. The radii of the possible orbits can be calculated from the postulate that the orbital angular momentum be quantized in units of $\hbar$, that is, the electrons form stationary de Broglie waves along the orbits [3]. We discuss Bohr's model in Excs. 22.1.6.6 and 22.1.6.7.

In the picture proposed by Bohr, the radiative decay happens as an abrupt transition of an electron between an outer (more energetic) orbit and an inner (less energetic) orbit. Since the energies of stationary orbits are very well defined, the emitted radiation is mono-energetic, i.e., the spectrum consists of discrete characteristic lines.

We note here that the picture of an abrupt transition of electrons between discrete states, called the *quantum jump*, did not receive Schrödinger's blessing. He rather imagined for electrons, within his theory of quantum wave mechanics, wave-shaped orbitals instead of planetary trajectories, thus avoiding the problem of radiation due to charge deceleration and the quantum jump concept. According to him, during a transition between electronic orbits, the energy is transformed into radiation *gradually* [4].

[3] A generalization of Bohr's theory was provided by *Arnold Johannes Wilhelm Sommerfeld*. Assuming elliptical orbits for the electrons he managed to explain some features of the fine structure, provided the motion of the electron was treated relativistically. The basic premises were 1. stable orbits when the Coulomb attraction is balanced by the centrifugal force, 2. quantization of phase space $\int r_q dq = n_q \hbar$, and 3. quantization of angular momentum $\int L d\theta = n_\theta \hbar$.

[4] We note here, that quantum jumps were observed much later!

22.1.6 Exercises

22.1.6.1 Ex: Analysis of Rutherford scattering

a. What conclusions can be drawn from the observation that Rutherford's formula describes well the scattering of charged particles traveling through matter over a wide range of parameters?
b. Why do we see a deviation from Rutherford's formula for large energies?
c. The scattering of protons with energy E crossing a thin film of thorium is well described up to energies of $E = 4.3\,\mathrm{MeV}$ by Rutherford's formula. Estimate for this case the range of nuclear forces.
d. For small scattering angles θ we observe large deviations from Rutherford's formula. Explain why?
e. Assume the thorium atoms of item (c) to form a periodic crystal with the lattice constant $d = 10a_B$. At which minimum angle θ Rutherford's formula loses its validity.

Solution: *a. Thomson's assumption of a heavy nuclear charge distributed across the atom is false. Instead they are the light-weighted electrons distributed through the atom.*
b. For large energies, i.e., small distances, the proton can feel the finite extension of the nucleus as well as nuclear forces.
c. When the shock parameter b tends to zero, the distance $2a$ between the proton and the nucleus depends on the kinetic energy as,

$$E_{\mathrm{kin}} = \frac{Z_p Z_{tg} e^2}{4\pi\varepsilon_0}\frac{1}{2a} \ .$$

With $Z_p = 1$, $Z_{tg} = 90$ and the given energy limit we obtain $2a = 15\,\mathrm{fm}$.
d. When the collision parameter b is large, we need to take into account the proximity of other nuclei as well as screening effects.
e. For this case we set $b = 5a_B$. From Eq. (22.5) we find,

$$\cot\tfrac{\theta}{2} = \frac{8\pi\varepsilon_0 E}{Z_\alpha Z_{thorium} e^2} b \ ,$$

yielding $\theta = 1.14 \cdot 10^{-4}\,\mathrm{rad} = 6.5 \cdot 10^{-3}\ ^\circ$.

22.1.6.2 Ex: Rutherford scattering

a. A beam of α-particles with energy $E_{\mathrm{kin}} = 3\,\mathrm{MeV}$ and flux $I = 5 \cdot 10^3\,\mathrm{s}^{-1}$ impinges on a thick gold film $x = 1\,\mu\mathrm{m}$. Using Rutherford's formula, calculate how many particles are scattered in $\Delta t = 10\,\mathrm{minutes}$ in the range of angles $10^\circ \le \theta \le 30^\circ$.
b. Now, the gold film is replaced with an aluminum film of the same thickness. How many α-particles are scattered under equal circumstances?

Solution: *a. The atomic mass of gold $^{197}_{79}Au$ being $m_{Au} = 196.966570\ u$ contains and its density being $\rho_{Au} = 19.3\,\mathrm{g/cm^3}$, we expect $n_{tg} = \rho_{Au}/m_{Au} = 5.9 \cdot 10^{28}\,\mathrm{m^3}$*

atoms per volume. With this we calculate,

$$N_{Au} = I\Delta t \int_{10^\circ \le 30^\circ} \frac{dN}{N} = I\Delta t n_{tg} x \frac{Z_\alpha^2 Z_{tg}^2 e^4}{256\pi^2 \varepsilon_0^2 E_{\text{kin}}^2} \int_0^{2\pi} \int_{10^\circ}^{30^\circ} \frac{1}{\sin^4 \frac{\theta}{2}} \sin\theta d\theta d\phi$$
$$= 63.6 \cdot \frac{-4\pi}{\sin^2 \frac{\theta}{2}} \Bigg|_{10^\circ}^{30^\circ} = 105000 \ .$$

b. Aluminum $^{27}_{13}Al$ *has about the same number of atoms per volume. With this we calculate,*

$$N_{Al} = \frac{Z_{Al}^2}{Z_{Au}^2} N_{Au} = 3885 \ .$$

22.1.6.3 Ex: Screening of electrons

Consider thin layer of charge $-Z_{tg}e$ with radius R. This screening causes a scattering angle,

$$\tan\tfrac{\theta}{2} = \frac{D}{2b} \frac{\sqrt{1-(b/R)^2}}{1+D/2R} \ ,$$

with $D \equiv \frac{3Ze^2}{m_2 v^2/2}$ for $b < R$. Verify how the screening changes the differential cross section $\frac{d\sigma}{d\Omega}$.

Solution:

22.1.6.4 Ex: Radiation of an oscillating dipole

Calculate the angular distribution of the power radiated by an oscillating electric or magnetic dipole from expressions for the emitted electric and magnetic fields found in literature.

Solution: *We consider* [5] *an electric dipole with the dipole moment* p_0 *harmonically oscillating with the angular frequency* ω *along the direction* $\hat{\mathbf{e}}_z$*,*

$$\mathbf{p}(\mathbf{r},t) = \mathbf{p}(\mathbf{r}) e^{-\imath\omega t} = p_0 \hat{\mathbf{e}}_z e^{-\imath\omega t} \ .$$

In vacuum, the generated field can be derived exactly using the retarded potentials as,

$$\mathbf{E} = \frac{1}{4\pi\varepsilon_0} \left\{ \frac{\omega^2}{c^2 r} (\hat{\mathbf{e}}_r \times \mathbf{p}) \times \hat{\mathbf{e}}_r + \left(\frac{1}{r^3} - \frac{\imath\omega}{cr^2} \right) [3\hat{\mathbf{e}}_r (\hat{\mathbf{e}}_r \cdot \mathbf{p}) - \mathbf{p}] \right\} e^{\imath\omega r/c} e^{-\imath\omega t}$$
$$\mathbf{B} = \frac{\omega^2}{4\pi\varepsilon_0 c^3} \hat{\mathbf{e}}_r \times \mathbf{p} \left(1 - \frac{c}{\imath\omega r} \right) \frac{e^{\imath\omega r/c}}{r} e^{-\imath\omega t} \ .$$

[5] See script on *Electrodynamics* (2023), Excs. 7.6.1.2 and 8.2.1.2.

For $r\omega/c \gg 1$, the far field adopts the simplest form of a radiating spherical wave, but with the angular dependence incorporated in the vector product:

$$\mathbf{B} = \frac{\omega^2}{4\pi\varepsilon_0 c^3}(\hat{\mathbf{e}}_r \times \mathbf{p})\frac{e^{i\omega(r/c-t)}}{r} = \frac{\omega^2\mu_0 p_0}{4\pi c}(\hat{\mathbf{e}}_r \times \hat{\mathbf{e}}_z)\frac{e^{i\omega(r/c-t)}}{r} = -\frac{\omega^2\mu_0 p_0}{4\pi c}\sin\theta\frac{e^{i\omega(r/c-t)}}{r}\hat{\mathbf{e}}_\phi$$

$$\mathbf{E} = c\mathbf{B}\times\hat{\mathbf{e}}_r = -\frac{\omega^2\mu_0 p_0}{4\pi}\sin\theta(\hat{\mathbf{e}}_\phi\times\hat{\mathbf{e}}_r)\frac{e^{i\omega(r/c-t)}}{r} = -\frac{\omega^2\mu_0 p_0}{4\pi}\sin\theta\frac{e^{i\omega(r/c-t)}}{r}\hat{\mathbf{e}}_\theta \ .$$

In the temporal average, $\frac{\omega}{2\pi}\int_0^{2\pi}\cos^2\omega t dt = \frac{1}{2}$, the Poynting vector,

$$\langle\mathbf{S}\rangle = \frac{1}{\mu_0}\langle\mathbf{E}\times\mathbf{B}\rangle = \frac{\mu_0 p_0^2\omega^4}{32\pi^2 c}\frac{\sin^2\theta}{r^2}\hat{\mathbf{e}}_r$$

In the temporal average, it is not isotropically distributed, but concentrated in the directions perpendicular to the dipolar moment, as a result of the non-spherical nature of the electrical and magnetic waves. In fact, the spherical harmonic function ($\sin\theta$) responsible for this toroidal angular distribution is just the p-wave ($\ell = 1$). The total power radiated by the field can be derived from the vector Poynting vector as being,

$$P = \int_0^{2\pi}\int_0^{\pi}\langle\mathbf{S}\rangle\cdot\hat{\mathbf{e}}_r r^2\sin\theta d\theta d\phi = \frac{\mu_0 p_0^2\omega^4}{32\pi^2 c}\ 2\pi\ \int_0^{\pi}\sin^3\theta d\theta = \frac{\mu_0\omega^4 p_0^2}{12\pi c} \ .$$

22.1.6.5 Ex: Magnetic moments

a. Derive from the expression $\vec{\mu}_L = \frac{1}{2}\int_{\mathbb{R}^3}\mathbf{r}\times\mathbf{j}(\mathbf{r}')d^3r'$ of classical electrodynamics and an appropriate parametrization of the current density $\mathbf{j}$ the relation between the magnetic dipole moment $\vec{\mu}$ due to the orbiting electron and the angular momentum $\mathbf{L}$.
b. The length of the angular momentum vector being given by $|\mathbf{L}| = \hbar$, calculate the magnetic moment for an electron and for a proton.

Solution: *a. The rotational motion of a charge, $-e$, creates a current $I = -e/2\pi r$, corresponding to a current density,*

$$\mathbf{j}(\mathbf{r}') = I\hat{\mathbf{e}}_\phi\delta(r-r')\delta(z') = -e\frac{\mathbf{v}}{2\pi r}\delta(r-r')\delta(z') \ .$$

The dipole moment caused by a circular motion of an electron is,

$$\vec{\mu}_L = \frac{1}{2}\int_{\mathbb{R}^3}\mathbf{r}\times\mathbf{j}(\mathbf{r}')d^3r' = \frac{1}{4\pi}\mathbf{r}\times\int_0^{2\pi}d\phi'\int_{-\infty}^{\infty}dz'\int_0^{\infty}r'dr'\frac{-e\mathbf{v}}{r}\delta(r-r')\delta(z')$$
$$= \frac{-1}{2}e\mathbf{r}\times\mathbf{v} = \frac{-e}{2m_e}\mathbf{L} \ ,$$

with the angular momentum $\mathbf{L} = \mathbf{r}\times m_e\mathbf{v}$. The quotient $\gamma_e \equiv -e/2m_e$ is called the gyromagnetic ratio of the electron. We often use the Bohr magneton, $\mu_B \equiv \hbar e/2m_e$, which represents the elementary unit of angular momentum,

$$\vec{\mu}_L = -\frac{\mu_B}{\hbar}g_L\mathbf{L} \ ,$$

where $g_L \equiv \mu_L/L = 1$ is a factor taking into account possible corrections between the classical derivation and quantum mechanics.
b. We have,

$$\mu_e = \mu_B \quad , \quad \mu_p = \mu_K \ .$$

22.1.6.6 Ex: Bohr's atom

In 1913, Niels Bohr presented his atomic model adapting Rutherford's model to the quantization ideas proposed by Max Planck.
a. Impose the quantization rule for the angular momentum ($L = n\hbar$) of an electron orbiting an atom of atomic number Z to find an expression for the radii of the allowed orbits.
b. According to Bohr's model, the transition between different orbits is accompanied by the emission (or absorption) of a photon. Determine the energy of a photon emitted during a transition between the first excited state and the ground state of a hydrogen atom.
c. Consider an electron trapped in an infinite one-dimensional box potential of width a. Determine an expression for the electronic energy levels.
d. What should be the width a of this potential, in terms of the Bohr radius, so to ensure that a photon emitted during a transition between the first excited state and the ground state equals that obtained in item (b)?

Solution: *a. In equilibrium, the centrifugal force and the Culombian force between the electron and the Z positive charges of the nucleus must compensate. Hence,*

$$F_{cf} = F_{cou} \qquad \textit{therefore} \qquad \frac{m_e v^2}{r} = \frac{1}{4\pi\varepsilon_0}\frac{Ze^2}{r^2} \ .$$

But the quantization condition is $L = n\hbar$, which by the definition of angular momentum leads us to:

$$v = \frac{n\hbar}{m_e r} \ .$$

By replacing the velocity in centripetal force, we will have:

$$r_n = \frac{(4\pi\varepsilon_0)\hbar^2}{m_e e^2}\frac{n^2}{Z} = a_B\frac{n^2}{Z} \ ,$$

where we defined the radius of Bohr a_B.
b. The energy of the electron is $E = E_c + E_p = \frac{m_e}{2}v^2 - \frac{1}{4\pi\epsilon_0}\frac{Ze^2}{r}$. With the Coulomb force, we have,

$$E = -\frac{1}{2}\frac{1}{4\pi\varepsilon_0}\frac{Ze^2}{r} \ .$$

Inserting the possible radii r_n, we get:

$$E_n = -\frac{1}{2}\frac{1}{4\pi\varepsilon_0}\frac{Z^2e^2}{a_B n^2} = -\frac{m_e}{2}\left(\frac{1}{4\pi\varepsilon_0}\right)^2\frac{Z^2e^2}{\hbar^2 n^2} \ .$$

The energy E_f of the photon emitted is,

$$E_2 - E_1 = -\frac{1}{2}\left(\frac{1}{4\pi\varepsilon_0}\right)^2 \frac{m_e Z^2 e^2}{\hbar^2}\left[\frac{1}{4} - 1\right] \ .$$

Hence,

$$E_f = \frac{3}{8}\left(\frac{1}{4\pi\varepsilon_0}\right)^2 \frac{m_e e^2}{\hbar^2} \ .$$

c. Considering that the potential $V(x)$ is zero for $0 < x < a$ and infinity outside this region, we have the Schrödinger equation $-\frac{\hbar^2}{2m}\frac{d}{dx}\psi = E\psi$ which leads us to the solution:

$$\psi(x) = A\cos(kx) + B\sin(kx) \qquad \text{where} \qquad k^2 = \frac{2m_e E}{\hbar^2}$$

The boundary condition, $\psi(0) = 0$ leads to $A = 0$ and $\psi(a) = 0$ leads to $ka = n\pi$. With ansatz above, we conclude that

$$E_n = \frac{n^2\pi^2\hbar^2}{2ma^2} \ .$$

d. The energy of the emitted photon is,

$$E_f = E_2 - E_1 = \frac{\hbar^2\pi^2}{2ma^2}[4-1] = \frac{3\hbar^2\pi^2}{2ma^2} \ .$$

Thus, equating with the expression for E_f for the Bohr atom, we have

$$\frac{3\hbar^2\pi^2}{2m_e a^2} = \frac{3}{8}\left(\frac{1}{4\pi\varepsilon_0}\right)^2 \frac{me^2}{\hbar^2} \ .$$

Hence,

$$a = \frac{4\pi\varepsilon_0\hbar^2}{m_e e^2}2\pi \ .$$

But the Bohr radius a_B is just the orbit in which $n = 1$ in the expression of the Bohr radius. Then

$$a = 2\pi a_B \ .$$

That is, the width of the potential has the same order of magnitude as the diameter of a hydrogen atom (around $0.1\,\text{nm}$).

22.1.6.7 Ex: The hydrogen atom

The hydrogen atom can be seen as a point-like proton and an electron distributed over space with charge density $\rho = Ae^{-2r/a_B}$ around the proton that is in the center. Here, A is a constant and r is the distance from the center.
a. Calculate A considering the fact that the atom is electrically neutral.
b. Calculate the amplitude of the electric field at a radius $r = a_B$.

Solution: *a. The total charge of the electronic layer must give one unit of negative elementary charge,*

$$\begin{aligned}\frac{-e}{A} &= \int_{\mathbb{R}^3} e^{-2r/a_B} dV = 4\pi \int_0^\infty r^2 e^{-2r/a_B} dr \\ &= 4\pi \left(-\frac{1}{2} a_B e^{-2\frac{R}{a_B}} R^2 - \frac{1}{2} a_B^2 e^{-2\frac{R}{a_B}} R - \frac{1}{4} a_B^3 e^{-2\frac{R}{a_B}} + \frac{1}{4} a_B^3 \right) \Big|_0^\infty = \pi a_B^3 \ .\end{aligned}$$

Hence, $A = -e/\pi a_B^3$.
b. For a sphere with volume V *and surface* ∂V *we have according to Gauß' law,*

$$\oint_{\partial V} \vec{E} \cdot d\vec{f} = \frac{1}{\varepsilon_0} \int_V \frac{-e}{\pi a_B^3} e^{-2r/a_B} dV \ .$$

The surface integral in spherical coordinates is,

$$\oint_{\partial V} \vec{E} \cdot d\vec{f} = \oint_{\partial V} \vec{E} \cdot \hat{e}_r R^2 \sin\theta d\theta d\phi = 4\pi E_r R^2 \ .$$

The charge inside the sphere (including the proton) is,

$$\begin{aligned} e + \int_V \frac{-e}{\pi a_B^3} e^{-2r/a_B} dV &= e + \frac{-e}{\pi a_B^3} 4\pi \int_0^R r^2 e^{-2r/a_B} dr \\ &= e + \frac{-e}{\pi a_B^3} 4\pi \frac{-1}{2} a_B \left(e^{-2\frac{R}{a_B}} R^2 + a_B e^{-2\frac{R}{a_B}} R + \frac{1}{2} a_B^2 e^{-2\frac{R}{a_B}} - \frac{1}{2} a_B^2 \right) \\ &= \frac{2e}{a_B^2} \left(e^{-2\frac{R}{a_B}} R^2 + a_B e^{-2\frac{R}{a_B}} R + \frac{1}{2} a_B^2 e^{-2\frac{R}{a_B}} \right) \ . \end{aligned}$$

Hence,

$$\begin{aligned} E_r(R) &= \frac{e}{2\pi\varepsilon_0 a_B^2} \left(e^{-2\frac{R}{a_B}} + \frac{a_B}{R} e^{-2\frac{R}{a_B}} + \frac{1}{2} \frac{a_B^2}{R^2} e^{-2\frac{R}{a_B}} \right) \\ &\overset{R \to a_B}{\longrightarrow} \frac{e}{4\pi\varepsilon_0 a_B^2} \ 5e^{-2} \simeq 350\,\mathrm{GV/m} \ . \end{aligned}$$

22.2 The discovery of the photon

The concept of the nature of light has a variable history. Newton proposed around ~ 1650 a corpuscular model to explain Snellius' law on the refraction of a light beam penetrating a crystal. Around the same time Huygens found a wave-based interpretation. The two models predicted different speeds of light within the dense medium. Newton found, that the speed of light is greater in the medium than outside, while Huygens found the opposite [6]. In the late 1800's the wave nature of light was established through observations of interference effects confirming Huygens' hypothesis.

[6] Note that until today there remain doubts about the correct value of the momentum of light in dielectric media [898].

However, some observations made were incompatible with this simplistic ideas, for example, the spectrum of blackbody radiation, the Compton effect, the specific heat of the solid, the radiation pressure, and the photoelectric effect. All these observations are readily understood by assuming a corpuscular nature of the light [7].

Nowadays, knowing the theory of quantum mechanics, we are aware that both ideas have their range of validity and that the electromagnetic radiation is dual: In general, propagation and interference effects are best described by waves. However, when interacting with matter, light tends to localize into small energy packets that we call *photons*.

22.2.1 Radiation in a conductive cavity

In the age of lasers a classical treatment of the emission and absorption of light may seem an atavism. However, even with coherent and monochromatic radiation sources, the most commonly used physical picture is that of a classical optical field interacting with an atom or a molecule whose energetic structure is treated quantum mechanically. And even the atomic or molecular dipole is often treated like a classical oscillator. The exposition of such a dipole to simple boundary conditions prepares the analogous development of a quantum oscillator and provides a direct path to quantization of the radiation field.

Even if we rarely do experiments by throwing light into a small hole in a metallic box, the electromagnetic fields obtained by solving Maxwell's equation are particularly simple for boundary conditions, where the fields disappear on the inner surfaces of the box. Before discussing the physics of radiation in a perfectly conducting cavity, we have to introduce some basic relations between electromagnetic amplitudes, stored energy, and intensity.

The electric field of a plane wave oscillating with frequency ω and propagating through vacuum in the direction of propagation defined by the *wave vector*,

$$\mathbf{k} = \frac{2\pi}{\lambda}\hat{\mathbf{k}} \ , \tag{22.33}$$

can be written,

$$\vec{\mathcal{E}} = \vec{\mathcal{E}}_0 e^{\imath(\mathbf{k}\cdot\mathbf{r}-\omega t)} \ , \tag{22.34}$$

where $\vec{\mathcal{E}}_0 = \mathcal{E}_0\hat{\mathbf{e}}$ consists of an amplitude $\mathcal{E}_0$ and a polarization $\hat{\mathbf{e}}$. Since the field $\vec{\mathcal{E}}_0$ is transverse to the direction of propagation, the polarization has two components perpendicular to $\mathbf{k}$. The magnetic induction field associated with the wave is,

$$\mathcal{B}_0 = \tfrac{1}{c}\mathcal{E}_0 \ . \tag{22.35}$$

For a propagating wave $\vec{\mathcal{E}}$ and $\vec{\mathcal{B}}$ are in phase, while for a standing wave they are out of phase.

For a given cavity mode we can express the standing wave in this mode as,

$$\vec{\mathcal{E}} = \vec{\mathcal{E}}_0(\mathbf{r})e^{-\imath\omega t} \ . \tag{22.36}$$

[7] The corpuscular hypothesis is now called the second quantization of quantum theory or quantization of the electromagnetic field.

The energy of the electromagnetic field of a standing wave, averaged over one oscillation of the frequency ω is,

$$\bar{U} = \frac{1}{2}\int \left(\frac{\varepsilon_0}{2}|\vec{\mathcal{E}}|^2 + \frac{1}{2\mu_0}|\vec{\mathcal{B}}|^2\right) dV \ . \tag{22.37}$$

Now, the *energy density* of the oscillating electromagnetic field is given by,

$$\boxed{\bar{u} = \frac{d\bar{U}}{dV} = \frac{1}{4}\left(\varepsilon_0|\vec{\mathcal{E}}|^2 + \frac{1}{\mu_0}|\vec{\mathcal{B}}|^2\right)} \ . \tag{22.38}$$

From the equation (22.35) we can see that the contributions of the electric and magnetic fields are equal. Therefore,

$$\bar{U} = \tfrac{1}{2}\int \varepsilon_0|\vec{\mathcal{E}}|^2 dV \qquad \text{and} \qquad \bar{u} = \tfrac{1}{2}\varepsilon_0|\vec{\mathcal{E}}|^2 \ . \tag{22.39}$$

Another important quantity is the *flux of electromagnetic energy* through a surface. The *Poynting vector* describing this flux is defined by,

$$\mathbf{I} = \tfrac{1}{\mu_0}\vec{\mathcal{E}} \times \vec{\mathcal{B}} \ . \tag{22.40}$$

Again using the equation (22.35), we find the value averaged over a time period,

$$\boxed{\bar{I} = \tfrac{1}{2}\varepsilon_0 c|\vec{\mathcal{E}}|^2} \ . \tag{22.41}$$

This quantity, called *intensity*, describes the fact that the flux is a density of energy multiplied with the velocity of propagation in vacuum,

$$\bar{u}c = \tfrac{1}{2}\varepsilon_0 c|\vec{\mathcal{E}}|^2 = \bar{I} \ . \tag{22.42}$$

The intensity can also be written,

$$\bar{I} = \frac{1}{2}\sqrt{\frac{\varepsilon_0}{\mu_0}}|\vec{\mathcal{E}}|^2 \ . \tag{22.43}$$

where the factor $\sqrt{\mu_0/\varepsilon_0}$ is called *impedance of free space*, because it has the unit of a resistance and the last equation has the same form as the power dissipated in a resistor,

$$W = \frac{1}{2}\frac{V^2}{R} \ . \tag{22.44}$$

22.2.2 Black body radiation

We now want to calculate the energy density inside the cavity before using the result to describe the interaction between light and a sample of two-level atoms located inside the cavity. The basic idea is to say that the electrons inside the conducting surface of the cavity oscillate because of thermal motion. The oscillation generates a dipolar radiation leading to stationary waves developing within the cavity. As the walls of the cavity are conducting, the electric field $\vec{\mathcal{E}}$ must disappear inside the wall and on its

surfaces. The task is now twofold: first count the number of possible standing waves, which satisfy the boundary conditions as a function of frequency; second, determine the energy for each wave and then calculate the spectral distribution of the energy within the cavity.

The equations describing the radiated energy in free space are,

$$\nabla^2\vec{\mathcal{E}} = \frac{1}{c^2}\frac{\partial^2\vec{\mathcal{E}}}{\partial t^2} \qquad \text{and} \qquad \nabla\cdot\vec{\mathcal{E}} = 0\ . \tag{22.45}$$

The stationary waves solutions separate into terms oscillating in time and in space.

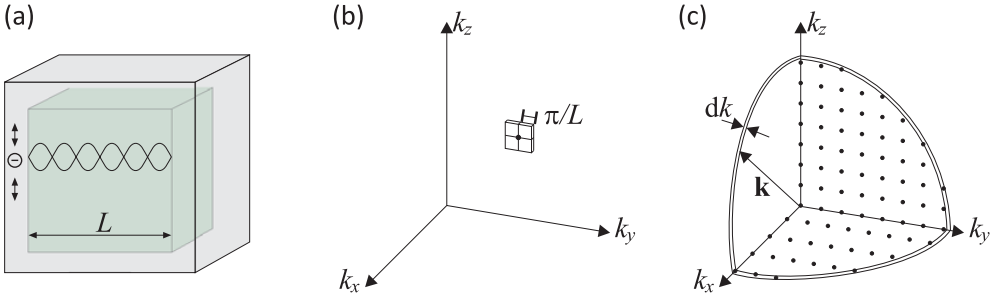

Figure 22.8: (a) Cavity in position space showing the thermal motion of the electrons inside the walls. (b and c) Density-of-states in a cavity in momentum space.

Now, respecting the boundary conditions for a three-dimensional box of length L, we have for the components of $\vec{\mathcal{E}}$ [8],

$$\begin{aligned}\vec{\mathcal{E}}(\mathbf{r},t) = e^{-\imath\omega t}[&\hat{\mathbf{e}}_x\cos(k_x x)\sin(k_y y)\sin(k_z z)\\ &+\hat{\mathbf{e}}_y\sin(k_x x)\cos(k_y y)\sin(k_z z)\\ &+\hat{\mathbf{e}}_z\sin(k_x x)\sin(k_y y)\cos(k_z z)]\ ,\end{aligned} \tag{22.46}$$

with the components,

$$k_x = \frac{\pi n_x}{L} \qquad \text{for} \qquad n_x = 0, 1, 2, ... \tag{22.47}$$

and similar for k_y and k_z. Note, that for each component $\mathcal{E}_{x,y,z}$ the transverse amplitudes disappear in 0 and L. By inserting this solution into Helmholtz's equation (22.45), we obtain,

$$k_x^2 + k_y^2 + k_z^2 = \frac{\omega^2}{c^2}\ . \tag{22.48}$$

The states $k_{x,y,z}$ (enumerated by integer numbers $n_{x,y,z}$) form a three-dimensional orthogonal lattice of points in space $\mathbf{k}$ separated by a distance along the axes k_x, k_y, k_z of $\frac{\pi}{L}$, as shown in Fig. 22.8. In principle, the number of states that can be placed within a sphere of radius k in the momentum space is,

$$N = \int_{\text{sphere}} dn_x dn_y dn_z\ . \tag{22.49}$$

[8] See script on *Electrodynamics* (2023).

However, the periodic boundary conditions for $|\mathbf{k}|$ limit the components k_x, k_y, k_z to positive values ($n \geq 0$), that is, the volume under consideration is limited to an octant. On the other hand, we must multiply the number of states by two because of the degeneracy of polarizations. Hence,

$$4N = \int_0^n 4\pi n^2 dn = \left(\frac{L}{\pi}\right)^3 \int_0^k 4\pi k^2 dk = \frac{4L^3}{\pi^2}\frac{k^3}{3} = \frac{4L^3\omega^3}{3\pi^2 c^3} \ . \tag{22.50}$$

With this, we obtain the *mode density*,

$$\frac{N}{L^3} = \frac{\omega^3}{3\pi^2 c^3} \ . \tag{22.51}$$

The *spectral density of modes* ϱ can be given in several units,

$$\int \varrho(n)dn = \int \varrho(k)dk = \int \varrho(\omega)d\omega = \frac{N}{L^3} \ , \tag{22.52}$$

such that,

$$\boxed{\varrho(n) = \frac{\pi n^2}{L^3} \quad \text{or} \quad \varrho(k) = \frac{k^2}{\pi^2} \quad \text{or} \quad \varrho(\omega) = \frac{\omega^2}{\pi^2 c^3}} \ . \tag{22.53}$$

The density of oscillating modes within the cavity grows like the square of the frequency. Now, the mean energy per mode in a sample of oscillators in thermal equilibrium is, following the equipartition law, equal to,

$$\bar{E} = k_B T \ , \tag{22.54}$$

where k_B is the Boltzmann constant. We conclude that the *spectral energy density* $u_{RJ}(\omega)$ in the cavity is,

$$\boxed{u_{RJ}(\omega)d\omega = k_B T \varrho(\omega)d\omega = k_B T \frac{\omega^2}{\pi^2 c^3}d\omega} \ . \tag{22.55}$$

This law is known as the *Rayleigh-Jeans law* of *black-body radiation*. As seen in Fig. 22.9, this law suggests the physically impossible fact, called *ultraviolet catastrophe*, that the energy storage in the cavity grows without limits like the square of frequency.

22.2.3 Planck's distribution of modes

We obtained the result (22.54) by multiplying the number of modes with the mean energy per mode. As there is no doubt about our method of counting the modes, the problem with the ultraviolet catastrophe can only root in the use of the equipartition principle for assigning energy to the oscillators.

Planck's idea to solve this problem was to first consider the probability distribution for exciting the modes (thermal states) for a sample of oscillators in thermal equilibrium at temperature T. This probability distribution p comes from mechanical

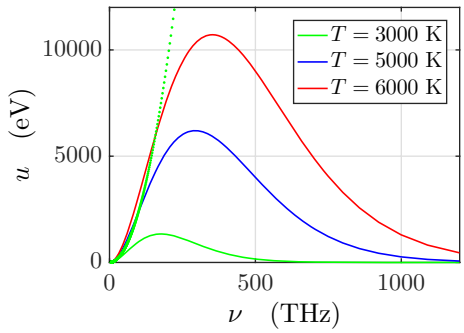

Figure 22.9: (code) Spectral energy density following Rayleigh-Jeans' and Planck's laws.

statistics and can be written in terms of the *Boltzmann factor*, e^{-E_n/k_BT}, and the partition function $q = \sum_{n=0}^{\infty} e^{-E_n/k_BT}$ as,

$$p_n = \frac{e^{-E_n/k_BT}}{q} \ . \tag{22.56}$$

Now Planck hypothesized that the energy be quantized, that is, it must be assigned in discrete portions, proportional to the frequency, such that,

$$\boxed{E_n = n\hbar\omega} \ , \tag{22.57}$$

where $n = 0, 1, 2, ..$ and the proportionality constant $\hbar$ is called *Planck's constant*. With the abbreviation $Z \equiv e^{-\hbar\omega/k_BT}$ and using the rule $\sum_{n=0}^{\infty} Z^n = (1-Z)^{-1}$, we find the average number,

$$\bar{n} = \sum_n n p_n = (1-Z)\sum_n n Z^n = (1-Z)Z\frac{\partial}{\partial Z}\sum_n Z^n = \frac{Z}{1-Z} = \frac{1}{e^{\hbar\omega/k_BT}-1} \ . \tag{22.58}$$

The probability of occupancy of state n is,

$$p_n = (1-Z)Z^n = \frac{\bar{n}^n}{(1+\bar{n})^{1+n}} \ , \tag{22.59}$$

and the average energy is,

$$\bar{E} = \sum_n E_n p_n = \sum_n n\hbar\omega e^{-n\hbar\omega/k_BT} = \frac{\hbar\omega}{e^{\hbar\omega/k_BT}-1} \ , \tag{22.60}$$

in contrast to the initial assumption (22.55).

Finally, we obtain Planck's expression for the energy density inside the cavity by replacing the energy (22.60) for the factor k_BT in Rayleigh-Jeans' law (22.55),

$$\boxed{u_P(\omega)d\omega = \bar{E}\varrho(\omega)d\omega = \frac{\omega^2}{\pi^2c^3}\frac{\hbar\omega}{e^{\hbar\omega/k_BT}-1}d\omega} \ . \tag{22.61}$$

This result, drawn in Fig. 22.9, is much more satisfactory, because now the energy density has an upper bound, and it coincides with the results of experiments. For high

temperatures or low excitation energies, $\hbar\omega \ll k_B T$, Planck's distribution converges to that of Rayleigh-Jeans', $u_P(\omega) \to u_{RJ}(\omega)$.

Note, that the form of the expression for the energy depends on the parametrization and must be derived respecting $u(\omega)d\omega = u(\lambda)d\lambda$, etc.. Often the blackbody radiation is expressed in terms of the *spectral radiance*,

$$L(\omega) \equiv \frac{c}{4\pi} u(\omega) \ , \tag{22.62}$$

which can be understood as the (isotropic) energy flux into all directions of space. Solve the Excs. 22.2.10.1 to 22.2.10.7.

22.2.4 The corpuscular nature of the photon

22.2.4.1 The photoelectric effect

Light incident on a metallic surface can expel electrons. For this to occur, the light must have a *minimum frequency*. If the frequency is below this value, there is no point in increasing the light intensity: the electrons won't be expelled. The main experimental observations are: 1. Electrons are ejected without apparent delay, i.e. it is not necessary (and it doesn't help) to accumulate a certain amount of energy. 2. Higher light intensities increase the number of electrons, but not their kinetic energy after expulsion. 3. Red light does not eject electrons, even at high intensities. 4. Weak ultraviolet light only ejects few electrons, but with high kinetic energy.

These observations challenge the classical electromagnetic model according to which the Lorentz acceleration of the electrons should be proportional to the field *amplitude*. The observations were explained by Einstein's theory of the *photoelectric effect*, which assumes the light to be quantized (unlike Planck, who preferred to quantize the process of light absorption),

$$E = h\nu \ . \tag{22.63}$$

Assuming a fixed exit work A for the extraction of an electron, we can measure the constant $\hbar$:

$$h\nu = A + \tfrac{mv^2}{2} = A + eV \qquad \to \qquad h = \frac{eV}{\nu - \nu_g} \ . \tag{22.64}$$

The energy of the fastest electrons is measured through the decelerating voltage by varying ν and I. We will discuss the photoelectric effect quantitatively later in the Exc. 27.4.5.7.

22.2.4.2 Bremsstrahlung and the Franck-Hertz experiment

Bremsstrahlung is, in a way, the inverse process of the photoelectric effect. Here, electrons are accelerated toward a cathode. Finding a target they are rapidly decelerated, a process in which they emit a continuous spectrum of X-rays (in addition to characteristic lines attributed to electronic transitions in the target atoms). For any given kinetic energy the spectra have a red threshold corresponding to photons that receive the entire energy of the electron.

In the *Franck-Hertz experiment* free electrons produced in a plasma are accelerated by a strong electric field. Having traveled a sufficiently long distance they have

acquired enough kinetic energy to excite electronic transitions in the atoms of the plasma. When an excitation occurs, the electron suddenly loses all its energy and must be accelerated again, starting from rest, before it can excite another atom.

22.2.4.3 Radiative pressure and Compton scattering

When light is scattered from a particle, it transfers momentum to it called *photonic recoil*. This effect, known as *radiation pressure*, occurs for example in *Compton scattering*.

X-rays scattered by the electrons of a carbon target are red-shifted by an amount, which increases with the scattering angle. This is the *Compton effect*. The data are understood assuming a corpuscular nature of light and applying the laws of conservation of energy and momentum to the collision processes between photons and electrons. The scattered photon sees its energy reduced and therefore its wavelength increased, as we have already seen in Sec. 20.2.3.

In a material where there are free electrons, this effect will occur at all photon energies. In other materials, it is only observed with high energy photons. For high energy photons, exceeding the atomic binding energy, the electrons can be considered free such that, in the scattering process, the photon is able to eject the electron from its atom. The photon receives the remaining energy and is deviated, such that the overall momentum of the system is conserved. The loss of energy for the photon results in a spectral shift to the red during its passage through the material.

Photons of visible light, on the other hand, do not have enough energy to eject bound electrons. In this case, the mass in the Compton formula must be replaced by the atomic mass, such that the spectral displacement becomes much smaller. This limit, which involves bound electrons, is that of Thomson and Rayleigh scattering.

The relevance of this effect lies in the fact that it shows that light exhibits properties commonly attributed to corpuscles, since Thomson's scattering model, based on the classical theory of charged particles accelerated by electromagnetic fields, can not explain any spectral shift. Compton scattering is discussed quantitatively in Exc. 20.2.6.5.

22.2.5 Einstein's transitions rates

Bohr's atom model explained for the first, time how light interacts with matter: Atoms have discrete excitation levels, and they absorb and emit discrete energy packets $\hbar\omega$. Unfortunately, Bohr's model can not predict transition rates. Here, Einstein helped out by developing a useful theory (see Fig. 22.10).

Figure 22.10: Bohr model and Einstein rate diagram.

We consider a two-level atom or a sample of atoms within a conducting cavity. We have N_1 atoms in the lower energy state E_1 and N_2 in the upper state E_2. Light interacts with these atoms through stimulated resonant absorption and emission. The rates, $B_{12}u(\omega)$ and $B_{21}u(\omega)$ are proportional to the energy spectral density $u(\omega)$ of the cavity modes. The central idea of Einstein is to postulate that atoms in the higher state can emit light spontaneously at a rate A_{21}, which depends only on the density of modes of the cavity, i.e. the volume of the cavity, but not the energy of the field of radiation. With the Einstein coefficients we can formulate valid rate equations in situations, where the spectral distribution of the radiation is wider than the spectral width of the atomic transition and where the spectral distribution of the light flux from the source, $\bar{I}(\omega)$, is weak compared to the saturation intensity of the atomic transition. Even if modern light sources generally have very narrow and intense spectral emission bands, Einstein's coefficients are often used in the spectroscopic literature to characterize the light-matter interaction with atoms and molecules.

The Einstein rate equations describe the energy flux between atoms and the optical modes of the cavity,

$$\begin{aligned} \frac{dN_1}{dt} = -\frac{dN_2}{dt} &= -R_{1\to 2} + R_{2\to 1} + \mathcal{S}_{2\to 1} \\ &= -N_1 B_{12} u(\omega) + N_2 B_{21} u(\omega) + N_2 A_{21} \ . \end{aligned} \tag{22.65}$$

$R_{1\to 2}$ is the *absorption rate*, $R_{2\to 1}$ the *stimulated emission rate* and $\mathcal{S}_{2\to 1}$ the *spontaneous emission rate*. The assumption of a third type of transition, called spontaneous emission, is necessary, if $B_{12} = B_{21}$ but $N_1 > N_2$ in thermal equilibrium. In thermal equilibrium we have the condition of stationarity, $\frac{dN_1}{dt} = -\frac{dN_2}{dt} = 0$ for a given energy density value $u(\omega) = u_{th}(\omega)$, such that,

$$u_{th}(\omega) = \frac{A_{21}}{\left(\frac{N_1}{N_2}\right) B_{12} - B_{21}} \ . \tag{22.66}$$

The *Boltzmann distribution law* controlling the distribution of the number of atoms in the lower and upper states is given by,

$$\frac{N_1}{N_2} = \frac{g_1}{g_2} e^{-(E_1 - E_2)/k_B T} \ , \tag{22.67}$$

where $g_{1,2}$ are the degeneracies of the lower and upper states and $E_2 - E_1 = \hbar\omega_0$. We find,

$$u_{th}(\omega) = \frac{A_{21}}{\frac{g_1}{g_2} e^{\hbar\omega_0/k_B T} B_{12} - B_{21}} \ . \tag{22.68}$$

But this result must be consistent with Planck's distribution (22.61). Therefore, by comparing this equation with the equation (22.68), it must be that,

$$\frac{g_1}{g_2}\frac{B_{12}}{B_{21}} = 1 \ . \tag{22.69}$$

and also,

$$\frac{A_{21}}{B_{21}} = \frac{\hbar\omega_0^3}{\pi^2 c^3} \ . \tag{22.70}$$

This equation shows that, once we know one of the three transition rates, we can always calculate the others.

It is useful to compare the rate A_{21} with B_{21} from the equation (22.68) inserting the equation (22.69),

$$\frac{A_{21}}{B_{21}u_{th}(\omega)} = e^{\hbar\omega_0/k_BT} - 1 \ . \tag{22.71}$$

This expression shows that, when $E_2 - E_1 \gg k_BT$, that is, for optical, UV, or X-ray frequencies, spontaneous emission dominates. But in low-frequency regimes, that is, IR, microwave, or radio waves, stimulated emission is more important. Note that even when stimulated emission dominates, spontaneous emission is always present and plays an important role, for example, in processes ultimately limiting the emission bandwidth of lasers.

22.2.6 Absorption spectrum for a single atom

Every light source has a certain spectral width. Conventional light sources, such as incandescent bulbs or plasmas have relatively broad emission bands compared to atomic or molecular absorbers, at least when the latter ones are studied in dilute gases. Even when we use pure spectral sources, such as a laser tuned to the peak of a resonance, the transition line always exhibits an intrinsic width associated with the interruption of the phase evolution of the excited state. Phase interruptions such as spontaneous or stimulated emission and collisions are common examples of line broadening mechanisms. The emission or absorption of radiation occurs within a frequency distribution centered about $\omega_0 \equiv \omega_2 - \omega_1$, and we must account for this spectral distribution in our calculation of the energy transfer.

On the other hand, as we will see in Sec. 34.1.3 and Sec. 34.5.1, spontaneous decay at a rate Γ of the excited level causes a finite linewidth for the atomic transition. Consequently, even perfectly monochromatic light will be absorbed according to a probability distribution given by the spectral absorption profile of the atomic transition. This profile is called the frequency-dependent *optical cross section* and reads [9],

$$\boxed{\sigma(\omega) = \frac{g_2}{g_1}\lambda^2\frac{\Gamma}{2\pi}\frac{\frac{1}{4}\Gamma}{(\omega-\omega_0)^2+\frac{1}{4}\Gamma^2} = \frac{g_2}{g_1}\lambda^2\frac{\Gamma}{4}\mathcal{L}_\Gamma(\omega-\omega_0)\ ,} \tag{22.72}$$

where we defined the Lorentzian profile as,

$$\mathcal{L}_\beta(\Delta) \equiv \frac{\beta}{2\pi}\frac{1}{\Delta^2+(\beta/2)^2} \qquad \text{with} \qquad \int_{-\infty}^{\infty}\mathcal{L}_\beta(\Delta)d\Delta = 1\ . \tag{22.73}$$

The total power P absorbed by a two-level atom with resonance frequency ω_0 from a radiation field with the spectral intensity distribution $I(\omega)$ and with the total intensity of the laser beam $\bar{I} = \int I(\omega)d\omega$ can now be expressed as the integral,

$$\boxed{P = \int \sigma(\omega)I(\omega)d\omega}\ , \tag{22.74}$$

[9] At low saturation.

Example 139 (*Limiting cases*): Let us analyze the two limiting cases when either one of the spectral distributions $I(\omega)$ or $\sigma(\omega)$ is much narrower than the other.
For a *narrow laser*, we may assume a δ-peaked spectral intensity distribution,

$$I(\omega) = \bar{I}\delta(\omega - \omega_L) \ . \tag{22.75}$$

When it drives a *broad transition* described by an optical cross section given by (22.72), the scattered power is,

$$P = \bar{I}\sigma(\omega_L) \ . \tag{22.76}$$

For a *narrow transition*, we may substitute the Lorentzian in (22.72) by a Dirac δ-function,

$$\sigma(\omega) \overset{\Gamma\to 0}{\longrightarrow} \frac{g_2}{g_1}\lambda^2\frac{\Gamma}{4}\delta(\Delta) \ . \tag{22.77}$$

When it is driven by a *broad laser*, for which we assume a spectral intensity distribution,

$$I(\omega) = \bar{I}\mathcal{L}_\beta(\omega - \omega_L) \qquad \text{with} \qquad \bar{I} = \int I(\omega)d\omega = \frac{I(\omega_L)}{\mathcal{L}_\beta(0)} = \frac{\pi\beta}{2}I(\omega_L) \tag{22.78}$$

we obtain for the scattered power,

$$P = \int \frac{g_2}{g_1}\lambda^2\frac{\Gamma}{4}\delta(\omega - \omega_0)\bar{I}\mathcal{L}_\beta(\omega - \omega_L)d\omega = \frac{g_2}{g_1}\lambda^2\frac{\Gamma}{4}\bar{I}\mathcal{L}_\beta(\omega_0 - \omega_L) \ . \tag{22.79}$$

22.2.6.1 Broad laser driving a broad transition

Until now we assumed a fixed laser frequency ω_L (with finite emission bandwidth) driving a fixed resonance frequency ω_0. What we call *absorption spectrum* is what we obtain when we tune either the laser frequency or when we (somehow) vary the resonance frequency, such that $\Delta \equiv \omega_L - \omega_0$ is ramped. Assuming Lorentzian profiles with finite linewidths for both, $\bar{I}$ and σ, we get,

$$\begin{aligned} P(\Delta) = P(\omega_L - \omega_0) &= \int \sigma(\omega)I(\omega)d\omega = \int \frac{g_2}{g_1}\frac{\lambda^2\Gamma}{4}\mathcal{L}_\Gamma(\omega - \omega_L)\bar{I}\mathcal{L}_\beta(\omega - \omega_0)d\omega \\ &= \frac{g_2}{g_1}\frac{\lambda^2\Gamma}{4}\bar{I}\int \mathcal{L}_\Gamma(\omega' + \omega_0 - \omega_L)\mathcal{L}_\beta(\omega')d\omega' \ . \end{aligned} \tag{22.80}$$

That is, the absorption spectrum is obtained as a convolution of both profiles,

$$\boxed{P(\Delta) = \frac{g_2}{g_1}\frac{\lambda^2\Gamma\bar{I}}{4}(\mathcal{L}_\Gamma \star \mathcal{L}_\beta)(\Delta)} \ . \tag{22.81}$$

This result reproduces the two limiting cases discussed in the above example, since for narrow transitions, $\Gamma \to 0$, that is $\mathcal{L}_\Gamma \to \delta$, we recover the results (22.79), and for narrow lasers, $\beta \to 0$, that is, $\mathcal{L}_\beta \to \delta$, we recover (22.76). Obviously, this formula holds for other line profiles e.g. when the resonance is broadened by some perturbations [10].

[10] Let us here remind the following identities holding for Lorentzian and Gaussian line profiles:

$$(\mathcal{L}_\gamma \star \mathcal{L}_\beta)(\Delta) = \mathcal{L}_{\gamma+\beta}(\Delta) \qquad \text{and} \qquad (\mathcal{G}_\Gamma \star \mathcal{G}_\beta)(\Delta) = \mathcal{G}_{\sqrt{\gamma^2+\beta^2}}(\Delta) \ .$$

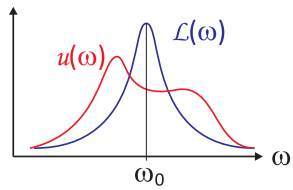

Figure 22.11: Absorption spectrum (blue) and spectral energy distribution of the source (red).

22.2.6.2 Two-level atom in a blackbody radiation field

When considering a two-level atom interacting with a blackbody a radiation field, we describe the spectral intensity distribution by (22.61),

$$I(\omega) = \frac{\omega^2}{\pi^2 c^2} \frac{\hbar\omega}{e^{\hbar\omega/k_B T} - 1} \tag{22.82}$$

$$\text{with} \qquad \bar{I} = \int I(\omega) d\omega = \frac{\hbar}{\pi^2 c^2} \left(\frac{k_B T}{\hbar}\right)^4 \int_0^\infty \frac{x^3 dx}{e^x - 1} = \frac{\pi^2}{15 c^2 \hbar^3} (k_B T)^4 \ .$$

Since the width of the transition is negligibly small in comparison with the blackbody spectrum, $\Gamma \to 0$, we may evaluate the scattered power as,

$$P = \int \frac{g_2}{g_1} \frac{\lambda^2 \Gamma}{4} \mathcal{L}_\Gamma(\omega - \omega_0) \frac{\omega^2}{\pi^2 c^2} \frac{\hbar\omega}{e^{\hbar\omega/k_B T} - 1} d\omega \tag{22.83}$$

$$\xrightarrow{\Gamma \to 0} \frac{g_2}{g_1} \frac{\lambda^2 \Gamma}{4} \frac{\omega_0^2}{\pi^2 c^2} \frac{\hbar\omega_0}{e^{\hbar\omega_0/k_B T} - 1} \ .$$

22.2.7 Absorption in a gas

We are often interested in the attenuation of the intensity of a beam of light traversing a dilute gas of resonant scattering atoms. The Einstein rate equation yields the *temporal* transition rates, but does not say how they relate to the *spatial* attenuation length of the light beam. Let us now generalize the previous results to a gas of two-level atoms. As long as the transition linewidth is narrow [case (22.77)], the power is removed from the system only by spontaneous emission; absorption only converts radiation into atomic excitation which, subsequently, can be returned to the radiation field by stimulated emission. At steady-state the Einstein rate equation (22.65) reads,

$$0 = -N_1 B_{12} u(\omega_0) + N_2 B_{21} u(\omega_0) + N_2 A_{21} \ . \tag{22.84}$$

Using the result (22.69), we can write the amount of power removed from the system by spontaneous emission as,

$$P = N_2 A_{21} \hbar\omega_0 = u(\omega_0) B_{12} (N_1 - \tfrac{g_1}{g_2} N_2) \hbar\omega_0 \ . \tag{22.85}$$

The second part of the equation describes the energy loss of the beam, i.e. the difference between energy removed by absorption and energy returned to the beam by stimulated emission.

On the other hand, the power absorbed from the radiation field $u(\omega_0)$ by atoms whose transition is described by the cross section (22.72), is given by,

$$P = \int (N_1 - \tfrac{g_1}{g_2} N_2)\sigma(\omega) I(\omega) d\omega \ . \tag{22.86}$$

Remembering $I(\omega) = cu(\omega)$ and assuming a *large radiation spectrum*, $I(\omega) \simeq I(\omega_0)$, a comparison of equations (22.85) and (22.86) yields,

$$\boxed{B_{12} = \frac{c}{\hbar\omega_0} \int \sigma(\omega) d\omega} \ . \tag{22.87}$$

22.2.7.1 Lambert-Beer law

In the expression (22.86) the absorption probability distribution $\sigma(\omega)$ is convoluted with the spectral energy distribution of the light source, $u(\omega) = d\bar{u}/d\omega$, which in turn is related to the energy *density* via, $\bar{U} = V\bar{u}$, where V is the mode volume of the light field. Considering a thin slab of the absorber with volume ΔV, we have $d\bar{U} = \Delta V d\bar{u}$. Assuming that the light propagates in z-direction across the absorber and converting the time dependence into a spatial dependence, we have on one hand,

$$P = -\frac{d\bar{U}}{dt} = -\frac{d\bar{u}}{dt}\Delta V = -c\frac{d\bar{u}}{dz}\Delta V = -\frac{d\bar{I}}{dz}\Delta V \ . \tag{22.88}$$

On the other hand, assuming that the light field be a *laser with narrow emission bandwidth*, $I(\omega) = \bar{I}\delta(\omega - \omega_L)$, we get from (22.86),

$$P = \int (N_1 - \tfrac{g_1}{g_2} N_2)\sigma(\omega) I(\omega) d\omega = \bar{I}(N_1 - \tfrac{g_1}{g_2} N_2)\sigma(\omega_L) \ , \tag{22.89}$$

Now comparing both results,

$$\frac{d\bar{I}}{\bar{I}} = -\frac{N_1 - \frac{g_1}{g_2} N_2}{\Delta V}\sigma(\omega_L) dz \simeq -n\sigma(\omega_L) dz \ , \tag{22.90}$$

where the approximation holds for low saturation, that it, if $N_1 \gg N_2$. The solution of this differential equation is,

$$\boxed{\bar{I} = \bar{I}_0 e^{-\sigma(\omega_L) n z}} \ . \tag{22.91}$$

Here, z is the total distance, over which absorption takes place. The last equation is the *Lambert-Beer law* for light absorption. It is very useful for measuring atomic densities in gas cells or of atomic beams [860, 816, 1364]. Solve the Excs. 22.2.10.9 to 22.2.10.11.

22.2.8 Saturation

Strong driving of a transition leads to its saturation and causes line broadening. To see this, we go back to Einstein's rate equations in steady-state (22.65) additionally

simplified by assuming $g_1 = 1 = g_2$, such that $B_{12} = B_{21}$. Resolving these equations by N_1 and N_2 and using $N_1 + N_2 = N$ and $N_1 - N_2 \equiv \Delta N$, we get,

$$N_1 = N\frac{B_{21}u(\omega) + A_{21}}{2B_{21}u(\omega) + A_{21}} \qquad \text{and} \qquad N_2 = N\frac{B_{12}u(\omega)}{2B_{21}u(\omega) + A_{21}} \ . \tag{22.92}$$

For vanishing pump rate we expect, $N_1 \overset{u\to 0}{\longrightarrow} N$ and $N_2 \overset{u\to 0}{\longrightarrow} 0$. In contrast, when the pump rate becomes much larger than the relaxation rates, $N_1, N_2 \overset{u\to\infty}{\longrightarrow} \frac{1}{2}$. This means that the absorption coefficient $\alpha = \sigma(N_1 - N_2)$ goes to zero, and the medium becomes completely transparent. The difference in the populations of the ground and excited states,

$$\Delta N = N\frac{A_{21}}{2B_{21}u(\omega) + A_{21}} = \frac{N}{1 + s(\omega)} \ , \tag{22.93}$$

can be expressed via a *saturation parameter*

$$s(\omega) \equiv \frac{2B_{12}u(\omega)}{A_{21}} \ , \tag{22.94}$$

which represents the ratio of pump rate to the relaxation rate. The pump rate due to a monochromatic wave with intensity $\bar{I}$ is obtained by comparing (22.85) with (22.89),

$$B_{12}u(\omega) = \frac{\sigma(\omega)\bar{I}}{\hbar\omega} \ . \tag{22.95}$$

We obtain for the saturation parameter,

$$s(\omega) = \frac{2\sigma(\omega)\bar{I}}{\hbar\omega A_{21}} \ . \tag{22.96}$$

According to (22.85) and (22.93) the power absorbed per unit volume on the transition by atoms with the populations $N_{1,2}$ in a radiation field with a broad spectral profile and spectral energy density $u(\omega)$ is,

$$P = \hbar\omega B_{12}u(\omega)\Delta N = \hbar\omega B_{12}u(\omega)\frac{N}{1 + s(\omega)} \ . \tag{22.97}$$

With (22.94) this can be written as,

$$P = \hbar\omega\frac{A_{21}}{2}\frac{N}{1 + s(\omega)^{-1}} \ . \tag{22.98}$$

Let us now remember that the absorption cross section (22.72) of a homogeneously broadened line is Lorentzian. This means that the saturation parameter (22.96) itself becomes Lorentzian. We can assume that the relaxation rate A_{21} is independent of ω within the frequency range of the line profile,

$$\boxed{s(\omega) = s(\omega_0)\frac{(\Gamma/2)^2}{\Delta^2 + (\Gamma/2)^2}} \ . \tag{22.99}$$

Substituting this into (22.98) yields the frequency dependence of the absorbed radiation power per unit frequency interval $d\omega$,

$$P = \hbar\omega \frac{A_{21}N}{2} \frac{s(\omega_0)(\Gamma/2)^2}{(\omega-\omega_0)^2 + (\Gamma/2)^2[1+s(\omega_0)]} = N\bar{I}\sigma(\omega_0)\frac{(\Gamma/2)^2}{\Delta^2 + (\gamma_s/2)^2} \ , \tag{22.100}$$

where we introduced the increased halfwidth of the Lorentzian profile,

$$\boxed{\gamma_s \equiv \Gamma\sqrt{1+s(\omega_0)}} \ . \tag{22.101}$$

Apparently, the halfwidth of the saturation-broadened line increases with the resonant saturation parameter $s(\omega_0)$. If according to (22.94) the induced transition rate at resonance equals the total relaxation rate $A_{21}/2$, the resonant saturation parameter becomes $s(\omega_0) = 1$, which increases the linewidth by a factor $\sqrt{2}$, compared to the unsaturated linewidth Γ for weak radiation fields. Starting from (22.100) we can define a *saturated* absorption cross section,

$$\boxed{\sigma_s(\omega) = \sigma_s(\omega_0)\frac{(\gamma_s/2)^2}{\Delta^2 + (\gamma_s/2)^2} = \sigma(\omega_0)\frac{(\Gamma/2)^2}{\Delta^2 + (\gamma_s/2)^2} = \sigma(\omega)\frac{1}{1+s(\omega)}} \ , \tag{22.102}$$

where the unsaturated absorption profile is,

$$\sigma(\omega) = \sigma(\omega_0)\frac{(\Gamma/2)^2}{\Delta^2 + (\Gamma/2)^2} \ . \tag{22.103}$$

This shows that the saturation decreases the absorption coefficient by the factor $1 + s(\omega)$. At the line center, this factor has its maximum value $1 + s(\omega_0)$, while it decreases to 1 for increasing $|\Delta|$, see (22.101), see Fig. 22.12. This is the reason why the line broadens.

From (22.96) we see, that unity saturation, $s(\omega_0) = 1$, corresponds to a light intensity of,

$$\bar{I}_{sat} \equiv \frac{\hbar\omega}{2\sigma(\omega_0)}\Gamma = \frac{2\pi^2 c\hbar}{3\lambda^3}\Gamma \ . \tag{22.104}$$

This intensity is called *saturation intensity*. Taking account of the degeneracies g_j of the levels the saturation intensity becomes [11],

$$\boxed{I_{sat} = \frac{g_1}{g_2}\frac{2\pi^2 c\hbar}{3\lambda_0^3}\Gamma} \ . \tag{22.105}$$

Finally, we anticipate that the resonant saturation parameter is basically a measure for the ratio between the stimulated population transfer rate, given by a quantity called *Rabi frequency* Ω, which will be thoroughly introduced in Secs. 27.4.3 and 34.4.2, and the spontaneous decay rate Γ,

$$s(\omega_0) = \frac{2\Omega^2}{\Gamma^2} \ . \tag{22.106}$$

We thus obtain the important relationship between laser intensity and Rabi frequency,

$$\boxed{\Omega^2 = \sigma(\omega_0)\frac{\bar{I}}{\hbar\omega_0}\Gamma} \ . \tag{22.107}$$

[11] Some authors define the saturation for $s = 2$, as happens when $\Omega = \Gamma$.

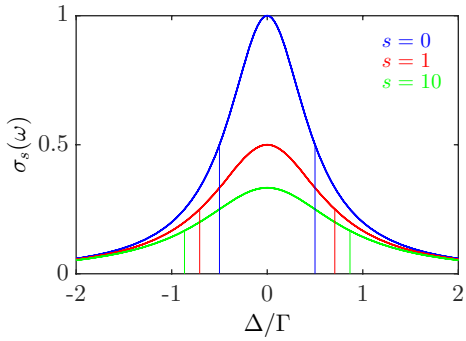

Figure 22.12: (code) Optical cross section for absorption at various saturation parameters. The reduction of absorption is understood by considerable depletion of the ground state at the profit of the excited state, $N_1, N_2 \overset{s\to\infty}{\longrightarrow} \frac{1}{2}$, in which case absorption is totally compensated by stimulated emission.

22.2.9 Specific heat of solids

The *Debye model* applies Planck's law on the distribution of energy in electromagnetic radiation, which treats radiation as a gas of *photons*, to the energy distribution of atomic vibrations in a solid, treating them as a gas of *phonons* in a box (the box being the solid). Most of the steps of the calculation are identical, as both are examples of a massless bosonic gas with linear dispersion relation.

According to the equipartition theorem, every atom has 3 degrees of freedom due to its translational motion. Thus, in a crystal lattice with N atoms, we expect the total energy $E = 3Nk_BT$ and the *specific heat* should be, following the *Dulong-Petit law*,

$$C_V = \left(\frac{\partial E}{\partial T}\right)_V = 3Nk_B \ , \tag{22.108}$$

for all solids regardless of temperature.

It was observed, however, that the specific heat of solids decreases like $C_V \propto T^3$ as T approaches zero. It was Einstein's idea to apply Planck's formula by treating the N atoms as three-dimensional harmonic oscillators vibrating in a lattice. The discrete energies $n\hbar\omega$ are identified with quasi-particles called *phonons*. The quantum nature of atoms does not matter, they just provide the medium supporting the phonons. Following the Bose-Einstein statistics, we must replace,

$$k_BT \to \hbar\omega/(e^{\hbar\omega/k_BT} - 1) \ , \tag{22.109}$$

such that the derivative of the energy,

$$C_V = \left(\frac{\partial}{\partial T}\frac{3Nk_B\hbar\omega}{e^{\hbar\omega/k_BT} - 1}\right)_V = 3Nk_B\left(\frac{\hbar\omega}{k_BT}\right)^2\frac{e^{\hbar\omega/k_BT}}{(e^{\hbar\omega/k_BT} - 1)^2} \ , \tag{22.110}$$

gives the specific heat. The disappearance of the specific heat at low temperatures,

$$C_V \simeq \frac{3N(\hbar\omega)^2}{k_BT^2}e^{-\hbar\omega/(k_BT)} \ , \tag{22.111}$$

which is related to the finite localization energy of harmonic oscillators, does not describe experimental observations very well, and the model had to be refined by Debye, later on.

22.2.9.1 Debye model for the specific heat

While Einstein assumed monochromatic lattice vibrations, Debye's approach was to allow a *spectrum* of vibrational frequencies. With the density of states,

$$\rho(\nu)d\nu = (4\pi V v^3)\nu^2 d\nu \ , \tag{22.112}$$

where v is the velocity of sound propagation, the formula is totally equivalent to the density-of-states for photons in a cavity. Assuming that there is an upper bound ν_m for the vibrational frequencies, we normalize as $3N_0 = \int_0^{\nu_m} \rho(\nu)d\nu$. The energy now is [12],

$$E = \int_0^{\nu_m} \frac{\hbar\omega}{e^{\hbar\omega/k_B T} - 1} \frac{4\pi V}{v^3} \nu d\nu = 9Nk_B \frac{T^4}{\theta^3} \int_0^{\theta/T} \frac{x^3 dx}{e^x - 1} \ . \tag{22.113}$$

The *Debye temperature* $\theta = h\nu_m/k_B$ is characteristic for the metal. The derivative is then,

$$C_V = 9Nk_B \left[4\left(\frac{T}{\theta}\right)^3 \int_0^{\theta/T} \frac{x^3 dx}{e^x - 1} - \frac{\theta}{T} \frac{1}{e^{\theta/T} - 1} \right] \ . \tag{22.114}$$

At low temperatures this formula reproduces the *Debye law*,

$$C_V = \frac{12\pi^4}{5} Nk_B \left(T/\theta\right)^3 \ . \tag{22.115}$$

22.2.10 Exercises

22.2.10.1 Ex: Resistance of vacuum

Show that $\sqrt{\mu_0/\varepsilon_0}$ has the dimension of a resistance and the value of $376.7\,\Omega$.

Solution: *Using the expressions* $\nabla \cdot \vec{\mathcal{E}} = \varrho/\varepsilon_0$, $\int \vec{\mathcal{E}} \cdot d\mathbf{l} = U$, $\dot{Q} = I$, *and* $U = RI$, *dimensional considerations yield,*

$$\left[\sqrt{\frac{\mu_0}{\varepsilon_0}}\right] = \left[\frac{1}{\varepsilon_0 c}\right] = \left[\frac{|\vec{\mathcal{E}}|}{l\varrho c}\right] = \left[\frac{Ul^3}{Ql^2 c}\right] = \left[\frac{U}{I}\right] = [R] = \Omega \ .$$

$\varepsilon_0 = 8.8542 \cdot 10^{12}\,\mathrm{As/Vm}$ *and* $\mu_0 = 4\pi \cdot 10^{-7}\,\mathrm{Vs/Am}$.

[12] The fact that the electron gas also has a heat capacity is neglected.

22.2.10.2 Ex: The laws of Planck and Rayleigh-Jeans

Show that Planck's law reproduces the Rayleigh-Jeans law in the low-frequency limit.

Solution: *Taylor Expansion of Planck's law:*

$$u_\omega^{Pl} = \frac{\omega^2}{\pi^2 c^3}\frac{\hbar\omega}{e^{\hbar\omega/k_B T}-1} = \frac{\omega^2}{\pi^2 c^3}\frac{\hbar\omega}{(1+\hbar\omega/k_B T+...)-1} \simeq \frac{\omega^2}{\pi^2 c^3}k_B T \ .$$

22.2.10.3 Ex: The laws of Wien and Stefan-Boltzmann

a. Derive the parametrization of Planck's law in terms of frequency ν and wavelength λ.
b. Derive the law of *Stefan-Boltzmann* according to which the total power radiated per unit surface area of a black body across all wavelengths (also known as the black-body radiant emittance) is given by σT^4, where $\sigma \equiv \pi^2 k_B^4/60c^2\hbar^3$ is called the Stefan-Boltzmann constant.
c. Derive *Wien's displacement law* according to which the maximum emission of a blackbody spectrum occurs at $\lambda_{\max} T = 2.898\times10^{-3}\,\mathrm{Km}$ in the wavelength parametrization and $\nu_{\max}/T = 0.0588\,\mathrm{THz/K}$ in the frequency parametrization. Determine the frequency of the maximum emission for the 2.7 K background radiation of the universe.

Solution: *a. The spectral energy density of a blackbody according to Planck's law is in the various parametrizations,*

$$\begin{aligned} u_{Pl}(\omega)d\omega &= \frac{\omega^2}{\pi^2 c^3}\frac{\hbar\omega}{e^{\beta\hbar\omega}-1}d\omega \\ = u_{Pl}(\nu)d\nu &= \frac{8\pi h\nu^3}{c^3}\frac{1}{e^{\beta h\nu}-1}d\nu \\ = u_{Pl}(\lambda)d\lambda &= \frac{8\pi ch}{\lambda^5}\frac{1}{e^{\beta hc/\lambda}-1}d\lambda \end{aligned}$$

b. The intensity of the light emitted from the blackbody surface is given by,

$$L_{Pl}(\omega) = \frac{c}{4\pi}u_{Pl}(\omega) = \frac{2h\nu^3}{c^2}\frac{1}{e^{\beta\hbar\omega}-1} \ .$$

The power emitted per unit area of the emitting body is,

$$\begin{aligned} \frac{P}{A} &= \int_{half\ sphere}\cos\theta d\Omega\int_0^\infty L_{Pl}(\nu)d\nu = \int_0^{2\pi}\int_0^{\pi/2}\cos\theta\sin\theta d\theta d\phi\int_0^\infty \frac{2h\nu^3}{c^2}\frac{1}{e^{\beta\hbar\omega}-1}d\nu \\ &= \pi\int_0^\infty \frac{2h}{c^2}\frac{1}{(\beta h)^4}\frac{x^3}{e^x-1}dx = \pi\frac{2h}{c^2}\frac{1}{(\beta h)^4}\frac{\pi^4}{15} = \frac{\pi^2 k_B^4}{60\hbar^3 c^2}T^4 \equiv \sigma T^4 \ . \end{aligned}$$

c. The spectral radiance in wavelength parametrization is

$$L_{Pl}(\lambda)d\lambda = \frac{c}{4\pi}u_{Pl}(\lambda)d\lambda = \frac{2c^2 h}{\lambda^5}\frac{1}{e^{\beta hc/\lambda}-1}d\lambda \ .$$

The peak follows from,

$$0 = \frac{\partial L(\lambda)}{\partial \lambda} = 2c^2 h \frac{-5\lambda e^{\beta h \frac{c}{\lambda}} + 5\lambda + ch\beta e^{\beta h \frac{c}{\lambda}}}{\lambda^7 \left(e^{\beta h \frac{c}{\lambda}} - 1\right)^2} \ .$$

Defining $x \equiv \beta h \frac{c}{\lambda}$ *we find the condition,*

$$0 = (x-5)e^x + 5$$

with the numerical solution $x = 4.965....$ *Hence,*

$$\lambda_{peak} = \frac{hc}{xk_B} \frac{1}{T} \ .$$

For $2.7\,\mathrm{K}$ *we expect* $\lambda_{peak} = 966\,\mu\mathrm{m}$*, or* $\nu_{peak} = 310\,\mathrm{GHz}$*.*
The spectral radiance in frequency parametrization is,

$$L(\nu)d\nu = \frac{c}{4\pi} u_{Pl}(\nu)d\nu = \frac{2h\nu^3}{c^2} \frac{1}{e^{\beta h\nu} - 1} d\nu \ .$$

The peak follows from,

$$0 = \frac{\partial L(\nu)}{\partial \nu} = 2h\nu^2 \frac{3e^{\beta h\nu} - 3 - \nu\beta h e^{\beta h\nu}}{c^2 \left(e^{\beta h\nu} - 1\right)^2} \ .$$

Defining $x \equiv \beta h\nu$ *we find the condition,*

$$0 = (x-3)e^x + 3$$

with the numerical solution $x = 4.965....$ *Hence,*

$$\nu_{peak} = \frac{xk_B}{h} T \ .$$

For $2.7\,\mathrm{K}$ *we expect* $\nu_{peak} = 280\,\mathrm{GHz}$*.*

22.2.10.4 Ex: Radiometric thermometry

Modern radiometric thermometers measure the blackbody radiation emitted by a hot body. Calculate the variation of the blackbody radiant emittance of a person having fever (40° instead of 37° body temperature). How much does the maximum emission wavelength change? In which spectral range should the thermometer be sensitive?

Solution: *The Stefan-Boltzmann law reads,*

$$\frac{P}{A} = \sigma T^4 \qquad with \qquad \sigma = \frac{\pi^2 k_B^4}{60c^2\hbar^3} \approx 5.67 \cdot 10^{-8} \frac{\mathrm{W}}{\mathrm{m^2 K^4}} \ .$$

Hence, around $T = (273 + 37)\,\mathrm{K}$ *and with* $\Delta T = 3\,\mathrm{K}$*,*

$$\frac{\Delta(P/A)}{P/A} = \frac{4\sigma T^3 \Delta T}{\sigma T^4} = \frac{4\Delta T}{T} \approx 0.0387 \ .$$

Wien's law reads,

$$\lambda_{max} T = C_{Wien} \qquad with \qquad C_{Wien} \approx 2.898 \cdot 10^{-3}\,\mathrm{Km} \ .$$

Hence, around $T = (273 + 37)\,\mathrm{K}$,

$$\lambda_{max} = \frac{C_{Wien}}{T} \approx 9.348\,\mu\mathrm{m} \ ,$$

and with $\Delta T = 3\,\mathrm{K}$,

$$\frac{\Delta\lambda_{max}}{\lambda_{max}} = -\frac{\Delta T}{T} \approx 0.0097 \ .$$

The thermometer should be sensitive in the infrared range around $10\,\mu\mathrm{m}$.

22.2.10.5 Ex: Photons in a resonator

a. The light power emitted by a laser ($\lambda = 633\,\mathrm{nm}$) be $P = 1\,\mathrm{nW}$. How many photons does the laser emit per second? How many photons of the emitted laser beam are in a mode volume of $L = 10\,\mathrm{cm}$ length?
b. How many photons on average are inside an optical cavity having the same mode volume at ambient temperature, when there is no incident light?

Solution: *a. The number of emitted photons per second is,*

$$\# = \frac{P}{h\nu} = \frac{\lambda P}{hc} \approx 3.2 \cdot 10^{9}\,\mathrm{s^{-1}} \ .$$

Using the expressions $I = 2P/\pi w^2$ *and* $V_m = \frac{\pi}{2} w^2 L$, *we get for the number of photons in the mode,*

$$n = \frac{E}{\hbar\omega} = \frac{uV_m}{\hbar\omega} = \frac{IV_m}{c\hbar\omega} = \frac{2P}{\pi w^2}\,\frac{V_m}{c\hbar\omega} = \frac{LP}{c\hbar\omega} = 1.06 \ photons \ .$$

b. The back-body radiation puts

$$\bar{n} = \frac{1}{e^{\hbar\omega/k_B T} - 1} = 10^{-33} \ photons$$

into the mode volume.

22.2.10.6 Ex: Number of modes in a cavity

a. How many modes do fit into a cubical box of $10\,\mathrm{cm}$ size for a frequency interval of $1000\,\mathrm{Hz}$ centered at a wavelength of $500\,\mathrm{nm}$?
b. How many photons are in the box supposing it has a temperature of $T = 300\,\mathrm{K}$, respectively, $T = 6000\,\mathrm{K}$?

Solution: *a. From Eq. (22.51) we get the total number of modes with frequencies between 0 and* ν,

$$N = \frac{\omega^3}{3\pi^2 c^3} L^3 = \frac{8\pi\nu^3}{3c^3} L^3 \ .$$

Hence, for the given range,

$$N = L^3 \int_{\nu-\Delta\nu/2}^{\nu+\Delta\nu/2} \varrho(\nu)d\nu = L^3 \int_{\nu-\Delta\nu/2}^{\nu+\Delta\nu/2} \frac{8\pi\nu^2}{c^3}d\nu$$
$$= \frac{8\pi L^3}{3c^3}\left[(\nu+\Delta\nu/2)^3 - (\nu-\Delta\nu/2)^3\right] \simeq \frac{8\pi L^3}{3c^3}6\nu^2\frac{\Delta\nu}{2} = \frac{8\pi L^3}{c\lambda^2}\Delta\nu = 335100 \ .$$

b. The number of photons follows from the spectral energy density Eq. (22.61),

$$N_{ph} = L^3 \int_{\nu-\Delta\nu/2}^{\nu+\Delta\nu/2} \frac{u(\nu)}{h\nu}d\nu = L^3 \int_{\nu-\Delta\nu/2}^{\nu+\Delta\nu/2} \varrho(\nu)\frac{h\nu}{e^{\beta h\nu}-1}d\nu$$
$$= L^3 \int_{\nu-\Delta\nu/2}^{\nu+\Delta\nu/2} \frac{4\nu^2}{c^3}\frac{1}{e^{\beta h\nu}-1}d\nu \simeq \frac{4L^3}{c\lambda^2}\Delta\nu\frac{1}{e^{\beta h\nu}-1} \ .$$

For $T = 300\,\mathrm{K}$ we expect only $4.6 \cdot 10^{-36}$ photons, but for $T = 6000\,\mathrm{K}$ we expect $1.8 \cdot 10^4$ photons. Integrated over all frequencies we would have,

$$N_{ph} = L^3 \int \frac{4\nu^2}{c^3}\frac{1}{e^{\beta h\nu}-1}d\nu = L^3\frac{1}{(\beta h)^3}\frac{4}{c^3}\int_0^\infty \frac{x^2}{e^x-1}dx = \left(\frac{2Lk_BT}{ch}\right)^3 \zeta(3) \ ,$$

hence $N_{ph} \approx 8.7 \cdot 10^{10}$ photons at $300\,\mathrm{K}$ and $N_{ph} \approx 7 \cdot 10^{14}$ photons at $6000\,\mathrm{K}$.

22.2.10.7 Ex: Number of photons emitted from lasers and blackbodies

a. Calculate the total number of photons per area per unit time emitted by a blackbody at temperature T.
b. The linewidth of a helium-neon laser is $\Delta\nu = 1000\,\mathrm{Hz}$. The operating wavelength is $\lambda = 632.8\,\mathrm{nm}$, the power is $P = 1\,\mathrm{mW}$, and the beam size $w_0 = 1\,\mathrm{mm}$. How many photons are emitted per second?
c. What would be the temperature of a blackbody radiator emitting the same number of photons from an equal area and over the same frequency interval as the laser?

Solution: *a. According to Wien's law the total radiance is,*

$$I = \sigma T^4 = \frac{2\pi^5 k_B^4}{15c^2h^3}T^4 \ .$$

The total number of photons per area per unit time is,

$$\frac{\partial N}{\partial A\partial t} = \int \frac{I_\nu}{h\nu}d\nu = \int_0^\infty \frac{2\pi\nu^2}{c^2}\frac{1}{e^{\beta h\nu}-1}d\nu$$
$$= \frac{2\pi}{c^2(\beta h)^3}\int_0^\infty \frac{x^2}{e^x-1}dx = \frac{2\pi(k_BT)^3}{c^2h^3}2\zeta(3) \ .$$

with $\zeta(3) = 1.202$.
b. The photon flux for the HeNe laser is,

$$\frac{\partial N_{HeNe}}{\partial t} = \frac{P}{h\nu} \approx 3.2 \cdot 10^{15}\,\mathrm{s^{-1}} \ .$$

c. The photon flux from the blackbody within the specified bandwidth is ($I_\nu = \frac{c}{4\pi} u_\nu$),

$$\frac{\partial N}{\partial A \partial t} = \int_\nu^{\nu+\Delta\nu} \frac{I_\nu}{h\nu} d\nu \simeq \frac{I_\nu}{h\nu}\Delta\nu = \frac{2}{\lambda^2}\frac{\Delta\nu}{e^{\beta h\nu}-1}$$
$$\Longrightarrow \frac{\partial N}{\partial t} = \frac{2}{\lambda^2}\frac{\Delta\nu}{e^{\beta h\nu}-1}\pi w_0^2 \ .$$

Hence,

$$T = \frac{h\nu/k_B}{\ln\left(1+\frac{2\pi w_0^2}{\lambda^2}\frac{\Delta\nu}{\partial_t N_{HeNe}}\right)} \approx 4.6\cdot 10^9\,\mathrm{K} \ .$$

22.2.10.8 Ex: Number of photons per radiation mode

Assume the isotropic emission of a pulsed flashlamp with spectral bandwidth $\Delta\lambda = 100\,\mathrm{nm}$ around $\lambda = 400\,\mathrm{nm}$ amounts to $P_0 = 100\,\mathrm{W}$ peak power out of a volume of $1\,\mathrm{cm}^3$. Calculate the spectral power density $u(\nu)$ and the spectral intensity $I(\nu)$ through a spherical surface $r = 2\,\mathrm{cm}$ away from the center of the emitting sphere. How many photons per mode are contained in the radiation field?

Solution: *The total intensity is,*

$$I = \frac{P_0}{4\pi r^2} \approx 2\cdot 10^4\,\mathrm{W/m^2} \ .$$

The spectral intensity is,

$$I(\nu) = \frac{I}{|\Delta\nu|} = \frac{I}{(c/\lambda^2)\Delta\lambda} \approx 1.1\cdot 10^{-10}\,\mathrm{J/m^2} \ ,$$

the spectral power density is,

$$u(\nu) = \frac{I(\nu)}{c} = 3.6\cdot 10^{-19}\,\mathrm{Js/m^2} \ ,$$

and the spectral mode density is,

$$\varrho(\nu) = \frac{8\pi\nu^2}{c^3} \ .$$

Within the volume of the sphere with radius r there are

$$N = \varrho(\nu)V\Delta\nu = \varrho(\nu)\tfrac{4}{3}\pi r^3\Delta\nu \approx 3\cdot 10^{15}$$

modes. The energy per mode is

$$W_m = \frac{u(\nu)V\Delta\nu}{N} \approx 7\cdot 10^{-25}\,\mathrm{J/mode} \ .$$

With the energy of a photon at λ *of* $E = h\nu = hc/\lambda \approx 3.1\,\mathrm{eV}$, *the average number of photons per mode is,*

$$n_{ph} = \frac{W_m}{h\nu} = \frac{u(\nu)}{\varrho(\nu)} = \approx 1.5\cdot 10^{-6} \ .$$

The average number of photons per mode is therefore very small.

22.2.10.9 Ex: Atoms in an optical cavity

a. Consider a closed optical cavity at $T = 600^\circ$ C. The cavity has the shape of a $L = 1$ m-long and $d = 3$ cm-diameter tube. Calculate the total energy of the black-body radiation inside the cavity.
b. Inside the cavity there is a gas with strontium atoms (1 fundamental level and 3 degenerate excited levels, $\lambda = 461$ nm). Using the expression (22.67), assuming thermal equilibrium, calculate the number of excited atoms for a partial pressure of the strontium gas of 10^{-3} mbar.
c. Calculate the optical density for a laser in resonance with the transition traversing the cavity along the symmetry axis.

Solution: *a. Following Planck's law the spectral energy density is,*

$$u_P(\omega) = \frac{\omega^2}{\pi^2 c^3} \frac{\hbar\omega}{e^{\hbar\omega/k_B T - 1}} \ .$$

The energy density is,

$$\begin{aligned} \bar{u}_P &= \int_0^\infty u_E^{Pl}(\omega) d\omega = \frac{k_B T}{\pi^2 c^3} \left(\frac{k_B T}{\hbar}\right)^3 \int_0^\infty \frac{x^3}{e^x - 1} dx \\ &= \frac{k_B T}{\pi^2 c^3} \left(\frac{k_B T}{\hbar}\right)^3 \frac{\pi^4}{15} = \frac{\pi^2}{15\hbar^3 c^3} (k_B T)^4 = \tfrac{4}{c}\sigma T^4 = 4.3 \cdot 10^{-4}\,\mathrm{J/m^3} \ , \end{aligned}$$

where $\sigma = 5.67 \cdot 10^{-8}\,\mathrm{W/m^2\ K^4}$ is the Stefan-Boltzmann constant. With the cavity volume $V = \pi L d^2/4$ the energy is,

$$\bar{u}_P V = 3 \cdot 10^{-7}\,\mathrm{J} \ .$$

b. In equilibrium the Einstein rate equation gives,

$$\frac{N_1}{N_2} = \frac{g_1}{g_2} e^{-(E_1 - E_2)/k_B T} \ .$$

Hence,

$$\frac{N_2}{N} = \frac{1}{N_1/N_2 + 1} = \frac{1}{\frac{g_1}{g_2} e^{-(E_1 - E_2)/k_B T} - 1} = 9.9 \cdot 10^{-16} \ .$$

At the pressure $p = 10^{-1}$ Pa, the total number of atoms is $N = \frac{pV}{k_B T} \simeq 5.8 \cdot 10^{15}$. Therefore, we expect $N = 57$ atoms.
c. With the density of the strontium gas $n = N/V \simeq 8.3 \cdot 10^{13}$ cm^{-3}, we obtain for optical density,

$$b_0 = \sigma_0 n L = \frac{g_2}{g_1} \frac{\lambda^2}{2\pi} n L \simeq 8.4 \cdot 10^5 \ .$$

22.2.10.10 Ex: Sodium atoms in an optical cavity

A sodium atom is placed in a cavity of volume $V = 1\,\mathrm{cm}^3$ with walls at the temperature T, producing a thermal radiation field with spectral energy density $u_P(\nu)$. At what temperature T are the spontaneous and induced transition probabilities equal
a. for the transition $3P \to 3S$ with the transition wavelength $\lambda = 589\,\mathrm{nm}$ and the excited state lifetime $\tau_{3P} = 16\,\mathrm{ns}$;
b. for the hyperfine transition $3S$ $(F = 3 \to F = 2)$ with the transition frequency $\nu = 1772\,\mathrm{MHz}$ and the excited state lifetime $\tau_{3F} \simeq 1\,\mathrm{s}$?

Solution: *Induced and spontaneous transition probabilities are equal when the radiation field contains one photon per mode. This means:*

$$\bar{n} = \frac{1}{e^{h\nu/k_B T} - 1} = 1 \ ,$$

hence $e^{h\nu/k_B T} = 2$ *and hence,*

$$T = \frac{hc}{\lambda k \ln 2} \ .$$

a. For $\lambda = 589\,\mathrm{nm}$ *we obtain for a thermal radiation field* $T = 35300\,\mathrm{K}$. *If a laser beam is sent through the cavity, the condition* $B_{ik}\rho = A_{ik}$ *can be fulfilled at modest laser intensities. This can be estimated as follows: The number of modes in the cavity within the frequency interval* $\Delta\nu = [2\pi\tau_{3P}]^{-1} \approx 10\,\mathrm{MHz}$, *which is the natural linewidth of the* $3P \to 3S$ *transition of Na, is,*

$$\varrho(\nu)\Delta\nu = \frac{8\pi}{c\lambda^2}\Delta\nu \approx 2.4 \cdot 10^6\,\mathrm{cm}^{-3} \ .$$

The energy of a photon at the transition wavelength is $h\nu$. *With 1 photon per mode, the radiation density in the cavity is,*

$$\bar{u} = \varrho_\nu h\nu\Delta\nu \approx 8 \cdot 10^{-8}\,\mathrm{J/cm}^{-13} \ .$$

The intensity of a laser beam with a spectral width equal to $\Delta\nu$ *is then inside the cavity* $I = c\bar{u} \approx 24\,\mathrm{mW/cm}^2$.
b. For $\nu = 1.772\,\mathrm{MHz}$ *we obtain* $T = 0.12\,\mathrm{K}$. *The energy density* $\bar{u}$ *of the thermal field within the natural linewidth* $\Delta\nu = [2\pi\tau_{3F}]^{-1} \approx 0.16\,\mathrm{s}^{-1}$ *is,*

$$\bar{u} = u_\nu\Delta\nu = \varrho_\nu h\nu\Delta\nu = \frac{8\pi\nu^2}{c^3}h\nu\Delta\nu \ .$$

With this we get, $\bar{u} = 5 \cdot 10^{-37}\,\mathrm{Ws/cm}^3$, *which is 24 orders of magnitude smaller than the visible radiation in (a).*

22.2.10.11 Ex: Applying the Lambert-Beer law

The beam of a monochromatic laser passes through an absorbing atomic vapor with path length $L = 5\,\mathrm{cm}$. If the laser frequency is tuned to the center of an absorbing transition $|i\rangle \to |k\rangle$ with absorption cross section $\sigma_0 = 10^{-14}\,\mathrm{cm}^2$, the attenuation

of the transmitted intensity is 10%. Assuming low saturation calculate the atomic density n_i in the absorbing level $|i\rangle$.

Solution: *The transmitted intensity is,*

$$I = I_0 e^{-\alpha L} = 0.9 I_0 \ .$$

Hence, $\alpha L = 0.1$. *With* $L = 5\,\mathrm{cm}$ *we expect* $\alpha = 0.02\,\mathrm{cm}^{-1}$. *Now with* $\alpha = n_i \sigma$,

$$n_i = \frac{\alpha}{\sigma} = 2 \cdot 10^{12}\,\mathrm{cm}^{-3} \ .$$

22.3 Further reading

W. Demtröder, *Atoms, Molecules and Photons: An Introduction to Atomic, Molecular, and Quantum Physics* [352]ISBN

J. Weiner et al., *Light-matter interaction, Fundamentals and applications* [1364]DOI

R. Loudon, Oxford Science Publications, Oxford (1982), *The quantum theory of light* [816]ISBN

Chapter 23

Foundations and mathematical tools

As we have seen in the precedent section, the important message of quantum mechanics is that matter propagates as a wave and light, when localized, only changes its energy in discrete units. Once we understand (or at least accept) this fact, a large part of quantum mechanics follows just as a corollary. The idea expressed by de Brogie, that matter would be a wave led to the first quantization. Interestingly, the concept of light underwent a reverse evolution. Classically described as a wave, it was divided by Planck and Einstein into quantized corpuscles, today called 'photons'.

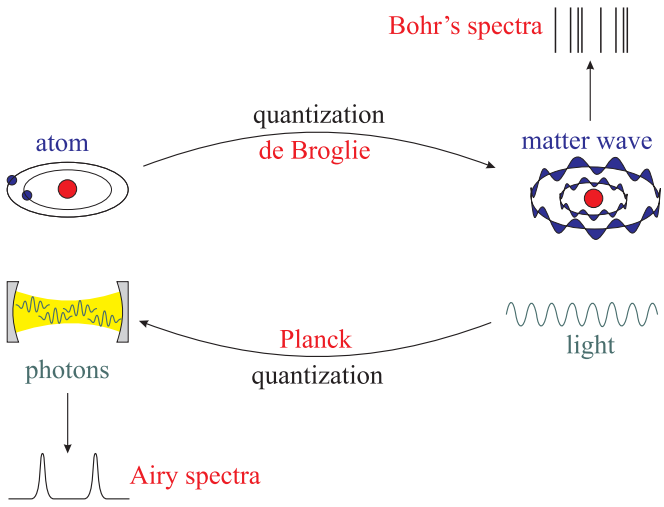

Figure 23.1: Illustration of particle-wave duality for matter and light.

In this chapter, we will introduce step by step the formalism of quantum mechanics by gradually increasing the degree of abstraction. Applications of the formalism will be shown in consecutive chapters (watch talk).

23.1 Basic notions

The aim of this section is to give 'feeling' for the new concepts introduced and used by quantum mechanics. We will first motivate the fundamental quantum equations of motion by linking them to classical dispersion relations and then spend some time to discuss the probabilistic concept proposed by Max Born.

23.1.1 Dispersion relation and Schrödinger equation

A fundamental problem in physics is the issue of the propagation of physical entities. On one hand, we have the light, whose propagation in the vacuum is described by the dispersion relation $\omega = ck$ or,

$$\omega^2 - c^2k^2 = 0 \ . \tag{23.1}$$

Since light is a wave, in the most general form, assuming the validity of the superposition principle, it can be described by a wave packet, $A(\mathbf{r},t) = \int e^{\imath(\mathbf{k}\cdot\mathbf{r}-\omega t)}a(\mathbf{k})d^3k$. It is easy to verify that the *wave equation*,

$$\frac{\partial^2}{\partial t^2}A - c^2\nabla^2 A = 0 \ , \tag{23.2}$$

reproduces the dispersion relation.

On the other hand, we have slow massive particles possessing kinetic energy,

$$E = \frac{p^2}{2m} \ . \tag{23.3}$$

With the hypothesis of de Broglie that even a massive particle has wave quality, we can try an *ansatz* [1] of a wave equation satisfying the dispersion relation (23.3). From Planck's formula, $E = \hbar\omega$, and the formula of *Louis de Broglie*, $\mathbf{p} = \hbar\mathbf{k}$, describing the particle by a wave packet $\psi(\mathbf{r},t) = \int e^{\imath(\mathbf{k}\cdot\mathbf{r}-\omega t)}\varphi(\mathbf{k})d^3k$ not subject to external forces, it is easy to verify that the equation,

$$\imath\hbar\frac{\partial}{\partial t}\psi = \left(-\frac{\hbar^2}{2m}\nabla^2\right)\psi \ , \tag{23.4}$$

reproduces the dispersion relation. If the particle is subject to a potential, its total energy is $E = \mathbf{p}^2/2m + V(\mathbf{r},t)$. This dispersion relation corresponds to the famous *Schrödinger equation*,

$$\imath\hbar\frac{\partial}{\partial t}\psi = \left(-\frac{\hbar^2}{2m}\nabla^2 + V(\mathbf{r},t)\right)\psi \ . \tag{23.5}$$

23.1.2 Relativistic particle waves

Despite the similarities between light particles and material particles, there are notable differences: The photon is a relativistic particle with no rest mass. How can we establish a relationship between such different objects?

[1] Trial, working hypothesis.

To clarify this relationship we now consider particles that are similar to light in the sense that they have high velocities, that is, relativistic particles. From the relativistic principle of the equivalence of mass and energy, we obtain for a massive particle $E^2 = m^2c^4 + c^2p^2$ or,

$$\omega^2 - c^2k^2 = \frac{m^2c^4}{\hbar^2} \ . \tag{23.6}$$

This dispersion relation can be obtained from the differential equation,

$$\frac{\partial^2}{\partial t^2}A - c^2\nabla^2 A = -\frac{m^2c^4}{\hbar^2}A \ , \tag{23.7}$$

inserting, for example, the already proposed wave packet $A(\mathbf{r},t) = \int e^{\imath(\mathbf{k}\cdot\mathbf{r}-\omega t)}a(\mathbf{k})d^3k$, supposed not to be subject to external forces. The equation (23.7) is a wave equation called *Klein-Gordon equation*. For particles without rest mass, as in the case of photons, the equation is reduced to the wave equation of light (23.2).

Now, making the transition to non-relativistic velocities, $v \ll c$, we can expand the dispersion relation,

$$E = \sqrt{m^2c^4 + c^2m^2v^2} = mc^2\left(1 + \frac{v^2}{2c^2} + ..\right) \qquad \text{or} \qquad \hbar\omega \simeq mc^2 + \frac{\hbar^2k^2}{2m} \ . \tag{23.8}$$

In analogy with the Klein-Gordon equation we can derive the approximate dispersion relation (23.8) from a wave equation,

$$\imath\hbar\frac{\partial}{\partial t}A = \left(mc^2 - \frac{\hbar^2}{2m}\nabla^2\right)A \ . \tag{23.9}$$

With the transformation $\psi = e^{-\imath mc^2t/\hbar}A$, we rediscover the Schrödinger equation (23.4),

$$\imath\hbar\frac{\partial}{\partial t}\psi = -\frac{\hbar^2}{2m}\nabla^2\psi \tag{23.10}$$

as the non-relativistic limit of the Klein-Gordon equation.

It is interesting to note that in all cases discussed, obviously the dispersion relations and the differential equations can be interconverted by the substitutions,

$$E \longrightarrow \imath\hbar\frac{\partial}{\partial t} \qquad \text{and} \qquad \mathbf{p} \longrightarrow -\imath\hbar\nabla \ . \tag{23.11}$$

We will discuss this later in the context of Ehrenfest's theorem in Secs. 23.1.6, 23.1.7, and 23.4.6.

> **Example 140 (*Demystifying Quantum Mechanics 1.0*):** The essence of quantum mechanics can be boiled down to the particle-wave duality. That is the fact that the building blocks of matter must be considered as de Broglie waves. Once this fact is understood and assimilated, quantum mechanics loses much of its mystery. For example delocalization of an atom, that is, the fact that it can be at two locations at the same time irritates us only as long as we try to imagine it as an indivisible solid block. In contrast we are not surprised

to encounter the same ocean wave or tsunami in different continents.
The misconception is already rooted in the statement that *a quantum particle can be simultaneously in two places*. What we really mean when we say a particle is delocalized is, that the way it is embedded in space-time (which is the frame in which we can (or cannot) attribute locations and velocities to it) resembles a wave, and that the way this wave evolves or propagates in space is wave-like and described by a Schrödinger equation. Note that position-velocity is just one property that a particle can have. Spin is another one, and the appropriate space in which a spin is embedded is not necessarily position space, but can be an abstract configuration space. An atom can have an internal structure, whose dynamics is totally independent of how the atom moves as a whole. Thus, a particle IS not a wave, but PROPAGATES like one in space-time. Still, its evolution will follow a Schrödinger-type equation.
At first the Schrödinger equation seems weird, because it is complex and thus rules the behavior of an unphysical quantity, the wave function. But we should keep in mind the Schrödinger equation is the non-relativistic approximation of the Klein-Gordon equation, which resembles much more a classical wave equation, and applies also to particles propagating at velocities nearly as fast as light.
With regard to these facts, a terminology that suits much better the features of quantum mechanics is simply wave mechanics, how Schrödinger termed it. This terminology also has the advantage of avoiding confusion with light wave effects erroneously attributed to quantum mechanics, such as light tunneling which is totally understood within Maxwell's theory.
We must however be aware that the simple wave picture is not sufficient to understand all of quantum mechanics. As we will see in the next sections, it is necessary to complement wave mechanics with a measurement theory, and phenomena genuine to what today is called Quantum Mechanics 2.0, in particular, entanglement are difficult to understand in wave mechanics.

23.1.3 Born's interpretation

The first part of this script is devoted to *individual particles* or systems of distinguishable *massive particles*, and we will only turn our attention to *light* and *indistinguishable particles* when discussing the (second) *quantization of fields*.

According to our current conviction, the complete reality (neglecting relativistic effects) on any system is contained in the Schrödinger equation (23.5). That statement does not make us smarter without having to explaining the meaning of the *wavefunction* ψ. In an attempt to marry the concepts of particles and waves, *Max Born* proposed in 1926 the interpretation of the quantity

$$\int_V |\psi(\mathbf{r},t)|^2 d^3r \tag{23.12}$$

as probability of finding the particle inside the volume V.

If $|\psi(\mathbf{r},t)|^2$ has the meaning of a *probability density* or *probability distribution*, the square of the wavefunction must be integrable,

$$\|\psi(\mathbf{r},t)\|^2 \equiv \int_{\mathbb{R}^3} |\psi(\mathbf{r},t)|^2 d^3r < \infty \ . \tag{23.13}$$

This allows us to proceed to a *normalization* of the wave function,

$$\tilde{\psi}(\mathbf{r},t) \equiv \frac{\psi(\mathbf{r},t)}{\sqrt{\int_{\mathbb{R}^3} |\psi(\mathbf{r},t)|^2 d^3r}} \ , \tag{23.14}$$

such that $\|\tilde{\psi}(\mathbf{r},t)\| = 1$.

23.1.4 Continuity equation

In quantum mechanics we associate the wavefunction that describes a quantum system to a *probability wave*. As the Schrödinger equation describes a time evolution, in order to be useful, the wavefunction must allow for probability flows. We define the probability density and the probability flow by,

$$\begin{aligned} \rho(\mathbf{r},t) &\equiv \psi^*(\mathbf{r},t)\psi(\mathbf{r},t) \ , \\ \mathbf{j}(\mathbf{r},t) &\equiv \frac{\hbar}{2m\imath} \left[\psi^*(\mathbf{r},t)\nabla\psi(\mathbf{r},t) - \psi(\mathbf{r},t)\nabla\psi^*(\mathbf{r},t)\right] \ . \end{aligned} \tag{23.15}$$

Starting from the Schrödinger equation we can easily derive the *continuity equation* (see Exc. 23.1.8.1),

$$\dot{\rho}(\mathbf{r},t) + \nabla\cdot\mathbf{j}(\mathbf{r},t) = 0 \ , \tag{23.16}$$

or in the integral form,

$$-\frac{d}{dt}\int_V \rho d^3r = \int_V \nabla\cdot\mathbf{j} d^3r = \oint_{\partial V} \mathbf{j}\cdot d\mathbf{S} \ , \tag{23.17}$$

using Gauß' law. With $I \equiv \int_S \mathbf{j}\cdot d\mathbf{S}$, the *probability current* which flows through the surface S delimiting the *probability charge* $Q \equiv \int_V \rho(\mathbf{r},t)d^3r$, we obtain,

$$-\dot{Q} = I \ . \tag{23.18}$$

The continuity equation is obviously similar to that of electromagnetism.

23.1.5 Distributions in space and time

So far we only spoke of spatial distributions, $\psi(\mathbf{r},t)$. But we could also consider velocity or moment distributions. In classical mechanics, a particle has a well-defined position and velocity. Knowing the position and velocity, Newton's equations allow predicting its coordinates at future times. Let us now investigate whether the Schrödinger equation allows this as well.

The more general solution of the Schrödinger equation can be written as a superposition of plane waves $e^{\imath(\mathbf{r}\cdot\mathbf{k}-\omega t)}$ with frequencies $\omega = \mathbf{p}^2/2\hbar m$ and wave vectors $\mathbf{k} = \mathbf{p}/\hbar$. Each plane wave has an individual amplitude $\varphi(\mathbf{p})$, such that,

$$\psi(\mathbf{r},t) = \tfrac{1}{h^{3/2}} \int d^3p\varphi(\mathbf{p})e^{\imath(\mathbf{r}\cdot\mathbf{k}-\omega t)} = \int d^3p \tfrac{1}{h^{3/2}}\varphi(\mathbf{p})e^{\imath(\mathbf{r}\cdot\mathbf{p}/\hbar - \mathbf{p}^2 t/2m\hbar)} \ , \tag{23.19}$$

with $h \equiv 2\pi\hbar$. At time $t = 0$, this expansion is nothing more than a Fourier transform,

$$\psi(\mathbf{r},0) = \tfrac{1}{h^{3/2}} \int d^3p\varphi(\mathbf{p})e^{\imath\mathbf{r}\cdot\mathbf{k}} \ , \tag{23.20}$$

that we can reverse,

$$\varphi(\mathbf{p}) = \tfrac{1}{h^{3/2}} \int d^3r \psi(\mathbf{r},0) e^{-\imath \mathbf{r}\cdot\mathbf{k}} \ . \tag{23.21}$$

In the absence of forces the momentum distribution becomes stationary. We can now use the momentum distribution $\varphi(\mathbf{p})$ as coefficients of the expansion of the temporal wavefunction $\psi(\mathbf{r},t)$, as shown above. Thus, the expansion represents a general solution of the time-dependent Schrödinger equation. The magnitude $|\varphi(\mathbf{p})|^2$ is the probability density in *momentum space*.

Example 141 (*Normalization of the wave function in momentum space*): It is easy to show that the probability density in momentum space is also normalized:

$$\begin{aligned}\int |\varphi(\mathbf{p})|^2 d^3p &= \tfrac{1}{h^3} \int d^3p \int d^3r \psi^*(\mathbf{r}) e^{\imath \mathbf{r}\cdot\mathbf{k}} \int d^3r' \psi(\mathbf{r}') e^{-\imath \mathbf{r}'\cdot\mathbf{k}} \\ &= \int d^3r \int d^3r' \psi^*(\mathbf{r}) \psi(\mathbf{r}') \tfrac{1}{(2\pi)^3} \int d^3k e^{\imath \mathbf{k}\cdot(\mathbf{r}-\mathbf{r}')} \\ &= \int d^3r \int d^3r' \psi^*(\mathbf{r}) \psi(\mathbf{r}') \delta^3(\mathbf{r}-\mathbf{r}') = \int |\psi(\mathbf{r})|^2 d^3r = 1 \ ,\end{aligned}$$

knowing that the Fourier transform of a plane wave is nothing more than the Dirac distribution.

Since the probability distributions $|\psi(\mathbf{r})|^2$ and $|\varphi(\mathbf{p})|^2$ are interconnected by Fourier transform, we already know that we can not localize [2] both simultaneously. If one is well localized, the other is necessarily delocalized. Do the Exc. 23.1.8.2.

23.1.6 Eigenvalues

We have already seen that the position and momentum distributions of a particle are spread. We calculate the mean values of these distributions, denoted by $\langle \mathbf{r} \rangle$ and $\langle \mathbf{p} \rangle$, as *first moments* of the respective distributions:

$$\langle \mathbf{r} \rangle = \int d^3r |\psi(\mathbf{r},t)|^2 \mathbf{r} \qquad \text{and} \qquad \langle \mathbf{p} \rangle = \int d^3p |\varphi(\mathbf{p},t)|^2 \mathbf{p} \ . \tag{23.22}$$

Using the expansions (23.19) and (23.20), we can calculate,

$$\begin{aligned}\langle \mathbf{p} \rangle = \int \varphi^*(\mathbf{p}) \mathbf{p} \varphi(\mathbf{p}) d^3p &= \int \tfrac{1}{h^{3/2}} \int \psi^*(\mathbf{r}) e^{\imath \mathbf{k}\cdot\mathbf{r}} d^3r \mathbf{p} \varphi(\mathbf{p}) d^3p \\ &= \tfrac{1}{h^{3/2}} \int \psi^*(\mathbf{r}) \int \varphi(\mathbf{p}) \mathbf{p} e^{\imath \mathbf{k}\cdot\mathbf{r}} d^3p d^3r \\ &= \tfrac{1}{h^{3/2}} \int \psi^*(\mathbf{r}) \tfrac{\hbar}{\imath} \nabla \int \varphi(\mathbf{p}) e^{\imath \mathbf{k}\cdot\mathbf{r}} d^3p d^3r = \int \psi^*(\mathbf{r}) \tfrac{\hbar}{\imath} \nabla \psi(\mathbf{r}) d^3r \ .\end{aligned}$$

This calculation shows that the expectation value, called *eigenvalue*, of the momentum can be expressed through an operator $\hat{p} \equiv (\hbar/\imath)\nabla$ acting on the wavefunction [3,4].

[2] Localize: Restrict the distribution volume indefinitely.

[3] From now on, the hat over a physical magnitude will denote quantum operators.

[4] We note here that the rules $\langle \psi | \hat{x} | \psi \rangle \leftrightarrow \langle \phi | - \tfrac{\hbar}{\imath} \nabla_p | \phi \rangle$ and $\langle \psi | \tfrac{\hbar}{\imath} \nabla_{\mathbf{r}} | \psi \rangle \leftrightarrow \langle \phi | \hat{p} | \phi \rangle$ from the Fourier transformation are useful for numerical simulations of the Schrödinger equation: Instead of calculating the spatial derivative $\left(\tfrac{\hbar}{\imath}\nabla\right)^2$ of the wavefunction, one makes a Fast Fourier Transform (FFT) to momentum space, multiplies with $\mathbf{p}$, and transforms back.

More generally, we can compute the eigenvalue of a function in $\mathbf{r}$ and $\mathbf{p}$ via,

$$\langle f(\hat{\mathbf{r}},\hat{\mathbf{p}})\rangle = \int d^3r\psi^*(\mathbf{r})f(\mathbf{r},\hat{\mathbf{p}})\psi(\mathbf{r}) \ . \tag{23.23}$$

However, it is important to note that the operators $\hat{\mathbf{r}}$ and $\hat{\mathbf{p}}$ do not necessarily commute.

Example 142 (*Non-commutation of space and momentum*): Considering a one-dimensional motion, we verify,

$$\hat{p}_x x\psi = \frac{\hbar}{\imath}\frac{d}{dx}x\psi = \frac{\hbar}{\imath}\psi + x\frac{\hbar}{\imath}\frac{d}{dx}\psi \neq x\frac{\hbar}{\imath}\frac{d}{dx}\psi = x\hat{p}_x\psi \ .$$

23.1.7 Temporal evolution of eigenvalues

We now consider the temporal evolution of the position of a particle. We will use in the following the partial integration rule $\int_V \psi\nabla\xi = \oint_{\partial V}\psi\xi - \int_V \nabla\psi\xi = -\int_V(\nabla\psi)\xi$, assuming that at least one of the functions, ψ or ξ, disappears at the edge of the volume, which can be guaranteed by choosing the volume large enough. To begin with, we will concentrate on the x-component of the position, the time derivative of which is computed using the continuity equation (23.16),

$$\frac{d}{dt}\langle\hat{x}\rangle = \int d^3r\frac{d}{dt}|\psi|^2 x = -\int d^3r\ x\nabla\cdot\mathbf{j} = -\cancelto{0}{\int d\mathbf{S}\cdot\mathbf{j}\,x} + \int d^3r\ \mathbf{j}\cdot\nabla x = \int d^3r\ \mathbf{j}_x \ , \tag{23.24}$$

Generalizing to three dimensions, we can write,

$$\begin{aligned}\frac{d}{dt}\langle m\hat{\mathbf{r}}\rangle &= m\int d^3r\ \mathbf{j} = m\int d^3r\frac{\hbar}{2m\imath}[\psi^*\nabla\psi - \psi\nabla\psi^*] \\ &= \tfrac{1}{2}\int d^3r[\psi^*\hat{\mathbf{p}}\psi + \psi\hat{\mathbf{p}}\psi^*] = \int d^3r\psi^*\hat{\mathbf{p}}\psi = \langle\hat{\mathbf{p}}\rangle \ ,\end{aligned} \tag{23.25}$$

since the eigenvalue of $\hat{\mathbf{p}}$ is a real quantity.

Now, we define the abbreviation:

$$\hat{H} \equiv -\frac{\hbar^2}{2m}\nabla^2 + V(\hat{\mathbf{r}},t) \ , \tag{23.26}$$

called the *Hamilton operator* or *Hamiltonian* and we calculate the second derivative of the position using the Schrödinger equation (23.5),

$$\frac{d}{dt}\langle\hat{\mathbf{p}}\rangle = \int d^3r\left[\left(\tfrac{1}{\imath\hbar}\hat{H}\psi\right)^*\hat{\mathbf{p}}\psi + \psi^*\hat{\mathbf{p}}\tfrac{1}{\imath\hbar}\hat{H}\psi\right] = \tfrac{\imath}{\hbar}\int d^3r\ \psi^*(\hat{H}\hat{\mathbf{p}} - \hat{\mathbf{p}}\hat{H})\psi = \tfrac{\imath}{\hbar}\langle[\hat{H},\hat{\mathbf{p}}]\rangle \ , \tag{23.27}$$

introducing the *commutator* $[\hat{a},\hat{b}] \equiv \hat{a}\hat{b} - \hat{b}\hat{a}$ as an abbreviation. After that,

$$\tfrac{\imath}{\hbar}\langle[\hat{H},\hat{\mathbf{p}}]\rangle = \tfrac{\imath}{\hbar}\langle[\hat{V},\hat{\mathbf{p}}]\rangle = \tfrac{\imath}{\hbar}\int d^3r\psi^*\left[\hat{V}\tfrac{\hbar}{\imath}\nabla\psi - \tfrac{\hbar}{\imath}\nabla(V\psi)\right] = -\int d^3r\psi^*\psi\nabla V = \langle\hat{\mathbf{F}}\rangle \ . \tag{23.28}$$

In summary, we found a law,

$$\langle \hat{\mathbf{F}} \rangle = \frac{d^2}{dt^2} \langle m\hat{\mathbf{r}} \rangle \ , \tag{23.29}$$

much like *Newton's law*, but instead of applying to localized particles, the law applies to the eigenvalues of probability distributions. Similar laws can be derived for angular momentum and energy conservation.

The observation made by *Paul Ehrenfest*, that in quantum mechanics the mean values follow the same laws of classical mechanics, is called *Ehrenfest theorem*.

23.1.8 Exercises

23.1.8.1 Ex: Conservation of probability

Demonstrate the conservation of local probability through the definitions of probability densities, $\rho(\mathbf{r}, t)$, and probability current $\mathbf{j}(\mathbf{r}, t)$.

Solution: *Assuming the validity of the Schrödinger equation, we obtain,*

$$\begin{aligned} \dot{\rho} &= \psi^* \dot{\psi} + \dot{\psi}^* \psi = \psi^* \frac{1}{\imath\hbar} \left(\frac{-\hbar^2}{2m} \nabla^2 \right) \psi + \left(\frac{1}{\imath\hbar} \frac{-\hbar^2}{2m} \nabla^2 \psi \right)^* \psi \\ &= -\frac{\hbar}{2mi} \nabla \cdot [\psi^* \nabla \psi - (\nabla \psi)^* \psi] = -\nabla \cdot \mathbf{j} \ . \end{aligned}$$

23.1.8.2 Ex: Fourier theorem

The spatial distribution of a particle is given by a Gaussian function with the width Δx. Calculate the momentum distribution and its width Δp. Just consider one spatial dimension. Show that $\Delta x \Delta p = \hbar$ using the *rms* definition for the widths.

Solution: *The distribution of the particle is given by* $\psi(x, 0) = Ae^{-x^2/2\Delta x^2}$. *The constant* A *is determined from the normalization condition,*

$$1 = \int_{-\infty}^{\infty} |\psi(x,0)|^2 dx = \int_{-\infty}^{\infty} A^2 e^{-x^2/\Delta x^2} dx = A^2 \sqrt{\pi} \Delta x \quad \Longrightarrow \quad A = \left(\frac{1}{\pi \Delta x^2} \right)^{1/4} .$$

Therefore, the momentum distribution is,

$$\varphi(p) = \frac{1}{(2\pi\hbar)^{1/2}} \int_{-\infty}^{\infty} \psi(x,0) e^{-\imath x k} dx = \frac{1}{(2\pi\hbar)^{1/2} \pi^{1/4}} \frac{1}{\sqrt{\Delta x}} \int_{-\infty}^{\infty} e^{-x^2/2\Delta x^2} e^{-\imath x k} dx \ .$$

With the definition of the Fourier transform,

$$g(k) = \frac{1}{\sqrt{2\pi}} \int_{-\infty}^{\infty} f(x) e^{-\imath k x} dx \ ,$$

the transformation of $f(x) = \frac{1}{\sqrt{2\pi}} \frac{1}{\sqrt{\Delta x}} e^{-x^2/2\Delta x^2}$ *is* $g(k) = \frac{1}{\sqrt{2\pi}} \sqrt{\Delta x} e^{-\Delta x^2 k^2/2}$. *Hence,*

$$\varphi(p) = \frac{1}{(2\pi\hbar)^{1/2} \pi^{1/4}} \sqrt{\Delta x} e^{-\Delta x^2 k^2/2} \ .$$

The width of this momentum distribution is $\Delta k \equiv \Delta x^{-1}$, which shows that position and momentum distributions can not be narrow simultaneously. The equation

$$\Delta x \Delta p = \hbar$$

corresponds to the Heisenberg uncertainty relation.

23.2 Postulates of quantum mechanics

In this section we will introduce the fundamentals and main methods of quantum mechanics. We will learn what are observables and get to know the postulates which establish the foundation of quantum mechanics, as well as Heisenberg's famous principle of uncertainty.

23.2.1 Superposition principle (1. postulate)

A physical system can be found in several states. For example, a particle may be at rest or in motion, an atom may be excited or deexcited. In quantum mechanics, every possible state is described by a *wavefunction* ψ. Wavefunctions can be functions of various types of coordinates, for example, of position $\psi = \psi(\mathbf{r})$, of momentum $\psi = \psi(\mathbf{p})$, or of energy $\psi = \psi(E)$. The choice of the coordinates is called *representation*.

One peculiarity of quantum systems is that they may be in a *superposition of states*. That is, if $\psi_1, \psi_2, ..., \psi_k$ are possible states with amplitudes c_k, automatically the functions,

$$\psi = \sum_k c_k \psi_k \qquad \text{or} \qquad \psi = \int dk\ c(k)\phi(k) \tag{23.30}$$

are possible states as well. This is called *superposition principle*, and means, for example, that a particle may be *simultaneously* in several places or that an atom may be *at the same time* excited and deexcited.

There are systems that can only exist in a *restricted number* of states, such as the two-level atom. Others may exist in an *infinite number* of states or even in a *continuous distribution* of states.

23.2.2 Interpretation of the wave function (2. postulate)

A *state function* (or wavefunction) characterizes a system of which we may calculate various properties. The function can adopt complex values devoid of immediate physical interpretation. In fact, the wavefunction is above all a mathematical construct. On the other hand, the norm $|\psi|^2$ has the meaning of a probability of the system to be in the state ψ. This is the famous interpretation of *Max Born* of the wave function (see Sec. 23.1.3).

If ψ_k with $k = 1, 2, \ldots$ are all possible states of a system, the interpretation as a probability requires,

$$\sum_k |\psi_k|^2 = 1\ . \tag{23.31}$$

Analogically, for a continuous distribution, for example, in spatial representation,

$$\int_{-\infty}^{\infty} |\psi(x)|^2 dx = 1 \ . \tag{23.32}$$

That is, the probability needs *normalization*.

23.2.3 Dirac bra-ket notation and vector representation

In order to distinguish more easily the amplitudes (which are complex numbers) and the wavefunctions we will now use the Bra-Ket notation introduced by *Paul Dirac*. The functions are represented by *kets*,

$$|\psi\rangle = \sum_k c_k |k\rangle \ . \tag{23.33}$$

The complex transpositions of these states are represented by *bras*,

$$\langle\psi| = |\psi\rangle^\dagger = \sum_k c_k^* \langle k| \ . \tag{23.34}$$

But the notation has other advantages. For example, let us suppose that we know the three possible states of a system, $|1\rangle$, $|2\rangle$, and $|3\rangle$, which are linearly independent. Then we can define the states as vectors:

$$|1\rangle = \begin{pmatrix} 1 \\ 0 \\ 0 \end{pmatrix} \quad , \quad |2\rangle = \begin{pmatrix} 0 \\ 1 \\ 0 \end{pmatrix} \quad , \quad |3\rangle = \begin{pmatrix} 0 \\ 0 \\ 1 \end{pmatrix} \ . \tag{23.35}$$

These three states can be interpreted as the basis of a *vector space* representing the system. Now, each wavefunction can be expanded on this basis and expressed by a vector. An arbitrary ket state of this system will then be,

$$|\psi\rangle = \begin{pmatrix} c_1 \\ c_2 \\ c_3 \end{pmatrix} \ . \tag{23.36}$$

The corresponding bra state will be,

$$\langle\psi| = \begin{pmatrix} c_1^* & c_2^* & c_3^* \end{pmatrix} \ . \tag{23.37}$$

Now we can easily calculate the probability for a system to be in a state $|\psi\rangle$,

$$||\psi\rangle|^2 = \langle\psi|\psi\rangle = \begin{pmatrix} c_1^* & c_2^* & c_3^* \end{pmatrix} \cdot \begin{pmatrix} c_1 \\ c_2 \\ c_3 \end{pmatrix} = |c_1|^2 + |c_2|^2 + |c_3|^2 \ . \tag{23.38}$$

23.2.4 Observables (3. postulate)

The only way to get information about a system is to *measure* the values of characteristic quantities of the system, e.g. energy or linear momentum. In classical mechanics we have learned that a system can be completely characterized by a set of measurable physical quantities. For example, the motion of a rigid body of mass m and inertial moment $\mathbf{I}$ is defined by its position $\mathbf{r}$, its moment $\mathbf{p}$, and its angular momentum $\mathbf{L}$. In quantum mechanics we describe observable physical quantities by *operators* acting on the *Hilbert space* of wavefunctions, $|\psi\rangle \mapsto \hat{\mathbf{p}}|\psi\rangle$, where $\hat{p}$ would be the operator of the linear momentum. To better distinguish the observables, we decorate their symbols with a hat. We will see more ahead (see Sec. 23.3.5) that every quantum system is completely described by a complete set of observables.

To find the current values a_ψ of any *observable* $\hat{A}$ in a specific situation given by a wave function ψ, we need to solve an equation of eigenvalues,

$$\hat{A}|\psi\rangle = a_\psi|\psi\rangle \ . \tag{23.39}$$

We can rewrite the equation as $a_\psi = \langle\psi|\hat{A}|\psi\rangle$. The values a_n are real numbers, if the observable is a *Hermitian operator*, that is,

$$\hat{A} = \hat{A}^\dagger \quad \Longrightarrow \quad a_\psi = a_\psi^* \ . \tag{23.40}$$

We leave proof of this for the Exc. 23.2.9.1.

Thus, we postulate the substitution of the *dynamic variables* characterizing a classical system by abstract objects called operators. These operators can be understood as mathematical prescriptions, e.g., differential operators acting on a state of the system. The expectation value of any operator $\hat{A}$ characterizing a system in a state $|\psi\rangle$ is $a_\psi \equiv \langle\hat{A}\rangle_\psi \equiv \langle\psi|\hat{A}|\psi\rangle/\langle\psi|\psi\rangle$. Such operators are specific for a system, but independent of its state. The dynamical variables for a specific state are obtained as eigenvalues of the respective variable in that specific state. The temporal evolution of the operators or of the states is governed by equations of motion (see Sec. 23.4) [5].

23.2.5 Representation of operators as matrices

In the same way as we already represented wavefunctions by vectors, we can also represent operators by matrices,

$$\hat{A} \equiv \sum_{i,j} |i\rangle a_{ij} \langle j| = \begin{pmatrix} & \vdots & \\ .. & a_{ij} & .. \\ & \vdots & \end{pmatrix} = \begin{pmatrix} & \vdots & \\ .. & \langle j|\hat{A}|i\rangle & .. \\ & \vdots & \end{pmatrix} \ . \tag{23.41}$$

To extract components from a matrix we do, $\langle i|\hat{A}|j\rangle$, for example,

$$\langle 1|\hat{A}|1\rangle = \begin{pmatrix} 1 & 0 & .. \end{pmatrix} \cdot \hat{A} \cdot \begin{pmatrix} 1 \\ 0 \\ \vdots \end{pmatrix} = a_{11} \ . \tag{23.42}$$

[5] Note that there are theoretical attempts to generalize the concept of observables to non-Hermitian operators [117, 118] only displaying $\mathcal{PT}$-symmetry.

Projectors are particular operators defined by,

$$\hat{P}_k \equiv |k\rangle\langle k| = \begin{pmatrix} 0 & : & 0 \\ .. & 1 & .. \\ 0 & : & 0 \end{pmatrix} \quad . \tag{23.43}$$

The eigenvalue of a projector, $\langle \hat{P}_k \rangle = \langle \psi | \hat{P}_k | \psi \rangle = |\langle k|\psi\rangle|^2$, is nothing more than the probability of finding a system, whose general state is $|\psi\rangle$, in the particular state, since expanding as done in (23.33), we have,

$$\langle \hat{P}_k \rangle = \sum_{m,n} c_m^* c_n \langle m|k\rangle\langle k|n\rangle = |c_k|^2 \ . \tag{23.44}$$

Using the matrix formalism we can define other interesting operators and verify their properties. For example, choosing the basis,

$$|1\rangle = \begin{pmatrix} 1 \\ 0 \end{pmatrix} \quad , \quad |2\rangle = \begin{pmatrix} 0 \\ 1 \end{pmatrix} \ , \tag{23.45}$$

we find,

$$\begin{array}{rclcrcl} |1\rangle\langle 1| & = & \begin{pmatrix} 1 & 0 \\ 0 & 0 \end{pmatrix} & , & |2\rangle\langle 2| & = & \begin{pmatrix} 0 & 0 \\ 0 & 1 \end{pmatrix} \\ |1\rangle\langle 2| & = & \begin{pmatrix} 0 & 1 \\ 0 & 0 \end{pmatrix} & , & |2\rangle\langle 1| & = & \begin{pmatrix} 0 & 0 \\ 1 & 0 \end{pmatrix} \end{array} \quad . \tag{23.46}$$

Obviously, these matrices can be used to expand any 2×2 matrix. An equivalent set of matrices are the *Pauli spin matrices*,

$$\boxed{\mathbb{I} \equiv \begin{pmatrix} 1 & 0 \\ 0 & 1 \end{pmatrix} \quad , \quad \hat{\sigma}^x \equiv \begin{pmatrix} 0 & 1 \\ 1 & 0 \end{pmatrix} \quad , \quad \hat{\sigma}^y \equiv \begin{pmatrix} 0 & \imath \\ -\imath & 0 \end{pmatrix} \quad , \quad \hat{\sigma}^z \equiv \begin{pmatrix} -1 & 0 \\ 0 & 1 \end{pmatrix}} \ . \tag{23.47}$$

An important property of the Pauli matrices is their behavior under commutation and anti-commutation,

$$\begin{aligned} [\hat{\sigma}_k, \hat{\sigma}_m]_- &\equiv \hat{\sigma}_k \hat{\sigma}_m - \hat{\sigma}_k \hat{\sigma}_m = \imath \epsilon_{kmn} \hat{\sigma}_n \\ [\hat{\sigma}_k, \hat{\sigma}_m]_+ &\equiv \hat{\sigma}_k \hat{\sigma}_m + \hat{\sigma}_k \hat{\sigma}_m = 2\delta_{km} \ . \end{aligned} \tag{23.48}$$

Defining so-called ladder operators or rising, respectively, lowering operators, depending on the arrangement of the level system via,

$$\boxed{\hat{\sigma}^{\pm} = \tfrac{1}{2}(\hat{\sigma}_x \pm \imath \hat{\sigma}_y)} \ , \tag{23.49}$$

we may represent the matrices as,

$$\begin{array}{rclcrcl} |1\rangle\langle 1| & = & \tfrac{1}{2}(\mathbb{I}_2 - \hat{\sigma}^z) = \hat{\sigma}^- \hat{\sigma}^+ & , & |2\rangle\langle 2| & = & \tfrac{1}{2}(\mathbb{I}_2 + \hat{\sigma}^z) = \hat{\sigma}^+ \hat{\sigma}^- \\ |2\rangle\langle 1| & = & \tfrac{1}{2}(\hat{\sigma}^x + \imath \hat{\sigma}^y) = \hat{\sigma}^+ & , & |1\rangle\langle 2| & = & \tfrac{1}{2}(\hat{\sigma}^x - \imath \hat{\sigma}^y) = \hat{\sigma}^- \end{array} \ , \tag{23.50}$$

and write down the *Pauli vector* [6],

$$\hat{\vec{\sigma}} \equiv \begin{pmatrix} \hat{\sigma}_x \\ \hat{\sigma}_y \\ \hat{\sigma}_z \end{pmatrix} = \begin{pmatrix} \hat{\sigma}^- + \hat{\sigma}^+ \\ \imath(\hat{\sigma}^- - \hat{\sigma}^+) \\ [\hat{\sigma}^+, \hat{\sigma}^-] \end{pmatrix} \tag{23.51}$$

and the vector

$$\vec{\rho} \equiv \begin{pmatrix} \langle\hat{\sigma}_x\rangle \\ \langle\hat{\sigma}_y\rangle \\ \langle\hat{\sigma}_z\rangle \end{pmatrix} , \tag{23.52}$$

which is called *Bloch vector* [7,8]. The eigenvalue of the Bloch vector has a fixed length (see Exc. 23.2.9.2).

The representation of physical quantities by matrices is essential for the description of quantum superposition states.

23.2.6 Correspondence principle (4. postulate)

Operators do not necessarily commute. We have already seen in Sec. 23.1.6, that in one dimension the position and the momentum operators do not commute. We can generalize to three dimensions via,

$$[\hat{p}_j, \hat{x}_k] = -\imath\hbar\delta_{jk} \qquad \text{and} \qquad [\hat{p}_j, \hat{p}_k] = 0 = [\hat{x}_j, \hat{x}_k] \ , \tag{23.53}$$

which is easily verified by replacing the operators with $\hat{x}_k = x_k$ and $\hat{p}_k = \frac{\hbar}{\imath}\nabla$ and allowing the commutators to act on a wavefunction $\psi(x)$.

Conversely, quantum mechanics follows from classical mechanics with the prescription [9], $A(q_k, p_k, t) \longrightarrow A(\hat{q}_k, \hat{p}_k, t) = \hat{A}$. Letting the smallest amount of energy possible go to zero, $\hbar \longrightarrow 0$, the commutator disappears, the energy spectrum becomes continuous, and we recover classical mechanics.

23.2.7 Schrödinger equation and quantum measurements (5. postulate)

The time evolution is given by the Schrödinger equation,

$$\boxed{\imath\hbar\frac{\partial}{\partial t}|\psi\rangle = \hat{H}|\psi\rangle} \ . \tag{23.54}$$

A closed system, disconnected from the rest of the world (we will now call the rest of the world *reservoir*) is not subject to dissipation, i.e., it does not lose energy

[6] Note that other definitions of the Pauli matrices, e.g. $\hat{\sigma}^y \to -\hat{\sigma}^y$ and $\hat{\sigma}^z \to -\hat{\sigma}^z$ are also found in literature. They simply correspond to a change of basis $|1\rangle \leftrightarrow |2\rangle$.

[7] The Bloch vector is widely used in describing the interaction of a two-level system with a light field.

[8] Schrödinger invented the *wave mechanics* when he derived his wave equation from the dispersion relation for massive particles. Heisenberg invented a mechanics (detailed in later sections), which he called *mechanics of matrices*. Later, he showed the formal equivalence of both theories.

[9] Considering the Weyl order.

to the reservoir. Such a system is always described by a hermitian Hamiltonian. Unfortunately, this system also does not allow information leakage, that is, we can not measure the system. This is reflected in the fact that the Schrödinger equation does not allow to describe the process of a *quantum measurement*. This is because before the measurement, the system can be in several states or even in a superposition of states, while after the measurement we know exactly the state. This amounts to a reduction of entropy, which is not allowed in a closed system.

The famous *postulate* of *state reduction* or *projection of the wavefunction* formulated by *John von Neumann* describes the quantum measurement process as a sequence of two distinct steps [10]. In a first step, the measuring apparatus projects the measured operator $\hat{A}$ on an eigenvector basis. That is, if the measurement is compatible with the operator [11], we obtain a distribution of probability amplitudes of the results,

$$\hat{A} \quad \curvearrowright \quad \langle \hat{A} \rangle = \langle \psi | \hat{A} | \psi \rangle = \langle \psi | \hat{A} | \sum_k c_k |k\rangle = \sum_k a_k c_k \langle \psi | k \rangle = \sum_k a_k |c_k|^2 \ , \quad (23.55)$$

with $\langle \psi | \psi \rangle = \sum_k |a_k|^2 = 1$. Therefore, we can understand $|\langle k | \psi \rangle|^2$ as the probability of the system to be in the eigenstate $|k\rangle$. In other words, this first step of the measurement process removes in an irreversible manner all coherences from the observable, $\hat{A} \curvearrowright \sum_k |k\rangle\langle k|\hat{A}|k\rangle\langle k|$.

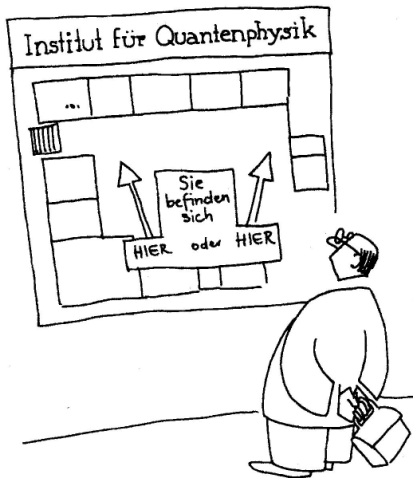

Figure 23.2: Superposition.

In a second step, the observing scientist will *read* the measuring device and note the result, which will necessarily be one of the possible a_k,

$$\langle \hat{A} \rangle \quad \curvearrowright \quad a_k \ . \quad (23.56)$$

If the state is stationary, it will never change any more. That is, each subsequent measurement will yield the same result. The Exc. 23.2.9.3 illustrates the process of

[10] For simplicity, we only consider pure state, here.

[11] To understand the meaning of *compatible*, we must establish a more complete theory of measurement including the reservoir in the quantum description.

quantum measurement at the example of a measurement of the excitation energy of a two-level atom.

23.2.8 Stationary Schrödinger equation

The general form of the Schrödinger equation in one dimension is,

$$\hat{H}\Psi(t,x) = \imath\hbar\frac{\partial}{\partial t}\Psi(t,x) \ , \tag{23.57}$$

with $\hat{H} \equiv \frac{\hat{p}^2}{2m} + V(x,t)$ and $\hat{p} \equiv -\imath\hbar\frac{\partial}{\partial x}$. If the potential is independent of time, $V(x,t) = V(x)$, we can do the following ansatz, $\Psi(x,t) \equiv \psi(x)f(t)$. Insertion into the Schrödinger equation yields,

$$\frac{1}{\psi(x)}\left(-\frac{\hbar^2}{2m}\frac{d^2}{dx^2} + V(x)\right)\psi(x) = \frac{\imath\hbar}{f(t)}\frac{d}{dt}f(t) = const. \equiv E \ . \tag{23.58}$$

The solution of the right-hand side of the equation is $\imath\hbar(\ln f - \ln f_0) = E(t - t_0)$. Hence,

$$f(t) = f(0)e^{-\imath E(t-t_0)/\hbar} \ . \tag{23.59}$$

Obviously, $|\Psi(x,t)|^2 = |\psi(x)|^2$.

Now, we can see that the stationary Schrödinger equation,

$$\hat{H}\psi(x) = E\psi(x) \ , \tag{23.60}$$

is nothing more than an eigenvalue equation. This means that the Schrödinger wave mechanics is equivalent to the mechanics of the Heisenberg matrices. The Excs. 23.2.9.4 and 23.2.9.5 are first simple calculations of the eigenvalues and eigenvectors of a two-level system.

23.2.9 Exercises

23.2.9.1 Ex: Reality of eigenvalues

Show that the eigenvalues of an observable are real.

Solution:

$$a_\psi = \langle\psi|\hat{A}|\psi\rangle = \langle\psi|\hat{A}^\dagger|\psi\rangle = (\langle\psi|\hat{A}|\psi\rangle)^* = a_\psi^* \ .$$

23.2.9.2 Ex: Normalization of the Bloch vector

Calculate the expectation value of the length of the Pauli vector and the length of the Bloch vector (23.49).

Solution: *With* $|\psi\rangle = a_1|1\rangle + a_2|2\rangle$ *the expectation value of the length of the Pauli vector is,*

$$\langle\hat{\vec{\sigma}}^\dagger\hat{\vec{\sigma}}\rangle = \langle\psi|\hat{\sigma}_x^2 + \hat{\sigma}_y^2 + \hat{\sigma}_z^2|\psi\rangle = 3\langle\psi|\mathbb{I}_2|\psi\rangle = 3 \ .$$

In contrast, the expectation value of the length of the Bloch vector is,

$$\begin{aligned}\vec{\rho}^{\dagger}\vec{\rho} &= \langle\psi|\hat{\sigma}_x|\psi\rangle^2 + \langle\psi|\hat{\sigma}_y|\psi\rangle^2 + \langle\psi|\hat{\sigma}_z|\psi\rangle^2 \\ &= (a_1^* a_2 + a_1 a_2^*)^2 - (a_1^* a_2 - a_1 a_2^*)^2 + (a_1^* a_1 - a_2^* a_2)^2 = |a_1|^2 + |a_2|^2 = 1 \ .\end{aligned}$$

23.2.9.3 Ex: Quantum measurement

Explain the idea of quantum measurement at the example of a measurement of the excitation energy of a two-level atom.

Solution: *With the general wavefunction* $|\psi(t)\rangle \equiv c_1(t)|1\rangle + c_2(t)|2\rangle$*, we obtain*

$$\langle\psi|\hat{H}|\psi\rangle = |c_1|^2 E_1 + |c_2|^2 E_2 \ .$$

Normalization requires $\langle\psi|\psi\rangle = |c_1|^2 + |c_2|^2 = 1$*. The measuring apparatus will give the result* E_1 *with the probability* $|c_1|^2$ *and the result* E_2 *with the probability* $|c_2|^2$*, even if in reality the system was in a superposition of the two states* [12]*.*

23.2.9.4 Ex: Two-level atom

Consider a two-level atom. The Hamiltonian is given by,

$$\hat{H} = \begin{pmatrix} 0 & 0 \\ 0 & \hbar\omega_0 \end{pmatrix} \ .$$

Using the stationary Schrödinger equation, calculate the eigenvalues and eigenvectors.

Solution: *The Hamiltonian has the eigenvalues,*

$$\det \begin{pmatrix} -E & 0 \\ 0 & \hbar\omega_0 - E \end{pmatrix} = -E(\hbar\omega_0 - E) = 0 \qquad \Longrightarrow \qquad E = 0, \hbar\omega_0 \ .$$

Solving the Schrödinger equation, $\hat{H}|\psi\rangle = E|\psi\rangle$*, we get the eigenvectors,*

$$\begin{pmatrix} 0 & 0 \\ 0 & \hbar\omega_0 \end{pmatrix} \begin{pmatrix} c_1 \\ c_2 \end{pmatrix} = 0 \begin{pmatrix} c_1 \\ c_2 \end{pmatrix} \Longrightarrow |1\rangle = \begin{pmatrix} 1 \\ 0 \end{pmatrix} \ ,$$

$$\begin{pmatrix} 0 & 0 \\ 0 & \hbar\omega_0 \end{pmatrix} \begin{pmatrix} c_1 \\ c_2 \end{pmatrix} = \hbar\omega_0 \begin{pmatrix} c_1 \\ c_2 \end{pmatrix} \Longrightarrow |2\rangle = \begin{pmatrix} 0 \\ 1 \end{pmatrix} \ .$$

[12] The quantum Monte Carlo wavefunction simulation method provides a useful picture of what happens in the process of projecting a wavefunction by a quantum measurement.

23.2.9.5 Ex: The ammonium molecule

Consider the two states $|1\rangle$ and $|2\rangle$ of the ammonium molecule outlined in the figure. Suppose they are orthonormal, $\langle i|j\rangle = \delta_{ij}$, and that only these two states are accessible to the system, so that we can describe it using the basis formed by $|1\rangle$ and $|2\rangle$. On this basis the Hamiltonian $\hat{H}$ of the system is given by,

$$\hat{H} = \begin{pmatrix} E_0 & -E_1 \\ -E_1 & E_0 \end{pmatrix} .$$

a. If the system is initially in state $|1\rangle$, will it remain in that state at a later time? How about if the initial state is $|2\rangle$?
b. Obtain the eigenvalues E_I and E_{II} and the respective eigenvectors $|I\rangle$ and $|II\rangle$ of $\hat{H}$, expressing them in terms of $|1\rangle$ and $|2\rangle$.
c. What is the probability of measuring an energy E_I in the following state,

$$|\psi\rangle = \tfrac{1}{\sqrt{5}}|1\rangle - \tfrac{2}{\sqrt{5}}|2\rangle \ ?$$

d. Based on the above result, we can predict at least one possible electromagnetic radiation emission frequency for an ammonia sample. What is this frequency?

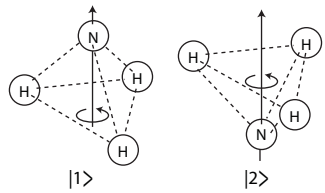

Figure 23.3: The two states of the ammonium molecule.

Solution: *a. No, because these states are not eigenstates of the Hamiltonian. The temporal evolution of the system mixes the two, and we have two specific combinations with well-defined energy, the eigenstates of $\hat{H}$. Starting in $|1\rangle$ or $|2\rangle$ we will be able to measure either one of the two possible energies depending of the time we wait, that is, $\langle 2|\hat{H}|1\rangle \neq 0$.*
b. We write

$$|1\rangle = \begin{pmatrix} 1 \\ 0 \end{pmatrix} \quad \textit{and} \quad |2\rangle = \begin{pmatrix} 0 \\ 1 \end{pmatrix} \quad \textit{and} \quad |\psi\rangle = \begin{pmatrix} c_1 \\ c_2 \end{pmatrix} .$$

With this,

$$0 = \hat{H}\begin{pmatrix} c_1 \\ c_2 \end{pmatrix} - \lambda \begin{pmatrix} c_1 \\ c_2 \end{pmatrix} = \begin{pmatrix} E_0 - \lambda - E_1 & \\ -E_1 & E_0 - \lambda \end{pmatrix} \begin{pmatrix} c_1 \\ c_2 \end{pmatrix} .$$

Hence,

$$\begin{vmatrix} E_0 - \lambda - E_1 & \\ -E_1 & E_0 - \lambda \end{vmatrix} = (E_0 - \lambda)^2 - E_1^2 = 0 \ ,$$

giving the eigenvalues

$$\lambda = E_{I,II} = E_0 \pm E_1 \ .$$

The eigenvectors follow from,

$$\hat{H}\begin{pmatrix} c_1 \\ c_2 \end{pmatrix} = E_I \begin{pmatrix} c_1 \\ c_2 \end{pmatrix} \Longrightarrow \begin{pmatrix} E_0 c_1 - E_1 c_2 \\ -E_1 c_1 + E_0 c_2 \end{pmatrix} = \begin{pmatrix} E_0 c_1 - E_1 c_1 \\ E_0 c_2 - E_1 c_2 \end{pmatrix} \Longrightarrow c_1 = c_2 \ .$$

Along with the normalization condition $\langle I|I\rangle = 1$ *this gives* $c_1 = c_2 = 1/\sqrt{2}$ *and*

$$|I\rangle = \tfrac{1}{\sqrt{2}}|1\rangle + \tfrac{1}{\sqrt{2}}|2\rangle \ .$$

Also,

$$\hat{H}\begin{pmatrix} c_1 \\ c_2 \end{pmatrix} = E_{II} \begin{pmatrix} c_1 \\ c_2 \end{pmatrix} \Longrightarrow \begin{pmatrix} E_0 c_1 - E_1 c_2 \\ -E_1 c_1 + E_0 c_2 \end{pmatrix} = \begin{pmatrix} E_0 c_1 + E_1 c_1 \\ E_0 c_2 + E_1 c_2 \end{pmatrix} \Longrightarrow c_1 = -c_2 \ .$$

Along with the normalization condition $\langle II|II\rangle = 1$ *this gives* $c_1 = -c_2 = 1/\sqrt{2}$ *and*

$$|II\rangle = \tfrac{1}{\sqrt{2}}|1\rangle - \tfrac{1}{\sqrt{2}}|2\rangle \ .$$

c. We calculate the superposition

$$\begin{aligned} P_{E_I} = |\langle I|\psi\rangle|^2 &= \left|\left(\tfrac{1}{\sqrt{2}}\langle 1| + \tfrac{1}{\sqrt{2}}\langle 2|\right)\left(\tfrac{1}{\sqrt{5}}|1\rangle - \tfrac{2}{\sqrt{5}}|2\rangle\right)\right|^2 \\ &= \left|\tfrac{1}{\sqrt{10}}\langle 1|1\rangle - \tfrac{2}{\sqrt{10}}\langle 2|2\rangle\right|^2 = \left|-\tfrac{1}{\sqrt{10}}\right|^2 = 10\% \ . \end{aligned}$$

d. The emission is due to the transition from E_{II} *to* E_I*, hence the emitted energy is:*

$$E_{II} - E_I = E_0 + E_1 - (E_0 - E_1) = 2E_1 \ .$$

Therefore the frequency of the emitted photons is $\nu = \frac{2E_1}{h}$.

23.3 Abstract formalism of quantum mechanics

The formal development of quantum mechanics will be the subject of this section. We will learn how to find a complete set of observables characterizing a system, discuss the role of symmetries in quantum mechanics and show how to switch between several representations of the same system.

23.3.1 Lie algebra

The quantum mechanical operators form a *Lie algebra* $\mathcal{L}^2$. This means that $\mathcal{L}^2$ is at the same time a complex and linear *vector space* with respect to addition and scalar multiplication and a *non-commutative ring* with scalar internal product. In

particular, $\mathcal{L}^2$ is unitary, normalized, and complete and acts on a *Hilbert space* of quantum states,

$$\begin{aligned}(\hat{A}+\hat{B})|\psi\rangle &= \hat{A}|\psi\rangle + \hat{B}|\psi\rangle, \\ (\alpha\hat{A})|\psi\rangle &= \alpha(\hat{A}|\psi\rangle)\ , \\ (\hat{A}\hat{B})|\psi\rangle &= \hat{A}(\hat{B}|\psi\rangle)\ .\end{aligned} \tag{23.61}$$

The properties of the Hilbert space are,

$$\begin{aligned}\hat{A}|\psi+\varphi\rangle &= \hat{A}|\psi\rangle + \hat{A}|\varphi\rangle\ , \\ \hat{A}|a\psi\rangle &= a\hat{A}|\psi\rangle\ .\end{aligned} \tag{23.62}$$

For a *Hermitian operator*, $\hat{A} = \hat{A}^\dagger$, we have $\langle\psi|\hat{A}|\psi\rangle = \langle\hat{A}\psi|\psi\rangle$ or $\langle\hat{A}\rangle \equiv \langle\psi|\hat{A}|\psi\rangle = \langle\hat{A}\rangle^*$, using the Dirac bra-ket notation,

$$\langle\psi|^\dagger \equiv |\psi\rangle\ . \tag{23.63}$$

There are identity and nullity operators,

$$\hat{1}|\psi\rangle = |\psi\rangle \qquad \text{and} \qquad \hat{0}|\psi\rangle = 0\ . \tag{23.64}$$

We define the *(anti-)commutator* as,

$$[\hat{A},\hat{B}]_\mp \equiv \hat{A}\hat{B} \pm \hat{B}\hat{A}\ , \tag{23.65}$$

which can be $\neq 0$. The sum of two Hermitian operators is Hermitian, but the product is not, since,

$$(\hat{A}+\hat{B})^\dagger = \hat{A}^\dagger + \hat{B}^\dagger = \hat{A}+\hat{B} \qquad \text{but} \qquad (\hat{A}\hat{B})^\dagger = \hat{B}^\dagger\hat{A}^\dagger = \hat{B}\hat{A} \neq \hat{A}\hat{B}\ . \tag{23.66}$$

On the other hand, the following relations of Hermitian operators are always Hermitian,

$$\hat{A}\hat{B} + \hat{B}\hat{A} \qquad \text{and} \qquad \imath(\hat{A}\hat{B} - \hat{B}\hat{A})\ . \tag{23.67}$$

We define the *scalar product* as,

$$\langle\psi|\varphi\rangle\ . \tag{23.68}$$

Two states are called *orthogonal*, if $\langle\psi|\varphi\rangle = 0$. The norm is written as,

$$|\psi|^2 = \langle\psi|\psi\rangle\ , \tag{23.69}$$

the deviation is,

$$\Delta A \equiv \sqrt{\langle\hat{A}^2\rangle - \langle\hat{A}\rangle^2}\ . \tag{23.70}$$

A *unitary operator* is defined by $\hat{A}^{-1} = \hat{A}^\dagger$.

23.3.2 Complete bases

If it is impossible to find a set of amplitudes c_n,

$$\nexists\{c_n\} \quad \text{such that} \quad \sum_n c_n|n\rangle = 0 \ , \tag{23.71}$$

the functions are called *linearly independent*. A set of linearly independent functions may form a *basis*. The space opened by a set of linearly independent functions is called *Hilbert space*.

An operator $\hat{A}$ is completely characterized by its *eigenvalues* and *eigenfunctions*. If a set of eigenfunctions $|n\rangle$ is *complete*, every allowed state of the system can be expanded in these eigenfunctions,

$$|\psi\rangle = \sum_n c_n|n\rangle \qquad \text{and} \qquad \hat{A}|n\rangle = a_n|n\rangle \ . \tag{23.72}$$

To calculate properties of a specific system, we often want to find a matrix representation for the operator $\hat{A}$. For this, we solve the stationary Schrödinger equation, that is, we calculate the eigenvalues and *eigenvectors*. When all eigenvalues are different, $a_n \neq a_m$, we know that the corresponding eigenvectors are orthogonal, $\langle n|m\rangle = 0$,

$$\begin{aligned} &\hat{A}|n\rangle = a_n|n\rangle \quad , \quad \hat{A}|m\rangle = a_n|m\rangle \quad , \quad \forall\{n,m\}\ a_n \neq a_m \\ \Longrightarrow\ &\forall\{n,m\}\ \langle n|m\rangle = \delta_{m,n} \ . \end{aligned} \tag{23.73}$$

Exc. 23.3.10.1 asks for demonstrating this.

Frequently, for example, in the case of a particle confined to a potential, there exist discrete eigenvalues (for $E < 0$) simultaneously with continuous eigenvalues (for $E > 0$). Assuming $\langle m|m'\rangle = \delta_{m,m'}$, $\langle m|\mathbf{k}\rangle = 0$ and $\langle \mathbf{k}|\mathbf{k'}\rangle = \delta^{(3)}(\mathbf{k}-\mathbf{k'})$, with a complete base,

$$\sum_m |m\rangle\langle m| + \int d^3k|\mathbf{k}\rangle\langle\mathbf{k}| = \hat{\mathbf{1}} \ , \tag{23.74}$$

an arbitrary vector can be expanded on an orthogonal basis,

$$|\psi\rangle = \sum_m |m\rangle\langle m|\psi\rangle + \int d^3k\ |\mathbf{k}\rangle\langle\mathbf{k}|\psi\rangle \ . \tag{23.75}$$

This also applies to observables,

$$\hat{A} = \sum_{m,n} |m\rangle\langle m|\hat{A}|n\rangle\langle n| + \int d^3k d^3l\ |\mathbf{k}\rangle\langle\mathbf{k}|\hat{A}|\mathbf{l}\rangle\langle\mathbf{l}| \ , \tag{23.76}$$

and functions of observables,

$$f(\hat{A}) = \sum_{m,n} |m\rangle f(\langle m|\hat{A}|n\rangle)\langle n| + \int d^3k d^3l\ |\mathbf{k}\rangle f(\langle\mathbf{k}|\hat{A}|\mathbf{l}\rangle)\langle\mathbf{l}| \ . \tag{23.77}$$

23.3.3 Degeneracy

The eigenvectors form a natural basis for the Hilbert space. However, a problem arises in the case of *degeneracy*, that is, when some eigenvalues are equal, $a_n = a_m$. In this case, the eigenvectors that correspond to degenerate eigenvalues are not completely defined, and we have to construct a basis verifying that all constructed eigenvectors are orthogonal. For this, there exists the method of *orthogonalization by Schmidt*, which works like this: We assume that we have already solved the eigenvalue equation, that we found a degenerate eigenvalue, $\hat{A}|a_k\rangle = a|a_k\rangle$ for every $k = 1, .., g_k$, where g_k is the degree of degeneracy, and that we also found a complete basis of eigenvalues $|a_m\rangle$, but which is not orthogonal, that is, $\exists\{m, n\}$ with $\langle a_n|a_m\rangle \neq 0$. The task is to build another basis $|b_m\rangle$ satisfying $\langle b_n|b_m\rangle = \delta_{n,m}$.

The first vector of the orthogonal base can be chosen freely, e.g.,

$$|b_1\rangle \equiv |a_1\rangle \ . \tag{23.78}$$

Since the basis $\{|a_k\rangle\}$ is assumed to be complete, the second vector is necessarily a linear combination of vectors $|a_k\rangle$, that is, $|b_2\rangle = |a_2\rangle + \lambda|b_1\rangle$. With the condition $\langle b_1|b_2\rangle = 0 = \langle b_1|a_2\rangle + \lambda\langle b_1|b_1\rangle$ we can determine the parameter λ, and obtain for the second vector,

$$|b_2\rangle \equiv |a_2\rangle - |b_1\rangle \frac{\langle b_1|a_2\rangle}{\langle b_1|b_1\rangle} \ . \tag{23.79}$$

In the same way, we can derive for a third vector, $|b_3\rangle = |a_3\rangle + \mu|b_1\rangle + \nu|b_2\rangle$, the conditions, $\langle b_1|b_3\rangle = 0 = \langle b_1|a_3\rangle + \mu\langle b_1|b_1\rangle$ and $\langle b_2|b_3\rangle = 0 = \langle b_2|a_3\rangle + \nu\langle b_2|b_2\rangle$, and obtain,

$$|b_3\rangle \equiv |a_3\rangle - |b_1\rangle \frac{\langle b_1|a_3\rangle}{\langle b_1|b_1\rangle} - |b_2\rangle \frac{\langle b_2|a_3\rangle}{\langle b_2|b_2\rangle} \ . \tag{23.80}$$

An overall way of writing this down is,

$$|b_k\rangle \equiv \left(1 - \frac{|b_1\rangle\langle b_1|}{\langle b_1|b_1\rangle} - \frac{|b_2\rangle\langle b_2|}{\langle b_2|b_2\rangle} - ... - \frac{|b_{k-1}\rangle\langle b_{k-1}|}{\langle b_{k-1}|b_{k-1}\rangle}\right)|a_k\rangle \ . \tag{23.81}$$

In the Exc. 23.3.10.2 we practice the orthogonalization of a set of three linearly independent but non-orthogonal vectors, and in the Exc. 23.3.10.3 we find an orthogonal basis for a partially degenerate three-level system.

23.3.4 Bases as unitary operators

One way to formulate the eigenvalue problem is as follows: Let $|n\rangle$ be an orthonormal basis with the respective eigenvalues a_n of an operator $\hat{A}$:

$$\hat{A}|n\rangle = a_n|n\rangle \qquad \text{with} \qquad \langle n|m\rangle = \delta_{mn} \ . \tag{23.82}$$

We construct the matrices,

$$U \equiv \begin{pmatrix} |1\rangle & |2\rangle & \cdots \end{pmatrix} \qquad \text{and} \qquad \hat{E} \equiv \begin{pmatrix} a_1 & 0 & \cdots \\ 0 & a_2 & \\ \vdots & & \ddots \end{pmatrix} \ . \tag{23.83}$$

With the definition of $U^\dagger$ we have,

$$U^\dagger = \begin{pmatrix} \langle 1| \\ \langle 2| \\ \vdots \end{pmatrix} \quad \text{and} \quad U^\dagger U = \begin{pmatrix} \langle 1|1\rangle & \langle 1|2\rangle & \cdots \\ \langle 2|1\rangle & \langle 2|2\rangle & \cdots \\ \vdots & \vdots & \ddots \end{pmatrix} = \hat{\mathbf{1}} \, . \tag{23.84}$$

Therefore,

$$\begin{aligned} U^\dagger U = \hat{\mathbf{1}} \quad &\Longrightarrow \quad U^\dagger U U^{-1} = \hat{1} U^{-1} \quad \Longrightarrow \quad U^\dagger = U^{-1} \\ U^\dagger U = \hat{\mathbf{1}} \quad &\Longrightarrow \quad U U^\dagger U U^{-1} = U \hat{1} U^{-1} \quad \Longrightarrow \quad U U^\dagger = \hat{\mathbf{1}} \, . \end{aligned} \tag{23.85}$$

Also,

$$\hat{A}|n\rangle = \hat{E}|n\rangle \quad \text{and} \quad \hat{A}U = U\hat{E} \, . \tag{23.86}$$

That is, by knowing the unitary matrix (or *transformation matrix*) U, we can solve the eigenvalue problem simply by $\hat{E} = U^{-1}\hat{A}U$.

Note, that this does not apply to a non-orthonormal basis. In this case, we need to do a Schmidt orthogonalization and use the condition $\det U = 1$. We apply the technique detailed in this section to solve Excs. 23.3.10.4, 23.3.10.5, and 23.3.10.6.

23.3.5 Complete set of commuting operators

Even for simple systems, we can ask various types of questions (measurements). Considering, for example, a particle flying freely in space, we can gather its position or its velocity. Let a be the result of a measurement of the observable $\hat{A}$, that is, $a = \langle\psi_a|\hat{A}|\psi_a\rangle$. Due to the measurement we know that the system is in the state $|\psi_a\rangle$. Immediately after this first measurement we perform another measurement of *another* observable $\hat{B}$ giving $\langle\psi_a|\hat{B}|\psi_a\rangle$. The result of this measurement can only yield an eigenstate, $b = \langle\psi_a|\hat{B}|\psi_a\rangle$, if the operators commute, $[\hat{A}, \hat{B}] = 0$. That is, *if two operators $\hat{A}$ and $\hat{B}$ commute, and if $|\psi\rangle$ is an eigenvector of $\hat{A}$, then $\hat{B}|\psi\rangle$ is also an eigenvector of $\hat{A}$ with the same eigenvalue*:

$$\begin{aligned} &[\hat{A}, \hat{B}] = 0 \quad , \quad a = \langle\psi|\hat{A}|\psi\rangle \\ \Longrightarrow \; &\hat{A}(\hat{B}|\psi\rangle) = a(\hat{B}|\psi\rangle) \quad \text{and} \quad \langle\psi|\hat{B}|\psi\rangle \in \mathbb{R} \, . \end{aligned} \tag{23.87}$$

In addition, we observe that, if two operators commute, the orthonormal basis constructed for one of the operators is also orthonormal for the other. That is, *if two operators $\hat{A}$ and $\hat{B}$ commute and if $|\psi_1\rangle$ and $|\psi_2\rangle$ are two eigenvectors of $\hat{A}$ with different eigenvalues, then the matrix element $\langle\psi_1|\hat{B}|\psi_2\rangle$ is equal to zero:*

$$\begin{aligned} &[\hat{A}, \hat{B}] = 0 \quad , \quad a_1 = \langle\psi_1|\hat{A}|\psi_1\rangle \neq \langle\psi_2|\hat{A}|\psi_2\rangle = a_2 \\ \Longrightarrow \; &\langle\psi_1|\hat{B}|\psi_2\rangle = 0 \, . \end{aligned} \tag{23.88}$$

Finally, we affirm that, *if two operators $\hat{A}$ and $\hat{B}$ commute, we can construct an orthonormal basis $\{|\psi_{a,b}\rangle\}$ with common eigenvectors of $\hat{A}$ and $\hat{B}$*:

$$\begin{aligned} &[\hat{A}, \hat{B}] = 0 \\ \Longrightarrow \; &\exists \, \{|\psi_{a,b}\rangle\} \quad \text{tal que} \quad \hat{A}|\psi_{a,b}\rangle = a|\psi_{a,b}\rangle \quad \text{and} \quad \hat{B}|\psi_{a,b}\rangle = b|\psi_{a,b}\rangle \, . \end{aligned} \tag{23.89}$$

The statements (23.87) to (23.89) are verified in Exc. 23.3.10.7.

The fact that commuting operators have a common system of eigenvectors authorizing sharp eigenvalues can be used to construct and characterize a state.

Example 143 (*Measuring momenta in orthogonal directions*): For example, the obvious solutions of the eigenvalue equations,

$$\hat{p}_x|\psi_{p_x}\rangle = \frac{\hbar}{\imath}\frac{d}{dx}|\psi_{p_x}\rangle = p_x|\psi_{p_x}\rangle \qquad \text{and} \qquad \hat{p}_y|\psi_{p_y}\rangle = \frac{\hbar}{\imath}\frac{d}{dy}|\psi_{p_y}\rangle = p_y|\psi_{p_y}\rangle$$

are the plane waves $e^{\imath p_x x/\hbar}$ and $e^{\imath p_y y/\hbar}$. Therefore, the total state of the particle can be described by,

$$|\psi_{p_x,p_y,p_z}\rangle = |\psi_{p_x}\rangle|\psi_{p_y}\rangle = e^{(\imath/\hbar)(p_x x+p_y y)} f(z) \ .$$

However, these eigenfunctions are infinitely degenerate, since the linear momentum in z-direction is not specified. A third operator $\hat{p}_z|\psi\rangle = p_z|\psi\rangle$ commutes with the others,

$$[\hat{p}_k, \hat{p}_m] = 0 \ .$$

Hence,

$$|\psi_{p_x,p_y,p_z}\rangle = e^{(\imath/\hbar)(p_x x+p_y y+p_z z)} \ ,$$

is a possible state of the system.
On the other hand, choosing $\hat{p}_z^2 = -\hbar^2\frac{\partial^2}{\partial z^2}$ as the third operator, giving the eigenvalues p_z^2, the state would have been,

$$|\psi_{p_x,p_y,p_z^2}\rangle = e^{(\imath/\hbar)(p_x x+p_y y)}\cos\tfrac{p_z z}{\hbar} \qquad \text{or} \qquad |\psi_{p_x,p_y,p_z^2}\rangle = e^{(\imath/\hbar)(p_x x+p_y y)}\sin\tfrac{p_z z}{\hbar} \ . \tag{23.90}$$

Therefore, there are two solutions with the same eigenvalues, p_x, p_y, p_z^2. To lift this degeneracy, we need to introduce yet another observable. This observable can be, for example, the *parity* $\hat{P}$, that is, the behavior of the wave function upon mirroring $z \longrightarrow -z$ in the x-y plane. The fact that the set of operators p_x, p_y, p_z on one hand and p_x, p_y, p_z^2, $\hat{P}$ on the other are equivalent, shows that the required number of observables for a complete characterization depends on their judicious choice.

Also, the number needed for a *complete set of commuting operators* (*CSCO*) depends on the number of *degrees of freedom* and the symmetry of the system. In the case of the free particle in one dimension it is enough to consider one observable only, for example, $\hat{x}$ or $\hat{p}$. In three dimensions, we already need at least three commuting observables. In Exc. 23.3.10.8 we will try to find a CSCO for a matrix with partially degenerate eigenvalues.

23.3.6 Uncertainty relation

We have already learned that observables that do not commute can not be measured with arbitrary precision. This principle can be quantified as follows: If $\hat{A}$ and $\hat{B}$ are two observables, then,

$$\boxed{\Delta\hat{A}\Delta\hat{B} \geq \tfrac{1}{2}|\langle[\hat{A},\hat{B}]\rangle|} \ . \tag{23.91}$$

This is Heisenberg's famous *uncertainty principle*. For example, $[\hat{p},\hat{x}] = -\imath\hbar$, and hence, $\Delta p\Delta x \geq \hbar/2$. We will see later (see Sec. 25.3.1), that $[\hat{l}_x,\hat{l}_y] = \imath\hbar\hat{l}_z$ such that $\Delta l_x \Delta l_y \geq \hbar|\langle l_z\rangle|/2$. More difficult to show, since time has no simple quantum operator, is $\Delta E\Delta t \geq \hbar/2$. In the Exc. 23.3.10.9 we will show the *Schwartz inequality*, and in the Exc. 23.3.10.10 we ask for a formal derivation of Heisenberg's uncertainty principle.

23.3.7 Representations

23.3.7.1 Spatial representation

A Hilbert space can be discrete or, as in the case of the momentum of a free particle, continuous. In this latter case, the eigenvalues are continuously distributed, since the equation,

$$-\imath\hbar\nabla_{\mathbf{r}}\psi(\mathbf{r}) = \mathbf{p}\psi(\mathbf{r}) \ , \tag{23.92}$$

has solutions for each value of E. The eigenfunctions are $\psi(\mathbf{r}) = ae^{\imath\mathbf{p}\cdot\mathbf{r}/\hbar}$. Eq. (23.92) clearly has the form of an eigenvalue equation, for which we have already introduced the Heisenberg matrix formalism. The question now is how these descriptions combine.

Observables that do not commute correspond to expansions on different bases and generate alternative representations. For example, we can represent quantum mechanics in *position space* or *linear momentum space*. If $|\mathbf{r}\rangle$ is a basis of the space of the particles' state,

$$\hat{\mathbf{r}}|\mathbf{r}\rangle = \mathbf{r}|\mathbf{r}\rangle \quad , \quad \langle\mathbf{r}'|\mathbf{r}\rangle = \delta^3(\mathbf{r}'-\mathbf{r}) \quad , \quad \int_{\mathbb{R}^3}|\mathbf{r}\rangle\langle\mathbf{r}|d^3r = \hat{\mathbf{1}} \ , \tag{23.93}$$

we can expand the position operator on a position basis as,

$$\hat{\mathbf{r}} = \int_{\mathbb{R}^3}\mathbf{r}|\mathbf{r}\rangle\langle\mathbf{r}|d^3r \ , \tag{23.94}$$

and any state vector as,

$$\boxed{|\psi(t)\rangle = \int_{\mathbb{R}^3}|\mathbf{r}\rangle\psi(t,\mathbf{r})d^3r} \ . \tag{23.95}$$

The quantities $\langle\mathbf{r}|\psi(t)\rangle = \psi(t,\mathbf{r})$ Schrödinger wave functions. We can also say that the wavefunctions are the coordinates of the state in the particular base $|\mathbf{r}\rangle$. Consequently,

$$\begin{aligned}\langle\mathbf{r}|\hat{\mathbf{r}}|\mathbf{r}'\rangle &= \mathbf{r}\delta^3(\mathbf{r}-\mathbf{r}') \\ \langle\mathbf{r}|f(\hat{\mathbf{r}})|\mathbf{r}'\rangle &= f(\mathbf{r})\delta^3(\mathbf{r}-\mathbf{r}') \ .\end{aligned} \tag{23.96}$$

It is also true that,

$$\boxed{\langle\mathbf{r}|\hat{A}|\psi(t)\rangle = \int_{\mathbb{R}^3}A(\mathbf{r},\mathbf{r}')\psi(t,\mathbf{r}')d^3r'} \ , \tag{23.97}$$

where the quantity $A(\mathbf{r},\mathbf{r}') \equiv \langle\mathbf{r}|\hat{A}|\mathbf{r}'\rangle$ is called *kernel* of the operator. The transition from Heisenberg's abstract mechanics to Schrödinger's wave mechanics is done by the substitutions $|\psi(t)\rangle \to \psi(t,\mathbf{r})$ and $\hat{A} \to A(\mathbf{r},\mathbf{r}')$.

23.3.7.2 Momentum representation

The uncertainty relation is symmetric in $\hat{\mathbf{r}}$ and $\hat{\mathbf{p}}$. Nothing prevents us from choosing as a basis,

$$\hat{\mathbf{p}}|\mathbf{p}\rangle = \mathbf{p}|\mathbf{p}\rangle \quad , \quad \langle\mathbf{p}'|\mathbf{p}\rangle = \delta^3(\mathbf{p}'-\mathbf{p}) \quad , \quad \int_{\mathbb{R}^3} |\mathbf{p}\rangle\langle\mathbf{p}|d^3p = \hat{\mathbf{1}} \ , \tag{23.98}$$

in which we can expand the momentum operator on a momentum basis as,

$$\hat{\mathbf{p}} = \int_{\mathbb{R}^3} \mathbf{p}|\mathbf{p}\rangle\langle\mathbf{p}|d^3p \ , \tag{23.99}$$

with the wavefunctions,

$$\boxed{|\psi(t)\rangle = \int_{R^3} |\mathbf{p}\rangle\varphi(\mathbf{p},t)d^3p} \ , \tag{23.100}$$

where $\langle\mathbf{p}|\psi(t)\rangle = \varphi(t,\mathbf{p})$. The formulas are analogous to the ones in the spatial representation. In particular, in the momentum representation the position operator is $\mathbf{r} = \imath\hbar\nabla_{\mathbf{p}}$.

The representations follow from one another by Fourier transformation. Since $-\imath\hbar\nabla_{\mathbf{r}}\langle\mathbf{r}|\mathbf{p}\rangle = \mathbf{p}\langle\mathbf{r}|\mathbf{p}\rangle$, we know,

$$\boxed{\langle\mathbf{r}|\mathbf{p}\rangle = \tfrac{1}{\hbar^{3/2}}\exp(\tfrac{\imath}{\hbar}\mathbf{r}\cdot\mathbf{p})} \ , \tag{23.101}$$

where the prefactor $\hbar^{-3/2}$ is introduced to take account of the unit of the states [13]. ψ and φ are different representations of the same quantum state related by,

$$\langle\mathbf{r}|\psi(t)\rangle = \int_{\mathbb{R}^3} \langle\mathbf{r}|\mathbf{p}\rangle\langle\mathbf{p}|\psi(t)\rangle d^3p = \tfrac{1}{h^{3/2}}\int_{\mathbb{R}^3} e^{\imath\mathbf{r}\cdot\mathbf{p}/\hbar}\varphi(\mathbf{p},t)d^3p = \psi(\mathbf{r},t) \tag{23.102}$$

$$\langle\mathbf{p}|\psi(t)\rangle = \int_{\mathbb{R}^3} \langle\mathbf{p}|\mathbf{r}\rangle\langle\mathbf{r}|\psi(t)\rangle d^3r = \tfrac{1}{h^{3/2}}\int_{\mathbb{R}^3} e^{-\imath\mathbf{r}\cdot\mathbf{p}/\hbar}\psi(\mathbf{r},t)d^3r = \varphi(\mathbf{p},t) \ .$$

Normalization ensures that $\psi = \mathcal{F}^{-1}\mathcal{F}\psi$ with the relation,

$$\delta(x) = \lim_{t\to\infty}\tfrac{1}{2\pi}\int_{-t}^{t} e^{\imath kx}dk \ . \tag{23.103}$$

Using the wavevector $\hbar\mathbf{k} = \mathbf{p}$ we can also write,

$$\psi(\mathbf{r}) = \tfrac{1}{(2\pi)^{3/2}}\int_{\mathbb{R}^3} e^{\imath\mathbf{r}\cdot\mathbf{k}}\tilde{\varphi}(\mathbf{k})d^3k \quad \text{and} \quad \tilde{\varphi}(\mathbf{k}) = \tfrac{1}{(2\pi)^{3/2}}\int_{\mathbb{R}^3} e^{-\imath\mathbf{r}\cdot\mathbf{k}}\psi(\mathbf{r})d^3r \ , \tag{23.104}$$

defining the function $\tilde{\varphi}(\mathbf{k}) \equiv \hbar^{3/2}\varphi(\mathbf{p})$. Applying the Fourier transform to functions of operator we can calculate,

$$\begin{aligned}\langle\mathbf{r}|G(\hat{\mathbf{p}})|\mathbf{r}'\rangle &= \int d^3p\langle\mathbf{r}|G(\hat{\mathbf{p}})|\mathbf{p}\rangle\langle\mathbf{p}|\mathbf{r}'\rangle = \int d^3pG(\mathbf{p})\langle\mathbf{r}|\mathbf{p}\rangle\langle\mathbf{p}|\mathbf{r}'\rangle \\ &= \tfrac{1}{\hbar^{3/2}}\int d^3pG(\mathbf{p})e^{\imath\mathbf{k}\cdot(\mathbf{r}-\mathbf{r}')} = \tfrac{1}{\hbar^3}(\mathcal{F}G)(\mathbf{r}-\mathbf{r}') \ .\end{aligned} \tag{23.105}$$

[13] Note that the units of the wavefunctions are defined by normalization: $\langle\mathbf{r}'|\mathbf{r}\rangle = \delta^3(\mathbf{r}-\mathbf{r}')$. Introducing the parenthesis [...] to extract the unit of a physical quantity, we find, $[|\mathbf{r}\rangle] = [\psi(\mathbf{r})] = [r^{-3/2}]$ and $[|\mathbf{p}\rangle] = [\varphi(\mathbf{p})] = [p^{-3/2}]$. We do not assign a unit to the abstract state $|\psi\rangle$, that is, $[|\psi\rangle] = 1$.

In Exc. 23.3.10.11 we will show $\langle \mathbf{r}|\hat{\mathbf{p}}|\psi\rangle = (\hbar/\imath)\nabla_{\mathbf{r}}\langle \mathbf{r}|\psi\rangle$, thus justifying that we can understand an operator as a rule to determine what happens to a function. For example, the rule $\hat{p}_x$ asks for a derivation of the wavefunction by x.

23.3.8 Quasi-classical approximation (WKB)

We can express the correspondence between classical and quantum mechanics by the following analogy between (i) the density matrices and observables depending on (ii) discrete variables and (iii) continuous variables,

$$\begin{array}{rclcrcl} \varrho(p,q) & = & \frac{1}{I}\sum_{i=1}^{I}\delta(p-p_i)\delta(q-q_i) & \text{(i)} & \hat{\varrho} & = & \frac{1}{I}\sum_{i=1}^{I}|p_iq_i\rangle\langle q_ip_i| \\ \langle A\rangle(p,q) & = & \frac{1}{I}\sum_{i=1}^{I}A(p_i,q_i) & \text{(ii)} & \langle\hat{A}\rangle & = & \frac{1}{I}\sum_{i=1}^{I}\langle p_iq_i|\hat{A}|q_ip_i\rangle \\ \Rightarrow \langle A\rangle(p,q) & = & \int A(p,q)\varrho(p,q)dpdq & \text{(iii)} & \langle\hat{A}\rangle & = & \sum_{i=1}^{I}\langle p_iq_i|\hat{\varrho}\hat{A}|q_ip_i\rangle \end{array} . \tag{23.106}$$

The objective is to bring this analogy to the point of assigning to the quantum functions $\hat{A}$ unequivocally corresponding classical functions $A(p,q)$ satisfying classical formula. We achieve this by,

$$\boxed{A(p,q) \equiv \langle p|\hat{A}|q\rangle\langle q|p\rangle \qquad \text{that is} \qquad \hat{A} \equiv \int |p\rangle\langle p|A(p,\hat{q})dp = \int A(\hat{p},q)|q\rangle\langle q|dp} \, , \tag{23.107}$$

with the normalization,

$$\langle q|q'\rangle = h^{I/2}\delta(q-q') \qquad \text{and} \qquad \langle p|p'\rangle = h^{I/2}\delta(p-p') \tag{23.108}$$
$$\text{as well as} \qquad \langle p|q\rangle = h^{-I/2}e^{ipq/\hbar} \qquad \text{and} \qquad \int |q\rangle\langle q|dq = \mathbb{I} = \int |p\rangle\langle p|dp \, ,$$

with $p,q \in \mathbb{R}^I$ and $|p\rangle = |p_1\rangle|p_2\rangle..|p_I\rangle$. We obtain for classical distributions for position and momentum,

$$\int \varrho(p,q)dpdq = 1 \tag{23.109}$$
$$\int \varrho(p,q)dp = \langle q|\hat{\varrho}|q\rangle = w(q) = \frac{1}{I}\sum_{i=1}^{I}\langle\delta(\hat{q}-q_i)$$
$$\int \varrho(p,q)dq = \langle p|\hat{\varrho}|p\rangle = w(p) = \frac{1}{I}\sum_{i=1}^{I}\langle\delta(\hat{p}-p_i) \, .$$

Now we expand the commutator $[\hat{A},\hat{B}]$ in powers of $\hbar$:

$$\begin{aligned}(AB)(p,q) &= \langle p|\hat{A}\hat{B}|q\rangle\langle q|p\rangle \\ &= \langle p|\int |p'\rangle\langle p'|A(p',\hat{q})dp'\int B(\hat{p},q')|q'\rangle\langle q'|dq'|q\rangle\langle q|p\rangle = \langle p|A(p,\hat{q})B(\hat{p},q)\langle q|p\rangle \, .\end{aligned} \tag{23.110}$$

We expand,

$$A(p,\hat{q}) = A|_q + \left.\frac{\partial A}{\partial q}\right|_q (\hat{q}-q) + ... + \frac{1}{n!}\frac{\partial^n A}{\partial q^n}(\hat{q}-q)^n + ... \tag{23.111}$$
$$B(\hat{p},q) = B|_p + \left.\frac{\partial B}{\partial p}\right|_p (\hat{p}-p) + ... + \frac{1}{m!}\frac{\partial^m B}{\partial p^m}(\hat{p}-p)^m + ... \ .$$

Now,

$$(AB)(p,q) = AB + A\frac{\partial B}{\partial p}\langle p|\hat{p}-p|q\rangle\langle q|p\rangle + \frac{\partial A}{\partial q}B\langle p|\hat{q}-q|q\rangle\langle q|p\rangle + ... \tag{23.112}$$
$$+ \frac{1}{m!n!}\frac{\partial^n A}{\partial q^n}\frac{\partial^m B}{\partial p^m}\langle p|(\hat{q}-q)^n(\hat{p}-p)^m|q\rangle\langle q|p\rangle + ... \ .$$

But now we have, $[(\hat{p}-p),(\hat{q}-q)] = [\hat{p},\hat{q}] = \hbar/\imath$ with the consequence,

$$[(\hat{p}-p),(\hat{q}-q)^n] = \frac{\hbar}{\imath}\frac{\partial(\hat{q}-q)^n}{\partial(\hat{q}-q)} = \frac{\hbar}{\imath}(\hat{q}-q)^{n-1}n \ . \tag{23.113}$$

Also,

$$[(\hat{q}-q)^n,(\hat{p}-p)^m] = (\hat{p}-p)[(\hat{q}-q)^n,(\hat{p}-p)^{m-1}]+[(\hat{q}-q)^n,(\hat{p}-p)](\hat{p}-p)^{m-1} \ . \tag{23.114}$$

Because of $\langle p|\hat{p}-p = 0$ all terms with $\hat{p}-p$ vanish,

$$(\hat{q}-q)^n(\hat{p}-p)^m = [(\hat{q}-q)^n,(\hat{p}-p)](\hat{p}-p)^{m-1} = \hbar\imath n(\hat{q}-q)^{n-1}(\hat{p}-p)^{m-1} \tag{23.115}$$
$$= \left\{ \begin{pmatrix} (\hbar\imath)^n n!(\hat{p}-p)^{m-n} & \text{for} & m \geq n \\ (\hbar\imath)^n m!(\hat{q}-q)^{n-m} & \text{for} & n \geq m \end{pmatrix} \right. = (\hbar\imath)^n n!\delta_{nm} \ .$$

Finally,

$$(AB)(p,q) = (\hbar\imath)^n n!\frac{\partial^n A}{\partial q^n}\frac{\partial^n B}{\partial p^n} \ . \tag{23.116}$$

23.3.9 Spanning a Hilbert space with several degrees of freedom

All systems analyzed up to this point were characterized by a single degree of freedom (e.g., energy, momentum, or angular momentum), which could have a continuous or discrete spectrum. Even when we treated systems exhibiting various degrees of freedom (motion of a particle in 3D space, electron orbitals in the hydrogen atom), we always found a way to separate the degrees of freedom into orthogonal Hilbert spaces, which allowed us to treat the dynamics of the degrees of freedom separately. In this chapter, we will establish the theoretical foundations allowing us to analyze systems, where degrees of freedom can not be separated because they are entangled or interact. In particular, we will consider the system of two spins and the coupling of angular momenta in general.

23.3.9.1 Projection and internal sum

A *projector* is an operator which *reduces* the domain of an operator, originally acting on a Hilbert space $\mathcal{H}$ to the *subspace* defined by the projector. We consider an operator $\hat{A}$ with the matrix representation,

$$\hat{A} \equiv \sum_{\substack{i,j \\ |i\rangle,|j\rangle\in\mathcal{H}}} |i\rangle A_{ij}\langle j| = \begin{pmatrix} & \vdots & \\ .. & A_{ij} & .. \\ & \vdots & \end{pmatrix} , \tag{23.117}$$

acting on wavefunctions $|\psi\rangle \in \mathcal{H}$ which can be expanded on a basis $|i\rangle$ of $\mathcal{H}$. Now, we consider a subspace $\mathcal{R} \subset \mathcal{H}$ defined by the base $|k\rangle$. Then the projector $\hat{P}_\mathcal{R}$ can be represented by,

$$\boxed{\hat{P}_\mathcal{R} \equiv \sum_{\substack{k \\ |k\rangle\in\mathcal{R}}} |k\rangle\langle k| = \begin{pmatrix} 0 & & 0 & & 0 \\ & 1 & & & \\ 0 & & .. & & 0 \\ & & & 1 & \\ 0 & & 0 & & 0 \end{pmatrix}} . \tag{23.118}$$

Applied to the operator $\hat{A}$,

$$\hat{A}_\mathcal{R} \equiv \hat{P}_\mathcal{R}\hat{A} = \hat{P}_\mathcal{R}\hat{A}_\mathcal{R} = \sum_{k,l} |k\rangle A_{kl}\langle l| = \begin{pmatrix} 0 & & 0 & & 0 \\ & & \vdots & & \\ 0 & .. & A_{kl} & .. & 0 \\ & & \vdots & & \\ 0 & & 0 & & 0 \end{pmatrix} . \tag{23.119}$$

Applied to a state $|i\rangle$,

$$|\psi\rangle_\mathcal{R} = \hat{P}_\mathcal{R}|\psi\rangle = \hat{P}_\mathcal{R}|\psi\rangle_\mathcal{R} = \sum_k c_k|k\rangle = \begin{pmatrix} 0 \\ \begin{pmatrix} \vdots \\ c_k \\ \vdots \end{pmatrix} \\ 0 \end{pmatrix} . \tag{23.120}$$

We study an example in the 23.3.10.12

Consequently, we can understand the Hilbert space as the sum of its subspaces,

$$\hat{A} = \bigoplus_\mathcal{R} \hat{A}_\mathcal{R} \qquad \text{and} \qquad \bigoplus_\mathcal{R} \hat{P}_\mathcal{R} = \mathbb{I} . \tag{23.121}$$

The dimensions of the subspaces are additive,

$$\dim \hat{A} = \sum_\mathcal{R} \dim \hat{A}_\mathcal{R} .$$

Example 144 (*Projection for a three-level atom*): The Hamiltonian of a three-level atom with excitation of two transitions is given by,

$$\hat{H} = \begin{pmatrix} \omega_1 & \Omega_{12} & 0 \\ \Omega_{12} & \omega_2 & \Omega_{23} \\ 0 & \Omega_{23} & \omega_3 \end{pmatrix} .$$

The projector,

$$\hat{P} = \begin{pmatrix} 1 & 0 & 0 \\ 0 & 1 & 0 \\ 0 & 0 & 0 \end{pmatrix}$$

reduces the Hamiltonian to a two-level transition,

$$\hat{H}_{\mathcal{R}} = \begin{pmatrix} \omega_1 & \Omega_{12} & 0 \\ \Omega_{12} & \omega_2 & 0 \\ 0 & 0 & 0 \end{pmatrix} .$$

Obviously, the concatenation (23.121) only serves to increase the Hilbert space of a given degree of freedom described by a given observable, e.g., when we add one more level of energy to the spectrum of an atom described by a Hamiltonian. If, in contrast, we want to add another degree of freedom, we need the external sum or external product discussed below.

23.3.9.2 Tensorial product

We have previously worked with systems exhibiting more than one degree of freedom and therefore having to be characterized by more than one observable with its spectrum of eigenstates. One example are the electronic orbitals of the hydrogen atom $|n\ell m\rangle$, which need three quantum numbers to be labeled unambiguously. Obviously, each quantum number increases the dimensionality of the Hilbert space. Another example is the system $|\alpha\beta\rangle$ of two particles with spin $\frac{1}{2}$, each spin being defined on its respective space,

$$|\alpha\rangle = \begin{pmatrix} \alpha_1 \\ \alpha_2 \end{pmatrix} = (\alpha_i)_i \in \mathcal{H}_A \qquad \text{and} \qquad |\beta\rangle = \begin{pmatrix} \beta_1 \\ \beta_2 \end{pmatrix} = (\beta_k)_k \in \mathcal{H}_B \ . \tag{23.122}$$

The combined state is,

$$|\alpha\beta\rangle \in \mathcal{H}_A \otimes \mathcal{H}_B \qquad \text{with} \qquad \dim \mathcal{H}_A \otimes \mathcal{H}_B = \dim \mathcal{H}_A \dim \mathcal{H}_B \ . \tag{23.123}$$

The symbol $\otimes$ denotes the *outer tensorial product* of two vectors (states) [14]. Now, in order to represent the multidimensional space $\mathcal{H}_A \otimes \mathcal{H}_B$ by a matrix, we use the fact

[14] The tensorial product of two states should not be confused with other definitions of products, such as the inner (or scalar) product of two states,

$$\langle\alpha|\beta\rangle \equiv \alpha_1\beta_1 + \alpha_2\beta_2 \ ,$$

that it is isomorphic to the space $\mathcal{H}_{\mathbb{I}} \otimes \mathcal{H}_{A\otimes B}$, that is, we proceed to a reorganization of the quantum numbers identifying,

$$|\gamma\rangle \equiv |\alpha\rangle|\beta\rangle = |\alpha\rangle \otimes |\beta\rangle = |\alpha\beta\rangle = \begin{pmatrix} \alpha_1|\beta\rangle \\ \alpha_2|\beta\rangle \end{pmatrix} = \begin{pmatrix} \alpha_1\beta_1 \\ \alpha_1\beta_2 \\ \alpha_2\beta_1 \\ \alpha_2\beta_2 \end{pmatrix} = (\gamma_m)_m \in \mathcal{H}_A \otimes \mathcal{H}_B \ , \tag{23.124}$$

where $m = 1, 2, 3, 4$ is identified with $(i, k) = (1, 1), (1, 2), (2, 1), (2, 2)$. The new vector is element of the 4-dimensional vector space $\mathcal{H}_A \otimes \mathcal{H}_B$. If $\{|\alpha\rangle_i\}$ and $\{|\beta\rangle_k\}$ are bases in their respective spaces $\mathcal{H}_A$ and $\mathcal{H}_B$, then $\{|\gamma\rangle_m\}$ is a basis of the product space $\mathcal{H}_A \otimes \mathcal{H}_B$.

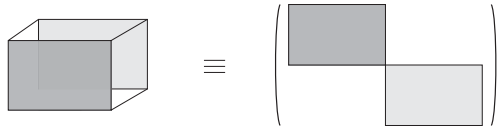

Figure 23.4: Illustration of the isomorphism between $\mathcal{H}_A \otimes \mathcal{H}_B$ and $\mathcal{H}_{\mathbb{I}} \otimes \mathcal{H}_{A\otimes B}$ for matrices of rank 2.

For observables we proceed in the same way: The external product of two commutators spans a Hilbert product space with the dimension corresponding to product of the dimensions of the sub-spaces. Assuming that,

$$\hat{A} \equiv \sum\nolimits_{i,j} |i\rangle A_{ij} \langle j| \quad \text{and} \quad \hat{B} \equiv \sum\nolimits_{k,l} |k\rangle B_{kl} \langle l| \ . \tag{23.125}$$

then

$$\hat{A} \otimes \hat{B} \equiv \sum_{(ik)(jl)} |ik\rangle A_{ij} B_{kl} \langle jl| \ , \tag{23.126}$$

---

the outer product,

$$|\alpha\rangle\langle\beta| \equiv \begin{pmatrix} \alpha_1\beta_1 & \alpha_1\beta_2 \\ \alpha_2\beta_1 & \alpha_2\beta_2 \end{pmatrix}$$

$$\begin{pmatrix} A_{11} \\ A_{12} \\ A_{21} \\ A_{22} \end{pmatrix} \begin{pmatrix} B_{11} \\ B_{12} \\ B_{21} \\ B_{22} \end{pmatrix}^{\dagger} = \begin{pmatrix} A_{11}B_{11} & A_{11}B_{12} & A_{11}B_{21} & A_{11}B_{22} \\ A_{12}B_{11} & A_{12}B_{12} & A_{12}B_{21} & A_{12}B_{22} \\ A_{21}B_{11} & A_{21}B_{12} & A_{21}B_{21} & A_{21}B_{22} \\ A_{22}B_{11} & A_{22}B_{12} & A_{22}B_{21} & A_{22}B_{22} \end{pmatrix} \ ,$$

the exterior (cross) product,

$$|\alpha\rangle \times |\beta\rangle = \begin{pmatrix} \alpha_2\beta_3 - \alpha_3\beta_2 \\ \alpha_3\beta_1 - \alpha_1\beta_3 \\ \alpha_1\beta_2 - \alpha_2\beta_1 \end{pmatrix} \ ,$$

nor the point-wise or *Hadamard product*,

$$\hat{A} \circ \hat{B} \equiv \begin{pmatrix} A_{11} & A_{12} \\ A_{21} & A_{22} \end{pmatrix} \circ \begin{pmatrix} B_{11} & B_{12} \\ B_{21} & B_{22} \end{pmatrix} = \begin{pmatrix} A_{11}B_{11} & A_{12}B_{12} \\ A_{21}B_{21} & A_{22}B_{22} \end{pmatrix} \ .$$

such that

$$\dim \hat{A} \otimes \hat{B} = \dim \hat{A} \dim \hat{B} \ .$$

For example, $|i\rangle\langle j| \otimes |k\rangle\langle l| = |ik\rangle\langle jl|$.

For two two-dimensional operators $\hat{A}$ and $\hat{B}$, the *tensorial external product* is defined by,

$$\hat{A} \otimes \hat{B} = \begin{pmatrix} A_{11}B_{11} & A_{11}B_{12} & A_{12}B_{11} & A_{12}B_{12} \\ A_{11}B_{21} & A_{11}B_{22} & A_{12}B_{21} & A_{12}B_{22} \\ A_{21}B_{11} & A_{21}B_{12} & A_{22}B_{11} & A_{22}B_{12} \\ A_{21}B_{21} & A_{21}B_{22} & A_{22}B_{21} & A_{22}B_{22} \end{pmatrix} \ , \tag{23.127}$$

and can be decomposed as,

$$\boxed{\hat{A} \otimes \hat{B} = (\hat{A} \otimes \mathbb{I})(\mathbb{I} \otimes \hat{B}) = \begin{pmatrix} A_{11} & & A_{12} & \\ & A_{11} & & A_{12} \\ A_{21} & & A_{22} & \\ & A_{21} & & A_{22} \end{pmatrix} \begin{pmatrix} B_{11} & B_{12} & & \\ B_{21} & B_{22} & & \\ & & B_{11} & B_{12} \\ & & B_{21} & B_{22} \end{pmatrix} .} \tag{23.128}$$

The concept (23.126) can be generalized to more degrees of freedom like,

$$\hat{A} \otimes \hat{B} \otimes \hat{C} \equiv \sum_{(ikm)(jln)} |ikm\rangle A_{ij} B_{kl} C_{mn} \langle jln| \ , \tag{23.129}$$

Obviously, the external product is associative $(\hat{A} \otimes \hat{B}) \otimes C = \hat{A} \otimes (\hat{B} \otimes C)$, but does not commute, even though the operators acting on different spaces do commute, $[\hat{A}, \hat{B}] = 0$. Nevertheless, we can reverse the order of the product of two operators using,

$$\hat{A} \otimes \hat{B} = \mathbb{S}(\hat{B} \otimes \hat{A})\mathbb{S} \qquad \text{with} \qquad \mathbb{S} \equiv \begin{pmatrix} 1 & & & \\ & 0 & 1 & \\ & 1 & 0 & \\ & & & 1 \end{pmatrix} \ . \tag{23.130}$$

The operator $\mathbb{S}$ is also called *SWAP-gate*.

We note, that it is important to distinguish from what space the vector came from. In our notation, the vector *before* the symbol of the tensorial product ($\otimes$) is belongs to the space $\mathcal{H}_A$, and the one *after* the $\otimes$ belongs to the space $\mathcal{H}_B$. With the definition (23.125) we can verify that the operators only act on their respective states:

$$(A \otimes B)(|\alpha\rangle \otimes |\beta\rangle) = A|\alpha\rangle \otimes B|\beta\rangle \ . \tag{23.131}$$

Example 145 (*Tensorial product*): We can check the relationship (23.131)

by the definitions (23.124) and (23.127) of the external product,

$$\left[\begin{pmatrix} A_{11} & A_{12} \\ A_{21} & A_{22} \end{pmatrix} \otimes \begin{pmatrix} B_{11} & B_{12} \\ B_{21} & B_{22} \end{pmatrix}\right]\left[\begin{pmatrix} \alpha_1 \\ \alpha_2 \end{pmatrix} \otimes \begin{pmatrix} \beta_1 \\ \beta_2 \end{pmatrix}\right] \tag{23.132}$$

$$= \begin{pmatrix} A_{11}B_{11} & A_{11}B_{12} & A_{12}B_{11} & A_{11}B_{12} \\ A_{11}B_{21} & A_{11}B_{22} & A_{12}B_{21} & A_{11}B_{22} \\ A_{21}B_{11} & A_{11}B_{12} & A_{22}B_{11} & A_{22}B_{12} \\ A_{21}B_{21} & A_{11}B_{22} & A_{22}B_{21} & A_{22}B_{22} \end{pmatrix} \begin{pmatrix} \alpha_{11}\beta_{11} \\ \alpha_{11}\beta_{21} \\ \alpha_{21}\beta_{11} \\ \alpha_{21}\beta_{21} \end{pmatrix}$$

$$= \begin{pmatrix} A_{11}B_{11}\alpha_{11}\beta_{11} + A_{11}B_{12}\alpha_{11}\beta_{21} + A_{12}B_{11}\alpha_{21}\beta_{11} + A_{11}B_{12}\alpha_{21}\beta_{21} \\ A_{11}B_{21}\alpha_{11}\beta_{11} + A_{11}B_{22}\alpha_{11}\beta_{21} + A_{12}B_{21}\alpha_{21}\beta_{11} + A_{11}B_{22}\alpha_{21}\beta_{21} \\ A_{21}B_{11}\alpha_{11}\beta_{11} + A_{11}B_{12}\alpha_{11}\beta_{21} + A_{22}B_{11}\alpha_{21}\beta_{11} + A_{22}B_{12}\alpha_{21}\beta_{21} \\ A_{21}B_{21}\alpha_{11}\beta_{11} + A_{11}B_{22}\alpha_{11}\beta_{21} + A_{22}B_{21}\alpha_{21}\beta_{11} + A_{22}B_{22}\alpha_{21}\beta_{21} \end{pmatrix}$$

$$= \begin{pmatrix} (A_{11}\alpha_1 + A_{12}\alpha_2)(B_{11}\beta_1 + B_{12}\beta_2) \\ (A_{11}\alpha_1 + A_{12}\alpha_2)(B_{21}\beta_1 + B_{22}\beta_2) \\ (A_{21}\alpha_1 + A_{22}\alpha_2)(B_{11}\beta_1 + B_{12}\beta_2) \\ (A_{21}\alpha_1 + A_{22}\alpha_2)(B_{21}\beta_1 + B_{22}\beta_2) \end{pmatrix}$$

$$= \begin{pmatrix} A_{11}\alpha_1 + A_{12}\alpha_2 \\ A_{21}\alpha_1 + A_{22}\alpha_2 \end{pmatrix} \otimes \begin{pmatrix} B_{11}\beta_1 + B_{12}\beta_2 \\ B_{21}\beta_1 + B_{22}\beta_2 \end{pmatrix} = \begin{pmatrix} A_{11} & A_{12} \\ A_{21} & A_{22} \end{pmatrix} \begin{pmatrix} \alpha_1 \\ \alpha_2 \end{pmatrix} \otimes \begin{pmatrix} B_{11} & B_{12} \\ B_{21} & B_{22} \end{pmatrix} \begin{pmatrix} \beta_1 \\ \beta_2 \end{pmatrix} .$$

Example 146 (*Mathematical definition of the tensor product*): If α belongs to the Hilbert space $\mathcal{H}_\alpha$ and β belongs to $\mathcal{H}_\beta$, then the equivalence class of (α, β) is denoted by $\alpha \otimes \beta$ and called the tensor product of α with β. This use of the $\otimes$-symbol refers specifically to the outer product operation. An element of $\mathcal{H}_\alpha \otimes \mathcal{H}_\beta$ that can be written in the form $\alpha \otimes \beta$ is called a pure tensor. In general, an element of the tensor product space is not a pure tensor, but rather a finite linear combination of pure tensors. For example, if α_1 and α_2 are linearly independent, and β_1 and β_2 are also linearly independent, then $\alpha_1 \otimes \beta_1 + \alpha_2 \otimes \beta_2$ cannot be written as a pure tensor. The number of pure tensors required to express an element of a tensor product is called the tensor rank. The rank should not be confused with the tensor order, which is the number of spaces one has taken the product of (in this case two), and which corresponds to the number of indices. For linear operators or matrices, thought of as $(1,1)$ tensors (elements of the space $\mathcal{H}_\alpha \otimes \mathcal{H}_\alpha^*$), the tensor rank agrees with matrix rank.
Given bases $\{\alpha_i\}$ and $\{\beta_j\}$ for $\mathcal{H}_\alpha$ and $\mathcal{H}_\beta$ respectively, the tensors $\{\alpha_i \otimes \beta_j\}$ form a basis for $\mathcal{H}_\alpha \otimes \mathcal{H}_\beta$. Therefore, if $\mathcal{H}_\alpha$ and $\mathcal{H}_\beta$ are finite-dimensional, the dimension of the tensor product is the product of dimensions of the original spaces; for instance $\mathbb{R}^m \otimes \mathbb{R}^n$ is isomorphic to $\mathbb{R}^{nm}$.
The tensor product also operates on linear maps (called operators in quantum mechanics) between vector spaces. Specifically, given two linear maps $\hat{A} : \mathcal{H}_\alpha \to \mathcal{H}'_\alpha$ and $\hat{B} : \mathcal{H}_\beta \to \mathcal{H}'_\beta$ between vector spaces, the tensor product of the two linear maps $\hat{A}$ and $\hat{B}$ is a linear map,

$$\hat{A} \otimes \hat{B} : \mathcal{H}_\alpha \otimes \mathcal{H}_\beta \to \mathcal{H}'_\alpha \otimes \mathcal{H}'_\beta ,$$

defined by,

$$(\hat{A} \otimes \hat{B})(\alpha \otimes \beta) = \hat{A}(\alpha) \otimes \hat{B}(\beta) .$$

In this way, the tensor product becomes a bifunctor from the category of vector spaces to itself, covariant in both arguments. If $\hat{A}$ and $\hat{B}$ are both injective, surjective or (in the case that $\mathcal{H}_\alpha$, $\mathcal{H}'_\alpha$, $\mathcal{H}_\beta$, and $\mathcal{H}'_\beta$ are normed vector spaces or topological vector spaces) continuous, then $\hat{A} \otimes \hat{B}$ is injective, surjective or continuous, respectively.
By choosing bases of all vector spaces involved, the linear maps $\hat{A}$ and $\hat{B}$ can be represented by matrices. Then, depending on how the tensor $\alpha \otimes \beta$ is vectorized, the matrix describing the tensor product $\hat{A} \otimes \hat{B}$ is the Kronecker product of the two matrices. For example, if $\mathcal{H}_\alpha$, $\mathcal{H}'_\alpha$, $\mathcal{H}_\beta$, and $\mathcal{H}'_\beta$ above are all two-dimensional and bases have been fixed for all of them, and $\hat{A}$ and $\hat{B}$ are given by the matrices,

$$\hat{A} = \begin{pmatrix} A_{11} & A_{12} \\ A_{21} & A_{22} \end{pmatrix} \quad , \quad \hat{B} = \begin{pmatrix} B_{11} & B_{12} \\ B_{21} & B_{22} \end{pmatrix}$$

respectively, then the tensor product of these two matrices is,

$$\begin{pmatrix} A_{11} & A_{12} \\ A_{21} & A_{22} \end{pmatrix} \otimes \begin{pmatrix} B_{11} & B_{12} \\ B_{21} & B_{22} \end{pmatrix} = \begin{pmatrix} A_{11} \begin{pmatrix} B_{11} & B_{12} \\ B_{21} & B_{22} \end{pmatrix} & A_{12} \begin{pmatrix} B_{11} & B_{12} \\ B_{21} & B_{22} \end{pmatrix} \\ A_{21} \begin{pmatrix} B_{11} & B_{12} \\ B_{21} & B_{22} \end{pmatrix} & A_{22} \begin{pmatrix} B_{11} & B_{12} \\ B_{21} & B_{22} \end{pmatrix} \end{pmatrix} .$$

The resultant rank is at most 4, and thus the resultant dimension is 4. Note that rank here denotes the tensor rank i.e. the number of requisite indices (while the matrix rank counts the number of degrees of freedom in the resulting array). Note $\mathrm{Tr}\ \hat{A} \otimes \hat{B} = \mathrm{Tr}\ \hat{A} \times \mathrm{Tr}\ \hat{B}$.
A dyadic product is the special case of the tensor product between two vectors of the same dimension.

23.3.9.3 Direct external sum

Using the nomenclature (23.125) we define the external direct sum by,

$$\hat{A} \oplus \hat{B} \equiv \sum_{(ik)(jl)} |ik\rangle (A_{ij} + B_{kl}) \langle jl| \ , \tag{23.133}$$

that is,

$$\hat{A} \oplus \hat{B} = \begin{pmatrix} A_{11} + B_{11} & A_{11} + B_{12} & A_{12} + B_{11} & A_{12} + B_{12} \\ A_{11} + B_{21} & A_{11} + B_{22} & A_{12} + B_{21} & A_{12} + B_{22} \\ A_{21} + B_{11} & A_{21} + B_{12} & A_{22} + B_{11} & A_{22} + B_{12} \\ A_{21} + B_{21} & A_{21} + B_{22} & A_{22} + B_{21} & A_{22} + B_{22} \end{pmatrix} . \tag{23.134}$$

It can be decomposed as,

$$\boxed{\hat{A} \oplus \hat{B} = \hat{A} \oplus \mathbb{O} + \mathbb{O} \oplus \hat{B} = \hat{A} \otimes \begin{pmatrix} 1 & 1 \\ 1 & 1 \end{pmatrix} + \begin{pmatrix} 1 & 1 \\ 1 & 1 \end{pmatrix} \otimes \hat{A} \ .} \tag{23.135}$$

Again, using the definition (23.130) of the unitary operator $\mathbb{S}$, we can reverse the order of the operator by,

$$\hat{A} \oplus \hat{B} = \mathbb{S}(\hat{B} \oplus \hat{A})\mathbb{S} \ . \tag{23.136}$$

Example 147 (*Direct external sum of two diagonal Hamiltonians*): As an example we consider a two-level atom excited by radiation and trapped in an external harmonic potential. We assume that the degrees of freedom do not interact. As the Hamiltonian of the HO is diagonal, the total Hamiltonian is organized into a diagonal matrix of quadratic subspaces,

$$\hat{H} = \hbar\omega(n+\tfrac{1}{2}) \oplus \begin{pmatrix} 0 & \hbar\Omega \\ \hbar\Omega & \hbar\Delta \end{pmatrix} = \begin{pmatrix} \frac{\hbar\omega}{2} & \frac{\hbar\omega}{2}+\hbar\Omega & 0 & 0 & \vdots \\ \frac{\hbar\omega}{2}+\hbar\Omega & \frac{\hbar\omega}{2}+\hbar\Delta & 0 & 0 & \vdots \\ 0 & 0 & \frac{3\hbar\omega}{2} & \frac{3\hbar\omega}{2}+\hbar\Omega & \vdots \\ 0 & 0 & \frac{3\hbar\omega}{2}+\hbar\Omega & \frac{3\hbar\omega}{2}+\hbar\Delta & \vdots \\ \cdots & \cdots & \cdots & \cdots & \ddots \end{pmatrix} .$$

It acts on the product state $|n\rangle|i\rangle$, where the first ket denotes the vibrational level and the second ket the electronic excitation of the atom.

Other examples are studied in 23.3.10.13 and 23.3.10.14.

23.3.9.4 Trace

The *trace* of an operator over a subspace reduces its domain to the remaining dimensions (the $\cdot$ -symbol is a place holder for the dimension over which we do NOT want to trace):

$$\mathrm{Tr}_B \hat{A}\otimes\hat{B} = \sum_{(ik)(jl)(\cdot m)} \langle \cdot\, m|ik\rangle A_{ij}B_{kl}\langle jl|\cdot m\rangle = \sum_{(ik)(jl)(\cdot m)} |i\rangle A_{ij}B_{kl}\langle j|\delta_{km}\delta_{lm}$$

$$= \sum_{(i)(j)(m)} |i\rangle A_{ij}B_{mm}\langle j| = \hat{A}\sum_m B_{mm} = \hat{A}\,\mathrm{Tr}_B\hat{B} \,. \tag{23.137}$$

For example, $\mathrm{Tr}_\rho \hat{A}\otimes\hat{\rho} = \hat{A}$. See the Excs. 23.3.10.15 and 23.3.10.16.

It can be shown,

$$\mathrm{Tr}\ \hat{A}\hat{B} = \mathrm{Tr}\ \hat{B}\hat{A} \,. \tag{23.138}$$

23.3.10 Exercises

23.3.10.1 Ex: Orthogonality

Show that two eigenvectors of a Hermitian operator associated with two different eigenvalues are orthogonal.

Solution:

$$\begin{aligned} &\hat{A}|1\rangle = a_1|1\rangle \quad , \quad \hat{A}|2\rangle = a_2|2\rangle \\ \Longrightarrow \quad &\langle 2|a_2|1\rangle = \langle 2|\hat{A}^\dagger|1\rangle = \langle 2|\hat{A}|1\rangle = \langle 2|a_1|1\rangle \\ \Longrightarrow \quad &\langle 2|1\rangle = \delta_{a_1,a_2} \,. \end{aligned}$$

23.3.10.2 Ex: Orthonormalization

Orthonormalize the base $\langle a_1| = \begin{pmatrix} 1 & -1 & 0 \end{pmatrix}$, $\langle a_2| = \begin{pmatrix} 0 & 1 & 0 \end{pmatrix}$, $\langle a_3| = \begin{pmatrix} 0 & 1 & 1 \end{pmatrix}$.

Solution: *The new base is,*

$$|b_1\rangle = \frac{|a_1\rangle}{||a_1\rangle|} = \tfrac{1}{\sqrt{2}}|a_1\rangle = \tfrac{1}{\sqrt{2}} \begin{pmatrix} 1 \\ -1 \\ 0 \end{pmatrix}$$

$$|b_2\rangle = \frac{(1 - |b_1\rangle\langle b_1|)|a_2\rangle}{|(1 - |b_1\rangle\langle b_1|)|a_2\rangle|} = \frac{1}{|.|} \left[1 - \tfrac{1}{2} \begin{pmatrix} 1 \\ -1 \\ 0 \end{pmatrix} \begin{pmatrix} 1 \\ -1 \\ 0 \end{pmatrix}^\dagger \right] \begin{pmatrix} 0 \\ 1 \\ 0 \end{pmatrix} = \tfrac{1}{\sqrt{2}} \begin{pmatrix} 1 \\ 1 \\ 0 \end{pmatrix}$$

$$|b_3\rangle = \frac{(1 - |b_1\rangle\langle b_1| - |b_2\rangle\langle b_2|)|a_3\rangle}{|(1 - |b_1\rangle\langle b_1| - |b_2\rangle\langle b_2|)|a_3\rangle|} = \frac{1}{|.|} \left[1 - \tfrac{1}{2} \begin{pmatrix} 1 \\ -1 \\ 0 \end{pmatrix} \begin{pmatrix} 1 \\ -1 \\ 0 \end{pmatrix}^\dagger - \begin{pmatrix} 1 \\ 0 \\ 0 \end{pmatrix} \begin{pmatrix} 1 \\ 0 \\ 0 \end{pmatrix}^\dagger \right] \begin{pmatrix} 0 \\ 1 \\ 1 \end{pmatrix} = \begin{pmatrix} 0 \\ 0 \\ 1 \end{pmatrix} .$$

23.3.10.3 Ex: Orthonormal base

Construct an orthonormal basis for the following operator describing a partially degenerate three-level system,

$$\hat{A} = \begin{pmatrix} 1 & 1 & 1 \\ 1 & 1 & 1 \\ 1 & 1 & 1 \end{pmatrix} .$$

Solution: *Obviously* $\langle a_1| = \begin{pmatrix} 1 & 1 & 1 \end{pmatrix}$ *is an eigenvector for the eigenvalue* $a = 3$ *without degeneracy. The other eigenvalue,* $a = 0$*, is twice degenerate, since it has the linearly independent eigenvectors* $\langle a_2| = \begin{pmatrix} 1 & -1 & 0 \end{pmatrix}$ *and* $\langle a_3| = \begin{pmatrix} 1 & 0 & -1 \end{pmatrix}$. *However,* $\langle a_2|$ *and* $\langle a_3|$ *are not orthonormal. But*

$$|b_1\rangle = \frac{|a_1\rangle}{\|\cdots\|} = \tfrac{1}{\sqrt{3}} \begin{pmatrix} 1 \\ 1 \\ 1 \end{pmatrix} \qquad \textit{and} \qquad |b_2\rangle = \frac{|a_2\rangle - |b_1\rangle\langle b_1|a_2\rangle}{\|\cdots\|} = \frac{|a_2\rangle}{\|\cdots\|} = \tfrac{1}{\sqrt{2}} \begin{pmatrix} 1 \\ -1 \\ 0 \end{pmatrix}$$

$$\textit{and} \qquad |b_3\rangle = \frac{|a_3\rangle - |b_1\rangle\langle b_1|a_3\rangle - |b_2\rangle\langle b_2|a_3\rangle}{\|\cdots\|} = \frac{|a_3\rangle - |b_2\rangle\frac{1}{\sqrt{2}}}{\|\cdots\|} = \tfrac{1}{\sqrt{6}} \begin{pmatrix} 1 \\ 1 \\ -2 \end{pmatrix} \qquad \textit{are.}$$

23.3.10.4 Ex: Eigenvalue equation

Calculate the unitary matrix U transforming the Hamiltonian $\hat{H} = \begin{pmatrix} 1 & -\imath \\ \imath & 1 \end{pmatrix}$ into a diagonal matrix $E = U^\dagger \hat{H} U$.

Solution: *The eigenvalue matrix is,*

$$E = \begin{pmatrix} 0 & 0 \\ 0 & 2 \end{pmatrix} .$$

The eigenvalue 0 *corresponds to the eigenvector* $\frac{1}{\sqrt{2}} \begin{pmatrix} \imath \\ 1 \end{pmatrix}$ *and the eigenvalue* 2 *to the eigenvector* $\frac{1}{\sqrt{2}} \begin{pmatrix} -\imath \\ 1 \end{pmatrix}$. *Hence,*

$$U = \frac{1}{\sqrt{2}} \begin{pmatrix} \imath & -\imath \\ 1 & 1 \end{pmatrix} .$$

This makes it easy to check $E = U^\dagger \hat{H} U$. *Note that the transformation matrix is not uniquely defined, since every matrix* $e^{\imath\phi} U$ *does the same job.*

23.3.10.5 Ex: Spin rotation operators

Prove the following relations for the spin rotation operator: $e^{-\imath\pi\hat{\sigma}_x/4} \hat{\sigma}_z e^{\imath\pi\hat{\sigma}_x/4} = -\hat{\sigma}_y$ and $e^{-\imath\pi\hat{\sigma}_x/4} \hat{\sigma}_y e^{\imath\pi\hat{\sigma}_x/4} = \hat{\sigma}_z$.

Solution: *The Hermitian operator* σ_x *can be diagonalized via,*

$$\hat{\sigma}_x = \begin{pmatrix} 0 & 1 \\ 1 & 0 \end{pmatrix} = \begin{pmatrix} -1 & 1 \\ 1 & 1 \end{pmatrix} \begin{pmatrix} -1 & 0 \\ 0 & 1 \end{pmatrix} \begin{pmatrix} -1 & 1 \\ 1 & 1 \end{pmatrix}^{-1} = U(-\hat{\sigma}_z)U^{-1} .$$

Hence, the unitary transformation $e^{-\imath\pi\sigma_x/4}$ *reads,*

$$e^{-\imath\pi\hat{\sigma}_x/4} = U e^{\imath\pi\hat{\sigma}_z/4} U^{-1} = \begin{pmatrix} -1 & 1 \\ 1 & 1 \end{pmatrix} \begin{pmatrix} e^{\imath\pi/4} & 0 \\ 0 & e^{-\imath\pi/4} \end{pmatrix} \begin{pmatrix} -1 & 1 \\ 1 & 1 \end{pmatrix}^{-1} = \begin{pmatrix} \frac{1}{\sqrt{2}} & -\frac{\imath}{\sqrt{2}} \\ -\frac{\imath}{\sqrt{2}} & \frac{1}{\sqrt{2}} \end{pmatrix} .$$

And so,

$$e^{-\imath\pi\hat{\sigma}_x/4} \hat{\sigma}_z e^{\imath\pi\hat{\sigma}_x/4} = \begin{pmatrix} \frac{1}{\sqrt{2}} & -\frac{\imath}{\sqrt{2}} \\ -\frac{\imath}{\sqrt{2}} & \frac{1}{\sqrt{2}} \end{pmatrix} \begin{pmatrix} 1 & 0 \\ 0 & -1 \end{pmatrix} \begin{pmatrix} \frac{1}{\sqrt{2}} & -\frac{\imath}{\sqrt{2}} \\ -\frac{\imath}{\sqrt{2}} & \frac{1}{\sqrt{2}} \end{pmatrix}^{-1} = \begin{pmatrix} 0 & \imath \\ -\imath & 0 \end{pmatrix} = \hat{\sigma}_y ,$$

and similar for the second expression.

23.3.10.6 Ex: Eigenvalues and eigenvectors

Find the eigenvalues and -vectors of the operator $\hat{A} = \begin{pmatrix} 1 & 1 & 1 \\ 1 & 1 & 1 \\ 1 & 1 & 1 \end{pmatrix}$ and construct the unitary matrix which transforms this operator into a diagonal matrix.

Solution: *The eigenvalues follow from,*

$$0 = \det(\hat{A} - E) = 3E^2 - E^3 \Longrightarrow E_1 = 0, E_2 = 3, E_3 = 0 \ .$$

The eigenvectors from,

$$\hat{A}\begin{pmatrix} a \\ b \\ c \end{pmatrix} = \begin{pmatrix} a+b+c \\ a+b+c \\ a+b+c \end{pmatrix} = 3\begin{pmatrix} a \\ b \\ c \end{pmatrix} \Longrightarrow \begin{array}{c} a = b = c \\ a^2+b^2+c^2 = 1 \end{array} \Longrightarrow u_2 = \begin{pmatrix} \frac{1}{\sqrt{3}} \\ \frac{1}{\sqrt{3}} \\ \frac{1}{\sqrt{3}} \end{pmatrix}$$

$$\hat{A}\begin{pmatrix} a \\ b \\ c \end{pmatrix} = \begin{pmatrix} a+b+c \\ a+b+c \\ a+b+c \end{pmatrix} = 0\begin{pmatrix} a \\ b \\ c \end{pmatrix} \Longrightarrow \begin{array}{c} b = -a-c \\ a^2+b^2+c^2 = 1 \end{array} \Longrightarrow c = -\frac{1}{2}\left(a \pm \sqrt{2-3a^2}\right)$$

$$\Longrightarrow u_1 = \begin{pmatrix} a \\ \frac{1}{2}\left(-a+\sqrt{2-3a^2}\right) \\ \frac{1}{2}\left(-a-\sqrt{2-3a^2}\right) \end{pmatrix} \ , u_3 = \begin{pmatrix} a \\ \frac{1}{2}\left(-a-\sqrt{2-3a^2}\right) \\ \frac{1}{2}\left(-a+\sqrt{2-3a^2}\right) \end{pmatrix} \ .$$

We define the unitary transformation matrix and the diagonal matrix of eigenvalues,

$$U \equiv \begin{pmatrix} |u_1\rangle & |u_2\rangle & |u_3\rangle \end{pmatrix} = \begin{pmatrix} a & \frac{1}{\sqrt{3}} & a \\ \frac{1}{2}\left(-a+\sqrt{2-3a^2}\right) & \frac{1}{\sqrt{3}} & \frac{1}{2}\left(-a-\sqrt{2-3a^2}\right) \\ \frac{1}{2}\left(-a-\sqrt{2-3a^2}\right) & \frac{1}{\sqrt{3}} & \frac{1}{2}\left(-a+\sqrt{2-3a^2}\right) \end{pmatrix}$$

$$E \equiv \begin{pmatrix} E_1 & 0 & 0 \\ 0 & E_2 & 0 \\ 0 & 0 & E_3 \end{pmatrix} = \begin{pmatrix} 0 & 0 & 0 \\ 0 & 3 & 0 \\ 0 & 0 & 0 \end{pmatrix} \ .$$

For the transformation matrix to be unitary, we need

$$1 = \det U = a\sqrt{3}\sqrt{2-3a^2} \ ,$$

with the solution $a = \frac{1}{\sqrt{3}}$*, that is,*

$$U = \begin{pmatrix} \frac{1}{\sqrt{3}} & \frac{1}{\sqrt{3}} & \frac{1}{\sqrt{3}} \\ \frac{1}{2} - \frac{1}{2\sqrt{3}} & \frac{1}{\sqrt{3}} & -\frac{1}{2} - \frac{1}{2\sqrt{3}} \\ -\frac{1}{2} - \frac{1}{2\sqrt{3}} & \frac{1}{\sqrt{3}} & \frac{1}{2} - \frac{1}{2\sqrt{3}} \end{pmatrix} \ .$$

It is easy to show,

$$U^\dagger U = UU^\dagger = \hat{1} \qquad \textit{and} \qquad \hat{A}U = UE \ .$$

23.3.10.7 Ex: Commuting operators

a. Show that if two operators $\hat{A}$ and $\hat{B}$ commute and if $|\psi\rangle$ is an eigenvector of $\hat{A}$, $\hat{B}|\psi\rangle$ also is an eigenvector of $\hat{A}$ with the same eigenvalue.
b. Show that if two operators $\hat{A}$ and $\hat{B}$ commute and if $|\psi_1\rangle$ and $|\psi_2\rangle$ are two eigenvector of $\hat{A}$ with different eigenvalues, the matrix element $\langle\psi_1|\hat{B}|\psi_2\rangle$ is equal to zero.
c. Show that if two operators $\hat{A}$ and $\hat{B}$ commute, we can construct an orthonormal basis of eigenvectors common to $\hat{A}$ and $\hat{B}$.

Solution: *a. The operators $\hat{A}$ and $\hat{B}$ commute:*

$$\begin{aligned} [\hat{A},\hat{B}] = 0 \quad &, \quad \hat{A}|\psi\rangle = a|\psi\rangle \\ \Longrightarrow \quad & \hat{A}\hat{B}|\psi\rangle = \hat{B}\hat{A}|\psi\rangle = \hat{B}a|\psi\rangle = a\hat{B}|\psi\rangle \ . \end{aligned}$$

b. If furthermore $|\psi_1\rangle$ and $|\psi_2\rangle$ are eigenvectors of $\hat{A}$,

$$\begin{aligned} [\hat{A},\hat{B}] = 0 \quad &, \quad \hat{A}|\psi_1\rangle = a_1|\psi_1\rangle \quad , \quad \hat{A}|\psi_2\rangle = a_2|\psi_2\rangle \\ \Longrightarrow \quad & \langle\psi_1|a_1\hat{B}|\psi_2\rangle = \langle\psi_1|\hat{A}\hat{B}|\psi_2\rangle = \langle\psi_1|\hat{B}\hat{A}|\psi_2\rangle = \langle\psi_1|\hat{B}a_2|\psi_2\rangle \\ \Longrightarrow \quad & \langle\psi_1|\hat{B}|\psi_2\rangle = \langle\psi_1|\hat{B}|\psi_2\rangle\delta_{a_1,a_2} \ . \end{aligned}$$

The result can be generalized to,

$$\langle\psi_m|\hat{B}|\psi_n\rangle = \delta_{m,n}\langle\psi_m|\hat{B}|\psi_m\rangle \ .$$

c. Using the last result we can make the following calculation,

$$\hat{B} = \sum_{m,n} |m\rangle\langle m|\hat{B}|n\rangle\langle n| = \sum_m |m\rangle\langle m|\hat{B}|m\rangle\langle m| \ ,$$

and,

$$\hat{B}|n\rangle = \sum_m |m\rangle\langle m|\hat{B}|m\rangle\langle m|n\rangle = \langle n|\hat{B}|n\rangle|n\rangle = b_n|n\rangle \ .$$

This shows that $|n\rangle$ is an eigenvector of $\hat{B}$, too.
c Alternative. The opposite is easy to show, since $\hat{A}|\psi_n\rangle = \psi_n|u_n\rangle$ and $\hat{B}|\psi_n\rangle = b_n|\psi_n\rangle$ we see that $[\hat{A},\hat{B}]|\psi_n\rangle = 0$.
To prove that observable commutators $[\hat{A},\hat{B}] = 0$ have a complete set of common eigenfunctions, we first consider the case where the eigenvalues of $\hat{A}$ are all non-degenerate. We let $\{|\psi_n\rangle\}$ be a complete base of eigenvectors of $\hat{A}$ with the eigenvalues a_n,

$$\hat{A}|\phi_n\rangle = a_n|a_n\rangle \qquad with \qquad a_n \neq a_m \ .$$

We can now write,

$$\hat{A}(\hat{B}|\psi_n>) = \hat{B}\hat{A}|\psi_n\rangle = a_n(\hat{B}|\psi_n\rangle) \ ,$$

such that we can say that $\hat{B}|\psi_n\rangle$ is an eigenvector of $\hat{A}$ with the corresponding eigenvalue a_n. As both, $\hat{B}|\psi_n\rangle$ and $psi_n\rangle$ are eigenvectors associated with the same eigenvalue a_n, which is unique, they may only be differ by a multiplicative constant, which we will call b_n. That is,

$$\hat{B}|\phi_n\rangle = b_n|\psi_n\rangle \ .$$

Now we treat the case, where $\hat{A}$ has degenerate eigenvalues, for example, the eigenvalue a_n being g times degenerate. We let $|\psi_{nr}>$ with $r = 1, 2, .., g$ be linearly independent eigenvectors of the eigenvalue. Since $[\hat{A}, \hat{B}] = 0$, we reason as we did above to find that $\hat{B}|\psi_{nr}\rangle$ is an eigenvector of $\hat{A}$ corresponding to the degenerate eigenvalue a. Therefore, we can expand $\hat{B}|\psi_{nr}\rangle$ on the basis of degenerate eigenvectors of a_n:

$$\hat{B}|\psi_{nr}\rangle = \sum_{s=1}^{g} c_{rs}|\psi_{ns}\rangle \ ,$$

with the expansion coefficients of c_{rs}. Now we apply the sum $\sum_r d_r$ with constants d_r to this equation,

$$\hat{B}\sum_{r=1}^{g} d_r|\psi_{nr}\rangle = \sum_{r=1}^{g}\sum_{s=1}^{g} d_r c_{rs}|\psi_{ns}\rangle \ .$$

Hence, $\sum_r d_r|\psi_{nr}\rangle$ will be an eigenvalue of $\hat{B}$ with the eigenvalue b_n, under the condition that,

$$\sum_{r=1}^{g} d_r c_{rs} = b_n d_s \qquad with \qquad s = 1, 2, .., g \ .$$

This constitutes a system of g linear equations for d_r constants. A non-trivial solution requires,

$$\det[c_{rs} - b_n\delta_{rs}] = 0 \ .$$

This is an equation of order g in b_n with g roots. For each root, $b_n = b_n^{(k)}$ with $k = 1, 2, .., g$, we get a value d_r, for example, $d_r^{(k)}$. Now, the ket,

$$|\phi_n^{(k)}\rangle = \sum_{r=1}^{g} d_r^{(k)}|\psi_{nr}\rangle$$

is simultaneously an eigenvector of $\hat{A}$ and of $\hat{B}$ with their respective eigenvalues a_n and $b_n^{(k)}$.

23.3.10.8 Ex: Eigenvalues

a. Find the eigenvalues and eigenvectors of the operator $\hat{A} = \begin{pmatrix} 1 & 0 & 1 \\ 0 & \mu & 0 \\ 1 & 0 & 1 \end{pmatrix}$ for $0 < \mu < 2$.
b. Write down the unitary matrix U satisfying the eigenvalue equation: $\hat{A}U = UE_A$, where E_A is the matrix that has all eigenvalues of $\hat{A}$ in its diagonal.
c. Now consider the case $\mu = 0$. Find a complete set of commuting operators (CSCO). That is, calculate the components of a second operator $\hat{B}$, which commutes with $\hat{A}$, as a function of its eigenvalues λ_1, λ_2, and λ_3, and verify $[\hat{A}, \hat{B}] = 0$. Find the most general form of operator $\hat{B}$.

Solution: *a. The eigenvalues are,*

$$\det\begin{pmatrix}1-\lambda & 0 & 1\\ 0 & \mu-\lambda & 0\\ 1 & 0 & 1-\lambda\end{pmatrix} = -2\lambda\mu + 2\lambda^2 + \lambda^2\mu - \lambda^3 = 0 \Longrightarrow \lambda = 0, \mu, 2\ .$$

The eigenvectors are,

$$\begin{pmatrix}1 & 0 & 1\\ 0 & \mu & 0\\ 1 & 0 & 1\end{pmatrix}\begin{pmatrix}a\\ b\\ c\end{pmatrix} = 0\begin{pmatrix}a\\ b\\ c\end{pmatrix} \Longrightarrow \begin{array}{c} a+c=0\\ \mu b = 0\\ a+c=0\end{array} \Longrightarrow \begin{array}{c} c=-a\\ b=0\end{array} \Longrightarrow u_1 = \begin{pmatrix}1/\sqrt{2}\\ 0\\ -1/\sqrt{2}\end{pmatrix}\ ,$$

$$\begin{pmatrix}1 & 0 & 1\\ 0 & \mu & 0\\ 1 & 0 & 1\end{pmatrix}\begin{pmatrix}a\\ b\\ c\end{pmatrix} = \mu\begin{pmatrix}a\\ b\\ c\end{pmatrix} \Longrightarrow \begin{array}{c} a+c=\mu a\\ \mu b = \mu b\\ a+c=\mu c\end{array} \Longrightarrow a=b \Longrightarrow u_2 = \begin{pmatrix}0\\ 1\\ 0\end{pmatrix}\ ,$$

$$\begin{pmatrix}1 & 0 & 1\\ 0 & \mu & 0\\ 1 & 0 & 1\end{pmatrix}\begin{pmatrix}a\\ b\\ c\end{pmatrix} = 2\begin{pmatrix}a\\ b\\ c\end{pmatrix} \Longrightarrow \begin{array}{c} a+c=2a\\ \mu b = 2b\\ a+c=2c\end{array} \Longrightarrow \begin{array}{c} c=a\\ b=0\end{array} \Longrightarrow u_3 = \begin{pmatrix}1/\sqrt{2}\\ 0\\ 1/\sqrt{2}\end{pmatrix}\ .$$

They form an orthonormal basis.
b. The eigenvalue matrix and the unitary matrix are,

$$E_A = \begin{pmatrix}0 & 0 & 0\\ 0 & \mu & 0\\ 0 & 0 & 2\end{pmatrix} \qquad \textit{and} \qquad U = \begin{pmatrix}1/\sqrt{2} & 0 & 1/\sqrt{2}\\ 0 & 1 & 0\\ -1/\sqrt{2} & 0 & 1/\sqrt{2}\end{pmatrix}\ .$$

It is easy to check $\hat{A}U = UE_A$.
c. As long as, $\mu \neq 0, 2$ *the observable* $\hat{A}$ *is sufficient to characterize the system, but if for example* $\mu = 0$*, we need another observable* $\hat{B}$ *which commutes with* $\hat{A}$ *and satisfies the condition,* $\hat{B}U = U\hat{E}_B$*,*

$$\begin{pmatrix}b_{11} & b_{12} & b_{13}\\ b_{21} & b_{22} & b_{23}\\ b_{31} & b_{32} & b_{33}\end{pmatrix}U = \begin{pmatrix}b_{11}/\sqrt{2} - b_{13}/\sqrt{2} & b_{12} & b_{11}/\sqrt{2} + b_{13}/\sqrt{2}\\ b_{21}/\sqrt{2} - b_{23}/\sqrt{2} & b_{22} & b_{21}/\sqrt{2} + b_{23}/\sqrt{2}\\ b_{31}/\sqrt{2} - b_{33}/\sqrt{2} & b_{32} & b_{31}/\sqrt{2} + b_{33}/\sqrt{2}\end{pmatrix}$$

$$= \begin{pmatrix}\lambda_1/\sqrt{2} & 0 & \lambda_3/\sqrt{2}\\ 0 & \lambda_2 & 0\\ -\lambda_1/\sqrt{2} & 0 & \lambda_3/\sqrt{2}\end{pmatrix} = U\begin{pmatrix}\lambda_1 & 0 & 0\\ 0 & \lambda_2 & 0\\ 0 & 0 & \lambda_3\end{pmatrix}\ ,$$

where b_{ij} *are the components and* λ_i *the eigenvalues of* $\hat{B}$*. The result is,*

$$\hat{B} = \begin{pmatrix}\frac{1}{2}(\lambda_1+\lambda_3) & 0 & \frac{1}{2}(\lambda_3-\lambda_1)\\ 0 & \lambda_2 & 0\\ \frac{1}{2}(\lambda_3-\lambda_1) & 0 & \frac{1}{2}(\lambda_1+\lambda_3)\end{pmatrix}\ .$$

It's easy to check $[\hat{A},\hat{B}]=0$. *Of course, in order to lift the degeneracy of* $\hat{A}$ *regarding the eigenvectors* u_1 *and* u_2, *the eigenvalues of* $\hat{B}$ *belonging to the same eigenvectors must be different, that is,* $\lambda_1 \neq \lambda_2$. *Note that the trivial case* $\lambda_2=\lambda_3$ *represents a possible observable.*

23.3.10.9 Ex: Schwartz inequality

Demonstrate the Schwartz inequality $|\langle u|v\rangle|^2 \leq \langle u|u\rangle\langle v|v\rangle$.

Solution: *Defining the wavefunction* $|\phi\rangle \equiv |v\rangle\langle u|u\rangle - |u\rangle\langle u|v\rangle$,

$$\begin{aligned}
0 \leq \langle\phi|\phi\rangle &= (-\langle v|u\rangle\langle u| + \langle u|u\rangle\langle v|)(|v\rangle\langle u|u\rangle - |u\rangle\langle u|v\rangle) \\
&= -\langle v|u\rangle\langle u|v\rangle\langle u|u\rangle + \langle v|u\rangle\langle u|u\rangle\langle u|v\rangle + \langle u|u\rangle\langle v|v\rangle\langle u|u\rangle - \langle u|u\rangle\langle v|u\rangle\langle u|v\rangle \\
&= \langle u|u\rangle\langle v|v\rangle\langle u|u\rangle - \langle u|u\rangle\langle v|u\rangle\langle u|v\rangle = \langle u|u\rangle(\langle u|u\rangle\langle v|v\rangle - |\langle u|v\rangle|^2) \ .
\end{aligned}$$

23.3.10.10 Ex: Heisenberg's uncertainty principle

Develop the formal derivation of Heisenberg's uncertainty principle.

Solution: *First we show,*

$$\Delta A^2 = \langle A^2\rangle - \langle A\rangle^2 = \langle A^2 - 2\langle A\rangle A + \langle A\rangle^2\rangle = \langle (A-\langle A\rangle)(A-\langle A\rangle)\rangle = \langle \delta A \delta A\rangle \ .$$

Now we calculate,

$$\begin{aligned}
\Delta A^2 \Delta B^2 = \langle\psi|\delta\hat{A}\delta\hat{A}|\psi\rangle\langle\psi|\delta\hat{B}\delta\hat{B}|\psi\rangle &= \langle\delta\hat{A}\psi|\delta\hat{A}\psi\rangle\langle\delta\hat{B}\psi|\delta\hat{B}\psi\rangle \\
&\geq |\langle\delta\hat{A}\psi|\delta\hat{B}\psi\rangle|^2 = \Big|\langle\psi|\delta\hat{A}\delta\hat{B}|\psi\rangle\Big|^2 \ ,
\end{aligned}$$

using Schwartz's inequality. Separating the real and imaginary part,

$$\begin{aligned}
\Delta A^2\Delta B^2 &\geq \mathfrak{Re}\ ^2\langle\psi|\delta\hat{A}\delta\hat{B}|\psi\rangle + \mathfrak{Im}\ ^2\langle\psi|\delta\hat{A}\delta\hat{B}|\psi\rangle \geq \mathfrak{Im}\ ^2\langle\psi|\delta\hat{A}\delta\hat{B}|\psi\rangle \\
&= \left[\tfrac{1}{2\imath}\Big(\langle\psi|\delta\hat{A}\delta\hat{B}|\psi\rangle - \langle\psi|\delta\hat{B}\delta\hat{A}|\psi\rangle\Big)\right]^2 = \left[\tfrac{1}{2\imath}\langle\psi|[\delta\hat{A},\delta\hat{B}]|\psi\rangle\right]^2 = \left[\tfrac{1}{2\imath}\langle\psi|[\hat{A},\hat{B}]|\psi\rangle\right]^2 \ .
\end{aligned}$$

$\imath[\hat{A},\hat{B}]$ *is always real when* $\hat{A}$ *and* $\hat{B}$ *are observable. This inequality has two roots:* $\Delta A\Delta B \geq \pm\frac{1}{2}|\langle[\hat{A},\hat{B}]\rangle|$, *but as the result must be valid when we exchange* $\hat{A}$ *and* $\hat{B}$, *we finally obtain,*

$$\Delta A\Delta B \geq \tfrac{1}{2}|\langle[\hat{A},\hat{B}]\rangle| \ .$$

23.3.10.11 Ex: Fourier transform

Show that $\langle \mathbf{r}|\hat{\mathbf{P}}|\psi\rangle = \frac{\hbar}{\imath}\nabla\langle \mathbf{r}|\psi\rangle$ reproduces the Schrödinger equation in position representation.

Solution: *Using the result (23.105) we calculate,*

$$\begin{aligned}\langle \mathbf{r}|\hat{\mathbf{P}}|\psi\rangle &= \int d^3r'\langle \mathbf{r}|\hat{\mathbf{P}}|\mathbf{r}'\rangle\langle \mathbf{r}'|\psi\rangle = \tfrac{1}{\hbar^{3/2}}\int\int d^3r'd^3p\ \mathbf{p}e^{\imath\mathbf{p}\cdot(\mathbf{r}-\mathbf{r}')/\hbar}\psi(\mathbf{r}') \\ &= \tfrac{1}{\hbar^{3/2}}\int\int d^3r'd^3p\tfrac{\hbar}{\imath}\nabla_{\mathbf{r}}e^{\imath\mathbf{p}\cdot(\mathbf{r}-\mathbf{r}')/\hbar}\psi(\mathbf{r}') = \tfrac{\hbar}{\imath}\nabla_{\mathbf{r}}\int d^3r'\delta^3(\mathbf{r}-\mathbf{r}')\psi(\mathbf{r}') = \tfrac{\hbar}{\imath}\nabla_{\mathbf{r}}\psi(\mathbf{r})\ .\end{aligned}$$

Alternatively we can explore the property of the Fourier transform, $\mathcal{F}[x^n f(x)] = \imath^n\frac{d^n\mathcal{F}f(k)}{dk^n}$, giving

$$\langle \mathbf{r}|\hat{P}_x|\mathbf{r}'\rangle = \int d^3p\langle \mathbf{r}|\hat{P}_x|\mathbf{p}\rangle\langle \mathbf{p}|\mathbf{r}'\rangle = \tfrac{\hbar}{\imath}\delta'(x-x')\delta(y-y')\delta(z-z')\ .$$

to calculate,

$$\begin{aligned}\langle \mathbf{r}|\hat{P}_x|\psi\rangle &= \int d^3r'\langle \mathbf{r}|\hat{P}_x|\mathbf{r}'\rangle\langle \mathbf{r}'|\psi\rangle \\ &= \tfrac{\hbar}{\imath}\int dx'\delta'(x-x')\int dy'\delta(y-y')\int dz'\delta(z-z')\psi(\mathbf{r}') = \frac{\hbar}{\imath}\frac{\partial}{\partial x}\psi(x,y,z)\ .\end{aligned}$$

With this result and the Hamiltonian $\hat{H} \equiv \hat{\mathbf{P}}^2/2m + V(\hat{\mathbf{R}})$ it is easy to verify the Schrödinger equation in spatial representation,

$$\imath\hbar\frac{d}{dt}\langle \mathbf{r}|\psi(t)\rangle = \left[-\frac{\hbar^2}{2m}\nabla^2_{\mathbf{r}} + V(\mathbf{r})\right]\langle \mathbf{r}|\psi(t)\rangle\ .$$

It is interesting to note that the Schrödinger equation in momentum representation is given by,

$$\begin{aligned}\imath\hbar\frac{d}{dt}\langle \mathbf{p}|\psi(t)\rangle &= \langle \mathbf{p}|\frac{\hat{\mathbf{P}}^2}{2m}\psi(t)\rangle + \langle \mathbf{p}|V(\hat{\mathbf{R}})|\psi(t)\rangle \\ &= \frac{\mathbf{p}^2}{2m}\langle \mathbf{p}|\psi(t)\rangle + \int\int\langle \mathbf{p}|V(\hat{\mathbf{R}})|\mathbf{r}\rangle\langle \mathbf{r}|\mathbf{p}'\rangle\varphi(\mathbf{p}',t)d^3rd^3p' \\ &= \frac{\mathbf{p}^2}{2m}\langle \mathbf{p}|\psi(t)\rangle + \frac{1}{h^{3/2}}\int\int V(\mathbf{r})e^{(\imath/\hbar)(\mathbf{p}'-\mathbf{p})\cdot\mathbf{r}}\varphi(\mathbf{p}',t)d^3rd^3p' \\ &= \frac{\mathbf{p}^2}{2m}\langle \mathbf{p}|\psi(t)\rangle + \int\tilde{V}(\mathbf{p}-\mathbf{p}')\varphi(\mathbf{p}',t)d^3p'\ ,\end{aligned}$$

where $\tilde{V}(\mathbf{p}) = \hbar^{-3/2}\int V(\mathbf{r})e^{-\imath\mathbf{k}\cdot\mathbf{r}}d^3r$.

23.3.10.12 Ex: Projection of the motion of a particle

Project the Hamiltonian of the motion of a free particle onto the plane x-y at the position $z = z_0$ using the projection operator $\hat{P} = |z_0\rangle\langle z_0|$ and the trace defined in

(23.137) generalized to continuous variables.

Solution: *The particle's Hamiltonian is,*

$$\hat{H} = \frac{\hat{\mathbf{p}}^2}{2m} = \int d^3r d^3r' |\mathbf{r}'\rangle\langle\mathbf{r}'| \frac{\hat{\mathbf{p}}^2}{2m} |\mathbf{r}\rangle\langle\mathbf{r}| \ .$$

The projector $\hat{P} = |z_0\rangle\langle z_0|$ *projects the Hamiltonian onto,*

$$\begin{aligned}
\hat{H}_{\mathcal{R}} &= |z_0\rangle\langle z_0| \int d^3r d^3r' |x'y'z'\rangle\langle x'y'z'| \frac{\hat{\mathbf{p}}^2}{2m} |xyz\rangle\langle xyz|z_0\rangle\langle z_0| \\
&= \int d^3r d^3r' \delta(z'-z_0) |x'y'\rangle\langle x'y'| \frac{\hat{p}_x^2 + \hat{p}_y^2 + \hat{p}_z^2}{2m} |xy\rangle\langle xy| \delta(z-z_0) \\
&= \int dx dy dx' dy' |x'y'\rangle\langle x'y'| \frac{\hat{p}_x^2 + \hat{p}_y^2}{2m} |xy\rangle\langle xy| = \frac{\hat{p}_x^2 + \hat{p}_y^2}{2m} \ .
\end{aligned}$$

23.3.10.13 Ex: Complete system of commuting operators

Construct the Hilbert space of two independent two-level systems a and b. Consider observables $\hat{X}_a$ and $\hat{Y}_b$ acting on their respective systems. What will be their shapes $\hat{X}_{ab}$, respectively $\hat{Y}_{ab}$, in the total Hilbert space? Construct the expanded state $|\psi_{ab}\rangle$ from the basis of the individual systems. Verify $[\hat{X}_{ab}, \hat{Y}_{ab}] = 0$. Verify that the expanded observables obey the same eigenvalue equations as the original ones.

Solution: *Be* $\hat{X}_a$ *and* $\hat{Y}_b$ *two operators related to the two atoms a and b with the eigenvalue spectra,*

$$\hat{X}_a |k\rangle_a = a_k |k\rangle_a \quad , \quad \hat{Y}_b |k\rangle_b = b_k |k\rangle_b \ ,$$

with $k = 1, 2$ *such that the general states are* $|\psi_a\rangle = a_1|1\rangle_a + a_2|2\rangle_a$ *and* $|\psi_b\rangle = b_1|1\rangle_b + b_2|2\rangle_b$. *Since* $[\hat{X}_a, \hat{Y}_b] = 0$, *we can build the operators,*

$$\hat{X}_{ab} = \hat{X}_a \otimes 1_2 = \begin{pmatrix} \hat{X}_a & 0 \\ 0 & 1_2 \end{pmatrix} \quad , \quad \hat{Y}_{ab} = 1_2 \otimes \begin{pmatrix} 1_2 & 0 \\ 0 & \hat{Y}_a \end{pmatrix} \quad , \quad \hat{Z}_{ab} = \begin{pmatrix} \hat{X}_a & 0 \\ 0 & \hat{Y}_b \end{pmatrix} \ .$$

We verify that $[\hat{X}_{ab}, \hat{Y}_{ab}] = 0$ *simply because of the construction of the total matrix. Also, we build states*

$$|\psi_{ab}\rangle = c_1 \begin{pmatrix} |1\rangle_a \\ |1\rangle_b \end{pmatrix} + c_2 \begin{pmatrix} |2\rangle_a \\ |1\rangle_b \end{pmatrix} + c_3 \begin{pmatrix} |1\rangle_a \\ |2\rangle_b \end{pmatrix} + c_4 \begin{pmatrix} |2\rangle_a \\ |2\rangle_b \end{pmatrix} = c_1|1\rangle_{ab} + c_2|2\rangle_{ab} + c_3|3\rangle_{ab} + c_4|4\rangle_{ab} \ .$$

The expanded operators satisfy the same eigenvalue equations:

$$\hat{X}_{ab}|1_{ab}\rangle = \begin{pmatrix} \hat{X}_a & 0 \\ 0 & 1_2 \end{pmatrix} \begin{pmatrix} |1\rangle_a \\ |1\rangle_b \end{pmatrix} = \begin{pmatrix} \hat{X}_a|1\rangle_a \\ |1\rangle_b \end{pmatrix} = \begin{pmatrix} a_1|1\rangle_a \\ |1\rangle_b \end{pmatrix} = a_1|1_{ab}\rangle \ .$$

such that $\hat{X}_{ab}|\psi_{ab}\rangle = c_k|\psi_{ab}\rangle$.

23.3.10.14 Ex: Liouville equation

Show that $\begin{pmatrix}1 & 0\\ 0 & 0\end{pmatrix}\otimes\hat{A}+\begin{pmatrix}0 & 0\\ 0 & 1\end{pmatrix}\otimes\hat{B}=\hat{A}\oplus\hat{B}$.

Solution:

23.3.10.15 Ex: Liouville equation

Show at the example of a two-level system that the von Neumann equation, $\dot{\hat{\rho}}=-\frac{\imath}{\hbar}[\hat{H},\hat{\rho}]$, can be written, $\dot{\vec{\rho}}=-\frac{\imath}{\hbar}(\hat{H}\otimes\mathbb{I}-\mathbb{I}\otimes\hat{H})\vec{\rho}$, using the definition of the external product and $\vec{\rho}\equiv\begin{pmatrix}\rho_{11}\\ \rho_{12}\\ \rho_{21}\\ \rho_{22}\end{pmatrix}$. **Help:** For this exercise the physical interpretation of $\hat{\rho}$ as the density operator does not matter. It may be regarded as a common observable.

Solution: *On one hand we have,*

$$\begin{aligned}[\hat{H},\hat{\rho}] &= \begin{pmatrix}H_{11} & H_{12}\\ H_{21} & H_{22}\end{pmatrix}\begin{pmatrix}\rho_{11} & \rho_{12}\\ \rho_{21} & \rho_{22}\end{pmatrix}-\begin{pmatrix}\rho_{11} & \rho_{12}\\ \rho_{21} & \rho_{22}\end{pmatrix}\begin{pmatrix}H_{11} & H_{12}\\ H_{21} & H_{22}\end{pmatrix}\\ &= \begin{pmatrix}H_{12}\rho_{21}-H_{21}\rho_{12} & H_{11}\rho_{12}+H_{12}\rho_{22}-H_{12}\rho_{11}-H_{22}\rho_{12}\\ H_{21}\rho_{11}+H_{22}\rho_{21}-\rho_{21}H_{11}-\rho_{22}H_{21} & H_{21}\rho_{12}-H_{12}\rho_{21}\end{pmatrix}.\end{aligned}$$

On the other hand, knowing,

$$\hat{H}\otimes\mathbb{I}=\begin{pmatrix}H_{11} & H_{12} & 0 & 0\\ H_{21} & H_{22} & 0 & 0\\ 0 & 0 & H_{11} & H_{12}\\ 0 & 0 & H_{21} & H_{22}\end{pmatrix}\quad,\quad \mathbb{I}\otimes\hat{H}=\begin{pmatrix}H_{11} & 0 & H_{12} & 0\\ 0 & H_{11} & 0 & H_{12}\\ H_{21} & 0 & H_{22} & 0\\ 0 & H_{21} & 0 & H_{22}\end{pmatrix},$$

we have,

$$\begin{aligned}(\mathbb{I}\otimes\hat{H}-\hat{H}\otimes\mathbb{I})\vec{\rho} &= \begin{pmatrix}H_{11} & 0 & H_{12} & 0\\ 0 & H_{11} & 0 & H_{12}\\ H_{21} & 0 & H_{22} & 0\\ 0 & H_{21} & 0 & H_{22}\end{pmatrix}-\begin{pmatrix}H_{11} & H_{12} & 0 & 0\\ H_{21} & H_{22} & 0 & 0\\ 0 & 0 & H_{11} & H_{12}\\ 0 & 0 & H_{21} & H_{22}\end{pmatrix}\begin{pmatrix}\rho_{11}\\ \rho_{12}\\ \rho_{21}\\ \rho_{22}\end{pmatrix}\\ &= \begin{pmatrix}H_{12}\rho_{21}-H_{12}\rho_{12}\\ -H_{21}\rho_{11}+(H_{11}-H_{22})\rho_{12}+H_{12}\rho_{22}\\ H_{21}\rho_{11}+(H_{22}-H_{11})\rho_{21}-H_{12}\rho_{22}\\ H_{21}\rho_{12}-H_{21}\rho_{21}\end{pmatrix},\end{aligned}$$

given that $\hat{H}^\dagger=\hat{H}$.

23.3.10.16 Ex: Unitary transformation of singlet states

Consider two spins a and b that do not interact. Applying to each spin the same transformation to another base, show that the singlet state has in each base the following form: $|\psi\rangle = \frac{1}{\sqrt{2}}\left(|\uparrow\rangle_a|\downarrow\rangle_b - |\downarrow\rangle_a|\uparrow\rangle_b\right)$.

Solution: *The change of base corresponds to a unitary transformation* $U = \begin{pmatrix} a & b \\ c & d \end{pmatrix}$, *where* $\det U = 1$. *Hence,*

$$\begin{aligned}
|0,0\rangle &= \tfrac{1}{\sqrt{2}}[|\uparrow\rangle_a|\downarrow\rangle_b - |\downarrow\rangle_a|\uparrow\rangle_b] \\
&= \tfrac{1}{\sqrt{2}}\left[(a|1\rangle_a + b|2\rangle_a)(c|1\rangle_b + d|2\rangle_b) - (c|1\rangle_a + d|2\rangle_a)(a|1\rangle_b + b|2\rangle_b)\right] \\
&= \tfrac{1}{\sqrt{2}}\left[ad(|1\rangle_a|2\rangle_b - |2\rangle_a|1\rangle_b) + bc(|2\rangle_a|1\rangle_b - |1\rangle_a|2\rangle_b)\right] = \tfrac{1}{\sqrt{2}}\left(|1\rangle_a|2\rangle_b - |2\rangle_a|1\rangle_b\right) \ .
\end{aligned}$$

23.4 Time evolutions

Quantum systems may evolve in time, as predicted by the time-dependent Schrödinger equation (23.54). In this section we show different equivalent but complementary descriptions of the temporal evolution of quantum systems depending on whether the time dependence is attributed to the state function of to observables.

23.4.1 Unitary transformations

The best we can do to characterize a system is, obviously, to measure all its observables. However, neither the state functions nor the observables are fixed unambiguously, since defining a unitary operator, $U^\dagger = U^{-1}$, we can do,

$$\langle\psi|\hat{A}|\psi\rangle = \langle\psi|U^\dagger U\hat{A}U^\dagger U|\psi\rangle = \langle U\psi|U\hat{A}U^\dagger|U\psi\rangle \ . \tag{23.139}$$

That is, exchanging $|\psi\rangle$ by $U|\psi\rangle$ and at the same time $\hat{A}$ by $U\hat{A}U^\dagger$, we obtain quantities describing the same physical reality, since the eigenvalues are unchanged. This allows us to choose the best mathematical representation for a specific problem. As an example, we will apply the temporal unitary transformation to solve the dynamics of a coupled two-level system in Exc. 23.4.7.1.

23.4.2 Schrödinger picture

Important examples of how the same system can be represented in different ways (related by unitary transformations) are the Heisenberg, Schrödinger, and interaction pictures.

The *Schrödinger picture*, denoted by the subscript S, is defined by the choice of a Hamiltonian,

$$\hat{H}_S = \hat{H}(t, \hat{p}_S, \hat{r}_S) \qquad \text{with} \qquad \frac{d}{dt}\hat{p}_S = \frac{d}{dt}\hat{r}_S = 0 \ . \tag{23.140}$$

That is, the observables of the system $\hat{A}_S(t, \hat{p}_S, \hat{r}_S)$ can only depend *explicitly* on time, but not via other operators, for instance $\hat{p}_S$ and $\hat{r}_S$, which are stationary,

$$\frac{d}{dt}\hat{A}_S = \frac{\partial \hat{A}_S}{\partial t} + \cancelto{0}{\dot{\hat{p}}_S}\frac{\partial \hat{A}_S}{\partial p_S} + \cancelto{0}{\dot{\hat{r}}_S}\frac{\partial \hat{A}_S}{\partial r_S} \ . \tag{23.141}$$

This is,

$$\boxed{\frac{d}{dt}\hat{A}_S(t) = \frac{\partial}{\partial t}\hat{A}_S(t)} \ . \tag{23.142}$$

In the context of a moving particle, this means that the Hamiltonian $\frac{1}{2m}\hat{p}_S^2 + V(\hat{r}_S)$ is time-independent (unless the potential $V(\hat{r}_S, t)$ is itself time-dependent). In this case, the formal solution of the Schrödinger equation,

$$\boxed{\imath\hbar\frac{d}{dt}|\psi_S(t)\rangle = \hat{H}_S|\psi_S(t)\rangle} \ , \tag{23.143}$$

can be written,

$$|\psi_S(t)\rangle = e^{-(\imath/\hbar)\hat{H}_S t}|\psi_S(0)\rangle \equiv U(t)|\psi_S(0)\rangle \ . \tag{23.144}$$

Apparently, the temporal dynamics is completely within the wave functions.

Example 148 (*The time evolution operator*): Generalizing to an arbitrary initial time t_0 we write the temporal translation operator,

$$U(t, t_0)|\psi(t_0)\rangle = |\psi(t)\rangle \ . \tag{23.145}$$

By the expression (23.144) we find immediately, with $t_0 < t_1 < t_2$,

$$U(t_2, t_0) = U(t_2, t_1)U(t_1, t_0) \quad \text{and} \quad U(t_0, t) = U^\dagger(t, t_0) = U^{-1}(t, t_0) = U(t, t_0)^{-1} \ .$$

The conjugate operator of time evolution acts on the vector 'bra',

$$\langle\psi(t)| = \langle\psi(t_0)|U^\dagger(t, t_0) \ .$$

23.4.3 Heisenberg picture

As unitary transformations do not change the physics, the system described by,

$$|\psi_S(t)\rangle \longrightarrow U(t)^\dagger|\psi_S(t)\rangle \equiv |\psi_H\rangle \qquad \text{and} \qquad \hat{A}_S(t) \longrightarrow U(t)^\dagger\hat{A}_S(t)U(t) \equiv \hat{A}_H(t) \tag{23.146}$$

with the transformation defined by equation (23.144), is equivalent. The subscript H means the *Heisenberg picture*. In particular, we obviously have,

$$\hat{H}_S = \hat{H}_H \equiv \hat{H} \ . \tag{23.147}$$

Thus, the matrix element of the operator $\hat{A}_S$ in Schrödinger's picture with the time-dependent base $\{|\psi_S\rangle\}$ is equal to the matrix element of the operator $\hat{A}_H = U^\dagger\hat{A}_S U$

in Heisenberg's picture with the time-independent base $\{|\psi_H\rangle\}$. In this picture the wavefunctions are independent of time,

$$\boxed{\frac{d}{dt}|\psi_H\rangle = \frac{d}{dt}|\psi_S(0)\rangle = 0}\,, \tag{23.148}$$

but the operators depend *im- and explicitly* on time,

$$\begin{aligned}\frac{d}{dt}\hat{A}_H(t) &= \frac{d}{dt}\left(U(t)^\dagger \hat{A}_S(t) U(t)\right) = \frac{dU^\dagger}{dt}\hat{A}_S(t)U(t) + U(t)^\dagger \hat{A}_S(t)\frac{dU}{dt} + U(t)^\dagger \frac{\partial \hat{A}_S(t)}{\partial t}U(t) \\ &= \frac{\imath}{\hbar}\hat{H}^\dagger U(t)^\dagger \hat{A}_S U(t) + U(t)^\dagger \hat{A}_S \frac{-\imath}{\hbar}\hat{H}U(t) + U^\dagger(t)\frac{\partial \hat{A}_S(t)}{\partial t}U(t)\,. \end{aligned} \tag{23.149}$$

That is,

$$\boxed{\frac{d}{dt}\hat{A}_H(t) = \frac{\imath}{\hbar}[\hat{H}, \hat{A}_H(t)] + \frac{\partial \hat{A}_H(t)}{\partial t}}\,. \tag{23.150}$$

This so-called *Heisenberg equation*, which describes the temporal evolution of an operator acting on time-independent states in the Heisenberg picture, is equivalent to the Schrödinger equation, which expresses the temporal evolution of a quantum state in Schrödinger's picture.

According to equation (23.150), the rate of temporal variation of an operator in the Heisenberg representation is given by the commutator of that operator with the total Hamiltonian of the system. Note that if an operator representing a dynamic variable commutes with the Hamiltonian in the Schrödinger representation, it will also commute with the Hamiltonian in the Heisenberg representation and thus with the complete set of commutating observables,

$$[\hat{H}, \hat{A}_S] = 0 \qquad \Longleftrightarrow \qquad [\hat{H}, \hat{A}_H] = 0\,. \tag{23.151}$$

We will show this in the Exc. 23.4.7.2. Note that we could interpret Eq. (23.148) as a Schrödinger equation with a Hamiltonian $\tilde{H}_H = 0$. That is, *the Hamiltonian used in the Schrödinger equation differs from the one used in the Heisenberg equation.* We will study this in more detail in Secs. 23.4.4 and 23.4.5.

> **Example 149 (*Position and momentum operators in the Heisenberg picture*):** We know that in Schrödinger's picture (23.140), the operators $\hat{p}_S$ and $\hat{r}_S$ are stationary. Using this fact in derivation (23.149), we can show for example for the momentum operator,
>
> $$\frac{\partial}{\partial t}\hat{p}_S = 0 \qquad \Longrightarrow \qquad \frac{\partial}{\partial t}\hat{p}_H = 0 \qquad \Longrightarrow \qquad \frac{d}{dt}\hat{p}_H = \frac{\imath}{\hbar}[\hat{H}, \hat{p}_H]\,.$$

In the Exc. 23.4.7.3 we will use the Heisenberg picture to derive the equations of motion for a particle confined to a potential.

23.4.4 Interaction picture

The *interaction picture* deals with problems where the total Hamiltonian is composed of a time-independent part and a time-dependent part,

$$\hat{H} = \hat{H}_0 + \hat{V}(t) \ . \tag{23.152}$$

Analogously to Eq. (23.144), we define a time evolution operator in terms of the *time-independent* part of the total Hamiltonian,

$$\boxed{|\psi_I(t)\rangle = e^{\imath \hat{H}_0 t/\hbar}|\psi_S(t)\rangle \qquad \text{and} \qquad \hat{A}_I(t) = e^{\imath \hat{H}_0 t/\hbar}\hat{A}_S e^{-\imath \hat{H}_0 t/\hbar}} \ . \tag{23.153}$$

Now we are interested in the temporal dependence of quantum states and operators in the interaction picture. Replacing the inverse function $|\psi_S(t)\rangle = e^{-\imath \hat{H}_0 t/\hbar}|\psi_I(t)\rangle$ in the Schrödinger equation (23.143) we immediately see,

$$\boxed{\hat{V}(t)|\psi_I(t)\rangle = \imath\hbar \frac{\partial}{\partial t}|\psi_I(t)\rangle} \ . \tag{23.154}$$

Apparently, in the interaction picture, only the perturbative term in Hamiltonian controls the temporal evolution. Taking the time derivative of both sides of the equation (23.153) transforming an operator from the Schrödinger to the interaction picture results in,

$$\boxed{\frac{d\hat{A}_I}{dt} = \frac{\imath}{\hbar}[\hat{H}_0, \hat{A}_I] + \frac{\partial \hat{A}_I}{\partial t}} \ . \tag{23.155}$$

Therefore, we see that the time derivative can be expressed in the form of a commutator, resembling the Heisenberg equation (23.150), except that only the unperturbed term of the Hamiltonian appears in the argument of the commutation operator. As already state in Sec. 23.4.3, different Hamiltonians are used in the Schrödinger and in the Heisenberg equation.

> **Example 150 (*Schrieffer-Wolff transformation*):** The *Schrieffer-Wolff transformation* is a unitary transformation used to perturbatively diagonalize the system Hamiltonian to first order in the interaction. As such, the Schrieffer-Wolff transformation is an operator version of second-order perturbation theory. The Schrieffer-Wolff transformation is often used to project out the high energy excitations of a given quantum many-body Hamiltonian in order to obtain an effective low energy model. The Schrieffer-Wolff transformation thus provides a controlled perturbative way to study the strong coupling regime of quantum-many body Hamiltonians.
> Consider a quantum system evolving under the time-independent Hamiltonian operator $\hat{H}$ of the form $\hat{H} = \hat{H}_0 + \hat{V}$, where H_0 is a Hamiltonian with known eigenstates $|m\rangle$ and corresponding eigenvalues E_m, and where V is a small perturbation. Moreover, it is assumed without loss of generality that $\hat{V}$ is purely off-diagonal in the eigenbasis of $\hat{H}_0$, i.e.,
>
> $$\langle m|\hat{V}|m\rangle = 0 \tag{23.156}$$
>
> for all m. Indeed, this situation can always be arranged by absorbing the diagonal elements of $\hat{V}$ into $\hat{H}_0$, thus modifying its eigenvalues to,
>
> $$E'_m = E_m + \langle m|\hat{V}|m\rangle \ . \tag{23.157}$$

The Schrieffer-Wolff transformation is a unitary transformation which expresses the Hamiltonian in a basis (the 'dressed' basis) where it is diagonal to first order in the perturbation $\hat{V}$. This unitary transformation is conventionally written as:

$$\hat{H}' = e^{\imath S}\hat{H}e^{-\imath S} \ . \tag{23.158}$$

When $\hat{V}$ is small, the generator S of the transformation will likewise be small. The transformation can then be expanded in S using the Baker-Campbell-Haussdorf formula,

$$\hat{H}' = \hat{H} + [\imath S, \hat{H}] + \tfrac{1}{2}[\imath S, [\imath S, \hat{H}]] + \dots \ . \tag{23.159}$$

In terms of $\hat{H}_0$ and $\hat{V}$, the transformation becomes,

$$\hat{H}' = \hat{H}_0 + \hat{V} + [\imath S, \hat{H}_0] + [\imath S, \hat{V}] + \tfrac{1}{2}[\imath S, [\imath S, \hat{H}_0]] + \tfrac{1}{2}[\imath S, [\imath S, \hat{V}]] + \dots \ . \tag{23.160}$$

The Hamiltonian can be made diagonal to first order in $\hat{V}$ by choosing the generator S such that,

$$[\hat{H}_0, \imath S] = \hat{V} \ . \tag{23.161}$$

This equation always has a definite solution under the assumption that $\hat{V}$ is off-diagonal in the eigenbasis of $\hat{H}_0$. Substituting this choice in the previous transformation yields:

$$\hat{H}' = \hat{H}_0 + \tfrac{1}{2}[\imath S, \hat{V}] + O(\hat{V}^3) \ . \tag{23.162}$$

This expression is the standard form of the Schrieffer-Wolff transformation. Note that all the operators on the right-hand side are now expressed in a new basis 'dressed' by the interaction $\hat{V}$ to first order.

In the general case, the difficult step of the transformation is to find an explicit expression for the generator S. Once this is done, it is straightforward to compute the Schrieffer-Wolff Hamiltonian by computing the commutator $[S, \hat{V}]$. The Hamiltonian can then be projected on any subspace of interest to obtain an effective projected Hamiltonian for that subspace. In order for the transformation to be accurate, the eliminated subspaces must be energetically well separated from the subspace of interest, meaning that the strength of the interaction $\hat{V}$ must be much smaller than the energy difference between the subspaces. This is the same regime of validity as in standard second-order perturbation theory.

23.4.5 Hamiltonian under arbitrary unitary transformation

In the preceding section we have studied particular unitary transformations between the Schrödinger, Heisenberg, and interaction pictures. Let us now have a look at *arbitrary* unitary transformations.

We have seen that the unitary transformation,

$$|\psi_U\rangle = U^\dagger|\psi\rangle \qquad , \qquad \hat{A}_U = U^\dagger \hat{A} U \ , \tag{23.163}$$

leaves the physics of a system unchanged. The question is now, how the Schrödinger equation,

$$\hat{H}|\psi\rangle = \imath\hbar\frac{d}{dt}|\psi\rangle \tag{23.164}$$

transforms into the new system, that is, what will the Hamiltonian $\hat{H}_U$ look like in the transformed equation,

$$\hat{H}_U|\psi_U\rangle \stackrel{?}{=} \imath\hbar\frac{d}{dt}|\psi_U\rangle \ . \tag{23.165}$$

We calculate,

$$\begin{aligned}\imath\hbar\frac{d}{dt}|\psi_U\rangle &= \imath\hbar U^\dagger\frac{d}{dt}|\psi\rangle + \imath\hbar\dot{U}^\dagger|\psi\rangle = (U^\dagger\hat{H} + \imath\hbar\dot{U}^\dagger)|\psi\rangle \\ &= (U^\dagger\hat{H} + \imath\hbar\dot{U}^\dagger)U|\psi_U\rangle = (U^\dagger\hat{H}U + \imath\hbar\dot{U}^\dagger U)|\psi_U\rangle = \hat{H}_U|\psi_U\rangle \ .\end{aligned} \tag{23.166}$$

Hence,

$$\boxed{\hat{H}_U = U^\dagger\hat{H}U + \imath\hbar\dot{U}^\dagger U} \ . \tag{23.167}$$

We will apply this concept in Exc. 23.5.6.2 to a particle in the field of gravity.

Example 151 (*Interaction picture*): The above derivation is general and holds for any unitary transformation. We will now apply it to transform the Hamiltonian $\hat{H} = \hat{H}_0 + \hat{V}(t)$ into the interaction picture via the transformation $U = e^{-(\imath/\hbar)\hat{H}_0 t}$. From

$$\dot{U}^\dagger = \frac{\imath}{\hbar}\hat{H}_0 e^{(\imath/\hbar)\hat{H}_0 t} = \frac{\imath}{\hbar}\hat{H}_0 U^\dagger \tag{23.168}$$

we calculate,

$$\begin{aligned}\hat{H}_U &= U^\dagger\hat{H}U + \imath\hbar\dot{U}^\dagger U = U^\dagger[\hat{H}_0 + \hat{V}(t)]U + \imath\hbar\frac{\imath}{\hbar}\hat{H}_0 U^\dagger U \\ &= U^\dagger[\hat{H}_0 + \hat{V}(t)]U - \hat{H}_0 = U^\dagger\hat{V}(t)U \ ,\end{aligned} \tag{23.169}$$

which confirms the validity of the Schrödinger equation (23.154) in the interaction picture, provided the Hamiltonian is taken to be the perturbation part $\hat{V}(t)$, only. In the Heisenberg picture $\hat{V}(t) = 0$, such that,

$$\hat{H}_U = 0 \ , \tag{23.170}$$

which confirms Eq. (23.148).

23.4.6 Ehrenfest's theorem

For linear operators satisfying $[\hat{A}, \hat{B}] = \imath$ we can give a generalization of the commutation relation:

$$\boxed{[\hat{A}, F(\hat{A}, \hat{B})] = \imath\frac{\delta F(\hat{A}, \hat{B})}{\delta\hat{B}}} \ . \tag{23.171}$$

This can be verified by a Taylor expansion of $F(\hat{A}, \hat{B})$ by $\hat{B}$ around $\hat{B} = 0$, as will be shown in Exc. 23.4.7.4. An immediate consequence of $[\hat{p}, \hat{r}] = -\imath\hbar$ is,

$$[\hat{p}, F(\hat{r})] = -\imath\hbar\frac{\delta F(\hat{r})}{\delta\hat{r}} \ . \tag{23.172}$$

The momentum observable is not singularly defined by the commutation relation, because each unitarily transformed operator satisfies the relation as well. We

can expand a unitarily equivalent momentum as $\tilde{p} = UpU^\dagger = e^{\imath F(r)} p e^{-\imath F(r)} = p + \imath[F(r), p] + \frac{1}{2!}[F(r), [F(r), p]] + ...$ using the relation (23.172).

The observables in the Heisenberg picture follow the same equations of motion as the corresponding classical quantities. This *correspondence principle* is called *Ehrenfest theorem*. For example, when working with position and momentum variables $[\hat{r}, \hat{k}] = \imath$ and $\hat{H} = \frac{\hbar^2}{2m}\hat{k}^2 + V(\hat{r})$, we obtain,

$$[\hat{r}, \hat{H}] = \imath\hbar \frac{\delta \hat{H}}{\delta \hat{p}} \qquad \text{and} \qquad [\hat{p}, \hat{H}] = -\imath\hbar \frac{\delta \hat{H}}{\delta \hat{r}} \ , \tag{23.173}$$

and using the Heisenberg equation (23.150),

$$\dot{\hat{r}} = \frac{\delta \hat{H}}{\delta \hat{p}} \qquad \text{and} \qquad \dot{\hat{p}} = -\frac{\delta \hat{H}}{\delta \hat{r}} \ . \tag{23.174}$$

We will demonstrate this in Exc. 23.4.7.5 for the case of a harmonic potential.

In the Schrödinger picture the equation of motion for the eigenvalues of the observables takes the form,

$$\frac{d}{dt}\langle \hat{A}_S \rangle = \langle \partial_t \psi | \hat{A}_S | \psi \rangle + \langle \psi | \partial_t \hat{A}_S | \psi \rangle + \langle \psi | \hat{A}_S | \partial_t \psi \rangle = \frac{\partial}{\partial t}\langle \hat{A}_S \rangle + \frac{\imath}{\hbar}\langle [\hat{H}, \hat{A}_S] \rangle \ . \tag{23.175}$$

The eigenvalues behave as Heisenberg observables in Eq. (23.149), that is, they follow the laws of Hamilton's and Newton's mechanics.

The important result now is that the equations that govern the eigenvalues of the observables are identical in the both pictures, since from the Heisenberg picture we obtain with Eq. (23.149),

$$\frac{d}{dt}\langle \hat{A}_H \rangle = \frac{\partial}{\partial t}\langle \hat{A}_H \rangle + \frac{\imath}{\hbar}\langle [\hat{H}, \hat{A}_H] \rangle \ .$$

23.4.7 Exercises

23.4.7.1 Ex: Coupled two-level atom

Calculate the time evolution of an atom with two levels coupled by a light field using the Hamiltonian,

$$\hat{H} = \begin{pmatrix} 0 & \frac{1}{2}\hbar\Omega \\ \frac{1}{2}\hbar\Omega & -\hbar\Delta \end{pmatrix} \ ,$$

where $\Delta = \omega - \omega_0$ is the detuning between the frequency of the light and the frequency of the transition and Ω the Rabi frequency. **Help:** Determine the matrix of the eigenvalues $\hat{E}$ and the unitary transformation U given by $U^\dagger \hat{H} U = \hat{E}$ and use the formal solution of the Schrödinger equation: $|\psi(t)\rangle = e^{-\imath \hat{H} t/\hbar}|\psi_0\rangle = e^{-\imath U^\dagger \hat{E} U t/\hbar}|\psi_0\rangle = U^\dagger e^{-\imath \hat{E} t/\hbar} U |\psi_0\rangle$.

Solution: *We find the eigenvalues via,*

$$0 = \det(\hat{H} - E\hat{1}) = \det \begin{pmatrix} -E & \frac{1}{2}\Omega \\ \frac{1}{2}\Omega & -\Delta - E \end{pmatrix} = E\Delta + E^2 - \tfrac{1}{4}\Omega^2 \Longrightarrow E_{1,2} = -\tfrac{1}{2}\Delta \pm \tfrac{1}{2}\sqrt{\Delta^2 + \Omega^2} \ .$$

The eigenvectors follow, introducing the generalized Rabi frequency, $G \equiv \sqrt{\Delta^2+\Omega^2}$, from,

$$\hat{H}\begin{pmatrix} a \\ b \end{pmatrix} = \begin{pmatrix} \frac{1}{2}\Omega b \\ \frac{1}{2}\Omega a - \Delta b \end{pmatrix} = -\tfrac{1}{2}\Delta \pm \tfrac{1}{2}G \begin{pmatrix} a \\ b \end{pmatrix} \quad \Longrightarrow \quad \begin{matrix} \Omega b = a(-\Delta \pm G) \\ a^2+b^2 = 1 \end{matrix} .$$

The second equation allows us to introduce an angle ϑ such, that for the first eigenvalue, $a_1 = \cos\vartheta$ and $b_1 = \sin\vartheta$. We find

$$\tan\vartheta = \frac{b_1}{a_1} = \frac{G-\Delta}{\Omega} = \frac{\Omega}{G+\Delta} = \frac{-a_2}{b_2} \ .$$

Joining the eigenvectors to form a unitary matrix and the eigenvalues into a diagonal matrix,

$$U \equiv \begin{pmatrix} a_1 & a_2 \\ b_1 & b_2 \end{pmatrix} = \begin{pmatrix} \cos\vartheta & \sin\vartheta \\ -\sin\vartheta & \cos\vartheta \end{pmatrix} \quad , \quad E = \begin{pmatrix} -\frac{1}{2}\Delta + \frac{1}{2}G & 0 \\ 0 & -\frac{1}{2}\Delta - \frac{1}{2}G \end{pmatrix} .$$

It is easy to show

$$\det U = 1 \quad , \quad U^{-1} = U^\dagger \quad , \quad U^\dagger \hat{H} U = E \ .$$

With the Schrödinger equation, $\frac{d}{dt}|\psi(t)\rangle = \frac{1}{\imath\hbar}|\psi(t)\rangle$, through its formal solution, we can finally calculate the temporal evolution,

$$\begin{aligned} |\psi(t)\rangle &= e^{-\imath\hat{H}t/\hbar}|\psi_0\rangle = e^{-\imath U^\dagger \hat{E} U t/\hbar}|\psi_0\rangle = U^\dagger e^{-\imath\hat{E}t/\hbar} U|\psi_0\rangle \\ &= \begin{pmatrix} \cos\vartheta & -\sin\vartheta \\ \sin\vartheta & \cos\vartheta \end{pmatrix} \begin{pmatrix} e^{\frac{1}{2}\imath t(-\Delta+G)} & 0 \\ 0 & e^{\frac{1}{2}\imath t(-\Delta-G)} \end{pmatrix} \begin{pmatrix} \cos\vartheta & -\sin\vartheta \\ \sin\vartheta & \cos\vartheta \end{pmatrix} |\psi_0\rangle \\ &= \begin{pmatrix} \cos^2\vartheta e^{\frac{1}{2}\imath t(-\Delta+G)} + \sin^2\vartheta e^{\frac{1}{2}\imath t(-\Delta-G)} & \sin\vartheta\cos\vartheta\left(e^{\frac{1}{2}\imath t(-\Delta+G)} - e^{\frac{1}{2}\imath t(-\Delta-G)}\right) \\ \sin\vartheta\cos\vartheta\left(e^{\frac{1}{2}\imath t(-\Delta+G)} - e^{\frac{1}{2}\imath t(-\Delta-G)}\right) & \sin^2\vartheta e^{\frac{1}{2}\imath t(-\Delta+G)} + \cos^2\vartheta e^{\frac{1}{2}\imath t(-\Delta-G)} \end{pmatrix} |\psi_0\rangle \ . \end{aligned}$$

Assuming the two-level system to be initially in its ground state, $|\psi_0\rangle = \binom{1}{0}$, we

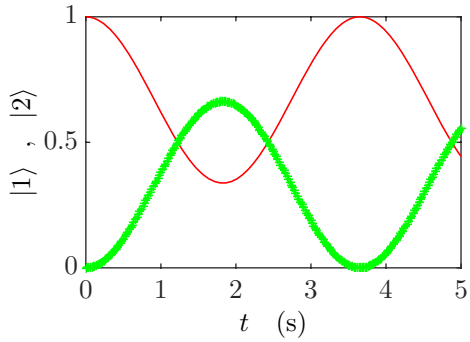

Figure 23.5: (code) Temporal evolution of the populations in a three-level system.

obtain,

$$a_1(t) = e^{-\imath t\Delta/2}\left(e^{\imath tG/2}\cos^2\vartheta + e^{-\imath tG/2}\sin^2\vartheta\right) = e^{-\imath t\Delta/2}\left[\cos\tfrac{Gt}{2} + \imath\left(\cos^2\vartheta - \sin^2\vartheta\right)\sin\tfrac{Gt}{2}\right]$$
$$a_2(t) = e^{-\frac{1}{2}\imath t\Delta}\sin\vartheta\cos\vartheta\left(e^{-\frac{1}{2}\imath tG} - e^{\frac{1}{2}\imath tG}\right) = 2ie^{-\imath t\Delta/2}\sin\vartheta\cos\vartheta\sin\tfrac{Gt}{2}\ .$$

With

$$\cos^2\vartheta - \sin^2\vartheta = \frac{1-\tan^2\vartheta}{1+\tan^2\vartheta} = \frac{\Omega^2-(G+\Delta)^2}{\Omega^2+(G+\Delta)^2} = -\frac{\Delta}{G}$$
$$\sin\vartheta\cos\vartheta = \frac{\tan\vartheta}{1+\tan^2\vartheta} = \frac{\Omega(G-\Delta)}{\Omega^2+(G-\Delta)^2} = \frac{\Omega}{2G}$$

we find

$$a_1(t) = e^{-\imath t\Delta/2}\left[\cos\tfrac{Gt}{2} - \imath\tfrac{\Delta}{G}\sin\tfrac{Gt}{2}\right] \qquad \textit{and} \qquad a_2(t) = \frac{\imath\Omega}{G}e^{-\imath t\Delta/2}\sin\tfrac{Gt}{2}$$

in accordance with the derivation of the Rabi formula (27.93).

23.4.7.2 Ex: Commutator in Schrödinger's and Heisenberg's picture

Show that operators which commute with the Hamiltonian in the Schrödinger picture also do it in the Heisenberg picture. Use the rule $[\hat{H}, \hat{A}\hat{B}] = \hat{A}[\hat{H},\hat{B}] + [\hat{H},\hat{A}]\hat{B}$.

Solution: *We calculate,*

$$0 = [\hat{H}, U\hat{A}_S U^\dagger] = U\hat{A}_S\cancelto{0}{[\hat{H},U^\dagger]} + U[\hat{H},\hat{A}_S]U^\dagger + \cancelto{0}{[\hat{H},U]}\hat{A}_S U^\dagger\ .$$

23.4.7.3 Ex: Motion in Heisenberg's picture

Consider the Hamiltonian $\hat{H} = \frac{\hat{p}^2}{2m} + \frac{m}{2}\omega^2\hat{r}^2$. Using the relation $[\hat{p},\hat{r}] = -\imath\hbar$ calculate in the Heisenberg picture the equations of motion for the observables $\hat{p}$, $\hat{r}$, and $\hat{p}\hat{r}$.

Solution: *a. We have*

$$\frac{d\hat{p}}{dt} = \frac{\imath}{\hbar}[\hat{H},\hat{p}] + \frac{\partial\hat{p}}{\partial t} = \frac{\imath}{\hbar}\left[\frac{\hat{p}^2}{2m} + \frac{m}{2}\omega^2\hat{r}^2, \hat{p}\right] = \frac{\imath m\omega^2}{2\hbar}[\hat{r}^2,\hat{p}] = \frac{\imath m\omega^2}{2\hbar}\left[\hat{r}\hat{r}\hat{p} - \left(\tfrac{\hbar}{\imath} + \hat{r}\hat{p}\right)\hat{r}\right] = -m\omega^2\hat{r}\ .$$

b. We have

$$\frac{d\hat{r}}{dt} = \frac{\imath}{\hbar}[\hat{H},\hat{r}] + \frac{\partial\hat{r}}{\partial t} = \frac{\imath}{\hbar}\left[\frac{\hat{p}^2}{2m} + \frac{m}{2}\omega^2\hat{r}^2, \hat{r}\right] = \frac{\imath}{2\hbar m}[\hat{p}^2,\hat{r}] = \frac{\imath}{2\hbar m}\left[\hat{p}\hat{p}\hat{r} - \left(\hat{p}\hat{r} - \tfrac{\hbar}{\imath}\right)\hat{p}\right] = \frac{\hat{p}}{m}\ .$$

c. We have

$$\frac{d(\hat{p}\hat{r})}{dt} = \frac{\imath}{\hbar}\left[\frac{\hat{p}^2}{2m} + \frac{m}{2}\omega^2\hat{r}^2, \hat{p}\hat{r}\right] + \frac{\partial(\hat{p}\hat{r})}{\partial t}$$
$$= \frac{\imath}{\hbar 2m}\left[\hat{p}\hat{p}\hat{p}\hat{r} - \hat{p}\left(\hat{p}\hat{r} - \tfrac{\hbar}{\imath}\right)\hat{p}\right] + \frac{\imath m\omega^2}{2\hbar}\left[\hat{r}\hat{r}\hat{p}\hat{r} - \left(\tfrac{\hbar}{\imath} + \hat{r}\hat{p}\right)\hat{r}\hat{r}\right] = \frac{\hat{p}^2}{m} - m\omega^2\hat{r}^2\ .$$

23.4.7.4 Ex: Commutator of a function of operators

Prove the relationship (23.171).

Solution: *We first calculate,*

$$\begin{aligned}
[\hat{A}, \hat{B}^n] &= \hat{B}^{n-1}[\hat{A}, \hat{B}] + [\hat{A}, \hat{B}^{n-1}]\hat{B} \\
&= \hat{B}^{n-1}[\hat{A}, \hat{B}] + \hat{B}^{n-2}[\hat{A}, \hat{B}]\hat{B} + [\hat{A}, \hat{B}^{n-2}]\hat{B}^2 \\
&= \hat{B}^{n-1}[\hat{A}, \hat{B}] + \hat{B}^{n-2}[\hat{A}, \hat{B}]\hat{B} + ... + [\hat{A}, \hat{B}]\hat{B}^{n-1} \\
&= \sum_{k=1}^{n} \hat{B}^{n-k}[\hat{A}, \hat{B}]\hat{B}^{k-1} = \imath n \hat{B}^{n-1} \ .
\end{aligned}$$

With this we can show,

$$\begin{aligned}
[\hat{A}, F(\hat{A}, \hat{B})] &= \left[\hat{A}, F(\hat{A}, 0) + \frac{\delta F(\hat{A}, 0)}{\delta \hat{B}}\hat{B} + ... + \frac{1}{n!}\frac{\delta^n F(\hat{A}, 0)}{\delta \hat{B}^n}\hat{B}^n + ...\right] \\
&= \frac{\delta F(\hat{A}, 0)}{\delta \hat{B}}[\hat{A}, \hat{B}] + ... + \frac{1}{n!}\frac{\delta^n F(\hat{A}, 0)}{\delta \hat{B}^n}[\hat{A}, \hat{B}^n] + ... \\
&= \imath\frac{\delta F(\hat{A}, 0)}{\delta \hat{B}} + ... + \imath\frac{1}{n!}\frac{\delta^n F(\hat{A}, 0)}{\delta \hat{B}^n}\imath n \hat{B}^{n-1} + ... \\
&= \imath\frac{\delta}{\delta \hat{B}}\left(1 + ... + \imath\frac{1}{(n-1)!}\frac{\delta^{n-1}}{\delta \hat{B}^{n-1}}\hat{B}^{n-1} + ...\right) F(\hat{A}, 0) = \imath\frac{\delta}{\delta \hat{B}}F(\hat{A}, B) \ .
\end{aligned}$$

23.4.7.5 Ex: Ehrenfest's theorem

Compare the equations of Ehrenfest's theorem with those of Hamilton-Jacobi for a classical particle subject to a time-independent potential. Discuss the classical limit, that is, when the Hamilton-Jacobi equations approach those of Ehrenfest.

Solution: *Are equivalent,*

$$\begin{aligned}
[\hat{r}, \hat{H}] &= \frac{1}{2m}\left(\hat{r}\hat{p}\hat{p} - \hat{p}\hat{p}\hat{r}\right) = \frac{1}{2m}\left((\hat{p}\hat{r} + \imath\hbar)\hat{p} - \hat{p}\left(-\imath\hbar + \hat{r}\hat{p}\right)\right) = \frac{\imath\hbar}{m}\hat{p} = \imath\hbar\frac{\delta \hat{H}}{\delta \hat{p}} \\
[\hat{p}, \hat{H}] &= \hat{p}V(\hat{r}) - V(\hat{r})\hat{p} = -\imath\hbar\frac{\delta \hat{H}}{\delta \hat{r}} \ .
\end{aligned}$$

For example, we take the harmonic potential, $V(\hat{r}) = \frac{m}{2}\omega^2\hat{r}^2$.

23.5 Symmetries in quantum mechanics

We already saw in Sec. 23.3.4 that, beyond observables, there is another category of operators that does not correspond to measurable physical quantities, but is very useful in the quantum formalism. These are the *unitary transformations*. In this section we will encounter some interesting examples.

23.5.1 Translation, rotation and momentum kick

23.5.1.1 Temporal translation operator

The temporal evolution of a system is described by the Schrödinger equation whose formal solution can be written as follows,

$$|\psi(t)\rangle = e^{-\imath\hat{H}t/\hbar}|\psi(0)\rangle \ . \tag{23.176}$$

With this we can define an *evolution operator* or temporal translation,

$$\boxed{U_{tp}(\tau) \equiv e^{-\imath\hat{H}t/\hbar} \qquad \text{such that} \qquad U_{tp}(\tau)|\psi(t)\rangle = |\psi(t+\tau)\rangle} \ . \tag{23.177}$$

The temporal evolution has already been discussed extensively in Sec. 23.4.

23.5.1.2 Spatial translation operator

In this section we look for a unitary *translation operator*,

$$\mathcal{T}_{tr}\mathbf{r} \equiv \mathbf{a} + \mathbf{r} \ . \tag{23.178}$$

Before this, we need to derive the following calculation rule for commutators, which will be done in Exc. 23.5.6.1:

$$e^{\hat{A}}\hat{B}e^{-\hat{A}} = \hat{B} + [\hat{A},\hat{B}] + \tfrac{1}{2!}[\hat{A},[\hat{A},\hat{B}]] + ... \ . \tag{23.179}$$

Applying this formula to the two operators $\hat{\mathbf{p}}$ and $\hat{\mathbf{r}}$ related by the commutation rule (23.53), we obtain,

$$e^{(\imath/\hbar)\mathbf{a}\cdot\hat{\mathbf{p}}}\hat{\mathbf{r}}e^{(-\imath/\hbar)\mathbf{a}\cdot\hat{\mathbf{p}}} = \hat{\mathbf{r}} + [(\imath/\hbar)\mathbf{a}\cdot\hat{\mathbf{p}},\hat{\mathbf{r}}] + \tfrac{1}{2!}\cancelto{0}{[(\imath/\hbar)\mathbf{a}\cdot\hat{\mathbf{p}},\mathbf{a}]} + ... = \hat{\mathbf{r}} + \mathbf{a} \ . \tag{23.180}$$

That is, the operator

$$\boxed{U_{tr}(\mathbf{a}) \equiv e^{(-\imath/\hbar)\mathbf{a}\cdot\hat{\mathbf{p}}}} \tag{23.181}$$

performs a spatial translation of the position operator. The operator is unitary,

$$U_{tr}(\mathbf{a})^{-1} = U_{tr}(\mathbf{a})^{\dagger} \ , \tag{23.182}$$

and forms a group since $U_{tr}(\mathbf{a})U_{tr}(\mathbf{b}) = U_{tr}(\mathbf{a}+\mathbf{b})$. Summarizing the impact of the translation on the operators of space,

$$\boxed{U_{tr}^{\dagger}(\mathbf{a})\hat{\mathbf{r}}U_{tr}(\mathbf{a}) = \hat{\mathbf{r}} + \mathbf{a} \qquad , \qquad U_{tr}^{\dagger}(\mathbf{a})\hat{\mathbf{p}}U_{tr}(\mathbf{a}) = \hat{\mathbf{p}}} \ , \tag{23.183}$$

where the second relation is obvious.

To demonstrate how the translation acts on a state, let us calculate,

$$\hat{\mathbf{r}} e^{(-\imath/\hbar)\mathbf{a}\cdot\hat{\mathbf{p}}}|\mathbf{r}\rangle = e^{(-\imath/\hbar)\mathbf{a}\cdot\hat{\mathbf{p}}}(\hat{\mathbf{r}}+\mathbf{a})|\mathbf{r}\rangle = (\mathbf{r}+\mathbf{a})e^{(-\imath/\hbar)\mathbf{a}\cdot\hat{\mathbf{p}}}|\mathbf{r}\rangle \ . \tag{23.184}$$

Hence,

$$\boxed{U_{tr}(\mathbf{a})|\mathbf{r}\rangle = e^{(-\imath/\hbar)\mathbf{a}\cdot\hat{\mathbf{p}}}|\mathbf{r}\rangle = |\mathbf{r}+\mathbf{a}\rangle} \ . \tag{23.185}$$

Therefore, if a particle is in an eigenstate $|\mathbf{r}\rangle$ of the position operator (i.e. located exactly at the position $\mathbf{r}$), then after $U_{tr}(\mathbf{a})$ acts on it, the particle is at the position $\mathbf{r}+\mathbf{a}$: The translation operator $U_{tr}(\mathbf{a})$ hence moves particles and fields by the distance $\mathbf{a}$.

Finally, we want to describe, how the translation operator acts on an arbitrary state $|\psi\rangle$ represented in position-space, remembering that the position-space wavefunction is obtained via $\psi(\mathbf{r}) \equiv \langle\mathbf{r}|\psi\rangle$, as already mentioned in Sec. 23.3.7. We get,

$$\psi'(\mathbf{r}) \equiv \mathcal{T}_{tr}\psi(\mathbf{r}) \equiv \langle\mathbf{r}|U_{tr}(\mathbf{a})|\psi\rangle = \langle U_{tr}^{\dagger}(\mathbf{a})\mathbf{r}|\psi\rangle = \langle\mathbf{r}-\mathbf{a}|\psi\rangle = \psi(\mathbf{r}-\mathbf{a}) \ . \tag{23.186}$$

This relation is easier to remember as $\psi'(\mathbf{r}+\mathbf{a}) = \psi(\mathbf{r})$, which can be read as: *The value of the new wavefunction at the new point equals the value of the old wavefunction at the old point.*

> **Example 152 (*Translation of spatial wavefunctions*):** Here is an example showing that these two descriptions (23.185) and (23.186) are equivalent. The state $|\mathbf{x}\rangle$ corresponds to the wavefunction $\psi(\mathbf{r}) = \delta^3(\mathbf{r}-\mathbf{x})$, while the state $U_{tr}(\mathbf{a})|\mathbf{x}\rangle = |\mathbf{x}+\mathbf{a}\rangle$ corresponds to the wavefunction $\psi'(\mathbf{r}) = \delta^3(\mathbf{r}-(\mathbf{x}+\mathbf{a}))$. These indeed satisfy $\psi'(\mathbf{r}) = \psi(\mathbf{r}-\mathbf{a})$.

Comparing the expansion of the translation operator,

$$\langle\mathbf{r}|U_{tr}(\mathbf{a})|\psi\rangle = \langle e^{(\imath/\hbar)\mathbf{a}\cdot\hat{\mathbf{p}}}\mathbf{r}|\psi\rangle = \left(1 + \frac{\imath}{\hbar}\mathbf{a}\cdot\hat{\mathbf{p}} - \frac{1}{\hbar^2}\frac{(\mathbf{a}\cdot\hat{\mathbf{p}})^2}{2!} + ..\right)\langle\mathbf{r}|\psi\rangle \ , \tag{23.187}$$

with the Taylor expansion of the wavefunction,

$$\langle\mathbf{r}+\mathbf{a}|\psi\rangle = \psi(\mathbf{r}+\mathbf{a}) = \left(1 + \mathbf{a}\cdot\nabla + \frac{(\mathbf{a}\cdot\nabla)^2}{2!} + ..\right)\psi(\mathbf{r}) \ . \tag{23.188}$$

we obtain

$$\hat{\mathbf{p}}|\mathbf{r}\rangle = \frac{\hbar}{\imath}\nabla|\mathbf{r}\rangle \ . \tag{23.189}$$

Finally, we note that the momentum operator can be defined via the translation operator,

$$\hat{\mathbf{p}} = \imath\hbar\,\nabla_{\mathbf{a}} U_{tr}(\mathbf{a})|_{\mathbf{a}=\mathbf{0}} \ . \tag{23.190}$$

23.5.1.3 Momentum kick operator

In this section we look for the unitary transformation into a frame moving a constant velocity $\mathbf{v}$,

$$\mathcal{T}_{kc}\mathbf{p} \equiv \mathbf{p} + m\mathbf{v} \ . \tag{23.191}$$

As this transformation corresponds to a 'translation' in momentum space, the form of the unitary transformation operator and the way it acts on operators and states are easy to derive by analogy to the spatial translation operator, simply interchanging the roles of the conjugate operators of space and momentum. The corresponding unitary operator in the so-called *kick operator*,

$$\boxed{U_{kc}(m\mathbf{v}) = e^{(\imath/\hbar)m\mathbf{v}\cdot\hat{\mathbf{r}}}} \ . \tag{23.192}$$

where $m\mathbf{v} = \mathbf{p} = \hbar\mathbf{k}$ is the gain in momentum due to the kick.

A common situation where such a kick occurs is the photonic recoil that an atom receives upon absorption of a photon. Using the relationship (23.179) derived in Exc. 23.5.6.1 it is easy to verify the following expressions of the left-hand panel,

$$\boxed{\begin{aligned} e^{\imath\mathbf{k}\cdot\hat{\mathbf{r}}}|\mathbf{r}\rangle &= e^{\imath\mathbf{k}\cdot\mathbf{r}}|\mathbf{r}\rangle \\ e^{\imath\mathbf{k}\cdot\hat{\mathbf{r}}}|\mathbf{p}\rangle &= |\mathbf{p}+\hbar\mathbf{k}\rangle \\ e^{-\imath\mathbf{k}\cdot\hat{\mathbf{r}}}\hat{\mathbf{r}}e^{\imath\mathbf{k}\cdot\hat{\mathbf{r}}} &= \hat{\mathbf{r}} \\ e^{-\imath\mathbf{k}\cdot\hat{\mathbf{r}}}\hat{\mathbf{p}}e^{\imath\mathbf{k}\cdot\hat{\mathbf{r}}} &= \hat{\mathbf{p}}+\hbar\mathbf{k} \\ e^{-\imath\mathbf{k}\cdot\hat{\mathbf{r}}}\frac{\hat{\mathbf{p}}^2}{2m}e^{\imath\mathbf{k}\cdot\hat{\mathbf{r}}} &= \frac{(\hat{\mathbf{p}}+\hbar\mathbf{k})^2}{2m} \end{aligned}} \quad , \quad \boxed{\begin{aligned} e^{-\imath\mathbf{b}\cdot\hat{\mathbf{p}}/\hbar}|\mathbf{r}\rangle &= |\mathbf{r}+\mathbf{b}\rangle \\ e^{-\imath\mathbf{b}\cdot\hat{\mathbf{p}}/\hbar}|\mathbf{p}\rangle &= e^{-\imath\mathbf{b}\cdot\mathbf{p}/\hbar}|\mathbf{p}\rangle \\ e^{\imath\mathbf{b}\cdot\hat{\mathbf{p}}/\hbar}\hat{\mathbf{r}}e^{-\imath\mathbf{b}\cdot\hat{\mathbf{p}}/\hbar} &= \hat{\mathbf{r}}+\mathbf{b} \\ e^{\imath\mathbf{b}\cdot\hat{\mathbf{p}}/\hbar}\hat{\mathbf{p}}e^{-\imath\mathbf{b}\cdot\hat{\mathbf{p}}/\hbar} &= \hat{\mathbf{p}} \\ e^{\imath\mathbf{b}\cdot\hat{\mathbf{p}}/\hbar}V(\hat{\mathbf{r}})e^{-\imath\mathbf{b}\cdot\hat{\mathbf{p}}/\hbar} &= V(\hat{\mathbf{r}}+\mathbf{b}) \end{aligned}} \tag{23.193}$$

The rule implies $[e^{\imath\mathbf{k}\cdot\hat{\mathbf{r}}}, \hat{\mathbf{p}}] \neq 0 \neq [e^{\imath\mathbf{k}\cdot\hat{\mathbf{r}}}, \hat{H}]$. That is, we describe the kick by simply adding the corresponding momentum $\hbar\mathbf{k}$ to the system and adjusting the kinetic energy accordingly.

The right-hand panel of Eq. (23.193) summarizes rules for calculating with the spatial *displacement operator*, $U_{tr}(\mathbf{b}) = e^{-\imath\mathbf{b}\cdot\hat{\mathbf{p}}/\hbar}$, introduced in Sec. 23.5.1. By analogy we find $[e^{-\imath\mathbf{b}\cdot\hat{\mathbf{p}}/\hbar}, \hat{\mathbf{r}}] \neq 0 \neq [e^{-\imath\mathbf{b}\cdot\hat{\mathbf{p}}/\hbar}, \hat{H}]$ when the particle is subject to a potential.

The 'kick' will play a prominent role in the discussion of photonic recoil (see Sec. 24.6.2). Of course the assumption of an infinitely fast transition is an idealization and the ultimate reason for the non-conservation of momentum and energy by the system. In real situations, such as in the case of photonic recoil, the dynamics should be described by a collision process which conserves momentum and energy.

23.5.1.4 Rotation operator

In this section we look for the unitary transformation corresponding to the *rotation operator* [1298],

$$\mathcal{T}_{rt}\mathbf{r} \equiv e^{\vec{\alpha}\times}\mathbf{r} \ . \tag{23.194}$$

We calculate,

$$\begin{aligned} e^{\vec{\alpha}\times}\mathbf{r} = \sum_n \frac{(\vec{\alpha}\times)^n}{n!}\mathbf{r} &= \mathbf{r} + \vec{\alpha}\times\mathbf{r} + \tfrac{1}{2}\vec{\alpha}\times(\vec{\alpha}\times\mathbf{r}) + .. \\ &= \hat{\mathbf{e}}_\alpha(\hat{\mathbf{e}}_\alpha\cdot\mathbf{r}) + \hat{\mathbf{e}}_\alpha\times\mathbf{r}\sin\alpha - \hat{\mathbf{e}}_\alpha\times(\hat{\mathbf{e}}_\alpha\times\mathbf{r})\cos\alpha \ , \end{aligned} \tag{23.195}$$

as we will see in Exc. 23.5.6.4. We define the unitary rotational transformation by,

$$\boxed{U_{rt}^\dagger(\vec{\alpha})\hat{\mathbf{r}}U_{rt}(\vec{\alpha}) = e^{\vec{\alpha}\times}\hat{\mathbf{r}} \quad , \quad U_{rt}(\vec{\alpha})|\mathbf{r}\rangle = |e^{\vec{\alpha}\times}\mathbf{r}\rangle} \ . \tag{23.196}$$

To derive the explicit form of the rotation operator, we consider two rotations about the same axis $\vec{\alpha} = \lambda_1 \hat{\mathbf{e}}_\alpha + \lambda_2 \hat{\mathbf{e}}_\alpha$, such that

$$U_{rt}(\lambda_1 \hat{\mathbf{e}}_\alpha) U_{rt}(\lambda_2 \hat{\mathbf{e}}_\alpha) = U_{rt}(\lambda_1 \hat{\mathbf{e}}_\alpha + \lambda_2 \hat{\mathbf{e}}_\alpha) \ . \tag{23.197}$$

Calculating the derivative of this equation by λ_1 and then setting $\lambda_1 = 0$, we have,

$$\begin{aligned} & \frac{dU_{rt}(\lambda_1 \hat{\mathbf{e}}_\alpha)}{d\lambda_1}\Big|_{\lambda_1=0} U_{rt}(\lambda_2 \hat{\mathbf{e}}_\alpha) &=& \frac{dU_{rt}(\lambda_1 \hat{\mathbf{e}}_\alpha + \lambda_2 \hat{\mathbf{e}}_\alpha)}{d(\lambda_1+\lambda_2)}\Big|_{\lambda_1=0} \frac{d(\lambda_1+\lambda_2)}{d\lambda_1}\Big|_{\lambda_1=0} \\ \Longrightarrow \quad & \frac{d\lambda_1 \hat{\mathbf{e}}_\alpha}{d\lambda_1}\Big|_{\lambda_1=0} \cdot \nabla_{\vec{\alpha}} U_{rt}(\vec{\alpha})|_{\vec{\alpha}=0} U_{rt}(\lambda_2 \hat{\mathbf{e}}_\alpha) &=& \frac{dU_{rt}(\lambda_2 \hat{\mathbf{e}}_\alpha)}{d\lambda_2} \\ \Longrightarrow \quad & \hat{\mathbf{e}}_\alpha \cdot \tfrac{\hat{\mathbf{L}}}{\imath\hbar} \ U_{rt}(\lambda_2 \hat{\mathbf{e}}_\alpha) &=& \frac{dU_{rt}(\lambda_2 \hat{\mathbf{e}}_\alpha)}{d\lambda_2} \end{aligned} \tag{23.198}$$

where we define the angular momentum operator,

$$\hat{\mathbf{L}} \equiv \imath\hbar \ \nabla_{\vec{\alpha}} U_{rt}(\vec{\alpha})|_{\vec{\alpha}=0} \ . \tag{23.199}$$

The solution of the last differential equation (23.198) is, with $\lambda_2 \hat{\mathbf{e}}_\alpha = \vec{\alpha}|_{\lambda_1=0}$,

$$\boxed{U_{rt}(\vec{\alpha}) = e^{(-\imath/\hbar)\hat{\mathbf{L}}\cdot\vec{\alpha}}} \ . \tag{23.200}$$

The explicit form of $\hat{\mathbf{L}}$ follows from its action on a state $|\psi\rangle$ projected into position space. In analogy with the derivation of the result (23.189), comparing the expansion of the operator (23.200),

$$\langle \mathbf{r}|U_{rt}(\vec{\alpha})|\psi\rangle = \langle e^{(\imath/\hbar)\vec{\alpha}\cdot\hat{\mathbf{L}}}\mathbf{r}|\psi\rangle = \left(1 + \frac{\imath}{\hbar}\vec{\alpha}\cdot\hat{\mathbf{L}} + ..\right)\langle \mathbf{r}|\psi\rangle \ , \tag{23.201}$$

with the Taylor expansion of the wavefunction,

$$\langle e^{\vec{\alpha}\times}\mathbf{r}|\psi\rangle = \psi(\mathbf{r} + \vec{\alpha}\times\mathbf{r} + ..) = [1 + (\vec{\alpha}\times\mathbf{r})\cdot\nabla_{\mathbf{r}} + ..]\,\psi(\mathbf{r}) \ , \tag{23.202}$$

we find,

$$\frac{\imath}{\hbar}\vec{\alpha}\cdot\hat{\mathbf{L}} = (\vec{\alpha}\times\mathbf{r})\cdot\nabla_{\mathbf{r}} = \vec{\alpha}\cdot(\mathbf{r}\times\nabla_{\mathbf{r}}) = \frac{\imath}{\hbar}\vec{\alpha}\cdot(\mathbf{r}\times\hat{\mathbf{p}}) \ , \tag{23.203}$$

that is,

$$\hat{\mathbf{L}} = \hat{\mathbf{r}}\times\hat{\mathbf{p}} \ . \tag{23.204}$$

Therefore, the observable $\hat{\mathbf{L}}$ is the *orbital angular momentum* of the particle producing the rotations.

Inserting the angular momentum expression (23.204) into the rotation operator (23.200) and using the rule (23.179) as well as the commutation relations for position and momentum operators, we can now verify the expression directly. Note also that the rotation transformation acts on the momentum operators and states in the same way as on position operators and states. This is not surprising, as the angular momentum operator is symmetric in $\mathbf{r}$ and $\mathbf{p}$.

23.5.2 Transformation to accelerated and rotating frames

23.5.2.1 Transformation to an accelerated frame

Transformation into a accelerated frame with acceleration $\mathbf{g}$ adds a homogeneous force term to the Hamiltonian. At non-relativistic velocities, the transformation can be performed via a unitary kick into a system instantaneously moving at velocity $\mathbf{g}t$,

$$\boxed{U_{ac}(\mathbf{g}) = e^{(\imath/\hbar)m\mathbf{g}t\cdot\hat{\mathbf{r}}}} \quad , \quad |\psi_{ac}\rangle = U_{ac}(\mathbf{g})|\psi\rangle \ . \tag{23.205}$$

This operator removes the force field from the Hamiltonian, since the Schrödinger equation,

$$\imath\hbar\frac{d}{dt}|\psi\rangle = \hat{H}|\psi\rangle \qquad \text{with} \qquad \hat{H} = \frac{\hat{\mathbf{p}}^2}{2m} + m\mathbf{g}\cdot\hat{\mathbf{r}} \ , \tag{23.206}$$

transforms into the Schrödiner equation,

$$\begin{aligned} \imath\hbar\frac{d}{dt}|\psi_{ac}\rangle &= \imath\hbar\frac{d}{dt}\left(e^{(\imath/\hbar)m\mathbf{g}t\cdot\hat{\mathbf{r}}}|\psi\rangle\right) \\ &= \imath\hbar e^{(\imath/\hbar)m\mathbf{g}t\cdot\hat{\mathbf{r}}}\frac{d}{dt}|\psi\rangle + \imath\hbar|\psi\rangle\frac{d}{dt}e^{(\imath/\hbar)m\mathbf{g}t\cdot\hat{\mathbf{r}}} \\ &= e^{(\imath/\hbar)m\mathbf{g}t\cdot\hat{\mathbf{r}}}\left(\frac{\hat{\mathbf{p}}^2}{2m} + m\mathbf{g}\cdot\hat{\mathbf{r}}\right)|\psi\rangle - m\mathbf{g}\cdot\hat{\mathbf{r}}e^{(\imath/\hbar)m\mathbf{g}t\cdot\hat{\mathbf{r}}}|\psi\rangle = \frac{\hat{\mathbf{p}}^2}{2m}|\psi_{ac}\rangle \ . \end{aligned} \tag{23.207}$$

23.5.2.2 Transformation to a rotating frame

Transformation into a frame rotating at angular velocity $\vec{\omega}$ adds ... to the Hamiltonian. At non-relativistic velocities, the transformation can be performed via a unitary rotation transformation into a system rotated by an angle $\vec{\omega}t$,

$$\boxed{U_{ar}(\vec{\omega}) = e^{(\imath/\hbar)m\vec{\omega}t\cdot\hat{\mathbf{L}}}} \quad , \quad |\psi_{ar}\rangle = U_{ar}(\vec{\omega})|\psi\rangle \ . \tag{23.208}$$

23.5.3 Composite transformations, Galilei boost

Some transformations are generated by several operators. The Galilei transform of a system into a moving frame, the displacement operator for coherent states (24.111), or the squeezing operator (35.88) are prominent examples. These transformations can be handled using Glauber's formula, which will be introduced below, before we turn our attention to the Galilei transform.

23.5.3.1 Glauber's and Baker-Campbell-Hausdorff's formulas

The *Baker-Campbell-Hausdorff formula* for operators $\hat{A}$ and $\hat{B}$ reads,

$$\ln(e^{\hat{A}}e^{\hat{B}}) = \hat{A} + \hat{B} + \tfrac{1}{2}[\hat{A},\hat{B}] + \tfrac{1}{12}[\hat{A},[\hat{A},\hat{B}]] - \tfrac{1}{12}[\hat{B},[\hat{A},\hat{B}]] + ... \ . \tag{23.209}$$

A useful special case called *Glauber's formula* follows when $\hat{A}$ and $\hat{B}$ commute with their commutator, i.e. $[\hat{A},[\hat{A},\hat{B}]] = [\hat{B},[\hat{A},\hat{B}]] = 0$,

$$\boxed{e^{[\hat{B},\hat{A}]/2}e^{\hat{A}}e^{\hat{B}} = e^{\hat{A}+\hat{B}} = e^{[\hat{A},\hat{B}]/2}e^{\hat{B}}e^{\hat{A}}} \ . \tag{23.210}$$

Example 153 (*The Baker-Hausdorff formula*): In order to prove the Baker-Hausdorff formula, we consider the operator,

$$\hat{G}(\tau) \equiv e^{\tau(\hat{A}+\hat{B})} e^{-\tau\hat{B}} e^{-\tau\hat{A}} \ .$$

The derivative is,

$$\begin{aligned}
\hat{G}'(\tau) &= (\hat{A}+\hat{B}) e^{\tau(\hat{A}+\hat{B})} e^{-\tau\hat{B}} e^{-\tau\hat{A}} - e^{\tau(\hat{A}+\hat{B})} \hat{B} e^{-\tau\hat{B}} e^{-\tau\hat{A}} - e^{\tau(\hat{A}+\hat{B})} e^{-\tau\hat{B}} \hat{A} e^{-\tau\hat{A}} \\
&= e^{\tau(\hat{A}+\hat{B})} \left[\hat{A} e^{-\tau\hat{B}} - e^{-\tau\hat{B}} \hat{A} \right] e^{-\tau\hat{A}} = e^{\tau(\hat{A}+\hat{B})} \left[\hat{A} - e^{-\tau\hat{B}} \hat{A} e^{\tau\hat{B}} \right] e^{-\tau\hat{B}} e^{-\tau\hat{A}} \\
&= e^{\tau(\hat{A}+\hat{B})} \left[\hat{A} - \left(\hat{A} + [-\tau\hat{B}, \hat{A}] + \tfrac{1}{2!}[-\tau\hat{B}, [-\tau\hat{B}, \hat{A}]] + .. \right) \right] e^{-\tau\hat{B}} e^{-\tau\hat{A}} \ ,
\end{aligned}$$

using the formula (23.179). If now $[\hat{A}, [\hat{A}, \hat{B}]] = 0 = [\hat{B}, [\hat{A}, \hat{B}]]$, then,

$$\hat{G}'(\tau) = e^{\tau(\hat{A}+\hat{B})} \tau [\hat{B}, \hat{A}] e^{-\tau\hat{B}} e^{-\tau\hat{A}} = -\tau [\hat{A}, \hat{B}] e^{\tau(\hat{A}+\hat{B})} e^{-\tau\hat{B}} e^{-\tau\hat{A}} = -\tau [\hat{A}, \hat{B}] \hat{G}(\tau) \ .$$

The solution of this differential equation is,

$$\hat{G}(\tau) \equiv e^{-(\tau^2/2)[\hat{A},\hat{B}]} \hat{G}(0) \ .$$

With $\hat{G}(0) = 1$ we obtain at the point $\tau = 1$,

$$e^{\hat{A}+\hat{B}} e^{-\hat{B}} e^{-\hat{A}} = e^{-(1/2)[\hat{A},\hat{B}]} \ .$$

23.5.3.2 Galilei and Lorentz boosts

The *Galilei transform* (or *Galilei boost*) is defined by,

$$\mathcal{T}_G \mathbf{r} = \mathbf{r} + \mathbf{v}t \qquad \text{and} \qquad \mathcal{T}_G \mathbf{p} = \mathbf{p} + m\mathbf{v} \ . \tag{23.211}$$

It describes the transformation of a system into a moving frame. Obviously, the Galilei transform must satisfy $\mathcal{T}_{\mathbf{v}_1} \mathcal{T}_{\mathbf{v}_2} = \mathcal{T}_{\mathbf{v}_1+\mathbf{v}_2}$, while this certainly does not hold for relativistic velocities.

In quantum mechanics we define,

$$\hat{\mathbf{G}} = \hat{\mathbf{p}}t - \hat{\mathbf{r}}m = \imath\hbar \nabla_{\mathbf{v}} U_G(\mathbf{v})|_{\mathbf{v}=0} \ , \tag{23.212}$$

with the Galilei boost,

$$\boxed{U_G(\mathbf{v}) = e^{(-\imath/\hbar)\mathbf{v}\cdot\hat{\mathbf{G}}}} \ . \tag{23.213}$$

We can simplify this unitary transform using Glauber's formula (23.210). To this end we first calculate the commutator,

$$[\mathbf{v}\cdot\hat{\mathbf{p}}, \mathbf{v}\cdot\hat{\mathbf{r}}] = -\imath\hbar\mathbf{v}^2 \ , \tag{23.214}$$

which does not depend on $\hat{\mathbf{p}}$ nor $\hat{\mathbf{r}}$, but may contribute a phase factors. With this we can rewrite the expression (23.213),

$$\begin{aligned}
U_G(\mathbf{v}) &= e^{(-\imath/\hbar)\mathbf{v}t\cdot\hat{\mathbf{p}} + (\imath/\hbar)\mathbf{v}m\cdot\hat{\mathbf{r}}} \qquad (23.215) \\
&= e^{(-\imath/\hbar)mt\mathbf{v}^2/2} e^{(\imath/\hbar)\mathbf{v}m\cdot\hat{\mathbf{r}}} e^{(-\imath/\hbar)\mathbf{v}t\cdot\hat{\mathbf{p}}} = e^{(\imath/\hbar)mt\mathbf{v}^2/2} e^{(-\imath/\hbar)\mathbf{v}t\cdot\hat{\mathbf{p}}} e^{(\imath/\hbar)\mathbf{v}m\cdot\hat{\mathbf{r}}} \\
U_G^\dagger(\mathbf{v}) &= e^{(\imath/\hbar)\mathbf{v}t\cdot\hat{\mathbf{p}} - (\imath/\hbar)\mathbf{v}m\cdot\hat{\mathbf{r}}} \\
&= e^{(-\imath/\hbar)mt\mathbf{v}^2/2} e^{(-\imath/\hbar)\mathbf{v}m\cdot\hat{\mathbf{r}}} e^{(\imath/\hbar)\mathbf{v}t\cdot\hat{\mathbf{p}}} = e^{(\imath/\hbar)mt\mathbf{v}^2/2} e^{(\imath/\hbar)\mathbf{v}t\cdot\hat{\mathbf{p}}} e^{(-\imath/\hbar)\mathbf{v}m\cdot\hat{\mathbf{r}}} \ .
\end{aligned}$$

We apply these expressions to transform the position and momentum operators,

$$\boxed{\begin{array}{rcl} U_G^\dagger(\mathbf{v})\hat{\mathbf{r}}U_G(\mathbf{v}) &=& e^{(\imath/\hbar)\mathbf{v}t\cdot\hat{\mathbf{p}}}\hat{\mathbf{r}}e^{(-\imath/\hbar)\mathbf{v}t\cdot\hat{\mathbf{p}}} = \hat{\mathbf{r}} + \mathbf{v}t \\ U_G^\dagger(\mathbf{v})\hat{\mathbf{p}}U_G(\mathbf{v}) &=& e^{(-\imath/\hbar)\mathbf{v}m\cdot\hat{\mathbf{r}}}\hat{\mathbf{p}}e^{(\imath/\hbar)\mathbf{v}m\cdot\hat{\mathbf{r}}} = \hat{\mathbf{p}} + m\mathbf{v} \end{array}} \ , \tag{23.216}$$

and consequently,

$$\begin{aligned} U_G^\dagger(\mathbf{v})\frac{\hat{\mathbf{p}}^2}{2m}U_G(\mathbf{v}) = \frac{\left[U_G^\dagger(\mathbf{v})\hat{\mathbf{p}}U_G(\mathbf{v})\right]^2}{2m} = \frac{(\hat{\mathbf{p}}+m\mathbf{v})^2}{2m} \\ U_G^\dagger(\mathbf{v})V(\hat{\mathbf{r}})U_G(\mathbf{v}) = V(U_G^\dagger(\mathbf{v})\hat{\mathbf{r}}U_G(\mathbf{v})) = V(\hat{\mathbf{r}}+\mathbf{v}t) \ . \end{aligned} \tag{23.217}$$

Setting $m = 0$ the Galilei boost simply reproduces a spatial translation by a vector $\mathbf{v}t$, and setting $t = 0$ the Galilei boost simply becomes the prescription for the momentum kick by an amount $m\mathbf{v}$.

Applying the Galilei boost expressions (23.215) to states, we find,

$$\boxed{\begin{array}{rcl} U_G(\mathbf{v})|\mathbf{r}\rangle &=& e^{(\imath/\hbar)m\mathbf{v}\cdot(\hat{\mathbf{r}}+\mathbf{v}t/2)}|\mathbf{r}+\mathbf{v}t\rangle \\ U_G(\mathbf{v})|\mathbf{p}\rangle &=& e^{-(\imath/\hbar)t\mathbf{v}\cdot(\hat{\mathbf{p}}+m\mathbf{v}/2)}|\mathbf{p}+m\mathbf{v}\rangle \end{array}} \ . \tag{23.218}$$

The prefactors do not shift the states, but only contribute irrelevant phase factors.

Finally, knowing the commutator of $\hat{\mathbf{p}}$ and $\hat{\mathbf{r}}$ we derive,

$$[\mathbf{G}\cdot\mathbf{a}, \mathbf{G}\cdot\mathbf{b}] = 0 \ , \tag{23.219}$$

for any vectors $\mathbf{a}$ and $\mathbf{b}$, and with that, using Glauber's formula (23.210), we verify,

$$U_G(\mathbf{v}_1)U_G(\mathbf{v}_2) = e^{(-\imath/\hbar)(\mathbf{v}_1+\mathbf{v}_2)\cdot\mathbf{G} - [\mathbf{v}_1\cdot\mathbf{G}, \mathbf{v}_2\cdot\mathbf{G}]/2\hbar^2} = U_G(\mathbf{v}_1+\mathbf{v}_2) \ . \tag{23.220}$$

Obviously, for very high velocities, the Galilei-boost should be replaced by the *Lorentz transform* (or *Lorentz boost*) [659]. Here, we only note, that the additivity of velocities expressed by equation (23.220) does not hold for non-collinear relativistic velocities (see Sec. 20.1.6).

23.5.4 Gauge transformations

We learn in electrodynamics [15], that the motion of a particle carrying the charge q and interacting with an electrical potential $\Phi(\mathbf{r}, t)$ and a magnetic vector potential $\mathbf{A}(\mathbf{r}, t)$ is governed by the electric and the magnetic field,

$$\vec{\mathcal{E}}(\mathbf{r}, t) = -\nabla\Phi - \partial_t\mathbf{A} \qquad \text{and} \qquad \vec{\mathcal{B}}(\mathbf{r}, t) = \nabla\times\mathbf{A} \ . \tag{23.221}$$

Also, we know that the fields are invariant under the substitution,

$$\Phi \to \Phi' \equiv \Phi - \partial_t\chi \qquad \text{and} \qquad \mathbf{A} \to \mathbf{A}' \equiv \mathbf{A} + \nabla\chi \ , \tag{23.222}$$

[15] See script on *Electrodynamics* (2023).

where $\chi(\mathbf{r},t)$ is a scalar field called *gauge field*.

In quantum mechanics the *gauge transformation* defined by,

$$\boxed{U_{gg}(\chi) = e^{-\imath q\chi(\mathbf{r},t)/\hbar}} \tag{23.223}$$

obviously must keep the Schrödinger equation invariant. However, since the gauge field may depend on time, as shown in Sec. 23.4.5, the Hamiltonian is different in the transformed system. Transforming operators and wave functions as,

$$\hat{H} \to U_{gg}\hat{H}U_{gg}^{-1} \equiv \hat{H}_U \qquad \text{and} \qquad |\psi\rangle \to U_{gg}|\psi\rangle \equiv |\psi_U\rangle \ , \tag{23.224}$$

we calculate for the energy,

$$\begin{aligned}\hat{H}_U|\psi_U\rangle = U_{gg}\imath\hbar\tfrac{d}{dt}U_{gg}^{-1}|\psi_U\rangle &= U_{gg}\imath\hbar U_{gg}^{-1}\tfrac{d}{dt}|\psi_U\rangle + U_{gg}\imath\hbar\left(\tfrac{-\imath q}{\hbar}U_{gg}^{-1}\tfrac{d\chi}{dt}\right)|\psi_U\rangle \\ &= \imath\hbar\left(\tfrac{d}{dt} - \tfrac{\imath q}{\hbar}\tfrac{d\chi}{dt}\right)|\psi_U\rangle \ ,\end{aligned} \tag{23.225}$$

in accordance with the transformation rule (23.167) for time-dependent unitary transformations. For the momentum, we get analogously,

$$\begin{aligned}\hat{\mathbf{p}}_U|\psi_U\rangle = U_{gg}(-\imath\hbar\nabla)U_{gg}^{-1}|\psi_U\rangle &= U_{gg}(-\imath\hbar)U_{gg}^{-1}(\nabla|\psi_U\rangle) + U_{gg}(-\imath\hbar)\left(\tfrac{-\imath q}{\hbar}U_{gg}^{-1}\nabla\chi\right)|\psi_U\rangle \\ &= (-\imath\hbar)\left[\nabla - \tfrac{\imath q}{\hbar}(\nabla\chi)\right]|\psi_U\rangle \ ,\end{aligned} \tag{23.226}$$

This corresponds to the substitutions [16],

$$\boxed{U_{gg}\imath\hbar\frac{d}{dt}U_{gg}^{-1} = \imath\hbar\frac{d}{dt} + q\frac{d\chi}{dt} \qquad \text{and} \qquad U_{gg}\hat{\mathbf{p}}U_{gg}^{-1} = \hat{\mathbf{p}} - q\nabla\chi} \ . \tag{23.227}$$

This shows that the gauge transformation applies to the *minimal coupling* rule (see Sec. 30.1.2),

$$\hat{H} = \hat{H}_{kin}+q\Phi \overset{U_{gg}}{\curvearrowright} \hat{H}_{kin}+q\Phi+q\partial_t\chi \quad \text{and} \quad m\hat{\mathbf{v}} = \hat{\mathbf{p}}-q\mathbf{A} \overset{U_{gg}}{\curvearrowright} \hat{\mathbf{p}}-q\mathbf{A}-q\nabla\chi \ , \tag{23.228}$$

confirming the rules (23.222). That is, the Hamiltonian of a particle carrying the charge q and interacting with an electric potential Φ and a magnetic vector potential $\mathbf{A}$ is,

$$\hat{H} = \tfrac{1}{2m}(\hat{\mathbf{p}} - q\mathbf{A} - q\nabla\chi)^2 + q\Phi + q\partial_t\chi \ . \tag{23.229}$$

23.5.5 Noether's theorem and conservation laws

The fundamental laws of physics are often expressed as symmetries. The knowledge of symmetries allows the characterization of a system and its behavior without the need to know its details. We can often deduce the differential equation of motion from the symmetries. The fundamental symmetries define the fundamental laws of physics. Following *Noether's theorem* each symmetry corresponds to a conserved quantity, that is, a quantities that remains invariant for all time. The invariance of a

[16] In quadrivetorial notation $\imath\hbar\partial_\mu \longrightarrow \imath\hbar\partial_\mu + q\partial_\mu\chi$.

system under symmetry transformation represents a *conservation law*. For example, the homogeneity of space corresponds to the conservation of linear momentum.

In quantum mechanics, a *symmetry transformation* is defined by,

$$|\psi\rangle \longrightarrow U|\psi\rangle \qquad \text{and} \qquad \hat{Q} \longrightarrow U\hat{Q}U^{\dagger} \ . \tag{23.230}$$

Therefore, to find a conservation law, i.e., an invariable observable (also called *constant of motion*), we must verify that the observable and the transformed wavefunctions simultaneously satisfy the same fundamental equations (that is, Schrödinger's or Heisenberg's equation) as the original observable and wavefunctions. For example, if the wavefunction $|\psi\rangle$ satisfies the Schrödinger equation, the wave function $U|\psi\rangle$ must do this too,

$$\hat{H}U|\psi\rangle \stackrel{!}{=} \imath\hbar\frac{d}{dt}U|\psi\rangle = \imath\hbar\frac{dU}{dt}|\psi\rangle + \imath\hbar U\frac{d}{dt}|\psi\rangle = \imath\hbar\frac{dU}{dt}|\psi\rangle + U\hat{H}|\psi\rangle \ . \tag{23.231}$$

Consequently, we obtain the relation,

$$[\hat{H}, U] = \imath\hbar\dot{U} \ . \tag{23.232}$$

As shown in (23.175) and (23.176), an operator that commutes with the Hamiltonian does not explicitly depend on time, that is, it is *conserved*.

23.5.5.1 Temporal homogeneity

Temporal homogeneity means invariance under translation in time by a fixed time interval τ, that is, under the unitary temporal transformation,

$$U(\tau) \equiv |\psi(\tau)\rangle\langle\psi(0)| = e^{(\imath/\hbar)\hat{E}\tau} \ . \tag{23.233}$$

Since $\frac{d}{dt}e^{(\imath/\hbar)\hat{E}\tau} = 0$, this means $[e^{(\imath/\hbar)\hat{E}\tau}, \hat{H}] = 0$, which implies conservation of energy $[\hat{E}, \hat{H}] = 0$. This will be verified in the Exc. 23.5.6.5.

> **Example 154 (*Homogeneity of time*):** We imagine the following mental experiment or *Gedankenexperiment*: We consider two attractive bodies that move away from each other until they reach the perihelia. At this point, before the bodies reapproach, we change the laws, for example, by modifying the force of attraction. As a consequence, when the bodies arrive at the initial point, the total energy is non-zero. Therefore, the conservation of energy indicates that the laws are invariant.

23.5.5.2 Temporal isotropy

The fundamental laws of classical physics and quantum mechanics are all symmetrical under *time reversal*. That is, they are remain invariant when we change the arrow of time, $t \to -t$.

23.5.5.3 Spatial homogeneity

Spatial homogeneity means invariance under spatial translation, that is, under the unitary translational transformation,

$$U_{tr}(\mathbf{a}) \equiv \int |\mathbf{r}+\mathbf{a}\rangle\langle\mathbf{r}| d^3r = e^{(-\imath/\hbar)\hat{\mathbf{p}}\cdot\mathbf{a}} \ . \tag{23.234}$$

This is equivalent to momentum conservation $[\hat{\mathbf{p}}, \hat{H}] = 0$ [17].

> **Example 155 (*Homogeneity of space*):** Ehrenfest's theorem says $[\hat{\mathbf{p}}, H] = -\imath\hbar\frac{\partial H}{\partial \hat{\mathbf{p}}}$. Therefore, the commutator is not zero when there is a potential, $\hat{H} = \hat{\mathbf{p}}^2/2m + V(\hat{\mathbf{r}})$. This is obvious, because the potential introduces an energy inhomogeneity to a particle interacting with the potential. However, this does not mean that the space itself is inhomogeneous, because in order to verify the translational invariance of space, we must displace the entire system, that is, the particle together with the potential. For example, if the potential is generated by another particle we must consider the Hamiltonian $\hat{H} = \hat{\mathbf{p}}_1^2/2m_1 + \hat{\mathbf{p}}_2^2/2m_2 + V(\hat{\mathbf{r}}_1 - \hat{\mathbf{r}}_2)$.

23.5.5.4 Spatial isotropy

Spatial isotropy means invariance under rotation, that is, under rotational unitary transformation,

$$U_{rt}(\phi) \equiv e^{(-\imath/\hbar)\hat{\mathbf{L}}\phi} \ . \tag{23.235}$$

This is equivalent to the conservation of angular momentum $[\hat{\mathbf{L}}, \hat{H}] = 0$.

23.5.5.5 Parity conservation

Besides continuous symmetry transformations there exist discrete transformations. Discrete symmetries are important in elementary particle physics. The *parity conservation* means invariance to spatial reflection: $\mathbf{r} \to -\mathbf{r}$. A parity transformation is defined by the mirroring of the wavefunction through a point in space, for example $\mathbf{r} = 0$,

$$\hat{P}|\psi(\mathbf{r})\rangle \equiv |\psi(-\mathbf{r})\rangle \ . \tag{23.236}$$

with

$$\hat{P}^2 = \hat{P} \ . \tag{23.237}$$

We talk about *even* parity when $\hat{P}|\psi(\mathbf{r})\rangle = |\psi(\mathbf{r})\rangle$ and *odd* parity when $\hat{P}|\psi(\mathbf{r})\rangle = -|\psi(\mathbf{r})\rangle$. See Exc. 23.5.6.6.

[17] Imagine that the forces attracting two bodies to each other are not equal: Contrary to Newton's third law, body A attracts body B, more than the body B attracts the body A. In that case after a while the two bodies have different momenta. With the unitary transformation $U_{tr}(\mathbf{a}) = e^{-\imath\hat{p}\cdot\mathbf{a}/\hbar} \simeq 1 - \imath\epsilon\mathbf{p}\cdot\mathbf{a}/\hbar + ...$ we have,

$$U_{tr}H|\psi\rangle = U_{tr}E_\psi|\psi\rangle = E_\psi U|\psi\rangle = H|\psi(\mathbf{r}+\mathbf{a})\rangle =? = H|\psi(\mathbf{r}\rangle \ .$$

Since, $[H, \hat{p}] = 0$, Heisenberg's equation yields,

$$\frac{\partial}{\partial t}\langle\psi|\hat{p}\cdot\mathbf{a}|\psi\rangle = \frac{1}{\imath\hbar}\langle\psi|[\hat{p}\cdot\mathbf{a}, \hat{H}]|\psi\rangle = 0 \ .$$

23.5.5.6 Invariance to the velocity of the inertial system

The *Galilei boost* asks for *Galilei invariance* regarding the transformation,

$$U_G(\mathbf{v}) \equiv \iint |\mathbf{r}+\mathbf{v}t, \mathbf{p}+m\mathbf{v}\rangle\langle \mathbf{r}, \mathbf{p}| d^3r d^3p \ , \tag{23.238}$$

that is, the equations of motion ruling the dynamics of the inertial system under consideration should not dependent on its velocity $\mathbf{v}$.

23.5.5.7 Charge conservation

Let us consider again the *gauge transform* (23.222). We know that the Lagrangian density in free space is given in terms of the potentials by,

$$\begin{aligned} \mathcal{L}(x^\mu) &= \tfrac{1}{4\mu_0} F^{\mu\nu}F_{\mu\nu} - A_\mu j^\mu = \tfrac{\varepsilon_0}{2}\vec{\mathcal{E}}^2 - \tfrac{1}{2\mu_0}\vec{\mathcal{B}}^2 - A_\mu j^\mu \\ &= \tfrac{\varepsilon_0}{2}[\nabla\Phi + \partial_t \mathbf{A}]^2 - \tfrac{1}{2\mu_0}[\nabla\times\mathbf{A}]^2 - \Phi\rho + \mathbf{A}\cdot\mathbf{j} \ , \end{aligned} \tag{23.239}$$

and the *action* is simply the fourth-dimensional integral,

$$S = \int \mathcal{L}(x^\mu) dV dt \ . \tag{23.240}$$

From the Lagrangian formulation, Maxwell's equations can be derived by requiring the action to be minimal, $\delta S = 0$, which yields the Euler-Lagrange equations. As the field equations do not change under gauge transformation, this implies that the action is also unchanged.

To find the relation with *charge conservation*, we simply have to compare the actions in different gauges. First, we express the Lagrangian transformed into the old gauge,

$$\begin{aligned} \mathcal{L}'(x^\mu) &= \tfrac{\varepsilon_0}{2}\{\nabla[\Phi - \cancel{\partial_t\chi}\,] + \partial_t[\mathbf{A} + \cancel{\nabla\chi}\,]\}^2 - \tfrac{1}{2\mu_0}\{\nabla\times[\mathbf{A} + \cancel{\nabla\chi}^{\,0}]\}^2 \\ &\quad - [\Phi - \partial_t\chi]\rho + [\mathbf{A}+\nabla\chi]\cdot\mathbf{j} \\ &= \mathcal{L} + (\partial_t\chi)\rho + \nabla\chi\cdot\mathbf{j} \ . \end{aligned} \tag{23.241}$$

With this result, we can calculate the difference between the actions under gauge transformation and recall, that they can not be different:

$$0 \stackrel{!}{=} S' - S = \int [(\partial_t\chi)\rho + \nabla\chi\cdot\mathbf{j}] dV dt = -\int \chi[\partial_t\rho + \nabla\cdot\mathbf{j}] dV dt \ , \tag{23.242}$$

using partial integration [18] and choosing volumes so large, that every charge is inside. This is the *continuity equation* derived from the gauge invariance of the action. The calculation really is nothing more than an application of Noether's theorem from which we could have derived directly the continuity equation, $\partial_\mu j^\mu = 0$.

In summary, the conservation of charge means invariance with respect to gauge transformations,

$$U_{cl}(\chi) \equiv e^{-\imath q\chi(\mathbf{r},t)/\hbar} \ , \tag{23.243}$$

[18] Think about the argument, because $\int \partial_t|\chi\rho dt = 0$!

where χ is the gauge field. We note that q and χ are conjugated observables. Therefore, if $[\chi, \hat{H}] = 0$, then the charge q is a conserved quantity.

Transformations can be combined. For example, we believe that nowadays all laws are invariant with respect to CPT transformation, that is, a combination of *charge conjugation*, *parity inversion*, and *θ-transform*.

23.5.6 Exercises

23.5.6.1 Ex: Calculus with commutator

Derive the rule (23.179) via a Taylor expansion of the operator $\hat{G}(\tau) \equiv e^{\tau\hat{A}}\hat{B}e^{-\tau\hat{A}}$.

Solution: *To derive the rule we make a Taylor expansion of the operator,*

$$\hat{G}(\tau) \equiv e^{\tau\hat{A}}\hat{B}e^{-\tau\hat{A}} = \sum_n \frac{\tau^n}{n!}\frac{d^n}{d\tau^n}\hat{G}(0) \ .$$

Derivatives are easily calculated,

$$\hat{G}'(\tau) = \hat{A}e^{\tau\hat{A}}\hat{B}e^{-\tau\hat{A}} - e^{\tau\hat{A}}\hat{B}\hat{A}e^{-\tau\hat{A}} = [\hat{A}, \hat{G}(\tau)] \ ,$$
$$\hat{G}''(\tau) = \hat{A}[\hat{A}, \hat{G}(\tau)] - [\hat{A}, \hat{G}(\tau)]\hat{A} = [\hat{A}, [\hat{A}, \hat{G}(\tau)]] \ .$$

At point $\tau = 1$ we get the result (23.179).

23.5.6.2 Ex: Particle in a homogenous gravitational field

a. Consider a particle free to move along the axis of gravity. Derive the time-dependent unitary operator describing the transformation into the particle's rest frame and check, whether the transformation satisfies the expression (23.167).
b. Solve the Schrödinger equation and derive the Heisenberg equations for $\hat{x}$ and $\hat{p}$.
c. Calculate the phase shift due to gravity from the solution of the Schrödinger equation.

Solution: *a. The force free-particle Schrödinger equation,*

$$\imath\hbar\frac{d}{dt}|\psi\rangle = \frac{\hat{p}^2}{2m}|\psi\rangle$$

describes the particle's evolution in the frame accelerated by gravity, where the particle does not sense external forces. With the time-dependent unitary transformation $|\tilde{\psi}\rangle = |\psi\rangle e^{-\imath mgzt/\hbar}$,

$$\begin{aligned}\imath\hbar\frac{d}{dt}|\tilde{\psi}\rangle &= \imath\hbar e^{-\imath mgzt/\hbar}\frac{d}{dt}|\psi\rangle + \imath\hbar|\psi\rangle\frac{d}{dt}e^{-\imath mgzt/\hbar} \\ &= \frac{\hat{p}^2}{2m}e^{-\imath mgzt/\hbar}|\psi\rangle + mgze^{-\imath mgzt/\hbar}|\psi\rangle = \left(\frac{\hat{p}^2}{2m} + mgz\right)|\tilde{\psi}\rangle = \hat{H}|\tilde{\psi}\rangle\end{aligned}$$

we transform back into the lab frame, where the particle is subject to a homogeneous potential.
b. Inserting into the Schrödinger equation,

$$\imath\hbar\frac{d}{dt}\tilde{\psi}(z,t) = \hat{H}\tilde{\psi}(z,t) = \left(-\frac{\hbar^2}{2m}\frac{d^2}{dz^2} + mg\hat{z}\right)\tilde{\psi}(z,t)$$

the ansatz,

$$\tilde{\psi}(z,t) \equiv \psi(z)e^{-\imath Et/\hbar}e^{-\imath mgzt/\hbar} \ ,$$

we get,

$$-\frac{d^2}{dz^2}\psi(z) = \frac{2mE}{\hbar^2}\psi(z) = k^2\psi(z) \ .$$

Hence,

$$\tilde{\psi}(z,t) = e^{-\imath Et/\hbar}e^{-\imath mgzt/\hbar}e^{\imath kz} \ .$$

The Heisenberg equations are,

$$\frac{d}{dt}\hat{z} = \frac{\imath}{\hbar}[\hat{H},\hat{z}] = \frac{\hat{p}}{m} \qquad \textit{and} \qquad \frac{d}{dt}\hat{p} = \frac{\imath}{\hbar}[\hat{H},\hat{p}] = mg \ .$$

c. The instantaneous phase is the exponent of the wavefunction,

$$\phi(t) = -\frac{Et}{\hbar} - \frac{mgzt}{\hbar} + kz = k\left(z - \frac{v}{2}t\right) - \frac{mgzt}{\hbar} \ ,$$

with $v = \hbar k/m$. Without gravity the de Broglie phase front would propagate with $z - \frac{v}{2}t = const$. Hence, the phase shift due to gravity depends quadratically on time,

$$\phi_{2z=vt}(t) = -\frac{mgvt^2}{2\hbar} = -\frac{kgt^2}{2} \ .$$

23.5.6.3 Ex: Phase shift in a Ramsey-Bordé interferometer

a. Calculate the time dependence of the dynamical phase accumulated by an atom in the field of gravity as a function of its initial momentum.
b. Derive the phase difference of a particle wavefunction passing through a *Ramsey-Bordé interferometer* [19].

Solution: *a. We assume plane waves. The momentum evolves as,*

$$p = mgt + p_0 \ .$$

Hence, the accumulated phase is,

$$\phi_{p_0} = \hbar^{-1}\int_0^t Edt = \hbar^{-1}\int_0^t \frac{p^2}{2m}dt = \frac{mg^2t^3}{6\hbar} + \frac{p_0gt^2}{2\hbar} + \frac{p_0^2t}{2m\hbar} \ .$$

[19] A Ramsey-Bordé interferometer consists of a $\pi/2$-π-$\pi/2$ laser pulse sequence (similar to photon echo in NMR) of Bragg diffraction pulses leading to a splitting and recombination of an atomic wavefunction in momentum space. Assume that every pulse transfers one unit of photonic recoil, $\hbar k$, to the atomic center-of-mass, where k is the wavevector of the laser light.

The phase difference with and without initial momentum is,

$$\Delta\phi = \phi_{p_0} - \phi_0 = \tfrac{1}{2\hbar}(p_0 g t^2 + \tfrac{1}{m} p_0^2 t) \ .$$

b. Using the obtained result, we calculate for each of the two arms of a Ramsey-Bordé interferometer, the upper and the lower one, two contributions: One phase shift accumulated between the first and second laser pulse and another phase shift accumulated between the second and third laser pulse,

$$\phi_{lower} = \phi_{p_0}|_{p_0=0} + \phi_{p_0}|_{p_0=\hbar k - mgt} \qquad \textit{and} \qquad \phi_{upper} = \phi_{p_0}|_{p_0=\hbar k} + \phi_{p_0}|_{p_0=\hbar k - mgt} \ ,$$

where t is the time interval between the first and second laser pulse. Apparently, the phase shifts accumulated during the time interval between the second and third laser pulse cancel out. Hence,

$$\Delta\phi = \phi_{upper} - \phi_{lower} = \phi_{p_0}|_{p_0=\hbar k} - \phi_{p_0}|_{p_0=0} = \frac{\hbar k g t^2}{2\hbar} + \frac{(\hbar k)^2 t}{2m\hbar} = \frac{k g t^2}{2} + \omega_{rec} t \ .$$

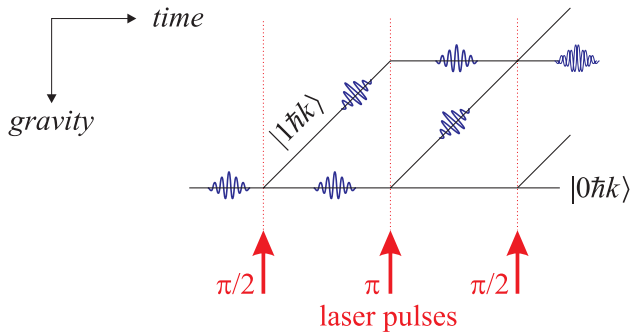

Figure 23.6: Scheme of a Ramsey-Bordé interferometer.

23.5.6.4 Ex: Rotation operator

Derive the rule $e^{\vec{\alpha}\times}\mathbf{r} = \sum_n \frac{(\vec{\alpha}\times)^n}{n!}\mathbf{r} = \hat{\mathbf{e}}_\alpha(\hat{\mathbf{e}}_\alpha\cdot\mathbf{r}) + \hat{\mathbf{e}}_\alpha\times\mathbf{r}\sin\alpha - \hat{\mathbf{e}}_\alpha\times(\hat{\mathbf{e}}_\alpha\times\mathbf{r})\cos\alpha$.

Solution: *We use,*

$$\begin{aligned}
&\vec{\alpha}\times(\vec{\alpha}\times\mathbf{r}) = \vec{\alpha}(\vec{\alpha}\cdot\mathbf{r}) - \alpha^2\mathbf{r} \\
&\vec{\alpha}\times[\vec{\alpha}\times(\vec{\alpha}\times\mathbf{r})] = -\alpha^2(\vec{\alpha}\cdot\mathbf{r}) \\
&\vec{\alpha}\times\{\vec{\alpha}\times[\vec{\alpha}\times(\vec{\alpha}\times\mathbf{r})]\} = -\alpha^2\vec{\alpha}\times(\vec{\alpha}\times\mathbf{r}) \ .
\end{aligned}$$

The odd terms of the sum give

$$\vec{\alpha}\times\mathbf{r} - \tfrac{\alpha^2}{3!}\vec{\alpha}\times\mathbf{r} + \tfrac{\alpha^4}{5!}\vec{\alpha}\times\mathbf{r} - ... = \vec{\alpha}\times\mathbf{r}\sin\alpha \ .$$

Even terms give

$$\mathbf{r} - \tfrac{1}{2!}\vec{\alpha}\times(\vec{\alpha}\times\mathbf{r}) - \tfrac{\alpha^2}{4!}\vec{\alpha}\times(\vec{\alpha}\times\mathbf{r}) - ... = \mathbf{r} + (1-\cos\alpha)\vec{\alpha}\times(\vec{\alpha}\times\mathbf{r}) \ .$$

Putting the terms together,

$$e^{\vec{\alpha}\times}\mathbf{r} = \mathbf{r} + \hat{\mathbf{e}}_\alpha \times \mathbf{r}\sin\alpha + \hat{\mathbf{e}}_\alpha \times (\hat{\mathbf{e}}_\alpha \times \mathbf{r})(1-\cos\alpha) \ ,$$

this is the equation we looked for.
The transformation represents a rotation about the angle $\vec{\alpha}$, which can be seen by separating $\mathbf{r}$ into vectors parallel or perpendicular to $\hat{\mathbf{e}}_\alpha$:

$$e^{\vec{\alpha}\times}\mathbf{r}_\parallel + e^{\vec{\alpha}\times}\mathbf{r}_\perp = \mathbf{r}_\parallel + \hat{\mathbf{e}}_\alpha \times \mathbf{r}_\perp \sin\alpha + \mathbf{r}_\perp \cos\alpha \ .$$

This equation is equivalent to,

$$e^{\vec{\alpha}\times}\mathbf{r}_\parallel = \mathbf{r}_\parallel \qquad \textit{and} \qquad e^{\vec{\alpha}\times}\mathbf{r}_\perp = \hat{\mathbf{e}}_\alpha \times \mathbf{r}_\perp \sin\alpha + \mathbf{r}_\perp \cos\alpha \ ,$$

the parallel component is conserved while for the perpendicular we have,

$$(e^{\vec{\alpha}\times}\mathbf{r}_\perp)^2 = \mathbf{r}_\perp^2 \sin^2\alpha + \mathbf{r}_\perp^2 \cos^2\alpha = \mathbf{r}_\perp^2 \qquad \textit{and} \qquad (e^{\vec{\alpha}\times}\mathbf{r}_\perp)\cdot\mathbf{r}_\perp - \cos\alpha \ .$$

23.5.6.5 Ex: Constants of motion

Show at the example of energy conservation using the relation (23.232), that energy commutes with the Hamiltonian if $\dot{E} = 0$.

Solution: *If $\dot{E} = 0$, we can deduce,*

$$0 = -e^{(\imath/\hbar)\hat{E}\tau}\frac{d\hat{E}}{dt} = \imath\hbar\frac{d}{dt}\left(e^{(\imath/\hbar)\hat{E}\tau}\right) = \imath\hbar\dot{U} = [\hat{H},U] = \left[\hat{H},\left(1+\frac{\imath\hat{E}\tau}{\hbar} - \frac{\hat{E}^2\tau^2}{2!\hbar^2} + ...\right)\right]$$
$$= \frac{\imath\tau}{\hbar}[\hat{H},\hat{E}] - \frac{\tau^2}{2!\hbar^2}[\hat{H},\hat{E}^2] + ... = \frac{\imath\tau}{\hbar}[\hat{H},\hat{E}] - \frac{\tau^2}{2!\hbar^2}\left[[\hat{H},\hat{E}]\hat{E} + \hat{E}[\hat{H},\hat{E}]\right] + ...,$$

which is valid when $[\hat{H},\hat{E}] = 0$.

23.5.6.6 Ex: Parity

Show that the eigenfunctions of the Hamiltonian $\hat{H} = -(\hbar/2m)(d^2/dx^2) + V(x)$ have well-defined parity, i.e., parity is a *good quantum number* in cases where the energy is an even function of position, $V(x) = V(-x)$.

Solution: *A state $|\psi\rangle$ has even parity when the wavefunction does not change under inversion of the position coordinate, $\hat{P}\langle x|\psi\rangle = \langle -x|\psi\rangle$. It has odd parity when*

$\hat{P}\langle x|\psi\rangle = \langle -x| - \psi\rangle$. *$\hat{P}$ is a* good quantum number *when is commutes with the Hamiltonian,*

$$0 = [\hat{P}, \hat{H}]\langle x|\psi\rangle = \left(-\frac{\hbar^2}{2m}\frac{d^2}{d(-x)^2} + V(-x)\right)\langle -x| \pm \psi\rangle - \left(-\frac{\hbar^2}{2m}\frac{d^2}{dx^2} + V(x)\right)\langle -x| \pm \psi\rangle$$
$$= [V(-x) - V(x)]\langle -x| \pm \psi\rangle \ .$$

That is, it should be, $V(x) = V(-x)$.

23.6 Further reading

Ph.W. Courteille (2020), *Script on Optical spectroscopy: A practical course* http

Ph.W. Courteille (2020), *Script on Electrodynamics: Electricity, magnetism, and radiation* http

Ph.W. Courteille (2020), *Script on Quantum mechanics applied to atomic and molecular physics* http

W.R. Theis, Teubner (1985), *Grundzüge der Quantentheorie* [1298]ISBN

C. Cohen-Tannoudji, B. Diu, F. Laloe, Wiley Interscience, *Quantum mechanics, vol. 1,2* [276]ISBN

L.I. Schiff, McGraw-Hill Book Company (1968), *Quantum mechanics* [1155]ISBN

J.J. Sakurai, J.J. Napolitano, 2^{nd} ed. Springer (2011), *Modern Quantum Mechanics* [1128]ISBN

H.A. Bethe, R. Jackiw, 3^{rd} ed. Taylor & Francis (1997), *Intermediate Quantum Mechanics* [135]ISBN

D.J. Griffiths, *Introduction to Quantum Mechanics* [546]ISBN

Photonics101, *How the Gauge Invariance of the Action implies Charge Conservation* http

Chapter 24

Linear motion / Separable potentials

In this chapter we will analyze the translational and vibrational motion of a quantum particle. We will give special consideration to the rectangular potential and the harmonic oscillator.

24.1 Translational motion

In one dimension the Hamiltonian of a free particle is,

$$\hat{H} = -\frac{\hbar^2}{2m}\frac{d^2}{dx^2} \ . \tag{24.1}$$

Therefore, the general solution of the Schrödinger stationary equation,

$$\hat{H}\psi(x) = E\psi(x) \ , \tag{24.2}$$

is,

$$\psi(x) = Ae^{\imath kx} + Be^{-\imath kx} \qquad \text{with} \qquad k = \sqrt{\tfrac{2mE}{\hbar^2}} \ . \tag{24.3}$$

Note that the $e^{\imath kx}$ functions are not quadratically integrable, since $\int_{-\infty}^{\infty} |e^{\imath kx}|^2 dx = \int_{-\infty}^{\infty} dx \to \infty$. On the other side, they do not represent actual physical systems. In practice, we need to consider wave packets or specify a finite volume for the particle. Note also that the spectrum of eigenvalues is continuous. Do the Exc. 24.1.4.1.

24.1.1 Quadratic integrability

To allow for an interpretation as probability density we need to ask for quadratic integrability,

$$\int |\psi|^2 d^3r = 1 \ . \tag{24.4}$$

This means that the wavefunction can not be infinite inside a finite volume. But it can be infinite within an infinitely small volume. Also, since the Schrödinger equation contains the second derivative by position, the wavefunction must be continuous and have a continuous derivative.

24.1.2 Separation of dimensions

Frequently, a 3D potential can be written in the way,

$$V(x,y,z) = V_x(x) + V_y(y) + V_z(z) \ . \tag{24.5}$$

This is the case, for example, for a rectangular well with $V_x(x) = V_y(y) = V_z(z) = V_0/3$ inside the well and $V(x,y,z) = 0$ outside. It also holds for a harmonic potential,

$$V(\mathbf{r}) = \frac{m}{2}\left(\omega_x^2 x^2 + \omega_y^2 y^2 + \omega_z^2 z^2\right) \ . \tag{24.6}$$

In these cases, the following ansatz for the wavefunction is generally useful,

$$\psi(\mathbf{r}) = \psi_x(x)\psi_y(y)\psi_z(z) \ , \tag{24.7}$$

since inserting the ansatz into the Schrödinger equation,

$$\left[-\frac{\hbar^2}{2m}\left(\frac{d^2}{dx^2} + \frac{d^2}{dy^2} + \frac{d^2}{dz^2}\right) + V_x(x) + V_y(y) + V_z(z)\right]\psi_x(x)\psi_y(y)\psi_z(z) = E\psi_x(x)\psi_y(y)\psi_z(z) \ , \tag{24.8}$$

the equation separates into three independent one-dimensional equations,

$$-\frac{\hbar^2}{2m}\frac{\psi_x''(x)}{\psi_x(x)} + V_x(x) = const. \equiv E_x \ , \tag{24.9}$$

and the same for y and z. Since, $E = E_x + E_y + E_z$ may have the same value for different combinations of E_x, E_y and E_z, multidimensional systems are often degenerate.

24.1.3 Homogeneous force fields, gravity

The behavior of a wavefunction in a homogeneous force field has been studied in Excs. 23.5.6.2 and 23.5.6.3.

24.1.4 Exercises

24.1.4.1 Ex: Trapped particle

Consider the problem of a particle of mass m forced to move in a single direction and completely confined to a box, with walls placed at the positions $x = 0$ and $x = a$.
a. The particle be in the ground state, what is its energy and its wavefunction?
b. Suppose the particle has the following wavefunction:

$$\psi_I(x) = \frac{1}{\sqrt{7a}}\left[2\cos\left(\frac{\pi}{2a}(6x-a)\right) - 3\imath\sin\left(\frac{2\pi}{a}x\right) + \cos\left(\frac{\pi}{2a}(2x-a)\right)\right] \ ,$$

what is the probability that a measurement of the energy yields the result $E = \frac{2\pi^2\hbar^2}{ma^2}$?
c. Considering again the ground state of item (a), what is the probability distribution for the momentum of the particle in this state?
d. Still starting from the ground state, suppose we remove (instantaneously) the walls,

leaving the particle free ($\hat{H} = \hat{p}^2/2m$). What is the energy of this free particle?
Formulae:

$$\int_0^L e^{\imath Bx} \sin\left(\frac{n\pi x}{L}\right) dx = \frac{n\pi L[1-(-1)^n e^{\imath BL}]}{n^2\pi^2 - B^2L^2} \qquad \text{for} \qquad n = 1, 2, 3, ...$$
$$\int_{-\infty}^{\infty} \frac{x^2}{(1-x^2)^2} \cos^2 \tfrac{\pi x}{2} dx = \frac{\pi^2}{4}$$

Solution: *a. This is the classical problem of an infinite potential well in 1D:*

$$\left[-\frac{\hbar^2}{2m}\frac{\partial^2}{\partial x^2} + V(x)\right]\psi(x) = E\psi(x) \ .$$

with $V(x) = 0$ for $0 < x < a$ and $V(x) = \infty$ for $x > a$ or $x < 0$. For $0 < x < a$ the ansatz

$$\psi(x) = Ae^{\imath kx} + Be^{-\imath kx}$$

gives $k = \sqrt{2mE}/\hbar$. For $x > a$ or $x < 0$ we have $\psi(x) = 0$. Hence, $\psi(a) = \psi(0) = 0$ and $\psi(0) = A + B = 0$, that is, $A = -B$. Also, $\psi(a) = A(e^{\imath ka} - e^{-\imath ka}) = 0$, that is, $A\sin(ka) = 0$ or $k = n\pi/a$ for $n = 1, 2, ...$ The result is,

$$\psi_n(x) = A_n \sin\frac{n\pi x}{a} \ .$$

Normalization requires $1 = \int_0^a |\psi_n(x)|^2 dx$, hence,

$$A_n^2 \int_0^a \sin^2\frac{n\pi x}{a} dx = \frac{A_n^2 a}{2} = 1 \ ,$$

or $A_n = \sqrt{2/a}$. The final result is,

$$\psi_n(x) = \sqrt{\frac{2}{a}} \sin\frac{n\pi x}{a} \ ,$$

for $0 < x < a$. With $k = \frac{\sqrt{2mE}}{\hbar} = \frac{n\pi}{a}$ we have

$$E = \frac{n^2\pi^2\hbar^2}{2ma^2} \ ,$$

for $n = 1, 2, 3, ...$
b. We can rewrite the cosines as sines [they are only written as cosines to not immediately deliver the solution of item (a)],

$$\psi_I(x) = \frac{1}{\sqrt{7a}}\left[2\sin\frac{3\pi x}{a} - 3\imath\sin\frac{2\pi x}{a} + \sin\frac{\pi x}{a}\right] \ .$$

The energy $E = \frac{2\pi^2\hbar^2}{ma^2}$ corresponds to the state with $n = 2$ and the wavefunction: $\psi_a(x) = \sqrt{\frac{2}{a}}\sin\frac{2\pi x}{a}$ and the overlap between this state and $\psi_I(x)$ is given by the

scalar product between them (see the given formulae). Only the product with the same period does not result in zero when integrated:

$$\langle\psi_2(x)|\psi_I(x)\rangle = \int_{-\infty}^{\infty}\psi_2^*(x)\psi_I(x)dx = \sqrt{\frac{2}{a}}\frac{-3\imath}{\sqrt{7a}}\int_0^a \sin\frac{2\pi x}{a}\sin\frac{2\pi x}{a}dx = \frac{-3\imath}{\sqrt{14}}\ .$$

The probability is given by:

$$P = |\langle\psi_2(x)|\psi_I(x)\rangle|^2 = \frac{9}{14} \approx 64\%\ .$$

c. We can go from the original wavefunction to the momentum space distribution:

$$\begin{aligned}\psi(p) &= \frac{1}{\sqrt{2\pi\hbar}}\int_{-\infty}^{\infty}\psi(x)e^{\imath px/\hbar}dx = \frac{1}{\sqrt{2\pi\hbar}}\int_0^a\sqrt{\frac{2}{a}}\sin\frac{\pi x}{a}e^{\imath px/\hbar}dx \\ &= \frac{1}{\sqrt{a\pi\hbar}}\frac{\pi a[1+e^{\imath pa/\hbar}]}{\pi^2-p^2a^2/\hbar^2} = \sqrt{\frac{a\pi}{\hbar}}\frac{1+e^{\imath pa/\hbar}}{\pi^2-p^2a^2/\hbar^2}\ ,\end{aligned}$$

using the given formulae. The probability distribution for moments is,

$$\begin{aligned}|\psi(p)|^2 &= \frac{a\pi}{\hbar}\frac{(1+e^{\imath pa}/\hbar)(1+e^{-\imath pa}/\hbar)}{(\pi^2-p^2a^2/\hbar^2)^2} = \frac{a\pi\hbar^3}{(\pi^2\hbar^2-p^2a^2)^2}(2+e^{\imath pa/\hbar}+e^{-\imath pa/\hbar}) \\ &= \frac{2a\pi\hbar^3}{(\pi^2\hbar^2-p^2a^2)^2}(1+\cos pa/\hbar) = \frac{4a\pi\hbar^3}{(\pi^2\hbar^2-p^2a^2)^2}\cos^2 pa/\hbar\ .\end{aligned}$$

d. The 'smart' way to respond is simply to argue that the idealized walls (infinitely high and instantaneously withdrawn) do not interact with the particle. Then by conservation of energy, the energy is the same as in item (a):

$$E_0 = \frac{\pi^2\hbar^2}{2ma^2}\ .$$

Or we can do the calculation. The Hamiltonian of the free particle is $\hat{H} = p^2/2m$. We can calculate the energy using the state prior to the removal of walls, and the new Hamiltonian is,

$$\begin{aligned}E &= \int_{-\infty}^{\infty}\frac{p^2}{2m}|\psi(p)|^2dp = \frac{1}{2m}4a\pi\hbar^3\int_{-\infty}^{\infty}\frac{p^2}{(\hbar^2\pi^2-p^2a^2)^2}\cos^2\frac{pa}{2\hbar}dp \\ &= \frac{2\hbar^2}{ma^2}\int_{-\infty}^{\infty}\frac{y^2}{(1-y^2)^2}\cos^2\frac{\pi y}{2}dy = \frac{\pi^2\hbar^2}{2ma^2}\ ,\end{aligned}$$

using the given formulae.

24.2 Rectangular potentials

The continuity equation (23.16) teaches us that the probability flux of a moving particle cannot make abrupt changes. That is, even if the particle encounters an obstacle represented by a smooth or abrupt variation of the potential depth, the wavefunction and its derivative must remain continuous, unless the potential step is infinitely high.

24.2.1 Box potential

Let us now place the particle into a rectangular potential well, such that the Hamiltonian is,

$$\hat{H} = -\frac{\hbar^2}{2m}\frac{d^2}{dx^2} + V(x) \qquad \text{with} \qquad V(x) = \begin{cases} 0 & \text{for} \quad x \in [0, L] \\ \infty & \text{for} \quad x \notin [0, L] \end{cases} . \tag{24.10}$$

As the potential barriers are high, the walls are hard, that is, the particle, even being a quantum particle, can not penetrate. The wavefunction and the possible energy values are,

$$\boxed{\psi(x) = \sqrt{\frac{2}{L}} \sin\frac{n\pi x}{L} \qquad \text{and} \qquad E_n = \frac{n^2\hbar^2\pi^2}{2mL^2}} . \tag{24.11}$$

The Exc. 24.2.5.1 asks to demonstrate the result (24.11) illustrated in Fig. 24.1.

Obviously the spectrum of eigenvalues is now discrete. They can be enumerated by an integer n called *quantum number*. Note that the energy levels are not equidistant.

> **Example 156 (*Localization energy*):** There is a minimal *energy* $E_1 = \frac{\hbar^2\pi^2}{2mL^2}$ which is called *zero point energy* or *localization energy*. This energy can be understood as a consequence of Heisenberg's *uncertainty principle*. We can make the following gross estimation of the zero point energy. Obviously, the particle is localized with an uncertainty lower than $\Delta x < L$. Hence, $\Delta p > \hbar/\Delta x > \hbar/L$. The average kinetic energy is,
>
> $$\frac{\langle p^2\rangle}{2m} = \frac{\langle p\rangle^2 + \Delta p^2}{2m} = \frac{\Delta p^2}{2m} > \frac{\hbar^2}{2mL^2} .$$
>
> The fact that the numerical value is different from the value calculated by the formula (24.11) comes from the particular geometry of the box potential.

24.2.2 Multidimensional box potential

In a multidimensional well there can be degeneracy if the well exhibits symmetries. In the case of a 2D quadratic well $L_x = L_y$, the eigenenergies are doubly degenerate, since $E_{n_x,n_y} = E_{n_y,n_x}$. In the case of a 3D cubic well $L_x = L_y = L_z$, the eigenenergies are 6-fold degenerate, because $E_{n_x,n_y,n_z} = E_{n_y,n_z,n_x} = E_{n_z,n_x,n_y} = E_{n_z,n_y,n_x} = E_{n_y,n_x,n_z} = E_{n_x,n_z,n_y}$. The states and energies of the 2D well are calculated in Exc. 24.2.5.2.

24.2.3 Potentials with several sections of constant depths

To find the global wavefunction in potentials with several sections of constant depths, we solve Schrödinger's equations separately for each section,

$$\left(-\frac{\hbar^2}{2m}\frac{d^2}{dx^2} + V_a\right)\psi_a(x) = E\psi_a(x) . \tag{24.12}$$

The general solution for a section a with potential energy V_a is,

$$\boxed{\psi_a(x) = A_a e^{\imath k_a x} + B_a e^{-\imath k_a x}} , \tag{24.13}$$

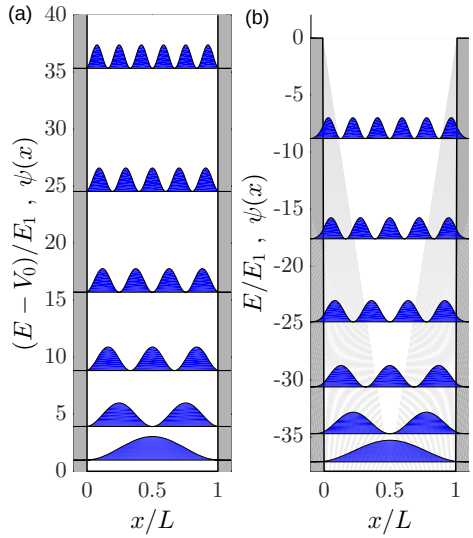

Figure 24.1: (code) (a) Wavefunctions and energies in the box potential. (b) The rectangular potential well with the reference energy set to the height of the well.

where $k_a = \frac{1}{\hbar}\sqrt{2m(E-V_a)}$. If $E > V_a$, the wave is propagating. k_a is the Broglie wavevector of the wave. If $E < V_a$, the wave is evanescent. That is, the wave decays within a distance $\kappa_a = -\imath k_a$.

If the particle is confined, that is, if $E < V(x \to \pm\infty)$, the possible energy levels are quantized and the spectrum is discrete.

For every transition between two sections $a = 1$ and $a = 2$ we require the boundary conditions,

$$\psi_1(x) = \psi_2(x) \qquad \text{and} \qquad \psi_1'(x) = \psi_2'(x)\ . \tag{24.14}$$

Together with the normalization, $1 = \int_{-\infty}^{\infty} |\psi|^2 dx$, these conditions are sufficient to determine the wavefunction unambiguously.

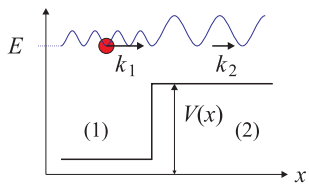

Figure 24.2: Scheme of a potential with several sections of constant depths.

24.2.4 Potential well

Consider a particle with energy E and a potential well of finite depth such that $V(x) = V_0 < 0$ for $-L/2 > x > L/2$ and $V(x) = 0$ otherwise, as illustrated in Fig. 24.3(a). The particle be confined, $E < 0$.

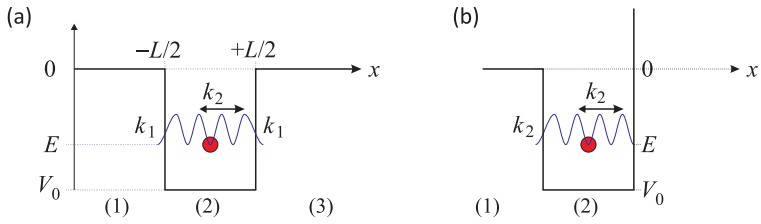

Figure 24.3: (a) Scheme of a two-sided and (b) one-sided potential well.

The wavevectors are

$$k_1 = k_3 = \tfrac{1}{\hbar}\sqrt{2mE} = \imath\tfrac{1}{\hbar}\sqrt{2m|E|} = \imath\kappa_1 \qquad \text{and} \qquad k_2 = \tfrac{1}{\hbar}\sqrt{2m(E-V_0)}\ . \tag{24.15}$$

with $\kappa_1 \in \mathbb{R}^+$. The boundary conditions yield,

$$\begin{aligned} A_1 e^{-\imath k_1 L/2} + B_1 e^{\imath k_1 L/2} &= A_2 e^{-\imath k_2 L/2} + B_2 e^{\imath k_2 L/2} \\ -\imath k_1 A_1 e^{-\imath k_1 L/2} + \imath k_1 B_1 e^{\imath k_1 L/2} &= -\imath k_2 A_2 e^{-\imath k_2 L/2} + \imath k_2 B_2 e^{\imath k_2 L/2} \\ A_2 e^{\imath k_2 L/2} + B_2 e^{-\imath k_2 L/2} &= A_3 e^{\imath k_1 L/2} + B_3 e^{-\imath k_1 L/2} \\ \imath k_2 A_2 e^{\imath k_2 L/2} - \imath k_2 B_2 e^{-\imath k_2 L/2} &= \imath k_1 A_3 e^{\imath k_1 L/2} - \imath k_1 B_3 e^{-\imath k_1 L/2}\ . \end{aligned} \tag{24.16}$$

For confined particles, $E < 0$, the problem is totally symmetric. In addition, the wavefunction must disappear for $x \to \pm\infty$. Therefore, we can simplify,

$$A_1 = 0 = B_3 \qquad \text{and} \qquad A_3 = B_1\ . \tag{24.17}$$

The first two equations (24.16) now give,

$$B_1 e^{\imath k_1 L/2} = A_2 e^{-\imath k_2 L/2} + B_2 e^{\imath k_2 L/2} = \frac{k_2}{k_1}\left(-A_2 e^{-\imath k_2 L/2} + B_2 e^{\imath k_2 L/2}\right)\ . \tag{24.18}$$

We now consider the quotient B_2/A_2. Using the right part of equation (24.18),

$$\frac{B_2}{A_2} = \frac{e^{-\imath k_2 L/2}(k_2 + k_1)}{e^{\imath k_2 L/2}(k_2 - k_1)} = \frac{e^{-\imath k_2 L}(k_2 + \imath\kappa_1)^2}{k_2^2 + \kappa_1^2}\ . \tag{24.19}$$

Since the amplitudes are real, the imaginary part of the quotient (24.19) should disappear, which is the case when,

$$\begin{aligned} 0 &= \mathfrak{Im}\ e^{-\imath k_2 L}(k_2 + \imath\kappa_1)^2 = 2\kappa_1 k_2 \cos k_2 L + (\kappa_1^2 - k_2^2)\sin k_2 L \\ &\Longrightarrow \tan k_2 L = \frac{2\kappa_1 k_2}{-\kappa_1^2 + k_2^2}\ . \end{aligned} \tag{24.20}$$

In order to construct graphically the values of the momenta k_2 of the particle associated with the allowed energy levels, we introduce a constant $\beta \equiv \hbar/(L\sqrt{2m|V_0|})$. Hence,

$$\tan k_2 L = \tan\frac{1}{\beta}\sqrt{1 - |E/V_0|} = \frac{2\sqrt{|E/V_0|}\sqrt{1-|E/V_0|}}{1 - 2|E/V_0|} = \frac{2\kappa_1 k_2}{-\kappa_1^2 + k_2^2}\ . \tag{24.21}$$

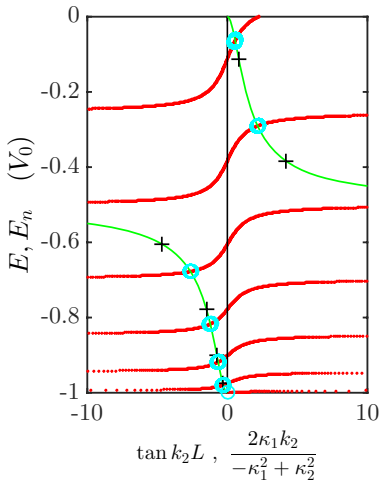

Figure 24.4: (code) Graphical solution for a finite bilateral potential well. The red dotted curves represent the tangents (left side of the equation (24.21)), the solid green curves the hyperbolas (right side of the equation), the circles in cyan are the eigenenergies. When $0 < E - V_0 \ll E$, they converge to the eigenenergies of the infinitely deep well (black crosses and vertical black line).

At the bottom of deep potentials, that is, when $0 < E - V_0 \ll E$, or equivalently, $E \simeq V_0$, we have $k_2 \ll \kappa_1$ and hence, $\tan k_2 L \to 0 \implies k_2 L = n\pi$. The energies are then,

$$E - V_0 = \frac{\hbar^2}{k_2^2} 2m = \frac{\hbar^2 \pi^2}{2mL^2} n^2 \ . \tag{24.22}$$

Apply the notions obtained in this section to solve Excs. 24.2.5.3 and 24.2.5.4.

24.2.5 Exercises

24.2.5.1 Ex: Particle in a box

Obtain the wavefunctions and associated energy levels of a particle confined in a box, where $V(x) = 0$ for $0 \leq x \leq l$ and $V(x) = \infty$ outside.

Solution: *In order to avoid abrupt variations near the walls, we require,*

$$\psi(0) = 0 = \psi(L) \ .$$

The general solution of the Schrödinger equation inside the well is,

$$\psi(t) = C \cos kx + D \sin kx \ .$$

With the boundary conditions,

$$C = 0 \qquad \textit{and} \qquad \sin kL = 0 \ .$$

The normalization condition results in,

$$1 = \int_0^L |\psi(x)|^2 dx = D^2 \int_0^L \sin^2 \frac{n\pi x}{L} dx = \frac{1}{2} L D^2 \ .$$

Therefore, the wave function and the possible values of energy are,

$$\psi(x) = \sqrt{\frac{2}{L}} \sin \frac{n\pi x}{L} \qquad \textit{and} \qquad E_n = \frac{n^2 \hbar^2 \pi^2}{2mL^2} \ .$$

24.2.5.2 Ex: Particle in a two-dimensional box

Obtain the wavefunctions and associated energy levels of a particle trapped in a two-dimensional box inside which the particle is confined to a rectangular surface with dimensions L_1 in x-direction and L_2 in y-direction, $V(x, y) = 0$ for $0 \le x \le L_1$ and $0 \le y \le L_2$ and $V(x, y) = \infty$ else.

Solution: *Since the dimensions of the potential separate, $V(x, y) = V_1(x) + V_2(y)$, we can simply use the solutions of the 1D problem,*

$$\langle n_1, n_2 | \psi \rangle \equiv \psi(x, y) = \frac{2}{\sqrt{L_1 L_2}} \sin \frac{n_1 \pi x}{L_1} \sin \frac{n_1 \pi x}{L_2} \qquad \textit{and} \qquad E_{n_1,n_2} = \frac{n_1^2 \hbar^2 \pi^2}{2mL_1^2} + \frac{n_2^2 \hbar^2 \pi^2}{2mL_2^2} \ .$$

In the case where $L_1 = L_2$, the eigenenergies are doubly degenerate, since $E_{n_1,n_2} = E_{n_2,n_1}$.

24.2.5.3 Ex: Particle in a well

Obtain the energies of the bound states of a particle in the potential well in which $V(x) = \infty$ for $x < 0$, $V(x) = -V_0$ for $0 \le x \le L/2$ and $V(x) = 0$ to $x > L/2$. Compare the obtained values with those of the symmetrical well discussed in Sec. 24.2.4 and the well with infinitely high walls discussed in Sec. 24.2.1.

Solution: *For the unilateral potential well we can simply apply the results of the bilateral potential well. However, with the condition $\psi(0) = 0$, even eigenfunctions are not allowed. That is, $n = 1, 3, ...$*

24.2.5.4 Ex: Least bound states and localization energy

Calculate, based on the discussion in Sec. 24.2.4, the minimum required potential depth V_0 of a three-dimensional finite rectangular well potential of size L to have a bound state capable of trapping an ^{87}Rb atom. Assuming a trap volume of $L = 10\,\text{nm}$, how deep should the trap be?

Solution: *We first consider the one-dimensional potential $V(r) = -V_0$ for $|x| < L/2$*

discussed in Sec. 24.2.4. When, varying the potential depth V_0, a bound state goes into the continuum, we have $E = 0$. With this condition Eq. (24.21) simplifies to,

$$\tan \tfrac{L}{\hbar}\sqrt{2mV_0} = 0 \qquad or \qquad V_0 = \frac{(n\hbar\pi)^2}{2mL^2} \ ,$$

which is just the energy spectrum (24.11) of an infinite box potential. In three dimensions,

$$E_{n_1,n_2,n_3} = \frac{\hbar^2\pi^2}{2mL^2}(n_1^2 + n_2^2 + n_3^2) \ .$$

Hence,

$$V_0 > \frac{3\hbar^2\pi^2}{2mL^2} \ .$$

That is, the more a particle is localized, the deeper must be the potential. For $L = 10\,\mathrm{nm}$, we get $V_0 > 17\,\mathrm{MHz} = 816\,\mu\mathrm{K}$.

24.3 Potential barrier

The linear momentum of a particle described by $\psi(x,t) = Ae^{\imath kx}$ is,

$$\langle\psi|\hat{p}|\psi\rangle = \langle\psi|\frac{\hbar}{\imath}\frac{d}{dx}|\psi\rangle = \hbar k \ . \tag{24.23}$$

Therefore, this particle propagates towards $+\infty$. On the contrary, the particle $Be^{-\imath kx}$ propagates towards $-\infty$. Thus, the two solutions (24.13) of the Schrödinger equation (24.12) correspond to propagating particle waves. From here on we will use the letter A (B) to denote the amplitudes of waves propagating in direction ∞ ($-\infty$).

In locations where the potential changes abruptly, the particle can be partially reflected.

24.3.1 $\mathcal{T}$-scattering matrix

As we have already shown in the previous section, we can write the transformation of the amplitudes due to a potential step at position L as,

$$\begin{aligned} A_2e^{\imath k_2L} + B_2e^{-\imath k_2L} &= A_1e^{\imath k_1L} + B_1e^{-\imath k_1L} \\ \imath k_2A_2e^{\imath k_2L} - \imath k_2B_2e^{-\imath k_2L} &= \imath k_1A_1e^{\imath k_1L} - \imath k_1B_1e^{-\imath k_1L} \ . \end{aligned} \tag{24.24}$$

We can summarize these two equations in a matrix formalism,

$$\boxed{\begin{pmatrix} A_2 \\ B_2 \end{pmatrix} = \mathcal{T}\begin{pmatrix} A_1 \\ B_1 \end{pmatrix}} \ , \tag{24.25}$$

with the *scattering matrix* $\mathcal{T}$ for a particle with energy E (see Fig. 24.2),

$$\begin{aligned}\mathcal{T} &= \frac{1}{2}\begin{pmatrix}\left(1+\frac{k_1}{k_2}\right)e^{\imath(k_1-k_2)L} & \left(1-\frac{k_1}{k_2}\right)e^{\imath(-k_1-k_2)L}\\ \left(1-\frac{k_1}{k_2}\right)e^{\imath(k_1+k_2)L} & \left(1+\frac{k_1}{k_2}\right)e^{\imath(-k_1+k_2)L}\end{pmatrix} \\ &= \frac{1}{2}\begin{pmatrix}e^{-\imath k_2 L} & 0\\ 0 & e^{\imath k_2 L}\end{pmatrix}\begin{pmatrix}1+\frac{k_1}{k_2} & 1-\frac{k_1}{k_2}\\ 1-\frac{k_1}{k_2} & 1+\frac{k_1}{k_2}\end{pmatrix}\begin{pmatrix}e^{\imath k_1 L} & 0\\ 0 & e^{-\imath k_1 L}\end{pmatrix} .\end{aligned} \tag{24.26}$$

If there are more zones with different depths, we may concatenate the scattering matrices. Denoting by $\mathcal{T}_{m\to n}$ the scattering matrix describing a transition at position $L_{m,n}$ of a potential of the depth V_m to another potential V_n, we write,

$$\mathcal{T} = \mathcal{T}_{2\to 3}\mathcal{T}_{1\to 2} . \tag{24.27}$$

24.3.2 $\mathcal{S}$-scattering matrix

Another common definition is the *scattering matrix* $\mathcal{S}$,

$$\boxed{\begin{pmatrix}A_2\\ B_1\end{pmatrix} = \mathcal{S}\begin{pmatrix}B_2\\ A_1\end{pmatrix}} . \tag{24.28}$$

To see how the scattering matrices are interconnected, we start with

$$\begin{pmatrix}A_2\\ B_2\end{pmatrix} = \mathcal{T}\begin{pmatrix}A_1\\ B_1\end{pmatrix} = \begin{pmatrix}\mathcal{T}_{11}A_1 + \mathcal{T}_{12}B_1\\ \mathcal{T}_{21}A_1 + \mathcal{T}_{22}B_1\end{pmatrix} , \tag{24.29}$$

Multiplying the first line with $\mathcal{T}_{22}$ and the second with $-\mathcal{T}_{12}$ and adding them,

$$\mathcal{T}_{22}A_2 - \mathcal{T}_{12}B_2 = \left(\mathcal{T}_{11}\mathcal{T}_{22} - \mathcal{T}_{12}\mathcal{T}_{21}\right)A_1 . \tag{24.30}$$

This equation resolved by A_2 along with the second equation (24.29) resolved by B_1 give,

$$\begin{pmatrix}A_2\\ B_1\end{pmatrix} = \mathcal{S}\begin{pmatrix}B_2\\ A_1\end{pmatrix} = \begin{pmatrix}\mathcal{T}_{12}/\mathcal{T}_{22} & \mathcal{T}_{11} - \mathcal{T}_{12}\mathcal{T}_{21}/\mathcal{T}_{22}\\ 1/\mathcal{T}_{22} & -\mathcal{T}_{21}/\mathcal{T}_{22}\end{pmatrix}\begin{pmatrix}B_2\\ A_1\end{pmatrix} . \tag{24.31}$$

The matrix $\mathcal{S}$ describes the causality of scattering process more adequately: The amplitude A_2 in region (2) results from the superposition of a wave B_2 being reflected by the barrier and a wave A_1 being transmitted by the barrier. The amplitude B_1 in region (1) results from the superposition of a wave A_1 being reflected by the barrier and a wave B_2 being transmitted by the barrier. Therefore, the matrix $\mathcal{S}$ is more appropriate for the description of the quantum reflection, as we will discuss in the next section. However, it has the disadvantage that it can not be concatenated in the same way as the $\mathcal{T}$ matrices.

Unlike the $\mathcal{T}$ matrix the $\mathcal{S}$ matrix is *unitary*, since

$$\det\mathcal{S} = \mathcal{S}_{11}\mathcal{S}_{22} - \mathcal{S}_{12}\mathcal{S}_{21} = -\frac{\mathcal{T}_{11}}{\mathcal{T}_{22}} = -e^{2\imath k_1 L} . \tag{24.32}$$

Also, it is possible to show,

$$\mathcal{S}^\dagger\mathcal{S} = \begin{pmatrix}\mathcal{S}_{11}^* & \mathcal{S}_{21}^*\\ \mathcal{S}_{12}^* & \mathcal{S}_{22}^*\end{pmatrix}\begin{pmatrix}\mathcal{S}_{11} & \mathcal{S}_{12}\\ \mathcal{S}_{21} & \mathcal{S}_{22}\end{pmatrix} = \begin{pmatrix}1 & 0\\ 0 & 1\end{pmatrix} . \tag{24.33}$$

24.3.3 Quantum reflection at a potential step

The *quantum reflection* is a non-classical property of the motion of a particle. An example is the *reflection* of a quantum particle by an *attractive* potential. To study this effect, we consider a plane wave $e^{\imath k_1 x}$ propagating in region (1) ($E_1 > V_1$) encountering a potential step up or down at position $x = 0$ leading to another region (2). Using the S matrix formalism introduced in the previous section,

$$\mathcal{S} = \frac{1}{k_1 + k_2} \begin{pmatrix} k_2 - k_1 & 2k_1 \\ 2k_2 & k_1 - k_2 \end{pmatrix} , \tag{24.34}$$

we find that one part of the wave is reflected into the region (1), another is transmitted into the region (2),

$$\begin{aligned} \begin{pmatrix} A_2 \\ B_1 \end{pmatrix} = \mathcal{S} \begin{pmatrix} 0 \\ 1 \end{pmatrix} = \begin{pmatrix} \mathcal{T}_{11} - \mathcal{T}_{12}\mathcal{T}_{21}/\mathcal{T}_{22} \\ -\mathcal{T}_{21}/\mathcal{T}_{22} \end{pmatrix} = \begin{pmatrix} \frac{(1+k_1/k_2)^2 - (1-k_1/k_2)^2}{2(1+k_1/k_2)} \\ -\frac{1-k_1/k_2}{1+k_1/k_2} \end{pmatrix} \\ = \frac{1}{k_1 + k_2} \begin{pmatrix} 2k_1 \\ k_1 - k_2 \end{pmatrix} . \end{aligned} \tag{24.35}$$

We use $B_2 = 0$, since no wave comes from the side of region (2), and $A_1 = 1$, because it simplifies the formulas and does not affect the generality of the results. The interesting results are:

- Even when $E_2 < V_2$, the particle enters the classically prohibited region: $\psi_2(x) \propto e^{-\kappa_2 x}$ with $\kappa_2 = \frac{1}{\hbar}\sqrt{2m(V_2 - E_2)}$, i.e. the transmission is non-zero, $|A_2| > 0$.

- Even with $E_2 > V_2$, the particle has a probability of being reflected at the step, $|B_1| > 0$.

Example 157 (*Contrast of a partially reflected wave*): Defining $K_\pm \equiv \frac{1}{2}\left(\max|\psi_1|^2 \pm \min|\psi_1|^2\right)$, the *contrast* of the wavefunction in region (1) is given by K_-/K_+. Writing the function as $\psi_1 = e^{\imath k_1 x} + B_1 e^{-\imath k_1 x}$ it is easy to show, that

$$|B_1| = \frac{\sqrt{K_+ + K_-} - \sqrt{K_+ - K_-}}{\sqrt{K_+ + K_-} + \sqrt{K_+ - K_-}} \simeq \frac{K_-}{2K_+} . \tag{24.36}$$

This formula can be understood as an analogue of *Fresnel formula* for matter waves [1].

In Exc. 24.3.7.1 we calculate the behavior of a Broglie wave passing through a potential step and entering a classically forbidden region. In Exc. 24.3.7.2 we investigate a model describing the collision between attracting or repelling particles via a partial reflection at a potential step.

[1] In this sense light reflection at an optical interface (with typical losses of 4% for glass) can be interpreted as quantum reflection of light

24.3.4 Continuity of probability flow

The continuity equation (23.16) requires that the *probability flux* be preserved in stationary situations,

$$0 = \frac{dj}{dx} = \frac{d}{dx}\frac{\hbar}{2m\imath}\left[\psi^*\left(\frac{d}{dx}\psi\right) - \left(\frac{d}{dx}\psi^*\right)\psi\right] \ . \tag{24.37}$$

Applying this to a potential step separating the regions $n = 1, 2$, we find,

$$\begin{aligned} j_n &= \frac{\hbar}{2mi}\left[\psi^*\frac{d}{dx}\psi - \psi\frac{d}{dx}\psi^*\right] \\ &= \frac{\hbar}{2m\imath}\left[(A_n^* e^{-\imath k_n x} + B_n^* e^{\imath k_n x})(\imath k_n A_n e^{\imath k_n x} - \imath k_n B_n e^{-\imath k_n x})\right. \\ &\quad \left. - (A_n e^{\imath k_n x} + B_n e^{-\imath k_n x})(-\imath k_n A_n^* e^{-\imath k_n x} + \imath k B_n^* e^{\imath k x})\right] \\ &= \frac{\hbar k_n}{m}(|A_n|^2 - |B_n|^2) \ . \end{aligned} \tag{24.38}$$

Hence, $j_1 = j_2$ implies $k_1|A_1|^2 - k_1|B_1|^2 = k_2|A_2|^2 - k_2|B_2|^2$. Assuming that the particle comes from side 1 and $B_2 = 0$, we have,

$$1 = |B_1|^2 + \tfrac{k_2}{k_1}|A_2|^2 = R + T \ , \tag{24.39}$$

defining the *transmission* T and the *reflection* R as,

$$T \equiv \tfrac{k_2}{k_1}|\mathcal{S}_{12}|^2 = \tfrac{k_2}{k_1}|A_2|^2 \qquad \text{and} \qquad R \equiv |\mathcal{S}_{22}|^2 = |B_1|^2 \ . \tag{24.40}$$

24.3.5 Tunneling and quantum reflection at a potential well

Particles thrown with a kinetic energy E against potential barriers can cross them even if $V_0 > E$ or be reflected even when $V_0 < E$, as illustrated in Fig. 24.5(a). This can be verified by considering a particle propagating from $x = -\infty$ towards $x = +\infty$ through a potential well located at $x \in [0, a]$. We determine the concatenation $\mathcal{T} = \mathcal{T}_{2\to3}\mathcal{T}_{1\to2}$. Then we find the $\mathcal{S}$ matrix that corresponds to the $\mathcal{T}$ matrix and solve the problem in the same way as in the previous section. For example, we can calculate the transmission and reflection probabilities. The formula is derived in Exc. 24.3.7.3,

$$\boxed{R = 1 - T = \left(1 + \frac{16E/V_0(1 - E/V_0)}{(e^{\kappa L} - e^{-\kappa L})^2}\right)^{-1}} \ , \tag{24.41}$$

and sketched in Fig. 24.5(b).

24.3.6 The delta-potential

In quantum mechanics the δ-potential can be used to simulate situations, where a particle is free to move in two regions of space with a barrier in between. For example, an electron can move almost freely in a conducting material, but when two conducting surfaces are put close together, the interface between them acts as a barrier for the electron that can be approximated by a δ-potential. The δ-potential is a limiting

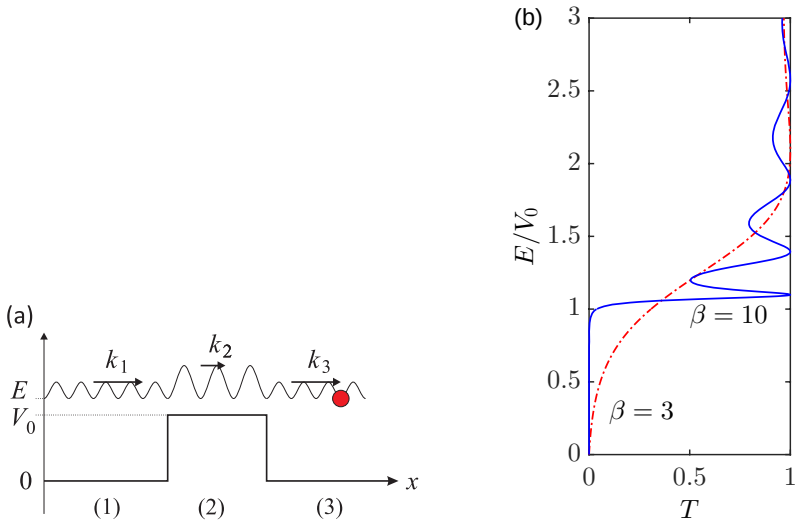

Figure 24.5: (code) (a) Tunnel effect and quantum transmission and reflection at a potential barrier. (b) Coefficients of transmission and reflection (horizontal) through the shown potential barrier as a function of the energy normalized to the height of the barrier E/V_0. The dashed red curve corresponds to a low barrier, $\beta \equiv \frac{1}{\hbar} L\sqrt{2mV_0} = 3$, the blue solid curve corresponds to a deep barrier $\beta = 10$.

case of the finite potential well when we decrease its width while maintained the product of its width and its depth constant. Here, for simplicity, we only consider a one-dimensional potential well, but the analysis can be expanded to more dimensions.

The time-independent Schrödinger equation for the wavefunction $\psi(x)$ of a particle in one dimension is,

$$-\frac{\hbar^2}{2m}\frac{d^2\psi(x)}{dx^2} + \alpha\delta(x)\psi(x) = E\psi(x) \ , \tag{24.42}$$

The potential is called a δ-potential well if α is negative and a δ-potential barrier if α is positive.

The potential splits the space in two parts ($x < 0$ and $x > 0$). In each of these parts the potential energy is zero, and the Schrödinger equation reduces to,

$$\frac{d^2\psi}{dx^2} = -\frac{2mE}{\hbar^2}\psi \ . \tag{24.43}$$

The solutions of this differential equation are linear combinations of $e^{\imath kx}$ and $e^{-\imath kx}$, where the wavenumber k is related to the energy by $k = \frac{\sqrt{2mE}}{\hbar}$. In general, due to the presence of the δ-potential in the origin, the coefficients of the solution need not be the same in both half-spaces:

$$\psi(x) = \begin{cases} \psi_1(x) = A_1 e^{\imath kx} + B_1 e^{-\imath kx} & \text{for } x < 0 \\ \psi_2(x) = A_2 e^{\imath kx} + B_2 e^{-\imath kx} & \text{for } x > 0 \end{cases} \ , \tag{24.44}$$

where, in the case of positive energies (real k), $e^{\imath kx}$ represents a wave traveling to the right, and $e^{-\imath kx}$ one traveling to the left. One obtains a relation between the coefficients by imposing that the wavefunction be continuous at the origin,

$$\psi(0) = \psi_1(0) = \psi_2(0) = A_1 + B_1 = A_2 + B_2 \ . \tag{24.45}$$

A second relation can be found by studying the derivative of the wavefunction. Normally, we could also impose differentiability at the origin, but this is not possible because of the δ-potential. However, if we integrate the Schrödinger equation around $x = 0$ over an interval $[-\epsilon, +\epsilon]$:

$$-\frac{\hbar^2}{2m}\int_{-\epsilon}^{+\epsilon}\psi''(x)dx + \int_{-\epsilon}^{+\epsilon}V(x)\psi(x)dx = E\int_{-\epsilon}^{+\epsilon}\psi(x)dx \ . \tag{24.46}$$

In the limit $\epsilon \to 0$ the right-hand side of this equation vanishes,

$$-\frac{\hbar^2}{2m}[\psi_2'(0) - \psi_1'(0)] + \alpha\psi(0) = 0 \ . \tag{24.47}$$

Substituting the definition of ψ into this expression, we obtain,

$$-\frac{\hbar^2}{2m}\imath k(A_1 - B_1 - A_2 + B_2) + \alpha(A_1 + B_1) = 0 \ . \tag{24.48}$$

The boundary conditions thus give the following restrictions on the coefficients,

$$\boxed{\begin{array}{rcl} A_1 + B_1 - A_2 - B_2 &=& 0 \\ A_1 - B_1 - A_2 + B_2 &=& \dfrac{2m\alpha}{\imath k\hbar^2}(A_1 + B_1) \end{array}} \ . \tag{24.49}$$

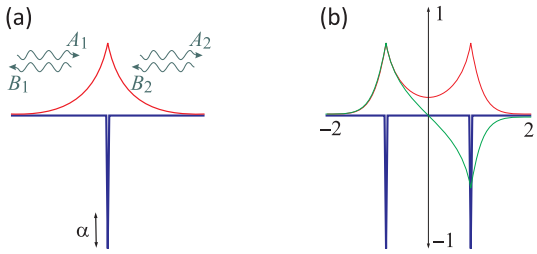

Figure 24.6: (a) The δ-potential (green) and the bound state wavefunction (blue). (b) Double δ-potential (green).

24.3.6.1 Bound states

The bound state wavefunction solution to the δ-function potential is continuous everywhere, but its derivative is not defined at $x = 0$.

In any one-dimensional attractive potential there will be a bound state. To find its energy, note that for negative energies, $E < 0$, the wavenumber $k = \imath\sqrt{2m|E|}/\hbar = \imath\kappa$

is imaginary and the wavefunctions are exponentially increasing or decreasing functions of x (see above). Requiring that the wavefunctions do not diverge at infinity eliminates half of the terms: $A_2 = B_1 = 0$. The wavefunction is then an evanescent wave,

$$\psi(x) = \begin{cases} \psi_1(x) = A_1 e^{\kappa x} & \text{for } x < 0 \\ \psi_2(x) = B_2 e^{-\kappa x} & \text{for } x > 0 \end{cases} . \tag{24.50}$$

From the boundary conditions and normalization conditions, it follows that,

$$A_1 = B_2 = \sqrt{\kappa} \quad \text{and} \quad \kappa = -\frac{m\alpha}{\hbar^2} , \tag{24.51}$$

from which follows that α must be negative, that is the bound state only exists for the well, and not for the barrier. The Fourier transform of this wavefunction is a Lorentzian function. The energy of the bound state is then,

$$E_b = -\frac{\hbar^2\kappa^2}{2m} = -\frac{m\alpha^2}{2\hbar^2} . \tag{24.52}$$

The δ-potential well and its wavefunction are exhibited in Fig. 24.6(a).

24.3.6.2 Scattering

For positive energies, the wavefunctions are oscillating functions of x. That is, the particle is free to move in either half-space: $x < 0$ or $x > 0$, but it may be scattered at the δ-potential. The quantum case can be studied in the following situation: a particle incident on the barrier from the left side (A_1) may be reflected (B_1) or transmitted (A_2). To find the amplitudes for reflection and transmission for incidence from the left, we set in the equations (24.49) $A_1 = 1$ (incoming particle), $B_1 = r$ (reflection), $B_2 = 0$ (no incoming particle from the right), and $A_2 = t$ (transmission), and solve for r and t,

$$t = \frac{1}{1 - \dfrac{m\alpha}{\imath\hbar^2 k}} \quad , \quad r = \frac{1}{\dfrac{\imath\hbar^2 k}{m\alpha} - 1} . \tag{24.53}$$

Due to the mirror symmetry of the model, the amplitudes for incidence from the right are the same as those from the left. The result is that there is a non-zero probability,

$$R = |r|^2 = \frac{1}{1 + \dfrac{\hbar^4 k^2}{m^2\alpha^2}} = \frac{1}{1 + \dfrac{2\hbar^2 E}{m\alpha^2}} . \tag{24.54}$$

for the particle to be reflected. This does not depend on the sign of α, that is, a barrier has the same probability of reflecting the particle as a well. This is a significant difference from classical mechanics, where the reflection probability would be 1 for the barrier (the particle simply bounces back), and 0 for the well (the particle passes through the well undisturbed). The probability for transmission is,

$$T = |t|^2 = 1 - R = \frac{1}{1 + \dfrac{m^2\alpha^2}{\hbar^4 k^2}} = \frac{1}{1 + \dfrac{m\alpha^2}{2\hbar^2 E}} . \tag{24.55}$$

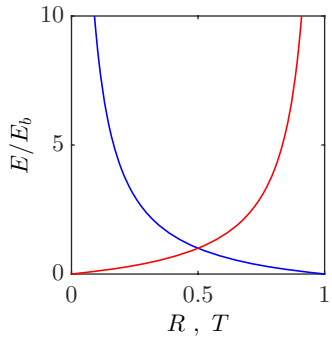

Figure 24.7: (code) Transmission (red) and reflection (blue) probability of a δ-potential well. The energy $E > 0$ is in units of $E_b = m\alpha^2/2\hbar^2$.

An application example regards the interfaces between two conducting materials. In the bulk of the materials, the motion of the electrons is quasi-free and can be described by the kinetic term in the above Hamiltonian with an effective mass m. Often, the surfaces of such materials are covered with oxide layers or are not ideal for other reasons. This thin, non-conducting layer may then be modeled by a local δ-function potential. Electrons may then tunnel from one material to the other giving rise to a current.

Example 158 (*Double delta potential*): The δ-function model is actually a one-dimensional version of the hydrogen atom. The model becomes particularly useful when applied to the hydrogen molecule ion, as shown in the following. The double-well δ-function models a diatomic hydrogen molecule by the corresponding Schrödinger equation:

$$-\frac{\hbar^2}{2m}\frac{d^2\psi}{dx^2}(x) + V(x)\psi(x) = E\psi(x) \ ,$$

where the potential is now:

$$V(x) = -q\lambda\left[\delta\left(x + \tfrac{R}{2}\right) + \delta\left(x - \tfrac{R}{2}\right)\right]$$

where $0 < R < \infty$ is the 'internuclear' distance with δ-function (negative) peaks located at $x = \pm R/2$ (shown in brown in the diagram). Keeping in mind the relationship of this model with its three-dimensional molecular counterpart, we use atomic units and set $\hbar = m = 1$. Here $0 < \lambda < 1$ is a formally adjustable parameter. From the single well case, we can infer the 'ansatz' for the solution to be:

$$\psi(x) = Ae^{-d\left|x+\frac{R}{2}\right|} + Be^{-d\left|x-\frac{R}{2}\right|} \ .$$

Matching of the wavefunction at the δ-function peaks yields the determinant:

$$\begin{vmatrix} q-d & qe^{-dR} \\ q\lambda e^{-dR} & q\lambda - d \end{vmatrix} = 0 \quad \text{where} \quad E = -\frac{d^2}{2} \ .$$

Thus, d is found to be governed by the pseudo-quadratic equation:

$$d_\pm(\lambda) = \tfrac{1}{2}q(\lambda+1) \pm \tfrac{1}{2}\left\{q^2(1+\lambda)^2 - 4\lambda q^2[1 - e^{-2d_\pm(\lambda)R}]\right\}^{1/2} \ ,$$

which has two solutions $d = d_{\pm}$. For the case of equal charges (symmetric homonuclear case), $\lambda = 1$ and the pseudo-quadratic reduces to:

$$d_{\pm} = q[1 \pm e^{-d_{\pm}R}] \ .$$

The '+' case corresponds to a wave function symmetric about the midpoint (shown in red in the diagram) where $A = B$ and is called gerade. Correspondingly, the '-' case is the wavefunction that is anti-symmetric about the midpoint where $A = -B$ is called ungerade (shown in green in the diagram). They represent an approximation of the two lowest discrete energy states of the three-dimensional H_2^+ and are useful in its analysis. Analytical solutions for the energy eigenvalues for the case of symmetric charges are given by:

$$d_{\pm} = q + W(\pm qRe^{-qR})/R \ ,$$

where W is the standard Lambert function. Note that the lowest energy corresponds to the symmetric solution d_+. In the case of unequal charges, and for that matter the three-dimensional molecular problem, the solutions are given by a generalization of the Lambert function (see section on generalization of Lambert function and references herein).
One of the most interesting cases is when $qR \leq 1$, which results in $d_- = 0$. Thus, one has a non-trivial bound state solution with $E = 0$. For these specific parameters, there are many interesting properties that occur, one of which is the unusual effect that the transmission coefficient is unity at zero energy.

24.3.7 Exercises

24.3.7.1 Ex: Tunneling

A rubidium-87 atom moves in free space (region 0) with velocity $v = 1\,\mathrm{cm/s}$ (see diagram). Suddenly it encounters a gap with depth $V_1 = -k_B \cdot 1\mu\mathrm{K}$.
a. What is the particle's Broglie wavelength in region 1?
b. Now the atom encounters a barrier of height $V_2 = -V_1$. What is the probability that the particle will enter region 2?
c. What is the probability of finding the particle inside region 2 up to a depth of $x_2 = 10\,\mathrm{nm}$?

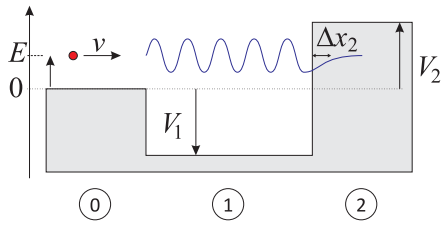

Figure 24.8: Particle in a potential landscape.

Solution: *a. The energy of the particle in region 0 is*

$$E = \frac{m}{2}v^2 = k_B \cdot 523\,\mathrm{nK} \ .$$

The wave vector in region 1 is

$$k_1 = \sqrt{\frac{2m}{\hbar^2}(E - V_1)} = \frac{\sqrt{m^2v^2 - 2mV_1}}{\hbar} \ ,$$

giving $\lambda = 2\pi/k_1 = 270\,\text{nm}$.
b. Writing the wavevector in region 2 as

$$k_2 = \sqrt{\frac{2m}{\hbar^2}(E - V_2)} = \imath\sqrt{\frac{2m}{\hbar^2}(V_2 - E)} = \imath\kappa_2 \ ,$$

we have $\kappa_2 = 2.34 \cdot 10^7\,\text{m}^{-1}$. *We have the conditions of continuity*

$$\psi_1(x) = Ae^{\imath k_1 x} + Be^{-\imath k_1 x} = Ce^{\imath k_2 x} + De^{-\imath k_2 x} = \psi_2(x)$$
$$\psi_1'(x) = \imath k_1 Ae^{\imath k_1 x} - \imath k_1 Be^{-\imath k_1 x} = \imath k_2 Ce^{\imath k_2 x} - \imath k_2 De^{-\imath k_2 x} = \psi_2'(x) \ .$$

Inserting $x = 0$ *and* $D = 0$,

$$A + B = C \quad , \quad \imath k_1 - \imath k_1 B = \imath k_2 C \ ,$$

giving

$$B = \frac{k_1 - k_2}{k_1 + k_2}A \quad , \quad C = \frac{2k_1}{k_1 + k_2}A \ .$$

We note that the dimension of the coefficients is that of a wavevector. The probability of finding the particle within region 2 is,

$$\int_0^\infty |\psi_2(x)|^2 dx = \int_0^\infty |Ce^{\imath k_2 x}|^2 dx = \left|\frac{2k_1}{k_1 + \imath\kappa_2}\right|^2 A^2 \int_0^\infty e^{-2\kappa_2 x} dx$$
$$= \frac{4k_1^2}{k_1^2 + \kappa_2^2}\frac{A^2}{-2\kappa_2}\, e^{-2\kappa_2 x}\Big|_0^\infty = \frac{4(E - V_1)}{-V_1 - V_1}\frac{A^2}{2\kappa_2} = 1.16 \cdot 10^{-7}\ A^2 \ .$$

c. The probability of finding the particle up to the depth x_2 *is,*

$$\int_0^{x_2} |\psi_2(x)|^2 dx = (1 - e^{-2\kappa_2 x_2}) \int_0^\infty |\psi(x_2)|^2 dx = 0.27 \cdot 10^{-7}\ A^2 \ .$$

24.3.7.2 Ex: Collisions

A *collision* between attractive or repulsive particles can be described by the Schrödinger equation as a one-dimensional scattering,

$$-\frac{\hbar^2}{2m}\psi''(x) + \alpha\delta(x)\psi(x) = E\psi(x) \ .$$

The energy spectrum may be a discrete spectrum of bound states and a continuum of free states.
a. Calculate the transmission coefficient for the case of a particle with energy E thrown against the potential energy barrier $V(x) = \alpha\delta(x)$. Does the result change for the

case when $V(x) = -\alpha\delta(x)$, with $\alpha > 0$?
b. For this last potential, find the energy of the bound state and its corresponding wavefunction.

Solution: *a. The general solution for $E > 0$ is simply,*

$$\psi_E(x) = \begin{cases} A_1 e^{\imath kx} + B_1 e^{-\imath kx} & for \quad x < 0 \\ A_2 e^{\imath kx} + B_2 e^{-\imath kx} & for \quad x > 0 \end{cases} \quad , \quad \frac{\hbar^2 k^2}{2m} = E \ .$$

The probability flow in the two regions 1 and 2,

$$\begin{aligned} j_n &= \frac{\hbar}{2m\imath}\left[\psi^* \frac{d}{dx}\psi - \psi \frac{d}{dx}\psi^*\right] \\ &= \frac{\hbar}{2m\imath}\left[(A_n^* e^{-\imath kx} + B_n^* e^{\imath kx})(\imath k A_n e^{\imath kx} - \imath k B_n e^{-\imath kx})\right. \\ &\quad \left. - (A_n e^{\imath kx} + B_n e^{-\imath kx})(-\imath k A_n^* e^{-\imath kx} + \imath k B_n^* e^{\imath kx})\right] \\ &= \frac{\hbar k}{m}(|A_n|^2 - |B_n|^2) \ , \end{aligned}$$

must be maintained, that is, $j_1 = j_2$, such that,

$$|A_1|^2 - |B_1|^2 = |A_2|^2 - |B_2|^2 \ .$$

Assuming that the particle comes from the region 1, $B_2 = 0$, we obtain,

$$\frac{|B_1|^2}{|A_1|^2} + \frac{|A_2|^2}{|A_1|^2} = R + T = 1 \ .$$

b.

24.3.7.3 Ex: Energy barrier

Consider a particle with energy E thrown (in the direction $\hat{\mathbf{e}}_x$) against a potential energy barrier of finite height and width, such that $V(x) = 0$ for $x < 0$ or $x > L$ and $V(x) = V_0$ for $0 \leq x \leq L$.
a. Obtain the reflection and transmission coefficients R and T for the case $E > V_0$. Discuss the result.
b. Do the same for the case $E < V_0$.

Solution: *We consider a particle with kinetic energy E moving from $x = -\infty$ to $x = \infty$ through a barrier (a well) of potential with the height (depth) $V(z) = V_0$ for $x \in [0, L]$. The wavevectors of the particle in the three zones are,*

$$k_1 = k_3 = \frac{1}{\hbar}\sqrt{2mE} \qquad and \qquad k_2 = \frac{1}{\hbar}\sqrt{2m(E - V_0)} \ . \tag{24.56}$$

The wavefunctions are,

$$\psi_1(x) = e^{\imath k_1 x} + B_1 e^{-\imath k_1 x} \quad and \quad \psi_2(x) = A_2 e^{\imath k_2 x} + B_2 e^{-\imath k_2 x} \quad and \quad \psi_3(x) = A_3 e^{\imath k_1 x} \ .$$

Boundary conditions must be met,

$$\begin{aligned}
\psi_1(0) = \psi_2(0) &\implies 1 + B_1 = A_2 + B_2 \\
\psi_1'(0) = \psi_2'(0) &\implies \imath k_1 - \imath k_1 B_1 = \imath k_2 A_2 - \imath k_2 B_2 \\
\psi_1(L) = \psi_2(L) &\implies A_2 e^{\imath k_2 L} + B_2 e^{-\imath k_2 L} = A_3 e^{\imath k_1 L} \\
\psi_1'(L) = \psi_2'(L) &\implies \imath k_2 A_2 e^{\imath k_2 L} - \imath k_2 B_2 e^{-\imath k_2 L} = \imath k_1 A_3 e^{\imath k_1 L} \ .
\end{aligned}$$

This gives,

$$1 + B_1 + \tfrac{k_1}{k_2}(1 - B_1) = 2A_2 \qquad \textit{and} \qquad 1 + B_1 - \tfrac{k_1}{k_2}(1 - B_1) = 2B_2$$

$$\textit{and} \qquad A_3 e^{\imath k_1 L} + \tfrac{k_1}{k_2} A_3 e^{\imath k_1 L} = 2A_2 e^{\imath k_2 L} \qquad \textit{and} \qquad A_3 e^{\imath k_1 L} - \tfrac{k_1}{k_2} A_3 e^{\imath k_1 L} = 2B_2 e^{-\imath k_2 L} \ .$$

And then

$$\begin{aligned}
1 + B_1 + \tfrac{k_1}{k_2}(1 - B_1) &= A_3 e^{\imath (k_1 - k_2) L} + \tfrac{k_1}{k_2} A_3 e^{\imath (k_1 - k_2) L} \\
1 + B_1 - \tfrac{k_1}{k_2}(1 - B_1) &= A_3 e^{\imath (k_1 + k_2) L} - \tfrac{k_1}{k_2} A_3 e^{\imath (k_1 + k_2) L} \ ,
\end{aligned}$$

yielding,

$$B_1 = \frac{(k_2^2 - k_1^2)(e^{2\imath k_2 L} - 1)}{(k_2 + k_1)^2 - (k_2 - k_1)^2 e^{2\imath k_2 L}} \qquad \textit{and} \qquad A_3 = \frac{(k_2 + k_1)^2 - (k_2 - k_1)^2}{(k_1 + k_2)^2 e^{\imath (k_2 - k_1) L} - (k_1 - k_2)^2 e^{\imath (k_2 + k_1) L}} \ .$$

From this we calculate the reflection,

$$R = |B_1|^2 = \frac{-(k_2^2 - k_1^2)^2 (e^{\imath k_2 L} - e^{-\imath k_2 L})^2}{2k_2^4 + 12 k_2^2 k_1^2 + 2k_1^4 - (k_2^2 - k_1^2)^2 (e^{2\imath k_2 L} + e^{-2\imath k_2 L})} = 1 - |A_3|^2 = 1 - T \ .$$

Substituting (24.56) and $\kappa \equiv \imath k_2$, we finally get,

$$R = 1 - T = \left(1 + \frac{16 E/V_0 (1 - E/V_0)}{(e^{\kappa L} - e^{-\kappa L})^2} \right)^{-1} \ .$$

The reflection $|B_1|^2$ and the transmission $|A_3|^2$ show resonances, when L or V_0 are varied. These are located at $2\kappa L = 2\pi \imath n$, where $n \in \mathbb{N}$.

24.3.7.4 Ex: Wavepacket reflected at a potential barrier

Simulate the reflection of a Gaussian wavepacket at a potential barrier for various kinetic energies using the Julia programming language.

Solution: *Fig. 24.9 shows the simulation.*

24.4 Numerical approaches for arbitrary potentials

In practice, many potentials are not box-shaped or harmonic, which renders an analytic treatment difficult or impossible. To some extend approximation methods can be

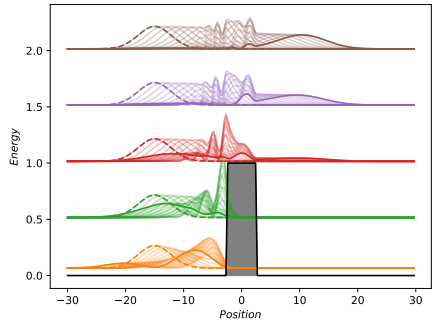

Figure 24.9: (code) Partial reflection of a wavepacket at a potential barrier.

used, as discussed in Sec. 27.5, but many problems can only be solved numerically. In Sec. 24.4.1 we will first show at the example of arbitrary one-dimensional potentials, how the Schrödinger equation can be solved numerically and how this allows one to determine the eigenenergies of bound states. In Sec. 24.4.2 we will introduce the very efficient Fourier grid method for calculating bound state energies and wavefunctions.

24.4.1 Calculation of free and bound states wavefunctions

Numerical routines or packages are available for solving ordinary differential equations (ODE). Generally it is advantageous to convert the one-dimensional second-order Schrödinger equation into two first-order differential equations via,

$$\varphi'(x) = \frac{2m}{\hbar^2}[E - V(x)]\psi(x) \qquad \text{and} \qquad \psi'(x) = \varphi(x)\ . \tag{24.57}$$

For free states, $E > V(x)$, we just solve equation (24.57) specifying the kinetic energy of the particle. The magenta curve in Fig 24.10(a) is an example of a collisional wavefunction in a Morse-type interatomic potential.

For bound states, we must additional satisfy the eigenvalue problem, since only specific discrete eigenenergies E are permitted. A possible procedure consists in guessing an eigenvalue E, calculating the associated wavefunction $\psi(x)$ using an ODE solver, check whether it diverges for $x \to \pm\infty$, and vary E until $\psi(x)$ no longer diverges. Then we repeat the procedure for are bound state energies, until we got them all. The red curve in Fig 24.10(a) shows the wavefunction of a vibrational state in a Morse-type potential obtained by solving the Schrödinger equation and adjusting the energy until the function stops diverging in the classically forbidden range. In this example the iteration process was stopped when the wavefunction diverged at around $R \approx 19a_B$. In Exc. 24.4.4.1 we will practice this technique at the example of Hermite's differential equation, and in Exc. 24.4.4.2 we will study the case of a potential whose depth linearly increases with the distance from origin.

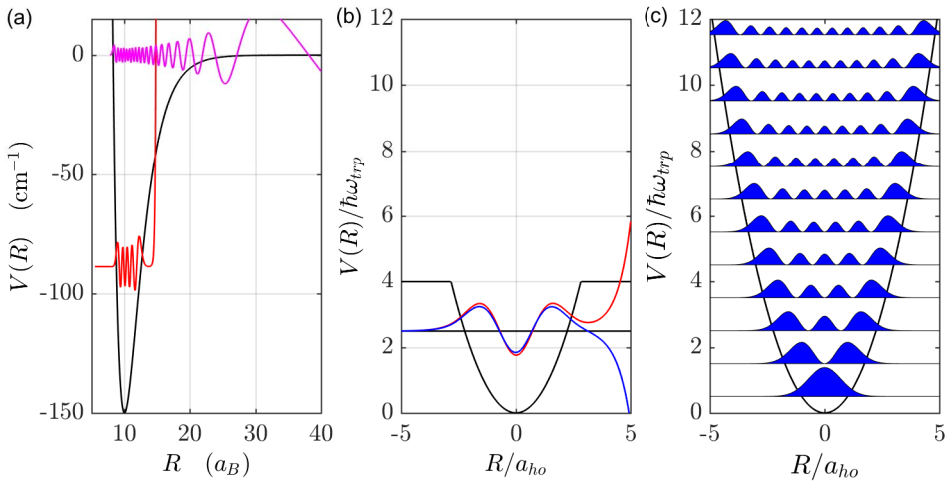

Figure 24.10: (code) (a) Free particle (magenta) and bound state wavefunction (red) calculated using a MATLAB ODE solver. (b) Bound state wavefunction of the harmonic oscillator calculated using a MATLAB ODE solver. For the red curve the eigenvalue has been slightly overestimated and for the blue curve underestimated. (c) Calculation of the harmonic oscillator energies and wave functions using the Fourier grid method.

24.4.2 The Fourier grid method for bound states

The objective of the *Fourier grid method* is to analytically solve the 1D Schrödinger equation with an arbitrary potential $V(r)$ on a grid of $2N+1$ equally spaced spatial points r_i, where $i = 0, \pm 1, ..., \pm N$. That is, we assume the potential $V(r_i)$ to be given at these points. Skaling by the spatial coordinate r by $r/L = x/2\pi$, we get for the dimensionless coordinate x the Schrödinger equation,

$$\left[-\frac{h^2}{2mL^2}\frac{d^2}{dx^2} + V(x)\right]\psi(x) = E\psi(x) \ , \tag{24.58}$$

with the grid given by,

$$x_i \equiv \frac{2\pi i}{2N+1} \ . \tag{24.59}$$

The main difficulty for numerically solving such eigenvalue equations is obviously the derivative. Numerical differentiation schemes can be cast into the following general form [884],

$$f'(x_i) = \sum_{j=-N}^{N} D_{ij} f(x_j) \ , \tag{24.60}$$

that is, they can be expressed as a multiplication of the discretized wavefunction represented as a vector $f(x_j)$ and a matrix D_{ij}. These schemes are usually based on interpolation polynomials and are the more accurate, the higher the order of these polynomials is chosen to be.

Instead of using interpolation polynomials, one may now consider over-all approximation of a function $f(x)$ by a Fourier series of N-th order, i.e. to assume (see

(21.126)),

$$f(x) = \sum_{k=-\infty}^{\infty} c_k e^{\imath kx} \simeq \sum_{k=-N}^{N} c_k e^{\imath kx} \ . \tag{24.61}$$

The highest harmonics of the Fourier expansion N is set by the distance between two grid points. The expansion coefficients are,

$$c_k = \frac{1}{2\pi}\int_0^{2\pi} f(x)e^{-\imath kx}dx \longrightarrow \frac{1}{2\pi}\sum_{j=-N}^{N} f(x_j)e^{-\imath kx_j}\Delta x = \frac{1}{2N+1}\sum_{j=-N}^{N} f(x_j)e^{-\imath kx_j} \ . \tag{24.62}$$

Now, substituting x by the discrete variable x_i, we take the derivative $f'(x_i)$ of the function (24.61), insert the expansion coefficients (24.62), and compare the resulting expression to the linear combination (24.60) of the functional values $f(x_j)$,

$$\begin{aligned} f'(x_i) &= \sum_{k=-N}^{N} \imath k c_k e^{\imath kx_i} = \frac{\imath}{2N+1}\sum_{k=-N}^{N} k \sum_{j=-N}^{N} f(x_j)e^{\imath k(x_i-x_j)} \\ &= \frac{2}{2N+1}\sum_{k=1}^{N} k \sum_{j=-N}^{N} f(x_j)\sin k(x_j-x_i) \equiv \sum_{j=-N}^{N} D_{ij}f(x_j) \ . \end{aligned} \tag{24.63}$$

From this we see, that the matrix elements $D_{j'j}$ are given by,

$$\boxed{D_{ij} = \frac{2}{2N+1}\sum_{k=1}^{N} k\sin k(x_j-x_i) = \frac{2}{2N+1}\sum_{k=1}^{N} k\sin\frac{2\pi k(i-j)}{2N+1}} \ . \tag{24.64}$$

The sum can be evaluated analytically, as shown in Exc. 24.4.4.3 [1244],

$$D_{ii} = 0 \qquad \text{and} \qquad D_{i\neq j} = \frac{(-1)^{i-j}}{2\sin\frac{x_i-x_j}{2}} = \frac{(-1)^{i-j}}{2\sin\frac{\pi(i-j)}{2N+1}} \ . \tag{24.65}$$

We may proceed similarly for the second derivative,

$$\begin{aligned} f''(x_i) &= -\sum_{k=-N}^{N} k^2 c_k e^{\imath kx_i} = \frac{-1}{2N+1}\sum_{k=-N}^{N} k^2 \sum_{j=-N}^{N} f(x_j)e^{\imath k(x_i-x_j)} \\ &= \frac{-2}{2N+1}\sum_{k=1}^{N} k^2 \sum_{j=-N}^{N} f(x_j)\cos k(x_j-x_i) \equiv \sum_{j=-N}^{N} (D^2)_{ij}f(x_j) \ , \end{aligned} \tag{24.66}$$

yielding,

$$\boxed{(D^2)_{ij} = \frac{-2}{2N+1}\sum_{k=1}^{N} k^2\cos k(x_j-x_i) = \frac{-2}{2N+1}\sum_{k=1}^{N} k^2\cos\frac{2\pi k(i-j)}{2N+1}} \ . \tag{24.67}$$

Again, the sum can be evaluated analytically, as shown in Exc. 24.4.4.3 [1244],

$$(D^2)_{ii} = -\frac{N^2+2}{12} \qquad \text{and} \qquad (D^2)_{i\neq j} = -\frac{(-1)^{i-j}}{2\sin^2\frac{\pi(i-j)}{2N+1}} \ . \tag{24.68}$$

With this scheme of differentiation, the set of difference equations representing the problem (24.68) is readily found to be [847, 395, 1244],

$$\boxed{\hat{H}\psi = E\psi \qquad \text{with} \qquad \hat{H}_{ij} = -\frac{h^2}{2mL^2}(D^2)_{ij} + V(x_j)\delta_{ij}} \ . \tag{24.69}$$

This eigenvalue problem can easily be solved on a computer, see Fig 24.10(b).

24.4.3 Steepest descent ot the ground state

The softwares 'Maple' or 'Mathematics' are useful for analytical calculations, that is, multiplying matrices or determining eigenvalues. For numerical calculations the software 'Matlab' is more adapted. For example, the time evolution of a Schrödinger equation,

$$|\psi(t)\rangle = e^{-\imath\hat{H}t/\hbar}|\psi(0)\rangle \ , \tag{24.70}$$

can be calculated in a single command line using the Matlab 'expm' function.

When the system varies temporally, $\hat{H}(t)$, we may divide time into small units dt and propagate the wavefunction as,

$$|\psi(t+dt)\rangle = e^{-\imath\hat{H}(t)dt/\hbar}|\psi(t)\rangle \simeq |\psi(t)\rangle\left(1 - \imath\frac{\hat{H}}{\hbar}dt\right) \ , \tag{24.71}$$

continuously reinserting the solution into the equation. This *Newton method* does not converge quickly (dt should be chosen small enough, when $\hat{H}(t)$ varies rapidly), but there are other more sophisticated methods like the *Runge-Kutta method*.

A variation of this method is called *steepest descent method*. This method is similar to the Newton Eq. (24.71), but replaces the time dt with an imaginary time. Thus, the coherent temporal evolution of the Schrödinger equation is replaced by a dissipative evolution. The loss of energy automatically takes the system to the ground state. However, in order to preserve the normalization of the wavefunction, it must be renormalized at each iteration step,

$$|\psi(t+dt)\rangle \to \frac{|\psi(t+dt)\rangle}{\sqrt{\langle\psi(t+dt)|\psi(t+dt)\rangle}} \ . \tag{24.72}$$

The method also applies to more complicated equations than the Schrödinger equation, for example, the *Gross-Pitaevskii equation*. We will deepen this technique in Sec. 45.3.3.

Another numerical method often used in quantum mechanics is the method called the quantum *Monte Carlo simulation* of the wavefunction [913]. This method simulates trajectories of quantum systems treating intrinsic quantum noise as random processes disrupting the uniformity of the trajectory. The advantage of this method is that it also applies to dissipative systems.

24.4.4 Exercises

24.4.4.1 Ex: Numerical resolution of the Hermite differential equation

Solve the Hermite differential equation (24.93) numerically for $n = 8$, e.g. using the 'ode45' ordinary differential equation solver of Matlab, or similar. Plot the wavefunction of the 8-th vibrational level of a harmonic oscillator.

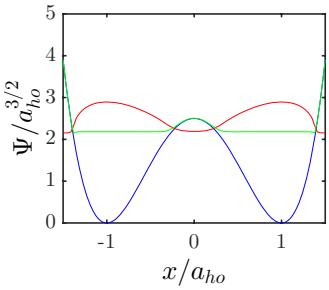

Figure 24.11: (code) Condensate wavefunction (red) in a double-well potential (blue) numerically calculated using the steepest descent method. Also shown is the chemical potential (green).

Solution: *The results are exhibited in Fig. 24.12.*

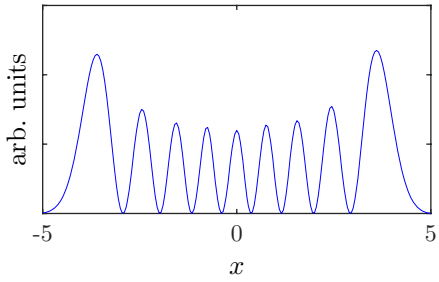

Figure 24.12: (code) Solution of the Hermite differential equation for $n = 8$.

24.4.4.2 Ex: Numerical resolution of the Schrödinger equation

Paramagnetic atoms, such as rubidium, can be confined in quadrupolar magnetic traps, which are characterized by a linear increase of the magnetic field in any direction of space. Let us consider one dimension of such a potential, given by $V(x) = \mu_B \partial_x B \, |x| - V_0$ wherever $V(x)$ is negative and $V(x) = 0$ else. Here μ_B is the Bohr magneton. Be $\partial_x B = 200\,\mathrm{G/cm}$ the magnetic field gradient and $V_0 = h\ 15\,\mathrm{kHz}$ the potential depth.
a. Calculate the energy and wavefunction of the lowest bound state of this potential by numerical integration of the stationary Schrödinger equation using Matlab or another software.
b. Obtain all bound state energies and wavefunctions using the Fourier grid method.

Solution: *The results are exhibited in Fig. 24.13.*

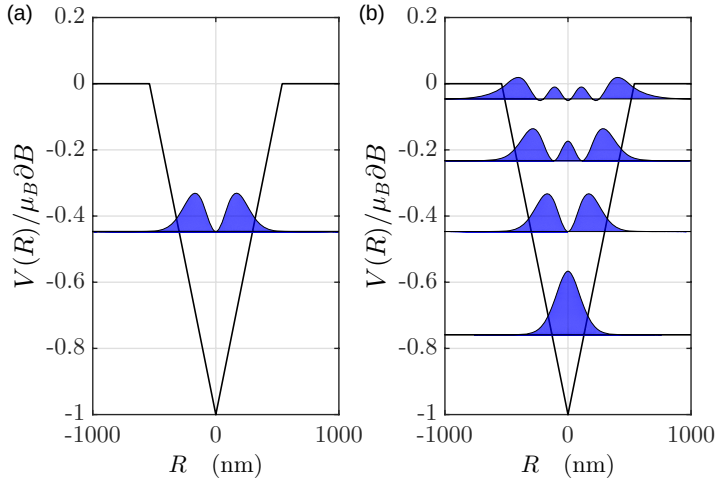

Figure 24.13: (code) Eigenenergies and wavefunctions of a quadrupolar potential.

24.4.4.3 Ex: The Fourier grid method

Derive (a) the formula (24.65) and (b) the formula (24.68) for $N \gg 1$ using the formula (1.352) from [532].

Solution: *a. Formula (1.352) [532] reads,*

$$\sum_{k=1}^{N} k \sin kx = \frac{\sin(N+1)x}{4\sin^2\frac{x}{2}} - \frac{(N+1)\cos\frac{2N+1}{2}x}{2\sin\frac{x}{2}} \ .$$

With this, inserting $x = \frac{2\pi(i-j)}{2N+1}$*, we find,*

$$D_{ij} = \frac{2}{2N+1}\sum_{k=1}^{N} k \sin\frac{2\pi k(i-j)}{2N+1} \ .$$

In particular we find,

$$D_{ii} = 0$$

$$D_{i\neq j} = \frac{2}{2N+1}\sum_{k=1}^{N} k \sin k\frac{2\pi(i-j)}{2N+1} = \frac{1}{2N+1}\left(\frac{\sin(N+1)\frac{2\pi(i-j)}{2N+1}}{2\sin^2\frac{\pi(i-j)}{2N+1}} - \frac{(N+1)\cos\pi(i-j)}{\sin\frac{\pi(i-j)}{2N+1}}\right) ,$$

in agreement with [1244]. Approximating $2N+1 \simeq 2N$*, we can simplify,*

$$D_{i\neq j} \simeq \frac{2}{2N+1}\left(\frac{\sin\pi(i-j)}{4\sin^2\frac{\pi(i-j)}{2N+1}} - \frac{(N+1)(-1)^{i-j}}{2\sin\frac{\pi(i-j)}{2N+1}}\right) = \frac{(-1)^{i-j}}{2\sin\frac{\pi(j-i)}{2N+1}} \ ,$$

recovering the result of [884].
b. Similarly,

$$(D^2)_{ij} = \frac{-2}{2N+1}\sum_{k=1}^{N} k^2 \cos\frac{2\pi k(i-j)}{2N+1} \ .$$

In particular we find [1244],

$$(D^2)_{ii} = \frac{-2}{2N+1}\sum_{k=1}^{N} k^2 = \frac{-2}{2N+1}\frac{N(N+1)(2N+1)}{6} = -\frac{N(N+1)}{3}$$

$$(D^2)_{i\neq j} = \frac{(-1)^{i-j}(N+1)\cos\frac{\pi(i-j)}{2N+1} + (N+1)\cos\frac{(N+1)2\pi(i-j)}{2N+1} - \sin\frac{(N+1)2\pi(i-j)}{2N+1}\cot\frac{\pi(i-j)}{2N+1}}{2(2N+1)\sin^2\frac{\pi(i-j)}{2N+1}} .$$

Approximating $2N+1 \simeq 2N$,

$$(D^2)_{i\neq j} \simeq (-1)^{i-j}\frac{\cos\frac{\pi(i-j)}{2N+1}+1}{4\sin^2\frac{\pi(i-j)}{2N+1}} .$$

24.4.4.4 Ex: Derivation of the Fourier grid method from the FFT

The Fast Fourier Transform (FFT) is defined by,

$$\begin{aligned} H_n &= \sum_{k=0}^{N-1} e^{-2\pi\imath nk/N} h_k \\ &= \sum_{k=0}^{N-1} e^{-2\pi\imath nk/(N/2)} h_{2k} + e^{-2\pi\imath k/N}\sum_{k=0}^{N/2-1} e^{-2\pi\imath nk/(N/2)} h_{2k+1} = even + odd . \end{aligned}$$

the inverse transform is,

$$h_k = \frac{1}{N}\sum\nolimits_{k=0}^{N-1} e^{2\pi\imath nk/N} H_n .$$

The sinus transform of a real vector s_k is,

$$S_n = \frac{2}{N}\sum\nolimits_{k=1}^{N-1} s_k \sin \pi nk/N .$$

Calculate the inverse transform of the matrix $T_{rs} = k_r^2\delta_{rs}$.

Solution: *See [884, 847, 395].*

24.4.4.5 Ex: Infinite rectangular double-well potential

a. Consider the rectangular double-well potential sketched in Fig. 24.14 and calculate the energy levels according to the procedure taught in Sec. 24.3.5.
b. For the same type of potential as in (a) prepare a numerical calculation of the wavefunctions, e.g. using the Fourier grid method introduced in Sec. 32.2.5, for ^{87}Rb using the following dimensions of the potential: $V_0 = h \times 15\,\text{MHz}$, $L = 40\,\text{nm}$, and $b = 3\,\text{nm}$.

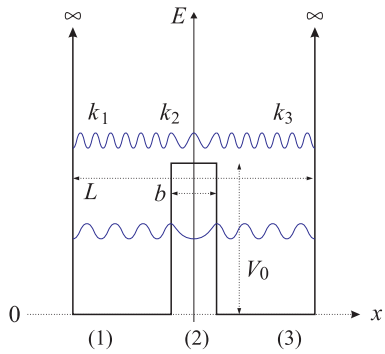

Figure 24.14: Scheme of the rectangular double-well potential.

Solution: *a. As usual, we set the wavefunctions in the various sections* $j = 1, 2, 3$ *as* $\psi_j(x) = A_j e^{\imath k_j x} + B_j e^{-\imath k_j x}$*, where for symmetry reasons* $k_1 = k_3$*, and* $\hbar k_1 = \sqrt{2mE}$ *and* $\hbar k_2 = \sqrt{2m(E - V_0)}$*. The boundary conditions are,*

$$\begin{aligned}
\psi_1(-\tfrac{L}{2}) = 0 = \psi_3(\tfrac{L}{2}) \\
\psi_1(-\tfrac{b}{2}) = \psi_2(-\tfrac{b}{2}) = \pm\psi_2(\tfrac{b}{2}) = \pm\psi_3(\tfrac{b}{2}) \\
\psi_1'(\tfrac{b}{2}) = \psi_2'(-\tfrac{b}{2}) = \pm\psi_2'(\tfrac{b}{2}) = \pm\psi_3'(\tfrac{b}{2}) \ .
\end{aligned}$$

Solving this system of equations, we get,

$$\begin{aligned}
\frac{B_1}{A_1} = -e^{\imath k_1 L} = \frac{A_3}{B_3} \\
\left(1 + \frac{k_1}{k_2}\right) A_1 e^{-\imath k_1 b/2} + \left(1 - \frac{k_1}{k_2}\right) B_1 e^{\imath k_1 b/2} = 2A_2 e^{-\imath k_2 b/2} \\
\left(1 - \frac{k_1}{k_2}\right) A_1 e^{-\imath k_1 b/2} + \left(1 + \frac{k_1}{k_2}\right) B_1 e^{\imath k_1 b/2} = 2B_2 e^{\imath k_2 b/2} \ ,
\end{aligned}$$

and from symmetry considerations,

$$A_1 = \pm B_3 \quad , \quad B_1 = \pm A_3 \quad , \quad A_2 = \pm B_2 \ .$$

After some algebra,

$$\pm \frac{e^{\imath k_1 (L+b/2) - \imath k_2 b/2} \pm e^{-\imath k_1 b/2 + \imath k_2 b/2}}{e^{\imath k_1 (L+b/2) + \imath k_2 b/2} \pm e^{-\imath k_1 b/2 - \imath k_2 b/2}} = \frac{k_2 - k_1}{k_2 + k_1} \ .$$

This equation must be solved numerically.
b. Fig. 24.15 shows the simulation.

24.4.4.6 Ex: Least bound states numerically

Calculate numerically the minimum required potential depth V_0 to have a bound state using the method detailed in Sec. 24.4.1 for the following three one-dimensional

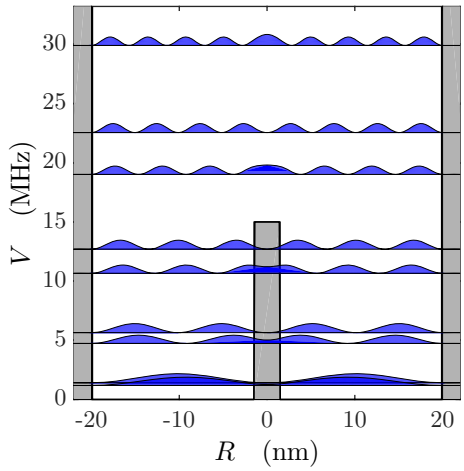

Figure 24.15: (code) Wavefunctions and energy levels of the rectangular double-well potential calculated by the Fourier grid method.

potentials (Θ is the Heavyside function):
a. For the square well potential $V(z) = -V_0\ \Theta(L-2|z|)$; compare with the calculated energy spectrum for the box potential and the square well potential of Secs. 24.2.1 and 24.2.4;
b. for the harmonic oscillator potential with given spill-over height V_0, that is, $V(z) = (\frac{m}{2}\omega_{ho}^2 z^2 - V_0)\ \Theta(2V_0 - m\omega_{ho}^2 z^2)$; compare with the calculated energy spectrum of an ordinary unlimited harmonic oscillator;
c. for the sinusoidal potential given by $V(z) = -V_0 \cos^2(kz)\ \Theta(\pi - 2k|z|)$; compare with the recoil energy $E_{rec} = \hbar^2 k^2/2m$.

Solution: *The results are exhibited in Fig. 24.16.*
a. The energy of the lowest bound state in a box potential with infinite walls is,

$$E_1 = \frac{\hbar^2 \pi^2}{2mL^2}\ .$$

We find that the square well potential must be deeper than $V_0 = 0.014E_1$ in order to support a bound state.
b. The energy of the lowest bound state in a harmonic potential is,

$$E_0 = \frac{\hbar\omega_{ho}}{2}\ .$$

We find that the spill-over height must be higher than $V_0 = 0.18\hbar\omega_{ho}$ in order to support a bound state.
c. The recoil energy is,

$$E_{rec} = \frac{\hbar^2 k^2}{2m}\ .$$

We find that the potential must be deeper than $V_0 = 0.54E_{rec}$.

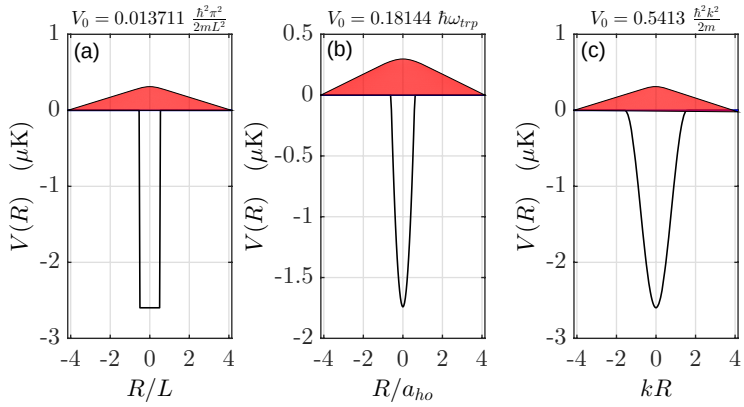

Figure 24.16: (code) Potential depth for having exactly one least bound state for (a) a square well, (b) a harmonic, and (c) a sine potential.

24.5 Harmonic oscillator

Many systems oscillate. Common examples are vibrations of atoms bound in a molecule or in a crystalline lattice, of particles trapped in applied electric or magnetic fields, or light in an electromagnetic mode. Most periodic movements are approximately harmonic for small amplitude vibrations and can be treated in a way that we will detail now.

We start with the unidimensional *harmonic oscillator* (OH),

$$\left[\frac{-\hbar^2}{2m}\frac{d^2}{dx^2} + V(x) - E\right]\psi(x) = 0 \qquad \text{where} \qquad V(x) = \frac{m}{2}\omega^2 x^2 \ . \tag{24.73}$$

24.5.1 Factorization of the Hamiltonian and Fock states

Respecting the fact that the operators $\hat{p}$ and $\hat{x}$ do not commute, $\frac{\imath}{\hbar}[\hat{p},\hat{x}] = 1$, we can rewrite the Hamiltonian of the harmonic oscillator in the following way,

$$\begin{aligned}\hat{H} &= -\frac{\hbar^2}{2m}\frac{d^2}{dx^2} + \frac{m}{2}\omega^2\hat{x}^2 = \hbar\omega\left[\left(\sqrt{\tfrac{m\omega}{2\hbar}}\hat{x} - \imath\sqrt{\tfrac{1}{2m\hbar\omega}}\hat{p}\right)\left(\sqrt{\tfrac{m\omega}{2\hbar}}\hat{x} + \imath\sqrt{\tfrac{1}{2m\hbar\omega}}\hat{p}\right) + \tfrac{1}{2}\right] \\ &= \hbar\omega\left(\hat{a}^\dagger\hat{a} + \tfrac{1}{2}\right) \ ,\end{aligned} \tag{24.74}$$

with the abbreviation

$$\hat{a} \equiv \sqrt{\frac{m\omega}{2\hbar}}\hat{x} + \imath\sqrt{\frac{1}{2m\hbar\omega}}\hat{p} \tag{24.75}$$

and its Hermitian transposition $\hat{a}^\dagger$. Now let's try to find out the properties of the operators $\hat{a}^\dagger$ and $\hat{a}$. First of all, the commutator is,

$$\begin{aligned}[\hat{a},\hat{a}^\dagger] &= \left[\sqrt{\frac{m\omega}{2\hbar}}\hat{x} + \imath\sqrt{\frac{1}{2m\hbar\omega}}\hat{p}, \sqrt{\frac{m\omega}{2\hbar}}\hat{x} - \imath\sqrt{\frac{1}{2m\hbar\omega}}\hat{p}\right] = \frac{\imath}{2\hbar}\left[\hat{x}+\hat{p}, \hat{x}-\hat{p}\right] \\ &= \tfrac{\imath}{\hbar}\left[\hat{p},\hat{x}\right] = 1 \ .\end{aligned} \tag{24.76}$$

Knowing $\hat{H}|\psi\rangle = E|\psi\rangle$ is it clear that $\hat{a}^\dagger\hat{a}$ is an observable with the eigenvalue $n \equiv \frac{E}{\hbar\omega} - \frac{1}{2}$,

$$\hat{a}^\dagger\hat{a}|\psi\rangle = \left(\tfrac{E}{\hbar\omega} - \tfrac{1}{2}\right)|\psi\rangle \equiv n|\psi\rangle \implies |\psi\rangle = |n\rangle \ . \tag{24.77}$$

Now, we show that the states $\hat{a}|\psi\rangle$ are eigenstates of the operator defined as $\hat{n} \equiv \hat{a}^\dagger\hat{a}$, since,

$$\begin{aligned}
\hat{a}^\dagger\hat{a}\hat{a}|\psi\rangle &= (\hat{a}\hat{a}^\dagger - [\hat{a},\hat{a}^\dagger])\hat{a}|\psi\rangle = (\hat{a}\hat{a}^\dagger\hat{a} - \hat{a})|\psi\rangle = \hat{a}(\hat{a}^\dagger\hat{a} - 1)|\psi\rangle = (n-1)\hat{a}|\psi\rangle \\
&\implies \hat{a}|\psi\rangle \propto |n-1\rangle \equiv C|n-1\rangle \\
&\implies n = \langle n|\hat{a}^\dagger\hat{a}|n\rangle = C^2\langle n-1|n-1\rangle \\
&\implies C = \sqrt{n} \ .
\end{aligned} \tag{24.78}$$

We note that the quantum number of the new $|n-1\rangle$ is decreased by 1. Similarly, we show for the state $\hat{a}^\dagger|\psi\rangle$,

$$\begin{aligned}
\hat{a}^\dagger\hat{a}\hat{a}^\dagger|\psi\rangle &= \hat{a}^\dagger([\hat{a},\hat{a}^\dagger] + \hat{a}^\dagger\hat{a})|\psi\rangle = \hat{a}^\dagger(1 + \hat{a}^\dagger\hat{a})|\psi\rangle = (n+1)\hat{a}^\dagger|\psi\rangle \\
&\implies \hat{a}^\dagger|\psi\rangle \propto |n+1\rangle \equiv C|n+1\rangle \\
&\implies n+1 = \langle n|\hat{a}^\dagger\hat{a} + [\hat{a},\hat{a}^\dagger]|n\rangle = C^2\langle n+1|n+1\rangle \\
&\implies C = \sqrt{n+1} \ .
\end{aligned} \tag{24.79}$$

Therefore, this new state is also an eigenvector $|n+1\rangle$, with a quantum number increased by one unit. $\hat{a}^\dagger$ and $\hat{a}$ are creation and annihilation operators of an energy packet,

$$\boxed{\hat{a}^\dagger|n\rangle = \sqrt{n+1}|n+1\rangle \qquad \text{and} \qquad \hat{a}|n\rangle = \sqrt{n}|n-1\rangle} \ . \tag{24.80}$$

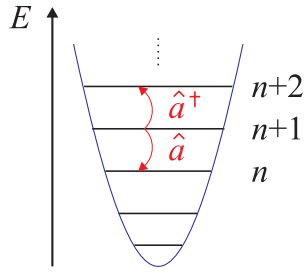

Figure 24.17: Equidistant ladder of vibrational levels showing the actions of the creation and the annihilation operator.

The matrix representation of the field operators is,

$$\hat{a}^\dagger = \sum_n \sqrt{n+1}|n+1\rangle\langle n| \qquad \text{and} \qquad \hat{a} = \sum_n \sqrt{n}|n-1\rangle\langle n| \ , \tag{24.81}$$

from which we deduce,

$$\hat{n} = \hat{a}^\dagger\hat{a} = \sum_n n|n\rangle\langle n| \qquad \text{and} \qquad \hat{H} = \hbar\omega\left(\hat{n} + \tfrac{1}{2}\right) \ . \tag{24.82}$$

Now it is clear, that $\hat{n}$ can be understood as a number operator [2]. The energy spectrum of the harmonic oscillator is equidistant,

$$\boxed{E_n = \hbar\omega\left(n + \tfrac{1}{2}\right)} \,. \tag{24.83}$$

The state with n quanta can be created from the vacuum,

$$|n\rangle = \frac{\hat{a}^\dagger}{\sqrt{n}}|n-1\rangle = \frac{\hat{a}^{\dagger n}}{\sqrt{n!}}|0\rangle \,. \tag{24.84}$$

The state $|n\rangle$ is called *number state* or *Fock state*.

24.5.1.1 Uncertainty in Fock states

We consider an OH of mass m and angular frequency ω prepared in the stationary state $|n\rangle$ which is an eigenstate of the Hamiltonian $\hat{H}$ with eigenvalue $(n+\frac{1}{2})\hbar\omega$. Defining the characteristic size of the OH, $a_{ho} = \sqrt{\hbar/m\omega}$, the annihilation and creation operators can be written,

$$\hat{a} = \frac{1}{\sqrt{2}}\left(\frac{\hat{x}}{a_{ho}} + \imath\frac{a_{ho}}{\hbar}\hat{p}\right) \qquad \text{and} \qquad \hat{a}^\dagger = \frac{1}{\sqrt{2}}\left(\frac{\hat{x}}{a_{ho}} - \imath\frac{a_{ho}}{\hbar}\hat{p}\right) \,. \tag{24.85}$$

Therefore, the position and momentum operators are,

$$\sqrt{2}\frac{1}{a_{ho}}\hat{x} = \hat{a} + \hat{a}^\dagger \qquad \text{and} \qquad \sqrt{2}\imath\frac{a_{ho}}{\hbar}\hat{p} = \hat{a} - \hat{a}^\dagger \,. \tag{24.86}$$

The mean squared deviations of the position $\hat{x}$ and the momentum $\hat{p}$ are,

$$\begin{aligned}
\Delta x^2 &= \langle n|\hat{x}^2|n\rangle = \frac{a_{ho}^2}{2}\langle n|\hat{a}\hat{a} + \hat{a}\hat{a}^\dagger + \hat{a}^\dagger\hat{a} + \hat{a}^\dagger\hat{a}^\dagger|n\rangle = \frac{a_{ho}^2}{2}\langle n|2\hat{n}+1|n\rangle \\
&= \frac{a_{ho}^2}{2}(2n+1) \qquad (24.87)\\
\Delta p^2 &= \langle n|\hat{p}^2|n\rangle = \frac{-\hbar^2}{2a_{ho}^2}\langle n|\hat{a}\hat{a} - \hat{a}\hat{a}^\dagger - \hat{a}^\dagger\hat{a} + \hat{a}^\dagger\hat{a}^\dagger|n\rangle = \frac{-\hbar^2}{2a_{ho}^2}\langle n| - 2\hat{n} - 1|n\rangle \\
&= \frac{\hbar^2}{2a_{ho}^2}(2n+1) \,.
\end{aligned}$$

From the results of the previous item we obtain the uncertainty relation $\Delta x\Delta p$ for the OH in the state $|n\rangle$,

$$\Delta p\Delta x = \tfrac{\hbar}{2}(2n+1) \,. \tag{24.88}$$

Example 159 (*Localization energy*): The non-vanishing energy of the fundamental state of the harmonic oscillator, $E_0 = \hbar\omega/2$, is an immediate consequence of the Heisenberg principle $\Delta x\Delta p \geq \hbar$, because in analogy with Example 156 we calculate,

$$\frac{\langle p^2\rangle}{2m} = \frac{\Delta p^2}{2m} > \frac{\hbar^2}{2m\Delta x^2} > \frac{\hbar^2}{2ma_{ho}^2} = \frac{\hbar\omega}{2} \,.$$

In the case of an electromagnetic field this energy is called *vacuum fluctuation*.

[2] Also, we can define phase operators by $\widehat{\exp}(\mp\imath\phi) = \sum_n |n \mp 1\rangle\langle n|$.

24.5.2 Harmonic oscillator in spatial representation

To simplify the Schrödinger equation in spatial representation,

$$\left[-\frac{\hbar^2}{2m}\frac{d^2}{dx^2}+\frac{m}{2}\omega^2 x^2\right]\psi(x)=\hbar\omega(n+\tfrac{1}{2})\psi(x)\ , \tag{24.89}$$

we use the scale $\tilde{x}\equiv x/a_{ho}$, where $a_{ho}=\sqrt{\hbar/m\omega}$ is the spatial extent of the ground state. Therefore,

$$\begin{aligned}\frac{2}{\hbar\omega}\left[-\frac{\hbar^2}{2m}\frac{d^2}{d(a_{ho}\tilde{x})^2}+\frac{m}{2}\omega^2(a_{ho}\tilde{x})^2\right]\tilde{\psi}(\tilde{x})&=\frac{2}{\hbar\omega}\left[-\frac{\hbar\omega}{2}\frac{d^2}{d\tilde{x}^2}+\frac{\hbar\omega}{2}\tilde{x}^2\right]\tilde{\psi}(\tilde{x})\\&=\left[-\frac{d^2}{d\tilde{x}^2}+\tilde{x}^2\right]\tilde{\psi}(\tilde{x})=(2n+1)\tilde{\psi}(\tilde{x})\ .\end{aligned}$$

Now we start looking for asymptotic solutions. For $\tilde{x}\to\pm\infty$, that is, when the particle enters the classically forbidden region, we can neglect the total energy of the particle,

$$\left[-\frac{d^2}{d\tilde{x}^2}+\tilde{x}^2\right]\tilde{\psi}_\infty(\tilde{x})\simeq 0\ . \tag{24.90}$$

The solution of this equation is $\tilde{\psi}_\infty(\tilde{x})=Ce^{-\tilde{x}^2/2}$, since

$$\begin{aligned}\left[-\frac{d^2}{d\tilde{x}^2}+\tilde{x}^2\right]e^{-\tilde{x}^2/2}&=-\frac{d}{d\tilde{x}}(-\tilde{x})e^{-\tilde{x}^2/2}+\tilde{x}^2e^{-\tilde{x}^2/2}\\&=-\tilde{x}^2e^{-\tilde{x}^2/2}+e^{-\tilde{x}^2/2}+\tilde{x}^2e^{-\tilde{x}^2/2}=e^{-\tilde{x}^2/2}\simeq 0\ .\end{aligned} \tag{24.91}$$

This motivates the ansatz $\tilde{\psi}(\tilde{x})\equiv e^{-\tilde{x}^2/2}H(\tilde{x})$ for the complete differential equation (24.89),

$$\begin{aligned}&\left[-\frac{d^2}{d\tilde{x}^2}+\tilde{x}^2\right]e^{-\tilde{x}^2/2}H(\tilde{x})=-e^{-\tilde{x}^2/2}\frac{d^2H(\tilde{x})}{d\tilde{x}^2}-2\frac{de^{-\tilde{x}^2/2}}{d\tilde{x}}\frac{dH(\tilde{x})}{d\tilde{x}}-\frac{d^2e^{-\tilde{x}^2/2}}{d\tilde{x}^2}H(\tilde{x})+\tilde{x}^2e^{-\tilde{x}^2/2}H(\tilde{x})\\&=-e^{-\tilde{x}^2/2}\frac{d^2H(\tilde{x})}{d\tilde{x}^2}-2(-x)e^{-\tilde{x}^2/2}\frac{dH(\tilde{x})}{d\tilde{x}}+\left[-\tilde{x}^2e^{-\tilde{x}^2/2}+e^{-\tilde{x}^2/2}\right]H(\tilde{x})+\tilde{x}^2e^{-\tilde{x}^2/2}H(\tilde{x})\\&\equiv(2n+1)e^{-\tilde{x}^2/2}H(\tilde{x})\ .\end{aligned} \tag{24.92}$$

Thus, the functions $H(\tilde{x})$ must satisfy the differential equation,

$$H''(\tilde{x})=2\tilde{x}H'(\tilde{x})-2nH(\tilde{x})\ . \tag{24.93}$$

We can verify that the Hermite polynomials defined by,

$$H_n(\tilde{x})=(-1)^ne^{\tilde{x}^2}\frac{d^n}{d\tilde{x}^n}e^{-\tilde{x}^2}\ , \tag{24.94}$$

transform the differential equation into a recursion formula,

$$H_{n+1}(\tilde{x})=2\tilde{x}H_n(\tilde{x})-2nH_{n-1}(\tilde{x})\ , \tag{24.95}$$

which allows us to easily calculate the polynomials,

$$H_0(\tilde{x})=1\quad,\quad H_1(\tilde{x})=2x\quad,\quad H_2(\tilde{x})=4x^2-2\quad,\quad ... \tag{24.96}$$

In summary, the eigenfunction of a harmonic oscillator in the state of excitation n is,

$$\boxed{\langle x|n\rangle = \psi_n(x) = C_n e^{-x^2/2a_{ho}^2} H_n(x/a_{ho})} \ , \tag{24.97}$$

where the constant C_n is determined by the normalization condition (28.22), $\langle \psi_m|\psi_n\rangle = \delta_{m,n}$,

$$C_n = \frac{1}{\sqrt{a_{ho}\sqrt{\pi}2^n n!}} \ . \tag{24.98}$$

The Hermite functions, H_n, are found in mathematical tables, see Sec. 28.3. The spatial and momentum wavefunctions for the vibrational ground state are,

$$\langle x|0\rangle = \frac{1}{\pi^{1/4}\sqrt{a_{ho}}} e^{-x^2/2a_{ho}^2} \quad \text{and} \quad \langle p|0\rangle = \frac{1}{\pi^{1/4}} \sqrt{\frac{a_{ho}}{\hbar}} e^{-a_{ho}^2 p^2/2\hbar^2} \ . \tag{24.99}$$

Here we will only show the graphical representation of $|\psi|^2$ in Fig. 24.18. The Exc. 24.5.6.1 asks to evaluate HO in a classically forbidden region and in Exc. 24.5.6.2 we will calculate the spectrum of a semi-harmonic HO.

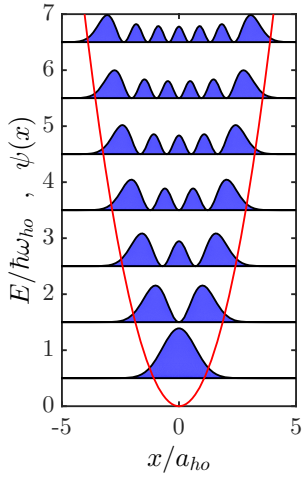

Figure 24.18: (code) Wavefunctions and energies for a harmonic potential.

24.5.3 Properties of the harmonic oscillator

We note that there are regions where $\psi(\tilde{x}) \neq 0$ even though $V(x) > E$. This effect is purely quantum. Classically, we can not find a particle in regions where its energy is below the potential.

We also note that for high quantum numbers, $n \to \infty$, we expect to recover the classical predictions, i.e.,

$$\lim_{n\to\infty} |\psi(x)|^2 = P_E(x) \ , \tag{24.100}$$

where P_E is the probability density of finding the oscillating particle at position x. The probability of finding the particle in a range dx close to the location x is easily

calculated,

$$E = \frac{m}{2}v^2 + \frac{m}{2}\omega^2 x^2 \tag{24.101}$$

$$\Rightarrow \qquad P_E(x)dx = \frac{t(x+dx)-t(x)}{T} = \frac{dx}{vT} = \frac{dx}{T}\frac{1}{\sqrt{2E/m-\omega^2x^2}} \ .$$

We see that for high energy values the wavefunction approaches the classical expectation.

We already mentioned that there exist solutions only for certain energies $E_n = \hbar\omega(2n+1)$. Consequently, the energy levels are equidistant, $E_{n+1} - E_n = \hbar\omega$, as if there were a box into which we add, one after the other, particles with the energy $\hbar\omega$ until we have accumulated n portions of energy. These particles are called *phonons* in the case of vibrations of massive particles, and *photons* in the case of a radiation field.

The fact that the energy distribution is the same as the one proposed by Planck for the black-body radiation suggests the use of the harmonic oscillator to describe the second quantization.

24.5.4 Time evolution of the unperturbed harmonic oscillator

Here we study the temporal evolution of a population distribution in a harmonic oscillator. The formal solution of the Schrödinger equation is,

$$|\psi(t)\rangle = e^{-\imath\hat{H}t/\hbar}|\psi(0)\rangle \ . \tag{24.102}$$

As the Hamiltonian is diagonal in the basis $|n\rangle$,

$$\hat{H} = \hbar\omega(\hat{n} + \tfrac{1}{2}) \ . \tag{24.103}$$

we can write,

$$e^{-\imath\hat{H}t/\hbar} = \sum_n |n\rangle e^{-\imath\omega t(n+1/2)}\langle n| \ . \tag{24.104}$$

If the initial state is $|\psi(0)\rangle = \sum_m c_m|m\rangle$, the final state and the eigenvalue of any observable will be,

$$|\psi(t)\rangle = \sum_n |n\rangle e^{-\imath\omega t(n+1/2)}\langle n|\psi(0)\rangle = \sum_n e^{-\imath\omega t(n+1/2)}c_n|n\rangle \tag{24.105}$$

$$\langle\psi(t)|\hat{A}|\psi(t)\rangle = \sum_m \langle m|e^{\imath\omega t(m+1/2)}c_m^*|\hat{A}|\sum_n e^{-\imath\omega t(n+1/2)}c_n|n\rangle = \sum_{m,n} c_m^* c_n e^{\imath\omega t(m-n)}\langle m|\hat{A}|n\rangle \ .$$

If the oscillator is initially in an eigenstate, $|\psi(0)\rangle = |k\rangle$, we obtain,

$$|\psi(t)\rangle = e^{-\imath\omega t(k+1/2)}|k\rangle \qquad \text{and} \qquad \langle\psi(t)|\hat{A}|\psi(t)\rangle = \langle k|\hat{A}|k\rangle \ , \tag{24.106}$$

that is, the *state remains stationary*. Motion needs non-diagonal elements of $\hat{A}$.

Another observation is that the populations do not change, even in the case of an initial superposition, since,

$$P_k(t) = |\langle k|\psi(t)\rangle|^2 = |e^{-\imath\omega t(k+1/2)}c_k|^2 = |c_k|^2 \ . \tag{24.107}$$

We conclude that

- movement of an observable $\hat{A}$ is possible, but only due to *variations of the phase factors*;
- to carry out transitions between the vibrational states is necessary to *perturb the oscillator*, e.g. by applying fields of electromagnetic radiation.

Example 160 (*Motion of a harmonic oscillator*): We now consider some specific examples. If the studied observable is the Hamiltonian and the initial state an arbitrary superposition, then

$$\langle\psi(t)|\hat{H}|\psi(t)\rangle = \hbar\omega \sum_{m,n} c_m^* c_n e^{\imath\omega t(m-n)} \langle m|\hat{n} + \tfrac{1}{2}|n\rangle = \hbar\omega \sum_n |c_n|^2 (n + \tfrac{1}{2}) \ .$$

That is, the total energy of the oscillator is the sum of the energies of the states weighted with the populations of those states. In the case of the position operator,

$$\begin{aligned}\langle\psi(t)|\hat{x}|\psi(t)\rangle &= \tfrac{a_{ho}}{\sqrt{2}} \sum_{m,n} c_m^* c_n e^{\imath\omega t(m-n)} \langle m|\hat{a} + \hat{a}^\dagger|n\rangle \\ &= \tfrac{a_{ho}}{\sqrt{2}} \sum_n \left(c_{n-1}^* c_n e^{-\imath\omega t}\sqrt{n} + c_{n+1}^* c_n e^{\imath\omega t}\sqrt{n+1}\right) \\ &\overset{m,n\to\infty}{\longrightarrow} a_{ho}\sqrt{2} \sum_n \sqrt{n}|c_n|^2 \cos\omega t \ .\end{aligned}$$

That is, *the particle can only oscillate, if there are populations in consecutive states*. If this is not the case, $\langle\psi(t)|\hat{x}|\psi(t)\rangle = 0$. The oscillation frequency is always ω, independent of the energy of the particle. We will study this in Excs. 24.5.6.3, leaving the discussion of the temporal evolution of perturbed oscillators to later sections.

24.5.5 Multidimensional harmonic oscillator

The 3D harmonic potential is given by

$$V_{ho}(\mathbf{r}) = \frac{m}{2}\omega_x^2 x^2 + \frac{m}{2}\omega_y^2 y^2 + \frac{m}{2}\omega_z^2 z^2 \ . \tag{24.108}$$

Making the ansatz

$$\psi(\mathbf{r}) = \psi_x(x)\psi_y(y)\psi_z(z) \ , \tag{24.109}$$

we can separate the spatial directions and obtain a one-dimensional equation for each coordinate, such that the coordinates can be considered separately. Each function $\psi_k(x_k)$ is of the form (24.97) and the energies are,

$$E_k = \hbar\omega_k(n_k + \tfrac{1}{2}) \ , \tag{24.110}$$

where $k = x, y, z$.

24.5.6 Exercises

24.5.6.1 Ex: Ground state of a harmonic oscillator

Equating the ground state energy of quantum HO to that of its classical analog, obtain the maximum elongation x_m. Now, knowing that the ground state wavefunction

is proportional to the Gaussian $\psi_0 \propto e^{-x^2/2x_m^2}$, obtain the expression for the probability of finding the HO outside the classical limits and estimate its value.

Solution: *The ground state energy is,*

$$\frac{1}{2}\hbar\omega = \frac{m}{2}\omega^2 x_m^2 \quad \Longrightarrow \quad x_m = \sqrt{\frac{\hbar}{m\omega}} = a_{ho} \ .$$

The ground state wave function is,

$$\psi_0(x) = Ce^{-x^2/2a_{ho}^2} H_0(x/a_{ho}) \ .$$

With the normalization,

$$1 = \int_{-\infty}^{\infty} |\psi_0(x)|^2 dx = C^2 a_{ho} \int_{-\infty}^{\infty} e^{-\tilde{x}^2} d\tilde{x} = C^2 a_{ho}\sqrt{\pi} \ ,$$

we get the probability of being in a classically forbidden region,

$$w = 1 - \int_{-a_{ho}}^{a_{ho}} |\psi_0(x)|^2 dx = 1 - \frac{1}{\sqrt{\pi}} \int_{-1}^{1} e^{-\tilde{x}^2} d\tilde{x} = 1 - erf(1) \approx 0.157 \ .$$

24.5.6.2 Ex: Particle in a semi-harmonic well

Find the energy levels of a particle in a potential energy well of the form $V(x) = \infty$ for $x < 0$ and $V(x) = \frac{m\omega^2 x^2}{2}$ for $x > 0$. What is the parity of the allowed states?

Solution: *They are simply states with $\psi_n(0) = 0$. That is, with n odd. Only states with odd parity are allowed.*

24.5.6.3 Ex: Vibration of a harmonic oscillator

Consider a HO of mass m and angular frequency ω. At time $t = 0$ the oscillator's state is $|\psi(0)\rangle = \sum_n c_n |n\rangle$, where $|n\rangle$ are the stationary states of the HO with energy $(n + 1/2)\hbar\omega$.
a. What is the probability P for measuring, at an arbitrary time $t > 0$, an energy of the HO higher than $2\hbar\omega$? For the case when $P = 0$, what are the non-zero coefficients c_n?
b. From now on, we assume that only c_0 and c_1 are nonzero. Write down the normalization condition for $|\psi(0)\rangle$ and the mean value $\langle\hat{H}\rangle$ of energy in terms of c_0 and c_1. With the additional requirement $\langle\hat{H}\rangle = \hbar\omega$, calculate $|c_0|^2$ and $|c_1|^2$.
c. Given that the normalized state vector $|\psi(0)\rangle$ is defined to less than an overall phase factor, we determine this factor by choosing the real and positive coefficients c_0 and $c_1 = |c_1|e^{\imath\theta}$. Assuming $\langle\hat{H}\rangle = \hbar\omega$ and $\langle\hat{x}\rangle = \frac{1}{2}\sqrt{\hbar/m\omega}$, calculate θ.
d. With $|\psi(0)\rangle$ determined (according to the previous item), write down $|\psi(t)\rangle$ for $t > 0$ and calculate the value θ at this time t. Deduce the average value $\langle\hat{x}\rangle(t)$ of the

position at time t.

Solution: *a. The probability is* $P_{n\geq 2}(t) = 1 - |c_0|^2 - |c_1|^2$. *For* $P = 0$ *we have* $c_n = c_0\delta_{n0} + c_1\delta_{n1}$.
b. Normalization requests $1 \equiv \langle\psi(0)|\psi(0)\rangle = |c_0|^2 + |c_1|^2$. *With the requirement*

$$\langle\hat{H}\rangle = \tfrac{1}{2}\hbar\omega|c_0|^2 + \tfrac{3}{2}\hbar\omega|c_1|^2 = \hbar\omega \ ,$$

we have the equations

$$|c_0|^2 + |c_1|^2 = 1 \qquad \textit{and} \qquad |c_0|^2 + 3|c_1|^2 = 2 \ ,$$

which gives $|c_0| = |c_1| = 2^{-1/2}$.
c. The expectation value for the position is,

$$\langle\hat{x}(t)\rangle = \tfrac{a_{ho}}{\sqrt{2}}\left(c_0^* c_1 e^{-\imath\omega t} + c_0 c_1^* e^{\imath\omega t}\right) \ .$$

Initially, $(t = 0)$ *we have the additional requirement,*

$$\langle\hat{x}(0)\rangle = a_{ho}\left(c_0^* c_1 + c_1^* c_0\right) \equiv \tfrac{1}{2}\sqrt{\tfrac{\hbar}{m\omega}} \ ,$$

setting $c_0 = |c_0|$ *and* $c_1 = |c_1|e^{\imath\theta}$ *we find,*

$$\cos\theta = \frac{1}{4c_0 c_1} = \frac{1}{\sqrt{2}} \ .$$

This means, $\theta = \pi/4$.
d. We can now write,

$$|\psi(t)\rangle = e^{-\imath\omega t/2}c_0|0\rangle + e^{-3\imath\omega t/2}c_1|1\rangle = \tfrac{1}{\sqrt{2}}e^{-\imath\omega t/2}\left(|0\rangle + e^{-\imath\omega t - \imath\pi/4}|1\rangle\right) \ .$$

The expectation value of the position is,

$$\begin{aligned}\langle\hat{x}(t)\rangle &= \tfrac{1}{2}\left(\langle 0| + e^{\imath\omega t + \imath\pi/4}\langle 1|\right)\tfrac{a_{ho}}{\sqrt{2}}(\hat{a}^\dagger + \hat{a})\left(|0\rangle + e^{-\imath\omega t - \imath\pi/4}|1\rangle\right) \\ &= \tfrac{a_{ho}}{\sqrt{2}}\cos(\omega t + \pi/4) \ .\end{aligned}$$

24.6 Superposition states of a harmonic oscillator

As any other quantum system, a harmonic oscillator does not need to be in a particular vibrational eigenstate. In fact, it is much more common to encounter them in superpositions of many states. In a system in thermal equilibrium, the energetic distribution of occupied states reflects the temperature of the system.

24.6.1 Coherent states

The most common superposition for a harmonic oscillation is a Poissonian probability distribution of occupied vibrational (Fock) states. This state, called coherent or Glauber state, has particular features that we will discuss in the following sections.

24.6.1.1 Displacement operator

We now consider the so-called *displacement operator*,

$$\boxed{D(\alpha) \equiv e^{\alpha\hat{a}^\dagger - \alpha^*\hat{a}}} \ , \tag{24.111}$$

which acts on the phase space of a harmonic oscillator spanned by the operators $\hat{a}$ and $\hat{a}^\dagger$, that is, $\hat{x} \propto \mathfrak{Re}\ \hat{a}$ and $\hat{p} \propto \mathfrak{Im}\ \hat{a}$, and try to discovers its features.

$D(\alpha)$ is a unitary operator, since using Glauber's formula (23.210) we get,

$$\begin{aligned} D^\dagger(\alpha)D(\alpha) &= e^{\alpha^*\hat{a}-\alpha\hat{a}^\dagger} e^{\alpha\hat{a}^\dagger-\alpha^*\hat{a}} = e^{\alpha^*\hat{a}-\alpha\hat{a}^\dagger+\alpha\hat{a}^\dagger-\alpha^*\hat{a}+[\alpha^*\hat{a}-\alpha\hat{a}^\dagger,\alpha\hat{a}^\dagger-\alpha^*\hat{a}]/2} \\ &= e^{[\alpha^*\hat{a}-\alpha\hat{a}^\dagger,\alpha\hat{a}^\dagger-\alpha^*\hat{a}]/2} = e^{[\alpha^*\hat{a},\alpha\hat{a}^\dagger]/2+[-\alpha\hat{a}^\dagger,\alpha\hat{a}^\dagger]/2+[\alpha^*\hat{a},-\alpha^*\hat{a}]/2+[-\alpha\hat{a}^\dagger,-\alpha^*\hat{a}]/2} \\ &= e^{|\alpha|^2[\hat{a},\hat{a}^\dagger]/2+|\alpha|^2[\hat{a}^\dagger,\hat{a}]/2} = e^0 = \hat{1} \ . \end{aligned} \tag{24.112}$$

We can rewrite the displacement operator using Glauber's formula:

$$\begin{aligned} D(\alpha) &= e^{\alpha\hat{a}^\dagger-\alpha^*\hat{a}} = e^{\alpha\hat{a}^\dagger} e^{-\alpha^*\hat{a}} e^{-[\alpha\hat{a}^\dagger,-\alpha^*\hat{a}]/2} = e^{\alpha\hat{a}^\dagger} e^{-\alpha^*\hat{a}} e^{|\alpha|^2[\hat{a}^\dagger,\hat{a}]/2} \\ &= e^{\alpha\hat{a}^\dagger} e^{-\alpha^*\hat{a}} e^{-|\alpha|^2/2} \ . \end{aligned} \tag{24.113}$$

The state resulting from the action of the operator $D(\alpha)$ onto the ground state of the HO is,

$$\begin{aligned} |\alpha\rangle \equiv D(\alpha)|0\rangle &= e^{-|\alpha|^2/2} e^{\alpha\hat{a}^\dagger} e^{-\alpha^*\hat{a}}|0\rangle = e^{-|\alpha|^2/2} \sum_{n=0}^{\infty} \frac{(\alpha\hat{a}^\dagger)^n}{n!}|0\rangle \\ &= e^{-|\alpha|^2/2} \left(1 + \alpha\hat{a}^\dagger + \frac{(\alpha\hat{a}^\dagger)^2}{2!} + ..\right)|0\rangle \\ &= e^{-|\alpha|^2/2} \left(|0\rangle + \frac{\alpha}{1!}\sqrt{1}|1\rangle + \frac{\alpha^2}{2!}\sqrt{2!}|2\rangle + ..\right) \ , \end{aligned} \tag{24.114}$$

that is, the state $|\alpha\rangle$ is a superposition distributed according to the *Poisson distribution*,

$$\boxed{|\alpha\rangle = e^{-|\alpha|^2/2} \sum_{n=0}^{\infty} \frac{\alpha^n}{\sqrt{n!}}|n\rangle} \ . \tag{24.115}$$

Applying the step-down operator $\hat{a}$ onto the state $|\alpha\rangle$, we find,

$$\begin{aligned} \hat{a}|\alpha\rangle &= e^{-|\alpha|^2/2} \sum_{n=0}^{\infty} \frac{\alpha^n}{\sqrt{n!}} \hat{a}|n\rangle = e^{-|\alpha|^2/2} \sum_{n=0}^{\infty} \frac{\alpha^n}{\sqrt{n!}} \sqrt{n}|n-1\rangle \\ &= e^{-|\alpha|^2/2} \sum_{n=0}^{\infty} \frac{\alpha^n}{\sqrt{(n-1)!}}|n-1\rangle \ , \end{aligned} \tag{24.116}$$

that is,

$$\boxed{\hat{a}|\alpha\rangle = \alpha|\alpha\rangle} \ . \tag{24.117}$$

We can also write,

$$\langle\alpha|\hat{a}^\dagger = (\hat{a}|\alpha\rangle)^\dagger = (\alpha|\alpha\rangle)^\dagger = \langle\alpha|\alpha^* \ . \tag{24.118}$$

The state $|\alpha\rangle$ is called *coherent state* or *Glauber state* [3]. We note that, in spite of its appearance, the equation (24.117) is not an eigenvalue equation, since $\hat{a}$ is not observable.

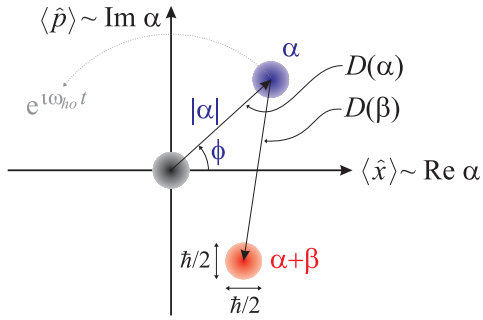

Figure 24.19: Illustration of the action of displacement operators $D(\alpha)$ and $D(\beta)$ on Glauber states in the phase space spanned by $\alpha = \mathfrak{Re}\ \alpha + \imath\, \mathfrak{Im}\ \alpha = |\alpha| e^{\imath\phi}$. The uncertainty of Glauber states Δx and Δp is represented by a finite distribution of the amplitude α in the phase space.

Using the formula (23.179), we verify immediately,

$$\boxed{D^\dagger(\alpha)\hat{a}D(\alpha) = \hat{a} + \alpha \quad , \quad D^\dagger(\alpha)\hat{a}^\dagger D(\alpha) = \hat{a}^\dagger + \alpha^*} \ . \tag{24.119}$$

Furthermore, the product of two displacement operators is, apart from a phase factor, another displacement operator satisfying,

$$\boxed{D(\alpha)D(\beta) = e^{(\alpha\beta^* - \alpha^*\beta)/2} D(\alpha+\beta)} \ , \tag{24.120}$$

as will be verified in Exc. 24.6.6.1. When acting on an eigenket, the phase factor $e^{(\alpha\beta^* - \alpha^*\beta)/2}$ appears in each term of the resulting state, which makes it physically irrelevant.

24.6.1.2 Uncertainty in Glauber states

Consider a HO prepared in a state $|\alpha\rangle$. The eigenvalues of the observables $\hat{x} \equiv \frac{a_{ho}}{\sqrt{2}}(\hat{a}^\dagger + \hat{a})$ and $\hat{p} \equiv \frac{\imath\hbar}{a_{ho}\sqrt{2}}(\hat{a}^\dagger - \hat{a})$ are,

$$\begin{aligned} \tfrac{\sqrt{2}}{a_{ho}}\langle\alpha|\hat{x}|\alpha\rangle &= \langle\alpha|\hat{a} + \hat{a}^\dagger|\alpha\rangle = \alpha + \alpha^* \\ \tfrac{\imath a_{ho}\sqrt{2}}{\hbar}\langle\alpha|\hat{p}|\alpha\rangle &= \langle\alpha|\hat{a} - \hat{a}^\dagger|\alpha\rangle = \alpha - \alpha^* . \end{aligned} \tag{24.121}$$

With this the eigenvalues of the quadratures become,

$$\begin{aligned} \tfrac{2}{a_{ho}^2}\langle\alpha|\hat{x}^2|\alpha\rangle &= \langle\alpha|(\hat{a}+\hat{a}^\dagger)^2|\alpha\rangle = \langle\alpha|\hat{a}\hat{a} + 1 + 2\hat{a}^\dagger\hat{a} + \hat{a}^\dagger\hat{a}^\dagger|\alpha\rangle \\ &= \alpha^2 + 1 + 2|\alpha|^2 + \alpha^{*2} = 1 + (\alpha+\alpha^*)^2 = 1 + \tfrac{2}{a_{ho}^2}\langle\alpha|\hat{x}|\alpha\rangle^2 \\ \tfrac{-a_{ho}^2}{\hbar^2}\langle\alpha|\hat{p}^2|\alpha\rangle &= \langle\alpha|(\hat{a}-\hat{a}^\dagger)^2|\alpha\rangle = \langle\alpha|\hat{a}\hat{a} - 1 - 2\hat{a}^\dagger\hat{a} + \hat{a}^\dagger\hat{a}^\dagger|\alpha\rangle \\ &= \alpha^2 - 1 - 2|\alpha|^2 + \alpha^{*2} = -1 + (\alpha-\alpha^*)^2 = -1 - \tfrac{2a_{ho}^2}{\hbar^2}\langle\alpha|\hat{p}|\alpha\rangle^2 \ . \end{aligned} \tag{24.122}$$

[3] We can also define a *Bargmann state* as the eigenstate corresponding to the step-up operator using the notation $\hat{a}^\dagger||\alpha\rangle = \alpha||\alpha\rangle$.

The uncertainties defined in (23.70) become,

$$\begin{aligned}\Delta x^2 &= \langle\alpha|\hat{x}^2|\alpha\rangle - \langle\alpha|\hat{x}|\alpha\rangle^2 = \tfrac{a_{ho}^2}{2} \\ \Delta p^2 &= \langle\alpha|\hat{p}^2|\alpha\rangle - \langle\alpha|\hat{p}|\alpha\rangle^2 = \tfrac{\hbar^2}{2a_{ho}^2}\ .\end{aligned} \tag{24.123}$$

And finally, we find the Heisenberg relation,

$$\Delta p \Delta x = \tfrac{\hbar}{2}\ . \tag{24.124}$$

Comparing with the uncertainty relation (24.88) derived for Fock states, we conclude that the uncertainty is always *smallest* for Glauber states. In this sense, the Glauber states are the ones which are closest to classical states characterized by the absence of uncertainty.

24.6.1.3 Orthogonality and completeness of Glauber states

Glauber are not orthogonal, since,

$$|\langle\alpha|\beta\rangle|^2 = e^{-|\alpha-\beta|^2}\ . \tag{24.125}$$

We leave the demonstration for Exc. 24.6.6.2, but we note here already that for $|\alpha-\beta| \gg 0$ the states are approximately orthogonal. The reason for this is, that the respective population distributions through the Fock states, $|\langle n|\alpha\rangle|^2$ and $|\langle n|\beta\rangle|^2$, do not overlap and hence do not interfere. Some more useful relationships are studied in Exc. 24.6.6.3. In Exc. 24.6.6.4 we show that the coherent state basis is not only complete,

$$\tfrac{1}{\pi}\int |\alpha\rangle\langle\alpha| d^2\alpha = \mathbb{I}\ , \tag{24.126}$$

but it is overcomplete. The state $|\alpha\rangle + |-\alpha\rangle$ is sometimes called *Schrödinger cat state*. In Exc. 24.6.6.5 we will show why such states are very difficult to detect.

24.6.2 Kicking a harmonic oscillator

Let us now study the dynamics of a harmonic oscillator subject to a *kick* or a dislocation or both in the same time. For this we need to remember the Galilei boost introduced in Sec. 23.5.3 and the unitary transformations corresponding to a spatial displacement (23.181) and to a kick (23.192),

$$U_{tr}(b) = e^{(-\imath/\hbar)b\hat{p}} \qquad \text{and} \qquad U_{kc}(k) = e^{\imath k\hat{x}}\ , \tag{24.127}$$

where we restrict to one dimension. The crucial point is that for a harmonic oscillator we know how to expand the operators $\hat{x}$ and $\hat{p}$ into linear combinations of the field operators $\hat{a}$ and $\hat{a}^\dagger$, which allows us to apply the whole formalism developed in the last sections to these transformation operators.

24.6.2.1 Transitions between vibrational states via momentum kick and dislocation

With the formalism developed in the last sections the displacement operator (24.114) can be decomposed in a combination of a spatial displacement and a kick operator (24.127). We can see this by simply substituting the field operators $\hat{a}$ and $\hat{a}^\dagger$ by linear combinations of position and momentum operators using (24.85),

$$\begin{aligned}\alpha\hat{a}^\dagger - \alpha^*\hat{a} &= \frac{\alpha}{\sqrt{2}}\left(\frac{\hat{x}}{a_{ho}} - \imath\frac{a_{ho}\hat{p}}{\hbar}\right) - \frac{\alpha^*}{\sqrt{2}}\left(\frac{\hat{x}}{a_{ho}} + \imath\frac{a_{ho}\hat{p}}{\hbar}\right) \\ &= -\imath\frac{\sqrt{2}a_{ho}\mathfrak{Re}\ \alpha}{\hbar}\ \hat{p} + \imath\frac{\sqrt{2}\mathfrak{Im}\ \alpha}{a_{ho}}\ \hat{x}\ .\end{aligned} \tag{24.128}$$

Using Glauber's rule,

$$D(\alpha) = e^{\alpha\hat{a}^\dagger - \alpha^*\hat{a}} = e^{\imath\ \mathfrak{Re}\ \alpha\mathfrak{Im}\ \alpha} e^{(-\imath a_{ho}\sqrt{2}/\hbar)\mathfrak{Re}\ \alpha\ \hat{p}} e^{(\imath\sqrt{2}/a_{ho})\mathfrak{Im}\ \alpha\ \hat{x}}\ . \tag{24.129}$$

Hence, similarly to the Galilei boost in time and space, the displacement operator $D(\alpha)$ transforms the state of a harmonic oscillator, for example the ground state, $|\alpha\rangle = D(\alpha)|0\rangle$, by kicking its momentum by an amount,

$$\hbar k = \frac{\hbar\sqrt{2}}{a_{ho}}\mathfrak{Im}\ \alpha\ , \tag{24.130}$$

and/or displacing its position suddenly by an amount,

$$b = \sqrt{2}a_{ho}\mathfrak{Re}\ \alpha\ , \tag{24.131}$$

such that,

$$\alpha = \frac{b}{\sqrt{2}a_{ho}} + \imath\frac{ka_{ho}}{\sqrt{2}}\ . \tag{24.132}$$

The real and imaginary parts of α decide which contribution predominates, the kick or the dislocation,

$$\boxed{D(\alpha) = e^{\imath\ \mathfrak{Re}\ \alpha\mathfrak{Im}\ \alpha}\ U_{tr}(\sqrt{2}a_{ho}\mathfrak{Re}\ \alpha)\ U_{kc}(\tfrac{\hbar\sqrt{2}}{a_{ho}}\mathfrak{Im}\ \alpha)}\ . \tag{24.133}$$

For example, if α is imaginary the operation describes a pure momentum kick by an amount $\hbar k$, which puts the harmonic oscillator into a coherent state with the mean occupation number,

$$n = |\alpha|^2 = |\mathfrak{Im}\ \alpha|^2 = \tfrac{1}{2}k^2a_{ho}^2\ , \tag{24.134}$$

On the other hand, if α is real the operation describes a pure dislocation by an amount b, which puts the harmonic oscillator into a coherent state with the mean occupation number,

$$n = |\alpha|^2 = |\mathfrak{Re}\ \alpha|^2 = \frac{b^2}{2a_{ho}^2}\ . \tag{24.135}$$

Now, let us focus on the kick operator and study how it acts on Fock states,

$$\begin{aligned}\langle n|e^{\imath k\hat{x}}|0\rangle = \langle n|\alpha\rangle &= \langle n|e^{-|\alpha|^2/2}\sum_{m=0}^{\infty}\frac{\alpha^m}{\sqrt{m!}}|m\rangle \\ &= e^{-|\alpha|^2/2}\frac{\alpha^n}{\sqrt{n!}} = e^{-|ka_{ho}|^2/4}\frac{(\imath k a_{ho})^n}{\sqrt{2^n n!}}\ ,\end{aligned} \tag{24.136}$$

using (24.132). This formula tells us that for small α, transitions may only occur to the vibrational states $|0\rangle$ and $|1\rangle$, since,

$$\langle n|e^{\imath k\hat{x}}|0\rangle \overset{ka_{ho}\to 0}{\longrightarrow} \frac{\alpha^n}{\sqrt{n!}} \simeq \delta_{n,0} + \alpha\delta_{n,1}\ . \tag{24.137}$$

On the other hand for very large α, the exponential in (24.136) pulls the transition rate to a particular vibrational state $|n\rangle$ to zero, but this is simply due to the fact that the population is redistributed over many states, since,

$$\sum_n |\langle n|e^{\imath k\hat{x}}|0\rangle|^2 = e^{-(ka_{ho})^2/2}\sum_{n=0}^{\infty}\frac{|\alpha|^{2n}}{n!} = e^{-(ka_{ho})^2/2}e^{|\alpha|^2} = 1\ . \tag{24.138}$$

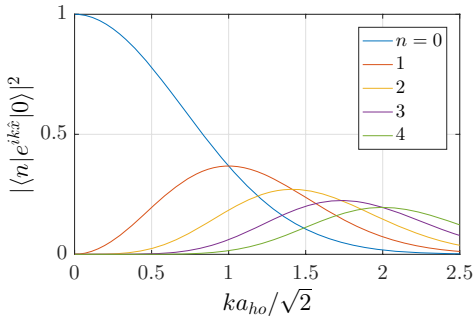

Figure 24.20: (code) Transition matrix element $|\langle n|e^{\imath k\hat{x}}|0\rangle|^2$ as a function of ka_{ho}. The curves are Poisson distributions of photon numbers in coherent states.

For small momentum kicks we may approximate the transition matrix elements by,

$$\begin{aligned}\langle m|e^{\imath k\hat{x}}|n\rangle &\simeq \langle m|1 + \imath k\tfrac{a_{ho}}{\sqrt{2}}(\hat{a}+\hat{a}^\dagger)|n\rangle \\ &= \delta_{m,n} + \tfrac{\imath k a_{ho}}{\sqrt{2}}(\sqrt{n}\delta_{m,n-1} + \sqrt{n+1}\delta_{m,n+1})\ ,\end{aligned} \tag{24.139}$$

such that,

$$\sum_{m\neq n}|\langle m|e^{\imath k\hat{x}}|n\rangle|^2 \simeq k^2 a_{ho}^2(n+\tfrac{1}{2})\ . \tag{24.140}$$

Formula (24.140) tell us that the probability for a transition between vibrational states depends on the parameter ka_{ho}, which we will discuss in the next section. For small ka_{ho} it gets increasingly more difficult for the system to leave the original

vibrational state $|n\rangle$ and to form a coherent state. After a momentum kick, the population is coherently distributed over several vibrational states in a way to fulfill momentum and energy conservation. Let us consider, for simplicity, an initial state $|0\rangle$. If the kick is weak or the trap strong (i.e. if $|\alpha| < 1$), the atom will stay in $|0\rangle$ with a high probability amplitude and go to $|1\rangle$ only with a small probability amplitude. We will derive in Exc. 24.6.6.6 the general expression for the transition matrix element for arbitrary values of α [4],

$$\boxed{\langle m|e^{\imath k\hat{x}}|n\rangle = e^{|\alpha|^2/2}\sum_{k=0}^{n}\sqrt{\binom{n}{k}\binom{m}{k}}\langle n-k|\alpha\rangle\langle m-k|\alpha\rangle} \ . \tag{24.141}$$

The formula satisfies,

$$\sum_m |\langle m|e^{\imath k\hat{x}}|n\rangle|^2 = \sum_m \langle n|e^{\imath kx}|m\rangle\langle m|e^{-\imath kx}|n\rangle = \langle n|e^{\imath kx}e^{-\imath kx}|n\rangle = 1 \ . \tag{24.142}$$

Kicking a harmonic oscillator initially in state $|0\rangle$ we obtain for the expectation value of position and momentum,

$$\boxed{\begin{array}{lcl} \langle\alpha|\hat{p}|\alpha\rangle & = & \langle 0|D(\alpha)^\dagger \hat{p} D(\alpha)|0\rangle = \langle 0|e^{\imath k\hat{x}}\hat{p}e^{-\imath k\hat{x}}|0\rangle = \langle 0|\hat{p}|0\rangle + \hbar k \\ \langle\alpha|\hat{x}|\alpha\rangle & = & \langle 0|\hat{x}|0\rangle \end{array}} \ .$$

24.6.2.2 Lamb-Dicke regime

We already introduced $|\alpha|$ as the amplitude (24.135) of the coherent vibrational state created by kicking a harmonic oscillator. Defined as,

$$\boxed{\eta \equiv |\alpha| = \tfrac{1}{\sqrt{2}} k a_{ho}} \qquad \text{with} \qquad a_{ho} \equiv \sqrt{\frac{\hbar}{m\omega_{ho}}} \ . \tag{24.143}$$

the so-called *Lamb-Dicke parameter* measures the *degree of confinement* of a particle in a harmonic trap with respect to the momentum kick. We say that we are in the *Lamb-Dicke regime*, when $\eta < 1$, that is when the particle is localized to a volume smaller than the wavelength, $2\pi x_0 \ll \lambda = 2\pi/k$, corresponding to the momentum change.

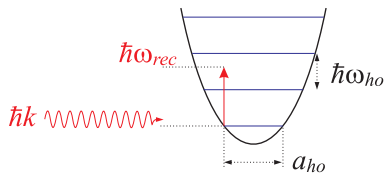

Figure 24.21: Illustration of the Lamb-Dicke parameter.

[4] See also 35.2.3.

We can also rewrite the Lamb-Dicke parameter in terms of the trap's secular frequency, ω_{ho}, and the recoil-shift,

$$\boxed{\eta = \sqrt{\frac{\omega_{rec}}{\omega_{ho}}}} \qquad \text{with} \qquad \omega_{rec} \equiv \frac{\hbar k^2}{2m} \ , \tag{24.144}$$

where we understand the recoil-energy $\hbar\omega_{rec}$ as the kinetic energy gained through the recoil acceleration. In this form the Lamb-Dicke parameter tells us that, in the Lamb-Dicke regime, the energy of the momentum kick is not sufficient to efficiently excite vibrational states,

$$(2n+1)\hbar k^2/m \ll \omega_{ho} \ . \tag{24.145}$$

That is, cold particles in low vibrational states n can not accommodate the recoil shift within the vibrational spectrum of the trap. Consequently, the recoil cannot be transferred to the particle itself, but must be absorbed by the entire trap. This is the case of the *strong binding regime* in ion traps, which is analogous to the *Mößbauer effect* discussed later in Sec. 38.3.3.

Finally, the Lamb-Dicke parameter can be rewritten in terms of the *inverse Doppler modulation index*,

$$\boxed{\eta = \frac{k v_{max}}{2\omega_{ho}}} \qquad \text{with} \qquad \frac{m}{2} v_{max}^2 = \hbar\omega_{ho} \ . \tag{24.146}$$

Accelerated by the momentum kick, the atom will execute harmonic oscillations with frequency ω_{ho} and with the maximum velocity-excursions v_{max}. Hence, any quantity depending on the atomic velocity, e.g. the Doppler-shift of light scattered from the atom, will be modulated. We will see in Sec. 38.3.3 that the modulation generates a spectrum of frequency sidebands which, in case of small $\eta < 1$, are restricted to first-order sidebands located at $\pm\omega_{ho}$ of the light frequency. Do the Exc. 24.6.6.7.

Example 161 (*Absorption of recoil by a molecular dimer*): To be able to discuss the validity of energy and momentum conservation in a kicked system, let us consider a molecule made of two atoms with masses m_1 and m_2 bound by a force obeying Hooke's law. Then we kick atom 1 via the momentum shift operator $e^{\imath k\hat{x}_1}$ (e.g. during a photon absorption process with the associated recoil) and analyze the motional dynamics of the whole system [5]. (We restrict ourselves to one dimension.)

The first step is to write down the Hamiltonian,

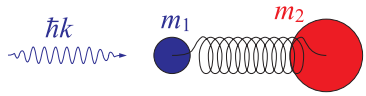

Figure 24.22: Illustration of a heteronuclear dimer kicked by photonic recoil.

$$\hat{H} = -\frac{\hbar^2}{2m_1}\frac{d^2}{dx_1^2} - \frac{\hbar^2}{2m_2}\frac{d^2}{dx_2^2} + \frac{\mu}{2}\omega_{ho}^2(x_1 - x_2)^2 \ ,$$

[5] The selective kicking is realistic if we image both atoms being of different species with different transitions responding differently to incident radiation.

We transform in the center-of-mass system via,

$$M \equiv m_1 + m_2 \quad \text{and} \quad \frac{1}{\mu} \equiv \frac{1}{m_1} + \frac{1}{m_2}$$
$$R = \frac{m_1 x_1 + m_2 x_2}{M} \quad \text{and} \quad r = x_1 - x_2 \ .$$

Applying the separation ansatz $\psi(x_1, x_2) = \Theta(R)\phi(r)$ to the Schrödinger equation,

$$\left[-\frac{\hbar^2}{2m_1}\frac{d^2}{dx_1^2} - \frac{\hbar^2}{2m_2}\frac{d^2}{dx_2^2} + \frac{\mu}{2}\omega_{ho}^2(\hat{x}_1 - \hat{x}_2)^2 \right] \psi(x_1, x_2) = E_{tot}\psi(x_1, x_2) \ ,$$

we calculate for $i = 1, 2$,

$$\frac{d}{dx_i} = \frac{dR}{dx_i}\frac{d}{dR} + \frac{dr}{dx_i}\frac{d}{dr} = \frac{m_i}{M}\frac{d}{dR} \pm \frac{d}{dr}$$
$$\frac{d^2}{dx_i^2} = \frac{m_i^2}{M^2}\frac{d^2}{dR^2} \pm 2\frac{m_i}{M}\frac{d}{dR}\frac{d}{dr} + \frac{d^2}{dr^2}$$
$$-\frac{\hbar^2}{2m_1}\frac{d^2}{dx_1^2} - \frac{\hbar^2}{2m_2}\frac{d^2}{dx_2^2} = -\frac{\hbar^2}{2M}\frac{d^2}{dR^2} - \frac{\hbar^2}{2\mu}\frac{d^2}{dr^2} \ .$$

Hence, we get,

$$-\frac{\hbar^2}{2M}\frac{d^2}{dR^2}\Theta(R) = (E_{tot} - E)\Theta(R) \quad , \quad \left[-\frac{\hbar^2}{2\mu}\frac{d^2}{dr^2} + \frac{\mu}{2}\omega_{ho}^2\hat{r}^2 \right] \phi(r) = E\phi(r) \ ,$$

with the vibrational energy E and the energy of the center-of-mass motion $E_{tot} - E$.
Now, we analyze the kick operator $e^{\imath k\hat{x}_1}$ with $\hat{x}_1 = \hat{R} - \frac{m_2}{M}\hat{r}$. We find that, because of $[\hat{R}, \hat{r}] = 0$,

$$e^{\imath k\hat{x}_1} = e^{\imath k\hat{R}} e^{-\imath k\frac{m_2}{M}\hat{r}} \ .$$

This means that the kick operator simultaneously acts on both: the center-of-mass receives a recoil accelerating it by an amount $p_{cm} = \hbar k$, and the vibrational relative motion receives a kick of an amount $p_{rl} = \hbar k m_2/M$ following the dynamics described in Sec. 24.6.2.
Obviously, the total system conserves momentum, which is imparted to the center-of-mass motion. Whether the kick also excites the relative motion depends on mass ratio. In the limit $m_1 \ll m_2$ we find $p_{rl} = \hbar k$, while in the limit $m_1 \gg m_2$ we get $p_{rl} \to 0$. In terms of the Lamb-Dicke parameter, we find,

$$\eta = \frac{p_{rl}a_{ho}}{\hbar\sqrt{2}} = \frac{km_2}{M\sqrt{2}}\sqrt{\frac{\hbar}{\mu\omega_{ho}}} = \frac{km_2}{m_1 + m_2}\sqrt{\frac{\hbar}{2\omega_{ho}}\left(\frac{1}{m_1} + \frac{1}{m_2}\right)} \ .$$

Hence, in the limit $m_1 \ll m_2$ we expect a much larger Lamb-Dicke parameter than for $m_1 \gg m_2$. In particular, considering the limit $m_2 \to \infty$, we recover the formula (24.144) holding for an atom confined in a harmonic potential,

$$\eta \overset{m_2\to\infty}{\longrightarrow} \sqrt{\frac{\hbar k^2}{\omega_{ho}2m_1}} = \sqrt{\frac{\omega_{rec}}{\omega_{ho}}} \ .$$

24.6.3 Shaking a harmonic oscillator

As we mentioned below the formulae (23.193), the transformation in momentum space is not a realistic concept for a *kick*. In practice, a kick will always be the results of a collision, which is understood here as a scattering of a free (massive or massless) particle at our harmonically trapped particle. And the scattering process will take a finite amount of time, e.g. the duration of a radiative π-pulse required to excite an atomic transition.

More realistic is to expose the harmonic oscillator to periodic forcing,

$$\boxed{\hat{H}(t) = \hat{H}^{(0)} + \hat{H}^{(1)} = -\frac{\hbar^2}{2m}\frac{d^2}{dx^2} + \frac{m}{2}\omega_{ho}^2\hat{x}^2 + \frac{\hbar\Omega}{2}(\hat{a}e^{\imath\nu t} + \hat{a}^\dagger e^{-\imath\nu t})} \,. \tag{24.147}$$

To study its time evolution we calculate,

$$|\psi(t)\rangle = e^{-(\imath/\hbar)\hat{H}t}\sum_n a_n|n\rangle \stackrel{a_n=\delta_{n,0}}{\longrightarrow} e^{-(\imath/\hbar)\hat{H}t}|0\rangle \,, \tag{24.148}$$

when the oscillator is initially in the state $|0\rangle$. We rewrite the time evolution propagator as,

$$e^{-(\imath/\hbar)\hat{H}t} = e^{-\imath\omega_{ho}t(\hat{n}+1/2)-(\imath\Omega t/2)(\hat{a}e^{\imath\nu t}+\hat{a}^\dagger e^{-\imath\nu t})} \,. \tag{24.149}$$

To simplify the propagator, we first have a closer look at the terms $\hat{a}e^{\imath\omega_{ho}t}$ and $\hat{a}^\dagger e^{-\imath\omega_{ho}t}$, which we evaluate through their action on the complete system of unperturbed eigenfunctions,

$$\begin{aligned} e^{-(\imath/\hbar)\hat{H}^{(0)}t}\hat{a}e^{(\imath/\hbar)\hat{H}^{(0)}t}|n\rangle &= e^{-(\imath/\hbar)\hat{H}^{(0)}t}\hat{a}e^{(\imath/\hbar)E_n^{(0)}t}|n\rangle \\ &= e^{-(\imath/\hbar)E_{n-1}^{(0)}t}e^{(\imath/\hbar)E_n^{(0)}t}\hat{a}|n\rangle = e^{\imath\omega_{ho}t}\hat{a}|n\rangle \,. \end{aligned} \tag{24.150}$$

Hence, defining the detuning $\Delta \equiv \nu - \omega_{ho}$,

$$\begin{array}{rcccl} \hat{a}e^{\imath\nu t} &=& e^{\imath\omega_{ho}t}\hat{a}e^{\imath\Delta t} &=& e^{-\imath\omega_{ho}t(\hat{n}+1/2)}\hat{a}e^{\imath\Delta t}e^{\imath\omega_{ho}t(\hat{n}+1/2)} \\ \hat{a}^\dagger e^{-\imath\nu t} &=& e^{-\imath\omega_{ho}t}\hat{a}^\dagger e^{-\imath\Delta t} &=& e^{-\imath\omega_{ho}t(\hat{n}+1/2)}\hat{a}^\dagger e^{-\imath\Delta t}e^{\imath\omega_{ho}t(\hat{n}+1/2)} \\ \hat{n} &=& & & e^{-\imath\omega_{ho}t(\hat{n}+1/2)}\hat{n}e^{\imath\omega_{ho}t(\hat{n}+1/2)} \end{array} \,. \tag{24.151}$$

Substituting these expression into the propagator (24.149) we get,

$$e^{-(\imath/\hbar)\hat{H}t} = e^{e^{-\imath\omega_{ho}t(\hat{n}+1/2)}\left[-\imath\omega_{ho}t(\hat{n}+1/2)-(\imath\Omega t/2)\hat{a}e^{\imath\Delta t}-(\imath\Omega t/2)\hat{a}^\dagger e^{-\imath\Delta t}\right]e^{\imath\omega_{ho}t(\hat{n}+1/2)}} \,. \tag{24.152}$$

Now, making use of the relationship,

$$e^{e^{-\hat{A}}\hat{B}e^{\hat{A}}} = \sum_n \frac{(e^{-\hat{A}}\hat{B}e^{\hat{A}})^n}{n!} = \sum_n \frac{e^{-\hat{A}}\hat{B}^n e^{\hat{A}}}{n!} = e^{-\hat{A}}e^{\hat{B}}e^{\hat{A}} \,, \tag{24.153}$$

which is easy to show by expansion of $e^{\hat{B}}$, we find [6],

$$e^{-(\imath/\hbar)\hat{H}t} = e^{-\imath\omega_{ho}t(\hat{n}+1/2)}e^{-\imath\omega_{ho}t(\hat{n}+1/2)-(\imath\Omega t/2)(\hat{a}e^{\imath\Delta t}+\hat{a}^\dagger e^{-\imath\Delta t})}e^{\imath\omega_{ho}t(\hat{n}+1/2)} \,. \tag{24.154}$$

[6] Note, that this formula can not be simplified using Glauber's formula, because $[\hat{n},[\hat{n},\hat{a}]] \neq 0$. Note also, that the unitary transformation corresponds to a transformation into Dirac's interaction picture, which will be studied in the context of quantized radiation fields in Sec. 35.4.

In particular, for $\Delta = 0$,

$$\boxed{\langle n|e^{-(\imath/\hbar)\hat{H}t}|0\rangle = e^{-n\imath\omega_{ho}t}\langle n|e^{-\imath\omega_{ho}t(\hat{n}+1/2)-(\imath\Omega t/2)(\hat{a}+\hat{a}^\dagger)}|0\rangle} \ . \tag{24.155}$$

The dynamics is illustrated in Fig. 24.23. Again, we notice that the state generated

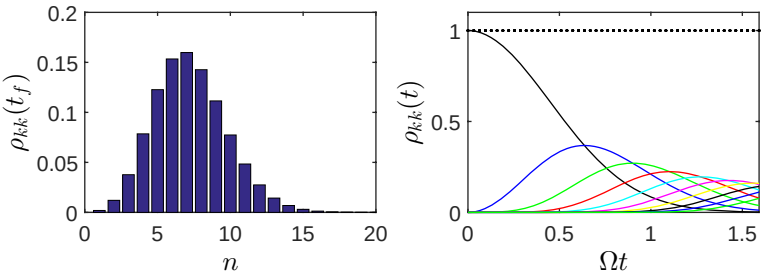

Figure 24.23: (code) (a) Populations of the vibrational states after a given interaction time. (b) Time evolution of the lowest populations.

is a coherent state. In Exc. 24.6.6.8 we will study how to generalize the problem to non-resonant excitation, $\Delta \neq 0$.

24.6.4 Forcing a harmonic oscillator

The transfer of momentum is the result of a (generally) constant force applied for a certain amount of time,

$$\hbar k = \int_{-\infty}^{\infty} mg\ \Theta_{[0,\Delta t]}(t)\ dt \ , \tag{24.156}$$

where g denotes the acceleration. That is, we expect that a harmonic oscillator,

$$\boxed{\hat{H}(t) = -\frac{\hbar^2}{2m}\frac{d^2}{dx^2} + \frac{m}{2}\omega_{ho}^2\hat{x}^2 - mg\hat{x}\ \Theta_{[0,\Delta t]}(t)} \ , \tag{24.157}$$

forced for a period of time Δt should have suffered a kick.

24.6.4.1 Displaced harmonic oscillator

To begin with, we will derive the dynamics of a harmonic oscillator suddenly exposed to a homogeneous constant force $F(t) = mg\ \Theta_{[0,\infty]}(t)$. It is easy to see, that the above perturbed Hamiltonian can be cast into the form,

$$\hat{H}(t) = -\frac{\hbar^2}{2m}\frac{d^2}{dx^2} + \frac{m}{2}\omega_{ho}^2\left(\hat{x} - \frac{g}{\omega_{ho}^2}\right)^2 - \frac{mg^2}{2\omega_{ho}^2} \ , \tag{24.158}$$

where the last constant term plays no role in the dynamics. That is, as we know from classical physics, the essential impact of a homogeneous force (e.g. gravity) on a harmonic oscillator consists in displacing its equilibrium position. Knowing the

eigenvalues and -states of the unperturbed Hamiltonian, the obvious solution of the perturbed eigenvalue problem is,

$$\begin{aligned} \hat{H}|\psi_n^{(1)}\rangle &= E_n^{(1)}|\psi_n^{(1)}\rangle \\ \text{with} \quad E_n^{(1)} &= E_n - \frac{mg^2}{2\omega_{ho}^2} \\ \text{and} \quad \langle x|\psi_n^{(1)}\rangle &= \psi_n^{(1)}(x) = \psi_n(x - \tfrac{g}{\omega_{ho}^2}) = \langle x - \tfrac{g}{\omega_{ho}^2}|n\rangle \ . \end{aligned} \tag{24.159}$$

Using the properties (23.181) and (23.183) we may write,

$$\langle x - \tfrac{g}{\omega_{ho}^2}|n\rangle = \langle x|U_{tr}^\dagger(-\tfrac{g}{\omega_{ho}^2})|n\rangle = \langle x|e^{-(\imath/\hbar)(g/\omega_{ho}^2)\hat{p}}|n\rangle \ , \tag{24.160}$$

and using the representation (24.86) of the momentum operator by the field operators and introducing the abbreviation $\beta \equiv \frac{g}{\omega_{ho}^2 a_{ho}\sqrt{2}}$ we can rewrite,

$$\langle x - \tfrac{g}{\omega_{ho}^2}|n\rangle = e^{-\beta(\hat{a}-\hat{a}^\dagger)}\langle x|n\rangle \ . \tag{24.161}$$

Note, that the transition from (24.157) to (24.159) can also be obtained by a redefinition of the field operators according to,

$$\hat{b} \equiv \hat{a} - \tfrac{mga_{ho}}{\hbar\omega_{ho}\sqrt{2}} \ , \tag{24.162}$$

since,

$$\hat{H} = \hbar\omega_{ho}(\hat{a}^\dagger\hat{a} + \tfrac{1}{2}) - \tfrac{mga_{ho}}{\sqrt{2}}(\hat{a} + \hat{a}^\dagger) = \hbar\omega_{ho}(\hat{b}^\dagger\hat{b} + \tfrac{1}{2}) - \tfrac{mg^2}{2\omega_{ho}^2} \tag{24.163}$$

and $\hat{a} - \hat{a}^\dagger = \hat{b} - \hat{b}^\dagger$.

The temporal evolution is given by the time-dependent Schrödinger equation. Since the jump is finite, the solution must be well behaved at time $t = 0$,

$$\begin{aligned} \langle x|\psi_n^{(1)}(t)\rangle &= \langle x|e^{-(\imath/\hbar)\hat{H}t}|\psi_n^{(1)}(0)\rangle \\ &= \langle x|e^{-(\imath/\hbar)\hat{H}t}e^{-\beta(\hat{a}-\hat{a}^\dagger)}|n\rangle \\ &= \langle x|e^{-(\imath/\hbar)\hat{H}t}e^{-\beta(\hat{a}-\hat{a}^\dagger)}e^{(\imath/\hbar)\hat{H}t}e^{-(\imath/\hbar)\hat{H}t}|n\rangle \ . \end{aligned} \tag{24.164}$$

To simplify the first three exponential functions, we use the relationships (24.153) and (24.150) [7],

$$e^{-(\imath/\hbar)\hat{H}t}e^{-\beta(\hat{a}-\hat{a}^\dagger)}e^{(\imath/\hbar)\hat{H}t} = e^{-\beta e^{-(\imath/\hbar)\hat{H}t}(\hat{a}-\hat{a}^\dagger)e^{(\imath/\hbar)\hat{H}t}} = e^{-\beta\left(e^{\imath\omega_{ho}t}\hat{a} - e^{-\imath\omega_{ho}t}\hat{a}^\dagger\right)} \ , \tag{24.165}$$

and write the temporal solution,

$$\begin{aligned} \psi_n^{(1)}(x,t) &= e^{-\beta(\hat{a}e^{\imath\omega_{ho}t} - \hat{a}^\dagger e^{-\imath\omega_{ho}t})}e^{-(\imath/\hbar)\hat{H}t}\psi_n(x) \\ &= e^{-\beta(\hat{a}-\hat{a}^\dagger)\cos\omega_{ho}t - \imath\beta(\hat{a}+\hat{a}^\dagger)\sin\omega_{ho}t}e^{-(\imath/\hbar)E_n^{(0)}t}\psi_n(x) \ . \end{aligned} \tag{24.166}$$

[7] We can use (24.150), because the shifted harmonic oscillator has, except from a constant offset the same eigenenergies.

Using Glauber's formula (23.210) we find,

$$\begin{aligned}\psi_n^{(1)}(x,t) &= e^{-\imath\beta(\hat{a}+\hat{a}^\dagger)\sin\omega_{ho}t}e^{-\beta(\hat{a}-\hat{a}^\dagger)\cos\omega_{ho}t}e^{\imath\beta^2\sin\omega_{ho}t\cos\omega_{ho}t}e^{-(\imath/\hbar)E_n^{(0)}t}\psi_n(x)\\ &= e^{-\imath(mg/\hbar\omega_{ho})\hat{x}\sin\omega_{ho}t}e^{-(\imath/\hbar)(g/\omega_{ho}^2)\hat{p}\cos\omega_{ho}t}e^{\imath\beta^2\sin\omega_{ho}t\cos\omega_{ho}t}e^{-(\imath/\hbar)E_n^{(0)}t}\psi_n(x)\\ &= e^{-\imath\beta(\hat{a}+\hat{a}^\dagger)\sin\omega_{ho}t}e^{\imath\beta^2\sin\omega_{ho}t\cos\omega_{ho}t}e^{-(\imath/\hbar)E_n^{(0)}t}\psi_n(x-b\cos\omega_{ho}t)\ . \end{aligned} \tag{24.167}$$

Finally,

$$\boxed{|\psi_n^{(1)}(x,t)|^2 = |\psi_n(x-\bar{x}(t))|^2 \qquad \text{where} \qquad \bar{x}(t)\equiv\tfrac{g}{\omega_{ho}^2}\cos\omega_{ho}t}\ . \tag{24.168}$$

This means that the spatial distribution of $\psi_n^{(1)}$ around $\bar{x}(t)$ is the same as of ψ_n around $\bar{x}=0$. The entire distribution oscillates without deformation. The momentum distribution follows from the Fourier transform,

$$\begin{aligned}\phi_n^{(1)}(p,t) &= \frac{1}{\sqrt{2\pi\hbar}}\int dx e^{-(\imath/\hbar)px}\psi_n^{(1)}(x,t)\\ &= \frac{1}{\sqrt{2\pi\hbar}}\int du\ e^{-(\imath/\hbar)pu}e^{-(\imath/\hbar)um\omega_{ho}\frac{g}{\omega_{ho}^2}\sin\omega_{ho}t}e^{\imath\gamma(p,t)}\psi_n\\ &= e^{\imath\gamma(p,t)}\phi_n(p+m\omega_{ho}\tfrac{g}{\omega_{ho}^2}\sin\omega_{ho}t)\ , \end{aligned} \tag{24.169}$$

where the abbreviation $\gamma=\gamma^*$ contains all unitary transformations of (24.167), that do not depend on x. We obtain,

$$\boxed{|\phi_n^{(1)}(p,t)|^2 = |\phi_n(p-\bar{p}(t))|^2 \qquad \text{where} \qquad \bar{p}(t)\equiv -m\tfrac{g}{\omega_{ho}}\sin\omega_{ho}t}\ . \tag{24.170}$$

24.6.4.2 Discussion of the kick dynamics

For the acceleration of the harmonic oscillator to resemble a 'kick', the time during which the perturbation is active must be much smaller than a trap oscillation period, $\omega_{ho}\Delta t \ll 1$. In this case, we may expand the oscillatory motion (24.168) and (24.170),

$$\bar{x}=\frac{g}{\omega_{ho}^2} \qquad \text{and} \qquad \bar{p}=-mg\Delta t\equiv-\hbar k\ , \tag{24.171}$$

which is consistent with the initial request (24.156). It is also clear that, for a given force mg, the maximum momentum that can be transmitted is limited, $\hbar k < mg/\omega_{ho}$.

As long as the kick-approximation $\omega_{ho}\Delta t \ll 1$ holds, we may simply describe the dynamics during the application of the force, via a time-dependent kick operator,

$$e^{\imath k(t)\hat{x}} = D(\alpha(t))\ , \tag{24.172}$$

where the acquired momentum increases linearly with time according to $k(t) = k\frac{\max(\min(t,\Delta t),0)}{\Delta t}$. I.e. the populations of the vibrational states evolve like (24.136) into a coherent state with increasing amplitude $|\alpha(t)|^2$. At the end of the kick, on a much slower time-scale ω_{ho}^{-1}, the wavefunctions will start to oscillate all in phase, according to (24.168).

The time-dependence of the states $|\alpha(t)\rangle$, as shown in Exc. 24.6.6.9 is given by,

$$|\alpha(t)\rangle = e^{-(\imath/\hbar)\hat{H}t}|\alpha(0)\rangle = \sum_n e^{-(\imath/\hbar)E_n t} e^{-|\alpha(0)|^2/2} \frac{\alpha(0)^n}{\sqrt{n!}}|n\rangle \tag{24.173}$$
$$= e^{-\imath\omega_{ho}t/2} \sum_n e^{-|\alpha(0)|^2/2} \frac{(\alpha(0)e^{-\imath\omega_{ho}t})^n}{\sqrt{n!}}|n\rangle = e^{-\imath\omega_{ho}t/2}|\alpha(0)e^{-\imath\omega_{ho}t}\rangle \ .$$

With (24.150) we find,

$$\hat{x}(t) = e^{-(\imath/\hbar)\hat{H}t}\hat{x}(0)e^{(\imath/\hbar)\hat{H}t} = \hat{x}(0)\cos\omega_{ho}t + \tfrac{\hat{p}(0)}{m\omega_{ho}}\sin\omega_{ho}t \qquad \text{and} \tag{24.174}$$
$$\hat{p}(t) = e^{-(\imath/\hbar)\hat{H}t}\hat{p}(0)e^{(\imath/\hbar)\hat{H}t} = m\omega_{ho}\hat{x}(0)\sin\omega_{ho}t + \hat{p}(0)\cos\omega_{ho}t \ ,$$

or with (24.173),

$$\boxed{\begin{array}{rcl} \langle\alpha(t)|\hat{x}|\alpha(t)\rangle & = & \langle\alpha(0)|\hat{x}|\alpha(0)\rangle\cos\omega_{ho}t + \frac{1}{m\omega_{ho}}\langle\alpha(0)|\hat{p}|\alpha(0)\rangle\sin\omega_{ho}t \\ \langle\alpha(t)|\hat{p}|\alpha(t)\rangle & = & m\omega_{ho}\langle\alpha(0)|\hat{x}|\alpha(0)\rangle\sin\omega_{ho}t + \langle\alpha(0)|\hat{p}|\alpha(0)\rangle\cos\omega_{ho}t \end{array}} \ . \tag{24.175}$$

We note, that the position and momentum wavefunctions $\langle x|n\rangle$ and $\langle p|n\rangle$ of the excited vibrational states are complicated Hermite polynomials, but we don't have to write them down explicitly to get to the last result. We will derive some further properties in Exc. 24.6.6.10.

24.6.4.3 Simulation of the displacement of a harmonic oscillator

The Hamiltonian of a harmonic oscillator subject to an external force can be cast into the form,

$$\hat{H}(t) = -\frac{\hbar^2}{2m}\frac{d^2}{dx^2} + \frac{m}{2}\omega_{ho}^2\hat{x}^2 + mg\hat{x} = \hbar\omega_{ho}(\hat{a}^\dagger\hat{a} + \tfrac{1}{2}) + mg\tfrac{a_{ho}}{\sqrt{2}}(\hat{a} + \hat{a}^\dagger)$$
$$= \begin{pmatrix} \ddots & \ddots & & 0 \\ \ddots & (n+\frac{1}{2})\hbar\omega_{ho} & mg\frac{a_{ho}}{\sqrt{2}}\sqrt{n+1} & \\ & mg\frac{a_{ho}}{\sqrt{2}}\sqrt{n+1} & (n+\frac{3}{2})\hbar\omega_{ho} & \ddots \\ 0 & & \ddots & \ddots \end{pmatrix} \ . \tag{24.176}$$

The temporal evolution of the state is given by,

$$|\psi(t)\rangle = e^{-(\imath/\hbar)\hat{H}t}|\psi(0)\rangle = e^{-(\imath/\hbar)\hat{H}t}\sum_n a_n|n\rangle \overset{a_n=\delta_{n,0}}{\longrightarrow} e^{-(\imath/\hbar)\hat{H}t}|0\rangle \ , \tag{24.177}$$

when the oscillator is initially in the state $|0\rangle$. Note that, without perturbation, $|\psi(t)\rangle = \sum_n e^{-\imath\omega_{ho}(\hat{n}+1/2)t}a_n|n\rangle$.

Various quantities now are interesting to plot as a function of time. Firstly, we calculate the populations $|\langle n|\psi(t)\rangle|^2$ of the various states and the total energy from,

$$\boxed{\begin{array}{rl} \langle n|\psi(t)\rangle & = \langle n|e^{-(\imath/\hbar)\hat{H}t}\sum_m a_m|m\rangle \\ E_{tot}(t) & = \sum_n \hbar\omega_{ho}(n+\frac{1}{2})|\langle n|\psi(t)\rangle|^2 \end{array}} \ . \tag{24.178}$$

Secondly, we get for the temporal evolution of the spatial wavefunction,

$$\langle x|\psi(t)\rangle = \sum_n \langle x|n\rangle\langle n|\psi(t)\rangle = \sum_n \langle x|n\rangle\langle n|e^{-(\imath/\hbar)\hat{H}t}\sum_m a_m|m\rangle \ , \tag{24.179}$$

where $|\langle x|n\rangle\langle n|\psi(t)\rangle|^2$ is the spatial representation of the wavefunction of the n-th eigenstate derived in (24.97),

$$\langle x|n\rangle = \frac{e^{-x^2/2a_{ho}^2}H_n(x/a_{ho})}{\sqrt{a_{ho}\sqrt{\pi}2^n n!}} \ , \tag{24.180}$$

weighed with instantaneous population (24.178) of this state. We thus obtain for the total wavefunction,

$$\boxed{\langle x|\psi(t)\rangle = \sum_n \frac{e^{-x^2/2a_{ho}^2}H_n(x/a_{ho})}{\sqrt{a_{ho}\sqrt{\pi}2^n n!}}\langle n|e^{-(\imath/\hbar)\hat{H}t}|n\rangle} \ . \tag{24.181}$$

Furthermore, we may calculate the expectation values of the position and the momentum of the harmonic oscillator from the total wavefunction $\langle x|\psi(t)\rangle$,

$$\begin{aligned} \langle\psi(t)|\hat{x}|\psi(t)\rangle &= \int\langle\psi(t)|\hat{x}|x\rangle\langle x|\psi(t)\rangle dx = \int x|\psi(x,t)|^2 dx \\ \langle\psi(t)|\hat{p}|\psi(t)\rangle &= \int\langle\psi(t)|\hat{p}|p\rangle\langle p|\psi(t)\rangle dp = \int p|\phi(p,t)|^2 dp \ , \end{aligned} \tag{24.182}$$

where $\phi(p,t)$ is the Fourier transform of $\psi(x,t)$ according to (23.102). In practice, it is however easier to calculate them from the populations $\langle n|\psi(t)\rangle$,

$$\boxed{\begin{array}{rl} \langle\psi(t)|\hat{x}|\psi(t)\rangle & = \frac{a_{ho}}{\sqrt{2}}\sum_n \langle\psi(t)|\hat{a}+\hat{a}^\dagger|n\rangle\langle n|\psi(t)\rangle \\ \langle\psi(t)|\hat{p}|\psi(t)\rangle & = \frac{\hbar}{\imath a_{ho}\sqrt{2}}\sum_n \langle\psi(t)|\hat{a}-\hat{a}^\dagger|n\rangle\langle n|\psi(t)\rangle \end{array}} \ . \tag{24.183}$$

The temporal evolution of the forced harmonic oscillator defined by (24.177) can be numerically propagated. In cases where the force varies in time, the propagation can be done iteratively by subdividing time in intervals $t_k - t_{k-1}$ for $k \in \mathbb{N}$ sufficiently small that the force can be considered constant within them,

$$|\psi(t_k)\rangle = e^{-(\imath/\hbar)\hat{H}(t_k-t_{k-1})}|\psi(t_{k-1})\rangle \ . \tag{24.184}$$

The results of such a simulation are illustrated in Fig. 24.24.

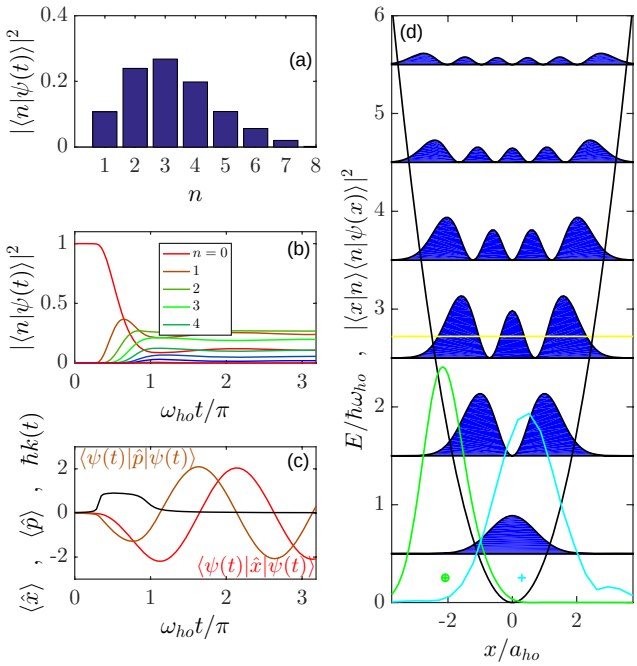

Figure 24.24: (code) Evolution of a harmonic oscillator subject to time-dependent forcing. (a) Histogram of the final population of the vibrational states. (b) Time evolution of the vibrational state populations. (c) Time evolution of the applied force (black) and of the expectation values of position (red) and momentum (brown). (d) Spatial wavefunctions $\langle n|\psi(x)\rangle|^2$ (Hermite polynomials) (blue) of the lowest vibrational states of the harmonic potential (black). The green Gaussian is the coherent sum of the spatial wavefunctions $|\sum_n\langle n|\psi(x)\rangle|^2$, and the cyan Gaussian the coherent sum of the momentum wavefunctions $|\sum_n\langle n|\psi(p)\rangle|^2$. The horizontal yellow line is the total energy of the system. You may also run a movie of the simulation clicking on (watch movie)! Furthermore, a presentation about the topic of recoil on trapped atoms is available at (watch talk)!

24.6.5 Quantization of the electromagnetic field

The quantization of light (also called *second quantization*) triggered by Max Planck's treatments of black-body radiation in 1905 resolved the problem of the ultraviolet divergence and explained the photoelectric effect. Twenty years later the quantization of the atom by Niels Bohr (also called *first quantization*) explained the internal structure of the atom.

The operator for the electric field of a laser mode is given by,

$$\hat{\mathcal{E}} = \imath\mathcal{E}_1[\hat{a}e^{\imath\mathbf{k}\cdot\mathbf{r}-\imath\omega t} - \hat{a}^\dagger e^{-\imath\mathbf{k}\cdot\mathbf{r}+\imath\omega t}] \,, \tag{24.185}$$

where $\mathcal{E}_1 = \sqrt{\hbar\omega/2\varepsilon_0 V}$ is the electric field generated by a single photon in the mode volume V. Exc. 24.6.6.11 asks to calculate the eigenvalues $\langle\hat{\mathcal{E}}\rangle$ and $\Delta\hat{\mathcal{E}}$.

It is sometimes convenient to represent the light field by its quadratures. With the definition $\hat{a} \equiv \hat{x}_1 + \imath\hat{x}_2$, where $\hat{x}_{1,2}$ are non-commuting observables ($[\hat{x}_1, \hat{x}_2] = \imath/2$),

we can write the field as,

$$\hat{\mathcal{E}} = -2\mathcal{E}_1[\hat{x}_1 \sin(\mathbf{k}\cdot\mathbf{r}-\omega t) + \hat{x}_2 \cos(\mathbf{k}\cdot\mathbf{r}-\omega t)] \ . \tag{24.186}$$

Heisenberg's uncertainty relations requires,

$$\Delta x_1 \Delta x_2 \geq \tfrac{1}{4} \ . \tag{24.187}$$

For coherent states, $\Delta x_1 = \Delta x_2 = \frac{1}{2}$.

24.6.6 Exercises

24.6.6.1 Ex: Sum of displacements operators

Prove formula (24.120). Find a geometric interpretation of the phase factor $(\alpha\beta^* - \alpha^*\beta)/2$ in the complex plane of Glauber states.

Solution: *The formula can be derived by utilizing the Baker-Campbell-Hausdorff formula,*

$$e^{\alpha\hat{a}^\dagger - \alpha^*\hat{a}} e^{\beta\hat{a}^\dagger - \beta^*\hat{a}} = e^{(\alpha+\beta)\hat{a}^\dagger - (\beta^*+\alpha^*)\hat{a}} e^{(\alpha\beta^* - \alpha^*\beta)/2} \ .$$

The phase factor measure the area in the Glauber plane enclosed by the amplitudes α, β, and $\alpha+\beta$. To see this we represent the amplitudes as vectors,

$$\alpha \to \begin{pmatrix} \mathfrak{Re}\ \alpha \\ \mathfrak{Im}\ \alpha \\ 0 \end{pmatrix} \qquad \textit{and} \qquad \beta \to \begin{pmatrix} \mathfrak{Re}\ \beta \\ \mathfrak{Im}\ \beta \\ 0 \end{pmatrix} \ .$$

Now, the area is given by,

$$A = \left| \begin{pmatrix} \mathfrak{Re}\ \alpha \\ \mathfrak{Im}\ \alpha \\ 0 \end{pmatrix} \times \begin{pmatrix} \mathfrak{Re}\ \beta \\ \mathfrak{Im}\ \beta \\ 0 \end{pmatrix} \right| = |\mathfrak{Re}\ \alpha \mathfrak{Im}\ \beta - \mathfrak{Im}\ \alpha \mathfrak{Re}\ \beta| = \left| \frac{\alpha^*\beta - \alpha\beta^*}{2\imath} \right| = |\mathfrak{Im}\ \alpha^*\beta| \ .$$

It has the meaning of a geometrical phase.

24.6.6.2 Ex: Harmonic oscillator and coherent states

a. Verify whether the Glauber states of a harmonic oscillator are orthogonal.
b. Show that $\langle\alpha|\hat{n}|\alpha\rangle = |\alpha|^2$, $\langle\alpha|\hat{n}^2|\alpha\rangle = |\alpha|^4 + |\alpha|^2$, and $\Delta\hat{n} = |\alpha|$.
c. What is the population of the state $|n\rangle$ of a harmonic oscillator in a Glauber state?

Solution: *a. This easily follows with*

$$\langle\alpha|\beta\rangle = e^{-|\alpha|^2/2 - |\beta|^2/2} \sum_n \frac{\alpha^{*n}\beta^n}{n!} = e^{-|\alpha|^2/2 - |\beta|^2/2 + \alpha^*\beta} \ ,$$

such that

$$|\langle\alpha|\beta\rangle|^2 = e^{-|\alpha-\beta|^2} \ .$$

b. We calculate

$$\langle\alpha|\hat{n}|\alpha\rangle = \langle\alpha|\hat{a}^\dagger\hat{a}|\alpha\rangle = |\alpha|^2 \ ,$$

and

$$\langle\alpha|\hat{n}^2|\alpha\rangle = \langle\alpha|\hat{a}^\dagger\hat{a}\hat{a}^\dagger\hat{a}|\alpha\rangle = \langle\alpha|\alpha^*\hat{a}\hat{a}^\dagger\alpha|\alpha\rangle = \langle\alpha|\alpha^*(1-\hat{a}^\dagger\hat{a})\alpha|\alpha\rangle = |\alpha|^2 + |\alpha|^4 \ ,$$

and

$$\Delta n = \sqrt{\langle n^2\rangle - \langle n\rangle^2} = |\alpha| \ .$$

c. The population is,

$$|\langle n|\alpha\rangle|^2 = e^{-|\alpha|^2}\frac{|\alpha|^{2n}}{n!} = e^{-\langle n\rangle}\frac{\langle n\rangle^n}{n!} \ .$$

This is a Poisson distribution which, for $\langle n\rangle$ very large, resembles a Gaussian.

24.6.6.3 Ex: Annihilation operator acting on Fock and Glauber states

Show that the annihilation operator $\hat{a}$ does not reduce the photon number of a Glauber state in contrast to a Fock state.

Solution: *We have,*

$$\frac{\langle n|\hat{a}^\dagger\hat{n}\hat{a}|n\rangle}{\langle n|\hat{n}|n\rangle} = n-1 \qquad \textit{but} \qquad \frac{\langle\alpha|\hat{a}^\dagger\hat{n}\hat{a}|\alpha\rangle}{\langle\alpha|\hat{n}|\alpha\rangle} = |\alpha|^2 = n \ .$$

24.6.6.4 Ex: Completeness of coherent states

a. Show,

$$\tfrac{1}{\pi}\int|\alpha\rangle\langle\alpha|d^2\alpha = \sum_{n=0}^{\infty}|n\rangle\langle n| = \mathbb{I} \ .$$

b. Show that coherent states can be expanded in terms of other coherent states and that, consequently, the coherent state basis is overcomplete.

Solution: *a. Using the expansion (24.115) of Glauber into Fock states and writing $\alpha = |\alpha|e^{\imath\theta}$ we find,*

$$\begin{aligned}\int|\alpha\rangle\langle\alpha|d^2\alpha &= \sum_{n,m=0}^{\infty}\frac{|n\rangle\langle m|}{\sqrt{m!}\sqrt{n!}}\int e^{-|\alpha|^2}\alpha^{*m}\alpha^n d^2\alpha \\ &= \sum_{n,m=0}^{\infty}\frac{|n\rangle\langle m|}{\sqrt{m!}\sqrt{n!}}\int_0^\infty e^{-|\alpha|^2}|\alpha|^{m+n+1}d|\alpha|\int_0^{2\pi}e^{\imath(n-m)\theta}d\theta \\ &= \sum_{n,m=0}^{\infty}\frac{|n\rangle\langle m|}{\sqrt{m!}\sqrt{n!}}\times\frac{n!}{2}\times 2\pi\delta_{nm} = \pi\sum_{n=0}^{\infty}|n\rangle\langle n| \ .\end{aligned}$$

b. [1184], p.55.

24.6.6.5 Ex: Schrödinger cat state

Calculate the probability of finding n photons in Schrödinger's cat state $|\psi\rangle = 2^{-1/2}(|\alpha\rangle \pm |-\alpha\rangle)$.

Solution: *The probability is,*

$$P_n = \left|\langle n|\tfrac{1}{\sqrt{2}}(|\alpha\rangle \pm |-\alpha\rangle)\right|^2 = \tfrac{1}{2}\left|e^{-|\alpha|^2/2}\frac{\alpha^n \pm (-\alpha)^n}{\sqrt{n!}}\right|^2 \ .$$

With this, for the sign $(+)$, we have $P_n^{cat} = 2P_n^{coherent}$ if n is even and $P_n^{cat} = 0$ if n is odd. But for the sign $(-)$ it is just the opposite. That is, the loss of a single photon turns the 'cat' $|\alpha\rangle + |-\alpha\rangle$ into a cat $|\alpha\rangle - |-\alpha\rangle$.

24.6.6.6 Ex: Transition elements for arbitrary Lamb-Dicke parameters

Calculate the general expression for $\langle m|e^{\imath k\hat{x}}|n\rangle$ with the abbreviation $\alpha \equiv \imath k a_{ho}/\sqrt{2}$ for arbitrary values of the Lamb-Dicke parameter using the following results of the discussion of the displacement operator $D(\alpha) = e^{\alpha\hat{a}^\dagger - \alpha^*\hat{a}} = e^{-|\alpha|^2/2}e^{\alpha\hat{a}^\dagger}e^{-\alpha^*\hat{a}}$ for Glauber states. The relations

$$|n\rangle = \frac{(\hat{a}^\dagger)^n}{\sqrt{n!}}|0\rangle \qquad \text{and} \qquad \langle n|\alpha\rangle = e^{-|\alpha|^2/2}\frac{\alpha^n}{\sqrt{n!}}$$

describe the relation between Fock and Glauber states. Furthermore,

$$D(-\alpha) = D^\dagger(\alpha) \qquad \text{and} \qquad D^\dagger(\alpha)\hat{a}^\dagger D(\alpha) = \hat{a}^\dagger + \alpha^* \ .$$

Solution: *From the rules for the displacement operator we immediately derive,*

$$D(\alpha)\hat{a}^\dagger = (\hat{a}^\dagger - \alpha^*)D(\alpha) = (\hat{a}^\dagger + \alpha)D(\alpha) \ ,$$

using that in this particular case $\alpha^* = -\alpha$. This allows us to do the following derivation,

$$e^{\imath k\hat{x}}|n\rangle = D(\alpha)|n\rangle = \tfrac{1}{\sqrt{n!}}D(\alpha)(\hat{a}^\dagger)^n|0\rangle = \tfrac{1}{\sqrt{n!}}(\hat{a}^\dagger + \alpha)^n D(\alpha)|0\rangle = \tfrac{1}{\sqrt{n!}}(\hat{a}^\dagger + \alpha)^n|\alpha\rangle \ .$$

Using the binomial expansion $(x+y)^n = \sum_{k=0}^n \binom{n}{k}x^k y^{n-k}$ we calculate,

$$e^{\imath k\hat{x}}|n\rangle = \frac{1}{\sqrt{n!}}\sum_{k=0}^{n}\binom{n}{k}\alpha^{n-k}(\hat{a}^\dagger)^k|\alpha\rangle \ ,$$

such that,

$$\begin{aligned}
\langle m|e^{\imath k\hat{x}}|n\rangle &= \frac{1}{\sqrt{n!}}\sum_{k=0}^{n}\binom{n}{k}\alpha^{n-k}\langle m|(\hat{a}^\dagger)^k|\alpha\rangle \\
&= \frac{1}{\sqrt{n!}}\sum_{k=0}^{n}\binom{n}{k}\alpha^{n-k}\left[\sqrt{m(m-1)}\hat{a}^{k-2}|m-2\rangle\right]^\dagger|\alpha\rangle \\
&= \frac{1}{\sqrt{n!}}\sum_{k=0}^{n}\binom{n}{k}\alpha^{n-k}\sqrt{\frac{m!}{[m-\min(k,m)]!}}\langle m-\min(k,m)|(\hat{a}^\dagger)^{k-\min(k,m)}|\alpha\rangle \ .
\end{aligned}$$

Let us restrict to the case $m \geq n$. Then necessarily $\min(k,m) = k$, *so that,*

$$\begin{aligned}\langle m|e^{\imath k\hat{x}}|n\rangle &= \frac{1}{\sqrt{n!}}\sum_{k=0}^{n}\binom{n}{k}\alpha^{n-k}\sqrt{\frac{m!}{(m-k)!}}\langle m-k|\alpha\rangle \\ &= \sum_{k=0}^{n}\sqrt{\binom{n}{k}}\frac{\alpha^{n-k}}{\sqrt{(n-k)!}}\sqrt{\binom{m}{k}}\langle m-k|\alpha\rangle \\ &= e^{|\alpha|^2/2}\sum_{k=0}^{n}\sqrt{\binom{n}{k}\binom{m}{k}}\langle n-k|\alpha\rangle\langle m-k|\alpha\rangle \ .\end{aligned}$$

The case $m \leq n$ can be calculated via,

$$\langle m|e^{\imath k\hat{x}}|n\rangle = \langle n|e^{-ik\hat{z}}|m\rangle^* = \langle n|D(-\alpha)|m\rangle^* = \langle n|D(\alpha)|m\rangle \ ,$$

which gives us the same formula.
With the last formula we recover the expression (24.136) for $\langle m|e^{-\imath k\hat{z}}|0\rangle$. We also recover the expressions (24.139),

$$\begin{aligned}\langle m|e^{\imath k\hat{x}}|m\rangle &\overset{\alpha\to 0}{\longrightarrow} \sum_{k=0}^{m}\frac{m!\alpha^{2m-2k}}{k!(m-k)!^2} \overset{\alpha\to 0}{\longrightarrow} 1 \\ \langle m|e^{\imath k\hat{x}}|m-1\rangle &\overset{\alpha\to 0}{\longrightarrow} \sum_{k=0}^{m-1}\frac{\sqrt{(m-1)!}\sqrt{m!}}{k!(m-1-k)!(m-k)!}\alpha^{2m-1-2k} \overset{\alpha\to 0}{\longrightarrow} \sqrt{m}\alpha \\ \langle m|e^{\imath k\hat{x}}|m+1\rangle &\overset{\alpha\to 0}{\longrightarrow} \sum_{k=0}^{m+1}\frac{\sqrt{(m+1)!}\sqrt{m!}}{k!(m+1-k)!(m-k)!}\alpha^{2m+1-2k} \overset{\alpha\to 0}{\longrightarrow} \sqrt{m+1}\alpha \ .\end{aligned}$$

24.6.6.7 Ex: Lamb-Dicke regime

A rubidium atom is trapped in an isotropic harmonic trap with secular frequency $\omega_{ho} = (2\pi)\ 1\,\text{kHz}$. Determine whether, driven on its D_2 line, it is within the Lamb-Dicke regime.

Solution: *The frequency of the D_2-line is* 780 nm. *Hence, the recoil frequency is,*

$$\omega_{rec} = \frac{\hbar k^2}{2m} \approx (2\pi)\ 3.54\,\text{kHz} \ ,$$

and the Lamb-Dicke parameter,

$$\eta = \sqrt{\frac{\omega_{rec}}{\omega_{ho}}} \approx 2 \ .$$

24.6.6.8 Ex: Resonantly excited harmonic oscillator

Write down the Hamiltonian of a harmonic oscillator subject to an oscillating homogenous force, and numerically simulate the evolution of the vibrational states starting from the ground state.

Solution: *Writing the force as,*

$$F = -\frac{d\hat{H}_F}{dx} = F_0 \cos\omega t \ ,$$

we see that it can be derived from the potential,

$$\hat{H}_F = -F_0 \hat{x} \cos\omega t \ .$$

Doing the RWA defining the Rabi frequency Ω as an abbreviation,

$$\hat{H}_F = -F_0 \tfrac{\sqrt{2}}{a_{ho}} (\hat{a} e^{\imath\omega t} + \hat{a}^\dagger e^{-\imath\omega t}) \equiv \tfrac{\hbar\Omega}{2} (\hat{a} e^{\imath\omega t} + \hat{a}^\dagger e^{-\imath\omega t}) \ .$$

In matrix formalism,

$$\begin{aligned}
\hat{H} &= \frac{\hat{p}^2}{2m} + V(\hat{x}) + \hat{H}_F \\
&= \sum_n \left[\hbar\omega_0 (n|n\rangle\langle n| + \tfrac{1}{2}) + \tfrac{\hbar\Omega}{2} e^{\imath\omega t} \sqrt{n} |n-1\rangle\langle n| + \tfrac{\hbar\Omega}{2} e^{-\imath\omega t} \sqrt{n+1} |n+1\rangle\langle n| \right] \\
&= \hbar \begin{pmatrix} \ddots & \ddots & & \\ \ddots & (n-1)\omega_0 & \frac{\Omega}{2} e^{\imath\omega t}\sqrt{n} & \\ & \frac{\Omega}{2} e^{-\imath\omega t}\sqrt{n} & n\omega_0 & \ddots \\ & & \ddots & \ddots \end{pmatrix} + \frac{\hbar\omega_0}{2} \mathcal{I} \ .
\end{aligned}$$

Transforming the eigenstates of the Schrödinger equation according to $|n'\rangle = e^{\imath n\omega t}|n\rangle$, or alternatively transforming the Hamiltonian according to,

$$\hat{H}' = U^\dagger \hat{H} U + i\hbar \dot{U}^\dagger U$$

with the unitary transformation,

$$U \equiv \begin{pmatrix} \ddots & \ddots & & \\ \ddots & e^{\imath(n-1)\omega t} & 0 & \\ & 0 & e^{\imath n\omega t} & \ddots \\ & & \ddots & \ddots \end{pmatrix} \ ,$$

we get,

$$\hat{H}' = \hbar \begin{pmatrix} \ddots & \ddots & & \\ \ddots & -(n-1)\Delta & \frac{\Omega}{2}\sqrt{n} & \\ & \frac{\Omega}{2}\sqrt{n} & -n\Delta & \ddots \\ & & \ddots & \ddots \end{pmatrix} + \frac{\hbar\omega_0}{2} \ ,$$

where we defined $\Delta \equiv \omega - \omega_0$.

24.6.6.9 Ex: Shifted harmonic oscillator

Consider a HO of mass m, angular frequency ω, and electric charge q immersed in a uniform electric field oriented parallel to the axis $\hat{\mathbf{e}}_x$ of the oscillator.
a. Get the energies of the stationary states of the HO and show how to get the corresponding eigenstates.
b. Calculate the expectation values $\langle x\rangle$ and $\langle p\rangle$ for the displaced oscillator now using Glauber states (or arbitrary superpositions of states) and taking advantage of the formulas (24.86), (24.119), and (23.179).
c. Now, the electric field is suddenly turned off. Calculate the time evolution of the oscillator.

Solution: *We consider an electron in a harmonic potential suddenly subject to an electric field,*

$$\hat{H} = \begin{cases} \hat{H}^{(1)} = \frac{p^2}{2m} + \frac{m}{2}\omega^2 x^2 + e\mathcal{E}x & for \quad t < 0 \\ \hat{H} = \frac{p^2}{2m} + \frac{m}{2}\omega^2 x^2 & for \quad t \geq 0 \end{cases} .$$

a. With the abbreviation $b \equiv \frac{e\mathcal{E}}{m\omega^2}$ *we can rewrite the Hamiltonian*

$$\hat{H}^{(1)} = \frac{p^2}{2m} + \frac{m}{2}\omega^2(x-b)^2 - \frac{m}{2}\omega^2 b^2 \ ,$$

with the obvious solution

$$\hat{H}^{(1)}|\psi_n^{(1)}\rangle = E_n^{(1)}|\psi_n^{(1)}\rangle \qquad , \qquad \psi_n^{(1)}(x) = \psi_n(x-b) \qquad , \qquad E_n^{(1)} = E_n - \frac{m}{2}\omega^2 b^2 \ .$$

b. With the Taylor expansion

$$\psi_n(x-b) = \psi_n(x) - b\psi_n'(x) + \frac{(-b)^2}{2!}\psi_n''(x) + .. = e^{-b(d/dx)}\psi_n(x) \ ,$$

and the abbreviation $\beta \equiv \frac{b}{a_{ho}\sqrt{2}}$ *we can rewrite,* $|\psi_n^{(1)}(x)\rangle = e^{-\beta(\hat{a}-\hat{a}^\dagger)}|\psi_n\rangle$. *The expectation value of* $\hat{a}$ *is therefore,*

$$\langle\psi_n^{(1)}|\hat{a}|\psi_n^{(1)}\rangle = \langle\psi_n|e^{-\beta(\hat{a}^\dagger-\hat{a})}\hat{a}e^{-\beta(\hat{a}-\hat{a}^\dagger)}|\psi_n\rangle \ .$$

Using the formula (23.179) we have

$$e^{-\beta(\hat{a}^\dagger-\hat{a})}\hat{a}e^{-\beta(\hat{a}-\hat{a}^\dagger)} = \hat{a} + \beta[\hat{a}-\hat{a}^\dagger, \hat{a}] = \hat{a} + \beta \ ,$$

which verifies the formula postulated in class (24.119). Hence, $\langle\psi_n^{(1)}|\hat{a}|\psi_n^{(1)}\rangle = \langle\psi_n|\hat{a}+\beta|\psi_n\rangle$ *and* $\langle\psi_n^{(1)}|\hat{a}^\dagger|\psi_n^{(1)}\rangle = \langle\psi_n|\hat{a}^\dagger+\beta|\psi_n\rangle$, *tal que,*

$$\langle\psi_n^{(1)}|\hat{x}|\psi_n^{(1)}\rangle = b \qquad and \qquad \langle\psi_n^{(1)}|\hat{p}|\psi_n^{(1)}\rangle = 0 \ .$$

c. The temporal evolution is given by the time-dependent Schrödinger equation. Since the jump is finite, the solution must be well behaved in time $t = 0$,

$$\psi_n^{(1)}(x,t) = \begin{cases} e^{-(\imath/\hbar)\hat{H}^{(1)}t}\psi_n^{(1)}(x) = e^{-(\imath/\hbar)E_n^{(1)}t}\psi_n^{(1)}(x) & \textit{for} \quad t < 0 \\ e^{-(\imath/\hbar)\hat{H}t}\psi_n^{(1)}(x) & \textit{for} \quad t \geq 0 \end{cases} .$$

For times $t \geq 0$ we write,

$$\psi_n^{(1)}(x,t) = e^{-(\imath/\hbar)Ht}e^{-\beta(\hat{a}-\hat{a}^\dagger)}\psi_n(x) = e^{-(\imath/\hbar)\hat{H}t}e^{-\beta(\hat{a}-\hat{a}^\dagger)}e^{(\imath/\hbar)\hat{H}t}e^{-(\imath/\hbar)\hat{H}t}\psi_n(x) .$$

We now use the relationship

$$e^{-\hat{A}}e^{\hat{B}}e^{\hat{A}} = \sum_n \frac{e^{-\hat{A}}\hat{B}^n e^{\hat{A}}}{n!} = \sum_n \frac{(e^{-\hat{A}}\hat{B}e^{\hat{A}})^n}{n!} = e^{e^{-\hat{A}}\hat{B}e^{\hat{A}}} ,$$

which is easy to show by expansion of $e^{\hat{B}}$. The expression $e^{-\hat{A}}\hat{B}e^{\hat{A}}$ can be evaluated through its action on the complete system of eigenfunctions,

$$e^{-(\imath/\hbar)\hat{H}t}\hat{a}e^{(\imath/\hbar)\hat{H}t}|\psi_n\rangle = e^{-(\imath/\hbar)\hat{H}t}\hat{a}e^{(\imath/\hbar)E_n^{(0)}t}|\psi_n\rangle = e^{-(\imath/\hbar)E_{n-1}^{(0)}t}e^{(\imath/\hbar)E_n^{(0)}t}\hat{a}|\psi_n\rangle .$$

Hence,

$$e^{-(\imath/\hbar)\hat{H}t}\hat{a}e^{(\imath/\hbar)\hat{H}t} = \hat{a}e^{\imath\omega t} \qquad \textit{and} \qquad e^{-(\imath/\hbar)\hat{H}t}\hat{a}^\dagger e^{(\imath/\hbar)\hat{H}t} = \hat{a}^\dagger e^{-\imath\omega t} .$$

Now we can write the temporal solution,

$$\psi_n^{(1)}(x,t) = e^{-\beta(\hat{a}e^{\imath\omega t}-\hat{a}^\dagger e^{-\imath\omega t})}e^{-(\imath/\hbar)\hat{H}t}\psi_n(x) = e^{-\beta\cos\omega t(\hat{a}-\hat{a}^\dagger)-\imath\beta\sin\omega t(\hat{a}+\hat{a}^\dagger)}e^{-(\imath/\hbar)E_n^{(0)}t}\psi_n(x) .$$

Using Glauber's formula (23.210) we find,

$$\begin{aligned}\psi_n^{(1)}(x,t) &= e^{-\imath\beta\sin\omega t(\hat{a}+\hat{a}^\dagger)}e^{-\beta\cos\omega t(\hat{a}-\hat{a}^\dagger)}e^{\imath\beta^2\sin\omega t\cos\omega t}e^{-(\imath/\hbar)E_n^{(0)}t}\psi_n(x) \\ &= e^{-\imath\beta\sin\omega t(\hat{a}+\hat{a}^\dagger)}e^{\imath\beta^2\sin\omega t\cos\omega t}e^{-(\imath/\hbar)E_n^{(0)}t}\psi_n(x - b\cos\omega t) .\end{aligned}$$

Finally,

$$|\psi_n^{(1)}(x,t)|^2 = |\psi_n(x - \bar{x}(t))|^2 ,$$

where $\bar{x}(t) \equiv b\cos\omega t$. This means that the spatial distribution of $\psi_n^{(1)}$ around $\bar{x}(t)$ is the same as of ψ_n around $\bar{x} = 0$. The entire distribution oscillates without deformation. The momentum distribution follows from the Fourier transform,

$$\begin{aligned}\phi_n^{(1)}(p,t) &= \frac{1}{\sqrt{2\pi\hbar}}\int dx e^{-(\imath/\hbar)px}\psi_n^{(1)} = \frac{1}{\sqrt{2\pi\hbar}}\int du\ e^{-(\imath/\hbar)pu}e^{-(\imath/\hbar)um\omega b\sin\omega t}e^{\imath\gamma(p,t)}\psi_n \\ &= e^{\imath\gamma(p,t)}\phi_n(p + m\omega b\sin\omega t) ,\end{aligned}$$

with $\gamma = \gamma^*$. We obtain,

$$|\phi_n^{(1)}(p,t)|^2 = |\phi_n(p - \bar{p}(t))|^2 ,$$

where $\bar{p}(t) \equiv -m\omega b\sin\omega t$.

24.6.6.10 Ex: Spatial wavefunction of a particle in a coherent state

a. Derive the following relations for the harmonic oscillator having received a recoil momentum,

$$\langle\psi_n^{(1)}|\hat{x}|\psi_n^{(1)}\rangle = 0 \qquad \text{and} \qquad \langle\psi_n^{(1)}|\hat{p}|\psi_n^{(1)}\rangle = \hbar k \ .$$

b. Calculate the temporal evolution of the oscillator after having received the recoil via,

$$\langle x|e^{-\imath\hat{H}t/\hbar}e^{-\imath k\hat{x}}|n\rangle \ .$$

c. Calculate the spatial wavefunction of a particle in a coherent state,

$$\langle x|\alpha\rangle = \sum_n e^{-|\alpha|^2/2}\frac{\alpha^n}{\sqrt{n!}}\langle x|n\rangle \ .$$

Solution: *a. We calculate,*

$$\begin{aligned}\langle\psi_n^{(1)}|\hat{x}|\psi_n^{(1)}\rangle &= \tfrac{a_{ho}}{\sqrt{2}}\langle n|e^{\imath k\hat{x}}(\hat{b}+\hat{b}^\dagger)e^{-\imath k\hat{x}}|n\rangle \\ &= \tfrac{a_{ho}}{\sqrt{2}}\langle\alpha|\hat{b}+\hat{b}^\dagger|\alpha\rangle = \tfrac{a_{ho}}{\sqrt{2}}(\alpha+\alpha^*)\langle\alpha|\alpha\rangle = 0 \ ,\end{aligned}$$

and,

$$\begin{aligned}\langle\psi_n^{(1)}|\hat{p}|\psi_n^{(1)}\rangle &= \tfrac{\hbar}{\imath\sqrt{2}a_{ho}}\langle n|e^{\imath k\hat{x}}(\hat{b}-\hat{b}^\dagger)e^{-\imath k\hat{x}}|n\rangle \\ &= \tfrac{\hbar}{\imath\sqrt{2}a_{ho}}(\alpha-\alpha^*)\langle\alpha|\alpha\rangle = -\hbar k \ .\end{aligned}$$

b.

24.6.6.11 Ex: Electric field amplitude and fluctuation

Calculate $\langle\hat{\mathcal{E}}\rangle$ and $\Delta\hat{\mathcal{E}}$ for a coherent state.

Solution: *The results are,*

$$\langle\hat{\mathcal{E}}\rangle = -2\hat{\mathcal{E}}_m|\alpha|\sin(\mathbf{k}\cdot\mathbf{r}-\omega t) \quad , \quad \langle\hat{\mathcal{E}}^2\rangle = \hat{\mathcal{E}}_m^2[4|\alpha|^2\sin(\mathbf{k}\cdot\mathbf{r}-\omega t)+1] \quad , \quad \Delta\hat{\mathcal{E}} = \hat{\mathcal{E}}_m \ .$$

24.6.6.12 Ex: Beam splitting a Fock state

A beam splitter is a device dividing an input mode (e.g. a laser beam) into two output modes 1 and 2. Assuming that a beam splitter sends every single photon with equal probability to one of the two output modes and that the input mode be a Fock state, what would be the photon statistics in the output mode? **Help:** Create the total output state $|n_1, n_2\rangle$ from vacuum by successive application of the photon creation operator $\hat{a}_1^\dagger + \hat{a}_2^\dagger$.

Solution: *See Sec. 35.8.2.*

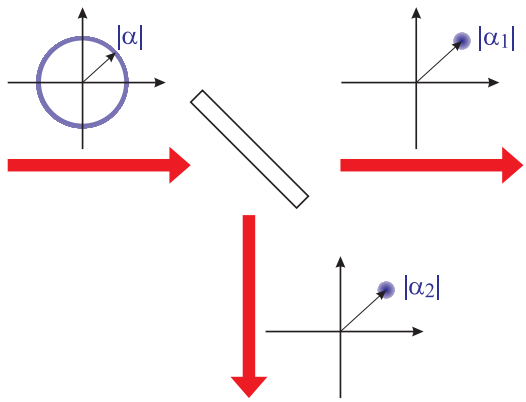

Figure 24.25: Beam splitting of a Fock state.

24.6.6.13 Ex: Wavefunction of a harmonic oscillator in a Glauber state

Derive the wavefunction for a harmonic oscillator in a coherent state using the exponential generating function of Hermite polynomials,

$$e^{2xt-t^2} = \sum_{n=0}^{\infty} \frac{t^n}{n!} H_n(x) \ .$$

Solution: *Starting from,*

$$\langle x|n\rangle = \frac{1}{\sqrt{a_{ho}\sqrt{\pi}2^n n!}} e^{-x^2/2a_{ho}^2} H_n(x/a_{ho}) \qquad \textit{and} \qquad |\alpha\rangle = e^{-|\alpha|^2/2} \sum_{n=0}^{\infty} \frac{\alpha^n}{\sqrt{n!}} |n\rangle$$

we obtain,

$$\langle x|\alpha\rangle = \frac{e^{-|\alpha|^2/2} e^{-x^2/2a_{ho}^2}}{\sqrt{a_{ho}\sqrt{\pi}}} \sum_{n=0}^{\infty} \frac{(\alpha/\sqrt{2})^n}{n!} H_n(x/a_{ho}) \ .$$

Using the given generating function we get,

$$\langle x|\alpha\rangle = \frac{1}{\sqrt{a_{ho}\sqrt{\pi}}} e^{-|\alpha|^2/2 - x^2/2a_{ho}^2 + \sqrt{2}\alpha x/a_{ho} - \alpha^2/2} \ ,$$

and,

$$|\langle x|\alpha\rangle|^2 = \frac{1}{a_{ho}\sqrt{\pi}} e^{-[(\alpha+\alpha^*)/\sqrt{2} + x/a_{ho}]^2} \ .$$

24.7 Further reading

A. Görlitz et al., *Observing the Position Spread of Atomic Wave Packets* [528]DOI

24.7.1 on the Fourier grid method

R. Meyer, *Trigonometric Interpolation Method for One-Dimensional Quantum-Mechanical Problems* [884]DOI

O. Dulieu, *Coupled channel bound states calculations for alkali dimers using the Fourier grid method* [395]DOI

J. Stare et al., *Fourier Grid Hamiltonian Method for Solving the Vibrational Schroedinger Equation in Internal Coordinates Theory and Test Applications* [1244]DOI

C. Clay Marston et al., *The Fourier grid Hamiltonian method for bound state eigenvalues and eigenfunctions* [847]DOI

24.7.2 on the harmonic oscillator

I. Bouchoule et al., *Neutral atoms prepared in Fock states of a one-dimensional harmonic potential* [182]DOI

M.O. Scully and M.S. Zubairy, Cambridge University Press, *Quantum Optics* [1184]ISBN

Chapter 25

Rotations / Central potentials

Rotations are, on the same rights as translations, symmetry operations in space. They are of fundamental importance for the discussion of composite particles, such as atoms because they help us to formulate appropriate boundary conditions facilitating the solution of the three-dimensional Schrödinger equation.

25.1 Particle in a central potential

Many potentials do not have Cartesian symmetry, but fortunately, many problems have *some* kind of symmetry, cylindrical, spherical or periodic. Those with cylindrical or spherical symmetry can be solved by separating the curvilinear coordinates, as we will show in the following. Particularly important are spherical potentials caused by central forces, for example, the Coulomb force between the proton and the electron in the hydrogen atom.

25.1.1 Transformation to relative coordinates

The hydrogen atom represents a *two-body problem*. We consider the two masses $m_{1,2}$ of a proton and an electron separated by a distance $\mathbf{r}$ and interacting through a potential $V(\mathbf{r})$. The Hamiltonian is

$$\hat{H} = \frac{-\hbar^2}{2m_1}\nabla_{r1}^2 + \frac{-\hbar^2}{2m_2}\nabla_{r2}^2 + V(\mathbf{r}_1 - \mathbf{r}_2) \ , \tag{25.1}$$

where $\mathbf{r}_{1,2}$ are the positions of the proton and the electron. With the ansatz $\Xi(t, \mathbf{r}_1, \mathbf{r}_2) = \Xi(\mathbf{r}_1, \mathbf{r}_2)e^{-\imath E_{tot}t/\hbar}$, the time-dependent Schrödinger equation

$$\hat{H}\Xi(t, \mathbf{r}_1, \mathbf{r}_2) = \imath\hbar\frac{d}{dt}\Xi(t, \mathbf{r}_1, \mathbf{r}_2) \ , \tag{25.2}$$

becomes stationary,

$$\left[\frac{-\hbar^2}{2m_1}\nabla_{r_1}^2 + \frac{-\hbar^2}{2m_2}\nabla_{r_2}^2 + V(\mathbf{r}_1 - \mathbf{r}_2)\right]\Xi(\mathbf{r}_1, \mathbf{r}_2) = E_{tot}\Xi(\mathbf{r}_1, \mathbf{r}_2) \ . \tag{25.3}$$

Now we transform into the center-of-mass system making for the total wavefunction the ansatz $\Xi(\mathbf{r}_1, \mathbf{r}_2) = e^{-\imath\mathbf{P}\cdot\mathbf{R}/\hbar}\Psi(\mathbf{r})$ with $\mathbf{R} \equiv \frac{m_1}{M}\mathbf{r}_1 + \frac{m_2}{M}\mathbf{r}_2$ and $\mathbf{r} \equiv \mathbf{r}_1 - \mathbf{r}_2$ and introducing the abbreviation $M = m_1 + m_2$. This corresponds to a product of a plane

wave, describing the linear motion of the center of the masses, and a radial wave function, which describes the relative motion of the atom. The kinetic energy of one mass is:

$$\begin{aligned}&\frac{-\hbar^2}{2m_1}\nabla_{r_1}^2 e^{-\imath\mathbf{P}\cdot\mathbf{R}/\hbar}\Psi(\mathbf{r}) \qquad (25.4)\\ &= \frac{-\hbar^2}{2m_1}\left[e^{-\imath\mathbf{P}\cdot\mathbf{R}/\hbar}\nabla_{r_1}^2\Psi(\mathbf{r}) + 2(-\tfrac{\imath m_1\mathbf{P}}{\hbar M})e^{-\imath\mathbf{P}\cdot\mathbf{R}/\hbar}\nabla_{r_1}\Psi(\mathbf{r}) + \Psi(\mathbf{r})(-\tfrac{\imath m_1}{\hbar^2 M}\mathbf{P})^2 e^{-\imath\mathbf{P}\cdot\mathbf{R}/\hbar}\right]\\ &= e^{-\imath\mathbf{P}\cdot\mathbf{R}/\hbar}\left[\frac{-\hbar^2}{2m_1}\nabla_{r_1}^2\Psi(\mathbf{r}) + \frac{\imath\hbar\mathbf{P}}{M}\nabla_{r_1}\Psi(\mathbf{r}) - \frac{m_1\mathbf{P}^2}{2M^2}\Psi(\mathbf{r})\right] .\end{aligned}$$

Hence, for two atoms,

$$\begin{aligned}&E_{tot}\Xi(\mathbf{r}_1,\mathbf{r}_2) - V(\mathbf{r})\Xi(\mathbf{r}_1,\mathbf{r}_2) \qquad (25.5)\\ &= e^{-\imath\mathbf{P}\cdot\mathbf{R}/\hbar}\left[\frac{-\hbar^2}{2m_1}\nabla_{r_1}^2\Psi(\mathbf{r}) + \frac{-\hbar^2}{2m_2}\nabla_{r_2}^2\Psi(\mathbf{r}) + \frac{\imath\hbar\mathbf{P}}{M}(\nabla_{r_1}+\nabla_{r_2})\Psi(\mathbf{r}) + \frac{\mathbf{P}^2}{2M}\Psi(\mathbf{r})\right] .\end{aligned}$$

Using $\nabla_{r_1} = -\nabla_{r_2} = \nabla_r$, we see that the third term cancels, such that,

$$\frac{P^2}{2M}\Psi(\mathbf{r}) + \frac{-\hbar^2}{2m_1}\nabla_r^2\Psi(\mathbf{r}) + \frac{-\hbar^2}{2m_2}\nabla_r^2\Psi(\mathbf{r}) + V(\mathbf{r})\Psi(\mathbf{r}) = E_{tot}\Psi(\mathbf{r}) . \qquad (25.6)$$

Subtracting the energy of the center-of-mass motion with $E = E_{tot} - \frac{P^2}{2M}$ and introducing the abbreviation $m^{-1} = m_1^{-1} + m_2^{-1}$, we finally get,

$$\boxed{\left[\frac{-\hbar^2}{2m}\nabla_r^2 + V(\mathbf{r})\right]\Psi(\mathbf{r}) = E\Psi(\mathbf{r})} . \qquad (25.7)$$

25.1.2 Particle in a cylindrical potential

The equation (25.7) is three-dimensional because $\Psi(\mathbf{r})$ is a *scalar field* and the momentum operator in Cartesian coordinates is given by,

$$\nabla_r^2 = \frac{\partial^2}{\partial x^2} + \frac{\partial^2}{\partial y^2} + \frac{\partial^2}{\partial z^2} . \qquad (25.8)$$

However, in some situations, the symmetry of the system allows to reduce dimensionality similarly to the cases of the box potential and the three-dimensional harmonic oscillator. Let us now discuss the cases of cylindrical and spherical symmetry.

Electrons in magnetic fields are subject to the Lorentz force, which keeps them in a rotating motion. We can rewrite the momentum operator in cylindrical coordinates,

$$x = \rho\cos\varphi \quad , \quad y = \rho\sin\varphi \quad , \quad z = z , \qquad (25.9)$$

as

$$\nabla_r^2 = \frac{\partial^2}{\partial\rho^2} + \frac{1}{\rho}\frac{\partial}{\partial\rho} + \frac{1}{\rho^2}\frac{\partial^2}{\partial\varphi^2} + \frac{\partial^2}{\partial z^2} . \qquad (25.10)$$

Now, with the assumption that the potential only depends on ρ, $V(\mathbf{r}) = V(\rho)$, we can try the ansatz,

$$\Psi(\mathbf{r}) = R(\rho)\xi(\varphi)\zeta(z) , \qquad (25.11)$$

and obtain,

$$\frac{1}{R(\rho)}\left[-\frac{\hbar^2}{2m}\left(\frac{\partial^2}{\partial\rho^2}+\frac{1}{\rho}\frac{\partial}{\partial\rho}+V(\rho)\right)\right]R(\rho)-\frac{\hbar^2}{2m}\frac{1}{\zeta(z)}\frac{\partial^2}{\partial z^2}\zeta(z)-\frac{\hbar^2}{2m\rho^2}\frac{1}{\xi(\varphi)}\frac{\partial^2}{\partial\varphi^2}\xi(\varphi)=E\,. \tag{25.12}$$

First, we separate the axial motion,

$$-\frac{\zeta''}{\zeta}=const\equiv\frac{2mE_z}{\hbar^2}\equiv k_z^2\,, \tag{25.13}$$

the solution of this equation being a superposition of two plane waves counterpropagating along the axis z, $\zeta(z)=Ae^{\imath k_z z}+Be^{-\imath k_z z}$. Now, we separate the azimuthal motion,

$$\frac{\rho^2}{R(\rho)}\frac{\partial R^2(\rho)}{\partial\rho^2}+\frac{\rho}{R(\rho)}\frac{\partial R(\rho)}{\partial\rho}+\frac{2m\rho^2}{\hbar^2}[E-V(\rho)]-\rho^2k_z^2=-\frac{\xi''}{\xi}=const\equiv m_\varphi^2\,. \tag{25.14}$$

The solution of the right-hand part of the equation is $\xi(\varphi)=Ce^{\imath m_\varphi\varphi}+De^{-\imath m_\varphi\varphi}$. Finally, we have the radial equation,

$$\frac{1}{R(\rho)}\frac{\partial R(\rho)^2}{\partial\rho^2}+\frac{1}{\rho R(\rho)}\frac{\partial R(\rho)}{\partial\rho}-\frac{2m}{\hbar^2}[E-V(\rho)]-k_z^2-\frac{m_\varphi^2}{\rho^2}=0\,, \tag{25.15}$$

with the effective potential $V_{eff}=V(\rho)+\frac{\hbar^2m_\varphi^2}{2m\rho^2}$. For a homogeneous potential, $V(\rho)=V_0$, the solution will be a superposition of Bessel functions.

Example 162 (*Rigid rotor in cylindrical coordinates*): To give an example, we disregard the potential, $V(\rho)=0$, and we consider for the particle an orbit with constant radius, $\rho=const$ such that $R(\rho)=\delta(\rho-\rho_0)$. In this case, we only need to treat the orbital motion described by the right part of Eq. (25.14). For the solution of this equation, $\xi(\varphi)=Ae^{\imath m_\varphi\varphi}$, to be well-defined, we need $\xi(\varphi)=\xi(\varphi+2\pi)$. This implies,

$$m_\varphi=0,\pm1,\pm2,..$$

and

$$E_\varphi=\frac{\hbar^2m_\varphi^2}{2m\rho^2}\,.$$

The allowed energies $E_{m_\varphi}=E_\varphi$ can be obtained by letting the Hamiltonian

$$\hat{H}=-\frac{\hbar^2}{2I}\frac{\partial^2}{\partial\varphi^2}\,,$$

with the moment of inertia $I=m\rho^2$ actuate on the azimuthal wavefunction $\xi(\varphi)$. We now define the operator,

$$\hat{l}_z=\frac{\hbar}{\imath}\frac{\partial}{\partial\varphi}\,.$$

This operator acts on the wavefunction ξ as follows,

$$\hat{l}_z\xi(\varphi)=\hbar m_\varphi\xi(\varphi)\,.$$

It is easy to show that wavefunctions with different values m_l are orthogonal.
Note: 1. The state $m_\varphi=0$ has zero energy; that is, it has no zero-point energy.
2. The particle is delocalized within a ring of radius r: $\Delta l_z\Delta\sin\varphi\geq\frac{\hbar}{2}|\langle\cos\varphi\rangle|$.

25.1.3 Hamiltonian in spherical coordinates

We can rewrite the momentum operator in spherical coordinates,

$$x = r\sin\vartheta\cos\varphi \quad , \quad y = r\sin\vartheta\sin\varphi \quad , \quad z = r\cos\vartheta \ , \tag{25.16}$$

as [1],

$$\nabla_r^2 = \frac{1}{r^2}\frac{\partial}{\partial r}\left(r^2\frac{\partial}{\partial r}\right) + \frac{1}{r^2}\frac{\hat{\mathbf{L}}^2}{\hbar^2} \qquad \text{where} \qquad \frac{\hat{\mathbf{L}}^2}{\hbar^2} \equiv \frac{1}{\sin\vartheta}\frac{\partial}{\partial\vartheta}\left(\sin\vartheta\frac{\partial}{\partial\vartheta}\right) + \frac{1}{\sin^2\vartheta}\frac{\partial^2}{\partial\varphi^2} \ , \tag{25.17}$$

is an abbreviation called *Legendre operator*. For an isotropic potential, $V(\mathbf{r}) = V(r)$, we can try the ansatz,

$$\Psi(\mathbf{r}) = R(r)Y(\vartheta,\varphi) \tag{25.18}$$

to solve the Schrödinger equation (23.60),

$$\frac{r^2}{R(r)}\left[-\frac{\hbar^2}{2m}\frac{1}{r^2}\frac{\partial}{\partial r}\left(r^2\frac{\partial}{\partial r}\right) + V(r) - E\right]R(r) = \frac{-1}{2m}\frac{\hat{\mathbf{L}}^2 Y(\vartheta,\varphi)}{Y(\vartheta,\varphi)} = const \equiv -\frac{\hbar^2}{2m}\ell(\ell{+}1) \ , \tag{25.19}$$

where we choose a separation constant, $\ell(\ell+1)$, the significance of which we shall soon learn. Considering only the angular part,

$$\boxed{\hat{\mathbf{L}}^2 Y(\vartheta,\varphi) = \hbar^2\ell(\ell+1)Y(\vartheta,\varphi)} \ , \tag{25.20}$$

and making another separation ansatz,

$$Y(\vartheta,\varphi) = \Theta(\vartheta)\Phi(\varphi) \ , \tag{25.21}$$

we obtain,

$$\sin^2\vartheta\left(\frac{1}{\Theta(\vartheta)}\frac{1}{\sin\vartheta}\frac{\partial}{\partial\vartheta}\sin\vartheta\frac{\partial}{\partial\vartheta}\Theta(\vartheta) + \ell(\ell+1)\right) = -\frac{1}{\Phi(\varphi)}\frac{\partial^2}{\partial\varphi^2}\Phi(\varphi) = const \equiv m^2 \ , \tag{25.22}$$

where we choose a separation constant, m^2. Introducing another abbreviation,

$$\hat{L}_z \equiv \frac{\hbar}{\imath}\frac{\partial}{\partial\varphi} \ , \tag{25.23}$$

the azimuthal equation takes the form

$$\boxed{\hat{L}_z\Phi(\varphi) = \hbar m\Phi(\varphi)} \ . \tag{25.24}$$

As in the case of the cylindrical potential, the solution of the *azimuthal equation* is, using the normalization,

$$\Phi(\varphi) = \tfrac{1}{\sqrt{2\pi}}e^{\imath m\varphi} \ , \tag{25.25}$$

with the *magnetic quantum number* $m = 0, \pm1, \pm2, ...$

[1] We may also write: $\mathbf{p}^2 = (\hat{\mathbf{e}}_r\cdot\mathbf{p})^2 + (\hat{\mathbf{e}}_r\times\mathbf{p})^2 = p_r^2 + \frac{\mathbf{L}^2}{r^2}$, where p_r^2 is the radial part of the Laplace operator and $\frac{\mathbf{L}^2}{r^2}$ the angular part.

The *polar equation*,

$$\frac{1}{\Theta(\vartheta)}\frac{1}{\sin\vartheta}\frac{\partial}{\partial\vartheta}\sin\vartheta\frac{\partial}{\partial\vartheta}\Theta(\vartheta)+\ell(\ell+1)=\frac{m^2}{\sin^2\vartheta}\ , \tag{25.26}$$

is called Legendre's differential equation and can be solved by a power series in $\cos^k\vartheta$. For $m=0$, the solutions are the *Legendre polynomials*, $P_\ell(\cos\vartheta)$ with

$$P_\ell(z)=\frac{1}{2^\ell\ell!}\frac{d^\ell}{dz^\ell}[(z^2-1)^\ell]\ . \tag{25.27}$$

The first polynomials are,

$$P_0(z)=1\quad,\quad P_1(z)=z\quad,\quad P_2(z)=\tfrac{1}{2}(3z^2-1)\quad,\quad P_3(z)=\tfrac{1}{2}(5z^3-3z)\ . \tag{25.28}$$

For $m>0$, the solutions are the associated polynomials,

$$P_\ell^m(z)=(-1)^m(1-z^2)^{m/2}\frac{d^m}{dz^m}P_\ell(z)=\frac{(-1)^m}{2^\ell\ell!}(1-z^2)^{m/2}\frac{d^{\ell+m}}{dz^{\ell+m}}[(z^2-1)^\ell] \tag{25.29}$$

$$P_\ell^{-m}(z)=(-1)^m\frac{(\ell-m)!}{(\ell+m)!}P_\ell^m(z)\ .$$

The polar function must still be normalized,

$$\Theta_\ell^m(\vartheta)=P_\ell^m(\cos\vartheta)\sqrt{\frac{2\ell+1}{2}\frac{(\ell-m)!}{(\ell+m)!}}\ . \tag{25.30}$$

The functions $Y_{\ell m}(\vartheta,\varphi)$ are the *spherical harmonics*. They form an orthonormal system,

$$\int_0^\pi\int_0^{2\pi}Y^*_{\ell'm'}(\vartheta,\varphi)Y_{\ell m}(\vartheta,\varphi)\sin\vartheta d\vartheta d\varphi=\delta_{\ell'\ell}\delta_{m'm}\ . \tag{25.31}$$

Finite solutions only exist when the *angular momentum quantum number* is $\ell=0,1,..$ and for $|m|\le\ell$.

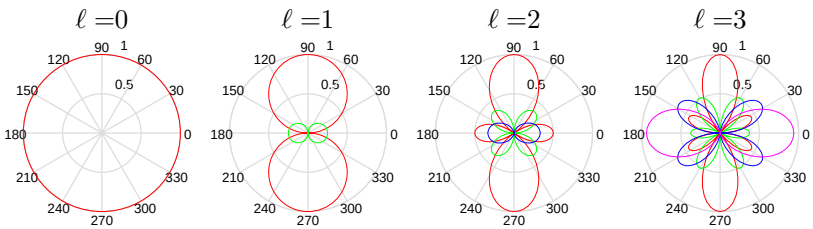

Figure 25.1: (code) Angular wavefunctions. Shown are the Legendre polynomials $P_\ell^m(\cos\vartheta)$ for $\ell=0,1,2,3$ and $m=0,..,\ell$. Red: $m=0$, green: $|m|=1$, blue: $|m|=2$, and magenta: $|m|=3$.

The solutions of the angular part of the Schrödinger equation for the hydrogen atom are finally,

$$\boxed{Y_{\ell m}(\vartheta,\varphi) = \frac{1}{\sqrt{2\pi}}\, P_\ell^m(\cos\vartheta)\sqrt{\frac{2\ell+1}{2}\frac{(\ell-m)!}{(\ell+m)!}}\, e^{\imath m\varphi}} \,. \tag{25.32}$$

The spherical harmonics are simultaneously eigenfunctions of the operators $\mathbf{L}^2$, as can be seen from Eq. (25.20), and of the operator L_z according to Eq. (25.24). The quantities represented by the quantum operators $\hat{H}, \hat{\mathbf{L}}^2, \hat{L}_z$ are conserved in the hydrogen system. The conservation of the angular momentum is due to the spherical symmetry of the Coulomb potential.

We will verify the parity of the spherical harmonics in Exc. 25.1.5.1.

25.1.4 Separation of radial motion

In Sec. 25.1.3 we derived, after having separated the motion of the center-of-mass (that is, of the heavy nucleus) and the angular coordinates, the radial equation (25.19) describing the radial component of the electronic motion,

$$\frac{1}{R(r)}\left[-\frac{\hbar^2}{2m}\frac{1}{r^2}\frac{\partial}{\partial r}\left(r^2\frac{\partial}{\partial r}\right) + V(r) - E\right] R(r) = -\frac{\hat{\mathbf{L}}^2}{2mr^2} \,, \tag{25.33}$$

Now, we make the substitution $R(r) = u(r)/r$ and the radial equation becomes,

$$\boxed{\left[-\frac{\hbar^2}{2m}\frac{\partial^2}{\partial r^2} + \frac{\hat{\mathbf{L}}^2}{2mr^2} + V(r)\right] u(r) = E u(r)} \,. \tag{25.34}$$

This equation is very similar to a one-dimensional Schrödinger equation, but there is an additional potential term called *centrifugal potential*,

$$V_\ell(r) \equiv \frac{\hat{\mathbf{L}}^2}{2mr^2} \,. \tag{25.35}$$

For example, for the potential of an electron orbiting a proton, we have,

$$\left[-\frac{\hbar^2}{2m}\frac{\partial^2}{\partial r^2} - \frac{Ze^2}{4\pi\epsilon_0 r} + \frac{\hbar^2\ell(\ell+1)}{2mr^2} - E\right] u_{E\ell}(r) = 0 \,. \tag{25.36}$$

We will discuss this equation intensely in the context of the hydrogen atom.

In Exc. 25.1.5.2 we derive the radial Gross-Pitaevskii equation for a Bose-Einstein condensate trapped in a spherical potential. In the Exc. 25.1.5.3 we will study particles inside a central potential of zero depth, in the Excs. 25.1.5.4 and 25.1.5.5 we consider 3D spherical box potentials and in Exc. 25.1.5.6 a spherical harmonic potential.

> **Example 163 (*Rigid rotor in spherical coordinates*):** We continue the discussion of the rigid rotor, now in spherical coordinates. In the case that the orbit of the particle is fixed to a radius R, we can neglect the kinetic energy due

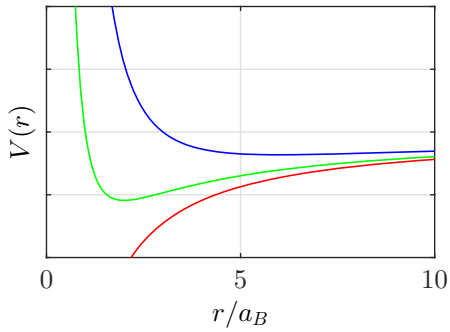

Figure 25.2: (code) Sum of a Coulomb potential and centrifugal potential for $\ell = 0$ (lower curve), $\ell = 1$ (center curve), and $\ell = 2$ (upper curve).

to the radial motion and the potential, both being constant. In this case the radial Schrödinger equation is,

$$\left[\frac{\hbar^2\ell(\ell+1)}{2mr^2}\right] u_{E\ell} = E_\ell u_{E\ell} \ .$$

The energies of the *rigid rotor* are

$$E_\ell = \frac{\hbar^2\ell(\ell+1)}{2I} \ ,$$

with the *momentum of inertia* $I = mR^2$.

25.1.5 Exercises

25.1.5.1 Ex: Parity of the spherical harmonic functions

We consider the parity transformation $\mathbf{P}$ with $(x, y, z) \xrightarrow{\mathbf{P}} (-x, -y, -z)$. Use spherical coordinates to show that $Y_{\ell m} \xrightarrow{\mathbf{P}} (-1)^\ell Y_{\ell m}$, and therefore that a spherical surface function has even parity when ℓ is even, and odd parity, when ℓ is odd.

Solution: *In spherical coordinates the parity transformation can be written* $(r, \theta, \phi) \xrightarrow{\mathbf{P}} (r, \pi-\theta, \pi+\phi)$. *On the azimuthal side, the spherical harmonics are* $\propto e^{im\phi}$. *Therefore, the transformation* $\phi \to \phi + \pi$ *yields a factor* $(-1)^m$. *On the polar side, the spherical harmonics are* $\propto P_\ell^m(\cos\theta)$. *The transformation* $\theta \to \pi - \theta$ *transforms* $z = \cos\theta$ *into* $-z$. *In the definition of polynomials via derivatives, (25.27) and (25.29), it is clear that this gives a factor* $(-1)^{\ell+m}$. *Therefore, we obtain,*

$$Y_{\ell m}(\pi - \theta, \pi + \phi) = (-1)^\ell Y_{\ell m}(\theta, \phi) \ .$$

That is, spherical harmonics are functions with well-defined parity.

25.1.5.2 Ex: Bose-Einstein condensate in an isotropic potential

The time-dependent Gross-Pitaevskii equation describing the wavefunction of a Bose-Einstein condensate reads,

$$\imath\hbar\frac{\partial\psi(\mathbf{r},t)}{\partial t} = \left(-\frac{\hbar^2}{2m}\nabla^2 + V_{trp}(r) + g|\psi(\mathbf{r},t)|^2\right)\psi(\mathbf{r},t) \ ,$$

where the factor g depends on the force of the interatomic interaction and V_{trp} is the potential trapping the atoms. Derive the stationary Gross-Pitaevskii equation via the transform $\psi(\mathbf{r},t) = \psi(\mathbf{r})e^{-\imath\mu t/\hbar}$, where the constant μ is called the chemical potential. For $V(\mathbf{r}) = V(r)$ the wavefunction will have radial symmetry, $\psi(\mathbf{r}) = \frac{\phi(r)}{r}$. Rewrite the Gross-Pitaevskii equation for the function ϕ.

Solution: *The transform immediately yields,*

$$\mu\psi(\mathbf{r}) = \left(-\frac{\hbar^2}{2m}\nabla^2 + V_{trp}(r) + g|\psi(\mathbf{r})|^2\right)\psi(\mathbf{r}) \ .$$

From this we obtain [626],

$$\mu\frac{\phi(r)}{r} = \left(-\frac{\hbar^2}{2m}\left[\frac{1}{r}\frac{\partial^2}{\partial r^2}r + \frac{1}{r^2\sin\vartheta}\frac{\partial}{\partial\vartheta}\left(\sin\vartheta\frac{\partial}{\partial\vartheta}\right) + \frac{1}{r^2\sin^2\vartheta}\frac{\partial^2}{\partial\varphi^2}\right] + V_{trp}(r) + g\left|\frac{\phi(r)}{r}\right|^2\right)\frac{\phi(r)}{r}$$

$$\mu\phi(r) = \left(-\frac{\hbar^2}{2m}\frac{\partial^2}{\partial r^2} + V_{trp}(r) + g\frac{|\phi(r)|^2}{r^2}\right)\phi(r) \ ,$$

with

$$\int|\psi(\mathbf{r})|^2 d^3r = 4\pi\int_0^\infty|\psi(\mathbf{r})|^2 r^2 dr = 4\pi\int_0^\infty|\phi(\rho,z)|^2 dr = 1 \ .$$

25.1.5.3 Ex: Motion of a free particle in spherical coordinates

Obtain the eigenfunctions of a free particle as the limiting case of its motion in a central force field with $V(r) \to 0$. Compare the derived eigenfunctions – associated with the complete set of observables $\hat{H}$, $\hat{L}^2$, and $\hat{L}_z$ – to those described by plane waves – associated with the motion characterized by the observables $\hat{p}_x$, $\hat{p}_y$, $\hat{p}_z$, and $\hat{H} = \hat{\mathbf{P}}^2/2m$ –, which also constitute a complete set of observables.

Solution: *The radial equation is,*

$$\left[-\frac{\hbar^2}{2mr^2}\frac{d}{dr}\left(r^2\frac{d}{dr}\right) + \frac{\hbar^2\ell(\ell+1)}{2mr^2} + V(r)\right]R(r) = ER(r) \ .$$

We consider $V(r) = 0$. Introducing a dimensionless variable $\rho \equiv kr$ with $k \equiv \sqrt{2mE/\hbar^2}$ the equation takes the form of a Bessel equation for $\mathcal{J}$ defined by $\mathcal{J}(\rho) \equiv \sqrt{\rho}R(r)$ (which motivates the choice of the notation $\mathcal{J}$):

$$\rho^2\frac{d^2\mathcal{J}}{d\rho^2} + \rho\frac{d\mathcal{J}}{d\rho} + \left[\rho^2 - (\ell+\tfrac{1}{2})^2\right]\mathcal{J} = 0 \ .$$

Regular solutions for positive energies are given by functions called Bessel functions of the first kind $\mathcal{J}_{\ell+1/2}(\rho)$ such that the solutions for R are the so-called spherical Bessel functions $R(r) = j_\ell(kr) \equiv \sqrt{\frac{\pi}{2kr}}\mathcal{J}_{\ell+1/2}(kr)$. The solutions of the Schrödinger equation in polar coordinates for a particle of mass m_0 in vacuum are enumerated by the discrete quantum numbers ℓ and m, while $k \in [0, \infty[$ varies continuously,

$$\psi(\mathbf{r}) = j_\ell(kr)Y_{\ell m}(\theta, \phi) \ ,$$

where $Y_{\ell m}$ are the spherical harmonics. These solutions represent states with defined angular momentum $\mathbf{L}$, contrary to the states corresponding to plane waves, $e^{\imath \mathbf{k}\cdot\mathbf{r}}$, which are characterized by defined linear momenta $\mathbf{p}$.
It is worth noting that plane waves can be expanded into spherical waves by,

$$e^{\imath \mathbf{k}\cdot\mathbf{r}} = \sum_{\ell=0}^{\infty}(2\ell+1)\imath^\ell j_\ell(kr)P_\ell(\hat{\mathbf{k}}\cdot\hat{\mathbf{r}}) = 4\pi\sum_{\ell=0}^{\infty}\sum_{m=-\ell}^{\ell}\imath^\ell j_\ell(kr)Y_{\ell m}(\hat{\mathbf{k}})Y^*_{\ell m}(\hat{\mathbf{r}}) \ .$$

25.1.5.4 Ex: Particle in a spherical box

Find the energy levels and wavefunctions of a particle confined in a spherical box described by potential energy, $V(r) = 0$ for $r < a$ and $V(r) = \infty$ for $r \geq a$ considering the angular momentum $\ell = 0$.

Solution: *The radial equation is,*

$$-\frac{\hbar^2}{2m}\frac{\partial^2}{\partial r^2}u = Eu \ .$$

This is a one-dimensional wave equation the general solution of which, $u(r) = Ae^{\imath kr} + Be^{-\imath kr}$, must meet the conditions,

$$u(0) = 0 = A + B \qquad \text{and} \qquad u(a) = 0 = Ae^{\imath ka} + Be^{-\imath ka} \ .$$

The first condition ensures that the radial function $R(r) = u(r)/r$ does not diverge in the center. We obtain, $ka = n\pi$ and, therefore, the energies,

$$E = \frac{\hbar^2 k^2}{2m} = \frac{\hbar^2\pi^2}{2ma^2}n^2 \ .$$

The wavefunctions are,

$$\psi(\mathbf{r}) = R_1(r)Y_{00}(\theta,\phi) = \frac{1}{\sqrt{4\pi}}\frac{u(r)}{r} = \frac{A}{\sqrt{4\pi}}\frac{e^{\imath kr} - e^{-\imath kr}}{r} = \frac{\imath A}{r\sqrt{\pi}}\sin\frac{n\pi r}{a} \ .$$

Normalization requests,

$$1 = \int|\psi(r)|^2 d^3r = 4\pi\frac{A^2}{\pi}\int_0^a \frac{\sin^2\frac{n\pi}{a}r}{r^2}r^2dr = 4A^2\int_0^a \sin^2\frac{n\pi r}{a}dr = 2aA^2 \ .$$

Finally,

$$\psi(\mathbf{r}) = \frac{\imath}{r\sqrt{2\pi a}}\sin\frac{n\pi r}{a} \ .$$

25.1.5.5 Ex: Finite spherical 3D potential well

a. Derive the possible energy levels and associated wavefunctions for a particle trapped in a spherical 3D potential well of depth V_0 and radius a. Note that this problem is analogous to *Mie scattering* of scalar waves.
b. Discuss the case of a well surrounded by infinitely high walls.

Solution: *a. We consider the potential $V(r) = V_0$ for $r < a$ and $V(r) = 0$ outside, and we first concentrate on bound states, that is, $E < 0$. We will see that there is a* discrete *number of such states (unlike for free states with $E > 0$ which form a continuous spectrum and describe the scattering of the particle by the sphere). Furthermore, the number of states is finite (unlike for Coulombian potentials). The resolution of this problem essentially follows that of free space with additionally a normalization of the total wave function. We solve two Schrödinger equations —inside and outside the sphere— with constant potential depths considering the following boundary conditions: 1. The wave function must be regular at the origin. 2. The wavefunction and its derivatives must be continuous at the potential discontinuity. 3. The wavefunction must converge at infinity.*
Inside the well, $r < a$, the radial Schrödinger equation

$$\left[-\frac{\hbar^2}{2m}\frac{1}{r^2}\frac{\partial}{\partial r}\left(r^2\frac{\partial}{\partial r}\right) + V(r) - E\right] R_{E\ell} = -\frac{\hbar^2\ell(\ell+1)}{2mr^2}R_{E\ell}$$

becomes with the substitutions $\rho \equiv kr$ and $k \equiv \frac{2m}{\hbar^2}(E - V_0)$,

$$R''_{E\ell} + \tfrac{2}{\rho}R'_{E\ell} + \left(1 - \tfrac{\ell(\ell+1)}{\rho^2}\right) R_{E\ell} = 0 \ .$$

Outside the radius, $r > a$, we obtain the same equation with the replacements $\rho \equiv \imath\kappa r$ and $\kappa \equiv \frac{2m}{\hbar^2}E$. The solutions are the spherical Bessel functions, the Hankel functions, and the Neumann functions [2]*. We note,*

$$j_\ell(\rho) = (-\rho)^\ell \left(\frac{1}{\rho}\frac{\partial}{\partial\rho}\right)^\ell \frac{\sin\rho}{\rho} \qquad \text{with} \qquad j_0(\rho) \overset{\rho\to 0}{\longrightarrow} 0$$

$$n_\ell(\rho) = -(-\rho)^\ell \left(\frac{1}{\rho}\frac{\partial}{\partial\rho}\right)^\ell \frac{\cos\rho}{\rho} \qquad \text{with} \qquad n_0(\rho) \overset{\rho\to 0}{\longrightarrow} \infty \ .$$

The first boundary condition excludes the Neumann and Hankel functions, which are singular at the origin. Therefore,

$$R_{E\ell}^{(r<a)} = A\ j_\ell\left(\sqrt{\tfrac{2m(E-V_0)}{\hbar^2}}r\right) \ ,$$

[2] The spherical Bessel and Neumann functions are related to the Bessel functions $\mathcal{J}$ by,

$$j_\ell(\rho) = \sqrt{\tfrac{\pi}{2\rho}}\mathcal{J}_{\ell+1/2}(\rho) \qquad \text{and} \qquad n_l(\rho) = (-1)^{\ell+1}\sqrt{\tfrac{\pi}{2\rho}}\mathcal{J}_{-\ell-1/2}(\rho) \ ,$$

where

$$\mathcal{J}''_\nu(\rho) + \tfrac{1}{\rho}\mathcal{J}'_\nu(\rho) + \left(1 - \tfrac{\nu^2}{\rho^2}\right)\mathcal{J}_\nu(\rho) = 0$$

is the differential Bessel equation.

with a constant A.
The fact that the energy of bound states is negative, together with the third boundary condition, selects the Hankel functions of the first type for the outside region, since they are those which converge at infinity,

$$R_{E\ell}^{(r>a)} = B\ h_\ell^{(1)}\left(\imath\sqrt{\tfrac{-2mE}{\hbar^2}}r\right)\ .$$

The possible energy values follow from the second boundary condition $R_{E\ell}^{(r<a)}(ka) = R_{E\ell}^{(r>a)}(\kappa a)$. That is, the continuity of the derivative (or conveniently of the logarithmic derivative) requires quantization of the energy. Along with the normalization, this condition allows the determination of the constants A and B.
b. The case of the well surrounded by infinite walls follows from the conditions $E - V_0 \ll -E, -V_0$. Obviously, $R_{E\ell}^{(r>a)} = 0$, such that we can impose the following boundary conditions to the Bessel functions,

$$R_{E\ell}(ka) = j_\ell(ka) = 0\ .$$

Each Bessel function with the index ℓ has several zero crossings corresponding to main quantum numbers n. We use zero crossings of the spherical Bessel functions to find

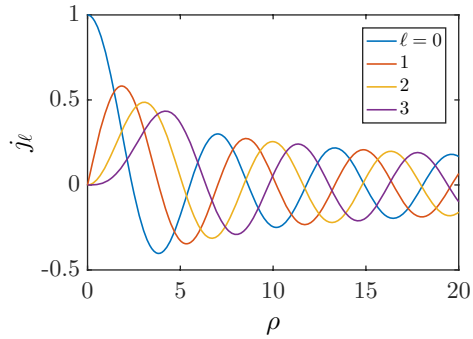

Figure 25.3: (code) Bessel functions.

the energy spectrum and the wavefunctions: Calling $u_{n,\ell}$ the n-th zero of j_ℓ we get,

$$E_{n\ell} = \frac{u_{n,\ell}^2\hbar^2}{2ma^2}\ .$$

The zero points generally have no analytical expression. However, for the particular case $\ell = 0$ (spherically symmetric orbitals), the spherical Bessel function is $j_0(x) = \frac{\sin x}{x}$, the zeros of which can easily be expressed by $u_{n,0} = k\pi$. The eigenenergies are consequently,

$$E_{n0} = \frac{(n\pi)^2\hbar^2}{2ma^2}\ .$$

25.1.5.6 Ex: Particle in a spherical harmonic potential

A quantum particle of mass m is subject to a potential

$$V = \tfrac{1}{2}m\omega^2(x^2+y^2+z^2) \ .$$

a. Obtain the energy levels of this particle. That is, determine the eigenvalues of

$$-\frac{\hbar^2}{2m}\nabla^2\psi + V\psi = E\psi \ .$$

b. Consider the fundamental level and the first two excited levels. Set up a table showing for each of these three levels the energy value, the degeneracy, and the respective states in terms of the quantum numbers.
c. Using

$$\nabla^2\psi = \left[\frac{1}{r^2}\frac{\partial}{\partial r}\left(r^2\frac{\partial}{\partial r}\right) - \frac{L^2}{\hbar^2 r^2}\right]\psi$$

and remembering $\hat{\mathbf{L}}^2 Y_{\ell m}(\theta,\phi) = \hbar^2\ell(\ell+1)Y_{\ell m}$, write down the differential equation of item (a) for the radial part of the wavefunction (it is not necessary to solve it). Identify in this equation the effective potential $V_{eff}(r)$.
d. Solve the differential equation of the previous item for the case where $\ell = 0$ and determine the corresponding eigenvalue. To do this, allow for a solution of the type $e^{-\alpha r^2}$ and determine α.

Solution: *a. The Hamiltonian with the harmonic potential is separable, that is, we can solve the one-dimensional equations,*

$$-\frac{\hbar^2}{2m}\frac{d^2}{dx^2}\psi_x(x) + \frac{m}{2}\omega^2\psi_x(x) = E\psi_x(x) \ .$$

and add the eigenenergies $E_x = \hbar\omega\left(n_x + \frac{1}{2}\right)$, giving

$$E = \hbar\omega\left(n_x + n_y + n_z + \frac{3}{2}\right) \ .$$

b. Sorting the states according to (n_x, n_y, n_z) under the condition $n_x + n_y + n_z = n$ we obtain,

level	*energy*	*states*	*degeneracy*
$n=0$	$E_0 = \frac{3\hbar\omega}{2}$	$(0,0,0)$	1
$n=1$	$E_1 = \frac{5\hbar\omega}{2}$	$(1,0,0);(0,1,0);(0,0,1)$	3
$n=2$	$E_2 = \frac{7\hbar\omega}{2}$	$(1,1,0);(1,0,1);(0,1,1);(2,0,0);(0,2,0);(0,0,2)$	6
n	$E_n = \frac{(2n+3)\hbar\omega}{2}$		$\frac{(n+1)(n+2)}{2}$

c. We can rewrite the Hamiltonian

$$H = \frac{\hat{p}^2}{2m} + \frac{m}{2}\omega^2 r^2 = -\frac{\hbar^2\nabla^2}{2m} + \frac{m}{2}\omega^2 r^2 \ .$$

Passing this expression into spherical coordinates and using $\psi(\mathbf{r}) = R_n(r)Y_{lm}(\theta,\phi)$, we have,

$$-\frac{\hbar^2}{2m}\left[\frac{1}{r^2}\frac{\partial}{\partial r}\left(r^2\frac{\partial}{\partial r}\psi(\mathbf{r})\right) - \frac{L^2}{\hbar^2 r^2}\psi(\mathbf{r})\right] + \frac{m}{2}\omega^2 r^2\psi(\mathbf{r}) = E\psi(\mathbf{r}) \ ,$$

from which,

$$Y_{\ell m}\left[-\frac{\hbar^2}{2m}\frac{1}{r^2}\frac{\partial}{\partial r}\left(r^2\frac{\partial}{\partial r}\right)+\frac{\hbar^2\ell(\ell+1)}{2mr^2}+\frac{m}{2}\omega^2r^2\right]R_n=ER_nY_{\ell m}\ ,$$

from where we can directly read the effective potential:

$$V_{eff}=\frac{m}{2}\omega^2r^2+\frac{\hbar^2\ell(\ell+1)}{2mr^2}\ .$$

The quantum numbers (n,ℓ,m) are equivalent to (n_x,n_y,n_z).
d. When $\ell=0$, the centrifugal term disappears, and we can eliminate the spherical functions from the differential equation:

$$\left[-\frac{\hbar^2}{2m}\frac{1}{r^2}\frac{\partial}{\partial r}\left(r^2\frac{\partial}{\partial r}\right)+\frac{m}{2}\omega^2r^2\right]R_n=ER_n\ .$$

Inserting the function $e^{-\alpha r^2}$ we obtain,

$$\begin{aligned}
&-\frac{\hbar^2}{2m}\frac{1}{r^2}\frac{\partial}{\partial r}\left(r^2\frac{\partial}{\partial r}\right)e^{-\alpha r^2}+\frac{m}{2}\omega^2r^2e^{-\alpha r^2}\\
&=-\frac{\hbar^2}{2m}\frac{1}{r^2}\frac{\partial}{\partial r}\left(-2\alpha r^3e^{-\alpha r^2}\right)+\frac{m}{2}\omega^2r^2e^{-\alpha r^2}\\
&=-\frac{\hbar^2}{2m}\frac{1}{r^2}\left(-2\alpha r^3\right)\left(-2\alpha re^{-\alpha r^2}\right)-\frac{\hbar^2}{2m}\frac{1}{r^2}e^{-\alpha r^2}\left(-6\alpha r^2\right)+\frac{m}{2}\omega^2r^2e^{-\alpha r^2}\\
&=-\frac{\hbar^2}{2m}\left[4\alpha^2r^2-6\alpha\right]e^{-\alpha r^2}+\frac{m}{2}\omega^2r^2e^{-\alpha r^2}=Ee^{-\alpha r^2}\ .
\end{aligned}$$

The constant α must satisfy the following equation for all values of r:

$$-\frac{\hbar^2}{2m}\left[4\alpha^2r^2-6\alpha\right]+\frac{m}{2}\omega^2r^2=E\ ,$$

which is only possible when

$$-\frac{\hbar^2}{2m}4\alpha^2+\frac{m}{2}\omega^2=0\ .$$

Hence,

$$\alpha=\pm\frac{m\omega}{2\hbar}\ ,$$

and eigenvalues are

$$E=\frac{3\hbar^2}{m}\alpha=\frac{3\hbar\omega}{2}\ .$$

25.2 Quantum treatment of hydrogen

According to Rutherford's and Bohr's planetary atomic model we may imagine an atom as a very heavy nucleus having a positive electric charge surrounded by a very light negatively charged charge electronic cloud. Since the nucleus is very small compared to the electronic cloud, we treat it as an entity with mass M and charge Ze, where Z is the number of protons and corresponds to the order of the element in the periodic system.

The canonical procedure for calculating all properties of an atom is to establish its Hamiltonian, that is, to determine the kinetic energies of all components and all interaction energies between them, and to solve the Schrödinger equation. For each component we write the kinetic energy,

$$T_{ncl} = \frac{P^2}{2M} \qquad \text{and} \qquad T_{ele} = \sum_{i=1}^{Z} \frac{p_i^2}{2m} \; . \tag{25.37}$$

Here, $(\mathbf{R}, \mathbf{P})$ are the nuclear coordinates and $(\mathbf{r}_i, \mathbf{p}_i)$ those of the electrons. The energies that corresponds to the interactions, that is, Coulombian attraction or repulsion, between the components of the atom are,

$$V_{ncl-ele} = -\sum_{i=1}^{Z} \frac{Ze^2}{4\pi\varepsilon_0 |\mathbf{R} - \mathbf{r}_i|} \qquad \text{and} \qquad V_{ele-ele} = \sum_{i \neq j=1}^{Z} \frac{e^2}{4\pi\varepsilon_0 |\mathbf{r}_i - \mathbf{r}_j|} \; . \tag{25.38}$$

There are also interactions due to the spin of the particles, which we will deal with later.

Obviously, the solution to this many-body problem is very complicated. For this reason, we will in this chapter, based on the Schrödinger equation, calculate the complete spectrum of the simplest possible atom, hydrogen. This atom consists of a proton and an electron, only.

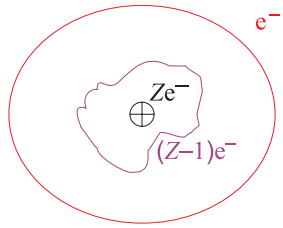

Figure 25.4: The hydrogen model applies to other atoms having a single valence electron occupying a sufficiently large space, that it sees the nucleus together with rest of the electrons shielding the nucleus as a single positive charge.

25.2.1 Bohr's model

Let us now turn our attention to the radial part of the Schrödinger equation describing a particle in a radial potential. We expect that the quantum solutions for the hydrogen atom are similar to the predictions of Bohr's model. Following this model, the orbit

is stable when the attraction force is equal to the centrifugal force. But in addition, Bohr postulated, that only certain energies are allowed. For the hydrogen atom he found,

$$E_n = -\frac{1}{2}\frac{Ze^2}{4\pi\varepsilon_0}\frac{1}{r_n} = -\frac{Z^2\hbar^2}{2ma_B^2}\frac{1}{n^2} = -\frac{Z^2e^2}{4\pi\varepsilon_0}\frac{1}{2a_Bn^2} = -\frac{Z^2}{n^2}\ 13.6\,\mathrm{eV}\ , \tag{25.39}$$

with the *Bohr radius*

$$a_B \equiv 4\pi\varepsilon_0\frac{\hbar^2}{me^2}\ . \tag{25.40}$$

With this equation he was able to explain the spectral observations. Electrons can only jump from one level to another, while emitting or absorbing a photon. The series observed in the hydrogen spectrum $(E_n - E_m)/\hbar$ are the Lyman ($m = 1$), the Balmer ($m = 2$), the Paschen ($m = 3$) an the Brackett series ($m = 4$).

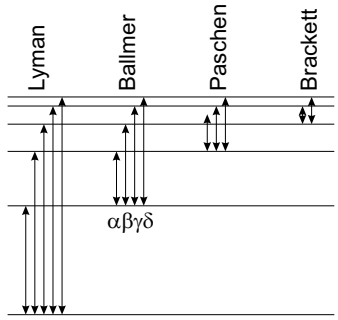

Figure 25.5: The hydrogen transitions.

The discussion of the hydrogen atom within quantum mechanics can start from the radial Schrödinger equation (25.36) with the Coulomb attraction potential,

$$\left[-\frac{\hbar^2}{2m}\frac{\partial^2}{\partial r^2} - \frac{Ze^2}{4\pi\varepsilon_0 r} + \frac{\hbar^2\ell(\ell+1)}{2mr^2} - E\right] u_{E\ell}(r) = 0\ . \tag{25.41}$$

In order to facilitate comparison with Bohr's classical model, let us express the energy in terms of Bohr's energy, $E \equiv E_n = E_1/n^2$, and write the radius in units of a_B, that is, $\tilde{r} \equiv Zr/a_B$. This yields,

$$u''_{n\ell}(\tilde{r}) + \left(-\frac{\ell(\ell+1)}{\tilde{r}^2} + \frac{2}{\tilde{r}} - \frac{1}{n^2}\right) u_{n\ell}(\tilde{r}) = 0\ . \tag{25.42}$$

To ensure that for large radii, $r \to \infty$, the solution is finite, we need an asymptotic behavior like $u_{n\ell}(\tilde{r} \to \infty) = e^{-\tilde{r}/n}$. To ensure that for small radii, $r \to 0$, the solution is finite, we need $u_{n\ell}(\tilde{r} \to 0) = \tilde{r}^{\ell+1}$. We derive the asymptotic solutions in Exc. 25.2.3.1. The resulting differential equation only has solutions for an integer and positive *main quantum number* n and when $\ell = 0, 1, .., n-1$. That is, in the relation $E = E_1/n^2$ the parameter n is integer and positive, such that energy levels remain

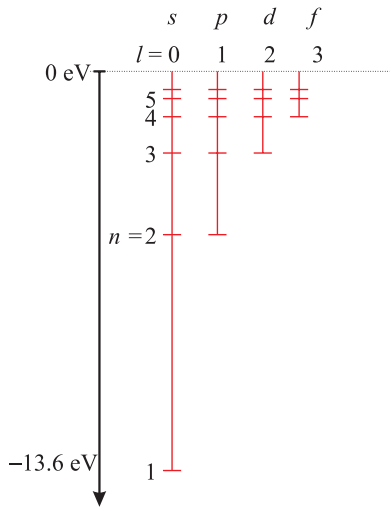

Figure 25.6: Level scheme.

degenerate in ℓ and m. This means that Bohr's postulate of discrete (i.e. quantized) energy levels is valid (uff!)

Substituting the ansatz,

$$u_{n\ell}(\tilde{r}) = D_{n\ell}\tilde{r}^{\ell+1}e^{-\tilde{r}/n}L(\tilde{r}) \ , \tag{25.43}$$

it's easy to show (see Exc. 25.2.3.2), that the differential equation (25.42) reduces to,

$$\tilde{r}L''(\tilde{r}) + 2\left[(\ell+1) - \tfrac{1}{n}\tilde{r}\right]L'(\tilde{r}) + 2\left[1 - \tfrac{1}{n}(\ell+1)\right]L(\tilde{r}) = 0 \ . \tag{25.44}$$

Still with the abbreviation $\rho \equiv 2\tilde{r}/n = 2Zr/na_B$ the ansatz

$$u_{n\ell}(\rho) = D_{n\ell}\rho^{\ell+1}e^{-\rho/2}L(\rho) \ , \tag{25.45}$$

leads to the differential equation [3]

$$\rho L''(\rho) + [2(\ell+1) - \rho]\,L'(\rho) + [n-\ell-1]L(\rho) = 0 \ . \tag{25.46}$$

The solutions of this differential equation, $L^{(2\ell+1)}_{n-\ell-1}(\rho)$, are the *Laguerre polynomials*. These polynomials are listed in mathematical tables. Using the properties of these polynomials it is possible to show that the radial functions are orthogonal and can be normalized (see Exc. 25.2.3.3). Fig. 25.7 shows the curves for the lowest orbitals.

[3] *Laguerre's associated differential equation* is,

$$\rho\partial_\rho^2 L^{(\alpha)}_\nu + (\alpha+1-\rho)\partial_\rho L^{(\alpha)}_\nu + \nu L^{(\alpha)}_\nu = 0 \ .$$

The Laguerre polynomials are generated by

$$L^{(\alpha)}_\nu(\rho) = \frac{e^\rho\rho^{-\alpha}}{\alpha!}\frac{d^\nu}{d\rho^\nu}\left(e^{-\rho}\rho^{\nu+\alpha}\right) \ .$$

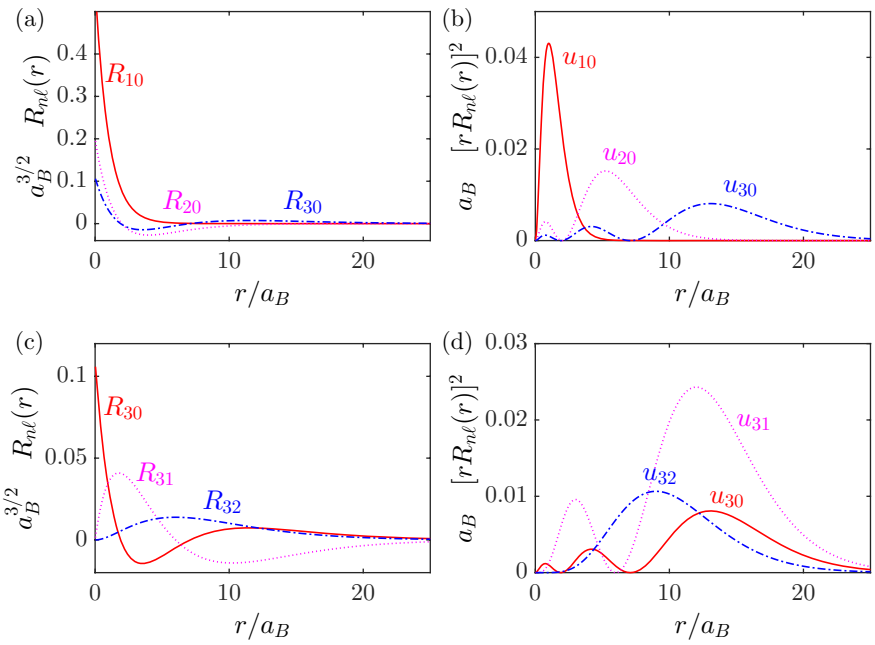

Figure 25.7: (code) (a,c) Radial wavefunctions $R_{n\ell}(r)$ and (b,d) square of the radial wavefunctions $u_{n\ell}(r)$ for various quantum numbers n and ℓ.

Finally, we can write the complete solutions of the Schrödinger equation $\hat{H}\psi = E\psi$,

$$\boxed{\psi_{n\ell m}(r,\theta,\phi) = \frac{u_{n\ell}(r)}{r} Y_{\ell m}(\theta,\phi) \qquad \text{and} \qquad E_n = -\frac{\hbar^2}{2ma_B^2}\frac{Z^2}{n^2}} \,, \tag{25.47}$$

where $n = 1, 2, 3, ..$ and $\ell = 0, 1, .., n-1$ and $m = -\ell, -\ell+1, .., \ell$. Of course, each energy level n is,

$$\sum_{\ell=0}^{n-1} (2\ell+1) = n^2 \tag{25.48}$$

times degenerate.

From the normalization condition,

$$\begin{aligned} 1 &= \int_{\mathbb{R}^3} |\psi_{n\ell m}(r,\theta,\phi)|^2 d^3r \\ &= \int_0^\infty |u_{n\ell}(r)|^2 dr \int_{\mathbb{R}^2} |Y_{\ell m}(\theta,\phi)|^2 \sin\theta d\theta d\phi = \int_0^\infty |u_{n\ell}(r)|^2 dr \,, \end{aligned} \tag{25.49}$$

we obtain the constants,

$$D_{n\ell} = \sqrt{\left(\frac{2Z}{na_B}\right)^3 \frac{(n-\ell-1)!}{2n(n+\ell)!}} \,, \tag{25.50}$$

and the radial wavefunctions finally read,

$$R_{n\ell}(r) = D_{n\ell}\left(\frac{2\tilde{r}}{n}\right)^{\ell} e^{-\tilde{r}/n} L_{n-\ell-1}^{(2\ell+1)}(\tfrac{2\tilde{r}}{n}) = D_{n\ell}\rho^{\ell}e^{-\rho/2}L_{n-\ell-1}^{(2\ell+1)}(\rho)\ , \tag{25.51}$$

using the previously introduced abbreviations.

Here is a list of the first wavefunctions of the hydrogen atom,

$$\begin{aligned}
\psi_{100} &= \tfrac{1}{\sqrt{\pi}}\left(\tfrac{Z}{a_B}\right)^{3/2} e^{-\tilde{r}} \\
\psi_{200} &= \tfrac{1}{4\sqrt{2\pi}}\left(\tfrac{Z}{a_B}\right)^{3/2} (2-\tilde{r})e^{-\tilde{r}/2} \\
\psi_{210} &= \tfrac{1}{4\sqrt{2\pi}}\left(\tfrac{Z}{a_B}\right)^{3/2} \tilde{r}e^{-\tilde{r}/2}\cos\theta \\
\psi_{21\pm1} &= \tfrac{1}{8\sqrt{\pi}}\left(\tfrac{Z}{a_B}\right)^{3/2} \tilde{r}e^{-\tilde{r}/2}\sin\theta e^{\pm\imath\varphi} \\
\psi_{300} &= \tfrac{1}{81\sqrt{3\pi}}\left(\tfrac{Z}{a_B}\right)^{3/2} (27-18\tilde{r}+2\tilde{r}^2)e^{-\tilde{r}/3} \\
\psi_{31\pm1} &= \tfrac{\sqrt{2}}{81\sqrt{3\pi}}\left(\tfrac{Z}{a_B}\right)^{3/2} (6-\tilde{r})\tilde{r}e^{-\tilde{r}/3}\sin\theta e^{\pm\imath\varphi} \\
\psi_{320} &= \tfrac{1}{81\sqrt{6\pi}}\left(\tfrac{Z}{a_B}\right)^{3/2} \tilde{r}^2e^{-\tilde{r}/3}(3\cos^2\theta-1)\ ,
\end{aligned} \tag{25.52}$$

where we use the abbreviation $\tilde{r} \equiv Zr/a_B$. Using these wavefunctions we can now calculate important eigenvalues such as, for example,

$$\begin{aligned}
\langle 1\rangle_{n\ell m} &= 1 \\
\langle \delta^{(3)}(\tilde{r})\rangle_{n\ell m} &= \frac{\delta_{\ell,0}}{\pi n^3} \\
\langle \tilde{r}\rangle_{n\ell m} &= n^2\left[1+\frac{1}{2}\left(1-\frac{\ell(\ell+1)}{n^2}\right)\right] \\
\langle \tilde{r}^2\rangle_{n\ell m} &= n^4\left[1+\frac{3}{2}\left(1-\frac{\ell(\ell+1)-\frac{1}{3}}{n^2}\right)\right] \\
\langle \tilde{r}^3\rangle_{n\ell m} &= n^6\left[\frac{35}{8}-\frac{35}{8n^2}-\frac{15}{4n^2}(\ell+2)(\ell-1)+\frac{3}{8n^4}(\ell+2)(\ell+1)\ell(\ell-1)\right] \\
\langle \tilde{r}^4\rangle_{n\ell m} &= n^8\left[\frac{63}{8}+\frac{35}{8n^2}(2\ell^2+2\ell-3)+\frac{5}{8n^4}5\ell(\ell+1)(3\ell^2+3\ell-10)+\frac{12}{n^8}\right] \\
\left\langle\frac{1}{\tilde{r}}\right\rangle_{n\ell m} &= \frac{1}{n^2} \\
\left\langle\frac{1}{\tilde{r}^2}\right\rangle_{n\ell m} &= \frac{1}{n^3(\ell+\frac{1}{2})} \\
\left\langle\frac{1}{\tilde{r}^3}\right\rangle_{n\ell m} &= \frac{n}{n^4\ell(\ell+\frac{1}{2})(\ell+1)} \\
\left\langle\frac{1}{\tilde{r}^4}\right\rangle_{n\ell m} &= \frac{\frac{3}{2}n^2-\frac{1}{2}\ell(\ell+1)}{n^5(\ell+\frac{3}{2})(\ell+1)(\ell+\frac{1}{2})\ell(\ell-\frac{1}{2})}\ .
\end{aligned} \tag{25.53}$$

These results will become important later. In Exc. 25.2.3.4 we will calculate the eigenvalue $\langle r \rangle$ for several orbitals $|\psi_{n\ell m}\rangle$.

25.2.2 The virial theorem

Originally derived for classical mechanics, the *virial theorem* also holds for quantum mechanics, as shown for the first time by *Fock*. We evaluate the commutator between the Hamiltonian

$$\hat{H} = \hat{\mathbf{p}}^2/2m + V(\hat{\mathbf{r}}) \ , \tag{25.54}$$

and the product of the position operator $\hat{\mathbf{r}}$ with the momentum operator $\hat{\mathbf{p}} = -\imath\hbar\nabla$ of the particle:

$$[\hat{H}, \hat{\mathbf{r}} \cdot \hat{\mathbf{p}}] = [\hat{H}, \hat{\mathbf{r}}] \cdot \hat{\mathbf{p}} + \hat{\mathbf{r}} \cdot [\hat{H}, \hat{\mathbf{p}}] = -\imath\hbar \frac{\hat{\mathbf{p}}^2}{m} + \imath\hbar \hat{\mathbf{r}} \cdot \nabla V \ , \tag{25.55}$$

using the theorems of Ehrenfest. Therefore, we find for the operator $\hat{Q} = \hat{\mathbf{r}} \cdot \hat{\mathbf{p}}$ the commutator,

$$\frac{\imath}{\hbar}[\hat{H}, \hat{Q}] = 2E_{kin} - \hat{\mathbf{r}} \cdot \nabla V \ . \tag{25.56}$$

The left side of this equation is precisely $-d\hat{Q}/dt$, following the Heisenberg equation of motion. The eigenvalue $\langle d\hat{Q}/dt \rangle$ of the temporal derivative vanishes in steady state, therefore we obtain the virial theorem,

$$2\langle E_{kin} \rangle = \langle \hat{\mathbf{r}} \cdot \nabla V \rangle \ . \tag{25.57}$$

Example 164 (*Virial theorem applied to a central potential*): For example, for a central potential $V(r) \propto r^s$ we obtain,

$$2\langle E_{kin} \rangle = \langle \hat{\mathbf{r}} \cdot \hat{\mathbf{e}}_r \frac{\partial V}{\partial r} \rangle = \langle r \frac{\partial V}{\partial r} \rangle = s\langle V \rangle \ .$$

In Exc. 25.2.3.5 we calculate the eigenvalues $\langle r^{-1} \rangle$ and $\langle p^2 \rangle$ and we verify the virial theorem. Finally, in Exc. 25.2.3.6 we calculate transition matrix elements between different orbitals.

25.2.3 Exercises

25.2.3.1 Ex: Asymptotes of Laguerre's polynomials

Derive the asymptotic solutions of equation (25.42).

Solution: *For $\tilde{r} \to 0$ the approximate equation is,*

$$u''_{n,\ell}(\tilde{r}) - \frac{\ell(\ell+1)}{\tilde{r}^2} u_{n,\ell}(\tilde{r}) = 0 \ .$$

The ansatz $u_{n,\ell} = \xi(\tilde{r})\tilde{r}^{\ell+1}$ transforms this equation into,

$$\xi''(\tilde{r})\tilde{r} + 2(\ell+1)\xi'(\tilde{r}) = 0 \ ,$$

which is satisfied in the center ($\tilde{r} \to 0$) for all polynomials $\xi(\tilde{r})$.
For $r \to \infty$ the equation becomes,

$$n^2 u''_{n,\ell}(\tilde{r}) - u_{n,\ell}(\tilde{r}) = 0 \ .$$

The solution of this differential equation is $u_{n,\ell} = e^{\pm\tilde{r}/n}$, the option with positive sign being non-normalized.

25.2.3.2 Ex: Laguerre equation

Show that the equation (25.42) transforms with the ansatz (25.43) into equation (25.44).

Solution: *The derivatives of the ansatz are,*

$$\begin{aligned}
\frac{\partial}{\partial\tilde{r}}\frac{u_{n\ell}(\tilde{r})}{D_{n\ell}} &= (\ell+1)\tilde{r}^{\ell}e^{-\tilde{r}/n}L(\tilde{r}) - \tfrac{1}{n}\tilde{r}^{\ell+1}e^{-\tilde{r}/n}L(\tilde{r}) + \tilde{r}^{\ell+1}e^{-\tilde{r}/n}L'(\tilde{r}) \\
\frac{\partial^2}{\partial\tilde{r}^2}\frac{u_{n\ell}(\tilde{r})}{D_{n\ell}} &= \tilde{r}^{\ell}e^{-\tilde{r}/n}\left[\tilde{r}L''(\tilde{r}) + 2(\ell+1)L'(\tilde{r}) - \tfrac{2}{n}\tilde{r}L'(\tilde{r}) + \ell(\ell+1)\tfrac{1}{\tilde{r}}L(\tilde{r})\right. \\
&\quad \left. -\tfrac{2}{n}(\ell+1)L(\tilde{r}) + \tfrac{1}{n^2}\tilde{r}L(\tilde{r})\right] \ .
\end{aligned}$$

With this,

$$0 = \tilde{r}\partial_{\tilde{r}}^2 L(\tilde{r}) + 2\left[(\ell+1) - \tfrac{1}{n}\tilde{r}\right]\partial_{\tilde{r}}L(\tilde{r}) + 2\left[1 - \tfrac{1}{n}(\ell+1)\right]L(\tilde{r}) \ .$$

25.2.3.3 Ex: Laguerre functions

Using the orthogonality relation of associated Laguerre polynomials,

$$\begin{aligned}
\int_0^\infty \rho^\alpha e^{-\rho}L_n^{(\alpha)}(\rho)L_m^{(\alpha)}(\rho)d\rho &= \frac{\Gamma(n+\alpha+1)}{n!}\delta_{n,m} \\
\int_0^\infty \rho^{\alpha+1}e^{-\rho}L_n^{(\alpha)}\rho^2 d\rho &= \frac{(n+\alpha)!}{n!}(2n+\alpha+1) \ ,
\end{aligned}$$

and the recursion formula,

$$\begin{aligned}
nL_n^{(\alpha+1)}(\rho) &= (n-\rho)L_{n-1}^{(\alpha+1)}(\rho r) + (n+\alpha)L_{n-1}^{(\alpha)}(\rho) \\
\rho L_n^{(\alpha+1)}(\rho) &= (n+\alpha)L_{n-1}^{(\alpha)}(\rho) - (n-\rho)L_n^{(\alpha)}(\rho) \ ,
\end{aligned}$$

a. calculate the normalization constant $D_{n,l}$ for a hydrogen-like atom with atomic number Z;
b. calculate the mean value

$$\langle r\rangle_{nlm} = \frac{n^2 a_B}{Z}\left[1 + \frac{1}{2}\left(1 - \frac{\ell(\ell+1)}{n^2}\right)\right] \ ;$$

c. calculate the mean value

$$\left\langle \frac{1}{r} \right\rangle_{n\ell m} = \frac{Z}{n^2 a_B} \ .$$

Solution: *a. To obtain the normalization, we write*

$$1 = \langle 1 \rangle_{n\ell m} = \int \psi^*_{n\ell m} \psi_{r\ell m} d^3r = \int R_{n\ell} Y^*_{\ell m} R_{n\ell} Y_{\ell m} r^2 \sin\theta dr d\theta d\phi$$
$$= \int |Y_{\ell m}|^2 d\Omega \int_0^\infty R^2_{n\ell} r^2 dr = \int_0^\infty u^2_{n\ell} dr = \frac{a_B}{2Z} \int_0^\infty \left(D_{n\ell} \rho^{\ell+1} e^{-\rho/2} L^{(2\ell+1)}_{n-\ell-1}(\rho) \right)^2 d\rho \ .$$

Using the orthogonality relation of the Laguerre polynomials,

$$1 = \frac{n a_B}{2} D^2_{n\ell} \int_0^\infty \rho^{(2l+1)+1} e^{-\rho} L^{(2\ell+1)}_{n-\ell-1}(\rho)^2 d\rho = \frac{n a_B}{2} D^2_{n\ell} \frac{(n+\ell)!}{(n-\ell-1)!} 2n \ ,$$

We find

$$D_{n\ell} = \left(\frac{2Z}{n a_B} \right)^3 \frac{(n-\ell-1)!}{2n(n+\ell)!^3} \ .$$

b. We write,

$$\langle r \rangle_{n\ell m} = \int \psi^*_{n\ell m} r \psi_{r\ell m} d^3r = \int R_{n\ell} Y^*_{\ell m} r R_{n\ell} Y_{\ell m} r^2 \sin\theta dr d\theta d\phi$$
$$= \int |Y_{\ell m}|^2 d\Omega \int_0^\infty R^2_{n\ell} r^3 dr = \int_0^\infty R^2_{n\ell} r^3 dr \ .$$

we find the normalization of the radial functions,

$$R_{n\ell}(r) = -\left(\frac{2Z}{n a_B} \right)^3 \frac{(n-\ell-1)!}{2n(n+\ell)!^3} \rho^\ell e^{-\rho/2} L^{2\ell+1}_{n+\ell}(\rho) \qquad \textit{with} \qquad \rho \equiv \frac{2Z}{n a_B} r \ .$$

With this we obtain,

$$\langle r \rangle_{n\ell m} = \left[\frac{2Z}{n a_B} \frac{(n-\ell-1)!}{2n(n+\ell)!^3} \right]^2 \int_0^\infty \rho^{2l+3} e^{-\rho} L^{2\ell+1}_{n+\ell}(\rho)^2 \ d\rho \ .$$

which is the desired result.
c. In the same way we write

$$\left\langle \frac{1}{r} \right\rangle_{n\ell m} = \int \psi^*_{n\ell m} \frac{1}{r} \psi_{r\ell m} d^3r = \int_0^\infty R^2_{n\ell} r d^3r \ .$$

25.2.3.4 Ex: Orbital radii in Bohr's model

Using the results of 25.2.3.3, obtain the expectation values $\langle r \rangle$ for the states ψ_{100}, ψ_{210} and ψ_{320} of the hydrogen atom. Compare the results with those of Bohr's model.

Solution: *We write,*

$$\langle r\rangle_{100} = \frac{a_0}{Z}\frac{3}{2} \quad , \quad \langle r\rangle_{210} = \frac{2^2 a_B}{Z}\frac{5}{4} \quad , \quad \langle r\rangle_{320} = \frac{3^2 a_B}{Z}\frac{7}{6} \ .$$

The values obtained from Bohr's model are,

$$r_n = \frac{n^2 a_B}{Z} \ .$$

That is, the second term containing the angular momentum represents a correction. But the correction diminishes when $n, l \to \infty$.

25.2.3.5 Ex: The virial theorem and Bohr's model

Calculate, for the state ψ_{320} of the hydrogen atom, the expectation values $\langle \frac{1}{r}\rangle$, $\langle \frac{\mathbf{L}^2}{r^2}\rangle$, and $\langle \mathbf{p}^2\rangle$.
From the results, obtain the expectation values for the kinetic and potential energies, $\langle T\rangle$ and $\langle V\rangle$, and show that, consistent with the virial theorem, $\langle T\rangle = -(1/2)\langle V\rangle$. Compare the results with Bohr's model.

Solution: *Using the formulas (25.53), we find,*

$$\left\langle \frac{1}{\tilde{r}} \right\rangle_{320} = \frac{1}{n^2} = \frac{1}{9} \ .$$

Thus, the expectation value of the potential is,

$$\langle V(r)\rangle_{320} = -\frac{Ze^2}{4\pi\epsilon_0}\frac{Z}{a_B}\left\langle \frac{1}{\tilde{r}} \right\rangle_{320} = -\frac{Z^2 e^2}{4\pi\epsilon_0 a_B}\frac{1}{9} = -\frac{Z^2\hbar}{m a_B^2}\frac{1}{9} \ .$$

Also we can rewrite the kinetic energy operator as the sum of a radial term and a centrifugal term,

$$\hat{\mathbf{p}}^2 = \hat{p}_r^2 + \frac{\hat{\mathbf{L}}^2}{r^2} \ .$$

The expectation value of the centrifugal term is,

$$\left\langle \frac{\hat{\mathbf{L}}^2}{\tilde{r}^2} \right\rangle_{320} = \left\langle \frac{1}{\tilde{r}^2} \right\rangle_{320} \hbar^2\ell(\ell+1) = \frac{6\hbar^2}{n^3(\ell+\frac{1}{2})} = \frac{4\hbar^2}{45} \ .$$

To evaluate the radial term we need the wavefunction,

$$\psi_{320} = \frac{1}{81\sqrt{6\pi}}\left(\frac{Z}{a_B}\right)^{3/2} \tilde{r}^2 e^{-\tilde{r}/3}(3\cos^2\vartheta - 1) \qquad \textit{with} \qquad \tilde{r} \equiv \frac{rZ}{a_B} \ .$$

We now calculate,

$$\begin{aligned}\langle p_{\tilde{r}}^2\rangle_{320} &= \int \psi_{320}^* p_{\tilde{r}}^2 \psi_{320} d^3r \\ &= \frac{1}{81^2 6\pi}\left(\frac{Z}{a_B}\right)^3 \int_0^{2\pi} d\varphi \int_0^{\pi} (3\cos^2\vartheta - 1)^2 \sin\vartheta d\vartheta \int_0^{\infty} \tilde{r}^2 e^{-\tilde{r}/3} p_r^2 \left[\tilde{r}^2 e^{-\tilde{r}/3}\right] r^2 dr \\ &= \frac{1}{81^2 6\pi}\cdot 2\pi \cdot \frac{8}{5}\cdot(-\hbar^2)\int_0^{\infty} \tilde{r}^4 e^{-\tilde{r}/3}\frac{1}{\tilde{r}}\left(\frac{\partial^2}{\partial\tilde{r}^2}\tilde{r}\tilde{r}^2 e^{-\tilde{r}/3}\right) d\tilde{r} = \frac{\hbar^2}{45} \ .\end{aligned}$$

Thus, the expectation value of the kinetic energy is

$$\langle E_{kin}\rangle_{320} = \frac{Z^2}{a_B^2}\frac{\langle p_{\tilde{r}}^2\rangle_{320}}{2m} + \frac{Z^2}{a_B^2}\frac{1}{2m}\left\langle\frac{L^2}{\tilde{r}^2}\right\rangle_{320} = \frac{Z^2\hbar^2}{2ma_B^2}\frac{1}{9} = -\frac{1}{2}\langle V(r)\rangle_{320} \ ,$$

in agreement with the virial theorem. We also check that, in agreement with Bohr's model,

$$\left\langle\frac{\hat{\mathbf{p}}^2}{2m}\right\rangle_{320} + \langle V(r)\rangle_{320} = -\frac{1}{2}\frac{Z^2e^2}{4\pi\epsilon_0 a_B}\frac{1}{3^2} = E_3 \ .$$

25.2.3.6 Ex: Transition matrix elements

Using the following (non-normalized) wavefunctions of hydrogen, $\psi_{100}(\mathbf{r}) = e^{-\tilde{r}}$, $\psi_{210}(\mathbf{r}) = \tilde{r}e^{-\tilde{r}/2}\cos\theta$ and $\psi_{21\pm1}(\mathbf{r}) = \tilde{r}e^{-\tilde{r}/2}\sin\theta e^{\pm\imath\phi}$, calculate the matrix elements (a) $\langle\psi_{100}|\tilde{z}|\psi_{210}\rangle$, (b) $\langle\psi_{100}|\tilde{z}|\psi_{211}\rangle$, (c) $\langle\psi_{100}|\tilde{x}-\imath\tilde{y}|\psi_{210}\rangle$, and (d) $\langle\psi_{100}|\tilde{x}-\imath\tilde{y}|\psi_{211}\rangle$ using the formulae:

$$\begin{aligned}&\int_0^{\infty} x^4 e^{-3x/2}dx = \tfrac{256}{81} \quad , \quad \int_0^{\pi}\sin^3 x dx = \tfrac{4}{3} \ , \\ &\int_0^{\pi}\cos x\sin^2 x dx = 0 \quad , \quad \int_0^{\pi}\cos^2 x\sin x dx = \tfrac{2}{3} \ .\end{aligned}$$

Try to interpret the results.

Solution: *a. With $\tilde{z} = \tilde{r}\cos\theta$ we calculate,*

$$\begin{aligned}\langle\psi_{100}|\tilde{z}|\psi_{210}\rangle &= \int e^{-\tilde{r}}\cdot\tilde{z}\cdot\tilde{r}e^{-\tilde{r}/2}\cos\theta d^3\tilde{r} \\ &= \int \tilde{z}\tilde{r}e^{-3\tilde{r}/2}\cos\theta\tilde{r}^2\sin\theta d\theta d\phi d\tilde{r} \\ &= \int_0^{\pi}\cos^2\theta\sin\theta d\theta\int_0^{2\pi} d\phi\int_0^{\infty}\tilde{r}^4 e^{-3\tilde{r}/2}d\tilde{r} = \tfrac{2}{3}\cdot 2\pi\cdot\tfrac{256}{81} = \tfrac{2^{10}}{3^5}\pi \ .\end{aligned}$$

b. With $\tilde{z} = \tilde{r}\cos\theta$ we calculate,

$$\begin{aligned}\langle\psi_{100}|\tilde{z}|\psi_{211}\rangle &= \int e^{-\tilde{r}}\cdot\tilde{z}\cdot\tilde{r}e^{-\tilde{r}/2}\sin\theta e^{\imath\phi}d^3\tilde{r}\\ &= \int \tilde{z}\tilde{r}e^{-3\tilde{r}/2}\sin\theta e^{\imath\phi}\tilde{r}^2\sin\theta d\theta d\phi d\tilde{r}\\ &= \int_0^\pi \cos\theta\sin^2\theta d\theta\int_0^{2\pi}e^{i\phi}d\phi\int_0^\infty \tilde{r}^4e^{-3\tilde{r}/2}d\tilde{r} = 0\ .\end{aligned}$$

c. With $\tilde{x}-\imath\tilde{y} = \tilde{r}\sin\theta e^{-\imath\phi}$ we calculate,

$$\begin{aligned}\langle\psi_{100}|\tilde{x}-\imath\tilde{y}|\psi_{210}\rangle &= \int e^{-\tilde{r}}\cdot(\tilde{x}-\imath\tilde{y})\cdot\tilde{r}e^{-\tilde{r}/2}\cos\theta d^3\tilde{r}\\ &= \int(\tilde{x}-\imath\tilde{y})\tilde{r}e^{-3\tilde{r}/2}\cos\theta\tilde{r}^2\sin\theta d\theta d\phi d\tilde{r}\\ &= \int_0^\pi \cos\theta\sin^2\theta d\theta\int_0^{2\pi}e^{-\imath\phi}d\phi\int_0^\infty \tilde{r}^4e^{-3\tilde{r}/2}d\tilde{r} = 0\ .\end{aligned}$$

d. With $\tilde{x}-\imath\tilde{y} = \tilde{r}\sin\theta e^{-\imath\phi}$ we calculate,

$$\begin{aligned}\langle\psi_{100}|\tilde{x}-\imath\tilde{y}|\psi_{211}\rangle &= \int e^{-\tilde{r}}\cdot(\tilde{x}-\imath\tilde{y})\cdot\tilde{r}e^{-\tilde{r}/2}\sin\theta e^{\imath\phi}d^3\tilde{r}\\ &= \int(\tilde{x}-\imath\tilde{y})\tilde{r}e^{-3\tilde{r}/2}\sin\theta e^{\imath\phi}\tilde{r}^2\sin\theta d\theta d\phi d\tilde{r}\\ &= \int_0^\pi \sin^3\theta d\theta\int_0^{2\pi}d\phi\int_0^\infty \tilde{r}^4e^{-3\tilde{r}/2}d\tilde{r} = \tfrac{4}{3}\cdot 2\pi\cdot\tfrac{256}{81} = \tfrac{2^{11}}{3^5}\pi\ .\end{aligned}$$

The matrix elements describe transitions between electronic states induced by dipole radiation. The selection rules are $|\Delta\ell| = 1$ and $\Delta m = 0$ for linear polarization and $\Delta m = \pm 1$ for circular polarization (always with respect to the $\hat{\mathbf{e}}_z$-axis). The linear polarization corresponds to the transition operator $\hat{z}$ and the circular polarization to the operator $\hat{x}-\imath\hat{y}$.

25.3 Angular momentum

25.3.1 The orbital angular momentum operator

The definition of *orbital angular momentum* is adopted from classical mechanics:

$$\hat{\mathbf{l}} = \hat{\mathbf{r}}\times\hat{\mathbf{p}} = -\imath\hbar\hat{\mathbf{r}}\times\hat{\nabla} = -\imath\hbar\begin{vmatrix}\hat{\mathbf{e}}_x & \hat{\mathbf{e}}_y & \hat{\mathbf{e}}_z\\ x & y & z\\ \partial_x & \partial_y & \partial_z\end{vmatrix}\ . \tag{25.58}$$

To better understand the properties of the angular momentum operator in quantum mechanics we will derive in the Excs. 25.3.4.1 and 25.3.4.2 some of its properties.

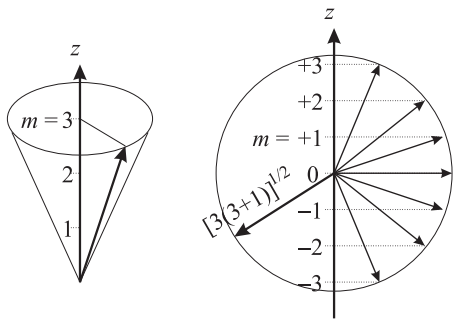

Figure 25.8: Illustration of angular momentum in quantum mechanics.

25.3.1.1 Constants of motion

The preceding chapter dealt with the resolution of the radial and angular equations for the case of a radial potential. The radial equation allowed to calculate the eigenenergies of the Hamiltonian $\hat{H}$,

$$\hat{H}|\psi\rangle = E_{n\ell}|\psi\rangle \ . \tag{25.59}$$

We also found the common eigenvalues and eigenfunctions of operators $\hat{\mathbf{l}}^2$ and $\hat{l}_z$ [see Eqs. (25.20) and (25.24)]. We now use the notation $|\ell, m\rangle \equiv Y_{\ell m}(\theta, \phi)$ for the eigenfunctions,

$$\hat{\mathbf{l}}^2|\ell, m\rangle = \hbar^2\ell(\ell+1)|\ell, m\rangle \qquad \text{and} \qquad \hat{l}_z|\ell, m\rangle = \hbar m|\ell, m\rangle \ . \tag{25.60}$$

With this we have,

$$\begin{aligned} & [\hat{H}, \hat{\mathbf{l}}^2]|\psi\rangle = \hat{H}\hbar^2\ell(\ell+1)|\psi\rangle - \hat{\mathbf{l}}^2 E|\psi\rangle = 0 \\ \text{and} \quad & [\hat{H}, \hat{l}_z]|\psi\rangle = \hat{H}\hbar m|\psi\rangle - \hat{l}_z E|\psi\rangle = 0 \ . \end{aligned} \tag{25.61}$$

Therefore, the operators $\hat{\mathbf{l}}^2$ and $\hat{l}_z$ are constants of motion,

$$[\hat{H}, \hat{l}_z] = 0 = [\hat{H}, \hat{\mathbf{l}}^2] \ . \tag{25.62}$$

Exc. 25.3.4.3 asks to show explicitly, at the example of an isotropic three-dimensional harmonic oscillator, that $\hat{\mathbf{l}}^2$ and $\hat{l}_z$ are constants of motion.

25.3.2 SU(2) algebra of angular momentum and spin

So far, we have solved the angular eigenvalue equation in the spatial representation for an orbital angular momentum, $\hat{\mathbf{l}} = \hat{\mathbf{r}} \times \hat{\mathbf{p}}$. But it is not clear, whether *every* angular momentum has this representation, which is derived from classical notions. Using the orbital angular momentum expression (25.58) it is easy to verify,

$$\hat{\mathbf{l}} \times \hat{\mathbf{l}} = \imath\hbar\hat{\mathbf{l}} \ . \tag{25.63}$$

However, it is not clear a priori, whether *any* quantity $\hat{\mathbf{j}}$ satisfying

$$\boxed{\hat{\mathbf{j}} \times \hat{\mathbf{j}} = \imath\hbar\hat{\mathbf{j}}} \qquad \text{or equivalently} \qquad [\hat{j}_m, \hat{j}_n] = \imath\hbar\epsilon_{kmn}\hat{j}_k \tag{25.64}$$

using the Levi-Civita symbol, can be represented like (25.58). In fact, we will see that the electron has an intrinsic spin with no orbiting charges, and cannot be represented as an orbital angular momentum. What needs to be done now is to show that (25.64) generates a consistent algebra even in cases beyond the representation (25.58).

Since $\hat{\mathbf{j}}^2$ and $\hat{j}_z$ commute (we show this from Eq. (25.64) in Exc. 25.3.4.4), they have common eigenfunctions $|j,m\rangle$. We can write the eigenvalues as,

$$\hat{\mathbf{j}}^2|j,m\rangle = \hbar^2 j(j+1)|j,m\rangle \qquad \text{and} \qquad \hat{j}_z|j,m\rangle = \hbar m|j,m\rangle \ , \tag{25.65}$$

where, for now, we only know that m is real and $j \geq 0$. But since $\langle j,m|\hat{\mathbf{j}}^2|j,m\rangle \geq \langle j,m|\hat{j}_z^2|j,m\rangle$, it is clear that $j(j+1) \geq m^2$.

25.3.2.1 Rising and lowering operator

Now we introduce the *rising operator* $\hat{j}_+$ and the *lowering operator* $\hat{j}_-$ via

$$\hat{j}_\pm \equiv \hat{j}_x \pm \imath \hat{j}_y \qquad \text{such that} \qquad \hat{j}_- = \hat{j}_+^\dagger \ . \tag{25.66}$$

It is easy to check the following relationships

$$[\hat{j}_z, \hat{j}_\pm] = \pm\hbar\hat{j}_\pm \qquad \text{and} \qquad [\hat{\mathbf{j}}^2, \hat{j}_\pm] = 0 \qquad \text{and} \qquad \hat{j}_\mp\hat{j}_\pm = \hat{\mathbf{j}}^2 - \hat{j}_z^2 \mp \hbar\hat{j}_z \ . \tag{25.67}$$

With this we find

$$\begin{aligned} &\hat{j}_z\hat{j}_\pm|j,m\rangle = ([\hat{j}_z,\hat{j}_\pm] + \hat{j}_\pm j_z)|j,m\rangle = \hbar(m\pm 1)\hat{j}_\pm|j,m\rangle \\ \text{and} \quad &\hat{\mathbf{j}}^2 j_\pm|j,m\rangle = \hat{j}_\pm\hat{\mathbf{j}}^2|j,m\rangle = \hbar^2 j(j+1)\hat{j}_\pm|j,m\rangle \ . \end{aligned} \tag{25.68}$$

That is, $\hat{j}_\pm|j,m\rangle$ is a eigenstate of $\hat{\mathbf{j}}^2$ and $\hat{j}_z$ with the eigenvalues j and $m \pm 1$, respectively, if $j_\pm|j,m\rangle \neq 0$. Hence,

$$\hat{j}_+|j,m\rangle \propto |j,m+1\rangle \ . \tag{25.69}$$

In order not to violate the condition $m^2 \leq j(j+1)$, we need to fix $\hat{j}_\pm|j,\pm j\rangle = 0$. Therefore, for a specified j, the m can have only one of the $2j+1$ possible values $m = -j, -j+1, .., j$. Since $2j+1$ is an integer, j can only have values $j = 0, \frac{1}{2}, 1, \frac{3}{2}, ...$ Thus, the eigenvalue equation of the observables $\hat{\mathbf{j}}^2$, $\hat{\mathbf{j}}$ is solved, since we could have chosen instead of $\hat{j}_z$ any one of the components of $\hat{\mathbf{j}}$, knowing that the others do not commute with the chosen one.

All spin components $\hat{j}_z$ and the scalar $\hat{\mathbf{j}}^2$ can only have discrete eigenvalues. The smallest unit is $\hbar/2$. With the normalization $\langle j,m|j',m'\rangle = \delta_{j,j'}\delta_{m,m'}$ we have,

$$\langle j,m|\hat{j}_\mp\hat{j}_\pm|j,m\rangle = \langle j,m|(\hat{\mathbf{j}}^2 - \hat{j}_z^2 \mp \hbar\hat{j}_z)|j,m\rangle = \hbar^2[j(j+1) - m(m\pm 1)] \ , \tag{25.70}$$

and

$$\boxed{\hat{j}_\pm|j,m\rangle = \hbar\sqrt{j(j+1) - m(m\pm 1)}|j,m\pm 1\rangle} \ . \tag{25.71}$$

In Exc. 25.3.4.5 we calculate the uncertainty of the angular momentum components, in Exc. 25.3.4.6 we write the operator $\hat{j}_x$ in a matrix form, and in Excs. 25.3.4.7 and 25.3.4.8 we calculate projections of the spin of the electron in different directions of the quantization axis.

25.3.3 The electron spin

Every angular momentum $\hat{\mathbf{l}}$ generates a *magnetic dipole moment* $\vec{\mu}_\ell \propto \hat{\mathbf{l}}$, which interacts with external magnetic fields, $V(\vec{\mathcal{B}}) = \vec{\mu}_\ell \cdot \vec{\mathcal{B}}$. *Inhomogeneous* magnetic fields exert forces on dipole moments, $\mathbf{F} = -\nabla(\vec{\mu}_\ell \cdot \vec{\mathcal{B}})$, which are detected by the *Stern-Gerlach experiment*. This experiment reveals not only the quantization of angular momentum, but also the presence of semi-integral values for the magnetic quantum number.

In 1925 Uhlenbeck and Goudsmit proposed that the electron could have an intrinsic angular momentum with the quantum number $s = 1/2$. This angular momentum, called *spin*, would not correspond to any orbiting mass or charge distribution within the classical radius of the electron of the type $\mathbf{l} = \mathbf{r} \times \mathbf{p}$. The spin is a purely quantum phenomenon because it disappears when $\hbar \to 0$. It is believed nowadays that the electron is actually point-like with no detectable deviation from Coulomb's law at any distance. The spin of the electron does not follow from the Schrödinger equation, but can be included, ad hoc. On the other hand, it is interesting that it is a necessary consequence of the stringent relativistic derivation of quantum mechanics by *Paul Dirac*.

To characterize the spin, we can use the whole SU(2) formalism of the quantum mechanics of angular momentum:

$$\hat{\mathbf{s}} \times \hat{\mathbf{s}} = \imath\hbar\hat{\mathbf{s}} \ , \tag{25.72}$$

and

$$\begin{aligned} &\hat{\mathbf{s}}^2|\tfrac{1}{2},\pm\tfrac{1}{2}\rangle = \hbar^2\tfrac{3}{4}|\tfrac{1}{2},\pm\tfrac{1}{2}\rangle \quad , \quad \hat{s}_z|\tfrac{1}{2},\pm\tfrac{1}{2}\rangle = \pm\tfrac{\hbar}{2}|\tfrac{1}{2},\pm\tfrac{1}{2}\rangle \quad , \\ &\hat{s}_\pm = \hbar\hat{\sigma}_\pm = \hbar|\tfrac{1}{2},\pm\tfrac{1}{2}\rangle\langle|\tfrac{1}{2},\mp\tfrac{1}{2}| \ . \end{aligned} \tag{25.73}$$

The operators $\hat{\sigma}_\pm$ are the *Pauli spin matrices* defined in (23.47) for the basis chosen as,

$$|\tfrac{1}{2},+\tfrac{1}{2}\rangle = \begin{pmatrix} 1 \\ 0 \end{pmatrix} \quad \text{and} \quad |\tfrac{1}{2},-\tfrac{1}{2}\rangle = -\tfrac{1}{2}\begin{pmatrix} 0 \\ 1 \end{pmatrix} \ . \tag{25.74}$$

25.3.4 Exercises

25.3.4.1 Ex: Properties of the angular orbital momentum

Show that $\hat{\mathbf{l}} \times \hat{\mathbf{l}} = \imath\hbar\hat{\mathbf{l}}$ and $[\hat{l}_x, \hat{l}_y] = \imath\hbar\hat{l}_z$.

Solution: *For the x-component we have,*

$$\begin{aligned} (\hat{\mathbf{l}} \times \hat{\mathbf{l}})_x = [\hat{l}_y, \hat{l}_z] &= (\hat{z}\hat{p}_x - \hat{x}\hat{p}_z)(\hat{x}\hat{p}_y - \hat{y}\hat{p}_x) - (\hat{x}\hat{p}_y - \hat{y}\hat{p}_x)(\hat{z}\hat{p}_x - \hat{x}\hat{p}_z) \\ &= (\hat{y}\hat{p}_z - \hat{z}\hat{p}_y)(\hat{x}\hat{p}_x - \hat{p}_x\hat{x}) = \imath\hbar\hat{l}_x \ , \end{aligned}$$

where we used $[\hat{p}_k, \hat{x}_m] = -\imath\hbar\delta_{km}$. For the other components we can do the same calculation.

25.3.4.2 Ex: Levi-Civita tensor

a. Demonstrate $[\hat{l}_k, \hat{r}_m] = \imath\hbar\hat{r}_n\epsilon_{kmn}$ where the Levi-Civita tensor is defined by $\epsilon_{kmn} = 1$ when (kmn) is an even permutation of (123), $\epsilon_{kmn} = -1$ for an odd permutation, and $\epsilon_{kmn} = 0$ when two of the indices are equal.
b. Verify $\hat{j}_m\hat{j}_n = \frac{1}{4}\delta_{mn} + \frac{\imath}{2}\epsilon_{kmn}\hat{j}_k$.

Solution: *a. Using*

$$\hat{l}_k = (\hat{r}\times\hat{p})_k = (\hat{r}_m\hat{p}_n - \hat{r}_n\hat{p}_m)\epsilon_{kmn} \qquad \textit{and} \qquad [\hat{p}_k, \hat{r}_m] = -\imath\hbar\delta_{km} \ ,$$

it is easy to show

$$\begin{aligned}[\hat{l}_k, \hat{r}_m] &= (\hat{r}_m\hat{p}_n - \hat{r}_n\hat{p}_m)\epsilon_{kmn}\hat{r}_m - \hat{r}_m(\hat{r}_m\hat{p}_n - \hat{r}_n\hat{p}_m)\epsilon_{kmn} \\ &= [\hat{r}_n\hat{r}_m\hat{p}_m - \hat{r}_n\hat{p}_m\hat{r}_m]\,\epsilon_{kmn} = \imath\hbar\hat{r}_n\epsilon_{kmn} \ .\end{aligned}$$

b.

25.3.4.3 Ex: Angular orbital momentum of a harmonic oscillator

Show for an isotropic three-dimensional harmonic oscillator: $[\hat{H}, \hat{\mathbf{l}}^2] = [\hat{H}, \hat{l}_z] = 0$. Make explicit calculations, that is, show

$$\left[\tfrac{\hat{p}^2}{2m}, \hat{l}_z\right] = 0 = \left[\frac{m}{2}\omega^2\hat{r}^2, \hat{l}_z\right] \qquad \text{and} \qquad \left[\tfrac{\hat{p}^2}{2m}, \hat{\mathbf{l}}^2\right] = 0 = \left[\frac{m}{2}\omega^2\hat{r}^2, \hat{\mathbf{l}}^2\right] \ .$$

Solution: *In general way, we can show*

$$\begin{aligned}\left[\tfrac{\hat{p}^2}{2m}, \hat{l}_z\right] &= \tfrac{1}{2m}[\hat{p}_x^2 + \hat{p}_y^2 + \hat{p}_z^2, \hat{x}\hat{p}_y - \hat{y}\hat{p}_x] = \tfrac{1}{2m}[\hat{p}_x^2, \hat{x}]\hat{p}_y - \frac{1}{2m}[\hat{p}_y^2, \hat{y}]\hat{p}_x \\ &= \tfrac{1}{2m}\left(\hat{p}_x\hat{p}_x\hat{x}\hat{p}_y - \hat{p}_x\hat{x}\hat{p}_x\hat{p}_y - \imath\hbar\hat{p}_x\hat{p}_y - [\hat{p}_y^2, \hat{y}\hat{p}_x]\right) = \tfrac{1}{2m}\left(-2\imath\hbar\hat{p}_x\hat{p}_y + 2\imath\hbar\hat{p}_x\hat{p}_y\right) = 0 \ ,\end{aligned}$$

and in the same way $\left[\tfrac{\hat{p}^2}{2m}, \hat{\mathbf{l}}^2\right] = 0$. *For a harmonic potential,*

$$\begin{aligned}\left[\frac{m}{2}\omega^2\hat{r}^2, \hat{l}_z\right] &= \frac{m}{2}\omega^2[\hat{x}^2 + \hat{y}^2 + \hat{z}^2, \hat{x}\hat{p}_y - \hat{y}\hat{p}_x] = \frac{m}{2}\omega^2[\hat{y}^2, \hat{p}_y]\hat{x} - \frac{m}{2}\omega^2[\hat{x}^2, \hat{p}_x]\hat{y} \\ &= \frac{m}{2}\omega^2(\hat{y}\hat{p}_y\hat{y}\hat{x} + \hat{y}\imath\hbar\hat{x} - \hat{p}_y\hat{y}\hat{y}\hat{x} - [\hat{x}^2, \hat{p}_x]\hat{y}) = \frac{m}{2}\omega^2(2\imath\hbar\hat{x}\hat{y} - 2\imath\hbar\hat{x}\hat{y}) = 0 \ .\end{aligned}$$

25.3.4.4 Ex: Commutation of the absolute value and the components of the orbital angular momentum

Show $[\hat{\mathbf{j}}^2, \hat{\mathbf{j}}] = 0$.

Solution: *With* $\hat{\mathbf{j}}^2 = \hat{j}_x^2 + \hat{j}_y^2 + \hat{j}_z^2$ *and* $[\hat{A}\hat{B}, \hat{C}] = \hat{A}[\hat{B}, \hat{C}] + [\hat{A}, \hat{C}]\hat{B}$ *we find, using the formal definition of angular momentum* $[\hat{j}_m, \hat{j}_n] = i\hbar\epsilon_{kmn}\hat{j}_k$, *that*

$$-[\hat{j}_x^2, \hat{j}_z] = \imath\hbar(\hat{j}_x\hat{j}_y + \hat{j}_y\hat{j}_x) = [\hat{j}_y^2, \hat{j}_z] \qquad \textit{and} \qquad [\hat{j}_z^2, \hat{j}_z] = 0 \ .$$

For the components $\hat{j}_x$ *and* $\hat{j}_y$ *we find the same results.*

25.3.4.5 Ex: Uncertainty of angular momentum components

Show that if $\hat{j}_z$ is precise, then $\hat{j}_x$ and $\hat{j}_y$ are imprecise.

Solution: *The definition of the operators* $\hat{j}_\pm \equiv \hat{j}_x \pm \imath\hat{j}_y$ *implies that* $\hat{j}_z$ *is an observable. Therefore,*

$$\begin{aligned}
(\Delta j_z)^2 &= \langle j,m|\hat{j}_z^2|j,m\rangle - \langle j,m|\hat{j}_z|j,m\rangle^2 = 0 \\
(\Delta j_x)^2 &= \langle j,m|\hat{j}_x^2|j,m\rangle - \langle j,m|\hat{j}_x|j,m\rangle^2 = \langle j,m|\hat{j}_x^2|j,m\rangle = \tfrac{1}{4}\langle j,m|(\hat{j}_+ + \hat{j}_-)^2|j,m\rangle \\
&= \tfrac{1}{4}\langle j,m|\hat{j}_+\hat{j}_- + \hat{j}_-\hat{j}_+|j,m\rangle = \tfrac{\hbar^2}{2}[j(j+1) - m^2] \geq \tfrac{\hbar^2}{2}j \ .
\end{aligned}$$

25.3.4.6 Ex: Matrix representation of the components of the angular momentum

Calculate the matrix elements of $\hat{j}_x$ and $\hat{j}_x^2$ in the basis where $\hat{j}_z$ is observable. Give the general formula and examples for $j = \frac{1}{2}$ and $j = 1$.

Solution: *We show,*

$$\begin{aligned}
\langle j',m'|\hat{j}_x|j,m\rangle &= \tfrac{1}{2}\langle j',m'|\hat{j}_+ + \hat{j}_-|j,m\rangle \\
&= \tfrac{\hbar}{2}\sqrt{j(j+1) - m(m+1)}\delta_{j',j}\delta_{m',m+1} + \tfrac{\hbar}{2}\sqrt{j(j+1) - m(m-1)}\delta_{j',j}\delta_{m',m-1} \ .
\end{aligned}$$

Similarly using $\hat{j}_x^2 = \frac{1}{4}(\hat{j}_+^2 + \hat{j}_-^2 + \hat{j}_+\hat{j}_- + \hat{j}_-\hat{j}_+) = \frac{1}{4}(\hat{j}_+^2 + \hat{j}_-^2 + 2\hat{\mathbf{j}}^2 - 2\hat{j}_z^2)$, *we get,*

$$\begin{aligned}
\langle j',m'|\hat{j}_x^2|j,m\rangle &= \tfrac{\hbar^2}{4}\sqrt{j(j+1) - (m+1)(m+2)}\sqrt{j(j+1) - m(m+1)}\delta_{j',j}\delta_{m',m+2} \\
&+ \tfrac{\hbar^2}{4}\sqrt{j(j+1) - (m-1)(m-2)}\sqrt{j(j+1) - m(m-1)}\delta_{j',j}\delta_{m',m-2} \\
&+ \tfrac{\hbar^2}{2}[j(j+1) - m^2]\delta_{j',j}\delta_{m',m} \ .
\end{aligned}$$

For example for $j = 1/2$ *we get,*

$$\hat{j}_x = \tfrac{\hbar}{\sqrt{2}}\hat{\sigma}_x \qquad \textit{and} \qquad \hat{j}_x^2 = \tfrac{\hbar^2}{2}\mathbb{I} \ .$$

And for $j = 1$ *we get,*

$$\hat{j}_x = \tfrac{\hbar}{2}\begin{pmatrix} 0 & 1 & 0 \\ 1 & 0 & 1 \\ 0 & 1 & 0 \end{pmatrix} \qquad \textit{and} \qquad \hat{j}_x^2 = \tfrac{\hbar^2}{4}\begin{pmatrix} 1 & 0 & 1 \\ 0 & 2 & 0 \\ 1 & 0 & 1 \end{pmatrix} \ .$$

25.3.4.7 Ex: Spin-1/2-particle in a magnetic field

Consider a spin-1/2-particle whose magnetic moment is $\vec{\mu} = \gamma \mathbf{s}$ (where γ is a constant). We can describe the quantum state of this particle in terms of the space generated by the eigenvectors $|+\rangle$ and $|-\rangle$ of the operator $\hat{s}_z$, which measures the spin projection in z-direction:

$$\hat{s}_z|+\rangle = \tfrac{\hbar}{2}|+\rangle \quad , \quad \hat{s}_z|-\rangle = -\tfrac{\hbar}{2}|-\rangle$$

Initially ($t = 0$) the particle is in the state $\psi(t=0)\rangle = |+\rangle$ and is subject to a uniform magnetic field $\vec{\mathcal{B}} = \mathcal{B}\hat{\mathbf{e}}_y$, so that:

$$\hat{H} = -\vec{\mu} \cdot \vec{\mathcal{B}} = -\gamma \mathcal{B} \hat{s}_y \ .$$

a. What are the possible measurements of the spin projection on the y-axis?
b. Find the eigenvectors of $\hat{s}_y$.
c. Get $|\psi(t)\rangle$ at $t > 0$ in terms of the eigenvectors $|+\rangle$ and $|-\rangle$ defined above.
d. Obtain the mean expectation values of the observables $\hat{s}_x$, $\hat{s}_y$ and $\hat{s}_z$ as a function of time.

Solution: *a. In any axis the possible projections are: $+\hbar/2$ and $-\hbar/2$.*
b. We have,

$$\hat{s}_y = \tfrac{\hbar}{2} \begin{pmatrix} 0 & -\imath \\ \imath & 0 \end{pmatrix} \ .$$

With this,

$$\hat{s}_y \begin{pmatrix} a \\ b \end{pmatrix} = \tfrac{\hbar}{2} \begin{pmatrix} -\imath b \\ \imath a \end{pmatrix} = \tfrac{\hbar}{2} \begin{pmatrix} a \\ b \end{pmatrix} \implies a = -\imath b \implies |+_y\rangle = b \begin{pmatrix} -\imath \\ 1 \end{pmatrix} \ .$$

Normalization, $|\langle +_y|+_y\rangle|^2 = 1$, requires,

$$|+_y\rangle = \tfrac{1}{\sqrt{2}} \begin{pmatrix} -\imath \\ 1 \end{pmatrix} \ .$$

Also,

$$\hat{s}_y \begin{pmatrix} a \\ b \end{pmatrix} = \frac{\hbar}{2} \begin{pmatrix} -\imath b \\ \imath a \end{pmatrix} = -\frac{\hbar}{2} \begin{pmatrix} a \\ b \end{pmatrix} \implies a = \imath b \implies |-_y\rangle = b \begin{pmatrix} \imath \\ 1 \end{pmatrix} \ .$$

Normalization, $|\langle -_y|-_y\rangle|^2 = 1$, requires,

$$|-_y\rangle = \tfrac{1}{\sqrt{2}} \begin{pmatrix} \imath \\ 1 \end{pmatrix} \ .$$

Finally,

$$|\pm_y\rangle = \mp \tfrac{\imath}{\sqrt{2}}|+\rangle + \tfrac{1}{\sqrt{2}}|-\rangle \ .$$

c. We have the solution,

$$|\psi(t)\rangle = e^{-\imath\hat{H}t/\hbar}|\psi(0)\rangle = e^{\imath\gamma\mathcal{B}\hat{s}_y t/\hbar}|+\rangle \ .$$

We can express $|+\rangle$ *in terms of the eigenvectors of* $\hat{s}_y$*:*

$$|+\rangle = \tfrac{\imath}{\sqrt{2}}(|+_y\rangle - |-_y\rangle) \ .$$

Finally, since $\hat{s}_y|\pm_y\rangle = \pm\frac{\hbar}{2}|\pm_y\rangle$ *engenders* $f(\hat{s}_y)|\pm_y\rangle = f(\pm\frac{\hbar}{2})|\pm_y\rangle$*,*

$$|\psi(t)\rangle = e^{\imath\gamma\mathcal{B}\hat{s}_y t/\hbar}\tfrac{\imath}{\sqrt{2}}(|+_y\rangle - |-_y\rangle) = \tfrac{\imath}{\sqrt{2}}(e^{\imath\gamma\mathcal{B}t/2}|+_y\rangle - e^{-\imath\gamma\mathcal{B}t/2}|-_y\rangle) \ .$$

Expressing the eigenvectors of $\hat{s}_y$ *by the eigenvectors of* $\hat{s}_z$*:*

$$\begin{aligned}|\psi(t)\rangle &= \tfrac{\imath}{\sqrt{2}}e^{\imath\gamma\mathcal{B}t/2}\left(\tfrac{-\imath}{\sqrt{2}}|+\rangle + \tfrac{1}{\sqrt{2}}|-\rangle\right) - e^{-\imath\gamma\mathcal{B}t/2}\left(\tfrac{\imath}{\sqrt{2}}|+\rangle + \tfrac{1}{\sqrt{2}}|-\rangle\right)\\ &= \tfrac{\imath}{2}\left[-2\imath\cos\tfrac{\gamma\mathcal{B}t}{2}|+\rangle + 2\imath\sin\tfrac{\gamma\mathcal{B}t}{2}|-\rangle\right] = \cos\tfrac{\gamma\mathcal{B}t}{2}|+\rangle - \sin\tfrac{\gamma\mathcal{B}t}{2}|-\rangle \ .\end{aligned}$$

d. We want $\langle\psi(t)|\hat{s}_i|\psi(t)\rangle$ *with* $i = x, y, z$*. We have,*

$$|\psi(t)\rangle = \begin{pmatrix}\cos\frac{\gamma\mathcal{B}t}{2}\\ -\sin\frac{\gamma\mathcal{B}t}{2}\end{pmatrix} \ .$$

Now,

$$\begin{aligned}\langle\hat{s}_x\rangle &= \begin{pmatrix}\cos & -\sin\end{pmatrix}\tfrac{\hbar}{2}\begin{pmatrix}0 & 1\\ 1 & 0\end{pmatrix}\begin{pmatrix}\cos\\ -\sin\end{pmatrix} = \tfrac{\hbar}{2}(-\cos\sin - \cos\sin) = -\tfrac{\hbar}{2}\sin(\gamma\mathcal{B}t)\\ \langle\hat{s}_y\rangle &= \begin{pmatrix}\cos & -\sin\end{pmatrix}\tfrac{\hbar}{2}\begin{pmatrix}0 & -\imath\\ \imath & 0\end{pmatrix}\begin{pmatrix}\cos\\ -\sin\end{pmatrix} = \tfrac{\hbar}{2}(\imath\cos\sin - \imath\cos\sin) = 0\\ \langle\hat{s}_z\rangle &= \begin{pmatrix}\cos & -\sin\end{pmatrix}\tfrac{\hbar}{2}\begin{pmatrix}1 & 0\\ 0 & -1\end{pmatrix}\begin{pmatrix}\cos\\ -\sin\end{pmatrix} = \tfrac{\hbar}{2}(\cos^2 - \sin^2) = \tfrac{\hbar}{2}\cos(\gamma\mathcal{B}t) \ .\end{aligned}$$

25.3.4.8 Ex: Spin expectation value for a two-level system

Consider an arbitrary state of a two-level system $|\vartheta,\varphi\rangle = \cos\frac{\vartheta}{2}|+\rangle + e^{\imath\varphi}\sin\frac{\vartheta}{2}|-\rangle$ and calculate the expectation values of the ladder operators $\hat{s}_\pm$ and of the spin operator $\hat{\mathbf{s}}$. Also calculate the expectation values of $\hat{s}_\pm^2$, $\hat{s}_\pm\hat{s}_\mp$, $\hat{s}_\alpha^2$ with $\alpha = x, y, z$. Finally, calculate the uncertainties of $\hat{s}_\alpha$ and check the uncertainty relation.

Solution: *Using* $\hat{s}_\pm|\mp\rangle = |\pm\rangle$*,* $\hat{s}_\mp|\mp\rangle = 0$*, and* $\hat{s}_z|\pm\rangle = \pm\frac{1}{2}|\pm\rangle$*, we first calculate,*

$$\langle\vartheta,\varphi|\hat{s}_+|\vartheta,\varphi\rangle = \left(\langle+|\cos\tfrac{\vartheta}{2} + \langle-|e^{-\imath\varphi}\sin\tfrac{\vartheta}{2}\right)\hat{s}_+\left(\cos\tfrac{\vartheta}{2}|+\rangle + e^{\imath\varphi}\sin\tfrac{\vartheta}{2}|-\rangle\right) = \tfrac{1}{2}e^{\imath\varphi}\sin\vartheta$$

$$\langle\vartheta,\varphi|\hat{\mathbf{s}}|\vartheta,\varphi\rangle = \begin{pmatrix}\frac{1}{2}(\hat{s}_+ + \hat{s}_-)\\ \frac{1}{2\imath}(\hat{s}_+ - \hat{s}_-)\\ \frac{1}{2}[\hat{s}_+, \hat{s}_-]\end{pmatrix} = \begin{pmatrix}\frac{1}{2}\cos\varphi\sin\vartheta\\ \frac{1}{2}\sin\varphi\sin\vartheta\\ \frac{1}{2}\cos\vartheta\end{pmatrix} \ ,$$

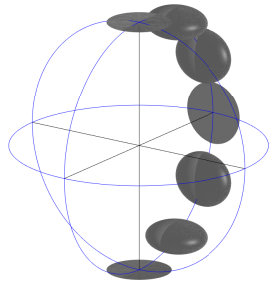

Figure 25.9: (code) Illustration of the uncertainties for various states on the Bloch sphere.

We also calculate,

$$\begin{aligned}
\langle\vartheta,\varphi|\hat{s}_+^2|\vartheta,\varphi\rangle &= 0 = \langle\vartheta,\varphi|\hat{s}_-^2|\vartheta,\varphi\rangle \\
\langle\vartheta,\varphi|\hat{s}_+\hat{s}_-|\vartheta,\varphi\rangle &= \left(\langle+|\cos\tfrac{\vartheta}{2} + \langle-|e^{-\imath\varphi}\sin\tfrac{\vartheta}{2}\right)\hat{s}_+\hat{s}_-\left(\cos\tfrac{\vartheta}{2}|+\rangle + e^{\imath\varphi}\sin\tfrac{\vartheta}{2}|-\rangle\right) = \cos^2\tfrac{\vartheta}{2} \\
\langle\vartheta,\varphi|\hat{s}_-\hat{s}_+|\vartheta,\varphi\rangle &= \sin^2\tfrac{\vartheta}{2} \\
\langle\vartheta,\varphi|\hat{s}_x^2|\vartheta,\varphi\rangle &= \tfrac{1}{4}\left(\hat{s}_+\hat{s}_- + \hat{s}_+\hat{s}_- + \hat{s}_+^2 + \hat{s}_-^2\right) = \tfrac{1}{4} \\
\langle\vartheta,\varphi|\hat{s}_y^2|\vartheta,\varphi\rangle &= \tfrac{1}{4}\left(\hat{s}_+\hat{s}_- + \hat{s}_+\hat{s}_- - \hat{s}_+^2 - \hat{s}_-^2\right) = \tfrac{1}{4} \\
\langle\vartheta,\varphi|\hat{s}_z^2|\vartheta,\varphi\rangle &= \left(\langle+|\cos\tfrac{\vartheta}{2} + \langle-|e^{-\imath\varphi}\sin\tfrac{\vartheta}{2}\right)\hat{s}_z^2\left(\cos\tfrac{\vartheta}{2}|+\rangle + e^{\imath\varphi}\sin\tfrac{\vartheta}{2}|-\rangle\right) = \tfrac{1}{4}\ ,
\end{aligned}$$

Finally,

$$\begin{aligned}
\langle\vartheta,\varphi|\Delta\hat{s}_x|\vartheta,\varphi\rangle &= \sqrt{\tfrac{1}{4} - \tfrac{1}{4}\cos^2\varphi\sin^2\vartheta} \\
\langle\vartheta,\varphi|\Delta\hat{s}_y|\vartheta,\varphi\rangle &= \sqrt{\tfrac{1}{4} - \tfrac{1}{4}\sin^2\varphi\sin^2\vartheta} \\
\langle\vartheta,\varphi|\Delta\hat{s}_z|\vartheta,\varphi\rangle &= \sqrt{\tfrac{1}{4} - \tfrac{1}{4}\cos^2\vartheta}\ .
\end{aligned}$$

The uncertainty relation demands,

$$\langle\vartheta,\varphi|\Delta\hat{s}_x|\vartheta,\varphi\rangle\langle\vartheta,\varphi|\Delta\hat{s}_y|\vartheta,\varphi\rangle \geq \tfrac{1}{4}|\cos\vartheta|\ ,$$

which can be verified by simple algebraic calculation. The uncertainties are illustrated in Fig. 25.9.

25.4 Coupling of angular momenta

25.4.1 Singlet and triplet states with two electrons

In this section we first consider the spin states of two electrons, which can be combined into two groups with well-defined total spin. With this we can understand the energy spectrum of helium, which is very much dominated by Pauli's principle and quantum statistics. The introduced concepts can be extended to atoms with many electrons.

Angular momentum is an important quantum number in the treatment of the internal structure of atoms. The two electrons in the helium electronic shell each

contribute a spin of $S = \frac{1}{2}$, which couple to a total angular momentum. Let us consider, for simplicity, two free electrons. The state of the two-particle system is an element of the product space of the two Hilbert spaces in which the individual electrons are described. We will now apply the formalism of Sec. 23.3.9 explicitly to a pair of electrons. The states that the two electrons can occupy are:

$$|\gamma_1\rangle = \begin{pmatrix}1\\0\end{pmatrix} \otimes \begin{pmatrix}1\\0\end{pmatrix} = \begin{pmatrix}1\\0\\0\\0\end{pmatrix} \equiv |\uparrow\uparrow\rangle \quad , \tag{25.75}$$

$$|\gamma_2\rangle = |\uparrow\downarrow\rangle \quad , \quad |\gamma_3\rangle = |\downarrow\uparrow\rangle \quad , \quad |\gamma_4\rangle = |\downarrow\downarrow\rangle \; .$$

The Pauli matrices act on the spin of the individual electrons. They can be extended to the product Hilbert space as follows,

$$\begin{aligned}
\tfrac{\hbar}{2}\hat{\sigma}_x \otimes \mathbb{I}_2 &= \tfrac{\hbar}{2}\begin{pmatrix}0 & \mathbb{I}_2\\ \mathbb{I}_2 & 0\end{pmatrix} \quad , \quad \tfrac{\hbar}{2}\mathbb{I}_2 \otimes \hat{\sigma}_x = \tfrac{\hbar}{2}\begin{pmatrix}\hat{\sigma}_x & 0\\ 0 & \hat{\sigma}_x\end{pmatrix} \\
\tfrac{\hbar}{2}\hat{\sigma}_y \otimes \mathbb{I}_2 &= \tfrac{\hbar}{2}\begin{pmatrix}0 & \imath\mathbb{I}_2\\ -\imath\mathbb{I}_2 & 0\end{pmatrix} \quad , \quad \tfrac{\hbar}{2}\mathbb{I}_2 \otimes \hat{\sigma}_y = \tfrac{\hbar}{2}\begin{pmatrix}\hat{\sigma}_y & 0\\ 0 & \hat{\sigma}_y\end{pmatrix} \\
\tfrac{\hbar}{2}\hat{\sigma}_z \otimes \mathbb{I}_2 &= \tfrac{\hbar}{2}\begin{pmatrix}-\mathbb{I}_2 & 0\\ 0 & \mathbb{I}_2\end{pmatrix} \quad , \quad \tfrac{\hbar}{2}\mathbb{I}_2 \otimes \hat{\sigma}_z = \tfrac{\hbar}{2}\begin{pmatrix}\hat{\sigma}_z & 0\\ 0 & \hat{\sigma}_z\end{pmatrix} \; .
\end{aligned} \tag{25.76}$$

With these operators we can now build other operators. We first consider the three components of the total angular momentum,

$$\hat{S}_k = \tfrac{\hbar}{2}(\hat{\sigma}_k \otimes \mathbb{I}_2 + \mathbb{I}_2 \otimes \hat{\sigma}_k) \qquad \text{such that} \tag{25.77}$$

$$\hat{S}_x = \tfrac{\hbar}{2}\begin{pmatrix}0&1&1&0\\1&0&0&1\\1&0&0&1\\0&1&1&0\end{pmatrix} \; , \; \hat{S}_y = \tfrac{\imath\hbar}{2}\begin{pmatrix}0&1&1&0\\-1&0&0&1\\-1&0&0&1\\0&-1&-1&0\end{pmatrix} \; , \; \hat{S}_z = \hbar\begin{pmatrix}-1&0&0&0\\0&0&0&0\\0&0&0&0\\0&0&0&1\end{pmatrix} \; .$$

The operator for the square of the absolute value of the total angular momentum is calculated as follows:

$$\hat{\mathbf{S}}^2 = \hat{S}_x^2 + \hat{S}_y^2 + \hat{S}_z^2 = \hbar^2\begin{pmatrix}2&0&0&0\\0&1&1&0\\0&1&1&0\\0&0&0&2\end{pmatrix} \; . \tag{25.78}$$

Now, we look for the eigenvalues of the total angular momentum. The equation for the eigenvalues of $\hat{S}_z$,

$$\hat{S}_z|\gamma_k\rangle = M_S|\gamma_k\rangle \; , \tag{25.79}$$

is already diagonal in the introduced basis $\{\gamma_k\}$ with the eigenvalues,

$$M_S = -\hbar, 0, 0, \hbar \ . \tag{25.80}$$

For $\hat{\mathbf{S}}^2$ the situation is more interesting: The states $|\gamma_1\rangle$ and $|\gamma_4\rangle$ *are* eigenstates of $\mathbf{S}^2$ for the eigenvalue $2\hbar^2$, but the states $|\gamma_2\rangle$ and $|\gamma_3\rangle$ are *not* eigenstates. On the other hand, we know that the linear combination of two eigenstates with the same eigenvalue is also a eigenstate. Therefore, the states

$$|\tilde{\gamma}_1\rangle \equiv |\gamma_1\rangle \quad , \quad |\tilde{\gamma}_4\rangle \equiv |\gamma_4\rangle \quad , \quad |\tilde{\gamma}_a\rangle \equiv \tfrac{1}{\sqrt{2}}(|\gamma_2\rangle - |\gamma_3\rangle) \quad , \quad |\tilde{\gamma}_s\rangle \equiv \tfrac{1}{\sqrt{2}}(|\gamma_2\rangle + |\gamma_3\rangle) \ , \tag{25.81}$$

are *still* eigenstates of $\hat{S}_z$, but they *also* are eigenstates of $\hat{\mathbf{S}}^2$, since we can easily verify,

$$\hat{\mathbf{S}}^2|\gamma_s\rangle = 2\hbar^2|\gamma_s\rangle \qquad \text{and} \qquad \hat{\mathbf{S}}^2|\gamma_a\rangle = 0\hbar^2|\gamma_a\rangle \ , \tag{25.82}$$

using the matrices (25.77). In summary, for the eigenvalue $\langle\hat{\mathbf{S}}^2\rangle = 2\hbar^2$ there exist the following three states:

$$\left.\begin{array}{ll} |\gamma_1\rangle & M_s = 1 \\ |\gamma_4\rangle & M_s = -1 \\ |\gamma_s\rangle & M_s = 0 \end{array}\right\} \qquad \text{triplet} \ , \ S = 1 \tag{25.83}$$

For $\langle\mathbf{S}^2\rangle = 0$ there is only one state:

$$|\gamma_a\rangle \quad M_s = 0 \qquad \text{singlet} \ , \ S = 0 \ . \tag{25.84}$$

By exchanging the two electrons, the vectors $|\gamma_1\rangle$ and $|\gamma_4\rangle$ retain their shape, while the mixed vectors change their shape: $\gamma_2 \longleftrightarrow \gamma_3$. Under particle exchange $|\gamma_a\rangle$ reverses its sign, that is, it is antisymmetric, while $|\gamma_1\rangle$, $|\gamma_4\rangle$ and $|\gamma_c\rangle$ conserve their signs, that is, they are symmetrical.

In summary, the triplet states have the quantum number of the total angular momentum (with the expected value for $\hat{\mathbf{S}}^2$ of $\hbar^2 S(S+1) = 2\hbar^2$), and they are symmetrical about the exchange of particles. The singlet state has the quantum number of the total angular momentum $S = 0$, and it is antisymmetric about the exchange of particles. The transition from the original basis $\{|\gamma_1\rangle, |\gamma_2\rangle, |\gamma_3\rangle, |\gamma_4\rangle\}$ to the new basis $\{|\tilde{\gamma}_1\rangle, |\tilde{\gamma}_s\rangle, |\tilde{\gamma}_a\rangle, |\tilde{\gamma}_4\rangle\}$ described by Eqs. (25.81) is done by a unitary transformation,

$$|\tilde{\gamma}\rangle = U_{CGC}|\gamma\rangle \qquad \text{with} \qquad U_{CGC} = \begin{pmatrix} 1 & & & \\ & \frac{1}{\sqrt{2}} & \frac{1}{\sqrt{2}} & \\ & \frac{1}{\sqrt{2}} & -\frac{1}{\sqrt{2}} & \\ & & & 1 \end{pmatrix} \ , \tag{25.85}$$

whose components are known as Clebsch-Gordan coefficients. A similar treatment can be done with bosons, as will be discussed in Sec. 31.1.

25.4.2 Coupling two spins

We now consider a perturbation of the system which, for some reason, only affects the first spin. In the absence of the second atom we would have,

$$\hat{H}_1 = \begin{pmatrix} 0 & \Omega^* \\ \Omega & 0 \end{pmatrix} . \tag{25.86}$$

Including the second atom,

$$\hat{H} = \hat{H}_1 \otimes \mathbb{I} = \begin{pmatrix} & & \Omega^* & \\ & & & \Omega^* \\ \Omega & & & \\ & \Omega & & \end{pmatrix} . \tag{25.87}$$

In this case, the perturbation Hamiltonian does not commute with the total angular momentum,

$$[\hat{\mathbf{S}}^2, \hat{H}] \neq 0 . \tag{25.88}$$

Another type of perturbation affects both spin symmetrically (e.g., Dicke superradiance with two atoms in the same radiative mode or two counterpropagating modes in a ring cavity). The interaction Hamiltonian is now the sum of the individual perturbations,

$$\hat{H} = \hat{H}_1 \otimes \mathbb{I} + \mathbb{I} \otimes \hat{H}_1 = \begin{pmatrix} & \Omega^* & \Omega^* & \\ \Omega & & & \Omega^* \\ \Omega & & & \Omega^* \\ & \Omega & \Omega & \end{pmatrix} . \tag{25.89}$$

This Hamiltonian commutes with the total angular momentum,

$$[\hat{\mathbf{S}}^2, \hat{H}] = 0 . \tag{25.90}$$

S now is a good quantum number. Singlet states do not couple with triplets. This is the idea behind Dicke's superradiance. The absolute value of the total angular momentum is conserved. The quantum number S is called *Dicke cooperativity* [366]. In Exc. 42.5.7.1 we will discuss the coupling of two counterpropagating modes in a ring cavity. In Sec. 41.1 we will discuss Dicke states.

Example 165 (*Two atoms interacting through their dipole moments*): As an example of a system exhibiting coupling of the type described in (25.89) we consider two two-level atoms $j = 1, 2$. As long as the atoms do not interact, the Hamiltonian will be,

$$\hat{H} = \hbar\omega_0 \hat{S}_z , \tag{25.91}$$

with $\hat{S}_z$ given by (25.77). Now, if the atoms interact via their dipole moments with an electromagnetic field assumed to be the same for both atoms,

$$\begin{aligned} \hat{H}_{int} = &- \tfrac{q}{m}\mathbf{A}(\mathbf{r}_1) \cdot (p_x \hat{\mathbf{e}}_x \hat{\sigma}^x \otimes \mathbb{I} + p_y \hat{\mathbf{e}}_y \hat{\sigma}^y \otimes \mathbb{I}) \\ &- \tfrac{q}{m}\mathbf{A}(\mathbf{r}_2) \cdot (p_x \hat{\mathbf{e}}_x \mathbb{I} \otimes \hat{\sigma}^x + p_y \hat{\mathbf{e}}_y \mathbb{I} \otimes \hat{\sigma}^y) , \end{aligned} \tag{25.92}$$

with $\mathbf{r}_1 \simeq \mathbf{r}_2$. By the rules (25.76) we find in matrix notation a Hamiltonian equivalent to (25.89). Using the abbreviations $\Omega_x \equiv \frac{q}{m} A_x p_x$, $\Omega_y \equiv \frac{q}{m} A_y p_y$, $\Omega_\pm \equiv \Omega_x \pm \imath\Omega_y$, and $\Omega \equiv \sqrt{\Omega_x^2 + \Omega_y^2}$,

$$\hat{H} = \begin{pmatrix} 0 & \Omega_- & \Omega_- & 0 \\ \Omega_+ & 0 & 0 & \Omega_- \\ \Omega_+ & 0 & 0 & \Omega_- \\ 0 & \Omega_+ & \Omega_+ & 0 \end{pmatrix} . \tag{25.93}$$

Using symbolic algebra software we find the eigenvector and eigenvalue matrices,

$$U = \begin{pmatrix} \frac{\Omega_-}{\Omega_+} & -\frac{\Omega_-}{\Omega_+} & 0 & \frac{\Omega_-}{\Omega_+} \\ -\sqrt{\frac{\Omega_-}{\Omega_+}} & 0 & -1 & \sqrt{\frac{\Omega_-}{\Omega_+}} \\ -\sqrt{\frac{\Omega_-}{\Omega_+}} & 0 & 1 & \sqrt{\frac{\Omega_-}{\Omega_+}} \\ 1 & 1 & 0 & 1 \end{pmatrix} \quad \text{and} \quad \hat{E} = \begin{pmatrix} -2\Omega & 0 & 0 & 0 \\ 0 & 0 & 0 & 0 \\ 0 & 0 & 0 & 0 \\ 0 & 0 & 0 & 2\Omega \end{pmatrix} . \tag{25.94}$$

Now, we get for the evolution of the various states,

$$U e^{\imath \hat{E} t} U^{-1} \begin{pmatrix} 0 \\ 1 \\ 1 \\ 0 \end{pmatrix} = \begin{pmatrix} -\sqrt{\frac{-\Omega_-}{\Omega_+}} \sin 2\Omega t \\ \cos 2\Omega t \\ \cos 2\Omega t \\ \sqrt{\frac{\Omega_+}{-\Omega_-}} \sin 2\Omega t \end{pmatrix} \quad \text{and} \quad U e^{\imath \hat{E} t} U^{-1} \begin{pmatrix} 0 \\ 1 \\ -1 \\ 0 \end{pmatrix} = \begin{pmatrix} 0 \\ 1 \\ -1 \\ 0 \end{pmatrix} . \tag{25.95}$$

That is, the Hamiltonian (25.92) does not mix antisymmetric singlet states and symmetric triplet states.

25.4.3 Decoupled and coupled bases

Electrically charged orbiting particles produce a magnetic field. This field can influence the motion of other particles. In the same way, the spin of an electron can influence its own orbital motion. That is, angular momenta can couple and interact in a complicated way. Even to describe the behavior of an atom as simple as hydrogen in an external field, we need to construct the eigenstates of the total angular momentum resulting from a coupling of the electron's intrinsic spin and its orbital motion.

On the other side, we have hitherto considered predominantly hydrogen and hydrogen-like atoms, that is, atoms with a nucleus and a single (valence) electron. But in fact atoms can have more than 100 electrons, which complicates the exact description. In atoms with many electrons, one of the most common coupling schemes is when the angular momenta of all electrons couple to a *total angular momentum*, $\hat{\mathbf{L}} = \sum_k \hat{\mathbf{l}}_k$, which then couples to the *total spin*, $\hat{\mathbf{S}} = \sum_k \hat{\mathbf{s}}_k$, to form the complete total angular momentum, $\hat{\mathbf{J}} = \hat{\mathbf{L}} + \hat{\mathbf{S}}$. We generally assign total momenta to capital letters.

Adopting an unbiased notation we study some properties of the total angular momentum, $\hat{\mathbf{j}} \equiv \hat{\mathbf{j}}_1 + \hat{\mathbf{j}}_2$. In Exc. 25.4.5.1 we find that the addition of angular momenta produces a quantity which is also an angular momentum, but not the subtraction.

The angular momenta of two particles or two angular momenta of different origins in a single particle represent independent degrees of freedom, $[\mathbf{j}_1, \mathbf{j}_2] = 0$. Without

interaction between angular momenta the Hilbert spaces are orthogonal:

$$\mathcal{H}_1 \otimes \mathcal{H}_2 = \begin{pmatrix} \mathcal{H}_1 & 0 \\ 0 & \mathcal{H}_2 \end{pmatrix} . \tag{25.96}$$

The eigenfunctions act on a space of dimension, $\dim \mathcal{H}_1 \cdot \dim \mathcal{H}_2$:

$$|j_1, m_{j1}; j_2, m_{j2}\rangle . \tag{25.97}$$

That is, there is a complete set of commuting operators $\{\hat{\mathbf{j}}_1^2, \hat{j}_{1z}, \hat{\mathbf{j}}_2^2, \hat{j}_{2z}\}$. Therefore, we can specify quantum numbers j_1, j_2, m_{j1}, and m_{j2} simultaneously. On the other hand, the group $\{\hat{\mathbf{j}}_1^2, \hat{\mathbf{j}}_2^2, \hat{\mathbf{j}}^2, \hat{j}_z\}$ also represents a complete set of commuting operators, as shown in Exc. 25.4.5.2. It has the basis

$$|(j_1, j_2)j, m_j\rangle . \tag{25.98}$$

To describe the two angular momenta simultaneously, we must opt between the decoupled picture $|j_1, m_{j1}; j_2, m_{j1}\rangle$ and the coupled picture $|(j_1, j_2)j, m_j\rangle$. For now, the choice of the picture makes no difference, but we will see later that there may be an energy associated with the coupling [4]. In this case, as we will show, the choice of the coupled base is more natural, because generally the energy commutes like $[\hat{H}, \hat{\mathbf{j}}^2] = 0 = [\hat{H}, \hat{j}_z]$ and $[\hat{H}, \hat{\mathbf{j}}_1^2] = 0 = [\hat{H}, \hat{\mathbf{j}}_2^2]$, but $[\hat{H}, \hat{j}_{1z}] \neq 0 \neq [\hat{H}, \hat{j}_{2z}]$.

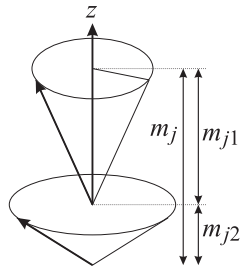

Figure 25.10: Illustration of the coupling of two angular momenta.

Example 166 (*Coupled basis*): For example, using the Hamiltonian (25.94) it is easy to see that,

$$[\hat{H}, (\hat{\sigma}_x \otimes \mathbb{I})^2 + (\hat{\sigma}_y \otimes \mathbb{I})^2 + (\hat{\sigma}_z \otimes \mathbb{I})^2] = 0 = [\hat{H}, (\mathbb{I} \otimes \hat{\sigma}_x)^2 + (\mathbb{I} \otimes \hat{\sigma}_y)^2 + (\mathbb{I} \otimes \hat{\sigma}_z)^2]$$
$$[\hat{H}, \hat{\sigma}_z \otimes \mathbb{I}] \neq 0 \neq [\hat{H}, \mathbb{I} \otimes \hat{\sigma}_z] .$$

25.4.3.1 Allowed values of total angular momentum

As long as we do not specify an interaction energy between the spins or between spins and external fields, all states are energetically degenerate. In the decoupled image

[4] That is, the Hamiltonian of the system does not contain terms of type $\hat{\mathbf{j}}_1 \cdot \hat{\mathbf{j}}_2$, but may have terms proportional to $\hat{\mathbf{j}}_1 + \hat{\mathbf{j}}_2$.

the degeneracy is easily calculated,

$$\# = \sum_{m_{j1}=-j_1}^{j_1} \sum_{m_{j2}=-j_2}^{j_2} 1 = (2j_1+1)(2j_2+1) \ . \tag{25.99}$$

Now, we want to find the possible values of j and m_j in the coupled picture. The values of m_j follow immediately from $\hat{\mathbf{j}}_1 + \hat{\mathbf{j}}_2 = \hat{\mathbf{j}}$,

$$m_j = m_{j1} + m_{j2} \ . \tag{25.100}$$

With $|m_{j1}| \leq j_1$ and $|m_{j2}| \leq j_2$ the values of m_j are limited to

$$|m_j| \leq j_1 + j_2 \ . \tag{25.101}$$

We often know the two angular momenta j_1 and j_2 and all their projections in the decoupled base,

$$|m_{j1}| \leq j_1 \qquad \text{and} \qquad |m_{j2}| \leq j_2 \ . \tag{25.102}$$

To find the quantum numbers in the coupled base, we arrange the states ordering them by their total magnetic quantum number m_j. We can, without loosing generality, concentrate on the situation $j_1 \geq j_2$. The following table reproduces the possible combinations. The x-symbols represent Clebsch-Gordan coefficients:

m_{j1} $+m_{j2}=$ m_j	j	j	$j-1$	j	$j-1$	$j-2$		j	$j-1$	j
		$j-1$	$j-1$	$j-2$	$j-2$	$j-2$		$-j+1$	$-j+1$	$-j$
j_1 j_2	x									
j_1 j_2-1		x	x							
j_1-1 j_2		x	x							
j_1 j_2-2				x	x	x				
j_1-1 j_2-1				x	x	x				
j_1-2 j_2				x	x	x				
							$\ddots$			
$-j_1+1$ $-j_2$								x	x	
$-j_1$ j_2+1								x	x	
$-j_1$ $-j_2$										x

The possible values for j are all those allowing for $j \geq |m_j| = |m_{j1} + m_{j2}|$, that is,

$$|j_1 - j_2| \leq j \leq j_1 + j_2 \ . \tag{25.103}$$

Each value of j has the degeneracy $2j+1$. Therefore, as will be verified in Exc. 25.4.5.3, the total degeneracy is,

$$\sum_{j=|j_1-j_2|}^{j_1+j_2} 2j+1 = (2j_1+1)(2j_2+1) \ . \tag{25.104}$$

Example 167 (*Spin states in the presence of* $\mathbf{L}\cdot\mathbf{S}$ *coupling*): As an example we consider two electrons occupying the $(5p)^2$ orbital. That is, both electrons have $s_i = \frac{1}{2}$ and $\ell_i = 1$. As illustrated in Fig. 25.11, the coupling first gives $S = s_1 + s_2 = 0, 1$ and $L = \ell_1 + \ell_2 = 0, 1, 2$. Then we determine the possible values of the total angular momentum $J = L + S = 0, 1, 2$ depending on the values of L and S.

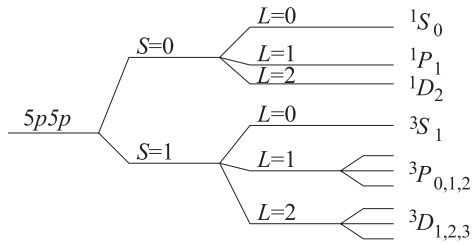

Figure 25.11: Possible spin states of two electrons occupying the $(5p)^2$ orbital. Spin-orbit coupling $\mathbf{L}\cdot\mathbf{S}$ leads to a splitting of the energy levels.

25.4.4 Clebsch-Gordan coefficients

Let us now describe how to add *two* angular momenta, $\hat{\mathbf{j}}_1$ and $\hat{\mathbf{j}}_2$. Since they act on different degrees of freedom,

$$[\vec{\alpha}_1\cdot\hat{\mathbf{j}}_1, \vec{\alpha}_2\cdot\hat{\mathbf{j}}_2] = 0 \tag{25.105}$$

for arbitrary vectors $\vec{\alpha}_1$ and $\vec{\alpha}_2$. We have a system of common eigenvectors, $|\eta, j_1, j_2, m_1, m_2\rangle$, where η are the eigenvalues of other observables commuting with $\hat{\mathbf{j}}_1$ and $\hat{\mathbf{j}}_2$. These eigenvectors give the values $\hbar^2 j_1(j_1+1)$ and $\hbar^2 j_2(j_2+1)$ for the observables $\hat{\mathbf{j}}_1^2$ and $\hat{\mathbf{j}}_2^2$, as well as $\hbar m_1$ and $\hbar m_2$ for the observables j_{z1} and j_{z2}. The number of states is $(2j_1+1)(2j_2+1)$. Now we want to construct the eigenstates of the total angular momentum $\hat{\mathbf{j}} = \hat{\mathbf{j}}_1 + \hat{\mathbf{j}}_2$. Since

$$[\hat{\mathbf{j}}, \hat{\mathbf{j}}_1^2] = 0 = [\hat{\mathbf{j}}, \hat{\mathbf{j}}_2^2]\ , \tag{25.106}$$

there exist common eigenstates $|j_1, j_2, j, m\rangle$ for the set of observables $\hat{\mathbf{j}}_1^2$, $\hat{\mathbf{j}}_2^2$, $\hat{\mathbf{j}}^2$ and $\hat{j}_z$. These eigenstates are linear combinations of the individual states,

$$\begin{aligned} |(j_1,j_2)j,m\rangle &= \sum_{m_1,m_2} |j_1,j_2,m_1,m_2\rangle\langle j_1,j_2,m_1,m_2|(j_1,j_2)j,m\rangle \\ &= \sum_{m_1,m_2} |j_1,j_2,m_1,m_2\rangle \left(\begin{array}{cc|c} j_1 & j_2 & j \\ m_1 & m_2 & m \end{array}\right)\ . \end{aligned} \tag{25.107}$$

The matrix coefficient is called *Clebsch-Gordan coefficient*. The Clebsch-Gordans disappear when the conditions [5]

$$|j_1-j_2| \le j \le j_1+j_2 \qquad \text{and} \qquad m = -j_1-j_2, -j_1-j_2+1, .., j_1+j_2 \tag{25.108}$$

are not satisfied.

The unitary transformation matrices between decoupled and coupled bases,

$$|(j_1,j_2)j,m\rangle = U_{CGC}|j_1,m_1;j_2,m_2\rangle\ , \tag{25.109}$$

are listed in tables of the Clebsch-Gordan coefficients.

[5] The Clebsch-Gordans are related to the $(3j)$ de Wigner symbols.

Example 168 (*Clebsch-Gordans for the coupling of two spins* $\frac{1}{2}$): For example, for the system consisting of two $\frac{1}{2}$ spins we have,

$$\begin{pmatrix} |(\frac{1}{2},\frac{1}{2})1,+1\rangle \\ |(\frac{1}{2},\frac{1}{2})1,0\rangle \\ |(\frac{1}{2},\frac{1}{2})0,0\rangle \\ |(\frac{1}{2},\frac{1}{2})1,-1\rangle \end{pmatrix} = \begin{pmatrix} 1 & 0 & 0 & 0 \\ 0 & \sqrt{\frac{1}{2}} & \sqrt{\frac{1}{2}} & 0 \\ 0 & \sqrt{\frac{1}{2}} & -\sqrt{\frac{1}{2}} & 0 \\ 0 & 0 & 0 & 1 \end{pmatrix} \begin{pmatrix} |\frac{1}{2},+\frac{1}{2};\frac{1}{2},+\frac{1}{2}\rangle \\ |\frac{1}{2},-\frac{1}{2};\frac{1}{2},+\frac{1}{2}\rangle \\ |\frac{1}{2},+\frac{1}{2};\frac{1}{2},-\frac{1}{2}\rangle \\ |\frac{1}{2},-\frac{1}{2};\frac{1}{2},-\frac{1}{2}\rangle \end{pmatrix} .$$

In the Excs. 25.4.5.4 and 25.4.5.5 we write all possible states of two angular momenta in decoupled and coupled bases. In Excs. 25.4.5.6, 25.4.5.7, we derive the matrix representation of two spins in the decoupled and the coupled base. In 25.4.5.8, and 25.4.5.9 we practice the transformation between decoupled and coupled bases, and in Exc. 25.4.5.10 we verify a rule guaranteeing the unitarity of the Clebsch-Gordan transformation. Finally in 25.4.5.11, 25.4.5.12, and 25.4.5.13 we study $\mathbf{L}\cdot\mathbf{S}$-coupling.

25.4.4.1 Coupling of three angular moments

Three angular momenta can be coupled in three different configurations: First j_1 with j_2, then the total spin $(j_1,j_2)j_{12}$ with the third one j_3. We use the notation $|[(j_1,j_2)j_{12},j_3]J\rangle$ or $|[(j_1,j_3)j_{13},j_2]J\rangle$ or $|[(j_2,j_3)j_{23},j_1]J\rangle$. The recoupling of three spins

$$\begin{array}{ccccc} \mathbf{j}_1 & + & \mathbf{j}_2 & = & \mathbf{j}_{12} \\ + & & & & + \\ \mathbf{j}_3 & & & & \mathbf{j}_3 \\ = & & & & = \\ \mathbf{j}_{13} & + & \mathbf{j}_2 & = & \mathbf{J} \end{array} \tag{25.110}$$

is described by $\{6j\} = \begin{Bmatrix} j_1 & j_3 & j_{13} \\ J & j_{12} & j_2 \end{Bmatrix}$-symbols, for example,

$$|[(j_1,j_2)j_{12},j_3]J\rangle = \sum_{j_{13}} \{6j\} |[(j_1,j_3)j_{13},j_2]J\rangle \ . \tag{25.111}$$

25.4.4.2 Notation for atomic states with LS-coupling

In an atom, the spins of the electrons often couple to a total spin, $\mathbf{S} = \sum_k \mathbf{s}_k$, and separately the orbital angular momenta to a total orbital angular momentum, $\mathbf{L} = \sum_k \mathbf{l}_k$. These two total spins now couple to a total angular momentum, $\mathbf{J} = \mathbf{L}+\mathbf{S}$. When this **LS**-*coupling* happens, the following notation is used to characterize the electronic states in atoms:

$$^{2S+1}L_J \ . \tag{25.112}$$

25.4.4.3 jj-coupling

There is also the case that for each electron its spin couples to its own orbital angular momentum, $\mathbf{j}_k = \mathbf{l}_k + \mathbf{s}_k$, before coupling to the total angular momenta of other

electrons, $\mathbf{J} = \sum_k \mathbf{j}_k$. This is called **jj**-*coupling*. In the case of two electrons the recoupling of the four involved spins

$$\begin{array}{ccccc} \mathbf{l}_1 & + & \mathbf{l}_2 & = & \mathbf{L} \\ + & & + & & + \\ \mathbf{s}_1 & + & \mathbf{s}_2 & = & \mathbf{S} \\ = & & = & & = \\ \mathbf{j}_1 & + & \mathbf{j}_2 & = & \mathbf{J} \end{array} \tag{25.113}$$

is described by $\{9j\} = \begin{Bmatrix} l_1 & l_2 & L \\ s_1 & s_2 & S \\ j_1 & j_2 & J \end{Bmatrix}$-symbols,

$$|[(l_1, s_1)j_1, (l_2, s_2)j_2]J\rangle = \sum_{L,S} \{9j\} |[(l_1, l_2)L, (s_1, s_2)S]J\rangle \ . \tag{25.114}$$

25.4.5 Exercises

25.4.5.1 Ex: Addition/subtraction of angular momenta

Show that $\hat{\mathbf{j}}_1 + \hat{\mathbf{j}}_2$ is an angular momentum, but not $\hat{\mathbf{j}}_1 - \hat{\mathbf{j}}_2$.

Solution: *We find on one hand,*

$$i\hbar\hat{\mathbf{j}} = i\hbar\hat{\mathbf{j}}_1 \pm i\hbar\hat{\mathbf{j}}_2 \ .$$

On the other hand, using $\hat{\mathbf{j}}_1 \times \hat{\mathbf{j}}_2 = -\hat{\mathbf{j}}_2 \times \hat{\mathbf{j}}_1$*, we find,*

$$i\hbar\hat{\mathbf{j}} = \hat{\mathbf{j}} \times \hat{\mathbf{j}} = (\hat{\mathbf{j}}_1 \pm \hat{\mathbf{j}}_2) \times (\hat{\mathbf{j}}_1 \pm \hat{\mathbf{j}}_2) = \hat{\mathbf{j}}_1 \times \hat{\mathbf{j}}_1 + \hat{\mathbf{j}}_2 \times \hat{\mathbf{j}}_2 + \hat{\mathbf{j}}_1 \times \hat{\mathbf{j}}_2 + \hat{\mathbf{j}}_2 \times \hat{\mathbf{j}}_1 = i\hbar\hat{\mathbf{j}}_1 + i\hbar\hat{\mathbf{j}}_2 \ .$$

Only for the upper signs do we obtain equality of the two above expressions and therefore a total angular momentum.

25.4.5.2 Ex: CSCO for coupled angular momenta

Be $\hat{\mathbf{j}} = \hat{\mathbf{j}}_1 + \hat{\mathbf{j}}_2$. Show that $\{\hat{\mathbf{j}}_1^2, \hat{\mathbf{j}}_2^2, \hat{\mathbf{j}}^2, \hat{j}_z\}$ is a CSCO; that is, show that
a. $\hat{\mathbf{j}}^2$ commutes with $\hat{\mathbf{j}}_1^2$ and $\hat{\mathbf{j}}_2^2$;
b. $\hat{\mathbf{j}}^2$ does not commute with $\hat{j}_{1z}$ or $\hat{j}_{2z}$ and that we can not specify m_{j1} or m_{j2} together with j.

Solution: *a. We have,*

$$[\mathbf{j}^2, \mathbf{j}_1^2] = [(\mathbf{j}_1 + \mathbf{j}_2)^2, \mathbf{j}_1^2] = [\mathbf{j}_1^2 + \mathbf{j}_2^2 + \mathbf{j}_1\mathbf{j}_2 + \mathbf{j}_2\mathbf{j}_1, \mathbf{j}_1^2] = [\mathbf{j}_1\mathbf{j}_2 + \mathbf{j}_2\mathbf{j}_1, \mathbf{j}_1^2] = 2\mathbf{j}_2[\mathbf{j}_1, \mathbf{j}_1^2] = 0.$$

b. We have,

$$[\hat{\mathbf{j}}^2, j_{1z}] = [\hat{\mathbf{j}}_1^2 + \hat{\mathbf{j}}_2^2 + 2\hat{\mathbf{j}}_1\hat{\mathbf{j}}_2, \hat{j}_{1z}] = 2\hat{\mathbf{j}}_2[\hat{\mathbf{j}}_1, \hat{j}_{1z}] \neq 0 \ .$$

Therefore, we can not specify m_{j1} *or* m_{j2} *together with* j*.*

25.4.5.3 Ex: Multiplicity of coupled angular momenta

Verify $\# = (2j_1+1)(2j_2+1)$ within the coupled representation.

Solution: *We have,*

$$2\sum_{j=a}^{b} j + \sum_{j=a}^{b} 1 = 2\tfrac{(b-a+1)(a+b)}{2} + (b-a+1) = (b-a+1)(a+b+1)$$

$$\sum_{j=|j_1-j_2|}^{j_1+j_2} 2j+1 = ([j_1+j_2]-[j_1-j_2]+1)([j_1-j_2]+[j_1+j_2]+1)$$

$$= (j_2+j_2+1)(j_1+j_1+1) \ .$$

25.4.5.4 Ex: Possible states of two (de-)coupled angular momenta

Find all possible states with the angular momenta $j_1 = 1$ and $j_2 = 1/2$ in decoupled and coupled pictures.

Solution: *In the decoupled image we have,*

$$|j_1, m_{j1}; j_2, m_{j2}\rangle = |1,+1;\tfrac{1}{2},\pm\tfrac{1}{2}\rangle, |1,0;\tfrac{1}{2},\pm\tfrac{1}{2}\rangle, |1,-1;\tfrac{1}{2},\pm\tfrac{1}{2}\rangle \ .$$

In the coupled image we have,

$$|(j_1,j_2)j, m_j\rangle = |\tfrac{3}{2}(1,\tfrac{1}{2}),\pm\tfrac{3}{2}\rangle, |\tfrac{3}{2}(1,\tfrac{1}{2}),\pm\tfrac{1}{2}\rangle, |\tfrac{1}{2}(1,\tfrac{1}{2}),\pm\tfrac{1}{2}\rangle \ .$$

25.4.5.5 Ex: Fine and hyperfine structure of the rubidium atom ^{85}Rb

1. The rubidium atom ^{85}Rb has one valence electron. In the first excited state this electron has the orbital angular momentum, $L = 1$. What are the possible states?
2. In the fundamental state of this atom the total electronic angular momentum J couples with the spin of the nucleus, $I = 5/2$, to form the total angular momentum $\mathbf{F} = \mathbf{J} + \mathbf{I}$. Determine the possible values for the angular momentum F and the magnetic quantum number m_F.

Solution: *a. The states are,*

$$^2P_{1/2} \ \ with \ \ m_j = \pm\tfrac{1}{2} \ \ and \ \ ^2P_{3/2} \ \ with \ \ m_j = \pm\tfrac{1}{2}, \pm\tfrac{3}{2} \ .$$

b. The states are,

$$F = 2 \ \ with \ \ m_F = -2,..,2 \ \ and \ \ F = 3 \ \ with \ \ m_F = -3,..3 \ .$$

25.4.5.6 Ex: Expansion of the hyperfine structure of the rubidium atom ^{87}Rb

Determine for the states $S_{1/2}$ and $P_{3/2}$ of an atom with nuclear spin $I = 3/2$ and hyperfine coupling $\hat{\mathbf{J}} \cdot \hat{\mathbf{I}}$ how the eigenstates of the coupled base expand into the decoupled base. Do not consider external magnetic fields.

Solution: *For the state $S_{1/2}$, we have $J = 1/2$ and $I = 3/2$ which coupled to $F = 1, 2$. The transformation is done via,*

$$|(J,I)F,m_F\rangle = |(\tfrac{1}{2},\tfrac{3}{2})2 \pm 2\rangle = U_{CGC}|\pm\tfrac{3}{2}\pm\tfrac{1}{2}\rangle = U_{CGC}\sum_{m_I,m_J}|I,m_I,J,m_J\rangle$$

that is,

$$\begin{pmatrix} |(\frac{3}{2},\frac{1}{2})2,\pm2\rangle \\ |(\frac{3}{2},\frac{1}{2})2,\pm1\rangle \\ |(\frac{3}{2},\frac{1}{2})1,\pm1\rangle \\ |(\frac{3}{2},\frac{1}{2})2,0\rangle \\ |(\frac{3}{2},\frac{1}{2})1,0\rangle \end{pmatrix} = \begin{pmatrix} 1 & & & & \\ & \sqrt{\frac{1}{4}} & \sqrt{\frac{3}{4}} & & \\ & \pm\sqrt{\frac{3}{4}} & \mp\sqrt{\frac{1}{4}} & & \\ & & & \sqrt{\frac{1}{2}} & \sqrt{\frac{1}{2}} \\ & & & \sqrt{\frac{1}{2}} & -\sqrt{\frac{1}{2}} \end{pmatrix} \begin{pmatrix} |\frac{3}{2},\pm\frac{3}{2},\frac{1}{2},\pm\frac{1}{2}\rangle \\ |\frac{3}{2},\pm\frac{3}{2},\frac{1}{2},\mp\frac{1}{2}\rangle \\ |\frac{3}{2},\pm\frac{1}{2},\frac{1}{2},\pm\frac{1}{2}\rangle \\ |\frac{3}{2},+\frac{1}{2},\frac{1}{2},-\frac{1}{2}\rangle \\ |\frac{3}{2},-\frac{1}{2},\frac{1}{2},+\frac{1}{2}\rangle \end{pmatrix}.$$

For the state $P_{3/2}$, the transformation is done by

$$\begin{aligned}
|3\pm3\rangle &= |\pm\tfrac{3}{2}\pm\tfrac{1}{2}\rangle \\
|3\pm2\rangle &= \sqrt{\tfrac{1}{2}}|\pm\tfrac{3}{2}\pm\tfrac{1}{2}\rangle + \sqrt{\tfrac{1}{2}}|\pm\tfrac{3}{2}\pm\tfrac{1}{2}\rangle \\
|3\pm1\rangle &= \sqrt{\tfrac{1}{5}}|\pm\tfrac{3}{2}\mp\tfrac{1}{2}\rangle + \sqrt{\tfrac{3}{5}}|\pm\tfrac{1}{2}\pm\tfrac{1}{2}\rangle + \sqrt{\tfrac{1}{5}}|\mp\tfrac{3}{2}\pm\tfrac{1}{2}\rangle \\
|30\rangle &= \sqrt{\tfrac{1}{20}}|\tfrac{3}{2}-\tfrac{3}{2}\rangle + \sqrt{\tfrac{9}{20}}|\tfrac{1}{2}-\tfrac{1}{2}\rangle + \sqrt{\tfrac{9}{20}}|-\tfrac{1}{2}\tfrac{1}{2}\rangle + \sqrt{\tfrac{1}{20}}|-\tfrac{3}{2}\tfrac{3}{2}\rangle \\
|2\pm2\rangle &= \sqrt{\tfrac{1}{2}}|\pm\tfrac{3}{2}\pm\tfrac{1}{2}\rangle - \sqrt{\tfrac{1}{2}}|\pm\tfrac{3}{2}\pm\tfrac{1}{2}\rangle \\
|2\pm1\rangle &= \mp\sqrt{\tfrac{3}{4}}|\mp\tfrac{1}{2}\pm\tfrac{3}{2}\rangle \pm \sqrt{\tfrac{1}{2}}|\pm\tfrac{3}{2}\mp\tfrac{1}{2}\rangle \\
|20\rangle &= \tfrac{1}{2}|\tfrac{3}{2}-\tfrac{3}{2}\rangle + \tfrac{1}{2}|\tfrac{1}{2}-\tfrac{1}{2}\rangle - \tfrac{1}{2}|-\tfrac{1}{2}\tfrac{1}{2}\rangle - \tfrac{1}{2}|-\tfrac{3}{2}\tfrac{3}{2}\rangle
\end{aligned}$$

25.4.5.7 Ex: Transition amplitudes between Zeeman sub-states

a. We consider the atom of ^{87}Rb having the nuclear angular momentum $I = 3/2$. What are the possible hyperfine states F resulting from a coupling of I with the total electronic state angular momentum of the ground state $^2S_{1/2}$? What are the possible Zeeman sub-states of F?
b. What are the possible hyperfine states F' resulting from a coupling of I with the total electronic angular momentum of the excited state $^2P_{3/2}$, $F' = 2$? What are the

possible Zeeman sub-states of F'?
c. A transition between a ground hyperfine state and an excited hyperfine state can be described by a coupling of the total angular momentum F with the angular momentum of the photon κ forming the angular momentum of the excited state F'. To see this, we now consider the levels $F = 1$ and $F' = 2$. Expand the coupled angular momentum $|(F, \kappa)F', m_{F'}\rangle = |(1, 1)2, m_{F'}\rangle$ on a decoupled basis for every possible value $m_{F'}$. Use the table in Fig. 25.13 to determine the Clebsch-Gordan coefficients.
Note: The Clebsch-Gordans only compare the oscillator strengths of transitions between Zeeman sub-states of a given set (F, F'). In order to compare the oscillator strengths to other transitions (F, F') it is necessary to calculate $6j$-coefficients.

Solution: *a. With $J = \frac{1}{2}$ we obtain $F = |J - I|, ..J + I = 1, 2$ and $m_F = -F, .. + F$*

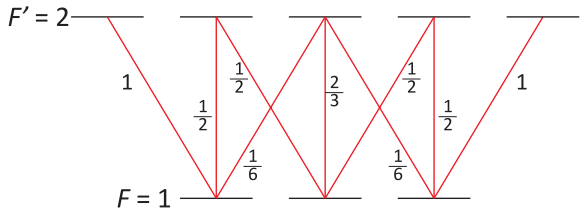

Figure 25.12: Transitions between hyperfine states.

for each F.
b. With $J' = 3/2$ we obtain $F' = 0, 1, 2, 3$ and $m_{F'} = -F', .. + F'$ for each F'.
c. We apply the formula (25.107),

$$|(F, \kappa)F', m_{F'}\rangle = \sum_{m_\kappa=-1}^{+1} |F, \kappa, m_{F'} - m_\kappa, m_\kappa\rangle \left(\begin{array}{cc|c} F & \kappa & F' \\ m_{F'} - m_\kappa & m_\kappa & m_{F'} \end{array}\right) .$$

Thereby,

$$|(1,1)2, \pm 2\rangle = \sum_{m_\kappa} |1, 1, \pm 2 - m_\kappa, m_\kappa\rangle \left(\begin{array}{cc|c} 1 & 1 & 2 \\ \pm 2 - m_\kappa & m_\kappa & \pm 2 \end{array}\right) = \sqrt{1}|1, 1, \pm 1, \pm 1\rangle$$

$$|(1,1)2, \pm 1\rangle = \sum_{m_\kappa} |1, 1, \pm 1 - m_\kappa, m_\kappa\rangle \left(\begin{array}{cc|c} 1 & 1 & 2 \\ \pm 1 - m_\kappa & m_\kappa & \pm 1 \end{array}\right) = \sqrt{\tfrac{1}{2}}|1, 1, \pm 1, 0\rangle + \sqrt{\tfrac{1}{2}}|1, 1, 0, \pm 1\rangle$$

$$\begin{aligned} |(1,1)2, 0\rangle &= \sum_{m_\kappa} |1, 1, 0 - m_\kappa, m_\kappa\rangle \left(\begin{array}{cc|c} 1 & 1 & 2 \\ -m_\kappa & m_\kappa & 0 \end{array}\right) \\ &= \sqrt{\tfrac{1}{6}}|1, 1, +1, -1\rangle + \sqrt{\tfrac{2}{3}}|1, 1, 0, 0\rangle + \sqrt{\tfrac{1}{6}}|1, 1, -1, +1\rangle \ . \end{aligned}$$

25.4.5.8 Ex: Gymnastics of angular momentum operators

Consider the problem of adding angular momenta $j_1 = 1$ and $j_2 = 1/2$:
a. What are the possible values of m and j, in which $\hat{j}^2|j, m\rangle = j(j + 1)\hbar^2|j, m\rangle$ and

$j_z|j,m\rangle = m\hbar|j,m\rangle$?
b. What are the degeneracy $g_{j_1,j_2}(m)$?
c. Find the base states $\{|j,m\rangle\}$, which are common to the operators $\mathbf{j}_1^2$, $\mathbf{j}_2^2$, $\mathbf{j}$, j_z, expanded in the base $\{|j_1,m_1\rangle \otimes |j_2,m_2\rangle\}$ of the eigenstates of $\mathbf{j}_1^2$, $\mathbf{j}_2^2$, j_{1z}, j_{2z}.

Solution: *a. The quantum numbers j and m can have the values,*

$$\begin{array}{lll} & j = 1/2 \quad & \textit{with} \quad m = \pm 1/2 \\ \textit{or} \quad & j = 3/2 \quad & \textit{with} \quad m = \pm 1/2, \pm 3/2 \ . \end{array}$$

*b. Every state m can be the result of several combinations of j_1 and j_2. The states with $m = \pm 3/2$ only correspond to $j = j_1 + j_2$ (*fully stretched *states), but the states $m = \pm 1/2$ correspond to $j = j_1 + j_2 = 3/2$ or $j = j_1 - j_2 = 1/2$. Hence, the degeneracies are $g_{1,1/2}(\pm 3/2) = 1$ and $g_{1,1/2}(\pm 1/2) = 2$.*
c. The states are

$$\left.\begin{array}{l} |(j_1,j_2)j = \frac{3}{2}, m = \pm\frac{3}{2}\rangle \\ |(j_1,j_2)j = \frac{3}{2}, m = \pm\frac{1}{2}\rangle \\ |(j_1,j_2)j = \frac{1}{2}, m = \pm\frac{1}{2}\rangle \end{array}\right\} = \left\{\begin{array}{c} |j_1 = 1, m_1 = \pm 1\rangle |j_2 = \frac{1}{2}, m_2 = \pm\frac{1}{2}\rangle \\ |j_1 = 1, m_1 = \pm 1\rangle |j_2 = \frac{1}{2}, m_2 = \mp\frac{1}{2}\rangle \\ |j_1 = 1, m_1 = 0\rangle |j_2 = \frac{1}{2}, m_2 = \pm\frac{1}{2}\rangle \end{array}\right. .$$

25.4.5.9 Ex: (Un-)coupled bases of the spherical harmonics

Expand the triplet state ${}^3P_J$ of strontium in a decoupled basis and write down the transformation matrix between the bases.

Solution: *We have*

$$|(L,S)J,M_J\rangle = \sum_{m_L,m_S} \left(\begin{array}{cc|c} L & S & J \\ m_L & m_S & m_J \end{array}\right) |L,m_L;S,m_S\rangle \ ,$$

such that,

$$\begin{pmatrix} |(1,1)2,+2\rangle \\ |(1,1)2,+1\rangle \\ |(1,1)1,+1\rangle \\ |(1,1)2,0\rangle \\ |(1,1)1,0\rangle \\ |(1,1)0,0\rangle \\ |(1,1)2,-1\rangle \\ |(1,1)1,-1\rangle \\ |(1,1)2,-2\rangle \end{pmatrix} = \begin{pmatrix} 1 & & & & & & & & \\ & \sqrt{1/2} & \sqrt{1/2} & & & & & & \\ & \sqrt{1/2} & -\sqrt{1/2} & & & & & & \\ & & & \sqrt{1/6} & \sqrt{1/2} & \sqrt{1/3} & & & \\ & & & \sqrt{2/3} & 0 & -\sqrt{1/3} & & & \\ & & & \sqrt{1/6} & -\sqrt{1/2} & \sqrt{1/3} & & & \\ & & & & & & \sqrt{1/2} & \sqrt{1/2} & \\ & & & & & & \sqrt{1/2} & -\sqrt{1/2} & \\ & & & & & & & & 1 \end{pmatrix} \begin{pmatrix} |1,+1;1,+1\rangle \\ |1,+1;1,0\rangle \\ |1,0;1,+1\rangle \\ |1,+1;1,-1\rangle \\ |1,0;1,0\rangle \\ |1,-1;1,+1\rangle \\ |1,0;1,-1\rangle \\ |1,-1;1,0\rangle \\ |1,-1;1,-1\rangle \end{pmatrix}$$

25.4.5.10 Ex: Properties of Clebsch-Gordan coefficients

Given the momenta j_1 and j_2, and C_{m_1,m_2} denoting the Clebsch-Gordan coefficients, prove that $\sum_{m_1,m_2} |C_{m_1,m_2}|^2 = 1$.

Solution: *The Clebsch-Gordans are defined by,*

$$|j,m\rangle = \sum_{m_1,m_2} |m_1,m_2\rangle\langle m_1,m_2|j,m\rangle \ ,$$

where we left out the $j_{1,2}$ to simplify the notation. Since the $|j,m\rangle$ and the $|m_1,m_2\rangle$ are orthogonal,

$$\begin{aligned} 1 = \langle j,m|j,m\rangle &= \sum_{m_1,m_2,m_1',m_2'} \langle j,m|m_1',m_2'\rangle\langle m_1',m_2'|m_1,m_2\rangle\langle m_1,m_2|j,m\rangle \\ &= \sum_{m_1,m_2} |\langle m_1,m_2|j,m\rangle|^2 \ . \end{aligned}$$

25.4.5.11 Ex: Spin-orbit coupling

a. Show that the operator $\hat{\mathbf{L}}\cdot\hat{\mathbf{S}}$ associated with the spin-orbit coupling, satisfies the relation $\hat{\mathbf{L}}\cdot\hat{\mathbf{S}} = \hat{L}_z\hat{S}_z + (\hat{L}_+\hat{S}_- + \hat{L}_-\hat{S}_+)/2$.
Obtain the matrix representation of the operator $\mathbf{L}\cdot\mathbf{S}$, considering the bases:
b. $\{|m_L\rangle\otimes|m_S\rangle\}$ of the eigenstates which are common to the operators $\hat{\mathbf{L}}^2$, $\hat{\mathbf{S}}^2$, $\hat{L}_z$, $\hat{S}_z$;
c. $\{|J,M\rangle\}$, which is associated with the operators $\hat{\mathbf{L}}^2$, $\hat{\mathbf{S}}^2$, $\hat{\mathbf{J}}^2$, $\hat{J}_z$.
d. Give the explicit matrices for the case $L=1$ and $S=\frac{1}{2}$ in the representations (b) and (c) and verify that the two representations yield the same eigenvalue spectrum.

Solution: *a. This is trivial using the definition, $\hat{L}_\pm \equiv \hat{L}_x \pm i\hat{L}_y$, and similarly for $\hat{S}$.*
b. In the decoupled base,

$$\begin{aligned} &\langle m_L'm_S'|\hat{\mathbf{L}}\cdot\hat{\mathbf{S}}|m_Lm_S\rangle \\ &= \langle m_L'm_S'|\hat{L}_z\hat{S}_z|m_Lm_S\rangle + \tfrac{1}{2}\langle m_L'm_S'|\hat{L}_+\hat{S}_-|m_Lm_S\rangle + \tfrac{1}{2}\langle m_L'm_S'|\hat{L}_-\hat{S}_+|m_Lm_S\rangle \\ &= \hbar^2 m_L m_S \delta_{m_L,m_L'}\delta_{m_S,m_S'} \\ &+ \tfrac{1}{2}\hbar^2\sqrt{L(L+1)+m_L(m_L+1)}\sqrt{S(S+1)+m_S(m_S-1)}\delta_{m_L+1,m_L'}\delta_{m_S-1,m_S'} \\ &+ \tfrac{1}{2}\hbar^2\sqrt{L(L+1)+m_L(m_L-1)}\sqrt{S(S+1)+m_S(m_S+1)}\delta_{m_L-1,m_L'}\delta_{m_S+1,m_S'} \ . \end{aligned}$$

c. In the coupled base,

$$\begin{aligned} \langle J'm_J|\hat{\mathbf{L}}\cdot\hat{\mathbf{S}}|Jm_J\rangle &= \tfrac{1}{2}\langle J'm_J|\hat{\mathbf{J}}^2 - \hat{\mathbf{L}}^2 - \hat{\mathbf{S}}^2|Jm_J\rangle \\ &= \tfrac{1}{2}\hbar^2\left[J(J+1) - L(L+1) - S(S+1)\right]\delta_{J',m_J,J,m_J} \ . \end{aligned}$$

To obtain the eigenvalues of the spin-orbit coupling in the decoupled base we must diagonalize the matrix. Doing so, we find exactly the eigenvalues resulting form a calculation in the coupled base.

d. The matrices are,

$$\langle m'_L m'_S|\hat{\mathbf{L}}\cdot\hat{\mathbf{S}}|m_L m_S\rangle = \frac{\hbar^2}{2}\begin{pmatrix} |+1,+\frac{1}{2}\rangle \\ |+1,-\frac{1}{2}\rangle \\ |0,+\frac{1}{2}\rangle \\ |0,-\frac{1}{2}\rangle \\ |-1,+\frac{1}{2}\rangle \\ |-1,-\frac{1}{2}\rangle \end{pmatrix}^t \begin{pmatrix} +1 & 0 & 0 & 0 & 0 & 0 \\ 0 & -1 & \sqrt{2} & 0 & 0 & 0 \\ 0 & \sqrt{2} & 0 & 0 & 0 & 0 \\ 0 & 0 & 0 & 0 & \sqrt{2} & 0 \\ 0 & 0 & 0 & \sqrt{2} & -1 & 0 \\ 0 & 0 & 0 & 0 & 0 & +1 \end{pmatrix} \begin{pmatrix} |+1,+\frac{1}{2}\rangle \\ |+1,-\frac{1}{2}\rangle \\ |0,+\frac{1}{2}\rangle \\ |0,-\frac{1}{2}\rangle \\ |-1,+\frac{1}{2}\rangle \\ |-1,-\frac{1}{2}\rangle \end{pmatrix}$$

and

$$\langle J' m_J|\hat{\mathbf{L}}\cdot\hat{\mathbf{S}}|J m_J\rangle = \frac{\hbar^2}{2}\begin{pmatrix} |\frac{1}{2},+\frac{1}{2}\rangle \\ |\frac{1}{2},-\frac{1}{2}\rangle \\ |\frac{3}{2},+\frac{3}{2}\rangle \\ |\frac{3}{2},+\frac{1}{2}\rangle \\ |\frac{3}{2},-\frac{1}{2}\rangle \\ |\frac{3}{2},-\frac{3}{2}\rangle \end{pmatrix}^t \begin{pmatrix} -2 & 0 & 0 & 0 & 0 & 0 \\ 0 & -2 & 0 & 0 & 0 & 0 \\ 0 & 0 & 1 & 0 & 0 & 0 \\ 0 & 0 & 0 & 1 & 0 & 0 \\ 0 & 0 & 0 & 0 & 1 & 0 \\ 0 & 0 & 0 & 0 & 0 & 1 \end{pmatrix} \begin{pmatrix} |\frac{1}{2},+\frac{1}{2}\rangle \\ |\frac{1}{2},-\frac{1}{2}\rangle \\ |\frac{3}{2},+\frac{3}{2}\rangle \\ |\frac{3}{2},+\frac{1}{2}\rangle \\ |\frac{3}{2},-\frac{1}{2}\rangle \\ |\frac{3}{2},-\frac{3}{2}\rangle \end{pmatrix} .$$

The eigenvalues of the first matrix are $1, -2$.

25.4.5.12 Ex: Expansion of the spin-orbit coupling

Consider the problem of adding the orbital angular momentum ℓ and a spin $1/2$. Obtain the $2\ell+1$ states $|\ell+1/2, m_j\rangle$, in addition to the 2ℓ states $|\ell-1/2, m_j\rangle$ (which constitute a common basis for the operators $\mathbf{l}_1^2$, $\mathbf{s}_2^2$, $\mathbf{j}^2$, j_z), expanded in the base $|m_1, m_2\rangle$ of the eigenstates of the operators $\mathbf{l}^2$, $\mathbf{s}^2$, l_z, s_z. You can simplify the procedure by deriving two recurrence relationships from which the desired states follow [6].

Solution: *The states are, for all* $m_j = -(\ell \pm \frac{1}{2}), .., \ell \pm \frac{1}{2}$,

$$|(\ell,s)j,m_j\rangle = |(\ell,\tfrac{1}{2})\ell\mp\tfrac{1}{2},m_j\rangle = \sum_{m_s=\pm 1/2} |\ell,\tfrac{1}{2},m_j-m_s,m_s\rangle \left(\begin{array}{cc|c} \ell & \frac{1}{2} & \ell\mp\frac{1}{2} \\ m_j-m_s & m_s & m_j \end{array}\right)$$

$$= |\ell,\tfrac{1}{2},m_j+\tfrac{1}{2},-\tfrac{1}{2}\rangle \left(\begin{array}{cc|c} \ell & \frac{1}{2} & \ell\mp\frac{1}{2} \\ m_j+\frac{1}{2} & -\frac{1}{2} & m_j \end{array}\right) + |\ell,\tfrac{1}{2},m_j-\tfrac{1}{2},\tfrac{1}{2}\rangle \left(\begin{array}{cc|c} \ell & \frac{1}{2} & \ell\mp\frac{1}{2} \\ m_j-\frac{1}{2} & \frac{1}{2} & m_j \end{array}\right)$$

$$= |\ell,\tfrac{1}{2},m_j+\tfrac{1}{2},-\tfrac{1}{2}\rangle\sqrt{\frac{\ell\pm m+\frac{1}{2}}{2\ell+1}} + |\ell,\tfrac{1}{2},m_j-\tfrac{1}{2},\tfrac{1}{2}\rangle\sqrt{\frac{\ell\mp m+\frac{1}{2}}{2\ell+1}} ,$$

using the formulae (28.5).

25.4.5.13 Ex: External product of two spins

Derive the matrix representation of the spin-orbit coupling operator $\mathbf{L}\cdot\mathbf{S}$ for $L=1$ and $S=1/2$ from the definition of the outer product.

[6] See Cohen-Tannoudji, Vol.2, Complement A_X.

Solution: *Choosing the base* $\langle \ell m| = \begin{pmatrix} 1 & 0 & -1 \end{pmatrix}$ *the matrix representation of the rising and lowering operators,*

$$\hat{l}_+ = \hbar\sqrt{2}\begin{pmatrix} 0 & 1 & 0 \\ 0 & 0 & 1 \\ 0 & 0 & 0 \end{pmatrix} \quad , \quad \hat{l}_- = \hbar\sqrt{2}\begin{pmatrix} 0 & 0 & 0 \\ 1 & 0 & 0 \\ 0 & 1 & 0 \end{pmatrix}$$

yields the matrix representation of the Cartesian coordinates of $\mathbf{l}$*,*

$$\hat{l}_x = \tfrac{\hat{l}_+ + \hat{l}_-}{2} = \tfrac{\hbar}{\sqrt{2}}\begin{pmatrix} 0 & 1 & 0 \\ 1 & 0 & 1 \\ 0 & 1 & 0 \end{pmatrix} \quad , \quad i\hat{l}_y = \tfrac{\hat{L}_+ - \hat{L}_-}{2} = \tfrac{\hbar}{\sqrt{2}}\begin{pmatrix} 0 & 1 & 0 \\ -1 & 0 & 1 \\ 0 & -1 & 0 \end{pmatrix} \quad ,$$

$$\hat{l}_z = \hbar\begin{pmatrix} 1 & 0 & 0 \\ 0 & 0 & 0 \\ 0 & 0 & -1 \end{pmatrix} .$$

We can verify that $\hat{\mathbf{l}}^2 = \hat{l}_x^2 + \hat{l}_y^2 + \hat{l}_z^2 = \hbar^2 l(l+1) = 2\hbar^2 \mathbb{I}_3$*. The matrix representation of* $\hat{\mathbf{s}}$ *are simply the Pauli matrices,*

$$\hat{s}_x = \tfrac{1}{2}\begin{pmatrix} 0 & 1 \\ 1 & 0 \end{pmatrix} \quad , \quad \hat{s}_y = \tfrac{1}{2}\begin{pmatrix} 0 & -\imath \\ \imath & 0 \end{pmatrix} \quad , \quad \hat{s}_z = \begin{pmatrix} 1 & 0 \\ 0 & -1 \end{pmatrix}.$$

We can verify that $\hat{\mathbf{s}}^2 = \hat{s}_x^2 + \hat{s}_y^2 + \hat{s}_z^2 = \hbar^2 s(s+1) = \frac{3}{4}\hbar^2 \mathbb{I}_3$*. The spin-orbit coupling can now be written* $\hat{\mathbf{l}} \otimes \hat{\mathbf{s}} = \hat{l}_x \otimes \hat{s}_x + \hat{l}_y \otimes \hat{s}_y + \hat{l}_z \otimes \hat{s}_z$*. Choosing the base* $\langle \ell m| = \begin{pmatrix} 1,+\frac{1}{2} & 1,-\frac{1}{2} & 0,+\frac{1}{2} & 0,-\frac{1}{2} & -1,+\frac{1}{2} & -1,-\frac{1}{2} \end{pmatrix}$ *the matrix representation of* $\hat{L}_x\hat{S}_x$ *in the full Hilbert space reads,*

$$\hat{L}_x\hat{S}_x = \tfrac{\hbar}{\sqrt{2}}\begin{pmatrix} & & 1 & & & \\ & & & 1 & & \\ 1 & & & & 1 & \\ & 1 & & & & 1 \\ & & 1 & & & \\ & & & 1 & & \end{pmatrix} \tfrac{\hbar}{2}\begin{pmatrix} & 1 & & & & \\ 1 & & & & 1 & \\ & & & & & 1 \\ & & & & & \\ & & 1 & & & \\ & & & 1 & & \end{pmatrix} = \tfrac{\hbar^2}{2\sqrt{2}}\begin{pmatrix} & & 1 & & 1 & \\ & 1 & & & & 1 \\ 1 & & & & 1 & \\ & & & & & \\ & 1 & & & & \\ & & 1 & & & \end{pmatrix} .$$

Similarly,

$$\hat{L}_y\hat{S}_y = \tfrac{\hbar}{\sqrt{2}}\begin{pmatrix} & & -\imath & & & \\ & & & -\imath & & \\ \imath & & & & -\imath & \\ & \imath & & & & -\imath \\ & & \imath & & & \\ & & & \imath & & \end{pmatrix} \tfrac{\hbar}{2}\begin{pmatrix} & -\imath & & & & \\ \imath & & & & -\imath & \\ & & & & & -\imath \\ & & & & & \\ & & \imath & & & \\ & & & \imath & & \end{pmatrix} = \tfrac{\hbar^2}{2\sqrt{2}}\begin{pmatrix} & & 1 & & -1 & \\ & 1 & & & & -1 \\ -1 & & & & 1 & \\ & & & & & 1 \\ & & -1 & & & \\ & & & 1 & & \end{pmatrix} ,$$

and,

$$\hat{L}_z\hat{S}_z = \hbar\begin{pmatrix} 1 & & & & & \\ & 1 & & & & \\ & & 0 & & & \\ & & & 0 & & \\ & & & & -1 & \\ & & & & & -1 \end{pmatrix} \tfrac{\hbar}{2}\begin{pmatrix} 1 & & & & & \\ & -1 & & & & \\ & & 1 & & & \\ & & & -1 & & \\ & & & & 1 & \\ & & & & & -1 \end{pmatrix} = \tfrac{\hbar^2}{2}\begin{pmatrix} 1 & & & & & \\ & 1 & & & & \\ & & & & & \\ & & & & & \\ & & & & -1 & \\ & & & & & -1 \end{pmatrix} .$$

Finally,

$$\hat{\mathbf{L}}\cdot\hat{\mathbf{S}} = \begin{pmatrix} \frac{1}{2} & 0 & 0 & 0 & 0 & 0 \\ 0 & -\frac{1}{2} & \frac{1}{\sqrt{2}} & 0 & 0 & 0 \\ 0 & \frac{1}{\sqrt{2}} & 0 & 0 & 0 & 0 \\ 0 & 0 & 0 & 0 & \frac{1}{\sqrt{2}} & 0 \\ 0 & 0 & 0 & \frac{1}{\sqrt{2}} & -\frac{1}{2} & 0 \\ 0 & 0 & 0 & 0 & 0 & \frac{1}{2} \end{pmatrix} .$$

25.4.5.14 Ex: Coupling three spins

Express the states of three coupled $\frac{1}{2}$ spins in the uncoupled basis using the Clebsch-Gordan coefficients. Proceed by first coupling two spins and then coupling the result to the third spin. Compare the dimensions of the Hilbert spaces in both basis and discuss your findings.

Solution: *We first couple two spins and then couple the result to the third one. The general procedure is summarized by,*

$$\begin{aligned} |(j_1,j_2)j_{12},m_{12}\rangle &= \sum_{m_1,m_2} U_{CGC}^{(1/2\times 1/2)} |j_1,m_1,j_2m_2\rangle \\ |(j_1,j_2)j_{12},j_3)j,m\rangle &= \sum_{m_{12},m_3} U_{CGC}^{(1\times 1/2)} |(j_1,j_2)j_{12},m_{12},j_3,m_3\rangle \\ &= \sum_{m_1,m_2,m_3} U_{CGC}^{(1\times 1/2)} U_{CGC}^{(1/2\times 1/2)} |j_1,m_1,j_2m_2,j_3,m_3\rangle \ . \end{aligned}$$

For the particular case of spin $\frac{1}{2}$ systems, the coupling of spin j_1 with j_2, we have,

$$\begin{pmatrix} |1,+1\rangle \\ |1,0\rangle \\ |0,0\rangle \\ |1,-1\rangle \end{pmatrix} = \begin{pmatrix} 1 & & & \\ & \frac{1}{\sqrt{2}} & \frac{1}{\sqrt{2}} & \\ & \frac{1}{\sqrt{2}} & -\frac{1}{\sqrt{2}} & \\ & & & 1 \end{pmatrix} \begin{pmatrix} |+\frac{1}{2}\rangle|+\frac{1}{2}\rangle \\ |+\frac{1}{2}\rangle|-\frac{1}{2}\rangle \\ |-\frac{1}{2}\rangle|+\frac{1}{2}\rangle \\ |-\frac{1}{2}\rangle|-\frac{1}{2}\rangle \end{pmatrix} = \begin{pmatrix} |+\frac{1}{2}\rangle|+\frac{1}{2}\rangle \\ \frac{1}{\sqrt{2}}|+\frac{1}{2}\rangle|-\frac{1}{2}\rangle + \frac{1}{\sqrt{2}}|-\frac{1}{2}\rangle|+\frac{1}{2}\rangle \\ \frac{1}{\sqrt{2}}|+\frac{1}{2}\rangle|-\frac{1}{2}\rangle - \frac{1}{\sqrt{2}}|-\frac{1}{2}\rangle|+\frac{1}{2}\rangle \\ |-\frac{1}{2}\rangle|-\frac{1}{2}\rangle \end{pmatrix} .$$

Now, we couple the spin $(j_1, j_2)j_{12}$ with the spin j_3,

$$\begin{pmatrix} |((\frac{1}{2},\frac{1}{2})1,\frac{1}{2})\frac{3}{2}+\frac{3}{2}\rangle \\ |((\frac{1}{2},\frac{1}{2})1,\frac{1}{2})\frac{3}{2},+\frac{1}{2}\rangle \\ |((\frac{1}{2},\frac{1}{2})0,\frac{1}{2})\frac{1}{2},+\frac{1}{2}\rangle \\ |((\frac{1}{2},\frac{1}{2})0,\frac{1}{2})\frac{3}{2},-\frac{1}{2}\rangle \\ |((\frac{1}{2},\frac{1}{2})1,\frac{1}{2})\frac{1}{2},-\frac{1}{2}\rangle \\ |((\frac{1}{2},\frac{1}{2})1,\frac{1}{2})\frac{3}{2},-\frac{3}{2}\rangle \end{pmatrix} = \begin{pmatrix} 1 & & & & & \\ & \sqrt{\frac{1}{3}} & \sqrt{\frac{2}{3}} & & & \\ & \sqrt{\frac{2}{3}} & -\sqrt{\frac{1}{3}} & & & \\ & & & \sqrt{\frac{2}{3}} & \sqrt{\frac{1}{3}} & \\ & & & \sqrt{\frac{1}{3}} & -\sqrt{\frac{2}{3}} & \\ & & & & & 1 \end{pmatrix} \begin{pmatrix} |1,+1\rangle|+\frac{1}{2}\rangle \\ |1,+1\rangle|-\frac{1}{2}\rangle \\ |0,0\rangle|+\frac{1}{2}\rangle \\ |0,0\rangle|-\frac{1}{2}\rangle \\ |1,-1\rangle|+\frac{1}{2}\rangle \\ |1,-1\rangle|-\frac{1}{2}\rangle \end{pmatrix}$$

$$= \begin{pmatrix} |1,+1\rangle|+\frac{1}{2}\rangle \\ \sqrt{\frac{1}{3}}|1,+1\rangle|-\frac{1}{2}\rangle + \sqrt{\frac{2}{3}}|0,0\rangle|+\frac{1}{2}\rangle \\ \sqrt{\frac{1}{3}}|1,+1\rangle|-\frac{1}{2}\rangle - \sqrt{\frac{2}{3}}|0,0\rangle|+\frac{1}{2}\rangle \\ \sqrt{\frac{2}{3}}|0,0\rangle|-\frac{1}{2}\rangle + \sqrt{\frac{1}{3}}|1,-1\rangle|+\frac{1}{2}\rangle \\ \sqrt{\frac{2}{3}}|0,0\rangle|-\frac{1}{2}\rangle - \sqrt{\frac{1}{3}}|1,-1\rangle|+\frac{1}{2}\rangle \\ |1,-1\rangle|-\frac{1}{2}\rangle \end{pmatrix} = \begin{pmatrix} |+++\rangle \\ \sqrt{\frac{1}{3}}(|++-\rangle + |+-+\rangle - |-++\rangle) \\ \sqrt{\frac{1}{3}}(|++-\rangle - |+-+\rangle + |-++\rangle) \\ \sqrt{\frac{1}{3}}(|+--\rangle - |-+-\rangle + |--+\rangle) \\ \sqrt{\frac{1}{3}}(|+--\rangle - |-+-\rangle - |--+\rangle) \\ |---\rangle \end{pmatrix},$$

where we simplified the notation for the last vector. Apparently, the Hilbert space for three spins is larger (dimension 2^3) than the one of a spin $\frac{3}{2}$ state, whose dimension is 6,

$$\begin{pmatrix} |(\frac{1}{2},\frac{1}{2})1,\frac{1}{2})\frac{3}{2},+\frac{3}{2}\rangle \\ |(\frac{1}{2},\frac{1}{2})1,\frac{1}{2})\frac{3}{2},+\frac{1}{2}\rangle \\ |(\frac{1}{2},\frac{1}{2})0,\frac{1}{2})\frac{1}{2},+\frac{1}{2}\rangle \\ ? \\ ? \\ |(\frac{1}{2},\frac{1}{2})0,\frac{1}{2})\frac{3}{2},-\frac{1}{2}\rangle \\ |(\frac{1}{2},\frac{1}{2})1,\frac{1}{2})\frac{1}{2},-\frac{1}{2}\rangle \\ |(\frac{1}{2},\frac{1}{2})1,\frac{1}{2})\frac{3}{2},-\frac{3}{2}\rangle \end{pmatrix} = \begin{pmatrix} 1 & & & & & & & \\ & \sqrt{\frac{1}{3}} & \sqrt{\frac{1}{3}} & -\sqrt{\frac{1}{3}} & & & & \\ & \sqrt{\frac{1}{3}} & -\sqrt{\frac{1}{3}} & \sqrt{\frac{1}{3}} & & & & \\ & & & & \sqrt{\frac{1}{3}} & -\sqrt{\frac{1}{3}} & \sqrt{\frac{1}{3}} & \\ & & & & \sqrt{\frac{1}{3}} & -\sqrt{\frac{1}{3}} & -\sqrt{\frac{1}{3}} & \\ & & & & & & & 1 \end{pmatrix} \begin{pmatrix} |+++\rangle \\ |++-\rangle \\ |+-+\rangle \\ |-++\rangle \\ |+--\rangle \\ |-+-\rangle \\ |--+\rangle \\ |---\rangle \end{pmatrix}.$$

This it due to the fact that, apart from the particular coupling $((j_1, j_2)j_{12}, j_3)j$, there are two more coupling schemes, $((j_1, j_3)j_{13}, j_2)j$ and $((j_2, j_3)j_{23}, j_1)j$, which can be transformed into each other via $\{6j\}$-coefficients.

25.5 Further reading

C. Cohen-Tannoudji, B. Diu, F. Laloe, Wiley Interscience, *Quantum mechanics, vol. 1,2* [276]ISBN

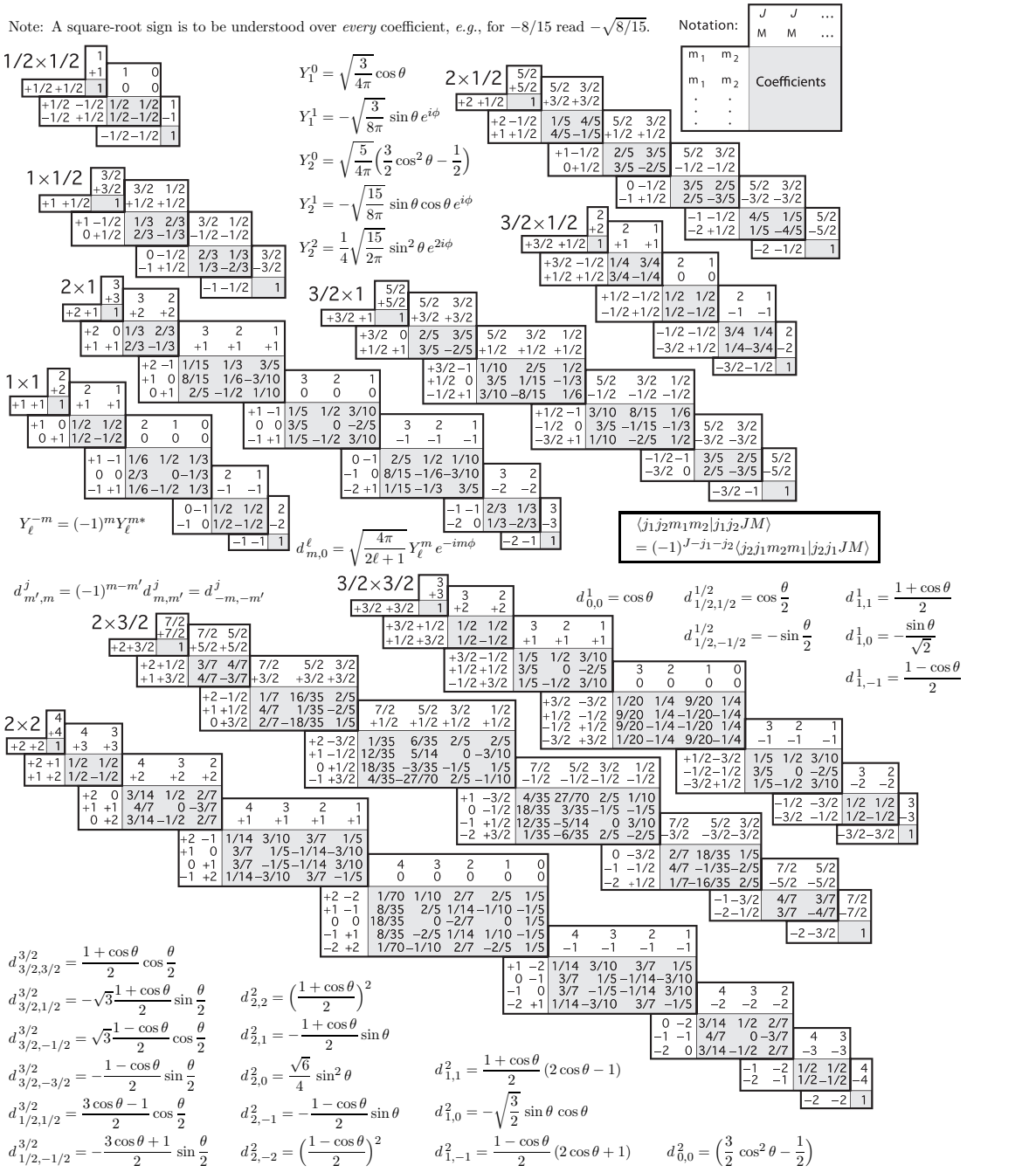

Figure 25.13: Clebsch-Gordan coefficients.

Chapter 26

Periodic systems

Many physical systems treat quantum particles in periodic potential. Examples are electrons in crystals or cold atoms in optical lattices. The periodicity gives rise to a wealth of new phenomena, such as Bragg scattering, the formation of energy bands, Mott insulators, or Bloch oscillations. Various theoretical approaches have been developed leading to a deep understanding of the features of crystals, metals, and optical lattices for atomic gases.

In the following sections we will mainly focus on the Bloch model, which is based on introducing periodic boundary conditions to the Schrödinger equation. In the Secs. 26.1 we will give a brief introduction into the Bloch model for electrons in solids, where the periodicity is imposed by the crystalline structure of the material. We will, however, no go into details leaving a comprehensive treatment to specialized textbooks [53, 726]. In the Secs. 26.2 we will concentrate on optical lattices for atomic gases formed by counterpropagating laser beams. The physical realization of these lattices, which can be realized with nearly perfect periodicity, have permitted the experimental observation of phenomena which had been elusive in solid state physics.

26.1 The Bloch model for electrons

The motion of an electron inside a crystal is ruled by a spatially periodic potential $V(\mathbf{r})$ originating from the positively charged crystal atoms and the mean field produced by the quasi-free electrons,

$$V(\mathbf{r}) = V(\mathbf{r} + \mathbf{R}) \ , \tag{26.1}$$

where $\mathbf{R}$ is a vector connecting two arbitrarily chosen atoms of the lattice. With the Hamiltonian

$$\hat{H} = -\frac{\hbar^2}{2m}\nabla^2 + V(\mathbf{r}) \tag{26.2}$$

we can write the Schrödinger equation,

$$[\hat{H} + V(\mathbf{r})]\psi(\mathbf{r}) = E\psi(\mathbf{r}) \ . \tag{26.3}$$

Since V and ∇ are invariant under translations $U_{tr}(\mathbf{R})\psi(\mathbf{r}) \equiv \psi(\mathbf{r} + \mathbf{R})$ by a fixed distance $\mathbf{R}$, where the translation operator has been defined in Eq. (23.181), we have,

$$\hat{H}U_{tr}(\mathbf{R})\psi(\mathbf{r}) = EU_{tr}(\mathbf{R})\psi(\mathbf{r}) \ . \tag{26.4}$$

That is, for a non-degenerate eigenvalue [1],

$$\psi(\mathbf{r}+\mathbf{R}) = f(\mathbf{R})\psi(\mathbf{r}) \ . \tag{26.5}$$

This relation holds for all vectors $\mathbf{R}$ of the lattice, such that,

$$f(\mathbf{R}_1+\mathbf{R}_2)\psi(\mathbf{r}) = \psi(\mathbf{r}+\mathbf{R}_1+\mathbf{R}_2) = f(\mathbf{R}_1)\psi(\mathbf{r}+\mathbf{R}_2) = f(\mathbf{R}_1)f(\mathbf{R}_2)\psi(\mathbf{r}) \ . \tag{26.6}$$

The relationship $f(\mathbf{R}_1+\mathbf{R}_2) = f(\mathbf{R}_1)f(\mathbf{R}_2)$ is satisfied by the ansatz $f(\mathbf{R}) \equiv e^{\imath\mathbf{k}\cdot\mathbf{R}}$, where $\mathbf{k}$ is an arbitrary vector of reciprocal space. We get the famous *Bloch theorem*,

$$\boxed{\psi_{\mathbf{k}}(\mathbf{r}+\mathbf{R}) = e^{\imath\mathbf{k}\cdot\mathbf{R}}\psi_{\mathbf{k}}(\mathbf{r})} \ , \tag{26.7}$$

which represents a necessary condition for any eigenfunction $\psi_{\mathbf{k}}$ of the Schrödinger equation with periodic potential. Bloch's theorem simply postulates that, apart from a phase factor, the wavefunction has the same periodicity as the potential.

The *Bloch function*,

$$\boxed{\psi_{\mathbf{k}}(\mathbf{r}) \equiv u_{\mathbf{k}}(\mathbf{r})e^{\imath\mathbf{k}\cdot\mathbf{r}} \qquad \text{with} \qquad u_{\mathbf{k}}(\mathbf{r}+\mathbf{R}) = u_{\mathbf{k}}(\mathbf{r})} \ , \tag{26.8}$$

automatically satisfies Bloch's theorem. That is, the wave function of the electron ψ is a plane wave $e^{\imath\mathbf{k}\cdot\mathbf{r}}$ modulated by a function $u_{\mathbf{k}}$ having the same periodicity as the lattice [741]. Although the vector of the electronic wave is arbitrary, it is possible (and useful) to restrict its value to the first *Brillouin zone* defined by $\mathbf{k} \in [-\pi/\mathbf{a}, \pi/\mathbf{a}]$, where $\mathbf{a}$ is an elementary vector of the lattice. The reason is that we can reduce a wavevector $\mathbf{k}$ in a wavefunction trespassing the first Brillouin zone by an appropriate vector $\mathbf{G}$ of *reciprocal lattice*,

$$\mathbf{k}' = \mathbf{k} + \mathbf{G} \ , \tag{26.9}$$

yielding,

$$\psi_{\mathbf{k}}(\mathbf{r}) = u_{\mathbf{k}}(\mathbf{r})e^{\imath\mathbf{k}\cdot\mathbf{r}} = u_{\mathbf{k}}(\mathbf{r})e^{-\imath\mathbf{G}\cdot\mathbf{r}}e^{\imath\mathbf{k}'\cdot\mathbf{r}} \ . \tag{26.10}$$

We now define another function $u_{\mathbf{k}'}(\mathbf{r}) \equiv u_{\mathbf{k}}(\mathbf{r})e^{-\imath\mathbf{G}\cdot\mathbf{r}}$, which also satisfies the requirement (26.8), knowing that $\mathbf{G}\cdot\mathbf{R} = n2\pi$, we see,

$$u_{\mathbf{k}'}(\mathbf{r}+\mathbf{R}) = u_{\mathbf{k}}(\mathbf{r}+\mathbf{R})e^{-\imath\mathbf{G}\cdot(\mathbf{r}+\mathbf{R})} = u_{\mathbf{k}}(\mathbf{r})e^{-\imath\mathbf{G}\cdot\mathbf{r}} = u_{\mathbf{k}'}(\mathbf{r}) \ . \tag{26.11}$$

Hence,

$$\psi_{\mathbf{k}}(\mathbf{r}) = u_{\mathbf{k}'}(\mathbf{r})e^{\imath\mathbf{k}'\cdot\mathbf{r}} = \psi_{\mathbf{k}'}(\mathbf{r}) \ . \tag{26.12}$$

26.1.1 Approximation for quasi-bound electrons

We now assume that the behavior of the electron near an atom is not influenced by atoms farther apart,

$$\psi_{\mathbf{k}}(\mathbf{r}) = \sum_{i\in\text{lattice}} c_i(\mathbf{k})\phi(\mathbf{r}-\mathbf{R}_i) \ . \tag{26.13}$$

That is, we neglect superposition states of the electron at various sites of the lattice. The atom is subject to a potential $U_{at}(\mathbf{r}-\mathbf{R}_i)$ located near the atom at the position

[1] This also holds true for degenerate eigenvalues if we choose suitable basis of eigenvectors.

$\mathbf{R}_i$, and it is described by the eigenfunction $\phi(\mathbf{r}-\mathbf{R}_i)$ (only defined for the site i) with energy E_0,

$$\left[-\frac{\hbar^2}{2m}\nabla^2 + U_{at}(\mathbf{r}-\mathbf{R}_i)\right]\phi(\mathbf{r}-\mathbf{R}_i) = E_0\phi(\mathbf{r}-\mathbf{R}_i)\ . \tag{26.14}$$

Even so, the function $\psi_{\mathbf{k}}(\mathbf{r})$ must satisfy Bloch's theorem. This is the case when $c_i(\mathbf{k}) = e^{\imath\mathbf{k}\cdot\mathbf{R}_i}$ and therefore,

$$\psi_{\mathbf{k}}(\mathbf{r}) = \sum_{i\in\text{lattice}} e^{\imath\mathbf{k}\cdot\mathbf{R}_i}\phi(\mathbf{r}-\mathbf{R}_i)\ . \tag{26.15}$$

Example 169 (*Ansatz for a quasi-bound electron wavefunction*): The ansatz (26.15) satisfies Bloch's theorem because,

$$\psi_{\mathbf{k}}(\mathbf{r}+\mathbf{R}_j) = \sum_i e^{\imath\mathbf{k}\cdot\mathbf{R}_i}\phi(\mathbf{r}-(\mathbf{R}_i-\mathbf{R}_j)) = e^{i\mathbf{k}\cdot\mathbf{R}_j}\sum_i e^{\imath\mathbf{k}\cdot(\mathbf{R}_i-\mathbf{R}_j)}\phi(\mathbf{r}-(\mathbf{R}_i-\mathbf{R}_j)) = e^{\imath\mathbf{k}\cdot\mathbf{R}_j}\psi_{\mathbf{k}}(\mathbf{r})\ .$$

We now calculate the energy $E(\mathbf{k})$ of an electron with the wavevector $\mathbf{k}$ inserting the function $\psi_{\mathbf{k}}(\mathbf{r})$ of (26.15) in the Schrödinger equation and obtain,

$$\left[-\frac{\hbar^2}{2m}\nabla^2 + U(\mathbf{r})\right]\sum_i e^{\imath\mathbf{k}\cdot\mathbf{R}_i}\phi(\mathbf{r}-\mathbf{R}_i) = E(\mathbf{k})\sum_i e^{\imath\mathbf{k}\cdot\mathbf{R}_i}\phi(\mathbf{r}-\mathbf{R}_i)\ . \tag{26.16}$$

$U(\mathbf{r})$ is the potential energy of the electron illustrated in Fig. 26.1 together with the energy $U_{at}(\mathbf{r}-\mathbf{R}_i)$ of a free electron.

Substituting the kinetic energy term of (26.16) by the kinetic energy of (26.14), we calculate,

$$\sum_i e^{\imath\mathbf{k}\cdot\mathbf{R}_i}[-U_{at}(\mathbf{r}-\mathbf{R}_i) + E_0 + U(\mathbf{r}) - E(\mathbf{k})]\phi(\mathbf{r}-\mathbf{R}_i) = 0\ . \tag{26.17}$$

Now, multiplying this equation with $\psi^*_{\mathbf{k}}(\mathbf{r}) = \sum_j e^{\imath\mathbf{k}\cdot\mathbf{R}_j}\phi^*(\mathbf{r}-\mathbf{R}_j)$ and integrating over the volume of the crystal, we obtain,

$$\begin{aligned}[E(\mathbf{k}) - E_0]\sum_{i,j} e^{\imath\mathbf{k}\cdot(\mathbf{R}_i-\mathbf{R}_j)}\int \phi^*(\mathbf{r}-\mathbf{R}_j)\phi(\mathbf{r}-\mathbf{R}_i)dV \\ = \sum_{i,j} e^{\imath\mathbf{k}\cdot(\mathbf{R}_i-\mathbf{R}_j)}\int \phi^*(\mathbf{r}-\mathbf{R}_j)[U(\mathbf{r}) - U_{at}(\mathbf{r}-\mathbf{R}_i)]\phi(\mathbf{r}-\mathbf{R}_i)dV\ .\end{aligned} \tag{26.18}$$

The functions $\phi^*(\mathbf{r}-\mathbf{R}_j)$ and $\phi(\mathbf{r}-\mathbf{R}_i)$ overlap only a little, even for adjacent atoms, such that we can neglect the terms $i \neq j$ on the left side. The sum then corresponds to the number N of sites in the lattice. On the right side we can not neglect the terms involving other sites, because even if the wavefunctions of adjacent sites overlap little, the contribution of the potential difference $|U(\mathbf{r}) - U_{at}(\mathbf{r}-\mathbf{R}_i)|$ is much lower for $\mathbf{r} = \mathbf{R}_i$ than for $\mathbf{r} = \mathbf{R}_j$. On the other hand, as the wavefunctions $\phi(\mathbf{r}-\mathbf{R}_i)$

disappear quickly when $|\mathbf{r}-\mathbf{R}_i| > |\mathbf{R}_m-\mathbf{R}_i|$, we can focus on adjacent sites (called $\mathbf{R}_m$),

$$N[E(\mathbf{k})-E_0] = N\int \phi^*(\mathbf{r}-\mathbf{R}_i)[U(\mathbf{r})-U_{at}(\mathbf{r}-\mathbf{R}_i)]\phi(\mathbf{r}-\mathbf{R}_i)dV \tag{26.19}$$
$$+N\sum_{m=\text{adjacent}} e^{\imath\mathbf{k}\cdot(\mathbf{R}_i-\mathbf{R}_m)}\int \phi^*(\mathbf{r}-\mathbf{R}_m)[U(\mathbf{r})-U_{at}(\mathbf{r}-\mathbf{R}_i)]\phi(\mathbf{r}-\mathbf{R}_i)dV\ .$$

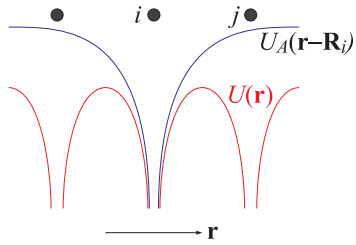

Figure 26.1: Potential energy $U(\mathbf{r})$ of a crystal electron (red) and potential energy $U_A(\mathbf{r}-\mathbf{R}_i)$ of the electron of a free atom (blue).

Now we further suppose that the eigenfunction ϕ exhibits radial symmetry corresponding to an s orbital. We obtain for the eigenvalues from the Schrödinger equation,

$$E(\mathbf{k}) = E_0-\alpha-\gamma\sum_{m\ \text{adjacent of}\ i} e^{\imath\mathbf{k}\cdot(\mathbf{R}_i-\mathbf{R}_m)} \tag{26.20}$$
$$\text{with}\quad \alpha = \int \phi^*(\mathbf{r}-\mathbf{R}_i)[U_{at}(\mathbf{r}-\mathbf{R}_i)-U(\mathbf{r})]\phi(\mathbf{r}-\mathbf{R}_i)dV$$
$$\text{and}\quad \gamma = \int \phi^*(\mathbf{r}-\mathbf{R}_m)[U_{at}(\mathbf{r}-\mathbf{R}_i)-U(\mathbf{r})]\phi(\mathbf{r}-\mathbf{R}_i)dV\ .$$

The interpretation is as follows: The combination of the atoms in a lattice produces an energy displacement α. In addition, it generates a spitting into a continuous band of energies as a function of reduced wavevector $\mathbf{k}$...

26.1.2 Approximation for quasi-free electrons

Here we assume an essentially homogeneous potential acting on the free electrons and consider the impact of the periodic lattice as a small perturbation. The periodic potential can be decomposed into a Fourier series by the vectors $\mathbf{G}$ of the reciprocal lattice,

$$U(\mathbf{r}) = \sum_{\mathbf{G}} U_{\mathbf{G}} e^{\imath\mathbf{G}\cdot\mathbf{r}}\ . \tag{26.21}$$

Consequently, we can make for Bloch functions (26.10) the following periodic ansatz,

$$\psi_{\mathbf{k}}(\mathbf{r}) = u_{\mathbf{k}}(\mathbf{r})e^{\imath\mathbf{k}\cdot\mathbf{r}} \qquad \text{with} \qquad u_{\mathbf{k}}(\mathbf{r}) = \tfrac{1}{\sqrt{V_c}}\sum_{\mathbf{G}} u_{\mathbf{G}}(\mathbf{k})e^{\imath\mathbf{G}\cdot\mathbf{r}}\ , \tag{26.22}$$

where V_c is the volume of the crystal.

Without periodic potential, the eigenfunctions would be those of a free particle,

$$\psi_{\mathbf{k}}(\mathbf{r}) = \tfrac{1}{V_c} e^{\imath \mathbf{k}\cdot\mathbf{r}} \tag{26.23}$$

with the eigenenergies

$$E_0(\mathbf{k}) = V_0 + \frac{\hbar^2 k^2}{2m} \ . \tag{26.24}$$

Inserting the functions (26.21) and (26.22) in the Schrödinger equation, we obtain,

$$\left[-\tfrac{\hbar^2}{2m}\nabla^2 + \sum_{\mathbf{G}''} U_{\mathbf{G}''} e^{\imath \mathbf{G}''\cdot\mathbf{r}} \right] \tfrac{1}{\sqrt{V_c}} e^{\imath \mathbf{k}\cdot\mathbf{r}} \sum_{\mathbf{G}'} u_{\mathbf{G}'}(\mathbf{k}) e^{\imath \mathbf{G}'\cdot\mathbf{r}} = E(\mathbf{k}) \tfrac{1}{\sqrt{V_c}} e^{\imath \mathbf{k}\cdot\mathbf{r}} \sum_{\mathbf{G}} u_{\mathbf{G}'}(\mathbf{k}) e^{\imath \mathbf{G}'\cdot\mathbf{r}} \ , \tag{26.25}$$

that is,

$$\tfrac{1}{\sqrt{V_c}} \sum_{\mathbf{G}'} \left[-\tfrac{\hbar^2}{2m}(\mathbf{k}+\mathbf{G}')^2 - E(\mathbf{k}) \right] u_{\mathbf{G}'}(\mathbf{k}) e^{\imath(\mathbf{k}+\mathbf{G}')\cdot\mathbf{r}} + \tfrac{1}{\sqrt{V_c}} \sum_{\mathbf{G}''} U_{\mathbf{G}''} e^{\imath \mathbf{G}''\cdot\mathbf{r}} \sum_{\mathbf{G}'} u_{\mathbf{G}'}(\mathbf{k}) e^{\imath(\mathbf{k}+\mathbf{G}')\cdot\mathbf{r}} = 0 \ . \tag{26.26}$$

Now multiplying with $\frac{1}{\sqrt{V_c}} e^{\imath(\mathbf{k}+\mathbf{G})\cdot\mathbf{r}}$ and integrating over the volume of the crystal (knowing $\frac{1}{V_c}\int_{V_c} e^{\imath \mathbf{G}\cdot\mathbf{r}} dV = \delta_{\mathbf{G},0}$), we obtain,

$$\left[\tfrac{\hbar^2}{2m}(\mathbf{k}+\mathbf{G})^2 - E(\mathbf{k}) \right] u_{\mathbf{G}}(\mathbf{k}) + \sum_{\mathbf{G}'} U_{\mathbf{G}-\mathbf{G}'} u_{\mathbf{G}'}(\mathbf{k}) = 0 \ , \tag{26.27}$$

for any value of $\mathbf{G}$.

To estimate the dependence of the Fourier components $u_{\mathbf{G}}(\mathbf{k})$ for $\mathbf{G} \neq 0$ we insert the unperturbed eigenenergies into the equation (26.27) only considering, in the sum over $\mathbf{G}'$, the terms of the first perturbative order, that is, those containing U_0 or $u_0(\mathbf{k})$,

$$\frac{\hbar^2}{2m}[(\mathbf{k}+\mathbf{G})^2 - k^2] u_{\mathbf{G}}(\mathbf{k}) - U_0 u_{\mathbf{G}}(\mathbf{k}) + U_0 u_{\mathbf{G}}(\mathbf{k}) + U_{\mathbf{G}} u_0(\mathbf{k}) = 0 \tag{26.28}$$

$$u_{\mathbf{G}}(\mathbf{k}) = \frac{U_{\mathbf{G}} u_0(\mathbf{k})}{\frac{\hbar^2}{2m}[k^2 - (\mathbf{k}+\mathbf{G})^2]} \ . \tag{26.29}$$

Since the Fourier coefficients $U_{\mathbf{G}}$ have, for $\mathbf{G} \neq 0$, small values, the function $u_{\mathbf{G}}(\mathbf{k})$ is not negligible only for $k^2 \simeq (\mathbf{k}+\mathbf{G})^2$ that is,

$$-2\mathbf{k}\cdot\mathbf{G} \simeq |\mathbf{G}|^2 \ . \tag{26.30}$$

We now want to find out the meaning of this condition ...

For the coefficients $u_0(\mathbf{k})$ and $u_{\mathbf{G}}(\mathbf{k})$ we obtain,

$$\left[\tfrac{\hbar^2}{2m} k^2 - E(\mathbf{k}) \right] u_0(\mathbf{k}) + U_0 u_0(\mathbf{k}) + U_{-\mathbf{G}}(\mathbf{k}) u_{\mathbf{G}}(\mathbf{k}) = 0 \tag{26.31}$$

$$\left[\tfrac{\hbar^2}{2m} k^2 - E(\mathbf{k}) \right] u_{\mathbf{G}}(\mathbf{k}) + U_{\mathbf{G}} u_0(\mathbf{k}) + U_0(\mathbf{k}) u_{\mathbf{G}}(\mathbf{k}) = 0 \ .$$

From this follows,

$$\left[\tfrac{\hbar^2}{2m} k^2 + U_0 - E(\mathbf{k}) \right]^2 = U_{\mathbf{G}} U_{-\mathbf{G}} = 0 \ . \tag{26.32}$$

Since the potential $U(\mathbf{r})$ is real, $U_{-\mathbf{G}} = U^*_{\mathbf{G}}$. Therefore, introducing the eigenenergies $E_0(\mathbf{k})$ of free electrons (26.24),

$$E(\mathbf{k}) = E_0(\mathbf{k}) \pm |U_{\mathbf{G}}| \ . \tag{26.33}$$

Under the influence of the periodic perturbation potential we find at the surfaces of a Brillouin zone an energy splitting developing a forbidden gap in the spectrum. We can understand this observation as follows: In the crystal all electronic waves with wavevectors ending on a surface of a Brillouin zone are reflected by Bragg reflection. In the example of a one-dimensional lattice we understand that the superposition of an incident wave ($k = n\pi/a$) with the reflected one ($k = -n\pi/a$) produces a standing electronic probability density wave ρ being proportional to $\rho_1 \propto \cos^2 n\pi/a$ or $\rho_2 \propto \sin^2 n\pi/a$. The charge density ρ_1 is maximal at the location of the atom in this site, which corresponds to an increased interaction energy; the density ρ_2 is minimal at the location of the atom. This explains the splitting.

The Bloch model can explain many properties of metals, semiconductors and insulators.

26.1.3 One-dimensional periodic potentials

In the following, we restrict ourselves to a one-dimensional potential, $V(z) = V(z+a)$, acting on (the center-of-mass of) atoms. How such potentials can be realized in practice will be shown in Sec. 26.2. For now, we just assume that we can write the potential as,

$$V(z) = -2V_0 \cos^2 Kz \ . \tag{26.34}$$

In the Fourier expansion, $V(z) = \sum_K U_K e^{\imath Kz}$, this potential corresponds to the Fourier coefficients $U_0 = -V_0$ and $U_{\pm K} = -\frac{V_0}{2}$,

$$V(z) = -V_0(1 + \tfrac{1}{2}e^{2\imath k_L z} + e^{-2\imath k_L z}) \ . \tag{26.35}$$

We also expand the wavefunction into plane waves,

$$\psi(z) = \sum_q c_q e^{\imath qz} \ , \tag{26.36}$$

and we insert these expansions into Schrödinger's stationary equation $\hat{H}\psi = \varepsilon\psi$, yielding,

$$\left[\frac{-\hbar^2}{2m}\frac{\partial^2}{\partial z^2} + \sum_K U_K e^{\imath Kz}\right] \sum_q c_q e^{\imath qz} = \varepsilon \sum_q c_q e^{\imath qz} \ . \tag{26.37}$$

Defining $q = k + nK$, where $k \in [-K/2, K/2]$ and $n \in \mathbb{Z}$,

$$\left[\tfrac{\hbar^2}{2m}(nK+k)^2 - V_0\right] c_{nK+k} - \tfrac{1}{2}V_0 c_{nK+k-K} - \tfrac{1}{2}V_0 c_{nK+k+K} = \varepsilon c_{nK+k} \ . \tag{26.38}$$

In matrix notation,

$$\hat{H}\mathbf{c} = \varepsilon\mathbf{c} \ . \tag{26.39}$$

where the matrix is around $n = .., -1, 0, +1, ..$:

$$\hat{H} = \begin{pmatrix} \ddots & & & & \\ & \frac{\hbar^2}{2m}(k-K)^2 - V_0 & -\frac{1}{2}V_0 & & \\ & -\frac{1}{2}V_0 & \frac{\hbar^2}{2m}k^2 - V_0 & -\frac{1}{2}V_0 & \\ & & -\frac{1}{2}V_0 & \frac{\hbar^2}{2m}(k+K)^2 - V_0 & \\ & & & & \ddots \end{pmatrix} \quad , \quad \mathbf{c} = \begin{pmatrix} \vdots \\ c_{k-K} \\ c_k \\ c_{k+K} \\ \vdots \end{pmatrix} . \tag{26.40}$$

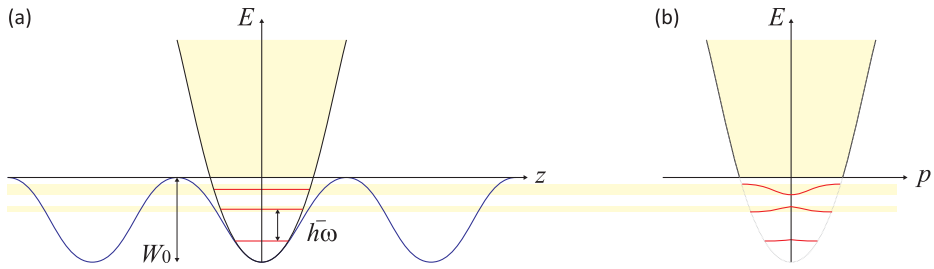

Figure 26.2: (a) Approximation of a periodic potential by a potential harmonic. (b) Dispersion relation in momentum space.

For shallow potentials, $V_0 \ll \hbar^2 K^2/2m$, we can neglect the coefficients V_0 in the Eq. (26.39) and we find,

$$\varepsilon \simeq \hbar^2 q^2/2m \ , \tag{26.41}$$

which corresponds to the dispersion relation for free particles. On the other hand, looking *at the bottom* of deep potentials, $V_0 \gg \hbar^2 K^2/2m$, we can harmonically approximate the cosine potential by $V(z) \approx -2V_0 + \frac{m}{2}\omega^2 z^2$ with $\omega = K\sqrt{V_0/m} = \hbar^{-1}\sqrt{2V_0 E_{rec}}$. For this case we expect,

$$\varepsilon \simeq -2V_0 + \hbar\omega\left(n + \tfrac{1}{2}\right) \ . \tag{26.42}$$

The exact spectrum of eigenvalues ε can be calculated by numerically determining the eigenvalues of the matrix (26.40) for the first Brillouin zone, $k \in [-K/2, K/2]$, and the above limits are confirmed.

To estimate the width of the forbidden band, we cut out a 2×2 matrix within the matrix $\hat{H}$ and neglect its coupling with the others submatrices,

$$\hat{H}_s = \begin{pmatrix} \frac{\hbar^2}{2m}(k-K)^2 - V_0 & -\frac{1}{2}V_0 \\ -\frac{1}{2}V_0 & \frac{\hbar^2}{2m}k^2 - V_0 \end{pmatrix} \ . \tag{26.43}$$

At the edges of the Brillouin zone, $k = \frac{1}{2}K$, we get the eigenvalues $\varepsilon = \frac{\hbar^2 K^2}{m} - V_0 \pm \frac{V_0}{2}$, that is, the band gap is $\Delta\varepsilon = V_0$. Bloch's theorem says that Schrödinger's equation can be solved for any *Bloch states*. These are superpositions of plane wave momentum states [53],

$$\psi_k(z) = e^{\imath kz} u_k(z) \ , \tag{26.44}$$

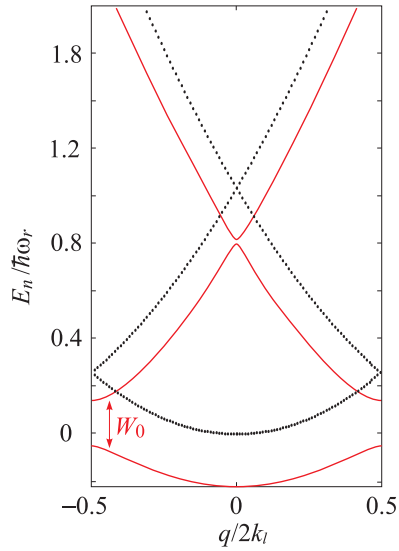

Figure 26.3: (code) Bloch bands with coupling potential (continuous red line) and without potential, $V_0 = 0$ (dotted black line). The parameters are $\omega_r = (2\pi)\ 20\,\text{kHz}$, $\omega_{ho} = (2\pi)\ 12\,\text{kHz}$, $\lambda_L = 689\,\text{nm}$, and $V_0 = 0.2\hbar\omega_r$.

with $u_k(z) = u_k(z + a)$.

The requirement that $\psi(z)$ satisfies the Schrödinger equation is equivalent to the condition that $\mathbf{c}$ satisfies an eigenvalue equation. Let U be the matrix of the eigenvectors of $\hat{H}$ and $\hat{E}$ the diagonal matrix of eigenvalues: $\hat{H} = U^{-1}\hat{E}U$ gives $\hat{E}U\mathbf{c} = \varepsilon U\mathbf{c}$, such that $U\mathbf{c}$ can be understood as eigenvectors.

Alternatively, we define $d_{nK+k} \equiv c_{nK+k+K}/c_{nK+k}$, consequently Eq. (26.39) becomes,

$$d_{nK+k-K} = \frac{V_0}{\frac{\hbar^2}{m}(nK+k)^2 - 2\varepsilon - V_0(2 + d_{nK+k})} \ . \tag{26.45}$$

26.1.4 Bloch oscillations

A *Bloch oscillation* is a phenomenon in solid state physics. It is the oscillation of a particle (e.g., an electron) confined to a periodic potential (e.g. a crystal), when a constant force (e.g., generated by a continuous electric field) acts on it. This phenomenon is very difficult to observe in solid crystals because, due to electron scattering by defects of the lattice [316, 1007], the coherent evolution is limited to a small fraction of the Brillouin zone. However, Bloch oscillations were observed in semiconducting superlattices, in ultrathin *Josephson junctions*, and with cold atoms in optical lattices [583, 851].

Let us first show a simple treatment for electrons subject to a constant electric field $\mathcal{E}$. The one-dimensional equation of motion is,

$$\hbar\frac{dk}{dt} = -e\mathcal{E} \ , \tag{26.46}$$

with the solution,

$$k(t) = k(0) - \frac{e\mathcal{E}}{\hbar} t \ . \tag{26.47}$$

The velocity v of the electron is given by,

$$v(k) = \frac{1}{\hbar} \frac{d\mathcal{E}}{dk} \ , \tag{26.48}$$

where $\mathcal{E}(k)$ denotes the *dispersion relation* for a given energy band. We now assume that it has the following form (tight-binding limit),

$$\mathcal{E} = A \cos ak \ , \tag{26.49}$$

where a is the lattice parameter and A a constant. Then, $v(k)$ is given by,

$$v(k) = -\frac{Aa}{\hbar} \sin ak \ , \tag{26.50}$$

and the position of the electron by,

$$x(t) = \int v(k(t))dt = -\frac{A}{e\mathcal{E}} \cos\left(\frac{ae\mathcal{E}}{\hbar} t\right) \ . \tag{26.51}$$

This shows, that the electron is oscillating in real space. The oscillation frequency, called *Bloch frequency* is given by,

$$\omega_{blo} = \frac{ae|\mathcal{E}|}{\hbar} \ . \tag{26.52}$$

26.1.5 Exercises

26.2 Optical lattices

Periodic potentials for quantum particles can be realized artificially. A prominent example are *optical lattices* formed by the interference patterns of intersecting laser beams. Tuned sufficiently far away from atomic resonances the periodically structured light field exerts optical forces on the atoms which can be derived from potentials being proportional to the local light intensity. As these forces are relatively weak, the kinetic energy of the atoms must be very low (typically μK) to allow for their impact to be relevant. In many cases, the depth of the optical lattice only allows for a small number of localized quantum states, so that the quantum nature of the atomic motion becomes highly relevant. Famous examples are the Bloch oscillations and the Mott insulating states.

We are not yet prepared to understand, how these potential arise from the light-atom interaction, as this topic will only be treated in the Secs. 38.2 and in Chp. 42.8.2. However, this is not necessary to understand many of the features of the atomic dynamics in optical lattices. We will thus simply impose a known periodic potential to a cold atomic cloud and study its energetic band structure and the atomic motion.

Various three-dimensional crystalline geometries have been realized and studied [673, 558, 153]. In the following, we will mainly focus on one-dimensional lattices, leaving a discussion of phenomena specific to three-dimensional lattices to future sections.

26.2.1 Atoms in 1D optical lattices

As already pointed out, a periodic optical potential can be generated by two counter-propagating plane wave laser beams, $e^{\pm \imath k_l z}$, with wavevectors k_l and $-k_l$ and tuned to the red side of an atomic transition. In this situation the atoms are attracted to the maxima of the light intensity, the antinodes,

$$V(z) = \tfrac{V_0}{4}|e^{\imath k_l z} + e^{-\imath k_l z}|^2 = \tfrac{V_0}{2}[1 + \cos(2k_l z)] \ . \tag{26.53}$$

Applying the procedure unfolded in Sec. 26.1.3 to the optical lattice, we expand the motional atomic wavefunction into plane (Bloch) waves,

$$\psi(z) = \sum_{n=-\infty}^{\infty} c_n e^{2\imath q z} e^{2\imath n k_l z} \ , \tag{26.54}$$

where $|c_n(t)|^2$ are the population of momentum states separated by $2k_l$ in momentum space. Inserting this expansion and the potential (26.53), after removing the constant energy $V_0/2$, into the stationary Schrödinger equation,

$$E\psi = -\frac{\hbar^2}{2m}\frac{\partial^2 \psi}{\partial z^2} + \frac{V_0}{2}\cos(2k_l z)\psi \ , \tag{26.55}$$

we obtain, collecting terms oscillating with the same exponential $e^{2\imath n k_l z}$,

$$\boxed{E_n c_n = 4\hbar\omega_{rec}\left(n + \frac{q}{k_l}\right)^2 c_n + \frac{V_0}{4}(c_{n+1} + c_{n-1})} \ , \tag{26.56}$$

where we defined an abbreviation,

$$\omega_{rec} = \frac{\hbar k_l^2}{2m} \tag{26.57}$$

called *recoil frequency* [2]. The eigenvalue problem (26.56) can be solved numerically for any value of q, yielding the dispersion relation already exhibited in Fig. 26.3.

To reproduce the dynamics of the matter wave, we start from the time-dependent Schrödinger equation with the same periodic potential. We again expand the time-dependent wavefunction into plane waves via,

$$\psi(z,t) = \sum_{n=-\infty}^{\infty} c_n(t) e^{2\imath n k_l z} \ , \tag{26.58}$$

and insert this ansatz into the Schrödinger equation,

$$\imath\hbar\frac{\partial \psi}{\partial t} = -\frac{\hbar^2}{2m}\frac{\partial^2 \psi}{\partial z^2} + \frac{V_0}{4}\cos(2k_l x)\psi \ , \tag{26.59}$$

obtaining a set of equations of motion for the expansion coefficients c_n,

$$\boxed{\dot{c}_n = -4\imath\omega_{rec} n^2 c_n + \frac{V_0}{4\imath\hbar}(c_{n+1} + c_{n-1})} \ . \tag{26.60}$$

The temporal evolution of the coefficients $c_n(t)$ can be simulated numerically.

[2] The reason of the terminology, which will become clear after a study of Sec. 38.2, is that the $\hbar\omega_{rec}$ is the kinetic energy of an atom having received two units of photonic momenta.

26.2.2 Bloch oscillations of atoms in 1D optical lattices

Neutral atoms in a vertical optical lattice are accelerated by gravity, and this accelerated motion leads to Bloch oscillations [316, 1007]. To treat this case, we could simply replace the electric force $-e\vec{\mathcal{E}}$ in the expression (26.52) by the gravitational force mg and obtain the result,

$$\omega_{blo} = \frac{mg\lambda_l}{2\hbar} \ , \tag{26.61}$$

with the wavelength $\lambda_l = 2a$ of the counterpropagating lasers generating the standing wave.

For didactic reasons, however, let us formulate the problem in the language introduced in the previous section extending the Hamiltonian by the gravitational potential [3] (see also Exc. 23.5.6.2),

$$\hat{H} = -\frac{\hbar^2}{2m}\frac{\partial^2}{\partial z^2} + \frac{V_0}{2}\cos 2k\hat{z} + mg\hat{z} \ . \tag{26.62}$$

We define the transformation $U \equiv e^{-\imath mg\hat{z}t/\hbar}$ and find with (23.167) and (23.213) the Hamiltonian in the accelerated frame,

$$\tilde{H} = U^\dagger \hat{H} U + \imath\hbar\dot{U}^\dagger U = \frac{\tilde{p}^2}{2m} + \frac{V_0}{4}\left(e^{2\imath k\hat{z}} + e^{-2\imath k\hat{z}}\right) \ . \tag{26.63}$$

with

$$\tilde{p} \equiv \hat{p} - mgt = U^\dagger \hat{p} U \ . \tag{26.64}$$

Now, we expand the operators using the rules (23.99) and (23.213) [4],

$$\begin{aligned} \tilde{p} &= \int p|p\rangle\langle p|dp \longrightarrow \sum_n (p + 2n\hbar k)|p + 2n\hbar k\rangle\langle p + 2n\hbar k| \\ e^{2\imath k\hat{z}} &= \int |p + 2\hbar k\rangle\langle p|dp \longrightarrow \sum_n |p + 2(n+1)\hbar k\rangle\langle p + 2n\hbar k| \ , \end{aligned} \tag{26.65}$$

based on the assumption that every atom can only exist in a superposition of discrete momentum states separated by $2\hbar k$, but can have an 'offset' momentum $p = mv$, e.g. due to thermal motion. Disregarding thermal motion, we may set in the accelerated frame $p = 0$. Then,

$$\tilde{p} = \sum_n 2n\hbar k|2n\hbar k\rangle\langle 2n\hbar k| \qquad \text{and} \qquad e^{2\imath k\hat{z}} = \sum_n |2n\hbar k + 2\hbar k\rangle\langle 2n\hbar k| \ , \tag{26.66}$$

such that,

$$\tilde{H} = \sum_n 4n^2\hbar\omega_{rec}|2n\hbar k\rangle\langle 2n\hbar k| + \tfrac{V_0}{4}\sum_n \left(|2n\hbar k + 2\hbar k\rangle\langle 2n\hbar k| + |2n\hbar k\rangle\langle 2n\hbar k + 2\hbar k|\right) \ . \tag{26.67}$$

[3] For Bose-Einstein condensates, the procedure should be generalized taking into account the energy of the mean field due to interatomic collisions.

[4] See also (42.149) and (42.156).

With the expansion of the wavefunction $|\tilde{\psi}\rangle = \sum_n c_n |2n\hbar k\rangle$ the Schrödinger equation becomes [1138, 1139],

$$\begin{aligned} \imath\hbar \frac{d}{dt}|\tilde{\psi}\rangle &= \imath\hbar \sum_n \dot{c}_n |2n\hbar k\rangle \\ &= \sum_n \left(4n^2\hbar\omega_{rec} c_n + \tfrac{V_0}{4}(c_{n-1} + c_{n+1})\right) |2n\hbar k\rangle = \tilde{H}|\tilde{\psi}\rangle \ , \end{aligned} \tag{26.68}$$

that is,

$$\dot{c}_n = -4\imath n^2 \omega_{rec} c_n + \frac{V_0}{4\imath\hbar}(c_{n-1} + c_{n+1}) \ . \tag{26.69}$$

In the lab frame the wavefunction reads,

$$\begin{aligned} |\psi\rangle = U|\tilde{\psi}\rangle &= e^{-\imath m g \hat{z} t/\hbar} \sum_n c_n |2n\hbar k\rangle \\ &= \sum_n c_n |2n\hbar k - mgt\rangle = \sum_n c_n |2\hbar k(n - \nu_{blo} t)\rangle \ , \end{aligned} \tag{26.70}$$

where we introduced the *Bloch frequency*,

$$\boxed{\nu_{blo} = \frac{mg}{2\hbar k}} \ . \tag{26.71}$$

Finally,

$$\boxed{\dot{c}_n = -4\imath (n - \nu_{blo} t)^2 \omega_{rec} c_n + \frac{V_0}{4\imath\hbar}(c_{n-1} + c_{n+1})} \ . \tag{26.72}$$

The center-of-the mass momentum of the atomic matter wave is,

$$\frac{\langle p \rangle_{lab}}{\hbar k_l} = \sum_n n |c_n(t)|^2 + \nu_{blo} t \ . \tag{26.73}$$

The Bloch oscillations can be understood in various pictures. The first one, illustrated in 26.4(a), is based on *Bragg reflection*: A resting atom has infinite de Broglie wavelength. Being constantly accelerated by gravity, the matter wave reduces its de Broglie wavelength from ∞ to a value, where it becomes commensurate with the periodicity of the standing light wave potential. At this moment Bragg scattering comes into play, reflecting the atomic motion back into upward direction, and the process starts over again. The atoms evolve like jumping on a trampoline with a frequency given by ν_{blo}.

To understand the second picture, we need to address a question we have left aside so far, as this requires a notion of optical forces. It is the question in which way the matter wave interacts with the standing light wave. For the present discussion, it is sufficient to know that the atom must have an internal transition capable of scattering photons from the light beams. As any absorption and emission process transfers a recoil momentum of $\hbar k_l$ to the atom, we can understand the Bragg scattering process as a so-called *Raman scattering* process: a photon of the laser beam generating the optical lattice coming from the left is absorbed and re-emitted to the left. This is best illustrated in the momentum domain sketched in Fig. 26.4(b). This Raman scattering

transfers twice the photonic recoil to the atom. The requirement for commensurability of the Broglie wavelength and wavelength of the standing light wave is equivalent to saying that the matter wave momentum is equal to the recoil of a single photon. In other words, the matter wave always Bragg-reflected at the edge of a Brillouin zone.

Finally, in the *Bloch state picture*, the dispersion relation of a free particle is distorted due to the periodicity of the potential generated by the standing light wave such as to open a forbidden band. As a consequence, instead of being accelerated without limits, the atom enters the second Brillouin zone, which is to say that it is reflected to the other side of the first Brillouin zone.

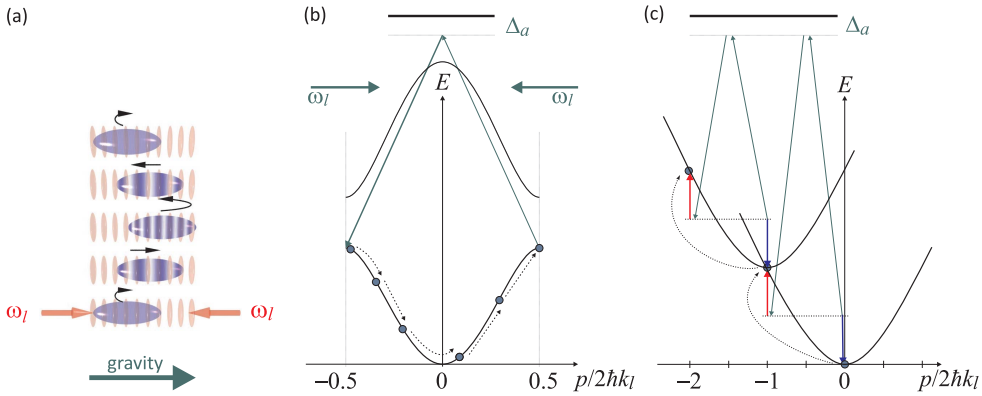

Figure 26.4: Illustration of Bloch oscillations (a) in real space, (b) in momentum space, and (c) in the moving frame. You may also run a movie of Bloch oscillations clicking on (watch movie)!

The additional term, which contains the frequency of the Bloch oscillation ν_{blo}, increases linearly over time. As time goes by, a resonance is crossed when $t = -n\tau_{blo}$, and the crossing is periodically repeated at every $n = -1, -2, 0, ...$ Tracing the matter wave evolution in the laboratory system, we see that whenever the resonance is crossed, the momentum undergoes a change of sign corresponding to a reflection of its motion. We expand the population of the momentum states into plane (Bloch) waves with $|c_n(t)|^2$.

Of course there are some conditions that need to be met to observe Bloch oscillations. The transfer of momentum is efficient only in the rapid adiabatic passage (ARP) regime characterized by the conditions $2(\nu_{blo}/\omega_{rec}) \ll (W_0/4\omega_{rec})^2 \ll 16$. The first condition requires that the force that drives the atoms to perform the Bloch oscillations must be weak enough to avoid transitions between Bloch bands, which guarantees the adiabaticity of the process. The other condition requires that the optical lattice be weak enough so that the dynamics involves only two adjacent momentum states at the same time and the transfer between the two is successful. A talk on this subject can be watched at (watch talk). Do the Exc. 26.2.3.1.

We will come back to the topic of optical lattices holding matter waves in Sec. 46.4.2 in the context of Mott insulating states of Bose-Einstein condensates.

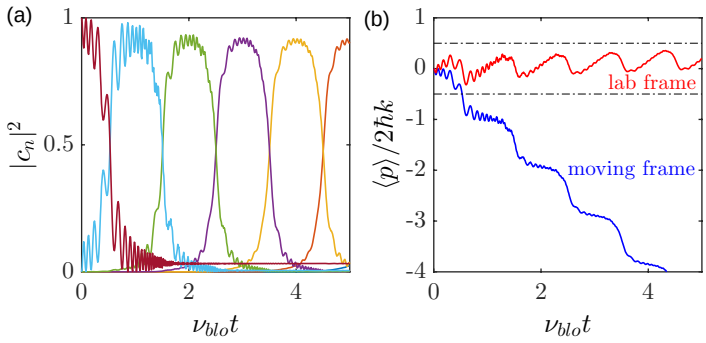

Figure 26.5: (code) Dynamics of Bloch's oscillations calculated from Eq. (26.57). (a) The colored curves show successively populated momentum states. (b) Center-of-mass motion of the wave packet in the lab frame (red) and in the moving frame (blue). The used parameters are $\omega_{rec} = (2\pi)\ 4.8\,\mathrm{kHz}$, $\nu_{blo} = 0.05\omega_{rec}$, and $W_0 = -0.7\omega_{rec}$.

26.2.3 Exercises

26.2.3.1 Ex: Purification of Bloch oscillations

Simulations of Bloch oscillations of atoms in an optical lattice for $W_0 = 0.4\omega_{rec}$ and $0.8\omega_{rec}$ produce the dynamics exhibited in Fig. 26.6. Interpret the different behaviors.

Solution: *(a-b) If the lattice is too shallow ($W_0 = 0.4\omega_{rec}$), the band gap is too narrow. The atom is then likely to tunnel into the next Bloch band staying inside its actual accelerated momentum state. I.e. stationary populations pile up in every c_n. Because the atom is not completely reflected at the edge of the Brillouin zone, its center of mass begins to drift.*
(e-f) If the lattice is too deep ($W_0 = 1.6\omega_{rec}$), the atom does not even reach the band gap. It stays confined to the standing wave potential oscillating like in a harmonic potential.
(c-d) If the lattice is just right ($W_0 = 0.8\omega_{rec}$), the atom is almost completely reflected. Fast initial oscillations damp out, because only the fastest atoms undergo Landau-Zener transitions confining them to the first momentum state c_0.
Approximating the lattice by a harmonic oscillator potential,

$$U_{dip}(z) = -\tfrac{\hbar W_0}{2}\cos 2kz \simeq -\tfrac{\hbar W_0}{2}(1 + k^2 z^2) \equiv \tfrac{m}{2}\omega_{ho}^2 z^2 \ ,$$

we expect the vibration frequency,

$$\omega_{ho} = \sqrt{2W_0\omega_{rec}} \ .$$

Using this formula it is possible to check that the fast vibrations observed in Figs. 26.6 have frequencies that correspond to $\omega_{ho}/2$.

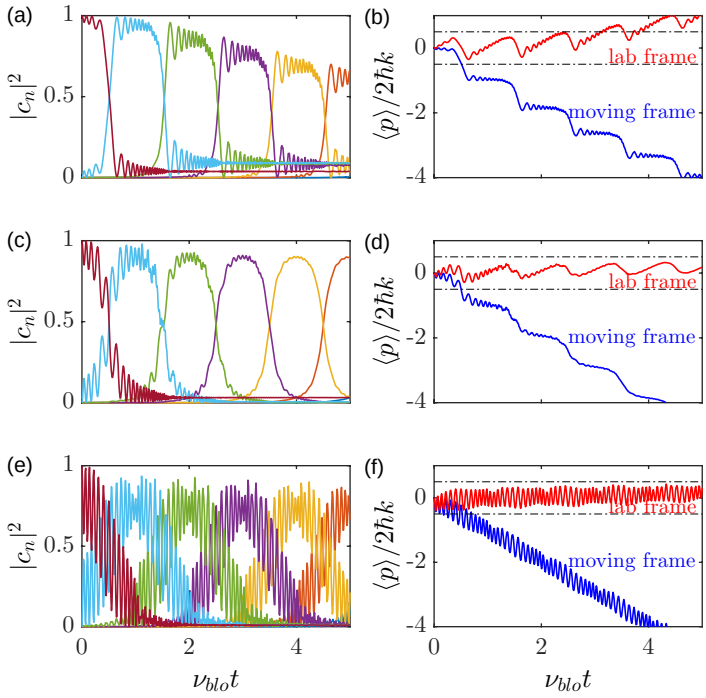

Figure 26.6: (code) Dynamics of Bloch oscillations (a-b) for $W_0 = 0.4\omega_{rec}$, (c-d) for $W_0 = 0.8\omega_{rec}$, and (e-f) for $W_0 = 1.6\omega_{rec}$. Furthermore, $\omega_{rec} = (2\pi)\ 4.8\,\mathrm{kHz}$ and $\nu_{blo} = 0.05\omega_{rec}$.

26.2.3.2 Ex: Gaussian approximation for Wannier function

Consider a standing light wave producing a dipolar potential of the shape $V(x) = W_0 \sin^2 kx = \frac{W_0}{2} - \frac{W_0}{2}\cos 2kx$ with $W_0 \gg E_{rec} = (\hbar k)^2/2m$.
a. Approximate the potential of a single lattice site around $x = 0$ by a harmonic potential. Calculate for which depth of the dipolar potential the approximated potential supports at least one bound state. What is the spacing of the levels and the characteristic size of the harmonic oscillator a_{ho}. Write down the normalized ground state wavefunction of the harmonic oscillator.
b. Now, let us consider a 3D cubic lattice made of three identical orthogonal standing light waves. Approximate the ground state Wannier function of a lattice site by appropriately normalized ground state wavefunctions of a harmonic oscillator. Derive the formula $U^{3d} = \frac{8}{\pi} k a_d \left(\frac{W_0}{E_{rec}}\right)^{3/4}$ starting from,

$$U^{3D} = g^{3D} \int \omega^4_{(0,0)}(x,y,z) d^3r$$

with $g^{3D} = \frac{4\pi\hbar a_d}{m}$.

Solution: *a. The harmonic approximation for the sinusoidal potential is,*

$$U(x) = W_0 (kx)^2 + \dots \ .$$

With $\omega \equiv \sqrt{\frac{2W_0k^2}{m}}$, *we can approximate the potential by,*

$$U_{ho}(x) = \frac{m}{2}\omega^2 x^2 \qquad for \qquad |x| \leq \sqrt{\frac{2\hbar U_0}{m\omega^2}} \qquad and \qquad U_{ho}(x) = 0 \qquad else\ .$$

The ground state of the harmonic oscillator is,

$$E_0 = \hbar\omega\left(0 + \frac{1}{2}\right) = \frac{\hbar\omega}{2}\ .$$

The condition of having at least one bound state, $E_0 < W_0$, *yields*

$$W_0 > E_0 = \frac{\hbar\omega}{2} = \frac{\hbar}{2}\sqrt{\frac{2W_0k^2}{m}} \qquad \Longrightarrow \qquad W_0 > \frac{\hbar k}{2m}\ .$$

This is precisely the energy of the photonic recoil of the light generating the standing wave. The spacing of the levels is $\hbar\omega$ *and the size of the harmonic oscillator is,*

$$a_{ho} = \sqrt{\frac{\hbar}{m\omega}}\ .$$

The normalized ground state wavefunction is given by,

$$\psi_{0,0}(x) = Ce^{-x^2/2a_{ho}^2} \qquad where \qquad C = \frac{1}{\sqrt{a_{ho}\sqrt{\pi}}}\ .$$

b. For the 3D harmonic oscillator the ground state wave function becomes simply,

$$\psi_{0,0}(\mathbf{r}) = C\psi_{0,0}(x)\psi_{0,0}(y)\psi_{0,0}(z)\ .$$

With the normalization condition,

$$1 = \int_{-\lambda/2}^{\lambda/2}\int_{-\lambda/2}^{\lambda/2}\int_{-\lambda/2}^{\lambda/2}\omega_{0,0}(\mathbf{r})d^3\mathbf{r} = \left(\int_{-\lambda/2}^{\lambda/2} C\sqrt{2}a_{ho}e^{-\tilde{x}^2}d\tilde{x}\right)^3$$
$$= (C\sqrt{2}a_{ho})^3\left(\int_{-\lambda/2}^{\lambda/2} e^{-\tilde{x}^2}d\tilde{x}\right)^3\ .$$

With this, ...

26.2.3.3 Ex: Perturbative treatment of a weak lattice

A weak lattice potential with $V_0 < E_{rec}$ can be treated in perturbation theory to motivate the resulting opening of a gap in the refolded energy parabola. The unperturbed Hamiltonian $\hat{H}_0 = p^2/2m$ contains only the kinetic energy and the perturbation is $V(x) = V_0\sin^2(kx) = \frac{1}{2}V_0 - \frac{1}{4}V_0(e^{2\imath kx} + e^{-2\imath kx})$.
a. Calculate $\hat{V}(x)\phi_p(x)$ and show that $\langle\phi_{p\pm\hbar k}|\hat{V}|\phi_p\rangle$ are the only non-zero matrix elements of the perturbation $V(x)$ between the eigenstates of $\hat{H}_0$ (which are the orthonormal plane waves $\phi_p = e^{\imath px/\hbar}$). Neglect the constant term of the potential,

which only yields a global energy shift.
b. This coupling is relevant around those momenta p, where ϕ_p has the same energy $\phi_{p+\hbar k}$ or $\phi_{p-\hbar k}$. Show that these momenta are $p = \mp\hbar k$.
c. Consider the perturbed system restricted to the basis $\{|p = -\hbar k\rangle, |p = +\hbar k\rangle\}$ and give the Hamiltonian as 2×2 matrix.
d. Diagonalize the matrix and consider the difference of the eigenenergies. Use them to estimate the size of the gap, that the lattice opens between the two lowest bands.
e. Calculate the eigenstates and interpret them by comparing the probability density to the lattice potential.

Solution:

26.3 The Kronig-Penney model

The *Kronig-Penney model* describes the band structure of a lattice. Let us assume a periodic potential of rectangular wells with valleys of widths a and peaks of widths b,

$$V(x) = U_0 \theta_{\mathrm{mod}(x,a+b)\in[a,a+b]} \ . \tag{26.74}$$

Inserting into the Schrödinger equation the plane wave ansatz $\psi = Ae^{\imath Kx} + Be^{-\imath Kx}$ for the wavefunction in the valley, $0 < x < a$, and $\psi = Ce^{Qx} + De^{-Qx}$ in the peak, $-b < x < 0$, we obtain $\varepsilon = \hbar^2 K^2/2m$ and $U_0 - \varepsilon = \hbar^2 Q^2/2m$. Choosing the constants A, B, C, D such that ψ and $\dot{\psi}$ are continuous in $x = 0, a$, we derive, using the periodicity of the Bloch wave $\psi(a < x < a + b) = \psi(-b < x < 0)e^{\imath k(a+b)}$,

$$\begin{pmatrix} 1 & 1 & -1 & -1 \\ \imath K & -\imath K & -Q & Q \\ e^{\imath Ka} & e^{-\imath Ka} & -e^{-Qb+\imath k(a+b)} & -e^{Qb+\imath k(a+b)} \\ \imath K e^{\imath Ka} & -\imath K e^{-\imath Ka} & -Qe^{-Qb+\imath k(a+b)} & Qe^{Qb+\imath k(a+b)} \end{pmatrix} \begin{pmatrix} A \\ B \\ C \\ D \end{pmatrix} = 0 \ . \tag{26.75}$$

The determinant of the matrix must be zero, or,

$$\frac{Q^2 - K^2}{2QK} \sinh Qb \sin Ka + \cosh Qb \cos Ka = \cos k(a + b) \ . \tag{26.76}$$

For δ-shaped peaks, we let $b = 0$ and $U_0 = \infty$ such that $Q^2 ba/2 = P$, this simplifies to,

$$\frac{P}{Ka} \sin Ka + \cos Ka = \cos ka \ . \tag{26.77}$$

The dispersion relation for light is different. According to [864],

$$-\frac{\sqrt{\varepsilon} + \sqrt{\varepsilon}^{-1}}{2} \sin(\sqrt{\varepsilon}\omega a/c) \sin(\omega a/c) + \cos(\sqrt{\varepsilon}\omega a/c) \cos(\omega a/c) = \cos ka \ . \tag{26.78}$$

For $\varepsilon = 1$ the equation simplifies to $ka = 2\omega a/c$.

26.3.1 Photonic density of states

The *photonic density of states* in free space in three dimensions is evaluated from [1324],

$$dN = 2\left(\frac{L}{2\pi}\right)^3 \int d^3k = 2\left(\frac{L}{2\pi}\right)^3 k^2 dk \int d\phi d\cos\theta = \frac{L^3\omega^2}{\pi^2 c^3} d\omega \equiv D(\omega)d\omega \ . \quad (26.79)$$

In one dimension,

$$dN = 2\frac{L}{2\pi}dk = \frac{L}{\pi c}d\omega \ . \quad (26.80)$$

The density is normalized $\int_0^{\pi c/L} D(\omega)d\omega = 1$ and the total energy, if all states are populated, is $E \equiv \int_0^{\pi c/L} \omega D(\omega)d\omega = \pi c/L$. However, this applies only if $\omega = ck$. If the dispersion relation is more complicated, for example, inside a cavity or a forbidden photonic band, $\omega = \omega(k)$, we must generalize,

$$D(\omega) = \frac{L}{\pi}\frac{dk}{d\omega} \ . \quad (26.81)$$

Assuming that the dispersion relation is given by the Kronig-Penney model, we obtain gaps in the density-of-states for those values of ω which do not belong to any k.

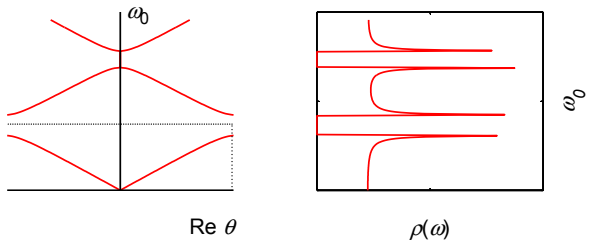

Figure 26.7: Dispersion ratio and state density for a one-dimensional optical lattice.

26.3.2 Exercises

26.3.2.1 Ex: Mass of photons in a lattice

The effective mass of particles in a lattice is defined as,

$$\frac{1}{m^*} = \frac{1}{\hbar^2}\frac{d^2E(k)}{dk^2} \ .$$

Calculate the effective mass of a rubidium atom in a far-detuned optical standing wave.

Solution: *For free electrons, $E = \hbar^2k^2/2m$, such that $1/m^* = 1/m$. For free photons $E = \hbar k/c$, such that $1/m^* = 0$!*

26.4 Further reading

B. Pelle et al., *State-labeling Wannier-Stark atomic interferometers* [1008]DOI

Min-Kang Zhou et al., *Atomic multiwave interferometer in an optical lattice* [1433]DOI

T. Hartmann et al., *Dynamics of Bloch oscillations* [583]DOI

N. Marzari et al., *Maximally localized Wannier functions: Theory and applications* [851]DOI

L. Guidoni et al., *Optical Lattices: Cold Atoms Ordered by Light* [558]DOI

N. Marzari et al., *Nonlinear Landau-Zener tunneling* [1390]DOI

E. Peik et al., *Bloch Oscillations of Atoms, Adiabatic Rapid Passage, and Monokinetic Atomic Beams* [1007]DOI

I. Bloch, *Ultracold quantum gases in optical lattices* [153]DOI

Chapter 27

Approximation methods

Virtually every problem going beyond the potential well, the harmonic oscillator, or the hydrogen atom without spin and external fields is impossible to solve analytically. In this chapter we will talk about techniques to solve approximately problems in more realistic situations. There are a number of methods of which we will discuss the only following: 1. The stationary or time-dependent perturbation method is useful for evaluating small perturbations of the system, for example, caused by external electric or magnetic fields; 2. the variational method, which serves to find and improve trial wavefunctions, the initial shapes of which are generally motivated by the symmetries of the system; 3. the semi-classical WKB method; 4. and finally the method of self-consistent fields, which is an iterative method of solving the Schrödinger equation.

27.1 Stationary perturbations

27.1.1 Time-independent perturbation theory

We first introduce *time-independent perturbation theory* (TIPT) for multilevel systems. We separate the Hamiltonian into an unperturbed part,

$$\hat{H}^{(0)}|\psi^{(0)}\rangle = E^{(0)}|\psi^{(0)}\rangle \ , \tag{27.1}$$

and perturbations, which are proportional to a small parameters λ,

$$\hat{H} = \hat{H}^{(0)} + \lambda\hat{H}^{(1)} + \lambda^2\hat{H}^{(2)} + .. \ . \tag{27.2}$$

The perturbed wavefunctions are,

$$|\psi\rangle = |\psi^{(0)}\rangle + \lambda|\psi^{(1)}\rangle + \lambda^2|\psi^{(2)}\rangle + .. \ , \tag{27.3}$$

and the energies

$$E = E^{(0)} + \lambda E^{(1)} + \lambda^2 E^{(2)} + .. \ . \tag{27.4}$$

The contributions $\propto \lambda^n$ are the *corrections* of order n. The equation we need to solve now is,

$$\hat{H}|\psi\rangle = E|\psi\rangle \ . \tag{27.5}$$

By inserting all the expansions above and segregating all orders of λ^k, we find the following system of equations,

$$\begin{aligned} \hat{H}^{(0)}|\psi^{(0)}\rangle &= E^{(0)}|\psi^{(0)}\rangle \\ (\hat{H}^{(0)} - E^{(0)})|\psi^{(1)}\rangle &= (E^{(1)} - \hat{H}^{(1)})|\psi^{(0)}\rangle \\ (\hat{H}^{(0)} - E^{(0)})|\psi^{(2)}\rangle &= (E^{(2)} - \hat{H}^{(2)})|\psi^{(0)}\rangle + (E^{(1)} - \hat{H}^{(1)})|\psi^{(1)}\rangle \\ &\dots \ . \end{aligned} \tag{27.6}$$

27.1.1.1 First order energy correction

We now consider eigenstates $|\psi_n^{(1)}\rangle$ of the perturbed system and expand the first-order correction of the wavefunction in a linear combination of unperturbed eigenvectors $|\psi_n^{(0)}\rangle \equiv |n\rangle$,

$$|\psi_n^{(1)}\rangle = \sum_m |m\rangle\langle m|\psi_n^{(1)}\rangle \ . \tag{27.7}$$

We insert this expansion into the second equation (27.6) and multiply with $\langle n|$,

$$\langle n|(\hat{H}^{(0)} - E_n^{(0)})\sum_m |m\rangle\langle m|\psi_n^{(1)}\rangle = 0 = \langle n|E_n^{(1)} - \hat{H}^{(1)}|n\rangle \ . \tag{27.8}$$

We obtain for the first order correction of the energy of unperturbed states,

$$\boxed{E_n^{(1)} = \langle n|\hat{H}^{(1)}|n\rangle} \ . \tag{27.9}$$

As a first example we will calculate in Exc. 27.1.3.1 the first order correction for the energy of a slightly deformed one-dimensional box potential.

27.1.1.2 First order correction for the wavefunction

Now let us have a look at the first-order correction for the wavefunction again considering the second equation (27.6),

$$\langle m|\hat{H}^{(0)} - E_n^{(0)}|\psi_n^{(1)}\rangle = \langle m|E_n^{(1)} - \hat{H}^{(1)}|n\rangle \ . \tag{27.10}$$

When $n = m$, the left side of this equation disappears. Therefore, $E_n^{(1)} - \langle n|\hat{H}^{(1)}|n\rangle = 0$, and we can restrict to the terms $n \neq m$ discarding the terms in $E_n^{(1)}$,

$$\langle m|\psi_n^{(1)}\rangle = \frac{E_n^{(1)}\delta_{mn} - \langle m|\hat{H}^{(1)}|n\rangle}{\hat{E}_m^{(0)} - E_n^{(0)}} = \frac{\langle m|\hat{H}^{(1)}|n\rangle}{E_n^{(0)} - E_m^{(0)}} \ . \tag{27.11}$$

We obtain for the first-order correction for the energy of the states,

$$\boxed{|\psi_n^{(1)}\rangle = \sum_m |m\rangle\langle m|\psi_n^{(1)}\rangle = \sum_{m\neq n} |m\rangle \frac{\langle m|\hat{H}^{(1)}|n\rangle}{\hat{E}_n^{(0)} - E_m^{(0)}}} \ . \tag{27.12}$$

This procedure simulates the distortion of the state by blending it with other states. The perturbation induces virtual transitions to other states. The perturbation is large when the blended levels are close.

See Exc. 27.1.3.2. In Exc. 27.1.3.3 we calculate the first order correction due to the finite extension of the hydrogen nucleus. In Exc. 27.1.3.4 we treat the coupling of the energy levels of a two-level system as a first order perturbation, and compare the result with the exact solution. The Stark effect for an electron confined in a box can be discussed (see Exc. 27.1.3.5) in first order TIPT.

27.1.1.3 Second order correction for the energy

To calculate the second order correction for the energy we expand the second order correction,

$$|\psi_n^{(2)}\rangle = \sum_m |m\rangle\langle m|\psi_n^{(2)}\rangle \ , \tag{27.13}$$

import it into the third equation (27.6) and multiply with $\langle n|$,

$$\langle n|(\hat{H}^{(0)}-E_n^{(0)})\sum_m |m\rangle\langle m|\psi_n^{(2)}\rangle = \langle n|(E_n^{(2)}-\hat{H}^{(2)})|n\rangle+\langle n|(E_n^{(1)}-\hat{H}^{(1)})\sum_m |m\rangle\langle m|\psi_n^{(1)}\rangle \ . \tag{27.14}$$

Now,

$$\sum_m \langle m|\psi_n^{(2)}\rangle(E_n^{(0)}-E_m^{(0)})\delta_{nm} = 0 = E_n^{(2)}-\langle n|\hat{H}^{(2)}|n\rangle+\sum_m \langle m|\psi_n^{(1)}\rangle\left(E_n^{(1)}\delta_{nm} - \langle n|\hat{H}^{(1)}|m\rangle\right) \ . \tag{27.15}$$

The left-hand side of this equation disappears. Also, on the right-hand side, for $n \neq m$, the term $E_n^{(1)}\delta_{nm}$ disappears, and for $n = m$ the whole parenthesis disappears. Therefore, we can discard the term $E_n^{(1)}$ and restrict the sum to terms with $n \neq m$. Inserting the coefficients $\langle m|\psi_n^{(1)}\rangle$ calculated in (27.11), we finally obtain,

$$\boxed{E_n^{(2)} = \langle n|\hat{H}^{(2)}|n\rangle + \sum_{m\neq n} \frac{\langle n|\hat{H}^{(1)}|m\rangle\langle m|\hat{H}^{(1)}|n\rangle}{E_n^{(0)} - E_m^{(0)}}} \ . \tag{27.16}$$

The first term is similar to the first order correction; the eigenvalue of the second order perturbation calculated in the base of the unperturbed states. The second term describes the shift of the energies through possible temporary transitions to other states.

In Exc. 27.1.3.6 we treat a system of three coupled levels up to the second perturbative order. The Stark effect discussed in Exc. 27.1.3.7 needs the TIPT calculation up to the second order.

27.1.2 TIPT with degenerate states

Exact calculations show that the effect of a perturbation is larger – but finite – for degenerate states. On the other hand, from the above expressions for the corrections of both energies and wavefunctions, we would infer that these corrections can become very large for small perturbations or even diverge.

Fortunately, the fact that every linear combination of degenerate wavefunctions is an eigenfunction of the Hamiltonian as well gives us the freedom to choose the combination, which is most similar to the final form of the perturbed wavefunctions.

For example, considering a perturbation by a magnetic field it may be advantageous to expand the spherical functions Y_{lm} on a basis of cylindrical coordinates [1]. We will see in the following that we can solve both problems, the selection of the initial combination and the prevention of divergent denominators at once, without explicitly specifying the expansion.

We consider eigenstates $|n,\nu\rangle$ with the energy $E_n^{(0)}$ being r times degenerate with respect to the quantum number ν, where $\nu = 1,..,r$. All states satisfy

$$\hat{H}^{(0)}|n,\nu\rangle = E_n^{(0)}|n,\nu\rangle \ . \tag{27.17}$$

We construct linear combinations that most resemble the perturbed states

$$|\psi_{n\mu}^{(0)}\rangle = \sum_{\nu=1}^{r} c_{\mu\nu}|n,\nu\rangle \ . \tag{27.18}$$

When the perturbation $\hat{H}^{(1)}$ is applied, we assume that the state $|\psi_{n\mu}^{(0)}\rangle$ is distorted towards the similar state $|\psi_{n\mu}\rangle$, and the energy changes from $E_n^{(0)}$ to $E_{n\mu}$. We now need the index μ to label the energy, since the degeneracy can be removed by the perturbation. As before, we write now,

$$\begin{aligned} \hat{H} &= \hat{H}^{(0)} + \lambda\hat{H}^{(1)} + .. \\ |\psi_{n\mu}\rangle &= |\psi_{n\mu}^{(0)}\rangle + \lambda|\psi_{n\mu}^{(1)}\rangle + .. \\ E_{n\mu} &= E_n^{(0)} + \lambda E_{n\mu}^{(1)} + .. \ . \end{aligned} \tag{27.19}$$

The replacement of these expansions in $\hat{H}|\psi_{n\mu}\rangle = E_{n\mu}|\psi_{n\mu}\rangle$, and a collection of the terms in λ up to first order gives,

$$\begin{aligned} \hat{H}^{(0)}|\psi_{n\mu}^{(0)}\rangle &= E_n^{(0)}|\psi_{n\mu}^{(0)}\rangle \\ (E_n^{(0)} - \hat{H}^{(0)})|\psi_{n\mu}^{(1)}\rangle &= (E_{n\mu}^{(1)} - \hat{H}^{(1)})|\psi_{n\mu}^{(0)}\rangle \ . \end{aligned} \tag{27.20}$$

As before, we try to express the first-order corrections for the wavefunctions through degenerate unperturbed wavefunctions $|\psi_{n\mu}^{(0)}\rangle$ and non-degenerate wavefunctions [2] $|\psi_m^{(0)}\rangle$:

$$|\psi_{n\mu}^{(1)}\rangle = \sum_{\nu} b_{\mu\nu}|\psi_{n\nu}^{(0)}\rangle + \sum_{m} a_{nm}|\psi_m^{(0)}\rangle \ . \tag{27.21}$$

Inserting this into the first-order equation (27.20), we obtain,

$$\sum_{\nu} b_{\mu\nu}(E_n^{(0)} - E_n^{(0)})|\psi_{n\nu}^{(0)}\rangle + \sum_{m} a_{nm}(E_m^{(0)} - E_n^{(0)})|\psi_m^{(0)}\rangle = (E_{n\mu}^{(1)} - \hat{H}^{(1)})|\psi_{n\mu}^{(0)}\rangle \ . \tag{27.22}$$

The first term disappears. Inserting the expansion (27.18),

$$\sum_{m} a_{nm}(E_m^{(0)} - E_n^{(0)})|\psi_m^{(0)}\rangle = (E_{n\mu}^{(1)} - \hat{H}^{(1)})\sum_{\nu} c_{\mu\nu}|n,\nu\rangle \ , \tag{27.23}$$

[1] Another example would be the preference for the coupled base $|(l,s)j,m_j\rangle$ in comparison to the decoupled base $|l,m_l,s,m_s\rangle$ knowing that the degeneracy in j is lifted, when there is an energy associated with interacting angular momenta and the degeneracy in m_j is lifted, when we apply a magnetic field.

[2] Note that we label all states *which are not degenerate with the state under investigation* $|\psi_{n\mu}^{(1)}\rangle$ with the index m, even if there are degeneracies between them.

and multiplying the two sides with $\langle n,\mu|$, we get zero on the left-hand side, since we can choose the non-degenerate states to be orthogonal $\langle n,\nu|m\rangle = \delta_{m,n}$. Hence,

$$\boxed{\sum_\nu c_{\mu\nu}\left[E^{(1)}_{n\mu}\langle n,\mu|n,\nu\rangle - \langle n,\mu|\hat{H}^{(1)}|n,\nu\rangle\right] = 0} \ . \tag{27.24}$$

This *secular equation* (one for each μ) represents, in fact, a set of r linear equations for the coefficients $c_{\mu\nu}$. The condition for having non-trivial solutions is,

$$\det\left(\langle n,\nu|\hat{H}^{(1)}|n,\mu\rangle - E^{(1)}_{n\mu}\delta_{\mu,\nu}\right)_{\mu,\nu} = 0 \ . \tag{27.25}$$

The solution of this *secular determinant* yields the solicited energies $E^{(1)}_\mu$. Now, the solution of the secular equation (27.24) *for each energy value* produces those coefficients, which represent the best linear combinations adapted to the perturbation. Unlike in previous calculations with degenerate states, here we consider linear combinations of vectors of the degenerate subspace prior to switching on the perturbation.

In practice, we apply perturbation theory only to the lowest relevant order. That is, we only calculate the second order correction if first order corrections vanish. One famous example is the *quadratic Stark effect* discussed in Sec. 30.3. In the case of eigenvalues, which are degenerate in the absence of perturbation, the first order will always produce a remarkable correction, as in the example of the *linear Stark effect*, also discussed in Sec. 30.3. For this reason, we need not discuss higher perturbation orders in the case of degenerate eigenvalues.

Example 170 (*Perturbation in a system with two degenerate states*): As an example, we consider the following Hamiltonian,

$$\hat{H} = \begin{pmatrix} \Delta & \Omega \\ \Omega & \Delta \end{pmatrix} \ .$$

The exact solution gives the eigenvalues and eigenvectors,

$$E_1 = \Delta+\Omega \quad , \quad E_2 = \Delta-\Omega \quad , \quad |\psi_1\rangle = \tfrac{1}{\sqrt{2}}\begin{pmatrix}1\\1\end{pmatrix} \quad , \quad |\psi_2\rangle = \tfrac{1}{\sqrt{2}}\begin{pmatrix}-1\\1\end{pmatrix} \ .$$

Now we divide the Hamiltonian into an unperturbed part and a perturbation,

$$\hat{H} \equiv \hat{H}^{(0)} + \hat{H}^{(1)} = \begin{pmatrix} \Delta & 0 \\ 0 & \Delta \end{pmatrix} + \begin{pmatrix} 0 & \Omega \\ \Omega & 0 \end{pmatrix} \ .$$

We get in zero order,

$$E^{(0)}_1 = \Delta = E^{(0)}_2 \quad , \quad |1\rangle = \begin{pmatrix}1\\0\end{pmatrix} \quad , \quad |2\rangle = \begin{pmatrix}0\\1\end{pmatrix} \ ,$$

The application of non-degenerate perturbation theory in first order would give,

$$\langle 1|\hat{H}^{(1)}|1\rangle = 0 = \langle 2|\hat{H}^{(1)}|2\rangle \quad , \quad |\psi^{(1)}_1\rangle = |1\rangle\frac{\langle 1|\hat{H}^{(1)}|2\rangle}{E^{(0)}_1 - E^{(0)}_2} \to \infty \leftarrow -|\psi^{(1)}_2\rangle \ .$$

That is, the correction of the energy vanishes in first order, while the correction of the wavefunction diverges. Obviously, the $|\nu\rangle$ obtained by the diagonalization of the matrix $\hat{H}^{(0)}$ is not adapted to the calculation of the matrix elements $\hat{H}^{(1)}$. Now, applying degenerate perturbation theory, we obtain by the secular determinant,

$$0 = \det\left[\langle\nu|\hat{H}^{(1)}|\mu\rangle - E_\mu^{(1)}\delta_{\mu,\nu}\right] = \det\begin{pmatrix} -E_\mu^{(1)} & \Omega \\ \Omega & -E_\mu^{(1)} \end{pmatrix} = (E_\mu^{(1)})^2 - \Omega^2 \ ,$$

eigenvalues are $E_1^{(1)} = \Omega$ and $E_2^{(1)} = -\Omega$ allowing the establishment of the secular equation,

$$c_{11}\left[E_1^{(1)} - \langle 1|\hat{H}^{(1)}|1\rangle\right] - c_{12}\langle 1|\hat{H}^{(1)}|2\rangle = c_{11}[\Omega - 0] - c_{12}\Omega = 0$$
$$-c_{21}\langle 2|\hat{H}^{(1)}|1\rangle + c_{22}\left[E_2^{(1)} - \langle 2|\hat{H}^{(1)}|2\rangle\right] = -c_{21}\Omega + c_{22}[-\Omega - 0] = 0 \ .$$

We obtain $c_{11} = c_{12}$ and $c_{21} = -c_{22}$ and with this,

$$|\psi_1^{(0)}\rangle = \sum_\nu c_{1\nu}|\nu\rangle = c_{11}|1\rangle + c_{12}|2\rangle = \tfrac{1}{\sqrt{2}}\begin{pmatrix}1\\1\end{pmatrix} \quad , \quad |\psi_2^{(0)}\rangle = c_{21}|1\rangle + c_{22}|2\rangle = \tfrac{1}{\sqrt{2}}\begin{pmatrix}-1\\1\end{pmatrix} \ .$$

Thus, we can verify that the corrections for the eigenenergies,

$$E_1 = E_1^{(0)} + \langle\psi_1^{(0)}|\hat{H}^{(1)}|\psi_1^{(0)}\rangle = \Delta + \Omega \quad , \quad E_2 = E_2^{(0)} + \langle\psi_2^{(0)}|\hat{H}^{(1)}|\psi_2^{(0)}\rangle = \Delta - \Omega \ ,$$

coincides with the exact calculation made at the beginning. The eigenfunctions $|\psi_1^{(0)}\rangle$ should be already corrected in zeroth order, which we verify by calculating,

$$|\psi_1^{(1)}\rangle = |\psi_1^{(0)}\rangle \frac{\langle\psi_1^{(0)}|\hat{H}^{(1)}|\psi_2^{(0)}\rangle}{E_1 - E_2} = 0 = |\psi_2^{(1)}\rangle \ .$$

In Exc. 27.1.3.8 we study a partially degenerate three-level system and the breakdown of the degeneracy due to a perturbation. And in Exc. 27.1.3.9 we will treat a perturbation in a box potential with degenerate energy levels.

27.1.3 Exercises

27.1.3.1 Ex: One-dimensional well with a deformation in the centre

Consider a one-dimensional potential well between $-L/2$ and $L/2$ with infinitely high walls. In the center of the well is a small deformation,

$$H^{(1)} = \begin{cases} \varepsilon \text{ for } \frac{-a}{2} \le x \le \frac{a}{2} \\ 0 \text{ outside that region} \ . \end{cases}$$

Calculate the correction for the eigenenergies in first order and discuss the limits $a \ll L$ and $a \to L$.

Solution: *The energies and wavefunctions for* $\varepsilon \longrightarrow 0$ *are,*

$$E_n^{(0)} = \frac{\pi^2\hbar^2 n^2}{2mL^2} \quad , \quad \psi^{(0)}_{n=impar}(x) = \sqrt{\frac{2}{L}}\cos\frac{n\pi x}{L} \quad , \quad \psi^{(0)}_{n=par}(x) = \sqrt{\frac{2}{L}}\sin\frac{n\pi x}{L} \ ,$$

because it is easy to check,

$$\psi_n^{(0)}(\pm L/2) = 0 \qquad \textit{and} \qquad \frac{2}{L}\int_{-L/2}^{L/2} \cos^2\frac{n\pi x}{L}dx = 1 = \frac{2}{L}\int_{-L/2}^{L/2} \sin^2\frac{n\pi x}{L}dx \ .$$

The first order correction is,

$$\begin{aligned} E_n^{(1)} = \langle n|H^{(1)}|n\rangle &= \int_0^L \psi_n^{*(0)}(x)H^{(1)}(x)\psi_n^{(0)}(x)dx = \frac{2}{L}\int_{-a/2}^{a/2} \varepsilon \begin{pmatrix} \cos^2\frac{n\pi x}{L} \\ \sin^2\frac{n\pi x}{L} \end{pmatrix} dx \\ &= \frac{4\varepsilon}{L}\int_0^{a/2}\left(\frac{1}{2} \pm \frac{1}{2}\cos\frac{2n\pi x}{L}\right)dx = \frac{2\varepsilon}{L}\frac{L}{2n\pi}\int_0^{n\pi a/L}(1 \pm \cos z)dz \\ &= \varepsilon\left(\frac{a}{L} - \frac{(-1)^n}{n\pi}\sin\frac{n\pi a}{L}\right) \ , \end{aligned}$$

where the upper (lower) signs correspond to the odd (even) n. When $a \ll L$, we can approximate by $E^{(1)}_{n=impar} \simeq \varepsilon 2a/L$ and $E^{(1)}_{n=par} \simeq 0$. Apparently, the perturbation is stronger when the wavefunction has a large overlap with the perturbation. By analogy we can consider the strings of a violin. When we perturb the strings near the nodes, we do not influence the vibration. When we perturb away from the nodes, the frequency is altered. When $a \to L$ but $\varepsilon \ll E_1^{(0)}$, we can approximate by $E_n^{(1)} \simeq \varepsilon$. In this case, all energies are shifted up by the same amount.

27.1.3.2 Ex: Perturbation

Show that the scalar product $\langle\psi_n^{(0)}|\psi_n^{(1)}\rangle$ (from the first-order correction to the state of the 'perturbed' system with the n-th state of the free Hamiltonian), cancels out when we impose that the 'perturbed' state $|\psi(\lambda)\rangle$ be normalized and the the product $\langle\psi_n^{(0)}|\psi(\lambda)\rangle$ be real.[3]

Solution:

27.1.3.3 Ex: Extended nucleus

The expression $V(r) = -e^2/4\pi\epsilon_0 r$ for the potential energy of an electron in the hydrogen atom implies that the nucleus (the proton) is treated as a point particle. Now suppose that, on the contrary, the charge of the proton $+e$ is evenly distributed over a sphere of radius $R = 10^{-13}$ cm.
a. Derive the modified potential V_m, which corresponds to this distribution of the nuclear charge.
b. Assume that the wavefunction of the hydrogen atom does not change much due to the modified potential. Calculate in lowest order in R/a_B the average energetic displacement $\langle\Delta V\rangle$ for the state $(n = 1, \ell = 0, m = 0)$. How will the energy displacement be in comparison to the states $(n = 2, \ell = 0, m = 0)$ and $(n = 2, \ell = 1, m = 0)$?
c. Calculate in the same way $\langle\Delta V\rangle$ for muonic hydrogen in the ground state.

[3] See [276], Cap XI, A-2.

Solution: *a. Using Gauss' law,*

$$\int_{\partial V} \mathbf{E}\cdot d\mathbf{S} = \tfrac{1}{\epsilon_0}\int_V \rho dV \qquad with \qquad \rho = \frac{e}{4\pi R^3/3}\ ,$$

we obtain for the electric field,

$$4\pi r^2 E_r = \begin{cases} \frac{1}{\varepsilon_0}4\pi\int_0^r \frac{e}{4\pi R^3/3} r'^2 dr' & for \quad r<R \\ \frac{e}{\varepsilon_0} & for \quad r>R \end{cases}\ .$$

Resolving by E_r,

$$E_r = \begin{cases} \frac{e}{4\pi\varepsilon_0}\frac{r}{R^3} & for \quad r<R \\ \frac{e}{4\pi\varepsilon_0 r^2} & for \quad r>R \end{cases}\ .$$

The potentials follow with,

$$V_m = e\int E_r dr = \begin{cases} \frac{e^2}{4\pi\varepsilon_0}\frac{r^2}{2R^3} + const & for \quad r<R \\ -\frac{e^2}{4\pi\varepsilon_0 r} & for \quad r>R \end{cases}\ .$$

Continuity at the position R requires, $const = \frac{3e^2}{4\pi\varepsilon_0 2R}$. Hence,

$$V_m = \begin{cases} \frac{-e^2}{8\pi\varepsilon_0 R}\left(3-\frac{r^2}{R^2}\right) & for \quad r<R \\ \frac{-e^2}{4\pi\varepsilon_0 r} & for \quad r>R \end{cases}\ .$$

b. We consider the difference of this potential from a Coulomb potential,

$$\Delta V(r) \equiv V_m(r) - V(r) = \begin{cases} -\frac{3e^2}{8\pi\epsilon_0 R} + \frac{e^2 r^2}{8\pi\epsilon_0 R^3} + \frac{e^2}{4\pi\epsilon_0 r} & for \ \ r<R \\ 0 \ \ for \ \ r>R \end{cases}\ .$$

being a perturbation of the Coulombian case, which has already been solved. Using perturbation theory we calculate the first-order correction of ground state energy,

$$\Delta E_1^{(1)} = \langle\psi_{100}|\Delta V(r)|\psi_{100}\rangle = 4\pi\int_0^R \psi_{100}^* \Delta V(r)\psi_{100} r^2 dr = \frac{4}{10}\frac{e^2}{4\pi\epsilon_0 a_B^3}R^2\ .$$

To solve the integral we can approximate the exponential appearing in the function ψ_{100} by $e^{-\tilde{r}} \simeq 1$, since the radius within which $\Delta V(r) \neq 0$ is very small: $R \approx a_B/10^4$. We obtain, $\frac{\Delta E_1^{(1)}}{E_1} \approx 10^{-8}$, which is a very small energy correction. Because of the smaller $\langle r\rangle$ and being consequently closer to the nucleus, the fundamental state (100) is most affected by the finite size of the nucleus. As the other states are further apart, they will have even smaller corrections of their energies.
The same calculation made for muonic hydrogen gives,

$$\frac{\Delta E_e}{\Delta E_\mu} = \left(\frac{a_\mu}{a_B}\right)^3 = \left(\frac{m_e}{m_\mu}\right)^3 \approx 1.25\cdot 10^{-7}\ .$$

27.1.3.4 Ex: Perturbation of a two-level system

We consider a two-level system. Without perturbation the system would have the Hamiltonian $H^{(0)}$, the eigenenergies $E^{(0)}_{1,2}$ and the eigenfunctions $\psi^{(0)}_{1,2}$. Now we switch on a stationary perturbation of the form $H^{(1)} = \epsilon(|1\rangle\langle 2| + |2\rangle\langle 1|)$.
a. Calculate the eigenenergies directly solving the perturbed Schrödinger equation.
b. Calculate the perturbed energies using TIPT and compare to the exact calculation of the eigenenergies.
c. Calculate the eigenstates directly solving the perturbed Schrödinger equation.
d. Calculate the perturbed states using TPIT and compare to the exact calculation of the eigenfunctions.

Solution: *a. We have already dealt with the two-level system with coupling in Exc. 23.4.7.1. Here we rephrase the problem assuming that the coupling represents a perturbation. The Hamiltonian is*

$$\hat{H} = \begin{pmatrix} H^{(0)}_{11} & 0 \\ 0 & H^{(0)}_{22} \end{pmatrix} + \begin{pmatrix} 0 & H^{(1)}_{12} \\ H^{(1)}_{21} & 0 \end{pmatrix} = \begin{pmatrix} E^{(0)}_1 & \varepsilon \\ \varepsilon & E^{(0)}_2 \end{pmatrix} .$$

To find the perturbed eigenvalues $E^{(1)}_{1,2}$ we solve the eigenvalue equation $\det(\hat{H} - E^{(1)}_{\pm}) = 0$, giving

$$E^{(1)}_{1,2} = \tfrac{1}{2}(E^{(0)}_1 + E^{(0)}_2) \pm \tfrac{1}{2}\sqrt{(E^{(0)}_1 - E^{(0)}_2)^2 + 4\varepsilon^2} .$$

Obviously, for $\varepsilon \to 0$ we get the unperturbed energies. If the distance from unperturbed levels, $\Delta E \equiv E^{(0)}_1 - E^{(0)}_2$, decreases, the perturbation gets more important and causes a minimum distance $E^{(1)}_1 - E^{(1)}_2 = 2\varepsilon$. That is, the perturbation drives the levels away from each other. This is called avoided crossing. For small perturbations we can expand,

$$E^{(1)}_{1,2} = \tfrac{1}{2}\left(E^{(0)}_1 + E^{(0)}_2\right) \pm \tfrac{1}{2}\left(E^{(0)}_1 - E^{(0)}_2\right)\left(1 + \frac{2\varepsilon^2}{\Delta E^2} + ...\right) \simeq E^{(0)}_{1,2} \pm \frac{\varepsilon^2}{\Delta E} .$$

b. Using first-order perturbation theory,

$$E^{(1)}_n = \langle\psi^{(0)}_n|\hat{H}^{(1)}|\psi^{(0)}_n\rangle = 0 ,$$

since $H^{(1)}$ has no diagonal components. In second order,

$$E^{(2)}_n = \langle\psi^{(0)}_n|\hat{H}^{(2)}|\psi^{(0)}_n\rangle + \sum_{m\neq n} \frac{\langle n|\hat{H}^{(1)}|m\rangle\langle m|\hat{H}^{(1)}|n\rangle}{E^{(0)}_n - E^{(0)}_m} = 0 \pm \frac{\varepsilon^2}{\Delta E} ,$$

giving the same result as in a Taylor expansion of the exact energies by the perturbation ε.
c. Now we take a look at the wavefunctions

$$\begin{pmatrix} E^{(0)}_1 & H^{(1)}_{12} \\ H^{(1)}_{21} & E^{(0)}_2 \end{pmatrix} \begin{pmatrix} \cos\zeta & \sin\zeta \\ -\sin\zeta & \cos\zeta \end{pmatrix} = \begin{pmatrix} \cos\zeta & \sin\zeta \\ -\sin\zeta & \cos\zeta \end{pmatrix} \begin{pmatrix} E^{(1)}_+ & 0 \\ 0 & E^{(1)}_- \end{pmatrix} .$$

We obtain

$$|\psi^{(1)}\rangle = \begin{pmatrix} \psi_+^{(1)} \\ \psi_-^{(1)} \end{pmatrix} = \begin{pmatrix} \cos\zeta & \sin\zeta \\ -\sin\zeta & \cos\zeta \end{pmatrix} \begin{pmatrix} \psi_1^{(0)} \\ \psi_2^{(0)} \end{pmatrix} = \begin{pmatrix} \psi_1^{(0)}\cos\zeta + \psi_2^{(0)}\sin\zeta \\ -\psi_1^{(0)}\sin\zeta + \psi_2^{(0)}\cos\zeta \end{pmatrix} ,$$

with $\tan\zeta = \frac{2|H_{12}^{(1)}|}{\Delta E} \simeq \zeta$. *In first order,*

$$\psi_+^{(1)} = \psi_1^{(0)}\cos\zeta + \psi_2^{(0)}\sin\zeta \simeq \psi_1^{(0)} + \zeta\psi_2^{(0)} \simeq \psi_1^{(0)} + \frac{\varepsilon}{\Delta E}\psi_2^{(0)}$$

and $$\psi_-^{(1)} = -\psi_1^{(0)}\sin\zeta + \psi_2^{(0)}\cos\zeta \simeq \psi_2^{(0)} - \zeta\psi_2^{(0)} \simeq \psi_2^{(0)} - \frac{\varepsilon}{\Delta E}\psi_1^{(0)} .$$

d. Using first-order perturbation theory,

$$|\psi_n^{(1)}\rangle = \sum_{m\neq n} |m\rangle \frac{\langle m|\hat{H}^{(1)}|n\rangle}{E_n^{(0)} - E_m^{(0)}} = \pm|m\rangle \frac{\varepsilon}{\Delta E} .$$

giving the same result as in a Taylor expansion of the exact energies by the perturbation ε.

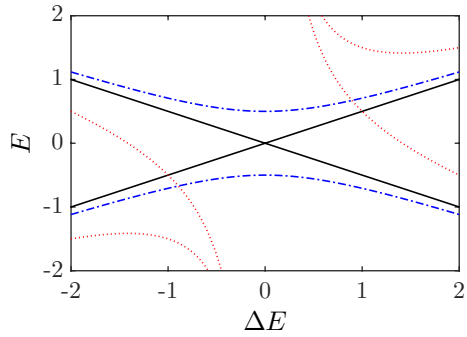

Figure 27.1: Avoided crossing of coupled two levels. Black solid: uncoupled states, blue dash-dotted: exact solution, red dotted: first order correction TIPT.

27.1.3.5 Ex: Stark effect for an electron in a box

Consider an electron in a one-dimensional box, that is, in a well inside the interval $x \in [0, a]$ delimited by infinite walls. When a uniform electric field $\mathcal{E}$ is applied, also in x-direction, the electron experiences a force equal to $-e\mathcal{E}$, being $-e$ the electron charge, so that the potential energy inside the box becomes $e\mathcal{E}x$.
a. What is the energy of the ground state of the electron (in first order approximation)? We can assume that $e\mathcal{E}a$ is much smaller than the ground state energy the electron would have in the absence of electric fields.
b. Use first-order TIPT to get an approximation for the ground state wavefunction by calculating the first term of the correction.

Solution: *a. In zeroth order we have,*

$$E_n^{(0)} = \frac{\pi^2\hbar^2 n^2}{2m_e a^2} \qquad \textit{and} \qquad \psi_n^{(0)}(x) = \sqrt{\frac{2}{a}} \sin\frac{n\pi x}{a} \ ,$$

with $n = 1$. *In the first order we obtain for the energy,*

$$E_n^{(1)} = \langle n|e\mathcal{E}x|n\rangle = \frac{2}{a} e\mathcal{E} \int_0^a x \sin^2\frac{n\pi x}{a} dx = \frac{2}{a} e\mathcal{E}\frac{a^2}{4} = \frac{a}{2} e\mathcal{E} \ .$$

b. In the first order we obtain the eigenfunctions,

$$\begin{aligned}
|\psi_n^{(1)}\rangle &= \sum_{m\neq n} |m\rangle \frac{\langle m|H^{(1)}|n\rangle}{E_n^{(0)} - E_m^{(0)}} = \sum_{m\neq n} |\psi_m^{(0)}\rangle \frac{\int\int \langle m|x\rangle\langle x|e\mathcal{E}x|x'\rangle\langle x'|n\rangle d^3x d^3x'}{E_n^{(0)} - E_m^{(0)}} \\
&= \sum_{m\neq n} |\psi_m^{(0)}\rangle \frac{1}{E_n^{(0)} - E_m^{(0)}} \frac{2}{a} e\mathcal{E} \int_0^a x \sin\frac{m\pi x}{a} \sin\frac{\pi x}{a} dx \\
&= \sum_{m\neq n} |\psi_m^{(0)}\rangle \frac{2m_e a^2}{\pi^2\hbar^2 n^2 - \pi^2\hbar^2 m^2} \frac{2}{a} e\mathcal{E} \frac{2mna^2}{\pi^2} \frac{(-1)^{m+n} - 1}{(m^2 - n^2)^2} \\
&= \sum_{m\neq n} |\psi_m^{(0)}\rangle \frac{8m_e a^3 e\mathcal{E}}{\pi^4\hbar^2} \frac{mn[1 - (-1)^{m+n}]}{(m^2 - n^2)^3} \ .
\end{aligned}$$

27.1.3.6 Ex: Perturbed 3-level system until second order TIPT

Consider the following perturbed Hamiltonian:

$$H = H_0 + H_\lambda = \begin{pmatrix} E_1 & 0 & 0 \\ 0 & E_2 & 0 \\ 0 & 0 & E_3 \end{pmatrix} + \begin{pmatrix} 0 & \lambda & 0 \\ \lambda & 0 & \lambda \\ 0 & \lambda & 0 \end{pmatrix} \ .$$

a. Determine the perturbed eigenvalues and eigenfunctions in first order TIPT.
b. Determine the eigenvalues in second order TIPT.

Solution: *a. In zeroth order,*

$$E_n^{(0)} = E_{1,2,3} \qquad \textit{and} \qquad |n\rangle = \hat{e}_n \ .$$

The eigenvalues in first order are,

$$E_n^{(1)} = \langle n|H_\lambda|n\rangle = \hat{e}_n^\dagger H_\lambda \hat{e}_n = 0 \ .$$

The perturbed eigenfunctions in first-order are $|\psi_n\rangle = |n\rangle + |\psi_n^{(1)}\rangle + ...$, *where*

$$|\psi_n^{(1)}\rangle = \sum_{m\neq n} |m\rangle \frac{\langle m|H_\lambda|n\rangle}{E_n - E_m}$$

$$|\psi_1^{(1)}\rangle = |2\rangle \frac{\hat{e}_2^\dagger H_\lambda \hat{e}_1}{E_1 - E_2} + |3\rangle \frac{\hat{e}_3^\dagger H_\lambda \hat{e}_1}{E_1 - E_3} = |2\rangle \frac{\lambda}{E_1 - E_2}$$

$$|\psi_2^{(1)}\rangle = |1\rangle \frac{\hat{e}_1^\dagger H_\lambda \hat{e}_2}{E_2 - E_1} + |3\rangle \frac{\hat{e}_3^\dagger H_\lambda \hat{e}_2}{E_2 - E_3} = |1\rangle \frac{\lambda}{E_2 - E_1} + |3\rangle \frac{\lambda}{E_2 - E_1}$$

$$|\psi_3^{(1)}\rangle = |1\rangle \frac{\hat{e}_1^\dagger H_\lambda \hat{e}_3}{E_3 - E_1} + |2\rangle \frac{\hat{e}_2^\dagger H_\lambda \hat{e}_3}{E_3 - E_2} = |2\rangle \frac{\lambda}{E_3 - E_2} \ .$$

b. The eigenvalues in second order are,

$$E_n^{(2)} = \sum_{m\neq n} \frac{\langle n|H_\lambda|m\rangle\langle m|H_\lambda|n\rangle}{E_n^{(0)} - E_m^{(0)}}$$

$$E_1^{(2)} = \frac{\langle 1|H_\lambda|2\rangle\langle 2|H_\lambda|1\rangle}{E_1^{(0)} - E_2^{(0)}} + \frac{\langle 1|H_\lambda|3\rangle\langle 3|H_\lambda|1\rangle}{E_1^{(0)} - E_3^{(0)}} = \frac{\lambda^2}{E_1^{(0)} - E_2^{(0)}} \ .$$

27.1.3.7 Ex: Stark effect for a charge in a harmonic oscillator

Consider a charged harmonic oscillator, immersed in a uniform electric field $\mathcal{E}$, described by the Hamiltonian $\hat{H}^{(1)} = \hat{H} + e\mathcal{E}\hat{x}$, being $\hat{H} = \hat{p}^2/2m + m\omega^2\hat{x}^2/2$ the Hamiltonian of the free one-dimensional oscillator, and e the charge of the oscillator.
a. Obtain, through TIPT, the eigenenergies (first and second order corrections). Compare the results obtained by TIPT with the analytical ones [4].
b. Same thing for a perturbation of the form $\rho m\omega^2\hat{x}^2/2$.
c. Same thing for a perturbation $\sigma\hbar\omega\hat{x}^3$.

Solution: *a. We already calculated in Exc. 24.6.6.9 the influence of a constant force on a harmonic oscillator,*

$$\hat{H}^{(1)}|\psi_n^{(1)}\rangle = E_n^{(1)}|\psi_n^{(1)}\rangle \quad , \quad |\psi_n^{(1)}(x)\rangle = |\psi_n(x-b)\rangle \quad , \quad E_n^{(1)} = E_n - \frac{m}{2}\omega^2 b^2 \ ,$$

with $b \equiv e\mathcal{E}/m\omega^2$. *With TIPT we calculate the first order correction,*

$$E_n^{(1)} = \langle n|\hat{H}^{(1)}|n\rangle = e\mathcal{E}\langle n|\hat{x}|n\rangle = 0 \ .$$

In second order,

$$E_n^{(2)} = \langle n|\hat{H}^{(2)}|n\rangle + \sum_{m\neq n} \frac{\langle m|\hat{H}^{(1)}|n\rangle\langle n|\hat{H}^{(1)}|m\rangle}{E_n^{(0)} - E_m^{(0)}} = e^2\mathbf{E}^2 \sum_{m\neq n} \frac{|\langle m|\hat{x}|n\rangle|^2}{\hbar\omega(n-m)} \ .$$

[4] See [276], Complement A_XI.

With

$$\langle m|\hat{x}|n\rangle = \frac{a_{ho}}{\sqrt{2}}\langle m|\hat{a}+\hat{a}^\dagger|n\rangle = \frac{a_{ho}}{\sqrt{2}}(\sqrt{n}\delta_{m,n-1}+\sqrt{n+1}\delta_{m,n+1}) \ ,$$

we find,

$$E_n^{(2)} = e^2\mathcal{E}^2\frac{a_{ho}^2}{\hbar\omega}\left[\frac{n}{2}+\frac{n+1}{-2}\right] = -\frac{1}{2}b^2m^2\omega^4\ \frac{\hbar}{m\omega}\frac{1}{\hbar\omega} = -\frac{m}{2}\omega^2b^2 \ .$$

This coincides with the exact result calculated above.
b. With a quadratic perturbation, the exact solutions will be,

$$E_n = \hbar\omega(1+\rho)(n+1/2) \ .$$

With TIPT, we calculate the first order correction,

$$E_n^{(1)} = \langle n|\hat{H}^{(1)}|n\rangle = \rho\frac{m}{2}\omega^2\langle n|\hat{x}^2|n\rangle = \rho\frac{m}{2}\omega^2a_{ho}^2(n+1/2) = \frac{\rho}{2}\hbar\omega(n+1/2) = \frac{\rho}{2}E_n^{(0)} \ .$$

In second order, with

$$\langle m|\hat{x}^2|n\rangle = \sqrt{n(n-1)}\delta_{m,n-2}+\sqrt{n^2}\delta_{m,n}+\sqrt{(n+1)(n+1)}\delta_{m,n}+\sqrt{(n+1)(n+2)}\delta_{m,n+2}$$

we find

$$\begin{aligned}
\langle m|\hat{x}^2|n\rangle &= \frac{a_{ho}^2}{2}\langle m|(\hat{a}+\hat{a}^\dagger)(\hat{a}+\hat{a}^\dagger)|n\rangle \\
&= \frac{a_{ho}^2}{2}\left(\sqrt{n(n-1)}\delta_{m,n-2}+n\delta_{m,n}+(n+1)\delta_{m,n}+\sqrt{(n+1)(n+2)}\delta_{m,n+2}\right) \\
E_n^{(2)} &= \langle n|\hat{H}^{(2)}|n\rangle + \sum_{m\neq n}\frac{\langle m|\hat{H}^{(1)}|n\rangle\langle n|\hat{H}^{(1)}|m\rangle}{E_n^{(0)}-E_m^{(0)}} = \frac{m^2}{4}\rho^2\omega^4\sum_{m\neq n}\frac{|\langle m|x^2|n\rangle|^2}{\hbar\omega(n-m)} \\
&= \frac{m^2}{4}\rho^2\omega^4\frac{a_{ho}^4}{4}\frac{1}{\hbar\omega}\left(\frac{n(n-1)}{n-(n-2)}+\frac{(n+1)(n+2)}{n-(n+2)}\right) = -\frac{\rho^2}{8}\hbar\omega(n+1/2) = -\frac{\rho^2}{8}E_n^{(0)} \ .
\end{aligned}$$

c. We calculate

$$E_n^{(1)} = \langle n|\hat{H}^{(1)}|n\rangle = \sigma\hbar\omega\langle n|\hat{x}^3|n\rangle \propto \langle n|(\hat{a}+\hat{a}^\dagger)^3|n\rangle = 0 \ ,$$

and

$$\begin{aligned}
E_n^{(2)} &= (\sigma\hbar\omega)^2\sum_{m\neq n}\frac{|\langle m|\hat{x}^3|n\rangle|^2}{E_n^{(0)}-E_m^{(0)}} \\
&= \frac{\sigma^2\hbar\omega}{2^3}a_{ho}^6\sum_{m\neq n}\frac{|\langle m|(\hat{a}^\dagger)^3+3(\hat{a}^\dagger)^2\hat{a}+3\hat{a}^\dagger-3\hat{a}+3\hat{a}^2\hat{a}^\dagger+\hat{a}^3|n\rangle|^2}{n-m} \\
&= \frac{\sigma^2\hbar^4}{8m^3\omega^2}\sum_{m\neq n}\frac{1}{n-m}\Big|\sqrt{(n+3)(n+2)(n+1)}\delta_{m,n+3}+\sqrt{n(n-1)(n-2)}\delta_{m,n-3}+ \\
&\qquad +3\sqrt{n^2(n+1)}\delta_{m,n+1}+\sqrt{n(n+1)^2}\delta_{m,n-1}\Big|^2 \\
&= \frac{\sigma^2\hbar^4}{8m^3\omega^2}\left[-\tfrac{1}{3}(n+3)(n+2)(n+1)+\tfrac{1}{3}n(n-1)(n-2)-3n^2(n+1)+3n(n+1)^2\right] \\
&= -\frac{\sigma^2\hbar^4}{4m^3\omega^2} \ .
\end{aligned}$$

27.1.3.8 Ex: Three-level system with degeneracy

Consider the following Hamiltonian $\hat{H}^{(0)}$ and its perturbation $\hat{H}^{(1)}$

$$\hat{H}^{(0)} + \hat{H}^{(1)} = \begin{pmatrix} \Delta & 0 & 0 \\ 0 & \Delta & 0 \\ 0 & 0 & \Delta' \end{pmatrix} + \begin{pmatrix} 0 & \Omega & 0 \\ \Omega & 0 & \Omega \\ 0 & \Omega & 0 \end{pmatrix} \ .$$

Calculate the corrections for the eigenvalues and eigenfunctions up to first order.

Solution: *For the unperturbed system we have* $(E_n^{(0)} - \hat{H}^{(0)})|n,\nu\rangle = 0$*, that is,*

$$\langle 1,1|\hat{H}^{(0)})|1,1\rangle = \langle 1,2|\hat{H}^{(0)}|1,2\rangle = \Delta \qquad \textit{and} \qquad \langle 2|\hat{H}^{(0)}|2\rangle = \Delta' \ ,$$

where ν *is the degenerate quantum number. Applying the non-degenerate TIPT, we would get* $(E_n^{(1)} - \hat{H}^{(1)})|n,\nu\rangle = 0$*,*

$$\langle 1,1|\hat{H}^{(1)})|1,1\rangle = \langle 1,2|\hat{H}^{(1)}|1,2\rangle = \langle 2|\hat{H}^{(0)}|2\rangle = 0 \ .$$

The first two eigenvalues are degenerate. To find the first-order corrections in this subspace, we calculate,

$$0 = \det\left[\langle n,\nu|\hat{H}^{(1)})|n,\mu\rangle - E_{n\mu}^{(1)}\delta_{\mu,\nu}\right] = \det\left[\begin{pmatrix} 0 & \Omega \\ \Omega & 0 \end{pmatrix} - \begin{pmatrix} E^{(1)} & 0 \\ 0 & E^{(1)} \end{pmatrix}\right] = (E^{(1)})^2 - \Omega^2 \ .$$

That is, the corrections for the eigenvalues are $E^{(1)} = \pm\Omega$*. The corrections for the eigenfunctions follow with* $\sum_n c_{\mu\nu}[E_{n\mu}^{(1)}\langle n,\mu|n,\nu\rangle - \langle n,\mu|\hat{H}^{(1)})|n,\nu\rangle] = 0$*, that is,*

$$\begin{aligned} c_{11}[\Omega - \langle 1|H^{(1)}|1\rangle] + c_{12}[-\langle 1|H^{(1)}|2\rangle] &= c_{11}\Omega - c_{12}\Omega = 0 \\ c_{21}[-\langle 2|H^{(1)}|1\rangle] + c_{22}[-\Omega - \langle 2|H^{(1)}|2\rangle] &= -c_{21}\Omega - c_{22}\Omega = 0 \ . \end{aligned}$$

Therefore, the normalized eigenfunctions are,

$$|\psi_1^{(0)}\rangle = c_{11}|1\rangle + c_{12}|2\rangle = \tfrac{1}{\sqrt{2}}\begin{pmatrix} 1 \\ 1 \\ 0 \end{pmatrix} \qquad \textit{and} \qquad |\psi_2^{(0)}\rangle = c_{21}|1\rangle + c_{22}|2\rangle = \tfrac{1}{\sqrt{2}}\begin{pmatrix} 1 \\ -1 \\ 0 \end{pmatrix} \ .$$

Finally we obtain the corrections for the eigenvalues $\langle\psi^{(0)}_{n,\mu}|H^{(1)}|\psi^{(0)}_{n,\mu}\rangle$,

$$\langle\psi^{(0)}_1|\hat{H}^{(1)}|\psi^{(0)}_1\rangle = \tfrac{1}{2}\begin{pmatrix}1\\1\\0\end{pmatrix}^T\begin{pmatrix}0&\Omega&0\\\Omega&0&\Omega\\0&\Omega&0\end{pmatrix}\begin{pmatrix}1\\1\\0\end{pmatrix} = \Omega$$

$$\langle\psi^{(0)}_2|\hat{H}^{(1)}|\psi^{(0)}_2\rangle = \frac{1}{2}\begin{pmatrix}1\\-1\\0\end{pmatrix}^T\begin{pmatrix}0&\Omega&0\\\Omega&0&\Omega\\0&\Omega&0\end{pmatrix}\begin{pmatrix}1\\-1\\0\end{pmatrix} = -\Omega$$

$$\langle\psi^{(0)}_3|\hat{H}^{(1)}|\psi^{(0)}_3\rangle = \begin{pmatrix}0\\0\\1\end{pmatrix}^T\begin{pmatrix}0&\Omega&0\\\Omega&0&\Omega\\0&\Omega&0\end{pmatrix}\begin{pmatrix}0\\0\\1\end{pmatrix} = 0\ .$$

Thus, the energies of the perturbed Hamiltonian are: $E^{(0)}_1 + E^{(1)}_1 = \Delta+\Omega, \Delta-\Omega, \Delta'$. *Finally, the wavefunctions are up to first order,*

$$|\psi^{(1)}_1\rangle = \sum_{m\neq 1}|\psi^{(0)}_1\rangle\frac{\langle\psi^{(0)}_m|\hat{H}^{(1)}|\psi^{(0)}_1\rangle}{E^{(0)}_1-E^{(0)}_m} = |\psi^{(0)}_1\rangle\frac{\langle\psi^{(0)}_2|\hat{H}^{(1)}|\psi^{(0)}_1\rangle}{E^{(0)}_1-E^{(0)}_2} + |\psi^{(0)}_1\rangle\frac{\langle\psi^{(0)}_3|\hat{H}^{(1)}|\psi^{(0)}_1\rangle}{E^{(0)}_1-E^{(0)}_3}$$

$$= \frac{1}{(\Delta+\Omega)-(\Delta-\Omega)}\tfrac{1}{\sqrt{2}}\begin{pmatrix}1\\1\\0\end{pmatrix}\tfrac{1}{\sqrt{2}}\begin{pmatrix}1\\-1\\0\end{pmatrix}\begin{pmatrix}0&\Omega&0\\\Omega&0&\Omega\\0&\Omega&0\end{pmatrix}\tfrac{1}{\sqrt{2}}\begin{pmatrix}1\\1\\0\end{pmatrix}$$

$$+\frac{1}{(\Delta+\Omega)-\Delta'}\tfrac{1}{\sqrt{2}}\begin{pmatrix}1\\1\\0\end{pmatrix}\begin{pmatrix}0\\0\\1\end{pmatrix}\begin{pmatrix}0&\Omega&0\\\Omega&0&\Omega\\0&\Omega&0\end{pmatrix}\tfrac{1}{\sqrt{2}}\begin{pmatrix}1\\1\\0\end{pmatrix} = \frac{\Omega}{2(\Delta-\Delta'+\Omega)}\begin{pmatrix}1\\1\\0\end{pmatrix}$$

$$|\psi^{(1)}_2\rangle = |\psi^{(0)}_2\rangle\frac{\langle\psi^{(0)}_1|\hat{H}^{(1)}|\psi^{(0)}_2\rangle}{E^{(0)}_2-E^{(0)}_1} + |\psi^{(0)}_2\rangle\frac{\langle\psi^{(0)}_3|\hat{H}^{(1)}|\psi^{(0)}_2\rangle}{E^{(0)}_2-E^{(0)}_3} = \frac{-\Omega}{2(\Delta-\Delta'-\Omega)}\begin{pmatrix}1\\-1\\0\end{pmatrix}$$

$$|\psi^{(1)}_3\rangle = |\psi^{(0)}_3\rangle\frac{\langle\psi^{(0)}_1|\hat{H}^{(1)}|\psi^{(0)}_3\rangle}{E^{(0)}_3-E^{(0)}_1} + |\psi^{(0)}_3\rangle\frac{\langle\psi^{(0)}_2|\hat{H}^{(1)}|\psi^{(0)}_3\rangle}{E^{(0)}_3-E^{(0)}_2} = \frac{-\sqrt{2}\Omega^2}{(\Delta'-\Delta)^2-\Omega^2}\begin{pmatrix}0\\0\\1\end{pmatrix}\ .$$

Note that we can alternatively separate the Hamiltonian as follows,

$$\hat{H}^{(0)}+\hat{H}^{(1)} = \begin{pmatrix}\Delta&\Omega&0\\\Omega&\Delta&0\\0&0&\Delta'\end{pmatrix} + \begin{pmatrix}0&0&0\\0&0&\Omega\\0&\Omega&0\end{pmatrix}\ .$$

the advantage being that, already without perturbation, the eigenvalues $E^{(0)}_n$ *are not degenerate:*

$$|1\rangle = \begin{pmatrix}1\\1\\0\end{pmatrix} \leftrightarrow E^{(0)}_1 = \Delta+\Omega \quad , \quad |2\rangle = \begin{pmatrix}1\\-1\\0\end{pmatrix} \leftrightarrow E^{(0)}_1 = \Delta-\Omega \quad , \quad |3\rangle = \begin{pmatrix}0\\0\\1\end{pmatrix} \leftrightarrow E^{(0)}_3 = \Delta'\ .$$

In this case none of the first order corrections contributes: $\langle n|\hat{H}^{(1)}|n\rangle = 0$.

27.1.3.9 Ex: Perturbation in a 3D well with degeneracy

Consider a particle confined to a three-dimensional, infinite cubic well described by the potential energy $V(x,y,z) = 0$ for $0 < x < a$, $0 < y < a$ and $0 < z < a$ and $V(x,y,z) = \infty$ outside this region. We know that the particle's stationary states are $\Psi^{(0)}_{n_x,n_y,n_z}(x,y,z) = \left(\frac{2}{a}\right)^{3/2} \sin\left(\frac{n_x\pi}{a}x\right) \sin\left(\frac{n_y\pi}{a}y\right) \sin\left(\frac{n_z\pi}{a}z\right)$, being n_x, n_y, n_z positive integers. The associated energies are $E^{(0)}_{n_x,n_y,n_z} = \frac{\pi^2\hbar^2}{2ma^2}(n_x^2 + n_y^2 + n_z^2)$. Note that the ground state is not degenerate while the first excited state is three times degenerate. Consider that the particle in this box is subject to a perturbation of the shape $H^{(1)} = V_0$ for $0 < x < a/2$ and $0 < y < a/2$ and $H^{(1)} = 0$ outside this region.
a. Obtain the first-order correction for the ground state energy.
b. Obtain the first-order correction for the (degenerate) energy of the first excited state, in addition to the *optimal base* (which follows from the linear combinations of degenerate states) which most closely approximates the perturbed states.

Solution: *a. The perturbation potential increases by* V_0 *in a quarter of the box. The ground state is not degenerate. Therefore, the first order correction for the ground state is simply,*

$$E^{(1)}_0 = \langle 111|H^{(1)}|111\rangle = \left(\tfrac{2}{a}\right)^3 V_0 \int_0^{a/2} \sin^2\tfrac{\pi x}{a}dx \int_0^{a/2} \sin^2\tfrac{\pi y}{a}dy \int_0^{a} \sin^2\tfrac{\pi z}{a}dz = \tfrac{V_0}{4} \ ,$$

such that the corrected value is,

$$E^{(1)}_0 = E^{(1)}_0 + \tfrac{V_0}{4} \ .$$

b. For the first excited state we need the complete degenerate TIPT machinery. We start by constructing the matrix, $W_{\mu\nu} = \langle\mu|H^{(1)}|\nu\rangle$*, com* $\mu,\nu \in \{(211),(121),(112)\}$*. We find,*

$$W_{211,211} = W_{121,121} = W_{112,112} = \tfrac{V_0}{4}$$
$$W_{121,112} = \left(\tfrac{2}{a}\right)^3 V_0 \int_0^{a/2} \sin^2\tfrac{\pi x}{a}dx \int_0^{a/2} \sin\tfrac{\pi y}{a}\sin\tfrac{2\pi y}{a}dy \int_0^{a} \sin\tfrac{2\pi z}{a}\sin\tfrac{\pi z}{a}dz = 0$$
$$W_{211,112} = 0 \ ,$$

because the integral in z *vanishes.*

$$W_{211,121} = \left(\tfrac{2}{a}\right)^3 V_0 \int_0^{a/2} \sin\tfrac{\pi x}{a}\sin\tfrac{2\pi x}{a}dx \int_0^{a/2} \sin\tfrac{\pi y}{a}\sin\tfrac{2\pi y}{a}dy \int_0^{a} \sin\tfrac{\pi z}{a}dz = \tfrac{16}{9\pi^2}V_0 \ .$$

Therefore,,

$$W = \tfrac{V_0}{4}\begin{pmatrix} 1 & 0 & 0 \\ 0 & 1 & (8/3\pi)^2 \\ 0 & (8/3\pi)^2 & 1 \end{pmatrix} \ .$$

The characteristic equation in W/V_0 gives the eigenvalues

$$w_1 = 1 \quad , \quad w_{2,3} = 1 \pm (8/3\pi)^2 \ .$$

In first-order the corrected value for the first excited state, therefore, is

$$E_1^{(1)} = E_1^{(0)} + \frac{V_0}{4} w_k \ .$$

That is, the perturbation removes the degeneracy to three distinct levels. If we had applied non-degenerate TIPT, we would have concluded that the first-order correction would be the same for all three states. The non-persturbed 'good' states are linear combinations of the form

$$|\psi^{(0)}\rangle = \alpha|112\rangle + \beta|211\rangle + \gamma|121\rangle \ .$$

where the coefficients form the eigenvectors of the matrix W,

$$W|\psi^{(0)}\rangle = \begin{pmatrix} 1 & 0 & 0 \\ 0 & 1 & (8/3\pi)^2 \\ 0 & (8/3\pi)^2 & 1 \end{pmatrix} \begin{pmatrix} \alpha \\ \beta \\ \gamma \end{pmatrix} = w \begin{pmatrix} \alpha \\ \beta \\ \gamma \end{pmatrix} = w|\psi^{(0)}\rangle \ .$$

For $w = 1$, we obtain $\alpha = 1$, $\beta = \gamma = 0$ and for $w = 1 \pm (8/3\pi)^2$ we obtain $\alpha = 0$, $\beta = \pm\gamma = 1/\sqrt{2}$. Therefore the good states are,

$$|\psi^0\rangle = |112\rangle, \tfrac{1}{\sqrt{2}}(|211\rangle \pm |121\rangle) \ .$$

27.1.3.10 Ex: Vanishing perturbation orders

Show that it is impossible to design a perturbation Hamiltonian of the form,

$$\hat{H} = \hat{H}^{(0)} + \hat{H}^{(1)} = \begin{pmatrix} 0 & 0 & 0 \\ 0 & E_2 & 0 \\ 0 & 0 & E_3 \end{pmatrix} + \begin{pmatrix} 0 & \Omega_{12} & \Omega_{13} \\ \Omega_{12}^* & 0 & \Omega_{23} \\ \Omega_{13}^* & \Omega_{23}^* & 0 \end{pmatrix}$$

such that the first and second order corrections vanish.

Solution: *The first order corrections $E_n^{(1)} = \langle n|\hat{H}^{(1)}|n\rangle$ obviously vanishes. For the second order corrections to vanish,*

$$0 = E_n^{(2)} = \sum_{m \neq n} \frac{\langle n|\hat{H}^{(1)}|m\rangle\langle m|\hat{H}^{(1)}|n\rangle}{E_n^{(0)} - E_m^{(0)}} \ ,$$

we have to guarantee,

$$0 = \frac{|\Omega_{12}|^2}{-E_2} + \frac{|\Omega_{13}|^2}{-E_3} \quad , \quad 0 = \frac{|\Omega_{12}|^2}{E_2} + \frac{|\Omega_{23}|^2}{E_2 - E_3} \quad , \quad 0 = \frac{|\Omega_{13}|^2}{E_3} + \frac{|\Omega_{23}|^2}{E_3 - E_2} \ .$$

Resolving the first equation by E_3 and substituting into the third, we obtain,

$$E_3 = -\frac{|\Omega_{13}|^2}{|\Omega_{12}|^2} E_2 \quad , \quad 0 = |\Omega_{12}|^2 + |\Omega_{13}|^2 + |\Omega_{23}|^2 \ ,$$

which is impossible to satisfy.

27.2 Variational method

27.2.1 The Rayleigh fraction

Let us assume that we want to calculate the ground state energy E_g of a system described by a Hamiltonian $\hat{H}$, but we do not know the wavefunction, and we do not know how to solve the Schrödinger equation. If at least we had a good idea of the generic form of the solution (Gaussian, sinusoidal, ..), we could choose a trial function with a free parameter and optimize this parameter minimizing the energy, which ought to be minimal for the ground state. This is precisely the idea of the *variational method*. Note that the variational method only works for the ground state.

For any function ψ we know that the *Rayleigh fraction* $\mathcal{E}$ satisfies,

$$E_g \leq \frac{\langle\psi|\hat{H}|\psi\rangle}{\langle\psi|\psi\rangle} \equiv \mathcal{E} \ , \tag{27.26}$$

not only when ψ is the wavefunction of an excited state, but even when it represents a (imperfect) trial to the ground state. Assuming normalized wavefunctions we can discard the denominator $\langle\psi|\psi\rangle = 1$. To verify the theorem, we expand the function ψ into orthonormal (unknown) eigenfunctions, $|\psi\rangle = \sum_n c_n|\psi_n\rangle$. Since ψ is normalized,

$$1 = \langle\psi|\psi\rangle = \sum_{m,n}\langle\psi_m|c_m^* c_n|\psi_n\rangle = \sum_n |c_n|^2 \ . \tag{27.27}$$

In the same way,

$$\langle\psi|\hat{H}|\psi\rangle = \sum_{m,n}\langle\psi_m|c_m^* \hat{H} c_n|\psi_n\rangle = \sum_n E_n|c_n|^2 \ . \tag{27.28}$$

As the ground state is that of the lowest energy, $E_g \leq E_n$, we have demonstrated the relationship (27.26)

$$E_g = E_g \sum_n |c_n|^2 \leq \sum_n E_n|c_n|^2 = \langle\hat{H}\rangle \ . \tag{27.29}$$

In practice, the ansatz ψ_α for the ground state allows us to calculate an energy that must be minimized via

$$\boxed{\frac{\partial\langle\psi_\alpha|\hat{H}_\alpha|\psi_\alpha\rangle}{\partial\alpha} = 0} \ . \tag{27.30}$$

In the Excs. 27.2.3.1 and 27.2.3.2 we will approach the fundamental state of a quartic potential and a harmonic oscillator, respectively, by trying several trial wavefunctions and optimizing their free parameters.

27.2.2 Rayleigh-Ritz method

A modification of the variational method is the *Rayleigh-Ritz method*. Here, instead of using a trial function, we use a linear combination of eigenfunctions with variable coefficients: $|\psi\rangle = \sum_k c_k|k\rangle$. These variables are then optimized to minimize the Rayleigh fraction,

$$E_g \leq \frac{\sum_{k,m} c_k^* c_m \langle k|\hat{H}|m\rangle}{\sum_{k,m} c_k^* c_m \langle k|m\rangle} = \mathcal{E} \ , \tag{27.31}$$

where we assume real coefficients and eigenfunctions. For this, the derivatives with respect to all coefficients must vanish:

$$\begin{aligned} 0 \equiv \frac{\partial \mathcal{E}}{\partial c_q} &= \frac{\sum_{k,m} \frac{\partial}{\partial c_q} c_k^* c_m \langle k|\hat{H}|m\rangle}{\sum_{k,m} c_k^* c_m \langle k|m\rangle} - \frac{\sum_{k,m} c_k^* c_m \langle k|\hat{H}|m\rangle \sum_{k,m} \frac{\partial}{\partial c_q} c_k^* c_m \langle k|m\rangle}{\left(\sum_{k,m} c_k^* c_m \langle k|m\rangle\right)^2} \\ &= \frac{\sum_{k,m} c_k^* \delta_{qm} \langle k|\hat{H}|m\rangle}{\sum_{k,m} c_k^* c_m \delta_{km}} - \mathcal{E} \frac{\sum_{k,m} c_k^* \delta_{qm} \delta_{km}}{\sum_{k,m} c_k^* c_m \delta_{km}} = \sum_k c_k^* \langle k|\hat{H}|q\rangle - \mathcal{E} c_q^* \ , \end{aligned} \tag{27.32}$$

using the definition of $\mathcal{E}$ (27.31). For the expression $\partial\mathcal{E}/\partial c_q^*$ we get analogous results. Hence,

$$\boxed{0 = \sum_m c_m (\langle q|\hat{H}|m\rangle - \mathcal{E}\langle q|m\rangle)} \ . \tag{27.33}$$

The condition for the existence of solutions is that the secular determinant disappears,

$$0 = \det(\langle q|\hat{H}|m\rangle - \mathcal{E}\langle q|m\rangle) \ . \tag{27.34}$$

The solution of this equation leads to a set of values $\mathcal{E}$, and the lowest value, $\mathcal{E}_{min}$, is the best approximation for the ground state energy. The coefficients of the wavefunction are obtained by solving the eigenvalue equation (27.33) with $\mathcal{E}_{min}$.

In Exc. 27.2.3.3 we derive the regression formulas for a linear *least squares fit* from a Rayleigh-Ritz variational. In Exc. 27.2.3.4 we will use the Rayleigh-Ritz method to estimate the effect of a finite nuclear mass of the hydrogen atom on the energy levels. In Exc. 27.2.3.5 we will use the Rayleigh-Ritz method to find the maximum number of atoms allowing for a stable Bose-Einstein condensate made of atoms subject to an attractive interatomic force.

27.2.3 Exercises

27.2.3.1 Ex: Variational method applied to a quartic potential

Determine the ground state energy of the quartic potential $V(x) = bx^4$ making the variational ansatz $\psi_\alpha(x) = (\alpha/\pi)^{1/4} e^{-\alpha x^2/2}$. **Formulae**:

$$\int_{-\infty}^{\infty} e^{-x^2} dx = \sqrt{\pi} \quad , \quad \int_{-\infty}^{\infty} x^2 e^{-x^2} dx = \tfrac{1}{2}\sqrt{\pi} \quad , \quad \int_{-\infty}^{\infty} x^4 e^{-x^2} dx = \tfrac{3}{4}\sqrt{\pi}$$

Solution: *The ansatz is already normalized, since*

$$\langle\psi_\alpha|\psi_\alpha\rangle = \sqrt{\frac{\alpha}{\pi}}\int_{-\infty}^{\infty} e^{-\alpha x^2}dx = 1 \ .$$

The energy follows from,

$$\begin{aligned}\langle\psi_\alpha|\hat{H}|\psi_\alpha\rangle &= \sqrt{\frac{\alpha}{\pi}}\int_{-\infty}^{\infty} e^{-\alpha x^2/2}\left(-\frac{\hbar^2}{2m}\frac{d^2}{dx^2}+bx^4\right)e^{-\alpha x^2/2}dx \\ &= -\frac{\hbar^2}{2m}\sqrt{\frac{\alpha}{\pi}}\int_{-\infty}^{\infty}(-\alpha+\alpha^2x^2)e^{-\alpha x^2}dx + b\sqrt{\frac{\alpha}{\pi}}\int_{-\infty}^{\infty}x^4e^{-\alpha x^2}dx = \frac{\hbar^2\alpha}{4m}+\frac{3b}{4\alpha^2} \ .\end{aligned}$$

The energy is minimal when,

$$0 = \frac{d\langle\psi_\alpha|\hat{H}|\psi_\alpha\rangle}{d\alpha} = \frac{d}{d\alpha}\left(\frac{\hbar^2\alpha}{4m}+\frac{3b}{4\alpha^2}\right) = \frac{1}{4}\frac{\hbar^2\alpha^3-6bm}{m\alpha^3} \ .$$

Hence, $\alpha = \left(\frac{6bm}{\hbar^2}\right)^{1/3}$ *and,*

$$\langle\psi_\alpha|\hat{H}|\psi_\alpha\rangle = \frac{3}{4}\left(\frac{3b\hbar^2}{4m^2}\right)^{1/3} \ .$$

27.2.3.2 Ex: Variational method applied to the harmonic oscillator

Obtain, through the variational method, the ground state energy of the one-dimensional harmonic oscillator described by the Hamiltonian $\hat{H} = -\frac{\hbar^2}{2m}\frac{d^2}{dx^2}+\frac{1}{2}m\omega^2x^2$, and the corresponding wavefunction from the test functions
a. $\psi(x) = Ae^{-\alpha x^2}$ being α a constant;
b. $\psi(x) = A/(x^2+\beta^2)$ being β a constant;
c. $\psi(x) = A\cos(\pi x/a)$ between the limits $\pm a/2$ being a a constant.

Solution: *a. Normalization requires*

$$1 = |A|^2\int_{-\infty}^{\infty}e^{-2\alpha x^2}dxA = |A|^2\sqrt{\frac{\pi}{2\alpha}} \ .$$

Now,

$$\begin{aligned}\langle\hat{H}\rangle &= -\frac{\hbar^2}{2m}|A|^2\int_{-\infty}^{\infty}e^{-\alpha x^2}\frac{d^2}{dx^2}e^{-\alpha x^2}dx + \frac{m}{2}\omega^2|A|^2\int_{-\infty}^{\infty}e^{-\alpha x^2}x^2e^{-\alpha x^2}dx \\ &= -\frac{\hbar^2}{2m}\sqrt{\frac{2\alpha}{\pi}}\int_{-\infty}^{\infty}2\alpha e^{-2\alpha x^2}\left(-1+2\alpha x^2\right)dx + \frac{m}{2}\omega^2\sqrt{\frac{2\alpha}{\pi}}\int_{-\infty}^{\infty}e^{-2\alpha x^2}x^2dx \\ &= \frac{\hbar^2}{2m}\sqrt{\frac{2\alpha}{\pi}}(2\alpha)^{1/2}\int_{-\infty}^{\infty}e^{-x^2}dx + \left(-\frac{\hbar^2}{2m}\sqrt{\frac{2\alpha}{\pi}}(2\alpha)^2+\frac{m}{2}\omega^2\sqrt{\frac{2\alpha}{\pi}}\right)\frac{1}{(2\alpha)^{3/2}}\int_{-\infty}^{\infty}e^{-x^2}x^2dx \\ &= \frac{\hbar^2}{2m}\sqrt{\frac{2\alpha}{\pi}}(2\alpha)^{1/2}\sqrt{\pi} + \left(-\frac{\hbar^2}{2m}\sqrt{\frac{2\alpha}{\pi}}(2\alpha)^2+\frac{m}{2}\omega^2\sqrt{\frac{2\alpha}{\pi}}\right)\frac{1}{(2\alpha)^{3/2}}\frac{1}{2}\sqrt{\pi} = \frac{\hbar^2\alpha}{2m}+\frac{m\omega^2}{8\alpha} \ .\end{aligned}$$

Now we vary $\hat{H}$ by α,

$$0 = \frac{d}{d\alpha}\langle\hat{H}\rangle = \frac{d}{d\alpha}\left(\frac{\hbar^2\alpha}{2m} + \frac{m\omega^2}{8\alpha}\right) = \frac{\hbar^2}{2m} - \frac{m\omega^2}{8\alpha^2} \ ,$$

and we estimate $\langle\hat{H}\rangle$ at the position of the minimum, $\alpha = \frac{m\omega}{2\hbar}$,

$$\langle\hat{H}\rangle = \frac{\hbar\omega}{2} \ .$$

b. Normalization requires

$$1 = |A|^2 \int_{-\infty}^{\infty} \frac{1}{(x^2+\beta^2)^2} dx = |A|^2 \left[\frac{1}{2}\frac{x}{\beta^2(x^2+\beta^2)} + \frac{1}{2\beta^3}\arctan\frac{x}{\beta}\right]_{-\infty}^{\infty} = \frac{\pi}{2\beta^3} \ .$$

With this

$$\begin{aligned}
\langle\hat{H}\rangle &= -\frac{\hbar^2}{2m}|A|^2 \int_{-\infty}^{\infty} \frac{1}{x^2+\beta^2}\frac{d^2}{dx^2}\frac{1}{x^2+\beta^2} dx + \frac{m}{2}\omega^2|A|^2 \int_{-\infty}^{\infty} \frac{1}{x^2+\beta^2} x^2 \frac{1}{x^2+\beta^2} dx \\
&= -\frac{\hbar^2}{2m}\frac{2\beta^3}{\pi} \int_{-\infty}^{\infty} \frac{6x^2-2\beta^2}{(x^2+\beta^2)^4} dx + \frac{m}{2}\omega^2\frac{2\beta^3}{\pi} \int_{-\infty}^{\infty} \frac{x^2}{(x^2+\beta^2)^2} dx \\
&= -\frac{\hbar^2}{2m}\frac{2\beta^3}{\pi}\left[-\frac{4}{3}\frac{x}{(x^2+\beta^2)^3} - \frac{1}{6}\frac{x}{\beta^2(x^2+\beta^2)^2} - \frac{1}{4\beta^4}\frac{x}{x^2+\beta^2} - \frac{1}{4\beta^5}\arctan\frac{x}{\beta}\right]_{-\infty}^{\infty} \\
&+ \frac{m}{2}\omega^2\frac{2\beta^3}{\pi}\left[-\frac{1}{2}\frac{x}{x^2+\beta^2} + \frac{1}{2\beta}\arctan\frac{x}{\beta}\right]_{-\infty}^{\infty} \\
&= \frac{\hbar^2}{2m}\frac{2\beta^3}{\pi}\frac{\pi}{4\beta^5} + \frac{m}{2}\omega^2\frac{2\beta^3}{\pi}\frac{\pi}{2\beta} = \frac{\hbar^2}{m4\beta^2} + \frac{m}{2}\omega^2\beta^2 \ .
\end{aligned}$$

Now we vary $\hat{H}$ by β,

$$0 = \frac{d}{d\beta}\langle\hat{H}\rangle = \frac{d}{d\beta}\left(\frac{\hbar^2}{m4\beta^2} + \frac{m}{2}\omega^2\beta^2\right) = -\frac{1}{2}\frac{\hbar^2 - 2m^2\omega^2\beta^4}{m\beta^3} \ ,$$

and we estimate $\langle\hat{H}\rangle$ at the position of the minimum, $\beta^2 = \frac{\hbar}{\sqrt{2}m\omega}$,

$$\langle\hat{H}\rangle = \frac{\hbar\omega}{\sqrt{2}} \ .$$

This estimate is $\sqrt{2}$ times larger than the estimate using a Gaussian trial function, which indicates that the Gaussian ansatz be closer to the exact wavefunction than the Lorentzian.

c. Normalization requires

$$1 = |A|^2 \int_{-a/2}^{a/2} \cos\frac{\pi x}{a}\cos\frac{\pi x}{a} dx = |A|^2\frac{a}{2} \ .$$

With this

$$\begin{aligned}\langle\hat{H}\rangle &= -\frac{\hbar^2}{2m}|A|^2\int_{-a/2}^{a/2}\cos\frac{\pi x}{a}\frac{d^2}{dx^2}\cos\frac{\pi x}{a}dx + \frac{m}{2}\omega^2|A|^2\int_{-a/2}^{a/2}x^2\cos^2\frac{\pi x}{a}dx \\ &= \sqrt{\frac{2}{a}}^2\left(\frac{\hbar^2}{2m}\frac{\pi^2}{a^2}\int_{-a/2}^{a/2}\cos^2\frac{\pi x}{a}dx + \frac{m}{2}\omega^2\int_{-a/2}^{a/2}x^2\cos^2\frac{\pi x}{a}dx\right) \\ &= \frac{2}{a}\left(\frac{\hbar^2}{2m}\frac{\pi^2}{a^2}\frac{a}{2} + \frac{m}{2}\omega^2\frac{a^3}{24}\frac{\pi^2-6}{\pi^2}\right) = \frac{\hbar^2}{2m}\frac{\pi^2}{a^2} + \frac{m}{2}\omega^2\frac{a^2}{12}\frac{\pi^2-6}{\pi^2}\ .\end{aligned}$$

Now we vary $\hat{H}$ by a,

$$0 = \frac{d\langle\hat{H}\rangle}{da} = \frac{d}{da}\left(\frac{\hbar^2}{2m}\frac{\pi^2}{a^2} + \frac{m}{2}\omega^2\frac{a^2}{12}\frac{\pi^2-6}{\pi^2}\right) = \frac{1}{12}\frac{-12\hbar^2\pi^4 + m^2\omega^2a^4\pi^2 - 6m^2\omega^2a^4}{ma^3\pi^2}\ ,$$

and we estimate $\langle\hat{H}\rangle$ at the position of the minimum, $a^4 = a_{ho}^4\frac{12\pi^4}{\pi^2-6}$,

$$\langle\hat{H}\rangle = \frac{\hbar\omega}{2}\sqrt{\frac{\pi^2-6}{3}}\ .$$

This estimate is $\sqrt{(\pi^2-6)/3} \approx 1.14$ times larger than the estimate using a Gaussian trial function, which indicates that the Gaussian ansatz be closer to the exact wavefunction than the cosine.

27.2.3.3 Ex: Linear least squares

Use the Raleigh-Ritz method to derive the regression coefficients for a linear fit $f(x_k) = ax_k + b$ to a set of data points (x_k, y_k).

Solution: *The sum of the squared deviations is,*

$$\chi = \sum_{k=1}^{N}[f(x_k) - y_k]^2 = \sum_{k=1}^{N}[ax_k + b - y_k]^2\ .$$

Its minimum with respect to b is given by,

$$0 = \frac{\partial\chi}{\partial b} = \sum_k 2(ax_k + b - y_k)\ .$$

Hence,

$$b = \frac{1}{N}\sum_k y_k - \frac{a}{N}\sum_k x_k = \bar{y} - a\bar{x}\ .$$

Its minimum with respect to a is now given by,

$$0 = \frac{\partial\chi}{\partial a} = \sum_k \frac{\partial}{\partial a}(ax_k + b - y_k)^2 = \sum_k 2(ax_k - a\bar{x} - y_k + \bar{y})(x_k - \bar{x})\ .$$

Hence,

$$a = \frac{\sum_k (x_k - \bar{x})(y_k - \bar{y})}{\sum_k (x_k - \bar{x})(x_k - \bar{x})} = \frac{\sum_k (x_k - \bar{x}) y_k}{\sum_k (x_k - \bar{x})^2} \ .$$

27.2.3.4 Ex: Effect of finite nuclear mass on hydrogen via Rayleigh-Ritz

Use the Rayleigh-Ritz method to estimate the impact of the finite mass of the nucleus of the hydrogen atom. To do this, calculate the ground state energy using the exact Hamiltonian, but a basis of wavefunctions assuming an infinitely heavy nucleus. Only take into account the states ψ_{100} and ψ_{200}. **Help:** Express the exact Hamiltonian in terms of the infinite-mass Hamiltonian approximating for small corrections of the reduced mass: $m \equiv m_e/(1+\gamma) \simeq (1-\gamma)m_e$, where $\gamma \equiv m_e/m_p$.

Solution: *The exact radial Hamiltonian follows from the transformation to the center-of-mass system,*

$$\hat{H}_m = -\frac{\hbar^2}{2m}\frac{d^2}{dr^2} - \frac{e^2}{4\pi\epsilon_0 r} \ ,$$

where $m = (1/m_e + 1/m_p)^{-1} = m_e/(1+\gamma) \simeq (1-\gamma)m_e$, *where* $\gamma \equiv m_e/m_p$. *However, when we solve the Schrödinger equation for the hydrogen atom, we use the approximate Hamiltonian* $\hat{H}_{m_e}$ *substituting* m *by* m_e. *We can rewrite the exact Hamiltonian in terms of the approximate one:*

$$\hat{H}_m = (1+\gamma)\hat{H}_{m_e} + \gamma\frac{e^2}{4\pi\varepsilon_0 r} \ .$$

The functions of the $1s$ *and* $2s$ *orbitals were derived for the approximate Hamiltonian,*

$$\psi_{100} = \sqrt{\tfrac{1}{\pi a_B^3}} e^{-r/a_B} \qquad \textit{and} \qquad \psi_{200} = \sqrt{\tfrac{1}{32\pi a_B^3}} \left(2 - \tfrac{r}{a_B} e^{-r/2a_B}\right) \ ,$$

where $a_B = \frac{4\pi\epsilon_0\hbar^2}{m_e e^2}$. *That is, the Bohr radius is calculated with the* real *mass of the electron and not the* reduced *mass,*

$$\langle 2|\hat{H}_m|1\rangle = (1+\gamma)E_n + \gamma\frac{e^2}{4\pi\varepsilon_0}\langle 2|\tfrac{1}{r}|1\rangle = (1+\gamma)E_n + \gamma\frac{e^2}{4\pi\varepsilon_0} 4\pi \int \psi^*_{200} r \psi_{100} d^3r = \frac{16E_1}{27\sqrt{2}}\gamma \ .$$

The other elements of the matrix are,

$$\langle k|m\rangle = \delta_{k,m} \qquad \textit{and} \qquad \langle 1|\hat{H}_m|2\rangle = \langle 2|\hat{H}_m|1\rangle = \frac{16\gamma}{27\sqrt{2}}E_1$$
$$\langle 1|\hat{H}_m|1\rangle = (1-\gamma)\frac{E_1}{1^2} \qquad \textit{and} \qquad \langle 2|\hat{H}_m|2\rangle = (1-\gamma)\frac{E_1}{2^2} \ .$$

with $E_1 = -\frac{m_e e^4}{32\pi^2\epsilon_0^2\hbar^2} = -\frac{\hbar^2}{2m_e a_B^2}$ *and* $E_n = \frac{E_1}{n^2}$. *Now,*

$$0 = \det(\langle k|\hat{H}_m|m\rangle - \mathcal{E}\langle k|m\rangle) = \begin{vmatrix} \langle 1|\hat{H}_m|1\rangle - \mathcal{E} & \langle 1|\hat{H}_m|2\rangle \\ \langle 2|\hat{H}_m|1\rangle & \langle 1|\hat{H}_m|1\rangle - \mathcal{E} \end{vmatrix}$$
$$= \begin{vmatrix} (1-\gamma)E_1 - \mathcal{E} & \frac{16}{27\sqrt{2}}\gamma E_1 \\ \frac{16}{27\sqrt{2}}\gamma E_1 & (1-\gamma)\frac{1}{4}E_1 - \mathcal{E} \end{vmatrix}$$
$$= \frac{1}{4}E_1^2 - \frac{1}{2}E_1^2\gamma - \frac{5}{4}E_1\mathcal{E} + \frac{1}{4}E_1^2\gamma^2 + \frac{5}{4}E_1\gamma\mathcal{E} + \mathcal{E}^2 - \frac{2^7}{3^6}\gamma^2 E_1^2 \ ,$$

with the solutions,

$$\mathcal{E} = E_1\left(\frac{5}{8}(1-\gamma) \pm \frac{3}{8}\sqrt{(1-\gamma)^2 + \frac{2^{13}}{3^8}\gamma^2}\right) = -\frac{\hbar^2}{2ma_{B^2}}\begin{cases} 0.999\ 46 \\ 0.249\ 95 \end{cases} .$$

The solution with the lower energy is obtained for the + sign, because E_1 *is negative. Hence, expanding this solution,*

$$\mathcal{E} \simeq E_1\left(1 - \gamma + \frac{1}{2}\frac{2^{13}}{3^8}\gamma^2 + ...\right) .$$

With the proton nucleus, the lowest energy $\mathcal{E}$ *is just a bit above the energy* E_1 *of the infinitely heavy nucleus. The coefficients follow from,*

$$c_1^2 + c_2^2 = 1 \qquad \textit{and} \qquad c_1(\langle 1|\hat{H}_m|1\rangle - \mathcal{E}) + c_2\langle 2|\hat{H}_m|1\rangle = 0$$
$$\textit{and} \qquad c_1\langle 1|\hat{H}_m|2\rangle + c_2(\langle 2|\hat{H}_m|2\rangle - \mathcal{E}) = 0 \ .$$

We find the solutions $c_1 = 1.000\ 00$ *and* $c_2 = -0.000\ 54 \simeq -\gamma$. *The* $2s$ *orbital mixes a little into the* $1s$ *and reduces its amplitude near the nucleus because of the finite mass.*

27.2.3.5 Ex: Collapse of a condensate with attractive interactions

A Bose-Einstein condensate of ^{7}Li may become unstable due to attractive interatomic force, the scattering length being $a_s = -27.3a_B$. Consider the radial Gross-Pitaevskii Hamiltonian derived in Exc. 25.1.5.2 with an external harmonic potential with the oscillation frequency $\omega_{trp}/(2\pi) = 50$ Hz. Using the variational method to determine the maximum number of atoms allowing for a stable condensate. (Note that the derived minimization condition must be evaluated numerically.)

Solution: *We want to minimize the radial Gross-Pitaevskii Hamiltonian,*

$$\hat{H}_\alpha = -\frac{\hbar^2}{2m}\frac{d^2}{dr^2} + \frac{m}{2}\omega^2 r^2 + \frac{g|\phi_\alpha(r)|^2}{r^2} \ ,$$

with $\psi_\alpha(\mathbf{r}) = \frac{\phi_\alpha(r)}{r}$ *and* $g = N\frac{4\pi\hbar^2 a_s}{m}$ *doing the ansatz* $\psi_\alpha(\mathbf{r}) = Ae^{-\alpha r^2}$. *Normaliza-*

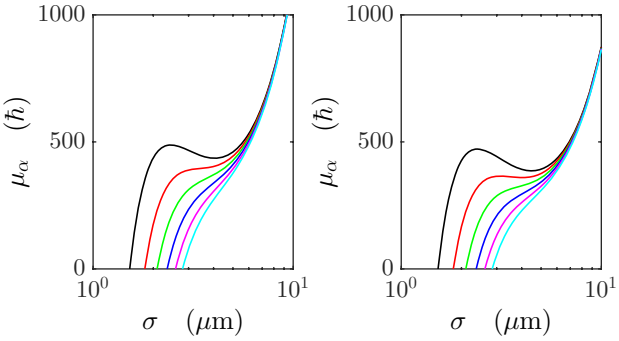

Figure 27.2: (code) Chemical potential as a function of the size of the BEC for various atom numbers between 1000 and 2000 calculated using the variational method (left) and by numerical integration (right).

tion requests,

$$1 = \langle\psi_\alpha|\psi_\alpha\rangle = 4\pi\int_0^\infty |\psi_\alpha(\mathbf{r})|^2 r^2 dr = 4\pi\int_0^\infty |\phi_\alpha(r)|^2 dr$$
$$= 4\pi\int_0^\infty A^2 e^{-2\alpha r^2} r^2 dr = A^2\sqrt{\frac{\pi}{2\alpha}}^3 .$$

Hence, $A^2 = \sqrt{2\alpha/\pi}^3$*. The ground state energy is now,*

$$\mu_\alpha = \langle\phi_\alpha|\hat{H}_\alpha|\phi_\alpha\rangle = 4\pi\int_0^\infty \phi_\alpha(r)\hat{H}_\alpha\phi_\alpha(r)dr$$
$$= 4\pi A^2\int_0^\infty re^{-\alpha r^2}\left[-\tfrac{\hbar^2}{2m}(-6\alpha+4r^2\alpha^2)+\tfrac{m}{2}\omega^2 r^2+gA^2e^{-2\alpha r^2}\right]re^{-\alpha r^2}dr$$
$$= \tfrac{4\pi A^2}{\alpha\sqrt{\alpha}}\tfrac{6\hbar^2\alpha}{2m}\int_0^\infty \zeta^2 e^{-2\zeta^2}d\zeta + \tfrac{4\pi A^2}{\alpha^2\sqrt{\alpha}}\left(-\tfrac{4\hbar^2\alpha^2}{2m}+\tfrac{m\omega^2}{2}\right)\int_0^\infty \zeta^4 e^{-2\zeta^2}d\zeta + \tfrac{4\pi A^2}{\alpha\sqrt{\alpha}}gA^2\int_0^\infty \zeta^2 e^{-4\zeta^2}d\zeta$$
$$= \tfrac{4\pi A^2}{\alpha\sqrt{\alpha}}\tfrac{6\hbar^2\alpha}{2m}\tfrac{1}{8}\sqrt{\tfrac{\pi}{2}} + \tfrac{4\pi A^2}{\alpha^2\sqrt{\alpha}}\left(-\tfrac{4\hbar^2\alpha^2}{2m}+\tfrac{m\omega^2}{2}\right)\tfrac{3}{32}\sqrt{\tfrac{\pi}{2}} + \tfrac{4\pi A^2}{\alpha\sqrt{\alpha}}gA^2\tfrac{\sqrt{\pi}}{32} = \tfrac{3\hbar^2\alpha}{2m}+\tfrac{m\omega^2}{2\alpha}+g\left(\tfrac{\alpha}{\pi}\right)^{3/2} .$$

Minimizing [262],

$$0 = \frac{\partial\mu_\alpha}{\partial\alpha} = \frac{\partial}{\partial\alpha}\left[\frac{3\hbar^2\alpha}{2m}+\frac{m\omega^2}{2\alpha}+g\left(\frac{\alpha}{\pi}\right)^{3/2}\right] = \frac{3\hbar^2\alpha^2 - m^2\omega^2 + 3\pi^{-3/2}g\alpha^{\frac{5}{2}}m}{2m\alpha^2}$$

we obtain

$$0 = 3\hbar^2\alpha^2 - m^2\omega^2 + 3\pi^{-3/2}g\alpha^{\frac{5}{2}}m .$$

This equation must be evaluated numerically. The challenge is to find the number of atoms for which μ_α *has no local minimum. Instead of doing this, here we simply trace some curves for various atom numbers. The figure above shows the chemical potential as a function of the size of the condensate* $\sigma = \alpha^{-1/2}$ *for atom numbers between 1000 (lower curve) and 2000 (upper curve).*

27.3 WKB approximation

The *WKB approximation* (from Wentzel-Kramers-Brillouin) [197, 751, 1370] is a method to find approximate solutions for linear differential equations with spatially variable coefficients. It is typically used for calculations in quantum mechanics where the wavefunction is reformulated as an exponential semi-classically expanded function, and then the amplitude or phase is slowly changed. In the following, we present the WKB approximation applied to the Schrödinger equation and exemplify it in some canonical systems.

27.3.1 WKB approximation applied to the Schrödinger equation

Starting from the time-independent Schrödinger equation,

$$-\frac{\hbar^2}{2m}\frac{d^2}{dx^2}\psi(x) + V(x)\psi(x) = E\psi(x) \ , \tag{27.35}$$

and rewrite it as follows,

$$\frac{d^2\psi}{dx^2} = k(x)\psi(x) \ . \tag{27.36}$$

with $k(x) = \sqrt{2m[E - V(x)]/\hbar^2}$. For now, we will restrict ourselves to energies $E > V(x)$. In this scheme, the wavefunctions are usually complex functions, so that we can write them in polar coordinates, containing an amplitude $A(x)$ and a phase $\phi(x)$, which are both real numbers:

$$\psi(x) = A(x)e^{\imath\phi(x)} \ . \tag{27.37}$$

Substituting this function into the Schrödinger equation we obtain a system of coupled equations in terms of $A(x)$ and $\phi(x)$,

$$A'' = A\Big[(\phi')^2 - k^2\Big] \qquad \text{and} \qquad (A^2\phi')' = 0 \ . \tag{27.38}$$

The equations (27.39) and (27.37) are completely equivalent to the Schrödinger equation. The second Eq. (27.38) is easy to solve,

$$A = \frac{C}{\sqrt{\phi'}} \ , \tag{27.39}$$

being C a real constant. We can not say the same thing about the solution of the first Eq. (27.38). In order to solve it we are going to use the WKB approach, assuming that A varies slowly, so the term $A'' \to 0$. By doing this approximation we can rewrite Eq. (27.39) in this way:

$$(\phi')^2 = k^2 \ . \tag{27.40}$$

Solving this last expression we obtain two linearly independent solutions, $\phi' = \pm k$. So we get the expression for the phase:

$$\phi(x) = \pm \int k(x)dx \ . \tag{27.41}$$

We write this indefinite integral, because the constant term can be absorbed by the constant C. Finally, we obtain the expression for the wavefunction in the WKB approximation:

$$\boxed{\psi(x) = \frac{C}{\sqrt{|k(x)|}} e^{\pm \int |k(x)| dx}} \ . \tag{27.42}$$

Here, taking the absolute value of the wavevector, we have already generalized for the case that the energy E of the particle is lower than the potential $V(x)$ (classically forbidden region).

Example 171 (*WKB approximation*): The WKB approach is a semiclassical method for the solution of the Schrödinger equation that does not require the potential to be a perturbation of a soluble problem. Instead, it only assumes that certain classical quantities having the dimension of an action (energy per time) are much larger than Planck's constant. Inserting the ansatz

$$\psi(x) = A e^{\imath S(x)/\hbar} \ ,$$

into the one-dimensional time-independent Schrödinger equation, we find,

$$-\tfrac{i\hbar}{2m} S''(x) + \tfrac{1}{2m} S'(x)^2 + V(x) - E = 0 \ .$$

Now we expand the exponent in orders of $\hbar$,

$$S(x) = S_0(x) + \hbar S_1(x) + \tfrac{\hbar^2}{2} S_2(x) + \dots \ ,$$

and insert it in the above equation. Collecting the orders in $\hbar$, we find in the first orders,

$$\begin{aligned} \left[\tfrac{1}{2m} S_0'(x)^2 + V(x) - E\right] \hbar^0 &= 0 \\ \left[-\tfrac{\imath\hbar}{2m} S_0''(x) + \tfrac{1}{m} S_0'(x) S_1'(x)\right] \hbar^1 &= 0 \\ \left[\tfrac{1}{2m} S_1'(x)^2 - \tfrac{\imath}{2m} S_1''(x)\right] \hbar^2 &= 0 \ . \end{aligned}$$

The solution of the zeroth order equation, $S_0(x) = \pm \int^x \sqrt{2m[E - V(x')}dx'$, gives

$$\psi(x) = A e^{\pm \frac{\imath}{\hbar} \int^x \sqrt{2m[E - V(x')}dx'} \ .$$

The WKB approximation can be used to describe continuous potentials (or barriers) by stepwise constant potentials. The transmission $|T|^2$ through these parts can be obtained by multiplying the individual tunneling probabilities,

$$\ln |T|^2 \simeq -2 \int_{barrier} \kappa(x) dx \ ,$$

with $\kappa(x) = \frac{1}{\hbar} \sqrt{2m[V(x) - E]}$.

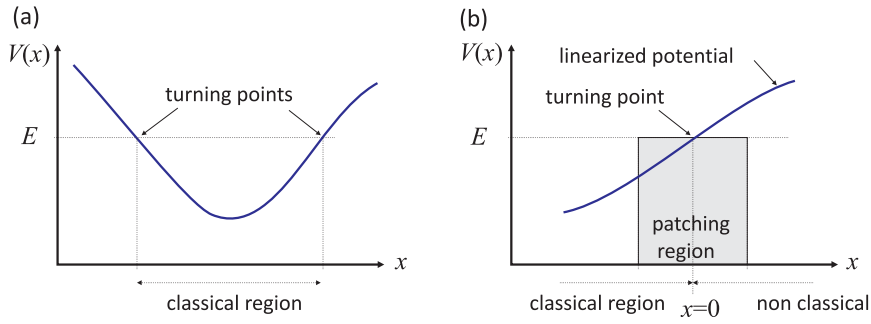

Figure 27.3: (a) Potential for which we want to obtain the connection formula. (b) Turning point.

27.3.2 Connection formulas

Now let us derive the connection formulas that interconnect solutions with E above and below $V(x)$ at the turning points, precisely those regions where WKB fails. We will apply the derivation to a generic confining potential shown in Fig. 27.3.

Let us start with the right turning point Fig. 27.3(a)]. First, we shift the coordinate system so that the turning point coincides with zero, as shown in Fig. 27.3(b). As seen above, the WKB solutions will be given by the following equations:

$$\psi(x) \approx \begin{cases} \frac{1}{\sqrt{k(x)}}\left[Be^{\imath\int_x^0 k(x')dx'} + Ce^{-\imath\int_x^0 k(x')dx'}\right] & \text{if} \quad x \leq 0 \\ \frac{1}{\sqrt{k(x)}} De^{-\int_0^x |k(x')|dx'} & \text{if} \quad x \geq 0 \end{cases} . \tag{27.43}$$

In the vicinity of the turning point we approximate the potential by a straight line (Taylor series expansion up to first order) with the following functional dependence,

$$V(x) \approx E + V'(0)x \ . \tag{27.44}$$

The Schrödinger equation for this potential acquires the following format,

$$\frac{d^2\psi_t}{dx^2} = \alpha^3 x\psi_t \ , \tag{27.45}$$

with $\alpha = [\frac{2m}{\hbar^2}V'(0)]^{1/3}$. Through a change of variables, $z = \alpha x$, we fall back on Airy's equation,

$$\frac{d^2\psi_t}{dz^2} = z\psi_t \ , \tag{27.46}$$

having as solution a linear combination of the two solutions of the Airy equation,

$$\psi_t(x) = a\text{Ai}(\alpha x) + b\text{Bi}(\alpha x) \ . \tag{27.47}$$

Now let's have a look at the WKB solutions in the two regions in the vicinity of the turning point. In the classically forbidden region we have $k(x) = \alpha^{3/2}\sqrt{-x}$, thus being $\int_0^x |k(x')|dx' = \frac{2}{3}(\alpha x)^{3/2}$. Thus, the WKB solution in the classically forbidden region near the turning point will be given by:

$$\psi(x) \approx \frac{D}{\sqrt{\hbar}\alpha^{3/4}x^{1/4}} e^{-\frac{2}{3}(\alpha x)^{3/2}} \ . \tag{27.48}$$

Using the asymptotic forms of Airy functions in the solution (27.47) we obtain the following expression for $\psi_t(x)$,

$$\psi_p(x) \approx \frac{a}{2\sqrt{\pi}(\alpha x)^{1/4}} e^{-\frac{2}{3}(\alpha x)^{3/2}} + \frac{b}{\sqrt{\pi}(\alpha x)^{1/4}} e^{\frac{2}{3}(\alpha x)^{3/2}} , \tag{27.49}$$

which when compared to equation (27.48) shows us that $a = \sqrt{\frac{4\pi}{\alpha\hbar}} D$ and $b = 0$. Repeating the previous steps in the negative region we see that the WKB solution in the asymptotic forms of the Airy solutions for approximately linear potentials takes the following format (with $b = 0$):

$$\psi(x) \approx \frac{1}{\sqrt{\hbar}\alpha^{3/4}(-x)^{1/4}} \left[B e^{\imath\frac{2}{3}(-\alpha x)^{3/2}} + C e^{-\imath\frac{2}{3}(-\alpha x)^{3/2}} \right] , \tag{27.50}$$

and

$$\psi_p(x) \approx \frac{a}{\sqrt{\pi}(-\alpha x)^{1/4}} \frac{1}{2\imath} \left[e^{\imath\pi/4} e^{\imath\frac{2}{3}(-\alpha x)^{3/2}} - e^{-\imath\pi/4} e^{-\imath\frac{2}{3}(-\alpha x)^{3/2}} \right] . \tag{27.51}$$

When compared, $\frac{a}{2\imath\sqrt{\pi}} e^{\imath\pi/4} = \frac{B}{\sqrt{\hbar\alpha}}$ and $-\frac{a}{2\imath\sqrt{\pi}} e^{-\imath\pi/4} = \frac{C}{\sqrt{\hbar\alpha}}$. Having all this information we can rewrite the WKB solutions for all positions in the potential, including the turning points [5]:

$$\psi(x) \approx \begin{cases} \frac{2D}{\sqrt{k(x)}} \sin\left[\int_x^{x_2} k(x')dx' + \frac{\pi}{4} \right] , & \text{if } x \le x_2 \\ \frac{D}{\sqrt{k(x)}} e^{-\int_{x_2}^{x} |k(x')|dx'} , & \text{if } x \ge x_2 \end{cases} . \tag{27.52}$$

Repeating the process for a decreasing turning point [left turning point of the potential of Fig. 27.3(a)], we obtain the following expression:

$$\psi(x) \approx \begin{cases} \frac{D'}{\sqrt{k(x)}} e^{-\int_{x}^{x_1} |k(x')|dx'} , & \text{if } x \le x_1 \\ \frac{2D'}{\sqrt{k(x)}} \sin\left[\int_{x_1}^{x} k(x')dx' + \frac{\pi}{4} \right] , & \text{if } x \ge x_1 \end{cases} . \tag{27.53}$$

Example 172 (*Harmonic oscillator*): Now we apply the WKB method to a well-known system: the harmonic oscillator. We will calculate its energy levels and the respective eigenfunctions.

Eigenenergies: First, note that for a confining potential, and more specifically in the region where $E \ge V(x)$, we have the solutions obtained for the left and right turning point, these two solutions must match each other, that is,

$$\frac{2D}{\sqrt{k(x)}} \sin\left[\int_x^{x_2} k(x')dx' + \frac{\pi}{4} \right] \simeq \frac{2D'}{\sqrt{k(x)}} \sin\left[\int_{x_1}^{x} k(x')dx' + \frac{\pi}{4} \right] ,$$

and hence the zeros of these functions, so the arguments of those sines must be equal (except for a multiple of π),

$$\begin{aligned} \int_x^{x_2} k dx' + \frac{\pi}{4} &= -\int_{x_1}^{x_1} k dx' - \frac{\pi}{4} + n\pi \qquad (27.54) \\ \left(\int_{x_1}^{x} + \int_x^{x_2} \right) k dx' &= \left(n - \frac{1}{2} \right)\pi \\ \int_{x_1}^{x_2} k dx' &= \left(n - \frac{1}{2} \right)\pi , \end{aligned}$$

[5] Note that we shifted the turning point to an arbitrary position x_2.

with $n = 1, 2...$ [6]. With this information we take a harmonic potential of the type $V(x) = \frac{1}{2}\kappa x^2$. In this case, the turning points for a given energy E will be at $-\sqrt{\frac{2E}{\kappa}}$ and $\sqrt{\frac{2E}{\kappa}}$. For this potential we will have that $k(x) = \sqrt{\frac{2m}{\hbar^2}(E - \frac{1}{2}\kappa x^2)}$. Calculating the integral of $k(x)$ between these two turning points we get,

$$\int_{x_1}^{x_2} k(x)dx = \frac{2m}{\hbar}\int_{-\sqrt{2E/k}}^{\sqrt{2E/k}} \sqrt{E - \frac{1}{2}\kappa x^2}dx = \pi E\frac{m}{\kappa} = \left(n - \frac{1}{2}\right)\pi\hbar \ ,$$

isolating E and taking $\omega = \sqrt{\kappa/m}$ we have,

$$E = (n - \tfrac{1}{2})\hbar\omega \ ,$$

with $n = 1, 2...$, the exact spectrum of the harmonic oscillator, but this is just a coincidence.

Eigenstates: Now we will calculate the eigenstates of the harmonic oscillator. The eigenfunctions were calculated on a computer. The first graph (Fig. 27.4) compares the first exact excited state with that obtained using the WKB method.

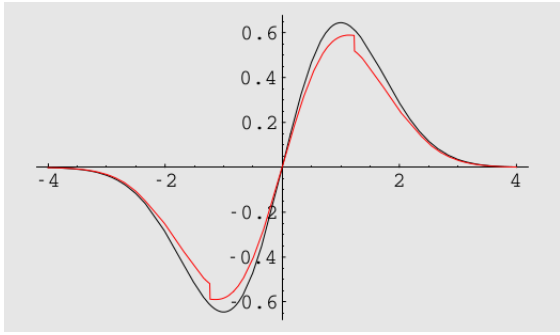

Figure 27.4: First excited state calculated accurately and through the WKB approximation.

Note that the WKB approach is very good when $x \to 0$ and $x \to \infty$, regions where the difference between the oscillator energy and the potential are large ($E \gg V(x \to 0)$ and $E \ll V(x \to \infty)$), because in these regions the wavelength $\lambda(x)$ acquires the lowest values, since it is proportional to $|1/\sqrt{E - V(x)}|$. Hence, the spatial region in which the potential needs to be practically constant is smaller, which explains why the approximation is closer to the exact solution. In the intermediate regions the difference between E and $V(x)$ begins to decrease, and the WKB approximation delivers its worst results.

As we increase the energy of the harmonic oscillator, the approximation becomes better (for the same reason as discussed in the previous paragraph). The following graph illustrates this effect for $n = 10$.

Example 173 (*Hydrogen atom*): Eigenenergies: For the hydrogen atom the effective potential is given by,

$$V(x) = -\frac{e^2}{4\pi\epsilon_0}\frac{1}{r} + \frac{\hbar^2}{2m}\frac{l(l+1)}{r^2} \ .$$

[6] Note that $n \neq 0$, because the integral (27.54) has to be greater than zero.

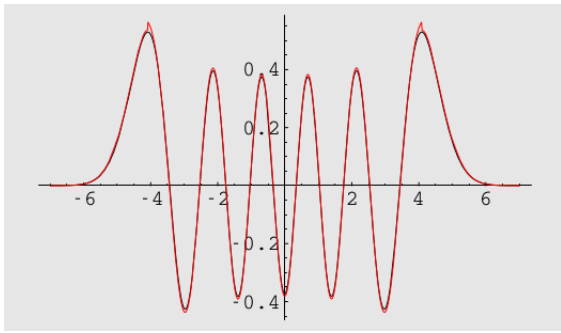

Figure 27.5: Wavefunction of the vibrational state $n = 10$ calculated exactly and using the WKB approximation.

Note that the WKB method for this case obeys the relation (27.54), hence we get,

$$\int_{r_1}^{r_2} p(r)dr = \sqrt{2m}\int_{r_1}^{r_2}\sqrt{E + \frac{e^2}{4\pi\epsilon_0}\frac{1}{r} - \frac{\hbar^2}{2m}\frac{l(l+1)}{r^2}}dr$$
$$= \sqrt{-2mE}\int_{r_1}^{r_2}\frac{1}{r}\sqrt{-r^2 - \frac{e^2}{4\pi\epsilon_0 E}r + \frac{\hbar^2}{2mE}l(l+1)}dr\ .$$

Notice that $E < 0$. Let us make the following substitution to facilitate algebraic manipulations,

$$B = -\frac{e^2}{4\pi\epsilon_0 E} \qquad \text{and} \qquad C = -\frac{\hbar^2}{2mE}l(l+1)\ .$$

The turning points r_1 and r_2 are given by the following expressions,

$$r_1 = \frac{B - \sqrt{B^2 - 4C}}{2} \qquad \text{and} \qquad r_2 = \frac{B + \sqrt{B^2 - 4C}}{2}\ .$$

Thus, returning to the integral we will have the following:

$$\int_{r_1}^{r_2} p(r)dr = \sqrt{-2mE}\int_{r_1}^{r_2}\frac{1}{r}\sqrt{(r-r_1)(r_2-r)}dr = \sqrt{-2mE}\frac{\pi}{2}(\sqrt{r_2} - \sqrt{r_1})^2$$
$$= \sqrt{-2mE}\frac{\pi}{2}(r_1 + r_2 - 2r_1r_2) = \sqrt{-2mE}\frac{\pi}{2}(B - 2\sqrt{C})$$
$$= \frac{\pi}{2}\Big(-\frac{e^2\sqrt{2m}}{4\pi\epsilon_0\sqrt{-E}} - 2\hbar\sqrt{l(l+1)}\Big) = \Big(n - \frac{1}{2}\Big)\pi\hbar\ .$$

Isolating E we obtain the energy spectrum of the hydrogen atom in the WKB approximation:

$$E = -\frac{m}{2\hbar}\Big(\frac{e^2}{4\pi\epsilon_0}\Big)^2\frac{1}{\Big[n - 1/2 + l(l+1)\Big]^2} = -\frac{13.6}{\Big[n - 1/2 + l(l+1)\Big]^2}eV\ .$$

For high energies ($n \gg l$), we recover Bohr's expression.

27.3.3 Exercises

27.3.3.1 Ex: Energy levels of hydrogen via WKB

Use the WKB approach to calculate the energy levels of the hydrogen atom.

Solution:

27.4 Time-dependent perturbations

Temporal perturbations typically occur when we suddenly switch on an external field that influences the motion or spin of the particles, or when the field varies over time, for example, an electromagnetic field. Let us first study a two-level system subject to a temporal perturbation.

27.4.1 Two-level systems

We write the perturbation as

$$\hat{H} = \hat{H}^{(0)} + \hat{H}^{(1)}(t) \ . \tag{27.55}$$

As in the case of a stationary perturbation, we write the eigenenergies and -functions of the unperturbed system as

$$\hat{H}^{(0)}|n\rangle = E_n|n\rangle \ . \tag{27.56}$$

Recalling that this stationary Schrödinger equation was obtained from the time-dependent Schrödinger equation via a separation ansatz (23.59), the temporal evolution of these eigenfunctions is given by,

$$|\psi_n^{(0)}(t)\rangle = |n\rangle e^{-\imath E_n t/\hbar} \ . \tag{27.57}$$

For small perturbations we can expect that the ansatz,

$$|\psi^{(1)}(t)\rangle = a_1(t)|\psi_1^{(0)}(t)\rangle + a_2(t)|\psi_2^{(0)}(t)\rangle \ , \tag{27.58}$$

be good. Note that not only do eigenfunctions oscillate, but the coefficients also depend on time, because the composition of the states can change. The instantaneous probability of finding the system in state n is $|a_n(t)|^2$. Importing the above linear combination into the Schrödinger equation,

$$\left[\hat{H}^{(0)} + \hat{H}^{(1)}(t)\right]|\psi^{(1)}(t)\rangle = \imath\hbar\frac{\partial}{\partial t}|\psi^{(1)}(t)\rangle \ , \tag{27.59}$$

we find,

$$\begin{aligned} &a_1\hat{H}^{(0)}|\psi_1^{(0)}\rangle + a_2\hat{H}^{(0)}|\psi_2^{(0)}\rangle + a_1\hat{H}^{(1)}|\psi_1^{(0)}\rangle + a_2\hat{H}^{(1)}|\psi_2^{(0)}\rangle \\ &\qquad = \imath\hbar\left[\frac{\partial a_1}{\partial t}|\psi_1^{(0)}\rangle + \frac{\partial a_2}{\partial t}|\psi_2^{(0)}\rangle + a_1\frac{\partial|\psi_1^{(0)}\rangle}{\partial t} + a_2\frac{\partial|\psi_2^{(0)}\rangle}{\partial t}\right] \\ \implies &a_1\hat{H}^{(1)}|\psi_1^{(0)}\rangle + a_2\hat{H}^{(1)}|\psi_2^{(0)}\rangle = \imath\hbar\dot{a}_1|\psi_1^{(0)}\rangle + \imath\hbar\dot{a}_2|\psi_2^{(0)}\rangle \ , \end{aligned} \tag{27.60}$$

because the other terms satisfy the Schrödinger equation of zero order. Replacing the stationary eigenfunctions,

$$a_1 e^{-\imath E_1 t/\hbar}\hat{H}^{(1)}|1\rangle + a_2 e^{-\imath E_2 t/\hbar}\hat{H}^{(1)}|2\rangle = \imath\hbar\dot{a}_1 e^{-\imath E_1 t/\hbar}|1\rangle + \imath\hbar\dot{a}_2 e^{-\imath E_2 t/\hbar}|2\rangle \ , \quad (27.61)$$

and multiplying this equation with $\langle 1|\times$ and $\langle 2|\times$, we find with the abbreviation $\hbar\omega_0 \equiv E_2 - E_1$,

$$\imath\hbar\dot{a}_1 = a_1\langle 1|\hat{H}^{(1)}|1\rangle + a_2 e^{-\imath\omega_0 t}\langle 1|\hat{H}^{(1)}|2\rangle \quad (27.62)$$

$$\text{and} \qquad \imath\hbar\dot{a}_2 = a_1 e^{\imath\omega_0 t}\langle 2|\hat{H}^{(1)}|1\rangle + a_2\langle 2|\hat{H}^{(1)}|2\rangle \ .$$

Frequently, the perturbation induces only a coupling, but does not directly influence the energies very much, $\langle n|\hat{H}^{(1)}|n\rangle \simeq 0$,

$$\boxed{\dot{a}_1 = a_2\frac{e^{-\imath\omega_0 t}}{\imath\hbar}\langle 1|\hat{H}^{(1)}|2\rangle \qquad \text{and} \qquad \dot{a}_2 = a_1\frac{e^{\imath\omega_0 t}}{\imath\hbar}\langle 2|\hat{H}^{(1)}|1\rangle} \ . \quad (27.63)$$

Without perturbation, $\langle m|\hat{H}^{(1)}|n\rangle = 0$, no dynamics develops; the eigenfunctions evolve independently.

27.4.2 The time-dependent perturbation method

Now, let us turn our attention to systems with many levels.

In *time-dependent perturbation theory* (TDPT) we separate the Hamiltonian into a stationary part and a time-dependent part [7,8],

$$\hat{H}(t) = \hat{H}^{(0)} + \lambda\hat{H}^{(1)}(t) \ . \quad (27.64)$$

As usual, this Hamiltonian satisfies the Schrödinger equation,

$$\imath\hbar\frac{\partial}{\partial t}|\psi(t)\rangle = \hat{H}(t)|\psi(t)\rangle \ . \quad (27.65)$$

Now, we do a unitary transformation into the *interaction picture* with $S(t) = e^{-\imath\hat{H}^{(0)}t/\hbar}$ substituting $|\psi(t)\rangle \equiv S(t)|\psi_I(t)\rangle$ and $\hat{H}^{(1)}(t) \equiv S(t)\hat{W}(t)S^{-1}(t)$ in the Schrödinger equation. This procedure removes the stationary part, as shown in Sec. 23.4.4,

$$\imath\hbar\frac{\partial}{\partial t}|\psi_I(t)\rangle = \lambda\hat{W}(t)|\psi_I(t)\rangle \ . \quad (27.66)$$

If $\hat{W}(t)$ is also independent of time, the solution simply is $|\psi_I(t)\rangle = e^{-\imath\hat{W}t/\hbar}|\psi_I(0)\rangle$. Otherwise, we integrate the equation,

$$|\psi_I(t)\rangle = |\psi_I(0)\rangle + \frac{\lambda}{\imath\hbar}\int_0^t \hat{W}(\tau)|\psi_I(\tau)\rangle d\tau \ . \quad (27.67)$$

[7] See Becker-Sauter II, p.118ff and [1298], p.104ff. An alternative treatment is found in [816], p.191ff or in Blochinzew, p.332ff.

[8] Note that by substituting $\hat{W}$ by $\hat{H}^{(1)}$, the equation (27.66), $\imath\hbar\partial_t|\psi_I(t)\rangle = \hat{H}^{(1)}(t)|\psi_I(t)\rangle$, corresponds to a first-order perturbative approximation, i.e., the perturbation eigenvalues $\hat{H}(1)$ are calculated with the eigenvectors of the unperturbed system. Thus, in first order TDPT we can substitute $\hat{W}$ for $\hat{H}^{(1)}$.

Substituting $|\psi_I(\tau)\rangle$ by $|\psi_I(t)\rangle$ we iterate this equation,

$$|\psi_I(t)\rangle = |\psi_I(0)\rangle + \frac{\lambda}{\imath\hbar}\int_0^t \hat{W}(\tau_1)\left(|\psi_I(0)\rangle + \frac{\lambda}{\imath\hbar}\int_0^{\tau_1}\hat{W}(\tau_2)|\psi_I(\tau_2)\rangle d\tau_2\right)d\tau_1 \tag{27.68}$$
$$= |\psi_I(0)\rangle + \frac{\lambda}{\imath\hbar}\int_0^t \hat{W}(\tau_1)d\tau_1|\psi_I(0)\rangle + \left(\frac{\lambda}{\imath\hbar}\right)^2\int_0^t\hat{W}(\tau_1)\int_0^{\tau_1}\hat{W}(\tau_2)|\psi_I(\tau_2)\rangle d\tau_2 d\tau_1\rangle$$
$$= \left[\sum\nolimits_{n=1}^{N}\left(\frac{\lambda}{\imath\hbar}\right)^n\int_0^t\hat{W}(\tau_1)\int_0^{\tau_1}\hat{W}(\tau_2)...\int_0^{\tau_{n-1}}\hat{W}(\tau_n)d\tau_1 d\tau_2...d\tau_n\right]|\psi_I(0)\rangle + o(\lambda^{N+1})\ .$$

This is called the *Dyson series*. For $N = 1$, we get the first order of the perturbation series [9],

$$|\psi_I(t)\rangle = \left(1 + \frac{\lambda}{\imath\hbar}\int_0^t\hat{W}(\tau)d\tau\right)|\psi_I(0)\rangle\ . \tag{27.69}$$

The stationary states of the unperturbed Hamiltonian are given by $\hat{H}^{(0)}|f\rangle = E_f|f\rangle$. Now, the perturbed states are expanded on this basis, $|\psi_I(t)\rangle = \sum_f |f\rangle a_f(t)$. The expansion coefficients are [10],

$$a_f(t) = \langle f|\psi_I(t)\rangle = \langle f|\psi_I(0)\rangle + \frac{\lambda}{\imath\hbar}\langle f|\int_0^t S^{-1}(\tau)\hat{H}^{(1)}(\tau)S(\tau)|\psi_I(0)\rangle d\tau\ . \tag{27.70}$$

Now, we assume that the system be initially in the eigenstate $|\psi_I(0)\rangle = |i\rangle$. The amplitudes then are,

$$a_{i\to f}(t) = \langle f|i\rangle + \frac{\lambda}{\imath\hbar}\int_0^t e^{\imath E_f\tau/\hbar}\langle f|\hat{H}^{(1)}(\tau)|i\rangle e^{-\imath E_i\tau/\hbar}d\tau \tag{27.71}$$
$$= \delta_{if} + \frac{\lambda}{\imath\hbar}\int_0^t\langle f|\hat{H}^{(1)}(\tau)|i\rangle e^{\imath\omega_{if}\tau}d\tau\ .$$

The time-varying potential generates a perturbation causing a variation of the system's state. As the energy is not conserved, $[\partial_t, \hat{H}(t)] \neq 0$, the time-dependence is not separable and the system exchanges energy with the potential. In first-order perturbation theory we only consider weak perturbations, i.e. the initial state is emptied only slowly, $a_{i\to i}(dt) \simeq a_{i\to i}(0) = 1$. On the other hand, for an initially empty state f the gain is obviously considerable. For $i \neq f$ we have,

$$\boxed{da_{i\to f}(t) = a_{i\to f}(t+dt) - a_{i\to f}(t) = \frac{\lambda}{\imath\hbar}\langle f|\hat{H}^{(1)}(t)|i\rangle e^{\imath\omega_{if}t}dt}\ . \tag{27.72}$$

This formula is nothing more than a generalization of the formula (27.63) obtained for a two-level system assuming that the initial state does not deplete considerably. In Exc. 27.4.5.1 we calculate the dynamics of a harmonic oscillator perturbed by a decaying force.

[9] For higher orders,

$$|\psi_I(t)\rangle \approx \left[\sum\nolimits_{n=1}^{N}\left(\frac{\lambda}{\imath\hbar}\right)^n\left(\int_0^t\hat{W}(\tau)d\tau\right)^n\right]|\psi_I(0)\rangle = T\left[\exp\left(\frac{\lambda}{\imath\hbar}\int_0^t\hat{W}(\tau)d\tau\right)\right]|\psi_I(0)\rangle\ .$$

[10] We could define the coefficients in Schrödinger's picture, $a_f \equiv \langle f|\psi\rangle$, but this would only introduce a phase factor, $a_{i\to f} \to a_{i\to f}e^{\imath(E_f-E_i)t/\hbar}$, which is unimportant for absolute values $|a_{i\to f}|^2$. This corresponds to a transformation to a rotating system, which will be discussed in Sec. 34.4.1.

27.4.3 Specific perturbations

27.4.3.1 Sudden switch-on of a constant perturbation

To begin with, we consider a constant perturbation $\hat{H}^{(1)}$ suddenly switched on at $t = 0$. In Schrödinger's picture we can rewrite Eq. (27.71),

$$a_{i\to f}(t) = \delta_{if} + \frac{\lambda}{\imath\hbar}\langle f|\hat{H}^{(1)}|i\rangle \int_0^t e^{\imath\omega_{if}\tau} d\tau = \delta_{if} + \frac{\lambda}{\imath\hbar}\langle f|\hat{H}^{(1)}|i\rangle \frac{-1+e^{\imath\omega_{if}t}}{\imath\omega_{if}} \ . \quad (27.73)$$

We obtain for $i \neq f$,

$$\boxed{|a_{i\to f}(t)|^2 = \frac{\lambda^2}{\hbar^2}|\langle f|\hat{H}^{(1)}|i\rangle|^2 \frac{\sin^2(\omega_{if}t/2)}{(\omega_{fi}/2)^2}} \ . \quad (27.74)$$

For long times we calculate the rate [11],

$$\frac{d}{dt}|a_{i\to f}(t)|^2 = \frac{\lambda^2}{\hbar^2}|\langle f|\hat{H}^{(1)}|i\rangle|^2 \frac{\sin\omega_{fi}t}{\omega_{fi}/2} \overset{t\to\infty}{\longrightarrow} \frac{2\pi\lambda^2}{\hbar^2}|\langle f|\hat{H}^{(1)}|i\rangle|^2 \delta(\omega_f - \omega_i) \ , \quad (27.75)$$

where we use the representation of the Dirac function,

$$\delta(x) = \lim_{t\to\infty} \tfrac{1}{2\pi} \int_{-t}^{t} e^{\imath kx} dk = \lim_{t\to\infty} \tfrac{t}{\pi} \mathrm{sinc}\ xt \ . \quad (27.76)$$

The δ-function in (27.75) ensures that, for infinitely sharp steps, transitions are impossible, unless the energy of the final state is the same as the one of the initial state. This points to the fact that infinitely sharp steps are not a realistic physical concept.

In practice, the changes applied to a system are often slow and the observation times are long, because the frequencies of the transitions are high $\omega_{fi}/2\pi \simeq$ THz. Let us assume that the perturbation be switched on within a time constant γ^{-1}. In Exc. 27.4.5.2 we will study how the rapidity of a perturbation influences the transition rate. We will see via a temporal analysis of $|a_{i\to f}(t)|^2$, that for slow variations, $\gamma \ll \omega_{fi}$, the system adiabatically approaches the final situation. For $\gamma \simeq \omega_{fi}$, the system receives a shock and exhibits oscillating transients. For $\gamma > \omega_{fi}$, we observe violent oscillations with largest amplitudes.

27.4.3.2 Periodic perturbations

We now consider the case of an oscillatory perturbation, for example an electromagnetic field. In principle, knowledge of the system's response to periodic perturbations allows us to treat arbitrary perturbations, since we can expand them in Fourier series. We first treat transitions between discrete levels, before considering states embedded in continua,

$$\hat{H}^{(1)}(t) = \begin{cases} 0 \quad \text{for} \quad t < 0 \\ 2\hbar\hat{\Omega}_0 \cos\omega t \quad \text{for} \quad t \geq 0 \end{cases} \ . \quad (27.77)$$

[11] We use the trigonometric rule $\sin x = 2\sin\frac{x}{2}\cos\frac{x}{2}$.

With the abbreviation $\Omega_{fi} \equiv \langle f|\hat{\Omega}_0|i\rangle$ the transition rate is,

$$a_{i\to f}(t) = -\imath\Omega_{fi}\int_0^t 2e^{\imath\omega_{fi}\tau}\cos\omega\tau d\tau \tag{27.78}$$
$$= -\imath\Omega_{fi}\left[\cancelto{0}{\frac{e^{\imath(\omega_{fi}+\omega)t}-1}{\imath(\omega_{fi}+\omega)}} + \frac{e^{\imath(\omega_{fi}-\omega)t}-1}{\imath(\omega_{fi}-\omega)}\right] .$$

The first term being small, we neglect it doing a so-called *rotating wave approximation* (RWA). We obtain,

$$|a_{i\to f}(t)|^2 = |\Omega_{fi}|^2\frac{\sin^2\frac{1}{2}(\omega_{fi}-\omega)t}{\frac{1}{4}(\omega_{fi}-\omega)^2} . \tag{27.79}$$

This result coincides with the formula (27.74), except that the energy difference between the states ω_{fi} is shifted by the frequency of the perturbation ω. The quantity $\Delta_{fi} \equiv \omega - \omega_{fi}$ is called a detuning. The transition probability is maximal, when we are at resonance, that is $\Delta_{fi} = 0$. In this case,

$$|a_{i\to f}(t)|^2 \longrightarrow |\Omega_{fi}|^2t^2 . \tag{27.80}$$

This can be seen by expanding the numerator in a Taylor series for small $(\omega_{fi}-\omega)t$.

Note, that the probability exceeds 1 for long times, which can not be. In fact, the restriction to the first order in the Taylor expansion used in the derivation of the last equation is no longer valid for long times, when $(\omega_{fi}-\omega)t > 1$, and we need to take into account higher orders.

Example 174 (*The Rabi formula*): Let us now come back to the two-level system studied in Sec. 27.4.1 and consider a periodic perturbation oscillating at frequency $\omega = \omega_0 + \Delta$, where Δ is called the *detuning* from the resonance whose frequency is ω_0,

$$H^{(1)} = -e\mathbf{E}(\mathbf{r},t)\cdot\mathbf{r} = -eE_0\hat{\varepsilon}\cos(kz-\omega t)\cdot\mathbf{r} . \tag{27.81}$$

Then,

$$\langle 2|H^{(1)}|1\rangle = -eE_0\cos(kz-\omega t)\langle 2|r|1\rangle = \hbar\Omega\cos(kz-\omega t) , \tag{27.82}$$

where we call

$$\Omega \equiv \frac{-eE_0\langle 2|r|1\rangle}{\hbar} \tag{27.83}$$

the *Rabi frequency*. With this abbreviation the Eqs. (27.63) become,

$$\dot{a}_1 = -\imath\Omega a_2e^{-\imath\omega_0t}\cos(kz-\omega t) \quad \text{and} \quad \dot{a}_2 = -\imath\Omega^*a_1e^{\imath\omega_0t}\cos(kz-\omega t) . \tag{27.84}$$

Neglecting fast-rotating terms doing the so-called *rotating wave approximation* (RWA) and choosing the position of the atom to be $z = 0$ we derive,

$$\dot{a}_1 \simeq -\frac{\imath\Omega}{2}a_2e^{\imath\Delta t} \quad \text{and} \quad \dot{a}_2 \simeq -\frac{\imath\Omega^*}{2}a_1e^{-\imath\Delta t} , \tag{27.85}$$

which coincides with the formulas derived in Sec. 27.4.1. With the equations of motion we can, starting from initial values for $a_1(0)$ and $a_2(0)$, calculate the temporal evolution.

We solve this system of differential equations by differentiating one and substituting the other,

$$\ddot{a}_2 = -\imath\dot{a}_1\frac{\Omega^*}{2}e^{-\imath\Delta t} - a_1\Delta\frac{\Omega^*}{2}e^{-\imath\Delta t} = -\frac{|\Omega|^2}{4}a_2 - \imath\Delta\dot{a}_2 \ . \tag{27.86}$$

We find solutions via the ansatz $a_2 = e^{-\imath\Delta t/2}(Ae^{\imath Gt/2}+Be^{-\imath Gt/2})$. The equation for a_2 yields,

$$\begin{aligned}(\tfrac{\imath}{2}G - \tfrac{\imath}{2}\Delta)^2 Ae^{\imath(G-\Delta)t/2} + (-\tfrac{\imath}{2}G - \tfrac{\imath}{2}\Delta)^2 Be^{\imath(-G-\Delta)t/2} \\ = -\tfrac{|\Omega|^2}{4}(Ae^{\imath(G-\Delta)t/2} + Be^{\imath(-G-\Delta)t/2} \\ - \imath\Delta\left[(\tfrac{\imath}{2}G - \tfrac{\imath}{2}\Delta)Ae^{\imath(G-\Delta)t/2} + (-\tfrac{\imath}{2}G - \tfrac{\imath}{2}\Delta)Be^{\imath(-G-\Delta)t/2}\right] \ .\end{aligned} \tag{27.87}$$

Separating the parts in A and in B we obtain two equations with the same result,

$$G^2 = |\Omega|^2 + \Delta^2 \ . \tag{27.88}$$

G is called the *generalized Rabi frequency*. Using the initial conditions, $a_1(0) = 1$ and $a_2(0) = 0$, we can fix one of the coefficients A and B, since $a_2(0) = A + B = 0$,

$$a_2 = 2\imath Ae^{-\imath\Delta t/2}\sin\tfrac{G}{2}t \ . \tag{27.89}$$

We now import this solution into the differential equation for a_1,

$$\dot{a}_1 = -\imath\frac{\Omega}{2}a_2e^{\imath\Delta t} = \Omega Ae^{\imath\Delta t/2}\sin\tfrac{G}{2}t \ . \tag{27.90}$$

The integral is,

$$a_1(t) = \int_0^t \Omega Ae^{\imath\Delta t'/2}\sin\tfrac{G}{2}t'dt' = -\frac{2A}{\Omega^*}e^{\imath\Delta t/2}\left(G\cos\tfrac{G}{2}t - \imath\Delta\sin\tfrac{G}{2}t\right) \ . \tag{27.91}$$

Using the normalization condition,

$$\begin{aligned}1 = |a_1|^2 + |a_2|^2 = \left|-\frac{2A}{\Omega^*}e^{\imath\Delta t/2}\left(G\cos Gt - \imath\Delta\sin\tfrac{G}{2}t\right)\right|^2 + \left|2\imath Ae^{-\imath\Delta t/2}\sin Gt\right|^2 \\ = \frac{4A^2}{|\Omega|^2}\left(G^2\cos^2\tfrac{G}{2}t + \Delta^2\sin^2\tfrac{G}{2}t\right) + 4A^2\sin^2\tfrac{G}{2}t = 4A^2\frac{G^2}{|\Omega|^2} \ .\end{aligned} \tag{27.92}$$

Hence, $A = |\Omega|/2G$. In general, we can choose Ω real, and the final solution is,

$$\boxed{a_1(t) = -e^{\imath\Delta t/2}\left(\cos\tfrac{G}{2}t + \tfrac{-\imath\Delta}{G}\sin\tfrac{G}{2}t\right) \quad \text{and} \quad a_2(t) = \tfrac{\imath\Omega}{G}e^{-\imath\Delta t/2}\sin\tfrac{G}{2}t} \ . \tag{27.93}$$

This results has already been obtained in Exc. 23.4.7.1 using an exact (i.e. not perturbative) calculus. When the energies E_n are degenerate, under the influence of the perturbation, the populations of the system oscillate with the Rabi frequency Ω. When the energies are different, the oscillation frequency G is higher, but the amplitude decreases as well. The initially empty state never reaches unitary population. In Exc. 27.4.5.3 we calculate the time required to allow the perturbation to invert the population of a two-level system, in Exc. 27.4.5.4 we study the maximum achievable inversion as a function of detuning, and in Exc. 27.4.5.5 we analyze the dynamics of a system subject to sequences of pulses.
In Exc. 27.4.5.6 we show a derivation using the Laplace transformation method.

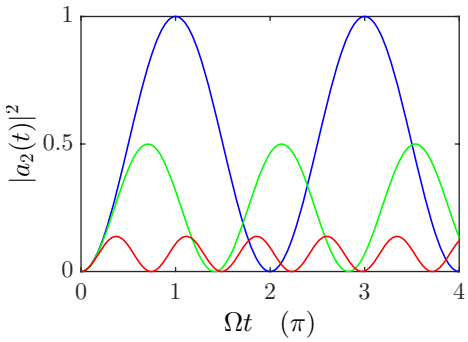

Figure 27.6: (code) Probability $|a_2(t)|^2$ for the atom to be in the excited state for $\Omega = \Gamma$ and $\Delta = 0$ (blue), $\Delta = \Gamma$ (green), and $\Delta = 2.5\Gamma$ (red). Time is in units of $1/\Gamma$.

27.4.3.3 Transitions to continuous levels

When there are several final states, $f \in F$, the formula (27.79) must be generalized. The total transition probability,

$$P_{i\to F}(t) = \sum_{f\in F} |a_{i\to f}(t)|^2 \ , \tag{27.94}$$

corresponds to the probability of the initial state $|i\rangle$ to be depleted. When the final state lies within a continuum, the sum in (27.94) must be replaced by an integral. With the *density of states* written in the form $\rho(E)$, where $\rho(E)dE$ is the number of states found in the energy range between E and $E + dE$, the transition probability is [12],

$$P_{i\to F}(t) = \int_{E_{min}}^{E_{max}} |a_{i\to f}(t)|^2 \rho(E_f) dE_f \ , \tag{27.95}$$

where $E \in [E_{min}, E_{max}]$ is the regime of energies within reach of the periodic perturbation. Now, plugging in the expression (27.79),

$$P_{i\to F}(t) = \int_{E_{min}}^{E_{max}} |\Omega_{fi}|^2 \frac{\sin^2 \frac{1}{2\hbar}(E_{fi} - E)t}{\frac{1}{4\hbar^2}(E_{fi} - E)^2} \rho(E_f) dE_f \ . \tag{27.96}$$

Again using the representation (27.76) of the Dirac function with the substitution $x \equiv (E_{fi} - E)/2\hbar$, we obtain after sufficiently long times [13],

$$P_{i\to F}(t) = \int_{E_{min}}^{E_{max}} |\Omega_{fi}|^2 t^2 \frac{\pi}{t} \delta(\tfrac{E_{fi}-E}{2\hbar}) \rho(E_f) dE_f = 2\pi\hbar t |\Omega_{fi}|^2 \rho(E_i + E) \ . \tag{27.97}$$

The transition rate is,

$$\frac{dP_{i\to F}(t)}{dt} = \pi\hbar |\Omega_{fi}|^2 \rho(E_i + E) \ . \tag{27.98}$$

[12] With $\rho(E) \equiv \sum_{f\in F} \delta(E_f - E)$ the integral is converted back into a sum.
[13] Remember $\delta(ax) = \frac{1}{a}\delta(x)$.

For a narrow distribution of final energies E centered around E_f we may substitute the density of states by a δ-distribution, $\rho(E) = \delta(E - E_f)$, so that,

$$\boxed{\frac{dP_{i\to F}}{dt} = \frac{2\pi}{\hbar}|\langle f|\hat{H}^{(1)}|i\rangle|^2\delta(E_{fi} - E)} \,, \tag{27.99}$$

where we went back to the definition of the perturbation Hamiltonian (27.77). This expression is called *Fermi's Golden rule*. In Exc. 27.4.5.7 we will calculate the *photoelectric effect*.

27.4.3.4 Continuous frequency distribution

To derive Eq. (27.79), we considered perturbations with fixed oscillation frequencies. To handle frequency distributions $\varrho(\omega)$, we must generalize this equation by calculating the integral,

$$\begin{aligned} |a_{i\to f}(t)|^2 &= |\Omega_{fi}|^2 \int \varrho(\omega)\frac{\sin^2\frac{1}{2}(\omega_{fi}-\omega)t}{\frac{1}{4}(\omega_{fi}-\omega)^2}d\omega \\ &\simeq |\Omega_{fi}|^2 t\varrho(\omega_{fi})\int_{-\infty}^{\infty}\mathrm{sinc}^2 x dx = \pi t|\Omega_{fi}|^2\varrho(\omega_{fi}-\omega) \,, \end{aligned} \tag{27.100}$$

again using the representation (27.76) of the Dirac function. The approximation $\varrho(\omega) = \varrho(\omega_{fi})$ can be used if the width of the sinc function is much narrower than the frequency distribution, which is the case for sufficiently long times, $t \gg \pi/2\Delta_{fi}$.

27.4.4 Transition rates for higher-order perturbations

The evolution from an initial state $|i\rangle$ that the system occupies at time t_0 to some final state $|\psi\rangle$, which may be a superposition, occupied at time t, is ruled by the solution of the Schrödinger equation,

$$|\psi\rangle = e^{-\imath\hat{H}(t-t_0)/\hbar}|i\rangle \,. \tag{27.101}$$

The probability to encounter $|\psi\rangle$ in a given state $|f\rangle$ is $|\langle f|\psi\rangle|^2$, and the *transition rate* is simply the derivative of this. The transition rate *out of the initial state* into any other final state is, consequently

$$\boxed{\frac{1}{\tau} = \sum_f \frac{d}{dt}|\langle f|e^{-\imath\hat{H}(t-t_0)/\hbar}|i\rangle|^2} \,. \tag{27.102}$$

From this formula we can already see, that at short times, when we can expand the exponential to first order, we will recover the results of (27.72).

Let us now consider a time-independent perturbation in the Schrödinger picture,

$$\hat{H}(t) = \hat{H}^{(0)} + \hat{H}^{(1)} \,, \tag{27.103}$$

where the time dependence is entirely left to the wavefunction. Now, we expand the propagator $e^{-\imath\hat{H}(t-t_0)}$ in a perturbative series [14]. Unfortunately, generally $[\hat{H}^{(0)}, \hat{H}^{(1)}] \neq$

[14] We drop the $\hbar = 1$ for the following calculation to simplify the notation.

0, so that we cannot simply assume $e^{-\imath\hat{H}t} \neq e^{-\imath\hat{H}^{(0)}t}e^{-\imath\hat{H}^{(1)}t}$. But we can calculate,

$$\imath\frac{d}{dt}e^{\imath\hat{H}^{(0)}t}e^{-\imath\hat{H}t} = -\hat{H}^{(0)}e^{\imath\hat{H}^{(0)}t}e^{-\imath\hat{H}t} + e^{\imath\hat{H}^{(0)}t}\hat{H}e^{-\imath\hat{H}t} = e^{\imath\hat{H}^{(0)}t}\hat{H}^{(1)}e^{-\imath\hat{H}t} \ . \quad (27.104)$$

Integrating both sides and resolving for $e^{-\imath\hat{H}t}$,

$$e^{-\imath\hat{H}t} = e^{-\imath\hat{H}^{(0)}t}\left\{e^{\imath\hat{H}^{(0)}t_0}e^{-\imath\hat{H}t_0} - \imath\int_{t_0}^{t} e^{\imath\hat{H}^{(0)}t_1}\hat{H}^{(1)}e^{-\imath\hat{H}t_1}dt_1\right\} \ . \quad (27.105)$$

We want to analyze a steady-state situation, that is, we assume that the interaction as gradually built up in an infinitely remote past. Hence, we can set $\hat{H} = \hat{H}^{(0)}$ for $t_0 \to -\infty$,

$$e^{-\imath\hat{H}t} = e^{-\imath\hat{H}^{(0)}t}\left\{1 - \imath\int_{-\infty}^{t} e^{\imath\hat{H}^{(0)}t_1}\hat{H}^{(1)}e^{\varepsilon t_1}e^{-\imath\hat{H}t_1}dt_1\right\} \ , \quad (27.106)$$

where the term $e^{\varepsilon t_1}$, with $\varepsilon \to 0$, is inserted to guarantee a smooth switch-on. We iterate,

$$\boxed{\begin{aligned} e^{-\imath\hat{H}t} &= e^{-\imath\hat{H}^{(0)}t}\left\{1 - \imath\int_{-\infty}^{t} e^{\imath\hat{H}^{(0)}t_1}\hat{H}^{(1)}e^{\varepsilon t_1}\times\right. \\ &\times \left. e^{-\imath\hat{H}^{(0)}t}\left[1 - \imath\int_{-\infty}^{t_1} e^{\imath\hat{H}^{(0)}t_2}\hat{H}^{(1)}e^{\varepsilon t_2}e^{-\imath\hat{H}t_2}dt_2\right]dt_1\right\} \end{aligned}} \ . \quad (27.107)$$

We calculate the matrix elements up to second order substituting $\hat{H}$ with $\hat{H}^{(0)}$ in the last integral,

$$\begin{aligned} &\langle f|e^{-\imath\hat{H}t}|i\rangle \quad (27.108)\\ &\simeq \langle f|e^{-\imath\hat{H}^{(0)}t}\left\{1 - \imath\int_{-\infty}^{t} e^{\imath\hat{H}^{(0)}t_1}\hat{H}^{(1)}e^{\varepsilon t_1}e^{-\imath\hat{H}^{(0)}t_1}\left[1 - \imath\int_{-\infty}^{t_1} e^{\imath\hat{H}^{(0)}t_2}\hat{H}^{(1)}e^{\varepsilon t_2}e^{-\imath\hat{H}^{(0)}t_2}dt_2\right]dt_1\right\}|i\rangle \\ &= e^{-\imath\omega_f t}\langle f|i\rangle - \imath e^{-\imath\omega_f t}\int_{-\infty}^{t} e^{\imath\omega_f t_1}\langle f|\hat{H}^{(1)}|i\rangle e^{\varepsilon t_1}e^{-\imath\omega_i t_1}dt_1 \\ &\quad - e^{-\imath\omega_f t_1}\int_{-\infty}^{t} e^{\imath\omega_f t_1}\langle f|\hat{H}^{(1)}e^{\varepsilon t_1}e^{-\imath\omega_i t_1}\sum_m |m\rangle\langle m|\int_{-\infty}^{t_1} e^{\imath\hat{H}^{(0)}t_2}\hat{H}^{(1)}|i\rangle e^{\varepsilon t_2}e^{-\imath\omega_i t_2}dt_2 dt_1 \ . \end{aligned}$$

where we separated the perturbation orders and inserted $\sum_m |m\rangle\langle m| = 1$ using the

closure relation. Using the time-independence of $\hat{H}^{(1)}$,

$$\begin{aligned}
\langle f|e^{-\imath\hat{H}t}|i\rangle &\simeq e^{-i\omega_{fi}t}\delta_{fi} - \imath e^{-\imath\omega_f t}\langle f|\hat{H}^{(1)}|i\rangle \int_{-\infty}^{t} e^{(\imath\omega_f - \imath\omega_i+\varepsilon)t_1}dt_1 \qquad (27.109)\\
&\quad - e^{-\imath\omega_f t}\sum_m \langle f|\hat{H}^{(1)}|m\rangle\langle m|\hat{H}^{(1)}|i\rangle \int_{-\infty}^{t} e^{(\imath\omega_f - \imath\omega_i+\varepsilon)t_1}\int_{-\infty}^{t_1} e^{(\imath\omega_m - \imath\omega_i+\varepsilon)t_2}dt_2dt_1\\
&= e^{-\imath\omega_{fi}t}\delta_{fi} - \imath e^{-\imath\omega_f t}\langle f|\hat{H}^{(1)}|i\rangle \frac{e^{(\imath\omega_f - \imath\omega_i+\varepsilon)t}}{\imath(\omega_f-\omega_i)+\varepsilon}\\
&\quad - e^{-\imath\omega_f t}\sum_m \langle f|\hat{H}^{(1)}|m\rangle\langle m|\hat{H}^{(1)}|i\rangle \int_{-\infty}^{t} e^{(\imath\omega_f - \imath\omega_m+\varepsilon)t_1}\frac{e^{(\imath\omega_m - \imath\omega_i+\varepsilon)t_1}}{\imath(\omega_m-\omega_i)+\varepsilon}dt_1\\
&= e^{-\imath\omega_{fi}t}\delta_{fi} - \imath\langle f|\hat{H}^{(1)}|i\rangle \frac{e^{(-\imath\omega_i+\varepsilon)t}}{\imath(\omega_f-\omega_i)+\varepsilon}\\
&\quad - e^{-\imath\omega_f t}\sum_m \frac{\langle f|\hat{H}^{(1)}|m\rangle\langle m|\hat{H}^{(1)}|i\rangle}{\imath(\omega_m-\omega_i)+\varepsilon}\int_{-\infty}^{t} e^{(\imath\omega_f - \imath\omega_i+2\varepsilon)t_1}dt_1\\
&= e^{-\imath\omega_{fi}t}\delta_{fi} - \imath\langle f|\hat{H}^{(1)}|i\rangle \frac{e^{(-\imath\omega_i+\varepsilon)t}}{\imath(\omega_f-\omega_i)+\varepsilon} - \sum_m \frac{\langle f|\hat{H}^{(1)}|m\rangle\langle m|\hat{H}^{(1)}|i\rangle}{\imath(\omega_m-\omega_i)+\varepsilon}\frac{e^{(-\imath\omega_i+2\varepsilon)t}}{\imath(\omega_f-\omega_i)+2\varepsilon}\,.
\end{aligned}$$

These three terms represent the zeroth, first, and second perturbation orders of the propagation operator (27.101). They are also called *Feynman propagators*. Now, we can calculate the transition rate up to second order,

$$\begin{aligned}
\frac{1}{\tau} &= \frac{d}{dt}\sum_f \left|\langle f|e^{-\imath\hat{H}t}|i\rangle\right|^2 \qquad (27.110)\\
&= \lim_{\varepsilon\to 0}\sum_f \left|\langle f|\hat{H}^{(1)}|i\rangle - \sum_m \frac{\langle f|\hat{H}^{(1)}|m\rangle\langle m|\hat{H}^{(1)}|i\rangle}{-\imath\imath(\omega_m-\omega_i)-\imath\varepsilon}\right|^2 \frac{d}{dt}\left|\frac{e^{(-\imath\omega_i+\varepsilon)t}}{\imath(\omega_f-\omega_i)+\varepsilon}\right|^2\\
&= \sum_f \left|\langle f|\hat{H}^{(1)}|i\rangle - \sum_m \frac{\langle f|\hat{H}^{(1)}|m\rangle\langle m|\hat{H}^{(1)}|i\rangle}{(\omega_m-\omega_i)}\right|^2 \lim_{\varepsilon\to 0}\frac{2\varepsilon e^{2\varepsilon t}}{(\omega_f-\omega_i)^2+\varepsilon^2}\,.
\end{aligned}$$

The last fraction is a representation of the δ-function. Reintroducing $\hbar$, we finally obtain,

$$\boxed{\frac{1}{\tau} = \frac{2\pi}{\hbar^2}\sum_f \left|\langle f|\hat{H}^{(1)}|i\rangle + \frac{1}{\hbar}\sum_m \frac{\langle f|\hat{H}^{(1)}|m\rangle\langle m|\hat{H}^{(1)}|i\rangle}{\omega_i-\omega_m}\right|^2 \delta(\omega_f-\omega_i)}\,. \qquad (27.111)$$

The first term is *Fermi's Golden rule*, the second order corresponds to the *Kramers-Heisenberg formula*, which serves to describe Thomson, Rayleigh and Raman scattering. The generalization of this transition rate to all perturbation orders can be written,

$$\begin{aligned}
\frac{1}{\tau} = \frac{2\pi}{\hbar^2}\sum_f \Bigg|\langle f|\Bigg(\hat{H}^{(1)} + \frac{1}{\hbar}\sum_m \frac{\hat{H}^{(1)}|m\rangle\langle m|\hat{H}^{(1)}}{\omega_i-\omega_m} + \ \ldots \qquad (27.112)\\
+\frac{1}{\hbar^{n-1}}\sum_{m_1,\ldots,m_{n-1}} \frac{\hat{H}^{(1)}|m_1\rangle\langle m_1|\ldots|m_{n-1}\rangle\langle m_{n-1}|\hat{H}^{(1)}}{(\omega_i-\omega_{m_1})\ldots(\omega_i-\omega_{m_{n-1}})}\Bigg)|i\rangle\Bigg|^2 \delta(\omega_{fi})\,.
\end{aligned}$$

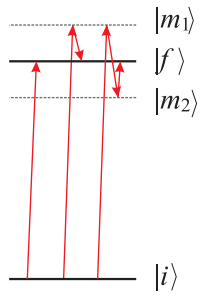

Figure 27.7: Graphical illustration of the various transitions orders. From left to right: absorption, Raman transition via an intermediate virtual state $|m_1\rangle$, three-photon process via two intermediate virtual states $|m_1\rangle$ and $|m_2\rangle$.

27.4.5 Exercises

27.4.5.1 Ex: Perturbed harmonic oscillator

Consider a one-dimensional harmonic oscillator (HO) initially prepared ($t = -\infty$) in the ground state $|0\rangle$ of the unperturbed Hamiltonian $H^{(0)} = \hbar\omega\hat{a}^\dagger\hat{a}$, such that $H^{(0)}|n\rangle = E_n|n\rangle$ with $E_n = n\hbar\omega$.
a. Through the expression, $a_f(t) \approx \frac{1}{i\hbar}\int_{t_i}^{t_f} W_{fi}e^{i\omega_{fi}t}dt$, and the perturbative Hamiltonian $W(t) = -e\mathcal{E}xe^{-t^2/\tau^2}$ (x is the position operator of the HO), applied between $t = -\infty$ and $t = +\infty$, calculate the probability of the system to be in the excited state $|n\rangle$, specifying n, at $t = +\infty$. Analyze the result.
b. Do the same for a shape-changing perturbation, $W(t) = \Lambda x^2 e^{-t^2/\tau^2}$.

Solution: *a. For this perturbation, the probability is,*

$$P_n = |\langle n|\psi\rangle|^2 = |a_{0\to n}(\infty)|^2 = \left|\delta_{0n} + \frac{1}{\imath\hbar}\int_{-\infty}^{\infty}\langle n|W|0\rangle e^{\imath\omega_{n0}t}dt\right|^2$$
$$= \left|\delta_{0n} - \frac{1}{\imath\hbar}e\mathcal{E}\int_{-\infty}^{\infty}\langle n|\hat{x}|0\rangle e^{-t^2/\tau^2}e^{\imath\omega_{n0}t}dt\right|^2 = \left|\delta_{0n} - \frac{e\mathcal{E}}{\imath\hbar}\frac{a_{ho}}{\sqrt{2}}\delta_{n1}\int_{-\infty}^{\infty}e^{-t^2/\tau^2}e^{\imath\omega t}dt\right|^2$$
$$= \left|\delta_{0n} - \frac{e\mathcal{E}}{\imath\hbar}\frac{a_{ho}}{\sqrt{2}}\delta_{n1}\sqrt{\pi}\tau e^{-\tau^2\omega^2/4}\right|^2 = \left|\delta_{0n} + \imath\delta_{n1}\frac{\sqrt{\pi}e\mathcal{E}\tau}{\sqrt{2m\hbar\omega}}e^{-\tau^2\omega^2/4}\right|^2 ,$$

such that,

$$P_{0\to 1} = \frac{\pi e^2\mathcal{E}^2\tau^2}{2m\hbar\omega}e^{-\tau^2\omega^2/2} .$$

To obtain transitions, the time scale τ of the perturbation must be adapted to provide Fourier components near the transition frequency. The rate is maximal for $\tau = \sqrt{2}/\omega$.

b. For this perturbation the probability is

$$\begin{aligned} P_n &= \left| \delta_{0n} + \frac{1}{\imath\hbar}\Lambda(1-\delta_{0n}) \int_{-\infty}^{\infty} \langle n|\hat{x}^2|0\rangle e^{-t^2/\tau^2} e^{\imath\omega_{n0}t} dt \right|^2 \\ &= \left| \delta_{0n} + \frac{\Lambda}{\imath\hbar} \frac{a_{ho}^2}{2} 2\delta_{n2} \int_{-\infty}^{\infty} e^{2i\omega t} e^{-t^2/\tau^2} dt \right|^2 \\ &= \left| \delta_{0n} + \frac{\Lambda}{\imath\hbar} \frac{a_{ho}^2}{2} 2\delta_{n2} \frac{\tau\sqrt{\pi}}{\sqrt{2}} e^{-\tau^2\omega^2} \right|^2 = \left| \delta_{0n} - \frac{\imath\sqrt{\pi}\Lambda\tau}{\sqrt{2}m\omega} \delta_{n2} e^{-\tau^2\omega^2} \right|^2 . \end{aligned}$$

such that,

$$P_{0\to 1} = \frac{\pi\Lambda^2\tau^2}{2m^2\omega^2} e^{-2\tau^2\omega^2} .$$

27.4.5.2 Ex: Impact of the rapidity of a perturbation

Here we consider a slow variation,

$$\hat{W}(t) = \begin{cases} 0 & \text{for} \quad t < 0 \\ W_0(1-e^{-\gamma t}) & \text{for} \quad t \geq 0 \end{cases} ,$$

with $\gamma \ll \omega_{fi}$.
a. Calculate the transition rate for long times, $t \gg \gamma^{-1}$.
b. Analyze the transition rate at a given time as a function of γ.

Solution: *Review this exercise!!!*
We calculate,

$$a_{i\to f}(t) = \frac{\langle f|\hat{W}_0|i\rangle}{\imath\hbar} \int_0^t (1-e^{-\gamma\tau}) e^{\imath\omega_{fi}\tau} d\tau = \frac{\langle f|\hat{W}_0|i\rangle}{\imath\hbar} \left[\frac{e^{\imath\omega_{fi}t}-1}{\imath\omega_{fi}} + \frac{e^{-\gamma t+\imath\omega_{fi}t}-1}{\gamma-\imath\omega_{fi}} \right] .$$

For $\gamma \ll \omega_{fi}$ we neglect the γ in the denominator,

$$a_{i\to f}(t) \simeq \frac{\langle f|\hat{W}_0|i\rangle}{\hbar\omega_{fi}} e^{\imath\omega_{fi}t} \left[-1+e^{-\gamma t}\right] .$$

a. For long times, $t \gg \gamma^{-1}$, we get,

$$a_{i\to f}(t) \overset{\gamma t\gg 0}{\longrightarrow} \frac{\langle f|\hat{W}_0|i\rangle}{\hbar\omega_{fi}} (-e^{\imath\omega_{fi}t}) ,$$

which joins the limit of the time-independent perturbation theory (27.12),

$$|a_{i\to f}(t)|^2 \overset{\gamma t\gg 0}{\longrightarrow} \left| \frac{\langle f|\hat{H}^{(1)}|i\rangle|}{\hbar\omega_{fi}} \right|^2 .$$

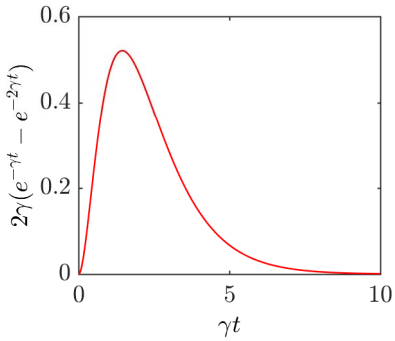

Figure 27.8: Transition rate for fixed $t = 1$ as a function of γ.

b. At a given time, the transition rate is,

$$\frac{d|a_{i\to f}|^2}{dt} = \left|\frac{\langle f|\hat{H}^{(1)}|i\rangle|}{\hbar\omega_{fi}}\right|^2 (2\gamma e^{-\gamma t} - 2\gamma e^{-2\gamma t}) \ .$$

27.4.5.3 Ex: Rabi oscillation

The population of a degenerate two-level system be initially in state $|1\rangle$. What should be the duration of a perturbation to transfer the population to state $|2\rangle$?

Solution: *Since $\omega_0 = 0$, the population of state $|2\rangle$ is,*

$$|a_2(t)|^2 = \frac{\Omega^2}{G^2}\sin^2 Gt = \sin^2 \Omega t \ .$$

For the sinus to reach 1, we need to wait for the time $t = \pi/2\Omega$ [15].

27.4.5.4 Ex: Rabi method

Free atoms be illuminated by light pulses characterized by the Rabi frequency Ω, whose pulse area is (i) $\int_0^t \Omega\ dt = \pi$ and (ii) $= 2\pi$. For which frequency tuning $\Delta = \omega - \omega_0$ the excited state population is maximum? Draw the spectral profile of the population in the range $-5 < \Delta/\Omega < 5$.

Solution: *The Schrödinger equation gives,*

$$\frac{\partial}{\partial t}|\psi\rangle = \begin{pmatrix} 0 & \frac{1}{2}\Omega \\ \frac{1}{2}\Omega & -\Delta \end{pmatrix} |\psi\rangle \ .$$

Deriving the second line and inserting it into the first one, we get,

[15] This is called π-*pulse*, because the frequency of Rabi is often defined as$\Omega/2$.

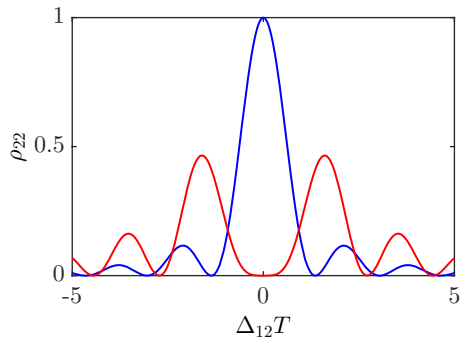

Figure 27.9: (code) Rabi fringes for (blue) a π-pulse and (red) a 2π-pulse.

$$\ddot{c}_2 = i\Delta\dot{c}_2 - \tfrac{1}{4}\Omega^2 c_2 \ .$$

The trial $c_2(t) = c_{20} + c_{2+}e^{\imath\chi t} + c_{2-}e^{-\imath\chi t}$ *gives the characteristic equation,*

$$-\chi^2 + \Delta\chi + \tfrac{1}{4}\Omega^2 = 0 \ .$$

With the initial conditions $c_2(0) = 0$ *the solution is,*

$$c_2(t) = c_2(0)e^{\imath\Delta t/2}(e^{\imath Gt/2} - e^{-\imath Gt/2}) \ ,$$

where $G \equiv \sqrt{\Delta^2 + \Omega^2}$*. Here,* $|c_2|^2 = \rho_{22}$ *is the population of the upper state. Therefore,*

$$|c_2|^2 \propto 2 - 2\cos(Gt) = 4\sin^2\tfrac{1}{2}Gt \ .$$

Considering, in particular, $n = \pi, 2\pi$*, the solution becomes,*

$$|c_2|^2 = \frac{\Omega^2}{G^2}\sin^2\tfrac{1}{2}G^2t = \frac{1}{1+(\Delta/\Omega)^2}\sin^2\frac{1}{2}\sqrt{1+(\Delta/\Omega)^2}n\pi \ .$$

27.4.5.5 Ex: Ramsey fringes

a. Consider a two-level atom illuminated by a $\frac{\pi}{2}$-pulse of nearly resonant light, $G \simeq \Omega$, and calculate the ground and excited state amplitudes.
b. How do the amplitudes evolve after the pulse if the detuning Δ is small but non-zero?
c. Derive the solution for $|a_2(t)|^2$ of the equations (27.63) for the resonant case ($\Delta = 0$) assuming the following initial conditions, $a_2(0) = \frac{e^{\imath\phi}}{\sqrt{2}}$ and $a_2(t = \frac{\pi}{2\Omega}) = 0$ if $\phi = 0$.
d. Discuss the case of two consecutive $\frac{\pi}{2}$-pulses separated by a time interval T.

Solution: *a. We exploit Eqs. (27.93), which holds for the initial condition that the atoms be in their ground state,*

$$a_1(t) = -e^{\imath\Delta t/2}\left(\cos\frac{G}{2}t + \frac{-\imath\Delta}{2G}\sin\frac{G}{2}t\right) \qquad \textit{and} \qquad a_2(t) = \frac{\imath\Omega}{G}e^{-\imath\Delta t/2}\sin\frac{G}{2}t \ .$$

Inserting $G \simeq \Omega = \frac{\pi}{2t}$ *we get after the first pulse,*

$$a_1(\tfrac{\pi}{2\Omega}) = -\frac{1}{\sqrt{2}} \qquad \text{and} \qquad a_2(\tfrac{\pi}{2\Omega}) = \frac{\imath}{\sqrt{2}} \ .$$

b. The coherence precesses according to,

$$a_1(t) = -\frac{1}{\sqrt{2}} e^{\imath \Delta T/2} \qquad \text{and} \qquad a_2(t) = \frac{\imath}{\sqrt{2}} e^{-\imath \Delta T/2} \ .$$

c. We use the same ansatz as in Eq. (27.87),

$$a_2 = e^{-\imath \Delta t/2}(A e^{\imath G t/2} + B e^{-\imath G t/2}) \ .$$

Inserting the first initial condition, $a_2(0) \equiv \frac{e^{\imath\phi}}{\sqrt{2}} = A + B$*, we get for the resonant case,*

$$a_2 = A e^{\imath \Omega t/2} + \left(\tfrac{e^{\imath\phi}}{\sqrt{2}} - A \right) e^{-\imath \Omega t/2} \ .$$

Now, we use the second initial condition setting $\phi = 0$*,*

$$0 \equiv a_2(t = \frac{\pi}{2\Omega}) = A e^{\imath \pi/4} + \left(\tfrac{1}{\sqrt{2}} - A \right) e^{-\imath \pi/4} \ ,$$

yielding $A = \frac{e^{\imath\pi/4}}{2}$*. Hence,*

$$a_2 \simeq \frac{e^{\imath\pi/4}}{2} e^{\imath \Omega t/2} + \left(\frac{e^{\imath\phi}}{\sqrt{2}} - \frac{e^{\imath\pi/4}}{2} \right) e^{-\imath \Omega t/2}$$

and

$$|a_2|^2 = 1 - \cos\phi \ .$$

d. Setting $\phi \equiv \Delta T$ *we see that the excited state population after the Ramsey pulse sequence oscillates with the free precession time period* T*.*

27.4.5.6 Ex: Two-level atom via Laplace transformation

Solve the problem of a two-level atom interacting with a laser using the Laplace transformation method.

Solution: *We consider the two-level system* $|\psi(t)\rangle = a(t)|1\rangle + b(t)|2\rangle$ *with the Hamiltonian in the rotating wave approximation,*

$$\hat{H} = \hat{H}^{(0)} + \hat{V} = \begin{pmatrix} 0 & c.c. \\ \frac{1}{2}\Omega e^{\imath\omega t} & \omega_0 \end{pmatrix} = \omega_0 |2\rangle\langle 2| + \tfrac{1}{2}\Omega e^{-\imath\omega t}|2\rangle\langle 1| + c.c. \ .$$

Entering into Schrödinger's equation, $|\dot{\psi}(t)\rangle = -\frac{\imath}{\hbar}\hat{H}(t)|\psi(t)\rangle$*, yields,*

$$\dot{a}|1\rangle + \dot{b}|2\rangle = -\frac{\imath}{\hbar}\left[\omega_0|2\rangle\langle 2| + \tfrac{1}{2}\Omega e^{-i\omega t}|2\rangle\langle 1| + \tfrac{1}{2}\Omega e^{\imath\omega t}|1\rangle\langle 2|\right]\left[a|1\rangle + b|2\rangle\right] \ .$$

Follows,

$$\dot{a} = -\tfrac{\imath\Omega}{2} e^{\imath\omega t} b \qquad \textit{and} \qquad \dot{b} = -\tfrac{\imath\Omega}{2} e^{-\imath\omega t} a - \imath\omega_0 b \ .$$

And by Laplace transformation,

$$p\tilde{a}(p) - a(t_0) = -\tfrac{\imath\Omega}{2}\tilde{b}(p-\imath\omega) \qquad \textit{and} \qquad p\tilde{b}(p) - b(t_0) = -\tfrac{\imath\Omega}{2}\tilde{a}(p+\imath\omega) - \imath\omega_0\tilde{b}(p) \ .$$

Now substitute $p \to p + \imath\omega$ and define $\Delta \equiv \omega - \omega_0$, $G = \sqrt{\Omega^2 + \Delta^2}$,

$$\tilde{b}(p) = \frac{(p+\imath\omega_0)b(t_0) - \frac{\imath\Omega}{2}a(t_0)}{(G/2)^2 + [p + \imath(\omega_0 + \Delta/2)]^2} \ .$$

The backward transformation is,

$$b(t) = e^{-\imath(\omega_0+\Delta/2)t}\left\{ b(0)\cos\frac{Gt}{2} - \frac{\imath}{G}\left[\Omega a(0) + \Delta b(0)\right]\sin\frac{Gt}{2}\right\} \ .$$

The population of the excited level is precisely $\rho_{22}(t) = |b(t)|^2$. In the same way we obtain the population of the ground level,

$$\tilde{a}(p) = \frac{(p-\imath\omega_0)a(t_0) - \frac{\imath\Omega}{2}b(t_0)}{(p-\imath\Delta)p + (\Omega/2)^2} \ ,$$

and

$$a(t) = e^{\imath(\Delta/2)t}\left\{ a(0)\cos\frac{Gt}{2} - \frac{\imath}{G}\left[\Omega b(0) + \Delta a(0)\right]\sin\frac{Gt}{2}\right\} \ .$$

We consider the particular case, $\Omega = 0$. The atom precedes in an unperturbed way,

$$a(t) = a(0) \qquad \textit{and} \qquad b(t) = b(0)e^{-\imath\omega t} \ .$$

27.4.5.7 Ex: Photoelectric effect

A hydrogen atom ground state in the ground state $1s$ is placed in an electric field $\mathbf{E}(t) = \mathbf{E}_0\cos\omega t$, such that $W(t) = -e\mathbf{r}\cdot\mathbf{E}(t) = W_0 e^{-\imath\omega t} + W_0^\dagger e^{\imath\omega t}$ with $W_0 = e\mathbf{r}\cdot\mathbf{E}_0/2$. Find, via Fermi's Golden rule,

$$R = \frac{2\pi}{\hbar}|\langle f|W(t)|i\rangle|^2\rho(E_f - E_i \mp \hbar\omega) \ ,$$

using the density of states $\rho(E_k)dE_k = V/(2\pi)^3 k^2 dk d\Omega$, the probability per unit of time for the atom to be ionized, by exciting from the ground state $\psi_{100}(\mathbf{r}) = e^{-r/a_B}/(\pi a_B^3)^{1/2}$ to the state described by the plane wave $\psi_{\mathbf{k}}(\mathbf{r}) = e^{-\imath\mathbf{k}\cdot\mathbf{r}}/V^{1/2}$. Simplify the calculation by assuming $\mathbf{E}_0 = E_0\hat{\mathbf{e}}_z$ and $\mathbf{k} = k\hat{\mathbf{e}}_z$.

Solution: *Transforming into the rotating system we realize that only one of the components $e^{\pm\imath\omega t}$ is resonant, such that we can discard the other:*

$$W(t) = W_0 e^{-\imath\omega t} \ .$$

Without loss of the generality we now choose $\mathbf{E}_0 = E_0\hat{\mathbf{e}}_z$,

$$\begin{aligned}\langle f|\hat{W}_0|i\rangle &= \int_{\mathbb{R}^3} d^3r' \frac{e^{\imath\mathbf{k}\cdot\mathbf{r}'}}{\sqrt{V}} \frac{e\mathcal{E}_0 z'}{2} \frac{1}{\sqrt{\pi a_B^3}} e^{-r'/a_B} \\ &= \frac{1}{\sqrt{V}} \frac{e\mathcal{E}_0}{2} \frac{1}{\sqrt{\pi a_B^3}} \int_0^\infty dr' r'^2 \int_{\mathbb{R}^2} d\Omega' e^{\imath\mathbf{k}\cdot\mathbf{r}'} r' \cos\theta' e^{-r'/a_B} \ .\end{aligned}$$

We need to expand the plane wave in terms of the spherical harmonics,

$$e^{\imath\mathbf{k}\cdot\mathbf{r}'} = 4\pi \sum_{\ell=0}^{\infty} \sum_{m=-\ell}^{\ell} \imath^\ell j_l kr' [Y_\ell^m(\theta,\phi)]^* Y_\ell^m(\theta',\phi') \ .$$

Inserting this above,

$$\langle f\hat{W}_0|i\rangle = \frac{4\pi e\mathcal{E}_0}{2(V\pi a_B^3)^{1/2}} \sum_{\ell=0}^{\infty} \imath^\ell \int_0^\infty dr' r'^3 e^{-r'/a_B} j_l(kr') \sum_{m=-\ell}^{\ell} [Y_\ell^m(\theta,\phi)]^* \int_{\mathbb{R}^2} d\Omega' Y_\ell^m(\theta',\phi') \cos\theta' \ .$$

Writing $\cos\theta'$ *as a function of the harmonics,* $\cos\theta' = \left(\frac{4\pi}{3}\right)^{1/2} [Y_1^0(\theta,\phi)]^*$, *due to the orthogonality of the spherical harmonics, we can simplify,*

$$\int_{\mathbb{R}^2} d\Omega' Y_\ell^m(\theta',\phi') \cos\theta' = \left(\tfrac{4\pi}{3}\right)^{1/2} \int_{\mathbb{R}^2} d\Omega' [Y_1^0(\theta,\phi)]^* Y_\ell^m(\theta',\phi') = \delta_{l,1}\delta_{m,0} \ .$$

This causes the matrix element to be,

$$\langle f\hat{W}_0|i\rangle = \frac{2\pi\imath e\mathcal{E}_0 \cos\theta}{(V\pi a_B^3)^{1/2}} \int_0^\infty dr' r'^3 e^{-r/a_B} \left(\frac{\sin kr'}{k^2 r'^2} - \frac{\cos kr'}{kr'} \right) \ .$$

We use the following tabulated integrals,

$$\int_0^\infty dr' r' e^{-r/a_B} \sin kr' = \frac{2ka_B^3}{(1+k^2a_B^2)^2} \quad \text{and} \quad \int_0^\infty dr' r'^2 e^{-r/a_B} \cos kr' = \frac{2a_B^3(1-3k^2a_B^2)}{(1+k^2a_B^2)^3} \ .$$

Therefore the radial integral is,

$$\int_0^\infty dr' r'^3 e^{-r/a_B} \left(\frac{\sin kr'}{k^2 r'^2} - \frac{\cos kr'}{kr'} \right) = \frac{8ka_B^5}{(1+k^2a_B^2)^3} \ ,$$

and the matrix element,

$$\langle f\hat{W}_0|i\rangle = 16\imath e\mathcal{E}_0 \cos\theta \left(\frac{\pi a_B^5}{V}\right)^{1/2} \frac{8ka_B}{(1+k^2a_B^2)^3} \ .$$

For the density of states we calculate, $\rho(E_k)dE_k = \rho(E_k)\frac{\hbar^2}{m}kdk \equiv \frac{V}{(2\pi)^3}k^2 dk d\Omega$, *yielding*

$$\rho(E_k) = \frac{V}{(2\pi)^3} \frac{m_e k}{\hbar^2} d\Omega \ .$$

The transition rate now becomes,

$$\frac{dR}{d\Omega} = \frac{2\pi}{\hbar^2}\frac{V}{(2\pi)^3}\frac{m_e k}{\hbar^2}\frac{256\pi e^2\mathcal{E}_0^2 a_B^5\cos^2\theta}{V}\frac{(ka_B)^2}{(1+(ka_B)^2)^6} = \frac{64\mathcal{E}_0^2 a_B^3\cos^2\theta}{\pi}\frac{(ka_B)^3}{(1+(ka_B)^2)^6} .$$

With the energy of the ground state of hydrogen,

$$E_1 = -\frac{\hbar^2}{2m_e a_B^2} \equiv \hbar\omega_0 ,$$

and energy conservation,

$$\hbar\omega = \frac{\hbar^2 k^2}{2m_e} + \hbar\omega_0 ,$$

we derive the abbreviation $(ka_B)^2 = \frac{\omega-\omega_0}{\omega_0}$ *which allows rewriting of the transition rate as,*

$$\frac{dR}{d\Omega} = \frac{4\pi\varepsilon_0 64\mathcal{E}_0^2 a_B^3}{\hbar}\frac{\omega_0^6}{\omega^6}\left(\frac{\omega}{\omega_0}-1\right)^{3/2}\cos^2\theta .$$

Only need to integrate over the solid angle, $\int d\Omega\cos^2\theta = 4\pi/3$,

$$R = \frac{256\mathcal{E}_0^2 a_B^3}{3\hbar}\frac{\omega_0^6}{\omega^6}\left(\frac{\omega}{\omega_0}-1\right)^{3/2} .$$

The frequency dependency is shown in the figure. Note, that the rate is zero directly above the ionization threshold. .

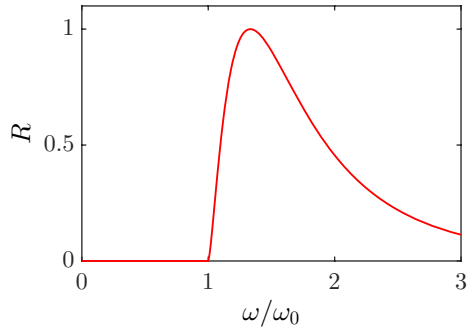

Figure 27.10: Photoelectric effect

27.4.5.8 Ex: Kicked harmonic oscillator in second order perturbation

Consider a one-dimensional harmonic oscillator initially in its ground state kicked via the $\hat{H}^{(1)}(t) = e^{\imath k\hat{x}}\Theta(t)$, as discussed in Sec. 24.6.2. Calculate the transition rate (27.102) to the final state $|f\rangle = |0\rangle$ in first and second order perturbation theory.

Solution: *The transition rate is given as,*

$$\frac{1}{\tau} = \frac{d}{dt}|\langle f|e^{-\imath\hat{H}(t-t_0)/\hbar}|0\rangle|^2 = \frac{2\pi}{\hbar^2}\left|\langle f|\hat{H}^{(1)}|0\rangle + \sum_m \frac{\langle f|\hat{H}^{(1)}|m\rangle\langle m|\hat{H}^{(1)}|0\rangle}{\omega_i - \omega_m}\right|^2 \delta(\omega_f - \omega_i) \ .$$

From (3.113) with $\alpha = \imath k a_{ho}/\sqrt{2}$,

$$\langle f|e^{ik\hat{x}}|0\rangle = \langle f|\alpha\rangle = e^{-|\alpha|^2/2}\frac{\alpha^f}{\sqrt{f!}} \ .$$

Hence, in first order,

$$\frac{1}{\tau_{0\to f}} = \frac{2\pi}{\hbar^2}|\langle f|e^{\imath k\hat{x}}|0\rangle|^2\delta(\omega_f - \omega_i) = \frac{2\pi}{\hbar^2}e^{-|\alpha|^2}\frac{|\alpha|^{2f}}{f!}\delta(\omega_f - \omega_i) \xrightarrow{f=0} \frac{2\pi}{\hbar^2}e^{-|\alpha|^2} \ .$$

In second order,

$$\begin{aligned}\frac{1}{\tau_{0\to f}} &= \frac{2\pi}{\hbar^2}\left|\sum_m \frac{\langle f|e^{\imath k\hat{x}}|m\rangle\langle m|e^{\imath k\hat{x}}|0\rangle}{\omega_i - \omega_m}\right|^2 \delta(\omega_f - \omega_i) \xrightarrow{f=0} \frac{2\pi}{\hbar^2}\left|\sum_m \frac{|\langle m|\alpha\rangle|^2}{\omega_i - \omega_m}\right|^2 \delta(0) \\ &= \frac{2\pi}{\hbar^2}e^{-2|\alpha|^2}\left|\sum_m \frac{|\alpha|^{2m}}{m!}\frac{1}{\omega_i - \omega_m}\right|^2 \delta(0) \ .\end{aligned}$$

27.4.5.9 Ex: Dynamic Stark shift induced by blackbody radiation

Calculate the dynamic Stark shift induced by blackbody radiation at $T = 300\,\mathrm{K}$ on the 1 mHz large strontium intercombination line at 698 nm.

Solution:

27.5 Further reading

C. Cohen-Tannoudji, B. Diu, F. Laloe, Wiley Interscience, *Quantum mechanics, vol. 1,2* [276]ISBN

Chapter 28

Appendices to 'Quantum Mechanics'

This chapter compiles some fundamental functions and polynomials, which are relevant in quantum theory.

28.1 Quantities and formulas in quantum mechanics

28.1.1 Atomic units

A system of units commonly used in atomic physics is the one of *atomic units*. This system is based on the system of Gaussian units (CGS) [1] defined by,

$$e_{cgs} = e/\sqrt{4\pi\varepsilon_0} \quad , \quad a_B = 1/\alpha \times \hbar/m_e c = \hbar^2/m_e e_{cgs}^2 \quad , \quad \hbar = 1 \ . \tag{28.1}$$

With this fixing we give the energy in terms of e_{cgs}^2/a_B, the wavevector in terms of $1/a_B$, the distance in terms of a_B and the mass in terms of m_e, such that,

$$\begin{aligned} \tilde{E} &= E/(e_{cgs}^2/a_B) \ , \\ \tilde{k} &= k a_B \ , \\ \tilde{R} &= R/a_B \ , \\ \tilde{\mu} &= \mu/m_e \ . \end{aligned} \tag{28.2}$$

This notation simplifies formulas in atomic physics. For example:

$$\begin{aligned} k = \sqrt{\tfrac{2\mu}{\hbar^2}(E-V)} \quad &\text{becomes} \quad \tilde{k} = \sqrt{2\tilde{\mu}(\tilde{E}-\tilde{V})} \ , \\ V = C_6 \tfrac{e_{cgs}^2 a_B^5}{R^6} \quad &\text{becomes} \quad \tilde{V} = \tfrac{C_6}{\tilde{R}^6} \ . \end{aligned} \tag{28.3}$$

[1] See script on *Electrodynamics* (2023).

28.2 Clebsch-Gordan and Wigner symbols

28.2.1 Clebsch-Gordan symbols

Clebsch-Gordan coefficients are used to describe spin coupling [2],

$$\langle j_1, m_1; j_2, m_2 | (j_1 j_2) j, m\rangle = \left(\begin{array}{cc|c} j_1 & j_2 & j \\ m_1 & m_2 & m \end{array}\right) = (-1)^{j_1 - j_2 + m}\sqrt{\Delta(j_1 j_2 j)}\times \tag{28.4}$$

$$\times \sqrt{(j_1+m_1)!(j_1-m_1)!(j_2+m_2)!(j_2-m_2)!(j+m)!(j-m)!}$$

$$\sum_t \frac{(-1)^t}{t!(-j_2+m_1+j+t)!(-j_1-m_2+j+t)!(j_1+j_2-j-t)!(j_1-m_1-t)!(j_2+m_2-t)!} .$$

28.2.2 $\{3j\}$-symbols

The Clebsch-Gordans are related to Wigner's *$\{3j\}$-symbols*,

$$\left(\begin{array}{cc|c} j_1 & j_2 & j \\ m_1 & m_2 & m \end{array}\right) = (-1)^{-j_1+j_2-m}\sqrt{2j+1}\begin{pmatrix} j_1 & j_2 & j \\ m_1 & m_2 & -m \end{pmatrix} , \tag{28.5}$$

with the abbreviation,

$$\Delta(j_1 j_2 j_3) \equiv \frac{(j_1+j_2-j_3)!(j_1-j_2+j_3)!(-j_1+j_2+j_3)!}{(j_1+j_2+j_3+1)!} . \tag{28.6}$$

Particular $\{3j\}$-symbols are,

$$\begin{pmatrix} j_1 & j_2 & j \\ 0 & 0 & 0 \end{pmatrix} = \frac{(-1)^{(j_1+j_2+j)/2}}{j_1/2+j_2/2+j/2+1}\frac{\sqrt{\Delta(j_1 j_2 j)}}{\Delta(\frac{j_1}{2}\frac{j_2}{2}\frac{j}{2})} , \tag{28.7}$$

and

$$\begin{pmatrix} 0 & j & j \\ 0 & 0 & 0 \end{pmatrix} = \frac{(-1)^j}{\sqrt{2j+1}} . \tag{28.8}$$

28.2.3 $\{6j\}$-symbols

$\{6j\}$-symbols describe the recoupling of two spins. They can be evaluated by,

$$\begin{Bmatrix} j_1 & j_2 & j_3 \\ J_1 & J_2 & J_3 \end{Bmatrix} = \sqrt{\Delta(j_1 j_2 j_3)\Delta(j_1 J_2 J_3)\Delta(J_1 j_2 J_3)\Delta(J_1 J_2 j_3)}\sum_t \frac{(-)^t(t+1)!}{f(t)} , \tag{28.9}$$

where,

$$f(t) = (t-j_1-j_2-j_3)!(t-j_1-J_2-J_3)!(t-J_1-j_2-J_3)!(t-J_1-J_2-j_3)! \tag{28.10}$$
$$(j_1+j_2+J_1+J_2-t)!(j_2+j_3+J_2+J_3-t)!(j_3+j_1+J_3+J_1-t)! .$$

[2] See [60], p.111 or [1298], p.119.

28.2.4 $\{9j\}$-symbols

$\{3j\}$-*symbols* describe the recoupling of three spins. They can be evaluated by,

$$\begin{Bmatrix} j_1 & j_2 & J_{12} \\ j_3 & j_4 & J_{34} \\ J_{13} & J_{24} & J \end{Bmatrix} = \sum_g (-)^{2g}(2g+1) \begin{Bmatrix} j_1 & j_2 & J_{12} \\ J_{34} & J & g \end{Bmatrix} \begin{Bmatrix} j_3 & j_4 & J_{34} \\ j_2 & g & J_{24} \end{Bmatrix} \begin{Bmatrix} J_{13} & J_{24} & J \\ g & j_1 & j_3 \end{Bmatrix} . \tag{28.11}$$

$\{9j\}$-symbols satisfy the following orthogonality relation,

$$\sum_{J_{12},J_{34}} \hat{J}_{12}\hat{J}_{34}\hat{H}_{13}\hat{H}_{24} \begin{Bmatrix} j_1 & j_2 & J_{12} \\ j_3 & j_4 & J_{34} \\ H_{13} & H_{24} & J \end{Bmatrix} \begin{Bmatrix} j_1 & j_2 & J_{12} \\ j_3 & j_4 & J_{34} \\ J_{13} & J_{24} & J \end{Bmatrix} = \delta_{J_{13}H_{13}}\delta_{J_{24}H_{24}} . \tag{28.12}$$

28.3 Functions and polynomials

28.3.1 The Gauss function

Indefinite integrals:

$$\int_{-\infty}^{\infty} e^{-ax^2} dx = \sqrt{\pi/a} \quad \text{and} \quad \int_0^{\infty} x^n e^{-ax^2} dx = \frac{\Gamma(\frac{n+1}{2})}{2a^{\frac{n+1}{2}}} . \tag{28.13}$$

Higher momenta:

$$\int_{x_0}^{x_1} e^{-ax^2} dx = xe^{-ax^2}\Big|_{x_0}^{x_1} + 2a\int_{x_0}^{x_1} x^2 e^{-ax^2} dx . \tag{28.14}$$

28.3.2 Bessel functions

The integral definition of the *Bessel function*, the *von Neumann function*, and the *Hankel function* of the first and second kind are:

$$\begin{aligned} J_k(x) &= \frac{1}{\pi}\int_0^{\pi} \cos(k\tau - x\sin\tau)d\tau = \frac{1}{2\pi}\int_{-\pi}^{\pi} e^{\imath(x\sin\tau - k\tau)} d\tau \\ N_k(x) &= ... \\ H_k^{(1,2)} &= J_k \pm \imath N_k . \end{aligned} \tag{28.15}$$

The derivative,

$$2\frac{dJ_k(x)}{dx} = J_{k-1}(x) - J_{k+1}(x) . \tag{28.16}$$

Sum rules (empirically found),

$$\sum_{k=-\infty}^{\infty} J_k(x) = \sum_{k=-\infty}^{\infty} J_k(x)^2 = 1 \neq \sum_{k=-\infty}^{\infty} |J_k(x)|^2 . \tag{28.17}$$

The *spherical Bessel function*, the *spherical von Neumann function*, and the *spherical Hankel function* of the first and second kind are defined by:

$$\begin{aligned} j_k(x) &= \sqrt{\frac{\pi}{2x}} J_{k+1/2}(x) \\ n_k(x) &= \sqrt{\frac{\pi}{2x}} N_{k+1/2}(x) = (-1)^{k+1} \sqrt{\frac{\pi}{2x}} J_{-k-1/2}(x) \\ h_k^{(1,2)} &= j_k \pm \imath n_k \ . \end{aligned} \tag{28.18}$$

The series,

$$j_k(x) = (-x)^k \left(\frac{1}{x} \frac{d}{dx} \right)^k \frac{\sin x}{x} \quad , \quad n_k(x) = -(-x)^k \left(\frac{1}{x} \frac{d}{dx} \right)^k \frac{\cos x}{x} \ . \tag{28.19}$$

The derivative,

$$j_k'(x) = \frac{k}{x} j_k(x) - j_{k+1}(x) \ . \tag{28.20}$$

28.3.3 Hermite polynomials

The definition of the *Hermite polynomials*:

$$\begin{aligned} H_n(x) &= \left(2x - \frac{d}{dx} \right)^n \cdot 1 = (-1)^n e^{x^2} \frac{d^n}{dx^n} e^{-x^2} = \frac{2^n}{\sqrt{\pi}} \int_{-\infty}^{\infty} (x + \imath t)^n e^{-t^2} dt \\ He_n(x) &\equiv 2^{-n/2} H_n(x) \ . \end{aligned} \tag{28.21}$$

Orthogonality and normalization:

$$\int_{-\infty}^{\infty} e^{-x^2} H_m(x) H_n(x) dx = \sqrt{\pi} 2^n n! \delta_{mn} \ . \tag{28.22}$$

Recursion:

$$\begin{aligned} \frac{d}{dx} H_n(x) &= 2 H_{n-1}(x) \\ \frac{d}{dx} e^{-x^2} H_n(x) &= e^{-x^2} H_{n+1}(x) \\ H_{n+1}(x) &= 2x H_n(x) - 2n H_{n-1}(x) \ . \end{aligned} \tag{28.23}$$

Particular values:

$$\begin{aligned} H_{2n+1}(0) &= 0 \\ H_{2n+1}(0) &= (-1)^n 2^n (2n-1)!! \end{aligned} \tag{28.24}$$

Series:

$$H_{2n}(x) = \sum_{k=0}^{\infty} \frac{(2n)!}{(2k)!} \frac{(-1)^{n-k}}{(n-k)!} (2x)^{2k} \tag{28.25}$$
$$H_{2n-1}(x) = \sum_{k=0}^{\infty} \frac{(2n+1)!}{(2k+1)!} \frac{(-1)^{n-k}}{(n-k)!} (2x)^{2k+1}$$
$$H_n(x) = n! \sum_{k=0}^{\text{int}(n/2)} \frac{1}{k!} \frac{(-1)^k}{(n-2k)!} (2x)^{n-2k} \ .$$

28.3.4 Laguerre polynomials

The definition of the *Laguerre polynomials* is:

$$L_n^{(m)}(x) \equiv \frac{e^x x^{-m}}{m!} \frac{d^n}{dx^n} (e^{-x} x^{n+m}) \tag{28.26}$$
$$L_n \equiv L_n^{(0)}(x) \ .$$

Series:

$$L_n^{(m)}(x) = \sum_{k=0}^{n} \binom{n+m}{n-k} \frac{(-x)^k}{k!} \ . \tag{28.27}$$

Recursion:

$$\frac{d}{dx} L_n^{(m)}(x) = -L_{n-1}^{(m+1)}(x) \ . \tag{28.28}$$

Related functions:

$$u_{mn}(\varepsilon) \equiv e^{-\varepsilon^2} \cdot (\imath\varepsilon)^{n-m} \cdot \sqrt{\tfrac{m!}{n!}} \cdot L_m^{n-m}(\varepsilon^2) \tag{28.29}$$
$$u_{mn}(0) \approx (\imath\varepsilon)^{n-m} \cdot \sqrt{\tfrac{n!}{m!(n-m)!^2}}$$
$$u_{n+1,n}(0) \approx \imath\varepsilon \cdot \sqrt{n+1} \ .$$

Fourier transforms:

$$\int_{-\infty}^{\infty} e^{-ax^2} x^{2k} \cos xp \cdot dx = \tfrac{(-1)^k \sqrt{\pi}}{2^k \sqrt{a^{2k+1}}} \cdot e^{p^2/4a} \cdot He_{2k}(p/\sqrt{2a}) \tag{28.30}$$
$$\int_{-\infty}^{\infty} e^{-x^2/2} x^{2m} L_n^{2m}(x^2) \cos xp \cdot dx = \tfrac{(-1)^m \sqrt{\pi}}{\sqrt{2}n!} \cdot e^{-p^2/2} \cdot He_n(p) He_{n+2m}(p)$$
$$\int_{-\infty}^{\infty} e^{-x^2/2} x^{2m+1} L_n^{2m+1}(x^2) \sin xp \cdot dx = \tfrac{(-1)^m \sqrt{\pi}}{\sqrt{2}n!} \cdot e^{-p^2/2} \cdot He_n(p) He_{n+2m+1}(p)$$
$$\int_{-\infty}^{\infty} e^{-ax-bp} f(|x-p|) \cdot dxdp = \tfrac{1}{a+b} \left[\int_{-\infty}^{\infty} e^{-ax} f(x) dx + \int_{-\infty}^{\infty} e^{-bp} f(p) dp \right] \ .$$

28.3.5 Legendre polynomials

The definition of *Legendre polynomials* is:

$$P_n(x) \equiv \frac{1}{2^n n!}\frac{d^n}{dx^n}(x^2-1)^n \tag{28.31}$$
$$P_n^{(-m)}(x) \equiv (1-x^2)^{m/2}\frac{d^m}{dx^m}P_l(x) \ .$$

Series:

$$P_n^{(m)}(x) = \frac{(-1)^m(n+m)!}{2^m m!(n-m)!}(1-x^2)^{m/2}\left[\begin{array}{c} 1-\frac{(n-m)!(m+n+1)!}{1!(m+1)!}\frac{1-x}{2}+ \\ +\frac{(n-m)!(n-m+1)!(m+n+1)!(m+n+2)!}{2!(m+1)!(m+2)!}\left(\frac{1-x}{2}\right)^2-...\end{array}\right] . \tag{28.32}$$

28.3.6 Spherical harmonics

The definition of *spherical harmonics* is [1368]:

$$Y_{\ell m}(\vartheta,\varphi) \equiv \sqrt{\frac{2\ell+1}{4\pi}}\sqrt{\frac{(\ell-|m|)!}{(\ell+|m|)!}}P_\ell^{|m|}(\cos(\vartheta)e^{im\varphi} \ . \tag{28.33}$$

The lowest *spherical harmonics* are:

$$\begin{array}{lcllcl} Y_0^{(0)} & = & \frac{1}{2}\sqrt{\frac{1}{\pi}} & Y_0^{(1)} & = & \frac{1}{2}\sqrt{\frac{3}{\pi}}\cos\theta \\ Y_{\pm1}^{(1)} & = & \mp\frac{1}{2}\sqrt{\frac{3}{2\pi}}\sin\theta e^{\pm i\phi} & Y_0^{(2)} & = & \frac{1}{4}\sqrt{\frac{5}{\pi}}(3\cos^2\theta-1) \\ Y_{\pm1}^{(2)} & = & \mp\frac{1}{2}\sqrt{\frac{15}{2\pi}}\sin\theta\cos\theta e^{\pm i\phi} & Y_{\pm2}^{(2)} & = & \frac{1}{4}\sqrt{\frac{15}{2\pi}}\sin^2\theta e^{\pm 2i\phi} \end{array} \tag{28.34}$$

28.3.7 Vector spherical harmonics

The definition of *vector spherical harmonics* is [1368]:

$$\mathbf{Y}_{j\ell m}(\mathbf{r}) \equiv (-1)^{1-\ell-m}\sqrt{2j+1}\sum_q \begin{pmatrix} \ell & 1 & j \\ m-q & q & -m \end{pmatrix} Y_{\ell\ m-q}(\vartheta,\varphi)\hat{\mathbf{e}}_q \ . \tag{28.35}$$

28.3.7.1 The Gamma function

The definition of the *Gamma function* is:

$$\Gamma(x+1) = x\Gamma(x) \quad , \quad \Gamma(1/2) = \sqrt{\pi} \ . \tag{28.36}$$

28.3.8 Riemann zeta-function

The definition of the *Riemann zeta-function* is,

$$g_\eta(1) = \zeta(\eta) \ , \tag{28.37}$$

where,

$$g_\eta(z) = \sum_{t=1}^{\infty} \pm \frac{(\pm z)^t}{t^\eta} = \frac{1}{\Gamma(\eta)} \int_0^\infty \frac{x^{\eta-1} dx}{z^{-1} e^x \pm 1} \ , \tag{28.38}$$

is also called the Bose/Fermi function. The upper sign holds for bosons, the lower for fermions. The *Sommerfeld expansion*,

$$\begin{aligned} \int_0^\infty \frac{g(x)dx}{e^{x-y}+1} &= \int_0^y g(x)dx + \int_0^\infty \frac{g(y+x)^{\eta-1}dx}{e^x+1} - \int_0^x \frac{g(y-x)^{\eta-1}dx}{e^x+1} \\ &\approx \int_0^y g(x)dx + \frac{\pi^2}{6} g'(x) + ... \end{aligned} \tag{28.39}$$

holds for $z \gg 1$ and yields,

$$f_\eta(e^y) \approx \frac{x^\eta}{\Gamma(\eta+1)} \left(1 + \frac{\pi^2 \eta(\eta-1)}{6x^2} + \frac{7\pi^4 \eta(\eta-1)(\eta-2)(\eta-3)}{360x^4} + ... \right) \ . \tag{28.40}$$

For small z both functions converge towards,

$$c_\eta(z) = \frac{1}{\Gamma(\eta)} \int_0^\infty \frac{x^{\eta-1} dx}{z^{-1} e^x} = c_{\eta-1}(z) = z \ . \tag{28.41}$$

The derivative is,

$$\frac{\partial f_\eta(Z)}{\partial Z} = \frac{\partial}{\partial Z} \sum_{t=1}^{\infty} -\frac{(-Z)^t}{t^\eta} = \sum_{t=1}^{\infty} \frac{(-Z)^{t-1}}{t^{\eta-1}} = \frac{1}{Z} \sum_{t=1}^{\infty} -\frac{(-Z)^t}{t^{\eta-1}} = \frac{f_{\eta-1}(Z)}{Z} \ , \tag{28.42}$$

or,

$$\begin{aligned} \frac{\partial f_\eta(Z)}{\partial Z} &= \frac{1}{\Gamma(\eta)} \frac{\partial}{\partial Z} \int_0^\infty \frac{x^{\eta-1} dx}{Z^{-1} e^x + 1} = \frac{1}{\Gamma(\eta)} \int_0^\infty \frac{x^{\eta-1} Z^{-2} e^x dx}{(Z^{-1} e^x + 1)^2} \\ &= \frac{1}{Z\Gamma(\eta)} \int_0^\infty x^{\eta-1} \frac{d}{dx} \frac{-1}{Z^{-1} e^x + 1} dx = \frac{\eta - 1}{Z\Gamma(\eta)} \int_0^\infty \frac{x^{\eta-2}}{Z^{-1} e^x + 1} dx = \frac{f_{\eta-1}(Z)}{Z} \ . \end{aligned} \tag{28.43}$$

28.4 Further reading

I.S. Gradshteyn and I.M. Ryzhik, *Table of integrals, series, and products* [532]ISBN

Part IV

Atomic and Molecular Physics

Chapter 29

Electron spin and the atomic fine structure

The energy structure of hydrogen calculated by Bohr's model from the non-relativistic Hamiltonian agrees very well with the experimental measurements. However, in high-resolution experiments, small deviations were observed as energy shifts and splittings of spectral lines. These deviations, called *fine structure*, were not predicted by theory, which suggests that there are weak additional effects that do not strongly affect the position of the spectral lines but remove the energy degeneracy of the orbital quantum number ℓ: $E = E_{n,\ell}$.

As a possible explanation we have the fact that the electrons present relativistic mass and momentum. In order to estimate the relevance of relativistic corrections let us estimate the electron velocity in the fundamental hydrogen states given by $E_1 = -\hbar^2/2m_e a_B^2$. Using the definitions of the Bohr radius, $a_B = 4\pi\varepsilon_0\hbar^2/(m_e e^2)$, and the *fine structure constant*

$$\alpha \equiv \frac{e^2}{4\pi\epsilon_0\hbar c} \simeq \frac{1}{137} \ , \tag{29.1}$$

we obtain,

$$v = \sqrt{\frac{2E_1}{m_e}} = \frac{\hbar}{m_e a_B} = \frac{e^2}{4\pi\varepsilon_0\hbar} = \alpha c \ , \tag{29.2}$$

which shows that the electron velocity is very high and that relativistic effects may indeed be *not negligible*.

29.1 The Dirac equation

29.1.1 The Klein-Gordon equation for bosons

The Schrödinger equation for a free particle is based on the non-relativistic energy-momentum dispersion relation,

$$E = \frac{p^2}{2m_e} \ . \tag{29.3}$$

and the definitions of the quantum operators for energy and momentum,

$$E = \imath\hbar\frac{\partial}{\partial t} \qquad \text{and} \qquad \mathbf{p} = -\imath\hbar\nabla \ . \tag{29.4}$$

As already discussed in Sec. 23.1.2 we can, in order to find a relativistic wave equation, try the approach of inserting the quantum operators into the relativistic energy-momentum relation [1].

$$E^2 = c^2p^2 + m_e^2c^4 \ . \tag{29.5}$$

We obtain,

$$\boxed{\left[\frac{1}{c^2}\frac{\partial^2}{\partial t^2} - \nabla^2 + \left(\frac{m_e c}{\hbar}\right)^2\right]\psi = 0} \ . \tag{29.6}$$

This is the *Klein-Gordon equation*. The stationary solution of this equation is a spherical wave,

$$\psi = \psi_0 \frac{1}{r} e^{-2\pi r/\lambda_C} \ , \tag{29.7}$$

where $\lambda_C = h/m_e c$ is the *Compton wavelength*. We show this in Exc. 29.1.5.1. For example, in the case of heavy bosonic particles, such as a field of π-mesons, ψ is the *Yukawa potential*.

In the framework of the *standard model*, it is believed that matter is composed of two fundamental types of particles, bosons and fermions. Bosons are exchanged between fermions conveying the interaction between them. A typical example is the one of two electrons whose Coulomb interaction is mediated by the exchange of photons. Bosons obey the Klein-Gordon equation, fermions the Dirac equation derived in the following section.

29.1.2 The Dirac equation for fermions

In 1928 Paul Dirac, at the age of 26, developed an approach to a relativistic wave equation which differed from the Klein-Gordon equation. Motivated by the observation that the photon, being the relativistic particle *par excellence*, obeys a linear energy-momentum relation of the form $\omega = ck$, he attempted to derive a linear dispersion relation in E and p for heavy particles via the following ansatz:

$$E = \alpha_0 m_e c^2 + \alpha_1 c p_x + \alpha_2 c p_y + \alpha_3 c p_z \ . \tag{29.8}$$

Replacing energy and momentum with their respective operators [2],

$$\imath\hbar\frac{\partial}{\partial t}\phi = \alpha_0 m_e c^2 \phi - \imath c\hbar\left(\alpha_1\frac{\partial}{\partial x} + \alpha_2\frac{\partial}{\partial y} + \alpha_3\frac{\partial}{\partial z}\right)\phi \ . \tag{29.9}$$

We must now ensure that the relativistic energy-momentum condition (29.5) be satisfied.

Example 175 (*Derivation of the Dirac equation*): Taking the square on the right-hand side of the equation (29.9),

$$\begin{aligned}
&[\alpha_0 m_e c^2 - \imath c\hbar(\alpha_1\partial_x + \alpha_2\partial_y + \alpha_3\partial_z)][\alpha_0 m_e c^2 - \imath c\hbar(\alpha_1\partial_x + \alpha_2\partial_y + \alpha_3\partial_z)] \\
&= m_e^2c^4\alpha_0^2 - ic\hbar m_e c^2[(\alpha_0\alpha_1 + \alpha_1\alpha_0)\partial_x + (\alpha_0\alpha_2 + \alpha_2\alpha_0)\partial_y + (\alpha_0\alpha_3 + \alpha_3\alpha_0)\partial_z] \\
&\quad - c^2\hbar^2[\alpha_1^2\partial_x^2 + \alpha_2^2\partial_y^2 + \alpha_3^2\partial_z^2] \\
&\quad - c^2\hbar^2[(\alpha_1\alpha_2\partial_x\partial_y + \alpha_2\alpha_1\partial_y\partial_x) + (\alpha_2\alpha_3\partial_y\partial_z + \alpha_3\alpha_2\partial_z\partial_y) + (\alpha_3\alpha_1\partial_z\partial_x + \alpha_1\alpha_3\partial_x\partial_z)] \ .
\end{aligned}$$

[1] Using the covariant notation with $p_\mu \equiv (E/c, \mathbf{p})$: $p_\mu p^\mu = E^2/c^2 - p^2 = m_e^2c^2$ is a Lorentz invariant.

[2] We introduce the abbreviation $\partial_k \equiv \frac{\partial}{\partial x_k}$

For this expression to be identical to the relativistic energy-momentum condition (29.5),

$$m_e^2c^4 - c^2\hbar^2[\partial_x^2 + \partial_y^2 + \partial_z^2] \ ,$$

we need to postulate for all $i = 0, .., 4$, that $\alpha_i\alpha_j + \alpha_j\alpha_i = 2\delta_{ij}$.

Obviously, the condition

$$[\alpha_i, \alpha_j]_+ = 2\delta_{ij} \tag{29.10}$$

can not be satisfied if the α_i are numbers. The idea of Dirac was to interpret the variables α_i as matrices. These matrices act as operators on appropriate states, which are no longer scalar wavefunctions but vectors. Each component of the vector is a wavefunction in the usual sense. The Hilbert space is extended to be the product space of the usual spatial wavefunctions and a finite-dimensional vector space.

Example 176 (*Calculation with matrices of operator*): To give an idea of how the algebra works we consider a general situation. As the operator we choose the product,

$$\begin{pmatrix} 0 & 1 \\ 1 & 0 \end{pmatrix} \frac{\partial}{\partial x}$$

and as the wavefunction vector we choose,

$$\begin{pmatrix} e^{\imath k_1 x} \\ e^{\imath k_2 x} \end{pmatrix} .$$

Applying the operator on the state vector we get,

$$\begin{pmatrix} 0 & 1 \\ 1 & 0 \end{pmatrix} \frac{\partial}{\partial x} \begin{pmatrix} e^{\imath k_1 x} \\ e^{\imath k_2 x} \end{pmatrix} = \begin{pmatrix} 0 & \frac{\partial}{\partial x} \\ \frac{\partial}{\partial x} & 0 \end{pmatrix} \begin{pmatrix} e^{\imath k_1 x} \\ e^{\imath k_2 x} \end{pmatrix} = \begin{pmatrix} 0 + \frac{\partial}{\partial x} e^{\imath k_2 x} \\ \frac{\partial}{\partial x} e^{\imath k_1 x} + 0 \end{pmatrix} = \begin{pmatrix} \imath k_2 e^{\imath k_2 x} \\ \imath k_1 e^{\imath k_1 x} \end{pmatrix} .$$

The matrices α_i must satisfy the condition (29.10). It is possible to show that this requires at least four-dimensional matrices of the following form:

$$\alpha_0 = \begin{pmatrix} -\mathbb{I} & 0 \\ 0 & \mathbb{I} \end{pmatrix} \quad \text{and} \quad \alpha_j = \begin{pmatrix} 0 & \sigma_j \\ \sigma_j & 0 \end{pmatrix} , \tag{29.11}$$

where $j = x, y, z = 1, 2, 3$. In this notation the components of the matrices are themselves matrices, i.e. the *Pauli spin matrices* defined in (23.47). The state vector must also have four dimensions,

$$\vec{\vec{\Phi}}(\mathbf{r}, t) = \begin{pmatrix} \vec{\phi}(\mathbf{r}, t) \\ \vec{\chi}(\mathbf{r}, t) \end{pmatrix} \quad \text{with} \quad \vec{\phi}(\mathbf{r}, t) = \begin{pmatrix} \phi_1(\mathbf{r}, t) \\ \phi_2(\mathbf{r}, t) \end{pmatrix} \quad \text{and} \quad \vec{\chi}(\mathbf{r}, t) = \begin{pmatrix} \chi_1(\mathbf{r}, t) \\ \chi_2(\mathbf{r}, t) \end{pmatrix} . \tag{29.12}$$

ϕ_j are called *large components*, χ_j are called *small components*. This designation is explained later. Combining the matrices α_j to a three-dimensional vector $\vec{\alpha}$, we can now write the Dirac equation (29.9) like,

$$\boxed{\imath\hbar\partial_t \vec{\vec{\Phi}}(\mathbf{r}, t) = \left(m_e c^2 \alpha_0 + c\vec{\alpha} \cdot \mathbf{p}\right) \vec{\vec{\Phi}}(\mathbf{r}, t)} \ . \tag{29.13}$$

Or, using the notation (29.11) and combining the Pauli matrices σ_j to a three-dimensional vector $\vec{\sigma}$, we can write the Dirac equation as:

$$\boxed{\imath\hbar\frac{\partial}{\partial t}\begin{pmatrix}\vec{\phi}\\ \vec{\chi}\end{pmatrix} = \left[m_e c^2\begin{pmatrix}-\mathbb{I} & 0\\ 0 & \mathbb{I}\end{pmatrix} + c\begin{pmatrix}0 & \vec{\sigma}\cdot\mathbf{p}\\ \vec{\sigma}\cdot\mathbf{p} & 0\end{pmatrix}\right]\begin{pmatrix}\vec{\phi}\\ \vec{\chi}\end{pmatrix}} \ . \tag{29.14}$$

The non-diagonal matrix,

$$\begin{pmatrix}0 & \vec{\sigma}\cdot\mathbf{p}\\ \vec{\sigma}\cdot\mathbf{p} & 0\end{pmatrix} \tag{29.15}$$

couples large and small components.

Example 177 (*Covariant and relativistically invariant form of Dirac's equation*): To demonstrate its relativistic invariance it is useful to rewrite the Dirac equation in a way in which time and space appear on equal footings. For this we introduce new matrices,

$$\gamma^0 \equiv \alpha_0 \qquad \text{and} \qquad \gamma^k = \gamma^0\alpha_k \ . \tag{29.16}$$

We obtain,

$$\gamma^0 = \begin{pmatrix}-\mathbb{I} & 0\\ 0 & \mathbb{I}\end{pmatrix} \qquad \text{and} \qquad \gamma^k = \begin{pmatrix}0 & \sigma_k\\ -\sigma_k & 0\end{pmatrix} \ . \tag{29.17}$$

We also define another important matrix by,

$$\gamma_5 \equiv \imath\gamma_0\gamma_1\gamma_2\gamma_3 = \begin{pmatrix}0 & \mathbb{I}\\ \mathbb{I} & 0\end{pmatrix} \ . \tag{29.18}$$

With this, using Einstein's notation [3], the Dirac equation (29.12) adopts the form,

$$\imath\hbar\gamma^\mu\partial_\mu\psi - mc\psi = 0 \ . \tag{29.19}$$

The complete system is summarized in the Minkowski metrics of time-space in the form,

$$[\gamma^\mu, \gamma^\nu]_+ = 2\eta^{\mu\nu} \ , \tag{29.20}$$

for $\mu, \nu = 0, .., 5$, that is, all matrices γ_k anticommute.
The Dirac equation can now be interpreted as an eigenvalue equation, where the rest mass is proportional to the eigenvalue of a momentum quadrivector, the proportionality constant being the speed of light:

$$P_{\text{op}}\psi = mc\psi \ , \tag{29.21}$$

Using $\not{\phi}$ in the Feynman slash notation, which includes the γ-matrices, as well as a summation over the components of the spinor in the derivative, the Dirac equation becomes:

$$\imath\hbar\not{\partial}\psi - mc\psi = 0 \ . \tag{29.22}$$

A fundamental theorem states that, if two distinct sets of matrices are given, which both satisfy Clifford's relations, then they are connected to each other by a similarity transformation:

$$\gamma'^\mu = S^{-1}\gamma^\mu S \ . \tag{29.23}$$

[3] $\partial_0 \equiv \frac{1}{c}\partial_t$

If, in addition, the matrices are all unitary, as is the case of Dirac's set, then S is unitary,

$$\gamma'^{\mu} = U^{\dagger}\gamma^{\mu}U \ . \tag{29.24}$$

29.1.2.1 Anti-particles

Disregarding for a moment the non-diagonal matrix, the Dirac equation separates into two independent equations,

$$\imath\hbar\frac{\partial\vec{\phi}}{\partial t} = m_e c^2\vec{\phi} \quad \text{and} \quad \imath\hbar\frac{\partial\vec{\chi}}{\partial t} = -m_e c^2\vec{\chi} \ . \tag{29.25}$$

These are eigenenergy equations with the eigenvalues $m_e c^2$ and $-m_e c^2$. The state with negative energy is interpreted as *anti-particle*. Therefore, the non-diagonal matrix mixes particles and anti-particles. We will study in Exc. 29.1.5.2 the so-called *Zitterbewegung* as a solution of the Dirac equation.

29.1.2.2 Particles and anti-particles in the non-relativistic limit

To reduce the Dirac equation to the non-relativistic Schrödinger equation, we first need to get rid of the rest energy. To do so, we separate a fast oscillation, whose frequency corresponds to the rest mass of the electron via the following ansatz, where $\mathbf{u}$ and $\mathbf{v}$ vary slowly in time:

$$\vec{\Phi}(\mathbf{r},t) = e^{-\imath\omega_0 t}\begin{pmatrix}\mathbf{u}(\mathbf{r},t)\\ \mathbf{v}(\mathbf{r},t)\end{pmatrix} \quad , \quad \hbar\omega_0 = m_e c^2 \ , \tag{29.26}$$

with the temporal derivative,

$$\imath\hbar\dot{\vec{\Phi}} = \left[m_e c^2\begin{pmatrix}\mathbf{u}\\ \mathbf{v}\end{pmatrix} + \imath\hbar\begin{pmatrix}\dot{\mathbf{u}}\\ \dot{\mathbf{v}}\end{pmatrix}\right] e^{-\imath\omega_0 t} \ . \tag{29.27}$$

We insert this into the Dirac equation,

$$\left[m_e c^2\begin{pmatrix}\mathbf{u}\\ \mathbf{v}\end{pmatrix} + \imath\hbar\begin{pmatrix}\dot{\mathbf{u}}\\ \dot{\mathbf{v}}\end{pmatrix}\right] e^{-\imath\omega_0 t} = \left[m_e c^2\begin{pmatrix}\mathbf{u}\\ -\mathbf{v}\end{pmatrix} + c\vec{\sigma}\cdot\mathbf{p}\begin{pmatrix}\mathbf{v}\\ \mathbf{u}\end{pmatrix}\right] e^{-\imath\omega_0 t} \tag{29.28}$$

finally obtaining,

$$\imath\hbar\dot{\mathbf{u}} = c(\vec{\sigma}\cdot\mathbf{p})\mathbf{v} \quad , \quad \imath\hbar\dot{\mathbf{v}} = c(\vec{\sigma}\cdot\mathbf{p})\mathbf{u} - 2m_e c^2\mathbf{v} \ . \tag{29.29}$$

Since $\mathbf{u}$ and $\mathbf{v}$ only vary slowly in time, the derivatives on the left-hand side are small quantities. However, the condition that both derivatives must zero is too strong, because it leads to the trivial solution $\mathbf{u} = 0$ and $\mathbf{v} = 0$. We find the first non-trivial solution by the condition $\dot{\mathbf{v}} = 0$. The second equation then becomes,

$$\mathbf{v} = \frac{1}{2m_e c}(\vec{\sigma}\cdot\mathbf{p})\mathbf{u} \ . \tag{29.30}$$

Inserted into the first equation,

$$\imath\hbar\dot{\mathbf{u}} = c\frac{(\vec{\sigma}\cdot\mathbf{p})^2}{2m_e c}\mathbf{u}\ . \tag{29.31}$$

We need, therefore, to evaluate the expression $(\vec{\sigma}\cdot\mathbf{p})^2$,

$$\vec{\sigma}\cdot\mathbf{p} = \begin{pmatrix} p_z & p_x - \imath p_y \\ p_x + \imath p_y & -p_z \end{pmatrix} \qquad \text{and} \qquad (\vec{\sigma}\cdot\mathbf{p})^2 = \mathbf{p}^2\begin{pmatrix} 1 & 0 \\ 0 & 1 \end{pmatrix}\ . \tag{29.32}$$

Inserted into the differential equation (29.31) for $\mathbf{u}$ we obtain precisely the Schrödinger equation for a free particle,

$$\boxed{\imath\hbar\dot{\mathbf{u}} = \frac{\mathbf{p}^2}{2m_e}\mathbf{u}}\ . \tag{29.33}$$

Let us return to the question, why we call $\mathbf{u}$ the *strong* component. We have from the equation (29.30),

$$\mathbf{v}^\dagger\mathbf{v} = \frac{1}{(2m_e c)^2}(\vec{\sigma}\cdot\mathbf{p})^2\mathbf{u}^\dagger\mathbf{u} = \frac{1}{2m_e c^2}\frac{\mathbf{p}^2}{2m_e}\mathbf{u}^\dagger\mathbf{u}\ , \tag{29.34}$$

and since $\frac{\mathbf{p}^2}{2m_e} \ll m_e c^2$ follows immediately $\mathbf{v}^\dagger\mathbf{v} \ll \mathbf{u}^\dagger\mathbf{u}$.

In this non-relativistic approximation the components $\mathbf{u}$ are much larger than the components $\mathbf{v}$. The mixture between particles and antiparticles only matters when $\frac{\mathbf{p}^2}{2m_e} \simeq m_e c^2$, resp., $\frac{1}{2}m_e v^2 \simeq m_e c^2$ or $|v| \simeq c$. The electron only receives small positronic contributions as it approaches the speed of light. In the ground state of the hydrogen atom the electron has a velocity of of $v = \alpha c \simeq c/137$. That is, the contribution of the weak components is small, but present.

Example 178 (*Vanishing rest mass*): Let us note that for the case of vanishing rest mass, $m_e = 0$, the Dirac equation (29.14) dramatically simplifies. Taking the time derivative of the upper equation (29.14) and inserting the lower equation (29.14), we find,

$$\frac{1}{c^2}\frac{\partial^2}{\partial t^2}\vec{\phi} = \frac{1}{c^2}\frac{c\vec{\sigma}\cdot\mathbf{p}}{\imath\hbar}\frac{\partial}{\partial t}\vec{\chi} = -\frac{(\vec{\sigma}\cdot\mathbf{p})^2}{\hbar^2}\vec{\phi} = -\frac{\mathbf{p}^2}{\hbar^2}\vec{\phi} = \nabla^2\vec{\phi}\ . \tag{29.35}$$

I.e. we recover a Helmholtz type wave equation.

29.1.2.3 The spin

We consider the operator defined by [372, 373],

$$\hat{\mathbf{s}} \equiv \tfrac{\hbar}{2}\vec{\sigma}\ , \tag{29.36}$$

and we calculate the commutation relations between its components. From the definitions of the Pauli matrices (23.47) we obtain the rule,

$$[\hat{s}_x, \hat{s}_y] = \tfrac{\hbar^2}{4}\begin{pmatrix} 0 & 1 \\ 1 & 0 \end{pmatrix}\begin{pmatrix} 0 & \imath \\ -\imath & 0 \end{pmatrix} - \tfrac{\hbar^2}{4}\begin{pmatrix} 0 & \imath \\ -\imath & 0 \end{pmatrix}\begin{pmatrix} 0 & 1 \\ 1 & 0 \end{pmatrix} = \frac{\hbar^2}{4}\begin{pmatrix} -2\imath & 0 \\ 0 & 2\imath \end{pmatrix} = \imath\hbar\hat{s}_z\ . \tag{29.37}$$

In general terms the following holds true: $[s_i, s_j] = \epsilon_{ijk}\imath\hbar s_k$. It is interesting to compare this with the commutation relation for the orbital angular momentum $[\hat{l}_i, \hat{l}_j] = \epsilon_{ijk}\imath\hbar\hat{l}_k$. The coincidence suggests a generalization of the concept of angular momentum: We now call *angular momentum operator* every three-dimensional vector operator satisfying this commutation relation [4]. We consider the eigenvalue equation for $\hat{s}_z$, which is incorporated in the Dirac equation,

$$\hat{s}_z\vec{\phi} = \tfrac{\hbar}{2}\begin{pmatrix} -1 & 0 \\ 0 & 1 \end{pmatrix}\begin{pmatrix} \phi_1 \\ \phi_2 \end{pmatrix} = m_s\hbar\begin{pmatrix} \phi_1 \\ \phi_2 \end{pmatrix} . \tag{29.38}$$

The eigenvalues are obviously $m_s = \pm\frac{1}{2}$. The angular momentum related to the matrices $\mathbf{S}$ is obviously half-integer. We are dealing here with a new type of angular momentum, which is not included in the usual definition of *orbital* angular momentum $\mathbf{L} = \mathbf{r} \times \mathbf{p}$. The new angular momentum is called *intrinsic* angular momentum or *spin* of the particle. The spin represents a new structure or dimension additional to space comparable to the polarization of light. The photons of a circularly polarized light beam also contribute to an intrinsic angular momentum, which however in this case is integer.

In Exc. 29.1.5.3 we will see that neither $\hat{l}_z$ nor $\hat{s}_z$ are constants of motion of the Hamiltonian (29.14), but the sum $\hat{j}_z \equiv \hat{l}_z + \hat{s}_z$,

$$[\hat{j}_z, \hat{H}] = 0 . \tag{29.39}$$

29.1.2.4 The stationary Dirac equation

By a similar treatment as in the Schrödinger equation one can deduce a stationary Dirac equation (29.13) via a separation of the time variable. Making for the time an exponential ansatz,

$$\vec{\phi}(\mathbf{r}, t) = \vec{\phi}(\mathbf{r})e^{-\imath Et/\hbar} \quad \text{and} \quad \vec{\chi}(\mathbf{r}, t) = \vec{\chi}(\mathbf{r})e^{-\imath Et/\hbar} , \tag{29.40}$$

we obtain coupled stationary equations for the large and small components,

$$(E - m_e c^2)\vec{\phi}(\mathbf{r}) = c\sigma \cdot \mathbf{p}\vec{\chi}(\mathbf{r}) \quad \text{and} \quad (E + m_e c^2)\vec{\chi}(\mathbf{r}) = c\sigma \cdot \mathbf{p}\vec{\phi}(\mathbf{r}) . \tag{29.41}$$

29.1.3 The relativistic electron in a central Coulomb field

29.1.3.1 Minimal coupling

In atomic physics we are mainly interested in electrons bound to a potential (e.g., generated by an atomic nucleus), that is, we must introduce electromagnetic forces into the Dirac equation. Therefore, we now consider the interaction of a charged particle with an electromagnetic field given by the vector potential $\mathbf{A}$ and by the electrostatic potential U, such that the electric and magnetic fields,

$$\vec{\mathcal{E}} = -\nabla U - \frac{\partial \mathbf{A}}{\partial t} \quad \text{and} \quad \vec{\mathcal{B}} = \nabla \times \mathbf{A} , \tag{29.42}$$

[4] This concept can be derived from the requirement of symmetry under rotation of space as discussed in Sec. 23.5.

allow to calculate the Coulomb-Lorentz force. In the Hamiltonian formulation of electrodynamics the interaction can be described simply by the transition [5],

$$\boxed{\hat{\mathbf{p}} \longrightarrow \hat{\mathbf{p}} - q\mathbf{A} \equiv \vec{\pi} \quad \text{and} \quad \hat{H} \longrightarrow \hat{H} + qU} \ . \tag{29.43}$$

called the *minimal coupling*. We briefly mentioned this already in Sec. 23.5.4, and the rules will be derived in Sec. 30.1. In addition to the substitution of the momentum, we must add the scalar potential qU, and we obtain the Dirac equation for a particle inside an applied electromagnetic field,

$$\imath\hbar\dot{\vec{\Phi}} = \left(m_e c^2\alpha_0 + c\vec{\alpha}\cdot\vec{\pi} + qU\right)\vec{\Phi} \ , \tag{29.44}$$

in generalization of Eq. (29.13).

29.1.3.2 Solving the stationary Dirac equation

Let us, for now, disregard external magnetic fields, $\mathbf{A} = 0$. Then, the stationary Dirac equation (29.41) becomes,

$$\begin{aligned} [E - qU(\mathbf{r}) - m_e c^2]\vec{\phi}(\mathbf{r}) &= c\sigma\cdot\mathbf{p}\vec{\chi}(\mathbf{r}) \\ [E - qU(\mathbf{r}) + m_e c^2]\vec{\chi}(\mathbf{r}) &= c\sigma\cdot\mathbf{p}\vec{\phi}(\mathbf{r}) \ . \end{aligned} \tag{29.45}$$

For the Coulomb potential,

$$qU(r) = -\frac{1}{4\pi\epsilon_0}\frac{e^2}{r} \tag{29.46}$$

the Dirac equation can be solved algebraically [374, 541, 548, 471] [6]. The calculation is more complicated than the resolution of the Schrödinger equation for hydrogen derived in Secs. 25.1.4 and 25.2.1 and will be sketched in the following.

> **Example 179 (*Dirac equation in spherical coordinates*):** The goal of the following calculation is to express the Dirac equation for an electron in a central Coulomb field in spherical coordinates, i.e. r and $p_r = -\imath\hbar\partial_r$ instead of $\mathbf{p}$. The starting point is the Dirac equation (29.14),
>
> $$\imath\hbar\partial_t\vec{\Phi}(\mathbf{r},t) = \hat{H}\vec{\Phi}(\mathbf{r},t) \ , \tag{29.47}$$
>
> with the Hamiltonian in the minimal coupling (29.43),
>
> $$\hat{H} \equiv m_e c^2\alpha_0 + c\vec{\alpha}\cdot[\mathbf{p} - q\mathbf{A}(\mathbf{r})] + qU(\mathbf{r}) \tag{29.48}$$
> $$\text{with} \quad \mathbf{A} = 0 \quad \text{and} \quad U(\mathbf{r}) = -\frac{e^2}{4\pi\varepsilon_0 r} \ .$$
>
> We adopt the standard procedure from non-relativistic physics, which consists in rewriting the Hamiltonian in terms of observables, which commute with the Hamiltonian [7].

[5] In quadrivetorial notation: $\pi_\mu = p_\mu - qA_\mu$ with $p_\mu = \begin{pmatrix} E/c \\ \mathbf{p} \end{pmatrix}$ and $A_\mu = \begin{pmatrix} U/c \\ \mathbf{A} \end{pmatrix}$.

[6] See also http://einstein.drexel.edu/~bob/Term_Reports/Whitehead_3.pdf

[7] Typical examples are the Hamiltonian of the harmonic oscillator (24.75) written in terms of $\hat{n} \equiv \hat{a}^\dagger\hat{a}$ or the Hamiltonian of the hydrogen atom (25.34) written in terms of $\mathbf{L}^2$.

The goal is to calculate the quantity $\vec{\alpha}\cdot\mathbf{p}$ appearing in the above Hamiltonian. As a first steps we define the following quantities,

$$\boxed{\begin{array}{rcll} \mathbf{L} & \equiv & \mathbf{r}\times\mathbf{p} \quad \text{satisfying} & \mathbf{L}\times\mathbf{L} = \imath\hbar\mathbf{L} \\ \mathbf{S} & \equiv & \frac{\hbar}{2}\vec{\varsigma} \equiv \frac{\hbar}{2}\gamma_5\vec{\alpha} & \\ \mathbf{J} & \equiv & \mathbf{L}+\mathbf{S} & \\ \hbar j' & \equiv & \alpha_0(\gamma_5\vec{\alpha}\cdot\mathbf{L}+\hbar) & \\ r\varepsilon & \equiv & \vec{\alpha}\cdot\mathbf{r} & \end{array}} \ . \tag{29.49}$$

remembering that $\gamma_5 = -\imath\alpha_1\alpha_2\alpha_3 = \begin{pmatrix} 0 & \mathbb{I} \\ \mathbb{I} & 0 \end{pmatrix}$ is the transformation exchanging particles and anti-particles. The first important relationship we have to derive is,

$$(\vec{\alpha}\cdot\mathbf{B})(\vec{\alpha}\cdot\mathbf{C}) = (\mathbf{B}\cdot\mathbf{C}) + \imath\gamma_5\vec{\alpha}\cdot(\mathbf{B}\times\mathbf{C}) \ . \tag{29.50}$$

It holds for $[\vec{\alpha},\mathbf{B}] = 0 = [\vec{\alpha},\mathbf{C}]$ and will be proven in 29.1.5.4. Exploiting this relationship, we see that the scalar quantity ε satisfies,

$$\varepsilon^2 = \frac{1}{r^2}(\vec{\alpha}\cdot\mathbf{r})^2 = \frac{1}{r^2}[\mathbf{r}\cdot\mathbf{r} + \imath\vec{\alpha}\cdot(\mathbf{r}\times\mathbf{r})] = 1 \ . \tag{29.51}$$

Furthermore, with the definition of j' we show,

$$\begin{aligned} r\varepsilon\vec{\alpha}\cdot\mathbf{p} = (\vec{\alpha}\cdot\mathbf{r})(\vec{\alpha}\cdot\mathbf{p}) &= \mathbf{r}\cdot\mathbf{p} + \imath\gamma_5\vec{\alpha}\cdot(\mathbf{r}\times\mathbf{p}) \\ &= \mathbf{r}\cdot\mathbf{p} + \imath\gamma_5\vec{\alpha}\cdot\mathbf{L} = rp_r + \imath\alpha_0\hbar j' - \imath\hbar \ , \end{aligned} \tag{29.52}$$

where the relationship $\mathbf{r}\cdot\mathbf{p} = rp_r$ is verified in Exc. 29.1.5.5(c). Hence,

$$\vec{\alpha}\cdot\mathbf{p} = \varepsilon\left(p_r + \frac{\imath\hbar(\alpha_0 j' - 1)}{r}\right) \ , \tag{29.53}$$

The final radial Hamiltonian is,

$$\boxed{\hat{H} = m_e c^2\alpha_0 + c\varepsilon\left(p_r - \imath\frac{\hbar}{r}\right) + \frac{\imath c\varepsilon\alpha_0\hbar j'}{r} - \frac{e^2}{4\pi\varepsilon_0 r}} \ . \tag{29.54}$$

For now the choice of the quantities ε and j' must seem arbitrary, so we will have to discover their properties. We will see that j' is a non-zero integer related to the total angular momentum j. The following properties will be proven in Exc. 29.1.5.5(a) and (b),

$$\begin{aligned} (\hbar j')^2 &= \mathbf{J}^2 + \tfrac{\hbar^2}{4} \\ [\hbar j', \hat{H}]_- = [\varepsilon, \hat{H}]_- &= [\alpha_0, \hat{H}]_- = 0 \ . \end{aligned} \tag{29.55}$$

Hence, we got a collection of radial variables being constants of motion of the Dirac Hamiltonian.

Example 180 (*Resolving the spherical Dirac equation*): We will now search a solution to the spherical Dirac equation with the Hamiltonian (29.54). Noticing that the matrix α_0 is diagonal and the matrix ε counter-diagonal (just

like the Dirac matrices $\vec{\alpha}$), we may break down the stationary radial Dirac equation into 2 by 2 matrices. Using the fact that ε commutes with all other terms and anti-commutes with α_0 and that $\varepsilon^{-1} = \varepsilon^\dagger$ is a unitary transformation, we may go to a new basis via,

$$\begin{pmatrix} m_e c^2 - \frac{e^2}{4\pi\varepsilon_0 r} & -\imath c p_r - c\frac{\hbar}{r} - c\frac{\hbar j'}{r} \\ \imath c p_r + c\frac{\hbar}{r} - c\frac{\hbar j'}{r} & -m_e c^2 - \frac{e^2}{4\pi\varepsilon_0 r} \end{pmatrix} \begin{pmatrix} \vec{\phi} \\ \varepsilon\vec{\chi} \end{pmatrix} = E \begin{pmatrix} \vec{\phi} \\ \varepsilon\vec{\chi} \end{pmatrix} . \tag{29.56}$$

Substituting $\alpha = \frac{e^2}{4\pi\varepsilon_0\hbar c}$ and $a_\pm \equiv \frac{\hbar}{m_e c \mp E/c}$ (that is, $\pm m_e c^2 - E \equiv \pm\frac{\hbar c}{a_\pm}$), we find,

$$\begin{pmatrix} \frac{1}{a_+} - \frac{\alpha}{r} & -\frac{d}{dr} - \frac{j'+1}{r} \\ \frac{d}{dr} - \frac{j'-1}{r} & -\frac{1}{a_-} - \frac{\alpha}{r} \end{pmatrix} \begin{pmatrix} \vec{\phi} \\ \varepsilon\vec{\chi} \end{pmatrix} = 0 . \tag{29.57}$$

Assuming the existence of solutions of the form,

$$\begin{pmatrix} \vec{\phi} \\ \varepsilon\vec{\chi} \end{pmatrix} = \frac{e^{-r/a}}{r} \begin{pmatrix} \vec{f} \\ \vec{g} \end{pmatrix} , \tag{29.58}$$

where $a \equiv \sqrt{a_+ a_-} = \hbar\left(m_e^2 c^2 - \frac{E^2}{c^2}\right)^{-1}$ [that is, $\frac{d}{dr}\frac{e^{-r/a}}{r} = \frac{e^{-r/a}}{r}\left(-\frac{1}{a} - \frac{1}{r}\right)$], we find,

$$\begin{pmatrix} \frac{1}{a_+} - \frac{\alpha}{r} & -\frac{d}{dr} - \frac{1}{a} - \frac{j'}{r} \\ \frac{d}{dr} - \frac{1}{a} - \frac{j'}{r} & -\frac{1}{a_-} - \frac{\alpha}{r} \end{pmatrix} \begin{pmatrix} \vec{f} \\ \vec{g} \end{pmatrix} = 0 . \tag{29.59}$$

Next we expand the unknown function $\vec{f}$ and $\vec{g}$ as series,

$$\vec{f}(r) = \sum_{s=-\infty}^{\infty} f_s r^s \qquad \text{and} \qquad \vec{g}(r) = \sum_{s=-\infty}^{\infty} g_s r^s . \tag{29.60}$$

These are then substituted into our system of equations. In order for the equation to go to zero as required, each term in the resulting series must separately go to zero. The coefficient of the r_s terms are,

$$\begin{aligned} \frac{f_s}{a_+} - \alpha f_{s+1} - (s+1+j')g_{s+1} + \frac{g_s}{a} &= 0 \\ \frac{g_s}{a_-} - \alpha g_{s+1} - (s+1-j')f_{s+1} + \frac{f_s}{a} &= 0 . \end{aligned} \tag{29.61}$$

These can be combined by multiplying the first equation (29.61) by a and and the second by a_- and then subtracting the former from the latter. Exploiting $\frac{a}{a_+} = \frac{a_-}{a}$, this gives us an expression directly relating the f_s coefficients with the g_s coefficients,

$$[\alpha a - a_+(s-j')]f_s + [\alpha a_- + a(s+j')]g_s = 0 . \tag{29.62}$$

To obtain the values of the coefficients we consider the boundary conditions. The functions $\vec{f}(r)$ and $\vec{g}(r)$ must go to zero at $r = 0$, because the functions $\vec{\phi}$ and $\vec{\chi}$ would otherwise diverge there due to the r^{-1} term. This means that there is some smallest s below which the series does not continue. We call this s_0, and it has the property,

$$f_{s_0-1} = g_{s_0-1} = 0 . \tag{29.63}$$

Plugging this into the equations (29.61), we find,

$$\begin{aligned} \alpha f_{s_0} + (s_0 + j')g_{s_0} &= 0 \\ \alpha g_{s_0} - (s_0 - j')f_{s_0} &= 0 \ . \end{aligned} \tag{29.64}$$

Combining these equations we can write the value s_0 in a very simple form,

$$s_0 = \sqrt{j'^2 - \alpha^2} \ . \tag{29.65}$$

This places a lower bound on the series. Note that this bound becomes imaginary if $\alpha > j'$. This will be discussed in more detail shortly.
The upper bound of the series is also useful. It can be shown that the series must terminate if the energy eigenvalue is to be less than $m_e c^2$ [374]. The implication of this result is that if the series terminates at index s_1 such that,

$$f_{s_1+1} = g_{s_1+1} = 0 \ . \tag{29.66}$$

Then, using equations (29.61) and (29.62), we have,

$$\frac{s_1}{a} = \frac{1}{2}\left(\frac{1}{a_-} - \frac{1}{a_+}\right)\alpha = \frac{E}{\hbar c}\alpha \ , \tag{29.67}$$

where we have used the definitions of the coefficients $a_\pm$ to expand them. Squaring this expression and expanding a using its definition, we get,

$$s_1^2\left(m_e c^2 - \frac{E^2}{c^2}\right) = \alpha^2 \frac{E^2}{c^2} \ . \tag{29.68}$$

This can be solved for the energy eigenvalues,

$$E = \pm m_e c^2 \left(1 + \frac{\alpha^2}{s_1^2}\right)^{-1/2} \ . \tag{29.69}$$

Note that the 'negative energy' solution corresponds to positron energy levels. From here forward, we drop the negative root and look only at the electron solution.
The two end points of the series, the indices s_0 and s_1 are separated by an integer number of steps. Calling this integer n' we can write,

$$s_1 = n' + s_0 = n' + \sqrt{j'^2 - \alpha^2} \ . \tag{29.70}$$

Plugging this into (29.69) gives a result for the energy eigenvalues in terms of only the two quantum numbers n' and j',

$$E_{n',j'} = m_e c^2 \left[1 + \frac{\alpha^2}{\left(n' + \sqrt{j'^2 - \alpha^2}\right)^2}\right]^{-1/2} \ .$$

This is the final result quoted for the energy eigenvalues of the hydrogenic atom by Dirac [374]. It turns out that later developments in the field [541, 548] prefer to use an equivalent set of quantum numbers that maps more closely to the familiar ones. The number j' is closely related to the total angular momentum quantum number j. j' has the range 1, 2, 3, while j has the range $\frac{1}{2}$, $\frac{3}{2}$, $\frac{5}{2}$. It is natural, and in fact correct, to make the identifications,

$$j' = j + \tfrac{1}{2} \ , \tag{29.71}$$

and

$$n' = n - j' = n - j - \tfrac{1}{2} \ , \tag{29.72}$$

for the principal quantum number n [541]. Combining these two adjustments with equation (29.71), we get the *Sommerfeld fine-structure formula*,

$$\boxed{E_{n,j} = m_e c^2 \left[1 + \frac{\alpha^2}{\left(n - j - \frac{1}{2} + \sqrt{(j+\frac{1}{2})^2 - \alpha^2} \right)^2} \right]^{-1/2}} \ , \tag{29.73}$$

with $j = \left| \ell \pm \frac{1}{2} \right|$ and $\ell = 0, 1, ...$ The derivation of the form of the actual wave functions $\vec{\phi}(r)$ and $\vec{\chi}(r)$ is very tedious [541] and will not be reproduced here.

The energy predicted by the Sommerfeld fine-structure formula (29.73) depends on two quantum numbers. The degeneracy of the orbital angular momentum $\mathbf{j}$ is lifted, and the new quantum number besides the main quantum number n is that of the total angular momentum j. The intransparent expression can be expanded by α,

$$\boxed{E_{n,j} \simeq m_e c^2 \left[1 - \frac{\alpha^2}{2n^2} - \frac{\alpha^4}{2n^3} \left(\frac{1}{j+1/2} - \frac{3}{4n} \right) \right]} \ . \tag{29.74}$$

The second term reproduces the energy of Bohr's model, but there are correction terms proportional to α^4. We will show in Secs. 29.1.4, that the energy levels, called *fine structure*, result from several relativistic corrections of different origins.

In the expression (29.74) for the electron energy in the Coulomb potential, the last term is positive and proportional to $1/n^4$. It describes relaxation of the binding due to the contribution of weak components. The term containing the quantum number j is called the spin-orbit coupling. To better understand this contribution we must first analyze more deeply the matrices $\vec{\sigma}$.

29.1.3.3 Dirac's Hamiltonian in the sub-relativistic limit

Defining the energy $E' = E - m_e c^2$, the stationary Dirac equation (29.45) for an electron of charge $q = -e$ in an external electrostatic potential $U(\mathbf{r})$ can be written,

$$[E' - qU(\mathbf{r})]\vec{\phi} = c\vec{\sigma} \cdot \mathbf{p}\vec{\chi} \qquad \text{and} \qquad [E' - qU(\mathbf{r}) + 2m_e c^2]\vec{\chi} = c\vec{\sigma} \cdot \mathbf{p}\vec{\phi} \ . \tag{29.75}$$

resolving the second equation for the wavefunction $\vec{\chi}$ and substituting it into the first,

$$\boxed{E'\vec{\phi} = qU(\mathbf{r})\vec{\phi} + \vec{\sigma} \cdot \mathbf{p} \frac{1}{2m_e} \left(1 + \frac{E' - qU(\mathbf{r})}{2m_e c^2} \right)^{-1} \vec{\sigma} \cdot \mathbf{p}\vec{\phi}} \ . \tag{29.76}$$

In the non-relativistic limit,

$$E' - qU \simeq \frac{\mathbf{p}^2}{2m_e} \ll m_e c^2 \ , \tag{29.77}$$

we get by Taylor expansion of the second term in the bracket,

$$E'\vec{\phi} \simeq qU(\mathbf{r})\vec{\phi} + \vec{\sigma} \cdot \mathbf{p} \frac{1}{2m_e} \left(1 - \frac{E' - qU(\mathbf{r})}{2m_e c^2} \right) \vec{\sigma} \cdot \mathbf{p}\vec{\phi} \ . \tag{29.78}$$

Now, $\vec{\sigma}\cdot\mathbf{p}$ is an operator entity, which acts on the subsequent operators and wavefunctions. We thus have to apply the product rule, $(\vec{\sigma}\cdot\mathbf{p})V\psi = V(\vec{\sigma}\cdot\mathbf{p})\psi + [(\vec{\sigma}\cdot\mathbf{p})V]\psi$, to the first occurrence of operator this operator in equation (29.76),

$$E'\vec{\phi} \simeq qU(\mathbf{r})\vec{\phi} + \tfrac{1}{2m_e}\left(1 - \tfrac{E'-qU(\mathbf{r})}{2m_e c^2}\right)(\vec{\sigma}\cdot\mathbf{p})^2\,\vec{\phi} + \tfrac{q}{4m_e^2c^2}[(\vec{\sigma}\cdot\mathbf{p})U(\mathbf{r})](\vec{\sigma}\cdot\mathbf{p})\vec{\phi}\,. \quad (29.79)$$

In the following we will make use of a general relationship which is similar to (29.50),

$$(\vec{\sigma}\cdot\mathbf{B})(\vec{\sigma}\cdot\mathbf{C}) = (\mathbf{B}\cdot\mathbf{C}) + \imath\vec{\sigma}\cdot(\mathbf{B}\times\mathbf{C})\,. \quad (29.80)$$

It holds for $[\vec{\sigma},\mathbf{B}] = 0 = [\vec{\sigma},\mathbf{C}]$ and will be demonstrated in Exc. 29.1.5.4. The relationship yields,

$$(\vec{\sigma}\cdot\mathbf{p})^2 = \mathbf{p}^2 \qquad \text{and} \qquad [\vec{\sigma}\cdot\mathbf{p}U(\mathbf{r})](\vec{\sigma}\cdot\mathbf{p}) = \mathbf{p}U(\mathbf{r})\cdot\mathbf{p} + \imath\vec{\sigma}\cdot[\mathbf{p}U(\mathbf{r})\times\mathbf{p}]\,, \quad (29.81)$$

so that expressing the momentum operator by $\mathbf{p} = -\imath\hbar\nabla$ wherever it acts on the potential,

$$E'\vec{\phi} \simeq qU(\mathbf{r})\vec{\phi} + \tfrac{1}{2m_e}\left(1 - \tfrac{E'-qU(\mathbf{r})}{2m_e c^2}\right)\mathbf{p}^2\vec{\phi} - \tfrac{\hbar^2 q}{4m_e^2c^2}\nabla U(\mathbf{r})\cdot\nabla\vec{\phi} + \tfrac{\hbar}{4m_e^2c^2}\vec{\sigma}\cdot[\nabla U(\mathbf{r})\times\mathbf{p}]\vec{\phi}\,. \quad (29.82)$$

Also, with $U(\mathbf{r}) = U(r)$,

$$\nabla U(r) = \frac{\partial U}{\partial r}\nabla r = \frac{\partial U}{\partial r}\frac{\mathbf{r}}{r} \qquad \text{and} \qquad \nabla U(r)\cdot\nabla = \frac{\partial U}{\partial r}\hat{\mathbf{e}}_r\cdot\nabla = \frac{\partial U}{\partial r}\frac{\partial}{\partial r}\,. \quad (29.83)$$

We get,

$$\begin{aligned} E'\vec{\phi} &= qU(\mathbf{r})\vec{\phi} + \frac{1}{2m_e}\left(1 - \frac{E'-qU(\mathbf{r})}{2m_e c^2}\right)\mathbf{p}^2\vec{\phi} - \frac{\hbar^2}{4m_e^2c^2}\frac{\partial qU}{\partial r}\frac{\partial}{\partial r}\vec{\phi} + \frac{\hbar q}{4m_e^2c^2}\vec{\sigma}\cdot\left[\frac{1}{r}\frac{\partial U}{\partial r}\mathbf{r}\times\mathbf{p}\vec{\phi}\right] \\ &\simeq \left(\frac{\mathbf{p}^2}{2m_e} + qU(r) - \frac{\mathbf{p}^4}{8m_e^3c^2} + \frac{q}{2m_e^2c^2}\frac{1}{r}\frac{\partial U}{\partial r}\mathbf{s}\cdot\mathbf{l} - \frac{\hbar^2 q}{4m_e^2c^2}\frac{\partial U}{\partial r}\frac{\partial}{\partial r}\right)\vec{\phi}\,. \end{aligned} \quad (29.84)$$

where we again applied the non-relativistic approximation (29.77) in the second line and made use of the definitions $\mathbf{s} = \frac{\hbar}{2}\vec{\sigma}$ and $\mathbf{l} = \mathbf{r}\times\mathbf{p}$. The term in the bracket can be used as the Hamiltonian allowing to calculate the fine structure as first-order perturbations to the non-relativistic energy levels obtained from non-relativistic theory,

$$\boxed{\hat{H} \simeq \frac{\mathbf{p}^2}{2m_e} - \frac{1}{4\pi\varepsilon_0}\frac{e^2}{r} - \frac{\mathbf{p}^4}{8m_e^3c^2} - \frac{e}{2m_e^2c^2}\frac{1}{r}\frac{\partial U}{\partial r}\mathbf{s}\cdot\mathbf{l} - \frac{\hbar^2 e}{4m_e^2c^2}\frac{\partial U}{\partial r}\frac{\partial}{\partial r}}\,. \quad (29.85)$$

The first two terms are those arising from Bohr's atom model, the third one is a correction due to the relativistic velocity of the electron, the forth comes from the electron's spin-orbit coupling, and the fifth is called the Darwin term. All contributions represent perturbations to the non-relativistic Schrödinger theory of Bohr's atom and will be discussed extensively in Secs. 29.2. We will show in 29.1.5.6 that $\hat{\mathbf{l}}^2$, $\hat{\mathbf{s}}^2$, and $\hat{\mathbf{j}}^2$ are constants of motion of the above Hamiltonian.

29.1.4 The Pauli equation

When we calculated the electron's energy in the Coulomb potential (29.85), we only considered the electrostatic potential of the nucleus, letting the potential vector $\mathbf{A}$ be zero. As long as we do not apply an external magnetic field this is correct, because the internal magnetism of the atom is already completely enclosed in the Dirac equation. On the other hand, we know that the atom contains moving charges, that is, currents which generate magnetic fields [8]. Furthermore, the spins of the electron and of the proton produce magnetic moments, which ought to interact with the magnetic fields. Hence, the existence of magnetic effects in an atom is to be expected.

These magnetic effects can be discussed in a more transparent way applying a Schrödinger-like equation with minimal coupling to electromagnetic fields (29.43) to a two-component spinor $\vec{\phi}$. This Schrödinger-like equation can be obtained from Dirac's equation (29.75) via a stronger non-relativistic approximation, which consists in completely neglecting the weak component $[E' - qU(\mathbf{r})]\vec{\chi}$. On the other hand, we allow for the existence of magnetic fields via the substitution $\mathbf{p} \to \vec{\pi}$. The equation for the strong component (29.76) then becomes,

$$\boxed{E'\vec{\phi} = qU(\mathbf{r})\vec{\phi} + \frac{(\vec{\sigma}\cdot\vec{\pi})^2}{2m_e}\vec{\phi}} \,. \tag{29.86}$$

We can again apply the formula (29.80) to calculate,

$$\begin{aligned}(\vec{\sigma}\cdot\vec{\pi})^2\psi &= \vec{\pi}^2\psi + \imath\vec{\sigma}\cdot(\vec{\pi}\times\vec{\pi})\psi = \vec{\pi}^2\psi + \imath q\vec{\sigma}\cdot[-\mathbf{p}\times\mathbf{A}(\mathbf{r}) - \mathbf{A}(\mathbf{r})\times\mathbf{p}]\psi \\ &= \vec{\pi}^2\psi - \hbar q\vec{\sigma}\cdot\{\nabla\times[\mathbf{A}(\mathbf{r})\psi] + \mathbf{A}(\mathbf{r})\times\nabla\psi\} \\ &= \vec{\pi}^2\psi - \hbar q\vec{\sigma}\cdot[\nabla\times\mathbf{A}(\mathbf{r})]\psi = [\mathbf{p} - q\mathbf{A}(\mathbf{r})]^2\psi - \hbar q\vec{\sigma}\cdot\vec{\mathcal{B}}(\mathbf{r})\psi \,.\end{aligned} \tag{29.87}$$

In the case of an electron ($e = -q$) we obtain the so-called *Pauli equation*,

$$E'\vec{\phi} = \left[\frac{1}{2m_e}\left(-\imath\hbar\nabla + e\mathbf{A}\right)^2 + \frac{e\hbar}{2m_e}\vec{\sigma}\cdot\vec{\mathcal{B}} - eU(\mathbf{r})\right]\vec{\phi} \,, \tag{29.88}$$

which corresponds to a Schrödinger-like equation for a two-component spinor $\vec{\phi}$ with the Hamiltonian,

$$\boxed{\hat{H} \simeq \frac{\mathbf{p}^2}{2m_e} - \frac{1}{4\pi\varepsilon_0}\frac{e^2}{r} - \frac{\imath\hbar e}{2m_e}(\nabla\cdot\mathbf{A} + \mathbf{A}\cdot\nabla) + \frac{e}{m_e}\mathbf{s}\cdot\vec{\mathcal{B}}} \,, \tag{29.89}$$

neglecting terms in $\mathbf{A}^2$. Note however, that the kinetic energy is calculated with the *momentum projected onto the spin*, $\vec{\sigma}\cdot\vec{\pi}$. The third term can be simplified within the Coulomb gauge $\nabla\cdot\mathbf{A} = 0$ yielding,

$$\hat{H}_{int} = \frac{e}{m_e}(\mathbf{A}\cdot\mathbf{p}) \,. \tag{29.90}$$

The Pauli equation serves for a classical (non-relativistic) approach to the electron's spin-orbit coupling, as we will see below and in the discussion of the fine structure in Sec. 29.2.2.

[8] The spin of the electron does not generate a magnetic field, in contrast to the angular momentum caused by its *orbital motion*. It only interacts with the environment through the requirement of symmetrization for being a fermion.

29.1.4.1 Dipole moment of the orbital angular momentum

The rotational motion of a charge, $-e$, creates a current I, corresponding to a current density,

$$\mathbf{j}(\mathbf{r}') = I\hat{\mathbf{e}}_\phi \delta(r-r')\delta(z') = -e\frac{\mathbf{v}}{2\pi r}\delta(r-r')\delta(z') \ . \tag{29.91}$$

Hence, the dipole moment caused by the circular motion of an electron is,

$$\begin{aligned}\vec{\mu}_\ell &= \frac{1}{2}\int_V \mathbf{r}\times\mathbf{j}(\mathbf{r}')d^3r' \qquad (29.92)\\ &= \frac{1}{4\pi}\mathbf{r}\times\int_0^{2\pi}d\phi'\int_{-\infty}^{\infty}dz'\int_0^{\infty}r'dr'\frac{-e\mathbf{v}}{r}\delta(r-r')\delta(z') = \tfrac{-1}{2}e\mathbf{r}\times\mathbf{v} = \frac{-e}{2m_e}\mathbf{l}\ ,\end{aligned}$$

with the angular momentum $\mathbf{l} = \mathbf{r}\times m_e\mathbf{v}$. The quotient $\gamma_e \equiv -e/2m_e$ is called *gyromagnetic ratio* of the electron. We often use the *Bohr magneton*, $\mu_B \equiv \hbar e/2m_e$, which represents the elementary unit of spin,

$$\boxed{\frac{\vec{\mu}_\ell}{\mu_B} = -g_l\frac{\mathbf{l}}{\hbar}} \ . \tag{29.93}$$

The *g-factor* of a system having any angular momentum $\mathbf{l}$ is defined as a proportionality constant between the normalized dipole moment and the normalized angular momentum. $g_\ell \equiv \frac{\mu_\ell}{\ell\mu_B} = 1$ takes into account possible corrections between our classical derivation and quantum mechanics.

29.1.4.2 Pauli's model of spin-orbit coupling

The aim of this section is to demonstrate the relationship between the spin-orbit coupling term in Dirac's Hamiltonian (29.85) and the spin-magnetic field coupling term in Pauli's Hamiltonian (29.89).

A comparison of Pauli's expression with the energy of a magnetic moment in the field $\vec{\mathcal{B}}$,

$$\hat{H}_{\ell s} = -\vec{\mu}_s\cdot\vec{\mathcal{B}} \ , \tag{29.94}$$

suggests the following connection between the spin and the magnetic moment:

$$-\vec{\mu}_s\cdot\vec{\mathcal{B}} = \frac{e\hbar}{2m_e}\vec{\sigma}\cdot\vec{\mathcal{B}} = \frac{e}{m_e}\mathbf{s}\cdot\vec{\mathcal{B}} \ . \tag{29.95}$$

We conclude, that the electron carries, besides mass, charge and spin, also a magnetic dipole moment,

$$\boxed{\frac{\vec{\mu}_s}{\mu_B} = -\frac{e}{m_e\mu_B}\mathbf{s} = -2\frac{\mathbf{s}}{\hbar}} \ , \tag{29.96}$$

For the g-factor of the electron, we obtain $g_e = 2$ [9]. Neutron and proton are also fermions with spin $\frac{1}{2}$, but they do not obey the Dirac equation! Their g-factors are

[9] The exact value is $g_e \equiv \frac{\mu_s}{s\mu_B} = 2.002319314...$ The deviation $g_e - 2 \simeq \frac{\alpha}{\pi} - 0.164\frac{\alpha^2}{\pi^2}$ is due to the coupling of the spin to the fluctuations of the electromagnetic vacuum. We need to use quantum electrodynamical methods to calculate the corrections.

$g_{proton} = 5.5858$ and $g_{neutron} = -3.8261$. The large deviation from $g = 2$ points to the existence of an internal structure.

The rapid motion of the electron within the electrostatic field $\vec{\mathcal{E}}$ of the nucleus produces, following the theory of relativity, in the electron's reference frame a magnetic field $\vec{\mathcal{B}}'$ with which the electronic spin can interact. As we will show in Exc. 29.1.5.7, the field seen by the electron can be approximated in first order in v/c by,

$$\vec{\mathcal{B}}' \simeq \frac{\mathbf{v}}{c^2} \times \vec{\mathcal{E}} \, . \tag{29.97}$$

With this the interaction energy (29.94) becomes,

$$\begin{aligned} \hat{H}_{\ell s} = -\vec{\mu}_s \cdot \vec{\mathcal{B}}' = \frac{e}{m_e c^2} \mathbf{s} \cdot (\mathbf{v} \times \vec{\mathcal{E}}) = -\frac{e}{m_e^2 c^2} \mathbf{s} \cdot (\mathbf{p} \times \nabla U) \\ = -\frac{e}{m_e^2 c^2} \mathbf{s} \cdot \left(\mathbf{p} \times \frac{\mathbf{r}}{r} \frac{\partial U}{\partial r} \right) = -\frac{1}{m_e^2 c^2 r} \mathbf{s} \cdot \mathbf{l} \frac{\partial V(r)}{\partial r} \, , \end{aligned} \tag{29.98}$$

with $V(r) = -eU(r)$.

The resulting interaction energy coincides, apart from a factor $\frac{1}{2}$ [1299], with the one obtained in the from Dirac's equation (29.85). The deviation, called *Thomas factor*, is due to the necessity to transform back into the inertial system of the nucleus. This transformation, called *Thomas precession*, must be done by a Lorentz transformation, which is not trivial with electron continuously changing its propagation direction on its circular orbit. The transformation introduces the additional factor of $\frac{1}{2}$ [10].

29.1.5 Exercises

29.1.5.1 Ex: Yukawa potential

Show, that Yukawa's potential satisfies the Klein-Gordon equation.

Solution: *We have,*

$$\frac{1}{r^2} \frac{\partial}{\partial r} r^2 \frac{\partial}{\partial r} \frac{e^{mcr/\hbar}}{r} = \frac{m^2 c^2}{\hbar^2} \frac{e^{2\pi mcr/h}}{r} \, .$$

29.1.5.2 Ex: Zitterbewegung

Zitterbewegung is a hypothetical rapid motion of elementary particles, in particular electrons, that obey the Dirac equation. The existence of such motion was first proposed by Erwin Schrödinger in 1930 as a result of his analysis of the wave packet solutions of the Dirac equation for relativistic electrons in free space, in which an interference between positive and negative energy states produces what appears to be a fluctuation (at the speed of light) of the position of an electron around the median,

[10] This is a kinematic effect in space-time: the Lorentz transformations for systems moving with non-collinear velocities can not simply be concatenated, but must be rotated, too [471, 659].

with a frequency of $2m_ec^2/\hbar$, or approximately $1.6 \cdot 10^{21}$ rad/s. For the hydrogen atom, the Zitterbewegung produces the Darwin term which plays the role in the fine structure as a small correction of the energy level of the s-orbitals.
Use the Heisenberg equation to derive, from Dirac's Hamiltonian, equations of motion for the position operator $\hat{\mathbf{r}}$ and the 'velocity operator' $\hat{\vec{\alpha}}$. Solve the equation of motion and identify the Zitterbewegung.
Zitterbewegung of a free relativistic particle has never been observed experimentally. However, it has been simulated twice. First, with a trapped ion, by putting it in an environment such that the non-relativistic Schrödinger equation for the ion has the same mathematical form as the Dirac equation (although the physical situation is different) [503]. Then, in 2013, it was simulated in a setup with Bose-Einstein condensates [778].

Solution: *For a free electron, the time-dependent Dirac equation (29.13) is written as,*

$$\hat{H}\vec{\vec{\Phi}}(\mathbf{r},t) = \imath\hbar\frac{\partial\vec{\vec{\Phi}}}{\partial t}(\mathbf{r},t) \ ,$$

where $\vec{\vec{\Phi}}(\mathbf{r},t)$ is the wavefunction (bispinor) of the electron, and $\hat{H} = m_ec^2\alpha_0 + c\vec{\alpha}\cdot\mathbf{p}$ is Dirac's Hamiltonian. The Heisenberg picture implies that any operator $\hat{Q}$ obeys the equation,

$$-\imath\hbar\frac{\partial\hat{Q}}{\partial t} = [\hat{H},\hat{Q}] \ .$$

In particular, the time-dependence of the position operator is given by

$$\hbar\frac{\partial\mathbf{r}(t)}{\partial t} = \imath[\hat{H},\mathbf{r}] = \hbar c\vec{\alpha} \ ,$$

where $\mathbf{r}(t)$ is the position operator at time t. The above equation shows that the operator $\vec{\alpha}$ can be interpreted as a 'velocity operator'. To add time-dependence to $\vec{\alpha}$, one implements the Heisenberg picture, which says,

$$\vec{\alpha}(t) = e^{\imath\hat{H}t/\hbar}\vec{\alpha}e^{-\imath\hat{H}t/\hbar} \ .$$

The time-dependence of the velocity operator is given by

$$\hbar\frac{\partial\vec{\alpha}(t)}{\partial t} = \imath[\hat{H},\vec{\alpha}]_- = \imath m_ec^2[\alpha_0,\vec{\alpha}]_- + c[\vec{\alpha}\cdot\mathbf{p},\vec{\alpha}]_- \ .$$

This expression can be simplified using $[\alpha_m,\alpha_n]_+ = 2\delta_{mn}$ for all $m,n = 0,..,3$, since with $k = 1,..,3$,

$$\begin{aligned}
\imath[\hat{H},\alpha_k] &= \imath m_ec^2[\alpha_0,\alpha_k]_- + \imath c[\alpha_np_n,\alpha_k]_- \\
&= 2\imath m_ec^2\alpha_0\alpha_k + \imath cp_n[\alpha_n,\alpha_k]_- \\
&= 2\imath m_ec^2\alpha_0\alpha_k + 2\imath cp_n\alpha_n\alpha_k(1-\delta_{nk}) \\
&= -2\imath m_ec^2\alpha_k\alpha_0 + 2\imath cp_k - 2\imath c\alpha_k\alpha_np_n \\
&= 2\imath cp_k - 2\imath m_ec^2\alpha_k\alpha_0 - 2\imath c\alpha_k\vec{\alpha}\cdot\mathbf{p} \\
&= 2\imath\left[cp_k - \alpha_k(m_ec^2\alpha_0 + c\vec{\alpha}\cdot\mathbf{p})\right] = 2\imath(cp_k - \alpha_k\hat{H}) \ .
\end{aligned}$$

With this we get,

$$\hbar\frac{\partial\vec{\alpha}(t)}{\partial t} = 2\imath(c\mathbf{p} - \vec{\alpha}\hat{H}) \ .$$

Now, because both $\mathbf{p}$ *and* $\hat{H}$ *are time-independent, the above equation can easily be integrated twice to find the explicit time-dependence of the position operator. First:*

$$\vec{\alpha}(t) = \left(\vec{\alpha}(0) - c\mathbf{p}\hat{H}^{-1}\right)e^{-\frac{2\imath\hat{H}t}{\hbar}} + c\mathbf{p}\hat{H}^{-1} \ ,$$

and finally

$$\mathbf{r}(t) = \mathbf{r}(0) + c^2\mathbf{p}\hat{H}^{-1}t + \tfrac{1}{2}\imath\hbar c\hat{H}^{-1}(\vec{\alpha}(0) - c\mathbf{p}\hat{H}^{-1})\left(e^{-2\imath\hat{H}t/\hbar} - 1\right) \ .$$

The resulting expression consists of an initial position, a motion proportional to time, and an unexpected oscillation term with an amplitude equal to the Compton wavelength, $hc/\hat{H} \simeq h/m_e c \equiv \lambda_C$*. That oscillation term is the so-called Zitterbewegung. The Zitterbewegung term vanishes on taking expectation values for wave-packets that are made up entirely of positive- (or entirely of negative-) energy waves. This can be achieved by taking a Foldy-Wouthuysen transformation. Thus, we arrive at the interpretation of the Zitterbewegung as being caused by interference between positive- and negative-energy wave components.*

29.1.5.3 Ex: Constants of motion of Dirac's Hamiltonian 1

Show that $\hat{L}_z$ with $\hat{\mathbf{L}} \equiv \mathbf{r} \times \hat{\mathbf{p}}$ and $\hat{S}_z$ with $\hat{\mathbf{S}} \equiv \frac{\hbar}{2}\gamma_5\vec{\alpha}$ defining $\gamma_5 \equiv -\imath\alpha_1\alpha_2\alpha_3$ are not constants of motions, but $\hat{\mathbf{J}} = \hat{\mathbf{L}} + \hat{\mathbf{S}}$, that is,

$$[\hat{H}, \hat{J}_z] = [\hat{H}, \hat{L}_z + \hat{S}_z] = 0 \ . \tag{29.99}$$

Solution: *Explicitly we have* $\hat{S}_z = \frac{\hbar}{2}\begin{pmatrix}\sigma_z & 0\\ 0 & \sigma_z\end{pmatrix}$*. Now we calculate with Dirac's Hamiltonian (29.13),*

$$\begin{aligned}[\hat{H}, \hat{L}_z] &= [\cancelto{0}{m_e c^2\alpha_0} + c\vec{\alpha}\cdot\mathbf{p}, \hat{L}_z] = \sum_k c\alpha_k p_k(xp_y - yp_x) - c(xp_y - yp_x)\alpha_k p_k \\ &= c\alpha_1 p_x xp_y - cxp_y\alpha_1 p_x - c\alpha_2 p_y yp_x + cyp_x\alpha_2 p_y = -\imath\hbar c(\alpha_1 p_y - \alpha_2 p_x) \\ &= -\imath\hbar c(\vec{\alpha}\times\mathbf{p})_z \ .\end{aligned}$$

Hence, $[\hat{H}, \mathbf{L}] = -\imath\hbar c\vec{\alpha}\times\mathbf{p}$*. With* $\alpha_j = \alpha_j^{-1} = \alpha_j^\dagger$ *for all* $j = 1, .., 3$ *and for* γ_5 *it is obvious to verify,*

$$\gamma_5\alpha_3\alpha_1 = \imath\alpha_2 = -\alpha_1\gamma_5\alpha_3 \qquad , \qquad \alpha_2\gamma_5\alpha_3 = \imath\alpha_1 = -\gamma_5\alpha_3\alpha_2 \ .$$

With this,

$$\begin{aligned}[\hat{H}, \hat{S}_z] &= [\cancelto{0}{m_e c^2\alpha_0} + c\vec{\alpha}\cdot\mathbf{p}, \gamma_5\hat{S}_z] = \sum_k c\alpha_k p_k\tfrac{\hbar\gamma_5}{2}\alpha_3 - \tfrac{\hbar\gamma_5}{2}\alpha_3 c\alpha_k p_k \\ &= \tfrac{\hbar}{2}c(\alpha_1\gamma_5\alpha_3 - \gamma_5\alpha_3\alpha_1)p_x + \tfrac{\hbar}{2}c(\alpha_2\gamma_5\alpha_3 - \gamma_5\alpha_3\alpha_2)p_y \\ &= \tfrac{\hbar}{2}c(-\imath\alpha_2 - \imath\alpha_2)p_x + \tfrac{\hbar}{2}c(\imath\alpha_1 + \imath\alpha_1)p_y = \hbar c\imath\alpha_1 p_y - \imath\hbar c\alpha_2 p_x = \imath\hbar c(\vec{\alpha}\times\mathbf{p})_z \ .\end{aligned}$$

Comparing the results of the two calculations, we conclude,

$$[\hat{H}, \hat{J}_z] = [\hat{H}, \hat{L}_z + \hat{S}_z] = 0 \ .$$

29.1.5.4 Ex: Calculating with Dirac matrices

a. Prove that, if $[\mathbf{B}, \vec{\sigma}] = 0 = [\mathbf{C}, \vec{\sigma}]$ where $\vec{\sigma}$ are the Pauli matrices, then,

$$(\vec{\sigma} \cdot \mathbf{B})(\vec{\sigma} \cdot \mathbf{C}) = \mathbf{B} \cdot \mathbf{C} + \imath \vec{\sigma} \cdot (\mathbf{B} \times \mathbf{C}) \ . \tag{29.100}$$

b. Prove that, if $[\mathbf{B}, \vec{\alpha}] = 0 = [\mathbf{C}, \vec{\alpha}]$ where $\vec{\alpha}$ are the Dirac matrices, then,

$$(\vec{\alpha} \cdot \mathbf{B})(\vec{\alpha} \cdot \mathbf{C}) = \mathbf{B} \cdot \mathbf{C} + \imath\gamma_5 \vec{\alpha} \cdot (\mathbf{B} \times \mathbf{C}) \ . \tag{29.101}$$

c. Show that the spin defined as,

$$\mathbf{S} = \tfrac{\hbar}{2} \vec{\varsigma} \qquad \text{where} \qquad \vec{\varsigma} \equiv \gamma_5 \vec{\alpha} = \mathbb{I} \otimes \vec{\sigma} \tag{29.102}$$

obeys different commutation rules than the Dirac matrices.
d. Conclude that,

$$(\vec{\varsigma} \cdot \mathbf{B})(\vec{\varsigma} \cdot \mathbf{C}) = \mathbf{B} \cdot \mathbf{C} + \imath \vec{\varsigma} \cdot (\mathbf{B} \times \mathbf{C}) \ . \tag{29.103}$$

Solution: *a. Using* $[\sigma_k, \sigma_m]_+ = 2\delta_{km}$ *we derive,*

$$\begin{aligned}
&(\sigma_x B_x + \sigma_y B_y + \sigma_z B_z)(\sigma_x C_x + \sigma_y C_y + \sigma_z C_z) \\
&= \sum_j \sigma_j^2 B_j C_j + \sigma_y B_y \sigma_z C_z + \sigma_z B_z \sigma_y C_y + \sigma_z B_z \sigma_x C_x + \sigma_x B_x \sigma_z C_z + \sigma_x B_x \sigma_y C_y + \sigma_y B_y \sigma_x C_x \\
&= \mathbf{B} \cdot \mathbf{C} + \sigma_y \sigma_z (\mathbf{B} \times \mathbf{C})_x + \sigma_z \sigma_x (\mathbf{B} \times \mathbf{C})_y + \sigma_x \sigma_y (\mathbf{B} \times \mathbf{C})_z \\
&= \mathbf{B} \cdot \mathbf{C} + \imath \sigma_x (\mathbf{B} \times \mathbf{C})_x + \imath \sigma_y [(\mathbf{B} \times \mathbf{C})_y + \imath \sigma_z (\mathbf{B} \times \mathbf{C})_z \ .
\end{aligned}$$

b. Using $[\alpha_i, \alpha_j]_+ = 2\delta_{ij}$ *we derive,*

$$\begin{aligned}
&(\alpha_x B_x + \alpha_y B_y + \alpha_z B_z)(\alpha_x C_x + \alpha_y C_y + \alpha_z C_z) \\
&= \sum_j \alpha_j^2 B_j C_j + \alpha_y B_y \alpha_z C_z + \alpha_z B_z \alpha_y C_y + \alpha_z B_z \alpha_x C_x + \alpha_x B_x \alpha_z C_z + \alpha_x B_x \alpha_y C_y + \alpha_y B_y \alpha_x C_x \\
&= \mathbf{B} \cdot \mathbf{C} + \alpha_y \alpha_z (\mathbf{B} \times \mathbf{C})_x + \alpha_z \alpha_x (\mathbf{B} \times \mathbf{C})_y + \alpha_x \alpha_y (\mathbf{B} \times \mathbf{C})_z \\
&= \mathbf{B} \cdot \mathbf{C} + \imath\gamma_5 \alpha_x (\mathbf{B} \times \mathbf{C})_x + \imath\gamma_5 \alpha_y [(\mathbf{B} \times \mathbf{C})_y + \imath\gamma_5 \alpha_z (\mathbf{B} \times \mathbf{C})_z \ .
\end{aligned}$$

c. Using the commutation rules for $m, n = 0, .., 3$,

$$[\alpha_m, \alpha_n]_+ = 2\delta_{mn} \qquad \textit{and} \qquad [\gamma_5, \alpha_0]_+ = 0 = [\gamma_5, \vec{\alpha}]_- = 0 \ ,$$

we deduce for $m, n = 1, .., 3$,

$$[\varsigma_m, \varsigma_n]_+ = [\alpha_m, \alpha_n]_+ = 2\delta_{mn} \qquad \textit{and} \qquad [\vec{\varsigma}, \alpha_0]_- = 0 = [\vec{\alpha}, \alpha_0]_+ \ .$$

On the other hand,

$$\begin{aligned}[\varsigma_m, \varsigma_n]_- &= \imath\hbar(\mathbb{I}_2 \otimes \sigma_m)(\mathbb{I}_2 \otimes \sigma_n) - \imath\hbar(\mathbb{I}_2 \otimes \sigma_n)(\mathbb{I}_2 \otimes \sigma_m) \\ &= \imath\hbar(\mathbb{I}_2 \otimes \sigma_m\sigma_n) - \imath\hbar(\mathbb{I}_2 \otimes \sigma_n\sigma_m) = \imath\hbar I_2 \otimes [\sigma_m, \sigma_n] \\ &= \imath\hbar\epsilon_{kmn}(\mathbb{I}_2 \otimes \sigma_k) = \imath\hbar\epsilon_{kmn}\varsigma_k \ ,\end{aligned}$$

and

$$\begin{aligned}[\alpha_m, \alpha_n]_- &= [\gamma_5\varsigma_m, \gamma_5\varsigma_n]_- = [\varsigma_m, \varsigma_n]_- = \imath\hbar\epsilon_{kmn}\varsigma_k \\ &= \imath\hbar\epsilon_{kmn}\gamma_5\alpha_k \neq \imath\hbar\epsilon_{kmn}\alpha_k \ .\end{aligned}$$

d. Follows trivially from (b) and (c).

29.1.5.5 Ex: Constants of motion of Dirac's Hamiltonian 2

In this exercise we will prove the relationships (29.55):
a. Prove,

$$(\hbar j')^2 = \mathbf{J}^2 + \tfrac{\hbar^2}{4} \ . \tag{29.104}$$

b. Prove,

$$[\hbar j', \hat{H}]_- = 0 \ . \tag{29.105}$$

c. Prove,

$$\mathbf{r}\cdot\mathbf{p} = -\imath\hbar r\frac{\partial}{\partial r} \ . \tag{29.106}$$

d. Prove,

$$[\varepsilon, \hat{H}]_- = 0 \ . \tag{29.107}$$

Solution: *a. We start inserting the definition of* $\hbar j' \equiv [\alpha_0(\gamma_5\vec{\alpha}\cdot\mathbf{L} + \hbar)$,

$$\begin{aligned}(\hbar j')^2 &= [\alpha_0(\gamma_5\vec{\alpha}\cdot\mathbf{L} + \hbar)]^2 \\ &= (\alpha_0\gamma_5\vec{\alpha}\cdot\mathbf{L})(\alpha_0\gamma_5\vec{\alpha}\cdot\mathbf{L}) + (\alpha_0\hbar)(\alpha_0\gamma_5\vec{\alpha}\cdot\mathbf{L}) + (\alpha_0\gamma_5\vec{\alpha}\cdot\mathbf{L})(\alpha_0\hbar) + \hbar^2\alpha_0^2 \ .\end{aligned}$$

Using the commutation rules $[\alpha_m, \alpha_n]_+ = 2\delta_{mn}$ *for* $m, n = 0, .., 3$ *and* $[\gamma_5, \alpha_m]_- = 0$ *for* $m = 1, 2, 3$*, but* $[\gamma_5, \alpha_0]_+ = 0$*, we can simplify,*

$$\begin{aligned}(\hbar j')^2 &= (\vec{\alpha}\cdot\mathbf{L})(\vec{\alpha}\cdot\mathbf{L}) + 2\hbar\gamma_5\vec{\alpha}\cdot\mathbf{L} + \hbar^2 \\ &= \mathbf{L}\cdot\mathbf{L} + \imath\gamma_5\vec{\alpha}\cdot(\mathbf{L}\times\mathbf{L}) + 2\hbar\gamma_5\vec{\alpha}\cdot\mathbf{L} + \hbar^2\end{aligned}$$

using the formula (29.101). Using $\mathbf{L}\times\mathbf{L} = \imath\hbar\mathbf{L}$ *we find,*

$$(\hbar j')^2 = \mathbf{L}^2 + \hbar\gamma_5\vec{\alpha}\cdot\mathbf{L} + \hbar^2 = (\mathbf{L} + \hbar\gamma_5\vec{\alpha})\cdot\mathbf{L} + \hbar^2 \ ,$$

and substituting $\mathbf{J} = \mathbf{L} + \frac{\hbar}{2}\gamma_5\vec{\alpha}$*,*

$$(\hbar j')^2 = \left(\mathbf{J} + \tfrac{\hbar}{2}\gamma_5\vec{\alpha}\right)\cdot\left(\mathbf{J} - \tfrac{\hbar}{2}\gamma_5\vec{\alpha}\right) + \hbar^2 = \mathbf{J}^2 - \tfrac{\hbar^2}{4}\vec{\alpha}^2 + \hbar^2 = \mathbf{J}^2 + \tfrac{\hbar^2}{4} \ ,$$

where we finally used $\vec{\alpha}\cdot\vec{\alpha}=3$ [11].
b. Using the formula derived in 29.1.5.3 we find quickly,

$$(\vec{\alpha}\cdot\mathbf{p})(\vec{\alpha}\cdot\mathbf{L})=\cancelto{0}{\mathbf{p}\cdot\mathbf{L}}+\imath\vec{\alpha}\cdot(\mathbf{p}\times\mathbf{L})$$
$$(\vec{\alpha}\cdot\mathbf{L})(\vec{\alpha}\cdot\mathbf{p})=\cancelto{0}{\mathbf{L}\cdot\mathbf{p}}+\imath\vec{\alpha}\cdot(\mathbf{L}\times\mathbf{p})\ .$$

The premisses for the formula (29.100) to be applicable, $[\alpha_j,p_j]=0=[\alpha_j,L_j]$ *are satisfied, because* α_j *are constants and* p_j *and* L_j *are scalars. With this, respecting* $[x_k,p_m]=\imath\hbar\delta_{km}$*,*

$$\begin{aligned}
&(\vec{\alpha}\cdot\mathbf{p})(\vec{\alpha}\cdot\mathbf{L})+(\vec{\alpha}\cdot\mathbf{L})(\vec{\alpha}\cdot\mathbf{p})=\imath\vec{\alpha}\cdot(\mathbf{p}\times\mathbf{L})+\imath\vec{\alpha}\cdot(\mathbf{L}\times\mathbf{p})\\
&=\imath\alpha_x p_y L_z-\imath\alpha_x p_z L_y+\imath\alpha_x L_y p_z-\imath\alpha_x L_z p_y+\ldots\textit{terms in }\alpha_y\textit{ and }\alpha_z\\
&=\imath\alpha_x p_y(xp_y-yp_x)-\imath\alpha_x p_z(zp_x-xp_z)+\imath\alpha_x(zp_x-xp_z)p_z-\imath\alpha_x(xp_y-yp_x)p_y+\\
&\quad+\ldots\textit{terms in }\alpha_{y,z}\\
&=\imath\alpha_x xp_y^2-\imath\alpha_x xp_y^2+\imath\alpha_x xp_z^2-\imath\alpha_x xp_z^2-\imath\alpha_x p_y yp_x-\imath\alpha_x p_z zp_x+\imath\alpha_x zp_x p_z+\imath\alpha_x yp_x p_y+\\
&\quad+\ldots\textit{terms in }\alpha_{y,z}\\
&=\imath\alpha_x[y,p_y]p_x+\imath\alpha_x[z,p_z]p_x+\ldots\textit{terms in }\alpha_{y,z}\\
&=-2\hbar\alpha_x p_x+\ldots\textit{terms in }\alpha_{y,z}=-2\hbar\vec{\alpha}\cdot\mathbf{p}\ .
\end{aligned}$$

This result can be rewritten as,

$$[\vec{\alpha}\cdot\mathbf{p},\vec{\alpha}\cdot\mathbf{L}+\hbar]_+=0\ .$$

Consequently,

$$[\vec{\alpha}\cdot\mathbf{p},\alpha_0(\gamma_5\vec{\alpha}\cdot\mathbf{L}+\hbar)]_-=[\vec{\alpha}\cdot\mathbf{p},\hbar j']_-=0\ .$$

It is easy to see,

$$[\hbar j',m_e c^2\alpha_0]_-=0=\left[\hbar j',-\frac{e^2}{4\pi\varepsilon_0 r}\right]\ .$$

Finally, $[\hbar j',\hat{H}]_-=0$ *.*
c. Using the representation of the gradient in spherical coordinates,

$$\mathbf{r}\cdot\mathbf{p}=r\hat{\mathbf{e}}_r\cdot(-\imath\hbar)\left(\hat{\mathbf{e}}_r\frac{\partial}{\partial r}+\frac{\hat{\mathbf{e}}_\theta\vartheta}{r}\frac{\partial}{\partial\vartheta}+\frac{\hat{\mathbf{e}}_\theta\varphi}{r\sin\vartheta}\frac{\partial}{\partial\varphi}\right)=-\imath\hbar r\frac{\partial}{\partial r}\ .$$

d. It is easy to see,

$$r\varepsilon\alpha_0=\vec{\alpha}\cdot\mathbf{r}\alpha_0=\vec{\alpha}\alpha_0\cdot\mathbf{r}=-\alpha_0\vec{\alpha}\cdot\mathbf{r}=-\alpha_0\vec{\alpha}\cdot\mathbf{r}=-\alpha_0 r\varepsilon\ .$$

We also calculate,

$$[\vec{\alpha}\cdot\mathbf{r},\mathbf{r}\cdot\mathbf{p}]=(\vec{\alpha}\cdot\mathbf{r})(\mathbf{r}\cdot\mathbf{p})-(\mathbf{r}\cdot\mathbf{p})(\vec{\alpha}\cdot\mathbf{r})=\vec{\alpha}\cdot[\mathbf{r}(\mathbf{r}\cdot\mathbf{p})-(\mathbf{r}\cdot\mathbf{p})\mathbf{r}]=\vec{\alpha}\cdot[\mathbf{r},\mathbf{r}\cdot\mathbf{p}]=\vec{\alpha}\cdot(\mathbf{r}\cdot[\mathbf{r},\mathbf{p}])=\imath\hbar\vec{\alpha}\cdot\mathbf{r}\ ,$$

or $[r\varepsilon,rp_r]_-=\imath\hbar\varepsilon r$*. Hence,*

$$\left[\varepsilon,\varepsilon\left(p_r-\imath\frac{\hbar}{r}\right)\right]_-=0\ .$$

[11] Not to confuse with $\vec{\alpha}^\dagger\vec{\alpha}=1$.

29.1.5.6 Ex: Constants of motion in the $\mathbf{L}\cdot\mathbf{S}$-coupling

Consider a particle of mass μ described by the Hamiltonian $\hat{H} = -\frac{\hbar^2}{2\mu}\nabla^2 + V(r) + \xi(r)\mathbf{L}\cdot\mathbf{S}$, being $V(r)$ a central potential, $\mathbf{L}$ and $\mathbf{S}$ its orbital angular momentum and spin.
a. Obtain the commutation relations $[\mathbf{L}, \hat{H}]$, $[\mathbf{S}, \hat{H}]$ and $[\mathbf{L}+\mathbf{S}, \hat{H}]$ for the cases without and with spin-orbit interaction $\xi(r)\mathbf{L}\cdot\mathbf{S}$ introduced by relativistic corrections.
b. Calculate $[\mathbf{L}^2, \hat{H}]$, $[\mathbf{S}^2, \hat{H}]$ and $[\mathbf{J}^2, \hat{H}]$.

Solution: *a. Without spin-orbit interaction we have,*

$$[\mathbf{L}, -\tfrac{\hbar^2}{2\mu}\nabla^2 + V(r)] = [\mathbf{S}, -\tfrac{\hbar^2}{2\mu}\nabla^2 + V(r)] = [\mathbf{J}, -\tfrac{\hbar^2}{2\mu}\nabla^2 + V(r)] = 0 \ .$$

This is obvious, since we know $[L_z, \hat{H}_0] = 0$, and since without spin-orbit interaction the atom is completely round, the same has to be valid for any other axis: $[L_x, \hat{H}_0] = [L_y, \hat{H}] = 0$. With interaction,

$$[\mathbf{L}, H] = [\mathbf{L}, -\frac{\hbar^2}{2\mu}\nabla^2 + V(r) + \xi(r)\mathbf{L}\cdot\mathbf{S}] = \xi(r)[\mathbf{L}, L_xS_x + L_yS_y + L_zS_z]$$
$$= \xi(r)\left\{\left[\begin{pmatrix}L_x\\L_y\\L_z\end{pmatrix}, L_x\right]S_x + \left[\begin{pmatrix}L_x\\L_y\\L_z\end{pmatrix}, L_y\right]S_y + \left[\begin{pmatrix}L_x\\L_y\\L_z\end{pmatrix}, L_z\right]S_z\right\} = \imath\hbar\xi(r)\mathbf{S}\times\mathbf{L} \ ,$$

using $[L_x, L_y] = \imath\hbar L_z$. Analogously,

$$[\mathbf{S}, \hat{H}] = \imath\hbar\xi(r)\mathbf{L}\times\mathbf{S} \ .$$

Finally,

$$[\mathbf{J}, \hat{H}] = [\mathbf{J}, -\frac{\hbar^2}{2\mu}\nabla^2 + V(r) + \xi(r)\mathbf{L}\cdot\mathbf{S}] = \frac{\xi(r)}{2}[\mathbf{J}, \mathbf{J}^2 - \mathbf{L}^2 - \mathbf{S}^2] = 0 \ .$$

Using the results of Excs. 25.4.5.2 and 25.4.5.11.
b. In the same way,

$$[\mathbf{L}^2, \hat{H}] = \mathbf{L}\cdot[\mathbf{L}, \hat{H}] + [\mathbf{L}, \hat{H}]\cdot\mathbf{L} = \imath\hbar\xi(r)\mathbf{L}\cdot(\mathbf{S}\times\mathbf{L}) + \imath\hbar\xi(r)(\mathbf{S}\times\mathbf{L})\cdot\mathbf{L} = 0 \ .$$

In the same way,

$$[\mathbf{S}^2, \hat{H}] = 0 = [\mathbf{J}^2, \hat{H}] \ .$$

29.1.5.7 Ex: Magnetic field generated by the orbiting proton at the location of the electron

Calculate the magnetic field generated by the orbiting proton as it is perceived by the electron.

Solution: *In relativistic mechanics defined by the metric and Lorentz transform,*

$$\eta_{\mu\nu} \equiv \begin{pmatrix} 1 & 0 & 0 & 0 \\ 0 & -1 & 0 & 0 \\ 0 & 0 & -1 & 0 \\ 0 & 0 & 0 & -1 \end{pmatrix} \quad , \quad \Lambda_{\mu\nu} \equiv \begin{pmatrix} \gamma & 0 & 0 & -\gamma\beta \\ 0 & 1 & 0 & 0 \\ 0 & 0 & 1 & 0 \\ -\gamma\beta & 0 & 0 & \gamma \end{pmatrix}$$

where $\beta \equiv v/c$ *and* $\gamma \equiv 1/\sqrt{1-\beta^2}$*, the Maxwell field tensor is given by*

$$F_{\mu\nu} \equiv \begin{pmatrix} 0 & -\frac{1}{c}\vec{\mathcal{E}}_x & -\frac{1}{c}\vec{\mathcal{E}}_y & -\frac{1}{c}\vec{\mathcal{E}}_z \\ \frac{1}{c}\vec{\mathcal{E}}_x & 0 & -\vec{\mathcal{B}}_z & \vec{\mathcal{B}}_y \\ \frac{1}{c}\vec{\mathcal{E}}_y & \vec{\mathcal{B}}_z & 0 & -\vec{\mathcal{B}}_x \\ \frac{1}{c}\vec{\mathcal{E}}_z & -\vec{\mathcal{B}}_y & \vec{\mathcal{B}}_x & 0 \end{pmatrix} .$$

With this we can calculate the transformed field in an inertial system,

$$\begin{aligned} F'_{\mu\nu} &= \Lambda_\mu{}^\alpha F_{\alpha\beta}\Lambda^\beta{}_\nu = \eta_{\mu\eta}\Lambda^{\eta\alpha}F_{\alpha\beta}\Lambda^{\beta\kappa}\eta_{\kappa\nu} \\ &= \begin{pmatrix} 0 & -\frac{\gamma}{c}\vec{\mathcal{E}}_x + \gamma\beta\vec{\mathcal{B}}_y & -\frac{\gamma}{c}\vec{\mathcal{E}}_y - \gamma\beta\vec{\mathcal{B}}_x & -\frac{1}{c}\vec{\mathcal{E}}_z \\ \frac{\gamma}{c}\vec{\mathcal{E}}_x - \gamma\beta\vec{\mathcal{B}}_y & 0 & -\vec{\mathcal{B}}_z & -\gamma\frac{\beta}{c}\vec{\mathcal{E}}_x + \gamma\vec{\mathcal{B}}_y \\ \frac{\gamma}{c}\vec{\mathcal{E}}_y + \gamma\beta\vec{\mathcal{B}}_x & \vec{\mathcal{B}}_z & 0 & -\gamma\frac{\beta}{c}\vec{\mathcal{E}}_y - \gamma\vec{\mathcal{B}}_x \\ \frac{1}{c}\vec{\mathcal{E}}_z & \gamma\frac{\beta}{c}\vec{\mathcal{E}}_x - \gamma\vec{\mathcal{B}}_y & \gamma\frac{\beta}{c}\vec{\mathcal{E}}_y + \gamma\vec{\mathcal{B}}_x & 0 \end{pmatrix} , \end{aligned}$$

giving at low velocities ($\gamma \to 1$) *and knowing* $\mathbf{v} = v_z\hat{\mathbf{e}}_z$*,*

$$\begin{aligned} \vec{\mathcal{E}}' &= \begin{pmatrix} \vec{\mathcal{E}}'_x \\ \vec{\mathcal{E}}'_y \\ \vec{\mathcal{E}}'_z \end{pmatrix} = \begin{pmatrix} \vec{\mathcal{E}}_x - \beta c\vec{\mathcal{B}}_y \\ \vec{\mathcal{E}}_y + \beta c\vec{\mathcal{B}}_x \\ \vec{\mathcal{E}}_z \end{pmatrix} = \begin{pmatrix} \vec{\mathcal{E}}_y + v_y\vec{\mathcal{B}}_z - v_z\vec{\mathcal{B}}_y \\ \vec{\mathcal{E}}_y + v_z\vec{\mathcal{B}}_x - v_x\vec{\mathcal{B}}_z \\ \vec{\mathcal{E}}_z + v_x\vec{\mathcal{B}}_y - v_y\vec{\mathcal{B}}_x \end{pmatrix} = \vec{\mathcal{E}} + \mathbf{v}\times\vec{\mathcal{B}} \\ \vec{\mathcal{B}}' &= \begin{pmatrix} \vec{\mathcal{B}}'_x \\ \vec{\mathcal{B}}'_y \\ \vec{\mathcal{B}}'_z \end{pmatrix} = \begin{pmatrix} \vec{\mathcal{B}}_x + \frac{\beta}{c}\vec{\mathcal{E}}_y \\ \vec{\mathcal{B}}_y - \frac{\beta}{c}\vec{\mathcal{E}}_x \\ \vec{\mathcal{B}}_z \end{pmatrix} = \begin{pmatrix} \vec{\mathcal{B}}_x + \frac{1}{c^2}v_z\vec{\mathcal{E}}_y - \frac{1}{c^2}v_y\vec{\mathcal{E}}_z \\ \vec{\mathcal{B}}_y + \frac{1}{c^2}v_x\vec{\mathcal{E}}_z - \frac{1}{c^2}v_z\vec{\mathcal{E}}_x \\ \vec{\mathcal{B}}_z + \frac{1}{c^2}v_y\vec{\mathcal{E}}_x - \frac{1}{c^2}v_x\vec{\mathcal{E}}_y \end{pmatrix} = \vec{\mathcal{B}} + \frac{\mathbf{v}}{c^2}\times\vec{\mathcal{E}} . \end{aligned}$$

The first equation is the Lorentz force. The second only becomes important for relativistic velocities. Thus, the field seen by the electron can be approximated in first order in v/c *by,*

$$\vec{\mathcal{B}}' \simeq \frac{\mathbf{v}}{c^2}\times\vec{\mathcal{E}} .$$

29.2 Fine structure of hydrogen-like atoms via TIPT

The wave equation that simultaneously satisfies the requirements of quantum mechanics and special relativity is the *Dirac equation*. In free space including electromagnetic

interactions it describes all massive particles of semi-integer spin with parity as a symmetry, such as electrons and quarks. It was the first theory to fully explain special relativity in the context of quantum mechanics. The Dirac equation describes the fine structure of the hydrogen spectrum in a completely rigorous manner. The equation also implied the existence of a new form of matter, antimatter, previously unsuspected and unobserved. The equation also justifies a posteriori the introduction of spinors, that is, of the vector wavefunctions introduced by Pauli in a heuristic way. We have seen in the last section that, in the limit of high but non-relativistic velocities, the Dirac equation adopts the form of a Schrödinger equation with the modified Hamiltonian (29.85),

$$\begin{aligned}\hat{H} &= \hat{H}_0 + \hat{H}_{rl} + \hat{H}_{\ell s} + \hat{H}_{dw} + \hat{H}_{lamb} \\ &= \left(\frac{p^2}{2m_e} - \frac{Ze^2}{4\pi\varepsilon_0 r}\right) - \frac{p^4}{8m_e^3c^2} + \frac{1}{2m_e^2c^2}\frac{1}{r}\frac{dV}{dr}\mathbf{l}\cdot\mathbf{s} + \frac{\pi\hbar^2}{2m_e^2c^2}\frac{Ze^2}{4\pi\varepsilon_0}\delta^3(\mathbf{r}) + \hat{H}_{lamb}\ .\end{aligned} \tag{29.108}$$

We will discuss the various terms in the following sections. Note that the expression for the Darwin term differs from that of (29.85). We will see in Exc. 29.2.6.1, that they are, in fact, equivalent.

29.2.1 Correction for relativistic velocities

The first correction in the expression, $\hat{H}_{rl}$ in Eq. (29.108), comes from the expansion of the relativistic energy for small velocities up to second order,

$$E_{kin} = \sqrt{p^2c^2 + m_e^2c^4} \simeq m_ec^2 + \frac{p^2}{2m_e} - \frac{p^4}{8m_e^3c^2} + \dots\ . \tag{29.109}$$

The correction is of the order of magnitude,

$$\frac{H_{rl}}{H_0} = \frac{\frac{p^4}{8m_e^3c^2}}{\frac{p^2}{2m_e}} = \frac{v^2}{4c^2} \simeq \frac{\alpha^2}{4} \approx 0.01\%\ . \tag{29.110}$$

Due to the degeneracy of these states, it would be appropriate to use perturbation theory with degenerate states. However, as $\hat{H}_{rl}$ only depends on spatial coordinates commuting with $\mathbf{l}$ and $\mathbf{s}$, the degeneracy is not very important, since $\hat{H}_{rl}$ is already diagonal in the base $|n,\ell,m\rangle$, that is, $\langle n,\ell,m|n',\ell',m'\rangle = \delta_{\ell\ell'}\delta_{mm'}$. Starting from,

$$\begin{aligned}\hat{H}_{rl} &= -\frac{p^4}{8m_e^3c^2} = -\frac{1}{2m_ec^2}\left(\frac{p^2}{2m_e}\right)^2 = -\frac{1}{2m_ec^2}\left(\hat{H}_0 + \frac{Ze^2}{4\pi\varepsilon_0 r}\right)^2 \\ &= -\frac{1}{2m_ec^2}\left(\hat{H}_0 - \frac{2E_n n^2}{\tilde{r}}\right)^2\ ,\end{aligned} \tag{29.111}$$

with $\tilde{r} \equiv \frac{Zr}{a_B}$ and using as an abbreviation the energies of hydrogen following Bohr's model,

$$E_n = \langle n,\ell|\hat{H}_0|n,\ell\rangle = -\frac{Z^2e^2}{4\pi\varepsilon_0}\frac{1}{2a_Bn^2} = -\frac{m_ec^2}{2}\frac{Z^2\alpha^2}{n^2}\ . \tag{29.112}$$

We have

$$\begin{aligned}\Delta E_{rl} &= \langle n,\ell|\hat{H}_{rl}|n,\ell\rangle \qquad (29.113)\\ &= -\frac{1}{2m_ec^2}\left[\langle n,\ell|\hat{H}_0^2|n,\ell\rangle - \langle n,\ell|\frac{4E_nn}{\tilde{r}}\hat{H}_0|n,\ell\rangle + \langle n,\ell|\left(\frac{2E_nn}{\tilde{r}}\right)^2|n,\ell\rangle\right]\\ &= \frac{Z^2\alpha^2}{4E_nn^2}\left[E_n^2 - 4E_n^2n^2\frac{1}{n^2} + 4E_n^2n^4\frac{1}{n^3(\ell+\frac{1}{2})}\right]\ ,\end{aligned}$$

using the eigenvalues calculated in (25.53). Finally, we obtain the following relativistic correction,

$$\boxed{\Delta E_{rl} = E_n(Z\alpha)^2\left[\frac{1}{n(\ell+\frac{1}{2})} - \frac{3}{4n^2}\right]}\ . \qquad (29.114)$$

Obviously, the degeneracy with respect to the angular momentum ℓ is lifted by this correction.

29.2.2 Correction due to spin-orbit coupling

The second correction, $\hat{H}_{\ell s}$ in the expression (29.108), called *spin-orbit interaction*, is a relativistic correction due to the fact that the electron moves rapidly within the electrostatic field $\vec{\mathcal{E}}$ generated by the nucleus. Considering the fundamental orbit and the fact that the angular momenta are of the order of $\hbar$ we can estimate the importance of this effect,

$$\frac{H_{\ell s}}{H_0} = \frac{\frac{1}{2m_e^2c^2}\frac{1}{r}\frac{e^2}{4\pi\varepsilon_0 r^2}\mathbf{l}\cdot\mathbf{s}}{\frac{p^2}{2m_e}} \simeq \frac{\frac{1}{2m_e^2c^2}\frac{e^2}{4\pi\varepsilon_0}\frac{1}{a_B^3}\hbar^2}{\frac{e^2}{4\pi\varepsilon_0 a_B}} = \frac{1}{2m_e^2c^2}\frac{\hbar^2}{a_B^2} = \frac{\alpha^2}{2} \approx 0.01\%\ . \qquad (29.115)$$

Example 181 (*Classical derivation of the spin-orbit interaction*): In the following, we will derive the expression from classical arguments borrowed from electrodynamic theory. Seen from the rest system of the electron being at position $\mathbf{x} = 0$, it is the proton that orbits around the electron. This orbit creates a current, $-\mathbf{j}(\mathbf{r}')$, which generates a magnetic field. Following the *Biot-Savart's law* the potential vector and the amplitude of the field are,

$$\mathbf{A}(\mathbf{x}) = \frac{\mu_0}{4\pi}\int_V \frac{-\mathbf{j}(\mathbf{r}')d^3r'}{|\mathbf{x}-\mathbf{r}'|}\ , \qquad (29.116)$$

respectively,

$$\begin{aligned}\vec{\mathcal{B}}(\mathbf{x}) = \nabla_x\times\mathbf{A}(\mathbf{x}) &= \frac{\mu_0}{4\pi}\int_V\frac{(\mathbf{x}-\mathbf{r}')\times\mathbf{j}(\mathbf{r}')}{|\mathbf{x}-\mathbf{r}'|^3}d^3r' \qquad (29.117)\\ &= -\frac{\mu_0}{4\pi}\int_{-\infty}^{\infty}dz'\int_0^{\infty}r'dr'\int_0^{2\pi}d\phi\frac{(\mathbf{x}-\mathbf{r}')\times\mathbf{v}}{|\mathbf{x}-\mathbf{r}'|^3}\frac{Ze}{2\pi r}\delta(r-r')\delta(z')\\ &= \frac{Ze\mu_0}{4\pi}\frac{(\mathbf{x}-\mathbf{r})\times\mathbf{v}}{|\mathbf{x}-\mathbf{r}|^3}\ ,\end{aligned}$$

where we replaced the expression for the current density (29.91). With the expression for the *Coulomb potential* between the electron and the proton and its radial derivative,

$$V(r) = \frac{-Ze^2}{4\pi\varepsilon_0 r}\quad ,\quad \frac{1}{r}\frac{dV(r)}{dr} = \frac{Ze^2}{4\pi\varepsilon_0 r^3}\ , \qquad (29.118)$$

we have at the position of the electron,

$$\vec{\mathcal{B}}(\mathbf{0}) = \frac{Ze\mu_0}{4\pi}\frac{-\mathbf{r}\times\mathbf{v}}{r^3} = -\frac{\varepsilon_0\mu_0}{e}\frac{\mathbf{r}\times\mathbf{v}}{r}\frac{dV(r)}{dr} \qquad (29.119)$$
$$= -\frac{1}{ec^2}\frac{\mathbf{r}\times\mathbf{v}}{r}\frac{dV(r)}{dr} = -\frac{1}{em_e c^2 r}\frac{dV(r)}{dr}\mathbf{l}\ .$$

The advantage of introducing the potential V is, that this expression also holds for more complicated atoms with many electrons, where the potential may deviate considerably from the Coulombian potential. Note, that the magnetic field is very strong, $B \simeq \xi(a_B)\hbar/\mu_B \approx 5$ T. Inserting the magnetic field into Pauli's expression (29.94) together with the magnetic moment of the spin (29.96),

$$\hat{H}_{\ell s} = -\vec{\mu}_s\cdot\vec{\mathcal{B}}(\mathbf{0}) = \frac{1}{m_e^2c^2}\mathbf{s}\cdot\mathbf{l}\frac{1}{r}\frac{dV(r)}{dr}\ . \qquad (29.120)$$

where we still have to apply the corrective *Thomas factor* of $\frac{1}{2}$.

The interaction operator can be written,

$$\hat{H}_{\ell s} = \xi(r)\mathbf{l}\cdot\mathbf{s}\ , \qquad (29.121)$$

with the abbreviation,

$$\xi(r) \equiv \frac{-1}{2m_e^2c^2r}\frac{dV}{dr} = -\frac{Ze^2}{8\pi\varepsilon_0 m_e^2c^2}\frac{1}{r^3} = \frac{E_nZ^2\alpha^2n^2}{\hbar^2}\frac{1}{\tilde{r}^3}\ , \qquad (29.122)$$

with $\tilde{r} \equiv Zr/a_B$ and using the formulas (25.53).

After the introduction of the spin, the Hilbert space of the particles' wavefunctions must be extended. The wavefunctions are now products of spatial wavefunctions and spin eigenvectors:

$$|n,\ell,m_\ell,m_s\rangle = R_{n\ell}(r)Y_{\ell m}(\theta,\phi)\begin{pmatrix}s_1\\s_2\end{pmatrix}\ . \qquad (29.123)$$

The new Hilbert space is the tensorial product of position space and spin space. The *radial* Hamiltonian for the hydrogen atom including the centrifugal term and the spin-orbit coupling now takes the form:

$$\hat{H} = \frac{p^2}{2m} + V(r) + \frac{\mathbf{l}^2}{2m_e r^2} + \xi(r)\mathbf{l}\cdot\mathbf{s}\ . \qquad (29.124)$$

We may again consider the energy term $V_{\ell s}$ as a small perturbation, and calculate it using unperturbed wavefunctions,

$$\Delta E_{\ell s} = \langle n,\ell,s,m_\ell,m_s|V_{\ell s}|n,\ell,s,m_\ell,m_s\rangle = \langle n,\ell|\xi(r)|n,\ell\rangle\langle\ell,s,m_\ell,m_s|\mathbf{s}\cdot\mathbf{l}|\ell,s,m_\ell,m_s\rangle\ . \qquad (29.125)$$

Assuming a Coulombian potential, we first look at the radial part (29.122), which can easily be calculated using the formulae (25.53),

$$\langle n,\ell|\xi(r)|n,\ell\rangle = \frac{E_nZ^2\alpha^2n^2}{\hbar^2}\frac{1}{n^3\ell(\ell+\frac{1}{2})(\ell+1)}\ . \qquad (29.126)$$

To diagonalize the angular part of the Hamiltonian, we need the common wavefunctions of $\mathbf{l}^2$ and $\mathbf{l}\cdot\mathbf{s}$. We can rewrite the coupling term as:

$$\mathbf{l}\cdot\mathbf{s} = \tfrac{1}{2}(\mathbf{j}^2 - \mathbf{l}^2 - \mathbf{s}^2) \ . \tag{29.127}$$

In the common eigensystem of $\mathbf{j}^2$, $\mathbf{l}^2$, and $\mathbf{s}^2$ the Hamiltonian, therefore, is diagonal. We know the basis of this system from the theory of the addition of angular momenta. The states of the basis are linear combinations of the functions $|n,\ell,m_\ell,m_s\rangle$. Since the spins precess around each other, ℓ_z and s_z are not good observables, the non-coupled base is not appropriate. But $\mathbf{s}^2$, $\mathbf{l}^2$, and $\mathbf{j}^2$ are good observables. In the coupled basis $\{n,(\ell,s)j,m_j\}$,

$$\langle n,(\ell,s)j,m_j|\mathbf{s}\cdot\mathbf{l}|n,(\ell,s)j,m_j\rangle = \tfrac{\hbar^2}{2}[j(j+1)-\ell(\ell+1)-s(s+1)] \ . \tag{29.128}$$

Since $j=\ell\pm 1/2$, we find that every level splits into two levels, one with the energy $E_{n\ell}+\ell\zeta_{n\ell}$ and the degeneracy $2\ell+2$ and the other with the degeneracy $E_{n\ell}-(\ell+1)\zeta_{n\ell}$ with the degeneracy 2ℓ, where we introduced the abbreviation,

$$\zeta_{n\ell} \equiv \tfrac{\hbar^2}{2}\langle\xi(r)\rangle \ . \tag{29.129}$$

All in all, we get an energy correction due to the spin-orbit interaction of,

$$\boxed{\Delta E_{\ell s} = -E_n(Z\alpha)^2\frac{j(j+1)-\ell(\ell+1)-\frac{3}{4}}{2n\ell(\ell+1/2)(\ell+1)}} \ . \tag{29.130}$$

Note, that the coupling $\mathbf{l}\cdot\mathbf{s}$ lifts the degeneracy with respect to $\mathbf{l}$, but not with respect to ℓ_z (see Fig. 29.1). As we have already seen in Exc. 29.1.5.6, in the presence of an energy associated with the coupling $\mathbf{l}\cdot\mathbf{s}$, only the total angular momentum $\mathbf{l}+\mathbf{s}$ is a constant of motion.

29.2.3 Non-local electron-core interaction

Let us now discuss the third correction in the expression (29.108). The electron-nucleus interaction that we have considered so far is *local*, that is, the interaction at the point $\mathbf{r}$ sensed by the electron depends essentially on the field at that point in space. However, when relativistic theory is correctly applied, the electron-nucleus interaction becomes *non-local*, and the electron is then affected by all values of the nuclear field in a region around $\mathbf{r}$ [12]. The size of this region is of the order of the *Compton wavelength* of the electron, $\lambda_C/2\pi \equiv \hbar/m_e c$. This correction was introduced by *Sir Charles Galton Darwin* through a substitution in the Dirac equation that solved the problem of normalization of the wavefunction.

Imagine that instead of the potential $V(\mathbf{r})$, the potential of the electron is given by the integral,

$$\int f(r')V(\mathbf{r}+\mathbf{r}')d^3r' \ , \tag{29.131}$$

[12] The smearing out of the electron's position is also known as *Zitterbewegung*. See Exc. 29.1.5.2.

where $f(r')$ is a radially symmetric and normalized density-type function that takes significant values only in the vicinity of $\mathbf{r}$ within a volume $(\lambda_C/2\pi)^3$ centered at $\mathbf{r}' = 0$. Expanding the potential $V(\mathbf{r}+\mathbf{r}')$ near the origin,

$$V(\mathbf{r}+\mathbf{r}') = V(\mathbf{r}) + [\mathbf{r}'\cdot\nabla_r]V(\mathbf{r}) + \tfrac{1}{2!}[\mathbf{r}'\cdot\nabla_r]^2 V(\mathbf{r}) + \dots\ , \tag{29.132}$$

and inserting into the integral,

$$\begin{aligned}&\int f(r')V(\mathbf{r}+\mathbf{r}')d^3r' \\ &= V(\mathbf{r})\int f(r')d^3r' + \int \mathbf{r}' f(r')d^3r'\cdot\nabla_r V(\mathbf{r}) + \tfrac{1}{2!}\int r'^2 f(r')[\hat{\mathbf{e}}_{r'}\cdot\nabla_r]^2 d^3r' V(r) + \dots \\ &= V(\mathbf{r}) + 0 + \tfrac{1}{2!}\int r'^2 f(r')d^3r'\nabla^2 V(r) + \dots\ .\end{aligned} \tag{29.133}$$

The second term is null due to the parity of $f(r')$ and the third produces the Darwin correction using $V(\mathbf{r}) = V(r)$. Letting the function be constant within the volume, $f(\mathbf{r}) \simeq f_0$, and with the normalization,

$$1 = \int_{-\hbar/2m_ec}^{\hbar/2m_ec}\int_{-\hbar/2m_ec}^{\hbar/2m_ec}\int_{-\hbar/2m_ec}^{\hbar/2m_ec} f(r)dxdydz = f_0\left(\frac{\hbar}{m_ec}\right)^3\ , \tag{29.134}$$

we get the integral

$$\int r^2 f(r)d^3r = \int_{-\hbar/2m_ec}^{\hbar/2m_ec}\int_{-\hbar/2m_ec}^{\hbar/2m_ec}\int_{-\hbar/2m_ec}^{\hbar/2m_ec} f(r)r^2 dxdydz = \left(\frac{\hbar}{2m_ec}\right)^2\ . \tag{29.135}$$

Also,

$$\nabla^2 V(\mathbf{r}) = -e\nabla^2\frac{Ze}{4\pi\varepsilon_0 r} = -e\frac{\varrho(\mathbf{r})}{\varepsilon_0} = -\frac{Ze^2\delta^3(\mathbf{r})}{\varepsilon_0}\ . \tag{29.136}$$

Hence,

$$\int f(r')V(\mathbf{r}+\mathbf{r}')d^3r' = -\frac{Ze^2}{4\pi\varepsilon_0 r} + \frac{\pi\hbar^2}{2m_e^2c^2}\frac{Ze^2}{4\pi\varepsilon_0}\delta^3(\mathbf{r}) + \dots\ , \tag{29.137}$$

which is precisely the electrostatic energy with the Darwin correction in the expressions (29.85) and (29.108).

To estimate the importance of this effect we inserting the wavefunctions (25.52) evaluated at the origin,

$$\begin{aligned}\langle\hat{H}_{dw}\rangle &= \int d^3r\psi^*_{n\ell m}(\mathbf{r})\frac{\pi\hbar^2}{2m_e^2c^2}\frac{Ze^2}{4\pi\varepsilon_0}\delta^3(\mathbf{r})\psi_{n\ell m}(\mathbf{r}) \\ &= \frac{\pi\hbar^2}{2m_e^2c^2}\frac{Ze^2}{4\pi\varepsilon_0}|\psi_{n00}(0)|^2\delta_{\ell 0}\delta_{m0} = \frac{\pi\hbar^2}{2m_e^2c^2}\frac{Ze^2}{4\pi\varepsilon_0}\frac{Z^3}{\pi n^3 a_B^3}\delta_{\ell 0}\ .\end{aligned} \tag{29.138}$$

We obtain,

$$\frac{H_{dw}}{H_0} = \frac{\frac{\pi\hbar^2}{2m_e^2c^2}\frac{Ze^2}{4\pi\varepsilon_0}\frac{1}{\pi a_B^3}}{\frac{e^2}{4\pi\varepsilon_0 a_B}} = \frac{\hbar^2}{2m_e^2c^2}\frac{Z}{a_B^2} = \frac{\alpha^2}{2} \approx 0.01\%\ . \tag{29.139}$$

Darwin's correction vanishes for angular momentum $\mathbf{l} > 0$, such that,

$$\boxed{\Delta E_{dw} = \langle\hat{H}_{dw}\rangle = -E_n\frac{(Z\alpha)^2}{n}\delta_{\ell 0}\ .} \tag{29.140}$$

29.2.4 Summary of the corrections

Combining the $\mathbf{l}\cdot\mathbf{s}$ and relativistic corrections, we obtain,

$$\begin{aligned}\Delta E_{fs} &= \Delta E_{rl} + \Delta E_{\ell s} + \Delta E_{dw} \qquad (29.141)\\ &= E_n(Z\alpha)^2\left[\frac{1}{n(\ell+\frac{1}{2})} - \frac{3}{4n^2}\right] - E_n(Z\alpha)^2\frac{j(j+1)-\ell(\ell+1)-\frac{3}{4}}{2n\ell(\ell+\frac{1}{2})(\ell+1)} - E_n(Z\alpha)^2\\ &= E_n(Z\alpha)^2\begin{cases}\frac{1}{nj} - \frac{3}{4n^2} - \frac{j(j+1)-(j-\frac{1}{2})(j+\frac{1}{2})-\frac{3}{4}}{2n(j-\frac{1}{2})j(j+\frac{1}{2})} - 1 & \text{para} \quad \ell = j-\frac{1}{2}\\ \frac{1}{n(j+1)} - \frac{3}{4n^2} - \frac{j(j+1)-(j+\frac{1}{2})(j+\frac{3}{2})-\frac{3}{4}}{2n(j+\frac{1}{2})(j+1)(j+\frac{3}{2})} - 1 & \text{para} \quad \ell = j+\frac{1}{2}\end{cases}\\ &= E_n(Z\alpha)^2\left[\frac{1}{n(j+\frac{1}{2})} - \frac{3}{4n^2} - 1\right] .\end{aligned}$$

That is, the levels are now degenerate in j (see Fig. 29.1) [13]. Obviously the levels which are most affected by relativistic corrections are those with low values of n and ℓ.

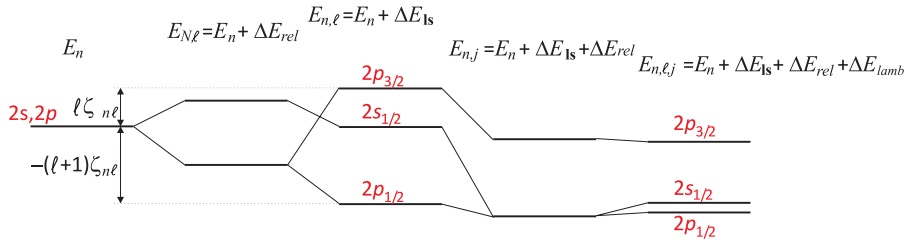

Figure 29.1: Hydrogen levels.

The levels are labeled by $n\ell_j$. For example, the state $3d_{5/2}$ has the main quantum number $n=3$, the orbital angular momentum $\ell=2$, and the total angular momentum $j=5/2$. For large n or j the fine structure disappears. The new energy scheme is shown in Fig. 29.1. We note that, taking into account all relativistic corrections (but without the Lamb shift), we still have a partial degeneracy of the quantum number j. For example, the states $^2s_{1/2}$ and $^2p_{1/2}$ have the same energy. This is a particularity of the hydrogen atom.

29.2.5 Lamb shift

Only remains to discuss the fourth correction, $\hat{H}_{lamb}$ in the expression (29.6). The origin of the *Lamb shift* lies in quantum electrodynamics. Being due to the quantum nature of the electromagnetic field, this correction is not predicted within the Dirac equation.

We may imagine the Coulomb force between charged particles being mediated by a continuous exchange of virtual photons. But each isolated charge also continuously emits and reabsorbs virtual photons, with the result that the position of the electron is smeared over a region of 0.1 fm. This reduces the overlap between the electronic

[13] It is interesting that the quantum treatment presented here, including relativistic corrections, coincidentally agrees with the corrections of *Arnold Johannes Wilhelm Sommerfeld*.

orbits and the nucleus. Hence, the Lamb shift causes corrections that are stronger for small n and small ℓ. For example in hydrogen, the $2p_{1/2}$ is $4.4 \cdot 10^{-6}\,\mathrm{eV} = 1\,\mathrm{GHz}$ below the $2s_{1/2}$ (see Fig. 29.1).

29.2.6 Exercises

29.2.6.1 Ex: The Darwin term

Show that the expressions for the Darwin correction (29.85) and (29.108) are equivalent.

Solution: *The Darwin term in (29.85) is given as,*

$$\hat{H}_{dw} = -\frac{\hbar^2 e}{4m_e^2c^2}\frac{\partial U(r)}{\partial r}\frac{\partial}{\partial r} = -\frac{\hbar^2 e}{4m_e^2c^2}\nabla U(r)\cdot\nabla \ .$$

The expectation value is,

$$\begin{aligned}\langle H_{dw}\rangle &= \int \psi^*(r)\nabla U(r)\cdot\nabla\psi(r)d^3r = \cancelto{0}{\int \nabla\psi^*(r)U(r)\psi(r)dS} - \int \nabla\left[\psi^*(r)\nabla U(r)\right]\psi(r)d^3r \\ &= -\int \left[\nabla\psi^*(r)\right]\nabla U(r)\psi(r)d^3r - \int \psi^*(r)\left[\nabla^2 U(r)\right]\psi(r)d^3r \ .\end{aligned}$$

Hence,

$$\int \psi^*(r)\nabla U(r)\cdot\nabla\psi(r)d^3r = -\tfrac{1}{2}\int \psi^*(r)\left[\nabla^2 U(r)\right]\psi(r)d^3r \ .$$

Therefore, we can rewrite the Darwin term as,

$$\hat{H}_{dw} = -\frac{1}{2}\frac{-\hbar^2}{4m_e^2c^2}\nabla^2 eU = \frac{\hbar^2}{8m_e^2c^2}\frac{-Ze^2}{\varepsilon_0}\delta^3(\mathbf{r}) = \frac{\pi\hbar^2}{2m_e^2c^2}\frac{Ze^2}{4\pi\varepsilon_0}\delta^3(\mathbf{r}) \ .$$

29.3 Hyperfine structure

Rutherford's measurements suggested a point-like and infinitely heavy atomic nucleus. In fact, the mass is finite and the nuclear charge is distributed over a finite volume and often in a non-isotropic manner, which leads to multipolar interactions with the electrons. In addition, many nuclei have a spin that can interact with the magnetic moment of the electrons. The energy corrections due to these effects are called *hyperfine structure* [14].

Because many of the following considerations will remain valid for many-electron systems to be discussed later, we will switch to a notation denoting by $\mathbf{L}$ the total orbital angular momentum of the electronic shell, $\mathbf{S}$ the total spin of the electronic shell, and $\mathbf{J}$ the total angular momentum of the electronic shell, remembering that for hydrogen $\mathbf{S} = \frac{\hbar}{2}\vec{\sigma}$.

[14] See [276] p. 1229 and [1329] p. 23 for further reading.

29.3.1 Coupling to the nuclear spin

29.3.1.1 Dipole moment of the nuclear spin

The nucleus may also have an angular momentum interacting with the angular momentum of the electrons. However, the momentum depends inversely on the masses. That is, the angular momentum of the nucleus is $\mu_N/\mu_B = m_e/m_p \simeq 10^{-3}$ times smaller, where $\mu_N = \hbar e/2m_p$ is an abbreviation called *nuclear magneton*. Thus, we can assume that the interaction between the nucleus and the electron will not interfere with the $\mathbf{L}\cdot\mathbf{S}$-coupling between the orbital angular momentum and the spin of the electron. The spin of the nucleus will be oriented along the total momentum of the electrons $\mathbf{J}$. However, this interaction will have the ability to lift the hydrogen degeneracy, even though the *splitting* will only be *hyperfine*. Indeed, the order of magnitude of *hyperfine splitting* is 10^{-6} eV.

Analogously to the expressions (29.93) and (29.96), we write the dipole moment of the nucleus,

$$\boxed{\frac{\vec{\mu}_I}{\mu_N} = \frac{e}{2m_p\mu_N} g_p \mathbf{I} = g_p \frac{\mathbf{I}}{\hbar}} \,, \tag{29.142}$$

where $g_p \equiv \mu_I/I$ is once again a factor taking into account possible corrections between the classical derivation and quantum mechanics [15].

29.3.1.2 Hyperfine splitting

In the derivation of the Pauli equation (29.89) from the Dirac equation (29.76) we discarded non-relativistic terms and reintroduced electronic spin-orbit coupling by hand allowing for $\mathbf{A}(\mathbf{r},t) \neq 0$. By an analogous calculation directly applied to the Dirac equation we may unravel the *hyperfine structure*. Instead of setting the vector potential to $\mathbf{A}(\mathbf{r},t) = 0$, as we did in (29.45), we now generalize the Dirac equation (29.76),

$$E'\vec{\phi} = qU(\mathbf{r})\vec{\phi} + \vec{\sigma}\cdot\vec{\pi}\frac{1}{2m_e}\left(1 + \frac{E'-U(\mathbf{r})}{2m_ec^2}\right)^{-1}\vec{\sigma}\cdot\vec{\pi}\vec{\phi} \,. \tag{29.143}$$

Assuming $\langle q\mathbf{A}\rangle \ll \langle \mathbf{p}\rangle$, we may only retain terms to the lowest order in $\mathbf{A}$ and neglect terms containing $q\mathbf{A}\frac{E'-U(\mathbf{r})}{2m_ec^2}$. Using the result of the calculation (29.87),

$$(\vec{\sigma}\cdot\vec{\pi})(\vec{\sigma}\cdot\vec{\pi}) = [\mathbf{p} - q\mathbf{A}]^2 - \hbar q\vec{\sigma}\cdot\vec{\mathcal{B}} \,, \tag{29.144}$$

we find the generalization of the total energy (29.85),

$$\hat{H} \simeq \frac{[\mathbf{p}-q\mathbf{A}(\mathbf{r})]^2}{2m_e} - \frac{1}{4\pi\varepsilon_0}\frac{e^2}{r} - \frac{\mathbf{p}^4}{8m_e^3c^2} - \frac{e}{2m_e^2c^2}\frac{1}{r}\frac{\partial U}{\partial r}\mathbf{S}\cdot\mathbf{L} - \frac{\hbar^2 e}{4m_e^2c^2}\frac{\partial U}{\partial r}\frac{\partial}{\partial r} - \frac{\hbar q}{2m_e}\vec{\sigma}\cdot\vec{\mathcal{B}}(\mathbf{r}) \,, \tag{29.145}$$

and expanding the bracket

$$[\mathbf{p}-q\mathbf{A}]^2 \simeq \mathbf{p}^2 - q\mathbf{p}\cdot\mathbf{A} - q\mathbf{A}\cdot\mathbf{p} = \mathbf{p}^2 - 2q\mathbf{A}\cdot\mathbf{p} \tag{29.146}$$

[15] In fact, the proton factor g is anomalous, $g_p = 5.58$, which reduces the fraction μ_l/μ_I. For the neutron we have: $g_n = -3.83$

in the Coulomb gauge, we see that two new terms are added to the energy called the hyperfine structure,

$$\boxed{\begin{array}{rcl} \hat{H} & = & \hat{H}_B + \hat{H}_{fs} + \hat{H}_{hfs} \\ \text{with} \quad \hat{H}_{hfs} & = & \hat{H}_{LI} + \hat{H}_{SI} = \frac{e}{m_e}\mathbf{A}(\mathbf{r})\cdot\mathbf{p} + \frac{2\mu_B}{\hbar}\mathbf{S}\cdot\vec{\mathcal{B}}(\mathbf{r}) \end{array}} \ , \tag{29.147}$$

with $\vec{\mu}_S = -\frac{e}{m_e}\mathbf{S}$.

Up to now we did not say anything about the origin of the magnetic field. We only notice that any magnetic field will interact with the electron's orbit and with its spin. We now make use of our knowledge that the proton has a spin of its own which produces, at the position of the electrons, a magnetic vector potential,

$$\mathbf{A}(\mathbf{r}) = \frac{\mu_0}{4\pi}\frac{\vec{\mu}_I \times \mathbf{r}}{r^3} \ , \tag{29.148}$$

interacting with the angular momentum of the electron $\mathbf{L}$ in the form,

$$\begin{aligned} \hat{H}_{LI} &= \frac{e}{m_e}\mathbf{A}\cdot\hat{\mathbf{p}} = \frac{e}{m_e}\frac{\mu_0}{4\pi r^3}(\vec{\mu}_I \times \mathbf{r})\cdot\mathbf{p} \\ &= \frac{e}{m_e}\frac{\mu_0}{4\pi r^3}\frac{\mu_N}{\hbar}g_p(\mathbf{I}\times\mathbf{r})\cdot\mathbf{p} = \frac{\mu_0}{2\pi r^3}\frac{\mu_B}{\hbar}\frac{\mu_N}{\hbar}g_p\mathbf{L}\cdot\mathbf{I} \ , \end{aligned} \tag{29.149}$$

using the definition of Bohr's magneton.

In addition, the potential vector (29.148) generated by the nuclear spin produces a magnetic field [659],

$$\vec{\mathcal{B}} = \nabla\times\mathbf{A} = \frac{\mu_0}{4\pi r^3}\left[3(\vec{\mu}_I\cdot\hat{\mathbf{r}})\hat{\mathbf{r}} - \vec{\mu}_I\right] + \tfrac{2}{3}\mu_0\vec{\mu}_I\delta^3(\mathbf{r}) \ , \tag{29.150}$$

as will be shown in Exc. 29.3.3.1. This field interacts with the spin of the electron $\mathbf{S}$ in the form,

$$\begin{aligned} \hat{H}_{SI} &= -\vec{\mu}_S\cdot\vec{\mathcal{B}} = -\frac{\mu_0}{4\pi r^3}\left[3(\vec{\mu}_I\cdot\hat{\mathbf{r}})(\vec{\mu}_S\cdot\hat{\mathbf{r}}) - (\vec{\mu}_S\cdot\vec{\mu}_I)\right] - \tfrac{2}{3}\mu_0\vec{\mu}_S\cdot\vec{\mu}_I\delta^3(\mathbf{r}) \\ &= \frac{\mu_0}{4\pi r^3}\frac{\mu_B}{\hbar}g_e\frac{\mu_N}{\hbar}g_p\left[3(\mathbf{I}\cdot\hat{\mathbf{r}})(\mathbf{S}\cdot\hat{\mathbf{r}}) - (\mathbf{S}\cdot\mathbf{I})\right] + \tfrac{2}{3}\mu_0 g_e\mu_B\frac{\mathbf{S}}{\hbar}\cdot g_p\mu_N\frac{\mathbf{I}}{\hbar}\delta^3(\mathbf{r}) \ , \end{aligned} \tag{29.151}$$

inserting the expressions (29.96) and (29.142). The first term gives the energy of the nuclear dipole in the field due to the electronic orbital angular momentum. The second term gives the energy of the 'finite distance' interaction of the nuclear dipole with the field due to the electron spin magnetic moments. The final term, often known as the *Fermi contact term* relates to the direct interaction of the nuclear dipole with the spin dipoles and is only non-zero for states with a finite electron spin density at the position of the nucleus (those with unpaired electrons in s-subshells).

We now discuss the two cases in which $L = 0$ or $L \neq 0$ separately in the following subsections [276, 1128, 659].

29.3.1.3 Orbital angular momentum $L = 0$

For vanishing orbital angular momenta, $L = 0$, we only need to consider the contribution $\hat{H}_{SI}$. Furthermore, this contribution will be dominated by the Dirac term,

because the s-orbitals have a high probability at the nuclear region, but fall off quickly at larger distances. Hence,

$$\hat{H}_{SI} \simeq \tfrac{2}{3}\mu_0 g_e \mu_B \frac{\mathbf{S}}{\hbar} \cdot g_p \mu_N \frac{\mathbf{I}}{\hbar} \delta^3(\mathbf{r}) \ . \tag{29.152}$$

Defining the complete total angular momentum of the atom,

$$\mathbf{F} \equiv \mathbf{I} + \mathbf{S} \ , \tag{29.153}$$

we calculate from (29.151),

$$\begin{aligned} \Delta E^{\ell=0}_{hfs} &= \langle (S,I)F, m_F | \hat{H}_{SI} | (S,I)F, m_F \rangle = \frac{2\mu_0 g_e g_p \mu_B \mu_N}{3\hbar^2} \langle \mathbf{S}\cdot\mathbf{I} \rangle \langle \delta^3(\mathbf{r}) \rangle \qquad (29.154) \\ &= \tfrac{2}{3}\mu_0 g_e g_p \mu_B \mu_N [F(F+1) - I(I+1) - S(S+1)] \int \psi^*_{n00}(\mathbf{r}) \delta^3(\mathbf{r}) \psi_{n00}(\mathbf{r}) d^3r \\ &= \tfrac{2}{3}\mu_0 g_e g_p \mu_B \mu_N [F(F+1) - I(I+1) - S(S+1)] \left| \tfrac{1}{\sqrt{\pi}} \left(\tfrac{Z}{n a_B} \right)^{3/2} \right|^2 \ . \end{aligned}$$

As an example consider the hyperfine structure of the state $1s_{1/2}$ of the hydrogen atom. With $J = I = \frac{1}{2}$ and $Z = n = 1$ we obtain (see Exc. 29.3.3.2),

$$\begin{aligned} \Delta E^{L=0}_{hfs}(F=1) - \Delta E^{\ell=0}_{hfs}(F=0) &= \tfrac{2}{3}\mu_0 g_e \mu_B g_p \mu_N \ 2 \ \tfrac{1}{\pi} \left(\tfrac{Z}{n a_B} \right)^3 \qquad (29.155) \\ &= \frac{2 g_e g_p m_e^2 c^2}{3 m_p} \alpha^4 \approx (2\pi\hbar) \cdot 1.420 \, \text{GHz} \ . \end{aligned}$$

The experimental value is 1.4204057518 GHz. This frequency corresponds to the spectral line used in radio astronomy, where the measurement of the angular distribution of this radiation allows the mapping of the spatial distribution of interstellar hydrogen.

29.3.1.4 Orbital angular momenta $L \neq 0$

In the case $L \neq 0$ both contributions, $\hat{H}_{SI}$ and $\hat{H}_{LI}$ have to be considered, however, we may neglect the Dirac term, because the orbitals with orbital angular momentum have vanishing probabilities at the nuclear region. Combining the two terms (29.149) and (29.151), we obtain,

$$\begin{aligned} \hat{H}_{JI} = \hat{H}_{LI} + \hat{H}_{SI} &= \frac{\mu_0}{4\pi r^3} \frac{\mu_B}{\hbar} g_e \frac{\mu_N}{\hbar} g_p \left[3(\mathbf{I}\cdot\hat{\mathbf{r}})(\mathbf{S}\cdot\hat{\mathbf{r}}) + \mathbf{L}\cdot\mathbf{I} - \mathbf{S}\cdot\mathbf{I} \right] \qquad (29.156) \\ &= \frac{\mu_0}{4\pi r^3} \frac{\mu_B}{\hbar} g_e \frac{\mu_N}{\hbar} g_p \mathbf{N}\cdot\mathbf{I} \ , \end{aligned}$$

introducing $\mathbf{N}$ as a quantity that only depends on the electronic shell:

$$\mathbf{N} \equiv 3(\mathbf{S}\cdot\hat{\mathbf{r}})\hat{\mathbf{r}} + \mathbf{L} - \mathbf{S} \ . \tag{29.157}$$

Generalizing the complete total angular momentum of the atom (29.153),

$$\mathbf{F} \equiv \mathbf{I} + \mathbf{J} \ , \tag{29.158}$$

is useful for calculating the coupling $\mathbf{I}\cdot\mathbf{J} = \frac{1}{2}(\mathbf{F}^2 - \mathbf{I}^2 - \mathbf{J}^2)$. Now, as the $\mathbf{L}\cdot\mathbf{S}$-coupling is strong, we project the two angular momenta onto the total electronic angular momentum $\mathbf{J}$,

$$\mathbf{N} \longrightarrow \frac{\mathbf{N}\cdot\mathbf{J}}{|\mathbf{J}|}\frac{\mathbf{J}}{|\mathbf{J}|} \quad , \qquad \mathbf{I} \longrightarrow \frac{\mathbf{I}\cdot\mathbf{J}}{|\mathbf{J}|}\frac{\mathbf{J}}{|\mathbf{J}|} \; . \tag{29.159}$$

We get for the coupling between the projected spins (29.159) of the electronic layer and the nucleus,

$$\mathbf{N}\cdot\mathbf{I} \longrightarrow \frac{(\mathbf{N}\cdot\mathbf{J})(\mathbf{I}\cdot\mathbf{J})}{|\mathbf{J}|^2} = \frac{(\mathbf{N}\cdot\mathbf{J})(\mathbf{F}^2 - \mathbf{I}^2 - \mathbf{J}^2)}{2|\mathbf{J}|^2} \; . \tag{29.160}$$

We calculate

$$\begin{aligned}\Delta E_{hfs}^{L\neq 0} &= \langle((L,S)J,I)F,m_F|\hat{H}_{JI}|((L,S)J,I)F,m_F\rangle \qquad (29.161)\\ &= \frac{\mu_0}{4\pi}\frac{\mu_B}{\hbar}g_e\frac{\mu_N}{\hbar}g_p\left\langle\frac{\mathbf{N}\cdot\mathbf{I}}{r^3}\right\rangle \\ &\longrightarrow \frac{\mu_0}{4\pi}\frac{\mu_B}{\hbar}g_e\frac{\mu_N}{\hbar}g_p\frac{\mathbf{N}\cdot\mathbf{J}[F(F+1)-I(I+1)-J(J+1)]}{2J(J+1)}\left(\frac{Z}{a_B}\right)^3\frac{n}{n^4L(L+\frac{1}{2})(L+1)} \; .\end{aligned}$$

Introducing the *interval factor*,

$$A_J \equiv \frac{\mu_0}{4\pi}\frac{\mu_B}{\hbar}g_e\frac{\mu_N}{\hbar}g_p\left(\frac{Z}{a_B}\right)^3\frac{\mathbf{N}\cdot\mathbf{J}}{2J(J+1)}\frac{n}{n^4L(L+\frac{1}{2})(L+1)} \; , \tag{29.162}$$

as a quantity that only depends on the electronic shell, we can write

$$\boxed{\Delta E_{hfs}^{L\neq 0} = \tfrac{A_J}{2}[F(F+1) - J(J+1) - I(I+1)]} \; . \tag{29.163}$$

Note, that the $\mathbf{J}\cdot\mathbf{I}$-coupling breaks the degeneracy of $\mathbf{J}$ in the hydrogen atom, but not of J_z. We can derive the following *interval rule*,

$$\Delta E_{F+1} - \Delta E_F = A_J(F+1) \; . \tag{29.164}$$

Besides the magnetic interaction between the angular momenta of the nucleus and the electronic shell there is an interaction between the nucleus, when it is not spherically symmetric, and the shell. This interaction causes deviations from the interval rule and an additional splitting of the hyperfine states.

29.3.2 Electric quadrupole interaction

The fact that the nucleus is not perfectly spherical gives rise to new electron-nucleus corrections that are called *quadrupolar interaction*. The starting point is,

$$\hat{H}_{qud} = -\frac{1}{4\pi\epsilon_0}\frac{e^2}{|\mathbf{r}_e - \mathbf{r}_N|} - \frac{1}{4\pi\epsilon_0}\frac{e^2}{|\mathbf{r}_e|} \; , \tag{29.165}$$

where $\mathbf{r}_e$ is the electronic coordinate and $\mathbf{r}_N$ is the nuclear coordinate, both having their origin in the center mass of the nucleus. For $\mathbf{r}_e > \mathbf{r}_N$ this interaction can be obtained after several mathematical steps as [860],

$$\hat{H}_{qud} = B_J \frac{3(\hat{\mathbf{I}}\cdot\hat{\mathbf{J}})(2\hat{\mathbf{I}}\cdot\hat{\mathbf{J}}+1) - 2\hat{\mathbf{I}}^2\hat{\mathbf{J}}^2}{2I(I-1)2J(J-1)} \ , \tag{29.166}$$

where B_J is called the *constant of the quadrupolar electron-nucleus interaction*. With this expression we can calculate,

$$\Delta E_{qud} = \langle IJKm_K|\hat{H}_{qud}|IJKm_K\rangle = B_J \frac{\frac{3}{2}K(K+1) - 2I(I+1)J(J+1)}{2I(2I-1)2J(2J-1)} \ , \tag{29.167}$$

where $K \equiv 2\langle\hat{\mathbf{J}}\cdot\hat{\mathbf{I}}\rangle = F(F+1) - I(I+1) - J(J+1)$. It is important to remember that a nucleus with $I = 0$ or $I = \frac{1}{2}$ has no quadrupole moment, $B_J = 0$. Also for $J = \frac{1}{2}$ there will be no contribution.

Joining the contributions $\hat{\mathbf{J}}\cdot\hat{\mathbf{I}}$ of Eq. (29.163) and the quadrupolar contribution (29.167), the hyperfine structure can be described by,

$$\begin{aligned}\Delta E_{hfs} &= \Delta E_{JI} + \Delta E_{qud} \\ &= \frac{A_J}{2}K + \frac{B_J}{8IJ(2I-1)(2J-1)}[3K(K+1) - 4I(I+1)J(J+1)] \ ,\end{aligned} \tag{29.168}$$

where the constants A_J and B_J depend on the atom and the total electronic angular momentum.

Table 29.1: List of atomic data [1245] showing the natural linewidth of the D_2 line, frequencies of the D_1 and D_2 lines, and the hyperfine splitting.

Element	$\gamma_{D2}/2\pi$	$D1$	$D2$	$\nu_{HFS}[S_{1/2}]$
	[MHz]	[cm^{-1}]	[cm^{-1}]	[MHz]
^{1}H	99.58	82264.000	82264.366	1420.4
^{2}H	99.58	82264.000	82264.366	
^{6}Li	5.92	14901.000	14901.337	228.2
^{7}Li	5.92	14901.000	14901.337	803.5
^{23}Na	10.01	16956.000	16973.190	1771.6
^{39}K	6.09	12985.170	13042.876	461.7
^{40}K	6.09	12985.170	13042.876	-1285.8
^{41}K	6.09	12985.170	13042.876	254.0
^{85}Rb	5.98	12578.920	12816.469	3035.7
^{87}Rb	5.98	12578.920	12816.469	6834.7
^{133}Cs	5.18	11182.000	11737.000	9192.6
^{135}Cs	5.18	11182.000	11737.000	

In Excs. 29.3.3.3 and 29.3.3.4 we determine the hyperfine structures of sodium and rubidium atoms.

29.3.3 Exercises

29.3.3.1 Ex: Field of a magnetic moment

a. Calculate the vector potential $\mathbf{A}(\mathbf{r})$ and the magnetic dipole moment $\vec{\mu}$ produced by an orbiting electron by Biot-Savart's law using the expansion of $|\mathbf{r}-\mathbf{r}'|^{-1}$ in Legendre polynomials.
b. Calculate the magnetic field $\vec{\mathcal{B}}(\mathbf{r})$.

Solution: *a. We parametrize the current of a loop around the z-axis by,*

$$\mathbf{j}(\mathbf{r}') = I\hat{e}_\phi \delta(z')\delta(\rho' - R) \ .$$

With this, the vector potential is,

$$\mathbf{A}(\mathbf{r}) = \frac{\mu_0}{4\pi}\int_V \frac{\mathbf{j}(\mathbf{r}')}{|\mathbf{r}-\mathbf{r}'|}d^3r' = \frac{\mu_0 I}{4\pi}\int_V \frac{\delta(z')\delta(\rho'-R)}{|\mathbf{r}-\mathbf{r}'|}d\rho'\hat{\mathbf{e}}_{\phi'}\rho' d\phi' dz' = \frac{\mu_0 I}{4\pi}\oint_C \frac{d\mathbf{s}'}{|\mathbf{r}-\mathbf{r}'|} \ ,$$

using $\hat{\mathbf{e}}_{\phi'}\rho' d\phi' = d\mathbf{s}'$. *We expand the integral in terms of Legendre polynomials,*

$$\frac{1}{|\mathbf{r}-\mathbf{r}'|} = \frac{1}{\sqrt{r^2+r'^2-2rr'\cos\theta'}} = \frac{1}{r\sqrt{1-2\frac{r'}{r}\cos\theta'+\frac{r'^2}{r^2}}} = \frac{1}{r}\sum_{n=0}^{\infty} P_n(\cos\theta')\left(\frac{r'}{r}\right)^n \ ,$$

Table 29.2: Hyperfine constants of some alkaline atoms.

atom	n	$A_J(n^2S_{1/2})$	$A_J(n^2P_{1/2})$	$A_J(n^2P_{3/2})$	$B_J(n^2P_{3/2})$
		[MHz·h]	[MHz·h]	[MHz·h]	[MHz·h]
^{1}H, $I=\frac{1}{2}$	1	1420	46.17	−3.07	−0.18
^{7}Li, $I=\frac{3}{2}$	2	401.75	46.17	−3.07	−0.18
	3		13.5	−0.96	
^{23}Na, $I=\frac{3}{2}$	3	885.82	94.3	18.65	2.82
	4	202	28.85	6.00	0.86
^{85}Rb, $I=\frac{5}{2}$	5	1011.9	120.7	25.029	26.03
	6	239.3	39.11	8.25	8.16
^{87}Rb, $I=\frac{3}{2}$	5	3417.3	409.1	84.852	12.510
	6	809.1	132.5	27.70	3.947

where θ' is the angle between the vectors $\mathbf{r}$ and $\mathbf{r}'$ and $r'=\rho'$. With this, the vector potential is,

$$\mathbf{A}(\mathbf{r})=\frac{\mu_0 I}{4\pi}\sum_{n=0}^{\infty}\frac{1}{r^{n+1}}\oint_C P_n(\cos\theta')r'^n d\mathbf{s}'=\frac{\mu_0 I}{4\pi r}\oint_C 1 d\mathbf{s}'+\frac{\mu_0 I}{4\pi r^2}\oint_C r'\cos\theta' d\mathbf{s}'+\dots\ .$$

The monopole term vanishes, while the dipole term is (considering a vector $\mathbf{r}$ within the x-y plane, such that $\theta'=\phi-\phi'$),

$$\mathbf{A}(\mathbf{r})=\frac{\mu_0 I}{4\pi}\frac{1}{r^2}\oint_C r'\cos(\phi-\phi')\hat{\mathbf{e}}_{\phi'}r'd\phi'=\frac{\mu_0 I}{4\pi r^2}R^2\oint_C\cos(\phi-\phi')\begin{pmatrix}-\sin\phi'\\ \cos\phi'\\ 0\end{pmatrix}d\phi'$$

$$=\frac{\mu_0}{4\pi}\frac{1}{r^3}I\pi R^2\begin{pmatrix}-r\sin\phi\\ r\cos\phi\\ 0\end{pmatrix}=\frac{\mu_0}{4\pi}\frac{\vec{\mu}\times\mathbf{r}}{r^3}\ ,$$

with

$$\mathbf{r}=\begin{pmatrix}r\sin\theta\cos\phi\\ r\sin\theta\sin\phi\\ r\cos\theta\end{pmatrix}\qquad\text{and}\qquad\vec{\mu}=I\pi R^2\hat{\mathbf{e}}_z\ .$$

b. The magnetic field is,

$$\vec{\mathcal{B}}=\nabla\times\mathbf{A}=\frac{\mu_0}{4\pi}\nabla\times\left(\vec{\mu}\times\frac{\mathbf{r}}{r^3}\right)=\tfrac{\mu_0}{4\pi}\left[\cancelto{0}{\left(\tfrac{\mathbf{r}}{r^3}\cdot\nabla\right)\vec{\mu}}-(\vec{\mu}\cdot\nabla)\tfrac{\mathbf{r}}{r^3}+\vec{\mu}\left(\nabla\cdot\tfrac{\mathbf{r}}{r^3}\right)-\cancelto{0}{\tfrac{\mathbf{r}}{r^3}(\nabla\cdot\vec{\mu})}\right]\ .$$

Now we calculate on one hand for the x-component of the first non-vanishing term,

$$(\vec{\mu}\cdot\nabla)\frac{x}{r^3}=\vec{\mu}\cdot\left(\nabla\frac{x}{r^3}\right)=\vec{\mu}\cdot\left(x\nabla\frac{1}{r^3}+\frac{1}{r^3}\nabla x\right)=\vec{\mu}\cdot\left(x\hat{\mathbf{e}}_r\frac{\partial}{\partial r}\frac{1}{r^3}+\frac{1}{r^3}\hat{\mathbf{e}}_x\right)=\vec{\mu}\cdot\left(x\hat{\mathbf{e}}_r\frac{-3}{r^4}+\frac{1}{r^3}\hat{\mathbf{e}}_x\right)\ ,$$

so that,

$$-(\vec{\mu}\cdot\nabla)\frac{\mathbf{r}}{r^3} = \frac{1}{r^3}\left[3(\vec{\mu}\cdot\hat{\mathbf{e}}_r)\hat{\mathbf{e}}_r - \vec{\mu}\right] \ .$$

However, this result only holds for $r > 0$, because the derivation only holds for this case. For $r > 0$ the other term vanishes,

$$\vec{\mu}\left(\nabla\cdot\frac{\mathbf{r}}{r^3}\right) = \vec{\mu}4\pi\delta^3(\mathbf{r}) \longrightarrow 0 \ .$$

The problem can be resolved by noticing that the average magnetic field on a finite sized sphere is known, and that the field must be obtained by volume integration of $\vec{\mathcal{B}}_{dip}(\mathbf{r})$ even in the limit of infinitesimally small r. This can be achieved by adding a δ-function term normalized such that,

$$\bar{\mathbf{B}} = \frac{2\mu_0\vec{\mu}}{4\pi R^3} = \frac{\frac{2}{3}\mu_0\vec{\mu}\int_{\mathbb{R}^3}\delta^3(\mathbf{r})d^3r}{\frac{4\pi}{3}R^3} \ .$$

With this we finally obtain (see 15.4.2.10),

$$\vec{\mathcal{B}} = \frac{\mu_0}{4\pi r^3}\left[3(\vec{\mu}\cdot\hat{\mathbf{r}})\hat{\mathbf{r}} - \vec{\mu}\right] + \frac{2}{3}\mu_0\vec{\mu}\delta^3(\mathbf{r}) \ .$$

29.3.3.2 Ex: Probability for finding the electron near the nucleus

Calculate the expectation value $\langle\delta^{(3)}(\mathbf{r})\rangle_{n\ell m}$ for encountering the electron of a hydrogen atom close to the nucleus.

Solution: *With,*

$$\begin{aligned}
\psi_{n\ell m}(r,\vartheta,\varphi) &= R_{n\ell}(r)Y_{\ell m}(\vartheta,\varphi)\\
R_{n\ell}(r) &= \sqrt{\left(\frac{2Z}{na_B}\right)^3\frac{(n-\ell-1)!}{2n(n+\ell)!}}\left(\frac{2\tilde{r}}{n}\right)^\ell e^{-\tilde{r}/n}L_{n-\ell-1}^{(2\ell+1)}(\tfrac{2\tilde{r}}{n})\\
Y_{\ell m}(\vartheta,\varphi) &= \frac{1}{\sqrt{2\pi}}P_\ell^m(\cos\vartheta)\sqrt{\frac{2\ell+1}{2}\frac{(\ell-m)!}{(\ell+m)!}}e^{\imath m\varphi} \ ,
\end{aligned}$$

we find, using the formula (28.27),

$$\begin{aligned}
R_{n0}(0) &= \sqrt{\left(\frac{Z}{na_B}\right)^3\left(\frac{2}{n}\right)^2}L_{n-1}^{(1)}(0)\delta_{\ell,0}\\
&= \sqrt{\frac{Z}{na_B}}^3\frac{2}{n}\sum_{k=0}^{n-1}\binom{n}{n-1-k}\frac{(-0)^k}{k!}\delta_{\ell,0} = \sqrt{\frac{Z}{na_B}}^3 2\delta_{\ell,0} \ ,
\end{aligned}$$

and

$$Y_{00}(\vartheta,\varphi) = \frac{P_0^0(\cos\vartheta)}{2\sqrt{\pi}} = \frac{1}{2\sqrt{\pi}} \ ,$$

and hence,

$$\langle \delta^{(3)}(\mathbf{r}) \rangle_{n\ell m} = |\psi_{n\ell m}(\mathbf{0})|^2 = \frac{1}{\pi} \left(\frac{Z}{n a_B} \right)^3 \delta_{\ell,0} \ .$$

29.3.3.3 Ex: Hyperfine structure of sodium

Determine the hyperfine structure of the ^2S and ^2P states of the sodium atom including energy shifts. See Tab. 34.1 for the hyperfine constants A_J and B_J.

Solution: *With $I = \frac{3}{2}$ the state $^2S_{1/2}$ has two hyperfine levels, $F = 1, 2$. The quadrupole coefficient vanishes,*

$$\Delta E_{hfs} = \frac{A_J}{2} K = \frac{885.82\,\mathrm{MHz}}{2} K \ ,$$

such that

$$\Delta E_{hfs}(^{23}Na,^2 S_{1/2}, F = 1) \stackrel{K=-5/2}{\longrightarrow} -\frac{5}{4} \cdot 885.82\,\mathrm{MHz}$$
$$\Delta E_{hfs}(^{23}Na,^2 S_{1/2}, F = 2) \stackrel{K=3/2}{\longrightarrow} \frac{3}{4} \cdot 885.82\,\mathrm{MHz}$$
$$\Delta E_{hfs}(^{23}Na,^2 S_{1/2}, F = 2) - \Delta E_{hfs}(^{23}Na,^2 S_{1/2}, F = 1) = 2A_J = 1771.64\,\mathrm{MHz} \ .$$

The state $^2P_{1/2}$ has two hyperfine levels, $F = 1, 2$. The quadrupole coefficient vanishes,

$$\Delta E_{hfs} = \frac{A_J}{2} K = \frac{94.3\,\mathrm{MHz}}{2} K \ ,$$

such that

$$\Delta E_{hfs}(^{23}Na,^2 P_{1/2}, F = 1) \stackrel{K=-5/2}{\longrightarrow} -\frac{5}{4} \cdot 94.3\,\mathrm{MHz}$$
$$\Delta E_{hfs}(^{23}Na,^2 P_{1/2}, F = 2) \stackrel{K=3/2}{\longrightarrow} \frac{3}{4} \cdot 94.3\,\mathrm{MHz}$$
$$\Delta E_{hfs}(^{23}Na,^2 P_{1/2}, F = 2) - \Delta E_{hfs}(^{23}Na,^2 S_{1/2}, F = 1) = 2A_J = 188.6\,\mathrm{MHz} \ .$$

The state $^2P_{3/2}$ has four hyperfine levels, $F = 0, 1, 2, 3$. The quadrupole coefficient does not vanish,

$$\begin{aligned} \Delta E_{hfs} &= \frac{A_J}{2} K + \frac{B_J[3K(K+1) - 4I(I+1)J(J+1)]}{8I(2I-1)(2J-1)} \\ &= \frac{18.65\,\mathrm{MHz}}{2} K + \frac{2.82\,\mathrm{MHz}[3K(K+1) - \frac{225}{4}]}{48} \ , \end{aligned}$$

such that

$$\Delta E_{hfs}(^{23}Na,^2P_{3/2},F=0) \overset{K=-15/2}{\longrightarrow} \frac{-15}{4}\cdot 18.65\,\text{MHz} - \frac{135}{256}\cdot 2.82\,\text{MHz}$$
$$\Delta E_{hfs}(^{23}Na,^2P_{3/2},F=1) \overset{K=-11/2}{\longrightarrow} \frac{-11}{4}\cdot 18.65\,\text{MHz} - \frac{223}{256}\cdot 2.82\,\text{MHz}$$
$$\Delta E_{hfs}(^{23}Na,^2P_{3/2},F=2) \overset{K=-3/2}{\longrightarrow} \frac{-3}{4}\cdot 18.65\,\text{MHz} - \frac{303}{256}\cdot 2.82\,\text{MHz}$$
$$\Delta E_{hfs}(^{23}Na,^2P_{3/2},F=3) \overset{K=9/2}{\longrightarrow} \frac{9}{4}\cdot 18.65\,\text{MHz} - \frac{209}{256}\cdot 2.82\,\text{MHz}\ .$$

We verify that $\sum_F (2F+1)\Delta E_{hfs}(^{23}Na,^{2S+1}L_J,F)=0$.

29.3.3.4 Ex: Hyperfine structure of rubidium

Given the following energy distances $\nu_{F,F'}$ of the hyperfine levels of the rubidium isotopes ^{87}Rb and ^{85}Rb [104],

^{87}Rb, $S_{1/2}$ splits into $\nu_{1,2}=6834.7\,\text{MHz}$
^{87}Rb, $P_{3/2}$ splits into $\nu_{0,1}=72.3\,\text{MHz}, \nu_{1,2}=157.1\,\text{MHz}, \nu_{2,3}=267.2\,\text{MHz}$
^{85}Rb, $S_{1/2}$ splits into $\nu_{1,2}=3035.7\,\text{MHz}$
^{85}Rb, $P_{3/2}$ splits into $\nu_{1,2}=29.4\,\text{MHz}, \nu_{2,3}=63.4\,\text{MHz}, \nu_{3,4}=120.7\,\text{MHz}$,

calculate the positions of the barycenters.

Solution: *The rubidium hyperfine structure is,*

^{87}Rb, $S_{1/2}$ *gives* $E_{bc}=\frac{\hat{1}+\hat{2}\nu_{1,2}}{\hat{1}+\hat{2}}=4272.1\,\text{MHz}$
^{87}Rb, $P_{3/2}$ *gives* $E_{bc}=\frac{\hat{0}+\hat{1}\nu_{0,1}+\hat{2}\nu_{0,2}+\hat{3}\nu_{0,3}}{\hat{0}+\hat{1}+\hat{2}+\hat{3}}=\frac{(\hat{1}+\hat{2}+\hat{3})\nu_{0,1}+(\hat{2}+\hat{3})\nu_{1,2}+\hat{3}\nu_{2,3}}{\hat{0}+\hat{1}+\hat{2}+\hat{3}}=302.5\,\text{MHz}$
^{85}Rb, $S_{1/2}$ *gives* $E_{bc}=\frac{\hat{2}+\hat{3}\nu_{2,3}}{\hat{2}+\hat{3}}=1771.2\,\text{MHz}$
^{85}Rb, $P_{3/2}$ *gives* $E_{bc}=\frac{\hat{1}+\hat{2}\nu_{1,2}+\hat{3}\nu_{1,3}+\hat{4}\nu_{1,4}}{\hat{1}+\hat{2}+\hat{3}+\hat{4}}=\frac{(\hat{2}+\hat{3}+\hat{4})\nu_{1,2}+(\hat{3}+\hat{4})\nu_{2,3}+\hat{4}\nu_{3,4}}{\hat{1}+\hat{2}+\hat{3}+\hat{4}}=113.3\,\text{MHz}$.

29.3.3.5 Ex: Two particles

Consider a two-particle system of masses μ_1 and μ_2, exposed to a central potential $V(r)$ and an interaction potential $V(|\mathbf{r}_1-\mathbf{r}_2|)$ which only depends on the distance between the particles. The Hamiltonian of the system in the interaction representation is $H=H_1+H_2+V(|\mathbf{r}_1-\mathbf{r}_2|)$ with $H_\ell=-\frac{\hbar^2}{2\mu_\ell}\nabla_\ell^2+V(r_\ell)$, $\ell=1,2,...$ Show that the individual angular momenta $\mathbf{L}_\ell$ are not, in general, constants of the motion, unlike the *total* angular momentum $\mathbf{L}=\mathbf{L}_1+\mathbf{L}_2$.

Solution: *We have,*

$$[\hat{H},\hat{\mathbf{L}}_\mathbf{1}^2]=[V(|\mathbf{r}_1-\mathbf{r}_2|),(\hat{\mathbf{r}}_\mathbf{1}\times\hat{\mathbf{p}}_\mathbf{1})^2]\neq 0\ .$$

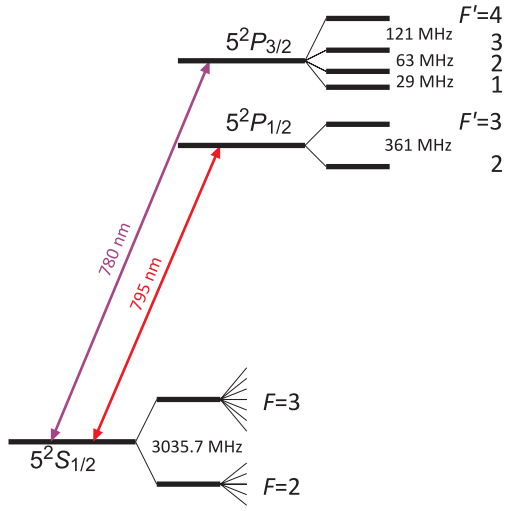

Figure 29.2: Rb hyperfine structure.

On the other side,

$$[\hat{H}, (\hat{\mathbf{L}}_\mathbf{1} + \hat{\mathbf{L}}_\mathbf{1})^2] = [V(|\mathbf{r}_1 - \mathbf{r}_2|), (\hat{\mathbf{r}}_\mathbf{1} \times \hat{\mathbf{p}}_\mathbf{1} + \hat{\mathbf{r}}_\mathbf{2} \times \hat{\mathbf{p}}_\mathbf{2})^2] \neq 0 \ .$$

We showed in the derivation of the radial Schrödinger equation (25.34), that the given Hamiltonian can be transformed into relative coordinates.

29.4 Exotic atoms

'Normal' atoms consist of a nucleus made of protons and neutrons and an electronic shell. But other two-particle systems are possible, e.g. where the nucleus or electron is replaced by another hadron or lepton (anti-proton, positron, muon, etc.). Such a system is called *exotic atom*. Atoms in Rydberg states also belong to this category.

29.4.1 Positronium and muonium

Positronium (e^+e^-) is a hydrogen-like system consisting of leptons, that is, an electron and a positron, which is the antiparticle of the electron. The muonium (μ^+e^-) is similar to positronium, except that here the positron is replaced by a muon whose mass is $m_{\mu^+} = 207m_e$. Leptons are, according to the present understanding, particles without internal structure. Both systems are unstable: the two particles annihilate each other producing γ-photons. The energy levels and orbits of the two particles are similar to that of the hydrogen atom. However, because of the reduced mass, the frequencies of the spectral lines are less than half of the corresponding hydrogen lines.

The fundamental state of positronium, like that of hydrogen, has two possible configurations depending on the relative orientation of the electron and positron spins.

The singlet state with antiparallel spins ($S = 0$, $M_s = 0$) is known as para-positronium (p-Ps) and denoted by $^1S_0$. It has an average lifetime of

$$\tau = \frac{2\hbar}{m_e c^2 \alpha^5} = 124.4\,\text{ps} \tag{29.169}$$

and decays preferably in two gamma rays with energy of 511 keV each (in the center-of-mass). The triplet state with parallel spins ($S = 1, M_s = -1, 0, 1$) is known as ortho-positronium (o-Ps) and denoted as $^3S_1$. It has an average life of 138.6 ns, and the most common form of decay produces three photons. Other forms of decay are negligible. For example, the decay channel producing five photons is 10^{-6} times less likely. Measurements of these lifetimes and the positronium energy levels have been used in precision tests of quantum electrodynamics.

While the precise calculation of the positronium energy levels is based on the Bethe-Salpeter equation, the similarity between positronium and hydrogen allows for an approximate estimate. In this approach, the energy levels are suppodsed to be different from those of hydrogen because of the difference in the value of the reduced mass μ, used in the energy equation. Since $\mu = m_e/2$ for positronium, we have

$$E_n = -\frac{\mu q_e^4}{8h^2\epsilon_0^2}\frac{1}{n^2} = -\frac{1}{2}\frac{m_e q_e^4}{8h^2\epsilon_0^2}\frac{1}{n^2} = \frac{-6.8\,\text{eV}}{n^2}\ . \tag{29.170}$$

A di-positronium molecule, that is, a system of two bound positronium atoms, has already been observed. Positronium in high energy states has been conjectured to become the dominant form of atomic matter in the universe in the very distant future if the proton decay becomes tangible.

29.4.2 Hadronic atoms

In contrast to *leptons* (such as the electron e^-, the positron e^+ and the muons μ^+ and μ^-) that participate only in electromagnetic interactions and weak interactions, *hadrons* also participate in strong (nuclear type) interactions. There are two types of hadrons, *baryons* (such as the proton p and antiproton $\bar{p}$, the neutron n and antineutron $\bar{n}$, hyperons Σ, Ξ, ...) that have semi-integer spin and behave like fermions and *mesons* (like the π-meson, K-meson, ...) that have an integer spin. Every negatively charged hadron can be used to form a hydrogen-type *hadronic atom*. These systems contain a nucleus and negative hyperon and are known as hyperonic atoms. All of these are unstable and due to the fact that they have a sufficiently long lifetime, some of their spectral lines have now been observed.

Since the hadrons interact strongly with the nucleus, the theory developed for hydrogen systems (in which only exist Coulomb interaction) can not be directly applied. In this way the values shown in Tab. 29.3 give only an estimate of the 'radius' and the ionization potential of the hadronic atoms $p\pi^-$, $p\kappa^-$, $p\bar{p}$ and $p\Sigma^-$.

29.4.3 Muonic hydrogen

The muon mass is $m_\mu = 207 m_e$. When a muon is attached to a proton we have *muonic hydrogen*. Its size is smaller because of the reduced mass $a_\mu = a_B \frac{1/m_e}{1/m_\mu + 1/m_p}$

Table 29.3: *Main features of some exotic atoms.*

system	reduced mass	radius 'a'	I_p
pe^-	$1836/1837 \approx 1$	$\approx a_B = 1$	$e^2/2a_B \approx 0.5$
e^+e^-	0.5	2	0.25
μ^+e^-	$207/208 \approx 1$	1	0.5
$p\mu^-$	≈ 186	$5.4 \cdot 10^{-3}$	93
$p\pi^-$	≈ 238	$4.2 \cdot 10^{-3}$	119
$p\kappa^-$	≈ 633	$1.6 \cdot 10^{-3}$	317
$p\bar{p}$	≈ 928	$1.1 \cdot 10^{-3}$	459
$p\Sigma^-$	≈ 1029	$9.7 \cdot 10^{-3}$	515

and the binding energy and the energies of excitation are greater for the same reason. F.ex. while for $H = p^+e^-$ the transition $2S - 2P_{1/2}$ is at 10 eV $\triangleq$ 121 nm, for $p^+\mu^-$ it is at 1900 eV. Muonic atoms are interesting because they have amplified Lamb shifts, hyperfine interactions, and quantum electrodynamical corrections. Therefore, the displacement due to the finite distribution of charges in the proton $r_p = 0.8$ fm should influence the spectrum. While in p^+e^- the $2S$ level is shifted upward by the Lamb shift by a value of 4.4×10^{-6} eV, in $p^+\mu^-$ it is shifted down by a value of 0.14 eV. In Exc. 29.4.5.2 we calculate the spectrum of the muonic hydrogen and in Exc. 27.1.3.3 we compare the energy corrections due to the finite extension of the nuclei for muonic and for standard hydrogen in first order TIPT.

29.4.4 Rydberg atoms

An atom excited to a state whose main quantum number is very high is called *Rydberg atom*. These atoms have a number of peculiar properties, including high sensitivity to electric and magnetic fields, long decay times, and wavefunctions that approximate classical electron orbits. The inner electrons protect the outer electron from the electric field of the nucleus such that, from a distance, the electric potential looks identical to that seen by the electron of a hydrogen atom.

Despite its flaws, Bohr's atom model is useful in explaining these properties. In Exc. 22.1.6.6 we derive Bohr's expression for the orbital radius in terms of the principal quantum number n:

$$r = \frac{4\pi\epsilon_0 n^2 \hbar^2}{e^2 m} \ . \tag{29.171}$$

Thus, it is clear why Rydberg atoms have peculiar properties: the radius goes as n^2 (such that for example the state with $n = 137$ of hydrogen has a radius of ~ 1 mm) and the geometric cross section goes as n^4. Thus, Rydberg atoms are extremely large, with loosely bound valence electrons that are easily perturbed or ionized by collisions or external fields.

Since the binding energy of a Rydberg electron is proportional to $1/r$, and therefore

falls as $1/n^2$, the spacing between energy levels falls as

$$\Delta E = E_1 \left(\frac{1}{(n+1)^2} - \frac{1}{n^2} \right) \stackrel{n\to\infty}{\longrightarrow} E_1 \left(-\frac{2}{n^3} + \frac{3}{n^4} + ... \right) \tag{29.172}$$

leading to less and less spaced levels. These Rydberg states form the *Rydberg series*.

29.4.4.1 Correspondence principle in Rydberg atoms

To calculate the oscillation frequency of an electron confined to a proton, we use the classical planetary model,

$$m\omega_n^2 = \frac{e^2}{4\pi\epsilon_0 r} \qquad \text{and} \qquad m\omega r^2 = n\hbar \ . \tag{29.173}$$

Eliminating r,

$$\omega_n = \frac{me^4}{(4\pi\epsilon_0)^2 n^3 \hbar^3} \ . \tag{29.174}$$

Radiation of this frequency will be emitted by an atomic antenna. On the other hand, the Bohr model predicts frequencies between orbitals,

$$\omega_n = \frac{E_{n+1} - E_n}{\hbar} = \frac{me^4}{2(4\pi\epsilon_0)^2\hbar^2} \left(\frac{1}{(n+1)^2} - \frac{1}{n^2} \right) \stackrel{n\to\infty}{\longrightarrow} \frac{me^4}{2(4\pi\epsilon_0)^2\hbar^2} \frac{2}{n^3} \ . \tag{29.175}$$

29.4.4.2 Production of Rydberg atoms

In the hydrogen atom only the ground state ($n = 1$) is actually stable. Other states must be excited by various techniques such as electron impact or charge exchange. In contrast to these methods, which produce a distribution of excited atoms at various levels, the optical excitation method allows to produce specific states, but only for alkali metals whose transitions fall into frequency regimes which are accessible to lasers.

29.4.4.3 Potential in a Rydberg atom

The valence electron in a Rydberg atom with Z protons in the nucleus and $Z - 1$ electrons in closed layers sees a spherically symmetric Coulomb potential:

$$U_{cou} = -\frac{e^2}{4\pi\varepsilon_0 r} \ . \tag{29.176}$$

The similarity of the effective potential 'seen' by the outer electron and the authentic hydrogen potential suggests a classical treatment within the planetary model. There are three notable exceptions:

- An atom can have two (or more) electrons in highly excited states with comparable orbital radii. In this case, the electron-electron interaction gives rise to a significant deviation from the hydrogen potential. For an atom in a multiple Rydberg state the additional term U_{ee} includes a sum over each pair of highly excited electrons:

$$U_{ee} = \frac{e^2}{4\pi\varepsilon_0} \sum_{i<j} \frac{1}{|\mathbf{r}_i - \mathbf{r}_j|} \ . \tag{29.177}$$

- If the valence electron has very low angular momentum (interpreted classically as an extremely eccentric elliptical orbit), it can pass close enough to the nucleus to polarize it, giving rise to an additional term,

$$U_{pol} = -\frac{e^2\alpha_d}{(4\pi\varepsilon_0)^2 r^4} \ . \tag{29.178}$$

- If the outer electron penetrates the inner electronic shells, it *sees* more of the charge of the nucleus and therefore feels a larger force. In general, the modification of the potential energy is not simple to calculate and should be based on some knowledge of the nucleus' geometry.

In hydrogen the binding energy is given by:

$$E_B = -\frac{E_1}{n^2} \ . \tag{29.179}$$

The binding energy is weak at high values of n, which explains the fragility of the Rydberg states that can easily be ionized, e.g. by collisions.

Additional terms modifying the potential energy of a Rydberg state require the introduction of a *quantum defect*, $\delta\ell$, in the expression for the binding energy:

$$E_B = -\frac{E_1}{(n-\delta_\ell)^2} \ . \tag{29.180}$$

The long lifetimes of Rydberg states with high orbital angular momentum can be explained in terms of overlapping wavefunctions. The wavefunction of an electron in a state with high ℓ (large angular momentum, 'circular orbit') has little overlap with the wavefunctions of the internal electrons and therefore stays relatively unperturbed. Also, the small energy difference between adjacent Rydberg states decreased the decay rate according to the result (34.40).

29.4.4.4 Rydberg atoms in external fields

The large distance between the electron and ionic nucleus in a Rydberg atom gives rise to an extremely large electric dipole moment d. There is an energy associated with the presence of an electric dipole in an electric field $\vec{\mathcal{E}}$, known as *Stark shift*,

$$E_S = -\mathbf{d}\cdot\vec{\mathcal{E}} \ . \tag{29.181}$$

Depending on the sign of the projection of the dipole moment onto the vector of the local electric field, the energy of a state increases or decreases with the intensity of the field. The narrow spacing between adjacent levels n in the Rydberg series means that the states can approach degeneracy even for relatively weak fields. Theoretically, the force of the field in which a level crossing would occur (assuming no coupling between the states) is given by the *Inglis-Teller limit*,

$$F_{IT} = \frac{e}{12\pi\varepsilon_0 a_0^2 n^5} \ . \tag{29.182}$$

In hydrogen the pure Coulomb potential does not couple the Stark states of an n level, which results in a *real crossover*. In other elements, deviations from the ideal $1/r$-potential allow for *avoided crossings*.

29.4.5 Exercises

29.4.5.1 Ex: Positronium

Calculate and compare the fine and hyperfine structure of positronium.

Solution: *The energy between states* $^1S_{1/2}, F = 0$ *and* $^1S_{1/2}, F = 1$ *is* $5.9 \cdot 10^{-6}\,\mathrm{eV}$. *The energy between states* $^3S_1$ *(ortho) and* $^1S_0$ *(para) is* $8.9 \cdot 10^{-4}\,\mathrm{eV}$.

29.4.5.2 Ex: Muonic hydrogen

Muonic hydrogen consists of a proton and a negatively charged muon. Calculate the binding energy of the ground state of muonic hydrogen in eV and write down the ground state's wavefunction.

Solution: *Following Bohr's model the hydrogen energy spectrum is,*

$$E_n = -\frac{\hbar^2}{2ma_B^2}\frac{1}{n^2} \qquad with \qquad a_B = 4\pi\epsilon_0\frac{\hbar^2}{me^2}\ ,$$

where m *is the reduced mass. In the case of the electron we have* $m = 0.9995m_e$. *The mass of the muon is approximately* $m_\mu = 207m_e$. *Thus, in the case of the muon we have* $m = 0.8981m_\mu$. *The ground state energy is,*

$$E_1^\mu \simeq -2.82\,\mathrm{keV} \qquad with \qquad a_B \simeq 2.56 \cdot 10^{-13}\,\mathrm{m}\ .$$

29.5 Further reading

T. Mayer-Kuckuk, *Atomphysik, Teubner Studienbücher (1985)* [860]ISBN

Chapter 30

Atoms with spin in external fields

The atomic fine structure was derived in the last chapter under the assumption that all electric and magnetic fields arise from the motion and spin of the electrons in the atomic shell and the nuclear spin. In this chapter, we will extend the treatment to include the reaction of the electrons to external electrostatic or electromagnetic fields. In this context, we will discuss the Zeeman and the Stark effect.

30.1 Charged particles in electromagnetic fields

30.1.1 Lagrangian and Hamiltonian of charged particles

A charge subject to an electromagnetic field feels the Lorentz force,

$$\mathbf{F} = q\vec{\mathcal{E}} + q\dot{\mathbf{r}} \times \vec{\mathcal{B}} \,, \tag{30.1}$$

where

$$\vec{\mathcal{E}} = -\nabla\Phi - \frac{\partial \mathbf{A}}{\partial t} \qquad \text{and} \qquad \vec{\mathcal{B}} = \nabla \times \mathbf{A} \,, \tag{30.2}$$

where Φ and $\mathbf{A}$ are called scalar and vector potential, respectively.

It is important to realize here, that the momentum $\mathbf{p}$ not only involves the momentum of the particle $m\mathbf{v}$, but the field also carries a momentum $q\mathbf{A}(\mathbf{r})$. As we learned in electrodynamics it is possible to derive the Lorentz force from a Lagrangian for the electronic motion,

$$\boxed{\mathcal{L}(r_i, \dot{r}_i) = \frac{m}{2}\dot{\mathbf{r}}^2 - q\Phi(\mathbf{r}) + q\dot{\mathbf{r}} \cdot \mathbf{A}(\mathbf{r})} \,. \tag{30.3}$$

With this aim we first determine the momentum by,

$$p_i = \frac{\partial \mathcal{L}}{\partial \dot{r}_i} = m\dot{r}_i + qA_i \,, \tag{30.4}$$

and the Hamiltonian by,

$$\mathcal{H} = \sum\nolimits_i p_i \dot{r}_i - \mathcal{L}(r_i, \dot{r}_i) = (m\mathbf{v} + q\mathbf{A}) \cdot \dot{\mathbf{r}} - \frac{m}{2}\dot{\mathbf{r}}^2 + q\Phi - q\dot{\mathbf{r}} \cdot \mathbf{A} = \frac{m}{2}\mathbf{v}^2 + q\Phi \,. \tag{30.5}$$

That is,

$$\boxed{\mathcal{H}(r_i, p_i) = \frac{1}{2m}(\mathbf{p} - q\mathbf{A})^2 + q\Phi} \ . \tag{30.6}$$

The following equations hold,

$$\dot{r}_i = \frac{\partial \mathcal{H}}{\partial p_i} \qquad \text{and} \qquad \dot{p}_i = -\frac{\partial \mathcal{H}}{\partial r_i} \ . \tag{30.7}$$

The first equation is easily verified by inserting the Hamiltonian (30.5). The second leads to the Lorentz force,

$$F_i = m\dot{v}_i = \dot{p}_i - q\dot{A}_i = -\frac{\partial \mathcal{H}}{\partial r_i} - q\dot{A}_i = q\mathcal{E}_i + q(\mathbf{v} \times \vec{\mathcal{B}})_i \ , \tag{30.8}$$

where the last step of the derivation will be shown in the Exc. 30.1.3.1 using the Coulomb gauge $\nabla \cdot \mathbf{A} = 0$.

30.1.2 Minimal coupling

Note that the same result (30.6) can be obtained by a canonical substitution,

$$m\mathbf{v} \longrightarrow \mathbf{p} - q\mathbf{A} \qquad \text{and} \qquad \mathcal{H} \longrightarrow \mathcal{H} + q\Phi \ . \tag{30.9}$$

This substitution rule, called *minimal coupling*, can be applied in quantum mechanics,

$$m\hat{\mathbf{v}} \longrightarrow -\imath\hbar\nabla - q\mathbf{A} \qquad \text{and} \qquad \hat{H} \longrightarrow \hat{H} + q\Phi \ . \tag{30.10}$$

In the case of the electron ($q = -e$) trapped in a central Coulomb potential $q\Phi = -\frac{Ze^2}{4\pi\varepsilon_0 r}$ and in the presence of any magnetic potential $\mathbf{A}$, we thus obtain,

$$\boxed{\hat{H} = \frac{m_e}{2}\hat{\mathbf{v}}^2 + q\Phi = \frac{-\hbar^2}{2m_e}\nabla^2 - \frac{\imath\hbar e}{2m_e}\mathbf{A}\cdot\nabla - \frac{\imath\hbar e}{2m_e}\nabla\cdot\mathbf{A} + \frac{e^2\mathbf{A}^2}{2m_e} + q\Phi} \ . \tag{30.11}$$

The fourth term called *diamagnetic term* is quadratic in $\mathbf{A}$ and usually so small that it can be neglected. The second and third terms describe the interaction of the electron through its momentum $\hat{\mathbf{p}}$ with the potential vector $\mathbf{A}$ produced by magnetic moments inside the atom or outer magnetic fields. Within the Coulomb gauge we have $(\nabla \cdot \mathbf{A})\psi = (\mathbf{A}\cdot\nabla)\psi + \psi(\nabla\cdot\mathbf{A}) = (\mathbf{A}\cdot\nabla)\psi$, such that,

$$\boxed{\hat{H}_{int} = \tfrac{e}{m_e}\mathbf{A}\cdot\hat{\mathbf{p}}} \ . \tag{30.12}$$

Example 182 (*Interaction Hamiltonian in dipolar approximation*): Note that the Hamiltonian (30.11) has been obtained from a gauge transformation in (23.229). With the particular choice for the gauge field,

$$\chi(\mathbf{r}, t) \equiv -\mathbf{A}(\mathbf{r}, t)\cdot\mathbf{r} \ ,$$

assuming that the potential only weakly varies in space, such that,

$$\nabla\chi(\mathbf{r}, t) \simeq -\mathbf{A}(\mathbf{r}, t) \qquad \textit{and} \qquad \frac{\partial\chi(\mathbf{r}, t)}{\partial t} = -\mathbf{r}\cdot\frac{\partial\mathbf{A}(\mathbf{r}, t)}{\partial t} = -\mathbf{r}\cdot\vec{\mathcal{E}}(\mathbf{r}, t) \ ,$$

we get with $\mathbf{d} \equiv q\mathbf{r}$,

$$\begin{aligned}\hat{H} &= \frac{1}{2m_e}(\hat{\mathbf{p}} - q\mathbf{A} + \nabla\chi)^2 + q\Phi + q\frac{\partial\chi(\mathbf{r},t)}{\partial t} \\ &\simeq \frac{\hat{\mathbf{p}}^2}{2m_e} + q\Phi - \mathbf{d}\cdot\vec{\mathcal{E}}(\mathbf{r},t)\ .\end{aligned} \tag{30.13}$$

This is the interaction Hamiltonian in the dipolar approximation.

30.1.3 Exercises

30.1.3.1 Ex: Lagrangian of an electron in the electromagnetic field

a. Show that the Lagrangian (30.3) reproduces the Lorentz force (30.1).
b. Show that the Hamiltonian (30.5) reproduces the Lorentz force (30.1).

Solution: *a. Starting from the Lagrangian (30.3) we derive,*

$$\frac{\partial\mathcal{L}}{\partial\dot{r}_i} = mv_i + qA_i \qquad \textit{and} \qquad \frac{\partial\mathcal{L}}{\partial r_i} = -q\partial_i\Phi + \partial_i\mathbf{v}\cdot\mathbf{A}\ .$$

Exploring the Lagrange equation,

$$\frac{d}{dt}\frac{\partial\mathcal{L}}{\partial\dot{r}_i} = \frac{\partial\mathcal{L}}{\partial r_i}$$

we calculate,

$$F_i = m\dot{v}_i = \frac{d}{dt}\frac{\partial\mathcal{L}}{\partial\dot{r}_i} - q\frac{dA_i}{dt} = \frac{\partial\mathcal{L}}{\partial r_i} - q\frac{dA_i}{dt} = -q\partial_i\Phi + \partial_i\mathbf{v}\cdot\mathbf{A} - q\frac{dA_i}{dt}\ .$$

Using,

$$\frac{d\mathbf{A}}{dt} = \frac{\partial\mathbf{A}}{\partial t} + (\mathbf{v}\cdot\nabla)\mathbf{A} \qquad \textit{and} \qquad \nabla(\mathbf{v}\cdot\mathbf{A}) = \mathbf{v}\times(\nabla\times\mathbf{A}) + (\mathbf{v}\cdot\nabla)\mathbf{A}\ ,$$

we obtain,

$$\mathbf{F} = m\dot{\mathbf{v}} = -q\nabla\Phi + q\mathbf{v}\times(\nabla\times\mathbf{A}) + q(\mathbf{v}\cdot\nabla)\mathbf{A} - q\frac{\partial\mathbf{A}}{\partial t} - q(\mathbf{v}\cdot\nabla)\mathbf{A} = q\vec{\mathcal{E}} + q\mathbf{v}\times\vec{\mathcal{B}}\ .$$

b. Inserting the Hamiltonian (30.5) into the equation (30.7) we obtain,

$$\begin{aligned}F_i &= -\frac{\partial}{\partial r_i}\left[\sum\nolimits_j \frac{1}{2m}(p_j - qA_j)^2 + q\Phi\right] - q\dot{A}_i = q\sum\nolimits_j \tfrac{1}{m}(p_j - qA_j)\partial_i A_j - q\partial_i\Phi - q\dot{A}_i \\ &= q\sum\nolimits_j v_j\partial_i A_j - q\partial_i\Phi - q\dot{A}_i\ .\end{aligned}$$

We derive using $\frac{d\mathbf{A}}{dt} = \frac{\partial \mathbf{A}}{\partial t} + (\mathbf{v}\cdot\nabla)\mathbf{A}$,

$$\begin{aligned}\mathbf{F} &= q\begin{pmatrix} v_2\partial_1 A_2 + v_3\partial_1 A_3 + v_1\partial_1 A_1 \\ v_3\partial_2 A_3 + v_1\partial_2 A_1 + v_2\partial_2 A_2 \\ v_1\partial_3 A_1 + v_2\partial_3 A_2 + v_3\partial_3 A_3 \end{pmatrix} - q\nabla\Phi - q\frac{\partial \mathbf{A}}{\partial t} - q(\mathbf{v}\cdot\nabla)\mathbf{A} \\ &= q\begin{pmatrix} -\partial_t A_1 + v_2(\partial_1 A_2 - \partial_2 A_1) - v_3(\partial_3 A_1 - \partial_1 A_3) \\ -\partial_t A_2 + v_3(\partial_2 A_3 - \partial_3 A_2) - v_1(\partial_1 A_2 - \partial_2 A_1) \\ -\partial_t A_3 + v_1(\partial_3 A_1 - \partial_1 A_3) - v_2(\partial_2 A_3 - \partial_3 A_2) \end{pmatrix} - q\nabla\Phi \\ &= -q\nabla\Phi - q\frac{\partial \mathbf{A}}{\partial t} + q\mathbf{v}\times(\nabla\times\mathbf{A}) = q\vec{\mathcal{E}} + q\mathbf{v}\times\vec{\mathcal{B}}\,.\end{aligned}$$

30.2 Interaction with magnetic fields

30.2.1 Normal Zeeman effect of the fine structure

The dipole moments of atoms can interact with external magnetic fields. The interaction leads to a shift of levels, which depends on the magnetic quantum number. Thus, the ultimate degeneracy in the energetic structure of the atom is lifted. This is called *Zeeman splitting*. We consider a uniform magnetic field $\vec{\mathcal{B}} = \mathcal{B}\hat{\mathbf{e}}_z$ with the potential vector,

$$\mathbf{A} = \tfrac{1}{2}\vec{\mathcal{B}}\times\mathbf{r} = -\tfrac{\mathcal{B}}{2}(-y\hat{\mathbf{e}}_x + x\hat{\mathbf{e}}_y)\,. \tag{30.14}$$

Thus the interaction energy between the electron and the field is given by the Hamiltonian (30.12),

$$\begin{aligned}\hat{V}_{zee}(B) &= -\frac{\imath\hbar e}{m_e}\mathbf{A}\cdot\nabla = -\frac{\imath\hbar e}{2m_e}(\vec{\mathcal{B}}\times\mathbf{r})\cdot\nabla = -\frac{\imath\hbar e}{2m_e}\vec{\mathcal{B}}\cdot(\mathbf{r}\times\nabla) \\ &= -\frac{e}{2m_e}\vec{\mathcal{B}}\cdot\hat{\mathbf{L}} = -\frac{\mu_B}{\hbar}g_L\hat{\mathbf{L}}\cdot\vec{\mathcal{B}} = -\vec{\mu}_L\cdot\vec{\mathcal{B}} = -\frac{\mu_B}{\hbar}\hat{L}_z\mathcal{B}\,,\end{aligned} \tag{30.15}$$

with $g_L = 1$ using the relation (29.93), $\vec{\mu}_L = \frac{e}{2m_e}\mathbf{L}$, between the angular momentum of the electron and the resulting magnetic moment. This relationship holds for an atom without spin (two electrons can couple their spins to a singlet state) and no hyperfine structure (or an unresolved hyperfine structure). The energies are therefore,

$$\boxed{\Delta E_{zee}(\mathcal{B}) = -\frac{\mu_B}{\hbar}\mathcal{B}\langle n,L,m_L|\hat{L}_z|n,L,m_L\rangle = -\mu_B m_L\mathcal{B}}\,. \tag{30.16}$$

In the Excs. 30.2.8.1 and 30.2.8.2 we represent the interaction between an atomic angular momentum and a magnetic field in different bases characterized by different quantization axes.

30.2.2 Anomalous Zeeman effect

The anomalous Zeeman effect occurs when the ensemble of electrons has a spin. Using the already known expressions for the dipole moments of the orbital momentum and

the spin of the electron, we obtain for the magnetic dipole moment,

$$\hat{\vec{\mu}}_J = \hat{\vec{\mu}}_L + \hat{\vec{\mu}}_S = \frac{\mu_B}{\hbar} g_L \hat{\mathbf{L}} + \frac{\mu_B}{\hbar} g_S \hat{\mathbf{S}} = \frac{\mu_B}{\hbar}(\hat{\mathbf{L}} + 2\hat{\mathbf{S}}) \ , \tag{30.17}$$

with $g_L = 1$ and $g_S = g_e = 2$. We can see that the dipole moment of the atom is not parallel to the total momentum, $\hat{\mathbf{J}} = \hat{\mathbf{L}} + \hat{\mathbf{S}}$.

When the magnetic field is weak, $\hat{V}_{ls} \gg \hat{V}_{zee}(\mathcal{B})$, the total momentum $\hat{\mathbf{J}}$ will be a good observable. Therefore, we must first project the momenta $\hat{\mathbf{L}}$ and $\hat{\mathbf{S}}$ onto $\hat{\mathbf{J}}$,

$$\hat{\mathbf{L}} \longrightarrow \left(\hat{\mathbf{L}} \cdot \tfrac{\hat{\mathbf{J}}}{|\hat{\mathbf{J}}|}\right) \tfrac{\hat{\mathbf{J}}}{|\hat{\mathbf{J}}|} \qquad \text{and} \qquad \hat{\mathbf{S}} \longrightarrow \left(\hat{\mathbf{S}} \cdot \tfrac{\hat{\mathbf{J}}}{|\hat{\mathbf{J}}|}\right) \tfrac{\hat{\mathbf{J}}}{|\hat{\mathbf{J}}|} \ , \tag{30.18}$$

before projecting the result onto the $\vec{\mathcal{B}}$-field. The potential is,

$$\begin{aligned}
\hat{V}_{zee}(\mathcal{B}) &= -\hat{\vec{\mu}}_J \cdot \vec{\mathcal{B}} = -\frac{\mu_B}{\hbar}(\hat{\mathbf{L}} + 2\hat{\mathbf{S}}) \cdot \vec{\mathcal{B}} \longrightarrow -\frac{\mu_B}{\hbar}\left[\left(\hat{\mathbf{L}} \cdot \tfrac{\hat{\mathbf{J}}}{|\hat{\mathbf{J}}|}\right)\tfrac{\hat{\mathbf{J}}}{|\hat{\mathbf{J}}|} \cdot \vec{\mathcal{B}} + 2\left(\hat{\mathbf{S}} \cdot \tfrac{\hat{\mathbf{J}}}{|\hat{\mathbf{J}}|}\right)\tfrac{\hat{\mathbf{J}}}{|\hat{\mathbf{J}}|} \cdot \vec{\mathcal{B}}\right] \\
&= -\frac{\mu_B}{\hbar|\mathbf{J}|^2}\left[\hat{\mathbf{L}} \cdot \hat{\mathbf{J}} + 2\hat{\mathbf{S}} \cdot \hat{\mathbf{J}}\right]\hat{\mathbf{J}} \cdot \vec{\mathcal{B}} = -\frac{\mu_B}{\hbar|\mathbf{J}|^2}\frac{1}{2}\left[\hat{\mathbf{J}}^2 + \hat{\mathbf{L}}^2 - \hat{\mathbf{S}}^2 + 2(\hat{\mathbf{J}}^2 + \hat{\mathbf{S}}^2 - \hat{\mathbf{L}}^2)\right]\hat{\mathbf{J}} \cdot \vec{\mathcal{B}} \\
&= -\frac{\mu_B}{\hbar}\frac{1}{2}\frac{3\hat{\mathbf{J}}^2 - \hat{\mathbf{L}}^2 + \hat{\mathbf{S}}^2}{|\hat{\mathbf{J}}|^2}\hat{\mathbf{J}} \cdot \vec{\mathcal{B}} \ .
\end{aligned} \tag{30.19}$$

And the energy is,

$$\Delta E_{zee}(\mathcal{B}) = \left\langle \frac{\mu_B}{\hbar}\left(1 + \frac{J(J+1) - L(L+1) + S(S+1)}{2J(J+1)}\right)\hat{\mathbf{J}} \cdot \vec{\mathcal{B}} \right\rangle \ . \tag{30.20}$$

Introducing the *Landé factor*,

$$g_J \equiv 1 + \frac{J(J+1) + S(S+1) - L(L+1)]}{2J(J+1)} \ , \tag{30.21}$$

we can write

$$\boxed{\Delta E_{zee}(\mathcal{B}) = -\frac{\mu_B}{\hbar} g_J \langle \hat{J}_z \rangle \mathcal{B} = -\mu_B g_J m_J \mathcal{B}} \ . \tag{30.22}$$

This expression describes the *anomalous Zeeman effect*, for which $S \neq 0$. For the *normal Zeeman effect*, for which the spin is zero, we find again $g_J = 1$.

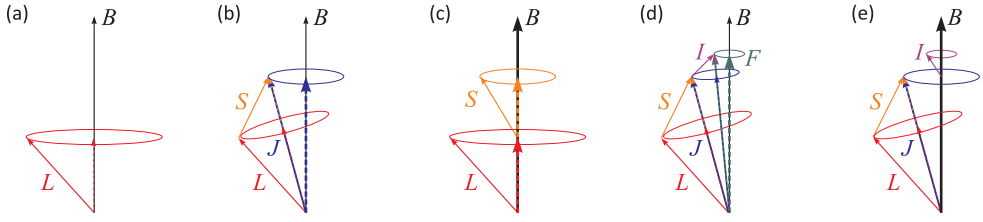

Figure 30.1: Coupling angular moments for the effect (a) Normal Zeeman effect, (b) anomalous Zeeman effect, (c) Paschen-Back effect, (d) Zeeman effect of the hyperfine structure, and (e) Paschen-Goudsmith effect.

30.2.3 Paschen-Back effect and intermediate magnetic fields

A very strong external magnetic field (> 1 T), such that $\hat{V}_{ls} \ll \hat{V}_{zee}(\mathcal{B})$, can break the $\hat{\mathbf{L}} \cdot \hat{\mathbf{S}}$-coupling. Both spins $\hat{\mathbf{L}}$ and $\hat{\mathbf{S}}$ now couple separately to the field,

$$\hat{\mathbf{L}} \longrightarrow \left(\hat{\mathbf{L}} \cdot \frac{\vec{\mathcal{B}}}{|\vec{\mathcal{B}}|}\right) \frac{\vec{\mathcal{B}}}{|\vec{\mathcal{B}}|} \qquad \text{and} \qquad \hat{\mathbf{S}} \longrightarrow \left(\hat{\mathbf{S}} \cdot \frac{\vec{\mathcal{B}}}{|\vec{\mathcal{B}}|}\right) \frac{\vec{\mathcal{B}}}{|\vec{\mathcal{B}}|} \ . \tag{30.23}$$

Therefore,

$$\hat{V}_{pb}(\mathcal{B}) = -\frac{\mu_B}{\hbar}(\hat{\mathbf{L}} + 2\hat{\mathbf{S}}) \cdot \vec{\mathcal{B}} \longrightarrow -\frac{\mu_B}{\hbar}\left[\left(\hat{\mathbf{L}} \cdot \frac{\vec{\mathcal{B}}}{|\vec{\mathcal{B}}|}\right) \frac{\vec{\mathcal{B}}}{|\vec{\mathcal{B}}|} + 2\left(\hat{\mathbf{S}} \cdot \frac{\vec{\mathcal{B}}}{|\vec{\mathcal{B}}|}\right) \frac{\vec{\mathcal{B}}}{|\vec{\mathcal{B}}|}\right] \cdot \vec{\mathcal{B}} \ , \tag{30.24}$$

such that

$$\boxed{\Delta E_{pb}(\mathcal{B}) = -\mu_B(m_L + 2m_S)\mathcal{B}} \ . \tag{30.25}$$

This is the *Paschen-Back effect*.

The derivations we have made so far have focused on simple situations well described by CSCOs in various coupling schemes. The projections on the different quantization axes [the total spin (30.18) in the Zeeman case or the applied magnetic field (30.23) in the Paschen-Back case] ensure that the Hamiltonians $\hat{V}_{ls}$ and $\hat{V}_{zee}(\mathcal{B})$ in these CSCOs are described by diagonal matrices. However, in regimes *intermediate* between Zeeman and Paschen-Back, $\hat{V}_{ls} \simeq \hat{V}_{zee}(\mathcal{B})$, it is generally not possible to find a diagonal representation.

In order to calculate the energy spectrum in intermediate regimes we must, therefore, determine all the components of the matrix,

$$\hat{V}_{ls} + \hat{V}_{zee}(\mathcal{B}) = \xi(r)\hat{\mathbf{L}} \cdot \hat{\mathbf{S}} + \frac{\mu_B}{\hbar}(\hat{\mathbf{L}} + 2\hat{\mathbf{S}}) \ . \tag{30.26}$$

Using $\hat{L}_\pm \equiv \hat{L}_x \pm \imath \hat{L}_y$ and $\hat{S}_\pm \equiv \hat{S}_x \pm \imath \hat{S}_y$, we can easily rewrite the energy in the following way,

$$\hat{V}_{ls} + \hat{V}_{zee}(\mathcal{B}) = \xi(r)\left(\hat{L}_z\hat{S}_z + \tfrac{1}{2}\hat{L}_+\hat{S}_- + \tfrac{1}{2}\hat{L}_-\hat{S}_+\right) + \frac{\mu_B}{\hbar}(\hat{\mathbf{L}} + 2\hat{\mathbf{S}}) \cdot \vec{\mathcal{B}} \ . \tag{30.27}$$

This operator acts on the uncoupled states,

$$\begin{aligned} &\Delta E_{ls} + \Delta E_{zee}(\mathcal{B}) \\ &= \langle L' m'_L; S' m'_S | \xi_{nl}(\hat{L}_z\hat{S}_z + \tfrac{1}{2}\hat{L}_+\hat{S}_- + \tfrac{1}{2}\hat{L}_-\hat{S}_+) + \mu_B(\hat{L}_z + 2\hat{S}_z)\mathcal{B} | L m_L; S m_S \rangle \\ &= \hbar^2 \xi_{nl}\left(m_L m_S \delta_{m_L,m'_L}\delta_{m_S,m'_S} + \tfrac{1}{2}L_+S_-\delta_{m_L,m'_L-1}\delta_{m_S-1,m'_S} + \tfrac{1}{2}L_-S_+\delta_{m_L-1,m'_L}\delta_{m_S,m'_S-1}\right) \\ &\quad + \hbar\mu_B(m_L + 2m_S)\mathcal{B}\delta_{m_L,m'_L}\delta_{m_S,m'_S} \ , \end{aligned} \tag{30.28}$$

with the abbreviations $L_\pm \equiv \sqrt{L(L+1) - m_L(m_L \pm 1)}$. The energies are now the eigenvalues of this matrix. The factor ξ_{nl} is usually determined experimentally by letting $\mathcal{B} = 0$. In Exc. 30.2.8.3 we calculate the re-coupling of the spins of two electrons in an external magnetic field.

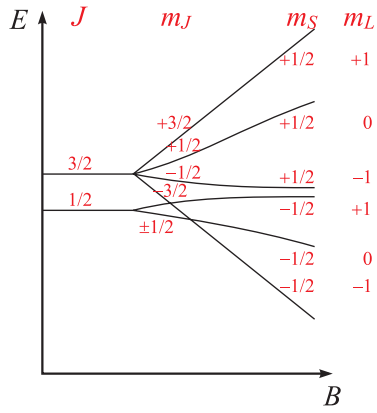

Figure 30.2: Transition between the Zeeman regime and the Paschen-Back regime for the case $L = 1$ and $S = 1/2$.

30.2.4 Zeeman effect of the hyperfine structure

When the energy of the interaction with the magnetic field is comparable to the hyperfine interactions, but much weaker than that of the fine interactions, the fields do not disturb the coupling between the total electronic momentum $\hat{\mathbf{J}}$ and the spin of the nucleus $\hat{\mathbf{I}}$. Hence, J, I, F, and m_F are good quantum numbers. Therefore, to calculate the interaction energy,

$$\hat{V}_{hfs} + \hat{V}_{zee}(\mathcal{B}) = \hat{V}_{hfs} - \hat{\vec{\mu}}_F \cdot \vec{\mathcal{B}} \,, \tag{30.29}$$

where $\hat{\vec{\mu}}_F$ is the total magnetic momentum,

$$\hat{\vec{\mu}}_F = \hat{\vec{\mu}}_J + \hat{\vec{\mu}}_I = -\frac{\mu_B}{\hbar} g_J \hat{\mathbf{J}} + \frac{\mu_N}{\hbar} g_p \hat{\mathbf{I}} \,. \tag{30.30}$$

we project the nuclear spin and the total electronic momentum separately in the direction of $\hat{\mathbf{F}}$,

$$\hat{\mathbf{J}} \longrightarrow \left(\hat{\mathbf{J}} \cdot \frac{\hat{\mathbf{F}}}{|\mathbf{F}|}\right) \frac{\hat{\mathbf{F}}}{|\mathbf{F}|} \qquad \text{and} \qquad \hat{\mathbf{I}} \longrightarrow \left(\hat{\mathbf{I}} \cdot \frac{\hat{\mathbf{F}}}{|\mathbf{F}|}\right) \frac{\hat{\mathbf{F}}}{|\mathbf{F}|} \,. \tag{30.31}$$

Note the negative sign in (30.30) due to the negative charge of the electron. The Landé factor g_J [see (30.21)] is the one caused by the coupling of the orbital angular momentum $\hat{\mathbf{L}}$ and the electron spin $\hat{\mathbf{S}}$ and depends on the state under consideration. Thereby,

$$\begin{aligned} \hat{V}_{zee}(\mathcal{B}) &= \left[-\frac{\mu_B}{\hbar} g_J \left(\hat{\mathbf{J}} \cdot \frac{\hat{\mathbf{F}}}{|\mathbf{F}|}\right) \frac{\hat{\mathbf{F}}}{|\mathbf{F}|} + \frac{\mu_N}{\hbar} g_p \left(\hat{\mathbf{I}} \cdot \frac{\hat{\mathbf{F}}}{|\mathbf{F}|}\right) \frac{\hat{\mathbf{F}}}{|\mathbf{F}|}\right] \vec{\mathcal{B}} \\ &= \left(-\frac{\mu_B}{\hbar |\hat{\mathbf{F}}|^2} g_J \hat{\mathbf{J}} \cdot \hat{\mathbf{F}} + \frac{\mu_N}{\hbar |\hat{\mathbf{F}}|^2} g_p \hat{\mathbf{I}} \cdot \hat{\mathbf{F}}\right) (\mathcal{B} \cdot \hat{F}_z) \,. \end{aligned} \tag{30.32}$$

Using $\hat{\mathbf{J}} \cdot \hat{\mathbf{F}} = \frac{1}{2}(\hat{\mathbf{F}}^2 + \hat{\mathbf{J}}^2 - \hat{\mathbf{I}}^2)$ and $\hat{\mathbf{I}} \cdot \hat{\mathbf{F}} = \frac{1}{2}(\hat{\mathbf{F}}^2 - \hat{\mathbf{J}}^2 + \hat{\mathbf{I}}^2)$ we write,

$$\hat{V}_{zee}(\mathcal{B}) = -\frac{\mu_B}{\hbar} g_J \frac{\hat{\mathbf{F}}^2 + \hat{\mathbf{J}}^2 - \hat{\mathbf{I}}^2}{2|\mathbf{F}|^2} \mathcal{B}\hat{F}_z + g_p \frac{\mu_N}{\hbar} \frac{\hat{\mathbf{F}}^2 - \hat{\mathbf{J}}^2 + \hat{\mathbf{I}}^2}{2|\hat{\mathbf{F}}|^2} \mathcal{B}\hat{F}_z \,, \tag{30.33}$$

such that

$$\boxed{\Delta E_{hfs} + \Delta E_{zee}(\mathcal{B}) \simeq \Delta E_{hfs} + \mu_B g_F m_F \mathcal{B}} \,, \tag{30.34}$$

using the *Landé factor* g_F for the state F,

$$g_F \simeq g_J \frac{F(F+1) + J(J+1) - I(I+1)}{2F(F+1)} - g_p \frac{\mu_N}{\mu_B} \frac{F(F+1) - J(J+1) + I(I+1)}{2F(F+1)} \,, \tag{30.35}$$

where the second term can be neglected.

The splitting of electronic states with the momentum $\hat{\mathbf{F}}$ into $2F+1$ sublevels $m_F = -F, .., F$ is called *Zeeman effect of the hyperfine structure*. The result (30.32) only applies to weak magnetic fields. For strong fields the Zeeman splitting becomes a Paschen-Back splitting of the hyperfine structure.

30.2.5 Paschen-Back effect of the hyperfine structure

When the interaction with the magnetic field exceeds the hyperfine interaction, the nuclear spin $\hat{\mathbf{I}}$ decouples from the total momentum $\hat{\mathbf{J}}$, and both couple separately to the external magnetic field,

$$\hat{\mathbf{J}} \longrightarrow \left(\hat{\mathbf{J}} \cdot \frac{\vec{\mathcal{B}}}{|\vec{\mathcal{B}}|}\right) \frac{\vec{\mathcal{B}}}{|\vec{\mathcal{B}}|} \qquad \text{and} \qquad \hat{\mathbf{I}} \longrightarrow \left(\hat{\mathbf{I}} \cdot \frac{\vec{\mathcal{B}}}{|\vec{\mathcal{B}}|}\right) \frac{\vec{\mathcal{B}}}{|\vec{\mathcal{B}}|} \,. \tag{30.36}$$

The Zeeman effect of the hyperfine structure becomes a hyperfine structure of the Zeeman effect, also called *Paschen-Back effect of the hyperfine structure* or *Paschen-Goudsmith effect*. We can diagonalize the potential on a basis, where I, m_I, J, and m_J are good quantum numbers. Using the expression (29.168) but disregarding the quadrupolar contribution to the hyperfine interaction, $B_J \simeq 0$, we obtain,

$$\begin{aligned} \hat{V}_{hfs} + \hat{V}_{zee}(\mathcal{B}) &= \hat{V}_{hfs} - (\hat{\vec{\mu}}_J + \cancelto{\simeq 0}{\hat{\vec{\mu}}_I}) \cdot \vec{\mathcal{B}} \simeq \frac{A_J}{\hbar^2} \hat{\mathbf{J}} \cdot \hat{\mathbf{I}} - \hat{\vec{\mu}}_J \cdot \vec{\mathcal{B}} \\ &\longrightarrow \frac{A_J}{\hbar^2} \left(\hat{\mathbf{J}} \cdot \frac{\vec{\mathcal{B}}}{\mathcal{B}}\right) \frac{\vec{\mathcal{B}}}{\mathcal{B}} \cdot \left(\hat{\mathbf{I}} \cdot \frac{\vec{\mathcal{B}}}{\mathcal{B}}\right) \frac{\vec{\mathcal{B}}}{\mathcal{B}} - \mu_{J_z} \mathcal{B} = \frac{A_J}{\hbar^2} \hat{J}_z \hat{I}_z + \frac{\mu_B}{\hbar} g_J \hat{J}_z \mathcal{B} \,, \end{aligned} \tag{30.37}$$

where we neglect the interaction of the dipole moment of the nucleus with the external magnetic field, $\vec{\mu}_I \simeq 0$. We obtain for strong magnetic fields,

$$\boxed{\Delta E_{hfs} + \Delta E_{zee}(\mathcal{B}) \simeq A_J m_J m_I + \mu_B g_J m_J \mathcal{B}} \,. \tag{30.38}$$

The re-coupling of the state $|F m_F\rangle$ to $|m_I m_J\rangle$ in strong magnetic fields is described by Clebsch-Gordan coefficients,

$$|F m_F\rangle = \sum\nolimits_{m_I + m_J = m_F} |m_I m_J\rangle \langle m_I m_J | F m_F\rangle \,. \tag{30.39}$$

Example 183 (*Nuclear magnetic resonance*): In Eq. (30.37) we have neglected the nuclear dipole moment for being small in comparison to the electronic one. Taking it into account, we get an additional term $\hat{V}_{nmr}$,

$$\hat{V}_{hfs} + \hat{V}_{zee} + \hat{V}_{nmr} = \frac{A_J}{\hbar^2} \hat{\mathbf{J}} \cdot \hat{\mathbf{I}} + \vec{\mu}_J \cdot \vec{\mathcal{B}} + \vec{\mu}_I \cdot \vec{\mathcal{B}} = \frac{A_J}{\hbar^2} \hat{J}_z \hat{I}_z + \mu_{J_z} \mathcal{B} + \mu_{I_z} \mathcal{B} \,. \tag{30.40}$$

Considering a hydrogen atom ^{1}H in a $\vec{\mathcal{B}} = 10\,\mathrm{T}$ strong magnetic field, we have the following hierarchy of energies:

$$\begin{aligned}\Delta E_{zee}(\mathcal{B}) &= \mu_B g_e m_J \simeq h \cdot 140\,\mathrm{GHz} \\ \Delta E_{hfs}(\mathcal{B}) &\simeq h \cdot 1.4\,\mathrm{GHz} \\ \Delta E_{nmr}(\mathcal{B}) &= \mu_N g_p m_I \simeq h \cdot 213\,\mathrm{MHz}\ ,\end{aligned} \tag{30.41}$$

where $g_e = 2.002..$ is the g-factor of the electron and $g_p = 5.586..$ of the proton. Now, in large molecules the most electrons are paired, such that $\hat{\mathbf{J}} = 0$. In that case, we are left with the interaction between the nuclear spin and the applied magnetic field,

$$\Delta E_{nmr}(\mathcal{B}) = \mu_N g_I m_I \mathcal{B}\ , \tag{30.42}$$

where the g-factor of the nucleus g_I must be looked up in data tables. This is the regime where *nuclear magnetic resonances* (NMR) can be excited with a large variety of applications in spectroscopy and imaging.

30.2.6 Hyperfine structure in the intermediate field regime

Knowing the dipolar magnetic A_J and quadrupolar B_J interval factors, it is possible to calculate the Zeeman shift of the hyperfine structure in magnetic fields intermediate between the Zeeman and Paschen-Back regimes. For this, we must determine all the components of the matrix $\hat{V}_{hfs} + \hat{V}_{zee}(B)$ and calculate the eigenvalues. The relevant terms of the Eqs. (29.168) and the Eq. (30.36) are,

$$\hat{V}_{hfs} + \hat{V}_{zee}(\mathcal{B}) = \frac{A_J}{\hbar^2}\hat{\mathbf{I}}\cdot\hat{\mathbf{J}} + \frac{B_J}{\hbar^2}\frac{6(\hat{\mathbf{I}}\cdot\hat{\mathbf{J}})^2 + 3\hat{\mathbf{I}}\cdot\hat{\mathbf{J}} - 2\hat{\mathbf{J}}^2\hat{\mathbf{I}}^2}{2I(2I-1)2J(2J-1)} + g_J\mu_B\vec{\mathcal{B}}\cdot\hat{\mathbf{J}} - g_I\mu_N\vec{\mathcal{B}}\cdot\hat{\mathbf{I}}\ . \tag{30.43}$$

We develop the complete matrix representation of this Hamiltonian within the uncoupled base, where m_J, m_I are good quantum numbers, introducing the abbreviations $I_\pm \equiv \sqrt{I(I+1) - m_I(m_I \pm 1)}$ and $I_{\pm\pm} \equiv \sqrt{I(I+1) - (m_I \pm 1)(m_I \pm 2)}$. The SU(2) algebra provides useful expressions, $\hat{\mathbf{I}}\cdot\hat{\mathbf{J}} = \hat{I}_z\hat{J}_z + \frac{1}{2}(\hat{I}_+\hat{J}_- + \hat{I}_-\hat{J}_+)$. The elements of the matrix are,

$$\begin{aligned}&\langle m_I' m_J'|H_{hfs} + H_B|m_I m_J\rangle = \left[A_J + \tfrac{3B_J}{2I(2I-1)2J(2J-1)}\right]\times \\ &\times\left\{m_I m_J \delta_{m_I'\ m_I}\delta_{m_J'\ m_J} + \tfrac{1}{2}I_+J_-\delta_{m_I'\ m_I+1}\delta_{m_J'\ m_J-1} + \tfrac{1}{2}I_-J_+\delta_{m_I'\ m_I-1}\delta_{m_J'\ m_J+1}\right\} \\ &+ \tfrac{6B_J}{2I(2I-1)2J(2J-1)}\langle m_I' m_J'|\left(\tfrac{\mathbf{I}\cdot\mathbf{J}}{\hbar}\right)^2|m_I m_J\rangle \\ &+ \left[-\tfrac{B_J 2I(I+1)J(J+1)}{2I(2I-1)2J(2J-1)} + (g_J m_J - g_I\mu_N m_I)\mu_B B\right]\delta_{m_I'\ m_I}\delta_{m_I'\ m_I}\end{aligned} \tag{30.44}$$

where

$$\begin{aligned}\langle m_I' m_J'|\left(\tfrac{\hat{\mathbf{I}}\cdot\hat{\mathbf{J}}}{\hbar}\right)^2|m_I m_J\rangle = &\left[(m_I m_J)^2 + \tfrac{1}{4}I_-^2J_+^2 + \tfrac{1}{4}I_+^2J_-^2\right]\delta_{m_I'\ m_I}\delta_{m_J'\ m_J} + \\ &+ \tfrac{1}{2}\left(m_I' m_J' + m_I m_J\right)I_+J_-\delta_{m_I'\ m_I+1}\delta_{m_J'\ m_J-1} + \\ &+ \tfrac{1}{2}\left(m_I' m_J' + m_I m_J\right)I_-J_+\delta_{m_I'\ m_I-1}\delta_{m_J'\ m_J+1} + \\ &+ \tfrac{1}{4}I_+J_-I_{++}J_{--}\delta_{m_I'\ m_I+2}\delta_{m_J'\ m_J-2} + \\ &+ \tfrac{1}{4}I_-J_+I_{--}J_{++}\delta_{m_I'\ m_I-2}\delta_{m_J'\ m_J+2}\ .\end{aligned} \tag{30.45}$$

The matrix $\langle m_I' m_J' | H_{hfs} + H_B | m_I m_J \rangle$ is divided into $2F+1$ diagonal blocks, each labeled m_F. The total number of levels is,

$$\sum_{F=|I-J|,..,I+J} 2F{+}1 = (2I{+}1)(2J{+}1) = \sum_{m_F=|-F,..,F|} \left(\sum_{m_I=|-I,..,I|,\ m_J=|-J,..,J|,\ m_I+m_J=m_F} 1 \right) .$$

In this form the matrix can be programmed, e.g. using computational software such as MATLAB, and all eigenvalues of the Hamiltonian for any state $^{2S+1}X_J$ and nuclear spin I can be calculated numerically. Obviously, the eigenvalues follow from a diagonalization of the matrix and do not depend on the chosen base. Fig. 30.3 shows the result obtained for ^{6}Li ($I = \frac{3}{2}$) in the state $2s\ ^2P_{3/2}$ knowing that $A_J/h = -1.17$ MHz and $B_J = 0$.

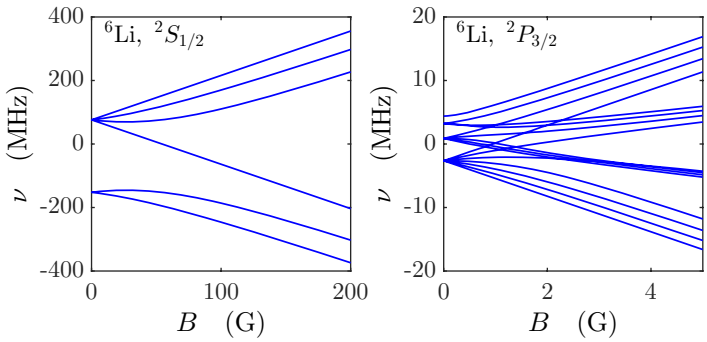

Figure 30.3: (code) Hyperfine and Zeeman structure of the state $^2P_{3/2}$ of ^{6}Li.

Example 184 (*Fully stretched states*): It is interesting to analyze the so-called *fully stretched Zeeman states* defined by $F = I + J$ and $|m_F| = F$. For these states, the spin K defined in (29.167) becomes,

$$\begin{aligned} K \equiv 2\langle \hat{\mathbf{J}} \cdot \hat{\mathbf{I}} \rangle &= F(F+1) - I(I+1) - J(J+1) \\ &= (I+J)(I+J+1) - I(I+1) - J(J+1) = 2JI \ , \end{aligned}$$

and the hyperfine structure (29.168) becomes,

$$\Delta E_{hfs} = \frac{A_J}{2} K + \frac{B_J}{8I(2I-1)J(2J-1)} [3K(K{+}1) - 4I(I{+}1)J(J{+}1)] = A_J IJ + \tfrac{B_J}{4} \ .$$

That is, the hyperfine structure does not depend on the F quantum number at any $\mathcal{B}$-field amplitude, which means that the m_J, m_I, and m_F will be good quantum numbers at arbitrary $\mathcal{B}$-field strengths. So see this, we calculate the Landé-factor (30.35),

$$g_F = g_J \frac{J}{F} - g_J \frac{\mu_N}{\mu_B} \frac{I}{F} \ ,$$

and consider the particular Zeeman state $m_F = F$, $m_J = J$, and $m_I = I$,

$$\begin{aligned} \hat{V}_{hfs} + \hat{V}_{zee}(\mathcal{B}) &= A_J IJ + \tfrac{B_J}{4} + g_J \mu_B \vec{\mathcal{B}} \cdot \hat{\mathbf{J}} - g_I \mu_N \vec{\mathcal{B}} \cdot \hat{\mathbf{I}} \\ &= A_J IJ + \tfrac{B_J}{4} + \mu_B g_F m_F \mathcal{B} = A_J IJ + \tfrac{B_J}{4} + (\mu_B g_J J - \mu_N g_J I)\mathcal{B} \ . \end{aligned}$$

The energy displacement of the fully stretched states is always linear in the magnetic field. We can also look at the matrix elements $I_+ = 0$ and $I_- = \sqrt{2I}$ and note that all non-diagonal terms vanish.

When one of the spins, J or I, is equal to $1/2$ only two possible hyperfine states exist: $F = I \pm J$. For this case there is an approximate analytic formula called the *Breit-Rabi formula* [81], which will be derived in Exc. 30.2.8.4,

$$\begin{aligned}\Delta E_{hfs} + \Delta E_{zee}(\mathcal{B}) &= \langle \tfrac{A_J}{\hbar^2}\hat{\mathbf{I}}\cdot\hat{\mathbf{J}} + g_J\mu_B\vec{\mathcal{B}}\cdot\hat{\mathbf{J}} - g_I\mu_N\vec{\mathcal{B}}\cdot\hat{\mathbf{I}}\rangle \\ &= -\frac{A_J}{4} + \mu_N g_N m_F \mathcal{B} \pm \frac{A_J(I+\frac{1}{2})}{2}\sqrt{1+\frac{4m_F}{2I+1}x+x^2}\ ,\end{aligned} \tag{30.46}$$

with the abbreviation $x \equiv \frac{2(\mu_B g_J - \mu_N g_I)\mathcal{B}}{A_J}$. Resolve also Exc. 30.2.8.5.

Atoms with paired electrons have no spin and therefore no magnetic dipole moment. For example, helium or strontium in their ground state $^1S_0$. These systems are diamagnetic due to the Hamiltonian term (30.11) being quadratic in $\vec{\mathcal{B}}$, as we shall see in Exc. 30.2.8.6.

30.2.7 Landau levels in two-dimensional systems subject to magnetic fields

Magnetic field can also have interesting effects in *artificial atoms*, e.g. quantum dots. An important example is the formation of *Landau levels*. We consider a two-dimensional system of non-interacting particles with charge q and spin S confined to an area $A = L_x L_y$ in the x-y plane. We apply a uniform magnetic field,

$$\vec{\mathcal{B}} = \mathcal{B}\hat{\mathbf{e}}_z \tag{30.47}$$

along the z axis. The Hamiltonian of this system is,

$$\hat{H} = \tfrac{1}{2m}(\hat{\mathbf{p}} - q\hat{\mathbf{A}})^2\ , \tag{30.48}$$

where $\hat{\mathbf{p}}$ is the operator of the canonical momentum and $\hat{\mathbf{A}}$ is the potential vector, related to the magnetic field by $\vec{\mathcal{B}} = \nabla\times\hat{\mathbf{A}}$. The vector potential,

$$\mathbf{A} = \tfrac{1}{2}\begin{pmatrix}-\mathcal{B}y\\ \mathcal{B}x\\ 0\end{pmatrix} \tag{30.49}$$

reproduces the field (30.47). However, we have the freedom in choosing the potential vector, given by the gauge transformation, to add the gradient of a scalar field, for example,

$$\chi \equiv \tfrac{1}{2}\mathcal{B}xy \quad\Longrightarrow\quad \nabla\chi = \tfrac{1}{2}\begin{pmatrix}\mathcal{B}y\\ \mathcal{B}x\\ 0\end{pmatrix} \quad\Longrightarrow\quad \mathbf{A}' \equiv \mathbf{A} + \nabla\chi = \mathcal{B}x\hat{\mathbf{e}}_y\ . \tag{30.50}$$

The potential vector $\mathbf{A}'$ gives the same magnetic field and only changes the general phase of the wavefunction, but the physical properties do not change. In this gauge, which is called *Landau gauge*, the Hamiltonian is,

$$\hat{H} = \frac{\hat{p}_x^2}{2m} + \frac{1}{2m}\left(\hat{p}_y - \frac{q\mathcal{B}}{c}\hat{x}\right)^2 . \tag{30.51}$$

The operator $\hat{p}_y$ commutes with this Hamiltonian, since the $\hat{y}$ operator is absent due to the choice of the gauge. Thus, the operator $\hat{p}_y$ can be replaced by its eigenvalue $\hbar k_y$. Hence, by introducing the *cyclotron frequency*,

$$\omega_c \equiv \frac{q\mathcal{B}}{mc} , \tag{30.52}$$

we obtain,

$$\boxed{\hat{H} = \frac{\hat{p}_x^2}{2m} + \frac{m\omega_c^2}{2}\left(\hat{x} - \frac{\hbar k_y}{m\omega_c}\right)^2} . \tag{30.53}$$

This is exactly the Hamiltonian of the quantum harmonic oscillator, except that the minimum of the potential is displaced in position space by the value,

$$x_0 \equiv \frac{\hbar k_y}{m\omega_c} . \tag{30.54}$$

To find the energies, we note that the translation of the potential of the harmonic oscillator does not affect the energies. The energies of this system are therefore identical to those of the standard quantum harmonic oscillator,

$$E_n = \hbar\omega_c\left(n + \tfrac{1}{2}\right) , \tag{30.55}$$

for $n \geq 0$. Since the energy does not depend on the quantum number k_y, we will have degeneracy. To derive the wavefunctions, we remember that $\hat{p}_y$ commutes with the Hamiltonian. Then the wavefunction splits into a product of eigenstates of the momentum in y-direction and eigenstates of the harmonic oscillator $|\phi_n\rangle$ shifted by a value x_0 in x-direction:

$$\Psi(x, y) = e^{\imath k_y y}\phi_n(x - x_0) . \tag{30.56}$$

That is, the state of the electron is characterized by two quantum numbers, n and k_y.

Each set of wavefunctions with the same n is called *Landau level*. Effects due to Landau levels are only observed, when the average thermal energy is lower than the separation of the energy levels, which means that low temperatures and strong magnetic fields are required. Each Landau level is degenerate, because of the second quantum number k_y, which can adopt the values,

$$k_y = \frac{2\pi N}{L_y} , \tag{30.57}$$

with $N \in \mathbb{N}$. The allowed values of N are further restricted by the condition that the center of mass of the oscillator, x_0, must be physically inside the system, $0 \leq x_0 < L_x$. Using (30.54) this gives the following range for N,

$$0 \leq N < \frac{m\omega_c L_x L_y}{2\pi\hbar} . \tag{30.58}$$

For particles with charge $q = Ze$, the upper limit in N can simply be written as a ratio of fluxes,

$$Z\frac{\Phi}{\Phi_0} = \frac{Z\mathcal{B}L_xL_y}{(hc/e)} = N_{max} \ , \tag{30.59}$$

where $\Phi_0 = h/2e$ is the fundamental *flux quantum* and $\Phi = \mathcal{B}A$ the flux through the system (with area $A = L_xL_y$). Thus, for particles with spin S, the maximum number of particles per Landau level is,

$$N_{max} = Z(2S+1)\frac{\Phi}{\Phi_0} \ . \tag{30.60}$$

30.2.7.1 Integer and fractional quantum Hall effect

In general, Landau levels are observed in electronic systems with $Z = 1$ and $S = 1/2$. As the magnetic field increases, more and more electrons can fit a certain Landau level. The occupation of the highest Landau level ranges from entirely full to entirely empty, leading to oscillations in various electronic properties (see *de Haas-van Alphen effect*, *Shubnikov-de Haas effect* and *quantum Hall effect*. The most direct observation of the

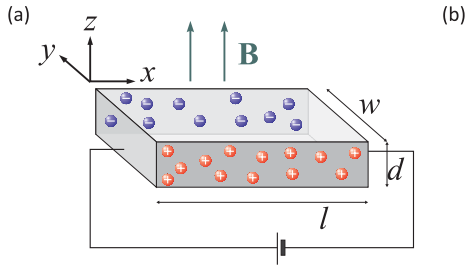

Figure 30.4: Scheme of the Quantum Hall effect.

Landau levels is done via the quantum Hall effect. To discuss this effect let us briefly recapitulate the Hall effectoriginally studied in Sec. 15.1.1. In the scheme of Fig. 30.4, charges are deviated by the Lorentz force exerted by an applied magnetic field $\vec{\mathcal{B}}$ from a driven current density j_x into a current density j_y until a sufficient amount of surface charge density has accumulated to generate an electric field exerting a Coulomb force on the charges which neutralizes the Lorentz force, $\mathbf{F} = q(\vec{\mathcal{E}} + \mathbf{v} \times \vec{\mathcal{B}}) = 0$. Resolving this condition by $\mathbf{v}$, we obtain for the current density,

$$\mathbf{j} = \varrho q\mathbf{v} = \varrho q\frac{\mathcal{E}}{\mathcal{B}}\hat{\mathbf{e}}_x = \varsigma\vec{\mathcal{E}} \ , \tag{30.61}$$

where the last equation is Ohm's law and

$$\varsigma = \begin{pmatrix} \varsigma_{xx} & \varsigma_{xy} \\ -\varsigma_{xy} & \varsigma_{yy} \end{pmatrix} \qquad \text{and} \qquad \varrho = \varsigma^{-1} = \frac{1}{\varsigma_{xx}^2 + \varsigma_{yy}^2}\begin{pmatrix} \varsigma_{xx} & -\varsigma_{xy} \\ \varsigma_{xy} & \varsigma_{yy} \end{pmatrix} \tag{30.62}$$

the conductivity and the resistivity, respectively. The Hall resistivity does therefore depend linearly on the magnetic field,

$$\varrho_{xy} = \frac{\mathcal{E}}{j} = \frac{\mathcal{B}}{\varrho q} \ . \tag{30.63}$$

In two-dimensional systems this is, however, not observed. Instead, plateaus emerge whenever the magnetic field is ramped across a value where a new Landau level is possible binding one more electron,

$$\varrho_{xy} = \frac{2\pi\hbar}{e^2}\frac{1}{\nu} \qquad \text{with} \qquad \nu \in \mathbb{Z} \ . \tag{30.64}$$

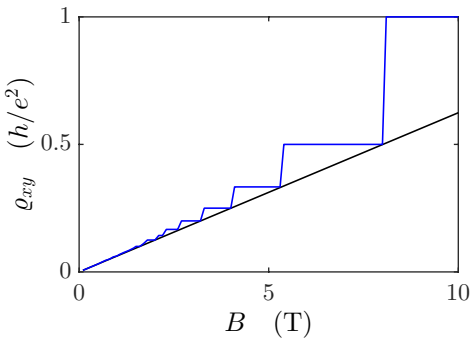

Figure 30.5: (code) Scheme of the quantum Hall effect.

30.2.8 Exercises

30.2.8.1 Ex: Zeeman effect with different quantization axes

The Zeeman effect can be described in several ways depending on the choice of the quantization axis. Consider a magnetic field $\vec{\mathcal{B}} = \mathcal{B}_x\hat{\mathbf{e}}_x$ and calculate the interaction Hamiltonian $V(\mathcal{B}) = -\vec{\mu}_J \cdot \vec{\mathcal{B}}$
a. choosing the quantization axis $\hat{\mathbf{e}}_x$ in the direction of the magnetic field,
b. choosing the quantization axis $\hat{\mathbf{e}}_z$ perpendicular to the direction of the magnetic field.

Solution: *a. Choosing the quantization axis* $\hat{\mathbf{e}}_x$ *in the direction of the magnetic field, the interaction Hamiltonian becomes,*

$$V(\mathcal{B}) = -\tfrac{1}{\hbar}\mu_B\mathcal{B}_x\hat{J}_x = -\tfrac{1}{\hbar}\mu_B\mathcal{B}_x\sum_{m_x,m_x'}|J,m_x'\rangle\langle J,m_x'|\hat{J}_x|J,m_x\rangle\langle J,m_x| \ ,$$

with the matrix elements,

$$\langle J,m_x'|\hat{J}_x|J,m_x\rangle = \hbar m_x\delta_{m_x',m_x} \ .$$

For the example of a spin $J = 1/2$*, we have,*

$$V(\mathcal{B}) = -\tfrac{1}{2}\mu_B\mathcal{B}_x\begin{pmatrix}1 & 0\\ 0 & -1\end{pmatrix}$$

with the eigenvalues,

$$\langle V(\mathcal{B})\rangle = \mp\tfrac{1}{2}\mu_B\mathcal{B}_x \qquad for \qquad |\psi_\pm\rangle = |\tfrac{1}{2},\pm\tfrac{1}{2}\rangle_x \ .$$

b. Now we choose the quantization axis $\hat{\mathbf{e}}_z$ *perpendicular to the direction of the magnetic field,*

$$V(\mathcal{B}) = -\tfrac{1}{\hbar}\mu_B\mathcal{B}_x\hat{J}_x = -\tfrac{1}{\hbar}\mu_B\mathcal{B}_x\sum_{m_z,m_z'}|J,m_z'\rangle\langle J,m_z'|\hat{J}_+ + \hat{J}_-|J,m_z\rangle\langle J,m_z| \ ,$$

with the matrix elements,

$$\begin{aligned}&\langle J,m_z'|\hat{J}_+ + \hat{J}_-|J,m_z\rangle\\ &\quad = \hbar\sqrt{J(J+1)-m_z(m_z+1)}\delta_{m_z',m_z+1} + \hbar\sqrt{J(J+1)-m_z(m_z-1)}\delta_{m_z',m_z-1} \ .\end{aligned}$$

For the example of a spin $J = 1/2$*, we have,*

$$V(\mathcal{B}) = -\tfrac{1}{2}\mu_B\mathcal{B}_x\begin{pmatrix}0 & 1\\ 1 & 0\end{pmatrix}$$

with the eigenvalues $\langle V(\mathcal{B})\rangle = \mp\frac{1}{2}\mu_B\mathcal{B}_x$ *for the eigenvectors* $|\psi_\pm\rangle = \frac{1}{\sqrt{2}}|\frac{1}{2},\frac{1}{2}\rangle_z + \frac{1}{\sqrt{2}}|\frac{1}{2},-\frac{1}{2}\rangle_z$.

30.2.8.2 Ex: Zeeman shift and quantization axes

Choosing the fixed quantization axis $\hat{\mathbf{e}}_z$ and a magnetic field $\vec{\mathcal{B}}(\mathbf{r})$ in an arbitrary direction, calculate the Hamiltonian of the Zeeman interaction with an angular momentum $J = 1$ and show that the energy shift depends only on absolute value $|\vec{\mathcal{B}}(\mathbf{r})|$.

Solution: *The energy is,*

$$\begin{aligned}V(\mathcal{B}) &= -\vec{\mu}_J\cdot\vec{\mathcal{B}} = -\tfrac{1}{\hbar}\mu_B(\mathcal{B}_x\hat{J}_x + \mathcal{B}_y\hat{J}_y + \mathcal{B}_z\hat{J}_z)\\ &= -\tfrac{1}{\hbar}\mu_B\sum_{m_z,m_z'}|J,m_z'\rangle\Big[\tfrac{1}{2}\mathcal{B}_x\langle J,m_z'|(\hat{J}_+ + \hat{J}_-)|J,m_z\rangle\\ &\qquad +\tfrac{1}{2\imath}\mathcal{B}_y\langle J,m_z'|(\hat{J}_+ - \hat{J}_-)|J,m_z\rangle + \mathcal{B}_z\langle J,m_z'|\hat{J}_z|J,m_z\rangle\Big]\langle J,m_z|\\ &= -\mu_B\sum_{m_z,m_z'}|J,m_z'\rangle\Big[\tfrac{1}{2}(\mathcal{B}_x - \imath\mathcal{B}_y)\sqrt{J(J+1)-m_z(m_z+1)}\delta_{m_z',m_z+1}\\ &\qquad +\tfrac{1}{2}(\mathcal{B}_x + \imath\mathcal{B}_y)\sqrt{J(J+1)-m_z(m_z-1)}\delta_{m_z',m_z-1} + \mathcal{B}_z m_z\delta_{m_z',m_z}\Big]\langle J,m_z| \ .\end{aligned}$$

For an angular momentum $J = 1$ *we have,*

$$V(\mathcal{B}) = -\mu_B\begin{pmatrix}\mathcal{B}_z & \frac{1}{\sqrt{2}}(\mathcal{B}_x - \imath\mathcal{B}_y) & 0\\ \frac{1}{\sqrt{2}}(\mathcal{B}_x + \imath\mathcal{B}_y) & 0 & \frac{1}{\sqrt{2}}(\mathcal{B}_x - \imath\mathcal{B}_y)\\ 0 & \frac{1}{\sqrt{2}}(\mathcal{B}_x + \imath\mathcal{B}_y) & -B_z\end{pmatrix}$$

with the eigenvalues $\langle V(\mathcal{B})\rangle = 0, \mp\mu_B|\vec{\mathcal{B}}|$.

30.2.8.3 Ex: Coupling of two electrons

Consider a two-electron system.
a. Show that the operator $(\hbar A/\hbar^2)\hat{\mathbf{s}}_1 \cdot \hat{\mathbf{s}}_2$ distinguishes the triplet from the singlet states.
b. Consider now, that the electrons are exposed to a magnetic field B applied in the direction $\hat{\mathbf{e}}_z$, so that they acquire the interaction energies with the field $(\mu_B\mathcal{B}/\hbar)(g_1\hat{s}_{1z}+g_2\hat{s}_{2z})$. Obtain the matrix associated with the total Hamiltonian and demonstrate that in the regime $\hbar A \gg \mu_B\mathcal{B}$, the representation that favors the total momentum is more adequate.
c. Show that in the regime $\hbar A \ll \mu_B\mathcal{B}$, it is convenient to use the representation that privileges the *individual* spins of the total momentum.
d. Analyze the intermediate regime $\hbar A \simeq \mu_B\mathcal{B}$.

Solution: *a. We first deal with the case of strong spin-spin coupling, $\hbar A \gg \mu_B\mathcal{B}$. We have,*

$$V_{ss} = \tfrac{\hbar A}{\hbar^2}\hat{\mathbf{s}}_1 \cdot \hat{\mathbf{s}}_2 = \tfrac{\hbar A}{2\hbar^2}(\hat{\mathbf{S}}^2 - \hat{\mathbf{s}}_1^2 - \hat{\mathbf{s}}_2^2) \ .$$

This gives,

$$V_{ss}|(s_1,s_2)S,m_S\rangle = \tfrac{\hbar A}{2}[(s_1 \pm s_2)(s_1 \pm s_2 + 1) - s_1(s_1+1) - s_2(s_2+1)]|(s_1,s_2)S,m_S\rangle$$
$$= \hbar A \left\{ \begin{array}{c} +2s_1s_2 \\ -2(s_1+1)s_2 \end{array} \right\} |(s_1,s_2)S,m_S\rangle \ .$$

The upper line corresponds to the triplet state, the lower state to the singlet state.
b. The coupling of the spins to the magnetic field is analogous to the discussion of the Zeeman effect and the Paschen-Back effect. In the case of strong spin-spin coupling, the energy of the spin-spin coupling is unaffected, such that we obtain the Zeeman effect,

$$V_{zee}(\mathcal{B}) = -\hat{\vec{\mu}}_S \cdot \vec{\mathcal{B}} = -\frac{\mu_B}{\hbar}(g_1\hat{\mathbf{s}}_1 + g_2\hat{\mathbf{s}}_2)\cdot\vec{\mathcal{B}} = -\frac{\mu_B\mathcal{B}}{\hbar}\left(g_1\frac{\hat{\mathbf{s}}_1\cdot\hat{\mathbf{S}}}{\hat{\vec{S}}^2} + g_2\frac{\hat{\mathbf{s}}_2\cdot\hat{\mathbf{S}}}{\hat{\vec{S}}^2}\right)\hat{\mathbf{S}}\cdot\vec{\mathcal{B}}$$
$$= -\frac{\mu_B}{2\hbar}\frac{g_1(\mathbf{S}^2+\mathbf{s}_1^2-\mathbf{s}_2^2)+g_2(\mathbf{S}^2+\mathbf{s}_2^2-\mathbf{s}_1^2)}{\hat{\vec{S}}^2}\hat{\mathbf{S}}\cdot\vec{\mathcal{B}}$$
$$= -\frac{\mu_B}{2\hbar}\frac{(g_1+g_2)(s_1\pm s_2)(s_1\pm s_2+1)+(g_1-g_2)s_1(s_1+1)+(g_2-g_1)s_2(s_2+1)}{(s_1\pm s_2)(s_1\pm s_2+1)}\hat{\mathbf{S}}\cdot\vec{\mathcal{B}}$$
$$= -\frac{\mu_B\mathcal{B}}{2\hbar}4\hat{S}_z \ ,$$

using $g_1 = g_2 = 2$. This gives the total energy,

$$[V_{ss} + V_{zee}(\mathcal{B})]|(s_1,s_2)S,m_S\rangle = \left[\hbar A\left\{\begin{array}{c}+2s_1s_2\\-2(s_1+1)s_2\end{array}\right\} - 2\mu_B\mathcal{B}m_S\right]|(s_1,s_2)S,m_S\rangle \ .$$

c. For weak spin-spin coupling, $\hbar A \ll \mu_B\mathcal{B}$, we have,

$$V_{ss} = \frac{\hbar A}{\hbar^2}\hat{\mathbf{s}}_1\cdot\hat{\mathbf{s}}_2 = \frac{\hbar A}{2\hbar^2}\left(\frac{\hat{\mathbf{s}}_1\cdot\vec{\mathcal{B}}}{\mathcal{B}^2}\right)\vec{\mathcal{B}}\cdot\left(\frac{\hat{\mathbf{s}}_2\cdot\vec{\mathcal{B}}}{\mathcal{B}^2}\right)\vec{\mathcal{B}} = \frac{\hbar A}{2\hbar^2}\hat{s}_{1z}\hat{s}_{2z} \ ,$$

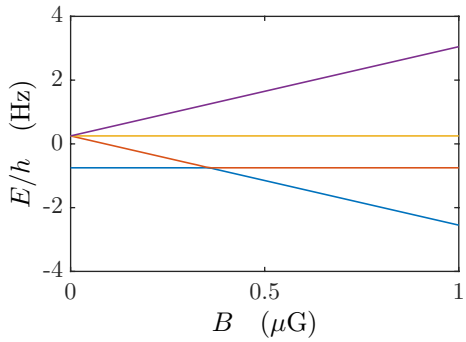

Figure 30.6: Zeeman splitting of coupled electrons.

giving

$$V_{ss}|s_1,m_1;s_2,m_2\rangle = \tfrac{\hbar A}{2} m_1 m_2 |s_1,m_1;s_2,m_2\rangle \ .$$

The reaction to a magnetic field is now that of the Paschen-Back effect,

$$V_{PB}(\mathcal{B}) = -\hat{\vec{\mu}}_S \cdot \vec{\mathcal{B}} = -\tfrac{\mu_B \mathcal{B}}{\hbar}(g_1 \hat{s}_{1z} + g_2 \hat{s}_{2z}) = -\tfrac{2\mu_B \mathcal{B}}{\hbar}(\hat{s}_{1z} + \hat{s}_{2z}) \ ,$$

using $g_1 = g_2 = 2$. *This gives,*

$$[V_{ss} + V_{zee}(\mathcal{B})]|s_1,m,1;s_2,m_2\rangle = \left[\tfrac{\hbar A}{2} m_1 m_2 - 2\mu_B \mathcal{B}(m_1+m_2)\right] |s_1,m_1;s_2,m_2\rangle \ .$$

d. For an intermediate spin-spin coupling, $\hbar A \simeq \mu_B \mathcal{B}$, *we have,*

$$\begin{aligned} V_{ss} + V_{zee}(\mathcal{B}) &= \tfrac{\hbar A}{\hbar^2} \hat{\mathbf{s}}_1 \cdot \hat{\mathbf{s}}_2 - \tfrac{\mu_B \mathcal{B}}{\hbar}(g_1 \hat{s}_{1z} + g_2 \hat{s}_{2z}) \\ &= \tfrac{\hbar A}{\hbar^2}\left(\hat{s}_{1z}\hat{s}_{2z} + \tfrac{1}{2}\hat{s}_{1+}\hat{s}_{2-} + \tfrac{1}{2}\hat{s}_{1-}\hat{s}_{2+}\right) - \tfrac{\mu_B \mathcal{B}}{\hbar}(g_1 \hat{s}_{1z} + g_2 \hat{s}_{2z}) \ . \end{aligned}$$

This gives,

$$\begin{aligned} &\langle s_1', m_1'; s_2', m_2' | [V_{ss} + V_{zee}(\mathcal{B})] | s_1, m_1; s_2, m_2 \rangle \\ &= \hbar A \left(m_1 m_2 \delta_{m_1,m_1'}\delta_{m_2,m_2'} + \tfrac{1}{2} s_{1+} s_{2-} \delta_{m_1,m_1'-1}\delta_{m_2-1,m_2'} + \tfrac{1}{2} s_{1-} s_{2+} \delta_{m_1-1,m_1'}\delta_{m_2,m_2'-1} \right) \\ &- \mu_B \mathcal{B}(g_1 m_1 + g_2 m_2)\delta_{m_1,m_1'}\delta_{m_2,m_2'} \ , \end{aligned}$$

with $s_{k\pm} \equiv \sqrt{s_k(s_k+1) - m_k(m_k \pm 1)}$. *Choosing the base* $|m_1, m_2\rangle = \begin{pmatrix} 1/2, 1/2 \\ 1/2, -1/2 \\ -1/2, 1/2 \\ -1/2, -1/2 \end{pmatrix}$

and with $g_k = 2$, $s_k = \frac{1}{2}$ *we find the following matrix representation,*

$$V_{ss} + V_{zee}(\mathcal{B}) = \begin{pmatrix} \frac{1}{4}\hbar A - 2\mu_B \mathcal{B} & 0 & 0 & 0 \\ 0 & -\frac{1}{4}\hbar A & \frac{1}{2}\hbar A s_{1-} s_{2+} & 0 \\ 0 & \frac{1}{2}\hbar A s_{1+} s_{2-} & -\frac{1}{4}\hbar A & 0 \\ 0 & 0 & 0 & \frac{1}{4}\hbar A + 2\mu_B \mathcal{B} \end{pmatrix} \ ,$$

with $s_{1-}s_{2+} = s_{1+}s_{2-} = 1$. The characteristic equation is,

$$0 = det\,[V_{ss}+V_{zee}(\mathcal{B})] = (\tfrac{1}{4}\hbar A-2\mu_B\mathcal{B}-E)(\tfrac{1}{4}\hbar A+2\mu_B\mathcal{B}-E)\left[(-\tfrac{1}{4}\hbar A-E)^2-(\tfrac{1}{2}\hbar A)^2\right] .$$

The eigenvalues are,

$$E = \tfrac{1}{4}\hbar A \pm 2\mu_B\mathcal{B}, -\tfrac{3}{4}\hbar A, \tfrac{1}{4}\hbar A .$$

This is nothing more than the Breit-Rabi formula for the specific case that both spin are $\frac{1}{2}$, that is, all states are fully stretched.

30.2.8.4 Ex: Breit-Rabi formula

Derive the analytical Breit-Rabi formula for the hyperfine structure (30.46) supposing $J = \frac{1}{2}$.

Solution: *The purpose is to diagonalize the following matrix,*

$$\begin{aligned}\langle m_I' m_J'|V_{hfs}+V_{zee}(\mathcal{B})|m_I m_J\rangle &= \langle m_I' m_J'|\tfrac{A_J}{\hbar^2}\mathbf{I}\cdot\mathbf{J}+g_J\mu_B\vec{\mathcal{B}}\cdot\mathbf{J}-g_I\mu_N\vec{\mathcal{B}}\cdot\mathbf{I}|m_I m_J\rangle \\ &= \langle m_I' m_J'|A_J(I_zJ_z+\left(\tfrac{1}{2}I_+J_-+\tfrac{1}{2}I_-J_+\right)+g_J\mu_B\mathcal{B}J_z-g_I\mu_N\mathcal{B}I_z|m_I m_J\rangle .\end{aligned}$$

Now, since $J = \frac{1}{2}$ we know that there are only two hyperfine states $F = I \pm J = I \pm \frac{1}{2}$. We also know $m_F = m_I + m_J$ and $m_J \pm \frac{1}{2}$. Using the formula,

$$\hat{J}_\pm|m_I, m_J\rangle = \hbar\sqrt{J(J+1)-m_J(m_J\pm 1)}|m_I, m_J\pm 1\rangle ,$$

we find,

$$\hat{J}_\pm|m_I, \pm\tfrac{1}{2}\rangle = 0 \qquad and \qquad \hat{J}_\pm|m_I, \mp\tfrac{1}{2}\rangle = |m_I, \mp\tfrac{1}{2}\rangle .$$

With this, we can calculate the components of the matrix:

$$\begin{aligned}\langle m_I', \tfrac{1}{2}|V_{hfs}+V_{zee}(B)|m_I, \tfrac{1}{2}\rangle &= (A_J m_I\tfrac{1}{2}+\hbar g_J\mu_B\mathcal{B}\tfrac{1}{2}-\hbar g_I\mu_N\mathcal{B}m_I)\delta_{m_I' m_I} \\ &= \left[\tfrac{A_J}{2}(m_F-\tfrac{1}{2})+\tfrac{\hbar}{2}(g_J\mu_B-g_I\mu_N)\mathcal{B}-\hbar g_I\mu_N\mathcal{B}m_F\right]\delta_{m_I' m_I} \\ \langle m_I', -\tfrac{1}{2}|V_{hfs}+V_{zee}(B)|m_I, -\tfrac{1}{2}\rangle &= (-A_J m_I\tfrac{1}{2}-\hbar g_J\mu_B\mathcal{B}\tfrac{1}{2}-\hbar g_I\mu_N\mathcal{B}m_I)\delta_{m_I' m_I} \\ &= \left[-\tfrac{A_J^2}{2}(m_F+\tfrac{1}{2})-\tfrac{\hbar}{2}(g_J\mu_B-g_I\mu_N)\mathcal{B}-\hbar g_I\mu_N\mathcal{B}m_F\right]\delta_{m_I' m_I} \\ \langle m_I', \tfrac{1}{2}|V_{hfs}+V_{zee}(\mathcal{B})|m_I, -\tfrac{1}{2}\rangle &= \tfrac{A_J}{2}\sqrt{I(I+1)+m_I(m_I-1)}\delta_{m_I' m_I-1} \\ &= \tfrac{A_J}{2}\sqrt{I(I+1)+(m_F^2-\tfrac{1}{4})}\delta_{m_I' m_I-1} \\ \langle m_I', -\tfrac{1}{2}|V_{hfs}+V_{zee}(\mathcal{B})|m_I, \tfrac{1}{2}\rangle &= \tfrac{A_J}{2}\sqrt{I(I+1)+m_I(m_I+1)}\delta_{m_I' m_I+1} \\ &= \tfrac{A_J}{2}\sqrt{I(I+1)+(m_F^2-\tfrac{1}{4})}\delta_{m_I' m_I+1} .\end{aligned}$$

The eigenvalues of this 2×2 matrix are,

$$\Delta E_{hfs}+\Delta E_{zee}(\mathcal{B}) = -\tfrac{A_J}{4}-g_I\mu_N\mathcal{B}m_F \pm \tfrac{A_J}{4}\sqrt{-1+8m_F^2+4A_J^2I(I+1)+4m_Fx+x^2} ,$$

with the abbreviation $x \equiv \frac{2(\mu_B g_J-\mu_N g_I)\mathcal{B}}{A_J}$. This is the Breit-Rabi formula. Note that the derivation can also be made in the base $|(I,J),F,m_F\rangle$ using the formula $\mathbf{I}\cdot\mathbf{J} = \frac{1}{2}(\mathbf{F}^2-\mathbf{J}^2-\mathbf{I}^2)$.

30.2.8.5 Ex: Reciprocal pollution of the Paschen-Back and Zeeman regimes

a. Determine the interaction matrix $\langle \tilde{m}_J \tilde{m}_I | \hat{V}_{hfs} + \hat{V}_{zee}(B) | m_J m_I \rangle$ of an atom with electron spin **J** and nuclear spin **J** in the decoupled base without considering the quadrupolar terms.
b. Determine the interaction matrix explicitly for the case of ^{6}Li ($I = 1$) in its ground state $^2S_{1/2}$ ($A_J = h \cdot 152.137$ MHz) for a magnetic field of $\mathcal{B} = 100$ G.
c. For the system defined in (b) determine the eigenvalues $E(\mathcal{B})$ of the interaction matrix and the eigenvectors $|\alpha(\mathcal{B})\rangle$ on the decoupled base $|m_J m_I\rangle$.
d. For the system defined in (c) determine the eigenvectors $|\alpha(\mathcal{B})\rangle$ in the coupled base $|F m_F\rangle$.
e. How good are the selection rules for transitions $S_{1/2} - P_{3/2}$ in the intermediate regime between Zeeman and Paschen-Back? We start by calculating the Zeeman shifts for both levels (s denotes the structure $S_{1/2}$, p the structure $P_{3/2}$)

$$
\begin{aligned}
{}_B\langle m_J^s m_I^s | H_{hfs} + H_B | m_J^s m_I^s \rangle_B &= E^s(\mathcal{B}) \\
{}_B\langle m_J^p m_I^p | H_{hfs} + H_B | m_J^p m_I^p \rangle_B &= E^p(\mathcal{B}) \ .
\end{aligned}
$$

For the level $P_{3/2}$ the interval factor is less. In particular for ^{6}Li it is so small that we are immediately in the Paschen-Back scheme. This means that the matrix $\overline{{}_\infty\langle \tilde{m}_J^p \tilde{m}_I^p | m_J^p m_I^p \rangle_B} = \delta_{m_J^p, \tilde{m}_J^p} \delta_{m_I^p, \tilde{m}_I^p}$ is diagonal. The element of the transition matrix is then,

$$
\begin{aligned}
&{}_B\langle m_J^p m_I^p | T_q^{(E\kappa)} | m_J^s m_I^s \rangle_B \\
&\quad = \sum_{\tilde{m}_J^s \tilde{m}_I^s} \sum_{\tilde{m}_J^p \tilde{m}_I^p} \overline{{}_\infty\langle \tilde{m}_J^p \tilde{m}_I^p | m_J^p m_I^p \rangle_B} \ {}_\infty\langle \tilde{m}_J^s \tilde{m}_I^s | m_J^s m_I^s \rangle_B \ {}_\infty\langle \tilde{m}_J^p \tilde{m}_I^p | T_q^{(E\kappa)} | \tilde{m}_J^s \tilde{m}_I^s \rangle_\infty \\
&\quad = \sum_{\tilde{m}_J^s \tilde{m}_I^s} {}_\infty\langle \tilde{m}_J^s \tilde{m}_I^s | m_J^s m_I^s \rangle_B \ {}_\infty\langle m_J^p m_I^p | T_q^{(E\kappa)} | \tilde{m}_J^s \tilde{m}_I^s \rangle_\infty \ .
\end{aligned}
$$

The matrix elements in the pure Zeeman regime can be expressed by [Deh07, unpublished],

$$
\begin{aligned}
\langle F^p m_F^p | T_q^{(E\kappa)} | F^s m_F^s \rangle &=_0 \langle m_J^p m_I^p | \, T_q^{(E\kappa)} \, | m_J^s m_I^s \rangle_0 \\
&= \begin{pmatrix} J^s & \kappa & J^p \\ m_J^s & \mathrm{sign}(m^p - m^s) & -m_J^p \end{pmatrix}^2 \begin{Bmatrix} J^p & J^s & \kappa \\ F^s & F^p & I \end{Bmatrix}^2 \frac{(2F^s+1)(2J^p+1)(2\kappa+1)}{2I+1} \ .
\end{aligned}
$$

Discuss the pure Paschen-Back regime via ${}_\infty\langle m_J^p m_I^p | T_q^{(E\kappa)} | m_J^s m_I^s \rangle_\infty$.

Solution: *a. The level shifts in a magnetic field are calculated in a regime, where m_J and m_I are good quantum numbers. Therefore, the diagonalization of the interaction matrix gives the eigenvalues (Zeeman shifts), and in strong magnetic fields, the corresponding eigenvectors are orthonormal. As the quadrupole interaction can usually be neglected, $B_J = 0$, we get,*

$$
\hat{H}_{hfs} + \hat{H}_B = \tfrac{A_J}{\hbar^2} \mathbf{I} \cdot \mathbf{J} + g_J \mu_B \vec{\mathcal{B}} \cdot \mathbf{J} - g_I \mu_N \vec{\mathcal{B}} \cdot \mathbf{I} \ .
$$

The elements of the matrix are,

$$
\begin{aligned}
&\langle \tilde{m}_I \tilde{m}_J | \hat{H}_{hfs} + \hat{H}_B | m_I m_J \rangle = (g_J m_J - g_I \mu_N m_I) \mu_B \mathcal{B} \delta_{\tilde{m}_I, m_I} \delta_{\tilde{m}_J, m_J} \\
&+ A_J \left\{ m_I m_J \delta_{\tilde{m}_I, m_I} \delta_{\tilde{m}_J, m_J} + \tfrac{1}{2} I_+ J_- \delta_{\tilde{m}_I, m_I+1} \delta_{\tilde{m}_J, m_J-1} + \tfrac{1}{2} I_- J_+ \delta_{\tilde{m}_I, m_I-1} \delta_{\tilde{m}_J, m_J+1} \right\} \ .
\end{aligned}
$$

b. In particular, for the given system we obtain,

$$\langle \tilde{m}_I \tilde{m}_J | \hat{H}_{hfs} + \hat{H}_B | m_I m_J \rangle = \begin{pmatrix} 0 & 0 & 0 & 0 & 0 & 0 \\ 0 & 0 & 0 & 0 & 0 & 0 \\ 0 & 0 & 0 & 0 & 0 & 0 \\ 0 & 0 & 0 & 0 & 0 & 0 \\ 0 & 0 & 0 & 0 & 0 & 0 \\ 0 & 0 & 0 & 0 & 0 & 0 \end{pmatrix} ,$$

using the following base: $\{|m_J, m_I\rangle\} = \{|\frac{1}{2}, 1\rangle, |\frac{1}{2}, 0\rangle, |\frac{1}{2}, -1\rangle, |-\frac{1}{2}, 1\rangle, |-\frac{1}{2}, 0\rangle, |-\frac{1}{2}, -1\rangle\}$.
c. We express the eigenfunctions corresponding to the eigenvalues by,

$$|\alpha(\mathcal{B})\rangle = \sum_{m_J m_I} |m_J m_I\rangle\langle m_J m_I | \alpha(\mathcal{B})\rangle \ .$$

We find, for example, for the ground state $^6Li\ S_{1/2}$,

$$|\alpha_{PB,1}(150\,\mathrm{G})\rangle = 0.987|m_J = -\tfrac{1}{2}, m_I = 1\rangle + 0.162|m_J = \tfrac{1}{2}, m_I = 0\rangle$$
$$|\alpha_{PB,2}(500\,\mathrm{G})\rangle = 0.999|m_J = -\tfrac{1}{2}, m_I = 1\rangle + 0.055|m_J = \tfrac{1}{2}, m_I = 0\rangle \ .$$

d. We express the eigenfunctions corresponding to the eigenvalues by,

$$|\alpha(\mathcal{B})\rangle = \sum_{m_J m_I} |m_J m_I\rangle\langle m_J m_I | \alpha(\mathcal{B})\rangle = \sum_{m_J m_I} \sum_{F m_F} |F m_F\rangle\langle F m_F | m_J m_I\rangle\langle m_J m_I | \alpha(\mathcal{B})\rangle \ ,$$

where $\langle F m_F | m_J m_I\rangle$ *are the Clebsch-Gordans and the* $\langle m_J m_I | \alpha(\mathcal{B})\rangle$ *were determined in (c). We find, for example, for the ground state* $^6Li\ S_{1/2}$,

$$|\alpha_{Z,1}(150\,\mathrm{G})\rangle = 0.xxx|F = 0, m_F = 0\rangle + 0.yyy|F = 1, m_F = 0\rangle$$
$$|\alpha_{Z,1}(500\,\mathrm{G})\rangle = 0.xxx|F = 0, m_F = 0\rangle + 0.yyy|F = 1, m_F = 0\rangle \ .$$

e.

30.2.8.6 Ex: Diamagnetism of the ground states of H atoms

Calculate the quadratic Zeeman effect for the ground state of the hydrogen atom caused by the (usually neglected) diamagnetic term of the Hamiltonian in first order TPIT. Write down the energy shift as $\Delta E = -\frac{\chi}{2}\mathcal{B}^2$ assuming a constant magnetic field in order to obtain the diamagnetic susceptibility χ.

Solution: *The diamagnetic term of the interaction Hamiltonian with electromagnetic fields is,*

$$\hat{H}_{int} = \frac{e^2 \mathbf{A}^2}{2m} \ .$$

Assuming a homogeneous magnetic field, $\mathbf{A} = \frac{\mathcal{B}}{2}(y\hat{\mathbf{e}}_x - x\hat{\mathbf{e}}_y) = \frac{\mathcal{B}}{2}\rho\hat{\mathbf{e}}_\phi$ *with* $\rho = r\sin\theta$, *we make a first coarse approximation substituting* ρ *by* a_B,

$$\langle \hat{H}_{int}\rangle_{ap} \simeq \mathcal{B}^2 \frac{e^2 a_B^2}{8m} \approx h\mathcal{B}^2\ 96\,\mathrm{mHz/G}^2 \ .$$

The theoretical value is 5.5 mHz/G². For a better estimate based on the 1s orbital wavefunction, $\psi_{100} = \frac{1}{\sqrt{\pi}}(Z/a_B)^{3/2}e^{-Zr/a_B}$. *We get for the first electron,*

$$\begin{aligned}\langle\psi_{100}|\hat{H}_{int}|\psi_{100}\rangle &= \frac{e^2\mathcal{B}^2}{8m}\frac{Z^3}{\pi a_B^3}\int_{\mathbb{R}^3} e^{-Zr/a_B}\rho^2 e^{-Zr/a_B}d^3r \\ &= \frac{e^2\mathcal{B}^2}{8m}\frac{Z^3}{\pi a_B^3}2\pi\int_0^\pi \sin^3\theta d\theta\int_0^\infty e^{-u}u^4du\left(\frac{a_B}{2Z}\right)^5 \\ &= \frac{e^2\mathcal{B}^2}{8m}\frac{Z^3}{\pi a_B^3}2\pi\frac{4}{3}\ 24\ \left(\frac{a_B}{2Z}\right)^5 = \frac{8e^2\mathcal{B}^2a_B^2}{mZ^2} = \frac{64}{Z^2}\langle\hat{H}_{int}\rangle_{ap}\ .\end{aligned}$$

Hence,

$$\chi = -\frac{16e^2a_B^2}{mZ^2}\ .$$

30.3 Interaction with electric fields

30.3.1 Stark Effect

Electric fields interact with the electrons of the atom. Describing the atom by its dipole moment, according to (30.13), the interaction energy is,

$$\hat{V}_{stark} = -\hat{\mathbf{d}}\cdot\vec{\mathcal{E}}\ . \tag{30.65}$$

This is the *Stark effect*. This effect is usually weak, and its observation requires strong fields or high spectral resolution. Stationary perturbation theory TIPT gives,

$$E_n^{(1)} = \langle\psi_n^{(0)}|-\hat{\mathbf{d}}\cdot\mathcal{E}|\psi_n^{(0)}\rangle = e\mathcal{E}_z\int_{\mathbb{R}^3} z|\psi_n^{(0)}|^2d^3r = 0\ , \tag{30.66}$$

with $\mathbf{d} = -e\mathbf{r}$ and $\vec{\mathcal{E}}_z = \mathcal{E}_z\hat{\mathbf{e}}_z$. This only applies when the states have well-defined parity and are NOT degenerate in ℓ. When they ARE degenerate in ℓ, which is the case of hydrogen, the states have no defined parity $(-1)^\ell$. For example, the states s and p contributing to the same state $|\psi_{n,j}\rangle$ have different parities. In this case, the condition (30.66) is not automatically satisfied, and the first perturbation order yields a value. This is the case of the *linear Stark effect*. In the Excs. 30.3.2.1 and 30.3.2.2 we explicitly calculate the Stark energy shift for a hydrogen atom subject to an electric field.

Other atoms do not have this degeneracy, and we must calculate the *quadratic Stark effect* in second order TIPT,

$$|\psi_n^{(1)}\rangle = e\mathcal{E}_z\sum_{n'\neq n}|\psi_{n'}^{(0)}\rangle\frac{\langle\psi_{n'}^{(0)}|\hat{z}|\psi_n^{(0)}\rangle}{E_n-E_{n'}}\ . \tag{30.67}$$

and

$$E_n^{(2)} = e^2\mathcal{E}_z^2\sum_{n'\neq n}\frac{|\langle\psi_{n'}^{(0)}|\hat{z}|\psi_n^{(0)}\rangle|^2}{E_n-E_{n'}}\ . \tag{30.68}$$

To simplify the matrix elements, we separate the radial part from the angular part,

$$\langle\psi_{n'}^{(0)}|\hat{z}|\psi_n^{(0)}\rangle = \langle n'J'm'_J|\hat{z}|nJm_J\rangle = \int_0^\infty r^3 R_{n'J'}R_{nJ}dr \int Y^*_{J'm'_J}\tfrac{z}{r}Y_{Jm_J}d\Omega \ . \quad (30.69)$$

The radial part, written as

$$\langle n'_J J'||\hat{z}||n_J J\rangle \equiv \int_0^\infty r^3 R_{n'_J J'}R_{n_J J}dr \ , \quad (30.70)$$

and called the *irreducible matrix element*, no longer depends on the magnetic quantum number. On the other hand, the angular part may be expressed by Clebsch-Gordan coefficients, as will be discussed more extensively in Sec. 34.2.3. The result is called *Wigner-Eckart theorem*,

$$\boxed{\frac{\langle n'_J J'm'_J|\hat{z}|n_J Jm_J\rangle}{\langle n'_J J'||\hat{z}||n_J J\rangle} = \int Y^*_{J'm'_J}\tfrac{z}{r}Y_{Jm_J}d\Omega = \frac{1}{2J'+1}\begin{pmatrix} J & 1 & J' \\ m_J & 0 & -m'_J\end{pmatrix}} \ . \quad (30.71)$$

With $[\hat{z},\hat{L}_z]=0$, which was shown in Exc. 25.3.4.2, and obviously $[\hat{z},\hat{S}_z]=0$ we find,

$$0 = \langle J'm'_J|[\hat{z},\hat{J}_z]|Jm_J\rangle = (m_J - m'_J)\langle J'm'_J|\hat{z}|Jm_J\rangle \ . \quad (30.72)$$

This means that for $m_J \neq m'_J$, the matrix elements $\langle J'm'_J|\hat{z}|Jm_J\rangle$ should disappear. Therefore, the matrix is diagonal in m_J. We consider dipole transitions with $|J-J'| \leq 1$ [1],

$$\begin{pmatrix} J & 1 & J+1 \\ m_J & 0 & -m_J\end{pmatrix} = \frac{(J+1)^2-m_J^2}{(2J+1)(J+1)}, \quad (30.73)$$
$$\begin{pmatrix} J & 1 & J \\ m_J & 0 & -m_J\end{pmatrix} = \frac{m_J^2}{J(J+1)} \ ,$$
$$\begin{pmatrix} J & 1 & J-1 \\ m_J & 0 & -m_J\end{pmatrix} = \frac{J^2-m_J^2}{J(2J+1)} \ .$$

States with the same $|m_J|$ lead to the same quadratic Stark effect,

$$\Delta E \sim A + B|m_J|^2 \ . \quad (30.74)$$

The factors A and B depend on the main quantum number n and also on L,S,J. Moreover, they depend on the energy distance of all contributing levels, because of the denominator in the perturbation equation (30.67). Only levels with different parity $(-1)^L$ contribute. The formulae (30.73) will be derived explicitly in Exc. 30.3.2.3.

30.3.2 Exercises

30.3.2.1 Ex: Stark effect in hydrogen

Consider the hydrogen atom immersed in a uniform electric field $\vec{\mathcal{E}}$ applied along the $\hat{\mathbf{e}}_z$-direction. The term corresponding to this interaction in the total Hamiltonian

[1] For it is possible to show that $\langle n'_J J'||\hat{z}||n_J J\rangle = 0$ for $|J-J'|>1$.

is $\hat{H}^{(1)} = -e\vec{\mathcal{E}}\hat{z}$. For typical electric fields produced in laboratory, the condition $\hat{H}^{(1)} \ll \hat{H}_0$, which allows the use of TIPT, is satisfied. The effect of the perturbation $\hat{H}^{(1)}$, called Stark effect, is the removal of the degeneracy of some of the hydrogen atom states. Calculate the Stark effect for the state $n = 2$.

Solution: *Before explicitly calculating the elements of the perturbation matrix, we note that the perturbation matrix has nonzero components only between states of opposite parity. As we are considering the level $n = 2$, the relevant states are $\ell = 0$ and $\ell = 1$. Hence,*

$$\langle n'\ell'm'|\hat{z}|n\ell m\rangle = 0 \qquad for \qquad \ell = \ell' \ .$$

In addition, knowing

$$0 = \langle n'\ell'm'|[\hat{L}_z, \hat{z}]|n\ell m\rangle = (m - m')\langle n'\ell'm'|\hat{z}|n\ell m\rangle \ ,$$

we deduce that,

$$\langle n'\ell'm'|\hat{z}|n\ell m\rangle = 0 \qquad para \qquad m \neq m' \ .$$

Therefore, by choosing the basis as $\Big(2s \quad 2p, m = 0 \quad 2p, m = 1 \quad 2p, m = -1\Big)$, we obtain the matrix,

$$W_s = \begin{pmatrix} 0 & \langle 2s|W|2p, m = 0\rangle & 0 & 0 \\ \langle 2p, m = 0|W|2s\rangle & 0 & 0 & 0 \\ 0 & 0 & 0 & 0 \\ 0 & 0 & 0 & 0 \end{pmatrix} \ .$$

We calculate explicitly,

$$\begin{aligned} \langle \phi_{200}|z|\phi_{100}\rangle &= \frac{a_B}{32\pi}\int_0^\infty \int_0^\pi \int_0^{2\pi} \tilde{r}e^{-\tilde{r}/2}\cos\theta \ \tilde{r}\cos\theta \ (2-\tilde{r})e^{-\tilde{r}/2}\tilde{r}^2\sin\theta d\theta d\phi d\tilde{r} \\ &= \frac{a_B}{16}\int_{-1}^1 \cos^2\theta d(\cos\theta)\int_0^\infty (2-\tilde{r})\tilde{r}^4 e^{-\tilde{r}}d\tilde{r} = \frac{a_B}{16}\frac{2}{3}(-72) = -3a_B \ . \end{aligned}$$

The characteristic equation for degenerate TIPT gives,

$$0 = \det(W_s - E\delta_{\ell\ell'}\delta_{mm'}) = E^2(E^2 - W_s^2) \ ,$$

such that we get four energies,

$$E = 0, \pm 3ea_B|\vec{\mathcal{E}}| \ .$$

Note that the matrix element is linear in $|\vec{\mathcal{E}}|$. Therefore, this correction is called the linear Stark effect. Transforming into the base diagonalizing the perturbation, we obtain the four vectors,

$$|2p, m = \pm 1\rangle \qquad and \qquad \tfrac{1}{\sqrt{2}}|2p, m = 0\rangle \pm |2s, m = 0\rangle \ .$$

30.3.2.2 Ex: Stark effect in the $1s$ hydrogen level

Calculate the Stark shift of the hydrogen ground state by taking into account the contributions of the excited states $n = 2, 3, ...$

Solution: *The energy term in second order perturbation theory for the* $1s$ *state of hydrogen is given by,*

$$E^{(2)} = e^2\mathcal{E}^2 \sum_{n\neq 1,\ell,m} \frac{|\langle 100|z|n\ell m\rangle|^2}{E_1 - E_n} \ ,$$

where E_n *is the eigenvalue associated with* $|n\ell m\rangle$ *taken from Bohr's model. As there are states* $|n\ell m\rangle$ *with parity opposite to* $|100\rangle$*, the term* $E^{(2)}$ *will not be zero and there will, in fact, be a quadratic contribution to the energy shift, which will be negative because* $E_1 - E_n < 0$*. An upper limit for the magnitude of this reduction can be obtained, noting that* $|E_1 - E_n| \geq \Delta E$*, where* $\Delta E \equiv |E_1 - E_2|$ *and hence,*

$$\begin{aligned} |E^{(2)}| &\leq \frac{e^2\mathcal{E}^2}{\Delta E} \sum_{n\neq 1,\ell,m} \langle 100|z|n\ell m\rangle\langle n\ell m|z|100\rangle \\ &= \frac{e^2\mathcal{E}^2}{\Delta E} \langle 100|z \left(\sum_{n\neq 1,\ell,m} |n\ell m\rangle\langle n\ell m| \right) z|100\rangle \ , \end{aligned}$$

Using the completeness relation for the base $|n\ell m\rangle$*,*

$$\sum_{n\neq 1,\ell,m} |n\ell m\rangle\langle n\ell m| = \mathbb{I} - |100\rangle\langle 100| \ ,$$

the inequality can be written in the form,

$$|E^{(2)}| \leq \frac{e^2\mathcal{E}^2}{\Delta E} [\langle 100|z^2|100\rangle - \langle 100|z|100\rangle^2] \ ,$$

As mentioned above, $\langle 100|z|100\rangle = 0$*, and the other term can be easily calculated,*

$$\langle 100|z^2|100\rangle = \int d\Omega \sin\theta \cos^2\theta \int dr r^4 \left(\frac{e^{-r/a_B}}{\sqrt{\pi a_B^3}} \right)^2 = a_B^2 \ .$$

Replacing the value $\Delta E = 3e^2/32\pi\epsilon_0 a_B$*, the limit for the reduction of energy is obtained,*

$$|E^{(2)}| \leq \frac{32\pi}{3} \epsilon_0 a_B^3 \mathcal{E}^2 \simeq 10.667\pi\epsilon_0 a_B^3 \mathcal{E}^2 \ .$$

To obtain the real energy correction from the starting equation, the matrix elements of z *must be calculated,*

$$\langle 100|z|n\ell m\rangle = \int d^3r R^*_{n\ell}(r) Y^*_{\ell m}(\theta,\phi)(r\cos\theta)\tfrac{1}{\sqrt{4\pi}} R_{10}(r) \ ,$$

where $\langle \mathbf{r}|n\ell m\rangle = R_{n\ell}(r)Y_{\ell m}(\theta,\phi)$. *Using* $\cos\theta = \sqrt{\frac{4\pi}{3}}Y_{10}(\theta,\phi)$, *we obtain,*

$$\langle 100|z|n\ell m\rangle = \int drr^3 R^*_{n\ell}(r)R_{10}(r)\int d\Omega Y^*_{\ell m}(\theta,\phi)\tfrac{1}{\sqrt{3}}Y_{10}(\theta,\phi)\ ,$$

and with the orthogonality relations for the spherical harmonics, the angular part is easily solved,

$$\langle 100|z|n\ell m\rangle = \frac{\delta_{\ell 1}\delta_{m0}}{\sqrt{3}}\int drr^3 R^*_{n\ell}(r)R_{10}(r)\ ,$$

Therefore, the second order energy correction is given by,

$$E^{(2)} = \frac{-8\pi\epsilon_0 a_B\mathcal{E}^2}{3}\sum_{n\neq 1}\left[\left(\int drr^3 R^*_{n\ell}(r)R_{10}(r)\right)^2\frac{n^2}{n^2-1}\right]\ .$$

The calculation of the radial integrals in general is not trivial, but the result for the sum can be estimated by taking the first terms. For example, for $n = 1,...,4$, *we have the radial wavefunctions,*

$$R_{10}(r) = \frac{2}{\sqrt{a_B^3}}e^{-r/a_B}\quad ,\quad R_{21}(r) = \frac{1}{2\sqrt{6a_B^3}}\frac{r}{a_B}e^{-r/2a_B}$$
$$R_{31}(r) = \frac{4}{81\sqrt{6a_B^3}}\left(6-\frac{r}{a_B}\right)\frac{r}{a_B}e^{-r/3a_B}\quad ,\quad R_{41}(r) = \frac{1}{8\sqrt{15a_B^3}}\left(\frac{r^2}{8a_B^2}-\frac{5r}{2a_B}+10\right)\ ,$$

and the integrals result in,

$$\int_0^\infty drr^3 R_{21}(r)R_{10}(r) = \frac{2^8}{3^4\sqrt{6}}a_B\quad ,\quad \int_0^\infty drr^3 R_{21}(r)R_{10}(r) = \frac{3^4}{2^6\sqrt{6}}a_B$$
$$\int_0^\infty drr^3 R_{21}(r)R_{10}(r) = \frac{2^8 3^3}{5^5\sqrt{15}}a_B\ .$$

With these terms, the energy shift is,

$$E^{(2)} = \frac{-8\pi\epsilon_0 a_B\mathcal{E}^2}{3}(2.220+0.300+0.157+..) \simeq -7.139\pi\epsilon a_B^3\mathcal{E}\ .$$

The exact result for this energy correction is $-9\pi\epsilon_0 a_B^3\mathcal{E}$ *[136].*

30.3.2.3 Ex: Stark effect

Derive the Eqs. (30.73) from the formula (28.5).

Solution: *We have*

$$\begin{pmatrix} J & 1 & J' \\ m_J & 0 & -m_J\end{pmatrix} = (-1)^{J-1+m_J}\sqrt{\frac{(J+1-J')!(J-1+J')!(-J+1+J')!}{(J+J'+2)!}}\times$$
$$\times\sum_t \frac{(-1)^t\sqrt{(J+m_J)!(J-m_J)!(J'-m_J)!(J'+m_J)!}}{t!(m_J-1+J'+t)!(-J+J'+t)!(J+1-J'-t)!(J-m_J-t)!(1-t)!}\ .$$

For $J' = J - 1$ we have

$$\begin{pmatrix} J & 1 & J-1 \\ m_J & 0 & -m_J \end{pmatrix} = (-1)^{J-1+m_J} \sqrt{\frac{2!(2J-2)!}{(2J+1)!}} \times \sum_t \frac{(-1)^t \sqrt{(J+m_J)!(J-m_J)!(J-1-m_J)!(J-1+m_J)!}}{t!(m_J-2+J+t)!(t-1)!(2-t)!(J-m_J-t)!(1-t)!} \times$$

$$\begin{pmatrix} J & 1 & J-1 \\ m_J & 0 & -m_J \end{pmatrix}^2 = \frac{2}{(2J+1)(2J)(2J-1)} \left[J^2 - m_J^2\right] \ .$$

For $J' = J$ we have

$$\begin{pmatrix} J & 1 & J \\ m_J & 0 & -m_J \end{pmatrix} = (-1)^{J-1+m_J} \sqrt{\frac{(2J-1)!}{(2J+2)!}} \sum_t \frac{(-1)^t (J+m_J)!(J-m_J)!}{t!^2(1-t)!^2(m_J-1+J+t)!(J-m_J-t)!}$$

$$\begin{pmatrix} J & 1 & J \\ m_J & 0 & -m_J \end{pmatrix}^2 = \frac{4}{(2J+2)(2J+1)2J} m_J^2 \ .$$

For $J' = J + 1$ we have

$$\begin{pmatrix} J & 1 & J+1 \\ m_J & 0 & -m_J \end{pmatrix} = (-1)^{J-1+m_J} \sqrt{\frac{(J+1-J')!(J-1+J')!(-J+1+J')!}{(J+J'+2)!}} \times \sum_t \frac{(-1)^t \sqrt{(J+m_J)!(J-m_J)!(J'-m_J)!(J'+m_J)!}}{t!(m_J-1+J'+t)!(-J+J'+t)!(J+1-J'-t)!(J-m_J-t)!(1-t)!}$$

$$\begin{pmatrix} J & 1 & J+1 \\ m_J & 0 & -m_J \end{pmatrix}^2 = \frac{2}{(2J+3)(2J+2)(2J+1)} \left[(J+1)^2 - m_J^2\right] \ .$$

30.4 Further reading

T. Mayer-Kuckuk, *Atomphysik, Teubner Studienbücher (1985)* [860]ISBN

Chapter 31

Atoms with many electrons

31.1 Symmetrization of bosons and fermions

Quantum mechanics must be formulated in a way to avoid any possibility of distinguishing identical particles. However, the language of mathematics automatically assigns a particle to a wavefunction; for example, $\psi_a(x_1)$ is the wavefunction a of particle 1 and $\psi_b(x_2)$ the wavefunction b of particle 2. In the absence of interactions, the total wavefunction, $\Psi = \psi_a(x_1)\psi_b(x_2)$, solves the Schrödinger equation of two particles. Now, by changing the coordinates of the particles we get a different state $\Psi' = \psi_a(x_2)\psi_b(x_1)$ [1]. This erroneously suggests that the wavefunction of a particle plays the role of a *label* (or 'soul') characterizing the particle beyond its set of quantum numbers. Why this is a problem, we will see in the following example [2].

Example 185 (*Indistinguishability of particles*): We consider a system of two non-interacting spinless particles in an infinite potential well. The total wavefunction is,

$$\Psi^{(1,2)} \equiv \psi_a(x_1)\psi_b(x_2) = C\cos\frac{n_a\pi x_1}{L}\cos\frac{n_b\pi x_2}{L} \tag{31.1}$$

with the energy,

$$E_{a,b} = \frac{\pi^2 n_a^2}{2mL^2} + \frac{\pi^2 n_b^2}{2mL^2} \ .$$

For observable quantities, such as $|\Psi^{(1,2)}|^2$, we must ensure, $|\Psi^{(1,2)}|^2 = |\Psi^{(2,1)}|^2$, that is,

$$C^2\cos^2\tfrac{n_a\pi x_1}{L}\cos^2\tfrac{n_b\pi x_2}{L} = C^2\cos^2\tfrac{n_a\pi x_2}{L}\cos^2\tfrac{n_b\pi x_1}{L} \ ,$$

[1] We note that the states are orthogonal, because

$$\int \Psi^{*(1,2)}\Psi^{(2,1)}dx_1dx_2 = \int \psi_a^*(x_1)\psi_b^*(x_2)\psi_a(x_2)\psi_b(x_1)dx_1dx_2$$
$$= \int \psi_a^*(x_1)\psi_b(x_1)dx_1 \int \psi_b^*(x_2)\psi_a(x_2)dx_2 = \delta_{n_a,n_b} \ .$$

[2] Ultimately, all this is simply a consequence of the uncertainty principle, which forbids us to specify a wavefunction as a function of two non-commuting coordinates: We have to choose one coordinate on which the wavefunction depends and treat the other as a quantum number, for example, $\psi_{\mathbf{k}}(\mathbf{r}) = e^{\imath\mathbf{k}\cdot\mathbf{r}}$ or $\psi_n(x) = \cos\frac{n\pi x}{L}$. When we now exchange the coordinates of two particles without changing their quantum numbers, we get obviously different states. In classical physics, the wavefunction of a particle would be written $\psi(x,p)$. If two classical particles are not distinct by any other mean, an exchange of *all* their coordinates would reproduce exactly the same state.

but this is not valid for $n_a \neq n_b$. If $n_a = n_b$, we have $\psi_a = \psi_b$. That is, the particles stay in the same state, and we do not need to worry about indistinguishability:

$$\Psi^{(2,1)} = \psi_a(x_2)\psi_b(x_1) = \Psi^{(1,2)} \qquad \text{and} \qquad E_{a,b} = E_{b,a} \ .$$

However, the fact that this state is never observed with two electrons shows, that theory must be corrected to allow a true description of reality. Will deepen this argument in Exc. 31.1.3.1.

We need to construct the total wavefunction in another way. Let us consider linear combinations of $\Psi^{(1,2)}$,

$$\Psi^{S,A} \equiv \tfrac{1}{\sqrt{2}}(\Psi^{(1,2)} \pm \Psi^{(2,1)}) = \tfrac{1}{\sqrt{2}}\left[\psi_a(x_1)\psi_b(x_2) \pm \psi_a(x_2)\psi_b(x_1)\right] \ . \tag{31.2}$$

This *symmetrized wavefunction* (or anti-symmetrized) represents a trick to eradicate the *label* sticking to the particles. For, under position exchange described by the operator $\mathcal{P}_x\psi_a(x_1)\psi_b(x_2) \equiv \psi_a(x_2)\psi_b(x_1)$, the (anti-)symmetrized functions behave like [3],

$$\mathcal{P}_x\Psi^{S,A} = \pm\Psi^{S,A} \qquad \text{while} \qquad \mathcal{P}_x\Psi^{(1,2)} = \Psi^{(2,1)} \neq \mp\Psi^{(1,2)} \ . \tag{31.3}$$

The (anti-)symmetrized function solves the Schrödinger equation, as well. As $[\hat{H}, \mathcal{P}_x] = 0$, we can say that the system exhibits an *exchange symmetry* or *exchange degeneracy* upon particle exchange. Observables such as $\Psi^{*S,A}\Psi^{S,A}$ stay conserved, for example, the probability

$$\begin{aligned} |\Psi^{S,A}|^2 &= \tfrac{1}{2}\left[|\psi_a(x_1)\psi_b(x_2)|^2 + |\psi_a(x_2)\psi_b(x_1)|^2\right] \\ &\pm \tfrac{1}{2}\left[\psi_a^*(x_1)\psi_b^*(x_2)\psi_a(x_2)\psi_b(x_1) + \psi_a^*(x_2)\psi_b^*(x_1)\psi_a(x_1)\psi_b(x_2)\right] = \mathcal{P}_x|\Psi^{S,A}|^2 \end{aligned} \tag{31.4}$$

does not change, when we exchange x_1 for x_2. For $x_1 = x_2$, we observe,

$$|\Psi^{S,A}|^2 = |\psi_a(x)\psi_b(x)|^2 \pm |\psi_a(x)\psi_b(x)|^2 \ . \tag{31.5}$$

That is, for a symmetric system, the probability of finding two particles at the same location is doubled, whereas for an anti-symmetric system, this probability is zero.

Wolfgang Pauli showed that the (anti-)symmetric character is related to the spin of the particles. Particles with *integer spin* called *bosons* must be symmetric. Particles with *semi-integer spin* called *fermions* must be anti-symmetric. Electrons are fermions. Therefore, in an atom, they can not be in the same state (location), but must be distributed over a complicated shell of orbitals. We note, that this applies not only to elementary particles, but also to composed particles such as, for example, atoms. We will determine in Exc. 31.1.3.2 the bosonic or fermionic character of several atomic species.

31.1.1 Pauli's Principle

Two electrons with anti-parallel spins can be separated by inhomogeneous magnetic fields, even if they are initially in the same place. Therefore, they are distinguishable

[3] To guarantee $|\mathcal{P}_x\Psi^{(1,2)}|^2 = |\Psi^{(1,2)}|^2$, we have $\mathcal{P}_x\Psi^{(1,2)} = e^{\imath\phi}\Psi^{(1,2)}$. From this, $\mathcal{P}_x\mathcal{P}_x\Psi^{(1,2)} = e^{2\imath\phi}\Psi^{(1,2)} = \Psi^{(1,2)}$. Hence, $\mathcal{P}_x\Psi^{(1,2)} = \pm\Psi^{(1,2)}$.

and the wavefunction need not be anti-symmetric. But if we exchange the spin along with the position, the particles must be indistinguishable. This must be taken into account in the wavefunction by assigning a spin coordinate, $\psi_a(x_1, s_1)$. The exchange operator should now be generalized,

$$\mathcal{P}_{x,s}\Psi^{(1,2)} \equiv \mathcal{P}_{x,s}\psi_a(x_1, s_1)\psi_b(x_2, s_2) = \psi_a(x_2, s_2)\psi_b(x_1, s_1) = \Psi^{(2,1)} \ . \tag{31.6}$$

We now assume that the electrons not only do *not* interact with each other, but there is also *no interaction* between the position and the spin of each electron. That is, for a while we will discard $\mathbf{L}\cdot\mathbf{S}$-coupling [4]. We can then write the total wavefunction of an electron as the *product* of a spatial function, $\psi(x)$, and a spin function, $\chi(s) = \alpha\uparrow + \beta\downarrow$, where α and β are probability amplitudes of finding the electron in the respective spin state, such that,

$$\psi(x, s) = \psi(x)\chi(s) \ . \tag{31.7}$$

For two particles, the total spin function is,

$$X^{(1,2)} = \chi_a(s_1)\chi_b(s_2) \ . \tag{31.8}$$

The (anti-)symmetrized version is

$$X^{S,A} = \tfrac{1}{\sqrt{2}}(X^{(1,2)} \pm X^{(2,1)}) = \tfrac{1}{\sqrt{2}}[\chi_a(s_1)\chi_b(s_2) \pm \chi_a(s_2)\chi_b(s_1)] \ , \tag{31.9}$$

as we have already seen in Sec. 25.4.1. Since there are only two spin directions, there are four possibilities to attribute the spins $\uparrow$ and $\downarrow$ to the functions $\chi_m(s_n)$,

$$X^S = \begin{cases} \uparrow\uparrow & = \chi_{1,1} \\ \frac{1}{\sqrt{2}}(\uparrow\downarrow + \downarrow\uparrow) & = \chi_{1,0} \\ \downarrow\downarrow & = \chi_{1,-1} \end{cases} \qquad \text{and} \qquad X^A = \tfrac{1}{\sqrt{2}}\,(\uparrow\downarrow - \downarrow\uparrow) = \chi_{0,0} \tag{31.10}$$

For the total wavefunction, which must be anti-symmetric for electrons, there are two possibilities,

$$\Theta^A = \begin{cases} \Psi^S X^A = \frac{1}{2}(\Psi^{(1,2)} + \Psi^{(2,1)})(X^{(1,2)} - X^{(2,1)}) = \frac{1}{\sqrt{2}}[\psi_a(x_1)\psi_b(x_2) + \psi_a(x_2)\psi_b(x_1)]\chi_{0,0} \\ \Psi^A X^S = \frac{1}{2}(\Psi^{(1,2)} - \Psi^{(2,1)})(X^{(1,2)} + X^{(2,1)}) = \frac{1}{\sqrt{2}}[\psi_a(x_1)\psi_b(x_2) - \psi_a(x_2)\psi_b(x_1)] \begin{cases} \chi_{1,1} \\ \chi_{1,0} \\ \chi_{1,-1} \end{cases} \end{cases} . \tag{31.11}$$

That is, the two electrons may be in a *triplet* state with the anti-symmetric spatial wavefunction, or in a *singlet* state with the symmetric spatial wavefunction [5].

How to generalize these considerations to N particles? The symmetric wavefunctions contain all permutations of the label a_k, where we understand by a_k the set of quantum numbers unambiguously specifying the state of the particle k,

$$\Theta^S = \mathcal{N} \sum_{\mathcal{P}_{x,s}a_k} \psi_{a_1}(x_1)...\psi_{a_N}(x_N) \ , \tag{31.12}$$

[4] In the case of $\mathbf{L}\cdot\mathbf{S}$-coupling, the total wavefunction can not be written as a product of spatial and spin functions, but it must be anti-symmetric anyway.

[5] In the coupled image, the total spin $\mathbf{S} = \mathbf{s}_1 + \mathbf{s}_2$ can have the following values $S = |s_1 - s_2|, .., s_1 + s_2 = 0, 1$. In the case $S = 0$ the magnetic quantum number can only have one value (singlet), $m_S = 0$. In the case $S = 1$ it can have three values $m_S = -1.0, +1$ (triplet) (see Exc. 30.2.8.3).

with a normalization factor $\mathcal{N}$ [6]. The (anti-)symmetrized wavefunction is obtained from the *Slater determinant*,

$$\Theta^A = \tfrac{1}{N!} \det \psi_{a_k}(x_n) = \tfrac{1}{N!} \begin{vmatrix} \psi_{a_1}(x_1) & \cdots & \psi_{a_1}(x_N) \\ \vdots & \ddots & \vdots \\ \psi_{a_N}(x_1) & \cdots & \psi_{a_N}(x_N) \end{vmatrix} . \tag{31.13}$$

This function satisfies

$$\mathcal{P}_{x,s}\Theta^{A,(1,..,i,j,..,N)} = \Theta^{A,(1,..,j,i,..,N)} = -\Theta^{A,(1,..,i,j,..,N)} . \tag{31.14}$$

The Slater determinant is zero, when two sets of quantum numbers are identical, $a_i = a_j$. For example, for two electrons in an electronic shell, $|n_i, l_i, m_i, s_i\rangle = |n_j, l_j, m_j, s_j\rangle$. This is *Pauli's strong exclusion principle*:

> *The total wavefunction must be antisymmetric with respect to the exchange of any pair of identical fermions and symmetrical with respect to exchange of any pair of identical bosons.*

Pauli's weak exclusion principle (usually sufficient for qualitative considerations) says that two fermions in identical states can not occupy the same region in space. That is, their Broglie waves interfere destructively, as if Pauli's principle exerted a repulsive interaction on the particles. This 'force' has a great impact on the phenomenology of the bonds between atoms, as we will discuss in the following sections.

31.1.2 Consequences for quantum statistics

The indistinguishability of quantum particles has interesting consequences on the statistical behavior of bosons and fermions. This becomes obvious when we consider two particles 1 and 2 being able to adopt two different states a and b. Distinguishable particles can be in one of the following four states,

$$\Psi = \{\psi_a(x_1)\psi_a(x_2), \psi_a(x_1)\psi_b(x_2), \psi_b(x_1)\psi_a(x_2), \psi_b(x_1)\psi_b(x_2)\} \tag{31.15}$$

with the same probability of $p = 1/4$. When the quantum particles approach each other, $x_1 \simeq x_2$, they must become indistinguishable. Bosonic indistinguishable particles can stay in one of the following three states,

$$\Psi = \{\psi_a(x_1)\psi_a(x_2), \tfrac{1}{\sqrt{2}}[\psi_a(x_1)\psi_b(x_2) + \psi_b(x_1)\psi_a(x_2)], \psi_b(x_1)\psi_b(x_2)\} \tag{31.16}$$

with the same probability of $p = 1/3$. Finally, fermionic indistinguishable particles can only be in one state,

$$\Psi = \{\tfrac{1}{\sqrt{2}}[\psi_a(x_1)\psi_b(x_2) - \psi_b(x_1)\psi_a(x_2)]\} \tag{31.17}$$

with the probability of $p = 1$. We see that a simple two-particle system already exhibits qualitative modifications of its statistical behavior. These differences generate

[6] It is possible to show $\mathcal{N} = \sqrt{\frac{\Pi_{k=1}^{m} n_k!}{N!}}$, where n_k is the population of state ψ_{a_k}, that is, the number of particles with the same set of quantum numbers a_k.

different physics as we deal with systems of large numbers of particles, as we can see in the cases of the free electron gas and the Bose-Einstein condensate.For a broader discussion, see Chap. 50.1.

We finally note a result of the standard model of particle physics assigning a fermionic character to all fundamental constituent particles of matter while the mediators of fundamental forces are always bosons.

31.1.3 Exercises

31.1.3.1 Ex: Indistinguishability of particles

Consider the observable quantity $\int_0^{L/2}\int_0^{L/4}|\Psi(x_1,x_2)|^2dx_1dx_2$ for the case of the wavefunction defined in (31.1) and show, that it *does* depend on particle exchange.

Solution: *We use the normalized wavefunctions* $\psi_k(x_m)=\sqrt{\frac{2}{L}}\cos\frac{n_k\pi x_m}{L}$ *with* $k=a,b$ *and* $m=1,2$*, and we consider the orbitals* $n_a=1$ *and* $n_b=2$*. The probability* $\int_0^{L/2}\int_0^{L/4}|\Psi^{(1,2)}|^2dx_1dx_2$ *is certainly an observable. However, because of,*

$$\int_0^{L/2}\int_0^{L/4}|\psi_a(x_1)\psi_b(x_2)|^2dx_1dx_2=\frac{2}{L}\int_0^{L/2}\int_0^{L/4}\cos^2\frac{\pi x_1}{L}\cos^2\frac{2\pi x_2}{L}dx_1dx_2=\frac{1}{16}\frac{2+\pi}{\pi}L$$
$$\neq\int_0^{L/2}\int_0^{L/4}|\psi_a(x_2)\psi_b(x_1)|^2dx_1dx_2=\frac{2}{L}\int_0^{L/2}\int_0^{L/4}\cos^2\frac{\pi x_2}{L}\cos^2\frac{2\pi x_1}{L}dx_1dx_2=\frac{1}{16}L\ ,$$

it is not equal to $\int_0^{L/2}\int_0^{L/4}|\Psi^{(2,1)}|^2dx_1dx_2$*.*

31.1.3.2 Ex: Bosonic and fermionic isotopes

Consulting an isotope table determine the bosonic or fermionic character of the following atomic species: ^{87}Sr, ^{86}Sr, ^{87}Rb, ^{39}K, and ^{40}K.

Solution:

31.1.3.3 Ex: Interference of bosons and fermions

a. Consider two clouds of ultracold bosonic atoms (BECs at temperature $T=0$) moving into opposite direction with velocities $v_\pm=\pm v$, respectively. Describe the matter wave interference pattern.
b. Repeat the consideration for the case of (i) fermionic clouds and (ii) only two counterpropagating atoms. Is matter wave interference possible at all for fermions?

Solution: *a. Neglecting the finite spatial extension and assuming the same number of atoms in both bosonic clouds, we describe the condensates as plane matter waves. We expect matter wave interference pattern with the periodicity* $2\pi\hbar/mv$*. Repeating the experiment the interference pattern will always have the same periodicity, but different phases. The total symmetrized wavefunction is* $\Psi(1,2)=\ldots\ \ldots$

Table 31.1: Nuclear spin, ground state, and quantum statistical nature of some atomic species.

atom	I	ground state	type
^{6}Li	0	$^{2}S_{1/2}$	fermion
^{7}Li	$\frac{3}{2}$	$^{2}S_{1/2}$	boson
^{23}Na	$\frac{3}{2}$	$^{2}S_{1/2}$	boson
^{39}K	$\frac{3}{2}$	$^{2}S_{1/2}$	boson
^{40}K	0	$^{2}S_{1/2}$	fermion
^{87}Sr	$\frac{7}{2}$	$^{1}S_{0}$	fermion
^{88}Sr	0	$^{1}S_{0}$	boson
^{85}Rb	$\frac{5}{2}$	$^{2}S_{1/2}$	boson
^{87}Rb	$\frac{3}{2}$	$^{2}S_{1/2}$	boson
^{133}Cs	$\frac{9}{2}$	$^{2}S_{1/2}$	boson

b. In the case of fermions, the total anti-symmetrized wavefunction is $\Psi(1,2) = ...$, hence, two fermions can interference. However, as the phase of the patterns for each pair of colliding atoms is arbitrary, no overall interference patterns will form. Nevertheless, fermions can interfere with themselves in matter wave interferometers [853, 344].

31.2 Helium

The simplest atom to discuss Pauli's principle is helium. The helium atom has a charged nucleus $Z = +2e$ and mass $m_{He} \approx 4m_H$.

31.2.1 The ground state

The ground state of the *helium* atom brings together the two electrons, that is, $(1s)^2$. To treat the helium atom, we can, as a first trial, describe the atom by the Bohr model, assuming independent electrons. Neglecting the electronic repulsion term (which depends on $r_{12} = |\mathbf{r}_1 - \mathbf{r}_2|$), we can separate the total wavefunction:

$$\Psi(\mathbf{r}_1, \mathbf{r}_2) = \Psi_1(\mathbf{r}_1)\Psi_2(\mathbf{r}_2) \ , \tag{31.18}$$

and we get two Schrödinger equations, the Hamiltonian being equal to the one of hydrogen-like atoms:

$$\left[-\frac{\hbar^2}{2\mu}\nabla_i^2 - \frac{e^2}{4\pi\varepsilon_0}\frac{Z}{r_i} \right] \Psi_i(\mathbf{r}_i) = E_n^{(i)}\Psi_i(\mathbf{r}_i) \ , \tag{31.19}$$

with $i = 1, 2$. For hydrogen-like atoms we have,

$$E = E_n^{(1)} + E_n^{(2)} = E_B Z^2 \left(\frac{1}{n_1^2} + \frac{1}{n_2^2} \right) \ , \tag{31.20}$$

with $E_B = -13.6\,\text{eV}$. With this, we get the energy for the ground state:

$$E_{He}(1s) = -2Z^2 E_B = -108.8\,\text{eV} \ . \tag{31.21}$$

The value predicted by Bohr's model is far from experimental reality: The ionization energy measured for the first electron is 24.6 eV, for the second 54.4 eV, totalizing a binding energy for two electrons of −78.983 eV . This corresponds to an error of about 38%. The lower energy of the first electron is due to the shielding of the nucleus by the second.

31.2.1.1 First-order perturbation of the energy

Treating the repulsion term between the electrons as a perturbation [60] and using the eigenfunctions of hydrogen atoms $|n, \ell, m_\ell\rangle$, the total wavefunction is $|n_1, \ell_1, m_{\ell_1}; n_2, \ell_2, m_{\ell_2}\rangle$, we obtain as first order TIPT correction for the energy:

$$\Delta E = \langle n_1, \ell_1, m_{\ell_1}; n_2, \ell_2, m_{\ell_2}| \frac{e^2}{4\pi\varepsilon_0 r_{12}} |n_1, \ell_1, m_{\ell_1}; n_2, \ell_2, m_{\ell_2}\rangle \ . \tag{31.22}$$

This correction is called the *Coulomb integral* and has the value:

$$\Delta E = \frac{e^2}{4\pi\varepsilon_0} \int |\Psi_{n_1,\ell_1,m_{\ell_1}}(\mathbf{r}_1)|^2 \left(\frac{1}{r_{12}}\right) |\Psi_{n_2,\ell_2,m_{\ell_2}}(\mathbf{r}_2)|^2 dV_1 dV_2 \ . \tag{31.23}$$

This integral is always positive. The term $|\Psi_{n_1,\ell_1,m_{\ell_1}}(\mathbf{r}_1)|^2 dV_1$ is the probability of finding the electron inside the volume element dV_1 and, when multiplied by $-e$, gives the charge associated with that region. Thus, the integral represents the Coulombian interaction energy of the confined charges within the two volume elements dV_1 and dV_2. ΔE is the total contribution to the potential energy. Calculating the Coulomb integral for the ground state, which will be done in Exc. 31.2.3.1, we obtain,

$$\Delta E = \frac{5Z}{4}\left(\frac{e^2}{4\pi\varepsilon_0 2a_B}\right) = \frac{5Z}{4} E_B \ , \tag{31.24}$$

with a_B the Bohr radius. ΔE corresponds to 34 eV. Thus, the ground state energy is $E_{He}(1s) = -108.8\,\text{eV} + 34\,\text{eV} = -74.8\,\text{eV}$. Comparing with the experimental value of $-78.983\,\text{eV}$ we have an error around 5.3%.

31.2.1.2 Shielding of the nuclear charge

We can make the approximation in which we consider that each electron moves in a Coulombian potential, with respect to the nucleus, shielded by the charge distribution of the other electron [352]. The resulting potential will be generated by an effective charge $\zeta e \equiv (Z - B)e$. The quantity $B \in [0, 1]$ is called the shielding constant.

The first electron feels a total nuclear charge Ze, while the second feels an effective nuclear charge ζe. We exchange Z for ζ in the energy term for hydrogen-like atoms,

$$E_n = -\zeta \frac{E_B}{n^2} \ , \tag{31.25}$$

and the energy for the ground state becomes, assuming total shielding, $B = 1$,

$$E = E_1 + E_2 = -Z^2 E_B - \zeta^2 E_B = -4E_B - E_B = -5E_B = -67.5\,\text{eV} \ . \qquad (31.26)$$

Comparing with the experimental value of -78.983 eV we have an error around 15%. For a shielding constant of around $B = 0.656$ the experimental value is reproduced. This means that the effective nuclear charge felt by the second electron is only *partly* shielded by the former. The TPIT method (31.22) and the shielding concept (31.25) can be combined in a variational calculation, where the effective charge ζ is the variational parameter. In Exc. 31.2.3.2 we study the reciprocal shielding of the electrons at the example of the helium-type ion H^-.

31.2.2 Excited states

Let us now investigate the excited states of helium, in particular those, where *only one electron* is excited, the other one being in the ground state, $(1s)^1(2s)^1$ and $(1s)^1(2p)^1$. All energies are considerably higher (weaker binding) than predicted by Bohr's model with $Z = 2$, because of the interaction with the other electron. Also, the $(2s)$ and $(2p)$ levels are no longer degenerate, because the electrostatic potential is no longer Coulombian (see Fig. 31.1).

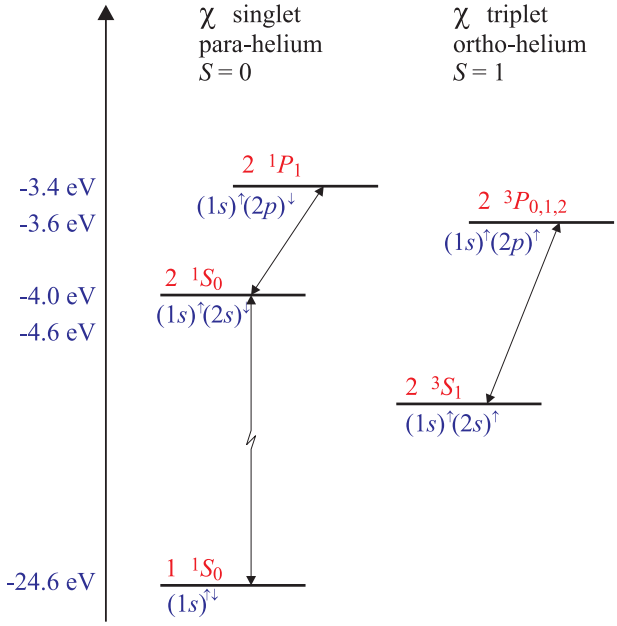

Figure 31.1: Helium levels for the excitation of the first electron and allowed singlet and triplet transitions. Note that the state $(1s)^{\uparrow\uparrow}$ does not exist.

As we have seen in the discussion of the fine structure of hydrogen, the energy of the $\mathbf{l} \cdot \mathbf{s}$-coupling given by (29.130) is $\propto E_n(Z\alpha)^2 \propto Z^4$. For helium which still has a small Z, the energy of the coupling is weak ($\sim 10^{-4}$ eV), so that we can count on a direct coupling of the spins of the two electrons. If in an excited state the

orbits of the electrons are different, we can construct combinations of symmetric **or** antisymmetric spatial wavefunctions $\Psi^{S,A}$, are therefore combinations $X^{A,S}$ of anti-parallel or parallel spins. When the spins are parallel ($S = 1$), the spatial wavefunction is antisymmetric, when they are antiparallel ($S = 0$), it is symmetric. From the symmetry of the wavefunction depends the energy of the Coulombian interelectronic interaction, because in the symmetric state the average distance of the electrons is much smaller than in the antisymmetric state, where *the total spatial function disappears for zero distance*. Consequently, the configuration $(1s)^1(2s)^1$ has two states with $S = 0$ and $S = 1$, with energy $E_{S=0} > E_{S=1}$. Likewise, all configurations are split, as shown in Fig. 31.1. The energy difference ($\sim 0.6\,\mathrm{eV}$) is considerable and larger than the energy of fine structure interaction. This explains why the two spins first couple to a total spin, $\mathbf{s}_1 + \mathbf{s}_2 = \mathbf{S}$, before this spin couples to the total orbital angular momentum, $\mathbf{S} + \mathbf{L} = \mathbf{J}$. This is the $\mathbf{L} \cdot \mathbf{S}$-coupling.

31.2.2.1 Exchange energy

The energy difference between the two states $S = 0$ and $S = 1$ is called *exchange energy*. It comes out of a first-order perturbation calculation. For example, for the two possible states $(1s)^1(2s)^1$, we write the total anti-symmetric wavefunctions,

$$\Theta^A_\pm = \tfrac{1}{\sqrt{2}} \left[\psi_{100}(\mathbf{r}_1)\psi_{200}(\mathbf{r}_2) \pm \psi_{100}(\mathbf{r}_2)\psi_{200}(\mathbf{r}_1)\right] \cdot \chi^{A,S} \ , \tag{31.27}$$

where the $(+)$ sign holds for χ^A $(S = 0)$ and the $(-)$ sign for χ^S $(S = 1)$. The energies are,

$$\begin{aligned} \Delta E^{S,A} &= \tfrac{1}{2} \int dr_1^3 \int dr_2^3 \Theta^{*A}_\pm \frac{e^2}{4\pi\varepsilon_0 |\mathbf{r}_1 - \mathbf{r}_2|} \Theta_p m^A \\ &= \tfrac{1}{2} \int dr_1^3 \int dr_2^3 \frac{e^2}{4\pi\varepsilon_0 |\mathbf{r}_1 - \mathbf{r}_2|} [|\psi_{100}(\mathbf{r}_1)|^2 |\psi_{200}(\mathbf{r}_2)|^2 + |\psi_{100}(\mathbf{r}_2)|^2 |\psi_{200}(\mathbf{r}_1)|^2] \\ &\quad \pm \tfrac{1}{2} \int dr_1^3 \int dr_2^3 \frac{e^2}{4\pi\varepsilon_0 |\mathbf{r}_1 - \mathbf{r}_2|} 2\psi^*_{100}(\mathbf{r}_1)\psi^*_{200}(\mathbf{r}_2)\psi_{100}(\mathbf{r}_2)\psi_{200}(\mathbf{r}_1) \\ &\equiv \Delta E_{coulomb} \pm \Delta E_{exchange} \ . \end{aligned} \tag{31.28}$$

The first integral,

$$\Delta E_{coulomb} = \int dr_1^3 \int dr_2^3 \frac{e^2}{4\pi\varepsilon_0 |\mathbf{r}_1 - \mathbf{r}_2|} |\psi_{100}(\mathbf{r}_1)|^2 |\psi_{200}(\mathbf{r}_2)|^2 \ , \tag{31.29}$$

is the Coulomb energy (31.23) between the electronic orbitals. We note that this part can be calculated from the Hamiltonian using *non-symmetrized* orbitals. The second integral,

$$\Delta E_{exchange} = \int dr_1^3 \int dr_2^3 \frac{e^2}{4\pi\varepsilon_0 |\mathbf{r}_1 - \mathbf{r}_2|} \psi^*_{100}(\mathbf{r}_1)\psi^*_{200}(\mathbf{r}_2)\psi_{100}(\mathbf{r}_2)\psi_{200}(\mathbf{r}_1) \ , \tag{31.30}$$

called *exchange energy* corresponds to the interference terms of the symmetrization and must be added or subtracted according to their symmetry character. It is interesting to note that up to this point the spin does not enter directly into the helium

Hamiltonian,

$$\hat{H}^{S,A} = \frac{p_1^2}{2m} + \frac{p_2^2}{2m} + V(r_1) + V(r_2) + V(|\mathbf{r}_1 - \mathbf{r}_2|) \pm \Delta E_{exchange} \ , \tag{31.31}$$

but only through the symmetry character of the spatial wavefunction. On the other hand, on a much smaller energy scale, the spin enters through the $\mathbf{L} \cdot \mathbf{S}$-interaction.

The potential is not spherically symmetric, the term r_{12} depends on the angle between $\mathbf{r}_1$ and $\mathbf{r}_2$. Thus, the total wavefunction $\Psi(\mathbf{r}_1, \mathbf{r}_2)$ is not separable into a radial and an angular part. By consequence, unlike for hydrogen, the Schrödinger equation with the Hamiltonian (31.21) has no analytical solution.

Example 186 (*TIPT for excited helium states*): We consider the two electrons of a helium atom occupying different orbits described by wavefunctions denoted by $\psi_a(1) \equiv \psi_{n_1,\ell_1,m_{\ell_1}}(\mathbf{r}_1)$ and $\psi_b(2) \equiv \psi_{n_2,\ell_2,m_{\ell_2}}(\mathbf{r}_2)$. Applying the Hamiltonian without the interelectronic interaction term, the total states $\Theta = \psi_a(1)\psi_b(2)$ and $\psi_a(2)\psi_b(1)$ have the same energy $E_a + E_b$. To calculate the energy correction, we use TIPT for degenerate states. We have to calculate the secular determinant $\det(\langle n, \nu | H^{(1)} | n, \mu \rangle - E^{(1)}_{n,\mu}\delta_{\mu,\nu})$. The terms of the perturbation matrix $H^{(1)}$ are:

$$\begin{aligned}
H^{(1)}_{11} &= \langle \psi_a(1)\psi_(2)| \frac{e^2}{4\pi\varepsilon_0 r_{12}} |\psi_a(1)\psi_b(2)\rangle \\
H^{(1)}_{22} &= \langle \psi_a(2)\psi_b(1)| \frac{e^2}{4\pi\varepsilon_0 r_{12}} |\psi_a(2)\psi_b(1)\rangle \\
H^{(1)}_{12} &= \langle \psi_a(1)\psi_b(2)| \frac{e^2}{4\pi\varepsilon_0 r_{12}} |\psi_a(2)\psi_b(1)\rangle = H^{(1)}_{21} \ .
\end{aligned}$$

The terms $J \equiv H^{(1)}_{11} = H^{(1)}_{22}$ are Coulomb integrals. The term $K \equiv H^{(1)}_{12}$ is called *exchange integral*:

$$K = \frac{e^2}{4\pi\varepsilon_0} \langle \psi_a(1)\psi_b(2)| \frac{1}{r_{12}} |\psi_a(2)\psi_b(1)\rangle \ .$$

Hence, as J and K are positive, the determinant is:

$$\begin{vmatrix} J - E & K \\ K & J - E \end{vmatrix} = 0 \ ,$$

yielding,

$$E^{(1)} = J \pm K \ .$$

That is, the states that were previously degenerate with energy $E = E_a + E_b$ are now split into two states with energies $E = E_a + E_b + J \pm K$. And the corresponding eigenfunctions are:

$$\Psi^{S,A}(1,2) = \frac{1}{\sqrt{2}} [\psi_a(1)\psi_b(2) \pm \psi_b(1)\psi_a(2)] \ .$$

This result shows that the repulsion between the two electrons breaks the degeneracy (of separable functions written in product form) into states with an energy difference $2K$. Note that the eigenfunctions are symmetric, which is discussed in the next section.

31.2.2.2 The spectrum of helium

So far we have seen that, if the electrons are in the same orbital, we have an energy term $E = 2E_a + J$ and, when they are in *different orbitals*, we have $E = E_a + E_b + J \pm K$, with a separation between levels of $2K$.

In practice, we consider only the excitation of *one* electron, because the energy to excite the two electrons exceeds the ionization energy of the helium atom. To find the selection rules for transitions between symmetric and antisymmetric states, we calculate the dipole moment of the transition. For a two-electron system the dipole moment is $\hat{\mathbf{d}} = -e\mathbf{r}_1 - e\mathbf{r}_2$, which is symmetric with respect to a permutation of the two electrons. The matrix element for the dipolar transition is:

$$\langle \Psi^A | \hat{\mathbf{d}} | \Psi^S \rangle = -e \int \Psi^{*A}(\mathbf{r}_1, \mathbf{r}_2)(\mathbf{r}_1 + \mathbf{r}_2)\Psi^S(\mathbf{r}_1, \mathbf{r}_2) dV_1 dV_2 \ . \tag{31.32}$$

If we exchange the electrons, the above integral changes sign, because $\Psi^A(\mathbf{r}_1, \mathbf{r}_2)$ changes sign. But the integral can not depend on the nomenclature of the integration variables, so *it must be zero*. The transition between a symmetric and an antisymmetric state can not occur. Looking at the spin wavefunction in $\Theta = \Psi^S\chi^A$ or $\Psi^A\chi^S$, we find that transitions are only allowed between singlet states or between triplet states. That is, there is a *selection rule* for the spin postulating $\Delta S = 0$ [7,8].

Because of the differences observed in the singlet and the triplet spectrum of helium, illustrated in Fig. 31.1, it was first believed that they belong to different atomic species, called *para-helium* and *ortho-helium*. A chemical analysis showed later that it was the same element.

31.2.3 Exercises

31.2.3.1 Ex: Helium atom

Compare the measured binding energy with the prediction of Bohr's model considering the inter-electronic interaction up to first order TIPT.

Solution: *Here, we consider the perturbation due to the Coulomb interaction between the electrons,*

$$V_{ee} = \frac{-e^2}{4\pi\varepsilon_0 |\mathbf{r}_1 - \mathbf{r}_2|} \ .$$

We focus on the ground state. As the total spatial wavefunction must necessarily be symmetrical (the orbitals of the electrons are identical), the total spin is antisymmet-

[7] Moreover, transitions between the states ${}^1S_0$ and ${}^3S_1$ are impossible, because they violate the selection rule for the angular momentum, $\Delta L = \pm 1$.

[8] We can understand the selection rules as follows: As long as the wavefunction can be written as a product, $\Theta = \Psi(x)\chi(s)$, the symmetry character is preserved for the two functions separately. The eigenvalues of the operators $\mathcal{P}_x$ and $\mathcal{P}_s$ are then good quantum numbers. But this only holds for weak $\mathbf{L}\cdot\mathbf{S}$-coupling. The electric dipole operator for the transition does not act on the spin (which prevents the recoupling $S = 1 \leftrightarrow S = 0$ via $E1$-radiation) and also does not act on the symmetry character of the orbitals (which prevents transitions $\Psi^S \leftrightarrow \Psi^A$).
In principle, this holds for any species of atoms with two valence electrons. In reality however, the influence of the $\mathbf{L}\cdot\mathbf{S}$-coupling grows with Z, which weakens the interdiction of the intercombination transition. In this case, only the operator $\mathcal{P}_{x,s}$ yields good eigenvalues.

ric. The list (25.52) gives us the radial wavefunction ψ_{100}*,*

$$\Theta^A = \psi_{100}(\mathbf{r}_1)\psi_{100}(\mathbf{r}_2)\chi_{00} = \frac{1}{\pi}\left(\frac{Z}{a_B}\right)^{3/2} e^{-Zr_1/a_B}\frac{1}{\pi}\left(\frac{Z}{a_B}\right)^{3/2} e^{-Zr_2/a_B}\times\uparrow\downarrow \ .$$

The perturbation energy calculated with unperturbed wavefunctions is,

$$\begin{aligned}
E_1^{(1)} &= \langle\Theta^A|V_{ee}|\Theta^A\rangle \\
&= \left\langle \frac{1}{\pi}\frac{Z^{3/2}}{a_B^{3/2}}e^{-Zr_1/a_B}\frac{1}{\pi}\frac{Z^{3/2}}{a_B^{3/2}}e^{-Zr_2/a_B}\right| \frac{e^2}{4\pi\varepsilon_0|\mathbf{r}_1-\mathbf{r}_2|}\left|\frac{1}{\pi}\frac{Z^{3/2}}{a_B^{3/2}}e^{-Zr_1/a_B}\frac{1}{\pi}\frac{Z^{3/2}}{a_B^{3/2}}e^{-Zr_2/a_B}\right\rangle \\
&= \frac{e^2}{4\pi\varepsilon_0}\frac{1}{\pi^4}\frac{Z^6}{a_B^6}\int\int\frac{e^{-2Z(r_1+r_2)/a_B}}{|\mathbf{r}_1-\mathbf{r}_2|}d^3r_1d^3r_2 = mc^2\alpha^2a_B\frac{1}{32\pi^4}\frac{Z}{a_B}\int\int\frac{e^{-\tilde{r}_1-\tilde{r}_2}}{|\tilde{\mathbf{r}}_1-\tilde{\mathbf{r}}_2|}d^3\tilde{r}_1d^3\tilde{r}_2 \\
&= \frac{mc^2\alpha^2Z}{32\pi^4}\int_0^{2\pi}d\varphi_2\int_0^\infty d\tilde{r}_2\tilde{r}_2^2\int_0^\pi d\vartheta_2\sin\vartheta_2\int_0^{2\pi}d\varphi_1\int_0^\infty d\tilde{r}_1\tilde{r}_1^2\int_0^\pi d\vartheta_1\sin\vartheta_1\frac{e^{-\tilde{r}_1-\tilde{r}_2}}{|\tilde{\mathbf{r}}_1-\tilde{\mathbf{r}}_2|} \ .
\end{aligned}$$

We write the distance between the electrons in spherical coordinates,

$$\begin{aligned}
&|\tilde{\mathbf{r}}_1-\tilde{\mathbf{r}}_2| \\
&= \sqrt{(\tilde{r}_1\sin\vartheta_1\cos\varphi_1-\tilde{r}_2\sin\vartheta_2\cos\varphi_2)^2+(\tilde{r}_1\sin\vartheta_1\sin\varphi_1-\tilde{r}_2\sin\vartheta_2\sin\varphi_2)^2+(\tilde{r}_1\cos\vartheta_1-\tilde{r}_2\cos\vartheta_2)^2} \\
&= \sqrt{\tilde{r}_1^2+\tilde{r}_2^2-2r_1r_2\left[\sin\vartheta_1\sin\vartheta_2\cos(\varphi_1-\varphi_2)+\cos\vartheta_1\cos\vartheta_2\right]} = R \ .
\end{aligned}$$

Since the two orbitals are spherical, we can solve the angular integrals in $\vartheta_2, \varphi_1, \varphi_2$ *letting* $\vartheta_2 = \varphi_1 = \varphi_2 = 0$ *at a distance*

$$R = \sqrt{\tilde{r}_1^2+\tilde{r}_2^2-2\tilde{r}_1\tilde{r}_2\cos\vartheta_1} \qquad \textit{with} \qquad \frac{dR}{d\vartheta_1} = \frac{\tilde{r}_1\tilde{r}_2\sin\vartheta_1}{R} \ .$$

Hence,

$$\begin{aligned}
E_1^{(1)} &= \frac{mc^2\alpha^2Z}{32\pi^4}8\pi^2\int_0^\infty d\tilde{r}_2\tilde{r}_2^2\int_0^\infty d\tilde{r}_1\tilde{r}_1^2\int_0^\pi d\vartheta_1\sin\vartheta_1\frac{e^{-\tilde{r}_1-\tilde{r}_2}}{R} \\
&= \frac{mc^2\alpha^2Z}{32\pi^4}8\pi^2\int_0^\infty d\tilde{r}_2\tilde{r}_2^2\int_0^\infty d\tilde{r}_1\tilde{r}_1^2\int_{\tilde{r}_1-\tilde{r}_2}^{\tilde{r}_1+\tilde{r}_2}dR\frac{e^{-\tilde{r}_1-\tilde{r}_2}}{\tilde{r}_1\tilde{r}_2} \\
&= \frac{mc^2\alpha^2Z}{4\pi^2}\int_0^\infty d\tilde{r}_2\tilde{r}_2e^{-\tilde{r}_1}\int_0^\infty d\tilde{r}_1\tilde{r}_1(\tilde{r}_1+\tilde{r}_2-\tilde{r}_1+\tilde{r}_2)e^{-\tilde{r}_2} = \frac{mc^2\alpha^2Z}{\pi^2} \\
&= .. = \frac{5}{4}\frac{m}{2}c^2\alpha^2Z = 34.0\,\text{eV} \ .
\end{aligned}$$

The corrected energy, $E_1 = (-108.8+34.0)\,\text{eV} = -74.8\,\text{eV}$ *is much closer to the measured value.*

31.2.3.2 Ex: Shielding in helium

The helium atom (or helium-like atoms such as H^-) has two interacting electrons in its composition, which means that these systems have no exact solution. To circumvent this problem we have to come up with a series of approximate methods for calculating their eigenstates and their respective eigenenergies. Among these methods, a widely

used one, due mainly to its ease and practicality, is the variational method, in which we calculate the fundamental state of a given problem through a test function that is not a solution of the original problem. This method, when applied to a helium atom, uses as test function the solution of the problem without coulombian interaction between the electrons, which only feel the interaction with the original charge of the nucleus. However, this method could be further improved if we considered an effective nuclear charge, due to its interaction with the electrons themselves, and then obtaining the test function. Apply this correction to the case of helium. Interpret the result. **Help:**

$$\int \frac{\sin\theta_2}{\sqrt{r_1^2+r_2^2-2r_1^2r_2^2\cos\theta_2}}d\theta_2 = \frac{\sqrt{r_1^2+r_2^2-2r_1^2r_2^2\cos\theta_2}}{r_1r_2} \qquad \text{and} \qquad \left\langle\frac{1}{r}\right\rangle = \frac{Z}{a_B}\ .$$

Solution: *This is the Hamiltonian of a helium-type atom (2 electrons) subjected to a nuclear charge of Z_0e:*

$$\hat{H} = -\frac{\hbar^2}{2m}(\nabla_1^2+\nabla_2^2) - \frac{e^2}{4\pi\varepsilon_0}\left(\frac{Z_0}{r_1}+\frac{Z_0}{r_2}-\frac{1}{|\mathbf{r}_1-\mathbf{r}_2|}\right)\ .$$

The term that prevents this problem from being calculated exactly is given by V_{ee}:

$$V_{ee} = \frac{e^2}{4\pi\varepsilon_0}\frac{1}{|\mathbf{r}_1-\mathbf{r}_2|}\ .$$

Applying the variational method in the traditional way, we would use the following test function:

$$\psi_{MV}(r_1,r_2) = \frac{Z_0^3}{\pi a_B^3}e^{-Z_0(r_1+r_2)/a_B}\ ,$$

which is the solution of the Hamiltonian with $V_{ee}=0$. But since we want to obtain the shielding effects in the problem, we will rewrite the Hamiltonian in the following format,

$$\hat{H} = -\frac{\hbar^2}{2m}(\nabla_1^2+\nabla_2^2) - \frac{e^2}{4\pi\varepsilon_0}\left(\frac{Z}{r_1}+\frac{Z}{r_2}\right) + \frac{e^2}{4\pi\varepsilon_0}\left[\frac{Z-Z_0}{r_1}+\frac{Z-Z_0}{r_2}+\frac{1}{|\mathbf{r}_1-\mathbf{r}_2|}\right]\ .$$

Now the test function of the variational method will be the solution of a problem of non-interacting electrons, but now with a nucleus having an effective charge different from the original one. The test function acquires a similar format as the previous one, but with Z_0 replaced by Z.

$$\psi_{MV}(r_1,r_2) = \frac{Z^3}{\pi a_B^3}e^{-Z(r_1+r_2)/a_B}\ .$$

Note that the adjustment parameter in this test function is Z, so we will minimize the energy in relation to Z. Once we have the test function at hand, we proceed with the variational method, calculating the mean value of H,

$$\langle H\rangle = 2Z^2E_1 + 2(Z-Z_0)\frac{e^2}{4\pi\varepsilon_0}\left\langle\frac{1}{r}\right\rangle + \langle V_{ee}\rangle\ ,$$

with $\langle 1/r\rangle$ being the expectation value of $1/r$ in the ground state ψ_{100} of a hydrogen-type atom with charge Z.

$$\frac{e^2}{4\pi\varepsilon_0}\Big\langle\frac{1}{r}\Big\rangle = \frac{e^2}{4\pi\varepsilon_0}\frac{Z}{a_B} = \langle V(r)\rangle = -2E_1 \ ,$$

and $E_1 = -13.6eV$. Now we have to calculate the mean value of V_{ee}:

$$\begin{aligned}\langle V_{ee}\rangle &= \frac{e^2}{4\pi\varepsilon_0}\Big(\frac{Z^3}{\pi a_B^3}\Big)^2\int\frac{e^{-2Z(r_1+r_2)/a_B}}{|\mathbf{r}_1-\mathbf{r}_2|}d^3r_1d^3r_2 \\ &= \frac{e^2}{4\pi\varepsilon_0}\Big(\frac{Z^3}{\pi a_B^3}\Big)^2\int\frac{e^{-2Z(r_1+r_2)/a_B}}{\sqrt{r_1^2+r_2^2-2r_1^2r_2^2\cos\theta_2}}d^3r_1d^3r_2 \ .\end{aligned}$$

Let us first calculate the integral in r_2. Without loss of generality we can rotate the coordinate system in r_2 such that its z-axis points along r_2, which facilitates integration. The integral in ϕ_2 is equal to 2π, the integral in θ_2 is given by,

$$\begin{aligned}\int_0^\pi\frac{\sin\theta_2}{\sqrt{r_1^2+r_2^2-2r_1^2r_2^2\cos\theta_2}}d\theta_2 &= \frac{1}{r_1r_2}\Big(\sqrt{r_1^2+r_2^2+2r_1^2r_2^2}-\sqrt{r_1^2+r_2^2-2r_1^2r_2^2}\Big) \\ &= \frac{1}{r_1r_2}[(r_1+r_2)-|r_1-r_2|] = \begin{cases}2/r_1, & \text{if } r_2<r_1\\ 2/r_2, & \text{if } r_2>r_1\end{cases} \ .\end{aligned}$$

Taking again the radial part r_2 we will have,

$$\begin{aligned}&= 4\pi\Big(\frac{1}{r_1}\int_0^{r_1}e^{-2Zr_2/a_B}r_2^2dr_2+\int_{r_1}^\infty e^{-2Zr_2/a_B}r_2dr_2\Big) \\ &= \frac{\pi a_B^3}{8Zr_1}\Big[1-\Big(1+\frac{2r_1}{a_B}\Big)e^{-4r_1/a_B}\Big] \ .\end{aligned}$$

Hence, $\langle V_{ee}\rangle$

$$\begin{aligned}\langle V_{ee}\rangle &= \frac{e^2}{4\pi\varepsilon_0}\frac{Z^2}{\pi a_B^3}\int\Big[1-\Big(1+\frac{2r_1}{a_B}\Big)e^{-4r_1/a_B}\Big]e^{-4r_1/a_B}r_1\sin\theta_1dr_1d\theta_1d\phi_1 \\ &= \frac{5Z}{8a_B}\frac{e^2}{4\pi\varepsilon_0} = -\frac{5Z}{4}E_1 \ .\end{aligned}$$

The average energy can then be written,

$$\langle H\rangle = [2Z^2-4Z(Z-Z_0)-\tfrac{5}{4}Z]E_1 = [-2Z^2+4ZZ_0-\tfrac{5}{4}Z]E_1 \ .$$

Minimizing $\langle H\rangle$ we obtain,

$$\frac{\partial\langle H\rangle}{\partial Z} = [-4Z+4Z_0-\tfrac{5}{4}]E_1 = 0 \ ,$$

yielding $Z = Z_0 - \frac{5}{16}$. Thus, for He, $Z_0 = 2$, the effective charge is $Z \approx 1.68$. This result seems to be correct, because it is the negatively charged electrons of the ion, which cause the effective charge to be less than the original charge. This phenomenon is known as core shielding.
The correction of the energy is,

$$E = \langle\Phi|\hat{H}|\Phi\rangle = -2E_0\left(Z-\tfrac{5}{16}\right)^2 = -77.46\,\text{eV} \ .$$

This gives an error around 1.9% compared to the experimental value of -78.983 eV.

31.3 Electronic shell structure

The interelectronic interaction and the need to antissimetrize the wavefunction of the electrons both contribute to excessively increase the complexity of multielectronic atoms. The Hamiltonian describing a multielectronic atom of atomic number Z,

$$\hat{H} = E_{kin} + V_{ncl-ele} + V_{ele-ele} = \sum_{i=1}^{Z} \frac{p_i^2}{2m} - \sum_{i=1}^{Z} \frac{Ze^2}{4\pi\varepsilon_0 |\mathbf{r}_i|} + \sum_{i<j=1}^{Z} \frac{e^2}{4\pi\varepsilon_0 |\mathbf{r}_i - \mathbf{r}_j|} \ , \quad (31.33)$$

is extremely complicated to solve, even for the simplest case ($Z = 2$) we must use approximation methods.

31.3.1 TIPT method

Note that, if we assume independent electrons ($V_{ele-ele} = 0$), that is, each electron moves independently of the others within the electrostatic potential generated by the nucleus and the other $Z-1$ electrons, the problem would be solvable: We could solve the Schrödinger equation for a product state of all the electronic wavefunctions, and we would know the eigenfunctions and individual eigenenergies of each electron (as for the hydrogen atom). In principle, we should use antisymmetric wavefunctions, but as a first approach we can choose to only respect Pauli's weak principle, that is, assign an *individual and unique* set of quantum numbers to each electron. The total energy would be the sum of the energy of every electron, and the associated physical eigenstates would be obtained by means of an antisymmetrization of the tensor product of the multielectronic state.

Thus, as a first approximation, we use the states of individual electrons (orbital approximation) and consider $V_{ele-ele}(|\mathbf{r}_i - \mathbf{r}_j|)$ as a perturbation making use of *time-independent perturbation theory*. However, this term is not small enough to justify this procedure, since approximating

$$V_{ncl-ele} \simeq \frac{Z^2 e^2}{a_B} \quad \text{and} \quad V_{ele-ele} \simeq \frac{Z(Z-1)e^2}{2a_B} \ , \quad (31.34)$$

we realize that $V_{ele-ele}/V_{ncl-ele}$ varies between $\frac{1}{4}$ for $Z = 2$ and $\frac{1}{2}$ for $Z \gg 1/2$. For this reason the use of alternative methods to describe multielectronic atoms is necessary. Nevertheless, the set of quantum numbers derived from Bohr's atomic model are still the same as those used for many-electron atoms, and the orbitals are used as starting points for more sophisticated methods.

To calculate most of the atomic properties we need reasonably realistic potentials. The most important terms of the Hamiltonian are the Coulombian potential between the nucleus and the electrons, V_{ne}, being naturally spherical, and the interaction potentials between the electrons, V_{ee}, which we will try to approximate by a spherical potential and treat the deviations caused by the approximation afterward. Knowing the effect of the shielding of the nucleus by electronic charges, we already know the asymptotes (see Fig. 31.2),

$$V_{eff} = -\frac{Ze^2}{4\pi\varepsilon_0 r} \quad \text{for} \quad r \to 0 \quad \text{and} \quad V_{eff} = -\frac{e^2}{4\pi\varepsilon_0 r} \quad \text{for} \quad r \to \infty. \quad (31.35)$$

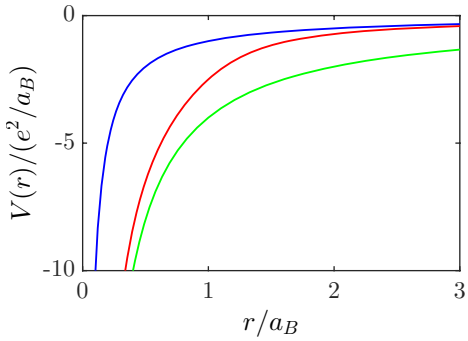

Figure 31.2: (code) External potential (shielded Coulombian) $V_{cl} \propto \frac{e^2}{r}$ (blue, upper curve), interior potential (non-shielded Coulombian for $Z = 4$) $V_{bl} \propto \frac{Ze^2}{r}$ (green, lower curve), and effective potential (red, middle curve).

31.3.2 Thomas-Fermi model for an electron gas

A first approach to getting a reasonable *effective potential* V_{eff} is provided by the *Thomas-Fermi model*. This is a semi-classical model that aims to roughly describe the total energy of the electrons as a *density functional* of atomic/molecular electrons. It serves as a basis for more sophisticated methods aiming at determining the electronic structure, such as *density functional theory* (DFT), and the wavefunctions determined by this method often serve as a starting point for the Hartree method discussed below. One of the important predictions of the *Thomas-Fermi model* is that the average radius of an atom depends on the nuclear charge as $\bar{R} \propto Z^{-1/3}$.

The Thomas-Fermi model allows us to understand the electronic configuration of the fundamental states and provides the basis for the periodic system of elements. In this model, the electrons are treated as independent particles, on one side forming an effective radial electric potential, on the other side being subjected to this potential. Instead of requiring anti-symmetry of the wavefunction, it is only necessary to ensure that all electrons are distinguished by at least one quantum number. The orbitals of complex atoms are similar to the wavefunctions of hydrogen. So, we can use these quantum numbers n, ℓ, m_ℓ, and m_s for every electron.

However, the effective radial potential depends very much on the species and is quite different from the Coulomb potential. So, the degeneracy in ℓ is lifted. In general, electrons with small ℓ are more strongly bound, because they have a higher probability of being near the nucleus, where the potential is deeper (see Fig. 31.2). The same argument explains why electrons with small n are more strongly bound. We will discuss these effects in more depth in Sec. 31.4.1 by comparing the excitation levels of the valence electron in different alkalis.

31.3.2.1 Density of states in the Fermi gas model

Even though the real potential sensed by the electrons bound to a nucleus is very different from the three-dimensional well, we can roughly imagine that the atom is subdivided into small volumes, understood as box potentials, all filled with electrons. From this we can calculate the distribution of the electronic charge, such that the

average local energy is homogeneous and the electronic cloud in equilibrium. The distribution, in turn, serves to determine the shape of the electrostatic potential which, when subdivided into small volumes filled with electrons, produces the same charge distribution. This principle is called *self-consistency*.

According to the Fermi gas model, we consider an infinite potential well, that we gradually fill up with electrons. The Pauli principle allows us to place at most two electrons in each orbital,

$$\Psi = \psi_{1,\uparrow}(x_1)\psi_{1,\downarrow}(x_2)\psi_{2,\uparrow}(x_3)\psi_{2,\downarrow}(x_4)\cdot\ldots\ . \tag{31.36}$$

This total wavefunction satisfies the weak Pauli principle, but is obviously not antisymmetric. The approximation is good, when the interaction between the electrons is negligible. Otherwise, we need to consider the exchange energy terms. This model, called *Fermi gas model*, is often used to describe the behavior of electrons that can freely move within the conductance band of a metal.

We divide the atom into small volumes (cells) containing uniformly distributed non-interacting electrons, whose total number is N, and we analyze each cell individually. The whole volume can be modeled by a box potential: $V(\mathbf{r}) = 0$ for $0 \le x, y, x \le L$ and $V(\mathbf{r}) = \infty$ in all other places. In this case we find the possible states $\{|n_x, n_y, n_z\rangle\}$ with $n_x, n_y, n_z = 1, 2, 3$ and the single electron energies,

$$E_{n_x,n_y,n_z} = \frac{\pi^2\hbar^2}{2m_eL^2}(n_x^2 + n_y^2 + n_z^2) = \frac{\hbar^2}{2m_e}\mathbf{k}^2_{n_x,n_y,n_z}\ , \tag{31.37}$$

where $\mathbf{k}^2_{n_x,n_y,n_z} = k_x^2 + k_y^2 + k_z^2 = (\frac{n_x\pi}{L})^2 + (\frac{n_y\pi}{L})^2 + (\frac{n_z\pi}{L})^2$. Each set of values $\mathbf{k} = (k_x, k_y, k_z)$ corresponds to an accessible state of the system, and each state is associated with a volume element $(\pi/L)^3$ in k-space. Defining the density of states $\eta(E)$, we can express the total number of states below a particular energy E by,

$$\begin{aligned} n(E) &= \int_0^E \eta(E')dE' \equiv \frac{1}{(2\pi)^3}\int d^3r d^3k = \frac{L^3}{(2\pi)^3}4\pi\int k^2dk \\ &= \frac{L^3}{(2\pi)^3}4\pi\left(\frac{2m_e}{\hbar^3}\right)^{3/2}\int_0^E\sqrt{E'}dE' = \frac{L^3}{3\pi^2}\left(\frac{2m_eE}{\hbar^3}\right)^{3/2}\ . \end{aligned} \tag{31.38}$$

$\eta(E)dE$ is the number of states with energies between E and $E + dE$.

At temperature $T = 0$ K all N electrons are in their energetically lowest available state, obeying the Pauli exclusion principle and considering the spin. The energy of the N-th electron (the most energetic one) is then called the *Fermi energy* E_F. That is, below E_F all states are occupied, and all states above E_F are unoccupied. The total energy is given by the sum of the energies of the N less energetic states, and the final physical state is given by the antisymmetrization of the corresponding wavefunction. With the formula (31.38), we can express the Fermi energy via $n(E_F) \equiv N$, such that,

$$E_F = \frac{\hbar^2}{2m_eL^2}(3\pi^2N)^{2/3}\ , \tag{31.39}$$

so that the density of states can be expressed as,

$$\boxed{\eta(E) = \frac{dn(E)}{dE} = \frac{L^3}{2\pi^2}\left(\frac{2m_e}{\hbar^2}\right)^{3/2}E^{1/2} = \frac{3N}{2}\frac{E^{1/2}}{E_F^{3/2}}}\ . \tag{31.40}$$

31.3.2.2 Thomas-Fermi energy

Fermi's box potential trick allowed us to model the impact of Pauli's principle on the spatial distribution of fermions in a restricted volume, but we did not take into account yet the fact that electrons are charged and will interact. Hence, the energy calculated so far is purely kinetic and will have to be complemented by potential energy.

The total kinetic energy of the electrons with the system in its ground state is,

$$\begin{aligned} E_{tot} &= \int_0^{E_F} E\eta(E)dE = \frac{L^3}{2\pi^2}\left(\frac{2m_e}{\hbar^2}\right)^{3/2}\int_0^{E_F} E^{3/2}dE \\ &= \frac{L^3}{5\pi^2}\left(\frac{2m_e}{\hbar^2}\right)^{3/2} E_F^{5/2} = \frac{\hbar^2 3^{5/3}\pi^{4/3}}{10m_e}L^3\left(\frac{N}{L^3}\right)^{5/3} = CL^3\rho^{5/3} \ , \end{aligned} \tag{31.41}$$

where $\rho \equiv N/L^3$ is the density of electrons per unit volume and C just a proportionality constant. Now understanding ρ as a quantity depending on position in space, we calculate the total number of electrons as,

$$N = \int_{\mathbb{R}^3} \rho(\mathbf{r})d^3r \ , \tag{31.42}$$

and the kinetic energy density by,

$$u_{kin}(\mathbf{r}) = C\rho^{5/3}(\mathbf{r}) \ , \tag{31.43}$$

such that the total kinetic energy of the electrons in the electronic shell is,

$$T[\rho] = C\int \rho^{5/3}(\mathbf{r})d^3r \ . \tag{31.44}$$

The potential associated with the electron-nucleus interaction is,

$$V_{ep}[\rho] = -\frac{Ze^2}{4\pi\varepsilon_0}\int \frac{\rho(\mathbf{r}')}{r'}d^3r' = \int V_p(\mathbf{r}')\rho(\mathbf{r}')d^3r' \ , \tag{31.45}$$

with the electrical potential generated by the nucleus,

$$\Phi_p(\mathbf{r}) = \frac{V_p(\mathbf{r})}{-e} = \frac{Ze}{4\pi\varepsilon_0}\frac{1}{r} \tag{31.46}$$

The potential associated with the electron-electron interaction is,

$$V_{ee}[\rho] = \frac{1}{2}\frac{e^2}{4\pi\varepsilon_0}\int \frac{\rho(\mathbf{r})\rho(\mathbf{r}')}{|\mathbf{r}-\mathbf{r}'|}d^3rd^3r' = \int V_e(\mathbf{r}')\rho(\mathbf{r}')d^3r' \ , \tag{31.47}$$

with the electrical potential generated by the electron cloud,

$$\Phi_e(\mathbf{r}) = \frac{V_e(\mathbf{r})}{-e} = -\frac{1}{2}\frac{e}{4\pi\varepsilon_0}\int \frac{\rho(\mathbf{r}')}{|\mathbf{r}-\mathbf{r}'|}d^3r' \tag{31.48}$$

Thus, the total energy (*Thomas-Fermi energy*) can be written as a functional of the electronic density of the atom,

$$\boxed{H_{TF}[\rho] = T[\rho] + V_{ep}[\rho] + V_{ee}[\rho]} \ . \tag{31.49}$$

31.3.2.3 Electronic density and the Thomas-Fermi equation

Exploiting the variational principle, we are interested in the electronic density $\rho(\mathbf{r})$ which minimizes the Thomas-Fermi energy. We can perform this process via Lagrange multipliers under the constraint, that the number of electrons remains constant in the atom. Thus,

$$0 = \delta \left\{ H_{TF}[\rho] - \mu \left(\int \rho(\mathbf{r}) d^3r - N \right) \right\} \ . \tag{31.50}$$

Inserting the Thomas-Fermi energy (31.49) we calculate,

$$\mu = \frac{\delta}{\delta\rho(\mathbf{r})} \left\{ C\rho^{5/3}(\mathbf{r}) + V_p(\mathbf{r})\rho(\mathbf{r}) + V_e(\mathbf{r})\rho(\mathbf{r}) \right\} = \tfrac{5}{3} C\rho^{2/3}(\mathbf{r}) + V_p(\mathbf{r}) + V_e(\mathbf{r}) \ . \tag{31.51}$$

Resolving for the electronic density,

$$\rho(\mathbf{r}) = \left(\frac{3}{5C} \right)^{3/2} [\mu - V_p(\mathbf{r}) - V_e(\mathbf{r})]^{3/2} \ . \tag{31.52}$$

The above expression is called the *Thomas-Fermi equation* and describes the electron density of the atom in its ground state. The expression (31.48) can be rewritten as a Poisson equation,

$$\nabla^2 V_e(\mathbf{r}) = \frac{e^2}{2\varepsilon_0} \rho(\mathbf{r}) \ , \tag{31.53}$$

so that,

$$\nabla^2 V_e(\mathbf{r}) = \frac{e^2}{2\varepsilon_0} \left(\frac{3}{5C} \right)^{3/2} [\mu - V_p(\mathbf{r}) - V_e(\mathbf{r})]^{3/2} \ . \tag{31.54}$$

For the effective potential introduced via $V_{eff} = V_p + V_e$, we find,

$$\begin{aligned} \nabla^2 V_{eff}(\mathbf{r}) &= \nabla^2 \left(-\frac{Ze^2}{4\pi\varepsilon_0} \frac{1}{r} \right) + \nabla^2 V_e(\mathbf{r}) \\ &= -\frac{Ze^2}{\varepsilon_0} \delta^3(\mathbf{r}) + \frac{e^2}{2\varepsilon_0} \left(\frac{3}{5C} \right)^{3/2} [\mu - V_{eff}(\mathbf{r})]^{3/2} \ . \end{aligned} \tag{31.55}$$

We note that, with (31.50), we can identify the Lagrange multiplier μ as a *chemical potential*. In particular, for non-interacting neutral atoms, we have $\mu = 0$. In addition, since for an atom both the potential and the electronic density must have spherical symmetry, we can write for $r \neq 0$,

$$\frac{1}{r} \frac{\partial^2}{\partial r^2} [r V_{eff}(r)] = \frac{e^2}{2\varepsilon_0} \left(\frac{3}{5C} \right)^{3/2} [-V_{eff}(\mathbf{r})]^{3/2} \ . \tag{31.56}$$

We now make the ansatz,

$$V_{eff}(r) \equiv -\frac{Z}{r} \chi(\alpha r) \qquad \text{setting} \qquad \alpha \equiv \frac{3e^{4/3}}{5C\varepsilon_0^{2/3}} Z^{1/3} \ . \tag{31.57}$$

This transforms the expression (31.56) into,

$$\frac{\partial^2}{\partial r^2} \chi(\alpha r) = -\frac{e^2}{Z\varepsilon_0} \left(\frac{3Z}{5C} \right)^{3/2} \frac{\chi^{3/2}(\alpha r)}{r^{1/2}} \ , \tag{31.58}$$

or, substituting $x \equiv \alpha r$,

$$\frac{d^2\chi}{dx^2} = -\frac{\chi^{3/2}}{x^{1/2}} \ . \tag{31.59}$$

It is important to note the last equation does not depend on the parameter Z, thus being a general result for any neutral atom. The function $\chi(x)$ is determined numerically, but we can analyze its asymptotic values given the expected behavior of the effective potential $V_{eff}(r)$: for $r \to 0$ we expect that $V_{eff}(r) = V_p(r)$, hence $\chi(0) = 1$. On the other hand, for $r \to \infty$, we expect $V_{eff}(r) = 0$, hence $\chi(\infty) = 0$. Do the Exc. 31.3.5.1.

With $\chi(x)$ known, we obtain the charge density $\rho(x)$, and hence we are able to calculate the total energy of the atom under investigation. Thus, it is possible to show that [60],

$$H_{TF}[\rho] = -0.7687\frac{e^2}{4\pi\varepsilon_0 a_B}Z^{7/3} \ . \tag{31.60}$$

It is important to highlight some points:

1. The result holds for neutral atoms.

2. There is no electronic shell structure assumed; apart from the fact that the kinetic energy was derived in a way as to respect Pauli's principle, the whole calculation was done within the laws of classical electromagnetism; no quantum mechanics was involved and, hence, no set of quantum numbers has been found.

3. Apart from the Pauli principle used to calculate the density of states (31.40), quantum statistical effects of identical particles (such as wavefunction anti-symmetrization) are not taken into account.

A more refined model which deals with third criticism and, in addition, is closer to density functional theory (DFT) is the Thomas-Fermi-Dirac model.

31.3.3 Hartree method

The effective potential obtained from the Thomas-Fermi model can serve as a starting point for quantum treatments. Assuming that all electrons are subject to the same effective potential V_{eff}, we numerically solve the Schrödinger equation for each electron independently,

$$\hat{H}_i = \left(-\frac{\hbar^2}{2m}\nabla_i^2 + V_{eff}\right)\psi_i(\mathbf{r}_i) = e_i\psi_i(\mathbf{r}_i) \ . \tag{31.61}$$

With this we calculate all energies and eigenfunctions (only the radial parts are of interest) minimizing the total energy and respecting the weak Pauli principle, that is, we classify the states in the order of increasing energies e_i and fill them successively with electrons. For the total wavefunction we obtain,

$$\left(\sum_{i=1}^{N}\hat{H}_i\right)\Psi_N = E_n\Psi_N \quad \text{with} \quad \Psi_N = \psi_1 \cdot .. \cdot \psi_N \quad \text{and} \quad E_n = \sum_{i=1}^{N} e_i \ . \tag{31.62}$$

With the eigenfunctions we calculate the charge densities $e|\psi_j(\mathbf{r}_j)|^2$. We integrate the interaction energy between these charge densities and the potentials exerted by the nucleus and all other electrons $j \neq i$ to obtain an effective potential that represents an improved estimation for the electronic mean field,

$$V_{eff} \longleftarrow -\frac{Ze^2}{4\pi\varepsilon_0 r_i} + \sum_{j\neq i} \int d^3r_j \frac{e^2}{4\pi\varepsilon_0|\mathbf{r}_i - \mathbf{r}_j|}|\psi_j(\mathbf{r}_j)|^2 \ . \tag{31.63}$$

We replace that potential in the Schrödinger equation, and repeat the whole process from the beginning, until the total energy $\sum_i e_i$ does not get any lower. This self-consistent method is called *Hartree method*. Fock improved these calculations using antisymmetric wavefunctions for the valence electrons. This method is called *Hartree-Fock method*.

31.3.4 Hartree-Fock method

The Hartree-Fock method used to treat atomic or molecular many-body systems aims at obtaining the electronic wavefunction of the system. Dealing with anti-symmetrized wavefunctions, it represents a refinement of the Hartree method. The method is based on the variational principle and on the assumption that we can write the global wavefunction as a Slater determinant, with each electron occupying a specific orbital state (spin-orbital) and interacting with an effective potential stemming from the electrons which occupy other orbitals. Instead of solving the Schrödinger equation, we must now solve a set of equations called Hartree-Fock equations of the type $\hat{F}\psi_k(1) = \epsilon_k\psi_k(1)$. The method is performed iteratively until convergence of the atomic orbitals and their respective energies is reached. The procedure is then called *self-consistent*: Starting from an initial trial global wavefunction we calculate the effective potential in each orbital and a new set of wavefunctions which, in turn, generate a new effective potential. This new potential is then used in a new set of Hartree-Fock equations.

31.3.4.1 Hartree-Fock equations

To start with, we write the Hamiltonian (31.33) of a multi-electronic atom as [60],

$$\hat{H} = \sum_{i=1}^{Z} \hat{h}_i + \tfrac{1}{2}\sum_{i\neq j} \hat{V}_{ij} \ , \tag{31.64}$$

where $\hat{h}_i$ is the Hamiltonian only of the electron i, and $\hat{V}_{ij}$ is the interaction term between the electrons i and j. To implement the method we must suppose that the multi-electronic state can be written as the product of the individual states of each electron:

$$\Psi'(1,...,Z) = \psi_1(1)\psi_2(2)...\psi_Z(Z) \ , \tag{31.65}$$

where $\psi_i(1) = \phi_i(r_1)\chi(\alpha) = \psi_i^\alpha(r_1)$ represents the spin-orbital state of electron 1, that is, the spatial wavefunction of the electron in the state i and with spin α. However, due to the symmetrization postulate, the physical state of the system must be expressed by a Slater determinant,

$$\Psi(1,...,Z) = \frac{1}{\sqrt{Z!}} \det\ [\psi_1(1)\psi_2(2)...\psi_Z(Z)] \ . \tag{31.66}$$

Now, we use the variational principle to minimize the expectation value of the ground state energy by varying the functions $\psi_k(n)$. In this way, the correct orbitals are those that minimize the energy. The expectation value is written as,

$$E = \langle\Psi|\hat{H}|\Psi\rangle = \langle\Psi|\sum_{i=1}^{Z}\hat{h}_i|\Psi\rangle + \langle\Psi|\tfrac{1}{2}\sum_{i\neq j}\hat{V}_{ij}|\Psi\rangle \ . \tag{31.67}$$

It is possible to show that,

$$\langle\Psi|\sum_{i=1}^{Z}\hat{h}_i|\Psi\rangle = \sum_{i=1}^{Z}\langle\psi_i|\hat{h}_i|\psi_i\rangle \qquad \text{and} \tag{31.68}$$

$$\langle\Psi|\tfrac{1}{2}\sum_{i\neq j}\hat{V}_{ij}|\Psi\rangle = \tfrac{1}{2}\sum_{i,j}^{Z}[\langle\psi_i\psi_j|\hat{V}_{ij}|\psi_i\psi_j\rangle - \langle\psi_j\psi_i|\hat{V}_{ij}|\psi_j\psi_i\rangle] \ .$$

Hence,

$$E = \sum_{i=1}^{Z}\langle\psi_i|\hat{h}_i|\psi_i\rangle + \tfrac{1}{2}\sum_{i,j}^{Z}[\langle\psi_i\psi_j|\hat{V}_{ij}|\psi_i\psi_j\rangle - \langle\psi_j\psi_i|\hat{V}_{ij}|\psi_j\psi_i\rangle] \ . \tag{31.69}$$

The above expression can be minimized via Lagrange multipliers under the constraint that the states are orthogonal $\langle\psi_i|\psi_j\rangle = \delta_{ij}$,

$$\delta\left\{\langle\Psi|\hat{H}|\Psi\rangle - \sum_{i,j}\epsilon_{ij}[\langle\psi_i\psi_j|\hat{V}_{ij}|\psi_i\psi_j\rangle - \langle\psi_j\psi_i|\hat{V}_{ij}|\psi_j\psi_i\rangle]\right\} \tag{31.70}$$

Thus, we obtain the following set of *Hartree-Fock equations*:

$$\hat{F}\psi_k(1) = \epsilon_k\psi_k(1) \qquad \text{where} \qquad \hat{F} = \hat{h}_1 + \sum_i(2\hat{J}_i - \hat{K}_i) \tag{31.71}$$

is the Fock operator and ϵ_k is the energy associated with the spin-orbital ψ_k. The operator $\hat{J}_i$, called *Coulomb operator*, represents the mean potential sensed by electron 1 in the orbital k due to the presence of electron 2 in the orbital i:

$$\hat{J}_i\psi_k(1) = \left\{\int \psi_i^*(2)V_{12}\psi_i(2)dr_2\right\}\psi_k(1) \ . \tag{31.72}$$

The operator $\hat{K}_i$, denominated *exchange operator*, is a consequence of the symmetrization process and therefore a purely quantum effect, that is, without classical analogue:

$$\hat{K}_i\psi_k(1) = \left\{\int \psi_i^*(2)V_{12}\psi_k(2)dr_2\right\}\psi_k(1) \ . \tag{31.73}$$

Once we know all wavefunctions, the energies of the orbitals can be obtained in the following way:

$$\int dr_1\psi_k^*(1)\left\{\hat{h}_1 + \sum_i(2\hat{J}_i - \hat{K}_i)\right\}\psi_k^*(1) = \epsilon_k\int dr_1\psi_k^*(1)\psi_k(1) = \epsilon_k \ , \tag{31.74}$$

that is,

$$\epsilon_k = \int dr_1 \psi_k^*(1)\hat{h}_1\psi_k^*(1) + \sum_i (2\hat{J}_{ki} - \hat{K}_{ki}) \ , \tag{31.75}$$

where,

$$\hat{J}_{ki} = \int dr_1 \psi_k^*(1)\hat{J}_i\psi_k(1) \qquad \text{is the Coulomb integral} \tag{31.76}$$

$$\hat{K}_{ki} = \int dr_1 \psi_k^*(1)\hat{K}_i\psi_k(1) \qquad \text{is the exchange integral .}$$

The total atomic energy can be calculated by,

$$E = 2\sum_k \epsilon_k - \sum_{k,i} (2\hat{J}_{ki} - \hat{K}_{ki}) \ . \tag{31.77}$$

Furthermore, if assuming that, taking an electron away from the orbital ψ_k the electronic distribution remains unchanged, it is possible to associate the energy ϵ_k with the ionization energy of the electron in this orbital, $I_k \simeq \epsilon_k$. This equality is known as *Koopman's theorem*.

31.3.5 Exercises

31.3.5.1 Ex: Effective potential in the Thomas-Fermi model

Calculate numerically and plot the effective potential in the Thomas-Fermi model from the differential equation (31.59) for $Z = 40$ [1419].

Solution: *We rewrite the equations as,*

$$\frac{d}{dt}\begin{pmatrix}\chi' \\ \chi\end{pmatrix} = \begin{pmatrix}-\chi^{3/2}/x^{1/2} \\ \chi'\end{pmatrix} \ .$$

Fig. 31.3 shows the calculated Thomas-Fermi potential and comparisons with the Coulombian nuclear and shielded potentials.

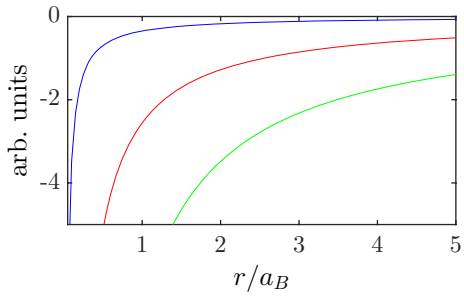

Figure 31.3: (code) (red) Effective potential in the Thomas-Fermi potential compared to the Coulombian nuclear (blue) and shielded (green) potentials.

31.4 The periodic system of elements

Completely filled principal layers n, ℓ are isotropic, $\Psi_N(\mathbf{r}) = \Psi(r)$, as we will show in Exc. 31.4.4.1. It is important to distinguish three different energetic sequences: 1. Tab. 31.6 shows, for a given atom, the excited orbitals of the *last electron*. 2. The energy sequence shown in Tab. 31.7 tells us in which orbital the next electron will be placed, when we go to the *next atom* in the periodic table 31.9 which has one more proton in the nucleus. 3. The inner electrons are subject to different potentials and, hence, follow a different sequence energetic sequence: While for the inner electrons we find,

$$E_{n,\ell} < E_{n,\ell+1} \ll E_{n+1,\ell} \ , \tag{31.78}$$

the sequence is partially inverted for the outermost electron. Note that it is the outermost electrons that determine the chemical reactivity of the atom. The sequence is illustrated in Fig. 31.5.

Noble gases have small radii, high excitation energies and high ionization energies. The outermost electrons in a noble gas atom must overcome a large energy gap to any higher quantum numbers. Halogens have strong electro-affinities, since the outer electron layer (n_{max}) is incomplete and therefore malleable, such that an electron approaching the halogen perceives the nuclear charge through a partially transparent shield. Alkalis are similar to hydrogen and have excitation energies in the optical regime. Their fundamental state $^2S_{1/2}$ is determined by a single valence electron in the $\ell = 0$ orbital. Unlike hydrogen, excitation energies are highly dependent on ℓ, since orbits with small ℓ correspond to eccentric ellipses and have higher probabilities to be in the unshielded region $-Z^2e^2/r$ than orbits with large ℓ, who spend more time in the shielded region $-e^2/r$. For the same reason, energies corresponding to larger n resemble more those of the hydrogen spectrum.

31.4.0.1 Inner shell electrons

The interior shell structure of the atoms can be analyzed by X-ray scattering. Electrons decelerated by atoms emit a continuous spectrum called *Bremsstrahlung*, but they can also expel electrons from the inner layers leaving a hole behind. When a hole is filled by cascades of electrons falling down from higher layers, the atom emits a specific X-ray spectrum ($\approx 10^4\,\mathrm{eV}$). The selection rules $\Delta\ell = \pm 1$ and $\Delta j = \pm 1$ split the lines in two components. X-ray spectra of neighboring elements in the periodic table are very similar, because the inner layers not being shielded, they see a potential close to $\propto Z^2/r$. Therefore, the Z-dependency of inner energy levels along a horizontal rows in the periodic table is more or less $\omega \propto Z^2$, as predicted by Bohr's atomic model.

31.4.1 Electronic shell model

In the Fermi gas model, each of the energy levels contains several states, and each of these states can be occupied by a single electron, according to the Pauli principle. In this way, we obtain the electronic configuration for the atoms of the periodic system. In this picture, the energies of the ground states of the elements, normalized by $1/Z^2$, can be arranged in the scheme of Fig. 31.4.

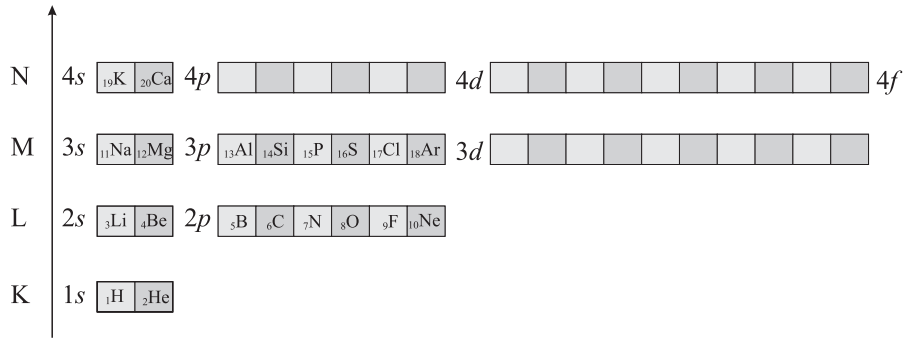

Figure 31.4: Periodic order.

This only works for atoms with up to 18 electrons. When the layer $3p$ is completely filled, the next to be occupied is not $3d$ but the $4s$. The new scheme is illustrated in Fig. 31.5. The anomalies beginning at $Z = 18$ arise due to electron-electron interaction. The real potential evolves from one to the other Coulombian potential, as distance from the nucleus is increased, as illustrated in Fig. 31.2. Near the nucleus, the electrons shield the positive charge less than for large distances r. Thus, those states that have a high probability near the nucleus are energetically lowered. That is,

$$E_{2s} < E_{2p} \qquad \text{and} \qquad E_{6s} < E_{6p} < E_{6d} \ . \tag{31.79}$$

The degeneracy of the orbital angular momentum in the Schrödinger model is thus lifted. The shielding is, as can be seen in the example of the excited states of lithium, a large effect in the range of some eV.

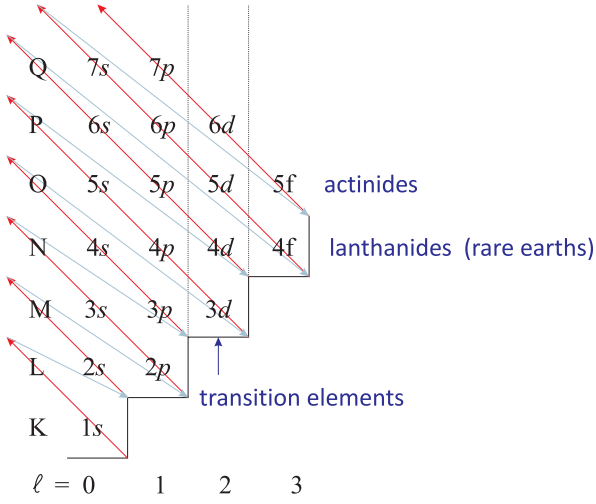

Figure 31.5: Illustration of the sequence of filling the orbitals with electrons.

The shielding also accounts for the anomalies in the periodic system, such as in K or Ca. Since $E_{4s} < E_{3d}$, the $4s$ state is filled before the $3d$. Similar anomalies

also occur in Rb ($5s$), Cs ($6s$), and Fr ($7s$). In rare earths the shielding effect is even more pronounced. Here, the energy of the state $6s$ is even below the energy of the $4f$, which means that the shells $6s$, $5s$, $5p$, and $5d$ protect the $4f$ shell very well [9]. Resolve Exc. 31.4.4.2.

31.4.1.1 Alkalines

The electronic shell structure of alkalines consists of a completed noble gas shell and an additional valence electron. Their spectrum is therefore very similar to hydrogen. An empirical approach can be stressed to describe this feature,

$$E_{n,\ell} = -\frac{\mu_{EG}c^2}{2}\frac{Z^2\alpha^2}{(n-\Delta_{n,\ell})^2} \ , \tag{31.80}$$

where μ_{EG} is the reduced mass relative to the noble gas shell and $\Delta_{n,\ell}$ is called *quantum defect*. The quantum defect is tabulated for most alkaline states and is particularly important for low energy states. For sodium, for example, the values are:

ℓ	$n=3$	$n=4$	$n=5$	$n=6$
s	1.37	1.36	1.35	1.34
p	0.88	0.87	0.86	0.86
d	0.10	0.11	0.13	0.11
f	-	0.00	-0.01	0.008

For states with a large angular momentum, the quantum defect disappears. In these states, the electron is far from the nucleus and the potential is similar to that of hydrogen. Alkalines are currently widely studied in quantum optics laboratories, for being comparatively simple, but having a sufficiently rich structure to be interesting. The fundamental electronic transitions typically lie in the visible and near-infrared spectral range and can be excited with comparatively simple laser sources. The lifetime of excited states is typically longer than 20 ns, which corresponds natural linewidths of approximately (2π) 10 MHz.

31.4.1.2 Excited states

The experimentally easiest and most precise approach to determining orbital energies consists in measuring excitation spectra of valence electrons. The diagram of Fig. 31.6 compares such excitation spectra for various alkaline atoms. Although this is not to be confused with the binding energies of valence electrons of different atoms, it gives us a qualitative idea of the impact of shielding and indicates, which orbital will be occupied by the additional valence electron of the next species in the periodic table.

[9] An example of this is Nd:YAG (Neodymium in Yttrium Aluminum Garnet). In this crystal, optical transitions can be excited within the $4f$ shell of the Nd. However, these transitions are only allowed due to perturbations of the crystalline field. The very strong shielding ensures a long life of the excited state. For this reason this crystal is an excellent laser material.

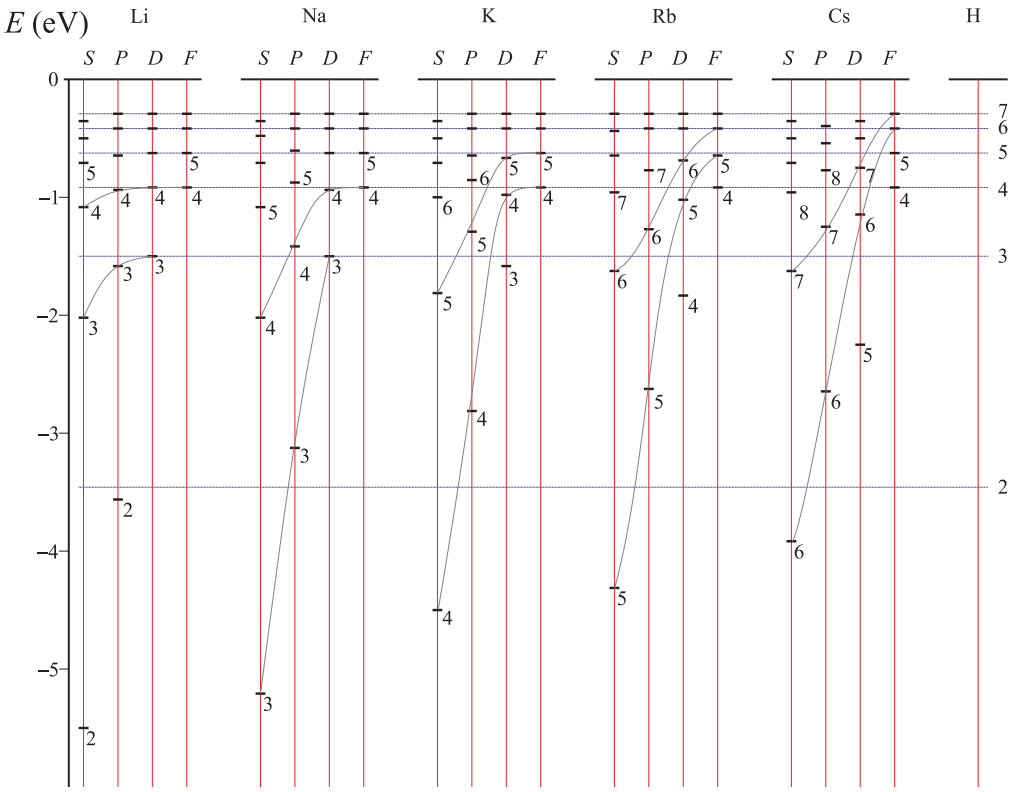

Figure 31.6: Comparison of the excitation energies of the *valence electron* for several alkaline atoms. Grey line are meant to guide the eye.

31.4.2 LS and jj-coupling

Following Hund's rule, the $\mathbf{L} \cdot \mathbf{S}$-coupling is energetically favorable compared to the $\mathbf{j} \cdot \mathbf{j}$-coupling, which means that the spins of the outermost electrons, that is, the electrons outside of filled subshells (n, ℓ), prefer to orient their spins in parallel in order to anti-symmetrize the spatial wavefunctions and thus maximize the distance between the electrons. Every sub-layer of the series shown in Fig. 31.5 must be filled in the listed order before placing new electrons in the next layer.

In the case of helium, we have seen that the Pauli principle first determines the relative orientation of the electron spins. The spins $\mathbf{s}_i$ of the individual electrons therefore add up to a total angular momentum $\mathbf{S}$. The *orbital* angular momenta $\mathbf{l}_i$ also adopt a relative orientation. It is determined by a residual spherically non-symmetric Coulomb interaction: A certain combination $\mathbf{L}$ of orbital angular momenta leads to a certain spatial distribution of the electrons and thus to a certain electrostatic energy distribution.

The total spin $\mathbf{S}$ and the total orbital angular momentum $\mathbf{L}$ subsequently couple to a total angular momentum $\mathbf{J}$ very similar to the $\mathbf{l} \cdot \mathbf{s}$ spin-orbit coupling in single electron systems. States with different $\mathbf{J}$ then have the respective energies that the

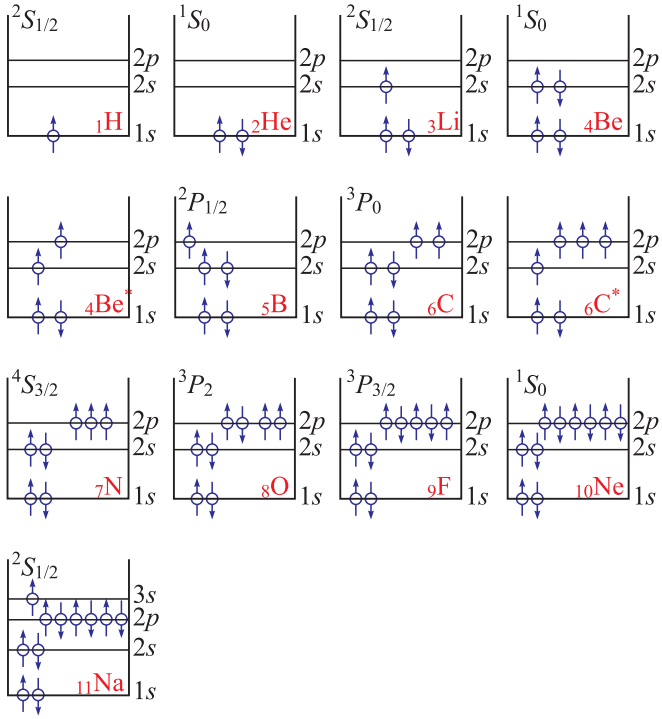

Figure 31.7: Illustration of Hund's rule.

total spin **S** adopts in the field generated by the total orbital angular momentum **L** [10].

The above coupling scheme is called *Russel-Saunders coupling* or *LS-coupling*. It works well when the spin-orbit coupling of individual electrons is small. In this case, intercombination is forbidden, which means that there can be no electromagnetic transition between states with different spins (see the case of metastable helium in Sec. 31.2.2).

Since $E_{LS} \simeq (Z\alpha)^4 \simeq Z^4$, as shown in (29.130), for heavy atoms, the coupling of an electronic spin to its own orbital momentum grows strongly with Z, as well as the symmetrization and the exchange energy, which mutually orient the spins, and the residual Coulomb interaction, which mutually couples the angular orbital momenta. In this case, the orientation of $\mathbf{L}_i$ relative to $\mathbf{S}_i$ delivers more energy than the exchange energy and the residual energy cost. Hence, the spin and the orbital angular momentum of an individual electron couple first,

$$\mathbf{j}_i = \mathbf{l}_i + \mathbf{s}_i \ . \tag{31.81}$$

We obtain a new Hamiltonian of fine structure of the form,

$$H_{FS} \propto \mathbf{j}_i \cdot \mathbf{j}_j \ . \tag{31.82}$$

[10] In addition, there are the small contributions due to $\mathbf{l}_i \cdot \mathbf{l}_j$-coupling and to $\mathbf{s}_i \cdot \mathbf{s}_j$-coupling, where $i \neq j$.

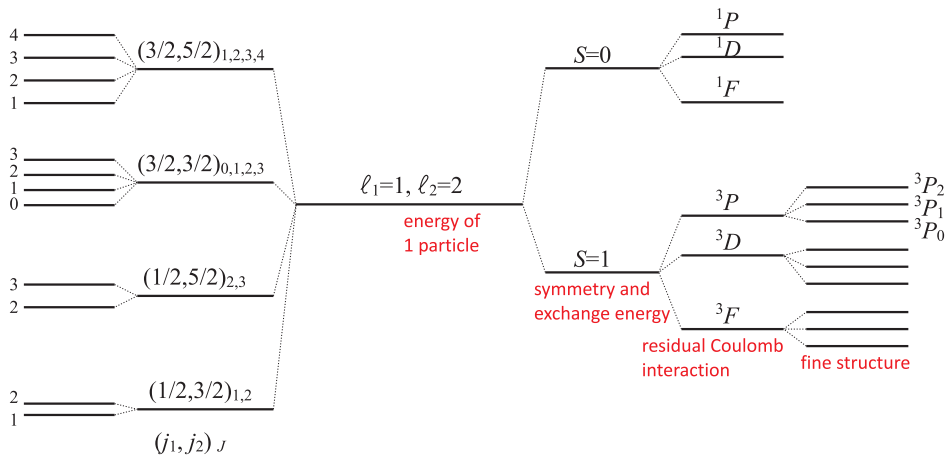

Figure 31.8: Hierarchy of coupling energies at the example of two electrons out of closed shells, $(2p)(3d)$, under the presumption of perfect jj-coupling (left) or LS-coupling (right).

Pure jj-coupling only exists for very heavy nuclei. Normally, we have a so-called *intermediate coupling*, which is a mixture of LS and jj-coupling. This can considerable relax the intercombination prohibition. When the coupling is pure, we have the following dipolar selection rules:

LS-coupling: $\Delta S = 0$, $\Delta L = \pm 1$, $\Delta \ell = \pm 1$

jj-coupling: $\Delta j = 0, \pm 1$ for one e^-, $\Delta j = 0$ for all others

In addition we have for the two couplings: $\Delta J = 0, \pm 1$, but $J, J' = 0$ is forbidden, $\Delta m_J = 0, \pm 1$ when $\Delta J = 0$ but $m_J, m_{J'} = 0$ is forbidden.

31.4.3 Summary of contributions to the atomic energy levels

The total Hamiltonian of a single atom is composed of the kinetic energy of the nucleus and the electrons, of various interaction potentials between the nucleus and the electrons, and of interactions with various types of external electromagnetic fields.

$$\hat{H} = -\frac{\hbar^2}{2m}\nabla_R^2 + \sum_{i=1}^{N}\left(-\frac{\hbar^2}{2m}\nabla_{r_i}^2\right) + V(\mathbf{r}_1, \mathbf{s}_1, .., \mathbf{r}_N, \mathbf{s}_N) + V_{ext} \ . \tag{31.83}$$

Of course, with the presence of other atoms, other interactions may generate other relevant contributions to the Hamiltonian.

The following interactions contribute to the potential V: The Coulomb interactions,

$$V_{ncl-ele} = -\sum_{i=1}^{Z}\frac{Ze^2}{4\pi\varepsilon_0|\mathbf{r} - \mathbf{r}_i|} \quad \text{and} \quad V_{ele-ele} = \sum_{i<j=1}^{Z}\frac{e^2}{4\pi\varepsilon_0|\mathbf{r}_i - \mathbf{r}_j|} \ , \tag{31.84}$$

the antisymmetry of the wavefunction, that is, exchange integrals,

$$V_{sym} \ , \tag{31.85}$$

the energies of spin-orbit couplings,

$$V_{ls} = -\sum_{i=1}^{Z} \frac{1}{e2m^2c^2} \frac{1}{|\mathbf{r}-\mathbf{r}_i|} \frac{dV_{cl}}{dr_i} (\mathbf{l}_i \cdot \mathbf{s}_i) \ , \tag{31.86}$$

the energies of spin-spin couplings,

$$V_{ss} = \sum_{i\neq j=1}^{Z} \frac{e^2}{m^2} \left[\frac{\sigma_\mathbf{i} \cdot \sigma_\mathbf{j}}{|r_i - r_j|^3} - 3\frac{[\sigma_\mathbf{i} \cdot (\mathbf{r}_i - \mathbf{r}_j)][\sigma_\mathbf{j} \cdot (\mathbf{r}_i - \mathbf{r}_j)]}{(\mathbf{r}_i - \mathbf{r}_j)^5} \right] \ , \tag{31.87}$$

the energies of orbit-orbit couplings,

$$V_{ll} = \sum_{i\neq j=1}^{Z} c_{ij} (\mathbf{l}_i \cdot \mathbf{l}_j) \ , \tag{31.88}$$

interactions between the spin of the electrons and the nuclear spin and between the orbital angular momentum of the electrons and the nuclear spin,

$$V_{hfs} = \frac{A}{\hbar^2} \mathbf{J} \cdot \mathbf{I} \ , \tag{31.89}$$

and relativistic corrections.

$$V_{rel} \ , \tag{31.90}$$

In addition, static external fields may displace energy levels and can influence the internal coupling of angular momenta and spins,

$$V_{ext} = -\mathbf{d} \cdot \vec{\mathcal{E}} \ , \ \ -\vec{\mu} \cdot \vec{\mathcal{B}} \ . \tag{31.91}$$

What quantum numbers are good depends on the relative amplitudes of intra-atomic interactions:
Case 1: fine structure with $\mathbf{L}\cdot\mathbf{S}$-coupling plus Zeeman splitting of hyperfine structure: $V_{ncl-ele}, V^r_{ele-ele} \gg V^a_{ele-ele}, V_{sym} \gg V_{\ell s} \gg V_{hfs} \gg V_B$ the quantum number are $|n_i, \ell_i, \mathbf{L}, \mathbf{S}, \mathbf{J}, \mathbf{F}, m_F\rangle$.
Case 2: fine structure with $\mathbf{j}\cdot\mathbf{j}$-coupling plus Zeeman splitting of hyperfine structure: $V_{ncl-ele}, V^r_{ele-ele} \gg V_{\ell s} \gg V^a_{ele-ele}, V_{sym} \gg V_{hfs} \gg V_B$ the quantum number are $|n_i, \ell_i, j_i, \mathbf{J}, \mathbf{F}, m_F\rangle$.
Case 3: fine structure with $\mathbf{L}\cdot\mathbf{S}$-coupling plus hyperfine structure of Zeeman splitting: $V_{ncl-ele}, V^r_{ele-ele} \gg V^a_{ele-ele}, V_{sym} \gg V_{\ell s} \gg V_B \gg V_{hfs}$ the quantum number are $|n_i, \ell_i, \mathbf{L}, \mathbf{S}, \mathbf{J}, m_J, m_I\rangle$.
Case 4: fine structure with $\mathbf{L}\cdot\mathbf{S}$-coupling plus Paschen-Back splitting of fine structure: $V_{ncl-ele}, V^r_{ele-ele} \gg V^a_{ele-ele}, V_{sym} \gg V_B \gg V_{\ell s} \gg V_{hfs}$ the quantum number are $|n_i, \ell_i, \mathbf{L}, \mathbf{S}, m_L, m_S, m_I\rangle$.

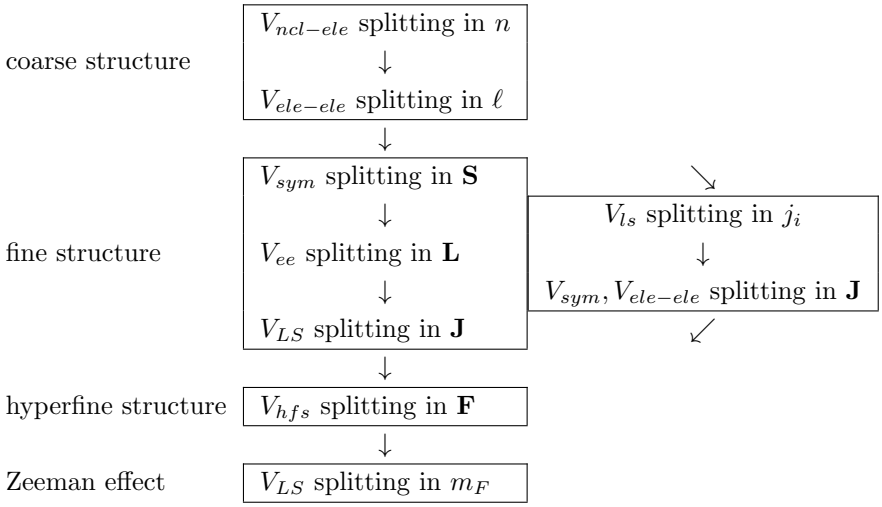

31.4.4 Exercises

31.4.4.1 Ex: Filled electronic shells

Show at the example of hydrogen that completely filled electronic layer are isotropic.

Solution: *An addition theorem for spherical harmonics states that,*

$$P_\ell(\hat{\mathbf{e}}_x \cdot \hat{\mathbf{e}}_y) = \frac{4\pi}{2\ell+1} \sum_{m=-\ell}^{\ell} Y_{\ell m}(\hat{\mathbf{e}}_y) Y^*_{\ell m}(\hat{\mathbf{e}}_x) \ ,$$

where P_ℓ is the Legendre polynomial of degree ℓ. In particular, for $\hat{\mathbf{e}}_y = \hat{\mathbf{e}}_x$,

$$\sum_{-\ell}^{\ell} |Y_{\ell m}|^2 d\Omega = \frac{2\ell+1}{4\pi} \ .$$

31.4.4.2 Ex: Electronic excitation levels of alkaline

Explain why
a. state [Li] $(2s)^2 S_{1/2}$ has lower energy than [H] $(2s)^2 S_{1/2}$;
b. state [Li] $(2s)^2 S_{1/2}$ has lower energy than [Li] $(2p)^2 P_J$;
c. state [Na] $(4s)^2 S_{1/2}$ has lower energy than [Na] $(3d)^2 D_J$.

Solution: *Looking at Fig. 31.6, we see:*
a. The nucleus is shielded by a filled $(1s)^2$ orbital, so that we could expect equivalence of both systems. However, the $(2s)$ valence electron still has a large probability of being near the nucleus, so that the shielding is only partial. The stronger attraction of the $Z = 3$ charge of the nucleus lowers the energy of the valence electron.

b. Higher orbital quantum numbers $\ell \gg 0$ have lower probabilities of near the nucleus, so that the shielding is more effective.
c. Same reason as in (b), only that the energy correction is now so large that the 'natural' ordering according to the main quantum number of Bohr's model is inverted.

31.5 Further reading

P.W. Atkins and R.S. Friedman, (3^{rd} ed. Oxford University (2001), *Molecular Quantum Mechanics* [60]ISBN

I.N. Levine, Allyn and Bacon, 7^{th} ed. Pearson (1983), *Quantum Chemistry* [796]ISBN

J.I. Steinfeld, The MIT Press, Cambridge (2005), *Molecules and Radiation* [1252]ISBN

B.H. Bransden, C.J. Joachain, John Wiley & Sons (1983), *Physics of Atoms and Molecules* [190]ISBN

p-table, *Periodic Table* http

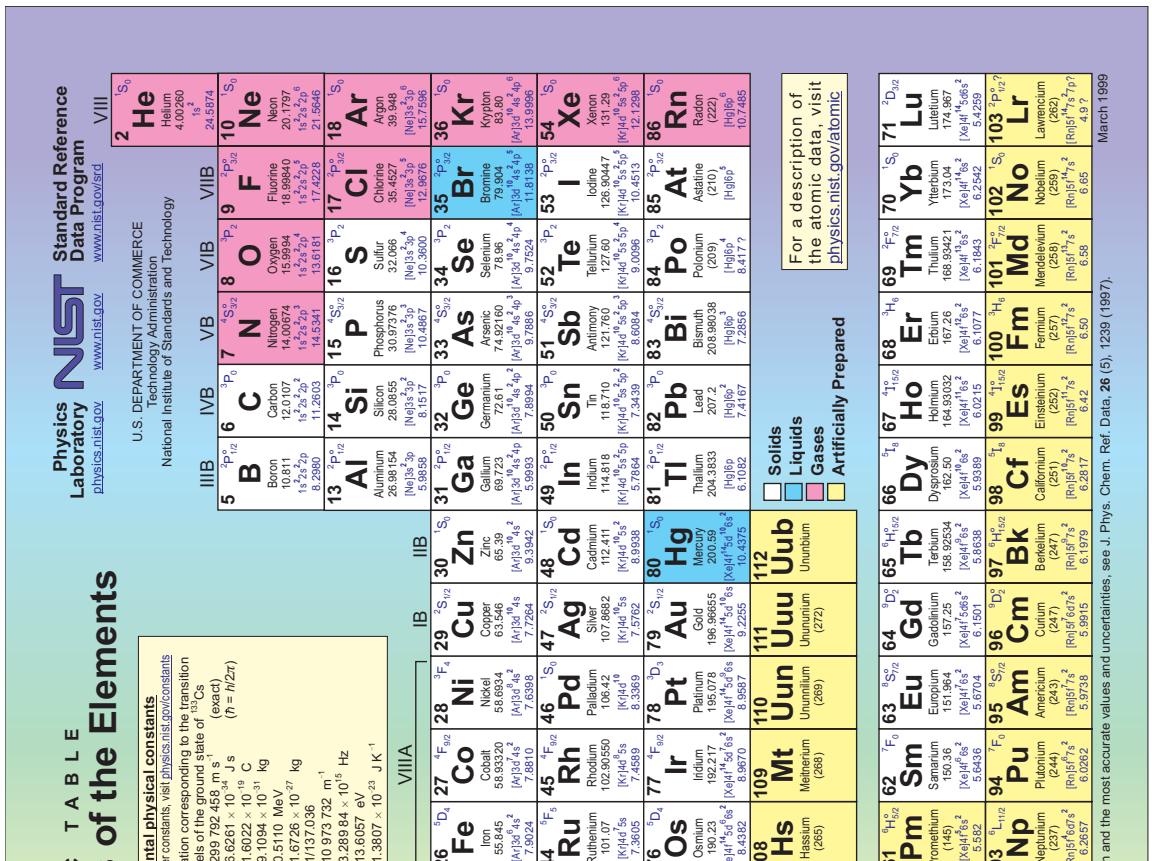

Figure 31.9: Periodic table.

Chapter 32

Molecular dimers

In systems of many particles (gases, fluids, or solids) interatomic interactions must be considered. These interactions usually have electrostatic origins, but generally can not be given in the form of closed expressions. For example, the collision of two atoms i and j can occur in a multitude of channels, that is, interaction potentials $V(\mathbf{r}_i - \mathbf{r}_j)$. Interatomic forces do not only govern collisions, but can sustain molecular bound states. This introduces new degrees of freedom in the systems of many particles through possible excitations of vibration or rotation movements.

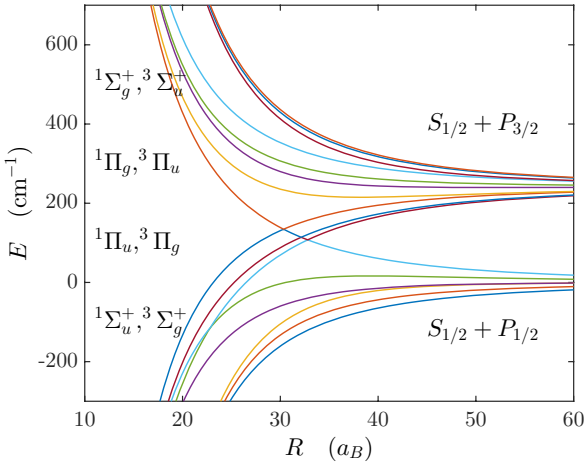

Figure 32.1: (code) Example of an interatomic potential spaghetti: The lowest states of the molecule $^{85}Rb_2$.

In this course, we will not go beyond homo- or heteronuclear dimers, that is, molecules consisting of two identical or different atoms.

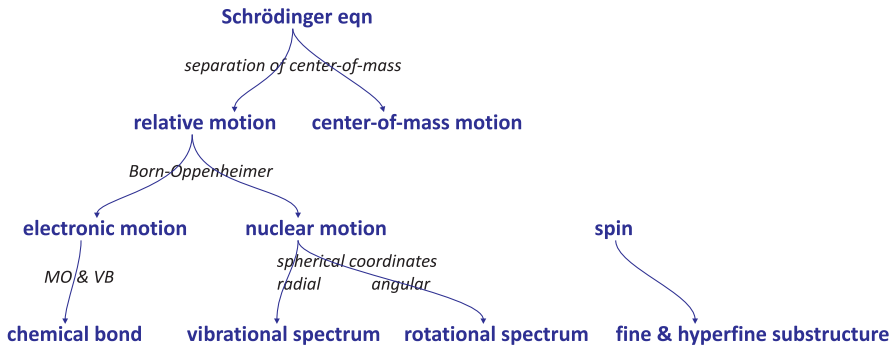

Figure 32.2: Approximations made in the molecular physics.

32.1 Molecular binding

32.1.1 Ionic and covalent binding

There are two fundamental ways of binding two atoms together, the ionic bond and the covalent bond [1]. The *ionic bond* is ruled by the quantities *electroaffinity* (EA), *electronegativity* (EN), and *ionization energy* (IE):

- **Ionization energy:** This energy is needed for the release of an electron by a neutral atom, e.g. $\mathrm{Na} + 5.1\,\mathrm{eV} \rightarrow \mathrm{Na}^+ + e^-$.
- **Electroaffinity**: This energy is released by the capture of an electron by a neutral atom, e.g. $\mathrm{Cl} + e^- \rightarrow \mathrm{Cl}^- + 3.8\,\mathrm{eV}$.
- **Electronegativity**: This quantity measures the stability of a valence orbital, e.g. that of fluorine (3.98) is more stable than that of cesium (0.79), such that fluorine holds its electrons tighter than cesium.

At short distances, the exchange of an electron between atoms can decrease energy. The so-called *ionic bond* is then sustained by the Coulombian attraction between two ions, and the binding energy can be estimated through electrostatic interaction.

Example 187 (*Ionic binding in NaCl*): For example, a sodium and a chlorine atom gain energy by forming a molecule,

$$\begin{aligned} \mathrm{Na} + 5.1\,\mathrm{eV} &\rightarrow \mathrm{Na}^+ + e^- \\ \mathrm{Cl} + e^- &\rightarrow \mathrm{Cl}^- + 3.8\,\mathrm{eV} \\ \mathrm{Na}^+ + \mathrm{Cl}^- &\rightarrow \mathrm{NaCl} + 4.9\,\mathrm{eV} \\ \hline \mathrm{Na} + \mathrm{Cl} &\rightarrow \mathrm{NaCl} + (-5.1 + 3.8 + 4.9)\,\mathrm{eV} \ . \end{aligned} \tag{32.1}$$

[1] We are not considering metallic bonds nor hydrogen bridge bonds, here.

The molecules are polar and, therefore, have a permanent electric dipole moment. The bond has no preferential direction, since each atom is perfectly isotropic. Therefore, this type is well suited for the construction of crystalline lattices.

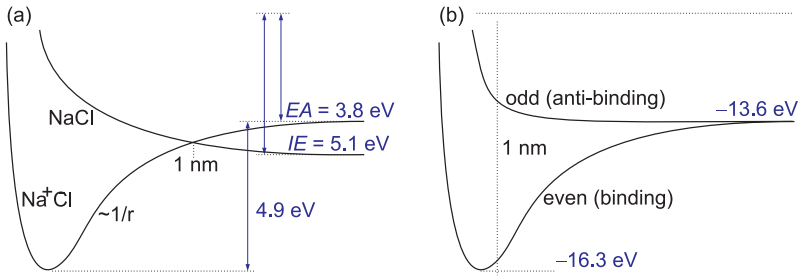

Figure 32.3: Scheme for (a) ionic binding of NaCl and (b) covalent binding of H_2.

To understand *covalent bond*, we consider the example H_2^+ and estimate the interaction energy for each distance R between the nuclei. In this case, in contrast to atoms, the spherical symmetry is broken, and therefore the energy degeneracy with respect to parity is abolished, that is, for wavefunctions $\psi(-x) = \pm\psi(x)$ the energies vary differently with R. The even wavefunction, which has an increased probability of the electron of being between the nuclei, is binding, which means that the interaction potential exhibits a minimum at a certain distance. The odd wavefunction, which disappears between the nuclei, is anti-binding, which means that the interaction potential is repulsive at all distances. In fact, an electron located at the center between two positive charges can overcome the Coulomb repulsion between the nuclei, whose mutual distance is twice. Obviously, the energy can not fall below that of the fundamental state of He^+, being approximately -4×13.6 eV. With two electrons, as in the case of the neutral molecule H_2, the anti-parallel orientation of the spins, $\uparrow\downarrow$, allows us to place the two electrons in the same orbital, while for parallel orientation, $\uparrow\uparrow$, we expect anti-binding. Each electron without a partner in an orbital can form a covalent bond, for example, phosphorus [P]=[Ne]$3s^2 3p^{\uparrow\uparrow\uparrow}$ has three available orbitals corresponding to different magnetic quantum numbers. The covalent bond is directional (sp^1, sp^2, or sp^3 hybridization), which is essential for the molecular structure such as in CH_4. Do the Exc. 32.1.6.1.

32.1.2 Born-Oppenheimer approximation and the H_2^+ molecule

The *Born-Oppenheimer approximation* in molecular physics consists in considering, at first, the positions of the nuclei as being fixed in space. This allows us to study the stationary states of the electrons subject to the potential created by the nuclei for a given internuclear distance R. Varying R, the electronic energies (computed for a fixed R) remain the same, because the electronic wavefunctions adjust instantaneously due to their mass being much lower than that of the nuclei. The non-varying electronic energies play the role of interaction potential energies between the nuclei [60].

32.1.2.1 Separation of the center-of-mass

Let us consider two heavy masses, $M_{a,b} = M$ separated by a distance R and interacting through a potential $V_{nn}(R)$. Furthermore, there is a light-weighted mass m_e interacting with the other masses through $V_{ne}(r)$. The Hamiltonian is,

$$\hat{H} = \frac{-\hbar^2}{2M}\nabla_a^2 + \frac{-\hbar^2}{2M}\nabla_b^2 + \frac{-\hbar^2}{2m_e}\nabla_e^2 + V_{nn}(|\mathbf{R}_a - \mathbf{R}_b|) + V_{ne}(|\mathbf{R}_a - \mathbf{R}_e|) + V_{ne}(|\mathbf{R}_b - \mathbf{R}_e|) \; . \tag{32.2}$$

We transform to the center-of-mass system of the two heavy masses anchored at

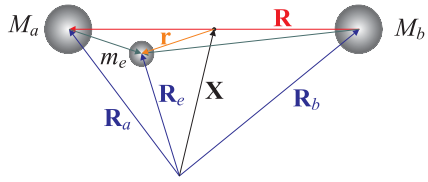

Figure 32.4: System with two heavy and one light mass.

$\mathbf{X} \equiv \frac{M_a\mathbf{R}_a + M_b\mathbf{R}_b}{M} = \frac{1}{2}(\mathbf{R}_a + \mathbf{R}_b)$. The distance of the *heavies* is $\mathbf{R} \equiv \mathbf{R}_a - \mathbf{R}_b$, and the coordinate of the light mass counting from the center-of-mass is $\mathbf{r} = \mathbf{R}_a - \frac{1}{2}\mathbf{R} - \mathbf{R}_e$. Introducing the reduced mass of the *heavies* $M_r = \frac{M}{2}$,

$$\left[\frac{-\hbar^2}{2M}\nabla_X^2 + \frac{-\hbar^2}{2M_r}\nabla_R^2 + V_{nn}(R) + \frac{-\hbar^2}{2m_e}\nabla_r^2 + V_{ne}(|\mathbf{r} + \tfrac{\mathbf{R}}{2}|) + V_{ne}(|\mathbf{r} - \tfrac{\mathbf{R}}{2}|)\right]\Theta(\mathbf{X})\Psi(\mathbf{R}, \mathbf{R}_e)$$
$$= E_{tot}\Theta(\mathbf{X})\Psi(\mathbf{R}, \mathbf{R}_e) \; , \tag{32.3}$$

Here, we made the ansatz for the total wavefunction $\Psi = \Theta(\mathbf{X})\Psi(\mathbf{R}, \mathbf{R}_e)$, assuming that the center-of-mass is only determined by the heavy masses,

$$\frac{-\hbar^2}{2M}\nabla_X^2\Theta(\mathbf{X}) = E_{cm}\Theta(\mathbf{X}) \tag{32.4}$$
$$\left[\frac{-\hbar^2}{2M_r}\nabla_R^2 + V_{nn}(R) + \frac{-\hbar^2}{2m_e}\nabla_r^2 + V_{ne}(|\mathbf{r} + \tfrac{1}{2}\mathbf{R}|) + V_{ne}(|\mathbf{r} - \tfrac{1}{2}\mathbf{R}|)\right]\Psi(\mathbf{R}, \mathbf{R}_e) = E\Psi(\mathbf{R}, \mathbf{R}_e) \; ,$$

where $E_{tot} = E_{cm} + E$.

32.1.2.2 Adiabatic approximation

The Born-Oppenheimer approximation now consists in assuming that the movement of the *heavies* is independent of the position of m_e, which allows us to separate the corresponding wavefunction ϕ via the ansatz $\Psi(\mathbf{R}, \mathbf{R}_e) = \psi(\mathbf{R}, \mathbf{r})\phi(\mathbf{R})$. On the other hand, the orbital ψ of the light mass m_e does not change much, when we vary the distance of the *heavies*, $\nabla_R\psi(\mathbf{R}, \mathbf{r}) \simeq 0$. This is only valid, as long as the *heavies* are inert on the time scale of the movement of m_e. Therefore, we can approximate the second derivative,

$$\nabla_R^2[\psi(\mathbf{R}, \mathbf{r})\phi(\mathbf{R})] = \phi(\mathbf{R})\nabla_R^2\psi(\mathbf{R}, \mathbf{r}) + 2[\nabla_R\phi(\mathbf{R})] \cdot [\nabla_R\psi(\mathbf{R}, \mathbf{r})] + \psi(\mathbf{R}, \mathbf{r})\nabla_R^2\phi(\mathbf{R})$$
$$\simeq \psi(\mathbf{R}, \mathbf{r})\nabla_R^2\phi(\mathbf{R}) \; , \tag{32.5}$$

postulating that the first two terms are negligible compared to the third. We can now separate the second equation (32.4) in two parts, the first being,

$$\boxed{\left[\frac{-\hbar^2}{2m_e}\nabla_r^2 + V_{ne}(|\mathbf{r}+\tfrac{1}{2}\mathbf{R}|) + V_{ne}(|\mathbf{r}-\tfrac{1}{2}\mathbf{R}|)\right]\psi(\mathbf{r},\mathbf{R}) = \varepsilon(R)\psi(\mathbf{r},\mathbf{R})}\,. \tag{32.6}$$

We solve this equation for the electronic degree of freedom $\mathbf{r}$ by choosing a fixed internuclear distance $\mathbf{R}$, and we substitute in the second expression (32.4), which gives,

$$\boxed{\left[\frac{-\hbar^2}{2M_r}\nabla_R^2 + V_{nn}(R) + \varepsilon(R)\right]\phi(\mathbf{R}) = E\phi(\mathbf{R})}\,. \tag{32.7}$$

Treating the interatomic distance R as a fixed parameter, the solution of Eq. (32.6) provides the electronic orbitals and their energies $\varepsilon(R)$. The *Born-Oppenheimer potential* is composed of the electrostatic repulsive potential of the nuclei and the kinetic energy of the electron, $V_{nn}(R) + \varepsilon(R)$. In other words, the presence of the electrons generates an additional interaction energy between the nuclei. By inserting this complete interatomic potential into Eq. (32.7), we can determine its vibrational structure $\phi_{vib}(\mathbf{R})$.

Fig. 32.5 shows an example of binary effective nuclear potentials, as a function of the distance R between the two nuclei. Each curve corresponds to a different solution of the electronic equation, that is, to a different electronic state. In many cases, such nuclear potentials have a stable equilibrium region. The bound states located in these regions are *molecular* bound states of two atoms.

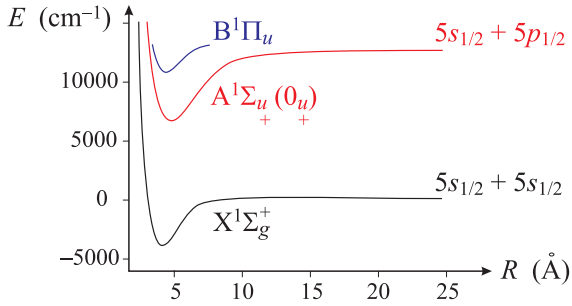

Figure 32.5: Effective nuclear potentials for the interaction between two rubidium atoms (Rb_2).

In practice, the calculation of adiabatic Born-Oppenheimer potentials is difficult and makes it the subject of sophisticated theories, such as the *molecular orbital model* or the *valence bond model* [2]. We study in Exc. 32.1.6.2 a generalization of the Born-Oppenheimer approximation.

[2] Note that the Born-Oppenheimer approximation is no longer good in the presence of relativistic or spin-orbit coupling effects.

32.1.3 Linear combination of orbitals and the H_2 molecule

In the following we will discuss the electronic structure of the simplest neutral molecule: H_2. For the low electron states of this molecule, the Born-Oppenheimer approximation is totally satisfactory, that is, we want to solve a Schrödinger type equation (32.6), but with two electrons. We are, therefore, interested in the electronic Hamiltonian,

$$\boxed{\hat{H} = -\frac{\hbar^2}{2m_e}(\nabla_1^2 + \nabla_2^2) + \frac{e^2}{4\pi\varepsilon_0}\left(\frac{1}{R_{ab}} - \frac{1}{|\mathbf{r}_1-\mathbf{R}_a|} - \frac{1}{|\mathbf{r}_1-\mathbf{R}_b|} - \frac{1}{|\mathbf{r}_2-\mathbf{R}_a|} - \frac{1}{|\mathbf{r}_2-\mathbf{R}_b|} + \frac{1}{r_{12}}\right)}\,, \tag{32.8}$$

where '1' and '2' denote the two electrons and 'a' and 'b' the nuclei.

This problem can not be solved analytically. The standard procedure begins with choosing a suitable basis, i.e. a very compact basis which does not depend on the configuration of the molecule. That is, we want the basis to be composed of functions that do not depend on the distance between the two nuclei, R_{ab}, to avoid calculations for different bond lengths.

The most natural basis functions are the available atomic orbitals of the individual hydrogen atoms. When the bond length is too large, the system approaches the limit of two non-interacting hydrogen atoms. In this case, the electron wavefunction can be approximated by the product of *atomic orbitals* (AO) of atom 'a' and atom 'b'. Therefore, the smallest basis that gives us a realistic picture of the fundamental state of the H_2 molecule must comprise two functions: $|1s_a\rangle$ and $|1s_b\rangle$. For finite bond lengths, it is advisable to allow the AOs to polarize and deform in response to the presence of the other electron (and the other nucleus). However, the $|1s_a\rangle$ and $|1s_b\rangle$ functions do not have to be exactly the hydrogenic eigenfunctions. It is sufficient to require them to be similar to the $1s$ orbitals and be centered on them. Since the actual shape of the orbitals is not yet fixed, we will give all the expressions in abstract matrix form, leaving the spatial integration for once the shape of the orbitals has been specified. This is the method of *linear combination of atomic orbitals* (LCAO).

32.1.4 Molecular orbital theory

We are now in a position to discuss the basic principles of the *molecular orbital method* (MO), which is the basis of the theory of the electronic structure of real molecules. The first step in any MO approach is to separate the Hamiltonian into two parts, one part describing the electrons '1' and '2' separately and one part counting for the interaction between them:

$$\hat{H} = \hat{h}(1) + \hat{h}(2) + \hat{V}_{12} + \frac{e^2}{4\pi\varepsilon_0}\frac{1}{R_{ab}} \qquad \text{with} \tag{32.9}$$

$$\hat{h}(i) = -\frac{\hbar^2\nabla_i}{2m_e} - \frac{e^2}{4\pi\varepsilon_0}\left(\frac{1}{|\mathbf{r}_i - \mathbf{R}_a|} + \frac{1}{|\mathbf{r}_i - \mathbf{R}_b|}\right) \qquad \text{and} \qquad \hat{V}_{12} = \frac{e^2}{4\pi\varepsilon_0}\frac{1}{r_{12}}\,,$$

where $i = 1, 2$. We must remember that, within the BO approximation, R_{ab} is just a number. We choose the Hamiltonian $h(i)$ as the one-electron part of the complete Hamiltonian in matrix representation on the minimum basis:

$$\begin{pmatrix} \langle 1s_a|\hat{h}|1s_a\rangle & \langle 1s_a|\hat{h}|1s_b\rangle \\ \langle 1s_b|\hat{h}|1s_a\rangle & \langle 1s_b|\hat{h}|1s_b\rangle \end{pmatrix} \equiv \begin{pmatrix} \epsilon & h_{ab} \\ h_{ab} & \epsilon \end{pmatrix}\,, \tag{32.10}$$

defining the average one-electron energy $\epsilon \equiv \langle 1s_a|\hat{h}|1s_a\rangle$ and the non-diagonal coupling (often called *resonance integral*) $h_{ab} \equiv \langle 1s_a|\hat{h}|1s_b\rangle = \langle 1s_a|\hat{h}|1s_b\rangle$. We can immediately diagonalize this matrix, the eigenvalues and the eigenvalues being:

$$\epsilon_\pm = \epsilon \pm h_{ab} \qquad \text{and} \qquad |\phi_\pm\rangle \propto \tfrac{1}{2}(|1s_a\rangle \pm |1s_b\rangle) \ . \tag{32.11}$$

The one-electron effective Hamiltonian eigenstates are called *molecular orbital* (MO). They are one-electron wavefunctions delocalized over the spatial regions of the molecule.

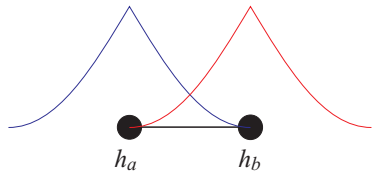

Figure 32.6: Illustration of the atomic orbitals.

We need to first normalize the MOs, which is more complicated than it might seem, because the AOs are not orthogonal. For example, when the atoms approach each other, their AOs may have the shape shown in Fig. 32.6. However, by defining the overlap integral by $S \equiv \langle 1s_a|1s_b\rangle$, we can normalize as follows:

$$|\phi_\pm\rangle = \tfrac{1}{\sqrt{2(1\pm S)}}(|1s_a\rangle \pm |1s_b\rangle) \ , \tag{32.12}$$

since,

$$\langle\phi_\pm|\phi_\pm\rangle = \tfrac{1}{2(1\pm S)}(\langle 1s_a|1s_a\rangle \pm \langle 1s_a|1s_b\rangle \pm \langle 1s_b|1s_a\rangle + \langle 1s_b|1s_b\rangle) = 1 \ . \tag{32.13}$$

These eigenfunctions merely show the symmetry of the molecule. The two hydrogen atoms are equivalent and, therefore, the eigenorbital must give equal weight to each $1s$ orbital. Thus, our choice of the one-electron Hamiltonian does not really matter that much, because every one-electron Hamiltonian exhibiting the symmetry of the molecule would give the same molecular orbitals. For historical reasons, $|\phi_+\rangle$ is denoted by $|\sigma\rangle$ and $|\phi_-\rangle$ by $|\sigma^*\rangle$.

The second step in MO theory consists of constructing the determinant from the MOs corresponding to the wanted states. For illustration we will look at the lowest singlet state constructed from molecular orbitals. We note that $h_{ab} < 0$, such that $|\sigma\rangle$ has an energy inferior to $|\sigma^*\rangle$. Neglecting the interaction, the lowest singlet state,

$$|\Phi_{MO}\rangle = |\sigma\rangle|\sigma^*\rangle \ , \tag{32.14}$$

is the molecular ground state of H_2. To estimate the validity of the approximation, we calculate the expectation value of the energy, $\left|\langle\sigma|\langle\sigma^*|\hat{H}|\sigma\rangle|\sigma^*\rangle\right|$, decomposing the wavefunction into spin and spatial parts, noting that the spin part is normalized:

$$\begin{aligned}\left|\langle\sigma|\langle\sigma^*|\hat{H}|\sigma\rangle|\sigma^*\rangle\right| &= \langle\sigma(1)|\langle\sigma(2)|\hat{H}|\sigma(1)\rangle|\sigma(2)\rangle\langle\Phi_{spin}|\Phi_{spin}\rangle \\ &= \langle\sigma(1)|\langle\sigma(2)|\hat{H}|\sigma(1)\rangle|\sigma(2)\rangle \ .\end{aligned} \tag{32.15}$$

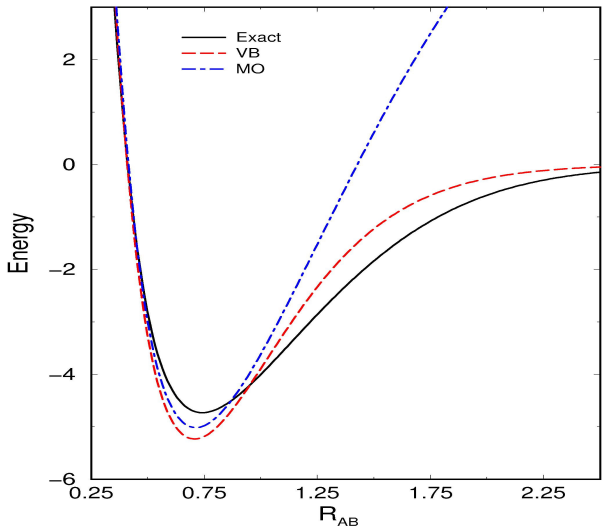

Figure 32.7: Total energy as a function of interatomic distance.

Hence, with (32.10) we get,

$$\begin{aligned}
\langle\sigma(1)|\langle\sigma(2)|\hat{h}(2)|\sigma(1)\rangle|\sigma(2)\rangle &= \langle\sigma(1)|\sigma(1)\rangle\langle\sigma(2)|h(2)|\sigma(2)\rangle = \langle\sigma(2)|h(2)|\sigma(2)\rangle \equiv \epsilon_\sigma \\
\langle\sigma(1)|\langle\sigma(2)|\hat{h}(1)|\sigma(1)\rangle|\sigma(2)\rangle &= \langle\sigma(1)|h(1)|\sigma(1)\rangle\langle\sigma(2)|\sigma(2)\rangle = \langle\sigma(1)|h(1)|\sigma(1)\rangle \equiv \epsilon_\sigma \\
\langle\sigma(1)|\langle\sigma(2)|\hat{V}_{12}|\sigma(1)\rangle|\sigma(2)\rangle &\equiv J_{\sigma\sigma} \ . \qquad (32.16)
\end{aligned}$$

Putting these facts together, we can write,

$$\begin{aligned}
\langle\Phi_{MO}|\hat{H}|\Phi_{MO}\rangle &= \langle\Phi_{MO}|\hat{h}_1|\Phi_{MO}\rangle + \langle\Phi_{MO}|\hat{h}_2|\Phi_{MO}\rangle + \langle\Phi_{MO}|\hat{V}_{12}|\Phi_{MO}\rangle + \frac{e^2}{4\pi\varepsilon_0 R_{ab}} \\
&= 2\epsilon_\sigma + J_{\sigma\sigma} + \frac{e^2}{4\pi\varepsilon_0 R_{ab}} \ . \qquad (32.17)
\end{aligned}$$

Each of the first two terms represents the energy of a single electron (either 1 or 2) in the field produced by both the nuclei ($\hat{h}$), while the third is the average repulsion between the two electrons. Note that the first and second term are both positive, such that the bond must come from the one-electron part. This is the MO energy for the ground state of the H_2. We can try a more reasonable ansatz for the $1s$-type basis functions [3] by determining the unknown quantities from above (ϵ_σ and $J_{\sigma\sigma}$) numerically and plot the total energy as a function of R_{ab} (blue dotted curve in Fig. 32.7). The exact adiabatic energy function determined from experimental data (solid black curve) agrees well at low energies. Summarizing the results with some key numbers, we note that MO theory predicts a bond distance of 0.072 nm in reasonable agreement with the exact value of 0.074 nm. We can also compare the

[3] It turns out that it is more convenient to adjust the exponential decomposition of the hydrogenic orbitals to a sum of Gaussians.

binding energies,

$$D_e = E_{H_2}(R_{equil}) - 2E_H \ . \tag{32.18}$$

MOs theory predicts a binding energy of 5.0 eV compared to the experimental value of 4.75 eV. In view of the simplicity of the wavefunction and the absence of adjustable parameters the agreement is not so bad. Unfortunately, far away from the equilibrium distance, we have an unpleasant surprise: the molecule does not dissociate into two hydrogen atoms!

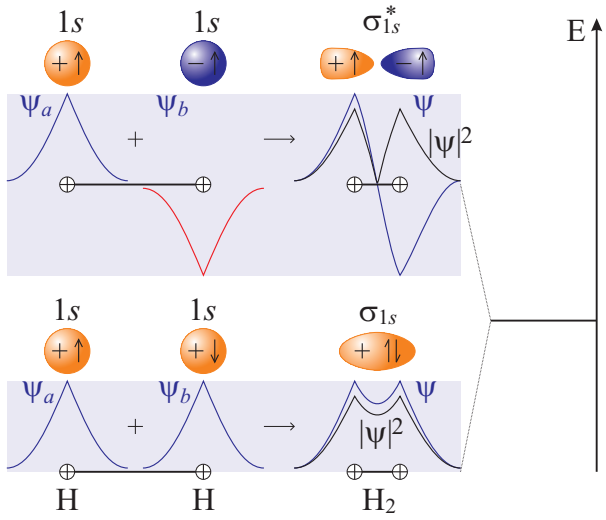

Figure 32.8: Illustration of MO theory for a dimer of two equal atoms, each one with a valence electron in the atomic 1s orbital: When the atoms approach, the atomic orbitals form new molecular binding and anti-biding orbitals.

To get an idea of what is happening near dissociation, we expand the fundamental MO state in terms of AO configurations:

$$\begin{aligned} |\Phi_{MO}\rangle &\propto |\sigma(1)\rangle|\sigma(2)\rangle|\Phi_{spin}\rangle \\ &= \tfrac{1}{2(1+S)}(|1s_a(1)\rangle + |1s_b(1)\rangle)(|1s_a(2)\rangle + |1s_b(2)\rangle)|\Phi_{spin}\rangle \\ &= \tfrac{1}{2(1+S)}(|1s_a(1)\rangle|1s_a(2)\rangle + |1s_a(1)\rangle|1s_b(2)\rangle + |1s_b(1)\rangle|1s_a(2)\rangle + |1s_b(1)\rangle|1s_b(2)\rangle)|\Phi_{spin}\rangle \ . \end{aligned} \tag{32.19}$$

The two terms in the middle of the last line, called *covalent configurations*, are exactly what we expect near dissociation: one electron in each hydrogen atom. However, the first and last term (which are called *ionic configurations*) correspond to having two electrons in one atom and none in the other, which gives us H^+ and H^- at dissociation! Since the weight of these terms is fixed, it is obvious that we got the wrong wavefunction (and therefore the wrong energy) when dissociating the molecule. Near the equilibrium point, the ionic terms contribute significantly to the true wavefunction, such that the MO theory is good at this point. But it is always terrible at dissociation.

32.1.5 Valence binding

An alternative to MO theory represents the *valence bond* theory (VB). Here, we use significantly more physical intuition and discard the ionic configurations from the MO wavefunction. Thus, the VB ground state wavefunction is:

$$\begin{aligned}|\Psi\rangle &\propto \frac{|1s_a(1)\rangle|1s_a(2)\rangle + |1s_b(1)\rangle|1s_a(2)\rangle}{\sqrt{2}} \frac{|\uparrow(1)\rangle|\downarrow(2)\rangle + |\downarrow(1)\rangle|\uparrow(2)\rangle}{\sqrt{2}} \\ &\equiv |\Psi_{space}\rangle|\Psi_{spin}\rangle \ . \end{aligned} \tag{32.20}$$

VB theory assumes that this wavefunction is a good approximation to the true wavefunction at *all* binding distances and not only at large distances R_{ab}. To verify this approximation, we can calculate the average energy for this VB state. First, we normalize the VB wavefunction,

$$\begin{aligned}\langle\Psi|\Psi\rangle &= \langle\Psi_{space}|\langle\Psi_{spin}|\Psi_{space}\rangle|\Psi_{spin}\rangle = \langle\Psi_{space}|\Psi_{space}\rangle \\ &= \tfrac{1}{2}\left(\langle 1s_a(1)|\langle 1s_b(2)| + \langle 1s_b(1)\langle 1s_a(2)|\right)\left(|1s_a(1)\rangle|1s_a(2)\rangle + |1s_b(1)\rangle|1s_a(2)\rangle\right) \\ &= \tfrac{1}{2}\left(\langle 1s_a(1)|1s_b(2)|1s_a(1)\rangle|1s_b(2)\rangle + \langle 1s_a(1)|1s_b(2)|1s_b(1)\rangle|1s_a(2)\rangle\right. \\ &\quad \left.+\langle 1s_b(1)|1s_a(2)|1s_a(1)\rangle|1s_b(2)\rangle + \langle 1s_b(1)|1s_a(2)|1s_b(1)\rangle|1s_a(2)\rangle\right) \\ &= \tfrac{1}{2}(1 + S^2 + S^2 + 1) = 1 + S^2 \ . \end{aligned} \tag{32.21}$$

Therefore, the correctly normalized VB wavefunction is:

$$|\Psi_{VB}\rangle = \frac{1}{2\sqrt{1+S^2}}\left(|1s_a(1)\rangle|1s_a(2)\rangle + |1s_b(1)\rangle|1s_a(2)\rangle\right)\left(|\uparrow(1)\rangle|\downarrow(2)\rangle - |\downarrow(1)\rangle|\uparrow(2)\rangle\right) \ . \tag{32.22}$$

Now we want to calculate $\langle\hat{H}_{el}\rangle$ for this state. We note that the spin part does not matter, since the Hamiltonian is independent of spin:

$$\begin{aligned}\langle\Psi_{VB}|\hat{H}|\Psi_{VB}\rangle &= \langle\Psi_{spin}|\langle\Psi_{space}|\hat{H}|\Psi_{space}\rangle|\Psi_{spin}\rangle \\ &= \langle\Psi_{space}|\hat{H}|\Psi_{space}\rangle\langle\Psi_{spin}|\Psi_{spin}\rangle = \langle\Psi_{space}|\hat{H}|\Psi_{space}\rangle \ . \end{aligned} \tag{32.23}$$

The only remnant of the spin state is the fact that the spatial wavefunction is symmetric, which is only possible when the spin part is antisymmetric. Treating each term in $\langle\hat{H}\rangle$ separately,

$$\begin{aligned}\langle\Psi|\hat{h}_1|\Psi\rangle &= \tfrac{1}{2}\left(\langle 1s_a(1)|\langle 1s_b(2)| + \langle 1s_b(1)|1s_a(2)|\right)\hat{h}_1\left(|1s_a(1)\rangle|1s_a(2)\rangle + |1s_b(1)\rangle|1s_a(2)\rangle\right) \\ &= \tfrac{1}{2}\Big(\langle 1s_a(1)|1s_b(2)|\hat{h}_1|1s_a(1)\rangle|1s_b(2)\rangle + \langle 1s_a(1)|1s_b(2)|\hat{h}_1|1s_b(1)\rangle|1s_a(2)\rangle \\ &\quad +\langle 1s_b(1)|1s_a(2)|\hat{h}_1|1s_a(1)\rangle|1s_b(2)\rangle + \langle 1s_b(1)|1s_a(2)|\hat{h}_1|1s_b(1)\rangle|1s_a(2)\rangle\Big) \\ &= \tfrac{1}{2}(\epsilon + Sh_{ab} + \epsilon + Sh_{ab}) \ , \end{aligned} \tag{32.24}$$

or,

$$\boxed{\langle\Psi_{VB}|\hat{h}_1|\Psi_{VB}\rangle = \frac{\epsilon + Sh_{ab}}{1+S^2}} \ . \tag{32.25}$$

Since the two electrons are identical, the elements of the $\hat{h}_2$ are the same as those of $\hat{h}_1$. The only remaining term is the average value of the interaction:

$$\langle\Psi|\hat{V}_{12}|\Psi\rangle = \tfrac{1}{2}\left(\langle 1s_a(1)|\langle 1s_b(2)| + \langle 1s_b(1)|1s_a(2)|\right)\hat{V}_{12}\left(|1s_a(1)\rangle|1s_a(2)\rangle + |1s_b(1)\rangle|1s_a(2)\rangle\right) \tag{32.26}$$

$$= \tfrac{1}{2}\Big(\langle 1s_a(1)|1s_b(2)|\hat{V}_{12}|1s_a(1)\rangle|1s_b(2)\rangle + \langle 1s_a(1)|1s_b(2)|\hat{V}_{12}|1s_b(1)\rangle|1s_a(2)\rangle$$
$$+ \langle 1s_b(1)|1s_a(2)|\hat{V}_{12}|1s_a(1)\rangle|1s_b(2)\rangle + \langle 1s_b(1)|1s_a(2)|\hat{V}_{12}|1s_b(1)\rangle|1s_a(2)\rangle\Big) \ .$$

The second and third terms are the same. They are called *exchange integrals*, because the 'bra' orbitals have switched order as compared to the 'kets':

$$K = \langle 1s_a(1)|1s_b(2)|\hat{V}_{12}|1s_b(1)\rangle|1s_a(2)\rangle = \langle 1s_b(1)|1s_a(2)|\hat{V}_{12}|1s_a(1)\rangle|1s_b(2)\rangle \ . \tag{32.27}$$

The first and forth terms are also the same. They are called *Coulomb integrals*, because they seem to be due to the Coulomb interaction between two charge densities:

$$J = \langle 1s_b(1)|1s_a(2)|\hat{V}_{12}|1s_a(1)\rangle|1s_b(2)\rangle = \langle 1s_a(1)|1s_b(2)|\hat{V}_{12}|1s_b(1)\rangle|1s_a(2)\rangle \ . \tag{32.28}$$

Therefore, we have the result,

$$\boxed{\langle\Psi_{VB}|\hat{V}_{12}|\Psi_{VB}\rangle = \frac{J+K}{1+S^2}} \ . \tag{32.29}$$

Adding all terms, we get:

$$\langle\Psi_{VB}|\hat{H}|\Psi_{VB}\rangle = \langle\Psi_{VB}|\hat{h}_1|\Psi_{VB}\rangle + \langle\Psi_{VB}|\hat{h}_2|\Psi_{VB}\rangle + \langle\Psi_{VB}|\hat{V}_{12}|\Psi_{VB}\rangle + \frac{1}{R_{ab}}$$
$$= 2\frac{\epsilon + Sh_{ab}}{1+S^2} + \frac{J+K}{1+S^2} + \frac{1}{R_{ab}} \ . \tag{32.30}$$

The Coulomb and exchange terms are positive. Nuclear repulsion is clearly positive. Thus, the only terms that lead to binding in this picture are the average energy of an electron ϵ and the resonance integral h_{ab}. If the first term is dominant, the bond is due to *electronic delocalization*, since an electron located near one of the atoms would only contribute the atomic value to ϵ, which does not imply a bound state. If h_{ab} is large, the bond involves some resonance character, which can be related to the familiar concept of resonance between different Lewis point structures.

A numerical evaluation of all integrals gives the potential curve presented in Fig. 32.7 for VB theory. As expected, this simple VB wavefunction gives the correct dissociation threshold, where MO theory fails. In addition, the accuracy of the simple VB result is surprisingly good even near the equilibrium distance: The VB predicts a bond distance of 0.071 nm (compared to the correct value of 0.074 nm) and $D_e = 5.2$ eV (compared to 4.75 eV). Thus, the VB wavefunction also gives a good agreement without adjustable parameters. But more importantly, it indicates a way of improving the wavefunction whenever we encounter an obvious error: in this case, we saw that the description of the dissociation was weak, and we constructed a VB ansatz curing the problem. This approach to VB is often generalized as follows

when dealing with polyatomic molecules. We write the wavefunction as a product of a spatial part and a spin:

$$|\Psi\rangle = |\Psi_{space}\rangle|\Psi_{spin}\rangle \ . \tag{32.31}$$

The main assumption in VB theory is that the spatial part can be well represented by a product of atomic-like functions. For example, for water, we would immediately write a spatial part as:

$$|\Psi_{space}\rangle \simeq |1s_{H_a}\rangle|1s_{H_b}\rangle|1s_O\rangle|1s_O\rangle|2s_O\rangle|2s_O\rangle|2p_{xO}\rangle|2p_{xO}\rangle|2p_{yO}\rangle|2p_{yO}\rangle \ . \tag{32.32}$$

However, there are two things wrong with this wavefunction. First, we know that atomic orbitals hybridize in a molecule. Therefore, we need to make appropriate linear combinations of AOs (in this case sp^3 hybrids) to obtain the hybridized AOs. In this case, the four sp^3 hybrids can be written symbolically as:

$$|sp^3\rangle = c_{s,i}|2s\rangle + c_{x,i}|2p_x\rangle + c_{y,i}|2p_y\rangle + c_{z,i}|2p_z\rangle \ . \tag{32.33}$$

and therefore, a more appropriate spatial configuration is:

$$|\Psi_{space}\rangle \simeq |1s_{H_a}\rangle|1s_{H_b}\rangle|1s_O\rangle|1s_O\rangle|sp^3_{1O}\rangle|sp^3_{1O}\rangle|sp^3_{2O}\rangle|sp^3_{2O}\rangle|sp^3_{3O}\rangle|sp^3_{4O}\rangle \ . \tag{32.34}$$

The other problem with this state is that it lacks the adequate symmetry to describe fermions; the general state must be antisymmetric. In the case of two electrons this concept is easy to apply - singlets have symmetric space parts and triplets antisymmetric ones. However, in the case of many electrons, the rules are not so simple; in fact, the time of numerical computation grows exponentially with the number of electrons.

Formally, we will leave the derivation at this point to defining an operator $\mathcal{A}$ which 'antisymmetrizes' the wavefunction. In this case,

$$|\Psi_{space}\rangle \simeq \mathcal{A}\left[|1s_{H_a}\rangle|1s_{H_b}\rangle|1s_O\rangle|1s_O\rangle|sp^3_{1O}\rangle|sp^3_{1O}\rangle|sp^3_{2O}\rangle|sp^3_{2O}\rangle|sp^3_{3O}\rangle|sp^3_{4O}\rangle\right] \ . \tag{32.35}$$

In general, the results of VB theory are very accurate for small systems, where it can be applied. The predicted bond lengths are rather short, and the binding energies tend to be too small, but the results are nevertheless qualitatively excellent. In addition, the correct hybridized atomic orbitals fall directly off the calculation, giving a good qualitative insight. Also, note that the atomic configurations should not change (or very little) when the geometry of the molecule changes (since the orbitals depend on the atom and not on the molecular structure). Therefore, these VB wavefunctions have a strong connection to the diabatic states discussed above. However, the exponential amount of time that one must invest to perform these calculations makes them impractical for most molecules of interest.

32.1.6 Exercises

32.1.6.1 Ex: Classical model of the covalent binding

Consider the molecule H_2^+ with the two nuclei separated by 1 nm and an electron located in the middle between the nuclei. Calculate the electrostatic force acting on the nuclei.

Solution:

32.1.6.2 Ex: Beyond the Born-Oppenheimer approximation for molecules

For molecules, the Born-Oppenheimer approximation may fail in some situations. Therefore, it is common to use another approach known as Born-Huang. To illustrate this approach, we consider a diatomic molecule in the laboratory frame.
a. Write down the many-body Hamiltonian of the molecule in atomic units.
b. If we change the coordinate system to the position of the center-of-mass of the nuclei of the molecule, we eliminate the dependency on the global translation of the molecule. The Hamiltonian is now given by,

$$-\frac{\nabla_R^2}{2\mu_{AB}} - \sum_{i,j}\frac{1}{2M}\nabla_i\nabla_j - \sum_i\frac{\nabla_i^2}{2} + V$$

where that the Coulombian interactions are included in the fifth term. Write down the time-independent Schrödinger equation for this molecule.
c. The Born-Huang approximation consists in assuming that the total wavefunction can be expanded on a basis of wavefunctions of the nuclei and the electrons, that is,

$$\Psi(\mathbf{r},\mathbf{R}) = \sum_k |\chi_k(\mathbf{R})\rangle|\phi_k(\mathbf{r},\mathbf{R})\rangle \ ,$$

where χ and ϕ are the wavefunctions of the nuclei and the electrons, respectively. For the Schrödinger equation calculated in the previous item, use the Born-Huang approximation and obtain the set of coupled equations

$$\left\{\sum_k\left[-\frac{1}{2\mu_{AB}}\left(\nabla_R^2 + \langle\phi_k|\nabla_R^2|\phi_k\rangle + 2\langle\phi_k|\nabla_R|\phi_k\rangle.\nabla_R|\right)\right] - \right.$$
$$\left.\sum_k\left[\frac{1}{2M}\left(\sum_{i,j}\langle\phi_i|\nabla_i.\nabla_j|\phi_k\rangle\right) + \frac{1}{2}\sum_i\langle\phi_i|\nabla_i^2|\phi_k\rangle - \langle\phi_i|V|\phi_k\rangle|\right]\right\}|\chi_k\rangle = E\sum_k|\chi_k\rangle$$

which includes, although approximately, the kinetic energy of nuclei and electrons.
Help: Use $\nabla^2(\alpha\beta) = \alpha\nabla^2\beta + \beta\nabla^2\alpha + 2\nabla\alpha\cdot\nabla\beta$.
d. Make a brief comparison between the Born-Huang approximation (and the coupled equations obtained in the previous equation) and the Born-Oppenheimer approximation.

Solution: *a. We have the kinetic energies of nucleus A, nucleus B and the electrons. We also consider the coulombian interaction nucleus-nucleus, nucleus-electron, and electron-electron. Therefore the Hamiltonian is given by,*

$$\hat{H} = -\frac{\nabla_A^2}{2M_A} - \frac{\nabla_B^2}{2M_B} - \sum_i\frac{\nabla_i^2}{2} + \frac{1}{2}\sum_{i\neq j}\frac{1}{|\mathbf{r_i}-\mathbf{r_j}|} + \sum_{i=A,B}\sum_j\frac{Z_i}{|\mathbf{r_j}-\mathbf{R_i}|} + \frac{Z_AZ_B}{\mathbf{R}} \ ,$$

being M_A and M_B the nuclear masses, Z_A e Z_B the charges of the nuclei, $\mathbf{R}$ the relative coordinate between the nuclei, and ∇_i the kinetic energy of the electron i.
b. The time-independent Schrödinger equation is given by,

$$\left[-\frac{\nabla_R^2}{2\mu_{AB}} - \sum_{i,j}\frac{1}{2M}\nabla_i\nabla_j - \sum_i\frac{\nabla_i^2}{2} + V\right]|\Psi(\mathbf{R},\mathbf{r})\rangle = E|\Psi(\mathbf{R},\mathbf{r})\rangle \ .$$

c. The Schrödinger equation obtained in the previous item is:

$$\left[-\frac{\nabla_R^2}{2\mu_{AB}} - \sum_{i,j}\frac{1}{2M}\nabla_i\nabla_j - \sum_i\frac{\nabla_i^2}{2} + V\right]\sum_k|\chi_k\rangle|\phi_k\rangle = E\sum_k|\chi_k\rangle|\phi_k\rangle\ ,$$

where V contains all Coulomb interactions. Using that

$$\nabla_R^2|\chi_k\rangle|\phi_k\rangle = (\nabla^2|\chi_k\rangle)|\phi_k\rangle + |\chi_k\rangle(\nabla^2|\phi_k\rangle) + 2|\nabla\chi_k\rangle\cdot\nabla|\phi_k\rangle$$

in the Schrödinger equation

$$\sum_i\left[-\frac{1}{2\mu_{AB}}\left(|\phi_i\rangle\nabla_R^2|\chi_i\rangle + |\chi_i\rangle\nabla_R^2|\phi_i\rangle + 2\nabla_R|\phi_i\rangle.\nabla_R|\chi_i\rangle\right)\right]$$
$$-\sum_k\left[\frac{1}{2M}\left(\sum_{i,j}\nabla_i\cdot\nabla_j|\phi_k\rangle\right)|\chi_k\rangle + \frac{1}{2}|\chi_k\rangle\sum_i\nabla_i^2|\phi_k\rangle - V|\phi_k\rangle|\chi_k\rangle\right] = E\sum_k|\phi_k\rangle|\chi_k\rangle$$

multiplying with $|\phi_n\rangle$ and considering that the base is orthonormal,

$$\sum_i\left[-\frac{1}{2\mu_{AB}}\left(\langle\phi_n|\phi_i\rangle\nabla_R^2|\chi_i\rangle + |\chi_i\rangle\langle\phi_n|\nabla_R^2|\phi_i\rangle + 2\langle\phi_n|\nabla_R|\phi_i\rangle.\nabla_R|\chi_i\rangle\right)\right]$$
$$-\sum_k\left[\frac{1}{2M}\left(\sum_{i,j}\langle\phi_n|\nabla_i\cdot\nabla_j|\phi_k\rangle\right)|\chi_k\rangle + \frac{1}{2}|\chi_k\rangle\sum_i\langle\phi_n|\nabla_i^2|\phi_k\rangle - \langle\phi_n|V|\phi_k\rangle|\chi_k\rangle\right] = E\sum_k\langle\phi_n|\phi_k\rangle|$$
$$\sum_i\left[-\frac{1}{2\mu_{AB}}\left(\nabla_R^2|\chi_i\rangle + |\chi_i\rangle\langle\phi_n|\nabla_R^2|\phi_i\rangle + 2\langle\phi_n|\nabla_R|\phi_i\rangle\cdot\nabla_R|\chi_i\rangle\right)\right]$$
$$-\sum_k\left[\frac{1}{2M}\left(\sum_{i,j}\langle\phi_n|\nabla_i.\nabla_j|\phi_k\rangle\right)|\chi_k\rangle + \frac{1}{2}|\chi_k\rangle\sum_i\langle\phi_n|\nabla_i^2|\phi_k\rangle - \langle\phi_n|V|\phi_k\rangle|\chi_k\rangle\right] = E\sum_k|\chi_k\rangle\ .$$

Hence, since, $\langle\phi_n|\phi_i\rangle = \delta_{ni}$

$$\left\{\sum_k\left[-\frac{1}{2\mu_{AB}}\left(\nabla_R^2 + \langle\phi_k|\nabla_R^2|\phi_k\rangle + 2\langle\phi_k|\nabla_R|\phi_k\rangle.\nabla_R|\right)\right]\right.$$
$$\left.-\sum_k\left[\frac{1}{2M}\left(\sum_{i,j}\langle\phi_i|\nabla_i.\nabla_j|\phi_k\rangle\right) + \frac{1}{2}\sum_i\langle\phi_i|\nabla_i^2|\phi_k\rangle - \langle\phi_i|V|\phi_k\rangle|\right]\right\}|\chi_k\rangle = E\sum_k|\chi_k\rangle\ .$$

d. In the Born-Oppenheimer approximation, the electrons do not influence the kinetic energy of the nuclei and the Hamiltonian becomes completely separable into one part due to the nuclei and another part due to the electrons. In the Born-Huang approximation the wavefunction of the nuclei depends on the wavefunctions of the electrons, which results in a system of coupled equations, but which contains information about the kinetic energy of the nuclei and how the electrons modify that energy. Although more complicated to solve than the equations obtained under the Born-Oppenheimer approximation, the Born-Huang approximation is the starting point for systems that require an approximation that takes into account non-adiabatic effects.

32.1.6.3 Ex: Classical model of the covalent bond

Calculate the energies of the ground state and the last bound state of the potential $V_n = -\frac{C}{r^n}$ for any n.

Solution:

32.1.6.4 Ex: Homonuclear collision

We consider the example of homonuclear collisions of ^{85}Rb atoms. For ground state collisions in the channel $^3\Sigma_+$, $|f = 2, m_f = -2\rangle$, the long-range part of the potential is fixed by $C_6 = 4550$, $C_8 = 550600$, and $C_{10} = 7.67 \times 10^7$ [300, 1108], where $R_m = 9.8a_B$, $D_m = 0.13$, and $B_m = 1/2.5a_B$. The potentials can be merged at a given distance $R_t = 27.6a_B$. Prepare a plot of potential.

Solution: *In atomic units: The green curve shows the short-range Morse potential, the blue curve shows the long-range potential, and the black curve the combined potential around the distance R_t, that is, at very large distances.*

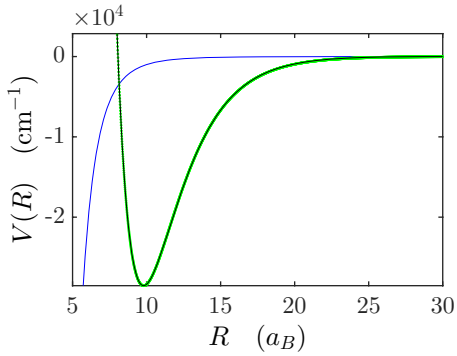

Figure 32.9: Short range potential.

32.2 Rovibrational structure of molecular potentials

The separation of the motion of the nuclei from the electronic dynamics made in the Born-Oppenheimer approximation led to equations (32.6) and (32.7). In a preceding section we analyzed in detail the equation (32.6) with the objective of understanding the phenomenon of molecular binding.

In the following section we will analyze the equation (32.7), which determines the motion of the nuclei. By separating the radii and angular parts of the motion, we will discover vibrational and rotational states.

32.2.1 The radial and angular equations

The interaction between two identical atoms is described by the following Hamiltonian, where $M_r = (M_a^{-1} + M_b^{-1})^{-1} = M/2$ is the *reduced mass* of the nuclei,

$$\hat{H} = \frac{\mathbf{P}^2}{2M_r} + V_{mol}(R) \qquad \text{with} \qquad V_{mol}(R) = \frac{e^2}{4\pi\epsilon_0 R} + V_{BO}(R) \ . \tag{32.36}$$

The interaction potential V_{mol} is composed of a repulsive internuclear Coulomb force and a Born-Oppenheimer adiabatic potential due to the interaction of the electrons with each other and with the two nuclei [4]. The kinetic energy is that of the relative motion (the center-of-mass motion has already been separated in Sec. 32.1.2, such that this inertial system is free of translational kinetic energy). In spherical coordinates,

$$\frac{\mathbf{P}^2}{2M_r}\phi(\mathbf{R}) = -\frac{\hbar^2}{2M_r}\left[\frac{1}{R}\frac{\partial^2}{\partial R^2}[R\phi(\mathbf{R})] + \frac{1}{R^2}\frac{\hat{\mathbf{L}}^2}{\hbar^2}\phi(\mathbf{R})\right] \ . \tag{32.37}$$

The wavefunction can be separated into an angular part and a radial part, $\phi(\mathbf{R}) = \mathcal{R}_v(R)Y_{\ell m}(\theta,\phi)$. The angular part, which was discussed in Sec. 25.1.3, describes a *rigid rotation* of the homonuclear atoms around their center-of-mass with the rotation energy,

$$\boxed{V_\ell(R) = \frac{\mathbf{L}^2}{2M_r R^2} = \frac{\hbar^2\ell(\ell+1)}{2M_r R^2}} \ , \tag{32.38}$$

also called *centrifugal barrier*. The radial part is ruled by,

$$\boxed{\left[-\frac{\hbar^2}{2M_r}\frac{\partial^2}{\partial R^2} + V_\ell(R) + V_{BO}(R)\right] u_v(R) = E u_v(R)} \ , \tag{32.39}$$

where $u_v(R) = r\mathcal{R}_v(R)$ is the radial wavefunction of nuclear motion. The interatomic potential causes a motion of *vibration*. The vibrational states of the adiabatic potential are quantized and characterized by a well-defined vibrational energy. We will discuss the ro-vibrational structure in the following sections.

32.2.1.1 Rotational and vibrational bands

Molecules have much more degrees of freedom than atoms. For example, the atoms of a molecular dimer may vibrate inside the mutual interaction potential. In the center-of-mass system we can imagine these vibrations as oscillations of an atom with reduced mass and quantized energy. The molecule can rotate and have a momentum of inertia. These degrees of freedom contribute energies to the molecule's Hamiltonian, either directly or through interactions with other degrees of freedom. Therefore, molecular spectra are characterized by a much greater complexity.

However, the energy regimes of the strongest excitations are quite different. A typical range for binding energies (depth of the interatomic potential) is $\Delta E_p \simeq$

[4] We note here that at great distances other forces called *van der Waals forces* dominate the interatomic interaction. These will be discussed in Sec. 32.3.

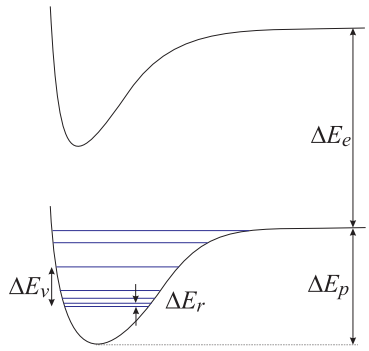

Figure 32.10: Molecular energy scales.

20..200 THz (0.1..1 eV) [5]. Electronic excitations occur in the regime $\Delta E_e \simeq 100..1000$ THz (1..10 eV). The spacing between vibrational excitations typically is $E_{v+1} - E_v \simeq$ THz (0.01 eV). Finally, the rotational excitations are on the scale of $E_{\ell+1} - E_\ell \simeq 100$ MHz (10^{-6} eV). Since at room temperature (a gas of molecules in thermal equilibrium at $T = 300$ K) the energy is on a scale of 2.5×10^{-2} eV, the degree of freedom of the electronic excitation is frozen, while a wide distribution of vibrational and rotational states can be excited (e.g. by intermolecular collisions). The large difference of scales facilitates their separation and, therefore, the identification of the origin of the observed states in experimental measurements.

32.2.2 Vibrational molecular states

The potential energy of a molecule grows when the nuclei are displaced from their equilibrium positions. When the displacement, $x \equiv R - R_e$ is small, we can expand the potential energy,

$$V_{mol}(x) = V_{mol}(0) + \frac{dV_{mol}(0)}{dx} x + \frac{1}{2} \frac{d^2 V_{mol}(0)}{dx^2} x^2 + .. \ . \tag{32.40}$$

The equilibrium energy is not of interest here, and the first derivative disappears in equilibrium. Therefore,

$$V_{mol}(x) \simeq \tfrac{1}{2} k^2 x^2 \qquad \text{with} \qquad k \equiv \frac{d^2 V_{mol}(0)}{dx^2} \ . \tag{32.41}$$

Using the effective mass we can write the Hamiltonian,

$$\hat{H}_{mol} = -\frac{\hbar^2}{2m_1} \frac{d^2}{dx_1^2} - \frac{\hbar^2}{2m_2} \frac{d^2}{dx_2^2} + \tfrac{1}{2} k x^2 = -\frac{\hbar^2}{2M_r} \frac{d^2}{dx^2} + \tfrac{1}{2} k x^2 \ . \tag{32.42}$$

The energy spectrum of this degree of freedom, therefore, is

$$\boxed{E_v = \hbar\omega(v + \tfrac{1}{2})} \ . \tag{32.43}$$

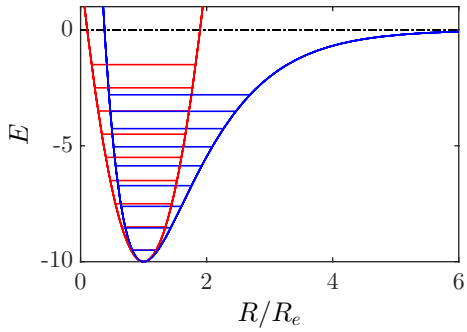

Figure 32.11: (code) Many potentials are approximately harmonic at the center such as, for instance, the Morse potential (blue). The red curve shows the approximate harmonic potential.

with $\omega = \sqrt{k/M_r}$. That is, at the bottom of deep potentials, the energy levels are equidistant.

32.2.2.1 Anharmonic vibrations in the Morse potential

For larger displacements we can no longer despise the anharmonic terms in the Taylor expansion. A better approximation is the *Morse potential*. This potential (blue in Fig. 32.11), unlike the harmonic potential (red in Fig. 32.11), is characterized by an asymptote for large interatomic distances. Therefore, it is often used as an analytical approximation to molecular potentials,

$$\boxed{V_{morse} = D_e(1 - e^{-a(R-R_e)})^2} \ , \tag{32.44}$$

where r is the interatomic distance, r_e the equilibrium bond distance, D_e the depth of the potential measuring from the *dissociation limit*, and a a parameter controlling the range of the potential. At the bottom of the potential we can make the harmonic approximation, $V_{morse}(R) \simeq \frac{k}{2}(R - R_e)^2$ with $k = 2a^2 D_e$. Rewriting the potential in the form,

$$\tilde{V}(R) \equiv V(R) - D_e = D_e(e^{-2a(R-R_e)} - 2e^{-a(R-R_e)}) \ , \tag{32.45}$$

we see, that it is a combination of a short-range repulsive potential and long-range attractive potential (similar to the Lennard-Jones's potential).

The calculation of the energy spectrum of this potential is more difficult [317],

$$E_v = \hbar\omega(v + 1/2) - \hbar\omega\chi_e(v + 1/2)^2 - D_e, \tag{32.46}$$

with $\omega\chi_e \equiv \frac{\hbar a^2}{2M_r}$ and $\omega \equiv \sqrt{k/M_r}$, but the availability of an analytical expression is interesting for the calibration of numerical methods. The second term of the expression (32.46), which is proportional to the anharmonicity constant χ_e, becomes dominant at high excitations. The potential is finite with a dissociation energy of,

$$D_0 = D_e - E_0 \ . \tag{32.47}$$

[5]Electronically excited states (that is, one of the valence electrons moves to an excited orbital) are more weakly bound, because the electrons are not in the most binding orbital.

The number of vibrational states is limited $v = 0, 1, .., v_{max}$. With $E < 0$, we find,

$$v_{max} < \tfrac{1}{x_e} - \tfrac{1}{2} \ . \tag{32.48}$$

Example 188 (*Morse potential*): To solve the Schrödinger equation

$$\left(-\frac{\hbar^2}{2m}\frac{\partial^2}{\partial R^2} + V(R) \right) \Psi(v) = E_v \Psi(v) \ ,$$

it is convenient to introduce new variables,

$$x \equiv aR \quad , \quad \lambda \equiv \frac{\sqrt{2mD_e}}{a\hbar} \quad , \quad \varepsilon_v \equiv \frac{2m}{a^2\hbar^2} E_v \ ,$$

such that,

$$\left(-\frac{\partial^2}{\partial x^2} + V(x) \right) \Psi_n(x) = \varepsilon_n \Psi_n(x) \quad \text{with} \quad V(x) = \lambda^2 \left(e^{-2(x-x_e)} - 2e^{-(x-x_e)} \right) \ .$$

The eigenvalues and eigenfunctions are [317]:

$$\varepsilon_n = 1 - \tfrac{1}{\lambda^2}\left(\lambda - n - \tfrac{1}{2}\right)^2 = \tfrac{2}{\lambda}(n+\tfrac{1}{2})^2 - \tfrac{1}{\lambda^2}(n+\tfrac{1}{2})^2 \quad \text{and} \quad \Psi_n(z) = N_n z^{\lambda-n-\frac{1}{2}} e^{-\frac{1}{2}z} L_n^{(2\lambda-2n-1)}(z) \ ,$$

where $z = 2\lambda e^{-(x-x_e)}$ e $N_n = \left[\frac{n!(2\lambda-2n-1)}{\Gamma(2\lambda-n)} \right]^{\frac{1}{2}}$ and,

$$L_n^{(\alpha)}(z) = \frac{z^{-\alpha}e^z}{n!}\frac{d^n}{dz^n}\left(z^{n+\alpha}e^{-z}\right) = \frac{\Gamma(\alpha+n+1)/\Gamma(\alpha+1)}{\Gamma(n+1)}\ {}_1F_1(-n, \alpha+1, z) \ ,$$

is the generalized Laguerre polynomial. The matrix elements of the spatial operator $\hat{x}$ are (assuming $m > n$ and $N = \lambda - \frac{1}{2}$),

$$\langle \Psi_m | x | \Psi_n \rangle = \frac{2(-1)^{m-n+1}}{(m-n)(2N-n-m)} \sqrt{\frac{(N-n)(N-m)\Gamma(2N-m+1)m!}{\Gamma(2N-n+1)n!}} \ .$$

In the original variables the eigenenergies are:

$$E_v = \hbar\omega(v+1/2) - \frac{[\hbar\omega(v+1/2)]^2}{4D_e} \ ,$$

where v is the vibrational quantum number and $\omega = a\sqrt{\frac{2D_e}{m}}$. The energy difference between adjacent levels decreases with v,

$$E_{v+1} - E_v = \hbar\omega - (\hbar\omega)^2 \frac{v+1}{2D_e} \ .$$

This fact describes well the vibrational structure of non-rotating molecules. However, the equation fails above some value of $v > v_{max}$, where $E_{v_{max}+1} - E_{v_{max}}$ is zero or negative,

$$v_{max} = \frac{2D_e - \hbar\omega}{\hbar\omega} \ .$$

This failure is due to the finite number v_{max} of bound states in the Morse potential. For energies above v_{max} all energies are possible, and the equation for E_v is no longer valid.

32.2.2.2 Vibrational selection rules

Electromagnetic fields of the type $E1$, e.g., black body radiation, can induce transitions between vibrational states and redistribute their populations such as to establish a thermal equilibrium. However, as the stronger transitions are induced by dipole migrations of charges, we need to analyze in more detail the selection rules imposed on the dipole moment $\langle f|\mathbf{d}|i\rangle$.

The states which are relevant for vibrational transitions are specified by $|\epsilon, v\rangle$, where ϵ denotes the electronic state of the molecule, since the vibrational spectrum depends on the electronic structure. The *Born-Oppenheimer approximation* allows us to consider the slow vibrations separately from the dynamics of the electrons. The time scale for electronic transitions is $1/\Delta E_e = 10^{-16}\,\mathrm{s}^{-1}$, and for a nuclear vibration it is $1/\Delta E_v = 10^{-13}\,\mathrm{s}^{-1}$. For each internuclear distance the electrons form an adapted stationary state, minimizing their energy for that distance. This is equivalent to the formation of an adiabatic interaction potential between the nuclei on which the nuclei can vibrate. To find out which vibrational transitions are possible, we need to calculate the matrix,

$$\langle \epsilon', v'|\hat{\mathbf{d}}|\epsilon, v\rangle = \langle v'|\hat{\mathbf{d}}_\epsilon|v\rangle \ . \tag{32.49}$$

The dipole moment, $\mathbf{d}_\epsilon = \langle\epsilon|\hat{\mathbf{d}}|\epsilon\rangle$, of the molecule depends on the distance of the nuclei, since the electronic orbitals $|\epsilon\rangle$ depend on distance. Therefore, we can expand,

$$\hat{\mathbf{d}} = \hat{\mathbf{d}}_0 + \frac{d\hat{\mathbf{d}}_0}{dx}\hat{x} + \frac{1}{2}\frac{d^2\hat{\mathbf{d}}_0}{dx^2}\hat{x}^2 + .. \ . \tag{32.50}$$

Therefore, the transition matrix is,

$$\langle \epsilon', v'|\hat{\mathbf{d}}|\epsilon, v\rangle = \hat{\mathbf{d}}_0\delta_{v,v'} + \frac{d\hat{\mathbf{d}}_0}{dx}\langle v'|\hat{x}|v\rangle + \frac{d^2\hat{\mathbf{d}}_0}{dx^2}\langle v'|\hat{x}^2|v\rangle + .. \ . \tag{32.51}$$

The first term disappears, that is, transitions can only occur, when the dipole moment varies with the distance. Therefore, *homonuclear dimers do not undergo vibrational transitions.*

For heteronuclear molecules with electronic charges that do not depend on the interatomic distance, the dipole moment varies linearly with small displacements. In this case, we only need the second term of the expansion. Within the harmonic approximation, the position operator can be expressed by, $\hat{x} \propto \hat{a} + \hat{a}^\dagger$. Therefore, only transitions $\Delta v = \pm 1$ are possible. However, due to anharmonicities, higher order terms, $\hat{x}^n \propto (\hat{a} + \hat{a}^\dagger)^n$ become influential, and transitions with $\Delta v = \pm 2, \pm 3, ..$ become possible.

Thus, in anharmonic potentials, the vibrational selection rules are replaced by the concept the overlapping wavefunctions called *Franck-Condon factor*.

Raman spectroscopy is a very useful tool to analyze ro-vibrational spectra. In this method, inelastic Raman scattering gives rise to Stokes and anti-Stokes lines in the spectrum at frequencies corresponding to $\Delta v = \pm 1, \pm 2$. The ground state spectrum is asymmetric, because of the absence of the lower state. In homonuclear dimers, the nuclear spins have a major impact on the Raman spectra. Parity considerations show that there can only be odd or even lines.

32.2.3 The Franck-Condon principle

The intensity of molecular transitions are, qualitatively, described by the *Franck-Condon principle*, whose *classical* formulation goes as follows:

> *The jump of an electron in a molecular transition occurs during a very small time compared to the time scale of the nuclear motion, so that immediately after the jump, the nuclei remain practically at the same positions and at the same velocities as before the jump* [614].

For this reason, the transitions are drawn vertically in the scheme of potentials shown in Fig. 32.12(right). To yield considerable rates, transitions must occur when the nuclear velocities in the two coupled states are similar, which is the case at the classical turning points. At these points, the wavefunctions are maximal [6].

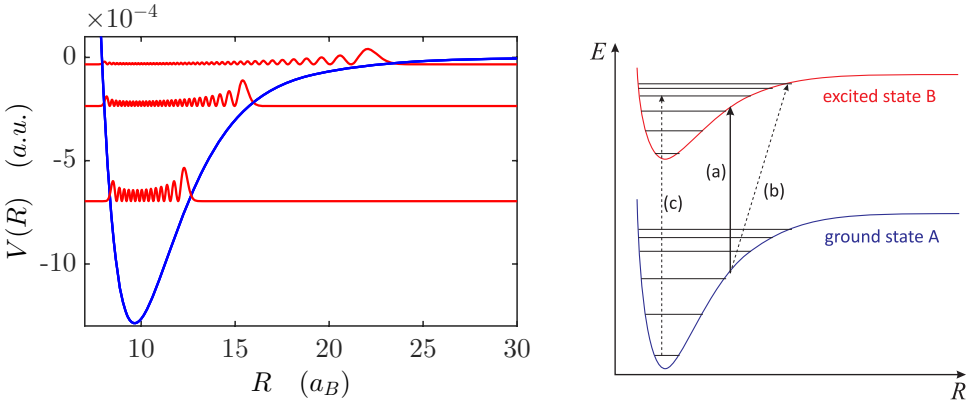

Figure 32.12: (Left, code) Molecular wavefunctions in a potential for three different vibrational states. (Right) Pictorial representation of the classical statement of the Franck-Condon principle. Transition (a) has high intensity (or probability), because here both, the position and the relative velocity of the nuclei do not change. Transitions (b) and (c) are unlikely, because they necessitate either a change in the position of the nuclei (case b) or in velocity (case c).

With this Franck-Condon principle, we can determine which are the strongest transitions between vibrational levels of a molecule, as represented in Fig. 32.12(left). In particular, we are interested in transitions between vibrational levels of different electronic states.

The exact transition probabilities are calculated via the square module of the *transition dipole moment* (TDM). The TDM is an out-of-diagonal matrix element of the electric dipole operator $\mathbf{M}$, given by:

$$\mathbf{M}_{AB} = \langle \Psi^{(A)} | \hat{\mathbf{M}} | \Psi^{(B)} \rangle \ , \tag{32.52}$$

being $|\Psi^{(A)}\rangle$ and $|\Psi^{(B)}\rangle$ two molecular states.

[6] Note that the presence of a hyperfine structure can modify the selection rules.

Still within the Born-Oppenheimer approximation, we can split the dipole moment operator into two terms, a nuclear and an electronic term, according to:

$$\hat{\mathbf{M}}(\mathbf{r},\mathbf{R}) = \hat{\mathbf{M}}_e(\mathbf{r},\mathbf{R}) + \hat{\mathbf{M}}_n(\mathbf{R}) \ . \tag{32.53}$$

Thus, the TDM is:

$$\begin{aligned}\mathbf{M}_{AB} &= \int \Psi^{(A)*}\hat{\mathbf{M}}\Psi^{(B)}dRdr \qquad (32.54)\\ &= \int \hat{\mathbf{M}}_e\psi_e^{(A)*}\ \psi_e^{(B)}\ \psi_n^{(A)*}\ \psi_n^{(B)}dRdr + \int \hat{\mathbf{M}}_n\psi_n^{(A)*}\ \psi_n^{(B)} \int \psi_e^{(A)*}\ \psi_e^{(B)}drdR \ .\end{aligned}$$

Since the electronic wavefunctions of different states are orthogonal, it follows that $\int \psi_e^{(A)*}\psi_e^{(B)}dr = 0$, canceling the second term.

Looking at the first term, we note that the electronic dipole moment $\hat{\mathbf{M}}_e(\mathbf{r},\mathbf{R})$ also depends on the nuclear coordinates as a parameter. The quantum formulation of the Franck-Condon principle consists in stating that, in a *molecular state, the electronic dipole moment varies little with the nuclear coordinates.* Thus, along with the condition of the Born-Oppenheimer approximation, we can split the first TDM term into electronic and nuclear integrals:

$$\mathbf{M}_{AB} = \int \hat{\mathbf{M}}_e\psi_e^{(A)*}\ \psi_e^{(B)}\ dr \int \psi_n^{(A)*}\ \psi_n^{(B)}dR \ . \tag{32.55}$$

Thus, we have a comparative expression for the transition probability given by:

$$P_{AB} \propto |\mathbf{M}_{AB}|^2 = \left|\int \hat{\mathbf{M}}_e\psi_e^{(A)*}\ \psi_e^{(B)}\ dr\right|^2 \left|\int \psi_n^{(A)*}\ \psi_n^{(B)}dR\right|^2 \ . \tag{32.56}$$

The second factor in equation (32.56) is called *Franck-Condon factor*. When we study the transitions between two electronic states, this factor compares the intensities of the transitions between distinct pairs of vibrational levels.

Example 189 (*Ultracold molecules*): Ultracold molecules have been proposed for a variety of applications, such as ultra high resolution spectroscopy [867], test of fundamental laws of physics [350, 1159], quantum computation [349] and others[236]. Most of these applications, however, require that the molecular sample be in a single quantum state. This is an experimental challenge, since molecules have more degrees of freedom than atoms, such as rotation and vibration.

To create a sample of molecules trapped in the ground state of vibration, a possible method is to first produce the molecules from ultracold atoms using a process called *photo association*, and then pump these molecules to the vibrational ground state.

Photoassociation consists in the excitation of a pair of free atoms to the bound state of an excited electronic potential by the absorption of a photon. The pair then decays by spontaneous emission either back to the state of two free atoms (which is not desirable), or to a bound state of the fundamental electronic potential. For Rb_2 molecules, photoassociation is efficient at certain frequencies

[875], with the $A^1\Sigma_u^+$ potential as the excited state (see Fig. 32.13).
Soon after being formed, the molecules are usually in levels of high vibrational energy (around $\nu \approx 80$), because these levels connect best (high Franck-Condon overlap) to the excited state. The transfer of population to the fundamental state of vibration is done by 'optical pumping'.
Vibrational cooling via optical pumping can be done by irradiating a broad frequency band of light that excites transitions to vibrational levels of the excited nuclear potential. These excited states are chosen such that their Franck-Condon overlap with the ground states of lower vibrational energy is larger. As a consequence, a molecule sent to an excited state returns with higher probability to a level of lower vibrational energy. The absorption and emission cycles are repeated, until the molecules reach the fundamental vibrational state.

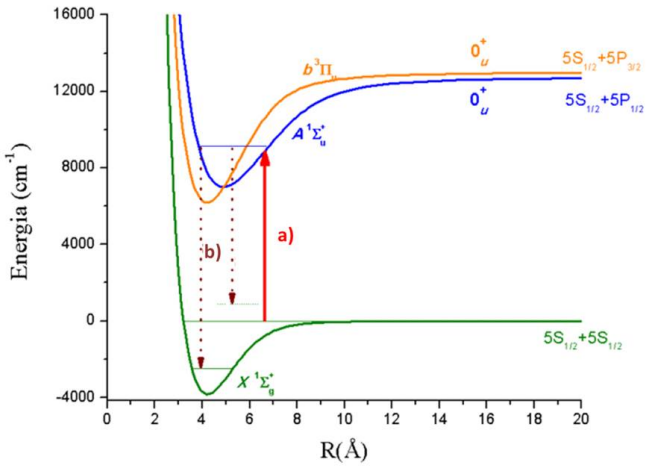

Figure 32.13: Photoassociation scheme to form Rb_2 molecules. In process (a), a pair of free atoms absorbs a photon of the incident radiation, forming a bound state in the excited potential. Then, in (b), the newly formed molecule decays by spontaneous emission to a bound state of the fundamental potential, or it can return to a state of two free atoms.

32.2.4 Rotational progression

Until now we neglected the centrifugal energy (32.38),

$$V_\ell(R) = \frac{\mathbf{L}^2}{2M_r R^2} = \frac{\hbar^2 \ell(\ell+1)}{2M_r R^2} \ . \tag{32.57}$$

As we shall now see, this energy creates a substructure of the vibrational levels.

The moments of inertia in the three axes of space are,

$$I_{qq} = \sum_i m_i r_i^2(q) \ . \tag{32.58}$$

The kinetic energy of the rotation is,

$$E_{rot} = \tfrac{1}{2}\sum_{q=1,2,3} m_q \mathbf{v}_q^2 = \tfrac{1}{2}\sum_{q=1,2,3} I_{qq}\omega_q^2 = \frac{L_x^2}{2I_{xx}} + \frac{L_y^2}{2I_{yy}} + \frac{L_z^2}{2I_{zz}} \ , \tag{32.59}$$

with the angular momentum $L_q = I_{qq}\omega_q$.

Many molecules have a symmetry axis, such that there are two different moments of inertia, $I_\perp \equiv I_{xx} = I_{yy}$ and $I_\parallel \equiv I_{zz}$. Interpreting angular momenta as quantum operators,

$$\hat{H} = \frac{\hat{\mathbf{L}}^2}{2I_\perp} + \left(\frac{1}{2I_\parallel} - \frac{1}{2I_\perp}\right)\hat{L}_z^2 \ . \tag{32.60}$$

We must first consider the rotation of the molecule relative to the symmetry axis of the molecule. Forgetting external fields we calculate the energy of the molecule associated with the observables $\hat{\mathbf{L}}^2$ with the quantum number ℓ and $\hat{\mathbf{L}}_z$ with the quantum number K. We find the eigenvalues,

$$E(\ell, K, M_\ell) = \frac{\hbar^2\ell(\ell+1)}{2I_\perp} + \left(\frac{1}{2I_\parallel} - \frac{1}{2I_\perp}\right)\hbar^2K^2 = B\ell(\ell+1) + (A-B)K^2 \ , \tag{32.61}$$

with $\ell = 0, 1, .., \ K = -\ell, .., \ell$, and $M_\ell = -\ell, .., \ell$ and introducing the *rotational constants*, $A \equiv \hbar^2/2I_\parallel$ and $B \equiv \hbar^2/2I_\perp$. We then analyze this equation in the context of applying an external field that defines both, the direction $\hat{\mathbf{e}}'_z$ in the laboratory as well as the projection of the angular motion $\hat{\mathbf{L}}^2$ on this direction, m_ℓ. That is, we have two axes, the internuclear axis $\hat{\mathbf{e}}_z$ and the rotation axis of the molecule $\hat{\mathbf{e}}'_z$.

Each level $|\ell, m_\ell\rangle$ is $2(2\ell+1)$ times degenerate, because $K = -\ell, .., \ell$ and K can be positive or negative. Each level ℓ contains $2\ell+1$ states. Note that for spherical molecules, $A = B$, and the degree of freedom K disappears. In Exc. 32.2.6.2 we calculate the rotational spectrum of a homonuclear diatomic molecule.

The rotational constant can be approximated by,

$$E_{rot} = \frac{\hbar^2\ell(\ell+1)}{2M_r\langle R^2\rangle} \ , \tag{32.62}$$

where $\sqrt{\langle R^2\rangle}$ is the expectation value for the outer turning point of the vibrational level. As an example, the rotational constant for the vibrational state of $^{87}Rb_2$ which is 5.9 cm^{-1} below the dissociation limit is $B_v = \nu_{rot}^{\ell=1} - \nu_{rot}^{\ell=0} = 81$ MHz. To be more precise, we would need to calculate $\langle R^2\rangle_v = \langle\psi_v|R^2|\psi_v\rangle$.

Transitions between vibrational levels occur together with rotational transitions $\Delta\ell = \pm 1$. Therefore, the frequencies of transitions depend on the rotational constant B_v, which depends on the vibrational state. The energies of the molecule are,

$$E_{v,\ell} = \hbar\omega(v+1/2) - \hbar\omega x_e(v+1/2)^2 + .. + hcB_v\ell(\ell+1) - hcD_v\ell^2(\ell+1)^2 + .. \ . \tag{32.63}$$

Under the influence of a rapid rotation, the atoms of the molecule are subjected to centrifugal force and, hence, are further away from each other [7].

Since at ambient temperatures many rotational levels are populated, we experimentally observe many lines known as P-branch, when $\Delta\ell = -1$, as Q-branch, when $\Delta\ell = 0$, and as R-branch, when $\Delta\ell = 1$. See Exc. 32.2.6.3.

[7] See [60], p.326

32.2.4.1 Rotational selection rules

For transitions between electronic states, the selection rules are $\Delta r = 0, \pm 1$. Rotational transitions can occur between levels $\Delta r = \pm 1$. $\Delta r = 0$ is not allowed, because it violates the conservation of parity. Note also that the nuclear isotope influences the ro-vibrational levels via the reduced mass.

We consider a linear molecule in the state $|\epsilon, \ell, M_\ell\rangle$, where ϵ denotes the electronic and vibrational state of the molecule. To find out which transitions are possible, we need to calculate the matrix,

$$\langle \epsilon', \ell', M'_\ell | \mathbf{d} | \epsilon, \ell, M_\ell \rangle = \langle \ell', M'_\ell | \mathbf{d}_\epsilon | \ell, M_\ell \rangle \ , \tag{32.64}$$

with $\mathbf{d}_\epsilon = \langle \epsilon | \mathbf{d} | \epsilon \rangle$. Here, we apply the *Born-Oppenheimer approximation*, which allows us to separate the dynamics of the electrons and also the vibrations of the molecule, because these movements are so fast, that they are always in a steady state, adiabatically following the slow movement of the rotation.

The selection rules can now be derived from the *Wigner-Eckart theorem*,

$$\frac{\langle \ell', M'_\ell | \mathbf{d}_\epsilon | \ell, M_\ell \rangle|^2}{|\langle \ell' \parallel \mathbf{d}_\epsilon \parallel \ell, M_\ell \rangle|^2} = \frac{1}{2\ell' + 1} \begin{pmatrix} \ell & 1 & \ell' \\ m_\ell & \kappa & -m'_\ell \end{pmatrix} \ . \tag{32.65}$$

We find $\Delta\ell = 1$ e $\Delta M_\ell = 0, \pm 1$. See Exc. 32.2.6.4.

32.2.5 Computation of vibrational states

32.2.5.1 Localization energy

One consequence of Heisenberg's uncertainty relation is that a certain *localization energy* is always required to localize a particle. As an example, we consider the attractive potential,

$$V = -\frac{C}{R^z \alpha} \ . \tag{32.66}$$

The space available for the particle is limited between the classical turning point, which for a given energy is $r_t = \left(\frac{C}{|E|}\right)^{1/\alpha}$. The momentum corresponding to this energy is $k_t = \left(\frac{2m|E|}{\hbar^2}\right)^{1/2}$. Heisenberg's uncertainty relation requires $k_t r_t > 2$, that is, at least half of the wavelength must fit within the potential (between 0 and r_t) at the height of the bound state. Therefore,

$$|E|^{1-2/\alpha} > \frac{2\hbar^2}{mC^{2/\alpha}} \ . \tag{32.67}$$

For a Coulomb potential, with $\alpha = 1$ and $C = e^2/4\pi\varepsilon_0$, we obtain the energy of the ground state of the hydrogen atom,

$$E > E_1 = -\frac{e^2}{4\pi\varepsilon_0 2a_B} \ , \tag{32.68}$$

but there is no state higher than all others. That is, all energies $E_n = E_1/n^2$ exist.

For $\alpha = 2$, we do not get a condition for the energy. For the Casimir-Polder potential, $\alpha = 3$, we obtain,

$$E < -\frac{8\hbar^6}{m^3 C^2} \ . \tag{32.69}$$

This means that, in contrast to the Coulomb potential, the *binding energy* must be *lower* than a certain limit.

32.2.5.2 The LeRoy-Bernstein method

The *LeRoy-Bernstein method* allows us to estimate the highest bound levels. It only applies near the dissociation limit, where the semi-classical formula of quantization is valid,

$$v + \frac{1}{2} = \sqrt{\frac{8M_r}{\hbar^2}} \int_0^{R_1} dR \sqrt{E(v) - V(R)} \ . \tag{32.70}$$

Inserting the potential

$$V(R) = D_e - \frac{C}{R^n} \ , \tag{32.71}$$

we get

$$E(v^*) = D_e - \left(\frac{(n-2)\Gamma\left(1+\frac{1}{n}\right)}{2\Gamma\left(\frac{1}{2}+\frac{1}{n}\right)} (v^* + v_D) \right)^{\frac{2n}{n-2}} \left(\frac{h^{2n}}{(2\pi M_r)^n C^2} \right)^{\frac{1}{n-2}} \ , \tag{32.72}$$

where v^* is a number counting the vibrational levels from the top to the bottom starting at the dissociation limit.

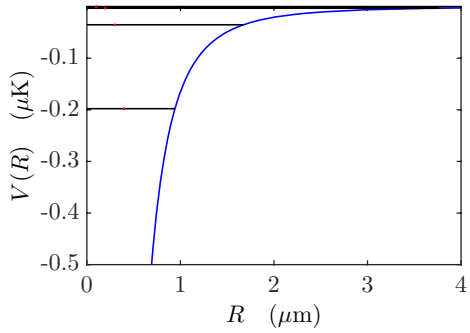

Figure 32.14: (code) Highest vibrational states obtained by the LeRoy-Bernstein method.

32.2.5.3 Open channels

For a given interatomic potential $V(R)$, neglecting the spin structure [690], the relative wavefunction of a two-atom system satisfies the Schrödinger equation,

$$\left[-\tfrac{1}{2\mu}\Delta + V(R) \right] \psi(\mathbf{R}) = E\psi(\mathbf{R}) \ . \tag{32.73}$$

Separating the radial and angular contributions, $\psi(\mathbf{R}) \equiv Y(\vartheta, \varphi) f(R)/R$, we obtain,

$$\left[-\frac{1}{2\mu} \frac{\partial^2}{\partial R^2} + V(R) + \frac{l(l+1)}{2\mu R^2} \right] f(R) = E f(R) \ . \tag{32.74}$$

Now, we introduce the local wavevector, $k(R) = \sqrt{2\mu[E - V(R)] - l(l+1)/R^2}$ and write,

$$f'' = -k^2 f \ . \tag{32.75}$$

This differential equation can be solved numerically [see Fig. 32.15(a)].

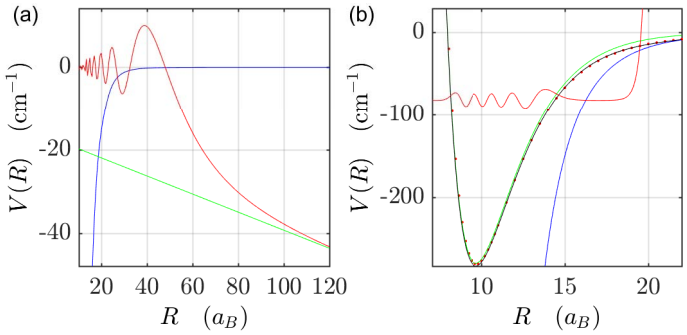

Figure 32.15: (code) (a) Numerical computation of the relative wavefunction for a low energy collision, $E \gtrsim 0$ and $\ell = 0$. The blue curve shows the interatomic Li-Rb potential (a)$^3\Sigma$, the red curve illustrates the relative Broglie wavefunction of the molecule. The asymptote of this extrapolated wavefunction (green curve) cuts the abscissa at $a_s = -120 a_B$, which is just the scattering length for collisions in this channel. (b) Numerical computation of the wavefunction for a vibrational state. The potential is an interpolation (black) between a short-range Morse potential (green), and a long range potential (blue). The red curve illustrates the relative wavefunction for the ninth vibrational state (counting from ground state).

32.2.5.4 Bound states

For bound states, we must simultaneously satisfy the eigenvalue problem. We can, for example, guess an eigenvalue E, calculate the associated wavefunction $f(R)$, check whether it diverges for $R \to \infty$, and vary E until $f(R)$ no longer diverges. Fig. 32.15(b) shows the wavefunction of a vibrational state obtained by solving the Schrödinger equation and adjusting the energy until the function stops diverging in the classically forbidden range.

32.2.5.5 The Fourier grid method

Another, extremely rapid, numerical method for determining the spectrum of vibrational states of a potential, is the *Fourier grid method*. It is based on the discretization of the Hamiltonian along the interatomic potential. We write the Hamiltonian as,

$$H\psi(R) = [T(R) + V(R)]\psi(R) = E\psi(R) \ , \tag{32.76}$$

and put it in a matrix form using the set of functions of the basis $\phi_i(R_j) = \delta(R_i - R_j)$ with $i = 1, .., N$, where $R_i = R_0 + i(R_N - R_0)/N$. This problem has N eigenvalues E_i. The Fourier grid method now evaluates the kinetic energy at each point in the grid. We insert the local terms $H_{ii} = H(R_i)$ and the non-local terms $H_{ij} = H(R_i, R_j)$ into the Hamiltonian, as well as the potential energies $V_{ij} = V(R_i)\delta_{ij}$. The kinetic energy is the inverse Fourier transform from momentum space of $T_{rs} = T(k_r)\delta_{rs} = (k_r^2/2\mu)\delta_{rs}$ and becomes [884, 847, 395],

$$H_{ij} = \frac{\pi^2}{4\mu(R_N - R_1)^2}(-1)^{i-j}\left(\frac{1}{\sin^2\frac{\pi(i-j)}{2N}} - \frac{1}{\sin^2\frac{\pi(i+j)}{2N}}\right) \quad \text{for} \quad i \neq j \tag{32.77}$$

$$H_{ij} = \frac{\pi^2}{4\mu(R_N - R_1)^2}\left(\frac{2N^2+1}{3} - \frac{1}{\sin^2\frac{\pi i}{2N}}\right) + V(R_i) \quad \text{for} \quad i = j \ .$$

To improve the wavefunction, we can interpolate,

$$\psi(q) = \sum\nolimits_{j=1}^{n} \psi(q_j)\ \mathrm{sinc}\frac{\pi(q - q_j)}{\Delta q} \ . \tag{32.78}$$

The method can be extended to coupled channels $\sigma = A, B$ via,

$$H_{\{i\sigma\}\{j\tau\}} = T_{ij}\delta_{\sigma\tau} + V_{\sigma\tau}(R_i)\delta_{ij} \ . \tag{32.79}$$

The Hamiltonian has the general form,

$$H = \begin{pmatrix} T & 0 \\ 0 & T \end{pmatrix} + \begin{pmatrix} V_A & 0 \\ 0 & V_B \end{pmatrix} + \begin{pmatrix} W_{AA} & W_{AB} \\ W_{AB} & W_{BB} \end{pmatrix} \ , \tag{32.80}$$

where all matrices V_k and W_k are diagonal [8].

32.2.6 Exercises

32.2.6.1 Ex: Transitions between vibrational states

Calculate the dipole moment between two arbitrary vibrational states of (a) a harmonic potential and (b) a Morse potential.

Solution:

32.2.6.2 Ex: Rotational spectrum of diatomic molecules

Calculate the rotational spectrum for a diatomic molecule from the result (32.59).

Solution: *We consider a diatomic molecule with R the distance between atoms and the symmetry axis $\hat{\mathbf{e}}_z$. The moments of inertia are then,*

$$I_{xx} = I_{yy} = M_r R^2 \quad , \quad I_{zz} = 0 \ ,$$

[8] Note that the Fourier grid method can be improved by using a grid with spacings adjusted to the potential gradient [739, 1304, 804].

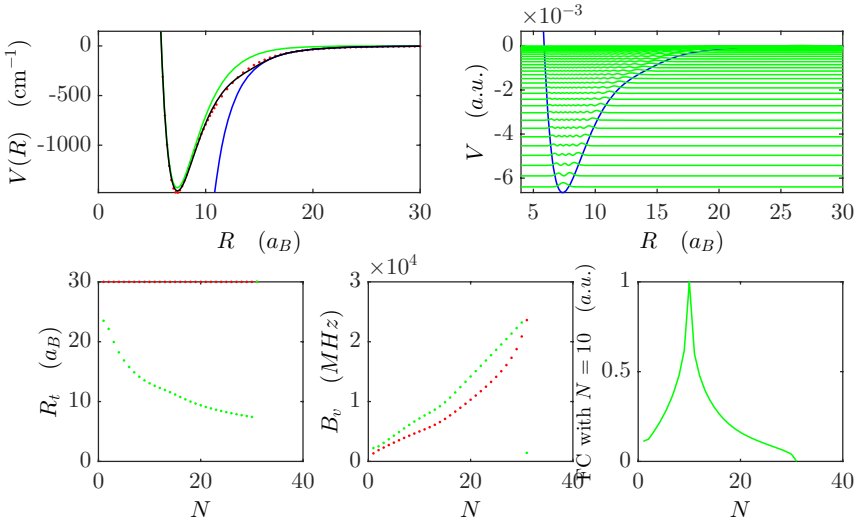

Figure 32.16: (code) Numerical computation of the wavefunction using the Fourier grid method at example of the interatomic potential Li-Rb $(1)^1\Pi$. (a) Short range Morse potential (green), long range (blue), interpolation (black) and [743]. (b) Vibrational wavefunctions, (c) external turning point (red) and center of mass (green), (d) rotational progression, and (e) Franck-Condon overlap with the tenth vibrational state.

where $\mu^{-1} \equiv M_1^{-1} + M_2^{-1}$. *The moment* I_{zz} *disappears because the spatial extent of atoms is negligible. For this case,*

$$A = \frac{\hbar}{4\pi c I_{\|}} = \infty \qquad \textit{and} \qquad B = \frac{\hbar}{4\pi c M_r R^2} \ .$$

This means that the excitations of rotations about the symmetry axis are inaccessible and frozen to the ground state $K = 0$. *Hence,*

$$E(J, M_J) = \frac{\hbar^2}{2M_r R^2} J(J+1) \ .$$

32.2.6.3 Ex: Ro-vibrational spectrum

Determine the frequency spectra of ro-vibrational transitions for the branches P, Q, and R.

Solution:

32.2.6.4 Ex: Rotational spectrum

Determine the rules and the spectrum of rotational transitions for a spherical molecule.

Solution:

32.3 Van der Waals forces and spin coupling

The individual atoms have a complex substructure due to the angular momenta of the electronic motion, its spins and the nuclear spin. All of these angular momenta can interact, couple and generate new energy terms, which need to be taken into account when calculating the various potentials of interatomic interaction,

$$\hat{H} = \frac{\mathbf{P}^2}{2M_r} + V_{coulomb}(R) + \sum_{k=1,2} \left(V_{hfs}^{(k)} + V_{zeeman}^{(k)} \right) + V_{dipole,spin-spin}(R) + V_{dipole,spin-orbit}(R) \; . \tag{32.81}$$

The Coulomb interaction for interacting alkaline gases can be expressed as:

$$V_{coulomb}(R) = V_{coulomb}^{S=0} \mathcal{P}_{S=0} + V_{coulomb}^{S=1} \mathcal{P}_{S=1} \; . \tag{32.82}$$

The projectors $\mathcal{P}_{S=0,1}$ will be required to expand the Hilbert space for the degrees of freedom of the spins.

The *van der Waals forces* include all intermolecular forces. These are long-range forces that occur between permanent and induced atomic dipoles $\sim 1/r^6$ [9]

32.3.1 Analytical models for short and long-range potentials

In general, the potentials are estimated by ab initio Hartree-Fock calculations. A short-range potential, or *Morse potential*, can be approximated by,

$$V_{morse} = D_m \left(\left[1 - e^{-B_m (R - R_m)} \right]^2 - 1 \right) \; . \tag{32.83}$$

Here, B_m is the width of the minimum, R_m the position of the minimum, D_m the length. A long-range potential can be written,

$$V_{vdw}(R) = D_e - \frac{C_6}{R^6} - \frac{C_8}{R^8} - \frac{C_{10}}{R^{10}} \; . \tag{32.84}$$

D_e is the energy of dissociation. The *van der Waals coefficients* C_k, which determine the potential shape at large distances, can be calculated using other methods with higher precision. To obtain a closed formula, the short and long range parts can be joined by,

$$V = V_{morse} F + V_{vdw}(1 - F) \; , \tag{32.85}$$

where $F \equiv e^{-(R/R_t)^{10}}$.

[9] They also occur, in a pure form, in optical resonators such as in the *Casimir effect*. Since the lowest frequency in a cavity is $\omega = \sqrt{2}\pi c/L$, the zero point energies inside and outside the cavity are different. This causes an attractive force between the cavity mirrors $\sim 1/r^3, 1/r^4$.

The situation is different for collisions of identical atoms in excited states, which has a much larger range because of the resonant interaction between dipoles. In this case, an additional *Movre-Pichler potential* dominated by a coefficient C_3 arises,

$$V^e_{vdw} = V^e_{movre} + V^e_{dispersion} \ . \tag{32.86}$$

In contrast, excited state collisions of different species are purely short ranged.

32.3.2 Spin coupling in dimers, molecular quantum numbers

We consider two interacting alkaline atoms, each being described by a set of quantum numbers of internal angular momenta, they couple their spins:

$$\begin{aligned}
\mathbf{l}_i & \quad \text{angular momentum of the individual atom} \\
\mathbf{s}_i & \quad \text{electronic spin} \\
\mathbf{i}_i & \quad \text{nuclear spin} \\
\mathbf{l}_i + \mathbf{s}_i = \mathbf{j}_i & \quad \text{total electronic angular momentum} \\
\mathbf{j}_i + \mathbf{i}_i = \mathbf{f}_i & \quad \text{total angular momentum .}
\end{aligned} \tag{32.87}$$

When the atoms approach each other, at intermediate distances, they couple their spins:

$$\begin{aligned}
\ell \perp \hat{\mathbf{e}}_z & \quad \text{molecular rotation} \\
\mathbf{\Lambda} \equiv |M_L| \hat{\mathbf{e}}_z & \quad \text{projection of } \mathbf{L} \text{ onto the interatomic } \hat{\mathbf{e}}_z \\
\mathbf{\Sigma} \equiv M_S \hat{\mathbf{e}}_z & \quad \text{projection of } \mathbf{S} \text{ onto the interatomic } \hat{\mathbf{e}}_z \\
\mathbf{\Omega} \equiv \mathbf{\Lambda} + \mathbf{\Sigma} & \quad \text{projection of } \mathbf{L} + \mathbf{S} \text{ onto the interatomic } \hat{\mathbf{e}}_z \ .
\end{aligned} \tag{32.88}$$

At short distances, they form a molecular dimer described by the quantum numbers:

$$\begin{aligned}
\mathbf{L} = \mathbf{l}_1 + \mathbf{l}_2 & \quad \text{total electronic angular momentum} \\
\mathbf{S} = \mathbf{s}_1 + \mathbf{s}_2 & \quad \text{electronic spin} \\
\mathbf{I} = \mathbf{i}_1 + \mathbf{i}_2 & \quad \text{nuclear spin} \\
\mathbf{f} = \mathbf{f}_1 + \mathbf{f}_2 & \quad \text{total angular momentum or } (\mathbf{L}, \mathbf{S})\mathbf{k} + \mathbf{I} \\
\mathbf{J} = \mathbf{\Omega} + \ell & \\
\mathbf{F} = \mathbf{f} + \ell & \ .
\end{aligned} \tag{32.89}$$

The quantum numbers couple like,

$$\begin{array}{ccccccccccccc}
\mathbf{l}_1 & + & \mathbf{l}_2 & = & \mathbf{L} & \xrightarrow{\hat{\mathbf{e}}_z} & \mathbf{\Lambda} & & & & & & \\
+ & & + & & + & & + & & & & & & \\
\mathbf{s}_1 & + & \mathbf{s}_2 & = & \mathbf{S} & \xrightarrow{\hat{\mathbf{e}}_z} & \mathbf{\Sigma} & & & & & & \\
= & & = & & = & & = & & & & & & \\
\mathbf{j}_1 & + & \mathbf{j}_2 & = & \mathbf{j} & \xrightarrow{\hat{\mathbf{e}}_z} & \mathbf{\Omega} & + & \ell & = & \mathbf{J} \\
+ & & + & & + & & & & & & + \\
\mathbf{i}_1 & + & \mathbf{i}_2 & = & \mathbf{I} & & & & & & \mathbf{I} \\
= & & = & & = & & & & & & = \\
\mathbf{f}_1 & + & \mathbf{f}_2 & = & \mathbf{f} & & & + & \ell & = & \mathbf{F}
\end{array} \tag{32.90}$$

Obviously, the atomic angular momentum is no longer a conserved quantity, but its projection onto the interatomic molecular axis is. The various possibilities how **L**, **S**, and **j** are projected onto the internuclear axis or directly couple to the rotational angular momentum ℓ are handled by Hund's cases (a) to (e). The spin coupling is described by $\{9j\}$-symbols, as discussed below.

32.3.3 Hund's coupling cases

The coupling force between atomic spins depends on the distance between the atoms. Due to the variety of spins appearing in atoms, there are many possibilities how they can couple. These were classified by Hund into five cases.

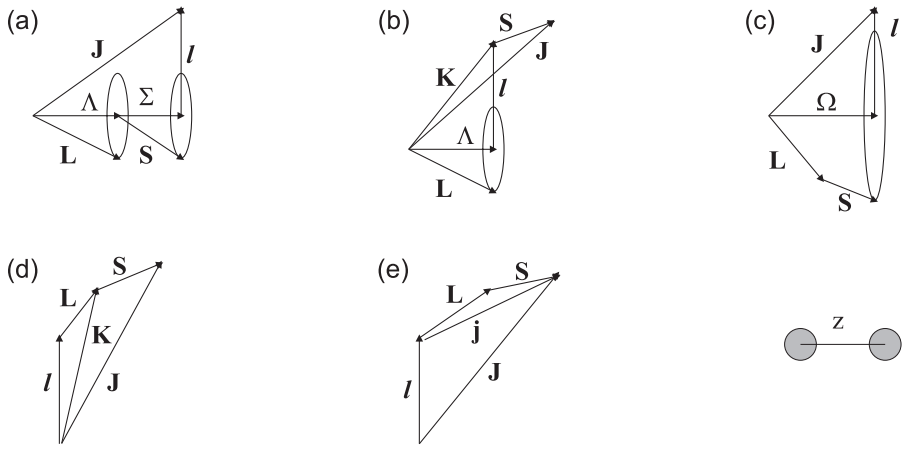

Figure 32.17: Hund's coupling cases.

32.3.3.1 Hund's case (a)

The molecular interaction is so strong that **L** and **S** couple to the z-axis instead of coupling to each other. This case is analogous to the Paschen-Back effect,

$$\begin{aligned} &\mathbf{L} \to \mathbf{\Lambda} \qquad \text{and} \qquad \mathbf{S} \to \mathbf{\Sigma} \\ &((\mathbf{\Lambda}, \mathbf{\Sigma})\mathbf{\Omega}, \ell)\mathbf{J} \ . \end{aligned} \tag{32.91}$$

A common notation is to label the states $\mathbf{\Lambda} = \mathbf{\Sigma}, \mathbf{\Pi}, \mathbf{\Delta}, ...$ That is, in the symbol $X(^{2S+1}\Lambda_\Omega)^{\pm}_{\sigma}$, where $\sigma = g, u$ is the inversion symmetry, $X, A, B, ..$ and $a, b, ..$ are the singlet and triplet series starting from the lowest energy levels. An alternative notation is to assign labels ordered by energy $X = (1), (2), ...$ Finally, $\pm$ is the symmetry upon reflection. For example, $X^1\Sigma_g^+$.

32.3.3.2 Hund's case (b)

L is projected onto the z-axis before coupling to ℓ. The resulting angular momentum afterward directly couples to **S**.

$$\begin{aligned} \mathbf{L} &\rightarrow \mathbf{\Lambda} \\ ((\mathbf{L},\ell)\mathbf{k},\mathbf{S})\mathbf{J} &. \end{aligned} \tag{32.92}$$

32.3.3.3 Hund's case (c)

L and **S** couple together instead of projecting themselves onto the z-axis. This case is analogous to the Zeeman effect,

$$\begin{aligned} (\mathbf{L},\mathbf{S})\mathbf{j} &\rightarrow \mathbf{\Omega} \\ (\mathbf{\Omega},\ell)\mathbf{J} &. \end{aligned} \tag{32.93}$$

A common notation is to label the states by $\mathbf{\Omega} = 0, 1, 2, ...$ That is, in the symbol $X(\Omega)_s^{\pm}$, the letter $X = 1, 2, ..$ is a label ordered by energy. For example $2(0_g^-)$.

32.3.3.4 Hund's case (d)

L is not projected on the z- axis, but directly couples to the rotational angular momentum. The resulting angular momentum afterward only couples to the **S**

$$((\mathbf{L},\ell)\mathbf{k},)\mathbf{J} \; . \tag{32.94}$$

32.3.3.5 Hund's case (e)

L and **S** mutually couple as in the case (c), but are not projected on the z-axis, but couple directly with ℓ, which is quantized,

$$((\mathbf{L},\mathbf{S})\mathbf{j},\ell)\mathbf{J} \; . \tag{32.95}$$

32.3.4 Molecular hyperfine struture

The scattering length in specific channels can be expressed via singlet and triplet scattering lengths,

$$a_{|f_1,m_{f1}\rangle+|f_2,m_{f2}\rangle} = P_{S=0}a_s + P_{S=1}a_t \; . \tag{32.96}$$

The projectors are $P_S = |\langle S|(f_1 f_2)f\rangle|$. According to [213, 889] the recoupling from the uncoupled hyperfine representation into the short range representation is given by,

$$\langle Sm_S \; Im_I \; \ell' m_{\ell'}|f_1 m_{f1} \; f_2 m_{f2} \; \ell m_\ell\rangle = \delta_{\ell\ell'}\delta_{m_\ell m'_\ell} \sum_{f,m_f} \langle Sm_S \; Im_I|fm_f\rangle\langle f_1 m_{f1} \; f_2 m_{f2}|fm_f\rangle \times$$

$$\times \begin{Bmatrix} s_1 & s_2 & S \\ i_1 & i_2 & I \\ f_1 & f_2 & f \end{Bmatrix} \sqrt{\hat{S}\hat{I}\hat{f}_1\hat{f}_2} \left(\frac{1-(1-\delta_{f_1 f_2})(-1)^{S+I+\ell}}{\sqrt{2-\delta_{f_1 f_2}}} \right) \; . \tag{32.97}$$

The last bracket is dropped for unsymmetrized recoupling. We will study examples of spin recoupling in the ground state channels in Exc. 32.3.5.1, 32.3.5.2, and 32.3.5.3.

32.3.5 Exercises

32.3.5.1 Ex: Spin recoupling of identical ^{87}Rb ground state channels

a. Unravel the molecular hyperfine structure of identical ^{87}Rb ground state channels.
b. Project the collisional channels $|f_1 m_{f1}\ f_2 m_{f2}\rangle = |1\,-1\ 1\,-1\rangle$ and $|22\ 22\rangle$ on the singlet and triplet potentials, $S = 0, 1$.

Solution: *a. With hyperfine structure we get for ^{87}Rb: According to Fig. 32.18 the*

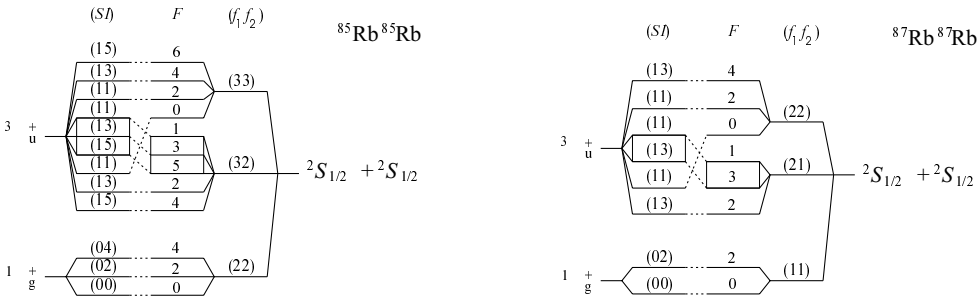

Figure 32.18: Hyperfine recoupling scheme.

levels $f = 1, 3, 4$ have pure triplet character, while $f = 0, 2$ have singlet admixtures. In the presence of hyperfine structure the potential curves split further. Collisions may occur on several levels simultaneously.
We test the recoupling procedure on ^{87}Rb, for which the following projectors are known [296]: $a_{|2,2\rangle+|2,2\rangle} = 0a_s + 1a_t$ and $a_{|1,-1\rangle+|1,-1\rangle} = \frac{3}{16}a_S + \frac{13}{16}a_t$. Now considering atoms with nuclear spin $i_1 = i_2 = 3/2$ in their electronic ground states, $s_1 = s_2 = 1/2$, colliding in identical channels, $f_1 = f_2$ and $m_{f1} = m_{f2}$,

$$\langle S m_S\ I m_I | f_1 m_{f1}\ f_1 m_{f1}\rangle = \sum_f \begin{pmatrix} S & I & f \\ m_S & 2m_{f1} - m_S & -2m_{f1} \end{pmatrix} \times$$
$$\times \begin{pmatrix} f_1 & f_1 & f \\ m_{f1} & m_{f1} & -2m_{f1} \end{pmatrix} \begin{Bmatrix} \frac{1}{2} & \frac{1}{2} & S \\ \frac{3}{2} & \frac{3}{2} & I \\ f_1 & f_1 & f \end{Bmatrix} \hat{f}_1 \sqrt{\hat{S}\hat{I}}\ ,$$

where we used $m_f = m_{f1} + m_{f2} = m_S + m_I$ and the fact that the sum of the lower row of a Clebsch-Gordan must be zero.
b. In the following, we calculate projections of the collisional channels $|f_1 m_{f1}\ f_2 m_{f2}\rangle = |1\,-1\ 1\,-1\rangle$ and $|22\ 22\rangle$ on the singlet and triplet potentials, $S = 0, 1$, separately. For this it suffices to calculate the above projections for various sets of $I = |i_1 - i_2|..i_1 + i_2$ and $m_I = -I..I$. The number $m_S = \min(\max(m_f - m_I, -S), S)$ is fixed by the previous ones. And the sum runs over $f = \max(|f_1 - f_2|, |I - S|)..\min(f_1 + f_2, I + S)$. Doing so, we obtain in the singlet channel (here $f = I$),

$$\langle 0 m_S\ I m_I | 22\ 22\rangle = 0\ ,$$

which gives $P_{S=0} = 0$, *and*

$$\langle 0 m_S \; I m_I | 1 - 1 \; 1 - 1 \rangle = \langle 00 \; 2 - 2 1 - 1 \; 1 - 1 \rangle = \tfrac{1}{4}\sqrt{3} \; ,$$

which gives $P_{S=0} = 3/16$. *Similarly, for the triplet states,* $S = 1$,

$$\langle 1 m_S \; I m_I | 22 \; 22 \rangle = \langle 11 \; 33 | 22 \; 22 \rangle = 1 \; ,$$

which gives $P_{1=0} = 1$, *and*

$$\langle 1 m_S \; I m_I | 1 - 1 \; 1 - 1 \rangle = \begin{cases} \langle 1 + 1 \; 3 - 3 | 1 - 1 \; 1 - 1 \rangle = 0.75 \\ \langle 1 + 0 \; 3 - 2 | 1 - 1 \; 1 - 1 \rangle = -0.4330 \\ \langle 1 - 1 \; 1 - 1 | 1 - 1 \; 1 - 1 \rangle = -0.1581 \\ \langle 1 - 1 \; 3 - 1 | 1 - 1 \; 1 - 1 \rangle = 0.1936 \end{cases} ,$$

which gives $P_{S=1} = \sum_{I,m_I} |\langle 1 m_S \; I m_I | 1 - 1 \; 1 - 1 \rangle|^2 = 13/16$.

32.3.5.2 Ex: Spin recoupling of ^{6}Li^{87}Rb ground state channels

a. Unravel the molecular hyperfine structure of ^{6}Li^{87}Rb ground state channels.
b. Project the collisional channels on short range potentials.

Solution: *As a second example consider* ^{6}*Li* ^{87}*Rb collisions. Apparently the coupling is diagonal in* f, *neglecting spin-spin interactions,*

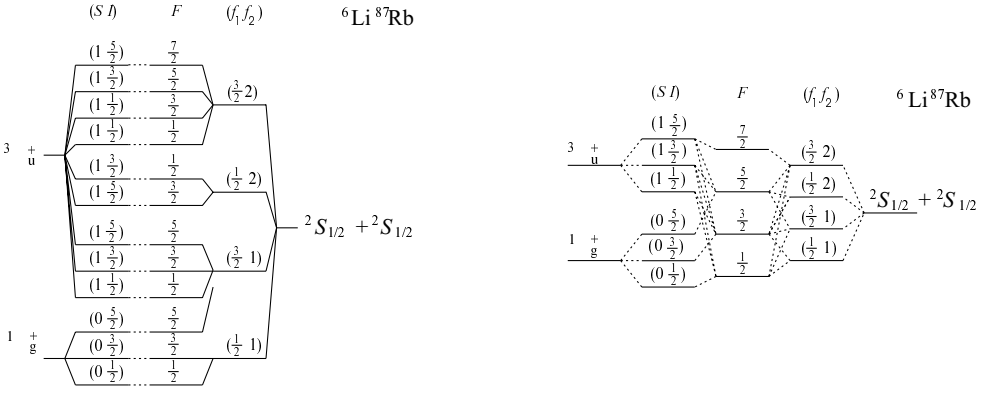

Figure 32.19: Hyperfine recoupling for heteronuclear collisions.

$$\begin{array}{c} (f_6 f_{87}) f \longrightarrow \\ (SI) f \downarrow \\ (0, \tfrac{1}{2})\tfrac{1}{2} \; (1, \tfrac{1}{2})\tfrac{1}{2} \; (1, \tfrac{3}{2})\tfrac{1}{2} \\ (0, \tfrac{3}{2})\tfrac{3}{2} \; (1, \tfrac{1}{2})\tfrac{3}{2} \; (1, \tfrac{3}{2})\tfrac{3}{2} \; (1, \tfrac{5}{2})\tfrac{3}{2} \\ (0, \tfrac{5}{2})\tfrac{5}{2} \; (1, \tfrac{3}{2})\tfrac{5}{2} \; (1, \tfrac{5}{2})\tfrac{5}{2} \\ (1, \tfrac{5}{2})\tfrac{7}{2} \end{array} \quad \begin{array}{ccccc} \tfrac{1}{2},1)\tfrac{1}{2} & (\tfrac{3}{2},1)\tfrac{1}{2} & (\tfrac{3}{2},2)\tfrac{1}{2} & & \\ & 3 \times 3 & & & \\ \tfrac{1}{2},1)\tfrac{3}{2} & (\tfrac{3}{2},1)\tfrac{3}{2} & (\tfrac{1}{2},2)\tfrac{3}{2} & (\tfrac{3}{2},2)\tfrac{3}{2} & \\ & & 4 \times 4 & & \\ & (\tfrac{3}{2},1)\tfrac{5}{2} & (\tfrac{1}{2},2)\tfrac{5}{2} & (\tfrac{3}{2},2)\tfrac{5}{2} & \\ & & & 3 \times 3 & \\ & & & & (\tfrac{3}{2},2)\tfrac{7}{2} \\ & & & & 1 \times 1 \end{array}$$

We start again from the general expression, but now insert the Li (label 1) and Rb (label 2) data,

$$\langle S m_S\ I m_I | f_1 m_{f1}\ f_2 m_{f2}\rangle = \sum_f \begin{pmatrix} S & I & f \\ m_S & m_I & -m_{f1}-m_{f2}\end{pmatrix} \times$$
$$\times \begin{pmatrix} f_1 & f_2 & f \\ m_{f1} & m_{f2} & -m_{f1}-m_{f2}\end{pmatrix} \begin{Bmatrix} \frac{1}{2} & \frac{1}{2} & S \\ 1 & \frac{3}{2} & I \\ f_1 & f_2 & f\end{Bmatrix} \sqrt{\hat{S}\hat{I}\hat{f}_1\hat{f}_2}\ .$$

b. Setting $S=0=m_S$, we get for the various channels,

$$\langle 00\ I m_I | \tfrac{3}{2}\tfrac{3}{2}\ 22\rangle = 0$$

which gives $P_{S=0}=0$, and

$$\langle 00\ I m_I | \tfrac{1}{2}-\tfrac{1}{2}\ 1-1\rangle = \langle 00\ \tfrac{3}{2}-\tfrac{3}{2} | \tfrac{1}{2}-\tfrac{1}{2}\ 1-1\rangle = 0.4564$$

which gives $P_{S=0}=0.2083$. Setting $S=1$, we get,

$$\langle 1 m_S\ I m_I | \tfrac{3}{2}\tfrac{3}{2}\ 22\rangle = \langle 11\ \tfrac{5}{2}\tfrac{5}{2} | \tfrac{3}{2}\tfrac{3}{2}\ 22\rangle = 1\ ,$$

and

$$\langle 1 m_S\ I m_I | \tfrac{1}{2}-\tfrac{1}{2}\ 1-1\rangle = \begin{cases} \langle 1+1\ \frac{5}{2}-\frac{5}{2} | \frac{1}{2}-\frac{1}{2}\ 1-1\rangle = \sqrt{\frac{1}{2}} \\ \langle 1+0\ \frac{5}{2}-\frac{3}{2} | \frac{1}{2}-\frac{1}{2}\ 1-1\rangle = -\sqrt{\frac{1}{5}} \\ \langle 1+0\ \frac{3}{2}-\frac{3}{2} | \frac{1}{2}-\frac{1}{2}\ 1-1\rangle = -0.0913 \\ \langle 1-1\ \frac{5}{2}-\frac{1}{2} | \frac{1}{2}-\frac{1}{2}\ 1-1\rangle = \sqrt{\frac{1}{20}} \\ \langle 1-1\ \frac{3}{2}-\frac{1}{2} | \frac{1}{2}-\frac{1}{2}\ 1-1\rangle = 0.0745 \\ \langle 1-1\ \frac{1}{2}-\frac{1}{2} | \frac{1}{2}-\frac{1}{2}\ 1-1\rangle = -\frac{1}{6} \end{cases},$$

which gives $P_{S=1}=\sum_{I,m_I} |\langle 1 m_S\ I m_I | \frac{1}{2}-\frac{1}{2}\ 1-1\rangle|^2 = 0.7917$.

32.3.5.3 Ex: Hyperfine structure of ^{6}Li^{23}Na and ^{6}Li^{87}Rb

a. Unravel the molecular hyperfine structure of ^{6}Li^{23}Na and ^{6}Li^{87}Rb bound state.
b. How about the open channels?

Solution: *a. The rank of the whole matrix follows from the following table:*

$\langle \vert V \vert S, m_S, i_6, m_6, i_{87}, m_{87}\rangle$	$(0,0)(1,-1..1)(\frac{3}{2},-\frac{3}{2}..\frac{3}{2})$	$(1,-1..1)(1,-1..1)(\frac{3}{2},-\frac{3}{2}..\frac{3}{2})$
$(0,0)(1,-1..1)(\frac{3}{2},-\frac{3}{2}..\frac{3}{2})$	12×12	
$(1,-1..1)(1,-1..1)(\frac{3}{2},-\frac{3}{2}..\frac{3}{2})$		36×36

For example, $^6Li^{87}Rb$ collisions in $S=1$ produce the curves in Fig. 32.20 [1242] using the tabulated values for i_k, $a_{hf,k}$ and g_k [43].

We consider ^6Li and the ground state $|1/2, \mp 1/2\rangle$ and ^{23}Na in $|1, \mp 1\rangle$. For the combined open channel we simply use the Breit-Rabi formula. According to [1242] using $S = 1$, $i_6 = 1$ and $i_{23} = 3/2$, $a_{hf,6} = 152.1368$ MHz and $a_{hf,23} = 885.8131$ MHz, and furthermore $E_B = -5550$ MHz. With $g_S = 2.000...$, $g_6 = -0.000447$ and $g_{23} = -0.000804$. The results can simply transferred to ^{87}Rb, in the same set of

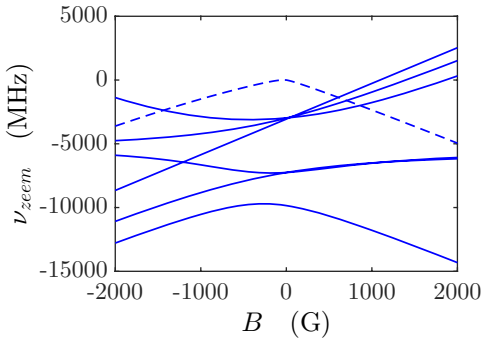

Figure 32.20: (code) Ground state level shift in a magnetic field for LiRb collisions. The binding energy is fitted to $E_B = -5550$ MHz. The dotted line denotes the open channel. Only those states with $m_f = m_{f1} + m_{f2} = -3/2$ are shown for $B < 0$ and $m_f = 3/2$ for $B > 0$.

quantum numbers, but with a different hf splitting, $a_{hf,87} = 3417.3413$ MHz, a different nuclear g-factor, $g_{87} = -0.000995$, and obviously a different orbital energy E_B. Note that the $(i_1, i_2)I$ coupling easily breaks up in a magnetic field. The magnetic field dependence of bound states is thus primarily determined by the total electronic spin. Singlet states $S = 0$ do not shift, triplet states $S = 1$ split up into three hyperfine multiplets [1242].
b. The total energy of a Zeeman-shifted open channel is just the sum of the Zeeman-shifted energy of the individual colliding atoms.

32.4 Further reading

et al., [?]DOI

Chapter 33

Collisions

Until now, we mostly restricted our studies to individual atoms or molecules. In practice, however, we investigate atomic or molecular gases by spectroscopic methods. The constituents of thermal gases are constantly in motion. They are subject to Doppler-shifts of their spectral lines and they collide with each other. Colliding atoms often get so close, that the electronic orbitals affect each other, which leads to distortions of the interaction potentials, spectral lineshifts and modifications of the interatomic forces. These are the topics to be addressed in the present chapter.

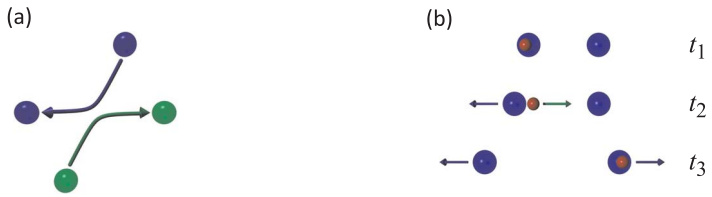

Figure 33.1: Atoms may interact via exchange of (a) virtual photons or (b) real photons.

33.1 Motion of interacting neutral atoms

The following sections, devoted to the relative motion of two neutral atoms, are adapted from J. Walraven's excellent lectures on *Quantum Gases* available at [1355]. The atoms are presumed to move slowly, typically at large separation, and to interact pair wise through a potential of the Van der Waals type. The term slowly refers to,

$$k_{therm} r_0 \ll 1 \qquad \text{where} \qquad \lambda_{therm} = \frac{2\pi}{k_{therm}} = \sqrt{\frac{2\pi\hbar^2}{m k_B T}} \tag{33.1}$$

is the *thermal de Broglie wavelength* and r_0 the range of the interaction potential. As the Van der Waals interaction gives rise to elastic collisions, the total energy of the relative motion is conserved in time. As the potential energy vanishes at large interatomic separation the total energy is usually expressed in the form $E = \hbar^2 k^2 / 2m_r$. This implies that also the wavenumbers for the relative motion before and after the collision must be the same and shows that, far from the potential center, the collision can only affect the phase of the wavefunction - not its wavelength. Apparently, the appearance of a shift in phase relative to the free atomic motion

provides the key to the quantum mechanical description of elastic collisions. This being said, we postpone the discussion of the actual collisional behavior to Sec. 33.2. First we prepare ourselves for this discussion by analyzing the stationary states for the motion in the presence of an interaction potential.

An important simplifying factor in the description of ultracold collisions is the emergence of universal behavior in the relative motion of the atoms. The latter applies to low-energy collisional states as well as to weakly bound states. Universal means in this context that, asymptotically (for $r \gg r_0$), the wavefunctions become independent of the details of the interaction potential but can be characterized in terms of a few parameters, each representing some characteristic length scale of the collisional system. In other words, very different short-range physics can give rise to the same scattering behavior. From a theory point of view this universality has the enormous advantage that the essential features of ultracold collisions can be described with the aid of simple model potentials for which analytical solutions can be obtained.

In our analysis of the collisional motion three characteristic length scales will appear, the interaction range r_0 the scattering length a and the effective range r_e, each expressing a different aspect of the interaction. The range r_0 is the distance beyond which the interaction may be neglected even for $k \to 0$. The second characteristic length, the s-wave scattering length a, acts as an effective hard-sphere diameter. It is a measure for the interaction strength and determines the collision cross section in the limit $k \to 0$ as will be elaborated on in Sec. 33.2. The third characteristic length, the effective range re expresses how the potential affects the energy dependence of the cross section and determines when the $k \to 0$ limit is reached.

The s-wave scattering length is the central parameter for the theoretical description of bosonic quantum gases. It determines both the thermodynamic and the collisional properties of these gases. In single-component fermionic gases the s-wave scattering length plays no role because the wavefunction for the relative motion of the atoms has to be antisymmetric. In two-component fermionic gases this restriction is absent for collisions between atoms of different components. As a consequence, in these systems the inter-component s-wave scattering length determines the collision related properties - for instance the thermalization rate.

In Sec. 33.1.1 we show how the phase shift appears as a result of interatomic interaction in the wavefunction for the relative motion of two atoms. For free particles the phase shift is zero. An integral expression for the phase shift is derived. In Sec. 33.1.2 and beyond we specialize to the case of low-energy collisions ($kr_0 \ll 1$). The basic phenomenology is introduced and analyzed for simple model potentials like the hard-sphere (Sec. 33.1.2) and the spherical well (Sec. 33.1.3), where the existence of a short range is manifest. For the discussion of arbitrarily shaped potentials, we refer to the script [1355].

33.1.1 The collisional phase shift

33.1.1.1 Schrödinger equation

The starting point for the description of the relative motion of two atoms at energy E is the Schrödinger equation (25.33),

$$\left[\frac{1}{2m_r}\left(p_r^2+\frac{\mathbf{L}^2}{r^2}\right)+V(r)\right]\psi(r,\vartheta,\varphi)=E\psi(r,\vartheta,\varphi)\ . \tag{33.2}$$

Here m_r is the reduced mass of the atom pair and $V(r)$ the interaction potential. As discussed in Sec. 25.1.3 the eigenfunctions $\psi(r,\vartheta,\varphi)$ can be separated in a radial and a angular part, $\psi = R_\ell(r)Y_{\ell m}(\vartheta,\varphi)$, where the functions $Y_{\ell m}$ are spherical harmonics and the functions $R_\ell(r)$ satisfy the radial wave equation,

$$\left[\frac{\hbar^2}{2m_r}\left(-\frac{d^2}{dr^2}-\frac{2}{r}\frac{d}{dr}+\frac{\ell(\ell+1)}{r^2}\right)+V(r)\right]R_\ell(r)=ER_\ell(r)\ . \tag{33.3}$$

By the separation procedure the angular momentum term is replaced by a repulsive effective potential,

$$V_{rot}(r)=\frac{\hbar^2\ell(\ell+1)}{2m_r r^2}\ , \tag{33.4}$$

representing the rotational energy of the atom pair at a given distance and for a given rotational quantum number ℓ. In combination with an attractive interaction it gives rise to a centrifugal barrier for the radial motion of the atoms. This is illustrated in Fig. 33.2 for the example of hydrogen.

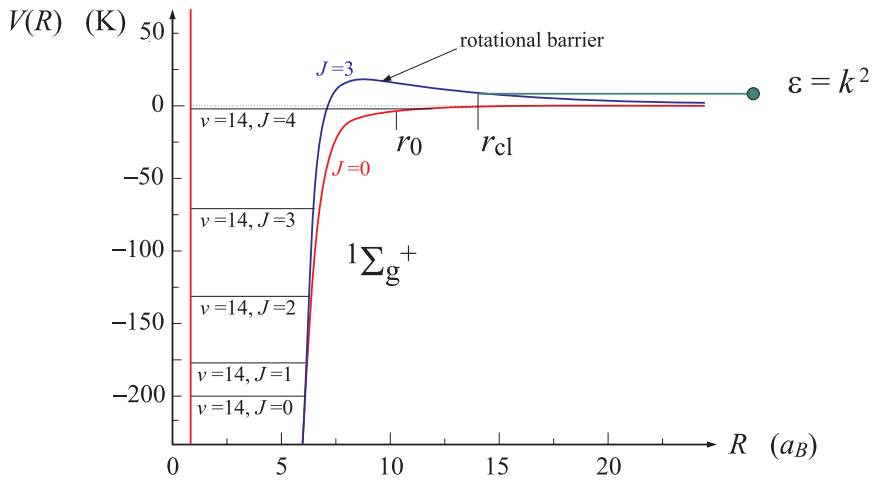

Figure 33.2: Example showing the high-lying bound states near the continuum of the singlet potential $^1\Sigma_g^+$ (the bonding potential) of the hydrogen molecule; v and J are the vibrational and rotational quantum numbers, respectively. The dashed line shows the effect of the $J = 3$ centrifugal barrier. The presence of a rotational barrier gives rise to an exponential suppression of the radial wavefunction for $r < r_{tp}$ and is negligible at distances where the interaction becomes noticeable $r \ll r_0$.

To analyze the radial wave equation we introduce reduced energies,

$$\varepsilon = \frac{2m_r E}{\hbar^2} = \begin{cases} k^2 & \text{for } k > 0 \\ -\kappa^2 & \text{for } k < 0 \end{cases} \quad \text{and} \quad \tilde{V}(r) = \frac{2m_r V(r)}{\hbar^2} \ , \tag{33.5}$$

choosing k and κ as real positive number. This puts Eq. (33.3) in the form,

$$\boxed{R_\ell'' + \frac{2}{r} R_\ell' + \left[\varepsilon - \tilde{V}(r) - \frac{\ell(\ell+1)}{r^2}\right] R_\ell = 0} \ . \tag{33.6}$$

With the substitution $u_\ell(r) = rR_\ell(r)$ it reduces to a 1D Schrödinger equation,

$$\boxed{u_\ell'' + \left[\varepsilon - \tilde{V}(r) - \frac{\ell(\ell+1)}{r^2}\right] u_\ell = 0} \ . \tag{33.7}$$

33.1.1.2 Low-energy limit: the s-wave regime

For two atoms with relative angular momentum $\ell > 0$ there exists a distance r_{tp}, called the classical turning point, below which the rotational energy exceeds the total energy E,

$$k^2 = \frac{\ell(\ell+1)}{r_{tp}^2} \ . \tag{33.8}$$

This is illustrated in Fig. 33.2. In the classically inaccessible region of space ($r < r_{tp}$) the radial wavefunction is exponentially suppressed [1]. Combining Eq. (33.8) with the condition (33.1) we obtain the inequality,

$$kr_0 = \sqrt{\ell(\ell+1)}\frac{r_0}{r_{tp}} \ll 1 \ , \tag{33.9}$$

which implies that, for $\ell \neq 0$, the classical turning point is found at a distance much larger than the range r_0 of the interaction. As the range r_0 defines the distance beyond which the potential can be neglected, this inequality shows that the radial motion is not affected by the presence of the potential $V(r)$ in the radial wave equation. The notable exception is the case $\ell = 0$, where the barrier is absent and the potential gives rise to a substantial distortion of the radial waves. In other words, for $kr_0 \ll 1$ phase shifts (i.e. scattering) can *only arise from collisions with zero angular momentum.* The range of collision energies where the inequalities (33.9) are valid is called the s-wave regime.

33.1.1.3 Free particle motion

We first have a look at the case of free particles or particles in a homogeneous potential, $V(r) = V_0$. By introducing the dimensionless variable $\varrho = kr$, where $k \equiv \sqrt{2m(E - V_0)/\hbar^2}$, the radial wave equation (33.6) can be rewritten in the form of the spherical Bessel differential equation,

$$R_\ell'' + \frac{2}{\varrho} R_\ell' + \left[1 - \frac{\ell(\ell+1)}{\varrho^2}\right] R_\ell = 0 \ . \tag{33.10}$$

[1] At this point we exclude tunneling through the barrier and the occurrence of shape resonances.

Here, the derivatives are with respect to the new variable.

The general solution of Eq. (33.10) for angular momentum ℓ is a linear combination of two particular solutions, one regular with amplitude A_ℓ, the spherical Bessel function $j_\ell(\varrho)$, and one irregular with amplitude B_ℓ, the spherical Neumann function $n_\ell(\varrho)$:

$$\boxed{R_\ell(\varrho) = A_\ell j_\ell(\varrho) + B_\ell n_\ell(\varrho) = c_\ell[\cos\eta_\ell\ j_\ell(\varrho) + \sin\eta_\ell\ n_\ell(\varrho)]}\ , \tag{33.11}$$

where the new parameters c_ℓ and η_ℓ, defined by

$$A_\ell \equiv c_\ell \cos\eta_\ell \qquad \text{and} \qquad B_\ell \equiv c_\ell \sin\eta_\ell\ , \tag{33.12}$$

represent the amplitude c_ℓ and the asymptotic phase η_ℓ of the wavefunction. Note that this equation is singular in the origin except for the case of vanishing phase shifts. Therefore, in the case of free particles we require $\eta_\ell = 0$ for all angular momentum values ℓ. This implies that the general solution reduces to the regular one,

$$R_\ell(\varrho) = c_\ell \cos\eta_\ell\ j_\ell(\varrho)\ . \tag{33.13}$$

33.1.1.4 Significance of the phase shifts

To investigate the effect of a short-range interaction potential $V(r)$ we return to the radial wave equation (33.6). As the potential is of short range it may be neglected for $r \gg r_0$ and the general solutions coincide with those of the spherical Bessel equation,

$$R_\ell(k,r) \underset{r\gg r_0}{\longrightarrow} c_\ell[\cos\eta_\ell\ j_\ell(kr) + \sin\eta_\ell\ n_\ell(kr)]\ . \tag{33.14}$$

For $r \gg 1/k$ the spherical Bessel and Neumann functions assume their asymptotic form and we find,

$$\begin{aligned} R_\ell(k,r) &\underset{kr\to\infty}{\longrightarrow} \frac{c_\ell}{kr}[\cos\eta_\ell \sin(kr - \tfrac{1}{2}\ell\pi) + \sin\eta_\ell \cos(kr - \tfrac{1}{2}\ell\pi)] \\ &= \frac{c_\ell}{kr}\sin(kr + \eta_\ell - \tfrac{1}{2}\ell\pi)\ . \end{aligned} \tag{33.15}$$

where we introduced a the constant η_ℓ representing the asymptotic phase shift. For a given value of k this phase shift fixes the general solution of the radial wavefunction $R_\ell(k,r)$ up to an ℓ dependent normalization constant c_ℓ. Note that in view of the k dependence of the phase shift, R_ℓ is a function of k and r rather than a function of the product kr. Whereas in the case of free particles the phase shifts must all vanish, in the presence of the interaction they provide the proper asymptotic form of the distorted waves. The non-zero asymptotic phase shift is the signature of the interaction at short distance; the motion becomes free-particle like (undistorted) only at large distance from the scattering center. In elastic scattering the relative energy $\hbar^2k^2/2m$ is conserved; hence, asymptotically also k and the de Broglie wavelength. This leaves only the asymptotic phase of the wave to be affected.

Example 190 (*Scattering matrix*): Rewriting Eq. (33.15) in complex notation,

$$R_\ell(k,r) \underset{r\to\infty}{\simeq} \frac{c_\ell}{2k} i \left[e^{-i\eta_\ell} \frac{e^{-i(kr-\frac{1}{2}\ell\pi)}}{r} - e^{i\eta_\ell} \frac{e^{i(kr-\frac{1}{2}\ell\pi)}}{r} \right]\ , \tag{33.16}$$

we see that for $r \to \infty$ the stationary solution $R_\ell(k,r)$ can be regarded as an 'incoming' spherical wave interfering with an 'outgoing' spherical wave. It is convention to choose the phase of the normalization constant such that the phase of the incoming wave is zero,

$$R_\ell(k,r) \underset{r\to\infty}{\simeq} \frac{c'_\ell}{2k} i \left[\frac{e^{-ikr}}{r} - e^{-i\ell\pi} e^{2i\eta_\ell} \frac{e^{ikr}}{r} \right] , \tag{33.17}$$

Apart from the sign, the ratio of the phase factors of the outgoing over the incoming wave is,

$$\mathcal{S}_\ell = e^{2i\eta_\ell} . \tag{33.18}$$

This quantity is called the scattering matrix ($\mathcal{S}$ matrix) or, better, the l-wave contribution to the $\mathcal{S}$ matrix. Being unitary it does not suffer from the divergences of the ratio $B_\ell/A_\ell = \tan\eta_\ell$. In the present context the name scattering matrix is a bit heavy because we only have a single matrix element (1×1 matrix). The term matrix finds its origin in the description of scattering of particles with an internal degree of freedom (like spin), for which the phase factor is replaced by a unitary matrix.

33.1.2 Hard-sphere potentials

We now turn to analytical solutions for model potentials in the limit of low energy. We first consider the case of two hard spheres of equal size. These can approach each other to a minimum distance equal to their diameter a. For $r \le a$ the radial wave function vanishes, $R_\ell(r) = 0$: Outside the hard sphere we have free atoms, $V(r) = 0$, with relative wave number $k = [2m_r E/\hbar^2]^{1/2}$. Thus, for $r \le a$ the general solution for the radial wave functions of angular momentum ℓ is given by the free atom expression (33.11), which asymptotically this takes the form (33.15) of a phase-shifted spherical Bessel function,

$$R_\ell(k,r) = c_\ell[\cos\eta_\ell\ j_\ell(kr) + \sin\eta_\ell\ n_\ell(kr)] \underset{r\to0}{\simeq} \frac{c_\ell}{kr} \sin(kr + \eta_\ell - \tfrac{1}{2}\ell\pi) . \tag{33.19}$$

To determine the phase shift we require as a boundary condition that $R_\ell(k,r)$ vanishes at the surface of the hard sphere (see Fig. 33.3),

$$\cos\eta_\ell\ j_\ell(ka) + \sin\eta_\ell\ n_\ell(ka) = 0 . \tag{33.20}$$

Hence, the phase shift follows from the expression,

$$\tan\eta_\ell = \frac{j_\ell(ka)}{n_\ell(ka)} . \tag{33.21}$$

This expression allows to derive asymptotic expressions (for $ka \ll 1$ and for $ka \gg 1$) for the radial wave function (33.19), as will be shown in Exc. 33.1.5.1.

33.1.2.1 s-wave phase shifts for hard spheres

For the case $\ell = 0$, inserting the analytical expressions for the Bessel and von Neumann function, (33.19) becomes without approximation,

$$R_0(k,r) = \frac{c_0}{kr}(\cos\eta_0 \sin kr + \sin\eta_0 \cos kr) = \frac{c_0}{kr} \sin(kr + \eta_0) . \tag{33.22}$$

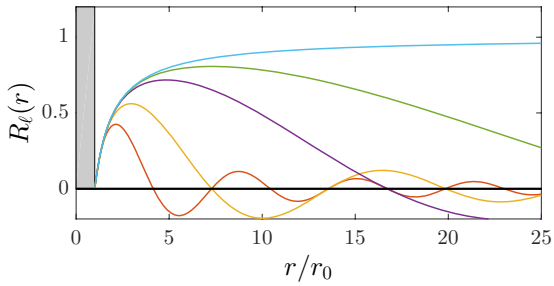

Figure 33.3: (code) Radial wavefunctions ($\ell = 0$) for various values of k (down to the $k \to 0$ limit) in the case of a hard sphere potential. The boundary condition is fixed by the requirement that the wavefunction vanishes at the edge of the hard sphere, $R_0(ka) = 0$.

The phase shift follows from the boundary condition $R_0(k, a) = 0$, which can be written in the form,

$$\cos\eta_0 \sin ka + \sin\eta_0 \cos ka = 0 \ . \tag{33.23}$$

Hence, the phase shift is

$$\eta_0 = -ka \ . \tag{33.24}$$

With this expression Eq. (33.22) reduces to

$$R_0(k, r) = \frac{c_0}{kr} \sin[k(r - a)] \ . \tag{33.25}$$

This expression is exact for any value of k, as announced above. The linear k dependence of η_0 simply expresses its definition in which the shift of the wave (by a) is compared to the de Broglie wavelength λ_{dB}, $\eta_0 = -2\pi a/\lambda_{dB}$. As a consequence the phase shift vanishes for $k \to 0$,

$$\lim_{k\to 0} \eta_0(k) = 0 \ . \tag{33.26}$$

This result is obvious when comparing the finite shift a to the diverging wavelength λ_{therm}. Interestingly, in the limit $k \to 0$ the expression (33.25) becomes k independent,

$$R_0(r) \underset{k\to 0}{\sim} 1 - \frac{a}{r} \qquad \text{for} \qquad a \le r \ll 1/k \ . \tag{33.27}$$

This important result is illustrated in Fig. 33.3. In the limit $k \to 0$ the wavefunction is essentially constant throughout space (up to a distance $1/k \to \infty$ at which it starts to oscillate), except for a small region of radius a around the potential center.

33.1.3 Spherical wells with a flat bottom

The second model potential to consider is the spherical well of range r_0 sketched in Fig. 33.4,

$$\tilde{V}(r) = \begin{cases} 2m_r V_0/\hbar^2 = \tilde{V}_0 = -\kappa_0^2 & \text{for } r \le r_0 \\ 0 & \text{for } r > r_0 \end{cases} \ . \tag{33.28}$$

Here $|U_0| = \kappa_0^2$ is called the well depth (κ_0 is chosen to be real and positive, $\kappa_0 > 0$). The energy of the continuum states is given by $\varepsilon = k^2$. In analogy, the energy of the bound states is written as,

$$\varepsilon_b = -\kappa^2 \ . \tag{33.29}$$

We now have to solve the radial wave equation (33.6) with the spherical well potential (33.28). Since the potential is constant inside the well ($r \leq r_0$) the wavefunction has to be free-particle like with the wave number given by,

$$K_+ = \sqrt{2m_r(E - V_0)/\hbar^2} = \sqrt{\kappa_0^2 + k^2} \ . \tag{33.30}$$

As the wavefunction has to be regular in the origin, inside the well it is given by,

$$R_\ell(r) = C_\ell j_\ell(K_+ r) \quad \text{for } r \leq r_0 \ , \tag{33.31}$$

where C_ℓ is a normalization constant. This expression holds for $E > V_0$ (both $E > 0$ and $E \leq 0$).

Outside the well ($r > r_0$) we have for $E > 0$ free atoms, $\tilde{V}(r) = 0$, with relative wavevector $k = [2m_r E/\hbar^2]^{1/2}$. Thus, for $r > r_0$ the general solution for the radial wave functions of angular momentum ℓ is given by the free atom expression (33.11),

$$R_\ell(k, r) = c_\ell[\cos\eta_\ell \ j_\ell(kr) + \sin\eta_\ell \ n_\ell(kr)] \quad \text{for } r > r_0 \ . \tag{33.32}$$

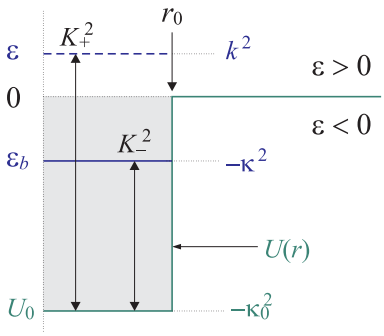

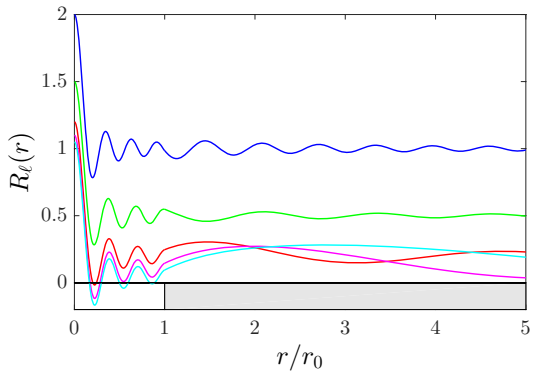

Figure 33.4: (code) (Left) Scheme of the flat bottom potential. (Right) (a) Radial wavefunctions for square wells: (a) continuum state ($\varepsilon = k^2 > 0$); (b) Zero energy state ($\varepsilon = k^2 = 0$) in the presence of an asymptotically bound level ($\varepsilon = -\kappa^2 = 0$); (c) bound state ($\varepsilon = -\kappa^2 < 0$). Note the continuity of $R_0(r)$ and $R_0'(r)$ at $r = r_0$. The wavefunctions are not normalized and are shifted relative to each other only for reasons of visibility.

The full solution [see Fig. 33.4(a)] is obtained by the continuity conditions for $R_\ell(r)$ and $R_\ell'(r)$ at the boundary $r = r_0$. These imply continuity of the logarithmic derivative with respect to r,

$$K_+ \frac{j_\ell'(\varrho_i)}{j_\ell(\varrho_i)} = \left.\frac{R_\ell'(r)}{R_\ell(r)}\right|_{r=r_0} = k \frac{\cos\eta_\ell \ j_\ell'(\varrho_e) + \sin\eta_\ell \ n_\ell'(\varrho_e)}{\cos\eta_\ell \ j_\ell(\varrho_e) + \sin\eta_\ell \ n_\ell(\varrho_e)} \ , \tag{33.33}$$

where we defined the abbreviations $\varrho_i \equiv K_+ r_0$ and $\varrho_e \equiv k r_0$. This ratio suffices to determine η_ℓ independently of the normalization constants C_ℓ and c_ℓ. Once the phase shift is known, the relation between C_ℓ and c_ℓ follows from the continuity condition for $R_\ell(r)$. Furthermore, it shows that the asymptotic phase shift η_ℓ can take any (real) value depending on the depth of the well. In view of the importance of the $\mathcal{S}$ matrix in scattering theory Sec. 33.2, it is advantageous to determine $e^{2i\eta_\ell}$ rather than η_ℓ itself. Expressing $\sin\eta_\ell$ and $\cos\eta_\ell$ in terms of $e^{i\eta_\ell}$ and $e^{-i\eta_\ell}$ Eq. (33.33) becomes,

$$K_+ \partial_\varrho \ln j_\ell(\varrho_i) = k \frac{e^{2i\eta_\ell} h_\ell^{(2)\prime}(\varrho_e) + h_\ell^{(1)\prime}(\varrho_e)}{e^{2i\eta_\ell} h_\ell^{(2)}(\varrho_e) + h_\ell^{(1)}(\varrho_e)} \ , \tag{33.34}$$

with the definition of the Hankel functions of the first and second kind: $h_\ell^{(1,2)} \equiv j_\ell \pm i n_\ell$. Solving for $e^{2i\eta_\ell}$ this leads to the following expression for the ℓ-wave contribution to the $\mathcal{S}$ matrix,

$$\boxed{e^{2i\eta_\ell} = -\frac{h_\ell^{(1)}(\varrho_e)}{h_\ell^{(2)}(\varrho_e)} \frac{K_+ \partial_\varrho \ln j_\ell(\varrho_i) - k \partial_\varrho \ln h_\ell^{(1)}(\varrho_e)}{K_+ \partial_\varrho \ln j_\ell(\varrho_i) - k \partial_\varrho \ln h_\ell^{(2)}(\varrho_e)}} \ , \tag{33.35}$$

where the expression $\partial_\varrho \ln$ stands for the logarithmic derivative. This expression may look a bit heavy, but is valuable as it represents the exact result for arbitrary ℓ. In Exc. 33.1.5.2 we simplify this formula for $\ell = 0$. As the formula (33.35) lacks transparency from the physical point of view, we analyze in the coming sections the case $\ell = 0$ directly discussing the radial wavefunctions u_ℓ.

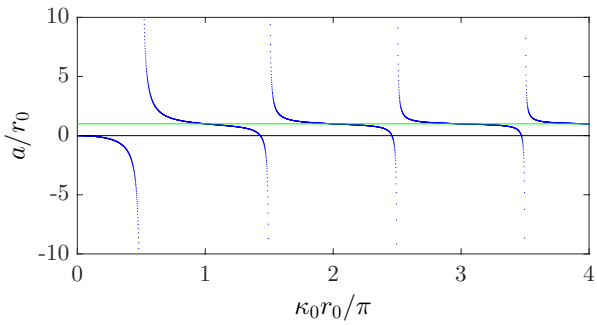

Figure 33.5: (code) The s-wave scattering length a normalized on r_0 as a function of the depth of a spherical square potential well (blue curve). Note that, typically, $a \simeq r_0$ (green line), except near the resonances at $\kappa_0 r_0 = (n + \frac{1}{2})\pi$ being an integer.

33.1.3.1 s-wave scattering ($E > 0$)

The analysis of spherical well potentials becomes particularly simple for the case $\ell = 0$. Let us first consider the case $E > 0$, for which the radial wave equation can be written as a 1D-Schrödinger equation (33.7) of the form,

$$u_0'' + [k^2 - \tilde{V}(r)] u_0 = 0 \ . \tag{33.36}$$

The solution is,

$$u_0(kr) = \begin{cases} C_0 \sin(K_+ r) & \text{for } r \leq r_0 \\ c_0 \sin(kr + \eta_0) & \text{for } r > r_0 \end{cases} . \tag{33.37}$$

To determine $\eta_0(k)$ it is sufficient to apply the boundary condition for continuity of the logarithmic derivative at the edge of the well,

$$\left.\frac{u_0'}{u_0}\right|_{r=r_0} = K_+ \cot K_+ r_0 = k \cot(kr_0 + \eta_0) . \tag{33.38}$$

Note that this expression coincides with the general result given by Eq. (33.33) for the case $\ell = 0$; i.e. the boundary condition of continuity for u_0'/u_0 coincides with that for R_0'/R_0, as we know from a calculation left to Exc. 33.1.5.3. Furthermore, for a vanishing potential ($\kappa_0 \to 0$) we have $K_+ \to k$ and the boundary condition properly yields a zero phase shift ($\eta_0 = 0$).

At this point we introduce the effective hard-sphere diameter $a(k)$ to describe, in analogy with Eq. (33.24), the behavior of the phase shift,

$$\eta_0(k) \equiv -ka(k) . \tag{33.39}$$

By this procedure we extract the linear k dependence as well as the negative sign from the phase shift. This is a good idea because the linear k-dependence does not arise from the potential but simply from the definition of the phase in which, as discussed earlier, the shift of the wave is compared to the de Broglie wavelength. In the limit $k \to 0$, we have $K_+ r_0 \to \kappa_0 r_0$ and with the definition,

$$a \equiv \lim_{k\to 0} a(k) = -\lim_{k\to 0} \eta(k)/k \tag{33.40}$$

the boundary condition (33.38) becomes,

$$\left.\frac{u_0'}{u_0}\right|_{r=r_0} = \kappa_0 \cot \kappa r_0 = \frac{1}{r_0 - a} . \tag{33.41}$$

Solving for a we find,

$$a = r_0 \left(1 - \frac{\tan\gamma}{\gamma}\right) , \tag{33.42}$$

where the dimensionless positive quantity,

$$\gamma \equiv \kappa_0 r_0 \tag{33.43}$$

is called the well parameter. As shown in Fig. 33.5, the value of a can be positive, negative or zero depending on the value of γ. Therefore, rather than using the pictorial term effective hard-sphere diameter the name scattering length is used for a. Next to the range, the scattering length represents the second characteristic length that can be associated with the interaction potential. As the name suggest, it is a measure for the scattering behavior of atoms, and we elaborate on this in Sec. 33.2. Also, in Sec. ?? we will show that a is also a measure for the effective strength of the interaction.

Fig. 33.5 and Eq. (33.42) show that a is typically a quantity of the size of r_0, although for $\gamma = \tan\gamma$ it is zero and for $\gamma = (\nu + \frac{1}{2})\pi$, with ν being an integer,

it diverges. The latter condition points to a resonance phenomenon occurring when (with increasing γ) a new bound level enters the potential well. For the square well potential the scattering length is mostly positive; it is negative in the regions with $\gamma < \tan\gamma$, which become narrower for increasing γ. This unlikely occurrence of negative a is atypical for the general case; e.g. for Van der Waals potentials the probability to find a negative scattering length is 25% .

For $r \geq r_0$ the radial wavefunction corresponding to Eq. (33.37) is of the form,

$$R_0(k,r) = \frac{c_0}{kr}\sin[kr - ka(k)] \ . \tag{33.44}$$

Recalling the definitions (33.39) and (33.40) we find that for $k \to 0$ this radial wavefunction becomes k-independent,

$$R_0(r) \underset{k\to 0}{\sim} 1 - \frac{a}{r} \qquad \text{for} \qquad r_0 < r \ll \frac{1}{k} \ . \tag{33.45}$$

The latter two expressions for the radial wavefunction have the same formal appearance as the hard sphere results (33.25) and (33.27). However, whereas the diameter of the hard-sphere has a fixed value, the scattering length for the well depends on γ. As shown in Fig. 33.6, for positive scattering length the s-wave has a characteristic node at $r = a$; for negative scattering length this becomes a virtual node.

Importantly, because Eq. (33.45) reaches the asymptotic value 1 only for distances $r \gg a$, the use of this equation in the modeling of dilute gases is only justified if a is much smaller than the interparticle spacing,

$$na^3 \ll 1 \ . \tag{33.46}$$

Otherwise, the interaction with neighboring atoms will distort the relative motion of the colliding pair. This violates the binary scattering approximation on which Eq. (33.45) is based. The dimensionless quantity na^3 is called the gas parameter. When its value is small, the gas is called nearly ideal or weakly interacting [2].

33.1.3.2 Bound s-levels ($E \leq 0$)

Let us turn to the case $E \leq 0$. We shall show that the divergences of the scattering length obtained by analyzing the continuum states ($E > 0$) result from the appearance of the next bound s-level when increasing the well parameter. The 1D Schrödinger equation takes the form,

$$u_0'' + [-\kappa^2 - \tilde{V}(r)]u_0(r) = 0 \ . \tag{33.47}$$

where $\varepsilon = -\kappa^2$ is the discrete energy eigenvalue of a bound state with $\ell = 0$. The solutions are of the type (see Fig. 33.30),

$$u_0(k,r) = \begin{cases} C_0 \sin K_- r & \text{for } r \leq r_0 \\ c_0 e^{-\kappa r} & \text{for } r \leq r_0 \end{cases} \tag{33.48}$$

[2] Note that weakly interacting does not mean that that the potential is 'shallow'. Any gas can be made weakly interacting by making the density sufficiently small.

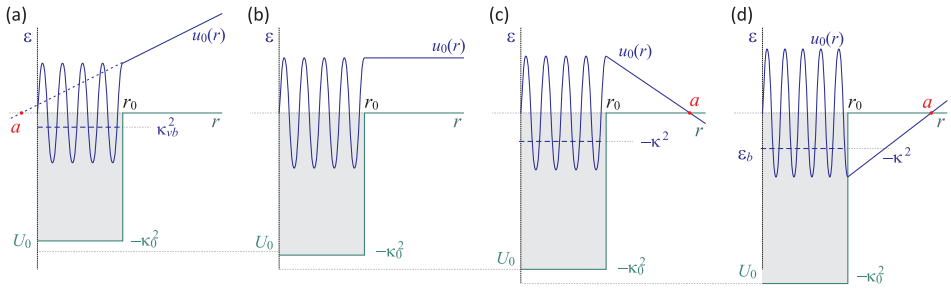

Figure 33.6: Reduced radial wavefunctions $u_0(r)$ for continuum states ($\varepsilon > 0$) in the $k \to 0$ limit for increasing well depth near the threshold value $\kappa_0 r_0 = (n + \frac{1}{2})\pi$: (a) presence of an almost bound state ($a < 0$); (b) presence of zero-energy resonance ($\kappa_{vb} = 0$, $a \to \pm\infty$); (c) presence of a weakly bound state ($a > 0$); (d) deeper binding of the least bound state. For $r > r_0$ the wavefunction is given by $u_0(r) = c_0(r - a)$; hence, the value of a is given by the intercept with the horizontal axis. This gives rise to a characteristic node at $r = a$, which is *real* for $a > 0$ (just as for hard spheres of diameter a), but *virtual* for $a < 0$. The wavefunctions are not normalized.

where $\kappa > 0$ because the bound state wavefunction has to be normalized. The bound state energy is obtained by requiring the continuity of the logarithmic derivative when connecting the inner part of the wavefunction to the outer part,

$$\left.\frac{u_0'(r)}{u_0(r)}\right|_{r=r_0} = K_- \cot K_- r_0 = -\kappa \ , \tag{33.49}$$

where $\kappa > 0$ and

$$K_- = [2m_r(E - V_0)/\hbar^2]^{1/2} = (\kappa_0^2 - \kappa^2)^{1/2} \ . \tag{33.50}$$

With decreasing γ, the least bound level disappears in the limit $\kappa \to 0$, $K_- \to \kappa_0$. In this limit Eq. (33.49) reduces to,

$$\left.\frac{u_0'(r)}{u_0(r)}\right|_{r=r_0} = \kappa_0 \cot \kappa_0 r_0 \underset{\kappa\to 0}{=} 0 \ , \tag{33.51}$$

Increasing from zero the vibrational levels appear sequentially for

$$\gamma = (v + \tfrac{1}{2})\pi \ , \tag{33.52}$$

where $v = 0, 1, .., r_{max}$ is the vibrational quantum number. This shows that a minimum well parameter ($\gamma = \pi/2$) is required to bind the first state [3]. For the least-bound level, v_{max}, we have,

$$(v_{max} + \tfrac{1}{2})\pi = \text{Int } (\tfrac{\gamma}{\pi} - \tfrac{1}{2}) \tag{33.53}$$

and the total number of bound s levels follows with,

$$N_b = v_{max} + 1 = \text{Int } (\tfrac{\gamma}{\pi} + \tfrac{1}{2}) \ . \tag{33.54}$$

[3]This conclusion cannot be extended to lower dimensions; in two dimensions bound states appear for arbitrarily shallow potentials.

The relation between κ and v for a given vibrational level depends on the ratio κ/K_- and is given by

$$\cot K_- r_0 = -\frac{\kappa}{K_-} \ . \tag{33.55}$$

Note that this relation corresponds to $K_- r_0 \simeq (v_{max} + \frac{1}{2})\pi$ for the least-bound state

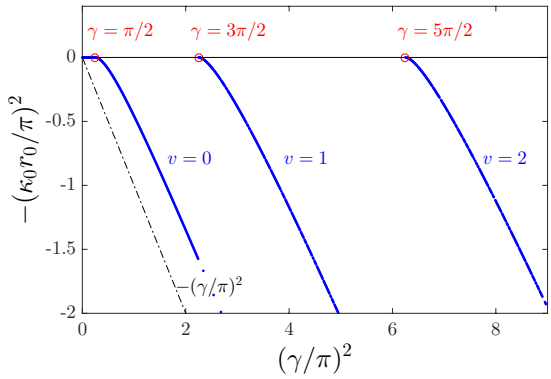

Figure 33.7: (code) Appearance and increase of binding of the first three bound levels for increasing well depth. The quadratic dependence near threshold is universal (i.e. independent of the well shape). The full crossover curve is obtained by numerical solution of Eq. (33.49) and corresponds to a $\pi/2$ phase shift of $K_+ r_0$ near threshold. The dashed line shows the increase in well depth.

$(\kappa/K- \ll 1)$ and to $K_- r_0 \simeq (v_{max} + 1)\pi$ for deeply bound levels $(K_-/\kappa \ll 1)$, as is illustrated in Fig. 33.8(a).

33.1.3.3 Weakly bound s-level: halo states

For weakly bound s levels $(0 < \kappa r_0 \ll 1)$ we have $K_- \to \kappa_0$ and Eq. (33.49) may be approximated by

$$\left.\frac{u_0'(r)}{u_0(r)}\right|_{r=r_0} = \kappa_0 \cot \kappa_0 r_0 = -\kappa \ , \tag{33.56}$$

Furthermore, we recall that in the presence of a weakly bound s-level the scattering length is large and positive, $a \gg r_0$. From Eq. (33.41) we recall that for $k \to 0$ the logarithmic derivative also satisfies the relation

$$\left.\frac{u_0'(r)}{u_0(r)}\right|_{r=r_0} = \kappa_0 \cot \kappa_0 r_0 = \frac{1}{r_0 - a} \simeq -\frac{1}{a} \ , \tag{33.57}$$

Interestingly, for $a \gg r_0$ the logarithmic derivative of the continuum states becomes independent of r_0 and κ_0; i.e. it becomes independent of the shape of the potential well. As we shall see it only depends on the well parameter γ and not on the well shape. This points to a universal limiting shape of the wavefunction for large scattering length. As is sketched in Fig. 33.8(b), for decreasing κ the least-bound state turns into a halo state; i.e. for $\kappa r_0 \ll 1$ most of the probability of the bound state is found in the classically inaccessible region outside the potential well, thus surrounding the

potential center like a halo. This behavior holds for arbitrary short-range potentials.

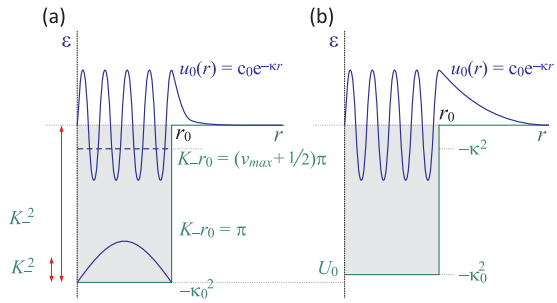

Figure 33.8: Bound states oscillate inside the well and decay exponentially outside the well: (a) the boundary condition depends on the ratio κ/K_-; (b) a slight reduction of the well depth can turn the least bound state into a halo state.

With Eqs. (33.56) and (33.57) we have obtained two expressions for $\kappa_0 \cot \kappa_0 r_0$ and arrive at the conclusion that in the presence of a weakly bound state the scattering length is given by,

$$a \underset{\kappa \to 0}{\simeq} 1/\kappa \ . \tag{33.58}$$

This expression reveals the tight relation between the binding energy of the least-bound state, given by Eq. (33.29), and the scattering length,

$$\boxed{E_b = -\frac{\hbar^2 \kappa^2}{2m_r} \underset{\kappa \to 0}{\longrightarrow} -\frac{\hbar^2}{2m_r a^2}} \ . \tag{33.59}$$

33.1.3.4 *s*-wave resonances in the continuum: The Breit-Wigner formula

To obtain the k-dependence of the phase shift for large but otherwise arbitrary well parameter ($\gamma \gg 1$) we rewrite the boundary condition (33.38) in the form,

$$\eta_0(k) = -kr_0 + \arctan \frac{kr_0}{K_+ r_0 \cot K_+ r_0} \equiv \eta_{bg} + \eta_{res} \ . \tag{33.60}$$

The first term of (33.60) is called the *background contribution* to the phase shift and the second term the *s*-wave *resonance contribution*. Note that the background contribution shows the same phase development as we found in Sec. 33.1.2 for hard spheres. The phase development of the resonance contribution is shown in Fig. 33.9(a) for the case of a large well parameter slightly detuned from the threshold value (at $\gamma = 31.5\pi \approx 98.960169$) such that the scattering length is negative ($\Delta_\gamma = -0.5$). For potentials with $\gamma \gg 1$ the argument of the arctangent is predominantly small, $kr_0/|K_+ r_0 \cot K_+ r_0| \ll 1$, because

$$K_+ r_0 = \kappa_0 r_0 (1 + k^2/\kappa_0^2)^{1/2} > \gamma \gg 1 \ . \tag{33.61}$$

However, the argument of the arctangent diverges when $\cot K_+ r_0$ passes through zero; i.e. for

$$K_+ r_0 = (\tilde{v} + \tfrac{1}{2})\pi \ , \tag{33.62}$$

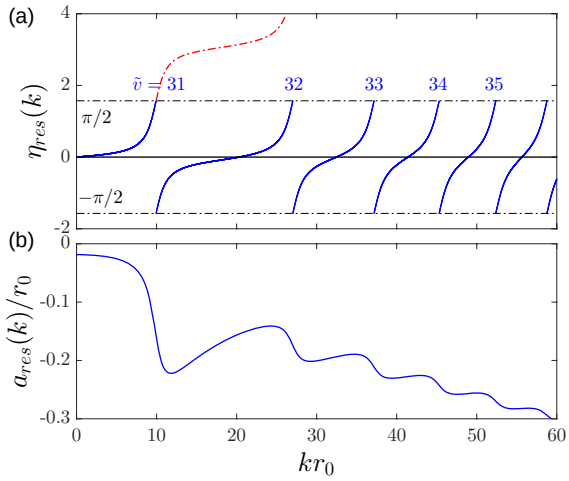

Figure 33.9: (code) (a) Resonance contribution to the s-wave phase shift $\eta_0(k)$ for a large well parameter slightly detuned from the threshold value (at $\gamma = 31.5\pi$), such that the scattering length is negative ($\Delta\gamma = -0.5$): The linear shift of the background contribution is not included in the plot. Note that the π phase jumps arise from the modulo-π representation of the arctangent and do not represent an observable phenomenon; the physical phase increases monotonically and equals $\eta_{res} = \frac{1}{2}$ (modulo π) at the center of the resonances; (b) contribution of the resonances to the effective hard sphere diameter $a(k) = -\eta_0(k)/k$. As (in this example) the lowest resonance is not close to threshold the resonant enhancement is small, $|a_{res}(k)| = r_0 \ll 1$.

where $\tilde{v}$ is an integer called the resonance index. This divergence is observed as a small resonant enhancement of $a(k)$, as shown in Fig. 33.9(b). The physical phase is a continuous function of k, which changes by π when sweeping across the resonance. Because the arctangent remains finite for $\cot K_+ r_0 = 0$ also the resonant phase shift remains finite, having the value $\eta_{res}(k) = \frac{1}{2}\pi$ (modulo π) at the center of each resonance.

In the remainder of this section we shall analyze the width and separation of the s-wave resonances for the case $\gamma \gg 1$. Since $K_+ \geq \kappa_0 \geq K_-$, we have,

$$\tilde{v} \geq \tfrac{\gamma}{\pi} - \tfrac{1}{2} \geq v_{max} \ , \tag{33.63}$$

which shows that for $\gamma \gg 1$ the value of $\tilde{v}$ is large ($\tilde{v}_{min} \geq \tilde{v}_{max} \gg 1$). Hence, the resonance numbering starts where the numbering of bound states ends. To discuss the resonances we denote the wavevectors k and K_+ at resonance by k_{res} and $K_{res} \equiv \sqrt{\kappa_0^2 + k_{res}^2}$, respectively. The resonance energies $\varepsilon_{res} = k_{res}^2$ satisfy the condition,

$$\varepsilon_{res} = K_{res}^2 - \kappa_0^2 = (\tilde{v} + \tfrac{1}{2})\pi(\tfrac{\pi}{r_0})^2 - \kappa_0^2 \geq 0 \ . \tag{33.64}$$

The exceptional case for which the equal sign applies ($\tilde{v} = v_{max}$) corresponds to a resonant bound state ($\kappa = 0$) and the resonance is called a resonance at threshold or zero-energy resonance ($k_{res} = 0$).

Let us first analyze s-wave resonances for large well parameters ($\tilde{v} = v_{max}$) and far from threshold, ($\kappa = 0$). The energy spacing between two subsequent resonances

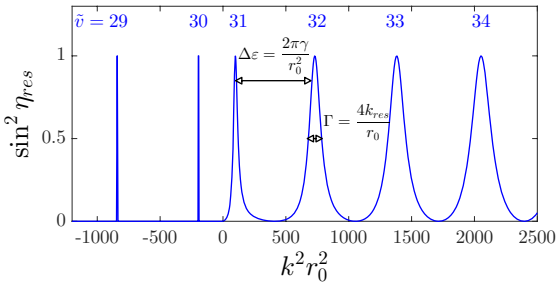

Figure 33.10: (code) (a) Transition from bound states to Breit-Wigner s-wave resonances plotted for $\Delta\gamma = -0.5$ with respect to the threshold at $\gamma = 31.5\pi$ (same conditions as Fig. 33.9). The bound states are indicated as zero-width spikes at energies $\varepsilon = -\kappa^2$, with κ following from Eq. (33.49). For $\varepsilon > 0$ the plot is based on Eqs. (33.60). The width of the resonances increases with the square root of the energy. Note that the band of energies typical for the quantum gases ($kr_0 \ll 1$) corresponds to a narrow zone, unresolved on the energy scale of the plot.

is,

$$\Delta\varepsilon_{res} = \varepsilon_{res}^{(\tilde{v}+1)} - \varepsilon_{res}^{(\tilde{v})} = 2(\tilde{v}+1)\tfrac{\pi^2}{r_0^2} \simeq \tfrac{2\pi\gamma}{r_0^2} \ . \tag{33.65}$$

To analyze a given resonance we expand $K_+ \cot K_+ r_0$ about the point of zero crossing. For this purpose we introduce the notation,

$$K_+ = \sqrt{\kappa_0^2 + (k_{res}+\delta k)^2} = K_{res} + \frac{\delta k\ k_{res}}{K_{res}} \ , \tag{33.66}$$

where $\delta k = k - k_{res}$ is called the detuning from resonance. Thus, restricting ourselves to the low-energy (but not zero energy) s-wave resonances ($1 < k_{res}r_0 \ll K_{res}r_0 \simeq \gamma$), we may approximate $K_+ \cot K_+ r_0 \simeq K_{res} \cot K_+ r_0$. Expanding $\cot K_+ r_0$ about the zero crossing at $K_+ r_0 = (\tilde{v}+1/2)\pi$ and retaining only the linear term we obtain (see Problem 3.4),

$$K_{res} \cot K_+ r_0 = -\delta k\ k_{res} r_0 \ . \tag{33.67}$$

Hence, the diverging argument of the arctangent becomes,

$$\tan\eta_{res} = \frac{k}{K_+ \cot K_+ r_0} \simeq -\frac{1}{\delta k\ r_0} = \frac{-(k+k_{res})}{(k^2-k_{res}^2)r_0} \simeq \frac{-2k_{res}/r_0}{\varepsilon-\varepsilon_0} \ . \tag{33.68}$$

The expansion (33.66) is valid over the full range of the resonant change in phase provided the following condition holds,

$$\delta k\ r_0 \ll \frac{K_{res}}{k_{res}} \simeq \tfrac{\gamma}{k_{res}r_0} \ , \tag{33.69}$$

which is satisfied for the lowest resonances as long as the well parameter is sufficiently large ($\gamma \gg k_{res}r_0$). As long as $\delta k \ll k_{res}$ we may further approximate $k \simeq k_{res}$. With these approximations and after restoring the dimensions, Eq. (33.68) can be written as a function of the energy $E = \hbar^2 2k^2/2m_r$,

$$\tan\eta_{res} = \frac{k}{K_+ \cot K_+ r_0} \simeq \frac{-\Gamma^2}{\varepsilon-\varepsilon_{res}} \ , \tag{33.70}$$

where

$$\Gamma/2 = 2k_{res}/r_0 \tag{33.71}$$

is called the spectral width of the resonance. Comparing the expressions for Γ and ΔE_{res} we find that for given r_0 the width Γ is independent of γ, whereas the resonance spacing is proportional to γ . Thus, only for sufficiently large well parameters ($\gamma \gg 1$) the spectral width becomes smaller than the resonance spacing,

$$\Gamma \ll \Delta\varepsilon_{res} \Longleftrightarrow k_{res} r_0 \ll \pi\gamma \ . \tag{33.72}$$

Knowing the tangent of η_{res}, we readily obtain the sine and Eq. (33.70) is replaced by the *Breit-Wigner formula*,

$$\sin^2 \eta_{res} = \frac{(\Gamma/2)^2}{(\varepsilon - \varepsilon_0)^2 + (\Gamma/2)^2} \ . \tag{33.73}$$

For optical resonances this energy dependence is known as the Lorentz lineshape. Note that Γ corresponds to the full-width-at-half-maximum (FWHM) of this line shape. The lowest energy resonances are plotted in Fig. 33.10 along with the highest-energy bound states.

The resonance near threshold (almost bound level) deserves special attention, as this type of resonance is the only one that can play an important role within the band of energies relevant for the quantum gases ($kr_0 \ll 1$). Fig. 33.10 shows that near the threshold (at $\gamma = 31.5\pi$) the resonance narrows down and becomes asymmetric, which means that the Breit-Wigner lineshape is lost. Using Eq. (33.54) we calculate $\tilde{v} = 31$. The narrow line is reminiscent of a bound level but the scattering length is negative (see Fig. 33.10). Under these conditions the wavefunction has a virtual node at $r = -|a|$ (see Fig. 33.30). Accordingly, the level is called a virtual level and the wavefunction is said to represent a virtual bound state. In analogy with the bound states its energy is written as $\varepsilon = \kappa_{res}^2$, where κ is to be defined later.

33.1.4 Other types of potentials

33.1.4.1 Zero-range potentials

An important model potential is obtained by considering a spherical well in the zero-range limit $r_0 \to 0$. As illustrated in Fig.33.11, it is possible to construct a zero-range well in such a way that the long-range properties of the wavefunction are unaffected; i.e. the scattering length a and the binding energy $\varepsilon = -\kappa^2$ of the least-bound state remain unchanged.

For $E < 0$ this can be demonstrated with the aid of the boundary condition (33.49),

$$-\kappa = K_- \cot K_- r_0 \ . \tag{33.74}$$

Reducing the radius r_0 the value of the binding energy $\varepsilon = -\kappa^2$, can be conserved by increasing κ_0. In the limit $r_0 \to 0$ the well depth should diverge in accordance with,

$$-\frac{\kappa}{K_-} = \cot K_- r_0 \to 0 \ . \tag{33.75}$$

This condition is satisfied for $K_- r_0 \simeq \pi/2$. To elucidate this point we consider the least-bound level with vibrational quantum number $v = v_{max}$, for which $K_- r_0 =$

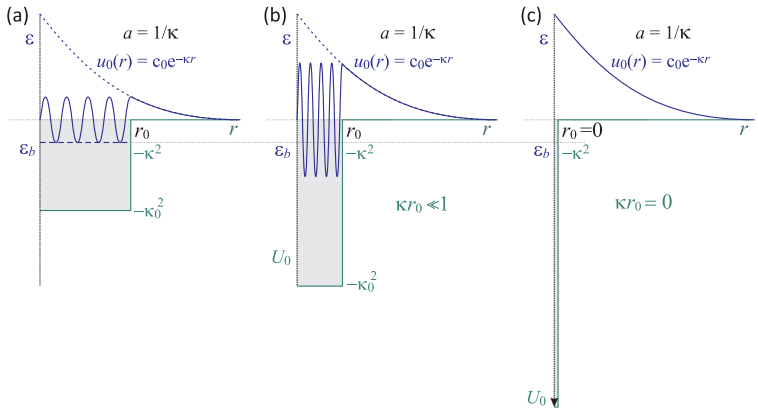

Figure 33.11: Wavefunctions corresponding to the same binding energy ($\varepsilon = -\kappa^2$) plotted for three different values of r_0. Outside r_0 the wavefunctions fall off exponentially, always with the same decay exponent κ; this is the essence of the Bethe-Peierls boundary condition. The dashed lines show the extrapolation for $r \to 0$. (a) reference case; (b) for $\kappa r_0 \ll 1$ most of the probability density of a bound state is found outside the well (halo state); (c) for zero-range potentials ($\kappa r_0 = 0$) the oscillating part of the wavefunction is compressed into a delta function and only the decaying exponent remains (universal limit). Note that these wavefunctions do not share the same normalization.

$(v_{max} + 1/2)\pi$. Reducing r_0 by a factor of 2 the wavenumber K_- has to be doubled to conserve the number of nodes in the wavefunction (i.e. to conserve v_{max}). This means that the kinetic energy inside the well has to increases by a factor 4. Since for the least-bound level we have $K_- r_0 \simeq \gamma$, it means that in this case the binding energy can be conserved at effectively constant well parameter. Obviously, the freedom to conserve (for decreasing r_0) the binding energy of one of the levels can only be used once. It does not hold for the other levels because the level separation diverges with κ_0. In the zero range limit the potential only supports a single bound state and the wavefunction of that state is given by,

$$R_0(r) = c_0 \frac{e^{-\kappa r}}{r} \qquad \text{for} \qquad r > 0 \ , \tag{33.76}$$

and with $\kappa > 0$. Unit normalization, $\int r^2 R_0^2(r) dr = 1$, is obtained for $c_0 = \sqrt{2\kappa}$. For $E > 0$ we can arrive at the same conclusion. The boundary condition for $k \to 0$ and given value of r_0 is given by Eq. (33.41), which we write in the form,

$$\frac{1}{r_0 - a} = \kappa_0 \cot \kappa_0 r_0 \ . \tag{33.77}$$

Reducing the radius r_0, the scattering length a can be conserved by increasing κ_0. In the limit $r_0 \to 0$ the well depth should diverge in accordance with,

$$-\frac{1}{\kappa_0 a} = \cot \kappa_0 r_0 \to 0 \ . \tag{33.78}$$

This is again satisfied for $\kappa_0 r_0 \simeq \pi/2$. In the zero-range limit the radial wavefunction

for $k \to 0$ is given by,

$$R_0(k,r) = \frac{1}{kr}\sin[k(r-a)] \qquad \text{for} \qquad r > 0 \ , \tag{33.79}$$

which implies $R_0(k,r) \simeq 1 - a/r$ for $0 < r \ll 1/k$.

33.1.4.2 Bethe-Peierls boundary condition

Note that Eq. (33.76) is the solution for $E < 0$ of the 1D-Schrödinger equation in the zero-range approximation,

$$u_0'' - \kappa^2 u_0 \qquad \text{for} \qquad r > 0 \ , \tag{33.80}$$

under the boundary condition,

$$\left.\frac{u_0'}{u_0}\right|_{r\to 0} = -\kappa \ . \tag{33.81}$$

The latter relation is called the *Bethe-Peierls boundary condition* and was first used to describe the deuteron, the weakly bound state of a proton with a neutron [**?**]. It shows that for weakly bound states the wavefunction has the universal form of a halo state, which only depends on the binding energy, $\varepsilon_0 = -\kappa^2$ (see Fig. 33.11).

For $E > 0$ the 1D-Schrödinger equation in the zero-range approximation is given by,

$$u_0' + k^2 u_0 = 0 \qquad \text{for} \qquad r > 0 \ . \tag{33.82}$$

The general solution is $u_0(k,r) = c_0 \sin[kr + \eta_0]$. Using the Bethe-Peierls boundary condition we obtain,

$$k \cot \eta_0(k) = -\kappa \ , \tag{33.83}$$

which yields after substituting $\eta_0(k \to 0) \simeq -ka$ the universal relation between the scattering length and the binding energy in the presence of a weakly bound s-level, $\varepsilon_0 = -\kappa^2 = -1/a^2$.

33.1.4.3 Power-law potentials

The general results obtained in the previous sections presumed the existence of a finite range of interaction, r_0. Thus far this presumption was based only on the heuristic argument presented in Sec. **??**. To derive a proper criterion for the existence of a finite range and to determine its value r_0 we have to analyze the asymptotic behavior of the interatomic interaction [929]. For this purpose we consider potentials of the power-law type,

$$V(r) = -\frac{C_s}{r^s} \ , \tag{33.84}$$

where $C_s = V_0 r_c^s$ is the power-law coefficient, with $V_0 \equiv |V(r_c)| \equiv \hbar^2\kappa_c^2/2m_r$ the well depth. These power-law potentials are important from the general physics point of view, because they capture major features of interparticle interactions.

For power-law potentials, the radial wave equation (33.6) takes the form,

$$R_\ell'' + \frac{2}{r}R_\ell' + \left[k^2 + \frac{\kappa_c^2 r_c^s}{r^s} - \frac{\ell(\ell+1)}{r^2}\right] = 0 \ . \tag{33.85}$$

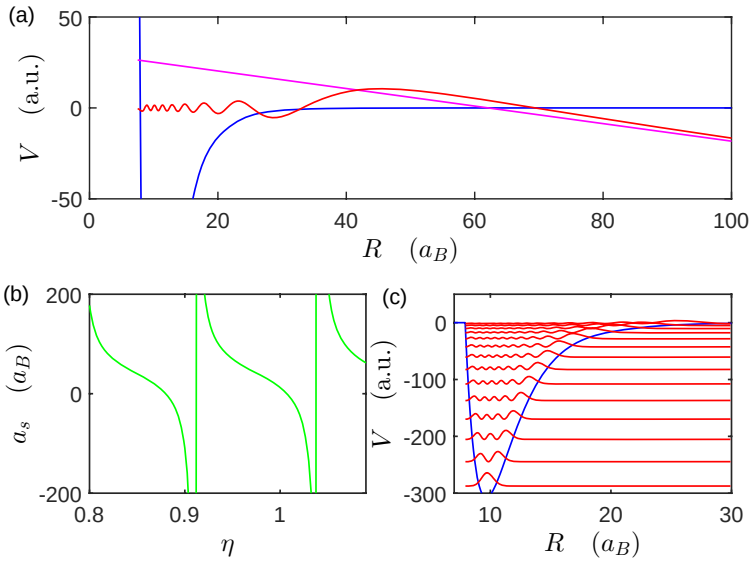

Figure 33.12: (code) Dependence of the scattering length on the potential depth.

Because this equation can be solved analytically in the limit $k \to 0$ it is ideally suited to analyze the conditions under which the potential $V(r)$ may be neglected and thus to determine r_0. To solve Eq. (33.85) we look for a clever substitution of the variable r and the function $R_\ell(r)$ to optimally exploit the known r dependence of the potential in order to bring the differential equation in a well-known form. To leave exibility in the transformation we search for functions of the type,

$$G_\ell(x) = r^{-\nu} R_\ell(r) \ , \tag{33.86}$$

where the power ν is to be selected in a later stage.

33.1.4.4 Computation of the scattering length

The scattering length depends on the *binding energy* E_v of weakly bound states. If a is positive and much greater than the range of the potential, then [542, 465] (33.59),

$$E_v = -\frac{\hbar^2}{2m_r a^2} \ . \tag{33.87}$$

More precisely, for a potential behaving at long range as,

$$V = -\frac{C_6}{R^6} \ , \tag{33.88}$$

we get,

$$E_v = -[(v_D - v)H(m_r, C_6)]^{-1/3} \ , \tag{33.89}$$

where v_D is the vibrational quantum number at the dissociation limit and H a constant. Also,

$$a = \frac{\Gamma(3/4)}{2\sqrt{2}\Gamma(5/4)} \left(\frac{2\mu C_6}{\hbar^2}\right)^{1/4} \left[1 - \tan \pi(v_D + \tfrac{1}{2})\right] \ . \tag{33.90}$$

33.1.4.5 Second method

It yields for $\gamma = \alpha, \beta$,

$$\tfrac{d^2}{dR^2}\varepsilon_\gamma(R) = 2m_r V(R)\varepsilon_\gamma(R) \ . \tag{33.91}$$

Successive approaches start with $\varepsilon_\alpha^{(0)} = R$ and $\varepsilon_\beta^{(0)} = 1$ and get superior orders via,

$$\tfrac{d^2}{dR^2}\varepsilon_\gamma^{(k+1)}(R) = 2m_r V(R)\varepsilon_\gamma^{(k)}(R) \ . \tag{33.92}$$

We define $\delta_\gamma^{(k)} \equiv \varepsilon_\gamma^{(k)} - \varepsilon_\gamma^{(k-1)}$ starting with $\delta_\gamma^{(0)} = \varepsilon_\gamma^{(0)}$, such that,

$$\tfrac{d^2}{dR^2}\delta_\gamma^{(k+1)}(R) = 2m_r V(R)\delta_\gamma^{(k)}(R) \ . \tag{33.93}$$

$\delta_\alpha(R \to \infty) = \delta_\beta(R \to \infty) = 0$. Since $\varepsilon_\alpha = \lim_{k\to\infty} \varepsilon_\alpha^{(k)}$, the wavefunction is thus obtained from,

$$U(R) = \alpha(1 + \delta_\alpha^{(1)} + \delta_\alpha^{(2)} + ..) + \beta(R + \delta_\beta^{(1)} + \delta_\beta^{(2)} + ..) \ . \tag{33.94}$$

This long-range expression must match the short-range value at a certain point R_0:

$$\begin{aligned} U(R_0) &= \alpha\varepsilon_\alpha(R_0) + \beta\varepsilon_\beta(R_0) \ . \\ U'(R_0) &= \alpha\tfrac{d}{dR}\varepsilon_\alpha(R_0) + \beta\tfrac{d}{dR}\varepsilon_\beta(R_0) \end{aligned} \tag{33.95}$$

and

$$a = -\frac{\beta}{\alpha} = \frac{U(R_0)\frac{d}{dR}\varepsilon_\alpha(R_0) - U'(R)\varepsilon_\alpha(R_0)}{U(R_0)\frac{d}{dR}\varepsilon_\beta(R_0) - U'(R)\varepsilon_\beta(R_0)} = \frac{\frac{d}{dR}\frac{\varepsilon_\alpha(R_0)}{U(R_0)}}{\frac{d}{dR}\frac{\varepsilon_\beta(R_0)}{U(R_0)}} \ . \tag{33.96}$$

Let us consider a specific potential,

$$\begin{aligned} V(R) &= \frac{1}{2}BR^{m_r}e^{-\eta R} - \left(\frac{C_6}{R^6} + \frac{C_8}{R^8} + \frac{C_{10}}{R^{10}}\right) f_c(R) \\ f_c(R) &= \theta(R_c - R)e^{-(R_c/R-1)^2} + \theta(R - R_c) \ . \end{aligned} \tag{33.97}$$

At very long range we have $V(R) \simeq -\frac{C_6}{R^6}$, such that,

$$\begin{aligned} \delta_\gamma^{(k+1)} &= \int_0^R 2m_r V\delta_\gamma^{(k+1)}dR = \delta_\gamma^{(k)}(\infty) - \int_R^\infty -\frac{2m_r C_6}{R^6}\delta_\gamma^{(k)}dR \\ &= 2m_r C_6 \int_R^\infty \frac{\delta_\gamma^{(k)}}{R^6}dR \ . \end{aligned} \tag{33.98}$$

In particular,

$$\begin{aligned} \delta_\alpha^{(1)} &= 2m_r C_6 \frac{-1}{4R^4} \quad , \quad \delta_\alpha^{(2)} = (2m_r C_6)^2 \frac{-1}{4\cdot 9R^9} \\ \delta_\beta^{(1)} &= 2m_r C_6 \frac{1}{5R^5} \quad , \quad \delta_\beta^{(2)} = (2m_r C_6)^2 \frac{1}{5\cdot 10R^{10}} \ . \end{aligned} \tag{33.99}$$

33.1.4.6 Third method

To estimate the scattering length for a particular interaction consult [844, **?**, 989]. Following [844] we write the Schrödinger equation in atomic units as,

$$\frac{d^2U}{dR^2} = 2m_r V(R)U(R) \ . \tag{33.100}$$

The ansatz $U(R) = \alpha\varepsilon_\alpha(R) + \beta\varepsilon_\beta(R)$ with $\varepsilon_\alpha(R \to \infty) = R$ and $\varepsilon_\beta(R \to \infty) = 1$ shows that $a = -\beta/\alpha$ is the desired scattering length.

33.1.4.7 Fourth method

The equation for the accumulated phase follows from the Schrödinger equation,

$$\begin{aligned} \phi(r_0) &\equiv \int_\infty^{r_0} k(r)dr \\ k^2(r) &= \frac{2m_r}{\hbar^2}\sqrt{E - V(r) - \frac{\hbar^2 l(l+1)}{2m_r r^2}} \ . \end{aligned} \tag{33.101}$$

According to [989] we start resolving,

$$\frac{d}{dR}\delta_{k,0}(R) = -k^{-1}V(R)\sin^2[kR + \delta_{k,0}(R)] \ . \tag{33.102}$$

33.1.4.8 Pseudo potentials

As in the low-energy limit ($k \to 0$) the scattering properties only depend on the asymptotic phase shift it is a good idea to search for the simplest mathematical form that generates this asymptotic behavior. The situation is similar to the case of electrostatics, where a spherically symmetric charge distribution generates the same far field as a properly chosen point charge in its center. Not surprisingly, the suitable mathematical form is a point interaction. It is known as the pseudo potential and serves as an important theoretical Ansatz at the two-body level for the description of interacting many-body systems [436, 641]. The existence of such pseudo potentials is not surprising in view of the zero-range square well solutions discussed in Sec. 33.6.2.

As the pseudo potential cannot be obtained at the level of the radial wave equation, we return to the full 3D Schrödinger equation for a pair of free atoms,

$$(\nabla^2 + k^2)\psi_k(r) = 0 \ , \tag{33.103}$$

where $k = \sqrt{2m_r E/\hbar^2}$ is the wavenumber for the relative motion. Restricting ourselves to s-wave collisions we derived earlier the solution of this equation as being given by $\psi_k(r) = \frac{c_0}{kr}\sin kr$. However, we are now looking a solution of the type (33.37), which includes a phase shift η_0,

$$\psi_k(r) = \frac{c_0}{kr}\sin(kr + \eta_0) \ . \tag{33.104}$$

Inserting this expression into the wave equation (33.103) we encounter the problem that the solution is irregular in the origin when $\eta_0 \neq 0$. Apparently, we need to complement the wave equation by a (pseudo-)potential to remove this problem.

Our claim is now that the operator,

$$-\frac{4\pi}{k\cot\eta_0}\delta^3(\mathbf{r})\frac{\partial}{\partial r}r \tag{33.105}$$

is the wanted s-wave *pseudo potential* $\tilde{V}(r)$. That is, the wave equation,

$$\boxed{\left(\nabla^2+k^2+\frac{4\pi}{k\cot\eta_0}\delta^3(\mathbf{r})\frac{\partial}{\partial r}r\right)\psi_k(r)=0} \tag{33.106}$$

lets the phase-shifted wavefunction (33.104) be regular at the origin.

The presence of the delta function makes the pseudo-potential act as a boundary condition at $r=0$,

$$\begin{aligned}\frac{4\pi\delta^3(\mathbf{r})}{k\cot\eta_0}\left[\frac{\partial}{\partial r}r\psi_k(r)\right]_{r=r_0} &= 4\pi\delta^3(\mathbf{r})\frac{c_0}{k}\sin\eta_0 \\ &= -4\pi\delta^3(\mathbf{r})\frac{c_0}{k}\sin(ka) \underset{k\to0}{\simeq} -4\pi a c_0\delta^3(\mathbf{r})\ ,\end{aligned} \tag{33.107}$$

where we used the expression for the s-wave phase shift, $\eta_0=-ka$. This is the alternative boundary condition we were looking for. Substituting this into Eq. (33.106) we obtain the inhomogeneous equation

$$(\nabla^2+k^2)\psi_k(r) \underset{k\to0}{\simeq} -4\pi a c_0\delta^3(\mathbf{r})\ . \tag{33.108}$$

This inhomogeneous equation has the solution (33.104), as demonstrated in Exc. 33.1.5.4.

For functions $f(\mathbf{r})$ with regular behavior in the origin we have [4],

$$\left[\frac{\partial}{\partial r}rf(\mathbf{r})\right]_{r=0} = f(\mathbf{0})+r\left[\frac{\partial}{\partial r}f(\mathbf{r})\right]_{r=0} = f(\mathbf{0})\ , \tag{33.109}$$

and the pseudo potential takes the form of a delta function potential [5],

$$\tilde{V}(r) = -\frac{4\pi}{k\cot\eta_0}\delta^3(\mathbf{r}) \underset{k\to0}{\simeq} 4\pi a\delta^3(\mathbf{r})\ , \tag{33.110}$$

or, equivalently, restoring the dimensions,

$$\boxed{V(r)=\frac{g}{2}\delta^3(\mathbf{r}) \qquad \text{with} \qquad g=\frac{4\pi\hbar^2}{m_r}}\ . \tag{33.111}$$

[4] Note that the wavefunction ψ_k is irregular,

$$\delta^3(\mathbf{r})\frac{\partial}{\partial r}[r\psi_k(r)] = \delta^3(\mathbf{r})\frac{\partial}{\partial r}\left(r\frac{c_0\sin(kr+\eta_0)}{kr}\right) = \delta^3(\mathbf{r})c_0\cos[k(r-a)] \underset{k\to0}{=} c_0\delta^3(\mathbf{r})\ .$$

On the other hand,

$$\delta^3(\mathbf{r})\frac{\partial}{\partial r}[r\psi_k(r)] = \delta^3(\mathbf{r})\frac{c_0\sin(kr+\eta_0)}{kr} = \delta^3(\mathbf{r})\frac{c_0\sin[k(r-a)]}{kr} \underset{k\to0}{=} c_0\delta^{(3)}(\mathbf{r})[1-\tfrac{a}{r}]\ .$$

[5] Note that the dependence on the relative position vector $\mathbf{r}$ rather than its modulus r is purely formal as the delta function restricts the integration to only zero-length vectors. This notation is used to indicate that normalization involves a 3-dimensional integration, $\int\delta^3(\mathbf{r})d^3r$. Pseudo potentials do not carry physical significance but are mathematical constructions that can chosen such that they provide wavefunctions with the proper phase shift.

This expression, for $na^3 \ll 1$ valid in the zero energy limit, is convenient for calculating the interaction energy, as will be shown in Sec. ??.

33.1.4.9 Coupling of potentials

When molecular potentials cross and couple via collisions, via radiative coupling, or via a Feshbach resonance (cf. Sec. 33.4.2), new adiabatic potentials are formed. These are obtained as the r-dependent eigenvalues of the coupling Hamiltonian,

$$\hat{H}_{cpl} = \begin{pmatrix} V_1(R) & \Omega \\ \Omega & V_2(R) \end{pmatrix} . \tag{33.112}$$

Such calculations are known as *coupled channels* calculations.

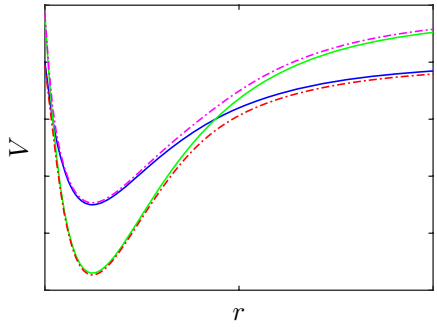

Figure 33.13: (code) The coupling of molecular potentials (solid lines) generates new adiabatic potentials (dash-dotted lines).

33.1.5 Exercises

33.1.5.1 Ex: Asymptotic radial function for hard-sphere potentials

Using asymptotic expressions for the Bessel and von Neumann functions derive the radial function $R_\ell(k,r)$ for the two limiting cases $ka \ll 1$ and $ka \gg 1$.

Solution: *i. For $ka \ll 1$ the phase shift can be written as,*

$$\tan\eta_\ell \underset{k\to 0}{\simeq} -\frac{2\ell+1}{[(2\ell+1)!!]^2}(ka)^{2\ell+1} \underset{k\to 0}{\simeq} \eta_\ell \ ,$$

and the radial wavefunction becomes,

$$R_\ell(k,r) \underset{r\to\infty}{\simeq} \frac{c_\ell}{kr}\sin\left(kr - \frac{2\ell+1}{[(2\ell+1)!!]^2}(ka)^{2\ell+1} - \tfrac{1}{2}\ell\pi\right) \ .$$

In particular, for s-waves we find

$$R_0(k,r) \underset{r\to\infty}{\simeq} \frac{c_\ell}{kr}\sin[k(r-a)] \ .$$

ii. For $ka \gg 1$ we find,

$$\tan\eta_\ell \underset{k\to\infty}{\simeq} -\tan(ka - \tfrac{1}{2}\ell\pi) \Longrightarrow \eta_\ell \underset{k\to\infty}{\simeq} -ka + \tfrac{1}{2}\ell\pi \ ,$$

and for the radial wavefunction,

$$R_\ell(k,r) \underset{r\to 0}{\simeq} \frac{c_\ell}{kr}\sin[k(r-a)] \ .$$

Note that this expression is independent of ℓ; i.e. for large k all wavefunctions are shifted by the diameter of the hard sphere. This is only the case for hard-sphere potentials.

33.1.5.2 Ex: s-wave collision on flat bottom potentials

Simplify the scattering matrix (33.35) for the collisional flat bottom potential for the case of s-wave collisions.

Solution: *We start from the expression (33.35) specifying $\ell = 0$,*

$$e^{2i\eta_0} = -\frac{h_0^{(1)}(\varrho_e)}{h_0^{(2)}(\varrho_e)}\frac{K_+\partial_\varrho \ln j_0(\varrho_i) - k\partial_\varrho \ln h_0^{(1)}(\varrho_e)}{K_+\partial_\varrho \ln j_0(\varrho_i) - k\partial_\varrho \ln h_0^{(2)}(\varrho_e)} \ ,$$

Coming from inside the potential we have at the boundary $\varrho_i = K_+ r_0$,

$$j_0(\varrho_i) = \frac{\sin\varrho_i}{\varrho_i} \qquad \Longrightarrow \qquad \partial_\varrho \ln j_0(\varrho_i) = \frac{j_0'(\varrho_i)}{j_0(\varrho_i)} = \cot\varrho_i - \frac{1}{\varrho_i} \ .$$

Coming from outside the potential we have at the boundary $\varrho_e = kr_0$,

$$n_0(\varrho_e) = -\frac{\cos\varrho_e}{\varrho_e} \qquad \Longrightarrow \qquad h_0^{(1)}(\varrho_e) = j_0(\varrho_e) + in_0(\varrho_e) = -\frac{ie^{i\varrho_e}}{\varrho_e}$$

$$\Longrightarrow \qquad h_0'^{(1)}(\varrho_e) = \frac{i+\varrho_e}{\varrho_e^2}e^{i\varrho_e} \qquad \Longrightarrow \qquad \partial_\varrho \ln h_0^{(1)}(\varrho_e) = -\frac{1-i\varrho_e}{\varrho_e}$$

$$\Longrightarrow \qquad \frac{h_0^{(1)}(\varrho_e)}{h_0^{(2)}(\varrho_e)} = -e^{2i\varrho_e} \ .$$

With this, the S matrix becomes,

$$e^{2i\eta_0} = e^{2i\varrho_e}\frac{K_+\left(\cot\varrho_i - \frac{1}{\varrho_i}\right) + k\frac{1-i\varrho_e}{\varrho_e}}{K_+\left(\cot\varrho_i - \frac{1}{\varrho_i}\right) + k\frac{1+i\varrho_e}{\varrho_e}} = e^{2ikr_0}\frac{K_+\cot K_+r_0 - ik}{K_+\cot K_+r_0 + ik}$$

$$\Longrightarrow \qquad \eta_0 = kr_0 + \frac{1}{2i}\ln\frac{K_+ - ik\tan K_+r_0}{K_+ + ik\tan K_+r_0} = kr_0 - \arctan\frac{k\tan K_+r_0}{K_+} \ ,$$

using $\arctan x = \frac{i}{2}\ln\frac{1-ix}{1+ix}$.
Alternatively, we may derive the same results from the continuity condition for the radial wavefunction $u_0(r)$, which reads,

$$K_+\frac{\cos\varrho_i}{\sin\varrho_i} = \frac{u_0'(r_0)}{u_0(r_0)} = k\frac{\cos\eta_0\cos\varrho_e + \sin\eta_0\sin\varrho_e}{\cos\eta_0\sin\varrho_e - \sin\eta_0\cos\varrho_e} \ ,$$

which can also be written as,

$$K_+ \cot \varrho_i = k \cot(\varrho_e - \eta_0) \ ,$$

or

$$\eta_0 = kr_0 - \arctan \frac{k \tan K_+ r_0}{K_+} \ .$$

With the definition of the scattering length we get,

$$\frac{\eta_0}{k} = r_0 - \frac{1}{k} \arctan \frac{k \tan(\sqrt{k^2 + \kappa_{0+}^2} r_0)}{\sqrt{k^2 + \kappa_0^2}} \underset{k \to 0}{\longrightarrow} r_0 - \frac{\tan \kappa_0 r_0}{\kappa_0} \equiv a \ .$$

33.1.5.3 Ex: Equivalence of boundary conditions

Show that the radial wavefunction R_ℓ and u_ℓ satisfy equivalent boundary conditions at the surface of the spherical box potential.

Solution: *The goal is to show that the following two boundary conditions are equivalent,*

$$\lim_{r \nearrow r_0} \frac{R'_\ell(r)}{R_\ell(r)} = \lim_{r \searrow r_0} \frac{R'_\ell(r)}{R_\ell(r)} \Longleftrightarrow \lim_{r \nearrow r_0} \frac{u'_\ell(r)}{u_\ell(r)} = \lim_{r \searrow r_0} \frac{u'_\ell(r)}{u_\ell(r)} \ .$$

This can be seen from,

$$\frac{u'_\ell(r)}{u_\ell(r)} = \frac{rR'_\ell(r) + R_\ell(r)}{rR_\ell(r)} = \frac{R'_\ell(r)}{R_\ell(r)} + \frac{1}{r} \ .$$

33.1.5.4 Ex: Derivation of a linear expansion

Derive the linear expansion (33.67).

Solution: *We calculate the linear expansion of* $K_{res} \cot K_+ r_0$ *near the zero crossing at* $K_+ r_0 = (\tilde{v}+1/2)\pi$*, where* $\cot K_+ r_0 = 0$*: This follows from the derivative evaluated at* $K_+ r_0 = (\tilde{v} + 1/2)\pi$*:*

$$\left. \frac{dK_{res} \cot K_+ r_0}{d\delta k} \right|_{K_+ r_0 = (\tilde{v}+1/2)\pi} = \left. -\frac{k_{res} r_0|^2}{\sin} K_+ r_0| \right|_{K_+ r_0 = (\tilde{v}+1/2)\pi} == -k_{res} r_0 \ .$$

Multiplying the derivative with δk *we obtain the desired result.*

33.1.5.5 Ex: Pseudo-potential for s-wave scattering

Verify the equation $(\nabla^2 + k^2)\psi_k(r) = 4\pi\delta^3(\mathbf{r})\frac{1}{k}\sin\eta_0$ by direct substitution of the solution (33.104) setting $c_0 = 1$.

Solution: *Integrating (33.108) by over a small sphere V of radius ϵ about the origin we have,*

$$\int_V (\nabla^2 + k^2)\frac{1}{kr}\sin(kr + \eta_0)d^3r = -\frac{4\pi}{k}\sin\eta_0 \ .$$

Here we used $\int_V \delta^3(\mathbf{r})d^3r$ for an arbitrarily small sphere about the origin. The second term on the l.h.s. of the last equation vanishes,

$$4\pi k \lim_{\epsilon\to 0}\int_0^\epsilon r\sin(kr + \eta_0)dr = 4\pi k\sin\eta_0 \lim_{\epsilon\to 0}\epsilon = 0 \ .$$

The first term follows with the divergence theorem (Gauss theorem),

$$\begin{aligned}\lim_{\epsilon\to 0}\int_V \nabla^2\frac{1}{kr}\sin(kr + \eta_0)d^3r &= \lim_{\epsilon\to 0}\oint_{\mathcal{S}} d\mathbf{S}\cdot\nabla\frac{1}{kr}\sin(kr + \eta_0) \\ &= \lim_{\epsilon\to 0} 4\pi\epsilon^2\left(\frac{1}{\epsilon}\cos(kr + \eta_0) - \frac{1}{k\epsilon^2}\sin(kr + \eta_0)\right) = -\frac{4\pi}{k}\sin\eta_0 \ .\end{aligned}$$

33.2 Scattering theory

In this chapter we discuss scattering by time independent potentials satisfying $rV(r \to \infty) \to 0$, that is short-range potentials. Such a potential may have attractive regions supporting bound states with energy $E < 0$. Here, however, we only consider states $E > 0$. Since the potential is supposed independent of time, $\partial_t\hat{H} = 0$, we will focus on time-independent problems,

$$\hat{H}\psi_{\mathbf{k}}(\mathbf{r}) = E_k\psi_{\mathbf{k}}(\mathbf{r}) \ , \tag{33.113}$$

with $\hat{H} = p^2/2m + V(\mathbf{r})$ and $E_{\mathbf{k}} = \hbar^2k^2/2m$. The boundary conditions are given by the scattering geometry in such a way that at long distances the wavefunction behaves as (see Fig. 33.14),

$$\psi_{\mathbf{k}}(\mathbf{r}) \sim e^{i\mathbf{k}\cdot\mathbf{r}} + f_k(\Omega)\frac{e^{ik_sr}}{r} \ . \tag{33.114}$$

For elastic scattering processes we have $k_s = k$. The *scattering amplitude* $f_k(\Omega)$ depends on the energy E_k and on the scattering solid angle. Experimentally, we scatter individual particles described by wave packets. Since the scattering theory is linear, we can describe the packets by superpositions of stationary solutions $\psi_{\mathbf{k}}$ [6].

[6] Note that $\mathbf{k}$ is not a quantum number, since $\psi_{\mathbf{k}}$ contains momentum components $\neq \mathbf{k}$.

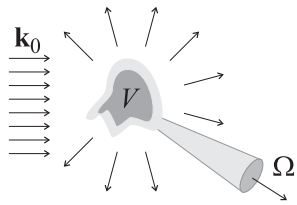

Figure 33.14: Scattering of incident light (wavevector $\mathbf{k}_0$) by a potential V.

33.2.1 Lippmann-Schwinger equation

In order to consider the example of two particles involved in a collision we may go into the center-of-mass system (using reduced masses), fix the origin of the coordinate system on one of the particles, and analyze the trajectory of the second particle inside the interaction potential.

The scattering theory is based on *Green's method*, which we already know from electrostatics. So, let us start of a brief reminder of the use of the *Green's function* as a method to solve electrostatic problems.

Example 191 (*Green's method in electrostatics*): From Maxwell's third equation we obtain,

$$\nabla^2\phi(\mathbf{r}) = -\varepsilon_0^{-1}\rho(\mathbf{r}) \ .$$

Being defined by,

$$\nabla^2 G(\mathbf{r}) = \delta^3(\mathbf{r}) \ ,$$

the Green function is,

$$G(\mathbf{r}) = \frac{-1}{4\pi}\frac{1}{|\mathbf{r}|} \ .$$

With this, we find the solution of the Maxwell equation,

$$\phi(\mathbf{r}) = \left(-G \star \varepsilon_0^{-1}\rho(\mathbf{r})\right)(\mathbf{r}) = -\frac{1}{\varepsilon_0}\int_V \rho(\mathbf{r}_0)G(\mathbf{r}-\mathbf{r}_0)d^3\mathbf{r}_0 = \frac{1}{4\pi\varepsilon_0}\int_V \frac{\rho(\mathbf{x})}{|\mathbf{r}-\mathbf{x}|}d^3\mathbf{x} \ ,$$

known as *Poisson's law*.

33.2.1.1 Green's method in quantum mechanics

Green's method can be used to solve Schrödinger's equation with the boundary condition (33.114). We start from the reduced stationary Schrödinger equation (33.113) [1298],

$$(\Delta + k^2)\psi_{\mathbf{k}}(\mathbf{r}) = \tfrac{2m}{\hbar^2}V(\mathbf{r})\psi_{\mathbf{k}}(\mathbf{r}) \ . \tag{33.115}$$

This equation is not a common eigenvalue problem, since any energy E_k generates a solution. The equation (33.115) is a partial inhomogeneous differential equation with the left side describing free propagation and the right side describing a source that depends on the solution. Such differential equations are usually solved using Green's functions. We choose a point source and we solve,

$$(\Delta + k^2)G(\mathbf{r}, k) = \delta^3(\mathbf{r}) \ , \tag{33.116}$$

along with the boundary conditions. The solution takes the form [151],

$$G(\mathbf{r},k) = -\frac{1}{4\pi}\frac{e^{ik|\mathbf{r}|}}{|\mathbf{r}|} \ , \tag{33.117}$$

such that,

$$\boxed{\psi_{\mathbf{k}}(\mathbf{r}) = e^{i\mathbf{k}\cdot\mathbf{r}} + \left(G \star \tfrac{2m}{\hbar^2} V\psi_{\mathbf{k}}\right)(\mathbf{r}) = e^{i\mathbf{k}\cdot\mathbf{r}} + \tfrac{2m}{\hbar^2}\int_V d^3\mathbf{r}' G(\mathbf{r}-\mathbf{r}',k)V(\mathbf{r}')\psi_{\mathbf{k}}(\mathbf{r}')} \ . \tag{33.118}$$

The equation (33.118) is called *Lippmann-Schwinger equation*. Of course, this equation does not solve, but only reformulate the problem taking into account the boundary conditions. It is more appropriate for an implementation of approximations. See Exc. 33.2.7.1 and 33.2.7.2.

Now let us consider the far field, $r \to \infty$, to verify the asymptotic behavior and find an expression for $f_k(\Omega)$ as a function of $V(\mathbf{r})$. For $r \to \infty$ we can approximate

$$k|\mathbf{r}-\mathbf{r}'| = kr\sqrt{(\hat{\mathbf{e}}_r - \mathbf{r}'/r)^2} = kr\sqrt{1 - 2\hat{\mathbf{e}}_r\cdot\mathbf{r}'/r + (r'/r)^2} \simeq kr - \mathbf{k}'\cdot\mathbf{r}' \simeq kr \ , \tag{33.119}$$

with $\mathbf{k}' \equiv k\hat{\mathbf{e}}_r$. With this the Lippmann-Schwinger equation (33.118) becomes,

$$\begin{aligned}\psi(\mathbf{r}) &\to e^{i\mathbf{k}\cdot\mathbf{r}} - \frac{2m}{\hbar^2}\int_V \frac{1}{4\pi}\frac{e^{ik|\mathbf{r}-\mathbf{r}'|}}{|\mathbf{r}-\mathbf{r}'|}V(\mathbf{r}')\psi(\mathbf{r}')d^3\mathbf{r}' \qquad (33.120)\\ &= e^{i\mathbf{k}\cdot\mathbf{r}} - \frac{2m}{4\pi\hbar^2}\frac{e^{ikr}}{kr}\int_V e^{-i\mathbf{k}'\cdot\mathbf{r}'}V(\mathbf{r}')\psi(\mathbf{r}')d^3\mathbf{r}' \equiv \psi_{in} + f_k(\Omega)\frac{e^{ikr}}{r} \ ,\end{aligned}$$

giving, in comparison with the expression (33.114), the *scattering amplitude*,

$$f_k(\Omega) = \frac{2m}{4\pi\hbar^2}\int_V e^{-i\mathbf{k}'\cdot\mathbf{r}'}V(\mathbf{r}')\psi(\mathbf{r}')d^3\mathbf{r}' \ . \tag{33.121}$$

Starting from the wavefunctions $\psi_{in} \equiv e^{i\mathbf{k}\cdot\mathbf{r}}$ and $\psi_s \equiv f_k(\Omega)e^{ikr}/r$ we can calculate the current densities,

$$\begin{aligned}\mathbf{J}_{in} &= \frac{\hbar}{2mi}(\psi_{in}^\dagger\nabla\psi_{in} - c.c.) = \frac{\hbar\mathbf{k}}{m} \qquad (33.122)\\ \mathbf{J}_s &= \frac{\hbar}{2mi}(\psi_s^\dagger\partial_r\psi_s - c.c.)\hat{\mathbf{e}}_r = \frac{\hbar\mathbf{k}'}{m}\frac{1}{r^2}|f_k(\Omega)|^2 + \mathcal{O}(r^{-3}) \ .\end{aligned}$$

The number $dI(\Omega)$ of particles scattered per second into the solid angle $d\Omega$ is simply $dI(\Omega) = |\mathbf{J}_s|r^2 d\Omega$. With this we can calculate the *differential effective cross section* defined by the ratio between $dI(\Omega)$ and the number $|\mathbf{J}_{in}|$ of incident particles per second,

$$\boxed{\frac{d\sigma}{d\Omega} \equiv \frac{dI(\Omega)}{|\mathbf{J}_{in}|d\Omega} = |f_k(\Omega)|^2} \ . \tag{33.123}$$

Finally we define the *total effective cross section*,

$$\sigma = \int d\Omega |f_k(\Omega)|^2 \ . \tag{33.124}$$

33.2.2 Wave packets

We now let a *wave packet* defined at a time $t = t_0$,

$$\psi(\mathbf{r}, t_0) = \int \frac{d^3k}{(2\pi)^3} a_{\mathbf{k}} e^{i\mathbf{k}\cdot\mathbf{r}} \ , \tag{33.125}$$

impinge on a scattering potential. The amplitude $a_{\mathbf{k}}$ be concentrated around $\mathbf{k}_0$, such that the wave packet approaches the scatterer with the velocity $\mathbf{v}_0 = \hbar\mathbf{k}_0/m$. The time evolution of the wavefunction $\psi(\mathbf{r}, t)$ determines the signal measured by a detector at a later time $t = t_0$. Our task is to determine $\psi(\mathbf{r}, t > t_0)$. The scattered states $\psi_{\mathbf{k}}$ solving the Schrödinger equation (33.113) are complete in the space of the extended wavefunctions, and we can write the temporal evolution as,

$$\psi(\mathbf{r}, t) = \int \frac{d^3k}{(2\pi)^3} A_{\mathbf{k}} \psi_{\mathbf{k}}(\mathbf{r}) e^{-iE_k(t-t_0)/\hbar} \ . \tag{33.126}$$

At time t_0 the results (33.125) and (33.126) must match. To verify this, we write (33.125) replacing the plane wave $e^{i\mathbf{k}\cdot\mathbf{r}}$ using the Lippmann-Schwinger equation (33.118) with Green's function (33.117), and then we compare the coefficients,

$$\psi(\mathbf{r}, t_0) = \int \frac{d^3k}{(2\pi)^3} a_{\mathbf{k}} \left[\psi_{\mathbf{k}}(\mathbf{r}) + \frac{m}{2\pi\hbar^2} \int d^3r' \frac{e^{ik|\mathbf{r}-\mathbf{r}'|}}{|\mathbf{r}-\mathbf{r}'|} V(\mathbf{r}') \psi_{\mathbf{k}}(\mathbf{r}') \right] \ . \tag{33.127}$$

The scattering process is illustrated in Fig. 33.15. To simplify the calculation of

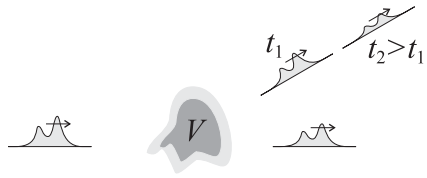

Figure 33.15: Scattering of wave packet at a potential.

the second term in this equation, we assume that $\psi_{\mathbf{k}}$ is smooth, that is, there are no resonances, such that we can approximate, $\psi_{\mathbf{k}} \simeq \psi_{\mathbf{k}_0}$. With $k \simeq \mathbf{k}\cdot\hat{\mathbf{e}}_{k_0}$ we obtain,

$$\begin{aligned} \int \frac{d^3k}{(2\pi)^3} a_{\mathbf{k}} e^{ik|\mathbf{r}-\mathbf{r}'|} \psi_{\mathbf{k}}(\mathbf{r}') &= \int \frac{d^3k}{(2\pi)^3} a_{\mathbf{k}} e^{i\mathbf{k}\cdot(\hat{\mathbf{e}}_{k_0}|\mathbf{r}-\mathbf{r}'|)} \psi_{\mathbf{k}_0}(\mathbf{r}') \\ &\overset{(33.125)}{=} \psi(\hat{\mathbf{e}}_{k_0}|\mathbf{r}-\mathbf{r}'|, t_0) \psi_{\mathbf{k}_0}(\mathbf{r}') \ . \end{aligned} \tag{33.128}$$

Here, $\psi(\hat{\mathbf{e}}_{k_0}|\mathbf{r}-\mathbf{r}'|, t_0)$ is the incident wave package evaluated to the right, where by definition it is $\simeq 0$. The expression (33.127) therefore has the form,

$$\psi(\mathbf{r}, t_0) = \int \frac{d^3k}{(2\pi)^3} a_{\mathbf{k}} \psi_{\mathbf{k}}(\mathbf{r}) \ , \tag{33.129}$$

and a comparison of the coefficients with (33.126) gives, $A_{\mathbf{k}} = a_{\mathbf{k}}$. Finally, we evaluate $\psi(\mathbf{r}, t)$ at the time of detection $t > t_0$ to understand, that the above stationary analysis

is actually physically correct. According to (33.126) we have,

$$\psi(\mathbf{r},t) = \int \frac{d^3k}{(2\pi)^3} A_{\mathbf{k}} \psi_{\mathbf{k}}(\mathbf{r}) e^{-iE_k(t-t_0)/\hbar} \tag{33.130}$$
$$\overset{(33.120)(33.125)}{\simeq} \psi_0(\mathbf{r},t) + \int \frac{d^3k}{(2\pi)^3} a_{\mathbf{k}} \frac{e^{ikr}}{r} f_k(\Omega) e^{-iE_k(t-t_0)/\hbar} \ .$$

Hence, $\psi_0(\mathbf{r},t)$ describes the evolution of the wave packet without scatterer,

$$\psi_0(\mathbf{r},t) = \underbrace{\int \frac{d^3k}{(2\pi)^3} a_{\mathbf{k}} e^{i\mathbf{k}\cdot\mathbf{r}}}_{\psi(\mathbf{r},t_0)} e^{-iE_k(t-t_0)/\hbar} \ . \tag{33.131}$$

If f_k it's smooth around $\mathbf{k} = \mathbf{k}_0$, which allows us to place this amplitude ($f_k \simeq f_{k_0}$) in front of the integral, and with $k \simeq \mathbf{k}\cdot\hat{\mathbf{k}}_0$ we obtain,

$$\psi(\mathbf{r},t) \overset{t \text{ large}}{\Longrightarrow} \underbrace{\psi_0(\mathbf{r},t)}_{\text{packet not scattered}} + \underbrace{\frac{f_{k_0}(\Omega)}{r} \psi_0(\hat{k}_0 r, t)}_{\text{packet scattered}} \ . \tag{33.132}$$

The scattering process is illustrated in Fig. 33.15: According to the last equation the scattering process involves the superposition of the non-scattered packet and a packet scattered in the direction Ω. The latter involves the amplitude $\Psi_0(\hat{k}_0 r, t)$ of a packet propagating in forward direction, which only needs to be evaluated at the right time and distance. This packet will then be multiplied with the amplitude describing the angular dependency f_{k_0}; the angle, therefore, only appears through this amplitude and not in the wavefunction ψ_0. In two situations the above analysis can not be applied :

- when V is long-ranged, f.ex., $V = 1/r$,
- when the incident energy E_k is resonant.

33.2.3 Born approximation

The Lippmann-Schwinger equation suggests the following perturbative iteration called *Born series* [151],

$$\begin{aligned} \psi(\mathbf{r}) &= \psi_i(\mathbf{r}) + \left(G \star \tfrac{2m}{\hbar^2} V\psi\right)(\mathbf{r}) \\ &= \psi_i(\mathbf{r}) + \tfrac{2m}{\hbar^2}(G \star V\psi_i)(\mathbf{r}) + \left(\tfrac{2m}{\hbar^2}\right)^2 [G \star V(G \star V\psi_i)](\mathbf{r}) \\ &= \psi_i(\mathbf{r}) + \tfrac{2m}{\hbar^2} \int_V G(\mathbf{r}-\mathbf{r}')V(\mathbf{r}')\psi_i(\mathbf{r}')d^3\mathbf{r}' \\ &\quad + \left(\tfrac{2m}{\hbar^2}\right)^2 \int_V G(\mathbf{r}-\mathbf{r}')V(\mathbf{r}')G(\mathbf{r}-\mathbf{r}'')V(\mathbf{r}'')\psi_i(\mathbf{r}'')d^3\mathbf{r}'d^3\mathbf{r}'' \ . \end{aligned} \tag{33.133}$$

In the so-called *Born approximation* we consider only the first perturbation order, and inserting a plane wave, $\psi_i(\mathbf{r}) = e^{ikz}/(2\pi)^{3/2}$, we obtain,

$$\psi(\mathbf{r}) = \frac{e^{ikz}}{(2\pi)^{3/2}} - \frac{m}{(2\pi)^{3/2} 2\pi\hbar^2} \int_V \frac{e^{ik|\mathbf{r}-\mathbf{r}'|}}{|\mathbf{r}-\mathbf{r}'|} V(\mathbf{r}') e^{ikz'} d^3\mathbf{r}' \ . \tag{33.134}$$

The asymptotic behavior $r \gg r'$, it follows with (33.119) using $z' = \mathbf{r}' \cdot \hat{\mathbf{e}}_z$ and defining $\mathbf{k}_s = k\hat{\mathbf{e}}_r$ e $\mathbf{k}_i = k\hat{\mathbf{e}}_z$,

$$\begin{aligned}\psi(\mathbf{r}) &\simeq \frac{e^{ikz}}{(2\pi)^{3/2}} - \frac{m}{(2\pi)^{3/2}2\pi\hbar^2}\int_V \frac{e^{ik\left(r-\mathbf{r}\cdot\mathbf{r}'/r\right)}}{r} V(\mathbf{r}')e^{i\mathbf{k}\cdot\mathbf{r}'}d^3\mathbf{r}' \\ &= \frac{e^{ikz}}{(2\pi)^{3/2}} + \frac{m}{(2\pi)^{3/2}2\pi\hbar^2}\frac{e^{ikr}}{r}\int_V V(\mathbf{r}')e^{i(\mathbf{k}_i-\mathbf{k}_s)\cdot\mathbf{r}'}d^3\mathbf{r}' \\ &\equiv \frac{1}{(2\pi)^{3/2}}\left(e^{ikz} + \frac{e^{ikr}}{r}f(k_i,k_s)\right) ,\end{aligned} \tag{33.135}$$

with

$$\boxed{f(k_i,k_s) \equiv \frac{m}{2\pi\hbar^2}\int_V V(\mathbf{r}')e^{i(\mathbf{k}_i-\mathbf{k}_s)\cdot\mathbf{r}'}d^3\mathbf{r}' = -\frac{m}{2\pi\hbar^2}\langle k_s|\tilde{V}|k_i\rangle} .$$

33.2.4 Spherical potentials

For spherically symmetric scattering potentials, $V(\mathbf{r}) = V(r)$, the Hamiltonian $\hat{H} = p^2/2m + V(r)$ commutes with the rotation operators $U_{\vec{\omega}} = e^{-i\vec{\omega}\cdot\mathbf{L}/\hbar}$ around any axis $\hat{\mathbf{e}}_{\vec{\omega}}$. Therefore, we can separate the angular problem and decompose the scattering problem following the irreducible representations of the rotation group. This *partial wave* decomposition can be written,

$$\psi_{\mathbf{k}}(\mathbf{r}) = \sum_{\ell=0}^{\infty}(2\ell+1)i^\ell P_\ell(\cos\theta)R_l(r) , \tag{33.136}$$

where the factor $(2\ell+1)i^\ell$ is a convention facilitating the calculation later on. By inserting this separation ansatz for the radial and angular variables into the stationary Schrödinger equation (33.113), we obtain the radial Schrödinger equation,

$$\left[\frac{\partial^2}{\partial r^2} - \frac{\ell(\ell+1)}{r^2} + k^2\right] rR_\ell(r) = \frac{2m}{\hbar^2}V(r)rR_\ell(r) , \tag{33.137}$$

where $\psi_{\mathbf{k}}$ must satisfy the boundary conditions (33.114). Fortunately, we can also expand the incident wave by partial waves [7],

$$e^{ikz} = e^{ir\cos\theta} = \sum_{\ell=0}^{\infty}(2\ell+1)i^\ell j_\ell(kr)P_\ell(\cos\theta) . \tag{33.138}$$

We now use the result (33.138) to find the boundary conditions for the radial waves R_ℓ. In the infinity we have $rV(r) \overset{r\to\infty}{\longrightarrow} 0$. For this reason,

$$R_\ell(r) \overset{r\to\infty}{\longrightarrow} \alpha_\ell[h_\ell^{(2)}(kr) + s_\ell h_\ell^{(1)}(kr)] , \tag{33.139}$$

[7] For the more general case of arbitrary vectors $\mathbf{k}$ e $\mathbf{r}$, we use the addition theorem for $Y_{\ell m}$ and express $P_\ell(\cos\theta)$ by spherical functions,

$$e^{i\mathbf{k}\cdot\mathbf{r}} = 4\pi\sum_{\ell=0}^{\infty}\sum_{m=-\ell}^{\ell} i^\ell j_\ell(kr)Y^*_{\ell m}(\Omega_{\mathbf{k}})Y_{\ell m}(\Omega_{\mathbf{r}}) .$$

where the Hankel functions $h_\ell^{(1,2)}(kr) \sim e^{\pm i(\rho-(\ell+1)\pi/2)}$ describe, respectively, incident ($h_\ell^{(2)}$) and outgoing ($h_\ell^{(1)}$) spherical waves.

To determine the coefficients α_ℓ and s_ℓ we note first that, without potential, $V(r) = 0$, the solution of the radial equation (33.137) is known,

$$R_\ell(r) = j_\ell(kr) = \tfrac{1}{2}[h_\ell^{(2)}(kr) + h_\ell^{(1)}(kr)] \ , \tag{33.140}$$

such that $\alpha_\ell = \frac{1}{2}$ and $s_\ell = 1$. For $V(r) \neq 0$ the incident wave $h_\ell^{(2)}$ is the same, but not the incident $h_\ell^{(1)}$, which results in $s_\ell \neq 1$. However, particle number conservation requires that the number of particles entering the potential is equal to the number of particles coming out. That is, the total radial flow must be,

$$0 = j_r^\ell(r) = \frac{\hbar}{2im}[R_\ell^* \partial_r R_\ell - R_\ell \partial_r R_\ell^*] = \frac{\hbar}{4mkr^2}[|s_\ell|^2 - 1] \ , \tag{33.141}$$

approximating $2R_\ell \simeq \frac{e^{-i(kr+w_\ell}}{kr} + s_\ell \frac{e^{i(kr+w_\ell}}{kr}$. Hence, $|s_\ell| = 1$, that is,

$$s_\ell = e^{2i\delta_\ell(k)} \ , \tag{33.142}$$

where $\delta_\ell(k)$ is the *scattering phase*. The scattering phase determines the solution of the scattering problem, because it fixes the scattering amplitude: Evaluating the solution (33.136) in the asymptotic limit by the formula (33.138),

$$\begin{aligned} \psi_{\mathbf{k}}(\mathbf{r}) &\sim \tfrac{1}{2}\sum_{\ell=0}^{\infty}(2\ell+1)i^\ell P_\ell(\cos\theta)[h_\ell^{(2)}(kr) + e^{2i\delta_\ell} h_\ell^{(1)}(kr)] \qquad (33.143) \\ &= e^{i\mathbf{k}\cdot\mathbf{r}} + \tfrac{1}{2}\sum_{\ell=0}^{\infty}(2\ell+1)i^\ell P_\ell(\cos\theta)[e^{2i\delta_\ell} - 1]h_\ell^{(1)}(kr) = e^{i\mathbf{k}\cdot\mathbf{r}} + f_k(\theta)\frac{e^{ikr}}{r} \ , \end{aligned}$$

we obtain the scattering amplitude in the form [8]

$$\boxed{f_k(\theta) = \tfrac{1}{k}\sum_\ell (2\ell+1)P_\ell(\cos\theta)e^{i\delta_\ell}\sin\delta_\ell} \ . \tag{33.144}$$

We call

$$\frac{e^{2i\delta_\ell} - 1}{2ik} = \frac{e^{i\delta_\ell}\sin\delta_\ell}{k} \equiv f_\ell \tag{33.145}$$

the *amplitude of the partial wave* [1363, 186].

33.2.5 Scattering phase and length

In summary, we can, within the Born approximation, express the collisional state of any type of particles by isotropic potentials,

$$\psi(\mathbf{r}) \sim e^{i\mathbf{k}\cdot\mathbf{r}} + \frac{e^{ikr}}{r} f_k(\Omega) \ . \tag{33.146}$$

[8] Com $h_\ell^{(1)} \sim (-i)^{\ell+1}\frac{e^{ikr}}{kr}$.

The scattering cross section can be written,

$$\sigma = \int d\Omega |f_{\mathbf{k}}(\Omega)|^2 = \tfrac{1}{k^2} \int d\Omega \Big| \sum_\ell (2\ell+1) P_\ell(\cos\theta) \sin\delta_\ell \Big|^2 \tag{33.147}$$
$$= \frac{4\pi}{k^2} \sum_\ell (2\ell+1) \sin^2\delta_\ell = 4\pi \sum_\ell (2\ell+1) |f_\ell|^2 \ .$$

The quantity

$$\boxed{\sigma_\ell = \frac{4\pi}{k^2}(2\ell+1)\sin^2\delta_\ell = \frac{4\pi}{k^2}(2\ell+1)|f_\ell|^2} \tag{33.148}$$

is called *effective partial cross section*. Obviously, $\sigma_\ell \leq \frac{4\pi}{k^2}(2\ell+1)$ holds. The phase shift $e^{2i\delta_\ell}$ has a simple physical interpretation: We consider the function,

$$e^{i\delta_\ell} j_\ell(kr+\delta_\ell) = \tfrac{e^{i\delta_\ell}}{2}[h_\ell^{(2)}(kr+\delta_\ell) + h_\ell^{(1)}(kr+\delta_\ell)] \tag{33.149}$$
$$\sim \frac{e^{i\delta_\ell}}{2}\left[\frac{(-i)^\ell e^{i(kr+\delta_\ell)}}{kr+\delta_\ell} + \frac{(+i)^\ell e^{-i(kr+\delta_\ell)}}{kr+\delta_\ell}\right] \overset{kr\gg\delta_\ell}{\longrightarrow} \tfrac{1}{2}[h_\ell^{(2)} + e^{2i\delta_\ell} h_\ell^{(1)}] \sim R_\ell \ .$$

Now comparing the case $V = 0$ giving $R_\ell(r) = j_\ell(kr)$ with the case $V \neq 0$ giving $R_\ell(r) \sim e^{i\delta_\ell} j_\ell(kr+\delta_\ell)$, we notice that a positive displacement, $\delta_\ell > 0$, pulls the wavefunction into the potential, while a negative displacement, $\delta_\ell < 0$, pushes the wavefunction out, as illustrated in Fig. 33.16.

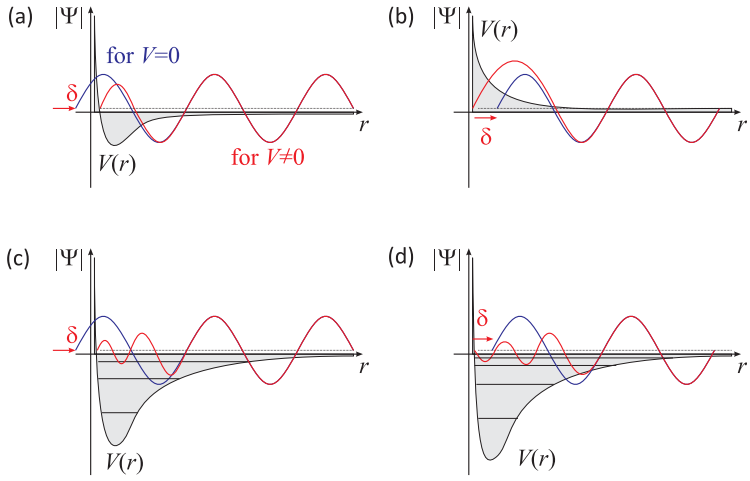

Figure 33.16: Phase shift $\delta_\ell(k)$ of the scattered wavefunction. (a) An attractive potential increases the kinetic energy and the wavefunction oscillates faster, which causes a positive phase shift and a negative scattering length. (b) A repulsive potential slows down the wavefunction oscillation and produces a positive scattering length. (c,d) In an attractive potential deep enough to support vibrational states, the wavefunction performs several oscillations. The sign of the scattering length then depends on the distance of the last bound state to the continuum.

Table 33.1: List of scattering length for various alkaline species.

Element	a_s^{mixed}	$a_s^{triplet}$	$a_p^{triplet}$	$B_{FB,s-wave}$	$B_{FB,p-wave}$
	$[a_B]$	$[a_B]$	$[a_B]$	[G]	[G]
^{1}H		1.23			
^{2}H		-6.8			
^{6}Li			-35		160, 186, 215
^{7}Li	10	-27.3			
^{23}Na	52	85			
^{39}K	118	81.1			
^{40}K	158	1.7	-100	200	200
^{41}K	225	286			
^{85}Rb	-450	-363		156	
^{87}Rb	105	109.3		685.43, 911.74, 1007.34	
^{133}Cs	-240	-350			
^{135}Cs	163	138			

33.2.6 Optical theorem

Consider the amplitude for forward scattering $f(0)$ by writing its imaginary part as,

$$\text{Im } f(0) = \tfrac{1}{k}\sum_k (2\ell+1)P_\ell(\cos\theta)\sin^2\delta_\ell\big|_{\theta=0} = \tfrac{1}{k}\sum_k (2\ell+1)\sin^2\delta_\ell \equiv \frac{k}{4\pi}\sigma\ . \quad (33.150)$$

With this we obtain the *optical theorem*,

$$\boxed{\sigma = \tfrac{4\pi}{k}\text{Im } f(0)}\ . \quad (33.151)$$

The deeper meaning of the optical theorem is the conservation of particle number: The flux of scattered particles, $(\hbar k/m)\sigma = I_{sct}$, must be extracted from the incident flux I_0 by scattering, and therefore, is missing in the forward direction. It is the interference of the scattered wave with the incident wave, which diminishes the non-scattered wave and therefore creates a shadow of the scatterer in the forward direction. The particles missing in the shadow of the scatterer are precisely those that have been scattered. This is the message of the optical theorem, which is always valid in the absence of possible (inelastic) processes leading to trapping or a transformation of the particles.

33.2.6.1 Born approximation for the scattering phase

The scattering problem can be considered as solved when we know the scattering amplitude $f_k(\theta)$, since this quantity gives us the flux measured by the detector. Now, $f_k(\theta)$ is known, when we know the scattering phases $\delta_{\ell,k}$. These are, in general,

determined by integrating the radial equation (33.137). Here, we expect that only angular momenta $\ell < kR_0$ (R_0 is the range of potential) produce significant phase shifts. Particles with larger angular momenta have collision parameters $b \sim \ell/k$ out of the potential reach. We notice that partial s-waves are always scattered, whereas partial p-waves (or higher) are only weakly scattered when the energy is weak, $E < \hbar^2/2mR_0^2$. In these cases an approximate calculation of δ_ℓ is sufficient: We insert (33.136) and $e^{ikz} = \sum_\ell \frac{1}{2}\sqrt{4\pi(2\ell+1)}\int_{-1}^{1} dz P_\ell(z)e^{ikz}$ into (33.121) and integration over Ω' yields,

$$\begin{aligned} f_k(\theta) &= \frac{2m}{4\pi\hbar^2}\int_V e^{-i\mathbf{k}'\cdot\mathbf{r}'}V(\mathbf{r}')\psi(\mathbf{r}')d^3\mathbf{r}' \\ &= -\tfrac{2m}{\hbar^2}\sum_{\ell=0}^{\infty}(2\ell+1)P_\ell(\cos\theta)\int_0^\infty dr\ r^2V(r)j_\ell(kr)R_\ell(r)\ . \end{aligned} \tag{33.152}$$

Comparing this formula with (33.144) we find,

$$e^{i\delta_\ell}\sin\delta_\ell = -\tfrac{2mk}{\hbar^2}\int_0^\infty dr\ r^2V(r)j_\ell(kr)R_\ell(r) \overset{R_\ell\simeq j_\ell}{\simeq} -\tfrac{2mk}{\hbar^2}\int_0^\infty dr\ r^2V(r)j_\ell^2(kr)\ . \tag{33.153}$$

The result (33.153) is the Born approximation for the scattering phase $\delta_\ell(k)$. Note that $R_\ell \simeq j_\ell$ is not a good approximation, in ranges where V is large and R_ℓ strongly suppressed (f.ex., inside hard cores). For ℓ large we have $j_\ell \sim r^\ell$, and $\delta\ell$ is small for a limited potential $V(r)$.

33.2.6.2 Analyticity of $s_\ell(E)$

We consider a short-range potential that disappears at $r > R_0$. The radial solution out of the reach of the potential will then be given by,

$$R_\ell(r) = \tfrac{1}{2}[h_\ell^{(2)}(kr) + s_\ell h_\ell^{(1)}(kr)]\ , \tag{33.154}$$

while for $r < R_0$ the solution R_ℓ must be found by integrating the radial equation (33.137). The scattering phase s_ℓ must be chosen in a way that R_ℓ and $\partial_r R_\ell$ be continuous at R_0. The normalization factor vanishes in the logarithmic derivative, such that,

$$\gamma_\ell \equiv \partial_r \ln R_\ell|_{R_0^-} = \left.\frac{1}{R_\ell}\frac{\partial R_\ell}{\partial r}\right|_{R_0^-} = \left.\frac{\partial_r h_\ell^{(2)} + s_\ell\partial_r h_\ell^{(1)}}{h_\ell^{(2)} + s_\ell h_\ell^{(1)}}\right|_{R_0^+}\ . \tag{33.155}$$

Now [9]

$$s_\ell - 1 = \left.\frac{2(\partial_r - \gamma_\ell)j_\ell}{(\gamma_\ell - \partial_r)h_\ell^{(1)}}\right|_{R_0} \tag{33.156}$$

or with $s_\ell - 1 = \frac{2i}{\cot\delta_\ell - i}$ expressing δ_ℓ by γ_ℓ,

$$\cot\delta_\ell = \left.\frac{(\partial_r - \gamma_\ell)n_\ell}{(\partial_r - \gamma_\ell)j_\ell}\right|_{R_0}\ . \tag{33.157}$$

[9] We have for the spherical Hankel functions: $h_\ell^{(1,2)}(x) = j_\ell(x) \pm iy_\ell(x)$.

The partial effective cross section is,

$$\sigma_\ell = \frac{4\pi}{k^2}(2\ell+1)\sin^2\delta_\ell = \frac{4\pi}{k^2}\frac{2\ell+1}{1+\cot^2\delta_\ell} \ . \tag{33.158}$$

Analyzing the expressions for $s_\ell(\cot\delta_\ell)$ and $\sigma_\ell(\cot\delta_\ell)$ we find that

- for $\cos\delta_\ell = i$ the scattering phase s_ℓ has a pole and $\sigma_\ell \to \infty$;
- for $\cos\delta_\ell = 0$ the scattering phase is $s_\ell - 1$ and $\sigma_\ell = 4\pi(2\ell+1)/k^2$ is maximal.

The poles of s_ℓ are just the bound states: A bound state asymptotically satisfies $R_\ell(r) \sim h_\ell^{(1)}(i\kappa r) \propto e^{-\kappa r}$ with the binding energy $E_B = -\hbar^2\kappa^2/2m$. The condition of continuity is given by,

$$\gamma_\ell = \left.\frac{\partial_r h_\ell^{(1)}}{h_\ell^{(1)}}\right|_{R_0} \ , \tag{33.159}$$

and the insertion into the general continuity condition (33.157) gives,

$$\cot\delta_\ell = \frac{h_\ell^{(1)}\partial_r n_\ell - n_\ell\partial_r h_\ell^{(1)}}{h_\ell^{(1)}\partial_r j_\ell - j_\ell\partial_r h_\ell^{(1)}} = i \ . \tag{33.160}$$

In the same way the zero crossings of $\cot\delta_\ell$ correspond precisely to the scattering resonances. To see this, we expand around a resonance,

$$\cot\delta_\ell(E) \simeq \cot\delta_\ell(E_r) - \frac{1}{\sin^2\delta_\ell}\left.\frac{d\delta_\ell}{dE}\right|_{E_r}(E-E_r) = -\left.\frac{d\delta_\ell}{dE}\right|_{E_r}(E-E_r) \equiv -\frac{2}{\Gamma_r}(E-E_r) \ , \tag{33.161}$$

defining the width $\Gamma_r = \left.\frac{2}{\partial_E\delta_\ell}\right|_{E_r}$ of the resonance peak in the effective section σ_ℓ in the form,

$$\sigma_\ell = \frac{4\pi}{k^2}(2\ell+1)\frac{(\Gamma_r/2)^2}{(E-E_r)^2+(\Gamma_r/2)^2} \ . \tag{33.162}$$

See Fig. 33.17,

$$s_\ell - 1 = \frac{-i\Gamma_r}{E-(E_r - i\gamma_r/2)} \ . \tag{33.163}$$

The scattering phase δ_ℓ increases by π. The value $\delta_\ell(E=0)$ gives the number of bound states, $\delta_\ell(0) = n^\ell_{\text{ligado}}\pi$.

33.2.7 Exercises

33.2.7.1 Ex: Green's method

Show that, knowing the solution of (33.116), that is, knowing the Green function, we can write the solution of the scattering problem (33.115) as,

$$\psi_{\mathbf{k}}(\mathbf{r}) = e^{i\mathbf{k}\cdot\mathbf{r}} + \tfrac{2m}{\hbar^2}\int d^3\mathbf{r}' G(\mathbf{r}-\mathbf{r}',k)V(\mathbf{r}')\psi_{\mathbf{k}}(\mathbf{r}) \ .$$

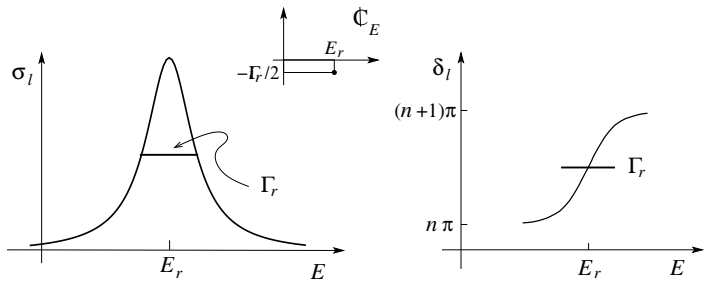

Figure 33.17: Peak of the resonance of width Γ_r: (Left) effective cross section $\sigma_\ell(E)$, (right) scattering phase $\delta_\ell(E)$, and (center) scheme of the position of the pole in the complex energy plane E.

Solution: *The solution of the homogeneous equation is just the incident wave and the solution of the inhomogeneous equation is the scattered wave. To show that this integral equation is equivalent to the problem (33.115) we define the free Hamiltonian* $\hat{H}_0 \equiv p^2/2m$ *and we apply the operator* $(E_k - \hat{H}_0)$ *to the integral equation:*

$$(E_k - \hat{H}_0)\psi_{\mathbf{k}}(\mathbf{r}) = (E_k - \hat{H}_0)e^{i\mathbf{k}\cdot\mathbf{r}} + \tfrac{2m}{\hbar^2}\int d^3r'(E_k - \hat{H}_0)G(\mathbf{r}-\mathbf{r}',k)V(\mathbf{r}')\psi_{\mathbf{k}}(\mathbf{r})$$
$$= \int d^3r'\delta^3(\mathbf{r}-\mathbf{r}',k)V(\mathbf{r}')\psi_{\mathbf{k}}(\mathbf{r}) = V(\mathbf{r})\psi_{\mathbf{k}}(\mathbf{r}) \ .$$

33.2.7.2 Ex: Green's function

Calculate the Green function of the equation (33.116).

Solution: *We make a Fourier transform of this equation,*

$$\int d^3r e^{-i\mathbf{q}\cdot\mathbf{r}}(E - \hat{H}_0)G(\mathbf{q},k) = \int d^3\mathbf{r} e^{-i\mathbf{q}\cdot\mathbf{r}}\tfrac{\hbar^2}{2m}\delta(\mathbf{r})$$
$$\left(E - \tfrac{\hbar^2 q^2}{2m}\right)G(\mathbf{q},k) = \tfrac{\hbar^2}{2m}$$
$$G(\mathbf{q},k) = \frac{\hbar^2}{2m(E-\hbar^2q^2/2m)} = \frac{1}{2mE/\hbar^2 - q^2} \ .$$

Transforming back,

$$G(\mathbf{r},k) = \frac{1}{(2\pi)^3}\int d^3\mathbf{q}\frac{e^{i\mathbf{q}\cdot\mathbf{r}}}{2mE/\hbar^2-q^2} = \frac{1}{(2\pi)^2}\int_0^\infty\int_0^\pi \frac{e^{iqr\cos\theta}}{2mE/\hbar^2-q^2}q^2\sin\theta d\theta dq$$
$$= \frac{1}{(2\pi)^2}\int_0^\infty \frac{q^2}{2mE/\hbar^2-q^2}\int_1^{-1}e^{iqrz}dzdq = \frac{-1}{(2\pi)^2}\int_0^\infty\frac{q^2}{2mE/\hbar^2-q^2}\frac{e^{iqr}-e^{-iqr}}{iqr}dq$$
$$= \frac{-1}{ir(2\pi)^2}\int_{-\infty}^{\infty}\frac{qe^{iqr}}{2mE/\hbar^2-q^2}dq \ .$$

This integral can be solved by the theorem of the residue,

$$G(\mathbf{r},k) = -\frac{e^{\sqrt{2mE}r/\hbar}}{4\pi r} \ .$$

33.2.7.3 Ex: Rutherford scattering

Consider the scattering of a particle of charge Q by a static charge distribution $\rho(\mathbf{r}) = \rho_0 e^{-\alpha r}$ totaling the charge Q'. Derive from (33.136) the formula (22.10) describing the Rutherford scattering.

Solution: *We consider the scattering of a particle of charge Q by a static charge distribution $\int \rho(\mathbf{r}')d^3r' = Q'$,*

$$\begin{aligned} Q' &= \int \rho_0 e^{-\alpha r} d^3r = 4\pi\rho_0 \int_0^\infty r^2 e^{-\alpha r} dr \\ &= -4\pi\rho_0 \left(\frac{r^2}{\alpha} + \frac{2r}{\alpha^2} + \frac{2}{\alpha^3}\right) e^{-\alpha r}\Big|_0^\infty = \frac{8\pi\rho_0}{\alpha^3} \ . \end{aligned}$$

Gauss' law requires, $\nabla^2 V = -4\pi\rho(\mathbf{r})$. Introducing the Fourier transform of the charge distribution,

$$\tilde{\rho}(\mathbf{q}) = \int d^3r e^{-i\mathbf{q}\cdot\mathbf{r}} \rho(\mathbf{r}) \equiv Q' F(\mathbf{q}) \ ,$$

where we defined the form factor $F(\mathbf{q})$ [10]. Thus the Fourier transform of Gauss's law is,

$$\mathbf{q}^2 \tilde{V}(\mathbf{q}) = 4\pi Q Q' F(\mathbf{q}) \ .$$

We calculate [1298],

$$\begin{aligned} \tilde{\rho}(\mathbf{q}) &= \int d^3r \rho_0 e^{-\alpha r} e^{-i\mathbf{q}\cdot\mathbf{r}} = 2\pi \int r^2 dr d(\cos\theta) \rho_0 e^{-\alpha r} e^{-iqr\cos\theta} = 2\pi \int r^2 dr \rho_0 e^{-\alpha r} \frac{e^{-iqr} - e^{iqr}}{-iqr} \\ &= \frac{2\pi}{iq}\rho_0 \int r dr e^{-\alpha r} e^{iqr} + c.c. = \frac{2\pi\rho_0}{iq}\left(-\frac{\partial}{\partial\alpha}\right)\int dr e^{i(q+i\alpha)r} + c.c. \\ &= \frac{2\pi\rho_0}{q}\left(-\frac{\partial}{\partial\alpha}\right)\left\{\frac{1}{q+i\alpha} + c.c.\right\} = 4\pi\rho_0\left(-\frac{\partial}{\partial\alpha}\right)\frac{1}{q^2+\alpha^2} = \frac{8\pi\rho_0\alpha}{(q^2+\alpha^2)^2} \ . \end{aligned}$$

Therefore,

$$F(\mathbf{q}) = \frac{\tilde{\rho}(\mathbf{q})}{\tilde{\rho}(0)} = \left(\frac{\alpha^2}{q^2+\alpha^2}\right)^2 \ .$$

Inserting into the equations (33.136) and (33.124) we obtain the effective differential section in the Born approximation,

$$\frac{d\sigma}{d\Omega} = \frac{4m^2Q^2Q'^2}{(\hbar^2q^2)^2}|F(\mathbf{q})|^2 \ .$$

[10] Always holds $F(0) = 1$

This shows that we can use measurements of effective cross sections to determine form factors and therefore charge distributions.
Particularly for the case $\alpha \to \infty$, when the density distribution describes a point potential by the form factor $F(\mathbf{q}) = 1$, we get the effective differential cross section,

$$\frac{d\sigma}{d\Omega} = \frac{4m^2Q^2Q'^2}{(\hbar^2q^2)^2} = \frac{4m^2Q^2Q'^2}{(\mathbf{p}' - \mathbf{p})^4} = \frac{m^2Q^2Q'^2}{4p^4 \sin^4 \frac{\theta}{2}} ,$$

since $\mathbf{p} \cdot \mathbf{p}' = p^2 \cos\theta$. This is Rutherford's famous scattering formula. It holds not only within the Born approximation, but follows from an exact quantum or classical derivation.

33.2.7.4 Ex: Scattering length for hard-core potentials

Calculate the scattering length for a spherical box barrier and a spherical box potential as a function of potential depth (see also Excs. 25.1.5.4 and 25.1.5.5 and [1354]).

Solution: *Do first for $V = 0$ introduce dephasing for $V \neq 0$, $R_\ell(r) = \frac{1}{2}\left[h_\ell^{(1)}(kr) + S_\ell h_\ell^{(2)}(kr)\right]$. Schrödinger $\psi = \frac{u}{r}$, $\frac{\partial^2 u}{\partial r^2} \equiv 0$ yields for $r \to 0$ $u(r) = c(r - a_s)$ and for $r \to \infty$ yields $u(r) = c' \sin(kr + \delta_0)$. Hence, $\delta_0 = -ka_s$ hard sphere.*

33.3 Cold atomic collisions

Modern techniques developed in the area of atomic optics allow to cool atomic gases to temperatures well below 1 μK. We use the expansions $j_\ell \sim x^\ell/(2\ell+1)!!$ and $n_\ell \sim (2\ell-1)!!/x^{\ell+1}$ in the equation (33.157), and obtain for $kR_0 \ll 1$,

$$\cos\delta_\ell \simeq \frac{2\ell+1)!!(2\ell-1)!!}{(kR_0)^{2\ell+1}} \frac{\ell + 1 + R_0\alpha_\ell(E)}{\ell - R_0\alpha_\ell(E)} . \tag{33.164}$$

A coarse approximation leads to

$$\cos\delta_\ell = \frac{\cos\delta_\ell}{\sin\delta_\ell} \overset{\delta_\ell \ll 1}{\simeq} \frac{1}{\sin\delta_\ell} \simeq \frac{1}{(R_0k)^{2\ell+1}} , \tag{33.165}$$

that is,

$$\sin\delta_\ell \simeq (R_0k)^{2\ell+1} . \tag{33.166}$$

In other words, the scattering phases decrease rapidly, in the regime of cold collisions, with increasing ℓ, and $\ell = 0$ type collisions dominate,

$$k\cot\delta_0 \overset{\alpha_\ell(E) \simeq \alpha_\ell(0)}{\simeq} -\frac{1 + R_0\alpha_0(0)}{R_0^2\alpha_\ell(E)} . \tag{33.167}$$

The s-wave *scattering length* defined by,

$$a_s \equiv \frac{R_0^2\alpha_\ell(E)}{1 + R_0\alpha_0(0)} = \frac{\sin\delta_0}{k} \tag{33.168}$$

then it is the only relevant parameter of the collision. For $R_0\alpha_0 \gg 1$ we find $a \simeq R_0$. For example, for a hard sphere we have $R_\ell(R_0) = 0$, $\alpha_\ell = \infty$, $a = R_0 > 0$ and $\cot\delta_0 = -1/kR_0$. For small kR_0 we obtain $\delta_0 \simeq -kR_0 < 0$, which corresponds to a negative phase shift for the repulsive potential, as expected. The effective cross section is,

$$\boxed{\sigma_0 = \frac{4\pi}{k^2}\frac{1}{1+\cot^2\delta_0} \simeq \frac{4\pi}{k^2+1/a_s^2}} \; . \tag{33.169}$$

In comparison to the effective cross section for higher angular momenta, $\sigma_\ell \propto \frac{\sin^2\delta_\ell}{k^2}$ behaves like,

$$\sigma_\ell \propto R_0^2(R_0k)^{4\ell} \to 0 \; . \tag{33.170}$$

In contrast, we find that the scattering at low energies has an s-wave character, σ being dominated by σ_0,

$$\sigma(E=0) = 4\pi a_s^2 \; . \tag{33.171}$$

For a hard sphere ($a = R_0$) we find an effective cross section *four times larger* than classically expected ($\sigma_{cl} = \pi R_0^2$).

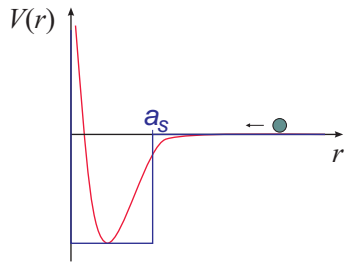

Figure 33.18: The cold collision can be described by a hard core potential.

In summary, for kinetic energies below the centrifugal barrier, only s-wave collisions are significant. The higher-order partial waves are *frozen* behind the centrifugal barrier. That is, the energy of cold collisions is not enough to excite a rotational motion, not even the one with the lowest rotational energy allowed by quantum mechanics. Such a collision is called *cold collision* or *s-wave collision*.

The relative wavefunction tends asymptotically to $\psi(R) \overset{R\to\infty}{\longrightarrow} k_{dB}^{-1}\sin\left[k_{dB}(R-a)\right] \overset{T\to 0}{\longrightarrow} R-a$. This means that for temperatures so low that the length of the Broglie wave of the relative motion is much longer than the potential range $k_{dB}^{-1} \gg R_{turning}$, the scattering becomes independent of temperature, and the scattering length a becomes well defined [11]

Generally, a repulsive interaction potential corresponds to a positive scattering length and an attractive potential to a negative one. However, if the attractive potential supports bound states, the value of the scattering length depends on the energy of the last bound state with respect to the dissociation threshold [1354, 1355].

[11] At temperatures at which the trajectory of atoms is described by de Broglie waves the only difference between an atom before and after an elastic collision is the phase shift δ_0 of this wave.

33.3.1 Collision cross section, unitarity regime

Note that the scattering length a may have a value quite different from r_e, especially in the presence of a Feshbach resonance. The meaning of *universality*, $|a| \gg r_e$, is that short-range properties play no role in the dynamics.

At low temperatures, $kr_e \to 0$, we have the equation (33.169). In contrast, in the *unitarity limit*, $k \to \infty$, but $r_e \to 0$, we have,

$$\sigma = \frac{8\pi}{k^2} \ , \tag{33.172}$$

and the cross section becomes independent of atomic particularities. What the equation (33.169) says is, that the maximum attainable cross-section is limited to the smallest of the values $8\pi a$ and $8\pi/k$. Even though $a(B)$ can be increased to divergent values near a Feshbach resonance, for finite collision energies it will never exceed an effective value $a_{eff} = 1/\sqrt{a^2 + 1/k^2}$. For a thermal gas, $k = \hbar^{-1}\sqrt{2\pi m k_B T}$, while for a pure condensate $k = 2\pi/L$, where L is the size of the condensate. Therefore, the effective scattering length can not exceed the size of the condensate. Unitarity also means that the kinetic energy exceeds the binding energy, $k_B T \equiv \frac{\hbar^2 k^2}{2m} \leq \frac{\hbar^2}{2ma^2}$.

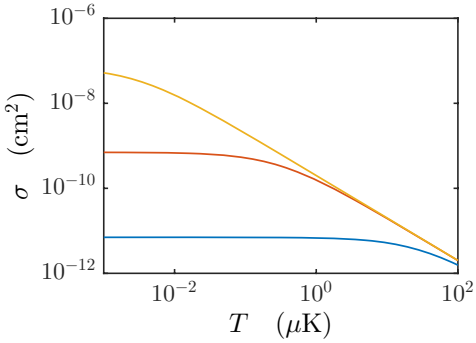

Figure 33.19: (code) Temperature dependence of the collision cross section for various scattering lengths. For higher scattering lengths, the unitarity limit is reached at lower temperatures.

The collision rate depends on the density, temperature and collisional cross section [711],

$$\begin{aligned} \gamma_{coll.peak} &= \sqrt{2}\sigma_{elast}\bar{v}n_0 \ , \\ \gamma_{coll.aver} &= \gamma_{coll.peak}/2\sqrt{2} \ . \end{aligned} \tag{33.173}$$

Note that at the unitary limit, as $\bar{v} \propto \sqrt{T}$, we have that $\sigma_{elas} \propto T$ and $n_0 \propto \bar{r}^{-3} \propto T^{-3/2}$, such that the collision rate is independent of temperature.

At low temperatures, $k \to 0$, the delocalization of the colliding particles is greater than its short-range structure. This is the *Wigner threshold law* [1374, 1363]. For elastic collisions of neutral ground state atoms, the cross section (33.169) becomes temperature-independent. Thus, the rate coefficient decreases as $\langle\sigma\bar{v}\rangle \propto \sqrt{T}$, while the collision rate increases as $\langle\sigma\bar{v}n_0\rangle \propto T^{-1}$.

For inelastic collisions, $\sigma \propto T^{-1}$. For three-body collisions see [424].

33.3.2 Collisions between identical particles

We consider collisions of two identical particles. Separating the center-of-mass coordinates, $\mathbf{R} = \mathbf{r}_1 + \mathbf{r}_2$, from the relative ones, $\mathbf{r} = \mathbf{r}_1 - \mathbf{r}_2$, we see that $\mathbf{R}$ is symmetric and $\mathbf{r}$ antisymmetric in $\mathbf{r}_1$ and $\mathbf{r}_2$. We separate the wavefunction into orbital and spin parts,

$$\Psi(x_1, x_2) = e^{i\mathbf{P}\cdot\mathbf{R}}\psi(\mathbf{r})\chi(s_1, s_2) \ . \tag{33.174}$$

For indistinguishable particles the result of the scattering has the asymptotic form,

$$\psi(\mathbf{r}) \sim e^{i\mathbf{k}\cdot\mathbf{r}} + f(\theta)\frac{e^{ikr}}{r} \ . \tag{33.175}$$

33.3.2.1 Spin 0 bosons

For bosons with spin 0 we have $\chi = 1$ and, because of the symmetry of Ψ, holds $\psi(\mathbf{r}) = \psi(-\mathbf{r})$. Consequently, we must symmetrize the result of the scattering. We make use of the fact that the exchange of particles via $\mathbf{r} \to -\mathbf{r}$ in polar coordinates corresponds to the transformation $\theta \to \pi - \theta$, $r \to r$,

$$\psi \sim (e^{i\mathbf{k}\cdot\mathbf{r}} + e^{-i\mathbf{k}\cdot\mathbf{r}}) + [f(\theta) + f(\pi - \theta)]\frac{e^{ikr}}{r} \ . \tag{33.176}$$

For the effective differential cross section we obtain,

$$\frac{d\sigma}{d\Omega} = |f(\theta) + f(\pi - \theta)|^2 = |f(\theta)|^2 + |f(\pi - \theta)|^2 + 2\mathfrak{Re}\ [f^*(\theta)f(\pi - \theta)] \ . \tag{33.177}$$

The first two terms are classical. The third (interference) term appears because of quantum statistics. The angles showing up in (33.177) are illustrated in Fig. 33.20. For bosons, the interference terms double the cross section as compared to the classical case, when $\theta = \pi/2$,

$$\boxed{\frac{d\sigma}{d\Omega} = 4|f(\tfrac{\pi}{2})|^2} \ . \tag{33.178}$$

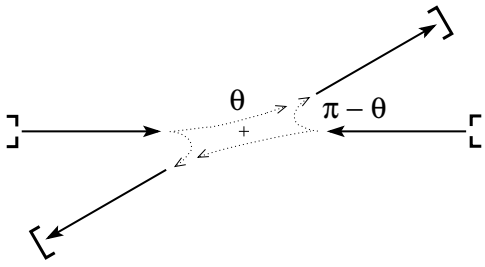

Figure 33.20: The symmetrization of the collision wavefunction produces two paths with angles θ and $\pi - \theta$, which must be added coherently.

For the isotropic potential $V(r)$ we use the partial wave representation,

$$f(\theta) = \sum_\ell i^\ell f_\ell P_\ell(\cos\theta) \ . \tag{33.179}$$

With $P_\ell(\cos\theta) = (-1)^\ell P_\ell(\pi - \cos\theta)$ we get,

$$f(\theta) - f(\pi - \cos\theta) = 2\sum_{\ell\text{par}} i^\ell f_\ell P_\ell(\cos\theta) \ , \tag{33.180}$$

and we find that only *even angular momenta* appear [12]

33.3.2.2 Spin 1/2 fermions

In the case of fermions with spin $\frac{1}{2}$ two situations are possible [13]:

1. The singlet spin state $\chi_s = \frac{1}{\sqrt{2}}[(|\uparrow\downarrow\rangle - |\downarrow\uparrow\rangle]$ is antisymmetric and, consequently, the orbital part,
$$\psi(\mathbf{r}) = \psi(-\mathbf{r}) \tag{33.181}$$
must be symmetric. The cross section is the same as for spin 0 bosons,
$$\left.\frac{d\sigma}{d\Omega}\right|_s = |f(\theta) + f(\pi - \theta)|^2 \ . \tag{33.182}$$

2. The triplet spin states,
$$\chi_s = \begin{cases} |\uparrow\uparrow\rangle \\ \frac{1}{\sqrt{2}}(|\uparrow\downarrow\rangle + |\downarrow\uparrow\rangle) \\ |\downarrow\downarrow\rangle \end{cases} \tag{33.183}$$
require an antisymmetric orbital wavefunction, $\psi(\mathbf{r}) = -\psi(-\mathbf{r})$, and we obtain a scattering amplitude, $f(\theta) \to f(\theta) - f(\pi - \theta)$, which only contains *odd angular momenta* ℓ. With this, the cross section becomes,
$$\left.\frac{d\sigma}{\Omega}\right|_t = |f(\theta) - f(\pi - \theta)|^2 \overset{\theta=\pi/2}{=} 0 \ , \tag{33.184}$$
Note that polarized fermions only scatter in channels of odd angular momenta: cold bosonic atoms show a *contact potential* due to s-wave collisions (33.180)), polarized fermionic atoms only interact weakly in the p-channel. In the case of a statistically mixed ensemble of non-polarized fermions we have a the weighted average,
$$\frac{d\sigma}{d\Omega} = \frac{3}{4}\left.\frac{d\sigma}{\Omega}\right|_t + \frac{1}{4}\left.\frac{d\sigma}{\Omega}\right|_s = |f(\theta)|^2 + |f(\pi - \theta)|^2 - \mathfrak{Re}\,[f^*(\theta) f(\pi - \theta)] \ . \tag{33.185}$$

33.3.2.3 Molecular spectra

Here we consider rotational spectra of low energies $E_{rot} = \hbar^2\ell(\ell+1)/2\Theta \ll E_{eletronico} \sim eV$. In slow time scales we can consider the electronic shell to be rigid. We look at two examples of molecules with bosonic and fermionic nuclei:

[12] For ℓ odd the Legendre polynomial changes sign, and the contributions vanish.

[13] This is analogous to the case of helium, where the spatial function of the state $2s^2\uparrow\uparrow$ is always antisymmetric, but for the $2s\uparrow 2p\uparrow$ exist symmetric spatial orbitals.

- Molecules $(C^{12})_2$: the nuclei are 0-spin bosons, so only collisions with even ℓ are allowed.
- Molecules H_2: the nuclei are spin-$\frac{1}{2}$ fermions, so we have for a spin wavefunction,

$$\chi = \chi_s : \ell = \text{even, para-hydrogen}, \chi = \chi_t : \ell = \text{odd, ortho-hydrogen.} \quad (33.186)$$

The transformation of ortho-hydrogen into para-hydrogen is difficult (the nuclei being well shielded), such that we observe two types of gases with,

$$E_{rot,para} = 0, \frac{3}{\Theta}, \frac{10}{\Theta}, \frac{21}{\Theta}, ... E_{rot,orto} = \frac{1}{\Theta}, \frac{6}{\Theta}, \frac{15}{\Theta}, \dots . \quad (33.187)$$

33.3.3 Collisions between hot atoms

Angular moments with $\ell \leq kR_0$ should contribute a lot to σ, since the collision parameter is inside R_0. For a hard sphere we have $\alpha_\ell = \infty$ and $\cot \delta_\ell = n_\ell(kR_0)/j_\ell(kR_0)$. With the asymptotic expressions of j_ℓ and n_ℓ we obtain $\cot \delta_\ell \sim -\cot(kR_0 - \ell\pi/2)$, that is, $\delta_\sim - kR_0 + \ell\pi/2$ $(+\pi)$. With these scattering phases we can calculate the scattering cross section,

$$\sigma \simeq \tfrac{4\pi}{k^2} \sum_{\ell=0}^{kR_0} (2\ell+1) \sin^2 \delta_\ell \quad (33.188)$$

$$\simeq \tfrac{4\pi}{k^2} \sum_{\ell=0}^{kR_0} (\ell+1) \cos^2[kR_0 - (\ell+1)\pi/2] + \ell \sin^2(kR_0 - \ell\pi/2)$$

$$= \tfrac{4\pi}{k^2} \sum_{\ell=0}^{kR_0} \ell(\cos^2 + \sin^2) = \tfrac{4\pi}{k^2} \frac{kR_0(kR_0+1)}{2} = 2\pi R_0^2 , \quad (33.189)$$

which is the double of the classical value.

33.3.4 Photoassociation during ultracold collisions

Ultra-cold collisions are an interesting example of how light can control the result of inelastic or reactive collisions. Here we discuss as a specific example the *photoassociation*, which illustrates the utility of the dressed states pictures. The upper panel of Fig. 33.22 shows schematic curves of (bare) potentials relevant to our discussion. Two atoms in the ground state form a relatively shallow molecular ground state characterized by electrostatic dispersion

$$V_1(r) = -\frac{C_6}{R^6} . \quad (33.190)$$

or long-range *van der Waals potential*. Two other molecular states arise from the interaction of an excited atom with the ground state atom. The predominant term of the interaction is the potential of resonant dipole-dipole interactions,

$$V_{2,3}(r) = - \mp \frac{C_3}{R^3} . \quad (33.191)$$

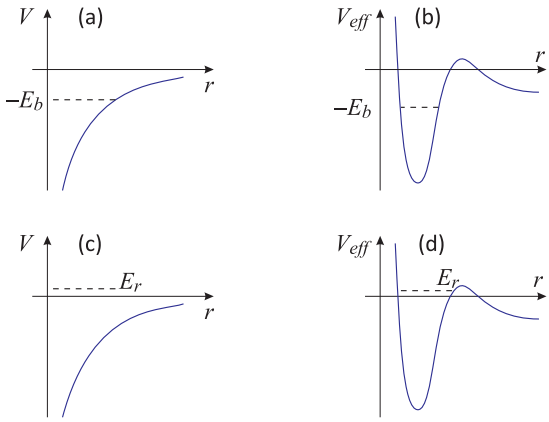

Figure 33.21: (a) Bound state for $\ell = 0$. (b) Bound state for $\ell > 0$ in a potential including the centrifugal barrier $\hbar^2\ell(\ell+1)/2mr^2$. (c) Resonances for $\ell = 0$ are broad and possibly not defined with $\Gamma_r > E_r$. A defined resonance with $\Gamma_r < E_r$ requires that $|\partial_E \alpha_0|$ be large. (d) For $\ell > 0$ we obtain narrow resonances called *shape resonance*s, because the decay of the state is suppressed by the centrifugal barrier.

which gives rise to an attractive and a repulsive potential. The R^{-3} dependence of the resonant dipole interaction means that the associated potentials greatly modify the asymptotic level even at internuclear distances where the ground state van der Waals potential is still relatively shallow. The photoassociation process involves a slow approach of two identical ground state atoms. A mono-modal optical field, tuned to the red of the atomic resonance, is applied. When the two atoms reach an internuclear distance R_C such that the energy of the applied field $\hbar\omega_C$ exactly coincides with the potential difference $V_2(R_c) - V_1(R_c)$, the probability of transferring population from the fundamental molecular state to the excited molecular state is maximal. This molecular resonance is sometimes called *Condon point*. The conventional way of calculating this probability follows the procedure elaborated in Sec. ?? for a two-level atom. First, we would solve the time-independent molecular Schrödinger equation to obtain the molecular wavefunctions. Then, write down the coupled differential equations by describing the time dependence of the expansion coefficients of the relevant molecular wavefunctions, solve for the coefficients and calculate the square of their absolute values. Finally, we would need to integrate the transition probability inside a region ΔR around the Condon point, where the transition probability is not be negligible. The dressed states picture allows to reduce this rather laborious program, essentially, to a problem of a curve crossing of two levels. The bottom panel of Fig. 33.22 illustrates the photoassociation in the dressed states picture. The basis states are now product states made up of the field and the molecular levels. Furthermore, we approximate the molecular states themselves as products of atomic states. This approximation is justified by the long range, weakly perturbative influence of the van der Waals and resonant dipoles interactions. Calling the ground and excited states $|1\rangle$ and $|2\rangle$, respectively, we have

$$|1, n\rangle = |1\|1\rangle|n\rangle \ , \tag{33.192}$$

and for the field-molecule excited state

$$|2, n-1\rangle = |2\|1\rangle|n-1\rangle \ . \tag{33.193}$$

The two molecular curves intersect at the Condon point and optically couple to the applied field. This optical coupling produces an *avoided crossing* near R_C and mixes the states of the molecule-field basis. The well-known *Landau-Zener* formula (LZ) expresses the probability of traversing from one adiabatic molecular state to another as a function of the interaction strength, the relative velocity of the collision partners, and the relative slopes of the two curves. The probability of LZ is given by,

$$\exp \frac{2\pi \langle 1, n|\frac{\Omega}{2}|2, n-1\rangle}{v\left|\frac{d}{dR}\Delta V_{12}(R_C)\right|} \ , \tag{33.194}$$

where v is the relative radial velocity of the approaching particles and $\frac{d}{dR}\Delta V_{12}(R_C)$ is the difference of slopes of the two non-interacting potentials at the Condon point. The dipole-field interaction operator Ω must be taken with the dipole of the molecular transition. A reasonable approximation is to take the moment of molecular transition as twice the atomic moment and average over the whole space. The result is,

$$\exp \frac{\frac{2\pi}{\sqrt{3}} \langle 1, n|\Omega_{at}|2, n-1\rangle}{v\left|\frac{d}{dR}\Delta V_{12}(R_C)\right|} \ , \tag{33.195}$$

where Ω_{at} denotes the atomic operator of the dipole-field interaction. In the case of a crossing of an essentially flat potential V_1 and $V_2(R) = -\frac{C_3}{R}^3$, the absolute value of the derivative of the slope difference is,

$$\left|\frac{d}{dR}\Delta V_{12}(R_C)\right| = \frac{3C_3}{R_C^3} \ . \tag{33.196}$$

Resolve Exc. 33.3.13.1.

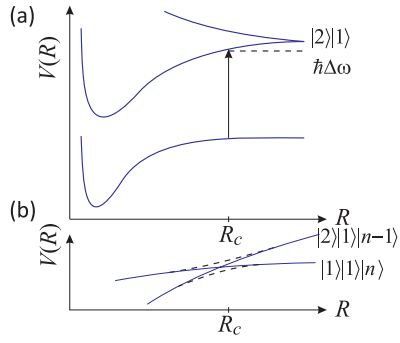

Figure 33.22: (Above) Molecular states resonantly coupled by a light field at the Condon point. (Below) Same coupling of the molecular states represented by an avoided intersection in the dressed states basis.

33.3.5 Ground state collisions

33.3.6 Hyperfine structure

We consider the scheme (32.90), we set $\mathbf{l}_j = 0$, and concentrate on s-waves, $\ell = 0$,

$$\begin{array}{ccccccc} \mathbf{s}_1 & + & \mathbf{s}_2 & = & \mathbf{S} & \xrightarrow{\hat{z}} & \mathbf{\Omega} \\ + & & + & & + & & \\ \mathbf{i}_1 & + & \mathbf{i}_2 & = & \mathbf{I} & & \\ = & & = & & = & & \\ \mathbf{f}_1 & + & \mathbf{f}_2 & = & \mathbf{f} & & \end{array} \tag{33.197}$$

At short distances the coupling $((S,I)f_1,f_2)f$ breaks up and a $((s_1,s_2)S,I)f$ coupling emerges. This does not hold for fully stretched spin states $f_1 + f_2 = f$, because f is a good quantum number at all distances (and small enough magnetic fields). In contrast m_f is a good quantum number at all distances and at all fields.

In order to obtain the potentials coupled by hyperfine interaction, we first calculate for a *single vibrational level* the relative wavefunctions $|\psi_{(f_1,f_2)f}(R)\rangle$ from the known perturbed but uncoupled potentials $V(R) + V_{hf}$, where,

$$V_{hf} = ha_{hf,1}\mathbf{s}_1\cdot\mathbf{i}_1 + ha_{hf,2}\mathbf{s}_2\cdot\mathbf{i}_2 \ . \tag{33.198}$$

The antisymmetric part is negligible [1339], so that $V_{hf} \simeq \frac{1}{2}ha_{hf,1}\mathbf{S}\cdot\mathbf{i}_1 + \frac{1}{2}ha_{hf,2}\mathbf{S}\cdot\mathbf{i}_2$. Then couple the channels via,

$$|\psi_{(S,I)f}(R)\rangle = A\sum_{f_1,f_2}\sqrt{\hat{S}\hat{I}\hat{f}_1\hat{f}_2}\begin{Bmatrix} s_1 & s_2 & S \\ i_1 & i_2 & I \\ f_1 & f_2 & f \end{Bmatrix}|\psi_{(f_1,f_2)f}(R)\rangle \tag{33.199}$$

$$|\psi_{(f_1,f_2)f}(R)\rangle = A^{-1}\sum_{S,I}\sqrt{\hat{S}\hat{I}\hat{f}_1\hat{f}_2}\begin{Bmatrix} s_1 & s_2 & S \\ i_1 & i_2 & I \\ f_1 & f_2 & f \end{Bmatrix}|\psi_{(S,I)f}(R)\rangle \ .$$

which satisfies the orthogonality relation (see Tables in 28.2).

33.3.7 Scattering length in specific channels

The scattering length in specific channels can be expressed via singlet and triplet scattering length,

$$a_{|f_1,m_{f1}\rangle+|f_2,m_{f2}\rangle} = P_{S=0}a_s + P_{S=1}a_t \ . \tag{33.200}$$

The projectors are $P_S = |\langle S|(f_1f_2)f\rangle|$. According to [213] or [889] the recoupling from the uncoupled hyperfine representation into the short range representation is

given by,

$$\langle Sm_S\ Im_I\ \ell' m_{\ell'}|f_1 m_{f1}\ f_2 m_{f2}\ \ell m_\ell\rangle = \delta_{\ell\ell'}\delta_{m_\ell m'_\ell}\sum_{f,m_f}\langle Sm_S\ Im_I|fm_f\rangle\langle f_1 m_{f1}\ f_2 m_{f2}|fm_f\rangle\times \tag{33.201}$$

$$\times\begin{Bmatrix} s_1 & s_2 & S \\ i_1 & i_2 & I \\ f_1 & f_2 & f \end{Bmatrix}\sqrt{\hat{S}\hat{I}\hat{f}_1\hat{f}_2}\left(\frac{1-(1-\delta_{f_1 f_2})(-1)^{S+I+\ell}}{\sqrt{2-\delta_{f_1 f_2}}}\right)\ .$$

The last bracket is dropped for unsymmetrized recoupling. Calculations have been done for ^{87}Rb collisions and for ^{6}Li^{87}Rb collisions. It turns out that the fully stretched states have pure triplet character.

Note that in strong magnetic fields the coupling $(i_1, i_2)I$ easily breaks up, and the recoupling to be considered is rather $\langle Sm_S\ m_{i1}\ m_{i2}\ \ell' m_{\ell'}|f_1 m_{f1}\ f_2 m_{f2}\ \ell m_\ell\rangle$.

33.3.8 Hyperfine coupling in magnetic fields

33.3.8.1 Zeeman splitting of bound states

The splitting of the bound state is described by [1339],

$$\begin{aligned} H^+_{int} &= V^+_{hf} + V_{Zeeman} \\ &= E_B + \frac{1}{2}ha_{hf,1}\mathbf{S}\cdot\mathbf{i}_1 + \frac{1}{2}ha_{hf,2}\mathbf{S}\cdot\mathbf{i}_2 + \mu_B\mathbf{B}(g_S\mathbf{S} + g_1\mathbf{i}_1 + g_2\mathbf{i}_2)\ , \end{aligned} \tag{33.202}$$

such that,

$$\begin{aligned} &\langle m'_{i1}m'_{i2}m'_S|H_{hfs}+H_B|m_S m_{i2}m_{i1}\rangle \\ &= E_B + (g_S m_S + g_{i1}m_{i1} + g_{i2}m_{i2})\mu_B B\delta_{m'_{i1}\ m_{i1}}\delta_{m'_{i2}\ m_{i2}}\delta_{m'_S\ m_S} \\ &+ \tfrac{1}{2}h(a_{hf,1}m_{i1}m_S + a_{hf,2}m_{i2}m_S)\delta_{m'_{i1}\ m_{i1}}\delta_{m'_{i2}\ m_{i2}}\delta_{m'_S\ m_S} \\ &+ \tfrac{1}{4}ha_{hf,1}(i_{1,+}S_-\delta_{m'_S\ m_S+1}\delta_{m'_{i1}\ m_{i1}-1} + i_{1,-}S_+\delta_{m'_{i1}\ m_{i1}-1}\delta_{m'_S\ m_S+1})\delta_{m'_{i2}\ m_{i2}} \\ &+ \tfrac{1}{4}ha_{hf,2}(i_{2,+}S_-\delta_{m'_S\ m_S+1}\delta_{m2\ m_{i2}-1} + i_{2,-}S_+\delta_{m'_{i2}\ m_{i2}-1}\delta_{m'_S\ m_S+1})\delta_{m'_{i1}\ m_{i1}}\ . \end{aligned} \tag{33.203}$$

For an example on how to evaluate the matrix at various magnetic fields and obtain the hyperfine structure of a bound state in the Zeeman and the Paschen-Back regime, we propose the systems ^{6}Li^{23}Na and ^{6}Li^{87}Rb.

33.3.8.2 Magnetic dipole interaction

Reads,

$$V_{dd} = \frac{\mu_0}{4\pi R^3}\left[\mu_1\cdot\mu_1 - 3(\mu_2\cdot\mathbf{R})(\mu_2\cdot\mathbf{R})\right] \tag{33.204}$$

neglecting nuclear spin.

33.3.8.3 Second-order spin-orbit interaction

First-order spin-orbit interaction disappears for ground state collisions. But second-order spin-orbit interaction may occur. These lead to inelastic losses (see next section).

33.3.8.4 Selection rules

The selection rules for bosonic homonuclear collisions are,

$$\begin{aligned} S &= 0, .., s_1 + s_2 \\ I &= 0, .., i_1 + i_2 \\ f_j &= |i_j - s_j|, .., i_j + s_j \\ |I - S| \leq F &\leq I + S \\ |f_1 - f_2| \leq F &\leq f_1 + f_2 \\ (-1)^I &= (-1)^S \quad \text{for all } F \\ (-1)^{f_1} &= -(-1)^{f_2} \quad \text{for all odd } F \ . \end{aligned} \tag{33.205}$$

What does they look like for fermions? What does they look like for heteronuclear collisions?

33.3.9 Inelastic collisions

33.3.9.1 Spin changing collisions

These have their origin in *spin exchange* and spin dipole-dipole processes. Spin exchange occurs when the colliding electronic clouds overlap. At short distances the $((S, I)f_1, f_2)f$ breaks up and a $((s_1, s_2)S, I)f$ coupling remixes, as shown in Exc. 32.3.5.1. Hence, collisions between atoms $|f_1, m_{f1}\rangle|f_2, m_{f2}\rangle$ are subject to spin exchange induced by coupling of the spin states via the exchange interaction, e.g. $|2, 1\rangle|2, 1\rangle \to |2, 2\rangle|2, 0\rangle$. Typical exchange rates are on the order of $10^{-10}\,\mathrm{cm}^3/\mathrm{s}$.

Since f is a good quantum number at all distances (for $B = 0$), spin exchange processes conserve ℓ and f. Hence, the fully stretched spin states $f_1 + f_2 = f$ cannot decay into other states, except by higher-order processes, such as dipolar relaxation. Consequently, the relaxation rates for $|2, 2\rangle + |2, 2\rangle$ or $|1, -1\rangle + |1, -1\rangle$ states are only on the order of $10^{-15}\,\mathrm{cm}^3/\mathrm{s}$.

The cross section for inelastic spin exchange collisions is [1367, 296],

$$\sigma = M_{if}\pi(a_t - a_s)^2 \ , \tag{33.206}$$

where,

$$\begin{aligned} M_{if} &= \left[\sum_{m_S, I, m_I} (C_{S=0} C'_{S=0} - C_{S=1} C'_{S=1}) \right]^2 \\ C &= \langle S, m_S; I, m_I | F_1 m_1; F_2 m_2 \rangle \ . \end{aligned} \tag{33.207}$$

See also [1207]. The reason for the above dependence can be understood as follows. a_s and a_t determine the energy of the last bounds states of the singlet and triplet potentials. The more those energies are different, the stronger the coupling $\propto |E_t - E_s|^{-1}$. An alternative, physical picture is given in [215].

33.3.9.2 Dipolar relaxation

The fully stretched spin states, such as ^{87}Rb $|f = 2, m_f = 2\rangle$ are expected to be quite stable. However, relativistic effects (retardation?) (and 2^{nd} order spin-orbit coupling) break the degeneracy of the molecule-fixed projection $|\Omega| = 0, 1$ of the $^3\Sigma$ potential [889]. When the atoms approach their spins recouple, i.e. from $[(s_1, i_1)f_1\ ,\ (s_2, i_2)f_2]f$ towards $[(s_1, s_2)s\ ,\ (i_1, i_2)i]f$ as described by the $9j$ coefficients Eq. (33.197). Due to the symmetry of the problem, f and its projection m_f are good quantum numbers at all distances. However, if there is a higher-order admixture of the orbit l_j, the symmetry is broken, and the quantum number depends on the coupling schemes. Consequently, transitions between different m_f become possible, i.e. dipolar relaxation may change f, m_f or $\ell = 0$, e.g. a collision can be s-wave in the entrance and d-wave in the exit channel.

33.3.9.3 Three-body collisions

The trapped low-field seeking alkali gases are metastable versus 3-body recombination. 3-body recombination is the combination of two colliding atoms to a dimer in presence of a third atom receiving the excess energy as kinetic energy and results in trap loss of the molecule and of the atom. They are suppressed as the gas gets more and more dilute since the rate goes like n^3. There might be interesting 3-body resonance phenomena like the *Efimov state* predicted for Helium droplets [407], [801] and recently seen in experiment [750, 1267, 186, 828].

3-body recombination is in contrast to the more controlled way of creating molecules via photoassociation or coherent free-bound coupling.

Ultracold collisions are crucial for BEC. They provide the thermalizing elastic collisions necessary for evaporative cooling, they are the cause for the condensate self-energy and give rise to nonlinearities in the condensate dynamics. But they are also interesting by themselves. The spectrum of two-body collisions exhibits interesting features like shape- and Feshbach resonances [300, 648]. Their analysis facilitates detailed conclusions on the nature of the interaction potentials. Three body collisions are important to investigate, because they constitute a decay mechanism of the intrinsically metastable system that represents a trapped Bose-gas.

Three body collisions are not a quantum statistical effect and don't require the presence of a BEC, but they occur only at very high densities comparable to those necessary for BEC. It should be possible to detect them in *photoassociation* (PA) spectra. Photoassociation provides a tool to explore the level structure of excited states by shining in a laser with frequency ν tuned between the colliding channel and a vibrational bound level of the excited state potential. Since the excited state preferentially decays into the continuum, where the atoms have high kinetic energy, the transition rate may be monitored via trap losses. Or we can shine in an additional laser that further excites the excited atoms into the ionized continuum where they can be registered by an ion detector.

Three-body photoassociation processes should reveal themselves by additional lines in the two-body photoassociation spectra. Those lines should only appear at very high densities and their strength should scale as the density cubed,

$$Rb + Rb + Rb + h\nu \rightarrow Rb_3^* \ . \tag{33.208}$$

33.3.9.4 Other processes

Majorana spin flips and collisions involving higher partial waves ℓ can eventually lead to spin relaxation. In Eq. (32.90) we see that f is not necessarily a good quantum number in contrast to F, $|2,2\rangle|2,2\rangle \to |2,1\rangle|2,0\rangle + E_{rot}$. However, the particles must tunnel across the centrifugal barrier, which sets temperature constraints.

33.3.9.5 Collisions between fermions

Very cold three-body collisions are suppressed for fermions, because two of them necessarily must have the same quantum state, which violates the Pauli exclusion principle. This is useful for employing Feshbach resonances to form molecular BECs made of fermions.

33.3.10 Excited states collisions

33.3.10.1 Adiabatic potentials

We consider the scheme (32.90), we set $\mathbf{I} = 0$, and we concentrate on s-waves, $\ell = 0$,

$$\begin{array}{ccccccc} \mathbf{l}_1 & + & \mathbf{l}_2 & = & \mathbf{L} & \xrightarrow{\hat{z}} & \mathbf{\Lambda} \\ + & & + & & + & & + \\ \mathbf{s}_1 & + & \mathbf{s}_2 & = & \mathbf{S} & \xrightarrow{\hat{z}} & \mathbf{\Sigma} \\ = & & = & & = & & = \\ \mathbf{j}_1 & + & \mathbf{j}_2 & = & \mathbf{j} & \xrightarrow{\hat{z}} & \mathbf{\Omega} \end{array} \tag{33.209}$$

The *spin-orbit interaction* splits the potential curves. The recoupling is described by,

$$|\psi_{(L,S)j}(R)\rangle \sim \sum_{j_1,j_2} \sqrt{\hat{L}\hat{S}j_1j_2} \begin{Bmatrix} l_1 & l_2 & L \\ s_1 & s_2 & S \\ j_1 & j_2 & j \end{Bmatrix} |\psi_{(j_1,j_2)j}(R)\rangle \ . \tag{33.210}$$

33.3.10.2 Homonuclear collisions

Let us consider the example of the fine structure in homonuclear ^{87}Rb collisions. Without hyperfine, rotational and Zeeman splitting the recoupling goes like illustrated in Fig. 33.23.

From Fig. 33.23 we see that the molecular states are remixed at long range: Every state $0_g^-, 0_u^-, 0_g^+, 0_u^+, 1_g, 1_u, 2_g, 2_u$ has several molecular states to which it connects, e.g. 0_g^- connects within the fine structure to $(2)^3\Sigma_g^+$ and $(2)^3\Pi_g$. Those multiplets form a closed interacting subspace. According to Movre and Pichler [930, 1305] we

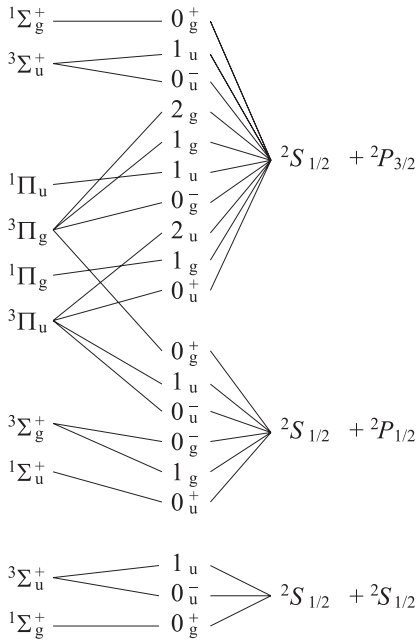

Figure 33.23: Movre coupling scheme.

get with $\Delta = E(^2P_{3/2}) - E(^2P_{1/2}) = \frac{3}{2}A_{so}$,

$$0_\sigma^- = \begin{pmatrix} E(^3\Pi_\sigma) - \frac{1}{3}\Delta & \frac{\sqrt{2}}{3}\Delta \\ -\frac{\sqrt{2}}{3}\Delta & E(^3\Sigma_\sigma^+) \end{pmatrix} \quad , \quad 0_\sigma^+ = \begin{pmatrix} E(^3\Pi_\sigma) - \frac{1}{3}\Delta & -\frac{\sqrt{2}}{3}\Delta \\ -\frac{\sqrt{2}}{3}\Delta & E(^1\Sigma_\sigma^+) \end{pmatrix} \tag{33.211}$$

$$1_\sigma = \begin{pmatrix} E(^3\Pi_\sigma) & \frac{1}{3}\Delta & -\frac{1}{3}\Delta \\ \frac{1}{3}\Delta & E(^1\Pi_\sigma) & -\frac{1}{3}\Delta \\ -\frac{1}{3}\Delta & -\frac{1}{3}\Delta & E(^3\Sigma_\sigma^+) \end{pmatrix} \quad , \quad 2_\sigma = \left(^3\Pi_\sigma\right) \ .$$

At short range the potentials approximately go like,

$$\begin{aligned} E(^1\Sigma_g^+), E(^3\Sigma_u^+) &\propto 2C_3/R^3 \\ E(^1\Pi_u), E(^3\Pi_g) &\propto C_3/R^3 \\ E(^1\Pi_g), E(^3\Pi_u) &\propto -C_3/R^3 \\ E(^1\Sigma_u^+), E(^3\Sigma_g^+) &\propto -2C_3/R^3 \ . \end{aligned} \tag{33.212}$$

Inserting the short range potentials and defining $X = \sigma C_3/3\Delta R^3$, $Y = E/\Delta$ and

$\sigma = +$ for g and $-$ for u,

$$0^-_\sigma = \begin{pmatrix} 3X+\frac{1}{3} & \frac{\sqrt{2}}{3} \\ \frac{\sqrt{2}}{3} & -6X+\frac{2}{3} \end{pmatrix} \quad , \quad 0^+_\sigma = \begin{pmatrix} 3X+\frac{1}{3} & \frac{\sqrt{2}}{3} \\ \frac{\sqrt{2}}{3} & 6X+\frac{2}{3} \end{pmatrix} \tag{33.213}$$
$$1_\sigma = \begin{pmatrix} 3X+\frac{1}{3} & \frac{1}{3} & -\frac{1}{3} \\ \frac{1}{3} & -3X+\frac{1}{3} & -\frac{1}{3} \\ -\frac{1}{3} & -\frac{1}{3} & -6X+\frac{2}{3} \end{pmatrix} \quad , \quad 2_\sigma = (3X+1) \; .$$

Note that the structure looks very much like the transition from the Zeeman to the Paschen-Back regime, where X plays the role of the magnetic field and Y the level shift. The characteristic equations are,

$$\begin{aligned} Y^2 - (1-3X)Y - 18X^2 &= 0 \quad \text{for} \quad 0^-_\sigma \\ Y^2 - (1+9X)Y + (4X+18X^2) &= 0 \quad \text{for} \quad 0^+_\sigma \\ Y^3 + (-2+6X)Y^2 + (1-8X-9X^2)Y + (2X+6X^2-54X^3) &= 0 \quad \text{for} \quad 1_\sigma \\ Y - (1+3X) &= 0 \quad \text{for} \quad 2_\sigma \end{aligned} \tag{33.214}$$

33.3.11 Heteronuclear collisions

For a collision in the channel ^{6}Li P ^{87}Rb S we get the $\{9j\}$-symbol,

$$\begin{Bmatrix} l_6 & l_{87} & L \\ s_6 & s_{87} & S \\ j_6 & j_{87} & j \end{Bmatrix} = \begin{Bmatrix} 0 & 1 & 1 \\ \frac{1}{2} & \frac{1}{2} & S \\ \frac{1}{2} & j_{87} & j \to \Omega \end{Bmatrix} \; . \tag{33.215}$$

We thus expect a fine structure $j_{87} = \frac{1}{2}, \frac{3}{2}$ at long range and exchange interactions $S = 0, 1$ at short range. For the projection onto the internuclear axis $|L-S| \leq \Omega \leq L+S$.

Let $V_k(R)$ be the uncoupled potentials and,

$$\Delta_{kl}(R) = D_{kl} + A_{kl}\left([1 - e^{-B_{kl}(R-R_{kl})}]^2 - 1\right) \tag{33.216}$$

the spin-orbit functions modeled as Morse potentials, where D_{kl} is related to the fine-structure splitting, $D_{kl} = \frac{1}{3}(E_k - E_l)$, for diagonal and, $D_{kl} = \frac{\sqrt{2}}{3}(E_k - E_l)$, for off-diagonal elements. For heteronuclear molecules like ^{6}Li^{87}Rb we have matrices like [129, 128],

H	$\vert^3\Sigma^+\rangle$	$\vert^3\Pi\rangle$	$\vert^1\Sigma^+\rangle$	$\vert^3\Pi\rangle$	$\vert^3\Sigma^+\rangle$	$\vert^1\Pi\rangle$	$\vert^3\Pi\rangle$	$\vert^3\Pi\rangle$
$\langle^3\Sigma^+_{\Omega=0^-}\vert$	$V(^3\Sigma)$	$\Delta_{cb}\sqrt{2}$						
$\langle^3\Pi_{\Omega=0^-}\vert$	$\Delta_{cb}\sqrt{2}$	$V(^3\Pi) - \Delta_{bb}$						
$\langle^1\Sigma^+_{\Omega=0^+}\vert$			$V(^1\Sigma)(-2\Delta_{bb})$	$-\Delta_{bb}$				
$\langle^3\Pi_{\Omega=0^+}\vert$			$-\Delta_{bb}$	$V(^3\Pi)\,(+\Delta_{bb})$				
$\langle^3\Sigma^+_{\Omega=1}\vert$					$V(^3\Sigma)$	Δ_{cB}	Δ_{cb}	
$\langle^1\Pi_{\Omega=1}\vert$					Δ_{cB}	$V(^1\Pi)$	$-\Delta_{bB}$	
$\langle^3\Pi_{\Omega=1}\vert$					Δ_{cb}	$-\Delta_{bB}$	$V(^3\Pi)$	
$\langle^3\Pi_{\Omega=2}\vert$								$V(^3\Pi) + \Delta_{bb}$

(33.217)

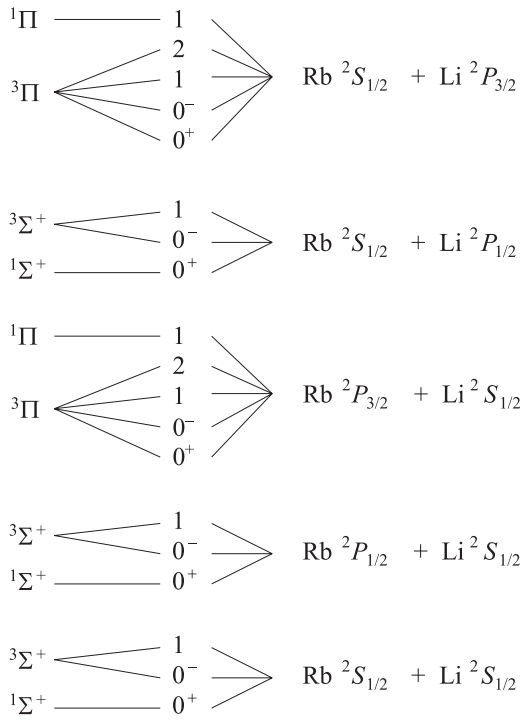

Figure 33.24: Movre type spin-orbit recoupling scheme for heteronuclear molecules.

for every fine structure. For example, there is a matrix for the two ^{6}Li $S_{1/2}$ ^{87}Rb$P_{1,3/2}$ asymptotes and another one for the ^{6}Li $P_{1/2,3/2}$ ^{87}Rb S_1 asymptotes. Additional terms enter via rotational effects [129].

Concretely,

$$\begin{aligned}
\Delta_{bb}(R\to\infty) &= \frac{1}{3}(E_{3/2}-E_{1/2}) \\
\Delta_{cB}(R\to\infty) &= \frac{1}{3}(E_{3/2}-E_{1/2}) \\
\Delta_{bB}(R\to\infty) &= \frac{1}{3}(E_{3/2}-E_{1/2}) \\
\Delta_{cb}(R\to\infty) &= \frac{1}{3}(E_{3/2}-E_{1/2})\ .
\end{aligned} \tag{33.218}$$

33.3.11.1 Inelastic trap losses

Between ground and excited states *fine changing collision*s and *radiative escape* are possible. Between two ground states only *hyperfine changing collision*s may occur.

The nature of the collision process, whether it is a one- [14], two-, or three-body collision, reveals itself via the temporal behavior of trap losses. Using the abbrevia-

[14] By one-body collision we mean collisions with atoms of the background gas.

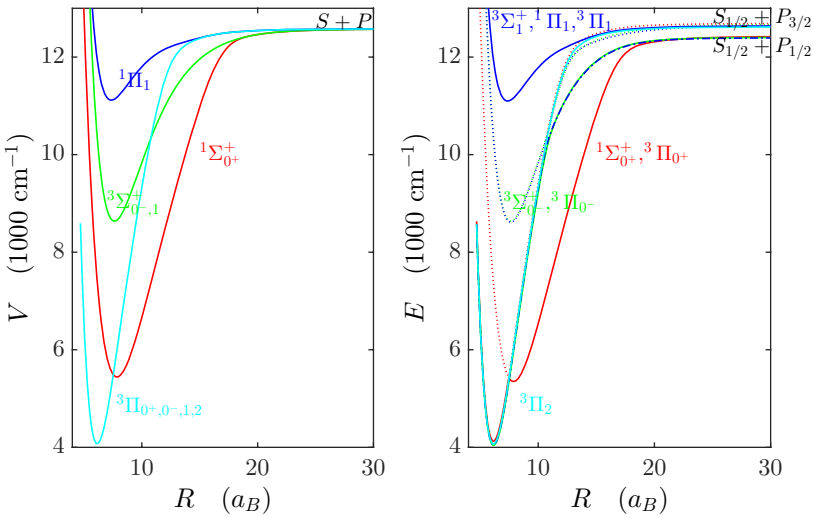

Figure 33.25: (code) Adiabatic potentials.

tion,

$$\langle \eta \rangle \equiv \frac{1}{N} \int \eta(\mathbf{r}) n(\mathbf{r}) d^3 r \ , \tag{33.219}$$

we can write the loss rates due to inelastic one-, two-, and three-body collisions,

$$B\langle 1 \rangle N \quad , \quad K\langle n \rangle N \quad , \quad L\langle n^2 \rangle N \ . \tag{33.220}$$

the prefactors depend on the collision velocity (that is, the temperature of the sample) and atomic parameters (for example, the collision cross section for two-body collisions, which may itself depend on temperature). Hence, the total number of trapped atoms evolves according to,

$$\boxed{\dot{N} = -B\langle 1 \rangle N - K\langle n \rangle N - L\langle n^2 \rangle N} \ . \tag{33.221}$$

Assuming a gaussian density distribution,

$$n(\mathbf{r}) = \frac{N}{(2\pi)^{3/2}\bar{r}^3} e^{-r^2/2\bar{r}^2} \ , \tag{33.222}$$

we calculate,

$$\dot{N} = -BN - \frac{K}{(4\pi)^{3/2}\bar{r}^3} N^2 - \frac{L}{3^{3/2}(2\pi)^3\bar{r}^6} N^3 \ . \tag{33.223}$$

Fig. 33.26 shows a simulation of Eq. (33.223).

For condensates in the Thomas-Fermi limit [1227] found the following differential equations for two- and three-body collisions,

$$\frac{\dot{N}}{N} = -Gc_2 N^{2/5} - \frac{1}{\tau} \quad \text{and} \quad \frac{\dot{N}}{N} = -Lc_3 N^{4/5} - \frac{1}{\tau} \ . \tag{33.224}$$

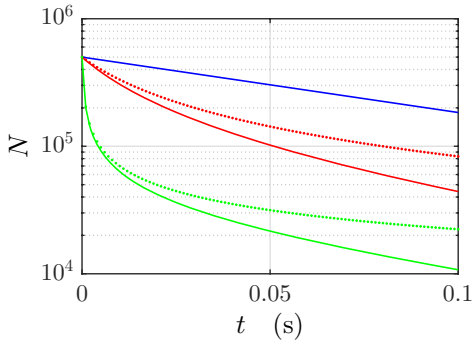

Figure 33.26: (code) One-, two-, and three-body losses.

33.3.12 Heteronuclear electric dipole moment

The *electric dipole moment* of a dimer is highest for big mass difference, as in the case of LiRb and for low vibrational quantum number [744, 63]. The electric dipole moment determines the rate for spontaneous and *black-body radiation*, $\bar{n} = (e^{-\beta\hbar\omega} - 1)^{-1}$, induced transitions between rovibrational states [745], $\Gamma^{tot}_{vlm} = \Gamma^{spnt}_{vlm} + \Gamma^{bb}_{vlm}$. With the transition rate between individual levels,

$$\Gamma^{\alpha}_{vlm\to v'l'm'} = \frac{8\pi}{3}\frac{\omega^3}{hc^3}|\langle|d|\rangle|^2 \ , \tag{33.225}$$

we can estimate the rates for spontaneous emission,

$$\Gamma^{spnt}_{vlm} = \sum\nolimits_{v'l'm'} \Gamma^{em}_{vlm\to v'l'm'} \ , \tag{33.226}$$

and for black-body radiation,

$$\Gamma^{bb}_{vlm} = \sum_{v'l'm'} \bar{n}\Gamma^{em}_{vlm\to v'l'm'} + \sum_{v''l''m''} \bar{n}\Gamma^{abs}_{vlm\to v''l''m''} \ . \tag{33.227}$$

Note that selection rules require $|l - l'| \leq 1$ and $|m - m'| \leq 1$, rotational transitions are inhibited by small ω^3, spontaneous emission is high for intermediate levels for which on one hand ω^3 is large enough and enough final states are available.

From calculations of the R-dependence of the electric dipole moments [63] the dipole moment of a specific vibrational state is easily estimated from,

$$d = \frac{\int \psi(R) R \psi(R) dR}{\int \psi(R)\psi(R) dR} \ . \tag{33.228}$$

In electric fields the dipole moments will lead to Stark shifts. For $|d| = 1$ Debye in a field of 1 V/m we expect a Stark shift of $H_{Stark} \approx 500$ kHz. It may be possible to measure this by photoassociation spectroscopy. Note also that since homonuclear dimers do not have a permanent electric dipole moment, transitions between vibrational ground states are forbidden.

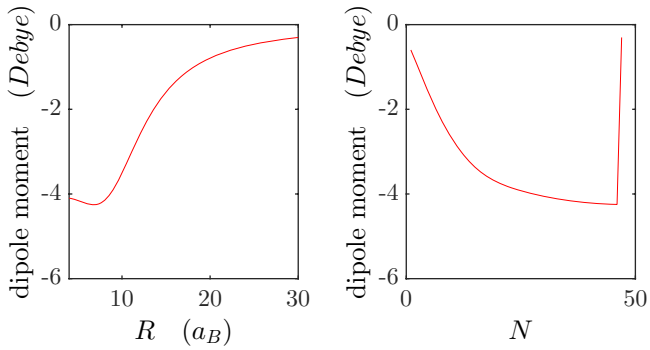

Figure 33.27: (code) (a) Dipole moment at the example of LiRb as a function of interatomic distance. (b) Dipole moment at the example of LiRb as a function of vibrational quantum number.

33.3.13 Exercises

33.3.13.1 Ex: Photoassociation

Consider a laser focused into a cold, confined cloud of Na atoms at a temperature of 450 μK. For a detuning of 600 MHz, calculate the laser intensity (in W/cm^2) required to produce a 25% probability of photoassociation. The transition moment (a.u.) of Na is 2.55.

Solution:

33.3.13.2 Ex: Vibrational structure of LiRb

Calculations of the vibrational structures of several ground states of the heteronuclear molecule LiRb.

Solution: *LiRbPotential_1Sigma:*
LiRbPotential_3Sigma:
LiRbPotential_1Pi:
LiRbPotential_3Pi:
LiRbPotential_13Delta:
LiRbStatesAdiabatic: Long-range interaction of Li with Rb, splitting at collision, Hunds Fall (c) via [Movre77].
LiRbStatesCompare: Compares ab-initio and fitted potentials.
LiRbStatesCoupledChannels: Fourier grid for solving a LiRb potential and mean distance.
LiRbStatesDipolemoment: R-dependent dipolemoment approximated from [Aymar05].
LiRbStatesFit: Fits adapted curve to ab-initio potential.
LiRbStatesFourierGrid: Fourier grid method for a specified LiRb potential.
LiRbStatesFranckCondon: Franck-Condon overlap for a specified LiRb potentials.
LiRbStatesOpenChannel: Finds wavefunction of open channel.

LiRbStatesPlot: Plots heteronuclear potentials [Korek00].
LiRbStatesRecouplingHfs: Recoupling due to hyperfine coupling by recoupling wavefunctions using 9j-coefficients.
LiRbStatesRecouplingHfs2,3: Recoupling due to hyperfine coupling by recoupling potentials using 9j-coefficients.
LiRbStatesRecouplingSo: Recoupling due to spin-orbit coupling using 9j-coefficients.
LiRbStatesSolve: Single eigenvalue and eigenstates in a given intervall.
LiRbStatesSpectrum: Complete eigenspectrum.
LiRbStatesSymb9jTest: Tests correctness of 9j-routine (not ready).
LiRbStates_9j: Subroutine returns 9j-coefficients.
LiRbStates_9jHfs: Subroutine returns 9j-coefficients put together as a matrix.
LiRbStates_Dipole: Subroutine loads R-dependence of dipole moment.
LiRbStates_DGl: Subroutine calculates wavefunction.
LiRbStates_Fit: Subroutine fits adapted curve to ab-initio potential.
LiRbStates_Grid: Subroutine returns wavefunction matrix using Fourier grid method for a specified LiRb potential.
LiRbStates_GridV: Subroutine like LiRbStates_Grid but the potential is provided by the main program.
LiRbStates_Lbl: Subroutine returns nomenclature of a potential.
LiRbStates_Par: Subroutine gets parameter of specified LiRb potential.
LiRbStates_Pot: Subroutine gets specified LiRb potential.
LiRbStates_Rot: Subroutine finds rotational constant, simple.
LiRbStates_RotW: Subroutine finds rotational constant, correct.
LiRbStates_Trn: Subroutine finds turning point.
LiRbStates_Vib: Subroutine counts vibrational quantum number and determines scattering length.
LiRbStates_Zeeman: Subroutine generates matrix for hyperfine splitting of LiRb ground state potentials.
LiRbStates_Zeeman2: Subroutine generates matrix for hyperfine splitting of LiRb ground state potentials.
LiRbScatteringLength: Finds scattering length for a given potential [Weiss00].
LiRbScatteringLength_DGl: Subroutine for Runge-Kutta integration.
LiRbScatteringLength2: Finds scattering length for a given potential [Marinescu99].
LiRbScatteringLength2_DGl: Subroutine for Runge-Kutta integration.
LiRbScatteringLength2_Cs: Subroutine for Cs reference potential.
LiRbScatteringVolume: Finds scattering length for a given potential [Ouerdane04].
LiRbScatteringVolume_DGl: Subroutine for Runge-Kutta integration.
LiRbMappedGrid: Mapped Fourier grid procedure.
LiRbMappedGrid2,3: Mapped Fourier grid procedure for coupled channels.
LiRbMapped_Couple: Subroutine for mapped Fourier grid for coupled channels with settable coupling.
LiRbWavefunctionWKB: Radial wavefunction at all interatomic distances for the groundstate potential.
RbPotentialAdiabatic: Long-range interaction of two 87Rb atoms, splitting at collision, Hunds Fall (c) via [930].
RbPotentialAdiabatic2: Long-range interaction of two 87Rb atoms, splitting at collision, Hunds Fall (c) via [930].

33.4 Resonances in cold collisions

33.4.1 Shape resonances

The 'centrifugal' term can give rise to repulsive walls for attractive potentials. Behind these walls, quasi-bound states can develop and give rise to collision resonances. That is, resonances emerge in the collision cross section as a function of the collision temperature called *shape resonance*s.

33.4.2 Feshbach resonances

The so-called *Feshbach resonance* is due to an energetic match between a collision channel and a bound molecular state [441, 1301, 1302, 906, 435, 907, 1340]. They allow to vary the scattering length a_s almost arbitrarily from zero, where the atomic cloud turns into an ideal gas, up to values exceeding the total size of the cloud.

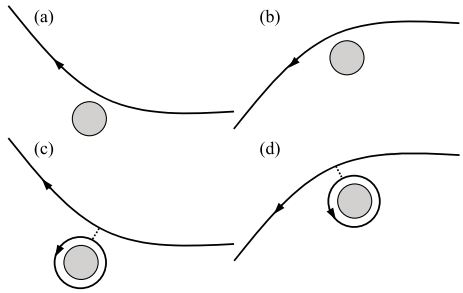

Figure 33.28: Classical illustration of a scattering resonance.

The impact of a Feshbach resonance can be understood as a perturbation of the collisional channel leading to a modification of the depth of the scattering potential. When this leads to the promotion of one more vibrational state into (or from) the continuum, this obviously leads to a dramatic modification of the scattering length a_s [15]

Let us consider two very cold atoms colliding on an attractive interatomic potential $V(R)$ (see Fig. 33.29,right). At long distances the relative wavefunction is a sine characterized by the Broglie wave vector k_{dB}. As the atoms approach each other, they mutually accelerate, and the Broglie wave performs some small and rapid oscillations within the potential. The number of nodes of the wavefunction within the potential corresponds to the number of bound vibrational levels that the potential with a given depth can support. The scattering length a_s is defined as the phase slip, which the Broglie wave would acquire during the collision at the boundary $k_{dB} \to \infty$.

With the possibility of gradually decreasing the depth of the molecular potential, at some point the last state below the ionization threshold goes to the continuum of

[15] Note that the divergence of the scattering length is an artifact of the hard core approximation, that is, the regularization of the interaction potential, since the matrix $\mathcal{T}$ by itself does not diverge.

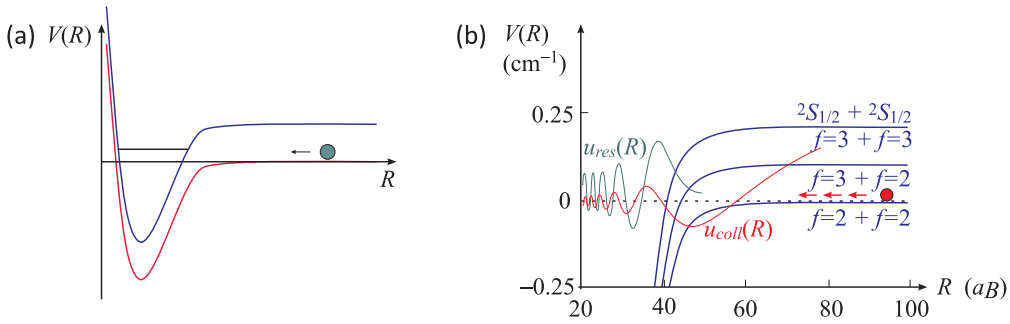

Figure 33.29: (a) The Feshbach resonance is due to a coincidence of collisional and bound channels. (b) Feshbach resonance in ^{85}Rb. The atoms collide in the hyperfine state $F = 2$, and the resonant bound state is in the $F = 3$ multiplet (courtesy [300]).

unbound states, the wavefunction decreases the number of nodes by one unit, while the scattering cross section crosses a singularity. In fact, the potential $V(R)$ *can be manipulated* with the help of radiation fields [435, 161, 907] or, near a collisional *Feshbach resonance*, by magnetic fields [1302, 1303]. Feshbach resonances were predicted in nuclear systems [441]. Its recent revival in the context of cold atomic collisions is due to the prospect of its use for manipulating the scattering length and thus controlling the mean-field energy of a Bose-Einstein condensate [16]

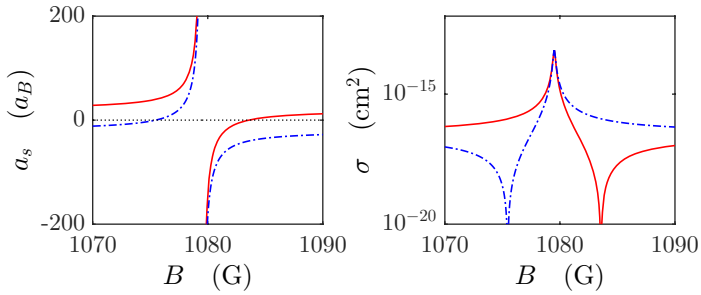

Figure 33.30: (code) (a) Scattering length and (b) collision cross section upon crossing a Feshbach resonance. The scattering length can be positive (solid red line) or negative (dashed blue line). A movie on a simulation of a Feshbach resonance can be watched here (watch movie).

The collisional *Feshbach resonance* arises when the energy of the state of two colliding atoms coincides with the energy of a vibrational molecular level belonging to a higher energy asymptote (see Fig. 33.29,right). This coincidence can strongly perturb the collisional channel, because the resonance shifts the phase of the relative de Broglie wavefunction and allows the atoms to tunnel into the molecular state

[16] It is even possible to invert the sign of the scattering length. This was a prerequisite for condensation of the atomic species of ^{85}Rb [1109]. In addition, Feshbach resonances are interesting because they can install a coherent free-bound coupling between an *open-channel* of colliding atoms and a bound molecular state of the same atoms, as shown in Fig. 33.29. This coupling can lead to the creation of molecular condensates.

for a short period of time, the duration of which is determined by the Heisenberg uncertainty relation. If the sum of the magnetic dipole moments of the atoms is different from the dipole moment of the molecule, the resonance can be tuned via external magnetic fields exploring the Zeeman effect. When a Feshbach resonance is crossed, the scattering length crosses a singularity, as shown in Fig. 33.30(left) [17].

33.4.2.1 Theory of Feshbach resonances

Feshbach resonances [441, 1301, 1302, 906, 435, 907, 1340] result from a coherent coupling between a collisional channel of free atoms and a quasi-bound molecular state. To describe this phenomenon, we first consider a global state consisting of two states located in the subspace of the open channel P and the closed channel Q,

$$|\Psi\rangle = |\Psi_P\rangle + |\Psi_Q\rangle \ , \tag{33.229}$$

with $|\Psi_P\rangle = \hat{P}|\Psi\rangle$ and $|\Psi_Q\rangle = \hat{Q}|\Psi\rangle$. The projection operators $\hat{P}$ and $\hat{Q}$ satisfy the conditions,

$$\hat{P} + \hat{Q} = 1 \qquad \text{and} \qquad \hat{P}\hat{Q} = 0 \ . \tag{33.230}$$

Hence, $\hat{P}^2 = \hat{P}$ and $\hat{Q}^2 = \hat{Q}$. Applying $\hat{P}$ to the Schrödinger equation

$$\hat{H}|\Psi\rangle = E|\Psi\rangle \tag{33.231}$$

and using the above equations, we get,

$$(E - \hat{H}_{PP})|\Psi_P\rangle = \hat{H}_{PQ}|\Psi_Q\rangle \qquad \text{and} \qquad (E - \hat{H}_{QQ})|\Psi_Q\rangle = \hat{H}_{QP}|\Psi_P\rangle \ , \tag{33.232}$$

where we defined $\hat{H}_{AB} \equiv \hat{A}\hat{H}\hat{B}$. This equation can be rewritten,

$$|\Psi_Q\rangle = (E - \hat{H}_{QQ})^{-1}\hat{H}_{QP}|\Psi_P\rangle \ . \tag{33.233}$$

Replacing this within the first Eq. (33.229),

$$(E - \hat{H}_{PP} - \hat{H}'_{PP})|\Psi_P\rangle = 0 \qquad \text{with} \qquad \hat{H}'_{PP} = \hat{H}_{PQ}(E - \hat{H}_{QQ})^{-1}\hat{H}_{QP} \ . \tag{33.234}$$

The term $\hat{H}'_{PP}$ can be interpreted as an effective interaction mediated by a transition from space P to Q and back to P.

The Hamiltonian of the open channel consists of a part $\hat{H}_0$ describing the two individual atoms including their Zeeman interactions with a magnetic field, and another part for the interaction between the two atoms $\hat{V}_1$. With the effective interaction potential through the bound channel $\hat{V}_2 \equiv \hat{H}'_{PP}$, we have,

$$(E - \hat{H}_0 - \hat{V}_1 - \hat{V}_2)|\Psi_P\rangle = 0 \ . \tag{33.235}$$

Now ...

Doing a little bit of algebra we find for the scattering length the following expression:

$$a = a_0 + \frac{\imath}{2k} \ln \frac{E - E_m - \frac{\imath}{2}\Gamma_m}{E - E_m + \frac{\imath}{2}\Gamma_m} = a_0 + \frac{1}{2k} \tan^{-1} \frac{\Gamma_m (E - E_m)}{(E - E_m)^2 + \frac{1}{4}\Gamma_m^2} \ . \tag{33.236}$$

[17] Explain better: The additional vibrational state distorting the collisional wavefunction during the singularity is entering the free-bound coupled-channel potential.

In reality, the channels are distinct due to their different hyperfine spin coupling. In general, the combination of the atoms generates a magnetic moment which is different from that of the molecule, $\mu_a \neq \mu_m$. This allows the resonance condition to be magnetically tuned,

$$a_{eff} = a_0 \left(1 - \frac{\Delta B}{B - B_{FB}}\right) . \tag{33.237}$$

The background scattering length $a_0 \equiv (B = 0)$ determines, on which side of the singularity the collision cross section $\sigma = 8\pi a_s^2$ goes through zero. The dependence of a_s on the magnetic field is monotonically increasing (decreasing), when $a_0 \Delta B > 0$ ($a_0 \Delta B < 0$). Note that ΔB is the distance between the singularity and the field where the scattering length crosses zero [1108]. Physically, a positive (negative) slope of the Feshbach resonance means that the energy of the bound state increases more (less) rapidly with the increase of the magnetic field, than the energy of the open channel, that is, $\mu_m < \sum \mu_a$ ($\mu_m > \sum \mu_a$) [906]. Note also that the divergence of the scattering length is an artifact of the hard-core approximation for the interaction potential, since the $\mathcal{T}$-matrix does not diverge.

33.4.2.2 Magnetic tuning of open and closed channels

The calculation of the Zeeman shift of bound states is relatively simple for a single channel, but this is an approximation. The Zeeman splitting of the open channel is simply the sum of the Zeeman structure of the collision partners. Therefore, it can be treated as shown in Sec. 30.2.4. It is sufficient to calculate the sum of the shifts for all pairs of individual atoms, $\nu_{Zeeman}^{m_F}(B) + \nu_{Zeeman}^{m'_F}(B) - \nu_{Zeeman}(0)$. For example, for $F = 2$ we have $m_F, m'_F = -2, ..., 2$, that is, we expect nine magnetic sublevels [18].

The Zeeman splitting of bound states has been demonstrated in Sec. 33.3.8. These calculations are however single-channel calculations and thus approximations.

The selection rule for coupling an open channel with total magnetic quantum number M_F and a bound channel M'_F is $M_F = M'_F \pm \ell$. I.e. s-wave collisions preserve the magnetic quantum number.

33.4.2.3 Photoassociative signature of Feshbach resonances

Near a Feshbach resonance the amplitude of the wavefunction is resonantly amplified, therefore we expect a larger Franck-Condon overlap, a larger transition rate, and a larger trap loss rate. The PA resonance enhancement has been calculated by [1323]:

$$\begin{aligned} K_{PA}(T, \Delta, B) &= \langle \nu \sigma_{PA}(E, \Delta, B) \rangle_T \\ &= \lambda_{therm}^3 \sum_{\ell=0}^{\infty} (2\ell + 1) \int_0^{\infty} |S_{PA}(E, \ell, \Delta, B)|^2 \exp(-E/k_B T) d(-E/2\pi\hbar) \\ &\xrightarrow{\ell=0} \lambda_{therm}^3 \int_0^{\infty} \frac{\frac{1}{4}\gamma_0 \gamma_L^{res}}{(\Delta + E)^2 + \frac{1}{4}\gamma_0^2} \frac{\sqrt{E/E_{res}}\Gamma^2}{(E - E_{res})^2 + \frac{1}{4}\Gamma^2} \exp(-E/k_B T) d(-E/2\pi\hbar) . \end{aligned} \tag{33.238}$$

[18] We may use this formula to fit the observed Zeeman splitting in the PA line, and calibrate our magnetic field. The excited 0_g^- has no hyperfine structure and does not exhibit Zeeman splitting. The precision of this method of calibration is limited due to line pulling effects induced by overlapping of rotational states.

The expression may be understood as a convolution of a Lorentzian term coming from the PA excitation, a Breit-Wigner resonance term resulting from the Feshbach enhancement, and a thermal Boltzmann velocity distribution. Experimental data are only available for the strong ^{85}Rb Feshbach resonance around 160 G [300]. In this experiment, ...

$$E_{res} = (2\mu_{atom} - \mu_{molecule})(B - B_0) \approx 2.45(B - B_0) \ , \tag{33.239}$$

where $\Gamma \approx 2.45\Delta B$, $T = 100$ μK, $\gamma_0/2\pi = 6$ MHz, $B_0 = 164$ G, $\Delta B = 5.9$ G. In this experiment, the excited state potential has been chosen to be a 0_g^- state, because of the absence of a hyperfine structure and therefore HF mixing. The rotational progression of vibrational states of this potential therefore looks simple and unperturbed. Figure xy shows the rotational spectrum of .... Higher partial waves contributions are small due to the low temperature of the atomic cloud.

33.4.2.4 Particular Feshbach resonances

A *p-wave Feshbach resonance* has been observed (see also Sec. 49.4) in channels of ^{6}Li [1426, **?**] and ^{40}K [1084] collisions. In homonuclear collisions, p-wave resonances occur in channels $|m_f, m_f'\rangle$, which are different form the channels for s-wave collisions. p-wave resonances are identified via inelastic collisions, since elastic collisions are frozen out. In heteronuclear collisions both types should be possible in all channels, only at different B-field values.

Heteronuclear Feshbach resonances have been found (see also Sec. **??**).

33.4.3 Efimov states and the exchange interaction

We assert that Efimov states in heteronuclear mixtures with large mass ratios are atom optical model systems for the very nature of chemical binding, the mechanism that ties atoms together to molecules. The type of chemical binding depends on whether the electrons are shared (covalent binding) or not (ionic binding). In the simplest imaginable molecule, H_2^+, two hydrogen atoms are bound by the exchange of an electron. In this case, the quantum statistical nature of H does not play a role, because the direct H-H interaction is dominated by Coulomb repulsion. The repulsion is overcome by the binding electron orbital, whose quantum nature does not play a role either, because there is only one electron. The same is true for Rb-Li-Rb with the difference that the atoms to not react via Coulomb but via short range van der Waals interactions. Hence, the Rb-Rb interaction is negligible at the long ranges, and the resonantly enhanced Li-Rb interaction is an exchange interaction.

Efimov states in optical lattices have been discussed [1267, 828].

33.4.3.1 Metals

Is exchange interaction by quasi-free electrons at the base of metallic binding? There may exist Bose-metals! How to calculate the lattice constant of a metal using the the Born-Oppenheimer approximation? Metallic binding is the exclusive mechanism for alkalis. $E_b \approx 1$ eV. For transition metals there is additional covalent binding due to exchange interaction $E_b \approx 9$ eV.

How about hydrogen bridge binding?

Table 33.2: List of famous Feshbach resonances. According to equation $a_s = a_{bg}\left(1 - \frac{\Delta B}{B-B_0}\right)$, the slope of a_s is rising with the increase of B, if a_{gb} and ΔB have the same signal. Otherwise it is decreasing. The resonances marked by p are p-wave resonances $|S, m_S, I, m_I\rangle$.

collisional channel	collision partner	a_s	B_{FB} and $[\Delta B]$
		$[a_B]$	[G]
$^{23}\mathrm{Na}_{\|1,1\rangle}$	idem	51.9	$907_{\|1,1,3,1\rangle}[+x]$
$^{85}\mathrm{Rb}_{\|2,-2\rangle}$	idem	-396	$155[-11.6]$
$^{87}\mathrm{Rb}_{\|1,1\rangle}$	idem	100	$685[?20m], 912[?1m], 1007[?0.2]$
$?^{6}\mathrm{Li}_{\|1/2,1/2\rangle}$	$^{6}\mathrm{Li}_{\|1/2,-1/2\rangle lf}$	-2160	$543[+0.2], 830[+x]$
$?^{40}\mathrm{K}_{\|9/2,-5/2\rangle}$	$^{40}\mathrm{K}_{\|9/2,-9/2\rangle}$	174	$224(9.7)$
$?^{6}\mathrm{Li}$	$^{7}\mathrm{Li}$		$226, 246, 540, 549$
$?^{85}\mathrm{Rb}_{\|2,-2\rangle}$	$^{87}\mathrm{Rb}_{\|1,-1\rangle}$	213	$265^*, 397^*$
$?^{40}\mathrm{K}_{\|9/2,-9/2\rangle}$	$^{87}\mathrm{Rb}_{\|1,1\rangle}$	-185	$492, 512, 543$
$?^{6}\mathrm{Li}_{\|1/2,1/2\rangle}$	$^{23}\mathrm{Na}_{\|1,1\rangle}$		$646, 746_{\|1,1,-1,3/2\rangle}, 759, 796$
$?^{6}\mathrm{Li}_{\|1/2,-1/2\rangle}$	$^{23}\mathrm{Na}_{\|1,-1\rangle}$		$12xx_{\|1,1,-1,-3/2\rangle}$
$?^{6}\mathrm{Li}_{\|1/2,1/2\rangle}$	$^{87}\mathrm{Rb}_{\|1,1\rangle}$	± 20	$158[\pm 0.4], 881[\pm 1.1], 1078[\pm 8.8]$
$?^{7}\mathrm{Li}_{\|1,1\rangle}$	$^{87}\mathrm{Rb}_{\|1,1\rangle}$	± 40	

33.4.3.2 Efimov states

The universal limit is reached, when the van der Waals length $\ell \equiv \left(mC_6/\hbar^2\right)^{1/4}$ is largely exceeded by the scattering length $a \gg \ell > 0$. This happens in case of Feshbach resonant enhancement, $a = a(B)$.

For $a > 0$ a shallow two-body bound state forms, whose energy for large a is given by $E_2 = -\frac{\hbar^2}{ma^2}$. Hence, in the universal limit the dimer binding energy is independent of the interaction potential. In a Feshbach resonance this universal bound state can tunnel into a real "chemical" bound state forming a molecule. For $a < 0$ there is no shallow dimer. In this regime three-body losses are only possible via the formation of deeply bound molecules.

There exist an infinite number of Efimov states with identical dependence on a. They accumulate at $a \to \pm\infty$. For a given a however the number of Efimov states is limited. In the diagram 33.31 an Efimov resonance occurs every time a solid line crosses the boundary to continuum (shaded line), $a_* = a(|E_2| = |E_3|)$. Tuning can be done via modifying a via a magnetic field near a Feshbach resonance. For $a < 0$ there are no bound dimers, the Efimov resonance is due to trimers. For $a > 0$ there are bound dimers, the Efimov resonance is due to atom-dimer resonances. There is a lowest Efimov state, which extends into non-universal regions. For this reason the energy offset of the Efimov series depends on the atomic potentials.

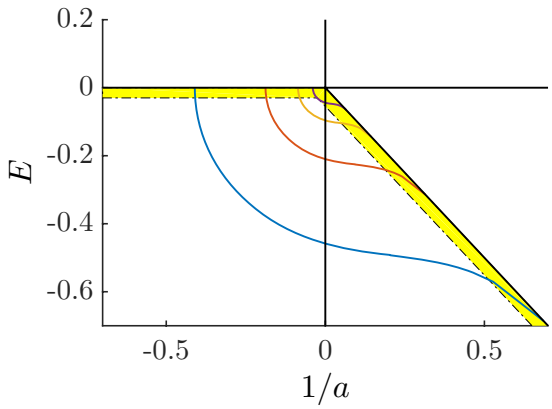

Figure 33.31: Spectrum of Efimov states as a function of $1/a$.

The energies of the Efimov states are given by the roots of,

$$\sin\left(\frac{s_0}{2}\ln(mE_3/\hbar^2\kappa_s^2)\right) \ . \tag{33.240}$$

Hence, the scaling factor for the distance between Efimov states is $e^{\pi/s_0} \simeq 22.7$, where $s_0 \approx 1.00624$ is the root of

$$s_0 \cosh\frac{\pi s_0}{2} - \frac{8}{\sqrt{3}}\sinh\frac{\pi s_0}{6} = 0 \ . \tag{33.241}$$

If one Efimov state is located near a_* then the others are located near $a_* e^{n\pi/s_0}$. I.e. $C(a_*) = C(a_* e^{\pi/s_0})$.

For binary heteronuclear mixtures the scaling factor for Efimov states can be very different. In this case it not only depends on the quantum statistical character of the two atoms (bosons, fermions, or distinguishable atoms), but on the mass ratio of the mixture and on the size of the various scattering lengths. In general, either the intraspecies scattering length between the two identical atoms is Feshbach resonantly enhanced or the interspecies scattering length, but not both simultaneously.

Let us define $\tan\gamma_{12} = \sqrt{(m_1+m_2+m_3)m_3/m_1m_1}$. For $R = 0$ and replacing $\lambda^{1/2} = -s_0$, the Eq. (389) of Ref. [186] can be written

$$\det\begin{pmatrix} \cosh(s_0\frac{\pi}{2}) & -2\frac{\sinh[s_0(\pi/2-\gamma_{12})]}{s_0\sin(2\gamma_{12})} & -2\frac{\sinh[s_0(\pi/2-\gamma_{13})]}{s_0\sin(2\gamma_{13})} \\ -2\frac{\sinh[\lambda^{1/2}(\pi/2-\gamma_{21})]}{s_0\sin(2\gamma_{21})} & \cosh\left(s_0\frac{\pi}{2}\right) & -2\frac{\sinh[s_0(\pi/2-\gamma_{23})]}{s_0\sin(2\gamma_{23})} \\ -2\frac{\sinh[s_0(\pi/2-\gamma_{31})]}{s_0\sin(2\gamma_{31})} & -2\frac{\sinh[s_0(\pi/2-\gamma_{32})]}{s_0\sin(2\gamma_{32})} & \cosh\left(s_0\frac{\pi}{2}\right) \end{pmatrix} = 0\ . \quad (33.242)$$

This holds when all scattering lengths are strong.

Figure 33.32: Various possibilities for Efimov states in binary mixtures of quantum gases.

On the other hand, for the case $m_1 = m_2 \neq m_3$ and $a_{13} = a_{23} \gg a_{12}$, the scaling factor is given by the root of

$$s_0\cosh\frac{\pi s_0}{2} \mp \frac{2\sinh(s_0(\frac{\pi}{2}-\gamma_{12})}{\sin 2\gamma_{12}} = 0\ . \quad (33.243)$$

The upper sign holds if $m_{1,2}$ are bosons, the lower sign for fermions, and a product of both terms if the atoms are distinguishable.

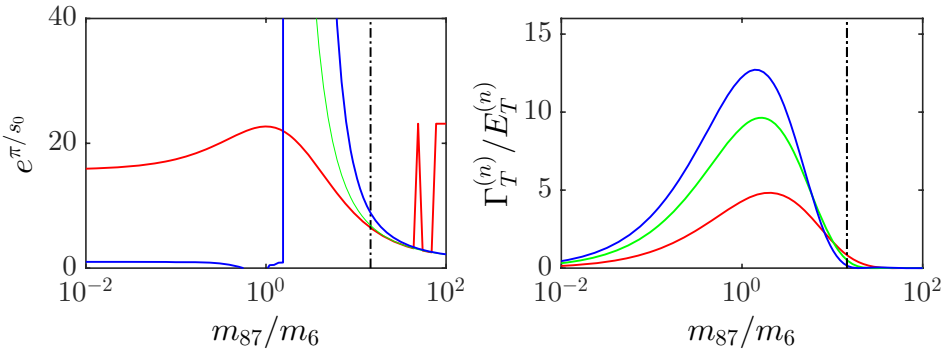

Figure 33.33: Scaling factor as a function of the mass ratio.

The three-body collision rate in the unitarity limit,

$$L_3 = \frac{3C(a)\hbar a^4}{m}\ , \quad (33.244)$$

can be expressed via the recombination length

$$\rho_3 \equiv \left(\frac{2mL_3}{\sqrt{3}\hbar}\right)^{1/4} . \tag{33.245}$$

Efimov states can be observed via L_3 or evtl. Bragg scattering?
According to [750],

$$C(a_{<0}) = \frac{4590 \sinh 2\eta_-}{\sin^2\left(s_0 \ln \frac{|a|}{a_-}\right) + \sinh^2 \eta_-} , \tag{33.246}$$
$$C(a_{>0}) = 67.1 e^{-2\eta_+}\left[\cos^2\left(s_0 \ln \frac{|a|}{a_+}\right) + \sinh^2 \eta_+\right] + 16.8(1 - e^{-4\eta_+}) .$$

$a_\pm$ describes the non-universal short-range potential, $\eta_\pm$ the three-body decay rate.

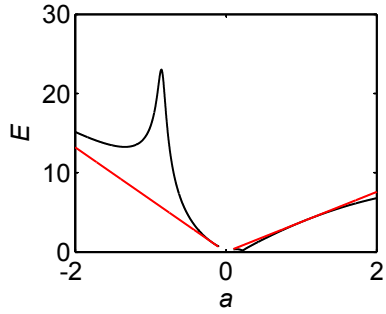

Figure 33.34: Calculated loss spectra for Cs Efimov trimers.

In the absence of Efimov states, we set $a = a_- e^{\pi/2s_0}$ and $a = a_+$, respectively and obtain,

$$C(a_{<0}) = 4590 \times 2 \tanh \eta_- , \tag{33.247}$$
$$C(a_{>0}) = 67.1 e^{-2\eta_+} \cosh^2 \eta_+ + 16.8(1 - e^{-4\eta_+}) .$$

Hence, three-body losses are scaling with a^4 without additional resonances. The decay via into deep bound states is summarized by the constants $\eta_\pm$. Interpolation formula of Shlyapnikov for two heavy bosons/fermions and a light atom. The interspecies scattering length is strong,

$$s_0 = \sqrt{.16M/m - 1/4} \quad \text{for bosons and} \quad s_0 = \sqrt{.16M/m - 9/4} \quad \text{for fermions} . \tag{33.248}$$

33.5 Light-assisted collisions

33.5.1 Photoassociation

Photoassociation is based on binary collisions. Transitions to excited states are followed by spontaneous decay and can be monitored in trap loss experiments. An

alternative way, which suits especially well for sodium is photoassociative ionization. The trap loss rate can be expressed as,

$$\dot{n} = -2K_{PA}n^2 \ . \tag{33.249}$$

The event rate for photoassociation in a thermal cloud with Boltzmann velocity distribution is:

$$\begin{aligned} K_{PA}(T,\Delta_1,I_1) &= \left\langle \frac{\pi v}{k^2}\sum_l (2l+1)|S(E,l,\Delta_1,I_1)|^2 \right\rangle \ , \\ &= \frac{2\pi\hbar}{\mu k}\sum_l (2l+1)\int_0^\infty |S(E,l,\Delta_1,I_1)|^2 e^{-\beta E}d(\beta E) \ , \end{aligned} \tag{33.250}$$

where the *S-matrix* is,

$$|S|^2 = \frac{\gamma_1\gamma_s}{(E-\Delta_1)^2 + \frac{1}{4}(\gamma_1+\gamma_s)^2} \ , \tag{33.251}$$

and γ_1 is the spontaneous linewidth and $\gamma_s(E,l,I_1)/2\pi \approx \Omega_1^2\,|\langle b_1|E,l\rangle|^2$ is the Franck-Condon overlap between the colliding channel and the excited state bound level. For cold ultra-cold collisions, we may only consider s-wave collisions, $l=0$. In the regime of Bose-Einstein condensation $T \lesssim 1$ μK and $n \gtrsim 10^{14}$ cm^{-3}, we can replace $e^{-\beta E} \to \delta(E)$ and $E \to 0$. The photoassociation rate then simplifies to [216],

$$K_{PA}(\Delta_1,I_1) \approx \frac{2\pi\hbar}{\mu k}\frac{\gamma_1\gamma_s}{\Delta^2 + \frac{1}{4}(\gamma_1+\gamma_s)^2} \ . \tag{33.252}$$

Thus the S-matrix is maximized in resonance and saturation, i.e. $\Delta_1 = E$ and $\gamma_s = \gamma_1$ so that $|S|^2 = 1$, which case is called the *unitarity limit*. Note that increasing the laser power beyond saturation, $\gamma_s > \gamma_1$, decreases the photoassociation efficiency again because of *Autler-Townes splitting* [**?**].

33.5.2 Two-color photoassociation

We can also shine in a second laser frequency tuned between the excited potential bound state and a ground potential bound state. This second laser power broadens the resonance and spoils the transition rate for the first laser. Following [161]:

$$K_{PA}(T,\Delta_1,\Delta_2,I_1,I_2) = \left\langle \frac{\pi v}{k^2}\sum_l (2l+1)|S(E,l,\Delta_1,\Delta_2,I_1,I_2)|^2 \right\rangle \ , \tag{33.253}$$

where,

$$|S|^2 = \frac{(E-\Delta_2)^2\gamma_1\gamma_s}{(E-\Delta_+)^2(E-\Delta_-)^2 + \frac{1}{4}(\gamma_1+\gamma_s)^2(E-\Delta_2)^2} \ , \tag{33.254}$$

where,

$$\Delta_\pm = \tfrac{1}{2}(\Delta_1+\Delta_2) \pm \tfrac{1}{2}\sqrt{(\Delta_1-\Delta_2)^2 + 4\Omega_{12}^2} \ . \tag{33.255}$$

Note that $\gamma_s(E,l,I_1)/2\pi \approx \Omega_1^2 \left|\langle b_1|E,l\rangle\right|^2$ and $\Omega_{12} = \Omega_2\langle b_1|b_2\rangle$. The one-color signal follows with $\Omega_{12} \to 0$. Assuming the unitarity limit for the free-bound transition, $\Delta_1 = E$ and $\gamma_s = \gamma_1$ the two-color signal reads:

$$|S|^2 = \frac{1}{1+\Omega_{12}^4/(\Delta_1-\Delta_2)^2\gamma_1^2} \ . \tag{33.256}$$

The width of the two-color spectral lines is mainly limited by the Boltzmann distribution of kinetic energies in the atomic cloud. At very low temperatures, we may .... and the two-color resonance dip may be interpreted as a true dark resonance.

Two-color PA lines have been observed for ^{85}Rb in a FORT [491]. In order to measure this for very low temperatures and even for condensates, one has to switch to ^{87}Rb in a dark MOT. A technical requirement is, of course, that the two lasers involved in the Raman process be very stable, at least with respect to each other. This is easiest achieved by using AOMs, which limits the range of levels to be studied to a few GHz binding energy.

Another important aspect is the requirement of a reasonable Raman transition probability, i.e. large Franck-Condon overlap between the collisional and the bound excited state and between the two bound states. Note also that selection rules hold.

33.5.3 Optical shielding

The adiabatic potential for ground state collisions can be manipulated using light to admix an another potential. The laser light can either be blue-detuned to the continuum of states of a repulsive excited state potential or red-detuned to vibrational resonances of an attractive excited state potential [435, 1349, 1363]. We can also admix another ground state potential with two-photon Raman transitions.

At cold collisions, the atom undergoes *Landau-Zehner transitions* between the mixed states with the probability $P_{LZ} = 1-\exp(-2\pi\hbar\Omega^2/\alpha v)$, where $\alpha = |d\Delta/dR|_{R_C} = |d(U_e(R) - U_g(R))/dR|_{R_C}$ is the slope of the difference potential evaluated at the Condon point. In the dressed states picture the dressed potentials display an avoided crossing. This modification of the collisional potential modifies the dynamics of the collision and the scattering length.

An example is the phenomenon of *optical suppression* or *shielding*. Here, two colliding atoms are inhibited to approach farther than a certain distance defined by the resonance condition set by a laser which is blue-detuned to a repulsive excited potential. The inhibition is probed by a photoassociation laser tuned to a resonance condition at smaller interatomic distances. The optical shielding scheme can be extended in the following way. Two lasers, one tuned to a repulsive another to an attractive excited state potential resonant at different interatomic distances.

33.5.4 Optical Feshbach resonances

We can view the modification of the colliding channel as a changed scattering length. Or do we introduce a temperature dependence $a(T)$? Anyway, if the goal is only to alter the a, we want to avoid spontaneous scattering, i.e. $(\Omega/\Delta)^2$ need to be small. Unfortunately, the effect of the light on the scattering length also scales with $(\Omega/\Delta)^2$. So that blue- or red-detuning optical shielding has small impact. An alternative is

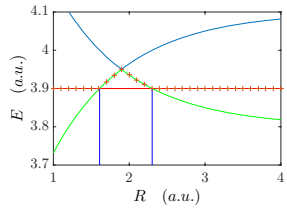

Figure 33.35: Optical shielding and anti-shielding.

resonant enhancement by a bound state for red-detuned shielding. For blue detuning and large Δ, shielding only works at short range R. This is called an *optical Feshbach resonance* [435, 161, 1297]. It can also occur in the microwave regime [907].

We can set up the following non-Hermitian Hamiltonian:

$$\begin{pmatrix} -\hbar^2/m \cdot \Delta_R + U(R) & \Omega\xi(R) \\ \Omega\xi(R) & -\hbar^2/m \cdot \Delta_R + U(R) - \imath R - \delta \end{pmatrix} \begin{pmatrix} \phi(R) \\ \psi(R) \end{pmatrix} = 0 \qquad (33.257)$$

results in a resonance described by the complex scattering length $a = a' - \imath a''$, where the real part governs the self energy and the imaginary part the spontaneous losses.

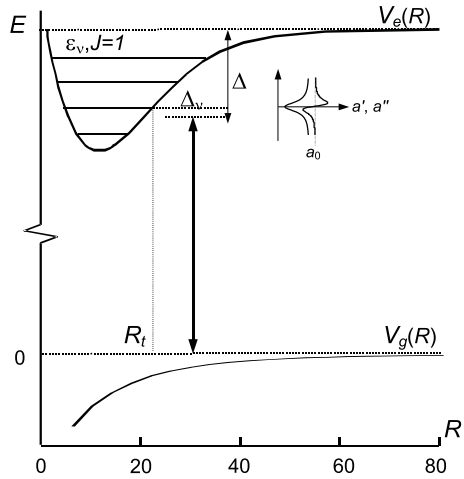

Figure 33.36: Optically induced Feshbach resonances.

33.5.5 Induced dipolar long-range forces

33.5.5.1 Electrostriction

The phenomenon of *electrostriction* is caused by static polarizability: Dipoles in an electric field gradient align themselves to the local field and the field gradient causes forces towards the field minimum. However forces may not only occur between dipoles

and inhomogeneous external fields, but also between pairs of dipoles. And this holds even if the dipole are induced by homogeneous fields. In this picture, *retardation* can induce electrostrictive long-range forces [**?**]. To see the effect, Rayleigh or Bragg scattering or superradiance have to be avoided, e.g. by minimizing the overlap between the dipole radiation pattern and the atomic cloud.

33.5.5.2 Effects due to dipole-dipole interaction

We assume isotropic real dispersion $\alpha_{pol} = \alpha_{pol}(k)$. The *Lippmann-Schwinger equation* is an integral equation describing the modification of the local electric field due to self-interaction including spatial retardation effects,

$$\mathbf{E}_{loc}(\mathbf{r},t) = \mathbf{E}_{ext}(\mathbf{r},t) + \frac{\alpha_{pol}(k)}{\varepsilon_0}\int d^3r' \mathbf{G}^0(\mathbf{r}-\mathbf{r}')n(\mathbf{r}')\mathbf{E}_{loc}(\mathbf{r}',t) \ , \tag{33.258}$$

where $\mathbf{G}^0(\mathbf{r})$ is the propagation tensor,

$$1\mathbf{G}^0(\mathbf{r}) = \frac{e^{\imath kr}}{4\pi r^3}\left[(\delta_{ij}-3\hat{\mathbf{r}}_i\hat{\mathbf{r}}_j)(1-\imath kr) - (\delta_{ij}-\hat{\mathbf{r}}_i\hat{\mathbf{r}}_j)(kr)^2\right] \ . \tag{33.259}$$

In the first Born approximation $\mathbf{E}_{loc}$ under the integral in Eq. (33.258) is replaced $\mathbf{E}_{ext}$. The expression is then used to calculate the polarization, which in term is used to calculate the interaction energy $H_{ind} = -\frac{1}{2}\int d^3\mathbf{r}\mathfrak{Re}\ \mathbf{P}\mathfrak{Re}\ \mathbf{E}_{ext}$. One obtains,

$$\hat{H}_{ind} = -\frac{\alpha_{pol}}{4}\mathbf{E}^2_{ext}\int d^3\mathbf{r} n(\mathbf{r}) + \frac{1}{2}\int d^3\mathbf{r}\int d^3\mathbf{r}' n(\mathbf{r})U(\mathbf{r}-\mathbf{r}')n(\mathbf{r}') \ , \tag{33.260}$$

where,

$$U(\mathbf{r}) = \frac{I\alpha_{pol}(k)^2}{4\pi c\varepsilon_0^2}\hat{\mathbf{E}}^*_i\hat{\mathbf{E}}_j V_{ij}(k,\mathbf{r})\cos\mathbf{kr} \ , \tag{33.261}$$

with $V_{ij}(k,\mathbf{r}) = -4\pi\mathfrak{Re}\ \mathbf{G}^0(\mathbf{r})$.

For $\mathbf{G}^0(\mathbf{r}) = \frac{1}{3}\delta(\mathbf{r})\mathbf{1}_3$,

$$\mathbf{E}_{loc}(\mathbf{r},t) = \mathbf{E}_{ext}(\mathbf{r},t) + \frac{\alpha_{pol}(k)}{3\varepsilon_0}n(\mathbf{r})\mathbf{E}_{loc}(\mathbf{r},t) \ , \tag{33.262}$$

we recover the Clausius-Mossotti formula. For dilute gases $n\alpha_{pol}/3\varepsilon_0 \ll 1$ and may be neglected. In [1118] it is shown that the Lorentz-Lorenz shift is the same for a BEC and therefore the quantum degeneracy does not modify the formula.

33.5.5.3 Rotons

The *Bijl-Feynman formula* links the dispersion relation to the static structure factor,

$$E(k) \le \frac{\hbar^2k^2}{2mS(k)} \ . \tag{33.263}$$

The equality holds for dilute gases. In generalization to thermal gases the structure factor is the Fourier transform of pair correlation functions. In the mean-field theory pair correlations are neglected. However, in the presence of dipole-dipole interactions this is not the case. Pair correlations lead to a maximum in the structure factor at quasi-momenta corresponding to the mean interparticle distance. Consequently there is a minimum in the Bogolubov dispersion relation $E(k)$, called *roton*.

33.6 Further reading

33.6.1 on cold collisions

J.M. Vogels et al., *Coupled Singlet-Triplet Analysis of Two-Color Cold-Atom Photoassociation Spectra* [1339]DOI

H. Ouerdane et al., *Scattering Parameters for Cold LiRb and NaRb Collisions Derived from Variable Phase Theory* [989]DOI

M. Marinescu et al., *Long-Range Potentials for Two-Species Alkali-Metal Atoms* [845]DOI

S.B. Weiss et al., *Calculation of the Interspecies S-Wave Scattering Length in an Ultracold Na-Rb Vapor* [1367]DOI

33.6.2 on Feshbach resonances

Ph.W. Courteille et al., *Observation of a Feshbach resonance in Cold Atom Scattering* [300]DOI

S. Inouye et al., *Observation of Feshbach resonances in a Bose-Einstein condensate* [648]DOI

C. Chin et al., *Feshbach Resonances in Ultracold Gases* [257]DOI

Part V

Quantum Optics

Chapter 34

Semiclassical theory of light-atom interaction

In Part IV of this script we solved the problem of a *stationary* atom using the formalism of quantum mechanics developed in Part III. We now come back to Bohr's original idea that *transitions* between atomic states be induced by absorption and emission of electromagnetic radiation and develop a semi-classical theory of light-atom interaction. That is, the atom will be treated as a quantum object, while the radiation is assumed to obey the rules of classical electrodynamics. The main objective of this chapter will be to derive an equation describing the temporal evolution of atoms interacting with a radiation field.

We begin with a perturbative approach to the excitation of atomic transitions in Sec. 34.1. In quantum mechanics we learned (see in Sec. 27.4) how time-dependent perturbations, such as suddenly applied force fields or periodic oscillations, can induce transitions between eigenstates. We will not repeat the concepts here. Rather we will focus on the calculation of transitions rates employing Fermi's Golden rule derived in Eq. (27.111). In Secs. 22.2 we introduced the Einstein coefficients A and B, which we associated with Planck's spectral distribution of black-body radiation. This procedure allowed us to connect the coefficients for spontaneous and stimulated transitions, but did not provide any method to calculate them from the intrinsic properties of the atoms. The purpose of Sec. 34.2 is to find expressions for the matrix elements coupling different atomic states using quantum mechanics and relate them to the Einstein coefficients in order to calculate the rates of absorption and emission of atomic radiation. In particular, we will dedicate some space to the dipolar approximation and to the derivation of selection rules allowing to quantify transition probabilities as a function of the quantum numbers characterizing the atomic states coupled by radiation.

Perturbation theory can describe the light-atom dynamics only at interaction times short enough, that the initially occupied atomic states is not noticeably depleted. An exception is the two-level atom, for which perturbation theory reproduces the exact results obtained by solving the time-dependent Schrödinger equation. This, however, only holds as long as spontaneous processes can be neglected. To portray systems that contain excitation and relaxation processes occurring simultaneously, a theory based on Schrödinger's equation is no longer sufficient, because it is only capable of explaining stimulated processes, such as the absorption of a monochromatic wave. Dissipative processes, such as spontaneous emission, require a more general approach

to describe the evolution of a system. A single wavefunction is, in general, not enough to represent such a system nor to quantify the probabilities associated with each of its states, but we rather need an ensemble of wavefunctions, which requires the description of the atom in terms of a density operator. This will be done in Sec. 34.3.

The equations of motion ruling the time evolution of the density operator are the so-called Bloch equations. They will be derived and studied in Sec. 34.4, and in Sec. 34.5 we will phenomenologically include spontaneous emission. In Sec. 34.6 we will discuss line broadening mechanisms and in Sec. 34.7 generalize the Bloch equation formalism to multilevel systems.

34.1 Perturbative approach to atomic excitation

In a model of an isolated atom, the atomic energy levels are eigenstates of the Hamiltonian and describe the system completely, i.e. they do not undergo any evolution. Transitions between atomic energy levels may, however, be induced by oscillatory perturbations, such as electromagnetic radiation accelerating bound electrons.

34.1.1 Time-dependent perturbation by a plane wave

Looking at the Hamiltonian (30.11) describing the interaction of a charged particle with an electromagnetic field, we find that the term $\mathbf{A}\cdot\nabla \propto e^{\imath\omega t}$ oscillates with frequency ω, while the term $\mathbf{A}^2 \propto e^{2\imath\omega t}$ oscillates with twice that frequency. We will only consider the interaction term (30.12), which is linear in $\mathbf{A}$, and we will treat this term as first-order perturbation by *time-dependent perturbation theory* (TPDT).

With this scope we separate the Hamiltonian in a stationary part and a time-dependent part [1],

$$\hat{H}(t) = \hat{H}^{(0)} + \hat{H}_{int}(t) \qquad \text{with} \qquad \hat{H}_{int} = \tfrac{e}{m}\mathbf{A}(\mathbf{r},t)\cdot\hat{\mathbf{p}}\ , \tag{34.1}$$

where $\hat{H}^{(0)}$ contains the kinetic energy and the Colombian potential of Eq. (30.11). In Sec. 27.4.4, inserting the expansion,

$$|\psi\rangle = \sum_k a_k(t)|k\rangle e^{-\imath E_k t/\hbar}\ , \tag{34.2}$$

along with the Hamiltonian (34.1) in the Schrödinger equation, we obtained the first order perturbative approximation (27.72). Setting the initial condition to $c_k(t\le 0) = \delta_{ki}$ and supposing that the probability of finding the atom initially in the ground state $|i\rangle$ for short times is 1, we got,

$$\boxed{a_f^{(1)}(t) \simeq \frac{1}{\imath\hbar}\int_0^t \langle f|\hat{H}_{int}|i\rangle e^{\imath\omega_{fi}t'}dt'}\ . \tag{34.3}$$

We now consider a perturbation by an electromagnetic plane wave within the Coulomb gauge,

$$\Phi = 0 \qquad \text{and} \qquad \nabla\cdot\mathbf{A} = 0\ . \tag{34.4}$$

[1] The energy of the light field is not considered in the Hamiltonian, because it is treated as classical, that is, its energy commutes with the other observables of the system.

The solution of the wave equation can be written,

$$\mathbf{A}(\mathbf{r},t) = \mathbf{A}_0^*(\mathbf{r})e^{\imath\omega t} + \mathbf{A}_0(\mathbf{r})e^{-\imath\omega t} \ . \tag{34.5}$$

For plane waves,

$$\mathbf{A}_0(\mathbf{r}) = \mathbf{A}_0 e^{\imath\mathbf{k}\cdot\mathbf{r}} \tag{34.6}$$

and $k = \omega/c$ and $\mathbf{k}\cdot\mathbf{A}_0 = 0$. With this, it is possible to show (see Exc. 34.1.4.1), that the energy density is,

$$u(\omega) = \tfrac{\varepsilon_0}{2}\vec{\mathcal{E}}^2 + \tfrac{1}{2\mu_0}\vec{\mathcal{B}}^2 = 2\varepsilon_0\omega^2 A_0^2 \ . \tag{34.7}$$

On the other hand, the energy density is proportional to the number of photons $N(\omega)$ inside the volume V,

$$u(\omega) = \frac{N(\omega)\hbar\omega}{V} \ . \tag{34.8}$$

The intensity corresponds to a flow of energy,

$$I(\omega) = u(\omega)c \ . \tag{34.9}$$

Separating the polarization $\hat{\epsilon}$ from the amplitude A_0,

$$\mathbf{A} = \hat{\epsilon}A_0 e^{\imath\mathbf{k}\cdot\mathbf{r}}e^{-\imath\omega t} + c.c. \ , \tag{34.10}$$

and inserting the perturbation (34.1) into the approximation (34.3),

$$\begin{aligned} a_f^{(1)}(t) &= -\tfrac{e}{m}\int_0^t dt'\langle f|\mathbf{A}\cdot\nabla|i\rangle e^{\imath\omega_{fi}t'}dt' \qquad (34.11)\\ &= -\tfrac{eA_0}{m}\langle f|e^{\imath\mathbf{k}\cdot\mathbf{r}}\hat{\epsilon}\cdot\nabla|i\rangle\int_0^t dt' e^{\imath(\omega_{fi}-\omega)t'}dt' - \tfrac{eA_0}{m}\langle f|e^{-\imath\mathbf{k}\cdot\mathbf{r}}\hat{\epsilon}\cdot\nabla|i\rangle\int_0^t dt' e^{\imath(\omega_{fi}+\omega)t'}dt' \ . \end{aligned}$$

Which one of the two processes described by Eq. (34.11) takes place, depends on the initial and final energies. For $E_f = E_i + \hbar\omega$ the first term describing the process of *absorption* will dominate, for $E_f = E_i - \hbar\omega$ the second term describing *emission* prevails.

34.1.2 Absorption and stimulated emission

34.1.2.1 Absorption

We define the *matrix element*,

$$M_{fi} \equiv \langle f|e^{\imath\mathbf{k}\cdot\mathbf{r}}\hat{\epsilon}\cdot\nabla|i\rangle \ , \tag{34.12}$$

and concentrate on the absorption process. Defining the detuning by $\Delta \equiv \omega - \omega_{fi}$ and evaluating the integral,

$$\left|\int_0^t e^{-\imath\Delta t'}dt'\right|^2 = \left|\frac{e^{-\imath\Delta t}-1}{-\imath\Delta}\right|^2 = 4\frac{\sin^2\frac{\Delta t}{2}}{\Delta^2} \simeq 2\pi t\delta(\Delta) \ , \tag{34.13}$$

at short times (see the formula (27.76)), the absorption probability becomes,

$$|a_f^{(1)}(t)|^2 = \frac{e^2}{m^2} A_0(\omega)^2 |M_{fi}|^2 \left| \int_0^t dt' e^{\imath(\omega_{fi}-\omega)t'} dt' \right|^2 = \frac{e^2}{m^2} A_0(\omega)^2 |M_{fi}|^2 2\pi t \delta(\Delta) \ . \tag{34.14}$$

The $\delta(\Delta = 0)$ function simply represents conservation of energy. Of course this is only an approximation not taking into account the finite width of the transition line.

Expressing the field by the intensity (34.10), we obtain the transition rate for absorption,

$$\boxed{W_{fi}^{(ab)} = \frac{d}{dt}|a_f^{(1)}(t)|^2 = 2\pi \left(\frac{eA_0}{m}\right)^2 |M_{fi}|^2 \delta(\omega - \omega_{fi}) = \frac{\pi e^2}{\varepsilon_0 m^2 c} \frac{I(\omega)}{\omega^2} |M_{fi}|^2 \delta(\omega - \omega_{fi})} \ . \tag{34.15}$$

We note that the absorption rate is proportional to the intensity of the radiation, which characterizes a typically linear effect.

If we want to express the rate of absorption by atoms in terms of energy, we simply multiply W_{fi} by $\hbar\omega$ and, hence, we can define the cross section for the absorption of radiative energy as,

$$\sigma_{i\to f} \equiv \frac{\text{absorption rate}}{\text{incident intensity}} = \frac{\hbar\omega W_{fi}}{I(\omega)} = \frac{\pi e^2}{\varepsilon_0 m^2 c} \frac{\hbar}{\omega} |M_{fi}(\omega_{fi})|^2 \delta(\omega - \omega_{fi}) \ . \tag{34.16}$$

34.1.2.2 Stimulated emission

For $E_f = E_i - \hbar\omega$ the equation describes the process of *stimulated emission*. Analogously to the calculation of the absorption, we obtain,

$$\boxed{W_{if}^{(st)} = \frac{\pi e^2}{\varepsilon_0 m^2 c} \frac{I(\omega)}{\omega^2} |M_{if}^*|^2 \delta(\omega + \omega_{fi})} \ , \tag{34.17}$$

with $M_{fi}^* = \langle f | e^{-\imath \mathbf{k}\cdot\mathbf{r}} \hat{\epsilon} \cdot \nabla | i \rangle$. Of course,

$$W_{if}^{(st)} = W_{fi}^{(ab)} \ . \tag{34.18}$$

The fact that, in a coupled atom-radiation system in equilibrium, the radiation field excites the same number of transitions in absorption $i \to f$ as in stimulated emission $f \to i$ is called the principle of *detailed balance*.

Obviously, the situation is different, if instead of two states we have several states that can be excited by radiation or decay.

34.1.3 Spontaneous emission

Absorption and stimulated emission are due to the interaction of an atom with a radiation field. However, even in the absence of radiation the atom couples to the field of the electromagnetic vacuum, and an accurate description of the atom must account for this fact. The total system has different eigenstates and their projection on the unperturbed eigenstates changes over time, as any excited atomic state has a constant probability, depending on the coupling to the electromagnetic field, to decay

to another state. The probability of measuring a specific lifetime thus follows a Poisson distribution. The decay process caused by atomic interaction with fluctuations of the electromagnetic vacuum is called *spontaneous emission*. It is understood in the framework of *quantum electrodynamics*, and a thorough discussion is postponed to Sec. 35.6. Here, we will adopt a preliminary heuristic treatment.

Replacing in Eq. (34.17) the intensity by the number of photons (34.8), we obtain,

$$W_{if}^{(st)} = \frac{\pi\hbar e^2 N(\omega)}{\varepsilon_0 m^2 \omega V} |M_{fi}|^2 \delta(\omega - \omega_{fi}) \ . \tag{34.19}$$

In fact, the introduction of the concept of photons already implies the quantization of the electromagnetic field. Adding to the number of photons a photon representing the vacuum fluctuations, $N(\omega) \longrightarrow N(\omega) + 1$, we are able to include spontaneous emission,

$$\boxed{W_{if}^{(st)} + W_{if}^{(sp)} = \frac{\pi\hbar e^2 [N(\omega) + 1]}{\varepsilon_0 m^2 \omega V} |M_{fi}|^2 \delta(\omega + \omega_{fi})} \ . \tag{34.20}$$

This means that even in the absence of a classical radiation field, $N(\omega) = 0$, there is an emission probability. We note that $W_{if}^{(sp)}$ depends on the volume confining the atom, that is, the cavity, since it describes the transfer of energy to this volume. Here, it is clear that an argument is still missing, because the transfer rate must depend in some way on the number of states available to accommodate the emitted photon, that is, on the *density of states* within the cavity. The calculation of this density of states should allow us to evaluate the quantization volume V.

34.1.3.1 Density of states

In Sec. 22.2.2 we calculated the isotropic spectral *density of modes* per volume (22.53),

$$\varrho(\omega) = \frac{\omega^2}{\pi^2 c^3} \ . \tag{34.21}$$

The density of modes in a specific direction of free space (i.e. no boundary conditions imposed e.g. by dielectric surfaces) regardless of the mode volume is then given by [2],

$$\int_{4\pi} \rho_{free}(\omega) d\Omega = V \varrho(\omega) \ , \tag{34.22}$$

that is,

$$\rho_{free}(\omega) = \frac{V}{(2\pi)^3} \frac{\omega^2}{c^3} \ . \tag{34.23}$$

Thus, the spontaneous emission rate of photons into the solid angle $d\Omega$ is,

$$\begin{aligned} \mathcal{W}_{if}^{(sp)} \ d\Omega &= \left(\int_\omega W_{if}^{(sp)} \rho_{free}(\omega) d\omega \right) \ d\Omega \\ &= \int_\omega \frac{\pi\hbar e^2}{\varepsilon_0 m^2 \omega V} |M_{fi}|^2 \delta(\omega + \omega_{fi}) \frac{V}{(2\pi)^3} \frac{\omega^2}{c^3} d\omega \ d\Omega = \frac{\hbar e^2}{8\pi^2 \varepsilon_0 m^2 c^3} |M_{fi}|^2 \omega_{fi} \ d\Omega \ , \end{aligned} \tag{34.24}$$

[2] See also (40.40) and (40.88) in Sec. 40.2.1.

This simplified treatment with only two atomic states considers light as a scalar field. In fact, light is a vector field and can have two independent orthogonal polarizations. The transition matrix may depend on polarization, such that,

$$\mathcal{W}_{if}^{(sp)} = \frac{\hbar e^2}{8\pi^2 \varepsilon_0 m^2 c^3} \int \sum_{\lambda=1,2} |M_{fi}^{\lambda}|^2 \omega_{fi} \, d\Omega \ . \tag{34.25}$$

Example 192 (*Natural linewidth of a transition*): Be $\Gamma \equiv \sum_f W_{if}^{(sp)}$ the spontaneous decay rate of a state $|i\rangle$. This means that its population is decreasing,

$$\dot{N}_i = -\Gamma N_i \ . \tag{34.26}$$

Since $N_i = \langle \psi_i | \psi_i \rangle$, we have $|\psi_i(t)\rangle = |\psi_i(0)\rangle e^{\imath \omega_{if} t - \Gamma t/2}$. The Fourier transform is,

$$\begin{aligned} |\xi(\omega)\rangle &= \frac{1}{\sqrt{2\pi}} \int_0^\infty |\psi_i(t)\rangle e^{-\imath\omega t} dt = \frac{1}{\sqrt{2\pi}} \int_0^\infty e^{\imath\omega_{if} t - \imath\omega t - \Gamma t/2} dt |\psi_i(0)\rangle \quad (34.27) \\ &= \frac{1}{\sqrt{2\pi}} \lim_{t\to\infty} \frac{e^{\imath(\omega_{if}-\omega)t - \Gamma t/2} - 1}{\imath(\omega_{if} - \omega) - \Gamma/2} |\psi_i(0)\rangle = \frac{1}{\sqrt{2\pi}} \frac{1}{\imath(\omega - \omega_{if}) + \Gamma/2} |\psi_i(0)\rangle \ . \end{aligned}$$

The spectrum,

$$|\xi(\omega)|^2 = \frac{1}{2\pi} \frac{1}{(\omega - \omega_{if})^2 + \Gamma^2/4} \ , \tag{34.28}$$

is a *Lorentz distribution*. Note, that the natural linewidth can be blurred by line broadening effects, such as the Doppler broadening or collisions between atoms. These effects will be discussed in the Sec. 34.6.

Excited states can sometimes decay into various states of lower energy. In this case the linewidth is simply given by the sum of the partial decay rates, since the convolution of Lorentz distributions $\mathcal{L}_{\Gamma_k}$ with widths Γ_k is again a Lorentzian with the total width $\Gamma = \sum_k \Gamma_k$.

34.1.4 Exercises

34.1.4.1 Ex: Energy density of plane waves

Derive the result (34.7) for the temporal averages of the squares of the fields $\overline{\vec{\mathcal{E}}(\mathbf{r},t)^2} = \overline{[-\partial_t \mathbf{A}(\mathbf{r},t)]^2}$ and $\overline{\vec{\mathcal{B}}(\mathbf{r},t)^2} = \overline{[\nabla \times \mathbf{A}(\mathbf{r},t)]^2}$.

Solution: *For the plane wave defined by (34.5) and (34.6) we have,*

$$\begin{aligned} \nabla \cdot \mathbf{A}(\mathbf{r},t) &= e^{\imath\omega t} \nabla \cdot \mathbf{A}_0 e^{-\imath \mathbf{k}\cdot\mathbf{r}} + e^{-\imath\omega t} \nabla \cdot \mathbf{A}_0 e^{\imath \mathbf{k}\cdot\mathbf{r}} = -\imath \mathbf{k} \cdot \mathbf{A}_0 (e^{\imath\omega t - \imath \mathbf{k}\cdot\mathbf{r}} - e^{-\imath\omega t + \imath \mathbf{k}\cdot\mathbf{r}}) \\ \frac{\partial \mathbf{A}(\mathbf{r},t)}{\partial t} &= \imath\omega \mathbf{A}_0 (e^{\imath\omega t - \imath \mathbf{k}\cdot\mathbf{r}} - e^{-\imath\omega t + \imath \mathbf{k}\cdot\mathbf{r}}) \\ \nabla \times \mathbf{A}(\mathbf{r},t) &= e^{\imath\omega t} \nabla \times \mathbf{A}_0 e^{-\imath \mathbf{k}\cdot\mathbf{r}} + e^{-\imath\omega t} \nabla \times \mathbf{A}_0 e^{\imath \mathbf{k}\cdot\mathbf{r}} = -\imath \mathbf{k} \times \mathbf{A}_0 (e^{\imath\omega t - \imath \mathbf{k}\cdot\mathbf{r}} - e^{-\imath\omega t + \imath \mathbf{k}\cdot\mathbf{r}}) \end{aligned}$$

and

$$\begin{aligned} \overline{\mathbf{A}(\mathbf{r},t)^2} &= \mathbf{A}_0^2 (2 + \overline{e^{2\imath\omega t - 2\imath \mathbf{k}\cdot\mathbf{r}}} + \overline{e^{-2\imath\omega t + 2\imath \mathbf{k}\cdot\mathbf{r}}}) = 2A_0^2 \\ \overline{[\partial_t \mathbf{A}(\mathbf{r},t)]^2} &= -\omega^2 \mathbf{A}_0^2 (-2 + \overline{e^{2\imath\omega t - 2\imath \mathbf{k}\cdot\mathbf{r}}} + \overline{e^{-2\imath\omega t + 2\imath \mathbf{k}\cdot\mathbf{r}}}) = 2\omega^2 A_0^2 \\ \overline{[\nabla \times \mathbf{A}(\mathbf{r},t)]^2} &= -(\mathbf{k} \times \mathbf{A}_0)^2 (-2 + \overline{e^{2\imath\omega t - 2\imath \mathbf{k}\cdot\mathbf{r}}} + \overline{e^{-2\imath\omega t + 2\imath \mathbf{k}\cdot\mathbf{r}}}) = 2(\mathbf{k} \times \mathbf{A}_0)^2 = 2k^2 A_0^2 \ , \end{aligned}$$

hence for $\mathbf{k}\cdot\mathbf{A}_0 = 0$ *we have* $(\mathbf{k}\times\mathbf{A}_0)^2 = k^2A_0^2$. *Therefore, using the relations (30.2) for electric and magnetic fields,*

$$u(\omega) = \frac{\varepsilon_0}{2}\mathcal{E}^2 + \frac{1}{2\mu_0}\mathcal{B}^2 = \frac{\varepsilon_0}{2}\overline{\partial_t \mathbf{A}(\mathbf{r},t)}^2 + \frac{1}{2\mu_0}\overline{\nabla\times\mathbf{A}(\mathbf{r},t)}^2 = \varepsilon_0\omega^2A_0^2 + \frac{1}{\mu_0}\frac{\omega^2}{c^2}A_0^2 = 2\varepsilon_0\omega^2A_0^2 \ .$$

34.2 The dipolar approximation and beyond

34.2.1 Dipolar transitions

So far, we have used the matrix element $M^\lambda_{fi}(\omega_{fi})$ without saying how it can be calculated, nor when it is significant. In many cases of interest the calculation of this matrix element is considerably simplified by an expansion of the term $e^{-\imath\mathbf{k}\cdot\mathbf{r}}$, which is part of the matrix element (34.12) [3],

$$e^{-\imath\mathbf{k}\cdot\mathbf{r}} = 1 - \imath\mathbf{k}\cdot\mathbf{r} - \tfrac{1}{2!}(\mathbf{k}\cdot\mathbf{r})^2 + \dots \ . \tag{34.29}$$

This expansion is justified by the fact that the wavelength ($\sim 600\,\text{nm}$ in the visible spectrum) is much larger than the size of the scattering atom, $ka_B \ll 1$. The *dipolar approximation* supposes,

$$e^{-\imath\mathbf{k}\cdot\mathbf{r}} \simeq 1 \ , \tag{34.30}$$

such that we can remove the spatial dependence. In this approximation there is only an interaction of the *electric field* of the radiation with the atom via an electric dipole term $\mathbf{d}\cdot\vec{\mathcal{E}}$. Thus,

$$M^\lambda_{fi}(\omega_{fi}) = \langle f|e^{-\imath\mathbf{k}\cdot\mathbf{r}}\hat\epsilon\cdot\nabla|i\rangle \simeq \hat\epsilon\tfrac{\imath}{\hbar}\langle f|\hat{\mathbf{p}}|i\rangle = \hat\epsilon\tfrac{\imath m}{\hbar}\langle f|\dot{\hat{\mathbf{r}}}|i\rangle \ . \tag{34.31}$$

We can calculate the expectation value of the velocity of the moving charge by the Heisenberg equation using the unperturbed Hamiltonian,

$$M^\lambda_{fi}(\omega_{fi}) \simeq \hat\epsilon\tfrac{\imath m}{\hbar}\langle f|\tfrac{1}{\imath\hbar}[\hat{\mathbf{r}},\hat H_0]|i\rangle = \hat\epsilon\tfrac{m}{\hbar^2}\langle f|\hat{\mathbf{r}}\hat H_0 - \hat H_0\hat{\mathbf{r}}|i\rangle = \hat\epsilon\tfrac{m}{\hbar^2}(E_i - E_f)\langle f|\hat{\mathbf{r}}|i\rangle \ . \tag{34.32}$$

The interpretation of the last equation is, that the states $|i\rangle$ and $|f\rangle$ are connected through a displacement of the electronic cloud which, therefore, represents the induction of an electric dipole during the electronic transition. It is convenient to introduce the *electric dipole moment* [4].

$$\mathbf{d}_{fi} \equiv -e\langle f|\hat{\mathbf{r}}|i\rangle \ . \tag{34.33}$$

As a result, the matrix element becomes,

$$\boxed{M^\lambda_{fi}(\omega_{fi}) \simeq \tfrac{m\omega_{fi}}{e\hbar}\hat\epsilon\cdot\mathbf{d}_{fi}} \tag{34.34}$$

[3] Note however, that doing the dipole approximation via $e^{\imath\mathbf{k}\cdot\hat{\mathbf{r}}} \simeq 1$ also deactivates the operator function of the recoil operator dipole, $e^{\imath\mathbf{k}\cdot\hat{\mathbf{r}}} = |\mathbf{p}+\hbar\mathbf{k}\rangle\langle\mathbf{k}|$. For discussions of photonic recoil the operator character must be maintained even in the dipole approximation, which can be done by reinserting the recoil operator in the Hamiltonian after the dipole approximation has been applied.

[4] In the presence of several atoms $\mathbf{d} = -e\sum_j \mathbf{r}_j$, where the $\mathbf{r}_j$ are the radii of the orbits of the various electrons of the atom.

and the absorption rate (34.15) is then, in the dipolar approximation,

$$W_{fi}^{(dp)} = \frac{\pi e^2}{\varepsilon_0 m^2 c}\frac{I(\omega_{fi})}{\omega_{fi}^2}|M_{fi}|^2\delta(\omega-\omega_{fi}) \tag{34.35}$$
$$= \frac{\pi}{\varepsilon_0\hbar^2 c}I(\omega_{fi})|\hat{\epsilon}\cdot\mathbf{d}_{fi}|^2\delta(\omega-\omega_{fi}) = \frac{4\pi^2\alpha}{\hbar}I(\omega_{fi})|\hat{\epsilon}\cdot\mathbf{r}_{fi}|^2\delta(\omega-\omega_{fi})\ .$$

using the definition of the fine structure constant $\alpha = e^2/4\pi\varepsilon_0\hbar c$.

34.2.1.1 Polarization dependence

Following Eq. (34.34) the absorption rate depends on the orientation of the dipole moment with respect to the polarization of light, which therefore plays an important role in this transition. When $\mathbf{d}_{fi}$ between two states is zero, the transition via electric dipole radiation is prohibited. This is not to say that there is no transition, since other terms of the expansion (34.29) are not necessarily zero, and there may be transitions of higher multipolar orders. Even the matrix element $M_{fi}^{\lambda}(\omega_{fi})$ being zero for transitions involving one photon, there is still the possibility of two-photon transitions.

Setting θ as the angle between $\hat{\epsilon}$ and $\mathbf{d}_{fi}$ we obtain,

$$W_{fi}^{(dp)} = \frac{\pi}{\varepsilon_0\hbar^2 c}I(\omega_{fi})|\mathbf{d}_{fi}|^2\cos^2\theta\ \delta(\omega-\omega_{fi})\ . \tag{34.36}$$

In case of unpolarized (or randomly polarized) radiation we can replace the angular distribution $\cos^2\theta$ by its average value,

$$\overline{\cos^2\theta} = \frac{1}{4\pi}\int_0^{2\pi}\int_0^{\pi}\cos^2\theta\sin\theta d\theta d\phi = \tfrac{1}{3}\ , \tag{34.37}$$

such that,

$$\boxed{W_{fi}^{(dp,no-pol)} = \frac{\pi}{3\varepsilon_0\hbar^2 c}I(\omega_{fi})|\mathbf{d}_{fi}|^2\delta(\omega-\omega_{fi})}\ . \tag{34.38}$$

This expression also represents the stimulated emission rate in the electric dipole approximation.

The total spontaneous emission rate can be obtained from Eq. (34.25) integrating over all possible orientations,

$$\mathcal{W}_{fi}^{(sp)} = \frac{\hbar e^2}{8\pi^2\varepsilon_0 m^2 c^3}\int\sum_{\lambda=1,2}|M_{fi}^{\lambda}|^2\omega_{fi}d\Omega \tag{34.39}$$
$$= 2\frac{\hbar e^2}{8\pi^2\varepsilon_0 m^2 c^3}\int_0^{2\pi}\int_0^{\pi}\left|\frac{m\omega_{fi}}{e\hbar}\hat{\epsilon}\cdot\mathbf{d}_{fi}\right|^2\omega_{fi}\sin\theta d\theta d\phi$$
$$= \frac{e^2}{4\pi^2\varepsilon_0\hbar c^3}\omega_{fi}^3|\mathbf{r}_{fi}|^2\int_0^{2\pi}\int_0^{\pi}\cos^2\theta\sin\theta d\theta d\phi = \frac{e^2}{3\pi\varepsilon_0\hbar c^3}\omega_{fi}^3|\mathbf{r}_{fi}|^2\ ,$$

such that, for non-polarized light,

$$\boxed{\mathcal{W}_{fi}^{(sp)} = \frac{4\alpha}{3c^2}\omega_{fi}^3|\mathbf{r}_{fi}|^2 = \frac{4\alpha}{3c^2}\omega_{fi}^3|\mathbf{r}_{fi}|^2 = \Gamma}\ . \tag{34.40}$$

This is the rate of spontaneous decay of an excited atomic state. It can be measured experimentally which, in turn, allows the calculation of the *induced dipole moment*,

$$d_{fi} = \sqrt{\frac{3\pi\varepsilon_0\hbar\Gamma}{k^3}} \ . \tag{34.41}$$

In Exc. 34.2.6.1 we calculate the Rabi frequency from the dipole moment of an atomic transition and the electric field of a radiation field.

34.2.2 Einstein transition rates

Considering the problem of the transfer of energy between the electromagnetic field and a sample of atoms in thermal equilibrium, Einstein realized that the processes of absorption and stimulated emission are not sufficient to understand the radiative coupling between two energy levels, that is, the coupling is not correctly described by Fermi's Golden rule, and we need to introduce the notion of spontaneous emission. Differently from the derivation of the preceding section, Einstein considered atoms whose populations of energy states are in thermal equilibrium with the electromagnetic field of a *black-body*. With this picture he came to the same result for the spontaneous emission rate (34.38), as we will show in the following.

The famous *Einstein coefficients* A_{fi} and B_{fi} are given by (22.70),

$$A_{fi}N_f = W_{fi}^{(sp)} \qquad \text{and} \qquad \frac{A_{fi}}{B_{fi}} = \frac{\hbar\omega_{fi}^3}{\pi^2 c^3} \ , \tag{34.42}$$

where N_f is the population of the excited state. This shows that, in fact, spontaneous emission is a necessary consequence of the interaction of an atom with a *thermal bath* (also called *reservoir*).

We now consider the problem of energy transfer between an electromagnetic field and a sample of atoms. The rate of *absorption* of a light field is,

$$R_{i\to f} \equiv \tfrac{1}{3}\dot{P}_{i\to f} = \frac{\pi}{6\hbar^2}\mathcal{E}_0^2|d_{fi}|^2\varrho(\omega_{fi}) \ , \tag{34.43}$$

with $W_0 = \mathcal{E}_0 d_{fi}$ and d_{fi} being the transition matrix element between atomic states. The factor $\frac{1}{3}$ comes from the fact that the vector $\vec{\mathcal{E}}$ of the electric field can have any polarization, but only polarizations along the direction of the oscillation of the dipole moment contribute.

For a single atom, the result (34.43) is symmetric with respect to an exchange of the initial and final states, that is, the rates for absorption and *induced emission* of light are the same. For a sample of atoms being in *thermal equilibrium*, the populations N_i of the ground state and N_f of the excited state are unequal according to Boltzmann's law. Therefore, as we have shown in Sec. 22.2.5,

$$N_f R_{f\to i} \neq N_i R_{i\to f} \ . \tag{34.44}$$

Thus, Einstein came to the conclusion that Fermi's golden rule correctly describes absorption, but does not contain all contributions of emission. The rates being related to the Einstein coefficients by the equation (22.65), we find,

$$R_{f\to i} = B_{fi}N_f u(\omega_{fi}) \tag{34.45}$$

and

$$\mathcal{S}_{f\to i} = A_{fi}N_f = \frac{\hbar\omega_{fi}^3}{\pi^2c^3}B_{if}N_f = \frac{\hbar\omega_{fi}^3}{\pi^2c^3}\frac{R_{i\to f}}{u(\omega_{fi})} = \frac{\omega_{fi}^3}{3\pi\epsilon_0\hbar c^3}|d_{fi}|^2 \ , \tag{34.46}$$

exploiting the relation (22.70).

Example 193 (*Line and oscillator strength*): Several disciplines such as spectrometry, spectroscopy and astrophysics have developed their own terminologies to describe absorption and emission of light by matter. We will explain how the most frequently used parameters are interrelated by placing particular emphasis on the simplest system, which is the two-level atom with no degeneracy and no spin.
In addition to the Einstein coefficients A_{21}, B_{21}, and B_{12}, the amplitude of the transition dipole moments d_{12} and the absorption cross-section $\sigma_{0a}(\omega)$, three other quantities are sometimes used to characterize atomic transitions: the oscillator strength f, the line strength S, and the spectral absorption cross section σ_ω. In the following sections, we will connect these different concepts.
The line strength S is defined as the square of the transition dipole moment summed over all degeneracies of the ground and excited states,

$$S_{12} = S_{21} = \sum_{m_1,m_2} |\langle\psi_{1,m_1}|d|\psi_{2,m_2}\rangle|^2 \ . \tag{34.47}$$

The notion of the line strength becomes significant when working with real atoms characterized by degenerate ground and excited states. In such cases we need to extend the meaning of d_{12} and consider transitions between each of the degenerate sublevels. For a non-degenerate two-level atom, the quantities d_{12} and A_{21} are simply related by,

$$A_{21} = \frac{\omega_0^3}{3\pi\epsilon_0\hbar c^3}d_{12}^2 \ . \tag{34.48}$$

If the lower level would be degenerate, the spontaneous emission rate coefficient would be given by the sum of all possible deexcitation rates. In this case, d_{12}^2 is defined as the sum of the elements of the transition matrix coupling the excited and the lower states,

$$d_{12}^2 = \sum_{m_1} |\langle\psi_{1,m_1}|d|\psi_2\rangle|^2 \ . \tag{34.49}$$

Now, it can be shown that the spontaneous emission rate from any sublevel of a degenerate excited state toward a lower level (that is, the sum over all lower sublevels) is the same for all excited sublevels [5] This statement reflects the intuitively plausible idea that spontaneous emission must be isotropic and unpolarized, if the sublevels of an excited state are uniformly populated. Therefore, the insertion of Eq. (34.49) into (34.48) should produce correct results, even when the excited state is degenerate. Comparing the sum over all upper and lower degeneracies with the line strength S,

$$S_{12} = \sum_{m_1,m_2} |\langle\psi_{1,m_1}|d|\psi_{2,m_2}\rangle|^2 = g_2d_{12}^2 \ . \tag{34.50}$$

[5] This applies to Zeeman sublevels (summing up $(3j)$-coefficients). Check for other degeneracy (also summing up $\{6j\}$-coefficients)!

Therefore, the insertion of Eq. (34.50) into (34.48) must be accompanied by a factor of $1/g_2$ to correct for the fact that all excited sub-levels radiate at the same rate. Therefore, using the S_{12} of Eq. (34.50) the correct expression relating the transition dipole between degenerate levels to the spontaneous emission rate is,

$$S_{12} = g_2 \frac{3\pi\epsilon_0 \hbar c^3}{\omega_0^3} A_{21} \ , \tag{34.51}$$

meaning that the line strength is proportional to the sum of the spontaneous emission rates A_{21} from each one of the g_2 excited levels toward all fundamental levels.

For an atom with two levels separated by an energy $\hbar\omega_0$ the *oscillator strength for emission* is defined as a measure for the radiative decay rate A_{21} as compared to the radiative decay rate γ_e of a classical electronic oscillator with frequency ω_0:

$$f_{21} = -\frac{1}{3}\frac{A_{21}}{\gamma_e} \ . \tag{34.52}$$

In case of degeneracy the *oscillator strength for absorption* is consequently defined by,

$$f_{12} = -\frac{g_2}{g_1} f_{21} = \frac{g_2}{3g_1}\frac{A_{21}}{\gamma_e} \ . \tag{34.53}$$

The transitions $S \leftrightarrow P$ in real atoms behave roughly as classical oscillators, that is, $A_{21} \simeq \gamma_e$. The factor $\frac{1}{3}$ in the definition compensates for the triple degeneracy of the P levels. So, a transition $S \leftrightarrow P$ which behaves exactly as a classical oscillator would be characterized by an oscillator strength for emission of $f_{21} = -\frac{1}{3}$ and an oscillator strength for absorption of $f_{12} = 1$. The classical expression for γ_e derived from the *Lorentz model* is [547],

$$\gamma_e = \frac{e^2\omega_0^2}{6\pi\epsilon_0 m_e c^3} \ . \tag{34.54}$$

Therefore, in terms of the A_{21} coefficient and of fundamental constants, the oscillator strength for absorption is given by,

$$f_{12} = A_{21}\frac{2\pi\epsilon_0 m_e c^3}{e^2\omega_0^2} \ . \tag{34.55}$$

Oscillator strengths obey certain sum rules that are useful for analyzing the relative intensities of atomic spectral lines. For example, atoms with single valence electrons (which are closer to the classical situation) obey the following sum rule,

$$\sum_k f_{ik} = 1 \ , \tag{34.56}$$

where the sum goes over all the excited states reached from the ground state. Alkaline atoms are approximately one-electron systems, and the oscillator strength of the first transition $S \longrightarrow P$ is typically of the order of $f_{12} = 0.7 - 0.95$. The sum rule tells us that most of the total transition probability for the excitation of the valence electron is concentrated in the first transition $S \to P$, and that transitions to higher states will be comparatively weaker. Another sum rule exists for the excitation and spontaneous emission from excited intermediate states j:

$$\sum_{i<j} f_{ji} + \sum_{k>j} f_{jk} = Z \ , \tag{34.57}$$

which is called the *Thomas-Reiche-Kuhn sum rule*. In the form of many electrons [Eq. (34.57)] this rule is very useful, when Z is the number of equivalent electrons, that is, electrons with the same quantum numbers n, l. Note also, that the numbers are intrinsically negative. Oscillator strengths are often used in astrophysics and plasma spectroscopy [6]. They are sometimes tabulated as $\log gf$, where,

$$g_1 f_{12} = -g_2 f_{21} \equiv gf \ . \tag{34.58}$$

34.2.3 Selection rules and electronic transitions

The selection rules that determine which transitions between two sets of quantum numbers $i \to f$ are allowed, reflect the symmetry properties of the system, e.g. the conservation of angular momentum (including the spin of the photon) or the change of parity, which can be understood by the fact that the emission of a photon in a particular direction must in some way alter the spatial isotropy of the atom. Note that radially symmetric oscillations of the shape of the charge distribution *do not radiate*.

Since the electronic transitions via electric dipole radiation are described by $|\hat{\epsilon} \cdot \mathbf{r}_{fi}|$, we expect a strong dependence of the transition rate on the orientation of the polarization state of the light with respect to the electronic displacement $\mathbf{r}_{fi}$. Let us express $\hat{\epsilon}$ and $\mathbf{r}_{fi}$ in spherical coordinates, which are more adapted to the problem [7]. For an arbitrary vector $\mathbf{r}$ we have,

$$x = \mathbf{r}\cdot\hat{\mathbf{e}}_x = r\sin\vartheta\cos\varphi \quad , \quad y = \mathbf{r}\cdot\hat{\mathbf{e}}_y = r\sin\vartheta\sin\varphi \quad , \quad z = \mathbf{r}\cdot\hat{\mathbf{e}}_z = r\cos\vartheta \ . \tag{34.59}$$

Defining,

$$\hat{\mathbf{e}}_{\pm1} \equiv \tfrac{1}{\sqrt{2}}(\mp\hat{\mathbf{e}}_x - \imath\hat{\mathbf{e}}_y) \qquad , \qquad \hat{\mathbf{e}}_0 \equiv \hat{\mathbf{e}}_z \ . \tag{34.60}$$

we obtain

$$r_{\pm1} \equiv \mathbf{r}\cdot\hat{\mathbf{e}}_\pm = \mathbf{r}\cdot\tfrac{1}{\sqrt{2}}(\mp\hat{\mathbf{e}}_x - \imath\hat{\mathbf{e}}_y) = \tfrac{1}{\sqrt{2}}(\mp x - \imath y) = \mp\tfrac{1}{\sqrt{2}} r\sin\vartheta e^{\pm\imath\varphi} = r\sqrt{\tfrac{4\pi}{3}}Y_{1,\pm1}(\vartheta,\varphi)$$
$$r_0 \equiv \mathbf{r}\cdot\hat{\mathbf{e}}_0 = \mathbf{r}\cdot\hat{\mathbf{e}}_z = z = r\cos\vartheta = r\sqrt{\tfrac{4\pi}{3}}Y_{1,0}(\vartheta,\varphi) \ . \tag{34.61}$$

Now, applying the expansion into spherical coordinates to the polarization, we get,

$$\epsilon_{\pm1} \equiv \hat{\epsilon}\cdot\hat{\mathbf{e}}_\pm \qquad , \qquad \epsilon_0 \equiv \hat{\epsilon}\cdot\hat{\mathbf{e}}_0 \ . \tag{34.62}$$

and applying the expansion to the matrix element $\mathbf{r}_{fi} = \langle f|\mathbf{r}|i\rangle$ with $\hat{\mathbf{e}}_q \cdot \hat{\mathbf{e}}_{q'} = \delta_{qq'}$, it is easy to check,

$$\hat{\epsilon}\cdot\mathbf{r}_{fi} = \sum_{q=0,\pm1}(\hat{\epsilon}\cdot\hat{\mathbf{e}}_q)\hat{\mathbf{e}}_q \cdot \sum_{q=0,\pm1}(\mathbf{r}_{fi}\cdot\hat{\mathbf{e}}_q)\hat{\mathbf{e}}_q = \sum_{q=0,\pm1}\epsilon_q\langle f|r_q|i\rangle = \sqrt{\tfrac{4\pi}{3}}\sum_{q=0,\pm1}\epsilon_q\langle f|rY_{1,q}|i\rangle \ . \tag{34.63}$$

[6] To find information about the atomic transition lines see 'http://www.nist.gov/pml/data/asd.cfm'.

[7] In the presence of a magnetic field it is often useful to choose the quantization axis along the field direction, because this simplifies the interpretation of π and $\sigma_\pm$ transitions in terms of light polarizations (see also Secs. 34.7.4 and 34.8.3).

The matrix elements are evaluated inserting the ansatz (25.18) separating the radial from the angular part of the wavefunction, where the angular part is solved by (25.32),

$$\begin{aligned}\langle f|r_q|i\rangle &= \sqrt{\tfrac{4\pi}{3}}\langle n_f\ell_f m_f|rY_{1,q}|n_i\ell_i m_i\rangle \\ &= \int_0^\infty r^3 R_{n_f,\ell_f}R_{n_i,\ell_i}dr\ \sqrt{\tfrac{4\pi}{3}}\int Y^*_{\ell_f,m_f}Y_{1,q}Y_{\ell_i,m_i}d\Omega\ .\end{aligned} \tag{34.64}$$

The angular integral,

$$\int Y^*_{\ell_f,m_f}Y_{\kappa,q}Y_{\ell_i,m_i}d\Omega = \sqrt{\tfrac{(2\ell_i+1)(2\ell_f+1)}{4\pi(2\kappa+1)}}\left(\begin{array}{cc|c}\ell_i & \kappa & \ell_f\\ 0 & 0 & 0\end{array}\right)\left(\begin{array}{cc|c}\ell_i & \kappa & \ell_f\\ m_i & q & m_f\end{array}\right)\ , \tag{34.65}$$

here with $\kappa = 1$, is only non-zero, if the values of ℓ_i, m_i, ℓ_f, m_f and q satisfy certain conditions called *selection rules* [8].

The radial integral, together with the coefficients of (34.65) which do not depend on the magnetic quantum numbers, is called *reduced matrix element* or *irreducible matrix element* with the notation,

$$\langle n_f\ell_f||r||n_i\ell_i\rangle \equiv \int_0^\infty r^3 R_{n_f,\ell_f}R_{n_i,\ell_i}dr\ \sqrt{\tfrac{(2\ell_i+1)(2\ell_f+1)}{3(2\kappa+1)}}\left(\begin{array}{cc|c}\ell_i & \kappa & \ell_f\\ 0 & 0 & 0\end{array}\right)\ . \tag{34.66}$$

Defining the electric dipole tensor operator,

$$Q^q_1(\mathbf{r}) = er_q(\mathbf{r}) = \sqrt{\tfrac{4\pi}{3}}Y_{1,q}(\vartheta,\varphi)er\ , \tag{34.67}$$

we can finally write,

$$\boxed{\langle n_f\ell_f m_f|Q^q_1(\mathbf{r})|n_i\ell_i m_i\rangle = \langle n_f\ell_f||er||n_i\ell_i\rangle\left(\begin{array}{cc|c}\ell_i & 1 & \ell_f\\ m_i & q & m_f\end{array}\right)}\ . \tag{34.68}$$

This is the *Wigner-Eckart theorem*. The electric dipole operator is a simpler example of a tensor operator $Q^q_\kappa(\mathbf{r})$ characterizing the transition between atomic states. In Excs. 34.2.6.2 and 34.2.6.3 we explicitly calculate, for a hydrogen atom subjected to a magnetic field, components of the electric dipole operator. Resolve Exc. 34.2.6.4.

Selection rules may be violated in higher orders, e.g. by multipolar radiation, as in the cases of *magnetic dipole transitions* or *electric quadrupole transitions*. This also is the case of the phenomenon of *phosphorescence*, which is a type of fluorescence emitted by metastable states.

34.2.3.1 Parity

The *parity* of a state has been defined as,

$$\mathcal{P}\psi_{n\ell m}(\mathbf{r}) = \psi_{n\ell m}(-\mathbf{r}) = (-1)^\ell\psi_{n\ell m}(\mathbf{r})\ , \tag{34.69}$$

[8] Frequently used are the $(3j)$-symbols connected to the Clebsch-Gordan coefficients by,

$$\langle j_i m_i, j_f m_f|J,M\rangle = (-1)^{j_i-j_f+M}\sqrt{2J+1}\left(\begin{array}{ccc}j_i & j_f & J\\ m_i & m_f & -M\end{array}\right)\ .$$

as shown above. That is, states with ℓ pair (impair) have even (odd) parity. Now the integral (34.67) only does not vanish, when $\ell_i + \ell_f + 1 = even$. Therefore, *dipole transitions must change the parity of the states.* F.ex. transitions $S \to P$ would be possible, while $S \to S$ would be prohibited.

34.2.3.2 Angular momentum

The irreducible matrix element (34.66) with $\kappa = 1$ is only non-zero, when $|\ell_f - \ell_i| \leq 1 \leq \ell_f + \ell_i$. That is, *dipole transitions can not change the angular momentum by more than one unit.*

34.2.3.3 Magnetic quantum number

In the decomposition (34.68) the Clebsch-Gordan coefficient is only non-zero, when $|q| \leq 1$. That is, *dipole transitions can not change the magnetic quantum number by more than one unit.* This can also be seen from,

$$\int Y^*_{\ell_f,m_f} Y_{\kappa,q} Y_{\ell_i,m_i} d\Omega \propto \int e^{\imath(m_i+q-m_f)} d\Omega \propto \delta_{m_i+q,m_f} \ . \tag{34.70}$$

34.2.3.4 Selection rules for emission in certain directions

As shown in Eq. (34.63), the excitation rate induced by a light field depends on the relative orientation of the laser polarization $\hat{\epsilon}$ and the atomic quantization axis (which may be set by the orientation of an applied magnetic field $\vec{\mathcal{B}}$). To take this dependence into account, we decompose the polarization vector (which can be linear or elliptical) on a coordinate basis, as shown in Eq. (34.62). Thus, the relative amplitude of the transitions $\Delta m_J = 0$ is proportional to the projection of the polarization vector onto the quantization axis, $\epsilon_0 \equiv \hat{\epsilon} \cdot \hat{\mathbf{e}}_0$. To estimate the amplitude of the transitions $\Delta m_J = \pm 1$, we must project onto the coordinates $\epsilon_{\pm 1} \equiv \hat{\epsilon} \cdot \hat{\mathbf{e}}_\pm$. Note that the direction of incidence of the beam, given by the wavevector $\mathbf{k}$, does not influence the transition probability directly (after all, the spatial dependence $e^{\imath \mathbf{k}\cdot\mathbf{r}}$ was removed by the dipolar approximation (34.29)); only through the fact, that the polarization is perpendicular to the propagation vector, $\hat{\epsilon} \perp \mathbf{k}$.

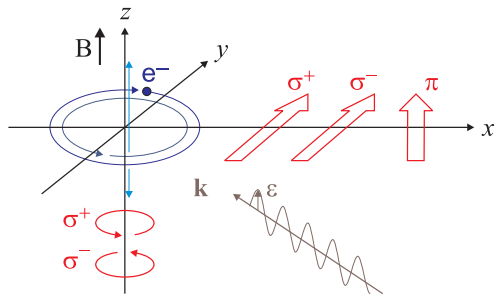

Figure 34.1: Selection rules due to polarization $\hat{\epsilon}$ of the incident light. The projection of this vector onto the axes $\pi = \hat{\epsilon} \cdot \hat{\mathbf{e}}_0$ and $\sigma_\pm = \hat{\epsilon} \cdot \hat{\mathbf{e}}_\pm$ is proportional to the excitation probability (and, obviously, also to the emission probability).

34.2.4 Reduction of the fine and hyperfine structure

In Sec. 34.2.3 we developed the Wigner-Eckart theorem for arbitrary angular momenta ℓ_i and ℓ_f. We will now be more specific identifying them with orbital angular momenta, $(\ell_i, \ell_f) = (\mathbf{L}, \mathbf{L}')$, total angular momenta of the electron shell, $(\ell_i, \ell_f) = (\mathbf{J}, \mathbf{J}')$, or total angular momenta including hyperfine structure, $(\ell_i, \ell_f) = (\mathbf{F}, \mathbf{F}')$.

34.2.4.1 Summary of selection rules including fine structure

The fine structure is due to a coupling of the type $\mathbf{L} + \mathbf{S} = \mathbf{J}$. The reduced matrix element (34.66) can then be recoupled as follows,

$$\boxed{\begin{aligned} \langle J', m'_J|\hat{\mathbf{d}}|J, m_J\rangle &= \langle J'||\hat{\mathbf{d}}||J\rangle \begin{pmatrix} J & \kappa & J' \\ m_J & q & m'_J \end{pmatrix} \quad \text{with} \\ \langle (L', S')J'||\hat{\mathbf{d}}||(L, S)J\rangle &= (-1)^{J+L'+1+S}\sqrt{(2J+1)(2L'+1)} \begin{Bmatrix} L' & L & 1 \\ J & J' & S \end{Bmatrix} \langle L'||\hat{\mathbf{d}}||L\rangle \end{aligned}} \,, \tag{34.71}$$

where the matrix in the second line represents a so-called *{6j}-symbol*, and the first line rewrites the Wigner-Eckart theorem (34.68) for total angular momenta. In this case,

$$\begin{aligned} \langle (L, S)Jm_J|er|(L', S')J'm'_J\rangle &= (-1)^{J+L'+1+S}\sqrt{2J+1}\sqrt{2L'+1} \times \\ &\times \delta_{S'S} \begin{Bmatrix} L & L' & 1 \\ J' & J & S \end{Bmatrix} \begin{pmatrix} J' & 1 & J \\ m'_J & q & -m_J \end{pmatrix} \langle n'L'||er||nL\rangle \\ &\propto \delta_{S'S} \begin{Bmatrix} L & L' & 1 \\ J' & J & S \end{Bmatrix} \begin{pmatrix} J' & 1 & J \\ m'_J & q & -m_J \end{pmatrix} \begin{pmatrix} L' & 1 & L \\ 0 & 0 & 0 \end{pmatrix} , \end{aligned} \tag{34.72}$$

Electric dipolar transitions are excited by Stark-like perturbations,

$$\hat{V}_{stark} = -e\mathbf{d} \cdot \mathcal{E} \,, \tag{34.73}$$

where $\mathcal{E} = \mathcal{E}_0 \cos(\mathbf{k} \cdot \mathbf{r} - \omega t)$ is the electric field of an electromagnetic oscillating wave with polarization $\mathcal{E}_0$. With $\mathbf{d} = ez\hat{\mathbf{e}}_z$, in order to determine which dipole transitions are possible, we must look at the matrix $\langle J'm'_J|\hat{z}|Jm_J\rangle$. Applying the Wigner-Eckart theorem (30.71), it is already possible to determine, between which magnetic quantum numbers m_J and m'_J transitions may occur.

We can compare the amplitudes of the various transitions between states $|m_J\rangle$ and $|m'_J\rangle$ via the Clebsch-Gordan coefficients (see Exc. 30.3.2.1). Again, transitions are only possible between states for which the corresponding Clebsch-Gordan coefficient does not zero. Looking at the equations (30.73), we find for dipolar transitions the following selection rules,

$$\begin{aligned} &\Delta J = 0, \pm 1 \quad \text{but} \quad (J = 0) \to (J' = 0) \quad \text{is prohibited} \\ &\Delta m_J = 0, \pm 1 \quad \text{but} \quad (m_J = 0) \to (m'_J = 0) \quad \text{is prohibited when} \quad \Delta J = 0 \,. \end{aligned} \tag{34.74}$$

In addition, we have for the $\mathbf{L} \cdot \mathbf{S}$ coupling,

$$\Delta S = 0, \Delta L = \pm 1 \quad \text{and for the electron undergoing the transition} \quad \Delta\ell = \pm 1 \,. \tag{34.75}$$

Table 34.1: Allowed transitions: (1-3) rigorous rules, (4-5) LS-coupling, and (6) intermediate coupling (https://en.wikipedia.org/wiki/Selection_rule).

	(E1)	(M1)	(E2)	(M2)	(E3)	(M3)
(1)	$\Delta J = 0, \pm 1$ ($\Delta J = 0 \nleftrightarrow 0$)		$\Delta J = 0, \pm 1, \pm 2$ ($\Delta J = 0 \nleftrightarrow 0, 1; \frac{1}{2} \nleftrightarrow \frac{1}{2}$)		$\Delta J = 0, \pm 1, \pm 2, \pm 3$ ($0 \nleftrightarrow 0, 1, 2; \frac{1}{2} \nleftrightarrow \frac{1}{2}, \frac{3}{2}; 1 \nleftrightarrow 1$)	
(2)	$\Delta M_J = 0, \pm 1$		$\Delta M_J = 0, \pm 1, \pm 2$		$\Delta M_J = 0, \pm 1, \pm 2, \pm 3$	
(3)	$\mathcal{P}_f = -\mathcal{P}_i$	$\mathcal{P}_f = \mathcal{P}_i$		$\mathcal{P}_f = -\mathcal{P}_i$		$\mathcal{P}_f = \mathcal{P}_i$
(4)	one e^- jump $\Delta L = \pm 1$	no e^- jump $\Delta L = 0; \Delta n \neq 0$	none or one e^- jump $\Delta L = 0, \pm 2$	one e^- jump $\Delta L = \pm 1$	one e^- jump $\Delta L = \pm 1, \pm 3$	one e^- jump $\Delta L = 0, \pm 2$
(5)	if $\Delta S = 0$ $\Delta L = 0, \pm 1$ ($L = 0 \nleftrightarrow 0$)	if $\Delta S = 0$ $\Delta L = 0$	if $\Delta S = 0$ $\Delta L = 0, \pm 1, \pm 2$ ($L = 0 \nleftrightarrow 0, 1$)		if $\Delta S = 0$ $\Delta L = 0, \pm 1, \pm 2, \pm 3$ ($L = 0 \nleftrightarrow 0, 1, 2; 1 \nleftrightarrow 1$)	
(6)	if $\Delta S = \pm 1$ $\Delta L = 0, \pm 1, \pm 2$		if $\Delta S = \pm 1$ $\Delta L = 0, \pm 1, \pm 2, \pm 3$ ($L = 0 \nleftrightarrow 0$)	if $\Delta S = \pm 1$ $\Delta L = 0, \pm 1$ ($L = 0 \nleftrightarrow 0$)	if $\Delta S = \pm 1$ $\Delta L = 0, \pm 1, \pm 2, \pm 3, \pm 4$ ($L = 0 \nleftrightarrow 0, 1$)	if $\Delta S = \pm 1$ $\Delta L = 0, \pm 1, \pm 2$ ($L = 0 \nleftrightarrow 0$)

In the presence of a strong magnetic field (Paschen-Back regime) breaking up the $\mathbf{L} \cdot \mathbf{S}$-coupling the selection rules are,

$$\Delta m_S = 0, \Delta m_L = 0, \pm 1 \ . \tag{34.76}$$

For $\mathbf{j} \cdot \mathbf{j}$-coupling,

$$\Delta j = 0, \pm 1 \ \text{ for one electron and } \ \Delta j = 0 \ \text{ for all others} \ . \tag{34.77}$$

For all dipole transitions the parity must change between even and odd.

Example 194 (*Transitions allowed and prohibited in the dipolar approximation*): Examples of allowed transitions are ${}^2S_{1/2} \leftrightarrow {}^2P_{1/2}$, ${}^1S_0 \leftrightarrow {}^1P_0$. Prohibited transitions are ${}^1S_0 \nleftrightarrow {}^3P_1$, ${}^2S_{1/2} \nleftrightarrow {}^2D_{3/2}$, $(5s)^2\ {}^3P_0 \nleftrightarrow (5s6s)\ {}^3P_0$.

34.2.4.2 Summary of selection rules including hyperfine structure

The fine structure is due to a coupling of the type $\mathbf{J} + \mathbf{I} = \mathbf{F}$. The reduced matrix element (34.66) can then be recoupled in a similar way as for the fine structure. Applying the Wigner-Eckart theorem (25.107) to the *hyperfine structure* [1368],

$$\begin{aligned}
\langle F', m'_F | \hat{\mathbf{d}} | F, m_F \rangle &= \langle F' || \hat{\mathbf{d}} || F \rangle \begin{pmatrix} F & \kappa & F' \\ m_F & q & m'_F \end{pmatrix} \quad \text{with} \\
\langle (J', I') F' || \hat{\mathbf{d}} || (J, I) F \rangle &= (-1)^{F+J'+1+I} \sqrt{(2F+1)(2J'+1)} \begin{Bmatrix} J' & J & 1 \\ F & F' & I \end{Bmatrix} \langle J' || \hat{\mathbf{d}} || J \rangle \\
\langle (L', S') J' || \hat{\mathbf{d}} || (L, S) J \rangle &= (-1)^{J+L'+1+S} \sqrt{(2J+1)(2L'+1)} \begin{Bmatrix} L' & L & 1 \\ J & J' & S \end{Bmatrix} \langle L' || \hat{\mathbf{d}} || L \rangle
\end{aligned} \ . \tag{34.78}$$

34.2.5 Irreducible tensor operators

Irreducible tensor operators are defined by their commutation relation with the angular momentum $\mathbf{J}$,

$$[\mathbf{J}, \mathbb{T}^{(k)}_q] = \sum_{q'} \langle kq | \mathbf{J} | kq' \rangle T^{(k)}_{q'} \ . \tag{34.79}$$

Using the spherical unit vectors $\hat{\mathbf{e}}_{\pm 1} = \frac{1}{\sqrt{2}}(\mp\hat{\mathbf{e}}_x - \imath\hat{\mathbf{e}}_y)$ and $\hat{\mathbf{e}}_0 = \hat{\mathbf{e}}_z$, we can reduce Cartesian vector operators to first-order tensor operators:

$$\vec{T} = \sum_q T_q^{(1)}\hat{\mathbf{e}}_q \qquad \text{resp.} \qquad T_q^{(1)} = \vec{T}\cdot\hat{\mathbf{e}}_q \ . \tag{34.80}$$

Examples for tensor operators are $\mathbb{I}_0^{(0)}$, $\hat{\mathbf{e}}_q^{(1)}$, $\mathbf{J}_q^{(1)}$, and $Y_q^{(k)}$. The most general tensor product is defined by:

$$(\mathbb{T}^{(k)} \times \mathbb{U}^{(k')})_m^{(j)} \equiv \sum_{q,q'} \begin{pmatrix} k & k' & j \\ q & q' & -m \end{pmatrix} \mathbb{T}_q^{(k)}\mathbb{U}_{q'}^{(k')} \ . \tag{34.81}$$

With this product it is possible to represent scalar, vector or tensor products of higher ranks,

$$\begin{aligned}
(\mathbb{T}^{(1)} \times \mathbb{U}^{(1)})_0^{(0)} &= \tfrac{1}{\sqrt{3}}\vec{\mathbb{T}}\cdot\vec{\mathbb{U}} \\
(\mathbb{T}^{(1)} \times \mathbb{U}^{(1)})_m^{(1)} &= \tfrac{1}{\sqrt{2}}(\vec{\mathbb{T}}\times\vec{\mathbb{U}})\cdot\hat{\mathbf{e}}_m \\
(\mathbb{T}^{(1)} \times \mathbb{U}^{(1)})_0^{(2)} &= -\tfrac{1}{\sqrt{6}}(3\mathbb{T}_z\mathbb{U}_z - \vec{\mathbb{T}}\cdot\vec{\mathbb{U}}) \\
(\mathbb{T}^{(1)} \times \mathbb{U}^{(1)})_{\pm 1}^{(2)} &= \pm\tfrac{1}{2}[(\mathbb{T}_x\mathbb{U}_z + \mathbb{T}_z\mathbb{U}_x) \pm \imath(\mathbb{T}_y\mathbb{U}_z + \mathbb{T}_z\mathbb{U}_y)] \\
(\mathbb{T}^{(1)} \times \mathbb{U}^{(1)})_{\pm 2}^{(2)} &= -\tfrac{1}{2}[(\mathbb{T}_x\mathbb{U}_x - \mathbb{T}_y\mathbb{U}_y) \pm \imath(\mathbb{T}_x\mathbb{U}_y + \mathbb{T}_y\mathbb{U}_x)] \ .
\end{aligned} \tag{34.82}$$

34.2.5.1 The Wigner-Eckart theorem

Be $\mathbb{T}_q^{(k)}$ an irreducible tensor of rank k. Then, there exists then an irreducible matrix element $\langle j||\mathbb{T}^{(k)}||j'\rangle$, which does not depend on the Zeeman sublevels:

$$\langle jm|\mathbb{T}_q^{(k)}|j'm'\rangle = \begin{pmatrix} j' & k & j \\ m' & q & -m \end{pmatrix} \frac{1}{\sqrt{2j+1}}\langle j||\mathbb{T}^{(k)}||j'\rangle \ . \tag{34.83}$$

From the possible values for the Clebsch-Gordan coefficients follow directly the selection rules for multipolar radiation:

$$\begin{aligned}
\langle jm|\mathbb{T}_q^{(k)}|j'm'\rangle = 0 \qquad \text{else} \qquad & E' - E = \hbar\omega \\
& |j'-j| \le k \le j'+j \\
& m' - m = q \\
& \tau'\tau = T \ .
\end{aligned} \tag{34.84}$$

For tensor products the reduced matrix element can be reduced:

$$\langle j||(\mathbb{T}^{(k)} \times \mathbb{U}^{(k')})^{(l)}||j'\rangle = (-)^{j+\ell+j'}\sqrt{2\ell+1}\sum_q \begin{Bmatrix} k & k' & \ell \\ j' & j & q \end{Bmatrix} \langle j||\mathbb{T}^{(k)}||q\rangle\langle q||\mathbb{U}^{(k')}||\mathbb{j}'\rangle \ . \tag{34.85}$$

In particular, it is possible to show,

$$\begin{aligned}\langle j||\mathbb{I}^{(0)}||j'\rangle &= \sqrt{2j+1}\delta_{jj'} \\ \langle j||\mathbb{J}^{(1)}||j'\rangle &= \sqrt{2j+1}\sqrt{j(j+1)}\delta_{jj'} \\ \langle j||\mathbb{Y}^{(k)}||j'\rangle &= \imath^{j+k+j'}\frac{\sqrt{2j+1}\sqrt{2k+1}\sqrt{2j'+1}}{4\pi}\begin{pmatrix} j & k & j' \\ 0 & 0 & 0\end{pmatrix} .\end{aligned} \tag{34.86}$$

34.2.5.2 Matrix element for angular momentum coupling

We consider states $|(l,s)j\rangle$. If the factors $\mathbb{T}$ and $\mathbb{U}$ of the tensor product act on different angular momenta, it can be reduced as follows:

$$\langle (l,s)j||(\mathbb{T}^{(k)}\times\mathbb{U}^{(k')})^{(l)}||(l',s')j'\rangle = \sqrt{2l+1}\sqrt{2j+1}\sqrt{2j'+1}\begin{Bmatrix} l' & s' & j' \\ k & k' & l \\ l & s & j\end{Bmatrix}\langle l||\mathbb{T}^{(k)}||l'\rangle\langle s||\mathbb{U}^{(k')}||s'\rangle . \tag{34.87}$$

Assuming, in particular, $\mathbb{U}^{(k')} \equiv \mathbb{I}^{(0)}$, we get, with $\mathbb{T}^{(k)} = \left(\mathbb{T}^{(k)}\times\mathbb{I}^{(0)}\right)^{(k)}$,

$$\langle (l,s)j||\mathbb{T}^{(k)}||(l',s')j'\rangle = (-)^{l+s+j'+k}\delta_{ss'}\sqrt{2j+1}\sqrt{2j'+1}\begin{Bmatrix} l & l' & k \\ j' & j & s\end{Bmatrix}\langle l||\mathbb{T}^{(k)}||l'\rangle . \tag{34.88}$$

The last equation therefore applies when $\mathbb{T}^{(k)}$ only acts on the angular momentum component ℓ. If on the other hand, $\mathbb{T}^{(k)}$ only acts on j, then we obviously have,

$$\langle (l,s)j||\mathbb{T}^{(k)}||(l',s')j'\rangle = \langle j||\mathbb{T}^{(k)}||j'\rangle . \tag{34.89}$$

34.2.6 Exercises

34.2.6.1 Ex: Rabi frequency

From the expression for the dipole moment d and the relationship between the intensity I and the electric field derive the Rabi frequency Ω produced by a laser beam of intensity I by exciting an atomic dipole transition with the wavelength λ and decay width Γ.

Solution: *The intensity is related to the electric field by,*

$$I = n\varepsilon_0 c\vec{\mathcal{E}}_1^2 .$$

Using the expression for the dipole moment,

$$d = \sqrt{\frac{3\pi\varepsilon_0\hbar\Gamma}{k^3}} ,$$

we find the Rabi frequency,

$$\Omega_n = \frac{d\mathcal{E}_1\sqrt{n}}{\hbar} = \frac{1}{\hbar}\sqrt{\frac{3\pi\varepsilon_0\hbar\Gamma}{k^3}}\sqrt{\frac{I}{n\varepsilon_0 c}}\sqrt{n} = \sqrt{\frac{3\lambda^2\Gamma I}{\hbar\omega 4\pi^2}} = \sqrt{\frac{\sigma_0\Gamma I}{2\hbar\omega}} ,$$

with the optical cross section $\sigma_0 = \frac{3\lambda^2}{2\pi}$.

34.2.6.2 Ex: Non-stationary state

Construct a non-stationary hydrogen wavefunction with equal contributions of $(n = 1, \ell = 0, m = 0)$ and $(n = 2, \ell = 1, m = 1)$. Calculate the expectation values $\langle|\mathbf{r}|\rangle$ and $\langle\mathbf{r}\rangle$ as a function of time.

Solution: *The wavefunction is,*

$$|\psi\rangle = \tfrac{1}{\sqrt{2}}|\psi_{100}\rangle + \tfrac{e^{-\imath\omega_{21}t}}{\sqrt{2}}|\psi_{211}\rangle = \tfrac{1}{\sqrt{2}}\tfrac{1}{\sqrt{\pi}}\left(\tfrac{Z}{a_B}\right)^{3/2} e^{-Zr/a_B} + \tfrac{e^{-\imath\omega_{21}t}}{\sqrt{2}}\tfrac{1}{8\sqrt{2\pi}}\left(\tfrac{Z}{a_B}\right)^{3/2}\tfrac{Zr}{a_B}e^{-Zr/2a_B}\sin\theta e^{\imath\phi} \ .$$

With this and using the result $\langle\tilde{r}\rangle = \tfrac{n^2 a_B}{Z}\left[1 + \tfrac{1}{2}\left(1 - \tfrac{\ell(\ell+1)}{n^2}\right)\right]$ *we calculate the integral,*

$$\begin{aligned}
\langle\psi|r|\psi\rangle &= \tfrac{1}{2}\langle\psi_{100}|r|\psi_{100}\rangle + \tfrac{1}{2}\langle\psi_{211}|r|\psi_{211}\rangle + \tfrac{e^{-\imath\omega_{21}t}}{2}\int \psi_{100} r \psi_{211} d^3r + c.c. \\
&= \tfrac{1}{2}\tfrac{1^2 a_B}{Z}\left[1 + \tfrac{1}{2}\left(1 - \tfrac{0(0+1)}{1^2}\right)\right] + \tfrac{1}{2}\tfrac{2^2 a_B}{Z}\left[1 + \tfrac{1}{2}\left(1 - \tfrac{1(1+1)}{2^2}\right)\right] \\
&+ \tfrac{e^{-\imath\omega_{21}t}}{2}\tfrac{1}{16\pi}\left(\tfrac{Z}{a_B}\right)^3 \int e^{-Zr/a_B}\tfrac{Zr}{a_B}e^{-Zr/2a_B}\sin\theta e^{\imath\phi} d^3r + c.c. \\
&= \tfrac{3a_B}{4Z} + \tfrac{5a_B}{2Z} + 0 = \tfrac{13a_B}{4Z} + 0 \ .
\end{aligned}$$

We also calculate the integral,

$$\langle\psi|\mathbf{r}|\psi\rangle = \tfrac{1}{2}\int |\psi_{100}|^2 \mathbf{r} d^3r + \tfrac{1}{2}\int |\psi_{211}|^2 \mathbf{r} d^3r + \tfrac{e^{-\imath\omega_{21}t}}{2}\int \psi_{100}\psi_{211}\mathbf{r} d^3r + c.c. \ .$$

The first term gives,

$$\tfrac{1}{2}\int_0^\infty \int_0^\pi \int_0^{2\pi} \tfrac{1}{2\pi}\left(\tfrac{Z}{a_B}\right)^3 e^{-2Zr/a_B}\begin{pmatrix} r\sin\theta\cos\phi \\ r\sin\theta\sin\phi \\ r\cos\theta \end{pmatrix} r^2\sin\theta d\theta d\phi dr = 0 \ ,$$

And the second,

$$\tfrac{1}{2}\int_0^\infty \int_0^\pi \int_0^{2\pi} \tfrac{1}{128\pi}\left(\tfrac{Z}{a_B}\right)^3\left(\tfrac{Zr}{a_B}\right)^2 e^{-Zr/a_B}\sin\theta^2\begin{pmatrix} r\sin\theta\cos\phi \\ r\sin\theta\sin\phi \\ r\cos\theta \end{pmatrix} r^2\sin\theta d\theta d\phi dr = 0 \ ,$$

such that we are left alone with the third,

$$\langle\psi|\mathbf{r}|\psi\rangle = \tfrac{e^{-\imath\omega_{21}t}}{2}\int_0^\infty\int_0^\pi\int_0^{2\pi}\tfrac{1}{16\pi\sqrt{2}}\left(\tfrac{Z}{a_B}\right)^3\tfrac{Zr}{a_B}e^{-3Zr/2a_B}\sin\theta e^{\imath\phi}\begin{pmatrix}r\sin\theta\cos\phi\\ r\sin\theta\sin\phi\\ r\cos\theta\end{pmatrix}r^2\sin\theta d\theta d\phi dr + c.c.$$

$$= \tfrac{\cos\omega_{12}t}{32\pi\sqrt{2}}\tfrac{a_B}{Z}\int_0^\infty\tilde{r}^4e^{-3\tilde{r}/2}dr\begin{pmatrix}\int_0^\pi\sin^3\theta d\theta\int_0^{2\pi}\cos^2\phi d\phi\\ \int_0^\pi\sin^3\theta d\theta\int_0^{2\pi}\sin\phi\cos\phi d\phi\\ 0\end{pmatrix}$$

$$- \tfrac{\sin\omega_{12}t}{32\pi}\tfrac{1}{\sqrt{2}}\tfrac{a_B}{Z}\int_0^\infty\tilde{r}^4e^{-3\tilde{r}/2}dr\begin{pmatrix}\int_0^\pi\sin^3\theta d\theta\int_0^{2\pi}\cos\phi\sin\phi d\phi\\ \int_0^\pi\sin^3\theta d\theta\int_0^{2\pi}\sin^2\phi d\phi\\ 0\end{pmatrix}$$

$$= \tfrac{\cos\omega_{12}t}{8\pi}\tfrac{1}{\sqrt{2}}\tfrac{a_B}{Z}\int_0^\infty\tilde{r}^4e^{-3\tilde{r}/2}dr\begin{pmatrix}\frac{4}{3}\int_0^{2\pi}\cos^2\phi d\phi\\ \frac{4}{3}\int_0^{2\pi}\sin\phi\cos\phi d\phi\\ 0\end{pmatrix}$$

$$+ \tfrac{\sin\omega_{12}t}{8\pi}\tfrac{1}{\sqrt{2}}\tfrac{a_B}{Z}\int_0^\infty\tilde{r}^4e^{-3\tilde{r}/2}dr\begin{pmatrix}\frac{4}{3}\int_0^{2\pi}\cos\phi\sin\phi d\phi\\ \frac{4}{3}\int_0^{2\pi}\sin^2\phi d\phi\\ 0\end{pmatrix}$$

$$= \frac{2^7}{3^3\sqrt{2}}[\hat{\mathbf{e}}_x\cos\omega_{12}t - \hat{\mathbf{e}}_y\sin\omega_{12}t]\ .$$

34.2.6.3 Ex: Transitions between Zeeman substates

Consider a hydrogen atom immersed in a uniform magnetic field, described by the Hamiltonian $\hat{H} = \hat{H}^{(0)} + \hat{H}^{(1)}$, being $\hat{H}^{(0)} = \hat{\mathbf{p}}^2/2m + V(r)$ and $H^{(1)} = -(\mu_B/\hbar)\hat{\mathbf{L}}\cdot\vec{\mathcal{B}}$ despising the spin [9].
a. Given the initial function, $|\psi_m(0)\rangle = \cos\alpha|\phi_{000}\rangle + \sin\alpha|\phi_{21m}\rangle$, determine its shape at time t.
b. Calculate the mean value $\langle\mathbf{d}\rangle_m(t) = \langle\psi_m(t)|\mathbf{d}|\psi_m(t)\rangle$ of the electric dipole operator of the atom $\mathbf{d} = q\mathbf{R}$.
c. Analyze the frequencies and polarizations of the emitted radiation by the transition of the excited states $|\phi_{21m}\rangle$ to the ground state.

Solution: *a. We derive the eigenenergies of the unperturbed Hamiltonian,*

$$E_n = -\tfrac{E_B}{n^2} \qquad with \qquad E_B = -\tfrac{m_e c^2}{2}\alpha^2\ .$$

and eigenfunctions $|\phi_{n\ell m}\rangle$ by Bohr's model. The perturbation causes normal Zeeman type energy shifts, which we calculate in first order TIPT,

$$\Delta E = \langle\phi_{n\ell m}|H^{(1)}|\phi_{n\ell m}\rangle = -\mu_B m\mathcal{B}\ .$$

[9] See Cohen-Tannoudji, Complemento D_VII

Thus, we have with the stationary perturbation,

$$|\psi_m(t)\rangle = e^{-iE_{100}t/\hbar}\cos\alpha|\phi_{100}\rangle + e^{-iE_{21m}t/\hbar}\sin\alpha|\phi_{21m}\rangle$$
$$\text{where} \qquad E_{100} = E_B \qquad \text{and} \qquad E_{21m} = \tfrac{E_B}{4} - \mu_B m\mathcal{B}\ .$$

Introducing the Larmor frequency $\omega_L \equiv \frac{\mu_B\mathcal{B}}{\hbar}$ *and the energy spacing* $\Delta \equiv E_{210} - E_{100}$, *we can write,*

$$|\psi_m(t)\rangle = \cos\alpha|\phi_{100}\rangle + e^{i(\Delta+m\omega_L)t}\sin\alpha|\phi_{21m}\rangle\ .$$

b. For the dipole moment we now expect,

$$\begin{aligned}\langle\psi_m(t)|\mathbf{d}|\psi_m(t)\rangle &= \cos^2\alpha\langle\phi_{100}|q\mathbf{R}|\phi_{100}\rangle + \sin^2\alpha\langle\phi_{21m}|q\mathbf{R}|\phi_{21m}\rangle\\ &+ \sin\alpha\cos\alpha e^{i(\Delta+m\omega_L)t}\langle\phi_{100}|q\mathbf{R}|\phi_{21m}\rangle + \sin\alpha\cos\alpha e^{-i(\Delta+m\omega_L)t}\langle|\phi_{21m}|q\mathbf{R}|\phi_{100}\rangle\\ &= q\cos^2\alpha\langle\phi_{100}|\mathbf{R}|\phi_{100}\rangle + q\sin^2\alpha\langle\phi_{21m}|\mathbf{R}|\phi_{21m}\rangle + q\sin 2\alpha\cos[(\Delta+m\omega_L)t]\langle\phi_{100}|\mathbf{R}|\phi_{21m}\rangle\ .\end{aligned}$$

Now, we need to calculate all elements of the matrix by choosing the quantization axis $\hat{\mathbf{e}}_z$. *Obviously,*

$$\langle\phi_{100}|\mathbf{R}|\phi_{100}\rangle = 0 \qquad \text{and} \qquad \langle\phi_{21m}|\mathbf{R}|\phi_{21m}\rangle = 0\ .$$

Besides that,

$$\begin{aligned}\langle\phi_{210}|\mathbf{R}|\phi_{100}\rangle &= \frac{a_B}{4\pi\sqrt{2}}\int_0^\infty\int_0^\pi\int_0^{2\pi}\tilde{r}e^{-\tilde{r}/2}\cos\theta\begin{pmatrix}\tilde{r}\sin\theta\cos\phi\\ \tilde{r}\sin\theta\sin\phi\\ \tilde{r}\cos\theta\end{pmatrix}e^{-\tilde{r}}\tilde{r}^2\sin\theta d\theta d\phi d\tilde{r}\\ &= \hat{\mathbf{e}}_z\frac{a_B}{2\sqrt{2}}\int_{-1}^1\cos^2\theta d(\cos\theta)\int_0^\infty\tilde{r}^4e^{-3\tilde{r}/2}d\tilde{r} = \hat{\mathbf{e}}_z\frac{a_B}{2\sqrt{2}}\frac{2}{3}\frac{2^8}{3^4} = \hat{\mathbf{e}}_z\frac{2^8a_B}{3^5\sqrt{2}}\ .\end{aligned}$$

and

$$\begin{aligned}\langle\phi_{21\pm1}|\mathbf{R}|\phi_{100}\rangle &= \frac{a_B}{8\pi\sqrt{2}}\int_0^\infty\int_0^\pi\int_0^{2\pi}\tilde{r}e^{-\tilde{r}/2}\sin\theta e^{\pm\imath\phi}\begin{pmatrix}\tilde{r}\sin\theta\cos\phi\\ \tilde{r}\sin\theta\sin\phi\\ \tilde{r}\cos\theta\end{pmatrix}e^{-\tilde{r}}\tilde{r}^2\sin\theta d\theta d\phi d\tilde{r}\\ &= \frac{a_B}{8\pi\sqrt{2}}\begin{pmatrix}\int_0^\pi\sin^3\theta d\theta(\int_0^{2\pi}\cos^2\phi d\phi \pm \imath\int_0^{2\pi}\cos\phi\sin\phi d\phi)\\ \int_0^\pi\sin^3\theta d\theta(\int_0^{2\pi}\cos\phi\sin\phi d\phi \pm i\int_0^{2\pi}\sin^2\phi d\phi)\\ \int_0^\pi\sin^2\theta\cos\theta d\theta\int_0^{2\pi}e^{\pm i\phi}d\phi\end{pmatrix}\int_0^\infty\tilde{r}^4e^{-3\tilde{r}/2}d\tilde{r}\\ &= \frac{a_B}{8\pi\sqrt{2}}\begin{pmatrix}\frac{4}{3}(\pi\pm 0\imath)\\ \frac{4}{3}(0\pm\imath\pi)\\ 0\end{pmatrix}\frac{2^8}{3^4} = \hat{\mathbf{e}}_\pm\frac{2^7a_B}{3^5\sqrt{2}}\ .\end{aligned}$$

c. Choosing $\alpha \equiv \pi/4$ *we get the final result,*

$$\langle\mathbf{d}\rangle_m(t) = \frac{2^7qa_B}{3^5\sqrt{2}}\cos[(\Delta+m\omega_L)t](\delta_{m,\pm1}\hat{\mathbf{e}}_\pm + 2\delta_{m,0}\hat{\mathbf{e}}_z)\ .$$

For $m = \pm1$ *the dipole moment is circular and* $\Delta = \mp m\omega_L$. *For* $m = 0$ *the dipole moment is linear and* $\Delta = 0$.

d. Assuming that the perturbation is suddenly switched on at time $t = 0$, we calculate the transition rates $\langle\phi_{100}|\psi_m(t)\rangle$,

$$\begin{aligned}
a_{i\to f}(t) &= \frac{1}{\imath\hbar}\int_0^t \langle\phi_{100}|W|\phi_{210}\rangle e^{\imath\omega_{if}\tau}d\tau \\
&= \langle\ell,m|\frac{1}{i\hbar}\int_0^t\int \frac{1}{4\pi\sqrt{2}}e^{-\tilde{r}}\frac{\mu_B}{\hbar}\mathbf{L}\cdot\vec{\mathcal{B}}\tilde{r}e^{-\tilde{r}/2}\cos\theta d^3\tilde{r}e^{\imath\omega_{if}\tau}d\tau|\ell,m\rangle \\
&= \frac{\mu_B}{\imath\hbar^2}\frac{1}{4\pi\sqrt{2}}\int_0^t\int e^{-\tilde{r}}\left(\langle 0,0|L_x|1,0\rangle\mathcal{B}\sin\theta\cos\phi + \langle 0,0|L_y|1,0\rangle\mathcal{B}\sin\theta\sin\phi\right. \\
&\quad \left.+\langle 0,0|L_z|1,0\rangle\mathcal{B}\cos\theta\right)\tilde{r}e^{-\tilde{r}/2}\cos\theta d^3\tilde{r}e^{\imath\omega_{if}\tau}d\tau = 0\ .
\end{aligned}$$

The same way,

$$\begin{aligned}
a_{i\to f}(t) &= \frac{1}{\imath\hbar}\int_0^t \langle\phi_{100}|W|\phi_{21\pm1}\rangle e^{\imath\omega_{if}\tau}d\tau \\
&= \langle\ell,m|\frac{1}{\imath\hbar}\int_0^t\int \frac{1}{4\pi\sqrt{2}}e^{-\tilde{r}}\frac{\mu_B}{\hbar}\mathbf{L}\cdot\vec{\mathcal{B}}\tilde{r}e^{-\tilde{r}/2}\sin\theta e^{\pm\imath\phi}d^3\tilde{r}e^{\imath\omega_{if}\tau}d\tau|\ell,m\rangle \\
&= \frac{\mu_B}{\imath\hbar^2}\frac{1}{4\pi\sqrt{2}}\int_0^t\int e^{-\tilde{r}}\left(\langle 0,0|L_x|1,\pm1\rangle\mathcal{B}\sin\theta\cos\phi + \langle 0,0|L_y|1,\pm1\rangle\mathcal{B}\sin\theta\sin\phi\right. \\
&\quad \left.+\langle 0,0|L_z|1,\pm1\rangle\mathcal{B}\sin\theta e^{\pm\imath\phi}\right)\tilde{r}e^{-\tilde{r}/2}\cos\theta d^3\tilde{r}e^{\imath\omega_{if}\tau}d\tau \\
&= \frac{\mu_B\mathcal{B}}{\imath\hbar}\frac{1}{4\pi\sqrt{2}}\int_0^t\int_0^{2\pi}\int_0^{\pi}\left(\frac{1}{\sqrt{2}}\sin\theta\cos\phi \mp \frac{\imath}{\sqrt{2}}\sin\theta\sin\phi + 0\right)\sin\theta e^{\pm\imath\phi}\sin\theta d\theta d\phi \\
&\quad \times\int_0^{\infty} e^{-3\tilde{r}/2}\tilde{r}^3 d\tilde{r}e^{\imath\omega_{if}\tau}d\tau = 0\ .
\end{aligned}$$

34.2.6.4 Ex: Derivation of selection rules

a. Prove $[L_k, r_m] = \imath\hbar r_n\epsilon_{kmn}$ for an *orbital angular momentum.*
b. Using the commutator derived in (a) derive the selection rules for transitions $\langle\alpha' L'm'|\vec{\varepsilon}\cdot\hat{\mathbf{r}}|\alpha Lm\rangle$, where $\vec{\varepsilon}$ is the polarization vector of the radiation field chosen to be $\hat{\mathbf{e}}_0$ or $\hat{\mathbf{e}}_\pm$.
c. Prove $[\hat{L}^2,[\hat{L}^2,\hat{\mathbf{r}}]] = 2\hbar^2(\hat{\mathbf{r}}\hat{L}^2 + \hat{L}^2\hat{\mathbf{r}})$ for an orbital angular momentum $\hat{\mathbf{L}}$.
d. Using the commutator derived in (b) derive the selection rule for $\hat{L}^2$.

Solution: *a. We calculate*

$$\begin{aligned}
[\hat{L}_x,\hat{x}] &= [\hat{\mathbf{r}}\times\hat{\mathbf{p}}_x,\hat{x}] = [\hat{y}\hat{p}_z,\hat{x}] - [z\hat{p}_y,\hat{x}] = 0 \\
[\hat{L}_y,\hat{x}] &= [\hat{\mathbf{r}}\times\hat{\mathbf{p}}_y,\hat{x}] = [\hat{z}\hat{p}_x,\hat{x}] - [x\hat{p}_z,\hat{x}] = \hat{z}[\hat{p}_x,\hat{x}] = -\imath\hbar\hat{z} \\
[\hat{L}_z,\hat{x}] &= [\hat{\mathbf{r}}\times\hat{\mathbf{p}}_z,\hat{x}] = [\hat{x}\hat{p}_y,\hat{x}] - [\hat{y}\hat{p}_x,\hat{x}] = -\hat{y}[\hat{p}_x,\hat{x}] = \imath\hbar\hat{y}\ ,
\end{aligned}$$

resulting in the specified formula.
b. From [880],

$$\begin{aligned}
0 &= \langle\alpha' L'm'|[\hat{L}_z,\hat{z}]|\alpha Lm\rangle = (m'-m)\langle\alpha' L'm'|\hat{z}|\alpha Lm\rangle \\
&= (m'-m)\langle\alpha' L'm'|-\hat{\mathbf{e}}_0\cdot\mathbf{r}|\alpha Lm\rangle\ ,
\end{aligned}$$

we conclude that the operator $-\hat{\mathbf{e}}_0 \cdot \mathbf{r}$ only drives transitions between corresponding Zeeman states: $m' = m$. From,

$$\begin{aligned}\hbar\langle\alpha' L' m'|\imath\hat{y} + \hat{x}|\alpha L m\rangle &= \langle\alpha' L' m'|[\hat{L}_z, \hat{x} + \imath\hat{y}]|\alpha L m\rangle(m' - m)\langle\alpha' L' m'|\hat{x} + \imath\hat{y}|\alpha L m\rangle \\ &= (m' - m)\langle\alpha' L' m'| - \hat{\mathbf{e}}_{-1} \cdot \mathbf{r}|\alpha L m\rangle \ ,\end{aligned}$$

we conclude that the operator $-\hat{\mathbf{e}}_\pm \cdot \mathbf{r}$ only drives transitions between adjacent Zeeman states: $m' = m \pm 1$.
c. We restrict without loss of generality to the x-dimension trying to show $[\hat{L}^2, [\hat{L}^2, \hat{x}]] = 2\hbar^2(\hat{x}\hat{L}^2 + \hat{L}^2\hat{x})$. Now,

$$[\hat{L}^2, [\hat{L}^2, \hat{x}]] = \ldots \ .$$

d. We have on one hand,

$$\begin{aligned}\langle L' m'|[L^2, [L^2, \hat{\mathbf{r}}]]|L, m\rangle &= \langle L' m'|[L^4\hat{\mathbf{r}} - 2L^2\hat{\mathbf{r}}L^2 + \hat{\mathbf{r}}L^4]|L, m\rangle \\ &= \langle L' m'|[\hbar^4 L'^2(L' + 1)^2\hat{\mathbf{r}} - 2\hbar^4 L'(L' + 1)\hat{\mathbf{r}}\hbar^4 L(L + 1) + \hat{\mathbf{r}}\hbar^4 L^2(L + 1)^2]|L, m\rangle \\ &= \hbar^4[L'(L' + 1) - L(L + 1)]^2\langle L' m'|\hat{\mathbf{r}}|L, m\rangle \ .\end{aligned}$$

On the other hand,

$$\langle L' m'|2\hbar^2(\hat{\mathbf{r}}L^2 + L^2\hat{\mathbf{r}})|L, m\rangle = 2\hbar^4[L(L + 1) + L'(L' + 1)]\langle L' m'|\hat{\mathbf{r}}|L, m\rangle \ .$$

By comparison,

$$\begin{aligned}0 &= [L'(L' + 1) - L(L + 1)]^2 - 2[L(L + 1) + L'(L' + 1)] \\ &= (L' + L + 1)^2(L' - L)^2 - 2L(L + 1) - 2L'(L' + 1) \\ &= (L' + L + 1)^2(L' - L)^2 - (L' + L + 1)^2 - (L' - L)^2 + 1 \\ &= [(L' + L + 1)^2 - 1][(L' - L)^2 - 1] \ .\end{aligned}$$

The first term can only be zero if $L = L' = 0$, but this is prohibited since L' is the vector sum of L and $\kappa = 1$ for the photon, and thus cannot be zero. The second term is zero only if $L = 1$. Hence, $\Delta L = 0, \pm 1$ is the selection rule.

34.3 Density matrix

As long as we are only interested in stimulated processes, such as the absorption of a monochromatic wave, the Schrödinger equation suffices to describe the light-atom interaction. A problem arises when we want to describe relaxation processes at the same time as excitation processes. Spontaneous emission (and any other dissipative process) must therefore be included in the physical description of the temporal evolution of our light-atom system. In this case, however, our system is no longer restricted to a single mode of the light field and the two atomic states of excitation. Spontaneous emission populates a statistical distribution of states of the light field and leaves the atom in a superposition of many momentum states. This situation can not be described by a single wavefunction, but only by a distribution of wavefunctions, and we can only expect to calculate the probability of finding the system

within this distribution. The Schrödinger equation, therefore, no longer applies, and we need to trace the time evolution of a system characterized by a density operator describing a statistical mixture of quantum states. The equations which describe the time evolution of the matrix elements of this density operator are the optical Bloch equations, and we must use them instead of the Schrödinger equation. In order to appreciate the origin and the physical content of the optical Bloch equations we begin by reviewing the rudiments of the density matrix theory.

34.3.1 The density operator

We define the *statistical operator* or *density operator* [10],

$$\boxed{\hat{\rho} \equiv \sum_k p_k \hat{P}_k \qquad \text{where} \qquad \hat{P}_k \equiv |\psi_k\rangle\langle\psi_k|} \ , \tag{34.90}$$

where $\{|\psi_k\rangle\}$ is a complete set of orthonormal states of the system under study. We consider a statistical distribution of these states with p_j being the probability of finding $|\psi_j\rangle$ in the set. Obviously, $\sum_k p_k = 1$. That is, the density operator acts on a member of the set $\{|\psi_k\rangle\}$ in a way to extract the probability of finding the system in $|\psi_j\rangle$,

$$\hat{\rho}|\psi_j\rangle = \sum_k p_k |\psi_k\rangle\langle\psi_k|\psi_j\rangle = p_j|\psi_j\rangle \ . \tag{34.91}$$

If all members of the set are in the same state, for example $|\psi_k\rangle$, the density operator reduces to,

$$\hat{\rho} = |\psi_k\rangle\langle\psi_k| \ , \tag{34.92}$$

and the system is in a *pure state* with $p_k = \delta_{1k}$. Each time a quantum state can be expressed by a single wave function, it is a pure state, but it does not have to be an eigenstate. Starting from the equation (34.91) we find,

$$\langle\psi_k|\hat{\rho}|\psi_j\rangle = p_j\delta_{kj} \ . \tag{34.93}$$

The diagonal elements of the density matrix are the probabilities of finding the system in $|\psi_j\rangle$, and assuming that all $|\psi_k\rangle$ are orthonormal, the non-diagonal elements of the incoherent sum (34.90) are necessarily zero [11], Besides that,

$$\sum_k \langle\psi_k|\hat{\rho}|\psi_k\rangle = 1 \ , \tag{34.94}$$

[10] In the presence of degeneracy or a continuous spectrum we can generalize the definition:

$$\hat{\rho} \equiv \sum_k p_k \hat{P}_k + \int p_\lambda \hat{P}_\lambda d\lambda \quad \text{where} \quad \hat{P}_k \equiv \sum_m |km\rangle\langle km| \quad \text{and} \quad \hat{P}_\lambda \equiv \int |\lambda\mu\rangle\langle\lambda\mu| d\mu \ .$$

Here, m and μ are degenerate quantum numbers, m, n are discrete, and λ, μ are continuous quantum numbers. The set of quantum numbers is complete, when

$$\sum\nolimits_{k,m} |km\rangle\langle km| = \hat{1} = \int |\lambda\mu\rangle\langle\lambda\mu| d\lambda d\mu \ .$$

The degree of degeneracy of a state $|k\rangle$ is $\mathrm{Tr}\ \hat{P}_k = \sum_m 1$. The probability of finding the system in the state $|k\rangle$ is $\langle\hat{P}_k\rangle = p_n \sum_m 1$.

[11] This is simply because we constructed the density operator to be diagonal in the basis $\{|\psi_k\rangle\}$. It does not mean, that the density operator cannot have non-diagonal elements in another basis.

so that $\hat{\rho}$ contains all *available* information about the system, that is, our *knowledge* about its state. When the state of the system is unknown, $\hat{\rho}$ describes the probability of finding the system in each state. When the state is fully known, $\hat{\rho}$ describes a pure state, that is, a vector in the Hilbert space, which is unequivocally determined by a complete set of observables with their respective quantum numbers.

The properties of the density operator are,

$$\boxed{\begin{array}{rcll} \hat{\rho} & = & \hat{\rho}^\dagger & \\ \langle\hat{\rho}\rangle & \geq & 0 & \\ \mathrm{Tr}\ \hat{\rho} & = & 1 & \\ \mathrm{Tr}\ \hat{\rho}^2 & \leq & 1 & \\ \det\hat{\rho} & = & 0 & \\ \hat{\rho} & = & \hat{\rho}^2 & \text{for a pure state} \end{array}} \ . \tag{34.95}$$

Example 195 (*Inhomogeneous atomic clouds*): For example, a thermal atomic cloud of N two-level atoms needs in general to be described by a density operator, because the state of every atom is independent of the state of the other atoms. If we knew that all atoms behave in the same way, for instance, when exposed to a radiation field, we could restrict to calculating the evolution of a single atom and extrapolate to N atoms. However, atomic motion and interatomic interactions often influence the dynamics.

34.3.1.1 Entropy

In a very general sense, the *entropy* determines in what direction a reversible process will take place. It is related to the size of the available phase space on both sides of the reaction. For example, the coupling of discrete and continuous modes is governed by entropy considerations.

Entropy measures of the lack of information about a system from which we only know $\langle\hat{H}\rangle$,

$$S \equiv -k_B\langle\ln\hat{\rho}\rangle = -k_B\ \mathrm{Tr}\ (\hat{\rho}\ln\hat{\rho})\ . \tag{34.96}$$

The *information entropy* (or *von Neumann entropy*) of statistically independent systems $\hat{\rho}\equiv\hat{\rho}_1\otimes\hat{\rho}_2$ is additive $S = S_1 + S_2$. We can also define absolute temperatures by $T^{-1}\equiv\partial S/\partial\langle\hat{H}\rangle$. The entropy of a pure state is 0. Hamiltonian processes conserve entropy, for they correspond to non-dissipative unitary transformations. On the other side, relaxation increases the entropy and the phase space volume. Another common definition is the so-called *purity* or *Renyi entropy*,

$$S_R \equiv \langle 1-\hat{\rho}\rangle = 1 - \mathrm{Tr}\ (\hat{\rho}^2)\ . \tag{34.97}$$

Quantum states can exhibit coherences. For example, if we express a state $|\psi\rangle$ on a basis of eigenstates $|1\rangle$ and $|2\rangle$:

$$\hat{\rho} = |\psi\rangle\langle\psi| = \begin{pmatrix} |\langle\psi|1\rangle|^2 & \langle 1|\psi\rangle\langle\psi|2\rangle \\ \langle 2|\psi\rangle\langle\psi|1\rangle & |\langle\psi|2\rangle|^2 \end{pmatrix}\ . \tag{34.98}$$

The evolution of such a state is described by the von Neumann equation,

$$i\hbar\partial_t\hat{\rho}(t) = [\hat{H}, \hat{\rho}(t)] \ . \tag{34.99}$$

The measurement process is not described by this equation. A pure state will always remain pure. If the eigenstates do not interact, the density operator will remain diagonal. The von Neumann equation conserves the properties of hermiticity, $\hat{\rho} = \hat{\rho}^\dagger$, completeness, Tr $\hat{\rho} = 1$, and purity $\det \hat{\rho} = 0$.

The density operator for a *statistical mixture* in a canonical ensemble (where S is maximum, U is variable, and N is fixed) follows from a variational problem with the Lagrange parameters $\delta(S - k_B\alpha\langle\hat{1}\rangle - k_B\beta\langle\hat{H}\rangle) = 0$, since Tr $\hat{\rho}$ and $\langle\hat{H}\rangle$ are fixed by boundary conditions. We find,

$$\boxed{\hat{\rho} = \frac{1}{Z}e^{-\hat{H}/k_BT} \qquad \text{with} \qquad Z \equiv \text{Tr } e^{-\hat{H}/k_BT}} \ . \tag{34.100}$$

We also have the expectation values, $\langle H\rangle = -\partial \ln Z/\partial\beta$ and $(\Delta H)^2 = -\partial\langle\hat{H}\rangle/\partial\beta$ with the abbreviation $\beta \equiv (k_BT)^{-1}$. All quantities are fixed, except the kinetic energy, which balances the interaction with a heat bath. T is the only equilibrium parameter. The density operator satisfies a Boltzmann distribution [12],

$$U = \langle\hat{H}\rangle = \frac{p^2}{2m} = -\frac{\partial}{\partial(1/k_BT)} \ln \int e^{-p^2/2mk_BT} dp = \frac{k_B}{2}T \ . \tag{34.101}$$

34.3.2 Matrix formalism

The next step is to develop matrix representations of the density operator by expanding the state vectors $|\psi_k\rangle$ in a complete orthonormal basis,

$$|\psi_k\rangle = \sum_n c_{nk}|n\rangle = \sum_n |n\rangle\langle n|\psi_k\rangle \ , \tag{34.102}$$

using the *completeness relation* (23.74), that is, $\sum_n |n\rangle\langle n| = \mathbb{I}$, and defining,

$$c_{nk} \equiv \langle n|\psi_k\rangle \tag{34.103}$$

as the projection of the state vector $|\psi_k\rangle$ on the basis vector $|n\rangle$. Now, we can write the density operator matrix representation within the basis $\{|n\rangle\}$ using the definition of $\hat{\rho}$ in Eq. (34.90) and replacing the expansions of $|\psi_k\rangle$ and $\langle\psi_k|$ of Eq. (34.102):

$$\hat{\rho} = \sum_k p_k|\psi_k\rangle\langle\psi_k| = \sum_k p_k \sum_{m,n} |n\rangle\langle n|\psi_k\rangle\langle\psi_k|m\rangle\langle m| = \sum_k p_k \sum_{m,n} c_{nk}c^*_{mk}|n\rangle\langle m| \ . \tag{34.104}$$

The matrix elements of $\hat{\rho}$ in this representation are

$$\rho_{nm} \equiv \langle n|\hat{\rho}|m\rangle = \sum_k p_k c_{nk}c^*_{mk} \tag{34.105}$$

[12] The von Neumann entropy S of a mixture can be expressed in terms of the eigenvalues or in terms of the trace and the logarithm of the density operator $\hat{\rho}$. Since $\hat{\rho}$ is a semi-definite positive operator, its spectrum λ_i, given by $\rho = \sum_i \lambda_i|\varphi_i\rangle\langle\varphi_i|$ where $\{|\varphi_i\rangle\}$ is an orthonormal basis, satisfies $\lambda_i > 0$ and $\sum\lambda_i = 1$. Then the entropy becomes $S = -\sum_i \lambda_i \ln\lambda_i = -\text{Tr } (\rho \ln\rho)$.

with the diagonal elements $\langle n|\hat{\rho}|n\rangle = \sum_k p_k |c_{nk}|^2$ and,

$$\rho^*_{nm} = \langle n|\hat{\rho}|m\rangle^* = \sum_k p_k c^*_{nk} c_{mk} = \sum_k p_k \langle m|\psi_k\rangle\langle\psi_k|n\rangle = \langle m|\rho|n\rangle = \rho_{mn} \ , \quad (34.106)$$

which means that the operator $\hat{\rho}$ is Hermitian.

Example 196 (*Density operator for a single atom*): For a very simple system such as a single atom with several levels, that without spontaneous emission can be described by a single wavefunction $|\psi_1\rangle$, we can let $p_k = \delta_{1k}$. That is, the equations (34.104) and (34.106) reduce to,

$$\hat{\rho} = \sum_{m,n} c_{n1} c^*_{m1} |n\rangle\langle m| \qquad \text{and} \qquad \langle n|\rho|m\rangle = c_{n1} c^*_{m1} \ . \quad (34.107)$$

34.3.3 Measurement and trace

The sum of the diagonal elements of a matrix representing an operator is called the *trace*. This quantity represents a fundamental property of the density operator, since it is invariant with respect to any unitary transformation:

$$\text{Tr } \hat{\rho} \equiv \sum_n \langle n|\hat{\rho}|n\rangle \ . \quad (34.108)$$

With the definition of the density operator (34.90) we can write the Eq. (34.108) as,

$$\text{Tr } \hat{\rho} \equiv \sum_{n,k} p_k \langle n|\psi_k\rangle\langle\psi_k|n\rangle \ . \quad (34.109)$$

Now, using the completeness relation,

$$\text{Tr } \hat{\rho} \equiv \sum_{n,k} p_k \langle\psi_k|n\rangle\langle n|\psi_k\rangle = \sum_k p_k \langle\psi_k|\psi_k\rangle = 1 \ , \quad (34.110)$$

which shows that the trace of the density operator representation is always 1 regardless of the basis of the matrix representation.

Example 197 (*Density operator for a statistical mixture*): Let us imagine an experiment with a single three-level atom coupling a state $|1\rangle$ to two other possible states $|2\rangle$ and $|3\rangle$ via a $\frac{\pi}{2}$-pulse, such that one of the two states,

$$|\psi_1\rangle = \tfrac{1}{\sqrt{2}}(|1\rangle + |2\rangle) \qquad \text{or} \qquad |\psi_2\rangle = \tfrac{1}{\sqrt{2}}(|1\rangle + |3\rangle)$$

be generated with equal probability. We also suppose that the performed experiment doesn't tell us which one of the two states was generated, so that we have to describe the system by a density operator,

$$\hat{\rho} = \sum_{k=1,2} \tfrac{1}{2} |\psi_k\rangle\langle\psi_k| = \tfrac{1}{2}\left[\frac{|1\rangle + |2\rangle}{\sqrt{2}} \frac{\langle 1| + \langle 2|}{\sqrt{2}}\right] + \tfrac{1}{2}\left[\frac{|1\rangle + |3\rangle}{\sqrt{2}} \frac{\langle 1| + \langle 3|}{\sqrt{2}}\right] \ .$$

Choosing an obvious basis, we can represent the density operator by a matrix,

$$\hat{\rho} = \begin{pmatrix} \frac{1}{2} & \frac{1}{4} & \frac{1}{4} \\ \frac{1}{4} & \frac{1}{4} & 0 \\ \frac{1}{4} & 0 & \frac{1}{4} \end{pmatrix} ,$$

for which we verify,

$$\hat{\rho} = \hat{\rho}^\dagger \quad \text{and} \quad \text{Tr } \hat{\rho} = 1 ,$$

but,

$$\hat{\rho}^2 \neq \hat{\rho} \quad \text{and} \quad \text{Tr } \hat{\rho}^2 = \tfrac{5}{8} \leq 1 .$$

Hence the state is not pure.

Expectation values of observables are expressed by,

$$\langle \hat{A} \rangle = \sum_k p_k \langle \psi_k | \hat{A} | \psi_k \rangle . \tag{34.111}$$

On the other side,

$$\hat{\rho}\hat{A} = \sum_k p_k |\psi_k\rangle\langle\psi_k|\hat{A} , \tag{34.112}$$

and in the basis $\{|n\rangle\}$,

$$\langle n|\hat{\rho}\hat{A}|m\rangle = \langle n| \sum_k p_k |\psi_k\rangle\langle\psi_k|\hat{A}|m\rangle = \sum_k p_k \langle n|\psi_k\rangle\langle\psi_k|\hat{A}|m\rangle = \sum_k p_k \langle\psi_k|\hat{A}|m\rangle\langle n|\psi_k\rangle . \tag{34.113}$$

Now, along the diagonal, we have,

$$\langle n|\hat{\rho}\hat{A}|n\rangle = \sum_k p_k \langle\psi_k|n\rangle\langle n|\hat{A}|\psi_k\rangle . \tag{34.114}$$

With the closure relation in the basis $\{|n\rangle\}$, we now have [13],

$$\boxed{\text{Tr } \hat{\rho}\hat{A} = \sum_k p_k \langle\psi_k|\hat{A}|\psi_k\rangle = \langle\hat{A}\rangle} . \tag{34.115}$$

The Eq. (34.115) says that the ensemble average of any dynamic observable $\hat{A}$ can be calculated from the diagonal elements of the operator matrix $\hat{\rho}\hat{A}$: Since the trace is independent of the basis (this will be shown in Exc. 34.3.5.1), each unitary transformation taking the matrix representation from a basis $\{|n\rangle\}$ to another one $\{|t\rangle\}$ leaves the trace invariant. Using the definition of a unitary transformation we can easily show that the trace of a cyclic permutation of a product is invariant. For example,

$$\text{Tr } [\hat{A}\hat{B}\hat{C}] = \text{Tr } [\hat{C}\hat{A}\hat{B}] = \text{Tr } [\hat{B}\hat{A}\hat{C}] , \tag{34.116}$$

and in particular

$$\text{Tr } [\hat{\rho}\hat{A}] = \text{Tr } [\hat{A}\hat{\rho}] = \langle\hat{A}\rangle . \tag{34.117}$$

In the Excs. 34.3.5.2 and 34.3.5.3 we apply the density operator to pure and mixed states of a two-level system. In Excs. 34.3.5.4 and 34.3.5.5 we study thermal mixtures and Exc. 34.3.5.6 Glauber states.

[13] In the presence of degeneracy or a continuous part of the spectrum we can generalize the definition of the expectation,

$$\langle\hat{X}\rangle \equiv \text{Tr } \hat{\rho}\hat{X} = \sum_{k,m} \langle km|\hat{\rho}\hat{X}|km\rangle .$$

34.3.3.1 Measurement process

If an observable $\hat{A}$ has a spectral representation $\hat{A} = \sum_n a_n |a_n\rangle\langle a_n| = \sum_n a_n \hat{P}_n$, with $\hat{P}_n = |a_n\rangle\langle a_n|$, the measurement process will transform the density operator to,

$$\hat{\rho}' = \sum_n \hat{P}_n \hat{\rho} \hat{P}_n \ . \tag{34.118}$$

That is, after the *measurement*, the density operator becomes diagonal on the basis of the eigenvalues of $\hat{A}$ [14], as explained in Sec. 23.2.7. The expression can be thought of as the mathematical formulation of von Neumann's state reduction postulate.

We note that the density operator (34.118) describes the whole ensemble after the measurement. The sub-ensemble corresponding to a particular result a_n of the measurement is described by a different density operator,

$$\hat{\rho}'_n = \frac{\hat{P}_n \hat{\rho} \hat{P}_n}{\text{Tr}\ [\hat{\rho}\hat{P}_n]} \ . \tag{34.119}$$

This is true, when $|a_n\rangle$ is the only eigenvector with the eigenvalue a_n. If not, $\hat{P}_n$ in the expression (34.119) should be replaced by the projection operator onto the sub-space of a_n [15]. In Exc. 34.3.5.7 we study the projection of Glauber states and in Exc. 34.3.5.8 of entangled states.

34.3.3.2 Systems and subsystems

Density operators are very useful for playing with systems and subsystems. Let us, for instance, assume that we have two quantum systems defined on the Hilbert spaces $\mathcal{H}_1$ and $\mathcal{H}_2$. The composite system is then the tensor product $\mathcal{H}_1 \otimes \mathcal{H}_2$. We now suppose that the compound system is in a pure state, $|\psi\rangle \in \mathcal{H}_1 \otimes \mathcal{H}_2$. If the state can be written in the form $|\psi\rangle = |\psi_1\rangle \otimes |\psi_2\rangle$, this means that the state of the first subsystem is $|\psi_1\rangle$. However, in general, $|\psi\rangle$ does not decompose like this. Of course, every vector in $\mathcal{H}_1 \otimes \mathcal{H}_2$ is a linear combination of tensorial products of $\mathcal{H}_1$ and $\mathcal{H}_2$. If $|\psi\rangle$ can not be decomposed as a tensor product, we say that the two systems are *entangled*. In this case, there is no reasonable way of associating a pure state $|\psi_1\rangle \in \mathcal{H}_1$ to the state $\psi \in \mathcal{H}_1 \otimes \mathcal{H}_2$. If, for example, in the case of a two particle wavefunction $\Psi(x_1, x_2)$ there is no way to construct a wavefunction (i.e. a pure state) $\psi_1(x_1)$ describing the state of the first particle, then $\Psi(x_1, x_2) \neq \psi_1(x_1)\psi_2(x_2)$.

[14] A projective measure always increases entropy. The entropy of a pure state is zero, while that of a mixture is always greater than zero. Therefore, a pure state can be converted into a mixture by a measurement, but the reverse can not happen. Thus, the action of measuring induces an irreversible change in the density matrix reminiscent of the collapse of the wavefunction. Strangely, the measurement *reduces* the amount of information by quenching the quantum interference of the compound system in a process called quantum decoherence. A subsystem can be taken from a mixed state to a pure state only at the price of increasing the von Neumann entropy elsewhere in the global system.

[15] In general, assuming that f is a function associating each observable $\hat{A}$ with a number $f(\hat{A})$ (which we may imagine as the expectation value), we can state the following: If f satisfies some natural properties (such as the one to produce positive values for positive operators), then there exists a unique density matrix $\hat{\rho}$, such that $f(\hat{A}) = \text{Tr}\ (\hat{\rho}\hat{A})$ for all $\hat{A}$. That is, every reasonable 'family' of expectation values' can be represented by a density matrix, which suggests that the density matrix provides the most general description of a quantum state.

The point of the discussion is that, even if the total system is in a pure state, the various subsystems that compose it will normally be in mixed states. On the other hand, regardless of whether the composite system is in a pure or mixed state, we can perfectly construct a density matrix that describes the state. Therefore, the use of density matrices is inevitable. Let $\hat{\rho}$ be the density matrix of the system composed of two subsystems. Then the state in $\mathcal{H}_2$ is described by a reduced density operator given by the partial trace of $\hat{\rho}$ over $\mathcal{H}_2$. In the particular case, where the state the density matrix has the form $\hat{\rho} = \hat{\rho}_1 \otimes \hat{\rho}_2$, where $\hat{\rho}_1$ and $\hat{\rho}_2$ are the density matrices in $\mathcal{H}_1$ and $\mathcal{H}_2$, then the partial trace is simply, $\text{Tr}_{\mathcal{H}_2} \hat{\rho}\hat{\rho}_1$.

34.3.4 Temporal evolution of the density operator

As shown in Secs. 23.4.2 to 23.4.4, the equations governing the temporal evolution of a quantum system depend on the choice of the picture, i.e. Schrödinger's (23.142), Heisenberg's (23.148), or the interaction picture (23.155). This, of course, also applies to a system represented by a density matrix.

Returning to the density operator definition (34.90), we can express its temporal dependence in terms of time-dependent quantum states and of the time evolution operator (23.145),

$$\hat{\rho}(t) = \sum_k p_k |\psi_k(t)\rangle\langle\psi_k(t)| = \sum_k p_k U(t,t_0)|\psi_k(t_0)\rangle\langle\psi_k(t_0)|U^\dagger(t,t_0) \ . \tag{34.120}$$

Writing,

$$\hat{\rho}(t_0) = \sum_k p_k |\psi_k(t_0)\rangle\langle\psi_k(t_0)| \ , \tag{34.121}$$

we see immediately,

$$\hat{\rho}(t) = U(t,t_0)\hat{\rho}(t_0)U^\dagger(t,t_0) \ , \tag{34.122}$$

where, for the common case of a time-independent Hamiltonian,

$$U(t,t_0) = e^{-\imath\hat{H}(t-t_0)/\hbar} \ . \tag{34.123}$$

Now we find the time derivative of the density operator differentiating the two sides of (34.122) and substituting the Eqs.

$$\frac{dU}{dt} = \frac{1}{\imath\hbar}\hat{H}U \qquad \text{and} \qquad \frac{dU^\dagger}{dt} = -\frac{1}{\imath\hbar}U^\dagger\hat{H} \tag{34.124}$$

for the time derivatives U and $U^\dagger$. The result is

$$\boxed{\frac{d\hat{\rho}(t)}{dt} = \frac{\imath}{\hbar}[\hat{\rho}(t),\hat{H}]} \ . \tag{34.125}$$

The commutator itself can be considered as a *superoperator* acting, not any more on states but on operators, that is, we can write,

$$\mathcal{L}\hat{\rho}(t) \equiv \frac{\imath}{\hbar}[\hat{\rho}(t),\hat{H}] \ , \tag{34.126}$$

where $\mathcal{L}$ is called *Liouville operator*. The equation (34.125) is called *Liouville equation* or *von Neumann equation*. The Liouville equation describes the *time evolution of the density operator* which, in turn, describes the distribution of an ensemble of quantum states. Even though the form of the Liouville equation resembles the Heisenberg equation, Eq. (34.120) shows that $\hat{\rho}(t)$ is in the *Schrödinger picture* [16].

34.3.4.1 Transformation to the interaction picture

For a two-level system perturbatively interacting with a light field, the Hamiltonian can be decomposed as in (23.152) into a stationary part and a time-dependent part,

$$\hat{H} = \hat{H}_{atom} + \hat{H}_{atom:field}(t) \ , \tag{34.127}$$

where $\hat{H}_{atom}$ is the part of the Hamiltonian describing the atomic structure and $\hat{H}_{atom:field}(t)$ the interaction of the dipole transition with the classical oscillating electric field. The interaction picture is the natural choice for this type of problem. In this case, we can transform the density operator into the interaction picture defined by (23.153),

$$\tilde{\rho}(t) = e^{\imath \hat{H}_{atom}(t-t_0)/\hbar} \hat{\rho}(t_0) e^{-\imath \hat{H}_{atom}(t-t_0)/\hbar} \ , \tag{34.128}$$

where the 'tilde' decoration (replacing the 'hat') emphasizes, that we are now in the *interaction picture*. We look for the time evolution rate of $\tilde{\rho}(t)$ analogously to the Liouville equation. Calculating the time derivatives on both sides of (34.128) and substituting Eq. (34.125) for $\frac{d\hat{\rho}}{dt}$ results in,

$$\boxed{\frac{d\tilde{\rho}(t)}{dt} = \frac{\imath}{\hbar}[\tilde{\rho}(t), \hat{H}_{atom:field}(t)]} \ . \tag{34.129}$$

This equation shows that the time evolution of the density operator in the interaction picture depends only on the time-dependent part of the total Hamiltonian.

In the following we will derive a ready-to-use form of the Hamiltonian governing the interaction of a weak single-mode light field with a two-level atom in the dipolar approximation.

34.3.4.2 Semi-classical two-level atom in the dipolar approximation

According to (34.127) the semi-classical light-atom interaction Hamiltonian comprises two terms which, in the dipolar approximation, can be written,

$$\hat{H} = \begin{pmatrix} 0 & 0 \\ 0 & \hbar\omega_0 \end{pmatrix} - \hat{\mathbf{d}} \cdot \vec{\mathcal{E}}(\mathbf{r}, t) \quad \text{where} \quad \hat{\mathbf{d}} = -e\hat{\mathbf{r}} = \begin{pmatrix} 0 & \langle 1|\mathbf{d}|2\rangle \\ \langle 2|\mathbf{d}|1\rangle & 0 \end{pmatrix} \tag{34.130}$$

is the dipole operator and

$$\vec{\mathcal{E}}(\mathbf{r}, t) = \frac{\vec{\epsilon}}{2}\left[\mathcal{E}_0(\mathbf{r}) e^{\imath(\mathbf{k}\cdot\mathbf{r}-\omega t)} + \mathcal{E}_0^*(\mathbf{r}) e^{-\imath(\mathbf{k}\cdot\mathbf{r}-\omega t)}\right] \tag{34.131}$$

[16] The Heisenberg equation for the density operator in the Schrödinger picture or the master equation in the Heisenberg picture are $d\hat{\rho}_H/dt = 0$.

the electric field. Note that via $\mathcal{E}_0(\mathbf{r}) \to \imath\sqrt{\frac{\hbar\omega}{2\varepsilon_0 V}}\hat{a}$, we can quantize the radiation mode, as will be shown in Sec. 35.1.2. Introducing the Rabi frequencies

$$\hbar\Omega(\mathbf{r}) \equiv -\mathcal{E}_0(\mathbf{r})\vec{\epsilon}\cdot\langle 2|\mathbf{d}|1\rangle \qquad \text{and} \qquad \hbar\Theta(\mathbf{r}) \equiv -\mathcal{E}_0(\mathbf{r})\vec{\epsilon}\cdot\langle 1|\mathbf{d}|2\rangle \tag{34.132}$$

as an abbreviation, we can write the Hamiltonian,

$$\hat{H} = \hbar\begin{pmatrix} 0 & \frac{\Theta(\mathbf{r})}{2}e^{\imath(\mathbf{k}\cdot\mathbf{r}-\omega t)} + \frac{\Omega^*(\mathbf{r})}{2}e^{-\imath(\mathbf{k}\cdot\mathbf{r}-\omega t)} \\ \frac{\Omega(\mathbf{r})}{2}e^{\imath(\mathbf{k}\cdot\mathbf{r}-\omega t)} + \frac{\Theta^*(\mathbf{r})}{2}e^{-\imath(\mathbf{k}\cdot\mathbf{r}-\omega t)} & \hbar\omega_0 \end{pmatrix} . \tag{34.133}$$

As shown in Sec. 23.4.5 the transformation from the Schrödinger to Dirac's interaction picture, is done via,

$$\hat{H}_{atom:field} \equiv U^\dagger \hat{H} U + \hbar\dot{U}^\dagger U \qquad \text{with} \qquad U = e^{-\imath\hat{H}_{atom}t/\hbar} . \tag{34.134}$$

Introducing the abbreviation $\Delta = \omega - \omega_0$ we obtain,

$$\begin{aligned}\hat{H}_{atom:field} = &\begin{pmatrix} 0 & \frac{\hbar}{2}\Omega^*(\mathbf{r})e^{-\imath(\mathbf{k}\cdot\mathbf{r}-\Delta t)} \\ \frac{\hbar}{2}\Omega(\mathbf{r})e^{\imath(\mathbf{k}\cdot\mathbf{r}-\Delta t)} & 0 \end{pmatrix} \\ &+ \begin{pmatrix} 0 & \frac{\hbar}{2}\Theta(\mathbf{r})e^{\imath(\mathbf{k}\cdot\mathbf{r}-\omega t-\omega_0 t)} \\ \frac{\hbar}{2}\Theta^*(\mathbf{r})e^{-\imath(\mathbf{k}\cdot\mathbf{r}-\omega t-\omega_0 t)} & 0 \end{pmatrix} \equiv \hat{H}^{(slow)}_{atom:field} + \hat{H}^{(fast)}_{atom:field} .\end{aligned} \tag{34.135}$$

34.3.4.3 The rotating wave approximation

The transition amplitude in first-order time-dependent perturbation theory is according to (27.71),

$$\begin{aligned} a_{i\to f}(t) &= \frac{1}{\imath\hbar}\int_0^t \langle 2|\hat{H}_{atom:field}(\tau)|1\rangle d\tau = \frac{\hbar}{2}\frac{1}{\imath\hbar}\int_0^t \left[\Omega(\mathbf{r})e^{\imath(\mathbf{k}\cdot\mathbf{r}-\Delta t)} + \Theta^*(\mathbf{r})e^{-\imath(\mathbf{k}\cdot\mathbf{r}-\omega t-\omega_0 t)}\right] d\tau \\ &= \frac{\Omega(\mathbf{r})e^{\imath\mathbf{k}\cdot\mathbf{r}}}{2\Delta}(e^{-\imath\Delta t}-1) + \frac{\Theta^*(\mathbf{r})e^{-\imath\mathbf{k}\cdot\mathbf{r}}}{2(\omega+\omega_0)}\left(e^{-\imath(\omega+\omega_0)\Delta t}-1\right) \\ &\simeq \frac{\Omega(\mathbf{r})e^{\imath\mathbf{k}\cdot\mathbf{r}}}{2\Delta}(e^{-\imath\Delta t}-1) , \end{aligned} \tag{34.136}$$

where the last step corresponds to the *rotating wave approximation*. This allows us to neglect $\hat{H}^{(fast)}_{atom:field}$.

34.3.4.4 Transformation into the rotating frame

Now, we further transform into rotating frame using,

$$\tilde{H}_{atom:field} = U^\dagger \hat{H}_{atom:field} U + \imath\hbar\dot{U}^\dagger U \qquad \text{with} \qquad U = \begin{pmatrix} 1 & 0 \\ 0 & e^{-\imath\Delta t} \end{pmatrix} . \tag{34.137}$$

This yields,

$$\tilde{H}_{atom:field} = \begin{pmatrix} 0 & \frac{\hbar}{2}\Omega^*(\mathbf{r})e^{-\imath\mathbf{k}\cdot\mathbf{r}} \\ \frac{\hbar}{2}\Omega(\mathbf{r})e^{\imath\mathbf{k}\cdot\mathbf{r}} & -\hbar\Delta \end{pmatrix} . \tag{34.138}$$

We always can write the Rabi frequency as $\Omega = |\Omega|e^{\imath\phi}$ and attribute the phase to the atomic position if necessary. Locating the atom in the center of the coordinate system, we finally get,

$$\tilde{H}_{atom:field} = \begin{pmatrix} 0 & \frac{\hbar}{2}\Omega \\ \frac{\hbar}{2}\Omega & -\hbar\Delta \end{pmatrix} , \tag{34.139}$$

yielding the new Liouville equation,

$$\boxed{\frac{d\rho(t)}{dt} = \frac{\imath}{\hbar}[\rho(t), \tilde{H}_{atom:field}]} . \tag{34.140}$$

The matrix representation of the Hamiltonian given in this section are given in the basis of the unperturbed states, but we still need to derive the matrix form of the Liouville equations (34.125), (34.129), and (34.129) in the various pictures. This will be the topic of the next section.

34.3.5 Exercises

34.3.5.1 Ex: Trace of an operator

The trace of an operator $\hat{A}$ is defined by Tr $\hat{A} = \sum_n \langle n|\hat{A}|n\rangle$.
a. Show that the trace is independent of the chosen basis!
b. Show that Tr $\hat{A}\hat{B}$ = Tr $\hat{B}\hat{A}$!

Solution: *a. The basis transformation* $|n\rangle = \sum_m |m\rangle\langle m|n\rangle$ *applied to the trace gives,*

$$Tr\ \hat{A} = \sum_n \langle n|\hat{A}|n\rangle = \sum_{n,m,m'} \langle n|m\rangle\langle m|\hat{A}|m'\rangle\langle m'|n\rangle = \sum_{m,m'} \langle m'|m\rangle\langle m|A|m'\rangle = \sum_m \langle m|\hat{A}|m\rangle .$$

b. Holds $Tr\ \hat{A}\hat{B} = \sum_n \langle n|\hat{A}\hat{B}|n\rangle = \sum_{n,m} \langle n|\hat{A}|m\rangle\langle m|\hat{B}|n\rangle = Tr\ \hat{B}\hat{A}$.

34.3.5.2 Ex: Pure states and mixtures

Consider a system of two levels coupled by a light mode. The Hamiltonian can be written ($\hbar \equiv 1$),

$$\hat{H} = \begin{pmatrix} 0 & \frac{1}{2}\Omega \\ \frac{1}{2}\Omega & \omega_0 \end{pmatrix} .$$

Calculate $\hat{\rho}$, $\hat{\rho}^2$ and $\langle\hat{H}\rangle$ for the following two cases:
a. The atom is in a superposition state, $|\psi\rangle = \alpha|1\rangle + \beta|2\rangle$ and
b. the atom is a statistical mixture of eigenstates, $\hat{\rho} = \mu|1\rangle\langle 1| + \nu|2\rangle\langle 2|$.

Solution: *a. In this case, the system is in a pure state. Therefore, the density*

operator is,

$$\rho = |\psi\rangle\langle\psi| = \alpha|1\rangle\langle 1| + \beta|2\rangle\langle 2| + \alpha\beta^*|1\rangle\langle 2| + \alpha^*\beta|2\rangle\langle 1| = \begin{pmatrix} |\alpha|^2 & \alpha^*\beta \\ \alpha\beta^* & |\beta|^2 \end{pmatrix}$$
$$= \begin{pmatrix} \langle 1|\rho|1\rangle & \langle 1|\rho|2\rangle \\ \langle 2|\rho|1\rangle & \langle 2|\rho|2\rangle \end{pmatrix} = \begin{pmatrix} \langle 1|\psi\rangle\langle\psi|1\rangle & \langle 1|\psi\rangle\langle\psi|2\rangle \\ \langle 2|\psi\rangle\langle\psi|1\rangle & \langle 2|\psi\rangle\langle\psi|2\rangle \end{pmatrix} .$$

Now the trace, which is the sum of the diagonal elements, must be normalized,

$$Tr\ \hat{\rho} = |\alpha|^2 + |\beta|^2 = 1 .$$

The square is,

$$\hat{\rho}^2 = \begin{pmatrix} |\alpha|^4 + \alpha^*\beta\alpha\beta^* & |\alpha|^2\alpha^*\beta + \alpha^*\beta|\beta|^2 \\ |\alpha|^2\alpha\beta^* + \alpha\beta^*|\beta|^2 & \alpha^*\beta\alpha\beta^* + |\beta|^4 \end{pmatrix} = \begin{pmatrix} |\alpha|^2 & \alpha^*\beta \\ \alpha\beta^* & |\beta|^2 \end{pmatrix} = \hat{\rho} .$$

The expectation value of the Hamiltonian is,

$$\langle\hat{H}\rangle = Tr\ \hat{\rho}\hat{H} = Tr \begin{pmatrix} |\alpha|^2 & \alpha^*\beta \\ \alpha\beta^* & |\beta|^2 \end{pmatrix} \begin{pmatrix} 0 & \Omega \\ \Omega & \omega_0 \end{pmatrix} = \alpha^*\beta\Omega + \alpha\beta^*\Omega + |\beta|^2\omega_0$$
$$= \langle\psi|\hat{H}|\psi\rangle = (\alpha^*\langle 1| + \beta^*\langle 2|)\,\hat{H}\,(\alpha|1\rangle + \beta|2\rangle)$$
$$= |\alpha|^2\langle 1|\hat{H}|1\rangle + |\beta|^2\langle 2|\hat{H}|2\rangle + \alpha^*\beta\langle 1|\hat{H}|2\rangle + \alpha\beta^*\langle 2|\hat{H}|1\rangle = |\beta|^2\omega_0 + \alpha^*\beta\Omega + \alpha\beta^*\Omega .$$

b. In the case of a mixture of eigenstates, the density operator is,

$$\hat{\rho} = \mu|1\rangle\langle 1| + \nu|2\rangle\langle 2| = \begin{pmatrix} \mu & 0 \\ 0 & \nu \end{pmatrix} .$$

The trace is always normalized,

$$Tr\ \hat{\rho} = Tr \begin{pmatrix} \mu & 0 \\ 0 & \nu \end{pmatrix} = \mu + \nu = 1 .$$

but the state is not pure, since,

$$\hat{\rho}^2 = \begin{pmatrix} \mu^2 & 0 \\ 0 & \nu^2 \end{pmatrix} \neq \hat{\rho} .$$

The average value of the Hamiltonian is now,

$$\langle\hat{H}\rangle = Tr\ \hat{\rho}\hat{H} = Tr \begin{pmatrix} \mu & 0 \\ 0 & \nu \end{pmatrix} \begin{pmatrix} 0 & \Omega \\ \Omega & \omega_0 \end{pmatrix} = Tr \begin{pmatrix} 0 & \mu\Omega \\ \nu\Omega & \nu\omega_0 \end{pmatrix} = \nu\omega_0 .$$

34.3.5.3 Ex: Mixture of states

A two-level atom is initially in a superposition of two states $|\psi\rangle = \frac{1}{\sqrt{2}}|1\rangle + \frac{1}{\sqrt{2}}|2\rangle$. An apparatus measures the populations of the states, but the experimenter forgot to read the indicated result.
a. Describe the state the atom by the density operator.
b. Now the experimenter returns to the device. Calculate with which probability he reads the state $|1\rangle$.

Solution: *a. The state is,*

$$\hat{\rho} = \tfrac{1}{2}|1\rangle\langle 1| + \tfrac{1}{2}|2\rangle\langle 2| \ .$$

Obviously, $\hat{\rho}^2 \neq \hat{\rho}$*, but* $Tr\ \hat{\rho} = 1$.
b. The probability is,

$$\langle \hat{P}_1 \rangle = Tr\ \hat{\rho}\hat{P}_1 = \sum_k \langle k|\hat{\rho}\hat{P}_1|k\rangle = \sum_k \langle k| \left(\tfrac{1}{2}|1\rangle\langle 1| + \tfrac{1}{2}|2\rangle\langle 2|\right)|1\rangle\langle 1|k\rangle = \tfrac{1}{2} \ .$$

34.3.5.4 Ex: Thermal mixture

We consider a thermal non-interacting atomic gas in one dimension. Instead of describing the state of the atomic ensemble, we can consider a single atom with a distributed probability of having a given velocity v. The density operator of the continuous degree of freedom can be written,

$$\hat{\rho} = \int dv \sqrt{\frac{m}{2\pi k_B T}} e^{-mv^2/2k_B T} |v\rangle\langle v| \ ,$$

and the trace of an arbitrary observable $\hat{A}$,

$$\langle \hat{A} \rangle = \mathrm{Tr}\ \hat{\rho}A = \int du \langle u|\hat{\rho}\hat{A}|u\rangle \ .$$

Now imagine a device capable of measuring the speed of a single atom randomly chosen within the cloud.
a. Express the probability of measuring a specific velocity v' for this atom using the density operator.
b. Express the expectation value of the average velocity by the density operator.

Solution: *a. The probability of measuring exactly the velocity* v' *for an atom is,*

$$\begin{aligned}\langle v'|\hat{\rho}|v'\rangle &= \langle v'| \int dv \sqrt{\frac{m}{2\pi k_B T}} e^{-mv^2/2k_B T} |v\rangle\langle v|v'\rangle \\ &= \int dv \sqrt{\frac{m}{2\pi k_B T}} e^{-mv^2/2k_B T} \delta(v - v') = \sqrt{\frac{m}{2\pi k_B T}} e^{-mv'^2/2k_B T} \ .\end{aligned}$$

b. The expectation value is,

$$\begin{aligned}\langle\hat{v}^2\rangle &= Tr\ \rho v^2 = \int du\langle u|\hat{\rho}\hat{v}^2|u\rangle = \int duu^2\langle u|\hat{\rho}|u\rangle \\ &= \sqrt{\frac{m}{2\pi k_BT}}\int duu^2\langle u|\int dve^{-mv^2/2k_BT}|v\rangle\langle v|u\rangle \\ &= \sqrt{\frac{m}{2\pi k_BT}}\int duu^2\langle u|e^{-mu^2/2k_BT}|u\rangle = \sqrt{\frac{m}{2\pi k_BT}}\int u^2e^{-mu^2/2k_BT}du \\ &= \sqrt{\frac{m}{2\pi k_BT}}\left(\frac{2k_BT}{m}\right)^{3/2}\int_{-\infty}^{\infty}z^2e^{-z^2}dz = \sqrt{\frac{1}{\pi}}\frac{2k_BT}{m}\frac{\sqrt{\pi}}{2} = \frac{k_BT}{m}\ .\end{aligned}$$

34.3.5.5 Ex: Thermal population of a harmonic oscillator

In thermal equilibrium the energy states of a system are populated following Boltzmann's law,

$$P_n = \frac{e^{-n\beta\hbar\omega}}{\sum_m e^{-m\beta\hbar\omega}} \qquad \text{with} \qquad \beta \equiv \frac{1}{k_BT}\ .$$

a. Consider a one-dimensional harmonic oscillator characterized by the secular frequency ω and, using the density operator, calculate the mean quantum number of the population and the mean energy.
b. For an energy spacing of $\omega/2\pi = 10\,\text{MHz}$, how many levels of the harmonic oscillator are necessary at room temperature to accumulate a population of at least 50%. How many for an energy spacing of $\omega/2\pi = 10\,\text{GHz}$. Repeat the calculation for a $1\,\mu\text{K}$ cold atomic cloud.

Solution: *a. The density operator,*

$$\hat{\rho} = \sum_n P_n|n\rangle\langle n|\ ,$$

satisfies $\hat{\rho}^2 \neq \hat{\rho}$ *and* $Tr\ \hat{\rho} = 1$. *It allows to calculate the most likely value for the population and is obtained using the rule* $\sum_{n=0}^{\infty}U^n = (1-U)^{-1}$ *with the abbreviation* $U \equiv e^{-\hbar\omega/k_BT}$,

$$\begin{aligned}\langle\hat{n}\rangle &= Tr\ \hat{\rho}\hat{n} = \sum_m\langle m|\hat{\rho}\hat{n}|m\rangle = \sum_m\langle m|\sum_n P_n|n\rangle\langle n|\hat{n}|m\rangle = \sum_m mP_m\langle m|m\rangle \\ &= \sum_m\frac{me^{-m\beta\hbar\omega}}{\sum_n e^{-n\beta\hbar\omega}} = (1-e^{-\beta\hbar\omega})\sum_m me^{-m\beta\hbar\omega} = (1-e^{-\beta\hbar\omega})\frac{-1}{\hbar\omega}\frac{\partial}{\partial\beta}\sum_m e^{-m\beta\hbar\omega} \\ &= (1-e^{-\beta\hbar\omega})\frac{-1}{\hbar\omega}\frac{\partial}{\partial\beta}\frac{1}{1-e^{-\beta\hbar\omega}} = \frac{e^{-\beta\hbar\omega}}{1-e^{-\beta\hbar\omega}} = \frac{1}{e^{\beta\hbar\omega}-1}\ .\end{aligned}$$

For the average energy, with $E_n = n\hbar\omega$,

$$\langle\hat{E}\rangle = \sum_n E_np_n = \frac{\hbar\omega}{e^{\beta\hbar\omega}-1}\ .$$

This is precisely the distribution proposed by Planck for the light modes in the black-body radiator. We can now express the occupation probability of state n as,

$$P_n = \frac{e^{-n\beta\hbar\omega}}{\sum_m e^{-m\beta\hbar\omega}} = (1 - e^{-\beta\hbar\omega})e^{-n\beta\hbar\omega} = \frac{\langle\hat{n}\rangle^n}{(1 + \langle\hat{n}\rangle)^{n+1}} \ .$$

b. Using the formulas,

$$\sum_{n=1}^{\infty} U^n = \frac{-1}{U-1} \qquad \textit{and} \qquad \sum_{n=1}^{N} U^n = \frac{U^{N+1} - 1}{U-1}$$

we find,

$$50\% = \sum_{n=0}^{N} \frac{e^{-n\beta\hbar\omega}}{\sum_m e^{-m\beta\hbar\omega}} = 1 - e^{-N\beta\hbar\omega} \ ,$$

that is,

$$N = -\frac{\ln 0.5}{\beta\hbar\omega} \ .$$

For the different situations we find,

T	$\omega/2\pi$	N
300 K	10 MHz	$4.3 \cdot 10^6$
300 K	10 GHz	4300
1 µK	10 MHz	0.014
1 µK	10 GHz	$1.4 \cdot 10^{-5}$

34.3.5.6 Ex: Density operator of a Glauber state

a. Write down the density operator of a Glauber state and calculate its purity.
b. How does the density operator look after a measurement of its vibrational level before acknowledging the result? Is it pure?
c. How does it look having acknowledged the result? Is it pure?

Solution: *The density operator is,*

$$\hat{\rho} = \sum_{m,n} \frac{\beta^{*m}\beta^n e^{-|\beta|^2}}{\sqrt{m!n!}} |n\rangle\langle m| \ ,$$

and its square,

$$\hat{\rho}^2 = e^{-2|\beta|^2} \sum_{n,n'} \frac{\beta^{*n'}\beta^n}{\sqrt{n!n'!}} |n\rangle\langle n'| \sum_{m,m'} \frac{\beta^{*m}\beta^{m'}}{\sqrt{m!m'!}} |m'\rangle\langle m|$$

$$= e^{-|\beta|^2} \sum_{m,n,n'} \frac{\beta^n\beta^{*m}}{\sqrt{n!m!}} |n\rangle\langle m| \sum_{n'} \frac{|\beta|^{2n'} e^{-|\beta|^2}}{n'!} = e^{-|\beta|^2} \sum_{m,n,n'} \frac{\beta^n\beta^{*m}}{\sqrt{n!m!}} |n\rangle\langle m|\langle\beta|\beta\rangle = \hat{\rho} \ .$$

b. After the measurement, the density operator reads,

$$\hat{\rho}' = \sum_k \hat{P}_k\hat{\rho}\hat{P}_k = \sum_k |k\rangle\langle k| e^{-|\alpha|^2} \sum_{m,n} \frac{\alpha^{*m}\alpha^n}{\sqrt{m!}\sqrt{n!}} |n\rangle\langle m|k\rangle\langle k| = \sum_k e^{-|\alpha|^2} \frac{|\alpha|^{2k}}{k!} |k\rangle\langle k| \ .$$

This the density operator is not pure, since,

$$\hat{\rho}'^2 = \sum_k \frac{|\alpha|^{2k} e^{-|\alpha|^2}}{k!} |k\rangle\langle k| \sum_n \frac{|\alpha|^{2n} e^{-|\alpha|^2}}{n!} |n\rangle\langle n| = \sum_n \frac{|\alpha|^{4n} e^{-2|\alpha|^2}}{n!^2} |n\rangle\langle n| \neq \hat{\rho} \ .$$

c. Having acknowledged the result, we get the Poisson distribution,

$$\hat{\rho}'' = e^{-|\alpha|^2} \frac{|\alpha|^{2k}}{k!} |k\rangle\langle k| \ ,$$

which obviously is a pure state.

34.3.5.7 Ex: Reduced density operator of a Glauber state

Project the density operator of a Glauber state onto its two lowest Fock states using the formula (34.119). Show that the resulting density operator is pure.

Solution: *With the density operator,*

$$\hat{\rho} = \sum_{m,n} \frac{\beta^{*m} \beta^n e^{-|\beta|^2}}{\sqrt{m!n!}} |n\rangle\langle m|$$

and the projector,

$$P_{1,2} = |0\rangle\langle 0| + |1\rangle\langle 1|$$

we find,

$$\begin{aligned} P_{1,2}\hat{\rho}P_{1,2} &= |0\rangle\langle 0|\hat{\rho}|0\rangle\langle 0| + |1\rangle\langle 1|\hat{\rho}|0\rangle\langle 0| + |0\rangle\langle 0|\hat{\rho}|1\rangle\langle 1| + |1\rangle\langle 1|\hat{\rho}|1\rangle\langle 1| \\ &= e^{-|\beta|^2} \left(|0\rangle\langle 0| + \beta|1\rangle\langle 0| + \beta^*|0\rangle\langle 1| + \beta\beta^*|1\rangle\langle 1|\right) \end{aligned}$$

and

$$Tr\ \hat{\rho}P_{1,2} = \sum_k \langle k|\hat{\rho}P_{1,2}|k\rangle = \sum_{k,m} \frac{\beta^{*m}\beta^k e^{-|\beta|^2}}{\sqrt{m!k!}} \langle m|(|0\rangle\langle 0| + |1\rangle\langle 1|)|k\rangle = e^{-|\beta|^2}(1+\beta^*\beta) \ .$$

Hence,

$$\hat{\rho}_{red} = \frac{P_{1,2}\hat{\rho}P_{1,2}}{Tr\ \hat{\rho}P_{1,2}} = \frac{|0\rangle\langle 0| + \beta|1\rangle\langle 0| + \beta^*|0\rangle\langle 1| + |\beta|^2|1\rangle\langle 1|}{1+|\beta|^2} \ .$$

The purity is given because of,

$$\begin{aligned} \hat{\rho}_{red}^2 &= \frac{|0\rangle\langle 0| + \beta|1\rangle\langle 0| + |\beta|^2|0\rangle\langle 0| + \beta|\beta|^2|1\rangle\langle 0| + \beta^*|0\rangle\langle 1| + |\beta|^2|1\rangle\langle 1| + \beta^*|\beta|^2|0\rangle\langle 1| + |\beta|^4|1\rangle\langle 1|}{(1+|\beta|^2)^2} \\ &= \hat{\rho}_{red} \ . \end{aligned}$$

34.3.5.8 Ex: Partial measurements

Consider the density operator describing the quantum state of two spins, $|\Psi\rangle = |\psi_a\rangle \otimes |\psi_b\rangle$, with $|\psi_a\rangle = a_1|\uparrow\rangle + a_2|\downarrow\rangle$ and $|\psi_b\rangle = b_1|\rightarrow\rangle + b_2|\leftarrow\rangle$.
a. Write down the density operator for the complete system in terms of the expansion coefficients $c_{ij} = a_i b_j$.
b. Assume that the spin $|\psi_b\rangle$ is measured and verify whether the new density operator describing our knowledge of the system is pure.
c. Now consider the entangled state $|\Psi_e\rangle = c_{11}|\uparrow\rangle|\rightarrow\rangle + c_{22}|\downarrow\rangle|\leftarrow\rangle$. Write down again the density operator for the complete system, measure the spin $|\psi_b\rangle$, and verify whether the new density operator describing our knowledge of the system is pure.

Solution: *a. The individual spin states are normalized,*

$$|a_1|^2 + |a_2|^2 = \langle\psi_a|\psi_a\rangle = 1 = \langle\psi_b|\psi_b\rangle = |b_1|^2 + |b_2|^2 \ .$$

The tensorial product is,

$$\begin{aligned}|\Psi\rangle &= a_1 b_1|\uparrow\rangle|\rightarrow\rangle + a_1 b_2|\uparrow\rangle|\leftarrow\rangle + a_2 b_1|\downarrow\rangle|\rightarrow\rangle + a_2 b_2|\downarrow\rangle|\leftarrow\rangle \\ &= c_{11}|\uparrow\rangle|\rightarrow\rangle + c_{12}|\uparrow\rangle|\leftarrow\rangle + c_{21}|\downarrow\rangle|\rightarrow\rangle + c_{22}|\downarrow\rangle|\leftarrow\rangle \ ,\end{aligned}$$

with the normalization,

$$1 = \langle\Psi|\Psi\rangle = |c_{11}|^2 + |c_{12}|^2 + |c_{21}|^2 + |c_{22}|^2 \ ,$$

and

$$|a_1|^2 = |c_{11}|^2 + |c_{12}|^2 \qquad \textit{and} \qquad |a_2|^2 = |c_{21}|^2 + |c_{22}|^2 \ .$$

The complete density operator now reads,

$$\hat{\rho} = \begin{pmatrix} |c_{11}|^2 & c_{11}c_{12}^* & c_{11}c_{21}^* & c_{11}c_{22}^* \\ c_{12}c_{11}^* & |c_{12}|^2 & c_{12}c_{21}^* & c_{12}c_{22}^* \\ c_{21}c_{11}^* & c_{21}c_{12}^* & |c_{21}|^2 & c_{21}c_{22}^* \\ c_{22}c_{11}^* & c_{22}c_{12}^* & c_{22}c_{21}^* & |c_{22}|^2 \end{pmatrix} \ .$$

b. The measurement corresponds to tracing over the measured spin yielding the new density operator,

$$\begin{aligned} Tr_b\ \hat{\rho} &= \sum_{j=\rightarrow,\leftarrow} \langle j|\Psi\rangle\langle\Psi|j\rangle = \langle\rightarrow|\Psi\rangle\langle\Psi|\rightarrow\rangle + \langle\leftarrow|\Psi\rangle\langle\Psi|\leftarrow\rangle \\ &= (c_{11}|\uparrow\rangle + c_{21}|\downarrow\rangle)(\langle\uparrow|c_{11}^* + \langle\downarrow|c_{21}^*) + (c_{12}|\uparrow\rangle + c_{22}|\downarrow\rangle)(\langle\uparrow|c_{12}^* + \langle\downarrow|c_{22}^*) \\ &= \begin{pmatrix} |c_{11}|^2 + |c_{12}|^2 & c_{11}c_{21}^* + c_{12}c_{22}^* \\ c_{11}^*c_{21} + c_{12}^*c_{22} & |c_{21}|^2 + |c_{22}|^2 \end{pmatrix} = \begin{pmatrix} |a_1|^2 & a_1 a_2^* \\ a_1^* a_2 & |a_2|^2 \end{pmatrix} = \hat{\rho}_a \ . \end{aligned}$$

Obviously,

$$Tr_a\ \hat{\rho}_a = 1 \qquad \textit{and} \qquad \hat{\rho}_a = \hat{\rho}_a^\dagger \qquad \textit{and} \qquad \hat{\rho}_a^2 = \hat{\rho}_a \ .$$

c. Normalization requests,

$$\langle\Psi_e|\Psi_e\rangle = |c_{11}|^2 + |c_{22}|^2 = 1 \ .$$

The complete density operator now reads,

$$\hat{\rho}_e = \begin{pmatrix} |c_{11}|^2 & 0 & 0 & c_{11}c_{22}^* \\ 0 & 0 & 0 & 0 \\ 0 & 0 & 0 & 0 \\ c_{11}^* c_{22} & 0 & 0 & |c_{22}|^2 \end{pmatrix}^2 = \hat{\rho}_e^2 \ ,$$

and satisfies,

$$\det \hat{\rho}_e = 0 \qquad \textit{and} \qquad Tr_{a,b}\ \hat{\rho}_e = 1 \ .$$

On the other hand,

$$Tr_b\ \hat{\rho}_e = \begin{pmatrix} |c_{11}|^2 & 0 \\ 0 & |c_{22}|^2 \end{pmatrix} \equiv \hat{\rho}_{e,a} \neq \hat{\rho}_{e,a}^2 \qquad \textit{and} \qquad \det \hat{\rho}_{e,a} \neq 0 \ .$$

Hence, in the entangled case, the traced density operator is not pure.

34.4 Bloch equations for two-level atoms

In this section we will begin to apply the ideas and tools developed in the previous sections. Let us first make use of the density matrix to describe a two-level atom coupled to a single-mode light field without spontaneous emission. We will then introduce the atomic Bloch vector as a convenient and suggestive method to describe the time evolution of a coupled two-level atom.

The internal structure of atoms is analyzed in atomic physics, where we find that the energy levels are discrete (Bohr's axiom). The center of mass motion of the atoms and collisions with other atoms are ignored, and concerning the interaction of the atoms with light, we are only interested in the aspect, that the interaction can induce transitions between internal states via absorption or emission of photons. It is the duty of atomic physics to calculate the frequencies and strengths of transitions (by Hartree-Fock or similar methods), as well as their behavior in external electric and magnetic fields. The results of these calculations are visualized in energy level schemes called *Grotrian diagrams*. In quantum optics we do not care, how the energies of the levels were calculated, but accept them as given. That is, we assume the Hamiltonian of the unperturbed atom to be diagonalized, so that its internal structure can be written as,

$$\hat{H}_{atom} = \sum_j \hbar\omega_j |j\rangle\langle j| \ . \tag{34.141}$$

34.4.1 The matrix elements of the density operator

Since the optical Bloch equations are coupled differential equations relating the elements of the density operator matrix, we must examine the temporal dependence of these matrix elements, based on our knowledge of the operator's properties. This can be done in the Schrödinger picture using Eq. (34.125), in the interaction picture

using Eq. (34.129), or directly in the co-rotating frame using Eq. (34.138). For didactic reason we will begin with the Schrödinger picture and then derive the interaction picture once again.

So, let us begin with the Liouville equation (34.125) and evaluate the elements of the matrix,

$$\begin{aligned}\langle m|\frac{d\hat{\rho}(t)}{dt}|n\rangle &= \tfrac{\imath}{\hbar}\langle m|[\hat{\rho}(t),\hat{H}]|n\rangle = \tfrac{\imath}{\hbar}\langle m|[\hat{\rho}(t),\hat{H}_{atom}+\hat{H}_{atom:field}(t)]|n\rangle \\ &= \tfrac{\imath}{\hbar}(E_n-E_m)\langle m|\hat{\rho}(t)|n\rangle + \tfrac{\imath}{\hbar}\langle m|[\hat{\rho}(t),\hat{H}_{atom:field}(t)]|n\rangle \ ,\end{aligned} \tag{34.142}$$

where $|m\rangle$ and $|n\rangle$ are members of a complete set of vectors of a basis $\{|k\rangle\}$ which are also eigen-kets of $\hat{H}_{atom}$ and span the space of $\hat{H}$. Now, we insert the closing expression $\sum_k |k\rangle\langle k| = \mathbb{I}$ in the commutator on the right-hand side of Eq. (34.142):

$$\begin{aligned}&\langle m|[\hat{\rho}(t),\hat{H}_{atom:field}(t)]|n\rangle \\ &= \sum_k [\langle m|\hat{\rho}(t)|k\rangle\langle k|\hat{H}_{atom:field}|n\rangle - \langle m|\hat{H}_{atom:field}|k\rangle\langle k|\hat{\rho}(t)|n\rangle] \ .\end{aligned} \tag{34.143}$$

For our two-level atom the complete set only includes two states: $|1(t)\rangle = |1\rangle$ and $|2(t)\rangle = e^{-\imath\omega_0 t}|2\rangle$. In addition, the matrix elements of the dipole coupling operator $\hat{H}_{atom:field}$ are only non-diagonal,

$$V \equiv \langle 1|\hat{H}_{atom:field}|2\rangle = \overline{\langle 2|\hat{H}_{atom:field}|1\rangle} = V^* \ . \tag{34.144}$$

Hence, Eq. (34.142) adopts the form,

$$\boxed{\begin{aligned}\frac{d\hat{\rho}_{11}}{dt} &= \tfrac{\imath}{\hbar}[\hat{\rho}_{12}V^* - \hat{\rho}_{21}V] \\ \frac{d\hat{\rho}_{22}}{dt} &= \tfrac{\imath}{\hbar}[\hat{\rho}_{21}V - \hat{\rho}_{12}V^*] = -\frac{d\hat{\rho}_{11}}{dt} \\ \frac{d\hat{\rho}_{12}}{dt} &= \imath\omega_0\hat{\rho}_{12} + \tfrac{\imath}{\hbar}[V(\hat{\rho}_{11}-\hat{\rho}_{22})] \\ \frac{d\hat{\rho}_{21}}{dt} &= -\imath\omega_0\hat{\rho}_{21} + \tfrac{\imath}{\hbar}[V^*(\hat{\rho}_{22}-\hat{\rho}_{11})] = \frac{d\hat{\rho}^*_{12}}{dt}\end{aligned}} \ , \tag{34.145}$$

remembering that the dash of the diagonal terms, called *populations*, must be unitary, and that the non-diagonal terms, called *coherences*, must be complex,

$$\hat{\rho}_{11} + \hat{\rho}_{22} = 1 \quad , \quad \hat{\rho}_{21} = \hat{\rho}^*_{12} \ . \tag{34.146}$$

The above set of equations constitutes the *optical Bloch equations* in the *Schrödinger picture*. It does not include loss terms due to spontaneous emission. We transform the Bloch equations to the *interaction picture* by replacing the Liouville equation (34.125) by (34.129), and calculating the matrix elements. We obtain,

$$\frac{d\tilde{\rho}_{22}}{dt} = \frac{\imath}{\hbar}(V\tilde{\rho}_{21} - V^*\tilde{\rho}_{12}) \quad \text{and} \quad \frac{d\tilde{\rho}_{12}}{dt} = \frac{\imath}{\hbar}V(\tilde{\rho}_{11}-\tilde{\rho}_{22}) \ . \tag{34.147}$$

We would also have obtained this expression via the substitution, $\hat{\rho}_{12} = \tilde{\rho}_{12}e^{\imath\omega_0 t}$. The interaction picture simplifies the expressions for the temporal dependence of the coherences by eliminating the first term on the right-hand side. Transforming to the interaction picture removes the temporal dependence of the basis vectors spanning the Hilbert space of the two-level atom.

We have derived the optical Bloch equations from the Liouville equation, which is the fundamental equation of motion of the density operator, and we have seen how a unitary transformation can be used to *represent* these equations in the Schrödinger, Heisenberg or interaction picture. So far, the Bloch equations do not include the possibility of spontaneous emission. We will learn later, how to include this phenomenon.

34.4.2 Rotating wave approximation

In the following, we will only consider exponentials rotating with the frequency $\Delta \equiv \omega - \omega_0$, and we will neglect terms rotating like $\Delta \equiv \omega + \omega_0$ in the time dependence of the coupling operator,

$$V(t) = \hbar\Omega \cos\omega t \to \tfrac{\hbar}{2}\Omega e^{-\imath\omega t} \ , \tag{34.148}$$

neglecting the part $\frac{1}{2}\hbar\Omega e^{\imath\omega t}$. The amplitude Ω is called *Rabi frequency*. This approximation, called *rotating wave approximation* (RWA) is good, when the is sufficiently small, $\Omega \ll \omega$. Otherwise, we observe an energy correction of the levels called *Bloch-Siegert shift*.

Once the RWA made, we can transform to the rotating system by the prescription,

$$\boxed{\rho_{12} \equiv \hat{\rho}_{12}e^{-\imath\omega t} \quad , \quad \rho_{22} \equiv \hat{\rho}_{22}} \ , \tag{34.149}$$

which, applied to the Bloch equations in the *Schrödinger picture* Eq. (34.145), yields,

$$\frac{d\rho_{22}}{dt} = \frac{\imath\Omega}{2}\rho_{21} - \frac{\imath\Omega^*}{2}\rho_{12} \quad , \quad \frac{d\rho_{12}}{dt} = -\imath\Delta\rho_{12} + \frac{\imath\Omega}{2}(\rho_{11} - \rho_{22}) \ . \tag{34.150}$$

In Exc. 34.4.6.1 we derive the Bloch equations from the equations of motion for the population amplitudes a_1 and a_2.

For arbitrary starting conditions, the solution of these equations is not simple. To solve the problem we write the equations in a matrix form,

$$\boxed{\vec{\rho} \equiv \begin{pmatrix} \rho_{11} \\ \rho_{22} \\ \rho_{12} \\ \rho_{21} \end{pmatrix} \quad , \quad \mathcal{M} \equiv \begin{pmatrix} 0 & 0 & \frac{\imath}{2}\Omega^* & -\frac{\imath}{2}\Omega \\ 0 & 0 & -\frac{\imath}{2}\Omega^* & \frac{\imath}{2}\Omega \\ \frac{\imath}{2}\Omega & -\frac{\imath}{2}\Omega & -\imath\Delta & 0 \\ -\frac{\imath}{2}\Omega^* & \frac{\imath}{2}\Omega^* & 0 & \imath\Delta \end{pmatrix} \quad , \quad \dot{\vec{\rho}} = \mathcal{M}\vec{\rho}} \ . \tag{34.151}$$

To solve this system of differential equations, we calculate the eigenvalues of the matrix,

$$\begin{aligned} \det(\mathcal{M} - \lambda\mathbb{I}_4) = \lambda^2(\Delta^2 + |\Omega|^2) + \lambda^4 = 0 \\ \lambda = 0, \pm\imath G \ , \end{aligned} \tag{34.152}$$

with the *generalized Rabi frequency* $G \equiv \sqrt{\Delta^2 + |\Omega|^2}$. Therefore, the general solution is,

$$\begin{aligned} \rho_{22}(t) &= \rho_{22}^{(1)} + \rho_{22}^{(2)} e^{\imath G t} + \rho_{22}^{(3)} e^{-\imath G t} \\ \rho_{12}(t) &= \rho_{12}^{(1)} + \rho_{12}^{(2)} e^{\imath G t} + \rho_{12}^{(3)} e^{-\imath G t} \ . \end{aligned} \tag{34.153}$$

The coefficients follow from the Bloch equations with particular starting conditions. With a little algebra we get

$$\begin{aligned} \rho_{22}^{(1)} &= \rho_{22}(0) + \tfrac{1}{2G^2}\left[|\Omega|^2\,(1-2\rho_{22}(0)) - \Delta\,(\Omega\rho_{12}^*(0) + \Omega^*\rho_{12}(0))\right] \\ \rho_{22}^{(2)} &= \tfrac{1}{4G^2}\left[-|\Omega|^2(1-2\rho_{22}(0)) + (\Delta+G)\Omega\rho_{12}^*(0) + (\Delta-G)\Omega^*\rho_{12}(0)\right] \\ \rho_{22}^{(3)} &= \tfrac{1}{4G^2}\left[-|\Omega|^2(1-2\rho_{22}(0)) + (\Delta-G)\Omega\rho_{12}^*(0) + (\Delta+G)\Omega^*\rho_{12}(0)\right] \\ \rho_{12}^{(1)} &= \tfrac{1}{2G^2}\left[\Delta\Omega(1-2\rho_{22}(0)) + \Omega\,(\Omega\rho_{12}^*(0) + \Omega^*\rho_{12}(0))\right] \\ \rho_{12}^{(2)} &= \tfrac{\Delta-G}{4G^2}\left[-\Omega(1-2\rho_{22}(0)) + (\Delta+G)\tfrac{\Omega}{\Omega^*}\rho_{12}^*(0) + (\Delta-G)\rho_{12}(0)\right] \\ \rho_{12}^{(3)} &= \tfrac{\Delta+G}{4G^2}\left[-\Omega(1-2\rho_{22}(0)) + (\Delta-G)\tfrac{\Omega}{\Omega^*}\rho_{12}^*(0) + (\Delta+G)\rho_{12}(0)\right] \ . \end{aligned} \tag{34.154}$$

We derive this solution in Exc. 34.4.6.2.

To begin the discussion of this solution, let us consider a sample of atoms initially in the ground state when the light field is switched on at time $t = 0$,

$$\rho_{11}(0) = 1 = 1 - \rho_{22}(0) \quad , \quad \rho_{12}(0) = 0 = \rho_{21}(0) \ . \tag{34.155}$$

In this case, the conditions (34.154) simplify to,

$$\begin{aligned} \rho_{22}^{(1)} &= \tfrac{|\Omega|^2}{2G^2} \quad , \quad \rho_{12}^{(1)} = \tfrac{1}{2G^2}\Delta\Omega \\ \rho_{22}^{(2)} &= \tfrac{-|\Omega|^2}{4G^2} \quad , \quad \rho_{12}^{(2)} = \tfrac{G-\Delta}{4G^2}\Omega \\ \rho_{22}^{(3)} &= \tfrac{-|\Omega|^2}{4G^2} \quad , \quad \rho_{12}^{(3)} = \tfrac{-G-\Delta}{4G^2}\Omega \ , \end{aligned} \tag{34.156}$$

such that,

$$\begin{aligned} \rho_{22} &= \rho_{22}^{(1)} + \rho_{22}^{(2)} e^{\imath G t} + \rho_{22}^{(3)} e^{-\imath G t} = \frac{|\Omega|^2}{4G^2}(2 - e^{\imath G t} - e^{-\imath G t}) \\ \rho_{12} &= \rho_{12}^{(1)} + \rho_{12}^{(2)} e^{\imath G t} + \rho_{12}^{(3)} e^{-\imath G t} = \frac{\Delta\Omega}{2G^2} - \frac{\Delta - G}{4G^2}\Omega e^{\imath G t} - \frac{\Delta + G}{4G^2}\Omega e^{-\imath G t} \\ &= \frac{2\Omega}{4G^2}(\Delta - \Delta\cos Gt + \imath G \sin Gt) \ . \end{aligned} \tag{34.157}$$

Using $\cos x = 1 - 2\sin^2\frac{x}{2}$ and $\sin x = 2\sin\frac{x}{2}\cos\frac{x}{2}$, we finally obtain,

$$\boxed{\rho_{22} = \frac{|\Omega|^2}{G^2}\sin^2\frac{Gt}{2} \quad , \quad \rho_{12} = \frac{\Omega}{G^2}\sin\frac{Gt}{2}\left(\Delta\sin\frac{Gt}{2} + \imath G\cos\frac{Gt}{2}\right)} \ . \tag{34.158}$$

And comparing with the solutions of the Schrödinger equation for a coupled two-level atom obtained in Exc. 23.4.7.1 and (27.93), we verify,

$$\begin{aligned} \rho_{22} &= \left|\tfrac{\imath\Omega}{G}e^{-\imath t\Delta/2}\sin\tfrac{Gt}{2}\right|^2 = |a_2|^2 \\ \rho_{12} &= -e^{-\imath t\Delta/2}\left[\cos\tfrac{Gt}{2} - \imath\tfrac{\Delta}{G}\sin\tfrac{Gt}{2}\right] \ \tfrac{-\imath\Omega}{G}e^{\imath t\Delta/2}\sin\tfrac{Gt}{2} = a_1^* a_2 \ . \end{aligned} \tag{34.159}$$

34.4.3 Pauli matrices and the atomic Bloch vector

Let us come back to the unperturbed atomic Hamiltonian (34.141). The electronic states are orthonormal $\langle i|j\rangle = \delta_{ij}$, and we define the transition operators by

$$\hat{\sigma}_{ij}|k\rangle = \delta_{jk}|i\rangle \ , \tag{34.160}$$

and $\hat{\sigma}_{ij}^{+} = \hat{\sigma}_{ji}$ satisfying the commutation relation,

$$[\hat{\sigma}_{ij}, \hat{\sigma}_{lk}] = \delta_{jl}\hat{\sigma}_{ik} - \delta_{ik}\hat{\sigma}_{lj} \ . \tag{34.161}$$

Many times we will restrict ourselves to atoms of two or three levels. For a two-level system we obtain the *Pauli spin matrix* defined in (23.45). Every 2×2 matrix can be expanded on a Pauli matrix basis (see Exc. 34.4.6.3),

$$\begin{aligned}\begin{pmatrix} \rho_{11} & \rho_{12} \\ \rho_{21} & \rho_{22} \end{pmatrix} &= |1\rangle\rho_{11}\langle 1| + |1\rangle\rho_{12}\langle 2| + |2\rangle\rho_{21}\langle 1| + |2\rangle\rho_{22}\langle 2| \\ &= \rho_{11}(\tfrac{1}{2} + \tfrac{1}{2}\hat{\sigma}_z) + \rho_{12}\hat{\sigma}^{-} + \rho_{21}\hat{\sigma}^{+} + \rho_{22}(\tfrac{1}{2} - \tfrac{1}{2}\hat{\sigma}_z) \\ &= \rho_{11}\hat{\sigma}^{-}\hat{\sigma}^{+} + \rho_{12}\hat{\sigma}^{-} + \rho_{21}\hat{\sigma}^{+} + \rho_{22}\hat{\sigma}^{+}\hat{\sigma}^{-} = \begin{pmatrix} \langle\hat{\sigma}^{-}\hat{\sigma}^{+}\rangle & \langle\hat{\sigma}^{-}\rangle \\ \langle\hat{\sigma}^{+}\rangle & \langle\hat{\sigma}^{+}\hat{\sigma}^{-}\rangle \end{pmatrix} \ .\end{aligned} \tag{34.162}$$

For the two-level case it is useful to introduce an alternative notation based on the *Bloch vector* defined in (23.46),

$$\langle\hat{\vec{\sigma}}\rangle \equiv \begin{pmatrix} 2\ \mathfrak{Re}\ \rho_{12} \\ 2\ \mathfrak{Im}\ \rho_{12} \\ \rho_{22} - \rho_{11} \end{pmatrix} = \begin{pmatrix} \langle\hat{\sigma}^{+}\rangle + \langle\hat{\sigma}^{-}\rangle \\ \imath(\langle\hat{\sigma}^{+}\rangle - \langle\hat{\sigma}^{-}\rangle) \\ \langle\hat{\sigma}^{+}\hat{\sigma}^{-}\rangle - \langle\hat{\sigma}^{-}\hat{\sigma}^{+}\rangle \end{pmatrix} = \begin{pmatrix} \langle\hat{\sigma}_x\rangle \\ \langle\hat{\sigma}_y\rangle \\ \langle\hat{\sigma}_z\rangle \end{pmatrix} \ . \tag{34.163}$$

We also define the torque vector,

$$\boxed{\mathbf{G} \equiv \begin{pmatrix} \mathfrak{Re}\ \Omega \\ \mathfrak{Im}\ \Omega \\ -\Delta \end{pmatrix} \qquad \text{with} \qquad \|G\| = G = \sqrt{|\Omega|^2 + \Delta^2}} \ , \tag{34.164}$$

the length of which is simply the generalized Rabi frequency. Note that here we allow for the possibility of complex Rabi frequency.

Now, using $\hat{\sigma}_z = [\hat{\sigma}^{+}, \hat{\sigma}^{-}]$, we may write the Hamiltonian of an unperturbed two-level system,

$$\hat{H}_0 = -\hbar\Delta\hat{\sigma}^{+}\hat{\sigma}^{-} = -\tfrac{\hbar}{2}\Delta(\hat{\sigma}_z + \mathbb{I}_2) = -\tfrac{\hbar}{2}\Delta\hat{\sigma}_z + \text{offset} \ . \tag{34.165}$$

For the perturbed system,

$$\hat{H} = \hat{\mathbf{s}} \cdot \mathbf{G} = \tfrac{\hbar}{2}\mathbf{G} \cdot \hat{\vec{\sigma}} = -\tfrac{\hbar}{2}\hat{\sigma}_z\Delta + \tfrac{\hbar}{2}\hat{\sigma}_x\mathfrak{Re}\ \Omega + \tfrac{\hbar}{2}\hat{\sigma}_y\mathfrak{Im}\ \Omega = \begin{pmatrix} \frac{\hbar}{2}\Delta & \frac{\hbar}{2}\Omega^{*} \\ \frac{\hbar}{2}\Omega & -\frac{\hbar}{2}\Delta \end{pmatrix} \ . \tag{34.166}$$

The Bloch equations (34.165) then follow as the Heisenberg equation with the Hamiltonian (34.167) using $[\hat{\sigma}_k, \hat{\sigma}_m] = 2\imath\epsilon_{klm}\hat{\sigma}_m$,

$$\frac{d\hat{\vec{\sigma}}}{dt} = \tfrac{\imath}{\hbar}[\hat{H}, \hat{\vec{\sigma}}] = \tfrac{\imath}{2}[\mathbf{G}\cdot\hat{\vec{\sigma}}, \hat{\vec{\sigma}}] \tag{34.167}$$

$$= \tfrac{\imath G_x}{2}[\hat{\sigma}_x, \hat{\vec{\sigma}}] + \tfrac{\imath G_y}{2}[\hat{\sigma}_y, \hat{\vec{\sigma}}] + \tfrac{\imath G_z}{2}[\hat{\sigma}_z, \hat{\vec{\sigma}}] = \begin{pmatrix} G_y\hat{\sigma}_z - G_z\hat{\sigma}_y \\ G_z\hat{\sigma}_x - G_x\hat{\sigma}_z \\ G_x\hat{\sigma}_y - G_y\hat{\sigma}_x \end{pmatrix} = \mathbf{G}\times\hat{\vec{\sigma}}\ .$$

The expectation values yield,

$$\boxed{\frac{d\vec{\varrho}}{dt} = \mathbf{G}\times\vec{\varrho}}\ . \tag{34.168}$$

As will be shown in Exc. 34.4.6.4, these equations are identical to the Liouville equations (34.151). ρ_{12} describes the polarization and $\rho_{22} - \rho_{11}$ the *population inversion* of the atom. The equation is analogous to the equation of motion for a *rigid rotor* or *spinning top* (for example, a dipole in a homogeneous field). It displays phenomena such as *precession* and *nutation*. The physical content and usefulness of the Bloch vector will become clearer when we use the formalism to analyze electric and magnetic couplings. In Exc. 34.4.6.5 we verify that the Bloch vector is normalized (as long as spontaneous emission is not considered).

34.4.4 State manipulations by sequences of radiation pulses

The temporal dependence of the three components of the atomic Bloch vector provides a useful illustration of the atom-field interaction. Resonant coupling, $\Delta = 0$ and $G = \Omega$, puts the solutions (34.158) into the form,

$$\rho_{22}(t) = \tfrac{1}{2}(1 - \cos\Omega t) \quad , \quad \rho_{12}(t) = \tfrac{\imath}{2}\sin\Omega t\ , \tag{34.169}$$

that is,

$$\vec{\varrho}(t) = \begin{pmatrix} 0 \\ \sin\Omega t \\ -\cos\Omega t \end{pmatrix}\ . \tag{34.170}$$

That is, a resonant pulse rotates a Bloch vector initially pointing in the direction $-z$ within the plane z-y, until it arrives, at time $t = \frac{\pi}{2\Omega}$, at the $+y$ direction and at time $t = \frac{\pi}{\Omega}$ at the $+z$ direction. This means that the entire population has been transferred to the excited state. The Bloch vector continues to rotate (the movement is called *nutation*) around the torque vector $\mathbf{G}$ which, as can be seen from Eq. (34.165), points at the $+x$ direction when $\Delta = 0$. The nutation frequency is proportional to the force Ω of the atom-field interaction. With the Eq. (34.158) we see that the population oscillates between the ground and excited state with the frequency Ω. This means that the energy $\hbar\omega$ is periodically exchanged between the atom and the field. A pulse of resonant light of duration such that $\tau = \pi/2\Omega$ is called a $\pi/2$-pulse. The nutation is illustrated in Fig. 34.2(a).

Once the coherence has been excited by a detuned radiation, $\Delta \neq 0$, the Bloch vector does not stand still, even after the radiation has been switched off. To see

this, we consider again the general solution (34.154) now entering $\Omega = 0$. If the Bloch vector is initially at a point in the unitary circle of the plane z-y, it will rotate according to the formula,

$$\rho_{22}(t) = \rho_{22}(0) \quad , \quad \rho_{12}(t) = \rho_{12}(0)e^{-\imath\Delta t} \, , \tag{34.171}$$

that is,

$$\vec{\varrho}(t) = \begin{pmatrix} \rho_{12}(0)\sin\Delta t \\ \rho_{12}(0)\cos\Delta t \\ 2\rho_{22}(0) - 1 \end{pmatrix} \, . \tag{34.172}$$

That is, the Bloch vector performs a motion of *precession* around the symmetry axis. The precession is illustrated in Fig. 34.2(b).

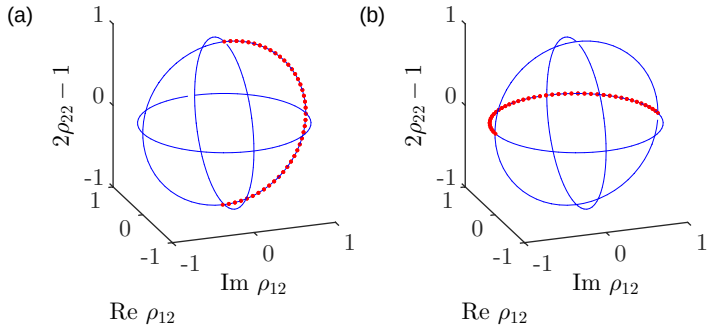

Figure 34.2: (code) (a) Nutation of the Bloch vector. The red circles show the evolution of the Bloch vector on the Bloch sphere for a resonant π-pulse. (b) Precession of the Bloch vector.

The evolution of the Bloch vector on the surface of the Bloch sphere under the influence of radiation fields can be considered a coherent trajectory of the wavefunction of the atomic state, which is therefore subject to interference phenomena [642]. Interferometers can be realized by sequences of consecutive pulses splitting populations, exciting coherences, and remixing populations.

Sensors based on interferometry of atomic excitation are nowadays among the most accurate and most sensitive. We will discuss the method of radiation pulse sequences in several exercises: In the Excs. 34.4.6.6, 34.4.6.7, and 34.4.6.8 the *Ramsey method*.

34.4.4.1 Atomic ensembles

While it is technically challenging to observe the dynamics of single atoms, it is relatively easy monitor the dynamics of ensembles of atoms, provided that they react synchronously to incident radiation. The concentration of a sufficient number of atoms in a small volume can, however, introduce additional (desirable or undesirable) effects. Collisions, for instance, induce (irreversible) decoherence. On the other hand, if the ensemble is sufficiently dense that the mean distance between atoms is less than a resonant wavelength, then the transition dipoles of the individual atoms will couple to produce a collective dipole moment and generate effects known as superradiance.

Thermal motion of the atoms is another undesired effect, because every atom will interact with the radiation on a different Doppler-shifted frequency. This leads to diffusion of the individual atomic Bloch vectors in the x-y-plane, which in turn limits the resolution of interferometric applications. We will discuss in Exc. 34.4.6.9 the *photon echo method*, which allows to circumvent this problem.

34.4.5 Nuclear magnetic resonance

Nuclear magnetic resonance (NMR) is a physical phenomenon in which nuclei in a strong constant magnetic field (up to 20 T) are perturbed by a weak oscillating magnetic field (in the near field) and respond by producing an electromagnetic signal with a frequency characteristic of the magnetic field at the nucleus. This process occurs near resonance, when the oscillation frequency (typically 60..1000 MHz) matches the intrinsic frequency of the nuclei, which depends on the strength of the static magnetic field, the chemical environment, and the magnetic properties of the isotope involved. NMR spectroscopy is widely used to determine the structure of organic molecules in solution and in advanced medical imaging techniques, such as in magnetic resonance imaging (MRI). The most commonly used nuclei are ^{1}H and ^{13}C.

NMR transitions can be excited, when the electron spins do not participate in the interaction, e.g. because they are paired (see Eq. (30.41)), and when the nucleus has an intrinsic nuclear magnetic moment $\hat{\vec{\mu}}_I$ and hence an angular momentum $\hat{\mathbf{I}}$. This is the case for an odd number of protons and/or neutrons. Nuclides with even numbers of both have a total spin of zero and are therefore NMR-inactive.

The principle of NMR usually involves three sequential steps: (i) The alignment of the magnetic nuclear spins in an applied, constant magnetic field $\vec{\mathcal{B}}_0$. (ii) The perturbation of this alignment of the nuclear spins by a weak oscillating magnetic field $\vec{\mathcal{B}}_1(t)$ called rf-pulse. (iii) The detection of the NMR signal during or after the rf-pulse via the voltage induced in a detection coil due to the precession of the nuclear spins around $\vec{\mathcal{B}}_0$. After an rf-pulse, the nuclear dipole moment precesses at the nuclei's intrinsic Larmor frequency without involving transitions between spin states. Choosing the two magnetic fields perpendicular to each other, one maximizes the NMR signal strength,

$$\vec{\mathcal{B}}(t) = \mathcal{B}_{rf}(t)\hat{\mathbf{e}}_x + \mathcal{B}_0\hat{\mathbf{e}}_z \ , \tag{34.173}$$

where, because of $|\mathcal{B}_{rf}(t)| \ll \mathcal{B}_0$, we choose the z-axis as the quantization axis and the rf-field as a perturbation along the x-axis.

The energy of a nuclear magnetic dipole moment placed in a magnetic field is [368],

$$\boxed{\hat{H} = -\hat{\vec{\mu}} \cdot \vec{\mathcal{B}} = -\gamma_I \hat{\mathbf{I}} \cdot \vec{\mathcal{B}}} \ , \tag{34.174}$$

where γ_I is the *gyromagnetic ratio* of the specific nucleus and $\hat{\mathbf{I}}$ the nuclear spin satisfying the usual commutation relation $[\hat{I}_m, \hat{I}_n] = \imath\hbar\epsilon_{kmn}\hat{I}_k$. Hence, as shown in Exc. 34.4.6.10, we can derive from the Heisenberg equation,

$$\imath\hbar\frac{d\hat{\vec{\mu}}}{dt} = [\hat{\vec{\mu}}, \hat{H}] \ , \tag{34.175}$$

the Bloch equations,

$$\boxed{\frac{d\hat{\vec{\mu}}}{dt} = \gamma_I \hat{\vec{\mu}} \times \vec{\mathcal{B}}} \ . \tag{34.176}$$

Now, let us restrict to a two-level system, $I = \frac{1}{2}$ such that $\hat{I}_z = \frac{\hbar}{2}\hat{\sigma}_z$. In thermal equilibrium, without time-dependent perturbation,

$$\hat{H}_0 = -\hat{\vec{\mu}} \cdot \vec{\mathcal{B}}_0 = -\hat{\mu}_z \mathcal{B}_0 = -\gamma_I \hat{I}_z \mathcal{B}_0 \equiv -\omega_L \hat{I}_z \ . \tag{34.177}$$

where we introduced the *Larmor frequency* ω_L. We expect energy levels,

$$E = -\hbar \gamma_I m \mathcal{B}_0 \ , \tag{34.178}$$

with $m = \pm\frac{1}{2}$. The energy difference between the two states, $\Delta E = \gamma_I \hbar \mathcal{B}_0$, results in a small population bias favoring the lower energy state in thermal equilibrium and, hence, in a net spin magnetization $\vec{\mathcal{M}} = \frac{1}{V}\sum_i \langle \vec{\mu}_i \rangle$ along the magnetic field $\vec{\mathcal{B}}_0$. For a thermal statistical mixture, as shown in (34.100), we write the density operator [17],

$$\boxed{\hat{\rho} = \frac{e^{-\hat{H}_0/k_B T}}{Z} = \frac{e^{-\frac{1}{2}\beta\hbar\omega_L \hat{\sigma}_z}}{Z} = \sum_{m=\pm 1/2} |I,m\rangle \frac{e^{-\beta\hbar\omega_L m}}{Z} \langle I,m|} \ , \tag{34.179}$$

with the partition function,

$$Z \equiv \mathrm{Tr}\ e^{-\hat{H}_0/k_B T} = \sum_{m=\pm 1/2} e^{-\beta\hbar\omega_L m} \ . \tag{34.180}$$

Now, as shown in (34.128), we can express the time-evolution of the density operator as,

$$\hat{\rho}(t) = e^{-\imath \hat{H}_0 t} \hat{\rho}(0) e^{\imath \hat{H}_0 t} = e^{-\imath\beta\hbar\omega_L \hat{I}_z t} \hat{\rho}(0) e^{\imath\beta\hbar\omega_L \hat{I}_z t} \ . \tag{34.181}$$

Then, as shown in Exc. 34.4.6.11,

$$\langle \hat{\mathbf{I}}(t) \rangle = \begin{pmatrix} \cos\omega_L t & -\sin\omega_L t & 0 \\ \sin\omega_L t & \cos\omega_L t & 0 \\ 0 & 0 & 1 \end{pmatrix} \langle \hat{\mathbf{I}}(0) \rangle \ , \tag{34.182}$$

which corroborates the result (34.176). Apparently, the nuclear magnetic dipole moment (and hence the spin magnetization) precesses around the magnetic field with the Larmor frequency leaving the populations of the energy levels unaffected.

A perturbation of nuclear spin orientations from equilibrium will occur when an oscillating magnetic field is applied whose frequency ω_{rf} sufficiently closely matches the Larmor precession frequency ω_L. The populations of the spin-up and -down energy levels then undergo Rabi oscillations. The stronger the oscillating field, the faster the Rabi oscillations or the precession around the effective field in the rotating

[17] Note that at high temperatures we get, $Z \simeq 1$ and may approximate,

$$\hat{\rho} - 1 \simeq \beta\hbar\omega_L \hat{I}_z \ .$$

frame. After a certain time (typically on the order of 2..1000 μs), a resonant rf-$\pi/2$-pulse flips the spin magnetization to the transverse plane, while after a twice longer time, the initial magnetization is inverted (π-pulse). It is the transverse magnetization generated by a resonant oscillating field which is usually detected in NMR.

The most important perturbation of the NMR frequency for applications of NMR is the 'shielding' effect of the surrounding shells of electrons. Electrons, similar to the nucleus, are also charged and rotate with a spin to produce a magnetic field opposite to the applied magnetic field. In general, this electronic shielding reduces the magnetic field at the nucleus. The corresponding shift in the NMR frequency due to the electronic molecular orbital coupling to the external magnetic field is called chemical shift, and it explains why NMR is able to probe the chemical structure of molecules, which depends on the electron density distribution in the corresponding molecular orbitals.

After perturbation the nuclear spins return to thermodynamic equilibrium due to relaxation processes. These are phenomenological included in the Bloch equations via decay time constants T_i,

$$\frac{d\hat{\vec{\mu}}}{dt} = \gamma_I \hat{\vec{\mu}} \times \vec{\mathcal{B}} - \frac{\hat{\mu}_z}{T_1}\hat{\mathbf{e}}_z - \frac{\hat{\mu}_x}{T_2}\hat{\mathbf{e}}_x \ . \tag{34.183}$$

$T_1 = \Gamma^{-1}$ is the time constant for 'longitudinal magnetic' relaxation and refers to the mean time for an individual nucleus to return to its thermal equilibrium state of the spins. The precessing nuclei can also fall out of alignment with each other and gradually stop producing a signal. This is called T_2 or transverse relaxation, where $T_2 = 2\gamma^{-1}$. Because of the difference in the actual relaxation mechanisms involved (for example, intermolecular versus intramolecular magnetic dipole-dipole interactions), T_1 is usually longer than T_2, which, in practice, also depends on significant static magnetic field inhomogeneities.

34.4.6 Exercises

34.4.6.1 Ex: Derivation of Bloch equations

Derive the Bloch equations explicitly based on the temporal evolutions of the coefficients $a_{1,2}$ (27.63) knowing that $\rho_{ij} = a_i^* a_j$.

Solution: *We differentiate the density operator,*

$$\frac{d\rho_{mn}}{dt} = a_m \frac{da_n^*}{dt} + \frac{da_m}{dt} a_n^* \ .$$

Substituting the derivatives of the population amplitudes by (27.63) and the transition elements by (27.77),

$$\frac{da_1}{dt} = -\imath\Omega \cos\omega t e^{-\imath\omega_0 t} a_2 \qquad \textit{and} \qquad \frac{da_2}{dt} = -\imath\Omega^* \cos\omega t e^{\imath\omega_0 t} a_1$$

for the time derivatives of (34.150) and letting $\Omega = \Omega^*$,

$$\begin{aligned}\frac{d\rho_{22}}{dt} &= \imath\Omega \cos\omega t e^{-\imath\omega_0 t} a_2 a_1^* - \imath\Omega^* \cos\omega t e^{\imath\omega_0 t} a_1 a_2^* = \imath\Omega_0 \frac{e^{\imath\omega t} + e^{-\imath\omega t}}{2} \left(a_2 a_1^* e^{-\imath\omega_0 t} - a_1 a_2^* e^{\imath\omega_0 t}\right) \\ &\simeq \frac{\imath\Omega}{2}\left(a_2 a_1^* e^{\imath\Delta t} - a_1 a_2^* e^{-\imath\Delta t}\right) = \frac{\imath\Omega}{2}\left(\rho_{21} e^{\imath\Delta t} - \rho_{12} e^{-\imath\Delta t}\right) = -\frac{d\rho_{11}}{dt} \ .\end{aligned}$$

and

$$\frac{d\rho_{12}}{dt} = \imath\Omega\cos\omega t e^{-\imath\omega_0 t}a_1 a_1^* - \imath\Omega\cos\omega t e^{-\imath\omega_0 t}a_2 a_2^* = \imath\Omega\frac{e^{\imath\omega t}+e^{-i\omega t}}{2}e^{-\imath\omega_0 t}(|a_1|^2-|a_2|^2)$$
$$\simeq \frac{\imath\Omega}{2}|a_1|^2 e^{\imath\Delta t} = \frac{\imath\Omega}{2}(\rho_{11}-\rho_{22})e^{\imath\Delta t} = \frac{d\rho_{21}^*}{dt}\ .$$

In this form the Bloch equations are in the interaction representation.

34.4.6.2 Ex: General solution of Bloch equations

Derive the solution (34.154) of the Bloch equations (34.151).

Solution: *We consider the ansatz,*

$$\rho_{22}(0) = \rho_{22}^{(1)} + \rho_{22}^{(2)}e^{\imath Gt} + \rho_{22}^{(3)}e^{-\imath Gt}$$
$$\rho_{12}(0) = \rho_{12}^{(1)} + \rho_{12}^{(2)}e^{\imath Gt} + \rho_{12}^{(3)}e^{-\imath Gt}$$
$$\rho_{21}(0) = \rho_{21}^{(1)} + \rho_{21}^{(2)}e^{\imath Gt} + \rho_{21}^{(3)}e^{-\imath Gt}\ .$$

Normalization and hermiticity require,

$$\rho_{11}^{(1)} + \rho_{11}^{(2)}e^{\imath Gt} + \rho_{11}^{(3)}e^{-\imath Gt} + \rho_{22}^{(1)} + \rho_{22}^{(2)}e^{\imath Gt} + \rho_{22}^{(3)}e^{-\imath Gt} = 1$$
$$\text{and} \qquad \rho_{21}^{(1)*} + \rho_{21}^{(2)*}e^{-\imath Gt} + \rho_{21}^{(3)*}e^{\imath Gt} = \rho_{12}^{(1)} + \rho_{12}^{(2)}e^{\imath Gt} + \rho_{12}^{(3)}e^{-\imath Gt}\ ,$$

such that,

$$\rho_{11}^{(1)} + \rho_{22}^{(1)} = 1 \quad , \quad \rho_{11}^{(2)} = -\rho_{22}^{(2)} \quad , \quad \rho_{11}^{(3)} = -\rho_{22}^{(3)}$$
$$\rho_{21}^{(1)*} = \rho_{12}^{(1)} \quad , \quad \rho_{21}^{(3)*} = \rho_{12}^{(2)} \quad , \quad \rho_{21}^{(2)*} = \rho_{12}^{(3)}\ .$$

Inserting the ansatz into the Bloch equations, we obtain

$$\begin{pmatrix} G\rho_{11}^{(2)}e^{\imath Gt} - G\rho_{11}^{(3)}e^{-\imath Gt} \\ G\rho_{22}^{(2)}e^{\imath Gt} - G\rho_{22}^{(3)}e^{-\imath Gt} \\ G\rho_{12}^{(2)}e^{\imath Gt} - G\rho_{12}^{(3)}e^{-\imath Gt} \\ G\rho_{21}^{(2)}e^{\imath Gt} - G\rho_{21}^{(3)}e^{-\imath Gt} \end{pmatrix}$$
$$= \begin{pmatrix} \frac{\Omega}{2}\left(\rho_{12}^{(1)} + \rho_{12}^{(2)}e^{\imath Gt} + \rho_{12}^{(3)}e^{-\imath Gt}\right) - \frac{\Omega}{2}\left(\rho_{21}^{(1)} + \rho_{21}^{(2)}e^{\imath Gt} + \rho_{21}^{(3)}e^{-\imath Gt}\right) \\ -\frac{\Omega}{2}\left(\rho_{12}^{(1)} + \rho_{12}^{(2)}e^{\imath Gt} + \rho_{12}^{(3)}e^{-\imath Gt}\right) + \frac{\Omega}{2}\left(\rho_{21}^{(1)} + \rho_{21}^{(2)}e^{\imath Gt} + \rho_{21}^{(3)}e^{-\imath Gt}\right) \\ \frac{\Omega}{2}\left(\rho_{11}^{(1)} + \rho_{11}^{(2)}e^{\imath Gt} + \rho_{11}^{(3)}e^{-\imath Gt}\right) - \frac{\Omega}{2}\left(\rho_{22}^{(1)} + \rho_{22}^{(2)}e^{\imath Gt} + \rho_{22}^{(3)}e^{-\imath Gt}\right) - \Delta\left(\rho_{12}' + \rho_{12}^{(2)}e^{\imath Gt} + \rho_{12}^{(3)}e^{-\imath Gt}\right) \\ -\frac{\Omega}{2}\left(\rho_{11}^{(1)} + \rho_{11}^{(2)}e^{\imath Gt} + \rho_{11}^{(3)}e^{-\imath Gt}\right) + \frac{\Omega}{2}\left(\rho_{22}^{(1)} + \rho_{22}^{(2)}e^{\imath Gt} + \rho_{22}^{(3)}e^{-\imath Gt}\right) + \Delta\left(\rho_{21}' + \rho_{21}^{(2)}e^{\imath Gt} + \rho_{21}^{(3)}e^{-\imath Gt}\right) \end{pmatrix}.$$

Since these equations must be valid for all times, we can separate the exponential functions,

	~ 1	$\sim e^{\imath Gt}$	$\sim e^{-\imath Gt}$
$\sim \rho_{11}$	$0 = \frac{\Omega}{2}\rho_{12}^{(1)} - \frac{\Omega}{2}\rho_{21}^{(1)}$	$G\rho_{11}^{(2)} = \frac{\Omega}{2}\rho_{12}^{(2)} - \frac{\Omega}{2}\rho_{21}^{(2)}$	$-\rho_{11}^{(3)}G = \frac{\Omega}{2}\rho_{12}^{(3)} - \frac{\Omega}{2}\rho_{21}^{(3)}$
$\sim \rho_{22}$	$0 = -\frac{\Omega}{2}\rho_{12}^{(1)} + \frac{\Omega}{2}\rho_{21}^{(1)}$	$G\rho_{22}^{(2)} = -\frac{\Omega}{2}\rho_{12}^{(2)} + \frac{\Omega}{2}\rho_{21}^{(2)}$	$-\rho_{22}^{(3)}G = -\frac{\Omega}{2}\rho_{12}^{(3)} + \frac{\Omega}{2}\rho_{21}^{(3)}$
$\sim \rho_{12}$	$0 = \frac{\Omega}{2}\rho_{11}^{(1)} - \frac{\Omega}{2}\rho_{22}^{(1)} - \Delta\rho_{12}^{(1)}$	$G\rho_{12}^{(2)} = \frac{\Omega}{2}\rho_{11}^{(2)} - \frac{\Omega}{2}\rho_{22}^{(2)} - \Delta\rho_{12}^{(2)}$	$-\rho_{12}^{(3)}G = \frac{\Omega}{2}\rho_{11}^{(3)} - \frac{\Omega}{2}\rho_{22}^{(3)} - \Delta\rho_{12}^{(3)}$
$\sim \rho_{21}$	$0 = -\frac{\Omega}{2}\rho_{11}^{(1)} + \frac{\Omega}{2}\rho_{22}^{(1)} + \Delta\rho_{21}^{(1)}$	$G\rho_{21}^{(2)} = -\frac{\Omega}{2}\rho_{11}^{(2)} + \frac{\Omega}{2}\rho_{22}^{(2)} + \Delta\rho_{21}^{(2)}$	$-\rho_{21}^{(3)}G = -\frac{\Omega}{2}\rho_{11}^{(3)} + \frac{\Omega}{2}\rho_{22}^{(3)} + \Delta\rho_{21}^{(3)}$

Consequently

$$\rho_{21}^{(1)} = \rho_{12}^{(1)} \quad , \quad \rho_{21}^{(2)} = \frac{-\Omega}{2(G-\Delta)}(1-2\rho_{22}^{(2)}) \quad , \quad \rho_{21}^{(3)} = \frac{\Omega}{2(G+\Delta)}(1-2\rho_{22}^{(3)})$$
$$\rho_{12}^{(1)} = \frac{\Omega}{2\Delta}(1-2\rho_{22}^{(1)}) \quad , \quad \rho_{12}^{(2)} = \frac{\Omega}{2(G+\Delta)}\left(1-2\rho_{22}^{(2)}\right) \quad , \quad \rho_{12}^{(3)} = \frac{-\Omega}{2(G-\Delta)}(1-2\rho_{22}^{(3)})\ .$$

With this, the starting conditions can be written,

$$\begin{pmatrix}\rho_{22}(0)\\ \rho_{12}(0)\\ \rho_{12}^*(0)\end{pmatrix} = \begin{pmatrix}\rho_{22}^{(1)}+\rho_{22}^{(2)}+\rho_{22}^{(3)}\\ \rho_{12}^{(1)}+\rho_{12}^{(2)}+\rho_{12}^{(3)}\\ \rho_{21}^{(1)}+\rho_{21}^{(2)}+\rho_{21}^{(3)}\end{pmatrix} = \begin{pmatrix}\rho_{22}^{(1)}+\rho_{22}^{(2)}+\rho_{22}^{(3)}\\ \frac{\Omega^2-2\Delta^2}{2\Delta\Omega}-\frac{\Omega}{\Delta}\rho_{22}^{(1)}-\frac{\Omega}{G+\Delta}\rho_{22}^{(2)}+\frac{\Omega}{G-\Delta}\rho_{22}^{(3)}\\ \frac{\Omega^2-2\Delta^2}{2\Delta\Omega}-\frac{\Omega}{\Delta}\rho_{22}^{(1)}+\frac{\Omega}{G-\Delta}\rho_{22}^{(2)}-\frac{\Omega}{G+\Delta}\rho_{22}^{(3)}\end{pmatrix} .$$

Now, all we have to do is to solve this system of equations to find the coefficients $\rho_{22}^{(1)}$, $\rho_{22}^{(2)}$, and $\rho_{22}^{(3)}$ in terms of the initial conditions. We calculate,

$$\begin{pmatrix}1-2\rho_{22}(0)\\ \rho_{12}(0)+\rho_{12}^*(0)\end{pmatrix} = \begin{pmatrix}1-2\left(\rho_{22}^{(1)}+\rho_{22}^{(2)}+\rho_{22}^{(3)}\right)\\ \frac{\Omega^2-2\Delta^2}{\Delta\Omega}-\frac{2\Omega}{\Delta}\rho_{22}^{(1)}+\frac{2\Delta}{\Omega}\rho_{22}^{(2)}+\frac{2\Delta}{\Omega}\rho_{22}^{(3)}\end{pmatrix} .$$

and then,

$$\rho_{22}(0)+\frac{1}{2G^2}\left[\Omega^2(1-2\rho_{22}(0))-\Delta\Omega\left(\rho_{12}(0)+\rho_{12}^*(0)\right)\right] = \frac{\Delta^2}{G^2}+\rho_{22}^{(1)} .$$

This confirms the first equation (34.154) [18]*. In the same way we can check $\rho_{22}^{(2)}$ and $\rho_{22}^{(3)}$ and then $\rho_{12}^{(1)}$, $\rho_{12}^{(2)}$, and $\rho_{12}^{(3)}$.*

34.4.6.3 Ex: Expansion in Pauli matrices

Show explicitly Tr $\hat{\rho}\hat{\sigma}^-\hat{\sigma}^+ = \rho_{11}$.

Solution: *We have,*

$$\begin{aligned}\langle\hat{\sigma}^-\hat{\sigma}^+\rangle = Tr\ \hat{\rho}\hat{\sigma}^-\hat{\sigma}^+ &= \sum_k\langle k|\begin{pmatrix}\rho_{11}&\rho_{12}\\ \rho_{11}&\rho_{12}\end{pmatrix}\begin{pmatrix}1&0\\0&0\end{pmatrix}|k\rangle\\ &= \sum_k\langle k|\left(\rho_{11}|1\rangle\langle 1|+\rho_{12}|1\rangle\langle 2|\right)|k\rangle = \rho_{11} .\end{aligned}$$

34.4.6.4 Ex: Bloch vector and Bloch equations

Show that Eq. (34.168) is equivalent to the Bloch equations (34.151).

Solution: *The explicit equations of motion for the components of the Bloch vector are,*

$$\begin{aligned}\frac{d}{dt}\langle\hat{\vec{\sigma}}\rangle = \vec{G}\times\langle\hat{\vec{\sigma}}\rangle &= \begin{pmatrix}\mathfrak{Re}\ \Omega\\ \mathfrak{Im}\ \Omega\\ \Delta\end{pmatrix}\times\begin{pmatrix}2\mathfrak{Re}\ \rho_{12}\\ 2\mathfrak{Im}\ \rho_{12}\\ \rho_{11}-\rho_{22}\end{pmatrix} = \begin{pmatrix}\frac{1}{2}(\Omega+\Omega^*)\\ \frac{1}{2\imath}(\Omega-\Omega^*)\\ \Delta\end{pmatrix}\times\begin{pmatrix}\rho_{12}+\rho_{21}\\ -\imath(\rho_{12}-\rho_{21})\\ \rho_{11}-\rho_{22}\end{pmatrix}\\ &= \begin{pmatrix}-\frac{\imath}{2}(\Omega-\Omega^*)(\rho_{11}-\rho_{22})+\imath\Delta(\rho_{12}-\rho_{21})\\ -\frac{1}{2}(\Omega+\Omega^*)(\rho_{11}-\rho_{22})+\Delta(\rho_{12}+\rho_{21})\\ -\frac{\imath}{2}\Omega^*\rho_{12}+\frac{\imath}{2}\Omega\rho_{21}\end{pmatrix} .\end{aligned}$$

[18] exception for a constant $\frac{\Delta^2}{G^2}$, I don't know where it comes from!

Hence,

$$\frac{d}{dt}\begin{pmatrix}\rho_{12}+\rho_{21}\\ \rho_{12}-\rho_{21}\\ \rho_{11}-\rho_{22}\end{pmatrix}=\begin{pmatrix}-\frac{\imath}{2}(\Omega-\Omega^*)(\rho_{11}-\rho_{22})+\imath\Delta(\rho_{12}-\rho_{21})\\ -\frac{\imath}{2}(\Omega+\Omega^*)(\rho_{11}-\rho_{22})+\imath\Delta(\rho_{12}+\rho_{21})\\ -\imath\Omega^*\rho_{12}+\imath\Omega\rho_{21}\end{pmatrix}\ ,$$

or,

$$\frac{d}{dt}\begin{pmatrix}\rho_{11}\\ \rho_{22}\\ \rho_{12}\\ \rho_{21}\end{pmatrix}=\begin{pmatrix}0 & 0 & -\frac{\imath}{2}\Omega^* & \frac{\imath}{2}\Omega\\ 0 & 0 & \frac{\imath}{2}\Omega^* & -\frac{\imath}{2}\Omega\\ -\frac{\imath}{2}\Omega & \frac{\imath}{2}\Omega & \imath\Delta & 0\\ \frac{\imath}{2}\Omega^* & -\frac{\imath}{2}\Omega^* & 0 & -\imath\Delta\end{pmatrix}\begin{pmatrix}\rho_{11}\\ \rho_{22}\\ \rho_{12}\\ \rho_{21}\end{pmatrix}\ .$$

34.4.6.5 Ex: Normalization of the Bloch vector

Verify $\|\vec{\rho}\|=1$.

Solution: *The Bloch vector is,*

$$\vec{\beta}=\begin{pmatrix}2\mathfrak{Re}\ \rho_{12} & 2\mathfrak{Im}\ \rho_{12} & \rho_{22}-\rho_{11}\end{pmatrix}=\begin{pmatrix}\rho_{12}+\rho_{21} & -\imath(\rho_{12}-\rho_{21}) & \rho_{22}-\rho_{11}\end{pmatrix}\ .$$

The length of the vector is,

$$\sqrt{\vec{\beta}^t\vec{\beta}}=\sqrt{4\rho_{12}\rho_{21}+\rho_{22}^2-2\rho_{22}\rho_{11}+\rho_{11}^2}=\sqrt{\rho_{22}^2+2\rho_{22}\rho_{11}+\rho_{11}^2}=1\ ,$$

using $\det\rho=\rho_{22}\rho_{11}-\rho_{12}\rho_{21}=0$ *and Tr* $\rho=\rho_{11}+\rho_{22}=1$.

34.4.6.6 Ex: Sequence of Ramsey pulses

Many atomic clocks work according to the Ramsey spectroscopy method: The two-level atom is resonantly excited by a microwave $\pi/2$-pulse. Then, the phase of atomic coherence precesses freely over a period of time T accumulating an angle ϕ. Finally, a second $\pi/2$-pulse is applied and the population of the upper-level is measured. Calculate this population as a function of the angle ϕ. Neglect spontaneous emission.

Solution: *To describe the dynamics of a two-level atom during a Ramsey cycle let us consider the general solutions (34.154) for two specific cases. For* $\Omega=0$, *we get*

$$\rho_{22}^{(1)}=\rho_{22}(0)\qquad\text{and}\qquad\rho_{12}^{(3)}=\rho_{12}(0)\qquad\text{and}\qquad\rho_{22}^{(2)}=0=\rho_{22}^{(3)}=\rho_{12}^{(1)}=\rho_{12}^{(2)}\ .$$

Hence,

$$\begin{aligned}\rho_{22}(t)&=\rho_{22}^{(1)}+\rho_{22}^{(2)}e^{\imath Gt}+\rho_{22}^{(3)}e^{-\imath Gt}=\rho_{22}(0)\\ \rho_{12}(t)&=\rho_{12}^{(1)}+\rho_{12}^{(2)}e^{\imath Gt}+\rho_{12}^{(3)}e^{-\imath Gt}=\rho_{12}(0)e^{-\imath\Delta t}\ .\end{aligned}$$

For $\Delta = 0$, we get

$$\begin{aligned}
\rho_{22}^{(1)} &= \tfrac{1}{2} \\
\rho_{22}^{(2)} &= \tfrac{1}{4}\left[-(1-2\rho_{22}(0)) + \rho_{12}^{*}(0) - \rho_{12}(0)\right] \\
\rho_{22}^{(3)} &= \tfrac{1}{4}\left[-(1-2\rho_{22}(0)) - \rho_{12}^{*}(0) + \rho_{12}(0)\right] \\
\rho_{12}^{(1)} &= \tfrac{1}{2}\left[\rho_{12}^{*}(0) + \rho_{12}(0)\right] \\
\rho_{12}^{(2)} &= \tfrac{1}{4}\left[(1-2\rho_{22}(0)) - \rho_{12}^{*}(0) + \rho_{12}(0)\right] \\
\rho_{12}^{(3)} &= \tfrac{1}{4}\left[-(1-2\rho_{22}(0)) - \rho_{12}^{*}(0) + \rho_{12}(0)\right] \ .
\end{aligned}$$

Hence,

$$\begin{aligned}
\rho_{22}(t) &= \rho_{22}^{(1)} + \rho_{22}^{(2)} e^{\imath\Omega t} + \rho_{22}^{(3)} e^{-\imath\Omega t} = \tfrac{1}{2} - \tfrac{1}{2}\left[1-2\rho_{22}(0)\right]\cos\Omega t + \mathfrak{Im}\ \rho_{12}(0)\sin\Omega t \\
\rho_{12}(t) &= \rho_{12}^{(1)} + \rho_{12}^{(2)} e^{\imath\Omega t} + \rho_{12}^{(3)} e^{-\imath\Omega t} = \mathfrak{Re}\ \rho_{12}(0) + \tfrac{\imath}{2}\left[1-2\rho_{22}(0)\right]\sin\Omega t + \imath\mathfrak{Im}\ \rho_{12}(0)\cos\Omega t \ .
\end{aligned}$$

At the beginning the atom is in $\rho_{22}(0) = 0 = \rho_{12}(0)$. For this case, the equations simplify to,

$$\rho_{22}(t) = \tfrac{1}{2} - \tfrac{1}{2}\cos\Omega t \qquad \textit{and} \qquad \rho_{12}(t) = \tfrac{\imath}{2}\sin\Omega t \ .$$

The application of the first $\pi/2$-pulse raises the population of the state to $\rho_{11}(0) = \rho_{22}(0) = \frac{1}{2}$ and the coherence is $\rho_{12}(0) = \frac{\imath}{2}$. We now imagine that the laser source is a little detuned, so little that the population of the coupled state is not affected. But if $\Delta \neq 0$, looking at solutions for $\Omega = 0$, we find that the Bloch vector begins to precess. After a time T, it rotated by a certain angle $\phi \equiv T\Delta$. After this time, we turn on the laser a second time and apply a second $\pi/2$-pulse. We look now at the solutions for $\Delta = 0$, using the new starting conditions, $\rho_{22}(0) = \frac{1}{2}$ and $\rho_{12}(0) = \frac{\imath}{2}e^{-\imath\phi}$,

$$\begin{aligned}
\rho_{22}(t) &= \tfrac{1}{2} + \mathfrak{Im}\ \tfrac{\imath e^{-\imath\phi}}{2}\sin\Omega t = \tfrac{1}{2} + \tfrac{1}{2}\cos\phi \\
\rho_{12}(t) &= \mathfrak{Re}\ \tfrac{\imath e^{-\imath\phi}}{2} + \imath\mathfrak{Im}\ \tfrac{\imath e^{-\imath\phi}}{2}\cos\Omega t = \tfrac{1}{2}\sin\phi \ .
\end{aligned}$$

That is, we find a phase-dependent oscillation of the excited state population between 0 and 1. Thus, this population, which can be measured experimentally, provides information about the laser detuning.

34.4.6.7 Ex: Analytical treatment of the Ramsey experiment

Derive the analytic formula for the final population ρ_{22} for the Rabi and Ramsey experiments. Derive and compare the line widths of the 'interference fringes' in these two experiments.

Solution: *We consider a two-level system without decay. Its optical Bloch equations are,*

$$\dot{\rho}_{22} = -\dot{\rho}_{11} = \imath\tfrac{\Omega}{2}e^{\imath\Delta t}\rho_{21} + c.c. \qquad , \qquad \dot{\rho}_{12} = -\dot{\rho}_{21}^{*} = \imath\tfrac{\Omega}{2}e^{\imath\Delta t}(\rho_{11} - \rho_{22}) \ ,$$

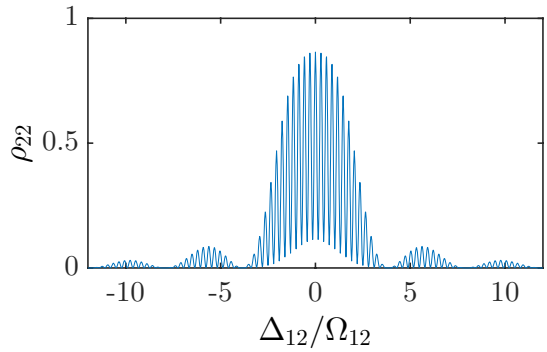

Figure 34.3: (code) Ramsey fringes.

and have the solution, when $\rho_{22}(0) = 0 = \rho_{12}(0)$,

$$\rho_{22} = \frac{|\Omega|^2}{G^2} \sin^2 \frac{Gt}{2} \quad , \quad \rho_{12} = \frac{\Omega}{G^2} \sin \frac{Gt}{2} \left(\Delta \sin \frac{Gt}{2} + \imath G \cos \frac{Gt}{2} \right) .$$

The population therefore oscillates with the generalized Rabi frequency, while the coherence precess with the detuning Δ. *The coherence determines the phase between the atomic dipole and the electromagnetic field. The vector* $(\rho_{12}, \rho_{21}, \rho_{22} - \rho_{11})$ *moves on a Bloch sphere with the radius 1.*
Shutting off the electromagnetic field suddenly at time $t = T$, *the solution of the Bloch equation for* $\Omega = 0$ *must be connected continuously:*

$$\dot{\rho}_{22} = 0 \quad \textit{and} \quad \dot{\rho}_{12} = -\imath \Delta \rho_{12} .$$

This means that the Bloch vector begins to precess without perturbation:

$$\rho_{22} = \frac{|\Omega|^2}{G^2} \sin^2 \frac{GT}{2} \quad , \quad \rho_{12} = \frac{\Omega}{G^2} \sin \frac{GT}{2} \left(\Delta \sin \frac{GT}{2} + \imath G \cos \frac{GT}{2} \right) e^{-\imath \Delta \tau} .$$

After a time τ, *when the phase accumulated an advancement by a factor of* $e^{-\imath \Delta \tau}$ *about the atomic dipole moment, we switch on the electromagnetic field again. Hence, we must solve the Bloch equation with the new boundary condition:*

$$\begin{aligned} \rho_{22} = \frac{\Omega^2}{2G^4} \{ & \left[\Delta^2 (1 - \cos GT)(1 - \cos \Delta\tau) + G^2 - \Delta G \sin GT \sin \Delta\tau \right] \\ & + \frac{e^{\pm \imath G t}}{2} \left[-\Delta^2 (1 - \cos GT) + \cos \Delta\tau \left\{ \Delta^2 (1 - \cos GT) \mp \imath G^2 \sin GT \right\} \right. \\ & \left. + \sin \Delta\tau \left\{ \Delta G \sin GT \pm \imath G \Delta (1 - \cos GT) \right\} \right] \} . \end{aligned}$$

If the second pulse also has the duration T, *the final excited state population is,*

$$\begin{aligned} \rho_{22} = \frac{\Omega^2}{2G^4} \{ & (G^2 + \Delta^2)(1 - \cos GT) + \cos \Delta\tau \left[G^2 \sin^2 GT - \Delta^2 (1 - \cos GT)^2 \right] \\ & + \sin \Delta\tau \left[-2\Delta G \sin GT (1 - \cos GT) \right] \} . \end{aligned}$$

The period of the Ramsey oscillations depends on the detuning Δ, the Rabi frequency Ω, the duration of the interaction T, and the time τ between the interaction periods. The following particular cases are interesting. For $\Omega \ll \Delta$:

$$\rho_{22} = \frac{4\Omega^2}{\Delta^2} \cos\frac{\Delta(\tau+T)}{2} \sin^2\frac{\Delta T}{2} \ .$$

For $\Omega \ll \Delta$:

$$\rho_{22} = \sin^2\frac{\Omega T}{2} + \cos\Delta\tau \sin^2\Omega T \ .$$

The approximation $\Omega \ll \Delta$ is analogous to a temporal double-slit experiment. The interference patterns are described by the approximate population ρ_{22}. This approximation corresponds to a perturbative derivation of the Born approximation.
To estimate the linewidth of the Rabi fringes, we choose the microwave pulses being π-pulses, that is, $\Omega T = \pi$. Then,

$$\rho_{22} = \frac{1}{1+\Delta^2/\Omega^2} \sin^2\frac{\pi}{2}\sqrt{1+\Delta^2/\Omega^2} \ .$$

The linewidth is dominated by Fourier broadening, respectively, power broadening:

$$\sqrt{2}\sin(\pi/2)x_h = x_h \qquad with \qquad x_h = \sqrt{1+\Delta_h^2/\Omega^2} \ .$$

Hence, $x_h = 1.28$, that is, $\Delta_h = 0.8\Omega = 2.5/T$.
To estimate the linewidth of the Ramsey patterns, we choose the microwave pulses to be $\pi/2$-pulses, that is, $\Omega T = \pi/2$. Then, in the approximation $\Omega \gg \Delta$,

$$\rho_{22} = \frac{1}{2} + \cos\Delta\tau \ .$$

The linewidth is neither broadened by the Fourier effect nor by power broadening:

$$\Delta_h = \frac{1}{\tau}\arccos\frac{1}{4} \ .$$

Numerical calculations show that natural decay limits the linewidth and decreases the contrast. A complete analysis (without decay) shows that the width is given by,

$$\Delta_h = \frac{1}{2\tau + 8T/\pi} \ .$$

That is, the width is dominated by the longest of the two times, τ and T.

34.4.6.8 Ex: Atomic clocks by the Ramsey method with spontaneous emission

In this exercise we study the Ramsey method used in atomic clocks. For this, we will consider a two-level system $|1\rangle$ and $|2\rangle$ excited by a microwave radiation field characterized by the Rabi frequency Ω_{12}, and we will compare two cases: without and with spontaneous emission:

a. Write down the Hamiltonian of the system, propose a sequence of pulses allowing the observation of the Ramsey fringes, do a numerical simulation of the Schrödinger equation (based on the prescription (34.287)), and prepare a graph of the type Fig. 34.2 illustrating the temporal evolution of the Bloch vector during the sequence.
b. Calculate numerically from the Schrödinger equation the population ρ_{22} immediately after the pulse sequence as a function of the detuning Δ_{12} of the radiation field, and prepare a graph of the spectrum. Also, assuming a decay rate of $\Gamma_{12} = 0.1\Omega_{12}$, calculate the population ρ_{22} as a function of detuning Δ_{12} from the Bloch equations (making sequences of type (34.287)), prepare a new graph, and compare it with the previous graph obtained by the Schrödinger equation.
c. What happens to the width of the fringes, when the free precession time τ between the Ramsey pulses is increased? Prepare a graph of the inversion $2\rho_{22} - 1$ as a function of Δ_{12} and τ and interprete the results.

Solution: *a. Choosing $\Omega_{12} = 1$ the duration of the $\pi/2$-pulse must be $T = \pi/2\Omega_{12}$. The Hamiltonian and the solution of the Schrödinger equation can be found in the numerical MATLAB code given in the file 'LM_Bloch_RamseySpontaneous.m'. Fig. 34.4(a) shows, that the final inversion $2\rho_{22}(2T + \tau) - 1$ depends on the detuning Δ_{12} and the free precession time τ between the pulses.*
b. The spectrum $\rho_{22,\infty}(\Delta_{12})$ can be obtained by simulation of the Schrödinger equation, but the inclusion of dissipation effects requires the use of Bloch equations. The code 'LM_Bloch_RamseySpontaneous.m' shows the simulations. We notice in Fig. 34.4(b), that the spontaneous emission reduces the contrast of the fringes.
c. A Fig. 34.4(c) shows the results of the simulations. We find that the width of the fringes decreases considerably, when we increase the time of free precession.

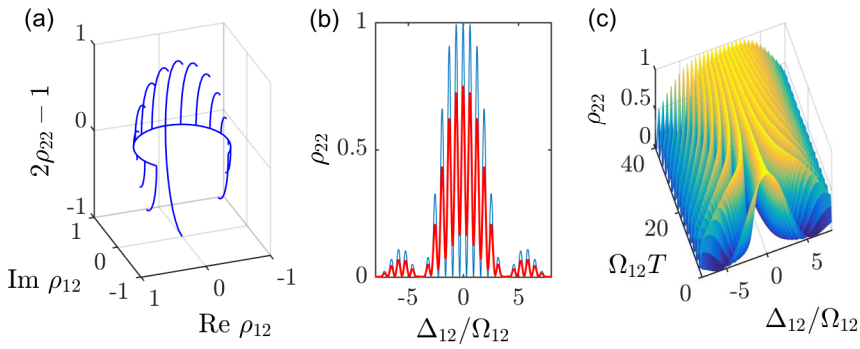

Figure 34.4: (code) (a) Time evolution of the Bloch vector for different detunings. (b) Spectra of the population ρ_{22} calculated by the Schrödinger (blue) and by the Bloch equations (red). (c) Ramsey fringes in the population ρ_{22} varying the time interval between the Ramsey pulses.

34.4.6.9 Ex: Photon echo

'Photon echo' is a powerful spectroscopic technique that allows circumvention of certain dephasing processes, for example, the Doppler shift due to the atomic motion in a thermal sample of atoms. The technique resembles the Ramsey method with the difference, that between the two Ramsey $\pi/2$-pulses, that is, during the free precession time, we apply an additional π-pulse, which inverts the imaginary part of the coherence. We will study this method by numerical simulation of the Schrödinger equation and the Bloch equations for a two-level system with and without spontaneous emission:
a. Write down the Hamiltonian of the system and do a numerical simulation of the Schrödinger equation (concatenating the pulses as explained in Eq. (34.287)) for the following temporal pulse sequence:
(i) resonant $\pi/2$-pulse ($\Delta_{12} = 0$) choosing $\Omega_{12} = 2$,
(ii) evolution for a time T without radiation ($\Omega_{12} = 0$),
(ii) resonant π-pulse using the same parameters as in (i),
(iv) evolution for a time T without radiation, and
(v) resonant $\pi/2$-pulse identical to the first pulse.
Prepare a graph of type Fig. 34.2 illustrating the temporal evolution of the Bloch vector during the sequence. Now, repeat the sequence taking into account a possible Doppler shift leading to $\Delta_{12} \neq 0$.
b. Repeat the calculation of (a), now numerically solving the Bloch equations, which allow the occurrence of spontaneous emission ($\Gamma_{12} = 0.03\Omega_{12}$). Interpret the results.

Solution: *a. Choosing $\Omega_{12} = 1$ the duration of the $\pi/2$-pulse must be $T = \pi/2\Omega_{12}$. The Hamiltonian and the solution of the Schrödinger equation can be found in the numerical MATLAB code given in the file 'LM_Bloch_PhotonEcho.m'. Fig. 34.5(a) shows, that the final inversion $2\rho_{22}(2T+\tau)-1$ depends on the detuning Δ_{12}, and the free precession time τ between the pulses*
b. The code 'LM_Bloch_PhotonEcho.m' shows the simulations.

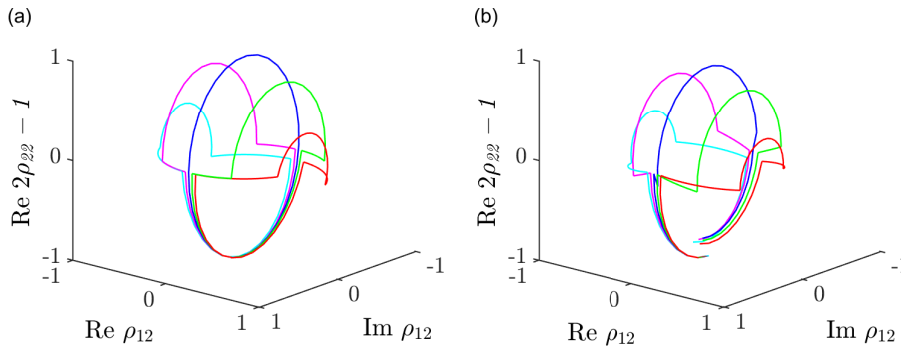

Figure 34.5: (code) (a) Time evolution of the Bloch vector for different detunings Δ_{12} calculated from the Schrödinger equation. (b) Same evolution now calculated from the Bloch equations with $\Gamma_{12} = 0.1\Omega_{12}$ the spontaneous emission rate.

Alternatively we can try an analytical approach: *We use the general solutions*

of the Bloch equations:

$$\begin{aligned}
\rho_{22}^{(1)} &= \rho_{22}(0) + \tfrac{1}{2G^2}\left[|\Omega|^2\left(1-2\rho_{22}(0)\right) - \Delta\left(\Omega\rho_{12}^*(0) + \Omega^*\rho_{12}(0)\right)\right] \\
\rho_{22}^{(2)} &= \tfrac{1}{4G^2}\left[-|\Omega|^2(1-2\rho_{22}(0)) + (\Delta+G)\Omega\rho_{12}^*(0) + (\Delta-G)\Omega^*\rho_{12}(0)\right] \\
\rho_{22}^{(3)} &= \tfrac{1}{4G^2}\left[-|\Omega|^2(1-2\rho_{22}(0)) + (\Delta-G)\Omega\rho_{12}^*(0) + (\Delta+G)\Omega^*\rho_{12}(0)\right] \\
\rho_{12}^{(1)} &= \tfrac{1}{2G^2}\left[\Delta\Omega(1-2\rho_{22}(0)) + \Omega\left(\Omega\rho_{12}^*(0) + \Omega^*\rho_{12}(0)\right)\right] \\
\rho_{12}^{(2)} &= \tfrac{\Delta-G}{4G^2}\left[-\Omega(1-2\rho_{22}(0)) + (\Delta+G)\frac{\Omega}{\Omega^*}\rho_{12}^*(0) + (\Delta-G)\rho_{12}(0)\right] \\
\rho_{12}^{(3)} &= \tfrac{\Delta+G}{4G^2}\left[-\Omega(1-2\rho_{22}(0)) + (\Delta-G)\frac{\Omega}{\Omega^*}\rho_{12}^*(0) + (\Delta+G)\rho_{12}(0)\right] \ ,
\end{aligned}$$

and consider the special cases $\Delta = 0$,

$$\begin{array}{lll}
\rho_{22}^{(1)} = \frac{1}{2} & \rho_{22}^{(2)} = -\frac{1}{4} + \frac{1}{2}\rho_{22}(0) + \frac{\imath}{2}\mathfrak{Im}\ \rho_{12}(0) & \rho_{22}^{(3)} = -\frac{1}{4} + \frac{1}{2}\rho_{22}(0) - \frac{\imath}{2}\mathfrak{Im}\ \rho_{12}(0) \\
\rho_{12}^{(1)} = \mathfrak{Re}\ \rho_{12}(0) & \rho_{12}^{(2)} = \frac{1}{4} - \frac{1}{2}\rho_{22}(0) + \frac{\imath}{2}\mathfrak{Im}\ \rho_{12}(0) & \rho_{12}^{(3)} = -\frac{1}{4} + \frac{1}{2}\rho_{22}(0) - \frac{\imath}{2}\mathfrak{Im}\ \rho_{12}(0)
\end{array}$$

with the solution

$$\begin{aligned}
\rho_{22}(t) &= \rho_{22}^{(1)} + \rho_{22}^{(2)}e^{\imath\Omega t} + \rho_{22}^{(3)}e^{-\imath\Omega t} \\
&= \tfrac{1}{2} + \left[-\tfrac{1}{4} + \tfrac{1}{2}\rho_{22}(0) - \tfrac{\imath}{2}\mathfrak{Im}\ \rho_{12}(0)\right]e^{\imath\Omega t} + \left[-\tfrac{1}{4} + \tfrac{1}{2}\rho_{22}(0) + \tfrac{\imath}{2}\mathfrak{Im}\ \rho_{12}(0)\right]e^{-\imath\Omega t} \\
\rho_{12}(t) &= \rho_{12}^{(1)} + \rho_{12}^{(2)}e^{\imath\Omega t} + \rho_{12}^{(3)}e^{-\imath\Omega t} \\
&= \mathfrak{Re}\ \rho_{12}(0) + \left[\tfrac{1}{4} - \tfrac{1}{2}\rho_{22}(0) + \tfrac{\imath}{2}\mathfrak{Im}\ \rho_{12}(0)\right]e^{\imath\Omega t} + \left[-\tfrac{1}{4} + \tfrac{1}{2}\rho_{22}(0) + \tfrac{\imath}{2}\mathfrak{Im}\ \rho_{12}(0)\right]e^{-\imath\Omega t}
\end{aligned}$$

and the case $\Omega = 0$

$$\begin{array}{lll}
\rho_{22}^{(1)} = \rho_{22}(0) & \rho_{22}^{(2)} = 0 & \rho_{22}^{(3)} = 0 \\
\rho_{12}^{(1)} = 0 & \rho_{12}^{(2)} = 0 & \rho_{12}^{(3)} = \rho_{12}(0)
\end{array}$$

with the solution

$$\begin{aligned}
\rho_{22}(t) &= \rho_{22}^{(1)} + \rho_{22}^{(1)}e^{\imath\Delta t} + \rho_{22}^{(1)}e^{-\imath\Delta t} = \rho_{22}(0) \\
\rho_{12}(t) &= \rho_{12}^{(1)} + \rho_{12}^{(1)}e^{\imath\Delta t} + \rho_{12}^{(1)}e^{-\imath\Delta t} = \rho_{12}(0)e^{-\imath\Delta t} \ .
\end{aligned}$$

We begin with the initial conditions

$$\begin{aligned}
\rho_{22}(0) &= 0 \\
\rho_{12}(0) &= 0 \ .
\end{aligned}$$

We apply a first resonant $\pi/2$*-pulse* ($\Omega t = \pi/2, \Delta = 0$),

$$\begin{aligned}
\rho_{22}(\tfrac{\pi}{2\Omega}) &= \tfrac{1}{2} - \tfrac{1}{2}\cos\Omega t = \tfrac{1}{2} \\
\rho_{12}(\tfrac{\pi}{2\Omega}) &= \tfrac{\imath}{2}\sin\Omega t = \tfrac{\imath}{2} \ .
\end{aligned}$$

Now, we turn off the laser and detune the transition ($\Omega = 0, \Delta_T$)*. After an arbitrary time* T *the state becomes,*

$$\begin{aligned}
\rho_{22}(\tfrac{\pi}{2\Omega} + T) &= \frac{1}{2} \\
\rho_{12}(\tfrac{\pi}{2\Omega} + T) &= \frac{\imath}{2}e^{-\imath\Delta_T T} = \tfrac{1}{2}\sin\Delta_T T + \tfrac{\imath}{2}\cos\Delta_T T \ .
\end{aligned}$$

Now we apply a resonant π-pulse ($\Omega t = \pi, \Delta = 0$),

$$\rho_{22}(\tfrac{\pi}{2\Omega} + T + \pi) = \tfrac{1}{2} - \tfrac{1}{2}\cos\Delta_T T \sin\Omega t = \tfrac{1}{2}$$
$$\rho_{12}(\tfrac{\pi}{2\Omega} + T + \pi) = \tfrac{1}{2}\sin\Delta_T T + \tfrac{\imath}{2}\cos\Delta_T T\cos\Omega t = \tfrac{1}{2}\sin\Delta_T T - \tfrac{\imath}{2}\cos\Delta_T T = -\frac{\imath}{2}e^{\imath\Delta_T T} \ .$$

We let the system evolve once more for a while T without laser ($\Omega = 0, \Delta_T$),

$$\rho_{22}(\tfrac{\pi}{2\Omega} + T + \pi + T) = \frac{1}{2}$$
$$\rho_{12}(\tfrac{\pi}{2\Omega} + T + \pi + T) = -\frac{\imath}{2}e^{\imath\Delta_T T}e^{-\imath\Delta_T t} = -\frac{\imath}{2} \ .$$

Finally, we apply the second $\pi/2$-pulse ($\Omega t = \pi/2, \Delta = 0$)

$$\rho_{22}(\tfrac{\pi}{2\Omega} + T + \tfrac{\pi}{\Omega} + T + \tfrac{\pi}{2\Omega}) = \tfrac{1}{2} + \tfrac{1}{2}\sin\Omega t = 1$$
$$\rho_{12}(\tfrac{\pi}{2\Omega} + T + \tfrac{\pi}{\Omega} + T + \tfrac{\pi}{2\Omega}) = \dots \ .$$

Therefore, for each value of them detuning Δ_T, which may in fact be different for each member of an atomic sample, the final value of the population of the excited state is always 1.
Photon echo is an interference effect in the radiation emitted by many atoms. We assume that many two-level atoms interact with the same radiation mode. To observe photon echoes, we apply a first $\pi/2$-pulse which brings every atom into a coherent superposition of the two energy states. However, because of the Doppler shift, the excitation of the individual atoms may be different, so that the individual Bloch vectors begin to precess at different paces. If after a certain time a π-pulse is applied, the state populations, and therefore the direction of the precession are reversed, so that after a certain time, the Bloch vectors are refocused.
The synchronization of the phases of the individual dipoles generates a cooperative spontaneous emission of the ensemble called photon echo. The signature of a photon echo is twofold: First, the appearance of a fluorescence pulse a delay of τ after the end of the applied π-pulse, and second, a fluorescence rate depending on the square of the excited state population. This unusual behavior emerges from a mutual coupling of the individual dipoles and results in a rapid depopulation of the excited state with a much shorter fluorescent lifetime than for individual atoms. This synchronization of the phases of the individual dipoles is called superradiance. It is important to keep in mind, that the photon echo does not allow to recover the coherence of an irreversible process. It only works for inhomogeneous broadening due to a well-defined distribution of the kinetic energy among the atoms, provided that the temporal evolutions of the individual atoms have not undergone random phase interruptions.

34.4.6.10 Ex: Time-evolution of NMR spin components

Derive the coherent part of the Bloch equations (34.175) from the Heisenberg equation (34.174).

Solution: *The nuclear spins satisfies the usual commutation relation $[\hat{I}_m, \hat{I}_n] =$*

$\imath\hbar\epsilon_{kmn}\hat{I}_k$. With this we obtain from the Heisenberg equation,

$$\imath\hbar\frac{d\hat{\vec{\mu}}}{dt} = [\hat{\vec{\mu}}, \hat{H}] = \hat{\vec{\mu}}(-\hat{\vec{\mu}}\cdot\vec{\mathcal{B}}) - (-\vec{\mu}\cdot\vec{\mathcal{B}})\hat{\vec{\mu}} = \gamma_I^2(\hat{\mathbf{I}}\cdot\vec{\mathcal{B}})\hat{\mathbf{I}} - \gamma_I^2\hat{\mathbf{I}}(\hat{\mathbf{I}}\cdot\vec{\mathcal{B}})$$
$$= \gamma_I^2([\hat{I}_x,\hat{\mathbf{I}}]\mathcal{B}_x + [\hat{I}_y,\hat{\mathbf{I}}]\mathcal{B}_y + [\hat{I}_z,\hat{\mathbf{I}}]\mathcal{B}_z) = \gamma_I^2\imath\hbar\begin{pmatrix}\hat{I}_y\mathcal{B}_z - \hat{I}_z\mathcal{B}_y\\ \hat{I}_z\mathcal{B}_x - \hat{I}_x\mathcal{B}_z\\ \hat{I}_x\mathcal{B}_y - \hat{I}_y\mathcal{B}_x\end{pmatrix} = \imath\hbar\gamma_I\hat{\vec{\mu}}\times\vec{\mathcal{B}}\ .$$

34.4.6.11 Ex: Precession of the nuclear spin in a magnetic field

Show for $\hat{H}_0 = -\frac{\hbar\omega_L}{2}\hat{\sigma}_z$ that,

$$\langle\hat{\vec{\sigma}}(t)\rangle = \begin{pmatrix}\cos\omega_L t & -\sin\omega_L t & 0\\ \sin\omega_L t & \cos\omega_L t & 0\\ 0 & 0 & 1\end{pmatrix}\langle\hat{\vec{\sigma}}(0)\rangle\ .$$

Solution: *For the x-component we calculate,*

$$\langle\hat{\sigma}_x(t)\rangle = Tr\ \hat{\rho}(t)\hat{\sigma}_x = Tr\ e^{-\frac{\imath}{2}\hbar\omega_L t\hat{\sigma}_z}\hat{\rho}(0)e^{\frac{\imath}{2}\hbar\omega_L t\hat{\sigma}_z}\hat{\sigma}_x$$
$$= Tr\begin{pmatrix}e^{-\imath\hbar\omega_L t/2} & 0\\ 0 & e^{\imath\hbar\omega_L t/2}\end{pmatrix}\begin{pmatrix}\rho_{11} & \rho_{12}\\ \rho_{21} & \rho_{22}\end{pmatrix}\begin{pmatrix}e^{\imath\hbar\omega_L t/2} & 0\\ 0 & e^{-\imath\hbar\omega_L t/2}\end{pmatrix}\begin{pmatrix}0 & 1\\ 1 & 0\end{pmatrix}$$
$$= Tr\begin{pmatrix}e^{-\imath\hbar\omega_L t}\rho_{12} & \rho_{11}\\ \rho_{22} & e^{\imath\hbar\omega_L t}\rho_{21}\end{pmatrix} = e^{-\imath\hbar\omega_L t}\rho_{12} + e^{\imath\hbar\omega_L t}\rho_{21}\ .$$

Similarly, we get for the y- and z-components,

$$\langle\hat{\sigma}_y(t)\rangle = \imath e^{-\imath\hbar\omega_L t}\rho_{12} - \imath e^{\imath\hbar\omega_L t}\rho_{21}$$
$$\langle\hat{\sigma}_z(t)\rangle = \rho_{11} - \rho_{22}\ .$$

These equations satisfy the initial conditions,

$$2\rho_{12} = \langle\hat{\sigma}_x(0)\rangle - \imath\langle\hat{\sigma}_y(0)\rangle$$
$$\rho_{11} - \rho_{22} = \langle\hat{\sigma}_z(0)\rangle\ ,$$

from which we immediately derive the result.

34.5 Bloch equations with spontaneous emission

In this section we will introduce spontaneous emission and the important concepts of polarization and susceptibility emanating from an excited sample of oscillating dipoles. Optical Bloch equations including spontaneous emission will be given and their stationary solutions will be discussed. Dissipative processes always broaden transition lines, and thus we will discuss various broadening mechanisms.

34.5.1 Phenomenological inclusion of spontaneous emission

To find the Bloch equations including spontaneous emission, we proceed similarly for Eq. (34.26) and insert the phenomenological decay term $-\imath\gamma a_2$ into the Eqs. (27.63),

$$\Omega^* \cos\omega t e^{\imath\omega_0 t} a_1 - \imath\gamma a_2 = \imath \frac{da_2}{dt} \ , \tag{34.184}$$

that is, the equations of motion can be corrected by simply replacing,

$$\frac{da_2}{dt} \curvearrowright \left(\frac{d}{dt} + \gamma\right) a_2 \ . \tag{34.185}$$

Knowing $\rho_{mn} = a_m^* a_n$, it is easy to check,

$$\frac{d\rho_{22}}{dt} \curvearrowright \left(\frac{d}{dt} + \Gamma\right) \rho_{22} \qquad \text{and} \qquad \frac{d\rho_{12}}{dt} \curvearrowright \left(\frac{d}{dt} + \gamma\right) \rho_{12} \ , \tag{34.186}$$

with $\gamma = \Gamma/2$, such that the Bloch equations become,

$$\boxed{\frac{d}{dt}\begin{pmatrix}\rho_{11}\\ \rho_{22}\\ \rho_{12}\\ \rho_{21}\end{pmatrix} = \begin{pmatrix} 0 & \Gamma & \frac{\imath}{2}\Omega & -\frac{\imath}{2}\Omega \\ 0 & -\Gamma & -\frac{\imath}{2}\Omega & \frac{\imath}{2}\Omega \\ \frac{\imath}{2}\Omega & -\frac{\imath}{2}\Omega & -\imath\Delta - \gamma & 0 \\ -\frac{\imath}{2}\Omega & \frac{\imath}{2}\Omega & 0 & \imath\Delta - \gamma \end{pmatrix}\begin{pmatrix}\rho_{11}\\ \rho_{22}\\ \rho_{12}\\ \rho_{21}\end{pmatrix}} \ . \tag{34.187}$$

Example 198 (*Langevin equation*): The *Heisenberg equation* for the evolution of the internal degrees of freedom, including the phenomenologically introduced decay, is also called *Langevin equation*. It can be written as,

$$\imath \frac{d\hat{\sigma}^-}{dt} = \tfrac{1}{\hbar}[\hat{\sigma}^-, \hat{H}] - \tfrac{\imath}{2}\Gamma\hat{\sigma}^- \ ,$$

and analogously for $\hat{\sigma}_z$. With the Hamiltonian $\hat{H} = \hbar\Delta\hat{\sigma}^+\hat{\sigma}^- + \frac{1}{2}\hbar\Omega(e^{\imath\omega t}\hat{\sigma}^- + h.c.)$ we obtain, using the Pauli spin matrices, exactly the Bloch equations,

$$\begin{aligned}
\imath\dot{\hat{\sigma}}^- &= \Delta[\hat{\sigma}^-, \hat{\sigma}^+\hat{\sigma}^-] + \tfrac{1}{2}\Omega e^{-\imath\omega t}[\hat{\sigma}^-, \hat{\sigma}^+] - \tfrac{\imath}{2}\Gamma\hat{\sigma}^- = \Delta\hat{\sigma}^- - \tfrac{1}{2}\Omega e^{-\imath\omega t}\hat{\sigma}_z - \tfrac{\imath}{2}\Gamma\hat{\sigma}^- \\
\imath\dot{\hat{\sigma}}_z &= \Delta[\hat{\sigma}_z, \hat{\sigma}^+\hat{\sigma}^-] + \tfrac{1}{2}\Omega e^{-\imath\omega t}[\hat{\sigma}_z, \hat{\sigma}^+] + \tfrac{1}{2}\Omega e^{\imath\omega t}[\hat{\sigma}_z, \hat{\sigma}^-] - \tfrac{\imath}{2}\Gamma\hat{\sigma}_z = \Omega(\hat{\sigma}^- - \hat{\sigma}^+) - \tfrac{\imath}{2}\Gamma\hat{\sigma}_z \ .
\end{aligned}$$

34.5.1.1 Stationary solution of the Bloch equations

The dissipation introduced by the spontaneous emission allows the system to reach a steady state. Letting the time derivatives be 0, we obtain the stationary solutions,

$$\boxed{\rho_{22}(\infty) = \frac{\frac{1}{4}|\Omega|^2}{\Delta^2 + \frac{1}{2}|\Omega|^2 + \frac{1}{4}\Gamma^2} \qquad \text{and} \qquad \rho_{12}(\infty) = e^{\imath\Delta t}\frac{\frac{1}{2}\Omega(\Delta - \frac{\imath}{2}\Gamma)}{\Delta^2 + \frac{1}{2}|\Omega|^2 + \frac{1}{4}\Gamma^2}} \ . \tag{34.188}$$

This will be shown in Exc. 34.5.4.1. We see that the populations and coherences both have a Lorentzian frequency dependence, which is similar to the one of the absorption

cross section σ derived in (22.72). However, the denominators have an extra term $\frac{1}{2}\Omega^2$ contributing to an *effective* widths of ρ_{22} and ρ_{12},

$$\Gamma_{\text{eff}} = \sqrt{2|\Omega|^2 + \Gamma^2} \ . \tag{34.189}$$

This effect, called *power broadening* or *saturation broadening*, has already been discussed in (22.102). The phase factor $e^{\imath\Delta t}$ describes the optical precession of the Bloch vector.

By introducing the *saturation parameter*,

$$s \equiv \frac{2|\Omega|^2}{4\Delta^2 + \Gamma^2} \ , \tag{34.190}$$

we can rewrite the stationary dipole moment and the excited state population (34.188) as,

$$\boxed{\rho_{22}(\infty) = \frac{s/2}{1+s} \quad , \quad \rho_{12}(\infty) = e^{\imath\Delta t}\frac{\Delta - \imath\Gamma/2}{\Omega}\frac{s}{1+s} \ .} \tag{34.191}$$

and

$$|\rho_{12}(\infty)|^2 = \frac{s/2}{(1+s)^2} \ . \tag{34.192}$$

Fig. 34.6(a) shows the Rabi oscillations damped by spontaneous emission. For long times the population of the excited state ρ_{22} converges to the asymptote (34.191). Fig. 34.6(b) shows the temporal evolution of the Bloch vector subject to spontaneous emission. In Exc. 34.5.4.2 we the behavior of the phase of the dipole moment ρ_{12} with respect to the driving field. In Exc. 34.5.4.3 and 34.5.4.4 we calculate the impact of

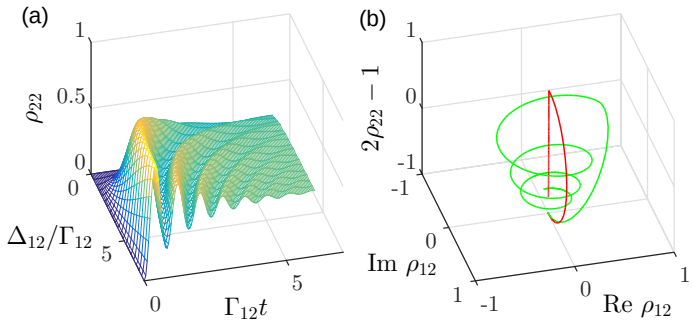

Figure 34.6: (code) (a) Rabi oscillations damped by spontaneous emission for Rabi frequencies between $\Omega/\Gamma = 0.2, .., 5$. (b) Evolution of the Bloch vector subject to spontaneous emission ($\Gamma_{12} = 0.05\Omega_{12}$) after application of a resonant π-pulse (red) and after a π-pulse with detuning $\Delta_{12} = \Omega_{12}/2$ (green).

the spontaneous emission on the determinant of the density operator. Solve the Excs. 34.5.4.5, 34.5.4.6, 34.5.4.7, and 34.5.4.8.

Example 199 (*Resonant excitation and weak excitation*): A case where the Bloch equations can be analytically treated is under resonant excitation,

$\Delta = 0$. In this case, for the initial conditions, $\rho_{12}(0) = \rho_{22}(0) = 0$, the solution including decay is,

$$\rho_{22}(t) = \frac{\Omega^2}{2|\Omega|^2 + \Gamma^2}\left[1 - e^{-3\Gamma t/4}\left(\cos\lambda t + \frac{3\Gamma}{4\lambda}\sin\lambda t\right)\right] \quad \text{and} \quad \rho_{12}(t) = 0 \ , \tag{34.193}$$

where $\lambda \equiv \sqrt{\Omega^2 - \Gamma^2}$. This solution (which will be derived in Exc. 34.5.4.9), describes the optical nutation of the Bloch vector along the ρ_z axis. We note here that, due to spontaneous emission, the norm of the Bloch vector is NOT conserved, i.e. the Bloch vector evolves to the interior of the Bloch sphere.
Another case that can be solved analytically is the weakly excited atom, $|\Omega| \ll \Gamma$,

$$\rho_{22} \simeq \frac{\Omega^2}{4G^2}\left(1 + e^{-2\Gamma t} - 2\cos\Delta t\right) \tag{34.194}$$

$$\text{and} \quad \rho_{12}(t) \simeq \frac{-\imath\Omega}{2\imath\Delta + 2\Gamma}\left(e^{-(\imath\Delta+\Gamma)t} - 1\right) + \rho_{12}(0)e^{-(\imath\Delta+\Gamma)t} \ .$$

34.5.1.2 Nonlinearity of the Bloch equations

Because the Bloch equation go beyond perturbation theory they contain nonlinear optics. We can see this by the simple fact that strong radiation field can saturate atomic transitions. For example, expanding the population and coherence (34.188) by the incident electric field amplitude $\mathcal{E} \propto \Omega$,

$$\rho_{22}(\infty) \simeq \frac{1}{4\Delta^2 + \Gamma^2}\Omega^2 - \frac{2}{(4\Delta^2 + \Gamma^2)^2}\Omega^4 + ... \tag{34.195}$$

$$\rho_{12}(\infty) \simeq e^{\imath\Delta t}\frac{2\Delta - \imath\Gamma}{4\Delta^2 + \Gamma^2}\Omega - 2e^{\imath\Delta t}\frac{2\Delta - \imath\Gamma}{(4\Delta^2 + \Gamma^2)^2}\Omega^3 + ... \ .$$

The theory of nonlinear optics will be developed in Sec. 35.7.2 and Chp. 37.

Example 200 (*Complex susceptibility and absorption coefficient*): The objective of this section is to obtain an expression for the susceptibility in the presence of spontaneous emission. For the present discussion we are only concerned with the temporal dependence of the actual light wave, which we write as,

$$\vec{\mathcal{E}}(t) = \vec{\mathcal{E}}_0 \cos\omega t = \tfrac{1}{2}[e^{\imath\omega t} + e^{-\imath\omega t}] \ . \tag{34.196}$$

Then we consider how to write the polarization in terms of a susceptibility when the field contains two conjugate frequencies, $\pm\omega$. Substituting into the polarization Eq. (14.20), we get,

$$\vec{\mathcal{P}}(t) = \varepsilon_0\chi_e\vec{\mathcal{E}} = \tfrac{1}{2}\varepsilon_0\vec{\mathcal{E}}_0[\chi_e(\omega)e^{\imath\omega t} + \chi_e(-\omega)e^{-\imath\omega t}] \ . \tag{34.197}$$

The polarization can also be expressed in terms of the density of the transition dipoles in a gas of two-level atoms,

$$\vec{\mathcal{P}}(t) = \frac{N}{V}\mathbf{d}_{12}(t) \longrightarrow \frac{N}{V}\langle\mathbf{d}_{12}(t)\rangle \ . \tag{34.198}$$

where $\mathbf{d}$ is the transition dipole of only one atom, N/V is the atomic density, and the quantum expectation value for the transition dipole moment is,

$$\langle\mathbf{d}_{12}\rangle = -e\int \Psi\sum_j \mathbf{r}_j\Psi d^3r \ . \tag{34.199}$$

Now, from Eq. (27.58),

$$\langle \mathbf{d}_{12} \rangle = -e \left[a_1^* a_2 \langle \psi_1 | \sum_j \mathbf{r}_j | \psi_2 \rangle e^{-\imath\omega_0 t} + a_1 a_2^* \langle \psi_2 | \sum_j \mathbf{r}_j | \psi_1 \rangle e^{\imath\omega_0 t} \right] . \quad (34.200)$$

To simplify the notation we define $\langle \mathbf{r}_{mn} \rangle \equiv \langle \psi_m | \sum_j \mathbf{r}_j | \psi_n \rangle$ and obtain,

$$\langle \mathbf{d}_{12} \rangle = -e[a_1^* a_2 \langle \mathbf{r}_{12} \rangle e^{-\imath\omega_0 t} + a_1 a_2^* \langle \mathbf{r}_{21} \rangle e^{\imath\omega_0 t}] . \quad (34.201)$$

Now, we only need to replace the solutions of the coupled equations by relating a_1 and a_2 of the Eqs. (27.63) in (34.201) which, in turn, can be inserted into the equation (34.197). Thus we obtain an expression for the polarization in terms of properties of the atoms and the incident field.
The crucial point now is, that the solution for a_2, Eq. (27.79), does not consider spontaneous emission. Therefore, as already done in Sec. 34.5.1, we will introduce an ad hoc modification of Eq. (27.63) by including a radiative loss constant γ,

$$\Omega^* \cos\omega t e^{\imath\omega_0 t} a_1 - \imath\gamma a_2 = \imath \frac{da_2}{dt} . \quad (34.202)$$

This term does NOT EXPLAIN spontaneous emission. It simply takes into account the existence of the effect and characterizes its amplitude through γ: If the incident field is turned off ($\Omega^* = 0$)

$$-\imath\gamma a_2 = \imath \frac{da_2}{dt} \quad (34.203)$$

and

$$a_2(t) = a_2(0) e^{-\gamma t} . \quad (34.204)$$

Then, the probability of finding an atom in the excited state (or the fraction of excited atoms in an ensemble) is,

$$N_2/N = |a_2(t)|^2 = |a_2(0)|^2 e^{-2\gamma t} . \quad (34.205)$$

Comparing this behavior with the result obtained from the Einstein rate equation, we see immediately,

$$A_{21} = 2\gamma \equiv \Gamma . \quad (34.206)$$

Now, the solution for our improved $a_2(t)$ coefficient is,

$$a_2(t) = -\tfrac{1}{2}\Omega^* \left[\frac{e^{\imath(\omega_0+\omega)t}}{\omega_0 + \omega - \imath\gamma} + \frac{e^{\imath(\omega_0-\omega)t}}{\omega_0 - \omega - \imath\gamma} \right] , \quad (34.207)$$

which solves the differential equation (34.202) in the weak field limit, $a_1(t) \simeq 1$, as will be verified in Exc. 34.5.4.10.
Making the weak field approach, replacing the values obtained for $a_{1,2}$ in the transition dipole (34.201) and replacing the average of the orientations, $|\langle r_{12} \rangle|^2 \longrightarrow \frac{1}{3}|\langle r_{12} \rangle|^2$, in the polarization (34.198), we obtain,

$$\vec{\tilde{\mathcal{P}}}(t) = \varepsilon_0 \tilde{\chi}_e \vec{\mathcal{E}} \quad (34.208)$$
$$= \frac{N}{V} \frac{e^2 |\langle r_{12} \rangle^2 \vec{\mathcal{E}}_0}{6\hbar} \left[\frac{e^{\imath\omega t}}{\omega_0 + \omega - \imath\gamma} + \frac{e^{\imath\omega t}}{\omega_0 - \omega + \imath\gamma} + \frac{e^{-\imath\omega t}}{\omega_0 - \omega - \imath\gamma} + \frac{e^{-\imath\omega t}}{\omega_0 + \omega + \imath\gamma} \right] .$$

Apparently, the presence of spontaneous emission turns the susceptibility into a complex number [see Eq. (18.132)].

Comparing this result with Eq. (34.197) and identifying the susceptibility $\tilde{\chi}_e(\omega)$ in terms of the atomic properties and the frequency of the incident field, we find,

$$\begin{aligned}\tilde{\chi}_e(\omega) &= \frac{Ne^2|\langle r_{12}\rangle|^2}{3\epsilon_0\hbar V}\left[\frac{1}{\omega_0-\omega-\imath\gamma}+\frac{1}{\omega_0+\omega-\imath\gamma}\right] \\ &= \frac{Ne^2|\langle r_{12}\rangle^2}{3\epsilon_0\hbar V}\left[\frac{\omega_0-\omega}{(\omega_0-\omega)^2+\gamma^2}+\frac{\omega_0+\omega}{(\omega_0+\omega)^2+\gamma^2}\right. \\ &\quad \left.+\imath\gamma\left(\frac{1}{(\omega_0-\omega)^2+\gamma^2}+\frac{1}{(\omega_0+\omega)^2+\gamma^2}\right)\right] .\end{aligned} \tag{34.209}$$

In most practical situations in the laboratory ω will not be tuned more than some 100 GHz away from ω_0, hence $|\omega_0-\omega| \lesssim 10^{11}$ Hz. With optical frequencies $\omega \simeq 10^{15}$ Hz, it is clear that the second term on the right hand side of Eq. (34.209) will be negligible compared to the first one. Therefore, we can discard the second term and write the susceptibility as,

$$\begin{aligned}\chi_e(\omega) &\simeq \frac{Ne^2|\langle r_{12}\rangle|^2}{3\epsilon_0\hbar V}\frac{1}{\omega_0-\omega-\imath\gamma} \\ &= \frac{Nd_{12}^2}{3\epsilon_0\hbar V}\frac{-\Delta+\imath\Gamma/2}{\Delta^2+(\Gamma/2)^2} = \frac{n\hbar\Omega^2}{3\epsilon_0 E_0^2}\frac{-\Delta+\imath\Gamma/2}{\Delta^2+(\Gamma/2)^2} .\end{aligned} \tag{34.210}$$

We identify the real and imaginary parts, $\tilde{\chi}_e = \chi_e' + \imath\chi_e''$, and express the absorption coefficient as (see (18.138)),

$$K = \frac{\omega}{c\eta}\chi_e''(\omega) = \frac{\pi N d_{12}^2\omega_0}{3\epsilon_0\hbar c V}\frac{\Gamma/2\pi}{\Delta^2+(\Gamma/2)^2} = \frac{\pi N d_{12}^2\omega_0}{3\epsilon_0\hbar c V}\mathcal{L}(\omega-\omega_0) . \tag{34.211}$$

The Lorentzian profile term governs the frequency dependence of the absorption coefficient. We see that K exhibits a peak at the resonance frequency ω_0 and a width of Γ. The factor of π inserted in the numerator and denominator of the right term of Eq. (34.211) allows to normalize the profile. We have also assumed in Eq. (34.211) that the gas is sufficiently dilute for $n \simeq 1$ to hold, and that the line is sufficiently narrow to be able to replace ω with ω_0, such that,

$$\frac{\omega}{c\eta} \longrightarrow \frac{\omega_0}{c} . \tag{34.212}$$

The absorption cross section has the same lineshape, since from Eqs. (22.72) and (34.211) we have,

$$\sigma_{0a} = \frac{\pi d_{12}^2\omega_0}{3\epsilon_0\hbar c V}\mathcal{L}(\omega-\omega_0) , \tag{34.213}$$

consistent with our previous expression for the frequency dependence of the absorption cross-section. We can also write the imaginary component of the susceptibility in terms of the cross section using the Eqs. (22.72) and (34.211)

$$\chi_e'' = \frac{cN}{\omega_0 V}\sigma_{0a} . \tag{34.214}$$

The frequency-dependent linear *susceptibility* completely describes the linear propagation of an electromagnetic wave within a medium. It is related to the index of refraction and the absorption coefficient. Nonlinear processes should be described by higher order susceptibilities. Electric fields $\vec{\mathcal{E}} = \vec{\mathcal{E}}_0 e^{\imath\omega t} + c.c.$ induce in media characterized by a given susceptibility $\tilde{\chi}_e$ the polarization $\vec{\mathcal{P}} = \varepsilon_0\tilde{\chi}_e\vec{\mathcal{E}}$.

The polarization is the sum of the dipole moments of the individual atoms, $\vec{\mathcal{P}} = n\langle \mathbf{d} \rangle$, where $n = N/V$ is the atomic density. The susceptibility can therefore be expressed by the Hamiltonian interaction $\hat{H} = -\mathbf{d} \cdot \vec{\mathcal{E}}$,

$$\chi_e = -\frac{n}{|\vec{\mathcal{E}}|^2} \langle \hat{H} \rangle \ . \tag{34.215}$$

Using the two-level Hamiltonian (34.209) we obtain,

$$\chi_e = -n \ \frac{\hbar\Omega}{2|\vec{\mathcal{E}}|^2} \ \rho_{12} e^{\imath\Delta t} + c.c. \tag{34.216}$$

for the polarization,

$$\vec{\mathcal{P}} = n \ \mathbf{d}\rho_{12} + c.c. \tag{34.217}$$

and for the susceptibility,

$$\chi_e(\omega) = \frac{2nd^2}{3\varepsilon_0\hbar} \frac{\Delta + \imath\Gamma}{4\Delta^2 + 2|\Omega|^2 + \Gamma^2} \qquad \text{with} \qquad d = \sqrt{\frac{3\pi\varepsilon_0\hbar\Gamma}{k^3}} \ . \tag{34.218}$$

We can insert the new expression (34.188) for ρ_{12} into our previous expression for $\langle d_{12} \rangle$ (34.201) and get new expressions for the polarization $\vec{\mathcal{P}}(t)$, (34.198) and (34.208), and the susceptibility χ (34.210). The modified expression for the susceptibility is,

$$\chi_e = \frac{Nd_{12}^2}{3\epsilon_0\hbar V} \frac{-\Delta + \frac{1}{2}\Gamma}{\Delta^2 + \frac{1}{2}|\Omega|^2 + \frac{1}{4}\Gamma^2} \ . \tag{34.219}$$

In the imaginary component we obtain the new absorption coefficient,

$$K = \frac{\omega}{cn}\chi_e''(\omega) = \frac{\pi N e^2 |\langle \mathbf{r}_{12} \rangle|^2 \omega_0}{3\epsilon_0\hbar c V} \frac{\Gamma/2\pi}{\Delta^2 + \frac{1}{2}\Omega^2 + \frac{1}{4}\Gamma^2} \ , \tag{34.220}$$

and the *optical cross-section* for absorption,

$$\sigma_{0a} = \frac{\pi e^2 |\langle \mathbf{r}_{12} \rangle|^2 \omega_0}{3\epsilon_0\hbar c} \frac{\Gamma/2\pi}{\Delta^2 + \frac{1}{2}\Omega^2 + \frac{1}{4}\Gamma^2} \ . \tag{34.221}$$

The important new property is the effective width $\Gamma_{\rm eff}$, which appears in χ_e, K, and σ_{0a}.

34.5.2 Liouville equation for two levels

In the previous section we chose to include spontaneous emission in the Bloch equations by phenomenological arguments. However, as we will show more ahead, dissipation can be treated from general principles. This treatment, named after *Weisskopf-Wigner*, derives from a Liouville type equation (34.125), but which holds for a total density operator $\rho_{atom\&field}$ describing the atom and the electromagnetic modes, an equation for the density operator of only the atom. The price to pay for this simplification is an additional term appearing in the equation now called *master equation*,

$$\boxed{\begin{array}{rcl} \dot{\hat{\rho}}(t) & = & (\mathcal{L}_0 + \mathcal{L}_{sp})\hat{\rho}(t) \qquad \text{with} \\ \mathcal{L}_0\hat{\rho}(t) & \equiv & \frac{\imath}{\hbar}[\hat{\rho}(t), \hat{H}] \qquad \text{and} \qquad \mathcal{L}_{sp} = \frac{\Gamma}{2}(2\hat{\sigma}\hat{\rho}^-\hat{\sigma}^+ - \hat{\sigma}^+\hat{\sigma}^-\hat{\rho} - \hat{\rho}\hat{\sigma}^+\hat{\sigma}^-) \end{array}} \ , \tag{34.222}$$

where $\hat{\sigma}^\pm$ are the Pauli matrices. We show in Exc. 34.5.4.11, that the known Bloch equations can be derived from the master equation.

34.5.3 The effective Hamiltonian approach

In Sec. 34.5.1 we have shown that spontaneous emission can be phenomenologically be included by substituting $\frac{d}{dt} \curvearrowright \frac{d}{dt} + \frac{\Gamma}{2}$ in the Schrödinger equation,

$$\imath \left(\tfrac{d}{dt} + \tfrac{\Gamma}{2} |2\rangle\langle 2| \right) |\psi\rangle = \hat{H}|\psi\rangle \ . \tag{34.223}$$

Rewriting the Schrödinger equation as,

$$\imath \tfrac{d}{dt}|\psi\rangle = (\hat{H} - \imath \tfrac{\Gamma}{2}|2\rangle\langle 2|)|\psi\rangle \equiv \hat{H}_{eff}|\psi\rangle \ , \tag{34.224}$$

it is tempting to study how far we can go [117, 118] with the emulation of dissipative processes by the Schrödinger equation using a non-Hermitian *effective Hamiltonian*.

More generally let us define,

$$\hat{H}_{eff} \equiv \hat{H} - \imath \hat{D} \ . \tag{34.225}$$

Rederiving the master equation from Schrödinger equation with this Hamiltonian, we get,

$$\begin{aligned} \dot{\hat{\rho}} &= |\psi\rangle \frac{d\langle\psi|}{dt} + \frac{d|\psi\rangle}{dt}\langle\psi| = \imath\hat{\rho}\hat{H}^*_{eff} - \imath\hat{H}_{eff}\hat{\rho} \\ &= \imath[\hat{\rho}, \hat{H}] - \{\hat{\rho}, \hat{D}\} \ . \end{aligned} \tag{34.226}$$

And for the Heisenberg equation,

$$\begin{aligned} \tfrac{d}{dt}\langle\hat{A}\rangle &= \langle\dot{\psi}|\hat{A}|\psi\rangle + \langle\psi|\hat{A}|\dot{\psi}\rangle = \imath\langle\psi|\hat{H}^*_{eff}\hat{A}|\psi\rangle - \imath\langle\psi|\hat{A}\hat{H}_{eff}|\psi\rangle \\ &= \imath\langle\psi|[\hat{H}, \hat{A}]|\psi\rangle - \langle\psi|\{\hat{D}, \hat{A}\}|\psi\rangle \ . \end{aligned} \tag{34.227}$$

Apparently, the dissipation term adds an anti-commutator to the evolution equations. It is now interesting to compare the dissipative terms of the expressions (34.222) and (34.226).

34.5.3.1 Saturation effects by the effective Hamiltonian

The eigenvalues of the *effective Hamiltonian* of a two-level system excited by radiation,

$$\hat{H}_{eff} = \begin{pmatrix} 0 & \frac{1}{2}\Omega \\ \frac{1}{2}\Omega & \Delta - \frac{\imath}{2}\Gamma \end{pmatrix} \ , \tag{34.228}$$

describe possible effects of line broadening and/or displacement due to coupling,

$$\boxed{E_\pm = \tfrac{1}{2}\left(\Delta - \tfrac{\imath}{2}\Gamma\right) \pm \tfrac{1}{2}\sqrt{\left(\Delta - \tfrac{\imath}{2}\Gamma\right)^2 + \Omega^2}} \ . \tag{34.229}$$

The real parts of the eigenvalues $\mathfrak{Re}\ E$ describe shifts and/or splittings of the transition line. The imaginary parts $\mathfrak{Im}\ E$ describe broadening effects of the lines.

In the simplest case, $\Delta = 0$ and $\Gamma > 4\Omega$, we find the *saturation broadening* already discussed in (34.189), and we will deepen it in Exc. 34.8.4.2. For the case $\Gamma < 4\Omega$, we observe a splitting of the line called *Autler-Townes splitting*, which will be studied

in Exc. 34.8.4.1. If $\Omega \neq 0$, the spectrum becomes asymmetrical. In the case of weak excitation, $\Gamma \gg 4\Omega$, we observe a shift of the transition line with dispersive dependence (near the resonance) on the frequency of the incident radiation. This is the *dynamic Stark shift* (or *light shift*). In the case of strong excitation, $\Gamma \ll 4\Omega$, we observe again at the split spectrum, but now the two lines exhibit an *avoided crossing*-type dependence on the radiation frequency. We study these effects in Excs. 34.5.4.12 and Exc. 34.5.4.13.

Obviously, these effects can be studied by the Bloch equation formalism containing the terms of spontaneous relaxation.

34.5.4 Exercises

34.5.4.1 Ex: Stationary solution of the Bloch equations

Derive the stationary solution of the Bloch equations including spontaneous emission. How does the spectrum $\rho_{22}(\Delta)$ change in the presence of phase noise, $\gamma = \frac{\Gamma}{2} + \beta$, in particular if $\beta \gg \frac{\Gamma}{2}$?

Solution: *Starting from the Bloch equations,*

$$0 = \frac{d}{dt}\begin{pmatrix}\rho_{11}\\ \rho_{22}\\ \tilde\rho_{12}\\ \tilde\rho_{21}\end{pmatrix} = \begin{pmatrix} 0 & \Gamma & \frac{\imath}{2}\Omega & -\frac{\imath}{2}\Omega \\ 0 & -\Gamma & -\frac{\imath}{2}\Omega & \frac{\imath}{2}\Omega \\ \frac{\imath}{2}\Omega & -\frac{\imath}{2}\Omega & \imath\Delta-\gamma & 0 \\ -\frac{\imath}{2}\Omega & \frac{\imath}{2}\Omega & 0 & -\imath\Delta-\gamma \end{pmatrix}\begin{pmatrix}\rho_{11}\\ \rho_{22}\\ \tilde\rho_{12}\\ \tilde\rho_{21}\end{pmatrix} ,$$

we find from the first and third line using the normalization condition,

$$0 = \Gamma\rho_{22} + \tfrac{\imath}{2}\Omega\tilde\rho_{12} - \tfrac{\imath}{2}\Omega\tilde\rho_{21} \qquad \textit{and} \qquad 0 = \tfrac{\imath}{2}\Omega - \imath\Omega\rho_{22} + (\imath\Delta-\gamma)\tilde\rho_{12} \ .$$

Solving,

$$\rho_{22} = \frac{\imath\Omega}{2\Gamma}(\tilde\rho_{21} - \tilde\rho_{12}) \qquad \textit{and} \qquad \tilde\rho_{12} = \frac{\imath\Omega}{2(\imath\Delta-\gamma)}(2\rho_{22}-1) \ .$$

Hence,

$$\rho_{22} = \frac{\Omega^2}{4\Gamma}\left(\frac{1}{\imath\Delta+\gamma} + \frac{1}{-\imath\Delta+\gamma}\right)(1-2\rho_{22}) = \frac{\frac{\gamma}{2\Gamma}\Omega^2}{\Delta^2 + \frac{\gamma}{\Gamma}\Omega^2 + \gamma^2}$$

$$\tilde\rho_{12} = \frac{\imath\Omega}{2(\imath\Delta-\gamma)}\left(\frac{\frac{\gamma}{\Gamma}\Omega^2}{\Delta^2 + \frac{\gamma}{\Gamma}\Omega^2 + \gamma^2} - 1\right) = \frac{\frac{\Omega}{2}(-\Delta+\imath\gamma)}{\Delta^2 + \frac{\gamma}{\Gamma}\Omega^2 + \gamma^2} \ .$$

For $\gamma = \frac{\Gamma}{2}$ *we get,*

$$\rho_{22} = \frac{\frac{1}{4}\Omega^2}{\Delta^2 + \frac{1}{2}\Omega^2 + \frac{1}{4}\Gamma^2} \qquad \textit{and} \qquad \tilde\rho_{12} = \frac{\frac{\Omega}{2}(-\Delta + \frac{\imath}{2}\Gamma)}{\Delta^2 + \frac{1}{2}\Omega^2 + \frac{1}{4}\Gamma^2} \ .$$

For $\gamma = \frac{\Gamma}{2} + \beta \gg \frac{\Gamma}{2}$ *we get,*

$$\rho_{22} \simeq \frac{\frac{\beta}{2\Gamma}\Omega^2}{\Delta^2+\beta^2} \overset{\Delta\to 0}{\longrightarrow} \frac{\Omega^2}{2\Gamma\beta} \qquad \textit{and} \qquad \tilde\rho_{12} \simeq \frac{\frac{\Omega}{2}(-\Delta+\imath\beta)}{\Delta^2+\beta^2} \overset{\Delta\to 0}{\longrightarrow} \frac{\imath\Omega}{2\beta} \ .$$

34.5.4.2 Ex: Detuning-dependent phase-shift of the dipole moment

Calculate the phase-shift of the dipole moment with respect to the driving field across resonance.

Solution: *The dipole moment in the interaction picture being given by (34.188),*

$$\rho_{12}(\infty) = e^{\imath\Delta t}\frac{\frac{1}{2}\Omega(\Delta - \frac{\imath}{2}\Gamma)}{\Delta^2 + \frac{1}{2}\Omega^2 + \frac{1}{4}\Gamma^2} \ ,$$

the phase-shift is,

$$\varphi = \arctan\frac{\mathfrak{Im}\ \rho_{12}e^{-\imath\Delta t}}{\mathfrak{Re}\ \rho_{12}e^{-\imath\Delta t}} = \arctan\frac{-\Gamma}{2\Delta} \overset{\Delta\to\pm\infty}{\longrightarrow} \pm\frac{\pi}{2} \ .$$

Note that the total phase-shift of π when sweeping across a resonance is consistent with the Lorentz model treating the oscillation of a bound electron like a harmonic oscillator. Apparently, this feature does not depend on saturation. Experimentally, the phase-shift may we extracted by a homodyne experiment [1219] as one of the quadratures. The other quadrature yields the amplitude,

$$|\hat{\rho}_{12}e^{-\imath\Delta t}| = \frac{\frac{1}{2}\Omega\sqrt{\Delta^2 + \frac{1}{4}\Gamma^2}}{\Delta^2 + \frac{1}{2}\Omega^2 + \frac{1}{4}\Gamma^2} \overset{\Delta\to\pm\infty}{\longrightarrow} \frac{\Omega}{2|\Delta|} \ .$$

34.5.4.3 Ex: Determinant of the Bloch matrix

In Sec. 34.3.1 we already saw that $\det\hat{\rho} = 0$ for conservative systems. Now, show explicitly for the Bloch matrix of a two-level system, that $\det\hat{\rho} = 0$ only holds in the absence of spontaneous emission.

Solution: *The system be initially in the ground state. So, the coherences are null and the determinant must disappear. But the Bloch equations contain the determinant, since,*

$$\begin{aligned}
\frac{d}{dt}\det\begin{pmatrix}\rho_{11} & \rho_{12}\\ \rho_{21} & \rho_{22}\end{pmatrix} &= \dot{\rho}_{gg}\rho_{22} + \rho_{11}\dot{\rho}_{22} - \dot{\rho}_{12}\rho_{21} - \rho_{12}\dot{\rho}_{21}\\
&= \Gamma_{\parallel}\rho_{22}^2 + \tfrac{1}{\imath\hbar}(V_{12}\rho_{21} - \rho_{12}V_{21})\rho_{22}\\
&= -\Gamma_{\parallel}\rho_{22}\rho_{11} + \tfrac{1}{\imath\hbar}(V_{21}\rho_{12} - \rho_{21}V_{12})\rho_{11}\\
&\quad + (-\imath\omega_0 + \Gamma_{\perp})\rho_{12}\rho_{21} + \tfrac{1}{\imath\hbar}V_{12}(\rho_{11} - \rho_{22})\rho_{21}\\
&\quad + (\imath\omega_0 + \Gamma_{\perp})\rho_{21}\rho_{12} - \tfrac{1}{\imath\hbar}V_{21}(\rho_{11} - \rho_{22})\rho_{12}\\
&= \Gamma_{\parallel}\rho_{22}(\rho_{22} - \rho_{11}) + 2\Gamma_{\perp}\rho_{12}\rho_{21} \ .
\end{aligned}$$

34.5.4.4 Ex: Density operator with dissipation

Discuss the phenomenon of dissipation at the example of
a. a thermal sample of two-level systems $|i\rangle = |1\rangle, |2\rangle$ characterized by the density operator $\hat{\rho} = |i\rangle\langle i| \otimes |v\rangle\langle v|$, where $|v\rangle$ is the velocity state of the atom and
b. a two-level atom coupled to a radiation field, $\hat{\rho} = |i\rangle\langle i| \otimes |n\rangle\langle n|$, where $|n\rangle$ is the number of photons inside the mode.

Solution: *We need to show that,*

$$Tr_{reserv}\rho_{atom} \to 0 \qquad while \qquad Tr_{reserv}\begin{pmatrix} \rho_{atom} & 0 \\ 0 & \rho_{reserv} \end{pmatrix} = 1 \ .$$

34.5.4.5 Ex: Bloch vector

A two-level atom with decay rate $\Gamma = 2\pi \times 6\,\mathrm{MHz}$ be excited by a light field detuned by $\Delta = 2\Gamma$ and whose intensity is a quarter of the saturation intensity. Write down the Bloch vector for $t \to \infty$.

Solution: *The Rabi frequency is* $\Omega = \sqrt{\Gamma^2/2 \times I/I_s}$ *and the detuning* $\Delta = 2\Gamma$. *The stationary solution of the Bloch equations are,*

$$\rho_{22} = \frac{\Omega^2}{4\Delta^2 + 2\Omega^2 + \Gamma^2} \qquad and \qquad \rho_{12} = \Omega\frac{2\Delta + \imath\Gamma}{4\Delta^2 + \Gamma^2}(\rho_{22} - \rho_{11}) \ .$$

Hence,

$$\vec{\rho} = \begin{pmatrix} \rho_{12} + \rho_{21} \\ \imath(\rho_{12} - \rho_{21}) \\ \rho_{22} - \rho_{11} \end{pmatrix} = (2\rho_{22} - 1)\begin{pmatrix} \Omega\frac{4\Delta}{4\Delta^2+\Gamma^2} \\ \Omega\frac{2\Gamma}{4\Delta^2+\Gamma^2} \\ 1 \end{pmatrix}$$
$$= \frac{-1}{4\Delta^2 + 2\Omega^2 + \Gamma^2}\begin{pmatrix} 4\Delta\Omega \\ 2\Gamma\Omega \\ 4\Delta^2 + \Gamma^2 \end{pmatrix} = \frac{-1}{17.25}\begin{pmatrix} \sqrt{8} \\ \sqrt{2}^{-1} \\ 17 \end{pmatrix} \ .$$

34.5.4.6 Ex: Purity of two-level atoms with spontaneous emission

Calculate for a driven two-level atom in the stationary limit Tr $\hat{\rho}$ and Tr $\hat{\rho}^2$.

Solution: *From* $1 = \rho_{11}(0) + \rho_{22}(0)$ *follows that Tr* $\rho = 1$ *always. With*

$$\hat{\rho}^2 = \begin{pmatrix} \rho_{11}^2 + \rho_{12}\rho_{21} & \rho_{11}\rho_{12} + \rho_{12}\rho_{22} \\ \rho_{11}\rho_{21} + \rho_{21}\rho_{22} & \rho_{12}\rho_{21} + \rho_{22}^2 \end{pmatrix}$$

follows

$$Tr\ \rho^2 = Tr\ \rho - 2\det\rho = 1 - 2\rho_{22} + 2\rho_{22}^2 + 2\rho_{12}\rho_{21}\ .$$

Inserting the stationary solution (34.188) of the Bloch equations,

$$\rho_{22} = \frac{\Omega^2}{4\Delta^2 + 2\Omega^2 + \Gamma^2} \qquad and \qquad \rho_{12} = e^{\imath\Delta t}\frac{\Omega(2\Delta + \imath\Gamma)}{4\Delta^2 + 2\Omega^2 + \Gamma^2}$$

we calculate,

$$\begin{aligned} Tr\ \rho^2 &= 1 - \frac{2\Omega^2(4\Delta^2 + 2\Omega^2 + \Gamma^2)}{(4\Delta^2 + 2\Omega^2 + \Gamma^2)^2} + \frac{2\Omega^4}{(4\Delta^2 + 2\Omega^2 + \Gamma^2)^2} + \frac{2\Omega^2(4\Delta^2 + \Gamma^2)}{(4\Delta^2 + 2\Omega^2 + \Gamma^2)^2} \\ &= 1 - 2\left(\frac{\Omega^2}{4\Delta^2 + 2\Omega^2 + \Gamma^2}\right)^2 = 1 - 2\rho_{22}^2 < 1\ . \end{aligned}$$

These quantities measure the purity of the state.

34.5.4.7 Ex: Bloch sphere

Check the temporal evolution of the norm of the Bloch vector defined by $\vec{\rho} \equiv (2\ \mathfrak{Re}\ \sigma_+\ ,\ 2\ \mathfrak{Im}\ \sigma_-\ ,\ \sigma_z)$, where the σ_k are the Pauli matrices, for a resonantly excited two-level system with and without spontaneous emission.

Solution:

34.5.4.8 Ex: Atomic beam

An atomic beam is illuminated perpendicular to its propagation direction by (quasi-)monochromatic, collimated laser pulses having the intensity $I = 1\,\mathrm{W/cm^2}$, the wavelength $\lambda = 780\,\mathrm{nm}$, and the duration 200 ns. The laser is tuned to the center of an atomic resonance line ($\Gamma/2\pi = 6\,\mathrm{MHz}$).
a. How does the population of the upper atomic state develop?
b. How does the dynamics change, when the light is detuned by 100 MHz?

Solution: *a. The Rabi frequency follows from,*

$$\Omega = \sqrt{\frac{\sigma_0 \Gamma I}{\hbar\omega}}\ .$$

With $\sigma_0 = 3\frac{\lambda^2}{2\pi}$ we obtain $\Omega/2\pi = 104\,\mathrm{MHz}$. The Rabi frequency is therefore much larger than the decay rate, such that the decay can be neglected at initial times. The solution of the Bloch equations is, therefore,

$$\rho_{22} = \frac{\Omega^2}{\Delta^2 + \Omega^2}\sin^2\frac{\sqrt{\Delta^2 + \Omega^2}}{2}t\ ,$$

that is, at the beginning, the atom is in the ground state, then the population inversion makes some rapid oscillations with maximum amplitude, which relax after a while.

The stationary population finally stabilizes to,

$$\rho_{22}(\infty) = \frac{\Omega^2}{4\Delta^2 + 2\Omega^2 + \Gamma^2} \to \frac{1}{2} \ .$$

When the pulse ends after 200 ns*, the population relaxes exponentially.*
b. When the light frequency is detuned, the generalized Rabi frequency drops to $G = \sqrt{\Delta^2 + \Omega^2} = 2\pi \times 144\,\text{MHz}$*, the amplitude of the Rabi oscillations decreases by half and the average stationary population drops to* $\rho_{22}(\infty) = 0.17$*.*

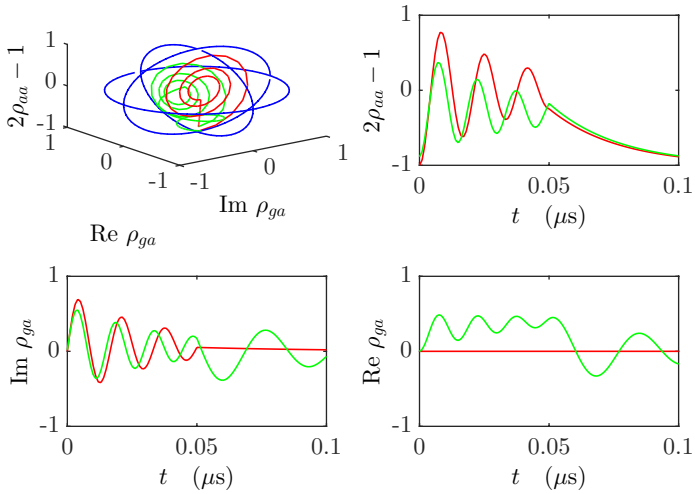

Figure 34.7: (code) Evolution on the sphere of Bloch.

34.5.4.9 Ex: Solution of the Bloch equations for resonant excitation

Derive the solution (34.193) of the Bloch equations with spontaneous emission for resonant excitation.

Solution: *See Exc. 35.6.4.4.*

34.5.4.10 Ex: Solution for the susceptibility

Show that the solution of Eq. (34.202) is given by the result (34.207).

Solution: *We assume weak excitation* $a_1 = 1$*,*

$$\frac{da_2}{dt} = -\imath\Omega^* \cos\omega t e^{\imath\omega_0 t} a_1 - \gamma a_2 \simeq -\imath\Omega^* \cos\omega t e^{\imath\omega_0 t} - \gamma a_2 \ ,$$

and we replace $a_2 \equiv \tilde{a}_2 e^{-\gamma t}$*. Thus the equation (34.202) becomes,*

$$\frac{d\tilde{a}_2}{dt} \simeq -\imath\Omega^* e^{\imath\omega_0 t + \gamma t} \cos\omega t \ .$$

Integrating this equation,

$$\tilde{a}_2 = -\imath\Omega^* \int e^{\imath\omega_0 t+\gamma t}\cos\omega t dt = -\frac{\Omega^*}{2}\left[\frac{e^{\imath(\omega_0+\omega)t+\gamma t}}{\omega_0+\omega+\imath\gamma}+\frac{e^{\imath(\omega_0-\omega)t+\gamma t}}{\omega_0-\omega+\imath\gamma}\right] ,$$

or

$$a_2 = -\frac{\Omega^*}{2}\left[\frac{e^{\imath(\omega_0+\omega)t}}{\omega_0+\omega-\imath\gamma}+\frac{e^{\imath(\omega_0-\omega)t}}{\omega_0-\omega-\imath\gamma}\right] .$$

34.5.4.11 Ex: General form of the master equation

Show that the general form of the master equation: $\dot{\hat{\rho}} = -\frac{\imath}{\hbar}[\hat{H},\hat{\rho}] - \frac{\Gamma}{2}(2\hat{\sigma}\hat{\rho}\hat{\sigma}^+ - \hat{\sigma}^+\hat{\sigma}\hat{\rho} - \hat{\rho}\hat{\sigma}^+\hat{\sigma})$, reproduces the Bloch equations including spontaneous emission.

Solution: *Inserting the Hamiltonian*

$$\hat{H} = \begin{pmatrix} 0 & \frac{1}{2}\hbar\Omega \\ \frac{1}{2}\hbar\Omega & \hbar\Delta \end{pmatrix}$$

into the master equation, we obtain,

$$-\frac{\imath}{\hbar}[\hat{H},\rho] = -\imath\begin{pmatrix} \frac{1}{2}\Omega\rho_{21} - \frac{1}{2}\Omega\rho_{12} & \frac{1}{2}\Omega\rho_{22} - \frac{1}{2}\Omega\rho_{11} - \rho_{12}\Delta \\ \frac{1}{2}\Omega\rho_{11} + \Delta\rho_{21} - \frac{1}{2}\Omega\rho_{22} & \frac{1}{2}\Omega\rho_{12} - \frac{1}{2}\Omega\rho_{21} \end{pmatrix}$$

and

$$\frac{\Gamma}{2}\left(2\sigma\rho\sigma^+ - \sigma^+\sigma\rho - \rho\sigma^+\sigma\right) = \frac{1}{2}\Gamma\begin{pmatrix} 2\rho_{22} & -\rho_{12} \\ -\rho_{21} & -2\rho_{22} \end{pmatrix} .$$

Thereby,

$$\frac{d\rho}{dt} = \begin{pmatrix} -\frac{\imath}{2}\Omega(\rho_{21}-\rho_{12}) + \Gamma\rho_{22} & -\imath\left(\frac{1}{2}\Omega\rho_{22} - \frac{1}{2}\Omega\rho_{11} - \rho_{12}\Delta\right) - \frac{1}{2}\Gamma\rho_{12} \\ -\imath\left(\frac{1}{2}\Omega\rho_{11} + \Delta\rho_{21} - \frac{1}{2}\Omega\rho_{22}\right) - \frac{1}{2}\Gamma\rho_{21} & -\frac{\imath}{2}\Omega(\rho_{12}-\rho_{21}) - \Gamma\rho_{22} \end{pmatrix} ,$$

or,

$$\frac{d}{dt}\begin{pmatrix}\rho_{11}\\ \rho_{22}\\ \rho_{12}\\ \rho_{21}\end{pmatrix} = \begin{pmatrix} 0 & \Gamma & \frac{\imath}{2}\Omega & -\frac{\imath}{2}\Omega \\ 0 & -\Gamma & -\frac{\imath}{2}\Omega & \frac{\imath}{2}\Omega \\ \frac{\imath}{2}\Omega & -\frac{\imath}{2}\Omega & -\frac{1}{2}\Gamma + \imath\Delta & 0 \\ -\frac{\imath}{2}\Omega & \frac{\imath}{2}\Omega & 0 & -\frac{1}{2}\Gamma - \imath\Delta \end{pmatrix}\begin{pmatrix}\rho_{11}\\ \rho_{22}\\ \rho_{12}\\ \rho_{21}\end{pmatrix} .$$

34.5.4.12 Ex: Light-shift

Calculate the light-shift in a driven two-level system from the *effective Hamiltonian*,

$$\hat{H}_{eff} = \begin{pmatrix} 0 & \frac{1}{2}\Omega \\ \frac{1}{2}\Omega & \Delta - \frac{\imath}{2}\Gamma \end{pmatrix} .$$

Prepare spectra of the eigenvalues for $\Gamma/\Omega = 0$, 0.5, and 2.

Solution: *It is easy to show,*

$$\Delta E = \tfrac{1}{2}\left(\Delta - \tfrac{\imath\Gamma}{2}\right) \pm \tfrac{1}{2}\sqrt{\left(\Delta - \tfrac{\imath\Gamma}{2}\right)^2 + \Omega^2}\ .$$

The asymptotes for $|\Delta| \gg \Gamma, \Omega$, *are found to be,*

$$\Delta E \simeq 0, \pm\Delta\ .$$

For $\Gamma \ll \Omega$ *we obtain avoided crossing,*

$$\Delta E \simeq \tfrac{1}{2}\Delta \pm \tfrac{1}{2}\sqrt{\Delta^2 + \Omega^2}\ .$$

And for $\Omega \ll \Gamma$ *we observe dispersive behavior,*

$$\Delta E \simeq \Delta - \tfrac{\imath\Gamma}{2}, \frac{\mp\Omega^2}{4\left(\Delta - \frac{\imath\Gamma}{2}\right)}\ .$$

The figure shows plots of the real and imaginary parts of ΔE.

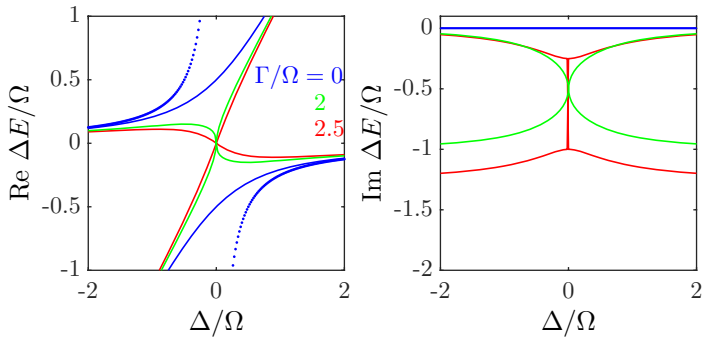

Figure 34.8: (code) Light shifts (dotted) approximated for $\Omega, \Gamma \ll |\Delta|$ and (solid) exact eigenvalues.

34.5.4.13 Ex: Light-shift

In this exercise we study the effect of the dynamic Stark shift (or light shift) of the energy levels of a two-level system $|1\rangle$ and $|2\rangle$ excited by a laser with the Rabi frequency Ω_{12} and the detuning Δ_{12}:
a. From the eigenvalues $E_{1,2}$ of the effective Hamiltonian (34.228) system, find approximations for weak coupling ($\Omega_{12} \ll \Gamma_{12}$) and strong coupling ($\Omega_{12} \gg \Gamma_{12}$). Prepare a graph showing the eigenvalue spectrum (separating the parts $\mathfrak{Re}\ E_{1,2}$ and $\mathfrak{Im}\ E_{1,2}$) as a function of detuning Δ_{12} for various values of Ω_{12}. Also search for approximations valid for large detunings $\Delta_{12} \gg \Gamma_{12}, \Omega_{12}$ and add them to the graph.
The light shift can be experimentally measured in a three-level system in Λ-configuration,

as illustrated in Fig. 34.17(a). To reproduce the experiment by numerical simulations of the Bloch equations (34.279),
b. write the Liouville matrix $\mathcal{M}_{red}$ reduced by the condition to the trace (34.284) and calculate the stationary Bloch vector from equation (34.286) varying the detunings of the two lasers Δ_{12} and Δ_{23}. Choosing the parameters $\Gamma_{23} = \Gamma_{12}$, $\Gamma_{13} = 0.01\Gamma_{12}$, $\Omega_{12} = 2\Gamma_{12}$, and $\Omega_{23} = 0.2\Gamma_{12}$, prepare a 3D curve [similar to Fig. 34.6(a)] of the stationary population $\rho_{22}(\infty)$. Interpret the results.

Solution: *a. The eigenvalues of the effective Hamiltonian (34.228),*

$$E = \tfrac{1}{2}\Lambda \pm \tfrac{1}{2}G_\Gamma \qquad with \qquad \Lambda \equiv \Delta - \tfrac{\imath}{2}\Gamma \qquad and \qquad G_\Gamma \equiv \sqrt{\Omega^2 + \Lambda^2}$$

describe the dynamic Stark shift. Expanding for weak coupling, $\Gamma \gg \Omega$,

$$E = \tfrac{\Lambda}{2} \pm \tfrac{1}{2}\sqrt{\Lambda^2 + \Omega^2} \quad \overset{\Omega \ll \Gamma}{\longrightarrow} \quad \tfrac{\Lambda}{2} \pm \tfrac{\Lambda}{2}\left(1 + \tfrac{\Omega^2}{2\Lambda^2}\right) = \tfrac{\Lambda}{2} \pm \tfrac{\Lambda}{2}(1+s) \ ,$$

with the definition (34.190) of the saturation parameter. Expanding for strong coupling, $\Gamma \ll \Omega$,

$$E = \mathfrak{Re}\ \left(\tfrac{1}{2}\Lambda \pm \tfrac{1}{2}G_\Gamma\right) = \tfrac{1}{2}\Delta \pm \tfrac{1}{2}\sqrt{\sqrt{\tfrac{1}{4}G^4 + \tfrac{1}{8}\Gamma^2\left(G^2 - 2\Omega^2 + \tfrac{1}{8}\Gamma^2\right)} + \tfrac{1}{2}G^2 - \tfrac{1}{8}\Gamma^2}$$
$$\overset{\Omega \gg \Gamma}{\longrightarrow} \quad \tfrac{1}{2}\Delta \pm \tfrac{1}{2}G \mp \tfrac{\Gamma^2\Omega^2}{16G^3} \ ,$$

where G is the common generalized Rabi frequency. For big detunings we can approximate,

$$E \overset{\Gamma \to 0}{\simeq} \tfrac{1}{2}\Delta \pm \tfrac{1}{2}G = \tfrac{1}{2}\Delta \pm \tfrac{\Delta}{2} \mp \tfrac{\Omega^2}{4\Delta} + \dots \ .$$

b. The Liouville matrix can be found in the numerical MATLAB code given in the file 'LM_Bloch_LightShift.m'. Fig. 34.9 shows the results of the simulations. The dynamic Stark splitting $E_1 - E_2$ is a consequence of the breaking of the degeneracy of the states dressed $|1, N\rangle$ and $|2, N-1\rangle$ for strong fields $\Gamma \ll \Omega$. The light shift is the expectation value of the perturbation of the atom by the light field. While the positions of the resonances follow from $\mathfrak{Re}\ (E)$, the linewidth follows from $\mathfrak{Im}\ (E)$. In the weak coupling regime, we observe a dispersive dependence of the energy shift. In the strong coupling regime we observe an avoided crossing.

34.5.4.14 Ex: Line broadening by optical repumping

Check for a two-level system that incoherent optical pumping from the ground into the excited state introduces a transverse decay rate R leading to line broadening.

Solution: *The Liouvillean reads,*

$$\mathcal{M} = \begin{pmatrix} -R & \Gamma & \frac{\imath}{2}\Omega & -\frac{\imath}{2}\Omega \\ R & -\Gamma & -\frac{\imath}{2}\Omega & \frac{\imath}{2}\Omega \\ \frac{\imath}{2}\Omega & -\frac{\imath}{2}\Omega & \imath\Delta - \frac{\Gamma}{2} - \frac{R}{2} & 0 \\ -\frac{\imath}{2}\Omega & \frac{\imath}{2}\Omega & 0 & -\imath\Delta - \frac{\Gamma}{2} - \frac{R}{2} \end{pmatrix} .$$

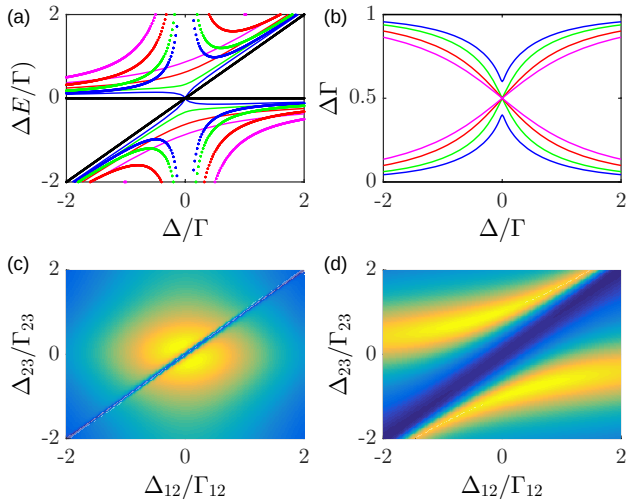

Figure 34.9: (code) (a) Light shift in a two level system varying Ω_{12} between $0.5\Gamma_{12}$ (internal blue curve) and $1\Gamma_{12}$ (external magenta curve). (b) Linewidth for the same parameters as in (a). (c,d) Population of the excited state in a three-level system in Λ-configuration, as shown in Fig. 34.17(a) sweeping the lasers. These figures are discussed later. For (c) $\Omega_{12}/\Gamma_{12} = 0.2$ and for (d) $\Omega_{12}/\Gamma_{12} = 2$.

In steady state,

$$\begin{aligned} 0 &= -R(1-\rho_{22}) + \Gamma\rho_{22} + \tfrac{\imath}{2}\Omega\rho_{12} - \tfrac{\imath}{2}\Omega\rho_{21} \\ 0 &= \tfrac{\imath}{2}\Omega(1-\rho_{22}) - \tfrac{\imath}{2}\Omega\rho_{22} + \left(\imath\Delta - \tfrac{\Gamma}{2} - \tfrac{R}{2}\right)\rho_{12} \ , \end{aligned}$$

so that,

$$\rho_{22} = \frac{\imath\Omega}{2(R+\Gamma)}(\rho_{21}-\rho_{12}) + \frac{R}{R+\Gamma} \qquad \textit{and} \qquad \rho_{12} = \frac{\imath\Omega}{2\imath\Delta - \Gamma - R}(2\rho_{22}-1) \ ,$$

yielding,

$$\rho_{22} = \frac{\frac{1}{4}\Omega^2 + \frac{1}{1+\Gamma/R}\left[\Delta^2 + \frac{1}{4}(\Gamma+R)^2\right]}{\Delta^2 + \frac{1}{2}\Omega^2 + \frac{1}{4}(\Gamma+R)^2} \ .$$

Some limits,

$$\begin{aligned} \rho_{22} &\xrightarrow{R=0} \frac{\frac{1}{4}\Omega^2}{\Delta^2 + \frac{1}{2}\Omega^2 + \frac{1}{4}\Gamma^2} \\ &\xrightarrow{\Gamma=0} 1 - \frac{\frac{1}{4}\Omega^2}{\Delta^2 + \frac{1}{2}\Omega^2 + \frac{1}{4}R^2} \\ &\xrightarrow{\Gamma=R} \frac{1}{2} \ . \end{aligned}$$

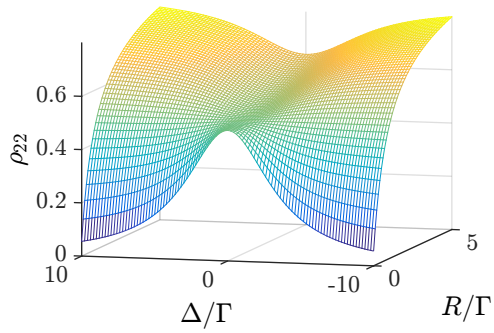

Figure 34.10: (code) Upper state population spectra for varied repumping rates.

34.6 Line broadening mechanisms

The resolution of atomic spectroscopy is generally limited by several perturbative effects, many of them originating in the atomic motion. They manifest themselves as broadening and/or shifts of atomic resonances. Free atoms, as well as atoms confined in potentials, have kinetic energy and evolve on extended phase space trajectories. If the spatial localization is less than the effective cross section of the exciting laser beam, then the interaction time is limited and the resonance lines are broadened by the Fourier effect in a process called *transit time broadening*, and the efficiency of fluorescence collection is reduced. The same happens with the *Doppler effect*: Only those atoms that have a specific velocity along the optical axis defined by the laser beam can interact. Free as well as confined atoms can only scatter when they are in specific cells of the phase space.

There are two different fundamental types of broadening. The so-called *homogeneous broadening* affects all atoms in the same way regardless of their positions or velocities. It usually gives rise to Lorentzian line profiles and can be included in the Bloch equations. It correspond to an acceleration of the relaxation. Examples are the natural linewidth, saturation broadening, and collision broadening.

The so-called *inhomogeneous broadening* is due to a displacement of atomic levels, which may be different for each atom. Averaging over a large sample of atoms, the displacements generate an *effective* broadening usually with a Gaussian line profile. It *can not* be included in the single-atom Bloch equations, but only as an average over all trajectories of all atoms. It does not correspond to an accelerated relaxation. Inhomogeneous broadening is often due to external perturbations, e.g., Doppler broadening and broadening due to temporal fluctuations or spatial inhomogeneities of external electric or magnetic fields. In Exc. 34.6.7.1 we calculate the optical density of atomic clouds. In Exc. 34.6.7.2 we present a spectroscopic technique bypassing the Doppler broadening called *Doppler-free spectroscopy* and calculate the *Lamb-dip* profile. Finally, in Exc. 34.6.7.3, we discuss a cooling technique allowing for the reduction of Doppler broadening, called *Zeeman slower*.

34.6.1 Saturation broadening

Eq. (34.189) shows that when the power of the incident light increases, the population of the excited state saturates at a limit value of $\rho_{22} = \frac{1}{2}$. The *saturation parameter* defined in (34.190) measures the degree of saturation. When the narrowband light source is tuned to resonance, the saturation parameter is basically a measure for the ratio between the stimulated population transfer rate Ω and the spontaneous decay rate A_{21}. We can rewrite the stationary population of the excited level as in (34.191). In resonance and with the saturation parameter $s = 1$, we obtain

$$\Omega = \tfrac{1}{\sqrt{2}}\Gamma \ . \tag{34.230}$$

We can use equation (34.230) to define the *saturation intensity* I_{sat} for an atom with the transition dipole d_{12}. From Eq. (22.41) we have,

$$\mathcal{E}_0 = \sqrt{\frac{2\bar{I}}{\varepsilon_0 c}} \ . \tag{34.231}$$

Therefore, using the definition of the Rabi frequency, $\hbar\Omega = d_{12}\mathcal{E}_0$, and the relationship between d_{12} and Γ given by Eq. (34.41), we have [19],

$$\boxed{I_{sat} = \frac{g_1}{g_2}\frac{2\pi^2 c\hbar}{3\lambda_0^3}\Gamma} \ , \tag{34.232}$$

taking into account the degeneracies g_j of the levels. In Excs. 34.6.7.4 and 34.6.7.5 we calculate the *saturation intensity* of popular atomic transitions.

34.6.2 Collision broadening

The theory of atomic collisions covers a large area of research, including elastic and inelastic, reactive and ionizing processes. In low-pressure gases at room temperature or hotter we need only consider the simpler processes: long-range van der Waals interactions that result in *elastic collisions*. The 'low pressure' criterion requires that the average free path between collisions be greater than any linear dimension of the gas volume. Under these conditions, collisions can be modeled with straight trajectories, along which the interaction time is short and the time between collisions is long in comparison with the radiative lifetime of the excited atomic state. Then, the impact of a collision on the emission of a radiating atom causes a loss of coherence due to a phase interruption of the excited state atomic wavefunction. The term 'elastic' means that the collision does not disturb the populations of the internal states, so we only need to consider the off-diagonal elements of the density matrix,

$$\frac{d\rho_{12}}{dt} = \imath\frac{\Omega_0}{2}e^{\imath(\omega-\omega_0)t}(\rho_{11} - \rho_{22}) - \gamma'\rho_{12} \ , \tag{34.233}$$

where γ' is the sum of the spontaneous emission γ and the collision rate γ_{col},

$$\boxed{\gamma' = \gamma + \gamma_{col}} \ . \tag{34.234}$$

[19] Some authors define the saturation for $s = 2$, as happens when $\Omega = \Gamma$.

The inverse of the collision rate is simply the time between phase interruptions or the time between collisions. Now, for collisions between hard cores of atoms of mass m (with reduced mass $m_{red} = m/2$) and with radius ρ in a gas with density n consisting of a single species, a standard analysis based on the kinetic theory of dilute gases shows that the time between collisions is given by the *collision rate*,

$$\gamma_{col} = \tau_{col}^{-1} = \sigma n \bar{v} \ , \tag{34.235}$$

where $\bar{v} = \sqrt{\frac{8k_BT}{\pi m_{red}}}$ is the average collision velocity in a homogeneous gas at the temperature T and $\sigma = \sqrt{8}\pi\rho^2$ the collision cross section. Thereby,

$$\boxed{\gamma_{col} = \frac{8\rho^2 n}{\sqrt{m_{red}/\pi k_B T}}} \ . \tag{34.236}$$

We can now relate this simple result of gas kinetics to the phase interruption rate by reinterpreting the meaning of the *collision radius*. When an excited atom propagating through space suffers a collision, the long-range interaction will produce a time-dependent perturbation of the energy levels of the radiating atom and a phase shift in the radiation,

$$\eta = \int_{-\infty}^{\infty} [\omega(t) - \omega_0] dt = \int_{-\infty}^{\infty} \Delta\omega(t) dt \ . \tag{34.237}$$

The long-range van der Waals interaction is expressed by,

$$\Delta E = \hbar\omega = \frac{C_n}{[b^2 + (vt)^2]^{n/2}} \ , \tag{34.238}$$

where b is the impact parameter of the collision trajectory and v the collision velocity. The phase shift is then

$$\eta = \frac{1}{\hbar} \int_{-\infty}^{\infty} \frac{C_n}{[b^2 + (vt)^2]^{n/2}} dt \ . \tag{34.239}$$

The integral is easily assessed for the two most frequent cases: non-resonant van der Waals interactions $n = 6$ and resonant van der Waals interactions $n = 3$. The phase shifts are,

$$\eta_6(b) = \frac{2\pi}{3\hbar} \frac{C_6}{b_6^5 v} \qquad \text{and} \qquad \eta_3(b) = \frac{4\pi}{3\sqrt{3}\hbar} \frac{C_3}{b_3^2 v} \ . \tag{34.240}$$

Now, if instead of using the *hard core approximation*, we define a collision as an encounter causing a phase shift of at least 1 radians, we have a new condition for the collision radius,

$$b_6 = \left(\frac{2\pi}{3\hbar} \frac{C_6}{v} \right)^{1/5} \qquad \text{and} \qquad b_3 = \left(\frac{4\pi}{3\sqrt{3}\hbar} \frac{C_3}{v} \right)^{1/2} \ . \tag{34.241}$$

Replacing these collision radiuses for the radius ρ in Eq. (34.236) and inserting the average collision velocity, we find the collision rate,

$$\gamma_{c6} = 4n \left(\frac{\sqrt{2}\pi^2 C_6}{3\hbar} \right)^{2/5} \left(\frac{4\pi k_B T}{\mu} \right) \qquad \text{and} \qquad \gamma_{c3} = 4n \left(\frac{2}{3} \right)^{3/2} \left(\frac{\pi^2 C_3}{\hbar} \right)^{3/10} \ . \tag{34.242}$$

Substituting the generalized γ' of (34.234) for γ in the Bloch equations (34.188), we find the stationary solutions,

$$\rho_{22} = \frac{\frac{1}{4}\frac{\gamma'}{\gamma}|\Omega|^2}{\Delta^2 + \frac{1}{2}\frac{\gamma'}{\gamma}|\Omega|^2 + \gamma'^2} \qquad \text{and} \qquad \rho_{12} = e^{\imath(\omega-\omega_0)t}\frac{\frac{1}{2}\Omega(\Delta - \imath\gamma')}{\Delta^2 + \frac{1}{2}\frac{\gamma'}{\gamma}|\Omega|^2 + \gamma'^2} \ . \quad (34.243)$$

The effective linewidth (radiative and collisions) is,

$$\Gamma'_{\text{eff}} = 2\sqrt{\gamma'^2 + \tfrac{1}{2}\tfrac{\gamma'}{\gamma}|\Omega|^2} \ . \quad (34.244)$$

When the excitation is sufficiently weak, so that power broadening can be neglected in comparison to collision broadening, the second term can be discarded,

$$\Gamma'_{\text{eff}} = 2(\gamma + \gamma_{col}) \ . \quad (34.245)$$

The equations (34.189) and (34.245) express the linewidths in the limits of dominating power and collision broadening, respectively. Note that the susceptibility, absorption coefficient, and absorption cross-section retain their Lorentzian profile, but with a larger width due to collisions. Since each atom is subject to the same broadening mechanism, the broadening is homogeneous. Solve Excs. 34.6.7.6.

34.6.3 Doppler broadening

The *Doppler broadening* is simply the apparent frequency distribution of a sample of radiating atoms at temperature T. The contribution of each atom to the radiation appears detuned by the *Doppler shift* because of its velocity. The frequency shift for a non-relativistically moving particle is $\omega = \omega_0/(1 - \frac{v}{c})$, such that,

$$\Delta \equiv \omega - \omega_0 \simeq \omega_0 \frac{v}{c} = \mathbf{k}\cdot\mathbf{v} = kv_z \ , \quad (34.246)$$

where $\mathbf{k}$ is the wavevector of the light and $\mathbf{v}$ is the velocity of the atom. This distribution of Doppler shifts of a gaseous sample in thermal equilibrium follows the probability distribution of velocities,

$$P(v_z)dv_z \propto e^{-mv_z^2/2k_BT}dv_z = e^{-mc^2\Delta^2/2\omega_0^2 k_BT}\frac{c}{\omega_0}d\omega \ . \quad (34.247)$$

This frequency distribution is a Gaussian centered at $\omega = \omega_0$ and with the width,

$$\text{FWHM} = 2\omega_0\left(\frac{2k_BT\ln 2}{mc^2}\right)^2 \ . \quad (34.248)$$

A measure of the width is also the *standard deviation*,

$$2\sigma = \frac{2\omega_0}{c}\sqrt{\frac{k_BT}{m}} = \frac{\text{FWHM}}{1.177} \ . \quad (34.249)$$

From Eq. (34.247) we can see that the line profile is,

$$\mathcal{D}(\omega - \omega_0) \equiv \frac{1}{\sqrt{2\pi}}\frac{m}{k_BT}e^{-(\omega-\omega_0)^2/2\sigma^2}d\omega \ . \quad (34.250)$$

The profile compares with the Lorentzian profile Eq. (22.73) associated with natural, power, or collision broadening. Doppler broadening is a property of the atomic ensemble, each atom suffering a unique but different displacement than the other atoms. Hence, it is called *inhomogeneous broadening*.

The Liouville equation (34.140) used to derive the Bloch equations assumes immobile atoms. However, we can easily apply the Galilei transformation to a system, where the atoms move with the given velocity $\mathbf{v}$,

$$(\partial_t + \mathbf{v}\cdot\nabla)\hat{\rho}(\mathbf{r},t) = -\tfrac{\imath}{\hbar}[\hat{H},\hat{\rho}(\mathbf{r},t)] \ . \tag{34.251}$$

Since the light fields propagate as $e^{\imath(\omega t - \mathbf{k}\cdot\mathbf{r})}$, the solution of the above equation simply follows from the immobile solution with the substitution $\Delta \to \Delta - \mathbf{k}\cdot\mathbf{v}$. For a cloud obeying Maxwell's velocity distribution, $P(v) \sim e^{-mv^2 k_B T}$,

$$\bar{\rho}(\Delta) = \frac{1}{\sqrt{2\pi}\delta}\int_{\mathbb{R}} e^{-(\mathbf{k}\cdot\mathbf{v})^2/2\delta^2}\hat{\rho}(\Delta - \mathbf{k}\cdot\mathbf{v})d(\mathbf{k}\cdot\mathbf{v}) \ . \tag{34.252}$$

The average of the density operator over all velocities, $\bar{\rho}$, therefore follows as the convolution of the density operator ρ (obtained as the solution of the Bloch equation) and the Gaussian function $G(\Delta) = (2\pi\delta^2)^{-1/2}e^{-\Delta^2/2\delta^2}$,

$$\boxed{\bar{\rho}(\Delta) = (G \star \hat{\rho})(\Delta)} \ . \tag{34.253}$$

34.6.4 Voigt profile

It is clear that in many practical circumstances homogeneous and inhomogeneous processes simultaneously contribute to the broadening of lines. In these cases, we can consider that the radiation of each atom, homogeneously broadened by phase-interruption processes (such as spontaneous emission or collisions), is displaced by the Doppler effect within the Maxwell-Boltzmann distribution corresponding to the temperature T. The profile of the gaseous sample, therefore, is a convolution of homogeneous and inhomogeneous profiles. The resulting profile is called *Voigt profile*:

$$\begin{aligned} V(\omega-\omega_0) &= \int_{-\infty}^{\infty}\mathcal{L}(\omega-\omega_0-\omega')\mathcal{D}(\omega-\omega_0)d\omega' \\ &= \frac{\gamma}{2\sigma\sqrt{2\pi}}\int_{-\infty}^{\infty}\frac{e^{-(\omega-\omega_0)^2/2\sigma^2}}{(\omega-\omega_0-\omega')^2+(\gamma/2)^2}d\omega' \ . \end{aligned} \tag{34.254}$$

This integral has no analytical solution, but it is easy to solve numerically. Resolve Excs. 34.6.7.7, 34.6.7.8, and 34.6.7.9.

34.6.5 Bloch equations with phase modulation

In some situations, the atom vibrates thus producing an oscillating Doppler shift. Also, external magnetic fields or oscillating laser frequencies can produce this effect. We incorporate this temporal modulation (frequency Ω_a) of the light frequency shifts,

induced by the Doppler effect, into the optical Bloch equations via the substitution [1170],

$$\Delta_{ij} \to \Delta_{ij} + \mathbf{k}_{ij} \cdot \mathbf{v} \ \cos \Omega_a t \ . \tag{34.255}$$

The Bloch equations can then be brought into the form,

$$\dot{\hat{\rho}} = (\mathbf{L} + 2\mathbf{X} \ \cos \Omega_a t)\hat{\rho} + \mathbf{b} \ , \tag{34.256}$$

where the matrix $\mathbf{X}$ contains the modulation index of the atomic motion $\mathbf{k}_{ij}\mathbf{v}$. The stationary solution of the differential equation, averaged over the time of an oscillation period, can be expressed as an infinite continuous fraction:

$$\hat{\rho}(\infty) = -(\mathbf{L} + \mathbf{S}^+ + \mathbf{S}^-)^{-1}\mathbf{b} \tag{34.257}$$
$$\text{where} \quad \mathbf{S}^{\pm} = -\mathbf{X}\frac{1}{\mathbf{L} \pm \imath\Omega_a \mathbf{1} - \mathbf{X}\frac{1}{\mathbf{L}\pm\imath\Omega_a\mathbf{1}-\mathbf{X}\frac{1}{\cdots}\mathbf{X}}\mathbf{X}} \ .$$

This solution replicates the correct excitation spectra even for a multilevel system.

Let us be more specific for a two-level system. In this case the Hamiltonian is given by $\hat{H}_{int} = \frac{1}{2}\hbar\Omega e^{-\imath[\omega t - \mathbf{k}\cdot\mathbf{v}/\Omega_a \ \sin \Omega_a t]}$, such that the Bloch equation is,

$$\begin{pmatrix} \dot{\rho}_{22} \\ \dot{\rho}_{12} \\ \dot{\rho}_{21} \end{pmatrix} = \left[\begin{pmatrix} -\Gamma & -\frac{\imath}{2}\Omega & \frac{\imath}{2}\Omega \\ -\frac{\imath}{2}\Omega & -\Lambda & 0 \\ \frac{\imath}{2}\Omega & 0 & -\Lambda^* \end{pmatrix} + 2\cos\Omega_a t \begin{pmatrix} 0 & 0 & 0 \\ 0 & -\frac{\imath}{2}kv & 0 \\ 0 & 0 & \frac{\imath}{2}kv \end{pmatrix} \right] \begin{pmatrix} \rho_{22} \\ \rho_{12} \\ \rho_{21} \end{pmatrix} + \begin{pmatrix} 0 \\ \frac{\imath}{2}\Omega \\ -\frac{\imath}{2}\Omega \end{pmatrix} \ . \tag{34.258}$$

We look for the stationary solution by expanding $\hat{\rho} = \sum_{n=-\infty}^{\infty} \hat{\rho}_n e^{-\imath n\Omega_a t}$, letting $\dot{\hat{\rho}}_n = 0$, and projecting on $e^{-\imath n\Omega_a t}$ via,

$$(\mathbf{L} + \imath n\Omega_a \mathbf{1})\hat{\rho}_n + \mathbf{X}(\hat{\rho}_{n+1} + \hat{\rho}_{n-1}) + \mathbf{b}\delta_{n0} = 0 \ . \tag{34.259}$$

Now we define $\hat{\rho}_{n\pm1} = \mathbf{S}^{\pm}\hat{\rho}_n$ for $n \gtrless 0$. Then, equation (34.259) becomes,

$$\hat{\rho}_0 = -[\mathbf{L} + \mathbf{X}(\mathbf{S}_0^+ + \mathbf{S}_0^-)]^{-1}\mathbf{b} \qquad \text{for} \qquad n = 0, \tag{34.260}$$
$$\mathbf{S}^{\pm}_{n\mp1} = -[\mathbf{L} + \imath n\Omega_a \mathbf{1} + \mathbf{X}\mathbf{S}^{\pm}_n]^{-1}\mathbf{b} \qquad \text{for} \qquad n \gtrless 0 \ .$$

Substituting the equation below into the equation above,

$$\hat{\rho}_0 = -\left[\mathbf{L} + \left(\frac{-\mathbf{X}|}{|\mathbf{L} + \imath\Omega_a} + \frac{-\mathbf{X}|}{|\mathbf{L} + 2\imath\Omega_a} + \dots\right) + \left(\frac{-\mathbf{X}|}{|\mathbf{L} + \imath\Omega_a} + \frac{-\mathbf{X}|}{|\mathbf{L} + 2\imath\Omega_a} + \dots\right)\right]^{-1}\mathbf{b} \ . \tag{34.261}$$

34.6.6 Two-level system interacting with several light fields

When several light fields excite a two-level atom,

$$\hat{H}_{int} = \frac{\hbar\Omega_a}{2}e^{-\imath\omega_a t} + \frac{\hbar\Omega_b}{2}e^{-\imath\omega_b t} \ , \tag{34.262}$$

the transformation into a co-rotating frame is impossible. The density operator must then be expanded into a Taylor series in the field amplitudes and a Fourier series in

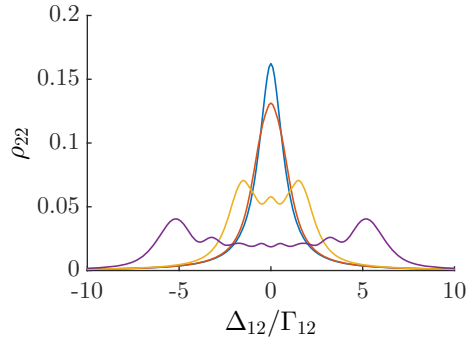

Figure 34.11: (code) Spectral broadening due to the periodic movement of the atom.

the laser frequencies, as well as the sum and difference frequencies:

$$\begin{aligned}\rho_{12}(t) = &[\rho_{12}^{(1)}(\omega_a) + \rho_{12}^{(3)}(\omega_a) + ...]e^{-\imath\omega_a t} \\ &+ [\rho_{12}^{(1)}(\omega_b) + \rho_{12}^{(3)}(\omega_b) + ...]e^{-\imath\omega_b t} \\ &+ [\rho_{12}^{(3)}(2\omega_a - \omega_b) + ...]e^{-\imath(2\omega_a-\omega_b)t} + ...\end{aligned} \tag{34.263}$$

and

$$\begin{aligned}\rho_{22}(t) - \rho_{11}(t) \equiv w_{12}(t) = &[-1 + w_{12}^{(2)}(0)] \\ &+ [w_{12}^{(2)}(\omega_a - \omega_b) + ...]e^{-\imath(\omega_a-\omega_b)t} \\ &+ [w_{12}^{(2)}(\omega_b - \omega_a) + ...]e^{-\imath(\omega_b-\omega_a)t} + ... \ .\end{aligned} \tag{34.264}$$

The solution of the Bloch equations is obtained in successive perturbation steps. The zero order in (34.264) is inserted into the Bloch equation,

$$\dot{\hat{\rho}} = -\frac{\imath}{\hbar}[\hat{H}_{int}, \hat{\rho}] \ , \tag{34.265}$$

and form this the first order in (34.263) is obtained. This in turn is inserted again into the Bloch equation, and so on. In this way the components $\rho_{12}^{(m)}(\omega_x)$ and $w_{12}^{(m)}(\omega_x)$ are calculated and from this the density operator $\hat{\rho}(t)$.

34.6.7 Exercises

34.6.7.1 Ex: Optical density of a cold cloud

The cross section of an atom with the resonant frequency ω_0 moving with velocity v and irradiated by a laser beam of frequency ω is,

$$\sigma(v) = \frac{6\pi}{k^2}\frac{\Gamma^2}{4(\omega - \omega_0 - kv)^2 + \Gamma^2} \ .$$

The normalized one-dimensional Maxwell distribution,

$$\rho(v)dv = \sqrt{\frac{m}{2\pi k_B T}}e^{-mv^2/2k_B T}dv \ .$$

a. Calculate the absorption profile of the resonance line at 461 nm ($\Gamma_{461} = (2\pi)\ 30.5$ MHz) of a strontium gas cooled to the Doppler limit ($k_B T_D = \hbar\Gamma$) of this transition.
b. Calculate the absorption profile of the resonance line at 689 nm ($\Gamma_{689} = (2\pi)\ 7.6$ kHz) of a strontium gas cooled to the Doppler limit of the transition at 461 nm.
c. Compare the optical densities in case of resonance.
Help: To evaluate the convolution integral approximate the narrower distribution by a δ-function maintaining the integral over the distribution normalized.

Solution: *The optical density with Doppler broadening is,*

$$\begin{aligned} OD(T,\omega) &= Ln(T)(\sigma \star \rho)(\omega) = Ln(T)\int_{-\infty}^{\infty}\sigma(v)\rho(v)dv \\ &= L\frac{P}{k_B T}\sqrt{\frac{m}{2\pi k_B T}}\frac{6\pi}{k^2}\int_{-\infty}^{\infty} e^{-mv^2/2k_B T}\frac{\Gamma^2}{4(\omega-\omega_0-kv)^2+\Gamma^2}dv\ . \end{aligned}$$

The Doppler limit yields,

$$k\bar{v} = k\sqrt{\frac{k_B T_D}{m}} = k\sqrt{\frac{\hbar\Gamma}{m}}\ ,$$

where $\bar{v} = \sqrt{k_B T/m}$ is the mean atomic velocity (or the rms*-width) of the Maxwell distribution.*
a. For the transition at 461 nm we get $k\bar{v} = 5.2$ MHz, which is much narrower than the natural linewidth. Therefore, we can approximate the Gaussian by the δ-distribution:

$$\int_{-\infty}^{\infty} e^{-mv^2/2k_B T}dv = \sqrt{\frac{2k_B T}{m}}\int_{-\infty}^{\infty} e^{-x^2}dx = \sqrt{\frac{2\pi k_B T}{m}} = \int_{-\infty}^{\infty}\sqrt{\frac{2\pi k_B T}{m}}\delta(kv)d(kv)\ .$$

Hence,

$$\begin{aligned} OD_{461}(T_D,\omega) &= Ln(T_D)\sqrt{\frac{m}{2\pi k_B T_D}}\frac{6\pi}{k^2}\int_{-\infty}^{\infty}\frac{\Gamma_{461}^2}{4(\omega-\omega_0-kv)^2+\Gamma_{461}^2}\sqrt{\frac{2\pi k_B T_D}{m}}\delta(kv)d(kv) \\ &= Ln(T_D)\frac{6\pi}{k^2}\frac{\Gamma_{461}^2}{4(\omega-\omega_0)^2+\Gamma_{461}^2}\ , \end{aligned}$$

which means that we retrieve the default expression for optical density,

$$OD_{461}(0,\omega) = Ln(T_D)\sigma(T_D)\ .$$

b. The natural width of the transition at 689 nm is much narrower than the Doppler width. Therefore, we can approximate the Lorentzian by the δ-distribution:

$$\int_{-\infty}^{\infty}\frac{\Gamma_{689}^2}{4(\omega-\omega_0-kv)^2+\Gamma_{689}^2}dv = \frac{\Gamma_{689}}{k}\int_{-\infty}^{\infty}\frac{dx}{1+4x^2} = \frac{\pi\Gamma_{689}}{2k} = \int_{-\infty}^{\infty}\frac{\pi\Gamma_{689}}{2k}\delta(\omega-\omega_0-kv)d(kv)\ .$$

Hence,

$$\begin{aligned} OD_{689}(T_D,\omega) &= Ln(T_D)\sqrt{\frac{m}{2\pi k_B T_D}}\frac{6\pi}{k^2}\int_{-\infty}^{\infty} e^{-mv^2/2k_B T_D}\frac{\pi\Gamma_{689}}{2k}\delta(\omega-\omega_0-kv)d(kv) \\ &= Ln(T_D)\sqrt{\frac{m}{2\pi k_B T_D}}\frac{6\pi}{k^2}\frac{\pi\Gamma_{689}}{2k}e^{-m(\omega-\omega_0)^2/2k_B T_D k^2}\ . \end{aligned}$$

In resonance,

$$OD_{689}(T_D, \omega_0) = Ln(T_D)\sqrt{\frac{\pi}{2}}\frac{\sigma_0 \Gamma_{689}}{2k\bar{v}_D} \ ,$$

The fraction $\Gamma_{689}/2k\bar{v}_D$ *can be interpreted as the spectral overlap between the Lorentzian-shaped absorption profile and the Maxwell distribution.*
c. The ratio is,

$$\frac{OD_{689}(T_D, \omega_0)}{OD_{461}(T_D, \omega_0)} = \sqrt{\frac{\pi}{8}}\frac{\Gamma_{689}}{k\bar{v}_D} \ .$$

34.6.7.2 Ex: Saturated absorption spectroscopy

Saturated absorption spectroscopy is a technique to avoid Doppler broadening. The setup, shown in Fig. 34.12, consists of a cell filled with a rubidium gas (resonance frequency $\omega_0 = ck = 2\pi c/780\,\text{nm}$, decay rate $\Gamma = (2\pi)\ 6\,\text{MHz}$) and two laser beams with the same frequency ω but counterpropagating, one called saturation and another called probe. The one-dimensional and normalized Maxwell velocity distribution is,

$$\rho(v)dv = \sqrt{\frac{m}{2\pi k_B T}} e^{-mv^2/2k_B T} dv \ .$$

The gas is at $T = 300\,\text{K}$, where the partial pressure of rubidium is around $P = 10^{-1}\,\text{mbar}$. The length of the cell is $L = 10\,\text{cm}$. The probe laser has an intensity below the saturation limit, such that the cross section of an atom moving at velocity v is,

$$\sigma(v) = \frac{6\pi}{k^2}\frac{\Gamma^2}{4(\omega - \omega_0 - kv)^2 + \Gamma^2} \ .$$

The saturation laser has high intensity. We suppose here, $\Omega \equiv 10\Gamma$, where Ω is the frequency of Rabi caused by the saturation beam. In this way it creates a population N_e of atoms in the excited state. As this population lacks in the ground state, $N_g = N - N_e$, the absorption of the probe beam is decreased by the factor,

$$\frac{N_e}{N} = \frac{\Omega^2}{4(\omega - \omega_0 + kv)^2 + 2\Omega^2 + \Gamma^2} \ .$$

To obtain the laser probe transmission spectrum, first calculate the optical density, $OD(\omega) = Ln\int_{-\infty}^{\infty}\frac{N_g - N_e}{N}\sigma(v)\rho(v)dv$ where n is the gas density, and then the intensity of light transmitted through the cell using the Lambert-Beer law $\frac{I}{I_0} = e^{-OD}$.

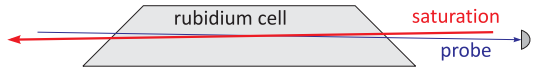

Figure 34.12: Scheme of saturation spectroscopy.

Solution: *The optical density with Doppler broadening is,*

$$\begin{aligned} OD(T,\omega) &= Ln(T)\int_{-\infty}^{\infty}\tfrac{N-2N_e}{N}\sigma(v)\rho(v)dv \\ &= L\frac{P}{k_BT}\sqrt{\frac{m}{2\pi k_BT}}\frac{6\pi}{k^2}\int_{-\infty}^{\infty}\left(1-\frac{2\Omega^2}{4(\Delta+kv)^2+2\Omega^2+\Gamma^2}\right)\times \\ &\qquad\times\frac{\Gamma^2}{4(\Delta-kv)^2+\Gamma^2}e^{-mv^2/2k_BT}dv\ , \end{aligned}$$

with $\Delta\equiv\omega-\omega_0$. The widths of the three velocity distributions are, respectively,

$$\begin{aligned} k\Delta v &= \sqrt{\tfrac{1}{2}\Omega^2+\tfrac{1}{4}\Gamma^2}\approx(2\pi)\ 68\,\text{MHz} \qquad \textit{for the saturation beam} \\ k\bar{v} &= k\sqrt{\tfrac{k_BT}{m}}\approx(2\pi)\ 217\,\text{MHz} \qquad \textit{for Doppler broadening} \\ k\Delta v &= \tfrac{1}{2}\Gamma\approx(2\pi)\ 3\,\text{MHz} \qquad \textit{for the probe beam} \end{aligned}$$

where $\bar{v}=\sqrt{k_BT/m}$ is the mean atomic velocity (or the rms width) of the Maxwell distribution. Since the probe beam spectral width is much smaller, we can substitute

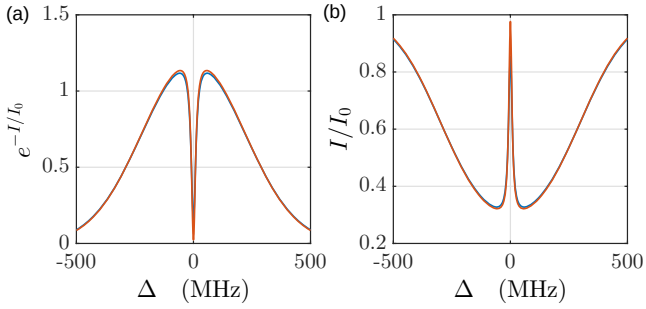

Figure 34.13: (code) (a) Optical density and (b) absorption. (Blue) Integral formula and (green) high temperature approach and high saturation.

a δ-function,

$$\frac{\Gamma^2}{4(\Delta-kv)^2+\Gamma^2}\longrightarrow\frac{\pi\Gamma}{2}\delta(\Delta-kv)\ ,$$

giving,

$$\begin{aligned} OD(T,\omega) &\simeq L\frac{P}{k_BT}\sqrt{\frac{m}{2\pi k_BT}}\frac{6\pi}{k^3}\int_{-\infty}^{\infty}\left(1-2\frac{2\Omega^2}{4(\Delta+kv)^2+2\Omega^2+\Gamma^2}\right)\times \\ &\qquad\times\frac{\pi\Gamma}{2}\delta(\Delta-kv)e^{-mv^2/2k_BT}dkv \\ &= L\frac{P}{k_BT}\sqrt{\frac{m}{2\pi k_BT}}\frac{6\pi}{k^3}\frac{\pi\Gamma}{2}\left(1-\frac{4\Omega^2}{8\Delta^2+2\Omega^2+\Gamma^2}\right)e^{-m(\Delta/k)^2/2k_BT}\ . \end{aligned}$$

34.6.7.3 Ex: The Zeeman slower

Consider a tube through which passes a collimated beam of atoms, all having the same initial velocity $v = v_0$. In the opposite direction to the atomic motion travels a collimated and monochromatic light beam with frequency $\omega = kc$. The absorption rate for photons by an atom has a Lorentzian profile, which can be written as:

$$W(v) = \frac{W_0}{2\pi} \frac{\Gamma^2}{(\omega - \omega_0 + kv)^2 + (\Gamma/2)^2} \ ,$$

where Γ is the natural width of the spectral line at ω_0, and W_0 is a constant. The frequency of the light is tuned in order to compensate for the Doppler effect at the beginning of the tube, $\delta = \omega - \omega_0 = -kv_0$ (the light is tuned to the red of the resonance). As the atoms are decelerated, they cease to be resonant with the light beam and fail to absorb photons. This can be avoided by employing the so-called Zeeman-slowing technique, which compensates for the effect using the Zeeman-shift induced by magnetic fields. In this exercise, we will study what happens if this technique is not used.

a. For an atom with velocity v, write an expression for the mean travel distance

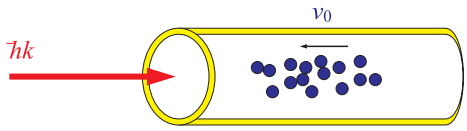

Figure 34.14: Zeeman slower scheme.

$\Delta s(v)$ before it absorbs a photon as a function of the parameters Γ, v_0, k, and W_0. (The mean time it takes to absorb a photon is $W(v)^{-1}$).

b. The velocity of the atom as a function of the number of absorbed photons is $v_n = v_0 - n\frac{\hbar k}{m}$, the second term being the recoil due to the absorption of a single photon. The average total distance traveled by an atom after absorbing N photons is estimated by:

$$S = \sum_{n=0}^{N} \Delta s(v_n) \simeq \int_0^N \Delta s(v_n) dn \ .$$

Calculate the average distance required for the atoms to be slowed down to $v = 0$ (ignoring the Doppler limit). Write the expression as a function of Γ, v_0, k, and W_0.
Help: Do the following change of variables to simplify the evaluation of the integral: $n \to v$.

c. Typically, the detuning of the light, $|\delta| = kv_0$, is much larger than the natural width Γ of the transition. What happens to S in the limit when $kv_0 \gg \Gamma$? Interpret this result, justifying the need for the Zeeman-slowing technique.

Solution: *a. Between two consecutive photon absorptions, the velocity of the atoms is constant. Therefore, the average distance traveled is simply the velocity times the average time:*

$$\Delta s(v) = v \frac{1}{W(v)} = \frac{2\pi v}{W_0 \Gamma^2} [(\omega - \omega_0 + kv)^2 + (\Gamma/2)^2] \ .$$

Using that $\omega - \omega_0 = -kv_0$*:*

$$\Delta s(v) = \frac{2\pi v}{W_0\Gamma^2}[k^2(v-v_0)^2 + (\Gamma/2)^2] \ .$$

b. We must calculate the shown integral for a number of photons N *such that the final velocity is zero. For this, we make the suggested variable change:*

$$v = v_0 - n\frac{\hbar k}{m}$$
$$dv = -\frac{\hbar k}{m}dn \ ,$$

such that $v(n=0) = v_0$ *and* $v(n=N) = 0$*. The integral is then:*

$$S = \int_0^N \Delta s(v_n)dn = \int_{v_0}^0 \Delta s(v)\left(-\frac{dv}{\hbar k/m}\right) = \int_0^{v_0} \frac{2\pi}{W_0\Gamma^2\hbar k/m}[k^2(v-v_0)^2 + (\Gamma/2)^2]dv$$
$$= \frac{2\pi}{W_0\Gamma^2\hbar k/m}\int_0^{v_0} v[k^2v^2 - 2k^2vv_0 + k^2v_0^2 + (\Gamma/2)^2]dv$$
$$= \frac{2\pi}{W_0\Gamma^2\hbar k/m}\left[\frac{k^2v_0^4}{4} - \frac{2k^2v_0v_0^3}{3} + \frac{k^2v_0^2v_0^2}{2} + \left(\frac{\Gamma}{2}\right)^2\frac{v_0^2}{2}\right] = \frac{2\pi v_0^2}{W_0\hbar k/m}\left[\left(\frac{kv_0}{\Gamma}\right)^2\frac{1}{12} + \frac{1}{8}\right] \ .$$

c. If $\Gamma \ll kv_0$*, the numerical factor in the above equation becomes very large, so that the distance required for a complete deceleration of the atoms is very large (Note: an underestimation of the dimensional factor* $v_0^2/(W_0\hbar k/m)$ *gives distances of at least a meter, so that this simplified model predicts that a tube of many meters would be needed to slow down the atoms in this scheme). The interpretation is that if the spectral line is sufficiently narrow, the atoms leave the resonance condition with the light beam in a short time, practically not absorbing photons any more. This justifies the need for a correction (for example) of the spectral line via the Zeeman effect, with fields that vary in space, so as to keep the atoms always in resonance with the light beam.*

34.6.7.4 Ex: Saturation intensity

Calculate the saturation intensity for the sodium transition $3s\ ^2S_{1/2}, F = 2 \longleftrightarrow 3p\ ^2P_{3/2}, F' = 3$. The natural width of the transition is $\Gamma/2\pi = 9.89\,\mathrm{MHz}$ and the wavelength $\lambda = 590\,\mathrm{nm}$.

Solution: *The degeneracies of the levels are* $g_1 = 5$ *and* $g_2 = 7$*. Hence, we get* $I_{sat} = 4.3\,\mathrm{mW/cm^2}$*.*

34.6.7.5 Ex: Saturation intensity of an octupole transition

Calculate the saturation intensity for the $^2S_{1/2}$-$^2F_{7/2}$ transition in Yb^+-ions (neglecting the Zeeman substructure) at $\lambda = 467\,\mathrm{nm}$ (decay time $\tau = 8\,\mathrm{a}$) and the Rabi frequency, when the transition is resonantly driven by a laser beam of $P = 10\,\mathrm{mW}$ power focused into a $w_0 = 20\,\mu\mathrm{m}$ waist.

Solution: *The saturation intensity is,*

$$I_{sat} = \frac{2\pi^2 c\hbar}{3\lambda^3}\Gamma \approx 48\,\mathrm{fW} \ ,$$

and the power broadening,

$$\Omega = \Gamma\sqrt{\frac{I}{2I_{sat}}} = \Gamma\sqrt{\frac{P}{\pi w_0^2 I_{sat}}} \approx 32\,\mathrm{kHz} \ .$$

Hence, it sounds feasible to drive the transition, provided the laser emission bandwidth is narrow than 32 kHz.

34.6.7.6 Ex: Pressure broadening

At what pressure the collision broadening [given by the expression (34.236)] between sodium atoms in the ground state dominates the width of the D2-transition at ambient temperature. The natural width of the D2-line is $\Gamma/2\pi = 6\,\mathrm{MHz}$.

Solution: *The mass of the sodium is* $m = 23u$. *We approximate the radius with* $\rho \simeq a_B$. *Then, with* $pV = Nk_BT$,

$$\tau_{col} = \frac{1}{8\rho^2 n}\sqrt{\frac{m}{2\pi k_B T}} = \frac{1}{8a_B^2 p}\sqrt{\frac{mk_BT}{2\pi}} \ .$$

Hence,

$$p = \frac{\gamma_{col}}{8a_B^2}\sqrt{\frac{mk_BT}{2\pi}} > \frac{\Gamma/2}{8a_B^2}\sqrt{\frac{mk_BT}{2\pi}} \equiv p_{crit} \ ,$$

which gives $p_{crit} = 4200\,\mathrm{Pa} = 42\,\mathrm{mbar}$.

34.6.7.7 Ex: Optical density of a hot cloud

Calculate and draw the effective Lorentz profile, Gauss profile and Voigt profile for the resonance line at 461 nm ($\Gamma = (2\pi)\ 32\,\mathrm{MHz}$) of a strontium gas heated to the temperature 400 C and the pressure $P = 10^{-4}$ mbar inside a 15 cm long cell.

Solution: *The cross-section of an atom with the resonance frequency* ω_0 *moving with velocity* v *and irradiated by a laser beam of frequency* ω *is,*

$$\sigma(v) = \frac{6\pi}{k^2}\frac{\Gamma^2}{4(\omega - \omega_0 - kv)^2 + \Gamma^2} \ .$$

The one-dimensional Maxwell distribution,

$$\rho(v)dv = \sqrt{\frac{m}{2\pi k_B T}}e^{-mv^2/2k_BT}dv \ ,$$

is normalized. The density of the atoms is,

$$n(T) = \frac{P}{k_B T} \approx 10^{18}\,\mathrm{m}^{-3} \ .$$

The optical density is,

$$\begin{aligned} OD(T,\omega) &= Ln(T)(\sigma \star \rho)(\delta) = Ln(T)\int_{-\infty}^{\infty}\sigma(v)\rho(v)dv \\ &= L\frac{P}{k_B T}\sqrt{\frac{m}{2\pi k_B T}}\frac{6\pi}{k^2}\int_{-\infty}^{\infty} e^{-mv^2/2k_B T}\frac{\Gamma^2}{4(\omega-\omega_0-kv)^2+\Gamma^2}dv \ . \end{aligned}$$

At zero temperature, we can approximate the Gaussian by the δ-distribution:

$$\int_{-\infty}^{\infty} e^{-mv^2/2k_B T}dv = \sqrt{\frac{2k_B T}{m}}\int_{-\infty}^{\infty} e^{-x^2}dx = \sqrt{\frac{2\pi k_B T}{m}} = \int_{-\infty}^{\infty}\sqrt{\frac{2\pi k_B T}{m}}\delta(kv)d(kv) \ .$$

Hence,

$$\begin{aligned} OD(0,\omega) &= Ln(T)\sqrt{\frac{m}{2\pi k_B T}}\frac{6\pi}{k^2}\int_{-\infty}^{\infty}\frac{\Gamma^2}{4(\omega-\omega_0-kv)^2+\Gamma^2}\sqrt{\frac{2\pi k_B T}{m}}\delta(kv)d(kv) \\ &= Ln(T)\frac{6\pi}{k^2}\frac{\Gamma^2}{4(\omega-\omega_0)^2+\Gamma^2} \ , \end{aligned}$$

which means that we retrieve the default expression for the optical density,

$$OD(0,\omega) = Ln(T)\sigma(T) \ .$$

When the natural width is very narrow, we can approximate the Lorentzian by the δ-distribution:

$$\int_{-\infty}^{\infty}\frac{\Gamma^2}{4(\omega-\omega_0-kv)^2+\Gamma^2}dv = \frac{\Gamma}{k}\int_{-\infty}^{\infty}\frac{dx}{1+4x^2} = \frac{\pi\Gamma}{2k} = \int_{-\infty}^{\infty}\frac{\pi\Gamma}{2k}\delta(\omega-\omega_0-kv)d(kv) \ .$$

Hence,

$$\begin{aligned} OD(T,\omega) &= Ln(T)\sqrt{\frac{m}{2\pi k_B T}}\frac{6\pi}{k^2}\int_{-\infty}^{\infty} e^{-mv^2/2k_B T}\frac{\pi\Gamma}{2k}\delta(\omega-\omega_0-kv)d(kv) \\ &= Ln(T)\sqrt{\frac{m}{2\pi k_B T}}\frac{6\pi}{k^2}\frac{\pi\Gamma}{2k}e^{-m(\omega-\omega_0)^2/2k_B T k^2} \ . \end{aligned}$$

In resonance,

$$OD(T,\omega_0) = Ln(T)\sqrt{\frac{\pi}{2}}\frac{\sigma_0\Gamma}{2k\bar{v}} \ ,$$

where $\bar{v} = \sqrt{k_B T/m}$ is the average atomic velocity (or the rms*-width of the Maxwell distribution. The fraction $\Gamma/2k\bar{v}$ can be interpreted as the spectral overlap between the Lorentzian absorption profile and the Maxwell distribution.*

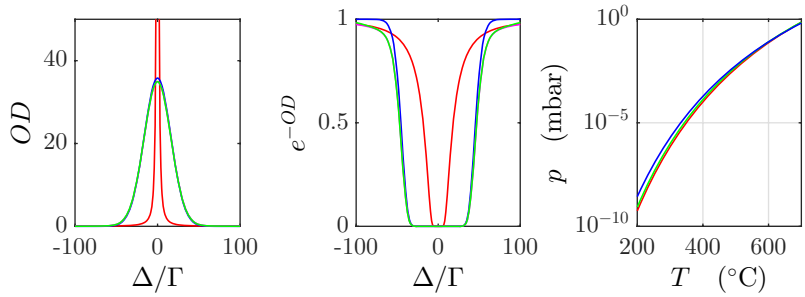

Figure 34.15: (code) (a) Optical density profiles, (red) exact, (green) in the limit $\Gamma = 0$, and (blue) in the limit $T = 0$. (b) Same as (a) but exponential.

34.6.7.8 Ex: Rate equations as a limiting case of Bloch equations

We show in this exercise that, in the limit $\Gamma \gg \Omega$, we can derive, from the Bloch equations, the Einstein rate equations. Proceed as follows:
a. Apply the condition $\dot{\rho}_{12} = 0$ to the Bloch equations for a two-level system (34.188), determine $\rho_{12}(\infty)$, and replace this stationary value in the equations for the populations $\rho_{kk}(t)$ using, as an abbreviation, the transition rate $R \equiv \gamma s$, where s is the saturation parameter (34.190).
b. Integrate the rate equations over the entire spectrum, i.e. $\Delta \in [-\infty, \infty]$, and derive Einstein's equations using the relations (34.7), (34.41), and (34.42).

Solution: *a. The Einstein rate equations can be derived from the Bloch equations following the Wilcox-Lamb procedure [1375, 4]. This consists in applying the condition $\dot{\rho}_{12} = 0$ to the Bloch equation,*

$$\frac{d}{dt}\begin{pmatrix}\rho_{11}\\ \rho_{22}\\ \rho_{12}\\ \rho_{21}\end{pmatrix} = \begin{pmatrix} 0 & \Gamma & \frac{\imath}{2}\Omega & -\frac{\imath}{2}\Omega \\ 0 & -\Gamma & -\frac{\imath}{2}\Omega & \frac{\imath}{2}\Omega \\ \frac{\imath}{2}\Omega & -\frac{\imath}{2}\Omega & \imath\Delta - \gamma & 0 \\ -\frac{\imath}{2}\Omega & \frac{\imath}{2}\Omega & 0 & -\imath\Delta - \gamma \end{pmatrix}\begin{pmatrix}\rho_{11}\\ \rho_{22}\\ \rho_{12}\\ \rho_{21}\end{pmatrix} ,$$

giving,

$$\rho_{12}(\infty) = \frac{-\Omega/2}{\imath\gamma + \Delta}(\rho_{11} - \rho_{22}) .$$

Substituting the coherences in the equations for the populations yields,

$$\frac{d}{dt}\rho_{11} = -\frac{\gamma\Omega^2/2}{\Delta^2 + \gamma^2}\rho_{11} + \Gamma\rho_{22} + \frac{\gamma\Omega^2/2}{\Delta^2 + \gamma^2}\rho_{22}$$

with the abbreviation,

$$R \equiv \frac{\gamma\Omega^2/2}{\Delta^2 + \gamma^2} = \gamma s ,$$

where s is the saturation parameter. We obtain the rate equations,

$$\frac{d}{dt}\begin{pmatrix}\rho_{11}\\ \rho_{22}\end{pmatrix} = \begin{pmatrix} -R & \Gamma + R \\ R & -\Gamma - R \end{pmatrix}\begin{pmatrix}\rho_{11}\\ \rho_{22}\end{pmatrix} .$$

b. Finally, integrating over the entire spectrum,

$$\int_{-\infty}^{\infty} R d\Delta \equiv \int_{-\infty}^{\infty} \frac{\gamma\Omega^2/2}{\Delta^2+\gamma^2} d\Delta = \tfrac{\pi}{2}\Omega^2 \ .$$

Using relationships $\bar{u} = \frac{1}{2}\varepsilon_0 E^2$, $\hbar\Omega = dE$, *and* $B_{12} = \frac{\pi d^2}{3\varepsilon_0\hbar^2}$ *we see,*

$$\tfrac{\pi}{2}\Omega^2 = 3B_{12}\bar{u} \ .$$

Hence, with $N_k/N = \rho_{kk}$,

$$\frac{d}{dt}\begin{pmatrix} N_1 \\ N_2 \end{pmatrix} = \begin{pmatrix} -B_{12}\bar{u} & A_{21} + B_{21}\bar{u} \\ B_{12}\bar{u} & -A_{21} - B_{21}\bar{u} \end{pmatrix}\begin{pmatrix} N_1 \\ N_2 \end{pmatrix} \ .$$

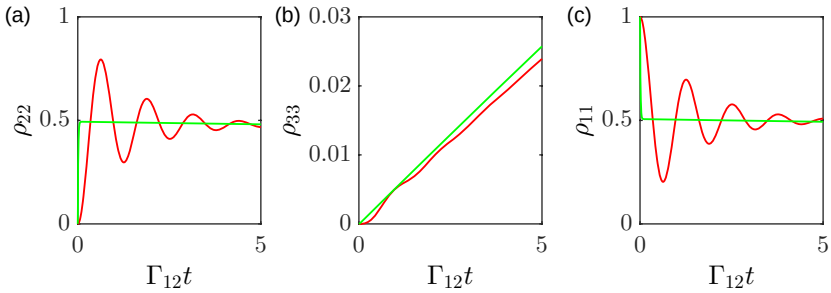

Figure 34.16: (code) Example for temporal evolution of the populations calculated from Bloch and from rate equations.

34.6.7.9 Ex: Blackbody radiation-induced transitions

Blackbody radiation induces incoherent transitions (see Exc. 34.6.7.8). Show that the Lindbladian of the master equation,

$$\dot{\hat{\rho}} = \mathcal{L}_{bb}\hat{\rho} = -\tfrac{R}{2}\left([\hat{\rho}\hat{\sigma}, \hat{\sigma}^\dagger] + [\hat{\sigma}, \hat{\sigma}^\dagger\hat{\rho}]\right) - \tfrac{R+\Gamma}{2}\left([\hat{\rho}\hat{\sigma}^\dagger, \hat{\sigma}] + [\hat{\sigma}^\dagger, \hat{\sigma}\hat{\rho}]\right)$$

reproduces the Einstein rate equation for $\Gamma = 2A_{12}$ and $R = B_{12}u(\omega)$.

Solution: *We calculate from the given expression,*

$$\begin{aligned}\dot{\hat{\rho}} &= -\tfrac{\Gamma}{2}\left(\hat{\rho}\hat{\sigma}^\dagger\hat{\sigma} + \hat{\sigma}^\dagger\hat{\sigma}\hat{\rho} - 2\hat{\sigma}\hat{\rho}\hat{\sigma}^\dagger\right) - \tfrac{R}{2}\left(\hat{\rho}\hat{\sigma}\hat{\sigma}^\dagger + \hat{\rho}\hat{\sigma}^\dagger\hat{\sigma} + \hat{\sigma}\hat{\sigma}^\dagger\hat{\rho} + \hat{\sigma}^\dagger\hat{\sigma}\hat{\rho} - 2\hat{\sigma}^\dagger\hat{\rho}\hat{\sigma} - 2\hat{\sigma}\hat{\rho}\hat{\sigma}^\dagger\right) \\ &= \Gamma\left(|1\rangle\rho_{22}\langle 1| - \tfrac{1}{2}\hat{\rho}|2\rangle\langle 2| - \tfrac{1}{2}|2\rangle\langle 2|\hat{\rho}\right) - R\left(|2\rangle\langle 1|\hat{\rho}|1\rangle\langle 2| + |1\rangle\langle 2|\hat{\rho}|2\rangle\langle 1| - \hat{\rho}\right) \ ,\end{aligned}$$

yielding,

$$\begin{aligned}\dot{\rho}_{22} &= -\dot{\rho}_{11} = -\Gamma\rho_{22} - R(\rho_{11} - \rho_{22}) \\ \dot{\rho}_{12} &= \dot{\rho}_{21}^* = \left(-\tfrac{\Gamma}{2} + R\right)\rho_{12} \ .\end{aligned}$$

The first equation is just the Einstein rate equation. The second equation is decoupled from the first one.

34.6.7.10 Ex: Lorentzian versus Gaussian line profile

Beyond what detuning is a Doppler-broadened transition dominated by the Lorentzian profile of the transition?

Solution: *We consider a cell of length L at temperature T. With the optical cross section,*

$$\sigma = \frac{6\pi}{k^2} \frac{\Gamma^2}{4(\omega - \omega_0 - kv)^2 + 2\Omega^2 + \Gamma^2}$$

and the Maxwell-Boltzmann distribution,

$$\rho dv = \sqrt{\frac{m}{2\pi k_B T}} e^{-mv^2/2k_B T} dv$$

the optical density is,

$$OD(T, \omega) = L \frac{P}{k_B T} \sqrt{\frac{m}{2\pi k_B T}} \frac{6\pi}{k^2} \int_{-\infty}^{\infty} e^{-mv^2/2k_B T} \frac{\Gamma^2}{4(\omega - \omega_0 - kv)^2 + 2\Omega^2 + \Gamma^2} dv \ .$$

Considering normalized profiles,

$$\sigma = \frac{a/\pi}{x^2 + a^2} \qquad \textit{respectively} \qquad \rho = \frac{1}{b\sqrt{\pi}} e^{-x^2/b^2} \ .$$

Expanding by $1/x$?

34.7 Bloch equations for multi-level systems

The two-level system represents an idealization of the real atom, since at least one of the levels is usually degenerate. Many important phenomena in quantum optics are not found in this system, but conditioned to the existence of a third level. Examples are optical pumping (essential for laser operation), quantum jumps or dark resonances [which are at the basis of the phenomenon of electromagnetically induced transparency (EIT)].

To derive the Bloch equations for atoms with several levels excited by several lasers and coupled to free space (i.e. without external cavity), we can use the same master equation (34.222), but with a generalized Hamiltonian in the semiclassical

approximation [20] and a Lindblad operator,

$$\boxed{\begin{aligned}
\hat{H}_{atom} &= \textstyle\sum_i \hbar\omega_i \hat{\sigma}_{ji}\hat{\sigma}_{ij} = \sum_i |i\rangle\hbar\omega_i\langle i| \\
\hat{H}_{atom:field} &= \tfrac{\hbar}{2}\Omega_{ij}\,(e^{-\imath\omega_{ij}t}\hat{\sigma}_{ij} + e^{\imath\omega_{ij}t}\hat{\sigma}_{ji}) = \textstyle\sum_{i<j} |i\rangle \tfrac{\hbar}{2}\Omega_{ij}\langle j|e^{\imath\omega_{ij}t} + c.c. \\
\mathcal{L}_{decay}\hat{\rho} &= \mathcal{L}_\gamma + \mathcal{L}_R + \mathcal{L}_\beta \\
\mathcal{L}_\gamma &= \textstyle\sum_{i,j} \gamma_{ij}\left([\hat{\sigma}_{ij}, \hat{\rho}\hat{\sigma}^\dagger_{ij}] + [\hat{\sigma}_{ij}\hat{\rho}, \hat{\sigma}^\dagger_{ij}]\right) \\
\mathcal{L}_R &= \textstyle\sum_{i,j} R_{ij}\left([\hat{\sigma}^\dagger_{ij}, \hat{\rho}\hat{\sigma}_{ij}] + [\hat{\sigma}^\dagger_{ij}\hat{\rho}, \hat{\sigma}_{ij}]\right) \\
\mathcal{L}_\beta &= \textstyle\sum_{i,j} 2\beta_{ij}\left([\hat{\sigma}_{ij}\hat{\sigma}^\dagger_{ij}, \hat{\rho}\hat{\sigma}_{ij}\hat{\sigma}^\dagger_{ij}] + [\hat{\sigma}_{ij}\hat{\sigma}^\dagger_{ij}\hat{\rho}, \hat{\sigma}_{ij}\hat{\sigma}^\dagger_{ij}]\right)
\end{aligned}} \quad . \tag{34.266}$$

Here, $\hat{\sigma}_{ij} \equiv |i\rangle\langle j| = \hat{\sigma}^\dagger_{ji}$. The constants R_{ij} are eventual incoherent pump rates due to optical pumping, β_{ij} take account of homogeneous broadening, e.g. due to finite laser linewidths. The levels have the energy $\hbar\omega_i$ above the ground level. The Rabi frequency Ω_{ij} is a measure for the force at which the levels $|i\rangle$ and $|j\rangle$ are coupled by the resonantly irradiated light field. The master equation can be simplified by applying the rotating wave approximation and transforming to the coordinate system which rotates with the light frequencies ω_{ij}:

$$\rho_{ij} \to \hat{\rho}_{ij}e^{\imath\omega_{ij}t} \quad , \quad \hat{H}_{atom:field} \to e^{-\imath\hat{H}t/\hbar}\hat{H}_{atom:field}e^{\imath\hat{H}t/\hbar} \; . \tag{34.267}$$

34.7.1 Liouville equation for many levels

The indices for the atomic levels are joined to a single index, such that the master equation takes a simpler form after having introduced a *Liouville operator*:

$$\begin{aligned}
\hat{\rho} &= (...\rho_k...) \equiv \sum\nolimits_{i,j} |i\rangle\rho_{ij}\langle j| \; , \\
\dot{\hat{\rho}} &= \mathcal{L}\hat{\rho}, \\
\hat{\rho} &= e^{\mathcal{L}_{atom}t}\hat{\rho}_0 \; .
\end{aligned} \tag{34.268}$$

The relation with the *von Neumann equation* with $\hat{H} = \sum_{i,j} |i\rangle H_{ij}\langle j|$ and $\hat{\rho} = \sum_{k,l} |k\rangle\rho_{kl}\langle l|$ and $\hat{\sigma}_{ij} = |i\rangle\langle j|$ is:

$$\mathcal{L}_{atom}\hat{\rho} = -\tfrac{\imath}{\hbar}[\hat{H}, \hat{\rho}] = -\imath\sum\nolimits_{k,l,j} H_{kl}\rho_{lj}|k\rangle\langle j| + \imath\sum\nolimits_{k,l,j} H_{lj}\rho_{kl}|k\rangle\langle j| \; . \tag{34.269}$$

For example, for the two-level system with the definition of the external product (23.127):

$$\mathcal{L}_{atom}\hat{\rho} = -\imath\hat{H}\otimes\mathbb{I}\hat{\rho} + \imath\mathbb{I}\otimes\hat{H}\hat{\rho} \; . \tag{34.270}$$

The relaxation terms for spontaneous decay obtained from (34.266) are,

$$\mathcal{L}_{decay}\hat{\rho} = \sum\nolimits_{i,j,k} \left(2\gamma_{ji}\delta_{kj}\rho_{ii} - \gamma_{ij}\rho_{kj} - \gamma_{ik}\rho_{kj}\right)|k\rangle\langle j| \; . \tag{34.271}$$

[20] That is, the atom is quantized and consists of several levels $|i\rangle$ with energies $\hbar\omega_i$, while the light fields are described by factors $e^{\imath\omega_{ij}t}$, with frequencies ω_{ij} tuned near the transitions $|i\rangle - |j\rangle$.

Example 201 (*Liouville equation for two levels*): For example, for the two-level system,

$$\mathcal{L}_{atom} = \begin{pmatrix} 2\gamma_{11} & 0 & 0 & 2\gamma_{21} \\ 0 & 0 & 0 & 0 \\ 0 & 0 & 0 & 0 \\ 2\gamma_{12} & 0 & 0 & 2\gamma_{22} \end{pmatrix} - \begin{pmatrix} 2(\gamma_{11}+\gamma_{12}) & 0 & 0 & 0 \\ 0 & \sum_{(kj)}\gamma_{(kj)} & 0 & 0 \\ 0 & 0 & \sum_{(kj)}\gamma_{(kj)} & 0 \\ 0 & 0 & 0 & 2(\gamma_{22}+\gamma_{21}) \end{pmatrix} .$$

Here, we consider $(kj) = (11\ 12\ 21\ 22)$ as a single index.

34.7.1.1 Derivation of the multilevel Bloch equation

Now, inserting the Hamiltonian in the RWA,

$$\hat{H} = \hat{H}_{atom} + \hat{H}_{atom:field} = \sum_i \hbar\omega_i |i\rangle\langle i| + \tfrac{\hbar}{2}\sum_{i<j} \Omega_{ij}\hat{\sigma}_{ij} + h.c. \ , \tag{34.272}$$

into the von Neumann equation together with the dissipative Lindbladian (34.271) and $\rho_{jk} \equiv \langle j|\hat{\rho}|k\rangle$, we derive the multilevel master equation,

$$\dot{\rho}_{jk} = \frac{\imath}{\hbar}\langle j|[\hat{\rho}, \hat{H}]|k\rangle + \langle j|\mathcal{L}_{decay}\hat{\rho}|k\rangle \ . \tag{34.273}$$

First we calculate the unperturbed Hamiltonian part,

$$\begin{aligned} \langle k|[\hat{\rho}, \hat{H}_{atom}]|m\rangle &= \hbar\langle k|\hat{\rho}\sum_a |a\rangle\langle a|\sum_i \omega_i|i\rangle\langle i|m\rangle - \hbar\langle k|\sum_i \omega_i|i\rangle\langle i|\sum_a |a\rangle\langle a|\hat{\rho}|m\rangle \\ &= \hbar(\omega_m - \omega_k)\rho_{km} \ . \end{aligned} \tag{34.274}$$

For the interaction part we get,

$$\begin{aligned} &\langle k|[\hat{\rho}, \hat{H}_{atom-field}]|m\rangle \\ &= \tfrac{\hbar}{2}\sum_a\sum_{i<j}\left[\langle k|\hat{\rho}|a\rangle\langle a|\left(\Omega_{ij}|i\rangle\langle j| + \Omega^*_{ij}|j\rangle\langle i|\right)|m\rangle - \langle k|\left(\Omega_{ij}|i\rangle\langle j| + \Omega^*_{ij}|j\rangle\langle i|\right)|a\rangle\langle a|\hat{\rho}|m\rangle\right] \\ &= \tfrac{\hbar}{2}\sum_{i<j}\left(\Omega_{ij}\rho_{ki}\delta_{jm} + \Omega^*_{ij}\rho_{kj}\delta_{im} - \Omega_{ij}\rho_{jm}\delta_{ki} - \Omega^*_{ij}\rho_{im}\delta_{kj}\right) \ , \end{aligned} \tag{34.275}$$

and for the dissipative part,

$$\begin{aligned} \langle k|\mathcal{L}_{decay}\hat{\rho}|m\rangle &= \langle k|\sum_{i,j}\gamma_{ij}(2|i\rangle\langle j|\hat{\rho}|j\rangle\langle i| - |j\rangle\langle i|i\rangle\langle j|\hat{\rho} - \hat{\rho}|j\rangle\langle i|i\rangle\langle j|)|m\rangle \\ &= \sum_j 2\gamma_{mj}\delta_{km}\rho_{jj} - \sum_i(\gamma_{ik}+\gamma_{im})\rho_{km} \ . \end{aligned} \tag{34.276}$$

So all in all,

$$\boxed{\begin{aligned} \dot{\rho}_{km} &= 2\sum_j \gamma_{mj}\rho_{jj}\delta_{km} - \left[\sum_i(\gamma_{ik}+\gamma_{im}) + \imath(\omega_k - \omega_m)\right]\rho_{km} \\ &+ \tfrac{\imath}{2}\sum_{i<j}\left(\Omega_{ij}\rho_{ki}\delta_{jm} + \Omega^*_{ij}\rho_{kj}\delta_{im} - \Omega_{ij}\rho_{jm}\delta_{ki} - \Omega^*_{ij}\rho_{im}\delta_{kj}\right) \end{aligned}} \ , \tag{34.277}$$

where the index j runs over all levels $|j\rangle$ into which a population ρ_{kk} can decay and the index i runs over all levels $|i\rangle$ into which the levels $|k\rangle$ and $|m\rangle$ of a dipole moment ρ_{km} can decay. In Exc. 34.7.5.1 we will apply this formula to three-level systems.

Finally, the master equation can be reformulated by introducing a *generalized Bloch vector* $\vec{\rho}$, and the matrix representation of the Liouville superoperator $\mathcal{L}$ as a linear system of n^2 coupled differential equations,

$$\frac{d}{dt}\vec{\rho} = \mathcal{M}\vec{\rho} \quad , \quad \vec{\rho} = (\rho_{11} \;\; .. \;\; \rho_{nn} \; \rho_{12} \; \rho_{21} \;\; .. \;\; \rho_{n-1\;\;n} \;\; \rho_{n\;\;n-1}) \; , \tag{34.278}$$

where the Bloch matrix $\mathcal{M}$ is obtained from the Liouvillean $\mathcal{L}$ simply by rearranging the matrix elements.

Alternatively to the complex formulation, the differential equations can be written for the real and imaginary part of the Bloch vector. The components ρ_{ii} correspond to the population probabilities of the levels $|i\rangle$, the non-diagonal elements ρ_{ij} describe the coherences between $|i\rangle$ and $|j\rangle$. Now, we must insert the Hamiltonian (34.266) and the density operator ρ_{ij} into the Liouville equation (34.125) in order to derive the generalized Bloch equations. In practice, these calculations are simple but heavy. Therefore, we describe in Sec. 34.7.4 a simplified recipe for compiling Bloch equations for arbitrary level systems for real atoms.

34.7.2 Bloch equations for three levels

In principle, three-level system can exist in there possible configurations, shown in Fig. 34.17. Note that it is not possible to describe a three-level system with all levels pairwise coupled by three lasers within the formalism of Bloch's equations [21].

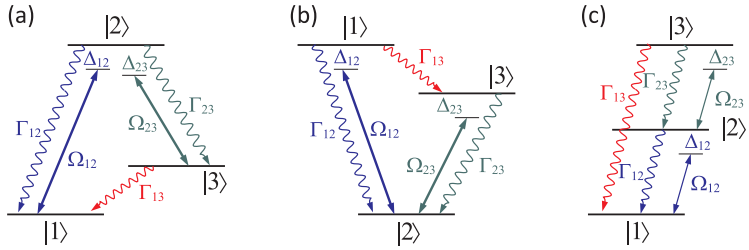

Figure 34.17: Three level system (a) in Λ-configuration, (b) in V-configuration, and (c) in cascade configuration.

Defining the Bloch vector by $\vec{\rho}$, the Bloch equation matrix for three levels in Raman

[21] For the same reason that the three-body problem has no general analytic solution.

configuration (that is, in Λ-configuration) using the labeling of Fig. 34.17(a), is,

$$\dot{\vec{\rho}} = \mathcal{M}\vec{\rho} = \tag{34.279}$$

$$\left(\begin{array}{ccc|ccccccc}
0 & \Gamma_{12} & \Gamma_{13} & \frac{\imath}{2}\Omega_{12} & -\frac{\imath}{2}\Omega_{12} & 0 & 0 & 0 & 0 \\
0 & -\Gamma_{12}-\Gamma_{23} & 0 & -\frac{\imath}{2}\Omega_{12} & \frac{\imath}{2}\Omega_{12} & 0 & 0 & \frac{\imath}{2}\Omega_{23} & -\frac{\imath}{2}\Omega_{23} \\
0 & \Gamma_{23} & -\Gamma_{13} & 0 & 0 & 0 & 0 & -\frac{\imath}{2}\Omega_{23} & \frac{\imath}{2}\Omega_{23} \\
\hline
\frac{\imath}{2}\Omega_{12} & -\frac{\imath}{2}\Omega_{12} & 0 & -\Lambda_{12} & 0 & \frac{\imath}{2}\Omega_{23} & 0 & 0 & 0 \\
-\frac{\imath}{2}\Omega_{12} & \frac{\imath}{2}\Omega_{12} & 0 & 0 & -\Lambda_{12}^* & 0 & -\frac{\imath}{2}\Omega_{23} & 0 & 0 \\
0 & 0 & 0 & \frac{\imath}{2}\Omega_{23} & 0 & -\Lambda_{13} & 0 & -\frac{\imath}{2}\Omega_{12} & 0 \\
0 & 0 & 0 & 0 & -\frac{\imath}{2}\Omega_{23} & 0 & -\Lambda_{13}^* & 0 & \frac{\imath}{2}\Omega_{12} \\
0 & \frac{\imath}{2}\Omega_{23} & -\frac{\imath}{2}\Omega_{23} & 0 & 0 & -\frac{\imath}{2}\Omega_{12} & 0 & -\Lambda_{23} & 0 \\
0 & -\frac{\imath}{2}\Omega_{23} & \frac{\imath}{2}\Omega_{23} & 0 & 0 & 0 & \frac{\imath}{2}\Omega_{12} & 0 & -\Lambda_{23}^*
\end{array}\right)
\left(\begin{array}{c}
\rho_{11} \\ \rho_{22} \\ \rho_{33} \\ \rho_{12} \\ \rho_{21} \\ \rho_{13} \\ \rho_{31} \\ \rho_{23} \\ \rho_{32}
\end{array}\right)$$

with $\Lambda_{mn} = \imath\Delta_{mn} + \gamma_{mn}$ and,

$$\begin{aligned}
&\Delta_{13} = \Delta_{12} - \Delta_{23} \qquad\qquad (34.280)\\
&\gamma_{12} = \tfrac{1}{2}(\Gamma_{12}+\Gamma_{23}) \quad , \quad \gamma_{23} = \tfrac{1}{2}(\Gamma_{12}+\Gamma_{23}+\Gamma_{13}) \quad , \quad \gamma_{13} = \tfrac{1}{2}\Gamma_{13}\ .
\end{aligned}$$

In Exc. 34.7.5.2 we will derive the matrix (34.279).

The coherent terms of the same matrix can be used for the V- and the cascade configurations shown in Figs. 34.17(b,c). Obviously, the incoherent terms, that is, the submatrix 3×3 separated in the matrix (34.279) containing the population decay rates must be adjusted, as well as the decay rates of the coherences on the diagonal. Finally, the definition of the Raman detuning Δ_{13} must be adjusted. For the system in V-configuration we have,

$$\begin{aligned}
&\mathcal{M}_{incoh} = \begin{pmatrix} -\Gamma_{12}-\Gamma_{13} & 0 & 0 \\ \Gamma_{12} & 0 & \Gamma_{23} \\ \Gamma_{13} & 0 & -\Gamma_{23} \end{pmatrix} \quad , \quad \Delta_{13} = \Delta_{12} - \Delta_{23} \qquad (34.281)\\
&\gamma_{12} = \tfrac{1}{2}(\Gamma_{12}+\Gamma_{13}) \quad , \quad \gamma_{23} = \tfrac{1}{2}\Gamma_{23} \quad , \quad \gamma_{13} = \tfrac{1}{2}(\Gamma_{12}+\Gamma_{13}+\Gamma_{23})\ .
\end{aligned}$$

For the cascade system we have,

$$\begin{aligned}
&\mathcal{M}_{incoh} = \begin{pmatrix} 0 & \Gamma_{12} & \Gamma_{13} \\ 0 & -\Gamma_{12} & \Gamma_{23} \\ 0 & 0 & -\Gamma_{13}-\Gamma_{23} \end{pmatrix} \quad , \quad \Delta_{13} = \Delta_{12} - \Delta_{23} \qquad (34.282)\\
&\gamma_{12} = \tfrac{1}{2}\Gamma_{12} \quad , \quad \gamma_{23} = \tfrac{1}{2}(\Gamma_{12}+\Gamma_{23}+\Gamma_{13}) \quad , \quad \gamma_{13} = \tfrac{1}{2}(\Gamma_{13}+\Gamma_{23})\ .
\end{aligned}$$

These matrices serve to describe quantitatively a wealth of phenomena, some of them to be discussed in Sec. 34.8.

34.7.3 Numerical treatment of Bloch equations

Since the differential Bloch equations are linear, they can be easily solved. For example, the prescription

$$\boxed{\vec{\rho}(t) = e^{\mathcal{M}t}\vec{\rho}(0)} \tag{34.283}$$

propagates the Bloch vector to later times.

The matrix $\mathcal{M}$ is not invertible, but by applying the condition Tr $\rho = 1$, a component of the density matrix can be eliminated, for example by letting,

$$\rho_{11} = 1 - \sum_k \rho_{kk} \ . \tag{34.284}$$

The resulting state vector, $\vec{\rho}_{red}$, has the length $n^2 - 1$, and from $\mathcal{M}$ we obtain the (trace-)reduced, now invertible matrix $\mathcal{M}_{red}$ and the inhomogeneity vector $\mathbf{b}$. The differential equation is now,

$$\frac{d}{dt}\vec{\rho}_{red} = \mathcal{M}_{red}\vec{\rho}_{red} + \mathbf{b} \ , \tag{34.285}$$

with the stationary and time-dependent solutions,

$$\boxed{\vec{\rho}_{red}(\infty) = -\mathcal{M}_{red}^{-1}\mathbf{b} \quad , \quad \vec{\rho}_{red}(t) = e^{\mathcal{M}_{red}t}\vec{\rho}_{red}(0) + (1 - e^{\mathcal{M}_{red}t})\vec{\rho}_{red}(\infty)} \ . \tag{34.286}$$

Once the matrix $\mathcal{M}$ or the matrix $\mathcal{M}_{red}$ and the inhomogeneity vector $\mathbf{b}$ are determined for a system, the state of the atom can be calculated at any time, as well as the populations and coherences. The system's free parameters are the natural transition linewidths and the detunings, as well as the intensities and emission bandwidths of the incident light fields.

34.7.3.1 Simulation of the Schrödinger and Bloch equation

Once we have written the solution of the Schrödinger equation in the form (23.144) with a time-independent Hamiltonian $\hat{H}$, or of the Bloch equations in the form (34.283) or (34.286) with a time-independent Liouvillian $\mathcal{M}$, we can easily simulate temporal evolutions of quantum systems. If the Hamiltonian or Liouvillian depend on time, for example, when the Rabi frequencies are pulsed or the detunings are ramped, we must solve the equations iteratively. That is, we chose time intervals Δt sufficiently short, so that the Hamiltonian (or the Liouvillian) can be considered constant during this interval, and we propagate the wavefunction (or the Bloch vector) to later times via:

$$|\psi(t + \Delta t)\rangle = e^{\imath\hat{H}(t)\Delta t}|\psi(t)\rangle \qquad \text{or} \qquad \vec{\rho}(t + \Delta t) = e^{\mathcal{M}(t)\Delta t}\vec{\rho}(t) \ , \tag{34.287}$$

and insert the solution obtained again into equations (34.287) with the Hamiltonian $\hat{H}(t + \Delta t)$ (or the Liouvillian $\mathcal{M}(t + \Delta t)$) adjusted to the new time.

34.7.4 General rules for setting up multilevel Bloch equations

The canonical way of deriving multi-level Bloch equations starts from a von Neumann equation for the total density operator for the atom embedded in the electromagnetic mode structure of the environment including incident laser beams. After tracing over the degrees of freedom of the electromagnetic vacuum and using the Markov and the Born approximations [487], one arrives at a master equation of the form (34.266). Simple but tedious algebraic transformations of the master equation lead,

in the rotating wave approximation, to a set of linear first-order differential equations in the populations of the atomic excitation levels and the coherences between them. The equations are called the optical Bloch equations.

Alternatively, the Bloch equations may be found by breaking down the multi-level scheme into a set of three-level systems. Respecting a few symmetry considerations, the multi-level Bloch equations can then be reassembled from the three-level Bloch equations corresponding to every possible combination of three levels. Based on such considerations, we provide in the following a simple recipe for setting up Bloch matrices for arbitrary level schemes. A movie showing a simulation of multi-level Bloch equations for Li atoms can be watched under the following link: (watch movie).

Let us regard a n-level atom. Its internal state is fully described by the populations ρ_{kk} and the (complex) coherences ρ_{kl}, with $k, l = 1, .., n$. In this work we describe the coherences by their real and imaginary parts. The labeling is such that the levels are sorted according to their excitation energy, $E_k < E_l$ for $k < l$. We define the Bloch vector,

$$\begin{aligned}\vec{\rho} \equiv (&\rho_{11}...\rho_{nn}\mathfrak{Im}\ \rho_{12}\mathfrak{Re}\ \rho_{12}\mathfrak{Im}\ \rho_{13}\ \mathfrak{Re}\ \rho_{13}... \\ &...\mathfrak{Im}\ \rho_{1n}\mathfrak{Re}\ \rho_{1n}\mathfrak{Im}\ \rho_{23}\mathfrak{Re}\ \rho_{23}... \\ &...\mathfrak{Im}\ \rho_{n-1,n}\mathfrak{Re}\ \rho_{n-1,n})\ .\end{aligned} \tag{34.288}$$

The Bloch equations then formally read,

$$\dot{\vec{\rho}} = \mathcal{M}\vec{\rho}\ , \tag{34.289}$$

where in the given Bloch vector basis the matrix $\mathcal{M}$ has the following structure,

$$\mathcal{M} = \begin{pmatrix} (A) & (B_1) \\ (B_2) & \begin{pmatrix} (C) & (D) \\ (D) & (C) \end{pmatrix} \end{pmatrix}\ . \tag{34.290}$$

The different blocks of the matrix have the following significations. Block A handles the transfer of populations by spontaneous decay. Its rank corresponds to the number of levels n. The diagonal elements of this block are the decay rates Γ of the excited states. The off-diagonal elements Γ_{kl} denote the gain of level k from a decaying level l. Conservation of energy thus requires that the sum of the transition rates cancels for every column of matrix A, $\Gamma = \sum_k \Gamma_{kl}$, as it is the case for the two-level Bloch matrix. If the levels are sublevels of a Zeeman and/or hyperfine split multiplet, the rates have to be weighted with Wigner's $(3j)$ and $\{6j\}$ symbols, $\Gamma_{kl} = \Gamma S_{kl}$. The relative oscillator strengths S_{kl} are given in Sec. 34.7.4.2.

The blocks B_k treat the interdependence of the populations and the coherences. B_1 describes how the coherence between any pair of states driven by a light field generating a Rabi frequency Ω_{kl} influences the populations. The block consists of convoluted 2×2 matrices of the form,

$$\begin{pmatrix} \dot{\rho}_{kk} \\ \dot{\rho}_{ll} \end{pmatrix} \sim \begin{pmatrix} -\Omega_{kl} & 0 \\ \Omega_{kl} & 0 \end{pmatrix} \begin{pmatrix} \mathfrak{Im}\ \rho_{kl} \\ \mathfrak{Re}\ \rho_{kl} \end{pmatrix}\ . \tag{34.291}$$

B_2 describes how the populations in turn influence the coherences,

$$\begin{pmatrix} \mathfrak{Im}\ \dot{\rho}_{kl} \\ \mathfrak{Re}\ \dot{\rho}_{kl} \end{pmatrix} \sim \begin{pmatrix} \frac{1}{2}\Omega_{kl} & -\frac{1}{2}\Omega_{kl} \\ 0 & 0 \end{pmatrix} \begin{pmatrix} \rho_{kk} \\ \rho_{ll} \end{pmatrix} \ . \tag{34.292}$$

The Rabi frequencies have to be weighted not only with the relative oscillator strength S_{kl}, but also with the projection H_{kl} of the laser polarization onto the orientation of the magnetic field and the laser polarization, $\Omega_{kl} = \Omega_x S_{kl} H_{kl}$. Here Ω_x is the Rabi frequency generated by a laser on a transition, whose oscillator strength is 1. The projection is calculated in Sec. 34.7.4.3 for the three possible laser polarizations, i.e. for $\sigma^{\pm}$ and for π light.

The matrix C rules the influence of the decays of the coherences, of the detunings $\Delta_{kl} = \omega_x - \omega_{atom}$, and the laser linewidths β_{kl}. Note that the detuning of the laser frequency ω_x is negative for red-detuned light. In the chosen basis it breaks down into an array 2×2 matrices aligned along the diagonal of $\mathcal{M}$. Their shape is,

$$\begin{pmatrix} \mathfrak{Im}\ \dot{\rho}_{kl} \\ \mathfrak{Re}\ \rho_{kl} \end{pmatrix} \sim \begin{pmatrix} -\frac{\gamma_{kl}}{2} & -\Delta_{kl} \\ \Delta_{kl} & -\frac{\gamma_{kl}}{2} \end{pmatrix} \begin{pmatrix} \mathfrak{Im}\ \dot{\rho}_{kl} \\ \mathfrak{Re}\ \rho_{kl} \end{pmatrix} \ . \tag{34.293}$$

where $\gamma_{kl} = \sum_{m,E_m<E_k,E_l} (\Gamma_{km} + \Gamma_{lm}) + 2\beta_{kl}$. Often the levels are sublevels of a Zeeman and/or hyperfine split multiplets. In this case the frequency shift Z_{kl} of the level is added to the detuning Δ_{kl}. The shift is calculated in Sec. 34.7.4.4 for the example of the ^{6}Li D_2 line.

The block D governs the interdependences of all laser-driven coherences of the atom. The block contains 2×2 submatrices at any place of the matrix $\mathcal{M}$, where the row index pair (mn) and the column index pair (kl) have one index in common provided the two different indices correspond to the Rabi frequency of an incident laser:,

$$\begin{pmatrix} \mathfrak{Im}\ \dot{\rho}_{mn} \\ \mathfrak{Re}\ \dot{\rho}_{mn} \end{pmatrix} \sim \begin{pmatrix} 0 & \pm\frac{1}{2}\Omega_{kl} \\ \pm\frac{1}{2}\Omega_{kl} & 0 \end{pmatrix} \begin{pmatrix} \mathfrak{Im}\ \rho_{pq} \\ \mathfrak{Re}\ \rho_{pq} \end{pmatrix} \ . \tag{34.294}$$

The submatrix elements indexed by column (pq) and row (mn) are non-zero if one of the indices p or q is equal to one of the indices m or n and the unequal indices correspond to a laser-driven transition. In order to find the correct signs of the submatrix elements, we distinguish four cases: 1. For $m = p$, $n = k$, and $q = l$ the signs are: $(_-\ ^+)$; 2. for $n = q$, $m = k$, and $p = l$ the signs are: $(_+\ ^-)$; 3. for $m = q$, $n = k$, and $p = l$ the signs are: $(_+\ ^+)$; and 4. for $n = p$, $m = k$, and $q = l$ the signs are: $(_-\ ^-)$. A proper parametrization is proposed in the next section.

34.7.4.1 Recipe for D transitions in alkalines

In order to give a simple algorithm we parametrize the particular choice of sorting the components of the vector, we define a new index μ running from 1 to n^2 by setting $(\varrho_\mu) \equiv (\rho_{kl})$, where,

$$\begin{aligned} \mu(k,k) &= k \\ \mu(k,l) &= 2nk - n - k^2 - k + 2l - 1 \ , \end{aligned} \tag{34.295}$$

so that,

$$\begin{aligned} \varrho_{\mu(k,k)} &= \rho_{kk} \\ \varrho_{\mu(k,l)} &= \mathfrak{Im}\ \rho_{kl} \\ \varrho_{\mu(k,l)+1} &= \mathfrak{Re}\ \rho_{kl}\ . \end{aligned} \tag{34.296}$$

The Bloch equations then formally read,

$$\dot{\varrho}_\mu = \mathcal{M}_{\mu\nu}\varrho_\nu\ . \tag{34.297}$$

We illustrate the procedure by considering the case of the ^{6}Li D_2 line with 6 ground states $k \in G \equiv \{1, ..., 6\}$ belonging to the $^2S_{1/2}$ hyperfine levels $F = \frac{1}{2}, \frac{3}{2}$ and 12 excited states $k \in E \equiv \{7, ..., 18\}$ belonging to the $^2P_{3/2}$ hyperfine levels $F = \frac{1}{2}, \frac{3}{2}, \frac{5}{2}$.

According to the parametrization (34.289) the block A of the matrix $\mathcal{M}$ is filled with the following components,

$$\begin{aligned} \mathcal{M}_{\mu(kk),\mu(kk)} &= -\Gamma \quad \text{for} \quad k \in E \\ \mathcal{M}_{\mu(kk),\nu(ll)} &= \Gamma S_{kl} \quad \text{for} \quad k \in G \quad \text{and} \quad l \in E\ , \end{aligned} \tag{34.298}$$

where the relative oscillator strength S_{kl} is given by Eq. (34.305).

The blocks B_k of the matrix $\mathcal{M}$ are filled with the components,

$$\begin{aligned} &\mathcal{M}_{\mu(k,k),\nu(k,l)} = -\mathcal{M}_{\mu(l,l),\nu(k,l)} \\ &= -2\mathcal{M}_{\mu(k,l),\nu(k,k)} = 2\mathcal{M}_{\mu(k,l),\nu(l,l)} \\ &= -\Omega_{kl}S_{kl}H_{kl}\ , \end{aligned} \tag{34.299}$$

for $k \in G$ and $l \in E$. The projection onto the quantization axis $H_{kl} = H_{kl}\left(\frac{\hat{\epsilon}_{kl}}{|\hat{\epsilon}_{kl}|}, \vec{\mathcal{B}}, m_l - m_k\right)$ is given by Eq. (34.308).

The block C contains the components,

$$\begin{aligned} &\mathcal{M}_{\mu(k,l)\mu(k,l)} = \mathcal{M}_{\mu(k,l)+1\mu(k,l)+1} \\ &= -\tfrac{\Gamma}{2} - \tfrac{\Gamma}{2}\delta_{k\geq 7} - \beta_{pb}\delta_{2<k<7} - \beta_{rp}\delta_{k\leq 2} \end{aligned} \tag{34.300}$$

for $k \in G \cup E$ and $l \in E$ and ,

$$\begin{aligned} &\mathcal{M}_{\mu(k,l),\mu(k,l)+1)} = -\mathcal{M}_{\mu(k,l)+1,\mu(k,l))} \\ &= -\Delta_{pb}\delta_{k>2} - \Delta_{rp}\delta_{k<3} + Z_{kl}(B) \end{aligned} \tag{34.301}$$

for $k \in G$ and $l \in E$,

$$\begin{aligned} &\mathcal{M}_{\mu(k,f),\mu(k,f)+1)} = -\mathcal{M}_{\mu(k,f)+1,\mu(k,f))} \\ &= -\Delta_{pb} + \Delta_{rp} + Z_{k,10}(B) - Z_{f,10}(B) \end{aligned} \tag{34.302}$$

for $k \in \{1, 2\}$ and $f \in \{3, .., 6\}$. The Zeeman shift Z_{kl} is given by Eq. (34.309).

Finally, the block D is filled with the components,

$$\begin{aligned} \mathcal{M}_{\mu(k,f),\mu(f,l)+1} &= (\delta_{f<k} - \tfrac{1}{2})\Omega_{kl}S_{kl}H_{kl} \\ \mathcal{M}_{\mu(k,f)+1,\mu(f,l)} &= (\delta_{l<f} - \tfrac{1}{2})\Omega_{kl}S_{kl}H_{kl} \\ \mathcal{M}_{\mu(l,f),\mu(f,k)+1} &= (\delta_{l<f} - \tfrac{1}{2})\Omega_{kl}S_{kl}H_{kl} \\ \mathcal{M}_{\mu(l,f)+1,\mu(f,k)} &= (\delta_{f<k} - \tfrac{1}{2})\Omega_{kl}S_{kl}H_{kl}\ , \end{aligned} \tag{34.303}$$

where,

$$\begin{aligned}\Omega_{kl} &\equiv (\Omega_{rp}\delta_{k\leq 2} + \Omega_{pb}\delta_{k\geq 3})\delta_{l\geq 7} \\ \hat{\epsilon}_{kl} &\equiv (\hat{\epsilon}_{rp}\delta_{k\leq 2} + \hat{\epsilon}_{pb}\delta_{k\geq 3})\delta_{l\geq 7}\ .\end{aligned} \tag{34.304}$$

for $k \in G \cup E$ and $l \in E$ and $f \in G \cup E$ but $f \neq k, l$. The projection onto the quantization axis $H_{kl} = H_{kl}\left(\frac{\hat{\epsilon}_{kl}}{|\hat{\epsilon}_{kl}|}, \vec{\mathcal{B}}, m_l - m_k\right)$ is given by Eq. (34.308).

The Eqs. (34.298)-(34.303) form together an algorithm to generate the matrix allowing one to numerically solve the Bloch equations (34.297), as has been done in the main text.

34.7.4.2 Relative forces of oscillators

Spontaneous transitions between hyperfine- and Zeeman split levels have to be weighted according to the Wigner-Eckardt theorem using Clebsch-Gordan $(3j)$ and Wigner $\{6j\}$ symbols. Consider the transition $|(J_k, I)F_k, m_k\rangle \leftrightarrow |(J_l, I)F_l, m_l\rangle$. The relative oscillator strength is,

$$\begin{aligned}S_{kl} = &\begin{pmatrix} F_k & \kappa & F_l \\ m_k & \text{sign}\ (m_l - m_k) & -m_l \end{pmatrix}^2 \\ &\begin{Bmatrix} J_l & J_k & \kappa \\ F_k & F_l & I \end{Bmatrix}^2 \frac{(2F_k+1)(2J_l+1)(2\kappa+1)}{2I+1}\ .\end{aligned} \tag{34.305}$$

34.7.4.3 Elliptical laser polarization

The transition rates additionally depend on the relative orientation of the laser polarizations and the magnetic field direction. This dependence is accounted for by decomposing the polarization vector into the,

$$\hat{\mathbf{e}}_3 = \frac{\vec{\mathcal{B}}}{B} \quad , \quad \hat{\mathbf{e}}_2 = \frac{\hat{\mathbf{e}}_3 \times \hat{\mathbf{g}}}{|\hat{\mathbf{e}}_3 \times \hat{\mathbf{g}}|} \quad , \quad \hat{\mathbf{e}}_1 = \frac{\hat{\mathbf{e}}_2 \times \hat{\mathbf{e}}_3}{|\hat{\mathbf{e}}_2 \times \hat{\mathbf{e}}_3|}\ , \tag{34.306}$$

where $\hat{\mathbf{g}}$ is an arbitrarily chosen direction, e.g. gravity. The relative amplitude of the transitions $\Delta m_J = 0$ is proportional to the projection of the polarization vector on the magnetic field axis $\zeta_0 = (\hat{\varepsilon} \cdot \hat{\mathbf{e}}_3)^2$ for π-polarized light. To estimate the amplitude of the transitions $\Delta m_J = \pm 1$, we must project onto the coordinates,

$$\hat{\mathbf{e}}_\pm = \tfrac{1}{\sqrt{2}}(\mp\hat{\mathbf{e}}_1 - \imath\hat{\mathbf{e}}_2)\ , \tag{34.307}$$

and we obtain $\zeta_{\pm 1} = (\hat{\varepsilon} \cdot \hat{\mathbf{e}}_\pm)^2$ for $\sigma^\pm$-polarized light. Hence,

$$H_{kl} = \zeta_{\Delta m_J} = \zeta_{m_l - m_k}\ . \tag{34.308}$$

With this generalization the Bloch equations can e.g. be employed to calculate Hanle resonances quantum mechanically. The Hanle effect occurs when a magnetic and an optical field compete for the quantization axis.

34.7.4.4 Hyperfine and Zeeman splitting

The nuclear spin of the ^{6}Li atom is $I = 1$, its electron spin is $S = \frac{1}{2}$. The excitation states are characterized by quantum numbers J_k, F_k, m_k. The electron angular orbital momentum is $L_k = \delta_{k\geq 7}$, and the electron angular orbital momentum is $J_k = \frac{1}{2}\delta_{k\leq 6} + \frac{3}{2}\delta_{k\geq 7}$. The hyperfine structure of the excited state $^2P_{3/2}$ can be written as $\nu_{hf1} = -2.8$ MHz, $\nu_{hf2} = 0$ MHz, and $\nu_{hf3} = 1.7$ MHz. Hence, the hyperfine splitting is inferior to the natural decay rate $\Gamma = (2\pi)\ 6$ MHz,

$$\begin{aligned} Z_{kl} &= \tfrac{\mu_B|\vec{\mathcal{B}}|}{2\pi\hbar}(g_{F_k}m_k - g_{F_l}m_l) \\ &+ \nu_{hf1}\delta_{7\leq l\leq 8} + \nu_{hf2}\delta_{8\leq l\leq 13} + \nu_{hf3}\delta_{13\leq l\leq 16}\ , \end{aligned} \tag{34.309}$$

where g_{F_k} is the Landé factor of hyperfine level F_k.

34.7.5 Exercises

34.7.5.1 Ex: Derivation of three-level Bloch equations

Derive from the general formula (34.277) the three-level Bloch equations for the system $|1\rangle \overset{\Omega_{12}}{\longleftrightarrow} |2\rangle \overset{\Omega_{23}}{\longleftrightarrow} |3\rangle$.

Solution: *In the case of three-level systems the sum in (34.277) runs over* $(ij) = (12), (13), (23)$*, so that we get,*

$$\begin{aligned} \dot\rho_{km} &= 2\sum_j \gamma_{mj}\rho_{jj}\delta_{km} - [\sum_i(\gamma_{ik}+\gamma_{im}) + \imath(\omega_k - \omega_m)]\rho_{km} \\ &+ \tfrac{\imath}{2}\left(\Omega_{12}\rho_{k1}\delta_{2m} + \Omega_{12}^*\rho_{k2}\delta_{1m} - \Omega_{12}\rho_{2m}\delta_{k1} - \Omega_{12}^*\rho_{1m}\delta_{k2}\right) \\ &+ \tfrac{\imath}{2}\left(\Omega_{13}\rho_{k1}\delta_{2m} + \Omega_{13}^*\rho_{k2}\delta_{1m} - \Omega_{13}\rho_{2m}\delta_{k1} - \Omega_{13}^*\rho_{1m}\delta_{k2}\right) \\ &+ \tfrac{\imath}{2}\left(\Omega_{23}\rho_{k2}\delta_{3m} + \Omega_{23}^*\rho_{k3}\delta_{2m} - \Omega_{23}\rho_{3m}\delta_{k2} - \Omega_{23}^*\rho_{2m}\delta_{k3}\right)\ . \end{aligned}$$

For example, for the components ρ_{11} *and* ρ_{12}*, assuming* $\Omega_{jm}^* = \Omega_{mj} = \Omega_{jm}$*, and* $\Omega_{13} = 0$*,*

$$\begin{aligned} \dot\rho_{11} &= 2\sum_j \gamma_{1j}\rho_{jj} - 2\sum_i(\gamma_{i1}+\gamma_{i1})\rho_{km} + \tfrac{\imath\Omega_{12}}{2}(\rho_{12}-\rho_{21}) \\ \dot\rho_{12} &= -[\sum_i(\gamma_{i1}+\gamma_{i2}) + \imath(\omega_1-\omega_2)]\rho_{12} + \tfrac{\imath\Omega_{12}}{2}(\rho_{11}-\rho_{22}) + \tfrac{\imath\Omega_{23}}{2}\rho_{13}\ . \end{aligned}$$

in agreement with (34.279). The decay terms actually depend on the level configuration. For a λ*-system we have* $E_1, E_2 < E_3$*, for a* V*-system we have* $E_1, E_2 > E_3$*, and for a cascade system* $E_1 < E_2 < E_3$*.*

34.7.5.2 Ex: Bloch equations for three levels

An excited Λ-shaped atom consists of two ground states $|1\rangle$ and $|3\rangle$, which are coupled by two lasers with Rabi frequencies and detunings Ω_{12} and Δ_{12} respectively Ω_{23} and Δ_{23} through an excited level $|2\rangle$. Derive the Bloch equations from this system from the general master equation.

Solution: *Let us first verify that the Bloch equations for two levels follow the formula (34.222). The Hamiltonian is* $\hat{H} = \hbar\omega_0|2\rangle\langle 2| + \frac{\hbar}{2}\Omega e^{-\imath\omega t}|1\rangle\langle 2| + \frac{\hbar}{2}\Omega e^{\imath\omega t}|2\rangle\langle 1|$ *the operator of Liouville is*

$$\begin{aligned}
\mathcal{L}\rho &= \sum\nolimits_{i,j}\gamma_{ij}\Big(|j\rangle\langle i|\sum\nolimits_{m,n}|m\rangle\rho_{mn}\langle n|i\rangle\langle j| - \sum\nolimits_{m,n}|m\rangle\rho_{mn}\langle n|i\rangle\langle j|j\rangle\langle i| \\
&+ |j\rangle\langle i|\sum\nolimits_{m,n}|m\rangle\rho_{mn}\langle n|i\rangle\langle j| - |i\rangle\langle j|j\rangle\langle i|\sum\nolimits_{m,n}|m\rangle\rho_{mn}\langle n|\Big) \\
&= \gamma\Big(|2\rangle\langle 1|\sum\nolimits_{m,n}|m\rangle\rho_{mn}\langle n|1\rangle\langle 2| - \sum\nolimits_{m,n}|n\rangle\rho_{nm}\langle m|1\rangle\langle 2|2\rangle\langle 1| \\
&+ |2\rangle\langle 1|\sum\nolimits_{m,n}|m\rangle\rho_{mn}\langle n|1\rangle\langle 2| - |1\rangle\langle 2|2\rangle\langle 1|\sum\nolimits_{m,n}|n\rangle\rho_{nm}\langle m|\Big) \\
&= \gamma\Big(2|2\rangle\rho_{11}\langle 2| - \sum\nolimits_{n}|n\rangle\rho_{n1}\langle 1| - \sum\nolimits_{m}|1\rangle\rho_{m1}\langle m|\Big)\ .
\end{aligned}$$

Follows the master equation,

$$\begin{aligned}
&\frac{d}{dt}\rho = -\frac{\imath}{\hbar}[H,\rho] + \mathcal{L}\rho \\
&= -\imath\begin{pmatrix} \frac{1}{2}\Omega e^{-\imath\omega t}\rho_{21} - \frac{1}{2}\Omega e^{\imath\omega t}\rho_{12} & \frac{1}{2}\Omega e^{-\imath\omega t}\rho_{22} - \frac{1}{2}\Omega e^{-\imath\omega t}\rho_{11} - \omega_0\rho_{12} \\ \frac{1}{2}\Omega e^{\imath\omega t}\rho_{11} - \frac{1}{2}\Omega e^{\imath\omega t}\rho_{22} + \omega_0\rho_{21} & \frac{1}{2}\Omega e^{\imath\omega t}\rho_{12} - \frac{1}{2}\Omega e^{-\imath\omega t}\rho_{21} \end{pmatrix} + \gamma\begin{pmatrix} 2\rho_{22} & -\rho_{12} \\ -\rho_{21} & -2\rho_{22} \end{pmatrix} \\
&= -\imath\begin{pmatrix} \frac{\Omega}{2}\tilde{\rho}_{21} - \frac{\Omega}{2}\tilde{\rho}_{12} & \frac{\Omega}{2}e^{-\imath\omega t}\rho_{22} - \frac{\Omega}{2}\rho_{11}e^{-\imath\omega t} - \omega_0\tilde{\rho}_{12}e^{-\imath\omega t} \\ \frac{\Omega}{2}e^{\imath\omega t}\rho_{11} - \frac{\Omega}{2}e^{\imath\omega t}\rho_{22} + \omega_0\tilde{\rho}_{21}e^{\imath\omega t} & \frac{\Omega}{2}\tilde{\rho}_{12} - \frac{1}{2}\Omega\tilde{\rho}_{21} \end{pmatrix} + \gamma\begin{pmatrix} 2\rho_{22} & -\rho_{12} \\ -\rho_{21} & -2\rho_{22} \end{pmatrix}
\end{aligned}$$

transforming to the rotating frame, $\tilde{\rho}_{12}e^{-\imath\omega t} = \rho_{12}$,

$$\frac{d}{dt}\tilde{\rho} = \begin{pmatrix} -\frac{\imath}{2}\Omega\tilde{\rho}_{21} + \frac{\imath}{2}\Omega\tilde{\rho}_{12} & -\frac{\imath}{2}\Omega\rho_{22} + \frac{\imath}{2}\Omega\rho_{11} - \imath\Delta\tilde{\rho}_{12} \\ -\frac{\imath}{2}\Omega\rho_{11} + \frac{\imath}{2}\Omega\rho_{22} + \imath\Delta\tilde{\rho}_{21} & -\frac{\imath}{2}\Omega\tilde{\rho}_{12} + \frac{\imath}{2}\Omega\tilde{\rho}_{21} \end{pmatrix} + \gamma\begin{pmatrix} 2\rho_{22} & -\rho_{12} \\ -\rho_{21} & -2\rho_{22} \end{pmatrix}\ .$$

Moving to the Bloch vector notation we find the well-known expression (34.188).
We now generalize to three levels using the equations (34.266). For three levels the Hamiltonian is,

$$\hat{H} = \hbar\omega_2|2\rangle\langle 2| + \hbar\omega_3|3\rangle\langle 3| + \frac{\hbar}{2}\Omega_{12}e^{-\imath\omega_a t}|1\rangle\langle 2| + \frac{\hbar}{2}\Omega_{12}e^{\imath\omega_a t}|2\rangle\langle 1| + \frac{\hbar}{2}\Omega_{23}e^{\imath\omega_b t}|2\rangle\langle 3| + \frac{\hbar}{2}\Omega_{23}e^{-\imath\omega_b t}|3\rangle\langle 2|\ ,$$

and the Liouville operator is,

$$\begin{aligned}
\mathcal{L}\rho = &\gamma_{12}\left(2|1\rangle\rho_{22}\langle 1| - 2|2\rangle\rho_{22}\langle 2| - |1\rangle\rho_{12}\langle 2| - |2\rangle\rho_{21}\langle 1|\right) \\
&+ \gamma_{23}\left(2|3\rangle\rho_{22}\langle 3| - 2|2\rangle\rho_{22}\langle 2| - |2\rangle\rho_{23}\langle 3| - |3\rangle\rho_{32}\langle 2|\right) \\
&+ \gamma_{13}\left(2|1\rangle\rho_{33}\langle 1| - 2|3\rangle\rho_{33}\langle 3| - |1\rangle\rho_{13}\langle 3| - |3\rangle\rho_{31}\langle 1|\right)\ .
\end{aligned}$$

Follows the master equation,

$$\begin{aligned}
&\frac{d}{dt}\rho = -\frac{\imath}{\hbar}[H,\rho] + \mathcal{L}\rho \\
&= -\imath\left[\begin{pmatrix} 0 & \frac{\Omega_{12}}{2}e^{-\imath\omega_a t} & 0 \\ \frac{\Omega_{12}}{2}e^{\imath\omega_a t} & -\imath\omega_2 & -\frac{\imath\Omega_{23}}{2}e^{\imath\omega_b t} \\ 0 & \frac{\Omega_{23}}{2}e^{-\imath\omega_b t} & -\imath\omega_3 \end{pmatrix}, \begin{pmatrix} \rho_{11} & \rho_{12} & \rho_{13} \\ \rho_{21} & \rho_{22} & \rho_{23} \\ \rho_{31} & \rho_{32} & \rho_{33} \end{pmatrix}\right] \\
&+ \begin{pmatrix} 2\gamma_{12}\rho_{22} + 2\gamma_{13}\rho_{33} & -\gamma_{12}\rho_{12} & -\gamma_{13}\rho_{13} \\ -\gamma_{12}\rho_{21} & -2(\gamma_{12}+\gamma_{23})\rho_{22} & -\gamma_{23}\rho_{23} \\ -\gamma_{13}\rho_{31} & -\gamma_{23}\rho_{32} & 2\gamma_{23}\rho_{22} - 2\gamma_{13}\rho_{33} \end{pmatrix}
\end{aligned}$$

Using MAPLE we derive the Bloch equations,

$$\dot\rho_{11} = \tfrac{\imath}{2}\Omega_{12}\left(e^{\imath\omega_a t}\rho_{12} - e^{-\imath\omega_a t}\rho_{21}\right) + 2\gamma_{12}\rho_{22} + 2\gamma_{13}\rho_{33} = 1 - \rho_{22} - \rho_{33}$$
$$\dot\rho_{22} = -\tfrac{\imath}{2}\Omega_{12}\left(e^{\imath\omega_a t}\rho_{12} - e^{-\imath\omega_a t}\rho_{21}\right) + \tfrac{\imath}{2}\Omega_{23}\left(e^{-\imath\omega_b t}\rho_{23} - e^{\imath\omega_b t}\rho_{32}\right) - 2\gamma_{12}\rho_{22} - 2\gamma_{23}\rho_{22}$$
$$\dot\rho_{12} = \tfrac{\imath}{2}\Omega_{12}e^{-\imath\omega_a t}(\rho_{11} - \rho_{22}) + \tfrac{\imath}{2}\Omega_{23}e^{-\imath\omega_b t}\rho_{13} + (\imath\omega_2 - \gamma_{12})\rho_{12} = \dot\rho_{21}^*$$
$$\dot\rho_{13} = \tfrac{\imath}{2}\Omega_{23}e^{-\imath\omega_b t}\rho_{12} - \tfrac{\imath}{2}\Omega_{12}e^{-\imath\omega_a t}\rho_{23} + (\imath\omega_3 - \gamma_{13})\rho_{13} = \dot\rho_{31}^*$$
$$\dot\rho_{23} = -\tfrac{\imath}{2}\Omega_{12}e^{\imath\omega_a t}\rho_{13} + \tfrac{\imath}{2}\Omega_{23}e^{\imath\omega_b t}(\rho_{22} - \rho_{33}) + (\imath\omega_3 - \imath\omega_2 - \gamma_{23})\rho_{23} = \dot\rho_{32}^* \ .$$

This result can be cast into a matrix form.

34.7.5.3 Ex: Adiabatic elimination

Derive the effective two-level Bloch equations for a Λ-type three-level system adiabatically eliminating the excited state under the Raman condition. **Help**: Start from the Liouvillean (34.279), set $\rho_{22} = 0$, assume $\Gamma_{13} \ll \Gamma_{12}, \Gamma_{23} \ll |\Delta_{12}|, |\Delta_{23}|$, and $\Delta_{12} = -\Delta_{23}$.

Solution: *To study adiabatic elimination we start from the Liouvillean (34.279) for a Λ-system and set $\rho_{22} = 0$, which is justified for large detunings, $|\Delta_{12}|$, $|\Delta_{23}| \gg \Gamma_{12}$, Γ_{23} . We also assume $\Gamma_{13} \ll \Gamma_{12}, \Gamma_{23}$,*

$$\dot{\tilde\rho} = \begin{pmatrix}
0 & \Gamma_{13} & \frac{\imath}{2}\Omega_{12} & -\frac{\imath}{2}\Omega_{12} & 0 & 0 & 0 & 0 \\
0 & -\Gamma_{13} & 0 & 0 & 0 & 0 & -\frac{\imath}{2}\Omega_{23} & \frac{\imath}{2}\Omega_{23} \\
\frac{\imath}{2}\Omega_{12} & 0 & -\imath\Delta_{12} - \frac{1}{2}\Gamma & 0 & \frac{\imath}{2}\Omega_{23} & 0 & 0 & 0 \\
-\frac{\imath}{2}\Omega_{12} & 0 & 0 & \imath\Delta_{12} - \frac{1}{2}\Gamma & 0 & -\frac{\imath}{2}\Omega_{23} & 0 & 0 \\
0 & 0 & \frac{\imath}{2}\Omega_{23} & 0 & -\imath\Delta_{13} - \frac{1}{2}\Gamma_{13} & 0 & -\frac{\imath}{2}\Omega_{12} & 0 \\
0 & 0 & 0 & -\frac{\imath}{2}\Omega_{23} & 0 & \imath\Delta_{13} - \frac{1}{2}\Gamma_{13} & 0 & \frac{\imath}{2}\Omega_{12} \\
0 & -\frac{\imath}{2}\Omega_{23} & 0 & 0 & -\frac{\imath}{2}\Omega_{12} & 0 & -\imath\Delta_{23} - \frac{1}{2}\Gamma & 0 \\
0 & \frac{\imath}{2}\Omega_{23} & 0 & 0 & 0 & \frac{\imath}{2}\Omega_{12} & 0 & \imath\Delta_{23} - \frac{1}{2}\Gamma
\end{pmatrix}
\begin{pmatrix} \rho_{11} \\ \rho_{33} \\ \rho_{12} \\ \rho_{21} \\ \rho_{13} \\ \rho_{31} \\ \rho_{23} \\ \rho_{32} \end{pmatrix},$$

with $\Delta_{13} = \Delta_{12} + \Delta_{23}$ and defining $\Gamma \equiv \Gamma_{12} + \Gamma_{23}$. We set the Raman condition $\Delta \equiv \Delta_{12} = -\Delta_{23}$, such that $\Delta_{13} = 0$, and assume the coherences to the excited state to be stationary,

$$\dot\rho_{12} = 0 = \tfrac{\imath}{2}\Omega_{12}\rho_{11} - \left(\imath\Delta + \tfrac{1}{2}\Gamma\right)\rho_{12} + \tfrac{\imath}{2}\Omega_{23}\rho_{13}$$
$$\dot\rho_{23} = 0 = -\tfrac{\imath}{2}\Omega_{23}\rho_{33} - \left(-\imath\Delta + \tfrac{1}{2}\Gamma\right)\rho_{23} - \tfrac{\imath}{2}\Omega_{12}\rho_{13}$$

such that

$$\rho_{12} = \frac{\imath\Omega_{12}\rho_{11} + \imath\Omega_{23}\rho_{13}}{2\imath\Delta + \Gamma} \quad , \quad \rho_{23} = \frac{-\imath\Omega_{23}\rho_{33} - \imath\Omega_{12}\rho_{13}}{-2\imath\Delta + \Gamma} \ .$$

Now substituting this into the remaining Bloch equations,

$$\begin{aligned}
\dot\rho_{11} &= \Gamma_{13}\rho_{33} + \tfrac{\imath}{2}\Omega_{12}\rho_{12} - \tfrac{\imath}{2}\Omega_{12}\rho_{21} \\
&= -\frac{\Omega_{12}^2\Gamma}{4\Delta^2 + \Gamma^2}\rho_{11} + \Gamma_{13}\rho_{33} - \frac{\Omega_{12}\Omega_{23}}{4\imath\Delta + 2\Gamma}\rho_{13} - \frac{\Omega_{12}\Omega_{23}}{-4\imath\Delta + 2\Gamma}\rho_{31} \\
\dot\rho_{33} &= -\Gamma_{13}\rho_{33} - \tfrac{\imath}{2}\Omega_{23}\rho_{23} + \tfrac{\imath}{2}\Omega_{23}\rho_{32} \\
&= -\Gamma_{13}\rho_{33} - \frac{\Omega_{23}^2\Gamma}{4\Delta^2 + \Gamma^2}\rho_{33} - \frac{\Omega_{12}\Omega_{23}}{-4\imath\Delta + 2\Gamma}\rho_{13} - \frac{\Omega_{12}\Omega_{23}}{4\imath\Delta + 2\Gamma}\rho_{31} \\
\dot\rho_{13} &= -\tfrac{1}{2}\Gamma_{13}\rho_{13} + \tfrac{\imath}{2}\Omega_{23}\rho_{12} - \tfrac{\imath}{2}\Omega_{12}\rho_{23} \\
&= \left(-\tfrac{1}{2}\Gamma_{13} - \frac{\Omega_{23}^2}{4\imath\Delta + 2\Gamma} - \frac{\Omega_{12}^2}{-4\imath\Delta + 2\Gamma}\right)\rho_{13} - \frac{\Omega_{12}\Omega_{23}}{4\imath\Delta + 2\Gamma}\rho_{11} - \frac{\Omega_{12}\Omega_{23}}{-4\imath\Delta + 2\Gamma}\rho_{33} \ .
\end{aligned}$$

Neglecting the terms 2Γ *in all denominators and defining* $\Omega \equiv \frac{\Omega_{12}\Omega_{23}}{2\Delta}$,

$$\mathcal{L} \simeq \begin{pmatrix} -\frac{\Omega_{12}^2\Gamma}{4\Delta^2} & \Gamma_{13} & \frac{\imath}{2}\Omega & -\frac{\imath}{2}\Omega \\ 0 & -\Gamma_{13} - \frac{\Omega_{23}^2\Gamma}{4\Delta^2} & -\frac{\imath}{2}\Omega & \frac{\imath}{2}\Omega \\ \frac{\imath}{2}\Omega & -\frac{\imath}{2}\Omega & -\frac{1}{2}\Gamma_{13} + \imath\frac{\Omega_{12}^2-\Omega_{23}^2}{4\Delta} & 0 \\ -\frac{\imath}{2}\Omega & \frac{\imath}{2}\Omega & 0 & -\frac{1}{2}\Gamma_{13} - \imath\frac{\Omega_{12}^2-\Omega_{23}^2}{4\Delta} \end{pmatrix} .$$

34.8 Multi-level phenomena

The multi-level Bloch equations, and in particular the three-level Bloch equations (34.279), allow for the theoretical description of many phenomena beyond the two-level approximation. Among them are the phenomena of *light shift* treated in Excs. 34.5.4.12 and 34.5.4.13, the *Autler-Townes splitting* treated in Exc. 34.8.4.1, the *dark resonances* treated in Excs. 34.8.4.3 to 34.8.4.6, the *STIRAP* method treated in Exc. 34.8.4.7, *adiabatic sweeps* treated in Exc. 34.8.4.8, the dispersive interaction between atoms and light treated in Exc. 34.8.4.9, *Fano resonance*-type line profiles of dark resonances treated in Exc. 34.8.4.10, and the *quantum jumps*, which will be studied in later chapters. In Excs. 34.8.4.11 and 34.8.4.12 we will show, that an atomic gas may have *negative permittivity* and *negative permeability* and, consequently, properties usually only found in artificial metamaterials, as for example, a *negative refractive index*.

34.8.1 Electromagnetically induced transparency

In some special cases, the three-level Bloch equations can be solved analytically. The system in Λ-configuration schematized in Fig. 34.17(a), where the two lasers satisfy the condition $\Delta_{12} = \Delta_{23}$ can exhibit a *dark resonance* leading to the phenomena of *electromagnetically induced transparency* (*EIT*) and *electromagnetically induced absorption*. In these resonances a dramatic change of the refractive index is observed despite the fact that the atom becomes transparent, $\mathfrak{Re}\ \chi \gg 0$ and $|\mathfrak{Im}\ \chi| \ll \mathfrak{Re}\ \chi$:

$$\mathfrak{Re}\ n = \sqrt{1 + \mathfrak{Re}\ \chi} \gg 1 \ , \tag{34.310}$$

resulting in a high group velocity,

$$v_g = \frac{c}{n + \omega\frac{dn}{d\omega}} \ . \tag{34.311}$$

EIT is usually studied in Λ-type systems, but similar phenomena can be found in cascade-type systems [1414, 1395], which will be studied here. Disregarding the decay rate Γ_{13}, the Bloch equations (34.279) and (34.282) give the coherences,

$$\begin{aligned} \dot\rho_{12} &= -\Lambda_{12}\rho_{12} + \tfrac{\imath\Omega_{12}}{2}(\rho_{11} - \rho_{22}) - \tfrac{\imath\Omega_{23}}{2}\rho_{13} \\ \dot\rho_{13} &= -\Lambda_{13}^*\rho_{13} - \tfrac{\imath\Omega_{12}}{2}\rho_{23} - \tfrac{\imath\Omega_{23}}{2}\rho_{12} \\ \dot\rho_{23} &= -\Lambda_{23}\rho_{23} + \tfrac{\imath\Omega_{23}}{2}(\rho_{22} - \rho_{33}) - \tfrac{\imath\Omega_{12}}{2}\rho_{13} \ . \end{aligned} \tag{34.312}$$

Assuming stationarity and negligible depletion of the ground state, $\rho_{11} = 1$,

$$\begin{aligned} 0 &= -\Lambda_{12}\rho_{12} + \tfrac{\imath\Omega_{12}}{2} - \tfrac{\imath\Omega_{23}}{2}\rho_{13} \\ 0 &= -\Lambda_{13}^{*}\rho_{13} - \tfrac{\imath\Omega_{12}}{2}\rho_{23} - \tfrac{\imath\Omega_{23}}{2}\rho_{12} \\ 0 &= -\Lambda_{23}\rho_{23} - \tfrac{\imath\Omega_{12}}{2}\rho_{13} \ . \end{aligned} \tag{34.313}$$

Substituting the third into the first equation,

$$\begin{aligned} 0 &= -\Lambda_{12}\rho_{12} + \tfrac{\imath\Omega_{12}}{2} - \tfrac{\imath\Omega_{23}}{2}\rho_{13} \\ 0 &= -\Lambda_{13}^{*}\rho_{13} - \tfrac{\Omega_{12}^{2}}{4\Lambda_{23}}\rho_{13} - \tfrac{\imath\Omega_{23}}{2}\rho_{12} \ . \end{aligned} \tag{34.314}$$

and finally,

$$\boxed{\rho_{12} = \frac{\imath\Omega_{12}}{2}\frac{4\Lambda_{13}^{*}\Lambda_{23} + \Omega_{12}^{2}}{\Lambda_{12}\left(4\Lambda_{13}^{*}\Lambda_{23} + \Omega_{12}^{2}\right) + \Omega_{23}^{2}\Lambda_{23}}} \ . \tag{34.315}$$

The macroscopic polarization is now $\mathcal{P} = \frac{N}{V} d_{12}\rho_{21}$, with the number of atoms N. In the limit of weak probes, the *dressed* susceptibility follows from $\mathcal{P} = \varepsilon_0\chi\mathcal{E}_{12} = \frac{N}{V} d_{12}\rho_{21}$,

$$\chi = \frac{N d_{12}}{V\varepsilon_0\mathcal{E}_{12}}\rho_{21} = \frac{N|d_{12}|^2}{V\varepsilon_0\hbar\Omega_{12}}\rho_{21} \ . \tag{34.316}$$

For a resonant probe laser, $\Delta_{23} = 0$ and with $\Gamma_{13} \simeq 0$, we have $\Lambda_{13} = \frac{1}{2}\Gamma_{23} + \imath\Delta_{12}$ and $\Lambda_{23} = \frac{1}{2}(\Gamma_{23} + \Gamma_{12})$. The susceptibility in the probe transition is now, using $\Theta \equiv \Gamma_{23} + \frac{\Omega_{12}^{2}}{2\Lambda_{23}}$,

$$\begin{aligned} \chi &= \frac{N|d_{12}|^2}{V\varepsilon_0\hbar\Omega_{12}}\imath\Omega_{12}\frac{\Gamma_{23} + \frac{\Omega_{12}^{2}}{2\Lambda_{23}} - 2\imath\Delta_{12}}{\left(\Gamma_{23} + \frac{\Omega_{12}^{2}}{2\Lambda_{23}} - 2\imath\Delta_{12}\right)(\Gamma_{12} + 2\imath\Delta_{12}) + \Omega_{23}^{2}} \\ &= \frac{N|d_{12}|^2}{V\varepsilon_0\hbar\Omega_{12}}\imath\Omega_{12}\frac{\Theta - 2\imath\Delta_{12}}{(\Theta - 2\imath\Delta_{12})(\Gamma_{12} + 2\imath\Delta_{12}) + \Omega_{23}^{2}} = \chi' + \imath\chi'' \ . \end{aligned} \tag{34.317}$$

Example 202 (*EIT in a cascade system*): We consider, for example, the intercombination line of atomic strontium ${}^{1}S_0$-${}^{3}P_1$ ($\lambda_{12} = 689\,\text{nm}$ and $\Gamma_{12} = (2\pi)\ 7.6\,\text{kHz}$) be the 'dressing' transition ${}^{3}P_1$-(5s4d)${}^{3}D_1$ ($\lambda_{23} = 2700\,\text{nm}$ and $\Gamma_{23} = (2\pi)\ 90.3\,\text{kHz}$), be the 'dressing' transition ${}^{3}P_1$-(5s5d)${}^{3}D_1$ ($\lambda_{23} = 497\,\text{nm}$ and $\Gamma_{23} = (2\pi)\ 2.3\,\text{MHz}$), both characterized by $\Gamma_{23} \gg \Omega_{12}, \Gamma_{12}, |\Delta_{12}|$, such that $\Theta \simeq \Gamma_{23}$. Hence,

$$\chi' + \imath\chi'' = \frac{N|d_{12}|^2}{V\varepsilon_0\hbar}\frac{2\Delta_{12} + \imath\Gamma_{23}}{\Omega_{23}} \ .$$

The refraction index follows with,

$$n = \sqrt{1+\chi} \simeq 1 + \tfrac{1}{2}\chi \ .$$

Its imaginary part originates from the decay term of the atom: it is here responsible for the absorbing nature of the cloud. EIT is characterized by a pronounced dispersion and a small concomitant absorption.

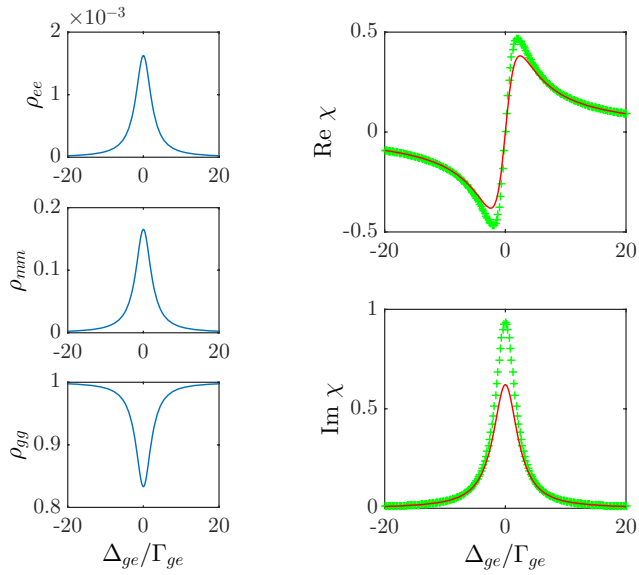

Figure 34.18: (code) EIT signal for the cascade system of strontium with the transitions at 689 nm and 497 nm with $\Omega_{12} = \Gamma_{12}$, $\Omega_{23} = \Gamma_{23}$ and $\Delta_{23} = 0$. The red lines are calculated by numerical integration of the Bloch equations. The dotted lines are obtained from analytical formulas based on the assumptions of weak ground state depletion (which is not really correct in the chosen parameter regime.

34.8.2 Polarization, alignment, and orientation

34.8.2.1 Polarization and helicity

Photons may have the angular momenta $\hat{\mathbf{L}}$, $\hat{\mathbf{S}}$, and $\hat{\mathbf{J}}$, but due to the fact that photons have zero mass, only $\hat{\mathbf{J}}$ is of importance. The *helicity* is defined as,

$$\hat{\mathbf{J}} \cdot \mathbf{k} = (\hat{\mathbf{L}} + \hat{\mathbf{S}}) \cdot \mathbf{k} = \hat{\mathbf{S}} \cdot \mathbf{k} = m_s = \pm 1 \ , \tag{34.318}$$

in beam direction and the *polarization* is,

$$\hat{\mathbf{J}} \cdot \hat{\mathbf{e}}_z = m_j = -j, ...j \ . \tag{34.319}$$

Polarizers prepare the photon in its eigenstate. The angular momentum with respect to $\hat{\mathbf{J}}$ in a basis $\hat{\mathbf{e}}_z$ orthogonal to $\mathbf{k}$ is,

$$\hat{\mathbf{J}} \cdot \mathbf{k}|m\rangle_y = a_m|1\rangle_z + b_m|-1\rangle_z \ . \tag{34.320}$$

The state $|0\rangle_z$ does not exist. For example,

$$\hat{\mathbf{J}} \cdot \mathbf{k}|1\rangle_y = \hat{J}_z \left(\tfrac{1}{2}|1\rangle_z + \imath|0\rangle_z - \tfrac{1}{2}|-1\rangle_z\right) = \tfrac{1}{2}(|1\rangle_z + |-1\rangle_z) \ . \tag{34.321}$$

34.8.2.2 Orientation and alignment

A level $|j\rangle$ with Zeeman degeneracy $|jm\rangle$ can be irreducibly described by Cartesian polarization tensors. Those are the *orientation* and the *alignment* [716, 1292],

$$\boxed{\begin{array}{rcl} O_i & \equiv & \langle \hat{J}_i \rangle \\ A_{ij} & \equiv & \frac{3}{2}\langle [\hat{J}_i, \hat{J}_j]_+ \rangle - \langle \hat{\mathbf{J}}^2 \rangle \delta_{ij} \end{array}} \ , \tag{34.322}$$

with $i, j = x, y, z$. The expectation value is calculated as usual, $\langle ... \rangle = \text{Tr}\ \hat{\rho} ... = \sum_m \langle jm|\hat{\rho}...|jm\rangle$. If $O_i \neq 0$ then the system is said *oriented*, if $A_{ij} \neq 0$ the system is said *aligned* and if either $O_i \neq 0$ or $A_{ij} \neq 0$ then the system is said *polarized*.

The orientation and the alignment depend on the choice of the quantization axis and on the Zeeman splitting of level $|j\rangle$. Choosing z as quantization axis and disregarding Zeeman coherences $\langle m|\hat{\rho}|m'\rangle \sim \delta_{mm'}$, we get the orientation,

$$\mathbf{O} = \hbar \hat{\mathbf{e}}_z \sum_m m \rho_{mm} \tag{34.323}$$

and the alignment,

$$(A_{ij}) = -\hbar^2 j(j+1) - \begin{pmatrix} -\frac{3}{2} & 0 & 0 \\ 0 & -\frac{3}{2} & 0 \\ 0 & 0 & 3 \end{pmatrix} \sum_m \hbar^2 m^2 \rho_{mm} \ , \tag{34.324}$$

if the atom is with certainty in level $|j\rangle$ so that $\text{Tr}\ \hat{\rho} = 1$. These results will be derived in Exc. 34.8.4.14.

34.8.3 Hanle effect

The *Hanle effect* occurs when a magnetic and an optical field compete for the quantization axis. Imagine an atom irradiated by a laser from direction $\mathbf{k} = k\hat{\mathbf{e}}_x$, linearly polarized $\varepsilon = \hat{\mathbf{e}}_y$ and subject to a magnetic field $\vec{\mathcal{B}} = \mathcal{B}\hat{\mathbf{e}}_z$. The fluorescence is detected in direction $\hat{\mathbf{e}}_y$ through a linear polarizer [351]. If $\mathcal{B} = 0$, no light is emitted into the detector since the dipole radiation pattern is a torus with symmetry axis $\hat{\mathbf{e}}_y$. If $\mathcal{B}$ is now increased, the quantization axis is tilted and the torus slowly precesses about the $\hat{\mathbf{e}}_x$ axis. Plotting the time-averaged fluorescence as a function of the magnetic field $\mathcal{B}$, we observe a *dark resonance*. These arguments are rather classical.

Quantum mechanically, Hanle resonances are easily calculated. The transition rates additionally depend on the relative orientation of the laser polarization and the magnetic field direction. This dependence is accounted for by decomposing the polarization vector into the coordinates defined by,

$$\hat{\mathbf{e}}_3 = \frac{\vec{\mathcal{B}}}{\mathcal{B}} \quad , \quad \hat{\mathbf{e}}_2 = \frac{\hat{\mathbf{e}}_3 \times \hat{\mathbf{g}}}{|\hat{\mathbf{e}}_3 \times \hat{\mathbf{g}}|} \quad , \quad \hat{\mathbf{e}}_1 = \frac{\hat{\mathbf{e}}_2 \times \hat{\mathbf{e}}_3}{|\hat{\mathbf{e}}_2 \times \hat{\mathbf{e}}_3|} \ , \tag{34.325}$$

where $\hat{\mathbf{g}}$ is an arbitrarily chosen direction, e.g. gravity. The relative amplitude of the transitions $\Delta m_J = 0$ is proportional to the projection of the polarization vector on

the magnetic field axis $\zeta_\pi = (\hat{\varepsilon} \cdot \hat{\mathbf{e}}_3)^2$. To estimate the amplitude of the transitions $\Delta m = \pm 1$, we must project onto the coordinates,

$$\hat{\mathbf{e}}_\pm = \tfrac{1}{\sqrt{2}}(\mp\hat{\mathbf{e}}_1 - \imath\hat{\mathbf{e}}_2) \ , \tag{34.326}$$

and we obtain $\zeta_{\sigma^\pm} = (\hat{\varepsilon} \cdot \hat{\mathbf{e}}_\pm)^2$.

Example 203 (*Hanle effect with rate equations*): The Hanle effect can be described without coherences, i.e. using only rate equations. Fig. 34.19 shows such a simulation for the case of three ground Zeeman states $|1\rangle = |g, m = +1\rangle$, $|2\rangle = |g, m = 0\rangle$, and $|3\rangle = |g, m = -1\rangle$, and one excited state $|4\rangle = |e, m = 0\rangle$. The rate equations are,

$$\dot{\rho}_{kk} = \mathcal{M}\rho_{kk} \tag{34.327}$$

$$\text{with} \quad \mathcal{M} = \begin{pmatrix} -\Omega_{14} & 0 & 0 & \Omega_{14} + \frac{1}{3}\Gamma \\ 0 & -\Omega_{24} & 0 & \Omega_{24} + \frac{1}{3}\Gamma \\ 0 & 0 & -\Omega_{34} & \Omega_{34} + \frac{1}{3}\Gamma \\ \Omega_{14} & \Omega_{24} & \Omega_{34} & -\Omega_{14} - \Omega_{24} - \Omega_{34} - \Gamma \end{pmatrix}$$

$$\text{and} \quad \Omega_{14} = \Omega_{34} = \zeta_{\sigma^\pm}\Omega \quad \text{and} \quad \Omega_{24} = \zeta_\pi \Omega \ .$$

In Exc. 34.8.4.15 we study the Hanle effect at the Ca^+ Zeeman degenerate level system.

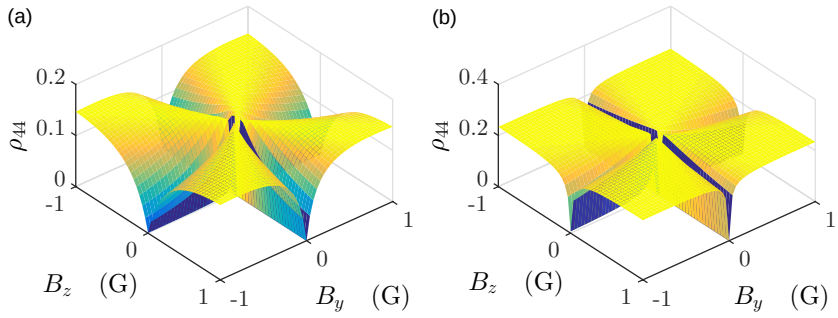

Figure 34.19: (code) Hanle effect in a four-level system with three ground and one excited state with $\hat{\varepsilon} = \hat{\mathbf{e}}_y$ and (a) $\Omega = 0.5\Gamma$ and (b) $\Omega = 5\Gamma$.

34.8.4 Exercises

34.8.4.1 Ex: Autler-Townes splitting

In this exercise we study the Autler-Townes effect in a two-level system $|1\rangle$ and $|2\rangle$ resonantly excited ($\Delta_{12} = 0$) by a laser with the Rabi frequency Ω_{12}:
a. From the eigenvalues $E_{1,2}$ of the effective Hamiltonian (34.228) of the system, describe the behavior of the real part (energy shift) and the imaginary part (linewidth) as a function of the Rabi frequency. Prepare diagrams Ω_{12} versus $\mathfrak{Re}\ E_{1,2}$ and versus $\mathfrak{Im}\ E_{1,2}$ and discuss the limits $\Omega_{12} > \frac{1}{2}\Gamma_{12}$ and $\Omega_{12} < \frac{1}{2}\Gamma_{12}$.
The Autler-Townes effect can be measured experimentally by probing the population

of level $|2\rangle$ via excitation of a third (higher) level by a second laser with the Rabi frequency Ω_{23}. Thus, we obtain a three-level system in cascade configuration, as shown in Fig. 34.17(c). In order to reproduce the experiment by numerical simulations of the Bloch equations (34.279),
b. write down the Liouville matrix $\mathcal{M}_{red}$ reduced by the trace condition (34.284) and c. compute the stationary Bloch vector from equation (34.286) varying the detuning of the probe laser Δ_{23} and the Rabi frequency Ω_{12} of the system under study ($|1\rangle$ and $|2\rangle$). Choosing the parameters $\Gamma_{23} = 0.5\Gamma_{12}$, $\Gamma_{13} = 0.01\Gamma_{12}$, $\Omega_{23} = 0.1\Gamma_{12}$, prepare a 3D curve [similar to Fig. 34.6(a)] of the stationary population $\rho_{22}(\infty)$. Interpret the results.

Solution: *a. The eigenvalues of the effective Hamiltonian (34.228) excited in resonance,*

$$E = -\tfrac{\imath}{4}\Gamma \pm \tfrac{\imath}{4}\sqrt{\Gamma^2 - 4\Omega^2} \ ,$$

describe possible effects of line broadening and/or shift due to the coupling. Two cases are interesting: In the case $\Gamma > 2\Omega$ *we get,*

$$E = \mathfrak{Re}\ E = 0 \qquad , \qquad \Gamma_{eff} = -2\mathfrak{Im}\ E = \tfrac{1}{2}\Gamma \mp \tfrac{1}{2}\sqrt{\Gamma^2 - 4\Omega^2} \to \Gamma \ .$$

That is, the resonance is not shifted or split, but undergoes a line broadening, as already shown in (34.189).
In the case $\Gamma < 2\Omega$*,*

$$E = \mathfrak{Re}\ E = \pm\tfrac{1}{2}\sqrt{\Omega^2 - \tfrac{1}{4}\Gamma^2} \to \pm\Omega \qquad , \qquad \Gamma_{eff} = -2\mathfrak{Im}\ E = \tfrac{1}{2}\Gamma \ .$$

we observe an splitting of the line called Autler-Townes splitting. When saturation is strong, the two new lines are separated by Ω*, each having the natural width* Γ*. Figs. 34.20(a,b) show the bifurcation of the spectrum at the point* $\Omega_{12} = \frac{1}{2}\Gamma$*.*
b. The Liouville matrix can be found in the numerical MATLAB code in given in the file 'LM_Bloch_AutlerTownes.m'.
c. Fig. 34.20(c) shows the results of the simulations. The laser Ω_{23} *probes the population* ρ_{22} *by excitation to a higher level, that is, the fluorescence emitted by the population* ρ_{33} *is representative for the population* ρ_{22}*.*

34.8.4.2 Ex: Quantum Zeno effect and saturation broadening

In this exercise we study saturation broadening effect in a three-level system $|1\rangle$, $|2\rangle$, and $|3\rangle$ in V-configuration, as shown in Fig. 34.17(b), excited by two resonant lasers with the Rabi frequencies Ω_{12} and Ω_{23}.
a. From the eigenvalues $E_{1,2}$ of the effective Hamiltonian (34.228) of the system, describe the behavior of the real part (energy shift) and the imaginary part (linewidth) as a function of the Rabi frequency. Prepare diagrams Ω_{12} versus $\mathfrak{Re}\ E_{1,2}$ and versus $\mathfrak{Im}\ E_{1,2}$ and discuss the limits $\Omega_{12} > \frac{1}{2}\Gamma_{12}$ and $\Omega_{12} < \frac{1}{2}\Gamma_{12}$.
Saturation broadening can be measured experimentally in a three-level system in V-configuration. To reproduce the experiment by numerical simulations of the Bloch equations (34.279),

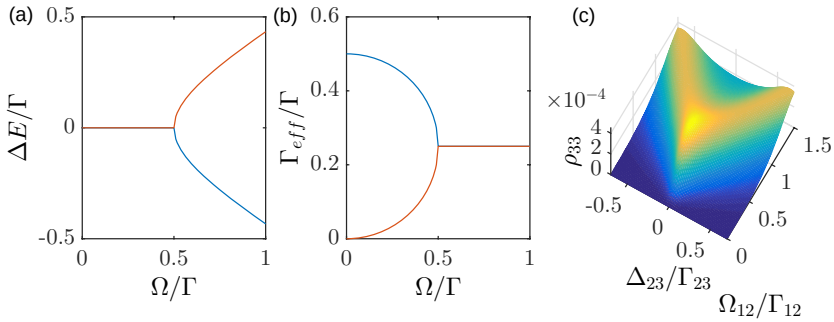

Figure 34.20: (code) (a) Autler-Townes splitting and (b) linewidths as a function of the Rabi frequency. (c) Population of the excited state in a three-level system in cascade configuration, as shown in Fig. 34.17(c) in a function of the Rabi frequencies Ω_{23} and Ω_{12}. The parameters are, $\Gamma_{23} = 0.5\Gamma_{12}$, $\Gamma_{13} = 0.01\Gamma_{12}$, $\Omega_{23} = 0.1\Gamma_{12}$.

b. write down the Liouville matrix $\mathcal{L}$ of the system and calculate the time evolution of the Bloch vector via equation (34.283) varying the Rabi frequency Ω_{12}. Choosing the parameters $\Gamma_{23} = 0.01\Gamma_{12}$, $\Gamma_{13} = 0.0001\Gamma_{12}$, $\Omega_{23} = 400\Gamma_{23}$, and $\Delta_{12} = 0 = \Delta_{23}$, prepare a 3D curve [similar to Fig. 34.6(a)] of the population $\rho_{33}(t)$ as a function of time and the Rabi frequency Ω_{12}.
c. Interpret the results in terms of broadening by saturation. The broadening can also be understood in terms of the quantum Zeno effect, where the transition $|1\rangle$-$|2\rangle$ plays the role of the 'observed system' and the transition $|2\rangle$-$|3\rangle$ the role of the measuring device or 'meter' (for example, we can observe the light scattered on the 'meter transition' to infer the evolution of the 'system transition').

Solution: *a. See the solution of Exc. 34.8.4.1(a).*
b. The Liouville matrix and the results of the simulations can be found in the numerical MATLAB code in given in the file 'LM_Bloch_ZenoEffect.m'.
c. When the 'meter transition' $|1\rangle$-$|2\rangle$ is weakly excited, $\Omega_{12} \ll \Gamma_{12}$, the 'system transition' $|2\rangle$-$|3\rangle$ evolves normally, as expected for an isolated two-level system. As we increase Ω_{12} to be able to observe the light scattered on the 'meter transition' more easily and extract information on the state of the system more quickly, we perturb the evolution of the system and prevent it from evolving: The population ρ_{33} is getting weaker.

34.8.4.3 Ex: EIT and dark resonances

In this exercise we study so-called *dark resonances*, which are responsible for the phenomenon of *electromagnetically induced transparency* (EIT). Such resonances are observed in three-level systems $|1\rangle$-$|2\rangle$-$|3\rangle$ in Λ-configuration, as shown in Fig. 34.17(a), when the laser detunings are chosen so as to satisfy $\Delta_{12} = \Delta_{23}$.
a. From the Bloch equations (34.279) show analytically that, in a stationary situation, the population of the excited state is $\rho_{22}(\infty) = 0$ in the center of the dark resonance. Dark resonances can be observed experimentally. To reproduce the experiment by

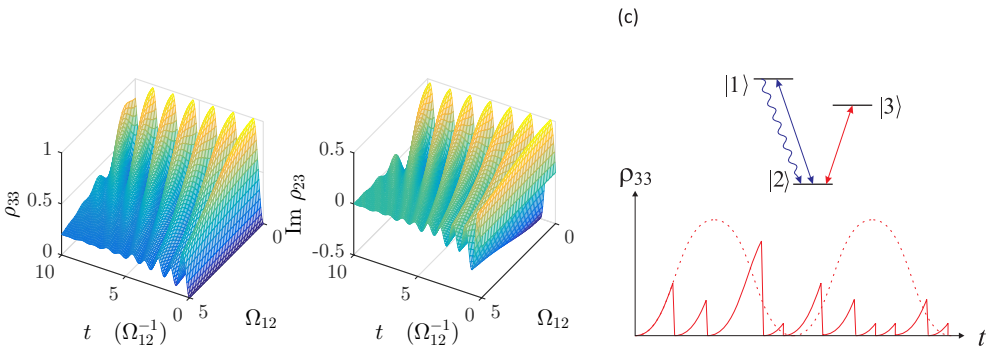

Figure 34.21: (code) (a) Temporal evolution of the excited state population ρ_{33} in a three-level system in V-configuration, as shown in Fig. 34.17(b), as a function of the Rabi frequency Ω_{12} of the 'meter' laser. (b) Temporal evolution of the coherence ρ_{23}. (c) Illustration of the interrupted evolution of the coherence.

numerical simulations of the Bloch equations (34.279), write down the Liouville matrix $\mathcal{M}_{red}$ reduced by the trace condition (34.283) and calculate the stationary Bloch vector from equation (34.284) varying the detunings of the two lasers Δ_{12} and Δ_{23}. Choosing the parameters such that $\Gamma_{23} = \Gamma_{12}$, $\Gamma_{13} = 0.01\Gamma_{12}$, $\Omega_{12} = 2\Gamma_{12}$, and $\Omega_{23} = 0.2\Gamma_{12}$, prepare a 3D curve [similar to Fig. 34.6(a)] of the population $\rho_{22}(\infty)$. Interpret the results.

Solution: *a. We put $\Delta_{12} = \Delta_{23}$ and we consider the stationary solution $\dot{\rho} = 0$. The Bloch equations are,*

$$
\begin{aligned}
0 &= \Gamma_{12}\rho_{22} + \tfrac{\imath}{2}\Omega_{12}(\rho_{12} - \rho_{21}) \\
0 &= \Gamma_{23}\rho_{22} - \tfrac{\imath}{2}\Omega_{23}(\rho_{23} - \rho_{32}) \\
0 &= \left(-\tfrac{1}{2}\Gamma_{12} - \tfrac{1}{2}\Gamma_{13} + \imath\Delta_{12}\right)\rho_{12} + \tfrac{\imath}{2}\Omega_{12}(\rho_{11} - \rho_{22}) + \tfrac{\imath}{2}\Omega_{23}\rho_{13} \\
0 &= \left(-\tfrac{1}{2}\Gamma_{12} - \tfrac{1}{2}\Gamma_{23} + \imath\Delta_{12}\right)\rho_{23} + \tfrac{\imath}{2}\Omega_{23}(\rho_{22} - \rho_{33}) - \tfrac{\imath}{2}\Omega_{12}\rho_{13} \\
0 &= \tfrac{\imath}{2}\Omega_{23}\rho_{12} - \tfrac{\imath}{2}\hbar\Omega_{12}\rho_{23} \ ,
\end{aligned}
$$

Eliminating ρ_{22} in equations I and II gives,

$$
\frac{\Omega_{12}}{\Gamma_{12}}\rho_{12} - \frac{\Omega_{12}}{\Gamma_{12}}\rho_{21} = \frac{\Omega_{23}}{\Gamma_{23}}\rho_{23} - \frac{\Omega_{23}}{\Gamma_{23}}\rho_{32} \ .
$$

Insertion of equation V into this equation gives,

$$
\frac{\Omega_{12}}{\Gamma_{12}}(\rho_{12} - \rho_{21}) = \frac{\Omega_{23}}{\Gamma_{23}}\left(\frac{\Omega_{23}}{\Omega_{12}}\rho_{21} - \frac{\Omega_{23}}{\Omega_{12}}\rho_{12}\right) \ .
$$

Since $\rho_{12} = \rho_{21} = \rho_{12}^*$, the last expression can only be true for arbitrary Rabi frequencies and decay rates if $\mathfrak{Im}\ \rho_{12} = 0$ and, hence, $\rho_{22} = 0$.
b. The Liouville matrix can be found in the numerical MATLAB code given in the file 'LM_Bloch_DarkResonance.m'. Fig. 34.22 shows the results of the simulations. The curves in Fig. 34.22(a) show that the contrast of the dark resonance decreases as the decay rate of coherence increases.

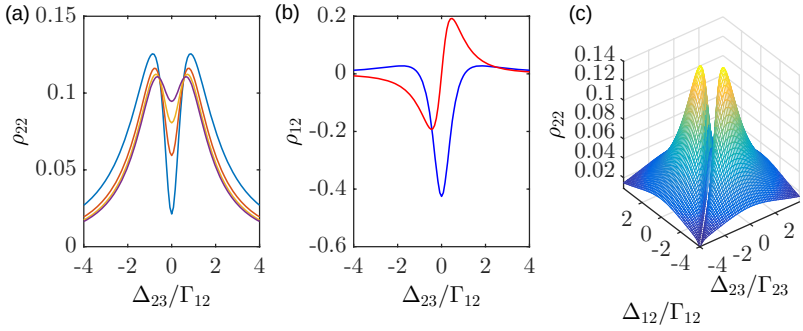

Figure 34.22: (code) (a) Population of the state excited as a function of the detuning Δ_{23} for several decay rates γ_{13} of the coherence. (b) Real and imaginary part of the susceptibility. (c) Population of the excited state as a function of the detunings Δ_{12} and Δ_{23}.

34.8.4.4 Ex: Coherent trapping and dark states

Consider a three-level system $|1\rangle$, $|2\rangle$, and $|3\rangle$ in Λ-configuration interacting with two electromagnetic fields with frequencies ω_a and ω_b. The two states $|1\rangle$ and $|3\rangle$ of lower energies $\hbar\omega_1$ and $\hbar\omega_3$ are coupled to a state $|2\rangle$ of higher energy $\hbar\omega_2$, as illustrated in Fig. 34.17(a). Assume that the transition $|1\rangle \leftrightarrow |3\rangle$ is forbidden and that the Hamiltonian of the system has the form $\hat{H} = \hat{H}_0 + \hat{H}_{int}$ where,

$$\hat{H}_0 = E_1|1\rangle\langle 1| + E_2|2\rangle\langle 2| + E_3|3\rangle\langle 3|$$
$$\hat{H}_{int} = -\tfrac{\hbar}{2}(\Omega_{12}e^{-\imath\omega_a t}|2\rangle\langle 1| + \Omega_{12}^* e^{\imath\omega_a t}|1\rangle\langle 2|) - \tfrac{\hbar}{2}(\Omega_{23}e^{-\imath\omega_b t}|2\rangle\langle 3| + \Omega_{23}^* e^{\imath\omega_b t}|3\rangle\langle 2|)\ .$$

a. Assuming that the system's state is described by $|\psi\rangle = c_1|1\rangle + c_2|2\rangle + c_3|3\rangle$ find the system of equations that describe the dynamics of probability amplitudes c_i with $(i = 1, 2, 3)$.
b. Rewrite the equations for the case where the frequencies of the applied fields are resonant (that is, $\omega_a = \omega_2 - \omega_1$ and $\omega_b = \omega_2 - \omega_3$). Simplify the system by writing in terms of the variables $u_i = c_i e^{\imath\omega_i t}$.
c. Assuming the initial condition $|\psi(0)\rangle = (|1\rangle + |3\rangle)/\sqrt{2}$, solve the system of equations for the resonant case and interpret the result.

Solution: *a. From the Schrödinger equation*

$$\imath\hbar\frac{d|\psi\rangle}{dt} = (\hat{H}_0 + \hat{H}_{int})|\psi\rangle$$

where $|\psi\rangle$ is the state given by the problem, we find the following system of equations,

$$\frac{dc_1}{dt} = -\imath\omega_1 c_1 + \tfrac{\imath\Omega_{12}^*}{2}e^{\imath\omega_a t}c_2$$
$$\frac{dc_2}{dt} = -\imath\omega_2 c_2 + \tfrac{\imath\Omega_{12}}{2}e^{-\imath\omega_a t}c_1 + \tfrac{\imath\Omega_{23}}{2}e^{-\imath\omega_b t}c_3$$
$$\frac{dc_3}{dt} = -\imath\omega_3 c_3 + \tfrac{\imath\Omega_{23}^*}{2}e^{\imath\omega_b t}c_2$$

b. By making the suggested substitutions, the system can be written as,

$$\begin{aligned}\frac{du_1}{dt} &= \frac{\imath\Omega_{12}^*}{2}u_2\\ \frac{du_2}{dt} &= \frac{\imath\Omega_{12}}{2}u_1 + \frac{\imath\Omega_{23}}{2}u_3\\ \frac{du_3}{dt} &= \frac{\imath\Omega_{23}^*}{2}u_2\end{aligned}$$

c. The initial conditions are as $u_2(0) = 0$ *and* $u_1(0) = u_3(0) = 1/\sqrt{2}$*, which will give us solutions of the type,*

$$\begin{aligned}u_1(t) &\simeq \frac{\Omega_{23}}{\sqrt{|\Omega_{12}|^2 + |\Omega_{23}|^2}}\cos\frac{\sqrt{(|\Omega_{12}|^2+|\Omega_{23}|^2)}t}{2}\\ u_2(t) &\simeq 0\\ u_3(t) &\simeq -\frac{\Omega_{12}}{\sqrt{|\Omega_{12}|^2 + |\Omega_{23}|^2}}\cos\frac{\sqrt{(|\Omega_{12}|^2+|\Omega_{23}|^2)}t}{2}\ .\end{aligned}$$

Hence, the final state can be written as $|\psi(t)\rangle = u_1(t)|1\rangle + u_3(t)|3\rangle$*. It is called a dark state, because it is independent of the excited state. This result implies that the population is trapped in the states with lower energy and the phenomenon of absorption will not occur even in the presence of external fields. The coherent trapping occurs due to the destructive quantum interference of the two transitions.*

34.8.4.5 Ex: Cascade EIT scheme in strontium

Consider the Bloch equations for the ^{88}Sr 7-level system consisting of the following levels: $|1\rangle \equiv (5s^2)\ ^1S_0$, $|2-4\rangle \equiv (5s5p)\ ^3P_1$, and $|5-7\rangle \equiv (5s5d)\ ^3D_1$, and check under which circumstances it is possible to observed dark resonances. The Sr level scheme can be consulted under (Sr level scheme). The Liouvillean can be consulted at (Sr Liouvillean).

Solution: *The results are shown in Fig. 34.23.*

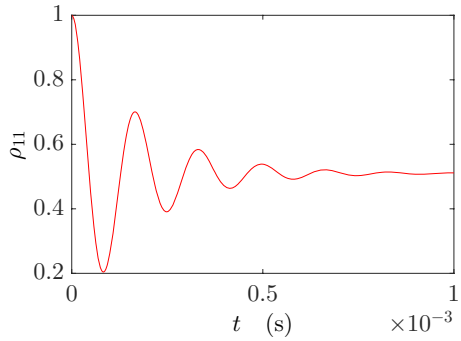

Figure 34.23: (code) Time evolution of the Sr system.

34.8.4.6 Ex: Dark resonances with Zeeman splitting

Calculate the dark resonance spectrum for the Ca^+ three-level system with Zeeman sub-structure consisting of the levels $|1\rangle \equiv {}^2S_{1/2}$, $|2\rangle \equiv {}^2P_{1/2}$, and $|3\rangle \equiv {}^2D_{3/2}$ using optical Bloch equations. **Help:** The decay rates are $\Gamma_{12}/2\pi = 23\,\text{MHz}$, $\Gamma_{23}/2\pi = 1.6\,\text{MHz}$, and $\Gamma_{13}/2\pi = 1\,\text{Hz}$. Assume that both incident lasers saturate the transitions, $\Omega_{12} = \Gamma_{12}$ and $\Omega_{23} = \Gamma_{23}$.

Solution: *The results are shown in Fig. 34.24.*

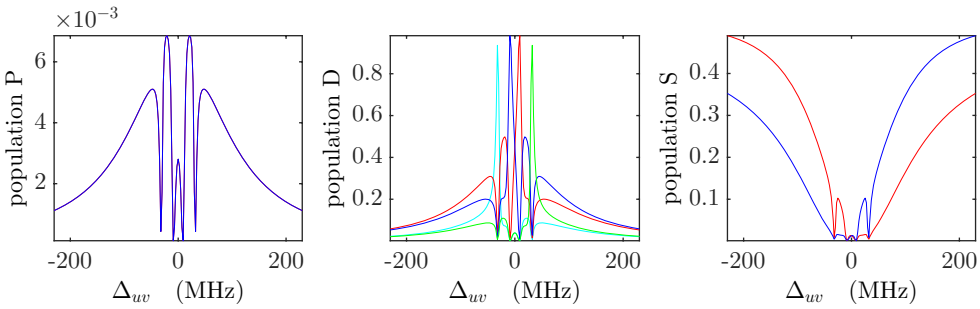

Figure 34.24: (code) Dark resonances in the Ca 3-level system. (red) $m = +1/2$, (blue) $m = -1/2$, (cyan) $m = +3/2$, and (green) $m = -3/2$.

34.8.4.7 Ex: STIRAP

In experiments with cold atoms it is often necessary to transfer populations between ground states, for example, between specific levels of a hyperfine structure. One possible procedure is the method of optical pumping, from the initial ground state to an excited state, which subsequently decays to the final state by spontaneous emission. The problem with this incoherent procedure is, that one can control into which ground state level the atom will decay, and that it heats atoms due to the photonic recoil associated with the scattering of light. In this exercise we studied an alternative method, called *Stimulated Raman Adiabatic Passage* (STIRAP), which allows the coherent transfer of population between two states by counter-intuitive pulse sequences:
a. Consider a three-level system in Λ-configuration, as shown in Fig. 34.17(a), initially being in the state $|1\rangle$. Write the system's Hamiltonian in the interaction picture. Now, choose $\Delta_{12} = 0 = \Delta_{23}$, and a temporal variation of the Rabi frequencies described by $\Omega_{12}(t) = \Gamma_{12}(\frac{1}{2} + \frac{1}{\pi}\arctan\Gamma_{12}t)$ and $\Omega_{23}(t) = \Gamma_{12}(\frac{1}{2} - \frac{1}{\pi}\arctan\Gamma_{12}t)$. With this, solve the Schrödinger equation (34.287) iteratively within the time interval $t \in [-40/\Gamma_{12}, 40/\Gamma_{12}]$, while continuously adjusting the Rabi frequencies.
b. The dynamics can also be calculated via a numerical simulations of the Bloch equations (34.279). Write down the Liouville matrix and prepare a simulation using the same parameters as in (b) and additionally $\Gamma_{23} = \Gamma_{12}/2$, $\Gamma_{13} = \Gamma_{12}/500$.
c. Interpret the results.

Solution: *a. The Hamiltonian is,*

$$\hat{H} = \hbar \begin{pmatrix} 0 & \frac{1}{2}\Omega_{12} & 0 \\ \frac{1}{2}\Omega_{12} & 0 & \frac{1}{2}\Omega_{23} \\ 0 & \frac{1}{2}\Omega_{23} & 0 \end{pmatrix} .$$

It is implemented in the numerical MATLAB code given in the file 'LM_Bloch_Stirap.m'. Fig. 34.25(a) shows the temporal variation of the Rabi frequencies. The result of the simulations is shown in Fig. 34.25(b).
b. The Liouville matrix can be found in the MATLAB numerical code given in the file 'LM_Bloch_Stirap.m'.
c. Fig. 34.25(c) shows the results of the simulations.

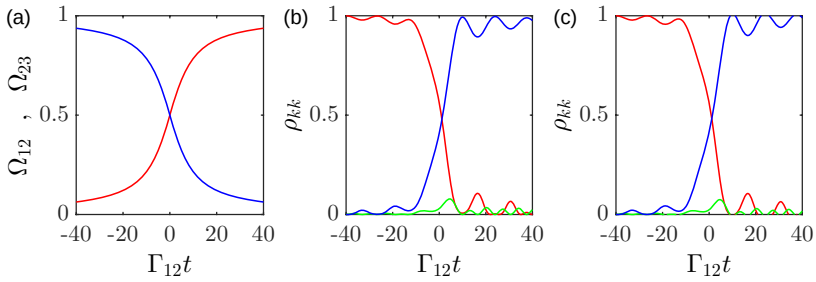

Figure 34.25: (code) (a) Temporal variation of laser intensities. (b) Variation of the populations obtained by simulation of the Schrödinger equation, and (c) of the Bloch equations: ρ_{11} in red, ρ_{22} in green, and ρ_{33} in blue. (Note that the solutions tend to diverge when the time steps are not significantly shorter than all characteristic time scales of the system, e.g. the decay rates $1/\Gamma_{12}$.)

34.8.4.8 Ex: Adiabatic sweeps

In experiments with cold atoms it is often necessary to transfer populations between ground states, for example, between specific levels of a Zeeman structure. One possible procedure is the method of optical pumping, from the initial ground state to an excited state, which subsequently decays to the final state by spontaneous emission. The problem with this incoherent procedure is, that one can control into which ground state level the atom will decay, and that it heats atoms due to the photonic recoil associated with the scattering of light. In this exercise we study an alternative method, called *adiabatic sweep*, which allows the coherent transfer of population between the two outer states of a degenerate multiplet, as shown in Fig. 34.26, via an adiabatic ramp of the frequency of the incident radiation:
a. Write down the Hamiltonian of the system in the interaction picture. Now, choose $\Omega/2\pi = 8\,\text{kHz}$ and apply a linear ramp of the radiation detuning between $-50\,\text{kHz} < \Delta(t)/2\pi < 50\,\text{kHz}$ during a time interval of 2 ms. With this, solve the Schrödinger equation (34.279) iteratively varying the detuning.
b. Write down the Liouville matrix of the system and do a numerical simulation of

the Bloch equations (34.279) using the same parameters as in (a). Interpret the results. What you observe when you introduce a decay rate between adjacent levels of $\Gamma/2\pi = 200\,\mathrm{Hz}$?

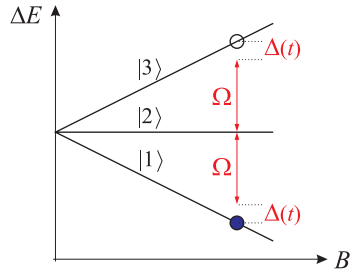

Figure 34.26: Energy levels of an atom in the ground state with Zeeman structure (for example, $|J = 1, m_J = -1, 0, +1\rangle$) as a function of the applied magnetic field.

Solution: *a. The Hamiltonian is,*

$$\hat{H} = \begin{pmatrix} 0 & \frac{1}{2}\Omega & 0 \\ \frac{1}{2}\Omega & \Delta & \frac{1}{2}\Omega \\ 0 & \frac{1}{2}\Omega & 2\Delta \end{pmatrix} .$$

The numerical MATLAB code in is given in the file 'LM_Bloch_AdiaSweep.m'. A Fig. 34.27(a) shows the result of the simulations.
b. The numerical MATLAB code in is given in the file 'LM_Bloch_AdiaSweep.m'. A Fig. 34.27(b) shows the result of the simulations.

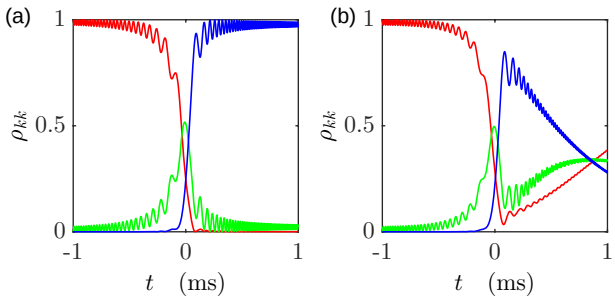

Figure 34.27: (code) Adiabatic sweep of the detuning of the radiation through resonance. The curves show the populations of the states $|1\rangle$ (red), $|2\rangle$ (green), and $|3\rangle$ (blue). (a) Schrödinger equation approach and (b) Bloch equation approach.

34.8.4.9 Ex: Dispersive interaction between an atom and light

Radiation which is tuned far from a resonance can change the phase of an atomic dipole moment without changing the populations [22]. We study this effect in a three-level system in cascade configuration excited by two radiation fields, as illustrated in Fig. 34.17(c), simulating the Schrödinger equation and the Bloch equations.
a. Write down the Hamiltonian $\hat{H}$ for this system letting $\Delta_{12} = 0$.
b. Now, consider the subsystem $|2\rangle$-$|3\rangle$, write down its Hamiltonian $\hat{H}_{23}$, determine the eigenvalues, and assume that this transition be excited very far-off resonance. That is, for $\Delta_{23} \gg \Omega_{23}, \Gamma_{23}$ expand the eigenvalues of $\hat{H}_{23}$ up to second order in Ω_{23}. Finally, replace the submatrix $\hat{H}_{23}$ in the complete Hamiltonian $\hat{H}$ by the matrix of the expanded eigenvalues. This procedure corresponds to treating the transition $|2\rangle$-$|3\rangle$ as a perturbation of the transition $|1\rangle$-$|2\rangle$ until second order.
c. Assume that the atom is initially in the ground state and compute the time evolution of the state via the Schrödinger equation (34.287) using (a) the perturbed Hamiltonian and (b) the exact Hamiltonian for the following *sequence of pulses*:
(i) a $\pi/2$-pulse on the transition $|1\rangle$-$|2\rangle$,
(ii) a pulse with a variable duration between 0 and $\Delta t = \Omega_{23}^2/4\pi\Delta_{23}$ applied to the transition $|2\rangle$-$|3\rangle$,
(iii) a $\pi/2$-pulse on the transition $|1\rangle$-$|2\rangle$. What you observe?
d. Establish the Liouville matrix $\mathcal{L}$ for the same system and calculate the time evolution of the Bloch vector during the sequence by the Bloch equations (34.287) choosing the same parameters as in (c) and additionally $\Gamma_{23} = 1$, $\Gamma_{13} = \Gamma_{23}$, $\Gamma_{12} = 0.01\Gamma_{23}$, and $\Omega_{12} \lll \Delta_{23}, \Gamma_{23}$. Prepare a 3D curve [similar to Fig. 34.6(b)] of the population $\rho_{22}(t)$. Interpret the results.

Solution: *a. The Hamiltonian for the system is,*

$$\hat{H}_{12} = \begin{pmatrix} 0 & \frac{1}{2}\Omega_{12} & 0 \\ \frac{1}{2}\Omega_{12} & 0 & \frac{1}{2}\Omega_{23} \\ 0 & \frac{1}{2}\Omega_{23} & \Delta_{23} \end{pmatrix} .$$

b. The Hamiltonian of the subsystem of the two upper levels is,

$$\hat{H}_{23} = \begin{pmatrix} 0 & \frac{1}{2}\Omega_{23} \\ \frac{1}{2}\Omega_{23} & \Delta_{23} \end{pmatrix} .$$

When excited very far-off resonance, we can expand its eigenvalues for small Ω_{23},

$$E_{1,2} = \tfrac{1}{2}(\Delta_{23} \pm G_{23}) = \frac{1}{2}\Delta_{23} \pm \frac{1}{2}\Delta_{23}\left(1 + \frac{\Omega_{23}^2}{2\Delta_{23}}\right) .$$

By substituting the matrix of corrected eigenvalues in the complete Hamiltonian, we obtain,

$$\hat{H} \simeq \begin{pmatrix} 0 & \frac{1}{2}\Omega_{12} & 0 \\ \frac{1}{2}\Omega_{12} & -\frac{\Omega_{23}^2}{4\Delta_{23}} & 0 \\ 0 & 0 & \Delta_{23} + \frac{\Omega_{23}^2}{4\Delta_{23}} \end{pmatrix} .$$

[22] This type of interaction is used in the implementation of quantum gates in quantum computing.

c. We simulate the evolution of the state to be,

$$|\psi(t)\rangle = e^{\imath\hat{H}^{(3)}\Delta t_3/\hbar}e^{\imath\hat{H}^{(2)}\Delta t_2/\hbar}e^{\imath\hat{H}^{(1)}\Delta t_1/\hbar}|\psi_(0)\rangle \ .$$

The numerical MATLAB code is given in the file 'LM_Bloch_Dispersive'.
d. We simulate the evolution of the Bloch vector to be,

$$\vec{\rho}(t) = e^{\mathcal{L}_3\Delta t_3}e^{\mathcal{L}_2\Delta t_2}e^{\mathcal{L}_1\Delta t_1}\vec{\rho}(0) \ .$$

The numerical MATLAB code is given in the file 'LM_Bloch_Dispersive'. Fig. 34.28 shows the result of the simulations. We find that Δ_{23} must be chosen very large (> 300) to obtain a really dispersive dynamics.

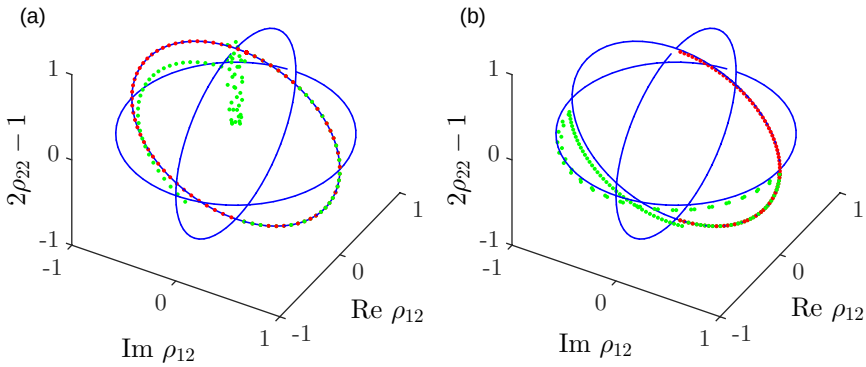

Figure 34.28: (code) (red) Evolution of Bloch vector for a sequence of resonant Ramsey pulses. (blue) Evolution for the occurrence of a dispersive pulse on a transition coupling an upper level.

34.8.4.10 Ex: Fano profile of a dark resonance

The dark resonance studied in Exc. 34.8.4.3 may in some circumstances adopt an asymmetric profile. Calculate, for a three-level system in Λ-configuration, as shown in Fig. 34.17(a), starting from the Bloch equations (34.279) with the Liouville matrix $\mathcal{M}_{red}$ reduced by the trace condition (34.283), the spectrum $\rho_{22}(\Delta_{23})$ for the following set of parameters: $\Gamma_{12} = 2$, $\Gamma_{23} = \Gamma_{12}/2$, $\Gamma_{23} = 0.1\Gamma_{12}$, $\Omega_{12} = 10\Gamma_{12}$, $\Omega_{23} = 5\Gamma_{23}$, $\Delta_{12} = -5\Gamma_{12}$ and $\Delta_{23} = [-1 : .01 : 1]\Gamma_{23}$. Interpret the spectrum in terms of a Fano resonance.

Solution: *a. The numerical MATLAB code is given in the file 'LM_Bloch_FanoResonance'. Fig. 34.29 shows the result of the simulations. For strong Rabi frequencies, the position of the dark resonance is shifted by the light-shift induced in the two transitions by a value of $\delta = \Delta_{12} - \Delta_{23}$. This value corresponds to a two-photon light-shift. The dark resonance is due to the destructive interference between two* one-photon *scattering processes: $|3\rangle \longrightarrow |i\rangle \xrightarrow{spnt} |1\rangle$ and $|1\rangle \longrightarrow |i\rangle \xrightarrow{spnt} |3\rangle$, where $|i\rangle$ is the virtual*

intermediate level. For large detunings, $\Delta_{12} \gg \Gamma_{12}, \Omega_{12}$, a small peak appears next to the dark resonance, which can be interpreted as a Fano resonance. It is due to the constructive interference between a one-photon *scattering process, $|3\rangle \to |i\rangle \xrightarrow{spnt} |1\rangle$, and a* three-photons *scattering process, $|3\rangle \to |i\rangle \to |1\rangle \to |i\rangle \xrightarrow{spnt} |1\rangle$.*

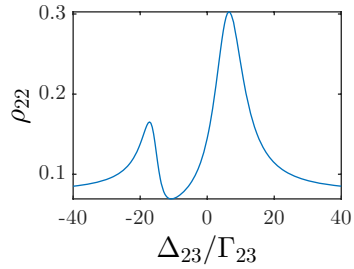

Figure 34.29: (code) Fano resonance.

34.8.4.11 Ex: Gas with negative permittivity

Study EIT on the strontium cascade system consisting of the transitions 689 nm and 497 nm and draw a spectrum of the permittivity. Compare with the permittivity of the 689 nm two-level system. What densities are necessary to get a negative permittivity?

Solution: *The curves are shown in Fig. 34.30.*

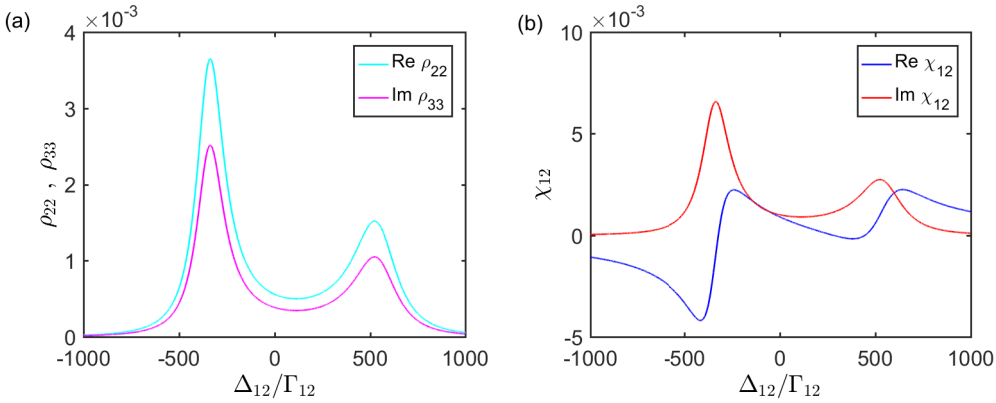

Figure 34.30: (code) Negative permittivity.

34.8.4.12 Ex: Gas with negative permeability

Theoretically, under certain conditions, gases may exhibit *negative* permittivity and permeability, and therefore refraction [1196, 1194, 1195, 968, 769]. To study this phenomenon we consider a three-level system in Λ-configuration with an electric dipole transition and another magnetic dipole transition. The objective is to balance the electrical dipole moment excited by a probe laser and the magnetic dipole moment excited via a Raman transition by both, the probe laser and a control laser. The Raman transition simulates an effective magnetic field. Since the magnetic moment is smaller by a factor of α^2, the electric moment must be reduced by detuning the probe laser, as shown in Fig. 34.31.

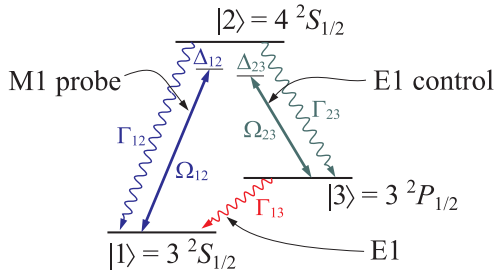

Figure 34.31:

a. Consider a three-level system in Λ-configuration. The transitions $|1\rangle$-$|2\rangle$ and $|2\rangle$-$|3\rangle$ are assumed to be electric dipoles and $|1\rangle$-$|3\rangle$ a magnetic dipole, such that, $\Gamma_{12}, \Gamma_{23} \gg \Gamma_{13}$. Extract from the Bloch equation (34.279) the equations for the coherences ρ_{12}, ρ_{13}, and ρ_{23}.
b. Suppose, that the excitation on the probe transition be so weak, $\Omega_{12} \ll \Gamma_{12}$, that it does not succeed to empty the ground state. In this approximation eliminate the dynamics of ρ_{23} and deduce the stationary solution for ρ_{12} and ρ_{13}.
c. Calculate the magnetic susceptibility χ_m [1195] with the following parameters $\Gamma_{12} = 7 \cdot 10^7\,\mathrm{s}^{-1}$, $\Gamma_{23} = 3 \cdot 10^7\,\mathrm{s}^{-1}$, $\Gamma_{13} = 2 \cdot 10^7\,\mathrm{s}^{-1}$, $\Omega_{12} = 0.1\Gamma_{12}$, $\Omega_{23} = 2 \cdot 10^8\,\mathrm{s}^{-1}$, $\Delta_{23} = 0$ in the regime $\Delta_{12} = [-15\Gamma_{23}, 15\Gamma_{23}]$.
d. Simulate the Bloch equations (34.279) and compare with the numerical solution.

Solution: *a. Assuming stationary populations, we begin by extracting from the equations (34.279) the equations for coherences,*

$$\begin{pmatrix}\dot\rho_{12}\\ \dot\rho_{13}\\ \dot\rho_{23}\end{pmatrix} = \begin{pmatrix}-\Lambda_{12} & \frac{\imath}{2}\Omega_{23} & 0\\ \frac{\imath}{2}\Omega_{23} & -\Lambda_{13} & -\frac{\imath}{2}\Omega_{12}\\ 0 & -\frac{\imath}{2}\Omega_{12} & -\Lambda_{23}\end{pmatrix}\begin{pmatrix}\rho_{12}\\ \rho_{13}\\ \rho_{23}\end{pmatrix} + \begin{pmatrix}\frac{\imath}{2}\Omega_{12}(\rho_{11}-\rho_{22})\\ 0\\ \frac{\imath}{2}\Omega_{23}(\rho_{22}-\rho_{33})\end{pmatrix},$$

where $\Lambda_{12} \equiv \imath\Delta_{12} + \frac{1}{2}(\Gamma_{12}+\Gamma_{23})$, $\Lambda_{23} \equiv \imath\Delta_{23} + \frac{1}{2}(\Gamma_{12}+\Gamma_{23}+\Gamma_{13})$ *and* $\Lambda_{13} \equiv i(\Delta_{12}-\Delta_{23}) + \frac{1}{2}\Gamma_{13}$.
b. Now we let $\Omega_{12} \ll \Gamma_{12}$, *such that* $\rho_{11} \simeq 1$ *the system of equations reduces to,*

$$\begin{pmatrix}\dot\rho_{12}\\ \dot\rho_{13}\end{pmatrix} = \begin{pmatrix}-\Lambda_{12} & \frac{\imath}{2}\Omega_{23}\\ \frac{\imath}{2}\Omega_{23} & -\Lambda_{13}\end{pmatrix}\begin{pmatrix}\frac{\imath}{2}\Omega_{12}\\ 0\end{pmatrix}.$$

The steady state is,

$$\rho_{12} = \frac{\frac{i}{2}\Lambda_{13}\Omega_{12}}{\frac{1}{2}\Omega_{23}^2 + \Lambda_{12}\Lambda_{13}} \quad , \quad \rho_{13} = \frac{-\frac{1}{4}\Omega_{12}\Omega_{23}}{\frac{1}{2}\Omega_{23}^2 + \Lambda_{12}\Lambda_{13}} \ .$$

c. The electrical and magnetic susceptibilities [1196] of the atom are observed in the probe transition,

$$\chi_e = \frac{2Nd_{23}^*\rho_{23}}{\varepsilon_0\mathcal{E}_{23}} = \varepsilon_r - 1$$
$$\chi_m = \frac{2N\mu_{13}^*\rho_{13}}{\mathcal{H}} = \mu_r - 1 \ .$$

The Rabi frequencies are $\hbar\Omega_{12}$ and,

$$\mathcal{H} = \mathcal{E}\sqrt{\varepsilon_0\varepsilon_r/\mu_0\mu_r}$$

d. Simulations of the complete Bloch equations give the results shown in Fig. 34.32. [1196]10.1631/jzus.2004.1322 believes that in practice very high densities of the order

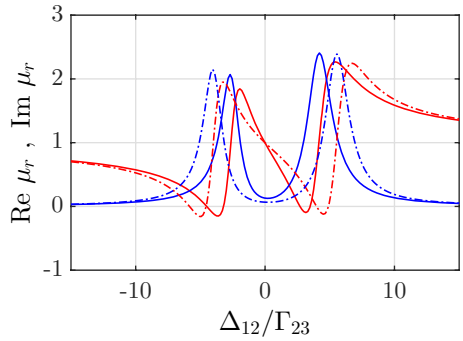

Figure 34.32:

of $10^{18}\,\mathrm{cm}^{-3}$ *are required.*

34.8.4.13 Ex: Magnetic dipole transitions in strontium

Magnetic dipole transitions are characterized by the selection rules $\Delta J = 0, \pm 1$, $\Delta S = 0$, $\Delta L = 0$, and $\Delta n = 0$. There are several transitions starting from the $5s5p\ ^3P_J$ metastable states going to the $5p^2\ 3P_J$ states with strong linewidths:

- $5s5p\ ^3P_1^o \leftrightarrow 5p^2\ ^3P_2$ at 472.2278 nm with $\Gamma = (2\pi)\ 5.7\,\mathrm{MHz}$
- $5s5p\ ^3P_1^o \leftrightarrow 5p^2\ ^3P_1$ at 478.4320 nm with $\Gamma = (2\pi)\ 4.8\,\mathrm{MHz}$

Check whether it is possible to reach negative permeability in a cold strontium gas.

Solution: *The strontium level scheme can be consulted in ⊙. The strontium levels are listed in ⊙.*

34.8.4.14 Ex: Orientation and alignment

Derive the formulas (34.323) and (34.324).

Solution: *We calculate orientation,*

$$\mathbf{O} = \langle \hat{\mathbf{J}} \rangle = Tr\ \hat{\rho}\hat{\mathbf{J}} = \sum_m \langle jm|\hat{\rho}\hat{\mathbf{J}}|jm\rangle = \sum_{m,m'} \langle jm|\hat{\rho}|jm'\rangle\langle jm'|\hat{\mathbf{J}}|jm\rangle \ .$$

If the atom is in a superposition of eigenstates ($\langle jm|\hat{\rho}|jm'\rangle = \rho_{mm}\delta_{m,m'}$), we get,

$$\mathbf{O} = \begin{pmatrix} 0 \\ 0 \\ \langle \hat{J}_z \rangle \end{pmatrix} = \sum_m \hbar m\ {}_z\langle m|\hat{\rho}|m\rangle_z \begin{pmatrix} 0 \\ 0 \\ 1 \end{pmatrix} \ .$$

Using the rules of the SU(2) algebra for angular momenta Sec. 25.3.2 we find for the alignment,

$$\begin{aligned}(A_{ij}) &= \begin{pmatrix} \langle 3\hat{J}_x^2 - \mathbf{J}^2 \rangle & \langle [\hat{J}_x, \hat{J}_y]_+ \rangle & \langle [\hat{J}_x, \hat{J}_z]_+ \rangle \\ \langle [\hat{J}_x, \hat{J}_y]_+ \rangle & \langle 3\hat{J}_y^2 - \hat{\mathbf{J}}^2 \rangle & \langle [\hat{J}_y, \hat{J}_z]_+ \rangle \\ \langle [\hat{J}_x, \hat{J}_z]_+ \rangle & \langle [\hat{J}_y, \hat{J}_z]_+ \rangle & \langle 3\hat{J}_z^2 - \hat{\mathbf{J}}^2 \rangle \end{pmatrix} \\ &= \begin{pmatrix} -\frac{1}{2}\langle 3\hat{J}_z^2 - \hat{\mathbf{J}}^2 \rangle & 0 & 0 \\ 0 & -\frac{1}{2}\langle 3\hat{J}_z^2 - \hat{\mathbf{J}}^2 \rangle & 0 \\ 0 & 0 & \langle 3\hat{J}_z^2 - \hat{\mathbf{J}}^2 \rangle \end{pmatrix} \ ,\end{aligned}$$

if the atom is in a superposition of eigenstates ($\langle jm|\hat{\rho}|jm'\rangle = \rho_{mm}\delta_{m,m'}$). We finally get,

$$(A_{ij}) = \sum_m \hbar^2[3m^2 - j(j+1)]\ {}_z\langle m|\hat{\rho}|m\rangle_z \begin{pmatrix} -1/2 & 0 & 0 \\ 0 & -1/2 & 0 \\ 0 & 0 & 1 \end{pmatrix} \ .$$

34.8.4.15 Ex: Hanle effect in Ca

Simulate the Hanle effect for the Ca^+ three-level system of Exc. 34.8.4.6 using optical Bloch equations.

Solution: *The results are shown in Fig. 34.33.*

34.9 Further reading

J. Weiner and P-T. Ho, Springer-Verlag, Berlin (2003), *Light-Matter Interaction: Fundamentals and Applications* [1364]ISBN

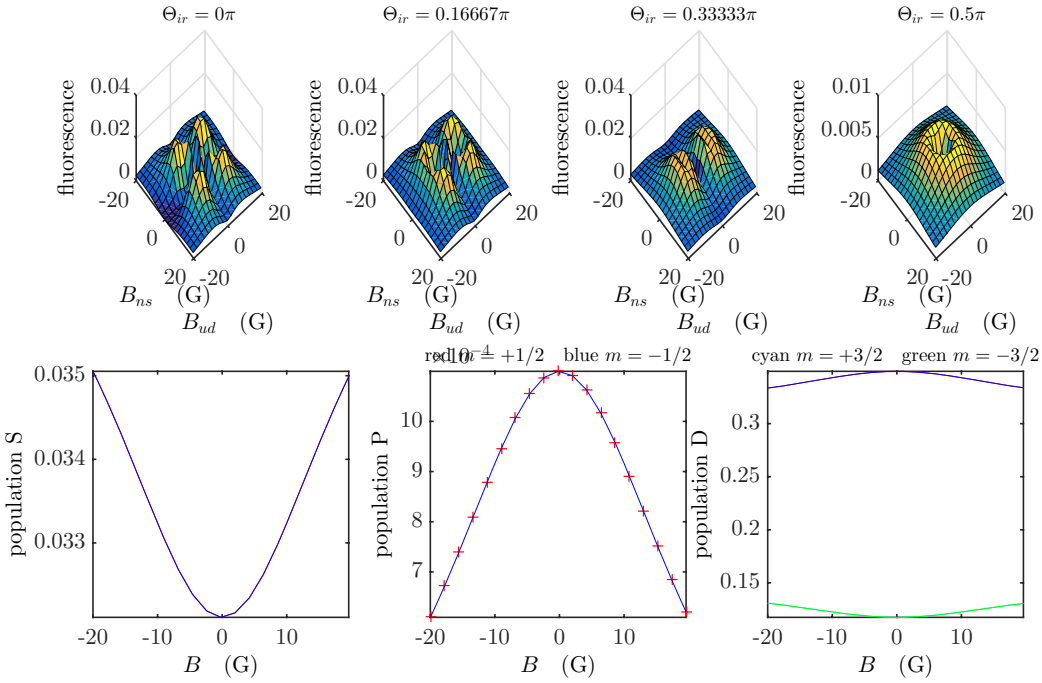

Figure 34.33: (code) Hanle effect for the Ca 3-level system.

R. Loudon, Oxford Science Publications, Oxford (1982), *The quantum theory of light* [816]ISBN

M.O. Scully, *From lasers and masers to phaseonium and phasers* [1176]DOI

I.I. Sobelman, Springer Verlag, Berlin (1972), *Introduction to the Theory of Atomic Spectra* [1226]ISBN

M. Weissbluth, (Academic Press, Boston, 1989), *Photon-Atom Interactions* [1368]ISBN

M. Weissbluth, *Atoms and Molecules* [1368]ISBN

A. Corney, Clarendon Press, Oxford (1977), *Atomic and Laser Spectroscopy* [292]ISBN

M. Tanifuji, World Scientific (2018), *Polarization Phenomena in Physics* [1292]ISBN

C.M. Tokarsky Dieguez et al., *Os fundamentos quânticos da Ressonância Magnética Nuclear* [368]DOI

Y. Stalgies et al., *Light shift and Fano resonances in a single cold ion* [1236]DOI

M. Fleischhauer et al., *Electromagnetically induced transparency, Optics in coherent media* [454]DOI

L.V. Hau et al., *Light Speed Reduction to 17 Metres per Second in an Ultracold Atomic Gas* [586]DOI

34.9.1 on negative refraction

A. Poddubny et al., *Hyperbolic metamaterials* [1040]DOI

Jian-Qi Shen et al., *How to realize a negative refractive index material at the atomic level in an optical frequency range* [1196]DOI

Jian-Qi Shen et al., *Negatively refracting atomic vapour* [1194]DOI

Jian-Qi Shen et al., *Negative permeability in a Λ-type three-level atomic vapor* [1195]DOI

F. Bello, *Negative index of refraction in a four-level system with magnetoelectric cross coupling and local field corrections* [116]DOI

Yi S. Ding et al., *Possible realization of negative refraction in Bose-Einstein condensates* [370]DOI

A. Alù et al., *Pairing an Epsilon-Negative Slab With a Mu-Negative Slab Resonance, Tunneling and Transparency* [26]DOI

M.Ö. Oktel et al., *Electromagnetically induced left-handedness in a dense gas of three-level atoms* [968]DOI

P.P. Orth et al., *Negative refraction with tunable absorption in an active dense gas of atoms* [979]DOI

D.E. Sikes et al., *Negative refraction using Raman transitions and chirality* [1205]DOI

P. Shekhar et al., *Strong Coupling in Hyperbolic Metamaterials* [1192]DOI

Chapter 35

Atoms in quantized radiation fields

So far we have treated the optical field only as a stationary or propagating classical wave, while our two-level atom has been regarded as an entity obedient to the laws of quantum mechanics and subject to an induced perturbation by an oscillatory electromagnetic field. This procedure naturally leads to oscillations of the atomic states' populations and the coherences between them. However, in strong fields, when atomic energy spectrum is significantly modified, a non-perturbative, time-independent approach can be fruitful. Time-independent solutions for the Schrödinger equation for atoms coupled to fields is called *dressed states*. They were used for the first time to interpret the *splitting* of rotational molecular spectra in the presence of intense classical radiofrequency fields. While the semiclassical treatment is suitable for a wide variety of phenomena and has the virtue of mathematical simplicity and familiarity, it is sometimes worth considering the field as a quantum entity as well. In the dressed states picture, the atom-field interaction corresponds to an exchange of energy quanta between the field (photons) and the atom. This approach allows us to express photonic *number states*, also called *Fock states*, on equal footings with the discrete states of atom excitation and to write the state functions of the coupled atom-field system in a basis of photonic and atomic product states. Diagonalization of the dipole coupling terms in the system's Hamiltonian generates time-independent solutions of dressed states in a completely quantum Schrödinger equation.

We begin this chapter with the quantization of the light field and then express the atom-field interaction in a fully quantized form. We will examine some examples illustrating how the dressed states picture can provide useful information on the light-matter interactions.

35.1 Quantization of the electromagnetic field

We have already seen that the energy of a monochromatic light field with frequency ω is quantized in small equal portions, such that the total energy is $N\hbar\omega$, where N is an integer number. The energy spectrum is the same as the one of the harmonic oscillator. Therefore, we can identify a light mode with an oscillator and adopt the entire formalism developed for the harmonic oscillator. The formalism will be assumed as known in the following. We will, for simplicity use the term *photon* (respectively *phonon*) for excitations of a harmonic oscillator mode. It is however important to be

aware that a photon is not a particle, as it simply *disappears when performing the transition from quantum to classical mechanics* [770].

35.1.1 Field operators

The basic idea behind field quantization is the replacement of the classical harmonic oscillators discussed in Sec. 24.5 by quantum oscillators. The simplest approach to perform this quantization is to introduce the scalar potential Φ and the potential vector $\mathbf{A}$ as done in electrodynamic theory [1]. In free space, without charges nor currents, and within the *Coulomb gauge* we have the solution of the wave equation (34.5) generalized to a distribution of wavevectors $\mathbf{k}$ [2],

$$\mathbf{A}(\mathbf{r},t) = \sum_{\mathbf{k}} \vec{\epsilon}_{\mathbf{k}} [A^{+}_{0\mathbf{k}} e^{-\imath(\mathbf{k}\cdot\mathbf{r}-\omega_{\mathbf{k}}t)} + A^{-}_{0\mathbf{k}} e^{\imath(\mathbf{k}\cdot\mathbf{r}-\omega_{\mathbf{k}}t)}] \; , \tag{35.1}$$

where we already isolated the vectorial character due to the polarization $\vec{\epsilon}_{\mathbf{k}}$ of the light mode $\mathbf{k}$. Obviously, $A^{-}_{0\mathbf{k}} = (A^{+}_{0\mathbf{k}})^{*}$. As each amplitude and polarization of the wave given by the vector potential $\mathbf{A}_{\mathbf{k}}$ and $\mathbf{A}^{*}_{\mathbf{k}}$ must satisfy the wave equation separately, we arrive at the dispersion relation,

$$\omega_{\mathbf{k}} = ck \; . \tag{35.2}$$

With the results (34.7) and (34.8) we know that the energy in each radiative mode containing $n_{\mathbf{k}}$ photons is,

$$E_{\mathbf{k}} = \hbar\omega_{\mathbf{k}} N_{\mathbf{k}} = u_{\mathbf{k}} V = 2\varepsilon_0 V \omega^2_{\mathbf{k}} \overline{\mathbf{A}^2_{0\mathbf{k}}} = 2\varepsilon_0 V \omega^2_{\mathbf{k}} (A^{-}_{0\mathbf{k}} A^{+}_{0\mathbf{k}} + A^{+}_{0\mathbf{k}} A^{-}_{0\mathbf{k}}) \; , \tag{35.3}$$

where the bar denotes cycle-averaging. The second quantization now consists in interpreting the mode as a *quantum harmonic oscillator*, that is, we understand the observables as *operators* satisfying commutation rules, such as $[\hat{A}^{-}_{0\mathbf{k}}, \hat{A}^{+}_{0\mathbf{k}'}] \propto \delta_{\mathbf{k},\mathbf{k}'}$, and hence being affected by quantum fluctuations:

$$\hat{H}_{\mathbf{k}} = \hbar\omega_{\mathbf{k}} (\hat{n}_{\mathbf{k}} + \tfrac{1}{2}) = 2\varepsilon_0 V \omega^2_{\mathbf{k}} (\hat{A}^{-}_{0\mathbf{k}} \hat{A}^{+}_{0\mathbf{k}} + \hat{A}^{+}_{0\mathbf{k}} \hat{A}^{-}_{0\mathbf{k}}) \; . \tag{35.4}$$

We introduce normalized field operators following the commutation rule (24.76) via,

$$\hat{a}_{\mathbf{k}} \sqrt{\tfrac{\hbar}{4\varepsilon_0 V \omega_{\mathbf{k}}}} \equiv \hat{A}^{+}_{0\mathbf{k}} \qquad \text{and} \qquad \hat{a}^{\dagger}_{\mathbf{k}} \sqrt{\tfrac{\hbar}{4\varepsilon_0 V \omega_{\mathbf{k}}}} \equiv \hat{A}^{-}_{0\mathbf{k}} \; , \tag{35.5}$$

such that,

$$\hat{H}_{\mathbf{k}} = \hbar\omega_{\mathbf{k}} (\hat{a}^{\dagger}_{\mathbf{k}} \hat{a}_{\mathbf{k}} + \tfrac{1}{2}) \; . \tag{35.6}$$

The analogy allows us to interpret them as *creation operator* and *annihilation operator* of photons. Finally, we can rewrite (35.1) as,

$$\boxed{\hat{\mathbf{A}}_{\mathbf{k}}(\mathbf{r},t) = \sqrt{\tfrac{\hbar}{4\varepsilon_0 V \omega_{\mathbf{k}}}} \vec{\epsilon}_{\mathbf{k}} \left[\hat{a}_{\mathbf{k}} e^{-\imath(\mathbf{k}\cdot\mathbf{r}-\omega_{\mathbf{k}}t)} + \hat{a}^{\dagger}_{\mathbf{k}} e^{\imath(\mathbf{k}\cdot\mathbf{r}-\omega_{\mathbf{k}}t)} \right]} \; . \tag{35.7}$$

[1] See Sec. 17.3

[2] The atom-light interaction may depend on the polarization of the light with respect to the quantization axis of the atom, as defined e.g. by a magnetic field. In these cases we need to extend the index $\mathbf{k}$ to include the polarization state $(\mathbf{k}, \lambda)$.

We already know such combinations of operators and their complex conjugates from the quantum harmonic oscillator (24.86).

In the Coulomb gauge, the electric and magnetic field operators for the cavity modes can be constructed from,

$$\boxed{\begin{aligned}\hat{\vec{\mathcal{E}}}_{\mathbf{k}} &= -\frac{\partial \hat{\mathbf{A}}_{\mathbf{k}}}{\partial t} = \imath\sqrt{\tfrac{\hbar\omega_{\mathbf{k}}}{2\varepsilon_0 V}}\left(\hat{a}_{\mathbf{k}} e^{-\imath(\mathbf{k}\cdot\mathbf{r}-\omega_{\mathbf{k}}t)} - \hat{a}^{\dagger}_{\mathbf{k}} e^{\imath(\mathbf{k}\cdot\mathbf{r}-\omega_{\mathbf{k}}t)}\right)\vec{\epsilon}_k \\ \hat{\vec{\mathcal{B}}}_{\mathbf{k}} &= \nabla\times\mathbf{A}_{\mathbf{k}} = \imath\sqrt{\tfrac{\hbar\omega_{\mathbf{k}}}{2\varepsilon_0 V}}\left(\hat{a}_{\mathbf{k}} e^{-\imath(\mathbf{k}\cdot\mathbf{r}-\omega_{\mathbf{k}}t)} - \hat{a}^{\dagger}_{\mathbf{k}} e^{\imath(\mathbf{k}\cdot\mathbf{r}-\omega_{\mathbf{k}}t)}\right)\mathbf{k}\times\vec{\epsilon}_k\end{aligned}} \quad . \tag{35.8}$$

We can calculate the cycle-averaged energy of the $\mathbf{k}$-th cavity mode from a quantum version of Eq. (35.3),

$$\bar{E}_{\mathbf{k}} = \tfrac{\varepsilon_0}{2}\int \langle n_{\mathbf{k}}|\hat{\vec{\mathcal{E}}}_{\mathbf{k}}\cdot\hat{\vec{\mathcal{E}}}_{\mathbf{k}}|n_{\mathbf{k}}\rangle dV \ . \tag{35.9}$$

The result (35.6) is exactly Planck's quantum hypothesis (although strictly speaking, he rather suggested a quantization of oscillators in the conducting walls of the cavity, not of the field) on the distribution of the spectral intensity radiated by a black body. We now can see that it follows naturally from the quantization of the cavity field modes. Solve Excs. 35.1.5.1 and 35.1.5.2.

35.1.2 Interaction of quantized fields with atoms

With the results of the previous section the complete field Hamiltonian reads,

$$\hat{H}_{field} = \sum_{\mathbf{k}} \hbar\omega_{\mathbf{k}}(\hat{a}^{\dagger}_{\mathbf{k}}\hat{a}_{\mathbf{k}} + \tfrac{1}{2}) \ . \tag{35.10}$$

Now, that we have a clear picture of the quantized field with the energies in the modes given by Eq. (35.9) and the photon number states given by the eigenstates $|n\rangle$ of the quantized harmonic oscillator, we are in a position to consider our two-level atom interacting with this quantized radiation field. If for the moment, we exclude spontaneous emission and stimulated processes, the Hamiltonian of the combined atom-field system is,

$$\hat{H} = \hat{H}_{atom} + \hat{H}_{field} + \hat{H}_{atom:field} \ . \tag{35.11}$$

We describe the atom by a two-level system,

$$\hat{H}_{atom} = \hbar\omega_g|g\rangle\langle g| + \hbar\omega_e|e\rangle\langle e| = \hbar\omega_g|g\rangle\langle g| + \hbar(\omega_g+\omega_0)|e\rangle\langle e| \ , \tag{35.12}$$

where $\hat{H}_{field}$ is the Hamiltonian of the quantized field, expressed by Eq. (35.6), and $\hat{H}_{atom:field}$ the atom-field interaction. For the Hamiltonian without interaction, $\hat{H} = \hat{H}_{atom} + \hat{H}_{field}$, the eigenstates are simply product states of the atomic states and the photon number states,

$$|g,n\rangle = |g\rangle|n\rangle \qquad \text{and} \qquad |e,n\rangle = |e\rangle|n\rangle \ . \tag{35.13}$$

The left side of Fig. 35.1 shows, how the eigenenergies of the product states consist of two ladders, being displaced by the energy difference $\hbar\Delta$, which corresponds to the

detuning. We write the Hamiltonian of the atom Eq. (35.12) as the sum of projectors on unperturbed eigenstates using the completeness relation and the orthogonality of eigenstates. With the same idea we can rewrite the dipole operator defined in Eq. (34.33),

$$\hat{\mathbf{d}} = \sum_i |\psi_i\rangle\langle\psi_i|\hat{\mathbf{d}}| \sum_j |\psi_j\rangle\langle\psi_j| = \sum_{i,j} |i\rangle\langle i|e^{\imath(\omega_i-\omega_j)t}\hat{\mathbf{d}}|j\rangle\langle j| \tag{35.14}$$
$$= \sum_{i,j} e^{\imath(\omega_i-\omega_j)t}\mathbf{d}_{ij}|i\rangle\langle j| = \sum_{i<j} e^{\imath(\omega_i-\omega_j)t}\mathbf{d}_{ij}|i\rangle\langle j| + e^{-\imath(\omega_i-\omega_j)t}\mathbf{d}_{ij}|j\rangle\langle i| \equiv \hat{\mathbf{d}}^{(+)} + \hat{\mathbf{d}}^{(-)} \ .$$

using $|\psi_n(t)\rangle = e^{-\imath\omega_n t}|n\rangle$. Note that $\hat{\mathbf{d}}$ only has non-diagonal elements.

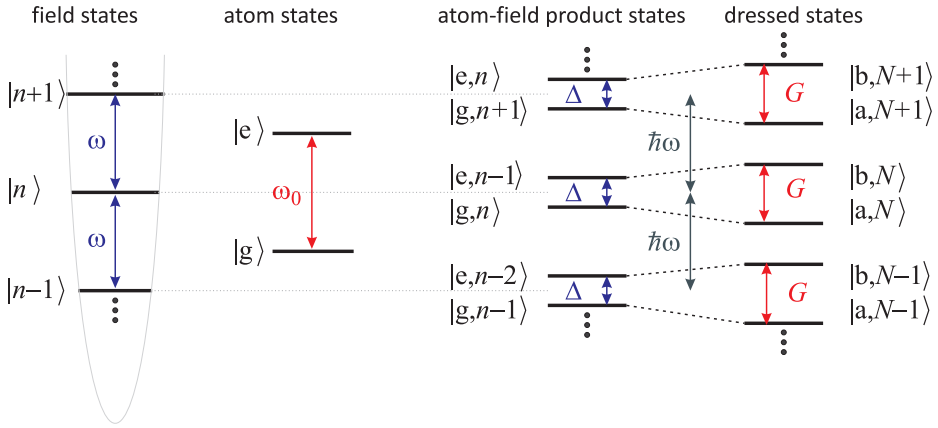

Figure 35.1: (Left) Photons number states and the two stationary states of the two-levels atom. (Center) Double ladder showing the basis of products states of photon number and atomic states. (Right) Dressed states constructed by diagonalization of the full Hamiltonian in the basis of the product states.

Now, let us use the electric field of Eqs. (35.8) to describe the atom-field interaction through the Hamiltonian $\hat{H}_{atom:field} = -\hat{\mathbf{d}} \cdot \hat{\vec{\mathcal{E}}}$,

$$\hat{H}_{atom:field} = \imath \sum_{\mathbf{k}} \sum_{i,j} \sqrt{\frac{\hbar\omega_{\mathbf{k}}}{2\varepsilon_0 V}} \mathbf{d}_{ij} e^{\imath(\omega_j-\omega_i)t}|i\rangle\langle j| \cdot \vec{\epsilon}_{\mathbf{k}} \left[\hat{a}_{\mathbf{k}} e^{-\imath(\mathbf{k}\cdot\mathbf{r}-\omega_{\mathbf{k}}t)} - \hat{a}^\dagger_{\mathbf{k}} e^{\imath(\mathbf{k}\cdot\mathbf{r}-\omega_{\mathbf{k}}t)}\right] \ . \tag{35.15}$$

For our two-level atom interacting with a single mode radiation field, we only have,

$$\hat{H}_{atom:field} = \imath\sqrt{\frac{\hbar\omega_{\mathbf{k}}}{2\varepsilon_0 V}} \mathbf{d}_{ge} \left[e^{\imath(\omega_e-\omega_g)t}|g\rangle\langle e| + e^{\imath(\omega_g-\omega_e)t}|e\rangle\langle g|\right] \cdot \tag{35.16}$$
$$\cdot \vec{\epsilon}_{\mathbf{k}} \left[\hat{a}_{\mathbf{k}} e^{-\imath(\mathbf{k}\cdot\mathbf{r}-\omega_{\mathbf{k}}t)} - \hat{a}^\dagger_{\mathbf{k}} e^{\imath(\mathbf{k}\cdot\mathbf{r}-\omega_{\mathbf{k}}t)}\right] \ .$$

35.1.2.1 Rotating wave approximation for dressed states

We can simplify the notation by identifying $\hat{\sigma}^+ = |e\rangle\langle g|$ and $\hat{\sigma}^- = |g\rangle\langle e|$ of the Eqs. (34.161) and introducing as an abbreviation the *Rabi frequency*,

$$\tfrac{1}{2}\hbar\Omega_1(\mathbf{r}) \equiv \sqrt{\frac{\hbar\omega_{\mathbf{k}}}{2\varepsilon_0 V}} \mathbf{d}_{ge} \cdot \vec{\epsilon}_{\mathbf{k}} e^{\imath\mathbf{k}\cdot\mathbf{r}} \ . \tag{35.17}$$

The interaction Hamiltonian then becomes,

$$\hat{H}_{atom:field} = \tfrac{\imath}{2}\hbar\Omega_1(\mathbf{r})e^{\imath(\omega_{\mathbf{k}}-\omega_0)t}\hat{\sigma}^+\hat{a}_{\mathbf{k}} + \tfrac{\imath}{2}\hbar\Omega_1(\mathbf{r})e^{\imath(\omega_{\mathbf{k}}+\omega_0)t}\hat{\sigma}^-\hat{a}_{\mathbf{k}} - \tfrac{\imath}{2}\hbar\Omega_1^*(\mathbf{r})e^{-\imath(\omega_{\mathbf{k}}+\omega_0)t}\hat{\sigma}^+\hat{a}_{\mathbf{k}}^\dagger - \tfrac{\imath}{2}\hbar\Omega_1^*(\mathbf{r})e^{-\imath(\omega_{\mathbf{k}}-\omega_0)t}\hat{\sigma}^-\hat{a}_{\mathbf{k}}^\dagger \,. \tag{35.18}$$

This Hamiltonian contains four terms describing the following processes [3],

$|g,n\rangle \longrightarrow |e,n-1\rangle$ the atom is excited by the absorption of a photon;

$|e,n\rangle \longrightarrow |g,n-1\rangle$ the atom is deexcited by the absorption of a photon;

$|g,n\rangle \longrightarrow |e,n+1\rangle$ the atom is excited by the emission of a photon;

$|e,n\rangle \longrightarrow |g,n+1\rangle$ the atom is deexcited by the emission of a photon.

Obviously, only the first and forth terms respect energy conservation (in first-order processes) and can serve as initial and final states in real physical processes. Fig. 35.3 shows schemes of these four terms. We see, that neglecting the second and third process (i.e., terms $\propto \hat{\sigma}^\pm\hat{a}^\pm$ of the Hamiltonian) is equivalent to making the rotating wave approximation (RWA), where we despise the terms rotating with the frequency $\pm(\omega_{\mathbf{k}}+\omega_0)$, and that we really only need to consider the coupling between the two dressed states $|g,n\rangle$ and $|e,n-1\rangle$.

Finally, within the RWA the Hamiltonian reads,

$$\boxed{\hat{H}_{atom:field} = \tfrac{\imath}{2}\hbar\Omega_1(\mathbf{r})e^{-\imath\Delta_{\mathbf{k}}t}\hat{\sigma}^+\hat{a}_k - \tfrac{\imath}{2}\hbar\Omega_1^*(\mathbf{r})e^{\imath\Delta_{\mathbf{k}}t}\hat{\sigma}^-\hat{a}_k^\dagger} \,, \tag{35.19}$$

where we introduced the detuning $\Delta_{\mathbf{k}} \equiv \omega_{\mathbf{k}} - \omega_0$ as short hand notation.

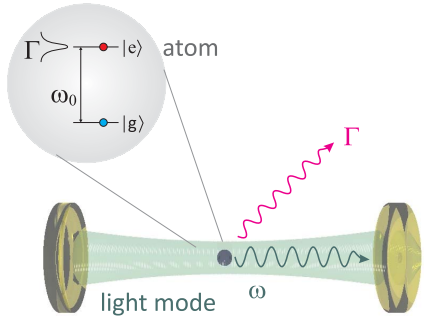

Figure 35.2: Two-level atom interacting with a cavity mode.

It is important to note that the first and fourth term can be important in higher order processes, such as multiphotonic absorption or Raman scattering processes, where the excited state would be a virtual level. In fact, when the Rabi frequency is very large, $\Omega_1 \simeq \omega$, the excitation and deexcitation processes follow each other so rapidly, that energy conservation can be violated for short times. The energy shift caused by terms neglected in the RWA are called *Bloch-Siegert shift* [4].

[3] Remember that the four processes contained in the Hamiltonian are all coherent (absorption and stimulated emission), and that spontaneous emission must be treated separately see next Sec. 35.6.

[4] The shift is not observed, when the non-rotating terms $\sigma^\pm a^\pm$ are forbidden by other conservation or selection rules. For example, when a resonance is excited by $\sigma^\pm$ light, the RWA is accurate.

35.1.3 Dressed states

Within the new dressed states basis, the atom-light coupling problem is reduced to diagonalizing the Hamiltonian of a quasi-degenerate two-level atom ($|\Delta| \ll \omega_0$), in which the non-diagonal elements are given by $\frac{1}{2}\hbar\Omega_1$. The eigenenergies of the complete Hamiltonian $\hat{H}$ are,

$$E_\pm = \tfrac{\hbar}{2}(\omega_{g,n} + \omega_{e,n-1}) \pm \tfrac{\hbar}{2} G_n \ . \tag{35.20}$$

where $\hbar\omega_{g,n}$ and $\hbar\omega_{e,n-1}$ are the energies of the product states $\hbar\omega_g + n\hbar\omega_{\mathbf{k}}$ and $\hbar\omega_e + (n-1)\hbar\omega_{\mathbf{k}}$. The separation between constituents of the same dressed state is $G_n = \sqrt{n\Omega_1^2 + \Delta^2}$. Fig. 35.4 illustrates how the coupling between a field mode and a two-level atom leads to an avoided crossing.

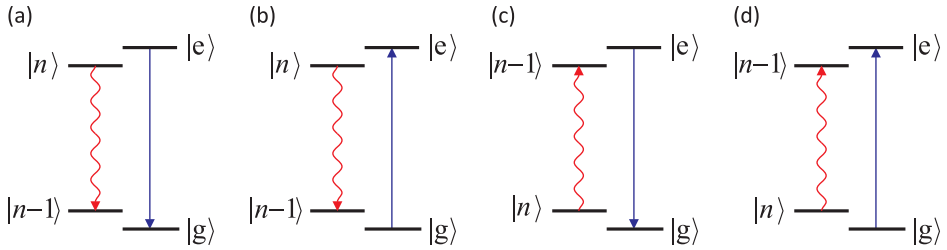

Figure 35.3: Illustration of the four processes in the atom-field interaction. Terms (b) and (c) conserve energy in first-order processes, while (a) and (d) do not conserve.

The atom-field product states offer a natural basis for the Hamiltonian of Eq. (35.11). The states resulting from the diagonalization of the Hamiltonian on this basis are called *dressed states*. As indicated in Fig. 35.1, the neighboring doublets the double ladder 'repel' each other under the influence of the interaction $\hat{H}_{atom:field}$ in Eq. (35.11). The mixed coefficients form the familiar problem of two levels, now called $|a\rangle$ and $|b\rangle$. Note that the semiclassical product state picture and the dressed states picture follow from each other via unitary transformation,

$$\boxed{\begin{pmatrix} |a,N\rangle \\ |b,N\rangle \end{pmatrix} = U \begin{pmatrix} |g,n\rangle \\ |e,n-1\rangle \end{pmatrix}} \ , \tag{35.21}$$

and, hence, are equivalent descriptions of the same reality. But while in the product state picture the system Hamiltonian is diagonal in the *absence* of atom-light interaction, in the dressed states picture the Hamiltonian is diagonal in the *presence* of interaction. The numbers n denote the amount of photons in the laser beam, the numbers N denote the amount of energy packets within the system, that is, the photons *plus* the possible excitation of the atom. The expression of the unitary transformation matrix will be derived in Sec. 35.4.1.

35.1.4 Dipole moments for vector transitions

Until now, we restricted to transitions between two levels without accounting for their possible substructure, which interacts with the vectorial nature of the driving

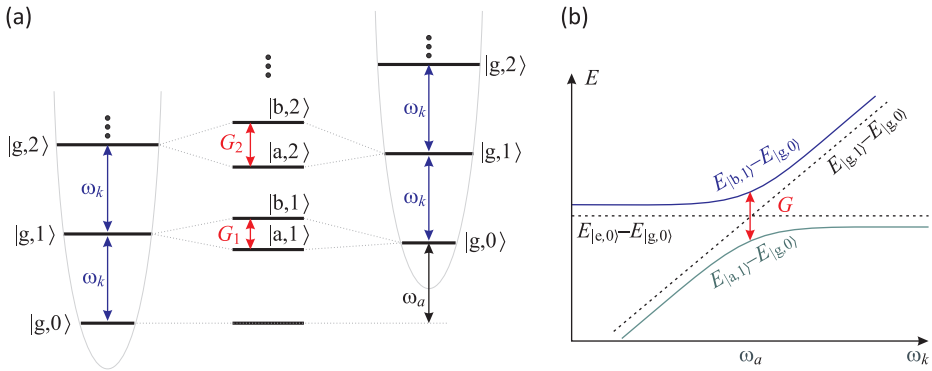

Figure 35.4: (a) Rabi splitting of the lowest dressed states. (b) Avoided crossing of dressed states.

light fields. Resuming the discussion of Sec. 34.2.3, we generalize the treatment of the preceding section considering a two-level atom with an arbitrary hyperfine level substructure $|g,(I,J)F,m\rangle \leftrightarrow |e,(I,J')F',m'\rangle$. The Hamiltonian is,

$$\hat{H} = \sum_{\alpha,\beta} \hbar\omega_{g\alpha}|g_\alpha\rangle\langle g_\alpha| + \hbar\omega_{e\beta}|g_\beta\rangle\langle g_\beta| \ . \tag{35.22}$$

Generalizing the expression (35.14) to vectorial transitions, the electric dipole operator reads,

$$\begin{aligned}\hat{\mathbf{d}} &= \sum_{i,j} |i\rangle\langle i|e^{\imath(\omega_i-\omega_j)t}\hat{\mathbf{d}}|j\rangle\langle j| \qquad (35.23)\\ &= \sum_{\alpha,\beta} |g_\alpha\rangle\langle g_\alpha|e^{\imath(\omega_{g\alpha}-\omega_{e\beta})t}\hat{\mathbf{d}}|e_\beta\rangle\langle e_\beta| + |e_\beta\rangle\langle e_\beta|e^{-\imath(\omega_{g\alpha}-\omega_{e_\beta})t}\hat{\mathbf{d}}|g_\alpha\rangle\langle g_\alpha| \ .\end{aligned}$$

Example 204 (*Vector transition in strontium*): The simplest possible vectorial level scheme consists of one ground and three excited Zeeman states, such as realized, for instance, in the strontium $^1S_0$-$^1P_1$ transition,

$$\hat{H}_{strontium} = \sum_{\beta} \hbar\omega_{e\beta}|g_\beta\rangle\langle g_\beta| \ , \tag{35.24}$$

setting $\omega_{ga} \equiv 0$. For strontium, we may introduce the vectorial lowering operator [365],

$$\hat{\vec{\sigma}} = \hat{\sigma}_x\hat{\mathbf{e}}_x + \hat{\sigma}_y\hat{\mathbf{e}}_y + \hat{\sigma}_z\hat{\mathbf{e}}_z \quad \text{with} \quad \hat{\sigma}_\beta = |g\rangle\langle e_\beta| \quad \text{with} \quad \beta = x,y,z \ . \tag{35.25}$$

In this case, the electric dipole operator reads,

$$\begin{aligned}\hat{\mathbf{d}}_{strontium} &= \sum_{\beta} |g\rangle\langle g|e^{-\imath\omega_{e\beta}t}\hat{\mathbf{d}}|e_\beta\rangle\langle e_\beta| + |e_\beta\rangle\langle e_\beta|e^{\imath\omega_{e\beta}t}\hat{\mathbf{d}}|g\rangle\langle g| \qquad (35.26)\\ &= d\sum_{\beta} e^{-\imath\omega_{e\beta}t}|g\rangle\langle e_\beta|\hat{\mathbf{e}}_\beta + c.c. = de^{-\imath\omega_e t}\hat{\vec{\sigma}} + c.c. \ ,\end{aligned}$$

with $\langle g|\hat{\mathbf{d}}|e_\beta\rangle = d\hat{\mathbf{e}}_\beta$ and $\omega_{e\beta} = \omega_e$.

35.1.5 Exercises

35.1.5.1 Ex: Photon statistics

An optical resonator contains on average 10 photons in the mode TEM_{00q}. What is the probability of finding, at any time, 1 photon resp. 10 photons, when the light is (a) thermal, (b) coherent? For case (a), what is the temperature of the light for $\lambda = 633\,\mathrm{nm}$?

Solution: *a. For thermal light,*

$$P_n = \frac{\bar{n}^n}{(1+\bar{n})^{n+1}} \ ,$$

such that $P_1 = 0.083$ *and* $P_{10} = 0.035$. *The temperature of the light can be evaluated from,*

$$\bar{n} = \frac{1}{e^{\hbar\omega/k_B T} - 1} \ ,$$

yielding $T_1 = 32800\,\mathrm{K}$, *respectively,* $T_{10} = 238000\,\mathrm{K}$.
b. For coherent light,

$$P_n = e^{\bar{n}} \frac{\bar{n}^n}{n!} \ ,$$

such that $P_1 = 4.5 \times 10^{-4}$ *and* $P_{10} = 0.13$.

35.1.5.2 Ex: Converting a pure state into a mixture by incomplete measurement

Consider a dressed two-level atom with the atomic states $|1\rangle$ and $|2\rangle$ and the photon number state $|n\rangle$.
a. Write down the general normalized dressed state and the density operator.
b. Now, perform a measurement of the atomic state tracing over the atomic degree of freedom and verify whether the resulting density operator represents a pure state.
c. Now, perform a measurement of the photon number and verify whether the resulting density operator represents a pure state.

Solution: *a. The state reads* $|\psi\rangle = \frac{1}{\sqrt{2}}|1,n\rangle + \frac{1}{\sqrt{2}}|2,n-1\rangle$. *The density operator*

$$\hat{\rho}_{AB} = |\psi\rangle\langle\psi| = \tfrac{1}{2}|1,n\rangle\langle 1,n| + \tfrac{1}{2}|2,n-1\rangle\langle 1,n| + \tfrac{1}{2}|1,n\rangle\langle 2,n-1| + \tfrac{1}{2}|2,n-1\rangle\langle 2,n-1|$$

obviously represents a pure state, $\hat{\rho}_{AB}^2 = \hat{\rho}_{AB}$.
b. Tracing over the atomic states,

$$\hat{\rho}_B \equiv Tr_A\ \hat{\rho}_{AB} = \sum_{i=1,2} \langle i|\hat{\rho}_{AB}|i\rangle = \tfrac{1}{2}|n\rangle\langle n| + \tfrac{1}{2}|n-1\rangle\langle n-1| \ ,$$

which is not a pure state,

$$\hat{\rho}_B^2 = \tfrac{1}{4}|n\rangle\langle n| + \tfrac{1}{4}|n-1\rangle\langle n-1| \neq \hat{\rho}_B \ .$$

c. Tracing over the photon numbers,

$$\hat{\rho}_A \equiv Tr_B\ \hat{\rho}_{AB} = \sum_m \langle m|\hat{\rho}_{AB}|m\rangle = \tfrac{1}{2}|1\rangle\langle 1| + \tfrac{1}{2}|2\rangle\langle 2|$$

with

$$\hat{\rho}_A^2 = \tfrac{1}{4}|1\rangle\langle 1| + \tfrac{1}{4}|2\rangle\langle 2| \neq \hat{\rho}_A\ .$$

35.1.5.3 Ex: Photon wavefunction

a. Show that for the *photonic wavefunction* $\mathbf{\Psi}$ and the current density $\mathbf{J}$ [1134],

$$\mathbf{\Psi} = \mathbf{\Psi}^+ + \mathbf{\Psi}^- \qquad \text{with} \qquad \mathbf{\Psi}^\pm = \sqrt{\tfrac{\varepsilon_0}{2}}\vec{\mathcal{E}}_\pm \pm \imath\sqrt{\tfrac{1}{2\mu_0}}\vec{\mathcal{B}}_\pm \qquad \text{and} \qquad \hat{\sigma}\mathbf{\Psi}^\pm = \pm\mathbf{\Psi}^\pm$$

$$\mathbf{J} = \mathbf{J}_f + \nabla\times\mathbf{M} + \frac{\partial\mathbf{P}}{\partial t}\ ,$$

where $\vec{\mathcal{E}} \equiv \vec{\mathcal{E}}_+ + \vec{\mathcal{E}}_-$ and $\vec{\mathcal{B}} \equiv \vec{\mathcal{B}}_+ + \vec{\mathcal{B}}_-$ are the real electric and magnetic fields of the photon and $\hat{\sigma}$ is the helicity, the Bialynicki-Birula-Sipe wave equation

$$\boxed{\imath\hbar\frac{\partial\mathbf{\Psi}}{\partial t} = \hbar c\hat{\sigma}\nabla\times\mathbf{\Psi} - \tfrac{\imath\hbar}{\sqrt{2\varepsilon_0}}\mathbf{J} \qquad \text{and} \qquad \nabla\cdot\mathbf{\Psi} = 0}$$

is equivalent to the Maxwell equations.
b. Use the plane wavefunction

$$\mathbf{\Psi} \equiv \sum_s \int d^3k \sqrt{\tfrac{\hbar\omega}{(2\pi)^3}} e^{\imath(\mathbf{k}\cdot\mathbf{r}-\omega t)}\hat{a}_{\mathbf{k}s}\hat{\mathbf{e}}_{\mathbf{k}s}$$

to calculate the total energy $\hat{H} = \frac{1}{2}\int d^3r[\mathbf{\Psi}^\dagger(\mathbf{r},t), \mathbf{\Psi}(\mathbf{r},t)]_+$.

Solution: *a. In vacuum, separating the Eq. by real and imaginary parts, we immediately verify,*

$$\imath\hbar\frac{\partial(\mathbf{\Psi}^+ + \mathbf{\Psi}^-)}{\partial t} = \hbar c\nabla\times(\mathbf{\Psi}^+ - \mathbf{\Psi}^-) \qquad \textit{and} \qquad \nabla\cdot\mathbf{\Psi}^\pm = 0$$

and substituting,

$$\tfrac{1}{\mu_0}\nabla\times\mathbf{B} = \varepsilon_0\frac{\partial\mathbf{E}}{\partial t} + \mathbf{J} \qquad \textit{and} \qquad \nabla\times\mathbf{E} = -\frac{\partial\mathbf{B}}{\partial t} \qquad \textit{and} \qquad \nabla\cdot\mathbf{E} = 0 = \nabla\cdot\mathbf{B}\ .$$

b. Inserting the plane wave we calculate,

$$\begin{aligned}
&\int d^3r\mathbf{\Psi}^\dagger(\mathbf{r},t)\mathbf{\Psi}(\mathbf{r},t)\\
&= \tfrac{1}{(2\pi)^3}\sum_{s,s'}\int d^3k\int d^3k'\left(\hbar\sqrt{\omega\omega'}\hat{a}^\dagger_{\mathbf{k}s}\hat{a}_{\mathbf{k}'s'}\epsilon_{\mathbf{k}s}\epsilon_{\mathbf{k}'s'}\int d^3r e^{-\imath[(\mathbf{k}-\mathbf{k}')\cdot\mathbf{r}-(\omega-\omega')t]}\right)\\
&= \sum_{s,s'}\int d^3k\int d^3k'\left(\hbar\sqrt{\omega\omega'}\hat{a}^\dagger_{\mathbf{k}s}\hat{a}_{\mathbf{k}'s'}\delta_{s,s'}\delta^3(\mathbf{k}-\mathbf{k}')\right) = \sum_s\int d^3k\ \hbar\omega|\hat{a}_{\mathbf{k}s}|^2\ ,
\end{aligned}$$

and consequently,

$$\hat{H} = \tfrac{1}{2}\int d^3r[\mathbf{\Psi}^\dagger(\mathbf{r},t),\mathbf{\Psi}(\mathbf{r},t)]_+ = \sum_s \int d^3k\ \hbar\omega(\hat{a}^\dagger_{\mathbf{k}s}\hat{a}_{\mathbf{k}s} + \tfrac{1}{2})\ .$$

35.2 (Quasi-)probability distribution functions of the coherent state basis

In the previous section we have seen that a light mode can be identified with a harmonic oscillator, which enabled us to harness the whole powerful formalism developed in Secs. 24.5 and 24.6 for the characterization of the quantum states of light. As we have seen in those sections, quantum observables are intrinsically affected by quantum noise, which leads to a spreading of their representation in phase space. For the case of Glauber states of a harmonic oscillator we illustrated in Fig. 24.19 the uncertainty of conjugate variables by circles around their expectation values whose areas are determined by the Heisenberg uncertainty relation. These circular areas represent phase space probability distribution functions. These are distribution functions measuring the probability to encounter the observables at specific points in phase space.

States other than Glauber states are possible, for instance Fock or cat states. Some of these states may exhibit quantum correlations, which we would like to identify in probability distributions. Quantum correlations in systems with small Hilbert spaces, such as the two-level atom, are conveniently represented by a density operator or by the Bloch vector introduced in Eq. (23.47). Large or infinite Hilbert spaces require different approaches. We have seen in Sec. 24.6.1 how to expand the state of a harmonic oscillator on a Fock state basis. On the other hand, we have seen that Glauber states are more 'natural' states for a harmonic oscillator, so that we would like to visualize expansions of arbitrary states into a coherent state basis.

The following sections are devoted to introducing various such distribution functions [1184, 1160] and to calculating them for a selection of particular states, such as the Fock and the Glauber state, the thermal state, and the Schrödinger cat state. We will mostly restrict the discussion to pure states, postponing a discussion of the representation of statistical mixtures to Sec. 35.4, where we will also extend the discussion to quantum correlations in light fields resulting from a Jaynes-Cummings type interaction of an atom with a light mode.

35.2.1 The density operator and distribution functions

35.2.1.1 The density operator

We define the *density operator* for a pure state as,

$$\hat{\rho} \equiv |\psi\rangle\langle\psi|\ . \tag{35.27}$$

A detailed discussion of the density operator for non pure states, that is, statistical mixtures has been given in Sec. 34.3. The definition (35.27) is independent from

a chosen basis, but a proper representation can be found by simply expanding the state $|\psi\rangle$ on a proper basis. The expansion we had in mind in Sec. 34.3.2 was on eigenstates of atomic excitations, which are typically discrete and limited in number. The expansion of the density operator in the infinite but discrete spectrum of Fock states is essentially the same as for atomic excitations and thus straightforward,

$$\begin{aligned} \hat{\rho} &= \sum_n |n\rangle\hat{\rho}\langle n| \equiv \sum_n p_n |n\rangle\langle n| \qquad (35.28)\\ \Longrightarrow p_m = \langle m|\hat{\rho}|m\rangle &= \sum_n p_n |\langle m|n\rangle|^2 \\ &= \sum_n p_n \delta_{mn} = p_m \ , \end{aligned}$$

where the first line can be read as a definition of the photon number distribution function p_n. An analogous expansion in the continuous Glauber basis is, however, more complicated, because the coherent states are not orthogonal,

$$\begin{aligned} \hat{\rho} &= \tfrac{1}{\pi}\int \hat{\rho}|\alpha\rangle\langle\alpha| d^2\alpha \equiv \int P(\alpha,\alpha^*)|\alpha\rangle\langle\alpha| d^2\alpha \qquad (35.29)\\ \Longrightarrow \pi Q(\beta,\beta^*) \equiv \langle\beta|\hat{\rho}|\beta\rangle &= \int P(\alpha,\alpha^*)|\langle\beta|\alpha\rangle|^2 d^2\alpha \\ &= \int P(\alpha,\alpha^*) e^{-|\alpha-\beta|^2} d^2\alpha \neq P(\beta,\beta^*) \ . \end{aligned}$$

That is, we end up with two distribution functions, the so-called *P-function* $P(\alpha,\alpha^*)$ (or *Glauber-Sudarshan representation*) and the *Q-function* $Q(\alpha,\alpha^*)$ (or *Husimi representation*) which, according to (35.29) they are not equal. Before we deepen the discussion in the upcoming sections let us already state here, that the reason for the complication is rooted in the non-commutativity of the field operators $[\hat{a},\hat{a}^\dagger] = 1$. Indeed, expressing the density operator of a system as a function of field operators we have (at least) two choices called the *normal-ordered* arrangement (label N) and the *antinormal-ordered* arrangement (label A),

$$\hat{\rho}_N(\hat{a},\hat{a}^\dagger) = \sum_{m,n} c_{m,n}\hat{a}^{\dagger m}\hat{a}^n \qquad \text{and} \qquad \hat{\rho}_A(\hat{a},\hat{a}^\dagger) = \sum_{m,n} c_{m,n}\hat{a}^m\hat{a}^{\dagger n} \ . \qquad (35.30)$$

Although both expressions can be converted into each other, the functional form of the density operator depends on the arrangement. We will show in Exc. 35.2.5.1 that the $P(\alpha,\alpha^*)$-function defined by the first line of (35.29) is more natural for the antinormal-ordered density operator $\hat{\rho}_A$, while the $Q(\alpha,\alpha^*)$-function defined by the second line of (35.29) is more natural for the normal-ordered density operator $\hat{\rho}_N$:

$$\rho_N(\alpha,\alpha^*) = \tfrac{1}{\pi}Q(\alpha,\alpha^*) \qquad \text{and} \qquad \rho_A(\alpha,\alpha^*) = \pi P(\alpha,\alpha^*) \ . \qquad (35.31)$$

We will discuss the distribution functions more deeply in the upcoming sections.

To prepare the subsequent derivations, let us define the two-dimensional complex Fourier transform by,

$$(\mathcal{F}\chi)(\beta,\beta^*) = \tfrac{1}{\pi}\int \chi(\alpha,\alpha^*) e^{\beta\alpha^* - \beta^*\alpha} d^2\alpha \ , \qquad (35.32)$$

with $d^2\lambda = d\mathfrak{Re}\ \lambda\ d\mathfrak{Im}\ \lambda = dr_\lambda dp_\lambda$. Twofold application of the Fourier transform reproduces the original function,

$$\begin{aligned}(\mathcal{F}\mathcal{F}\chi)(\gamma,\gamma^*) &= \tfrac{1}{\pi}\int(\mathcal{F}\chi)(\beta,\beta^*)e^{\gamma\beta^*-\gamma^*\beta}d^2\beta \\ &= \tfrac{1}{\pi^2}\int\chi(\alpha,\alpha^*)\int e^{\beta^*(\gamma-\alpha)-\beta(\gamma^*-\alpha^*)}d^2\beta d^2\alpha \\ &= \tfrac{1}{\pi^2}\int\chi(\alpha,\alpha^*)\pi^2\delta^{(2)}(\gamma-\alpha)d^2\alpha = \chi(\gamma,\gamma^*)\ ,\end{aligned} \tag{35.33}$$

where we used,

$$\delta^{(2)}(\alpha) = \tfrac{1}{\pi^2}\int e^{\lambda^*\alpha-\lambda\alpha^*}d^2\lambda\ . \tag{35.34}$$

The formula (35.34) can be extended to include field operators [1184],

$$\begin{aligned}\delta(\alpha^*-\hat{a}^\dagger)\delta(\alpha-\hat{a}) &= \tfrac{1}{\pi^2}\int e^{-\lambda(\alpha^*-\hat{a}^\dagger)}e^{\lambda^*(\alpha-\hat{a})}d^2\lambda \\ \delta(\alpha-\hat{a})\delta(\alpha^*-\hat{a}^\dagger) &= \tfrac{1}{\pi^2}\int e^{\lambda^*(\alpha-\hat{a})}e^{-\lambda(\alpha^*-\hat{a}^\dagger)}d^2\lambda\ ,\end{aligned} \tag{35.35}$$

which will be useful in the following.

35.2.1.2 The Glauber-Sudarshan P-distribution

The Glauber-Sudarshan P-function can be formally defined by [1184],

$$\boxed{P(\alpha,\alpha^*) \equiv \mathrm{Tr}\ \hat{\rho}\delta(\alpha^*-\hat{a}^\dagger)\delta(\alpha-\hat{a})}\ . \tag{35.36}$$

The definition (35.29) of the P-function, that is,

$$\boxed{\hat{\rho} \equiv \int P(\alpha,\alpha^*)|\alpha\rangle\langle\alpha|d^2\alpha}\ , \tag{35.37}$$

is equivalent to the definition (35.36), as will be verified in Exc. 35.2.5.2. From (35.37) we see, that the Glauber-Sudarshan P-function is just the distribution that leaves the density matrix diagonal in the coherent state basis. Since $\hat{\rho}$ is Hermitian, $P(\alpha,\alpha^*)$ is real, and since $\mathrm{Tr}\ \hat{\rho} = 1$, it is normalized, $\int P(\alpha,\alpha^*)d^2\alpha = 1$. Hence, the P-distribution functions can be interpreted as the probability of finding the coherent state $|\alpha\rangle$ within the statistical mixture given by (35.37).

In order to unravel its properties let us consider an arbitrary operator $\hat{O}$ being a function of the field operators $\hat{a}$ and $\hat{a}^\dagger$. Using the commutation rule $[\hat{a},\hat{a}^\dagger] = 1$ the operator can always be brought in normal-ordered form,

$$\hat{O}_N(\hat{a},\hat{a}^\dagger) = \sum_{m,n} o_{m,n}\hat{a}^{\dagger m}\hat{a}^n\ . \tag{35.38}$$

The expectation value of this operator is,

$$\langle\hat{O}_N(\hat{a},\hat{a}^\dagger)\rangle = \mathrm{Tr}\ \hat{\rho}\hat{O}_N(\hat{a},\hat{a}^\dagger) = \int P(\alpha,\alpha^*)O_N(\alpha,\alpha^*)d^2\alpha\ , \tag{35.39}$$

as we will show in Exc. 35.2.5.3.

35.2.1.3 The Husimi Q-distribution

The Husimi Q-function is formally defined by [1184],

$$\boxed{Q(\alpha,\alpha^*) \equiv \text{Tr } \hat{\rho}\delta(\alpha-\hat{a})\delta(\alpha^*-\hat{a}^\dagger)} \ . \tag{35.40}$$

The definition (35.29) of the Q-function, that is,

$$\boxed{\langle\alpha|\hat{\rho}|\alpha\rangle = \pi Q(\alpha,\alpha^*)} \ , \tag{35.41}$$

is equivalent to the definition (35.36), as will be verified in Exc. 35.2.5.2. From (35.41) we see, that the Q-distribution function can be interpreted as the expectation value of the density operator (35.27).

The expression resembles Eq. (35.36) except for the order of the δ-functions. We now consider the same arbitrary operator $\hat{O}$ as in (35.38), but now expressed in antinormal ordered form of the field operators $\hat{a}$ and $\hat{a}^\dagger$,

$$\hat{O}_A(\hat{a},\hat{a}^\dagger) = \sum_{m,n} o_{m,n}\hat{a}^m\hat{a}^{\dagger n} \ . \tag{35.42}$$

As we will show in Exc. 35.2.5.3, the expectation value of this operator is,

$$\langle\hat{O}_A(\hat{a},\hat{a}^\dagger)\rangle = \text{Tr } \hat{\rho}\hat{O}_A(\hat{a},\hat{a}^\dagger) = \int Q(\alpha,\alpha^*)O_A(\alpha,\alpha^*)d^2\alpha \ . \tag{35.43}$$

35.2.1.4 The Wigner-Weyl distribution

The *Wigner function* represents something like the spectrum of two-dimensional phase-space correlation function. For a pure state and a one-dimensional system it is defined by,

$$W(x,p) \equiv \tfrac{1}{\pi}\int_{-\infty}^{\infty}\langle\psi|x+y\rangle\langle x-y|\psi\rangle e^{2\imath py/\hbar}dy \ . \tag{35.44}$$

Example 205 (*Wigner function of a free particle in 3D*): For example, for a free particle described by the wavefunction in three-dimensional space,

$$\langle\mathbf{r}|\psi\rangle = \tfrac{1}{\sqrt{V}}e^{\imath\mathbf{k}\cdot\mathbf{r}} \ ,$$

the Wigner function is,

$$\begin{aligned} W(\mathbf{r},\mathbf{p}) &= \frac{1}{\pi^3}\int_{-\infty}^{\infty}\tfrac{1}{\sqrt{V}}e^{-\imath\mathbf{k}\cdot(\mathbf{r}+\mathbf{x})}\tfrac{1}{\sqrt{V}}e^{\imath\mathbf{k}\cdot(\mathbf{r}-\mathbf{x})}e^{(2\imath/\hbar)\mathbf{p}\cdot\mathbf{x}}d^3x \\ &= \frac{1}{\pi^3 V}\int_{-\infty}^{\infty}e^{-2\imath(\mathbf{k}-\mathbf{p}/\hbar)\cdot\mathbf{x}}d^3x = \tfrac{1}{V}\delta^3(\mathbf{p}-\hbar\mathbf{k}) \ . \end{aligned}$$

For a harmonic oscillator, we would like to embed the Wigner function into the formalism of the coherent states distribution functions, such that it can be used to evaluate expectation values,

$$\langle\hat{O}_S(\hat{a},\hat{a}^\dagger)\rangle = \text{Tr } \hat{\rho}\hat{O}_S(\hat{a},\hat{a}^\dagger) = \int W(\alpha,\alpha^*)O_S(\alpha,\alpha^*)d^2\alpha \ , \tag{35.45}$$

where the index S denotes *symmetric order*. How this can be done will be detailed in the next section and in Exc. 35.2.5.3.

Example 206 (*Symmetric order*): Simple examples for Wigner-Weyl ordering are,

$$\begin{aligned}
\hat{a}\hat{a}^\dagger &= \tfrac{1}{2}(\hat{a}\hat{a}^\dagger + \hat{a}^\dagger\hat{a}) - \tfrac{1}{2} \\
\hat{a}^\dagger\hat{a} &= \tfrac{1}{2}(\hat{a}\hat{a}^\dagger + \hat{a}^\dagger\hat{a}) + \tfrac{1}{2} \\
\hat{a}^2\hat{a}^\dagger &= \tfrac{1}{2}(\hat{a}^2\hat{a}^\dagger + \hat{a}^\dagger\hat{a}^2) + \hat{a} \\
\hat{a}\hat{a}^\dagger\hat{a} &= \tfrac{1}{2}(\hat{a}^2\hat{a}^\dagger + \hat{a}^\dagger\hat{a}^2) \\
\hat{a}^\dagger\hat{a}^2 &= \tfrac{1}{2}(\hat{a}^2\hat{a}^\dagger + \hat{a}^\dagger\hat{a}^2) - \hat{a}\ .
\end{aligned}$$

35.2.2 Relation between the P, Q, and Wigner distributions

All three distribution function studied here, the P, the Q, and the Wigner distributions can be brought into a common generic shape writing the density operator as [1184],

$$\boxed{\begin{aligned}
\hat{\rho} \;&=\; \pi \int F_X(\alpha,\alpha^*)\Delta_X(\alpha-\hat{a},\alpha^*-\hat{a}^\dagger)d^2\alpha \\
\text{with}\qquad &\Delta_N(\alpha-\hat{a},\alpha^*-\hat{a}^\dagger) = \tfrac{1}{\pi^2}\int e^{-\lambda(\alpha^*-\hat{a}^\dagger)+\lambda^*(\alpha-\hat{a})}e^{-|\lambda|^2/2}d^2\lambda \\
&\Delta_S(\alpha-\hat{a},\alpha^*-\hat{a}^\dagger) = \tfrac{1}{\pi^2}\int e^{-\lambda(\alpha^*-\hat{a}^\dagger)+\lambda^*(\alpha-\hat{a})}d^2\lambda \\
&\Delta_A(\alpha-\hat{a},\alpha^*-\hat{a}^\dagger) = \tfrac{1}{\pi^2}\int e^{-\lambda(\alpha^*-\hat{a}^\dagger)+\lambda^*(\alpha-\hat{a})}e^{|\lambda|^2/2}d^2\lambda
\end{aligned}}\ , \tag{35.46}$$

with the indices $X = N, S, A$ and the respective distribution functions $F_N = P$, $F_S = W$, and $F_A = Q$. A useful formula helping us to break down the exponential functions is obtained from Glauber's formula (23.210) applied to the displacement operator $D(\alpha) = e^{\lambda\hat{a}^\dagger - \lambda^*\hat{a}}$ defined in (24.111),

$$e^{\lambda\hat{a}^\dagger-\lambda^*\hat{a}} = e^{-\lambda^*\hat{a}}e^{\lambda\hat{a}^\dagger}e^{|\lambda|^2/2} = e^{\lambda\hat{a}^\dagger}e^{-\lambda^*\hat{a}}e^{-|\lambda|^2/2}\ . \tag{35.47}$$

as it allows us to rewrite the formulas (35.46) as,

$$\begin{aligned}
\Delta_N(\alpha-\hat{a},\alpha^*-\hat{a}^\dagger) &= \mathcal{F}[e^{-\lambda^*\hat{a}}e^{\lambda\hat{a}^\dagger}] \\
\Delta_S(\alpha-\hat{a},\alpha^*-\hat{a}^\dagger) &= \mathcal{F}[e^{\lambda\hat{a}^\dagger-\lambda^*\hat{a}}] \\
\Delta_A(\alpha-\hat{a},\alpha^*-\hat{a}^\dagger) &= \mathcal{F}[e^{\lambda\hat{a}^\dagger}e^{-\lambda^*\hat{a}}]\ .
\end{aligned} \tag{35.48}$$

Inserting the density operator (35.46) into definition (35.36) of the Glauber-Sudarshan P-function we calculate,

$$\begin{aligned}
P(\alpha,\alpha^*) &= \mathrm{Tr}\ \hat{\rho}\delta(\alpha^*-\hat{a}^\dagger)(\alpha-\hat{a}) \\
&= \tfrac{1}{\pi^2}\int e^{\lambda^*\alpha-\lambda\alpha^*}\,\mathrm{Tr}\ \hat{\rho}e^{\lambda\hat{a}^\dagger}e^{-\lambda^*\hat{a}}d^2\lambda = \mathcal{F}[\chi_N(\lambda,\lambda^*)]\ ,
\end{aligned} \tag{35.49}$$

where we defined the so-called normal-ordered *characteristic function* $\chi_N \equiv \mathrm{Tr}\ \hat{\rho} e^{\lambda \hat{a}^\dagger} e^{-\lambda^* \hat{a}}$. Similarly, inserting the density operator (35.46) into definition (35.40) of the Husimi Q-function we calculate,

$$\begin{aligned} Q(\alpha, \alpha^*) &= \mathrm{Tr}\ \hat{\rho} \delta(\alpha - \hat{a})(\alpha^* - \hat{a}^\dagger) \\ &= \tfrac{1}{\pi^2} \int e^{\lambda^* \alpha - \lambda \alpha^*} \mathrm{Tr}\ \hat{\rho} e^{-\lambda^* \hat{a}} e^{\lambda \hat{a}^\dagger} d^2\lambda = \mathcal{F}[\chi_A(\lambda, \lambda^*)] \ , \end{aligned} \tag{35.50}$$

where we defined the antinormal-ordered characteristic function $\chi_A \equiv \mathrm{Tr}\ \hat{\rho} e^{-\lambda^* \hat{a}} e^{\lambda \hat{a}^\dagger}$. By analogy we find for the Wigner distribution,

$$W(\alpha, \alpha^*) = \mathcal{F}[\chi_A(\lambda, \lambda^*)] = \tfrac{1}{\pi^2} \int e^{\lambda^* \alpha - \lambda \alpha^*} \mathrm{Tr}\ \hat{\rho} e^{\lambda \hat{a}^\dagger - \lambda^* \hat{a}} d^2\lambda \ . \tag{35.51}$$

In summary, the three coherent distribution functions are expressed by inverse Fourier transforms of the following characteristic functions [5],

$$\boxed{\begin{array}{rclcrcl} \chi_N(\lambda, \lambda^*) & = & \mathrm{Tr}\ \hat{\rho} e^{\lambda \hat{a}^\dagger} e^{-\lambda^* \hat{a}} & , & P & = & \mathcal{F}\chi_N \\ \chi_S(\lambda, \lambda^*) & = & \mathrm{Tr}\ \hat{\rho} e^{\lambda \hat{a}^\dagger - \lambda^* \hat{a}} & , & W & = & \mathcal{F}\chi_S \\ \chi_A(\lambda, \lambda^*) & = & \mathrm{Tr}\ \hat{\rho} e^{-\lambda^* \hat{a}} e^{\lambda \hat{a}^\dagger} & , & Q & = & \mathcal{F}\chi_A \end{array}} \ . \tag{35.52}$$

We see that the distribution functions $\chi_{N,S,A}$ are related to each other via (35.47). We derive in Exc. 35.2.5.4 the so-called disentangling theorem [504],

$$e^{-|\lambda|^2/2} \chi_N(\lambda) = \chi_S(\lambda) = e^{|\lambda|^2/2} \chi_A(\lambda) \ . \tag{35.53}$$

Thus, Q-function corresponds to a smoothed Wigner function, which in turn corresponds to a smoothed P-function. The inverse complex Fourier transformation converts the products in (35.53) into convolutions. Exploiting the useful integral formula,

$$\tfrac{1}{\pi} \int e^{-a|\lambda|^2 + b\lambda + c\lambda^*} d^2\lambda = \tfrac{1}{a} e^{bc/a} \ , \tag{35.54}$$

we find,

$$W = P \star \frac{2}{\pi} e^{-2|\lambda|^2} \qquad \text{and} \qquad Q = W \star \frac{2}{\pi} e^{-2|\lambda|^2} = P \star \frac{1}{\pi} e^{-|\lambda|^2} \ . \tag{35.55}$$

What still needs to be proven is, that the generic definition of the distribution function (35.49), (35.50), and (35.51) coincides with the earlier definitions (35.36), (35.40), and (35.44). This will be done in Exc. 35.2.5.5. Also solve the Excs. 35.2.5.6 to 35.2.5.7.

Example 207 (*Generalized phase space representations*): The fact that the probability distributions Q, W, and P are intrinsically connected suggests setting up a generalized formalism based on the displacement operator

[5] For pure states, the definition of the characteristic functions is simplified to,

$$\chi_X(\lambda, \lambda^*) = \langle \psi | ... | \psi \rangle \ .$$

$D(\alpha)|0\rangle = e^{\lambda\hat{a}^\dagger - \lambda^*\hat{a}}|0\rangle = |\alpha\rangle$ introduced in (24.111) and the parity operator Π_s [732]. Defining the s-parametrized probability distribution,

$$X_\rho(\alpha, s) = \text{Tr}\ \hat{\rho}D(\alpha)\Pi_s D^\dagger(\alpha) \longrightarrow \langle\psi|D(\alpha)\Pi_s D^\dagger(\alpha)|\psi\rangle\ , \tag{35.56}$$

where the second expression holds for pure states, we recover the probability distributions Q, W, and P from,

$$Q_\rho(\alpha) \equiv X_\rho(\alpha, -1) \qquad \text{with} \qquad \Pi_{-1} = \sum_{m,n} \delta_{n0}\delta_{mn}|m\rangle\langle n| \tag{35.57}$$

$$W_\rho(\alpha) \equiv X_\rho(\alpha, 0) \qquad \text{with} \qquad \Pi_0 = \sum_{m,n} 2e^{\imath\pi n}\delta_{mn}|m\rangle\langle n|$$

$$\text{so that} \qquad \Pi_0|\alpha\rangle = \sum_n 2e^{\imath\pi n}|n\rangle\langle n|\alpha\rangle = \sum_n 2e^{-|\alpha|^2/2}\frac{(-\alpha)^n}{\sqrt{n!}}|n\rangle = 2|-\alpha\rangle$$

$$P_\rho(\alpha) \equiv X_\rho(\alpha, 1) \qquad \text{with} \qquad \Pi_1 = \sum_{m,n} \infty\delta_{mn}|m\rangle\langle n|\ .$$

In particular, for the vacuum state we calculate,

$$Q_{|0\rangle}(\alpha) = \sum_n \langle 0|D(\alpha)\delta_{n0}|n\rangle\langle n|D^\dagger(\alpha)|0\rangle = |\langle 0|-\alpha\rangle|^2 = e^{-|\alpha|^2} \tag{35.58}$$

$$W_{|0\rangle}(\alpha) = \sum_n \langle 0|D(\alpha)2e^{\imath\pi n}|n\rangle\langle n|D^\dagger(\alpha)|0\rangle = 2\sum_n e^{\imath\pi n}|\langle n|-\alpha\rangle|^2 = 2e^{-2|\alpha|^2}$$

$$P_{|0\rangle}(\alpha) = ... = \delta^{(2)}(\alpha)\ .$$

The convolution of distribution functions yields,

$$[Y \star X](\alpha) = \int [D^{-1}(\alpha)Y(\alpha')]X(\alpha')d\alpha' = \int Y(\alpha' - \alpha)X(\alpha')d\alpha'$$

$$X_{|0\rangle}(\alpha, s') \star X_\rho(\alpha, s) = X_\rho(\alpha, s + s' - 1)\ . \tag{35.59}$$

For example,

$$P_{|0\rangle}(\alpha) \star X_\rho(\alpha, s) = X_{|0\rangle}(\alpha, 1) \star X_\rho(\alpha, s) = X_\rho(\alpha, s)\ . \tag{35.60}$$

identifying the Glauber-Sudarshan distribution as the identity operator, and

$$W_{|0\rangle}(\alpha) \star W_\rho(\alpha) = X_{|0\rangle}(\alpha, 0) \star X_\rho(\alpha, 0) = X_\rho(\alpha, -1) = Q_\rho(\alpha)\ . \tag{35.61}$$

35.2.3 Characteristic functions for arbitrary HO states in the Fock basis

The various states that a light field can adopt can now be expressed either by photon number distribution in a Fock state basis, or by two-dimensional weighting functions P, Q, W in a coherent state basis. Here, are some examples for these representations.

If a state of a harmonic oscillator can be expanded into Fock states,

$$|\psi\rangle = \sum_n c_n|n\rangle\ , \tag{35.62}$$

the normal-ordered characteristic function (35.52) will be composed of terms like $\langle m|e^{\lambda\hat{a}^\dagger}e^{-\lambda^*\hat{a}}|n\rangle$. To evaluate these terms, we begin calculating [6],

$$\hat{a}^k|n\rangle = \sqrt{\frac{n!}{(n-k)!}}|n-k\rangle \quad \text{for} \quad k \leq n \qquad \text{and} \qquad \hat{a}^k|n\rangle = 0 \quad \text{for} \quad k \geq n \ , \tag{35.63}$$

and,

$$e^{-\lambda^*\hat{a}}|n\rangle = \sum_{k=0}^{\infty}\frac{(-\lambda^*\hat{a})^k}{k!}|n\rangle = \sum_{k=0}^{n}\frac{(-\lambda^*)^k}{\sqrt{k!}}\sqrt{\binom{n}{k}}|n-k\rangle \ . \tag{35.64}$$

Hence, assuming $m \geq n$,

$$\begin{aligned}\langle m|e^{\lambda\hat{a}^\dagger}e^{-\lambda^*\hat{a}}|n\rangle &= \sum_{k=0}^{n}\frac{(-\lambda^*)^k\lambda^{m-n+k}}{\sqrt{k!(m-n+k)!}}\sqrt{\binom{n}{k}\binom{m}{m-n+k}} \\ &= \sqrt{\frac{n!}{m!}}\lambda^{m-n}\sum_{k=0}^{n}\binom{m}{k+m-n}\frac{(-|\lambda|^2)^k}{k!} = \sqrt{\frac{n!}{m!}}\lambda^{m-n}L_n^{m-n}(|\lambda|^2) \ ,\end{aligned} \tag{35.65}$$

where L_n^{m-n} are Laguerre polynomials. Now, exploiting the fact that

$$\begin{aligned}\langle m|e^{\lambda\hat{a}^\dagger}e^{-\lambda^*\hat{a}}|n\rangle &= (\langle n|e^{-\lambda\hat{a}^\dagger}e^{\lambda^*\hat{a}}|m\rangle)^\dagger = \overline{\langle n|e^{-\lambda\hat{a}^\dagger}e^{\lambda^*\hat{a}}|m\rangle} \\ &= \sqrt{\frac{m!}{n!}}(-\lambda^*)^{n-m}L_n^{n-m}(|\lambda|^2) \ ,\end{aligned} \tag{35.66}$$

and with the expansion (35.62) we obtain for the normally-ordered characteristic function,

$$\begin{aligned}\chi_N(\lambda) &= \sum_{m,n}c_m^*c_n\langle m|e^{\lambda\hat{a}^\dagger}e^{-\lambda^*\hat{a}}|n\rangle \\ &= \sum_{m\geq n}(1-\tfrac{1}{2}\delta_{m,n})\left(c_m^*c_n\langle m|e^{\lambda\hat{a}^\dagger}e^{-\lambda^*\hat{a}}|n\rangle + \overline{c_m^*c_n\langle m|e^{-\lambda\hat{a}^\dagger}e^{\lambda^*\hat{a}}|n\rangle}\right) \ .\end{aligned} \tag{35.67}$$

finally yielding,

$$\boxed{\chi_N(\lambda) = \sum_{m\geq n}(1-\tfrac{1}{2}\delta_{m,n})\left[c_m^*c_n\lambda^{m-n} + c_mc_n^*(-\lambda^*)^{m-n}\right]\sqrt{\tfrac{n!}{m!}}L_n^{m-n}(|\lambda|^2)} \ . \tag{35.68}$$

Remembering that the symmetrically ordered function is given by $\chi_S(\lambda) = e^{-|\lambda|^2}\chi_N(\lambda)$ we may obtain the Wigner function by a numerical two-dimensional FFT,

$$W(\alpha) = \tfrac{1}{\pi^2}\int e^{-|\lambda|^2}\chi_N(\lambda)e^{\lambda^*\alpha-\lambda\alpha^*}d^2\lambda \ . \tag{35.69}$$

We will use this result in Sec. 35.4.3 to characterize correlations in an optical mode emanating from a Jaynes-Cummings type coupling to an atom. In Exc. 35.2.5.8 we will try to find an analytic solution for this integral.

[6] See also 24.6.6.6.

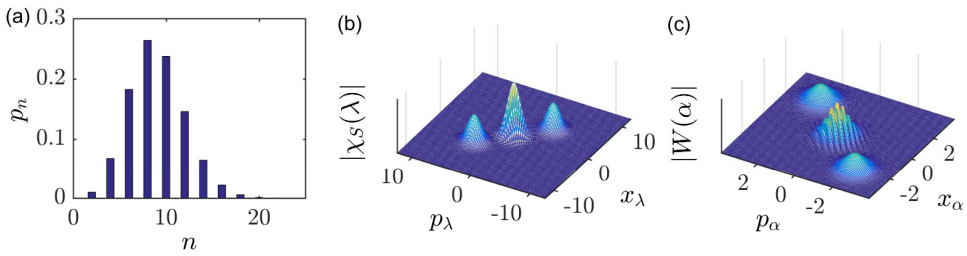

Figure 35.5: (code) Starting from a cat-state photon distribution, as shown in (a), we calculate the symmetrically ordered characteristic function (b) from the expression (35.67), and the Wigner function (c) by an FFT.

35.2.4 Representation of particular states in the Fock and Glauber basis

35.2.4.1 Representations of Glauber states

We have seen earlier that coherent states $|\beta\rangle$ can be expanded on a Fock state basis $|n\rangle$. For the state function, the density operator, and the photon number distribution we have,

$$\boxed{\begin{aligned} |\beta\rangle &= e^{-|\beta|/2}\sum_n \frac{\beta^n}{\sqrt{n!}}|n\rangle \\ \hat{\rho} &= e^{-|\beta|^2}\sum_{m,n}\frac{\beta^n\beta^{*m}}{\sqrt{m!n!}}|n\rangle\langle m| \\ P_n &= |\langle n|\beta\rangle|^2 = e^{-|\beta|^2}\frac{|\beta|^{2n}}{n!} \end{aligned}} \quad . \tag{35.70}$$

Expanding a coherent state on a basis of Glauber states, we will derive in Exc. 35.2.5.9 the P-function, the density matrix, the Q-function, and the Wigner function,

$$\boxed{\begin{aligned} |\psi\rangle &= |\beta\rangle \\ P_{|\beta\rangle}(\alpha) &= \delta^{(2)}(\alpha-\beta) \\ \hat{\rho} &= \int \delta^{(2)}(\alpha-\beta)|\alpha\rangle\langle\alpha|d^2\alpha = |\beta\rangle\langle\beta| \\ Q_{|\beta\rangle}(\alpha) &= \tfrac{1}{\pi}e^{-|\alpha-\beta|^2} \\ W_{|\beta\rangle}(\alpha) &= \tfrac{2}{\pi}e^{-2|\alpha-\beta|^2} \end{aligned}} \quad . \tag{35.71}$$

Example 208 (*State of a laser*): Following [1385, 1131], the correct *state of a laser* beam is not simply a coherent state, but rather,

$$\hat{\rho} = \int |\alpha e^{\imath\varphi}\rangle\langle\alpha e^{\imath\varphi}|\frac{d\varphi}{2\pi} \; . \tag{35.72}$$

After averaging, this state can be written as a superposition of Fock states [313],

$$\hat{\rho} = \sum_n P_n |n\rangle\langle n| \qquad \text{with} \qquad P_n = \frac{e^{-|\alpha|^2}|\alpha|^2 n}{n!} \ , \tag{35.73}$$

but without a specific phase,

$$\hat{\rho} \neq \sum_{m,n} c_m^* c_n |m\rangle\langle n| \ . \tag{35.74}$$

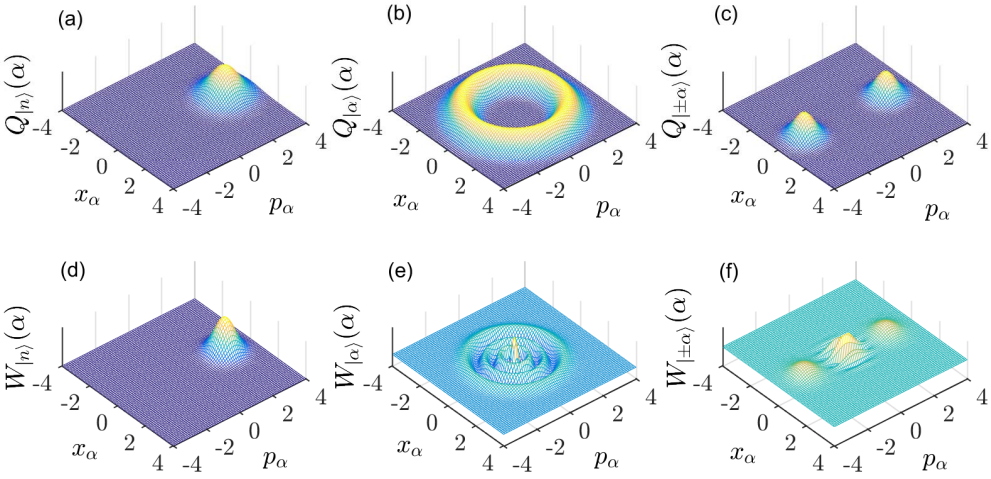

Figure 35.6: (code) (a-c) Q functions and (d-f) Wigner functions of a Glauber state (a,d), a Fock state (b,e), and a Schrödinger cat state (c,f).

35.2.4.2 Representations of Schrödinger cat states

Schrödinger cat states are correlated states of many particles (or quasi-particles). The expansion of the *Schrödinger cat state* $|\beta_0\rangle \pm |\beta_1\rangle$ on a Fock state basis yields, as we have seen in Exc. 24.6.6.5,

$$\boxed{\begin{aligned} |\psi_\pm\rangle &= \sum_n \frac{e^{-|\beta_0|^2/2}\beta_0^n \pm e^{-|\beta_1|^2/2}\beta_1^n}{\sqrt{2n!}}|n\rangle \\ P_n &= |\langle n|\psi_\pm\rangle|^2 \longrightarrow e^{-|\beta_0|^2}\frac{|\beta_0|^{2n}}{n!}\frac{|1\pm(-1)^n|^2}{2} \qquad \text{for} \quad \beta_0 = -\beta_1 \end{aligned}} \ . \tag{35.75}$$

Expanding a Schrödinger cat state on a basis of Glauber states, we will derive in Exc. 35.2.5.10 the P-function, the density matrix, the Q-function, and the Wigner

function,

$$\boxed{\begin{aligned} |\psi_\pm\rangle &= \tfrac{1}{C}(|\beta_0\rangle \pm |\beta_1\rangle) \qquad \text{with} \qquad C = \sqrt{2 \pm 2e^{-|\beta_0-\beta_1|^2}} \\ P_{|\beta_0\rangle|\beta_1\rangle}(\alpha) &= \delta^{(2)}(\alpha-\beta_0) + \delta^{(2)}(\alpha-\beta_1) \\ \hat{\rho} &= |\psi_\pm\rangle\langle\psi_\pm| \\ Q_{|\beta_0\rangle|\beta_1\rangle}(\alpha) &= \tfrac{1}{\pi}e^{-|\alpha-\beta_0|^2} + \tfrac{1}{\pi}e^{-|\alpha-\beta_1|^2} \\ W_{|\beta_0\rangle|\beta_1\rangle}(\alpha) &= \tfrac{2}{C^2\pi}\Big(e^{-2|\alpha-\beta_0|^2} + e^{-2|\alpha-\beta_1|^2} \\ &\pm 2e^{-|\beta_0|^2/2-|\beta_1|^2/2}\mathfrak{Re}\; e^{-2(\beta_1-\alpha)(\beta_0^*-\alpha^*)+\beta_0^*\beta_1}\Big) \end{aligned}} \quad . \tag{35.76}$$

We know from microscopic systems, for instance a two-level atom, that they can live in superposition states $|1\rangle + |2\rangle$. In contrast, the Schrödinger cat states discussed above occur in continuous Schrödinger fields involving many particles. Macroscopic quantum interferences (i.e. interferences that are detectable with macroscopic apparatuses, for example in heterodyne schemes) are named *fuzzy Schrödinger cats*, if the interfering states are conspicuously separated in phase space.

At this point, we have to emphasize the fundamental difference between Schrödinger cats and superpositions of modes,

$$\begin{aligned} |\psi\rangle &= |\alpha\rangle + |\beta\rangle && \neq |\alpha\rangle|\beta\rangle \\ \hat{\rho} &= |\alpha\rangle\langle\alpha| + |\beta\rangle\langle\beta| + |\alpha\rangle\langle\beta| + |\beta\rangle\langle\alpha| && \neq |\alpha\beta\rangle\langle\alpha\beta| \end{aligned} \quad . \tag{35.77}$$

Schrödinger cats exhibit interferences in phase space, whereas for mode superpositions, interferences only appear when a parameter is varied (e.g., the length of an interferometer arm).

Schrödinger cat states are very sensitive to dissipation and easily converted into statistical mixtures. For example, $|\alpha\rangle \pm |-\alpha\rangle$ contains only odd (even) photon numbers in the distribution function P_n. After some time $\sim \tau_{cav}/N$, the distribution is converted into a Poisson distribution. The higher the particle number N, the faster the decoherence will be. Consequently, *truely macroscopic* cat states have never been observed.

35.2.4.3 Representations of Fock states

On the Fock state basis $|n\rangle$, a number state is characterized by,

$$\boxed{\begin{aligned} |n\rangle &= (\hat{a}^\dagger)^n|0\rangle \\ \hat{\rho} &= |n\rangle\langle n| \\ P_k &= \delta_{nk} \end{aligned}} \quad . \tag{35.78}$$

This state can be expanded into Glauber states $|\alpha\rangle$ by following procedure. For large n we first calculate the P-distribution function,

$$P_{|n\rangle}(\alpha) = \delta^{(1)}(|\alpha| - \sqrt{n}) \;, \tag{35.79}$$

because it allows us to derive the density matrix via the formula (35.37),

$$\begin{aligned}\hat{\rho}_{|n\rangle} &= \int \delta^{(1)}(|\alpha| - \sqrt{n})|\alpha\rangle\langle\alpha| d^2\alpha \\ &= \int_0^\infty \int_0^{2\pi} \delta^{(1)}(|\alpha| - \sqrt{n})|\alpha\rangle\langle\alpha| \ |\alpha| d|\alpha| d\varphi_\alpha = \sqrt{n}\int_0^{2\pi} |\alpha\rangle\langle\alpha| d\varphi_\alpha \ .\end{aligned} \tag{35.80}$$

The Q-distribution function becomes, inserting the density operator obtained in (35.80),

$$\begin{aligned}Q_{|n\rangle}(\alpha) &= \tfrac{1}{\pi}\langle\alpha|\hat{\rho}_{|n\rangle}|\alpha\rangle \\ &= \tfrac{1}{\pi} n \int_0^{2\pi} |\langle\alpha|\beta\rangle|^2 d\varphi_\beta = \frac{1}{\pi} n \int_0^{2\pi} e^{-|\alpha - |\beta| e^{\imath\varphi_\beta}|^2} d\varphi_\beta \triangleq \frac{|\alpha|^{2n}}{\pi n!} e^{-|\alpha|^2} \ ,\end{aligned} \tag{35.81}$$

and finally the Wigner function is,

$$W_{|n\rangle}(\alpha) = \frac{2}{\pi} e^{-2|\alpha|^2} (-1)^n \sum_{m=0}^{n} \binom{n}{m} \frac{(-4|\alpha|^2)^m}{m!} = \frac{2}{\pi} e^{-2|\alpha|^2} (-1)^n L_n(4|\alpha|^2) \ , \tag{35.82}$$

where $L_m(4|\alpha|^2)$ are Laguerre polynomials. In Exc. 35.2.5.11 we will learn how to derive the above distribution functions directly from the characteristic functions. In summary, we have,

$$\boxed{\begin{aligned} |\psi\rangle &= |n\rangle \\ P_{|n\rangle}(\alpha) &= \delta^{(1)}(|\alpha| - \sqrt{n}) \\ \hat{\rho} &= \sqrt{n}\int_0^{2\pi} |\alpha\rangle\langle\alpha| d\varphi_\alpha \\ Q_{|n\rangle}(\alpha) &= \frac{|\alpha|^{2n}}{\pi n!} e^{-|\alpha|^2} \\ W_{|n\rangle}(\alpha) &= \frac{2}{\pi} e^{-2|\alpha|^2} (-1)^n L_n(4|\alpha|^2) \end{aligned}} \ . \tag{35.83}$$

35.2.4.4 Representations of thermal states

A light mode in a thermal mixture can not be represented by a pure state, but requires a density matrix description beyond (35.27). The concept of statistical mixtures has been introduced in Sec. 34.3. The following formulas will be derived in Exc. 35.2.5.12 [1184],

$$\boxed{\begin{aligned} \hat{\rho} &= \textstyle\sum_n \frac{\bar{n}^n}{(1+\bar{n})^{1+n}} |n\rangle\langle n| \\ P_n &= \frac{\bar{n}^n}{(1+\bar{n})^{1+n}} \end{aligned}} \ . \tag{35.84}$$

The coherent distribution P-function is,

$$\boxed{\begin{aligned} P_{therm}(\alpha) &= \tfrac{1}{\pi\bar{n}} e^{-|\alpha|^2/\bar{n}} \\ \hat{\rho} &= \tfrac{1}{\pi\bar{n}} \int e^{-|\alpha|^2/\bar{n}} |\alpha\rangle\langle\alpha| d^2\alpha \\ Q_{therm}(\alpha) &= \tfrac{1}{\pi(\bar{n}+1)} e^{-|\alpha|^2/(\bar{n}+1)} \\ W_{therm}(\alpha) &= \tfrac{1}{\pi(\bar{n}+1/2)} e^{-|\alpha|^2/(\bar{n}+1/2)} \end{aligned}} \quad . \tag{35.85}$$

35.2.5 Exercises

35.2.5.1 Ex: Glauber-Sudarshan and Husimi distribution

a. Show that $\rho_A(\alpha,\alpha^*) = \pi P(\alpha,\alpha^*)$ for an anti-normally ordered density operator $\hat{\rho}_A(\hat{a},\hat{a}^\dagger)$.
b. Show that $\rho_N(\alpha,\alpha^*) = \frac{1}{\pi} Q(\alpha,\alpha^*)$ for a normally ordered density operator $\hat{\rho}_N(\hat{a},\hat{a}^\dagger)$.

Solution: *a. For the anti-normal ordered density operator we calculate,*

$$\begin{aligned} \hat{\rho}_A(\hat{a},\hat{a}^\dagger) = \sum_{m,n} c_{m,n} \hat{a}^m \hat{a}^{\dagger n} &= \sum_{m,n} c_{m,n} \hat{a}^m \ \tfrac{1}{\pi} \int |\alpha\rangle\langle\alpha| d^2\alpha \ \hat{a}^{\dagger n} \\ &= \tfrac{1}{\pi} \int \sum_{m,n} c_{m,n} \alpha^j \alpha^{*k} |\alpha\rangle\langle\alpha| d^2\alpha \\ &= \tfrac{1}{\pi} \int \rho_A(\alpha,\alpha^*) |\alpha\rangle\langle\alpha| d^2\alpha = \int P(\alpha,\alpha^*) |\alpha\rangle\langle\alpha| d^2\alpha \ . \end{aligned}$$

b. For the normal ordered density operator we calculate,

$$\begin{aligned} \langle\alpha|\hat{\rho}_N(\hat{a},\hat{a}^\dagger)|\alpha\rangle = \langle\alpha| \sum_{m,n} c_{m,n} \hat{a}^{\dagger m} \hat{a}^n |\alpha\rangle &= \sum_{m,n} c_{m,n} \alpha^{*m} \alpha^n \\ = \rho_N(\alpha,\alpha^*) = \tfrac{1}{\pi} Q(\alpha,\alpha^*) \ . \end{aligned}$$

35.2.5.2 Ex: Glauber-Sudarshan and Husimi distribution

a. Show that the definitions of the Glauber-Sudarshan distribution given by (35.46) and (35.37) are equivalent.
b. Show that the definitions of the Husimi distribution given by (35.46) and (35.41) are equivalent.

Solution: *a. We get,*

$$\begin{aligned} \int P(\alpha,\alpha^*) |\alpha\rangle\langle\alpha| d^2\alpha = \int Tr\ \hat{\rho} \delta(\alpha^* - \hat{a}^\dagger) \delta(\alpha - \hat{a}) |\alpha\rangle\langle\alpha| d^2\alpha \\ = ... = \hat{\rho} \ . \end{aligned}$$

b. Using the completeness of the coherent state basis (24.126) we get,

$$\begin{aligned} Q(\alpha,\alpha^*) &= Tr\ \hat{\rho}\delta(\alpha-\hat{a})\ \tfrac{1}{\pi}\int |\beta\rangle\langle\beta| d^2\beta\ \delta(\alpha^*-\hat{a}^\dagger) \\ &= \tfrac{1}{\pi} Tr\ \int \hat{\rho}\delta(\alpha-\hat{a})|\beta\rangle\langle\beta|\delta(\alpha^*-\hat{a}^\dagger)d^2\beta \\ &= \tfrac{1}{\pi} Tr\ \int \hat{\rho}\delta(\alpha-\beta)|\beta\rangle\langle\beta|\delta(\alpha^*-\beta^*)d^2\beta = \tfrac{1}{\pi} Tr\ \hat{\rho}|\alpha\rangle\langle\alpha| = \tfrac{1}{\pi}\langle\alpha|\hat{\rho}|\alpha\rangle\ . \end{aligned}$$

35.2.5.3 Ex: Moments of Glauber states

a. Prove Eq. (35.39).
b. Prove Eq. (35.43).
c. Prove $\frac{1}{2}\langle\hat{a}\hat{a}^\dagger+\hat{a}^\dagger\hat{a}\rangle = \int W(\alpha,\alpha^*)\alpha\alpha^* d^2\alpha$.
d. Prove $\langle\{\hat{a}_j^{\dagger m}\hat{a}_k^n\}_S\rangle = \int W(\alpha)\alpha_j^m\alpha_k^{*n}\ d\alpha$, where the index S denotes *symmetric ordering*. Symmetric or *Weyl ordering* means that all products $\hat{r}\hat{p}$ must be replaced by the symmetric expressions, such as $(\hat{r}\hat{p}+\hat{p}\hat{r})/2$.
e. Then prove Eq. (35.45).

Solution: *a. The expectation value is,*

$$\begin{aligned} \langle\hat{O}_N(\hat{a},\hat{a}^\dagger)\rangle &= Tr\ \hat{\rho}\hat{O}_N(\hat{a},\hat{a}^\dagger) = \sum_{m,n} o_{m,n}\, Tr\ \hat{\rho}\hat{a}^{\dagger m}\hat{a}^n \\ &= ... = \sum_{m,n} c_{m,n}\, Tr\ \hat{\rho}\ \int \delta(\alpha^*-\hat{a}^\dagger)\delta(\alpha-\hat{a})\alpha^{*m}\alpha^n d^2\alpha \\ &= \int Tr\ \hat{\rho}\delta(\alpha^*\hat{a}^\dagger)\delta(\alpha-\hat{a})O_N(\alpha,\alpha^*)d^2\alpha \\ &= \int P(\alpha,\alpha^*)O_N(\alpha,\alpha^*)d^2\alpha\ . \end{aligned}$$

b. The expectation value is,

$$\begin{aligned} \langle\hat{O}_A(\hat{a},\hat{a}^\dagger)\rangle &= Tr\ \hat{\rho}\hat{O}_A(\hat{a},\hat{a}^\dagger) = \sum_{m,n} o_{m,n}\, Tr\ \hat{\rho}\hat{a}^m\hat{a}^{\dagger n} \\ &= \sum_{m,n} c_{m,n}\, Tr\ \hat{\rho}\hat{a}^m\ \tfrac{1}{\pi}\int |\alpha\rangle\langle\alpha| d^2\alpha\ \hat{a}^{\dagger n} = \tfrac{1}{\pi}\sum_{m,n} c_{m,n}\, Tr\ \int \hat{\rho}\alpha^m\alpha^{*n}|\alpha\rangle\langle\alpha| d^2\alpha \\ &= \tfrac{1}{\pi}\int O_A(\alpha,\alpha^*)\, Tr\ \hat{\rho}|\alpha\rangle\langle\alpha| d^2\alpha = \int Q(\alpha,\alpha^*)O_A(\alpha,\alpha^*)d^2\alpha\ . \end{aligned}$$

c.

35.2.5.4 Ex: Relationship between the characteristic functions

Derive the disentangling theorem (35.53) between the characteristic functions of the Glauber state basis.

Solution: *Using (24.113) we find,*

$$\begin{aligned} D(\lambda) &= e^{\lambda\hat{a}^\dagger - \lambda^*\hat{a}} = e^{-\lambda^*\hat{a}+\lambda\hat{a}^\dagger+[-\lambda^*\hat{a},\lambda\hat{a}^\dagger]/2}e^{|\lambda|^2/2} \\ &= e^{-\lambda^*\hat{a}+\lambda\hat{a}^\dagger-|\lambda|^2/2}e^{|\lambda|^2/2} = e^{-\lambda^*\hat{a}}e^{+\lambda\hat{a}^\dagger}e^{|\lambda|^2/2} \ , \end{aligned}$$

and,

$$\begin{aligned} D(\lambda) &= e^{\lambda\hat{a}^\dagger - \lambda^*\hat{a}} = e^{\lambda\hat{a}^\dagger-\lambda^*\hat{a}-[\lambda\hat{a}^\dagger,-\lambda^*\hat{a}]/2}e^{-|\lambda|^2/2} \\ &= e^{\lambda\hat{a}^\dagger-\lambda^*\hat{a}+|\lambda|^2/2}e^{-|\lambda|^2/2} = e^{\lambda\hat{a}^\dagger}e^{-\lambda^*\hat{a}}e^{-|\lambda|^2/2} \ . \end{aligned}$$

That is,

$$\langle\psi|e^{\lambda\hat{a}^\dagger}e^{-\lambda^*\hat{a}}e^{-|\lambda|^2/2}|\psi\rangle = \langle\psi|e^{\lambda\hat{a}^\dagger-\lambda^*\hat{a}}|\psi\rangle = \langle\psi|e^{-\lambda^*\hat{a}}e^{\lambda\hat{a}^\dagger}e^{|\lambda|^2/2}|\psi\rangle \ ,$$

or, inserting the definitions of the characteristic functions (35.52),

$$\chi_N(\lambda)e^{-|\lambda|^2/2} = \chi_S(\lambda) = \chi_A(\lambda)e^{|\lambda|^2/2} \ .$$

35.2.5.5 Ex: General form of the distribution functions

Show that from the definition (35.46) the common definition of the distribution functions (35.37) and (35.41) are recovered.

Solution: *For the Husimi P-distribution we find,*

$$\begin{aligned} \Delta_N(\alpha-\hat{a},\alpha^*-\hat{a}^\dagger) &= \tfrac{1}{\pi^2}\int e^{\lambda^*(\alpha-\hat{a})}e^{-\lambda(\alpha^*-\hat{a}^\dagger)}d^2\lambda \\ &= \tfrac{1}{\pi^2}\int e^{\lambda^*(\alpha-\hat{a})}\int|\beta\rangle\langle\beta|d^2\beta e^{-\lambda(\alpha^*-\hat{a}^\dagger)}d^2\lambda \\ &= \tfrac{1}{\pi^3}\int\int e^{\lambda^*(\alpha-\beta)}|\beta\rangle\langle\beta|e^{-\lambda(\alpha^*-\beta^*)}d^2\lambda d^2\beta \\ &= \tfrac{1}{\pi}\int\delta^{(2)}(\alpha-\beta)|\beta\rangle\langle\beta|d^2\beta = \tfrac{1}{\pi}|\alpha\rangle\langle\alpha| \ , \end{aligned}$$

and, using the coherent state basis,

$$\langle\beta|\Delta_N(\alpha-\hat{a},\alpha^*-\hat{a}^\dagger)|\beta\rangle = \tfrac{1}{\pi}e^{-|\alpha-\beta|^2} \ ,$$

and hence,

$$\langle\beta|\hat{\rho}|\beta\rangle = \int P(\alpha,\alpha^*)e^{-|\alpha-\beta|^2}d^2\alpha \ .$$

For the Wigner function, we find,

$$\Delta_S(\alpha-\hat{a},\alpha^*-\hat{a}^\dagger) = \tfrac{1}{\pi^2}\int e^{-\lambda(\alpha^*-\hat{a}^\dagger)+\lambda^*(\alpha-\hat{a})}d^2\lambda \ ,$$

and, using the coherent state basis,

$$\langle\beta|\Delta_S(\alpha-\hat{a},\alpha^*-\hat{a}^\dagger)|\beta\rangle = \tfrac{1}{\pi^2}\int\langle\beta|e^{-\lambda(\alpha^*-\hat{a}^\dagger)+\lambda^*(\alpha-\hat{a})}|\beta\rangle d^2\lambda \ ,$$

and hence,

$$\langle\beta|\hat{\rho}|\beta\rangle = \ .$$

For the Glauber-Sudarshan Q-distribution we find,

$$\Delta_A(\alpha-\hat{a},\alpha^*-\hat{a}^\dagger) = \tfrac{1}{\pi^2}\int e^{-\lambda(\alpha^*-\hat{a}^\dagger)}e^{\lambda^*(\alpha-\hat{a})}d^2\lambda \ ,$$

and, using the coherent state basis,

$$\langle\beta|\Delta_A(\alpha-\hat{a},\alpha^*-\hat{a}^\dagger)|\beta\rangle = \tfrac{1}{\pi^2}\int e^{-\lambda(\alpha^*-\beta^*)}e^{\lambda^*(\alpha-\beta)}d^2\lambda \ ,$$

and hence,

$$\begin{aligned}\langle\beta|\hat{\rho}|\beta\rangle &= \tfrac{1}{\pi}\int Q(\alpha,\alpha^*)\int e^{-\lambda(\alpha^*-\beta^*)+\lambda^*(\alpha-\beta)}d^2\lambda d^2\alpha \\ &= \int Q(\alpha,\alpha^*)\pi\delta^{(2)}(\alpha-\beta)d^2\alpha = \pi Q(\beta,\beta^*) \ .\end{aligned}$$

35.2.5.6 Ex: Characteristic functions

a. Evaluate the expression $\left.\frac{\partial^{m+n}\chi_X(\lambda)}{\partial\lambda^{*m}\partial(-\lambda)^n}\right|_{\lambda=0}$ for $X = N, S, A$.
b. Consider the particular case of a coherent state.

Solution: *a. For normal ordering we calculate,*

$$\left.\frac{\partial^{m+n}\chi_N(\lambda)}{\partial\lambda^{*m}\partial(-\lambda)^n}\right|_{\lambda=0} = \left.\langle\psi|\frac{\partial^n e^{-\lambda\hat{a}^\dagger}}{\partial(-\lambda)^n}\frac{\partial^m e^{\lambda^*\hat{a}}}{\partial\lambda^{*m}}|\psi\rangle\right|_{\lambda=0} = \left.\langle\psi|\hat{a}^{\dagger n}e^{-\lambda\hat{a}^\dagger}\hat{a}^m e^{\lambda^*\hat{a}}|\psi\rangle\right|_{\lambda=0} = \langle\hat{a}^{\dagger m}\hat{a}^n\rangle \ .$$

Similarly, we find for symmetric and anti-normal ordering,

$$\left.\frac{\partial^{m+n}\chi_S(\lambda)}{\partial\lambda^{*m}\partial(-\lambda)^n}\right|_{\lambda=0} = \langle\{\hat{a}^{\dagger m}\hat{a}^n\}_S\rangle \qquad \textit{and} \qquad \left.\frac{\partial^{m+n}\chi_A(\lambda)}{\partial\lambda^{*m}\partial(-\lambda)^n}\right|_{\lambda=0} = \langle\hat{a}^m\hat{a}^{\dagger n}\rangle \ ,$$

where the index S denotes symmetric ordering.
b. For a coherent state we find,

$$\langle\alpha|\hat{a}^{\dagger m}\hat{a}^n|\alpha\rangle = \alpha^{*m}\alpha^n \ .$$

35.2.5.7 Ex: Calculating with Wirtinger derivatives

Prove the following identities [504],

$$\hat{a}^\dagger - \alpha^* = \frac{\partial}{\partial \underrightarrow{\alpha}} \quad \text{and} \quad \hat{a}^\dagger - \alpha = \frac{\partial}{\partial \underleftarrow{\alpha}^*} \ .$$

Note, that with the bosonic operators we can construct the observables,

$$\hat{x} + \imath\hat{p} = \sqrt{2}\hat{a} \quad , \quad \partial_x - \imath\partial_p = 2\underrightarrow{\partial_\alpha} \quad , \quad \partial_x + \imath\partial_p = 2\underleftarrow{\partial_{\alpha^*}} \ .$$

In two dimensions [447], $d^2\alpha = d(\mathfrak{Re}\ \alpha)d(\mathfrak{Im}\ \alpha) = dxdp$.

Solution: *This is straightforward using the Fock state expansion. Alternatively, we may start representing,*

$$|\alpha\rangle\langle\alpha| = e^{\alpha\hat{a}^\dagger - \alpha^*\hat{a}}|0\rangle\langle 0|e^{-\alpha\hat{a}^\dagger + \alpha^*\hat{a}} \ .$$

Now,

$$\begin{aligned}\left(\alpha^* + \frac{\partial}{\partial\alpha}\right)|\alpha\rangle\langle\alpha| &= \alpha^*|\alpha\rangle\langle\alpha| + \frac{\partial e^{\alpha\hat{a}^\dagger - \alpha^*\hat{a}}}{\partial\alpha}|0\rangle\langle 0|e^{-\alpha\hat{a}^\dagger + \alpha^*\hat{a}} + e^{\alpha\hat{a}^\dagger - \alpha^*\hat{a}}|0\rangle\langle 0|\frac{\partial e^{-\alpha\hat{a}^\dagger + \alpha^*\hat{a}}}{\partial\alpha} \\ &= \alpha^*|\alpha\rangle\langle\alpha| + \hat{a}^\dagger e^{\alpha\hat{a}^\dagger - \alpha^*\hat{a}}|0\rangle\langle 0|e^{-\alpha\hat{a}^\dagger + \alpha^*\hat{a}} + e^{\alpha\hat{a}^\dagger - \alpha^*\hat{a}}|0\rangle\langle 0|e^{-\alpha\hat{a}^\dagger + \alpha^*\hat{a}}(-\hat{a}^\dagger) \\ &= \alpha^*|\alpha\rangle\langle\alpha| + \hat{a}^\dagger|\alpha\rangle\langle\alpha| + |\alpha\rangle\langle\alpha|(-\hat{a}^\dagger) = \hat{a}^\dagger|\alpha\rangle\langle\alpha| \ .\end{aligned}$$

As a corollary, we get,

$$\left(\alpha + \frac{\partial}{\partial\alpha^*}\right)|\alpha\langle\alpha| = |\alpha\rangle\langle\alpha|\hat{a} = |\alpha\rangle\langle\alpha|\hat{a} \ .$$

35.2.5.8 Ex: Wigner function for arbitrary HO states in the Fock basis

Search an analytic solution for the integral (35.68).

Solution: *The 2D Fourier transform of a radially symmetric function $u(|\lambda|)$ instead of $u_{nm}(\lambda)$ is,*

$$\begin{aligned}\int u(|\lambda|)e^{\alpha\lambda^* - \alpha^*\lambda}d^2\lambda &= \int u(\tfrac{1}{2}|x_\lambda + \imath p_\lambda|)e^{\imath p_\alpha x_\lambda - \imath x_\alpha p_\lambda}dx_\lambda dp_\lambda \\ &= \frac{1}{\imath p_\alpha - x_\alpha}\left[\int e^{+\imath p_\alpha x_\lambda}u(\tfrac{1}{2}x_\lambda)dx_\lambda - \int e^{-\imath x_\alpha p_\lambda}u(\tfrac{1}{2}p_\lambda)dp_\lambda\right] \ .\end{aligned}$$

With this,

$$\begin{aligned}\int e^{+\imath p_\alpha x_\lambda}u_{nm}(\tfrac{x_\lambda}{2})dx_\lambda &= \sqrt{\frac{n!}{m!}}\int e^{-x_\lambda^2/2}x_\lambda^{m-n}L_n^{m-n}(\tfrac{x_\lambda^2}{2})e^{\imath p_\alpha x_\lambda}dx_\lambda \\ &= \sqrt{\frac{n!}{m!}}\sqrt{\frac{\pi}{2}}\frac{1}{n!}(-1)^{int\frac{m-n}{2}}e^{-p_\alpha^2/2}He_n(p_\alpha)He_m(p_\alpha) \ .\end{aligned}$$

The Wigner function is now,

$$W(\alpha) = \sum_{m,n} \frac{1}{\pi^2} c_m^* c_n \frac{-1}{\alpha} \sqrt{\frac{\pi}{2}} \sqrt{\frac{1}{n!m!}} (-1)^{int\frac{m-n}{2}} \left[e^{-p_\alpha^2/2} He_n(p_\alpha) He_m(p_\alpha) + e^{-x_\alpha^2/2} He_n(x_\alpha) He_m(x_\alpha) \right] ,$$

where the He_n are probabilist's Hermite polynomials.

35.2.5.9 Ex: P-, Q-, and Wigner distribution functions for Glauber states

Starting from the characteristic functions $\chi_{A,S,N}(\lambda)$ derive for a coherent state $|\beta\rangle$ (a) the Husimi representation, (b) the Glauber-Sudarshan representation, and (c) the Wigner representation.

Solution: *In the following we will use the definition of the complex Fourier transform (35.46) and of the characteristic functions (35.52).*
a. For the P-representation we calculate,

$$\chi_N(\lambda) = \langle\beta| e^{\lambda \hat{a}^\dagger} e^{-\lambda^* \hat{a}} |\beta\rangle = e^{-\lambda^*\beta + \lambda\beta^*} ,$$

and hence, exploiting the formula (35.54),

$$P_{|\beta\rangle}(\alpha) = \tfrac{1}{\pi^2} \int e^{-\lambda^*(\beta-\alpha)+\lambda(\beta^*-\alpha^*)} d^2\lambda = \tfrac{1}{\pi^2} \int e^{-\lambda^*\eta + \lambda\eta^*} d^2\lambda$$
$$= \tfrac{1}{\pi^2} \int e^{-2\imath r_\lambda p_\eta + 2\imath p_\lambda r_\eta} dr_\lambda dp_\lambda = \delta(p_\eta)\delta(r_\eta) = \delta^{(2)}(\alpha - \beta) .$$

b. For the Q-representation we calculate, $\chi_A(\lambda) = e^{-|\lambda|^2} \chi_N(\lambda)$, and hence,

$$Q_{|\beta\rangle}(\alpha) = \tfrac{1}{\pi^2} \int e^{-\lambda^*(\beta-\alpha)+\lambda(\beta^*-\alpha^*)} e^{-|\lambda|^2} d^2\lambda = \tfrac{1}{\pi} e^{-|\alpha-\beta|^2} .$$

c. For the Wigner representation we calculate, $\chi_S(\lambda) = e^{-|\lambda|^2/2} \chi_N(\lambda)$, and hence,

$$W_{|\beta\rangle}(\alpha) = \tfrac{1}{\pi^2} \int e^{-\lambda^*(\beta-\alpha)+\lambda(\beta^*-\alpha^*)} e^{-|\lambda|^2/2} d^2\lambda = \tfrac{2}{\pi} e^{-2|\alpha-\beta|^2} .$$

35.2.5.10 Ex: P-, Q-, and Wigner distribution functions for cat states

Starting from the characteristic functions $\chi_{A,S,N}(\lambda)$ derive for a normalized cat state $C^{-1}(|\beta_0\rangle + |\beta_1\rangle)$ (a) the Husimi representation, (b) the Glauber-Sudarshan representation, and (c) the Wigner representation.

Solution: *The normalization of the cat state is given by,*

$$C = \sqrt{(\langle\beta_0| \pm \langle\beta_1|)(|\beta_0\rangle \pm |\beta_1\rangle)} = \sqrt{2 \pm 2e^{-|\beta_0-\beta_1|^2}} .$$

a. In Exc. 24.6.6.2 we already derived the expression,

$$\langle\beta_0|\beta_1\rangle = e^{-|\beta_0|^2/2-|\beta_1|^2/2+\beta_0^*\beta_1} \ .$$

With this we obtain,

$$\langle\beta_0|e^{\lambda\hat{a}^\dagger}e^{-\lambda^*\hat{a}}|\beta_1\rangle = e^{\lambda\beta_0^*-\lambda^*\beta_1}\langle\beta_0|\beta_1\rangle = e^{\lambda\beta_0^*-\lambda^*\beta_1-|\beta_0|^2/2-|\beta_1|^2/2+\beta_0^*\beta_1} \ ,$$

and the normally ordered characteristic function,

$$\chi_N(\lambda) = \tfrac{1}{C^2}(\langle\beta_0| \pm \langle\beta_1|)e^{\lambda\hat{a}^\dagger}e^{-\lambda^*\hat{a}}(|\beta_1\rangle \pm |\beta_0\rangle)$$
$$= \tfrac{1}{C^2}\left[e^{\lambda\beta_0^*-\lambda^*\beta_0} + e^{\lambda\beta_1^*-\lambda^*\beta_1} \pm e^{-|\beta_0|^2/2-|\beta_1|^2/2}\left(e^{\lambda\beta_0^*-\lambda^*\beta_1+\beta_0^*\beta_1} + e^{\lambda\beta_1^*-\lambda^*\beta_0+\beta_0\beta_1^*}\right)\right] \ .$$

Hence,

$$P_{|\beta_0\rangle|\beta_1\rangle}(\alpha) =$$

b. The anti-symmetrically ordered characteristic function being $\chi_A(\lambda) = e^{-|\lambda|^2}\chi_N(\lambda)$, we immediately get the Q-function using (35.54),

$$Q_{|\beta_0\rangle|\beta_1\rangle}(\alpha) =$$

c. The symmetrically ordered characteristic function being $\chi_S(\lambda) = e^{-|\lambda|^2/2}\chi_N(\lambda)$, we get the Wigner function using (35.54),

$$W_{|\beta_0\rangle|\beta_1\rangle}(\alpha) = \tfrac{1}{\pi^2}\int \chi_S(\lambda)e^{\lambda^*\alpha-\lambda\alpha^*}d^2\lambda$$
$$= \tfrac{1}{C^2\pi^2}\int\Big[e^{-|\lambda|^2/2-(\alpha^*-\beta_0^*)\lambda+(\alpha-\beta_0)\lambda^*} + e^{-|\lambda|^2/2-(\alpha^*-\beta_1^*)\lambda+(\alpha-\beta_1)\lambda^*}$$
$$\pm e^{-|\beta_0|^2/2-|\beta_1|^2/2}\left(e^{-|\lambda|^2/2-\lambda(\alpha^*-\beta_0^*)+\lambda^*(\alpha-\beta_1)+\beta_0^*\beta_1} + e^{-|\lambda|^2/2+\lambda^*(\alpha-\beta_0)-\lambda(\alpha^*-\beta_1^*)+\beta_0\beta_1^*}\right)\Big]d^2\lambda$$
$$= \tfrac{2}{C^2\pi}\left(e^{-2|\alpha-\beta_0|^2} + e^{-2|\alpha-\beta_1|^2} \pm 2e^{-|\beta_0|^2/2-|\beta_1|^2/2}\mathfrak{Re}\ e^{-2(\beta_1-\alpha)(\beta_0^*-\alpha^*)+\beta_0^*\beta_1}\right) \ .$$

We note that for $|\beta_0\rangle = |\beta_1\rangle$ we recover exactly the Glauber state calculated in Exc. 35.2.5.7(c).

35.2.5.11 Ex: *P*-, *Q*-, and Wigner distribution functions for Fock states

Starting from the characteristic functions $\chi_{A,S,N}(\lambda)$ derive for a number state $|n\rangle$ (a) the Husimi representation, (b) the Glauber-Sudarshan representation, and (c) the Wigner representation.

Solution: *From the expressions following the Fock state expansion (35.62), we derive immediately,*

$$\chi_N(\lambda) = \langle n|e^{\lambda\hat{a}^\dagger}e^{-\lambda^*\hat{a}}|n\rangle = \sum_{q,k=0}^{n}\frac{\lambda^q(-\lambda^*)^k}{\sqrt{q!k!}}\sqrt{\binom{n}{q}\binom{n}{k}}\langle n-q|n-k\rangle$$
$$= \sum_{k=0}^{n}\frac{(-|\lambda|^2)^k}{k!}\binom{n}{k} = L_n^0(|\lambda|^2) \ ,$$

where L_n^0 is a Laguerre polynomial. With this the symmetrically ordered characteristic function becomes,

$$\chi_S(\lambda) = \langle n|e^{\lambda\hat{a}^\dagger - \lambda^*\hat{a}}|n\rangle = e^{-|\lambda|^2/2}\chi_N(\lambda) = e^{-|\lambda|^2/2}L_n^0(|\lambda|^2) \ ,$$

and the anti-symmetrically ordered,

$$\chi_A(\lambda) = \langle n|e^{-\lambda^*\hat{a}}e^{\lambda\hat{a}^\dagger}|n\rangle = e^{-|\lambda|^2}\chi_N(\lambda) = e^{-|\lambda|^2}L_n^0(|\lambda|^2) \ .$$

a. Now, we calculate for the P-representation,

$$P_{|\beta\rangle}(\alpha) =$$

b. For the Q-representation, we get,

$$Q_{|\beta\rangle}(\alpha) =$$

c. Finally, the Wigner function is,

$$\begin{aligned} W_{|n\rangle}(\alpha) &= \tfrac{1}{\pi^2}\int \chi_S(\lambda)e^{-\alpha\lambda^* + \alpha^*\lambda}d^2\lambda = \tfrac{1}{\pi^2}\int e^{-|\lambda|^2/2}L_n^0(|\lambda|^2)e^{-\alpha\lambda^* + \alpha^*\lambda}d^2\lambda \\ &= \tfrac{1}{\pi^2}\int e^{(-\lambda_r^2-\lambda_i^2)/2}L_n^0(\lambda_r^2+\lambda_i^2)e^{2\imath(-\alpha_i\lambda_r + \alpha_r\lambda_i)}d\lambda_r d\lambda_i \ . \end{aligned}$$

35.2.5.12 Ex: Wigner distribution function of a Fock state

Calculate the Wigner function for a harmonic oscillator in a Fock state from its wavefunction $\langle x|n\rangle$.

Solution: *The wavefunction of a Fock state is,*

$$\langle x|n\rangle = \frac{e^{-x^2/2a_{ho}^2}H_n(x/a_{ho})}{\sqrt{a_{ho}\sqrt{\pi}2^n n!}} \ .$$

With this,

$$\begin{aligned} W(x,p) &= \frac{1}{\pi}\int_{-\infty}^{\infty}\langle n|x+y\rangle\langle x-y|n\rangle e^{2\imath py/\hbar}dy \\ &= \frac{1}{\pi a_{ho}\sqrt{\pi}2^n n!}\int_{-\infty}^{\infty}e^{(-x^2-y^2)/a_{ho}^2}H_n(\tfrac{x+y}{a_{ho}})H_n(\tfrac{x-y}{a_{ho}})e^{2\imath py/\hbar}dy \\ &= \frac{1}{\pi\sqrt{\pi}2^n n!}\int_{-\infty}^{\infty}e^{-\tilde{x}^2-\tilde{y}^2}H_n(\tilde{x}+\tilde{y})H_n(\tilde{x}-\tilde{y})e^{2\imath\tilde{p}\tilde{y}}d\tilde{y} \ , \end{aligned}$$

where we introduced $\tilde{x} \equiv x/a_{ho}$ and $\tilde{p} \equiv a_{ho}p/\hbar$. Now, we get from a Taylor expansion the rule,

$$H_n(x+y) = \sum_{k=0}^{n}\binom{n}{k}(2x)^{n-k}H_k(y) \ ,$$

allowing us to rewrite the Wigner function as,

$$W(x,p) = \frac{1}{\pi\sqrt{\pi}2^n n!}\sum_{k,q=0}^{n}\binom{n}{k}\binom{n}{q}(2\tilde{x})^{2n-k-q}e^{-\tilde{x}^2}\int_{-\infty}^{\infty}e^{-\tilde{y}^2}H_k(\tilde{y})H_q(-\tilde{y})e^{2\imath\tilde{p}\tilde{y}}d\tilde{y}\ .$$

This integral can be solved.

35.2.5.13 Ex: Thermal state

a. Show that $\langle-\beta|\hat{\rho}|\beta\rangle e^{|\beta|^2}$ and $P(\alpha,\alpha^*)e^{-|\alpha|^2}$ are related by Fourier transform.
b. Using the relationship of (a), derive the density operator and the distribution function of the Fock and the Glauber basis for a thermal state.

Solution: *a. Let us consider coherent states $|\beta\rangle$ and $|-\beta\rangle$. Then,*

$$\begin{aligned}\langle-\beta|\hat{\rho}|\beta\rangle e^{|\beta|^2} &= e^{|\beta|^2}\int P(\alpha,\alpha^*)\langle-\beta|\alpha\rangle\langle\alpha|\beta\rangle d^2\alpha\\ &= e^{|\beta|^2}\int P(\alpha,\alpha^*)e^{-|\beta|^2/2-|\alpha|^2/2-\beta\alpha^*}e^{-|\alpha|^2/2-|\beta|^2/2+\alpha\beta^*}d^2\alpha\\ &= \int P(\alpha,\alpha^*)e^{-|\alpha|^2}e^{\alpha\beta^*-\alpha^*\beta}d^2\alpha = \mathcal{F}[P(\alpha,\alpha^*)e^{-|\alpha|^2}]\ .\end{aligned}$$

b. With the photon number probability calculated in Eq. (22.59) we have,

$$\hat{\rho} = P_n = \sum_n \frac{\bar{n}^n}{(1+\bar{n})^{1+n}}|n\rangle\langle n|\ .$$

This allows us to calculate,

$$\begin{aligned}\langle-\beta|\hat{\rho}|\beta\rangle &= \sum_n \frac{\bar{n}^n}{(1+\bar{n})^{1+n}}\langle-\beta|n\rangle\langle n|\beta\rangle\\ &= \frac{e^{-|\beta|^2}}{1+\langle n\rangle}\sum_n\frac{(-|\beta|^2)^n}{n!}\left(\frac{\langle n\rangle}{1+\langle n\rangle}\right)^n = \frac{e^{-|\beta|^2}}{1+\langle n\rangle}e^{-|\beta|^2/(1+1/\langle n\rangle)}\ ,\end{aligned}$$

and finally,

$$P(\alpha,\alpha^*) = \tfrac{1}{\pi^2}\mathcal{F}[\langle-\beta|\hat{\rho}|\beta\rangle] = \tfrac{1}{\pi^2}\int\langle-\beta|\hat{\rho}|\beta\rangle e^{-\beta\alpha^*+\beta^*\alpha}d^2\beta = \frac{1}{\pi\langle n\rangle}e^{-|\alpha|^2/\langle n\rangle}\ .$$

35.3 Squeezed states of the harmonic oscillator

35.3.1 The squeezing operator

Let us consider a Hamiltonian of the following form,

$$\boxed{\hat{H}_{sqz} = \hbar\omega\hat{a}^\dagger\hat{a} + \tfrac{\imath}{2}\hbar\xi\hat{a}^{\dagger 2} + \tfrac{\imath}{2}\hbar\xi^*\hat{a}^2}\ . \tag{35.86}$$

leading to the equation of motion,

$$\dot{\hat{a}} = -\imath\omega\hat{a} + 2g\hat{a}^\dagger \ . \tag{35.87}$$

The non-linear, i.e. quadratic, appearance of the field operators suggests that the interaction should include correlated pair production, as is the case for parametric processes or four-wave mixing. We will see later that cavities are good for generating squeezing. However, the unused ports of a cavity let uncorrelated vacuum fluctuations enter, which partially overrule squeezing.

For now, we study, in analogy with the displacement operator (24.111), the propagator $e^{-\imath\hat{H}_{sqz}t/\hbar}$, i.e the operator given by,

$$\boxed{\hat{S}(\xi) \equiv e^{\xi\hat{a}^{\dagger 2}/2 - \xi^*\hat{a}^2/2}} \ , \tag{35.88}$$

which we will call the *squeezing operator* because, applied to the vacuum state, $|\xi\rangle = S(\xi)|0\rangle$, this operator will compress the uncertainty of one quadrature component, as we will see shortly.

In analogy with the calculation (24.112), using the commutation rules, it is possible to verify the unitarity of this operator [818] (see Exc. 35.3.4.1). In particular, using the relationship (??) and the abbreviation $\hat{A} \equiv \frac{\xi}{2}\hat{a}^{\dagger 2} - \frac{\xi^*}{2}\hat{a}^2$, we can show [1265] (see Exc. 35.3.4.2),

$$\begin{aligned}\hat{S}^\dagger(\xi)\hat{a}\hat{S}(\xi) = e^{\hat{A}}\hat{a}e^{-\hat{A}} &= \hat{a} + [\hat{A},\hat{a}] + \tfrac{1}{2!}\Big[\hat{A},[\hat{A},\hat{a}]\Big] + \tfrac{1}{3!}\Big[\hat{A},\Big[\hat{A},[\hat{A},\hat{a}]\Big]\Big] \ldots \\ &= \hat{a} + \xi\hat{a}^\dagger + \tfrac{1}{2!}\xi\xi^*\hat{a} + \tfrac{1}{3!}\xi\xi^*\xi\hat{a}^\dagger + \ldots = \hat{a}\cosh|\xi| + \frac{|\xi|}{\xi^*}\hat{a}^\dagger\sinh|\xi| \ ,\end{aligned} \tag{35.89}$$

and similarly for $\hat{a}^\dagger$, such that with $\xi \equiv re^{\imath\varphi}$,

$$\boxed{\begin{array}{rcl}\hat{S}^\dagger(\xi)\hat{a}\hat{S}(\xi) &=& \hat{a}\cosh r + e^{-\imath\varphi}\hat{a}^\dagger\sinh r \\ \hat{S}^\dagger(\xi)\hat{a}^\dagger\hat{S}(\xi) &=& \hat{a}^\dagger\cosh r + e^{\imath\varphi}\hat{a}\sinh r\end{array}} \ . \tag{35.90}$$

The formulas (35.90) describe a *Bogolubov transform*, as they can be cast into the form,

$$\boxed{\hat{b} \equiv u\hat{a} + v\hat{a}^\dagger \qquad , \qquad \hat{b}^\dagger \equiv u^*\hat{a}^\dagger + v^*\hat{a}} \ , \tag{35.91}$$

for complex numbers u and v. By postulating the same commutation relation for new operators, $[\hat{b},\hat{b}^\dagger] = 1$, we immediately get the condition,

$$|u|^2 - |v|^2 = 1 \ . \tag{35.92}$$

Comparing with the hyperbolic identity $\cosh^2 r - \sinh^2 r = 1$, we can parametrize the constants as,

$$u = \cosh r \qquad \text{and} \qquad v = e^{\imath\varphi}\sinh r \ . \tag{35.93}$$

This is interpreted as a linear simplectic transformation in phase space between pairs of annihilation and creation operators satisfying the same commutation relation $[\hat{a},\hat{a}^\dagger] = 1$.

35.3.1.1 Relation between squeezing and displacement operator

The squeezing operator *does not commute* with the displacement operator. However, from (35.90) we an derive the following simple relation,

$$\hat{S}(\xi)D(\alpha) \neq D(\alpha)\hat{S}(\xi) = \hat{S}(\xi)D(\alpha\cosh r + \alpha^* e^{\imath\theta}\sinh r) \ . \tag{35.94}$$

Solve the Exc. 35.3.4.3.

Squeezed coherent states are generated by coherent displacement of a *squeezed vacuum*,

$$|\alpha,\xi\rangle = \hat{S}(\xi)|0,\xi\rangle = D(\alpha)\hat{S}(\xi)|0\rangle \ . \tag{35.95}$$

On the other hand, from (35.94),

$$\begin{aligned} D(\alpha)\hat{S}(\xi)|0\rangle &= \hat{S}(\xi)D(\alpha\cosh r + \alpha^* e^{\imath\varphi}\sinh r)|0\rangle \\ &= S(\xi)|\alpha\cosh r + \alpha^* e^{\imath\varphi}\sinh r\rangle \ . \end{aligned} \tag{35.96}$$

35.3.1.2 Squeezing of the uncertainty relation

The real and imaginary parts of the transformed operators, defined by $\hat{b} = \hat{x}_b + \imath\hat{y}_b$, are Hermitian and satisfy the Heisenberg uncertainty relation (23.91),

$$[\hat{x}_b,\hat{y}_b] = \tfrac{\imath}{2} \qquad \text{and} \qquad \Delta\hat{x}_b\Delta\hat{y}_b \geq \tfrac{1}{2\imath}\langle[\hat{x}_b,\hat{y}_b]\rangle = \tfrac{1}{4} \ . \tag{35.97}$$

However, let us take a look at the uncertainties separately. They relate to the Glauber mode via,

$$\begin{aligned} \hat{x}_b &= \tfrac{1}{2}(\hat{b}+\hat{b}^\dagger) = \tfrac{1}{2}(\hat{a}\cosh r + \hat{a}^\dagger e^{\imath\varphi}\sinh r) + \tfrac{1}{2}(\hat{a}^\dagger\cosh r + \hat{a}e^{-\imath\varphi}\sinh r) \\ &= \hat{x}_a\cosh r + \tfrac{1}{2}\sinh r(\hat{a}^\dagger e^{\imath\varphi} + \hat{a}e^{-\imath\varphi}) \xrightarrow{\varphi=0} \hat{x}_a e^r \\ \hat{y}_b &= \tfrac{1}{2\imath}(\hat{b}-\hat{b}^\dagger) = \tfrac{1}{2\imath}(\hat{a}\cosh r + \hat{a}^\dagger e^{\imath\varphi}\sinh r) - \tfrac{1}{2\imath}(\hat{a}^\dagger\cosh r + \hat{a}e^{-\imath\varphi}\sinh r) \\ &= \hat{y}_a\cosh r + \tfrac{1}{2\imath}\sinh r(\hat{a}^\dagger e^{\imath\varphi} - \hat{a}e^{-\imath\varphi}) \xrightarrow{\varphi=0} \hat{y}_a e^{-r} \ . \end{aligned} \tag{35.98}$$

The individual fluctuations are (assuming $\varphi = 0$),

$$\begin{aligned} \Delta\hat{x}_b^2 &= \langle\hat{x}_b^2\rangle - \langle\hat{x}_b\rangle^2 = e^{2r}\left(\langle\hat{x}_a^2\rangle - \langle\hat{x}_a\rangle^2\right) \\ &= \tfrac{1}{4}e^{2r}\left(1 + \langle\hat{a}^2\rangle + \langle\hat{a}^\dagger\rangle^2 + 2\langle\hat{a}^\dagger\hat{a}\rangle - \langle\hat{a}\rangle^2 - \langle\hat{a}^\dagger\rangle^2 - 2\langle\hat{a}^\dagger\rangle\langle\hat{a}\rangle\right) \ . \end{aligned} \tag{35.99}$$

With $\langle\hat{a}\rangle = 0$,

$$\begin{aligned} \Delta\hat{x}_b^2 &= e^{2r}\left(\tfrac{1}{2}\mathfrak{Re}\ \langle\hat{a}^2\rangle + \tfrac{1}{4} + \tfrac{1}{2}\langle\hat{a}^\dagger\hat{a}\rangle\right) \\ \Delta\hat{y}_b^2 &= e^{-2r}\left(-\tfrac{1}{2}\mathfrak{Re}\ \langle\hat{a}^2\rangle + \tfrac{1}{4} + \tfrac{1}{2}\langle\hat{a}^\dagger\hat{a}\rangle\right) \ . \end{aligned} \tag{35.100}$$

Looking at the coherent vacuum, $\hat{a}|\alpha\rangle = 0$, hence,

$$\Delta\hat{x}_b = \tfrac{1}{2}e^r \qquad \text{and} \qquad \Delta\hat{y}_b = \tfrac{1}{2}e^{-r} \ , \tag{35.101}$$

and the squeezed state is at the uncertainty minimum.

35.3.2 Squeezed state in the Fock basis

The numbers of photons in the squeezed state is [818],

$$\langle n|\alpha,\xi\rangle = \frac{(\zeta/2)^{n/2}}{\sqrt{n!\cosh r}} e^{-\frac{1}{2}(|\alpha|^2+\alpha^*\zeta)} H_n\left(\frac{\alpha+\alpha^*\zeta}{\sqrt{2\zeta}}\right) , \tag{35.102}$$

with the abbreviation $\zeta \equiv e^{i\theta}\tanh r$. For squeezed vacuum $\alpha = 0$, noting that $H_n(0) = (-2)^{n/2}(n-1)!!$ for even n and $H_n(0) = 0$ for odd n, we find,

$$\langle n|0,\xi\rangle = \frac{(-\zeta)^{n/2}(n-1)!!}{\sqrt{n!\cosh r}} \tag{35.103}$$

for even photon number. Odd photon numbers are excluded. Hence,

$$\boxed{\begin{aligned} |\alpha,\xi\rangle &= \sum_n |n\rangle\langle n|\alpha,\xi\rangle \\ \hat\rho &= |\alpha,\xi\rangle\langle\alpha,\xi| \\ P_n &= |\langle n|\alpha,\xi\rangle|^2 \end{aligned}} . \tag{35.104}$$

In the photon representation we can easily see that the squeezed vacuum is (unlike the coherent and the Fock vacuum) not empty,

$$\begin{aligned} \langle\alpha,\xi|\hat n|\alpha,\xi\rangle &= |\alpha|^2 + \sinh^2|\xi| \overset{\alpha\to 0}{\longrightarrow} \sinh^2|\xi| \\ \Delta_{\alpha,\xi}\hat n &= |\alpha| + 2\cosh^2|\xi|\sinh^2|\xi| \overset{\alpha\to 0}{\longrightarrow} 2\cosh^2|\xi|\sinh^2|\xi| \ . \end{aligned} \tag{35.105}$$

Squeezed vacuum contains contributions from many $|n\rangle$.

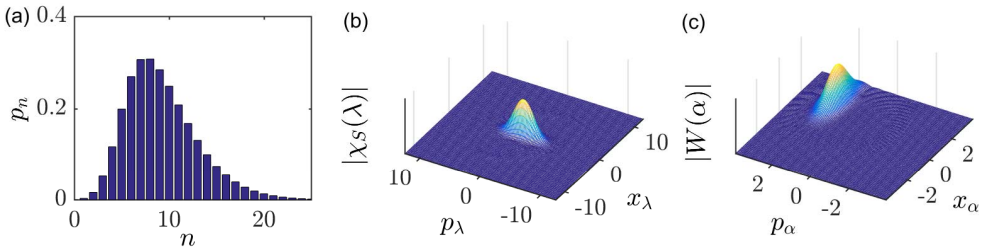

Figure 35.7: (code) Starting from a squeezed state photon distribution with $r = 0.5$, as shown in (a), we calculate the symmetrically ordered characteristic function (b) from the expression (35.68), and the Wigner function (c) by an FFT.

For the squeezed vacuum state the photon number distribution displays odd-even-oscillations. This can be explained by the mathematical form of the squeezing operator, that resembles the operator for two-photon generation and annihilation processes. Photons in a squeezed vacuum state are more likely to appear in pairs.

35.3.3 Squeezed state in the Glauber basis

The *squeezed state* contains non-classical quantum correlations, as we will show by calculating $g^{(1)}$ and $g^{(2)}$ for squeezed states,

$$g^{(2)}(0) = \frac{\langle \hat{b}^\dagger \hat{b} \hat{b}^\dagger \hat{b} \rangle}{\langle \hat{b}^\dagger \rangle^2 \langle \hat{b} \rangle^2} = 1 + \frac{\cosh 2r}{\sinh^2 r} \ . \tag{35.106}$$

The distribution functions in the coherent representation are,

$$\begin{aligned}
|\psi\rangle &= |\beta, \xi\rangle \\
P_{|\beta\rangle}(\alpha) &= \\
\hat{\rho} &= |\beta, \xi\rangle\langle\beta, \xi| \\
Q_{|\beta\rangle}(\alpha) &= \tfrac{\text{sech } r}{\pi} \ e^{-(|\alpha|^2+|\beta|^2)+(\alpha^*\beta+\alpha\beta^*)} \ \text{sech } r - \frac{1}{2}\left[e^{\imath\theta}(\alpha^{*2}-\beta^{*2})+e^{-\imath\theta}(\alpha^2-\beta^2)\right] \ \tanh r \\
W_{|\beta\rangle}(\alpha) &= \tfrac{1}{2\pi} \exp(-\tfrac{(\alpha+\alpha^*)^2}{2e^{-2r}} + \tfrac{(\alpha-\alpha^*)^2}{2e^{2r}})
\end{aligned} \tag{35.107}$$

35.3.4 Exercises

35.3.4.1 Ex: Unitarity of the squeezing operator

Calculate $\langle \hat{E} \rangle$ and $\Delta \hat{E}$.

Solution:

35.3.4.2 Ex: Transformation by the squeezing operator

Demonstrate the relationship (35.89).

Solution: *First we calculate,*

$$\begin{aligned}
[\hat{a}^{\dagger 2}, \hat{a}] &= \hat{a}^\dagger [\hat{a}^\dagger, \hat{a}] + [\hat{a}^\dagger, \hat{a}] \hat{a}^\dagger = -2\hat{a}^\dagger \\
[\hat{a}^2, \hat{a}^\dagger] &= \hat{a}[\hat{a}, \hat{a}^\dagger] + [\hat{a}, \hat{a}^\dagger]\hat{a} = 2\hat{a} \ .
\end{aligned}$$

Now we calculate,

$$\begin{aligned}
& e^{-\xi \hat{a}^{\dagger 2}/2 + \xi^* \hat{a}^2/2} \hat{a} e^{\xi \hat{a}^{\dagger 2}/2 - \xi^* \hat{a}^2/2} \\
&\quad = \hat{a} + \left[-\tfrac{\xi}{2}\hat{a}^{\dagger 2} + \tfrac{\xi^*}{2}\hat{a}^2, \hat{a} \right] + \tfrac{1}{2!}\left[-\tfrac{\xi}{2}\hat{a}^{\dagger 2} + \tfrac{\xi^*}{2}\hat{a}^2, \left[-\tfrac{\xi}{2}\hat{a}^{\dagger 2} + \tfrac{\xi^*}{2}\hat{a}^2, \hat{a} \right] \right] + ... \\
&\quad = \hat{a} + \hat{B}_1 + \hat{B}_2 + \hat{B}_3 ... \ ,
\end{aligned}$$

with $\hat{B}_n = \frac{1}{n}[\hat{a}, \hat{B}_{n-1}]$, *such that,*

$$\begin{aligned}
\hat{B}_1 &= \xi\hat{a}^\dagger \\
\hat{B}_2 &= \tfrac{1}{2}\left[-\tfrac{\xi}{2}\hat{a}^{\dagger 2} + \tfrac{\xi^*}{2}\hat{a}^2, \hat{B}_1\right] = \tfrac{1}{2}\tfrac{|\xi|^2}{2}\left[\hat{a}^2, \hat{a}^\dagger\right] = \tfrac{\xi\xi^*}{2}\hat{a} \\
\hat{B}_3 &= \tfrac{1}{3}\left[-\tfrac{\xi}{2}\hat{a}^{\dagger 2} + \tfrac{\xi^*}{2}\hat{a}^2, \hat{B}_2\right] = \tfrac{1}{3}\tfrac{|\xi|^2}{2}\tfrac{-\xi}{2}\left[\hat{a}^{\dagger 2}, \hat{a}\right] = \tfrac{1}{3}\tfrac{\xi\xi^*\xi}{2}\hat{a}^\dagger \ ,
\end{aligned}$$

confirming the result.

35.3.4.3 Ex: Squeezed states

Squeezed states may be introduced by the application of the operator $S(\xi) \equiv e^{\frac{\xi^*}{2}\hat{a}^2 - \frac{\xi}{2}\hat{a}^{\dagger\ 2}}$ on a Glauber state $|\alpha\rangle$, where ξ is the squeezing parameter.
Calculate $\langle\alpha, \xi|\hat{n}|\alpha, \xi\rangle$ and show with $\alpha \to 0$, that the squeezed vacuum is not empty.

Solution: *With the commutation rules and with* $e^A e^B = e^{A+[A,B]/2+B}$ *it is easy to show the unitarity of the squeezing operator. In particular,*

$$\begin{aligned}
\hat{b} &= S^\dagger(\xi)\hat{a}S(\xi) = e^{\hat{B}}\hat{a}e^{-\hat{B}} \\
&= \hat{a} + \left[\hat{B}, \hat{a}\right] + \tfrac{1}{2!}\left[\hat{B}, [\hat{B}, \hat{a}]\right] + \tfrac{1}{3!}\left[\hat{B}, \left[\hat{B}, [\hat{B}, \hat{a}]\right]\right] ... \\
&= \hat{a} + \xi\hat{a}^\dagger + \tfrac{1}{2!}\xi\xi^*\hat{a} + \tfrac{1}{3!}\xi\xi^*\xi\hat{a}^\dagger + ... = \hat{a}\cosh|\xi| + \frac{|\xi|}{\xi^*}\hat{a}^\dagger \sinh|\xi| \ .
\end{aligned}$$

Hence,

$$\begin{aligned}
\hat{b}^\dagger\hat{b} &= \left(\hat{a}^\dagger\cosh|\xi| + \frac{|\xi|}{\xi}\hat{a}\sinh|\xi|\right)\left(\hat{a}\cosh|\xi| + \frac{|\xi|}{\xi^*}\hat{a}^\dagger\sinh|\xi|\right) \\
&= \hat{a}^\dagger\hat{a}\cosh^2|\xi| + \hat{a}\hat{a}^\dagger\sinh^2|\xi| + \left(\frac{|\xi|}{\xi^*}\hat{a}^\dagger\hat{a}^\dagger + \frac{|\xi|}{\xi}\hat{a}\hat{a}\right)\sinh|\xi|\cosh|\xi| \\
&= \hat{a}^\dagger\hat{a} + \sinh^2|\xi| + \left(\frac{|\xi|}{\xi^*}\hat{a}^\dagger\hat{a}^\dagger + \frac{|\xi|}{\xi}\hat{a}\hat{a}\right)\sinh|\xi|\cosh|\xi| \ .
\end{aligned}$$

Finally,

$$\begin{aligned}
\langle\alpha, \xi|\hat{n}|\alpha, \xi\rangle &= |\alpha|^2 + \sinh^2|\xi| \overset{\alpha\to 0}{\longrightarrow} \sinh^2|\xi| \ , \\
\Delta_{\alpha,\xi}\hat{n} &= |\alpha| + 2\cosh^2|\xi|\sinh^2|\xi| \overset{\alpha\to 0}{\longrightarrow} 2\cosh^2|\xi|\sinh^2|\xi| \ .
\end{aligned}$$

35.3.4.4 Ex: Studying the squeezing operator

Using the Baker-Campbell-Hausdorff braiding identity,

$$e^{\hat{x}}e^{\hat{y}}e^{-\hat{x}} = e^{\hat{y}+[\hat{x},\hat{y}]+\frac{1}{2!}[\hat{x},[\hat{x},\hat{y}]]+...}$$

evaluate the expression $e^{\hat{a}^{\dagger 2}/2}e^{\hat{a}^2/2}e^{-\hat{a}^{\dagger 2}/2}$.

Solution: *We first calculate the commutators,*

$$[\hat{n}, \tfrac{\hat{a}^{\dagger 2}}{2}] = \hat{a}^{\dagger 2} \qquad \textit{and} \qquad [\hat{n}, \tfrac{\hat{a}^2}{2}] = -\hat{a}^2 \qquad \textit{and} \qquad [\tfrac{\hat{a}^2}{2}, \tfrac{\hat{a}^{\dagger 2}}{2}] = \hat{n} + \tfrac{1}{2} \ .$$

Now, identifying $\hat{x} \equiv \frac{\hat{a}^{\dagger 2}}{2}$ *and* $\hat{y} \equiv \frac{\hat{a}^2}{2}$,

$$e^{\hat{a}^{\dagger 2}/2}e^{\hat{a}^2/2}e^{-\hat{a}^{\dagger 2}/2} = e^{\hat{a}^2/2 + \hat{a}^{\dagger 2}/2 - \hat{n}} \ .$$

35.4 The Jaynes-Cummings model

The *Jaynes-Cummings model* describes the dynamics of a single dressed two-level atom in a single monochromatic laser mode in the absence of spontaneous emission processes. The model, illustrated in Fig. 35.2 has become a paradigm of quantum mechanics with applications in quantum information, where it applies to the formulation of entanglement protocols of atomic states and the implementation of quantum gates, which will be discussed in Sec. 41.4. In the following, we will first study the interaction of an atom with an optical mode neglecting dissipation effects and leave the discussion on the impact of dissipation processes to later sections.

The dynamic evolution of pure states is then obtained from the Schrödinger equation. The Hamiltonian of this system is given by (35.19). Letting $\hbar = 1$ and assuming that the atom is located at the origin [such that $\Omega_1(\mathbf{r})e^{\imath \mathbf{k}\cdot\mathbf{r}} = \Omega_1(\mathbf{0})$], we can write the time-dependent Hamiltonian in the *interaction picture* as,

$$\boxed{\begin{aligned} \hat{H}_{atom:field} &= \tfrac{\imath}{2}\Omega_1 e^{-\imath\Delta t}\hat{\sigma}^+\hat{a} - \tfrac{\imath}{2}\Omega_1 e^{\imath\Delta t}\hat{\sigma}^-\hat{a}^\dagger \\ &= \begin{pmatrix} 0 & \frac{\imath}{2}\Omega_1 e^{-\imath\Delta t}\hat{a} \\ -\frac{\imath}{2}\Omega_1 e^{\imath\Delta t}\hat{a}^\dagger & 0 \end{pmatrix} \end{aligned}} \ . \tag{35.108}$$

where ω is the frequency of the radiation, ω_0 the frequency of the atomic transition, $\Delta \equiv \omega - \omega_0$ the detuning, and Ω_1 the Rabi frequency generated by a single photon. The atomic operators $\sigma^\pm$ are related to the *Pauli spin matrices* (23.47), and we use the conventions $\hat{\sigma}^z = [\hat{\sigma}^+, \hat{\sigma}^-] = |2\rangle\langle 2| - |1\rangle\langle 1| = 2\hat{\sigma}^+\hat{\sigma}^- - \mathbb{I}$ and $\omega_0 \equiv \omega_2 - \omega_1 > 0$.

Starting from this Hamiltonian the Jaynes-Cummings model is translated into the *Schrödinger picture* via the unitary transform,

$$U = e^{-\imath(\hat{n}+1/2)\omega t}e^{\imath\hat{\sigma}^z\omega_0 t/2} \ , \tag{35.109}$$

for which we find the relationships,

$$\begin{aligned} -\imath U\dot{U}^\dagger &= \omega(\hat{n} + \tfrac{1}{2}) - \tfrac{1}{2}\omega_0\hat{\sigma}^z \\ U\hat{a}U^\dagger &= \Sigma_{n'}|n'\rangle e^{-\imath n'\omega t}\langle n'|\hat{a}\Sigma_n|n\rangle e^{\imath n\omega t}\langle n| = e^{\imath\omega t}\hat{a} \\ U\hat{\sigma}^- U^\dagger &= e^{\imath\omega_0 t}\hat{\sigma}^- \ . \end{aligned} \tag{35.110}$$

Obviously, the dynamics of the states is now given by $|\psi(t)\rangle = U|\psi_I(t)\rangle$, and the new Hamiltonian in the Schrödinger picture reads,

$$\boxed{\begin{array}{rcl} \tilde{H}_{atom:field} &=& U\hat{H}_{atom:field}U^\dagger - \imath U\dot{U}^\dagger \\ &=& \omega(\hat{n}+\frac{1}{2}) - \frac{1}{2}\omega_0\hat{\sigma}^z + \frac{1}{2}\Omega_1(\hat{a}\hat{\sigma}^+ + \hat{a}^\dagger\hat{\sigma}^-) \\ &=& \begin{pmatrix} (\hat{n}+\frac{1}{2})\omega - \frac{1}{2}\omega_0 & \frac{1}{2}\Omega_1\hat{a}^\dagger \\ \frac{1}{2}\Omega_1\hat{a} & (\hat{n}+\frac{1}{2})\omega + \frac{1}{2}\omega_0 \end{pmatrix} \end{array}} \; . \tag{35.111}$$

We choose the Fock representation (24.81) for the radiation mode, we represent the atomic transitions by the Pauli matrices (23.45), and we span the product space $\hat{\rho}_{field} \otimes \hat{\rho}_{atom}$ generalizing the operators $\hat{a}^\pm \curvearrowright \hat{a}^\pm \otimes \mathbb{I}$ and $\hat{\sigma}^\pm \curvearrowright \mathbb{I} \otimes \hat{\sigma}^\pm$. Explicitly we get,

$$\begin{array}{rclcrcl} \hat{a}^\dagger &=& \sum_n \sqrt{n+1}|n+1\rangle \begin{pmatrix} 1 & 0 \\ 0 & 1 \end{pmatrix} \langle n| & \text{and} & \hat{\sigma}^+ &=& \sum_n |n\rangle \begin{pmatrix} 0 & 0 \\ 1 & 0 \end{pmatrix} \langle n| \\ \hat{a} &=& \sum_n \sqrt{n}|n-1\rangle \begin{pmatrix} 1 & 0 \\ 0 & 1 \end{pmatrix} \langle n| & \text{and} & \hat{\sigma}^- &=& \sum_n |n\rangle \begin{pmatrix} 0 & 1 \\ 0 & 0 \end{pmatrix} \langle n| \; . \end{array} \tag{35.112}$$

35.4.1 Dressed states representation

The basis

$$|1,n\rangle = \begin{pmatrix} 1 \\ 0 \end{pmatrix} |n\rangle \quad , \quad |2,n-1\rangle = \begin{pmatrix} 0 \\ 1 \end{pmatrix} |n-1\rangle \tag{35.113}$$

spans a sub-space of two energetically nearly degenerate states with n photons in the system one out of which can have been absorbed by the atom. The density operator for the subspace is,

$$\hat{\rho}_n = \begin{pmatrix} |n\rangle|1\rangle\langle 1|\langle n| & |n\rangle|1\rangle\langle 2|\langle n-1| \\ |n-1\rangle|2\rangle\langle 1|\langle n| & |n-1\rangle|2\rangle\langle 2|\langle n-1| \end{pmatrix} \; . \tag{35.114}$$

We project the Hamiltonian onto that basis via the projectors $\hat{P} = |1,n\rangle\langle 1,n| + |2,n-1\rangle\langle 2,n-1|$,

$$\boxed{\hat{H}_n = \hat{P}\tilde{H}_{atom:field}\hat{P} = \begin{pmatrix} n\omega + \frac{\Delta}{2} & \frac{1}{2}\Omega_1\sqrt{n} \\ \frac{1}{2}\Omega_1\sqrt{n} & n\omega - \frac{\Delta}{2} \end{pmatrix}} \; . \tag{35.115}$$

That is, the Hamiltonian can be decomposed into sub-hyperspaces which are all orthogonal, because the Hamiltonian $\tilde{H}_{atom:field}$ only contains terms conserving the total number of photons + excitations.

Example 209 (*Orthogonality of submatrices with same numbers of excitations*): This can be seen by expanding the Hamiltonian matrix:

$$\tilde{H}_{atom:field} = \bigoplus_n \hat{H}_n \tag{35.116}$$

$$= \sum_n \left[|n\rangle \begin{pmatrix} n\omega + \frac{\Delta}{2} & 0 \\ 0 & n\omega - \frac{\Delta}{2} \end{pmatrix} + |n-1\rangle \begin{pmatrix} 0 & 0 \\ \frac{\Omega_1}{2}\sqrt{n} & 0 \end{pmatrix} + |n+1\rangle \begin{pmatrix} 0 & \frac{\Omega_1}{2}\sqrt{n+1} \\ 0 & 0 \end{pmatrix} \right] \langle n|$$

$$= \begin{pmatrix} \frac{\Delta}{2} & & & & & & \\ & \omega + \frac{\Delta}{2} & \frac{\Omega_1}{2} & & & & \\ & \frac{\Omega_1}{2} & \omega - \frac{\Delta}{2} & & & & \\ & & & 2\omega + \frac{\Delta}{2} & \frac{\Omega_1}{2}\sqrt{2} & & \\ & & & \frac{\Omega_1}{2}\sqrt{2} & 2\omega - \frac{\Delta}{2} & & \\ & & & & & 3\omega + \frac{\Delta}{2} & \cdots \\ & & & & & \vdots & \ddots \end{pmatrix} .$$

The eigenvalues can be easily calculated by [7],

$$\det \sum_n \hat{H}_n = \sum_n \det \hat{H}_n \ , \tag{35.117}$$

defining the generalized n-photon Rabi frequency, $\varpi_n \equiv \sqrt{\Delta^2 + n\Omega_1^2} = |\varpi_n| e^{\imath \mathbf{k}\cdot\mathbf{R}}$, which contains the spatial mode function of the radiation field. Using the standard procedure outlined in Sec. 23.3.4 we find the diagonal matrix of eigenvalues,

$$\hat{E}_n = \begin{pmatrix} n\omega + \frac{\varpi_n}{2} & 0 \\ 0 & n\omega - \frac{\varpi_n}{2} \end{pmatrix} . \tag{35.118}$$

From the transformation $\hat{H}_n U_n = U_n \hat{E}_n$, under the condition that U_n is unitary and Hermitian, $U_n^\dagger U_n$, and using the abbreviation $\tan 2\phi_n \equiv \sqrt{n}\Omega_1/\Delta$, we obtain:

$$U_n = \begin{pmatrix} \cos\phi_n & \sin\phi_n \\ -\sin\phi_n & \cos\phi_n \end{pmatrix} . \tag{35.119}$$

The unitary matrix U_n describes the transform from the product state basis (35.113) to the dressed state basis (35.21), as illustrated in Fig. 35.4.

The temporal evolution of the Jaynes-Cummings state, $|\psi(t)\rangle = e^{-\imath \tilde{H}_{atom:field} t} |\psi(0)\rangle$, is described by the transformation,

$$\boxed{\begin{aligned} & e^{-\imath \hat{H}_n t} = U_n e^{-\imath \hat{E}_n t} U_n^\dagger = e^{-\imath n\omega t} \times \\ & \times \begin{pmatrix} \cos^2\phi_n e^{-\imath\varpi_n t/2} + \sin^2\phi_n e^{\imath\varpi_n t/2} & \cos\phi_n \sin\phi_n (e^{\imath\varpi_n t/2} - e^{-\imath\varpi_n t/2}) \\ \cos\phi_n \sin\phi_n (e^{\imath\varpi_n t/2} - e^{-\imath\varpi_n t/2}) & \sin^2\phi_n e^{-\imath\varpi_n t/2} + \cos^2\phi_n e^{\imath\varpi_n t/2} \end{pmatrix} , \end{aligned}} \tag{35.120}$$

[7] The following rules apply to determinants,

$$\det(AB) = \det A \det B \qquad \text{and} \qquad (\det A)^{-1} = \det A^{-1} \ .$$

which is essentially the same formula as for the time evolution of a two-level atom driven by a classical light field derived in Exc. 23.4.7.1. The transition probability between dressed states is,

$$|\langle 2,n-1|e^{-\imath\hat{H}_n t}|1,n\rangle|^2 = \frac{n\Omega_1^2}{\varpi_n^2}\sin^2\frac{\varpi_n t}{2} \ . \tag{35.121}$$

The temporal evolution follows with [672],

$$\hat{\rho}(t) = e^{-\imath\hat{H}_n t}\hat{\rho}(0)e^{\imath\hat{H}_n t} \equiv \mathcal{L}(t)\hat{\rho}(0) \ . \tag{35.122}$$

Alternatively to the master equation (35.122) we could describe the time evolution of the system by Heisenberg equations, as done in Exc. 35.4.5.1.

35.4.2 Classical and quantum limits

35.4.2.1 The limit of high laser intensities and resonant interaction

The classical limit is recovered for $n \to \infty$, where a single photon makes no difference, that is, we can treat the states $|n\rangle$ and $|n+1\rangle$ as equivalent. Then, we can approximate the Hamiltonian of the system (35.113) by the trace of this same Hamiltonian taken over the number of photons,

$$\hat{H}_{semi} = \lim_{n\to\infty} \mathrm{Tr}_{field}\hat{\rho}\tilde{H}_{atom:field} = \sum_m \langle m|\hat{\rho}\tilde{H}_{atom:field}|m\rangle \ . \tag{35.123}$$

This situation, as illustrated in Fig. 35.8, describes well the state of a laser as a coherent state, $|\alpha\rangle = \sum_n \frac{\alpha^n}{\sqrt{n!}}|n\rangle e^{-|\alpha|^2/2}$. For $n \to \infty$, the uncertainty of the Poisson distribution is small, $\Delta n/\bar{n} = 1/\sqrt{n} \to 0$, such that the light mode is characterized by the average number of photons, and fluctuations are negligible. This allows us to replace the Poisson distribution, $P_n = |\langle n|\alpha\rangle|^2 = \delta_{n\bar{n}}$. The Hamiltonian (35.115) then becomes,

$$\begin{aligned}\hat{H}_{semi} &= \hat{H}_{field} + \hat{H}_{atom} + \hat{H}_{atom:field} = \sum_m \langle m|\alpha\rangle\langle\alpha|\hat{H}|m\rangle = \langle\alpha|\hat{H}|\alpha\rangle \simeq \langle\bar{n}|\hat{H}|\bar{n}\rangle \\ &= \hat{H}_{\bar{n}} = \begin{pmatrix}\bar{n}\omega & 0\\ 0 & (\bar{n}-1)\omega\end{pmatrix} + \begin{pmatrix}-\frac{\omega_0}{2} & 0\\ 0 & \frac{\omega_0}{2}\end{pmatrix} + \begin{pmatrix}0 & \frac{\varpi_{\bar{n}}}{2}\\ \frac{\varpi^*_{\bar{n}}}{2} & 0\end{pmatrix} \ .\end{aligned} \tag{35.124}$$

Now, in the case of a resonant interaction, $\Delta = 0$, the Jaynes-Cummings evolution is,

$$\boxed{e^{-\imath\hat{H}_{\bar{n}}t} = \frac{1}{\sqrt{2}}e^{-\imath(\bar{n}-1/2)\omega t}\begin{pmatrix}\cos\frac{1}{2}\varpi_{\bar{n}}t & \imath\sin\frac{1}{2}\varpi_{\bar{n}}t\\ \imath\sin\frac{1}{2}\varpi_{\bar{n}}t & \cos\frac{1}{2}\varpi_{\bar{n}}t\end{pmatrix}} \ , \tag{35.125}$$

which is a result already obtained in Exc. 23.4.7.1.

Example 210 (*Resonant* $\pi/2$*-pulse*): In this example, we consider resonant $\pi/2$-pulses, that is, $\sqrt{\bar{n}}\Omega_1 t = \frac{1}{2}\pi$. The Jaynes-Cummings evolution now simplifies to,

$$e^{-\imath\hat{H}_{\bar{n}}t} = \frac{1}{2}e^{-\imath(\bar{n}-1/2)\omega t}\begin{pmatrix}1 & \imath\\ \imath & 1\end{pmatrix} \ . \tag{35.126}$$

For large $\bar{n}$, a resonant $\pi/2$-pulse does (ignoring irrelevant dynamical phases),

$$\begin{pmatrix} |1\rangle|\bar{n}\rangle \\ |2\rangle|\bar{n}-1\rangle \end{pmatrix} \overset{\pi/2}{\curvearrowright} \begin{pmatrix} (\imath|2\rangle|\bar{n}-1\rangle + |1\rangle|\bar{n}\rangle) \\ (|2\rangle|\bar{n}-1\rangle + \imath|1\rangle|\bar{n}\rangle) \end{pmatrix} , \tag{35.127}$$

that is, for a coherent field,

$$\begin{pmatrix} |1\rangle|\alpha\rangle \\ |2\rangle|\alpha\rangle \end{pmatrix} \overset{\pi/2}{\curvearrowright} \begin{pmatrix} (\imath|2\rangle + |1\rangle)|\alpha\rangle \\ (|2\rangle + \imath|1\rangle)|\alpha\rangle \end{pmatrix} . \tag{35.128}$$

Obviously, the structure of the field $|\alpha\rangle$ is not affected, and we recover the dynamics of a two-level atom excited by a resonant classical *radiation* as described by the Bloch equations (34.151). In the language of quantum computation the operation (35.126) corresponds to a Hadamard gate.

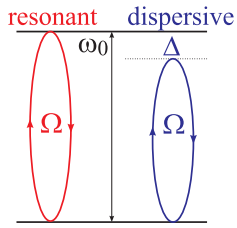

Figure 35.8: Atomic level scheme for the implementation of resonant interactions with classical radiation fields (on the lower transition) and dispersive interactions with quantum fields (on the upper transition).

35.4.2.2 Dispersive interaction, the limit of large detunings

The dispersive Jaynes-Cummings dynamics can be implemented by irradiating a light field, which is sufficiently detuned to avoid Rayleigh scattering processes, as shown in Fig. 35.8. This interaction results in a phase shift of the atomic levels. For $|\Delta| \gg \sqrt{n}\Omega_1$ we consider the radiative coupling as a small perturbation,

$$\hat{H}_n = \hat{H}_n^{(0)} + \hat{H}_n^{(1)} = \begin{pmatrix} n\omega - \frac{\Delta}{2} & 0 \\ 0 & n\omega + \frac{\Delta}{2} \end{pmatrix} + \begin{pmatrix} 0 & \frac{\Omega_1}{2}\sqrt{n} \\ \frac{\Omega_1}{2}\sqrt{n} & 0 \end{pmatrix} . \tag{35.129}$$

In the unperturbed case we have, $\hat{H}_n^{(0)}|\psi_{j,n}\rangle = E_{j,n}|\psi_{j,n}\rangle$, where the n-photon subspace is spanned by the basis $|j\rangle = (1\ 0)$ and $(0\ 1)$. In second perturbation order,

$$\langle\psi_{j,n}|\hat{H}_n^{(1)}|\psi_{j,n}\rangle \simeq \cancelto{0}{\langle j|\hat{H}_n^{(1)} + \hat{H}_n^{(2)}|j\rangle} + \sum_{j\neq i} \frac{\langle j|\hat{H}_n^{(1)}|i\rangle\langle i|\hat{H}_n^{(1)}|j\rangle}{E_{j,n}^{(0)} - E_{i,n}^{(0)}} = \mp\frac{n\Omega_1^2}{4\Delta} , \tag{35.130}$$

where the upper sign holds for $|j\rangle = (1\ 0)$. This result was already obtained in the Excs. 27.1.3.4 and 34.5.4.13. In matrix notation [8],

$$\hat{H}_n^{(1)} \simeq \begin{pmatrix} n\Omega_1^2/4\Delta & 0 \\ 0 & -n\Omega_1^2/4\Delta \end{pmatrix} . \tag{35.131}$$

The temporal propagation operator (35.120) then simplifies to,

$$\boxed{e^{-\imath\hat{H}_n^{(1)}t} = \begin{pmatrix} e^{\imath n\Omega_1^2 t/4\Delta} & 0 \\ 0 & e^{-\imath n\Omega_1^2 t/4\Delta} \end{pmatrix}} . \tag{35.132}$$

The fact that the ground and excited atomic states evolve with different phase factors is important, as we will show in the following example.

Example 211 (*Dispersive π-pulse*): As in the previous case, we consider a two-level atom subject to a coherent field, but now tuned out of resonance. Introducing the abbreviation $\varphi \equiv \Omega_1^2 t/4\Delta$, the Jaynes-Cummings evolution is,

$$e^{-\imath\hat{H}_n^{(1)}t} = \begin{pmatrix} e^{\imath n\varphi} & 0 \\ 0 & e^{-\imath n\varphi} \end{pmatrix} . \tag{35.133}$$

The fact that the phase shift $n\varphi$ depends on the number of photons, and that it goes in opposite directions for the ground and excited states, is crucial. We have already studied in Exc. 34.8.4.9, that the dispersive interaction of the atom with a radiation field can phase-shift the Bloch vector. Now, we observe that in addition, it causes a phase shift of the probability amplitude of having n photons in the radiation field by a value proportional to n, i.e. (ignoring irrelevant dynamical phases),

$$\begin{pmatrix} |1\rangle|n\rangle \\ |2\rangle|n-1\rangle \end{pmatrix} \overset{n\varphi}{\curvearrowright} \begin{pmatrix} e^{-\imath n\varphi}|1\rangle|n\rangle \\ e^{\imath n\varphi}|2\rangle|n-1\rangle \end{pmatrix} . \tag{35.134}$$

Applying this result to Glauber states,

$$\begin{pmatrix} |1\rangle|\alpha\rangle \\ |2\rangle|\alpha\rangle \end{pmatrix} \overset{n\varphi}{\curvearrowright} \begin{pmatrix} |1\rangle \sum_n \frac{\alpha^n}{\sqrt{n!}} e^{-\imath n\varphi}|n\rangle \\ |2\rangle \sum_n \frac{\alpha^n}{\sqrt{n!}} e^{\imath n\varphi}|n\rangle \end{pmatrix} = \begin{pmatrix} |1\rangle|\alpha e^{-\imath\varphi}\rangle \\ |2\rangle|\alpha e^{\imath\varphi}\rangle \end{pmatrix} . \tag{35.135}$$

Apparently, the phase of the radiation field is shifted by a value φ, which depends on the state of the atom.

[8] Note, that the same perturbation expansion applied to the complete Hamiltonian in the interaction picture yields,

$$\tilde{H}_I^{(1)} = \begin{pmatrix} 0 & \frac{1}{2}\Omega_1\hat{a}^\dagger \\ \frac{1}{2}\Omega_1\hat{a} & 0 \end{pmatrix} = \tfrac{1}{2}\Omega_1\hat{a}\hat{\sigma}^+ + \tfrac{1}{2}\Omega_1\hat{a}^\dagger\hat{\sigma}^-$$
$$\simeq \frac{\tilde{H}_I^{(1)}|2\rangle\langle 2|\tilde{H}_I^{(1)}}{\omega_2-\omega_1} + \frac{\tilde{H}_I^{(1)}|1\rangle\langle 1|\tilde{H}_I^{(1)}}{\omega_1-\omega_2} = \frac{\Omega_1^2}{4\Delta}(\hat{\sigma}^-\hat{\sigma}^+\hat{a}^\dagger\hat{a} - \hat{\sigma}^+\hat{\sigma}^-\hat{a}\hat{a}^\dagger) = \frac{\Omega_1^2}{4\Delta}\begin{pmatrix} -\hat{a}^\dagger\hat{a} & 0 \\ 0 & \hat{a}\hat{a}^\dagger \end{pmatrix} .$$

We note here, that the dynamics studied in the last example provides a method of *transferring coherence from an atomic superposition to a quantum correlation of a radiation field*. All we have to do, is to bring the atom into a superposition of states $|1\rangle + |2\rangle$, and the field will automatically evolve toward a Schrödinger cat state $|\alpha e^{\imath\varphi}\rangle + |\alpha e^{-\imath\varphi}\rangle$. The transfer of quantum correlations between coupled degrees of freedom can induce a temporal complete disappearance of any signatures of quantum coherence in the light field. This phenomenon termed *quantum collapse and revival* is genuine of the Jaynes-Cummings model and will be studied in Excs. 35.4.5.2 and 35.4.5.3. Another phenomenon is *vacuum Rabi splitting*, which will be studied in 35.4.5.4.

35.4.3 Observables and correlations of the Jaynes-Cummings dynamics

In the limit of low laser intensities we must consider photonic distributions that are not necessarily coherent. The stationary solution of the Schrödinger equation consists of the dressed states $|1, n\rangle$ and $|2, n-1\rangle$. If we now expand a general Jaynes-Cummings state in amplitudes $c_{jn}(t)$,

$$|\psi\rangle = \sum_n (c_{1,n}|1, n\rangle + c_{2,n-1}|2, n-1\rangle) \ , \tag{35.136}$$

they will follow the Schrödinger equation,

$$\imath\hbar \frac{d}{dt} \begin{pmatrix} c_{1,n} \\ c_{2,n-1} \end{pmatrix} = \hat{H}_n \begin{pmatrix} c_{1,n} \\ c_{2,n-1} \end{pmatrix} \ . \tag{35.137}$$

The evolution of the coefficients c_{jn} completely describes the Jaynes-Cummings dynamics of the system through the formula (35.120). Obviously, the Jaynes-Cummings state is normalized because,

$$\langle\psi|\psi\rangle = \mathrm{Tr}_{field}\ |\psi\rangle\langle\psi| = \sum_{n=0}^{\infty} (|c_{1,n}|^2 + |c_{2,n}|^2) = 1 \ . \tag{35.138}$$

As dissipation processes are neglected, we get a pure state described by,

$$\hat{\rho} = |\psi\rangle\langle\psi| \ . \tag{35.139}$$

The Jaynes-Cummings dynamics involves two coupled degrees of freedom characterized by with their respective observables. If we are interested in them, we can do two things: (a) We ignore the degrees of freedom NOT under study by NOT DOING a measurement of the other degrees. That is, we simply remove the non-interesting degrees of freedom from the state. For example, if our focus is on the optical mode, we ignore the atomic state,

$$|\gamma\rangle \equiv \sum_{j=1,2} \langle j|\psi\rangle = \sum_n c_{1,n}|n\rangle + c_{2,n-1}|n-1\rangle \ . \tag{35.140}$$

Our new density operator remains pure, that is,

$$\hat{\rho}^{(pure)}_{field} = \sum_{i,j=1,2} \langle j|\hat{\rho}|i\rangle = \sum_{i,j=1,2} \langle j|\psi\rangle\langle\psi|i\rangle = |\gamma\rangle\langle\gamma| \ . \tag{35.141}$$

On the other hand, ignoring the optical mode via,

$$|\gamma\rangle \equiv \sum_n \langle n|\psi\rangle = \sum_n c_{1,n}|1\rangle + c_{2,n-1}|2\rangle \ . \tag{35.142}$$

Again, our new density operator remains pure, that is,

$$\hat{\rho}_{atom}^{(pure)} = \sum_{m,n} \langle m|\hat{\rho}|n\rangle = \sum_{m,n} \langle m|\psi\rangle\langle\psi|n\rangle = |\gamma\rangle\langle\gamma| \ . \tag{35.143}$$

(b) We trace over the degrees of freedom NOT under study by DOING a measurement. For example, if again our focus is on the optical mode, we trace over the atomic states,

$$\begin{aligned} \hat{\rho}_{field}^{(mix)} &= \mathrm{Tr}_{atom}\ \hat{\rho} = \sum_{j=1,2} \langle j|\hat{\rho}|j\rangle = \sum_{j=1,2} \langle j|\psi\rangle\langle\psi|j\rangle \\ &= \sum_{n,m} c_{1,m}^* c_{1,n}|n\rangle\langle m| + c_{2,m-1}^* c_{2,n-1}|n-1\rangle\langle m-1| \neq \hat{\rho}_{field}^{(pure)} \ . \end{aligned} \tag{35.144}$$

It is clear, that this incomplete measurement converts the reduced density operator into a statistical mixture, which is free of inneratomic correlations of the type $c_{2,m}^* c_{1,n}$, but this means that we also loose possible field correlations. On the other hand, tracing over the field mode,

$$\begin{aligned} \hat{\rho}_{atom}^{(mix)} &= \mathrm{Tr}_{field}\ \hat{\rho} = \sum_{n=0}^{\infty} \langle n|\hat{\rho}|n\rangle = \sum_{n=0}^{\infty} \langle n|\psi\rangle\langle\psi|n\rangle \\ &= \sum_n \left(c_{1,n}|1\rangle + c_{2,n}|2\rangle\right)\left(c_{1,n}^*\langle 1| + c_{2,n}^*\langle 2|\right) \neq \hat{\rho}_{atom}^{(pure)} \ . \end{aligned} \tag{35.145}$$

After these preliminary remarks let us have a look a some interesting observables.

35.4.3.1 Temporal evolution of the Bloch vector

The expectation value for field observables $\hat{A}|n\rangle = A_n|n\rangle$ is,

$$\langle\psi|\hat{A}|\psi\rangle = \mathrm{Tr}\ \hat{\rho}\hat{A} \sum_{i,n} \langle i|\langle n|\psi\rangle\langle\psi|\hat{A}|n\rangle|i\rangle = \sum_n A_n(|c_{1,n}|^2 + |c_{2,n}|^2) \ . \tag{35.146}$$

An example for a field observable is the photon number operator $\hat{n}$. And for the annihilation operator $\hat{a}|n\rangle = \sqrt{n}|n\rangle$ we have,

$$\langle\psi|\hat{a}|\psi\rangle = \sum_n \sqrt{n}(c_{1,n-1}^* c_{1,n} + c_{2,n-1}^* c_{2,n}) \ . \tag{35.147}$$

To determine the internal state of the atom, we must trace over the light field. The populations and coherences are, therefore,

$$\boxed{\rho_{ij} = \langle i|\mathrm{Tr}_{field}\ \hat{\rho}|j\rangle = \langle i|\sum_n \langle n|\psi\rangle\langle\psi|n\rangle|j\rangle = \sum_n c_{i,n}c_{j,n}^*} \ . \tag{35.148}$$

The projection onto the atomic state is done by,

$$\frac{|j\rangle\langle j|\psi\rangle}{\langle\psi|j\rangle\langle j|\psi\rangle} = \frac{\sum_m c_{j,n}|j,n\rangle}{\sum_m |c_{j,m}|^2} \ . \tag{35.149}$$

With (35.148), we can calculate the atomic Bloch vector (34.163), whose norm is interestingly NOT preserved, since,

$$\begin{aligned} |\vec{\rho}| = \left\| \begin{pmatrix} 2\ \mathfrak{Re}\ \rho_{12} \\ 2\ \mathfrak{Im}\ \rho_{12} \\ \rho_{22}-\rho_{11} \end{pmatrix} \right\| &= 2|\rho_{12}|^2 - 2\rho_{11}\rho_{22} = -2\det\hat{\rho} \\ &= 2\sum_n c_{1,n}c_{2,n}^* \sum_n c_{1,n}^* c_{2,n} - 2\sum_n |c_{2,n}|^2 \sum_n |c_{1,n}|^2 \neq 1 \ . \end{aligned} \tag{35.150}$$

35.4.3.2 The photon number distribution

To determine the state of the light field, we must trace over the atomic state. For example, the probability amplitude of encountering the state $|\psi\rangle$ in $|n\rangle$ is,

$$\langle n|\psi\rangle = c_{1,n}|1\rangle + c_{2,n}|2\rangle \ , \tag{35.151}$$

such that,

$$\boxed{p_n = \langle n|\mathrm{Tr}_{atom}\ \hat{\rho}|n\rangle = \langle n|\sum_{i=1,2}\langle i|\psi\rangle\langle\psi|i\rangle|n\rangle = |\langle n|\psi\rangle|^2 = |c_{1,n}|^2 + |c_{2,n}|^2} \ . \tag{35.152}$$

35.4.3.3 The Glauber-Sudarshan Q-function

To characterize the optical field separately from the atomic state, we can try, by a calculation similar to (35.146), to project the Jaynes-Cummings state onto a basis of coherent states. Thus, the probability amplitude of encountering the state $|\psi\rangle$ in $|\alpha\rangle$ is,

$$\begin{aligned} \langle\alpha|\psi\rangle &= e^{-|\alpha|^2/2}\sum_n \frac{\alpha^{*n}}{\sqrt{n!}}(c_{1,n}|1\rangle + c_{2,n}|2\rangle) \\ |\langle\alpha|\psi\rangle|^2 &= e^{-|\alpha|^2}\sum_n \frac{\alpha^{*n}\alpha^m}{\sqrt{n!}\sqrt{m!}}(c_{1,m}^* c_{1,n} + c_{2,m}^* c_{2,n}) \ , \end{aligned} \tag{35.153}$$

such that,

$$\boxed{\pi Q(\alpha) \equiv \langle\alpha|\mathrm{Tr}_{atom}\ \hat{\rho}|\alpha\rangle = e^{-|\alpha|^2}\left(\left|\sum_n c_{1,n}\frac{\alpha^n}{\sqrt{n!}}\right|^2 + \left|\sum_n c_{2,n}\frac{\alpha^n}{\sqrt{n!}}\right|^2\right)} \ . \tag{35.154}$$

We will derive this result in Exc. 35.4.5.5. This quantity, called *Q-function*, allows the illustration of the state in a coordinate system spanned by $\mathfrak{Re}\ \alpha$ and $\mathfrak{Im}\ \alpha$ [157]. It is generally easy to calculate, but does not exhibit much information, e.g., on

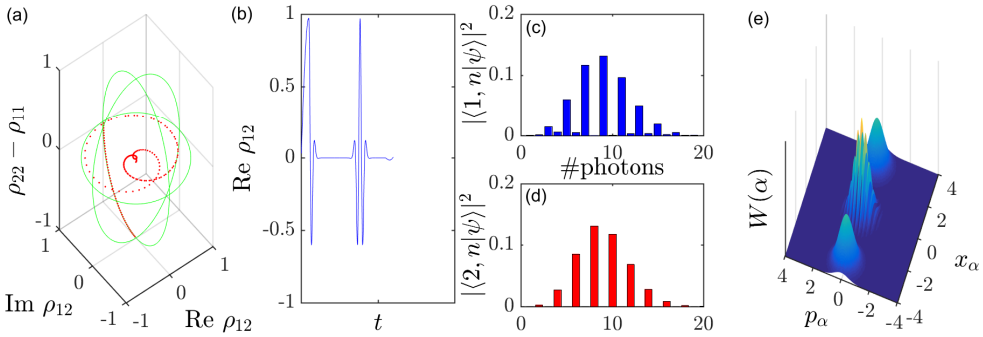

Figure 35.9: (code) Evolution of the state during a Jaynes-Cummings type interaction: (a) Bloch vector, (b,c) photon distribution after projection on the ground and excited atomic state, (d) time evolution of the coherence ρ_{12} showing the phenomenon of collapse and revival, and (e) $W(\alpha)$ function.

interference phenomena caused by quantum correlations. In the following section, we will calculate the Wigner function, which can also be evaluated from the Jaynes-Cummings coefficients [412].

The Jaynes-Cummings dynamics illustrated in Fig. 35.9 demonstrates the transfer of coherence between an atom and a light field. In Exc. 35.4.5.6 we study how to create, via a sequence of Ramsey pulses, a Schrödinger cat state in a light field.

35.4.3.4 The Wigner function in the Glauber picture

We found in (35.132) that a dispersive phase shift of the atomic state $|2\rangle$ leads to a time-dependent phase shift of the Glauber field,

$$|\psi\rangle = \sum_N (c_{1,n}|1,n\rangle + c_{2,n-1}|2,n-1\rangle) = |1,\beta\rangle + e^{\imath\varphi(t)}|2,\beta\rangle \qquad \text{or} \qquad \hat{\rho} = |\psi\rangle\langle\psi| \ , \tag{35.155}$$

with

$$c_{1,n} = e^{-|\beta|^2/2}\frac{\beta^n}{\sqrt{n!}} \qquad \text{and} \qquad c_{2,n} = e^{-|\beta|^2/2}\frac{(e^{\imath\varphi(t)}\beta)^n}{\sqrt{n!}} \ . \tag{35.156}$$

We will now concentrate on the field state by explicitly IGNORING the atomic states $|j\rangle$,

$$|\gamma\rangle = \sum_{j=1,2}\langle j|\psi\rangle = |\beta\rangle + |e^{\imath\varphi}\beta\rangle \qquad \text{or} \qquad \hat{\rho}^{(pure)}_{field} = \sum_{i,j=1,2}\langle j|\psi\rangle\langle\psi|i\rangle = |\gamma\rangle\langle\gamma| \ . \tag{35.157}$$

From the optical cat pure state wavefunction (35.157), we can easily calculate the Wigner function in the Glauber picture, as done in (35.76) and Exc. 35.2.5.10,

$$\boxed{W(\alpha) = \frac{2}{C^2\pi}\left(e^{-2|\alpha-\beta|^2} + e^{-2|\alpha-\beta e^{\imath\varphi}|^2} \pm 2e^{-|\beta|^2}\mathfrak{Re}\ e^{-2(\beta e^{\imath\varphi}-\alpha)(\beta^*-\alpha^*)+|\beta|^2 e^{\imath\varphi}}\right)} \ . \tag{35.158}$$

Now, what happens if we MEASURE the atomic state before we analyze the field state? The incomplete measurement corresponds to tracing over the atomic degrees of

freedom, which transforms our initially pure state (35.155) into a statistical mixture. With $|\psi\rangle$ given by (35.155),

$$\hat{\rho}_{field}^{(mix)} = \mathrm{Tr}_{atom}\hat{\rho} = \sum_{j=1,2}\langle j|\psi\rangle\langle\psi|j\rangle = |\beta\rangle\langle\beta| + |e^{\imath\varphi}\beta\rangle\langle e^{\imath\varphi}\beta| \neq |\gamma\rangle\langle\gamma| \ . \tag{35.159}$$

Calculating the Wigner function from this density operator consequently must yield a different result, because any correlations are lost. A movie of the dynamics can be watched here (watch movie) [228, 340, 16, 1321].

35.4.3.5 The Wigner function in the Fock picture

Let us now calculate the Wigner function in the Fock state picture. This will allow us to consider more general states later on. We start from the expansion,

$$|\psi\rangle = \sum_n c_{1,n}|1,n\rangle + c_{2,n-1}|2,n-1\rangle \ . \tag{35.160}$$

As before, we can now choose to DO or NOT DO a measurement of the atomic state. If we do a measurement tracing over the atomic states, we calculate the normally ordered characteristic function using the density operator (35.144),

$$\begin{aligned}\chi_N(\lambda) &= \mathrm{Tr}\ \hat{\rho}_{field}^{(mix)} e^{\lambda\hat{a}^\dagger} e^{-\lambda^*\hat{a}} = \sum_{n'}\langle n'|\hat{\rho}_{field}^{(mix)} e^{\lambda\hat{a}^\dagger} e^{-\lambda^*\hat{a}}|n'\rangle \\ &= \sum_{n,m} c_{1,m}^* c_{1,n}\langle m|e^{\lambda\hat{a}^\dagger} e^{-\lambda^*\hat{a}}|n\rangle + c_{2,m-1}^* c_{2,n-1}\langle m-1|e^{\lambda\hat{a}^\dagger} e^{-\lambda^*\hat{a}}|n-1\rangle \ .\end{aligned} \tag{35.161}$$

Obviously, this formula does not contain inneratomic correlations and, since non-classical field correlation would be entangled with atomic superposition states, we expect no interesting field correlations, neither.

If on the other hand we decide to ignore the atomic state, we calculate the normally ordered characteristic function using the density operator (35.141),

$$\begin{aligned}\chi_N(\lambda) &= \mathrm{Tr}\ \hat{\rho}_{field}^{(pure)} e^{\lambda\hat{a}^\dagger} e^{-\lambda^*\hat{a}} = \langle\gamma|e^{\lambda\hat{a}^\dagger} e^{-\lambda^*\hat{a}}|\gamma\rangle \\ &= \sum_{n,m}\Big(c_{1,m}^* c_{1,n}\langle m|e^{\lambda\hat{a}^\dagger} e^{-\lambda^*\hat{a}}|n\rangle + c_{2,m-1}^* c_{2,n-1}\langle m-1|e^{\lambda\hat{a}^\dagger} e^{-\lambda^*\hat{a}}|n-1\rangle \\ &\qquad + c_{1,m}^* c_{2,n-1}\langle m|e^{-\lambda\hat{a}^\dagger} e^{\lambda^*\hat{a}}|n-1\rangle + c_{2,m-1}^* c_{1,n}\langle m-1|e^{\lambda\hat{a}^\dagger} e^{-\lambda^*\hat{a}}|n\rangle\Big) \ ,\end{aligned} \tag{35.162}$$

which now contains field correlations. Inserting the results derived in (35.67) we can express the characteristic functions by Laguerre polynomials and obtain the Wigner function as the two-dimensional FFT according to Eq. (35.158). This will be done in Exc. 35.4.5.8.

35.4.4 Jaynes-Cummings model with dissipation

Applying the numerical method of *quantum Monte Carlo wavefunction simulation* to the Jaynes-Cummings model, we write the effective Hamiltonian of the light field as [493],

$$\hat{H}_{eff} = \omega\hat{a}^\dagger\hat{a} + \omega_0\left(\hat{\sigma}^+\hat{\sigma} - \tfrac{1}{2}\right) + \tfrac{\Omega_1}{2}\left(\hat{a}\hat{\sigma}^+ + \hat{a}^\dagger\hat{\sigma}^-\right) + \tfrac{\imath\Gamma}{2}\hat{\sigma}^+\hat{\sigma}^- \ . \tag{35.163}$$

Or in matrix notation,

$$H_{eff} = \begin{pmatrix} -\frac{1}{2}\omega_0 & 0 & & & & & & \\ 0 & \omega - \frac{1}{2}\omega_0 & \frac{1}{2}\Omega_1 & & & & & \\ & \frac{1}{2}\Omega_1 & \frac{1}{2}\omega_0 - \frac{\imath}{2}\Gamma & 0 & & & & \\ & & 0 & 2\omega - \frac{1}{2}\omega_0 & \sqrt{2}\frac{1}{2}\Omega_1 & & & \\ & & & \sqrt{2}\frac{1}{2}\Omega_1 & \omega + \frac{1}{2}\omega_0 - \frac{\imath}{2}\Gamma & 0 & & \\ & & & & 0 & 3\omega - \frac{1}{2}\omega_0 & & \\ & & & & & & \ddots & \end{pmatrix} . \tag{35.164}$$

The simulation flowchart is,

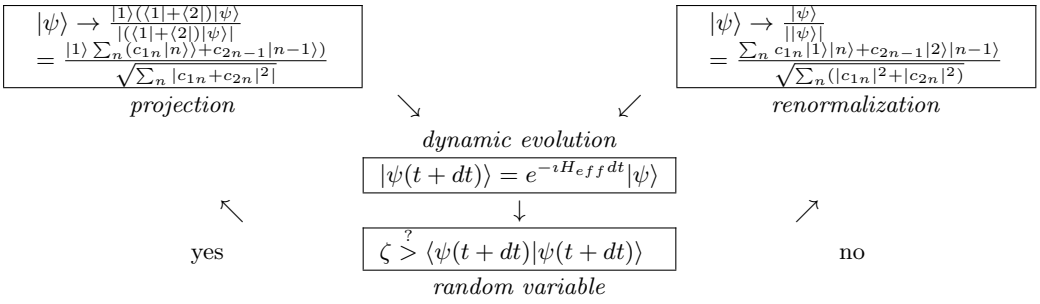

Absorption or scattering of light causes the optical field to decay as $\alpha(t) \propto e^{-\kappa t/2}$. The projection (in component notation) is implemented by,

$$c'_{jn} \equiv \frac{1}{\sqrt{\sum_n (|c_{1n}|^2 + |c_{2n}|^2)}} c_{jn} \ , \tag{35.165}$$

and the dynamical evolution by $c'_{jn} \equiv e^{-\kappa n t/2} c_{jn}$. Note, that the dissipation due to cavity losses can also be taken into account by a *master equation*. Do the Exc. 36.2.6.1.

35.4.4.1 Criticality in the Jaynes-Cummings model

The Jaynes-Cummings Hamiltonian (without counter-rotating terms) is,

$$\hat{H}_{JC} = \hbar\omega_c \hat{a}^\dagger \hat{a} + \hbar\omega_a \frac{\hat{\sigma}_z}{2} + \frac{\hbar\Omega_1}{2}(\hat{a}\hat{\sigma}_+ + \hat{a}^\dagger \hat{\sigma}_-) \ , \tag{35.166}$$

where Ω_1 is the single-photon Rabi frequency. The eigen-energies for the case of zero detuning, $\omega_c = \omega_a$, are

$$E_\pm(n) = \hbar\omega_a(n + \tfrac{1}{2}) \pm \tfrac{1}{2}\hbar\Omega_1\sqrt{n+1} \ . \tag{35.167}$$

One can approximately calculate the canonical partition function,

$$Z = \mathrm{Tr}\ e^{-\imath\beta\hat{H}} = \sum_{\pm,n} e^{-\beta E_\pm(n)} \simeq \int \left(e^{-\beta E_+(n)} + e^{-\beta E_-(n)}\right) dn \equiv \int e^{\Phi(n)} dn \ , \tag{35.168}$$

where the discrete sum was replaced by the integral. We get immediately,

$$\Phi(n) = \ln(e^{-\beta E_+(n)} + e^{-\beta E_-(n)}) = -\beta\hbar\omega_a(n+\tfrac{1}{2}) + \ln\left(2\cosh\tfrac{1}{2}\beta\hbar\Omega_1\sqrt{n+1}\right) \ . \tag{35.169}$$

The normal approach is that the latter integral is calculated by the Gaussian approximation around the maximum of the exponent:

$$0 = \frac{\partial\Phi(n)}{\partial n} = -\beta\hbar\left(\omega_a + \frac{\Omega_1}{4\sqrt{n+1}}\tanh\tfrac{1}{2}\beta\hbar\Omega_1\sqrt{n+1}\right) \ . \tag{35.170}$$

This *criticality* has solutions only if $\Omega > 4\omega_a$, which means that the normal and the superradiant phase, exist only if the field-atom coupling is significantly stronger than the energy difference between the atom levels. When the condition is fulfilled, the equation gives the solution for the order parameter n depending on the inverse of the temperature $1/\beta$, which means non-vanishing ordered field mode.

35.4.5 Exercises

35.4.5.1 Ex: Time-evolution in the Jaynes-Cummings model

Derive the equations of motion for $\hat{\sigma}^-$, $\hat{\sigma}_z$, and $\hat{a}$ in the Jaynes-Cummings model. Show that the number of photons is not a constant of motion, but the total number of excitations.

Solution: *Using the Jaynes-Cummings Hamiltonian,*

$$\hat{H} = \omega\hat{a}^\dagger\hat{a} + \omega_0(\hat{\sigma}^+\hat{\sigma}^- - \tfrac{1}{2}) + \tfrac{1}{2}\Omega_1(\hat{a}\hat{\sigma}^+ + \hat{a}^\dagger\hat{\sigma}^-) \ ,$$

we derive the Heisenberg equations,

$$\begin{aligned}
\dot{\hat{\sigma}}^- &= -\imath[\hat{\sigma}^-, \hat{H}] = -\imath\omega_0\hat{\sigma}_- - \tfrac{\imath}{2}\Omega_1\hat{a}\hat{\sigma}_z \\
\dot{\hat{\sigma}}_z &= -\imath[\hat{\sigma}_z, \hat{H}] = -\tfrac{\imath}{2}\Omega_1(\hat{a}\hat{\sigma}^+ - \hat{a}^\dagger\hat{\sigma}^-) \\
\dot{\hat{a}} &= -\imath[\hat{a}, \hat{H}] = -\imath\omega\hat{a} - \tfrac{\imath}{2}\Omega_1\hat{\sigma}^- \ .
\end{aligned}$$

We also find,

$$[\hat{n}, \hat{H}] = \tfrac{1}{2}\Omega_1[\hat{a}^\dagger\hat{a}, \hat{a}\hat{\sigma}^+ + \hat{a}^\dagger\hat{\sigma}^-] = -[\hat{\sigma}_z, \hat{H}] \ ,$$

which shows that only the total number of excitations $\langle\hat{a}^\dagger\hat{a} + \hat{\sigma}_z\rangle$ is a constant of motion.

35.4.5.2 Ex: The Jaynes-Cummings model

Consider the Jaynes-Cummings Hamiltonian.
a. Determine from the Schrödinger equation the system of differential equations for the temporal evolution of the coefficients $c_{2,n}(t)$ and $c_{1,n+1}(t)$ in the interaction picture within the rotating wave approximation (RWA).
b. Calculate the time evolution for the start condition $c_{2,n}(0) = 1$ and $c_{1,n+1}(0) = 0$ for the particular case $\omega = \omega_0$.

c. Generalize the result of item (a) for a multimode field, for which initially (i) all modes of field $\mathbf{k}$ are empty $|0\rangle$ and (ii) the atom is in the excited state $|a\rangle$. Use the ansatz,

$$|\psi(t)\rangle = c_2(t)e^{-\imath E_2 t/\hbar}|2,0\rangle + \sum_{\mathbf{k}} c_{1,\mathbf{k}}(t)e^{-\imath[E_1/\hbar+\omega_{\mathbf{k}}]t}|1,1_{\mathbf{k}}\rangle \ ,$$

and determine the equations of motion for the amplitudes c_2 and $c_{1,\mathbf{k}}$.

Solution: *a. The Schrödinger equation gives*

$$\begin{aligned}
&\frac{\partial}{\partial t}\left(c_{2,n}e^{-\imath(E_2/\hbar+n\omega)t}\right) = \frac{\partial}{\partial t}\langle 2,n|\psi(t)\rangle = \langle 2,n|\frac{\partial}{\partial t}|\psi\rangle = \tfrac{1}{\imath\hbar}\langle 2,n|\hat{H}|\psi\rangle \\
&= \langle 2,n| - \imath\textstyle\sum_n \frac{\omega_0}{2}c_{2,n}e^{-\imath(E_2/\hbar+n\omega)t}\hat{\sigma}_z|2,n\rangle + \\
&\quad + \langle 2,n| - \imath\textstyle\sum_n \frac{\omega_0}{2}c_{1,n+1}e^{-\imath(E_1/\hbar+(n+1)\omega)t}\hat{\sigma}_z|1,n+1\rangle + \\
&\quad + \langle 2,n| - \imath\textstyle\sum_n \omega c_{2,n}e^{-\imath(E_2/\hbar+n\omega)t}(\hat{a}^\dagger\hat{a}+\tfrac{1}{2})|2,n\rangle + \\
&\quad + \langle 2,n| - \imath\textstyle\sum_n \omega c_{1,n+1}e^{-\imath(E_1/\hbar+(n+1)\omega)t}(\hat{a}^\dagger\hat{a}+\tfrac{1}{2})|1,n+1\rangle + \\
&\quad + \langle 2,n| - \imath\textstyle\sum_n g c_{2,n}e^{-\imath(E_2/\hbar+n\omega)t}(\hat{a}\hat{\sigma}^+ + \hat{a}^\dagger\hat{\sigma}^-)|2,n\rangle + \\
&\quad + \langle 2,n| - \imath\textstyle\sum_n g c_{1,n+1}e^{-\imath(E_1/\hbar+(n+1)\omega)t}(\hat{a}\hat{\sigma}^+ + \hat{a}^\dagger\hat{\sigma}^-)|1,n+1\rangle \\
&= -\tfrac{\imath}{2}\omega_0 c_{2,n}e^{-\imath(E_2/\hbar+n\omega)t} + 0 - \imath(n+\tfrac{1}{2})\omega c_{2,n}e^{-\imath(E_2/\hbar+n\omega)t} + \\
&\quad + 0 - \imath\sqrt{n+1}\,g c_{1,n+1}e^{-\imath(E_1/\hbar+(n+1)\omega)t} \ ,
\end{aligned}$$

where $\hat{\sigma}_z|1\rangle = |1\rangle$ *and* $\hat{\sigma}_z|2\rangle = -|2\rangle$ *and* $\hat{a}|n\rangle = \sqrt{n}|n-1\rangle$ *and* $\hat{a}^\dagger|n\rangle = \sqrt{n+1}|n+1\rangle$. *Furthermore,*

$$\begin{aligned}
\frac{\partial}{\partial t}\left(c_{1,n+1}e^{-\imath(E_1/\hbar+(n+1)\omega)t}\right) &= -\tfrac{\imath}{2}\omega_0 c_{1,n+1}e^{-\imath(E_1/\hbar+(n+1)\omega)t} + 0 - \\
&\quad - \imath(n+\tfrac{1}{2})\omega c_{1,n+1}e^{-\imath(E_1/\hbar+(n+1)\omega)t} + \\
&\quad + 0 - \imath\sqrt{n+1}\,g c_{2,n}e^{-\imath(E_2/\hbar+n\omega)t} \ ,
\end{aligned}$$

also,

$$\begin{aligned}
\dot{c}_{2,n} + (E_2/\hbar + n\omega)c_{2,n} &= \tfrac{1}{2}\omega_0 c_{2,n} + (n+\tfrac{1}{2})\omega c_{2,n} + \sqrt{n+1}\,g c_{1,n+1}e^{\imath(\omega_0-\omega)t} \\
\dot{c}_{1,n+1} + (E_1/\hbar + (n+1)\omega)c_{1,n+1} &= \tfrac{1}{2}\omega_0 c_{1,n+1} + (n+\tfrac{1}{2})\omega c_{1,n+1} + \sqrt{n+1}\,g c_{2,n}e^{\imath(\omega-\omega_0)t} \ .
\end{aligned}$$

b. In short, we can write with $\omega_0 = E_2 - E_1$

$$\frac{\partial}{\partial t}\begin{pmatrix} c_{1,n+1} \\ c_{2,n}\end{pmatrix} = -\imath\begin{pmatrix} \frac{1}{2}\omega_0 - \frac{1}{2}\omega - \frac{1}{\hbar}E_1 & \sqrt{n+1}\,g e^{-\imath(\omega_0-\omega)t} \\ \sqrt{n+1}\,g e^{\imath(\omega_0-\omega)t} & \frac{1}{2}\omega_0 + \frac{1}{2}\omega - \frac{1}{\hbar}E_2\end{pmatrix}\begin{pmatrix} c_{1,n+1} \\ c_{2,n}\end{pmatrix}$$

in resonance we have,

$$\frac{\partial}{\partial t}\begin{pmatrix} c_{1,n+1} \\ c_{2,n}\end{pmatrix} = -\imath\begin{pmatrix} -\frac{1}{\hbar}E_1 & \sqrt{n+1}\,g \\ \sqrt{n+1}\,g & -\frac{1}{\hbar}E_2\end{pmatrix}\begin{pmatrix} c_{1,n+1} \\ c_{2,n}\end{pmatrix}$$

The eigenvalues of the matrix are $E = E_1 \pm g\sqrt{n+1}$. *Placing the ansatz,*

$$\begin{pmatrix} c_{1,n+1}(t) \\ c_{2,n}(t)\end{pmatrix} = \begin{pmatrix} \alpha_g e^{-\imath(-E_1+g\sqrt{n+1})t} + \beta_g e^{-\imath(-E_1-g\sqrt{n+1})t} \\ \alpha_a e^{-\imath(-E_1+g\sqrt{n+1})t} + \beta_a e^{-\imath(-E_1-g\sqrt{n+1})t}\end{pmatrix}$$

gives,

$$
\begin{aligned}
&-\imath(-E_1+g\sqrt{n+1})\alpha_g e^{-\imath gt\sqrt{n+1}}-\imath(-E_1+g\sqrt{n+1})\beta_g e^{\imath gt\sqrt{n+1}}\\
&\quad=\frac{\imath}{\hbar}E_1\alpha_g e^{-\imath gt\sqrt{n+1}}+\frac{\imath}{\hbar}E_1\beta_g e^{\imath gt\sqrt{n+1}}-\imath\sqrt{n+1}g\alpha_a e^{-\imath gt\sqrt{n+1}}-\imath\sqrt{n+1}g\beta_a e^{\imath gt\sqrt{n+1}}\\
&-\imath\left(-E_1+g\sqrt{n+1}\right)\alpha_a e^{-\imath gt\sqrt{n+1}}-\imath\left(-E_1+g\sqrt{n+1}\right)\beta_a e^{\imath gt\sqrt{n+1}}\\
&\quad=\frac{\imath}{\hbar}E_1\alpha_a e^{-\imath gt\sqrt{n+1}}+\frac{\imath}{\hbar}E_1\beta_a e^{\imath gt\sqrt{n+1}}-\imath\sqrt{n+1}g\alpha_g e^{-\imath gt\sqrt{n+1}}-\imath\sqrt{n+1}g\beta_g e^{\imath gt\sqrt{n+1}}
\end{aligned}
$$

and hence $\alpha_a=\alpha_g$ *and* $\beta_g=-\beta_a$. *The initial condition* $c_{2,n}(0)=1$ *and* $c_{1,n+1}(0)=0$ *gives* $\alpha_g+\beta_g=1$ *and* $\alpha_a+\beta_a=0$. *Hence, the solution is,*

$$
\begin{pmatrix}c_{1,n+1}(t)\\ c_{2,n}(t)\end{pmatrix}=e^{\imath E_1 t}\begin{pmatrix}\cos gt\sqrt{n+1}\\ \imath\sin gt\sqrt{n+1}\end{pmatrix}\ .
$$

c. The generalization of the result found in (a) to a multimode field $|\psi(t)\rangle=c_a(t)e^{-\imath E_2 t/\hbar}|a,0\rangle+\sum_{\mathbf{k}}c_{g,\mathbf{k}}(t)e^{-\imath(E_1/\hbar+\omega_{\mathbf{k}})t}|g,1_{\mathbf{k}}\rangle$ *yields,*

$$
\begin{aligned}
\frac{\partial}{\partial t}\left(c_a e^{-E_2 t/\hbar}\right)&=\langle 2,0|-\imath\tfrac{\omega_0}{2}c_a e^{-\imath E_2 t/\hbar}\sigma_z|a,0\rangle+\\
&+\langle 2,0|-\imath\sum_{\mathbf{k}}\tfrac{\omega_0}{2}c_{g,\mathbf{k}}e^{-\imath(E_1/\hbar+\omega_{\mathbf{k}})t}\sigma_z|g,1_{\mathbf{k}}\rangle+\\
&+\langle 2,0|-\imath\omega c_a e^{-\imath E_2 t/\hbar}\left(a^\dagger a+\tfrac{1}{2}\right)|a,0\rangle+\\
&+\langle 2,0|-\imath\sum_{\mathbf{k}}\omega c_{g,\mathbf{k}}e^{-\imath(E_1/\hbar+\omega_{\mathbf{k}})t}(a^\dagger a+\tfrac{1}{2})|g,1_{\mathbf{k}}\rangle+\\
&+\langle 2,0|-\imath g c_a e^{-\imath E_2 t/\hbar}(a\sigma^+ +a^\dagger\sigma^-)|a,0\rangle+\\
&+\langle 2,0|-\imath\sum_{\mathbf{k}}g c_{g,\mathbf{k}}e^{-\imath(E_1/\hbar+\omega_{\mathbf{k}})t}(a\sigma^+ +a^\dagger\sigma^-)|g,1_{\mathbf{k}}\rangle\\
&=-\tfrac{\imath}{2}\omega_0 c_a e^{-\imath E_2 t/\hbar}+0-\imath(0+\tfrac{1}{2})\omega c_a e^{-\imath E_2 t/\hbar}+\\
&+0-\imath g\sum_{\mathbf{k}}c_{g,\mathbf{k}}e^{-\imath(E_1/\hbar+\omega_{\mathbf{k}})t}\ ,
\end{aligned}
$$

and also,

$$\begin{aligned}
\frac{\partial}{\partial t}\left(c_{g,\mathbf{k}}e^{-\imath(E_1/\hbar+\omega_{\mathbf{k}})t}\right) &= \langle g,1_{\mathbf{k}}|-\imath\tfrac{\omega_0}{2}c_a e^{-\imath E_2 t/\hbar}\hat{\sigma}_z|a,0\rangle+\\
&+\langle g,1_{\mathbf{k}}|-\imath\sum_{\mathbf{k}}\tfrac{\omega_0}{2}c_{g,\mathbf{k}}e^{-\imath(E_1/\hbar+\omega_{\mathbf{k}})t}\hat{\sigma}_z|g,1_{\mathbf{k}}\rangle+\\
&+\langle g,1_{\mathbf{k}}|-\imath\omega c_a e^{-\imath E_2 t/\hbar}(a^\dagger a+\tfrac{1}{2})|a,0\rangle+\\
&+\langle g,1_{\mathbf{k}}|-\imath\sum_{\mathbf{k}}\omega c_{g,\mathbf{k}}e^{-\imath(E_1/\hbar+\omega_{\mathbf{k}})t}(\hat{a}^\dagger\hat{a}+\tfrac{1}{2})|g,1_{\mathbf{k}}\rangle+\\
&+\langle g,1_{\mathbf{k}}|-\imath g c_a e^{-\imath E_2 t/\hbar}(a\sigma^+ + a^\dagger\hat{\sigma}^-)|a,0\rangle+\\
&+\langle g,1_{\mathbf{k}}|-\imath\sum_{\mathbf{k}}g c_{g,\mathbf{k}}e^{-\imath(E_1/\hbar+\omega_{\mathbf{k}})t}(\hat{a}\hat{\sigma}^+ + \hat{a}^\dagger\sigma^-)|g,1_{\mathbf{k}}\rangle\\
=0-\imath\sum_{\mathbf{q}}\tfrac{\omega_0}{2}c_{g,\mathbf{q}}e^{-\imath(E_1/\hbar+\omega_{\mathbf{k}})t}\langle 1_{\mathbf{k}}|1_{\mathbf{q}}\rangle+0-&\\
-\imath\sum_{\mathbf{q}}\omega_{\mathbf{q}}c_{g,\mathbf{q}}e^{-\imath(E_1/\hbar+\omega_{\mathbf{k}})t}(1+\tfrac{1}{2})\langle 1_{\mathbf{k}}|1_{\mathbf{q}}\rangle-&\\
-\imath g c_a e^{-\imath E_2 t/\hbar}\langle 1_{\mathbf{k}}|a^\dagger|0\rangle+0\ .&
\end{aligned}$$

From this,

$$\begin{aligned}
\dot{c}_a-\tfrac{\imath}{\hbar}E_2 c_a &= -\tfrac{\imath}{2}(\omega_{\mathbf{k}}+\omega_0)c_a-\imath g\sum_{\mathbf{k}}c_{g,\mathbf{k}}e^{-\imath(-\omega_0+\omega_{\mathbf{k}})t}\\
\dot{c}_{g,\mathbf{k}}-\imath(E_1/\hbar+\omega_{\mathbf{k}})c_{g,\mathbf{k}} &= -\tfrac{\imath}{2}(\omega_0+3\omega_{\mathbf{k}})c_{g,\mathbf{k}}-\imath g c_a e^{-\imath(\omega_0-\omega_{\mathbf{k}})t}\ .
\end{aligned}$$

With a transformation to the interaction picture $\tilde{c}_a = c_a e^{\imath/2(\omega_{\mathbf{k}}-\omega_0)t}$ *and* $\tilde{c}_g = c_g e^{\imath/2(\omega_{\mathbf{k}}+\omega_0)t}$, *where without general restriction* $E_1\equiv 0$,

$$\begin{aligned}
\partial_t\tilde{c}_a &= -\imath g\sum_{\mathbf{k}}\tilde{c}_{g,\mathbf{k}}e^{-\imath(-\omega_0+\omega_{\mathbf{k}})t}\\
\partial_t\tilde{c}_{g,\mathbf{k}} &= -\imath g\tilde{c}_a e^{-\imath(\omega_0-\omega_{\mathbf{k}})t}\ .
\end{aligned}$$

With this we can calculate the spontaneous emission [1184].
d. Background: The formal solution is

$$c_{g,\mathbf{k}}(t) = -g\int_0^t dt'\ e^{\imath(\omega_{\mathbf{k}}-\omega_0)t'}c_a(t')\ .$$

When we introduce the density of the slowly varying states, $\sum_{\mathbf{k}}\to\int_0^\infty d\omega\ \rho(\omega)$, *we get,*

$$\begin{aligned}
\dot{c}_a(t) &= -g^2\sum_{\mathbf{k}}\int_0^t dt'\ e^{\imath(\omega_{\mathbf{k}}-\omega_0)(t-t')}c_a(t')\\
&\approx -g^2\rho(\omega_0)\int_0^t dt'\int_{-\infty}^{\infty}d\omega\ e^{\imath(\omega_{\mathbf{k}}-\omega_0)(t-t')}c_a(t')\\
&= -g^2\rho(\omega_0)\int_0^t dt' 2\pi\delta(t-t')c_a(t') = -\tfrac{\Gamma}{2}c_a(t)\ ,
\end{aligned}$$

with $\Gamma \equiv 4\pi g^2 \rho(\omega_0)$. The presence of many modes blurs the periodicity of the Rabi oscillations, until only remains a purely exponential decay, $|c_a(t)|^2 = e^{-\Gamma t}$, characterizing the spontaneous emission.

35.4.5.3 Ex: Quantum collapse and revival in the Jaynes-Cummings model

Consider the Jaynes-Cummings Hamiltonian and show that the quantum coherence between the two atomic levels can disappear altogether for long periods and reappear later. Explain how this is possible.

Solution: *The figure shows a simulation done in the Julia Language.*

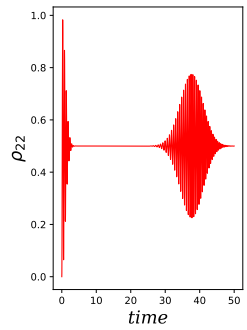

Figure 35.10: (code) Simulation of the time-evolution of the excited state population in the JCM for 200 photons.

35.4.5.4 Ex: Vacuum Rabi splitting

Calculate the Autler-Townes splitting for an excited atom interacting with an empty cavity.

Solution: *Without light in the cavity but with an initially excited atom, the Hamiltonian (35.113) is restricted to,*

$$\hat{H}_n = \begin{pmatrix} \frac{\omega_0}{2} & \frac{\Omega}{2} \\ \frac{\Omega}{2} & \omega - \frac{\omega_0}{2} \end{pmatrix} ,$$

with all the consequences. That is, even without photons in the mode, the atom starts to make a stimulated transition to the ground state. These are the well-known vacuum Rabi oscillations.

35.4.5.5 Ex: The Q-function in a Jaynes-Cummings state

Calculate the Q-function for a Jaynes-Cummings state from its definition (35.154).

Solution: *To begin with, we project the Glauber state onto a Fock state,*

$$\langle n|\alpha\rangle = \langle n|e^{-|\alpha|^2/2}\sum_{m=0}^{\infty}\frac{\alpha^m}{\sqrt{m!}}|m\rangle = e^{-|\alpha|^2/2}\frac{\alpha^n}{\sqrt{n!}}$$

and the Jaynes-Cummings state onto an atomic state,

$$\langle j|\psi\rangle = \langle j|\sum_n (c_{1,n}|1,n\rangle + c_{2,n-1}|2,n-1\rangle) = \sum_n (\delta_{j1}c_{1,n}|n\rangle + \delta_{j2}c_{2,n-1}|n-1\rangle) = \sum_n c_{j,n}|n\rangle \ .$$

With this we calculate the Q-function,

$$\pi Q(\alpha) = \langle\alpha|\, Tr_{atom}\ \hat{\rho}|\alpha\rangle = \langle\alpha|\sum_{j=1,2}\langle j|\psi\rangle\langle\psi|j\rangle|\alpha\rangle = \langle\alpha|\sum_{j=1,2}\sum_n c_{j,n}|n\rangle\sum_m c^*_{j,m}\langle m|\alpha\rangle$$

$$= \sum_{j=1,2}\sum_{n,m} c^*_{j,m}c_{j,n}e^{-|\alpha|^2/2}\frac{\alpha^{*n}}{\sqrt{n!}}\langle n|e^{-|\alpha|^2/2}\frac{\alpha^m}{\sqrt{m!}}|m\rangle = e^{-|\alpha|^2}\sum_{j=1,2}\sum_n |c_{j,n}|^2\frac{|\alpha|^n}{n!} \ .$$

35.4.5.6 Ex: Creation of quantum correlations in an optical mode

a. We will show in this exercise how, via coherent operations in a three-level system, we can create Schrödinger-type quantum-type correlations in an optical mode. In the system shown in Fig. 35.11 we imagine the lower transition excited by $\pi/2$-pulses of a classical resonant microwave radiation (as described by the operation (35.125)). The upper transition is excited by quantum laser pulses tuned very far out of resonance, thus creating a dispersive dynamics (as described by the operation (35.125)). At time $t = 0$ the atom is in state $|1\rangle$. Now, we apply the following pulse sequence: (i) a microwave pulse with $\sqrt{\bar{n}}\Omega_{12}t = \pi/2$, (ii) an optical pulse with $\Omega_{23}^2 t/4\Delta_{23} = \pi$, (iii) another microwave $\pi/2$-pulse, and finally (iv) an optical pulse of light which is resonant with the transition $|2\rangle$-$|3\rangle$ and projects the population of the atom into one of the states of the microwave transition. Describe the evolution of the state of the system during the sequence and determine the final state of the optical mode.
b. Calculate the number of photons for the two cases that, after a measurement, the atom is found in (i) the lower state and (ii) the upper state. Interprete the results.

Solution: *We denote the microwave radiation by $|\mu\rangle$ and the laser light by $|\beta\rangle$. Initially, before the atom interacts with the fields, we have the state,*

$$|\psi(0)\rangle = \begin{pmatrix}1\\0\end{pmatrix}|\mu\rangle|\beta\rangle \ .$$

We now apply a resonant $\pi/2$-pulse to the microwave transition ω_{12}. If the field is coherent, $|\mu|^2 \gg 1$, the atom goes to a superposition of atomic states,

$$|\psi(t)\rangle = \tfrac{1}{\sqrt{2}}\begin{pmatrix}1\\ \imath\end{pmatrix}|\mu e^{-\imath\omega_{12}t}\rangle \ .$$

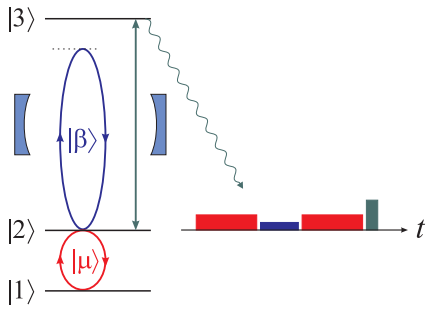

Figure 35.11: (a) Level scheme and (b) pulse sequence.

The microwave field being classical, the atomic state does not get entangled with the field, that is, the microwave field factors out. Now, we apply an optical pulse tuned far away from the resonance $|2\rangle - |3\rangle$*, such that* $|\Delta_{23}| \gg |\beta|^2\Omega_{23}$*. The laser-induced light shift is* $\Omega_{23}^2/4\Delta_{23}$*, such that the atom suffers phase shift of* $\varphi \equiv \Omega_{23}^2 t/4\Delta_{23}$ *provided it is in the state* $|2\rangle$*, but not if it is in the state* $|1\rangle$*. For* $\varphi = \pi$ *we obtain,*

$$|\psi(t+\tau)\rangle = \tfrac{1}{\sqrt{2}}\begin{pmatrix} |\beta'\rangle \\ -\imath|-\beta'\rangle \end{pmatrix} \qquad \textit{with} \qquad \beta' = \beta e^{-\imath\omega_{23}\tau} \ .$$

Therefore, the atomic state is entangled with the coherences of the optical field. Now, a second Ramsey $\pi/2$*-pulse is applied to the microwave transition, such that the correlated state is disentangled:*

$$|\psi(2t+\tau)\rangle = \tfrac{1}{2}\begin{pmatrix} 1 \\ \imath \end{pmatrix}|\beta'\rangle + \tfrac{1}{2}\begin{pmatrix} 1 \\ -\imath \end{pmatrix}|-\beta'\rangle \ .$$

Finally, a resonant optical light pulse measures the population of the state $|2\rangle$*. The measurement reduces the atomic state, and we are left with a pure Schrödinger cat state of the optical field:*

$$|\psi(T)\rangle = \tfrac{\imath}{\sqrt{2}}\begin{pmatrix} 0 \\ \imath \end{pmatrix}(|\beta'\rangle - |\beta'\rangle) \ ,$$

and analogously for the level $|1\rangle$ [9]*.*
b. With,

$$\begin{aligned} |\psi\rangle &= \tfrac{1}{2}\begin{pmatrix} 1 \\ \imath \end{pmatrix}|\beta\rangle + \tfrac{1}{2}\begin{pmatrix} 1 \\ -\imath \end{pmatrix}|-\beta\rangle \\ &= \tfrac{1}{2}|1,\beta\rangle + \tfrac{\imath}{2}|2,\beta\rangle + \tfrac{1}{2}|1,-\beta\rangle - \tfrac{\imath}{2}|2,-\beta\rangle \end{aligned}$$

[9] The detection of quantum correlations is much more complicated than their creation: In principle, it is sufficient to detect the quantum interference fringes appearing in the Wigner distribution via phase-sensitive homodyne detection [1164, 1352]. But in a Schrödinger cat state the number of fringes corresponds to the number of photons in the mode. If the number of photons is too large, the interference fringes are too thin to be resolved. In addition, scattering can wear out the fringes, such that large cats are much more sensitive to dissipation. Since the dissipation corresponds to photon annihilation, the cat is jumping between odd and even cat states.

we get for the photon numbers when the atom is in state $|1\rangle$*,*

$$\begin{aligned}\langle\psi|1\rangle\langle 1|\hat{a}^\dagger\hat{a}|1\rangle\langle 1|\psi\rangle &= \tfrac{1}{4}(\langle\beta| + \langle -\beta|)\hat{a}^\dagger\hat{a}(|\beta\rangle + |-\beta\rangle)\\ &= \tfrac{1}{4}|\beta|^2(\langle\beta| - \langle -\beta|)(\beta\rangle - |-\beta\rangle)\\ &= \tfrac{1}{4}|\beta|^2\left(2 - e^{-|\beta|^2/2-|-\beta|^2/2-\beta^*\beta} - e^{-|-\beta|^2/2-|-\beta|^2/2-\beta^*\beta}\right)\\ &= \tfrac{1}{2}|\beta|^2(1 - e^{-2|\beta|^2}) \simeq \tfrac{1}{2}|\beta|^2\end{aligned}$$

for $|\beta| \gg 1$*, and when the atom is in state* $|2\rangle$*,*

$$\begin{aligned}\langle\psi|2\rangle\langle 2|\hat{a}^\dagger\hat{a}|2\rangle\langle 2|\psi\rangle &= \tfrac{1}{4}(-\langle\beta|\imath + \langle -\beta|\imath)\hat{a}^\dagger\hat{a}(\imath|\beta\rangle - \imath|-\beta\rangle)\\ &= \tfrac{\imath^2}{4}|\beta|^2(-\langle\beta| - \langle -\beta|)(|\beta\rangle + |-\beta\rangle)\\ &= \tfrac{1}{4}|\beta|^2\left(2 + e^{-|\beta|^2/2-|-\beta|^2/2-\beta^*\beta} + e^{-|-\beta|^2/2-|-\beta|^2/2-\beta^*\beta}\right)\\ &= \tfrac{1}{2}|\beta|^2(1 + e^{-2|\beta|^2}) \simeq \tfrac{1}{2}|\beta|^2\ ,\end{aligned}$$

so that the total photon number is,

$$\langle\psi|\hat{a}^\dagger\hat{a}|\psi\rangle = \langle\psi|1\rangle\langle 1|\hat{a}^\dagger\hat{a}|1\rangle\langle 1|\psi\rangle + \langle\psi|2\rangle\langle 2|\hat{a}^\dagger\hat{a}|2\rangle\langle 2|\psi\rangle = |\beta|^2\ .$$

The system realizes a fully quantized model of a beam splitter and a Mach-Zehnder interferometer *with the difference, the two interferometer arms are not spatially separated. The fact that they are entangled is not different from a classical beam spitter (see Sec. 35.8.2). When the dispersive optical pulse realizes a* π *phase shift between the arms, we observe constructive interference in one arm and destructive in the other. In the same time we know that the cat states* $|\psi\rangle \pm |-\psi\rangle$ *are not empty of photons, but have probability distributions of even/odd photon numbers.*

35.4.5.7 Ex: Master equation derived from JC model Hamiltonian for two-level systems

Write down the Liouvillean for a JC system in matrix form for a density operator defined like,

$$\begin{pmatrix}\cdots & \rho_{11}^{n-1} & \rho_{22}^{n} & \rho_{12}^{n} & \rho_{21}^{n} & \rho_{11}^{n} & \rho_{22}^{n+1} & \cdots\end{pmatrix}\ .$$

Solution: *See [1440, 264, 339],*

$$\begin{pmatrix}
\ddots & & & & & & & \\
 & 0 & \Gamma & & & & & \\
 & 0 & -\Gamma & -\frac{\imath}{2}\sqrt{n}\Omega & \frac{\imath}{2}\sqrt{n}\Omega & 0 & & \\
 & & -\frac{\imath}{2}\sqrt{n}\Omega & -\Lambda & 0 & \frac{\imath}{2}\sqrt{n}\Omega & & \\
 & & \frac{\imath}{2}\sqrt{n}\Omega & 0 & -\Lambda^* & -\frac{\imath}{2}\sqrt{n}\Omega & & \\
 & & 0 & \frac{\imath}{2}\sqrt{n}\Omega & -\frac{\imath}{2}\sqrt{n}\Omega & 0 & \Gamma & \\
 & & & & & 0 & -\Gamma & \\
 & & & & & & & \ddots
\end{pmatrix}\ .$$

35.4.5.8 Ex: Laguerre polynomials

Calculate the Wigner function for the field generated by a Jaynes-Cummings dynamics in the photon picture.

Solution: *First we find the series expressions for the Laguerre polynomials* $L_n^{(\alpha)}(x)$ *and* $L_n^{(-\alpha)}(x)$*. According to Wikipedia,*

$$L_n^{(\alpha)}(x) = \sum_{m=0}^{n} \binom{n+\alpha}{n-m} \frac{(-x)^m}{m!} \qquad \text{and} \qquad \frac{(-x)^m}{m!} L_n^{(m-n)}(x) = \frac{(-x)^n}{n!} L_m^{(n-m)}(x) \ .$$

With this,

$$\begin{aligned} L_n^{(-\alpha)}(x) &= \frac{(n-\alpha)!}{n!}(-x)^\alpha L_{n-\alpha}^{(\alpha)}(x) \\ &= \frac{(n-\alpha)!}{n!}(-x)^\alpha \sum_{m=0}^{n-\alpha} \binom{n}{n-\alpha-m} \frac{(-x)^m}{m!} = \sum_{m=0}^{n-\alpha} \binom{n-\alpha}{m} \frac{(-x)^{m+\alpha}}{(m+\alpha)!} \ . \end{aligned}$$

Now, the normally ordered characteristic function is,

$$\begin{aligned} \chi_N(\lambda) = &\sum_{m,n} c_{1,m}^* c_{1,n} \sqrt{\frac{n!}{m!}} \left[\lambda^{m-n}\Theta_{m\geq n} + (-\lambda^*)^{m-n}\Theta_{m<n}\right] L_N^{m-n}(|\lambda|^2) \\ &+ \sum_{m-1,n-1} c_{2,m-1}^* c_{2,n-1} \sqrt{\frac{(n-1)!}{(m-1)!}} \left[\lambda^{m-n}\Theta_{m\geq n} + (-\lambda^*)^{m-n}\Theta_{m<n}\right] L_{n-1}^{m-n}(|\lambda|^2) \\ &+ \sum_{m,n-1} c_{1,m}^* c_{2,n-1} \sqrt{\frac{(n-1)!}{m!}} \left[\lambda^{m-n+1}\Theta_{m\geq n} + (-\lambda^*)^{m-n+1}\Theta_{m<n})\right] L_{n-1}^{m-n+1}(|\lambda|^2) \\ &+ \sum_{m-1,n} c_{2,m-1}^* c_{1,n} \sqrt{\frac{n!}{(m-1)!}} \left[\lambda^{m-1-n}\Theta_{m\geq n} + (-\lambda^*)^{m-1-n}\Theta_{m<n}\right] L_N^{m-1-n}(|\lambda|^2) \ . \end{aligned}$$

This yields after rearrangement,

$$\chi_N(\lambda) = \sum_{m,n} \sqrt{\frac{n!}{m!}} \left[\begin{array}{l} (c_{1,m}^* c_{1,n} + c_{2,m}^* c_{2,n})(\lambda^{m-n}\Theta_{m\geq n} + (-\lambda^*)^{m-n}\Theta_{n<m}) \\ +\lambda^{m-n}\left(c_{1,m}^* c_{2,n}\Theta_{m\geq n+1} + c_{2,m}^* c_{1,n}\Theta_{m\geq n-1}\right) \\ +(-\lambda^*)^{m-n}(c_{1,m}^* c_{2,n}\Theta_{m<n+1} + c_{2,m}^* c_{1,n}\Theta_{m<n-1}) \end{array} \right] L_N^{m-n}(|\lambda|^2) \ .$$

From here we get the Wigner function by numerical FFT according to Eq. (35.158).

35.5 Correlation functions

In the preceding sections and in Sec. 35.2 we have learned, how to characterize quantum fields by (quasi-)probability distribution functions, and how to represent correlations in the Fock or the Glauber basis. But we did not propose experimental schemes

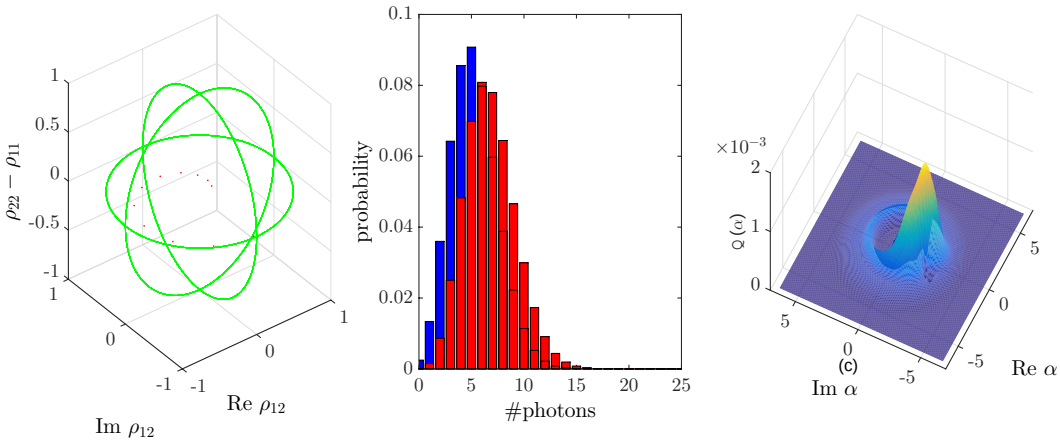

Figure 35.12: (code) Bloch vector, photon number distribution, and Wigner function for JC-coupling in the Fock state representation.

allowing to detect them. Experimental devices, such as interferometers or photon correlators, necessarily involve space or time coordinates. Hence, we need to devise quantities for the characterization of correlations, that are compatible with experimental devices. The *correlation functions* are such quantities, and in the next section we will focus our attention them.

In order to be able to distinguish classical from genuinely quantum correlations, we will first a classical description, before introducing a quantum description of the light field [816].

35.5.1 Classical first and second order coherence

The coherence properties of a light field (or a matter wave) are measured by n^{th} space time order correlation functions. In quantum mechanics, these are defined by,

$$g^{(n)}(\mathbf{r}_1,t_1,..,\mathbf{r}_{2n},t_{2n}) \equiv \frac{\langle \hat{\mathcal{E}}^-(\mathbf{r}_1,t_1)..\hat{\mathcal{E}}^-(\mathbf{r}_n,t_n)\hat{\mathcal{E}}^+(\mathbf{r}_{n+1},t_{n+1})..\hat{\mathcal{E}}^+(\mathbf{r}_{2n},t_{2n})\rangle}{\sqrt{\langle \hat{\mathcal{E}}^-(\mathbf{r}_1,t_1)\hat{\mathcal{E}}^+(\mathbf{r}_1,t_1)\rangle..\langle \hat{\mathcal{E}}^-(\mathbf{r}_{2n},t_{2n})\hat{\mathcal{E}}^+(\mathbf{r}_{2n},t_{2n})\rangle}} \,. \tag{35.171}$$

In the following, we will only consider temporal coherences, e.g. one or more collinear light beams, $\mathbf{k}_m \parallel \mathbf{k}_n$, impinging on a photodetector, $(t_m - \frac{z_m}{c}) - (t_n - \frac{z_n}{c}) = \tau$, since $\hat{\mathcal{E}}(\mathbf{r},t) = \hat{\mathcal{E}}(\omega t - \mathbf{k}\cdot\mathbf{r})$, we can define the the 1^{st} and 2^{nd} order correlation functions $g^{(1)}$ and $g^{(2)}$, which are particularly important,

$$\boxed{g^{(1)}(\tau) \equiv \frac{\langle \hat{\mathcal{E}}^-(t)\hat{\mathcal{E}}^+(t+\tau)\rangle}{\langle \hat{\mathcal{E}}^-(t)\hat{\mathcal{E}}^+(t)\rangle} \quad \text{and} \quad g^{(2)}(\tau) \equiv \frac{\langle \hat{\mathcal{E}}^-(t)\hat{\mathcal{E}}^-(t+\tau)\hat{\mathcal{E}}^+(t+\tau)\hat{\mathcal{E}}^+(t)\rangle}{\langle \hat{\mathcal{E}}^-(t)\hat{\mathcal{E}}^+(t)\rangle^2}} \,. \tag{35.172}$$

Ignoring the quantized nature of light, we may substitute the field operators by complex numbers, $\hat{\mathcal{E}}^+ \to \mathcal{E}$ and $\hat{\mathcal{E}}^- \to \mathcal{E}^*$ and interprete the brackets as pure time

averages,

$$\langle \cdots \rangle_t = \lim_{t\to\infty} \frac{1}{t} \int_0^t \cdots dt' \ . \tag{35.173}$$

Defining the intensity as $I = 2\varepsilon_0 c \mathcal{E}^* \mathcal{E}$, the coherences become,

$$g^{(1)}(\tau) \equiv \tfrac{2\varepsilon_0 c}{I} \langle \mathcal{E}^*(t)\mathcal{E}(t+\tau)\rangle \qquad \text{and} \qquad g^{(2)}(\tau) \equiv \left(\tfrac{2\varepsilon_0 c}{I}\right)^2 \langle I(t)I(t+\tau)\rangle \ . \tag{35.174}$$

The correlation functions must be calculated from the field operators simultaneously respecting *time order* and *normal order*. These functions are useful quantities to describe phenomena such as photon *bunching* or to understand the fluorescence spectra or the scattering of light from correlated atoms. $g^{(1)}$ measures the *coherence* of a light field (how much it resembles a sine wave). $g^{(2)}$ measures, for a given degree of coherence, the deviation of the light field from the quantum state that most closely approximates a classical light (how much it resembles a laser).

The correlation functions $g^{(1)}$ and $g^{(2)}$ are experimentally measured in *Young's experiment* and in the *Hanbury-Brown-Twiss experiment*. The experimental schemes are explained in Figs. 35.13.

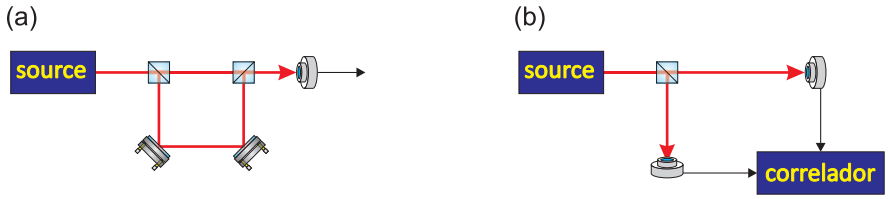

Figure 35.13: (a) Scheme of Young's experiment. (b) Scheme of the experiment of Hanbury, Brown, and Twiss. Young's experiment reveals the coherence of a field, that is, its ability to interfere. In contrast, the Hanbury-Brown-Twist experiment reveals correlations between the (quasi-)particles constituting the field, that is, effects due to quantum statistics or interactions.

Coherence and chaos are contrary properties of light. They leave their imprint in the spectrum of the light or in the autocorrelation functions. The emission spectrum of a light source generally emerges as a combination of various physical effects: The active medium gives rise resonances and broadenings, a resonator containing the active medium imprints a modal structure, and the coupling to a thermal bath gives rise to a thermal distribution of the radiation energy according to $P_n = e^{-\hbar\omega(n+1/2)/k_B T} / \sum_n e^{-\hbar\omega(n+1/2)/k_B T}$.

35.5.2 The Wiener-Khintchine theorem

When the time dependence of a wave is given by $\mathcal{E}(t)$, we call

$$R_{\mathcal{E}}(\tau) = \langle \mathcal{E}^*(t)\mathcal{E}(t+\tau)\rangle_t \tag{35.175}$$

the autocorrelation function and the power density

$$S_{\mathcal{E}}(\omega) = (\mathcal{F}R_{\mathcal{E}})(\omega) = |(\mathcal{F}\mathcal{E})(\omega)|^2 \tag{35.176}$$

the *spectrum*. This relation is called the *Wiener-Khintchine theorem*. We may also consider the normalized quantities, dividing (35.175) and (35.176) by $R_{\mathcal{E}}(0) = \langle \hat{\mathcal{E}}^*(t)\hat{\mathcal{E}}(t)\rangle_t = \int_{-\infty}^{\infty} |(\mathcal{F}\mathcal{E})(\omega)|^2 d\omega = \int_{-\infty}^{\infty} S_{\mathcal{E}}(\omega)d\omega$. We obtain,

$$g^{(1)}(\tau) = \frac{R_{\mathcal{E}}(\tau)}{R_{\mathcal{E}}(0)} \ , \tag{35.177}$$

and,

$$\boxed{F_{\mathcal{E}}(\omega) \equiv (\mathcal{F}g^{(1)})(\omega) = \frac{S_{\mathcal{E}}(\omega)}{R_{\mathcal{E}}(0)} = \frac{1}{2\pi}\int_{-\infty}^{\infty} g^{(1)}(\tau)e^{\imath\omega\tau}d\tau} \ . \tag{35.178}$$

The quantity $F_{\mathcal{E}}(\omega)$ is called line profile or *spectrum*. Note that, since,

$$g^{(1)}(-\tau) = g^{(1)}(\tau)^* \ , \tag{35.179}$$

we may also write,

$$F_{\mathcal{E}}(\omega) = \mathfrak{Re}\ \frac{1}{\pi}\int_0^{\infty} g^{(1)}(\tau)e^{\imath\omega\tau}d\tau \ . \tag{35.180}$$

35.5.3 Coherent and chaotic light

The temporal and spectral properties of a light field are largely determined by the processes leading to its generation in the light source, that is, whether the light is generated by stimulated or spontaneous emission, by a laser or by blackbody radiation, by a single atom or by atomic gases subject to collisional and Doppler-broadening.

35.5.3.1 Correlation functions for laser light

First-order coherent light satisfies $|g^{(1)}(\tau)| = 1$, incoherent light $|g^{(1)}(\tau)| = 0$, and for partially coherent light, we get intermediate values. Second-order coherent light satisfies $g^{(2)}(-\tau) = g^{(2)}(\tau)$ and $1 \leq g^{(2)}(0) \leq \infty$ and $0 \leq g^{(2)}(\tau) \leq \infty$ and $g^{(2)}(0) \geq g^{(2)}(\tau) \overset{\tau \gg \tau_c}{\to} 1$. Let us now look at some specific cases, for which the correlation functions and spectra can be calculated.

With the definitions (35.172) it is easy to calculate the autocorrelation functions and the spectrum of a *laser* light field,

laser

$$\boxed{\begin{aligned} \mathcal{E}(t) &= e^{\imath\omega_0 t} \\ \Longrightarrow \quad g^{(1)}(\tau) &= \frac{t^{-1}\int e^{-\imath\omega_0\tau}dt}{t^{-1}\int dt} = e^{-\imath\omega_0\tau} \\ \Longrightarrow \quad \mathcal{F}\left[g^{(1)}(\tau)\right] &= \frac{1}{2\pi}\int_{-\infty}^{\infty} e^{\imath(\omega-\omega_0)\tau}d\tau = \delta(\Delta) \\ g^{(2)}(\tau) &= 1 \end{aligned}} \ . \tag{35.181}$$

We see that the absolute values of the first and second-order coherences are constant, and that the spectrum is narrow like a δ-function.

35.5.3.2 Correlation functions for laser light subject to white noise

For a laser subject to *white phase noise* (ζ be a normally distributed random number) we have (see also Sec. 56.3.2),

noisy laser

$$\begin{aligned} \mathcal{E}(t) &= e^{\imath[\omega_0 t+\zeta(t)]} \\ \Longrightarrow \quad g^{(1)}(\tau) &= \frac{\int e^{-\imath[\omega_0\tau+\zeta(t+\tau)-\zeta(t)]}dt}{\int dt} = e^{\imath\omega_0\tau-\gamma|\tau|} \\ \Longrightarrow \quad \mathcal{F}[g^{(1)}(\tau)] &= \frac{\gamma/\pi}{\Delta^2+\gamma^2} \\ g^{(2)}(\tau) &= 1 \end{aligned} \quad . \tag{35.182}$$

We see, that the first-order coherence decays exponentially, $|g^{(1)}(\tau)| = e^{-\gamma|\tau|}$ [10], such that the spectrum has a *Lorentzian profile*. This result has already been derived in Eq. (34.28) for the natural linewidth of a transition subject to spontaneous emission. We understand the connection by interpreting spontaneous emission as being induced by *vacuum fluctuations, which do have a white noise spectrum*, indeed.

Example 212 (*Laser broadening due to spontaneous emission*): Laser light is generated by stimulated emission on a transition between two quantized levels. The alternance of absorption and stimulated emission induces coherent Rabi oscillations ensuring the coherence of the emitted light. But we have seen earlier that spontaneous emission leads to randomly occurring interruptions of the coherent Rabi oscillations. The probability of finding a coherent interval decreases exponentially with the evolution time,

$$p(\tau)d\tau = \gamma e^{-\gamma\tau}d\tau \ ,$$

where γ is the spontaneous decay rate of the dipole moment. From $\mathcal{E}(t) = e^{\imath\omega_0 t+\imath\zeta(t)}$ we calculate,

$$\begin{aligned} R_{\mathcal{E}}(\tau) &= \langle e^{\imath\omega_0 t+\imath\zeta(t)}e^{-\imath\omega_0(t+\tau)-\imath\zeta(t+\tau)}\rangle = e^{-\imath\omega_0\tau}\lim_{t\to\infty}\frac{1}{t}\int_0^t e^{\imath[\zeta(t)-\zeta(t+\tau)]}dt \\ &= e^{-\imath\omega_0\tau}\int_\tau^\infty p(\tau')d\tau' = e^{-\imath\omega_0\tau}e^{-\gamma|\tau|} \ , \end{aligned}$$

and,

$$F_{\mathcal{E}}(\omega) = \frac{1}{2\pi}\int_{-\infty}^{\infty}\frac{R_{\mathcal{E}}(\tau)}{R_{\mathcal{E}}(0)}e^{\imath\omega\tau}d\tau = \frac{1}{2\pi}\int_{-\infty}^{\infty}e^{-\imath\omega_0\tau}e^{-\gamma|\tau|}e^{\imath(\omega-\omega_0)\tau}d\tau = \frac{\gamma/\pi}{\Delta^2+\gamma^2} \ .$$

An alternative derivation from Bloch or rate equations is shown in Excs. 35.6.4.3 and 35.6.4.4.

[10] Note that, in order to satisfy (35.179), we must take the absolute value of the delay $|\tau|$.

35.5.3.3 Correlation functions with pressure broadening

In Sec. 34.6.2 we have already seen, that collision or *pressure broadening* can be treated by assuming that the light is emitted as a superposition of coherent waves all having the same frequency, but being randomly interrupted by phase jumps,

$$\mathcal{E}(t) = \sum_n \mathcal{E}_n(t) \qquad \text{with} \qquad \mathcal{E}_n(t) = e^{\imath\omega_0 t + \imath\phi_n(t)} \; . \tag{35.183}$$

The autocorrelation function is then,

$$\begin{aligned} \langle \mathcal{E}^*(t)\mathcal{E}(t+\tau)\rangle &= \frac{1}{t}\int \sum_n e^{-\imath\omega_0 t - \imath\phi_n(t)} \sum_m e^{\imath\omega_0 t + \imath\omega_0\tau + \imath\phi_m(t+\tau)} dt \\ &= e^{\imath\omega_0\tau} \sum_{n,m} \frac{1}{t}\int e^{\imath\phi_m(t+\tau) - \imath\phi_n(t)} dt = N\langle \mathcal{E}_n^*(t)\mathcal{E}_m(t+\tau)\rangle \delta_{nm} \; . \end{aligned} \tag{35.184}$$

The crossed terms $n \neq m$ of this expressions vanish. The pressure broadening is homogeneous, but the fact that the wavepackets are scattered by different atoms results in a modified first-order coherence,

$$\langle \mathcal{E}_n^*(t)\mathcal{E}_n(t+\tau)\rangle = e^{\imath\omega_0\tau} \sum_n \int e^{\imath\phi_n(t+\tau) - \imath\phi_n(t)} dt = e^{\imath\omega_0\tau} \int_\tau^\infty p(\tau) d\tau \; . \tag{35.185}$$

The probability density of finding a coherent interval of duration τ is $p(\tau)d\tau = \gamma_c e^{-\gamma_c\tau} d\tau$, which finally gives,

$$\langle \mathcal{E}^*(t)\mathcal{E}(t+\tau)\rangle = N e^{\imath\omega_0\tau - \gamma_c|\tau|} \; . \tag{35.186}$$

The calculation for the 2^{nd} order correlation function (35.174) is analogous,

$$\begin{aligned} &\langle \mathcal{E}^*(t)\mathcal{E}^*(t+\tau)\mathcal{E}(t+\tau)\mathcal{E}(t)\rangle = \sum_{n,m,n',m'} \langle \mathcal{E}_m^*(t)\mathcal{E}_n(t)\mathcal{E}_{m'}^*(t+\tau)\mathcal{E}_{n'}(t+\tau)\rangle \\ &= \sum_n \langle \mathcal{E}_n^*(t)\mathcal{E}_n(t)\mathcal{E}_n^*(t+\tau)\mathcal{E}_n(t+\tau)\rangle \\ &+ \left(\sum_{n\neq m} \langle \mathcal{E}_n^*(t)\mathcal{E}_n(t)\mathcal{E}_m^*(t+\tau)\mathcal{E}_m(t+\tau)\rangle + \langle \mathcal{E}_m^*(t)\mathcal{E}_n(t)\mathcal{E}_n^*(t+\tau)\mathcal{E}_m(t+\tau)\rangle \right) \; , \end{aligned} \tag{35.187}$$

neglecting all terms which do not satisfy either $\mathcal{E}_n^*(t)\mathcal{E}_n(t)$ or $\mathcal{E}_n^*(t)\mathcal{E}_n(t+\tau)$. Now, assuming a large amount of identical atoms,

$$\begin{aligned} &\langle \mathcal{E}^*(t)\mathcal{E}^*(t+\tau)\mathcal{E}(t+\tau)\mathcal{E}(t)\rangle \\ &= N\langle \mathcal{E}_n^*(t)\mathcal{E}_n(t)\mathcal{E}_n^*(t+\tau)\mathcal{E}_n(t+\tau)\rangle + N(N-1)\left(\langle \mathcal{E}_n^*(t)\mathcal{E}_n(t)\rangle^2 + |\langle \mathcal{E}_n(t)\mathcal{E}_n^*(t+\tau)\rangle|^2\right) \\ &\simeq N^2\left(\langle \mathcal{E}_n^*(t)\mathcal{E}_n(t)\rangle^2 + |\langle \mathcal{E}_n(t)\mathcal{E}_n^*(t+\tau)\rangle|^2\right) \; . \end{aligned} \tag{35.188}$$

Finally, exploiting the result (35.184) and the definitions of the 1^{st} and 2^{nd} order correlations functions,

$$g^{(2)}(\tau) = \frac{\langle \mathcal{E}_n^*(t)\mathcal{E}_n(t)\rangle^2 + |\langle \mathcal{E}_n(t)\mathcal{E}_n^*(t+\tau)\rangle|^2}{\langle \mathcal{E}_n^*(t)\mathcal{E}_n(t)\rangle^2} = 1 + |g^{(1)}(\tau)|^2 \; . \tag{35.189}$$

In summary,

pressure broadening

$$\boxed{\begin{aligned} \mathcal{E}(t) &= \textstyle\sum_n e^{\imath\omega_0 t+\imath\phi_n(t)} \\ \implies g^{(1)}(\tau) &= e^{\imath\omega_0\tau-\gamma_c|\tau|} \\ \implies \mathcal{F}\left[g^{(1)}(\tau)\right] &= \frac{\gamma/\pi}{\Delta^2+\gamma_c^2} \\ g^{(2)}(\tau) &= 1+e^{-\gamma_c|\tau|} \end{aligned}} \quad . \tag{35.190}$$

The spectrum is a Lorentzian with the full linewidth $\gamma' = \gamma + \gamma_c$.

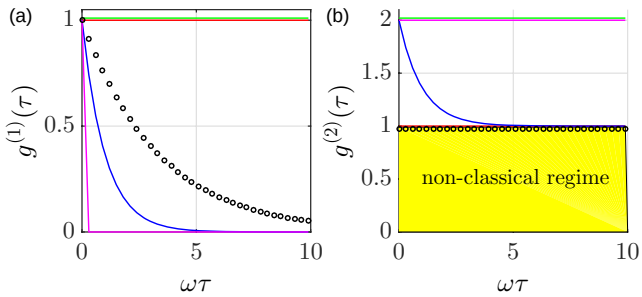

Figure 35.14: (code) First and second-order correlation functions for (red) a laser, (cyan) a laser subject to phase noise, (blue) a laser subject to collision broadening, (magenta) chaotic light, and (green) spectrally filtered thermal light.

35.5.3.4 Correlation functions with thermal broadening

For light emitted by an ensemble of non-colliding atoms in thermal motion, we must allow for different frequencies, $\mathcal{E}_n(t) = e^{\imath\omega_n t+\imath\phi_n}$, but time-independent phases,

$$\begin{aligned} \langle\mathcal{E}^*(t)\mathcal{E}(t+\tau)\rangle &= \int \sum_n e^{-\imath\omega_n t-\imath\phi_n} \sum_m e^{\imath\omega_m t+\imath\omega_m\tau+\imath\phi_m} dt \\ &= \sum_{n,m} \int e^{-\imath\omega_n t-\imath\phi_n+\imath\omega_m t+\imath\omega_m\tau+\imath\phi_m} dt = \sum_n e^{\imath\omega_n\tau} \quad . \end{aligned} \tag{35.191}$$

The crossed terms $n \neq m$ of this expressions vanish. *Doppler broadening* is inhomogeneous. Hence, the probability density for frequencies emitted by thermal atoms is

a Gaussian, $p(\omega)d\omega = (2\pi\delta)^{-1/2}e^{-(\omega_n-\omega_0)^2/2\delta^2}d\omega$, such that,

thermal ensemble

$$\boxed{\begin{aligned} \langle \mathcal{E}^*(t)\mathcal{E}(t+\tau)\rangle &= N(2\pi\delta)^{-1/2}\int e^{\imath\omega_n\tau}e^{-(\omega_n-\omega_0)^2/2\delta^2}d\omega_n \\ \Longrightarrow \quad g^{(1)}(\tau) &= e^{\imath\omega\tau-\delta^2\tau^2/2} \\ \Longrightarrow \quad \mathcal{F}[g^{(1)}(\tau)] &= \sqrt{\frac{\ln 2}{\pi\delta^2}}e^{-\ln 2\cdot\omega^2/\delta^2} \\ g^{(2)}(\tau) &= 1+e^{-\delta^2\tau^2/2} \end{aligned}} \quad . \tag{35.192}$$

For a totally emission *chaotic light*,

chaotic line

$$\boxed{\begin{aligned} g^{(1)}(\tau) &= \delta(0) \\ \mathcal{F}[g^{(1)}(\tau)] &= 1 \\ g^{(2)}(\tau) &= 1+|g^{(1)}(\tau)| \end{aligned}} \quad . \tag{35.193}$$

The last expression is known as *Bloch-Siegert relation*. Mono-mode chaotic light can be seen as incoherent multi-mode light, where all modes except a single mode are filtered by a Fabry-Pérot etalon. This light is characterized by $|g^{(1)}(\tau)| = 1$ and $g^{(2)}(\tau) = 2$, despite the coherence length being $\tau \to \infty$. Do the Excs. 35.5.5.1 to 35.5.5.3.

35.5.4 Photon counting statistics

35.5.4.1 Photon counting with classical fields

There is a nice introduction by [816], p.229. Irradiate a photon counter with efficiency η with a classical light beam of cycle-averaged intensity $I(t)$. The probability density of registering a count is $p(t) = \eta I(t)$. Now consider a time interval $[t, t+T]$. Be $P_m(t,T)$ the probability to encounter m counts. We now separate a time period dt which is too short to yield more than one photon, $[t, t+t'+dt]$. Then the probability of finding m photons in this interval is,

$$P_m(t,t'+dt) = P_m(t,t')[1-p(t)]dt + P_{m-1}(t,t')p(t)dt \ . \tag{35.194}$$

From this one derives a differential equation, whose solution is,

$$P_m(t,T) = \frac{\left(\int_t^{t+T}p(t')dt'\right)^m}{m!}\exp\left(-\int_t^{t+T}p(t')dt'\right) \ . \tag{35.195}$$

Defining $\bar{I}(t,T) \equiv T^{-1}\int_t^{t+T}I(t')dt'$ and averaging over a number of initial start times t,

$$P_m(T) \equiv \langle P_m(t,T)\rangle_t = \left\langle \frac{\left[\eta T\bar{I}(t,T)\right]^m}{m!}\,e^{-\eta T\bar{I}(t,T)}\right\rangle_t \ . \tag{35.196}$$

The probability follows as an approximation to a binomial distribution. One can show that for noise-free light as well as for chaotic light with short coherence length the distribution is Poissonian. For chaotic light with long coherence length it is thermal.

35.5.4.2 Photon counting with quantum fields

Quantum mechanically the probability is obtained by replacing the intensity by an operator and the starting time averaging by a trace over the density operator and the normal-ordered probability P_m [516, 515, 1310, 1154],

$$P_m(T) = \mathrm{Tr}\ \hat{\rho}\mathcal{N}\ \frac{\left[\eta T \hat{I}(T)\right]^m}{m!}\ e^{-\eta T \hat{I}(T)}\ , \tag{35.197}$$

where $\hat{I}(T) \equiv T^{-1}\int_0^T 2\varepsilon_0 c\hat{\mathcal{E}}^-(\mathbf{r},t)\hat{\mathcal{E}}^+(\mathbf{r},t)dt$. The field operators can be expanded, $\hat{\mathcal{E}}^+(\mathbf{r},t) = \imath\hat{\epsilon}\sqrt{\hbar\omega/2\varepsilon_0 V}e^{-\imath\omega t+\imath\mathbf{k}\cdot\mathbf{r}}\hat{b}$, only considering one mode. We obtain,

$$P_m(T) = \mathrm{Tr}\ \hat{\rho}\mathcal{N}\ \frac{(\xi\hat{b}^\dagger\hat{b})^m}{m!}\ e^{-\xi\hat{b}^\dagger\hat{b}}\ . \tag{35.198}$$

where $\xi \equiv \eta c\hbar\omega T/V$ is the quantum efficiency,

$$\begin{aligned} P_m(T) &= \frac{1}{m!}\sum_k \langle k|\,\hat{\rho}\sum_n |n\rangle\langle n|\mathcal{N}\ (\xi\hat{b}^\dagger\hat{b})^m \sum_l \frac{(-\xi\hat{b}^\dagger\hat{b})^l}{l!}|k\rangle \\ &= \sum_{k=m}^{\infty} P_k \sum_{l=0}^{k-m}\frac{\xi^m(-\xi)^l}{m!l!}\langle k|(\hat{b}^\dagger)^{m+l}(\hat{b})^{m+l}\,|k\rangle \\ &= \sum_{k=m}^{\infty} P_k \sum_{l=0}^{k-m}\frac{\xi^m(-\xi)^l}{l!}\frac{k!}{m!(k-m-l)!} \\ &= \sum_{k=m}^{\infty} P_k \binom{k}{m}\xi^m \sum_{l=0}^{k-m}\binom{k-m}{l}(-\xi)^l = \sum_{k=m}^{\infty} P_k\binom{k}{m}\xi^m(1-\xi)^{k-m}\ . \end{aligned} \tag{35.199}$$

Second-order correlation (for a single mode there is no time-dependence),

$$\begin{aligned} \frac{1}{\bar{m}^2}\sum_m m(m-1)P_m(T) &= \frac{1}{(\xi\bar{n})^2}\sum_m m(m-1)\sum_{n=m}^{\infty} P_n\binom{n}{m}\xi^m(1-\xi)^{n-m} \\ &= \frac{1}{\bar{n}^2}\sum_n n(n-1)P_n\sum_{m<n}\binom{n-2}{m-2}\xi^{m-2}(1-\xi)^{n-m} \\ &= \frac{1}{\bar{n}^2}\sum_n n(n-1)P_n = \frac{\langle n(n-1)\rangle}{\langle\bar{n}\rangle^2} \equiv g^{(2)}(\tau)\ . \end{aligned} \tag{35.200}$$

For a photon number state $\rho = |n\rangle\langle n|$ and $P_k = \delta_{nk}$,

$$\begin{aligned} P_m(T) &= \binom{n}{m}\xi^m(1-\xi)^{n-m} \\ g^{(2)}(\tau) &= \frac{1}{\bar{n}^2}\sum_k k(k-1)\delta_{nk} = \frac{1}{n^2}n(n-1) = 1-\frac{1}{n}\ . \end{aligned} \tag{35.201}$$

For a coherent state $\rho = \sum_n \frac{|\alpha|^n e^{-|\alpha|}}{\sqrt{n!}}|n\rangle\langle n|$ and $P_k = \frac{\bar{n}^k}{k!}e^{-\bar{n}}$,

$$P_m(T) = \sum_k \frac{\bar{n}^k}{k!}e^{-\bar{n}}\binom{k}{m}\xi^m(1-\xi)^{k-m} \tag{35.202}$$
$$= \frac{(\xi\bar{n})^m}{m!}e^{-\bar{n}}\sum_{k'=0}^{\infty}\frac{\bar{n}^{k'}(1-\xi)^{k'}}{k'!} = \frac{(\xi\bar{n})^m}{m!}e^{-\xi\bar{n}}$$
$$g^{(2)}(\tau)\frac{1}{\bar{n}^2}\sum_k k(k-1)\frac{\bar{n}^k}{k!}e^{-\bar{n}} = \sum_{k'}\frac{\bar{n}^{k'}}{k'!}e^{-\bar{n}} = 1 \ .$$

Similarly we get for a thermal state,

$$P_m(T) = \frac{(\xi\bar{n})^m}{(1+\xi\bar{n})^{1+m}}g^{(2)}(\tau) = \frac{1}{\bar{n}^2}\sum_k k(k-1)\frac{\bar{n}^k}{(1+\bar{n})^k} \tag{35.203}$$
$$= \frac{1}{(1+\bar{n})^2}\sum_{k'}(k+2)(k+1)\frac{\bar{n}^{k'}}{(1+\bar{n})^{k'}}$$
$$= \frac{1}{(1+\bar{n})^2}\frac{2}{\left[1-\bar{n}/(1+\bar{n})\right]^3} = 2(1+\bar{n}) \ .$$

35.5.4.3 Quantum correlations

Defining the intensity as $\hat{I} = 2\varepsilon_0 c\hat{\mathcal{E}}^+\hat{\mathcal{E}}^-$, the coherences become,

$$g^{(1)}(\tau) \equiv \tfrac{2\varepsilon_0 c}{I}\langle\mathcal{TN}\hat{\mathcal{E}}^-(t)\hat{\mathcal{E}}^+(t+\tau)\rangle \qquad \text{and} \qquad g^{(2)}(\tau) \equiv \left(\tfrac{2\varepsilon_0 c}{I}\right)^2\langle\mathcal{TN}\hat{I}(t)\hat{I}(t+\tau)\rangle \ . \tag{35.204}$$

The correlation functions must be calculated from the field operators simultaneously respecting *time order* and *normal order*.

35.5.4.4 Generalization for time-dependent fields and finite detector bandwidth

The measured count rate is then replaced by,

$$\xi\hat{b}^\dagger\hat{b} \to \int_0^T d\tau\int_0^T d\tau'\xi(\tau-\tau')\hat{b}^\dagger(\tau)\hat{b}(\tau') \tag{35.205}$$

with the spectral sensitivity,

$$\xi(\tau-\tau') \equiv \frac{1}{2\pi}\int_{-\infty}^{\infty}\xi(\omega)e^{-\imath\omega(\tau-\tau')}d\omega \ . \tag{35.206}$$

For large detector bandwidth $\xi(\omega) = \xi$, so that we may set $\xi\hat{b}^\dagger\hat{b} \to \xi\int_0^T d\tau\hat{b}^\dagger(\tau)\hat{b}(\tau)$. For this case the probability becomes,

$$P_m(T) = \mathrm{Tr}\ \hat{\rho}\mathcal{TN}\ \frac{1}{m!}\ \hat{B}(T)^m\ e^{-\hat{B}(T)} \ , \tag{35.207}$$

where $\hat{B}(T) \equiv \xi\int_0^T d\tau\hat{b}^\dagger(\tau)\hat{b}(\tau)$.

Carrying out the ordering we get now,

$$P_k(T) = \left\langle \sum_{l=0}^{\infty} \frac{(-\xi)^{k+l}}{k!l!} \mathcal{TN} \int_0^T d\tau_1 \int_0^T d\tau_2 .. \int_0^T d\tau_{k+l}\ \hat{b}^\dagger(\tau_1)\hat{b}(\tau_1)\hat{b}^\dagger(\tau_2)\hat{b}(\tau_2)..\hat{b}^\dagger(\tau_{k+l})\hat{b}(\tau_{k+l}) \right\rangle \tag{35.208}$$

$$= \left\langle \sum_{l=0}^{\infty} \frac{(-\xi)^{k+l}}{k!l!} \int_0^T d\tau_1 \int_0^{\tau_1} d\tau_2 .. \int_0^{\tau_{k+l-1}} d\tau_{k+l}\ \hat{b}^\dagger(\tau_1)\hat{b}^\dagger(\tau_2)..\hat{b}^\dagger(\tau_{k+l})\hat{b}(\tau_{k+l})..\hat{b}(\tau_2)\hat{b}(\tau_1) \right\rangle ,$$

when we assume $d\tau_1 < d\tau_2 < .. < d\tau_{n+l}$.

The expectation value for registering n counts is,

$$\langle n\rangle(T) = \sum_k k P_k(T) \stackrel{?}{=} \langle \mathcal{TN}\ \hat{B}(T)\rangle \tag{35.209}$$

$$= \sum_k \frac{1}{(k-1)!} \left\langle \mathcal{TN}\ \hat{B}(T)^k\ e^{-\hat{B}(T)} \right\rangle = \xi \int_0^T d\tau \left\langle \hat{b}^\dagger(\tau)\hat{b}(\tau) \right\rangle .$$

The variance is often described by Mandel's Q-function,

$$Q(T) \equiv \frac{\langle \Delta n^2\rangle(T) - \langle n\rangle(T)}{\langle n\rangle(T)} = \frac{\langle n(n-1)\rangle(T) - \langle n\rangle^2(T)}{\langle n\rangle(T)} . \tag{35.210}$$

We have,

$$\langle n(n-1)\rangle(T) = \sum_k k(k-1) P_k(T) \stackrel{?}{=} \langle \mathcal{TN}\ \hat{A}^2(T)\rangle \tag{35.211}$$

$$\stackrel{?}{=} \eta^2 \int_0^T d\tau \int_0^T d\tau' \left\langle \mathcal{TN} \hat{b}^\dagger(\tau)\hat{b}^\dagger(\tau')\hat{b}(\tau')\hat{b}(\tau) \right\rangle . \tag{35.212}$$

The conditional probability to detect a photon at time $t = \tau$ after a successful detection at time $t = 0$ is,

$$g^{(2)}(\tau) \equiv \frac{\left\langle \mathcal{TN} \hat{b}^\dagger(\tau)\hat{b}^\dagger(\tau')\hat{b}(\tau')\hat{b}(\tau) \right\rangle}{\left\langle \hat{b}^\dagger(\tau)\hat{b}(\tau) \right\rangle^2} , \tag{35.213}$$

hence,

$$Q(T) = \langle n\rangle(T) \left(\frac{\int_t^{t+T} d\tau \int_t^{t+T} d\tau' S^2(\tau - \tau')\, \langle \mathcal{TN} \mathcal{E}^-(\tau)\mathcal{E}^-(\tau')\mathcal{E}^+(\tau')\mathcal{E}^+(\tau)\rangle}{\left(S \int_t^{t+T} d\tau \langle \mathcal{E}^-(\tau)\mathcal{E}^+(\tau)\rangle \right)^2} - 1 \right)$$

$$= 2\frac{\langle n\rangle(T)}{T^2} \int_0^T d\tau (T-\tau)[g^{(2)}(\tau) - 1] . \tag{35.214}$$

I.e. we can follow the evolution of the photon number variance as time goes on [1310, 1232, 1266].

35.5.4.5 Waiting time distributions

The conditional probability $\tilde{P}(\tau)$ that after a detection at time 0 any other photon (not necessarily the next one) is detected at time τ is the sum of the probabilities to detect the first, the second, etc. photon,

$$\tilde{P}(\tau) = \sum_k P^{(k)}(\tau) \ . \tag{35.215}$$

Now $P^{(2)}(\tau) = \int_0^\tau P^{(1)}(t)P^{(1)}(\tau - t)dt$, so that

$$g^{(2)}(\tau) \propto \tilde{P}(\tau) \ . \tag{35.216}$$

35.5.5 Exercises

35.5.5.1 Ex: Correlation functions for two light modes

a. Calculate $|g^{(1)}(\tau)|$, $F_{\mathcal{E}}(\omega)$, and $|g^{(2)}(\tau)|$ for two interfering and non-interfering modes neglecting fluctuations.
b. What changes when one mode is broadened by random noise, e.g. induced by spontaneous emission?

Solution: *a. We denote the modes by $\mathcal{E}(t) = e^{\imath\omega_1 t} + e^{\imath\omega_2 t}$, and calculate subsequently the autocorrelation function,*

$$R_{\mathcal{E}}(\tau) = e^{-\imath\omega_1\tau} + e^{-\imath\omega_2\tau} \ ,$$

the $g^{(1)}$-function,

$$g^{(1)}(\tau) = \frac{R_{\mathcal{E}}(\tau)}{R_{\mathcal{E}}(0)} = \frac{e^{-\imath\omega_1\tau} + e^{-\imath\omega_2\tau}}{2}$$

and its absolute value,

$$|g^{(1)}(\tau)| = \sqrt{\tfrac{e^{-\imath\omega_1\tau}+e^{-\imath\omega_2\tau}}{2}\,\tfrac{e^{\imath\omega_1\tau}+e^{\imath\omega_2\tau}}{2}} = \sqrt{\tfrac{1}{2} + \tfrac{1}{2}\cos(\omega_1 - \omega_2)\tau} = \cos\tfrac{(\omega_1-\omega_2)\tau}{2} \ ,$$

and the spectrum,

$$F_{\mathcal{E}}(\omega) = \frac{1}{2\pi}\int_{-\infty}^{\infty} g^{(1)}(\tau)e^{\imath\omega\tau}d\tau = \frac{1}{4\pi}\int_{-\infty}^{\infty}(e^{-\imath\omega_1\tau}+e^{-\imath\omega_2\tau})e^{\imath\omega\tau}d\tau = \tfrac{1}{2}[\delta(\Delta_1)+\delta(\Delta_2)] \ .$$

Hence, while two non-interfering modes without fluctuations satisfy $|g^{(1)}(\tau)| = 1$, two interfering modes without fluctuations satisfy $|g^{(1)}(\tau)| = \cos\frac{1}{2}(\omega_1 - \omega_2)\tau$. The $g^{(2)}$-function is,

$$g^{(2)}(\tau) = \frac{\langle\mathcal{E}^*(t)\mathcal{E}^*(t+\tau)\mathcal{E}(t+\tau)\mathcal{E}(t)\rangle}{\langle\mathcal{E}^*(t)\mathcal{E}(t)\rangle^2} = \frac{\langle\cos^2\frac{(\omega_1-\omega_2)t}{2}\cos^2\frac{(\omega_1-\omega_2)(t+\tau)}{2}\rangle}{\langle\cos^4\frac{(\omega_1-\omega_2)t}{2}\rangle} \ .$$

Using,

$$\lim_{t\to\infty}\tfrac{1}{t}\int_0^t \cos^2 x\cos^2(x+y)dx = \tfrac{1}{4}\cos^2 y + \tfrac{1}{8} \ ,$$

we find,

$$g^{(2)}(\tau) = \tfrac{2}{3} + \tfrac{1}{3}\cos(\omega_1 - \omega_2)\tau \ .$$

b. In analogy to (a) we now consider $\mathcal{E}(t) = e^{\imath\omega_1 t} + e^{\imath\omega_2 t + \zeta(t)}$ *and calculate,*

$$\begin{aligned} R_{\mathcal{E}}(\tau) &= e^{-\imath\omega_1\tau} + e^{-\imath\omega_2\tau}\langle e^{\imath\zeta(t)-\imath\zeta(t+\tau)}\rangle + \cancelto{0}{\langle e^{-\imath\omega_1\tau}e^{\imath(\omega_2-\omega_1)t+\imath\zeta(t)}\rangle} + \cancelto{0}{\langle e^{-\imath\omega_2\tau}e^{\imath(\omega_1-\omega_2)t-\imath\zeta(t+\tau)}\rangle} \\ &= e^{-\imath\omega_1\tau} + e^{-\imath\omega_2\tau}e^{-\gamma\tau} \ , \end{aligned}$$

and

$$g^{(1)}(\tau) = \tfrac{1}{2}e^{-\imath\omega_1\tau} + e^{-\imath\omega_2\tau}e^{-\gamma\tau} \ ,$$

and

$$F_{\mathcal{E}}(\omega) = \delta(\Delta_1) + \frac{\gamma/\pi}{\Delta_2^2 + \gamma^2} \ .$$

35.5.5.2 Ex: Correlation functions and spectra of phase- and amplitude-modulated light

a. Calculate $g^{(1)}(\tau)$, $S_{\mathcal{E}}(\omega)$, and $g^{(2)}(\tau)$ for amplitude-modulated light: $\mathcal{E}_{am}(t) = e^{\imath\omega_0 t}(1 + M\cos\Omega t)$.
b. Calculate $g^{(1)}(\tau)$, $S_{\mathcal{E}}(\omega)$, and $g^{(2)}(\tau)$ for phase-modulated light: $\mathcal{E}_{pm}(t) = e^{\imath\omega_0 t + \imath M\cos\Omega t}$.
c. Repeat the calculation (a) for exponentially decaying amplitude-modulated light: $\mathcal{E}_{dam}(t) = e^{-\gamma t}e^{\imath\omega_0 t}(1 + M\cos\Omega t)$. See also 52.3.3.1.

Solution: *We use the definition of the first-order correlation function,*

$$g^{(1)}(\tau) \equiv \frac{\langle \mathcal{E}^*(t)\mathcal{E}(t+\tau)\rangle}{\langle \mathcal{E}^*(t)\mathcal{E}(t)\rangle} \qquad \textit{where} \qquad \langle ...\rangle \equiv \lim_{t\to\infty}\frac{1}{t}\int_0^t ...dt' \ .$$

a. The electric field of amplitude-modulated light is given by,

$$\mathcal{E}_{am}(t) = e^{\imath\omega_0 t}(1 + M\cos\Omega t) = e^{\imath\omega_0 t}(1 + \tfrac{M}{2}e^{\imath\Omega t} + \tfrac{M}{2}e^{-\imath\Omega t}) \ .$$

From this,

$$\begin{aligned} \langle \mathcal{E}^*_{am}(t)\mathcal{E}_{am}(t+\tau)\rangle &= e^{-\imath\omega_0\tau}\langle [1 + M\cos\Omega t)(1 + M\cos\Omega(t+\tau)]\rangle \\ &= e^{-\imath\omega_0\tau}\langle 1 + M\cos\Omega t + M\cos\Omega(t+\tau) + M^2\cos\Omega\tau\langle\cos^2\Omega t\rangle - M^2\sin\Omega\tau\langle\sin\Omega t\cos\Omega t\rangle \\ &= e^{-\imath\omega_0\tau}\left(1 + \tfrac{1}{2}M^2\cos\Omega\tau\right) \ . \end{aligned}$$

Hence,

$$\boxed{g^{(1)}_{am}(\tau) = e^{-\imath\omega_0\tau}\frac{2 + M^2\cos\Omega\tau}{2 + M^2}} \ . \tag{35.217}$$

The spectrum follows from (35.178),

$$S_{\mathcal{E}}(\omega) = \frac{1}{2\pi}\int_{-\infty}^{\infty} g^{(1)}(\tau)e^{\imath\omega\tau}d\tau \ .$$

Expanding the correlation function (35.217) for amplitude-modulated light in exponentials, using $\int_{-\infty}^{\infty} e^{-\imath\omega\tau}d\tau = \delta(\omega)$*, it is easy to see that,*

$$\boxed{S_{\mathcal{E}}(\omega) = \frac{1}{2\pi}\frac{1}{2+M^2}\left[2\delta(\Delta) + \tfrac{M^2}{2}\delta(\Delta+\Omega) + \tfrac{M^2}{2}\delta(\Delta-\Omega)\right]} \ ,$$

with $\Delta \equiv \omega - \omega_0$*.*
The $g^{(2)}(\tau)$ *function follows easily from its definition,*

$$g^{(2)}(\tau) = \frac{\langle E^*(t)E^*(t+\tau)E(t+\tau)E(t)\rangle}{\langle E^*(t)E(t)\rangle^2} = \frac{\langle (1+M\cos\Omega t)(1+M\cos\Omega(t+\tau))\rangle}{\langle (1+M\cos\Omega t)\rangle^2} \ .$$

Using,

$$\lim_{t\to\infty}\tfrac{1}{t}\int_0^t (1+M\cos x)(1+M\cos(x+y))dx = 1 + \tfrac{M^2}{2}\cos y \ ,$$

we find,

$$g^{(2)}(\tau) = 1 + \tfrac{M^2}{2}\cos\Omega\tau \ .$$

b. The electric field of phase-modulated light is given by,

$$\mathcal{E}_{pm}(t) = e^{\imath\omega t + \imath M\cos\Omega t} = e^{\imath\omega t}\sum_{k=-\infty}^{\infty} J_k(M)e^{\imath k\Omega t} \ .$$

From this,

$$\begin{aligned}\langle \mathcal{E}^-_{pm}(t)\mathcal{E}^+_{pm}(t+\tau)\rangle &= e^{-\imath\omega_0\tau}\langle e^{\imath M\cos\Omega t}e^{-\imath M\cos\Omega(t+\tau)}\rangle \\ &= e^{-\imath\omega_0\tau}\sum_{k,m=-\infty}^{\infty} J_k(M)J_m(-M)e^{\imath m\Omega\tau}\langle e^{\imath(k+m)\Omega t}\rangle = e^{-\imath\omega_0\tau}\sum_{k=-\infty}^{\infty} J_k(M)^2 e^{-\imath k\Omega\tau} \ ,\end{aligned}$$

with $\langle e^{\imath(k+m)\Omega t}\rangle = \delta_{k,-m}$ *and* $J_{-k}(M) = J_k(-M) = (-1)^k J_k(M)$*. Hence, using,*

$$\sum_{k=-\infty}^{\infty} J_k(x) = \sum_{k=-\infty}^{\infty} J_k(x)^2 = 1 \neq \sum_{k=-\infty}^{\infty} |J_k(x)|^2 \ ,$$

we find,

$$\boxed{g^{(1)}_{pm}(\tau) = e^{-\imath\omega_0\tau}\frac{\sum_{k=-\infty}^{\infty} J_k(M)^2 e^{-\imath k\Omega\tau}}{\sum_{k=-\infty}^{\infty} J_k(M)^2}} \ .$$

The spectrum is, in this case,

$$\boxed{S_{\mathcal{E}}(\omega) = \frac{1}{2\pi}\frac{1}{\sum_{k=-\infty}^{\infty} J_k(M)^2}\sum_{k=-\infty}^{\infty} J_k(M)^2\delta(\Delta+k\Omega)} \ .$$

The $g^{(2)}(\tau)$ *function is trivially calculated from its definition,*

$$g^{(2)}(\tau) = \frac{\langle \mathcal{E}^*(t)\mathcal{E}^*(t+\tau)\mathcal{E}(t+\tau)\mathcal{E}(t)\rangle}{\langle \mathcal{E}^*(t)\mathcal{E}(t)\rangle^2} = 1 \ .$$

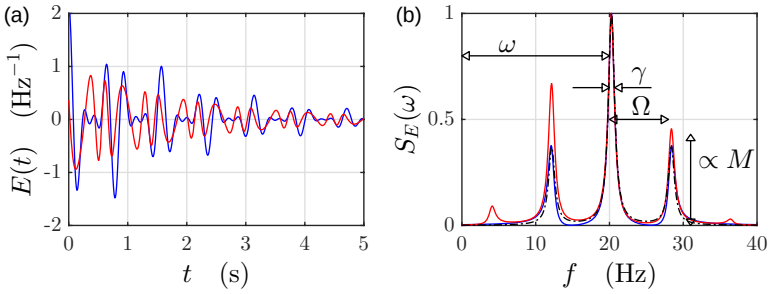

Figure 35.15: (code) (a) AM (blue) and PM-modulated field (red). (b) Numerically calculated pectra for AM (blue) and PM-modulated light (red). Analytically calculated spectrum (black).

c. The electric field of exponentially decaying amplitude-modulated light is given by,

$$\mathcal{E}_{dam}(t) = e^{-\gamma t} e^{\imath\omega_0 t}(1 + M\cos\Omega t) \ .$$

From this,

$$\begin{aligned}
&\langle \mathcal{E}^-_{dam}(t)\mathcal{E}^+_{dam}(t+\tau)\rangle \\
&= e^{-\imath\omega_0\tau-\gamma\tau} \lim_{t\to\infty} \frac{1}{t}\int_0^t e^{-2\gamma t}\left[1 + M\cos\Omega t + M\cos\Omega(t+\tau) + M\cos(\Omega t)M\cos(\Omega(t+\tau))\right] dt \\
&= e^{-\imath\omega_0\tau-\gamma\tau} \lim_{t\to\infty} \frac{1}{t}\int_0^t e^{-2\gamma t} M\cos(\Omega t)M\cos(\Omega(t+\tau))dt \\
&= e^{-\imath\omega_0\tau-\gamma\tau} \lim_{t\to\infty} \left[\begin{array}{l}
\frac{1-e^{-2\gamma t}}{2\gamma t} + \frac{M}{t}\frac{2\gamma - 2\gamma e^{-2\gamma t}\cos\Omega t + \Omega e^{-2\gamma t}\sin\Omega t}{4\gamma^2+\Omega^2} \\
+\frac{M}{t}\frac{2\gamma\cos\Omega\tau - \Omega\sin\Omega\tau - 2\gamma e^{-2\gamma t}\cos\Omega(t+\tau) + \Omega e^{-2\gamma t}\sin\Omega(t+\tau)}{4\gamma^2+\Omega^2} \\
-\frac{M^2}{4\gamma t}\frac{\left(-2\gamma^2-\Omega^2+\gamma^2 e^{-2\gamma t}+\Omega^2 e^{-2\gamma t}\right)\cos\Omega\tau + \gamma\Omega\sin\Omega\tau + e^{-2\gamma t}\gamma^2\cos\Omega(2t+\tau) - e^{-2\gamma t}\gamma\Omega\sin\Omega(2t+\tau)}{\gamma^2+\Omega^2}
\end{array}\right]
\end{aligned}$$

Hence,

$$\begin{aligned}
g^{(1)}_{dam}(\tau) &= e^{-\imath\omega_0\tau-\gamma\tau}\frac{\lim_{t\to\infty}\langle\mathcal{E}^*(t)\mathcal{E}(t+\tau)\rangle}{\lim_{t\to\infty}\langle\mathcal{E}^*(t)\mathcal{E}(t)\rangle} = e^{-\imath\omega_0\tau-\gamma\tau}\frac{\lim_{t\to\infty} t\langle\mathcal{E}^*(t)\mathcal{E}(t+\tau)\rangle}{\lim_{t\to\infty} t\langle\mathcal{E}^*(t)\mathcal{E}(t)\rangle} \\
&= e^{-\imath\omega_0\tau-\gamma\tau}\frac{1 + M\frac{4\gamma^2(1+\cos\Omega\tau) - 2\gamma\Omega\sin\Omega\tau}{4\gamma^2+\Omega^2} + \frac{M^2}{2}\frac{(2\gamma^2+\Omega^2)\cos\Omega\tau + \gamma\Omega\sin\Omega\tau}{\gamma^2+\Omega^2}}{1 + M\frac{8\gamma^2}{4\gamma^2+\Omega^2} + \frac{M^2}{2}\frac{2\gamma^2+\Omega^2}{\gamma^2+\Omega^2}} \ .
\end{aligned}$$

For $\gamma \ll \Omega$ we recover the result (35.217). For $\Omega \ll \gamma$ we get,

$$g^{(1)}_{dam} \overset{\Omega\ll\gamma}{\longrightarrow} e^{-\imath\omega\tau-\gamma\tau}\frac{1 + M + M^2 + M\cos\Omega\tau}{(1+M)^2} \ .$$

The spectrum is, in this case, similar to the amplitude-modulated one, only are the sidebands Lorentz-broadened.

35.5.5.3 Ex: Phase modulation

a. Show that it is not possible to construct a periodic phase modulation function such that the signal has only two sidebands.

b. From $1 = |e^{\imath M \sin \Omega t}|^2$ derive a sum rule for the Bessel functions.
c. Discuss the difference of the spectra $\sum_{k=-\infty}^{\infty} J_k(M) e^{\imath k \Omega t}$ and $\sum_{k=-\infty}^{\infty} |J_k(M)| e^{\imath k \Omega t}$.

Solution: *a. The question is whether there is a periodic function $f(t)$ such that*

$$e^{\imath \omega t + \imath f(t)} = e^{\imath \omega t} + M e^{\imath(\omega+\Omega)t} - M e^{\imath(\omega-\Omega)t}$$

or equivalently $e^{\imath f(t)} = 1 + 2\imath M \sin \Omega t$. Such a function would have to satisfy,

$$1 = |1 + 2\imath M \sin \Omega t|^2 = 1 + 4M^2 \sin^2 \Omega t \ ,$$

which only holds for $M = 0$.
b. In contrast, a sinusoidal phase modulation satisfies,

$$1 = |e^{\imath M \sin \Omega t}|^2 = \left| \sum_{k=-\infty}^{\infty} J_k(M) e^{\imath k \Omega t} \right|^2 = \sum_{k,m=-\infty}^{\infty} J_k(M) J_m(M) e^{\imath(k-m)\Omega t} \ .$$

This can only be true at all times if,

$$1 = \sum_{k=-\infty}^{\infty} J_k(M)^2 \ .$$

c. In Exc. 35.5.5.1(c) we have seen, that the spectrum of phase-modulated light, $\sum_{k=-\infty}^{\infty} J_k(M) e^{\imath k \Omega t}$, is given by,

$$S_{\mathcal{E}}(\omega) = \frac{1}{2\pi} \frac{1}{\sum_{k=-\infty}^{\infty} J_k(M)^2} \sum_{k=-\infty}^{\infty} J_k(M)^2 \delta(\Delta + k\Omega) \ .$$

Similarly, we obtain for $\sum_{k=-\infty}^{\infty} |J_k(M)| e^{\imath k \Omega t}$,

$$S_{\mathcal{E}}(\omega) = \frac{1}{2\pi} \frac{1}{\sum_{k=-\infty}^{\infty} |J_k(M)|^2} \sum_{k=-\infty}^{\infty} J_k(M)^2 \delta(\Delta + k\Omega) \ .$$

Thus, the spectra are indistinguishable, and one must resort to phase-sensitive spectroscopy to distinguish both cases.

35.5.5.4 Ex: Non-classicality of antibunched states

Quantized radiation fields can exhibit the feature of antibunching, which is incompatible with the classical concept of radiation. Show that $g^{(2)}(0) < 1$ entails the possibility of negative values for the Glauber-Sudarshan P-function, that is, $P(\alpha) < 0$ at least for some α.

Solution: *The Glauber-Sudarshan P-function defined via the density operator, $\hat{\rho} = \int P(\alpha) |\alpha\rangle\langle\alpha| d^2\alpha$, allows to express the expectation value as,*

$$\langle \hat{A} \rangle = Tr\ \hat{A}\hat{\rho} = \int P(\alpha) \langle\alpha|\hat{A}|\alpha\rangle d^2\alpha \ .$$

Antibunching, that is $g^{(2)}(0) < 1$, *implies*

$$0 > \langle \hat{a}^\dagger \hat{a}^\dagger \hat{a}\hat{a} \rangle - \langle \hat{a}^\dagger \hat{a} \rangle^2 = \int P(\alpha) |\alpha|^4 d^2\alpha - \left(\int P(\alpha) |\alpha|^2 d^2\alpha \right)^2$$
$$= \int P(\alpha) \left(|\alpha|^2 - \int P(\beta) |\beta|^2 d^2\beta \right)^2 d^2\alpha = \int P(\alpha) \left(|\alpha|^2 \langle \hat{a}^\dagger \hat{a} \rangle \right)^2 d^2\alpha$$

using the normalization condition $\int P(\alpha) d^2\alpha = 1$. *This is only possible to satisfy the quasi-probability distribution is negative at least for some* α.

35.6 Spontaneous emission and light scattering

35.6.1 Interaction of atoms with vacuum modes

The Jaynes-Cummings Hamiltonian (35.11), discussed in Sec. 35.4, describes the purely coherent dynamics of a single immobile two-level atom interacting with a single cavity mode. The model is simple enough to allow for analytical solutions. However, it does not include processes of spontaneous emission, which can be understood as the interaction of the atom with the light modes of the vacuum. That is, we must extend the Hamiltonian,

$$\hat{H} = \hat{H}_{atom} + \hat{H}_{field} + \hat{H}_{atom:field} + \hat{H}_{vacuum} + \hat{H}_{atom:vacuum} \ . \tag{35.218}$$

The evolution of the system represented by the Hamiltonian (35.218) is described by a total density operator, $\hat{\rho}_{total}(t)$, obeying the *von Neumann equation*,

$$\boxed{\frac{d\hat{\rho}_{total}}{dt} = -\frac{\imath}{\hbar}[\hat{H}, \hat{\rho}_{total}]} \ , \tag{35.219}$$

which has the solution,

$$\hat{\rho}_{total}(t) = e^{-\imath \hat{H} t/\hbar} \hat{\rho}_{total}(0) e^{\imath \hat{H} t/\hbar} \equiv e^{-\imath \mathcal{L} t} \hat{\rho}_{total}(0) \ . \tag{35.220}$$

Often, we are only interested in *either* the evolution of the light field, *or* the internal state of the atom. In these cases, we calculate the trace over all those degrees of freedom, which are we are NOT interested in,

$$\hat{\rho}_{atom} = \mathrm{Tr}_{vacuum} \ \hat{\rho}_{total} \ . \tag{35.221}$$

The procedure is the following. We begin choosing the initial state of the electromagnetic vacuum as the photonic vacuum $\hat{\rho}_{vacuum} = |\{0\}\rangle\langle\{0\}|$ and defining a projection operator onto this state, $\hat{P}... \equiv \hat{\rho}_{vacuum}(0)\mathrm{Tr}_{vacuum} ... = \hat{P}^2....$ Then we apply to the von Neumann equation the rotating wave, the Markov and the Born approximations. Finally, tracing over the vacuum field variables, we obtain after some calculations the *Bloch-Lindbladt equation* or *master equation* [1062] for the atom interacting with the driving field. For a discussion of the validity of the Born-Markov approximation [932]. For the relation between the Markov approximation and the Fermi's Golden Rule [17].

We emphasize that the Hamiltonian (35.218) describes the interaction of light with a *single immobile atom* at the most fundamental level. However, it excludes many-body effects introduced by quantum statistics or interatomic interactions (to be discussed in Chp. 45), as well as the center-of-mass motion of the atom and the impact of photonic recoil (to be discussed in Chp. 38).

In the following section we give a simplified derivation concentrating us on the situation of a single motionless atom, excited by a laser and emitting photons into the electromagnetic vacuum.

35.6.1.1 Spontaneous emission

Spontaneous emission can be understood as an energy diffusion process from a system with a restricted number of degrees of freedom into a large thermal bath. For example, although a two-dimensional Hilbert space is sufficient to describe a laser-driven two-level atom, this atom couples to a huge phase-space by spontaneously emitting photons into arbitrary directions. We account for his fact by including in the Hamiltonian not only the interaction of the atom with the incident laser (wavevector $\mathbf{k}_0$, frequency $\omega_{\mathbf{k}_0}$), but also with the modes of the electromagnetic vacuum (wavevector $\mathbf{k}$, frequency $\omega_{\mathbf{k}}$). We will see, that with this Hamiltonian, we can derive, in a calculation is known as *Weisskopf-Wigner theory*, the Schrödinger equation for the amplitudes of the atomic levels (34.184) including spontaneous emission.

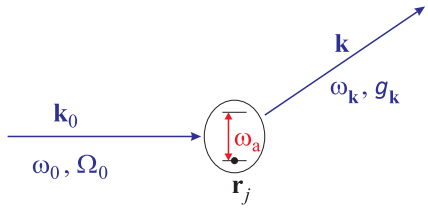

Figure 35.16: Scattering of a laser beam by an atom.

Denoting the frequency of the atomic resonance by ω_a, the interaction part of the Hamiltonian is,

$$\boxed{\begin{aligned}\hat{H} &= \hbar g_{\mathbf{k}_0}\left(\hat{\sigma}^- e^{-\imath\omega_a t}+\hat{\sigma}^+ e^{\imath\omega_a t}\right)\left(\hat{a}^\dagger_{\mathbf{k}_0} e^{\imath\omega_0 t-\imath\mathbf{k}_0\cdot\mathbf{r}}+\hat{a}_{\mathbf{k}_0} e^{-\imath\omega_0 t+\imath\mathbf{k}_0\cdot\mathbf{r}}\right)\\ &+ \sum_{\mathbf{k}}\hbar g_{\mathbf{k}}\left(\hat{\sigma}^- e^{-\imath\omega_a t}+\hat{\sigma}^+ e^{\imath\omega_a t}\right)\left(\hat{a}^\dagger_{\mathbf{k}} e^{\imath\omega_{\mathbf{k}} t-\imath\mathbf{k}\cdot\mathbf{r}}+\hat{a}_{\mathbf{k}} e^{-\imath\omega_{\mathbf{k}} t+\imath\mathbf{k}\cdot\mathbf{r}}\right)\end{aligned}} \quad . \tag{35.222}$$

$g_{\mathbf{k}_0}$ is the coupling strength of the interaction between the atom and the pump mode, $\hat{\sigma}^-$ is the atomic deexcitation operator, $\hat{a}_{\mathbf{k}}$ is the annihilation operator of a photon, and $g_{\mathbf{k}} = d\sqrt{\omega/(\hbar\varepsilon_0 V)}$ describes the coupling between the atom and a vacuum mode whose volume is V. The atom has two states, the ground state $|g\rangle$ and excited state $|e\rangle$. Since we are considering only one atom fixed in space [11], we can as well locate it at the origin $\mathbf{r} = 0$. In addition, considering a high power incident laser,

$$\hat{a}_{\mathbf{k}_0}|n_0\rangle_{\mathbf{k}_0} = \sqrt{n_0}|n_0-1\rangle_{\mathbf{k}_0} \simeq \sqrt{n_0}|n_0\rangle_{\mathbf{k}_0} \ , \tag{35.223}$$

[11] We do not let the atom be accelerated by photonic recoil.

$\hat{a}_{\mathbf{k}_0}$ is approximately an observable proportional to the root of the intensity. As $[\hat{a}_{\mathbf{k}_0}, \hat{a}^\dagger_{\mathbf{k}_0}] \simeq 0$, we can disregard the quantum nature of the incident field and replace, $\Omega_0 \equiv 2\sqrt{n_0} g_{\mathbf{k}_0}$. Within the rotating wave approximation (RWA), the Hamiltonian becomes,

$$\hat{H} = \tfrac{\hbar}{2}\Omega_0 \left[\hat{\sigma}^- e^{\imath\Delta_0 t} + h.c.\right] + \hbar \sum_{\mathbf{k}} \left[g_{\mathbf{k}} \hat{\sigma} \hat{a}^\dagger_{\mathbf{k}} e^{\imath\Delta_{\mathbf{k}} t} + h.c.\right] \ , \tag{35.224}$$

where we introduced the abbreviations,

$$\Delta_0 \equiv \omega_0 - \omega_a \qquad \text{and} \qquad \Delta_{\mathbf{k}} \equiv \omega_{\mathbf{k}} - \omega_a \ . \tag{35.225}$$

The general state of the system is given by,

$$|\Psi(t)\rangle = \alpha(t)|g\rangle_a|0\rangle_{\mathbf{k}} + \beta(t)|e\rangle_a|0\rangle_{\mathbf{k}} + \sum_{\mathbf{k}} \gamma_{\mathbf{k}}(t)|g\rangle_a|1\rangle_{\mathbf{k}} \ , \tag{35.226}$$

where $|j\rangle_a$ denotes the atomic state and $|n\rangle_{\mathbf{k}}$ the number of photons in the scattering mode.

The temporal evolution of the amplitudes is obtained by inserting the Hamiltonian (35.224) and the ansatz (35.226) into the Schrödinger equation,

$$\frac{\partial}{\partial t}|\Psi(t)\rangle = -\frac{\imath}{\hbar}\hat{H}|\Psi(t)\rangle \ . \tag{35.227}$$

As verified in Exc. 35.6.4.1, we obtain,

$$\begin{aligned} \dot{\alpha}(t) &= -\imath\tfrac{\Omega_0}{2} e^{\imath\Delta_0 t}\beta(t) \\ \dot{\beta}(t) &= -\imath\tfrac{\Omega_0}{2}\alpha(t)e^{-\imath\Delta_0 t} - \sum\nolimits_{\mathbf{k}} \imath g_{\mathbf{k}}\gamma_{\mathbf{k}}(t)e^{-\imath\Delta_{\mathbf{k}} t} \\ \dot{\gamma}_{\mathbf{k}}(t) &= -\imath g_{\mathbf{k}} e^{\imath\Delta_{\mathbf{k}} t}\beta(t) \ . \end{aligned} \tag{35.228}$$

Now, we chose the initial conditions,

$$\alpha(0) = 1 \qquad \text{and} \qquad \beta(0) = 0 \qquad \text{and} \qquad \gamma_{\mathbf{k}}(0) = 0 \ , \tag{35.229}$$

we integrate the third equation,

$$\gamma_{\mathbf{k}}(t) = -\imath g_{\mathbf{k}} \int_0^t e^{\imath\Delta_{\mathbf{k}} t'}\beta(t')dt' \ , \tag{35.230}$$

and we substitute it in the second equation,

$$\dot{\beta}(t) = -\imath\tfrac{\Omega_0}{2}\alpha(t)e^{-\imath\Delta_0 t} - \sum_{\mathbf{k}} g^2_{\mathbf{k}} \int_0^t e^{\imath\Delta_{\mathbf{k}}(t'-t)}\beta(t')dt' \ . \tag{35.231}$$

35.6.1.2 The Markov approximation

For small systems (which certainly is the case of a single atom), we can apply the *Markov approximation* [12] claiming that the temporal variation of the amplitudes

[12] The approximation does not necessarily hold for large clouds of atoms.

$\beta(t')$ is slower than the evolution of the system given by $e^{\imath(\omega_{\mathbf{k}}-\omega_a)t}$ in the integro-differential equation, which is equivalent to an arbitrarily high-order equation. Hence, substituting $\beta(t') \to \beta(t)$ into the integro-differential equation, we reduce it to a simple first-order differential equation.

In practice, we redefine the integration variable, $t'' \equiv t - t'$, to obtain,

$$\begin{aligned}\frac{d}{dt}\beta(t) &= -\imath\tfrac{\Omega_0}{2}\alpha(t) - \sum_{\mathbf{k}} g_k^2 \int_0^t e^{\imath(\omega_{\mathbf{k}}-\omega_a)(t'-t)}\beta(t')dt' \\ &= -\imath\tfrac{\Omega_0}{2}\alpha(t) - \sum_{\mathbf{k}} g_k^2 \int_0^t e^{-\imath(\omega_{\mathbf{k}}-\omega_a)t''}\beta(t-t'')dt'' \ ,\end{aligned} \tag{35.232}$$

and implement the Markov approximation by setting $\beta(t-t'') \simeq \beta(t)$, and with $\lim_{t\to\infty}\int_0^t e^{-\imath(\omega_{\mathbf{k}}-\omega_a)t'}dt' = \pi\delta(\omega_{\mathbf{k}}-\omega_a)$, and replacing $\sum_{\mathbf{k}} \longrightarrow \frac{V}{(2\pi)^3}\int d^3\mathbf{k}$, we arrive at,

$$\begin{aligned}\frac{d}{dt}\beta(t) &\simeq -\imath\tfrac{\Omega_0}{2}\alpha(t) - \sum_{\mathbf{k}} g_{\mathbf{k}}^2\beta(t)\pi\delta(\omega_{\mathbf{k}}-\omega_a) \\ &= -\imath\tfrac{\Omega_0}{2}\alpha(t) - \tfrac{V}{(2\pi)^3}\beta(t)\int g_{\mathbf{k}}^2\pi\delta(\omega_{\mathbf{k}}-\omega_a)d^3\mathbf{k} \\ &= -\imath\tfrac{\Omega_0}{2}\alpha(t) - \tfrac{V}{(2\pi)^3}\beta(t)4\pi g_{\mathbf{k}_a}^2\pi k_a^2\tfrac{1}{c} = -\imath\tfrac{\Omega_0}{2}\alpha(t) - \tfrac{\Gamma}{2}\beta(t) \ .\end{aligned} \tag{35.233}$$

In the last step we introduced, as an abbreviation, the spontaneous emission rate,

$$\Gamma \equiv \sum_{\mathbf{k}} 2g_{\mathbf{k}}^2\pi\delta(\omega_{\mathbf{k}}-\omega_a) = \tfrac{V}{\pi c}k_a^2 g_{\mathbf{k}_a}^2 \ , \tag{35.234}$$

Finally,

$$\boxed{\frac{d}{dt}\alpha(t) = -\imath\frac{\Omega_0}{2}\beta(t) \qquad \text{and} \qquad \frac{d}{dt}\beta(t) = -\imath\frac{\Omega_0}{2}\alpha(t) - \frac{\Gamma}{2}\beta(t)} \ . \tag{35.235}$$

These are exactly the equations for the probability amplitudes (34.184) derived from the Schrödinger equation, only that now, the spontaneous emission term has been derived explicitly. Solve the Exc. 35.6.4.2.

Example 213 (*Emission stimulated by vacuum fluctuations*): Spontaneous emission can be regarded as an emission stimulated by vacuum fluctuations. To see this, we write down the resonant optical cross section ($\omega_0 = \omega_a$) of a driven two-level atom without degeneracies, $\sigma_0 = \lambda^2/2\pi$, and the intensity of an incident laser field, $\bar{I} = cN\hbar\omega_0/V$, generating the Rabi frequency (see (22.107)),

$$\Omega_0^2 = \sigma_0\frac{\bar{I}}{\hbar\omega_a}\Gamma = \frac{2\pi c}{k_a^2}\frac{N}{V}\Gamma \ . \tag{35.236}$$

Now, we assume that the field is, in fact, a vacuum mode containing only half a photon, $N = 1/2$, which corresponds to vacuum fluctuations in the mode k_0. Then,

$$\Omega_{1/2}^2 = \frac{\pi c}{k_a^2 V}\Gamma = g^2 \ . \tag{35.237}$$

35.6.2 Resonance fluorescence and (in-)coherent light scattering

The typical situation for a spectroscopy experiment is illustrated in Fig. 35.17: When a beam of light, understood as a plane wave, strikes an atom (or a cloud of many atoms), a part of the light is absorbed and reemitted into a direction indicated by a solid angle $d\Omega$. Light scattering is, of course, a second order process involving two atomic transitions, one absorption and one emission.

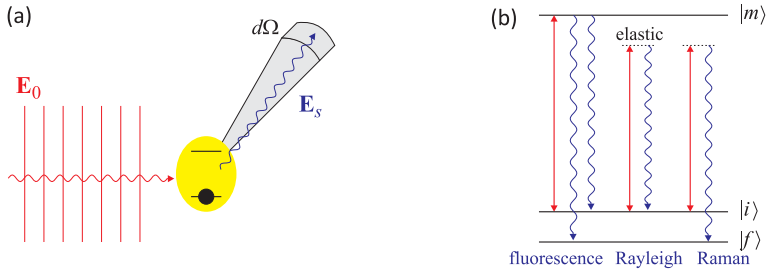

Figure 35.17: (a) Geometry of a scattering experiment. (b) Spectral contributions of light scattered elastically and inelastically by a three-level atom.

Radiation can be absorbed or scattered by an atom in different ways, depending on whether the interaction is an *elastic scattering* or an *inelastic scattering* process, a coherent or incoherent, a spontaneous or (bosonically) stimulated process. These properties characterize many processes, in particular, resonance fluorescence (i.e. absorption and reemission), *Rayleigh scattering*, or *Raman scattering*. In the following, we will clarify this classification.

Every scattering process is either spontaneous or stimulated [13]. Rayleigh scattering is elastic, that is, the kinetic energy of the scattering atom is the same, before and after the scattering process. In contrast, Raman scattering is inelastic. Spontaneous emission is due to the decay of population from an excited state, and spontaneous Rayleigh scattering is due to the decay of an induced dipole moment. Both spontaneous processes can be regarded as being stimulated by vacuum fluctuations.

35.6.2.1 Deriving the source field expression

We will now calculate the electric field due to spontaneous emission by an atom from the interaction Hamiltonian for atom-vacuum coupling (35.222) in the RWA,

$$\hat{H} = \sum_{\mathbf{k}} \hbar g_{\mathbf{k}} \hat{\sigma}^- \hat{a}^\dagger_{\mathbf{k}} e^{\imath\omega_{\mathbf{k}} t - \imath\omega_a t - \imath\mathbf{k}\cdot\mathbf{R}} + h.c. \ . \tag{35.238}$$

Now, we assume isotropic coupling, $g_{\mathbf{k}} = g_k$, and $\omega_{\mathbf{k}} = \omega_k$, and for simplicity we position the atom in the origin, $\mathbf{R} = 0$. We use the Heisenberg equation with the

[13] Classical theories of light scattering through the excitation of an electronic motion based on the models of Lorentz or Drude can be found in Secs. 18.2.3 . Although being classical, these model are useful for a deeper understanding of many aspects of *Compton scattering*, *Thomson scattering*, and *Rayleigh scattering*.

commutation rule $[\hat{a}_{\mathbf{k}}, \hat{a}^{\dagger}_{\mathbf{k}'}] = \delta_{\mathbf{k},\mathbf{k}'}$ to derive the temporal evolution of the field operators,

$$\frac{d\hat{a}_{\mathbf{k}}}{dt} = \tfrac{1}{\imath\hbar}[\hat{a}_{\mathbf{k}}, \hat{H}] = -\imath\hat{\sigma}^{-} g_k e^{\imath(\omega_k - \omega_a)t} \ . \tag{35.239}$$

Neglecting for simplicity polarization, the electric field is given by,

$$\hat{\mathcal{E}}^{+}_{sct}(\mathbf{r}, t) = \sum_{\mathbf{k}} \mathcal{E}_1 \hat{a}_{\mathbf{k}}(t) e^{\imath(\mathbf{k}\cdot\mathbf{r} - \omega_k t)} \ , \tag{35.240}$$

where $\mathbf{r}$ is now the observation point of the electric field. We restrict to the far-field and substitute the annihilation operator with the integral of Eq. (35.239) using the initial condition $\hat{a}_{\mathbf{k}}(0) = 0$,

$$\hat{\mathcal{E}}^{+}_{sct}(\mathbf{r}, t) = \sum_{\mathbf{k}} \mathcal{E}_1 g_k \int_0^t \hat{\sigma}^{-}(t') e^{\imath(\omega_k - \omega_a)t'} dt' e^{\imath(\mathbf{k}\cdot\mathbf{r} - \omega_k t)} \ . \tag{35.241}$$

Now, we substitute the sum over $\mathbf{k}$ by an integral, as done in (35.233),

$$\hat{\mathcal{E}}^{+}_{sct}(\mathbf{r}, t) = -\imath \frac{V}{(2\pi)^3} \int_{\mathbb{R}^3} \mathcal{E}_1 g_k \int_0^t \hat{\sigma}^{-}(t') e^{\imath(\omega_k - \omega_a)t'} dt' e^{\imath(\mathbf{k}\cdot\mathbf{r} - \omega_k t)} d^3k \ . \tag{35.242}$$

Using the relationships,

$$g_k = \frac{d_{12}\mathcal{E}_1}{\hbar} \qquad \text{and} \qquad \mathcal{E}_1 = \sqrt{\frac{\hbar\omega_k}{2\varepsilon_0 V}} \ , \tag{35.243}$$

the final result of the integration yields [816],

$$\hat{\mathcal{E}}^{+}_{sct}(\mathbf{r}, t) \simeq -\imath \frac{d_{12} k_a^2}{4\pi\varepsilon_0 r} \hat{\sigma}^{-}(t - \tfrac{r}{c}) \ . \tag{35.244}$$

35.6.2.2 Resonance fluorescence

When we introduced the second quantization (35.8) we learned that the field of light emitted by a radiator in the radiation zone ($\lambda \ll r$) is, taking into account retardation [14], given by,

$$\langle \hat{\vec{\mathcal{E}}}^{+}_s(\mathbf{r}, t) \rangle \propto \langle \hat{\sigma}^{-} \rangle \propto \tilde{\rho}_{21} \qquad \text{and} \qquad \langle \hat{\vec{\mathcal{E}}}^{-}_s(\mathbf{r}, t) \hat{\vec{\mathcal{E}}}^{+}_s(\mathbf{r}, t) \rangle \propto \langle \hat{\sigma}^{+}\hat{\sigma}^{-} \rangle \propto \rho_{22} \ . \tag{35.245}$$

Therefore, the electric field emitted by an atom and the intensity of scattered light are given by,

$$\boxed{\begin{aligned} \langle \hat{\vec{\mathcal{E}}}^{+}_s(\mathbf{r}, t) \rangle &= -\frac{e\omega_a^2 \hat{\epsilon}\cdot\mathbf{r}_{12}}{4\pi\varepsilon_0 c^2 r} \tilde{\rho}_{21}(t - \tfrac{r}{c}) e^{-\imath\omega(t - r/c)} \\ \bar{I}_s = c\varepsilon_0 \langle \hat{\vec{\mathcal{E}}}^{-}_s(\mathbf{r}, t) \hat{\vec{\mathcal{E}}}^{+}_s(\mathbf{r}, t) \rangle &= \frac{\alpha\hbar\omega_a^4 |\hat{\epsilon}\cdot\mathbf{r}_{12}|^2}{4\pi c^2 r^2} \rho_{22}(t - \tfrac{r}{c}) \end{aligned}} \ , \tag{35.246}$$

[14] The classical version of this formula is (19.41) .

with the definition of the Sommerfeld constant $\alpha = e^2/4\pi\varepsilon_0\hbar c$. We calculate the total flux of emitted photons,

$$W_{fi}^{(sp)} = \int \frac{\bar{I}_s r^2}{\hbar\omega_a} d\Omega = \frac{1}{\hbar\omega_a} \int \frac{\alpha\hbar\omega_a^4 |\mathbf{r}_{12}|^2 \cos^2\theta}{4\pi c^2} \rho_{22}(t - \tfrac{r}{c}) \sin\theta d\theta d\phi \qquad (35.247)$$
$$= \frac{8\pi}{3\hbar\omega_a} \frac{\alpha\hbar\omega_a^4 |\mathbf{r}_{12}|^2}{4\pi c^2} \rho_{22}(t - \tfrac{r}{c}) = \frac{2\alpha}{3c^2} \omega_a^3 |\mathbf{r}_{12}|^2 \rho_{22}(t - \tfrac{r}{c}) \ .$$

The result *coincides with the spontaneous emission rate* Γ calculated in (34.40).

A *differential scattering cross section* can be defined by,

$$\frac{d\sigma}{d\Omega} \equiv \frac{\omega \bar{I}_s r^2}{\omega_s \bar{I}_0} \ . \qquad (35.248)$$

35.6.2.3 Coherently scattered light and saturation

The total intensity of the scattered light being $\bar{I}_s$, the fraction of the coherently scattered light is,

$$\frac{\bar{I}_s^{\rm coh}}{\bar{I}_s} = \frac{\langle \hat{\vec{\mathcal{E}}}_s^-(\mathbf{r},t)\rangle \langle \hat{\vec{\mathcal{E}}}_s^+(\mathbf{r},t)\rangle}{\langle \hat{\vec{\mathcal{E}}}_s^-(\mathbf{r},t) \hat{\vec{\mathcal{E}}}_s^+(\mathbf{r},t)\rangle} \ . \qquad (35.249)$$

Inserting the expressions (35.246) and the stationary solution of the Bloch equations (34.188) with the saturation parameter defined in (34.190),

$$\frac{\bar{I}_s^{\rm coh}}{\bar{I}_s} = \frac{|\tilde{\rho}_{21}(\infty)|^2}{\rho_{22}(\infty)} = \frac{1}{1+s} = 1 - \frac{\bar{I}_s^{\rm incoh}}{\bar{I}_s} \ . \qquad (35.250)$$

That is, since the resonance fluorescence is proportional to the excited state population, we may define a quantity $S_{tot} \equiv \rho_{22}(\infty)$, so that the coherent and incoherent parts of the fluorescence are,

$$\boxed{S_{coh} = |\rho_{21}(\infty)|^2 = \frac{s/2}{(1+s)^2} \quad \text{and} \quad S_{incoh} = \rho_{22}(\infty) - |\rho_{21}(\infty)|^2 = \frac{s^2/2}{(1+s)^2}} \ . \qquad (35.251)$$

Hence, $S_{incoh} = s S_{coh}$.

The result (35.251), illustrated in Fig. 35.18(a), means that *below saturation* scattering is dominated by elastic scattering. Incident light excites the atomic dipole moment ρ_{12}, that is, charge oscillations which, in turn, emit electromagnetic radiation like a classical antenna. *Above saturation* the excited atomic state accumulates an considerable amount of population ρ_{22} giving rise to spontaneous emission, which is interpreted as inelastic scattering. This intrinsically quantum feature is a consequence of the quantized nature of the atomic energy levels and has no classical counterpart. Another interesting feature seen in Fig. 35.18(b) is that, when the incident light is tuned sufficiently far from resonance, elastic scattering will dominate at any saturation parameter.

35.6.3 The spectrum of resonance fluorescence

The *correlation functions* defined in (35.172) represent an interesting concept for describing resonance fluorescence and for phenomena such as *antibunching* observed in resonance fluorescence.

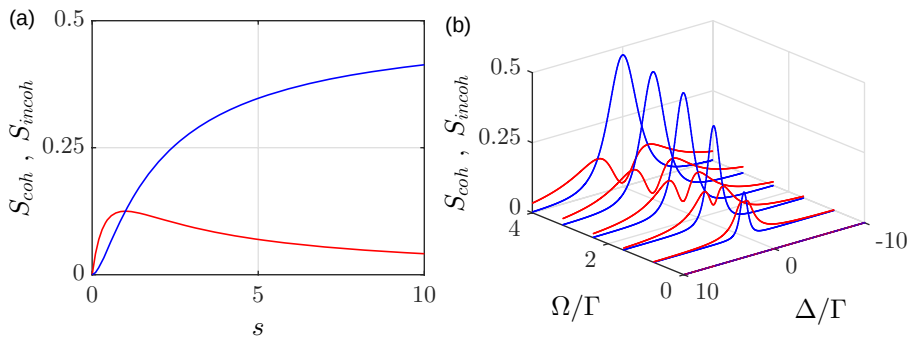

Figure 35.18: (code) Elastic (red) versus inelastic scattering (blue) as a function of the saturation parameter (a) at resonance and (b) for various detunings.

35.6.3.1 The quantum regression theorem

From (35.178) we see that, to compute the spectra of *resonance fluorescence*, we only need to compute the correlation function $g^{(1)}$, i.e. the amplitudes of the field $\hat{\mathcal{E}}(t)$, which in turn are related to the field operators (35.8). The field operators follow the solutions of the Bloch equation, which, being linear, have the following generic form,

$$\rho_{ij}(t+\tau) = \sum_{k,l} \alpha_{ijkl}(\tau)\rho_{ij}(t) + \beta_{ij}(\tau) \ . \tag{35.252}$$

The trace condition is satisfied, when $(i,j),(k,l) \neq (1,1)$.

To be able to explore the above relationship to calculate correlation functions, we have to invoke the so-called *quantum regression theorem*,

$$\boxed{\langle \hat{A}(t+\tau)\rangle = \sum_i \xi_i(\tau)\langle \hat{A}_i(t)\rangle \quad \Longrightarrow \quad \langle \hat{B}(t)\hat{A}(t+\tau)\hat{C}(t)\rangle = \sum_i \xi_i(\tau)\langle \hat{B}(t)\hat{A}_i(t)\hat{C}(t)\rangle} \ . \tag{35.253}$$

Example 214 (*Quantum regression applied to the Langevin equation*): We have,

$$\begin{aligned} \dot{A}_\mu &= D_\mu(t) + F_\mu(t) \\ \langle F_\mu(t)F_\nu(t)\rangle &= 2\langle D_{\mu\nu}\rangle\delta(t-t') \ . \end{aligned} \tag{35.254}$$

We know,

$$\langle A_\mu(t)F_\nu(t)\rangle = \langle D_{\mu\nu}\rangle \quad \text{and} \quad \langle F_\mu(t)A_\nu(t)\rangle = \langle D_{\mu\nu}\rangle \tag{35.255}$$

and the quantum regression theorem gives,

$$\frac{d}{dt}\langle A_\mu(t)A_\nu(t')\rangle = \langle D_\mu(t)A_\nu(t')\rangle \ , \tag{35.256}$$

because if $t' < t$, the term $\langle F_\mu(t)A_\nu(t')\rangle$ vanishes for a *Markovian process*.

35.6.3.2 Bloch equation for a two-level system

The Fourier transform of the first-order coherence, $g^{(1)}(\tau) = e^{-\imath\omega\tau}G(\tau)$, gives,

$$F(\nu) = (\mathcal{F}g^{(1)})(\nu) = \mathcal{F}[e^{-\imath\omega\tau}] \star \mathcal{F}[G(\tau)] = \delta(\nu-\omega) \star \mathcal{F}[G(\tau)] = (\mathcal{F}G)(\nu-\omega) \ . \tag{35.257}$$

Therefore, we can look at the unshifted spectrum, $(\mathcal{F}G)(\nu)$. Since the fluorescence spectrum is determined by the first-order coherence, which depends on the field operators, which in turn depend on the atomic populations and coherences, we have to solve the Bloch equation.

For a two-level atom the Bloch equations, having been reduced by the normalization condition (34.284) are,

$$\dot{\vec{\rho}}_{red} = \mathcal{M}\vec{\rho}_{red} + \mathbf{b} = \begin{pmatrix} -\Gamma & -\frac{\imath}{2}\Omega & \frac{\imath}{2}\Omega \\ -\imath\Omega & -\frac{1}{2}\Gamma - \imath\Delta & 0 \\ \imath\Omega & 0 & -\frac{1}{2}\Gamma + \imath\Delta \end{pmatrix} \begin{pmatrix} \rho_{22} \\ \rho_{12} \\ \rho_{21} \end{pmatrix} + \begin{pmatrix} 0 \\ \frac{\imath}{2}\Omega \\ -\frac{\imath}{2}\Omega \end{pmatrix} \tag{35.258}$$

with the solution (34.286), that is, $\vec{\rho}(t+\tau) = e^{\mathcal{M}\tau}\vec{\rho}(t) + (1-e^{\mathcal{M}\tau})\vec{\rho}(\infty)$ with $\rho(\infty) = -\mathcal{M}^{-1}b$. This solution can be cast in the following form,

$$\rho_{kl}(t+\tau) = \sum_{(mn)} \alpha_{(kl)(mn)}(\tau)\rho_{mn}(t) + \beta_{(kl)}(\tau) \ , \tag{35.259}$$

where $(mn), (kl) = (22), (12), (21)$ identifying,

$$\alpha_{(kl)(mn)}(\tau) = \begin{pmatrix} \alpha_{22,22} & \alpha_{12,22} & \alpha_{21,22} \\ \alpha_{22,12} & \alpha_{12,12} & \alpha_{21,12} \\ \alpha_{22,21} & \alpha_{12,21} & \alpha_{21,21} \end{pmatrix} \equiv \begin{pmatrix} (e^{\mathcal{M}\tau})_{11} & . & . \\ . & . & . \\ . & . & . \end{pmatrix} = e^{\mathcal{M}\tau} \tag{35.260}$$

$$\beta_{(kl)}(\tau) = \begin{pmatrix} \beta_{22} \\ \beta_{12} \\ \beta_{21} \end{pmatrix} \equiv \begin{pmatrix} -[(1-e^{\mathcal{M}\tau})\mathcal{M}^{-1}\mathbf{b}]_1 \\ . \\ . \end{pmatrix} = -(1-e^{\mathcal{M}\tau})\mathcal{M}^{-1}\mathbf{b} \ .$$

Using quantum operators in the interaction image, $|k\rangle\langle l| = \hat{\sigma}_{kl}$, we have,

$$\langle\hat{\sigma}_{12}(t)\rangle = \langle\hat{\sigma}_{21}^{\dagger}(t)\rangle = \rho_{12}(t)e^{\imath\omega_0 t} \qquad \text{and} \qquad \langle\hat{\sigma}_{22}(t)\rangle = \langle\hat{\sigma}_{12}(t)\hat{\sigma}_{21}(t)\rangle = \rho_{22}(t) \ . \tag{35.261}$$

yielding,

$$\langle e^{(k-l)\imath\omega_0(t+\tau)}\hat{\sigma}_{kl}(t+\tau)\rangle = \sum_{(mn)} \alpha_{(kl)(mn)}(\tau)\langle e^{(m-n)\imath\omega_0 t}\hat{\sigma}_{mn}(t)\rangle + \beta_{(mn)}(\tau)\langle 1\rangle \ , \tag{35.262}$$

or,

$$\langle\hat{\sigma}_{kl}(t+\tau)\rangle \tag{35.263}$$
$$= \sum_{(mn)} e^{(l-k)\imath\omega_0\tau}\alpha_{(kl)(mn)}(\tau)\langle e^{(l-k+m-n)\imath\omega_0 t}\hat{\sigma}_{mn}(t)\rangle + e^{(l-k)\imath\omega_0\tau}\beta_{(mn)}(\tau)\langle e^{(l-k)\imath\omega_0 t}\rangle \ .$$

Applying the quantum regression theorem to the Bloch equations, we get for an arbitrary time-dependent operator $\hat{B}(t)$,

$$\boxed{\begin{aligned}\langle \hat{B}(t)\hat{\sigma}_{kl}(t+\tau)\rangle &= \sum_{(mn)} e^{(l-k)\imath\omega_0\tau}\alpha_{(kl)(mn)}(\tau)\langle e^{(l-k+m-n)\imath\omega_0 t}\hat{B}(t)\hat{\sigma}_{mn}(t)\rangle \\ &\qquad + e^{(l-k)\imath\omega_0\tau}\beta_{(mn)}(\tau)\langle e^{(l-k)\imath\omega_0 t}\hat{B}(t)\rangle\end{aligned}} \ . \tag{35.264}$$

35.6.3.3 Correlation functions

We now look at the radiation field, which is related to the dipole moment operator via,

$$\hat{\mathcal{E}}^- = \gamma\hat{\sigma}_{21} \ , \tag{35.265}$$

where γ is simply a constant. Substituting this relation in the correlation functions (35.172) we obtain,

$$\begin{aligned} g^{(1)}(\tau) &= \frac{\langle\hat{\sigma}_{21}(t)\hat{\sigma}_{12}(t+\tau)\rangle}{\langle\hat{\sigma}_{21}(t)\hat{\sigma}_{12}(t)\rangle} = \frac{\langle\hat{\sigma}_{21}(t)\hat{\sigma}_{12}(t+\tau)\rangle}{\langle\hat{\sigma}_{22}(t)\rangle} \\ g^{(2)}(\tau) &= \frac{\langle\hat{\sigma}_{21}(t)\hat{\sigma}_{21}(t+\tau)\hat{\sigma}_{12}(t+\tau)\hat{\sigma}_{12}(t)\rangle}{\langle\hat{\sigma}_{21}(t)\hat{\sigma}_{12}(t)\rangle^2} = \frac{\langle\hat{\sigma}_{22}(t)\hat{\sigma}_{22}(t+\tau)\rangle}{\langle\hat{\sigma}_{22}(t)\rangle^2} \ . \end{aligned} \tag{35.266}$$

Now we can calculate, letting $\xi_i(\tau) \equiv \alpha_{(12)(mn)}$, $\hat{C}(t) \equiv 1$, and $\hat{B}(t) \equiv \hat{\sigma}_{21}(t)$,

$$g^{(1)}(\tau) = \frac{\sum_{(mn)} e^{\imath\omega_0(t+\tau)}e^{(m-n)\imath\omega_0 t}\alpha_{(12)(mn)}(\tau)\langle\hat{\sigma}_{21}(t)\hat{\sigma}_{mn}(t)\rangle + e^{\imath\omega_0(t+\tau)}\beta_{(12)}(\tau)\langle\hat{\sigma}_{21}(t)\rangle}{\langle\hat{\sigma}_{22}(t)\rangle} \tag{35.267}$$

$$g^{(2)}(\tau) = \frac{\sum_{(mn)} e^{(m-n)\imath\omega_0 t}\alpha_{(22)(mn)}(\tau)\langle\hat{\sigma}_{22}(t)\hat{\sigma}_{mn}(t)\rangle + \beta_{(22)}(\tau)\langle\hat{\sigma}_{22}(t)\rangle}{\langle\hat{\sigma}_{22}(t)\rangle^2} \ .$$

Using $\hat{\sigma}_{21}\hat{\sigma}_{mn} = \hat{\sigma}_{2n}\delta_{m1}$,

$$\begin{aligned} g^{(1)}(\tau) &= e^{\imath\omega_0\tau}\frac{\alpha_{(12)(12)}(\tau)\langle\hat{\sigma}_{21}(t)\hat{\sigma}_{12}(t)\rangle + \beta_{(12)}(\tau)\langle e^{\imath\omega_0 t}\hat{\sigma}_{21}(t)\rangle}{\langle\hat{\sigma}_{22}(t)\rangle} \\ g^{(2)}(\tau) &= \frac{\alpha_{(22)(21)}(\tau)\langle e^{\imath\omega_0 t}\hat{\sigma}_{22}(t)\hat{\sigma}_{21}(t)\rangle + \alpha_{(22)(22)}(\tau)\langle\hat{\sigma}_{22}(t)\hat{\sigma}_{22}(t)\rangle + \beta_{(22)}(\tau)\langle\hat{\sigma}_{22}(t)\rangle}{\langle\hat{\sigma}_{22}(t)\rangle^2} \ . \end{aligned} \tag{35.268}$$

Returning to the density operator and letting $t \to \infty$,

$$g^{(1)}(\tau) = e^{\imath\omega_0\tau}\left[\alpha_{(12)(12)}(\tau) + \beta_{(12)}(\tau)\frac{\rho_{21}(\infty)}{\rho_{22}(\infty)}\right] \qquad \text{and} \qquad g^{(2)}(\tau) = e^{\imath\omega_0\tau}\frac{\beta_{(22)}(\tau)}{\rho_{22}(\infty)} \ , \tag{35.269}$$

that is,

$$\boxed{\begin{aligned} g^{(1)}(\tau) &= e^{\imath\omega_0\tau}\left[\left[e^{\mathcal{M}\tau}\right]_{(12)(12)} - \left[(\mathbb{I}-e^{\mathcal{M}\tau})\mathcal{M}^{-1}\mathbf{b}\right]_{(12)}\frac{\left[\mathcal{M}^{-1}\mathbf{b}\right]_{(21)}}{\left[\mathcal{M}^{-1}\mathbf{b}\right]_{(22)}}\right] \\ g^{(2)}(\tau) &= e^{\imath\omega_0\tau}\frac{\left[(\mathbb{I}-e^{\mathcal{M}\tau})\mathcal{M}^{-1}\mathbf{b}\right]_{(22)}}{\left[\mathcal{M}^{-1}\mathbf{b}\right]_{(22)}} \end{aligned}} \ . \tag{35.270}$$

These correlation functions can easily be calculated via a numerical resolution of the Bloch equations (35.258). Fig. 35.19 shows the correlation functions and the fluorescence spectrum derived by Fourier transform of the first-order correlation function (35.177). Assuming resonant excitation, $\Delta = 0$, analytic formulas can be derived, as will be exercised in Excs. 35.6.4.3 and Exc. 35.6.4.4.

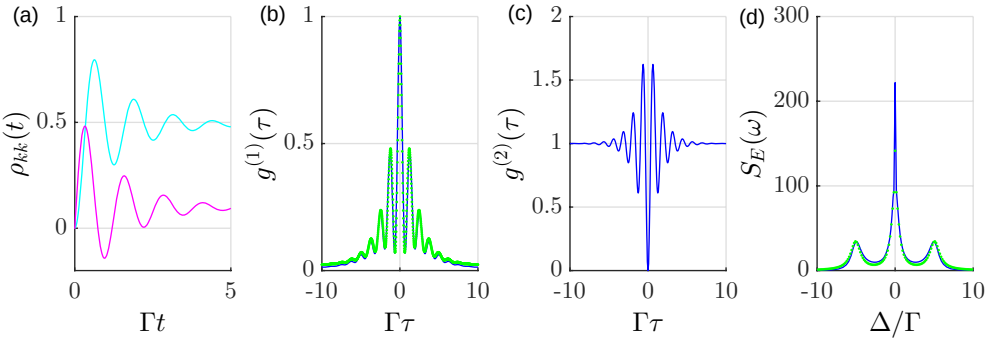

Figure 35.19: (code) (a) Temporal evolution of the excited state population $\rho_{22}(t)$ (cyan) and coherence $\rho_{12}(t)$ (magenta) of a laser-driven two-level atom with $\Omega = 5\Gamma$. (b) Correlation function $g^{(1)}(\tau)$ and (c) $g^{(2)}(\tau)$. The blue curves in (b-c) are obtained by numerical simulations of the Bloch equations and subsequent application of the quantum regression theorem (35.270). The green dots are obtained from an analytic solution derived in Exc. 35.6.4.3. (d) Mollow spectrum obtained by numerical FFT of $g^{(1)}(\tau)$.

The spectrum 35.19(d) exhibits three lines known as the *Mollow triplet*. Note that the spontaneous emission triplet is only observed in the presence of a driving laser, because it is the laser excitation which causes the splitting. Indeed, the splitting and the position of the lines are easily understood in the dressed states picture visualized in Fig. 35.1: The coupling of the two-level atom to a light field splits up the levels $|n\rangle$ and $|n+1\rangle$ by an amount corresponding to the Rabi frequency Ω. Now, the transition from the two excited state $|n+1\rangle$ levels to the ground state $|n\rangle$ levels can occur on three different frequencies. In Exc. 35.6.4.5 we calculate the Mollow spectrum for a transition between one ground and three excited Zeeman states. Fig. 35.20 illustrates the various methods to analyze scattered light, but not all of them yield information on the Mollow triplet.

35.6.3.4 Mollow spectrum from effective Hamiltonian

The Mollow triplet is easily understood in the dressed states picture. On the other hand, we know that (for classical light) the semi-classical picture is totally equivalent (its just a unitary transform of the dressed states picture). Developing a physical picture the Mollow triplet in the semi-classical framework may give us a deeper insight. Generally, the Mollow spectrum is anyhow calculated using the semi-classical Bloch equations, via the correlation function $g^{(1)}(\tau)$ and the Wiener-Khintchine theorem, but the on the way the physical intuition is lost.

For example, looking at the stationary solution of the Bloch equations (34.188), we see that $\vec{\rho}(\infty)$ is time-independent, so that we might be *surprised to see correla-*

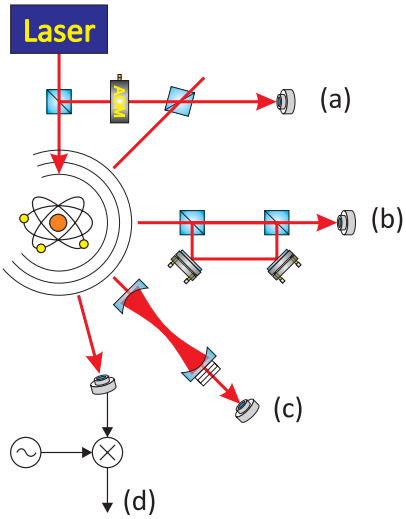

Figure 35.20: Schemes for analyzing resonance fluorescence: (a) Heterodyning [980], (b) temporal correlation, (c) spectrum [1235, 981], (d) demodulation. Only the schemes (b) and (c) yield information on the Mollow triplet.

tions in time domain (and consequently a structured spectrum) at all. This surprise results from a common misconception that may arise considering the damping of $\vec{\rho}(t)$ predicted by the Bloch model, as illustrated e.g. in Fig. 34.6: It seems that the atoms eventually cease oscillating between the ground and excited states. In most experiments, measurement are made on a large number of atoms and indeed the oscillations are damped.

In fact, however, every individual atom undergoes a complicated unpredictable trajectory alternating times of coherent evolution with spontaneous emission events (called quantum jumps). The damped behavior only results as an average over many such quantum trajectories. In this light, the reason for $g^{(1)}$-type correlations is a subtle interplay between coherently and incoherently scattered light: *The spontaneous emission probability is amplitude-modulated with the Rabi frequency.*

An alternative way to calculate the Mollow spectrum consists in solving the Schrödinger equation with the effective Hamiltonian, as done in Exc. 35.6.4.2 and 35.6.4.6. The results are shown in Fig. 35.21. While providing an intuitive picture of the origin of of the Mollow triplet a quantitatively correct treatment requires a Monte-Carlo wavefunction simulation [913] (see Sec. 36.1.2).

35.6.3.5 Weak excitation and the role of collisions

For the case of a weakly excited two-level atom, $|\Omega| \ll \Gamma$, we have analytic solutions (34.194) of the Bloch equation. We can then take the coefficients α_{ijkl} and β_{ij} and

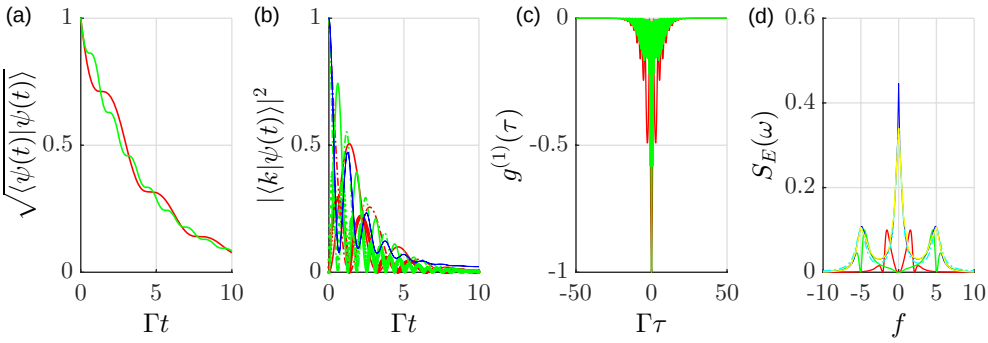

Figure 35.21: (code) (a) Time evolution of the norm of a decaying driven two-level atom. (b) Time evolution of the ground and excited state amplitudes. (c) First-order autocorrelation function, and (d) spectrum.

insert them into the correlation functions,

$$
\begin{aligned}
g^{(1)}(\tau) &= e^{-\imath\omega\tau} \ , \\
g^{(2)}(\tau) &= 1 + e^{-2\gamma\tau} - 2\cos\Delta\tau \ , \\
F(\omega_s) &= (\mathcal{F}g^{(1)})(\omega_s) = \delta(\omega_s - \omega) \ .
\end{aligned}
\tag{35.271}
$$

These functions show that the spectrum is essentially composed of *Rayleigh scattering* at the frequency of the incident light. The δ-shaped fluorescence spectrum shows, that the contribution of elastically scattered light dominates below saturation, which confirms the results (35.251) illustrated in Fig. 35.18. The light is 'antibunched' and, at higher τ exhibits a damped oscillation around the value 1.

If pressure broadening is taken into account, the two-level Bloch equations are given by (34.188), where $\gamma' = \gamma + \gamma_{coll}$ is the width of the collision-broadened line. Within this model and in the limit $\Omega \ll \Gamma$, the resonance fluorescence spectrum is given by [816],

$$
F(\omega_s) = \frac{\gamma' - \Gamma}{\gamma'} \frac{\gamma'/\pi}{(\omega_0 - \omega_s)^2 + \gamma'^2} + \frac{\Gamma}{\gamma'} \delta(\omega_s - \omega) \ . \tag{35.272}
$$

So, we find that, even at low intensities, a continuous spectrum due to *inelastic scattering* appears around the resonance frequency ω_0 additionally to the elastic Rayleigh peak.

35.6.4 Exercises

35.6.4.1 Ex: Derivation of the rate equations for two-level atoms

Inserting the ansatz (35.226) into the Schrödinger equation, derive the equations of motion (35.228) for the wavefunction amplitudes.

Solution: *The Schrödinger equation is,*

$$\begin{aligned}
&\dot\alpha|g\rangle_a|0\rangle_{\mathbf{k}} + \dot\beta|e\rangle_a|0\rangle_{\mathbf{k}} + \sum_{\mathbf{k}} \dot\gamma_{\mathbf{k}}|g\rangle_a|1\rangle_{\mathbf{k}} \\
&= -\frac{\imath}{\hbar}\left(\tfrac{\hbar}{2}\Omega_0|g\rangle_a\langle 1|e^{\imath\Delta_0 t} + \tfrac{\hbar}{2}\Omega_0|e\rangle_a\langle 0|e^{-\imath\Delta_0 t} + \hbar\sum_{\mathbf{k}} g_k|g\rangle_a\langle 1|\hat a^\dagger_{\mathbf{k}}e^{\imath\Delta_{\mathbf{k}}t} + \hbar\sum_{\mathbf{k}} g_k|e\rangle_a\langle 0|\hat a_{\mathbf{k}}e^{-\imath\Delta_k t}\right) \\
&\qquad \left(\alpha|g\rangle_a|0\rangle_{\mathbf{k}} + \beta|e\rangle_a|0\rangle_{\mathbf{k}} + \sum_{\mathbf{k}}\gamma_{\mathbf{k}}|g\rangle_a|1\rangle_{\mathbf{k}}\right) \\
&= -\imath\left(\tfrac{\Omega_0}{2}e^{-\imath\Delta_0 t} + \sum_{\mathbf{k}} g_k\hat a_{\mathbf{k}}e^{-\imath\Delta_k t}\right)\alpha|e\rangle_a|0\rangle_{\mathbf{k}} - \imath\left(\tfrac{\Omega_0}{2}e^{\imath\Delta_0 t} + \sum_{\mathbf{k}} g_k\hat a^\dagger_{\mathbf{k}}e^{\imath\Delta_k t}\right)\beta|g\rangle_a|0\rangle_{\mathbf{k}} \\
&\qquad -\imath\left(\tfrac{\Omega_0}{2}e^{-\imath\Delta_0 t} + \sum_{\mathbf{k}} g_k\hat a_{\mathbf{k}}e^{-\imath\Delta_k t}\right)\sum_{\mathbf{k}'}\gamma_{\mathbf{k}'}|e\rangle_a|1\rangle_{\mathbf{k}'} \\
&= -\imath\tfrac{\Omega_0}{2}e^{-\imath\Delta_0 t}\alpha|e\rangle_a|0\rangle_{\mathbf{k}} - \imath\tfrac{\Omega_0}{2}e^{\imath\Delta_0 t}\beta|g\rangle_a|0\rangle_{\mathbf{k}} - \imath\sum_{\mathbf{k}} g_k e^{\imath\Delta_k t}\beta|g\rangle_a|1\rangle_{\mathbf{k}} \\
&\qquad -\imath\tfrac{\Omega_0}{2}e^{-\imath\Delta_0 t}\sum_{\mathbf{k}}\gamma_{\mathbf{k}}|e\rangle_a|1\rangle_{\mathbf{k}} - \imath\sum_{\mathbf{k}} g_k e^{-\imath\Delta_k t}\gamma_{\mathbf{k}}|e\rangle_a|0\rangle_{\mathbf{k}}\ .
\end{aligned}$$

Note that the term $|e\rangle_a|1\rangle_{\mathbf{k}'}$ should be neglected, as it is not allowed within the RWA. We get,

$$\begin{aligned}
\dot\alpha|g\rangle_a|0\rangle_{\mathbf{k}} &= -\imath\tfrac{\Omega_0}{2}e^{\imath\Delta_0 t}\beta|g\rangle_a|0\rangle_{\mathbf{k}} \\
\dot\beta|e\rangle_a|0\rangle_{\mathbf{k}} &= -\imath\tfrac{\Omega_0}{2}e^{-\imath\Delta_0 t}\alpha|e\rangle_a|0\rangle_{\mathbf{k}} - \imath\sum_{\mathbf{k}} g_k e^{-\imath\Delta_k t}\gamma_{\mathbf{k}}|e\rangle_a|0\rangle_{\mathbf{k}} \\
\sum_{\mathbf{k}}\dot\gamma_{\mathbf{k}}|g\rangle_a|1\rangle_{\mathbf{k}} &= -\imath\sum_{\mathbf{k}} g_k e^{\imath\Delta_k t}\beta|g\rangle_a|1\rangle_{\mathbf{k}}\ .
\end{aligned}$$

The final result follows when we cut the states on both sides of the equation.

35.6.4.2 Ex: Non-Hermitian time evolution

Study the time evolution $|\psi(t)\rangle = e^{-\imath\hat H_{eff}t/\hbar}|\psi(0)\rangle$ with the effective Hamiltonian,

$$\hat H_{eff} = \begin{pmatrix} 0 & \frac{\hbar}{2}\Omega \\ \frac{\hbar}{2}\Omega & -\frac{\imath\hbar}{2}\Gamma \end{pmatrix}$$

starting from the initial condition $\langle 2|\psi(0)\rangle = 1$. Calculate the evolution of $|\psi(t)\rangle$ and the norm $\langle\psi(t)|\psi(t)\rangle$. Plot the time evolution of the norm for various ratios Ω/Γ and interpret the curves.

Solution: *To solve the Schrödinger equation,*

$$\imath\hbar\frac{d}{dt}|\psi\rangle = \hat H_{eff}|\psi\rangle \qquad with \qquad |\psi(t)\rangle = \begin{pmatrix} c_1(t) \\ c_2(t)\end{pmatrix} \qquad and \qquad \hat H_{eff} = \begin{pmatrix} 0 & \frac{\hbar}{2}\Omega \\ \frac{\hbar}{2}\Omega & -\frac{\imath\hbar}{2}\Gamma \end{pmatrix}\ ,$$

we need to solve the set of differential equation,

$$\begin{aligned}
\imath\dot c_1 &= \tfrac{\Omega}{2}c_2 \\
\imath\dot c_2 &= \tfrac{\Omega}{2}c_1 - \tfrac{\imath\Omega}{2}\Gamma c_2\ .
\end{aligned}$$

Differentiating the second equation and substituting the first,

$$\ddot c_2 = -\tfrac{\Gamma}{2}\dot c_2 - \tfrac{\Omega^2}{4}c_2\ .$$

The ansatz $c_2 = ae^{\lambda t}$ leads to the characteristic equation,

$$\lambda^2 + \tfrac{\Gamma}{2}\lambda + \tfrac{\Omega^2}{4} = 0 \qquad \Longrightarrow \qquad \lambda = -\tfrac{\Gamma}{4} \pm \tfrac{1}{4}\sqrt{\Gamma^2 - 4\Omega^2} \equiv -\tfrac{\Gamma}{4} \pm \tfrac{\Lambda}{4}$$

defining the abbreviation,

$$\Lambda \equiv \sqrt{\Gamma^2 - 4\Omega^2} \ .$$

Hence, our solution has the shape $c_2(t) = a_+ e^{\lambda_+ t} + a_- e^{\lambda_- t}$. Now,

$$\begin{aligned} c_2(t) &= e^{-\Gamma t/4}\left(a_+ e^{\Lambda t/4} + a_- e^{-\Lambda t/4}\right) \\ &\xrightarrow{\Omega\to 0} e^{-\Gamma t/2} \\ &\xrightarrow{\Gamma\to 0} a_+ e^{\imath\Omega t/2} + a_- e^{-\imath\Omega t/2} \ . \end{aligned}$$

The ground state amplitude follows by integration,

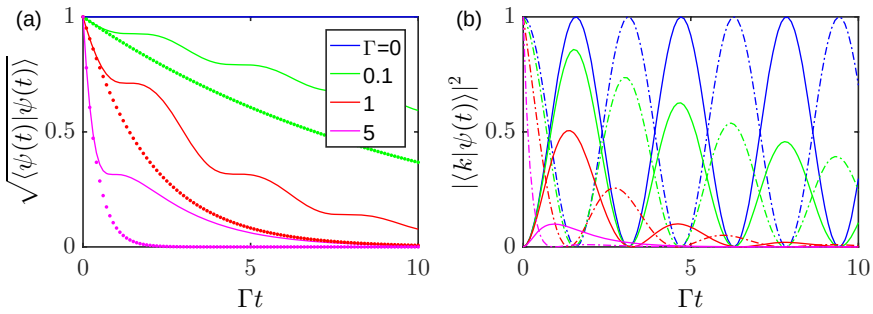

Figure 35.22: (code) (a) Time evolution of the norm of a resonantly driven two-level system with spontaneous emission for $\Omega = 2$ (solid lines) and $\Omega = 0$ (dotted lines). (b) Time evolution of the excited state (dash-dotted lines) and ground state (solid lines) populations.

$$c_1(t) = \tfrac{\Omega}{2\imath}\int_0^t c_2(t')dt' = 2\imath\Omega\left(a_+\frac{e^{-\Gamma t/4+\Lambda t/4}-1}{\Gamma-\Lambda} + a_-\frac{e^{-\Gamma t/4-\Lambda t/4}-1}{\Gamma+\Lambda}\right) \ .$$

Note the normalization condition cannot be used, here, to fix the coefficients. Instead, we use,

$$1 = c_2(0) = a_+ + a_- \qquad \textit{and} \qquad 0 = c_2(\infty) \ ,$$

yielding,

$$1 - a_- = a_+ = -\frac{2\Omega^2/\Lambda}{\Gamma+\Lambda} \ .$$

Finally,

$$\begin{pmatrix} c_1(t) \\ c_2(t) \end{pmatrix} = \begin{pmatrix} \frac{2\imath\Omega}{\Gamma+\Lambda}\left[\frac{2\Omega^2}{\Lambda}\left(\frac{1-e^{-(\Gamma-\Lambda)t/4}}{\Gamma-\Lambda} - \frac{1-e^{-(\Gamma+\Lambda)t/4}}{\Gamma+\Lambda}\right) - 1 + e^{-(\Gamma+\Lambda)t/4}\right] \\ e^{-\Gamma t/4}\left[\frac{2\Omega^2/\Lambda}{\Gamma+\Lambda}\left(e^{-\Lambda t/4} - e^{\Lambda t/4}\right) + e^{-\Lambda t/4}\right] \end{pmatrix} \ .$$

Introducing the new abbreviation $\Lambda = 2\imath\tilde{\Omega}$, we can simplify this expression,

$$\boxed{\begin{pmatrix} c_1(t) \\ c_2(t) \end{pmatrix} = e^{-\Gamma t/4} \begin{pmatrix} -\imath\frac{\Omega}{\tilde{\Omega}} \sin\frac{\tilde{\Omega}t}{2} \\ \cos\frac{\tilde{\Omega}t}{2} - \frac{\Gamma}{2\tilde{\Omega}} \sin\frac{\tilde{\Omega}t}{2} \end{pmatrix}} .$$

We readily find the following limits,

$$\begin{pmatrix} c_1(t) \\ c_2(t) \end{pmatrix} \stackrel{\Gamma\to 0}{\longrightarrow} \begin{pmatrix} -\imath \sin\frac{\Omega t}{2} \\ \cos\frac{\Omega t}{2} \end{pmatrix} \qquad \textit{and} \qquad \stackrel{\Omega\to 0}{\longrightarrow} \begin{pmatrix} 0 \\ e^{-\Gamma t/2} \end{pmatrix} .$$

The norm is,

$$\langle\psi(t)|\psi(t)\rangle = e^{-\Gamma t/2}\left(1 - \frac{\Gamma}{\tilde{\Omega}} \cos\frac{\tilde{\Omega}t}{2} \sin\frac{\tilde{\Omega}t}{2} + \frac{\Gamma^2}{2\tilde{\Omega}^2} \sin^2\frac{\tilde{\Omega}t}{2}\right)$$
$$\stackrel{\Gamma\to 0}{\longrightarrow} 1 \qquad \textit{and} \qquad \stackrel{\Omega\to 0}{\longrightarrow} e^{-\Gamma t} .$$

The decaying normalization and the exponential decay of the excited state population in the case of strong driving, $\Omega > \Gamma$, observed in Fig. 35.22 is, of course, not realistic, and points to the fact that the Schrödinger equation is unable to account for spontaneous emission. It is, however, possible to correct for the decay by continuously renormalization procedures [321].

Alternative solution:

We set $\hbar = 1$ and calculate the eigenvalues $E_\pm$ and the unitary transformation matrix U, where $U\hat{H}_{eff} = \hat{E}U$ and

$$\hat{E} \equiv \begin{pmatrix} E_+ & 0 \\ 0 & E_- \end{pmatrix} .$$

The eigenvalues are,

$$E_\pm = -\tfrac{\imath\Gamma}{4} \pm \tfrac{1}{4}\sqrt{4\Omega^2 - \Gamma^2} \stackrel{\Omega\to 0}{\longrightarrow} 0, -\tfrac{\imath}{2}\Gamma .$$

The unitary transformation matrix is nothing else than the eigenvector matrix,

$$U = \begin{pmatrix} \frac{2E_+ + \imath\Gamma}{\Omega} & \frac{2E_- + \imath\Gamma}{\Omega} \\ 1 & 1 \end{pmatrix} = \begin{pmatrix} \frac{\imath\Gamma}{2\Omega} + \sqrt{1 - \frac{\Gamma^2}{4\Omega^2}} & \frac{\imath\Gamma}{2\Omega} - \sqrt{1 - \frac{\Gamma^2}{4\Omega^2}} \\ 1 & 1 \end{pmatrix} .$$

We get for the evolution,

$$
\begin{aligned}
e^{-\imath\hat{H}_{eff}t}\begin{pmatrix}0\\1\end{pmatrix} &= Ue^{-\imath\hat{E}t}U^{-1}\begin{pmatrix}0\\1\end{pmatrix} \\
&= \begin{pmatrix}\frac{2E_+ +\imath\Gamma}{\Omega} & \frac{2E_- +\imath\Gamma}{\Omega}\\ 1 & 1\end{pmatrix}\begin{pmatrix}e^{-\imath E_+ t} & 0\\ 0 & e^{-\imath E_- t}\end{pmatrix}\begin{pmatrix}\frac{2E_+ +\imath\Gamma}{\Omega} & \frac{2E_- +\imath\Gamma}{\Omega}\\ 1 & 1\end{pmatrix}^{-1}\begin{pmatrix}0\\1\end{pmatrix} \\
&= \begin{pmatrix}-\frac{(2E_+ +\imath\Gamma)(2E_- +\imath\Gamma)}{2\Omega(E_+ -E_-)}(e^{-\imath E_+ t}-e^{-\imath E_- t}) \\ -\frac{(2E_- +\imath\Gamma)}{2(E_+ -E_-)}e^{-\imath E_+ t}+\frac{(2E_+ +\imath\Gamma)}{2(E_+ -E_-)}e^{-\imath E_- t}\end{pmatrix} \\
&= \begin{pmatrix}\frac{\Omega}{\sqrt{4\Omega^2-\Gamma^2}}(e^{-\imath E_+ t}-e^{-\imath E_- t}) \\ \frac{1}{2}\left(1-\frac{\imath\Gamma}{\sqrt{4\Omega^2-\Gamma^2}}\right)e^{-\imath E_+ t}+\frac{1}{2}\left(1+\frac{\imath\Gamma}{\sqrt{4\Omega^2-\Gamma^2}}\right)e^{-\imath E_- t}\end{pmatrix} \\
&= e^{-\Gamma t/4}\begin{pmatrix}\frac{-2\imath\Omega}{\sqrt{4\Omega^2-\Gamma^2}}\sin\frac{t\sqrt{4\Omega^2-\Gamma^2}}{4} \\ \cos\frac{t\sqrt{4\Omega^2-\Gamma^2}}{4}-\frac{\Gamma}{\sqrt{4\Omega^2-\Gamma^2}}\sin\frac{t\sqrt{4\Omega^2-\Gamma^2}}{4}\end{pmatrix}\ .
\end{aligned}
$$

The result is identical to the one previously derived.

35.6.4.3 Ex: Resonance fluorescence and antibunching via Bloch equations

a. Derive the analytic solution of the Bloch equations for a resonantly driven two-level atom.
b. Calculate the 1^{st}-order correlation function $g^{(1)}(\tau)$ from the formula (35.270).
c. Derive the spectrum of resonance fluorescence [912].
d. Derive the 2^{nd}-order correlation function $g^{(2)}(\tau)$ from the formula (35.270).

Solution: *a. The Bloch equations for a single driven two-level atom become, after elimination of the ground state population,*

$$\dot{\vec{\rho}}_{red} = \mathcal{M}\vec{\rho}_{red} + \mathbf{b}\ ,$$

where $\vec{\rho}_{red} = (\rho_{22}\ \rho_{21}\ \rho_{12})^\dagger$ *and*

$$\mathcal{M} = \begin{pmatrix}-\Gamma & -\frac{\imath}{2}\Omega & \frac{\imath}{2}\Omega \\ -\imath\Omega & -\frac{1}{2}\Gamma-\imath\Delta & 0 \\ \imath\Omega & 0 & -\frac{1}{2}\Gamma+\imath\Delta\end{pmatrix} \quad \textit{and} \quad \mathbf{b} = \begin{pmatrix}0\\ \frac{\imath}{2}\Omega \\ -\frac{\imath}{2}\Omega\end{pmatrix}\ .$$

The stationary solution is (using MAPLE) found to be,

$$\vec{\rho}_{red}(\infty) = -\mathcal{M}^{-1}\mathbf{b} = \frac{\imath\Omega}{4\Delta^2+2\Omega^2+\Gamma^2}\begin{pmatrix}-\imath\Omega \\ \Gamma-2\imath\Delta \\ -\Gamma-2\imath\Delta\end{pmatrix}\ .$$

We now simplify the calculation assuming $\Delta = 0$,

$$\mathcal{M} = \begin{pmatrix}-\Gamma & -\frac{\imath}{2}\Omega & \frac{\imath}{2}\Omega \\ -\imath\Omega & -\frac{1}{2}\Gamma & 0 \\ \imath\Omega & 0 & -\frac{1}{2}\Gamma\end{pmatrix} = UEU^{-1}$$

with

$$E=\begin{pmatrix}-\frac{3}{4}\Gamma+\frac{1}{4}\Lambda & 0 & 0\\ 0 & -\frac{3}{4}\Gamma-\frac{1}{4}\Lambda & 0\\ 0 & 0 & -\frac{1}{2}\Gamma\end{pmatrix} \quad \textit{and} \quad U=\begin{pmatrix}-\frac{\imath\Gamma}{4\Omega}+\frac{\imath\Lambda}{4\Omega} & -\frac{\imath\Gamma}{4\Omega}-\frac{\imath\Lambda}{4\Omega} & 0\\ 1 & 1 & 1\\ -1 & -1 & 1\end{pmatrix},$$

where we introduced the abbreviation $\Lambda\equiv\sqrt{\Gamma^2-16\Omega^2}$. *Now,*

$$e^{\mathcal{M}t}=Ue^{Et}U^{-1}=e^{-\gamma t}\times$$
$$\begin{pmatrix}\frac{-\Gamma+\Lambda}{2\Lambda}e^{-\frac{(\Gamma-\Lambda)t}{4}}+\frac{\Gamma+\Lambda}{2\Lambda}e^{-\frac{(\Gamma+\Lambda)t}{4}} & -\frac{\imath\Omega}{\Lambda}\left(e^{-\frac{(\Gamma-\Lambda)t}{4}}-e^{-\frac{(\Gamma+\Lambda)t}{4}}\right) & \frac{\imath\Omega}{\Lambda}\left(e^{-\frac{(\Gamma-\Lambda)t}{4}}-e^{-\frac{(\Gamma+\Lambda)t}{4}}\right)\\ -\frac{2\imath\Omega}{\Lambda}\left(e^{-\frac{(\Gamma-\Lambda)t}{4}}-e^{-\frac{(\Gamma+\Lambda)t}{4}}\right) & \frac{\Gamma+\Lambda}{4\Lambda}e^{-\frac{(\Gamma-\Lambda)t}{4}}+\frac{-\Gamma+\Lambda}{4\Lambda}e^{-\frac{(\Gamma+\Lambda)t}{4}}+\frac{1}{2} & \frac{-\Gamma-\Lambda}{4\Lambda}e^{-\frac{(\Gamma-\Lambda)t}{4}}+\frac{\Gamma-\Lambda}{4\Lambda}e^{-\frac{(\Gamma+\Lambda)t}{4}}+\frac{1}{2}\\ \frac{2\imath\Omega}{\Lambda}\left(e^{-\frac{(\Gamma-\Lambda)t}{4}}-e^{-\frac{t}{2}(\gamma+\lambda)}\right) & \frac{-\Gamma-\Lambda}{4\Lambda}e^{-\frac{(\Gamma-\Lambda)t}{4}}+\frac{\Gamma-\Lambda}{4\Lambda}e^{-\frac{(\Gamma+\Lambda)t}{4}}+\frac{1}{2} & \frac{\Gamma+\Lambda}{4\Lambda}e^{-\frac{(\Gamma-\Lambda)t}{4}}+\frac{-\Gamma+\Lambda}{4\Lambda}e^{-\frac{t(\gamma+\lambda)}{2}}+\frac{1}{2}\end{pmatrix}.$$

Hence,

$$(\mathbb{I}-e^{\mathcal{M}t})\vec{\rho}_{red}(\infty)$$
$$=\frac{\Omega}{2\Lambda(\Gamma^2+2\Omega^2)}\left[\begin{pmatrix}2\Omega\Lambda\\ 2\imath\Gamma\Lambda\\ -2\imath\Gamma\Lambda\end{pmatrix}+e^{-\frac{t}{4}(3\Gamma+\Lambda)}\begin{pmatrix}-(3\Gamma-\Lambda)\Omega\\ -\imath(\Gamma\Lambda-\Gamma^2+4\Omega^2)\\ \imath(\Gamma\Lambda-\Gamma^2+\Omega^2)\end{pmatrix}+e^{-\frac{t}{4}(3\Gamma-\Lambda)}\begin{pmatrix}-(3\Gamma+\Lambda)\Omega\\ -\imath(\Gamma\Lambda+\Gamma^2-4\Omega^2)\\ \imath(\Gamma\Lambda+\Gamma^2-\Omega^2)\end{pmatrix}\right].$$

After sufficiently long times t *the solution found in (34.286) becomes,*

$$\boxed{\vec{\rho}_{red}(t)=e^{\mathcal{M}t}\vec{\rho}_{red}(0)+(\mathbb{I}-e^{\mathcal{M}t})\vec{\rho}_{red}(\infty)\overset{\gamma t,\Omega t\gg 1}{\longrightarrow}(\mathbb{I}-e^{\mathcal{M}t})\vec{\rho}_{red}(\infty)}.$$

The same solution applies for arbitrary times choosing $\rho_{red}(0)=0$ *as the initial condition.*

b. With the expression for the correlation function (35.270),

$$g^{(1)}(\tau)=e^{\imath\omega_0\tau}\left[[e^{\mathcal{M}\tau}]_{(12)(12)}+[(\mathbb{I}-e^{\mathcal{M}\tau})\vec{\rho}_{red}(\infty)]_{(12)}\frac{[\vec{\rho}_{red}(\infty)]_{(21)}}{[\vec{\rho}_{red}(\infty)]_{(22)}}\right]$$

we get from the above solution of the Bloch equations,

$$g^{(1)}(\tau)=e^{\imath\omega_0\tau}\left[\frac{\Gamma^2}{\Gamma^2+2\Omega^2}+\frac{1}{2}e^{-\Gamma\tau/2}+\sum_{\pm}\frac{-\Gamma^2(\Lambda\pm\Gamma)+2\Omega^2(\Lambda\pm 5\Gamma)}{4\Lambda(\Gamma^2+2\Omega^2)}e^{-(3\Gamma\mp\Lambda)\tau/4}\right].$$

For weak driving, $\Omega\ll\Gamma$,

$$g^{(1)}(\tau)\simeq e^{\imath\omega_0\tau}\left(1+\tfrac{\Omega^2}{\Gamma^2}e^{-\Gamma\tau}\right).$$

For strong driving,

$$g^{(1)}(\tau)\simeq e^{\imath\omega_0\tau}\left[\tfrac{\Gamma^2}{2\Omega^2}+\tfrac{1}{2}e^{-\frac{1}{2}\Gamma\tau}+\tfrac{1}{2}e^{-\frac{3}{4}\Gamma\tau}\cos\Omega\tau\right].$$

Let us now rewrite the expression for $g^{(1)}(\tau)$ *introducing the abbreviation* $\tilde{\Omega}\equiv\sqrt{\Omega^2-\Gamma^2/16}=\imath\Lambda/4$. *Then,*

$$\boxed{g^{(1)}(\tau)=e^{\imath\omega_0\tau}\left[\frac{\Gamma^2}{\Gamma^2+2\Omega^2}+\frac{1}{2}e^{-\Gamma\tau/2}+\sum_{\pm}\frac{4\tilde{\Omega}(2\Omega^2-\Gamma^2)\pm\imath\Gamma(10\Omega^2-\Gamma^2)}{16\tilde{\Omega}(\Gamma^2+2\Omega^2)}e^{-3\Gamma\tau/4\mp\imath\tilde{\Omega}\tau}\right]}. \tag{35.273}$$

c. The spectrum is just the Fourier transform, for which the following rules hold,

$$(\mathcal{F})(\omega) = \frac{1}{\sqrt{2\pi}} \int_{-\infty}^{\infty} f(\tau) e^{-\imath\omega\tau} d\tau \quad , \quad (f * g)(\omega) = \int_{-\infty}^{\infty} f(t) g(\tau - t) dt$$

$$\mathcal{F}[1](\omega) = \sqrt{2\pi}\delta(\omega) \quad , \quad \mathcal{F}[\theta(\tau) e^{-a\tau}] = \frac{1}{\sqrt{2\pi}} \frac{1}{\imath\omega + a} \quad \Longrightarrow \quad \mathcal{F}[e^{-a|\tau|}] = \sqrt{\frac{2}{\pi}} \frac{a}{\omega^2 + a^2} \ .$$

Applying them to the above function $g^{(1)}(\tau)$ we get for $\tilde{\Omega} \in R$,

$$S_{\mathcal{E}}(\omega) = \mathcal{F}[g^{(1)}(\tau)] \ .$$

In the case of weak driving, the spectrum is readily obtained,

$$S_{\mathcal{E}}(\omega) = \frac{1}{2\pi} \int_{-\infty}^{\infty} e^{\imath\omega_0\tau} \left(1 + \frac{\Omega^2}{\Gamma^2} e^{-\Gamma\tau}\right) e^{-\imath\omega\tau} d\tau = \delta(\Delta) + \frac{\Omega^2}{\Gamma^2} \frac{\Gamma/\pi}{\Delta^2 + \Gamma^2} \ .$$

In the case of string driving, we must resort to Eq. (35.274). The first term gives,

$$T_1 = \delta(\omega - \omega_0) * \frac{\Gamma^2}{\Gamma^2 + 2\Omega^2} \frac{1}{\sqrt{2\pi}} \int_{-\infty}^{\infty} e^{-\imath\omega\tau} d\tau = \frac{\Gamma^2}{\Gamma^2 + 2\Omega^2} \delta(\omega - \omega_0) \ .$$

The second term gives,

$$T_2 = \delta(\omega - \omega_0) * \frac{1}{2} \frac{1}{\sqrt{2\pi}} \int_{-\infty}^{\infty} e^{-\imath\omega\tau} e^{-\Gamma\tau/2} d\tau = \frac{1}{2} \frac{1}{\sqrt{2\pi}} \frac{1}{\imath(\omega - \omega_0) + \Gamma/2} \ .$$

Finally, the third term is,

$$\begin{aligned} T_3 &= \delta(\omega - \omega_0 \pm \tilde{\Omega}) * \sum_{\pm} \frac{4\tilde{\Omega}\left(2\Omega^2 - \Gamma^2\right) \pm \imath\Gamma(10\Omega^2 - \Gamma^2)}{16\tilde{\Omega}(\Gamma^2 + 2\Omega^2)} \frac{1}{\sqrt{2\pi}} \int_{-\infty}^{\infty} e^{-\imath\omega\tau} e^{-3\Gamma\tau/4} d\tau \\ &= \frac{1}{\sqrt{2\pi}} \sum_{\pm} \frac{4\tilde{\Omega}(2\Omega^2 - \Gamma^2) \pm \imath\Gamma(10\Omega^2 - \Gamma^2)}{16\tilde{\Omega}(\Gamma^2 + 2\Omega^2)} \frac{1}{\imath(\omega - \omega_0 \pm \tilde{\Omega}) + \frac{3}{4}\Gamma} \ . \end{aligned}$$

The spectrum follows as the real part of these four terms,

$$\boxed{\begin{aligned} \mathfrak{Re}\ S_{\mathcal{E}}(\omega) &= \frac{\Gamma^2}{\Gamma^2 + 2\Omega^2} \delta(\omega - \omega_0) + \frac{1}{\sqrt{2\pi}} \frac{\Gamma/4}{(\omega - \omega_0)^2 + (\Gamma/2)^2} \\ &+ \frac{1}{\sqrt{2\pi}} \sum_{\pm} \frac{3\Gamma\tilde{\Omega}(2\Omega^2 - \Gamma^2) \mp (\omega - \omega_0 \pm \tilde{\Omega})\Gamma(10\Omega^2 - \Gamma^2)}{16\tilde{\Omega}(\Gamma^2 + 2\Omega^2)\left[(\omega - \omega_0 \pm \tilde{\Omega})^2 + (\frac{3}{4}\Gamma)^2\right]} \end{aligned}} \ . \tag{35.274}$$

Note that the sidebands are partially correlated (especially for strong driving) and partially anti-correlated [15]*. For strong driving, we get,*

$$\mathfrak{Re}\ S_{\mathcal{E}}(\omega) \simeq \frac{\Gamma}{4\sqrt{2\pi}} \frac{1}{\Delta^2 + (\frac{1}{2}\Gamma)^2} + \frac{3\Gamma}{16\sqrt{2\pi}} \sum_{\pm} \frac{1}{(\Delta \pm \Omega)^2 + (\frac{3}{4}\Gamma)^2} \ . \tag{35.275}$$

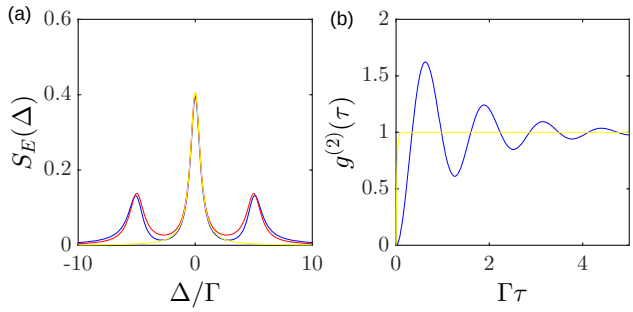

Figure 35.23: (code) (a) Analytical shape of the fluorescence spectrum for $\Omega = 5\Gamma$ calculated from the (blue) full formula (35.274), (red) high power limit (35.275). (b) $g^{(2)}(\tau)$.

The exact spectrum and its strong driving approximation are shown in Fig. 35.23(a).
d. With the expression for the correlation function (35.270),

$$g^{(2)}(\tau) = e^{\imath\omega_0\tau}\frac{[(\mathbb{I} - e^{\mathcal{M}\tau})\mathcal{M}^{-1}\mathbf{b}]_{(22)}}{[\mathcal{M}^{-1}\mathbf{b}]_{(22)}} \ .$$

we get from the above solution of the Bloch equations,

$$\boxed{g^{(2)}(\tau) = -e^{\imath\omega_0\tau}\left[1 + \left(\frac{1}{2} - \frac{3\Gamma}{2\Lambda}\right)e^{-\frac{\tau}{4}(3\Gamma+\Lambda)} - \left(\frac{1}{2} + \frac{3\Gamma}{2\Lambda}\right)e^{-\frac{\tau}{4}(3\Gamma-\Lambda)}\right]} \ .$$

The absolute value of $|g^{(2)}(\tau)|$ is shown in Fig. 35.23(b).

35.6.4.4 Ex: Resonance fluorescence via rate equations

Repeat Exc. 35.6.4.3 neglecting coherences, i.e. replacing the Bloch equations by rate equations,

$$\dot{\vec{\rho}} = \begin{pmatrix} -R & R+\Gamma & 0 & 0 \\ R & -R-\Gamma & 0 & 0 \\ 0 & 0 & -\gamma & 0 \\ 0 & 0 & 0 & -\gamma \end{pmatrix}\vec{\rho} \ ,$$

where $R = \Omega^2/2\gamma$ is the pump rate.

Solution: *a. Eliminating ρ_{11} from the rate equations, we write $\dot{\vec{\rho}}_{red} = \mathcal{M}\vec{\rho}_{red} + \mathbf{b}$, where,*

$$\mathcal{M} = \begin{pmatrix} -2R-\Gamma & 0 & 0 \\ 0 & -\gamma & 0 \\ 0 & 0-\gamma & \end{pmatrix} \qquad \textit{and} \qquad \mathbf{b} = \begin{pmatrix} R \\ 0 \\ 0 \end{pmatrix} \ .$$

[15] This is reminiscent to AM and PM: $|1 + Me^{\imath\Omega t} \pm Me^{-\imath\Omega t}|^2 = 1 + 2(1 \pm 1)M\cos\Omega t + 2M^2(1 \pm \cos 2\Omega t)$.

b. From this we obtain,

$$\vec{\rho}_{red}(\infty) = -\mathcal{M}^{-1}\mathbf{b} = \begin{pmatrix} (2+\frac{\Gamma}{R})^{-1} \\ 0 \\ 0 \end{pmatrix} \quad \textit{and} \quad e^{\mathcal{M}t} = \begin{pmatrix} e^{(-2R-\Gamma)t} & 0 & 0 \\ 0 & e^{-\gamma t} & 0 \\ 0 & 0 & e^{-\gamma t} \end{pmatrix} ,$$

which allows us the calculate, with the expression for the correlation function (35.270),

$$g^{(1)}(\tau) = e^{\imath\omega_0\tau}\left[[e^{\mathcal{M}t}]_{(12)(12)} + [(\mathbb{I}-e^{\mathcal{M}t})\vec{\rho}_{red}(\infty)]_{(12)}\frac{[\vec{\rho}_{red}(\infty)]_{(21)}}{[\vec{\rho}_{red}(\infty)]_{(22)}}\right] = e^{\imath\omega_0\tau-\gamma\tau} .$$

c. The spectrum is,

$$\mathfrak{Re}\ S_{\mathcal{E}}(\omega) = \frac{\gamma/\pi}{\Delta^2 + (\frac{1}{2}\Gamma)^2} .$$

d. With the expression for the correlation function (35.270),

$$g^{(2)}(\tau) = e^{\imath\omega_0\tau}\frac{[(\mathbb{I}-e^{\mathcal{M}\tau})\mathcal{M}^{-1}\mathbf{b}]_{(22)}}{[\mathcal{M}^{-1}\mathbf{b}]_{(22)}} .$$

we get from the above solution of the Bloch equations,

$$g^{(2)}(\tau) = e^{\imath\omega_0\tau}\left[1-e^{(-2R-\Gamma)\tau}\right] .$$

The absolute value of $|g^{(2)}(\tau)|$ is shown in Fig. 35.23(b).

35.6.4.5 Ex: Fluorescence spectrum of a four-level system

A more realistic transition, allowing for a vectorial nature of the radiation field, involves one ground and three excited Zeeman states (e.g. the strontium $^1S_0$-$^1P_1$ transition). In this case, the emitted light is,

$$\hat{\mathcal{E}}^-(t) = \hat{\mathcal{E}}^-_{\sigma^-}(t) + \hat{\mathcal{E}}^-_{\pi}(t) + \hat{\mathcal{E}}^-_{\sigma^+}(t) .$$

Calculate the first-order correlation function and the fluorescence spectrum of this transition.

Solution: *The correlation function is,*

$$\begin{aligned} g^{(1)}(\tau) &\equiv \frac{\langle\hat{\mathcal{E}}^-(t)\hat{\mathcal{E}}^+(t+\tau)\rangle}{\langle\hat{\mathcal{E}}^-(t)\hat{\mathcal{E}}^+(t)\rangle} \\ &= \frac{\langle[\hat{\mathcal{E}}^-_{\sigma^-}(t)+\hat{\mathcal{E}}^-_{\pi}(t)+\hat{\mathcal{E}}^-_{\sigma^+}(t)][\hat{\mathcal{E}}^+_{\sigma^-}(t+\tau)+\hat{\mathcal{E}}^+_{\pi}(t+\tau)+\hat{\mathcal{E}}^+_{\sigma^+}(t+\tau)]\rangle}{\langle[\hat{\mathcal{E}}^-_{\sigma^-}(t)+\hat{\mathcal{E}}^-_{\pi}(t)+\hat{\mathcal{E}}^-_{\sigma^+}(t)][\hat{\mathcal{E}}^+_{\sigma^-}(t)+\hat{\mathcal{E}}^+_{\pi}(t)+\hat{\mathcal{E}}^+_{\sigma^+}(t)]\rangle} . \end{aligned}$$

Labeling the states,

$$\hat{\mathcal{E}}^-_{\sigma^-} = \gamma\hat{\sigma}_{21} \quad , \quad \hat{\mathcal{E}}^-_{\pi} = \gamma\hat{\sigma}_{31} \quad , \quad \hat{\mathcal{E}}^-_{\sigma^+} = \gamma\hat{\sigma}_{41} ,$$

we arrive at,

$$
\begin{aligned}
g^{(1)}(\tau) &= \frac{\langle[\gamma\hat{\sigma}_{21}(t)+\gamma\hat{\sigma}_{31}(t)+\gamma\hat{\sigma}_{41}(t)][\gamma\hat{\sigma}_{12}(t+\tau)+\gamma\hat{\sigma}_{13}(t+\tau)+\gamma\hat{\sigma}_{14}(t+\tau)]\rangle}{\langle[\gamma\hat{\sigma}_{21}(t)+\gamma\hat{\sigma}_{31}(t)+\gamma\hat{\sigma}_{41}(t)][\gamma\hat{\sigma}_{12}(t)+\gamma\hat{\sigma}_{13}(t)+\gamma\hat{\sigma}_{14}(t)]\rangle} \\
&= \frac{\begin{array}{c}\sum_{(mn)}\alpha_{(12)(mn)}(\tau)\langle[\hat{\sigma}_{21}(t)+\hat{\sigma}_{31}(t)+\hat{\sigma}_{41}(t)]\,\hat{\sigma}_{12}(t)\rangle+\beta_{(12)}(\tau)\langle\hat{\sigma}_{21}(t)\rangle \\ +\sum_{(mn)}\alpha_{(13)(mn)}(\tau)\langle[\hat{\sigma}_{21}(t)+\hat{\sigma}_{31}(t)+\hat{\sigma}_{41}(t)]\,\hat{\sigma}_{13}(t)\rangle+\beta_{(13)}(\tau)\langle\hat{\sigma}_{31}(t)\rangle \\ +\sum_{(mn)}\alpha_{(14)(mn)}(\tau)\langle[\hat{\sigma}_{21}(t)+\hat{\sigma}_{31}(t)+\hat{\sigma}_{41}(t)]\,\hat{\sigma}_{14}(t)\rangle+\beta_{(14)}(\tau)\langle\hat{\sigma}_{41}(t)\rangle\end{array}}{\langle[\hat{\sigma}_{21}(t)+\hat{\sigma}_{31}(t)+\hat{\sigma}_{41}(t)]\,[\hat{\sigma}_{12}(t)+\hat{\sigma}_{13}(t)+\hat{\sigma}_{14}(t)]\rangle} \\
&= \frac{\begin{array}{c}\alpha_{(12)(12)}(\tau)\langle\hat{\sigma}_{21}(t)\hat{\sigma}_{12}(t)\rangle+\beta_{(12)}(\tau)\langle\hat{\sigma}_{21}(t)\rangle \\ +\alpha_{(13)(13)}(\tau)\langle\hat{\sigma}_{31}(t)\hat{\sigma}_{13}(t)\rangle+\beta_{(13)}(\tau)\langle\hat{\sigma}_{31}(t)\rangle \\ +\alpha_{(14)(14)}(\tau)\langle\hat{\sigma}_{41}(t)\hat{\sigma}_{14}(t)\rangle+\beta_{(14)}(\tau)\langle\hat{\sigma}_{41}(t)\rangle\end{array}}{\langle[\hat{\sigma}_{21}(t)+\hat{\sigma}_{31}(t)+\hat{\sigma}_{41}(t)][\hat{\sigma}_{12}(t)+\hat{\sigma}_{13}(t)+\hat{\sigma}_{14}(t)]\rangle} \\
&= \frac{\begin{array}{c}\alpha_{(12)(12)}(\tau)\rho_{22}(\infty)\rangle+\beta_{(12)}(\tau)\rho_{21}(\infty)+\alpha_{(13)(13)}(\tau)\rho_{33}(\infty) \\ +\beta_{(13)}(\tau)\rho_{31}(\infty)+\alpha_{(14)(14)}(\tau)\rho_{44}(\infty)+\beta_{(14)}(\tau)\rho_{41}(\infty)\end{array}}{\rho_{22}(\infty)+\rho_{33}(\infty)+\rho_{44}(\infty)+\rho_{23}(\infty)+\rho_{32}(\infty)+\rho_{24}(\infty)+\rho_{42}(\infty)+\rho_{34}(\infty)+\rho_{43}(\infty)} \,.
\end{aligned}
$$

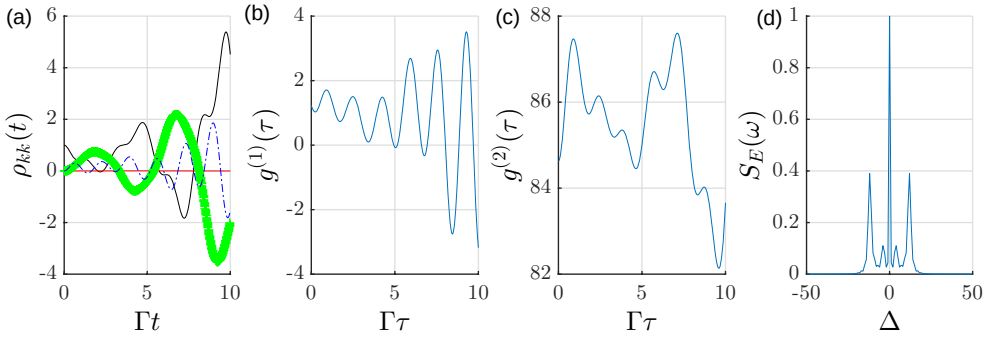

Figure 35.24: Resonance fluorescence spectrum of a degenerate four-level system.

35.6.4.6 Ex: Semi-classical picture of the Mollow triplet

Calculate the first-order correlation function from the solution of the Schrödinger equation with the effective Hamiltonian derived in Exc. 35.6.4.2.

Solution: *Solving the Schrödinger equation with the effective Hamiltonian we derived the following solution in Exc. 35.6.4.2,*

$$
|\psi(t)\rangle = e^{-\Gamma t/4}\begin{pmatrix} \frac{-\imath\Omega}{\tilde{\Omega}}\sin\frac{\tilde{\Omega}t}{2} \\ \cos\frac{\tilde{\Omega}t}{2}-\frac{\Gamma}{2\tilde{\Omega}}\sin\frac{\tilde{\Omega}t}{2}\end{pmatrix} \quad , \quad \tilde{\Omega}\equiv\sqrt{\Omega^2-\tfrac{\Gamma^2}{4}} \,.
$$

The populations and coherences are then,

$$\langle 2|2\rangle = e^{-\Gamma t/2}\left(\frac{\Omega^2}{2\tilde{\Omega}^2} + \frac{2\Omega^2-\Gamma^2}{\tilde{\Omega}^2}\cos\tilde{\Omega}t - \frac{\Gamma}{2\tilde{\Omega}}\sin\tilde{\Omega}t\right)$$
$$\langle 1|1\rangle = e^{-\Gamma t/2}\frac{\Omega^2}{2\tilde{\Omega}^2}(1-\cos\tilde{\Omega}t)$$
$$\langle 2|1\rangle = ie^{-\Gamma t/2}\frac{\Omega}{2\tilde{\Omega}}\left(\frac{\Gamma}{2\tilde{\Omega}} - \frac{\Gamma}{2\tilde{\Omega}}\cos\tilde{\Omega}t - \sin\tilde{\Omega}t\right) .$$

The field radiated by resonance fluorescence is $\mathcal{E} \propto \sigma^- = |1\rangle\langle 2|$. From this we can calculate the correlation,

$$\begin{aligned}&\langle t\mathcal{E}(t)\mathcal{E}^+(t+\tau)\rangle \\ &= e^{-\Gamma\tau/2}\left(\frac{\Omega}{2\tilde{\Omega}}\right)^2 \lim_{t\to\infty}\int_0^t e^{-\Gamma t}\left(\tfrac{\Gamma}{2\tilde{\Omega}} - \tfrac{\Gamma}{2\tilde{\Omega}}\cos\tilde{\Omega}t - \sin\tilde{\Omega}t\right)\left(\tfrac{\Gamma}{2\tilde{\Omega}} - \tfrac{\Gamma}{2\tilde{\Omega}}\cos\tilde{\Omega}(t+\tau) - \sin\tilde{\Omega}(t+\tau)\right)dt \\ &= e^{-\Gamma\tau/2}\frac{-\Omega^2}{2\tilde{\Omega}^2}\frac{\Gamma^2-(\Gamma^2+2\tilde{\Omega}^2)\cos\tilde{\Omega}\tau - \Gamma\tilde{\Omega}\sin\tilde{\Omega}\tau}{8\Gamma(\Gamma^2+\tilde{\Omega}^2)} .\end{aligned}$$

Hence,

$$g^{(1)}(\tau) = \frac{\langle t\mathcal{E}(t)\mathcal{E}^+(t+T)\rangle}{\langle t\mathcal{E}(t)\mathcal{E}^+(t)\rangle} = e^{-\Gamma\tau/2}\frac{-\Gamma^2+(\Gamma^2+2\tilde{\Omega}^2)\cos\tilde{\Omega}\tau + \Gamma\tilde{\Omega}\sin\tilde{\Omega}\tau}{2\tilde{\Omega}^2} .$$

35.6.4.7 Ex: Monte-Carlo simulation of the Mollow triplet

Implement a Monte-Carlo simulation of the Mollow triplet for a driven two-level atom according to [321, 913].

Solution: *We consider a single laser-driven two-level atom,*

$$\hat{H} = \tfrac{\hbar\Omega}{2}(\hat{\sigma}^+ + \hat{\sigma}^-) + (\hbar\omega_0 + \imath\hbar\Gamma)\hat{\sigma}_z = \begin{pmatrix} 0 & \frac{\hbar\Omega}{2} \\ \frac{\hbar\Omega}{2} & \hbar\omega_0 + \imath\frac{\Gamma}{2}\end{pmatrix} ,$$

where $\hat{\sigma}^- = |1\rangle\langle 2|$. We are interested in calculating the first-order correlation function $g^{(1)}(\tau) = \langle\hat{\sigma}^+(t+\tau)\hat{\sigma}^-(t)\rangle$. The MCWF is performed by starting with the atom in the ground state, $|\psi(0)\rangle = |1\rangle$, and applying the procedure,

$$|\psi(t_1)\rangle \to \begin{cases} e^{-\imath\hat{H}t_1/\hbar}|\psi(t_1)\rangle & \text{for} \quad \zeta < \sqrt{\langle\psi|\psi\rangle} \\ |\psi(0)\rangle & \text{for} \quad \zeta > \sqrt{\langle\psi|\psi\rangle}\end{cases}$$

Now, we consider new states,

$$|\chi_\pm(0)\rangle \equiv \tfrac{1}{\sqrt{\mu_\pm}}(1\pm\hat{\sigma}^-)|\psi(t)\rangle \qquad \text{and} \qquad |\chi'_\pm(0)\rangle \equiv \tfrac{1}{\sqrt{\mu'_\pm}}(1\pm\imath\hat{\sigma}^-)|\psi(t)\rangle ,$$

where $\mu_\pm = \langle\psi|(1\pm\hat{\sigma}^+)(1\pm\hat{\sigma}^-)|\psi\rangle$,

$$|\chi_\pm^{(\prime)}(\tau)\rangle \to \begin{cases} e^{-\imath\hat{H}t_1/\hbar}|\chi_\pm^{(\prime)}(t_1)\rangle & \text{for} \quad \zeta < \sqrt{\langle\psi|\psi\rangle} \\ |\chi_\pm^{(\prime)}(0)\rangle & \text{for} \quad \zeta > \sqrt{\langle\psi|\psi\rangle}\end{cases} .$$

The first-order correlation function is obtained from,

$$g^{(1)}(\tau) = \tfrac{1}{4}\left(\mu_+\overline{\langle\chi_+(\tau)|\hat{\sigma}^+|\chi_+(\tau)\rangle} - \mu_-\overline{\langle\chi_-(\tau)|\hat{\sigma}^+|\chi_-(\tau)\rangle} - \imath\mu'_+\overline{\langle\chi'_+(\tau)|\hat{\sigma}^+|\chi'_+(\tau)\rangle} + \imath\mu'_+\overline{\langle\chi'_-(\tau)|\hat{\sigma}^+|\chi'_-(\tau)\rangle}\right) .$$

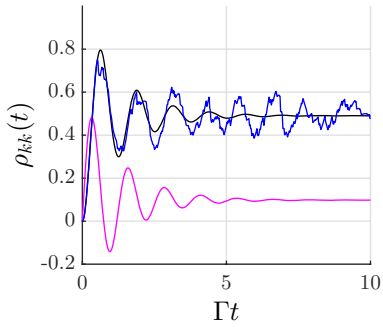

Figure 35.25: (code) Monte-Carlo simulation of the Mollow triplet.

35.7 Light scattering from multi-level atoms

35.7.1 Quantum beats

The phenomenon of *quantum beats* is another simple example of effects beyond semi-classical theory, requiring a full second-quantized calculation. In semi-classical theory (SCT), there is an interference or beat note term for both V-type and Λ-type atoms, while in quantum electrodynamics (QED) only V-type atoms exhibits a beat term.

In the semi-classical picture, the state vector of electrons is [1184],

$$\psi(t)\rangle = c_1 e^{-\imath\omega_1 t}|1\rangle + c_2 e^{-\imath\omega_2 t}|2\rangle + c_3 e^{-\imath\omega_3 t}|3\rangle \ . \tag{35.276}$$

Writing the non-vanishing dipole matrix elements as $d_{12} = e\langle 1|r|2\rangle$, $d_{23} = e\langle 2|r|3\rangle$ a three-level atom has two microscopic oscillating dipoles,

$$\mathcal{P}(t) = d_{12}(c_1^* c_2)e^{\imath\omega_{12}t} + d_{23}(c_2^* c_3)e^{\imath\omega_{23}t} + c.c. \ . \tag{35.277}$$

In the semi-classical picture, the radiated field will be a sum of these two terms,

$$\mathcal{E}^+ = \mathcal{E}_1 e^{-\imath\omega_{12}t} + \mathcal{E}_2 e^{-\imath\omega_{23}t} \ . \tag{35.278}$$

This leads to an interference or beat note term in a square-law detector,

$$|\mathcal{E}^+|^2 = |\mathcal{E}_{12}|^2 + |\mathcal{E}_{23}|^2 + \mathcal{E}_{12}^*\mathcal{E}_{23}e^{[\imath(\omega_{12}-\omega_{23})t]} + c.c. \ , \tag{35.279}$$

regardless of whether state $|2\rangle$ decays simultaneously to $|1\rangle$ and $|3\rangle$ or vice versa.

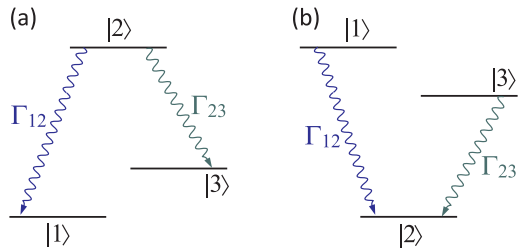

Figure 35.26: Level configuration of a Λ-system (left) and a V-system (right).

35.7.1.1 Quantum electrodynamics calculation

For the quantum electrodynamical calculation, we use the creation and annihilation operators from second quantization of quantum mechanics. Let $\hat{\mathcal{E}}_n^+ = \hat{a}_n e^{-\imath\omega_n t}$ be the annihilation operator and $\hat{\mathcal{E}}_n^- = \hat{a}_n^\dagger e^{\imath\omega_n t}$ be the creation operator with $n = (12)$ or $n = (23)$. Then the beat note becomes,

$$\langle\psi_V(t)|\hat{\mathcal{E}}_{12}^-(t)\hat{\mathcal{E}}_{23}^+(t)|\psi_V(t)\rangle \qquad \text{and} \qquad \langle\psi_\Lambda(t)|\hat{\mathcal{E}}_{12}^-(t)\hat{\mathcal{E}}_{23}^+(t)|\psi_\Lambda(t)\rangle \tag{35.280}$$

for the Λ and the V-system, respectively. The state vector for each type of system is,

$$|\psi_V(t)\rangle = \sum_{i=1,2,3} c_i|i,0\rangle + c_1|c,1_{12}\rangle + c_2|c,1_{23}\rangle \tag{35.281}$$

and,

$$|\psi_\Lambda(t)\rangle = \sum_{i=1,2,3} c_i'|i,0\rangle + c_1'|b,1_{12}\rangle + c_2'|c,1_{23}\rangle \ . \tag{35.282}$$

The beat note term becomes,

$$\begin{aligned}\langle\psi_V(t)|\hat{\mathcal{E}}_1^-(t)\hat{\mathcal{E}}_2^+(t)|\psi_V(t)\rangle &= \kappa\langle 1_{12}0_{23}|a_1^\dagger a_2|0_{12}1_{23}\rangle e^{[\imath(\omega_{12}-\omega_{23})t]}\langle 3|3\rangle \\ &= \kappa e^{[\imath(\omega_{12}-\omega_{23})t]}\langle 3|3\rangle\end{aligned} \tag{35.283}$$

for the V-system and

$$\begin{aligned}\langle\psi_\Lambda(t)|\hat{\mathcal{E}}_1^-(t)\hat{\mathcal{E}}_2^+(t)|\psi_\Lambda(t)\rangle &= \kappa'\langle 1_{12}0_{23}|a_1^\dagger a_2|0_{12}1_{23}\rangle e^{[\imath(\omega_{12}-\omega_{23})t]}\langle 2|3\rangle \\ &= \kappa' e^{[\imath(\omega_{12}-\omega_{23})t]}\langle 2|3\rangle\end{aligned} \tag{35.284}$$

for the Λ-system. However, orthogonality of the eigenstates requires $\langle 3|3\rangle = 1$ and $\langle 2|3\rangle = 0$. Therefore, there is a quantum beat note term for V-type atoms, but not for Λ-type atoms.

This difference originates in quantum mechanical uncertainty. A V-type atom decays to state $|3\rangle$ via the emission with ω_{12} and ω_{23}. Since both transitions decayed to the same state, one cannot determine along which path each decayed, similar to Young's double-slit experiment. However, Λ-type atoms decay to two different states. Therefore, in this case we can identify the path by the end product.

Quantum beat spectroscopy is a technique which allows for Doppler-free resolution provided the separation of the adjacent levels is less than the Doppler width. It consists in generating a coherently distributed population of two upper states, e.g. via a short laser pulse, and detecting the beat frequency.

35.7.2 Two-photon transitions

We will now apply the *Kramers-Heisenberg formula* (27.111) to photon scattering processes $\omega \to \omega_s$. The states are then product states of atomic excitations and photonic modes $|m, n, n_s\rangle$. In particular, the final state must take into account the mode into which light is scattered,

$$\frac{1}{\tau} = \frac{2\pi}{\hbar^2} \sum_f \sum_{\mathbf{k}_s} \Big| \langle f, n-1, 1|\hat{H}^{(2)}|i, n, 0\rangle + \frac{1}{\hbar} \sum_m \frac{\langle f, n-1, 1|\hat{H}^{(1)}|m\rangle\langle m|\hat{H}^{(1)}|i, n, 0\rangle}{\omega_i - \omega_m} \Big|^2 \delta(\omega_f - \omega_i) \; . \tag{35.285}$$

The initial energy is $\omega_i \to n\omega$, the final energy $\omega_f \to (n-1)\omega + \omega_s + \omega_f$, two intermediate states are possible, $|m\rangle \to |m, n-1, 0\rangle$ and $|m\rangle \to |m, n, 1\rangle$ over which we must sum, that is $\omega_m \to \omega_m + (n-1)\omega$ and $\omega_m \to \omega_m + n\omega + \omega_s$. They are illustrated by the Feyman diagrams in Fig. xx. Hence, and neglecting the non-linear contribution $\hat{H}^{(2)}$,

$$\frac{1}{\tau} = \frac{2\pi}{\hbar^3} \sum_f \sum_{\mathbf{k}_s} \Big| \sum_m \frac{\langle f, n-1, 1|\hat{H}^{(1)}|m, n, 0\rangle\langle m, n, 0|\hat{H}^{(1)}|i, n, 0\rangle}{\omega - \omega_m} + \frac{\langle f, n-1, 1|\hat{H}^{(1)}|m, n-1, 1\rangle\langle m, n-1, 1|\hat{H}^{(1)}|i, n, 0\rangle}{-\omega_m - \omega_s} \Big|^2 \delta(\omega_f - \omega + \omega_s) \; . \tag{35.286}$$

Evaluated far from resonance, $\omega \gg \omega_m$, this result leads to Thomson and Compton scattering. Close to resonance the second term of the sum may neglected.

The matrix elements can be evaluated by the electric dipole Hamiltonian in second quantization,

$$\frac{1}{\tau} = \frac{2\pi}{\hbar} \sum_{\mathbf{k}_s} \Big| \sum_m \frac{\Omega_{fm}\Omega_{mi}}{\omega - \omega_m} \Big|^2 \delta(\omega_f - \omega + \omega_s) \; . \tag{35.287}$$

We convert the transition rate into a cross section via,

$$\sum_{\mathbf{k}_s} \to \frac{V}{(2\pi)^3} \int\int k_s^2 dk_s d\Omega = \frac{V}{(2\pi c)^3} \int\int \omega_s^2 d\omega_s d\Omega \; . \tag{35.288}$$

35.7.2.1 Transition rates for n-photon processes

It is adequate to move to a continuum of final states of the field. The sum over the final states includes a sum over the modes $\mathbf{k}$ and the polarizations λ,

$$\sum_f = \sum_{\mathbf{k}} \sum_{\lambda} \longrightarrow \frac{1}{h^3} \int_{\mathbb{R}^6} d^3p d^3r \sum_{\lambda} = \frac{V}{(2\pi c)^3} \int_\Omega d\Omega \; d\omega \; \omega^2 \sum_{\lambda} \; . \tag{35.289}$$

We now insert for the matrix element (first term in ()) the cartesian multipole expansion () and obtain,

$$\frac{1}{\tau} = \frac{2\pi}{\hbar^2}\sum_f \left|\langle f| - \imath e\sqrt{\frac{\hbar\omega}{2\varepsilon_0 V}}[\hat{\varepsilon}\cdot\mathbf{d}_E + ...]|i\rangle\right|^2 \delta(\omega-\omega_f)\sum_\lambda \tag{35.290}$$
$$\longrightarrow \frac{2\pi}{\hbar^2}\frac{V}{(2\pi c)^3}\frac{e^2\hbar\omega}{2\varepsilon_0 V}\omega^2\sum_\lambda\int |\hat{\varepsilon}\cdot\langle g|\mathbf{d}_E|e\rangle + \imath\hat{\varepsilon}\cdot\langle g|\mathbf{q}_E|e\rangle\cdot\mathbf{k}...] - ...|^2\, d\Omega\ .$$

Finally, letting $\sum_\lambda = 2$,

$$\frac{1}{\tau} = \frac{\alpha\omega^3}{\pi c^2}\int |\hat{\varepsilon}\cdot\langle g|\text{multipole-tensor}|e\rangle\text{wavenumber-tensor}|^2\, d\Omega\ . \tag{35.291}$$

For example, for dipole radiation, letting $\hat{\varepsilon} = \hat{\mathbf{e}}_z$,

$$\frac{1}{\tau} = \frac{\alpha\omega^3}{\pi c^2}\int |\hat{\varepsilon}\cdot\langle g|\mathbf{d}_E|e\rangle|^2\, d\cos\theta d\phi \tag{35.292}$$
$$= \frac{\alpha\omega^3}{\pi c^2}|\langle g|\mathbf{d}_E|e\rangle|^2\int |\cos\theta|^2 d\cos\theta d\phi = \frac{4\alpha\omega^3}{3c^2}|\langle g|\mathbf{d}_E|e\rangle|^2\ .$$

35.7.2.2 Absorption

In first order perturbation theory we have Fermi's Golden rule,

$$\frac{1}{\tau} = \frac{2\pi}{\hbar^2}\sum_f |\langle f|\hat{H}_{int}|i\rangle|^2\delta(\omega_f-\omega_i)\ . \tag{35.293}$$

In the dipolar approximation, $\hat{H}_{int} = -\mathbf{d}\cdot\vec{\mathcal{E}}$, and separating the field and atomic degrees of freedom, $|f\rangle = |N_f\rangle|A_f\rangle$, we get for absorption processes,

$$\frac{1}{\tau} = \frac{2\pi e^2}{\hbar^2}\sum_{N_f}\left|\langle N_f|\hat{\mathcal{E}}^-|N_i\rangle\cdot\langle A_f|\hat{\varepsilon}\cdot\hat{\mathbf{d}}|A_i\rangle\right|^2\delta(\omega_f-\omega_i)\ . \tag{35.294}$$

Generalizing to a statistical mixture of Fock states via $\sum_{N_f,N_i}\langle N_i|\hat{E}^+|N_f\rangle p_i\langle N_f|\hat{E}^-|N_i\rangle = \text{Tr}\ (\hat{\rho}\hat{\mathcal{E}}^+\hat{\mathcal{E}}^-)$, we may also write,

$$\frac{1}{\tau} = \frac{2\pi e^2}{\hbar^2}|M_{abs}|^2\delta(\omega_f-\omega_i)\text{Tr}\ (\hat{\rho}\hat{\mathcal{E}}^+\hat{\mathcal{E}}^-)\ , \tag{35.295}$$

where

$$|M_{abs}|^2 \equiv \langle A_f|\hat{\varepsilon}\cdot\hat{\mathbf{d}}|A_i\rangle\ . \tag{35.296}$$

For an incoming photon ω, we get $\omega_f = E_f$ and $\omega_i = E_i + \omega$. See Fig. 35.27(a).

35.7.2.3 Spontaneous and stimulated emission

In complete analogy to the absorption process, but now using the scattered field, $\hat{H}_{int} = -\mathbf{d}\cdot\hat{\vec{\mathcal{E}}}_s$, we get for emission processes,

$$\frac{1}{\tau} = \frac{2\pi e^2}{\hbar^2}|M_{em}|^2\delta(\omega_f-\omega_i)\text{Tr}\ (\hat{\rho}\hat{\mathcal{E}}_s^+\hat{\mathcal{E}}_s^-)\ , \tag{35.297}$$

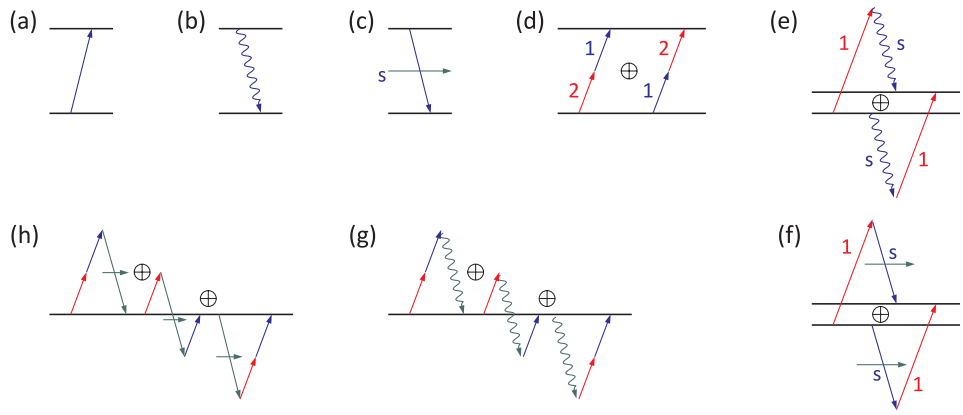

Figure 35.27: Feynman graphs for (a) absorption, (b) spontaneous emission, (c) stimulated emission, (d) two-photon absorption, (e) spontaneous Raman, (f) stimulated Raman, (g) spontaneous second harmonic generation, (h) and stimulated second harmonic generation.

where

$$|M_{em}|^2 \equiv \langle A_f|\hat{\varepsilon}_s \cdot \hat{\mathbf{d}}|A_i\rangle \ . \tag{35.298}$$

For an outgoing photon ω_s, we get $\omega_f = E_f + \omega_s$ and $\omega_i = E_i$.

35.7.2.4 Two-photon absorption

In second order perturbation theory we have the Kramers-Heisenberg rule,

$$\frac{1}{\tau} = \frac{2\pi}{\hbar^2}\sum_f \left|\sum_m \frac{\langle f|\hat{H}_{int}|m\rangle\langle m|\hat{H}_{int}|i\rangle}{\omega - \omega_m}\right|^2 \delta(\omega_f - \omega_i) \ . \tag{35.299}$$

In the dipolar approximation, $\hat{H}_{int} = -\mathbf{d}\cdot\hat{\vec{\mathcal{E}}}_1 - \mathbf{d}\cdot\hat{\vec{\mathcal{E}}}_2$, and separating the field and atomic degrees of freedom, $|f\rangle = |N_f\rangle|A_f\rangle$, we get for two-photon absorption processes,

$$\frac{1}{\tau} = \frac{2\pi e^4}{\hbar^4}\sum_{N_f}\left|\sum_{N_m,A_m}\frac{\langle N_f|\mathcal{E}_2^-|N_m\rangle\langle N_m|\mathcal{E}_1^-|N_i\rangle\langle A_f|\hat{\varepsilon}_2\cdot\hat{\mathbf{d}}|A_m\rangle\langle A_m|\hat{\varepsilon}_1\cdot\hat{\mathbf{d}}|A_i\rangle}{\omega_1 - \omega_m}\right. \tag{35.300}$$

$$\left. + \frac{\langle N_f|\mathcal{E}_1^-|N_m\rangle\langle N_m|\mathcal{E}_2^-|N_i\rangle\langle A_f|\hat{\varepsilon}_1\cdot\hat{\mathbf{d}}|A_m\rangle\langle A_m|\hat{\varepsilon}_2\cdot\hat{\mathbf{d}}|A_i\rangle}{\omega_2 - \omega_m}\right|^2 \delta(\omega_f - \omega_1 - \omega_2) \ .$$

Generalizing to a statistical mixture of Fock states via $\sum_{N_f,N_i} p_i|\langle N_f|\hat{\mathcal{E}}_2^-\hat{\mathcal{E}}_1^-|N_i\rangle = \mathrm{Tr}\ (\hat{\rho}\hat{\mathcal{E}}_1^+\hat{\mathcal{E}}_2^+\hat{\mathcal{E}}_2^-\hat{\mathcal{E}}_1^-)$, we may also write,

$$\frac{1}{\tau} = \frac{2\pi e^4}{\hbar^4}|M_{tpa}|^2\delta(\omega_f - \omega_i)\mathrm{Tr}\ (\hat{\rho}\hat{\mathcal{E}}_1^+\hat{\mathcal{E}}_2^+\hat{\mathcal{E}}_2^-\hat{\mathcal{E}}_1^-) \ , \tag{35.301}$$

where

$$M_{tpa} \equiv \langle A_f|\hat{\varepsilon}_2 \cdot \hat{\mathbf{d}} G(E_i + \omega_1)\hat{\varepsilon}_1 \cdot \hat{\mathbf{d}}|A_i\rangle + \langle A_f|\hat{\varepsilon}_1 \cdot \hat{\mathbf{d}} G(E_i + \omega_2)\hat{\varepsilon}_2 \cdot \hat{\mathbf{d}}|A_i\rangle \ . \quad (35.302)$$

For two incoming photons ω, we get $\omega_f = E_f$ and $\omega_i = E_i + \omega_1 + \omega_2$. Here, G denotes the *photon propagator*,

$$G(\omega) = \sum_m \frac{|A_m\rangle\langle A_m|}{\omega - E_m} \ . \quad (35.303)$$

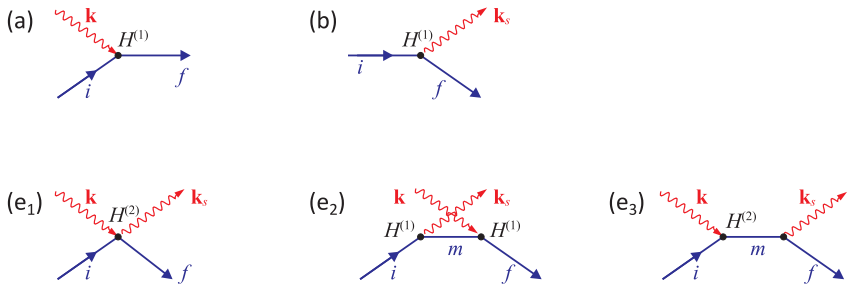

Figure 35.28: Feynman graphs for (a) absorption, (b) spontaneous emission, (c) stimulated emission, (e)(i-iii) spontaneous Raman.

35.7.2.5 Spontaneous and stimulated Raman process

In complete analogy to the two-photon absorption process, but now using the incident and the scattered fields, $\hat{H}_{int} = -\mathbf{d}\cdot\vec{\mathcal{E}}_1 - \mathbf{d}\cdot\vec{\mathcal{E}}_s$, we get for spontaneous and stimulated Raman processes,

$$\frac{1}{\tau} = \frac{2\pi e^4}{\hbar^4}|M_{ram}|^2\delta(\omega_f - \omega_i)\mathrm{Tr}\ (\hat{\rho}\hat{\mathcal{E}}_1^+\hat{\mathcal{E}}_s^-\hat{\mathcal{E}}_s^+\hat{\mathcal{E}}_1^-) \ , \quad (35.304)$$

where

$$M_{ram} \equiv \langle A_f|\hat{\varepsilon}_s \cdot \hat{\mathbf{d}} G(E_i + \omega_1)\hat{\varepsilon}_1 \cdot \hat{\mathbf{d}}|A_i\rangle + \langle A_f|\hat{\varepsilon}_1 \cdot \hat{\mathbf{d}} G(E_i - \omega_s)\hat{\varepsilon}_s \cdot \hat{\mathbf{d}}|A_i\rangle \ . \quad (35.305)$$

For an incoming photon ω_1 and a scattered photon ω_s, we get $\omega_f = E_f + \omega_s$ and $\omega_i = E_i + \omega_1$.

35.7.2.6 General n-photon processes

The transition probability in n-th order perturbation theory can be formulated in a general way as,

$$\frac{1}{\tau} = \frac{2\pi e^2}{\hbar^{2n}}|M_{fi}^{(n)}|^2\delta(\omega_f - \omega_i)\mathrm{Tr}\ (\hat{\rho}\hat{\mathcal{E}}_1^{\pm}\hat{\mathcal{E}}_2^{\pm}...\hat{\mathcal{E}}_2^{\mp}\hat{\mathcal{E}}_1^{\mp}) \ , \quad (35.306)$$

where

$$\begin{aligned} M_{fi}(\omega_n, ..., \omega_1) \equiv \mathcal{S}_p\langle A_f|\hat{\varepsilon}_n\hat{\mathbf{d}}G(E_i \pm \omega_1 \pm ... \pm \omega_{n-2} \pm \omega_{n-1})\ ... \quad (35.307)\\ ...\ \hat{\varepsilon}_{n-1}\hat{\mathbf{d}}G(E_i \pm \omega_1 \pm ... \pm \omega_{n-2})\ ...\\ ...\ \hat{\varepsilon}_1 \cdot \hat{\mathbf{d}}G(E_i \pm \omega_1)|A_i\rangle \ . \end{aligned}$$

The upper signs hold for absorbed photons (up to n), the lower for emitted photons, $\omega_f = E_f + \omega_1 + ... + \omega_n$ and $\omega_i = E_i + \omega_1 + ... + \omega_n$.

For n-photon processes, there are theoretically up to $n + 1$ different types, each one with $n!$ possible temporal sequences, which can be illustrated in Feynman graphs. Additionally, for every emitted photon can be either spontaneous or stimulated. The number of possible time sequences is reduced, if some absorbed or emitted photons have the same frequency by $m!$ (if m is the number og identical photons).

For example there are (3+1) different types of three-photon processes: 3 photons in, 2 photons in 1 out, 1 photon in 2 out, 3 photons out.

For example second harmonic generation: 3! possible time sequences, 2 processes, 2 equivalent photons = $\frac{3!2}{2!}$ possible Feynman graphs.

35.7.3 Exercises

35.7.3.1 Ex: Two-photon transitions in rubidium

Considering the following transitions of rubidium, $5S_{1/2} - 5P_{1/2}$ at 795 nm with $\Gamma_{795} = (2\pi)$ 6 MHz linewidth $5S_{1/2} - 5P_{3/2}$ at 780 nm with $\Gamma_{780} = (2\pi)$ 6MHz, and $5P_{3/2} - 5D_{5/2}$ at 776 nm with $\Gamma_{776} = (2\pi)$ 700 kHz linewidth. Calculate the rate for resonant two-photon transitions from the ground state to the $5D_{5/2}$ level without bothering about hyperfine splitting induced by a laser intensity of $I = 1$ mW/cm^2.

Solution:

35.7.3.2 Ex: Spin relaxation in a dipole trap

Consider a transition in a hypothetical atomic species without nuclear spin between two levels $^2S_{1/2}$ and $^2P_{1/2}$ driven far-off resonance. Calculate the spin relaxation rate as a function of the detuning.

Solution: *Spin relaxation means that atoms polarized in a specific Zeeman state, say $^2S_{1/2}$, $m_J = +\frac{1}{2}$, may transit to the $m_J = -\frac{1}{2}$ state due to spontaneous Raman scattering.*

35.7.3.3 Ex: Rayleigh scattering and spin relaxation

Derive the rates for Rayleigh scattering and spin relaxation for ^{87}Rb driven far-off resonance. **Help**: Determine the hyperfine structure of the D1 and D2 lines and calculate the transition rates between sublevels from the Kramers-Heisenberg formula.

Solution: *The hyperfine structure is [895, 271, 1245].*

35.8 Beam splitting and quantum amplification

The beam splitter is one of the most important devices not only in practical optical setups, but also for its conceptual role in quantum mechanics. It thus deserves a dedicated section.

A classical beam splitter divides a beam of light into two branches, which are distinct by their orientation in space or by other degrees of freedom. On the other hand, a photonic picture obviously requires a quantum description. For one reason, the photon numbers scattered into the two branches are quantum mechanically entangled. Furthermore, the very concept of the beam splitter necessitates a second entrance port which, even if empty, unavoidably introduces quantum noise. Finally, in quantum mechanics, as we already learned for the case of measurement devices, the beam splitting device needs to be included in a full description of the beam splitting dynamics, which has important concequences. In fact, quantum mechanically the beam splitting resembles more a scattering problem, where the light beam represents one entrance and output channel and the physical beam splitter the other one (see Fig. 35.29).

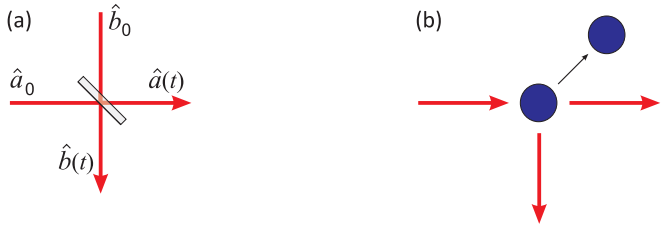

Figure 35.29: (a) Classical beam splitting. (b) Scattering of two modes.

This section is organized as follows. In Secs. 35.8.1 and 35.8.2 we discuss beam splitting at a macroscopic splitting device, i.e. we neglect backaction of the beam splitting event on the splitting device (e.g. recoil or transitions between electronic levels). Backaction on the splitting device is then treated in 35.8.3.

35.8.1 The beam splitter in various representations

We have learned in Sec. 35.4 how a two-level quantum systems couples to a harmonic oscillator via terms in the Hamiltonian containing expressions such as $\hat{\sigma}_+\hat{a}$. We will now see how two quantum harmonic oscillators couple together via terms such as $\hat{a}^\dagger\hat{b}$, where $\hat{a}$ and $\hat{b}$ are the field operators of two oscillator modes. A device providing such a coupling is called *beam splitter*. It *mixes two modes* according to the Hamiltonian,

$$\boxed{\hat{H} = \tfrac{\hbar}{2}\Omega(\hat{a}\hat{b}^\dagger + \hat{a}^\dagger\hat{b})}\,. \tag{35.308}$$

The beam splitter can be described in the Schrödinger or the Heisenberg picture exploiting the formalism introduced in Sec. 24.5.

35.8.1.1 Schrödinger picture

In the Schrödinger picture, if $|\psi_0\rangle = |\alpha_0\rangle|\beta_0\rangle$ is the state of the modes before the beam splitter, the Schrödinger equation, $\imath\hbar\partial_t|\psi(t)\rangle = \hat{H}|\psi(t)\rangle$, gives us the state after the splitter via its solution,

$$\boxed{|\psi(t)\rangle = e^{\imath\Omega t/2(\hat{a}\hat{b}^\dagger + \hat{a}^\dagger\hat{b})}|\psi_0\rangle} \ . \tag{35.309}$$

A 50% beam splitter corresponds to a $\Omega t = \pi/2$ pulse.

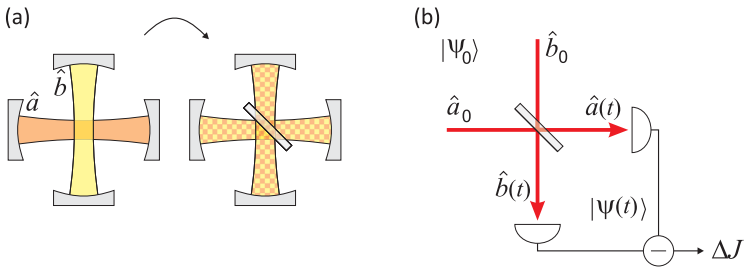

Figure 35.30: (a) Coupling of two cavity modes by insertion of a beam splitter. (b) Beam splitter mixing two propagating modes.

35.8.1.2 Heisenberg picture

We can also describe the beam splitter in the Heisenberg picture. With the commutation rules,

$$[\hat{a}, \hat{a}^\dagger] = 1 = [\hat{b}, \hat{b}^\dagger] \quad , \quad [\hat{a}, \hat{b}] = 0 \ , \tag{35.310}$$

and the Heisenberg equations,

$$\begin{aligned} \dot{\hat{a}} &= \tfrac{\imath}{\hbar}[\hat{H}, \hat{a}] = \tfrac{\imath}{2}\Omega[(\hat{a}\hat{b}^\dagger + \hat{a}^\dagger\hat{b}), \hat{a}] = -\tfrac{\imath}{2}\Omega\hat{b} \\ \dot{\hat{b}} &= \tfrac{\imath}{\hbar}[\hat{H}, \hat{b}] = \tfrac{\imath}{2}\Omega[(\hat{a}\hat{b}^\dagger + \hat{a}^\dagger\hat{b}), \hat{b}] = -\tfrac{\imath}{2}\Omega\hat{a} \ , \end{aligned} \tag{35.311}$$

we calculate,

$$\ddot{\hat{a}} = -\tfrac{1}{4}\Omega^2\hat{a} \quad \text{and} \quad \ddot{\hat{b}} = -\tfrac{1}{4}\Omega^2\hat{b} \ , \tag{35.312}$$

the solution of which is,

$$\begin{pmatrix} \hat{a}(t) \\ \hat{b}(t) \end{pmatrix} = \begin{pmatrix} \cos\frac{1}{2}\Omega t & -\imath\sin\frac{1}{2}\Omega t \\ -\imath\sin\frac{1}{2}\Omega t & \cos\frac{1}{2}\Omega t \end{pmatrix} \begin{pmatrix} \hat{a}_0 \\ \hat{b}_0 \end{pmatrix} \ . \tag{35.313}$$

Introducing the abbreviation $\eta \equiv \cos^2(\Omega t/2)$, we can describe the evolution as,

$$\boxed{\begin{pmatrix} \hat{a}(t) \\ \hat{b}(t) \end{pmatrix} = \begin{pmatrix} \sqrt{\eta} & -\imath\sqrt{1-\eta} \\ -\imath\sqrt{1-\eta} & \sqrt{\eta} \end{pmatrix} \begin{pmatrix} \hat{a}_0 \\ \hat{b}_0 \end{pmatrix}} \ . \tag{35.314}$$

For a $\Omega t = \pi/2$ pulse, we get,

$$\begin{pmatrix} \hat{a}(t) \\ \hat{b}(t) \end{pmatrix} = \sqrt{\tfrac{1}{2}} \begin{pmatrix} 1 & -\imath \\ -\imath & 1 \end{pmatrix} \begin{pmatrix} \hat{a}_0 \\ \hat{b}_0 \end{pmatrix} \ . \tag{35.315}$$

that each the reflected beam suffers a phase shift of $\pi/2$ [16]. Resolve the Excs. 35.8.9.1 to 35.8.9.3.

35.8.1.3 Glauber representation

In the Heisenberg picture, the wavefunctions of the quantum states (and hence the density operator and the Wigner function) remain unchanged during the evolution, i.e.,

$$\begin{aligned} |\psi\rangle \equiv |\alpha\rangle|\beta\rangle = |\alpha_0\rangle|\beta_0\rangle \equiv |\psi_0\rangle \ , \\ \rho_{|\psi\rangle} = \rho_{|\psi_0\rangle} \ , \\ W_{|\psi\rangle}(\gamma) = W_{|\psi_0\rangle}(\gamma) \ , \\ P_{|\psi\rangle}(\gamma) = P_{|\psi_0\rangle}(\gamma) \ , \\ Q_{|\psi\rangle}(\gamma) = Q_{|\psi_0\rangle}(\gamma) \ , \end{aligned} \tag{35.316}$$

where the $|\psi\rangle$ are arbitrary quantum states and the $|\gamma\rangle$ are Glauber's states. This means that two field modes mixed at a beam splitter do not interfere with phase space, i.e. do not develop quantum correlations. Of course, that would be too easy, indeed; we will soon see in Sec. 35.3, that we need to work a little harder to produce quantum correlations.

Setting $\theta \equiv \Omega t/2$ and $\hat{b} \curvearrowright -\imath\hat{b}$ in the propagator of Eq. (35.309), we may define a beam splitting operator in analogy to the displacement operator (24.111),

$$\boxed{\hat{B}(\theta) \equiv e^{\theta(\hat{a}^\dagger \hat{b} - \hat{a}\hat{b}^\dagger)}} \ , \tag{35.317}$$

which is an equivalent beam splitter description. We find,

$$\boxed{\begin{aligned} \hat{B}(\theta)^\dagger \hat{a} \hat{B}(\theta) &= \hat{a}\cos\theta + \hat{b}\sin\theta \\ \hat{B}(\theta)^\dagger \hat{b} \hat{B}(\theta) &= -\hat{a}\sin\theta + \hat{b}\cos\theta \end{aligned}} \ , \tag{35.318}$$

as will be shown in Exc. 35.8.9.4 [17].

35.8.1.4 Fock representation

Alternatively, we can describe the beam splitter in the Fock representation [18]. The Hamiltonian of the beam splitter couples two modes of harmonic oscillators. Expanding on a two-dimensional Fock basis via $|\psi\rangle \equiv (...|0\rangle|n_a\rangle....|n_b\rangle|0\rangle...)$ we can gain more

[16] This fact is a consequence of *time-reversal invariance* at the beam splitter. We will see later that, in fact, only the beam reflected at the surface of an optically denser medium suffers a phase-shift of π, while the beam reflected at an optically thinner medium does not suffer any phase shift.

[17] Compare to the formulas (24.119), (35.90), and (35.361).

[18] A more in-depth discussion is found in Ref. [791].

insight:

$$\begin{aligned}\hat{H} &= \tfrac{\hbar}{2}\Omega(\hat{a}\hat{b}^\dagger + \hat{a}^\dagger\hat{b}) \qquad (35.319)\\ &= \tfrac{\hbar}{2}\Omega\sum_{n_a,n_b}\sqrt{n_a(n_b+1)}|n_a-1,n_b+1\rangle\langle n_a,n_b| + \sqrt{(n_a+1)n_b}|n_a+1,n_b-1\rangle\langle n_a,n_b|\\ &= \sum_{n_a+n_b}\hat{H}_{a+b}\ ,\end{aligned}$$

where,

$$\hat{H}_{a+b} = \tfrac{\hbar}{2}\Omega\begin{pmatrix} 0 & \sqrt{1n_b} & & & & \\ \sqrt{1n_b} & 0 & \sqrt{2(n_b-1)} & & & \\ & \sqrt{2(n_b-1)} & \ddots & & & \\ & & & \ddots & \sqrt{n_a 1} & \\ & & & \sqrt{n_a 1} & 0 & \end{pmatrix}. \qquad (35.320)$$

The sub-spaces with n_a+n_b+1 photons are completely degenerate, since $\det(\lambda\mathbb{I}_{a+b} - \hat{H}_{a+b}) = \lambda^{n_a+n_b+1} = 0$. The degeneracy is removed, when we introduce loss mechanisms into one of the modes. Thus, the Hamiltonian can be understood as a Dicke system with the multiplicity $\frac{1}{2}\widehat{(n_a+n_b)} = n_a+n_b+1$. See also Exc. 35.8.9.2.

Example 215 (*Beam splitter with 0 or 1 photons*): As an example, we consider $n_a, n_b = 0, 1$. Then, in the basis $\begin{pmatrix}|0,0\rangle & |0,1\rangle & |1,0\rangle & |0,2\rangle & |1,1\rangle & |2,0\rangle & \cdots\end{pmatrix}^t$ the matrix of the Hamiltonian becomes,

$$\hat{H} = \tfrac{1}{2}\Omega\begin{pmatrix} 0 & & & & & & \\ & 0 & 1 & & & & \\ & 1 & 0 & & & & \\ & & & 0 & \sqrt{2} & 0 & \\ & & & \sqrt{2} & 0 & \sqrt{2} & \\ & & & 0 & \sqrt{2} & 0 & \end{pmatrix}.$$

It is easily verified that the matrix of eigenvectors and the matrix of eigenvalues,

$$U = \begin{pmatrix} 1 & 0 & 0 & 0 & 0 & 0 \\ 0 & -1 & 1 & 0 & 0 & 0 \\ 0 & 1 & 1 & 0 & 0 & 0 \\ 0 & 0 & 0 & -\frac{1}{2}\sqrt{2} & -1 & \frac{1}{2}\sqrt{2} \\ 0 & 0 & 0 & 1 & 0 & 1 \\ 0 & 0 & 0 & -\frac{1}{2}\sqrt{2} & 1 & \frac{1}{2}\sqrt{2} \end{pmatrix} \quad \text{respectively} \quad E = \tfrac{\hbar}{2}\Omega\begin{pmatrix} 0 & 0 & 0 & 0 & 0 & 0 \\ 0 & -1 & 0 & 0 & 0 & 0 \\ 0 & 0 & 1 & 0 & 0 & 0 \\ 0 & 0 & 0 & -2 & 0 & 0 \\ 0 & 0 & 0 & 0 & 0 & 0 \\ 0 & 0 & 0 & 0 & 0 & 2 \end{pmatrix}$$

satisfy $U^{-1}HU = E$. Hence,

$$|\psi\rangle = U^{-1}e^{\imath Et}U|\psi_0\rangle\ ,$$

and we find, that the state $|1,1\rangle = \begin{pmatrix}0 & 0 & 0 & 0 & 1 & 0\end{pmatrix}^T$ is transformed into a superposition,

$$\begin{pmatrix}0 & 0 & 0 & \frac{1}{\sqrt{2}}\imath\sin\Omega t & \cos\Omega t & \frac{1}{\sqrt{2}}\imath\sin\Omega t\end{pmatrix}^T \overset{\Omega t=\pi/2}{\longrightarrow} \frac{\imath}{\sqrt{2}}(|0,2\rangle + |2,0\rangle)\ .$$

Similarly, we find that the superposition state $\frac{1}{\sqrt{2}}(|1,0\rangle+|0,1\rangle) = \begin{pmatrix}0 & 1 & -1 & 0 & 0 & 0\end{pmatrix}^T$ is transformed into,

$$e^{-\frac{1}{2}\imath\Omega t}\begin{pmatrix}0 & 1 & -1 & 0 & 0 & 0\end{pmatrix}^T \overset{\Omega t=\pi/2}{\longrightarrow} e^{-\imath\pi/4}\frac{1}{\sqrt{2}}(|1,0\rangle + |0,1\rangle) \ .$$

35.8.2 Fock and Glauber states at a beam splitter

A beam splitter divides a Fock state containing N photons into two Glauber states,

$$\begin{aligned}|\psi\rangle &= \frac{1}{2^{N/2}\sqrt{N!}}(\hat{a}_1^\dagger + \hat{a}_2^\dagger)^N|0,0\rangle = \frac{1}{2^{N/2}\sqrt{N!}}\sum_{n=0}^{N}\binom{N}{n}(\hat{a}_1^\dagger)^n(\hat{a}_2^\dagger)^{N-n}|0,0\rangle \qquad (35.321)\\ &= \frac{1}{2^{N/2}}\sum_{n=0}^{N}\sqrt{\binom{N}{n}}|n,N-n\rangle = \sum_{n=0}^{N}\sqrt{\binom{N}{n}0.5^n 0.5^{N-n}}|n,N-n\rangle\\ &\simeq \sum_{n=0}^{N}\sqrt{\frac{(N/2)^n}{n!}e^{-N/2}}|n,N-n\rangle = e^{-|\alpha|/2}\sum_{n=0}^{N}\frac{\alpha^n}{\sqrt{n!}}|n,N-n\rangle \ ,\end{aligned}$$

approximating the binomial distribution by the Poisson distribution,

$$\binom{N}{n}p^n(1-p)^{N-n} \overset{N\to\infty}{\longrightarrow} \frac{(pN)^n}{n!}e^{-pN} \ . \qquad (35.322)$$

and defining $\alpha \equiv N/2$. The normalization is $\langle\psi|\psi\rangle = 1$. The population in an individual mode is,

$$\begin{aligned}\langle\hat{n}_1\rangle = \langle\psi|\hat{a}_1^\dagger\hat{a}_1|\psi\rangle &= \frac{1}{2^N}\langle m,N-m|\sum_{n,m=0}^{N}\sqrt{\binom{N}{m}}\hat{a}_1^\dagger\hat{a}_1\sqrt{\binom{N}{n}}|n,N-n\rangle \qquad (35.323)\\ &= \frac{1}{2^N}\sum_{n=0}^{N}\binom{N}{n}n = \frac{N}{2} \ .\end{aligned}$$

The result (35.321) shows that, ignoring (tracing over) one of the modes, the other mode automatically becomes a Glauber state [19].

Besides that,

$$\begin{aligned}\langle\hat{n}_1^2\rangle &= \frac{1}{2^n}\sum_{n=0}^{n}\binom{N}{n}n^2 = \frac{N}{2^n}\sum_{n=0}^{N-1}\binom{N}{n}(n+1) = \frac{N(N+1)}{4} \qquad (35.324)\\ \langle\hat{n}_1\hat{n}_2\rangle &= \frac{1}{2^n}\sum_{n=0}^{n}\sqrt{\binom{N}{n}}n(N-n) = N\langle\hat{n}_1\rangle - \langle\hat{n}_1^2\rangle = \frac{N(N-1)}{4}\end{aligned}$$

[19] This does not mean that the output modes are uncorrelated. For instance, if we measure n photons in one mode, we know that the other must contain exactly $N-n$ photons. However, the correlations are so dense in phase space that they are not resolvable or decohere rapidly. In fact, it can be shown that coherent states are the only pure states that produce uncorrelated outputs when mixed by a passive linear-optics device [16, 14].

The squeezing parameter is,

$$\xi_{12} = \frac{\sigma^2(\hat{n}_1 - \hat{n}_2)}{\langle \hat{n}_1 \rangle + \langle \hat{n}_2 \rangle} = \frac{\langle \hat{n}_1^2 - 2\hat{n}_1\hat{n}_2 + \hat{n}_2^2 \rangle}{N} = \frac{2\langle \hat{n}_1^2 \rangle - 2\langle \hat{n}_1\hat{n}_2 \rangle}{N} = 1 \ . \tag{35.325}$$

The correlation functions at equal times are,

$$g_{11} = \frac{\left\langle \hat{a}_1^\dagger \hat{a}_1^\dagger \hat{a}_1 \hat{a}_1 \right\rangle}{\langle \hat{n}_1 \rangle^2} = \frac{1}{\langle \hat{n}_1 \rangle^2} \frac{1}{2^n} \sum_{n=2}^{n} \binom{N}{n} n(n-1) = \frac{\langle \hat{n}_1^2 \rangle - \langle \hat{n}_1 \rangle}{\langle \hat{n}_1 \rangle^2} = 1 \tag{35.326}$$

$$g_{12} = \frac{\left\langle \hat{a}_1^\dagger \hat{a}_2^\dagger \hat{a}_2 \hat{a}_1 \right\rangle}{\langle \hat{n}_1 \rangle \langle \hat{n}_2 \rangle} = \frac{1}{\langle \hat{n}_1 \rangle^2} \frac{1}{2^n} \sum_{n=0}^{N} \binom{N}{n} n(N-n) = \frac{N\langle \hat{n}_1 \rangle - \langle \hat{n}_1^2 \rangle}{\langle \hat{n}_1 \rangle^2} = \frac{N-1}{N}$$

The Cauchy-Schwarz inequality and the quantum inequality are both met,

$$\begin{aligned} g_{12} &\leq \sqrt{g_{11} g_{22}} \\ g_{12} &\leq \sqrt{\left(g_{11} + \frac{1}{\langle \hat{n}_1 \rangle} \right) \left(g_{22} + \frac{1}{\langle \hat{n}_2 \rangle} \right)} \end{aligned} \tag{35.327}$$

In comparison, a Glauber state is normally divided,

$$\begin{aligned} |\psi\rangle = |\alpha_1\rangle|\alpha_2\rangle &= e^{-|\alpha_1|^2/2} \sum_n \frac{\alpha_1^n}{\sqrt{n!}} |n\rangle e^{-|\alpha_2|^2/2} \sum_m \frac{\alpha_2^m}{\sqrt{m!}} |m\rangle \\ &= e^{-|\alpha_1|^2/2 - |\alpha_2|^2/2} \sum_{n,m} \frac{\alpha_1^n \alpha_2^m}{\sqrt{n!}\sqrt{m!}} |n\rangle|m\rangle \ . \end{aligned} \tag{35.328}$$

35.8.2.1 Density matrix representation

The density matrix for a pure state is,

$$\hat{\rho} = |\psi\rangle\langle\psi| = \begin{pmatrix} |\langle\psi|1\rangle|^2 & \langle 1|\psi\rangle\langle\psi|2\rangle \\ \langle 2|\psi\rangle\langle\psi|1\rangle & |\langle\psi|2\rangle|^2 \end{pmatrix} \ . \tag{35.329}$$

The evolution of such a state is described by the von Neumann equation:

$$\imath\hbar\partial_t \hat{\rho}(t) = [\hat{H}, \hat{\rho}(t)] \ . \tag{35.330}$$

For the beam splitter we obtain,

$$\hat{\rho} = |\psi\rangle\langle\psi| = \begin{pmatrix} |\langle\psi|0,0\rangle|^2 & \langle 0,0|\psi\rangle\langle\psi|0,1\rangle & \langle 0,0|\psi\rangle\langle\psi|1,0\rangle & \\ \langle 0,1|\psi\rangle\langle\psi|0,0\rangle & |\langle\psi|0,1\rangle|^2 & \langle 0,1|\psi\rangle\langle\psi|1,0\rangle & \\ \langle 1,0|\psi\rangle\langle\psi|0,0\rangle & \langle 1,0|\psi\rangle\langle\psi|0,1\rangle & |\langle\psi|1,0\rangle|^2 & \\ & & & \ddots \end{pmatrix} \ . \tag{35.331}$$

Example 216 (*Density matrix for the beam splitter with 0 or 1 photons*): For the case of the superposition states, $|\psi\rangle = \frac{1}{\sqrt{2}}(|0,1\rangle \pm |1,0\rangle)$,

$$\hat{\rho} = \begin{pmatrix} 0 & 0 & 0 & \\ 0 & \frac{1}{2} & \pm\frac{1}{2} & \\ 0 & \pm\frac{1}{2} & \frac{1}{2} & \\ & & & \ddots \end{pmatrix} .$$

Obviously, $\hat{\rho} = \hat{\rho}^2$. For the above superposition state, $\partial_t \hat{\rho}(t) = 0$.

35.8.3 Backaction of the splitting device

In quantum mechanics, beam splitting is ALWAYS an interaction between two degrees of freedom, the mode suffering the splitting (which we already treated quantum mechanically in the preceding sections), and the splitting device (which we will treat as an ancilla in the following, similarly as we did for a quantum measurement). In classical beam splitters, the dynamics of the ancilla is neglected, but in quantum beam splitters the ancilla serves as a witness of a splitting event. In practice, it can be a recoiling atom, a phase shift of an internal atomic state, or something else.

We will now develop a generic model allowing us to describe quantum mechanically (i) strong measurement directly on the system or (ii) weak measurements via an ancilla. For simplicity, we will assume the beam splitting device to be a two-level atom including its internal and external degrees of freedom. The light mode may then interact with the atom (or not) and be scattered into different directions of space. In order to emulate a beam splitter we need to ensure the existence of only two scattered exit modes. This can be done by putting the atom in a ring cavity, where the only modes available are the forward and the backward scattered mode. It is fair to say that this model represents the simplest possible beam splitter description including backaction. In the same time, the system exhibits a dynamics known as collective atomic recoil lasing (CARL), which is extensively discussed in Chp. 42.

35.8.4 Shot noise

As any quantized degree of freedom, a light mode is subject to intrinsic quantum noise imposed by the Heisenberg uncertainty relation, as we have seen for the harmonic oscillator (24.124). The Heisenberg limit in the quadrature phases of a light field determines the *shot noise* noise in the intensity of the light beam. To measure this noise, we divide the laser beam by a beam splitter into two beams $\hat{a}$ and $\hat{b}$ and recombine them with a second beam splitter,

$$\hat{c} = \tfrac{1}{\sqrt{2}}(\hat{a} + \hat{b}) \quad , \quad \hat{d} = \tfrac{1}{\sqrt{2}}(\hat{a} - \hat{b}) \; . \tag{35.332}$$

Detected by photodetectors with the gain coefficient g, these two beams produce currents,

$$\hat{I}_c = g\hat{c}^\dagger \hat{c} \quad , \quad \hat{I}_d = g\hat{d}^\dagger \hat{d} \; . \tag{35.333}$$

We add and subtract these currents,

$$\hat{I}_+ \equiv \hat{I}_c + \hat{I}_d = g(\hat{a}^\dagger \hat{a} + \hat{b}^\dagger \hat{b}) \quad , \quad \hat{I}_- \equiv \hat{I}_c - \hat{I}_d = g(\hat{a}^\dagger \hat{b} + \hat{b}^\dagger \hat{a}) \; . \tag{35.334}$$

and,

$$\hat{I}_+^2 = g^2[\hat{n}_a^2+\hat{n}_b^2+2\hat{n}_a\hat{n}_b] \quad , \quad \hat{I}_-^2 = g^2[(\hat{a}^\dagger\hat{b})^2+(\hat{b}^\dagger\hat{a})^2+\hat{a}^\dagger\hat{a}+\hat{b}\hat{b}^\dagger+\hat{a}\hat{a}^\dagger+\hat{b}^\dagger\hat{b}] \ . \quad (35.335)$$

The expectation values are,

$$\begin{aligned} \langle\hat{I}_+\rangle = g\langle\hat{n}_a\rangle_a \quad &, \quad \langle\hat{I}_+\rangle = 0 \\ \langle\hat{I}_+^2\rangle = g\langle(\hat{a}^\dagger\hat{a})^2\rangle_a \quad &, \quad \langle\hat{I}_-^2\rangle = g^2\langle\hat{n}_a\rangle_a \ . \end{aligned} \quad (35.336)$$

Now, with the definition, $\langle(\Delta\hat{I})^2\rangle \equiv \langle\hat{I}^2\rangle - \langle\hat{I}\rangle^2$, we get the intensity noise of the field,

$$\langle\Delta\hat{I}_+^2\rangle = \langle(\Delta\hat{I}_+)^2\rangle = g^2\langle(\Delta\hat{n}_a)^2\rangle \ , \quad (35.337)$$

and the shot noise [20] ,

$$\langle\Delta\hat{I}_-^2\rangle = g^2 I_a \ . \quad (35.338)$$

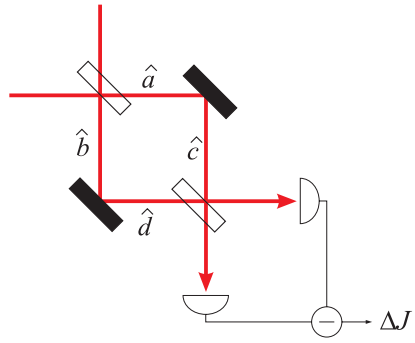

Figure 35.31: Shot noise measurement.

35.8.5 Quantum amplifier

We will call in the following as *quantum signals* degrees of freedom subject to quantum noise. Typically a quantum signal will be a mode of an electric field, represented by an annihilation operator $\hat{a}$. Such a mode can be enhanced by *quantum amplifier*, which is a device amplifying quantum signals according to the rules of quantum mechanics. Examples include the active elements of lasers and optical parametric amplifiers. A quantum amplifier is characterized by its gain and its own intrinsic quantum noise, which are interdependent parameters; the higher the gain, the larger the uncertainty noise. In the case of lasers, the uncertainty corresponds to the amplified spontaneous emission of the active medium.

Quantum amplification is a unitary transformation $\hat{U}$, acting in an initial state $|in\rangle$ and producing (in the Schrödinger figure) the amplified state,

$$|out\rangle = \hat{U}|in\rangle \ . \quad (35.339)$$

[20] Insert citation, f.ex., [Hans Marin Flores, PhD thesis].

The amplification depends on the mean value $\langle\hat{a}\rangle$ of the annihilation operator and its dispersion $\langle\hat{a}^\dagger\hat{a}\rangle - \langle\hat{a}^\dagger\rangle\langle\hat{a}\rangle$. A coherent state is a state with minimal uncertainty; when the state is transformed, the uncertainty may increase. This increase can be interpreted as noise in the amplifier. The gain G can be defined as follows:

$$G = \frac{\langle\hat{a}\rangle_{out}}{\langle\hat{a}\rangle_{in}} \ . \tag{35.340}$$

The quantum amplifier can also be described in the Heisenberg picture; the changes are attributed to the amplification of the field operator. Thus, the evolution of the operator $\hat{a}_{out}$ is given by

$$\hat{a}_{out} = \hat{U}^\dagger\hat{a}\hat{U} \ , \tag{35.341}$$

while the state vector remains unchanged. The gain is then given by,

$$G = \frac{\langle\hat{a}_{out}\rangle_{in}}{\langle\hat{a}\rangle_{in}} \ . \tag{35.342}$$

In general, the gain G may be complex, and it may depend on the initial state. For laser applications, the amplification of coherent states is important. Therefore, it is usually assumed that the initial state is a coherent state characterized by a complex-valued initial parameter α, such that $|in\rangle = |\alpha\rangle$. Even with such a restriction, the gain may depend on the amplitude or phase of the initial field.

In the following, the Heisenberg representation is used; all brackets are assumed to be evaluated with respect to the initial coherent state,

$$\text{noise} = \langle\hat{a}^\dagger_{out}\hat{a}_{out}\rangle - \langle\hat{a}^\dagger_{out}\rangle\langle\hat{a}_{out}\rangle - (\langle\hat{a}^\dagger\hat{a}\rangle - \langle\hat{a}^\dagger\rangle\langle\hat{a}\rangle) \ . \tag{35.343}$$

The expectation values are assumed to be evaluated with respect to the initial coherent state. This quantity characterizes the increase of the uncertainty of the field due to amplification. As the uncertainty of the field operator does not depend on its parameter, the quantity above shows how much output field differs from a coherent state.

35.8.5.1 Linear phase-invariant amplifier

Linear phase-invariant amplifiers may be described as follows. Assume that the unitary operator U amplifies in such a way that the input $\hat{a}$ and the output $\hat{a}_{out} = \hat{U}^\dagger\hat{a}\hat{U}$, are related by a linear equation,

$$\hat{a}_{out} = c\hat{a} + s\hat{b}^\dagger \ , \tag{35.344}$$

where c and s are c-numbers and $\hat{b}^\dagger$ is a creation operator characterizing the amplifier. Without loss of generality, it may be assumed that c and s are real. The commutator of the field operators is invariant under unitary transformation U:

$$[\hat{a}_{out}, \hat{a}^\dagger_{out}] = 1 = [\hat{a}, \hat{a}^\dagger] \quad , \quad [\hat{a}_{in}, \hat{a}^\dagger_{out}] = 0 = [\hat{a}_{out}, \hat{a}^\dagger_{in}] \ . \tag{35.345}$$

From the unitarity of U, it follows that $\hat{b}$ satisfies the same commutation relations. The c-numbers are then $c^2 - s^2 = 1$. Hence, the phase-invariant amplifier acts by

introducing an additional mode to the field, with a large amount of stored energy, behaving as a boson. Calculating the gain and the noise of this amplifier, one finds $G = c$, and

$$\text{noise} = \mathrm{c}^2 - 1 \ . \tag{35.346}$$

The coefficient $g = |G|^2$ is sometimes called the intensity amplification coefficient. The noise of the linear phase-invariant amplifier is given by $g - 1$. The gain can be dropped by splitting the beam; the estimate above gives the minimal possible noise of the linear phase-invariant amplifier. The linear amplifier has an advantage over the multi-mode amplifier: if several modes of a linear amplifier are amplified by the same factor, the noise in each mode is determined independently;that is, modes in a linear quantum amplifier are independent.

To obtain a large amplification coefficient with minimal noise, one may use homodyne detection, constructing a field state with known amplitude and phase, corresponding to the linear phase-invariant amplifier. The uncertainty principle sets the lower bound of quantum noise in an amplifier. In particular, the output of a laser system and the output of an optical generator are not coherent states.

The multiplicative amplifier D also adds additive noise F. We have $DD^\dagger = 1$,

$$\begin{pmatrix} \hat{a}^\dagger_{out} \\ \hat{a}_{out} \end{pmatrix} = D \begin{pmatrix} \hat{a}^\dagger_{in} \\ \hat{a}_{in} \end{pmatrix} + \begin{pmatrix} F_1 \\ F_2 \end{pmatrix} \ . \tag{35.347}$$

35.8.6 Homodyne detection and inverse Radon transform

In the method of *homodyne detection* or *phase-sensitive detection* the signal is obtained by superposing the field mode of interest with a local oscillator with a relative phase θ at a beam splitter and a subtraction of the photo currents in the two ports of the interferometer:

$$\begin{aligned} \Delta\hat{J} &= \hat{a}^\dagger_t \hat{a}_t - \hat{b}^\dagger_t \hat{b}_t \qquad (35.348) \\ &= (2\eta - 1)(\hat{a}^\dagger_0 \hat{a}_0 + \hat{b}^\dagger_0 \hat{b}_0) + 2\sqrt{(1-\eta)\eta}(\hat{a}^\dagger_0 \hat{a}_0 + \hat{b}^\dagger_0 \hat{b}_0) \overset{\eta \to 1/2}{\longrightarrow} \hat{a}^\dagger_0 \hat{a}_0 + \hat{b}^\dagger_0 \hat{b}_0 \ . \end{aligned}$$

If the local oscillator is a classical light field $\hat{b}_0 = \alpha_{LO} e^{-\imath\theta}$,

$$\begin{aligned} \Delta\hat{J} &= |\alpha_{LO}|(\hat{a}_0 e^{-\imath\theta} + \hat{a}^\dagger_0 e^{\imath\theta}) \qquad (35.349) \\ &= \sqrt{2}|\alpha_{LO}|\hat{x}_\theta \ , \end{aligned}$$

where the field mode is expressed by the Hermitian quadrature components $\hat{a}_0 = 2^{-1/2} \cdot (\hat{x}_\theta + \imath\hat{y}_\theta)$. The expectation value of $\Delta\hat{J}$ is afflicted with the Heisenberg uncertainty and can be expressed as the first moment of the Wigner function $W(\alpha)$:

$$\begin{aligned} \langle\psi|\Delta\hat{J}|\psi\rangle &= \int W_{|\psi\rangle}(\alpha)\Delta\hat{J}d^2\alpha \qquad (35.350) \\ &= \sqrt{2}|\alpha_{LO}| \int W_{|\psi\rangle}(x_\theta, p_\theta) x_\theta dx_\theta dp_\theta = \sqrt{2}|\alpha_{LO}| \int_{-\infty}^{\infty} w_\theta(x_\theta) x_\theta dx_\theta \ . \end{aligned}$$

Here, the distribution function integrated over a rotated quadrature component p_θ is given by,

$$w_\theta(x_\theta) \equiv \int_{-\infty}^{\infty} W_\theta(x_\theta, p_\theta) dp_\theta \ . \tag{35.351}$$

This is called the *radon transform*. The distribution function $w_\theta(p_\theta)$ as well as the Wigner function are normalized to 1. Multiple measurements of the expectation value $x_\theta = \langle\psi|\hat{x}_\theta|\psi\rangle$ now yields a histogram $H_{|\psi\rangle}(x_\theta)$ reflecting, if normalized, $w_{|\psi\rangle}(x_\theta) = H_{|\psi\rangle}(x_\theta)/\int H_{|\psi\rangle}(x_\theta)$ exactly the distribution function.

Considering the finite detector efficiency [791] $w_\theta(x_\theta)$ must be generalized to a convolution with an apparatus function $\zeta(x)$:

$$w_\theta^{\rm real}(\sqrt{\eta}x_\theta) = (w_\theta^{ideal} \star \zeta) \qquad \text{where} \qquad \zeta(x) = \frac{1}{\sqrt{\pi(1-\eta)}} e^{-\eta\alpha^2/(1-\eta)} \ . \tag{35.352}$$

A finite detector efficiency degrades the contrast of the quantum interference structures.

With the procedure of optical *homodyne tomography* or *quantum state endoscopy* the Wigner function for e.g. a Schrödinger cat state can be reconstructed from a set of distribution functions $w_\theta(x_\theta) = \int W(\alpha e^{\imath\theta})dp_\theta$ measured for various phases θ [791]. To do this the data set is exposed to an inverse *radon transform*:

$$W(\alpha) = \frac{1}{4\pi^2}\int_{-\infty}^{\infty}\int_0^\pi\int_{-\infty}^{\infty} w_\theta(x_\theta)|\zeta|e^{\imath\zeta\left[\mathfrak{Re}\ (2^{-1/2}\alpha e^{-\imath\theta})-x_\theta\right]}dx d\theta d\zeta \ . \tag{35.353}$$

In contrast to the conventional homodyne detection, where the phase dependency of amplitude noise is recorded, the homodyne tomography allows the complete reconstruction of a quantum state through measurement of the distribution of the amplitude noise power,

$$P_s = \frac{\omega_s}{2\pi}\int_0^{\omega_s/2\pi} dt|\langle I(t)\rangle|^2 \tag{35.354}$$

for various phases.

Alternatively, to the homodyne method, one may reconstruct the photon distribution in field modes from their temporal evolution [1352]. Another method could be to use atoms as sensors for the quantum state of a light field in a Jaynes-Cummings type dynamics.

35.8.6.1 Homodyne signature of squeezed states

Let us mix squeezed light $\hat{b}$ with a local oscillator $\hat{a}$ at a beam splitter,

$$\begin{pmatrix}\hat{x}\\ \hat{y}\end{pmatrix} = \frac{1}{\sqrt{2}}\begin{pmatrix}1 & -\imath\\ -\imath & 1\end{pmatrix}\begin{pmatrix}\hat{b}\\ \hat{a}\end{pmatrix} \ . \tag{35.355}$$

The homodyne signal is,

$$\begin{aligned} P_{hody} &\propto \hat{x}^\dagger\hat{x} - \hat{y}^\dagger\hat{y} \\ &= \imath\hat{a}^\dagger\hat{b} - \imath\hat{a}\hat{b}^\dagger \\ &= \imath(\hat{a}^\dagger - \hat{a})\hat{b}_r - (\hat{a}^\dagger + \hat{a})\hat{b}_p \\ &= 2|\alpha|\left(\hat{b}_r\sin\theta - \hat{b}_p\cos\theta\right) \ , \end{aligned} \tag{35.356}$$

if the local oscillator can be considered as classical, $\alpha = |\alpha|e^{\imath\theta}$. I.e. the phase of the local oscillator permits us to select either one of the quadrature components.

35.8.7 Multimode squeezing

Define,

$$\hat{b} = \mu\hat{a} + \nu\hat{c}^\dagger \ . \tag{35.357}$$

Again using $\mu^2 - \nu^2 = 1$, the standard commutation rules for $\hat{a}$ and $\hat{c}$ give,

$$\begin{aligned} [\hat{b}, \hat{b}^\dagger] &= 1 \\ [\hat{b}_r, \hat{b}_p] &= \tfrac{\imath}{2} \ . \end{aligned} \tag{35.358}$$

The individual variances read,

$$\begin{aligned} \Delta\hat{b}_r^2 &= \langle \hat{b}_r^2 \rangle - \langle \hat{b}_r \rangle^2 \\ &= \tfrac{1}{4}\langle (\hat{b} + \hat{b}^\dagger)^2 \rangle - \tfrac{1}{4}\langle \hat{b} + \hat{b}^\dagger \rangle^2 \\ &= \tfrac{1}{4}\langle (\mu\hat{a} + \mu\hat{a}^\dagger + \nu\hat{c} + \nu\hat{c}^\dagger)^2 \rangle \\ &= \tfrac{1}{4}\mu^2 + \tfrac{1}{4}\nu^2 + \tfrac{1}{2}\mu^2\langle \hat{a}^\dagger\hat{a} \rangle + \tfrac{1}{2}\nu^2\langle \hat{c}^\dagger\hat{c} \rangle + \tfrac{1}{2}\mu\nu \left(\langle \hat{a}\hat{c} \rangle + \langle \hat{a}^\dagger\hat{c}^\dagger \rangle \right) \rangle \ . \end{aligned} \tag{35.359}$$

using $\langle \hat{a} \rangle = \langle \hat{c} \rangle = \langle \hat{a}^\dagger\hat{c} \rangle = 0$.

Two-mode squeezing can exist even if the individual modes are not squeezed,

$$|r, \phi\rangle = \cosh^{-1} r \sum\nolimits_n \tanh^n r e^{\imath n\phi} |r, \phi\rangle_a |r, \phi\rangle_b \ . \tag{35.360}$$

A *two-mode squeezed vacuum state* can be generated by the squeezing operator

$$\boxed{S(\xi) \equiv \exp\left(\tfrac{\xi^*}{2}\hat{a}\hat{b} - \tfrac{\xi}{2}\hat{a}^\dagger b^\dagger \right)} \ . \tag{35.361}$$

Remember that the single-mode squeezing is obtained if $\hat{a} = \hat{b}$. In a number state base

$$|r, \phi\rangle = \frac{1}{\cosh r} \sum\nolimits_n (\tanh r)^n e^{\imath n\phi} |n\rangle_a |n\rangle_b \ . \tag{35.362}$$

Two-mode relative number squeezing parameter

$$\xi_{i,j} = \frac{\sigma^2(n_i - \langle n_j \rangle)}{\langle n_i \rangle + \langle n_j \rangle} \ . \tag{35.363}$$

35.8.8 Coupled quantum oscillators with/out counter-rotating terms

The Hamiltonian of a beam splitter resembles the one of a system of two *coupled oscillators* with identical eigenfrequencies. Here, we are interested in calculating the time evolution of such a system. We rewrite the Hamiltonian in terms of the *normal modes*. We start from the Hamiltonian with counter-rotating terms [426],

$$\boxed{\hat{H} = \hbar\omega(\hat{a}^\dagger\hat{a} + \tfrac{1}{2}) + \hbar\omega(\hat{b}^\dagger\hat{b} + \tfrac{1}{2}) + \tfrac{\hbar\Omega}{2}(\hat{a} + \hat{a}^\dagger)(\hat{b} + \hat{b}^\dagger)} \ , \tag{35.364}$$

which we rewrite in terms of the quadrature components given by,

$$\begin{pmatrix} \hat{x}_a \\ \hat{p}_a \\ \hat{x}_b \\ \hat{p}_b \end{pmatrix} = \mathcal{T}_{ab} \begin{pmatrix} \hat{a} \\ \hat{a}^\dagger \\ \hat{b} \\ \hat{b}^\dagger \end{pmatrix} \qquad \text{with} \qquad \mathcal{T}_{ab} \equiv \sqrt{\frac{\hbar\omega}{2}} \begin{pmatrix} \omega^{-1} & \omega^{-1} & 0 & 0 \\ \imath & -\imath & 0 & 0 \\ 0 & 0 & \omega^{-1} & \omega^{-1} \\ 0 & 0 & \imath & -\imath \end{pmatrix} , \tag{35.365}$$

as

$$\hat{H} = \tfrac{1}{2}(\hat{p}_a^2 + \omega^2 \hat{x}_a^2) + \tfrac{1}{2}(\hat{p}_b^2 + \omega^2 \hat{x}_b^2) + \Omega\omega \hat{x}_a \hat{x}_b \ . \tag{35.366}$$

Setting $\omega_\pm = \sqrt{\omega^2 \pm \Omega\omega}$ allows us to rewrite the Hamiltonian as,

$$\hat{H} = \tfrac{1}{4}(\hat{p}_a + \hat{p}_b)^2 + \tfrac{1}{4}\omega_+^2(\hat{x}_a + \hat{x}_b)^2 + \tfrac{1}{4}(\hat{p}_a - \hat{p}_b)^2 + \tfrac{1}{4}\omega_-^2(\hat{x}_a - \hat{x}_b)^2 \ . \tag{35.367}$$

Now, we apply the transform,

$$\begin{pmatrix} \hat{x}_A \\ \hat{p}_A \\ \hat{x}_B \\ \hat{p}_B \end{pmatrix} = \mathcal{M} \begin{pmatrix} \hat{x}_a \\ \hat{p}_a \\ \hat{x}_b \\ \hat{p}_b \end{pmatrix} \qquad \text{with} \qquad \mathcal{M} \equiv \sqrt{\frac{1}{2}} \begin{pmatrix} 1 & 0 & 1 & 0 \\ 0 & 1 & 0 & 1 \\ 1 & 0 & -1 & 0 \\ 0 & 1 & 0 & -1 \end{pmatrix} = M^{-1} , \tag{35.368}$$

and rewrite the Hamiltonian again as,

$$\hat{H} = \tfrac{1}{2}(\hat{p}_A^2 + \omega_+^2 \hat{x}_A^2) + \tfrac{1}{2}(\hat{p}_B^2 + \omega_-^2 \hat{x}_B^2) \ . \tag{35.369}$$

We go back from the quadrature components to the field mode operators via,

$$\begin{pmatrix} \hat{x}_A \\ \hat{p}_A \\ \hat{x}_B \\ \hat{p}_B \end{pmatrix} = \mathcal{T}_{AB} \begin{pmatrix} \hat{A} \\ \hat{A}^\dagger \\ \hat{B} \\ \hat{B}^\dagger \end{pmatrix} \qquad \text{with} \qquad \mathcal{T}_{AB} \equiv \sqrt{\frac{\hbar}{2}} \begin{pmatrix} 1/\sqrt{\omega_+} & 1/\sqrt{\omega_+} & 0 & 0 \\ \imath\sqrt{\omega_+} & -\imath\sqrt{\omega_+} & 0 & 0 \\ 0 & 0 & 1/\sqrt{\omega_-} & 1/\sqrt{\omega_+} \\ 0 & 0 & \imath\sqrt{\omega_-} & -\imath\sqrt{\omega_+} \end{pmatrix} , \tag{35.370}$$

and finally obtain,

$$\boxed{\hat{H} = \hbar\omega_+(\hat{A}^\dagger \hat{A} + \tfrac{1}{2}) + \hbar\omega_-(\hat{B}^\dagger \hat{B} + \tfrac{1}{2})} \ . \tag{35.371}$$

The Heisenberg equations of motion for the oscillator modes,

$$\frac{d}{dt} \begin{pmatrix} \hat{a} \\ \hat{a}^\dagger \\ \hat{b} \\ \hat{b}^\dagger \end{pmatrix} = -\tfrac{\imath}{\hbar} \left[\begin{pmatrix} \hat{a} \\ \hat{a}^\dagger \\ \hat{b} \\ \hat{b}^\dagger \end{pmatrix} , \hat{H} \right] = \mathcal{X} \begin{pmatrix} \hat{a} \\ \hat{a}^\dagger \\ \hat{b} \\ \hat{b}^\dagger \end{pmatrix} \qquad \text{with} \qquad \mathcal{X} \equiv \begin{pmatrix} -\imath\omega & 0 & -\frac{\imath\Omega}{2} & -\frac{\imath\Omega}{2} \\ 0 & \imath\omega & \frac{\imath\Omega}{2} & \frac{\imath\Omega}{2} \\ -\frac{\imath\Omega}{2} & -\frac{\imath\Omega}{2} & -\imath\omega & 0 \\ \frac{\imath\Omega}{2} & \frac{\imath\Omega}{2} & 0 & \imath\omega \end{pmatrix} , \tag{35.372}$$

are difficult to integrate. In contrast, the Heisenberg equations for the normal modes,

$$\frac{d}{dt}\begin{pmatrix}\hat{A}\\ \hat{A}^\dagger\\ \hat{B}\\ \hat{B}^\dagger\end{pmatrix} = -\tfrac{\imath}{\hbar}\left[\begin{pmatrix}\hat{A}\\ \hat{A}^\dagger\\ \hat{B}\\ \hat{B}^\dagger\end{pmatrix}, \hat{H}\right] = E_{\mathcal{X}}\begin{pmatrix}\hat{A}\\ \hat{A}^\dagger\\ \hat{B}\\ \hat{B}^\dagger\end{pmatrix} \tag{35.373}$$

$$\text{with} \qquad E_{\mathcal{X}} = U_{\mathcal{X}}^{-1}\mathcal{X}U_{\mathcal{X}} = \begin{pmatrix}-\imath\omega_+ & 0 & 0 & 0\\ 0 & \imath\omega_+ & 0 & 0\\ 0 & 0 & -\imath\omega_- & 0\\ 0 & 0 & 0 & \imath\omega_-\end{pmatrix}$$

$$\text{and} \qquad U_{\mathcal{X}} = \begin{pmatrix}-1-\frac{2}{\Omega}(\omega+\omega_+) & -1-\frac{2}{\Omega}(\omega-\omega_+) & 1-\frac{2}{\Omega}(\omega+\omega_-) & 1-\frac{2}{\Omega}(\omega-\omega_-)\\ 1 & 1 & -1 & -1\\ -1-\frac{2}{\Omega}(\omega+\omega_+) & -1-\frac{2}{\Omega}(\omega-\omega_+) & -1+\frac{2}{\Omega}(\omega+\omega_-) & -1+\frac{2}{\Omega}(\omega-\omega_-)\\ 1 & 1 & 1 & 1\end{pmatrix},$$

are easily solved by,

$$\begin{pmatrix}\hat{A}(t)\\ \hat{A}^\dagger(t)\\ \hat{B}(t)\\ \hat{B}^\dagger(t)\end{pmatrix} = e^{E_{\mathcal{X}}t}\begin{pmatrix}\hat{A}(0)\\ \hat{A}^\dagger(0)\\ \hat{B}(0)\\ \hat{B}^\dagger(0)\end{pmatrix} \qquad \text{with} \qquad e^{E_{\mathcal{X}}t} \equiv \begin{pmatrix}e^{-\imath\omega_+ t} & 0 & 0 & 0\\ 0 & e^{\imath\omega_+ t} & 0 & 0\\ 0 & 0 & e^{-\imath\omega_- t} & 0\\ 0 & 0 & 0 & e^{\imath\omega_- t}\end{pmatrix}. \tag{35.374}$$

Hence, the oscillator modes evolve as,

$$\begin{pmatrix}\hat{a}(t)\\ \hat{a}^\dagger(t)\\ \hat{b}(t)\\ \hat{b}^\dagger(t)\end{pmatrix} = e^{\mathcal{X}t}\begin{pmatrix}\hat{a}(0)\\ \hat{a}^\dagger(0)\\ \hat{b}(0)\\ \hat{b}^\dagger(0)\end{pmatrix} \qquad \text{with} \qquad e^{\mathcal{X}t} = \mathcal{T}_{ab}^{-1}\mathcal{M}^{-1}\mathcal{T}_{AB}e^{E_{\mathcal{X}}t}\mathcal{T}_{AB}^{-1}\mathcal{M}\mathcal{T}_{ab} = U_{\mathcal{X}}e^{E_{\mathcal{X}}t}U_{\mathcal{X}}^{-1}. \tag{35.375}$$

35.8.8.1 Rotating-wave approximation

The rotating-wave approximation is performed via $\omega_\pm \simeq \omega \pm \frac{1}{2}\Omega$. It leads to the Hamiltonian,

$$\boxed{\hat{H} = \hbar\omega(\hat{a}^\dagger\hat{a} + \tfrac{1}{2}) + \hbar\omega(\hat{b}^\dagger\hat{b} + \tfrac{1}{2}) + \tfrac{\hbar\Omega}{2}(\hat{a}\hat{b}^\dagger + \hat{a}^\dagger\hat{b})}\,. \tag{35.376}$$

In this approximation, we find $\mathcal{T}_{AB}^{-1}\mathcal{M}\mathcal{T}_{ab} \simeq \mathcal{M}$ and the transformation defined in (35.368),

$$\begin{pmatrix}\hat{A}\\ \hat{A}^\dagger\\ \hat{B}\\ \hat{B}^\dagger\end{pmatrix} = \mathcal{M}\begin{pmatrix}\hat{a}\\ \hat{a}^\dagger\\ \hat{b}\\ \hat{b}^\dagger\end{pmatrix}, \tag{35.377}$$

takes us directly from the Hamiltonian (35.376) to [21],

$$\boxed{\hat{H} = (\hbar\omega + \tfrac{\hbar\Omega}{2})(\hat{A}^\dagger\hat{A} + \tfrac{1}{2}) + (\hbar\omega - \tfrac{\hbar\Omega}{2})(\hat{B}^\dagger\hat{B} + \tfrac{1}{2})} \,. \tag{35.378}$$

Do the Excs. 35.8.9.5 and 35.8.9.6.

Note, that two coupled oscillator model becomes *criticality*, when the atom-field coupling strength exceeds the frequencies of the mode and the atomic two-level system.

35.8.8.2 Interaction-free measurement

Beam splitters and coupled cavities have been proposed for the realization of *interaction-free measurements* 35.8.9.7 and 35.8.9.8 [413, 1322, 764, 742].

35.8.9 Exercises

35.8.9.1 Ex: Conservation law at a beam splitter 1

Show that the beam-split transformation

$$\begin{pmatrix} \hat{c} \\ \hat{d} \end{pmatrix} = \begin{pmatrix} t & -r \\ r & t \end{pmatrix} \begin{pmatrix} \hat{a} \\ \hat{b} \end{pmatrix}$$

preserves the commutations relations and the photon number.

Solution: *From*

$$\hat{c} = t\hat{a} - r\hat{b} \qquad \textit{and} \qquad \hat{d} = r\hat{a} + t\hat{b}$$

follows

$$\begin{aligned} [\hat{c}, \hat{d}] &= [t\hat{a} - r\hat{b}, r\hat{a} + t\hat{b}] = 0 \\ [\hat{c}, \hat{c}^\dagger] &= [t\hat{a} - r\hat{b}, t\hat{a}^\dagger - r\hat{b}^\dagger] = |t|^2 + |r|^2 = 1 \end{aligned}$$

with

$$\det U = |t|^2 + |r|^2 = 1 \ .$$

Furthermore,

$$\begin{aligned} \hat{c}^\dagger\hat{c} + \hat{d}^\dagger\hat{d} &= (t^*\hat{a}^\dagger - r^*\hat{b}^\dagger)(t\hat{a} - r\hat{b}) + (r\hat{a}^\dagger + t\hat{b}^\dagger)(r\hat{a} + t\hat{b}) \\ &= (|t|^2 + |r|^2)(\hat{a}^\dagger\hat{a} + \hat{b}^\dagger\hat{b}) + (rt - rt)\hat{a}\hat{b}^\dagger + (rt - rt)\hat{a}^\dagger\hat{b} = \hat{a}^\dagger\hat{a} + \hat{b}^\dagger\hat{b} \ . \end{aligned}$$

[21] Note the different behavior of a beam splitter under this transformation,

$$\begin{aligned} \hat{H} &= \hbar\omega(\hat{a}^\dagger\hat{a} + \tfrac{1}{2}) + \hbar\omega(\hat{b}^\dagger\hat{b} + \tfrac{1}{2}) + \tfrac{\hbar\Omega}{2}\left(\hat{a}\hat{b}^\dagger - \hat{a}^\dagger\hat{b}\right) \\ &= \hbar\omega(\hat{A}^\dagger\hat{A} + \tfrac{1}{2}) + \hbar\omega(\hat{B}^\dagger\hat{B} + \tfrac{1}{2}) + \tfrac{\hbar\Omega}{2}(-\hat{A}\hat{B}^\dagger + \hat{A}^\dagger\hat{B}) \ . \end{aligned}$$

35.8.9.2 Ex: Conservation law at a beam splitter 2

Derive from the Hamiltonian (35.308) that $\hat{a}^\dagger\hat{a} + \hat{b}^\dagger\hat{b} = const.$

Solution: *With the Hamiltonian (35.308) we have,*

$$\frac{d}{dt}(\hat{a}^\dagger\hat{a}) = \frac{\imath}{\hbar}[\hat{H}, \hat{a}^\dagger\hat{a}] = \frac{\imath}{2}\Omega[\hat{a}\hat{b}^\dagger + \hat{a}^\dagger\hat{b}, \hat{a}^\dagger\hat{a}] = \frac{\imath}{2}\Omega(\hat{a}\hat{b}^\dagger - \hat{a}^\dagger\hat{b})$$
$$\frac{d}{dt}(\hat{b}^\dagger\hat{b}) = \frac{\imath}{\hbar}[\hat{H}, \hat{b}^\dagger\hat{b}] = \frac{\imath}{2}\Omega[\hat{a}\hat{b}^\dagger + \hat{a}^\dagger\hat{b}, \hat{b}^\dagger\hat{b}] = -\frac{\imath}{2}\Omega(\hat{a}\hat{b}^\dagger - \hat{a}^\dagger\hat{b}) \ .$$

Hence,

$$\hat{a}^\dagger\hat{a} + \hat{b}^\dagger\hat{b} = const \ .$$

35.8.9.3 Ex: Beam splitter

Show that $\hat{B}|1,0\rangle = \cos\theta|1,0\rangle - \sin\theta|0,1\rangle$ and $\hat{B}|0,n\rangle = \sum_{k=0}^{\infty}\sqrt{\binom{n}{k}}\cos^k\theta\sin^{n-k}\theta|n-k,k\rangle$.

Solution: *a. From*

$$(\hat{a}\hat{b}^\dagger - \hat{a}^\dagger\hat{b})|1,0\rangle = |0,1\rangle \qquad and \qquad (\hat{a}\hat{b}^\dagger - \hat{a}^\dagger\hat{b})|0,1\rangle = -|1,0\rangle$$

we deduce

$$(\hat{a}\hat{b}^\dagger - \hat{a}^\dagger\hat{b})^{2k}|1,0\rangle = (-1)^k|1,0\rangle \qquad and \qquad (\hat{a}\hat{b}^\dagger - \hat{a}^\dagger\hat{b})^{2k+1}|1,0\rangle = -(-1)^k|0,1\rangle$$

and then

$$\begin{aligned} e^{\theta(\hat{a}\hat{b}^\dagger - \hat{a}^\dagger\hat{b})}|1,0\rangle &= \sum_k \frac{\theta^k}{k!}(\hat{a}\hat{b}^\dagger - \hat{a}^\dagger\hat{b})^k|1,0\rangle \\ &= \sum_k \frac{\theta^{2k}}{(2k)!}(\hat{a}\hat{b}^\dagger - \hat{a}^\dagger\hat{b})^{2k}|1,0\rangle + \sum_k \frac{\theta^{2k+1}}{(2k+1)!}(\hat{a}\hat{b}^\dagger - \hat{a}^\dagger\hat{b})^{2k+1}|1,0\rangle \\ &= \sum_k \frac{\theta^{2k}}{(2k)!}(-1)^k|1,0\rangle - \sum_k \frac{\theta^{2k+1}}{(2k+1)!}(-1)^k|0,1\rangle \\ &= \cos\theta|1,0\rangle - \sin\theta|0,1\rangle \ . \end{aligned}$$

b. We can express the vacuum state via a Fock state by,

$$|n,0\rangle = \frac{\hat{a}^{\dagger n}}{\sqrt{n!}}|0,0\rangle \qquad and \qquad |0,n\rangle = \frac{\hat{b}^{\dagger n}}{\sqrt{n!}}|0,0\rangle \ .$$

Using the results of a. we calculate,

$$\begin{aligned} \hat{B}\hat{a}^{\dagger n}\hat{B}^\dagger &= (\hat{B}\hat{a}^n\hat{B}^\dagger)^\dagger = (\hat{B}\hat{a}\hat{B}^\dagger)^{n\dagger} = (\hat{a}^\dagger\cos\theta + \hat{b}^\dagger\sin\theta)^{n\dagger} \\ &= \sum_k \binom{n}{k}\hat{a}^{k\dagger}\cos^k\theta + (\hat{b}^{n-k})^\dagger\sin^{n-k}\theta \ . \end{aligned}$$

Finally, because of,

$$(\hat{a}\hat{b}^\dagger - \hat{a}^\dagger\hat{b})|0,0\rangle = 0 \qquad \Longrightarrow \qquad \hat{B}|0,0\rangle = e^{\theta(\hat{a}\hat{b}^\dagger - \hat{a}^\dagger\hat{b})}|0,0\rangle = 1$$

we get

$$\begin{aligned}\hat{B}|n,0\rangle = \hat{B}\frac{\hat{a}^{\dagger n}}{\sqrt{n!}}|0,0\rangle &= \frac{1}{\sqrt{n!}}\left(\sum_k \binom{n}{k}\hat{a}^{k\dagger}\cos^k\theta + (\hat{b}^{n-k})^\dagger \sin^{n-k}\theta\right)\hat{B}|0,0\rangle \\ &= \frac{1}{\sqrt{n!}}\sum_k \binom{n}{k}\hat{a}^{k\dagger}\cos^k\theta(\hat{b}^{n-k})^\dagger \sin^{n-k}\theta \ .\end{aligned}$$

35.8.9.4 Ex: Beam splitter

Show that for $\hat{B} \equiv e^{\theta(\hat{a}\hat{b}^\dagger - \hat{a}^\dagger\hat{b})}$ holds,

$$\hat{B}\hat{a}\hat{B}^\dagger = \hat{a}\cos\theta + \hat{b}\sin\theta \qquad \text{and} \qquad \hat{B}\hat{b}\hat{B}^\dagger = -\hat{a}\sin\theta + \hat{b}\cos\theta \ .$$

Solution: *The two expressions can be recombined to,*

$$\hat{B}(\hat{a} \pm \imath\hat{b})\hat{B}^\dagger = (\hat{a} \pm \imath\hat{b})e^{\mp\imath\theta} \ .$$

Now, we define the new quantities,

$$\hat{x} \equiv \hat{a} + \imath\hat{b} \qquad \textit{and} \qquad \hat{A} \equiv \hat{a}\hat{b}^\dagger - \hat{a}^\dagger\hat{b} \ ,$$

for which,

$$[\hat{A}, \hat{x}] = -\imath\hat{x} \ ,$$

and rewrite one of the expressions as,

$$e^{\theta\hat{A}}\hat{x}e^{-\theta\hat{A}} = \hat{x}e^{-\imath\theta} \ .$$

Now, we use (23.179) which has been derived in Exc. 23.5.6.1,

$$e^{\hat{A}}\hat{x}e^{-\hat{A}} = \hat{x} + [\hat{A}, \hat{x}] + \tfrac{1}{2!}[\hat{A}, [\hat{A}, \hat{x}]] + ... \ ,$$

and obtain,

$$\begin{aligned}e^{\hat{A}}\hat{x}e^{-\hat{A}} &= \hat{x} + \theta[\hat{A}, \hat{x}] + \tfrac{\theta^2}{2!}[\hat{A}, [\hat{A}, \hat{x}]] + ... \\ &= \hat{x} - \theta\imath\hat{x} + \tfrac{\imath\theta^2}{2!}\imath\hat{x} + ... = \hat{x}e^{-\imath\theta} \ .\end{aligned}$$

35.8.9.5 Ex: Coupled harmonic oscillators with different eigenfrequencies and damping

Here, we generalize the calculation of Sec. 35.8.8 for coupling of oscillators with different eigenfrequencies.
a. From,

$$\hat{H} = \hbar\omega_a(\hat{a}^\dagger\hat{a} + \tfrac{1}{2}) + \hbar\omega_b(\hat{b}^\dagger\hat{b} + \tfrac{1}{2}) + \tfrac{\hbar\Omega}{2}(\hat{a}\hat{b}^\dagger + \hat{a}^\dagger\hat{b}) + \tfrac{\hbar\Omega'}{2}(\hat{a}\hat{b} + \hat{a}^\dagger\hat{b}^\dagger)$$

derive the Hamiltonian in terms of the quadrature components $\hat{x}_{a,b}$ and $\hat{p}_{a,b}$.
b. Set up the Heisenberg equations for the field operators $\hat{a}$, $\hat{a}^\dagger$, $\hat{b}$, and $\hat{b}^\dagger$ and determine the eigenvalues of the matrix $\mathcal{X}$ defined by,

$$\frac{d}{dt}\begin{pmatrix}\hat{a}\\ \hat{a}^\dagger\\ \hat{b}\\ \hat{b}^\dagger\end{pmatrix} = X\begin{pmatrix}\hat{a}\\ \hat{a}^\dagger\\ \hat{b}\\ \hat{b}^\dagger\end{pmatrix} \ .$$

c. Extend the Heisenberg equations by including loss terms for the cavity modes κ_a and κ_b and determine the corresponding matrix $\mathcal{X}_\kappa$, as well as its eigenvalues for the simplifying case $\Omega' \equiv \Omega$.

Solution: *a. Transforming like,*

$$\begin{pmatrix}\hat{x}_a\\ \hat{p}_a\\ \hat{x}_b\\ \hat{p}_b\end{pmatrix} = \mathcal{T}_{ab}\begin{pmatrix}\hat{a}\\ \hat{a}^\dagger\\ \hat{b}\\ \hat{b}^\dagger\end{pmatrix} \qquad \textit{with} \qquad \mathcal{T}_{ab} \equiv \begin{pmatrix}\sqrt{\frac{\hbar}{2\omega_a}} & \sqrt{\frac{\hbar}{2\omega_a}} & 0 & 0\\ \imath\sqrt{\frac{\hbar\omega_a}{2}} & -\imath\sqrt{\frac{\hbar\omega_a}{2}} & 0 & 0\\ 0 & 0 & \sqrt{\frac{\hbar}{2\omega_b}} & \sqrt{\frac{\hbar}{2\omega_b}}\\ 0 & 0 & \imath\sqrt{\frac{\hbar\omega_b}{2}} & -\imath\sqrt{\frac{\hbar\omega_b}{2}}\end{pmatrix} ,$$

we obtain,

$$\hat{H} = \tfrac{1}{2}(\hat{p}_a^2 + \omega_a^2\hat{x}_a^2) + \tfrac{1}{2}(\hat{p}_b^2 + \omega_b^2\hat{x}_b^2) + \tfrac{(\Omega+\Omega')\sqrt{\omega_a\omega_b}}{2}\hat{x}_a\hat{x}_b + \tfrac{\Omega-\Omega'}{2\sqrt{\omega_a\omega_b}}\hat{p}_a\hat{p}_b \ .$$

b. The Heisenberg equations are,

$$\frac{d}{dt}\begin{pmatrix}\hat{a}\\ \hat{a}^\dagger\\ \hat{b}\\ \hat{b}^\dagger\end{pmatrix} = -\tfrac{\imath}{\hbar}\left[\begin{pmatrix}\hat{a}\\ \hat{a}^\dagger\\ \hat{b}\\ \hat{b}^\dagger\end{pmatrix}, \hat{H}\right] = \mathcal{X}\begin{pmatrix}\hat{a}\\ \hat{a}^\dagger\\ \hat{b}\\ \hat{b}^\dagger\end{pmatrix} \qquad \textit{with} \qquad \mathcal{X} \equiv \begin{pmatrix}-\imath\omega_a & 0 & -\frac{\imath\Omega}{2} & -\frac{\imath\Omega'}{2}\\ 0 & \imath\omega_a & \frac{\imath\Omega'}{2} & \frac{\imath\Omega}{2}\\ -\frac{\imath\Omega}{2} & -\frac{\imath\Omega'}{2} & -\imath\omega_b & 0\\ \frac{\imath\Omega'}{2} & \frac{\imath\Omega}{2} & 0 & \imath\omega_b\end{pmatrix} .$$

The eigenvalues are $\pm\omega_\pm$ with,

$$\omega_\pm \equiv \tfrac{1}{\sqrt{2}}\sqrt{\omega_a^2 + \omega_b^2 + \tfrac{\Omega^2-\Omega'^2}{2} \pm \sqrt{(\omega_a^2-\omega_b^2)^2 + (\omega_a+\omega_b)^2\Omega^2 - (\omega_a-\omega_b)^2\Omega'^2}} \ .$$

For $\Omega = \Omega'$ we recover,

$$\omega_\pm = \tfrac{1}{\sqrt{2}}\sqrt{\omega_a^2 + \omega_b^2 \pm \sqrt{(\omega_a^2-\omega_b^2)^2 + 4\omega_a\omega_b\Omega^2}} \ ,$$

for $\omega_a = \omega_b$ we recover,

$$\omega_\pm = \sqrt{\omega^2 \pm \omega\Omega + \tfrac{\Omega^2 - \Omega'^2}{4}} \ ,$$

and finally for $\Omega = \Omega'$ and $\omega_a = \omega_b$ we recover $\omega_\pm = \sqrt{\omega^2 \pm \omega\Omega}$.
c. The extended Heisenberg-Liouville equations are,

$$\frac{d}{dt}\hat{a} = -\tfrac{\imath}{\hbar}[\hat{a}, \hat{H}] - \kappa_a \hat{a} \qquad with \qquad \frac{d}{dt}\hat{b} = -\tfrac{\imath}{\hbar}[\hat{b}, \hat{H}] - \kappa_b \hat{b} \ ,$$

such that,

$$\mathcal{X}_\kappa = \begin{pmatrix} -\imath\omega_a - \kappa_a & 0 & -\frac{\imath\Omega}{2} & -\frac{\imath\Omega'}{2} \\ 0 & \imath\omega_a - \kappa_a & \frac{\imath\Omega'}{2} & \frac{\imath\Omega}{2} \\ -\frac{\imath\Omega}{2} & -\frac{\imath\Omega'}{2} & -\imath\omega_b - \kappa_b & 0 \\ \frac{\imath\Omega'}{2} & \frac{\imath\Omega}{2} & 0 & \imath\omega_b - \kappa_b \end{pmatrix} \ .$$

The eigenvalues for the case $\Omega' \equiv \Omega$ are,

$$\omega_{1,2,3,4} = -\tfrac{\kappa_a + \kappa_b}{2} \pm \sqrt{(\tfrac{\kappa_a - \kappa_b}{2})^2 - \omega^2 \pm \omega\sqrt{\Omega^2 - (\kappa_a - \kappa_b)^2}} \ .$$

35.8.9.6 Ex: Equivalence of beam splitter and coupled oscillator models

Show that the beam splitter and the coupled oscillators model for degenerate frequencies are equivalent.

Solution: *The prescription $\hat{A} \equiv \hat{a}$ and $\hat{B} = -\imath\hat{b}$ transforms the Hamiltonian between the beam splitter and coupled oscillators model,*

$$\begin{aligned} \hat{H} &= \hbar\omega(\hat{a}^\dagger\hat{a} + \tfrac{1}{2}) + \hbar\omega(\hat{b}^\dagger\hat{b} + \tfrac{1}{2}) + \Omega(\hat{a}\hat{b}^\dagger + \hat{a}^\dagger\hat{b}) \\ &= \hbar\omega(\hat{A}^\dagger\hat{A} + \tfrac{1}{2}) + \hbar\omega(\hat{B}^\dagger\hat{B} + \tfrac{1}{2}) + \imath\Omega(\hat{A}\hat{B}^\dagger - \hat{A}^\dagger\hat{B}) \ . \end{aligned}$$

In matrix notation we may write,

$$\begin{pmatrix} \hat{x}_a \\ \hat{p}_a \\ \hat{x}_b \\ \hat{p}_b \end{pmatrix} = \mathcal{T} \begin{pmatrix} \hat{a} \\ \hat{a}^\dagger \\ \hat{b} \\ \hat{b}^\dagger \end{pmatrix} \qquad with \qquad \mathcal{T} \equiv \begin{pmatrix} 1 & 1 & 0 & 0 \\ \imath & -\imath & 0 & 0 \\ 0 & 0 & 1 & 1 \\ 0 & 0 & \imath & -\imath \end{pmatrix}$$

$$\begin{pmatrix} \hat{A} \\ \hat{A}^\dagger \\ \hat{B} \\ \hat{B}^\dagger \end{pmatrix} = \mathcal{M} \begin{pmatrix} \hat{a} \\ \hat{a}^\dagger \\ b \\ b^\dagger \end{pmatrix} \qquad where \qquad \mathcal{M} \equiv \begin{pmatrix} 1 & 0 & 0 & 0 \\ 0 & 1 & 0 & 0 \\ 0 & 0 & -\imath & 0 \\ 0 & 0 & 0 & \imath \end{pmatrix}$$

$$\begin{pmatrix} \hat{x}_A \\ \hat{p}_A \\ \hat{x}_B \\ \hat{p}_B \end{pmatrix} = \mathcal{T}\mathcal{M}\mathcal{T}^{-1} \begin{pmatrix} \hat{x}_a \\ \hat{p}_a \\ \hat{x}_b \\ \hat{p}_b \end{pmatrix} \qquad with \qquad \mathcal{T}\mathcal{M}\mathcal{T}^{-1} = \begin{pmatrix} 1 & 0 & 0 & 0 \\ 0 & 1 & 0 & 0 \\ 0 & 0 & 0 & -\imath \\ 0 & 0 & -\imath & 0 \end{pmatrix} \ .$$

We verify the commutation rules,

$$[\hat{A},\hat{A}^\dagger]=[\hat{a},\hat{a}^\dagger]=1 \quad , \quad [\hat{B},\hat{B}^\dagger]=[-\imath\hat{B},\imath\hat{B}^\dagger]=[\hat{b},\hat{b}^\dagger]=1 \ ,$$

and the conservation laws,

$$[\hat{H},\hat{a}^\dagger\hat{a}+\hat{b}^\dagger\hat{b}]=\Omega[\hat{a}b^\dagger+\hat{a}^\dagger b,\hat{a}^\dagger\hat{a}+\hat{b}^\dagger\hat{b}]=0$$
$$[\hat{H},\hat{A}^\dagger\hat{A}+\hat{B}^\dagger\hat{B}]=\Omega[\hat{A}\hat{B}^\dagger-\hat{A}^\dagger\hat{B},\hat{A}^\dagger\hat{A}+\hat{B}^\dagger\hat{B}]=0 \ .$$

35.8.9.7 Ex: Elitzur and Vaidman bomb tester

a. Write down the beam splitter Hamiltonian in the Fock representation for a the case of a single photon, diagonalize it, and determine the propagator $e^{\imath\hat{H}t/\hbar}$ for a 50/50 beam splitter.
b. Based on the propagator derived in (a) draw an analogy between a Mach-Zehnder interferometer and a resonantly driven two-level system. Interpreting the interferometer as a qubit explain the *Elitzur and Vaidman bomb testing problem*. What is the probability?
c. Reformulate the interaction-free bomb tester in a quantum computing language.

Solution: *a. Knowing that there is exactly 1 photon in the interferometer, we may reduce the Hamiltonian (35.320) to,*

$$\hat{H}_{a+b}=\hat{H}_1=\frac{\hbar\Omega}{2}\begin{pmatrix}0&1\\1&0\end{pmatrix}=\hat{U}\begin{pmatrix}-\frac{\hbar}{2}\Omega&0\\0&\frac{\hbar}{2}\Omega\end{pmatrix}\hat{U}^\dagger$$
$$with \qquad \hat{U}=\begin{pmatrix}\cos\frac{\pi}{4}&\sin\frac{\pi}{4}\\-\sin\frac{\pi}{4}&\cos\frac{\pi}{4}\end{pmatrix} \ .$$

Hence, the propagator reads,

$$e^{\imath\hat{H}t/\hbar}=\hat{U}\begin{pmatrix}e^{-\imath\Omega t/2}&0\\0&e^{\imath\Omega t/2}\end{pmatrix}\hat{U}^\dagger \overset{\Omega t=\pi/2}{\longrightarrow} \tfrac{1}{\sqrt{2}}\begin{pmatrix}1&\imath\\\imath&1\end{pmatrix} \ .$$

This propagator also describes nutations in a driven two-level atom.
b. We define the states,

$$|1\rangle\equiv|1,0\rangle=\begin{pmatrix}1\\0\end{pmatrix} \qquad and \qquad |2\rangle\equiv|0,1\rangle=\begin{pmatrix}0\\1\end{pmatrix}$$

as those in which a photon is moving, respectively, horizontally and vertically. Then, we can describe the action of the beam splitter as,

$$|1\rangle \xrightarrow{BS} e^{\imath\hat{H}t/\hbar}|1\rangle=\tfrac{1}{\sqrt{2}}(|1\rangle+\imath|2\rangle)$$
$$|2\rangle \xrightarrow{BS} e^{\imath\hat{H}t/\hbar}|1\rangle=\tfrac{1}{\sqrt{2}}(|2\rangle+\imath|1\rangle) \ .$$

A path difference between the interferometer arms acts like,

$$|1\rangle \xrightarrow{L} |1\rangle \qquad \textit{and} \qquad |2\rangle \xrightarrow{L} e^{\imath k\Delta L}|2\rangle \ .$$

An obstacle in the second interferometer arms acts like,

$$|2\rangle \xrightarrow{O} |0\rangle \ .$$

Hence, without obstacle the interferometer does,

$$\begin{aligned}
|1\rangle &\xrightarrow{BS} \tfrac{1}{\sqrt{2}}(|1\rangle + \imath|2\rangle) \\
&\xrightarrow{L} \tfrac{1}{\sqrt{2}}(|1\rangle + \imath e^{\imath k\Delta L}|2\rangle) \\
&\xrightarrow{BS} \tfrac{1}{\sqrt{2}}\left[\tfrac{1}{\sqrt{2}}(|1\rangle + \imath|2\rangle) + \imath e^{\imath k\Delta L}\tfrac{1}{\sqrt{2}}(|2\rangle + \imath|1\rangle)\right] = \tfrac{1}{2}\left[(1 - e^{\imath k\Delta L})|1\rangle + \imath(1 + e^{\imath k\Delta L})|2\rangle\right] \ .
\end{aligned}$$

We align the interferometer such that $e^{\imath k\Delta L} = -1$. Then,

$$|1\rangle \xrightarrow{BS} \xrightarrow{L} \xrightarrow{BS} |1\rangle \ .$$

This means that the photon only interferes constructively on detector D_{constr}, but destructively on detector D_{destr}.
Now, the presence of an obstacle in the second arm spoils the interference,

$$\begin{aligned}
|1\rangle &\xrightarrow{BS} \tfrac{1}{\sqrt{2}}(|1\rangle + \imath|2\rangle) \\
&\xrightarrow{O} \tfrac{1}{\sqrt{2}}(|1\rangle + |0\rangle) \\
&\xrightarrow{BS} \tfrac{1}{\sqrt{2}}\left[\tfrac{1}{\sqrt{2}}(|1\rangle + \imath|2\rangle) + |0\rangle\right] = \tfrac{1}{2}(|1\rangle + \imath|2\rangle) + \tfrac{1}{\sqrt{2}}|0\rangle) \ .
\end{aligned}$$

That is, the probability for counting a photon on detector D_{destr} is $\frac{1}{4}$. A detection of a photon on detector D_{destr} tells us the presence of an obstacle (bomb) in the second interferometer arm, despite the fact that photon went to the first arm and, hence, didn't hit the bomb.
The probability for counting a photon on detector D_{constr} is $\frac{1}{4}$, but in this case we don't know by which interferometer arm it passed. We have to repeat the test with another photon, which will tell us the presence of a bomb with the accumulated probability $\frac{1}{4}\frac{1}{4}$. For n consecutive photons we calculate the probability for detecting the obstacle without hitting it as (see Thorlabs educational kit),

$$\sum_{k=1}^{n} \tfrac{1}{4^k} \overset{n\to\infty}{\longrightarrow} \tfrac{1}{3} \ .$$

c. Fig. 35.32(c) shows a representation of the bomb tester in the quantum computing language: The qubit q_1 represents the interferometer and the qubit q_0 the bomb. The first Hadamard gate and the subsequent cNOT gate entangle both qubits. The bomb's release mechanism represents a measurement of q_0, which projects it to the ground state, $q_0 \to |0\rangle$. Meanwhile, q_1 is remixed, and the interferometer output ports measured,

$$|\psi_{out}\rangle = (H \otimes \mathbb{I})\overset{c}{X}_{10}(H \otimes \mathbb{I})|0\rangle \ .$$

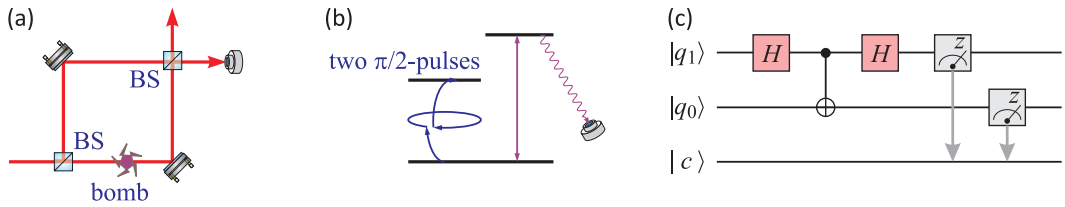

Figure 35.32: The main reason for the analogy between a Mach-Zehnder-Interferometer (a) and a driven two-level atoms (b) is the existence of a coherence between two states residing in the wave nature of light in (a) and of electronic orbitals in (b). (c) Quantum computing language formulation of the bomb tester.

35.8.9.8 Ex: Multiple beam splitters for improved bomb testing

In the original Elitzur and Vaidman bomb tester photons are sent through a single interferometer. Now, let the photons be sent repeatedly through the same beam splitter. Assume the photon wavepacket to be shorter than the length of the interferometer arms so that it *does not interfere with itself*. How many times must the photons be sent to the beam splitter to be totally transferred?

Solution: *We use the transfer matrix model describing the beam splitting by,*

$$\begin{pmatrix} a_n \\ b_n \end{pmatrix} = T \begin{pmatrix} a_{n-1} \\ b_{n-1} \end{pmatrix} = T^n \begin{pmatrix} a_0 \\ b_0 \end{pmatrix} \qquad \text{with} \qquad T = \begin{pmatrix} r & t \\ -t & r \end{pmatrix} .$$

In order to conserve energy, $a_n^2+b_n^2 = a_{n-1}^2+b_{n-1}^2$*, the matrix must satisfy,* $r^2+t^2 = 1$*. We may therefore introduce a new variable* θ *such that* $r = \cos\theta$ *and* $t = \sin\theta$*. The beam splitting matrix can be unitarily transformed into a diagonal matrix via,*

$$T = U \begin{pmatrix} e^{\imath\theta} & 0 \\ 0 & e^{-\imath\theta} \end{pmatrix} U^{-1} \qquad \text{with} \qquad U \equiv \tfrac{1}{\sqrt{2}} \begin{pmatrix} -\imath & \imath \\ 1 & 1 \end{pmatrix} ,$$

satisfying $\det U = 1$*. Hence, the multiple beam splitting is described by,*

$$T^n = U \begin{pmatrix} e^{\imath n\theta} & 0 \\ 0 & e^{-\imath n\theta} \end{pmatrix} U^{-1} = \begin{pmatrix} \cos n\theta & \sin n\theta \\ -\sin n\theta & \cos n\theta \end{pmatrix} .$$

With the initial condition $a_0 = 1$ *and* $b_0 = 0$ *and supposing the reflectivity of the beam splitter to be adjusted such that after* n *round trips,* $a_n = 0$ *and* $b_n = 1$*, we find,*

$$\begin{pmatrix} a_n \\ b_n \end{pmatrix} = \begin{pmatrix} \cos n\theta \\ -\sin n\theta \end{pmatrix} \equiv \begin{pmatrix} 0 \\ 1 \end{pmatrix} .$$

Hence,

$$0 \equiv \cos n\theta \Longrightarrow n = \frac{\pi}{2 \arccos r} .$$

Note, that the transfer matrix model can be extended to account for finite transmissions of the in- and output coupling mirrors,

$$\begin{pmatrix} a_n \\ b_n \end{pmatrix} = R_{in} T \begin{pmatrix} a_{n-1} \\ b_{n-1} \end{pmatrix} + T_{in} \begin{pmatrix} a_{in} \\ b_{in} \end{pmatrix} \qquad \text{with} \qquad R_{in} = \begin{pmatrix} r_a & 0 \\ 0 & r_b \end{pmatrix} \quad , \quad T_{in} = \begin{pmatrix} t_a & 0 \\ 0 & t_b \end{pmatrix} .$$

35.8.9.9 Ex: Hamiltonian approach to coupled cavities for improved bomb testing

a. Consider two identical weakly coupled cavities. Solving the Heisenberg equations with the Hamiltonian for two coupled oscillators calculate how the photon number evolves in each cavity (see Exc. 35.8.9.5). How does the field amplitudes change after one cavity round trip?
b. How does the photon number in cavity 'b' evolve if an absorber is inserted into the cavity 'a' [764]? How does the field amplitudes change in this case after one cavity round trip?
c. Now, we model the absorber by a two-level atom being in resonance with the light field and subject to spontaneous emission. Set up the Hamiltonian, derive the equations of motion, and solve them numerically. Interpret the results.
Comments: The multiple path model leading to the Airy formulas describes a physical process involving beam propagation and reflection and transmission at a real object like an atom or a beam splitter. The complete dynamics is only partially grasped by a Hamiltonian and a master equation treating the cavity as a closed system and being restricted to describing energy fluxes into and out of the system.
One manifestation of it is the necessity of approximating the Airy function close to resonance by a Lorentzian in order to link the cavity transmission to a decay rate.
Another manifestation is the discrepancy in the coupled cavity description via multiple paths and via Hamiltonian for coupled oscillators: The models only coincide of $r = \sqrt{R} \stackrel{!}{=} 1$.

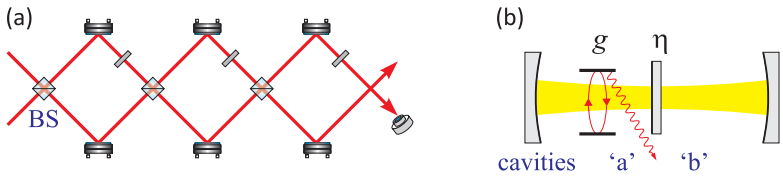

Figure 35.33: (a) Illustration of the multiple paths model and (b) the coupled cavities model for improved bomb testing.

Solution: *a. The Hamiltonian of the coupled system is,*

$$\hat{H} = -\Delta_c \hat{a}^\dagger \hat{a} - \Delta_c \omega \hat{b}^\dagger \hat{b} + \tfrac{\Omega}{2}(\hat{a}\hat{b}^\dagger + \hat{a}^\dagger \hat{b}) \ .$$

The Heisenberg-Liouville equations are,

$$\dot{\hat{a}} = -\imath[\hat{a}, \hat{H}] = \imath\Delta_c \hat{a} - \imath\tfrac{\Omega}{2}\hat{b} - \kappa_a \hat{a}$$
$$\dot{\hat{b}} = -\imath[\hat{b}, \hat{H}] = \imath\Delta_c \hat{b} - \imath\tfrac{\Omega}{2}\hat{a} - \kappa_b \hat{b} \ .$$

On resonance, $\Delta_a = 0$, and without decay, $\kappa_a = 0 = \kappa_b$, they read,

$$\begin{pmatrix} \dot{\hat{a}} \\ \dot{\hat{b}} \end{pmatrix} = -\imath \begin{pmatrix} 0 & \frac{\Omega}{2} \\ \frac{\Omega}{2} & 0 \end{pmatrix} \begin{pmatrix} \hat{a} \\ \hat{b} \end{pmatrix} = -\imath U \hat{E} U^{-1} \begin{pmatrix} \hat{a} \\ \hat{b} \end{pmatrix}$$

$$\text{with} \quad U = \begin{pmatrix} -\frac{1}{\sqrt{2}} & \frac{1}{\sqrt{2}} \\ \frac{1}{\sqrt{2}} & \frac{1}{\sqrt{2}} \end{pmatrix} \quad \text{and} \quad \hat{E} = \begin{pmatrix} -\frac{\Omega}{2} & 0 \\ 0 & \frac{\Omega}{2} \end{pmatrix} ,$$

and have the solution,

$$\begin{pmatrix} \hat{a}(t) \\ \hat{b}(t) \end{pmatrix} = U e^{-\imath \hat{E} t} U^{-1} = \begin{pmatrix} \cos\frac{\Omega t}{2} & -\imath \sin\frac{\Omega t}{2} \\ -\imath \sin\frac{\Omega t}{2} & \cos\frac{\Omega t}{2} \end{pmatrix} \begin{pmatrix} \hat{a}(0) \\ \hat{b}(0) \end{pmatrix} .$$

The photon numbers are now,

$$\hat{n}_a(t) = \hat{a}^\dagger(t)\hat{a}(t) = \hat{n}_a(0)\cos^2\tfrac{\Omega t}{2} + \hat{n}_b(0)\sin^2\tfrac{\Omega t}{2} + [\hat{b}^\dagger(0)\hat{a}(0) - \hat{a}^\dagger(0)\hat{b}(0)]\imath \sin\tfrac{\Omega t}{2}\cos\tfrac{\Omega t}{2}$$
$$\hat{n}_b(t) = \hat{b}^\dagger(t)\hat{b}(t) = \hat{n}_a(0)\sin^2\tfrac{\Omega t}{2} + \hat{n}_b(0)\cos^2\tfrac{\Omega t}{2} - [\hat{b}^\dagger(0)\hat{a}(0) - \hat{a}^\dagger(0)\hat{b}(0)]\imath \sin\tfrac{\Omega t}{2}\cos\tfrac{\Omega t}{2} .$$

That is, the total photon number is conserved, $\hat{n}_a(t) + \hat{n}_b(t) = \hat{n}_a(0) + \hat{n}_b(0)$. If initially $\hat{n}_b(0) = 0$, we get,

$$\hat{n}_a(t) = \hat{n}_a(0)\cos^2\tfrac{\Omega t}{2} = \hat{n}_a(0) - \hat{n}_b(t) .$$

One cavity round trip lasts δ_{fsr}^{-1}, where δ_{fsr} is the cavities' free spectral range. After one round trip the field amplitudes become,

$$\begin{pmatrix} \hat{a}(t + \delta_{fsr}^{-1}) \\ \hat{b}(t + \delta_{fsr}^{-1}) \end{pmatrix} = \begin{pmatrix} \cos\frac{\Omega}{2\delta_{fsr}} & -\imath \sin\frac{\Omega}{2\delta_{fsr}} \\ -\imath \sin\frac{\Omega t}{2\delta_{fsr}} & \cos\frac{\Omega t}{2\delta_{fsr}} \end{pmatrix} \begin{pmatrix} \hat{a}(t) \\ \hat{b}(t) \end{pmatrix} ,$$

or

$$\begin{pmatrix} \hat{a}_n \\ \hat{b}_n \end{pmatrix} = \begin{pmatrix} r & -\imath t \\ -\imath t & r \end{pmatrix} \begin{pmatrix} a_{n-1} \\ b_{n-1} \end{pmatrix} ,$$

with the identification,

$$t \equiv \sin\tfrac{\Omega}{2\delta_{fsr}} \qquad \text{and} \qquad r \equiv \cos\tfrac{\Omega}{2\delta_{fsr}} = \sqrt{1 - t^2} .$$

See Fig. 35.34.

b. Now, we insert an absorber into the cavity 'b'. This obviously destroys the coherent coupling between both cavities, which means that we are left with cavity 'a' and a loss rate κ_a,

$$\hat{H} = -\Delta_c \hat{a}^\dagger \hat{a} ,$$

described by the Heisenberg-Liouville equation,

$$\dot{\hat{a}} = -\imath[\hat{a}, \hat{H}] = \imath\Delta_c \hat{a} - \kappa_a \hat{a} .$$

On resonance, the solution is an exponential decay of the photon number,

$$\hat{n}_a(t) = \hat{n}_a(0) e^{-2\kappa_a t} .$$

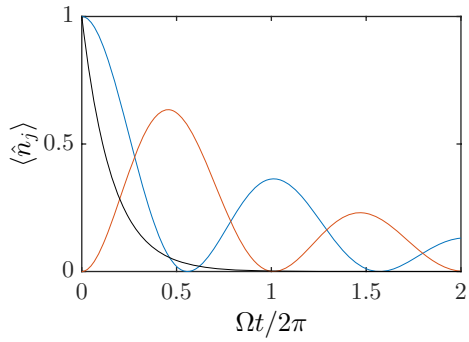

Figure 35.34: (code) (blue) Photon number in a cavity 'a' coupled to a cavity 'b' subject to losses. (red) Photon number in a cavity 'b'. (black) Photon number in a cavity 'a' coupled to an absorber.

After one round trip the field amplitudes become,

$$a(t + \delta_{fsr}^{-1}) = e^{-\kappa_a/\delta_{fsr}} a(t) \ ,$$

or

$$a_{n+1} = e^{-\kappa_a/\delta_{fsr}} a_n = r^2 a_n \ .$$

From this we deduce the identities,

$$r^2 = e^{-\kappa_a/\delta_{fsr}} \simeq 1 - \frac{\kappa_a}{\delta_{fsr}} \ ,$$

that is,

$$T = 1 - R = 1 - r^2 = \frac{\kappa_a}{\delta_{fsr}} = \frac{\pi}{F} \ .$$

However, we constantly evaluate the photo detector signal. As long as no photon is registered, we know that the intracavity photon number did not change.
In the bomb tester language, having let the cavities interact for a time corresponding to $2\pi/\Omega$, there are three possible outcomes: (i) No photon is observed in cavity 'a': This tells us that there is no bomb in cavity 'b'. (ii) A photon is observed in cavity 'a': This tells us that there is a 'bomb' in cavity 'b', although the photon never had a chance to interact with the it. (iii) The bomb explodes.
c. From the Hamiltonian,

$$\hat{H} = -\Delta_c \hat{a}^\dagger \hat{a} - \Delta_a \hat{\sigma}^z + g(\hat{\sigma}^- \hat{a}^\dagger + \hat{\sigma}^+ \hat{a}) - \Delta_c \hat{b}^\dagger \hat{b} + \tfrac{\Omega}{2}(\hat{a}\hat{b}^\dagger + \hat{a}^\dagger \hat{b}) \ ,$$

we derive the equations of motion,

$$\begin{aligned}
\dot{\hat{a}} &= -\imath[\hat{a}, \hat{H}] - \kappa_a \hat{a} = (\imath\Delta_c - \kappa_a)\hat{a} - \imath\tfrac{\Omega}{2}\hat{b} - \imath g\hat{\sigma}^- \\
\dot{\hat{b}} &= -\imath[\hat{b}, \hat{H}] - \kappa_b \hat{b} = (\imath\Delta_c - \kappa_b)\hat{b} - \imath\tfrac{\Omega}{2}\hat{a} \\
\dot{\hat{\sigma}}^- &= -\imath[\hat{\sigma}^-, \hat{H}] - \tfrac{\Gamma}{2}\hat{\sigma}^- = (\imath\Delta_a - \tfrac{\Gamma}{2})\hat{\sigma}^- + \imath g\hat{a}\hat{\sigma}^z \\
\dot{\hat{\sigma}}^z &= -\imath[\hat{\sigma}^z, \hat{H}] - \Gamma\hat{\sigma}^z = -2\imath g\hat{a}\hat{\sigma}^+ + 2\imath g\hat{a}^\dagger\hat{\sigma}^- - \Gamma(\mathbb{I}_2 + \hat{\sigma}^z) \ .
\end{aligned}$$

For simplicity we assume resonant excitation and no cavity decay,

$$\begin{aligned}\dot{\hat{a}} &= -\imath\tfrac{\Omega}{2}\hat{b} - \imath g\hat{\sigma}^- \\ \dot{\hat{b}} &= -\imath\tfrac{\Omega}{2}\hat{a} \\ \dot{\hat{\sigma}}^- &= -\tfrac{\Gamma}{2}\hat{\sigma}^- + \imath g\hat{a}\hat{\sigma}^z \\ \dot{\hat{\sigma}}^z &= -2\imath g\hat{a}\hat{\sigma}^+ + 2\imath g\hat{a}^\dagger\hat{\sigma}^- - \Gamma(\mathbb{I}_2 + \hat{\sigma}^z)\ .\end{aligned}$$

Treating cavity 'a' like a reservoir by setting $\eta \equiv \frac{\Omega}{2\imath}\alpha$ *the Hamiltonian for cavity 'b' becomes,*

$$\hat{H} = -\Delta_c\hat{b}^\dagger\hat{b} + \tfrac{\Omega}{2}(\alpha^*\hat{b} + \alpha\hat{b}^\dagger) = -\Delta_c\hat{b}^\dagger\hat{b} - \imath(\eta^*\hat{b} - \eta\hat{b}^\dagger)\ .$$

Fig. 35.34 shows the time evolution.

35.8.9.10 Ex: Simulation of the quantum Zeno effect with qubit gates

Design a quantum circuit simulating the quantum Zeno effect ruling the bomb tester and its extension to multiple paths.

Solution: *In matricial language the bomb tester reads,*

$$(H\otimes\mathbb{I})\overset{c}{X}_{10}(H\otimes\mathbb{I})|0\rangle\ .$$

The multiple paths extension reads,

$$\left([\mathbb{I}\otimes|0\rangle\langle 0|]\left[R_x(\tfrac{\pi}{n})\otimes\mathbb{I}\right]\overset{c}{X}_{10}\right)^n\left[R_x(\tfrac{\pi}{n})\otimes\mathbb{I}\right]|0\rangle\ .$$

As seen in Fig. 35.35 the detection efficiency increases with n asymptotically approaching 1.
Now [764, 765], instead of Hadamard gates, we consider a small rotation by $\vartheta = \frac{\pi}{2n}$,

$$U_3(\vartheta,0,0) = \begin{pmatrix}\cos\vartheta & -\sin\vartheta\\ \sin\vartheta & \cos\vartheta\end{pmatrix} \quad \textit{so that} \quad U_3(\vartheta,0,0)\otimes\mathbb{I} = \begin{pmatrix}\cos\vartheta & 0 & -\sin\vartheta & 0\\ 0 & \cos\vartheta & 0 & -\sin\vartheta\\ \sin\vartheta & 0 & \cos\vartheta & 0\\ 0 & \sin\vartheta & 0 & \cos\vartheta\end{pmatrix}\ .$$

With,

$$\mathbb{I}\otimes|0\rangle\langle 0| = \begin{pmatrix}1&0&0&0\\0&0&0&0\\0&0&1&0\\0&0&0&0\end{pmatrix} \quad \textit{and} \quad \overset{c}{X}_{10} = \begin{pmatrix}1&0&0&0\\0&1&0&0\\0&0&0&1\\0&0&1&0\end{pmatrix}\ ,$$

we find,

$$T = (\mathbb{I}\otimes|0\rangle\langle 0|)\ \ (U_3(\vartheta,0,0)\otimes\mathbb{I})\ \ \overset{c}{X}_{10} = \begin{pmatrix}\cos\vartheta & 0 & 0 & -\sin\vartheta\\ 0&0&0&0\\ \sin\vartheta&0&0&\cos\vartheta\\ 0&0&0&0\end{pmatrix}\ .$$

Finally,

$$|\psi\rangle = T^n \;\; (U_3(\vartheta,0,0)\otimes\mathbb{I}) \;\; |0\rangle = \cos^n\vartheta \begin{pmatrix} \cos\vartheta \\ 0 \\ \sin\vartheta \\ 0 \end{pmatrix} \;\; ,$$

respectively, $\hat{\rho}_{out} = T\;\hat{\rho}_{in}\;T^\dagger$.

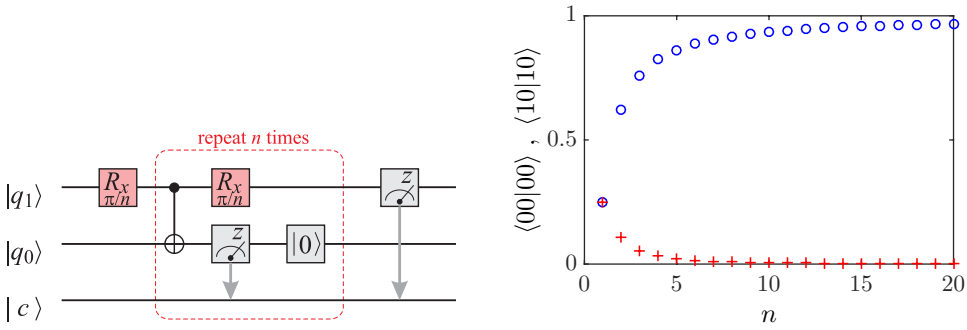

Figure 35.35: (code) Detection efficiency of the multiple path bomb tester as a function of the number of paths n.

35.8.9.11 Ex: Link between entanglement and squeezing

Prove that, if $\hat{a}_1$ and $\hat{a}_2$ are EPR-entangled beams with respect to quadrature components, then beams $\hat{b}_{1,2} = \frac{1}{\sqrt{2}}(\hat{a}_1 \pm \hat{a}_2)$ are squeezed with respect to two orthogonal quadrature components and vice versa [1087, 1088, 822].

Solution: *We consider independent modes characterized by their field operators,*

$$[\hat{a}_m, \hat{a}_n^\dagger] = \delta_{mn} = [\hat{b}_m, \hat{b}_n^\dagger] \qquad but \qquad [\hat{a}_1, \hat{b}_1^\dagger] = \tfrac{1}{\sqrt{2}} \;\; .$$

The Hamiltonian,

$$\hat{H} = \imath\hbar g\alpha(\hat{a}_1^\dagger\hat{a}_2^\dagger - \hat{a}_1\hat{a}_2)$$

describes parametric down-conversion in the non-degenerate configuration and in the approximation of a classical undepleted pump α. As is well known, in the non-degenerate configuration the two beams $\hat{a}_1$ and $\hat{a}_2$ are entangled both with respect to the photon number and with respect to the two quadrature components. The entanglement can be explicitly shown by applying the time evolution operator corresponding to the Hamiltonian to the uncorrelated vacuum state, for an interaction time τ,

$$e^{-\imath/\hbar\hat{H}\tau}|0\rangle_1|0\rangle_2 = \sum_{n=0}^{\infty} \frac{\tanh^n g\tau/\hbar}{\cosh g\tau/\hbar}|n\rangle_1|n\rangle_2 \;\; .$$

On the other hand, the Hamiltonian obtained by the transformation,

$$\hat{a}_{1,2} = \tfrac{1}{\sqrt{2}}(\hat{b}_1 \pm \hat{b}_2)$$

is

$$\hat{H} = \frac{\imath\hbar g\alpha}{2}(\hat{b}_1^{\dagger 2} - \hat{b}_1^2) - \frac{\imath\hbar g\alpha}{2}(\hat{b}_2^{\dagger 2} - \hat{b}_2^2) \ ,$$

which corresponds to the sum of two interaction Hamiltonians for parametric down-conversion in the degenerate configuration. Hence the beams $\hat{b}_1$ and $\hat{b}_2$ are squeezed, and because of the minus sign in front of the second term, the squeezing is in orthogonal quadrature components. For example, when α is real $\hat{b}_1$ is squeezed with respect to the Y quadrature (imaginary part of the annihilation operator) and $\hat{b}_2$ is squeezed with respect to the X quadrature (real part of the annihilation operator).

35.9 Further reading

Ch.C. Gerry and P.L. Knight, Cambridge University Press (2005), *Introductory Quantum Optics* [504]ISBN

P. Meystre and M. Sargent III, Springer-Verlag, Berlin (1990), *Elements of Quantum Optics* [886]ISBN

M.O. Scully and M.S. Zubairy, Cambridge University Press (1997), *Quantum Optics* [1184]ISBN

E.T. Jaynes et al., *Comparison of quantum and semiclassical radiation theories with application to the beam maser* [672]DOI

F. Albarelli et al., *Nonlinearity as a resource for nonclassicality in anharmonic systems* [16]DOI

J.P. Bartolotta et al., *Entropy transfer from a quantum particle to a classical coherent light field* [103]DOI

K.E. Cahill et al., *Density Operators and Quasiprobability Distributions* [228]DOI

C.M. Caves et al., *Quantum-mechanical noise in an interferometer* [241]DOI

J. Dalibard et al., *Wave-Function Approach to Dissipative Processes in Quantum Optics* [321]DOI

R.G. DeVoe et al., *Observation and Superradiant and Subradiant Spontaneous Emission of Two Trapped Ions* [364]DOI

R. Dum et al., *Monte Carlo simulation of master equations in quantum optics for vacuum, thermal, and squeezed reservoirs* [396]DOI

J. Eschner et al., *Light interference from single atoms and their mirror images* [423]DOI

Z. Ficek et al., *Effect of interatomic interactions on resonance fluorescence of two atoms coherently driven by strong resonant laser field* [443]DOI

J.C. García-Melgarejo et al., *A Numerical Perspective on the Jaynes-Cummings Model Wigner Function* [485]DOI

K. Nakayama et al., *Precise intensity correlation measurement for atomic resonance fluorescence from optical molasses* [944]DOI

U. Leonhardt et al., *Measuring the quantum state of light* [791]DOI

P. Longo et al., *Far-Field Signatures of a Two-Body Bound State in Collective Emission from Interacting Two-Level Atoms on a Lattice* [813]DOI

R. Loudon et al., *Squeezed light* [818]DOI

L.A. Lugiato et al., *Quantum imaging* [822]DOI

B.R. Mollow et al., *Power spectrum of light scattered by two-level systems* [910]DOI

K. Mølmer et al., *Monte Carlo wave-function method in quantum optics* [913]DOI

F.A. de Oliveira et al., *Properties of displaced number states* [340]DOI

M.D. Reid, *Quantum Correlations of Phase in Nondegenerate Parametric Oscillation* [1087]DOI

M.D. Reid, *Demonstration of the Einstein-Podolsky-Rosen paradox using nondegenerate parametric amplification* [1088]DOI

D. Stoler, *Equivalence Classes of Minimum Uncertainty Packets* [1265]DOI

M. Uria et al., *Deterministic Generation of Large Fock States* [1321]DOI

H.P. Yuen et al., *Two-photon coherent states of the radiation field* [1415]DOI

M. Schubert et al., *Photon antibunching and non-Poissonian fluorescence of a single three-level ion* [1171]DOI

Y. Stalgies et al., *The Spectrum of Single-Atom Resonance Fluorescence* [1235]DOI

Y. Gutiérrez et al., *Mollow triplet in cold atoms* [981]DOI

G.S. Agarwal et al., *Inhibition of Decoherence due to Decay in a Continuum* [10]DOI

Ho Trung Dung et al., *Electromagnetic-field quantization and spontaneous decay in left-handed media* [398]DOI

35.9.1 on second quantization

W.E.Jr. Lamb, *Anti-Photon* [770]DOI

35.9.2 on the Jaynes-Cummings model

J. Eiselt et al., *Quasiprobability distributions for the Jaynes-Cummings model with cavity damping* [412]DOI

M. Brune et al., *Manipulation of photons in a cavity by dispersive atom-field coupling: Quantum-nondemolition measurement and generation of "Schrödinger cat" states* [203]DOI

K. Gietka et al., *Quantum-enhanced interferometry with cavity QED-generated nonclassical light* [509]DOI

M. Mohammad et al., *Cavity quantum electrodynamics with atom-like mirrors* [909]DOI

35.9.3 on beam splitters

L.E. Estes et al., *Quantum-Mechanical Description of Two Coupled Harmonic Oscillators* [426]DOI

U. Leonhardt, *Quantum physics of simple optical instruments* [789]DOI

Chapter 36

Quantum measurement

Since its foundation, the theory of quantum mechanics was driven by the urge to clarify the relationship between the world and what we can learn about it, that is, between reality and the observer. Scientists such as Bohr, Heisenberg, Schrödinger, and Einstein defended controversial positions and struggled for the correct interpretation of quantum mechanics. The *measurement* process is supposed to provide information about the world out there, but it is not clear whether this information can be complete and accurate, or whether there are limitations or hidden variables. Also, it was unclear, to what extend a measurement can be non-invasive or whether it would always perturb the phenomenon under investigation. The most important step in this question was the *Copenhagen interpretation* formulated by Bohr, Heisenberg and Born in 1927 and elaborated later by von Neumann and Dirac. Although contested many times in the past, it's essence still remains valid today.

In this chapter we will study the measurement process from the viewpoint quantum mechanics and discuss some seemingly paradoxical effects, that will allow us to deepen our understanding. Among them are the quantum jump, Schrödinger's cat, the quantum Zeno effect, and the Einstein-Podolski-Rosen paradox.

36.1 The reality and the observer

According to the Copenhagen interpretation, theoretical predictions have a probabilistic character. However, this is not an expression of the imperfection of the theory, but of the intrinsically indeterministic character of quantum processes [1]. Moreover, the Copenhagen interpretation desists to attribute to objects of the quantum formalism, such as wavefunctions and operators, an immediate reality. Instead, the objects of the formalism only represent vehicles for a probabilistic prediction of the results of measurements. These results are *only truly real* elements of quantum theory. It is obvious, that the quantum theory and its interpretations are of fundamental importance to the scientific view of the world and our concept of nature.

36.1.1 Schrödinger's cat

In the microscopic world, the relationship between the sample and the observer is very delicate. And this delicacy is at the origin of quantum effects that seem paradoxical

[1] Note that it is problematic to identify unpredictability and indeterminism. We may be unable to predict specific events, without having to assume that these events occur in a random manner.

through our classical concept of the world. It is, thus, not surprising that one of the most fascinating areas of investigations is the *interface* between the classical and the quantum, the macroscopic and the microscopic worlds. For the pioneers of quantum mechanics the most important questions were of the type: 'How is it possible that a microscopic particle flies simultaneously through two slits?' Nowadays, we are accustomed to such paradoxes, and we simply accept the fact that we have to consider a particle as a wave. Nevertheless, we still do not understand very well, why the classical and the quantum world behave so differently. 'Why does quantum mechanics allow for quantum superpositions states, which are absolutely forbidden in classical physics?', 'Why are the fundamental laws of the quantum world invariant to the arrow of time, while the macroscopic world always evolves from the past to the future?, 'How can it be that quantum mechanics allows for effects having no cause, like spontaneous emission, while the everyday world seems to be deterministic?'

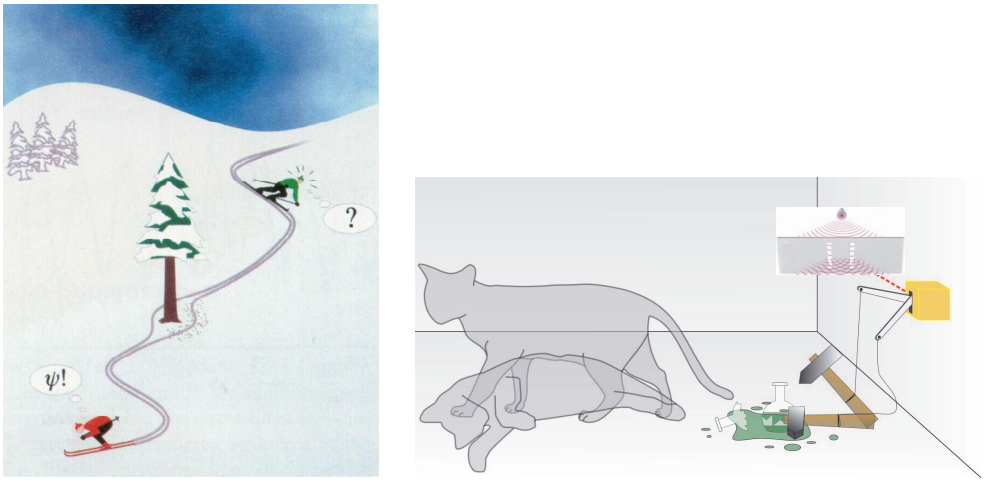

Figure 36.1: Double slit and Schrödinger's cat.

Quantum mechanics must, in some limit, clearly encompass classical physics. But in spite of *Ehrenfest's correspondence principle*, this fact is far from being trivial. Some predictions of classical and quantum physics are fundamentally different and, in some cases, even contradictory. The famous *Schrödinger cat* states are the epitome of this fact: In one version of this paradox, a particle crosses a double slit. Behind one of the slits is a detector which, as soon as it registers a particle, actuates a device killing a cat. We know that in quantum reality the particle crosses both slits in a superposition state, so that the cat should be in a superposition state as well. Hence, quantum cats can be in a superposition of 'dead' and 'alive'.

We believe nowadays that the answers to the above questions are somehow buried in processes that destroy the quantum superposition of Schrödinger cats during the transition from the microscopic to the macroscopic world. However, the details of these quantum coherence destruction processes, called *decoherence*, are very complicated and the subject of serious efforts in contemporary research. It is one of the motivations for trying to create in laboratories the largest possible (quasi-macroscopic) quantum systems, bring them in Schrödinger cat-like superposition states and study

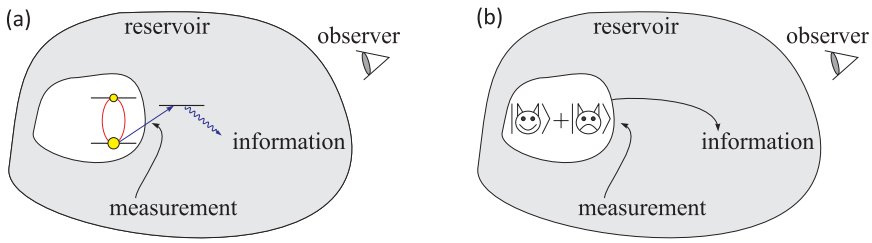

Figure 36.2: The measurement of a quantum system presupposes the interaction of the system with a reservoir, which disturbs its dynamics.

their decoherence [2].

36.1.1.1 Quantum measurement

Every unperturbed system follows the Schrödinger equation. Once its Hamiltonian has been determined, the formal solution,

$$|\psi\rangle = e^{-\imath\hat{H}t/\hbar}|\psi_0\rangle \ , \tag{36.1}$$

allows to calculate the time evolution, that is, the trajectory of the wavefunction. The evolution is *coherent and reversible* in time.

Now, the process of measuring a pure quantum state includes –according the Copenhagen interpretation and as discussed in Sec. 23.2.7– two consecutive steps: In the *first step*, the interaction of the quantum sample with the measuring device (which from now on we will call *meter*) destroys all coherences and projects the pure state into a statistical mixture of eigenstates of the meter. Following von Neumann, the impact of the meter on the quantum system is so strong, that its coherent evolution is interrupted and it is projected onto the degree of freedom that the apparatus wants to measure, e.g. its position or its momentum, but not both in the same time. The projection transforms a pure quantum state $|\psi\rangle$ into a statistical mixture ρ of eigenstates,

$$\hat{\rho}_{sample} = |\psi(t)\rangle\langle\psi(t)| \curvearrowright \hat{\rho}_{proj} = \sum\nolimits_k |\langle\psi|k\rangle|^2 |k\rangle\langle k| \ . \tag{36.2}$$

This process is irreversible, that is, it separates the past from the future. The projection is *not* described by the Schrödinger equation. Instead, the sudden reduction of the state must be postulated, as done by von Neumann's famous axiom.

In a *second step*, the observer looks at the measuring device and confirms one of the possible results. Thus, he transforms the state into a eigenstate of the device [3]:

$$\hat{\rho}_{proj} \curvearrowright \hat{\rho}_{meter} = |k\rangle\langle k| \ . \tag{36.3}$$

From this moment, we can again leave the quantum system alone until the next measure.

[2] There are attempts to introduce the concept of the time arrow also in the microscopic world: 'In an isolated system, spontaneous processes occur in the direction of increasing entropy.' [896, 500].

[3] We note that, only if *all* commuting observables of the system are measured *and* acknowledged, $\hat{\rho}_{meter}$ becomes a pure state. Otherwise ρ_{meter} remains a partial mixture.

From the viewpoint of the quantum system, the evolution of the measurement process appears *discontinuous*, because it destroys all possible coherences between its states. In fact, the problem comes from the non-ideal behavior of the measuring device (symbolized by $|\uparrow\rangle$ before the measurement). An ideal non-invasive measurement [4] would leave the quantum state $|\psi\rangle$ unchanged:

$$|\psi\rangle|\uparrow\rangle \xrightarrow{H} |\psi\rangle|\nearrow\rangle \ , \tag{36.4}$$

while the measuring device changes to a state ($|\nearrow\rangle$ after the measurement) indicating the current state of the system. However, this is normally impossible without previously established correlation between $|\psi\rangle$ and $|\uparrow\rangle$. In a real meter device, the coupling between $|\psi\rangle$ and $|\uparrow\rangle$ requires that the meter and the system to be non-orthogonal.

36.1.1.2 Measurement-induced decoherence

A more modern view of the quantum measurement is the following: When the outer world (called reservoir, observer or meter) *reads* a quantum system, it causes, due to this transfer of information, an irreversible demolition of coherence. Consequently, the density operator condenses to its diagonal. On the other hand, the system as a whole (including the sample and the reservoir) always evolves coherently according to the von Neumann equation with the Hamiltonian of everything $\hat{H}_{all}$:

$$\dot{\hat{\rho}} = \frac{\imath}{\hbar}[\hat{\rho}, \hat{H}_{all}] \ . \tag{36.5}$$

If $\hat{H}_{sample}$ is the small quantum system under investigation, a complete description of the measurement process requires the inclusion of the observer, that is, the total Hamiltonian is,

$$\hat{H} = \hat{H}_{sample} \otimes \hat{H}_{meter} = \begin{pmatrix} \text{sample} & 0 \\ 0 & \text{meter} \end{pmatrix} \ . \tag{36.6}$$

Ideally, the system evolves independently without being disturbed by the meter. Unfortunately, this also means that the meter evolves independently, that is, it is not influenced by the system and thus does not provide information about the system. To allow a transfer of information, we need to couple the respective spaces by an interaction Ω, such that,

$$\hat{H} = \begin{pmatrix} \text{sample} & \Omega \\ \Omega & \text{meter} \end{pmatrix} \ . \tag{36.7}$$

Tracing over all degrees of freedom of the universe *except* those of the quantum system, the von Neumann equation (36.5) turns into a master equation,

$$\dot{\hat{\rho}}_{sample} = \frac{\imath}{\hbar}[\hat{\rho}, \hat{H}_{sample}] + \mathcal{L}_{reserv}\rho \ . \tag{36.8}$$

[4] See the discussion of the *quantum non-demolition measurement*.

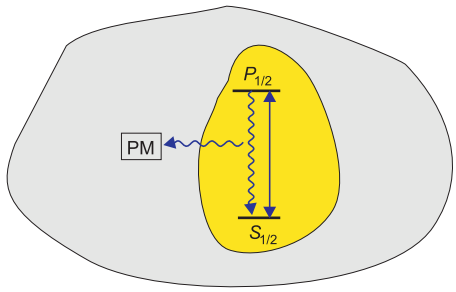

Figure 36.3: Spontaneous emission can be seen as a coupling of the system under investigation to an external meter, because it delivers information to the meter, even if only to tell us: 'The system was in an excited state, but now it's in a ground state.'

Example 217 (*Quantum measurement in a two-qubit system*): To discuss this at an example, we consider the simplest imaginable system: Two two-level atoms, the first one representing the quantum system under investigation and the second the meter. We introduce the following basis:

$$|1\rangle \equiv |\downarrow\rangle|\downarrow\rangle = \begin{pmatrix}1\\0\\0\\0\end{pmatrix} , \; |2\rangle \equiv |\uparrow\rangle|\downarrow\rangle = \begin{pmatrix}0\\1\\0\\0\end{pmatrix} , \; |3\rangle \equiv |\downarrow\rangle|\uparrow\rangle = \begin{pmatrix}0\\0\\1\\0\end{pmatrix} , \; |4\rangle \equiv |\uparrow\rangle|\uparrow\rangle = \begin{pmatrix}0\\0\\0\\1\end{pmatrix} .$$

The Hamiltonian of independent atoms is,

$$\hat{H} = |\downarrow\rangle\langle\downarrow| \otimes |\uparrow\rangle\langle\uparrow| .$$

The discussion about the correct interpretation of the measurement process is still ongoing. Modern theories describe the state reduction in terms of *quantum decoherence* due to interactions of the system with the environment. Other interpretations involve *decoherent histories* or assume *multiple worlds* [1004]. On the practical side, the current interest in quantum decoherence is motivated by the fact that this phenomenon may turn out to be the fundamental factor limiting the useful operation of quantum computers. Another interesting area where quantum mechanics meets classical physics is the phenomenon of quantum chaos.

36.1.2 The quantum jump

Obviously, the whole quantum measurement process, including the discontinuity of the state projection, could be fully understood within a grand model of the complete system, which would include the measuring device. In practice, this is illusory, because of the excessive number of degrees of freedom of the classical measuring device (e.g. a Schrödinger cat).

On the other hand, many characteristics of quantum measurement can be illustrated in a simple *three-level atom* with a weak transition representing the quantum sample and a strong transition representing the meter. The assertion defended in

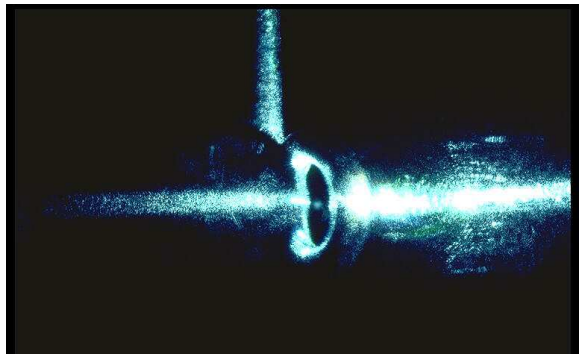

Figure 36.4: One of the first pictures of a single Ba^+ ion.

the following is, that this three-level system, called *quantum amplifier*, gives a deep insight into what happens during the process of state reduction and, therefore, can be considered as paradigmatic for theories on quantum measurement.

To be able to discuss the dynamics of this system on a firmer ground, we will first introduce the quantum Monte Carlo wavefunction simulation method (MCWF).

36.1.2.1 Quantum Monte-Carlo wavefunction simulation of a two-level system

The possible occurrence of spontaneous emission produces a dynamics called *quantum trajectory*, which can be described by a non-hermitian *effective Hamiltonian*,

$$\hat{H}_{eff} = \hbar\Delta\sigma_z + \hbar\Omega\sigma^+ + c.c. - \frac{\imath}{2}\Gamma\sigma_z = \begin{pmatrix} 0 & \Omega \\ \Omega & \Delta - \imath\frac{\Gamma}{2} \end{pmatrix} , \tag{36.9}$$

aiming at including energy dissipation processes. The problem with this Hamiltonian is that, for being non-hermitian, $[\hat{H}_{eff}, \hat{H}^\dagger_{eff}] \neq 0$, it also generates a non-unitary dynamics, $e^{-\imath\hat{H}_{eff}t} \neq e^{\imath\hat{H}^\dagger_{eff}t}$. This means that the mere *possibility* of spontaneous emission prevents the reversibility of the dynamics. We observe a temporal decrease of the norm $\langle\psi(t)|\psi(t)\rangle$ indicating a loss of energy,

$$\langle\psi|\psi\rangle = \langle\psi_0|e^{-\imath\hat{H}_{eff}t}e^{\imath\hat{H}_{eff}t}|\psi_0\rangle \longrightarrow e^{-\Gamma t} . \tag{36.10}$$

The loss of normalization during the evolution, until the next quantum jump occurs, is due to the dissipation of energy toward the reservoir,

$$\text{Tr } \rho_{sample} \to 0 \qquad \text{while} \qquad \text{Tr} \begin{pmatrix} \rho_{sample} & 0 \\ 0 & \rho_{reserv} \end{pmatrix} = 1 , \tag{36.11}$$

and represents a measure of the probability that an irreversible process has occurred during the evolution time.

Dissipative processes can be simulated by playing dices with random numbers ζ. We divide time into small intervals dt and propagate the wavefunction from $\psi(t)$

to $\psi(t+dt)$. After each interval we evaluate the probability $p = 1 - \langle\psi(t)|\psi(t)\rangle$ accumulated during the time period $[0, t+dt]$ that a dissipative process (such as spontaneous emission) has occurred. Now, we generate a random number ζ, uniformly distributed between 0 and 1, which we compare to probability the probability p. In case, $\zeta > 1 - \langle\psi(t)|\psi(t)\rangle$, we conclude that there was no dissipative process, and we let the system proceed in peace, only renormalizing the wavefunction to compensate for the losses [893, 321]. Otherwise, if $\zeta < 1 - \langle\psi(t)|\psi(t)\rangle$, we conclude that there was a dissipative process, and the system is projected into the eigenstate ψ_0. This projection is abrupt and called *quantum jump*. Now, the evolution restarts from zero, ruled by the effective Hamiltonian. The simulation implemented via,

$$|\psi(t)\rangle \curvearrowright |\psi(t+dt)\rangle \equiv \begin{pmatrix} \frac{(1-\imath\hat{H}dt)|\psi(t+dt)\rangle}{\sqrt{\langle\psi(t)|\psi(t)\rangle}} & \text{if} \quad \zeta > 1 - \langle\psi(t)|\psi(t)\rangle \\ |\psi_0\rangle \quad \text{if} \quad \zeta < 1 - \langle\psi(t)|\psi(t)\rangle \end{pmatrix} . \tag{36.12}$$

This is the method called *quantum Monte Carlo wavefunction simulation*.

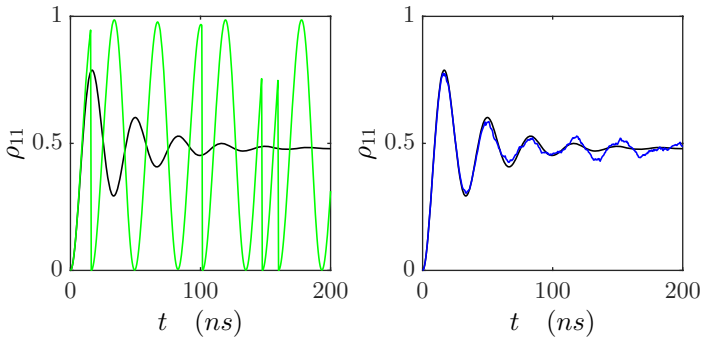

Figure 36.5: (code) a) Quantum Monte Carlo wavefunction simulation. It is important to be aware, that a trajectory generated by a MCWF simulation (36.12) only represents *one* of many possible trajectories of the system. (b) The evolution of the density matrix $\rho(t) = |\psi(t)\rangle\langle\psi(t)|$ (blue curve) is nothing else, than the average (black curve) over all possible MCWF trajectories for the system. A movie of this simulation can be watched here (watch movie).

The effective two-level Hamiltonian (36.9) dissipates via spontaneous emission, which is included in the dynamics through the *possibility* for the system to suffer a *state reduction*. The modification of $|\psi(t)\rangle$ by *non-observation* of spontaneous emission, reduces the population of the state excited by $1 - \frac{1}{2}\Gamma dt$, while the ground state population remains unchanged. Every quantum jump projecting the system into the ground state constitutes a measurement, because it corresponds to a detected fluorescence photon.

36.1.2.2 Three-level systems: The epitome of quantum measurement

Let us now return to the mysterious interaction between the sample and the meter, which we want to unravel by comparing two possible procedures: 1. treating the

sample and the meter separately and explain the extraction of information following the von Neumann postulate; 2. treating the sample and the meter by a global theory.

As said above, the inclusion of the meter in a global theory is, in general, difficult. For this reason, to perform the comparison, we choose the simplest imaginable system: the *three-level system* with two transitions connecting to a common ground state and excited by radiation fields. As shown in Fig. 36.6(a) this three-level system can be an atom with a strong transition and a weak transition, for example, the dipolar transition $S_{1/2} - P_{1/2}$ and the forbidden quadrupolar transition $S_{1/2} - D_{5/2}$ in a single Ba^+ ion. We will now name the 'strong transition' as *meter* and the 'weak transition' as *sample* and show that this system allows to study the von Neumann measurement process including the direct observation of quantum jumps [5]. At the same time, the system is simple enough for a complete theoretical description. In this sense, the three-level system becomes the *epitome of a quantum measurement device.*

We turn our attention to the three-level atom: Obviously, the atom will preferentially scatters photons on its strong dipolar transition. However, at times when the valence electron is 'shelved' in the metastable state excited by the quadrupole transition, no fluorescence can be observed on the strong transition.

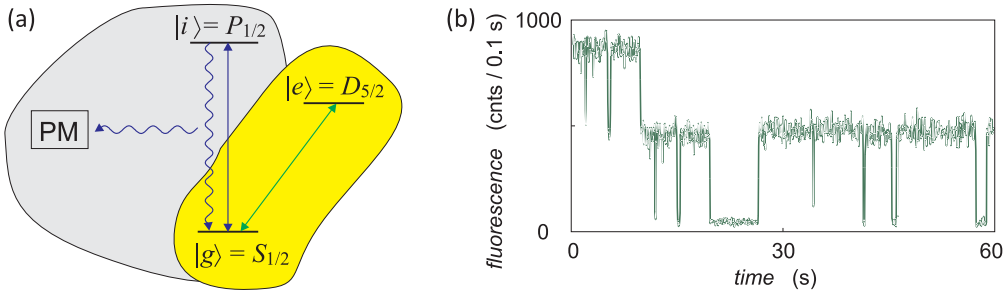

Figure 36.6: (a) Quantum measurement at the example of a three-level atom incorporating a weak (sample) transition and a strong (meter) transition. (b) *Random Telegraph signal* in the resonance fluorescence due to quantum jumps.

Quantum jumps were experimentally observed in single trapped ions, whose lowest energies form a three-level systems [943, 1147, 1148, 130].

36.1.2.3 Quantum Monte-Carlo wavefunction simulation of the quantum amplifier

When both lasers driving the weak and the strong transition are irradiated simultaneously, the coherence on the weak transition is easily perturbed by the dynamics of the strong transition. To resolve this problem *Dehmelt* invented what he called the *quantum amplifier*. The idea consists in alternately irradiating the *sample* laser (at stage $S - D$ in Fig. 36.7) and the *meter* laser (at stage $S - P$ in Fig. 36.7) [6].

[5] The observability of quantum jumps as manifestations of sudden state reductions has been the object of long-standing debates: 'If we have to go on with these damned quantum jumps, then I'm sorry that I ever got involved with quantum mechanics.' [1169].

[6] The absence of the 'meter' laser during the 'sample' stage avoids saturation broadening and light-shifts of the ground state. Since the ground state is shared by both transitions, its broadening

The alternating irradiation of the lasers $S-D$ and $S-P$ can also be treated by the Monte Carlo quantum wavefunction simulation method (36.12) using the effective Hamiltonian,

$$\hat{H}_{eff} = \begin{pmatrix} 0 & \frac{1}{2}\Omega_{sp} & \frac{1}{2}\Omega_{sd} \\ \frac{1}{2}\Omega_{sp} & -\Delta_{sp} - \frac{i}{2}\Gamma_{sp} & 0 \\ \frac{1}{2}\Omega_{sd} & 0 & -\Delta_{sd} \end{pmatrix} , \tag{36.13}$$

where the Rabi frequencies Ω_{sd} and Ω_{sd} are switched on alternately.

In the simulation 36.7 the quantum jumps to the shelved metastable state $D_{5/2}$ appear as long periods without population in the $P_{1/2}$ level (first period $S-P$, where the population of $S_{1/2}$, illustrated by the red curve, gradually tends to 0 for long times). The reduction of the system to the shelved state actually occurs by *non-observation* of fluorescence on the strong transition. The projection needs a finite time, simply because we can not be sure whether the non-observation is actually due to shelving or the incidental absence of scattering events on the $S-P$ transition: After all, it is not predictable, when the next photon will be spontaneously emitted, even though the lifetime of the excited state is short. But for longer observation times it becomes increasingly unlikely that the absence of photons is *not* due to shelving. It is this unlikeliness, which lets the population rapidly converge towards the metastable state. In the second $S-P$ period, Fig. 36.7 shows fast transitions to the $P_{1/2}$ followed by sudden decays to the ground state. These processes correspond to photon absorption and spontaneous reemission by the strong transition. The succession of the photon scattering events is so fast, that the signal recorded by photodetectors appears as a continuous fluorescence. The sudden transitions between bright and dark periods shown in Fig. 36.6(b), which occur totally randomly, are interpreted as quantum jumps.

36.1.2.4 Comparison with Bloch equations and interpretation of quantum jumps

We already mentioned in Fig. 36.5, that a trajectory generated by a MCWF simulation (36.12) represents *one* possible evolution of the system. In Chp. 34 we got to know an alternative way of predicting the evolution of a system, based on density operator obeying a *master equation*, which in the context of atomic excitation levels is called Bloch equation. Comparing MCWF trajectories (red curves in Fig. 36.7) with Bloch vector evolutions (green curves) it becomes apparent, that the Bloch vector evolution does not produce quantum jumps, but is always smooth and continuous.

In most cases, our knowledge about the actual state of an atom comes from the collection of spontaneously emitted photons. The observation of a photon projects the atomic state into the ground state. However, this concept is not included in the Bloch equations, as we just saw in Fig. 36.7. So, as it seems, we have to take back our statement, that the three-level Bloch equation describe the complete system, although they somehow contain spontaneous emission.

---

would reduce the spectral overlap between the 'sample' transition and the driving laser and therefore the probability to excite the metastable level. This inhibition of the coherent dynamic by too strong or too frequent measurements is known as *quantum Zeno effect*: The more an observer tries to extract information from a system, the more he inhibits its evolution. We will discuss this effect in more detail in Sec. 56.3.2.2.

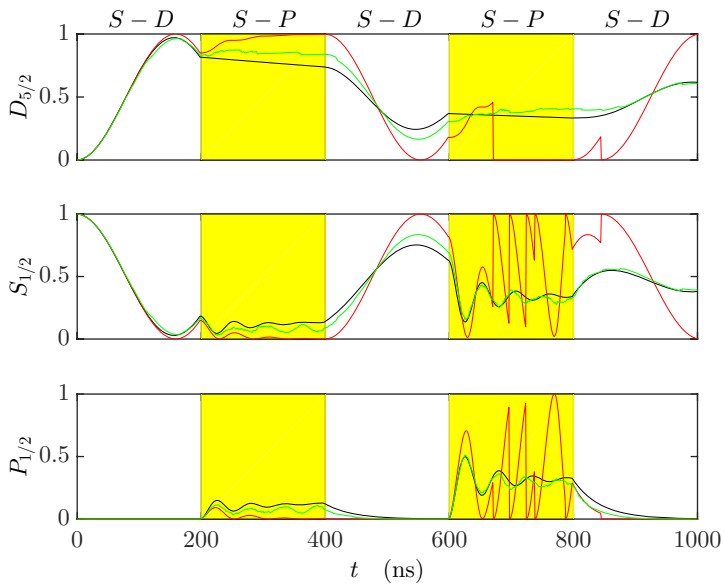

Figure 36.7: (code) Quantum amplifier comparing Monte-Carlo quantum simulations (red lines) and Bloch equations (black lines), which coincide well with the averages over 100 Monte-Carlo trajectories (green lines). The periods $S-D$ (white background) represent the free evolution of the quantum system, the periods $S-P$ (yellow background) represent the measurement periods.

Let us go one step back and ask, where the Bloch equations came from. In fact, as we learned in Sec. 35.6 and will deepen in Sec. 36.2, they are derived from a von Neumann equation for the three-level system *plus* the degrees of freedom of the vacuum modes receiving the spontaneously emitted photons by *tracing over the latter ones*.

We will not be able to handle all degrees of freedom. However, we can generalize the Bloch equations in the following way [912, 1440]. We project the total density operator ρ_{AFR} of the atom plus the driving field plus the reservoir of vacuum modes into the subspace of the atom and the driving field consisting of exactly n photons,

$$\rho^{(n)} = \mathrm{Tr}_R \left(P^{(n)} \rho_{AFR} \right) , \tag{36.14}$$

and derive, from the von Neumann equation, the master equation for the atomic state $\rho^{(n)}$ under the constraint of a fixed number of photons n in the field. The master equation differs only in one term from the usual Bloch equations: The expression $\Gamma_{12}\rho_{22}^{(n)}$, which describes the spontaneous decay of the population of the excited state of the meter transition, is replaced by the expression $\Gamma_{12}\rho_{22}^{(n-1)}$:

$$\frac{d}{dt}\rho^{(n)} = (\mathcal{L}|1\rangle\Gamma_{12}\langle 2|)\rho_{(n)} + |1\rangle\Gamma_{12}\langle 2|\rho^{(n-1)} , \tag{36.15}$$

The substate with of n photons violates the trace condition, $\sum_j \rho_{jj}^{(n)} \neq 1$. The physical explanation for this is the following: While induced emission and absorption

maintain the number of photons in the combined light-atom system (like in the Jaynes-Cummings model), spontaneous emission decreases the number of photons, leading to an irreversible loss of energy. The quantum jump observed in MCWF model corresponds, in the modified equations (36.15), to a collapse of the subspace described by $\rho^{(n)}$ with the time constant Γ_{12} and a birth of another subspace $\rho^{(n-1)}$, whose evolution is guided by another (analogous) Bloch equation, now for $n-1$ photons. Each fluorescence detection at time $t = 0$ determines the initial condition for the future development of the system: $\rho^{(n)}(0) = 0$ and $\rho^{(n-1)}(0) = |1\rangle\langle 1|$. The probability density $c(t)$ for a new observation of spontaneous emission at time t with detection efficiency η, or in other words, the histogram of the durations of dark periods in the fluorescence signal is related to the solution $\rho^{(n)}$ of the homogeneous part of the equation (36.14) via,

$$c(t) = \eta\Gamma_{12}\tilde{\rho}_{22}^{(n)}(t) = \eta\sum_{j=1}^{4}\frac{d}{dt}\tilde{\rho}_{jj}^{(n)}(t)\ , \tag{36.16}$$

The second step immediately follows from the homogeneous part of equation (36.15).

36.1.2.5 Final remarks

The explanations of the last sections show that Bohr's and Schrödinger's views can be reconcealed. They simply depend on whether the measuring transition is excluded or included in the description of the dynamics. *The quantum jump is an* ***artifact*** *arising from the separation of the quantum system under study (object) from the meter (observer) assumed to strongly interact with the system!* In any case (strong or weak interaction), this separation is not compulsory once a more complete model including the meter is at hand. However, as the dynamics of the meter and the object evolve on different time scales, a separation of the dynamics leading to apparently discontinuous trajectories is *only meaningful for strong meter interactions.*

As soon as this has been understood, that is since the 1980-th, the apparent paradox is simply not on the agenda any more. Recent claims of having unraveled the mystery [901] are just not timely and only show that the author did not understand the full meaning of a 'quantum jump' or, at most, did not read the pertinent literature.

36.1.3 Weak measurements

Strong measurements leave the measured quantum system in a eigenstate without uncertainty. But it is possible to imagine a situation, where the measured device does not strongly interact with the quantum system, so that the system is not heavily perturbed. The price to pay will, however, be an uncertain result of the measurement (*no free lunch theorem*).

We consider the use of an ancilla, i.e. an adjunct degree of freedom, for example, a field or a current, to probe a quantum system. The interaction between the system and the probe correlates the two systems.

36.1.3.1 Weak interaction and measurement by coupling to an ancilla

Let us consider a system initially in the quantum state $|\psi\rangle$ and an ancilla initially in the state $|\phi\rangle$, such that the combined state is, $|\Psi\rangle = |\psi\rangle \otimes |\phi\rangle$. The two systems

interact through the Hamiltonian $\hat{H} = \hat{A} \otimes \hat{B}$, which generates the temporal evolution $U(t) = e^{-\imath x t \hat{H}}$ (in units where $\hbar = 1$), where x is the *strength of the interaction* (in angular frequency unit). We assume a fixed interaction time $t = \Delta t$ such that, $\lambda = x\Delta t$ is very small, that is, $\lambda^3 \approx 0$. The expansion of U λ gives,

$$U \approx \mathbb{I} \otimes \mathbb{I} - \imath\lambda\hat{H} - \tfrac{\lambda^2}{2}\hat{H}^2 + O(\lambda^3) = \mathbb{I} \otimes \mathbb{I} - \imath\lambda\hat{A} \otimes \hat{B} - \tfrac{\lambda^2}{2}\hat{A}^2 \otimes \hat{B}^2 \ . \tag{36.17}$$

In cases, where it is sufficient to expand the unitary transformation into low perturbation orders, we speak of *weak interaction*. Since λ and λ^2 are small, the combined state after the interaction will not be very different from the initial state,

$$|\Psi'\rangle = (\mathbb{I} \otimes \mathbb{I} - \imath\lambda\hat{A} \otimes \hat{B} - \tfrac{\lambda^2}{2}\hat{A}^2 \otimes \hat{B}^2)|\Psi\rangle \ . \tag{36.18}$$

Now, we make a measurement on the ancilla to extract information from the system. This is called *ancilla-mediated measurement*. We consider measurements in the basis $|q\rangle$ (of the ancilla system), such that $\sum_q |q\rangle\langle q| = \mathbb{I}$. The action of the measurement on the total system is described by the action of the projector $\Pi_q = \mathbf{1} \otimes |q\rangle\langle q|$ onto $|\Psi'\rangle$. According to the theory of quantum measurement, the conditional state after the measurement is,

$$|\Psi_q\rangle = \frac{\Pi_q|\Psi'\rangle}{\sqrt{\langle\Psi'|\Pi_q|\Psi'\rangle}} = \frac{\mathbf{1} \otimes |q\rangle\langle q| \left(\mathbb{I} \otimes \sum_k |k\rangle\langle k| - \imath\lambda\hat{A} \otimes \hat{B} - \frac{\lambda^2}{2}\hat{A}^2 \otimes \hat{B}^2\right)}{\mathcal{N}}|\psi\rangle \otimes |\phi\rangle \tag{36.19}$$

$$= \frac{\mathbb{I} \otimes \sum_k |q\rangle\langle q|k\rangle\langle k| - \imath\lambda\hat{A} \otimes |q\rangle\langle q|\hat{B} - \frac{\lambda^2}{2}A^2 \otimes |q\rangle\langle q|B^2}{\mathcal{N}}|\psi\rangle \otimes |\phi\rangle$$

$$= \frac{\mathbb{I}\langle q|\phi\rangle - \imath\lambda\hat{A}\langle q|\hat{B}|\phi\rangle - \frac{\lambda^2}{2}\hat{A}^2\langle q|\hat{B}^2|\phi\rangle}{\mathcal{N}}|\psi\rangle \otimes |q\rangle \ ,$$

where $\mathcal{N} = \sqrt{\langle\Psi'|\Pi_q|\Psi'\rangle}$ is the normalization factor for the wavefunction. Note, that the status of the ancilla records the result of the measurement. The object,

$$M_q \equiv \langle q|e^{-\imath\hat{A}\otimes\hat{B}}|\phi\rangle \simeq \mathbb{I}\langle q|\phi\rangle - \imath\lambda\hat{A}\langle q|\hat{B}|\phi\rangle - \tfrac{\lambda^2}{2}\hat{A}^2\langle q|\hat{B}^2|\phi\rangle \tag{36.20}$$

is an operator acting on the total Hilbert space and called the *Kraus operator*. With respect to Kraus operators the state of the combined system after the measurement is,

$$|\Psi_q\rangle = \frac{M_q|\psi\rangle}{\sqrt{\langle\psi|M_q^\dagger M_q|\psi\rangle}} \otimes |q\rangle \ . \tag{36.21}$$

The objects $E_q = M_q^\dagger M_q$ are elements of the so-called *positive operator valued (probability) measurement* (POVM) and must obey $\sum_q E_q = \mathbb{I}$, such that the corresponding probabilities add up to unity: $\sum_q \Pr(q|\psi) = \sum_q \langle\psi|E_q|\psi\rangle = 1$. The ancilla system is no longer correlated with the primary system. It simply records the result of the measurement, such that we can calculate the trace over it. Doing so, we come to the conditional state of the primary system alone,

$$|\psi_q\rangle = \frac{M_q|\psi\rangle}{\sqrt{\langle\psi|M_q^\dagger M_q|\psi\rangle}} \ , \tag{36.22}$$

which we still label with the result q of the measurement. In fact, these considerations allow us to derive a *quantum trajectory*.

36.1.3.2 Kraus operator for position measurement

As a canonical example of a Kraus operator [91, 242] we take $\hat{H} = \hat{x} \otimes \hat{p}$, where the position and the momentum satisfy the commutation relation, $[\hat{x}, \hat{p}] = i$. The initial state of the ancilla be a Gaussian distribution,

$$|\phi\rangle = \frac{1}{(2\pi\sigma^2)^{1/4}} \int dq' e^{-q'^2/4\sigma^2} |q'\rangle \ . \tag{36.23}$$

The position wavefunction of the ancilla is,

$$\phi(q) = \langle q|\phi\rangle = \frac{1}{(2\pi\sigma^2)^{1/4}} e^{-q^2/4\sigma^2} \ . \tag{36.24}$$

The Kraus operators are (compared to the previous discussion, we now let $\lambda = 1$),

$$M(q) = \langle q|e^{-\imath\hat{x}\otimes\hat{p}}|\phi\rangle = \frac{1}{(2\pi\sigma^2)^{1/4}} e^{-(q-x)^2/4\sigma^2} \ , \tag{36.25}$$

since the operator $e^{-\imath\hat{x}\otimes\hat{p}}$ makes a spatial translation when applied to the degree of freedom of the position. The corresponding POVM elements are,

$$E(q) = M_q^\dagger M_q = \frac{1}{\sqrt{2\pi\sigma^2}} e^{-(q-x)^2/2\sigma^2} \ , \tag{36.26}$$

which obey $\int dq E(q) = \mathbb{I}$.

Calculate $\langle\psi_q|\psi_q\rangle = \langle\psi'|M(q)^\dagger M(q)|\psi'\rangle$.

Note that $\lim_{\sigma\to 0} E(q) = |x = q\rangle\langle x = q|$. That is, in a particular limit, these operators converge to a strong measurement of position. For $\sigma \to \infty$, we speak of weak measurement.

Another example would be the three-level atom of Dehmelt's quantum amplifier.

36.1.4 *Welcher Weg* information

36.1.4.1 The Elitzur and Vaidman bomb testing problem

Mixing the concepts of particles and waves we sometimes arrive at seemingly paradoxical conclusions. One example is Elitzur and Vaidman's *bomb testing problem*. They imagined a Mach-Zehnder interferometer with the particularity that the reflecting mirror of one of the arms be connected to a device measuring the photonic recoil. That is, when a photon passes through this arm, the mirror undergoes a small acceleration, which is sufficient to activate an explosive bomb.

Now, we distinguish two cases: 1. The recoil detector *does not work*, i.e. the bomb is not armed. 2. The bomb is *armed*. We now adjust the interferometer in a way to produce destructive interference in one of the two interferometer output ports. If, having sent many photons through the interferometer, we never saw any photons in the 'dark' port, we can be almost sure that the bomb is *not operational*.

In case the bomb is operational, the observation of a photonic recoil destroys the interference pattern at the interferometer outputs. It *has* to do so, because the exploding bomb informs us, in which arm the photon has passed. However, with an operational bomb the interference pattern is *also* destroyed, when the photon passes through the other arm, since the fact that the bomb didn't explode tells us, that the photon went the other way.

The funny conclusion is now, that it may happen, that a photon traverses the interferometer in the arm that does *not* contain the bomb and exits through the 'dark port'. The probability of this happening is only 25%, but nevertheless the observation of a photon in the 'dark port' informs to us that the pump is operative without ever having interacted with it [7].

36.1.5 Exercises

36.1.5.1 Ex: Schwartzeneggers cat

Explain why we will never observe a real cat in a dead-alive superposition.

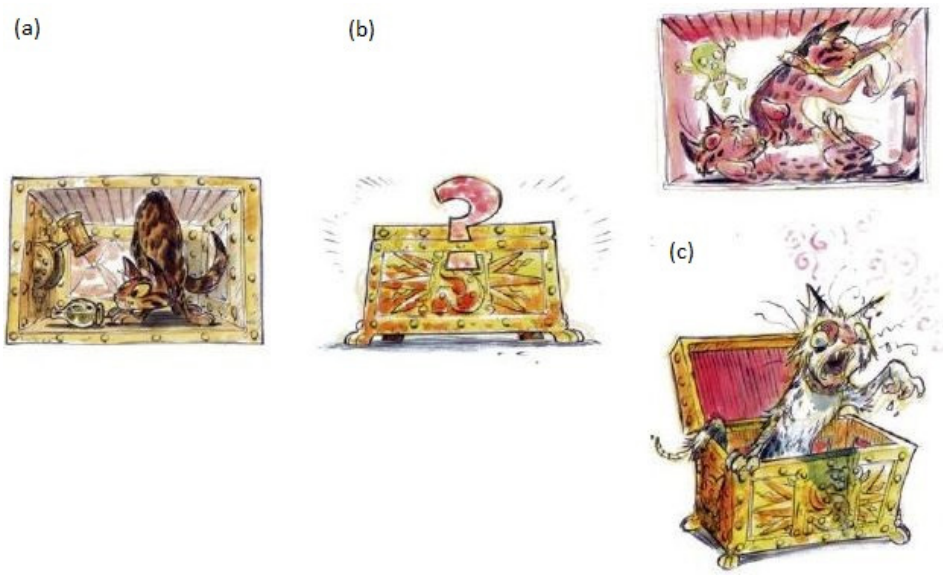

Figure 36.8: Schrödinger's cat according to *Ekhö, Le monde miroir* by Arleston and Barbucco: Quantum superposition or zombie cat?

Solution:

[7] See https://www.thorlabs.com/newgrouppage9.cfm?objectgroup_id=6635

36.1.5.2 Ex: Dispersive quantum jumps

Consider a three-level system in V-configuration, as depicted in Fig. 34.17(b), with an unstable state $|1\rangle$, a ground state $2\rangle$, and a metastable state $|3\rangle$. Discuss whether the atom shelved in state $|3\rangle$ is sensitive to light-shift and power broadened induced by a laser resonant to the $|1\rangle - |2\rangle$ transition. E.g. will power-broadening only effect the transition rate $|1\rangle \longrightarrow |3\rangle$ or also $|3\rangle \longrightarrow |1\rangle$?

Solution: *We assume that both transitions $|1\rangle - |2\rangle$ and $|1\rangle - |3\rangle$ are simultaneously driven. The probability to find the system in the shelved state $|3\rangle$ is then [952],*

$$n_{33}(t) = \frac{R_+}{R_+ + R_-}(1 - e^{-(R_+ + R_-)t}) \ .$$

The rates $R_\pm$ are easily obtained via numerical fit to the solution of the optical Bloch equations.
Then the 'dark' state is not a reached by projection, because it corresponds to a non-observation *of photons. ρ_{33} only increases gradually, ruled by $\hat{H}_{eff}$ and under steady renormalization of the total wavefunction, until a stationary superposition $|1\rangle - |3\rangle$ is reached with a small admixture of $|2\rangle$. This admixture guarantees that R_+ as well as R_- are light-shifted. For the ensemble the Bloch equations must hold. The decay of the 'dark' state is induced by the admixture of ρ_{22}. The light-shift is obtained as an eigenvalue of $\hat{H}_{eff}$ and, hence, is conceptually stationary. That is, it depends on the parameters Ω_{ij}, Δ_{ij}, and Γ_{ij}, which also determine toward which stationary populations and coherences the atom will evolve.*

36.2 Open systems and the master equation

Let us now derive the master equation for an open quantum system. We assume that the environment (also called *bath* or *reservoir*) and the system under consideration are quantum systems in the sense that (1) the relevant degrees of freedom are completely characterized by state vectors (or density matrices), and (2) the temporal evolution of the total system is unitary $U(t) = e^{-\imath \hat{H} t}$. The total Hamiltonian, $\hat{H} = \hat{H}_{sys} + \hat{H}_{res} + V$ is assumed to be independent of time and consists of three parts, namely the Hamiltonian of the system $\hat{H}_{sys}$, the Hamiltonian of the bath $\hat{H}_{res}$, and the interaction V between the system and the bath. The purpose of the master equation is to find the dynamics of the system by tracing over all degrees of freedom of the bath. This is not always possible, and we will assume that the interaction V is sufficiently weak, so that perturbation theory is applicable.

In the interaction representation the evolution of the total density matrix $\hat{\rho}_{tot}$ becomes,

$$\boxed{\imath\hbar \frac{d\tilde{\rho}_{tot}}{dt} = [\tilde{V}(t), \tilde{\rho}_{tot}]} \ . \tag{36.27}$$

where $\tilde{\rho}_{tot}(t) \equiv U_0^\dagger \rho_{tot} U_0$ and $\tilde{V}(t) \equiv U_0^\dagger V U_0$ and $U_0 = e^{-\imath(\hat{H}_{sys} + \hat{H}_{res})t/\hbar}$. This

evolution is, for the time being, very general, and the solution can be formally written,

$$\tilde{\rho}_{tot}(t) = \tilde{\rho}_{tot}(0) + \frac{1}{\imath\hbar}\int_0^t dt_1[\tilde{V}(t_1), \tilde{\rho}_{tot}(t_1)] \ . \tag{36.28}$$

Iterating once again:

$$\tilde{\rho}_{tot}(t) = \tilde{\rho}_{tot}(0)+\frac{1}{\imath\hbar}\int_0^t dt_1[\tilde{V}(t_1), \tilde{\rho}_{tot}(0)]+\frac{1}{(\imath\hbar)^2}\int_0^t dt_1\int_0^{t_1} dt_2\left[\tilde{V}(t_1), [\tilde{V}(t_2), \tilde{\rho}_{tot}(t_2)\right] \ . \tag{36.29}$$

In the following, we will call several approximations to simplify the calculations, in particular, the Born approximation, the assumption that the initial state is a product state and, later-on, the Markov approximation.

36.2.1 Born approximation for weak coupling

We will now assume the interaction $\tilde{V}$ to be weak. We can then expect that, repeating the iterative process, the series will converge and write the general solution as,

$$\tilde{\rho}_{tot}(t) = \tilde{\rho}_{tot}(0) + \sum_{n\geq 1}\frac{1}{(\imath\hbar)^n}\int_0^t dt_1 ... \int_0^{t_{n-1}} dt_n\left[\tilde{V}(t_1), ..., [\tilde{V}(t_n), \tilde{\rho}_{tot}(0)]\right] \ . \tag{36.30}$$

This way of terminating an iterative equation by $\rho_{tot}(0)$ is generally known as the *Born approximation*. Here, we will just go to second order in $\tilde{V}$. Tracing over the bath,

$$\tilde{\rho}_{sys}(t) = \mathrm{Tr}_{res}\ \tilde{\rho}_{tot}(t) \ , \tag{36.31}$$

we extract the density matrix for only the system,

$$\begin{aligned}\tilde{\rho}_{sys}(t) = \tilde{\rho}_{sys}(0) + \frac{1}{\imath\hbar}\int_0^t dt_1 \mathrm{Tr}_{res}[\tilde{V}(t_1), \tilde{\rho}_{tot}(0)] \\ + \frac{1}{(\imath\hbar)^2}\int_0^t dt_1\int_0^{t_1} dt_2 \mathrm{Tr}_{res}\left[\tilde{V}(t_1), [\tilde{V}(t_2), \tilde{\rho}_{tot}(0)]\right] \ .\end{aligned} \tag{36.32}$$

36.2.2 Assumption of an initial product state

Next, we need to make the quite important assumption, that the initial state between the system and the environment are not correlated, or mathematically speaking, they can be written as product states,

$$\tilde{\rho}_{tot}(0) = \tilde{\rho}_{sys}(0) \otimes \rho_{res}(0) \ . \tag{36.33}$$

Another assumption, which is not essential but often valid, is that $\mathrm{Tr}_{res}[\tilde{V}(t_1), \tilde{\rho}_{tot}(0)] = 0$. If this is the case, then the first-order term will vanish. In second order, we can write,

$$\begin{aligned}&\tilde{\rho}_{sys}(t) = e^{\mathcal{M}(t)}\tilde{\rho}_{sys}(0) \\ &\text{where} \quad \mathcal{M}(t)\chi \equiv \frac{1}{(\imath\hbar)^2}\int_0^t dt_1\int_0^{t_1} dt_2 \mathrm{Tr}_{res}\left[\tilde{V}(t_1), [\tilde{V}(t_2), \chi\otimes\rho_{res}]\right] \ ,\end{aligned} \tag{36.34}$$

is a *superoperator* acting on the operator density of the system. Taking the temporal derivative, we have the explicit master equation,

$$\boxed{\begin{array}{rcl}\frac{d\tilde{\rho}_{sys}(t)}{dt} = \mathcal{L}\rho_{sys}(t) &=& \frac{d}{dt}\left(\mathcal{M}(t)\tilde{\rho}_{sys}(t)\right) \\ &=& \frac{1}{(\imath\hbar)^2}\int_0^t d\tau\ \mathrm{Tr}_{res}\left[\tilde{V}(t),[\tilde{V}(\tau),\tilde{\rho}_{sys}(t)\otimes\rho_{res}]\right]\end{array}} \ . \tag{36.35}$$

The superoperator $\mathcal{L}$ is called *Lindblad operator*.

36.2.3 Markov approximation for short memory

Here, we have to evaluate the terms involving the average with respect to the thermal bath, which is assumed to have a short memory, in the sense that the correlation time is very short. Mathematically,

$$\begin{aligned}\int_0^t d\tau\ \mathrm{Tr}_{res}\left(\tilde{V}(t)\tilde{V}(\tau)\rho_{res}\right) &= \int_0^t d\tau\ \mathrm{Tr}_{res}\left(\tilde{V}(t-\tau)\tilde{V}(0)\rho_{res}\right) \\ &\simeq \int_0^\infty d\tau\ \mathrm{Tr}_{res}\left(\tilde{V}(t-\tau)\tilde{V}(0)\rho_{res}\right)\ .\end{aligned} \tag{36.36}$$

In other words, the two-point correlation function is significant only, when $t \simeq \tau$, and it is valid to extend the upper bound to infinity. This is the *Markov approximation*.

36.2.4 Example: Damped harmonic quantum oscillator

As an example, we let us consider the master equation for the *Brownian motion of a quantum harmonic oscillator*. It can be written,

$$\frac{d\tilde{\rho}_{sys}}{dt} = \frac{1}{(\imath\hbar)^2}\int_0^t d\tau\ \mathrm{Tr}_{res}\left\{\begin{array}{c}\tilde{V}(t)\tilde{V}(\tau)\tilde{\rho}(t)\otimes\rho_{res} - \tilde{V}(t)\tilde{\rho}_{sys}(t)\otimes\rho_{res}\tilde{V}(\tau) \\ -\tilde{V}(\tau)\tilde{\rho}_{sys}(t)\otimes\rho_{res}\tilde{V}(t) + \tilde{\rho}_{sys}(t)\otimes\rho_{res}\tilde{V}(\tau)\tilde{V}(t)\end{array}\right\} . \tag{36.37}$$

The coupling of the system to the bath is assumed to be of the form,

$$\tilde{V} = \hbar\left(\hat{a}^\dagger\hat{\Gamma}(t)e^{\imath\Omega t} + \hat{a}\hat{\Gamma}^\dagger(t)e^{-\imath\Omega t}\right)\ , \tag{36.38}$$

where $\hat{\Gamma}(t) = \sum_k g_k\hat{b}_k e^{-\imath\omega_k t}$, the bosonic operators $\hat{a}$ and $\hat{b}_k$ act, respectively, on the system (with the frequency Ω) and the bath (with the frequency ω_k). Here, g_k characterizes the coupling force between the oscillators of the system and the bath. Hence,

$$\frac{d\tilde{\rho}_{sys}}{dt} = -\int_0^t d\tau\ \mathrm{Tr}_{res}\left\{\begin{array}{l}\left(\hat{a}^\dagger\hat{\Gamma}(t)e^{\imath\Omega t} + \hat{a}\hat{\Gamma}^\dagger(t)e^{-\imath\Omega t}\right)\left(\hat{a}^\dagger\hat{\Gamma}(\tau)e^{\imath\Omega\tau} + \hat{a}\hat{\Gamma}^\dagger(\tau)e^{-\imath\Omega\tau}\right)\tilde{\rho}(t)\otimes\rho_{res} \\ -\left(\hat{a}^\dagger\hat{\Gamma}(t)e^{\imath\Omega t} + \hat{a}\hat{\Gamma}^\dagger(t)e^{-\imath\Omega t}\right)\tilde{\rho}(t)\otimes\rho_{res}\left(\hat{a}^\dagger\hat{\Gamma}(\tau)e^{\imath\Omega\tau} + \hat{a}\hat{\Gamma}^\dagger(\tau)e^{-\imath\Omega\tau}\right) \\ -\left(\hat{a}^\dagger\hat{\Gamma}(\tau)e^{\imath\Omega\tau} + a\hat{\Gamma}^\dagger(\tau)e^{-\imath\Omega\tau}\right)\tilde{\rho}(t)\otimes\rho_{res}\left(\hat{a}^\dagger\hat{\Gamma}(t)e^{\imath\Omega t} + a\hat{\Gamma}^\dagger(t)e^{-\imath\Omega t}\right) \\ +\tilde{\rho}(t)\otimes\rho_{res}\left(\hat{a}^\dagger\hat{\Gamma}(\tau)e^{\imath\Omega\tau} + \hat{a}\hat{\Gamma}^\dagger(\tau)e^{-\imath\Omega\tau}\right)\left(\hat{a}^\dagger\hat{\Gamma}(t)e^{\imath\Omega t} + \hat{a}\hat{\Gamma}^\dagger(t)e^{-\imath\Omega t}\right)\end{array}\right\} . \tag{36.39}$$

Let's take a closer look at one of the terms,

$$\hat{T} \equiv -\int_0^t d\tau \mathrm{Tr}_{res}\left\{\hat{a}^\dagger\hat{\Gamma}(t)e^{\imath\Omega t}\hat{a}\hat{\Gamma}^\dagger(\tau)e^{-\imath\Omega\tau}\tilde{\rho}(t)\otimes\rho_{res}\right\} \tag{36.40}$$
$$= -\hat{a}^\dagger\hat{a}\tilde{\rho}(t)\int_0^t d\tau\langle\hat{\Gamma}(t)\hat{\Gamma}^\dagger(\tau)\rangle_{res}e^{\imath\Omega t}e^{-\imath\Omega\tau} \ .$$

We will have to evaluate quantities such as

$$\mathrm{Tr}_{res}\left(V(t)V(s)\rho_{res}\right) = \hbar^2\hat{a}^\dagger\hat{a}\langle\hat{\Gamma}(t)\hat{\Gamma}^\dagger(t)\rangle_{res}e^{\imath\Omega(t-s)} + \hbar^2\hat{a}\hat{a}^\dagger\langle\hat{\Gamma}^\dagger(t)\hat{\Gamma}(t)\rangle_{res}e^{-\imath\Omega(t-s)} \ , \tag{36.41}$$

where $\langle\hat{\Gamma}(t)\hat{\Gamma}^\dagger(t)\rangle_{res} \equiv \mathrm{Tr}_{res}[\hat{\Gamma}(t)\hat{\Gamma}^\dagger(t)\rho_{res}]$, and for the thermal bath, $\langle\hat{b}_j^\dagger\hat{b}_k\rangle = \delta_{jk}n_k$ and $\langle\hat{b}_j\hat{b}_k^\dagger\rangle = \delta_{jk}(1+n_k)$ and $n_k = (e^{\beta\hbar\omega_k}-1)^{-1}$. Hence,

$$\hat{T} = -\hat{a}^\dagger\hat{a}\tilde{\rho}(t)\sum_{j,k}g_jg_k\langle b_jb_k^\dagger\rangle_{res}\int_0^t d\tau e^{\imath(\omega_jt-\omega_k\tau)}e^{\imath\Omega(t-\tau)} \tag{36.42}$$
$$\simeq -\hat{a}^\dagger\hat{a}\tilde{\rho}(t)\sum_k g_k^2n_k\int_0^\infty d\tau e^{\imath(\omega_k-\Omega)(t-\tau)} \ .$$

Then we will have to use the relationship,

$$\int_0^\infty d\tau e^{\pm\imath\varepsilon\tau} = \pi\delta(\varepsilon) \pm \imath PV \ , \tag{36.43}$$

where PV denotes Cauchy part of the principal value. These correspond to a 'Lamb shift' and a 'Stark shift' of the frequency, which are considered to be small in comparison to Ω and should be neglected here,

$$\hat{T} = -\hat{a}^\dagger\hat{a}\tilde{\rho}(t)\sum_k g_k^2\left(e^{\beta\hbar\omega_k}-1\right)^{-1}\int_0^\infty d\tau e^{\imath(\omega_k-\Omega)(t-\tau)} \tag{36.44}$$
$$= -\hat{a}^\dagger\hat{a}\tilde{\rho}(t)\sum_k g_k^2\left(e^{\beta\hbar\omega_k}-1\right)^{-1}\pi\delta(\omega_k-\Omega)$$
$$= -\hat{a}^\dagger\hat{a}\tilde{\rho}(t)\sum_k g_k^2\left(e^{\beta\hbar\Omega}-1\right)^{-1}\pi = -\pi\bar{n}\hat{a}^\dagger\hat{a}\tilde{\rho}(t)\sum_k g_k^2\delta(\omega_k-\Omega) = \bar{n}\hat{a}\hat{a}^\dagger\tilde{\rho}(t)\pi\frac{\gamma}{2} \ .$$

where $\bar{n} \equiv \left(e^{\beta\hbar\Omega}-1\right)^{-1}$. We define $\frac{\gamma}{2} \equiv \sum_k g_k^2\delta(\omega_k-\Omega)$. The procedure can be repeated for all terms in the master equation. We then obtain the master equation for a damped harmonic oscillator,

$$\frac{d\tilde{\rho}}{dt} = \tfrac{\gamma}{2}(\bar{n}+1)\left(2\hat{a}\tilde{\rho}\hat{a}^\dagger - \hat{a}^\dagger\hat{a}\tilde{\rho} - \tilde{\rho}\hat{a}^\dagger\hat{a}\right) - \tfrac{\gamma}{2}\bar{n}\left(2\hat{a}^\dagger\tilde{\rho}\hat{a} - \hat{a}\hat{a}^\dagger\tilde{\rho} - \tilde{\rho}\hat{a}\hat{a}^\dagger\right) \ . \tag{36.45}$$

36.2.4.1 Thermalization

To complete the discussion, let us consider the evolution time of the mean number of photons $\langle\hat{a}^\dagger\hat{a}\rangle$. Note that $\mathrm{Tr}_{res}\hat{a}\hat{a}^\dagger\tilde{\rho} = \mathrm{Tr}_{res}\hat{a}\hat{a}^\dagger\rho$, which can be useful (with $\hat{n} = \hat{a}^\dagger\hat{a}$ and $\hat{n}\hat{a} = \hat{a}\hat{n} - \hat{a}$) for simplifying the right-hand side of the master equation. We get,

$$\frac{d\langle\hat{a}^\dagger\hat{a}\rangle}{dt} = -\gamma\langle\hat{a}^\dagger\hat{a}\rangle + \gamma N \ , \tag{36.46}$$

and the solution of this equation is,

$$\langle \hat{n}(t) \rangle = \langle \hat{n}(0) \rangle e^{-\gamma t} + \bar{n}(1 - e^{-\gamma t}) \ , \tag{36.47}$$

which suggests that $\langle n(t \to \infty) \rangle \to \bar{n} = (e^{\beta\hbar\Omega} - 1)^{-1}$, as expected for the thermalization rate [1062]. For a discussion of the validity of the Born-Markov approximation, see [932]. For the relationship between the Markov approximation and Fermi's Golden Rule, see [17].

36.2.5 Deriving the Heisenberg-Langevin from the master equation

The Heisenberg-Langevin equation for the operators $\hat{A}$ of a system subject to dissipation with rates γ_k via the degrees of freedom $\hat{L}_k$ and the *master equation* for the density operator $\hat{\rho}$ are equivalent descriptions for the time-evolution of a system,

$$\boxed{\begin{array}{rcccl} \frac{d\hat{\rho}}{dt} & = & \mathcal{L}\hat{\rho} & = & -\frac{\imath}{\hbar}[\hat{H}, \hat{\rho}] + \sum_k \gamma_k \left(\hat{L}_k \hat{\rho} \hat{L}_k^\dagger - \frac{1}{2} \hat{L}_k^\dagger \hat{L}_k \hat{\rho} - \frac{1}{2} \hat{\rho} \hat{L}_k^\dagger \hat{L}_k \right) \\ \frac{d\hat{A}}{dt} & = & \mathcal{L}^\dagger \hat{A} & = & \frac{\imath}{\hbar}[\hat{H}, \hat{A}] + \sum_k \gamma_k \left(\hat{L}_k^\dagger \hat{A} \hat{L}_k - \frac{1}{2} \hat{L}_k^\dagger \hat{L}_k \hat{A} - \frac{1}{2} \hat{A} \hat{L}_k^\dagger \hat{L}_k \right) \end{array}} \ , \tag{36.48}$$

as we will show in Exc. 36.2.6.2. The former stresses the Schrödinger picture and the latter the Heisenberg picture. In particular, the dissipative *Lindblad terms* are equivalent. That is, open systems are sufficiently characterized by the system Hamiltonian $\hat{H}$ and a set of the so-called *jump operators* $\hat{L}_k$ with their corresponding rates γ_k.

36.2.6 Exercises

36.2.6.1 Ex: Master equation for cavities

Consider a cavity laser-pumped at a rate η, subject to losses by transmission through the mirrors at a rate κ, and incoherently pumped by thermal photons at a rate $\kappa\bar{n}$, where $\bar{n}$ is the number of thermal photons.
a. Write down the Hamiltonian and the Heisenberg-Liouville equation for an arbitrary operator $\hat{a}$ of the system.
b. Derive the equation of motion for the field annihilation operator $\hat{a}$ and for the photon number operator $\hat{n}$.
c. Solve the equation of motion for the photon number operator for the case of no coherent pumping, $\eta = 0$.
d. Write down the master equation of the system.
e. Derive the equation of motion for the components of the density operator $\rho_{m,n}$.
f. Calculate the phton number evolution from (e).

Solution: *a. The Hamiltonian is,*

$$\hat{H} = -\Delta_c \hat{a}^\dagger \hat{a} - \imath\eta(\hat{a} - \hat{a}^\dagger) \ ,$$

and the Heisenberg-Liouville equation for an arbitrary operator $\hat{A}$ of the system is,

$$\frac{d\hat{A}}{dt} = -\imath[\hat{A}, \hat{H}] + \tfrac{\kappa}{2}(\bar{n} + 1)(\hat{a}^\dagger[\hat{A}, \hat{a}] + [\hat{a}^\dagger, \hat{A}]\hat{a}) + \tfrac{\kappa}{2}\bar{n}(\hat{a}[\hat{A}, \hat{a}^\dagger] + [\hat{a}, \hat{A}]\hat{a}^\dagger) \ .$$

b. Using the standard commutation rules we derive the equation of motion for the field annihilation operator,

$$\begin{aligned}\frac{d\hat{a}}{dt} &= -\imath[\hat{a},\hat{H}] + \tfrac{\kappa}{2}(\bar{n}+1)(\hat{a}^\dagger[\hat{a},\hat{a}] + [\hat{a}^\dagger,\hat{a}]\hat{a}) + \tfrac{\kappa}{2}\bar{n}(\hat{a}[\hat{a},\hat{a}^\dagger] + [\hat{a},\hat{a}]\hat{a}^\dagger) \\ &= (\imath\Delta_c - \tfrac{\kappa}{2})\hat{a} + \eta \ .\end{aligned}$$

The equation of motion for the photon number operator is [8]*,*

$$\begin{aligned}\frac{d\hat{n}}{dt} &= -\imath[\hat{a}^\dagger\hat{a},\hat{H}] + \tfrac{\kappa}{2}(\bar{n}+1)(\hat{a}^\dagger[\hat{a}^\dagger\hat{a},\hat{a}] + [\hat{a}^\dagger,\hat{a}^\dagger\hat{a}]\hat{a}) + \tfrac{\kappa}{2}\bar{n}(\hat{a}[\hat{a}^\dagger\hat{a},\hat{a}^\dagger] + [\hat{a},\hat{a}^\dagger\hat{a}]\hat{a}^\dagger) \\ &= -\eta[\hat{a}^\dagger\hat{a},\hat{a}-\hat{a}^\dagger] - \kappa(\bar{n}+1)\hat{a}^\dagger\hat{a} + \kappa\bar{n}\hat{a}\hat{a}^\dagger = \eta(\hat{a}^\dagger+\hat{a}) - \kappa\hat{n} + \kappa\bar{n} \ .\end{aligned}$$

c. The solution for the case $\eta = 0$ is,

$$\hat{n}(t) = \hat{n}(0)e^{-\kappa t} + \bar{n}(1-e^{-\kappa t}) \ .$$

d. The master equation for the density operator defined by $\hat{\rho} \equiv \sum_{m,n}\rho_{m,n}|m\rangle\langle n|$ is,

$$\frac{d\hat{\rho}}{dt} = \imath[\hat{\rho},\hat{H}] + \kappa_+(2\hat{a}\hat{\rho}\hat{a}^\dagger - \hat{a}^\dagger\hat{a}\hat{\rho} - \hat{\rho}\hat{a}^\dagger\hat{a}) + \kappa_-(2\hat{a}^\dagger\hat{\rho}\hat{a} - \hat{a}\hat{a}^\dagger\hat{\rho} - \hat{\rho}\hat{a}\hat{a}^\dagger) \ .$$

using the abbreviations $\kappa_+ \equiv \frac{\kappa}{2}(\bar{n}+1)$ and $\kappa_- \equiv \frac{\kappa}{2}\bar{n}$.
e. For the components we get,

$$\begin{aligned}\dot{\rho}_{n,m} &= \langle n|\dot{\hat{\rho}}|m\rangle \\ &= \imath\langle n|[\hat{\rho}, -\Delta_c\hat{a}^\dagger\hat{a} - \imath\eta(\hat{a}-\hat{a}^\dagger)]|m\rangle \\ &\quad + \kappa_+[\langle n|2\hat{a}\hat{\rho}\hat{a}^\dagger|m\rangle - \langle n|\hat{a}^\dagger\hat{a}\hat{\rho}|m\rangle - \langle n|\hat{\rho}\hat{a}^\dagger\hat{a}|m\rangle] \\ &\quad + \kappa_-[\langle n|2\hat{a}^\dagger\hat{\rho}\hat{a}|m\rangle - \langle n|\hat{a}\hat{a}^\dagger\hat{\rho}|m\rangle - \langle n|\hat{\rho}\hat{a}\hat{a}^\dagger|m\rangle] \\ &= \imath\Delta_c(n-m)\rho_{n,m} + \eta[\sqrt{m}\rho_{n,m-1} - \sqrt{m+1}\rho_{n,m+1} - \sqrt{n+1}\rho_{n+1,m} + \sqrt{n}\rho_{n-1,m}] \\ &\quad + \kappa_+[2\sqrt{n+1}\sqrt{m+1}\rho_{n+1,m+1} - (n+m)\rho_{n,m}] \\ &\quad + \kappa_-[2\sqrt{nm}\rho_{n-1,m-1} - (n+m)\rho_{n,m} - 2\rho_{n,m}] \ .\end{aligned}$$

In particular, for the diagonal,

$$\begin{aligned}\dot{\rho}_{n,n} = \eta\left(\sqrt{n}(\rho_{n,n-1}+\rho_{n-1,n}) - \sqrt{n+1}(\rho_{n,n+1}+\rho_{n+1,n})\right) \\ + 2\kappa_+\left[(n+1)\rho_{n+1,n+1} - n\rho_{n,n}\right] + 2\kappa_-\left[n\rho_{n-1,n-1} - (n+1)\rho_{n,n}\right] \ .\end{aligned}$$

f. The photon number evolves like,

$$\begin{aligned}\frac{d}{dt}\langle\hat{n}\rangle &= \frac{d}{dt}\,Tr\,\hat{\rho}\hat{n} = \frac{d}{dt}\sum_n\langle n|\hat{\rho}\hat{n}|n\rangle = \sum_n n\dot{\rho}_{n,n} \\ &= \sum\nolimits_n n\eta\left(\sqrt{n}\rho_{n,n-1} - \sqrt{n+1}\rho_{n,n+1} - \sqrt{n+1}\rho_{n+1,n} + \sqrt{n}\rho_{n-1,n}\right) \\ &\quad + 2\kappa_+\left[n(n+1)\rho_{n+1,n+1} - n^2\rho_{n,n}\right] + 2\kappa_-\left[n^2\rho_{n-1,n-1} - n(n+1)\rho_{n,n}\right] \\ &= \sum\nolimits_n \eta\langle n|\hat{a}^\dagger\hat{\rho} + \hat{a}\hat{\rho}|n\rangle - 2\tfrac{\kappa}{2}(\bar{n}+1)n\rho_{n,n} + 2\tfrac{\kappa}{2}\bar{n}(n+1)\rho_{n,n} \\ &= \eta(\langle\hat{a}^\dagger\rangle + \langle\hat{a}\rangle) - \kappa\langle\hat{n}\rangle + \kappa\bar{n} \ ,\end{aligned}$$

[8] Curiously this not equal to,

$$\dot{\hat{a}}^\dagger\hat{a} + \hat{a}^\dagger\dot{\hat{a}} = \hat{a}^\dagger\left[(\imath\Delta_c - \tfrac{\kappa}{2})\hat{a} + \eta\right] + \left[(-\imath\Delta_c - \tfrac{\kappa}{2})\hat{a}^\dagger + \eta\right]\hat{a} = \eta(\hat{a}^\dagger + \hat{a}) - \kappa\hat{n} \ .$$

in accordance with the result of (b).

36.2.6.2 Ex: Deriving the Heisenberg-Langevin from the master equation

Derive the Heisenberg-Langevin from the master equation including the dissipative Lindblad terms.

Solution: *To derive the Heisenberg-Langevin from the master equation we simply demand that the expectation value of an operator $\hat{A}$ is the same in the Schrödinger picture (density matrix evolves) and the Heisenberg picture (operator evolves). That is,*

$$\langle \hat{A} \rangle = Tr\ \hat{A}(0)\hat{\rho}(t) = Tr\ \hat{A}(t)\hat{\rho}(0)\ ,$$

where $\hat{A}(t)\hat{\rho}(0)$ is the operator in the Heisenberg picture, while $\hat{A}(0)\hat{\rho}(t)$ is the operator in the Schrödinger picture. The Lindblad equation can be written in the Schrödinger picture as,

$$\frac{d\hat{\rho}}{dt} = \mathcal{L}\hat{\rho} = -\tfrac{i}{\hbar}[\hat{H},\hat{\rho}] + \sum_k \gamma_k \left(\hat{L}_k \hat{\rho} \hat{L}_k^\dagger - \tfrac{1}{2}\hat{L}_k^\dagger \hat{L}_k \hat{\rho} - \tfrac{1}{2}\hat{\rho}\hat{L}_k^\dagger \hat{L}_k \right)\ .$$

The formal solution of the Lindblad equation can then be written as,

$$\hat{\rho}(t) = e^{\mathcal{L}t}\hat{\rho}(0)\ ,$$

where the exponential of the superoperator $\mathcal{L}$ is defined as usual by its Taylor series expansion. Now, we define the adjoint Liouvillian $\mathcal{L}^\dagger$ by,

$$Tr\ \hat{P}[\mathcal{L}\hat{Q}] = Tr\ [\mathcal{L}^\dagger \hat{P}]\hat{Q}\ ,$$

where $\hat{P}$ and $\hat{Q}$ are arbitrary operators. It follows from the definitions that,

$$Tr\ \hat{A}(0)\hat{\rho}(t) = Tr\ \hat{A}(0)e^{\mathcal{L}t}\hat{\rho}(0) = Tr\ [e^{\mathcal{L}^\dagger t}\hat{A}(0)]\hat{\rho}(0)\ ,$$

from which we identify

$$\hat{A}(t) = e^{\mathcal{L}^\dagger t}\hat{A}(0)$$

as the operator $\hat{A}$ in the Heisenberg picture, which obviously satisfies the differential equation,

$$\frac{d\hat{A}}{dt} = \mathcal{L}^\dagger \hat{A}\ .$$

All that remains is to check that indeed,

$$\mathcal{L}^\dagger \hat{A} = \tfrac{i}{\hbar}[\hat{H},\hat{A}] + \sum_k \gamma_k \left(\hat{L}_k^\dagger \hat{A} \hat{L}_k - \tfrac{1}{2}\hat{L}_k^\dagger \hat{L}_k \hat{A} - \tfrac{1}{2}\hat{A}\hat{L}_k^\dagger \hat{L}_k \right)\ ,$$

which can be shown using the definition of $\mathcal{L}^\dagger$ and the cyclicity of the trace.

36.3 Repeated measurements

36.3.1 The quantum Zeno effect

A famous problem raised by the Greek philosopher (490-430 AC) *Zeno* goes like this: Achilles and a turtle organize a race. The arrogant Achilles leaves a 100-meter lead to the turtle. The race begins. Achilles soon covers the 100 meters, only to find out that meanwhile the turtle has advanced by 10 meters. He continues running to cover the 10 meters, only to find out that meanwhile the turtle has advanced by 1 meter, and so on [9]. A presentation on the subject is available at (watch talk).

Interestingly, Zeno's problem has a counterpart in quantum mechanics. Let us do the following Gedankenexperiment: A laser beam passes through a dense series of n polarizers, each one being rotated by an angle $\frac{\pi}{2n}$ with respect to the preceding one. Each polarizer performs a local measurement of beam polarization. The result of this arrangement is that, in the limit of an infinitely dense series, the continuous measurement of the system completely governs its evolution and rotates the polarization by an angle of $\pi/2$ [10].

In every version of the *Zeno effect*, the system is inhibited from evolving freely, because of too frequent measurements of its current state. Achilles would surely be able to overtake the turtle, if he did not always check on her to assess the remaining distance [654] [11].

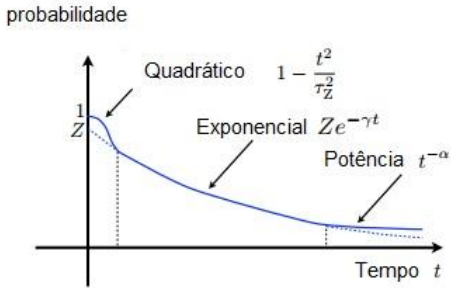

Figure 36.9: Quadratic time dependence of an excited state population.

The temporal evolution of the wavefunction of a system described by the Hamiltonian $\hat{H}$ is $|\psi(t)\rangle = e^{-i\hat{H}t/\hbar}|\psi_0\rangle$. We can then calculate the amplitude and probability

[9] In another version of his paradox, Zeno questions the possibility of motion at the example of a flying arrow: At any instant of time it occupies a space equal to its size. That is, at any particular moment of its flight, it is at rest, in a space that does not move. That is, any kind of motion is impossible. Nowadays, we know that this paradox is false, because time and motion are not discrete. But this can only be understood on the basis of infinitesimal calculus [902].

[10] An analogous experiment can be imagined by a series of Stern-Gerlach measurements of the spin of an atom.

[11] The quantum Zeno effect was often used to justify the physical relevance of the state reduction postulate. It was shown, however, that this postulate is not essential for understanding the quantum Zeno effect [112]. The effect already follows directly from the Schrödinger equation and therefore has a purely dynamical nature. This shows that the projection is a purely mathematical construct without physical reality (see Sec. 36.1.2).

for the system to stay in the initial state,

$$\langle\psi_0|\psi(t)\rangle = \langle\psi_0|e^{-\imath\hat{H}t/\hbar}|\psi_0\rangle \qquad \text{and} \qquad P(t) = |\langle\psi_0|\psi(t)\rangle|^2 \ . \tag{36.49}$$

For short times we can expand,

$$\langle\psi_0|\psi(\delta t)\rangle = |\psi_0\rangle - \frac{\imath}{\hbar}\hat{H}\delta t/\hbar|\psi_0\rangle - \frac{1}{2\hbar^2}\hat{H}^2\delta t^2|\psi_0\rangle + ... = |\psi_0\rangle + |\delta\psi\rangle \ , \tag{36.50}$$

such that,

$$\langle\psi_0|\psi(\delta t)\rangle \simeq 1 - \frac{\imath}{\hbar}\hat{H}\delta t - \frac{1}{2\hbar^2}\hat{H}^2\delta t^2 \quad \text{and} \quad P(\delta t) \simeq 1 - \frac{1}{\hbar^2}(\langle\hat{H}^2\rangle_0 - \langle\hat{H}\rangle_0^2)\delta t^2 \ . \tag{36.51}$$

In this way we can extract the Zeno time from the above equations, $\tau_Z = \hbar^2/\sqrt{\langle\hat{H}^2\rangle_0 - \langle\hat{H}\rangle_0^2}$. We now make N successive von Neumann measurements within a time t, which leads to a measurement frequency of τ^{-1}. The measurements are conceived as to verify, whether the system is still in its initial state, but each measurement projects our system back to its initial state, from where it has to start the transition process from scratch. Under these conditions, the population of the initial state will evolve like,

$$P^{(N)}(\tau) = P^{(N)}(t/N)^N \ . \tag{36.52}$$

Fig. 36.10 shows the evolution for five measurements separated by time intervals τ. In comparison with the evolution, when no measurements are taken (dashed line), the evolution with measurements inhibits the depletion of the initial state. Extrapolating the number of measurements to infinity, the probability (36.52) converges to 1,

$$\left[1 - \left(\frac{t}{N\tau_Z}\right)^2\right]^N \overset{N\ large}{\longrightarrow} e^{-t^2/N\tau_Z^2} \overset{N\to\infty}{\longrightarrow} 1 \ . \tag{36.53}$$

See Excs. 36.3.4.1 and 36.3.4.2.

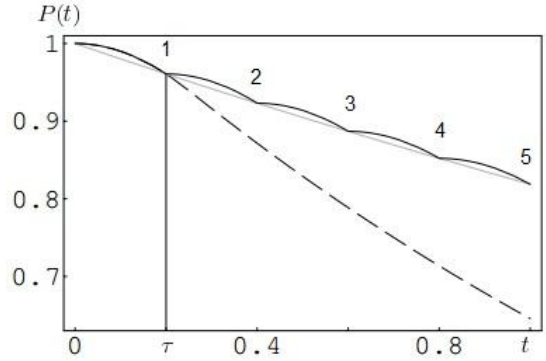

Figure 36.10: Inhibition of the decay of a state by repeated measurements (here $N = 5$). The dashed (solid) line represents the survival probability with (without) measurements. The gray line represents an exponential interpolation function.

Suppression of the evolution of a quantum system due to the quantum Zeno effect was observed experimentally [654] using beryllium ions. Nevertheless, the discussion about the correct interpretation of this effect and its relationship to trivial power broadening is not closed. Some works have even proposed the possibility of an anti-Zeno effect [25, 1344], where observation would accelerate the evolution of the system. Currently the quantum Zeno effect is also studied for possible applications in metrology, computation, and quantum information [717].

When the quantum Zeno effect was proposed for the first time, it was considered a paradox: How could an unstable particle never decay, just by being continually observed? And what would happen to Schrödinger's cat, whose live depends on state of the particle? Could we save it from its cruel fate just by observing it?

Another interesting question concerns the quantum nature of the quantum Zeno effect. Is it really non-classical? On one hand, the quantum Zeno effect supposes the complete reduction of the system to an eigenstate. However, we can imagine classical measurements that also reduce the state (such as the above-mentioned measurement of the polarization of a beam of light).

36.3.2 Quantum projection noise

The intrinsic indeterminism of quantum mechanics has serious consequences for metrology. To show this, we consider the example of a system of two levels $|+\rangle$ and $|-\rangle$. This system can be in a superposition state $|\psi\rangle$. The probability [12] to find the system in one of the two states $|\pm\rangle$ is,

$$p_\pm = \langle \hat{P}_\pm \rangle = |\langle \psi | \pm \rangle|^2 = 1 - p_\mp \ , \tag{36.54}$$

where $\hat{P}_\pm$ is the projection operator. The result of a measurement of the population is afflicted by an inherent uncertainty expressed by the variance,

$$(\Delta p_\pm)^2 = \langle \hat{P}_\pm^2 \rangle - \langle \hat{P}_\pm \rangle^2 = \langle \pm|\psi\rangle\langle\psi|\psi\rangle\langle\psi|\pm\rangle - (\langle \pm|\psi\rangle\langle\psi|\pm\rangle)^2 = p_\pm(1-p_\pm) \ . \tag{36.55}$$

In other words, the random projection of the system on the eigenstate basis induces a noise called *quantum projection noise* [13]. This noise inhibits the determination of the probabilities $p_\pm$ in a single measurement. On the other hand, by measuring populations on a sample of N atoms or by repeating the measurement N times with a single atom under identical conditions, we can reduce the uncertainty. The probability of finding an atom r times in the state $|+\rangle$ is [653],

$$\boxed{P_{N,r,+} = \binom{N}{r} p_+^r (1-p_+)^{N-r}} \ . \tag{36.56}$$

The expectation value and variance of this binomial distribution are [653],

$$\bar{r} = \sum_{r=0}^{N} r P_{N,r,+} = N p_+ \quad , \quad (\Delta r)^2 = \sum_{r=0}^{N} (r - N p_+)^2 P_{N,r,+} = N p_+ (1-p_+) \ . \tag{36.57}$$

[12] We adopt here the viewpoint of the Copenhagen interpretation of the quantum state reduction, but we note that a discussion based on statistical mixtures described by density matrices gives the same results.

[13] Projection noise can be interpreted as *shot noise*. However, the optical shot noise in photodetectors is generated by the repartition of the field energy into discrete photons, the projection noise is the consequence of the discretization of the electronic excitation levels.

Thus, the standard deviation decreases with the number of atoms or measurements,

$$\sigma = \frac{\Delta r}{\bar{r}} \sim \frac{1}{\sqrt{N}} \,. \tag{36.58}$$

The increase of knowledge on the population of a two-level system by repeated measurements can be illustrated by a simple simulation exhibited in Fig. 36.11(a). Experiments are performed by comparing p_2 with a random number η. Two outcomes are possible $r = 0, 1$. The histograms narrow as the number of experiments increases. In practice, a measurement is performed using the quantum amplifier method illus-

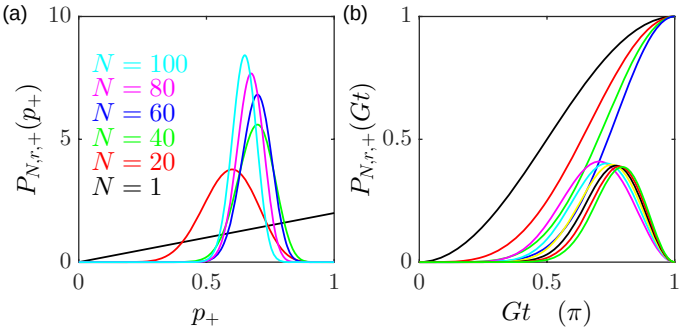

Figure 36.11: (code) (a) Simulation of the increase of knowledge on the population of a two-level system by repeated measurement, $P_{N,r,+}(p_+)/\int_0^1 P_{N,r,+}(p_+)dp_+$. The population of the state $|+\rangle$ was set to $p_+ = 0.2$. (b) Determination of the most likely Rabi pulse length $Gt = 2\arcsin(r/N)^{1/2}$.

trated in Fig. 36.6 [642].

36.3.2.1 Rabi experiments

The method of repeated measurements can be extended to map time-dependent dynamics of the two-level system. Under the influence of a radiation field, the population of the two-level system (which we assume free of spontaneous emission) performs Rabi oscillations, $\rho_{++}(t) = \frac{\Omega^2}{G^2}\sin^2\frac{Gt}{2}$, where $G = \sqrt{\Delta^2 + \Omega^2}$. The probability of finding the system in state $|2\rangle$, therefore, varies in time, $p_+(t) = \rho_{++}(t)$, and the binomial distribution (36.56) becomes,

$$P_{N,r,+}(t) = \binom{N}{r} \left(\tfrac{\Omega}{G}\right)^{2N} \sin^{2r}\tfrac{Gt}{2} \cos^{2N-2r}\tfrac{Gt}{2} \,. \tag{36.59}$$

When we increase the number of measurements, $N \to \infty$, this function condenses around a narrow peak at the position $Gt = 2\arcsin\sqrt{r/N}$. The width of the peak evolves like $2\arccos(2^{-1/2N})$. Fig. 36.11(b) shows a simulation demonstrating how repeated measurements gradually pin down the pulse area Ωt.

In summary, even for perfectly efficient population measurements (e.g. using the microwave-optical double resonance method) it is impossible to measure the probability p_+ with a single atom in a single experiment. As such an observation only

admits two possible results, 'fluorescence observed' or 'fluorescence not observed', i.e. $\rho_{++} = 1$ or $\rho_{++} = 0$, a whole range of possible populations between 0 and 1 is excluded. Therefore, a single observation only provides 'partial' information, which can be gradually improved with each consecutive observation.

A presentation on this topic is available here (watch talk).

36.3.2.2 Ramsey experiments

The Ramsey experiment is basically equivalent to the Rabi experiment described above except for an additional rotation in configuration space allowing for the measurement of the phase precession of the coherence between the Ramsey pulses via population spectroscopy. The Ramsey fringes are approximated by $p_+ = 0.5(1 + \cos[(\omega - \omega_0)T])$. The interesting magnitude is the frequency uncertainty,

$$\frac{\Delta r}{(\partial r/\partial\omega)|_{(\omega-\omega_0)T=\pi/2}} = \frac{\sqrt{Np_+(1-p_+)}}{N(\partial p_+/\partial\omega)} = \frac{1}{T\sqrt{N}} \ . \tag{36.60}$$

36.3.2.3 Spin squeezing and the Heisenberg limit

The above considerations apply to *independent measurements*. When the atoms are maximally correlated they occupy EPR-like states, $|\psi\rangle = p_+|+++..\rangle + p_-|---..\rangle$, such that it is sufficient to measure a single atom to know the state of all others. This means that the ratio $\Delta r/\bar{r}$ is just the one of a single measurement, but the signal strength and hence the signal-to-noise ratio increase by the factor N. Thus the standard deviation scales with $1/N$ rather than with $1/\sqrt{N}$. This is the so-called *Heisenberg limit*. For Ramsey interferometers we get [1380, 166, 184, 885],

$$\frac{\Delta r}{(\partial r/\partial\omega)|_{(\omega-\omega_0)T=\pi/2}} = \frac{1}{TN} \ . \tag{36.61}$$

Example 218 (*Interferometry with condensates*): It is an interesting question, whether condensates can improve metrology and enhance the precision of atomic clocks. The answer is *no*, if we only replace the thermal atomic cloud by a condensate! To see this, we consider an interferometer in configuration space measuring a phase (and therefore a frequency shift) by the method of Ramsey spectroscopy. The states are coupled by a radiation adjusted for $\pi/2$ pulses. The condensate *Fock state* factorizes the Schrödinger equation with the Hamiltonian $\hat{H} = \sum_{i=1}^{N}(H^{(i)} + V_{12}^{(i)})$ into N identical equations for every single atom. The dynamic evolution of this state will be the same as the one for a thermal state. However, this is not true for two Fock state condensates in both entrance channels of the interferometer.

The first radiative beamsplitter divides N_1. This division produces an atom number uncertainty in each state, which come together with a well-defined phase relationship between the two states. By providing at the second port of the interferometer another Fock state N_2, one increases the atom number uncertainty and therefore (because entropy must be conserved in coherent processes) the phase precision. It's a bit like a massive parallel computing for every possible repartition of the populations of both states. Of course the two Fock states cannot be obtained by dividing a single condensate in two in a coherent manner,

except if the repartition is measured afterward.
The Fock state is a maximally *spin-squeezed state* (sub-Poissonian statistics). The beam-splitters (which only perform unitary rotations) create starting from the Fock state a quantum entanglement, which is the deeper reason for the improvement of the resolution of the interferometer up the the Heisenberg limit by reducing the *quantum projection noise* [184].

Quantum correlations and spin-squeezed states are the same phenomena seen in different bases. Often the term of *quantum entanglement* is used in an energy bases, while spin squeezing is described in a Dicke state bases.

We may also consider real space interferometers. This allows us to use for creating the Fock states the recently discovered method of transforming BECs into *Mott insulator* states. Of course it is important to use condensates. First of all, we need Fock states, i.e. states with strong on-site quantum correlations with well-defined phase relations between every pair of atoms from the same site. Furthermore, Mott insulators have thus far only been seen with CBEs. Solve Exc. 36.3.4.4.

36.3.2.4 Noise in light fields

Quantum noise in lasers limit their emission bandwidth to the so-called *Schawlow-Townes limit*, while *shot noise* comes in additionally through the detection process. Let us define the stability by,

$$\boxed{\sigma = \frac{1}{Q}\frac{1}{S/N_{noise}} \qquad \text{with} \qquad Q = \frac{\omega}{\Gamma_{nat}+\Gamma_{pert}}} \ , \tag{36.62}$$

for a laser oscillator optimally stabilized on an atomic resonance with quality factor Q, when we directly detect the fluorescence $S = \Gamma\tau$ (neglecting background). The photon shot noise is then,

$$N_\Gamma = \sqrt{S} = \sqrt{\Gamma\tau} \ . \tag{36.63}$$

Assume now, that we discretize the measurement process, e.g. in order to perform a Ramsey type experiment on a single ion using the *microwave-optical double-resonance* (MODR) detection scheme. The signal is $S = KN$, where K is the number of photons detected on the monitor transition for a single attempt and N is the number of attempts *assumed to be independent*. K and N are both subject to stochastic fluctuations

$$N_{shot} = \sqrt{S} = \sqrt{KN} \qquad , \qquad N_{proj} = K\sqrt{N} \ .$$

We have again the photon shot noise, but we also have *projection noise* [653] due to the random result of the projection of hyperfine resonance coherence. If the MODR detection scheme is cyclic, $K \gg 1$, we may neglect the uncertainty du to photon shot noise. But if not (in the case of $^{171}Yb^+$ a leak in the detection cycle results in $K \lesssim 1$), projection noise will be covered.

Example 219 (*Schawlow-Townes limit*): When a laser is locked to an external cavity, its spectral noise density is,

$$S_r = \frac{\delta\nu^2}{\zeta^2}\frac{4\hbar}{\omega P\eta} \ ,$$

where $\delta\nu/2\pi$ is the cavity linewidth, ζ is a factor accounting for losses in the signal generation, η the quantum efficiency of the detector, and P the light power coupled into the resonator. The corresponding emission bandwidth is,

$$\beta = \frac{\delta\nu^2}{\zeta^2}\frac{\hbar\omega}{P\eta} \ .$$

36.3.3 Quantum non-demolition measurements

36.3.4 Exercises

36.3.4.1 Ex: The quantum Zeno effect

Discuss the quantum Zeno effect at the example of a laser beam passing through a birefringent medium. Compare the situations without polarizers and with an infinite number of vertical polarizers.

Solution: *When we subdivide a rotation into n small rotations by angles of $\pi/2n$, we can calculate, using the Jones matrices, the polarization of the laser beam after its passage through the birefringent medium,*

$$\lim_{n\to\infty}\left[\begin{pmatrix}\cos\frac{\pi}{2n} & -\sin\frac{\pi}{2n}\\ \sin\frac{\pi}{2n} & \cos\frac{\pi}{2n}\end{pmatrix}^n\right]\begin{pmatrix}1\\0\end{pmatrix} = \lim_{n\to\infty}\begin{pmatrix}\cos\frac{\pi}{2} & -\sin\frac{\pi}{2}\\ \sin\frac{\pi}{2} & \cos\frac{\pi}{2}\end{pmatrix}\begin{pmatrix}1\\0\end{pmatrix} = \begin{pmatrix}0\\1\end{pmatrix} \ .$$

Inserting after every tiny rotation a polarizer,

$$\lim_{n\to\infty}\left\{\left[\begin{pmatrix}\cos\frac{\pi}{2n} & -\sin\frac{\pi}{2n}\\ \sin\frac{\pi}{2n} & \cos\frac{\pi}{2n}\end{pmatrix}\begin{pmatrix}1 & 0\\0 & 0\end{pmatrix}\right]^n\right\}\begin{pmatrix}1\\0\end{pmatrix} = \lim_{n\to\infty}\begin{pmatrix}\cos^n\frac{\pi}{2n} & 0\\ \sin\frac{\pi}{2n}\cos^{n-1}\frac{\pi}{2n} & 0\end{pmatrix}\begin{pmatrix}1\\0\end{pmatrix}$$
$$= \lim_{n\to\infty}\begin{pmatrix}1-\frac{n}{2}\left(\frac{\pi}{2n}\right)^2+\ldots\\ \frac{\pi}{2n}-\ldots\end{pmatrix} = \begin{pmatrix}1\\0\end{pmatrix} \ .$$

36.3.4.2 Ex: The quantum Zeno effect

A two-level atom resonantly driven by a laser can be described by the Hamiltonian:

$$H = \begin{pmatrix}0 & \frac{1}{2}\Omega\\ \frac{1}{2}\Omega & 0\end{pmatrix} \ .$$

The solution of the Schrödinger equation gives,

$$|\psi(t)\rangle = e^{-\imath t\hat{H}/\hbar}|\psi_0\rangle = \begin{pmatrix}\cos\frac{1}{2}\Omega t & \imath\sin\frac{1}{2}\Omega t\\ \imath\sin\frac{1}{2}\Omega t & \cos\frac{1}{2}\Omega t\end{pmatrix}\begin{pmatrix}1\\0\end{pmatrix}$$

provided the atom is initially in the ground state $\langle\psi_0| = \begin{pmatrix}1 & 0\end{pmatrix}$. A measurement of the ground state population can only be done by a projection of the wavefunction,

that is, the measurement yields the result $\| |1\rangle\langle 1|\psi(t)\rangle \|^2$. What is the final state of the atom,
a. when the ground state population is measured once after an evolution time of $t = \pi/\Omega$;
b. when the ground state population is measured once after n time intervals $t_n = \pi/n\Omega$;
c. when the ground state population is measured n times after evolution times of $t_n = \pi/n\Omega$;
d. when $n \to \infty$.

Solution: *a. The measurement of the ground state is described by,*

$$|\psi(t)\rangle = |1\rangle\langle 1|e^{-it\hat{H}/\hbar}|\psi_0\rangle = \begin{pmatrix} 1 & 0 \\ 0 & 0 \end{pmatrix} \begin{pmatrix} \cos\frac{1}{2}\Omega t & -\imath \sin\frac{1}{2}\Omega t \\ -\imath\sin\frac{1}{2}\Omega t & \cos\frac{1}{2}\Omega t \end{pmatrix} \begin{pmatrix} 1 \\ 0 \end{pmatrix} = \begin{pmatrix} \cos\frac{1}{2}\Omega t \\ 0 \end{pmatrix}$$

After a time $t = \pi/\Omega$, we obtain $\| |\psi(t)\rangle \|^2 = \cos^2\frac{\pi}{2} = 0$, that is, the atom is inverted.
b. The measurement after n consecutive evolutions during intervals $t_n = \pi/n\Omega$ is,

$$|\psi(t)\rangle = |1\rangle\langle 1| \left(e^{-it_n\hat{H}/\hbar}\right)^n |\psi_0\rangle = \begin{pmatrix} 1 & 0 \\ 0 & 0 \end{pmatrix} \begin{pmatrix} \cos\frac{n}{2}\Omega t & -\imath \sin\frac{n}{2}\Omega t \\ -\imath\sin\frac{n}{2}\Omega t & \cos\frac{n}{2}\Omega t \end{pmatrix} \begin{pmatrix} 1 \\ 0 \end{pmatrix} = \begin{pmatrix} \cos\frac{n}{2}\Omega t \\ 0 \end{pmatrix}$$

After n time periods of $t = \pi/n\Omega$, we have $\| |\psi(t)\rangle \|^2 = \cos^2\frac{\pi}{2} = 0$, which is the same result as above.
c. The repeated measurement of ground state is described by,

$$\begin{aligned} |\psi(t)\rangle &= \left(|1\rangle\langle 1|e^{-\imath t\hat{H}/n\hbar}\right)^n |\psi_0\rangle = \begin{pmatrix} \cos\frac{\pi}{2n} & -\imath\sin\frac{\pi}{2n} \\ 0 & 0 \end{pmatrix}^n \begin{pmatrix} 1 \\ 0 \end{pmatrix} \\ &= \begin{pmatrix} \cos^n\frac{\pi}{2n} & -\imath\sin\frac{\pi}{2n}\cos^{n-1}\frac{\pi}{2n} \\ 0 & 0 \end{pmatrix} \begin{pmatrix} 1 \\ 0 \end{pmatrix} = \begin{pmatrix} \cos^n\frac{\pi}{2n} \\ 0 \end{pmatrix} \end{aligned}$$

Therefore, the probability of finding the atom in the ground state is $\| |\psi(t)\rangle \|^2 = \cos^{2n}\frac{\pi}{2n}$.
d. For an infinite number of measurements,

$$|\psi(t)\rangle = \lim_{n\to\infty} \left(|1\rangle\langle 1|e^{-\imath t\hat{H}/n\hbar}\right)^n |\psi_0\rangle = \lim_{n\to\infty} \begin{pmatrix} \cos^n\frac{\pi}{2n} \\ 0 \end{pmatrix}$$

Therefore, the probability of finding the atom in the ground state is,

$$\| |\psi(t)\rangle \|^2 = \lim_{n\to\infty} \cos^{2n}\frac{\pi}{2n} = \lim_{n\to\infty} \left(1 - \frac{1}{2}\left(\frac{\pi}{2n}\right)^2 + ...\right)^{2n} = \lim_{n\to\infty} \left[1 - \frac{2n}{2}\left(\frac{\pi}{2n}\right)^2 + ...\right] = 1\ .$$

That is, the atom is not excited at all.

36.3.4.3 Ex: The quantum Zeno effect

Consider a system described by a time-independent Hamiltonian $\hat{H}$.
a. Calculate the probability $P(t)$ of the system to remain in its initial state $|\Psi_0\rangle$ in the short time approximation, that is, considering until the second-order expression expansion term for the probability. Use the simplification:

$$\tau_z = \frac{\hbar}{\sqrt{\langle \hat{H}^2 \rangle - \langle \hat{H} \rangle^2}} \ ,$$

where the term τ_z is called the Zeno time.
b. If N measurements are performed during a time t, we have the time interval $T = t/N$ between measurements. When a measurement is performed, the system is projected on the initial state and the temporal evolution must start from zero. Thus, after N measurements, the probability of the system remaining in the initial state is given by $[P(T)]^N$. Show that for an infinite number of measurements, $N \to \infty$, the system remains in the initial state without loss of probability: $[P(T)]^N = 1$. Interpret the result.
c. One of the simplest imaginable systems, a laser-driven two-level system executing Rabi oscillation, is described by the Hamiltonian:

$$\hat{H} = \begin{pmatrix} 0 & \Omega \\ \Omega & 0 \end{pmatrix} \ .$$

Find the expression for τ_z as a function of the Rabi frequency Ω for the initial state $(1 \ \ 0)^\dagger$.
d. Choosing the evolution time $t = 0.01\tau_z \ll \tau_z$ and performing $N = 5$ measurements during this time interval, how likely is the system to remain in the initial state?
e. Let us now include a decay channel for the state $(0 \ \ 1)^\dagger$ with $\Gamma = 4\gamma$, such as to simulate a system with continuous measurement. The system is initially prepared in the state $(1 \ \ 0)^\dagger$. If we now observe emission by decay, it means that the system *left* the initial state. We now have the effective Hamiltonian:

$$\hat{H} = \begin{pmatrix} 0 & \Omega \\ \Omega & -2\imath\gamma \end{pmatrix} \ .$$

For this system, the probability amplitude for the initial state is:

$$\langle \Psi_0 | \Psi(t) \rangle = \frac{1}{2}\left(1 + \frac{\gamma}{\Delta}\right) e^{-(\gamma - \Delta)t/\hbar} + \frac{1}{2}\left(1 - \frac{\gamma}{\Delta}\right) e^{-(\gamma + \Delta)t/\hbar} \ ,$$

with $\Delta = \sqrt{\gamma^2 - \Omega^2}$. For a decay rate $\gamma \ll \Omega$, calculate the probability that the system remains in the initial state. Interpret the result.
Formulas:

$$e^x = 1 + x + \tfrac{x^2}{2} + \mathcal{O}(x^3) \quad , \quad (1-x)^N = 1 - Nx + \mathcal{O}(x^2)$$

$$\cos^2(x) = 1 - x^2 + \mathcal{O}(x^3) \quad , \quad \hat{H} = \begin{pmatrix} 0 & \Omega \\ \Omega & 0 \end{pmatrix} \to e^{-i\hat{H}t/\hbar} = \begin{pmatrix} \cos\frac{\Omega t}{\hbar} & -\imath \sin\frac{\Omega t}{\hbar} \\ -\imath \sin\frac{\Omega t}{\hbar} & \cos\frac{\Omega t}{\hbar} \end{pmatrix} \ .$$

Solution: *a. The initial state is denoted by* $|\Psi_0\rangle$*, the temporal evolution is* $|\Psi(t)\rangle = e^{-\imath\hat{H}t/\hbar}|\Psi_0(t)\rangle$*. The probability amplitude for remaining in the initial state is,*

$$A(t) = \langle\Psi_0|\Psi(t)\rangle = \langle\Psi_0|e^{-\imath\hat{H}t/\hbar}|\Psi_0\rangle$$

Expanding the exponential and considering terms up to second order in t *(see formulas):*

$$A(t) \approx \langle\Psi_0|1 - \frac{i\hat{H}t}{\hbar} - \frac{\hat{H}^2t^2}{2\hbar^2}|\Psi_0\rangle = 1 - \imath\langle\hat{H}\rangle t/\hbar - \langle\hat{H}^2\rangle t^2/2\hbar^2 \ .$$

The probability is:

$$\begin{aligned} P(t) = |A(t)|^2 &= \left(1 - \langle\hat{H}^2\rangle t^2/2\hbar^2 - \imath\langle\hat{H}\rangle t/\hbar\right)\left(1 - \langle\hat{H}^2\rangle t^2/2\hbar^2 + \imath\langle\hat{H}\rangle t/\hbar\right) \\ &= \left(1 - \langle\hat{H}^2\rangle t^2/2\hbar^2\right)^2 + \left(\langle\hat{H}\rangle t/\hbar\right)^2 \ . \end{aligned}$$

Neglecting the term in t^4*:*

$$P(t) = 1 - \langle\hat{H}^2\rangle t^2/\hbar^2 + \langle\hat{H}\rangle^2 t^2/\hbar^2 = 1 - t^2\left(\langle\hat{H}^2\rangle - \langle\hat{H}\rangle^2\right)/\hbar^2 = 1 - t^2/\tau_z^2 \ .$$

b. We have $T = t/N$*, hence,*

$$P(T) = 1 - \frac{t^2}{N^2\tau_z^2} \ ,$$

and,

$$[P(T)]^N = \left(1 - \frac{t^2}{N^2\tau_z^2}\right)^N \simeq 1 - \frac{t^2}{N\tau_z^2} \ ,$$

where we expand the power for large N *and only retain terms of up to first order (see formulas). For* $N \to \infty$*, we have* $[P(T)]^N = 1$*. Thus, if we perform a sufficiently large number of measurements during a time interval* t*, the system stays in the initial state and evolution is inhibited. This is the Zeno Effect.*
c. Building the exponential of the given Hamiltonian (see formulas),

$$e^{-\imath\hat{H}t/\hbar} = \begin{pmatrix} \cos\frac{\Omega t}{\hbar} & -\imath\sin\frac{\Omega t}{\hbar} \\ -\imath\sin\frac{\Omega t}{\hbar} & \cos\frac{\Omega t}{\hbar} \end{pmatrix} \ .$$

The probability amplitude for the state $(1\ ,\ 0)$ *is,*

$$A(t) = \begin{pmatrix} 1 & 0 \end{pmatrix} e^{-\imath\hat{H}t/\hbar}\begin{pmatrix} 1 \\ 0 \end{pmatrix} = \cos\frac{\Omega t}{\hbar} \ .$$

And the probability,

$$P(t) = |A(t)|^2 = \cos^2(\Omega t/\hbar) \simeq 1 - \Omega^2 t^2/\hbar^2 \ ,$$

where we expand the $\cos^2 x$ *for small* t *(see formulas). Comparing with the expression of item (a):*

$$\tau_z = \frac{\hbar}{\Omega}$$

d. With $t \ll \tau_z$*, we expand the power and use the expression already calculated in item (b):*

$$[P(T)]^N = 1 - \frac{t^2}{N\tau_z^2} \ .$$

With $N = 5$ *and* $t = 0.01\tau_z$ *we obtain,*

$$[P(T)]^N = 1 - \frac{0.01^2}{5} = 1 - 2.0 \times 10^{-5} = 0.99998$$

Thus, if we know the Rabi frequency for the driven two-level system, we can choose a sufficiently short time interval and inhibit the evolution of the system.
e. The expression for the probability amplitude has already been given. We have to calculate the probability $P(t) = |A(t)|^2$ *in the limit* $\gamma \gg \Omega$*. Calculating the square of the given expression, we get,*

$$P(t) = \frac{1}{4}\left(1 + \frac{\gamma}{\Delta}\right)^2 e^{-2(\gamma-\Delta)t/\hbar} + \frac{1}{4}\left(1 - \frac{\gamma}{\Delta}\right)^2 e^{-2(\gamma+\Delta)t/\hbar} + \frac{1}{2}\left(1 - \frac{\gamma^2}{\Delta^2}\right) e^{-2\gamma t/\hbar} \ .$$

Looking at the term γ/Δ*, remembering that* $\Delta = \sqrt{\gamma^2 - \Omega^2}$*,*

$$\frac{\gamma}{\Delta} = \frac{1}{\sqrt{1 - \Omega^2/\gamma^2}}$$

As $\gamma \gg \Omega$*, we have* $1 - \Omega^2/\gamma^2 \approx 1$*. Hence,* $\gamma/\Delta \approx 1$*, and we can consider only the first term of the above expression, since:*

$$\left(1 + \frac{\gamma}{\Delta}\right) \gg \left(1 - \frac{\gamma}{\Delta}\right) \quad \textit{and} \quad \left(1 + \frac{\gamma}{\Delta}\right) \gg \left(1 - \frac{\gamma^2}{\Delta^2}\right)$$

Thus, looking at the exponential term:

$$\gamma - \Delta = \gamma(1 - \sqrt{1 - \Omega^2/\gamma^2}) \ ,$$

expanding the root,

$$\gamma - \Delta = \gamma(1 - [1 - \Omega^2/2\gamma^2]) = \Omega^2/2\gamma \ ,$$

we get for the exponential,

$$e^{-2(\gamma-\Delta)t/\hbar} \approx e^{-\Omega^2 t/\gamma\hbar} \ .$$

The multiplicative term is,

$$\frac{1}{4}\left(1 + \frac{\gamma}{\Delta}\right)^2 = \left(\frac{1}{2} + \frac{\gamma}{2\Delta}\right)^2 = \left(\frac{1}{2} + \frac{1}{2\sqrt{1 - \Omega^2/\gamma^2}}\right)^2 = \left(\frac{\sqrt{1 - \Omega^2/\gamma^2} + 1}{2\sqrt{1 - \Omega^2/\gamma^2}}\right)^2 \ .$$

Expanding the root we get,

$$\left(\frac{2-\Omega^2/2\gamma^2}{2(1-\Omega^2/2\gamma^2)}\right)^2 = \left(\frac{2-\Omega^2/2\gamma^2}{2-\Omega^2/\gamma^2)}\right)^2 = \left(1+\frac{\Omega^2/2\gamma^2}{2-\Omega^2/\gamma^2}\right)^2 .$$

Doing $2-\Omega^2/\gamma^2 \approx 2$ *and expanding the power up to first order* ($\Omega/\gamma \ll 1$),

$$\left(1+\frac{\Omega^2/2\gamma^2}{2-\Omega^2/\gamma^2}\right)^2 = \left(1+\frac{\Omega^2}{4\gamma^2}\right)^2 = 1+\frac{\Omega^2}{2\gamma^2} .$$

Finally, the probability is:

$$P(t) = \left(1+\frac{\Omega^2}{2\gamma^2}\right) e^{-\Omega^2 t/\gamma\hbar} .$$

For $t = 0$ *there is a small error in the normalization due to the approximations made. Looking at the exponential term, the probability decay rate is* $t_d = \Omega^2/\gamma\hbar$. *This means that, if we increase* γ, *the probability of the system to leave the initial state decays more slowly.*
Once we prepare the system in the initial state $(1\ ,\ 0)$, *the system starts oscillating between the initial state and the state* $(0\ ,\ 1)$ *with the Rabi frequency* Ω. *In the presence of a decay channel to* $(0\ ,\ 1)$ *with* $\Gamma = 4\gamma$, *intuitively, we expect to observe a faster emission, i.e. the system leaves its initial state sooner when* Γ *is increased. However, due to the quantum Zeno effect, the opposite is true!*

36.3.4.4 Ex: Scaling with the number of measurements

Imagine you have a coin which you suspect to be manipulated so that, when tossed, it doesn't provide a 50% chance to show the face side. Assuming that all flip trials are independent, how many trials are necessary to prove that the probability for "face" is 60%? How many for 51%? What would be necessary to obtain a more favorable scaling with the number of trials?

Solution: *For independent measurements the probability distribution is binomial. In order to detect a deviation of* $\Delta p = 10\%$ *(*1%*) from* $p_+ = \frac{1}{2} = p_-$ *we need to perform enough measurements* N *that*

$$\frac{\Delta r}{r} = \frac{\sqrt{Np_+p_-}}{Np_+} \simeq \tfrac{1}{\sqrt{N}} < \Delta p .$$

That is we need $N = 100$ *(*10000*) measurements. A more favorable scaling necessarily requires some sort of correlation between the trials.*

36.4 Geometric and topological phases

We consider a Hamiltonian $\hat{H}(\mathbf{R}(t))$, which only depends implicitly on time, that is, via some time-dependent parameter $\mathbf{R}(t)$. Then the Hamiltonian evolves by developing a *non-measurable* dynamic phase and additionally accumulates a *geometric phase*

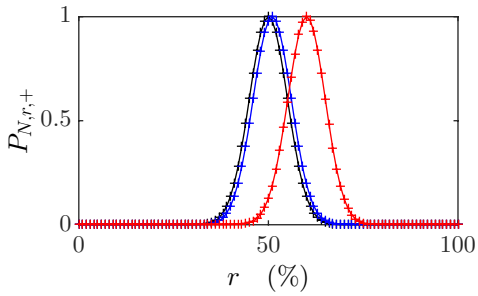

Figure 36.12: (code) Binomial distributions for tossing a coin $N = 100$ times with (black) $p_+ = 0.5$, (blue) $p_+ = 0.6$, and (red) $p_+ = 0.51$.

(also called *topological phase* or *Berry phase*. This geometric phase, which *depends on the trajectory*, is adiabatically followed in parameter space. Let us consider the time-evolution of a state $|\psi(t)\rangle$ [134],

$$\hat{H}|\psi(t)\rangle = \imath\hbar\partial_t|\psi(t)\rangle \ , \tag{36.64}$$

assuming that at any instant of time the system stays in a eigenstate $|n(\mathbf{R})\rangle$,

$$\hat{H}|n(\mathbf{R})\rangle = E_n(\mathbf{R})|n(\mathbf{R})\rangle \ . \tag{36.65}$$

When $\hat{H}$ moves along a trajectory $C : t \to \mathbf{R}(t)$, then we see from,

$$\boxed{|\psi(t)\rangle = \exp\left[-\tfrac{\imath}{\hbar}\int_0^t E_n(\mathbf{R}(t'))dt'\right]\exp(\imath\gamma_n(C))|n(\mathbf{R}(t))\rangle} \ , \tag{36.66}$$

that, while the first exponential describes the standard dynamical phase, the phase $\gamma_n : C \to \gamma_n(C)$ is not integrable, i.e. γ_n cannot be expressed as a function of $\mathbf{R}(t)$ and is not single-valued meaning that from $\mathbf{R}(T) = \mathbf{R}(0)$ we cannot infer $\gamma_n(T) = \gamma_n(0)$. Substituting (36.66) in (36.64), we find,

$$\hat{H}(\mathbf{R}(t))|\psi(t)\rangle = \imath\hbar|\dot{\psi}(t)\rangle = \left(E_n + \imath\hbar\dot{\imath}\dot{\gamma}_n(t) + \imath\hbar\dot{\mathbf{R}}(t)\cdot\nabla_{\mathbf{R}}\right)|\psi(t)\rangle \ . \tag{36.67}$$

Since for a particular eigenstate,

$$\hat{H}(\mathbf{R}(t))|n(\mathbf{R}(t))\rangle = E_n|n(\mathbf{R}(t))\rangle \ , \tag{36.68}$$

we infer,

$$\dot{\gamma}_n(t) = \imath\dot{\mathbf{R}}(t)\cdot\langle n(\mathbf{R}(t))|\nabla_{\mathbf{R}}|n(\mathbf{R}(t))\rangle \ . \tag{36.69}$$

The integrated phase change upon evolution of the state from $|\psi(0)\rangle$ to $|\psi(T)\rangle$ around a closed loop is then,

$$\boxed{\gamma_n(C) = \imath\oint_C \langle n(\mathbf{R})|\nabla_{\mathbf{R}}|n(\mathbf{R})\rangle\cdot d\mathbf{R} \equiv \oint_C \vec{\mathcal{A}}(\mathbf{R})\cdot d\mathbf{R}} \ , \tag{36.70}$$

where $\vec{\mathcal{A}}$ is known as *Berry connection*.

The condition of adiabaticity is essential for emergence of geometric phases. The system always remains in an eigenstate (fixed quantum numbers) when we vary parameters of the environment more slowly than all characteristic constants of the system, even when the Hamiltonian is time-dependent (variable eigenvalues).

36.4.1 Properties of the Berry phase

36.4.1.1 Gauge invariance

We have seen in 23.5.4 that the gauge transformation (??), $U_{cl}(\xi) = e^{-\imath\xi(\mathbf{R})}$, leaves the Schrödinger equation invariant. Applied to an eigenstate,

$$|\tilde{n}(\mathbf{R})\rangle = e^{-\imath\xi(\mathbf{R})}|n(\mathbf{R})\rangle \ , \tag{36.71}$$

the Berry connection becomes,

$$\tilde{\vec{\mathcal{A}}}(\mathbf{R}) = \imath\langle e^{\imath\xi(\mathbf{R})}n(\mathbf{R})|\nabla_{\mathbf{R}}|e^{-\imath\xi(\mathbf{R})}n(\mathbf{R})\rangle = \vec{\mathcal{A}}(\mathbf{R}) + \nabla_{\mathbf{R}}\xi(\mathbf{R}) \ . \tag{36.72}$$

It is apparently gauge-dependent, so that the local Berry connection $\vec{\mathcal{A}}_n(\mathbf{R})$ can never be physically observable. On the other hand, the Berry phase is,

$$\tilde{\gamma}_n(C) = \gamma_n(C) + \int_C \nabla_{\mathbf{R}}\xi \cdot d\mathbf{R} = \gamma_n(C) + \xi(t) - \xi(0) \ . \tag{36.73}$$

For a *closed loop*, continuity of the gauge field requires $\xi(T) - \xi(0) = 2\pi m$. Hence, up to an integer multiple of 2π, *closed loop Berry phases remain gauge-invariant* under arbitrary gauge transformation and may be related to physical observables.

36.4.1.2 Berry curvature

It is often advantageous to convert the path integral (36.70) into a surface integral using Stokes' theorem. Defining the Berry curvature as,

$$\vec{\mathcal{V}}_n(\mathbf{R}) \equiv \nabla_{\mathbf{R}} \times \mathbf{A}_n(\mathbf{R}) \ , \tag{36.74}$$

we obtain,

$$\gamma_n(C) = \iint_S \vec{\mathcal{V}}_n(\mathbf{r}) \cdot d\mathbf{S} \ . \tag{36.75}$$

The Berry curvature can be expressed as [134],

$$\mathbf{V}_n(\mathbf{r}) = \mathrm{Im} \sum_{m\neq n} \frac{\langle n(\mathbf{r})|\nabla_{\mathbf{r}}\hat{H}(\mathbf{r})|m(\mathbf{r})\rangle \cdot \langle m(\mathbf{r})|\nabla_{\mathbf{r}}\hat{H}(\mathbf{r})|n(\mathbf{r})\rangle}{(E_m(\mathbf{r}) - E_n(\mathbf{r}))^2} \ . \tag{36.76}$$

This will be shown in Exc. 36.4.3.1.

Example 220 (*Geometric phase in a two-level system*): We consider the following state [1086],

$$n_\pm(\mathbf{r}) = \cos\theta|g\rangle \pm e^{\pm\imath\phi}\sin\theta|e\rangle \ .$$

Now, we want to calculate the geometric phase,

$$\gamma_\pm = \oint_C \imath\langle n_\pm(\mathbf{r})|\nabla_{\mathbf{r}}|n_\pm(\mathbf{r})\rangle d\mathbf{r} \ .$$

Applying the gradient in spherical coordinates,

$$\nabla_{\mathbf{r}} = \hat{\mathbf{e}}_\theta \frac{1}{r}\frac{\partial}{\partial\theta} + \hat{\mathbf{e}}_\phi \frac{1}{\mathbf{r}\sin\theta}\frac{\partial}{\partial\phi} + \hat{\mathbf{e}}_r \frac{\partial}{\partial r}$$

to the function $|n_+\rangle$, we find,

$$\nabla_{\mathbf{r}}|n_+(\mathbf{r})\rangle = -\hat{\mathbf{e}}_\theta \frac{\sin\theta}{r}|g\rangle + \hat{\mathbf{e}}_\theta \frac{e^{\pm\imath\phi}\cos\theta}{\mathbf{r}}|e\rangle + \hat{\mathbf{e}}_\phi \frac{\imath e^{\imath\phi}}{r}|e\rangle \ ,$$

and,

$$\imath\langle n_\pm(\mathbf{r})|\nabla_{\mathbf{r}}|n_\pm(\mathbf{r})\rangle = \imath\hat{\mathbf{e}}_\phi \frac{\imath\sin\theta}{r} \ .$$

Finally,

$$\gamma_+ = \oint_C \frac{-\sin\theta}{r}\hat{\mathbf{e}}_\phi d\mathbf{R} = \oint_C \frac{-\sin\theta}{r} r\sin\theta d\phi = \oint_C \sin^2\theta\dot{\phi}dt \ .$$

Example 221 (*Berry phase on the Bloch sphere*): We consider the example of a two-level system without decay described by the Bloch vector $\vec{\varrho}$ defined in (34.163) and whose evolution is govern by the Hamiltonian (34.166),

$$\hat{H} = \tfrac{1}{2}\mathbf{G}\cdot\sigma \equiv \begin{pmatrix} \mathfrak{Re}\ \Omega \\ \mathfrak{Im}\ \Omega \\ \Delta/2 \end{pmatrix}\begin{pmatrix} \sigma_x \\ \sigma_y \\ \sigma_z \end{pmatrix} \ .$$

Now, we change the parameters regrouped in $\mathbf{G}$ adiabatically. It is easy to see that,

$$E_\pm = \pm R/2 \qquad \text{and} \qquad \nabla_{\mathbf{G}}\hat{H} = \vec{\sigma}/2 \ ,$$

such that,

$$\mathbf{V}_n(\mathbf{r}) = \mathrm{Im}\frac{\langle n_\pm(\mathbf{G})|\nabla_{\mathbf{G}}\hat{H}(\mathbf{G})|n_\mp(\mathbf{G})\rangle\cdot\langle n_\mp(\mathbf{G})|\nabla_{\mathbf{G}}\hat{H}(\mathbf{G})|n_\pm(\mathbf{G})\rangle}{(E_+(\mathbf{G})-E_-(\mathbf{G})^2} = \pm\frac{\mathbf{G}}{2G^3} \ .$$

The geometric phase accumulated on a closed loop $C = \partial S$ surrounding an area $S = 4\pi\Omega_S$ on the surface of the Bloch sphere is,

$$\gamma_n(C) = \mp\oint_C \frac{dS}{2G^2} = 4\pi \mp \oint_C dR = \mp\frac{\Omega_S(C)}{2}$$

and thus equal to half the enclosed solid angle Ω_S. The Berry phase can be measured in Ramsey experiments, as discussed in Exc. 36.4.3.2.

36.4.1.3 Generalization of the Berry phase according to Aharonov

We will now drop the conditions imposed to the Hamiltonian with regard to its adiabatic behavior and request that the state must be a eigenstate [274]:

$$\hat{H}|\psi(t)\rangle = \imath\hbar|\dot{\psi}(t)\rangle \ . \tag{36.77}$$

A process is cyclic, when there is a τ, such that,

$$|\psi(\tau\rangle = e^{\imath[f(\tau)-f(0)]}|\psi(0)\rangle \ . \tag{36.78}$$

Defining the space of radii by $|\tilde{\psi}(t)\rangle = e^{-\imath f(t)}|\psi(t)\rangle$, we obtain,

$$|\tilde{\psi}(\tau)\rangle = |\tilde{\psi}(0)\rangle \ , \tag{36.79}$$

and from the Schrödinger equation we obtain,

$$f(t) - f(0) = -\tfrac{1}{\hbar}\int_0^t \langle\psi(t)|\hat{H}(t)|\psi(t)\rangle dt + \int_0^t \langle\tilde{\psi}(t)|\imath\tfrac{d}{dt}|\tilde{\psi}(t)\rangle \equiv \delta + \beta \ . \tag{36.80}$$

Therefore, in the space of radii we have a closed curve:

$$\begin{array}{c} C : [0,\tau] \longrightarrow \psi(t) \in \mathcal{H} \\ \downarrow e^{-\imath f(t)} \\ C' : [0,\tau] \longrightarrow \tilde{\psi}(t) \in \mathcal{P} \ . \end{array} \tag{36.81}$$

The dynamic phase δ can be zeroed by an appropriate choice of $\hat{H}(t)$, but not the topological phase β. β does not depend on $\hat{H}(t)$, but is a geometric property of the curve, which projects $\mathcal{H}$ onto $\mathcal{P}$. In contrast to $e^{\imath\beta}$, the phase β is only determined modulo $2\pi n$.

36.4.2 Aharonov-Bohm effect

A particular case for topological phases is the *Aharonov-Bohm effect*, which we will discuss in the following. The only observables of electromagnetism are the forces of Coulomb and Lorentz which, in the theory of electrodynamics, are described by electric and magnetic fields. Electromagnetic potentials can be introduced to simplify calculations, but they are not observables with a physical reality. In contrast, in quantum mechanics, electromagnetic potentials are more fundamental than electromagnetic fields. This is demonstrated by the Aharonov-Bohm effect.

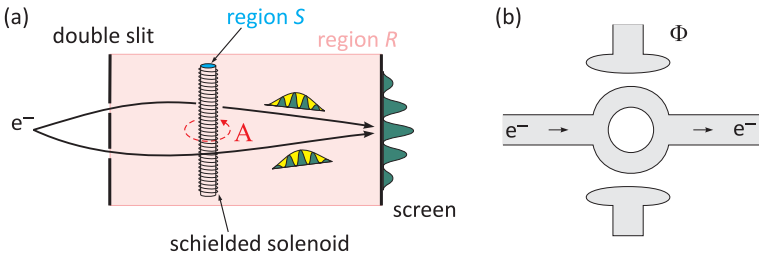

Figure 36.13: (a) Scheme for measuring the Aharonov-Bohm effect. The electrons propagate as wavepackets whose centers-of-mass are not subject to forces, but whose de Broglie waves are phase-shifted by the vector potential. (b) Aharonov-Casher effect: the electrodes Φ do not produce electric fields inside the conductors; even so, one observes constructive or destructive interference at the output of the interferometer, depending on the applied potential.

The idea of this effect is schematized in Fig. 36.13. An electron beam is coherently divided into two arms (e.g. by a double slit) passing both sides of an infinitely extended and perfectly shielded solenoid. In this way the magnetic field $\vec{\mathcal{B}}$ vanishes in the region outside the solenoid, but there must exist nonetheless a potential vector $\mathbf{A}$, because

we observe on the screen an interference pattern of the two arms of the electronic interferometer. When pass a current through the solenoid, we observe a displacement of the interference pattern.

36.4.2.1 Aharonov-Bohm effect and gauge transformation

Let R and S be two disconnected spatial regions. Suppose that the electric and magnetic fields are kept zero in region R. Then, it is *classically impossible* to measure some change in the dynamics of a body confined to the region R resulting from a change of the magnetic field confined to the region S. The Aharonov-Bohm effect shows that the *opposite* is true: Electrons in the magnetic field-free region R do sense magnetic field fluxes in a region S, despite the regions R and S having no intersection!

In the classical theory of electromagnetism, in a region of empty space (except for electric charges and electric currents), the electric $\vec{\mathcal{E}}(\mathbf{r},t)$ and magnetic fields $\vec{\mathcal{B}}(\mathbf{r},t)$ are related to the electric charge $\rho(\mathbf{r},t)$ and current densities $\mathbf{j}(\mathbf{r},t)$ according to the *Maxwell equations*. When we know for a spatial region the sources ρ and $\mathbf{j}$ and the boundary conditions that the fields $\vec{\mathcal{E}}$ and $\vec{\mathcal{B}}$ must fulfill, we can determine the fields as solutions of Maxwell's system of partial differential equations.

In classical electrodynamics, observed from some inertial frame, the electromagnetic force $\mathbf{F}_{em}$ acting on a point-like body with charge q, at position $\mathbf{r}$, and with velocity $\mathbf{v}$, is given by the Lorentz force:

$$\mathbf{F}_{em}(\mathbf{r}(t),t) = q\vec{\mathcal{E}}(\mathbf{r}(t),t) + q\mathbf{v}(t)\times\vec{\mathcal{B}}(\mathbf{r}(t),t)\ . \tag{36.82}$$

Electrodynamic theory affirms the existence of two functions $\Phi(\mathbf{r},t)$ and $\mathbf{A}(\mathbf{r},t)$, such that,

$$\vec{\mathcal{B}}(\mathbf{r},t) = \nabla\times\mathbf{A}(\mathbf{r},t) \qquad \text{and} \qquad \vec{\mathcal{E}}(\mathbf{r},t) = -\nabla\Phi(\mathbf{r},t) - \frac{\partial\mathbf{A}(\mathbf{r},t)}{\partial t}\ . \tag{36.83}$$

Thus, we can use the equations (36.83) to rewrite the Maxwell equations.

The so-defined potentials Φ and $\mathbf{A}$ are not unique, but any Φ and $\mathbf{A}$ leading to the same fields $\vec{\mathcal{E}}$ and $\vec{\mathcal{B}}$, and thus to the same physics, are equivalent. We will, however, fix Φ and $\mathbf{A}$ adopting an additional condition that must be obeyed, i.e. we will adopt a particular gauge. For the discussion of the Aharonov-Bohm effect, we will adopt the *Lorentz gauge* defined by,

$$\nabla\cdot\mathbf{A}(\mathbf{r},t) + \frac{1}{c^2}\frac{\partial\Phi(\mathbf{r},t)}{\partial t} = 0\ , \tag{36.84}$$

where c is the propagation velocity of light in vacuum.

36.4.2.2 Equation for quantum particle exposed to a vector potential A

Assume a particle (without spin) of mass m and charge q, whose wavefunction is confined to a region R (connected by paths). We demand $\Phi = 0$ and $\vec{\mathcal{E}} = 0 = \vec{\mathcal{B}}$, but we let $\mathbf{A}\neq 0$, that is, $\nabla\times\mathbf{A}(\mathbf{r},t) = 0$. Note that along with (36.83) this forces $\mathbf{A}$ to be stationary. According to quantum mechanics the wavefunction Ψ of the particle must obey the following Schrödinger equation:

$$\frac{1}{2m}\left(\frac{\hbar}{\imath}\nabla - q\mathbf{A}(\mathbf{r})\right)^2\Psi(\mathbf{r},t) + V(\mathbf{r})\Psi(\mathbf{r},t) = \imath\hbar\frac{\partial\Psi(\mathbf{r},t)}{\partial t}\ . \tag{36.85}$$

In (36.85) the potential vector $\mathbf{A}$ is present, even if ϕ, $\vec{\mathcal{E}}$, and $\vec{\mathcal{B}}$ are kept zero throughout the region R.

Since the rotation $\mathbf{A}$ vanishes in R, considering that the integral can be calculated for any path contained in R that is deformable to a (arbitrarily chosen) point $O \in R$, we can define the following scalar field:

$$g(\mathbf{r}) \equiv \frac{q}{\hbar} \int_0^{\mathbf{r}} \mathbf{A}(\mathbf{x}) \cdot d\mathbf{x} \ . \tag{36.86}$$

From (36.86) we have:

$$\nabla g(\mathbf{r}) = \frac{q}{\hbar} \mathbf{A}(\mathbf{r}) \ . \tag{36.87}$$

Now, we have already shown in Sec. 23.5.4, that the wavefunction

$$\psi(\mathbf{r}, t) \equiv e^{-\imath g(\mathbf{r})} \Psi(\mathbf{r}, t) \tag{36.88}$$

corresponds to the gauge transform (??) and, given the condition (??), satisfies the same Schrödinger equation as $\Psi(\mathbf{r}, t)$. We showed this explicitly in Exc. 36.4.3.3. Thus, the presence of a potential vector in the region R, even in the absence of fields, causes a phase shift $e^{\imath g(\mathbf{r})}$ of the wavefunction. An interesting issue studied in Exc. 36.4.3.4 is, whether this implies that the freedom of choice of the gauge field is lost.

Example 222 (*Observation of the Aharonov-Bohm effect*): Imagine an electron beam passing through a double-slit, as shown in Fig. 36.13(a). The electronic wavefunction diffracts through both slits, which produces an interference pattern on a subsequent screen. Now, just after the double-slit, in the shade of the region separating the two slits, we place an ideal infinitely long solenoid traversed on its axis by a constant, however, adjustable flux of magnetic field. The magnetic (and also the electric) field of the solenoid is confined to a region S, and the confinement can be guaranteed, e.g. with layers of shielding materials, including superconductors. On the other hand, the wavefunctions of the electrons are manifestly zero in this S region. In the R region, where the electronic wavefunction may be non-zero, the fields are kept zero. R and S have no overlap, both R and S are *separately* connected by paths.
We will show that the flux of the magnetic field in S can be measured through the electronic dynamics in the region R, although the electron is *never* in the region S, but confined to the field-free region R. This is the Aharonov-Bohm (magnetic) effect.
The field $\vec{\mathcal{B}}$ in the inner region of the solenoid is given by (I is the electric current in the wire, N is the density of windings),

$$\vec{\mathcal{B}}(\mathbf{r}, t) = \mu_0 I N \hat{\mathbf{e}}_z \ .$$

Outside the solenoid, that is, for $\rho > a$, we have,

$$\mathbf{A}(\mathbf{r}, t) = \frac{\Phi_B}{2\pi\rho} \hat{\mathbf{e}}_\phi \ ,$$

where $\Phi_B = \pi a^2 B(0, t)$ is the magnetic field flux $\vec{\mathcal{B}}$ through the cross section of the solenoid.
At a point $\mathbf{r}_{sim}$ of the screen, located in the plane of symmetry of the system,

we calculate $g(\mathbf{r}_{sim})$ from Eq. (36.86) for two different paths: both starting at the source and ending at the screen, but one going through the left slit, the other through the right slit:

$$g(\mathbf{r}_{sim}) = \frac{q}{\hbar}\int_0^{\mathbf{r}_{sim}} \mathbf{A}(\mathbf{x})\cdot d\mathbf{x} = \frac{q\Phi_B}{2\pi\hbar}\int\left(\frac{1}{\rho}\hat{\phi}\right)\cdot(\rho\hat{\phi}d\phi) = \pm\frac{q\Phi_B}{2\hbar}\ .$$

The + sign means, that the integration was done in the sense parallel to $\mathbf{A}$, and thus in the sense of I in the solenoid. The sign - holds for the other integration path. The phase difference, at point $\mathbf{r}_{sim}$, between these two paths will be:

$$\delta = \frac{q\Phi_B}{\hbar}\ .$$

That is, the phase difference (experimentally observable via a shift of the interference pattern) is directly proportional to the magnetic field flux $\vec{\mathcal{B}}$, even though the wavefunction is zero in the region S, where the $\vec{\mathcal{B}}$ field is confined. Let us also imagine another situation: Instead of an electron source producing a beam, let us confine an electronic wavefunction on a closed path circling the solenoid at a distance b, but inside the region of R. That is, the electron follows a field line $BA \propto \hat{\mathbf{e}}_\phi$. Then it can be shown, that the flow Φ_B removes the degeneracy of the energy levels of the electron:

$$E_n = \frac{\hbar^2}{2mb}\left(n - \frac{q\Phi_B}{2\pi\hbar}\right)^2\ ,$$

with integer, that is, $n = 0, \pm1, \pm2, ...$ [546].

The *Aharonov-Bohm phase is a (topological) Berry-phase* [134]. This is shown explicitly in Exc. 36.4.3.5.

36.4.2.3 Generalizations of the Aharonov-Bohm effect

The Aharonov-Bohm effect can be generalized to the internal degrees of freedom of a single atom, that is, from real space to configuration space. Let us imagine a Mach-Zehnder interferometer, where one of the arms crosses a constant homogeneous field region. The corresponding Lorentz force $\mathbf{F} = \int d^3r\ \rho(\mathbf{r})\vec{\mathcal{E}}(\mathbf{r}) + \mathbf{j}(\mathbf{r})\times\vec{\mathcal{B}}(\mathbf{r})$ vanishes, but the de Broglie wave undergoes a phase shift $\chi = \int \hat{H}_{int}dt$:

scalar potentials		
$\chi = -\int e\phi dt$	$\nabla\phi = 0$	for e^-
$-\int \mathbf{d}\cdot\vec{\mathcal{E}}dt$	$\nabla\times\vec{\mathcal{E}} = \nabla\cdot\vec{\mathcal{E}} = 0$	Mg, Yb^+
$-\int \vec{\mu}\cdot\vec{\mathcal{B}}dt$	$\nabla\times\vec{\mathcal{B}} = \nabla\cdot\vec{\mathcal{B}} = 0$	n, Yb^+
vector potentials		
$-\oint e\mathbf{A}d\mathbf{r}$	$\nabla\times\mathbf{A} = 0$	e^-, (ABE)
$-\oint d\times\vec{\mathcal{B}}d\mathbf{r}$		?
$-\oint \mu\times\vec{\mathcal{E}}d\mathbf{r}$		n, Ca, (ACE)

Example 223 (*Topological phase in configuration space*): We consider a temporal Ramsey experiment with a single trapped ion by exciting a hyperfine

transition. Between the pulses we apply a magnetic field for a time t. The accumulated phase will be $\phi = (\vec{\mu} \cdot \vec{\mathcal{B}}/\hbar)t$. This phase corresponds to the precession of the dipole moment excited by the first Ramsey pulse. The phase can be interpreted in analogy to Aharonov-Bohm effect, considering that 1. the magnetic field is homogeneous, and 2. despite this fact still acts on the spin, not exerting a force, but causing a phase shift.

36.4.3 Exercises

36.4.3.1 Ex: Derivation of the Berry curvature

Derive the expression (36.76) for the Berry curvature.

Solution: *We rewrite the Berry curvature from its definition (36.74),*

$$\vec{\mathcal{V}}_{n,\mu\nu} = \frac{\partial}{\partial R^\mu}\vec{\mathcal{A}}_{n,\nu} - \frac{\partial}{\partial R^\nu}\vec{\mathcal{A}}_{n,\mu} \ .$$

Using the Stokes theorem and expanding on a basis $\{|m\rangle\}$, we recover the expressions (36.76).

36.4.3.2 Ex: Measurement of the Berry phase in a two-level system

Discuss how the Berry phase in a two-level system can be measured via a Ramsey experiment.

Solution: *Following [12] we consider the Hamiltonian,*

$$\hat{H} = \hbar \begin{pmatrix} \Delta/2 & \Omega \\ \Omega/2 & -\Delta/2 \end{pmatrix} \ .$$

The solution of the Schrödinger equation is $|\psi(t)\rangle e^{-\imath \hat{H} t/\hbar}|\psi(0)\rangle$. The eigenvalue matrix is,

$$\hat{E} = \frac{\hbar}{2} G \hat{\sigma}_z \qquad with \qquad G \equiv \sqrt{\Delta^2 + \Omega^2} \qquad and \qquad \hat{\sigma}_z = \begin{pmatrix} 1 & 0 \\ 0 & -1 \end{pmatrix} \ .$$

The total phase shift after a precession cycle is,

$$\phi = \tfrac{\hat{H}}{\hbar} t = \tfrac{1}{2} G t = \pi \ .$$

The dynamic phase is,

$$\delta = \tfrac{1}{\hbar} \int_0^{2\pi/G} \langle \psi(t)|\hat{H}|\psi(t)\rangle dt = \tfrac{1}{\hbar} \int_0^{2\pi/G} \langle e^{\imath G t/2}\psi(0)|\tfrac{\hbar}{2} G|e^{-\imath G t/2}\psi(0)\rangle dt \ .$$

Starting from the initial state $\psi = \begin{pmatrix} \cos\theta \\ \imath \sin\theta \end{pmatrix}$,

$$\delta = \tfrac{1}{\hbar} \frac{\hbar}{2} \int_0^{2\pi/G} (\cos^2\theta - \sin^2\theta) > dt = -\pi \cos\theta \ .$$

The geometric phase corresponds to the enclosed solid angle,

$$\beta = \phi - \delta = \pi(1 - \cos\theta) = \tfrac{1}{2}\Omega(C) \ ,$$

although the atom is not in an eigenstate and has no adiabatic variation of the parameters.
After a first Ramsey pulse we introduce a short perturbation shifting the energies of the two-levels.

36.4.3.3 Ex: The Aharonov-Bohm effect as a gauge transform

Show explicitly that the wavefunction transformed by a gauge transformation (36.88) satisfies the Schrödinger equation.

Solution: *We assume that the wavefunction $\Psi(\mathbf{r})$ satisfies the Schrödinger equation. The objective is to show that $\psi(\mathbf{r},t) \equiv e^{\imath g(\mathbf{r})}\Psi(\mathbf{r},t)$ also satisfies it. In (36.86) we have,*

$$\nabla g(\mathbf{r}) = \frac{q}{\hbar}\mathbf{A}(\mathbf{r}) \ .$$

Hence,

$$\frac{1}{2m}\left(\frac{\hbar}{\imath}\nabla - q\mathbf{A}(\mathbf{r})\right)^2 \Psi(\mathbf{r},t) + V(\mathbf{r})\Psi(\mathbf{r},t) = \imath\hbar\frac{\partial\Psi(\mathbf{r},t)}{\partial t} \ .$$

In (36.85) the vector potential $\mathbf{A}$ is present, even if ϕ, $\vec{\mathcal{E}}$ and $\vec{\mathcal{B}}$ are kept zero throughout the region R.

36.4.3.4 Ex: Aharonov-Bohm effect and gauge transformation

The phase of the interference pattern in the Aharonov-Bohm effect is fixed by the magnetic flux through the solenoid. Does that mean, that we lose the freedom of choosing an arbitrary gauge potential?

Solution: *No! See the discussion of Griffiths,* Quantum Mechanics*, p.390.*

36.4.3.5 Ex: Aharonov-Bohm effect as a geometric phase

Show that the Aharonov-Bohm effect represents a particular case of a geometric phase.

Solution: *The state of a charge q confined to a volume centered around $\mathbf{R}$ in the vicinity of a magnetic flux line is given by the Schrödinger equation (36.85). That is, in the presence of flux, we may write,*

$$\hat{H}(\hat{\mathbf{r}} - \mathbf{R}, \mathbf{p} - q\mathbf{A}(\hat{\mathbf{r}}))|n(\mathbf{R})\rangle = E_n|n(\mathbf{R})\rangle \ ,$$

with eigenenergies independent of $\mathbf{r}$*. The spatial wavefunction of this state is found by adding a Dirac phase factor,*

$$\langle \mathbf{r}|n(\mathbf{R})\rangle = e^{(\imath q/\hbar)\int_R^r \mathbf{A}(\mathbf{r}')\cdot d\mathbf{r}'}\Psi_n(\mathbf{r}-\mathbf{R}) \ .$$

Now, we calculate the gradient,

$$\begin{aligned}\nabla_{\mathbf{R}}\langle \mathbf{r}|n(\mathbf{R})\rangle &= e^{(\imath q/\hbar)\int_{\mathbf{R}}^{\mathbf{r}} \mathbf{A}(\mathbf{r}')\cdot d\mathbf{r}'}\frac{-\imath q}{\hbar}\mathbf{A}(\mathbf{r})\Psi_n(\mathbf{r}-\mathbf{R}) + e^{(\imath q/\hbar)\int_{\mathbf{R}}^{\mathbf{r}} \mathbf{A}(\mathbf{r}')\cdot d\mathbf{r}'}\nabla_{\mathbf{R}}\Psi_n(\mathbf{r}-\mathbf{R}) \\ &= e^{(\imath q/\hbar)\int_{\mathbf{R}}^{\mathbf{r}} \mathbf{A}(\mathbf{r}')\cdot d\mathbf{r}'}\left(\frac{-\imath q}{\hbar}\mathbf{A}(\mathbf{r}') + \nabla_{\mathbf{R}}\right)\Psi_n(\mathbf{r}-\mathbf{R}) \ ,\end{aligned}$$

and the Berry connection,

$$\begin{aligned}\vec{\mathcal{A}}_n(\mathbf{r}) &= \imath\langle n(\mathbf{r})|\nabla_{\mathbf{R}} n(\mathbf{R})\rangle = \imath\langle n(\mathbf{r})|\int_V d^3r|\mathbf{r}\rangle\langle\mathbf{r}|\nabla_{\mathbf{R}} n(\mathbf{r})\rangle \\ &= \imath\int_V d^3r e^{(-\imath q/\hbar)\int_{\mathbf{R}}^{\mathbf{r}} \mathbf{A}(\mathbf{r}')\cdot d\mathbf{r}'}\Psi_n^*(\mathbf{r}-\mathbf{R})e^{(\imath q/\hbar)\int_{\mathbf{R}}^{\mathbf{r}} \mathbf{A}(\mathbf{r}')\cdot d\mathbf{r}'}\times \\ &\quad\times\left[\frac{-\imath q}{\hbar}\mathbf{A}(\hat{\mathbf{r}})\Psi_n(\mathbf{r}-\mathbf{R}) + \nabla_{\mathbf{R}}\Psi_n(\mathbf{r}-\mathbf{R})\right] \\ &= \frac{q}{\hbar}\int_V d^3r'\Psi_n^*(\mathbf{r}-\mathbf{R})\left[\mathbf{A}(\hat{\mathbf{r}})\Psi_n^*(\mathbf{r}-\mathbf{R}) + \nabla_{\mathbf{r}}\Psi_n^*(\mathbf{r}-\mathbf{R})\right] = \frac{q}{\hbar}\mathbf{A}(\hat{\mathbf{r}}) \ .\end{aligned}$$

Hence, $\gamma_n(C) = \frac{q}{\hbar}\int \mathbf{A}(\mathbf{r}')\cdot d\mathbf{r}'$ *is the geometric Aharonov-Bohm phase. Furthermore, for trajectories around a singularity, it is topological.*

36.5 Frequency metrology and sensing in quantum mechanics

Absolute space and time do not exist. According to the restricted and the general theory of relativity they are interconnected by velocity and they depend on the presence of masses exerted gravitational forces. These relationships and the question how quantum mechanics can be harnessed to improve measurements of time and forces, in particular gravity, will be treated in the following sections.

36.5.1 Atomic clocks

Before we start talking about clocks, we should spend a few words on the physical quantity they are supposed to measure: *time*. In the same way as it is meaningless to talk about space with nothing in it, time is only there, because things are happening. Space is the distance between things and time is nothing else than the distance between events.

In our current physical understanding of the universe the most elementary events are collisions between (real or virtual) particles. Obviously, our universe is full of time. In order to bring any succession of such events into a logical and causal order, a reference time line is needed. It allows for historical book keeping of sequences of

Figure 36.14: (left) 'Time persistence' by Salvatore Dali. (center) Recurrent events. (right) Periodic astronomical cycles.

events, that we may call *histories*. And in order to facilitate a comparison between different histories, this reference time line should follow a simple deterministic rule, e.g. be periodic or exponentially decaying. In fact, both types of processes are currently used for time measurements. E.g. exponential processes, such as radioactive decay is commonly used in radioactive dating.

The most common practical approach to the measurement of time, however, is based on the observation of recurrent phenomena that we think of being periodic, such as a day on Earth, the dripping of a water pipe, or the oscillation of a pendulum or of an atomic excitation. Assuming the time intervals separating the recurrent phenomena as being all the same, we build a ruler for time which we call *clock*.

But now comes a tricky question: How do we know whether a clock is really periodic? In fact, we never know for sure whether the time intervals are really all the same. We only know that some clocks deserve a greater degree of confidence based on the fact that *more care has been taken in their design and construction*, or based on the observation that clocks built in a certain manner tend to deviate less from each other than clocks built in a different manner. The other approach would be to compare several totally *independent* clocks and to give preference to those who deviate less from each other.

An important criterion for a useful clock concerns its duty cycle. The shorter the cycling time, the faster we can extract information from the clock, and the higher is the accuracy we can reach in a given integration time. Ancient time standards had been link to the periodic motion of celestial bodies, e.g. the revolution time of the Earth around the sun. Therefore, clocks with smaller duty cycles have been engineered, such as the clepsydra or the hour glass. But their calibration to periodical astronomical cycles remained tedious and slow. Historically, the development of ever precise clocks has been motivated by navigation. Indeed, 1 minute of inaccuracy in the clock generates an uncertainty of 28 km in global positioning. And this motivation still prevails nowadays, although, meanwhile, atomic clocks are reaching uncertainties of below 10^{-18} and extremely short duty cycles on the order of femto-seconds.

The left part of Fig. 36.15 shows the basic idea of any human-made clock, which consists in locking an oscillating mechanism, whose time constant can be manipulated,

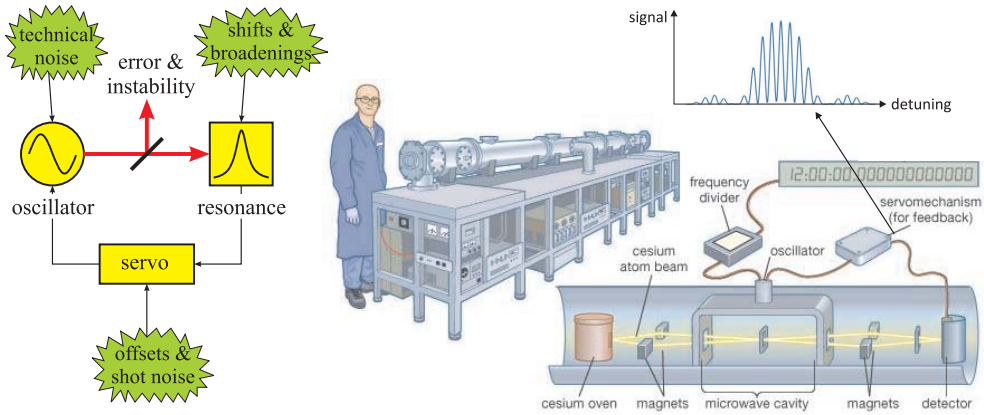

Figure 36.15: (left) Principle of any clock and possible perturbations. (right) Cesium beam atomic clock and Ramsey interference fringes.

for instance a pendulum or a laser, by a very precise periodic process, that we call *resonance*. This resonance can be an astronomic period or the transition of an atomic between two states of excitation. Expressing the stability of a clock that can be obtained in a given integration time as,

$$\sigma = \frac{\Gamma_{nat} + \Gamma_{pert}}{\omega} \frac{1}{S/N_{noise}} \ , \tag{36.89}$$

we see that we better look for oscillators and resonances operating at high frequencies ω, having very narrow widths Γ_{nat}, being subject to very weak perturbations and line broadenings Γ_{pert}, and delivering a good signal-to-noise ratio. The right part of Fig. 36.15 shows the concept of a cesium beam *atomic clock*. A microwave oscillator operating at $\omega/2\pi = 9.1\,\mathrm{GHz}$ excites cesium atoms passing through a microwave cavity thus generating in a detector a frequency-dependent error signal which can be used to correct the oscillator frequency.

36.5.2 Gravitational red-shift

Clocks and gravimeters are intrinsically related the gravitational redshift. The *gravitational red-shift* is that phenomenon in which electromagnetic waves or photons traveling out of a gravitational well (seem to) lose energy. This loss of energy corresponds to a decrease in the wave frequency and increase in the wavelength. Gravitational redshift can be interpreted (i) as a consequence of the *equivalence principle* stating that gravity and acceleration are equivalent and the redshift is caused by the Doppler effect. It can also be understood (ii) as a consequence of the mass-energy equivalence stating that 'falling' photons gain energy (though there are numerous subtleties that complicate a rigorous derivation). Finally, it can be understood (iii) in terms of gravitational time dilation at the source of the radiation: an oscillator (producing electromagnetic radiation) will seem to 'tick' faster when exposed to a stronger gravitational potential.

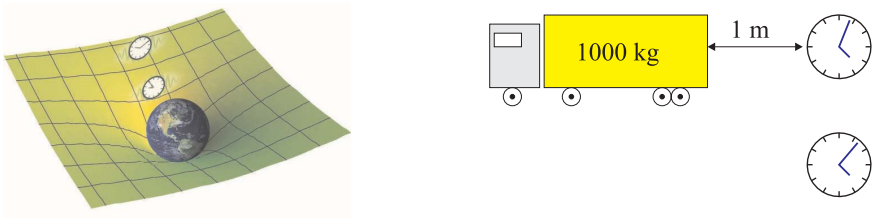

Figure 36.16: Gravitational redshift is due to the dilation of time near heavy masses.

To first approximation, the gravitational redshift is proportional to the difference in gravitational potential. In a homogeneous field(see Sec. ??),

$$\frac{\Delta\nu}{\nu} = \frac{\Delta\lambda}{\lambda} \simeq \frac{g\Delta z}{c^2} \ , \tag{36.90}$$

where Δz is the change in height. Accounting for the accompanying gravitational time dilation affecting the atomic clock in the satellite is crucially important for accurate navigation. For this reason, *metrology* of time and *gravimetry* are closely interrelated. Do the Exc. 36.5.4.1.

Example 224 (*Prediction by the equivalence principle and general relativity for a uniform gravitational field or acceleration*): Einstein's theory of general relativity incorporates the equivalence principle, which can be stated in various different ways. One such statement is that gravitational effects are locally undetectable for a free-falling observer. Therefore, in a laboratory experiment at the surface of the earth, all gravitational effects should be equivalent to the effects that would have been observed if the laboratory had been accelerating through outer space at g. One consequence is a gravitational Doppler effect. If a light pulse is emitted at the floor of the laboratory, then a free-falling observer says that by the time it reaches the ceiling, the ceiling has accelerated away from it, and therefore when observed by a detector fixed to the ceiling, it will be observed to have been Doppler shifted toward the red end of the spectrum. This shift, which the free-falling observer considers to be a kinematic Doppler shift, is thought of by the laboratory observer as a gravitational redshift. Such an effect was verified in the 1959 Pound-Rebka experiment. Since this prediction arises directly from the equivalence principle, it does not require any of the mathematical apparatus of general relativity, and its verification does not specifically support general relativity over any other theory that incorporates the equivalence principle.

36.5.3 Quantum sensing

Let us first define what we mean by a *sensor* in general before discussing what quantum mechanics has to do with it. A *sensor* is a device, module, machine, or subsystem whose purpose is to detect events or changes in its environment and send the information to other electronics, frequently a computer processor. Progress in engineering, science, medicine, and other disciplines is unavoidably conditioned to sensing: What

you cannot measure, you cannot improve! In many areas of applications, however, conventional sensing techniques have met fundamental limitations, and novel disruptive approaches are required in order to reach higher sensitivity and precision.

In many cases, limitations are imposed by the macroscopic, i.e. *classical*, nature of the sensor, and much can be gained by using microscopic sensors. These however, follow different rules of physics given by *quantum mechanics*. Nuclear magnetic resonance spectroscopy (NMR), magnetic resonance imaging, and the development of transistors, LEDs, solar panels, and lasers are examples of technologies developed during the first so-called quantum revolution in the 20th century, which was based on the exploitation of the particle-wave duality. However, the full potential of quantum mechanics goes much further. Today *quantum sensing* is, together with quantum computation and quantum communication (see Sec. 41.6.5), one of the key technologies anticipated to drive the quantum revolution 2.0.

Let us discuss the disruptive role of quantum mechanics at the example of an *atom*, which is a paradigmatic example for a sensor subject to quantum laws. The reasons for this are numerous: (i) Because all atoms of a given species are strictly identical (that is, indistinguishable in the quantum statistical sense) they can be used in different sensing devices, places and countries. We do not need to duplicate reference standards, such as the Original Meter or the Original Kilogram safely kept in Paris. We simply recommend to people wishing to construct their own clock standard to gather cesium atoms (wherever you can find them) and try to excite the 9.1 GHz hyperfine transition (with whatever technique you prefer). In the end, you just need to prove that your clock is sufficiently good. (ii) Some atomic species have ultranarrow transitions outperforming any imaginable artificial device by many orders of magnitude, which makes them ideal candidates for clock resonances. (iii) Atoms can easily be moved in space with extremely high precision, which makes them suitable for matter wave interferometers, which are useful for the measurement of distances and the sensing of forces.

The main reason, however, for the superiority of atoms (and other quantum devices, such as SQUIDs, quantum dots or nitrogen-vacancy (NV) centers in diamond) with respect to classical objects in sensing applications is, that they can exist in superposition states (of their internal excitation or of their center-of-mass motion) whose evolution delicately depends on external parameters, such as forces. We can now define a *quantum sensor* as a measurement device exploiting quantum correlations in order to enhance sensitivity and resolution, f.ex. quantum superpositions or entanglement [343]. Typically its core is a single atomic two-level system (or any other kind of qubit), whose superposition states (i) are sensitive to some environment parameter, (ii) can be manipulated in a controlled way, and (iii) can be read out.

In fact, quantum sensors already exist since the invention of atomic clocks and matter wave interferometers, which build on the control and detection of quantum states in individual qubits, even though in practice, most of these device are operated with large incoherent ensembles of qubits. Even if perturbations related to uncontrolled inter-qubit interactions (collisions, thermal excitations, etc.) can be avoided, the sensitivity that can be reached with such ensembles is bound to the standard quantum limit imposed by quantum projection noise (see Secs. 36.3.2 and 41.1.4). Novel approaches investigate the possibilities of overcoming these limits via the creation of strong interparticle correlations via entanglement, spin-squeezing [1380], or

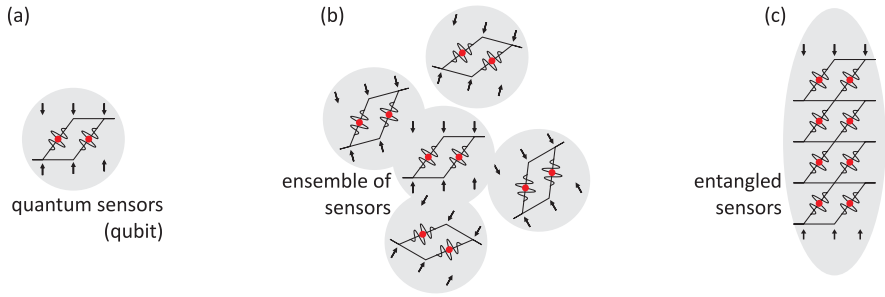

Figure 36.17: (left) Single qu-bit. (center) Larger signals can be observed using ensemble of qu-bits. (right) Collective manipulations on entangled qu-bits allow precisions beyond the standard quantum limit.

superradiant lasing [1005]. Such correlations have been created with atoms, which therefore qualify as building blocks of quantum computers or sensing devices capable of overruling the standard quantum limit.

36.5.3.1 Working principle of a quantum sensor

As mentioned above, in order to measure a weak force it is not sufficient to sense it, one also has to read the result. In the field of atom optics, this can conveniently be done with light fields taking the information from an atom isolated in a vacuum chamber to the macroscopic world. In order not to loose information already at the level of the light-atom interaction, one generally tries to avoid dissipation and keep the interaction coherent [14].

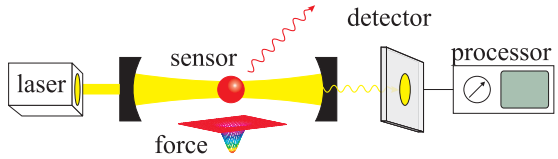

Figure 36.18: Taking information from the sensor to the detector.

A typical quantum sensor can be described by the generic Hamiltonian [343],

$$\hat{H}(t) = \hat{H}_{qbit} + \hat{H}_{cntrl}(t) + \hat{H}_{int}(t) \ , \tag{36.91}$$

composed of a (known) internal Hamiltonian $\hat{H}_{qbit}$, a control Hamiltonian $\hat{H}_{cntrl}$ allowing to manipulate or tune the sensor, and a signal Hamiltonian $\hat{H}_{int}$ allowing to pass information about the state of the system to the outside world.

Typically, the internal Hamiltonian is static and defines the energy eigenstates $|0\rangle$ and $|1\rangle$,

$$\hat{H}_{qbit} = E_0|0\rangle\langle 0| + E_1|1\rangle\langle 1| \ . \tag{36.92}$$

[14] E.g. by using two-level systems not subject to motion, collisions, spontaneous emission, etc.. Sometimes spontaneous emission can be controlled by confining both, the atom and the interrogating light field, in a cavity.

The qubit internal Hamiltonian may contain additional interactions, such as couplings to other qubits or time-dependent stochastic terms due to interactions with an environment.

Many quantum sensing protocols require to manipulate the qubit either before, during, or after the sensing process. This is achieved via a control Hamiltonian, which allows implementing a sequence of appropriate quantum gates, such as the Hadamard gate or Pauli X and Y gates. These gates are nothing else than what, in the language of atom interferometry is known as $\pi/2$ or π-pulses around different axes. Advanced sensing schemes employing more than one sensor qubit may further require conditional gates, especially controlled-NOT gates to generate entanglement, swap gates to exploit memory qubits, and controlled phase shifts in quantum phase estimation (see Sec. 41.6). Finally, the control Hamiltonian can include control fields for systematically tuning the transition frequency $\hbar\omega_0 = E_1 - E_2$.

Finally, the signal Hamiltonian represents the coupling between the sensor qubit and a signal $V(t)$ to be measured. When the signal is weak (which is assumed here) $\hat{H}_{int}$ adds a small perturbation to the internal Hamiltonian. The signal Hamiltonian can then be separated into two qualitatively different contributions,

$$\hat{H}_{int} = \hat{H}_{int,\parallel} + \hat{H}_{int,\perp} \ , \tag{36.93}$$

where $\hat{H}_{int,\parallel}$ is the parallel (commuting) and $\hat{H}_{int,\perp}$ the transverse (non-commuting) components, respectively. The two components can quite generally be captured by,

$$\begin{aligned} \hat{H}_{int,\parallel} &= \tfrac{\gamma}{2} V_\parallel(t)[|1\rangle\langle 1| - |0\rangle\langle 0|] \\ \hat{H}_{int,\perp} &= \tfrac{\gamma}{2}[V_\perp(t)|1\rangle\langle 0| + V_\perp^\dagger(t)|0\rangle\langle 1|] \ , \end{aligned} \tag{36.94}$$

where γ is the coupling or transduction parameter of the qubit to the signal $V(t)$. Examples of coupling parameters include the Zeeman shift parameter or the Stark shift parameter of electric dipoles in an electric field. The parallel and transverse components of a signal have distinctly different effects on the quantum sensor. A commuting perturbation $\hat{H}_{int,\parallel}$ leads to shifts of the energy levels and an associated change of the transition frequency ω_0. A non-commuting perturbation $\hat{H}_{int,\perp}$, by contrast, can induce transitions between levels, manifesting through an increased transition rate. Most often, this requires the signal to be time-dependent (resonant with the transition) in order to have an appreciable effect on the quantum sensor.

An important class of signals are vector signal $\mathbf{V}(t)$, in particular, those provided by electric or magnetic fields. The interaction between a vector signal and a qubit can be described by the signal Hamiltonian,

$$\hat{H}_{int} = \gamma \mathbf{V}(t) \cdot \hat{\vec{\sigma}} \ , \tag{36.95}$$

where $\hat{\vec{\sigma}}$ is the vector of Pauli matrices (23.46). For a vector signal, the two signal functions $V_\parallel(t)$ and $V_\perp(t)$ are,

$$\begin{aligned} V_\parallel(t) &= V_z(t) \\ V_\perp(t) &= V_x(t) + \imath V_y(t) \ , \end{aligned} \tag{36.96}$$

where the z-direction is defined by the qubit's quantization axis. The corresponding signal Hamiltonian,

$$\hat{H}_V(t) = \gamma\hat{\sigma}_x \mathfrak{Re}\ V_\perp(t) + \gamma\hat{\sigma}_y \mathfrak{Im}\ V_\perp(t) + \gamma\hat{\sigma}_z V_\parallel(t) \ , \tag{36.97}$$

is just the one of the Rabi model extensively discussed in Sec. 34.4.

36.5.3.2 Sensing forces by matter wave interferometry

Matter wave interferometry is ideal for sensing weak forces or sensing strong forces with high precision. Many interferometers employ the Ramsey scheme, which consists in sandwiching the sensing Hamiltonian between two $\pi/2$-control Hamiltonian pulses $\hat{H}_{cntrl}$ preparing and reading out the atomic coherence. Between the pulses (or interaction zones), the atomic coherence is influenced by the parallel part of the sensing Hamiltonian $\hat{H}_{int,\parallel}$.

The basic idea is the following: One takes a matter wave and lets it fall in the Earth's gravitational field. But before that, apply a laser pulse separating the matter wave into two parts taking different paths. Thus, the Broglie waves of the two parts will accumulate different phases, which results in an interference pattern when the waves are superimposed again. As illustrated in Fig. 36.19, the matter wave interferometry works similarly to the Ramsey method used in atomic clocks with the difference that in the former the trajectories of the atomic center-of-mass motion must be separated in real space as much as possible (see Sec. 34.4.5 on Ramsey pulses and NMR, Sec. 24.1.3 on gravity with Excs. 23.5.6.2 and 23.5.6.3, Sec. 47.2.2 on Bragg interferometry and photon echos with Excs. 47.2.4.1) [15].

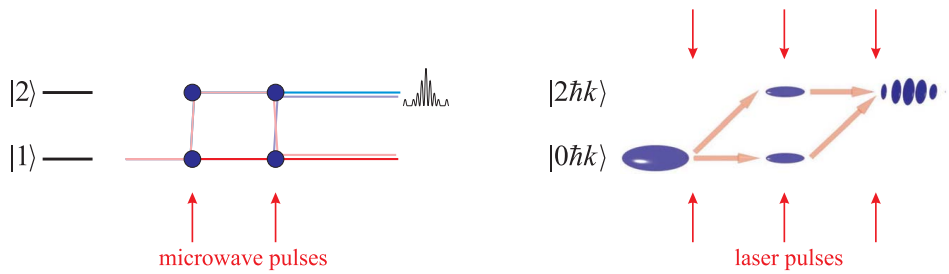

Figure 36.19: Difference between clocks and interferometers. (left) Ramsey-type clock. (right) Ramsey-Bordé interferometer. A movie can be seen at (watch movie).

A particularly smart way to do matter wave interferometry is via the observation of Bloch oscillations of matter waves in a periodic lattice (see Sec. 26.2.2). The Bloch oscillations can be understood in the following picture: A resting atom has infinite de Broglie wavelength. Being constantly accelerated by gravity, the matter wave reduces its de Broglie wavelength from ∞ to a value, where it becomes commensurate with the periodicity of the standing light wave potential. At this moment Bragg scattering comes into play, reflecting the atomic motion back into upward direction, and the process starts over again. The atoms evolve like jumping on a trampoline with a frequency given,

$$\nu_{blo} = \frac{mg}{2\hbar k_{lat}} \ . \tag{36.98}$$

[15] See also Sec. 53.5 and 54.5 on interferometric and spectroscopic techniques.

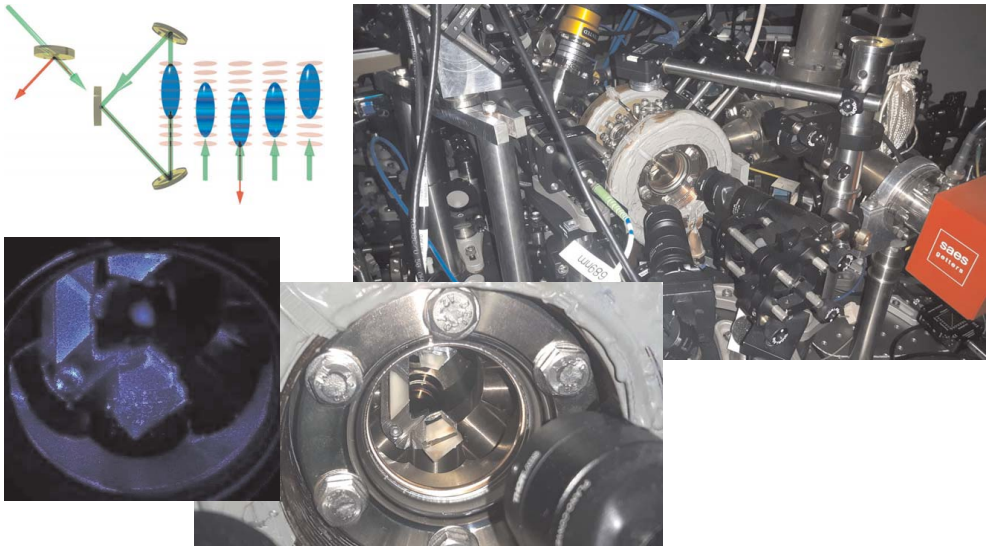

Figure 36.20: Working principle and pictures of the Sr Bloch oscillation interferometer constructed at the IFSC, USP.

36.5.4 Exercises

36.5.4.1 Ex: Red-shift of sun light and on Earth

a. Calculate the gravitational redshift of light escaping from the sun.
b. Calculate the blue-shift of navigational signals from GPS satellites orbiting at 20000 km altitude with respect to the surface of Earth. Compare it to the Doppler shift resulting from their orbital velocity.
c. In astronomy, the magnitude of a gravitational redshift is often expressed as the velocity that would create an equivalent shift through the relativistic Doppler effect. Calculate the sunlight redshift and the GPS signal blue-shift in terms of this velocity.

Solution: *a. Light escaping from the surface of the sun was predicted by Einstein in 1911 to be red-shifted by roughly* $2 \cdot 10^{-6}$.
b. The signals emitted from GPS satellites are perceived as blue-shifted by approximately $5 \cdot 10^{-10}$ *corresponding to an increase of less than* 1 Hz *in the frequency of a* 1.5 GHz *signal.*
c. In such units, sunlight redshift corresponds to a 633 m/s *receding velocity, roughly of the same magnitude as convective motions in the sun, thus complicating the measurement. In astronomical objects with strong gravitational fields the redshift can be much greater; for example, light from the surface of a white dwarf is gravitationally red-shifted on average by around* 50 km/s/c.

36.6 Further reading

P.L. Saldanha et al., *Inconsistency of a realistic interpretation of quantum measurements a simple example* [1133]DOI

B. Hacker et al., *Deterministic creation of entangled atom-light Schrödinger-cat states* [566]DOI

36.6.1 on quantum jumps

A. Schenzle et al., *Macroscopic quantum jump in a single atom* [1152]DOI

A. Schenzle et al., *Possibility of quantum jumps* [1154]DOI

W. Nagourney et al., *Shelved Optical Electron Amplifier: Observation of Quantum Jumps* [943]DOI

P. Zoller et al., *Quantum jumps in atomic systems* [1440]DOI

T. Erber et al., *Resonance Fluorescence and Quantum Jumps in Single Atoms, Testing the Randomness of Quantum Mechanics* [418]DOI

J. Dalibard et al., *Wave-Function Approach to Dissipative Processes in Quantum Optics* [321]DOI

K. Mølmer et al., *Monte-Carlo Wave-Function Method in Quantum Optics* [913]DOI

Z. K. Minev et al., *To catch and reverse a quantum jump mid-flight* [901]DOI

36.6.2 on projection noise

R.H. Dicke, *Coherence in Spontaneous Radiation Processes* [366]DOI

M. Kitagawa et al., *Spin-squeezed states* [724]DOI

W.M. Itano et al., *Quantum projection noise: Population fluctuations in two-level systems* [653]DOI

D.J. Wineland et al., *Squeezed atomic states and projection noise in spectroscopy* [1380]DOI

Ph. Bouyer et al., *Heisenberg-Limited Spectroscopy with Degenerate Bose-Einstein Gases* [184]DOI

R. Huesmann et al., *Single-Atom Interferometry* [642]DOI

L. Salvi et al., *Squeezing on Momentum States for Atom Interferometry* [1135]DOI

36.6.3 on sensing

A.D. Cronin et al., *Optics and interferometry with atoms and molecules* [310]DOI

L. Pezzè et al., *Quantum metrology with nonclassical states of atomic ensembles* [1026]DOI

D. Braun et al., *Quantum-enhanced measurements without entanglement* [191]DOI

J. Kitching et al., *Atomic sensors - A review* [725]DOI

C.L. Degen et al., *Quantum sensing* [343]DOI

36.6.4 on geometric phases

M.V. Berry, *Quantal Phase Factors Accompanying Adiabatic Changes* [134]DOI

Y. Aharonov et al., *Significance of Electromagnetic Potentials in the Quantum Theory* [13]DOI

E. Cohen et al., *Geometric phase from Aharonov-Bohm to Pancharatnam-Berry and beyond* [274]DOI

Chapter 37

Nonlinear optics

The discipline of *nonlinear optics* studies phenomena that occur as a consequence of modifications of the optical properties of materials by the presence of light. Such modifications are appreciable only, when the interacting light is sufficiently intense, i.e. of the order of the interatomic electric field,

$$\mathcal{E}_{at} = \frac{e^2}{4\pi\varepsilon_0 a_B^2} \simeq 5.14 \cdot 10^{11}\,\mathrm{V/m}\ , \tag{37.1}$$

which explains that nonlinear effects could only be studied properly after the advent of the laser.

In general, light-matter interaction is expressed through the relationship between the polarization induced in the medium, $\mathcal{P}(\omega)$, with the optical light field, $\mathcal{E}(\omega)$. In linear optics this relation can be expressed as,

$$\tilde{\mathcal{P}}(\omega) = \varepsilon_0 \chi(\omega)\tilde{\mathcal{E}}(\omega)\ . \tag{37.2}$$

But in the perturbative regime of non-linear optics this expression must be generalized to a series of powers of the electric field,

$$\tilde{\mathcal{P}}(\omega) = \varepsilon_0[\chi^{(1)}(\omega)\tilde{\mathcal{E}}(\omega) + \chi^{(2)}(\omega)\tilde{\mathcal{E}}^2(\omega) + \chi^{(3)}(\omega)\tilde{\mathcal{E}}^3(\omega) + ...]\ , \tag{37.3}$$

so that higher order polarization terms, $\mathcal{P}^{(n)}(\omega) = \varepsilon_0\chi^{(n)}\mathcal{E}^N(\omega)$, are considered. Therefore, the phenomena are non-linear in the sense that they depend non-linearly on the optical field applied to the material. In a more complete treatment, in terms of the optical properties of materials, $\tilde{\mathcal{P}}$ and $\tilde{\mathcal{E}}$ are vector fields and the electric susceptibility is a tensor. However, to simplify the treatment, we consider the fields as scalars and $\chi^{(n)}$ as constants independent of the frequency ω.

Examples of non-linear optical phenomena are: parametric processes of sum and difference frequency generation, as shown in Fig. 37.1, optical parametric oscillation, and the dependence of the refractive index with the optical intensity. Examples of non-parametric processes are: multi-photonic absorption, stimulated Raman scattering, and saturated absorption. In the latter example, the absorption coefficient of the material decreases with increasing light intensity:

$$\alpha = \frac{\alpha_0}{1 + I/I_s}\ . \tag{37.4}$$

Saturated absorption is an example where a perturbative approach is not capable of providing good results, and its most reliable description is given by the approximation of a two-level quantum system.

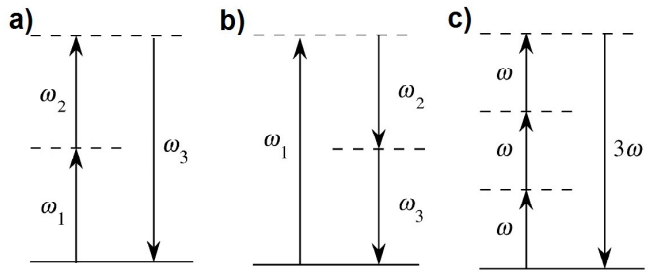

Figure 37.1: Parametric (a) sum and (b) difference frequency generation. (c) Third harmonic generation.

It is also important to emphasize that parametric processes are those, in which the initial and final quantum states of a system are identical. Consequently, the population of an initial state can only be moved to a virtual state, different in energy by ΔE, for a short time lapse limited by Heisenberg's uncertainty principle ($\hbar/\Delta E$). Nonparametric processes are those involving population transfer between real energy levels, eigenstates of the system's Hamiltonian. In terms of the electrical susceptibility of the medium, $\chi^{(n)}$ is a real quantity for parametric and an imaginary one for non-parametric processes.

37.1 The nonlinear optical susceptibility

The description of nonlinear optical phenomena can be approached from a variety of perspectives, most of which are semi-classical in the sense that the matter is treated quantum mechanically, while the electromagnetic radiation is treated classically. One possible description explores the wave nature of the radiation, using Maxwell's equations to describe the generation of new spectral components by the nonlinear terms of the polarization. More generally, this description explains how different frequencies can be coupled through their nonlinear interaction with the material. It can be shown that the electromagnetic wave equation in the nonlinear regime is,

$$\nabla\tilde{\mathcal{E}} - \frac{n^2}{c^2}\frac{\partial^2}{\partial t^2}\tilde{\mathcal{E}} = \frac{1}{\varepsilon_0 c^2}\frac{\partial^2}{\partial t^2}\tilde{\mathcal{P}} \ , \tag{37.5}$$

such that $\tilde{\mathcal{P}} = \tilde{\mathcal{P}}^{(1)} + \tilde{\mathcal{P}}^{nl}$. In this view, $\tilde{\mathcal{P}}^{nl}$ acts as a source of frequencies, several of that are incident.

Although electromagnetic theory is capable of explaining several aspects of nonlinear optics, it is the quantum description that provides explicit expressions for nonlinear optical susceptibility. There are three main motivations for obtaining quantum expressions:

- They reveal a functional form of the nonlinear optical susceptibility and show how they depend on microscopic parameters of the material, such as transition dipole moments and atomic energy levels.
- They exhibit the intrinsic symmetries of nonlinear susceptibility.

- They can be used to calculate numerically the values of nonlinear susceptibilities.

The numerical predictions of quantum theory for nonlinear optical susceptibilities are particularly accurate in the case of atomic vapors, because the atomic parameters of these are known with sufficient precision for the theory to provide reliable results.

Two quantum mechanical formalisms can be used for the calculation of nonlinear optical susceptibilities. Perturbation theory is used to make predictions on non-resonant systems, i.e. situations where the photon energy is much smaller than the energy separation between two eigenstates of the material. On the other hand, when the interactions are close to resonance, such that it becomes necessary to include relaxation processes, the state-density matrix formalism is used. Although this approach is more complex, it provides better results.

37.1.1 Expansion of the nonlinear susceptibility

In non-linear anisotropic media the *susceptibility* $\chi(\vec{\mathcal{E}})$ can depend on the electric field in a complicated manner. Often it is possible to expand it in orders of the field amplitude,

$$\boxed{\begin{array}{rcl} \chi(\vec{\mathcal{E}}) & = & \chi^{(1)}\vec{\mathcal{E}} + \chi^{(2)}\vec{\mathcal{E}} : \vec{\mathcal{E}} + \chi^{(3)}\vec{\mathcal{E}} : \vec{\mathcal{E}} : \vec{\mathcal{E}} + ... \\ \text{with} \quad (\chi^{(n)}\vec{\mathcal{E}}^n)_\mu & = & \sum_{\nu_1,...,\nu_n} \chi^{(n)}_{\mu,\nu_1,...,\nu_n} \vec{\mathcal{E}}_{\nu_1} ... \vec{\mathcal{E}}_{\nu_n} \end{array}} , \tag{37.6}$$

where μ and ν are components of Cartesian coordinates. That is, all the products in the first line of equation (37.6) are, in fact, tensor products. In isotropic media, only the first-order susceptibility contributes. We can Fourier transform in equation (37.2) the polarization $\vec{\mathcal{P}}$ and the field amplitude $\vec{\mathcal{E}}$. Since the susceptibilities $\chi^{(n)}$ are time-dependent, in the frequency domain the product turns into a convolution,

$$\vec{\mathcal{P}}(\mathbf{r}, t) = \int_{-\infty}^{\infty} e^{-\imath\omega t} \vec{\mathcal{P}}(\mathbf{r}, \omega) dt \ , \tag{37.7}$$

where $\vec{\mathcal{P}}^*(\mathbf{r}, \omega) = \vec{\mathcal{P}}(\mathbf{r}, -\omega)$.

Hence,

$$\vec{\mathcal{P}}(\mathbf{r}, \omega) = \sum_{n=1}^{\infty} [\chi^{(n)} * \vec{\mathcal{E}}(\mathbf{r}) * ... * \vec{\mathcal{E}}(\mathbf{r})](\omega) \tag{37.8}$$

$$= \sum_{n=1}^{\infty} \int_{\mathbb{R}^n} \chi^{(n)}(-\omega, \omega_1, ..., \omega_n) * \vec{\mathcal{E}}(\mathbf{r}, \omega_1) * ... * \vec{\mathcal{E}}(\mathbf{r}, \omega_n) \delta(\omega - \omega_1 - ... - \omega_n) d\omega_1 ... d\omega_n \ .$$

The δ-function expressed energy conservation. For the susceptibilities holds,

$$\chi^*(-\omega, \omega_1, ..., \omega_n) = \chi(\omega, -\omega_1, ..., \omega_n) \ . \tag{37.9}$$

There is a $n = 0$ term, which disappears for isotropic media...! Eq. (37.8) only holds in the dipole approximation, since $\mathbf{r}$ is supposed equal on both sides (local response).

Now, we suppose for $\vec{\mathcal{E}}(t) = \frac{1}{2}\sum_{\omega>0}(\vec{\mathcal{E}}_\omega e^{-\imath\omega t} + \vec{\mathcal{E}}_{-\omega} e^{\imath\omega t})$ a sum of monochromatic waves. Then we must substitute in Eq. (37.7) $\vec{\mathcal{E}}(\omega) = \frac{1}{2}\sum_{\mu_i} \vec{\mathcal{E}}_{\mu_i}\delta(\omega - \mu_i)$:

$$\begin{aligned}\vec{\mathcal{P}}(\mathbf{r},\omega) &= \sum_{n=1}^{\infty} \sum_{\mu_1,...,\mu_n} \tfrac{1}{2^n}\chi^{(n)}(-\omega,\mu_1,...,\mu_n)\vec{\mathcal{E}}_{\mu_1}...\vec{\mathcal{E}}_{\mu_n}\delta(\omega-\mu_1-...-\mu_n) \qquad (37.10)\\ &= \sum_{n=1}^{\infty} \sum_{\substack{\omega_1,\,...,\,\omega_n \\ \omega_1+...+\omega_n=\omega}} \tfrac{1}{2^{n-1}}\chi^{(n)}(-\omega,\omega_1,...,\omega_n)\vec{\mathcal{E}}_{\omega_1}...\vec{\mathcal{E}}_{\omega_n}\ .\end{aligned}$$

The frequencies ω_i do not have to be all different, but the modes can also differ by their polarizations. We have,

$$\chi^*(-\omega,\omega_1,\omega_2,...,\omega_n) = \chi(-\omega,\omega_2,\omega_1,...,\omega_n)\ . \qquad (37.11)$$

Therefore we can, using the number of permutations $n!/m_1!m_2!...$, where $m_1, m_2, ...$ are the numbers of equal frequencies $\omega_1, \omega_2, ...$, rewrite the sum in Eq. (37.10),

$$\sum_{\substack{\omega_1,\,...,\,\omega_n \\ \omega_1+...+\omega_n=\omega}} = \sum_{\substack{\omega_1,\,...,\,\omega_n \\ \omega_1+...+\omega_n=\omega \\ \omega_1\le...\le\omega_n}} \frac{n!}{m!}\ . \qquad (37.12)$$

From stationary perturbation theory we can deduce,

$$\chi^{(n)}(-\omega_{n+1},\omega_n,...,\omega_1) = \frac{N}{n!V\varepsilon_0\hbar^n}\sum_i \rho(E_i)\overline{M_{ii}^{(n+1)}}\ , \qquad (37.13)$$

where the transition hyperpolarizability is,

$$\begin{aligned}M_{fi}^{(n+1)} = \mathrm{Tr}\ \langle f|\hat{\epsilon}_{n+1}\cdot\hat{\mathbf{d}}\ G(E_i+\omega_1+...+\omega_{n-1}+\omega_n)\times \qquad (37.14)\\ \times\ \hat{\epsilon}_n\cdot\hat{\mathbf{d}}\ G(E_i+\omega_1+...+\omega_{n-1})\times...\times\hat{\epsilon}_1\cdot\hat{\mathbf{d}}\ G(E_i+\omega_1)|i\rangle\ .\end{aligned}$$

Here $G(\omega) \equiv \sum_i \int \frac{|A_i\rangle\langle A_i|}{\omega - E_\ell}$ is the photon propagator for the intermediate level $|A_\ell\rangle$. γ_{fi} describes thus the temporal succession of the absorption processes of the photons ω_1 to ω_n.

Since after the total process the atoms again needs to be in the initial state $|A_i\rangle$ we have $\omega_{n+1} = \omega_1 + ... + \omega_n$. The permutation operator described in (37.12) guarantees that every permutation of intermediate states appears in the sum. The matrix element $M_{fi}^{(n)}$ also appears in the transition probability $1/\tau$.

Here are a few nonlinear processes and their susceptibilities:

absorption and stimulated emission	$\chi^{(1)}(-\omega;\omega)$
two-photon emission	$\chi^{(1)}(-\omega;\omega)$
spontaneous Rayleigh or Raman scattering	$\chi^{(1)}(-\omega;\omega)$
self focusing and defocusing (nonlinear index of refraction)	$\chi^{(3)}(-\omega;\omega,-\omega,\omega)$
phase conjugation	$\chi^{(3)}(-\omega;\omega,-\omega,\omega)$
stimulated Rayleigh or Raman scattering (CARS)	$\chi^{(3)}(-\omega;\omega_s,-\omega_s,\omega)$
Kerr effect	$\chi^{(3)}(-\omega;\omega_s,-\omega_s,\omega)$
third harmonic generation	$\chi^{(3)}(-3\omega;\omega,\omega,\omega)$
four wave mixing (4WM)	$\chi^{(3)}(-\omega;\omega_1,\omega_2,\omega_3)$
hyper Raman scattering	$\chi^{(3)}$
two-photon absorption	$\chi^{(3)}(-\omega;\omega_s,-\omega_s,\omega)$
enhanced spontaneous emission	

37.1.1.1 Non-linear spectroscopy

Several light field create in an atom a dielectric polarization $\hat{\mathbf{d}}$. The polarization of the medium is calculated via $\vec{\mathcal{P}} = \frac{N}{V}\mathrm{Tr}\,\hat{\rho}\hat{\mathbf{d}}$. Hence, the density operator must be calculated from the non-linear Bloch equations. It can be expanded in perturbation orders of susceptibilities, $\vec{\mathcal{P}} = \sum_n \chi^{(n)}\vec{\mathcal{E}}_1 \cdot ... \cdot \vec{\mathcal{E}}_n$. The polarization radiates a light field according to $\Box\vec{\mathcal{E}}_d = \ddot{\vec{\mathcal{P}}}$.

37.1.2 Four-wave mixing

Assume motionless atoms. In a gas cell, a non-linear polarization develops,

$$\mathcal{P}(\omega) = \chi^{(1)}(\omega)\mathcal{E}_p(\omega) + \chi^{(3)}(\omega)\mathcal{E}_s^*(\omega_s)\mathcal{E}_p(\omega)\mathcal{E}_s(\omega_s)\ . \tag{37.15}$$

The *four-wave mixing* (4WM) procedure by $\chi^{(3)}(\omega)$ can be interpreted as a perturbation series,

$$\rho_{22} \xrightarrow{\mathcal{E}_s} \rho_{21} \xrightarrow{\mathcal{E}_s^*} \rho_{11} \xrightarrow{\mathcal{E}_p} \rho_{02} \xrightarrow{\mathcal{P}} \rho_{00}\ . \tag{37.16}$$

The time-reversed undergoing *phase-conjugation* wave is perfectly anti-collinear and has the same frequency. The phase-matching condition $\mathbf{k}\mathbf{k}_s \to 1$ must only hold for one-photon transitions. For two-photon transition arbitrary $\mathbf{k}\mathbf{k}_s$ are acceptable.

The *coherent anti-Stokes Raman scattering* (CARS) is related to 4WM. Phase-matching is necessary if the atomic states are unchanged by the process.

37.1.3 Optical parametric oscillator

An *optical parametric oscillator* is a device exhibiting a resonance, which driven with a specific phase lag displays amplification. The optical parametric oscillators (OPO) and the *optical parametric amplifier* (OPA) are common devices of nonlinear optics. In quantum language terms like $\hat{a}^\dagger\hat{c}^\dagger$, which describe the creation of entangled pairs of particles are typical for OPAs.

37.1.4 Optical bistability

The phenomenon of *optical bistability* can be observed in lasers and passive cavities [886]. Optical bistability can also be induced by atomic motion [942].

37.1.4.1 Dispersive bistability

Consider a ring cavity with a two-level medium inside resonantly pumped by a laser. The *dispersive optical bistability* is easily explained as the medium under the influence of the pump laser shifting the refractive index and thus the cavity resonance away from the incoupled laser beam, so the pump transmission ceases. Assume the phase shift is $\beta = \beta_0 + \beta_2 I_T$. The transmitted intensity follows an Airy-function, which close to resonance resembles a Lorentzian,

$$\frac{I_T}{I} = \frac{1}{1 + R\beta^2/T^2} \tag{37.17}$$

or,

$$I = I_T \left[1 + (\beta_0 + \beta_2 I_T)^2 \, R/T^2\right] \ . \tag{37.18}$$

This expression gives the typical bistable curve.

37.1.4.2 Absorptive bistability

The *absorptive optical bistability* occurs upon bleaching of the medium. With $\alpha = \alpha_0/(1 + I_T)$,

$$\frac{I_T}{I} = \frac{1}{(1 + \alpha l/T)^2} \tag{37.19}$$

or,

$$I = I_T \left[1 + \frac{\alpha_0 l}{T(1 + I_T)}\right]^2 \ . \tag{37.20}$$

This expression gives the typical bistable curve.

37.1.5 Exercises

37.2 Quantum interference

We have seen earlier that a *dark resonance* in Λ-shaped three-level systems create superposition states between the two stable ground states which allow the adiabatic elimination of the excited state. Dark resonances may be understood as destructively interfering excitation paths at Raman-coherences between inneratomic transitions. Quantum interference is at the origin of various other phenomena which are discussed in the following sections.

37.2.1 Lasing without inversion

The question of the necessity of population inversion to construct a laser has been the subject of debates. Indeed, even an ordinary two-level system may exhibit gain with a small frequency interval [911] known as *Mollow gain*. Lasing without population inversion may also result from a splitting of emission and absorption spectra caused by atomic recoil as in the example of CARL [173].

Various schemes of a *laser without inversion* (LWI) have been proposed. Here is one of them [947]. We will discuss an example in Exc. 37.2.7.1.

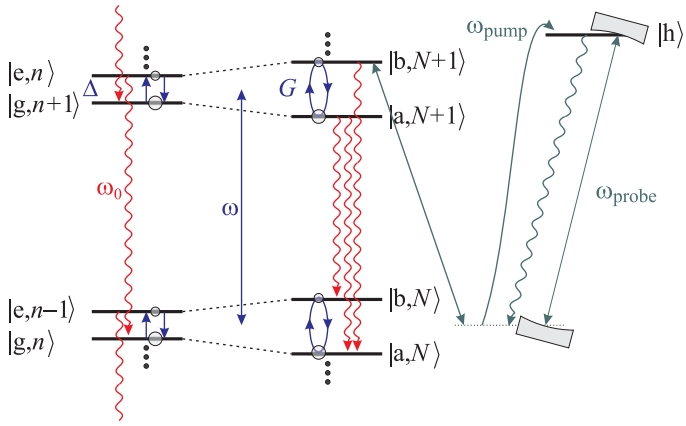

Figure 37.2: Dressed states level scheme for LWI. Quantum interference between two possible Raman transitions (green) leads to a cancellation of the ground state population. When the upper level $|h\rangle$ is incoherently pumped, gain can be reached for a weak probe field. Inserting the atoms in a cavity one can reach lasing [636].

37.2.2 Correlated spontaneous emission lasing

In a V-shaped three-level system in which the excited levels are coherently coupled, the spontaneous emission is correlated under certain circumstances. This feature may be used to suppress the relative noise beneath the shot noise limit and has triggered the idea of *correlated spontaneous emission* (CEL) lasing. The CEL is described by a complicated laser theory. Various simplifications allow to boil it down to an *Adler-Langevin equation* (this is similar to simplifying CARL into Kuramoto), describing the evolution of the phase difference $\theta \equiv \theta_1 - \theta_2$ between the lasers,

$$\frac{d\theta}{dt} = a - b\sin\theta + \xi_1(t) + \xi_2(t) \tag{37.21}$$
$$\langle \xi_k(t) \rangle = 0 \qquad \text{and} \qquad \langle \xi_k^\dagger(t)\xi_l(s) \rangle = 2D_{kl}\delta(t-s) \ ,$$

where a is the frequency difference and b the coupling constant.

For the case of purely additive noise $D_{k\neq l} = 0$ [1161], the equation is identical to the Kuramoto equations for two coupled oscillators, as shown in Sec. 42.6.4. This case which describes the *phase-locked laser* (PLL) is a Kuramoto system. The CEL in

contrast is defined by the fact that the noise is multiplicative (maximum correlation is obtained for $D_{11} + D_{22} = 2\mathfrak{Re}\ D_{12}$).

The fact that the laser coupling reduces the drift of $\theta(t)$ leading to a stationary value $\theta(\infty)$ is not necessarily due to CEL, but already occurs in Kuramoto systems. In fact phase-locking may occur independently from phase noise reduction. For interferometric purposes noise reduction without locking is preferable [1251].

37.2.2.1 Stochastic modulation peak

The random occurence of quantum jumps gives rise to a sharp Lorentzian peak called *stochastic resonance* on top of a fluorescence peak [594].

37.2.3 Superluminal group velocity

The *phase velocity* $v_{ph} = \omega/k$ of Fourier components of a light pulse is certainly not limited to the speed of light. But even the group velocity can, in highly non-dispersive media exceed the speed of light $v_g = d\omega/dk > c$, or even be negative. The *superluminal group velocity* without deformation of the pulse shape has been observed [762] via double-peaked Raman amplification. It has been argued that a properly defined *signal velocity* of signal transfer is limited by increased quantum noise to the subluminal regime, $v_s < c$.

37.2.4 Dark-state polaritons

We consider a gaseous medium made up of λ-shaped three-level system whose one transition is driven by a low-atomnumber photonic quantum field and the other by a classical laser. We define collective slowly-varying atomic operators, setup the Hamiltonian, write down the propagation equation for the optical field Heisenberg operators in the slowly-varying amplitude approximation and the Heisenberg-Langevin equation for the atomic evolution. If we assume very low photonnumbers in the optical quantum mode, and a rather slow variation of the classical mode Rabi frequency (perturbative and adiabatic approximation), we obtain simple equations describing the propagation of the light pulse and the atomic excitation. The canonical transformation to the bosonic quasi-particle quantum field allows the interpretation of the propagating perturbation in terms of the *dark-state polariton* [455]. This type of polaritons can be viewed as mixtures of photonic and Raman-like matter branches.

The propagation velocity depends on the classical control field, which should allow the slowing, stopping and reaccelerating of the light pulse [586, **?**], where we define the propagation velocity as $v_g = (d\mathcal{E}/dt)/(d\mathcal{E}/dz)$. This is achieved by mapping the shape of the light pulse, i.e. the photonic quantum correlations, to collective atomic (internal) (Raman) coherences. This does not require degeneracy of the external atomic states. We have seen the transfer of coherence between different types of degrees of freedoms earlier at the example of quantum collaps and revival in Jaynes-Cummings type couplings.

Unlike solitons polaritons are not shape-dependent. Look up analogy to excitons in solids !

Particularly interesting is the possible use of dark-state polaritons for creating non-classical atomic quantum states, entangling distant atomic samples, studying quan-

tum scattering in systems involving coherent cold collisions and investigating their impact collective excitations of the center-of-mass motion like solitons and vortices.

37.2.5 Brillouin scattering

Stimulated scattering of phonons is called *stimulated Brillouin scattering* (SBS). Like *Raman-scattering* (SRS) Brillouin-scattering is a limiting factor for the transmission efficiency in optical fibers. It is used in acousto-optic modulators (AOM). While SBS is based on the exchange of phonons between atoms bound in crystals, SRS is based on the exchange of phonons between atoms bound in molecules.

Raman-scattering (in a restricted historical sense) is very common technique of molecular spectroscopy. The process is Rayleigh-scattering at an electronic transition, but towards a different vibrational substate. Brillouin-scattering also involves the motional state of the scatterer, but its center-of-mass motion rather than some internal degree of freedom. It is also related to *polariton scattering* in solids, which produces optical phonons, rather than acoustic phonons.

If a strong electromagnetic field (pump laser) is irradiated into a medium (typically a crystal or a fluid) it produces a time-varying *electrostrictive strain*, which can be understood as the reaction force of particles dislocated from their equilibrium position. The strain is quantized into *phonons* and may drive a sound wave. This wave modulates the optical dielectric constant ε and thus create a periodic polarization $\vec{\mathcal{P}}$. This polarization may now interact with the incident electric field (pump laser $\omega_2, \mathbf{k}_2, \vec{\mathcal{E}}_2$). The resulting energy exchange can, under suitable circumstances, lead to simultaneous amplification of a probe wave $(\omega_2, \mathbf{k}_2, \vec{\mathcal{E}}_2)$ and a sound wave $(\omega_s, \mathbf{k}_s, u_s)$.

Let us consider a $1D$ geometry, $\mathbf{k}_j = k_j \hat{\mathbf{e}}_z$ and $\vec{\mathcal{E}}_j = \mathcal{E}_j \hat{\mathbf{e}}_x$. (More general geometries can be considered [1407]). The pump field $\mathcal{E}_2(t,z)$ causes a strain $\partial u_s/\partial z$ via longitudinal displacements $u_s(z,t)$ of test volumes. This strain produces a modulation of ε by $\delta\varepsilon = -\gamma \partial u_s/\partial z$, where γ is the strain coefficient (or coupling strength). The modulation of the dielectric constant $\delta\varepsilon$ now modulates the interaction energy $\delta U = -\frac{1}{2}\delta\varepsilon \mathcal{E}_2$, which exerts work $p\partial u_s/\partial z = \delta U$ against the pressure p. The pressure modulation creates a force $F = -\partial p/\partial z = \frac{1}{2}\gamma \partial \mathcal{E}_2^2/\partial z$. We can now set up a Fokker-Planck type force equation,

$$\rho \frac{\partial^2 u_s}{\partial t^2} = \frac{\gamma}{2}\frac{\partial \mathcal{E}_2^2}{\partial z} - \eta \frac{\partial u_s}{\partial t} + T \frac{\partial^2 u_s}{\partial z^2} \ , \tag{37.22}$$

where ρ is the mass density, T the elastic constant and η acoustic dissipation. $v_s \equiv \omega_s/k_s = \sqrt{T/\rho}$ is the free propagation velocity of sound. Simultaneously we know that the light wave propagates like,

$$\frac{\partial^2 \mathcal{E}_j}{\partial z^2} + \mu\varepsilon \frac{\partial^2 \mathcal{E}_j}{\partial t^2} + \mu \frac{\partial^2 \mathcal{P}_{NL,j}}{\partial t^2} \ . \tag{37.23}$$

We insert the ansatz $\mathcal{E}_j(t,z) = \frac{1}{2}\mathcal{E}_{0j}(z) e^{\imath(\omega_j t - k_j z)} + c.c.$ and $u_s(t,z) = \frac{1}{2} u_{0s}(z) e^{\imath(\omega_s t - k_s z)} + c.c.$ first into the above equations. We use the approximations $k_s^2 u_s \gg d^2 u_s/dz^2 \ll k_s du_s/dz$ and $|\partial(\mathcal{E}_2 \mathcal{E}_1^*)/\partial z| \ll |k_s \mathcal{E}_2 \mathcal{E}_1^*|$ and focus on the real parts. Assuming that the pump field $\mathcal{E}_2$ is undepleted, stimulated Brillouin-scattering is described by the

following set of equations,

$$\frac{d\mathcal{E}_1^*}{dz} = -\frac{\alpha}{2}\mathcal{E}_1^* - \frac{\gamma k_1 k_s}{4\varepsilon_1}\mathcal{E}_2^* u_s \qquad (37.24)$$
$$\frac{du_s}{dz} = -\frac{\eta}{2\rho v_s}u_s - \frac{\gamma}{8\rho v_s^2}\mathcal{E}_2\mathcal{E}_1^* \ .$$

Here ρ is the mass density, optical losses are described by α, and η is the dissipation constant for phonons. $\varepsilon_1 \approx \varepsilon_0$. The scattering satisfies the *Bragg condition* $\mathbf{k}_2 - \mathbf{k}_1 = \mathbf{k}_s$. The above equations describe *exponential gain* and *threshold behavior* for $\mathcal{E}_1$ and u_s. For backscattering $\mathbf{k}_1\mathbf{k}_2 = -k_1 k_2$ the rate of growth for the probe $\mathcal{E}_1$ is influenced by the values of $\mathcal{E}_1$ lying ahead in the direction $\mathbf{k}_1$. This is by virtue of the sound beam propagating in opposite direction to E_1 and provides the positive feedback being at the origin of exponential gain.

The equations are reminiscent to the CARL equations. The difference is the nature of the mediating force field: The CARL force is mediated by photons. The mediation is thus instantaneous. Photons do not require a medium in order to propagate. In contrast, the Brillouin-gain is mediated by phonons. Phonons propagate through a gas by collisions. Sound needs a medium to propagate. In dilute gases where CARL is observed, collisions are totally neglegible. Brillouin-scattering may lead to bunching, which propagates along $\mathbf{k}_s$. But similar to water waves, which do not transport the water molecules, the bunching does not lead to a net transport of atoms.

Just like CARL and the superradiant Rayleigh scattering in BECs SBS can be understood as being mediated by dipole-dipole interactions (i.e. the exchange of real or virtual photons between atoms). In a BECs SBS can be interpreted as phonon-like excitations (smaller momentum transfer) due to dipole-dipole interactions [514], while CARL are particle-like excitations due to dipole-dipole interactions (the nature of scattered particles changes from recoiling atoms to phonons). Note that while ultralow temperatures are necessary, these effects are not base on superfluidity, i.e. binary collisions. Thus the speed of sound is not the Bogolubov sound. The question is whether quantum degeneracy plays a role.

37.2.6 Selective reflection spectroscopy

The considered system is light at the interface of a dielectric and a gas phase. The gas may influence the reflection behavior of the light [165, 1206, 953, 1028], but the light may also influence the atomic excitation and motional state.

The range of interesting questions include: 1. The gas may absorb resonant light from an evanescent wave, it should be possible to image this. 2. Non-resonant light is phase-shifted by the gas and in the same time generates a dipole potential. Is it possible to do phase-contrast imaging. 3. Light force in near-fields: What is the force acting on atoms: $\mathbf{S}$ or $\mathbf{k}$? The response may be tested via the Goos-Hänchen shift.

The propagation direction of the phase fronts of a field $\arctan \frac{\Im\mathfrak{m}\ \mathcal{E}}{\Re\mathfrak{e}\ \mathcal{E}} = kz - \omega t$ may be different from the flux $\mathbf{S} = \vec{\mathcal{E}} \times \vec{\mathcal{B}}$. In the evanescent wave $\mathbf{k}$ is parallel to the surface [1233].

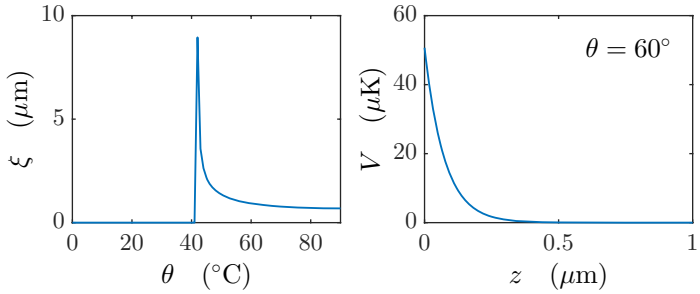

Figure 37.3: (code) Evanescent wave.

37.2.6.1 Fresnel's formulas

The reflected light comes from interference of reflection at the interface and the gas polarization [953]. The reflection at the interface is given by the Fresnel formulae, the response of the gas polarization is labeled S,

$$\vec{\mathcal{E}}_1(\mathbf{r}) = \mathcal{E}_0 \begin{pmatrix} \frac{2nb}{n\beta+b}\sin\phi \\ \frac{2nb}{nb+\beta} \\ -\frac{2nb}{n\beta+b}\cos\phi \end{pmatrix} \quad \text{and} \quad \vec{\mathcal{E}}_2(\mathbf{r}) = \mathcal{E}_0 \begin{pmatrix} \frac{n\beta-b}{n\beta+b}\sin\phi \\ \frac{nb-\beta}{nb+\beta} \\ -\frac{n\beta-b}{n\beta+b}\cos\phi \end{pmatrix} + S \begin{pmatrix} \frac{\beta^2-\alpha^2}{n\beta+b} \\ \frac{1}{nb+\beta} \\ \frac{\beta^2-\alpha^2}{n\beta+b} \end{pmatrix} . \tag{37.25}$$

For small angles of incidence ϕ (partial reflection, no evanescent wave) $\beta = \sqrt{1-n^2\sin^2\phi}$ is real. Then,

$$S = \frac{\imath k}{\epsilon_0}\int_0^\infty dz_0 e^{\imath\beta k z_0}\mathcal{P}_0(z_0) \ , \tag{37.26}$$

is the sum of the contributions of the polarizations at different places shifted by the displacement factor $e^{\imath\beta k z_0}$ away from the surface. In the evanescent case, S is the Laplace transform of the polarization at different phases kz_0 yields the spectrum of the response arising from different penetration depths $\imath\beta$.

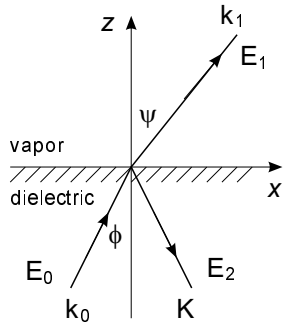

Figure 37.4: Selective reflection.

The polarization at a given location,

$$\frac{1}{\epsilon_0 \mathcal{E}_1}\mathcal{P}_0(z) = \frac{\hbar\Omega N}{I_1}\int d^3\mathbf{v} W(\mathbf{v}) e^{\imath\beta kz}\left[\theta(v_z)\sigma_+(\mathbf{v}, z/v_z) + \theta(-v_z)\bar{\sigma}_+(\mathbf{v})\right] \ . \quad (37.27)$$

The Maxwell-Boltzmann velocity distribution $W(\mathbf{v}) = \left(3/2\pi v_0^2\right)^{3/2} e^{-3\mathbf{v}^2/2v_0^2}$ is normalized, where mean velocity $v_0 = \sqrt{k_B T/m}$. The definition of the Laplace transform is,

$$\hat{\sigma}_+(\mathbf{v}, s) = \int_0^\infty dt e^{-st}\sigma_+(\mathbf{v}, t) \ . \quad (37.28)$$

Solution of two-level Bloch equations,

$$s\hat{\sigma}_+(\mathbf{v}, s) = \frac{\imath\Omega}{2}\frac{\imath\left(\Delta - \mathbf{kv}\right) + \gamma + s}{\left(\Delta - \mathbf{kv}\right)^2 + \frac{\gamma+s}{\Gamma+s}\Omega^2 + \left(\gamma + s\right)^2} \ . \quad (37.29)$$

The steady-state simply follows from $\bar{\sigma}_+(\mathbf{v}) = \lim_{s\to 0} s\hat{\sigma}_+(\mathbf{v}, s)$. We chose $\Gamma = (2\pi)6$ MHz and $\gamma = \frac{\Gamma}{2}$,

$$\frac{S}{\mathcal{E}_1} = -\frac{N\hbar\Omega}{2\beta I_1}\int d^3\mathbf{v} W(\mathbf{v})\left[\theta(v_z)(-2\imath\beta k v_z)\hat{\sigma}_+(\mathbf{v}, -2\imath\beta k v_z) + \theta(-v_z)\bar{\sigma}_+(\mathbf{v})\right] \ . \quad (37.30)$$

37.2.6.2 Gas of two-level atoms

Plugging in the solution of the Bloch equations,

$$\begin{aligned}\mathfrak{Re}\ \frac{S}{\mathcal{E}_1} = -\frac{N\hbar\Omega}{2\beta I_1}\left(\frac{3}{2\pi v_0^2}\right)^{3/2}\mathrm{Re}\int dv_x dv_y dv_z e^{-3v_x^2/2v_0^2} e^{-3v_y^2/2v_0^2} e^{-3v_z^2/2v_0^2}\times \quad (37.31)\\ \times\frac{\imath\Omega}{2}\left[\theta(v_z)\frac{\imath(\Delta - k_x v_x - k_y v_y - k_z v_z) + \gamma - 2\imath\beta k v_z}{(\Delta - k_x v_x - k_y v_y - k_z v_z)^2 + \frac{\gamma - 2\imath\beta k v_z}{\Gamma - 2\imath\beta k v_z}\Omega^2 + (\gamma - 2\imath\beta k v_z)^2}\right.\\ \left. + \theta(-v_z)\frac{\imath(\Delta - k_x v_x - k_y v_y - k_z v_z) + \gamma}{(\Delta - k_x v_x - k_y v_y - k_z v_z)^2 + \frac{\gamma}{\Gamma}\Omega^2 + \gamma^2}\right] \ .\end{aligned}$$

For normal incidence $k_x = k_y = 0$, $k_z = k$, and $\beta = 1$ and neglecting collisions $\gamma = \frac{1}{2}\Gamma$,

$$\begin{aligned}\mathfrak{Re}\ \frac{S}{\mathcal{E}_1} = -\frac{N\hbar\Omega^2}{4I_1}\left(\frac{3}{2\pi v_0^2}\right)^{1/2}\int dv_z e^{-3v_z^2/2v_0^2}\times \quad (37.32)\\ \times\ \mathfrak{Re}\left[\theta(v_z)\frac{-\Delta + 3kv_z + \frac{\imath}{2}\Gamma}{(\Delta - kv_z)^2 + \frac{\frac{1}{2}\Gamma - 2\imath\beta k v_z}{\Gamma - 2\imath\beta k v_z}\Omega^2 + \left(\frac{1}{2}\Gamma - 2\imath k v_z\right)^2}\right.\\ \left. +\theta(-v_z)\frac{-\Delta + kv_z + \frac{\imath}{2}\Gamma}{(\Delta - kv_z)^2 + \frac{1}{2}\Omega^2 + \gamma^2}\right] \ .\end{aligned}$$

Define a normalized function $\Phi = \frac{k^4 v_0}{NA}\mathrm{Re}\frac{S}{\mathcal{E}_1} = \frac{2\pi I_1 k v_0}{N\hbar\Omega^2}\mathrm{Re}\frac{S}{E_1}$,

$$\Phi = -\sqrt{\frac{3\pi}{8}}\int dk v_z e^{-3v_z^2/2v_0^2}\mathrm{Re}\left[\frac{\theta(v_z)\left(-\Delta+3kv_z+\frac{\imath}{2}\Gamma\right)}{(\Delta-kv_z)^2+\frac{\frac{1}{2}\Gamma-2\imath\beta k v_z}{\Gamma-2\imath\beta k v_z}\Omega^2+\left(\frac{1}{2}\Gamma-2\imath k v_z\right)^2}\right.$$
$$\left.+\frac{\theta(-v_z)\left(-\Delta+kv_z+\frac{\imath}{2}\Gamma\right)}{(\Delta-kv_z)^2+\frac{1}{2}\Omega^2+\gamma^2}\right] . \tag{37.33}$$

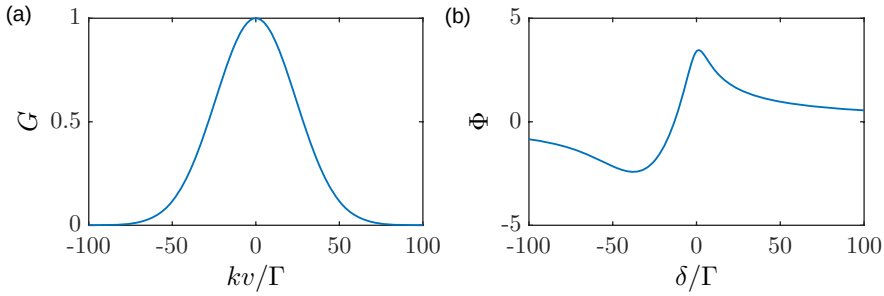

Figure 37.5: (code) Selective reflection profile.

37.2.6.3 Cold atoms

The vapor pressure of Rb at 100 C is $P = 1.5\times10^{-4}$ hPa. The density is then $n = p/k_BT = 3\times10^{18}\,\mathrm{m}^{-3}$. If there is no buffer gas the distance covered between two collisions is $\sqrt{k_BT/m}/\gamma_{coll} = 1/\sigma n = 1$ mm.

The atomic excitation reaches its steady-state value during a time on the order of $1/\Gamma$. In a thermal gas the distance covered by a thermal gas atom during this time is much larger than an optical wavelength, $\sqrt{k_BT/m}/\Gamma \approx 4$ μm. In contrast, if the atoms move less than a wavelength during this time, the Voigt theory of complex refraction index is recovered. In Eq. (37.30) we may set $kv_z = 0$,

$$\frac{S}{\mathcal{E}_1} = -\frac{N\hbar\Omega}{2\beta I_1}\int d^3\mathbf{v} W(\mathbf{v})\bar{\sigma}_+(\mathbf{v}) . \tag{37.34}$$

As long as $k\bar{v} \gg \Gamma$, the Voigt profile is dominated by temperature, the Lorentz profile $\bar{\sigma}_+$ can be approximated by a δ-distribution and the dependence on detuning is averaged out by the integral.

37.2.6.4 Ultracold atoms

At even lower temperatures, $k\bar{v} \ll \Gamma$, the Doppler width is narrower than the natural linewidth. E.g. at 1 μK the atom moves less than 0.3 nm during a radiative lifetime. Let us assume low velocities and far detunings $\Delta \gg \mathbf{kv}$, so that the internal dynamics does not depend much on atomic motion. Eq. (37.27) then reads,

$$\frac{1}{\epsilon_0\mathcal{E}_1}\mathcal{P}_0(z) = \frac{\hbar\Omega N}{I_1}\left(\frac{3}{2\pi v_0^2}\right)^{1/2} e^{\imath\beta kz}\int dv_z e^{-3v_z^2/2v_0^2}\bar{\sigma}_+(\mathbf{0}) . \tag{37.35}$$

If the atoms were immobile, they would all be in steady-state, regardless of their motion. Using,

$$\delta(x-x_0)=\lim_{\varepsilon\to 0}\frac{1}{\sqrt{\pi\varepsilon}}e^{-(x-x_0)^2/\varepsilon}\ , \tag{37.36}$$

Eq. (37.35) can be rewritten,

$$\frac{\mathcal{P}_0(z)}{\epsilon_0\mathcal{E}_1}=\frac{\hbar\Omega N}{I_1}e^{\imath\beta kz}\int dv_z\delta(v_z)\left[\theta(v_z)\sigma_+(\mathbf{0},z/v_z)+\theta(-v_z)\frac{\imath\Omega}{2}\frac{\imath\Delta+\gamma}{\Delta^2+\frac{1}{2}\Omega^2+\frac{1}{4}\Gamma^2}\right]\ . \tag{37.37}$$

Finally,

$$\frac{1}{\epsilon_0\mathcal{E}_1}\mathcal{P}_0(z)=\frac{\hbar\Omega N\bar{\sigma}_+}{I_1}e^{\imath\beta kz}\ . \tag{37.38}$$

Hence, for $z>v_zt_{ss}$ or $v_z<0$ there is no z-dependence. The only case when z dependence can occur is immediately after a collision, i.e. during the time $t_{ss}=2\pi/\sqrt{\Delta^2+\Omega^2}$ it takes to approach steady state. The distance v_0t_{ss} covered during this time is short. *The polarization is homogeneous without atomic motion.*

37.2.6.5 Crossed Kerr effect

The most interesting thing is the fact that matter wave phases are proportional to the light field intensity and the light phases to the matter wave intensity: $\delta\phi_\psi\propto\delta|\mathcal{E}|^2$ and $\delta\phi_\mathcal{E}\propto\delta|\psi|^2$. This leads to quantum nondemolition measurements [1033, 1034, 55, 304].

The question arises, why only a narrow region near the surface contributes to the selective reflection signal, and whether this fact gives rise to a dipole force. Let us first find out the reason for spatially inhomogeneous polarization near the surface.

Spatial dispersion only results from the symmetry-breaking effect of the wall on the atomic motion. Hence, we need to keep the atomic motion in consideration. Anyway, even if there were spatial dispersion leading to inhomogeneous density, is would be washed out by thermal motion quickly.

Looking at the selective reflection signal, the lineshape is approximately the derivative of a Gaussian distorted by an asymmetry, which disappears for lower temperatures. The width is on the order of the Doppler-width kv_0. As the temperature is reduced the lineshape narrows until it has becomes the derivative of a Lorentzian with the natural linewidth Γ, as predicted by formula (37.37).

The knackpoint is now using Eq. (37.26),

$$S=\mathcal{E}_1\frac{\hbar\Omega N}{2I_1}\int_0^\infty d(2\imath kz_0)\bar{\sigma}_+e^{2\imath\beta kz_0}=\mathcal{E}_1\frac{\hbar\Omega N}{2I_1}\bar{\sigma}_+\int_0^\infty dse^{-\beta s}=\mathcal{E}_1\frac{\hbar\Omega N}{2I_1}\bar{\sigma}_+\frac{1}{\beta}\ . \tag{37.39}$$

Substituting $s\equiv-2\imath kz_0$.

The question about the width of the contributing region is probably in the Laplace transform, which is known to exhibit memory-like behavior.

37.2.7 Exercises

37.2.7.1 Ex: Lasing without inversion

Explain the phenomenon of lasing without inversion in the dressed states picture for a V-type three-level system.

Solution:

37.3 Further reading

G. Kurizki et al., *Free-electron lasing without inversion by interference of momentum states* [761]$_{\text{DOI}}$

D. Bloch et al., *Atom-wall interaction* [152]$_{\text{DOI}}$

G. Nienhuis, *Nonlinear selective reflection from an atomic vapor at arbitrary incidence angle* [953]$_{\text{DOI}}$

E. Pleghaar, *Quantitative investigation of the effect of resonant absorbers on the Goos-Hänchen shift* [1028]$_{\text{DOI}}$

Chapter 38

Atomic motion in force fields

So far – and especially in Sec. 24.7.2– we analyzed the motion of quantum particles in potential landscapes without specifying the physical origin of the potentials. We know the *gravitational force*, which can be derived from the Earth's homogeneous attraction,

$$\mathbf{F} = -\nabla V_{grav} = -\nabla(mgz) = -gm\hat{\mathbf{e}}_z \ . \tag{38.1}$$

Another fundamental force comes from electromagnetism. We have already studied – mainly in Sec. 30.4– the reaction of the electronic shell in atoms subjected to applied electromagnetic fields.

In contrast, the present chapter is devoted to the motion of the *atomic center-of-mass* subject to forces resulting from interactions with *electromagnetic fields*. We will begin, in the first section, with electromagnetic forces of the Coulomb-Lorentz type acting on charges (e.g. ions), permanent electric dipoles (e.g. polar molecules), or permanent magnetic dipoles (e.g. paramagnetic atoms). Also, more complex situations will be discussed, such as the scattering of light by confined atoms, atoms interacting with optical cavities, and adiabatic potentials.

The second section will entirely be devoted to the forces exerted by light beams, in particular the *radiation pressure* and the *optical dipole force*, which are nowadays widely used in atomic cooling and trapping experiments. We will leave the issue of the application of these forces to Chp. 43 and concentrate here on the (semiclassical or quantum) derivation and the interpretation of the forces. In fact, to understand optical forces acting on atoms, we need to consider their internal degrees of freedom.

Apart from the degrees of freedom related to their center-of-mass motion (kinetic or potential energy), many quantum objects are endowed with internal degrees of freedom, for example, the motion of electrons inside atoms or molecules. In the simplest case, the Hamiltonian of such a system is composed of an outer part, comprising the kinetic and the potential energy, and an inner part counting for the excitation energy $\hbar\omega_0$ of an internal state $|e\rangle$,

$$\hat{H}_{atom} = \frac{\mathbf{p}^2}{2m} + V(\mathbf{r}) + \hbar\omega_0 |e\rangle\langle e| \ . \tag{38.2}$$

The time scale of the electronic motion is usually very rapid compared to the motion of the nucleus, where (almost) the entire mass of the atom is concentrated. Therefore, the external (nuclear) dynamics decouples from the internal (electronic) one, which allows the separation of the total wavefunction in two parts,

$$|\psi\rangle = |\psi\rangle_{ext}|\psi\rangle_{ele} \ , \tag{38.3}$$

where for a simple two-level atom, $|\psi(t)\rangle_{ele} = c_g(t)|g\rangle + c_e(t)|e\rangle$, with the atomic ground state $|g\rangle$ and the excited state $|e\rangle$. The external states are eigenstates of the momentum in the case of a free particle, $|\psi\rangle_{ext} = |\mathbf{p}\rangle$. For particles confined in a potential the external states are the vibrational eigenstates, $|\psi\rangle_{ext} = |n\rangle$. The temporal evolutions of the internal and external degrees of freedom are governed by independent Schrödinger equations. For cold atomic clouds the kinetic energy is much smaller than the excitation energy, which allows the separation of the energy scales. That is, the internal degrees of freedom are frozen in the ground state. Many phenomena, for example, Bose-Einstein condensation and the dynamics of condensates are described in this regime.

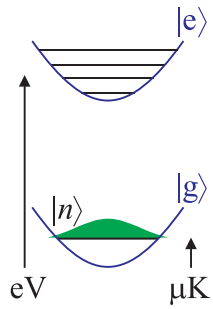

Figure 38.1: The internal degrees of freedom of cold atoms are thermally frozen.

Nevertheless, the fact that it is thermally frozen does not prevent the intentional excitation of the internal degree of freedom by irradiating electromagnetic fields tuned close to resonances and coupling electronic energy levels. In the case of coupling, the external and internal degrees of freedom must both be considered.

38.1 Electromagnetic forces

Obviously, in order to allow for forces acting on the atomic center-of-mass, the atomic Hamiltonian must contain terms depending on the center-of-mass coordinates:

$$\mathbf{F} = -\langle \nabla \hat{H}_{atom:field} \rangle \ . \tag{38.4}$$

We will see shortly that some of the terms may be dissipative, other conservative.

The impact of electromagnetic fields on the internal dynamics of atoms has already been studied in the Chp. 30. Here, we will focus on the force on the center-of-mass exerted by the gradient of *electromagnetic potentials*, where the Hamiltonian in Eq. (38.4) of a charge interacting with electromagnetic fields is obtained in minimum coupling (30.11) by,

$$\boxed{\hat{H}_{atom:field} = \frac{1}{2m}(-\imath\hbar\nabla - q\mathbf{A})^2 + q\Phi \simeq \frac{-\hbar^2}{2m}\nabla^2 + \frac{\imath\hbar q}{m}\mathbf{A}\cdot\nabla + q\Phi} \ . \tag{38.5}$$

From this formula we can, in principle, calculate all electromagnetic forces.

The coupling of external and internal degrees of freedom is mediated by the photonic recoil transferred to the atom during absorption and emission processes. That

is, the feature that the interaction with light simultaneously *excites* the atom and exerts a *force* couples the degrees of freedom. This fact manifests itself in the Hamiltonian of the atom interacting with a light field (35.17) by the appearance of terms joining operators acting on different degrees of freedom,

$$\hat{H} = \hbar\omega\hat{a}^\dagger\hat{a} + \hat{H}_{atom:field} + \hat{H}_{atom} \qquad (38.6)$$
$$\text{where} \qquad \hat{H}_{atom:field} = \hbar g(\hat{\mathbf{r}})e^{\imath\mathbf{k}\cdot\hat{\mathbf{r}}}\hat{a}^\dagger\hat{\sigma} + c.c. \ ,$$

where $\hat{\sigma} \equiv |g\rangle\langle e|$ and $\hat{a} \equiv \sum_n n|n\rangle\langle n+1|$ and $\hbar g(\hat{\mathbf{r}}) \equiv \mathbf{d}_{12}\cdot\vec{\mathcal{E}}_1(\hat{\mathbf{r}})$ is the coupling constant or one-photon *Rabi frequency* derived from (14.10). The Hamiltonian is that of the Jaynes-Cummings model, except that in addition to the field operators $\hat{a}$ and the atom transition operators $\hat{\sigma}$, appears an operator for the position of the atom $\hat{\mathbf{r}}$, whose quantum features we have not taken very seriously so far. It appears in the Rabi frequency and also in the term $e^{\imath\mathbf{k}\cdot\hat{\mathbf{r}}}$. Now, we must remember, that

$$U_{recoil} = e^{-\imath\mathbf{k}\cdot\hat{\mathbf{r}}} = |\mathbf{p}+\hbar\mathbf{k}\rangle\langle\mathbf{p}| \qquad (38.7)$$

is the unitary operator of the photonic recoil in the absorption process introduced in Sec. 23.5.3 and extensively discussed in Sec. 24.6.2. We shall shortly see, that it is precisely this term in the Hamiltonian that gives rise to all phenomena related to light forces on atoms.

The presence of the position operator in the Jaynes-Cummings Hamiltonian introduces a new degree of freedom. With no external potential (that is, the system is invariant to spatial translations), this degree of freedom is simply the atomic center-of-mass momentum, such that the new set of quantum numbers is $|j, n, \mathbf{p}\rangle$. Strictly speaking we have to span the whole Hilbert space by an external product, $\hat{H}_{ele} \otimes \hat{H}_{field} \otimes \hat{H}_{ext}$.

Often a *semi-classical* description treating the light field a classically is sufficient, $\hat{a} \simeq \sqrt{n}$ with n the number of photons. Then the Hamiltonian (38.6) simplifies to,

$$\hat{H}_{atom:field} = \hbar\Omega(\hat{\mathbf{r}})e^{\imath\mathbf{k}\cdot\hat{\mathbf{r}}}\hat{\sigma} + c.c. \ , \qquad (38.8)$$

with the Rabi frequency $\Omega(\mathbf{r}) = \sqrt{n}g(\mathbf{r})$.

38.1.1 Forces on charges and electric dipole moments

As shown in Eq. (30.8), the equations (38.4) and (38.5) (obviously) lead to Coulomb-Lorentz forces on charges and currents.

In atomic optics, the Coulomb-Lorentz force is used, for example, to accelerate or trap ions (see Sec. 43.5) and other electrically charged particles.

Atoms naturally do not exhibit *permanent electric dipole moments*, when they are not subject to external electric fields. In contrast, polar molecules (such as heteronuclear dimers), which have permanent electric dipole moments can have their motion be influenced by inhomogeneous electric fields (see Sec. 43.5.3).

38.1.2 Forces on magnetic dipole moments

Neutral atoms are insensitive to electric fields. But as we have already seen in Chp. 30, the orbital motion of the electrons corresponds to a circular current generating a permanent magnetic dipole moment $\vec{\mu}$, which can interact with external magnetic fields. We have already shown in the calculation (30.15) and (30.19) that the interaction energy (38.5) can be written as,

$$\hat{H}_{magn} = -\vec{\mu}_J \cdot \vec{\mathcal{B}} = -\frac{g_J \mu_B}{\hbar} \mathbf{J} \cdot \vec{\mathcal{B}} \longrightarrow -\frac{g_J \mu_B}{\hbar} |\mathbf{J}| \cdot |\vec{\mathcal{B}}| = -g_J \mu_B m_J \mathcal{B} \ , \tag{38.9}$$

where the *Landé factor* is given by the formula (30.21),

$$g_J = 1 + \frac{J(J+1) + S(S+1) - L(L+1)}{2J(J+1)} \ . \tag{38.10}$$

Here, $\mathbf{J} = \mathbf{L} + \mathbf{S}$ is the total angular momentum resulting from the coupling of the total angular orbital momentum and the total spin of all electrons. If the atom has a nuclear spin I other than zero, then $\mathbf{F} = \mathbf{J} + \mathbf{I}$ replaces $\mathbf{J}$ in Eq. (38.9), and the g-factor generalizes to (30.35) [1],

$$g_F \simeq g_J \frac{F(F+1) + J(J+1) - I(I+1)}{2F(F+1)} \ . \tag{38.11}$$

In Sec. 30.2 we used the formula (38.9) to calculate the Zeeman shift of internal energy levels. But, according to the formula (38.4), the interaction also generates a force acting on the center-of-mass of atom,

$$\boxed{\mathbf{f} = -g_F \mu_B m_F \nabla \mathcal{B}} \ . \tag{38.12}$$

In case of absence of hyperfine structure we simply replace F by J.

Obviously, force is conditioned by the existence of a gradient of the absolute value of the magnetic field. It was first used in the famous *Stern-Gerlach experiment*, which led to the discovery of the electron (see Sec. 25.3.3). In atomic optics (see Sec. 43.4), this force is widely used to create *magnetic traps* for cold atoms. Resolve the Excs. 30.2.8.2, 38.1.4.1, and 38.1.4.2.

38.1.3 Adiabatic potentials

Adiabatic potentials can be used to realize more complicated trapping geometries [299]. To study adiabatic potentials we consider the two-level system $|\frac{1}{2}, \frac{1}{2}\rangle \leftrightarrow |\frac{1}{2}, -\frac{1}{2}\rangle$ coupled by an incident radiation (e.g. a radiofrequency). A generalization to multilevel systems $F > \frac{1}{2}$ is simple. The dressed states Hamiltonian of our two-level system is a 2×2 matrix,

$$\hat{H}_{adiab}(z) = \begin{pmatrix} \frac{1}{2}\mu_B g_F \mathcal{B}(z) - \frac{1}{2}\hbar\omega & \frac{1}{2}\hbar\Omega \\ \frac{1}{2}\hbar\Omega & -\frac{1}{2}\mu_B g_F \mathcal{B}(z) + \frac{1}{2}\hbar\omega \end{pmatrix} \ . \tag{38.13}$$

[1] Note that the formula only applies to weak fields. For strong fields the Zeeman unfolding changes to the Paschen-Back unfolding of the hyperfine structure.

For simplicity, we assume a one-dimensional geometry, $\mathcal{B} = \mathcal{B}(z)$, but we can easily generalize to three dimensions. The eigenvalues of $\hat{H}$ are,

$$E_{\pm}(z) = \pm\tfrac{1}{2}\sqrt{\hbar^2\Omega^2 + \left[\mu_B g_F \mathcal{B}(z) - \hbar\omega\right]^2} \,. \tag{38.14}$$

Sufficiently far from resonance, $\hbar\Omega \ll |\mu_B g_F \mathcal{B}(z) - \hbar\omega|$, we obtain,

$$E_{\pm}(z) \simeq \pm\tfrac{1}{2}[\mu_B g_F \mathcal{B}(z) - \hbar\omega] \pm \frac{\hbar^2\Omega^2}{4[\mu_B g_F \mathcal{B}(z) - \hbar\omega]} \,, \tag{38.15}$$

where the second term can be interpreted as the dynamic Stark shift of the energy levels.

To illustrate the influence of the radiofrequency, we calculate the potential energy and the dressed states assuming a linear $1D$ magnetic field gradient $\mathcal{B}(z) \equiv zb$. Fig. 38.2(a) illustrates the radiofrequency coupling and Fig. 38.2(b) the dressed states for two magnetic substates coupled by a radiofrequency. The minimum emerging in

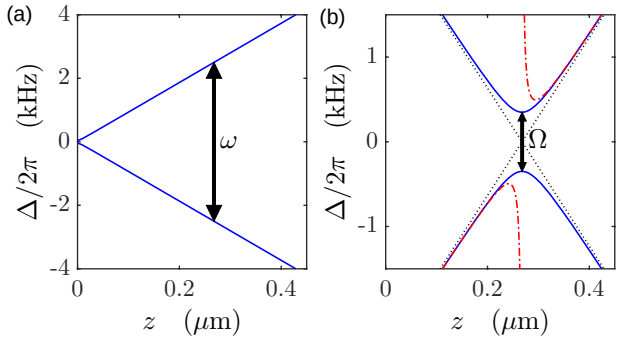

Figure 38.2: (code) (a) Potential energies for a hyperfine structure $F = \frac{1}{2}$ with a g-fator of $g = -\frac{2}{3}$ (as e.g. in the ground state ${}^2S_{1/2}$ of ^{6}Li). A radiofrequency (arrow) couples the substates $m_F = \pm\frac{1}{2}$. Here, $b = 200\,\mathrm{G/cm}$ and $\omega = 2\pi \times 5\,\mathrm{kHz}$. (b) Uncoupled dressed states (dotted line), coupled dressed states (solid line), and dynamic Stark shifts (dash-dotted) approximated far away from resonance. The Rabi frequency is $\Omega = 2\pi \times 700\,\mathrm{Hz}$.

the upper curve of Fig. 38.2(a) may serve as a confinement potential. Using an rf-radiation composed by several frequencies, potential minima can be realized at several distances z. In Exc. 38.1.4.3 we calculate an example.

In the dressed states basis with the Hamiltonian (38.13), the force is calculated from,

$$\mathbf{F}(\mathbf{r}) = \langle\hat{\mathbf{F}}(\mathbf{r})\rangle = -\mathrm{Tr}_{\,atom:laser}\,\hat{\rho}\nabla_{\mathbf{r}}\hat{H}_{adiab} = -\sum_{n,j}\langle n,j|\hat{\rho}\nabla_{\mathbf{r}}\hat{H}_{adiab}|j,n\rangle \,. \tag{38.16}$$

We consider only one dimension and disregard the degrees of freedom of the radiation field,

$$F(z) = -\mathrm{Tr}_{\,atom:laser}\,\hat{\rho}\partial_z\hat{H}_{adiab} \tag{38.17}$$
$$= -\sum_j \langle j|\hat{\rho}\partial_z\left(\tfrac{\mu_B g_F\mathcal{B}}{2}|1\rangle\langle 1| - \tfrac{\hbar\omega}{2}|1\rangle\langle 1| - \tfrac{\mu_B g_F\mathcal{B}}{2}|2\rangle\langle 2| + \tfrac{\hbar\omega}{2}|2\rangle\langle 2| + \tfrac{\hbar\Omega}{2}e^{\imath kz}\hat{\sigma}^+ + c.c.\right)|j\rangle \,.$$

Here we neglect any possible position dependence of Ω,

$$F(z) = -\tfrac{1}{2}\mu_B g_F \partial_z \mathcal{B} \sum_j \langle j|\hat{\rho}(|1\rangle\langle 1| - |2\rangle\langle 2|)|j\rangle = -\tfrac{1}{2}\mu_B g_F \partial_z \mathcal{B}(\rho_{11} - \rho_{22}) \ . \quad (38.18)$$

If the atoms enter the coupling area adiabatically, the populations of the adiabatic potentials will only depend on z. This is analogous to the *adiabatic transfer* via adiabatic sweeps or STIRAP pulse sequences. If the atoms are too fast, the populations also depend on history (i.e. the recent trajectory of the atoms), which can result in Landau-Zener transitions to other (possibly untrapped) states.

38.1.4 Exercises

38.1.4.1 Ex: The Stern-Gerlach effect

Consider initially motionless ^{87}Rb atoms trapped in a superposition of two the trappable Zeeman states $|F, m_F\rangle = |2, +2\rangle$ and $|1, -1\rangle$. Suddenly a magnetic gradient of $\partial_z \mathcal{B} = 100\,\mathrm{G/cm}$ is applied for 2 ms. Calculate the spatial separation of the atoms being in either one of the two states after 10 ms of ballistic expansion.

Solution: *We first need to calculate the Landé-factors for the states using $I = \frac{3}{2}$. From formulae (30.21) and (30.35) we get for the ground state $^2S_{1/2}$,*

$$g_J = 2 \qquad \textit{and} \qquad g_F = \begin{cases} -\frac{1}{2} & \textit{for} \quad F = 1 \\ +\frac{1}{2} & \textit{for} \quad F = 2 \end{cases} .$$

Hence, atoms in the state $|2, +2\rangle$ are accelerated by the force,

$$F = -\partial_z(-\mu_B g_F m_F \mathcal{B}) = \mu_B \partial_z \mathcal{B} \begin{cases} -\frac{1}{2}(-1) & \textit{for} \quad F = 1 \\ +\frac{1}{2}(2) & \textit{for} \quad F = 2 \end{cases} .$$

After $t_{frc} = 2$ ms the force has accelerated the atoms to a final velocity,

$$v = \frac{F}{m} t_{frc} \ ,$$

and after $t_{bll} = 10$ ms ballistic expansion the displacement is,

$$z = \frac{F}{2m} t_{frc} t_{bll} = 1.3\,\mathrm{mm} \begin{cases} \frac{1}{2} & \textit{for} \quad F = 1 \\ 1 & \textit{for} \quad F = 2 \end{cases} .$$

38.1.4.2 Ex: Potential for magnetic trapping

Invent a potential for magnetic confinement.

Solution: *The simplest example is, of course, the quadrupolar potential generated by a magnetic field produced by current-carrying coils in anti-Helmholtz configuration,*

$$\vec{\mathcal{B}} = \begin{pmatrix} x \\ y \\ -2z \end{pmatrix} \partial\mathcal{B} \ ,$$

yielding,

$$\mathcal{B} = \partial\mathcal{B}\sqrt{r^2 + 4z^2} \ .$$

Another example, is the Ioffe-Pritchard trap generated by a magnetic field such as,

$$\vec{\mathcal{B}} = \begin{pmatrix} x\partial\mathcal{B} \\ -y\partial\mathcal{B} \\ \mathcal{B}_0 + \alpha z^2 \end{pmatrix} \ .$$

This corresponds to a linear quadrupole along the z-axis superposed to a magnetic bottle along the same direction and yields,

$$\begin{aligned} |\mathbf{B}| &= \sqrt{x^2\partial\mathcal{B}^2 + y^2\partial\mathcal{B}^2 + (\mathcal{B}_0 + \alpha z^2)^2} \\ &\simeq \sqrt{\mathcal{B}_0^2 + r^2\partial\mathcal{B}^2 + 2\alpha\mathcal{B}_0 z^2} \simeq \mathcal{B}_0 + \frac{\partial B^2}{2B_0^2} r^2 + \frac{\alpha}{B_0} z^2 \ , \end{aligned}$$

for small enough field curvature α close to the center of the potential.

38.1.4.3 Ex: Adiabatic potentials

An *adiabatic potential* can be used to create more complicated trapping potentials [299]. To study these potentials we consider a system of two Zeeman states $m = \frac{1}{2}$ coupled by a radiofrequency radiation $\hbar\omega$. The dressed states Hamiltonian of our two-level system is a 2×2 matrix,

$$\hat{H} = \begin{pmatrix} \frac{1}{2}\mu_B\mathcal{B} - \frac{1}{2}\hbar\omega & \frac{1}{2}\hbar\Omega \\ \frac{1}{2}\hbar\Omega & -\frac{1}{2}\mu_B\mathcal{B} + \frac{1}{2}\hbar\omega \end{pmatrix} \ ,$$

defining the energetic zero in the middle between the states. Now, assume that the magnetic field grows linearly along the axis z, $\mathcal{B}(z) = z\partial_z\mathcal{B}$, where $\partial_z\mathcal{B}$ is the gradient. Also assume that the radiofrequency is tuned in resonance with the difference of the energies of the Zeeman states at some distance z_0 such that, $\hbar\omega = \mu_B z_0 \partial_z\mathcal{B}$.
a. Calculate the eigenenergies of the coupled system as a function of z.
b. Expands eigenenergies around the position z_0.
c. What would be the oscillation frequency of the trapped atoms inside the adiabatic potential?
d. Expands the eigenenergies in $\hbar\Omega$ for locations away from resonance.

Solution: *a. The eigenvalues of H are,*

$$E_{1,2}(z) = \pm\frac{1}{2}\sqrt{(\mu_B z\partial_z\mathcal{B} - \hbar\omega)^2 + \hbar^2\Omega^2} = \pm\frac{1}{2}\sqrt{(\mu_B\partial_z\mathcal{B})^2(z - z_0)^2 + \hbar^2\Omega^2} \ .$$

b. The expansion around z_0 gives,

$$E_{1,2}(z) = \pm\frac{1}{2}\left(\hbar\Omega + \frac{1}{2}\frac{(\mu_B\partial_z\mathcal{B})^2}{\hbar\Omega}(z-z_0)^2 + ...\right) .$$

c. We obtain a harmonic adiabatic potential,

$$E_{1,2}(z) = \frac{1}{2}\frac{(\mu_B\partial_z\mathcal{B})^2}{\hbar\Omega}(z-z_0)^2 = \frac{m}{2}\omega_{ho}^2(z-z_0)^2 ,$$

such that,

$$\omega_{ho} = \frac{\mu_B\partial_z\mathcal{B}}{\sqrt{m\hbar\Omega}}$$

is the oscillation frequency.
d. Sufficiently far away from resonance, $\hbar\Omega \ll |\mu_B\mathcal{B}(z) - \hbar\omega|$, we obtain

$$E_{1,2}(z) \approx \pm\frac{1}{2}\left[\mu_B z\partial_z\mathcal{B} - \hbar\omega\right] \pm \frac{\hbar^2\Omega^2}{4\left[\mu_B z\partial_z\mathcal{B} - \hbar\omega\right]} ,$$

where the second term can be interpreted as the dynamic Stark shift of the energy levels.
To illustrate the impact of the radiofrequency, we calculate the potential energy and the dressed states for ^6Li atoms. For simplicity, we assume a linear $1D$ magnetic field gradient $\mathcal{B}(z) \equiv zb$. Fig. 38.2(a) shows the radiofrequency coupling and Fig. 38.2(b) dressed states for two magnetic substates coupled by a radiofrequency.
Fig. 38.2(a) shows the potential energies for a level scheme $F = \frac{1}{2}$ with a g-factor of $g = -\frac{2}{3}$ (as in the case of the ground state $^2S_{1/2}$ of ^6Li). A radiofrequency (arrow) couples the substates $m_F = \pm\frac{1}{2}$. Here, $b = 200\,\mathrm{G/cm}$ and $\omega = 2\pi\times 5\,\mathrm{kHz}$. Fig. 38.2(b) shows the uncoupled dressed states (dotted line), the dressed states (solid line), and dynamic Stark shifts (dash-dotted) calculated in the approximation for far detuning. The Rabi frequency is $\Omega = 2\pi \times 700$ Hz. The minimum appearing on the upper curve of Fig. 38.2(a) may serve a confinement potentials. Using rf-radiation with several frequency components potential minima can be generated at various distances z.

38.2 Optical forces

Light carries momentum, and the scattering of light by an object produces a force on that object. Although these properties of light are direct consequences of Maxwell's classical theory of electromagnetism, they were only verified in 1933 by *Frisch*, who observed a very small transverse deviation ($3 \cdot 10^{-5}$ rad) of an atomic sodium beam exposed to the light of a lamp. With the invention of the laser, it became easier to observe the light's mechanical effects, because the more intense and highly directional laser light exerts much larger forces. Although these results sparked the interest in using light forces to control the motion of neutral atoms, the fundamental bases for understanding the physics of light forces were not developed before the late 1970s. Unequivocal experimental demonstrations of cooling and trapping of atoms were not performed before the mid-1980s. In this section we will discuss some fundamental

aspects of light forces. Practical schemes used to cool and trap neutral atoms will be presented in Secs. 43.2 and 43.3.

The light force acting on an atom can be of two types: a spontaneous dissipative force and a conservative dipole force. The spontaneous force arises from the recoil experienced by an atom when it absorbs or emits a quantum of light. As we saw in Sec. 22.2.6, when an atom scatters light, the resonant scattering cross section can be written as in Eq. (22.72), $\sigma_{0a} = \frac{g_2}{g_1}\frac{\lambda_0^2}{2\pi}$, where λ_0 is the resonant wavelength. In the optical region of the electromagnetic spectrum the wavelengths of light are of the order of several hundred nanometers, and the resonant cross sections for scattering become very large, ($\sim 10^{-9}\,\mathrm{cm}^2$). Each absorbed photon transfers a quantum of momentum $\hbar k$ to the atom in the direction of propagation. Spontaneous emission following an absorption process occurs in random directions and, hence, averaged over many absorption-emission cycles, it cancels to zero. Consequently, the total spontaneous force acts on the atom in the propagation direction of the light, as shown schematically in the diagram of Fig. 38.3. The saturated photon scattering rate via spontaneous emission (the reciprocal value of the excited state's lifetime) sets the upper limit for the magnitude of the force. This force is called *radiation pressure* force.

The *dipolar gradient force* can be easily understood by considering light as a classical wave. It is simply the time-averaged force resulting from the interaction of the transition dipole –induced by the oscillating electric field of the light– with the gradient of the electric field amplitude. The strength of this gradient can be controlled, e.g. by focusing the light beam. By tuning the optical frequency below or above an atomic transition, we can control the sign of the force acting on the atom: Tuning the light below resonance attracts the atom to the center of the light beam, tuning it above resonance repels it. The dipole force is a stimulated process without energy exchange between the field and the atom. Photons are absorbed in one light mode and reappear by stimulated emission in another one. However, conservation of momentum requires that the change in the propagation direction of the scattered photons from an initial mode to a final mode leaves the atom with a recoil. Contrary to spontaneous force, there is, in principle, no upper limit for the magnitude of the dipole force, since it is a function of the field gradient only and the detuning.

Within the theory of electromagnetism we calculate radiative forces on charges via *Maxwell's stress tensor* [2]. The interaction of radiation with atoms having internal degrees of freedom exhibiting resonances can be treated qualitatively by the *Lorentz model* [3].

In the following, we will show quantitative semi-classical and quantum calculations: The force of a light beam on an atom can be calculated in many different ways, each emphasizing a slightly different aspect: From the classical Lorentz force exerted on an atom by electromagnetic fields we can derive a semi-classical Fokker-Planck equation [1263]. In Sec. 38.2.1 we will derive the two contributions (dipole force and radiative pressure) within a semi-classical theory [526]. Wineland *et al.* [1382] chose as starting point the cross section for an elementary scattering process (Sec. 38.2.3).

[2] See script on *Electrodynamics* (2023), Sec. 6.2.3.
[3] See script on *Electrodynamics* (2023), Sec. 7.2.4.

Dalibard *et al.* [322] developed a quantum theory using the dressed states representation (Sec. 38.2.2). And Cirac *et al.* [265] showed an approach based on the master equation (Sec. 38.2.3).

38.2.1 The dipolar gradient force and the radiation pressure force

To compute the forces of light on an atom, we describe the atom as a two-level system: A fundamental level $|1\rangle$ and an excited level $|2\rangle$ decaying to the fundamental level with the rate Γ. The energy difference between the levels is $\omega_0 \equiv E_2 - E_1$. The light with frequency ω is derived from a laser beam, which can be detuned from the atomic transition, $\Delta \equiv \omega - \omega_0$. To describe the interaction, we consider the part (38.6) of the total Hamiltonian describing the interaction [322]. Using the semi-classical density operator $\hat{\rho}$ [4], we can calculate the force that the light field exerts on the atom,

$$\begin{aligned}\mathbf{F}(\mathbf{r}) = \langle\hat{\mathbf{F}}(\mathbf{r})\rangle &= -\mathrm{Tr}_{at}\ \hat{\rho}\nabla_{\mathbf{r}}\hat{H}_{atom:field} \\ &= -\tfrac{1}{2}\hbar\sum\nolimits_j \langle j|\hat{\rho}|\nabla_{\mathbf{r}}\left(\Omega(\mathbf{r})e^{\imath\mathbf{k}\cdot\mathbf{r}-\imath\Delta t}|2\rangle\langle 1| + \Omega(\mathbf{r})e^{-\imath\mathbf{k}\mathbf{r}+\imath\Delta t}|1\rangle\langle 2|\right)|j\rangle \\ &= -\tfrac{1}{2}\hbar\nabla_{\mathbf{r}}\Omega(\mathbf{r})\left(\langle 1|\hat{\rho}e^{\imath\mathbf{k}\cdot\mathbf{r}-\imath\Delta t}|2\rangle + \langle 2|\hat{\rho}e^{-\imath\mathbf{k}\cdot\mathbf{r}+\imath\Delta t}|1\rangle\right) \\ &\quad - \tfrac{\imath}{2}\hbar\mathbf{k}\Omega(\mathbf{r})\left(\langle 1|\hat{\rho}e^{\imath\mathbf{k}\cdot\mathbf{r}-\imath\Delta t}|2\rangle - \langle 2|\hat{\rho}e^{-\imath\mathbf{k}\cdot\mathbf{r}+\imath\Delta t}|1\rangle\right)\ .\end{aligned} \tag{38.19}$$

Now, we let the atom be at the position $\mathbf{r} = 0$,

$$\mathbf{F}(\mathbf{0}) = -\tfrac{1}{2}\hbar\nabla_{\mathbf{r}}\Omega(\mathbf{0})(\rho_{12}e^{-\imath\Delta t} + \rho_{21}e^{\imath\Delta t}) - \tfrac{\imath}{2}\hbar\mathbf{k}\Omega(\mathbf{0})(\rho_{12}e^{-\imath\Delta t} - \rho_{21}e^{\imath\Delta t})\ . \tag{38.20}$$

The quantities $\rho_{12} \equiv \langle 1|\hat{\rho}|2\rangle = \rho_{21}^*$ are the coherences, which develop in a two-level system excited by a laser beam. Inserting the stationary solutions of the Bloch equations (34.188),

$$\rho_{22} = \frac{\Omega^2}{4\Delta^2 + 2\Omega^2 + \Gamma^2} \qquad \text{and} \qquad \rho_{12} = \frac{(2\Delta - \imath\Gamma)\Omega}{4\Delta^2 + 2\Omega^2 + \Gamma^2}e^{-\imath\Delta t}\ . \tag{38.21}$$

we obtain

$$\mathbf{F}(\mathbf{0}) = -\tfrac{1}{2}\hbar\frac{4\Delta\Omega}{4\Delta^2 + 2\Omega^2 + \Gamma^2}\nabla_{\mathbf{r}}\Omega + \hbar\mathbf{k}\frac{\Gamma\Omega^2}{4\Delta^2 + 2\Omega^2 + \Gamma^2}\ . \tag{38.22}$$

With the definition of the cross section, $\sigma_a(\Delta) = \sigma_{a0}\frac{\Gamma^2}{4\Delta^2+2\Omega^2+\Gamma^2}$,

$$\mathbf{F}(\mathbf{0}) = -\tfrac{1}{2}\hbar\Delta\nabla_{\mathbf{r}}\ln\left(1 + \frac{2\Omega^2}{4\Delta^2 + \Gamma^2}\right) + \hbar\mathbf{k}\frac{\Omega^2}{\Gamma}\frac{\sigma_a(\Delta)}{\sigma_{a0}}\ . \tag{38.23}$$

The resonant cross section for a 'classical' transition is $\sigma_{a0} = 3\lambda^2/2\pi$.

Apparently, the force comprises two contributions. The *dipolar gradient force* can be derived from a potential. It is proportional to the intensity gradient and can

[4] Treating the motional and the optical degrees of freedom as classical the density operator only contains the atomic excitation.

be interpreted as resulting from absorption processes immediately followed by self-stimulated emission. Near resonance it is dispersive. Far from resonance it can be approximated by,

$$\boxed{\mathbf{F}_{dp} = \nabla_{\mathbf{r}} \frac{-\hbar\Delta\Omega^2}{4\Delta^2+\Gamma^2} \overset{|\Delta|\gg\Gamma}{\longrightarrow} -\nabla_{\mathbf{r}} \frac{\hbar\Omega^2}{4\Delta}} \ . \tag{38.24}$$

The *radiation pressure* force is dissipative. Close to resonance it is absorbing. It is proportional to the phase gradient and the only force exerted by plane waves. It can be interpreted as resulting from absorption processes followed by spontaneous emission. With $\Omega^2 = \sigma_{a0}\Gamma I/\hbar\omega$ we get a formula,

$$\boxed{\mathbf{F}_{rp} = \hbar\mathbf{k}\frac{I}{\hbar\omega}\sigma_a(\Delta) = \hbar\mathbf{k}\gamma_{sct}} \ , \tag{38.25}$$

which describes the force as a product of the number of photons in the incident beam, $I/\hbar\omega$, the absorption cross section, $\sigma_a(\Delta)$, and the recoil momentum per photon, $\hbar k$. γ_{sct} is the scattering rate. Fig. 38.3(a) illustrates the radiation pressure force.

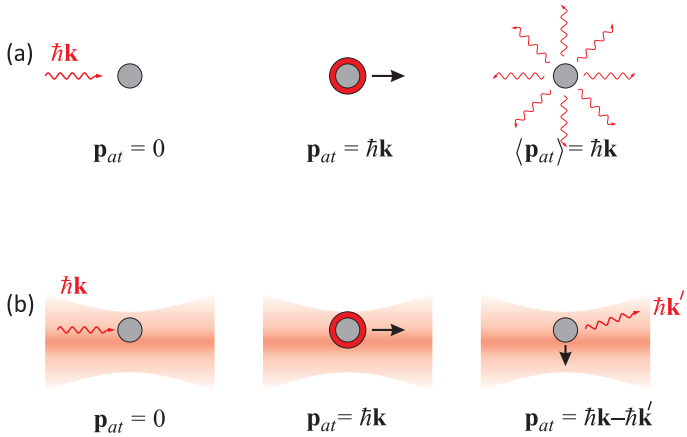

Figure 38.3: (a) Upon absorption of a photon an initially resting atom receives a recoil momentum kick $\hbar k_L$. As the re-emission is isotropic, averaged over many absorption-emission cycles, the net force is only given by the absorption process. (b) The dipole force may be interpreted as a coherent redistribution of photons between spatial modes of a focused light beam.

The dipole gradient force (and the associated potential) is often used to spatially confine atoms, and the radiation pressure force is often used to cool them down. Note that we still need to correct Eqs. (38.24) and (38.25) to take into account the square of the average over the possible spatial orientations of the transition matrix element $d_{12}/3$. As illustrated in Fig. 38.3(b), the dipole force may be interpreted as being due to coherent redistribution of photons between partial spatial modes of a non-uniform (e.g. focused) light beam. The orientation of the force depends on the sign of the detuning and can be understood in terms of the Lorentz model treating the atom as classical radiator (see Sec. 18.2.4).

The saturation parameter,

$$s = \frac{\frac{1}{2}\Omega^2}{\Delta^2 + \frac{1}{4}\Gamma^2} \ , \tag{38.26}$$

allows to write the dipolar gradient force and the radiative pressure force as,

$$\mathbf{F}_{dp} = -\frac{\hbar\Delta}{6}\frac{1}{1+s}\nabla s = \frac{\hbar\Delta}{6}\nabla \ln[1+s] \quad \text{and} \quad \mathbf{F}_{rp} = \frac{\hbar\mathbf{k}\Gamma}{6}\frac{s}{1+s} \ . \tag{38.27}$$

Eq. (38.27) shows that the radiation pressure force 'saturates' as s increases, and is therefore limited by the spontaneous emission rate. The saturation parameter essentially describes the relative importance of terms appearing in the denominator of the line profile function for the light forces. The spontaneous emission rate is an intrinsic property of the atom, proportional to the square of the atomic transition dipole moment, whereas the square of the Rabi frequency is a function of the incident laser intensity. If $s \ll 1$, the spontaneous emission is fast compared to any stimulated process, and the light field is said to be weak. If $s \gg 1$, the Rabi oscillation is fast compared to spontaneous emission and the field is considered as strong. The line profile factor indicates a 'power broadening' by saturation of a factor of $\sqrt{2}$. Note that the dipolar gradient force and potential, Eqs. (38.27), do not saturate when the intensity of the light field is increased. Usually $\mathbf{F}_{dp}$ and U_{dp} are used to manipulate and trap atoms in a laser beam tuned far away from resonance in order to avoid absorption.

Often, the transition moment can be oriented using circularly polarized light. In this case, all previous expressions for $\mathbf{F}_{dp}$, $\mathbf{F}_{rp}$, and U_{dp} should be multiplied by 3. From now on we will abandon the average over the orientations and only use d_{12}^2 for the square of the transition dipole moment. Solve Excs. 38.2.5.1 and 38.2.5.2.

38.2.2 Semiclassical calculation of dipole force and radiative pressure

In quantum mechanics we calculate the force from the Heisenberg equation [526],

$$\hat{\mathbf{F}} = \frac{d}{dt}\hat{\mathbf{p}} = \frac{\imath}{\hbar}[\hat{H}, \hat{\mathbf{p}}] = -\nabla_{\mathbf{r}}\hat{H}_{atom:field} \ . \tag{38.28}$$

Thus, the force is given by the gradient of the interaction energy between the atom and the light field. Within the dipole approximation the interaction energy is given by $\mathbf{d}\cdot\vec{\mathcal{E}}(\mathbf{r})$. The force is now,

$$\begin{aligned}\mathbf{F}(\mathbf{r}) = \langle\hat{\mathbf{F}}(\mathbf{r})\rangle = \langle\nabla_{\mathbf{r}}[\mathbf{d}\cdot\vec{\mathcal{E}}(\mathbf{r})]\rangle = \langle(\mathbf{d}\cdot\nabla_{\mathbf{r}})\vec{\mathcal{E}}(\mathbf{r})\rangle - \langle\mathbf{d}\times(\nabla_{\mathbf{r}}\times\vec{\mathcal{E}}(\mathbf{r}))\rangle \\ \equiv \mathbf{F}_C(\mathbf{r}) + \mathbf{F}_L(\mathbf{r}) \ .\end{aligned} \tag{38.29}$$

The first contribution can be interpreted as the Coulomb force acting on the electron performing rapid oscillations at the position $\mathbf{r}(t) = \mathbf{r}_0 + e^{-1}\vec{\mathcal{P}}(\mathbf{r}_0, t)$. The second term is the time-averaged Lorentz force acting on the oscillating electric dipolar moment [604, 607, 605],

$$\mathbf{F}_C = e\langle\vec{\mathcal{E}}\rangle \quad \text{and} \quad \mathbf{F}_L = -\langle\mathbf{d}\times\partial_t\vec{\mathcal{B}}\rangle = \langle\partial_t\mathbf{d}\times\vec{\mathcal{B}}\rangle \ . \tag{38.30}$$

The relation between the light-induced electric dipole moment and the polarizability, $\mathbf{d} = \alpha(\vec{\mathcal{E}})\vec{\mathcal{E}}$, where $\alpha_{\nu\nu} \equiv \alpha_\nu + \imath\beta_\nu$ and $\mathcal{E}_\nu \equiv \sqrt{I_\nu}e^{\imath\psi_\nu}$, becomes,

$$\mathbf{F} = \sum_{\nu=1}^{3} \alpha_\nu \nabla I_\nu + 2\sum_{\nu=1}^{3} \beta_\nu I_\nu \nabla\psi_\nu \ . \tag{38.31}$$

38.2.3 Force exerted by a quantized radiation field

Photons carry one unit of momentum $\mathbf{p} = \hbar\mathbf{k}$, which they transfer to the atom during an absorption or emission process. That is, the light exerts a recoil on the atoms. Spontaneous emission couples to all radiative modes of the electromagnetic vacuum, $\hat{H}_{cm:vacuum} = \sum_j \hat{H}_{cm:laser}(\mathbf{k}_j)$. We can trace over these variables and only keep those of the atom and the laser. Following Cirac *et al.* [1382, 265], the randomness of the recoil by spontaneous emission is accounted for by,

$$\hat{\rho} \to \int_{4\pi\mathbb{R}^2} S(\mathbf{r}) e^{\imath\mathbf{k}\cdot\mathbf{r}} \hat{\rho} e^{-\imath\mathbf{k}\cdot\mathbf{r}} d\Omega \ , \tag{38.32}$$

such that the *Lindblad operator* becomes,

$$\begin{aligned} \mathcal{L}_{atom}\hat{\rho} &= -\Gamma\{\hat{\sigma}^\dagger\hat{\sigma}\hat{\rho}(t) - \tfrac{3}{4\pi}\int S(\mathbf{r}) e^{\imath\mathbf{k}\cdot\mathbf{r}}\hat{\sigma}\hat{\rho}(t)\hat{\sigma}^\dagger e^{-\imath\mathbf{k}\cdot\mathbf{r}} d\Omega + \hat{\rho}(t)\hat{\sigma}^\dagger\hat{\sigma}\} \\ \mathcal{L}_{cavity}\hat{\rho} &= -\kappa\{\hat{a}^\dagger\hat{a}\hat{\rho}(t) - 2\hat{a}\rho(t)\hat{a}^\dagger + \hat{\rho}(t)\hat{a}^\dagger\hat{a}\} \ , \end{aligned} \tag{38.33}$$

where $e^{\pm\imath\mathbf{k}\cdot\mathbf{r}} = \sum_{\mathbf{p}} |\mathbf{p} \mp \imath\mathbf{k}\cdot\mathbf{r}\rangle\langle\mathbf{p}|$ and $S(\mathbf{r}) = \frac{1}{2}\left(1 + (\frac{\mathbf{k}\cdot\mathbf{r}}{kr})^2\right)$ and $d\Omega = d\varphi d\cos\vartheta$. From this they calculate the force and establish a *Fokker-Planck equation* for the *Wigner function*.

38.2.4 Refraction of atoms by light and of light by atoms

Non-resonant light acts on the external degrees of freedom of atoms by a *phase shift of the Broglie wave*, $\exp\left[\imath\hbar^{-1}\int U(\mathbf{r},t)dt\right]$, and simultaneously on the internal degrees of freedom by a *dynamic Stark shift* or *light shift* of the energy levels by the value of $U(\mathbf{r})$. The Bloch vector defined by,

$$\rho \equiv \begin{pmatrix} \frac{1}{\sqrt{2}} c_g c_e^* \\ \frac{1}{\sqrt{2}} c_g^* c_e \\ |c_e|^2 - |c_g|^2 \end{pmatrix} \tag{38.34}$$

describes, under the influence of the dispersive interaction, a precession around the polar axis. This was discussed in Exc. 34.8.4.9. The Stark shift causes a rotation of $\hbar^{-1}U(\mathbf{r})t$. Simultaneously, the atom is subjected to a force, which corresponds to the gradient of the potential $-\nabla U(\mathbf{r})$, as illustrated in Fig. 38.4(a). We see that the phase shifts of the Broglie wave and the Bloch vector are equal. Finally, the light mode phase is also shifted by the same amount in an effect called *refraction*. That is, the internal, external, and optical degrees of freedom are entangled.

This fact has a practical use in atomic interferometers, because it is often easier to detect an interference of internal excitation states rather than of Broglie waves.

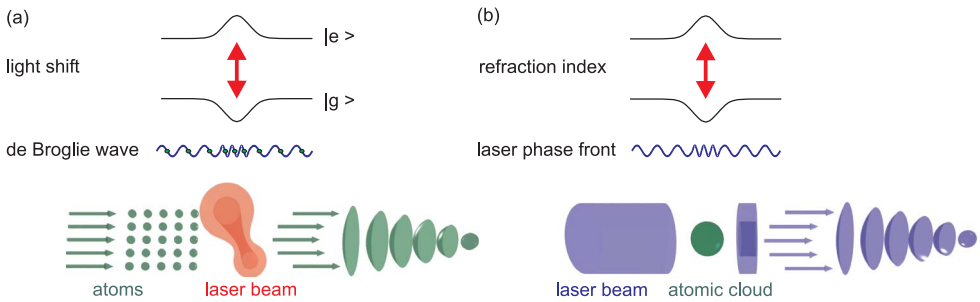

Figure 38.4: Diagram (a) shows product states and dressed states for blue detuning. Note that the population is in the upper level and that the atom is subject to a repulsive weak field seeking force when it enters the laser beam. Diagram (b) is similar, but for red detuning. The population is in the lower level and the atom is subject to an attractive high field seeking force.

Because of the entanglement, it is sufficient to measure *one* interference pattern to know the *other one*.

By local variations of the potential $U(\mathbf{r})$, e.g. induced by a focused laser beam, it is possible to manipulate a Broglie wavefront in the same way that, in classical optics, we manipulate the wavefront of a light beam by lenses or other objects, such as for instance, the refractive index represented by an atomic cloud near resonance, as illustrated in Fig. 38.4(b).

The orientation of the force depends on the light frequency as compared to the resonant frequency. The dipolar force attracts the atom to regions where the light field is strong, when the frequency is tuned below ω_0, and it attracts the atom to regions of weak fields, when tuned above ω_0. Integration over the relevant spatial coordinates results in an effective potential or barrier to the atom. The qualitative behavior of the dipolar potential and its effect on the motion of atoms is easily visualized in the dressed states picture. Fig. 38.5 shows what happens when an atom enters a well defined region of an optical field, for example a focused laser beam.

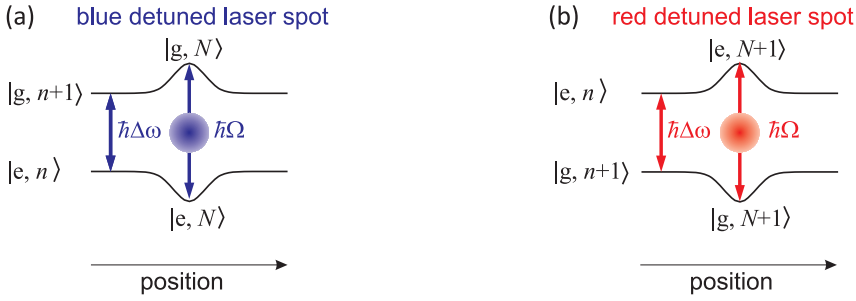

Figure 38.5: Analogy between light optics and atomic optics.

Outside the atom-dipole coupling zone the expression $\hbar\Omega$ is despicable and the 'dressed states' are just the atom-field product states. When the atom enters the

field, this expression becomes nonzero and the atom-field states combine to produce a set of dressed states. The energy levels of the product states 'repel' each other and approach the dressed states levels. Assuming that the laser is sufficiently detuned to maintain the absorption rate negligible, the population remains in the ground state. We see that blue (red) detuning leads to a repulsive (attractive) potential for atoms remaining in the grounded state. In addition, since $\hbar\Omega$ is directly proportional to the root of the laser intensity, an increase in that intensity (optical power per unit area) obviously amplifies the force on the atom ($\mathbf{F} \simeq \nabla_R \Omega$).

38.2.5 Exercises

38.2.5.1 Ex: Dipole force for large detunings

Verify that in the limit of large detunings the dipole potential Eq. (38.23) tends to $\longrightarrow \frac{\Omega^2}{4\Delta}$.

Solution:

38.2.5.2 Ex: Radiation pressure

Calculate the radiation pressure force exerted on a strontium atom by a laser beam in plane wave geometry ($I = 10\,\mathrm{mW/cm^2}$) tuned 50 MHz below the resonance at 461 nm ($\Gamma/2\pi = 30.5\,\mathrm{MHz}$).

Solution: *The force is,*

$$F = \hbar k \frac{\Gamma}{2} \frac{I/I_s}{1 + I/I_s} \simeq \hbar k \frac{\Gamma}{2} \approx 1.3 \cdot 10^{-19}\,\mathrm{N} \ ,$$

because the saturation intensity,

$$I_s = \frac{2\pi^2 c\hbar\Gamma}{3\lambda^3} \approx 38.6\,\mathrm{mW/cm^2} \ ,$$

is much higher than the intensity I of the laser beam. The acceleration becomes $a = F/m \approx 10^5 g$.

38.2.5.3 Ex: lin-lin standing wave

Calculate the electric field of two counter-propagating linearly polarized laser beams of equal intensities,

$$\vec{\mathcal{E}}_{lat}(\mathbf{r}, t) = \tfrac{1}{2} \sum_{\mathbf{k}=\pm k\hat{\mathbf{e}}_z} \mathcal{E}_0 \vec{\varepsilon}_{\mathbf{k}} e^{\imath(\mathbf{k}\cdot\mathbf{r} - \omega_{\mathbf{k}} t + \phi_{\mathbf{k}})} + c.c. \ ,$$

but different polariztions in the spherical basis.

Solution: *The spherical basis is defined by,*

$$\hat{\mathbf{e}}_{\pm 1} = \tfrac{1}{\sqrt{2}}(\mp\hat{\mathbf{e}}_x - \imath\hat{\mathbf{e}}_y) \quad , \quad \hat{\mathbf{e}}_0 = \hat{\mathbf{e}}_z \quad , \quad \hat{\mathbf{e}}_x = \tfrac{1}{\sqrt{2}}(\hat{\mathbf{e}}_{-1} - \hat{\mathbf{e}}_1) \quad , \quad \hat{\mathbf{e}}_y = \tfrac{\imath}{\sqrt{2}}(\hat{\mathbf{e}}_1 + \hat{\mathbf{e}}_{-1}) \ .$$

Hence, we get (focussing only on the $e^{-\imath\omega_{\mathbf{k}}t}$ terms),

$$\begin{aligned}\vec{\mathcal{E}}_{lat}(\mathbf{r}) &= \mathcal{E}_0 \begin{pmatrix}1\\0\\0\end{pmatrix} e^{\imath kz} + \mathcal{E}_0 \begin{pmatrix}\cos\theta\\ \sin\theta\\ 0\end{pmatrix} e^{-\imath kz} \\ &= \mathcal{E}_0 \left(e^{\imath kz} + \tfrac{e^{\imath\theta}+e^{-\imath\theta}}{2} e^{-\imath kz}\right)\hat{\mathbf{e}}_x + \mathcal{E}_0 \tfrac{e^{\imath\theta}-e^{-\imath\theta}}{2\imath} e^{-\imath kz}\hat{\mathbf{e}}_y \\ &= \tfrac{\mathcal{E}_0}{\sqrt{2}}\left[-(e^{\imath kz}+e^{-\imath kz-\imath\theta})\hat{\mathbf{e}}_1 + (e^{\imath kz}+e^{-\imath kz+\imath\theta})\hat{\mathbf{e}}_{-1}\right] \\ &= \sqrt{2}\mathcal{E}_0\left[-e^{-\imath\theta/2}\cos(kz+\tfrac{\theta}{2})\hat{\mathbf{e}}_1 + e^{\imath\theta/2}\cos(kz-\tfrac{\theta}{2})\hat{\mathbf{e}}_{-1}\right] .\end{aligned}$$

38.2.5.4 Ex: Sub-lattices

Consider two laser standing wave laser beams crossing each other under an angle of 90°,

$$\vec{\mathcal{E}}_1 = \vec{\varepsilon}_1 e^{\imath(kx-\omega t)} \qquad \text{and} \qquad \vec{\mathcal{E}}_2 = \vec{\varepsilon}_2 e^{\imath(ky-\omega t)} ,$$

with arbitrary elliptical polarizations $\vec{\varepsilon}_i$ and study the scalar light-shift potential,

$$U_s = -\frac{\alpha_s}{4}|\vec{\mathcal{E}}|^2 ,$$

as well as the vector light-shift potential,

$$U_v = \vec{\mathcal{B}}_{eff}\cdot\mathbf{F} \qquad \text{where} \qquad \vec{\mathcal{B}}_{eff} = \imath\alpha_v\vec{\varepsilon}^{*}\times\vec{\varepsilon}$$

in the xy-plane. α_v is the vector part of the atomic polarizability and $\vec{\mathcal{B}}_{eff}$ an effective magnetic field [362, 783, 28].

Solution: *See the figure 38.6.*

38.3 Photonic recoil on free and confined atoms

A trap confining the atomic motion can dramatically modify the way in which they interact with light [5]. For instance, a trapping potential may alter the scattering rate, the scattering angle, and the transfer of photonic recoil. However, *potentials do not exist* in microscopic reality, not more than friction forces do. What exists, as we learn in electrodynamics, are *electromagnetic fields* exerting Coulomb and Lorentz forces. When we write down the Hamiltonian $\hat{H} = \mathbf{p}^2/2m + V(\mathbf{r})$ in quantum mechanics, we already make an important approximation, because the potential $V(\mathbf{r})$ is an artifact obtained by tracing over all those degrees of freedom, which are necessary to generate a force field that can be approximated by a conservative potential.

[5] The interaction also depends on other parameters, such as the geometry of the confinement potential and on cooperative effects (bosonic stimulation), but this will be discussed later.

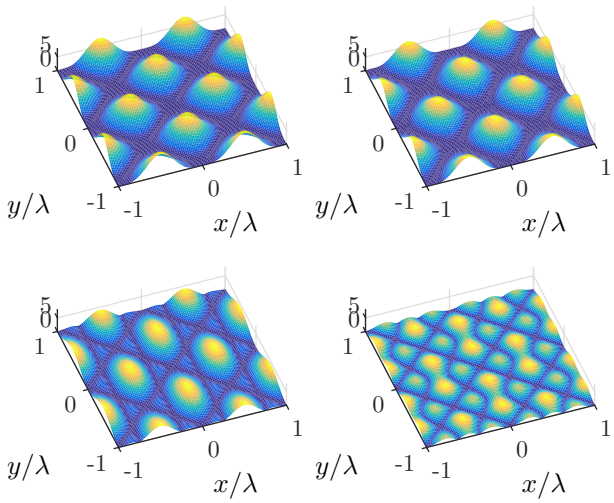

Figure 38.6: (code) Lattice potential for different polarizations.

In the great majority of situations, the approximation is very good. Problems may however arise, when the momentum conservation comes into play, which is the case e.g. of light scattering from ultracold atoms being accelerated by the photonic recoil and shifting the scattered light via the Doppler effect. We then have to address the issue of photonic recoil conserving (or not) the momentum.

Let us begin with a recapitulation of the classical picture of the scattering process applying the rules of energy and momentum conservation to the elastic collision between a free atom and a photon. This process is known as *Compton scattering*.

38.3.1 Recoil- and Doppler-shift in classical mechanics

In classical mechanics we speak of *elastic scattering* when no energy is transferred to internal degrees of freedom of the collision partners, so that *kinetic* energy and momentum stay conserved. This concept can be transferred to quantum particles (e.g. atoms) and photons. In elastic Compton scattering, if the atoms keep their initial internal excitation, the law of momentum conservation requires the transfer of photonic momentum to the scattering atom which, consequently, changes its kinetic energy. To compensate for this kinetic energy change, the frequency of the scattered light must change in order to preserve the total energy, as illustrated in Fig. 38.7(b).

We will calculate in the following the frequency distribution of the light scattered by an atom as a function of its initial velocity $\mathbf{p}_1$, of the frequency ω_1 of the incident light and of the scattering angle, that is, the angle between the modes $\mathbf{k}_1$ and $\mathbf{k}_2$. We begin by writing the laws of conservation of energy and momentum,

$$\begin{aligned} \hbar\mathbf{k}_1 + \mathbf{p}_1 &= \hbar\mathbf{k}_2 + \mathbf{p}_2 \\ \hbar\omega_1 + \frac{p_1^2}{2m} &= \hbar\omega_2 + \frac{p_2^2}{2m} \ . \end{aligned} \tag{38.35}$$

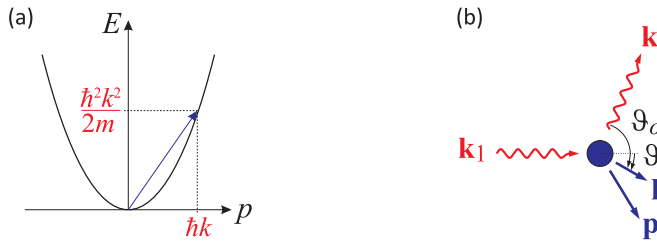

Figure 38.7: (a) Kicking an atom along its dispersion relation. (b) Scheme of the Compton-scattering of light.

Eliminating $\mathbf{p}_2$ from the second equations, we obtain,

$$\hbar\omega_1 - \frac{\hbar^2 k_1^2}{2m} - \frac{\hbar \mathbf{k}_1 \cdot \mathbf{p}_1}{m} = \hbar\omega_2 + \frac{\hbar^2 k_2^2}{2m} - \frac{(\hbar \mathbf{k}_1 + \mathbf{p}_1) \cdot \hbar \mathbf{k}_2}{m} \ . \tag{38.36}$$

The photonic recoils of the incident and of the scattered light are almost equal,

$$\omega_{rec} \equiv \frac{\hbar k_1^2}{2m} \simeq \frac{\hbar k_2^2}{2m} \ , \tag{38.37}$$

such we can approximate,

$$\omega_2 = \omega_1 \frac{1 - \frac{\hbar\omega_1}{mc^2} - \frac{p_1}{mc}\cos\sphericalangle(k_1, p_1)}{1 - \frac{\hbar\omega_1}{mc^2}\cos\sphericalangle(k_1, k_2) - \frac{p_1}{mc}\cos\sphericalangle(p_1, k_2)} \ , \tag{38.38}$$

using $\omega_1 = ck_1$, or also,

$$\omega_2 - \omega_1 = \omega_1 \frac{\frac{\hbar\omega_1}{mc^2}\left[-1 + \cos(\vartheta_{in} - \vartheta_{out})\right] + \frac{p_1}{mc}(\cos\vartheta_{out} + \cos\vartheta_{in})}{1 - \frac{\hbar\omega_1}{mc^2}\cos(\vartheta_{in} - \vartheta_{out}) - \frac{p_1}{mc}\cos\vartheta_{out}} \ , \tag{38.39}$$

where we call the angles $\vartheta_{in} = \sphericalangle(k_1, p_1)$, $\vartheta_{out} = \sphericalangle(k_2, p_1)$, and $\vartheta = \vartheta_{in} - \vartheta_{out} = \sphericalangle(k_1, k_2)$. For non-relativistic velocities, the denominator is approximately 1:

$$\boxed{\omega_2 - \omega_1 = 2\omega_{rec}(-1 + \cos\vartheta) + k_1 v_1(\cos\vartheta_{out} + \cos\vartheta_{in})} \ , \tag{38.40}$$

with $\mathbf{p}_1 = m\mathbf{v}_1$. The first term describes the recoil shift and the second term the Doppler shift.

The second term vanishes for initially at resting atoms, $\mathbf{p}_1 = 0$, and Eq. (38.40) simplifies to,

$$\omega_2 - \omega_1 = 2\omega_{rec}(-1 + \cos\vartheta) \ . \tag{38.41}$$

It also vanishes for atoms which have no velocity component in the scattering plane spanned by the wavevectors $\mathbf{k}_1$ and $\mathbf{k}_2$, that is $\vartheta_{out} = 180° - \vartheta_{in}$ [6], for which case we get the maximum recoil shift,

$$\omega_2 - \omega_1 = -4\omega_{rec} \ . \tag{38.42}$$

[6] This situation is often realized in Bragg scattering from optical lattices [1219, 1221, 1220].

The recoil shift is a consequence of momentum conservation.

The recoil shift is typically on the order of $\omega_2 - \omega_1 \approx (2\pi)\ 10$ kHz, which in many situations is negligible (e.g. when we deal with thermal atomic clouds), such that we can consider the scattering as elastic., i.e. the first term can be disregarded. Considering, for simplicity, only backscattering, $\cos\vartheta_{out} = \cos\vartheta_{in} = 1$, then Eq. (38.40) simplifies to,

$$\omega_2 - \omega_1 = 2k_1 v_1 \ . \tag{38.43}$$

Obviously, the frequency shift depends on the initial velocity through the Doppler shift $k_1 v_1$. In a thermal gas, the velocities are distributed according to the Maxwell-Boltzmann distribution. Therefore, Rayleigh scattering of light off a cloud of free thermal atoms is subject to Doppler broadening [7].

38.3.1.1 Roadmap

For the discussion of optical forces on confined atoms we will consecutively discuss the following questions:

1. Energy and momentum conservation upon scattering of light from a single atom confined in **weak** or **strong** trapping potentials (inhomogeneous systems);

2. scattering from atoms confined in anisotropic traps (strong confinement in one and weak confinement in the other direction);

3. cooperativity (bosonic stimulation) (of the scattered light, not of the atomic momentum) shapes the static structure factor [8];

4. discrete translation invariant (periodic) systems, where quasi-momentum (Bloch bands, lattices);

5. lattices made of laser beams with fixed phase, explicit pots. $V(\mathbf{r}) = \hbar g e^{\imath \mathbf{k}\cdot\mathbf{r}} \hat{b} + c.c.$;

6. lattices made of laser beams with mobile phase.

7. how does the trap modify scattering rates, scattering angles (in particular in case of anisotropic traps), dynamic structure factor?

8. how to calculate a dynamic structure factor?

9. differentiate the term elastic scattering with respect to resonance fluorescence (internal) and recoil (external).

[7] This Doppler broadening is explored e.g. in RIR spectroscopy, where the momentum distribution in p_1 reveals as a frequency distribution $\Delta\omega = \omega_2 - \omega_1$ of Bragg-scattered light, which can be measured by beating with an irradiated idler mode, which can be chosen as being identical to $\mathbf{k}_2$.

[8] In [1219, 1220], we argue that $\mathbf{p}_f = 0$ and that $\hat{\mathbf{e}}_z \cdot \mathbf{k}_i = -\hat{\mathbf{e}}_z \cdot \mathbf{k}_f$, so that we can disregard momentum conservation. The scattering is elastic although (electronically) on resonance, because it is not vibrationally on resonance.

38.3.2 Kicking a free atom

A conceptual difficulty arises from the incompatibility of scattering picture (generally described in homogeneous space with momentum conservation) and the trapping picture (when it is described in inhomogeneous space without momentum conservation). The difficulty can be avoided by separating the processes into a 'kick' followed by a harmonic oscillation, for which we have to calculate the time-dependence of the states and the observables. We will leave the discussion of such a scattering process to 38.3.3 and for the time being just focus on the time evolution of a harmonic oscillator that just received a kick.

By a 'kicking' an atom we denote a change of momentum within an arbitrarily short amount of time. The shorter the kick-time the larger is, according to Heisenberg's uncertainty relation, the spectrum of possible kinetic energies that can be reached by the kick (see Sec. 27.4.3). However, the spectrum is restricted by the free-particle dispersion relation, as illustrated in Fig. 38.7(a).

The kick is not a realistic physical concept, as it corresponds to an infinitely strong and infinitely short force [9]. In a microscopic scattering process it assumes an infinitely heavy collision partner, while we are more interested in photon scattering. Consequently, in this case the spectrum of reachable energies is determined by the frequency of the photon *and* the free-particle dispersion relation. We will now turn our attention to the (Compton-)scattering of light by free atoms.

38.3.3 (In-)elastic light scattering from a single weakly or strongly confined atom

We mentioned in the last subsection that a scattering process is elastic when none of the collision partners changes its internal excitation energy. The situation becomes, however, more complex when one of the collision partners is confined in a potential, as we will show in the following.

38.3.3.1 Cooperativity in light scattering

In light scattering *cooperativity* means *breaking of the isotropic symmetry* for the angular distribution of scattered modes. In this sense, the anisotropic scattering from an atom confined in an anisotropic trap is cooperative. But there are other cooperative scattering effects messing with isotropy and shaping the density-of-states, like the Purcell effect in the presence of an optical cavity or a photonic band gap concentrating optical modes in a specific solid angles [596]. Another cooperative effect, which is observed in the presence of other atoms, has to do with bosonic stimulation by the optical output mode (as in Bragg scattering [1219, 1221, 1220]) or the momentum sidemode (as in stimulated matter wave 4WM). These effects, which all need to be considered in calculations of the static structure factor ruling the scattering of light, are often strong enough to hide the role of an anisotropic trapping potential. In the following subsections we will disregard all these effects and concentrate on a *single trapped atom*.

The simple picture of Compton scattering presented in Sec. 38.3.1 holds for *free atoms*, whose dynamics is totally understood in terms of their internal electronic

[9] which is what allows us to write down a potential

excitation ($\hat{H}_{ele}$), the kinetic energy of their center-of-mass ($\hat{H}_{cm} = \frac{\mathbf{p}^2}{2m}$), the radiation field ($\hat{H}_{rad}$) (which may be treated classically under the circumstances discussed here), and the coupling ($\hat{H}_{int}$) of all three degrees of freedom,

$$\hat{H}_{free} = \hat{H}_{ele} + \hat{H}_{cm} + \hat{H}_{rad} + \hat{H}_{int} \ . \tag{38.44}$$

Transition probabilities are readily calculated using Fermi's Golden rule, because the density-of-states distributions for the final radiation modes receiving the scattered photons (photonic density-of-states) and the recoil modes receiving the scattered atoms (phononic density-of-states) are white, that is, without resonances, and isotropic.

In the presence of an imposed trapping potential, an additional term appears in the Hamiltonian, which has the capacity of dramatically changing the scattering features,

$$\hat{H}_{cm} = \frac{\mathbf{p}^2}{2m} + \hat{V}_{trap}(\mathbf{r}) \ . \tag{38.45}$$

The confining potential may or may not depend on the internal state of the atom. For ions in a Paul trap it does not depend, but for atoms in magnetic traps it usually depends,

$$\begin{aligned} \hat{H}_{atom} &= |g\rangle \hat{H}_{cm,g} \langle g| + |e\rangle (\hat{H}_{cm,e} + \hbar\omega_0) \langle e| \\ \hat{H}_{cm,j} &= \frac{\hat{p}^2}{2m} + V_j(\mathbf{r}) \ , \end{aligned} \tag{38.46}$$

where ω_0 is the frequency of the atomic transition. In the following, however, we will treat potentials that are independent of the internal atomic state.

38.3.3.2 Resolved sideband regime

As discussed in Sec. 34.6.5, incident light is absorbed by an atom harmonically oscillating in a trap with frequency ω_{trp} on a spectrum of discrete sidebands separated by ω_{trp} with amplitudes given by $J_n(kv_0/\omega_{trp})$. The modulation index $kv_0/\omega_{trp} = kx_0 = 2\pi x_0/\lambda$ corresponds to the Lamb-Dicke parameter. When the modulation amplitude is within the so-called *Lamb-Dicke regime*, $kv_0 \ll \omega_{trp}$, the first sidebands become smaller than the carrier, $J_1(kv_0/\omega_{trp}) < J_0(kv_0/\omega_{trp})$ and, therefore, do not contribute to the Doppler width of the frequency distribution. That is, the linear Doppler effect vanishes.

The relative size of the characteristic frequencies ω_{rec}, ω_{trp}, and Γ define characteristic regimes, as illustrated in the table.

confinement		sidebands	
weak	$\eta > 1$	unresolved	$\frac{\omega_{trp}}{\Gamma} < 1$
strong	$\eta < 1$	resolved	$\frac{\omega_{trp}}{\Gamma} > 1$

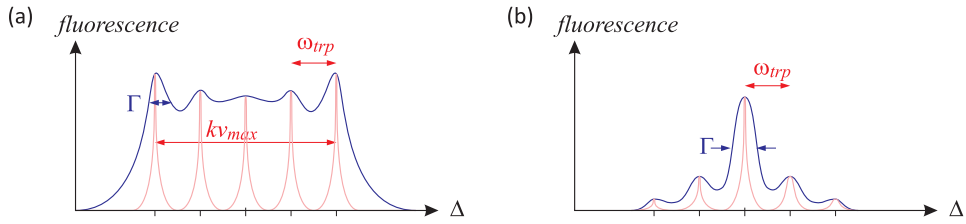

Figure 38.8: Absorption profile in the regimes of (a) weak binding ($\eta > 1$) for the cases of and unresolved sidebands (blue curve) and resolved sidebands (red curve), and (b) strong binding (Lamb-Dicke regime $\eta < 1$) for the same cases as in (a).

38.3.3.3 The Mößbauer effect

The role of photonic recoil in the scattering of light by confined atoms has been unraveled by *Mößbauer*, who performed scattering experiments of γ-photons on a ^{57}Fe crystal on a narrow transition of this isotope at 14 keV (0.086 nm). The linewidth of this transition, $\Gamma \approx (2\pi)\ 1\,\text{MHz}$, is much narrower than the recoil-shift, $\omega_{rec} \approx (2\pi)\ 500\,\text{MHz} \gg \Gamma$, so that we should expect the scattered light to be considerably recoil-shifted and Doppler-broadened. In fact, the recoil-shift should be so large, that scattered photons cannot be reabsorbed by other atoms on this transition being at rest. This is *not* what Mößbauer observed in his experiments. He found that scattered photons can be reused for subsequent scattering, which means that the scattering must be elastic.

The explanation for this unexpected observation is that, if the nucleus is embedded in a crystal, the vibrational frequencies, which are even higher than the photonic recoil frequency, $\omega_{trp} \approx 2\pi \cdot 3\,\text{THz}$, are unreachable. That is to say, we are in the *resolved sidebands Lamb-Dicke regime*, $\omega_{trp} \gg \omega_{rec} \gg \Gamma$. Here, the phonons corresponding to the vibrations cannot be excited, so that the recoil momentum must be absorbed by the whole lattice, whose entire mass is so large, that the photon frequency is not recoil-shifted by the scattering process. Hence, the first-order *Doppler effect* is avoided and the measured width of the transition is just the natural linewidth. Furthermore, the atom remains in the same vibrational state of their localizing potential. This is the *Mößbauer effect*.

	γ for ^{57}Fe	optical for $^{172}Yb^{+}$
photon energy	$\approx 14\,\text{keV} \quad \approx 4 \times 10^{18}\,\text{Hz}$	$\approx 3\,\text{eV} \quad \approx 640\,\text{THz}$
recoil	$\approx 2\,\text{meV} \quad \approx 500\,\text{MHz} \quad \approx 10^{-10}$	$\approx 20\,\text{peV} \quad \approx 5\,\text{kHz} \quad \approx 10^{-11}$
linewidth	$\approx 5\,\text{neV} \quad \approx 1\,\text{MHz} \quad \approx 2 \times 10^{-13}$	$\approx 5\,\text{feV} \quad \approx 1\,\text{Hz} \quad \approx 2 \times 10^{-15}$
lattice vibrations	$\approx 10\,\text{meV} \quad \approx 3\,\text{THz}$	$\approx 3\,\text{neV} \quad \approx 1\,\text{MHz}$

Table 38.1: Comparison of γ-radiation and the optical regime.

A similar effect can be observed with trapped atoms driven on very narrow transitions, as we will discuss in the following.

38.3.3.4 Coupling of internal and external motion by photonic recoil, tracing over the internal excitation

When discussing the transfer of momentum to a harmonic oscillator in 24.6.2, we did not say how the momentum shift could be realized in practice. As we have seen in the example of the Mößbauer effect, a possible way is via the photonic recoil received on a light scattering process. The coupling of the relevant degrees of freedom of the system induced by the absorption of a photon by an atom is accounted for by an additional interaction term $\hat{H}_{int}$ in the Hamiltonian. The relevant degrees of freedom are the electronic orbital $|i\rangle$, the vibrational state $|n\rangle$, and the number of photons $|N\rangle$ in the light mode, assumed to be a plane wave $\vec{\mathcal{E}}(\mathbf{r},t) = E_0\hat{\mathbf{e}}_y e^{\imath k_z z - \imath\omega t}$. Neglecting the quantum nature of the light, we will disregard this degree of freedom in the following. Assuming that the trapping potential is the same for all electronic orbitals, as in (38.46), the total state can be expressed as a product state, $|n,i\rangle \equiv |i\rangle \otimes |n\rangle$. The interaction Hamiltonian,

$$\hat{H}_{int} = \frac{\hbar\Omega}{2}(e^{\imath k\hat{z}}\hat{a}|e\rangle\langle g| + e^{-\imath k\hat{z}}\hat{a}^\dagger|g\rangle\langle e|) - |e\rangle\hbar\omega\langle e| \ , \tag{38.47}$$

couples the dynamics on the internal transition, given by the Rabi frequency $\hbar\Omega \equiv \langle e|d_y|g\rangle\mathcal{E}_0$, with the absorption (or stimulated emission) of a photon $\hat{a}$, and the transfer of a recoil momentum. The last term comes from the transformation into the interaction picture [10]. With this our total Hamiltonian (38.46) becomes,

$$\boxed{\hat{H} = \hbar\omega_{trp}(\hat{b}^\dagger\hat{b} + \tfrac{1}{2}) + |e\rangle\hbar(\omega_0-\omega)\langle e| + \tfrac{\hbar\Omega}{2}(e^{\imath k\hat{z}}|e\rangle\langle g| + e^{-\imath k\hat{z}}|g\rangle\langle e|)} \ . \tag{38.48}$$

So, vibrational states are only coupled via electronic transitions,

$$\langle n,g|\hat{H}_{int}|0,g\rangle = 0 \qquad \text{and} \qquad \langle n,e|\hat{H}_{int}|0,g\rangle = \tfrac{1}{2}\hbar\Omega\langle n,e|e^{\imath k\hat{z}}|0,g\rangle \ . \tag{38.49}$$

Hence, we have to span the complete Hilbert space of all operators like $\hat{\sigma}^\dagger = \sum_n |n\rangle\langle n| \otimes |e\rangle\langle g|$.

We can expand the system's state into,

$$|\psi(t)\rangle = \sum_{n=0}^{\infty}(c_{n,g}|n,g\rangle + c_{n,e}|n,e\rangle \ , \tag{38.50}$$

and insert it together with the Hamiltonian (38.48) into the Schrödinger equation. Projecting onto the states $\langle n,g|$ and $\langle n,e|$, we easily derive the following equations of motion,

$$\boxed{\begin{aligned} \frac{dc_{n,g}}{dt} &= -\imath\omega_{trp}(n+\tfrac{1}{2})c_{n,g} - \frac{\imath\Omega}{2}\sum_{m=0}^{\infty} c_{m,e}\langle n|e^{-\imath k\hat{z}}|m\rangle \\ \frac{dc_{n,e}}{dt} &= -\imath\omega_{trp}(n+\tfrac{1}{2})c_{n,e} - \imath(\omega_0-\omega)c_{n,e} - \frac{\imath\Omega}{2}\sum_{m=0}^{\infty} c_{m,g}\langle n|e^{\imath k\hat{z}}|m\rangle \end{aligned}} \ . \tag{38.51}$$

[10] Note, that this Hamiltonian cannot be used to describe spontaneous emission. To do so, we need to allow for 3D systems and decay modes,

$$\hat{H} = \hbar\omega_{trp}(|\mathbf{n}\rangle\langle\mathbf{n}| + \tfrac{1}{2}) + \hbar(\omega_0-\omega)|e\rangle\langle e| + \tfrac{\hbar\Omega}{2}(e^{-\imath\mathbf{k}_i\cdot\hat{\mathbf{r}}}\hat{\sigma}^\dagger\hat{a}_{\mathbf{k}_i} + c.c.) + \hbar g\sum_{\mathbf{k}_f}(e^{\imath\mathbf{k}_f\cdot\hat{\mathbf{r}}}\hat{\sigma}\hat{a}^\dagger_{\mathbf{k}_f} + c.c.) \ .$$

The fact that only terms proportional to $\langle n|e^{ik\hat{z}}|m\rangle$ contribute can be understood in terms of the *Franck-Condon overlap* between the vibrational states to be coupled. And the fact that the energy of the harmonic oscillator, and thus the effective detuning $\Delta_n \equiv \omega - \omega_0 - \omega_{trp}(n + \frac{1}{2})$, depend on the vibrational state couples the internal and the external dynamics.

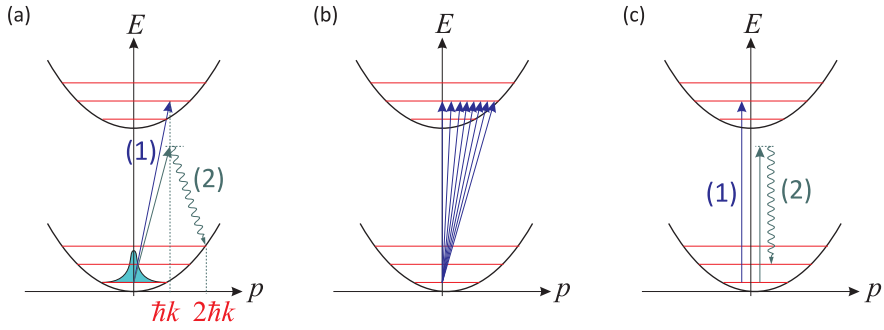

Figure 38.9: (a) Absorption (1) and Rayleigh scattering (2) in a weakly confining trap, where the momentum must stay conserved. (b) Illustration of the regime $\omega_{rec} > \Gamma$, where the atom moves during the absorption process. (c) Absorption and Rayleigh scattering in a strongly confining trap.

Nevertheless, the off-diagonal coupling elements only contain the degrees of freedom of the harmonic oscillator.

38.3.3.5 Momentum kick by photonic recoil

We said earlier that a momentum kick can drive an atom from the vibrational ground state $|0\rangle$ into a coherent superposition of states $|\alpha\rangle$, except when the Lamb-Dicke parameter is very small. When the kick is realized via photonic recoil, e.g. when an electronically excited atom decays to the ground state, the frequency of the emitted photon depends on the final vibrational state of the atom. That is we expect a coherent superposition of light frequencies, which in the limit $\eta > 1$ generates a *Doppler broadening* and in the limit $\eta < 1$ stays unshifted as for *elastic scattering*.

Let us now consider a single confined atom and address the question of the absorption probability. In first-order perturbation, using the Hamiltonian (38.48), the transition rate for absorption of a photon incident in z-direction is given by Fermi's Golden Rule,

$$\begin{aligned}\frac{1}{\tau} &= \frac{d}{dt}|\langle n,e|e^{\imath\hat{H}t/\hbar}|0,g\rangle|^2 \simeq \frac{2\pi}{\hbar^2}|\langle n,e|\hat{H}|0,g\rangle|^2 \\ &= \frac{2\pi}{\hbar^2}|\langle n,e|\tfrac{\hbar\Omega}{2}(e^{\imath k\hat{z}}\hat{\sigma}^\dagger + e^{-\imath k\hat{z}}\hat{\sigma})|0,g\rangle|^2 = \frac{\pi\Omega^2}{2}|\langle n,e|e^{\imath k\hat{z}}|0,e\rangle|^2 \ .\end{aligned} \tag{38.52}$$

Obviously, it is thus sufficient to calculate $\langle n|e^{ik\hat{z}}|0\rangle$, i.e. we can trace over the internal degrees of freedom. Using our previous results (24.136), we find with $\alpha = -ika_{trp}/\sqrt{2}$,

$$\boxed{\frac{1}{\tau} = \frac{\pi\Omega^2}{2}|\langle n|\alpha\rangle|^2 = \frac{\pi\Omega^2}{2}e^{-|\alpha|^2}\frac{|\alpha^n|^2}{n!}} \ . \tag{38.53}$$

The interpretation of this result is that the absorption of a photon by an atom in state $|0,g\rangle$ transfers recoil by *leaving the vibrational state of the atom in a coherent superposition state*. Inversely, for the emission process from state $|0,e\rangle$ within the Lamb-Dicke regime, most of the time we will encounter the emitted photon at the resonance frequency ω_0, and rarely at $\omega_0 - \omega_{trp}$. In any case, energy conservation is satisfied, since,

$$\sum_n n\hbar\omega_{trp}\langle n|\alpha\rangle\langle\alpha|n\rangle = \sum_n n\hbar\omega_{trp}e^{-|\alpha|^2}\frac{|\alpha|^{2n}}{n!} = \hbar\omega_{trp}|\alpha|^2\sum_n ne^{-|\alpha|^2}\frac{|\alpha|^{2n-2}}{(n-1)!}$$
$$= \frac{\hbar^2k^2}{2m}\langle\alpha|\alpha\rangle = \hbar\omega_{rec}\ . \tag{38.54}$$

Thus energy and momentum conservation are automatically satisfied by the way the kick is implemented.

38.3.3.6 A single anisotropically trapped atom in first-order perturbation

Let us now consider a single atom (e.g. a trapped ion) confined in an 3-dimensional anisotropic trap (e.g. strong confinement in one and weak confinement in the other direction) and address the question, whether the scattering will be anisotropic, as well. We generalize the problem to three dimensions by allowing for quantized vibrational states in three dimensions, $\hat\sigma^\dagger = \sum_{\mathbf{n}}|\mathbf{n}\rangle\langle\mathbf{n}|\otimes|e\rangle\langle g|$ with $|\mathbf{n}\rangle = |n_x,n_y,n_z\rangle$.

In first-order perturbation, using the Hamiltonian (38.48), the transition rate for absorption or emission is given by Fermi's Golden Rule,

$$\frac{1}{\tau} = \frac{d}{dt}|\langle\mathbf{n},e|e^{\imath\hat Ht/\hbar}|\mathbf{0},g\rangle|^2 \simeq \frac{2\pi}{\hbar^2}|\langle\mathbf{n},e|\tfrac{\hbar\Omega}{2}(e^{\imath\mathbf{k}\cdot\hat{\mathbf{r}}}\hat\sigma^\dagger + e^{-\imath\mathbf{k}\cdot\hat{\mathbf{r}}}\hat\sigma)|\mathbf{0},g\rangle|^2 \tag{38.55}$$
$$= \frac{\pi\Omega^2}{2}|\langle n_x,e|e^{\imath k\hat x}|0,e\rangle\langle n_y,e|e^{\imath k\hat y}|0,e\rangle\langle n_z,e|e^{\imath k\hat z}|0,e\rangle|^2\ .$$

Obviously, it is thus sufficient to calculate $\langle n_j|e^{\imath k\hat z}|0\rangle$, i.e. we can trace over the internal degrees of freedom. Using our previous results (24.136), we find with $\alpha_j = -\imath k_j a_{trp,j}/\sqrt{2}$,

$$\boxed{\frac{1}{\tau} = \frac{\pi\Omega^2}{2}|\langle n_x|\alpha_x\rangle\langle n_y|\alpha_y\rangle\langle n_z|\alpha_z\rangle|^2 = \frac{\pi\Omega^2}{2}e^{-|\alpha_x|^2-|\alpha_y|^2-|\alpha_z|^2}\frac{|\alpha_x^{n_x}\alpha_y^{n_y}\alpha_z^{n_z}|^2}{n_x!n_y!n_z!}}\ .$$

In Exc. 38.3.5.1 we calculate and illustrate the transition matrix elements $\langle\mathbf{0}|e^{\imath k\hat z}|0\rangle$ and $\langle\mathbf{n}|e^{\imath k\hat z}|0\rangle$.

38.3.3.7 A single anisotropically trapped atom in second-order perturbation

To understand Rayleigh scattering, we need to go to second perturbation order summing over all intermediate vibrational states according to the Kramers-Heisenberg

formula,

$$\begin{aligned}\frac{d\sigma}{d\Omega} &= \frac{d}{dt}|\langle \mathbf{n}, g, \mathbf{k}_f|e^{\imath\hat{H}t/\hbar}|\mathbf{0}, g, \mathbf{k}_i\rangle|^2 \simeq \frac{2\pi}{\hbar^2}|\langle \mathbf{n}, g, \mathbf{k}_f|\sum_{\mathbf{m}}\frac{\hat{H}^{(1)}|\mathbf{m}, e\rangle\langle \mathbf{m}, e|\hat{H}^{(1)}}{\omega_i - \omega_m}|\mathbf{0}, g, \mathbf{k}_i\rangle|^2 \\ &= \frac{\pi\hbar^2\Omega^4}{8}\left|\sum_{\mathbf{m}}\frac{\langle \mathbf{n}, \mathbf{k}_f|e^{-\imath\mathbf{q}\cdot\hat{\mathbf{r}}}|\mathbf{m}\rangle\langle \mathbf{m}|e^{\imath\mathbf{q}\cdot\hat{\mathbf{r}}}|\mathbf{0}, \mathbf{k}_i\rangle}{E_i/\hbar + (0\omega_x + 0\omega_y + 0\omega_z + \frac{3}{2}) - E_m/\hbar - (m_x\omega_x + m_y\omega_y + m_z\omega_z + \frac{3}{2})}\right|^2 \\ &= \frac{\pi\hbar^2\Omega^4}{8}\left|\sum_{m_x,m_y,m_z}\frac{\langle n_x, n_y, n_z|e^{-i\mathbf{k}_f\cdot\hat{\mathbf{r}}}|m_x, m_y, m_z\rangle\langle m_x, m_y, m_z|e^{\imath\mathbf{k}_i\cdot\hat{\mathbf{r}}}|0, 0, 0\rangle}{(E_i - E_m)/\hbar - m_x\omega_x - m_y\omega_y - m_z\omega_z}\right|^2 \\ &= \frac{\pi\hbar^2\Omega^4}{8}\left|\sum_{m_x,m_y,m_z}\prod_{j=x,y,z}\frac{\langle n_j|e^{-ik_{jf}r_j}|m_j\rangle\langle m_j|e^{ik_{ji}\mathbf{r}_j}|0\rangle}{(E_i - E_m)/\hbar - m_x\omega_{mx} - m_y\omega_{my} - m_z\omega_{mz}}\right|^2 .\end{aligned} \tag{38.56}$$

The transition matrix elements can be calculated via (24.141). This expression represents (in the same time) the *dynamic structure factor* of the single trapped atom.

Example 225 (*Axial incidence*): Let us consider the particular case of Rayleigh scattering from the ground state of light incident in the direction $\mathbf{k}_i \equiv k_{iz}\hat{\mathbf{e}}_z$. We can then simplify,

$$\begin{aligned}\frac{d\sigma}{d\Omega} &= \frac{\pi\hbar^2\Omega^4}{8}\left|\sum_{m_z}\frac{\langle 0|e^{-\imath k_{xf}\hat{x}}|0\rangle\langle 0|e^{-\imath k_{yf}\hat{y}}|0\rangle\langle 0|e^{-\imath k_{zf}\hat{z}}|m_z\rangle\langle m_z|e^{\imath k_{zi}\hat{z}}|0\rangle}{-m_z\omega_{trp}}\right|^2 \\ &= \frac{\pi\hbar^2\Omega^4}{8}e^{-|\alpha_{fx}|^2-|\alpha_{fy}|^2-|\alpha_{fz}|^2-|\alpha_{iz}|^2}\left|\sum_{m_z}\frac{1}{(E_m - E_i)/\hbar - m_z\omega_{trp,z}}\frac{\alpha_{fz}^{m_z}\alpha_{iz}^{m_z}}{m_z!}\right|^2 \\ &= \frac{\pi\hbar^2\Omega^4}{8}e^{-(\mathbf{k}_f\cdot\mathbf{a}_{trp})^2/2-(\mathbf{k}_i\cdot\mathbf{a}_{trp})^2/2}\left|\sum_{m_z}\frac{1}{(E_m - E_i)/\hbar - m_z\omega_{trp,z}}\frac{(-\frac{1}{2}k_{fz}k_{iz}a_{trp,z}^2)^{m_z}}{m_z!}\right|^2 ,\end{aligned}$$

where $\mathbf{a}_{trp} \equiv (a_{trp,x}\ a_{trp,y}\ a_{trp,z})$. Looking into scattering into transverse direction, $\mathbf{k}_{f,z} = 0$, we get,

$$\left(\frac{d\sigma}{d\Omega}\right)_{\perp} = \frac{\pi\hbar^4\Omega^4}{8|E_m - E_i|^2}e^{-\mathbf{k}_{fx}^2a_{trp,x}^2/2-\mathbf{k}_{fy}^2a_{trp,y}^2/2-\mathbf{k}_{iz}^2a_{trp,z}^2/2} .$$

Looking into backscattering, $\mathbf{k}_{f,z} = -\mathbf{k}_{i,z}$,

$$\left(\frac{d\sigma}{d\Omega}\right)_{\parallel} = \frac{\pi\hbar^2\Omega^4}{8}e^{-\mathbf{k}_i a_{trp,z})^2}\left|\sum_{m_z}\frac{1}{(E_m - E_i)/\hbar - m_z\omega_{trp,z}}\frac{(-\frac{1}{2}k_{iz}^2a_{trp,z}^2)^{m_z}}{m_z!}\right|^2 .$$

we expect a spectrum with vibrational resonances.

38.3.3.8 Discussion of scattering from a single weakly or strongly confined particle

We assume that the lifetime of an atomic transition is much shorter than an oscillation period (or the Rabi-frequency), $\Gamma, \Omega \gg \omega_{trp}$, the position of the atoms does not change

during a transition process, i.e. we have a *Franck-Condon transition* in position space [853] [11].
For weakly confined particles:

- Energy and momentum conservation holds during absorption or scattering process. Absorption, fluorescence, and Rayleigh scattering are just like for free particles (i.e. inelastic because of photon recoil). Thus, transitions must start and end on the dispersion curve, e.g. for scattering at an initially resting atom,

$$\hbar\omega_i = \hbar\omega_f + \frac{p_f^2}{2m} - \hbar\Delta\omega_{trap} \qquad \text{and} \qquad \mathbf{k}_i = \hbar\mathbf{k}_f + \mathbf{p}_f \ . \tag{38.57}$$

- U-shaped absorption spectrum
- Doppler-cooling picture of shrinking ellipse in phase space [655], but not during the oscillation of the atom in the trap.
- Message: *If your atom is weakly confined, you may not neglect the recoil-shift.*
- The momentum is conserved during the scattering process, provided the process is fast enough, i.e. $\Gamma \gg \omega_{trp}$. What the trap does afterward with the momentum is its own problem [1383], not the one of the light field.

For strongly confined particles:

- Momentum conservation does not hold during the scattering process, it is absorbed by the trap. Light scattering is totally elastic (no recoil shift). Nevertheless, absorption and fluorescence, Rayleigh and Raman scattering must end up on vibrational sidebands.
- motional sideband spectrum
- in the resolved sideband regime, we may achieve sideband cooling [422]
- when the sidebands are not resolved, we still can do stimulated Raman sideband cooling (Bragg spectroscopy)
- Message: *If your atom is strongly confined, you may do Rayleigh or Raman.*

Discuss momentum conservation from (??) comparing $\hbar^2k^2/2m$ and $m\omega_{trp}^2\hat{z}^2/2$.

38.3.3.9 Rigid lattice: single atom in a standing wave cavity mode

Let us restrict to a single dimension and discuss the problem of kicking a single atom confined in a standing plane light wave. We want to describe the physical situation after an attempted kick *including* the optical lattice system and *satisfying all conservation laws*. The problem is that we need to describe the atomic motion quantum-mechanically! [12].

[11] Vertical transitions in the potential curve.
[12] The harmonic oscillator picture cannot we used for shallow potentials supporting only 0 or 1 vibrational states.

The situation in a linear optical cavity is different, because the counterpropagating light modes just form a single one,

$$\hat{a}_- = \hat{a}_+ \ , \tag{38.58}$$

so a photon backscattered between the two modes always ends up in original mode after having been reflected from a cavity mirror. Then, the dipole potential terms simplifies to,

$$2\hbar U_0 |\alpha_+|^2 \sin 2k_{lat}\hat{z} \ . \tag{38.59}$$

Now, the momentum of the cavity light fields is certainly *not conserved*, since the photonic recoil upon reflection of light at a mirror is absorbed by the mirror, which is not included in our model. However, the atom does (probably) not know about the photon's problems: when, accelerated by the dipole force, it redistributes photons between counterpropagating light modes, it wants to see its momentum conserved. But if both light modes are identical, then the momentum transfer can only be in exact units of $2\hbar k_{lat}$, without frequency- or phase-shifts of the light modes possible. Or in other words: Either the momentum kick satisfies $\Delta p = 2\hbar k_{lat}$, or it simply *does not occur*, the atom gets transparent with respect any attempt of motional excitation.

In practice, this means nothing else, than that the process of scattering a photon incident from an arbitrary direction at an optical lattice needs to fulfill the Bragg condition *not only for the optical modes, but also for the recoil modes*, and that the scattering must be elastic, as in the Mößbauer effect.

For the case that the momentum kick is commensurate with twice the photonic recoil of the laser beams,

$$\Delta p = 2\hbar k_{lat} \ , \tag{38.60}$$

we have a simple picture in terms of a coherent redistribution of photons between lattice beams. But what happens, if this is not the case?

In the case of an atom vibrationally embedded in a crystal, the distribution of phononic modes is so dense and broad, that the interesting questions are: 'Where does the momentum go?' and 'How is it distributed over the modes?' In the case of a single atom sitting in a 1D optical lattice, the distribution of phononic modes is sparse and sharp, since it is shaped by the commensurability condition. Here, the interesting questions should be: 'How likely is it, that the atom really responds to my momentum kick attempt?' and 'How does this probability depend on the amplitude Δp of the kick?'

The second term of the Hamiltonian (38.58) is the dipole potential generated by the counterpropagating laser beams. It contains the *phononic* reservoir. Its expression is more complicated than that of a harmonic oscillator, which can easily be quantized in a canonical way. Nevertheless, hence, should be possible to derive from it (i) the vibrational structure of the standing wave potential and (ii) the transition probability between vibrational states, when the atom is kicked.

The scattering of light off a rigid lattice is totally understood in terms of the dynamic structure factor [878]. Indeed, the dynamic structure factor includes all kind of cooperative effects: those due to 'bosonic stimulation', to peculiarities of the spatial distribution, and of the photonic density of states [878]. We want to calculate the scattering rate. For internal energetic excitation we would calculate,

$$\frac{1}{\tau} \propto |\langle f|e^{-i\hat{H}t}|i\rangle|^2 \ . \tag{38.61}$$

In first order, the expansion of the expression yields Fermi's Golden rule (in second order the Kramers-Heisenberg rule). From there we get the photonic density of states ...

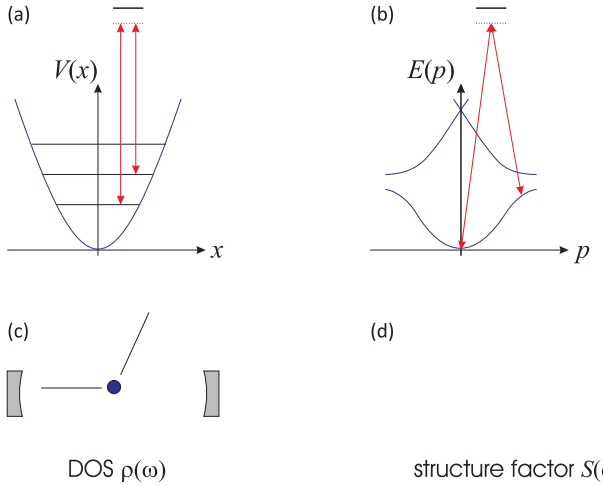

Figure 38.10: (a) Raman anti-Stokes transition on a particle confined in a trapping potential V(z). (b) Raman anti-Stokes transition on a free particle between motional states determined by the dispersion relation $E(p)$.

For momentum kicks it would be,

$$\frac{d\sigma}{d\Omega} \propto |\langle f|e^{-i\mathbf{k}\cdot\hat{\mathbf{r}}}|i\rangle|^2 \ . \tag{38.62}$$

Expanding this do we get in first order the structure factor? And the phononic density of states?

How elastic is the scattering from an atom trapped in the Lamb-Dicke regime in a ring cavity standing wave?

The dynamic structure factor is measured by Bragg spectroscopy. We did NOT Bragg spectroscopy [1219, 1157] and we found elastic scattering (no recoil-shift). How is this possible? Also we measured the static structure factor in [1219]. How about the dynamic?

What are the question we want to respond?

- Bragg spectroscopy from trapped particles avoids to have to treat spontaneous emission!
- Imagine an excited atom in the vibrational ground state of an anisotropic trap. Will it emit preferentially in particular directions? I.e. will light be preferentially scattered within a frozen dimension?
- What is the relationship to Hemmerich's ring cavity quantum computer [606] (see Sec. 42.2.5)?

38.3.4 Optical cooling in of trapped atoms

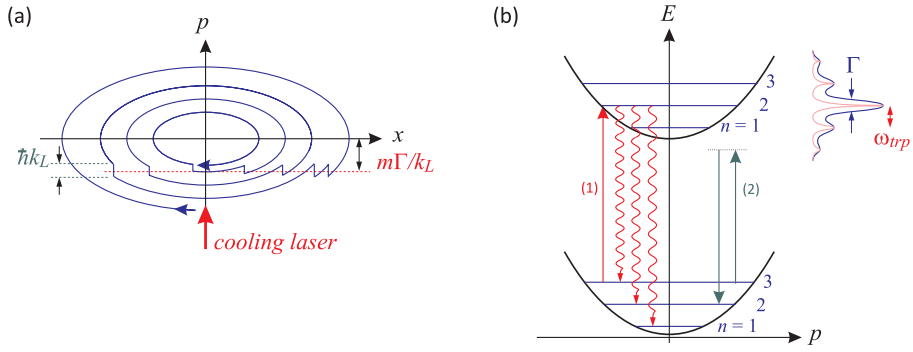

Figure 38.11: (a) Illustration of Doppler cooling of strongly trapped ions via a shrinking of the phase-space ellipse, (b) sideband cooling.

38.3.5 Exercises

38.3.5.1 Ex: Transition elements in anisotropic harmonic traps

a. Calculate and illustrate $\langle \mathbf{0}|e^{-\imath \mathbf{k}\cdot\hat{\mathbf{r}}}|\mathbf{0}\rangle$ for an anisotropic trap with cylindrical symmetry.
b. Calculate $\langle \mathbf{n}|e^{-\imath \mathbf{k}\cdot\hat{\mathbf{r}}}|\mathbf{0}\rangle$ and $\sum_{n_x,n_y,n_z}\langle \mathbf{n}|e^{-\imath \mathbf{k}\cdot\hat{\mathbf{r}}}|\mathbf{0}\rangle$.

Solution: *a. We characterize our trap by* $\mathbf{a}_{trp} = (a_{r,trp}\ a_{r,trp}\ a_{z,trp})$ *and calculate,*

$$\begin{aligned}\langle \mathbf{0}|e^{-\imath \mathbf{k}\cdot\hat{\mathbf{r}}}|\mathbf{0}\rangle &= \langle 0|e^{-\imath k_x\hat{x}}|0\rangle\langle 0|e^{-\imath k_y\hat{y}}|0\rangle\langle 0|e^{-\imath k_z\hat{z}}|0\rangle = \langle 0|\alpha_x\rangle\langle 0|\alpha_y\rangle\langle 0|\alpha_z\rangle \\ &= e^{-|\alpha_x|^2/2}e^{-|\alpha_y|^2/2}e^{-|\alpha_z|^2/2} = e^{-k_r^2a_{trp,r}^2}e^{-k_z^2a_{trp,z}^2/2}\ .\end{aligned}$$

The result exhibited in Fig. 38.12 shows that the transition between vibrational ground states is facilitated in directions, where the Lamb-Dicke parameter is small. This is simply, because for large Lamb-Dicke parameter higher vibrational states may be excited.
b. The results are exhibited in Fig. 38.13.

38.3.5.2 Ex: Periodicity of a lattice

Calculate $e^{\imath a\hat{p}}e^{2\imath k\hat{z}}e^{-\imath a\hat{p}}$.

Solution: *Using the Baker-Hausdorff formula,*

$$\begin{aligned}e^{\imath a\hat{p}/\hbar}e^{2\imath k\hat{z}}e^{-\imath a\hat{p}/\hbar} &= e^{\imath a\hat{p}/\hbar}e^{2\imath k\hat{z}-\imath a\hat{p}+[2\imath k\hat{z},-\imath a\hat{p}/\hbar]/2} \\ &= e^{\imath a\hat{p}/\hbar}e^{-\imath a\hat{p}/\hbar+2\imath k\hat{z}+[-\imath a\hat{p}/\hbar,2\imath k\hat{z}]/2-2ak[\hat{p}/\hbar,\hat{z}]} \\ &= e^{\imath a\hat{p}/\hbar}e^{-\imath a\hat{p}/\hbar}e^{2\imath k\hat{z}}e^{-2\imath ak} = e^{2\imath k(\hat{z}-a)}\ .\end{aligned}$$

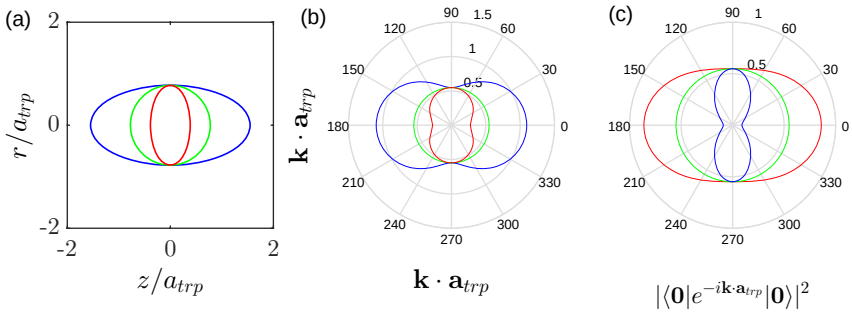

Figure 38.12: (code) (a) Equipotential line of the trapping potential. (b) Angular distribution of the Lamb-Dicke parameter for $\lambda = 689$ nm, $m = 88u$, $\omega_x = \omega_y = 10^5\,\mathrm{s}^{-1}$, and $\omega_z/\omega_x = 1, 2, 3$ (red,green,blue). (c) Corresponding angular distribution of the transition matrix element.

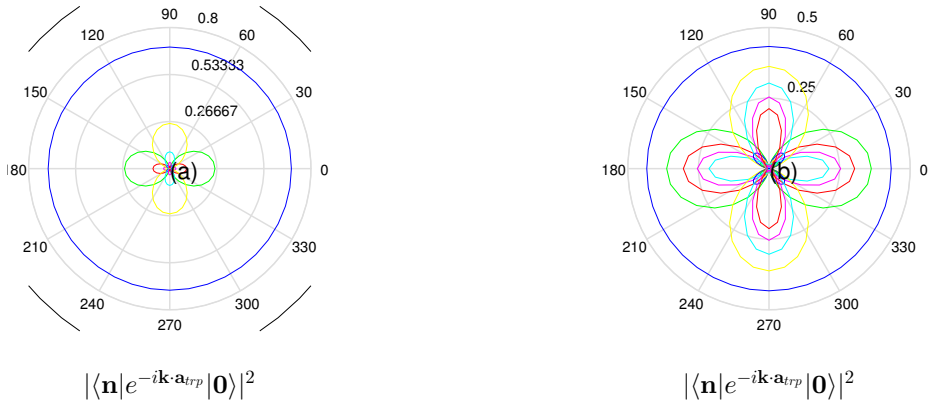

Figure 38.13: (code) (Left) Angular distribution of the transition matrix elements.

38.3.5.3 Ex: Energy commutators

Calculate the commutator between the kinetic and the potential energy for (a) a harmonic oscillator and (b) a standing wave dipolar potential.

Solution: *a. For a harmonic oscillator we have,*

$$\begin{aligned}\hat{H} &= \frac{\hat{p}^2}{2m} + \frac{m}{2}\omega^2\hat{z}^2 \\ \hat{z}(t) &= e^{-\imath\hat{H}t/\hbar}\hat{z}(0)e^{\imath\hat{H}t/\hbar} \\ \hat{p}(t) &= e^{-\imath\hat{H}t/\hbar}\hat{p}(0)e^{\imath\hat{H}t/\hbar}\ .\end{aligned}$$

With this we calculate the commutator between kinetic and potential energy for a harmonic oscillator,

$$[\frac{\hat{p}^2}{2m}, \frac{m}{2}\omega^2\hat{z}^2] = \frac{\omega^2}{4}[\hat{p}^2, \hat{z}^2] = \frac{\omega^2}{4}\left(\hat{p}[\hat{p},\hat{z}]\hat{z} + \hat{p}\hat{z}[\hat{p},\hat{z}] + [\hat{p},\hat{z}]\hat{z}\hat{p} + \hat{z}[\hat{p},\hat{z}]\hat{p}\right) = -\imath\frac{\hbar\omega^2}{2}(\hat{p}\hat{z}+\hat{z}\hat{p}) \ .$$

b. For a standing wave dipolar potential we have,

$$\begin{aligned}
\hat{H} &= \frac{\hat{p}^2}{2m} + U_0 \sin^2 k\hat{z} = \frac{\hat{p}^2}{2m} + U_0\left(k^2\hat{z}^2 - \frac{1}{3}k^4\hat{z}^4 + \frac{2}{45}k^6\hat{z}^6 + ...\right) \\
\hat{z}(t) &= e^{-\imath\hat{H}t/\hbar}\hat{z}(0)e^{\imath\hat{H}t/\hbar} \\
\hat{p}(t) &= e^{-\imath\hat{H}t/\hbar}\hat{p}(0)e^{\imath\hat{H}t/\hbar} \ .
\end{aligned}$$

With Baker-Hausdorff $e^{\hat{A}}e^{\hat{B}} = e^{\hat{A}+\hat{B}+[\hat{A},\hat{B}]/2}$ *we find,*

$$\begin{aligned}
[\hat{A},\hat{B}] = \left[\frac{\hat{p}^2}{2m}, U_0\sin^2 k\hat{z}\right] &= \frac{U_0}{2m}\left[\hat{p}^2, (k\hat{z})^2 - \tfrac{(k\hat{z})^4}{3} + ...\right] \\
&= \frac{k^2U_0}{2m}\left(\hat{p}[\hat{p},\hat{z}]\hat{z} + \hat{p}\hat{z}[\hat{p},\hat{z}] + [\hat{p},\hat{z}]\hat{z}\hat{p} + \hat{z}[\hat{p},\hat{z}]\hat{p}...\right) \\
&= \frac{-\imath\hbar k^2U_0}{m}(2\hat{p}\hat{z} - \imath\hbar...) = ... \\
e^{-\imath\hat{H}t/\hbar} &= e^{-(\imath/\hbar)t\left(\frac{\hat{p}^2}{2m} + U_0\sin^2 k\hat{z}\right)} = ... \ .
\end{aligned}$$

38.4 Driven atomic motion

The degree of freedom of atomic motion can be used for interesting studies of a new kind. For them being a microscopic object we expect the emergence of quantum effects in some circumstances. In free space the spectrum of atomic motion is continuous.

38.4.1 Map representations

38.4.1.1 Poincaré map

Given is the differential equation,

$$\dot{x} = f(x,t) \ , \tag{38.63}$$

with the initial condition $x(\tau) = x_0$ with the solution $x(x_0, t, \tau)$. Be $t = a$ and $t = b$ two fixed points. The *Poincaré map* ϕ relates in initial value a to the value of the solution at point b, i.e. $x_0 \leftarrow \phi x_0 = x(x_0, b, a)$. In other words, if one can find the system function Φ of the time-discrete dynamical system, $\phi_{n+1} = \Phi(\phi_n)$, then P is the Poincaré map.

In dynamical systems, a Poincaré map or Poincaré section, is the intersection of a trajectory which moves periodically (or quasi-periodically, or chaotically), in

a space of at least three dimensions, with a transversal hypersurface of one fewer dimension. More precisely, one considers a trajectory with initial conditions on the hyperplane and observes the point at which this trajectory returns to the hyperplane. Imagine as stroboscopic illumination. The Poincaré section refers to the hyperplane, and the Poincaré map refers to the map of points in the hyperplane induced by the intersections.

It differs from a recurrence plot in that space, not time, determines when to plot a point. For instance, the locus of the moon when the earth is at perihelion is a recurrence plot; the locus of the moon when it passes through the plane perpendicular to the earth's orbit and passing through the sun and the earth at perihelion is a Poincaré map.

38.4.1.2 Circle map and annulus map for periodic forcing

The equation of motion of a periodically forced dynamical system, e.g. a self-sustained oscillator, in the vicinity of a limit cycle can be reduced to [1031],

$$\dot{\phi} = \omega_0 + \epsilon F(\phi, t) \ . \tag{38.64}$$

Note that this equation does not describe a real motion, since there is only one spatial variable. Nevertheless, it is useful whenever inertia can be neglected. The r.h.s. of this equation is a 2π periodic function of phase ϕ and a T periodic function of time t. Thus the phase space of the dynamical system is a two-dimensional torus (see Fig. 38.14).

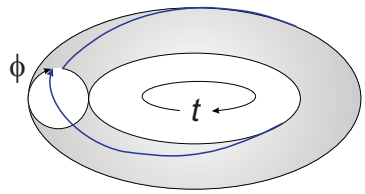

Figure 38.14: Toroidal phase space of the limit-cycle oscillator. Time goes along the ring, phase winds around the cross section.

If $\epsilon \ll 1$, then $\dot{\phi} \approx (\phi(t+T) - \phi(t))/T$, and the phase space can be reduced to a one-dimensional map called *circle map* by stroboscopic mapping with time interval T,

$$\phi(t+T) = \phi(t)+\omega_0 T+\epsilon \int_t^{t+T} F dt = \phi(t)+\omega_0 T+\epsilon[G(t+T)-G(t)] \simeq \phi(t)+\omega_0 T+\epsilon T G(t) \ . \tag{38.65}$$

Defining $\phi_n \equiv \phi(t+nT)$,

$$\phi_{n+1} = \mathrm{mod}_{2\pi} \left[\phi_n + \omega_0 T + \epsilon F(\phi_n)\right] \ . \tag{38.66}$$

If $\epsilon = 0$, we get a circle shift. For rational periods $\omega_0 T = 2\pi p/q$, each point of the circle is periodic with period q. The *rotation number* is,

$$\rho(\phi_0) = \lim_{n\to\infty} \frac{\phi_n - \phi_0}{2\pi n} \ . \tag{38.67}$$

The observed frequency is $\Omega = \rho\omega_0$. Close to rational periods it tends to lock. This is visualized by the *devil's staircase* and the *Arnold tongue*.

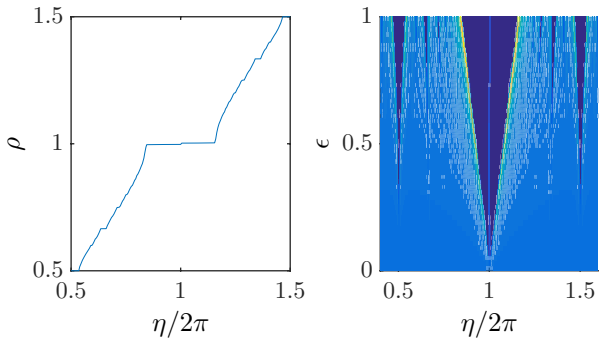

Figure 38.15: (code) (a) Devil's staircase of locking ranges and (b) Arnold tongues in the circle map $\phi_{n+1} = \phi_n + \omega_0 T + \epsilon \sin\phi_n$.

The *annulus map* is used in 2D. As an example, the standard map for the equation $\ddot{\phi} + K\sin\phi = 0$ would be $\phi_{n+1} = \phi_n + P_{n+1}$ and $P_{n+1} = P_n + K\sin\phi_n$.

38.4.2 Driven oscillators

A driven *self-sustained oscillator* or *limit-cycle oscillator* are described by circle maps, as shown above. Their dynamics is described by the so-called *Kuramoto model* explained below. Although forced rotators are not self-sustained, they behave in a similar way, if driven by a constant force. Examples are the δ-kicked rotor and the resistively shunted Josephson junction discussed in Sec. 21.4.4.

38.4.2.1 Self-sustained oscillators and the Kuramoto model

The Kuramoto model is given by the following equation [667] [13],

$$\boxed{\dot{\theta}_n = \frac{K}{N}\sum_m \sin(\theta_n - \theta_m) - \xi_n(t)} \ . \tag{38.68}$$

The Kuramoto model describes, how an ensemble of coupled harmonic oscillators oscillating at different frequencies will synchronize, if their number and their mutual coupling exceeds a critical value. This paradigm is very rich of examples, since it applies as well to physical systems like Huygens' coupled pendulums (illustrated in

[13] For *two coupled limit-cycle oscillators* the Kuramoto equations read,

$$\dot{\theta}_1 = \omega_1 + \tfrac{1}{2}K\sin(\theta_2 - \theta_1) \qquad \text{and} \qquad \dot{\theta}_2 = \omega_2 + \tfrac{1}{2}K\sin(\theta_1 - \theta_2) \ ,$$

such that, defining $\theta \equiv \theta_1 - \theta_2$, we obtain the so-called *Adler equation* (see (21.99) and 37.2.2),

$$\dot{\theta} = \Delta\omega - K\sin\theta \ .$$

.

Fig. 38.16) and arrays of Josephson junctions or lasers, as it describes biological systems like the cardiac pacemakers cells, firing neurons, firefly flashes and cricket concerts [1273]. The variance of the oscillator frequencies introduces a random mixing of the phase space, which may be described by a stochastic Langevin force, which introduces fluctuations in the (otherwise deterministic) center-of-motion. Another prominent system is the collective atomic recoil laser discussed in Sec. 42.2. The Kuramoto model corresponds to a mean-field theory. It has been shown that this leads to a phase transition (in time domain). Cooperative action starts at a threshold value.

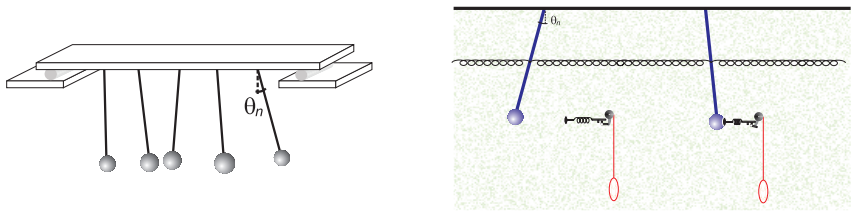

Figure 38.16: Huygen's pendulum.

38.4.2.2 Synchronization of limit-cycle oscillators

It is an interesting question, why the Kuramoto model is able to map physical systems anyway! While it is clear, that it predicts synchronization of the phases θ_n in equation (38.68), its application to coupled pendulums is less obvious. Indeed, we would rather expect coupled pendulums to beat, rather then synchronize their oscillations. Synchronization would lower entropy, which is not possible in closed systems. In fact, Huygens did his observation with *pendulum clocks* rather than physical pendulums, which is totally different, because each clock provides energy and friction in such a way as to maintain the oscillation at a constant amplitude. Hence, the physical system is not closed, as the Kuramoto model suggests.

But even for pendulum clocks synchronization seems to be an artefact of the Kuramoto model, because in order to synchronize two pendulums, one has to speed up the first and slow down the second. If the pendulums have finite mass, this requires inertial terms, which are absent from the Kuramoto model. Hence, the Kuramoto equation does not follow immediately from a mechanical model, but at some limit or approximation.

The Kuramoto model does *not* map exactly a real physical system, but grasps some of their features and exhibits them in an illustrative way. In this sense, its applicability to a vast variety of systems is not surprising.

Even in the case of coupled driven pendulums, a derivation of the Kuramoto equation from first principles is not obvious. One might start from the mechanical eequations of motion,

$$\ddot{x}_n + \beta\dot{x}_n + \omega_n^2 x_n + g\sum_m (x_n - x_m) = F\cos\omega t \ , \tag{38.69}$$

where we let the oscillators have different frequencies ω_n, but they couple with the same strength g to all other oscillators, where $\omega_n^2 \gg g$. As a simplification we only

consider *limit-cycle oscillation* of the individual oscillators. The role of the force is reduced to assuring this boundary condition, so that if we impose solutions like $x_n \equiv e^{\imath\omega t+\imath\theta_n}$ we do not need an explicit force term, $F \equiv 0$,

$$\imath\ddot{\theta}_n e^{\imath\omega t+\imath\theta_n} - (\omega^2 + \dot{\theta}_n^2)e^{\imath\omega t+\imath\theta_n} + \imath\beta\left(\omega + \dot{\theta}_n\right)e^{\imath\omega t+\imath\theta_n} + \omega_n^2 e^{\imath\omega t+\imath\theta_n} + g\sum_m \left(e^{\imath\omega t+\imath\theta_n} - e^{\imath\omega t+\imath\theta_m}\right) = 0 \ . \tag{38.70}$$

The imaginary part is,

$$\ddot{\theta}_n + \beta\dot{\theta}_n + \beta\omega - g\sum_m \sin(\theta_m - \theta_n) = 0 \ . \tag{38.71}$$

Neglect inertia and defining $K \equiv g/\beta$ and $re^{\imath\psi} \equiv N^{-1}\sum_m e^{\imath\theta_m}$,

$$\dot{\theta}_n = \omega + Kr\sin(\psi - \theta_n) \ . \tag{38.72}$$

This shows that dissipation is an essential ingredient for the Kuramoto model. The assumption of a driving and a friction force is necessary to ensure a constant kinetic energy for every oscillator despite the existence of a coupling, i.e. an energy exchange between the oscillators. Every oscillator is coupled to a reservoir, and this coupling provides or receives the excess energy and entropy resulting from the mutual coupling between the oscillators. The model also has been extended to include inertial effect [3],

$$m\ddot{\theta}_n + \dot{\theta}_n = \omega + Kr\sin(\psi - \theta_n) \ . \tag{38.73}$$

The numerical simulation of Eq. (38.68) with *real coupling* does not exhibit synchronization (be careful to avoid numerical errors). This is not astonishing, because it is a *linear closed system not driven by any dissipative force*. Energy is not lost, the evolution is deterministic, thus reversible, thus no entropy is produced or reduced. In contrast synchronization would indicate that entropy has been reduced. Therefore synchronization must have something to do with imaginary coupling...? And nonlinearity in the case of Huygens' pendulum.

38.4.3 Forced rotator

38.4.3.1 Constant forcing

The phase space of a free undamped rotator is shown in Fig. 38.17.

By adding a torque and friction, we obtain the *forced rotator*. Its behavior is similar that of the δ-kicked rotor. The damped rotator equation has many applications in various domains. In the form,

$$\frac{d^2\varphi}{dt^2} + \gamma\frac{d\varphi}{dt} + \frac{g}{l}\sin\varphi = T/I \ , \tag{38.74}$$

it describes a physical pendulum of length l and moment of inertia I, if a friction force and a torque T are applied (see Sec. 4.1.7). In the form,

$$\frac{d^2\varphi}{dt^2} + \frac{1}{\tau}\frac{d\varphi}{dt} + KAB\sin\varphi = -\frac{1}{\tau}(\omega_{lo} - \omega_0) \ , \tag{38.75}$$

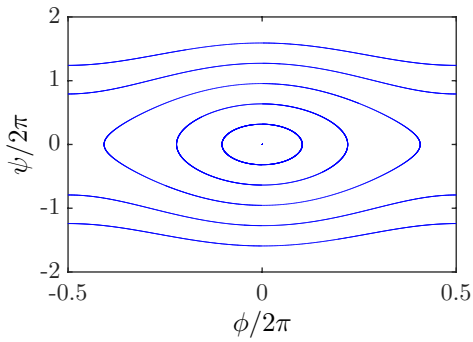

Figure 38.17: (code) Phase space trajectories of undamped pendulum.

it describes a phase-locked loop (PLL) (see Sec. 55.3.5). Here τ is the integration time of the low-pass filter, A and B are the amplitudes of the master and slave lasers, K the amplitude of the local oscillator, ω_{lo} its frequency, and ω the center frequency of the VCO. In the form,

$$C\frac{\Phi_0}{2\pi}\frac{d^2\varphi}{dt^2}+\frac{1}{R}\frac{d\varphi}{dt}+I_c\sin\varphi=i\ , \tag{38.76}$$

it describes resistively shunted Josephson junctions (see Sec. 21.4.4). Here $\Phi_0=h/2e$, C is the capacitance of the junction, R its resistance, and I_c the critical current through the junction. In the form,

$$\frac{1}{2U}\frac{d^2\varphi}{dt^2}+\frac{8\nu g^2N^2\kappa}{\left(\kappa^2+4\nu^2\right)^2}\frac{d\varphi}{dt}+\frac{\Omega_{mw}N}{2}\sin\varphi=\frac{g^2N^2\kappa}{\kappa^2+4\nu^2}\ , \tag{38.77}$$

it describes merging BECs in a ring cavity (see Sec. 47.5.4). The synchronizing degrees of freedom are relative phases of the Broglie waves. Irreversible dissipation is obtained via coupling to an optical cavity followed cavity decay.

Harmonically forced rotators are described by annulus maps. In the presence of dissipation, the rotator can be overdamped, e.g. vanishing capacitance in the JJ. The equation of motion then reduces to that of a self-sustained oscillator described by a circle map. Phase-locking of the dipole moments of the transitions in a V-type three-level system, like for the *Correlated spontaneous Emission Laser* (CEL) is such an example. The Adler equation, which describes the CEL, resembles the equation for a resistively shunted Josephson junction [663] for the approximation $\ddot{\Phi}=0$. For the CEL irreversibility, is achieved via optical pumping followed by spontaneous emission.

In all cases, quantum systems synchronize, provided there is some resistive dissipation (spontaneous emission, cavity friction, ..). I.e. *forcing against friction is a necessary precondition for synchronization.*

38.4.3.2 Periodic forcing

Expect classically chaotic behavior.

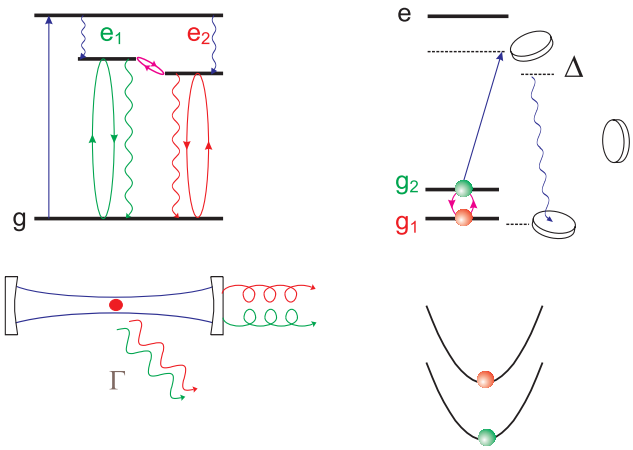

Figure 38.18: (a) Schemes for PLL/CEL and (b) merging BEC (right). PLL corresponds to a locking of the induced dipole moments (green and red elliptic curves). CEL corresponds to a correlation of the spontaneous emission (green and red waves). Noise reduction by synchronization analogous to CEL.

An interesting question is whether the Kuramoto phase transitions considered here are quantum phase transitions, i.e. whether they occur at $T = 0$. For the merging BEC system the temperature resides in thermal excitations. How about the PLL, where *inversion* is a precondition for lasing?

A rich system to study *dynamical localization*, *quantum resonance*, and *quantum synchronization* is the *δ-kicked rotor*.

38.4.4 Periodically kicked quantum rotor

The *δ-kicked rotor* is the paradigm of Hamiltonian chaos. Experimentally, 100 μK cold atoms are released from a MOT, and a fast succession of light pulses is applied. The light is a far-detuned standing wave.

Atom optical systems have a number of advantages: 1. It is relatively simple to generate highly nonlinear potentials, in which the dynamics of trapped particles exhibits classical chaos. 2. The duration of an experiment can easily exceed the quantum break time. 3. The isolation from environment is sufficient to allow for persistent quantum interferences. 4. Negligible dissipation permits quantum effects to get visible.

A presentation on the subject is available here (watch talk).

38.4.4.1 Classical evolution

At short times (shorter than the quantum break time) the δ-kicked rotor behaves classically. I.e. the initial spatial distribution of the MOT diffuses into a Gaussian momentum distribution. The energy growth is diffusive. These are signatures of

chaotic behavior. The Hamiltonian of a δ-kicked rotor is,

$$\hat{H}' = \frac{\hat{p}'^2}{2m} + V_0 \cos 2k_L \hat{x}' \sum_{n=-\infty}^{\infty} \delta(t - nT) \ , \tag{38.78}$$

where T is the time interval between the pulses, t is an integer counting the pulses. The equation of motion follows from $\dot{\hat{x}}' = \partial \hat{H}/\partial \hat{p}'$ and $\dot{\hat{p}}' = -\partial H/\partial \hat{x}'$,

$$m\ddot{\hat{x}}' = 2k_L V_0 \sin 2k_L \hat{x} \sum_{n=-\infty}^{\infty} \delta(t - n) \ . \tag{38.79}$$

With the abbreviations $\omega_r \equiv 2\hbar k_L^2/m$ and $\bar{k} \equiv 2\omega_r T$, we go to dimensionless units via $\hat{H} = \hat{H}'\bar{k}^2/2\hbar\omega_r$, $K = V_0\bar{k}^2/2\hbar\omega_r$, $t = t'/T$, $\hat{x} = 2k_L\hat{x}'$, and $\hat{p} = \hat{p}'\bar{k}/2\hbar k_L$, we get,

$$\hat{H} = \frac{\hat{p}^2}{2} + K \cos \hat{x} \sum_{n=-\infty}^{\infty} \delta(t - n) \ . \tag{38.80}$$

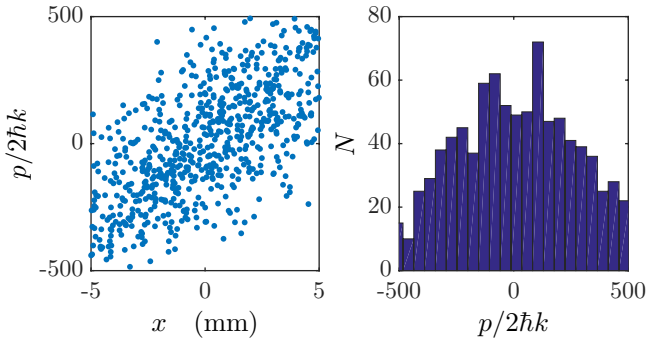

Figure 38.19: (code) (a) Phase diagram and (b) histogram of the classical kicked rotor.

38.4.4.2 Dynamical localization

At longer times the momentum distribution turns exponential, which is a clear indication of dynamical localization. This is quantum suppression of chaotic diffusion, i.e. of stochasticity. This is at first surprising, because all quantum problems have probabilistic, i.e. stochastic interpretations. Apparently, the fact that the density of states in quantum mechanics is discrete, leads to periodic time evolutions. (This is because the Fourier spectrum of a periodic motion is discrete.) This gives rise to periodic orbits in situations, where classical mechanics predicts chaos.

The suppression of energy transport in the rotor can be interpreted as Anderson localization (in angular momentum rather than in space) [450]. The randomness of disordered lattices in the Anderson problem is replaced by pseudo-randomness in the phase of the δ-kicks. Dynamical localization suppressed chaotic diffusion by coherence effects. Typical pulse lengths for δ-kicks are 300 ns. This would work in the ring cavity at low finesse.

The classical dynamics of the δ-kicked rotor is solely determined by the stochasticity parameter K. For $K > 4$ the dynamics is predominantly chaotic. The quantum mechanics are additionally specified by $\bar{k}$. The scaled version of commutation relation, $[\hat{x}', \hat{p}'] = \imath\hbar$, reads,

$$[\hat{x}, \hat{p}] = \imath\bar{k} \ . \tag{38.81}$$

Obviously, k has the meaning of a scaled Planck constant measuring the action scale of our system.

Technical issues are: 1. Finite pulse shapes reduce chaos and hence dynamical localization [728, 729]. 2. Noise and dissipation also lead to delocalization, i.e. the classical limits are recovered, i.e. instead of localization after the quantum break time, momentum continues to diffuse with a coefficient dependent on the amount of noise.

38.4.4.3 Quantum resonance

However, at specific periods between the kicks, i.e. when time interval equals the inverse of the recoil shift, the ballistic expansion is observed, i.e. there is a constant and uniform acceleration force. There is no localization any more, but a quadratic increase of energy. This is due to quantum resonance. Quantum resonances occur when $\bar{k}/2\pi$ is integer or a simple rational number. This can be understood as follows: The kicks occur when $Tv = \lambda/4 \times m/n$, the Bragg condition is fulfilled, i.e. the transitions takes place at the edges of a Brillouin zone. While quasimomentum is always conserved, with every kick the atoms jump into the next higher band increasing their energy by one recoil unit. These are the accelerator modes.

38.4.4.4 δ-kicked rotor in the gravitational field

Gravitation [451, 1163] helps stabilizing quantum resonances.

In the gravitational field, $-mg\hat{x}'$, the equation of motion reads,

$$m\ddot{\hat{x}}' = 2k_L V_0 \sin 2k_L\hat{x} \sum_{n=-\infty}^{\infty} \delta(t-n) + mg \ . \tag{38.82}$$

The scaled Hamiltonian of a δ-kicked rotor is, using $f \equiv mgT/\hbar k_L$,

$$\hat{H} = \frac{\hat{p}^2}{2} - f\hat{x} + K\cos\hat{x} \sum_{n=-\infty}^{\infty} \delta(t-n) \ , \tag{38.83}$$

We transform into the accelerated frame via $\hat{P} = \hat{p} - ft$,

$$\hat{H}_g = e^{\imath f\hat{x}t}\hat{H}e^{-\imath f\hat{x}t} = \frac{1}{2}(\hat{P} + ft)^2 + K\cos\hat{x} \sum_{n=-\infty}^{\infty} \delta(t-n) \ . \tag{38.84}$$

Separate band and quasimomentum via $\hat{P} = N + \beta$, $N = -\imath\frac{\partial}{\partial\theta}$. The evolution over one period is then,

$$e^{-\imath\hat{H}_g t} = e^{-\imath K\cos\hat{x}_{\mathrm{mod}2\pi} - \frac{\imath\tau}{2}(N+\beta+fn+f/2)^2} \ . \tag{38.85}$$

38.4.4.5 Impact of noise and dissipation

The standard map of a δ-kicked rotor is [451, 206]

$$\begin{aligned} J_{n+1} &= J_n - k\sin\theta_{n+1} - \mathrm{sgn}(\epsilon)\tau\eta \\ \theta_{n+1} &= \theta_n \mathrm{sgn}(\epsilon) J_n \mathrm{mod} 2\pi \ . \end{aligned} \tag{38.86}$$

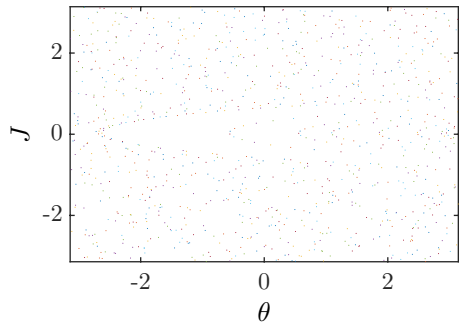

Figure 38.20: (code) Standard map of the gravitationally accelerated δ-kicked rotor. The parameters are $\tau = 6.26$, $k = 1.329$, $\eta = \tau * pi/20$, $\theta_0 = 0.42$, and $J_0 = 0$.

In the presence of dissipation, the *dissipative map* is derived [1431]

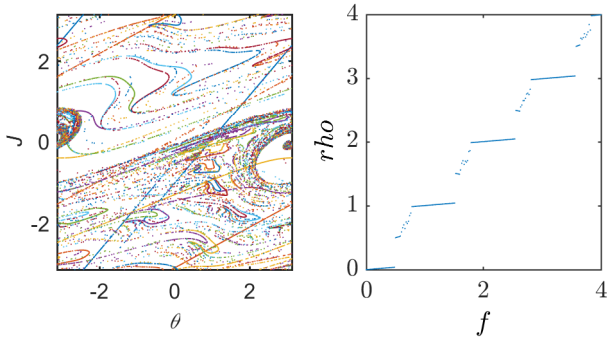

Figure 38.21: (code) Dissipative map of the gravitationally accelerated δ-kicked rotor.

38.4.4.6 Quantum synchronization

Quantum accelerator modes are the non-dissipative counterparts of mode locking: The δ-kicked rotor with gravity leads to the same map as the Josephson junction with dissipation. Hence, the classical mode locking mechanism underlying quantum accelerator modes renders them a robust tool for efficient quantum state control, deep in the quantum realm [206]. Accelerator modes are due to stability islands in pseudo-classical phase space.

All map are necessarily classical constructs. To get quantum maps, a master equation treating dissipation via additional Lindblad terms can be simulated by quantum Monte-Carlo procedures [1431]. As an example, one may consider the formation of Shapiro steps in δ-kicked atomic clouds in the presence of dissipation. For strong dissipation, quantum fluctuations can be suppressed by *quantum synchronization* when the system is close to the classical limit. In the quantum limit, there is a steady phase slip washing out the synchronization plateaus. For weak dissipation in the classical limit, chaotic behavior can lead to multivalued synchronization frequencies (the dissipative map can have different attractors). In the quantum limit, chaos is stabilized.

A dissipative quantum system at zero temperature can only tunnel towards its lowest energy state when a biasing dc-signal is applied. As the bias periodically changes its sign due to the action of a driving field, tunneling makes the particle move periodically towards its corresponding lowest energy state, as long as the driving period is much *longer* than the typical tunneling time. In contrast, a *short* driving periods, finite temperature quantum noise promotes and assists synchronization. This is similar to the stochastic resonance.

One could have the impression that the whole quantum synchronization business is nothing else a reinvention of the CEL [1251].

One of the defining features of quantum mechanics in entanglement, i.e. the impossibility to factorize a system into its constituents. It seems, that in an appropriate classical limit only chaotic systems can preserve a significant amount of entanglement [429]. E.g. as long as two coupled oscillators are classically uncorrelated and behave chaotically, quantum entanglement can exist no matter the value of $\hbar$. As soon as they synchronize, chaos disappears and so does entanglement. In fact chaos disappears mainly in the classical limit, since it does really exist in the quantum limit, where quantum noise is large enough to drive the system away from periodic attractors and swamp the fractal structure found in the chaotic classical attractor.

The quantum correlations do not have classical counterparts yet they persist in the classical limit. Some understanding can be gained if we consider that in order to obtain the classical limit, it is sufficient that the state of the system be localized relative to a large classical action. However, in order to guarantee that the entanglement between the two oscillators can be eliminated from the system, we require that the localization of the wavefunction be of the order of $\hbar$. Hence, satisfying the classical limit does not imply that entanglement will be removed.

38.4.5 Chaos

'Chaos is found in greatest abundance wherever order is being sought. It always defeats order, because it is better organized.' [T. Pratchett, Diskworld novela, 'Interesting times']

38.4.5.1 Classical chaos versus quantum chaos

The *classical chaos* or *deterministic chaos* arises of unprecisely known initial conditions. The signatures of chaos are an exponential sensitivity of the systems' trajectory

to initial conditions and *self-similarity*. The first one is measured by the *Lyapunov exponent*. *Hopf bifurcation*.

While in the classical world chaos is encountered everywhere, in quantum mechanics this is not obvious, because the fundamental equation of motion, the Schrödinger equation, is linear. Counterintuatively, and although quantum mechanics is intrinsically probabilistic, there are systems at the boundary of quantum and classicality where chaos is inhibited and stabilized by quantum mechanics. The *quantum chaos* thus behaves very differently from classical chaos.

38.4.5.2 Quantum synchronization

How to find a system that suits for quantum synchronization? Start checking the following requirements: 1. In the classical limit the system should behave chaotic (this is fulfilled with the CARL). 2. There must be a continuous degree of freedom that can be quantized, e.g. atomic motion, tunneling flux, etc.. 3. Feasibility of weak dissipation. 4. ...

A particularity of atoms interacting with optical ring cavities is that they are literally haunted by synchronization. Examples are: 1. Kuramoto type synchronization of the motion of individual atoms. This effects is known as CARL. 2. Mode locking of the optical fields to resonances of the cavity. This effect is at the origin of laser cooling. 3. Fusion of independent but coupled BECs under the action of an irreversible cycling scheme. This effects is analogous to resistively shunted Josephson junctions. 4. Tunneling between adjacent wells of the standing wave in the cavity, and the interplay of superfluidity and Mott insulation.

Some of the synchronization phenomena are essentially classical. Nevertheless, the protagonists of the system are all quantum objects. For example, 1. the momentum of individual atoms is discretized when $k_B T < \hbar\omega_r$. 2. Quantum statistical effects, quantum correlations and entanglement come into play when $T < T_c$. 3. BECs are zero-temperature objects, and (at optical wavelengths) the universe represents an effective zero-temperature reservoir to which the cavity couples. Hence, it is an obvious question whether and in what sense quantum effects are going to effect the synchronization process itself. It is important to be aware that the fact that the synchronizing modes are quantum objects does not mean that the coupling force exhibits quantum behavior.

To construct an approach to quantum synchronization in the ring cavity system, in the following, we will start recalling another well-studied system, the atom optical δ-kicked rotor. This system bears analogies with an array of coupled Josephson junctions. Both, the coupled JJs and the δ-kicked rotor, have been proposed for studies of quantum synchronization [533]. We will try to find out analogies with ring cavity dynamics, e.g. the JJ like fusion of BECs [663].

The question addressed is that of classical-quantum mechanical correspondence, i.e. what happens if $\hbar \to 0$?

For strong coupling, classical nonlinear synchronization phenomena emerge on microscopic scales. Is mode locking necessarily strictly a (semi-)classical effect? No! An example is the atom optical quantum accelerator, i.e. δ-kicked atoms in the field of gravity. The δ-kicked rotor serves as prototype for classical and quantum chaos. In Sec. 42.8.2 we show how to simulate quantized motion.

38.5 Further reading

H.J. Metcalf, P. van der Straten, Graduate Texts in Contemporary Physics, Springer (1999), *Laser Cooling and Trapping* http

Ch.J. Foot, (Oxford Master Series in Atomic, Optical and Laser Physics, 2005), *Atomic physics* http

G. Vandegrift, *The Moessbauer effect explained* [1328]DOI

38.5.1 on optical forces

T.W. Hänsch et al., *Cooling of Gases by Laser Radiation* [581]DOI

D.J. Wineland et al, *Laser Cooling of Atoms* [1382]DOI

A. Ashkin, *Trapping of atoms by resonance radiation pressure* [51]DOI

E.L. Raab et al., *Trapping of Neutral Sodium Atoms with Radiation Pressure* [1065]DOI

Ph.W. Courteille et al., *Highly Versatile Atomic Micro Traps Generated by Multi-frequency Magnetic Field Modulation* [299]DOI

38.5.2 on nonlinear dynamics

D.L. Shepelyanski, *Localization of diffusive excitation in multi-level systems* [1199]DOI

G. Behinaein et al., *Exploring the phase space of the quantum delta kicked accelerator* [111]DOI

A. Buchleitner et al., *Quantum Accelerator Modes from the Farey Tree* [206]DOI

G.G. Carlo et al., *Dissipative Quantum Chaos: Transition from Wave Packet Collapse to Explosion* [233]DOI

F.S. Cataliotti et al., *Josephson Junction Arrays with Bose-Einstein Condensates* [240]DOI

Qijin Chen et al., *Shapiro steps observed in a dc superconducting quantum interference device with multiple junctions in each arm* [249]DOI

G.J. Duffy et al., *Experimental investigation of early-time diffusion in the quantum kicked rotor using a Bose-Einstein condensate* [394]DOI

M.J. Everitt et al., *Persistent entanglement in the classical limit* [429]DOI

S. Fishman et al., *Chaos, quantum recurrences, and Anderson localization* [450]DOI

S. Fishman et al., *Stable quantum resonances in atom optics* [451]DOI

B.G. Klappauf et al., *Quantum chaos with cesium atoms: pushing the boundaries* [729]DOI

F.L. Moore et al., *Atom optics realization of the quantum δ-kicked rotor* [916]DOI

J. Ringot et al., *Experimental Evidence of Dynamical Localization and Delocalization in a Quasiperiodic Driven System* [1098]DOI

S. Schlunk et al., *Experimental observation of high-order quantum accelerator modes* [1163]DOI

D.A. Steck et al., *Quantum Feedback Control of Atomic Motion in an Optical Cavity* [1247]DOI

I. Steiner et al., *Quenching Phase Noise: Correlated Spontaneous Emission versus Phase Locking* [1251]DOI

O.V. Zhirov et al., *Quantum synchronization* [1431]DOI

R. Kohlhaas et al., *Phase Locking a Clock Oscillator to a Coherent Atomic Ensemble* [?]DOI

T.E. Lee et al., *Quantum Synchronization of Quantum van der Pol Oscillators with Trapped Ions* [?]DOI

Minghui Xu et al., *Conditional Ramsey Spectroscopy with Synchronized Atoms* [?]DOI

Part VI

Collective Scattering of Light

Chapter 39

Cooperativity in light scattering

In Chp. 34 we discussed the interaction of light with individual atoms. In the practice of spectroscopy, however, we often work with ensembles of scatterers. Depending on their *spatial distribution* (e.g. disordered, quasi-continuous, periodic), their *motion* (hot gas or cold cloud), the possible existence of *correlations* between them, the presence of *boundary conditions* (e.g., free space, cavities, or photon bands), and finally, in case of degenerate quantum gases, of a possible *bosonic stimulation* of the scattering process, we expect new collective effects. In this chapter we will discuss several examples, in particular, localization effects induced by disorder, super- and subradiance, Bragg scattering, and the formation of forbidden photonic bands in periodic lattices. Phenomena leading to self-organization, such as the collective atomic recoil laser, will be discussed in Chp. 42.

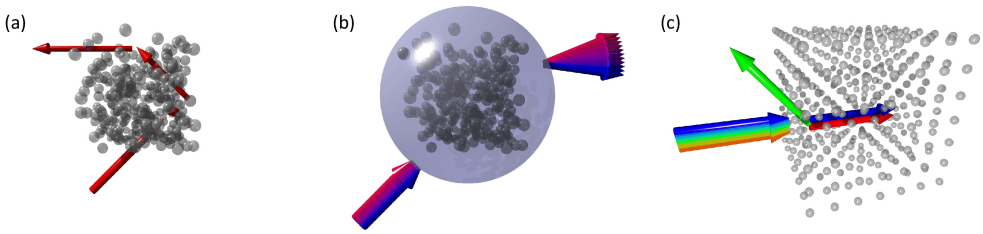

Figure 39.1: (a) Artist's view of multiple scattering of a photon through a dilute cloud. (b) Atomic cloud as a bulk object characterized by a refraction index $n(\mathbf{r})$. (c) Illustration of a photonic band in an optical lattice.

This chapter starts with introducing as the main theoretical tools the *structure factor* and the *coupled dipoles model*. In Sec. 39.1 we will derive the formalism and learn, how to employ it to calculate, e.g. the spatial distribution of light scattered by an atomic cloud and the radiation pressure force on the atoms focusing on situations, where interatomic interactions induced by the incident light can be neglected. In Sec. 39.2 we will, disregarding the atomic's cloud graininess and disorder, introduce the *smooth density approximation* and compare it to macroscopic Mie scattering. In Sec. 39.3 we will focus on cooperative effects inducing collective lineshifts and broadenings, such as the Lorentz-Lorenz and the Lamb shift. We will also discuss disorder-induced localization effects, super- and subradiance. In Sec. 39.2 we investi-

gate Bragg scattering, i.e. scattering from periodically ordered atoms, and finally in Sec. 40.2 we study scattering from correlated atoms.

39.1 Theoretical tools and models

As mentioned above, the process of light scattering by an atomic cloud depends on several factors, many of which can be summarized by a quantity called the *structure factor*. This structure factor, obtained in perturbation theory, describes the probability for the light to be scattered into a particular direction as a function of the properties of the atomic cloud (spatial distribution, motion, etc.). The quantity is well suited for dealing with stationary situations.

On the other hand we have at our disposal a microscopic theory called the *coupled dipole model*. In this model we treat every individual atom as a dipole, which interacts with all other atoms by rescattering the incident light. The resolution of the Schrödinger equation allows, several approximations having been made, to calculate the dynamics of the system.

39.1.1 The structure factor and definition of cooperativity

One way of characterizing the scattering process is by structure factor. The *static structure factor* is the normalized response of a system to a perturbation with the wave vector $\mathbf{q}$. It can be understood as the final density of states for the atom after the scattering process. In contrast, the *dynamic structure factor* also considers the final density of states for the emitted or scattered photon. That is, on one hand, the frequency and momentum of the photon must satisfy the Bragg condition. On the other hand, the density of available states can also be structured, for example, when the scattering process takes place inside a cavity.

In lowest-order perturbation theory (Fermi's Golden Rule) we get the general expressions [713],

$$\boxed{\frac{d\sigma}{d\Omega_s d\omega} = \left(\frac{d\sigma}{d\Omega_s}\right)_1 S(\mathbf{q},\omega)}\,, \tag{39.1}$$

that is, the effective scattering cross section is reduced to the effective Rayleigh scattering cross section by an isolated atom times a geometric term called *dynamic structure factor*,

$$\boxed{S(\mathbf{q},\omega) \equiv \tfrac{1}{2\pi}\int dt e^{\imath\omega t}\langle\hat{\rho}(\mathbf{q},t)\hat{\rho}^\dagger(\mathbf{q},0)\rangle}\,, \tag{39.2}$$

where,

$$\hat{\rho}(\mathbf{q},t) = \int_V \hat{n}(\mathbf{r},t)e^{\imath\mathbf{q}\cdot\mathbf{r}}d^3r \tag{39.3}$$

is Fourier transform of the atomic density. Thus, $S(\mathbf{q},\omega)$ is the Fourier transform of the density-density correlation function. On the other hand, $\int e^{\imath\omega t}d\omega = 2\pi\delta(t)$, and we calculate the *static structure factor*,

$$\boxed{S(\mathbf{q}) \equiv \int S(\mathbf{q},\omega)d\omega = \langle\hat{\rho}(\mathbf{q},0)\hat{\rho}^\dagger(\mathbf{q},0)\rangle}\,. \tag{39.4}$$

In the equations (39.2) and (39.3) we have written the quantities $\hat{\rho}(\mathbf{q},t)$ and $\hat{n}(\mathbf{r},t)$ as operators, in order to allow for the possibility, that the atomic ensemble is a quantum gas, i.e. a Bose-Einstein condensate characterized by a single wavefunction $\hat{\psi}(\mathbf{r},t)$ normalized to the density distribution, $\hat{\rho}(\mathbf{r},t)=\hat{\psi}^\dagger(\mathbf{r},t)\hat{\psi}(\mathbf{r},t)$. We shall return to this subject in Sec. 47.1.1. In the following, we will restrict ourselves to atoms localized in space with well-defined velocities and calculate the structure factor (i) for disordered clouds of atoms excited by the passage of a photon in Sec. 39.1.6 and (ii) for Bragg scattering by optical lattices in Sec. 39.4. In these cases, we find in the literature often another definition of the structure factor as the expectation value of the Fourier transform of the atomic density,

$$\mathcal{S}(\mathbf{q})=\langle\hat{\rho}(\mathbf{q})\rangle\ , \tag{39.5}$$

Thus, it describes the amplitude of the electric field of the scattered radiation. In order to avoid confusion we will call this quantity *structure coefficient* and denote it by a calligraphic $\mathcal{S}$. We study the structure factor for various atomic density distributions in Excs. 39.1.8.1 to 39.1.8.3.

Example 226 (*Structure factor of a discrete cloud*): In case of discrete clouds, $n(\mathbf{r},t)=\sum_j\delta^{(3)}(\mathbf{r}-\mathbf{r}_j)$, we can disregard the quantum nature of the operators. The relationship (39.3) immediately gives,

$$\rho(\mathbf{q},t)=\sum_j e^{\imath\mathbf{q}\cdot\mathbf{r}_j(t)} \tag{39.6}$$

and the relationship (39.2),

$$S(\mathbf{q},\omega)=\tfrac{1}{2\pi}\int dt e^{\imath\omega t}\rho(\mathbf{q},t)\rho^*(\mathbf{q},0)=\tfrac{1}{2\pi}\int dt e^{\imath\omega t}\sum_{j,k}e^{\imath\mathbf{q}\cdot[\mathbf{r}_j(t)-\mathbf{r}_k(0)]}\ . \tag{39.7}$$

Assuming atoms fixed in space, $\mathbf{r}_j(t)=\mathbf{r}_j$,

$$S(\mathbf{q},\omega)=\sum_{j,k}e^{\imath\mathbf{q}\cdot(\mathbf{r}_j-\mathbf{r}_k)}\delta(\omega)\ . \tag{39.8}$$

That is, without recoil the light must be scattered elastically.

The notion of *cooperativity* is fundamental for any problem involving scattering of radiation and, depending on the specific area of physics, is called by many different names, such as Purcell factor, cavity-to-free-space scattering ratio, or phase matching condition. Here, we will regard cooperativity as any ***deviation of the structure factor from isotropy***. For example, Bragg scattering and optical cavities are highly cooperative, because they favor scattering in particular directions [1].

39.1.2 The scalar coupled dipoles model

In the following, we develop the coupled dipoles model, within which we define the structure factor for light scattering by a cloud of scatterers making the following assumptions:

[1] Note that cooperativity does not request the atoms to interact and exists in the single scattering regime. In the multiple scattering regime other forms of collective phenomena, such as collective Lamb shifts emerge, as we will see later on.

- The light is (mostly) treated as a scalar field. That is, we disregard effects due to the polarization of light and assume two-level atoms. Generalizations are shown in Sec. 39.5.4 [1214, 859].
- Atoms are supposed to be fixed in space. That is, we disregard the Doppler shift of moving atoms and the photonic recoil. Therefore, it will suffice to consider the static structure factor.
- Atoms are initially uncorrelated and not degenerate. That means that we neglect effects such as bosonic stimulation or Fermi blocking [2].

Be ω_0 the frequency of the incident light, ω_a the frequency of the atomic resonance, and ω the frequency of the scattered light. The Hamiltonian is nothing more than the generalization of (35.222) to several assumed atoms located at the positions r_j,

$$\boxed{\begin{aligned}\hat{H} &= \sum_{j=1}^{N} \hbar g_{\mathbf{k}_0}(\hat{\sigma}_j e^{-\imath\omega_a t} + \hat{\sigma}_j^\dagger e^{\imath\omega_a t})(\hat{a}_{\mathbf{k}_0}^\dagger e^{\imath\omega_0 t - \imath\mathbf{k}_0\cdot\mathbf{r}_j} + \hat{a}_{\mathbf{k}_0} e^{-\imath\omega_0 t + \imath\mathbf{k}_0\cdot\mathbf{r}_j}) \\ &+ \sum_{\mathbf{k}}\sum_{j=1}^{N} \hbar g_{\mathbf{k}}(\hat{\sigma}_j e^{-\imath\omega_a t} + \hat{\sigma}_j^\dagger e^{\imath\omega_a t})(\hat{a}_{\mathbf{k}}^\dagger e^{\imath\omega_k t - \imath\mathbf{k}\cdot\mathbf{r}_j} + \hat{a}_{\mathbf{k}} e^{-\imath\omega_k t + \imath\mathbf{k}\cdot\mathbf{r}_j})\end{aligned}} \quad . \tag{39.9}$$

Here, $\Omega_0 = 2g_{k_0}\sqrt{n_0}$ is the Rabi frequency of the interaction between an atom and the incident light (which is treated as a classical field with n_0 photons), $\hat{\sigma}_j$ is the deexcitation operator for the j-th atom, $\hat{a}_{\mathbf{k}}$ is the photon annihilation operator, and $g_k = d\sqrt{\omega/(\hbar\epsilon_0 V_{ph})}$ describes the coupling between the atom and the vacuum modes the volume of which is V_{ph}. The j-th atom has its lower and upper states denoted by $|g_j\rangle$ and $|e_j\rangle$, respectively. That is, we treat the atoms as simple two-level systems. We also assume that all atoms are excited by the same unperturbed incident laser beam, thus neglecting their dephasing along the laser path or induced by near-field effects (which could arise for large spatial densities).

Within the *rotating wave approximation* RWA the Hamiltonian simplifies to,

$$\begin{aligned}\hat{H} &= \hbar\sum_{j=1}^{N}[g_{k_0}\hat{\sigma}_j\hat{a}_{\mathbf{k}_0}^\dagger e^{\imath(\omega_0-\omega_a)t - \imath\mathbf{k}_0\cdot\mathbf{r}_j} + h.c.] \\ &+ \hbar\sum_{j=1}^{N}\sum_{\mathbf{k}}[g_k\hat{\sigma}_j\hat{a}_{\mathbf{k}}^\dagger e^{\imath(\omega_k-\omega_a)t - \imath\mathbf{k}\cdot\mathbf{r}_j} + h.c.] \ .\end{aligned} \tag{39.10}$$

The RWA only considers energy-conserving terms in single-photon processes. But this is an artifact from the field quantization. Energy conservation can be warranted by considering multi-photon virtual processes, which as a whole, conserve energy. These terms appear in the full Hamiltonian, but are neglected in the RWA. While the RWA often is a good assumption in single atom quantum optics, this is frequently not the case for collective scattering. Here, we adopt the RWA to a simplify the subsequent solution of the Schrödinger equation, but we will need to generalize the results obtained a posteriori, as shown in the discussion of Sec. 39.1.4.

[2] Spontaneous emission by an atom in a Fermi gas of temperature $T = 0$ can not occur if the photon wave vector is inside the Fermi lake, $q < k_F$.

We call $|0\rangle_a = |g_1,..,g_N\rangle$ the atomic ground state, $|j\rangle_a = |g_1,..,e_j,..,g_N\rangle$ the state where only the atom j is excited, and we assume that the system is in a the superposition of states described by [3],

$$|\Psi(t)\rangle = \alpha(t)|0\rangle_a|n_0\rangle_{\mathbf{k}_0}|0\rangle_{\mathbf{k}} + \sum_{j=1}^{N}\beta_j(t)|j\rangle_a|n_0-1\rangle_{\mathbf{k}_0}|0\rangle_{\mathbf{k}} + \sum_{\mathbf{k}}\gamma_{\mathbf{k}}(t)|0\rangle_a|n_0-1\rangle_{\mathbf{k}_0}|1\rangle_{\mathbf{k}} \ . \tag{39.11}$$

With this ansatz we imply that at every instant of time, there can be at most only one excitation in the atomic cloud. The temporal evolution of the amplitudes is obtained by inserting the Hamiltonian and the ansatz into the Schrödinger equation, $\imath\hbar\partial_t|\Psi(t)\rangle = \hat{H}|\Psi(t)\rangle$. Once the evolution of the amplitudes is calculated, we can determine the observables of the system, such as the radiative pressure force or the amplitudes of the scattered radiation fields or the fields inside the cloud.

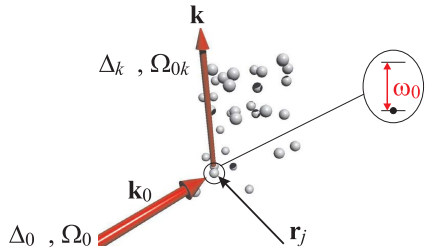

Figure 39.2: Scheme of the interaction of a light beam with a sample of atoms.

Example 227 (*Interaction Hamiltonian in the rotating frame*): The Hamiltonian in the rotating wave approximation is,

$$\hat{H} = \hbar g\left(\hat{\sigma}e^{-\imath\omega_a t} + \hat{\sigma}^\dagger e^{\imath\omega_a t}\right)\left(\hat{a}^\dagger e^{\imath\omega_0 t} + \hat{a}e^{-\imath\omega_0 t}\right) \simeq \hbar g\left(\hat{\sigma}\hat{a}^\dagger e^{\imath\Delta_0 t} + \hat{\sigma}^\dagger\hat{a}e^{-\imath\Delta_0 t}\right) \ .$$

For the Pauli matrices we have the following rules,

$$[\hat{\sigma}_z,\hat{\sigma}] = -\hat{\sigma} \qquad \text{and} \qquad [\hat{\sigma}_z,\hat{\sigma}^\dagger] = \hat{\sigma}^\dagger \ ,$$

such that,

$$\begin{aligned}
[\hat{\sigma}_z,\hat{H}] &= \hbar g\left(-e^{\imath\Delta_0 t}\hat{a}^\dagger\hat{\sigma} + e^{-\imath\Delta_0 t}\hat{a}\hat{\sigma}^\dagger\right)\\
[\hat{\sigma}_z,[\hat{\sigma}_z,\hat{H}]] &= \hbar g\left(e^{\imath\Delta_0 t}\hat{a}^\dagger\hat{\sigma} + e^{-\imath\Delta_0 t}\hat{a}\hat{\sigma}^\dagger\right) = \hat{H}\\
[\hat{\sigma}_z,[...[\hat{\sigma}_z,\hat{H}]]...] &= \hbar g\left[(-1)^n e^{\imath\Delta_0 t}\hat{a}^\dagger\hat{\sigma} + e^{-\imath\Delta_0 t}\hat{a}\hat{\sigma}^\dagger\right] \ .
\end{aligned}$$

[3] This ansatz is well adapted to situations where the RWA holds. Otherwise, additional counter-rotating terms must be included [458].

Using the Baker-Haussdorff formula,

$$\begin{aligned} e^{\imath\omega_0 t\hat{\sigma}_z}\hat{H}e^{-\imath\omega_0 t\hat{\sigma}_z} &= \hat{H} + [\imath\omega_0 t\hat{\sigma}_z, \hat{H}] + \tfrac{1}{2!}[\imath\omega_0 t\hat{\sigma}_z, [\imath\omega_0 t\hat{\sigma}_z, \hat{H}]] + ... \\ &= \hbar g \sum_{n=0}^{\infty} \tfrac{(\imath\omega_0 t)^n}{n!} \left[(-1)^n e^{\imath\Delta_0 t}\hat{a}^\dagger\hat{\sigma} + e^{-\imath\Delta_0 t}\hat{a}\hat{\sigma}^\dagger\right] \\ &= \hbar g e^{\imath\Delta_0 t}\hat{a}^\dagger\hat{\sigma}\sum_{n=0}^{\infty}\tfrac{(-\imath\omega_0 t)^n}{n!} + \hbar g e^{-\imath\Delta_0 t}\hat{a}\hat{\sigma}^\dagger\sum_{n=0}^{\infty}\tfrac{(\imath\omega_0 t)^n}{n!} \\ &= \hbar g\left(e^{-\imath\omega_a t}\hat{a}^\dagger\hat{\sigma} + e^{\imath\omega_a t}\hat{a}\hat{\sigma}^\dagger\right) . \end{aligned}$$

39.1.2.1 Temporal evolution of the amplitudes

The time evolution of the amplitudes is obtained by inserting the Hamiltonian $\hat{H}$ and the ansatz $|\Psi(t)\rangle$ into the Schrödinger equation,

$$\frac{\partial}{\partial t}|\Psi(t)\rangle = -\frac{\imath}{\hbar}\hat{H}|\Psi(t)\rangle \ . \tag{39.12}$$

one obtains with $\Omega_0 = 2g_{k_0}\sqrt{n_0}$,

$$\begin{aligned} \dot{\alpha}(t) &= -\imath\tfrac{\Omega_0}{2}e^{\imath\Delta_0 t}\sum_{j=1}^{N}\beta_j(t)e^{-\imath\mathbf{k}_0\cdot\mathbf{r}_j} \\ \dot{\beta}_j(t) &= -\imath\tfrac{\Omega_0}{2}\alpha(t)e^{-\imath\Delta_0 t+\imath\mathbf{k}_0\cdot\mathbf{r}_j} - \sum_{\mathbf{k}}\imath g_k\gamma_{\mathbf{k}}(t)e^{-\imath\Delta_k t+\imath\mathbf{k}\cdot\mathbf{r}_j} \\ \dot{\gamma}_{\mathbf{k}}(t) &= -\imath g_k e^{\imath\Delta_k t}\sum_{j=1}^{N}\beta_j(t)e^{-\imath\mathbf{k}\cdot\mathbf{r}_j} \ . \end{aligned} \tag{39.13}$$

We set the initial conditions,

$$\alpha(0) = 1 \quad , \quad \beta_j(t) = 0 \quad , \quad \gamma_{\mathbf{k}}(t) = 0 \ . \tag{39.14}$$

For low excitation rate, we can set $\alpha(t) \simeq 1$. Integrating the third equation,

$$\gamma_{\mathbf{k}}(t) = -\imath g_k\sum_{j=1}^{N}e^{-\imath\mathbf{k}\cdot\mathbf{r}_j}\int_0^t e^{\imath\Delta_k t'}\beta_j(t')dt' \ , \tag{39.15}$$

and substituting it into the second equation,

$$\dot{\beta}_j(t) = -\imath\tfrac{\Omega_0}{2}\alpha(t)e^{-\imath\Delta_0 t+\imath\mathbf{k}_0\cdot\mathbf{r}_j} - \sum_{\mathbf{k}}g_k^2\sum_{m=1}^{N}e^{\imath\mathbf{k}\cdot(\mathbf{r}_j-\mathbf{r}_m)}\int_0^t e^{\imath\Delta_k(t'-t)}\beta_m(t')dt' \ . \tag{39.16}$$

39.1.3 The Markov approximation

For small systems, $R < \lambda$, we can make use of the Markov approximation, which holds when the collective decay time $t_{decay} < R/c$. Larger systems persist memory effects, which may lead to (Rabi) *collective Rabi oscillations*. In the Markov approximation given by $\beta_j(t') \simeq \beta_j(t)$ the integro-differential equation (which is equivalent to a differential equation of arbitrarily high order) reduces to a simple first order differential equation. Defining [4],

$$\beta_j \equiv \tilde{\beta}_j e^{-\imath\Delta_0 t + \imath \mathbf{k}_0\cdot\mathbf{r}_j} \ , \tag{39.17}$$

we obtain,

$$\frac{d}{dt}\alpha(t) = -\imath\frac{\Omega_0}{2}\sum_{j=1}^{N}\tilde{\beta}_j(t) \tag{39.18}$$

$$\frac{d}{dt}\tilde{\beta}_j(t) = \imath\Delta_0\tilde{\beta}_j(t) - \frac{\Omega_0^2}{4}\sum_{m=1}^{N}\int_0^t \tilde{\beta}_m(t')dt' - \sum_{\mathbf{k}} g_k^2 \sum_{m=1}^{N} e^{\imath(\mathbf{k}-\mathbf{k}_0)\cdot(\mathbf{r}_j-\mathbf{r}_m)}\int_0^t e^{-\imath(\omega_k-\omega_0)t''}\tilde{\beta}_m(t-t'')dt'' \ ,$$

where we substituted $t'' \equiv t - t'$ in the last integral. Now, using the Markov approximation $\tilde{\beta}_m(t-t'') \simeq \tilde{\beta}_m(t)$, with $\lim_{t\to\infty}\int_0^t e^{-\imath(\omega_k-\omega_0)t'}dt' = \pi\delta(\omega_k-\omega_0)$, and with the rate of spontaneous emission,

$$\boxed{\Gamma \equiv \frac{V_{ph}}{\pi c}k_0^2 g_{k_0}^2} \ , \tag{39.19}$$

the third term becomes for the case $m = j$,

$$\sum_{\mathbf{k}} g_k^2\int_0^t e^{-\imath(\omega_k-\omega_0)t''}\tilde{\beta}_j(t-t'')dt'' \simeq \sum_{\mathbf{k}} g_k^2\tilde{\beta}_j(t)\pi\delta(\omega_k-\omega_0) \tag{39.20}$$

$$= \frac{V_{ph}}{(2\pi)^3}\tilde{\beta}_j(t)\int g_k^2\pi\delta(\omega_k-\omega_0)d^3k = \frac{V_{ph}}{(2\pi)^3}\tilde{\beta}_j(t)4\pi g_{k_0}^2\pi k_0^2\frac{1}{c} = \frac{\Gamma}{2}\tilde{\beta}_j(t) \ .$$

The third term becomes for the case $m \neq j$, evaluating the sum over the wavevectors by $\sum_{\mathbf{k}} \to \frac{V_{ph}}{(2\pi)^3}\int d^3k$,

$$\sum_{\mathbf{k}} g_k^2\sum_{m\neq j}^{N} e^{\imath(\mathbf{k}-\mathbf{k}_0)\cdot(\mathbf{r}_j-\mathbf{r}_m)}\int_0^t e^{-\imath(\omega_k-\omega_0)t''}\tilde{\beta}_m(t-t'')dt'' \tag{39.21}$$

$$\simeq \sum_{\mathbf{k}} g_k^2\sum_{m\neq j}^{N} e^{\imath(\mathbf{k}-\mathbf{k}_0)\cdot(\mathbf{r}_j-\mathbf{r}_m)}\tilde{\beta}_m(t)\pi\delta(\omega_k-\omega_0)$$

$$= \frac{V_{ph}}{(2\pi)^3}\sum_{m\neq j}^{N}\tilde{\beta}_m(t)\int g_k^2 e^{\imath(\mathbf{k}-\mathbf{k}_0)\cdot(\mathbf{r}_j-\mathbf{r}_m)}\pi\delta(\omega_k-\omega_0)d^3k = \frac{\Gamma}{2}\sum_{m\neq j}^{N}\gamma_{jm}\tilde{\beta}_m(t) \ ,$$

[4] Later on we will be particularly interested in so-called *timed Dicke states* characterized by $\tilde{\beta}_j = \tilde{\beta}$ independent on j.

with

$$\gamma_{jm} \equiv \frac{2}{\Gamma}\frac{V_{ph}}{(2\pi)^3}\int_0^\infty\int_0^\pi\int_0^{2\pi} g_k^2 e^{\imath(\mathbf{k}-\mathbf{k}_0)\cdot(\mathbf{r}_j-\mathbf{r}_m)}\frac{\pi}{c}\delta(k-k_0)k^2\sin\theta dk d\theta d\phi \ . \quad (39.22)$$

Finally,

$$\frac{d}{dt}\tilde{\beta}_j(t) = \imath\Delta_0\tilde{\beta}_j(t) - \frac{\Omega_0^2}{4}\sum_{m=1}^N\int_0^t\tilde{\beta}_m(t')dt' - \frac{\Gamma}{2}\sum_{m=1}^N\gamma_{jm}\tilde{\beta}_m(t) \ , \quad (39.23)$$

or

$$\frac{d}{dt}\alpha(t) = -\imath\frac{\Omega_0}{2}\sum_{j=1}^N\tilde{\beta}_j(t) \quad (39.24)$$

$$\frac{d}{dt}\tilde{\beta}_j(t) = \imath\Delta_0\tilde{\beta}_j(t) - \imath\frac{\Omega_0}{2}\alpha(t) - \frac{\Gamma}{2}\sum_{m=1}^N\gamma_{jm}\tilde{\beta}_m(t) \ .$$

This means that the problem is reduced to finding the γ_{jm}. Continuing the evaluation of Eq. (39.22),

$$\begin{aligned}\gamma_{jm} &= \frac{1}{\Gamma}g_k^2\frac{V_{ph}}{4\pi^2 c}e^{-\imath\mathbf{k}_0\cdot(\mathbf{r}_j-\mathbf{r}_m)}\int_0^\infty\int_0^{2\pi}\int_{-1}^1 e^{\imath k|\mathbf{r}_j-\mathbf{r}_m|\cos\theta}d\cos\theta d\phi\delta(k-k_0)k^2dk \\ &= \frac{1}{\Gamma}g_k^2\frac{V_{ph}}{\pi c}e^{-\imath\mathbf{k}_0\cdot(\mathbf{r}_j-\mathbf{r}_m)}\int_0^\infty\frac{\sin k|\mathbf{r}_j-\mathbf{r}_m|}{k|\mathbf{r}_j-\mathbf{r}_m|}\delta(k-k_0)k^2dk \\ &= e^{-\imath\mathbf{k}_0\cdot(\mathbf{r}_j-\mathbf{r}_m)}\frac{\sin k_0|\mathbf{r}_j-\mathbf{r}_m|}{k_0|\mathbf{r}_j-\mathbf{r}_m|} \ . \end{aligned} \quad (39.25)$$

Isolating the self-decaying term and assuming low saturation, $\alpha(t) = 1$, we get,

$$\boxed{\dot{\tilde{\beta}}_j = \left(\imath\Delta_0 - \frac{\Gamma}{2}\right)\tilde{\beta}_j - \frac{\imath\Omega_0}{2} - \frac{\Gamma}{2}\sum_{m\neq j}\gamma_{jm}\tilde{\beta}_m} \ . \quad (39.26)$$

In Exc. 39.1.8.4 we will analyze the validity of the Markov approximation for typical cold atoms experiments.

39.1.4 General solution with exponential kernel, validity of the RWA

The RWA is valid for $\max(\Omega, \Gamma_n) \ll \omega$,

$$\int_0^t dt\cdot e^{-\imath(\omega_k-\omega_0)t} \simeq \mathcal{P}\left(\frac{1}{\omega_k+\omega_0}\right) - \imath\mathcal{P}\left(\frac{1}{\omega_k-\omega_0}\right) + \pi\delta(\omega_k-\omega_0) \ . \quad (39.27)$$

The whole expression leads to the exponential kernel, the first two terms are the cosine part, the third term is the sine part. The rotating wave approximation consists in neglecting the first term, i.e. it only concerns the cosine part of the kernel.

Within the RWA we got [5,6],

$$\gamma_{jm} = e^{-\imath \mathbf{k}_0 \cdot (\mathbf{r}_j - \mathbf{r}_m)} \frac{\imath \sin(k_0 |\mathbf{r}_j - \mathbf{r}_m|)}{\imath k_0 |\mathbf{r}_j - \mathbf{r}_m|} \ . \tag{39.28}$$

Without the RWA we would have found [1186, 1178, 1180, 1283],

$$\gamma_{jm} = e^{-\imath \mathbf{k}_0 \cdot (\mathbf{r}_j - \mathbf{r}_m)} \frac{e^{\imath k_0 |\mathbf{r}_j - \mathbf{r}_m|}}{\imath k_0 |\mathbf{r}_j - \mathbf{r}_m|} \ . \tag{39.29}$$

An alternative derivation from a Green function approach to the master equation is presented in Sec. 41.3.2 (see Eq. (41.94)).

There has been a controversy between Friedberg and Scully about the role of virtual photons (or *collective Lamb-shift*) [468, 1282, 469, 1181]. These terms result from counterrotating terms in the rotating wave approximation. Scully assumes timed Dicke states in *infinitely large* clouds and finds the contributions weak. Friedberg does a mode expansion of the cloud and finds that different modes decay at different velocities. This yields time-dependent radiation patterns, which can be temporarily larger in backward direction.

Normally, the RWA is a good approximation, when $\Omega \ll \omega$. Deviations from this approximations lead e.g. to the Bloch-Siegert shift and important corrections for very far-detuned (quasi-electrostatic) optical trapping. The above requirement is not well satisfied for our experiment, since $\Omega_N = \sqrt{N}\Omega \simeq 1..10$ THz.

Be $|b_1 b_2 ... a_j ... b_N\rangle$ the state with all atoms in the ground state except atom j being in the excited state. Hence, the cloud's state is simply expressed by the wavefunction,

$$\Psi_{atom}(t) = \sum_{j=1}^{N} \beta_j(t) |b_1 b_2 ... a_j ... b_N\rangle \ . \tag{39.30}$$

For large σ the radiation pressure is independent on the choice of the kernel. In fact we may even set the kernel to 0. For small σ there appears a considerable deviation. Interestingly, the imaginary part of the kernel gets important for higher densities, even when the optical density is maintained, e.g. by compressing the cloud in z-direction. This means that the collective Lamb shift becomes more apparent is small compressed clouds. But we postpone a more thorough discussion to Sec. 39.3.

The analytic expansion into eigenmodes assumes the RWA. Hence, the numerics deviate from the analytics for small σ and large N. Is it possible to generalize the expansion to the exponential kernel (see [1283])? The authors also suggest that the scattered radiation be frequency-shifted due to the imaginary part of the kernel. This might be an interesting observable for experiments.

39.1.4.1 Low collective saturation

Note that for low *saturation*, $\alpha(t) = 1$, the first term simply becomes $-\frac{\imath}{2}\Omega_0$. Even though the single atom excitation rate may be small in case of large detuning, the

[5] Note that dipole-dipole interactions are mediated by the exchange of virtual photons. Hence, they are included in the Hamiltonian when the RWA is NOT applied.

[6] Note that Maxwell's equations contain non-RWA terms.

collective Rabi frequency $\sqrt{N}\Omega$ can be large. The presence of many excitations in the cloud means, that higher Dicke states are populated. Then we may expect a complicated many-body dynamics, if decay into other states than the timed Dicke state is possible.

Even though the single atom excitation rate may be small in case of large detuning, the *collective* Rabi frequency $\sqrt{N}\Omega$ can be large. The presence of many excitations in the cloud means, that higher Dicke states are populated. Then we may expect a complicated many-body dynamics, if decay into other states than the timed Dicke state is possible.

The model we use (ground state + first excited state in the times Dicke basis) does not allow more than 1 photon for N atoms. For such a model, neglecting saturation means 'much' less than 1 atom in the excited state, i.e. the probability of having the any atom in the excited state is less than 1. But having N atoms, this means that each atoms should have a excited state population of much less than $1/N$. Including the saturation in the naive way, means that when this term $N\Omega_0^2$ is not negligible, than we will have less atoms in the first excited state of the timed Dicke basis, than if when we would neglect saturation. This is precisely why we call this saturation, we cannot take more atoms away from the ground state, because the system cannot absorb more than one photon. But when this term is not longer negligible, then in a cloud of N atoms, this does not prevent us from taking atoms away from the ground state (we have N atoms which each can take one photon). Either the term is negligible (and we could drop it) or we will try to keep its contribution (even at first order in $N\Omega_0^2$), but then we cannot neglect the possibility of having 2 atoms excited.

39.1.4.2 Steady-state solution

In steady-state the equations of the coupled dipoles model can be solved numerically for an arbitrary (ordered or disordered) cloud of immobile atoms located at positions $\mathbf{r}_j$ illuminated by an electric field.

Assuming scalar light and the validity of the Markov approximation, and furthermore defining $\bar{\beta}_j \equiv \tilde{\beta}_j e^{\imath \mathbf{k}_0 \cdot \mathbf{r}_j}$ and $\bar{\Omega}_0(\mathbf{r}_j) \equiv \Omega_0(\mathbf{r}_j) e^{\imath \mathbf{k}_0 \cdot \mathbf{r}_j}$, and using the exponential kernel,

$$\bar{\gamma}_{jm} = \frac{e^{\imath k_0 |\mathbf{r}_j - \mathbf{r}_m|}}{\imath k_0 |\mathbf{r}_j - \mathbf{r}_m|} \ , \tag{39.31}$$

the Eq. (39.26) for the atomic states reads,

$$\frac{d}{dt}\bar{\beta}_j = \left(\imath\Delta_0 - \frac{\Gamma}{2}\right)\bar{\beta}_j - \frac{\imath\bar{\Omega}_0(\mathbf{r}_j)}{2} - \frac{\Gamma}{2}\sum_{m\neq j}\bar{\gamma}_{jm}\bar{\beta}_m \ . \tag{39.32}$$

Defining the matrix,

$$M_{jm} \equiv (\imath\Delta_0 - \tfrac{\Gamma}{2})\delta_{jm} - \tfrac{\Gamma}{2}(1-\delta_{jm})\bar{\gamma}_{jm} = \begin{pmatrix} \imath\Delta_0 - \frac{\Gamma}{2} & \imath\gamma_{12}\frac{\Gamma}{2} & \cdots \\ \imath\gamma_{21}\frac{\Gamma}{2} & \imath\Delta_0 - \frac{\Gamma}{2} & \\ \vdots & & \ddots \end{pmatrix} \ , \tag{39.33}$$

we can rewrite Eq. (39.34) as,

$$\boxed{\frac{d}{dt}\bar{\beta}_j = \sum_m M_{jm}\bar{\beta}_m - \frac{\imath}{2}\bar{\Omega}_0(\mathbf{r}_j)} \; . \tag{39.34}$$

The steady-state solution of is simply obtained by $\dot{\bar{\beta}}_j = 0$ [298, 225],

$$M_{jm}\bar{\beta}_m(\infty) = \tfrac{\imath}{2}\bar{\Omega}_0(\mathbf{r}_j) \; . \tag{39.35}$$

This equation can now be solved by the dipole moment amplitudes,

$$\boxed{\bar{\beta}_m(\infty) = (M_{jm})^{-1} \; \tfrac{\imath}{2}\bar{\Omega}_0(\mathbf{r}_j)} \; , \tag{39.36}$$

where we use the exponential kernel,

$$\gamma_{jm} = \frac{e^{\imath k_0(|\mathbf{r}_j - \mathbf{r}_m| + \delta_{jm})}}{\imath k_0(|\mathbf{r}_j - \mathbf{r}_m| + \delta_{jm})} \; , \tag{39.37}$$

where the trick with the δ_{jm}-symbol helps to remove divergences for equal atom positions.

In this form the solution is immediately suitable for numerical implementation of the coupled dipoles model, although in practice the number of atoms is limited to $N < 10000$ for ordinary PCs.

39.1.4.3 Limit of dilute clouds

Dilute clouds are characterized by a large interatomic distance $k_0|\mathbf{r}_j - \mathbf{r}_m| \gg 1$. In this case, the non-diagonal elements of the kernel (39.33) quickly vanish, and the equations of motion (39.34) decouple to,

$$\frac{d}{dt}\bar{\beta}_j = \left(\imath\Delta_0 - \frac{\Gamma}{2}\right)\bar{\beta}_j - \frac{\imath}{2}\bar{\Omega}_0(\mathbf{r}_j) \; . \tag{39.38}$$

39.1.4.4 Characterization of the atomic cloud in steady-state

Plot the spacial dependence of the phases of the atomic dipoles, $\phi(\mathbf{r}_j) = \mathfrak{Im}\,(\ln\tilde{\beta}_j)$.

39.1.4.5 Time-dependence

In order to calculate the time-dependence, we reconsider the equation (39.34) for the excitation amplitudes. Its solution is formally given by the sum of the general solution of the homogeneous equation and a particular (e.g. the asymptotic) solution of the inhomogeneous equation,

$$\bar{\beta}_j(t) = e^{M_{jm}t}\bar{\beta}_m(0) + (\mathbb{I} - e^{M_{jm}t})\bar{\beta}_m(\infty) \; . \tag{39.39}$$

Inserting the steady-state solution we finally get,

$$\boxed{\bar{\beta}_j(t) = e^{M_{jm}t}\bar{\beta}_m(0) + (\mathbb{I} - e^{M_{jn}t})M^{-1}_{mn} \; \tfrac{\imath}{2}\bar{\Omega}_0(\mathbf{r}_m)} \; . \tag{39.40}$$

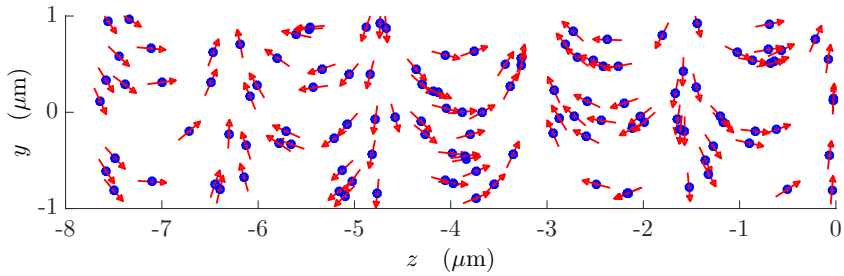

Figure 39.3: Phase delay in the excitation of the atomic dipoles (a) without rescattering ($\gamma_{jm} = 0$) and (b) with rescattering.

39.1.5 Calculation of light scattering in steady-state

To calculate the distribution of scattered light, we start from the Heisenberg equation for the field operator [458],

$$\frac{d\hat{a}_{\mathbf{k}}}{dt} = \frac{1}{\imath\hbar}[\hat{a}_{\mathbf{k}}, \hat{H}] = -\imath g_{\mathbf{k}} e^{\imath(\omega_{\mathbf{k}}-\omega_a)t} \sum_{j=1}^{N} \hat{\sigma}_j e^{-\imath\mathbf{k}\cdot\mathbf{r}_j} \ . \tag{39.41}$$

where the fast oscillating term proportional to $e^{\imath(\omega_{\mathbf{k}}+\omega_a)t}$ has been neglected. Now,

$$\hat{\mathcal{E}}_{sct}(\mathbf{r}, t) = \sum_{\mathbf{k}} \mathcal{E}_k \hat{a}_{\mathbf{k}}(t) e^{\imath(\mathbf{k}\cdot\mathbf{r}-\omega_k t)} \ , \tag{39.42}$$

where $\mathcal{E}_k = \sqrt{\hbar\omega_k/2\varepsilon_0 V_{ph}}$. Integrating Eq. (39.41) with $\hat{a}_{\mathbf{k}}(0) = 0$, inserting it in Eq. (39.42), and approximating the sum over the modes $\mathbf{k}$ by an integral, we obtain,

$$\hat{\mathcal{E}}_{sct}(\mathbf{r}, t) = -\imath \frac{V_{ph}}{8\pi^3} \sum_{j=1}^{N} \int_0^t dt' \hat{\sigma}_j(t-t') e^{\imath\omega_a t} \int d^3k \ \mathcal{E}_k g_k e^{\imath\mathbf{k}\cdot(\mathbf{r}-\mathbf{r}_j)-\imath ckt'} \ . \tag{39.43}$$

Introducing spherical coordinates, $d^3k = dkk^2 d\phi d\theta \sin\theta$, and integrating the angular part Eq. (39.43) becomes,

$$\begin{aligned} \hat{\mathcal{E}}_{sct}(\mathbf{r}, t) = -\imath \frac{V_{ph}}{4\pi^2} \sum_{j=1}^{N} \frac{1}{|\mathbf{r}-\mathbf{r}_j|} \int_0^t dt' \hat{\sigma}_j(t-t') e^{\imath\omega_a t'} \times \\ \times \int dk k \mathcal{E}_k g_k [e^{-\imath ck(t'-|\mathbf{r}'-\mathbf{r}_j|/c)} - e^{-\imath ck(t'+|\mathbf{r}'-\mathbf{r}_j|/c)}] \ . \end{aligned} \tag{39.44}$$

Assuming the radiation spectrum centered around $k \simeq k_0$, we approximate $k\mathcal{E}_k g_k \simeq k_0 \mathcal{E}_{k_0} g_{k_0}$. Then, extending the lower limit of integration of k to $-\infty$, we obtain for $t < |\mathbf{r}-\mathbf{r}_j|/c$ [1049, 816],

$$\hat{\mathcal{E}}_{sct}(\mathbf{r}, t) \simeq -\frac{dk_0^2}{4\pi\varepsilon_0} \sum_{j=1}^{N} \frac{e^{\imath k_0|\mathbf{r}-\mathbf{r}_j|}}{|\mathbf{r}-\mathbf{r}_j|} \hat{\sigma}_j(t-|\mathbf{r}-\mathbf{r}_j|/c) \ . \tag{39.45}$$

where we may neglect the radiation retardation in the limit $t \gg \sigma_R/c$. Using (39.19) and expressing the coupling strength,

$$\hbar g_k = d\mathcal{E}_k \qquad \text{with} \qquad \mathcal{E}_k = \sqrt{\frac{\hbar\omega_k}{2\varepsilon_0 V_{ph}}} \ , \tag{39.46}$$

we get,

$$\hat{\mathcal{E}}_{sct}(\mathbf{r},t) \simeq -\frac{\imath\hbar\Gamma}{2d}\sum_{j=1}^{N}\gamma_{oj}(\mathbf{r})\hat{\sigma}_j(t) \ , \tag{39.47}$$

where we defined the abbreviation,

$$\gamma_{oj}(\mathbf{r}) \equiv \frac{e^{\imath k_0|\mathbf{r}-\mathbf{r}_j|}}{\imath k_0|\mathbf{r}-\mathbf{r}_j|} \ . \tag{39.48}$$

When applied on the state of Eq. (39.11), neglecting virtual transitions, it yields $\hat{\mathcal{E}}_{sct}|\Psi\rangle = \mathcal{E}_{sct}|g_1,...,g_N\rangle$, where $\mathcal{E}_{sct}$ is the electric field radiated by the excited atoms. Once the excitation amplitudes $\beta_j(\infty)$ are known, the scattered light field and the total field can easily be calculated via [1137],

$$\boxed{\mathcal{E}_{sct}(\mathbf{r}) = \langle\hat{\mathcal{E}}_{sct}(\mathbf{r})\rangle = -\frac{\imath\hbar\Gamma}{2d}\sum_{j=1}^{N}\gamma_{oj}(\mathbf{r})\beta_j(\infty) \qquad \text{and} \qquad \mathcal{E}_{tot} = \mathcal{E}_{las} + \mathcal{E}_{sct}} \ , \tag{39.49}$$

Example 228 (*Light scattering from a Gaussian beam*): Fig. 39.4 shows an example of light scattering from an incident light field parametrized as a Gaussian beam, as shown in (18.293),

$$\mathcal{E}_{las}(\mathbf{r}) = \hat{\epsilon}\mathcal{E}_0\frac{w_0}{w(z)}e^{-r^2/w(z)^2+\imath kz+z\imath kr^2/2R(z)-\imath\varphi(z)} = \hat{\epsilon}\frac{\hbar}{|\mathbf{d}|}\Omega_0(\mathbf{r})e^{\imath\mathbf{k}_0\cdot\mathbf{r}} \ . \tag{39.50}$$

Note that, for the chosen parameters, the result does not depend on the interaction terms. I.e. we can as well set the kernel to 0.

Note, that the phase factor $e^{\imath\mathbf{k}_0\cdot\mathbf{r}}$ can either be attributed to the atomic dipole moments or to the field. Here, $N = 125$ atoms are periodically arranged in a three-dimensional cubic lattice.

39.1.6 Calculation of the steady-state radiation pressure force

Let us now calculate the radiative pressure force exerted by an incident beam of light $\mathbf{k}_0$ on an atom j located at position $\mathbf{r}_j$ inside an atomic cloud, as illustrated in Fig. 39.2,

$$\frac{d\hat{\mathbf{p}}_j}{dt} = \hat{\mathbf{F}}_j = -\nabla_{\mathbf{r}_j}\hat{H} \ . \tag{39.51}$$

Inserting the Hamiltonian in the RWA (39.10),

$$\begin{aligned}\hat{\mathbf{F}}_j = {} & \imath\hbar\mathbf{k}_0 g_{k_0}\left[\hat{\sigma}_j\hat{a}^\dagger_{\mathbf{k}_0}e^{\imath(\omega_0-\omega_a)t-\imath\mathbf{k}_0\cdot\mathbf{r}_j} - h.c.\right] \\ & + \sum_{\mathbf{k}}\imath\hbar\mathbf{k}g_k\left[\hat{\sigma}_j\hat{a}^\dagger_{\mathbf{k}}e^{\imath(\omega_k-\omega_a)t-\imath\mathbf{k}\cdot\mathbf{r}_j} - h.c.\right] \ .\end{aligned} \tag{39.52}$$

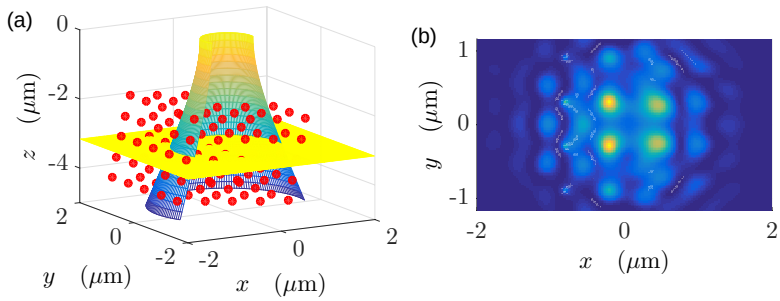

Figure 39.4: (code) (a) Geometry of light scattering from a cubic lattice with lattice constant $d = 100\,\mathrm{nm}$. The light is irradiated from below and is partially reflected. (b) Intensity distribution of scattered light along the yellow plane.

Introducing $\Delta_0 = \omega_0 - \omega_a$, the expectation value of the force separates in two contribution,

$$\begin{aligned}\langle \hat{\mathbf{F}}_j \rangle \equiv \mathbf{F}_{aj} + \mathbf{F}_{ej} &= \imath\hbar\mathbf{k}_0 g_{k_0} \left[\alpha^*(t)\beta_j(t)e^{\imath\Delta_0 t - \imath\mathbf{k}_0\cdot\mathbf{r}_j} - c.c.\right] \\ &\quad + \sum_{\mathbf{k}} \imath\hbar\mathbf{k} g_k \left[\beta_j(t)\gamma^*_{\mathbf{k}}(t)e^{\imath(\omega_k-\omega_a)t - \imath\mathbf{k}\cdot\mathbf{r}_j} - c.c.\right] \\ &= \imath\hbar\mathbf{k}_0 g_{k_0}[\alpha^*(t)\tilde{\beta}_j(t) - c.c.] \\ &\quad + \sum_{\mathbf{k}} \imath\hbar\mathbf{k} g_k \left[\tilde{\beta}_j(t)e^{-\imath(\omega_0-\omega_k)t + \imath(\mathbf{k}_0-\mathbf{k})\cdot\mathbf{r}_j}\gamma^*_{\mathbf{k}}(t) - c.c.\right] ,\end{aligned} \tag{39.53}$$

where we reintroduced the abbreviation (39.17). In particular, the term $m = j$ in the sum of $\mathbf{F}_{ej}$ vanishes since $\sum_{\mathbf{k}} \mathbf{k} = 0$. Substituting $\gamma_{\mathbf{k}}$ with equation (39.16),

$$\begin{aligned}\mathbf{F}_{aj} + \mathbf{F}_{ej} &= \imath\hbar\mathbf{k}_0 g_{k_0}[\alpha^*(t)\tilde{\beta}_j(t) - c.c.] \\ &\quad - \sum_{\mathbf{k}} \hbar\mathbf{k} g_k^2 \left[\tilde{\beta}_j(t)e^{-\imath(\omega_0-\omega_k)t + \imath(\mathbf{k}_0-\mathbf{k})\cdot\mathbf{r}_j} \sum_{m=1}^{N} e^{\imath\mathbf{k}\cdot\mathbf{r}_m} \int_0^t e^{-\imath(\omega_k-\omega_a)t'}\tilde{\beta}^*_m(t')dt' - c.c.\right] \\ &= -2\hbar\mathbf{k}_0 g_{k_0}\mathfrak{Im}\,[\alpha^*(t)\tilde{\beta}_j(t)] \\ &\quad - \sum_{\mathbf{k}} \hbar\mathbf{k} g_k^2 \sum_{m=1}^{N} \left[\tilde{\beta}_j(t)e^{\imath(\mathbf{k}_0-\mathbf{k})\cdot(\mathbf{r}_j-\mathbf{r}_m)} \int_0^t e^{\imath(\omega_0-\omega_k)(t'-t)}\tilde{\beta}^*_m(t')dt' - c.c.\right] ,\end{aligned} \tag{39.54}$$

and applying the Markov approximation (39.20),

$$\begin{aligned}\mathbf{F}_{aj} + \mathbf{F}_{ej} &= -2\hbar\mathbf{k}_0 g_{k_0}\mathfrak{Im}\,[\alpha^*(t)\tilde{\beta}_j(t)] \\ &\quad - \sum_{\mathbf{k}} \hbar\mathbf{k} g_k^2 \sum_{m=1}^{N} [e^{\imath(\mathbf{k}_0-\mathbf{k})\cdot(\mathbf{r}_j-\mathbf{r}_m)}\tfrac{\pi}{c}\delta(k-k_0)\tilde{\beta}_j(t)\tilde{\beta}^*_m(t) - c.c.] .\end{aligned} \tag{39.55}$$

This is the expression for the force acting on an atom at the position $\mathbf{r}_j$. Knowing the stationary excitation amplitudes $\beta_j(\infty)$ and assuming $\alpha(\infty) \simeq 1$, the radiation pressure force can numerically be calculated. Remembering $\Omega_0 = 2g_{k_0}$ we get for the

absorption force acting on atom j,

$$\mathbf{F}_{aj} = -2\hbar\mathbf{k}_0 g_{k_0} \Im\mathfrak{m}\ \tilde{\beta}_j(\infty)\ . \tag{39.56}$$

To evaluate the emission force acting on atom j, for every atom m of the sum, we need to average over all possible scattering angles. To do so, we choose a reference frame in which the z-component of $\mathbf{k}$ is directed along $\hat{\mathbf{r}}_{jm} = \frac{\mathbf{r}_j - \mathbf{r}_m}{|\mathbf{r}_j - \mathbf{r}_m|}$, that is,

$$\mathbf{k} = \hat{\mathbf{e}}_{x,jm} k \sin\theta_{jm}\cos\phi_{jm} + \hat{\mathbf{e}}_{y,jm} k \sin\theta_{jm}\sin\phi_{jm} + \hat{\mathbf{r}}_{jm} k\cos\theta_{jm}\ , \tag{39.57}$$

and evaluate the sum over the wavevectors by $\sum_{\mathbf{k}} \to \frac{V_{ph}}{(2\pi)^3}\int d^3k$,

$$\begin{aligned}
\mathbf{F}_{ej} &= -\sum_{m=1}^{N} \tilde{\beta}_j(\infty)\tilde{\beta}_m^*(\infty)\frac{V_{ph}}{(2\pi)^3}\frac{\pi}{c}\int_{\mathbb{R}^3} d\theta_{jm}d\phi_{jm}dk\ \hbar k \begin{pmatrix}\sin\theta_{jm}\cos\phi_{jm}\\ \sin\theta_{jm}\sin\phi_{jm}\\ \cos\theta_{jm}\end{pmatrix}\times \\
&\times g_k^2[e^{\imath(\mathbf{k}_0-\mathbf{k})\cdot(\mathbf{r}_j-\mathbf{r}_m)}\delta(k-k_0)k^2\sin\theta_{jm} - c.c. \\
&= -\hbar k_0\frac{\Gamma}{8\pi}\sum_{m=1}^{N} e^{\imath\mathbf{k}_0\cdot(\mathbf{r}_j-\mathbf{r}_m)}\tilde{\beta}_j(\infty)\tilde{\beta}_m^*(\infty)\int_0^{\pi}\int_0^{2\pi} d\theta_{jm}d\phi_{jm}\begin{pmatrix}\sin\theta_{jm}\cos\phi_{jm}\\ \sin\theta_{jm}\sin\phi_{jm}\\ \cos\theta_{jm}\end{pmatrix}\times \\
&\times e^{-\imath k\cdot|\mathbf{r}_j-\mathbf{r}_m|\cos\theta_{jm}}\sin\theta_{jm} - c.c.\ .
\end{aligned} \tag{39.58}$$

remembering $\Gamma = \frac{V_{ph}}{\pi c}k_0^2 g_{k_0}^2$ from Eq. (39.19). The integrals over ϕ_{jm} vanishes whereas the integral over θ_{jm} becomes, using,

$$\int_0^{\pi} d\theta \sin\theta\cos\theta e^{-\imath\alpha\cos\theta} = 2\imath\frac{\alpha\cos\alpha - \sin\alpha}{\alpha^2} = -2\imath j_1(\alpha)\ , \tag{39.59}$$

we find,

$$\begin{aligned}
\mathbf{F}_{ej} &= -\hbar k_0\frac{\Gamma}{4}\sum_{m=1}^{N} e^{\imath\mathbf{k}_0\cdot(\mathbf{r}_j-\mathbf{r}_m)}\tilde{\beta}_j(\infty)\tilde{\beta}_m^*(\infty)\hat{\mathbf{r}}_{jm}\times \\
&\times\int_0^{\pi}\cos\theta_{jm}\sin\theta_{jm}e^{-\imath k|\mathbf{r}_j-\mathbf{r}_m|\cos\theta_{jm}}d\theta_{jm} - c.c. \\
&= \imath\hbar k_0\frac{\Gamma}{2}\sum_{m=1}^{N} e^{\imath\mathbf{k}_0\cdot(\mathbf{r}_j-\mathbf{r}_m)}\tilde{\beta}_j(\infty)\tilde{\beta}_m^*(\infty)\hat{\mathbf{r}}_{jm}j_1(k|\mathbf{r}_j-\mathbf{r}_m|) - c.c. \\
&= -\imath\hbar k_0\frac{\Gamma}{2}\sum_{m=1}^{N}\mathbf{f}_{jm}\tilde{\beta}_j(\infty)\tilde{\beta}_m^*(\infty) - c.c.\ ,
\end{aligned} \tag{39.60}$$

where we defined [7],

$$\mathbf{f}_{jm} = -j_1(k|\mathbf{r}_j-\mathbf{r}_m|)e^{\imath\mathbf{k}_0\cdot(\mathbf{r}_j-\mathbf{r}_m)}\hat{\mathbf{r}}_{jm}\ . \tag{39.61}$$

[7] For exploitation in MATLAB we may express the spherical Bessel function by a Bessel function of the first kind: $j_n(x) = \sqrt{\pi/2x}J_{n+1/2}(x)$.

In summary we got,

$$\boxed{\begin{aligned}\mathbf{F}_{aj} &= -\imath\hbar k_0\Omega_0\Im\mathfrak{m}\ \tilde{\beta}_j(\infty)\\ \mathbf{F}_{ej} &= -\imath\hbar k_0\Gamma\sum_{m=1}^{N}\mathbf{f}_{jm}\Im\mathfrak{m}\ [\tilde{\beta}_j(\infty)\tilde{\beta}^*_m(\infty)]\end{aligned}}\ . \tag{39.62}$$

The steady state absorption and the emission part of the radiation pressure force on the *center of mass* of the atomic cloud follow from,

$$\mathbf{F}_a = \frac{1}{N}\sum_j\langle\hat{\mathbf{F}}_{aj}\rangle \qquad \text{and} \qquad \mathbf{F}_e = \frac{1}{N}\sum_j\langle\hat{\mathbf{F}}_{ej}\rangle\ . \tag{39.63}$$

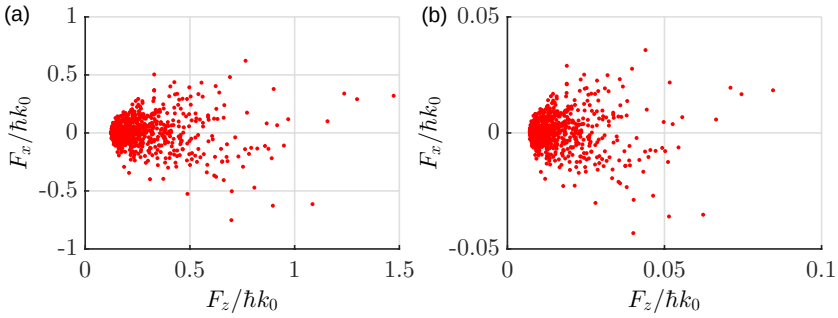

Figure 39.5: (code) Force distribution upon scattering of a photon by an atom of an spherical Gaussian cloud (a) without and (b) with rescattering according to Eqs. (39.63).

As long as the RWA and the Markov approximation are valid and only the lowest Dicke state is considered (no collective saturation), this simulation is supposed to be exact and contains all the physics including, e.g. multiple scattering. Fig. 39.5 shows a comparison of the cases when the off-diagonal components of the kernel (39.37) are present or not. Apparently, the presence of rescattering dramatically spoils the radiation pressure force, a phenomenon that we will extensively study in Secs. 39.1.7 and 39.2 [458, 66, 67, 1035, 139, 68].

39.1.7 The structure coefficient of the 'timed' Dicke state

When a beam of light passes through an atomic cloud, its phase fronts will excite the atomic dipole moments as it traverses the cloud. That is, understanding the beam as a plane wave $e^{\imath(\mathbf{k}_0\cdot\mathbf{r}-\omega t)}$, the dipoles start to oscillate with relative phase delays $e^{\imath\mathbf{k}_0\cdot(\mathbf{r}_j-\mathbf{r}_m)}$ depending on their position along the optical axis $\mathbf{k}_0$. The resulting collective state has been termed *timed Dicke state* [1182]. Assuming that this phase delay is the only parameter distinguishing two atoms, we may write with Eq. (39.17),

$$\tilde{\beta}_j(t) = \beta_j(t)e^{\imath(\Delta_0 t-\mathbf{k}_0\cdot\mathbf{r}_j)} \equiv \frac{1}{\sqrt{N}}\beta(t)\ , \tag{39.64}$$

where β is the macroscopic dipole moment. Note, that the fact that $\beta(t)$ does not depend on the atomic position does not imply a continuous density distribution. The atoms are still sitting at their positions $\mathbf{r}_j$; only are their dipole moments synchronized to the incident light wave.

The assumption of a timed Dicke state for the atomic cloud is, nevertheless, an approximation which is not always good [458]. For example, it neglects dispersive phase shifts of the excitation of the atomic dipole moments by the pump laser beam being delayed on its propagation due to its interaction with the atoms. If such phase shifts (and absorption as well) are radially inhomogeneous, this can lead to deformation of the pump laser beam's phase front and thus to lensing. We will discuss this in Exc. 39.1.8.5 and in Sec. 39.2.

39.1.7.1 Structure coefficient for 'timed' Dicke states

We start again with the Eqs. (39.24) inserting the ansatz of *timed Dicke* states,

$$\begin{aligned}\dot{\beta}(t) &= \frac{1}{N}\sum_{j=1}^{N}\dot{\beta}(t) = \frac{1}{\sqrt{N}}\sum_{j=1}^{N}\frac{d}{dt}\tilde{\beta}_j(t) \\ &= \frac{1}{\sqrt{N}}\sum_{j=1}^{N}\left(\imath\Delta_0\tilde{\beta}_j(t) - \imath\frac{\Omega_0}{2}\alpha(t) - \frac{\Gamma}{2}\sum_{m=1}^{N}\gamma_{jm}\tilde{\beta}_m(t)\right) \\ &= \left(\imath\Delta_0 - \frac{\Gamma}{2}Ns_N\right)\beta(t) - \imath\frac{\sqrt{N}\Omega_0}{2}\alpha(t)\ ,\end{aligned} \tag{39.65}$$

where we introduced the abbreviation,

$$s_N \equiv \frac{1}{N}\frac{1}{N}\sum_{j,m=1}^{N}\gamma_{jm}\ . \tag{39.66}$$

Taking the kernel from (39.25), we get,

$$\begin{aligned}s_N &= \frac{1}{N}\frac{2}{\Gamma}\frac{V_{ph}}{(2\pi)^3}\int_{\mathbb{R}^3} g_k^2\frac{1}{N}\sum_{j,m=1}^{N} e^{\imath(\mathbf{k}-\mathbf{k}_0)\cdot(\mathbf{r}_j-\mathbf{r}_m)}\frac{\pi}{c}\delta(k-k_0)k^2\sin\theta dk d\theta d\phi \\ &= \frac{1}{N}\frac{2}{\Gamma}\frac{V_{ph}}{(2\pi)^3}\int_0^\infty\int_0^\pi\int_0^{2\pi} g_k^2 N|S_N(k,\theta,\phi)|^2\frac{\pi}{c}\delta(k-k_0)k^2\sin\theta dk d\theta d\phi \\ &= \frac{1}{4\pi}\int_0^\pi\int_0^{2\pi}|S_N(k_0,\theta,\phi)|^2\sin\theta d\theta d\phi\ ,\end{aligned} \tag{39.67}$$

introducing the normalized *structure coefficient*,

$$\boxed{\mathcal{S}_N(\mathbf{k}) \equiv \rho(\mathbf{q}) = \frac{1}{N}\sum_{j=1}^{N} e^{\imath(\mathbf{k}-\mathbf{k}_0)\cdot\mathbf{r}_j}}\ , \tag{39.68}$$

where $\mathbf{q} = \mathbf{k} - \mathbf{k}_0$ and $\rho(\mathbf{q})$ is the structure coefficient defined in (39.3).

In steady state, $\dot{\beta}(t) = 0$, and disregarding saturation, $\alpha(t) \simeq 1$, the solution of (39.65) reads,

$$\boxed{\beta(\infty) = \frac{\sqrt{N}\Omega_0}{2\Delta_0 + \imath\Gamma N s_N}}\,, \tag{39.69}$$

such that,

$$\begin{aligned} |\beta(\infty)|^2 &= \frac{N\Omega_0^2}{4\Delta_0^2 + N^2\Gamma^2 s_N^2} \\ \mathfrak{Im}\left[\alpha(\infty)\beta^*(\infty)\right] &= \frac{N^{3/2}\Gamma\Omega_0 s_N}{4\Delta_0^2 + N^2\Gamma^2 s_N^2}\,. \end{aligned} \tag{39.70}$$

The time-dependent solution is easily obtained as,

$$\beta(t) = \beta(0)e^{(\imath\Delta_0 - \Gamma N s_n/2)t} + \beta(\infty)\,. \tag{39.71}$$

The evolution of the cloud very much depends on the initial conditions, e.g. $\beta_j(0) = 1$ for the uniformly excited *symmetric state* $\beta_j(0) = e^{\imath\mathbf{k}_0\cdot\mathbf{r}_j}$ for timed Dicke states.

In cylindrical coordinates the structure coefficient can be written,

$$\mathcal{S}(k,\theta,\phi) = \frac{1}{N}\sum_{j=1}^{N} e^{\imath(kx_j\sin\theta\cos\phi + ky_j\sin\theta\cos\phi + (k\cos\theta - k_0)z_j)}\,. \tag{39.72}$$

It basically tells the angular distribution of the scattered light. Fig. 39.6 shows numerical calculations and analytical approximations of the structure factor for various shapes and sizes of the atomic cloud. Obviously, the radiation pattern very much depends on the size of the spherical cloud. For $R < \lambda$ it is isotropic, for $R > \lambda$ scattering mainly occurs in forward direction. Furthermore, if the cloud is ellipsoidal the radiation pattern is shifted into forward direction.

39.1.7.2 Time evolution of radiation modes

We are interested in the power emitted into the solid angle $\Omega_{\mathbf{k}}$, $P(t) \propto |\gamma_{\mathbf{k}}(t)|^2$. For timed Dicke state (39.64) we get immediately from the equations of motion,

$$\begin{aligned} \dot{\gamma}_{\mathbf{k}}(t) &= -\imath g_k e^{\imath\Delta_k t}\sum_{j=1}^{N}\beta_j(t)e^{-\imath\mathbf{k}\cdot\mathbf{r}_j} \\ &= -\imath g_k e^{\imath(\Delta_k - \Delta_0)t}\frac{1}{\sqrt{N}}\beta(t)\sum_{j=1}^{N} e^{\imath(\mathbf{k}_0 - \mathbf{k})\cdot\mathbf{r}_j} = -\imath g_k e^{\imath(\Delta_k - \Delta_0)t}\sqrt{N}\mathcal{S}_N(\mathbf{k})\,. \end{aligned} \tag{39.73}$$

We see that the time-dependence factorizes from the structure factor, which is the only component containing an angular dependence. The same holds for *symmetric Dicke states* defined by $|\beta_j| = |\beta_m|$.

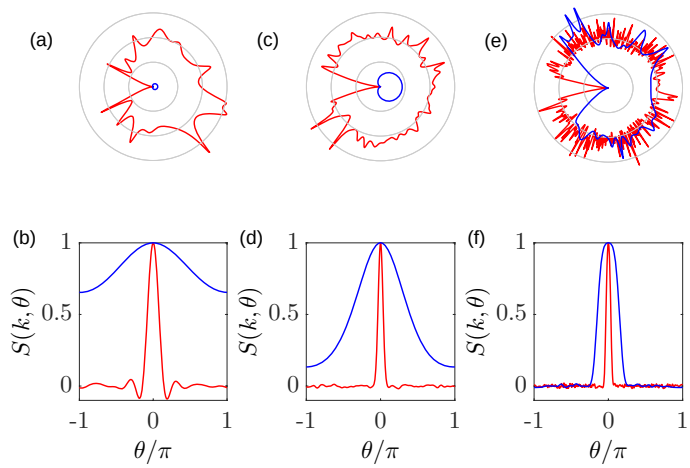

Figure 39.6: (code) Numerical calculation of $\mathcal{S}(k,\theta)$ according to (39.68) for 10^4 atomic positions r_j chosen by a random number generator. For the graphs (a-b) the cloud is *homogeneous and spherical* and has the sizes $R = \lambda$ (red) and $R = 10\lambda$ (blue). For the graphs (c-d) the cloud is *Gaussian and spherical* and has the same sizes as (a-b). For the graphs (d-e) the cloud is *homogeneous and ellipsoidal with aspect ratio* $R_z/R_\rho = 3$ and has the same radial sizes as in (a-b).

39.1.7.3 Light scattering in the 'timed Dicke state'

The scalar electric field scattered by an arbitrary distribution of atoms has been calculated in (39.49). Substituting the stationary timed Dicke state (39.69), we get,

$$\mathcal{E}_{sct}(\mathbf{r}) = -\frac{\imath\hbar\Gamma}{2d}\frac{\sqrt{N}\Omega_0}{2\Delta_0 + \imath\Gamma N s_N}\sum_{j=1}^{N}\frac{e^{\imath k_0|\mathbf{r}-\mathbf{r}_j|}}{\imath k_0|\mathbf{r}-\mathbf{r}_j|} \ . \tag{39.74}$$

Note that the 'timed Dicke' state starts from the assumption of an infinitely extended plane wave incident light field. This excludes situations where the incident beam size is smaller than the cloud's size.

39.1.7.4 Force in the 'timed Dicke state' on a particular atom in a cloud

The time-dependent expressions (39.56) for the forces in the coupled dipoles model can be further evaluated for timed Dicke states (39.64),

$$\begin{aligned}
&\mathbf{F}_{aj} + \mathbf{F}_{ej} \qquad\qquad (39.75)\\
&= -\frac{2\hbar\mathbf{k}_0 g_{k_0}}{\sqrt{N}}\mathfrak{Im}\ \beta(t) - \sum_{\mathbf{k}}\frac{\hbar\mathbf{k}g_k^2}{N}\sum_{m=1}^{N}\left[e^{\imath(\mathbf{k}_0-\mathbf{k})\cdot(\mathbf{r}_j-\mathbf{r}_m)}\frac{\pi}{c}\delta(k-k_0)|\beta(t)|^2 - c.c.\right]\\
&= -\frac{2\hbar\mathbf{k}_0 g_{k_0}}{\sqrt{N}}\mathfrak{Im}\ \beta(t) - \sum_{\mathbf{k}}\hbar\mathbf{k}g_k^2\left[\mathcal{S}_N(\mathbf{k})e^{-\imath(\mathbf{k}-\mathbf{k}_0)\cdot\mathbf{r}_j}\frac{\pi}{c}\delta(k-k_0)|\beta(t)|^2 - c.c.\right] \ .
\end{aligned}$$

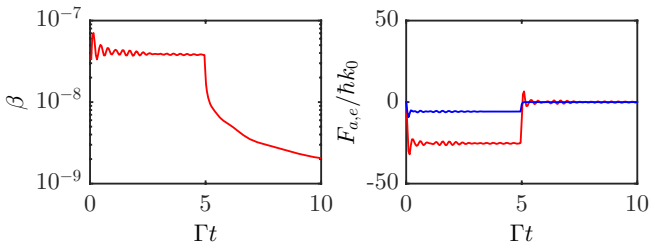

Figure 39.7: (code) Time-dependent of (a) the dipole amplitudes and (b) the forces for $\sigma = 1$, $\Delta_0 = 20\Gamma$, $\Omega_0 = 0.01\Gamma$, and $\eta = 1$.

Evaluating the sum over the wavevectors by $\sum_{\mathbf{k}} \to \frac{V_{ph}}{(2\pi)^3}\int d^3k$,

$$\mathbf{F}_{aj} + \mathbf{F}_{ej} = \frac{-2\hbar\mathbf{k_0} g_{k_0}}{\sqrt{N}} \Im\mathfrak{m}\ \beta(t) \tag{39.76}$$
$$- |\beta(t)|^2 \frac{V_{ph}}{(2\pi)^3}\int_0^\infty \int_0^\pi \int_0^{2\pi} \hbar\mathbf{k} g_k^2 \left[\mathcal{S}_N(k,\theta,\phi) e^{-i(\mathbf{k}-\mathbf{k}_0)\cdot\mathbf{r}_j} \frac{\pi}{c}\delta(k-k_0) - c.c.\right] k^2 \sin\theta d\theta d\phi dk\ .$$

Let us consider an atom sitting on axis, $\mathbf{r}_j = 0$, and use cylindrical coordinates, $\mathbf{k}_0 = k_0\hat{\mathbf{e}}_z$ and $\mathbf{k} = \hat{\mathbf{e}}_x k\sin\theta\cos\phi + \hat{\mathbf{e}}_y k\sin\theta\sin\phi + \hat{\mathbf{e}}_z k\cos\theta$, and using the definition (39.19) of Γ,

$$\mathbf{F}_{aj} + \mathbf{F}_{ej} = \frac{-2\hbar k_0 g_{k_0}}{\sqrt{N}} \hat{\mathbf{e}}_z \Im\mathfrak{m}\ \beta(t) \tag{39.77}$$
$$- |\beta(t)|^2 \frac{\Gamma}{8\pi}\hbar k_0 \int_0^\pi \int_0^{2\pi} (\hat{\mathbf{e}}_x \sin\theta\cos\phi + \hat{\mathbf{e}}_y \sin\theta\sin\phi + \hat{\mathbf{e}}_z\cos\theta)\left[\mathcal{S}_N(k,\theta,\phi) - c.c.\right]\sin\theta d\theta d\phi\ .$$

Using the abbreviation,

$$\tilde{f}_N \equiv \frac{1}{4\pi}\int_0^\pi \int_0^{2\pi} \Re\mathfrak{e}\ \mathcal{S}_N(k_0,\theta,\phi)\sin\theta\cos\theta d\theta d\phi\ , \tag{39.78}$$

the z-component becomes,

$$F_{zaj} + F_{zej} = -\frac{2\hbar k_0 g_{k_0}}{\sqrt{N}} \Im\mathfrak{m}\ \beta(t) - |\beta(t)|^2 \Gamma\hbar k_0 \tilde{f}_N\ . \tag{39.79}$$

In steady state and normalizing to the standard radiation pressure,

$$F_{z1j} = \Gamma\hbar k_0 \frac{\Omega_0^2}{4\Delta_0^2 + \Gamma^2} = \hbar k_0 \sigma(\Delta)\frac{I}{\hbar\omega}\ , \tag{39.80}$$

where $\sigma(\Delta_0)$ is the optical cross section and I the intensity of the incident light, we can write,

$$\frac{F_{zaj} + F_{zej}}{F_{z1j}} = \left(-\frac{2\hbar k_0 g_{k_0}}{\sqrt{N}} \Im\mathfrak{m}\ \beta(\infty) - |\beta(\infty)|^2 \Gamma\hbar k_0 \tilde{f}_N\right)\frac{4\Delta_0^2 + \Gamma^2}{\Gamma\hbar k_0 \Omega_0^2}\ . \tag{39.81}$$

Finally, inserting the the expression (39.69) for the dipole moment, we obtain for the timed Dicke state,

$$\boxed{\frac{F_{zaj} + F_{zej}}{F_{z1j}} = \frac{(2\Delta_0/\Gamma)^2 + 1}{(2\Delta_0/\Gamma)^2 + N^2 s_N^2} N(s_N - \tilde{f}_N)}\ , \tag{39.82}$$

using $\Omega_0 = 2g_{k_0}$.

The factors s_N and f_N can be calculated exactly, as will be done in Exc. 39.1.8.6,

$$s_N = \frac{1}{N^2}\sum_{j,m=1}^{N}\frac{\sin(k_0|\mathbf{r}_j-\mathbf{r}_m|)}{k_0|\mathbf{r}_j-\mathbf{r}_m|}\cos[k_0(z_j-z_m)] \tag{39.83}$$

$$f_N = \sqrt{\frac{\pi}{2}}\frac{1}{N^2}\sum_{j,m=1}^{N}\frac{J_{3/2}(k_0|\mathbf{r}_j-\mathbf{r}_m|)}{(k_0|\mathbf{r}_j-\mathbf{r}_m|)^{3/2}}k_0(z_j-z_m)\sin[k_0(z_j-z_m)]\ .$$

However, this is only practicable for atom numbers small enough for numerical simulations. For larger atom number we may use the analytic expressions including the disorder term [141].

39.1.7.5 Force on the center of mass of the cloud

The force acting on the center of mass of the atomic cloud is given by the average of the forces (39.76) sensed by particular atoms,

$$\begin{aligned}\mathbf{F}_a+\mathbf{F}_e &= \frac{1}{N}\sum_{j=1}^{N}(\mathbf{F}_{aj}+\mathbf{F}_{ej}) \qquad (39.84)\\ &= -\frac{2\hbar\mathbf{k_0}g_{k_0}}{\sqrt{N}}\mathfrak{Im}\ \beta(t)\\ &\quad -|\beta(t)|^2\frac{V_{ph}}{(2\pi)^3}\int_{\mathbb{R}^3}\hbar\mathbf{k}g_k^2\left[\mathcal{S}_N(k,\theta,\phi)\frac{1}{N}\sum_{j=1}^{N}e^{-\imath(\mathbf{k}-\mathbf{k}_0)\cdot\mathbf{r}_j}\frac{\pi}{c}\delta(k-k_0)-c.c.\right]k^2\sin\theta d\theta d\phi dk\\ &= \frac{-2\hbar\mathbf{k_0}}{\sqrt{N}}g_{k_0}\mathfrak{Im}\ \beta(t)-|\beta(t)|^2\frac{V_{ph}}{(2\pi)^3}\int_{\mathbb{R}^3}\hbar\mathbf{k}g_k^2 2|\mathcal{S}_N(k,\theta,\phi)|^2\frac{\pi}{c}\delta(k-k_0)k^2\sin\theta d\theta d\phi dk\ .\end{aligned}$$

Using cylindrical coordinates, $\mathbf{k}_0 = k_0\hat{\mathbf{e}}_z$ and $\mathbf{k} = \hat{\mathbf{e}}_x k\sin\theta\cos\phi + \hat{\mathbf{e}}_y k\sin\theta\sin\phi + \hat{\mathbf{e}}_z k\cos\theta$, and the definition of Γ,

$$\begin{aligned}\mathbf{F}_a+\mathbf{F}_e &= \frac{-2\hbar k_0}{\sqrt{N}}\hat{\mathbf{e}}_z g_{k_0}\mathfrak{Im}\ \beta(t) \qquad (39.85)\\ &\quad -|\beta(t)|^2\frac{\Gamma}{8\pi}\hbar k_0\int_0^{\pi}\int_0^{2\pi}(\hat{\mathbf{e}}_x\sin\theta\cos\phi+\hat{\mathbf{e}}_y\sin\theta\sin\phi+\hat{\mathbf{e}}_z\cos\theta)\,2|\mathcal{S}_N(k,\theta,\phi)|^2\sin\theta d\theta d\phi\ .\end{aligned}$$

Using the abbreviation,

$$f_N \equiv \frac{1}{4\pi}\int_0^{\pi}\int_0^{2\pi}|\mathcal{S}_N(k_0,\theta,\phi)|^2\sin\theta\cos\theta d\theta d\phi\ , \tag{39.86}$$

we get for the z-component an analogous formula to (39.79),

$$\begin{aligned}F_{za}+F_{ze} &= \frac{-2\hbar k_0 g_{k_0}}{\sqrt{N}}\mathfrak{Im}\ \beta(t)-|\beta(t)|^2\frac{\Gamma}{8\pi}\hbar k_0\int_0^{\pi}\int_0^{2\pi}2|\mathcal{S}_N(k,\theta,\phi)|^2\sin\theta\cos\theta d\theta d\phi\\ &= -\frac{2\hbar k_0 g_{k_0}}{\sqrt{N}}\mathfrak{Im}\ \beta(t)-|\beta(t)|^2\Gamma\hbar k_0 f_N\ . \qquad (39.87)\end{aligned}$$

In steady state and normalizing again to the standard radiation pressure (39.80),

$$\frac{F_{za}+F_{ze}}{F_{z1}} = \left(-\frac{2\hbar k_0 g_{k_0}}{\sqrt{N}}\mathfrak{Im}\ \beta(\infty)-|\beta(\infty)|^2\Gamma\hbar k_0 f_N\right)\frac{4\Delta_0^2+\Gamma^2}{\Gamma\hbar k_0\Omega_0^2}\ . \tag{39.88}$$

Finally, inserting the the expression (39.69) for the dipole moment, we obtain for the timed Dicke state,

$$\boxed{\frac{F_{za}+F_{ze}}{F_{z1}} = \frac{(2\Delta_0/\Gamma)^2+1}{(2\Delta_0/\Gamma)^2+N^2 s_N^2} N(s_N - f_N)} \,, \tag{39.89}$$

using $\Omega_0 = 2g_{k_0}$. Inserting the expressions (39.67) for s_N and (39.86) for f_N, we may also write,

$$\frac{F_{0a}+F_{0e}}{F_{z1}} = \frac{(2\Delta_0/\Gamma)^2+1}{(2\Delta_0/\Gamma)^2+N^2 s_N^2} N \frac{1}{4\pi} \int_0^\pi \int_0^{2\pi} |\mathcal{S}_N(k,\theta,\phi)|^2 (1-\cos\theta)\sin\theta d\theta d\phi \,. \tag{39.90}$$

Let us assume in the following that the scattering of every single photon can be treated independently [1180]. In particular, the density distribution may change between two scattering events. The force is something like the first moment of the structure factor. This makes it so adapted to measure fluctuation-induced deviations from the structure coefficient [8].

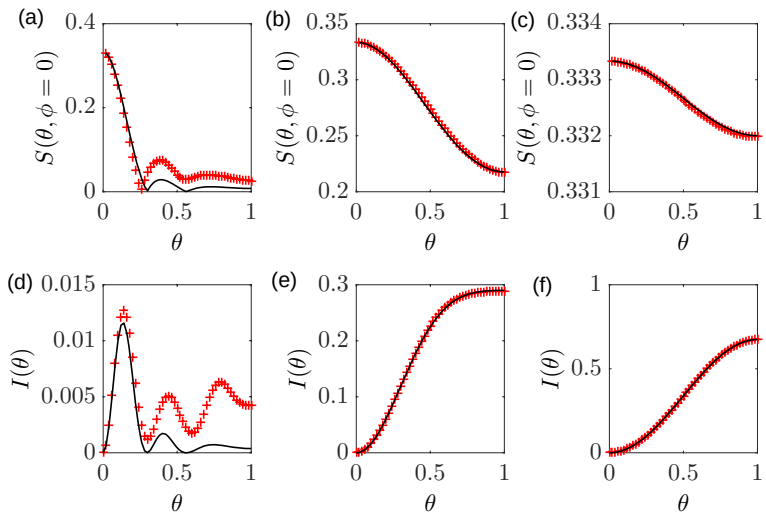

Figure 39.8: (code) (a-c) Calculation of the structure coefficient $|\mathcal{S}(k=k_0,\theta,\phi=0)|^2$ for an isotropic homogeneous density distribution. (d-f) Calculation of the force $I(\theta) = \int_0^{2\pi} |\mathcal{S}(k=k_0,\theta,\phi)|^2(1-\cos\theta)d\phi$. The red curves show numerical calculations based on (39.68), the green curves show analytical calculations according to (39.98). (a,d) $k_0R = 1$ and $N = 100$. (b,e) $k_0R = 5$ and $N = 100$. (c,f) $k_0R = 5$ and $N = 1000$.

We want to compare this force to the force acting on a cloud of N uncorrelated scatterers, i.e. atoms receiving recoil from the pump photons but reemitting isotrop-

[8] Insert a clarifying discussion of what we said in the EPDJ and what we did not: We said there is a collective effect coming from the structure factor of the cloud. We did NOT say that interatomic interactions are essential...!

ically,

$$\langle F_{unc,z}\rangle = \frac{V_{ph}}{(2\pi)^3}\sigma(\Delta)\frac{I}{\hbar\omega}\hbar k_0 \int_0^\infty \int_0^\pi \int_0^{2\pi} |\mathcal{S}_N(k,\theta,\phi)|^2 k^2 \sin\theta d\theta d\phi dk \ . \quad (39.91)$$

For such a cloud the structure coefficient is $\mathcal{S}_N = N^{-1/2}$. Note that this is unlike N atoms in the Dicke limit, where $\mathcal{S}_N = 1$.

A dense homogeneous cloud with $\mathcal{S}_N(\mathbf{k}) \propto \delta^3(\mathbf{k}_0 - \mathbf{k})$ does not scatter light and experiences no force, $\langle F_{hom}\rangle = 0$. This is however not true any more in the limit of small extended clouds, where fluctuations introduce disorder. This can be shown by simulating a random atomic distribution $\mathbf{r}_j$ and integrating the resulting force over all possible $\mathbf{k}$. For simplicity we assume a very sharp momentum distribution, $|\mathbf{k}| = |\mathbf{k}_0|$ or $\frac{V_{ph}}{2\pi^2}\int_0^\infty k^2 dk = 1$,

$$\langle F_z\rangle = \sigma(\Delta)\frac{I}{\hbar\omega}k_0(s_N - f_N) \ . \quad (39.92)$$

Finally to compare with experiment we evaluate the ratio,

$$\frac{\langle F_z\rangle}{\langle F_{unc,z}\rangle} = 1 - \frac{f_N}{s_N} \ . \quad (39.93)$$

We describe the cloud as being made of two fractions: An isotropically scattering fraction of $N_0 = \sqrt{N}$ disordered atoms, whose structure factor is $\mathcal{S}_{iso}(\mathbf{k}) = 1$, and a forward scattering homogeneous cloud with structure factor $\mathcal{S}_{hom}(\mathbf{k}) = \delta_{\mathbf{k}_0,\mathbf{k}}$. The surface integration of the total structure factor,

$$\mathcal{S}_N(\mathbf{k}) = \frac{N_0}{N}\mathcal{S}_{iso}(\mathbf{k}) + \frac{N-N_0}{N}\mathcal{S}_{hom}(\mathbf{k}) = \frac{N_0}{N} + \frac{N-N_0}{N}\delta_{\mathbf{k}_0,\mathbf{k}} \simeq \frac{N_0}{N} \quad (39.94)$$

yields the same N-dependence of the force,

$$\frac{\langle F_z\rangle}{\langle F_{iso,z}\rangle} = \frac{1}{4\pi N^2}\int_0^\pi \int_0^{2\pi} |\sqrt{N}|^2(1-\cos\theta)\sin\theta d\theta d\phi = \frac{1}{N} \ . \quad (39.95)$$

The interpretation is the following. In the experimentally realized situation, we are very far in the large cloud limit completely dominated by forward scattering, which means that *if the cloud were homogeneous no radiation pressure force should be expected* at all. However diffuse scattering from disordered atoms (or fluctuations) disturbs the forward scattering. It is this scattering which gives rise to radiation pressure.

There is an interesting analogy: Diffuse scattering not only inhibits forward scattering in homogeneous clouds, but also coherent backscattering from ordered structures. E.g. in optical lattices [1220] it disturbs the detection of photonic band gaps. In an optical lattice the atoms are in the Dicke limit and do not absorb photonic recoil. Hence, no displacement due to radiation pressure is expected. However, diffuse scattering is observed as absorptive features in the spectra [146, 1220].

The Bragg scattering is expressed by a periodic structure factor. A widely used approach to describe the impact of disordered atoms in lattices is to divide the cloud into a perfectly ordered part with density nf_{DW} and isotropically scattering part with density $n(1-f_{DW})$ [1220]. The factor f_{DW} is known as Debye-Waller factor. In Exc. 39.1.8.7 we try an alternative traetment of radiation pressure based on a Monte-Carlo simulation.

39.1.7.6 Cooperative scattering and single photon superradiance

A non-isotropic structure factor scattering light into a specific direction of space (e.g. the Bragg angle) at a rate scaling like N^α with $\alpha > 1$ needs several 'cooperating' particles. In this sense cooperation only means, that the particles be arranged in space in a particular way, i.e. in a lattice or in a particular bulk shape like a homogeneous sphere or a Gaussian cigar-shaped density distribution. It also immediately becomes clear that disorder ought to play a major role. However, cooperation goes further, since cooperative scattering can be observed in spontaneous emission of an atomic cloud being excited by just a single photon. Single-photon superradiance is the topic of the following sections.

For now let us state that a non-isotropic structure factor results in collective scattering. The density distribution (which is the Fourier transform of the structure factor) can adopt two extremes: A periodic lattice results in backscattering into specific directions, a homogeneous clouds shows nothing but forward scattering. Both situations are never perfectly realized, but are subject to density fluctuations (Debye-Waller factor in a lattice, radiation pressure in a homogeneous cloud).

A single photon on its trip through an atomic cloud successively excites the atomic dipole moment thus establishing a phase relation between potential radiators [404, 1284, 1181, 1286]. One could think that the scattering process localizes atom and photon, i.e. only one atom scatters. However, we don't know which atom scatters, and this introduces a correlation of the dipole moments along the propagation direction of the light beam.

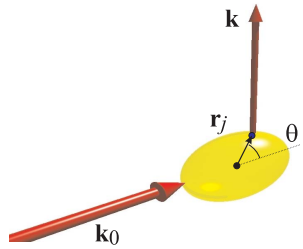

Figure 39.9: Scattering of a photon by an atom of an ellipsoidal cloud.

While normally the radiation rate of a dilute cloud is $\propto N$, in the presence of coherent interactions it scales as $\propto N^2$. Coherent interactions are not conditioned to overlapping space functions of the atoms, i.e. it is not compulsory that the density be $n^{-1/3} > \lambda$. For example, scattering from ordered structures also scales as $\propto N^2$ [691]. However, the scattering will be dramatically different if $n^{-1/3} < \lambda$.

Spontaneous emission radiation pattern from uncorrelated scatterers only depend on the relative orientation of $\hat{\sigma}$ and $\vec{\mathcal{B}}$, but not on the $\mathbf{k}$-vector of the incident light. This also holds for Dicke superradiance in the small cloud limit, but not for large clouds. Here forward scattering dominates.

We have seen in this section that, despite its simplicity, the coupled dipoles model has a large range of applications. It allows for a deeper understanding of known classical phenomena and, as we will study in Excs. 41.2.4.7 to 41.2.4.1 and in forthcoming sections, it allows to unravel new effects.

39.1.8 Exercises

39.1.8.1 Ex: Structure coefficient of a linear array

a. Based on the definition (39.1) compute the structure factor of a linear array of point-like scatterers.
b. Based on the definition (39.2) compute the structure factor of a linear array of 10 Gaussian density distributions.

Solution: *a. See Fig. 39.10. b. See Fig. 39.11.*

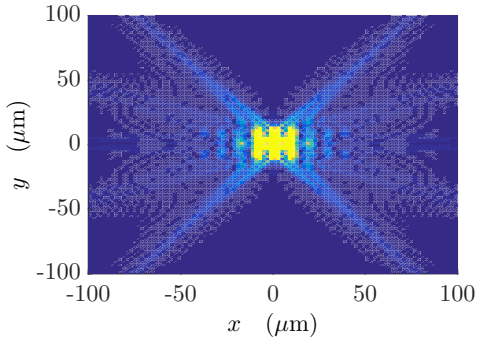

Figure 39.10: (code) Linear array of scatterers separated by 2 nm at $\lambda = 797$ nm.

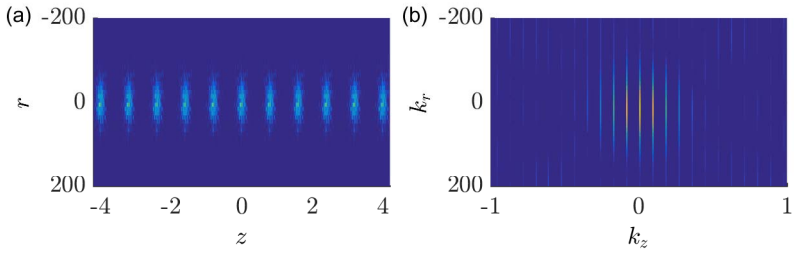

Figure 39.11: (code) Linear array of Gaussian density distributions separated by 2 nm at $\lambda = 797$ nm.

39.1.8.2 Ex: Structure factor of a cloud

a. Based on the definition (39.1) compute the structure coefficient of (i) a slit, (ii) a pinhole, and (iii) a homogeneous spherical cloud.
b. Based on the definition (39.3) compute the structure coefficient of a homogeneous spherical cloud.

Solution: *a. The structure coefficient is the Fourier transform of the density,* $\mathcal{S}(\mathbf{k}) =$

$\int n(\mathbf{r})e^{\imath\mathbf{k}\cdot\mathbf{r}}d^3r$. *In 1D it describes the diffraction through a slit,*

$$\int_{-R}^{R} e^{\imath kr}dr = \frac{2}{k}\sin kR \ .$$

In 2D it describes the diffraction by a pinhole,

$$\int_{disk} e^{\imath\mathbf{k}\cdot\mathbf{r}}d^2\mathbf{r} = \int_0^R\int_0^{2\pi} re^{\imath kr}d\phi dr = \frac{2\pi}{k^2}\left[\cos kR + kR\sin kR - 1 + \imath(\sin kR - kR\cos kR)\right] \ .$$

In 3D the structure factor is,

$$\int_{sphere} e^{\imath\mathbf{k}\cdot\mathbf{r}}d^3r = \int_0^R\int_0^{2\pi}\int_0^{\pi} r^2e^{\imath kr\cos\theta}\sin\theta d\theta d\phi dr = \frac{4\pi}{k^3}(\sin kR - kR\cos kR) \ .$$

b. The structure factor can be evaluated from $S(\mathbf{q}) = \langle\rho(\mathbf{q})\rho^*(\mathbf{q})\rangle$, *where* $\rho(\mathbf{q}) = \int_V n(\mathbf{r})e^{\imath\mathbf{q}\cdot\mathbf{r}}d^3r$ *[1085, 333],*

$$\begin{aligned} S(\mathbf{q}) &= \int d^3r\int d^3r' n(\mathbf{r})n(\mathbf{r}')e^{\imath q\cdot(\mathbf{r}-\mathbf{r}')} = \frac{4\pi}{V}\int_0^R r^2e^{\imath\mathbf{q}\cdot\mathbf{r}}dr\frac{4\pi}{V}\int_0^R r'^2e^{-\imath\mathbf{q}\cdot\mathbf{r}'}dr' \\ &= \left(\frac{4\pi}{q^3V}\right)^2(\sin qR - qR\cos qR)^2 = 9\frac{(\sin qR - qR\cos qR)^2}{(qR)^6} \ , \end{aligned}$$

with $V = \frac{4\pi}{3}R^3$ *and* $n(\mathbf{r}) = \frac{1}{V}$. *In particular we have,*

$$S(\mathbf{q}) \overset{R\ll\lambda}{\longrightarrow} 1 \qquad \textit{and} \qquad S(\mathbf{q}) \overset{R\gg\lambda}{\longrightarrow} 0 \ .$$

The structure factor is then identical to the collective cooperativity $\Upsilon_N = S(\mathbf{q})$.

39.1.8.3 Ex: Structure coefficient and Snell's law

Calculate the structure coefficient for a light beam passing through a plane interface between two dielectrics.

Solution: *We set the interface in the xy-plane and assume that for* $z < 0 >$ *the refraction index in 1, and for* $z > 0$ *it is* n_{rfr}. *The structure coefficient is the Fourier transform of the density. Hence,*

$$\begin{aligned} \mathcal{S}(\mathbf{k}) &= \int[1 + (n_{rfr} - 1)\Theta(z)]e^{\imath\mathbf{k}\cdot\mathbf{r}}d^3r = \delta(\mathbf{k}) + (n_{rfr} - 1)\delta(k_x)\delta(k_y)\int_0^\infty e^{\imath k_z z}dz \\ &= \delta(\mathbf{k}) + (n_{rfr} - 1)\delta(k_x)\delta(k_y)\frac{1}{\imath k_z} = \ldots \ . \end{aligned}$$

39.1.8.4 Ex: Validity of Markov approximation

a. Calculate the single-atom scattering rate for a rubidium cloud of $N = 10^6$ atoms driven with $P = 100\,\mathrm{mW}$ laser power focused into a waist of $w_0 = 100\,\mu\mathrm{m}$ and detuned by $\Delta = (2\pi)\ 100\,\mathrm{GHz}$ from the D_2-line at 780 nm [225].
b. Assume for the cloud a homogeneous spherical density distribution with radius $R = 250/k_0$. Based on Ref. [1284] estimate whether the Markov approximation is valid.

Solution: *a. The single-atom excitation rate is for the specified parameters,*

$$\gamma_{ex} = N\frac{\sigma(\Delta)I}{\hbar\omega} \simeq 6.5\cdot 10^9\ \ \mathrm{s}^{-1}\ .$$

b. The superradiant deexcitation rate is for $k_0R = 250$ assuming a homogeneous spherical cloud [1284],

$$\gamma_{deex} = N\frac{27\Gamma}{8(k_0R)^2} \simeq 2\cdot 10^9\,\mathrm{s}^{-1}\ .$$

Hence the assumption of single-photon Dicke superradiance is questionable. The condition for having less than one photon in the cloud is for smooth clouds $\gamma_{ex} \ll \gamma_{deex}$. This means,

$$\frac{N\Gamma}{(2\sigma)^2} \gg N\sigma_{opt}\frac{I}{\hbar\omega} = N\frac{\Gamma^2}{4\Delta_0^2+2\Omega_0^2+\Gamma^2}\frac{\Omega_0^2}{\Gamma} \ll \frac{N\Gamma}{(2\sigma)^2}$$

using $\Omega_0^2 = \sigma_0\Gamma\frac{I}{\hbar\omega}$. For $\Delta_0 \gg \Gamma, \Omega_0$ we get,

$$\frac{\Omega_0^2}{4\Delta_0^2}(2\sigma)^2 \ll 1\ .$$

For disordered clouds the condition reads

$$\frac{\Omega_0^2}{4\Delta_0^2}N \ll 1\ .$$

39.1.8.5 Ex: Lensing by a dense atomic cloud with the coupled dipoles model

Simulate the pump laser phase shift and lensing by a small dense cloud by the coupled dipoles model for red and blue detuning. Discuss the influence of rescattering by removing artificially the off-diagonal terms from the scattering kernel. Discuss whether lensing is observed within the timed Dicke approximation.

Solution: *The question is, whether the fact that the pump laser is depleted (partially absorbed) and phase-shifted is contained in the CDM, although we assumed in its derivation $\alpha \simeq 1$. As illustrated in Fig. 39.12, red detuning leads to focusing, blue*

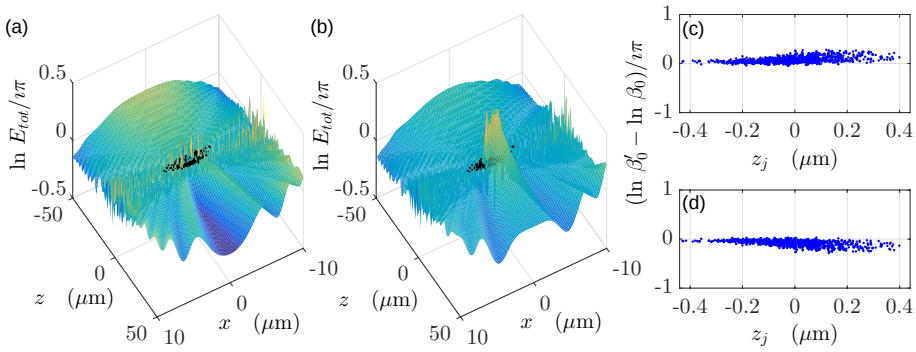

Figure 39.12: (code) Phase profile upon scattering from a (strontium) spherical Gaussian cloud $k_0\sigma_r = 15$ of 1000 atoms for (a) red detuning of $\Delta = -5\Gamma$ and (b) blue detuning $\Delta = 5\Gamma$. (c,d) Difference of the phase shifts of the atomic dipoles located at positions z_j of the optical axis calculated by Eqs. (39.36) and (39.69).

detuning to defocusing. Note, that removing the off-diagonal elements of the kernel does not change the result. Lensing also occurs when calculating the steady-state of the atomic cloud within the timed Dicke approximation. However, the phase shift will be underestimated by an amount depending on the cloud's optical density.

39.1.8.6 Ex: Exact calculation of projected structure coefficients

Calculated the integrals (39.66), (39.78), and (39.86).

Solution: *With the real part of the kernel (39.25), we see immediately,*

$$s_N \equiv \frac{1}{4\pi}\int_0^\pi\int_0^{2\pi} |\mathcal{S}_N(k_0,\theta,\phi)|^2 \sin\theta d\theta d\phi = \frac{1}{N^2}\sum_{j,m=1}^{N} \mathfrak{Re}\ \gamma_{jm}$$

$$= \frac{1}{N^2}\sum_{j,m=1}^{N} \frac{\sin k_0 r_{jm}}{k_0 r_{jm}} \cos k_0 z_{jm}\ .$$

Also,

$$f_N \equiv \frac{1}{4\pi}\int_0^\pi\int_0^{2\pi} |\mathcal{S}_N(k_0,\theta,\phi)|^2 \sin\theta\cos\theta d\theta d\phi = ...$$

$$= \frac{1}{N^2}\sum_{j,m=1}^{N} \frac{j_1(k_0 r_{jm})}{k_0 r_{jm}} k_0 z_{jm} \sin k_0 z_{jm}\ .$$

Finally,

$$\tilde{f}_N \equiv \frac{1}{4\pi}\int_0^\pi\int_0^{2\pi} \mathfrak{Re}\ \mathcal{S}_N(k_0,\theta,\phi) \sin\theta\cos\theta d\theta d\phi = ...$$

39.1.8.7 Ex: Monte-Carlo simulation of cooperative radiation pressure

In a regime of negligible interatomic interaction single photons are scattered by individual atoms, which thereby receive the entire photonic recoil. That is, the acceleration occurs in quantized steps, which can be easily resolved in experiments [649, 1217] with Bose-Einstein condensates. In the absence of collective effects, we generally observe halo-shaped momentum distributions. Because of the recoil received upon absorption, the halos are centered at $\hbar k$, and since the emission is generally isotropic, they have a radius of $\hbar k$. On the other hand, as we have seen earlier, cooperative effects can suppression radiation pressure. In the following we try a different approach based on a Monte-Carlo simulation with a Langevin force.
This approach starts from the idea that it is possible to simulate the radiation pressure without explicit calculation of the force by treating the scattering process as a Langevin force. The simulation describes the scattering of single photons by individual atoms. Cooperativity is included 1. in the scattering rate, which is *influenced by collective effects*, 2. by weighing the probability for the direction (θ, ϕ) into which the photons are scattered with the structure factor. The enhancement of the collective scattering rate corresponds to the rate of absorption part of the radiation pressure, [9,10]

$$\gamma_c = \gamma_R \frac{F_{c,abs}}{F_{1,abs}} = \sigma_{opt}(\Delta_0)\frac{I}{\hbar\omega} \cdot \frac{4\Delta_0^2 + \Gamma^2}{4\Delta_0^2 + N^2\Gamma^2 s_N^2} N \ ,$$

where $s_N = N^{-1} + (2\sigma)^{-2}$. The structure factor is numerically calculated for a randomly distributed cloud.

Solution: *We proceed as follows,*

1. *For a given push laser intensity, detuning and atom number we estimate the total number of scattered photons within a given time interval, $n_{ph} = \gamma_c \Delta t$.*

2. *We generate a random distribution of N atom in position space, $\{\mathbf{r}_j(0) | j \in [1, N]\}$.*

3. *We calculate the structure factor $S(\theta, \phi) = \frac{1}{N}\sum_{j=1}^{N} e^{i(\mathbf{k}_0 - \mathbf{k})\mathbf{r}_j}$.*

4. *We generate a random distribution of N atom in the momentum space $\{\mathbf{p}_j(0)\}$, e.g. for a BEC $\mathbf{p}_j(0) = 0$.*

5. *Now we simulate the scattering of a single photon by picking an atom labeled $\mu = int(N\zeta)$ chosen from a uniformly distributed random number $\zeta \in [0, 1]$.*

6. *Then we pick a randomly chosen direction for the emitted photon by identifying the azimuth $\phi = 2\pi\xi_\phi$ with a uniformly distributed random number $\xi_\phi \in [0, 1]$, and extracting the elevation θ from $2\pi \int_0^\theta |S(\theta, \phi)|^2 \sin\theta' d\theta' = \xi_\theta \in [0, 1]$.*

[9] Note that in reality the scattering of a photon converts the scattering atom into a coherent superposition of directions into which the atom might have scattered. This is of course not described by the simulation.

[10] Although the atomic motion is frozen, it is not correct to say that the external degree of freedom is not involved in the collective dynamics, since the spatial atomic distribution shapes the structure factor.

7. *The momentum of the μ^{th} atom is modified by $\mathbf{p}_\mu(t+dt) = \mathbf{p}_\mu(t) + \hbar\mathbf{k} - \hbar\mathbf{k}_0$, where the recoil is given by $\mathbf{k}-\mathbf{k}_0 = k_0\hat{\mathbf{e}}_x \sin\theta\cos\phi + k_0\hat{\mathbf{e}}_y \sin\theta\sin\phi + k_0\hat{\mathbf{e}}_z(\cos\theta - 1)$.*

8. *We repeat the steps 2 to 6 n_{ph} times.*

The final momentum distribution $\{\mathbf{p}_j(\Delta t)\}$ can now be converted into a density $n(\mathbf{r})$ by discretizing the space. The density is now projected onto a CCD camera by column-integration, $A(x,z) = \sum_y n(\mathbf{r})$. Finally, we calculate from this image the center-of-mass displacement, $\Delta z_{cm} = \sum_{x,z} zA(x,z)$. Note that in this picture we don't

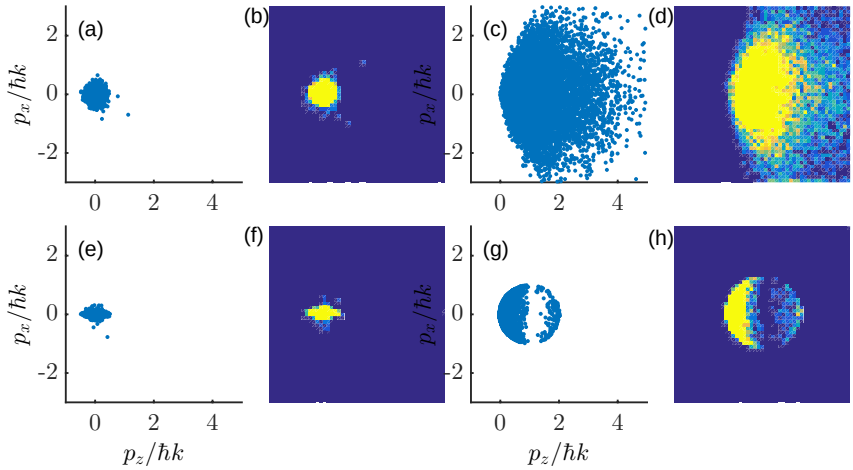

Figure 39.13: (code) Langevin simulation of radiation pressure for $N = 10000$ atoms and 50000 scattered photons with (a,b) $\sigma = 1$ and (b,d) $\sigma = 3$. $\eta = 30$. The figures (b,d) simulate time-of-flight absorption images taken from the momentum distributions (a,c). (d-h) Same as (a-d), but now every atom scatters exactly 1 photon.

need any knowledge about the collective optical cross section to predict the correct momentum pattern after a certain amount of scattering events. However, the rate at which photons are scattered (and hence the time scale to be chosen for the simulation) is subject to collective effects.
However, the Monte-Carlo simulations do not give the same quantitative results as the analytical calculations. Particularly the N-dependence is different. My present guess is that the calculation of the scattering rate and its N-dependence are oversimplified.

39.1.8.8 Ex: Super- and subradiance with two atoms

Super- and subradiance have been observed in two ion crystals [1047, 364]. In this exercise, we study this system in the framework of the coupled dipoles model.
a. Calculate the structure coefficient of this system.
b. Write down the equations of motion (39.26) and solve them in steady-state.

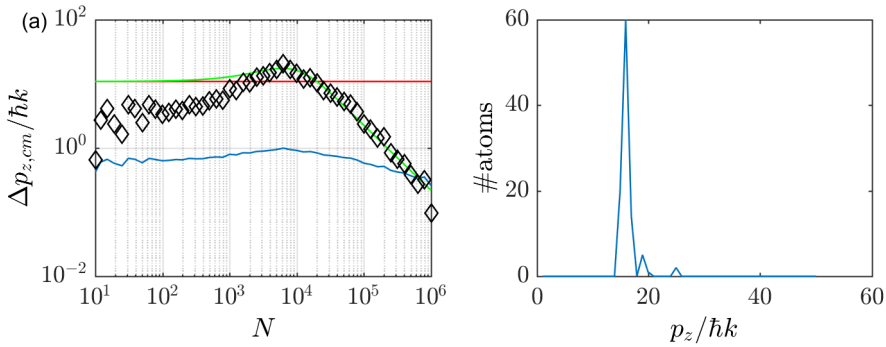

Figure 39.14: (code) (a) Simulated N-dependence of Δz_{cm}. The deviation from the theoretical expectation is quite large. In contrast $21\Delta z_{cm}^4$ (black diamonds) fits much better. Why? (b) Histogram of the axial momentum distribution.

Solution: *a. Two atoms separated by λ do not scatter only into forward and backward direction. Their structure factor is,*

$$\mathcal{S}_2(\mathbf{k}) = \tfrac{1}{2}\left(e^{\imath(\mathbf{k}-\mathbf{k}_0)\mathbf{r}_0} + e^{\imath(\mathbf{k}-\mathbf{k}_0)(\mathbf{r}_0+\lambda\hat{\mathbf{e}}_z)}\right) = \tfrac{1}{2}e^{\imath(\mathbf{k}-\mathbf{k}_0)\mathbf{r}_0}(1-e^{\imath\lambda\hat{\mathbf{e}}_z\mathbf{k}}) = \tfrac{1}{2}(1-e^{2\pi\imath\cos\theta}) \ ,$$

setting $\mathbf{r}_0 = 0$ and $k \simeq k_0$.
b. Let us consider two atoms separated by $d \equiv |\mathbf{r}_1 - \mathbf{r}_2|$. Then the equations of motion read,

$$\begin{aligned}\dot{\beta}_j(t) &= -\Gamma\sum_{m=1}^{N}\left(\frac{\sin k_0|\mathbf{r}_j-\mathbf{r}_m|}{k_0|\mathbf{r}_j-\mathbf{r}_m|} - \imath\frac{\cos k_0|\mathbf{r}_j-\mathbf{r}_m|}{k_0|\mathbf{r}_j-\mathbf{r}_m|}\right)\beta_m(t) \\ &= -\Gamma\beta_j(t) - \Gamma\sum_{m\neq j}^{N}\left(\frac{\sin k_0|\mathbf{r}_j-\mathbf{r}_m|}{k_0|\mathbf{r}_j-\mathbf{r}_m|} - \imath\frac{\cos k_0|\mathbf{r}_j-\mathbf{r}_m|}{k_0|\mathbf{r}_j-\mathbf{r}_m|}\right)\beta_m(t) \ .\end{aligned}$$

We find,

$$\beta_j(t) = e^{-\left(1\pm\frac{\sin k_0 d}{k_0 d}\right)\Gamma t} \ ,$$

in qualitative agreement with [364].

39.1.8.9 Ex: Signatures of subradiance

Super- and subradiance are contained in the coupled dipoles model. Try to identify the presence of subradiant states via a reduced decay rate of $\beta(t)$ starting from the timed Dicke state.

Solution: *Simplifying by $\Delta_0 = \Omega_0 = 0$, we recover from Eq. (39.26)) [1180, 1283, 1286],*

$$\dot{\beta}_j(t) = -\Gamma\beta_j(t) + \imath\Gamma\sum_{j'\neq j}^{N}\frac{e^{\imath k_0|\mathbf{r}_j-\mathbf{r}_m|}}{k_0|\mathbf{r}_j-\mathbf{r}_m|}\beta_m(t) \ .$$

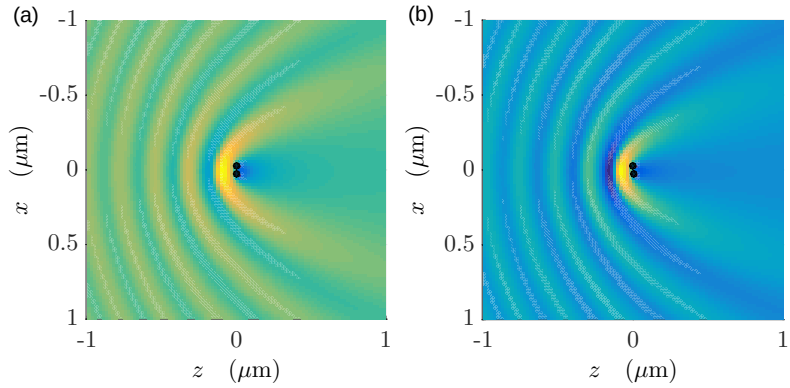

Figure 39.15: (code) Phase profile of the total light in the presence of two atoms illuminated by a Gaussian laser beam (a) without and (b) with off-diagonal elements of the kernel.

We numerically evaluate the equation in the Markov approximation. We find that the offset (see Fig. 39.16).
1. is much larger for homogeneous than for Gaussian distributions;
2. is smaller for large clouds than for small ones;
3. is much larger for large aspect ratios σ.

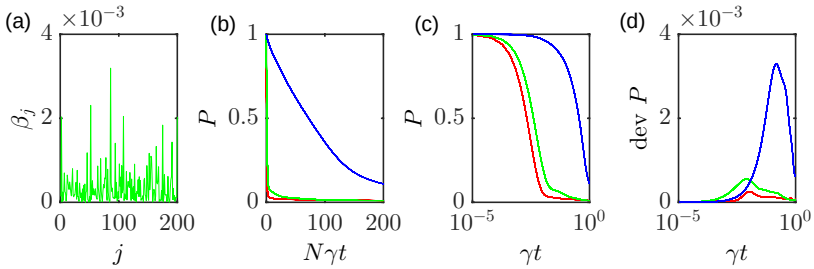

Figure 39.16: (code) Calculation of the time evolution of P within the Markov approximation for $N = 200$ atoms. Red: Gaussian distribution with $\sigma = 1$ and $R = 5/k_0$ starting from a timed Dicke state. Green: uniform distribution with $\sigma = 1$ and $R = 5/k_0$ starting from a timed Dicke state. Blue: uniform distribution with $\sigma = 5$ and $R = 5/k_0$ starting from a timed Dicke state. Yellow: uniform distribution with $\sigma = 1$ and $R = 20/k_0$ starting from a timed Dicke state. Cyan: uniform distribution with $\sigma = 1$ and $R = 20/k_0$ starting from a uniform excitation state.

39.1.8.10 Ex: Other applications of the coupled dipoles model

Discuss whether the coupled dipoles model can be extended to provide a microscopic description of gaseous metamaterials (negative refractive index) and the Goos-Hänchen, Imbert-Fedorov, Spin-Hall, and *Ewald-Oseen effects*, and interference with a LO. Is it possible to check Ewald-Oseen's theorem in media with negative refractive

index?

Solution:

39.2 Continuous density distributions and Mie scattering

In the last sections we developed the coupled dipoles model describing light scattering from ensembles of individual microscopic particles by a set of equations of motion, in the simplest case, one for every atomic dipole. This limits the number of atoms that can be considered in numerical simulations to a few 1000. On the other hand, most cold atom experiments nowadays are performed with 10^5 to 10^9 atoms. The following section are devoted to introducing concepts and approximations allowing us to understand light scattering from large atomic clouds.

The main step will consist in an approximation called smooth or *continuous density approximation*, where the discrete distribution of point-like scatterers is replaced by an inhomogeneous but smooth continuous density distribution characterized by a refraction index field $n_{rfr}(\mathbf{r})$. The interaction of this density distribution with light is then treated in the framework of Maxwell's equations, i.e. inhomogeneities are treated as macroscopic boundary conditions to the electromagnetic fields. In the following we will term this regime as *Mie scattering*.

At first sight Rayleigh scattering from point-like particles and Mie scattering from extended objects are quite different phenomena. Rayleigh scattering exhibits resonances due to the internal structure of the particles, e.g. an atom. Mie scattering shows resonances induced by the boundary conditions the scattering objects impose to the field. On the other hand, from a microscopic viewpoint, any extended object (e.g. a dielectric sphere) is nothing but an assembly of microscopic scattering particles. The question we need to study is then whether a description of the diffraction from this object as the sum of the radiation patterns scattered from the individual constituent particles is correct; or in how far the graininess of the cloud's density distribution and cooperative effects arising from the interaction *between* the individual particles play a role [225].

Interesting phenomena are expected in the transition regime between the limits of a dense bunch of individual scatterers and macroscopic dielectric objects. One of them is a strong modification of the radiation pressure force [298], which can conveniently be studied with atomic ensembles. The reason is that, in the smooth density approximation, the cloud can be understood as a macroscopic object characterized by a refraction index, which can be tuned over huge ranges by changing the cloud's density and volume, or by tuning the frequency of the incident light exploiting the existence of atomic resonances. We will see in the following that it is possible to study radiation pressure with cold atoms in the Rayleigh-Debye-Gans limit of small phase-shifts, as well as in the Mie limit of large phase shifts [66]. Despite the absence of sharp boundaries for the atomic cloud, we predict the occurrence of Mie resonances, which could be detected experimentally [67].

39.2.1 Continuous density approximation

In light scattering experiments, disorder (or granularity) plays a role when the number of atoms projected onto a cross section perpendicular to the incident beam is small enough so that a light mode focused down to the diffraction limit (that is $\sim \lambda^2$) would be able to resolve and count the atoms. In other words, the stochastic fluctuations induced by the random positions of the atoms can be neglected when the total number of atoms N is larger than the number of modes $\sim \sigma^2$ that fit into the cloud's cross section, i.e. when the optical density is $b_0 = 3N/\sigma^2 \gg 1$. Under this hypothesis, the differential equation (39.26) for $\tilde{\beta}_j$ can be simplified by replacing the discrete sum over atom positions by an integral over a density distribution $\rho(\mathbf{r})$,

$$\boxed{\sum_{j=1}^{N} \to \int \rho(\mathbf{r}')d^3r' \qquad \text{and} \qquad \tilde{\beta}_j(t) \to \tilde{\beta}(\mathbf{r}', t)} \,. \tag{39.96}$$

For example, the smoothed structure coefficient reads,

$$\mathcal{S}(\mathbf{k}) = \frac{1}{N}\sum_{j=1}^{N} e^{\imath(\mathbf{k}-\mathbf{k}_0)\mathbf{r}_j} = \frac{1}{N}\int d^3r' \; \rho(\mathbf{r}')e^{\imath(\mathbf{k}-\mathbf{k}_0)\mathbf{r}'} \,. \tag{39.97}$$

In the Exc. 39.2.5.1 we calculate the structure coefficients for a homogeneous spherical cloud of radius R and for a Gaussian ellipsoidal cloud with the *rms*-width $\sigma_{\rho,z}$:

$$\begin{aligned} \mathcal{S}_{\text{homog.sphere}}(\mathbf{k}) &= \tfrac{3}{q^3R^3}(\sin qR - qR\cos qR) \\ \mathcal{S}_{\text{gauss.ellipse}}(\mathbf{k}) &= e^{-\frac{1}{2}k^2\sigma_\rho^2\sin^2\theta - \frac{1}{2}\sigma_z^2(k\cos\theta - k_0)^2} \,. \end{aligned} \tag{39.98}$$

The simulated structure factor (red curve in Figs. 39.17) agrees well with the analytical expression (green curve). Since small clouds have a larger fluctuations, the fact that the total force is a sum of intensities rather than amplitudes leads to a finite value at large scattering angles θ.

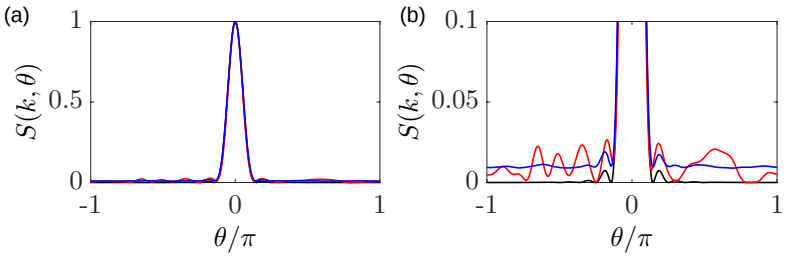

Figure 39.17: (code) (a) The red curve shows a calculation of the structure factor: $|\mathcal{S}(k = k_0, \theta, \phi = 0)|^2$ for 200 atoms randomly distributed in a homogeneous spherical cloud of size $R = 10/k_0$. The blue curve shows an average over 500 realizations of such a cloud according to $\sum_{m=1}^{200} |\mathcal{S}(k, \theta, \phi = 0)|^2$. The black curve is an analytical calculation according to Eq. (39.98) [1284]. (b) Same curves as in (a) but with a stretched y-axis.

In the continuous limit defined by (39.96) for the equations of motion (39.32) [11],

$$\dot{\tilde{\beta}}(\mathbf{r},t) = \imath\left(\Delta_0 + \imath\frac{\Gamma}{2}\right)\tilde{\beta}(\mathbf{r},t) - \frac{\imath}{2}\Omega_0 - \frac{\Gamma}{2}\int d^3r'\rho(\mathbf{r}')\frac{\sin(k_0|\mathbf{r}-\mathbf{r}'|)}{k_0|\mathbf{r}-\mathbf{r}'|}\tilde{\beta}(\mathbf{r}',t)e^{-\imath\mathbf{k}_0\cdot(\mathbf{r}-\mathbf{r}')} \,. \tag{39.99}$$

Transforming back to $\beta_j \equiv \tilde{\beta}e^{\imath\mathbf{k}_0\cdot\mathbf{r}}$, we obtain the fundamental equation for the dipolar excitation field,

$$\boxed{\dot{\beta}(\mathbf{r},t) = \imath\left(\Delta_0 + \imath\frac{\Gamma}{2}\right)\beta(\mathbf{r},t) - \frac{\imath\Omega_0}{2}e^{\imath\mathbf{k}_0\cdot\mathbf{r}} - \frac{\Gamma}{2}\int d^3r'\rho(\mathbf{r}')\frac{\sin(k_0|\mathbf{r}-\mathbf{r}'|)}{k_0|\mathbf{r}-\mathbf{r}'|}\beta(\mathbf{r}',t)} \,. \tag{39.100}$$

Example 229 (*Connection between coupled dipoles model and Helmholtz equation*): The steady-state solution of (39.100) can also be obtained from the *Helmholtz equation* of Maxwell's theory [458, 66, 67], as shown in Sec. 19.3.2,

$$\boxed{[\nabla^2 + k_0^2 n_{rfr}^2(\mathbf{r})]\beta(\mathbf{r}) = 0 \qquad \text{defining} \qquad n_{rfr}^2(\mathbf{r}) \equiv 1 - \frac{4\pi\rho(\mathbf{r})}{k_0^3(2\Delta_0/\Gamma + \imath)}} \,. \tag{39.101}$$

39.2.2 Simulations of the time evolution

We start from the second equation (39.18),

$$\dot{\tilde{\beta}}_j(t) = \imath\Delta_0\tilde{\beta}_j(t) - \frac{\Omega_0^2}{4}\sum_{m=1}^{N}\int_0^t \tilde{\beta}_m(t')dt' \tag{39.102}$$
$$- \sum_{\mathbf{k}} g_k^2 \sum_{m=1}^{N} e^{\imath(\mathbf{k}-\mathbf{k}_0)(\mathbf{r}_j-\mathbf{r}_m)}\int_0^t e^{-\imath(\omega_k-\omega_0)(t-t')}\tilde{\beta}_m(t')dt' \,.$$

Substituting the timed Dicke state (39.64),

$$\dot{\beta}(t) = \frac{1}{N}\sum_{j=1}^{N}\dot{\beta}(t) = \frac{1}{\sqrt{N}}\sum_{j=1}^{N}\dot{\tilde{\beta}}_j(t) \tag{39.103}$$
$$= \imath\Delta_0\beta(t) - \frac{N\Omega_0^2}{4}\int_0^t \beta(t')dt' - \frac{V_{ph}}{(2\pi)^3}\int d^3k\; g_k^2N^2|\mathcal{S}(\mathbf{k})|^2\int_0^t e^{-\imath(\omega_k-\omega_0)(t-t')}\frac{\tilde{\beta}_m(t')}{\sqrt{N}}dt' \,,$$

where we used $\sum_{m=1}^{N} e^{\imath(\mathbf{k}-\mathbf{k}_0)(\mathbf{r}_j-\mathbf{r}_m)} = N^2|\mathcal{S}(\mathbf{k})|^2$ from Eq. (39.67). Finally, at resonance and low saturation we may neglect the first two terms,

$$\dot{\beta}(t) = -N\frac{V_{ph}}{(2\pi)^3}\int_{\mathbb{R}} d^3k\int_0^t dt'\; g_k^2\beta(t')e^{\imath(\nu_k-\omega)(t-t')}|\mathcal{S}(\mathbf{k})|^2 \tag{39.104}$$
$$= -N\frac{V_{ph}}{(2\pi)^3}\int_0^t dt'\;\beta(t')\int_0^\infty\int_0^\pi g_k^2e^{\imath(\nu_k-\omega)(t-t')}|\mathcal{S}(k,\theta)|^2 2\pi k^2\sin\theta d\theta dk$$
$$= -N\frac{V_{ph}}{(2\pi)^3}g_k^2\int_0^t dt'\;\beta(t')\int_0^\infty e^{\imath(\nu_k-\omega)(t-t')}k^2I(k)dk = -\Omega_N^2\int_0^t dt'\;\beta(t')G(t-t') \,,$$

[11] Note that the 'timed Dicke' assumption (39.64) has not been used here.

with the collective Rabi frequency $\Omega_N = \sqrt{N} g_k$ and the surface integrated structure factor,

$$I(k) = \int_0^{2\pi} \int_0^{\pi} |\mathcal{S}(k,\theta,\phi)|^2 \sin\theta d\theta d\phi \ , \tag{39.105}$$

and

$$G(\tau) = \frac{V_{ph}}{(2\pi)^3} e^{-\imath\omega\tau} \int_0^{\infty} e^{\imath ck\tau} k^2 I(k) dk \ , \tag{39.106}$$

with $\omega = ck_0$ and $\nu_k = ck$. The integral $I(k)$ has been solved by Nicola for an ellipsoidal Gaussian density distribution. It is quite close to,

$$I(k) \simeq I(k_0) \simeq \sqrt{\frac{\pi}{2}} \frac{1}{k\sigma_z} e^{F^2/2} [1 - \mathrm{erf}\ (F/\sqrt{2})] \ , \tag{39.107}$$

with the Fresnel number $F = k\sigma_r^2/\sigma_z$.

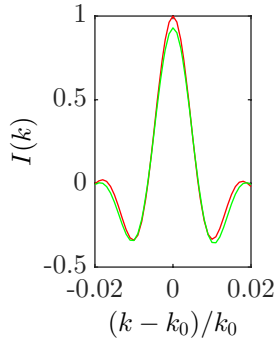

Figure 39.18: (code) Averaging of the structure factor over the whole k-space.

39.2.2.1 Analytical method

To evaluate the above integro-differential equation, we use the rule for differentiating integrals with variable boundaries,

$$\frac{\partial}{\partial t} \int_{\phi(t)}^{\psi(t)} f(x,t) dx = \int_{\phi(t)}^{\psi(t)} \frac{\partial f(x,t)}{\partial t} dx + f(\psi(t),t)\psi'(t) - f(\phi(t),t)\phi'(t) \ , \tag{39.108}$$

it is easy to show,

$$\frac{\partial}{\partial t} \int_0^t f(t')G(t-t')dt' = f(t)G(0) + \int_0^t f(t')\dot{G}(t-t')dt' \tag{39.109}$$

and to thusly evaluate the integral until $\frac{\partial^n}{\partial t^n} G(t-t')$ gets smooth enough to be neglected.

39.2.2.2 Numerical method

We can directly solve the integro-differential equation numerically using,

$$G(\tau) = \left[1 + \frac{3c}{4R}\tau - \frac{c^3}{16R^3}\tau^3\right]\Theta(3R - c\tau) \ , \tag{39.110}$$

for a homogeneous spherical cloud and,

$$G(\tau) = \frac{k\sigma_r^2}{k\sigma_r^2 + ic\tau} e^{-(c\tau/\sigma_z)^2/2} \ , \tag{39.111}$$

for an ellipsoidal Gaussian cloud. The iteration is done via,

$$\beta(t + dt) = \beta(t) - dt\ \Omega_N^2 \int_0^t \beta(t')G(t - t')dt' \ . \tag{39.112}$$

The discretization is done via,

$$\begin{aligned} t_{m+1} &= t_m + dt \\ \beta_{m+1} &= \beta_m - dt\ Ng_k^2 \sum_{m'=1}^{m} \beta_{m'} G(t_m - t_{m'})dt \ . \end{aligned} \tag{39.113}$$

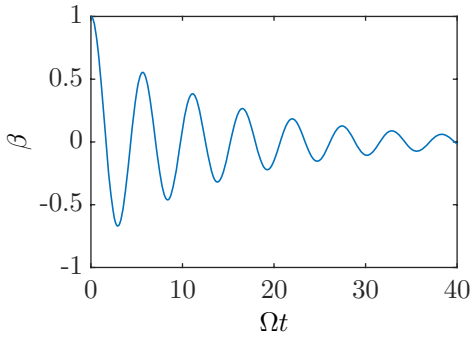

Figure 39.19: (code) Calculation of the time evolution of β for a homogeneous spherical cloud. The parameters are $\lambda \simeq 780\,\text{nm}$ and $c/\Omega \simeq 30\,\text{cm}$ with $\Omega = \sqrt{N}g_k$ for typically $g_k \simeq 1\,\text{MHz}$ and $N \simeq 10^6$.

With the solution of the integro-differential equation $\beta(t)$, we can calculate the probability that atoms are excited [1284] [12],

$$P(t) = |\beta(t)|^2 = \sum_j |\beta_j(t)|^2 = \int d^3r |\beta(t, \mathbf{r})|^2 \ . \tag{39.114}$$

[12]Compare to Jaynes-Cummings model in a CQED environment: A single photon is coherently exchanged between the cavity and the atomic excitation, we get Rabi oscillations. Here, the atomic cloud is the cavity.
We know that the Mollow triplet in the dressed states picture gives rive to an oscillating decay curve resembling that of Fig. 39.19. Does this curve also have an interpretation in terms of collective dressed states?

Example 230 (*Solutions for a homogeneous spherical cloud*): For a homogeneous spherical cloud, we find three regimes characterized by the size of the cloud compared to the two length scales λ and c/Ω:

$$\beta(t) = \beta(0) \begin{cases} e^{-N\Gamma t} & \text{for } R < \lambda \ll c/\Omega \\ e^{-27N\Gamma t/8(k_0 R)^2} & \text{for } \lambda < R \ll c/\Omega \\ \cos\Omega t e^{-3ct/8R} & \text{for } \lambda \ll c/\Omega < R \end{cases} .$$

39.2.2.3 Complete numerical simulation

In order to be independent from initial conditions, we generate a random distribution $\mathbf{r}_{j'}$ and solve the differential equation,

$$\dot{\beta}_j(t) = -Ng_k^2 \int_0^t dt' \, \frac{V_{ph}}{(2\pi)^3} \int d^3k \, \frac{1}{N} \sum_{j'=1}^{N} \beta_{j'}(t') e^{\imath(\nu_k - \omega)(t-t') + \imath \mathbf{k}(\mathbf{r}_j - \mathbf{r}_{j'})} . \quad (39.115)$$

We propagate the amplitudes in time via,

$$\beta_j(t+dt) = \beta_j(t) - dtg_k^2 \frac{V_{ph}}{(2\pi)^3} \int_0^t dt' \, \sum_{j'=1}^{N} \beta_{j'}(t') \int_0^\infty k^2 e^{\imath(ck-\omega)(t-t')} I_{jj'}(k) dk , \quad (39.116)$$

where $I_{jj'}(k) \equiv \int_0^\pi \int_0^{2\pi} e^{\imath k\left[(x_j - x_{j'})\sin\theta\cos\phi + (y_j - y_{j'})\sin\theta\sin\phi + (z_j - z_{j'})\cos\theta\right]} \sin\theta d\theta d\phi$, and discretize via,

$$t_{m+1} = t_m + dt \quad (39.117)$$

$$\beta_j(t_{m+1}) = \beta_j(t_m) - dt^2 g_k^2 \sum_{m'=1}^{m} \sum_{j'=1}^{N} \beta_{j'}(t_{m'}) G_{jj'}(t_m - t_{m'}) ,$$

with $G_{jj'}(t_m - t_{m'}) = \frac{V_{ph}}{(2\pi)^3} \int_0^\infty k^2 e^{\imath(ck-\omega)(t_m - t_{m'})} I_{jj'}(k) dk$.

39.2.3 Radiation pressure force in macro- and microscopic scattering

As mentioned at the beginning of this section, scattering of light by an extended object such as an atomic ensemble or a dielectric sphere is fundamentally different from scattering at a point-like scatterer such as a single atom. On one hand, the finite size of the object leads to Mie scattering. On the other hand, the spatial distribution of the scatterers rules the degree of cooperativity. Homogeneous and periodic distributions tend to scatter cooperatively, whereas disorder suppresses cooperativity. In an atomic cloud, the amount of disorder can be tuned via the optical density seen by the incident light, and its role can be studied via the radiation pressure exerted by the light on the atomic cloud. We present an analytic expression for the radiation pressure valid for any numbers of atoms and arbitrary density distributions, which interpolates between the regimes of dominating disorder and dominating cooperativity. Furthermore, we present first experimental signatures of radiation pressure reduction due to cooperative scattering.

The radiation pressure exerted by a plane wave laser beam with frequency ω_0 and wave vector $\mathbf{k}_0 = k_0\hat{\mathbf{e}}_z$ on a single two-level atom with resonance frequency $\omega_a = \omega_0 - \Delta_0$ is correctly described by the standard formula (39.80). Generalization to scattering by atomic ensembles and extended objects is only possible, if a number of effects is explicitly taken into account. The most important ones are named in the following. a. *Cooperativity* and b. *disorder*: Cooperativity is the tendency of atoms located in the same area of space, forming regular structures or being forced by the mode structure of the environment (e.g. optical cavities) to scatter light synchronously into the same direction, as in the case of Dicke superradiance. While homogeneously or periodically distributed atoms concentrate the scattered light in specific solid angles by forward or Bragg scattering, randomly distributed atoms do not cooperate and scatter light isotropically. In this respect, cooperativity and disorder are antagonists. c. *Mie scattering and refraction*: The finite volume and the shape of the cloud represent an inhomogeneity at which light is scattered in a global way. As long as the optical density is low, the pump mode depletion is mainly due to the fact, that the atomic cloud distorts the phase front of the incident light. For high optical density, scattering is predominantly absorptive. d. *Multiple scattering* and e. *resonance fluorescence*: Near resonance, multiple scattering leads to radiation trapping. Even off-resonance, inelastic scattering pumps resonant photons into the atomic cloud, which have a high probability to be reabsorbed. Taking account of all these effects, the real radiation pressure can differ by orders of magnitude from the naive prediction of the above formula.

For smooth density distributions F_c is only limited by Mie scattering at the inhomogeneity represented by the *finite extend* of the atomic cloud [298]. The radiation pressure depends on the number of atoms N in the volume, and the scaling $F_c(N)$ depends on the pump laser detuning and the radial cross section of the cloud. But small scale inhomogeneity *within the cloud*, i.e. disorder, can play an eminent role for collective scattering. This is the case, when the number of atoms is beyond a critical value, which mainly depends on the volume and shape of the cloud. In the following we will derive an analytic expression for the radiation pressure as a function of atom number, which interpolates between the regimes of dominating disorder (single-atom Rayleigh scattering) and dominating cooperativity (pure Mie scattering).

On the other hand, we point out, that we do not consider multiple scattering in our treatment. This is a good assumption far from resonance, where the scattering is predominantly Rayleigh scattering and inelastic scattering can safely be disregarded. In contrast, our extensions of single to multi-atom scattering are not valid near resonance.

The radiation pressure provides sensitive signatures for the impact of cooperativity and disorder. We describe an experiment measuring the displacement of cold atoms confined in a far-off resonance dipole trap and interpret our observations in terms of collective scattering.

39.2.3.1 Radiation pressure for timed Dicke states

As a first approach we will calculate the radiation pressure for a timed Dicke state from Eq. (39.89) by explicit analytical integration of the surface-integrated structure factors s_∞ and f_∞ in the smooth density limit (39.96) for an ellipsoidal Gaussian

smooth density distribution, as shown in Exc. 39.2.5.2. In the spherical case,

$$\rho(\mathbf{r}) = \rho_0 e^{-r^2/2\bar{r}^2} \qquad \text{with} \qquad \rho_0 = \frac{N}{(2\pi)^{3/2}\bar{r}^3} \ , \tag{39.118}$$

and introducing $\sigma \equiv k\bar{r}$, we get,

$$\begin{aligned} s_\infty &= \frac{1 - e^{-4\sigma^2}}{4\sigma^2} \overset{\sigma\gg1}{\longrightarrow} \frac{1}{4\sigma^2} \\ f_\infty &= \frac{1}{4\sigma^2}\left[1 - \frac{1}{2\sigma^2} + \left(1 + \frac{1}{2\sigma^2}\right) e^{-4\sigma^2}\right] \overset{\sigma\gg1}{\longrightarrow} s_\infty - 2s_\infty^2 \ . \end{aligned} \tag{39.119}$$

Hence,

$$\boxed{\frac{F_{za} + F_{ze}}{F_{z1}} = \frac{(2\Delta_0/\Gamma)^2 + 1}{(2\Delta_0/\Gamma)^2 + N^2 s_\infty^2} N(s_\infty - f_\infty)} \ . \tag{39.120}$$

Note that the radiation pressure calculated from Eq. (39.120) also holds for elongated ellipsoidal Gaussian clouds characterized by an aspect ratio $\eta > 1$, even though the expressions for the surface-integrated structure factors become more complicated.

It is revealing to compare the smooth density expressions (39.120) with numerical simulations based on randomly generated atomic distributions from which the structure factor is directly from the sum (39.68). Interestingly, we find in certain parameter regimes (in particular at low atom numbers) considerable deviations between s_N, f_N and s_∞, f_∞ and consequently between the numerical simulations and the analytic calculations of the radiation pressure. We attribute these deviations to disorder in the atomic cloud, which is not seen in the smooth density limit, but naturally incorporated in the numerical approach.

By comparison to numerical simulations [black solid lines and blue circles in Figs. 39.20(a)] we found that the surface-integrated structure factors in the presence of disorder are well described by [141],

$$s_N = \frac{1}{N} + s_\infty \qquad \text{and} \qquad f_N = f_\infty \ . \tag{39.121}$$

39.2.3.2 Cooperativity versus disorder

We expect disorder to play a dominant role, when the coarse graininess, which is related to the average distance between two atoms, $|\mathbf{r}_i - \mathbf{r}_j|$, can be resolved by the incident light. For the *absorption process*, this means that disorder gets important, when the number of spatial modes supported by the pump laser in a radial cross section of the atomic cloud,

$$N_{ca} = s_\infty^{-1} \simeq 4\sigma^2 \ , \tag{39.122}$$

(for voluminous clouds) surpasses the number of atoms, $N < N_{ca}$. This is just the case, when the mean resonant optical density (for a ray passing through the center of the cloud $x = y = 0$) is larger than 1,

$$b_0 = \int_{-\infty}^{\infty} dz \ \rho(z)\sigma_{opt} = \frac{3N}{\sigma^2} = \frac{12N}{N_{ca}} > 1 \ , \tag{39.123}$$

where $\sigma_{opt} = \frac{3\lambda^2}{2\pi}$ is the resonant optical cross section and $\rho(\mathbf{r})$ the spherical Gaussian density distribution (39.118). For the *scattering process*, the number of modes available for the reemitted light also counts. Hence, the critical number of atoms that can be resolved by light scattering is larger than N_{ca}:

$$N_{ce} = (s_\infty - f_\infty)^{-1} \simeq \tfrac{1}{2}(2\sigma)^4 = \tfrac{1}{2} N_{ca} \cdot \sigma^2 \ . \tag{39.124}$$

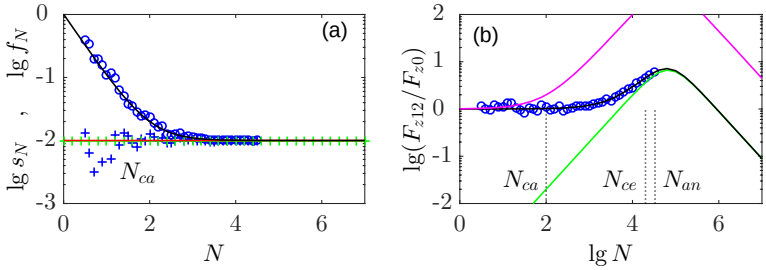

Figure 39.20: (code) (a) Numerical evaluation of s_N (blue circles) and f_N (blue crosses) [225]. Analytical calculation of s_N (black solid line) according to Eq. (39.121). Smooth density limit of s_∞ (red solid line) and f_∞ (green crosses). The cloud is assumed spherical, $\eta = 1$, and Gaussian with size $\sigma = 5$. (b) Numerical evaluation (blue circles) of the corresponding force ratio as a function of atom number N for $\Delta_0 = (2\pi)\ 2\,\mathrm{GHz}$ and small collective saturation, $\sqrt{N}\Omega_0 \ll \Delta_0$. Analytical calculation in the smooth density limit (green solid line) and according to Eq. (39.126) (black solid line). The magenta line traces the radiation pressure force resulting from pump photon absorption only.

In order to simplify the discussion, we neglect saturation, $\Omega_0 \to 0$. Using $\Delta_0 \gg \Gamma$ and defining a third characteristic atom number,

$$N_{cr} = \frac{2\Delta_0}{\Gamma s_\infty} \ , \tag{39.125}$$

Eq. (39.120) can be written,

$$\frac{F_c}{F_1} \simeq \frac{1 + N/N_{ce}}{1 + (N/N_{cr})^2} \ . \tag{39.126}$$

In the limit of very large detunings, $\Delta_0/\Gamma \gg \sigma^2 \gg 1$, the three introduced characteristic atom numbers introduced in Eqs. (39.122), (39.124) and (39.125) satisfy $N_{ca} < N_{ce} < N_{cr}$, and we obtain the N-dependence of the radiation pressure depicted in Fig. 39.20.

In the regime $N < N_{ca}$, radiation pressure is dominated by the absorption process, $s_N \gg f_N$, because the emission is isotropic. The absorption radiation pressure exerted on a hypothetical smooth density distribution occupying the same volume as the atomic cloud [green line in Fig. 39.20] is dramatically reduced with respect to the single-atom radiation pressure (cyan dash-dotted line). However, disorder suppresses cooperativity and increases the radiation pressure up to the single-atom value. The novelty as compared to Ref. [1180] is the fact that cooperativity and disorder not

only influence the collective emission of a photon by an atomic cloud, but also the collective *absorption* of a photon from a pump laser beam.

Neglecting the photon reemission at higher atom numbers would result in an increase of radiation pressure in the regime $N_{ca} < N < N_{ce}$ (magenta line). However, in this regime, the emission process becomes increasingly important, $s_N \simeq f_N$, because the emission changes its radiation pattern from isotropic to forward scattering. Consequently, the radiation pressure is reduced with respect to its purely absorptive component. This regime is still ruled by disorder, so that the critical atom number for the impact of disorder on the absorption process, N_{ca}, has no impact. It does not even show up in the formula (39.126).

In the regime $N_{ce} < N < N_{cr}$, disorder steps back and cooperativity wins, so that the radiation pressure approaches the smooth density limit. Since in this regime, the smooth density radiation pressure depends on atom number like $\propto N$, as already shown in Ref. [298], we observe an increase of the radiation pressure beyond the single-atom value. This is only possible, because the collective enhancement of absorption (magenta line) rises as fast with N, as the collective enhancement of emission.

For even higher atom numbers, $N_{cr} < N$, the radiation pressure dramatically alters its N-dependency from $\propto N$ to $\propto N^{-1}$. This change of behavior is *not* caused by the interplay of cooperativity and disorder, but can be understood within the framework of Mie scattering, as discussed in the next section.

39.2.3.3 Rayleigh-Debye-Gans versus Mie scattering

Radiation pressure is observed in many experiments, as it is the basis for optical cooling techniques (like magneto-optical traps) and limits the efficiency of resonant absorption imaging of cold atoms, because their acceleration leads to considerable Doppler-shifts. However, as stated before, the impact of disorder on radiation pressure can only be seen for large optical densities, $b \gg 1$, which may partially explain, why this effect has not been observed until two experiments explicitly searched for it [141, 119] (see Fig. 39.21).

Depending on the parameter regime chosen, the measurements exhibited in Fig. 39.21 present data for reduced or enhanced radiation pressure for larger N. As explained above, the reduction is understood as microscopic Rayleigh scattering at disordered atoms together with superradiant acceleration of the decay, while the enhancement is observed when the bulk cloud becomes so small and dense that it turns into an inhomogeneous dielectric sphere refracting and lensing incident light by macroscopic Mie scattering.

The question then remains why the radiation pressure, with increasing N, after an initial rise the drops again. To answer this question we must have a look at the phase shift induced in the pumjp light by the cloud's refraction index.. From calculations done in Secs. 18.2.4, 22.2.7 and 43.6.1 we know that (below saturation) the optical density b and the phase shift φ are linked to the refraction index n_{rfr} and the optical

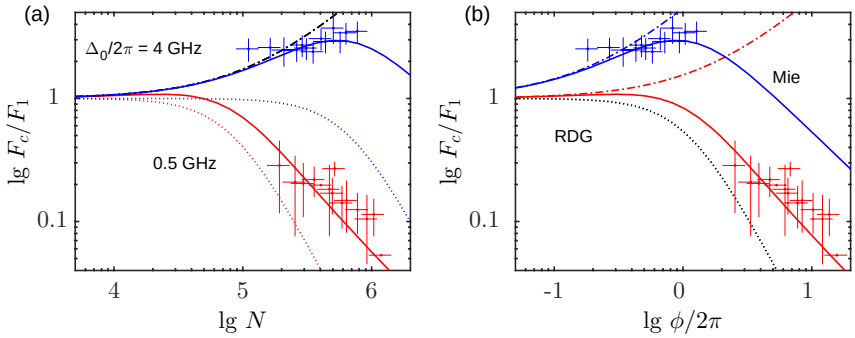

Figure 39.21: (code) (a) Double-logarithmic plot of the measured (symbols) and calculated (lines) N dependence of the radiation pressure force. The red symbols and lines correspond to the detuning $\Delta_0 = (2\pi)\ 0.5\,\mathrm{GHz}$ and the intensity $I_0 = 95\,\mathrm{mW/cm^2}$. For the blue symbols and lines, $\Delta_0 = (2\pi)4\,\mathrm{GHz}$ and $I_0 = 730\,\mathrm{mW/cm^2}$. The red (bottom) and blue (top) solid lines show calculations based on the full expression (39.120) without adjustable parameters. The red (bottom) and blue (top) dotted lines represent just the fraction of expression (39.120). The dash-dotted lines representing just the parentheses coincide for both values of Δ_0. (b) Same data as (a), but plotted as a function of the push beam phase shift φ. In this diagram the dotted lines representing the fraction coincide for both values of Δ_0 [119].

scattering cross section σ_{opt} via,

$$\frac{\imath b}{2} + \varphi = \frac{\omega}{c}\int_{-\infty}^{\infty}[n_{rfr}(\mathbf{r}) - 1]dz = \left(\imath - \frac{2\Delta_0}{\Gamma}\right)\sigma_{opt}(\Delta_0)\int_{-\infty}^{\infty}\rho(\mathbf{r})dz \qquad (39.127)$$

$$\text{where} \quad \sigma_{opt}(\Delta_0) = \frac{2\pi}{k^2}\frac{\Gamma^2}{4\Delta_0^2 + \Gamma^2} \qquad \text{and} \qquad n_{rfr}(\mathbf{r}) - 1 = -\frac{4\pi\rho(\mathbf{r})}{k_0^3(2\Delta_0/\Gamma + \imath)}\ ,$$

such that,

$$\boxed{b = -\sigma_{opt}(\Delta_0)\int_{-\infty}^{\infty}\rho(\mathbf{r})dz = b_0\frac{\Gamma^2}{4\Delta_0^2 + \Gamma^2} \qquad \text{and} \qquad \varphi = \frac{2\Delta_0}{\Gamma}b}\ . \qquad (39.128)$$

Estimating coarsely $k\int_{-\infty}^{\infty}[n_{rfr}(\mathbf{r}) - 1]dz \simeq \sigma[n_{rfr}(\mathbf{r}) - 1]$, where $\sigma \equiv k\bar{r}$, we may simplify,

$$\frac{\imath b}{2} + \varphi = \sigma[n_{rfr}(\mathbf{r}) - 1]\ . \qquad (39.129)$$

At high atom numbers (i.e. in the smooth density limit), the dependency of the radiation pressure on atom number (39.126) exhibits a maximum at N_{cr}. For an atomic cloud with density n and the resonant optical density b_0, the characteristic atom number can be expressed in terms of the phase shift φ experienced by the pump laser beam on its path across the cloud. Absorption losses for the pump beam (e.g. resonance fluorescence, whose differential cross section contributes σ_{opt} to the total scattering cross section [816]) is completely negligible at large detunings. Only elastic Rayleigh scattering occurs, which in the smooth density limit of Mie scattering becomes pure

diffraction (real part of the refraction index). We can than understand the atomic cloud as a non-absorbing dielectric sphere with a Gaussian index of refraction.

Rewriting Eq. (39.126) in terms of the refraction index,

$$\frac{F_c}{F_1} \simeq \frac{N}{1+(2\varphi)^2}\frac{2}{(2\sigma)^4} \ , \tag{39.130}$$

we see that, as long as $\varphi < \frac{1}{2}$, the force increases linearly like $\propto N$. The proportionality comes from the perfect (in the sense of not spoiled by disorder) cooperative enhancement of the scattering rate in the smooth density limit. The enhancement is only limited by the finite size σ of the cloud, which is accounted for in the second fraction. This regime, characterized by [13],

$$\sigma[n_{rfr}(\mathbf{r}) - 1] \ll 1 \tag{39.131}$$

is termed the *Rayleigh-Debye-Gans regime*.

For larger phase shifts, $\varphi > \frac{1}{2}$, refraction more and more distorts the wavefront of the pump beam, which spoils the pump mode depletion and hence reduces radiation pressure. Consequently, the radiation pressure decreases again like N^{-1}. This is the *Mie regime* of scattering. The maximum is thus a pure diffraction effect, a so-called Mie resonance. It corresponds to the n_{rfr}, where the Rayleigh-Debye-Gans scattering approximation looses its validity according to (39.131). In Excs. 39.2.5.3 and 39.2.5.4 we study Mie and Rayleigh-Debye-Gans scattering, and in 39.2.5.5 we discuss the question is whether recoil is imparted to individual atoms or to the center-of-mass of the whole cloud.

In the limit of the approximations made, our formula correctly describes the radiation pressure force on extended objects. These objects can either be ensembles of scatterers like homogeneous, ordered or disordered atomic clouds of arbitrary shapes and volumes, or macroscopic objects like dielectric spheres. The formula thus represents a bridge between microscopic Rayleigh scattering and macroscopic Mie scattering. At very low atom numbers, the atomic cloud basically represents a randomly distributed bunch of scatterers, whose intrinsic disorder spoils cooperativity. The radiation pressure is then well described by the single-atom value. At large atom numbers, the atomic cloud forms a smooth density distribution characterized by an almost perfect a cooperativity, which is only limited by Mie scattering.

39.2.3.4 Light scattering in the continuous density approximation

The scalar electric field scattered by an arbitrary distribution of atoms has been calculated in (39.49). In the continuous density approximation (39.96), we get,

$$\vec{\mathcal{E}}_{sct}(\mathbf{r}) = -\frac{\imath\hbar\Gamma}{2d}\sum_{j=1}^{N}\frac{e^{\imath k_0|\mathbf{r}-\mathbf{r}_j|}}{\imath k_0|\mathbf{r}-\mathbf{r}_j|}\beta_j(\infty) \to -\frac{\imath\hbar\Gamma}{2d}\int d^3r'\rho(\mathbf{r}')\frac{e^{\imath k_0|\mathbf{r}-\mathbf{r}'|}}{\imath k_0|\mathbf{r}-\mathbf{r}'|}\beta(\mathbf{r}',\infty) \ . \tag{39.132}$$

[13] Note the necessity of another condition $[n_{rfr}(\mathbf{r}) - 1] \ll 1$ termed Born approximation, which demands that the incident wave be not appreciably reflected.

In particular, for a timed Dicke state,

$$\vec{\mathcal{E}}_{sct}(\mathbf{r}) = -\frac{\imath\hbar\Gamma}{2d}\frac{\sqrt{N}\Omega_0}{2\Delta_0 + \imath\Gamma N s_N}\sum_{j=1}^{N}\frac{e^{\imath k_0|\mathbf{r}-\mathbf{r}_j|}}{\imath k_0|\mathbf{r}-\mathbf{r}_j|} \tag{39.133}$$
$$\to -\frac{\imath\hbar\Gamma}{2d}\frac{\sqrt{N}\Omega_0}{2\Delta_0 + \imath\Gamma(1+N s_\infty)}\int d^3r'\rho(\mathbf{r}')\frac{e^{\imath k_0|\mathbf{r}-\mathbf{r}'|}}{\imath k_0|\mathbf{r}-\mathbf{r}'|} \ .$$

39.2.4 Spherical harmonics expansion and generalized timed Dicke state

The results derived in (39.120) assumed the cloud to be in a timed Dicke state. As we have seen in Exc. 39.1.8.5, timed Dicke states do not account for pump laser phase shifts induced by the cloud's refraction index. The timed Dicke states might work well for homogeneous cylinders, but not for ellipsoidal clouds, which we assume in our analytical treatments. Therefore, a better approach consists in expanding the cloud into spherical harmonics. Under the assumption that the cloud is radially symmetric, $\rho(\mathbf{r}) = \rho(r)$, we get [458],

$$\beta(r,\theta,t) = \sum_{n=0}^{\infty}\sqrt{\frac{2n+1}{4\pi}}\alpha_n(t)j_n(k_0 r)P_n(\cos\theta)e^{-\imath k_0 r\cos\theta} \ , \tag{39.134}$$

where the coefficients α_n are the solutions of,

$$\dot{\alpha}_n = \left[\imath\Delta_0 - \frac{\Gamma}{2}(1+\lambda_n)\right]\left[\alpha_n - \alpha_n(\infty)\right] \ , \tag{39.135}$$

In steady state,

$$\alpha_n(\infty) = \frac{2\imath^n\sqrt{\pi(2n+1)}\Omega_0}{2\Delta_0 + \imath\Gamma(1+\lambda_n)} \ , \tag{39.136}$$

where,

$$\lambda_n \equiv 4\pi\int_0^\infty dr\rho(r)j_n^2(k_0 r) \tag{39.137}$$

is the decay rate of eigenmode n.

Inserting this into the steady-state solution (39.100) and integrating over the volume,

$$\langle\beta_\infty\rangle \equiv \frac{2\pi}{N}\int_0^{2\pi}d\theta\sin\theta\int_0^\infty dr^2\rho(r)\beta(r,\theta) = \frac{\Omega_0}{N}\sum_{n=0}^{\infty}\frac{(2n+1)\lambda_n}{2\Delta_0 + \imath\Gamma(1+\lambda_n)} \tag{39.138}$$
$$\langle|\beta_\infty|^2\rangle \equiv \frac{2\pi}{N}\int_0^{2\pi}d\theta\sin\theta\int_0^\infty dr^2\rho(r)|\beta(r,\theta)|^2 = \frac{\Omega_0^2}{N}\sum_{n=0}^{\infty}\frac{(2n+1)\lambda_n}{4\Delta_0^2 + \Gamma^2(1+\lambda_n)^2} \ .$$

Example 231 (*Spherical harmonics expansion for a Gaussian density distribution*): The density distribution determines the coefficients λ_n. For a Gaussian distribution $n(r) = N/[(2\pi)^{3/2}\sigma_R^3]e^{-r^2/2\sigma_R^2}$ using the sine kernel,

$$\lambda_n = N\sqrt{\frac{\pi}{2}}\frac{e^{-\sigma^2}}{\sigma}I_{n+1/2}(\sigma^2) \ .$$

For a homogeneous sphere, $n(r) = n_0$, of radius $\sigma = k_0 R$, using the sine kernel [[1283], Eq. (18)],

$$\lambda_n = \frac{3N}{2}[j_n^2(\sigma) - j_{n-1}(\sigma) j_{n+1}(\sigma)] \ .$$

39.2.4.1 Expansion of the radiation pressure forces

This allows us to calculate the forces,

$$F_a = -\hbar k_0 \Omega_0 \Gamma \Im\mathfrak{m} \, \langle \beta_\infty \rangle \tag{39.139}$$

$$F_e = -\hbar k_0 \Omega_0^2 \Gamma \sum_{n=0}^{\infty} \frac{2(n+1)\lambda_n \lambda_{n+1}[4\Delta_0^2 + \Gamma^2(1+\lambda_n)(1+\lambda_{n+1})]}{[4\Delta_0^2 + \Gamma^2(1+\lambda_n)(1+\lambda_{n+1})]^2 + 4\Delta^2\Gamma^2(\lambda_{n+1}-\lambda_n)^2} \ .$$

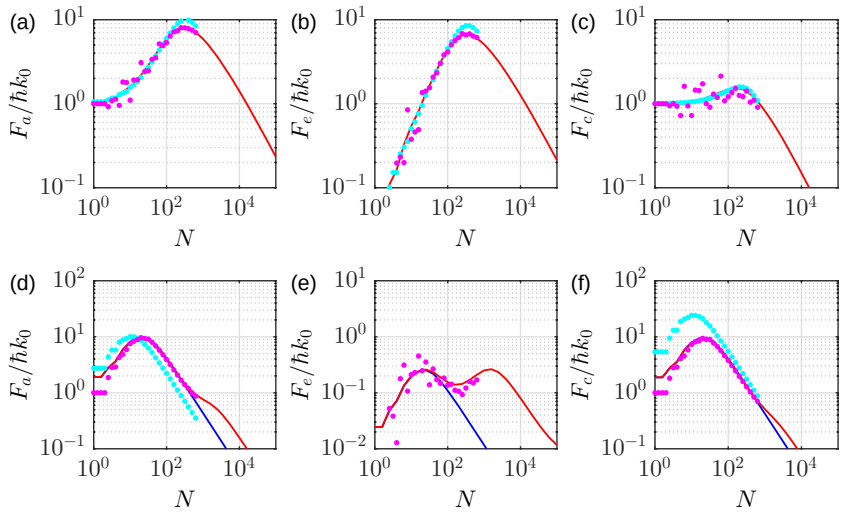

Figure 39.22: (code) (a) Absorption, (b) emission, and (c) total force for a Gaussian cloud with the following parameters: $\sigma = 2$, $\Delta_0 = 10\Gamma$, $\Omega_0 = 0.001\Gamma$, and $\eta = 1$. The magenta dots show a fully numerical calculation for a randomly generated cloud according to formula (39.63). The red lines show a calculation according to the complete formula (39.139). The cyan dots show a calculation assuming timed Dicke states according to (39.82) via numerical calculation of the structure factor according to (39.83) for the same randomly generated cloud as for the full simulation. The blue lines are obtained within the timed Dicke state approximation with structure factors estimated from formula (39.120). (d-f) Same as (a-c) but with $\sigma = 0.2$.

As seen in Fig. 39.22, the results obtained via the complete analytical formula (39.139) coincide with the fully numerical simulations according to formula (39.63). But both disagree with analytical and numerical results obtained within the timed Dicke state approximation.

It is possible to approximate the Bessel function $I_{n+1/2}(\sigma^2)$ and to obtain analytical solutions. The new formula works for $\sigma \gg 1$ and $\eta = 1$ [458],

$$F_a = \frac{\Omega_0^2}{\Gamma}\frac{\sigma^2}{N}\ln\left(1+\frac{N^2\Gamma^2 s_N}{\sigma^2(4\Delta_0^2+\Gamma^2)}\right) = \frac{\Omega_0^2}{4N\Gamma s_\infty}\ln\left(1+\frac{4N^2\Gamma^2 s_\infty s_N}{4\Delta_0^2+\Gamma^2}\right) \tag{39.140}$$

$$F_e = -F_a + \frac{\Omega_0^2}{\Delta_0}\frac{\sigma^2}{N}\arctan\frac{\Delta\Gamma N}{\sigma^2\left(4\Delta_0^2+\Gamma^2+\frac{\Gamma^2 N}{2\sigma^2}\right)} = \frac{\Omega_0^2}{4N\Delta_0 s_\infty}\arctan\frac{4\Delta_0\Gamma N s_\infty}{4\Delta_0^2+\Gamma^2+2\Gamma^2 N s_\infty}$$

$$b_0 = \frac{3N}{\sigma^2}$$

$$s_N = \frac{1}{N} + s_\infty = \frac{1}{N} + \frac{1}{(2\sigma)^2}\ .$$

39.2.4.2 Expansion of the scattered radiation intensity

The incident electric field is ...

The radiated electric field $\hat{\vec{\mathcal{E}}}^{(+)}(\mathbf{r},t)|\psi\rangle$ where $\hat{\vec{\mathcal{E}}}^{(+)}(\mathbf{r},t) = \sum_{\mathbf{k}} \varepsilon_{\mathbf{k}}\hat{a}_{\mathbf{k}}e^{\imath\mathbf{k}\cdot\mathbf{r}-\imath\omega_k t}$,

$$\begin{aligned}\hat{\vec{\mathcal{E}}}^{(+)}(\mathbf{r},t)|\psi\rangle &= \sum_{\mathbf{k}} \varepsilon_{\mathbf{k}}\gamma_{\mathbf{k}}(t)e^{\imath\mathbf{k}\cdot\mathbf{r}-\imath\omega_k t}|0\rangle|1\rangle_{\mathbf{k}} \\ &= -\imath\frac{V_{ph}g_{k_0}\varepsilon_{k_0}k_0}{4\pi c\sqrt{N}}e^{-\imath\omega_0 t}\sum_{j=1}^{N}\beta_j(t)e^{\imath\mathbf{k}_0\cdot\mathbf{r}_j}\frac{e^{\imath k_0|\mathbf{r}-\mathbf{r}_j|}-e^{-\imath k_0|\mathbf{r}-\mathbf{r}_j|}}{|\mathbf{r}-\mathbf{r}_j|}\ .\end{aligned} \tag{39.141}$$

We neglect the second term, which describes an incoming wave and go to smooth densities. We expand into spherical harmonics and obtain,

$$\hat{\vec{\mathcal{E}}}^{(+)}(\mathbf{r},t)|\psi\rangle = e^{-\imath\omega_0 t}\sum_{n=0}^{\infty}\frac{V_{ph}g_{k_0}\varepsilon_{k_0}}{c\sqrt{N}}\frac{\lambda_n}{2\Delta_0+\imath\Gamma(1+\lambda_n)}\Omega_0(2n+1)\imath^n h_n^{(1)}(k_0 r)P_n(\cos\theta)\ . \tag{39.142}$$

39.2.4.3 Mie resonances

It is an interesting question whether the maxima found in the curves of Fig. 39.22 can be associated with Mie resonances [164, 1228, 125]. To show this we need to apply the formalism of Mie scattering to atomic clouds with the smooth density approximation, where it is described by a continuous refraction index, as studied in Ref. [66]. The Mie formalism had been developed for homogeneous spheres, which can be dielectric or absorptive. For more general refractive index distribution the formalism gets quickly cumbersome [14]. Also Mie resonances are generally though of being conditioned to the existence of sharp boundaries.

The results of Ref. [66] surprisingly show that Mie resonances are expected for parabolic distributions of atoms, as is the case for example for Bose-Einstein condensates in the Thomas-Fermi limit. However, the spectra of Mie resonances exhibit much less structure. This is understood by the fact that 'whispering galery' Mie resonances may live on the surface of a sphere whose refraction index drops quadratically to zero, while cavity type Mie resonances may not.

[14] There is a treatment for parabolic radial variations [703].

39.2.5 Exercises

39.2.5.1 Ex: Structure coefficient of a homogeneous spherical and of a Gaussian ellipsoidal cloud

a. Calculate the structure coefficient of a homogeneous spherical cloud of radius R, and discuss the limits $qR < 1$ and $qR < 1$. Plot the structure coefficient as a function of θ for various radii R.
b. Calculate the structure coefficient of an ellipsoidal Gaussian cloud having the *rms*-widths σ_z and σ_r, and discuss the limits $qR < 1$ and $qR < 1$. Plot the structure coefficient as a function of θ for various aspect ratios σ_z/σ_ρ.

Solution: *a. The case of a homogeneous cloud with volume V is recovered by $n(\mathbf{r}) = \frac{N}{V}\chi_{[\mathbf{r}\in V]}$. For a homogeneous spherical cloud [1178] of volume $V = (4\pi/3)R^3$ the structure coefficient becomes with $\mathbf{q} \equiv \mathbf{k} - \mathbf{k}_0$,*

$$\begin{aligned}\mathcal{S}_\infty(\mathbf{k}) &= \frac{1}{V}\int_{sphere} e^{\imath\mathbf{q}\cdot\mathbf{r}} d^3r = \frac{3}{4\pi R^3}\int_0^R\int_0^{2\pi}\int_0^\pi r^2 e^{\imath qr\cos\theta}\sin\theta d\theta d\phi dr \\ &= \frac{3}{2R^3}\int_0^R r^2\int_{-1}^1 e^{\imath qru} du dr = \frac{3}{q^3R^3}(\sin qR - qR\cos qR)\ .\end{aligned}$$

In the small cloud limit, $qR \ll 1$, the density is well described by $n(\mathbf{r}) = N\delta^3(\mathbf{r})$, and the structure factor becomes,

$$\mathcal{S}_\infty(\mathbf{k}) = 1\ .$$

For large homogeneous clouds, $qR > 1$, of limited size V we get,

$$\mathcal{S}_\infty(\mathbf{k}) = \delta_{\mathbf{k},\mathbf{k}_0} = \frac{n_0}{N}\int_V e^{\imath(\mathbf{k}-\mathbf{k}_0)\mathbf{r}} d^3r = \frac{(2\pi)^3}{V}\delta^3(\mathbf{k}-\mathbf{k}_0) = \frac{6\pi^2}{R^3}\delta^3(\mathbf{k}-\mathbf{k}_0)\ .$$

b. The volume of an ellipsoidal Gaussian with the density distribution $n(\mathbf{r}) = n_0 e^{-\rho^2/2\bar\rho^2 - z^2/2\bar z^2}$ is $V = (2\pi)^{3/2}\sigma_\rho^2\sigma_z$. We write the incident wavevector as $\mathbf{k} = k\hat{\mathbf{e}}_z$ and the scattered wavevector as $\mathbf{k} = k\sin\theta(\hat{\mathbf{e}}_x\cos\phi + \hat{\mathbf{e}}_y\sin\phi) + k\hat{\mathbf{e}}_z\cos\theta$. With the Fourier transform $\int e^{-x^2/2\sigma^2} e^{\imath kx} dx = \sqrt{2\pi}\sigma\ e^{-\sigma^2x^2/2}$ the structure coefficient becomes,

$$\begin{aligned}\mathcal{S}_\infty(\mathbf{k}) &= \frac{1}{N}\int_{\mathbb{R}^3} n_0 e^{-\rho^2/2\sigma_\rho^2 - z^2/2\sigma_z^2} e^{\imath\mathbf{q}\cdot\mathbf{r}} d^3r \\ &= \frac{1}{(2\pi)^{3/2}\sigma_\rho^2\sigma_z}\int_{\mathbb{R}^3} e^{-\rho^2/2\sigma_\rho^2 - z^2/2\sigma_z^2} e^{\imath(\mathbf{k}-\mathbf{k}\hat{\mathbf{e}}_z)\cdot\mathbf{r}} d^3r \\ &= \frac{1}{(2\pi)^{3/2}\sigma_\rho^2\sigma_z}\int_{\mathbb{R}^3} e^{-x^2/2\sigma_\rho^2 + \imath kx\sin\theta\cos\phi} e^{-y^2/2\sigma_\rho^2 + \imath ky\sin\theta\sin\phi} e^{-z^2/2\sigma_z^2 + \imath kz(\cos\theta-1)} d^3r \\ &= e^{-\frac{1}{2}\sigma_\rho^2k^2\sin^2\theta\cos^2\phi} e^{-\frac{1}{2}\sigma_\rho^2k^2\sin^2\theta\sin^2\phi} e^{-\frac{1}{2}\sigma_z^2k^2(\cos\theta-1)^2} \\ &= e^{-\frac{1}{2}k^2\sigma_\rho^2\sin^2\theta - \frac{1}{2}k^2\sigma_z^2(\cos\theta-1)^2}\ .\end{aligned}$$

Again in the small cloud limit, $\sigma_\rho, \sigma_z < \lambda$, the structure coefficient becomes

$$\mathcal{S}_\infty(\mathbf{k}) = 1\ .$$

In the large cloud limit, we get,

$$\mathcal{S}_\infty(\mathbf{k}) = \delta_{\mathbf{k},\mathbf{k}_0} = \frac{(2\pi)^{3/2}}{\sigma_\rho^2 \sigma_z}\delta^3(\mathbf{k}-\mathbf{k}_0) \ .$$

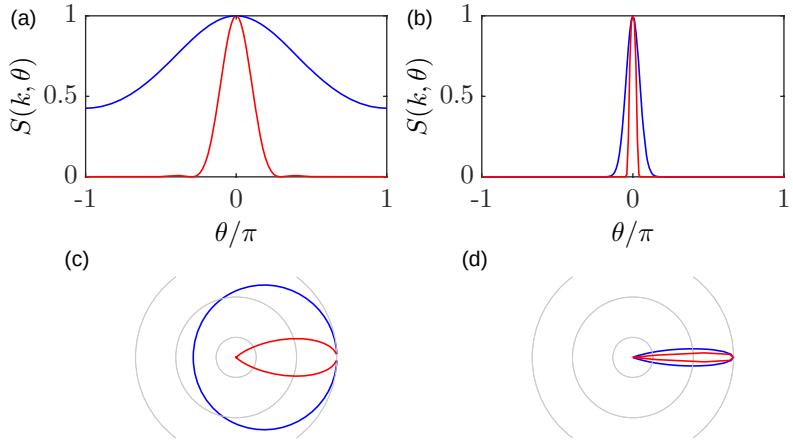

Figure 39.23: θ-dependence of the structure coefficients of (a) a homogeneous sphere for $kR = 1$ (blue) and $kR = 5$ (red) and of an ellipsoidal Gaussian cloud (b) for $\sigma_z/\sigma_\rho = 1$ (blue) and $\sigma_z/\sigma_\rho = 50$ (red). The figures (c) and (d) are polar representations of the curves in (a-b).

39.2.5.2 Ex: Force coefficients of a homogeneous spherical and of a Gaussian ellipsoidal cloud

a. Calculate the force coefficients s_N, $\tilde{f}_N$, and f_N from the Eqs. (39.66), Eqs. (39.78), and Eqs. (39.86), respectively, for a homogeneous spherical cloud of radius R.
b. Repeat the calculation of (a) for an ellipsoidal Gaussian cloud having the *rms*-widths σ_z and σ_r.

Solution: *a.*
b. The force coefficients are, setting $k \simeq k_0$ [298] and $\eta \equiv \sigma_z/\sigma_r$ and using the result from Exc. 39.2.5.1(a),

$$\begin{aligned} s_\infty &= \frac{1}{4\pi}\int_0^\pi \int_0^{2\pi} |\mathcal{S}_\infty(k_0,\theta,\phi)|^2 \sin\theta d\theta d\phi \\ &= \frac{\sqrt{\pi} e^{\sigma^2/(\eta^2-1)}}{4\sigma\sqrt{\eta^2-1}} \left[erf\left(\frac{\sigma(2\eta^2-1)}{\sqrt{\eta^2-1}}\right) - erf\left(\frac{\sigma}{\sqrt{\eta^2-1}}\right)\right] \\ &\xrightarrow{\eta=1} \frac{1-e^{-4\sigma^2}}{4\sigma^2} \xrightarrow{\sigma\gg 1} \frac{1}{4\sigma^2} \ . \end{aligned}$$

Also,

$$\tilde{f}_\infty = \frac{1}{4\pi}\int_0^\pi \int_0^{2\pi} \mathfrak{Re}\ \mathcal{S}_\infty(k_0,\theta,\phi)\sin\theta\cos\theta d\theta d\phi = \dots\ .$$

And,

$$\begin{aligned} f_\infty &= \frac{1}{4\pi}\int_0^\pi \int_0^{2\pi} |\mathcal{S}_\infty(k_0,\theta,\phi)|^2 \sin\theta\cos\theta d\theta d\phi \\ &= \frac{1}{\eta^2-1}\left[\eta^2 s_\infty - \frac{1}{4\sigma^2}(1-e^{-4\eta^2\sigma^2})\right] \\ &\xrightarrow{\eta=1} \frac{1}{4\sigma^2}\left[1-\frac{1}{2\sigma^2}+\left(1+\frac{1}{2\sigma^2}\right)e^{-4\sigma^2}\right] \xrightarrow{\sigma\gg 1} s_\infty - 2s_\infty^2\ . \end{aligned}$$

39.2.5.3 Ex: RDG and Mie

Estimate whether it is possible to distinguish Rayleigh-Debye-Gans scattering from Mie scattering in strontium spectra.

Solution: *We need,*

$$k\bar{v}, \omega_{rec} \ll \Gamma\ .$$

On the blue line,

$$\begin{aligned} k\bar{v} &= k\sqrt{\frac{k_B T}{m}} \simeq k\sqrt{\frac{\hbar\Gamma_{blue}}{2m}} \approx (2\pi)580\,\text{kHz} \\ \omega_{rec} &= \frac{\hbar k^2}{2m} = (2\pi)11\,\text{kHz}\ . \end{aligned}$$

It is easier on the red line

$$\begin{aligned} k\bar{v} &= k\sqrt{\frac{k_B T}{m}} \simeq k\sqrt{\frac{\hbar\Gamma_{red}}{2m}} \approx (2\pi)8.7\,\text{kHz} \\ \omega_{rec} &= \frac{\hbar k^2}{2m} = (2\pi)5\,\text{kHz}\ . \end{aligned}$$

39.2.5.4 Ex: Mie scattering from absorbing spheres

Calculate the force on a homogeneous dielectric sphere as a function of the absorptive and dispersive part of the refraction index [703].

Solution: *The result is shown in Fig. 39.24.*

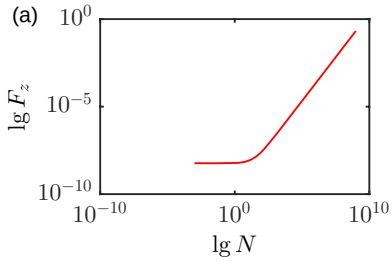

Figure 39.24: (code) Force on a homogeneous dielectric sphere as a function of n_{rfr}.

39.2.5.5 Ex: Momentum halos and heating, is the recoil cooperative?

Discuss the question is whether recoil is imparted to individual atoms or to the center-of-mass of the whole cloud.

Solution: *The individual recoil case corresponds to a product state, the shared recoil case to an entangled sum state. From radiation pressure force measurements it is impossible to distinguish between both, but perhaps analyzing fluctuations versus heating? On the other hand, even if a shared recoil state is generated, it may quickly decohere into individual recoil states.*
It might be necessary to include the external degrees of freedom into the formalism to see which degrees is really affected by cooperativity [15]*. There might be an interesting analogy between the transfer of recoil to individual particles and the photoeffect, where individual electrons are ejected from a solid..*
Let us consider cooperative scattering from two atoms. In the individual recoil case, the momentum halo should be a spherical shell with azimuthal modulation. In the shared recoil case, we expect a momentum blob somewhere inside the sphere. The effect is analogous to the Mössbauer effect, where the interatomic interaction is mediated by the lattice. In our case, it is induced by light (light shift imprinted by the dipole induced in atom j in atom m leads to level splitting gg, $eg + ge$, ee).

39.3 Scattering from disordered and dense clouds

39.3.1 Collective shifts and broadenings, vectorial light

The calculations show that the term identified as being responsible for disordered scattering comes from the self-decaying term (diagonal in the matrix γ_{jm}), i.e. when the excitation amplitude of the j-th atom decays by spontaneous emission. The other process, that the j-th atom decays because of the decay of the m-th atom, is described by the non-diagonal elements.

The classical radiation pressure formula is recovered for $\lambda_n = 0$, which means that the scattering is purely isotropic. The smooth density interpolation formula [298] is recovered when $\lambda_n \ll 1$ is assumed at all N.

[15] Note that the external degree of freedom is already contained in the Hamiltonian via the exponential $e^{\imath k\mathbf{r}}$. The coordinate just has to be interpreted as an operator.

The impact of *multiple scattering* gets important, when the off-resonant optical density exceeds 1, i.e. when,

$$b_0 > \frac{4\Delta_0^2}{\Gamma^2} \ . \tag{39.143}$$

We are interested in the question, whether it is possible to find signatures of collective Lamb shift in experiments with cold atoms. The Lamb shift should appear, e.g. in the spectra of the $\frac{1}{N}\sum_j |\beta_j|^2$ (calculated or simulated using exponential kernels). Indeed the dependence on Δ show asymmetries in certain parameter regimes. One of the features of the spectra is a strong central peak, which can be attributed to multiple scattering.

But what if we were able to inhibit multiple scattering? In the case of the strontium intercombination line, singly scattered photons are frequency-shifted by photonic recoil, such that they cannot be reabsorbed by other atoms. This feature is not contained in the coupled dipoles Hamiltonian, since in this model the external degrees of freedom are frozen. Then, how does the time-evolution have to be modified for Sr? Is it possible to construct the Hamiltonian in such a way that scattering intrinsically occurs only once without having to include external degrees of freedom, photonic recoil and the corresponding Doppler shift?

The eigenstates of the differential equation are found via $\beta_j(t) = \beta_j e^{-\lambda_n t}$, where $\mathfrak{Re}\ \lambda_n$ are the decay rates of the modes n and $\mathfrak{Im}\ \lambda_n$ are the frequency shifts [140].

According to [467] various frequency shifts may occur in ensembles of atoms due to a. collisions (of ground state atoms) and b. radiation-induced interactions (particularly resonant interactions). The shifts can be categorized as follows:
1. Coulomb shift (instantaneous interactions), for E1-radiation the Coulomb shift gives rise to the Lorentz shift for $\sigma \gg 0$, for $\sigma \ll 0$ the Lorentz shift goes to zero;
2. cooperative Lamb shift (exchange of virtual photons), photons are not only emitting and reabsorbing virtual photons, but the photons may be reabsorbed by adjacent atoms;
3. resonant collision shift (temporal correlations of dipole orientations), note that the scattering amplitude is non-linear in the potential;
4. van der Waals shift (due to buffer gas collisions or to non-resonant levels, the latter, however, being small).

39.3.1.1 Real and virtual photons

A virtual particle is a transient quantum fluctuation that exhibits some of the characteristics of an ordinary particle, while having its existence limited by the Heisenberg uncertainty principle. The concept of virtual particles arises in perturbation theory of quantum field theory, where interactions between ordinary particles (e.g. particle scattering or Casimir forces) are described in terms of exchanges of virtual particles with limited lifetime. A process involving virtual particles can be described by a schematic representation known as a *Feynman diagram*, in which virtual particles are represented by internal lines.

A virtual particle does not necessarily carry the same mass as the corresponding real particle, although it always conserves energy and momentum. The closer its characteristics come to those of ordinary particles, the longer its lifetime. Virtual photons

are the exchange particle for the electromagnetic interaction. I.e. electromagnetic repulsion or attraction between two charges can be thought of as due to the exchange of virtual photons between the charges.

As a consequence of quantum mechanical uncertainty, any object or process that exists for a limited time or in a limited volume cannot have a precisely defined energy or momentum. Hence, virtual particles which exist only temporarily do not typically obey the mass-shell relation $m^2c^2 = E^2 - p^2c^2$. The longer the lifetime of a virtual particle, the more the energy and momentum approach the mass-shell relation ruling the behavior of real particles. For instance, electromagnetic radiation consists of real photons which may travel light years between the emitter and absorber, but electrostatic attraction and repulsion is a relatively short-range force that is a consequence of the exchange of virtual photons.

By expressing an interaction in terms of the exchange of a virtual particle with four-momentum q, where q is given by the difference between the four-momenta of the particles entering and leaving the interaction vertex, both momentum and energy are conserved at the interaction vertices of the Feynman diagram. A virtual particle does not precisely obey the energy-momentum (or mass-shell) relation, that is, its kinetic energy may not have the usual relationship to velocity, as it can be negative. This is expressed by the expression *off mass shell*. The probability amplitude for a virtual particle to exist tends to be canceled out by destructive interference over longer distances and times. As a consequence, a real photon is massless and thus has only two polarization states, whereas a virtual one, being effectively massive, has three polarization states. Quantum field theory considers real particles as being *detectable* excitations of underlying quantum fields, while virtual particles appear only as forces, i.e. *non-detectable* excitations. Virtual particles are 'temporary' in the sense that they appear never appear as the observable inputs and outputs of a physical process.

Many observable physical phenomena can be interpreted in terms of virtual particles. For bosonic particles that exhibit rest mass when free and real, virtual interactions are characterized by a relatively short range of the interaction force. Confinement can lead to a short range, too. Examples of such short-range interactions are the strong and weak forces, and their associated field bosons. For the gravitational and electromagnetic forces, the zero rest-mass of the associated bosonic exchange particle allows for long-range forces. However, in the case of photons, power and information transfer by virtual particles is relatively short-ranged (restricted to only a few wavelengths of the field source), as is the case of inductive and capacitive coupling in the near field zone of coils and antennas.

Some field interactions which may be interpreted in terms of virtual particles are:

- The electrostatic Coulomb force between electric charges and the magnetostatic Lorentz force between magnetic dipoles are caused by the exchange of virtual photons. In symmetric 3-dimensional space this exchange results in the inverse square law for the electrostatic force and the inverse cube law for the magnetostatic force. Since the photon has no mass, the electric and magnetic potentials have infinite range.

- Electromagnetic induction transfers energy to and from a magnetic coil via a changing (electro)magnetic field. Much of the so-called near-field of radio

antennas, where the magnetic and electric effects of the changing current in the antenna wire and the charge effects of the wire's capacitive charge may be (and usually are) important contributors to the total EM field close to the source, but both of which effects are dipole effects that decay with increasing distance from the antenna much more quickly than do the influence of 'conventional' electromagnetic waves that are 'far' from the source. These far-field waves, for which $\mathcal{E}$ is (in the limit of long distance) equal to $c\mathcal{B}$, are composed of actual photons. Actual and virtual photons are mixed near an antenna, with the virtual photons responsible only for the 'extra' magnetic-inductive and transient electric-dipole effects, which cause any imbalance between $\mathcal{E}$ and $c\mathcal{B}$. As distance from the antenna grows, the near-field effects (as dipole fields) die out more quickly, and only the 'radiative' effects that are due to actual photons remain as important effects. Although virtual effects extend to infinity, they drop off in field strength as $1/r^2$ rather than the field of EM waves composed of actual photons, which drop as $1/r$. The electrical power in the fields, respectively, decrease as $1/r^4$ and $1/r^2$.

- Quantum tunneling and evanescent waves may be considered a manifestation of virtual particle exchanges. The range of forces carried by virtual particles is limited by the uncertainty principle, which regards energy and time as conjugate variables; thus, virtual particles of larger mass have more limited range.

- The strong nuclear force between quarks is the result of interaction of virtual gluons. The residual of this force outside of quark triplets (neutron and proton) holds neutrons and protons together in nuclei, and is due to virtual mesons such as the π meson and ρ meson. The weak nuclear force is the result of exchange by virtual W and Z bosons.

- The spontaneous emission of a photon due to the decay of an excited atom or nucleus can be traced back to the quantization of the electromagnetic field.

- The Casimir effect, where the ground state of the quantized electromagnetic field causes attraction between a pair of electrically neutral metal plates, and the van der Waals force, which is partly due to a (relativistic) Casimir effect between two atoms, are consequences of vacuum fluctuations.

- Vacuum polarization, which involves pair production or the decay of the vacuum, which is the spontaneous production of particle-antiparticle pairs (such as electron-positron).

- The Lamb shift of energies of atomic levels.

The calculation of scattering amplitudes in theoretical particle physics requires the use of some rather large and complicated integrals over a large number of variables. These integrals do, however, have a regular structure, and may be represented as Feynman diagrams. The appeal of the Feynman diagrams is strong, as it allows for a simple visual presentation of what would otherwise be a rather arcane and abstract formula. In particular, part of the appeal is that the outgoing legs of a Feynman diagram can be associated with actual, on-shell particles. Thus, it is natural to

associate the other lines in the diagram with particles as well, called the 'virtual particles'. In mathematical terms, they correspond to the propagators appearing in the diagram.

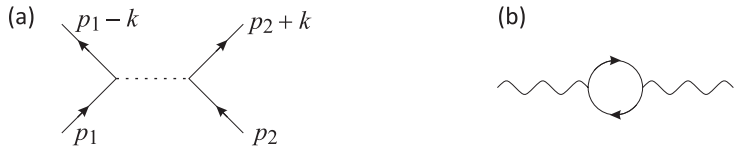

Figure 39.25: (a) Feynman diagram for one particle exchange scattering. The solid lines correspond to real particles, e.g. electrons (of momentum p_1 and so on), while the dotted line corresponds to a virtual particle carrying momentum k, e.g. a virtual photon. (b) One-loop diagram with fermion propagator. Virtual particles may be mesons or vector bosons, as in the example above; they may also be fermions. However, in order to preserve quantum numbers, most simple diagrams involving fermion exchange are prohibited. The image to the right shows an allowed diagram, a one-loop diagram. The solid lines correspond to a fermion propagator, the wavy lines to bosons.

In formal terms, a particle is considered to be an eigenstate of the particle number operator $\hat{a}^\dagger \hat{a}$. In many cases, the particle number operator does not commute with the Hamiltonian of the system, which implies that the particle number in an area of space is not a well-defined quantity. Instead, like other quantum observables, it must be represented by a probability distribution. Since these particles are not certain to exist, they are called virtual particles or vacuum fluctuations of vacuum energy. In a certain sense, they can be understood to be a manifestation of the time-energy uncertainty principle in a vacuum.

An important example of the 'presence' of virtual particles in a vacuum is the Casimir effect. Here, the explanation of the effect requires that the total energy of all of the virtual particles in a vacuum can be added together. Thus, although the virtual particles themselves are not directly observable, they do leave an observable effect: Their zero-point energy results in forces acting on suitably arranged metal plates or dielectrics.

Virtual particles are often popularly described as coming in pairs, a particle and antiparticle which can be of any kind. These pairs exist for an extremely short time, and then mutually annihilate, or in some cases, the pair may be boosted apart using external energy so that they avoid annihilation and become real particles. This may occur in one of two ways. In an accelerating frame of reference, the virtual particles may appear to be real to the accelerated observer; this is known as the Unruh effect. In short, the vacuum of a stationary frame appears to the accelerated observer, to be a warm gas of real particles in thermodynamic equilibrium.

39.3.1.2 Collective Lamb-shift

The *Lamb shift* results from the interaction of a (bound) valence electron with fluctuations of the electromagnetic vacuum. The fluctuations smear out the electronic orbit inside the Coulombian potential, thus leading to a shift. In the same time, if the electron is on an excited orbit, they incite radiative decay, thus leading to *spontaneous*

emission. The interaction takes place as an emission-reabsorption cycle of a *virtual photon* associated to a *transverse radiation field* [16].

The Lamb shift can be manipulated by tailoring the vacuum's mode structure, e.g. by a cavity or by the presence of antennas such as other atoms. The impact of a cavity on the Lamb shift and the spontaneous emission rate has been measured [596].

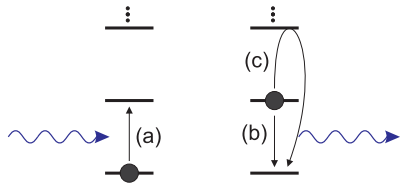

Figure 39.26: Scheme of collective Lamb shift.

Can we measure the collective Lamb-shift (impact of virtual photon processes)? Perhaps mixing the input and the scattered light using heterodyne techniques. Measure the collective Lamb shift in an ordered lattice, as Desy scientists do? A problem would be inhomogeneous light-shifts induced by the trapping potential and dipole-dipole interactions of the atoms excited by the lattice beams. Our calculations and simulations show that the impact of the exponential kernel decreases dramatically for large σ. How can [1112] have seen an effect in the X-ray regime? What distinguishes the collective Lamb-shift (impact of virtual photon processes) from shifts induced by atomic dipole interactions responsible for ground state collisions. After all all these are also mediated by virtual photons. Obviously, the interatomic interactions require an additional term in the Hamiltonian.

Can we derive a Lorentz-Lorenz formula from our theory analogously to [1119]? How to distinguish Lorentz-Lorenz shifts from collective dipole interactions? How are they related to collective line shifts [922, 470]?

According to [470] the total collective Lamb shift is [1286, 1285],

$$\Delta\omega_{lmb} = \left(\frac{4}{3} \mp 1\right) \frac{\rho\pi}{\hbar} \wp^2 \ , \tag{39.144}$$

where $\wp \equiv d/\sqrt{4\pi\varepsilon_0}$ and $d = \sqrt{3\pi\varepsilon_0\hbar\Gamma/k^3}$. The minus sign holds for a homogeneous slab, the plus sign for a homogeneous sphere.

$$\Delta\omega_{lmb} = \left(\frac{4}{3} \mp 1\right) \frac{\rho\pi}{4\pi\varepsilon_0\hbar} d^2 = \left(\frac{4}{3} \mp 1\right) \frac{\rho}{4} \frac{3\pi\Gamma}{k^3} = \frac{\pi\rho\Gamma}{4k^3} \ . \tag{39.145}$$

The $\frac{4}{3}$ term accounts for the Lorentz-Lorenz shift

$$\Delta\omega_{LL} = \frac{\rho\pi\Gamma}{k^3} \ . \tag{39.146}$$

Fig. 39.27 shows the collective Lamb shift calculated numerically and approximated analytically.

[16] What is the relationship between the Lamb shift and the *Bloch-Siegert shift* for single atoms without RWA and the collective Lamb-shift and the Lorentz-Lorenz shift with many atoms?

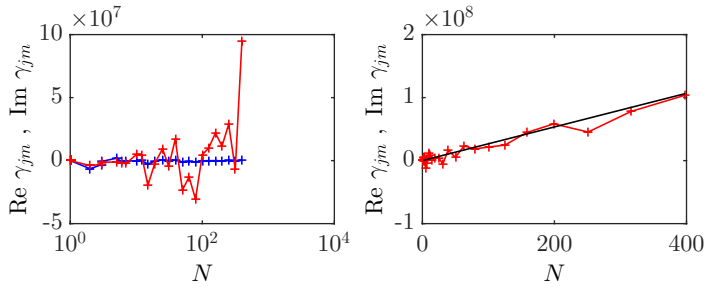

Figure 39.27: Collective Lamb shift.

39.3.1.3 Lorentz-Lorenz shift

The *Lorentz-Lorenz shift* follows from the *Clausius-Mossotti formula*[see Eqs. (14.28) and (16.29)],

$$n_{rfr}^2 - 1 = \frac{\frac{\rho\alpha_{pol}}{\varepsilon_0}}{1 - \frac{\rho\alpha_{pol}}{3\varepsilon_0}} \ . \tag{39.147}$$

The formula results from the fact that the polarization of a medium is induced by a local electric field resulting from a superposition of an external field and the field produced by the polarization of the neighboring atoms. In quantum optics near atomic resonances the polarisability can be approximated by [see (18.122)],

$$\alpha_{pol} = \frac{e^2}{m_e}\frac{1}{\omega_0^2 - \omega^2 - \imath\omega\gamma_\omega} = \frac{6\pi\varepsilon_0}{k_0^3}\frac{\omega_0\gamma_{\omega_0}}{\omega_0^2 - \omega^2 - \imath\omega\gamma_\omega} \simeq \frac{6\pi\varepsilon_0}{k_0^3}\frac{\Gamma}{2\Delta + \imath\Gamma} \ , \tag{39.148}$$

with

$$\gamma_\omega = \frac{e^2\omega^2}{6\pi\varepsilon_0 m_e c^3} = \frac{\omega^2}{\omega_0^2}\Gamma \ . \tag{39.149}$$

Inserting this into the susceptibility,

$$\chi_\varepsilon = \frac{3\pi\rho}{k_0^3}\frac{1}{\Delta/\Gamma - \pi\rho/k_0^3 + \imath/2} \equiv \frac{3\pi\rho}{k_0^3}\frac{1}{(\Delta - \Delta\omega_{LL})/\Gamma + \imath/2} \ , \tag{39.150}$$

defining the *Lorentz-Lorenz shift*

$$\boxed{\Delta\omega_{LL} = -\frac{\pi\rho}{k_0^3}\Gamma} \ . \tag{39.151}$$

For typical densities $\rho \simeq 10^{12}\,\mathrm{cm}^{-3}$, $\lambda = 780\,\mathrm{nm}$ and $\Gamma = (2\pi)\ 6\,\mathrm{MHz}$, we expect,

$$\Delta\omega_{LL} = (2\pi)\ 9\,\mathrm{kHz} \ . \tag{39.152}$$

In scalar approximation

$$\Delta\omega_{lmb} = \mp\frac{\rho\pi\Gamma}{2k^3} \approx \frac{N\Gamma}{R^3k^3} = \frac{N\Gamma}{\sigma^3} \ , \tag{39.153}$$

and there is no Lorentz-Lorenz contribution.

The Lorentz-Lorenz shift is due to static dipole-dipole interaction, not to virtual photon exchange.

39.3.1.4 Vectorial light

The procedure can be generalized to the vectorial case [1215, 1214, 859], where we get a similar steady-state solution as in (39.37),

$$\boxed{\vec{\beta}_j = (M_{jm})^{-1}\ \hat{\epsilon}\ \tfrac{\imath}{2}\Omega_0(\mathbf{r}_m)}\ , \tag{39.154}$$

only that the dipole moment amplitudes and the incident light field are now considered as vectors. The expression for the matrix M_{jm} is the same as in (39.36). However, the vectorial kernel must be calculated in a different way. Using the abbreviations,

$$\mathbf{r}_{jm} = \mathbf{r}_j - \mathbf{r}_m \quad , \quad r_{jm} = |\mathbf{r}_j - \mathbf{r}_m| + \delta_{jm} \quad , \quad c_{jm} = \frac{\imath}{k_0 r_{jm}} - \frac{1}{(k_0 r_{jm})^2}\ , \tag{39.155}$$

the new vectorial kernel can be written,

$$\gamma^{(3)}_{jm} = \frac{3\gamma_{jm}}{2}\ \frac{(1+c_{jm})r_{jm}^2\delta_{mn} - (1+3c_{jm})\mathbf{r}_{jm}\mathbf{r}^{\intercal}_{jm}}{r_{jm}^2}\ . \tag{39.156}$$

The steady-state scattered light field and the total field are now,

$$\vec{\mathcal{E}}_{sct}(\mathbf{r}) = -\frac{\imath\Gamma}{2}\sum_{j=1}^{N}\frac{3\gamma_{oj}(\mathbf{r})}{2}\ \frac{(1+c_{oj}(\mathbf{r}))k_0^2|\mathbf{r}-\mathbf{r}_j|^2\vec{\beta}_j - (1+3c_{oj}(\mathbf{r}))[(\mathbf{r}-\mathbf{r}_j)\cdot\vec{\beta}_j](\mathbf{r}-\mathbf{r}_j)}{|\mathbf{r}-\mathbf{r}_j|^2}\ . \tag{39.157}$$

A movie can be assisted at (watch movie).

39.3.2 Propagation of light within an absorber

The passage of coherent light through an absorber follows the *Lambert-Beer law*,

$$\boxed{I = I_0 e^{-\alpha z} \qquad \text{satisfying} \qquad I(mz) = I(z)^m}\ . \tag{39.158}$$

The *diffuse scattering* follows a different law. Imagine that the photons homogeneously fill a given volume $V = Az$. Per unit time, a given amount of energy E is pumped to the volume. The thicker the volume, the lower the energy density $u = E/Az$ and fewer photons reach the end of the absorber. This is the *Ohm's law*. The diffusively transmitted energy is,

$$\boxed{I = I_0\frac{a}{z} \qquad \text{satisfying} \qquad I(mz) = I(z)/m}\ . \tag{39.159}$$

39.3.2.1 Coherent backscattering

Shining coherent light on a homogeneous cloud, we expect no coherent scattering (exception made of multiple-atom scattering in backward direction, CBS and of fluctuations like speckle patterns). Like radiation trapping, *coherent backscattering* (CBS) is a manifestation of interference in multiple scattering. Just like photon echoes it is *not* due to interatomic correlations. While in radiation trapping this leads to an energy storage inside the atomic cloud connected to destructive interference of the radiation emitted to the cloud's outside, when the coherent beam is reflected at a diffuse

scattered, one observes *speckle patterns*. This holds as well for laser light reflection as for atomic wave reflections at a rough surface. See also (watch talk).

The coherent backscattering is an effect of constructive interference between two light scattering paths having the exact time-reversed single scattering sequence,

$$I = \left| \sum_j \vec{\mathcal{E}}_j e^{\imath\varphi_j} \right|^2 = \sum_j \left| \vec{\mathcal{E}}_j \right|^2 + \sum_{j \neq k} \vec{\mathcal{E}}_j \vec{\mathcal{E}}_k^* e^{\imath(\varphi_j - \varphi_k)} \ . \tag{39.160}$$

Only the second term makes speckles. However, the atomic motion smoothes out the speckle pattern in all directions. Only in the presence of correlations in the atomic positions they do not. E.g. in crystals or in the backscattering directions. Therefore, the constructive interference depends strongly on the backscattering angle ϑ. Fast atomic motion internal excitations can dynamically break the time-reversal symmetry of the scattering path, esp. when the laser is close to resonance and the phase delay per scattering process is long. Coherent backscattering is a weak form of *Anderson localization* (also strong localization) of light.

39.3.3 Localization of light

For a long time, people tried to observe strong localization with light. Many problems have been identified, some have been circumvented: Path irreversibilities due to internal structure, accumulated frequency shifts upon multiple photonic recoil, retardation combined to Doppler shifts, inelastic scattering, collisions. Recent simulations, however, suggest that strong localization would be impossible with vectorial light [1215, 1214, 859].

The higher the scattering order (number of scattering atoms), the deeper you can probe the cloud, involve higher-order correlation functions.

Strong localization is the inhibition of light propagation due to interference between multiple scattering paths. In fact the concept of a path for photons looses its sense, since a scattered photon is reabsorbed before it has time to leave the atom: We are approaching a regime where a dipolar description is more suited. The strong localization has been interpreted as a metal-insulator transition. Thinking of CBS with matter waves one is reminded the Mott insulating phase.

39.3.3.1 Anderson localization

In a disordered gas, interference between incident and reflected beams is averaged out. In the absence of interference phenomena the total transmission of a disordered medium is inversely proportional to the sample thickness (Ohm's law). In contrast, long-range spatial order can tolerate interferences, which may have dramatic influence on the propagation of light, such as a vanishing diffusion constant: in this situation, the medium behaves like an insulator (*strong localization of light* or *Anderson localization* in analogy to phase transitions to insulating states due to interference of electron wavefunctions) and its total transmission decreases exponentially with the samples thickness. Localization means that the transmission coefficient T of a plane wave decays exponentially with the system length L. The decay length is measured

by a so-called localization length $\lambda(k) = -L/\langle \ln T \rangle$ ($\lambda(k)^{-1}$ is also called the *Lyapunov exponent*). For $T \to 0, 1$, the localization length tends to $\lambda \to 0, \infty$. Multiple scattering experiments on strong localization of microwaves and light have been performed [1372]. A more accessible experimental situation is the so-called weak *weak localization of light* regime which manifests as coherent backscattering [768].

In dilute gases, single photon scattering will predominate. If L is the size of the sample and $l = 1/n\sigma$ the mean free path, this regime where the Lambert-Beer law, $I \sim e^{-\alpha z}$, holds is delimited by $1 < kL < kl$. At higher densities, multiple scattering leads to random walk of photons inside the sample resulting in *radiation trapping*. In this regimedelimited by $1 < kl < kL$, Ohm's law, $I \sim 1/z$, rules diffusive propagation of light. Interference effects may come into play when the sample is so dense that the mean free path for a photon is no larger than its wavelength. This so-called *Ioffe-Regel criterion*,

$$kl < 1 \ , \tag{39.161}$$

describes the regime of strong localization in $3D$ disordered samples. In this regime, ray optics does not apply. The propagation of radiation must rather be described by field amplitudes, which can interfere. Closed paths lead to standing waves, i.e. constructive interference. This hinders light propagation out of small regions: *The light gets localized* and the law is again exponential, $I \sim e^{-\tilde{\alpha} z}$. In other words localization arises from interference corrections to optical transport.

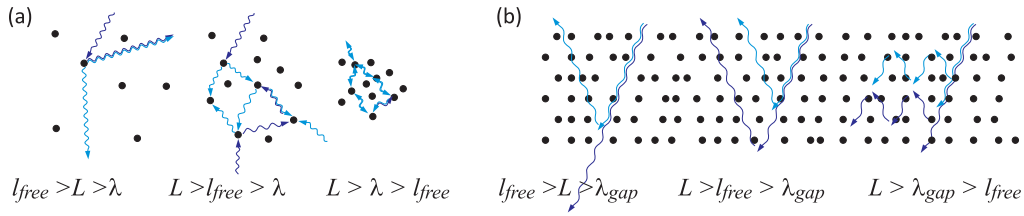

Figure 39.28: Illustration of the regime of single scattering, random walks, strong localization in (a) disordered gases and (b) photonic band gaps.

Now atoms have the important advantage that, due to their internal structure, the optical density can be tuned over wide ranges. However, for typical resonant cross sections σ the density must still be larger than $n > 10^{14}\,\mathrm{cm}^{-3}$, which is a lot.

Connection to superradiance [680], where directional bundling of radiation favors stimulated processes

Localization corresponds to a minimum in the density of states. E.g. PBGs arise from suppression of many states by destructive interference.

39.3.4 Exercises

39.3.4.1 Ex: The green flash

Discuss whether the '*green flash*' at sunset could be due to *superradiant extinction*. It can last seconds because refraction sweeps the ray through the spectrum (see the movie *Le rayon vert* by Éric Rohmer).

Solution:

39.3.4.2 Ex: Faraday effect with vectorial kernel in the coupled dipoles model

Try to simulate the pump laser phase shift and lensing by a small dense cloud by the coupled dipoles model for red and blue detuning. Discuss the influence of rescattering.

Solution:

39.4 Scattering from periodic structures and photonic bands

Long-range spatial ordering can have a dramatic influence on the propagation of light and the cooperativity of scattering, as we have already pointed out in the introduction of the structure factor in Sec. 39.1.1. This is true for the scattering of electronic waves in crystals. But atomic gases can also be arranged in periodic luminous potentials generated by dipolar forces (introduced in Sec. 38.2.2) exerted by counterpropagating laser beams. Such potentials, called *optical lattices*, can be realized with various geometries in 1, 2 or 3 dimensions. See also (watch talk).

Periodic structures are usually probed by Bragg scattering. This procedure can be applied to atoms ordered in optical lattices [146, 1361, 1219, 1221]: A test beam with wavevector $\mathbf{k}_{brg}$ and intensity I_{brg} is irradiated into the atomic cloud, and the power P_s of the first-order reflected beam by Bragg is detected under a solid angle Ω_s. Bragg diffraction is an interference effect of radiation patterns emitted by Rayleigh scattering from periodically aligned point-like antennas, the interference being constructive in only specified directions.

For optically dilute lattices, where multiple reflections can be neglected, the imaginary part of the atomic response is sufficient to describe Bragg reflection. For optically dense lattices, multiple reflections between consecutive atomic layers lead to interference phenomena between reflected and transmitted light fields and cause the emergence of frequency bands, inside which the propagation of light waves through the cloud is prohibited. These bands are known as *forbidden photonic bands*.

Photonic bands in optical lattices are interesting for several reasons:

1. They may facilitate the study of the phenomenon of Anderson localization. In fact, Anderson location of light in atomic gases requires very high densities or very large optical cross sections. Now, it is expected that, if the disorder is realized within periodic structures near the Bragg condition, the high density requirement is dramatically relaxed.

2. They modify the local density of states in a way to suppress spontaneous emission.

3. In optical lattices, unlike other systems, the scattering is very weak except when the light is tuned close to atomic resonances. Consequently, the expected forbidden bands are very narrow. This bears the advantage that we can adjust the optical density and tune the photon energy and the Bragg angle (i.e. the quasi-momentum) independently, which facilitates the mapping of the dispersion relation.

4. Crystals are always hampered by defects in the periodicity [733]. In latest-generation photonic crystals, the typical distance over which coherent light turns diffuse is limited to less than 20 μm. This limitation plays no role in optical lattices, where the delocalized photons rigorously guarantee perfect long-range order, even though the Debye-Waller factor may introduce local disorder.

Spectra of photonic bands in atomic clouds were detected experimentally [1158] in one-dimensional structures. Most of the above mentioned effects require omnidirectional photonic bands, but this is technically very difficult, mainly because of the narrow linewidth of the atomic transitions. We will develop this point in the course of this section. We also mention the prediction of forbidden photon bands in Bose condensates [852].

A presentation on this subject is available here (watch talk).

39.4.1 Bragg scattering

39.4.1.1 The reciprocal lattice

Let us consider a periodic *direct lattice* in real three-dimensional space whose elementary cells are located at positions,

$$\mathbf{R_n} = n_1\mathbf{a}_1 + n_2\mathbf{a}_2 + n_3\mathbf{a}_3 \ , \tag{39.162}$$

where $\mathbf{n} = (n_1, n_2, n_3)$ with $n_j \in \mathbb{Z}$ and $\mathbf{a}_j$ are linearly independent vectors describing the distance of two adjacent elementary cells [308]. Functions extended over the lattice, e.g. density distributions, are then supposed to be periodic,

$$n(\mathbf{r}) = n(\mathbf{r} + \mathbf{R_n}) \ , \tag{39.163}$$

such that they can be expanded in Fourier series similarly as we did for the introduction of the Bloch waves in Sec. 26.1,

$$n(\mathbf{r}) = \tfrac{1}{V}\sum_{\mathbf{m}} \rho_{\mathbf{m}} e^{\imath \mathbf{G_m}\cdot\mathbf{r}} \ , \tag{39.164}$$

where $\mathbf{m} = (m_1, m_2, m_3)$ with $m_j \in \mathbb{Z}$. The Fourier coefficients are [17],

$$\rho_{\mathbf{m}} = \int_0^{a_1}\int_0^{a_2}\int_0^{a_3} n(\mathbf{r}) e^{-2\pi\imath(m_1 x/a_1 + m_2 y/a_2 + m_3 z/a_3)} dxdydz = \int_0^1 n(\tilde{\mathbf{r}}) e^{2\pi\imath \mathbf{m}\cdot\tilde{\mathbf{r}}} d^3\tilde{r} \ . \tag{39.165}$$

[17] In crystallography $\rho_{\mathbf{m}}$ is called *structure factor*, but it is not to be confused with the structure factor defined in (39.5).

The condition (39.163) then yields,

$$n(\mathbf{r}) = \tfrac{1}{V}\sum_{\mathbf{m}} \rho_{\mathbf{m}} e^{\imath \mathbf{G_m}\cdot\mathbf{r}} = \tfrac{1}{V}\sum_{\mathbf{m}} \rho_{\mathbf{m}} e^{\imath \mathbf{G_m}\cdot\mathbf{r}} e^{\imath \mathbf{G_m}\cdot\mathbf{R_n}} = n(\mathbf{r}+\mathbf{R_n}) \ , \tag{39.166}$$

from which we conclude that the vectors $\mathbf{G_n}$ of the reciprocal lattice must satisfy,

$$\tfrac{1}{2\pi}\mathbf{G_m}\cdot\mathbf{R_n} \in \mathbb{Z} \ . \tag{39.167}$$

Example 232 (*The reciprocal lattice in crystallography*): In three dimensions the reciprocal lattice can be constructed by,

$$\begin{aligned} &\mathbf{G_m} = m_1\mathbf{b}_1 + m_2\mathbf{b}_2 + m_3\mathbf{b}_3 \qquad (39.168)\\ &\text{with} \quad \mathbf{b}_1 \equiv \frac{\mathbf{a}_2\times\mathbf{a}_3}{V} \quad , \quad \mathbf{b}_2 \equiv \frac{\mathbf{a}_3\times\mathbf{a}}{V} \quad , \quad \mathbf{b}_3 \equiv \frac{\mathbf{a}_1\times\mathbf{a}_2}{V} \\ &\text{and} \quad V \equiv \mathbf{a}_1\cdot(\mathbf{a}_2\times\mathbf{a}_3) \ . \end{aligned}$$

Knowing the density $n_1(\mathbf{r})$ within a single cell, which is often the case when the overlap between the density distributions of adjacent cells is negligible, we can write the global density distribution as,

$$\boxed{n(\mathbf{r}) = n_1(\mathbf{r}) \star \sum_{\mathbf{m}} \delta^{(3)}(\mathbf{r}-\mathbf{R_m})} \ . \tag{39.169}$$

Example 233 (*Elementary cell with Gaussian distribution*): With the ansatz $n_1(\mathbf{r}) = n_0 e^{-r^2/2\bar{r}^2}$, such that $\int n_1(\mathbf{r})d^3r = n_0(2\pi)^{3/2}\bar{r}^3 = N_1$,

$$\begin{aligned} \rho(\Delta\mathbf{k}) &= \sum_m e^{\imath m\Delta\mathbf{k}\cdot\mathbf{R}} \int_V n_1(\mathbf{r}) e^{\imath\Delta\mathbf{k}\cdot\mathbf{r}} d^3\mathbf{r} \qquad (39.170)\\ &= \frac{1-e^{\imath N_s\Delta kR}}{1-e^{\imath\Delta kR}} \times n_0 \int_V e^{-x^2/2\bar{r}^2} e^{-y^2/2\bar{r}^2} e^{-z^2/2\bar{r}^2} e^{\imath\Delta\mathbf{k}\cdot\mathbf{r}} d^3\mathbf{r} \\ &\approx N_s\delta(\Delta k - 2\pi/R) n_0 (2\pi)^{3/2}\bar{r}^3 e^{-6\Delta k^2\bar{r}^2} = N\delta(\Delta k - 2\pi/R) e^{-6\Delta k_x^2\bar{r}^2} \ . \end{aligned}$$

39.4.1.2 Impact of disorder in one-dimensional lattices

A wave be incident on a lattice in the direction $\mathbf{k}_0$ and scattered into the direction $\mathbf{k}_s \equiv \mathbf{k}_0 + \Delta\mathbf{k}$. The *structure coefficient* $\rho_{\mathbf{m}}$ describes the amplitude of radiation field scattered by the lattice,

$$\rho_{\mathbf{m}} = \int_V \rho(\mathbf{r}) e^{\imath\Delta\mathbf{k}\cdot\mathbf{r}} d^3\mathbf{r} \ . \tag{39.171}$$

Let the density distribution be,

$$n(\mathbf{r}) = \sum_j \rho_j(\mathbf{r}) \star \delta^{(3)}(\mathbf{r}-\mathbf{r}_j) = n_1(\mathbf{r}) \star \sum_j \delta(\mathbf{r} - j\hat{\mathbf{e}}_z \tfrac{\lambda_{dip}}{2}) \ , \tag{39.172}$$

that is, for perfect periodicity, introducing the density distribution of a unit cell and a $1D$ lattice.

The *Debye-Waller factor* describes the diffusion of the density over the sites of the lattice due to the thermal motion,

$$\begin{aligned}\overline{\rho_{\mathbf{m}}} &= \int_V n_1(\mathbf{r}) e^{\imath \Delta\mathbf{k}\cdot\mathbf{r}} d^3r \sum_j \overline{e^{\imath(j\hat{\mathbf{e}}_z\lambda_{dip}/2+\mathbf{u})\Delta\mathbf{k}}} \\ &= f_i \sum_j \overline{e^{\imath(j\hat{\mathbf{e}}_z\lambda_{dip}/2+\mathbf{u})\Delta\mathbf{k}}} = \rho_{\mathbf{m}} \overline{e^{\imath\mathbf{u}\Delta\mathbf{k}}} \ ,\end{aligned} \tag{39.173}$$

with

$$\overline{e^{\imath\mathbf{u}\Delta\mathbf{k}}} \approx e^{-|\mathbf{G}|^2\overline{u^2}/6} \ . \tag{39.174}$$

Example 234 (*Optical lattice*): The exponential distribution $e^{-6\Delta k_x^2 \bar{r}^2}$ is called Debye-Waller factor and describes the smearing out of the population over the lattice due to the thermal motion of the atoms. The δ-function sets the wavevector of emitted light. That is, the power of light is only emitted in particular directions given by the Bragg condition. Here, the solid angle $\Delta\Omega_s$ does not depend on the thermal distribution (as long as the atoms are within the Lamb-Dicke regime), but on the lattice size, which determines the goodness of the approximation of the Airy function (the sum in the above equation) by a Dirac δ-function. The width of the Airy function for a lattice of size w_0 is approximately $\Delta k = 2\sqrt{3}/w_0$. With this the solid angle is,

$$\Delta\Omega_s = \frac{12}{k^2 w_0^2} \ . \tag{39.175}$$

We can also estimate the solid angle from the diameter d of the Gaussian beam at a distance x away from a scattering medium of size w_0,

$$\begin{aligned} d &= w_0 \sqrt{1 + \left(\frac{\lambda x}{\pi w_0^2}\right)^2} \\ \Delta\Omega_s &= \frac{\pi d^2}{x^2} = \frac{\lambda^2}{\pi w_0^2} = \frac{4\pi}{k^2 w_0^2} \ . \end{aligned} \tag{39.176}$$

The power scattered into this solid angle is,

$$P_s = |A_s|^2 F^2 \Delta\Omega_s = |A_s|^2 e^{-2W} N^2 \Delta\Omega_s \ . \tag{39.177}$$

It depends quadratically on the number of atoms. Strictly speaking, the derivation only applies to perfectly ordered lattices, i.e. all the lattice sites are equally occupied. Defects lead to diffuse scattering, i.e. a background of isotropically distributed power at the expense of Bragg scattering. The sharpness of the Bragg radiation distribution remains intact.

We parametrize the density in an optical $1D$ lattice as follows:

$$\begin{aligned} n_l(\mathbf{r}) &= n_0 e^{(-x^2-y^2)/2\sigma_r^2} e^{-z^2/2\sigma_z^2} \\ n_a(\mathbf{r}) &= \sum_{m=1}^{N_s} \delta(\mathbf{r} - md\hat{\mathbf{e}}_z) \star n_l(\mathbf{r}) = \sum_{m=1}^{N_s} n_l(\mathbf{r} - md\hat{\mathbf{e}}_z) \ . \end{aligned} \tag{39.178}$$

We will show in Exc. 39.4.4.1, that the structure factor is then,

$$\boxed{\mathcal{S}_{\mathbf{k}_0}(\mathbf{k}) = \frac{n_0}{N}\frac{1-e^{\imath N_s dq_z}}{e^{-\imath dq_z}-1}e^{-q_x^2\sigma_r^2/2}e^{-q_y^2\sigma_r^2/2}e^{-q_z^2\sigma_z^2/2}} \ . \tag{39.179}$$

In Exc. 39.4.4.2 we derive the structure factor in spherical coordinates.

Some comments are needed:

1. The structure factor treatment assumes low optical density, which is not necessarily guaranteed when the laser is tuned close to a resonance [1219].

2. As the structure factor is independent of the laser detuning, it will not reveal any spectral structure, such as a band-gap or dip due to diffuse scattering. Also, absorption is not incorporated into the model.

39.4.1.3 The structure factor and the Bragg condition

The reciprocal space, obtained by Fourier transformation of the periodic density distribution, also adopts the shape of a periodic lattice. The Bragg condition requires that the difference between the incident and emitted wavevectors, $\Delta\mathbf{k} \equiv \mathbf{k}_s - \mathbf{k}_i$, matches a vector of the reciprocal lattice, $\mathbf{r}_j = j\mathbf{G}$. The Bragg condition is thus automatically incorporated into the structure factor (39.216).

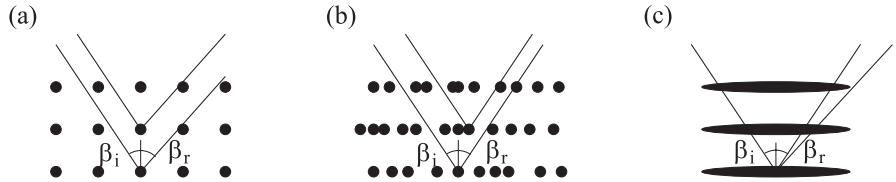

Figure 39.29: Several Bragg lattices.

With the lattice constant $d = \frac{1}{2}\lambda_{dip}$ the interference is constructive when the difference of the paths of two beams reflected by different layers is a multiple of the wavelength,

$$\tfrac{1}{2}\lambda_{dip}\cos\beta_i + \tfrac{1}{2}\lambda_{dip}\cos\beta_s = \lambda \ . \tag{39.180}$$

This is illustrated in Fig. 39.29(a). If the transverse distribution can be considered as homogeneous, as shown in Fig. 39.29(b), we have as second condition,

$$\beta_i = -\beta_s \ . \tag{39.181}$$

That is, the angles of incidence and reflection must be the same, as if we were dealing with a dielectric mirror. In contrast, if the transverse extent of the atomic layers gets smaller (until converging to the limit of a one-dimensional chain of point-scatterers, $\mathbf{G} \equiv 2k_{dip}\hat{\mathbf{e}}_z$), we return to the condition (39.180). In intermediate situations, illustrated in Fig. 39.29(c), and for $\lambda_{dip}\cos\beta_i \neq \lambda$ the reflection angle does not follow any of the relations (39.180) and (39.181).

39.4.1.4 Incoherent background

A finite size or defects in the periodic ordering of the atoms may lead to an isotropic background of Rayleigh-scattered light,

$$\frac{dP_s}{d\Omega_s} = |A_s|^2 \left[e^{-2W}|F|^2 + N_1 N(1 - e^{-2W})\right] \ . \tag{39.182}$$

The amount of photons scattered into the *same solid angle* as the one of Bragg scattering is typically for $1D$ lattices,

$$\frac{(1 - e^{-2W})N_1 N}{e^{-2W}|F|^2} = (e^{2W} - 1)\frac{N_1}{N} \approx 0.002 \ . \tag{39.183}$$

However, if we compare the total amount of coherently Bragg-scattered light, we obtain,

$$\frac{(1 - e^{-2W})N_1 N}{e^{-2W}|F|^2}\frac{4\pi}{d\Omega_s} \approx 2500 \ . \tag{39.184}$$

39.4.2 Transfer matrices calculation for $1D$-lattices

For one-dimensional optical lattices, that is, when the atoms are trapped in a potential dipole generated by a stationary light wave, we may consider applying the transfer matrix formalism developed in Secs. 18.1.7 and 24.3. The premisses of this model are the homogeneity and the infinite extent of the cloud in a direction transverse to the optical axis.

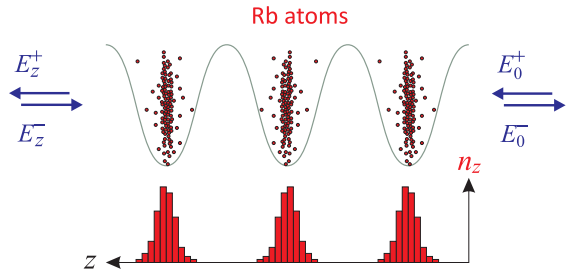

Figure 39.30: Scheme for transfer matrices calculations on $1D$-lattices.

With the notation introduced in Fig. 39.30 we find the equations relating the incident electric fields with the transmitted and reflected ones. If the T-matrix and the S-matrix are defined by [361],

$$\boxed{\begin{pmatrix} \mathcal{E}_z^+ \\ \mathcal{E}_0^- \end{pmatrix} = \mathcal{S}\begin{pmatrix} \mathcal{E}_0^+ \\ \mathcal{E}_z^- \end{pmatrix} \qquad \text{and} \qquad \begin{pmatrix} \mathcal{E}_z^+ \\ \mathcal{E}_z^- \end{pmatrix} = \mathcal{T}\begin{pmatrix} \mathcal{E}_0^+ \\ \mathcal{E}_0^- \end{pmatrix}}\ , \tag{39.185}$$

they are connected by,

$$\mathcal{S} = \begin{pmatrix} S_{11} & S_{12} \\ S_{21} & S_{22} \end{pmatrix} = \begin{pmatrix} T_{11} - \frac{T_{12}T_{21}}{T_{22}} & \frac{T_{12}}{T_{22}} \\ -\frac{T_{21}}{T_{22}} & \frac{1}{T_{22}} \end{pmatrix} \tag{39.186}$$

$$\text{and} \qquad \mathcal{T} = \begin{pmatrix} T_{11} & T_{12} \\ T_{21} & T_{22} \end{pmatrix} = \begin{pmatrix} S_{11} - \frac{S_{12}S_{21}}{S_{22}} & \frac{S_{12}}{S_{22}} \\ -\frac{S_{21}}{S_{22}} & \frac{1}{S_{22}} \end{pmatrix} .$$

From this follows,

$$\boxed{\mathcal{S} = \begin{pmatrix} t & r \\ r & t \end{pmatrix} \qquad \text{then} \qquad \mathcal{T} = \begin{pmatrix} t - \frac{r^2}{t} & \frac{r}{t} \\ -\frac{r}{t} & \frac{1}{t} \end{pmatrix}} , \tag{39.187}$$

satisfying by construction $\det \mathcal{S} = t^2 - r^2 \neq 1$ and $\det \mathcal{T} = 1$.

We calculate the reflection coefficient β of a classical polarizable sample from the microscopic polarizability (18.122) and the optical density (depth) of a thin layer, $n\delta z \sigma_0$, where σ_0 is the resonant optical cross section,

$$\beta = n\frac{k_{brg}\delta z}{2}\frac{\alpha_{pol}}{\varepsilon_0} = \frac{n\delta z}{2}\frac{6\pi}{k_{brg}^2}\frac{-1}{\imath + 2\Delta_{brg}/\Gamma} = \frac{n\delta z\sigma_0}{2}\frac{-1}{\imath + 2\Delta_{brg}/\Gamma} . \tag{39.188}$$

We remember that the polarizability is linked to the macroscopic susceptibility $\chi_e = n\alpha_{pol}/\varepsilon_0$ [18]. With

$$r = \frac{\imath\beta}{1 - \imath\beta} \qquad \text{and} \qquad t = \frac{1}{1 - \imath\beta} , \tag{39.189}$$

satisfying by construction $|t|^2 + |r|^2 = 1 = t - r$ and $rt^* + r^*t = 0$, we get

$$\boxed{\mathcal{S}_\beta = \frac{1}{1 - \imath\beta}\begin{pmatrix} 1 & \imath\beta \\ \imath\beta & 1 \end{pmatrix} \qquad \text{and} \qquad \mathcal{T}_\beta = \begin{pmatrix} 1 + \imath\beta & \imath\beta \\ -\imath\beta & 1 - \imath\beta \end{pmatrix}} . \tag{39.190}$$

We note that the employed model is classical, since we describe the gas by a sequence of layers, each characterized by a refractive index. Applying the transfer matrix model, we calculate how the incident and reflected light fields transform from one layer to another. The intrinsically 1D model allows to calculate the reflection, transmission, and absorption by the atomic lattice as a function of the incident laser frequency.

We still need to multiply with the transfer matrix describing the propagation of the incident beam through the layer,

$$\mathcal{T}_d = \begin{pmatrix} e^{\imath\mathbf{k}\cdot\mathbf{d}} & 0 \\ 0 & e^{-\imath\mathbf{k}\cdot\mathbf{d}} \end{pmatrix} , \tag{39.191}$$

[18] Note the analogy to the calculation (40.113) made for the reflection coefficient of an atom in a cavity in Sec. 40.2.2,

$$\beta = \frac{k}{\pi w^2}\frac{\alpha_{pol}}{\varepsilon_0} = \frac{6}{k^2w^2}\frac{-1}{2\Delta/\Gamma + \imath} = \frac{\sigma_0}{\pi w^2}\frac{-1}{2\Delta/\Gamma + \imath} .$$

such that the transfer matrix for passing the beam through an atomic layer is,

$$\mathcal{T} = \mathcal{T}_\beta \mathcal{T}_d \ . \tag{39.192}$$

For N_s layers we must obviously concatenate the matrices $\mathcal{M}^{N_s}$. The reflection coefficient is now simply,

$$r_{N_s} = \frac{(\mathcal{T}^{N_s})_{12}}{(\mathcal{T}^{N_s})_{22}} \ , \tag{39.193}$$

and can be evaluated numerically or analytically [361]. If the incident beam hits the cloud under an angle, $\mathbf{k}\cdot\mathbf{d} = kd\cos\theta = k_z d$, and furthermore, as shown in [363] Eq. (A10), the theory must be generalized by replacing,

$$\beta \to \frac{\beta}{2}(\cos^{-1}\theta + \cos\theta) \ . \tag{39.194}$$

However, for $\theta < 60^\circ$ the correction is small.

39.4.2.1 Limit of optically dilute clouds

For optically dilute clouds, $r \ll 1$, we expect standard Bragg scattering as described by equation (39.190),

$$\boxed{\mathcal{T} = \mathcal{T}_\beta \mathcal{T}_d \simeq \begin{pmatrix} e^{\imath k_z d} & \imath\beta e^{-\imath k_z d} \\ -\imath\beta e^{\imath k_z d} & e^{-\imath k_z d} \end{pmatrix}} \ , \tag{39.195}$$

with $\mathbf{k}\cdot\mathbf{d} = kd\cos\theta = k_z d$. Near the Bragg angle we have $\cos\theta \simeq \cos\theta_{brg} = \lambda_{sp}/\lambda_{dip}$ and near resonance we have $2\pi/k = \lambda \simeq \lambda_{sp}$, so that, with $d = \lambda_{dip}/2$, we obtain $k_z d \simeq \pi$ and,

$$\mathcal{T}^{N_s} \simeq \begin{pmatrix} e^{\imath\pi} & \imath\beta e^{-\imath\pi} \\ -\imath\beta e^{\imath\pi} & e^{-\imath\pi} \end{pmatrix}^{N_s} = \begin{pmatrix} -1 & -\imath\beta \\ \imath\beta & -1 \end{pmatrix}^{N_s} = (-1)^{N_s} \begin{pmatrix} 1 & N_s\imath\beta \\ -N_s\imath\beta & 1 \end{pmatrix} \ , \tag{39.196}$$

which we will verify in Exc. 39.4.4.3. The total reflectivity being $r_{N_s} \simeq N_s\imath\beta$, we get the reflection,

$$|r_{N_s}|^2 \simeq \frac{N_s^2\beta_{sp}^2\Gamma_{sp}^2}{4\Delta^2 + \Gamma_{sp}^2} \ . \tag{39.197}$$

Thus, the profile of the reflection curve is Lorentzian.

> **Example 235 (*Estimation of the reflectivity in the dilute cloud limit*):** In resonance we estimate for typical experimental values $N_s = 1000$, $n = 10^{17}\,\mathrm{cm}^3$, $\lambda_{dip} = 797\,\mathrm{nm}$, and $\Lambda_{brg} = 422\,\mathrm{nm}$,
>
> $$|r_{N_s}| = N_s\frac{nd\sigma_{sp}}{2} = N_s n\lambda_{dip}\frac{3\lambda_{sp}^2}{8\pi} \approx 1.7 \ .$$
>
> The high reflectivity is not physical, which shows that the assumption of optically diluted clouds is not necessarily satisfied in experimentally achievable parameter regimes. On the contrary we can expect to reach regimes, where the clouds are optically so dense, that photonic bands can be expected. That is, if the goal is to detect a band gap, it helps to have 1. many layers filled with atoms, 2. high atomic densities per layer.

39.4.2.2 Limit of optically dense clouds

In order to obtain analytical expressions in the regime of dense clouds, we write the transfer matrix for a single layer, using the expressions (39.190) and (39.191), as follows [363],

$$\boxed{\mathcal{T} = \mathcal{T}_\beta \mathcal{T}_d = \begin{pmatrix} (1+\imath\beta)e^{\imath \mathbf{k}\cdot\mathbf{d}} & \imath\beta e^{-\imath\mathbf{k}\cdot\mathbf{d}} \\ -\imath\beta e^{\imath\mathbf{k}\cdot\mathbf{d}} & (1-\imath\beta)e^{-\imath\mathbf{k}\cdot\mathbf{d}} \end{pmatrix}} \; . \tag{39.198}$$

Given that $\det \mathcal{T} = 1$, the matrix represents a unitary transformation and the eigenvalues can be cast into the form $e^{\pm\imath\phi}$. Letting,

$$\cos\Theta \equiv \tfrac{1}{2}\mathrm{Tr}\ \mathcal{T} = \cos k_z d - \beta \sin k_z d \; , \tag{39.199}$$

we can write the matrix,

$$\mathcal{T} = \mathbb{I}\cos\Theta + \imath A \sin\Theta = e^{\imath\Theta A} \tag{39.200}$$

with

$$A = \frac{1}{\sin\Theta}\begin{pmatrix} \beta\cos k_z d + \sin k_z d & \beta e^{-\imath k_z d} \\ -\beta e^{\imath k_z d} & -\beta\cos k_z d - \sin k_z d \end{pmatrix} \tag{39.201}$$

The eigenvectors of $\mathcal{T}$, and therefore of each power of $\mathcal{T}$, are *Bloch states of the periodic lattice*. We verify in Exc. 39.4.4.4, that the following relationships are satisfied,

$$\mathrm{Tr}\ A = 0 \quad , \quad A^2 = 1 \quad , \quad \det A = 1 \; . \tag{39.202}$$

The eigenvalues of $A\sin\Theta$ are $\lambda_A \pm 1$. The eigenvalues of the transfer matrix are,

$$\begin{aligned} \lambda &= \cos k_z d - \beta \sin k_z d \pm \imath\sqrt{1-(\cos k_z d - \beta\sin k_z d)^2} = \cos\Theta \pm \imath\sin\Theta \\ &= e^{\pm\imath \arccos(\cos k_z d - \beta \sin k_z d)} = e^{\pm\imath\theta} \; . \end{aligned} \tag{39.203}$$

This decomposition allows us to calculate the transfer matrix for a succession of μ layers. We get,

$$\begin{aligned} \mathcal{T}^\mu &= e^{\imath\mu\theta A} = \mathbb{I}\cos(\mu\theta) + \imath A \sin(\mu\theta) \\ &= \mathbb{I}\cos\left[\mu \arccos(\cos k_z d - \zeta \sin k_z d)\right] + iA\sin\left[\mu\arccos(\cos k_z d - \zeta\sin k_z d)\right] \; , \end{aligned} \tag{39.204}$$

which gives us the reflection coefficient,

$$\begin{aligned} r_\mu &= \frac{(\mathcal{T}^\mu)_{12}}{(\mathcal{T}^\mu)_{22}} = \frac{\imath\sin(\mu\theta)\mathcal{T}_{12}}{\cos(\mu\theta) + \imath\sin(\mu\theta)\mathcal{T}_{22}} \\ &= \frac{-\imath\beta e^{ik_z d}}{\sin\theta\cot(\mu\theta) - \imath\sin k_z d - \imath\beta\cos k_z d} \; . \end{aligned} \tag{39.205}$$

This is the final result. Near the Bragg angle, $\cos\theta \simeq 1$, we have,

$$\begin{aligned} r_{N_s} &= \frac{\imath\beta}{\sin\theta\cot(N_s\theta) - \imath\beta} \simeq \frac{\imath N_s\zeta}{1-\imath N_s\beta} \\ |r_{N_s}|^2 &\simeq \frac{N_s^2\beta_{sp}^2\Gamma_{sp}^2}{4\Delta^2 + (1+n\beta_{sp}^2)\Gamma_{sp}^2} \; . \end{aligned} \tag{39.206}$$

The intensity reflection profile, therefore, is a Lorentzian also in the limit of thick clouds. The additional condition for the occurrence of prohibited photonic bands is a large number of atomic layers, $N_s \gg 1$. We note that the model is an extension of the *Kronig-Penney model* introduced in Sec. 26.3.

39.4.2.3 Application of transfer matrices to real $1D$ optical lattices

The analytical treatment shown in the previous sections does not take account of possible lattice imperfections, since the atomic layers are assumed to be identical, infinitely thin, immobile and located at fixed periodic distances. Realistic optical lattices are different for several reasons:

1. Atomic clouds are not perfectly localized in ultra-thin layers, but distributed in a Gaussian way as a function of the cloud's temperature. The Debye-Waller factor (39.173) describes the impact of this distribution on the Bragg model.

2. The atoms are in thermal motion causing an inhomogeneous Doppler shift and are affected by the photonic recoil received in each scattering process. This causes a broadening of the reflection profiles and decreases the interference capability.

3. The number of atoms per layer may vary. Also, the global extent of the cloud is not infinite, that is, we have N_s layers filled with atoms with a gradual decrease at the confines of the cloud.

4. The atoms trapped in the optical potential are subjected to a dynamic Stark shift [19] causing an inhomogeneous broadening of the atomic transition as well.

5. The periodicity of the lattice is slightly modified because the refractive index experienced by the laser beams creating the dipole potential locally depends on the atomic density concentrated in the lattice's anti-nodes. The consequence is a local decrease of the lattice constant d [20].

All of the aforementioned imperfections may be included in a numerical treatment of the transfer matrices. For this we subdivide the atomic cloud into sufficiently thin sublayers, as shown in Fig. 39.30. Each sublayer, being characterized by its own 2D atomic density and its own shift from resonance, is described by an individual transfer matrix. The matrices are concatenated, and the reflection profile is computed, as shown in the expression (39.193) [1220]. Fig. 39.31 shows a numerical calculation of a photonic band in a rubidium optical lattice. The experimental variables are the incidence angle θ of the probe laser and its tuning Δ from a transition λ_{sp}. Δ determines σ and β via the polarizability (39.186) [21] and thus governs the propagation of light inside the layers. θ determines $k_z d$ and thus probes the periodicity *between* the layers.

Depending on the atomic density we can identify different behaviors [22]:

[19] Or 'light-shift', see Exc. 34.5.4.13.

[20] More correctly: If between λ_{dip} and λ_{D1} a photonic band were created for the laser beams that produce the optical lattice [363, 1360], these beams would be reflected without being able to penetrate the lattice. In fact, the periodicity changes in such a way, that the frequency of the beams is at the edge of the band gap. Deutsch *et al.* [363] showed that a self-consistent solution gives the modified lattice constant,

$$d' = \frac{\lambda_{dip}}{2}\left[1 + \frac{\phi_{dip}}{\pi}(1 - \mathrm{sign}\Delta_{dip})\right] ,$$

where $\phi_{dip} = \arctan\left(-\frac{\Delta_{dip}}{\Gamma} n d\, \sigma_{D1}(\Delta_{dip})\right)$.

[21] Δ also enters $k_z d$, but so weakly, that we can despise this dependence.

[22] The densities are assumed to be sufficiently low to eliminate collective effects such as, for example, superradiance.

1. At the limit of thin lattices, we do not expect multiple scattering. The absorptive (imaginary) part of polarizability dominates, $\beta \approx \mathfrak{Im}\ \beta$. Thus, the reflection coefficient is almost real, $re^{\imath\phi} \approx |r|$, the phase shifts are negligible, the profile of the reflection spectrum is symmetric. In this scheme, the interference of the radiation patterns of individual atoms is destructive in all directions, except under the Bragg angle. There are losses caused by scattering in non-paraxial modes. They are also due to elastic Rayleigh scattering but, because of the finite Debye-Waller factor, the radiation becomes diffuse and incoherent.

2. At the limit of thick lattices, we have multiple scattering. The (real) dispersive part of the polarizability is $\beta \approx \mathfrak{Re}\ \beta$. Thus, absorption is suppressed, we observe large phase shifts and the reflection spectrum profile is asymmetric. Multiple beam interference gives rise to global scattering.

Physically, the set parameters consistent of the quasi-momentum and the energy of the Bloch wave, (Θ, Δ), is more relevant because it allows analyzing the *dispersion relation* [23]. We observe the existence of energies Δ, where the real part of the quasi-momentum vanishes (modulo π). The 3D representation in Fig. 39.31(e) illustrates the occurrence of an *avoided crossing* due to the band gap at the edge of the Brillouin zone.

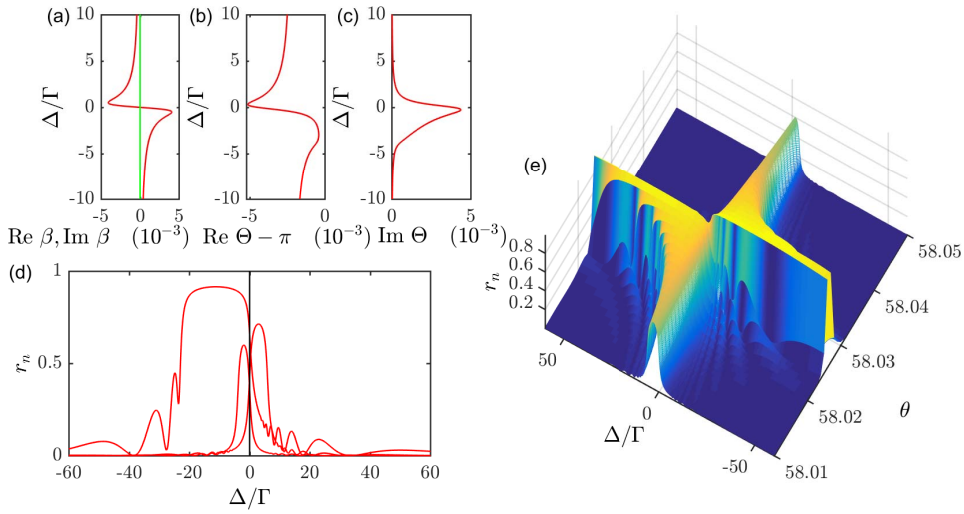

Figure 39.31: (code) Numerical calculation of a photonic band in a 1D optical lattice (wavelength $\Lambda_{dip} = 797$ nm) far-tuned from the rubidium D1 transition ($\lambda_{D1} = 795\,\text{nm}$). The probe laser exciting the Bragg resonance is tuned close to the rubidium resonance at $\lambda_{sp} = 422$ nm. We assume atomic densities of $n = 4 \cdot 10^{11}\,\text{cm}^{-3}$ and $N_s = 40000$ atomic layers. (a) Real and imaginary parts of the reflection index ($\propto$ polarizability) as a function of detuning Δ. (b,c) Real and imaginary parts of the quasi-momentum (x-axis) as a function of the detuning Δ. (d,e) 2D and 3D representation of the reflection coefficient.

[23] We note, that Θ via the relation (39.199) of the angle of incidence θ, but only weakly of the energy Δ.

In fact, Bragg resonances can be understood in reciprocal space as reflections at the edges of the Brillouin zone. Through the angle of incidence of the injected light beam, we adjust the quasi-momentum. The frequency of the light beam determines the energy. The forbidden photonic bands are caused by the formation of an energetic gap in the dispersion relation induced by the interaction of the atoms with the optical lattice.

39.4.2.4 Intensity distribution and LDOS within a lattice

The density matrix formalism outlined in Sec. 39.4.2 not only allows to calculate the overall reflectivity of the 1D optical lattice, but also the local intensity $I \propto |\mathcal{E}_a^+ + \mathcal{E}_a^-|^2$ at a point $z = a$ inside the lattice [1220].

To calculate this intensity we assume that the network is located between the points $z = 0$ and $z = b$ of the optical axis with $0 < a < b$. The transfer through the entire structure is given by,

$$\begin{pmatrix} \mathcal{E}_b^+ \\ \mathcal{E}_b^- \end{pmatrix} = \mathcal{T} \begin{pmatrix} \mathcal{E}_0^+ \\ \mathcal{E}_0^- \end{pmatrix} . \tag{39.207}$$

We use the boundary condition that, $\mathcal{E}_0^+$ being preset, there is no reflection of light behind the last layer, i.e., $\mathcal{E}_b^- = 0$. We obtain,

$$\mathcal{E}_0^- = -\frac{\mathcal{T}_{21}}{\mathcal{T}_{22}} \mathcal{E}_0^+ \qquad \text{and} \qquad \mathcal{E}_b^+ = \left(\mathcal{T}_{11} - \frac{\mathcal{T}_{12}\mathcal{T}_{21}}{\mathcal{T}_{22}} \right) \mathcal{E}_0^+ . \tag{39.208}$$

Now we separate the entire structure into two parts $\mathcal{T} = \mathcal{T}^{(b)}\mathcal{T}^{(a)}$, such that the field between the two parts is,

$$\begin{pmatrix} \mathcal{E}_1^+ \\ \mathcal{E}_1^- \end{pmatrix} = \mathcal{T}^{(a)} \begin{pmatrix} 1 \\ -\mathcal{T}_{21}/\mathcal{T}_{22} \end{pmatrix} \mathcal{E}_0^+ . \tag{39.209}$$

The sum gives,

$$\boxed{\mathcal{E}_1^+ + \mathcal{E}_1^- = \left(\mathcal{T}_{11}^{(a)} + \mathcal{T}_{21}^{(a)} - \frac{\mathcal{T}_{21}}{\mathcal{T}_{22}} (\mathcal{T}_{12}^{(a)} + \mathcal{T}_{22}^{(a)}) \right) \mathcal{E}_0^+} . \tag{39.210}$$

The *local density of states* (LDOS) in a photonic band can be evaluated from [1324, 507],

$$N(\omega) = 2\omega \sum_{\mathbf{k}} \delta(\omega^2 - \omega_{\mathbf{k}}^2) . \tag{39.211}$$

William found out:

$$k_{eff} = \frac{d\phi}{dz} , \tag{39.212}$$

with $\phi = \arctan(\mathfrak{Im}\ \mathcal{E}/\mathfrak{Re}\ \mathcal{E})$. The $\mathcal{E}$-field between two layers can be calculated using transfer matrices. The density of the states is given as the derivative of the inverse function of the dispersion relation:

$$N(\omega) = \frac{dk_{eff}(\omega)}{d\omega} . \tag{39.213}$$

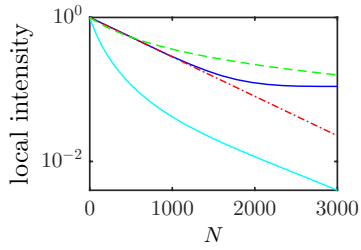

Figure 39.32: (code) The intensity decreases exponentially over a infinite lattice. For a finite lattice (here $N_s = 3000$), the intensity approaches a constant value at the end of the lattice. The graph shows in blue the intensity along the lattice, in red the exponential decay due to absorption in a homogeneous cloud (Lambert-Beer law), in green the hyperbolic decay following Ohm's law and in cyan the transmission assuming a lattice of N layers.

39.4.2.5 Suppression of spontaneous emission in forbidden photonic bands

The decrease in the LDOS is equivalent to the suppression of spontaneous emission [24], that is, an excited atom located inside the lattice will not be able to emit its photon. This is the condition for a forbidden photonic band to be *omnidimensional*. Omnidirectional bands need three-dimensional lattices. Nevertheless, the reduction of the spontaneous emission rate has already been observed in [596, 1387], which can be interpreted as $1D$ photonic crystals.

39.4.2.6 Impurities

The formula (39.210) allows the calculation of the impact of localized defects in numerical simulations. For example, it is instructive to look at the intensity profile along the structure in the presence of a localized lattice defect. In Fig. 39.33(c) we observe an intensity peak located at the 100-th atomic layer, exactly where the defect was introduced. This peak corresponds to a localized evanescent wave. Photons can not propagate freely through the lattice: they prefer to tunnel between lattice defects the rather than propagate by radiation.

The curves (a-b) of Fig. 39.33 illustrate how an empty photonic band fills up with localized states with well-defined energies when noise is added to the periodicity of the lattice. This situation is similar to that in semi-conductors doped by donor and acceptor states.

39.4.3 Photonic bands in the Bloch and the coupled dipoles models

The transfer matrix model is limited in several respects:

1. Firstly, being intrinsically 1D, the model does not apply to 2D or 3D lattices.

2. Also, it does not incorporate the possibility of transverse disorder or effects linked to the finite transverse extension of the atomic layers, for example, the

[24] For the same reason, resonant dipole-dipole interactions are suppressed [760].

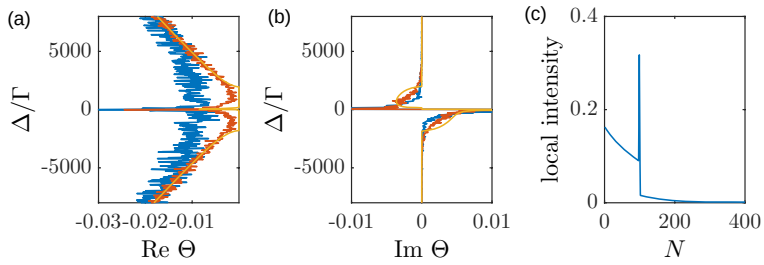

Figure 39.33: (code) (a,b) Dispersion relation as in Fig. 39.31, but in the presence of randomly distributed defects. (c) Intensity profile along the lattice with a defect located in the 100^{esima} atomic layer.

limitation of the number of layers participating in multiple reflection ('walk-off') [1221] or the impact of an imperfect mode matching [1219].

In contrast, the coupled dipoles model offers several advantages. An optical lattice is, after all, nothing more than a periodically ordered diluted sample of atoms. Hence, we can apply the coupled dipoles model introduced in Sec. 39.1.2 [1138, 1137]. The advantages of this model are its applicability to 3D systems and finite and disordered lattices. It also allows the inclusion of all kinds of inhomogeneities such as, for example, the spatial intensity distribution of a focused incident laser, or the deviation of the laser beam penetrating an atomic cloud due to refraction. On the other hand, the model only lends itself to heavy numerical simulations, limiting it to some 10000 atoms.

39.4.3.1 The Bloch model and forbidden electronic bands

The *Bloch model* is another model to describe 3D periodic systems [37]. It was introduced in Chp. 26 for 1D optical lattices. Its disadvantages are that it supposes infinite lattices and the absence of defects.

The Bloch model is commonly used to describe the scattering of electron waves in a solid, where the band gap originates from the Coulomb interaction of the electron with the atoms of the solid crystal. In contrast, in photonic crystals, the modes with high (low) frequency ω concentrate their energy in spatial regions with low (high) dielectric index ϵ. Close to geometric (Mie) resonances this causes a repulsion in the density distribution of photonic states, and the opening of a gap separating high frequency bands (air bands) from low frequency bands.

In optical lattices the photons interact with the atomic resonances. Photons and electrons are distinguished by their different dispersion relations and by the fact that electronic waves are scalar and photonic waves are vectorial. The electrons of a crystal are bound to an energy surface and follow the lines of the dispersion relation without leaving the metal. In contrast, photons are usually injected into the structure, which gives an additional degree of freedom. Therefore, any point in the phase diagram can be reached and the dispersion relation only informs, where at which point the transmission is stronger.

	photonic crystal	metal
lattice structure	atoms in a stationary wave	atoms in a crystal
particles	photons	electrons in a metal
equations of motion	Maxwell	Schrödinger
dispersion relation	$\hbar k/c$	$\hbar k^2/2m$
tune	Bragg angle and frequency	voltage
band gap origin	$\mathfrak{Im}\ \alpha$ absorption by atoms	e^- interacting with the atomic nuclei
band gap width	$< \omega_0 - \omega_{dip}$	interaction energy

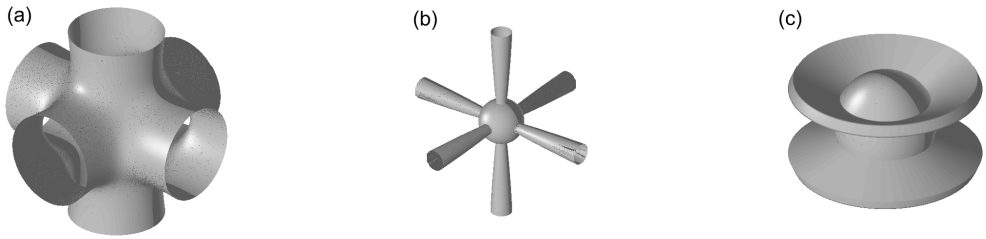

Figure 39.34: Attempt of an artistic illustration of the isoenergetic surfaces for electrons in a metal (left), photons in a 3D optical lattice (center), and photons in a 1D optical lattice (right). The interaction of atoms with the lattice is much weaker than the interaction of electrons with the metal, except close to resonances. Therefore, photonic bands are much narrower than electronic bands.

39.4.3.2 $3D$ photonic crystals

The reflection profile calculated in Fig. 39.31 resembles that of a dielectric mirror 18.6, for the calculation of which we also use the transfer matrix formalism. A dielectric coating consists of a periodic structure alternating high and low refractive index materials. Such structures are called *photonic crystals*.

The basic equation describing such material derives simply from Maxwell's equation, assuming macroscopic dielectric media, i.e., $\mathbf{D}(\mathbf{r}) = \varepsilon(\mathbf{r})\vec{\mathcal{E}}(\mathbf{r})$ with ε being real and scalar and $\mu \simeq 1$. After the expansion in $e^{\imath\omega t}$, we obtain a *master equation for dielectrics*,

$$\Theta\mathbf{H}(\mathbf{r}) \equiv \nabla \times \left(\frac{1}{\varepsilon(\mathbf{r})}\nabla \times \mathbf{H}(\mathbf{r})\right) = \frac{\omega^2}{c^2}\mathbf{H}(\mathbf{r}) \ , \tag{39.214}$$

with the condition of transversality $\nabla\mathbf{H}(\mathbf{r}) = 0 = \mathbf{D}(\mathbf{r})$ and $\vec{\mathcal{E}}(\mathbf{r}) = \left(\frac{-ic}{\omega\varepsilon(\mathbf{r})}\right)\nabla \times \mathbf{H}(\mathbf{r})$ [676]. The Θ operator is linear and Hermitian. We define the internal product analogously to quantum mechanics,

$$\langle \mathbf{F}|\mathbf{G}\rangle \equiv \int d\mathbf{r}\mathbf{F}(\mathbf{r})|\mathbf{G}(\mathbf{r}) \ . \tag{39.215}$$

The scalar product of modes with different frequencies vanishes, $\langle \mathbf{F}_{\omega_1}|\mathbf{G}_{\omega_2}\rangle = \delta_{\omega_1,\omega_2}$. The field can be found by minimizing the energy function $\frac{\langle \mathbf{H}|\Theta\mathbf{H}\rangle}{\langle \mathbf{H}|\mathbf{H}\rangle}$. We find that the displacement field $\langle \mathbf{D}\rangle$ is concentrated in regions, where $\epsilon(\mathbf{r})$ is large and is orthogonal to the lower frequency modes.

For periodic structures we can apply the reciprocal lattice theory in the same way as we do in solid-state physics or in optical lattices. But now, the state of Bloch is a vector: $\mathbf{H}_{\mathbf{k}}(\mathbf{r}) = e^{\imath \mathbf{k}\cdot\mathbf{r}} u_{\mathbf{k}}(\mathbf{r})$. Inserting in the master equation gives,

$$\Theta_{\mathbf{k}}\mathbf{u}_{\mathbf{k}}(\mathbf{r}) \equiv \left[(\imath\mathbf{k}+\nabla)\times\left(\frac{1}{\varepsilon(\mathbf{r})}(\imath\mathbf{k}+\nabla)\times\mathbf{u}_{\mathbf{k}}(\mathbf{r})\right)\right] = \frac{\omega(\mathbf{k})^2}{c^2}\mathbf{u}_{\mathbf{k}}(\mathbf{r}) \ , \tag{39.216}$$

together with $\mathbf{u}_{\mathbf{k}}(\mathbf{r}) = \mathbf{u}_{\mathbf{k}}(\mathbf{r}+\mathbf{r})$.

39.4.4 Exercises

39.4.4.1 Ex: Structure coefficient of a 1D lattice

Calculate the structure coefficient of the density distribution (39.178) and the square $|S_{\mathbf{k}_0}(\mathbf{k})|^2$.

Solution: *We calculate,*

$$\begin{aligned}
\mathcal{S}_{\mathbf{k}_0}(\mathbf{k}) &= \frac{1}{N}\int_{R^3} n_a(\mathbf{r}) e^{\imath(\mathbf{k}-\mathbf{k}_0)\cdot\mathbf{r}} d^3r \\
&= \frac{1}{N}\sum_{m=1}^{N_s} e^{\imath m d\mathbf{e}_z\cdot(k-\mathbf{k}_0)} \int_{R^3} n_l(\mathbf{r}) e^{\imath(\mathbf{k}-\mathbf{k}_0)\cdot\mathbf{r}} d^3r \\
&= \frac{1}{N} e^{\imath d\mathbf{e}_z\cdot(\mathbf{k}-\mathbf{k}_0)} \frac{1-e^{\imath N_s d\hat{\mathbf{e}}_z\cdot(\mathbf{k}-\mathbf{k}_0)}}{1-e^{\imath d\mathbf{e}_z\cdot(\mathbf{k}-\mathbf{k}_0)}} n_0 \int_{R^3} e^{(-x^2-y^2)/2\sigma_r^2} e^{-z^2/2\sigma_z^2} e^{\imath(\mathbf{k}-\mathbf{k}_0)\cdot\mathbf{r}} d^3r \\
&= \frac{n_0}{N}\frac{1-e^{\imath N_s dq_z}}{e^{-\imath dq_z}-1} \int_{-\infty}^{\infty} e^{-x^2/2\sigma_r^2} e^{\imath q_x x} dx \int_{-\infty}^{\infty} e^{-y^2/2\sigma_r^2} e^{\imath q_y y} dy \int_{-\infty}^{\infty} e^{-z^2/2\sigma_z^2} e^{\imath q_z z} dz \\
&= \frac{n_0}{N}\frac{1-e^{\imath N_s dq_z}}{e^{-\imath dq_z}-1} e^{-q_x^2\sigma_r^2/2} e^{-q_y^2\sigma_r^2/2} e^{-q_z^2\sigma_z^2/2} \ ,
\end{aligned}$$

and,

$$|\mathcal{S}_{\mathbf{k}_0}(\mathbf{k})|^2 = \frac{n_0^2}{N^2}\frac{1-\cos N_s(k_z-k_{0z})d}{1-\cos(k_z-k_{0z})d} e^{-(k_x-k_{0x})^2\sigma_r^2} e^{-(k_y-k_{0y})^2\sigma_r^2} e^{-(k_z-k_{0z})^2\sigma_z^2} \ .$$

39.4.4.2 Ex: Structure coefficient in spherical coordinates

Write the structure coefficient (39.178) in spherical coordinates.

Solution: *In spherical coordinates the structure coefficient can be written,*

$$\begin{aligned}
&\mathcal{S}_{k_0,\theta_0,0}(k_0,\theta,\phi)\\
&= \frac{1-e^{\imath N_s d(k_z-k_{0z})}}{1-e^{\imath d(k_z-k_{0z})}} e^{-(k_x-k_{0x})^2\sigma_r^2/2} e^{-(k_y-k_{0y})^2\sigma_r^2/2} e^{-(k_z-k_{0z})^2\sigma_z^2/2}\\
&= \frac{1-e^{\imath N_s d(k_0\cos\theta-k_0\cos\theta_0)}}{1-e^{\imath d(k_0\cos\theta-k_0\cos\theta_0)}} e^{-(k_0\cos\phi\sin\theta-k_0\cos\phi_0\sin\theta_0)^2\sigma_r^2/2}\times\\
&\quad\times e^{-(k_0\sin\phi\sin\theta-k_0\sin\phi_0\sin\theta_0)^2\sigma_r^2/2} e^{-(k_0\cos\theta-k_0\cos\theta_0)^2\sigma_z^2/2}\\
&= \frac{1-e^{\imath N_s dk_0(\cos\theta-\cos\theta_0)}}{1-e^{\imath dk_0(\cos\theta-\cos\theta_0)}} e^{-(\sin^2\theta-2\cos\phi\sin\theta\sin\theta_0+\sin^2\theta_0)k_0^2\sigma_r^2/2} e^{-(\cos\theta-\cos\theta_0)^2k_0^2\sigma_z^2/2} .
\end{aligned}$$

Assuming that we irradiate under the Bragg angle, $2dk_0\cos\theta_0 = 2\pi$, we obtain the solid angle into which light is scattered by,

$$\mathcal{S}_{k_0,\theta_{brg},0}(k_0,\theta,\phi) = \frac{1-e^{\imath N_s dk_0\cos\theta-\imath\pi N_s}}{1+e^{\imath dk_0\cos\theta}} \exp\left[-\left(\cos\theta-\frac{\pi}{dk_0}\right)^2\frac{k_0^2\sigma_z^2}{2}\right]\times$$
$$\times\exp\left[-\left(\sin^2\theta-2\cos\phi\sin\theta\sqrt{1-\left(\frac{\pi}{dk_0}\right)^2}+1-\left(\frac{\pi}{dk_0}\right)^2\right)\frac{k_0^2\sigma_r^2}{2}\right] .$$

39.4.4.3 Ex: Reflection in the dilute cloud limit

Verify the calculation (39.196).

Solution: *To calculate the total transfer matrix $\mathcal{T}^{N_s}$, we first diagonalize the matrix $\mathcal{T} = U\mathcal{D}U^{-1}$, where $\mathcal{D}$ is the matrix of eigenvalues and U a unitary transformation given by eigenvectors of $\mathcal{T}$. Under the Bragg angle this matrix adopts the form (39.190),*

$$\mathcal{T} = \begin{pmatrix} -1 & -\imath\beta \\ \imath\beta & -1 \end{pmatrix} .$$

We calculate,

$$U = \begin{pmatrix} -\imath & \imath \\ 1 & 1 \end{pmatrix} \qquad \textit{and} \qquad \mathcal{D} = \begin{pmatrix} -1+\beta & 0 \\ 0 & -1-\beta \end{pmatrix} .$$

We can now evaluate the transfer matrix for N_s layers,

$$\begin{aligned}
\mathcal{T}^{N_s} = U\mathcal{D}^{N_s}U^{-1} &\simeq (-1)^{N_s}\mathbf{U}\begin{pmatrix} 1-N_s\beta & 0 \\ 0 & 1+N_s\beta \end{pmatrix} U^{-1}\\
&= (-1)^{N_s}\begin{pmatrix} 1 & \imath N_s\beta \\ -\imath N_s\beta & 1 \end{pmatrix} .
\end{aligned}$$

For a finite Bragg angle we obtain,

$$\mathcal{T}^{N_s} = \begin{pmatrix} e^{\imath kd\cos\theta} & \imath\beta e^{-\imath kd\cos\theta} \\ -\imath\beta e^{\imath kd\cos\theta} & e^{-\imath kd\cos\theta} \end{pmatrix} ,$$

with the eigenvalues $\cos(kd\cos\theta) \pm \sqrt{\beta^2 - \sin^2(kd\cos\theta)}$.

39.4.4.4 Ex: Reflection in the dense cloud limit

Verify the representation (39.200).

Solution: *a. The expression (39.200) is composed of two parts. First, we compare the two sides of the equation,*

$$\begin{aligned}\mathcal{T} &= \begin{pmatrix} (1+\imath\beta)e^{\imath\mathbf{k}\cdot\mathbf{d}} & \imath\beta e^{-\imath\mathbf{k}\cdot\mathbf{d}} \\ -\imath\beta e^{\imath\mathbf{k}\cdot\mathbf{d}} & (1-\imath\beta)e^{-\imath\mathbf{k}\cdot\mathbf{d}} \end{pmatrix} \\ &= \begin{pmatrix} \cos k_z d - \beta\sin k_z d & 0 \\ 0 & \cos k_z d + \beta\sin k_z d \end{pmatrix} + \imath \begin{pmatrix} \beta\cos k_z d + \sin k_z d & \beta e^{-\imath k_z d} \\ -\beta e^{\imath k_z d} & -\beta\cos k_z d - \sin k_z d \end{pmatrix} \\ &= \mathbb{I}\cos\Theta + A\sin\Theta \ .\end{aligned}$$

Defining,

$$\begin{aligned}\cos\Theta &\equiv \cos k_z d - \beta\sin k_z d \\ \sin\Theta &= 1 - \cos\Theta = \sqrt{(\cos k_z d - \beta\sin k_z d)^2 - 1} \ ,\end{aligned}$$

it is easy to verify,

$$\begin{aligned} Tr\ A &= 0 \\ \det A &= -\frac{(1-\beta^2)\sin^2 k_z d + 2\beta\cos k_z d\sin k_z d}{\sin^2\Theta} = \frac{(\cos k_z d - \beta\sin k_z d)^2 - 1}{\sin^2\Theta} \equiv 1 \\ AA &= \frac{(1-\beta^2)\sin^2 k_z d + 2\beta\cos k_z d\sin k_z d}{\sin^2\Theta} \begin{pmatrix} 1 & 0 \\ 0 & 1 \end{pmatrix} = \mathbb{I} \ .\end{aligned}$$

b. Since the A matrix is nilpotent, $AA = \mathbb{I}$*, we calculate,*

$$\begin{aligned}\sin(\Theta A) &= A\sin\Theta = \Theta A - \frac{(\Theta A)^3}{3!} + ... = \Theta A - \frac{\Theta^3 A}{3!} + ... = A\sin\Theta \\ \cos(\Theta A) &= A\cos\Theta = 1 - \frac{(\Theta A)^2}{2!} + ... = 1 - \frac{\Theta^2 I}{2!} + ... = \imath\cos\Theta \ .\end{aligned}$$

39.4.4.5 Ex: Photonic band spectra

Plot the 1D-photonic band gap spectrum in a standing wave as a function of Δ_{pr} and n.

Solution: *The result is shown in Fig. 39.35.*

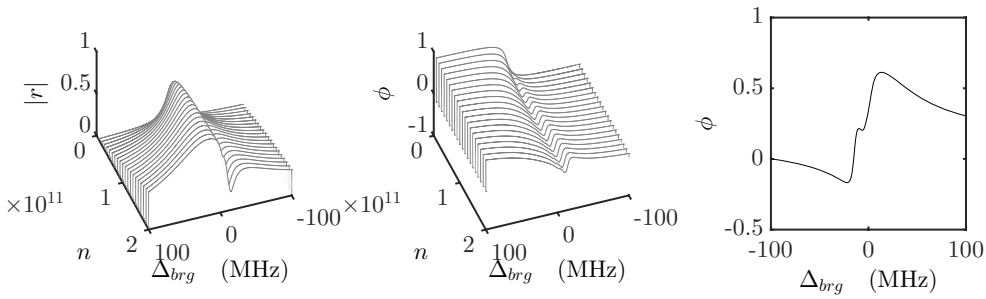

Figure 39.35: (code) 1D-photonic band gap spectrum in a standing wave as a function of Δ_{pr} and n.

39.4.4.6 Ex: Intensity drop inside photonic bands

Plot the intensity of the probe on its passage through the 1D optical lattice.

Solution: *The result is shown in Fig. 39.36.*

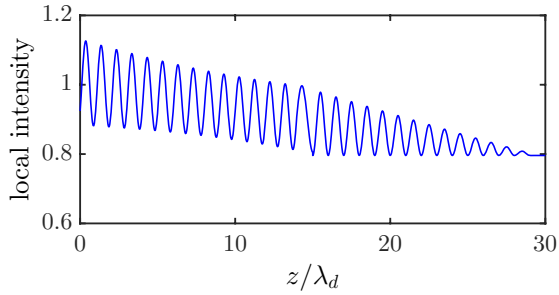

Figure 39.36: (code) Intensity of the probe on its passage through the 1D optical lattice.

39.4.4.7 Ex: Intensity drop inside photonic bands in the presence of disorder

Simulate the intensity of the probe on its passage through the 1D optical lattice inthe presence of disorder.

Solution: *The result is shown in Fig. 39.37.*

39.4.4.8 Ex: Photonic bands with sidebands

Plot the intensity of the probe on its passage through the 1D optical lattice as a function of detuning in the presence of modulation sidebands.

Solution: *The result is shown in Fig. 39.38.*

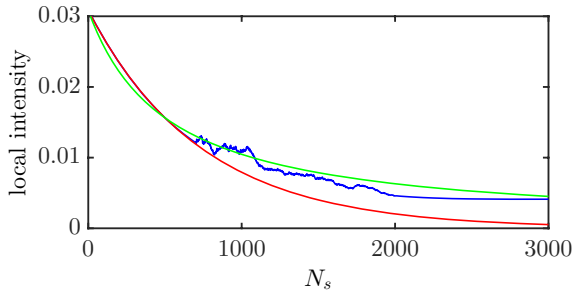

Figure 39.37: (code) Comparing the signatures of band gaps with absorption.

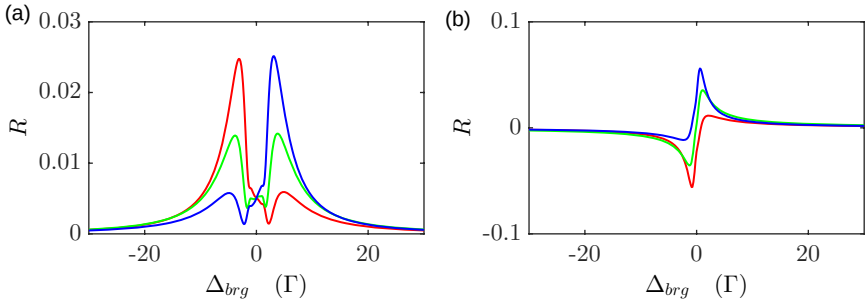

Figure 39.38: (code) Probing the band gap with MTS or FMS.

39.4.4.9 Ex: Photonic bands versus absorption

Compare the signatures of band gaps with absorption.

Solution: *The result is shown in Fig. 39.39.*

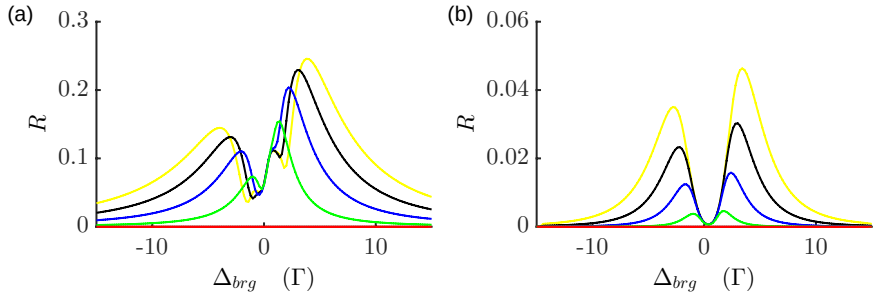

Figure 39.39: (code) Comparing the signatures of band gaps with absorption.

39.4.4.10 Ex: Structure of a diamond lattice

A geometric configuration of point-like scatterers that can exhibit a broad omnidirectional photonic bandgap is the one of a diamond lattice [273, 1146, 37]. In this exercise we will study such a diamond-shaped lattice.
a. Produce a geometric representation of the primitive cell and a Wigner-Seitz cell.
b. Study the optical lattice generated by the following configuration of incident lasers,

$$\mathbf{k}_0 = \tfrac{\pi}{a}(0,-2,-1) \quad , \quad \mathbf{k}_1 = \tfrac{\pi}{a}(2,0,1) \quad , \quad \mathbf{k}_2 = \tfrac{\pi}{a}(0,2,-1) \quad , \quad \mathbf{k}_3 = \tfrac{\pi}{a}(-2,0,1)$$

with $k_{laser} = \omega_{laser}/c = \sqrt{5}\pi/a$.
c. Calculate the forbidden band according to [273, 1146, 37].

Solution: *a. This configuration is based on the superposition of two fcc lattices [37],*

$$\hat{\mathbf{a}}_{1,2,3} = \left(0, \tfrac{a}{2}, \tfrac{a}{2}\right), \left(\tfrac{a}{2}, 0, \tfrac{a}{2}\right), \left(\tfrac{a}{2}, \tfrac{a}{2}, 0\right) \quad \textit{and} \quad \hat{\mathbf{a}}_{4,5,6} = \hat{\mathbf{e}}_{1,2,3} + \left(\tfrac{a}{4}, \tfrac{a}{4}, \tfrac{a}{4}\right) \ . \tag{39.217}$$

The vectors of the reciprocal lattice are obtained via,

$$\begin{pmatrix} b_{1x} & b_{2x} & b_{3x} \\ b_{1y} & b_{2y} & b_{3y} \\ b_{1z} & b_{2z} & b_{3z} \end{pmatrix}^{\mathsf{T}} 2\pi = \begin{pmatrix} a_{1x} & a_{2x} & a_{3x} \\ a_{1y} & a_{2y} & a_{3y} \\ a_{1z} & a_{2z} & a_{3z} \end{pmatrix}^{-1} \quad , \tag{39.218}$$

yielding,

$$\hat{\mathbf{b}} = \left(-\tfrac{2\pi}{a}, \tfrac{2\pi}{a}, \tfrac{2\pi}{a}\right), \left(\tfrac{2\pi}{a}, -\tfrac{2\pi}{a}, \tfrac{2\pi}{a}\right), \left(\tfrac{2\pi}{a}, \tfrac{2\pi}{a}, -\tfrac{2\pi}{a}\right) \ . \tag{39.219}$$

The Wigner-Seitz cell of the reciprocal lattice, referred as the first Brillouin zone, is bordered by faces which can be given as,

$$|k_x|+|k_y|+|k_z| = \tfrac{3}{2}\frac{2\pi}{a} \quad , \quad |k_x| = \frac{2\pi}{a} \quad , \quad |k_y| = \frac{2\pi}{a} \quad , \quad |k_z| = \frac{2\pi}{a} \ . \tag{39.220}$$

b. The optical lattice obtained is illustrated in Fig. 39.40(c). For large forbidden bands we choose $k_0 a < 5$, i.e. $\omega_{laser} > 1.4\omega_0$. This gives the intensity distribution in the optical lattice,

$$I(\mathbf{r}) = I_0 + I_1 \left[-\cos\left(\sum_{\gamma=1}^{3} \hat{\mathbf{e}}_\gamma \cdot \mathbf{r} \right) + \sum_{\gamma=1}^{3} \cos(\hat{\mathbf{e}}_\gamma \cdot \mathbf{r}) \right] \ . \tag{39.221}$$

c.

39.5 Further reading

39.5.1 on the coupled dipoles model

E. Akkermans et al., *Photon Localization and Dicke Superradiance in Atomic Gases* [15]DOI

R. Bachelard et al., *Cooperative scattering and radiation pressure force in dense atomic clouds* [458]DOI

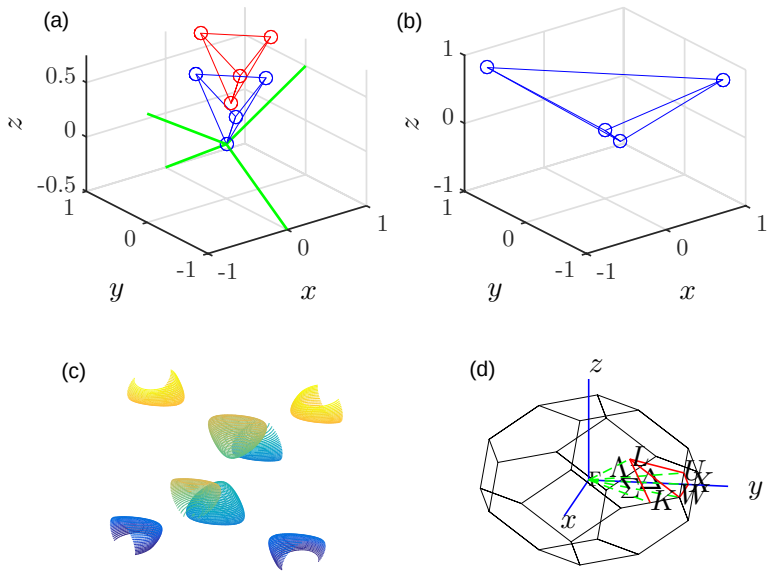

Figure 39.40: (code) Characterization of the diamond lattice. (a) laser configuration, (b) reciprocal space, (c) intensity distribution, and (d) Wigner-Seitz cell.

R. Bachelard et al., *Resonances in Mie scattering by an inhomogeneous atomic cloud* [67]DOI

R. Bachelard et al., *Collective effects in the radiation pressure force* [68]DOI

H. Bender et al., *Observation of cooperative Mie scattering from an ultracold atomic cloud* [120]DOI

T. Bienaimé et al., *Observation of cooperative radiation pressure in presence of disorder* [141]DOI

T. Bienaimé et al., *Atom and photon measurement in cooperative scattering by cold atoms* [142]DOI

T. Bienaimé et al., *Controlled Dicke Subradiance from a Large Cloud of Two-Level Systems* [143]DOI

R. Kaiser et al., *Quantum Multiple Scattering* [691]DOI

R. Friedberg et al., *Frequency shifts in emission and absorption by resonant systems ot two-level atoms* [467]DOI

R. Friedberg et al., *Effects of including the counterrotating term and virtual photons on the eigenfunctions and eigenvalues of a scalar photon collective emission theory* [468]DOI

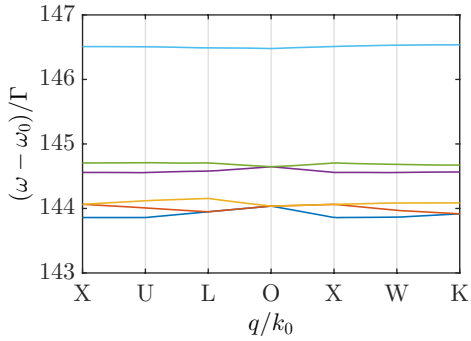

Figure 39.41: (code) Calculated forbidden bands (flawed).

R. Friedberg et al., *Reply to: Comment on: Effects of including the counterrotating term and virtual photons on the eigenfunctions and eigenvalues of a scalar photon collective emission theory; Phys. Lett. A 372 (2008) 2514; Phys. Lett. A 372 (2008) 5732* [469]DOI

R. Friedberg et al., *The dynamical Cooperative Lamb Shift in a system of two-level atoms* [836]DOI

R. Friedberg et al., *Cooperative Lamb shift in an ellipsoid* [470]DOI

M.O. Scully et al., *Directed Spontaneous Emission from an Extended Ensemble of N Atoms: Timing Is Everything* [1180]DOI

M.O. Scully et al., *The effects of the N atom collective Lamb shift on single photon superradiance* [1181]DOI

M.O. Scully et al., *The super of superradiance* [1182]DOI

M.O. Scully et al., *Collective Lamb Shift in Single Photon Dicke Superradiance* [1179]DOI

M.O. Scully et al., *The Lamb Shift-Yesterday, Today, and Tomorrow* [1183]DOI

A.A. Svidzinsky et al., *Dynamical Evolution of Correlated Spontaneous Emission of a from a Uniformly Excited Cloud of Atoms* [1284]DOI

A.A. Svidzinsky et al., *Cooperative spontaneous emission as a many-body eigenvalue problem* [1283]DOI

A.A. Svidzinsky et al., *Evolution of collective N atom states in single photon superradiance: Effect of virtual Lamb shift processes* [1286]DOI

A.A. Svidzinsky et al., *Cooperative spontaneous emission of N atoms: Many-body eigenstates, the effect of virtual Lamb shift processes, and analogy with radiation of N classical oscillators* [1285]DOI

J. Ruostekoski et al., *Lorentz-Lorenz shift in a Bose-Einstein condensate* [1119]DOI

R. Röhlsberger et al., *The collective Lamb shift in nuclear c-ray superradiance* [1111]$_{\text{DOI}}$

R. Röhlsberger et al., *Collective Lamb Shift in Single-Photon Superradiance* [1112]$_{\text{DOI}}$

S.E. Skipetrov et al., *Absence of Anderson Localization of Light in a Random Ensemble of Point Scatterers* [1215]$_{\text{DOI}}$

S.E. Skipetrov et al., *Red light for Anderson localization* [1213]$_{\text{DOI}}$

D. Pavolini et al., *Experimental evidence for subradiance* [1003]$_{\text{DOI}}$

C.E. Máximo et al., *Spatial and temporal localization of light in two dimensions* [859]$_{\text{DOI}}$

Ph.W. Courteille et al., *Modification of radiation pressure due to cooperative scattering of light* [298]$_{\text{DOI}}$

R.T. Sutherland et al., *Collective dipole-dipole interactions in an atomic array* [1280]$_{\text{DOI}}$

W.R. Garrett et al., *Large Multiple Collective Line Shifts Observed in Three-Photon Excitations of Xe* [494]$_{\text{DOI}}$

C.C. Kwong et al., *Cooperative Emission of a Coherent Superflash of Light* [766]$_{\text{DOI}}$

J. Keaveney et al., *Cooperative Lamb Shift in an Atomic Vapor Layer of Nanometer Thickness* [705]$_{\text{DOI}}$

E. Shahmoon et al., *Cooperative Resonances in Light Scattering from Two-Dimensional Atomic Arrays* [1188]$_{\text{DOI}}$

Ch. Weitenberg et al., *Coherent Light Scattering from a Two-Dimensional Mott Insulator* [1369]$_{\text{DOI}}$

39.5.2 on Bragg scattering

G. Birkl et al., *Bragg scattering from atoms in optical lattices* [146]$_{\text{DOI}}$

M. Weidemüller et al., *Bragg diffraction in an atomic lattice bound by light* [1361]$_{\text{DOI}}$

M. Weidemüller et al., *Local and global properties of light-bound atomic lattices investigated by Bragg diffraction* [1360]$_{\text{DOI}}$

S. Slama et al., *Dimensional crossover in Bragg scattering from an optical lattice* [1219]$_{\text{DOI}}$

S. Slama et al., *Multiple reflections and diffuse scattering in Bragg scattering at optical lattices* [1220]$_{\text{DOI}}$

39.5.3 on photonic bands

M. Woldeyohannes et al., *Coherent control of spontaneous emission near a photonic band edge* [1387]DOI

O. Toader et al., *Photonic band gap architectures for holographic lithography* [1311]DOI

G. Vandegrift et al., *The Moessbauer effect explained* [?]DOI

D. Mogilevtsev et al., *Light propagation and Anderson localization in disordered superlattices containing dispersive metamaterials Effects of correlated disorder* [908]DOI

M. Antezza et al., *Fano-Hopfield model and photonic band gaps for an arbitrary atomic lattice* [37]DOI

M. Antezza et al., *Spectrum of Light in a Quantum Fluctuating Periodic Structure* [38]DOI

M. Antezza et al., *Photonic band gap in an imperfect atomic diamond lattice: Penetration depth and effects of finite size and vacancies* [39]DOI

Deshui Yu, *Photonic band structure of the three-dimensional ^{88}Sr atomic lattice* [1414]DOI

D.V. van Coevorden et al., *Photonic band structure of atomic lattices* [1324]DOI

N.V. Cohan et al., *Band structure of diamond* [273]DOI

W. Saslow et al., *Band structure and optical properties of diamond* [1146]DOI

K. M. Ho et al., *Existence of a photonic gap in periodic dielectric structures* [621]DOI

K.I. Petsas et al., *Crystallography of optical lattices* [1024]DOI

I.H. Deutsch et al., *Photonic Band Gaps in Optical Lattices* [363]DOI

M. Artoni et al., *Resonantly absorbing one-dimensional photonic crystals* [48]DOI

G. Boedecker et al., *All-frequency effective medium theory of a photonic crystal* [158]DOI

M. Artoni et al., *Optically tunable photonic stop bands in homogeneous absorbing media* [47]DOI

A. Schilke et al., *Photonic Band Gaps in One-Dimensionally Ordered Cold Atomic Vapors* [1157]DOI

A. Schilke et al., *Optical parametric oscillation with distributed feedback in cold atoms* [1158]DOI

A. André et al., *Manipulating light pulses via dynamically controlled photonic band gap* [32]DOI

J.M. Bendickson et al., *Analytic expressions for the electromagnetic mode density in finite, one-dimensional, photonic band-gap structures* [?]DOI

D. Petrosyan, *Tunable photonic band gaps with coherently driven atoms in optical lattices* [1019]DOI

Jin-Hui Wu et al., *Controlling the photonic band structure of optically driven cold atoms* [1395]DOI

K. Ishizaki et al., *Realization of three-dimensional guiding of photons in photonic crystals* [652]DOI

D. Petrosyan, *Tunable photonic band gaps with coherently driven atoms in optical lattices* [1019]DOI

39.5.4 on noise analysis of Bragg scattering

M.O. Scully et al., *The Super of Superradiance* [1182]DOI

J. Chabé et al., *Experimental Observation of the Anderson Metal-Insulator Transition with Atomic Matter Waves* [245]DOI

I.B. Mekhov et al., *Cavity-Enhanced Light Scattering in Optical Lattices to Probe Atomic Quantum Statistics* [871]DOI

I.B. Mekhov et al., *Light scattering from ultracold atoms in optical lattices as an optical probe of atomic statistics* [873]DOI

I.B. Mekhov et al., *Quantum Nondemolition Measurements and State Preparation in Quantum Gases by Light Detection* [874]DOI

Ph.T. Ernst et al., *Probing superfluids in optical lattices by momentum-resolved Bragg spectroscopy* [419]DOI

Chapter 40

Coupling of atoms and optical cavities and the CQED regime

So far we have considered the coherent dynamics between atoms and radiation fields in free space, and we extended the theory to take into account the dissipative coupling to the electromagnetic vacuum by spontaneous emission and atomic motion. The vacuum represents a homogeneous and isotropic reservoir characterized by a continuous white energy spectrum. The situation changes completely when we place the atom inside an optical cavity which breaks the translational and rotational symmetries and imprints a resonance structure into the density of photonic states. Obviously, the cavity will profoundly change the atomic coupling to the electromagnetic vacuum, and hence the way in which the atom reacts to incident light, as much with respect to light scattering as with respect to optical forces.

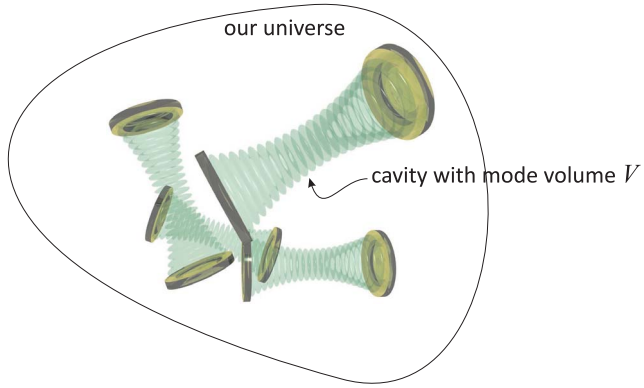

Figure 40.1: Illustration of the mode structure of empty space.

In this chapter we analyze the coupled dynamics of atoms interacting with the optical field modes of a cavity pumped by incident laser beams. We first concentrate in Sec. 40.1 on empty cavities. Then in Sec. 40.2 we turn our attention to the impact of atoms on the cavity dynamics, in particular its transmission spectrum. Cooperative and collective effects that may be induced by cavities will be discussed in Chps. 41

and 42.

40.1 Light fields in cavities without atoms

The quantization of the electromagnetic field has been introduced in Chp. 35. Nevertheless, we will consider the degree of freedom to be studied in this chapter, that is, the electric field amplitude of a light field developing in a mode of an optical cavity, as a classical entity. Therefore, there is no need to stress quantum mechanics to derive the fundamental equations of motion, and a classical derivation is shown in Sec. 40.2.5. Nevertheless, for reasons of consistency with later discussions, where quantization is required, we will reproduce here the standard procedure, which consists in constructing the Hamiltonian for the relevant degrees of freedom. The degree of freedom under study being a mode of a cavity, we will label it by the field operator $\hat{a}$ normalized to the electric field strength $\vec{\mathcal{E}}_1$ generated by a single photon, such that $|\langle\hat{a}\rangle|^2 = n$ represents the number of photons in the cavity.

In this first section of this chapter we will only consider a bare cavity not containing any matter which could interact with light. The mode of a linear cavity or the two counterpropagating modes of a ring cavity are pumped by incident laser light. We will first set up the equations of motion for the cavity fields and then discuss the main quantities characterizing a cavity, such as free spectral range, mode volume, decay rate, and single-photon field strength. Finally, we will calculate the density of states of cavities.

40.1.1 Master equation

The Hamiltonian of a laser-pumped linear cavity mode $\hat{a}$ coupled to the continuum of a heat bath represented by operators $\hat{a}_\omega$ is ($\hbar = 1$) (see Sec. 36.2.4 and Exc. 36.2.6.1),

$$\boxed{\begin{aligned}
\hat{H} &= \hat{H}_{cavity} + \hat{H}_{bath} + \hat{H}_{cavity:bath} + \hat{H}_{laser:cavity} \\
\hat{H}_{cavity} &= \omega_0 \hat{a}^\dagger \hat{a} \\
\hat{H}_{bath} &= \sum_\omega \omega \hat{a}^\dagger_\omega \hat{a}_\omega \\
\hat{H}_{cavity:bath} &= \sum_\omega g_{cavity:bath} \hat{a}^\dagger_\omega \hat{a} + h.c. \\
\hat{H}_{laser:cavity} &= \imath\eta \hat{a}^\dagger + h.c.
\end{aligned}} \quad , \tag{40.1}$$

with $[\hat{a}_\omega, \hat{a}^\dagger_{\omega'}] = \delta_{\omega,\omega'}$. The part of the Hamiltonian $\hat{H}_{laser:cavity}$ describes pumping of the cavity with an external light field matched to the cavity mode. The standard procedure consists in setting up the quantum Liouville equation for the total density operator $\hat{\rho}_{total} = \hat{\rho}_{cavity} \otimes \hat{\rho}_{bath}$ and tracing the over the bath's degrees of freedom [488, 283]. From this procedure, as shown in Sec. 36.2.4, we derive a master equation for the reduced density operator $\hat{\rho}_{cavity}$.

The inevitable coupling of the cavity to the environment, described by $\hat{H}_{cavity:bath}$, leads to irreversible losses. These losses can be described as spontaneous decay to the continuous vacuum heat bath. The irreversibility of the process is readily understood

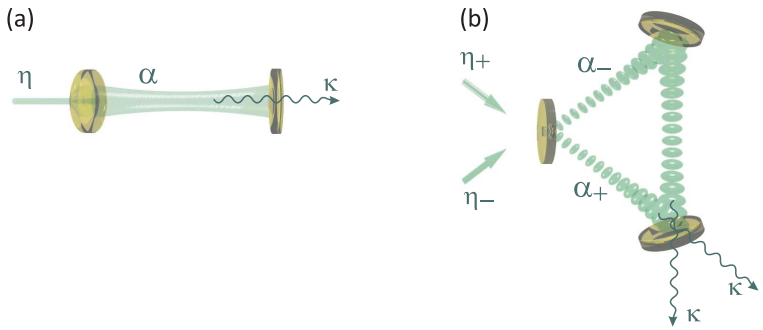

Figure 40.2: Scheme of (a) a linear cavity and (b) a ring cavity with optical modes $\alpha_\pm$ pumped by incident light fields $\eta_\pm$ and decaying into the void with rate κ.

in terms of the phase space offered by the vacuum being much larger. In fact, whenever discrete states are coupled to a continuum, the equilibrium is very much on the side of the continuum, that is, *discrete states decay*. Since an optical cavity can be considered a *temperature reservoir* T, where,

$$\bar{n} = \frac{1}{1 - e^{-\hbar\omega/k_B T)}} \ , \tag{40.2}$$

is the mean thermal photon number, the *Lindblad operator* is,

$$\begin{aligned} \mathcal{L}_{bath}\hat{\rho} = {} & \tfrac{\kappa}{2}(\bar{n}+1)(2\hat{a}\hat{\rho}\hat{a}^\dagger - \hat{a}^\dagger\hat{a}\hat{\rho} - \hat{\rho}\hat{a}^\dagger\hat{a}) + \tfrac{\kappa}{2}\bar{n}(2\hat{a}^\dagger\hat{\rho}\hat{a} - \hat{a}\hat{a}^\dagger\hat{\rho} - \hat{\rho}\hat{a}\hat{a}^\dagger) \\ & + \beta(2\bar{n}+1)(2\hat{a}^\dagger\hat{a}\hat{\rho}\hat{a}^\dagger\hat{a} - (\hat{a}^\dagger\hat{a})^2\hat{\rho} - \hat{\rho}(\hat{a}^\dagger\hat{a})^2) \ . \end{aligned} \tag{40.3}$$

We have already shown this in Exc. 36.2.6.1. The constants are the *cavity decay rate* κ and the pump rate β. Note that at room temperature in the microwave regime, $\bar{n}$ may be as large as a few hundred photons, whereas in the optical regime we may neglect the thermal excitation,

$$\boxed{\begin{aligned} \dot{\hat{\rho}} &= -\tfrac{\imath}{\hbar}[\hat{H},\hat{\rho}] + \mathcal{L}_{cav} \\ \mathcal{L}_{cav}\hat{\rho}(t) &= -\kappa\{\hat{a}^\dagger\hat{a}\hat{\rho}(t) - 2\hat{a}\rho(t)\hat{a}^\dagger + \hat{\rho}(t)\hat{a}^\dagger\hat{a}\} \end{aligned}} \ . \tag{40.4}$$

The expectation values are given by a *quantum Langevin equation* [283],

$$\boxed{\dot{\alpha} = \langle\dot{\hat{a}}\rangle = \frac{\imath}{\hbar}\langle[\hat{H},\hat{a}]\rangle - \kappa\langle\hat{a}\rangle = (-\kappa - \imath\Delta_c)\alpha + \eta} \ , \tag{40.5}$$

whose solution is easy to derive,

$$\boxed{\alpha(t) = \left(\alpha(0) - \frac{\eta}{\kappa + \imath\Delta_c}\right) e^{(-\kappa-\imath\Delta_c)t} + \frac{\eta}{\kappa + \imath\Delta_c}} \ , \tag{40.6}$$

or, using the electric field normalized to the amplitude of the field generated by a

single photon, $\vec{\mathcal{E}}^+_{cav} = \vec{\mathcal{E}}_1 \alpha$,

$$\begin{aligned}\vec{\mathcal{E}}_{cav}(z,t) &= \mathfrak{Re}\left[\vec{\mathcal{E}}_1 e^{\imath(kz-\omega t)}\alpha(t) + \vec{\mathcal{E}}_1 e^{\imath(-kz-\omega t)}\alpha(t)\right] \\ &= 2\vec{\mathcal{E}}_1 \cos kz \ \mathrm{Re}\left[e^{-\imath\omega t}\alpha(t)\right] \\ &= 2\vec{\mathcal{E}}_1 \cos kz \ \mathrm{Re}\left[\left(\alpha(0) - \frac{\eta}{\kappa + \imath\Delta_c}\right) e^{(-\kappa - \imath\omega_c)t} + \frac{\eta}{\kappa+\imath\Delta_c} e^{-\imath\omega t}\right] .\end{aligned} \tag{40.7}$$

The stationary solution is simply a Lorentzian,

$$|\alpha(\infty)|^2 = \frac{|\eta|^2}{\kappa^2 + \Delta_c^2} , \tag{40.8}$$

which represents an approximation of the Airy function(18.263).

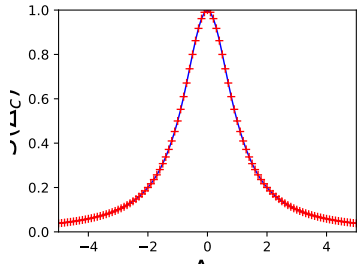

Figure 40.3: (code) Transmission spectrum of a cavity via numerical solution of the master equation (40.6) (solid line) and via the stationary solution (40.8) (crosses).

The result (40.7) shows that, letting $\eta = 0$, we see that the cavity field decays with the time constant κ from the stationary situation. κ also corresponds to the HWHM of the *field intensity*, $|\alpha(|\Delta_c| = \kappa)|^2 = \frac{1}{2}|\alpha(0)|^2$. Note, that the intensity decays as 2κ, and the HWHM of the *field amplitude* is $\left|\alpha(|\Delta_c| = \sqrt{3}\kappa)\right| = \frac{1}{2}|\alpha(0)|$.

> **Example 236 (*Evolution of the modes of a linear cavity*):** (40.7) also shows that a cavity initially filled with a strong resonant light field $|\alpha(0)| \gg \eta/\kappa$ begins to oscillate at its own frequency ω_c, before the pump dominates and imposes its own frequency ω. This is illustrated in Fig. 40.4. .

Frequently, we are interested in the light reflected from a cavity. The reflective response of the cavity to an incident pump beam E_{in} is,

$$\vec{\mathcal{E}}^+_{refl} = r_{in}\vec{\mathcal{E}}^+_{in} + t_{in}\vec{\mathcal{E}}^+_{cav} . \tag{40.9}$$

Also we may want to consider a temporal variation of the input field, for example of its detuning, $\Delta_c(t)$. In such cases, the equation (40.5) can not be integrated easily, and we need to resort to numerical methods. The simplest (and least convergent) method in a Newtonian iteration like,

$$\vec{\mathcal{E}}^+_{refl}(t+dt) = \vec{\mathcal{E}}^+_{refl}(t) + dt\ t_{in}\left[(-\kappa - \imath\Delta_c(t))\vec{\mathcal{E}}^+_{cav}(t) + \eta\vec{\mathcal{E}}^+_{in}(t)\right] . \tag{40.10}$$

We will study in Exc. 40.1.6.1 how a sudden change of the pump laser detuning may lead to *ringing* with a fixed frequency Δ_c. In Exc. 40.1.6.2 we will show, how it is possible to empty an optical cavity in times shorter than $1/\kappa$.

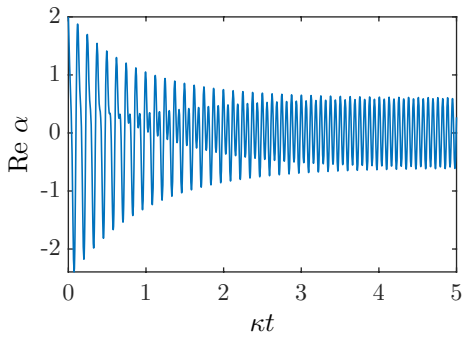

Figure 40.4: (code) Transient oscillations in a cavity pumped out of resonance.

40.1.2 Dynamics of an empty ring cavity

Linear cavities are characterized by the fact that they sustain standing light waves. That is, at every point of the mode volume, there are field components pointing into two counterpropagating orientations. In case of a ring cavity, we have two counterpropagating modes $\alpha_\pm$, which may be independently pumped by laser beams $\eta\pm$. Hence, the quantum Langevin equation (40.5) must be generalized to,

$$\boxed{\dot{\alpha}_\pm(t) = (-\kappa - \imath\Delta_c)\alpha_\pm + \eta_\pm} \,, \tag{40.11}$$

and the general solution (40.6) to,

$$\boxed{\alpha_\pm(t) = \left(\alpha_\pm(0) - \frac{\eta_\pm}{\kappa + \imath\Delta_c}\right) e^{(-\kappa-\imath\Delta_c)t} + \frac{\eta_\pm}{\kappa + \imath\Delta_c}} \,. \tag{40.12}$$

The two counterpropagating field modes will, provided they have the same polarization, interfere and form a standing light wave. In contrast to linear cavities, the phase of this standing wave is represents a degree of freedom, as it depends on the phases of the two field modes $\alpha_\pm$, which in turn can be controlled by the incident laser fields $\eta_\pm$. To better understand the behavior of the phase as a function of the pump beams, we analyze the interference of the two modes, which is described by,

$$\begin{aligned}\alpha_+\alpha_-^* = &\left(\alpha_+(0)\alpha_-^*(0) - \frac{\eta_-^*\alpha_+(0)}{\kappa - \imath\Delta_c} - \frac{\eta_+\alpha_-^*(0)}{\kappa + \imath\Delta_c} + \frac{\eta_+\eta_-^*}{\kappa^2 + \Delta_c^2}\right) e^{-2\kappa t} + \frac{\eta_+\eta_-^*}{\kappa^2 + \Delta_c^2} + \\ &+ \left(\alpha_+(0)\frac{\eta_-^*}{\kappa - \imath\Delta_c} - \frac{\eta_+\eta_-^*}{\kappa^2 + \Delta_c^2}\right) e^{(-\kappa-\imath\Delta_c)t} + \left(\alpha_-^*(0)\frac{\eta_+}{\kappa + \imath\Delta_c} - \frac{\eta_+\eta_-^*}{\kappa^2 + \Delta_c^2}\right) e^{(-\kappa+\imath\Delta_c)t} \,.\end{aligned} \tag{40.13}$$

To simplify this expression, we assume a symmetric pump, $\eta_\pm = \eta e^{\pm\imath\phi}$. We are interested in the reaction of the field's phase to a sudden change of ϕ. Now, we define the initial stationary conditions for $\phi = 0$ to be $\alpha_\pm(0) = \frac{\eta}{\kappa+\imath\Delta_c}$ and obtain,

$$\boxed{\alpha_+\alpha_-^* = \frac{\eta^2}{\kappa^2 + \Delta_c^2}\left[(1 - e^{\imath\phi})^2 e^{-2\kappa t} + e^{2\imath\phi} + 2e^{\imath\phi}(1 - e^{\imath\phi})e^{-\kappa t}\cos\Delta_c t\right]} \,. \tag{40.14}$$

In resonance, $\Delta_c = 0$, the expression (40.14) simplifies to,

$$\alpha_+\alpha_-^* = \frac{\eta^2}{\kappa^2}\left[(1 - e^{-\kappa t})e^{\imath\phi} + e^{-\kappa t}\right]^2 \,. \tag{40.15}$$

This results shows that the cavity phase adjusts itself to the pump field in exponential time κ^{-1}:

$$\tan\theta = \frac{\mathfrak{Im}\ \alpha_+\alpha_-^*}{\mathfrak{Re}\ \alpha_+\alpha_-^*} = \frac{(1-e^{-\kappa t})^2\sin 2\phi + 2(1-e^{-\kappa t})e^{-\kappa t}\sin\phi}{(1-e^{-\kappa t})^2\cos 2\phi + 2(1-e^{-\kappa t})e^{-\kappa t}\cos\phi + e^{-2\kappa t}} \ . \quad (40.16)$$

For small phase slips $\phi \ll \pi$, this reduces to,

$$\theta = 2\phi(1-e^{-\kappa t}) \quad , \quad \dot\theta \simeq \kappa(2\phi-\theta) \quad , \quad \ddot\theta \simeq -\kappa\dot\theta \ . \quad (40.17)$$

Hence, the pump represents a friction force for the phase.

Out of resonance but with negligible decay, $\kappa \simeq 0$, the expression (40.14) simplifies to,

$$\alpha_+\alpha_-^* = \frac{\eta^2}{\Delta_c^2}\left[1 + 2(e^{2\imath\phi} - e^{\imath\phi})(1-\cos\Delta_c t)\right] + \ , \quad (40.18)$$

such that,

$$\tan\theta = \frac{2(\sin 2\phi - \sin\phi)(1-\cos\Delta_c t)}{1 + 2(\cos 2\phi - \cos\phi)(1-\cos\Delta_c t)} \ , \quad (40.19)$$

which, for very small angles ϕ, reduces to,

$$\theta \simeq 4\phi\sin^2\frac{1}{2}\Delta_c t \ . \quad (40.20)$$

40.1.2.1 Transfer function of a ring cavity

Cavities have a finite response time to frequency or amplitude fluctuations of the pump light. To study this, we assume the light pumping a ring cavity to be subject to a phase modulation with frequency Ω and amplitude ϕ_0, that is, the quantum Langevin equation (40.5) is,

$$\boxed{(\partial_t + \kappa + \imath\Delta_c)\alpha_\pm = \eta e^{\pm\imath\phi_0\sin\Omega t}} \ , \quad (40.21)$$

and has the solution,

$$\alpha_\pm(t) = e^{(-\kappa-\imath\Delta_c)t}\left(\alpha_\pm(0) + \eta\int_0^T e^{(\kappa+\imath\Delta_c)\tau\pm\imath\phi_0\sin\Omega\tau}d\tau\right) \ . \quad (40.22)$$

For small amplitude oscillations, we can expand the pump term into a Fourier series of Bessel functions,

$$\begin{aligned}
\alpha_\pm(t) &= e^{(-\kappa-\imath\Delta_c)t}\left(\alpha_\pm(0) + \eta\int_0^T\left(e^{(\kappa+\imath\Delta_c)\tau} \pm \tfrac{\phi_0}{2}e^{(\kappa+\imath\Delta_c)\tau+\imath\Omega\tau} \mp \tfrac{\phi_0}{2}e^{(\kappa+\imath\Delta_c)\tau-\imath\Omega\tau}\right)d\tau\right) \\
&= e^{(-\kappa-\imath\Delta_c)t}\alpha_\pm(0) + \eta\frac{1-e^{(-\kappa-\imath\Delta_c)t}}{\kappa+\imath\Delta_c} \pm \tfrac{\phi_0}{2}\frac{e^{\imath\Omega t}-e^{(-\kappa-\imath\Delta_c)t}}{\kappa+\imath\Delta_c+\imath\Omega} \mp \tfrac{\phi_0}{2}\frac{e^{-\imath\Omega t}-e^{(-\kappa-\imath\Delta_c)t}}{\kappa+\imath\Delta_c-\imath\Omega} \\
&= \frac{\eta}{\kappa+\imath\Delta_c} \pm \tfrac{\phi_0\eta}{2}\frac{e^{\imath\Omega t}-e^{(-\kappa-\imath\Delta_c)t}}{\kappa+\imath\Delta_c+\imath\Omega} \mp \tfrac{\phi_0\eta}{2}\frac{e^{-\imath\Omega t}-e^{(-\kappa-\imath\Delta_c)t}}{\kappa+\imath\Delta_c-\imath\Omega} \\
&= \frac{\eta}{\kappa} \pm \imath\phi_0\eta\frac{\kappa\sin\Omega t - \Omega\cos\Omega t + \Omega e^{-\kappa t}}{\kappa^2+\Omega^2} \ .
\end{aligned} \quad (40.23)$$

In the last two steps, we defined for simplicity, $\alpha_\pm(0) = \frac{\eta}{\kappa + \imath\Delta_c}$ and set $\Delta_c = 0$. After some initial transients, when $t \gg \kappa^{-1}$, we can write,

$$\alpha_\pm \alpha_\pm^* = \frac{\eta^2}{\kappa^2} + \phi_0^2 \eta^2 \left(\frac{\kappa \sin \Omega t - \Omega \cos \Omega t}{\kappa^2 + \Omega^2} \right)^2 \tag{40.24}$$
$$\alpha_\pm \alpha_\mp^* = \left(\frac{\eta}{\kappa} \pm \imath \phi_0 \eta \frac{\kappa \sin \Omega t - \Omega \cos \Omega t}{\kappa^2 + \Omega^2} \right)^2 ,$$

giving in analogy to (40.16),

$$\theta = \arctan \frac{2\phi_0(\kappa^2 + \Omega^2)\left(\kappa^2 \sin \Omega t - \kappa\Omega \cos \Omega t\right)}{\left(\kappa^2 + \Omega^2\right)^2 - \phi_0^2 \left(\kappa^2 \sin \Omega t - \kappa\Omega \cos \Omega t\right)^2} \simeq 2\phi_0 \frac{\kappa^2 \sin \Omega t - \kappa\Omega \cos \Omega t}{\kappa^2 + \Omega^2} .$$

At low frequencies, $\Omega \ll \kappa$, the phase of the cavity field goes as, $\theta(\phi_0) \simeq 2\phi_0 \sin \Omega t$, and for high frequencies, $\Omega \gg \kappa$, as, $\theta(\phi_0) \simeq -2\phi_0 \frac{\kappa}{\Omega} \cos \Omega t$. Thus, we observe a low-pass behavior of the phase excursions of the cavity field with a cut-off frequency, κ^{-1}:

$$\boxed{\theta_m \simeq \frac{2\phi_0}{1 + \Omega/\kappa}} . \tag{40.25}$$

40.1.3 Characterization of the bare cavity

We first consider a linear cavity of length L pumped by a laser without any scatterer located inside the cavity. The cavity spectrum is an equidistant comb of eigenfrequencies separated by,

$$\delta_{fsr} \equiv \tau_{rt}^{-1} = \frac{c}{2L} . \tag{40.26}$$

The *free spectral range* δ_{fsr} is given in units of a real frequency. τ_{rt}^{-1} is the time for a photon to make a round trip in the cavity. The amplitude *decay rate of the cavity*,

$$\boxed{\kappa = \tau_\kappa^{-1} = \frac{\pi \delta_{fsr}}{F}} . \tag{40.27}$$

The intensity decay rate of the cavity, measured by 'cavity ring-down' is $\kappa_{int} = 2\kappa$. Note, that κ_{int} is also the FWHM width of the intensity transmission spectrum (see Exc. 18.3.7.18), such that the finesse

$$F = \frac{\delta_{fsr}}{\kappa_{int}/2\pi} \tag{40.28}$$

is simply the ratio between the free spectral range and the FWHM of the cavity intensity transmission curve, both measured in Hertz.

Example 237 (*Finesse of a cavity*): For example, for a cavity of length $L = 10$ cm an intensity decay time of $\tau_{int} = 20$ μs is measured, and we want to evaluate the finesse. We begin calculating the free spectral range $\delta_{fsr} = c/2L \approx 1.5$ GHz. Since the cavity field decays like $E(t) = E_0 e^{-\kappa t}$ and the intensity like $I(t) = E_0^2 e^{-2\kappa t}$, we get $\kappa = 1/\tau_\kappa = 1/2\tau_{int} \approx (2\pi)$ 4 kHz. Finally, the finesse is $F = \pi\delta_{fsr}/\kappa \approx 189000$.

For a cavity with a given geometry filled with a Gaussian mode of light with power P, the intensity is determined by Gaussian optics [1],

$$I(\mathbf{r}) = \frac{2P}{\pi w^2(z)} e^{-2\rho^2/w^2(z)} \qquad \text{and} \qquad w(z) = w_0\sqrt{1+\left(\frac{\lambda z}{\pi w_0^2}\right)^2} \ . \tag{40.29}$$

Defining the *mode volume* via $I(0)V_m \equiv \int I(\mathbf{r})dV$ and evaluating the spatial integral over the Gaussian mode along the cavity, we obtain,

$$\boxed{V_m = \frac{1}{I(0)}\int_0^L\int_0^\infty\int_0^{2\pi} \frac{2P}{\pi w^2(z)} e^{-2\rho^2/w^2(z)} d\phi\rho d\rho dz = \tfrac{\pi}{2} L w_0^2} \ . \tag{40.30}$$

Defining the amplitude of the electric field generated by a *single photon* via,

$$I(\mathbf{r}) = n\varepsilon_0 c\mathcal{E}_1^2(\mathbf{r}) \ , \tag{40.31}$$

where n is the number of photons in the cavity, we calculate for the energy stored in the cavity,

$$\frac{\hbar\omega}{2} = \int u_1(\mathbf{r})dV = \frac{1}{c}\int I_1(\mathbf{r})dV = \frac{1}{c} I_1(0)V_m \ . \tag{40.32}$$

Hence,

$$\boxed{|\vec{\mathcal{E}}_1(0)| = \sqrt{\frac{I_1(0)}{\varepsilon_0 c}} = \sqrt{\frac{\hbar\omega}{2\varepsilon_0 V_m}}} \ . \tag{40.33}$$

Resolve Exc. 18.4.4.2.The light power in the linear cavity can now be expressed using its free spectral range (40.26),

$$P = \frac{\pi w_0^2}{2} I(0) = \frac{2V_m}{L} n\varepsilon_0 c|\vec{\mathcal{E}}_1^2(0)| = 2V_m\delta_{fsr} n\varepsilon_0 \frac{\hbar\omega}{2\varepsilon_0 V_m} = \delta_{fsr} n\hbar\omega \ . \tag{40.34}$$

We assume that the cavity is pumped by a laser beam. To estimate the pump rate, we assume that the power P_{input} be measured in transmission. The coefficient η for resonant pumping is related to the number n of photons inside the cavity,

$$n = |\alpha|^2 = \frac{\eta^2}{\kappa^2} \ . \tag{40.35}$$

The intracavity field is resonantly amplified by the finesse,

$$\boxed{\alpha = \sqrt{\frac{F}{\pi}}\alpha_{input} = \sqrt{\frac{\delta_{fsr}}{\kappa}}\alpha_{input}} \ . \tag{40.36}$$

This gives,

$$\eta = \kappa\alpha = \kappa\sqrt{\frac{I}{c\hbar\omega}V_m} = \sqrt{\kappa\delta_{fsr}}\alpha_{input} = \sqrt{\kappa\delta_{fsr}}\sqrt{\frac{I_{input}}{c\hbar\omega}V_m} \ . \tag{40.37}$$

In practice, the pump rate will depend on the quality of the phase matching of the Gaussian beams and the impedance matching (in case of partially absorbing mirrors).

We will pursue the characterization of ring cavities including their interaction with scattering atoms in Sec. 40.2.2.

[1] See script on *Electrodynamics* (2023), Sec. 7.4.1 and Exc. 7.4.3.1.

40.1.3.1 The Schawlow-Townes limit

The *Schawlow-Townes limit* results from phase fluctuation of the standing light wave in the cavity demand $\Delta\phi = \frac{1}{n}$. Using the relationships (40.34) and (40.36), we find [1385],

$$\Delta\omega_{laser} = \frac{\kappa}{|\alpha|^2} = \kappa\frac{\delta_{fsr}\hbar\omega_{laser}}{P_{cav}} = \kappa\frac{\delta_{fsr}\hbar\omega_{laser}}{\frac{\delta_{fsr}}{\kappa}P_{out}} = \kappa^2\frac{\hbar\omega_{laser}}{P_{out}} \ . \tag{40.38}$$

Example 238 (*Schawlow-Townes limit of a HeNe laser*): For a typical HeNe laser, $F = 100$, $P_{out} = 1\,\mathrm{mW}$, $L = 20\,\mathrm{cm}$, we estimate,

$$\Delta\omega_{laser} = \left(\frac{\pi\delta_{fsr}}{F}\right)^2\frac{h\nu_{laser}}{P_{out}} = \left(\frac{\pi c}{2LF}\right)^2\frac{h\nu_{laser}}{P_{out}} \approx (2\pi)30\,\mathrm{mHz} \ .$$

40.1.4 Density of states in cavities

The density of states $\rho(\omega, \mathbf{k})$ of an optical cavity is defined by,

$$\int_{\mathcal{R}} \rho(\omega, \mathbf{k}) d\omega d\Omega = \frac{1}{(2\pi)^3}\int d^3\mathbf{x} d^3\mathbf{k} \ , \tag{40.39}$$

where $\mathcal{R}$ denotes the boundary imposed by the cavity. For free space photons we calculate (see Eq. (34.22)),

$$4\pi\int \rho_{free}(\omega, \mathbf{k}) d\omega = \frac{V}{(2\pi)^3}\int k^2 \sin\theta d\theta d\phi dk = \frac{Vk^3}{6\pi^2} = \frac{V\omega^3}{6\pi^2c^3} \ , \tag{40.40}$$

such that,

$$\rho_{free}(\omega, \mathbf{k}) = \rho_{free}(\omega) = \frac{V\omega^2}{(2\pi c)^3} \ , \tag{40.41}$$

is isotropic.

For light in a cavity, the density of states is modified with respect to free space, because it becomes frequency-dependent and anisotropic. The frequency dependence is expressed by the Airy formula,

$$\mathcal{L}(\omega) \equiv \frac{I_{cav}}{I_{in}} = \frac{\sqrt{1 + (2F/\pi)^2}}{1 + (2F/\pi)^2 \sin^2 kL} \ , \tag{40.42}$$

which will be derived in Excs. 40.1.6.3 and 40.1.6.4, and the anisotropy by,

$$\mathcal{R}(\hat{\mathbf{e}}_k) = 1 \qquad \forall \qquad \hat{\mathbf{e}}_k \in \Omega_{cav} \ , \tag{40.43}$$

where Ω_{cav} is the solid angle covered by the cavity mode. The formula,

$$\boxed{\rho_{cav}(\omega, \mathbf{k}) = \rho_{free}(\omega)[1 - \mathcal{R}(\hat{\mathbf{e}}_k)] + \rho_{free}(\omega)\mathcal{L}(\omega)\mathcal{R}(\hat{\mathbf{e}}_k)} \tag{40.44}$$

expresses that the density of states is nothing more than the *structure factor* of the cavity.

40.1.4.1 Confocal cavities

For a confocal cavity the solid angle is easy to calculate [596, 597]. Denoting by b is the clear aperture of the cavity mirrors, we get,

$$\Omega_{cav,con} = 2\int_0^{2\pi}\int_0^{\arcsin(2b/L)} \sin\theta d\theta d\phi = 4\pi\left(1-\sqrt{1-4\frac{b^2}{L^2}}\right) . \tag{40.45}$$

Expanding the root for small $b \ll L$, we get,

$$\boxed{\Omega_{cav,con} \simeq \frac{8\pi b^2}{L^2}} . \tag{40.46}$$

For non-degenerate geometries the functions $\mathcal{L}$ and $\mathcal{R}$ depend on the order mn of the transverse Gaussian modes:

$$\mathcal{L}_{mn}(\omega) = \frac{\sqrt{1+(2F/\pi)^2}}{1+(2F/\pi)^2\sin^2(kL+\varphi_{mn})} \qquad \text{and} \qquad \mathcal{R}_{mn}(\hat{\mathbf{e}}_k) = 1 \quad \forall \quad \hat{\mathbf{e}}_k \in \Omega_{mn} ,$$

where φ_{mn} is the frequency shift of the transverse modes.

40.1.4.2 Expansion into Hermite-Gaussian modes

More correctly, $\hat{\mathbf{e}}_k \in \Omega_{mn}$ means that we must weigh the density of states by the structure factor of the mode volume, which is nothing more than the Fourier transform of the cavity mode function,

$$\boxed{\mathcal{R}_{mn}(\hat{\mathbf{e}}_k) = \int_{\hat{\mathbf{e}}_k\in\Omega_{mn}} d^2k = \int_{\mathbb{R}^2} \mathcal{F}\left[\frac{u_{mn}(\mathbf{r})}{\hbar\omega}\right] d^2k} . \tag{40.47}$$

For a Hermite-Gaussian mode with waist $w(z)$ [see (18.313)],

$$u_{mn}(\mathbf{r}) = \hbar\omega\frac{w_0}{w}e^{-2(x^2+y^2)/w^2}H_m(\sqrt{2}x/w)^2H_n(\sqrt{2}y/w)^2 . \tag{40.48}$$

The Hermite polynomials are the eigenfunctions of the Fourier transform,

$$\mathcal{F}[e^{-x^2/2}H_n(x)] = (-\imath)^n e^{-k^2/2}H_n(k) . \tag{40.49}$$

Hence,

$$\begin{aligned}\mathcal{F}\left[\tfrac{1}{\hbar\omega}u_{mn}(\mathbf{r})\right] &= \frac{1}{\hbar\omega}\frac{w_0}{w}\mathcal{F}\left[e^{-2(x^2+y^2)/w^2}H_m(\sqrt{2}x/w)^2H_n(\sqrt{2}y/w)^2\right] \qquad (40.50)\\ &= \frac{1}{\hbar\omega}\frac{w_0}{w}\mathcal{F}\left[e^{-2x^2/w^2}H_m(\sqrt{2}x/w)^2\right]\mathcal{F}\left[e^{-2y^2/w^2}H_n(\sqrt{2}y/w)^2\right]\\ &= \frac{1}{\hbar\omega}\frac{w_0}{w}e^{-2k_x^2w^2}H_m(\sqrt{2}k_xw)^2e^{-2k_y^2w^2}H_n(\sqrt{2}k_yw)^2 \overset{m,n=0}{\longrightarrow} \frac{1}{\hbar\omega}\frac{w_0}{w}e^{-2\left(k_x^2+k_y^2\right)w^2} .\end{aligned}$$

Finally,

$$\begin{aligned}\mathcal{R}_{mn}(\hat{\mathbf{e}}_k) &= \int \mathcal{F}\left[\frac{u_{mn}(\mathbf{r})}{\hbar\omega}\right] d\left(\tfrac{k_x}{k}\right) d\left(\tfrac{k_y}{k}\right) \qquad (40.51)\\ &= \frac{1}{\hbar\omega}\frac{w_0}{w}\int e^{-2k_x^2w^2}H_m(\sqrt{2}k_xw)^2 d\left(\tfrac{k_x}{k}\right)\int e^{-2k_y^2w^2}H_n(\sqrt{2}k_yw)^2 d\left(\tfrac{k_y}{k}\right) .\end{aligned}$$

For the TEM_{00} mode, we get,

$$\mathcal{R}_{00}(\hat{\mathbf{e}}_k) = \frac{\pi}{2k^2w^2} \ , \tag{40.52}$$

using $P = \int I_{mn}(\mathbf{r})dxdy = \frac{1}{2}\pi w^2 I_0$. This coincides with the intuition, that for the TEM_{00}, the aperture is simply the divergence angle of the Gaussian mode.

The solid angle of a Gaussian mode in a non-degenerate cavity is calculated via,

$$\Omega_{cav} = 2 \cdot \frac{\pi w(z)^2}{z^2} = 2 \cdot \frac{\pi w_0^2}{z^2}\left(1 + \left(\frac{\lambda z}{\pi w_0^2}\right)^2\right) \ . \tag{40.53}$$

In the far field, we get,

$$\boxed{\Omega_{cav} \overset{z\to\infty}{\longrightarrow} \frac{8\pi}{k^2w_0^2}} \ . \tag{40.54}$$

Example 239 (*Solid angle for Hermite-Gaussian modes in a confocal cavity*): For confocal cavities, we must add $\sum_{mn}\mathcal{F}\left[\frac{1}{\hbar\omega}u_{mn}(\mathbf{r})\right]$ up to a limit, where the maximum $H_m(\sqrt{2}kw)$ is cut by the finite aperture of the mirrors of the cavity. Empirically, we find that $H_n(\xi)^2e^{-\xi^2}$ has its maximum at $\xi_{\max} = 13.7 \cdot n^{1/2}$. From the condition $u_{mn}(x, y, L) = 0$ for $xy > a^2$, we obtain,

$$x_{\max}y_{\max} < a^2$$
$$\left(13.7 \cdot n^{1/2}\right)^2 = \frac{\sqrt{2}x_{\max}}{w(L)}\frac{\sqrt{2}y_{\max}}{w(L)} < \frac{2a^2}{w(L)^2} \to \frac{a^2k^2w_0^2}{2L^2} \ ,$$

using $w(L) = w_0\sqrt{1 + \left(\frac{\lambda L}{\pi w_0^2}\right)^2} \to \frac{\lambda L}{\pi w_0}$. Finally,

$$\sum_{mn}\mathcal{F}\left[\frac{1}{\hbar\omega}u_{mn}(\mathbf{r})\right] = \frac{\pi}{2k^2w^2}\sum_{13.7^2 m,n<a^2k^2w_0^2/2L^2} = \frac{\pi}{2k^2w^2}\frac{1}{13.7^2}\frac{a^2k^2w_0^2}{2L^2} = \frac{1}{13.7^2}\frac{\pi a^2}{4L^2} \ .$$

40.1.5 Cumulant expansion of correlation functions and power spectra

40.1.5.1 Correlation functions

The evolution of the two-time correlation function of two operators $\hat{A}$ and $\hat{B}$ given by,

$$R(t,\tau) \equiv \langle\hat{A}(t+\tau)\hat{B}(t)\rangle \quad , \quad R(\tau) = \lim_{t\to\infty}\langle\hat{A}(t+\tau)\hat{B}(t)\rangle \ , \tag{40.55}$$

with respect to the time delay τ is determined by,

$$\frac{d}{d\tau}R(t,\tau) = \langle[\partial_\tau\hat{A}(t+\tau)]\hat{B}(t)\rangle \ . \tag{40.56}$$

Hence, the set of equations required to compute the correlation function can be derived from the equation of motion for the operator $\hat{A}$. The cumulant expansion of the correlation function then follows the same procedure as for a standard time evolution: the set of equations is expanded to a certain order and completed.

40.1.5.2 Steady state

If the original system is evolved up to a time t such that it is in steady state, i.e. expectation values no longer change after that time, the set of equations determining the correlation function has a special property. specifically, after the cumulant expansion has been performed, there can only be a single term in each product on the right-hand-side of the set of equations that depends on τ. All other terms depend on t alone, meaning that they are constant since they no longer change after the time t. Therefore, the system of equations from which the correlation function is computed is linear, in the sense that it can be written as,

$$\frac{d}{d\tau}\mathbf{y}(\tau) = \mathbf{M}\mathbf{y}(\tau) + \mathbf{d} \ , \tag{40.57}$$

where $\mathbf{y}(\tau)$ is the vector of τ-dependent variables. The elements of the matrix $\mathbf{M}$ as well as the vector $\mathbf{d}$ are given by steady-state expectation values and parameters, i.e. they are independent of τ.

40.1.5.3 Power spectra

According to the Wiener-Khinchin theorem. the spectral density associated with a correlation function is given by its Fourier transform,

$$S(t,\omega) = 2\mathfrak{Re} \int e^{-\imath\omega\tau} R(t,\tau) d\tau \ . \tag{40.58}$$

In order to compute this, we can solve the system of equations determining $R(t,\tau)$, subsequently taking the Fourier transform. However, if we are not interested in the temporal behavior of the correlation function, and if the system of which we want to compute the spectrum is in steady state, we can directly compute the spectrum from Eq. (40.57). To this end, we define

$$\mathbf{x}(s) = \mathcal{L}[y(\tau)] \ , \tag{40.59}$$

where $\mathcal{L}$ denotes the Laplace transform with respect to τ. Taking the Laplace transform of Eq. (40.57), we have,

$$(s\mathbb{I} - \mathbf{M})\mathbf{x}(s) = \mathbf{y}(0) + \frac{\mathbf{d}}{s} \ . \tag{40.60}$$

Note that the Laplace transform is equivalent to the Fourier transform at the point where $s = \imath\omega$, i.e. $S(\omega) = 2\mathfrak{Re}\ \mathbf{x}_1(\imath\omega)\}$. Hence, instead of computing the time evolution of the correlation function we can directly compute the spectrum by solving the linear equation,

$$\mathbf{x} = (\imath\omega\mathbb{I} - \mathbf{M})^{-1}[\mathbf{y}(0) + \tfrac{1}{\imath\omega}\mathbf{d}] \ . \tag{40.61}$$

For larger systems, the method using a Laplace transform is usually faster than integrating a system of equations of the same size. Additionally, it avoids numerical errors of the integration and the subsequent discrete Fourier transform.

40.1.6 Exercises

40.1.6.1 Ex: Quick ullage of an optical cavity

Consider a linear cavity resonantly pumped by a laser beam until a stationary state is reached. Suddenly, the phase of the incident light is changed by 180°. Based on equation (40.6), analyze the evolution of the light field inside the cavity.

Solution: *We have seen in class that the evolution of the light field in the cavity is given by (40.6). We now assume that the cavity is initially filled with the amplitude,*

$$\alpha(0) \equiv \frac{\eta_1}{\kappa + \imath\Delta_c} \ .$$

Suddenly, we change the phase and amplitude of the pumping wave, $\eta_1 \longrightarrow \eta_2$. The amplitude now evolves as,

$$\alpha(t) = (\alpha(0) - \frac{\eta_2}{\kappa + \imath\Delta_c})e^{(-\kappa - \imath\Delta_c)t} + \frac{\eta_2}{\kappa + \imath\Delta_c} = \frac{\eta_1 - \eta_2}{\kappa + \imath\Delta_c}e^{(-\kappa - \imath\Delta_c)t} + \frac{\eta_2}{\kappa + \imath\Delta_c} \ .$$

Therefore, the light amplitude vanishes at time,

$$t_0 = \frac{1}{\kappa + \imath\Delta_c} \ln \frac{\eta_2 - \eta_1}{\eta_2} \ .$$

Choosing $\eta_2 = -c\eta_1$ with large c we can minimize the time t_0.

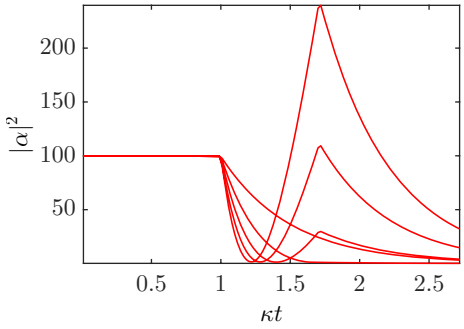

Figure 40.5: (code) Quick ullage of an optical cavity.

40.1.6.2 Ex: Ringing of an optical cavity

Consider a linear cavity with resonant frequency ω_c and the decay rate κ pumped by a laser beam whose frequency is swept linearly over a range $\omega \in [-10\kappa, 10\kappa]$. Prepare a numerical simulation varying the time Δt of the sweep.

Solution: *See Fig. 40.6.*

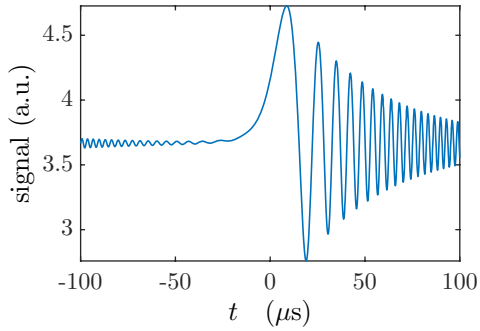

Figure 40.6: (code) Sweeping the laser frequency which pumps a cavity.

40.1.6.3 Ex: Derivation of the Airy formula

Derive the Airy formula (40.42).

Solution: *The electric field inside a cavity is,*

$$\mathcal{E}_{cav} = \mathcal{E}_{in} t_1 \frac{e^{\imath kx} - r_2 e^{\imath k(2L-x)}}{1 - r_1 r_2 e^{\imath k 2L}} \ .$$

This has been shown in Exc. 18.3.7.18. From this we calculate,

$$\mathcal{L}(\omega) = \frac{I_{cav}}{I_{in}} = t_1^2 \left| \frac{e^{\imath kx} - r_2 e^{\imath k(2L-x)}}{1 - r_1 r_2 e^{\imath k 2L}} \right|^2 = t_1^2 \frac{1 + r_2^2 - 2r_2 \cos(2k(L-x))}{1 + r_1^2 r_2^2 - 2r_1 r_2 \cos k2L} \ .$$

Averaging over the cavity field along the optical axis coordinate x, the cosine term in the numerator vanishes. Hence the expression simplifies to,

$$\mathcal{L}(\omega) = t_1^2 \frac{1 + r_2^2}{(1 - r_1 r_2)^2 + 4 r_1 r_2 \sin^2 kL} \ .$$

Assuming $r_1 = r_2 = \sqrt{R}$ and $t_1^2 = T = 1 - R$, we get,

$$\frac{I_{cav}}{I_{in}} = \frac{T}{1-R} \frac{\frac{1+R}{1-R}}{1 + \frac{4R}{(1-R)^2} \sin^2 kL} = \frac{\sqrt{1 + \left(\frac{2F}{\pi}\right)^2}}{1 + \left(\frac{2F}{\pi}\right)^2 \sin^2 kL} \ ,$$

using $F = \frac{\pi\sqrt{R}}{1-R}$. For sufficiently high finesse and close to resonance,

$$\frac{I_{cav}}{I_{in}} \simeq \frac{\frac{2F}{\pi}}{1 + \left(\frac{2F}{\pi}\right)^2 \sin^2 kL} \simeq \frac{\frac{2F}{\pi}}{1 + \left(\frac{2F}{\pi}\right)^2 (\frac{\Delta}{2\delta_{fsr}})^2} = \frac{\delta_{fsr} \kappa_{int}}{\Delta^2 + \left(\frac{\kappa_{int}}{2}\right)^2} \ ,$$

with

$$kL = \pi N + \frac{\Delta}{2\delta_{fsr}} \qquad \textit{and} \qquad F = \frac{\delta_{fsr}}{\kappa_{int}/2\pi} \ .$$

40.1.6.4 Ex: Airy formula for ring cavities

Derive the Airy formulas for a ring cavity laser-pumped through an incoupling mirror with reflectivity r_{ic} and comprising two more high-reflecting mirrors with reflectivity r_{hr}. Calculate (a) the intracavity intensity, (b) the intensity of the light reflected from the incoupler, and (c) the intensity of the light transmitted through the first encountered high reflector. For each for intensity study the cases that (i) the ring cavity is resonant and (ii) off-resonance. Also study the limit $r_{hr} \to 1$. Disregard absorption losses.

Solution: *a. The intracavity cavity field amplitude and intensity are,*

$$\frac{\mathcal{E}_{cav}(z)}{\mathcal{E}_{in}} = t_{ic}\sum_n (-r_{hr}^2 r_{ic})^n e^{\imath k(nL+x)} = t_{ic}\frac{e^{\imath kx}}{1+r_{ic}r_{hr}^2 e^{\imath kL}}$$
$$\frac{I_{cav}(z)}{I_{in}} = \frac{T_{ic}}{1+R_{hr}^2 R_{ic}+2R_{hr}\sqrt{R_{ic}}\cos kL} \ .$$

On resonance, $kL = \pi(2n+1)$,

$$\frac{I_{cav}^{(res)}(z)}{I_{in}} = \frac{1-R_{ic}}{(1-R_{hr}\sqrt{R_{ic}})^2} \overset{R_{hr}=1}{\longrightarrow} \frac{1+\sqrt{R_{ic}}}{1-\sqrt{R_{ic}}} \simeq \frac{2}{1-\sqrt{R_{ic}}} \gg 1 \ ,$$

and off resonance, $kL = \pi 2n$,

$$\frac{I_{cav}^{(off)}(z)}{I_{in}} = \frac{1-R_{ic}}{(1+R_{hr}\sqrt{R_{ic}})^2} \overset{R_{hr}=1}{\longrightarrow} \frac{1-\sqrt{R_{ic}}}{1+\sqrt{R_{ic}}} \simeq \frac{1-\sqrt{R_{ic}}}{2} \approx 0 \ .$$

b. The light amplitude and intensity reflected from the incoupler are,

$$\frac{\mathcal{E}_{rfl}(z)}{\mathcal{E}_{in}} = r_{ic} + t_{ic}r_{hr}^2 e^{\imath kL}\sum_n (-r_{ic}r_{hr}^2)^n e^{\imath nkL} t_{ic} = r_{ic} + \frac{t_{ic}^2 r_{hr}^2 e^{\imath kL}}{1+r_{ic}r_{hr}^2 e^{\imath kL}}$$
$$\frac{I_{rfl}(z)}{I_{in}} = \frac{R_{ic}+R_{hr}^2+2R_{hr}^2\sqrt{R_{ic}}\cos kL}{1+R_{hr}^2 R_{ic}+2R_{hr}\sqrt{R_{ic}}\cos kL} \ .$$

On resonance, $kL = \pi(2n+1)$,

$$\frac{I_{rfl}^{(res)}(z)}{I_{in}} = \frac{R_{ic}+R_{hr}^2-2R_{hr}^2\sqrt{R_{ic}}}{1+R_{hr}^2 R_{ic}-2R_{hr}\sqrt{R_{ic}}} \overset{R_{hr}=1}{\longrightarrow} 1 \ ,$$

and off resonance, $kL = \pi 2n$,

$$\frac{I_{rfl}^{(off)}(z)}{I_{in}} = \frac{R_{ic}+R_{hr}^2+2R_{hr}^2\sqrt{R_{ic}}}{1+R_{hr}^2 R_{ic}+2R_{hr}\sqrt{R_{ic}}} \overset{R_{hr}=1}{\longrightarrow} 1 \ .$$

c. The light amplitude and intensity transmitted through the first encountered high reflector are,

$$\frac{\mathcal{E}_{trns}(z)}{\mathcal{E}_{in}} = t_{ic}t_{hr}e^{\imath ka} + t_{ic}\sum_n (-r_{hr}^2 r_{ic})^n e^{\imath k(nL+a)} t_{hr} = t_{ic}t_{hr}e^{\imath ka}\left(1+\frac{1}{1+r_{ic}r_{hr}^2 e^{\imath kL}}\right)$$
$$\frac{I_{trns}(z)}{I_{in}} = T_{ic}T_{hr}\frac{4+R_{hr}^2 R_{ic}+4R_{hr}\sqrt{R_{ic}}\cos kL}{1+R_{hr}^2 R_{ic}+2R_{hr}\sqrt{R_{ic}}\cos kL} \ .$$

On resonance, $kL = \pi(2n+1)$,

$$\frac{I^{(res)}_{trns}(z)}{I_{in}} = T_{ic}T_{hr}\frac{R_{ic}+R^2_{hr}-2R^2_{hr}\sqrt{R_{ic}}}{1+R^2_{hr}R_{ic}-2R_{hr}\sqrt{R_{ic}}} \overset{R_{hr}=1}{\longrightarrow} T_{hr}\left(2-\sqrt{R_{ic}}\right)^2\frac{1+\sqrt{R_{ic}}}{1-\sqrt{R_{ic}}} \simeq T_{hr}\frac{I^{(res)}_{cav}(z)}{I_{in}} ,$$

and off resonance, $kL = \pi 2n$,

$$\frac{I^{(off)}_{trns}(z)}{I_{in}} = T_{ic}T_{hr}\frac{4+R^2_{hr}R_{ic}+4R_{hr}\sqrt{R_{ic}}}{1+R^2_{hr}R_{ic}+2R_{hr}\sqrt{R_{ic}}} \overset{R_{hr}=1}{\longrightarrow} \frac{9}{4}T_{ic}T_{hr} .$$

40.1.6.5 Ex: Filling rate for long cavities

Using the solution (40.6) try to calculate the transmission of a 15 km long cavity of finesse $F = 1000$ as a function of time, when it is pumped by a suddenly switched on laser. Analyze the results in the light of local causality.

Solution: *The free spectral range is $\delta_{fsr} = c/2L = 30\,\mathrm{kHz}$, the round-trip time $\tau_{rt} = \delta^{-1}_{fsr} = 0.33\,\mathrm{ms}$, the cavity linewidth $\kappa = \pi\delta_{fsr}/F = (2\pi)\ 15\,\mathrm{kHz}$, and the cavity decay time $\tau_\kappa = \kappa^{-1} = 10.6\,\mathrm{ms}$. Assuming resonance, $\Delta_c = 0$, the solution (40.6) predicts position-independent filling of the cavity at a rate $|\eta/\kappa|^2$. That is, we expect instantaneous transfer of information over a long distance, which is not possible. This means, that we must generalize the calculation leading to the solution (40.6).*
The problem is, that the single resonant mode assumption becomes invalid when the mode spacing is small and the step due to the sudden pump power increase so steep that is involves a large band of Fourier components, which can transiently excite several cavity modes.
The step response can be obtained as the Laplace transform of the frequency-dependent transfer function [1417, 489](see Sec. 56.2.1). The transfer function for transmission is just the Airy function, as shown in Exc. 18.3.7.18,

$$\mathcal{E}_{trns} = \mathcal{E}_{in}\frac{(1-R)e^{\imath kL}}{1-Re^{2\imath kL}} \simeq \mathcal{E}_{in}\sum_N \frac{1}{1+2\imath\Delta_c/\kappa} ,$$

with $\Delta_{c,N} \equiv \omega - \omega_N \equiv \omega - N2\pi\delta_{fsr}$ is the detuning from the N-th cavity ω_N. We describe the incident light by an oscillation suddenly switched on a time $t = 0$,

$$\mathcal{E}_{in}(t) = \mathcal{E}_0\theta(t)e^{\imath\omega t} .$$

Using the rules for the Laplace transform, $\mathcal{L}[\theta(t)] = \frac{1}{s}$ and $\mathcal{L}[e^{\imath\omega t}f(t)] = (\mathcal{L}f)(s-\imath\omega)]$, we get for the Laplace transform of this step signal,

$$\mathcal{L}[\mathcal{E}_{in}(t)] = \frac{\mathcal{E}_0}{s-\imath\omega} ,$$

showing that the sudden switch-on leads to a transient spectral broadening. In reality the broadening depends on the switching time constant γ^{-1}: the faster the switching, the larger the broadening. The general response of the cavity in transmission is,

$$\mathcal{E}_{trns}(t) = T_{Airy}(t) \star \mathcal{E}_{in}(t) ,$$

where the Laplace transform of the response function $T_{Airy}(t)$ is nothing else than the cavity's Airy function,

$$\mathcal{L}[T_{Airy}(t)] \equiv T_{Airy}(\omega) = \frac{\mathcal{E}_{trns}(\omega)}{\mathcal{E}_{in}(\omega)} \simeq \sum_N \frac{\kappa/2}{\kappa/2 + \imath\omega - \imath\omega_N} \ .$$

With these informations, we calculate,

$$\begin{aligned}\mathcal{E}_{trns}(t) &= \mathcal{L}^{-1}\left\{\mathcal{L}[T_{Airy}(t) \star \mathcal{E}_{in}(t)]\right\} = \mathcal{L}^{-1}\left\{\mathcal{L}[T_{Airy}(t)] \cdot \mathcal{L}[\mathcal{E}_{in}(t)]\right\} \\ &= \mathcal{E}_0 \sum_N \mathcal{L}^{-1}\left[\frac{\kappa/2}{\kappa/2 + s - \imath\omega_N} \cdot \frac{1}{s - \imath\omega_N}\right] \ .\end{aligned}$$

For simplicity, let us consider a single cavity mode labeled N_0 and resonant light, $\omega = \omega_{N_0}$. Then,

$$\begin{aligned}\mathcal{E}_{trns}(t) &= \mathcal{E}_0 \mathcal{L}^{-1}\left[\frac{\kappa/2}{\kappa/2 + s - \imath\omega_{N_0}} \frac{1}{s - \imath\omega_{N_0}}\right] \\ &= \mathcal{E}_0 e^{\imath\omega_{N_0} t} \mathcal{L}^{-1}\left[\frac{\kappa/2}{\kappa/2 + s} \frac{1}{s}\right] = \mathcal{E}_0 e^{\imath\omega_{N_0} t}(1 - e^{-\kappa t/2})\theta(t) \ ,\end{aligned}$$

which is exactly what we would expect for large mode spacing, $\delta_{fsr} \gg \gamma$. Otherwise, we need to consider the presence of non-resonant modes,

$$\begin{aligned}\mathcal{E}_{trns}(t) &= \mathcal{E}_0 \sum_N \mathcal{L}^{-1}\left[\frac{\kappa/2}{\kappa/2 + s - \imath\omega_N} \frac{1}{s - \imath\omega_{N_0}}\right] \\ &= \mathcal{E}_0 e^{\imath\omega_{N_0} t} \mathcal{L}^{-1}\left[\frac{\kappa/2}{\kappa/2 + s - \imath(N - N_0)2\pi\delta_{fsr}} \frac{1}{s}\right] \ .\end{aligned}$$

Introducing the abbreviation $\Delta_N \equiv (N - N_0)2\pi\delta_{fsr}$, we can also write,

$$\mathcal{E}_{trns}(t) = \mathcal{E}_0 e^{\imath\omega_{N_0} t} \sum_N \mathcal{L}^{-1}\left[\frac{\kappa/2}{(\kappa/2 - \imath\Delta_N)\, s + s^2}\right] = \mathcal{E}_0 e^{\imath\omega_{N_0} t} \sum_N \frac{\kappa/2}{(\kappa/2 - \imath\Delta_N)\, \partial_t + \partial_t^2} \ .$$

Hence,

$$\sum_N \ddot{\mathcal{E}}_{trns} + \left(\frac{\kappa}{2} - \imath\Delta_N\right) \dot{\mathcal{E}}_{trns} = \frac{\kappa}{2}\mathcal{E}_{in} \ .$$

Coming back to the case of large mode separation, we may approximate the differential equation by,

$$\ddot{\mathcal{E}}_{trns} + \frac{\kappa}{2}\dot{\mathcal{E}}_{trns} = \frac{\kappa}{2}\mathcal{E}_{in} \ ,$$

whose solution reproduces the previous result.

40.1.6.6 Ex: Fluorescence spectrum of an empty cavity

a. Calculate the fluorescence spectrum of an empty cavity pumped at a rate η classically via the autocorrelation function $\langle\alpha^*(t+\tau)\alpha(t)\rangle$.
b. Calculate the time evolution of the cumulants $\langle\hat{a}\rangle$, $\langle\hat{a}^\dagger\hat{a}\rangle$, $\langle\hat{a}^\dagger\hat{a}^\dagger\hat{a}\rangle$, $\langle\hat{a}\hat{a}^\dagger\hat{a}\rangle$, and

$\langle \hat{a}^\dagger \hat{a} \hat{a}^\dagger \hat{a} \rangle$ expanding up to forth order.
c. Based on the results obtained in (b) and applying the quantum regression theorem derive a set of linear differential equations for the autocorrelation functions $\langle \hat{a}(\tau) \rangle$, $\langle \hat{a}^\dagger(t+\tau)\hat{a}(t) \rangle$, $\langle \hat{a}^\dagger(t+\tau)\hat{a}^\dagger(t)\hat{a}(t) \rangle$, $\langle \hat{a}(t+\tau)\hat{a}^\dagger(t)\hat{a}(t) \rangle$, and $\langle \hat{a}^\dagger(t+\tau)\hat{a}(t+\tau)\hat{a}^\dagger(t)\hat{a}(t) \rangle$. Express them in matrix notation.
d. Calculate $g^{(1)}(\tau)$, the fluorescence spectrum, and $g^{(2)}(\tau)$ for the case $\eta = 0$.
e. Repeat the calculations in (c) to the case $\eta \neq 0$.

Solution: *a. The general solution of the inhomogeneous equation,*

$$[\partial_t + \kappa + \imath\Delta_c] f(t) = h \tag{40.62}$$

is,

$$\begin{aligned} f(t) &= [f(0) - f(\infty)] e^{-(\kappa+\imath\Delta_c)t} + f(\infty) \\ &= \left(f(0) - \tfrac{h}{\kappa+\imath\Delta_c} \right) e^{-(\kappa+\imath\Delta_c)t} + \tfrac{h}{\kappa+\imath\Delta_c} \ . \end{aligned} \tag{40.63}$$

Hence, the time-evolution according to (40.11) is,

$$\alpha e^{\imath\omega t} = \left(\alpha(0) e^{\imath\omega t} - \frac{\eta}{\kappa + \imath\Delta_c} \right) e^{(-\kappa+\imath\Delta_c)t} + \frac{\eta}{\kappa + \imath\Delta_c} \ , \tag{40.64}$$

or

$$\begin{aligned} \alpha(t) &= A e^{(-\kappa-\imath\omega_c)t} + B e^{-\imath\omega t} \\ \text{with} \quad A &= \alpha(0) - \frac{\eta}{\kappa + \imath\Delta_c} \qquad \text{and} \qquad B = \frac{\eta}{\kappa + \imath\Delta_c} \ . \end{aligned} \tag{40.65}$$

The autocorrelation is now,

$$\begin{aligned} \langle \alpha^*(t+\tau)\alpha(t) \rangle &= \lim_{t\to\infty} \frac{1}{t} \int_0^t \alpha^*(t'+\tau)\alpha(t') dt' \\ &= \lim_{t\to\infty} \frac{1}{t} \int_0^t \left(A^* e^{(-\kappa+\imath\omega_c)(t'+\tau)} + B^* e^{\imath\omega(t'+\tau)} \right) \left(A e^{(-\kappa-\imath\omega_c)t'} + B e^{-\imath\omega t'} \right) dt' \\ &= e^{(-\kappa+\imath\omega_c)\tau} \lim_{t\to\infty} \frac{1}{t} \int_0^t \left(|A|^2 e^{-2\kappa t'} + A^* B e^{(-\kappa-\imath\omega+\imath\omega_c)t'} \right) dt' \\ &\quad + e^{\imath\omega\tau} \lim_{t\to\infty} \frac{1}{t} \int_0^t \left(A B^* e^{(-\kappa+\imath\omega-\imath\omega_c)t'} + |B|^2 \right) dt' \\ &= \lim_{t\to\infty} \left[e^{(-\kappa+\imath\omega_c)\tau} \left(|A|^2 \frac{e^{-2\kappa t} - 1}{-2\kappa t} + A^* B \frac{e^{(-\kappa-\imath\omega+\imath\omega_c)t} - 1}{(-\kappa - \imath\omega + \imath\omega_c)t} \right) + \right. \\ &\quad \left. + e^{\imath\omega\tau} \left(A B^* \frac{e^{(-\kappa+\imath\omega-\imath\omega_c)t} - 1}{(-\kappa + \imath\omega - \imath\omega_c)t} + |B|^2 \right) \right] \\ &= \lim_{t\to\infty} \left[e^{(-\kappa+\imath\omega_c)\tau} (0+0) + e^{\imath\omega\tau} (0 + |B|^2) \right] = |B|^2 e^{\imath\omega\tau} \ . \end{aligned} \tag{40.66}$$

Hence, the $g^{(1)}(\tau)$ function is,

$$g^{(1)}(\tau) = \frac{\langle \alpha^*(t+\tau)\alpha(t) \rangle}{\langle \alpha^*(t)\alpha(t) \rangle} = e^{\imath\omega\tau} \ . \tag{40.67}$$

The spectrum should consist of an elastic peak at the Fourier frequency $\nu = \omega$. A broadened spectrum could only be observed as a transient at shorter times $t < \infty$.
b. From the Hamiltonian,

$$\hat{H} = -\Delta_c \hat{a}^\dagger \hat{a} + \imath\eta(\hat{a} - \hat{a}^\dagger) \ , \tag{40.68}$$

using the Heisenberg-Liouville equations, we derive the cumulant equations,

$$\begin{aligned}
[\partial_t + \kappa - \imath\Delta_c]\langle\hat{a}\rangle &= \eta \\
[\partial_t + 2\kappa]\langle\hat{a}^\dagger\hat{a}\rangle &= \eta(\langle\hat{a}^\dagger\rangle + \langle\hat{a}\rangle) \\
[\partial_t + 2\kappa + 2\imath\Delta_c]\langle\hat{a}^\dagger\hat{a}^\dagger\rangle &= 2\eta\langle\hat{a}^\dagger\rangle = 0 \\
[\partial_t + 3\kappa + \imath\Delta_c]\langle\hat{a}^\dagger\hat{a}^\dagger\hat{a}\rangle &= \eta\langle\hat{a}^\dagger\hat{a}^\dagger\rangle + 2\eta\langle\hat{a}^\dagger\hat{a}\rangle = 0 \\
[\partial_t + 4\kappa]\langle\hat{a}^\dagger\hat{a}^\dagger\hat{a}\hat{a}\rangle &= 2\eta(\langle\hat{a}^\dagger\hat{a}^\dagger\hat{a}\rangle + \langle\hat{a}^\dagger\hat{a}\hat{a}\rangle) = 0 \ .
\end{aligned} \tag{40.69}$$

The solution of the first equation (40.69) has already been derived in (40.64),

$$\begin{aligned}
\langle\hat{a}(t)\rangle &= (\langle\hat{a}_0\rangle - \langle\hat{a}_\infty\rangle)e^{-(\kappa+\imath\Delta_c)t} + \langle\hat{a}_\infty\rangle \\
&= \left(\langle\hat{a}_0\rangle - \tfrac{\eta}{\kappa+\imath\Delta_c}\right) e^{-(\kappa+\imath\Delta_c)t} + \tfrac{\eta}{\kappa+\imath\Delta_c} \ .
\end{aligned} \tag{40.70}$$

In matrix notation, $\partial_t \mathbf{y} = \mathcal{M}\mathbf{y} + \mathbf{d}$, with

$$\mathcal{M} = \begin{pmatrix}
\imath\Delta_c - \kappa & 0 & 0 & 0 & 0 & 0 & 0 \\
0 & -\imath\Delta_c - \kappa & 0 & 0 & 0 & 0 & 0 \\
\eta & \eta & -2\kappa & 0 & 0 & 0 & 0 \\
0 & 2\tilde{\eta} & 0 & 2\imath\Delta_c - 2\kappa & 0 & 0 & 0 \\
0 & 0 & 2\tilde{\eta} & \tilde{\eta} & \imath\Delta_c - 3\kappa & 0 & 0 \\
0 & 0 & 0 & 0 & 0 & -\imath\Delta_c - 3\kappa & 0 \\
0 & 0 & 0 & 0 & 2\tilde{\eta} & 2\tilde{\eta} & -4\kappa
\end{pmatrix}$$

$$\mathbf{y} = \begin{pmatrix}
\langle\hat{a}\rangle \\
\langle\hat{a}^\dagger\rangle \\
\langle\hat{a}^\dagger\hat{a}\rangle \\
\langle\hat{a}^\dagger\hat{a}^\dagger\rangle \\
\langle\hat{a}^\dagger\hat{a}^\dagger\hat{a}\rangle \\
\langle\hat{a}^\dagger\hat{a}\hat{a}\rangle \\
\langle\hat{a}^\dagger\hat{a}\hat{a}^\dagger\hat{a}\rangle
\end{pmatrix} \quad , \quad \mathbf{d} = \begin{pmatrix}
\eta \\ \eta \\ 0 \\ 0 \\ 0 \\ 0 \\ 0
\end{pmatrix} \ . \tag{40.71}$$

The steady-state solution can be obtained from $\mathbf{y} = -\mathcal{M}^{-1}\mathbf{d}$. Neglecting phase-invariant terms marked with $\tilde{\eta}$ vanish.
c. We can use the result to evaluate correlations such as $\langle\hat{a}^\dagger(t+\tau)\hat{a}(t)\rangle$. To this end we solve the second equation (40.69) using the quantum regression theorem, for example,

$$\begin{aligned}
\frac{d}{d\tau}\langle\hat{a}^\dagger(t+\tau)\hat{a}(t)\rangle &= \langle[\partial_\tau\hat{a}^\dagger(t+\tau)]\hat{a}(t)\rangle \\
&= \langle[\eta - (\kappa - \imath\Delta_c)\hat{a}^\dagger(t+\tau)]\hat{a}(t)\rangle \\
&= \eta\alpha(t) - (\kappa - \imath\Delta_c)\langle\hat{a}^\dagger(t+\tau)\hat{a}(t)\rangle \ .
\end{aligned} \tag{40.72}$$

The procedure can be extended to higher orders. Introducing the short-hand notation $\hat{a} \equiv \hat{a}(t+\tau)$ *and* $\hat{a}_0 \equiv \hat{a}(t)$ *we get,*

$$\begin{aligned}
[\partial_\tau + \kappa + \imath\Delta_c]\langle \hat{a}^\dagger \hat{a}_0\rangle &= \eta\langle \hat{a}_0\rangle = 0 \\
[\partial_\tau + \kappa + \imath\Delta_c]\langle \hat{a}^\dagger \hat{a}_0^\dagger \hat{a}_0\rangle &= \eta\langle \hat{a}_0^\dagger \hat{a}_0\rangle = 0 \\
[\partial_\tau + 2\kappa]\langle \hat{a}^\dagger \hat{a}\hat{a}_0^\dagger \hat{a}_0\rangle &= \eta(\langle \hat{a}^\dagger \hat{a}_0^\dagger \hat{a}_0\rangle + \langle \hat{a}\hat{a}_0^\dagger \hat{a}_0\rangle) = 0 \ .
\end{aligned} \tag{40.73}$$

In matrix notation, $\partial_\tau \mathbf{y} = \mathcal{M}\mathbf{y} + \mathbf{d}$*, with*

$$\mathcal{M} = \begin{pmatrix}
-\kappa + \imath\Delta_c & 0 & 0 & 0 & 0 \\
0 & -\kappa + \imath\Delta_c & 0 & 0 & 0 \\
0 & 0 & -\kappa + \imath\Delta_c & 0 & 0 \\
0 & 0 & 0 & -\kappa + \imath\Delta_c & 0 \\
0 & 0 & \eta & \eta & -2\kappa
\end{pmatrix} \tag{40.74}$$

$$\mathbf{y} = \begin{pmatrix}
\langle \hat{a}\rangle \\
\langle \hat{a}^\dagger \hat{a}_0\rangle \\
\langle \hat{a}^\dagger \hat{a}_0^\dagger \hat{a}_0\rangle \\
\langle \hat{a}\hat{a}_0^\dagger \hat{a}_0\rangle \\
\langle \hat{a}^\dagger \hat{a}\hat{a}_0^\dagger \hat{a}_0\rangle
\end{pmatrix} \quad , \quad \mathbf{d} = \eta \begin{pmatrix}
\langle \hat{a}_0\rangle \\
\langle \hat{a}_0^\dagger \hat{a}_0\rangle \\
\langle \hat{a}_0^\dagger \hat{a}_0^\dagger \hat{a}_0\rangle \\
\langle \hat{a}_0 \hat{a}_0^\dagger \hat{a}_0\rangle \\
\langle \hat{a}_0^\dagger \hat{a}_0 \hat{a}_0^\dagger \hat{a}_0\rangle
\end{pmatrix} \ .$$

d. Without pumping, $\eta = 0$*, the homogeneous equations are easy to solve,*

$$\begin{aligned}
\langle \hat{a}^\dagger \hat{a}_0\rangle &= \langle \hat{a}_0^\dagger \hat{a}_0\rangle e^{-(\imath\Delta_c + \kappa)\tau} \\
\langle \hat{a}^\dagger \hat{a}\hat{a}_0^\dagger \hat{a}_0\rangle &= \langle \hat{a}_0^\dagger \hat{a}_0 \hat{a}_0^\dagger \hat{a}_0\rangle e^{-(\imath\Delta_c + \kappa)\tau} \ ,
\end{aligned} \tag{40.75}$$

etc., so that,

$$g^{(1)}(\tau) = e^{-(\imath\Delta_c + \kappa)\tau} \qquad \textit{and} \qquad g^{(2)}(\tau) = e^{-(\imath\Delta_c + \kappa)\tau} \ . \tag{40.76}$$

The spectrum is a Lorentzian line,

$$\mathcal{F}(\langle \hat{a}^\dagger \hat{a}_0\rangle)(\omega) = \frac{1}{(\omega - \Delta_c)^2 + \kappa^2} \ . \tag{40.77}$$

e. In the presence of pumping, $\eta \neq 0$ *we get,*

$$\begin{aligned}
\langle \hat{a}_0\rangle &= \frac{\eta}{\kappa + \imath\Delta_c} \\
\langle \hat{a}^\dagger \hat{a}_0\rangle &= \left(\langle \hat{a}_0^\dagger \hat{a}_0\rangle - \eta\langle \hat{a}_0\rangle\right) e^{-(\kappa + \imath\Delta_c)\tau} + \eta\langle \hat{a}_0\rangle \\
&= \left(\langle \hat{a}_0^\dagger \hat{a}_0\rangle - \frac{\eta^2}{\kappa + \imath\Delta_c}\right) e^{-(\kappa + \imath\Delta_c)\tau} + \frac{\eta^2}{\kappa + \imath\Delta_c} \\
\langle \hat{a}^\dagger \hat{a}_0^\dagger \hat{a}_0\rangle &= \left(\langle \hat{a}_0^\dagger \hat{a}_0^\dagger \hat{a}_0\rangle - \eta\langle \hat{a}_0^\dagger \hat{a}_0\rangle\right) e^{-(\kappa + \imath\Delta_c)\tau} + \eta\langle \hat{a}_0^\dagger \hat{a}_0\rangle \\
\langle \hat{a}^\dagger \hat{a}\hat{a}_0^\dagger \hat{a}_0\rangle &= \left(\langle \hat{a}_0^\dagger \hat{a}_0 \hat{a}_0^\dagger \hat{a}_0\rangle - \eta(\langle \hat{a}^\dagger \hat{a}_0^\dagger \hat{a}_0\rangle + \langle \hat{a}\hat{a}_0^\dagger \hat{a}_0\rangle)\right) e^{-2\kappa\tau} + \eta(\langle \hat{a}^\dagger \hat{a}_0^\dagger \hat{a}_0\rangle + \langle \hat{a}\hat{a}_0^\dagger \hat{a}_0\rangle) \ .
\end{aligned} \tag{40.78}$$

40.2 Interaction of atoms with cavities

In Sec. 35.1 we have shown how to describe the dynamics of a single two-level atom driven by a quantized electromagnetic field and embedded in an electromagnetic vacuum under the assumption that the driving field be a plane wave and the vacuum be isotropic. In the following, we want to relax these conditions. We generalize Eq. (35.7) replacing the plane wave $e^{i\mathbf{k}\cdot\mathbf{r}}$ by a mode function $u_{\mathbf{k}}(\mathbf{r})$ and allowing the coupling constant (35.17) $g_{\mathbf{k}}$ to depend on $\mathbf{k}$. Such a situation corresponds to placing the atom inside an optical cavity whose macroscopic boundary conditions create a cooperative environment for the atom. We note that the role of the cavity can be understood as generating mirror images with which the atom interacts. Furthermore, both the atomic excitation and the radiation fields may decay. On the other hand, we restrict to non-interacting atoms, that is, free atoms or atoms trapped in external potentials that only interact with each other via re-scattering of an incident radiation field, i.e. no collisions and no properties requiring symmetrization of their wavefunctions.

In Sec. 40.2.1 we study a single atom or two atoms in a cooperative environment (e.g. a cavity). In particular, we will find that spontaneous emission is affected by the presence of a cavity. A wider discussion of scattering from correlated atoms is postponed to Sec. 41.1. Then, in Sec. 40.2.2 we will introduce some parameters characterizing the interaction between atoms and cavities. In particular, we will relate the important notions of the *cooperativity* of several atoms and the structure factor for light scattering introduced in 39.1.1 with the cavity-to-free space scattering ratio, the finesse and the density-of-states of a cavity, simply by pointing out that a cavity multiplies the number of atoms interacting with a light mode by the number of its mirror images. In Secs. 40.2.3, 40.2.4, and 40.2.6 we study the Hamiltonian governing the dynamics of a cavity mode interacting with a single immobile atom emphasizing the phenomenon of normal mode splitting. In Sec. 40.2.5 we simplify the equations of motion by adiabatically eliminating the internal atomic degree of freedom. Finally, in Secs. 40.2.7 and 40.2.8 we study the impact of the atomic center-of-mass degree of freedom (position and velocity) on the dynamics of the cavity fields. The discussion of backaction of the cavity fields on the atomic motion is postponed to Chp. 42.

40.2.1 Spontaneous emission in a cooperative environment

40.2.1.1 Atoms in a cooperative environment

The quantization of the electromagnetic field has been presented in Sec. 35.1.1 for the case of plane wave radiation modes. In the following, we want to generalize the treatment to arbitrary field modes characterized by mode functions $\mathbf{u}_{\mathbf{k}\lambda}(\mathbf{r})$ labeled by a wavevector and a polarization. These are classical vector functions satisfying the vector Helmholtz equation and the transversality condition,

$$[\nabla^2 + k_\lambda^2]\mathbf{u}_{\mathbf{k}\lambda}(\mathbf{r}) = 0 \qquad \text{and} \qquad \nabla\cdot\mathbf{u}_{\mathbf{k}\lambda}(\mathbf{r}) = 0\ , \tag{40.79}$$

with $k_\lambda = \omega_{\mathbf{k}\lambda}/c$ [897]. These classical functions are chosen to form an orthonormal set,

$$\int_V \mathbf{u}^*_{\mathbf{k}\lambda}(\mathbf{r})\cdot\mathbf{u}_{\mathbf{k}'\lambda'}(\mathbf{r})d^3r = \delta_{\mathbf{k}\mathbf{k}'}\delta_{\lambda,\lambda'}\ . \tag{40.80}$$

In free space, the plane wave approximation is generally good,

$$\mathbf{u}_{\mathbf{k}\lambda}^{free}(\mathbf{r}) = \frac{\vec{\epsilon}_\lambda}{\sqrt{V}} e^{\imath \mathbf{k}\cdot\mathbf{r}} \ , \tag{40.81}$$

where $\vec{\epsilon}_{\mathbf{k}\lambda}$ is a polarization vector such that $\mathbf{k}\cdot\vec{\epsilon}_{\mathbf{k}\lambda} = 0$ and V is the photon quantization volume.

Let us now rewrite the quantized transverse vector potential of the radiation field (35.7) as,

$$\boxed{\hat{\mathbf{A}}(\mathbf{r},t) = \sum_{\mathbf{k}\lambda} \sqrt{\tfrac{\hbar}{2\omega_{\mathbf{k}\lambda}\varepsilon_0}} [\mathbf{u}_{\mathbf{k}\lambda}(\mathbf{r})\hat{a}_{\mathbf{k}\lambda}(t) + \mathbf{u}^*_{\mathbf{k}\lambda}(\mathbf{r})\hat{a}^\dagger_{\mathbf{k}\lambda}(t)]} \ . \tag{40.82}$$

The quantum properties of the electric and magnetic field operators are determined by the bosonic annihilation and creation operators, $\hat{a}_{\mathbf{k}\lambda}(t)$ and $\hat{a}^\dagger_{\mathbf{k}\lambda}(t)$, respectively, with usual commutation relations: $[\hat{a}_{\mathbf{k}\lambda}(t), \hat{a}_{\mathbf{k}'\lambda'}(t)] = 0$ and $[\hat{a}_{\mathbf{k}\lambda}(t), \hat{a}^\dagger_{\mathbf{k}'\lambda'}(t)] = \delta_{\mathbf{k}\mathbf{k}'}\delta_{\lambda\lambda'}$.

For weak-coupling between the atoms and the field, one has the contributions to the Hamiltonian,

$$\boxed{\begin{aligned} \hat{H}_{atom} &= \hbar\omega_0 \hat{\sigma}^z \\ \hat{H}_{field} &= \sum_{\mathbf{k}} \hbar\omega_{\mathbf{k}} [\hat{a}^\dagger_{\mathbf{k}\lambda}(t)\hat{a}_{\mathbf{k}\lambda}(t) + \tfrac{1}{2}] \\ \hat{H}_{atom:field} &= -\imath\hbar \sum_{\mathbf{k},\lambda} (\hat{\sigma}^+ + \hat{\sigma}^-)[g_{\mathbf{k}\lambda}(\mathbf{r})\hat{a}_{\mathbf{k}\lambda} - g^*_{\mathbf{k}\lambda}(\mathbf{r})\hat{a}^\dagger_{\mathbf{k}\lambda}] \end{aligned}} \ , \tag{40.83}$$

and,

$$g_{\mathbf{k}\lambda}(\mathbf{r}) \equiv \sqrt{\frac{\omega_{\mathbf{k}}}{2\varepsilon_0\hbar}} \mathbf{d}\cdot\mathbf{u}_{\mathbf{k}\lambda}(\mathbf{r}) \tag{40.84}$$

is a complex function associated with the coupling strength between the atom and the field.

By solving the Heisenberg equations of motion for the atomic and field operators within the Born and Markov approximations (or using the procedure leading to the expression (35.234)), one obtains the spontaneous emission rate on a transition $|e\rangle \to |g\rangle$ of frequency ω_0:

$$\Gamma(\mathbf{r}) = 2\pi \sum_{\mathbf{k},\lambda} |g_{\mathbf{k}\lambda}(\mathbf{r})|^2 \delta(\omega_{\mathbf{k}} - \omega_0) \ . \tag{40.85}$$

which is the same result obtained by the Weisskopf-Wigner theory [897]. To evaluate the sum we need go to a continuous k-space via,

$$\sum_{\mathbf{k},\lambda} \longrightarrow \lim_{V\to\infty} \sum_\lambda \frac{V}{8\pi^3} \int d^3k \ . \tag{40.86}$$

Hence, in free space, inserting the mode function (40.82),

$$\begin{aligned}\Gamma(\mathbf{r}) &= \frac{\pi\omega_0}{\varepsilon_0\hbar}\sum_{\mathbf{k},\lambda}|\mathbf{d}\cdot\mathbf{u}_{\mathbf{k}\lambda}(\mathbf{r})|^2\delta(\omega_{\mathbf{k}}-\omega_0) \\ &= \frac{\hbar\omega_0}{8\pi^2\varepsilon_0\hbar^2}\lim_{V\to\infty}\sum_{\lambda}\int d^3k\ |\mathbf{d}\cdot\vec{\epsilon}_{\mathbf{k}\lambda}|^2\delta(\omega_{\mathbf{k}}-\omega_0) \\ &= \lim_{V\to\infty}\sum_{\lambda}\int\frac{|\mathbf{d}\cdot\vec{\epsilon}_{\mathbf{k}\lambda}|^2\vec{\mathcal{E}}_{\mathbf{k}}^2}{\hbar^2}2\pi\delta(\omega_{\mathbf{k}}-\omega_0)\frac{V}{8\pi^3c}k^2d\Omega_{\mathbf{k}}d\omega_{\mathbf{k}}\ .\end{aligned} \tag{40.87}$$

Plugging in the density of states for free space (22.53) and (34.23), we finally get,

$$\Gamma(\mathbf{r}) = \sum_{\lambda}\int\frac{|\mathbf{d}\cdot\vec{\epsilon}_{\mathbf{k}\lambda}|^2\vec{\mathcal{E}}_{\mathbf{k}}^2}{\hbar^2}2\pi\delta(\omega_{\mathbf{k}}-\omega_0)\rho(\omega_{\mathbf{k}},\mathbf{k})d\Omega_{\mathbf{k}}d\omega_{\mathbf{k}}\ , \tag{40.88}$$

where the density of states can now be arbitrarily shaped by the presence of boundary conditions, such as optical cavities or dielectric or metallic surfaces.

Example 240 (*Two atoms*): Let us now consider two excited atoms labeled by $q = 1, 2$, located at $\mathbf{r}_1$ and $\mathbf{r}_2$, and described by two of their eigenstates, $\{|g_q\rangle, |e_q\rangle\}$. As usual, $|g_q\rangle$ is the eigenstate with lowest energy ($E_{g_q} = -\frac{1}{2}\hbar\omega_q$) and longer lifetime, i.e. the ground state, whereas $|e_q\rangle$ is the eigenstate with highest energy ($E_{e_q} = +\frac{1}{2}\hbar\omega_q$). In presence of an external electromagnetic field, the Hamiltonian of the two atom-field system in the electric dipole approximation is,

$$\hat{H} = \sum_{q=1,2}[\hat{H}^{(q)}_{atom} + \hat{H}^{(q)}_{atom:field}] + \hat{H}_{field}\ ,$$

where $\hat{H}^{(q)}_{atom} \equiv \hbar\omega_q\hat{s}^z_q$ is the atomic Hamiltonian, with $\hat{s}^z_q \equiv \frac{1}{2}(|e_q\rangle\langle e_q| - |g_q\rangle\langle g_q|)$ being the energy operator of the q-th atom, and $\hat{H}^{(q)}_{atom:field} \equiv -\hat{\mathbf{d}}_q\cdot\hat{\vec{\mathcal{E}}}(\mathbf{r}_q)$ is the atom-field interaction Hamiltonian. The electric dipole moment operator satisfies $\langle e_q|\hat{\mathbf{d}}_q|e_q\rangle = \mathbf{0} = \langle g_q|\hat{\mathbf{d}}_q|g_q\rangle$ and has non-vanishing off-diagonal elements, i.e. the eigenstates have no permanent dipole moment. We define the dipole-moment matrix element as $\mathbf{d}_q \equiv \langle e_q|\hat{\mathbf{d}}_q|g_q\rangle$. The description of the field is identical to the case of one atom (40.81).
For weak-coupling between the atoms and the field, the interaction Hamiltonian becomes,

$$\hat{H}_{atom:field} = -\imath\hbar\sum_{\mathbf{k},\lambda}\sum_{q=1,2}(\hat{s}^+_q + \hat{s}^-_q)[g_{\mathbf{k}\lambda}(\mathbf{r}_q)\hat{a}_{\mathbf{k}\lambda} - g^*_{\mathbf{k}\lambda}(\mathbf{r}_q)\hat{a}^\dagger_{\mathbf{k}\lambda}]\ ,$$

where $\hat{s}^+_q \equiv |e_q\rangle\langle g_q|$ and $\hat{s}^-_q \equiv |g_q\rangle\langle e_q|$ are the electric dipole raising and lowering operators, respectively, satisfying the well-known commutation and anti-commutation relations: $[\hat{s}^+_q, \hat{s}^-_{q'}] = 2\hat{s}^z_q\delta_{qq'}$, $[\hat{s}^z_q, \hat{s}^\pm_{q'}] = \pm\hat{s}^\pm_q\delta_{qq'}$, and $[\hat{s}^+_q, \hat{s}^-_{q'}]_+ = 0$ with $(\hat{s}^\pm_q)^2 = 0$.
By solving the Heisenberg equations of motion for the atomic and field operators within the Born and Markov approximations, one obtains the spontaneous emission rate on a transition $|e_q\rangle \longrightarrow |g_q\rangle$ of frequency ω_q:

$$\Gamma_q = 2\pi\sum_{\mathbf{k},\lambda}|g_{\mathbf{k}\lambda}(\mathbf{r}_q)|^2\delta(\omega_{\mathbf{k}}-\omega_q) = \frac{\pi\omega_q}{\varepsilon_0\hbar}\sum_{\mathbf{k},\lambda}|\mathbf{d}_q\cdot\mathbf{u}_{\mathbf{k}\lambda}(\mathbf{r}_q)|^2\delta(\omega_{\mathbf{k}}-\omega_q)\ ,$$

which is the same result obtained by the Weisskopf-Wigner theory [897]. In addition, due to the coupling between the atoms through the vacuum field, one also has the cross-damping spontaneous emission rate:

$$\Gamma_q(\mathbf{r}_1,\mathbf{r}_2)=\Gamma_q(\mathbf{r}_2,\mathbf{r}_1)=\frac{\pi\omega_0}{\varepsilon_0\hbar}\sum_{\mathbf{k},\lambda}\Re\mathfrak{e}\ \left[\mathbf{d}_1\cdot\mathbf{u}_{\mathbf{k}\lambda}(\mathbf{r}_1)\mathbf{u}^*_{\mathbf{k}\lambda}(\mathbf{r}_2)\cdot\mathbf{d}_2^*\right]\delta(\omega_{\mathbf{k}}-\omega_q)\ ,$$

which shows explicitly the cooperative effect of the dipole-dipole interaction in the spontaneous emission rate.

40.2.1.2 Modification of the natural linewidth by cavities

The *cooperativity parameter* of a cavity is defined as the rate at which an atom emits into the volume of a cavity mode normalized to the rate at which it would scatter into free space,

$$\boxed{\Upsilon\equiv\frac{\Gamma_{cav}}{\Gamma_{free}}}\ . \tag{40.89}$$

In a cavity, spontaneous emission is strongly modified [596, 597, 598]. An atom interacting with a cavity will spontaneously emit into the cavity mode at an increased (reduced) rate, depending on whether the cavity is resonant or out of resonance. The natural width due to spontaneous decay and the line shift are calculated by integration over the coupling force between the atom and every available field mode [see (40.87)],

$$\boxed{\begin{aligned}\Gamma &= \iint\frac{|\mathbf{d}_{eg}\cdot\vec{\epsilon}_{\mathbf{k}}|^2|\vec{\mathcal{E}}_{\mathbf{k}}|^2}{\hbar^2}2\pi\delta(\omega_0-\omega_{\mathbf{k}})\rho(\omega_{\mathbf{k}},\mathbf{k})d\Omega_{\mathbf{k}}d\omega_{\mathbf{k}}\\ \Delta\omega &= \sum_i\iint\frac{|\mathbf{d}_{ei}\cdot\vec{\epsilon}_{\mathbf{k}}|^2|\vec{\mathcal{E}}_{\mathbf{k}}|^2}{\hbar^2}\frac{1}{\omega_{ei}-\omega_{\mathbf{k}}}\rho(\omega_{\mathbf{k}},\mathbf{k})d\Omega_{\mathbf{k}}d\omega_{\mathbf{k}}\end{aligned}}\ , \tag{40.90}$$

with the field amplitude per photon, $|\vec{\mathcal{E}}_{\mathbf{k}}|=\sqrt{\hbar\omega_{\mathbf{k}}/2\varepsilon_0 V}$, derived in (40.33), and the index i running over all internal atomic states. These formulas are simply applications of second-order perturbation theory (27.16) and of Fermi's golden rule (27.111) for transition probabilities both weighed with dynamic structure factor of the cavity.

We use the number of modes per unit of frequency range and per unit of solid angle in free space derived in (40.41) (ρ/V is the density of states),

$$\rho_{free}(\omega_{\mathbf{k}})=\frac{V\omega_{\mathbf{k}}^2}{(2\pi)^3c^3}\ . \tag{40.91}$$

Setting $\theta_{\mathbf{k}}$ as the angle between the atomic dipole moment and the cavity axis (which is not in place, yet, as we are still in free space), $\mathbf{d}\cdot\hat{\epsilon}_{\mathbf{k}}=d\cos\alpha_{\mathbf{k}}=d\cos(90^\circ-\theta_{\mathbf{k}})=d\sin\theta_{\mathbf{k}}$,

$$\begin{aligned}\Gamma_{free} &= \int\frac{d^2\sin^2\theta_{\mathbf{k}}}{\hbar^2}\frac{\hbar\omega_0}{2\varepsilon_0 V}2\pi\frac{V\omega_0^2}{(2\pi)^3c^3}\sin\theta d\theta d\phi\\ &= \frac{d^2k^3}{4\pi\varepsilon_0\hbar}\int_0^\pi\sin^3\theta d\theta=\frac{d^2k^3}{3\pi\varepsilon_0\hbar}\ .\end{aligned} \tag{40.92}$$

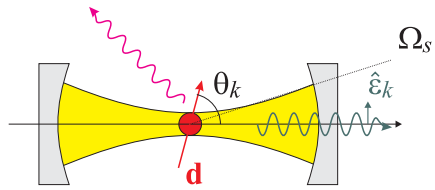

Figure 40.7: Illustration of cooperativity in a cavity. An excited atom can decay by emitting light into a cavity mode or into free space. Note that the cavity is not pumped directly by an incident laser beam.

Since the integration covers the whole solid angle of space 4π and the free space is isotropic, there is no preferred orientation, and we can perform the integration setting $\theta \equiv \theta_{\mathbf{k}}$. The result coincides with earlier calculations (34.46).

Now, we put the cavity in place, but tune it off resonance, such that no photons can be emitted into the solid angle covered by the cavity. That is, in the presence of the cavity, the solid angle of free space into which photons can be emitted is restricted. We repeat the calculation (40.92), but now we are not free to choose the axis of the coordinate system arbitrarily. Instead, we we assume that $\theta_{\mathbf{k}}(\theta,\phi) \simeq const$ over the small solid angle covered by the cavity, $\theta, \phi \in \Omega_{cav}$,

$$\begin{aligned}\Gamma_{free\notin cav} &= \int_{\hat{\mathbf{e}}_k \notin cav} \frac{d^2 \sin^2\theta_k}{\hbar^2} \frac{\hbar\omega_0}{2\varepsilon_0 V} 2\pi \frac{V\omega_0^2}{(2\pi)^3 c^3} \sin\theta d\theta d\phi \\ &\simeq \Gamma_{free} - \frac{d^2 k^3 \sin^2\theta_{\mathbf{k}}}{8\pi^2\varepsilon_0\hbar} \int_{\hat{\mathbf{e}}_k \in cav} \sin\theta d\theta d\phi = \Gamma_{free}\left(1 - \frac{3}{8\pi}\Omega_{cav}\sin^2\theta_{\mathbf{k}}\right) .\end{aligned} \tag{40.93}$$

Finally, we study the situation, when the cavity is in place but now tuned on resonance. Then the density of states in the photon emission directions $\mathbf{k} \in$ cavity is modulated by the Airy function (40.42),

$$\rho_{cav}(\omega_{\mathbf{k}}, \mathbf{k}) = \rho_{free}(\omega_{\mathbf{k}}) \mathcal{L}(\omega_{\mathbf{k}}) . \tag{40.94}$$

That is, photons can be emitted into the cavity mode with increased probability. Once again we repeat the calculation (40.92), but now inserting the density of states of the cavity,

$$\begin{aligned}\Gamma_{cav} &= \int_{\hat{\mathbf{e}}_k \in cav} \frac{d^2 \sin^2\theta_{\mathbf{k}}}{\hbar^2} \frac{\hbar\omega_0}{2\varepsilon_0 V} 2\pi \mathcal{L}(\omega_0) \frac{V\omega_0^2}{(2\pi)^3 c^3} \sin\theta d\theta d\phi \\ &\simeq \frac{d^2 k^3 \sin^2\theta_{\mathbf{k}}}{8\pi^2\varepsilon_0\hbar} \mathcal{L}(\omega_0) \int_{\hat{\mathbf{e}}_k \in cav} \sin\theta d\theta d\phi = \Gamma_{free}\mathcal{L}(\omega_0) \frac{3}{8\pi}\Omega_{cav}\sin^2\theta_{\mathbf{k}} ,\end{aligned} \tag{40.95}$$

where, in the last step, we substituted the free space decay rate (40.92). An analogous calculation for the *cooperative Lamb shift* $\Delta\omega_{cav}$ is left to the Exc. 40.2.9.1:

$$\boxed{\begin{aligned}\Gamma_{cav} &= \Gamma_{free} \tfrac{3}{8\pi}\Omega_{cav}\sin^2\theta_{\mathbf{k}} \mathcal{L}(\omega_0) \\ \Delta\omega_{cav} &= \Gamma_{free} \tfrac{3}{32\pi}\Omega_{cav}\sin^2\theta_{\mathbf{k}} \tfrac{\mathcal{L}'(\omega_0)}{\mathcal{L}(\omega_0)} 2\delta_{fsr}\end{aligned}} . \tag{40.96}$$

The quantities Γ_{cav} and $\Gamma_{free\in cav}$ are scattering rates into complementary solid angles. Now, the total spontaneous emission rate, which determines the lifetime of the radiating excited state and the spectral width of the transition is simply the sum of the partial scattering rates,

$$\begin{aligned}\Gamma &= \Gamma_{free\notin cav} + \Gamma_{cav} \\ &= \Gamma_{free}\left(1-\tfrac{3}{8\pi}\Omega_{cav}\right)\sin^2\theta_{\mathbf{k}} + \Gamma_{free}\mathcal{L}(\omega_0)\tfrac{3}{8\pi}\Omega_{cav}\sin^2\theta_{\mathbf{k}} \\ &= \Gamma_{free}\left[1+\left(\mathcal{L}(\omega_0)-1\right)\tfrac{3}{8\pi}\Omega_{cav}\right]\sin^2\theta_{\mathbf{k}}\ .\end{aligned} \tag{40.97}$$

Assuming for simplicity, $\theta_{\mathbf{k}} = \pi/2$, we find the extremes of the spontaneous emission rate, Γ_{enh} and Γ_{inh}, when the cavity is on or off resonance. With a resonant high finesse cavity the emission is obtained via $kL \to 0$,

$$\Gamma_{enh} = \Gamma_{free}\left[1+\left(\sqrt{1+\left(\tfrac{2F}{\pi}\right)^2}-1\right)\tfrac{3}{8\pi}\Omega_{cav}\right] \simeq \Gamma_{free}\left(1+\tfrac{3}{4\pi^2}F\Omega_{cav}\right)\ . \tag{40.98}$$

assuming high finesse, $F \gg 1$. With a non-resonant cavity, the emission is obtained via $kL \to \pi/2$,

$$\Gamma_{inh} = \Gamma_{free}\left[1+\left(\frac{1}{\sqrt{1+\left(\tfrac{2F}{\pi}\right)^2}}-1\right)\tfrac{3}{8\pi}\Omega_{cav}\right] \simeq \Gamma_{free}\left(1-\tfrac{3}{8\pi}\Omega_{cav}\right)\ . \tag{40.99}$$

For a small solid angle, we can expect a big increase of the scattering into the cavity, but without noticeable inhibition of the total decay, $\Gamma_{inh} \simeq \Gamma_{free}$.

If the atoms are saturated by an incident laser, they scatter light into the cavity at a rate (apart from a factor $\frac{1}{2}$),

$$\Gamma_{cav} = \Gamma_{free}\mathcal{L}(\omega_0)\tfrac{3}{8\pi}\Omega_{cav}\ . \tag{40.100}$$

Without cavity the emission into the same solid angle is obtained via $F \to 0$,

$$\Gamma_{free\in cav} = \Gamma_{free}\tfrac{3}{8\pi}\Omega_{cav}\ . \tag{40.101}$$

The scattering will fill the cavity with photons, until the leakage equalizes the pumping. When the balance is reached, Γ_{cav} will also be the rate at which photons are emitted by the cavity mode. We calculate an example in Exc. 40.2.9.2.

40.2.1.3 Purcell factor for confocal and concentric cavities

Using the solid angle of a confocal cavity (40.48), the cooperativity parameter is,

$$\Upsilon \simeq \frac{3F}{4\pi^2}\Omega_{cav} = \frac{3F}{4\pi^2}\frac{8\pi b^2}{L^2}\ , \tag{40.102}$$

where b is the clear aperture of the cavity mirrors. That is,

$$\boxed{\Upsilon = \frac{F}{\pi}\frac{6b^2}{L^2}\ .} \tag{40.103}$$

40.2.1.4 Purcell factor for the TEM_{00} cavity mode

With the solid angle (40.54) calculated for a this TEM_{00} cavity mode we calculate the *cooperativity parameter*,

$$\begin{aligned}\Upsilon \equiv \frac{\Gamma_{cav}}{\Gamma_{free}} &= \mathcal{L}(\omega_0)\tfrac{3}{8\pi}\Omega_{cav} = \sqrt{1+\left(\frac{2F}{\pi}\right)^2}\,\frac{3}{8\pi}\Omega_{cav} \\ &\simeq \frac{3F}{4\pi^2}\Omega_{cav} = \frac{\Gamma_{enh}}{\Gamma_{free}} - 1 = \frac{3F}{4\pi^2}\frac{8\pi}{k^2 w_0^2}\ ,\end{aligned} \tag{40.104}$$

that is,

$$\boxed{\Upsilon = \frac{F}{\pi}\frac{6}{k^2 w_0^2}}\ , \tag{40.105}$$

which is also called *Purcell factor*.

Now, exploiting the relationships (40.54), (40.105), and (40.27),

$$\Omega_{cav} = \frac{8\pi}{k^2 w_0^2} \quad , \quad \Upsilon = \frac{F}{\pi}\frac{6}{k^2 w_0^2} \quad , \quad \frac{F}{\pi} = \frac{\delta_{fsr}}{\kappa}\ , \tag{40.106}$$

and defining a new quantity,

$$g^2 = \Upsilon\kappa\Gamma_{free}\ , \tag{40.107}$$

which we will call the atom-field coupling strength, we may rewrite the prefactor $\Gamma_{free}\frac{3}{8\pi}\Omega_{cav}$ for the case of Gaussian cavity modes,

$$\Gamma_{free}\frac{3}{8\pi}\Omega_{cav} = \frac{g^2}{2\delta_{fsr}}\ . \tag{40.108}$$

Close to a cavity resonance, $kL = \omega/2\delta_{fsr} = (\omega_c + \Delta_c)/2\delta_{fsr} = 2\pi N + \Delta_c/2\delta_{fsr}$, the sine appearing in the Airy function (40.42) may be expanded $\sin kL = \sin \Delta_c/2\delta_{fsr} \simeq \Delta_c/2\delta_{fsr}$. Furthermore, assuming a high finesse, $F \gg 1$, the Airy function simplifies to,

$$\mathcal{L}(\omega_0) = \frac{\sqrt{1+(2F/\pi)^2}}{1+(2F/\pi)^2\sin^2\frac{\omega}{2\delta_{fsr}}} \simeq \frac{2F/\pi}{1+\Delta_a^2/\kappa^2}\ . \tag{40.109}$$

Inserting this into the formulae (40.96), where we set $\theta_{\mathbf{k}} = \frac{\pi}{2}$,

$$\boxed{\begin{aligned}\Gamma_{cav} &\simeq \tfrac{g^2\kappa}{\Delta_c^2+\kappa^2} \\ \Delta\omega_{cav} &\simeq \tfrac{-2g^2\Delta_c}{\Delta_c^2+\kappa^2}\end{aligned}}\ . \tag{40.110}$$

Obviously, the atom-field coupling strength g plays a central role in the modification of the emission spectra of atoms interaction with cavities. Therefore, we will have to study this quantity more deeply in the next sections.

Example 241 (*Cooperativity of non-degenerate and confocal cavities*): For example, for a non-degenerate linear cavity with finesse $F = 110000$ and waist $w_0 = 50\,\mu\mathrm{m}$ at 689 nm, the cooperativity is relatively weak, $\Upsilon \simeq 1$. Still, at this

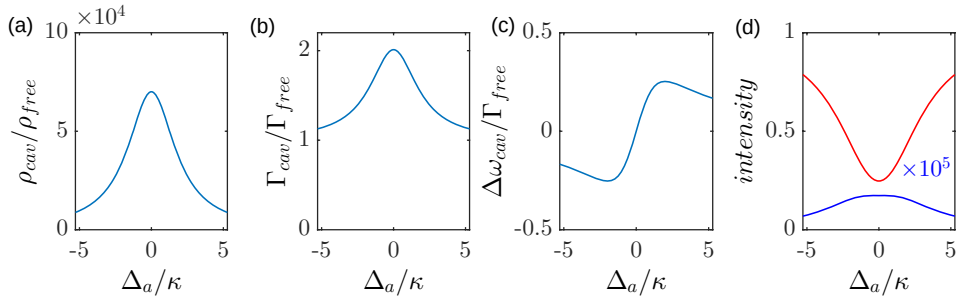

Figure 40.8: (code) Spontaneous emission on the strontium atom cooling transition ($\lambda = 689\,\text{nm}$, $\Gamma = (2\pi)\ 7.6\,\text{kHz}$) in a $L = 3.6\,\text{cm}$ long cavity with $F = 110000$ and $w_0 = 50\,\mu\text{m}$. (a) Cooperativity $\mathcal{L}(\omega)$ from Eq. (40.42) as a function of the detuning of the cavity. (b) Linewidth Γ_{cav} from (40.96)(ii) and (c) frequency shift of the strontium transition from Eq. (40.96)(ii). (d) Spontaneous emission into the cavity (blue) and into the open space (red).

cooperativity, half of the spontaneously emitted photons go into a tiny solid angle represented by the cavity. Confocal or concentric cavities may present more favorable geometries [596, 597, 598]. With $N_0 = 10^4$ saturated strontium atoms, the light power scattered into the cavity is $P_j = 20\,\text{fW}$. Estimation the cavity transmission by $T \simeq \pi/F$, we expect that a number of $T\frac{P_{cav}}{\hbar\omega} = 10^7\,\text{s}^{-1}$ photons can be detected by a photodetector recording the photon number leaking out of the cavity.

40.2.2 Characterization of the atom-field coupling

In Sec. 40.1.3 we started introducing a number of quantities characterizing empty cavities. We will now pursue this task including their interaction with atoms. In particular, we will introduce three important quantities allowing us to measure the degree of quantization of the system: the cooperativity Υ, the saturation parameter s, and the cavity resolution r.

40.2.2.1 The atomic dipole moment

As usual, the interaction strength of an atom with a light field is measured by the atom-field coupling constant, which is precisely HALF the single photon Rabi frequency. Using relationships derived in Sec. 40.1.3 and the expression (34.41) for the atomic dipole moment d, we find,

$$g \equiv \frac{d\mathcal{E}_1(0)}{\hbar} = \sqrt{\frac{3\pi\Gamma\omega}{2k^3V_m}} = \sqrt{\frac{3\Gamma\delta_{fsr}}{k^2w^2}}\ , \tag{40.111}$$

where $\mathcal{E}_1(0)$ the electric field produced by a single photon inside the cavity mode volume V_m calculated in (40.30) and Γ is the spontaneous decay rate. See also (watch talk).

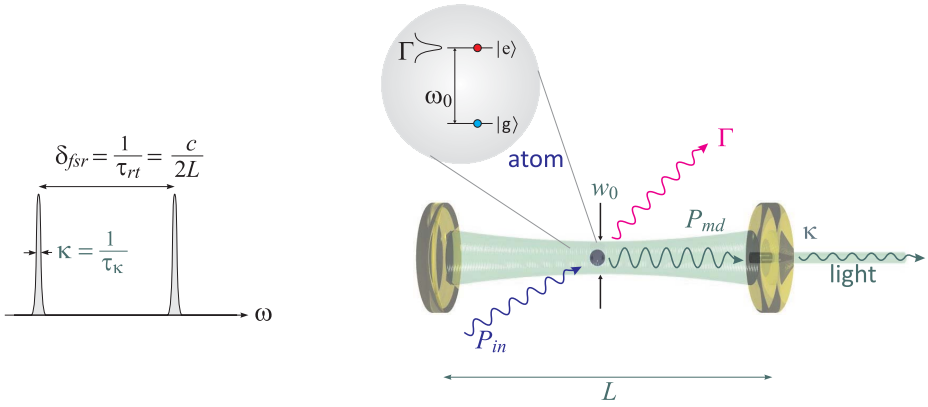

Figure 40.9: Relevant parameters for an atom interacting with a cavity.

40.2.2.2 Single atom reflection coefficient

Based on the complex atomic polarizability (18.122),

$$\frac{\alpha_{pol}}{\varepsilon_0} \simeq \frac{6\pi}{k^3} \frac{-1}{\imath + 2\Delta/\Gamma} \ , \tag{40.112}$$

the *single atom reflection coefficient* is defined as,

$$\beta_\Delta = \frac{k}{\pi w^2} \left| \frac{\mathfrak{Re}\ \alpha_{pol}}{\varepsilon_0} \right| = \frac{6}{k^2 w^2} \frac{2\Gamma|\Delta_a|}{4\Delta_a^2 + \Gamma} \overset{|\Delta| \gg \Gamma}{\longrightarrow} \frac{6}{k^2 w^2} \frac{\Gamma}{2|\Delta_a|} \ , \tag{40.113}$$

where $\Delta_a = \omega - \omega_0$. The resonant reflection coefficient can be interpreted in terms of a phase shift that depends on the matching between the resonant optical cross-section of the atom, $\sigma_0 = 3\lambda^2/2\pi$, and the cross section of the optical mode,

$$\beta_0 = \frac{\sigma_0}{\pi w^2} = \frac{6}{k^2 w^2} = \frac{2g^2}{\delta_{fsr}\Gamma} \ . \tag{40.114}$$

The total reflection coefficient is increased by the number of atoms N and the number of photon round trips F in the cavity, which gives out of resonance,

$$NF\beta_\Delta \simeq NF \frac{6}{k^2 w^2} \frac{\Gamma}{2\Delta_a} = NF \frac{g^2}{\Delta_a} \frac{kV}{\omega \pi w^2} = NU_0 \frac{L}{c} F = \frac{NU_0}{\kappa} \ , \tag{40.115}$$

where we introduced the *light-shift* produced by a single off-resonant photon and the Rayleigh scattering rate produced by a single photon,

$$U_0 \simeq \frac{g^2}{\Delta_a} \qquad \text{and} \qquad \gamma_0 \simeq \frac{g^2 \Gamma}{\Delta_a^2} \ . \tag{40.116}$$

Using the dipole moment $d = \sqrt{3\pi\varepsilon_0 \hbar \Gamma / k^3}$ and defining the electric field amplitude per photon $\mathcal{E}_1$ by the photon number n, the power P, and the intensity

$I = \varepsilon_0 c n_{ph} \mathcal{E}_1^2 = 2P/\pi w_0^2$, we calculate for the single-photon Rabi frequency (or atom-field coupling strength),

$$g = \frac{d\mathcal{E}_1}{\hbar} = \sqrt{\frac{1}{\hbar^2}\frac{3\pi\varepsilon_0\hbar\Gamma}{k^3}\frac{I}{\varepsilon_0 c n_{ph}}} = \sqrt{\frac{1}{\hbar^2}\frac{3\pi\varepsilon_0\hbar\Gamma}{k^3}\frac{1}{\varepsilon_0 c n_{ph}}\frac{2P}{\pi w_0^2}} = \sqrt{\frac{6}{k^2 w_0^2}\Gamma\frac{P}{n_{ph}\hbar\omega}} \ . \tag{40.117}$$

The single-photon light shift (or atom-atom coupling strength) is,

$$U_0 = \frac{g^2}{|\Delta_a|} = \frac{6}{k^2 w_0^2}\frac{\Gamma}{|\Delta_a|}\frac{P}{n_{ph}\hbar\omega} = \beta_\Delta \frac{P}{n_{ph}\hbar\omega} \ , \tag{40.118}$$

and the single-photon Rayleigh scattering rate,

$$\gamma_0 = \frac{g^2\Gamma}{\Delta_a^2} = \frac{6}{k^2 w_0^2}\frac{\Gamma^2}{\Delta_a^2}\frac{P}{n_{ph}\hbar\omega} \ . \tag{40.119}$$

In a cavity the flux $\delta_{fsr} = P/n_{ph}\hbar\omega$ is just the photon round trip rate (or free spectral range). $1/\delta_{fsr}$ is the time a photon interacts with an atom. In free space, this does not make sense to me, because I don't know how define the mode volume. I can however consider the interaction of a photon with an extended sample of length L. In this case, a photon interacts with the sample for the time L/c, so that,

$$U_0 = \frac{g^2}{|\Delta_a|} = \frac{6}{k^2 w_0^2}\frac{\Gamma}{|\Delta_a|}\frac{c}{L} = \beta_\Delta \frac{c}{L} \ , \tag{40.120}$$

and

$$\gamma_0 = \frac{g^2\Gamma}{\Delta_a^2} = \frac{6}{k^2 w_0^2}\frac{\Gamma^2}{\Delta_a^2}\frac{c}{L} \ . \tag{40.121}$$

This means, we can use the CARL equations derived for a ring cavity by just substituting $\kappa = \delta_{fsr} = c/L$, where L is now not the cavity but the sample length.

40.2.2.3 Optical density

Lambert-Beer's law relates the amplitude of the field transmitted to the incident (see also Eq. (43.140)),

$$\frac{\mathcal{E}_t}{\mathcal{E}_0} = \exp\left[\imath\sigma(\Delta_a)\left(\frac{\imath}{2} - \frac{\Delta_a}{\Gamma}\right)\int_{-\infty}^{\infty} n(\mathbf{r})dz\right] = e^{-b/2}e^{\imath\varphi} \ . \tag{40.122}$$

I.e. the field is shifted by an amount φ and absorbed by an amount b. The exponent (called optical density) can be rewritten, if we assume a number of N atoms homogeneously distributed over a cylinder with length L and radius $\bar{r} = w_0$,

$$\begin{aligned} OD &= \imath\sigma(\Delta_a)\left(\frac{\imath}{2} - \frac{\Delta_a}{\Gamma}\right)\int_{-\infty}^{\infty} n(\mathbf{r})dz = \sigma_0\frac{\Gamma^2}{\Delta_a^2}\left(-\frac{1}{2} - \frac{\imath\Delta_a}{\Gamma}\right)\int_0^L \frac{N}{\pi\bar{r}^2 L}dz \\ &= \sigma_0\frac{\Gamma^2}{\Delta_a^2}\left(-\frac{1}{2} - \frac{\imath\Delta_a}{\Gamma}\right)\frac{N}{\pi w_0^2} = \frac{6N}{k^2 w_0^2}\frac{\Gamma^2}{\Delta_a^2}\left(-\frac{1}{2} - \frac{\imath\Delta_a}{\Gamma}\right) \\ &= \frac{6N}{k^2 w_0^2}\left(-\frac{1}{2}\frac{\Gamma^2}{\Delta_a^2} - \frac{\imath\Gamma}{\Delta_a}\right) = N\frac{L}{c}(-\gamma_0 - \imath U_0) \ . \end{aligned} \tag{40.123}$$

Hence, the parameters $N\gamma_0$ and NU_0 are nothing else that the optical density per photon round trip time $\delta_{fsr} = c/L$,

$$\boxed{OD = \frac{-N(\gamma_0 + \imath U_0)}{\delta_{fsr}}} \,. \tag{40.124}$$

40.2.2.4 Collective cooperativity

The frequency shift accumulated during a round trip in the cavity, $\delta_{fsr}\beta_0$, becomes noticeable, when it exceeds the linewidth of the cavity κ. From this condition, we obtain the optical depth for a single passage through the atomic sample multiplied by the finesse of the cavity, which is precisely the *cooperativity parameter*,

$$\boxed{\Upsilon \equiv \frac{\delta_{fsr}\beta_0}{\kappa} = \frac{F}{\pi}\frac{6}{k^2 w^2} = \frac{2g^2}{\kappa\Gamma}} \,. \tag{40.125}$$

The sensitivity to the atom number can be measured in terms of a *critical atom number* N_{crt}, which the system can resolve,

$$N_{crt} = \frac{4\pi}{F\beta_0} = \frac{1}{\Upsilon} \,. \tag{40.126}$$

While the strong coupling regime of the CQED requires $\Upsilon > 1$ with a single atom, collective cooperativity is reached with N atoms if $N\Upsilon > 1$ [193, 285]. In this case, the atomic ensemble couples to the mode like a single 'super-atom', the coupling force being magnified to $g_N = g_1\sqrt{N}$. We have already obtained this result within the Jaynes-Cummings model for two indistinguishable atoms coupling to the same light mode and forming a *Dicke state* (see Sec. 41.1.1).

40.2.2.5 Saturation parameter in cavities

The *saturation parameter* for a single photon is given by,

$$\boxed{s = \frac{2\Omega_1^2}{\Gamma^2} = \frac{8g^2}{\Gamma^2}} \,, \tag{40.127}$$

where Ω_1 is the single photon Rabi frequency. Therefore, the number of photons needed to saturate an atomic transition is,

$$n_{sat} = \frac{1}{s} \,. \tag{40.128}$$

We see, that there is a *symmetry* between Υ and s, that is, between N_{crt} and n_{sat}. The regime $N\Upsilon > 1$ denotes the collective behavior of N atoms in the same way as $n_{sat} > 1$ indicates saturation. While Υ depends only on the phase matching between the atomic antenna and the cavity, s also depends on the cavity mode volume and the natural decay rate.

40.2.2.6 Cavity resolution parameter

Comparing the photonic recoil, which is given by,

$$\omega_{rec} = \frac{\hbar k^2}{2m} \ , \tag{40.129}$$

with the resolution power of a cavity κ, we can define the *resolution parameter*,

$$\boxed{r \equiv \frac{\omega_{rec}}{\kappa}} \ . \tag{40.130}$$

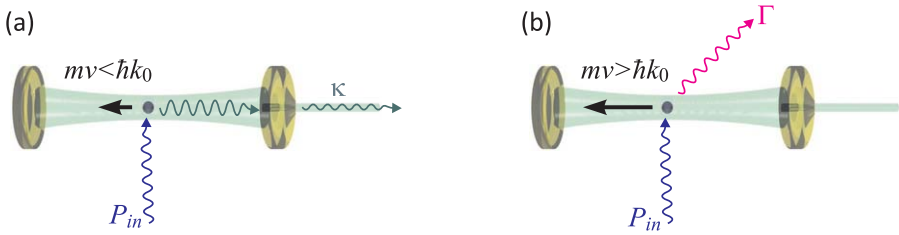

Figure 40.10: (a) If the recoil-induced Doppler shift of the atom moving along the cavity axis is smaller than the cavity linewidth, the light is preferentially scattered into the cavity mode. (b) Else it is scattered outside the mode.

With the three parameters defined in Eqs. (40.125), (40.127), and (40.130) we are able to measure the degree of quantization of the degrees of freedom involved in the matter-light interaction in a cavity. The cooperativity Υ measures the resolvability of single atoms in the atomic cloud, which depends on the phase matching between the atomic antenna (i.e. its optical cross section) and the focus of the optical mode. The saturation parameter s measures the resolvability of single photons in the cavity. And the cavity resolution parameter r measures the resolvability of the Doppler-shift due to the atomic center-of-mass motion caused by the absorption of a single photon. If one wants to operate in an environment, where all degrees of freedom involved in the atom-light interactions are fully quantized, the atoms need to be placed into a cavity whose characteristic quantities are all large, $\Upsilon, s, r \gg 1$.

In Exc. 40.2.9.3 we compare the coupling force and other characteristic parameters for various combinations of atomic species and optical cavities. In Exc. 40.2.9.4 we calculate the number of photons in a cavity pumped in or out of resonance.

40.2.3 Jaynes-Cummings model for one or two radiation modes

To study the dynamics of the coupled atom-cavity system, we consider the Jaynes-Cummings Hamiltonian (35.108) (or (40.83)), for a more concrete situation. That is, we allow for optical pumping and decay of internal states with the rates R and Γ, respectively, and we allow for inhomogeneous (however, mostly one-dimensional) mode functions $g(z) = ge^{\imath kz}$. On the other hand, we stick to a single atom (or N uncorrelated atoms), we disregard polarization and multi-mode excitation, and we will explicitly consider and compare two well distinct cases, linear and ring cavities.

40.2.3.1 Linear and ring cavities

From the Heisenberg equations with the Hamiltonian (40.83),

$$\boxed{\begin{aligned} \hat{H}_{atom} &= -\Delta_a \hat{\sigma}^+ \hat{\sigma}^- \\ \hat{H}_{cav} &= -\Delta_c \hat{a}^\dagger \hat{a} \\ \hat{H}_{atom:cav} &= g(z)\hat{a}^\dagger \hat{\sigma}^- + h.c. \\ \hat{H}_{laser:cav} &= -\imath\eta(\hat{a} - \hat{a}^\dagger) \end{aligned}} \; . \tag{40.131}$$

The Hamiltonian for a single motionless atom interacting with two cavity modes $|+\rangle$ and $|-\rangle$ (we may, for instance, consider the counterpropagating modes of a ring cavity) reads,

$$\boxed{\begin{aligned} \hat{H}_{atom} &= -\Delta_a \hat{\sigma}^+ \hat{\sigma}^- \\ \hat{H}_{cav} &= -\Delta_+ \hat{a}_+^\dagger \hat{a}_+ - \Delta_- \hat{a}_-^\dagger \hat{a}_- \\ \hat{H}_{atom:cav} &= g(z)\hat{a}_+^\dagger \hat{\sigma}^- + h.c. + g(z)\hat{a}_-^\dagger \hat{\sigma}^- + h.c. \\ \hat{H}_{laser:cav} &= -\imath\eta_+(\hat{a}_+ - \hat{a}_+^\dagger) - \imath\eta_-(\hat{a}_- - \hat{a}_-^\dagger) \end{aligned}} \; . \tag{40.132}$$

40.2.3.2 Time-evolution of an atom in a ring cavity

The coupling of the atom to the cavities $g(z)$ will, in general, depend on the atomic position. For simplicity let us, however, consider uniform and identical coupling, $g_+(z) = g_-(z) = g$, and furthermore assume that both cavities be on resonance, $\Delta_+ = \Delta_- = 0$. Finally, neglecting spontaneous emission and pumping, the total number of photons is conserved. With $\Delta_a = \omega - \omega_a$ we get,

$$\hat{H} = \omega \hat{a}_+^\dagger \hat{a}_+ + \omega \hat{a}_-^\dagger \hat{a}_- + \omega_0(\hat{\sigma}^+\hat{\sigma} - \tfrac{1}{2}) + g\hat{a}_+^\dagger \hat{\sigma}^- + g\hat{a}_-^\dagger \hat{\sigma}^- + h.c. \; . \tag{40.133}$$

Expanding the operators $\hat{a}_\pm = \sum_{n_\pm} |n_\pm - 1\rangle\langle n_\pm|$ and $\hat{\sigma}^- = |1\rangle\langle 2|$ we can, expand the state of the system like,

$$|\psi(t)\rangle = \sum_{k=0}^{n} c_{j,n_+,n_-} |j, n_+, n_-\rangle \; . \tag{40.134}$$

Alternatively, in analogy with Sec. 35.4.2, we may organize the Hilbert space in orthogonal subspaces, $\hat{H} = \bigoplus_n \hat{H}_n$, each one having $N \equiv j + n_+ + n_-$ energy units distributed over the atomic excitation state $j = 0, 1$ and the numbers of photons $n_\pm$ in each mode. Hence, every subspace is of dimension $2N + 1$. In this dressed states picture, introducing the photon imbalance $D \equiv n_+ - n_- = -N, ..., N$, we may expand the coupled state like,

$$\boxed{|\psi(t)\rangle = \sum_{N=0}^{\infty} \sum_{D=-N}^{N} \tilde{c}_{N,D} |N, D\rangle} \; . \tag{40.135}$$

Obviously, the set of three quantum numbers $\{j, n_+, n_-\}$ is equivalent to the set of two quantum numbers $\{N, D\}$ and can be recovered by,

$$j = 1 + (-1)^{N+D-1} \quad , \quad n_\pm = \tfrac{1}{2}(N \pm D - j) \ . \tag{40.136}$$

Hence, states with odd $N + D$ are excited atomic states, and states with even $N + D$ are ground states. We may now write down the Hamiltonian,

$$\hat{H}_N = (N - \tfrac{1}{2})\omega \mathbb{I}_{2N+1} + \tag{40.137}$$
$$+ \frac{1}{2} \begin{pmatrix} \Delta & g_+\sqrt{N} & & & & & & \\ g_+\sqrt{N} & -\Delta & g_-\sqrt{1} & & & & & \\ & g_-\sqrt{1} & \Delta & g_+\sqrt{N-1} & & & & \\ & & g_+\sqrt{N-1} & \ddots & g_-\sqrt{N-1} & & & \\ & & & g_-\sqrt{N-1} & \Delta & g_+\sqrt{1} & & \\ & & & & g_+\sqrt{1} & -\Delta & g_-\sqrt{N} & \\ & & & & & g_-\sqrt{N} & \Delta & \end{pmatrix} .$$

The subscripts of the coupling constants $g_+ = g_-$ are there only to clarify to which mode the photon belongs. Very far from resonance, where the interaction is dispersive, we may treat the light field perturbatively, as shown in (35.130),

$$\hat{H}_N = (N - \tfrac{1}{2})\omega \mathbb{I}_{2N+1} + \tag{40.138}$$
$$+ \begin{pmatrix} \frac{\Delta}{2} + \frac{Ng_+^2 + 0g_-^2}{4\Delta} & & & & \\ & -\frac{\Delta}{2} - \frac{Ng_+^2 + 1g_-^2}{4\Delta} & & & \\ & & \frac{\Delta}{2} + \frac{(N-1)g_+^2 + 1g_-^2}{4\Delta} & & \\ & & & -\frac{\Delta}{2} - \frac{(N-1)g_+^2 + 2g_-^2}{4\Delta} & \\ & & & & \ddots \end{pmatrix} ,$$

or with $g_+ = g_-$,

$$(\hat{H}_N)_{DD'} = \left[\left(N + \frac{1}{2} \right) \omega - \frac{1}{2} \frac{g^2}{4\Delta} + (-1)^{N+D} \left(\frac{\Delta}{2} + \left(N + \frac{1}{2} \right) \frac{g^2}{4\Delta} \right) \right] \delta_{DD'} \ . \tag{40.139}$$

If only the upper level of the atom interacts with both light fields, all terms with negative light shift disappear,

$$(\hat{H}_N)_{DD'} = \left[\left(N + \frac{1}{2} \right) \omega + \frac{1}{2} \frac{Ng^2}{4\Delta} + (-1)^{N+D} \left(\frac{\Delta}{2} + \frac{N}{2} \frac{g^2}{4\Delta} \right) \right] \delta_{DD'} \ . \tag{40.140}$$

As shown in Sec. 35.4.2, we propagate the evolution of the coupled state via $|\psi(t)\rangle = e^{-\imath \hat{H} t} |\psi(0)\rangle$. As the initial condition we may choose the atom to be in its ground state and the two field modes in uncorrelated Glauber states,

$$c_{j,n_+,n_-} = \langle j, n_+, n_- | \psi \rangle = e^{-|\alpha_+|^2/2 - |\alpha_-|^2/2} \frac{\alpha_+^{n_+} \alpha_-^{n_-}}{\sqrt{n_+! n_-!}} \delta_{j,0} \tag{40.141}$$
$$= \tilde{c}_{N,\delta} = e^{-|\alpha_+|^2/2 - |\alpha_-|^2/2} \frac{\alpha_+^{(N+\delta-j)/2} \alpha_-^{(N-\delta-j)/2}}{\sqrt{(\frac{N+\delta-j}{2})! (\frac{N-\delta-j}{2})!}} \delta_{1+(-1)^{N+\delta-1},0} \ .$$

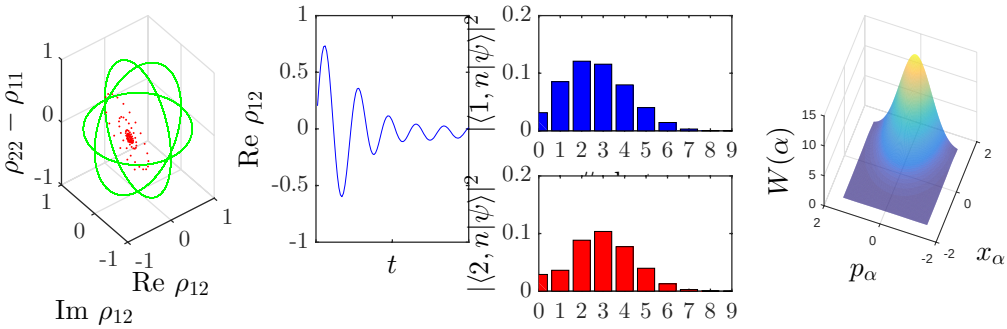

Figure 40.11: (code) Evolution of the coupled atom-ring cavity system. (a) Bloch vector, (b) photon distributions, and (c) Husimi function.

The observables of interest are the atomic Bloch vector (34.163), whose components are obtained from,

$$\rho_{ij} = \langle i|\mathrm{Tr}_{n_+,n_-}\hat{\rho}|j\rangle = \sum_{n_+,n_-}\langle i,n_+,n_-|\psi\rangle\langle\psi|j,n_+,n_-\rangle \tag{40.142}$$
$$= \sum_{n_+,n_-} c^*_{i,n_+,n_-}c_{j,n_+,n_-} = \sum_{n_+,n_-}\tilde{c}^*_{n_++n_-+i,n_+-n_-}\tilde{c}_{n_++n_-+j,n_+-n_-} \ ,$$

the photon statistics in each mode,

$$p_{n_+} = \langle n_+|\mathrm{Tr}_{i,n_-}\hat{\rho}|n_+\rangle = \sum_{j,n_-}\langle j,n_+,n_-|\psi\rangle\langle\psi|j,n_+,n_-\rangle \tag{40.143}$$
$$= \sum_{j,n_-}|c_{j,n_+,n_-}|^2 = \sum_{j,n_-}|\tilde{c}_{n_++n_-+j,n_+-n_-}|^2 \ ,$$

and analogously for p_{n_-}, and the field distribution functions, such as the Husimi function,

$$\pi Q_+(\alpha) \equiv \langle\alpha_+|\mathrm{Tr}_{\ i,n-}\hat{\rho}|\alpha_+\rangle \tag{40.144}$$
$$= e^{-|\alpha_+|^2}\sum_{n_-}\left(\left|\sum_{n_+}c_{1,n_+,n_-}\frac{\alpha^n}{\sqrt{n!}}\right|^2 + \left|\sum_{n_+}c_{2,n_+,n_-}\frac{\alpha^n}{\sqrt{n!}}\right|^2\right) \ ,$$

and analogously for $Q_-(\alpha)$, or the Wigner functions $W_\pm(\alpha)$ from the coefficients $\tilde{c}_{j,n_+,n_-}$, respectively, $\tilde{c}_{N,\delta}$, as shown in Secs. 35.2.2 and 35.4.3.

40.2.4 Normal-mode splitting in linear and ring cavities

The Jaynes-Cummings model introduced in Sec. 35.4 represents an idealized model of the interaction of a single cavity mode with a single atom. In this section we reconsider this model taking into account the facts that the coupling strength may vary in space

(via the introduction of mode functions) and that the cavity may interact with a reservoir (via the introduction of couplings to pump fields and losses.

We will also study the phenomenon of *normal mode splitting*, which is one of the most direct witnesses of an ongoing atom-cavity interaction (see the vacuum Rabi splitting discussed in Exc. 35.4.5.4).

40.2.4.1 Linear cavities

The starting point is the full Jaynes-Cummings Hamiltonian within the RWA (40.131) for an atom interacting with one mode of a linear optical cavity,

$$\boxed{\hat{H}_{JC} = -\Delta_a \hat{\sigma}^+\hat{\sigma}^- - \Delta_c \hat{a}^\dagger \hat{a} + g \sin kz(\hat{a}^\dagger\hat{\sigma}^- + \hat{a}\hat{\sigma}^+) - \imath\eta(\hat{a} - \hat{a}^\dagger)} \,. \tag{40.145}$$

For linear cavities normal mode splitting is derived in Exc. 40.2.9.5, where we compare the solution obtained by full numerical integration of the Jaynes-Cummings Hamiltonian (40.131) with an analytical approximation obtained in the weak excitation limit $g|\alpha|^2 \ll \Gamma, \Delta_a$ [2],

$$\alpha \simeq \frac{\eta}{\kappa - \imath\Delta_c + \frac{Ng^2}{\Gamma - \imath\Delta_a}} = \frac{\eta}{\kappa + N\gamma_0 + \imath(NU_0 - \Delta_c)} \,. \tag{40.146}$$

The solution coincides with one obtained for a system, where the atomic degree of freedom is adiabatically eliminated atom (see Sec. 40.2.5).

40.2.4.2 Ring cavities

The starting point is the full Jaynes-Cummings Hamiltonian within the RWA (40.132) for an atom interacting with two modes of an optical cavity. For two counter-propagating modes of a ring cavity it reads,

$$\boxed{\hat{H}_{JC} = -\Delta_a \hat{\sigma}^+\hat{\sigma}^- - \sum_{\pm} \Delta_c \hat{a}_\pm^\dagger \hat{a}_\pm + g(\hat{a}_\pm^\dagger \hat{\sigma}^- e^{\mp\imath kz} + \hat{a}_\pm \hat{\sigma}^+ e^{\pm\imath kz}) - \imath\eta_\pm(\hat{a}_\pm - \hat{a}_\pm^\dagger)} \,. \tag{40.147}$$

Note, that here, we do not treat the recoil $e^{\mp\imath kz}$ as a degree of freedom, but just as a parameter depending on the location of the atom. (We will come back to this in Chp. 42.) Decay processes can be considered in a master or in Heisenberg equations via jump operators $\hat{L}_k = \hat{\sigma}^-,\ \hat{\sigma}^+,\ \hat{a}_+, \hat{a}_-$ describing decay processes occurring, respectively, at rates $\gamma_k = 2\Gamma,\ 2R,\ 2\kappa,\ 2\kappa$.

40.2.4.3 (Anti-)Symmetric modes

Let us now introduce symmetric and anti-symmetric modes by,

$$\hat{b}_s = \tfrac{1}{\sqrt{2}}(\hat{a}_+ e^{\imath kz} + \hat{a}_- e^{-\imath kz}) \qquad \text{and} \qquad \hat{b}_a = \tfrac{1}{\sqrt{2}}(\hat{a}_+ e^{\imath kz} - \hat{a}_- e^{-\imath kz}) \,, \tag{40.148}$$

[2] Note that for N uncorrelated atoms, defining a bunching parameter via $b \equiv \frac{1}{N}\sum_j \sin kz_j$ and introducing the abbreviations $U_\gamma \equiv U_0 - \imath\gamma_0$ and $\Delta_\kappa \equiv \Delta_c + \imath\kappa$, the result (40.146) can be generalized to,

$$\alpha \simeq \frac{-\imath\eta}{NbU_\gamma - \Delta_\kappa} \,.$$

that is,

$$\hat{a}_+ = \frac{\hat{b}_s + \hat{b}_a}{\sqrt{2}e^{\imath kz}} \qquad \text{and} \qquad \hat{a}_- = \frac{\hat{b}_s - \hat{b}_a}{\sqrt{2}e^{-\imath kz}} \ , \tag{40.149}$$

which satisfy the commutations rules $[\hat{b}_s, \hat{b}_s^\dagger] = 1 = [\hat{b}_a, \hat{b}_a^\dagger]$. We can then rewrite the Hamiltonian,

$$\begin{aligned} \hat{H}_{JC} &= -\Delta_a \hat{\sigma}^+\hat{\sigma}^- + \sqrt{2}g(\hat{b}_s^\dagger\hat{\sigma}^- + \hat{b}_s\hat{\sigma}^+) - \sum_\pm \Delta_c \hat{a}_\pm^\dagger\hat{a}_\pm - \imath\eta_\pm(\hat{a}_\pm - \hat{a}_\pm^\dagger) \qquad (40.150) \\ &= \hat{H}_{atom} + \hat{H}_{atom:cav} + \hat{H}_{cav} + \hat{H}_{laser:cav} \ . \end{aligned}$$

We see that only the symmetric mode couples to the atom. On the other hand, both modes contribute to the field energy,

$$\hat{H}_{cav} = \Delta_c(\hat{a}_+^\dagger\hat{a}_+ + \hat{a}_-^\dagger\hat{a}) = \Delta_c(\hat{b}_s^\dagger\hat{b}_s + \hat{b}_a^\dagger\hat{b}_a) \ . \tag{40.151}$$

Now, let us check the pump terms,

$$\begin{aligned} \hat{H}_{laser:cav} &= \imath\eta_+(\hat{a}_+ - \hat{a}_+^\dagger) + \imath\eta_-(\hat{a}_- - \hat{a}_-^\dagger) \qquad (40.152) \\ &= \tfrac{\imath}{\sqrt{2}}\Big[(\eta_+e^{-\imath kz} + \eta_-e^{\imath kz})\hat{b}_s - (\eta_+e^{\imath kz} + \eta_-e^{-\imath kz})\hat{b}_s^\dagger \\ &\qquad +(\eta_+e^{-\imath kz} - \eta_-e^{\imath kz})\hat{b}_a - (\eta_+e^{\imath kz} - \eta_-e^{-\imath kz})\hat{b}_a^\dagger\Big] \ . \end{aligned}$$

For $\eta_+ = \eta_- = \eta$ we get,

$$\hat{H}_{laser:cav} = \eta\sqrt{2}\left[\imath(\hat{b}_s - \hat{b}_s^\dagger)\cos kz + (\hat{b}_a + \hat{b}_a^\dagger)\sin kz\right] \ . \tag{40.153}$$

Hence, for $kz = 0$ only the symmetric mode is pumped (no central peak). On the other hand, for $kz = \frac{\pi}{2}$ only the anti-symmetric mode is pumped, so that no normal-mode splitting is expected.

For $\eta_- = 0$ we get,

$$\hat{H}_{laser:cav} = \tfrac{\imath\eta_+}{\sqrt{2}}\left[e^{-\imath kz}(\hat{b}_s + \hat{b}_a) - e^{\imath kz}(\hat{b}_s^\dagger + \hat{b}_a^\dagger)\right] \ . \tag{40.154}$$

Hence, both modes are pumped and we observe three peaks. The normal-mode splitting can be observed in transmission spectra, as we will demonstrate in the following.

40.2.4.4 Normal modes of a ring cavity

We start from the Hamiltonian (40.147) and derive the Heisenberg equations,

$$\begin{aligned} \dot{\hat{\sigma}}^- &= (\imath\Delta_a - \tfrac{\Gamma}{2})\hat{\sigma}^- - \imath g(e^{\imath kz}\hat{a}_+ + e^{-\imath kz}\hat{a}_-)\hat{\sigma}^z \qquad (40.155) \\ \dot{\hat{\sigma}}^z &= 2\imath g(e^{\imath kz}\hat{a}_+ + e^{-\imath kz}\hat{a}_-)\hat{\sigma}^+ - 2\imath g\hat{\sigma}^-(e^{-\imath kz}\hat{a}_+^\dagger + e^{\imath kz}\hat{a}_-^\dagger) - \Gamma(\mathbb{I}_2 + \hat{\sigma}^z) \\ \dot{\hat{a}}_\pm &= (\imath\Delta_c - \kappa)\hat{a}_\pm - \imath g\hat{\sigma}^- e^{\mp\imath kz} + \eta_\pm \ . \end{aligned}$$

The stationary solution follows from the expectation values of these equations,

$$\begin{aligned} 0 &= (\imath\Delta_a - \tfrac{\Gamma}{2})\langle\hat{\sigma}^-\rangle + \imath g(e^{\imath kz}\langle\hat{a}_+\hat{\sigma}^z\rangle + e^{-\imath kz}\langle\hat{a}_-\hat{\sigma}^z\rangle) \qquad (40.156) \\ 0 &= 2\imath g(e^{\imath kz}\langle\hat{a}_+\hat{\sigma}^+\rangle + e^{-\imath kz}\langle\hat{a}_-\hat{\sigma}^+\rangle) - 2\imath g(e^{-\imath kz}\langle\hat{a}_+^\dagger\hat{\sigma}^-\rangle + e^{\imath kz}\langle\hat{a}_-^\dagger\hat{\sigma}^-\rangle) - \Gamma(1 + \langle\hat{\sigma}^z\rangle) \\ 0 &= (\imath\Delta_c - \kappa)\langle\hat{a}_\pm\rangle - \imath g\langle\hat{\sigma}^-\rangle e^{\mp\imath kz} + \eta_\pm \ . \end{aligned}$$

Neglecting all correlations, we derive from (40.156)(i),

$$\langle\hat{\sigma}^-\rangle = \frac{-\imath g}{\frac{\Gamma}{2}-\imath\Delta_a}(e^{\imath kz}\alpha_+ + e^{-\imath kz}\alpha_-)\langle\hat{\sigma}^z\rangle \ . \tag{40.157}$$

Substituting $\langle\hat{\sigma}^\pm\rangle$ in (40.156)(ii),

$$\left(1+\frac{2g^2}{\frac{\Gamma^2}{4}+\Delta_a^2}(|\alpha_+|^2+|\alpha_-|^2+e^{2\imath kz}\alpha_-^*\alpha_+ + e^{-2\imath kz}\alpha_+^*\alpha_-)\right)\langle\hat{\sigma}^z\rangle = -1 \ , \tag{40.158}$$

and in (40.156)(iii),

$$(\kappa-\imath\Delta_c)\alpha_\pm - \frac{g^2}{\frac{\Gamma}{2}-\imath\Delta_a}(e^{\imath kz\mp\imath kz}\alpha_+ + e^{-\imath kz\mp\imath kz}\alpha_-)\langle\hat{\sigma}^z\rangle = \eta_\pm \ . \tag{40.159}$$

Substituting $\langle\hat{\sigma}^z\rangle$ from (40.156) in (40.156),

$$(\kappa-\imath\Delta_c)\alpha_\pm - \frac{g^2(\frac{\Gamma}{2}+\imath\Delta_a)(\alpha_\pm + e^{\mp 2\imath kz}\alpha_\mp)}{\frac{\Gamma^2}{4}+\Delta_a^2+2g^2(|\alpha_+|^2+|\alpha_-|^2+e^{2\imath kz}\alpha_-^*\alpha_+ + e^{-2\imath kz}\alpha_+^*\alpha_-)} = \eta_\pm \ . \tag{40.160}$$

Assuming weak excitation, $g|\alpha_\pm|^2 \ll \Gamma, \Delta_a$, this last expression simplifies to,

$$\left(\kappa-\imath\Delta_c-\frac{g^2}{\frac{\Gamma}{2}-\imath\Delta_a}\right)\alpha_\pm - \frac{g^2}{\frac{\Gamma}{2}-\imath\Delta_a}e^{\mp 2\imath kz}\alpha_\mp \simeq \eta_\pm \ , \tag{40.161}$$

or, using the abbreviations,

$$U_\gamma \equiv U_0 - \imath\gamma_0 \equiv \frac{g^2}{\Delta_a+\imath\Gamma} = \frac{g^2(\Delta_a-\imath\frac{\Gamma}{2})}{\frac{\Gamma^2}{4}+\Delta_a^2} \ , \tag{40.162}$$

we write,

$$[\kappa+\imath(U_\gamma-\Delta_c)]\alpha_\pm + \imath U_\gamma e^{\mp 2\imath kz}\alpha_\mp \simeq \eta_\pm \ . \tag{40.163}$$

Resolving for $\alpha_\pm$,

$$\boxed{\alpha_\pm \simeq \frac{\eta_\pm\left[\kappa+\gamma_0+\imath(U_0-\Delta_c)\right]-\eta_\mp(\gamma_0+\imath U_0)e^{\mp 2\imath kz}}{\left[\kappa+\gamma_0+\imath(U_0-\Delta_c)\right]^2-(\gamma_0+\imath U_0)^2}} \ , \tag{40.164}$$

from which we can determine the transmission,

$$T_\pm = \left|\frac{\kappa\alpha_\pm}{\eta_\pm}\right|^2 \ . \tag{40.165}$$

This is illustrated in Fig. 40.12.

Example 242 (*Generalization for many atoms*): For N uncorrelated atoms, defining a bunching parameter via $b \equiv \frac{1}{N}\sum_j e^{2\imath kz_j}$ and introducing the abbreviations $U_\gamma \equiv U_0 - \imath\gamma_0$ and $\Delta_\kappa \equiv \Delta_c + \imath\kappa$, the result (40.146) can be generalized to,

$$\alpha_\pm \simeq -\imath\frac{\eta_\pm(NU_\gamma-\Delta_\kappa)-\eta_\mp NbU_\gamma}{(NU_\gamma-\Delta_\kappa)^2-(N|b|^2U_\gamma)^2} \ . \tag{40.166}$$

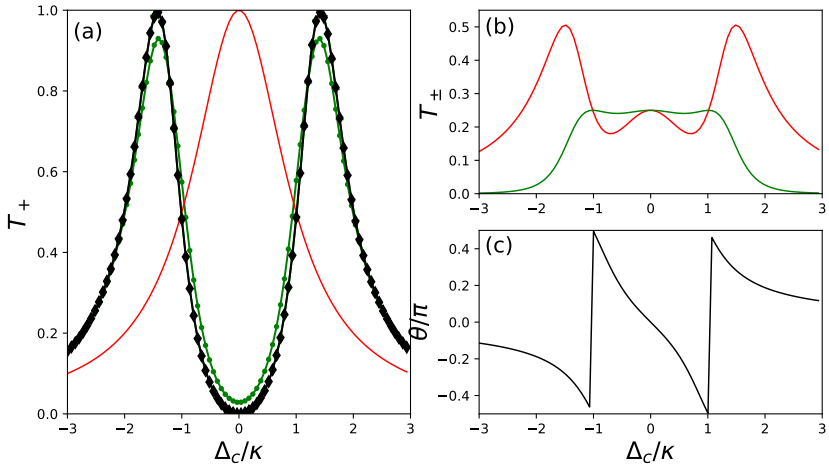

Figure 40.12: (code) Normal-mode splitting in a ring cavity observed in transmission spectra T_+ calculated from (40.165) with $g = \kappa$, $\eta_+ = 0.1\kappa$, and $\Gamma = R = 0$. (a) The blue curve is obtained for one-sided pumping ($\eta_- = 0$), the green curve for symmetric pumping ($\eta_- = \eta_+$ and $kz = 0$), and the red curve for anti-symmetric pumping ($\eta_- = \eta_+$ and $kz = \pi/2$). The green dots are obtained for symmetric pumping via numerical integration of the Hamiltonian (40.147). (b) Transmission spectra T_+ (green) and T_- (red) for one-sided pumping. (c) Phase of the standing wave formed by backscattering of probe light into the mode α_-.

Example 243 (*Level splitting for some limiting cases*): The first limiting case consists in setting $\eta_\pm = 0$ and assuming the light field to be classical. Then we obtain the Rabi Hamiltonian studied in previous sections,

$$\hat{H}_{Rabi} = -\Delta_a \hat{\sigma}^+\hat{\sigma}^- + \tfrac{1}{2}\Omega(\hat{\sigma}^+ + \hat{\sigma}^-) = \begin{pmatrix} 0 & \frac{1}{2}\Omega \\ \frac{1}{2}\Omega & -\Delta_a \end{pmatrix} .$$

Its eigenvalues: $E_{1,2} = -\frac{1}{2}\Delta_a \pm \sqrt{\Delta_a^2 + \Omega^2}$ exhibit the famous Autler-Townes splitting.
The second limiting case consists adiabatically eliminating the atomic states. This is valid if $|\Delta_a| \gg \Gamma$. Then we obtain the cavity Hamiltonian,

$$\hat{H}_{cav} = U_0(e^{-2\imath kz}\hat{a}_+^\dagger\hat{a}_- + e^{2\imath kz}\hat{a}_+\hat{a}_-^\dagger) + \sum_\pm (U_0 - \Delta_c)\hat{a}_\pm^\dagger\hat{a}_\pm - \imath\eta_\pm(\hat{a}_\pm - \hat{a}_\pm^\dagger) ,$$

with $L_k = \hat{a}_+, \hat{a}_-$ and $\gamma_k = 2\kappa, 2\kappa$, again for the case $z = \eta_\pm = 0$. The spectrum is asymmetric because $\Delta_a \neq 0$ [3,4]

[3] We note that, setting $z = \eta_\pm = 0$, the cavity Hamiltonian $\hat{H}_{cav} = U_0(\hat{a}_+^\dagger\hat{a}_- + \hat{a}_+\hat{a}_-^\dagger) - (\Delta_c - U_0)\sum_\pm \hat{a}_\pm^\dagger\hat{a}_\pm$ has the same structure as the Rabi Hamiltonian, which we can write, introducing annihilation and creation operators $\hat{\psi}_{g,e}$ and $\hat{\psi}_{g,e}^\dagger$ for atoms in ground and excited states, $\hat{H}_{Rabi} = \frac{1}{2}\Omega(\hat{\psi}_e^\dagger\hat{\psi}_g + \hat{\psi}_g^\dagger\hat{\psi}_e) - \Delta_a\sum_{j=g,e}\hat{\psi}_j^\dagger\hat{\psi}_j$. This emphasizes the analogy between Autler-Townes and normal-mode splitting.

[4] As the atomic degrees of freedom have been eliminated, spontaneous emission must be reintroduced by hand when required.

40.2.5 Adiabatic elimination of internal states

The equations of motion (40.11) describe the evolution of the light fields in counterpropagating modes of a ring cavity. Without scatterer located in the mode volume, the modes evolve independently. In contrast, a scatterer (e.g. an atom or a beam splitter) may redistribute photons between the modes, whose dynamics thereby becomes coupled.

We will in the following assume the scatterer as immobile, except for Sec. 40.5.1, where we consider a vibrating scatterer. Immobile scatterers can, for example, be heavy masses, such as imperfections on the surfaces of the mirrors of the cavity (scratches, dust particles, etc.), which can scatter light both, out of the cavity and into the reverse cavity mode. In *laser gyroscopes* this backscattering may induce a locking of counterpropagating modes and hamper their proper operation.

40.2.5.1 Classical derivation of coupled atom-ring cavity equations

The equations of motion (40.11) describe the light fields classically. Hence, it is not surprising that they can be derived with entirely classical arguments. Here, we will show this for a ring cavity in the presence of an atom sitting at a fixed position z on the cavity's optical axis. We understand the atom as a beamsplitter located within the mode volume of the resonator and partially reflecting and transmitting incident light with reflection and transmission coefficients $(r_\beta, t_\beta) = (\imath\beta, 1+\imath\beta)$ such that $r_\beta^2 + t_\beta^2 = 1$. Transmitted (forward scattered) photons may be phase-shifted, while reflected photons are backscattered into the counterpropagating mode of the resonator.

Similarly, we treat the incoupling mirror as a beam splitter with coefficients (r_{in}, t_{in}). The incident field E_{in} produces, in the cavity, field amplitudes of $\alpha_\pm$ for the co- and counterpropagating waves. As in (40.7), we normalize the amplitudes by the numbers of photons $n_\pm \equiv |\alpha_\pm|^2$. After a round-trip time $\tau = \delta_{fsr}^{-1}$ through the mode volume we have in the position of the incoupling mirror the field,

$$\begin{aligned}\alpha_+(t+\tau) &= r_{in}(1+\imath\beta)e^{\imath kL}\alpha_+(t) + \imath\beta r_{in}^2 e^{2\imath kL - 2\imath kz}\alpha_-(t) + t_{in}\alpha_+^{in}(t) \\ \alpha_-(t+\tau) &= r_{in}(1+\imath\beta)e^{\imath kL}\alpha_-(t) + \imath\beta e^{2\imath kz}\alpha_+(t) + t_{in}(1+\imath\beta)e^{\imath kL}\alpha_-^{in}(t)\ .\end{aligned} \tag{40.167}$$

L is the total length of the ring cavity. Obviously, we have $kL = \omega/\delta_{fsr}$. In the vicinity of a resonance we have, $\Delta_c \ll \delta_{fsr}$, and the quantity ω/δ_{fsr} is almost integer, $\omega \simeq 2\pi N\delta_{fsr} - \Delta_c$, such that we can expand the exponential, $e^{\imath kL} = 1 - \imath\Delta_c/\delta_{fsr}$. Thus, we obtain,

$$\begin{aligned}\tau\dot{\alpha}_+ &= -\left[1 - r_{in}(1+\imath\beta)e^{\imath kL}\right]\alpha_+ + \imath\beta r_{in}^2 e^{-2\imath kz}\alpha_- + t_{in}\alpha_+^{in} \\ \tau\dot{\alpha}_- &= -\left[1 - r_{in}(1+\imath\beta)e^{\imath kL}\right]\alpha_- + \imath\beta e^{2\imath kz}\alpha_+ + t_{in}(1+\imath\beta)\alpha_-^{in}\ .\end{aligned} \tag{40.168}$$

We now connect the transmission of the coupling mirror t_{in} with the decay constant κ assuming that the light can only leave the cavity through this mirror. We define,

$$\kappa \equiv \frac{T}{\tau} \tag{40.169}$$

as the part of the light lost during one round trip. Thus, $t_{in} = \sqrt{T} \simeq \sqrt{\pi/F} = \sqrt{\kappa/\delta_{fsr}}$. Besides that, t_{in} is very small, such that,

$$t_{in}^2 = 1 - r_{in}^2 \simeq 2(1 - r_{in}) \ . \tag{40.170}$$

Thus, the first factor is,

$$\begin{aligned} \delta_{fsr}\left[1 - r_{in}(1+\imath\beta)e^{\imath kL}\right] &\simeq \delta_{fsr} - \delta_{fsr}(1 - t_{in}^2/2)(1+\imath\beta)(1+\imath\Delta_c/\delta_{fsr}) \\ &\simeq \kappa/2 + \imath\beta - \imath\Delta_c \simeq -\kappa/2 \ . \end{aligned} \tag{40.171}$$

It gives the cavity losses for the two modes during one round trip. We assume here that losses can only occur via the coupling mirror. However, all losses can be included in a single appropriate κ. There are usually other losses due to scattering on the surface of the mirrors or absorption by the atoms. Finally, we obtain for weak atomic reflection and in resonance, that is, for $\beta \ll \kappa$ and $\Delta_c = 0$ the system of equations,

$$\begin{aligned} \dot{\alpha}_+ &= -\kappa\alpha_+ + \imath\delta_{fsr}\beta(1 - t_{in}^2)e^{-2\imath kz}\alpha_- + \sqrt{\kappa\delta_{fsr}}\alpha_+^{in} \\ \dot{\alpha}_- &= -\kappa\alpha_- + \imath\delta_{fsr}\beta e^{2\imath kz}\alpha_+ + (1+\imath\beta)\sqrt{\kappa\delta_{fsr}}\alpha_-^{in} \end{aligned} \tag{40.172}$$

To calculate the value of β, we need the reflection coefficient of a single atom. It depends on the polarizability,

$$r_\beta = \frac{k}{\pi w^2}\frac{\alpha_{pol}}{\varepsilon_0} \ \left(= \frac{\sigma_0}{\pi w^2}\frac{\Gamma}{2\Delta_a}\right) \ . \tag{40.173}$$

The optical potential to which the atom is exposed is,

$$\phi = \frac{I}{2c}\frac{\alpha_{pol}}{\varepsilon_0} \ , \tag{40.174}$$

where we write the intensity of light as,

$$I = 2\varepsilon_0 c\mathcal{E}_1^2|\alpha_+ e^{\imath kZ} + \alpha_- e^{-\imath kZ}| \ . \tag{40.175}$$

We normalize once more to the field generated by a single photon, $\mathcal{E}_1 = \sqrt{\hbar\omega/2\varepsilon_0 V_m}$ with the mode volume, $V_m = \frac{\pi}{2}Lw^2$. On the other hand, the potential can be determined directly through the Rabi frequency,

$$\phi(\mathbf{r}) = \frac{\hbar\Omega(\mathbf{r})^2}{4\Delta_a} \ , \tag{40.176}$$

The Rabi frequency $\Omega(\mathbf{r})^2 = 4g^2|\alpha_+ e^{\imath kZ} + \alpha_- e^{-\imath kZ}|^2$ is normalized to the frequency of Rabi generated by a photon g. Using the frequency shift (light-shift) by photon (40.116), $U_0 = \frac{g^2}{\Delta_a}$, we can also write,

$$\phi(\mathbf{r}) = \hbar U_0|\alpha_+ e^{\imath kZ} + \alpha_- e^{-\imath kZ}|^2 \ . \tag{40.177}$$

A comparison of the above equations gives,

$$r_\beta = \frac{\imath U_0}{\delta_{fsr}} \ . \tag{40.178}$$

With an atom in the resonator, we have,

$$\beta = \frac{\imath U_0}{\delta_{fsr}} \ . \tag{40.179}$$

We define for convenience, $\eta_\pm = \sqrt{\kappa\delta_{fsr}}\alpha_\pm^{in}$ and we suppose, that $t_{in} \ll 1$, $r_\beta \ll 1$ and $\beta \ll 1$. This ultimately leads to the result,

$$\dot{\alpha}_\pm = -\kappa\alpha_\pm - \imath U_0 e^{\mp 2\imath kz}\alpha_\mp + \eta_\pm \ . \tag{40.180}$$

Example 244 (*Classical CARL equations*): If we were to treat the atomic position z as a degree of freedom, we could calculate the classical potential of the stationary light wave, and therefore the dipole force,

$$F = -\nabla\phi = -\hbar U_0 \nabla_{Z=z} |\alpha_+ e^{\imath kZ} + \alpha_- e^{-\imath kZ}|^2 \ , \tag{40.181}$$

and, consequently, derive the dynamics of the scatterer via,

$$m\ddot{z} = -2\imath\hbar k U_0(\alpha_+\alpha_-^* e^{2\imath kz} - \alpha_+^*\alpha_- e^{-2\imath kz}) \ . \tag{40.182}$$

This will be studied in Chp. 42. In the remaining sections of this chapter we will assume the atom to be located at a fixed position.

In the above derivation we assumed, for simplicity, the pump laser on resonance with the cavity, $\Delta_c = 0$. Relaxing this condition, an analogous derivation yields [5],

$$\dot{\alpha}_\pm = (-\kappa + \imath\Delta_c - \imath U_0)\alpha_\pm - \imath U_0 e^{\mp 2\imath kz}\alpha_\mp + \eta_\pm \ . \tag{40.183}$$

40.2.5.2 Adiabatically simplified Hamiltonian

In a ring cavity, the simplified Hamiltonian,

$$\boxed{\hat{H} = (U_0 - \Delta_c)\sum_\pm \hat{a}_\pm^\dagger \hat{a}_\pm - \imath\eta_\pm(\hat{a}_\pm - \hat{a}_\pm^\dagger) + U_0(\hat{a}_+\hat{a}_-^\dagger e^{2\imath kz} + \hat{a}_+^\dagger \hat{a}_- e^{-2\imath kz})} \ , \tag{40.184}$$

which can be obtained from the full Hamiltonian via adiabatic elimination of the excited atomic state, already exhibits this phenomenon. With the above Hamiltonian we derive from the Heisenberg equation,

$$\dot{\hat{a}}_\pm = -\imath[\hat{a}_\pm, \hat{a}] - \kappa\hat{a}_\pm = (-\kappa + \imath\Delta_c - \imath U_0)\hat{a}_\pm - \imath U_0 e^{\mp 2\imath kz}\hat{a}_\mp + \eta_\pm \ , \tag{40.185}$$

which, after taking the expectation values and disregarding correlations, reproduces the equations of motion (40.183). Of course, as we eliminated the internal atomic degree of freedom, spontaneous emission is not accounted for. We may, however, include it phenomenologically via the substitution $U_0 \to U_\gamma \equiv U_0 - \imath\gamma_0$. The stationary solution of Eq. (40.185) is *exactly the same* as the one derived for the full Jaynes-Cummings model (40.164) under the assumption of weak excitation, $g|\alpha_\pm| \ll \Gamma, \Delta_a$,

$$\boxed{\alpha_\pm = -\imath\frac{\eta_\pm(U_\gamma - \Delta_\kappa) - U_\gamma e^{\mp 2\imath kz}\eta_\mp}{(U_\gamma - \Delta_\kappa)^2 - U_\gamma^2}} \tag{40.186}$$

[5] Note, that we have not allowed for spontaneous emission by the atomic scatterer out of the cavity mode. This approximation is only good far from resonance, $\Delta_a \gg \Gamma$. We will see in Sec. 42.1.3, how to generalize the equations of motion for near resonance cases.

with the abbreviations,

$$U_\gamma \equiv U_0 - \imath\gamma_0 \quad , \quad \Delta_\kappa \equiv \Delta_c + \imath\kappa \; . \tag{40.187}$$

Solve the Exc. 40.2.9.7.

40.2.6 Normal mode splitting induced by beam splitting

The fact that (in the weak excitation limit) normal mode splitting is fully described by the classical field equations (40.183) shows that the phenomenon clearly is *not a quantum effect*: a classical beam splitter inserted into the cavity does the same job. We will now discuss the normal mode splitting in detail based on the adiabatically simplified equations (40.187).

The equation (40.183) can be written as follows,

$$\imath\dot{\vec{\alpha}} = W\vec{\alpha} + \imath\vec{\eta} \; , \tag{40.188}$$

where $\vec{\alpha}$ and $\vec{\eta}$ regroup the amplitudes $\alpha_\pm$ and $\eta_\pm$. This equation takes the form of a Schrödinger equation, where,

$$W \equiv \begin{pmatrix} U_0 - \Delta_c - \imath\kappa & U_0 e^{-2\imath kz} \\ U_0 e^{2\imath kz} & U_0 - \Delta_c - \imath\kappa \end{pmatrix} \tag{40.189}$$

would be the Hamiltonian describing the coupling between counterpropagating modes. The eigenvalues of this matrix are,

$$W^{(1,2)} = 2U_0 - \Delta_c - \imath\kappa \quad , \quad -\Delta_c - \imath\kappa \; . \tag{40.190}$$

This *normal mode splitting* [6] of the cavity results from the coupling of the two cavity modes $\hat{a}_+^\dagger \hat{a}_-$. Obviously, the energies and widths of the eigenvalues do not depend neither on the pump intensities $\eta_\pm$ nor the z-position of the atom. On the other hand, the spectral behavior of $\alpha_\pm$, and hence the observable quantities, such as the transmission

$$T_\pm \equiv \left| \frac{\kappa\alpha_\pm}{\eta_\pm} \right|^2 \tag{40.191}$$

depend on these parameters. In the following, we will study normal mode splitting in a ring cavity by a discussion of the expression (40.164) for the cases of (i) anti-symmetric pumping, (ii) symmetric pumping, and (iii) uni-directional pumping.

(i) Assuming $\gamma_0 = 0$ and anti-symmetric pumping, $\eta_- = \eta_+$ and $kz = \pi/2$, the expression (40.164) becomes,

$$\begin{aligned} \alpha_+ &= \eta_+ \frac{\kappa - \imath(\Delta_c - 2U_0)}{[\kappa - \imath(\Delta_c - U_0)]^2 + U_0^2} \\ \Rightarrow \quad \left| \frac{\alpha_+}{\eta_+} \right|^2 &= \frac{1}{\kappa^2 + \Delta_c^2} \; . \end{aligned} \tag{40.192}$$

[6] The splitting is not exactly the *vacuum Rabi splitting*, which occurs when the excitation can not be eliminated adiabatically. The vacuum Rabi splitting results from the Jaynes-Cummings [1300, 312] and is caused by the coupling of internal and external states $\hat{a}^\dagger\hat{\sigma}$.

That is, the transmission profile is a Lorentzian.

(ii) For symmetric pumping, $\eta_- = \eta_+$ and $kz = 0$,

$$\alpha_+ = \eta_+ \frac{\kappa - \imath\Delta_c}{[\kappa - \imath(\Delta_c - U_0)]^2 + U_0^2} \qquad (40.193)$$
$$\Rightarrow \quad \left|\frac{\alpha_+}{\eta_+}\right|^2 = \frac{1}{\kappa^2 + (\Delta_c - 2U_0)^2} \ .$$

Setting $\Delta_c = \Delta_a$ we find from $0 \equiv \frac{d}{d\Delta_c}\left|\frac{\alpha_+}{\eta_+}\right|^2$ a minimum at $\Delta_c = 0$ and two maxima at $\Delta_c = 2U_0 = \sqrt{2}g$. This is the usual normal mode splitting for a ring cavity.

(iii) For uni-directional pumping, $\eta_- = 0$,

$$\alpha_+ = \eta_+ \frac{\kappa - \imath(\Delta_c - U_0)}{[\kappa - \imath(\Delta_c - U_0)]^2 + U_0^2} \qquad (40.194)$$
$$\Rightarrow \quad \left|\frac{\alpha_+}{\eta_+}\right|^2 = \frac{\kappa^2 + (\Delta_c - U_0)^2}{[\kappa^2 - \Delta_c(\Delta_c - 2U_0)]^2 + 4\kappa^2(\Delta_c - U_0)^2} \ .$$

That is, the transmission profile is a more complicated and may exhibit up to three peaks.

40.2.6.1 Unidirectional pumping

For unilateral pumping, $\eta_- = 0$, and approximating $\gamma_0 = 0$, the solution (40.164) simplifies to,

$$\alpha_+(\infty) = \eta_+ \frac{\chi}{\chi^2 + U_0^2} \qquad \text{and} \qquad \alpha_-(\infty) = \eta_+ \frac{\imath U_0 e^{2\imath kz}}{\chi^2 + U_0^2} \ . \qquad (40.195)$$

These formulas show that, for weak coupling, $U_0 \ll \kappa$, the counterpropagating mode receives little light. On the other side, for strong coupling (or very high finesse) and $\Delta_c = 0$, the intensity is equally distributed, $|\alpha_+|^2 = |\alpha_-|^2 = \frac{\eta_+}{2\kappa}$ [7]. We calculate the splitting of normal modes in Exc. 40.2.9.8.

The counterpropagating modes form, by interference, a standing light wave giving rise to a dipole potential in the form of a one-dimensional optical lattice. Defining the phase $\theta = \theta_1 - \theta_2$ through,

$$\alpha_+ \equiv |\alpha_+| e^{-\imath\theta_1} \qquad \text{and} \qquad \alpha_- \equiv |\alpha_-| e^{-\imath\theta_2} \ , \qquad (40.196)$$

we verify by the equation (40.7),

$$\mathcal{E}^+(\zeta, t) = \mathcal{E}_1 |\alpha_+(t)| e^{\imath k\zeta} + \mathcal{E}_1 |\alpha_-(t)| e^{-\imath\theta(t)} e^{-\imath k\zeta} \ , \qquad (40.197)$$

and,

$$\frac{1}{2\varepsilon_0 c \mathcal{E}_1^2} I(\zeta, t) = \frac{1}{\mathcal{E}_1^2} \mathcal{E}^+(\zeta, t) \mathcal{E}^-(\zeta, t) \qquad (40.198)$$
$$= |\alpha_+(t)|^2 + |\alpha_-(t)|^2 + 2|\alpha_+(t)||\alpha_-(t)| \cos(2k\zeta + \theta) \ .$$

[7] This observation explains why perturbing effects such as backscattering from mirrors imperfections are dramatically magnified when the finesse is high.

That is, the phase indicates the positions of the potential maxima. Inserting the stationary solution for unilateral pumping (40.195), we derive the expression,

$$\tan\theta = \frac{\mathfrak{Im}\ \alpha_+(\infty)\alpha_-^*(\infty)}{\mathfrak{Re}\ \alpha_+(\infty)\alpha_-^*(\infty)} = \frac{\mathfrak{Im}\ \chi\imath e^{-2\imath kz}}{\mathfrak{Re}\ \chi\imath e^{-2\imath kz}} = \frac{\kappa\cos 2kz + (U_0-\Delta_c)\sin 2kz}{\kappa\sin 2kz - (U_0-\Delta_c)\cos 2kz}\ . \tag{40.199}$$

Or in other words, the phase of light determines the equilibrium position of the atom (or vice versa). Two cases are interesting: (i) For $\Delta_c = 0$ and $U_0 \gg \kappa$ the condition (40.203) turns into $\tan\theta = -\tan 2kz$. In this case, the phase of the backscattered field adjusts in such a way, that the atom stays at the valleys of the anti-nodes. (ii) For $\Delta_c = U_0$ (or alternatively, when $\kappa \gg U_0, \Delta_c$) the condition (40.203) turns into $\tan\theta = -\tan(2kx + \frac{\pi}{2})$, such that the atom is at half height of the potential slope, exactly at the position, where it is able to backscatter the maximum of photons from the pumped mode α_+ to the mode α_-.

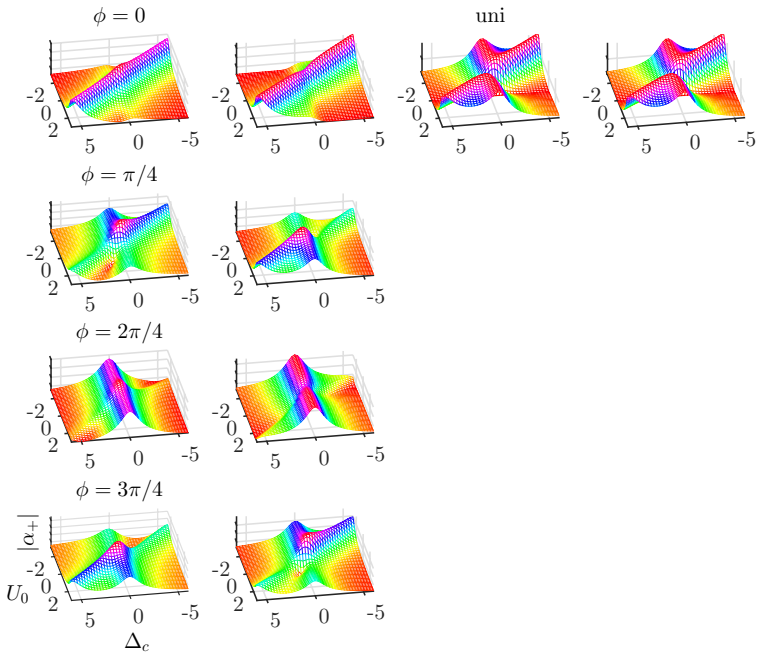

Figure 40.13: (code) (columns 1 and 2) Steady state field values according to (40.188) for bidirectional pumping with a single scatterer located at ϕ. (columns 3 and 4) Same for unidirectional pumping. Here the location of the scatterer does not matter.

40.2.6.2 (Anti-)Symmetric pumping

Let us assume equal intensities for the pumps, but variable phases, $\eta_\pm = \eta e^{\pm\imath\phi}$, such that $\xi = e^{-2\imath kz-\imath\phi}$. Then, equation (40.164) simplifies to,

$$\alpha_\pm(\infty) = \eta_\pm \frac{\chi - \imath U_\gamma \xi^\pm}{\chi^2 + U_\gamma^2} = \eta \frac{\chi - \imath U_\gamma e^{\mp 2\imath kz \mp \imath\phi}}{\chi^2 + U_\gamma^2}\ . \tag{40.200}$$

The potential is calculated in the same way as in (40.198). The coherences are,

$$\begin{aligned}
\alpha_\pm(\infty)\alpha_\pm^*(\infty) &= \eta^2 \tfrac{(\kappa-\imath\Delta_c\mp 2U_0 e^{\mp\imath kz}\sin kz)(\kappa+\imath\Delta_c\mp 2U_0 e^{\pm\imath kz}\sin kz)}{(\kappa^2+2U_0\Delta_c-\Delta_c^2)^2+4\kappa^2(U_0-\Delta_c)^2} \\
\alpha_\pm(\infty)\alpha_\mp^*(\infty) &= \eta^2 \tfrac{\kappa^2+(\Delta_c\mp 2\imath U_0 e^{\mp\imath kz}\sin kz)^2}{(\kappa^2+2U_0\Delta_c-\Delta_c^2)^2+4\kappa^2(U_0-\Delta_c)^2} \\
e^{\pm 2\imath kz} &= \tfrac{\alpha_\mp\alpha_\pm^*}{|\alpha_-\alpha_+^*|}
\end{aligned} \quad , \tag{40.201}$$

such that the relative phase of the counter-propagating waves adjusts itself to,

$$\tan\theta = \frac{\mathfrak{Im}\ \alpha_+(\infty)\alpha_-^*(\infty)}{\mathfrak{Re}\ \alpha_+(\infty)\alpha_-^*(\infty)} = \frac{\kappa^2\sin 2\phi + 4U_0^2\sin^2(kz+\phi)\sin 2kz}{\kappa^2\cos 2\phi - 4U_0^2\sin^2(kz+\phi)\cos 2kz} \ . \tag{40.202}$$

The quantity η^2/κ^2 denotes the number of intracavity photons. According to the formula (40.202), for a weak atom-field coupling, $U_0 \ll \kappa$, the phase adjusts itself to the external pumps, $\theta \to 2\phi$, while for strong coupling, it adjusts to the position of the atom, $\theta \to 2kz$.

Example 245 (*'Pulling' of the optical mode by the atom*): We study the case $U_0 \simeq \kappa$ considering $\gamma_0 = 0 = \Delta_c$ and a particular external phase [482], $\phi = \pi/2$,

$$\begin{aligned}
\alpha_\pm(\infty) &= \pm\imath\eta\frac{\kappa+\imath U_0 \pm U_0 e^{\mp 2\imath kz}}{\kappa^2+2\imath\kappa U_0} \\
\theta(\infty) &= \arctan\frac{-4U_0^2\cos^2 kz\sin 2kz}{\kappa^2+4U_0^2\cos^2 kz\cos 2kz} \simeq \arctan\frac{-8U_0^2}{\kappa^2+4U_0^2}kz \ ,
\end{aligned} \tag{40.203}$$

expanding the last formula around $kz = 0$. Fig. 40.14 shows how, with the increase in the coupling force between the field and the atoms, U_0, the phase tends to lock to the atomic position. However, the phase imposed by the external pump competes for this privilege. Curiously, this is independent of laser power, but depends only on the ratio between U_0 and κ.

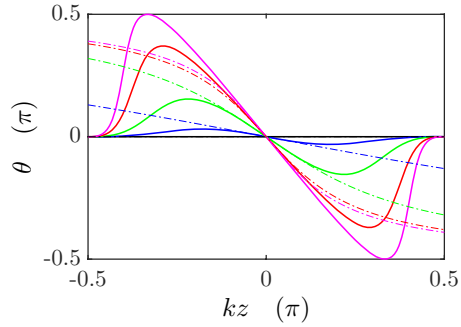

Figure 40.14: (code) 'Pulling' of the phase by the atoms for $U_0/\kappa = 0$, 0.2, 0.5, 1 and $\sqrt{2}$. The solid curves show the exact phase, the 'dash-dotted' curves the linear approximation (40.207).

Example 246 (*Resonant case*): Assuming that the cavity is in resonance, $\Delta_c = 0$, and pumped in a single direction, $\eta_- = 0$, neglecting spontaneous emission, $\gamma_0 = 0$, and assuming low backscattering rates, $U_s \ll \kappa$,

$$\alpha_+(\infty) \simeq \frac{\eta_+}{\kappa} \qquad \text{and} \qquad |\alpha_-(\infty)| = \frac{U_s}{\kappa}|\alpha_+(\infty)| \ .$$

Looking at short times, we find that the dynamics of the unpumped mode is delayed, since,

$$\dot\alpha_+(0) \simeq \eta_+ \qquad \text{and} \qquad \dot\alpha_-(0) \simeq -\imath U_s \alpha_+ e^{-2\imath k r_s} \ ,$$

giving,

$$\alpha_+(0) \simeq \eta_+ t \qquad \text{and} \qquad \alpha_-(0) \simeq -\imath U_s \eta_+ \frac{t^2}{2} e^{-2\imath k r_s} \ .$$

The complete solution of the equations (40.191) with unidirectional pumping, $\eta_- = 0$, will be derived in Exc. 40.2.9.9.

40.2.7 Time-dependent solutions

40.2.7.1 Time-dependent solution without pump

To calculate the homogeneous time-dependent solution of the equation of motion of the ring cavity with $\eta_\pm = 0$, we solve the Schrödinger equation (40.188) the way we learned in quantum mechanics. We start by diagonalizing the matrix (40.189),

$$\begin{aligned} W &= \begin{pmatrix} U_0 - \imath\kappa & U_0 e^{-2\imath kz} \\ U_0 e^{2\imath kz} & U_0 - \imath\kappa \end{pmatrix} \qquad (40.204) \\ &= \begin{pmatrix} e^{-2\imath kz} & -e^{-2\imath kz} \\ 1 & 1 \end{pmatrix} \begin{pmatrix} 2U_0 - \imath\kappa & 0 \\ 0 & -\imath\kappa \end{pmatrix} \begin{pmatrix} e^{-2\imath kz} & -e^{-2\imath kz} \\ 1 & 1 \end{pmatrix}^{-1} = U E_W U^{-1} \ , \end{aligned}$$

where E_W is the matrix of eigenvalues and U a unitary transformation. So,

$$\begin{aligned} \vec\alpha &= e^{-\imath W t}\vec\alpha_0 = U e^{-iE_W t} U^{-1}\vec\alpha_0 \qquad (40.205) \\ &= e^{-\kappa t - \imath U_0 t} \begin{pmatrix} \cos U_0 t & -\imath e^{-2\imath kz} \sin U_0 t \\ -\imath e^{2\imath kz} \sin U_0 t & \cos U_0 t \end{pmatrix} \vec\alpha_0 \ . \end{aligned}$$

In Exc. 40.2.9.7 we study the equation of motion numerically. We'll see an alternative calculation in Exc. 40.2.9.11. We calculate the coherence by,

$$\begin{aligned} \alpha_+(t)\alpha_-^*(t) &= e^{-2\kappa t}\left[\alpha_{0+}\alpha_{0-}(\cos^2 U_0 t + e^{-4\imath kz}\sin^2 U_0 t) + \tfrac{1}{2}(\alpha_{0+}^2 - \alpha_{0-}^2)\imath e^{-2\imath kz}\sin 2U_0 t\right] \\ &\xrightarrow{z\to 0} e^{-2\kappa t}\left[\alpha_{0+}\alpha_{0-} + \tfrac{1}{2}(\alpha_{0+}^2 - \alpha_{0-}^2)\imath \sin 2U_0 t\right] \ , \qquad (40.206) \end{aligned}$$

making the transition to the Lamb-Dicke regime by $z \to 0$. The phase of the standing wave is,

$$\tan\theta = \frac{\mathfrak{Im}\ \alpha_+(t)\alpha_-^*(t)}{\mathfrak{Re}\ \alpha_+(t)\alpha_-^*(t)} \xrightarrow{z\to 0} \frac{\alpha_{0+}^2 - \alpha_{0-}^2}{2\alpha_{0+}\alpha_{0-}} \sin 2U_0 t \ . \qquad (40.207)$$

We see that, in resonance and without pumping, the field adjusts its phase to the atom and also decays with the rate κ, while the atom redistributes the photons between

modes with the (Rabi-)frequency $2U_0$. The formula (40.207) does not show any damping of the phase dynamics in the Lamb-Dicke regime. Thus, in the absence of pumping, the cavity dissipation reduces only the field amplitudes, but does not damp the adjustment of the phase to the atomic position.

40.2.7.2 Time-dependent solution with fixed pump

To find the complete solution of the inhomogeneous Schrödinger equation (40.188), we first calculate the stationary solution,

$$\vec{\alpha}(\infty) = -\imath W^{-1}\vec{\eta}\ . \tag{40.208}$$

This particular solution of the inhomogeneous equation, added to the general solution of the homogeneous equation, gives the general solution of the inhomogeneous Schrödinger equation,

$$\vec{\alpha}(t) = e^{-\imath Wt}\vec{\alpha}(0) + (1 - e^{-\imath Wt})\vec{\alpha}(\infty)\ . \tag{40.209}$$

We derive and analyze this solution in the Exc. 40.2.9.12.

Analytical solutions only exist in particular cases. However, they allow a better understanding of the dynamics. So let's consider some limiting cases. In Exc. 40.2.9.13 we determine the steady state of an atom interacting with the modes of a unidirectionally pumped annular cavity and calculate the stationary position of the atom in a unidirectionally pumped ring cavity. In Exc. 40.2.9.14 we derive motion equations for the 'intensities' $\alpha_\pm\alpha_\pm^*$ and 'coherences' $\alpha_\pm\alpha_\mp^*$.

40.2.8 Forced atomic vibration in a ring cavity

We now assume, that the atom is forced to vibrate by an external force. The vibration is described by,

$$kz = kz_0 \sin\omega t\ . \tag{40.210}$$

We consider small modulation excursions, $1 \gtrsim kz_0 = \frac{kv}{\omega} = \frac{2\omega_{rec}}{\omega}$, which is equivalent to saying that the oscillation frequency should exceed to recoil shift. In this (Lamb-Dicke) regime the Bessel-expansion yields,

$$e^{\pm 2\imath kz_0 \sin\omega t} = \sum_n J_n(\pm 2kz_0)e^{\imath n\omega t} \simeq J_0(2kz_0) \pm 2\imath J_1(2kz_0)\sin\omega t \simeq 1 \pm 2\imath kz_0 \sin\omega t\ . \tag{40.211}$$

The differential equations for the two counterpropagating ring cavity-field (40.183) can then be written:

$$\boxed{\dot{\alpha}_\pm = (\mathbf{L} - 2\imath\mathbf{X}\sin\omega t)\alpha_\pm + \eta_\pm}\ , \tag{40.212}$$

where,

$$\mathbf{L} = \begin{pmatrix} -\kappa - \imath U_0 & -\imath U_0 J_0 \\ -\imath U_0 J_0 & -\kappa - \imath U_0 \end{pmatrix} \quad \text{and} \quad \mathbf{X} = \begin{pmatrix} 0 & -\imath U_0 J_1 \\ \imath U_0 J_1 & 0 \end{pmatrix}\ . \tag{40.213}$$

We insert the ansatz $\alpha_\pm = \sum_n \alpha_\pm^{(n)} e^{\imath n\omega t}$, where $\dot{\alpha}_\pm^{(n)} = 0$, into the equations and project onto the basis $e^{\imath n\omega t}$:

$$\begin{aligned} &\imath n\omega_x \sum_n \alpha_\pm^{(n)} e^{\imath n\omega t} = \big(\mathbf{L} - \mathbf{X}(e^{\imath\omega t} - e^{-\imath\omega t})\big) \sum_n \alpha_\pm^{(n)} e^{\imath n\omega t} + \eta_\pm \qquad (40.214)\\ &\Longrightarrow (\mathbf{L} - \imath n\omega)\alpha_\pm^{(n)} + \mathbf{X}(\alpha_\pm^{(n+1)} - \alpha_\pm^{(n-1)}) = -\eta_\pm \delta_{n0} \ . \end{aligned}$$

We define operators $\mathbf{S}_n^{\uparrow\downarrow}$ by $\alpha_\pm^{(n+1)} = \mathbf{S}_n^\uparrow \alpha_\pm^{(n)}$ for $n \geq 0$ and $\alpha_\pm^{(n-1)} = \mathbf{S}_n^\downarrow \alpha_\pm^{(n)}$ for $n \leq 0$ and obtain,

$$\big[\mathbf{L} - \imath n\omega + \mathbf{X}(\mathbf{S}_n^\uparrow - \mathbf{S}_n^\downarrow)\big]\, \alpha_\pm^{(n)} = -\eta_\pm \delta_{n0} \ . \qquad (40.215)$$

For $n = 0$, we get,

$$\alpha_\pm(\infty) = \alpha_\pm^{(0)} = -\left[\mathbf{L} + \mathbf{X}(\mathbf{S}_0^\uparrow - \mathbf{S}_0^\downarrow)\right]^{-1} \eta_\pm \ . \qquad (40.216)$$

If we substitute in equation (40.214) $\alpha_\pm^{(n)} = \mathbf{S}_{n-1}^\uparrow \alpha_\pm^{(n-1)} = \mathbf{S}_{n+1}^\downarrow \alpha_\pm^{(n+1)}$, we get for $n \gtrless 0$,

$$\mathbf{S}_{n-1}^\uparrow = \left[\mathbf{L} - \imath n\omega + \mathbf{X}\mathbf{S}_n^\uparrow\right]^{-1} \mathbf{X} \qquad \text{and} \qquad \mathbf{S}_{n+1}^\downarrow = \left[\mathbf{L} - \imath n\omega - \mathbf{X}\mathbf{S}_n^\downarrow\right]^{-1} \mathbf{X} \ . \quad (40.217)$$

By recursive substitution of the lower into the upper equation, the stationary solution can now be written by means of continued fractions,

$$\mathbf{S}_0^{\uparrow\downarrow} \equiv \frac{1}{\mathbf{L} - \imath\omega \pm \mathbf{X}\frac{1}{\mathbf{L} - 2\imath\omega \pm \mathbf{X}\frac{1}{\cdots}}\mathbf{X}}\mathbf{X} \ . \qquad (40.218)$$

$\alpha_\pm(\infty)$ in Eq. (40.216) gives us the stationary solution of the differential equation, time-averaged over an oscillation period.

If we are deep in the Lamb-Dicke regime, we need only consider the first order of the continued fractions. We set $\mathbf{S}_1^{\uparrow\downarrow} = \mathbf{1}$ and obtain the simplified equations,

$$\begin{aligned} &\mathbf{S}_0^\uparrow = [\mathbf{L} - \imath\omega + \mathbf{X}]^{-1}\mathbf{X} \qquad \text{and} \qquad \mathbf{S}_0^\downarrow = [\mathbf{L} - \imath\omega - \mathbf{X}]^{-1}\mathbf{X} \qquad (40.219)\\ &\alpha_\pm^{(0)} = -\left[\mathbf{L} + \mathbf{X}\left(\mathbf{S}_0^\uparrow - \mathbf{S}_0^\downarrow\right)\right]^{-1} \eta_\pm\\ &\alpha_\pm^{(1)} = \mathbf{S}_0^\uparrow \alpha_\pm^{(0)} \qquad \text{and} \qquad \alpha_\pm^{(-1)} = \mathbf{S}_0^\downarrow \alpha_\pm^{(0)} \ . \end{aligned}$$

Explicitly,

$$\begin{aligned} \mathbf{S}_0^{\uparrow\downarrow} &= \frac{U_0 k z_0}{(\kappa + \imath U_0 + \imath\omega)^2 + U_0^2(1 - k^2 x_0^2)} \begin{pmatrix} -U_0(1 \pm k z_0) & \imath(\kappa + \imath U_0 + \imath\omega) \\ -\imath(\kappa + \imath U_0 + \imath\omega) & -U_0(-1 \pm k z_0) \end{pmatrix}\\ \mathbf{S}_0^\uparrow - \mathbf{S}_0^\downarrow &= \frac{-2U_0^2 k^2 x_0^2}{(\kappa + \imath U_0 + \imath\omega)^2 + U_0^2(1 - k^2 x_0^2)} \mathbb{I}_2\\ \alpha_\pm &= \alpha_\pm^{(0)} + \alpha_\pm^{(1)} e^{\imath\omega t} + \alpha_\pm^{(-1)} e^{-\imath\omega t} \ . \qquad (40.220) \end{aligned}$$

Finally,

$$\boxed{\alpha_\pm = -[1 + \mathbf{S}_0^\uparrow e^{\imath\omega t} + \mathbf{S}_0^\downarrow e^{-\imath\omega t}][\mathbf{L} + \mathbf{X}(\mathbf{S}_0^\uparrow - \mathbf{S}_0^\downarrow)]^{-1}\eta_\pm} \ . \qquad (40.221)$$

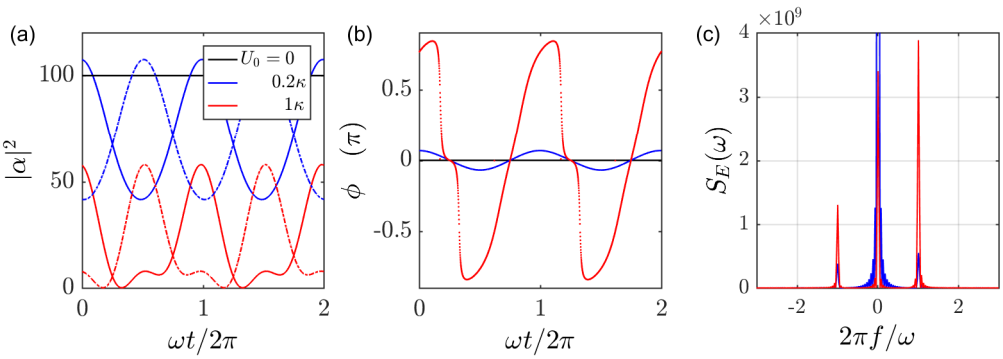

Figure 40.15: (code) (a) Photon number and (b) phase shift of the cavity in response to a modulated atomic position. The parameters are $kz_0 = 1$, $\kappa = (2\pi)\ 20\,\mathrm{kHz}$, $\omega = 2.5\kappa$, and $\eta_\pm = 10\kappa$. (c) Spectrum recorded behind a cavity mirror with the transmittivity t_{hr}. The spectrum is obtained as the Fourier transform of the $g^{(1)}(\tau)$ correlation function of the transmitted field $E_{out} = t_{hr}e^{\imath ka}E_{cav}$, where $e^{\imath ka}$ is a fixed phase factor depending on the mirror position a (see Sec. 35.5.2).

The Fig. 40.15 shows how the phase of the ring cavity behaves in time for various atom-field coupling constants.

It is interesting to study the oscillatory response of the cavity-field to a forced atomic vibration, because it yields information about the cavity backaction. In fact, as shown above, the vibrating atom imprints sidebands to the intracavity refractive index [1141, 9]. The sidebands appear in the cavity transmission spectrum. A more sophisticated method to detect the backaction could be to watch the response in the beat signal to a periodic modulation of the incoupled fields with a vibrating atom,

$$\dot{\alpha}_\pm = (-\kappa - \imath U_0)\alpha_\pm - \imath U_0 e^{\mp 2\imath k z_0 \sin\omega t}\alpha_\mp + \eta e^{\pm\imath\phi_0 \sin\omega_\phi t}\ . \tag{40.222}$$

We would expect a clear signature for resonance, $\omega_\phi = \omega$. The sidebands of the modulated pump would be coupled in, if they coincide. Instead of monitoring the cavity field, we could search the signature of the backaction in the atomic response. We will come back to this, when we discuss collective effects and the frequency shift of the center-of-mass motion. Do the Exc. 40.2.9.15. In Exc. 40.2.9.16 we study the spectrum of resonance fluorescence emitted by a ring cavity incorporating a beam splitter, and in Exc. 40.2.9.16 we study the spectrum of resonance fluorescence emitted by a linear cavity interacting with a single atom.

40.2.9 Exercises

40.2.9.1 Ex: Cooperative Lamb shift in a cavity

Calculate the cooperative Lamb shift in a cavity from the second formula (40.90) and plot the result as a function of the cavity detuning.

Solution: *The recipe to calculate the the cooperative Lamb shift is given by the second*

equation (40.90),

$$\Delta\omega = \sum_i \iint \frac{d^2 \sin^2\theta_{\mathbf{k}}}{\hbar^2} \frac{\hbar\omega_0}{2\varepsilon_0 V} \frac{1}{\omega_{ei} - \omega_{\mathbf{k}}} \rho(\omega_{\mathbf{k}}, \mathbf{k}) d\Omega_{\mathbf{k}} d\omega_{\mathbf{k}} \ .$$

Using previous results we can replace the density of states by (40.94), (40.91), and (40.42) and the integral over small solid angle by,

$$\int_{\hat{e}_k \in cav} \sin^2\theta_{\mathbf{k}} d\Omega_{\mathbf{k}} \simeq \tfrac{3}{8\pi}\Omega_{cav}$$

for $\theta_{\mathbf{k}} = \frac{\pi}{2}$. *Using the abbreviation (40.92), we obtain,*

$$\begin{aligned}\Delta\omega_{cav} &= \sum_i \Gamma_{free} \frac{3}{16\pi^2}\Omega_{cav} \int \frac{\mathcal{L}(\omega_{\mathbf{k}})}{\omega_{ei} - \omega_{\mathbf{k}}} d\omega_{\mathbf{k}} \\ &= \sum_i \Gamma_{free} \frac{3}{16\pi^2}\Omega_{cav} \int \frac{\sqrt{1 + (2F/\pi)^2}}{1 + (2F/\pi)^2 \sin^2 kL} \frac{1}{\omega_{ei} - \omega_{\mathbf{k}}} d\omega_{\mathbf{k}} \ .\end{aligned}$$

The only contribution to the difference in frequency shifts occurs near a resonance $\omega_{\mathbf{k}} \simeq \omega_{eg}$. *Therefore,*

$$\Delta\omega_{cav} \simeq \Gamma_{free} \frac{3}{32\pi}\Omega_{cav} \frac{\mathcal{L}'(\omega_{eg})}{\mathcal{L}(\omega_{eg})} 2\delta_{fsr} = \Gamma_{free} \frac{3}{32\pi}\Omega_{cav} \frac{(2F/\pi)^2 \sin(\omega_{eg}/\delta_{fsr})}{1 + (2F/\pi)^2 \sin^2(\omega_{eg}/2\delta_{fsr})} \ .$$

The spectrum is shown in Fig. 40.16

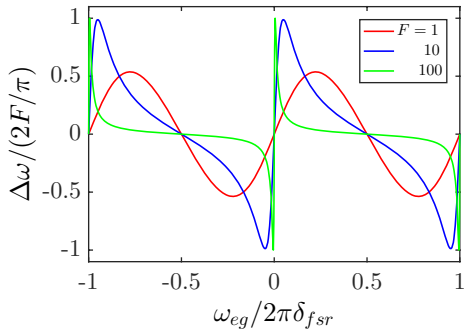

Figure 40.16: (code) Spectrum of the cooperative Lamb shift for three different finesses F.

40.2.9.2 Ex: Cooperative amplification for a rubidium gas in a cavity

Consider an non-degenerate cavity characterized by $\delta_{fsr} = 2\,\text{GHz}$, $F = 80$, and $w_0 = 6\,\mu\text{m}$. In order to benefit from the cooperativity of the cavity, the atoms must be within a volume axially delimited by the Rayleigh length and radially by the diameter of the mode near its waist.
a. Calculate the Rayleigh length for a wavelength of 780 nm and the mode volume.

b. For a given partial pressure of rubidium at room temperature of $p \approx 10^{-5}\,\mathrm{Pa}$, calculate the average number of atoms within the mode volume.
c. Of these atoms only those with an axial Doppler shift below $kv_z < \kappa$ emit resonantly into the cavity. Calculate the number of these atoms from the Maxwell-Boltzmann distribution.
d. Calculate the cooperative amplification of the emission rate into the cavity.

Solution: *a. The Rayleigh length is* $z_R = kw_0^2/2$. *This corresponds to a volume of* $V \simeq \pi w_0^2 z_R$.
b. The average number of atoms inside the mode volume is,

$$N_m = \frac{pV}{k_B T} \simeq 120 \ .$$

c. The number of atoms within the given velocity range is,

$$\begin{aligned} N_{kv_z} &= N_m \left(\frac{m}{2\pi k_B T}\right)^{3/2} \int e^{-m\mathbf{v}^2/2k_B T} d^3\mathbf{v} \\ &= N_m \left(\frac{\pi m}{2k_B T}\right)^{1/2} \int_0^{\kappa/k} e^{-mv_z^2/2k_B T} dv_z \\ &\simeq N_m \left(\frac{\pi m}{2k_B T}\right)^{1/2} \frac{\kappa}{k} = N_m \sqrt{\pi} \frac{\kappa}{k\bar{v}} \simeq 2 \ . \end{aligned}$$

Note that the interaction time of an atom transversely crossing the cavity mode is $w_0\sqrt{\frac{k_B T}{m}} \simeq 17\,\mathrm{ms}$.
d. The emission rate into the cavity is now,

$$R = \Gamma_{cav}|_{\hat{\mathbf{e}}_{\mathbf{k}} \in cav} \ N_{kv_z} = \Gamma_{free} \sqrt{1 + \left(\frac{2F}{\pi}\right)^2} \ \frac{3}{8\pi} \ \frac{8\pi}{k^2 w_0^2} \ N_m \sqrt{\pi} \frac{\kappa}{k\bar{v}} \ .$$

Without cavity,

$$R = \Gamma_{free} \cdot \frac{3}{8\pi} \cdot \frac{8\pi}{k^2 w_0^2} \cdot N_m \sqrt{\pi} \frac{\kappa}{k\bar{v}} \simeq 15000\,\mathrm{s}^{-1} \ .$$

With the cavity,

$$\Upsilon_{ndg} = \frac{F}{\pi} \cdot \frac{6}{k^2 w_0^2} \simeq 0.06 \ ,$$

we obtain,

$$R = \Gamma_{free} \cdot \eta \cdot N_m \sqrt{\pi} \frac{\kappa}{k\bar{v}} \simeq 780000 \ .$$

40.2.9.3 Ex: Characteristic parameters for various atom-cavity systems

Complete the following table calculating κ, V_m, ω_r, g_1, Υ, s, and r,

	rubidium	strontium
Γ	6 MHz	6.8 kHz
$\mathcal{F}$	250000	250000
L	100 μm	3 cm
w_0	20 μm	70 μm

Solution: *The completed table is,*

	rubidium	*strontium*
Γ	6 MHz	6.8 kHz
$\mathcal{F}$	250000	250000
L	100 μm	3 cm
w_0	20 μm	70 μm
κ	6 MHz	16 kHz
V_m	0.0002 mm^3	1 mm^3
ω_r	5 kHz	5 kHz
g_1	18 MHz	9 kHz
Υ	9	1
s	9	3
r	0.0008	0.3

40.2.9.4 Ex: Number of photons in a cavity

a. How many photons are in the mode of a cavity with finesse $F = 80000$ (i) in resonance and (ii) out of resonance resonantly pumped with a laser power of $P_{in} = 100\,\mu W$?
b. What power must be injected to produce 1 photon inside the cavity?
c. Resonant backscattering by the cavity mirrors can scatter photons into the reverse mode. Typically, $P_-/P_+ \simeq 0.005$. Hence, $n^{on}_{-,cav} = 1.5 \times 10^7$ and $n^{off}_{-,cav} = 0.01$. Using advanced techniques it is possible to reduce the number of backscattered photons by factor of > 20. Assuming that the losses due to backscattering are $S = 1$ ppm. Can the resonant backscattering by the mirrors destroy a BEC?
d. What is the amplitude of the output signal in terms of photons?

Solution: *a. The Airy formulas for the simplified case of a cavity with two identical mirrors give the intracavity intensity,*

$$\frac{P_{cav}}{P_{in}} = \frac{1}{T}\frac{(1-R)^2}{(1-R)^2 + 4R\sin^2\delta/2} \ ,$$

with $T = 1 - R$. For $\delta = 2\pi N$ and $\delta = 2\pi N + \pi$, we obtain respectively,

$$\frac{P^{on}_{cav}}{P_{in}} = \frac{1}{T} \qquad \textit{and} \qquad \frac{P^{off}_{cav}}{P_{in}} = \frac{1}{T}\frac{(1-R)^2}{(1+R)^2} \approx \frac{T}{2} \ .$$

From the finesse, $F = \pi\sqrt{R}/(1-R)$, we estimate the reflectivity of the mirrors $R \approx 1 - \pi/F$. Therefore, the fraction of the power injected in and out of resonance are, $P^{on}_{cav}/P_{in} \simeq 25000$ and $P^{off}_{cav}/P_{in} = 2 \times 10^{-5}$. Pumping the cavity mode with $P_{in} = 100\,\mu\mathrm{W}$ gives,

$$n^{on}_{+,cav} = \frac{P_{in}}{T\hbar\omega\delta_{fsr}} = 3 \times 10^9 \qquad \text{and} \qquad n^{off}_{+,cav} = 2.3 \ ,$$

photons.
b. We need $P_{in}/n^{on}_{+,cav} \simeq 0.3\,\mathrm{pW}$.
c. The photon number reflected from one mirror into the waist $(w_0/4L)^2 S n^{on}_{cav} \simeq 7 \times 10^{-3}$ into the cross section of a BEC $(\bar{r}/4L)^2 S n^{on}_{cav} \simeq 6 \times 10^{-6}$. The effect is negligible.
d. Assume an integration time of $\tau = 1\,\mu\mathrm{s}$. The count rate leaking out of the cavity is,

$$R = \frac{P_{-,out}}{\hbar\omega} = \frac{TP^{on}_{-,cav}}{\hbar\omega} = T\delta_{fsr} n^{on}_{-,cav} = \kappa n^{on}_{-,cav} \ .$$

Within τ we count $n_{-,out}\tau = \kappa n^{on}_{-,cav}\tau \simeq 2 \times 10^6$ photons. The photon counter can only count 10 photons per τ.

40.2.9.5 Ex: Saturation-induced bistability in a linear cavity

a. Derive the equations of motion for N immobile atoms located at positions z_j along the optical axis of and interacting with a linear cavity.
b. Assuming steady-state and doing the mean-field approximation isolate an equation for the cavity field $\alpha \equiv \langle \hat{a} \rangle$.
c. Simplify the equation for α for the case of perfect bunching $z_j = z$ and solve it analytically. Identify the instability.
d. Discuss the weak excitation limit.
e. Derive the transmission spectrum in the weak excitation limit.
f. Write down the equation for $n = |\alpha|^2$ for the resonant case, $\Delta_c = 0 = \Delta_a$, in terms of the single-atom cooperativity parameter $\Upsilon \equiv 4g^2/\gamma\Gamma$ and the single-photon saturation parameter $s_1 \equiv 8g^2/\Gamma^2$.

Solution: *a. The Hamiltonian for the open Dicke model applied to N atoms distributed over the mode volume of a ring cavity within the RWA is,*

$$\hat{H} = \hat{H}_{field} + \hat{H}_{pump} + \sum_{j=1}^{N} (\hat{H}^{(j)}_{atom} + \hat{H}^{(j)}_{atom:field}) \tag{40.223}$$

with

$$\begin{aligned} \hat{H}^{(j)}_{atom} &= -\Delta_a \hat{\sigma}^+_j \hat{\sigma}^-_j = -\tfrac{\Delta_a}{2}(\mathbb{I}_2 + \hat{\sigma}^z_j) \\ \hat{H}_{field} &= -\Delta_c \hat{a}^\dagger \hat{a} \\ \hat{H}_{pump} &= -\imath\eta(\hat{a} - \hat{a}^\dagger) \\ \hat{H}^{(j)}_{atom:field} &= g \sin kz_j (\hat{a}\hat{\sigma}^+_j + \hat{a}^\dagger \hat{\sigma}^-_j) \ . \end{aligned} \tag{40.224}$$

Using this Hamiltonian we derive the equations of motion for the individual atomic operators,

$$\begin{aligned}\dot{\hat{\sigma}}_i^- &= -\imath[\hat{\sigma}_i^-, \hat{H}] + \mathcal{L}_\Gamma \hat{\sigma}_i^- \\ &= \imath\Delta_a \sum_j [\hat{\sigma}_i^-, \hat{\sigma}_j^+]\hat{\sigma}_j^- - \imath g \sum_j \hat{a} \sin kz_j [\hat{\sigma}_i^-, \hat{\sigma}_j^+] - \tfrac{\Gamma}{2}\hat{\sigma}_i^- \\ &= (\imath\Delta_a - \tfrac{\Gamma}{2})\hat{\sigma}_i^- + \imath g \hat{a}\hat{\sigma}_i^z \sin kz_i \ ,\end{aligned} \tag{40.225}$$

and

$$\begin{aligned}\dot{\hat{\sigma}}_i^z &= -\imath[\hat{\sigma}_i^z, \hat{H}] + \mathcal{L}_\Gamma \hat{\sigma}_i^z \\ &= -\imath g \sum_j \hat{a} \sin kz_j [\hat{\sigma}_i^z, \hat{\sigma}_j^+] - \imath g \sum_j \hat{a}^\dagger \sin kz_j [\hat{\sigma}_i^z, \hat{\sigma}_j^-] + 2\Gamma \hat{\sigma}_i^+ \hat{\sigma}_i^- \\ &= -2\imath g \sin kz_i (\hat{a}\hat{\sigma}_i^+ - \hat{a}_+^\dagger \hat{\sigma}_i^-) - \Gamma(\mathbb{I}_2 + \hat{\sigma}_i^z) \ ,\end{aligned} \tag{40.226}$$

and for the field operators,

$$\begin{aligned}\dot{\hat{a}} &= -\imath[\hat{a}, \hat{H}] + \mathcal{L}_\kappa \hat{a} \\ &= \imath\Delta_c [\hat{a}, \hat{a}^\dagger \hat{a}] + \eta[\hat{a}, \hat{a}^\dagger] - \imath g \sum_j \hat{\sigma}_j^- \sin kz_j [\hat{a}, \hat{a}^\dagger] - \kappa\hat{a} \\ &= (\imath\Delta_c - \kappa)\hat{a} - \imath g \sum_j \hat{\sigma}_j^- \sin kz_j + \eta \ .\end{aligned} \tag{40.227}$$

b. The stationary solution follows from the expectation values of the Eqs. (40.225), (40.226), and (40.227),

$$\begin{aligned}&(i) \qquad 0 = (\imath\Delta_a - \tfrac{\Gamma}{2})\langle\hat{\sigma}_i^-\rangle - \imath g \langle\hat{a}\hat{\sigma}_i^z\rangle \sin kz_i \\ &(ii) \qquad 0 = 2\imath g \sin kz_i (\langle\hat{a}\hat{\sigma}_i^+\rangle - \langle\hat{a}^\dagger\hat{\sigma}_i^-\rangle) + \Gamma(\mathbb{I}_2 - \langle\hat{\sigma}_i^z\rangle) \\ &(iii) \qquad 0 = (\imath\Delta_c - \kappa)\langle\hat{a}\rangle - \imath g \sum_j \langle\hat{\sigma}_j^-\rangle \sin kz_j + \eta \ .\end{aligned} \tag{40.228}$$

Neglecting all correlations, we derive from (i),

$$\langle\hat{\sigma}_i^-\rangle = \frac{-\imath g}{\frac{\Gamma}{2} - \imath\Delta_a} \alpha \sin kz_i \langle\hat{\sigma}_i^z\rangle \ . \tag{40.229}$$

Substituting $\langle\hat{\sigma}_i^\pm\rangle$ in (ii),

$$\left(1 + \frac{2g^2}{\frac{\Gamma^2}{4} + \Delta_a^2} |\alpha|^2 \sin^2 kz_i\right) \langle\hat{\sigma}_i^z\rangle = 1 \ , \tag{40.230}$$

and in (iii),

$$-(\imath\Delta_c - \kappa)\alpha + \sum_j \frac{g^2}{\frac{\Gamma}{2} - \imath\Delta_a} \alpha \sin^2 kz_j \langle\hat{\sigma}_j^z\rangle = \eta \ . \tag{40.231}$$

Substituting $\langle\hat{\sigma}_j^z\rangle$,

$$-(\imath\Delta_c - \kappa)\alpha + \sum_j \frac{g^2(\frac{\Gamma}{2} + \imath\Delta_a)\alpha \sin^2 kz_j}{\frac{\Gamma^2}{4} + \Delta_a^2 + 2g^2|\alpha|^2 \sin^2 kz_j} = \eta \ . \tag{40.232}$$

or, using the abbreviations $U_\gamma \equiv U_0 - \imath\gamma_0$ *and* $\Delta_\kappa \equiv \Delta_c + \imath\kappa$,

$$\boxed{\sum_j \frac{U_\gamma \alpha \sin^2 kz_j}{1 + 2|U_\gamma/g|^2|\alpha|^2 \sin^2 kz_j} = \Delta_\kappa \alpha - \imath\eta} \ . \tag{40.233}$$

c. From this in the case of perfect bunching, $z_j = z$, *we get,*

$$\alpha = \frac{\imath\eta}{\Delta_\kappa - \frac{NU_\gamma \sin^2 kz}{1+2|U_\gamma/g|^2|\alpha|^2 \sin^2 kz}} \ . \tag{40.234}$$

With the abbreviation $g \longrightarrow g \sin kz$,

$$\alpha = \frac{\imath\eta}{\Delta_\kappa - \frac{NU_\gamma}{1+2|U_\gamma/g|^2|\alpha|^2}} \ , \tag{40.235}$$

and defining $\tilde{U}_\gamma \equiv U_\gamma/g_1$, $\tilde{\Delta}_\kappa \equiv \Delta_\kappa/g_1$, $\tilde{\eta} \equiv \eta/g_1$, $\tilde{N} \equiv N \sin^2 kz$, *and* $n \equiv |\alpha|^2$,

$$\alpha = \frac{\imath\tilde{\eta}}{\tilde{\Delta}_\kappa - \frac{N\tilde{U}_\gamma}{1+2|\tilde{U}_\gamma|^2 n}}. \tag{40.236}$$

From this we calculate the photon number,

$$n = \frac{\tilde{\eta}^2(1 + 2|\tilde{U}_\gamma|^2 n)^2}{|\tilde{\Delta}_\kappa|^2(1 + 2|\tilde{U}_\gamma|^2 n)^2 - N\left(\tilde{\Delta}_\kappa \tilde{U}_\gamma^* + \tilde{\Delta}_\kappa^* \tilde{U}_\gamma\right)(1 + 2|\tilde{U}_\gamma|^2 n) + N^2|\tilde{U}_\gamma|^2} \ . \tag{40.237}$$

Sorting the terms by powers of photon numbers we obtain a cubic equation, $0 = An^3 + Bn^2 + Cn + D$, *with the coefficients,*

$$\begin{aligned} A &= 4|\tilde{\Delta}_\kappa|^2|\tilde{U}_\gamma|^4 \\ B &= 4|\tilde{\Delta}_\kappa|^2|\tilde{U}_\gamma|^2 - 2N\left(\tilde{\Delta}_\kappa \tilde{U}_\gamma^* + \tilde{\Delta}_\kappa^* \tilde{U}_\gamma\right)|\tilde{U}_\gamma|^2 - 4\tilde{\eta}^2|\tilde{U}_\gamma|^4 \\ C &= |\tilde{\Delta}_\kappa|^2 - N\left(\tilde{\Delta}_\kappa \tilde{U}_\gamma^* + \tilde{\Delta}_\kappa^* \tilde{U}_\gamma\right) + N^2|\tilde{U}_\gamma|^2 - 4\tilde{\eta}^2|\tilde{U}_\gamma|^2 \\ D &= -\tilde{\eta}^2 \ . \end{aligned} \tag{40.238}$$

The roots of the cubic equation are given by,

$$R \equiv \sqrt[3]{36CBA - 108DA^2 - 8B^3 + 12\sqrt{3}A\sqrt{4C^3A - C^2B^2 - 18CBAD + 27D^2A^2 + 4DB^3}} \tag{40.239}$$

and

$$X_\pm \equiv \frac{R}{6A} \pm \frac{6AC - 2B^2}{3AR} \tag{40.240}$$

so that,

$$n_0 = X_- - \frac{B}{3A} \quad , \quad n_\pm = -\frac{1}{2}X_- - \frac{B}{3A} \pm \frac{\imath\sqrt{3}}{2}X_+ \ . \tag{40.241}$$

From this expression we numerically find $n = |\alpha_+ + \alpha_-|^2$, *which we ca use to finally obtain* α.

d. Assuming weak excitation, $g|\alpha_\pm| \ll \Gamma, \Delta_a$, *expression (40.233) simplifies to,*

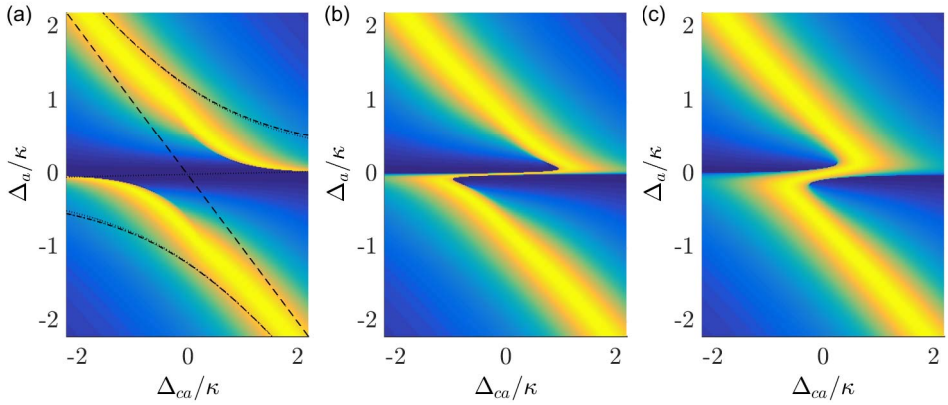

Figure 40.17: (code) Normal mode spectrum using the formula (40.244).

$$U_\gamma \alpha \sum_j \sin^2 kz_j = \Delta_\kappa \alpha - \imath\eta \ . \tag{40.242}$$

That is, defining the bunching parameter $b \equiv \frac{1}{N}\sum_j \sin^2 kz_j$,

$$NU_\gamma \alpha b = \Delta_\kappa \alpha - \imath\eta \ . \tag{40.243}$$

Resolving for α *we finally get,*

$$\alpha(\infty) \simeq \frac{-\imath\eta}{NU_\gamma b - \Delta_\kappa} = \frac{\eta}{\chi} = \frac{\eta}{\kappa + \imath(NbU_0 - \Delta_{ca} - \Delta_c)} \ , \tag{40.244}$$

defining $\chi \equiv \imath(NbU_\gamma - \Delta_\kappa)$ *and* $\Delta_{ca} \equiv \Delta_c - \Delta_a$. *Hence, finite bunching only effects the efficient number of atoms participating in the normal-mode splitting.*
e. The excitation spectrum for $\Gamma \simeq 0$ *is derived from the steady-state solution using the request,* $0 = \frac{d}{d\Delta_{ca}}|\alpha(\infty)|^2$. *We get,*

$$\Delta_{ca} = NbU_0 - \Delta_a = \frac{Nbg^2}{\Delta_a} - \Delta_a \ . \tag{40.245}$$

Assuming, $\Delta_{ca} = 0$, *we have the normal-mode splitting,*

$$\Delta_a = \pm g\sqrt{Nb} \ . \tag{40.246}$$

The transmission is illustrated in Fig. 40.18.
f. From Eq. (40.234) we get,

$$n = \frac{\eta^2}{\left|\Delta_\kappa - \frac{NU_\gamma}{1+2|U_\gamma/g|^2 n}\right|^2} \ , \tag{40.247}$$

and thus,

$$n = \frac{\eta^2}{\kappa^2}\left(\frac{1+s_1 n}{1+s_1 n + \frac{N\Upsilon}{2}}\right)^2 \ . \tag{40.248}$$

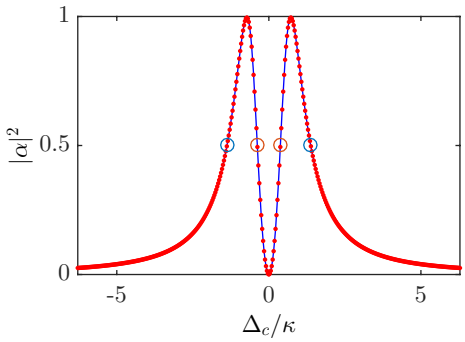

Figure 40.18: (code) Normal mode spectrum using the formula (40.244).

40.2.9.6 Ex: Emission spectrum of atoms in a linear cavity below saturation

a. Derive the mean-field evolution equation for the intracavity field $\alpha(t) = \langle \hat{a}(t) \rangle$ for a linear cavity driven below saturation.
b. Is it possible to calculate the autocorrelation spectrum and the emission spectrum of the cavity from $\langle \alpha^*(t+\tau)\alpha(t) \rangle$ [226, 1039]?
c. Calculate numerically the emission spectrum of a linear cavity interacting with many atoms using for the cavity mode a Fock state expansion up to a cut-off photon number of $n_{\rm cutoff} = 10$. Assume $(\eta, \Gamma, N, g_1, \Delta) = (0.1\kappa, 0.002\kappa, 100000, 0.002\kappa, 0)$. Interpret the result [949, 497].

Solution: *a. We use the steady-state solution, Eqs. (40.229) and (40.230), for the atomic state derived from the Maxwell-Bloch equations in Exc. 40.2.9.5,*

$$\langle \hat{\sigma}_i^- \rangle = \frac{-\imath g}{\frac{\Gamma}{2} - \imath \Delta_a} \alpha \sin kz_i \langle \hat{\sigma}_i^z \rangle = \frac{U_\gamma}{g} \alpha \sin kz_i \langle \hat{\sigma}_i^z \rangle \tag{40.249}$$

$$1 = \left(1 + \frac{2g^2 \sin^2 kz_i}{\frac{\Gamma^2}{4} + \Delta_a^2} |\alpha|^2 \right) \langle \hat{\sigma}_i^z \rangle = \left(1 + 2 \sin^2 kz_i \left| \frac{U_\gamma}{g} \right|^2 |\alpha|^2 \right) \langle \hat{\sigma}_i^z \rangle \ . \tag{40.250}$$

However, instead of inserting them into the steady-state equation of the field amplitude (40.228)(iii), we insert them into time-dependent mean-field equation (40.227),

$$\dot{\hat{a}} = \imath \Delta_\kappa \hat{a} - \imath g \sum_j \hat{\sigma}_j \sin kz_j + \eta \ . \tag{40.251}$$

This yields,

$$\dot{\alpha} = \imath \Delta_\kappa \alpha - \imath U_\gamma \alpha \sum_j \sin^2 kz_j \langle \hat{\sigma}_j^z \rangle + \eta \tag{40.252}$$

$$= \left(\imath \Delta_\kappa - \imath U_\gamma \sum_j \frac{\sin^2 kz_j}{1 + 2 \sin^2 kz_i |U_\gamma/g|^2 |\alpha|^2} \right) \alpha + \eta \ .$$

Below saturation, the denominator simplifies dramatically, and with $b \equiv \frac{1}{N}\sum_j \sin^2 kz_j$ *we obtain,*

$$\dot{\alpha} \simeq \imath(\Delta_\kappa - NbU_\gamma)\alpha + \eta = -\chi\alpha + \eta \ , \tag{40.253}$$

with $\chi \equiv \imath(NbU_\gamma - \Delta_\kappa) = \kappa + \imath(NbU_0 - \Delta_c)$*. For the initial condition* $\alpha(t) = 0$ *it is easy to see that this equation is solved by,*

$$\alpha(t) = \frac{\eta}{\chi}(1 - e^{-\chi t}) \ . \tag{40.254}$$

b. Naively, one might think that the autocorrelation function and the spectrum are given, respectively by,

$$g^{(1)}(\tau) \equiv \frac{\langle \alpha^*(t+\tau)e^{\imath\omega\tau}\alpha(t)\rangle}{\langle \alpha^*(t)\alpha(t)\rangle} \qquad with \qquad \langle ...\rangle \equiv \lim_{t\to\infty}\frac{1}{t}\int_0^t ...dt' \tag{40.255}$$
$$and \qquad S(\nu) = \mathcal{F}g^{(1)}(\tau) \ .$$

The autocorrelation function strongly dominated by an elastic peak, since,

$$\langle \alpha^*(t+\tau)e^{\imath\omega\tau}\alpha(t)\rangle = \frac{\eta^2}{|\chi|^2}e^{\imath\omega\tau}\lim_{t\to\infty}\frac{1}{t}\int_0^t (1 - e^{-\chi^*(t'+\tau)})(1 - e^{-\chi t'})dt' = \frac{\eta^2}{|\chi|^2}e^{\imath\omega\tau} \ , \tag{40.256}$$

which is not what we expect, because the fluorescence spectrum should contain inelastic contributions from two normal-modes. The problem is due to the fact that, deriving the expression we approximated the cavity field by its first-order mean-field, $\alpha = \langle\hat{a}\rangle$*, while the spectrum requires evaluation of second-order correlations. That is,* $\langle \alpha^*(t+\tau)e^{\imath\omega\tau}\alpha(t)\rangle$ *is NOT the correct way to calculate the autocorrelation, but* $\langle \hat{a}^*(t+\tau)e^{\imath\omega\tau}\hat{a}(t)\rangle$*.*
Actually, using the Julia package 'QuantumCumulants.jl', we can derive the following closed set of equations for the expectation values of the observables and their correlations,

$$\begin{aligned}
[\partial - \imath\Delta_c + \kappa]\langle\hat{a}\rangle &= \eta \\
[\partial + 2\kappa]\langle\hat{a}^\dagger\hat{a}\rangle &= \imath N g_1(\langle\hat{a}\hat{\sigma}_{1,21}\rangle - \langle\hat{a}^\dagger\hat{\sigma}_{1,12}\rangle) + \eta(\langle\hat{a}^\dagger\rangle + \langle\hat{a}\rangle) \\
[\partial + \Gamma]\langle\hat{\sigma}_{1,22}\rangle &= \imath g_1(\langle\hat{a}^\dagger\hat{\sigma}_{1,12}\rangle - \langle\hat{a}\hat{\sigma}_{1,21}\rangle) \\
[\partial + \imath\Delta_c + \tfrac{\Gamma}{2} + \kappa]\langle\hat{a}^\dagger\hat{\sigma}_{1,12}\rangle &= \imath g_1\left[\langle\hat{\sigma}_{1,22}\rangle + (2\langle\hat{\sigma}_{1,22}\rangle - 1)\langle\hat{a}^\dagger\hat{a}\rangle - 4\langle\hat{a}^\dagger\rangle\langle\hat{a}\rangle\langle\hat{\sigma}_{1,22}\rangle\right. \\
&\qquad \left. + (N-1)\langle\hat{\sigma}_{1,21}\hat{\sigma}_{2,12}\rangle\right] \\
[\partial + \Gamma]\langle\hat{\sigma}_{1,21}\hat{\sigma}_{2,12}\rangle &= \imath g_1(\langle\hat{a}^\dagger\hat{\sigma}_{1,12}\rangle - \langle\hat{a}\hat{\sigma}_{1,21}\rangle)(1 - 2\langle\hat{\sigma}_{1,22}\rangle) \ ,
\end{aligned} \tag{40.257}$$

as well as for the two-times correlations,

$$\begin{aligned}
[\partial + \imath\Delta_c + \kappa]\langle\hat{a}^\dagger a_0\rangle &= \imath N g_1\langle\hat{\sigma}_{1,21}\hat{a}_0\rangle \\
[\partial + \tfrac{\Gamma}{2}]\langle\hat{\sigma}_{1,21}\hat{a}_0\rangle &= \imath g_1[1 - 2\langle\hat{\sigma}_{1,22}\rangle]\langle\hat{a}^\dagger\hat{a}_0\rangle \ .
\end{aligned} \tag{40.258}$$

Here, phase-invariant expectation values have been set to zero and interatomic correlations ignored by dropping sums over atom number $\sum_{i=1}^N$ *and substituting the single-atom coupling strength* g_1 *by a collective coupling strength* $g_N = g_1\sqrt{N}$*. A numerical*

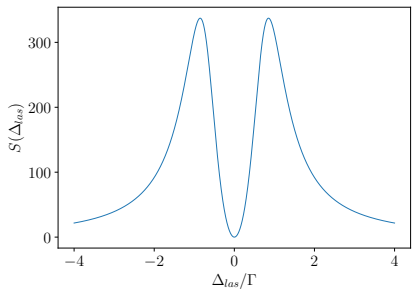

Figure 40.19: (code) Emission spectrum of a linear cavity driven below saturation using the quantum cumulants expansion.

calculation using the Julia 'QuantumCumulants.jl' package is shown in Fig. 40.19.

c. Alternatively, using the Julia package 'QuantumOptics.jl', we can numerically simulate the Hamiltonian for a single atom via a Fock state expansion of the cavity field up to a certain cut-off photon number. The result is exhibited in 40.21. It shows the appearance of an elastic peak and two Mollow triplets due to their beating with the normal modes. The normal modes are separated by g_N, Mollow sidebands are split by $g_N\sqrt{2}$.

The structure of the emission spectrum can be interpreted as follows. As we have already seen in Sec. 35.9.3, the Mollow splitting results from a modulation of spontaneous emission by Rabi flopping, whose frequency depends on the photon number as $g\sqrt{n}$. Similarly, normal-mode splitting would be modulation of cavity decay by Rabi-type flopping between counterpropagating modes. In a linear cavity this doesn't change n, hence we do not expect an n-dependence of normal mode splitting. In contrast the flopping between counterpropagating modes depends on the atom number as NU_0.

Transmission is modulated the collective Rabi oscillation of atoms.

The lowest eigen-energies of the Jaynes-Cummings ladder are,

$$\begin{aligned}\omega_0 &= 0\\ \omega_1 &= \omega \pm 2g\sqrt{1}\\ \omega_2 &= 2\omega \pm 2g\sqrt{2}\\ \omega_3 &= 3\omega \pm 2g\sqrt{3}\ ,\end{aligned}$$

as confirmed by the graph 40.21(b). Hence, the transition frequencies starting from the first excited state are,

$$\begin{aligned}\omega_1 - \omega_0 &= \omega + 2g\sqrt{1}\\ \omega_1 - \omega_0 &= \omega - 2g\sqrt{1}\ ,\end{aligned}$$

and including the second excited state,

$$\begin{aligned}
\omega_2 - \omega_1 &= \omega + 2g(\sqrt{2}+1) \\
\omega_2 - \omega_1 &= \omega + 2g \\
\omega_1 - \omega_0 &= \omega + 2g(\sqrt{2}-1) \\
\omega_1 - \omega_0 &= \omega + 2g(\sqrt{2}-1) \\
\omega_2 - \omega_1 &= \omega - 2g \\
\omega_2 - \omega_1 &= \omega - 2g(\sqrt{2}-1) \ .
\end{aligned}$$

In summary, Autler-Townes splitting is due to Rabi flopping of the degree of freedom

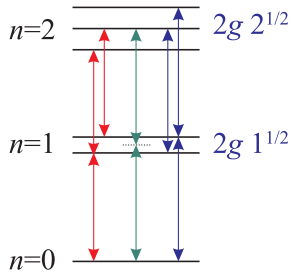

Figure 40.20: Eigenvalue spectrum of the Jaynes-Cummings model due to the first two excited states.

$\hat{\sigma}^-$ and depends on $\sqrt{n}$. Analogously, normal mode splitting is due to a flopping of α and depends on N. This might be interesting for calibrating $g\sqrt{N}$ via normal-mode splitting and, simultaneously $g\sqrt{n}$ via Mollow splitting.

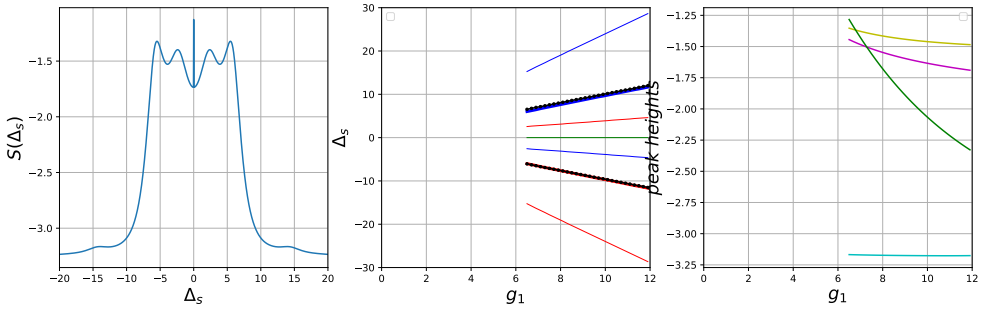

Figure 40.21: (code) (a) Emission spectrum of a linear cavity. (b) Dependence of the peaks's location observed in (a) on the atom-cavity coupling strength g. (thick red/blue lines) Lower and upper Mollow central peaks, respectively. They are separated by normal-mode splitting. (thin red/blue lines) Corresponding Mollow sidebands, (green) elastic peak due to cavity pumping, and (dotted) separations between Mollow central peaks and sidebands. (c) Dependence of the peaks' heights on g. (green) Elastic peak, (yellow) central Mollow peaks, (cyan) outer Mollow sideband, (magenta) inner Mollow sideband.

40.2.9.7 Ex: PDH-probing atoms in a ring cavity

Calculate the steady-state reflection of a phase-modulated laser beam from a ring cavity neglecting backscattering from the atoms. Demodulate the reflection signal with the modulation frequency.

Solution: *The steady-state solution (40.146) is,*

$$\alpha_+ = \frac{\eta_+ - \imath U_\gamma e^{-2\imath kz}\alpha_-}{\kappa - \imath(\Delta_c - U_\gamma)} \ ,$$

where we now neglect $\alpha_- \simeq 0$. Assuming that only the input coupler has finite transmission, with $\eta_+ = \sqrt{\kappa\delta_{fsr}}\beta_{in}$ from Eq. (40.37), the light leaking out of the cavity is then,

$$\beta_{out} = \sqrt{\frac{\kappa}{\delta_{fsr}}}\alpha_+ = \frac{\kappa\beta_{in}}{\kappa - \imath(\Delta_c - U_\gamma)} \ .$$

Note, that without atoms, $U_\gamma = 0$, we recover the Airy function derived in Exc. 18.3.7.18. If the incident light is described by,

$$\beta_{in} = \beta_{0,in}\left[J_0(M)e^{\imath\Delta_c t} + J_{+1}(M)e^{\imath(\Delta_c+\Omega)t} + J_{-1}(M)e^{\imath(\Delta_c-\Omega)t}\right] \ ,$$

the reflection signal becomes ($\Omega \gg \kappa$),

$$\beta_{refl} = \beta_{in} + \beta_{out} = \beta_{0,in}\sum_{n=0,\pm1} J_n(M)e^{\imath(\Delta_c+n\Omega)t}\left(1 + \frac{\kappa}{\kappa - \imath(\Delta_c + n\Omega - U_\gamma)}\right) \ .$$

Introducing the abbreviation,

$$L_n(\Delta_c, U_0) \equiv 1 + \frac{\kappa}{\kappa - \imath(\Delta_c + n\Omega - U_\gamma)} \ ,$$

the demodulated intensity is,

$$\begin{aligned}\mathfrak{Re}\ e^{\imath\Omega t+\imath\theta}\frac{|\beta_{refl}|^2}{\beta_{0,in}^2} &= \mathfrak{Re}\ e^{\imath\Omega t+\imath\theta}\left|\sum_{n=0,\pm1} J_n(M)e^{\imath n\Omega t}L_n(\Delta_c, U_0)\right|^2 \\ &= \mathfrak{Re}\ e^{\imath\theta}J_0(M)J_1(M)\left[L_0(\Delta_c, U_\gamma)L_1^*(\Delta_c, U_\gamma) - L_0^*(\Delta_c, U_\gamma)L_{-1}(\Delta_c, U_\gamma)\right] + \dots \ .\end{aligned}$$

After low-pass filtering, the oscillating terms disappear and we recover the standard PDH-signal, only that the error signal now is a measure for the one-photon light shift caused by the atoms.

40.2.9.8 Ex: Normal mode splitting of a ring cavity

Consider the stationary fields (40.166) developing in a ring cavity containing a homogeneous cloud of atoms and pumped in one direction, $\eta_- = 0$. For this system.
a. Calculate the transmission of the cavity in the direction of mode α_+ as a function of the detunings Δ_a and Δ_c and the number of atoms.

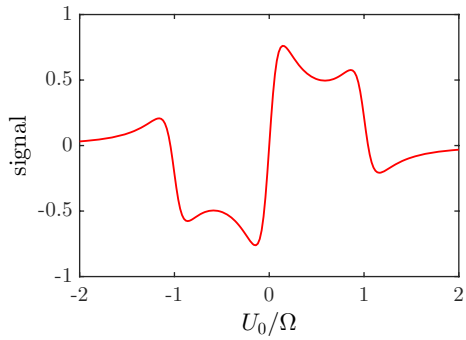

Figure 40.22: (code) PDH-signal induced by one-photon light shift. $\kappa = 0.1\Omega$, $\gamma_0 = 0.05\Omega$, and $\Delta_c = 0$.

Transmission spectra can be recorded under various boundary conditions. Calculate the transmission
b. keeping the laser at a fixed frequency ω and varying the cavity length ω_c;
c. tuning a cavity resonance to the atomic transition, $\omega_c = \omega_a$, and varying the laser frequency ω;
d. same as (d), but now calculate the detunings Δ_{ch} where the transmission drops to 1/2;
e. keeping the cavity constant at an *arbitrary* frequency ω_c and varying the laser frequency ω;
f. keeping the laser locked to the cavity, $\omega = \omega_c + NU_0$, and now ramping the cavity across the atomic resonance.

Solution: *a. The stationary solution for one-way pumping is,*

$$\alpha_+ \simeq -\imath \frac{\eta_+(NU_\gamma - \Delta_\kappa)}{(NU_\gamma - \Delta_\kappa)^2 - (N|b|^2 U_\gamma)^2} \ .$$

For a homogeneous cloud $b = \frac{1}{N}\sum_j e^{2\imath k z_j} = 0$, *so that,*

$$\alpha_+ \simeq \frac{-\imath\eta_+}{NU_\gamma - \Delta_\kappa} \ ,$$

or, substituting the abbreviations [312],

$$\boxed{\alpha_+ = \frac{\eta_+}{\kappa - \imath\Delta_c + \frac{g_N^2}{\Gamma - \imath\Delta_a}}} \ . \tag{40.259}$$

The transmission is given by (40.191),

$$\boxed{T_+ = \left|\frac{\kappa\alpha_+}{\eta_+}\right|^2 = \frac{\kappa^2(\Gamma^2 + \Delta_a^2)}{(\kappa\Gamma + g_N^2 - \Delta_c\Delta_a)^2 + (\Gamma\Delta_c + \kappa\Delta_a)^2}} \ . \tag{40.260}$$

Fig. 40.23 shows cavity transmission spectra.
Defining $\tilde{\Delta}_c \equiv \Delta_c/\kappa$ *and* $\tilde{\Delta}_a \equiv \Delta_a/\Gamma$ *and using the definition (40.125) of the*

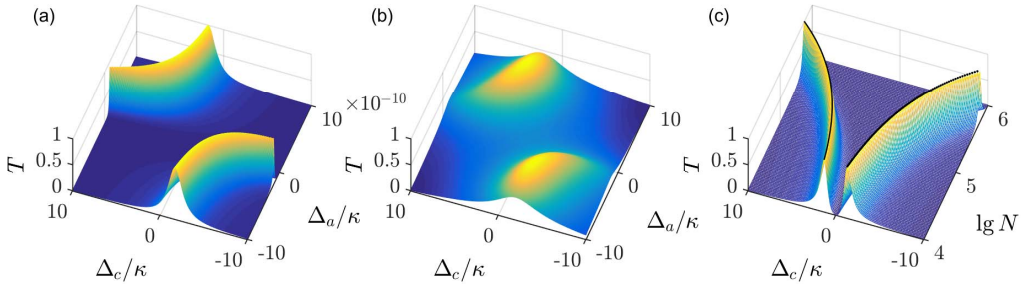

Figure 40.23: (code) Normal mode splitting of an annular cavity for the strontium intercombination line: $\kappa/2\pi = 690\,\mathrm{kHz}$, $\Gamma/2\pi = 7.6\,\mathrm{kHz}$ and $g/2\pi = 8.7\,\mathrm{kHz}$. (b) Convolution with a Lorentzian of 1 MHz width. (c) Dependence of the normal mode splitting on the atom number. The black lines are solutions of Eq. (40.262).

cooperativity, we can also write,

$$T_+ = \frac{1+\tilde{\Delta}_a^2}{\left(1+N\frac{\Upsilon}{2}-\tilde{\Delta}_c\tilde{\Delta}_a\right)^2+(\tilde{\Delta}_c+\tilde{\Delta}_a)^2} \ .$$

b. Keeping the laser at a fixed frequency ω (so that Δ_a is constant) and varying the cavity length Δ_c, we obtain from (40.260),

$$0 = \frac{\partial T_+}{\partial \Delta_c} = -\frac{[-2\Delta_a(\kappa\Gamma+g_N^2-\Delta_c\Delta_a)+2\Gamma(\kappa\Delta_a+\Gamma\Delta_c)]\kappa^2(\Gamma^2+\Delta_a^2)}{\cdots} \ ,$$

yielding,

$$\Delta_c = \frac{g_N^2\Delta_a}{\Gamma^2+\Delta_a^2} = U_0 \ . \tag{40.261}$$

c. Tuning a cavity resonance to the atomic transition, $\omega_c = \omega_a$, and varying the laser frequency, we obtain from (40.260),

$$\begin{aligned} 0 = \frac{\partial T_+}{\partial \Delta_a} &= \frac{\partial \Delta_a^2}{\partial \Delta_a}\frac{\partial T_+}{\partial \Delta_a^2} = 2\Delta_a \frac{\partial}{\partial \Delta_a^2}\frac{\kappa^2\Delta_a^2+\kappa^2\Gamma^2}{\Delta_a^4+(\kappa^2+\Gamma^2-2g_N^2)\Delta_a^2+(\kappa\Gamma+g^2)^2} \\ &= \frac{\kappa^2[\Delta_a^4+(\kappa^2+\Gamma^2-2g_N^2)\Delta_a^2+(\kappa\Gamma+g_N^2)^2]-[2\Delta_a^2+(\kappa^2+\Gamma^2-2g_N^2)][\kappa^2\Delta_a^2+\kappa^2\Gamma^2]}{\cdots} \ . \end{aligned}$$

The solution of this equation,

$$\Delta_a^2 = -\Gamma^2 \pm g_N\sqrt{2\Gamma^2+g_N^2+2\kappa\Gamma} \ , \tag{40.262}$$

is plotted in Fig. 40.23(c) as a black line. For cases of very narrow atomic resonances, $\kappa \gg \Gamma$, we may simplify,

$$\Delta_a^2 \simeq \pm g_N^2\sqrt{1+\frac{4\kappa\Gamma}{2g_N^2}} = \pm N g^2\sqrt{1+\frac{N_{crt}}{N}} \ , \tag{40.263}$$

where $N_{crt} = 4/\Upsilon$ is the critical atom number (40.126) and Υ the cooperativity (40.125).
d. For $\Delta_c = \Delta_a$ the transmission (40.260) simplifies to,

$$T(\Delta_a = \Delta_c) = \frac{\kappa^2(\Gamma^2 + \Delta_c^2)}{(\kappa\Gamma + g_N^2 - \Delta_c^2)^2 + (\Gamma + \kappa)^2\Delta_c^2} \ .$$

Then from $T(\Delta_{ch}) = \frac{1}{2}$ we get,

$$\begin{aligned}\Delta_{ch}^2 &= \tfrac{\kappa^2 - \Gamma^2 + 2g_N^2}{2} \pm \sqrt{\tfrac{(\kappa^2 - \Gamma^2 + 2g_N^2)^2}{4} + \kappa^2\Gamma^2 - 2\kappa\Gamma g_N^2 - g_N^4} \\ &\simeq \tfrac{\kappa^2}{2} + g_N^2 \pm \kappa\sqrt{\tfrac{\kappa^2}{4} + g_N^2} \ .\end{aligned}$$

The last approximation hold for $\Gamma \ll \kappa, g_N$. Now,

$$\Delta_{ch}^2 = \begin{cases} g_N^2 \pm \kappa g_N & for \ \ g_N \gg \kappa \\ \frac{\kappa^2}{2} + g_N^2 \pm \left(\frac{\kappa^2}{2} + g_N^2 - \frac{g_N^4}{\kappa^2}\right) & for \ \ g_N \ll \kappa \end{cases} \ .$$

such that for $g_N \ll \kappa$,

$$|\Delta_{ch}| = \kappa, \tfrac{g_N^2}{\kappa} \ .$$

The detunings are indicated as circles in Fig. 40.18.
e. Keeping the cavity constant at an arbitrary *frequency ω_c, and varying the laser frequency,*

$$0 = \frac{\partial T_+}{\partial \omega} = \frac{\partial}{\partial \omega} \frac{\kappa^2[\Gamma^2 + (\omega - \omega_a)^2]}{[\kappa\Gamma + g^2 - (\omega - \omega_c)(\omega - \omega_a)]^2 + [\kappa(\omega - \omega_a) + \Gamma(\omega - \omega_c)]^2} \ .$$

f. Typically, a locking electronics will maintain the pump laser locked to a cavity resonance, even if the cavity resonance is shifted by the refraction index imposed by atoms in the mode volume, that is,

$$\Delta_c = NU_0 = \omega - \omega_c = \frac{g_N^2\Delta_a}{\Gamma^2 + \Delta_a^2} \ .$$

Substituting the above boundary condition into the expression for the transmission,

$$T_+ = \frac{1}{\left(1 + \frac{g_N^2/\kappa\Gamma}{1 + \Delta_a^2/\Gamma^2}\right)^2} = \frac{1}{\left(1 + \frac{N\Upsilon/2}{1 + \Delta_a^2/\Gamma^2}\right)^2} \ .$$

We are now seeking transmission resonances upon varying the cavity length ω_c. However, we already see from the expression for T_+, that the transmission is maximized for $\Delta_a = 0$.

40.2.9.9 Ex: Time-dependent solution for a ring cavity pumped from one side below saturation

Derive the complete solution of the adiabatic field equations (40.183).

Solution: *For one-sided pumping with* $\chi \equiv \kappa + \imath(U_\gamma - \Delta_c)$ *the equations of motion read,*

$$\begin{aligned}\dot{\alpha}_+ &= -\chi\alpha_+ - \imath U_\gamma e^{-2\imath kz}\alpha_- + \eta_+ \\ \dot{\alpha}_- &= -\chi\alpha_- - \imath U_\gamma e^{2\imath kz}\alpha_+ \ .\end{aligned}$$

To decouple the differential equations from each other we derive one and insert the other,

$$\begin{aligned}\ddot{\alpha}_+ &= -\chi\dot{\alpha}_+ - \imath U_\gamma e^{-2\imath kz}\dot{\alpha}_- \\ &= -\chi\dot{\alpha}_+ + \imath U_\gamma e^{-2\imath kz}(\chi\alpha_- + \imath U_\gamma e^{2\imath kz}\alpha_+) \\ &= -\chi\dot{\alpha}_+ + \imath U_\gamma e^{-2\imath kz}\left(\chi\left[\frac{\dot{\alpha}_+ + \chi\alpha_+ - \eta_+}{-\imath U_\gamma e^{-2\imath kz}}\right] + \imath U_\gamma e^{2\imath kz}\alpha_+\right) \\ &= -2\chi\dot{\alpha}_+ - (U_\gamma^2 + \chi^2)\alpha_+ + \chi\eta_+\end{aligned}$$

and

$$\begin{aligned}\ddot{\alpha}_- &= -\chi\dot{\alpha}_- - \imath U_\gamma e^{2\imath kz}\dot{\alpha}_+ \\ &= -\chi\dot{\alpha}_- + \imath U_\gamma e^{2\imath kz}(\chi\alpha_+ + \imath U_\gamma e^{-2\imath kz}\alpha_- - \eta_+) \\ &= -\chi\dot{\alpha}_- + \imath U_\gamma e^{2\imath kz}\left(\chi\frac{\dot{\alpha}_- + \chi\alpha_-}{-\imath U_\gamma e^{2\imath kz}} + \imath U_\gamma e^{-2\imath kz}\alpha_- - \eta_+\right) \\ &= -2\chi\dot{\alpha}_- - (U_\gamma^2 + \chi^2)\alpha_- - \imath U_\gamma e^{2\imath kz}\eta_+ \ .\end{aligned}$$

This shows that we expect a damped oscillation tending toward the stationary solution. Making the ansatz,

$$\alpha_+ = e^{\lambda t} + \frac{\chi\eta_+}{\chi^2 + U_\gamma^2} \qquad \textit{and} \qquad \alpha_- = e^{\lambda t} + \frac{-\imath U_\gamma e^{2\imath kz}\eta_+}{\chi^2 + U_\gamma^2} \ ,$$

we obtain $\lambda = -\chi \pm \imath U_\gamma$*. Hence,*

$$\alpha_+ = e^{-\chi t}(A_+ e^{\imath U_\gamma t} + B_+ e^{-\imath U_\gamma t}) + \frac{\chi\eta_+}{\chi^2 + U_\gamma^2}$$

and

$$\alpha_- = e^{-\chi t}(A_- e^{\imath U_\gamma t} + B_- e^{-\imath U_\gamma t}) - \frac{\imath U_\gamma e^{2\imath kz}\eta_+}{\chi^2 + U_\gamma^2} \ .$$

Inserting the solutions into the original differential equations yields,

$$A_- = -A_+ e^{2\imath kz} \qquad \textit{and} \qquad B_- = B_+ e^{2\imath kz} \ .$$

$A_\pm$ *and* $B_\pm$ *depend on initial conditions. For example, setting* $\alpha_\pm(0) = 0$ *we get,*

$$A_+ = -\frac{1}{\chi - \imath U_\gamma}\frac{\eta_+}{2} \qquad \textit{and} \qquad B_+ = -\frac{1}{\chi + \imath U_\gamma}\frac{\eta_+}{2} \ ,$$

and finally,

$$\alpha_+(t) = \frac{\eta_+}{\chi^2 + U_\gamma^2}\left[\chi - e^{-\chi t}(\chi\cos U_\gamma t - U_\gamma \sin U_\gamma t)\right]$$
$$\alpha_-(t) = \frac{-\imath e^{2\imath kz}\eta_+}{\chi^2 + U_\gamma^2}\left[U_\gamma - e^{-\chi t}(U_\gamma\cos U_\gamma t + \chi \sin U_\gamma t)\right] \ .$$

Using the abbreviations,

$$U_\gamma \equiv U_0 - \imath\gamma_0 = \frac{g^2}{\Delta_a^2 + (\Gamma/2)^2} \quad , \quad \Delta_\kappa \equiv \Delta_c + \imath\kappa \quad , \quad \chi \equiv \imath(U_\gamma - \Delta_\kappa) \ ,$$

the time-dependent field amplitudes can also be written,

$$\boxed{\begin{array}{rcl} \frac{1}{\imath\eta_+}\alpha_+(t) & = & -\frac{\frac{1}{2}e^{\imath\Delta_\kappa t}}{\Delta_\kappa} + \frac{\frac{1}{2}e^{\imath(\Delta_\kappa - 2U_\gamma)t}}{2U_\gamma - \Delta_\kappa} + \frac{1}{\Delta_\kappa}\frac{U_\gamma - \Delta_\kappa}{2U_\gamma - \Delta_\kappa} \\ \frac{e^{-2\imath kz}}{\imath\eta_+}\alpha_-(t) & = & \frac{\frac{1}{2}e^{\imath\Delta_\kappa t}}{\Delta_\kappa} + \frac{\frac{1}{2}e^{\imath(\Delta_\kappa - 2U_\gamma)t}}{2U_\gamma - \Delta_\kappa} - \frac{1}{\Delta_\kappa}\frac{U_\gamma}{2U_\gamma - \Delta_\kappa} \end{array}} \ .$$

That is, we expect a sideband spectrum with frequency components at 0, Δ_c, *and* $\Delta_c - U_0$. *At long times,*

$$\frac{1}{\imath\eta_+}\begin{pmatrix}\alpha_+ \\ \alpha_-\end{pmatrix} \overset{t\to\infty}{\longrightarrow} \frac{1}{\Delta_\kappa(2U_\gamma - \Delta_\kappa)}\begin{pmatrix}U_\gamma - \Delta_\kappa \\ -U_\gamma e^{2\imath kz}\end{pmatrix} \ ,$$

we recover the usual steady-state solution. On resonance, $\Delta_c = 0 = \Delta_a$, *with the definition of the cooperativity,*

$$U_\gamma = \frac{-2\imath g^2}{\Gamma} \quad , \quad \Delta_\kappa = \imath\kappa \quad , \quad \Upsilon \equiv \frac{4g^2}{\kappa\Gamma}$$

we get,

$$\frac{\kappa}{\eta_+}\alpha_+(t) = -\frac{e^{-\kappa t}}{2} - \frac{\frac{1}{2}e^{-\kappa(1+\Upsilon)t}}{\Upsilon + 1} + \frac{\frac{1}{2}\Upsilon + 1}{\Upsilon + 1}$$
$$\frac{\kappa e^{-2\imath kz}}{\eta_+}\alpha_-(t) = \frac{e^{-\kappa t}}{2} - \frac{\frac{1}{2}e^{-\kappa(1+\Upsilon)t}}{\Upsilon + 1} - \frac{\frac{1}{2}\Upsilon}{\Upsilon + 1} \ .$$

40.2.9.10 Ex: Filling and drainage of a ring cavity with one fixed atom

Calculate by simulation of the classical cavity equations, how a laser-pumped ring cavity fills and looses photons in the presence of a single immobile atom.

Solution: *The result of the simulation is shown in Fig. 40.24. Only the mode* α_+ *is pumped until a time corresponding to* $\kappa t = 0.5$, *when it is switched off. The parameters are* $\kappa = (2\pi)\ 10\,\text{kHz}$, $U_0 = 2\kappa$, $\Delta_c = 0$, *and* $\eta = 10\kappa$. *We see that the intensities of the modes* $|\alpha_\pm|^2$ *do not depend on the atom's location, but the interference signal* $|\alpha_+ - \alpha_-|^2$ *does.*

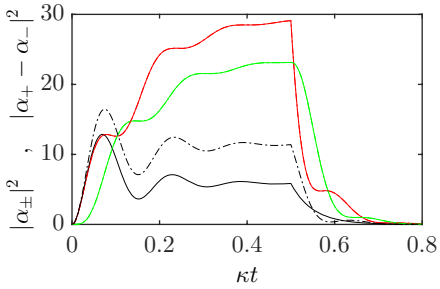

Figure 40.24: (code) Filling and drainage of the two counter-propagating modes of a laser-pumped ring cavity. Red curves show $|\alpha_+|^2$, green curves $|\alpha_-|^2$, and black curves $|\alpha_+ - \alpha_-|^2$. The atom is located at $kz = 0$ (solid line) and $kz = 0.1$ (dash-dotted line).

40.2.9.11 Ex: Position of the phase without pumping of the cavity

Solve the Schrödinger equation (40.189) by inserting ansatz,

$$\vec{\alpha} = \vec{\alpha}_1 e^{-\lambda_1 t} + \vec{\alpha}_2 e^{-\lambda_2 t} \ ,$$

where $\lambda_1 = \kappa + 2\imath U_0$ and $-\lambda_2 = \kappa$ are the eigenvalues of the matrix (40.189).

Solution: *We obtain,*

$$\begin{pmatrix} (-\kappa - 2\imath U_0)\alpha_{1+} e^{-\kappa t - 2\imath U_0 t} - \kappa \alpha_{2+} e^{-\kappa t} \\ (-\kappa - 2\imath U_0)\alpha_{1-} e^{-\kappa t - 2\imath U_0 t} - \kappa \alpha_{2-} e^{-\kappa t} \end{pmatrix}$$
$$= \begin{pmatrix} (-\imath U_0 - \kappa)(\alpha_{1+} e^{-\kappa t - 2\imath U_0 t} + \alpha_{2+} e^{-\kappa t}) - \imath U_0 e^{-2\imath kz}(\alpha_{1-} e^{-\kappa t - 2\imath U_0 t} + \alpha_{2-} e^{-\kappa t}) \\ -\imath U_0 e^{2\imath kz}(\alpha_{1+} e^{-\kappa t - 2\imath U_0 t} + \alpha_{2+} e^{-\kappa t}) + (-\imath U_0 - \kappa)(\alpha_{1-} e^{-\kappa t - 2\imath U_0 t} + \alpha_{2-} e^{-\kappa t}) \end{pmatrix} \ .$$

Separating the terms proportional to $e^{-\kappa t - 2\imath U_0 t}$ e $e^{-\kappa t}$, we obtain 4 relations,

$$\begin{pmatrix} \alpha_{1+} \\ \alpha_{2+} \\ \alpha_{1+} \\ \alpha_{2+} \end{pmatrix} = \begin{pmatrix} e^{-2\imath kz}\alpha_{1-} \\ -e^{-2\imath kz}\alpha_{2-} \\ e^{-2\imath kz}\alpha_{1-} \\ -e^{-2\imath kz}\alpha_{2-} \end{pmatrix} \ .$$

We can now write the solution as,

$$\vec{\alpha} = \begin{pmatrix} 1 \\ e^{2\imath kz} \end{pmatrix} \alpha_{1+} e^{-\kappa t - 2\imath U_0 t} + \begin{pmatrix} 1 \\ -e^{2\imath kz} \end{pmatrix} \alpha_{2+} e^{-\kappa t} \ ,$$

or, defining the abbreviation $\beta_n \equiv e^{\imath kz}\alpha_{n+}$,

$$\alpha_\pm = e^{\mp \imath kz}\beta_1 e^{-\kappa t - 2\imath U_0 t} \pm e^{-\imath kz}\beta_2 e^{-\kappa t} \ .$$

40.2.9.12 Ex: Dynamics of a standing wave in a symmetrically pumped ring cavity

Solve and discuss the equation (40.209).

Solution: *To obtain the inhomogeneous solution of the equation of motion for the ring cavity, we insert the general solution of the homogeneous equation into the equation of motion including a pump field, but assuming time-dependent coefficients $\beta_j(t)$. This gives,*

$$\dot{\beta}_1(t) = \tfrac{1}{2}e^{(\chi-\imath U_0)t}(\eta_+ e^{-\imath kz} - \eta_- e^{\imath kz}) = \imath\eta e^{(\chi-\imath U_0)t}\sin[-kz+\phi(t)] \ ,$$
$$\dot{\beta}_2(t) = \tfrac{1}{2}e^{(\chi+\imath U_0)t}(\eta_+ e^{-\imath kz} + \eta_- e^{\imath kz}) = \eta e^{(\chi+\imath U_0)t}\cos[-kz+\phi(t)] \ .$$

For a stationary pump, $\phi(t) = \phi$, a particular solution of the above differential equations is,

$$\beta_1(t) = \imath\frac{\eta}{\chi-\imath U_0}e^{(\chi-\imath U_0)t}\sin(-kz+\phi) \ ,$$
$$\beta_2(t) = \frac{\eta}{\chi+\imath U_0}e^{(\chi+\imath U_0)t}\cos(-kz+\phi) \ .$$

A particular solution of the inhomogeneous field equation is, therefore,

$$\begin{aligned} e^{\pm\imath kz}\alpha_\pm(t) &= \pm\beta_1(t)e^{-(\chi-\imath U_0)t} + \beta_2(t)e^{-(\chi+\imath U_0)t} \\ &= \pm\imath\frac{\eta}{\chi-\imath U_0}\sin(-kx+\phi) + \frac{\eta}{\chi+\imath U_0}\cos(-kz+\phi) \ . \end{aligned}$$

The general solution of the inhomogeneous equation is the sum of the general solution of the homogeneous equation and a particular solution of the inhomogeneous equation,

$$\begin{aligned} e^{\pm\imath kz}\alpha_\pm(t) &= \pm\beta_1(t)e^{-(\chi-\imath U_0)t} + \beta_2(t)e^{-(\chi+\imath U_0)t} \pm \beta_1 e^{-(\chi-\imath U_0)t} + \beta_2 e^{-(\chi+\imath U_0)t} \\ \alpha_\pm(t) &= \eta\frac{\pm\imath(\chi+\imath U_0)\sin(-kz+\phi) + (\chi-\imath U_0)\cos(-kz+\phi)}{\chi^2+U_0^2} \\ &\quad \pm \beta_1 e^{-(\chi-\imath U_0)t\mp\imath kz} + \beta_2 e^{-(\chi+\imath U_0)t\mp\imath kz} \ . \end{aligned}$$

Note that the specific initial condition, $\alpha_\pm(0) = \alpha_\pm(\infty)$, is realized for $\mp\beta_1 = \beta_2$. Further insight comes from the phase of the cavity field. The field adjusts to the atomic position by pulling its phase to the position of the atom, as long as the coupling is strong enough. Interestingly, the pumping force does not matter to the stationary situation. It only determines the speed of the self-adjustment process. This can be seen from a time-dependent analysis. We look at the phase $\phi = \pi/2$ and focus on $U_0 \ll \kappa$,

$$\begin{aligned} \alpha_\pm(t) &\simeq \imath\frac{\eta}{\kappa}\left(\pm 1 + \frac{2U_0}{\kappa}\sin(kz)e^{\mp\imath kz}\right) + (\beta_2 \pm \beta_1)e^{-\kappa t\mp\imath kz} \\ &\simeq \imath\frac{\eta}{\kappa}\left(\pm 1 + \frac{2U_0}{\kappa}kz\right) + (\beta_2 \pm \beta_1)e^{-\kappa t}(1 \mp \imath kz) \\ &\simeq \imath\frac{\eta}{\kappa}\left(\pm 1 + \frac{2U_0}{\kappa}kz\right) + (\beta_2 \pm \beta_1)e^{-\kappa t} \ . \end{aligned}$$

such that,

$$\alpha_+\alpha_-^* = \left(\imath\frac{\eta}{\kappa}\left(1+\frac{2U_0}{\kappa}kz\right)+(\beta_2+\beta_1)e^{-\kappa t}\right)\left(-\imath\frac{\eta}{\kappa}\left(1+\frac{2U_0}{\kappa}kz\right)+(\beta_2-\beta_1)e^{-\kappa t}\right)$$

$$\theta = \arctan\frac{-2\beta_1\frac{\eta}{\kappa}e^{-\kappa t}\left(1+\frac{2U_0}{\kappa}kz\right)}{(\beta_2^2-\beta_1^2)e^{-2\kappa t}+\frac{\eta^2}{\kappa^2}\left(1+\frac{2U_0}{\kappa}kz\right)^2} \ .$$

The time constant to reach the steady-state value is κ, and we retrieve the stationary formula for long times τ. During this period, small oscillations can occur with the period $2U_0$. To summarize, there is a competition between the phase of the field being defined by the coupling or by the atoms. The equilibrium depends on the ratio U_0/κ. Interestingly, the pump rate only matters during the transitional regime.

40.2.9.13 Ex: Stationary position of the atom in a unidirectionally pumped ring cavity

What is the steady state position of an atom interacting with the modes of a unidirectionally pumped ring cavity?

Solution: *To find the phase of the stationary wave we assume for simplicity, that the mode α_+ is stable, $\dot{\alpha}_+ = 0$. Also, we consider a scatterer fixed at a position Z, and look at the stationary solution,*

$$0 = -\kappa\alpha_- - \imath U_0 e^{2\imath kz}\alpha_+ \ ,$$

leading to,

$$|\alpha_+e^{\imath kZ}+\alpha_-e^{-\imath kZ}|^2 = \left|\alpha_+e^{\imath kZ}-\frac{\imath U_0}{\kappa}e^{-\imath kZ+2\imath kz}\alpha_+\right|^2 \sim 1+\frac{U_0^2}{\kappa^2}+\frac{2U_0}{\kappa}\sin 2k(z-Z) \ .$$

The slope of the standing wave is just where the sinus disappears, that is, $Z_{pente} = z$. Therefore, the scatterer is located right at the middle of the slope of the stationary wave, which it produced in the first place. The atoms are accelerated to the valley, that is, in the same direction as the wavevector of the pump field. Then, the standing wave again tries to regenerate itself at the new location of the scatterer. This means that the wave must continuously adjust its phase to the accelerated atoms. The atoms are always on the slope, etc. That is, the CARL starts running [8].

40.2.9.14 Ex: Equations of motion for intensities and coherences in a ring cavity

Derive from the equations (40.183) the equations of motion for intermodal coherences $\alpha_+\alpha_+^*$, $\alpha_-\alpha_-^*$, $\alpha_+\alpha_-^*$, and $\alpha_-\alpha_+^*$.

[8] Representations of numerical simulations can be contemplated here: http://www.ifsc.usp.br/~strontium/ → Research → Quantum Sensing → History of CARL → Children's corner.

Solution: *We obtain,*

$$\frac{d}{dt}(\alpha_\pm\alpha_\pm^* + 2\kappa) = \imath U_0(e^{\pm 2\imath kz}\alpha_\pm\alpha_\mp^* - e^{\mp 2\imath kz}\alpha_\mp\alpha_\pm^*) + \eta_\pm^*\alpha_\pm + \eta_\pm\alpha_\pm^*$$
$$\frac{d}{dt}(\alpha_\pm\alpha_\mp^* + 2\kappa) = (\alpha_\pm\alpha_\pm^* - \alpha_\mp\alpha_\mp^*) + \eta_\mp^*\alpha_\pm + \eta_\pm\alpha_\mp^* \ .$$

The quantities $\alpha_\pm\alpha_\mp^*$ describe a redistribution of photons between counterpropagating waves.

40.2.9.15 Ex: Backaction of atomic vibration on the modes of a symmetrically pumped ring cavity

a. Calculate the Lamb-Dicke parameter for gravitation-induced Bloch oscillations in a strontium gravimeter, as well as the modulation index. Is the continued fractions method applicable?
b. Study the dynamics of the counterpropagating light modes of a ring cavity in the presence of an atom whose position is periodically modulated with a given frequency by numerical integration of the equations of motion (40.183). Compare with the results obtained by the method of continued fractions proposed in Sec. 40.2.8.

Solution: *a. The recoil shift and the Bloch oscillation frequency are, respectively,*

$$\omega_{rec} = \frac{\hbar k^2}{2m} \quad , \quad \nu_{blo} = \frac{mg}{2\hbar k} \ .$$

With this we calculate for the gravitation-induced Bloch oscillations in a strontium gravimeter a Lamb-Dicke parameter of

$$\eta_{blo} = \sqrt{\frac{\omega_{rec}}{2\pi\nu_{ho}}} = \sqrt{\frac{\hbar k^2}{2m}\frac{\hbar k}{\pi mg}} \approx 2.4 \ .$$

The modulation index is,

$$kz_0 = \frac{kv}{2\pi\nu_{ho}} = \frac{2\omega_{rec}}{2\pi\nu_{ho}} = 2\eta_{blo}^2 \approx 12.5 \ .$$

Hence, the continued fractions method is NOT applicable. In contrast, the cavity linewidth does not matter.
b. The equations of motion (40.183), modified to account for the periodic vibration of the atom, are,

$$\dot\alpha_\pm = (-\kappa + \imath\Delta_c - \imath U_0)\alpha_\pm - \imath U_0 e^{\mp 2\imath kz_0 \sin\omega t}\alpha_\mp + \eta_\pm \ ,$$

ω being the vibration frequency and kz_0 the modulation excursion. The results of the simulation are exhibited in Fig. 40.25. Interestingly, we find that the cavity linewidth does not matter.

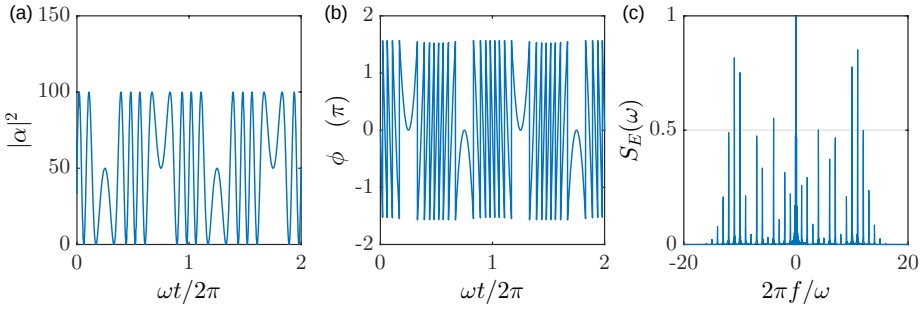

Figure 40.25: (code) (a) Photon number and (b) phase shift of the cavity in response to a modulated atomic position. The chosen parameters are $kz_0 = 2\pi$, $\kappa = (2\pi)\ 440\,\text{kHz}$, $\omega = (2\pi)\ 745\,\text{kHz}$, $\eta_\pm = 10\kappa$, $U_0 = -\kappa$. The initial photon number is $|\alpha|^2 = 16$. (c) Spectrum recorded behind a cavity mirror with the transmittivity t_{hr}. The spectrum is obtained as the Fourier transform of the $g^{(1)}(\tau)$ correlation function of the transmitted field $E_{out} = t_{hr}e^{\imath ka}E_{cav}$, where $e^{\imath ka}$ is a fixed phase factor depending on the mirror position a (see Sec. 35.5).

40.2.9.16 Ex: Fluorescent emission of a ring cavity for one-sided pumping in the adiabatic approximation

Based on the solution of the adiabatic field equations derived in Exc. 40.2.9.9 calculate the emission spectrum of the ring cavity driven below saturation (where the adiabatic approximation is good) from one side ($\eta_- = 0$) for both counter-propagating directions ($\alpha_\pm$). Compare with numerical solutions.

Solution: *In Exc. 40.2.9.9 we found,*

$$\begin{aligned}\alpha_\pm(t) &= A_\pm e^{(-\chi+\imath U_0)t} + B_\pm e^{(-\chi-\imath U_0)t} + C_\pm \\ &= A_\pm e^{(-\kappa+\imath\Delta_c)t} + B_\pm e^{[-\kappa+\imath(\Delta_c-2U_0)]t} + C_\pm\ ,\end{aligned}$$

where we assume $U_\gamma = U_0$ and $\chi = \kappa + \imath(U_0 - \Delta_c)$ and,

$$\begin{aligned}A_+ &= \frac{-\eta_+/2}{\chi - \imath U_0} \quad , \quad B_+ = \frac{-\eta_+/2}{\chi + \imath U_0} \quad , \quad C_+ = \frac{\chi\eta_+}{\chi^2 + U_\gamma^2} \\ A_- &= \frac{e^{2\imath kz}\eta_+/2}{\chi - \imath U_0} \quad , \quad B_+ = \frac{-e^{2\imath kz}\eta_+/2}{\chi + \imath U_0} \quad , \quad C_- = \frac{e^{2\imath kz}\imath U_0\eta_+}{\chi^2 + U_\gamma^2}\ .\end{aligned}$$

Now, we need to calculate the correlation function,

$$\langle t\alpha_+^*(t+\tau)e^{\imath\omega\tau}\alpha_+(t)\rangle = e^{\imath\omega\tau}\lim_{t\to\infty}\int_0^t \left[\begin{array}{c}\left(A_+^* e^{(-\kappa-\imath\Delta_c)(t+\tau)} + B_+^* e^{[-\kappa-\imath(\Delta_c-2U_0)](t+\tau)} + C_+^*\right)\times \\ \times\left(A_+ e^{(-\kappa+\imath\Delta_c)t} + B_+ e^{[-\kappa+\imath(\Delta_c-2U_0)]t} + C_+\right)\end{array}\right] dt'\ .$$

Using,

$$\lim_{t\to\infty}\int_0^t e^{-(a+\imath b)t}dt' = \lim_{t\to\infty}\frac{1-e^{-(a+\imath b)t}}{a+\imath b} = \frac{1}{a+\imath b}\ ,$$

we find,

$$\begin{aligned}
&\langle t\alpha_+^*(t+\tau)e^{\imath\omega\tau}\alpha_+(t)\rangle \\
&= e^{\imath\omega\tau}\begin{bmatrix} e^{(-\kappa-\imath\Delta_c)\tau}|A_+|^2\frac{1}{2\kappa}+e^{[-\kappa-\imath(\Delta_c-2U_0)]\tau}|B_+|^2\frac{1}{2\kappa}+|C_+|^2 t \\ +e^{(-\kappa-\imath\Delta_c)\tau}A_+^*B_+\frac{1}{2\kappa+2\imath U_0}+e^{[-\kappa-\imath(\Delta_c-2U_0)]\tau}A_+B_+^*\frac{1}{2\kappa-2\imath U_0} \\ +e^{(-\kappa-\imath\Delta_c)\tau}A_+^*C_+\frac{1}{\kappa+\imath\Delta_c}+A_+C_+^*\frac{1}{\kappa-\imath\Delta_c} \\ +e^{[-\kappa-\imath(\Delta_c-2U_0)]\tau}B_+^*C_+\frac{1}{\kappa+\imath(\Delta_c-2U_0)}+B_+C_+^*\frac{1}{\kappa-\imath(\Delta_c-2U_0)} \end{bmatrix} \\
&= e^{\imath\omega\tau}\begin{bmatrix} e^{(-\kappa-\imath\Delta_c)\tau}\left(\frac{|A_+|^2}{2\kappa}+\frac{A_+^*B_+}{2\kappa+2\imath U_0}+\frac{A_+^*C_+}{\kappa+\imath\Delta_c}\right) \\ +e^{[-\kappa-\imath(\Delta_c-2U_0)]\tau}\left(\frac{|B_+|^2}{2\kappa}+\frac{A_+B_+^*}{2\kappa-2\imath U_0}+\frac{B_+^*C_+}{\kappa+\imath(\Delta_c-2U_0)}\right) \\ +t|C_+|^2+\frac{A_+C_+^*}{\kappa-\imath\Delta_c}+\frac{B_+C_+^*}{\kappa-\imath(\Delta_c-2U_0)} \end{bmatrix}.
\end{aligned}$$

The autocorrelation function is now,

$$g^{(1)}(\tau)=\frac{\langle t\alpha_+^*(t+\tau)e^{\imath\omega\tau}\alpha_+(t)\rangle}{\langle t\alpha_+^*(t)\alpha_+(t)\rangle}=\frac{e^{-\kappa\tau}e^{\imath\omega\tau}\left(Xe^{-\imath\Delta_c\tau}+Ye^{\imath(2U_0-\Delta_c)\tau}+Z\right)}{X+Y+Z}$$

and the emission spectrum,

$$\begin{aligned}
S(\nu)&=\mathcal{F}g^{(1)}(\tau) \\
&=\frac{1}{X+Y+Z}\left(X\frac{\kappa}{(\nu-\omega+\Delta_c)^2+\kappa^2}+Y\frac{\kappa}{(\nu-\omega+2U_0-\Delta_c)^2+\kappa^2}+Z\delta(\nu-\omega)\right)
\end{aligned}$$

with $\Delta=\nu-\omega$ the detuning of the analyzing frequency filter.
The numerical solution is exhibited in Fig. 40.26.

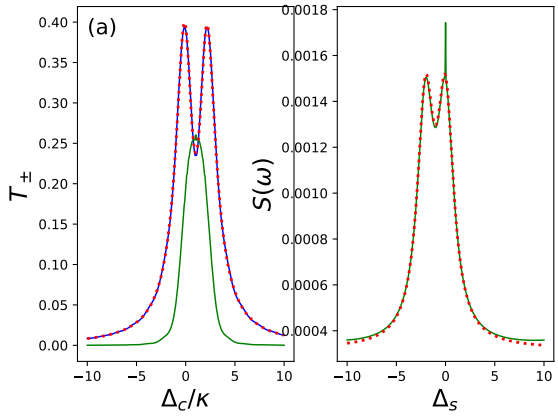

Figure 40.26: (code) (a) Transmission spectra and (b) emission spectra. The parameters are $\eta_+=0.1\kappa$, $\eta_-=0$, and $U_0=\kappa$.

40.3 Noise analysis of Bragg scattering in cavities

40.3.1 Fluorescence versus absorption

Consider a atoms in a cavity mode irradiated from the side [1295]. Every atom emits m photons, a fraction α of which goes into the cavity mode and is detected. Hence, $c = \alpha m a$ photons are counted, from which we infer the atom number and the noise,

$$a = \frac{c}{\alpha m} \tag{40.264}$$

$$\Delta a_f = a\frac{\Delta c}{c} = \frac{c}{\alpha m}\frac{\sqrt{c}}{c} = \sqrt{\frac{1}{\alpha m}a} \ . \tag{40.265}$$

For absorption $2\sigma/\pi w^2 = 4\alpha$ with $\sigma = 3\lambda^2/2\pi$. The photons missing in the transmitted beam are those scattered out of the cavity. If m_i photons come in, $ma = 4\alpha m_i a$ photons are scattered out. The main contribution to the absolute noise in the detected signal evidently comes from the shot noise of the incident probe beam, not from atom number fluctuations. Hence,

$$\Delta a_f = a\frac{\Delta c}{c} = \frac{c}{4\alpha m}\frac{\Delta c}{c} = \frac{1}{4\alpha m}\Delta c = \frac{1}{4\alpha m}\Delta m_i = \frac{1}{4\alpha m}\sqrt{4\alpha m} = \sqrt{1/4\alpha m} \ . \tag{40.266}$$

Consider a fluctuating number of atoms a. Each one scatters a fluctuating number of photons n, which are all detected. What information does the statistics of n containt about a? Let us first define the fluctuation and correlations function for the atom number,

$$\Delta a^2 = \langle a^2\rangle - \langle a\rangle^2 \tag{40.267}$$

$$g_{aa} \equiv \frac{\langle a^2\rangle - \langle a\rangle}{\langle a\rangle^2} = \frac{\Delta a^2 - \langle a\rangle}{\langle a\rangle^2} + 1 \ .$$

The probability to encounter a atoms is given by a distribution function $\rho(a)$. The probability to measure n_a photons at a fixed atom number is distribution according to $\varepsilon(n, a)$. Hence, the mean value of photon counts is,

$$\langle n\rangle = \sum_{a,n}\rho(a)\varepsilon(n,a)n = \sum_a \rho(a)\sum_n \varepsilon(n,a)n = \sum_a \rho(a)\langle n_a\rangle \ , \tag{40.268}$$

where $\langle n_a\rangle$ is the mean value of photon numbers at a fixed given atom number a and the fluctuation and correlations function are,

$$\Delta n_a^2 = \langle n_a^2\rangle - \langle n_a\rangle^2 \tag{40.269}$$

$$g_{nn} \equiv \frac{\langle n_a^2\rangle - \langle n_a\rangle}{\langle n_a\rangle^2} = \frac{\Delta n_a^2 - \langle n_a\rangle}{\langle n_a\rangle^2} + 1 \ .$$

It is reasonable to assume $\langle n_a\rangle = a\langle p\rangle$ where $\langle p\rangle$ is the mean number of photons scattered by an individual atom. We then get,

$$\langle n\rangle = \sum_a \rho(a)a\langle p\rangle = \langle p\rangle\sum_a \rho(a)a = \langle a\rangle\langle p\rangle \ . \tag{40.270}$$

Again we calculate the mean square of the counted photon numbers,

$$\begin{aligned}\langle n^2\rangle &= \sum_{a,n}\rho(a)\varepsilon(n,a)n^2 = \sum_a \rho(a)\langle n_a^2\rangle \\ &= \sum_a \rho(a)(\langle n_a\rangle^2 g_{nn} + \langle n_a\rangle) \\ &= \sum_a \rho(a)(\langle n_a\rangle^2 g_{nn} + a\langle p\rangle) = g_{nn}\sum_a \rho(a)\langle n_a\rangle^2 + \langle n\rangle \ .\end{aligned} \tag{40.271}$$

If the distribution $\varepsilon(n,a)$ is Poissonian with the mean value $a\langle p\rangle$,

$$\varepsilon(n,a) = e^{-a\langle p\rangle}\frac{(a\langle p\rangle)^n}{n!} \tag{40.272}$$

and the atom distribution is also Poissonian,

$$\rho(a) = e^{-\langle a\rangle}\frac{\langle a\rangle^n}{a!} \tag{40.273}$$

the total distribution is,

$$\kappa(n) = \sum_a \rho(a)\varepsilon(n,a) = \sum_a e^{-\langle a\rangle}\frac{\langle a\rangle^n}{a!}e^{-a\langle p\rangle}\frac{(a\langle p\rangle)^n}{n!} \ . \tag{40.274}$$

Hence

$$g_{nn} = g_{aa} + \frac{\langle p\rangle}{\langle n\rangle} \ . \tag{40.275}$$

40.3.2 Correlations in Bragg scattering

Light scattered from ultracold atoms arranged in a periodic optical lattice contains information about the quantum state of the system. The goal of the following calculations is to study the angular dependence and the coherence characteristics of the scattered light for the cases of propagating wave or cavity-enhanced input and output modes.

We consider a 1D grating with lattice constant d with N atoms distributed over M lattice sites. K of the lattice sites are illuminated by a pump laser. The full Hamiltonian for the problem of Bragg scattering at quantum correlated atoms is given in [870, 871, 873, 872]. The authors derive the Bose-Hubbard model and set up the Heisenberg equations of motion. Then however they dramatically simplify them by preventing tunneling. The correlations are then reintroduced ad hoc, when they assume particular wavefunctions, e.g. Mott insulator, superfluid or coherent states. The lattice is irradiated by a pump laser a_0, the scattered probe laser a_1 is detected. The angles of both modes with respect to the lattice can be chosen freely. The multiparticle Hamiltonian is, after adiabatic elimination of excited atomic states assumed to be valid for large detunings $\Delta_{la} = \omega_l - \omega_a$ between atomic resonance and light

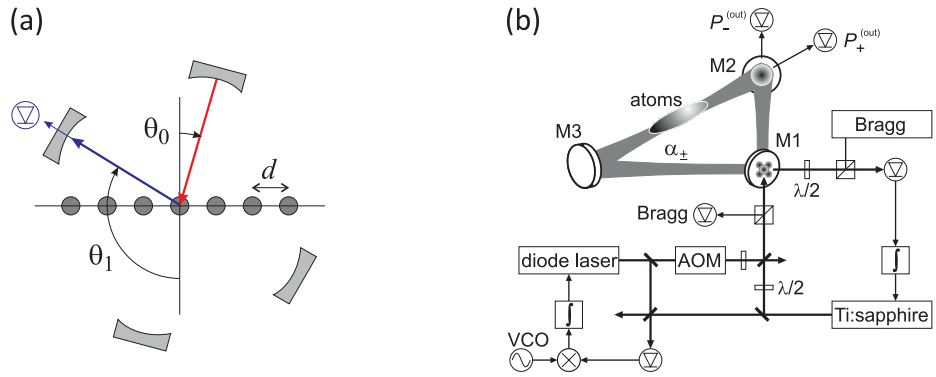

Figure 40.27: (a) Geometry of the scattering problem. (b) Possible experimental setup for measuring Bragg diffraction from CARL.

frequency,

$$\begin{aligned}
\hat{H} &= \hat{H}_f + \hat{H}_a \\
\text{with} \quad \hat{H}_f &= \sum_l \hbar\omega_l \hat{a}_l^\dagger \hat{a}_l - \imath\hbar \sum_l (\eta_l^* \hat{a}_l - \eta_l \hat{a}_l^\dagger) \\
\text{and} \quad \hat{H}_a &= \int d^3 r \hat{\Psi}^\dagger(\mathbf{r}) \hat{H}_{a_1} \hat{\Psi}(\mathbf{r}) + \frac{2\pi a_s \hbar^2}{m} \int d^3\mathbf{r} \hat{\Psi}^\dagger(\mathbf{r}) \hat{\Psi}^\dagger(\mathbf{r}) \hat{\Psi}(\mathbf{r}) \hat{\Psi}(\mathbf{r}) \\
\text{with} \quad \hat{h}_{a_1} &= \frac{\hat{p}^2}{2m_a} + V_{cl}(\mathbf{r}) + \hbar g_0^2 \sum_{l,m} \frac{u_l^*(\mathbf{r}) u_m(\mathbf{r}) \hat{a}_l^\dagger \hat{a}_m}{\Delta_{ma}} \; .
\end{aligned}$$

Here, $\hat{a}_i$ is the annihilation operator of mode i, η_l the pumping rate of mode 1, $\hat{\Psi}(\mathbf{r})$ the atomic field operator, a_s the s-wave scattering length, V_{cl} the lattice potential, and u_i the mode functions of the light fields.

For a strong potential and a weak pump, we derive the Bose-Hubbard-Hamiltonian with the ansatz of Wannier functions $\hat{\Psi}(\mathbf{r}) = \sum_i \hat{b}_i w(\mathbf{r} - \mathbf{r}_i)$,

$$\hat{H} = \hat{H}_f + \sum_{i,j=1}^{M} J_{i,j}^{cl} \hat{b}_i^\dagger \hat{b}_j + \hbar g_0^2 \sum_{l,m} \frac{\hat{a}_l^\dagger \hat{a}_m}{\Delta_{ma}} \left(\sum_{i,j=1}^{K} J_{i,j}^{lm} \hat{b}_i^\dagger \hat{b}_j \right) + \frac{U}{2} \sum_{i=1}^{M} \hat{b}_i^\dagger \hat{b}_i (\hat{b}_i^\dagger \hat{b}_i - 1) \quad (40.276)$$

and with the terms denoting the coefficients for the quantum motion of the atoms, the contribution of the light modes, and the interatomic interaction within a site, respectively

$$\begin{aligned}
J_{i,j}^{cl} &= \int d^3\mathbf{r} w(\mathbf{r} - \mathbf{r}_i) \left(-\frac{\hbar^2 \nabla^2}{2m} + V_{cl}(\mathbf{r}) \right) w(\mathbf{r} - \mathbf{r}_j) \qquad (40.277) \\
J_{i,j}^{lm} &= \int d^3\mathbf{r} w(\mathbf{r} - \mathbf{r}_i) u_l^*(\mathbf{r}) u_m(\mathbf{r}) w(\mathbf{r} - \mathbf{r}_j) \\
U &= \frac{4\pi a_s \hbar^2}{m_a} \int \mathrm{d}r |w(\mathbf{r})|^4 \; .
\end{aligned}$$

We now make the approximation that tunneling is only possible between nearest neighbors. Then the coefficients J^{cl} do not depend on index i of the potential site,

$$J^{cl}_{i,i} = J^{cl}_0 \quad , \quad J^{cl}_{i,i\pm1} = J^{cl} \ . \tag{40.278}$$

so that

$$\hat{H} = \hat{H}_f + J^{cl}_0 \hat{N} + J^{cl}\hat{B} + \hbar g_0^2 \sum_{l,m} \frac{\hat{a}^\dagger_l \hat{a}_m}{\Delta_{ma}} \left(\sum_{i=1}^{K} J^{lm}_{i,i} \hat{n}_i \right) \tag{40.279}$$
$$+ \hbar g_0^2 \sum_{l,m} \frac{\hat{a}^\dagger_l \hat{a}_m}{\Delta_{ma}} \left(\sum_{\langle i,j \rangle}^{K} J^{lm}_{i,j} \hat{b}^\dagger_i \hat{b}_j \right) + \frac{U}{2} \sum_{i=1}^{M} \hat{n}_i(\hat{n}_i - 1) \ .$$

where $\hat{n}_i = \hat{b}^\dagger_i \hat{b}_i$ is the atom number operator, $\hat{B} = \sum_{i=1}^{M} \hat{b}^\dagger_i \hat{b}_i + \text{h.c.}$, $\hat{N} = \sum_{i=1}^{K} \hat{n}_i$ the atom number is conserved g_0 is the atom-field coupling constant.

Let us calculate the Heisenberg equations from $\imath\hbar\dot{\hat{x}} = [\hat{x}, \hat{H}]$,

$$\dot{\hat{a}}_l = -\imath \left(\omega_l + \underbrace{\frac{g_0^2}{\Delta_{la}} \sum_{i=1}^{K} J^{ll}_{i,i} \hat{n}_i}_{\text{non-resonant dispersion}} + \underbrace{\frac{g_0^2}{\Delta_{la}} \sum_{\langle i,j \rangle}^{K} J^{ll}_{i,j} b^\dagger_i b_i}_{\text{tunneling}} \right) \hat{a}_l - \underbrace{i g_0^2 \sum_{m \neq l} \frac{a_m}{\Delta_{ma}} \left(\sum_{i=1}^{K} J^{lm}_{i,i} \hat{n}_i \right)}_{\text{scattering into } a_l}$$
$$- \underbrace{\imath g_0^2 \sum_{m \neq l} \frac{\hat{a}_m}{\Delta_{ma}} \left(\sum_{\langle i,j \rangle}^{K} J^{lm}_{i,j} \hat{b}^\dagger_i \hat{b}_i \right)}_{\text{correction to scattering due to tunneling}} + \eta_l \ . \tag{40.280}$$

and

$$\dot{\hat{b}}_i = -\frac{\imath}{\hbar} \left(J^{cl}_0 + \hbar g_0^2 \sum_{l,m} \frac{\hat{a}^\dagger_l \hat{a}_m}{\Delta_{ma}} J^{lm}_{i,i} + U \hat{n}_i \right) \hat{b}_i - \frac{\imath}{\hbar} \left(J^{cl} + \hbar g_0^2 \sum_{l,m} \frac{\hat{a}^\dagger_l \hat{a}_m}{\Delta_{ma}} J^{lm}_{i,i+1} \right) \hat{b}_{i+1}$$
$$- \frac{\imath}{\hbar} \left(J^{cl} + \hbar g_0^2 \sum_{l,m} \frac{\hat{a}^\dagger_l \hat{a}_m}{\Delta_{ma}} J^{lm}_{i,i-1} \right) \hat{b}_{i-1} \ . \tag{40.281}$$

The system contains additionally to the Bose-Hubbard model terms describing long-range interactions. This interaction is mediated by the light field.

40.3.3 Scattering from deep lattice

[873] derive the following Heisenberg equation for Bragg scattering reminiscent to the CARL model. The deep lattice is characterized by large V_{cl}, small overlap of Wannier functions, no tunneling ($J^{cl} = 0$, $J^{lm}_{i,j} = 0$ for $i \neq j$). With the approximation: $J^{lm}_{i,i} = u^*_l(r_i) u_m(r_i)$, neglect atomic localization,

$$\dot{\hat{a}}_1 = -\imath \left(\omega_1 + \frac{g_0^2}{\Delta_{1a}} \sum_{i=1}^{K} |u_1(r_i)|^2 \hat{n}_i \right) \hat{a}_1 - \imath \frac{g_0^2 a_0}{\Delta_{la}} \sum_{i=1}^{K} u^*_1(r_i) u_0(r_i) \hat{n}_i - \kappa \hat{a}_1 + \eta_1 \ . \tag{40.282}$$

In the equation for the matter wave only the first term doesn't vanish. This only concerns the phase, not the atom number operator. The term for dispersion $\frac{g_0^2}{\Delta_{1a}} \sum_{i=1}^{K} |u_1(r_i)|^2 \hat{n}_i$ be small compared to the the(weak coupling) rest. $\hat{a}_j \to a_j e^{-\imath\omega t}$ is a slowly varying envelope. A stationary solution is:

$$a_1 = C\hat{D} \tag{40.283}$$

with

$$\begin{aligned} C &\equiv -\frac{ig_0^2 a_0}{\Delta_{0a}(\kappa - \imath\Delta_{01})} \\ \hat{D} &\equiv \sum_{i=1}^{K} u_1^*(r_i) u_0(r_i) \hat{n}_i \equiv \sum_{i=1}^{K} A_i \hat{n}_i \ . \end{aligned} \tag{40.284}$$

Consider a 1D-lattice with sites at $x_m = m \cdot d$ $(m = 1, 2, ..., M)$. We scatter a running wave a_0 at the lattice and look at the expectation value of the scattered light field,

$$\begin{aligned} \langle a_1 \rangle = C\langle \hat{D} \rangle &= C \sum_{m=1}^{K} \mathrm{e}^{im\delta k_x d} \langle \hat{n}_m \rangle \\ &= Cn\mathrm{e}^{\imath(K+1)\alpha_-/2} \frac{\sin(K\alpha_-/2)}{\sin(\alpha_-/2)} \ . \end{aligned} \tag{40.285}$$

Here $\alpha_- = \delta k_x d$ and $\delta k_x = (k_0 - k_1)_x = k(\sin\Theta_0 - \sin\Theta_1)$. The above equation describes classical diffraction. The expectation value of the light field thus only depends of the atom number per lattice site n. The photon number and statistics however depend on higher moments of $\hat{n}_i$, i.e. on quantum correlations and quantum statistics.

The mode functions or traveling waves are

$$u_\beta(\mathbf{r}_m) = e^{\imath m k_{\beta x} d} \ , \tag{40.286}$$

where $\beta = 0, 1$. For standing waves

$$u_\beta(\mathbf{r}_m) = \cos(\imath m k_{\beta x} d) \ . \tag{40.287}$$

40.3.4 Correlations

We now assume all sites $\langle \hat{n}_i \rangle$ to be identical to an arbitrary specific site $\langle \hat{n}_a \rangle$, so that $\langle \hat{n}_i^2 \rangle = \langle \hat{n}_a^2 \rangle$. Furthermore, we assume a steep lattice, $\langle \hat{n}_i \hat{n}_{j \neq i} \rangle \equiv \langle \hat{n}_a \hat{n}_b \rangle$. The expectation value for the field is then,

$$\langle \hat{D} \rangle = \langle \hat{n}_a \rangle \sum_{i=1}^{K} A_i \equiv A \langle \hat{n}_a \rangle \ . \tag{40.288}$$

It can be measured by homodyne techniques. The photon count rate is,

$$\begin{aligned}\langle \hat{D}^* \hat{D} \rangle &= \sum_{i,j=1}^{K} A_i^* A_j \langle \hat{n}_i \hat{n}_j \rangle = \sum_{\imath \neq j}^{K} A_i^* A_j \langle \hat{n}_i \hat{n}_j \rangle + \sum_{i=1}^{K} |A_i|^2 \langle \hat{n}_i^2 \rangle \\ &= \langle \hat{n}_a \hat{n}_b \rangle \left(|A|^2 - \sum_{a}^{K} |A_a|^2 \right) + \langle \hat{n}_a^2 \rangle \sum_{i=1}^{K} |A_i|^2 \\ &= \langle \hat{n}_a \hat{n}_b \rangle |A|^2 + (\langle \hat{n}_a^2 \rangle - \langle \hat{n}_a \hat{n}_b \rangle) \sum_{i=1}^{K} |A_i|^2 \ ,\end{aligned} \tag{40.289}$$

and its variance is

$$\begin{aligned}\langle \hat{D}^* \hat{D} \rangle - |\langle \hat{D} \rangle|^2 &= \langle \hat{n}_a \hat{n}_b \rangle |A|^2 + (\langle \hat{n}_a^2 \rangle - \langle \hat{n}_a \hat{n}_b \rangle) \sum_{i=1}^{K} |A_i|^2 - \left| \sum_{i=1}^{K} A_i \langle \hat{n}_i \rangle \right|^2 \\ &= (\langle \hat{n}_a \hat{n}_b \rangle - \langle \hat{n}_a \rangle^2) |A|^2 + (\langle \hat{n}_a^2 \rangle - \langle \hat{n}_a \hat{n}_b \rangle) \sum_{i=1}^{K} |A_i|^2 \\ &= (\delta \hat{n}_a \delta \hat{n}_b) \, |A|^2 + (\langle \delta \hat{n}_a^2 \rangle - \langle \delta \hat{n}_a \delta \hat{n}_b \rangle) \sum_{i=1}^{K} |A_i|^2 \ .\end{aligned} \tag{40.290}$$

In the last equation we used the definition $\delta \hat{n}_i \equiv \hat{n}_i - \langle \hat{n}_i \rangle$ for which $\langle \delta \hat{n}_i \delta \hat{n}_j \rangle = \langle \hat{n}_i \hat{n}_j \rangle - \langle \hat{n}_a \rangle^2$ is easy to show.

40.3.4.1 Variance of photon number

The photon number variance is,

$$\begin{aligned}(\Delta n_{ph})^2 &= \langle n_{ph}^2 \rangle - \langle n_{ph} \rangle^2 = \langle \Delta n_{ph}^2 \rangle + \langle n_{ph} \rangle \\ &= |C|^4 (\langle \hat{D}^{*2} \hat{D}^2 \rangle - \langle \hat{D}^* \hat{D} \rangle) + |C|^2 \langle \hat{D}^* \hat{D} \rangle \ .\end{aligned}$$

40.3.5 Probing atomic correlations with traveling waves

Using the above relationships with traveling waves,

$$\langle a_1 \rangle = C \langle \hat{n}_a \rangle \sum_{i=1}^{K} u_1^*(\mathbf{r}_i) u_0(\mathbf{r}_i) = C \langle \hat{n}_a \rangle e^{i(K+1)d(k_{0x} - k_{1x})} \frac{\sin \frac{K}{2} d(k_{0x} - k_{1x})}{\sin \frac{1}{2} d(k_{0x} - k_{1x})} \ . \tag{40.291}$$

Analogously the correlation function gives,

$$\langle a_1^* a_1 \rangle = |C|^2 \left(\langle \hat{n}_a \hat{n}_b \rangle \left| \sum\nolimits_{m=1}^{K} u_1^*(\mathbf{r}_m) u_0(\mathbf{r}_m) \right|^2 + \left(\langle \hat{n}_a^2 \rangle - \langle \hat{n}_a \hat{n}_b \rangle \right) \sum\nolimits_{m=1}^{K} |u_0(\mathbf{r}_m)| |u_1(\mathbf{r}_m)| \right) \tag{40.292}$$

$$= |C|^2 \left(\frac{1 - \cos K d(k_{0x} - k_{1x})}{1 - \cos d(k_{0x} - k_{1x})} \langle \hat{n}_a \hat{n}_b \rangle + K \left(\langle \hat{n}_a^2 \rangle - \langle \hat{n}_a \hat{n}_b \rangle \right) \right) \ .$$

Its variance is

$$\langle a_1^* a_1\rangle - |\langle a_1\rangle|^2 = |C|^2 \left(\frac{1-\cos Kd(k_{0x}-k_{1x})}{1-\cos d(k_{0x}-k_{1x})} (\langle \hat{n}_a \hat{n}_b\rangle - |\langle \hat{n}_a\rangle|^2) + K(\langle \hat{n}_a^2\rangle - \langle \hat{n}_a \hat{n}_b\rangle) \right) . \tag{40.293}$$

Various techniques are possible, heterodyne or spectral measurements. Or one may tune the Bragg angle. The above Bragg technique may be applied to various types of quantum correlation [871, 873].

40.3.6 Quantum statistics for typical atomic distributions

If the number of illuminated lattice sites is much smaller than the total number of sites, then the coherent state is a good approximation for the calculation of the features of the scattered light in the limit $N, M \to \infty$ with finite $\frac{N}{M}$. Far from the diffraction maxima the approximation also holds for $M \propto K$. Now $n \equiv \frac{N}{M}$ is the expectation value of the atom number per potential site and $N_K \equiv K\frac{N}{M} = nK$.

40.3.6.1 Mott insulator

Products of Fock states at each lattice site, exactly n_i atoms per lattice site. The number of atoms per lattice site does not fluctuate $\hat{n}_i$, neither does the total number of atoms K. No quantum correlations between lattice sites.

The Mott insulating state is described by,

$$|\psi_{mi}\rangle = \prod_{m=1}^{N} |\psi_m\rangle_m . \tag{40.294}$$

Hence the atom numbers per site are uncorrelated. The correlation is,

$$\langle a_1^* a_1\rangle = |C|^2 \frac{1-\cos Kd(k_{0x}-k_{1x})}{1-\cos d(k_{0x}-k_{1x})} \langle \hat{n}_a\rangle^2 = |\langle a_1\rangle|^2 . \tag{40.295}$$

Its variance is $\langle a_1^* a_1\rangle - |\langle a_1\rangle|^2 = 0$. The behavior is identical to classical Bragg scattering,

$$\begin{aligned} \langle \hat{n}_a \hat{n}_b\rangle_{mi} &= \langle \hat{n}_a\rangle^2 \\ \langle \delta\hat{n}_a \delta\hat{n}_b\rangle_{mi} &= 0 \qquad \text{for} \qquad a \neq b \\ \langle \Delta\hat{n}_a\rangle_{mi} &= 0 . \end{aligned} \tag{40.296}$$

In $\langle \hat{D}^{*2}\hat{D}^2\rangle$, all terms with 2, 3, or 4 lattice sites factorize; are closest to the classical state. Consider uniform filling with $n = \frac{N}{M}$ atoms per lattice site.

40.3.6.2 Superfluid state

Every atom is delocalized over all sites. This causes fluctuating atom numbers in $K < M$ sites. All terms involving 2, 3, or 4 lattice sites do not factorize. The SF state is a superposition of all possible Fock states with N atoms in M sites.

The superfluid state,

$$|\psi_{sf}\rangle = \frac{1}{\sqrt{N!}}\left(\frac{1}{\sqrt{M}}\sum_{m=1}^{N} b_m^\dagger\right)^N |0\rangle \tag{40.297}$$

$$\hat{b}_i|\psi_{sf}(N,M)\rangle = \sqrt{\frac{N}{M}}|\psi_{sf}(N-1,M)\rangle_{sf}$$

$$\langle\psi_{sf}|\hat{b}_i^{\dagger m}\hat{b}_i^m|\psi_{sf}\rangle = \frac{N!}{M^m(N-m)!}\ .$$

In particular in the photon number variance there are terms like $\langle\hat{D}^{*2}\hat{D}^2\rangle$ containing contributions like $\langle n_a n_b n_c n_d\rangle$. With $[b_i, b_j^\dagger] = \delta_{ij}$ we find,

$$\begin{aligned}
\langle\hat{n}_i\rangle &= \langle b_i^\dagger b_i\rangle \qquad (40.298)\\
\langle\hat{n}_i^2\rangle &= \langle b_i^\dagger b_i b_i^\dagger b_i\rangle = \langle b_i^\dagger b_i\rangle + \langle b_i^\dagger 2 b_i^2\rangle\\
\langle\hat{n}_i^3\rangle &= \langle\hat{b}_i^\dagger\hat{b}_i\rangle 2 + \langle\hat{b}_i^{\dagger 2}\hat{b}_i^2\rangle + \langle\hat{b}_i^{\dagger 3}\hat{b}_i^3\rangle\\
\langle\hat{n}_i^4\rangle &= \langle b_i^\dagger b_i\rangle + 7\langle b_i^{\dagger 2} b_i^2\rangle + 6\langle b_i^{\dagger 3} b_i^3\rangle + \langle b_i^{\dagger 4} b_i^4\rangle\\
\langle\hat{n}_a\hat{n}_b\rangle &= \langle b_a^\dagger b_b^\dagger b_a b_b\rangle = \langle b_i^{\dagger 2} b_i^2\rangle\\
\langle\hat{n}_a\hat{n}_b\hat{n}_c\rangle &= \langle b_i^{\dagger 3} b_i^3\rangle\\
\langle\hat{n}_a\hat{n}_b\hat{n}_c\hat{n}_d\rangle &= \langle b_i^{\dagger 4} b_i^4\rangle\\
\langle\hat{n}_a^2\hat{n}_b\hat{n}_c\rangle &= \langle b_i^{\dagger 3} b_i^3\rangle + \langle b_i^{\dagger 4} b_i^4\rangle\\
\langle\hat{n}_a^3\hat{n}_b\rangle &= \langle b_i^{\dagger 2} b_i^2\rangle + 3\langle b_i^{\dagger 3} b_i^3\rangle + \langle b_i^{\dagger 4} b_i^4\rangle\\
\langle\hat{n}_a^2\hat{n}_b^2\rangle &= \langle b_i^{\dagger 2} b_i^2\rangle + 2\langle b_i^{\dagger 3} b_i^3\rangle + \langle b_i^{\dagger 4} b_i^4\rangle
\end{aligned}$$

This yields,

$$\begin{aligned}
2\langle\hat{n}_a\hat{n}_b\hat{n}_c\hat{n}_d\rangle - 3\langle\hat{n}_a^2\hat{n}_b\hat{n}_c\rangle + \langle\hat{n}_a^3\hat{n}_b\rangle &= N\frac{N-1}{M^2} \qquad (40.299)\\
-\langle\hat{n}_a\hat{n}_b\hat{n}_c\hat{n}_d\rangle + \langle\hat{n}_a^2\hat{n}_b\hat{n}_c\rangle &= N(N-1)\frac{N-2}{M^3}\\
\langle\hat{n}_a\hat{n}_b\hat{n}_c\hat{n}_d\rangle - 2\langle\hat{n}_a^2\hat{n}_b\hat{n}_c\rangle + \langle\hat{n}_a^2\hat{n}_b^2\rangle &= N\frac{N-1}{M^2}\\
-6\langle\hat{n}_a\hat{n}_b\hat{n}_c\hat{n}_d\rangle + 12\langle\hat{n}_a^2\hat{n}_b\hat{n}_c\rangle - 4\langle\hat{n}_a^3\hat{n}_b\rangle - 3\langle\hat{n}_a^2\hat{n}_b^2\rangle + \langle\hat{n}^4\rangle &= \frac{N}{M}
\end{aligned}$$

and hence the formula found by [873] simplifies to,

$$\begin{aligned}
\langle\hat{D}^{*2}\hat{D}^2\rangle = &\left|\sum_{i=1}^K A_i\right|^4 \frac{N!}{M^4(N-4)!} + \left[\left(\sum_{i=1}^K A_i^2\right)\left(\sum_{i=1}^K A_i^*\right)^2 + c.c. + 4\left|\sum_{i=1}^K A_i^2\right|^2 \sum_{i=1}^K |A_i|^2\right]\frac{N!}{M^3(N-3)!}\\
&+ 2\left[\left(\sum_{i=1}^K |A_i|^2\right)^2 + \frac{1}{2}\left|\sum_{i=1}^K A_i^2\right|^2\right]\frac{N!}{M^2(N-2)!} + 2\left[\left(\sum_{i=1}^K |A_i|^2 A_i\right)\sum_{i=1}^K A_i^* + c.c.\right]\frac{N!}{M(N-1)!}\\
&+ \sum_{i=1}^K |A_i|^4\frac{N}{M}\ . \qquad (40.300)
\end{aligned}$$

40.3.6.3 Coherent state

Approximation of the SF state. Product of local coherent states. Fluctuating atom numbers in $K \leq M$ sites, but also fluctuating total number (which is a drawback). No correlations between several different states. The approximation is good only for $K < M$.

Approximation to superfluid state,

$$|\psi_{co}\rangle = e^{-N/2} \prod_{m=1}^{N} e^{\hat{b}_i^\dagger \sqrt{N/M}} |0\rangle_m \tag{40.301}$$

$$\hat{b}_i |\psi_{co}(N,M)\rangle = \sqrt{\frac{N}{M}} |\psi_{co}(N-1,M)\rangle_{co}$$

$$\langle \psi_{co} | \hat{b}_i^{\dagger m} \hat{b}_i^m | \psi_{co} \rangle = \frac{N^m}{M^m} \ .$$

The correlation functions are derived analogously to the superfluid state.

	Mott insulator state	superfluid state	coherent state
$\langle \hat{n}_i^2 \rangle$	n^2	$n^2(1-\frac{1}{N})+n$	n^2+n
$(\Delta n_i)^2$	0	$n(1-\frac{1}{M})$	n
$\langle \hat{n}_K^2 \rangle$	N_K	$N_K^2(1-\frac{1}{N})+N_K$	$N_K^2+N_K$
$(\Delta \hat{n}_K)^2$	0	$N_K(1-\frac{K}{M})$	N_K
$\langle \hat{n}_a \hat{n}_b \rangle$	n^2	$n^2(1-\frac{1}{N})$	n^2
$\langle \delta\hat{n}_a \delta\hat{n}_b \rangle$	0	$-\frac{N}{M^2}$	0

40.3.6.4 Self-organized states

An interesting case occurs when self-organization populates only odd or even (Mott insulating) states as found by Vuletic. For us the more important cases are 1. thermal clouds with partial ordering into a lattice (CARL) and 2. arrays of BECs localized at different lattice sites. Try,

$$|\psi_{so}\rangle_{so} = \frac{1}{\sqrt{N!}} \prod_{m=1}^{M} \left(\frac{1}{\sqrt{N_m}} \sum_{i=1}^{N_m} b_i^\dagger \right) |0\rangle \ . \tag{40.302}$$

[1036] shows what correlations are building up under CARL action. Also Suppl. Carl, "Quantized motion" and "Coherence".

Let us interpret the observations: The expectation value of the field amplitude, $\langle a_1 \rangle$ only depends on the mean atom number. The angular dependence is like in for classical Bragg scattering.

Number of scattered photons $\langle a_1^* a_i \rangle$ (intensity depends for certain angles on the density correlation. From this one obtains the structure factor. Two terms contribute to the angular dependence of the intensity: the first one depends on $|A|^2$, i.e. it goes quadratically with the field amplitude. the second term is proportional to $\langle \hat{n}^2 \rangle - \langle \hat{n}_a \hat{n}_b \rangle$, i.e. contains quantum fluctuations.

Variance $R(\theta_0, \theta_1)$: the term with classical angular distribution $|A|^2$ only appears, when pair correlations $\langle \hat{n}_a \hat{n}_b \rangle$ do not vanish. So, not only the spatial structure of the lattice leads to diffraction, but also the distribution of the fluctuations. Here, the spatial distribution of the fluctuations $\langle \delta\hat{n}_a \delta\hat{n}_b \rangle$ can be either zero (MI) or identical with the density distribution. In the first case, only the fluctuation at each lattice site $\langle \delta\hat{n}^2 \rangle$ contributes to the noise, in the second case, pair correlations contribute to the classical distribution $|A|^2$.

The spatial distribution of the noise may differ from that of the average density. Additional peaks are obtained in the angular distribution.

40.3.7 Results and questions

40.3.7.1 1D optical lattice in transversely pumped cavity

System: Pump beam orthogonal to lattice ($\theta_0 = 0$), light scattered in the direction of the lattice $\left(\theta_1 = \frac{\pi}{2}\right)$, scattering into the resonator mode. Atoms at the distance $d = \lambda/2$ in the antinodes of a standing wave. Then:

$$\begin{aligned} \hat{D} &= \sum_{m=1}^{K} u_1^*(r_k) u_0(r_k) \hat{n}_k = \sum_{m=1}^{K} \cos(mdk_1 \sin\theta_1) \hat{n}_k \cos(mdk_0 \sin\theta_0) \hat{n}_k \\ &= \sum_{m=1}^{K} \cos(\pi m) \hat{n}_k = \sum_{m=1}^{K} (-1)^{2m-1} \hat{n}_k \ . \end{aligned} \tag{40.303}$$

$\langle \hat{D} \rangle$ disappears and thus also field amplitude (for both states). This corresponds to destructive interference (even K).

Photon number $\langle a_1^\dagger a_1 \rangle$ proportional to,

$$\langle \hat{D}^* \hat{D} \rangle = \langle \hat{n}_a \hat{n}_b \rangle |A|^2 + (\langle \hat{n}^2 \rangle - \langle \hat{n}_a \hat{n}_b \rangle) \sum_{i=1}^{K} |A_i|^2 = (\langle \hat{n}^2 \rangle - \langle \hat{n}_a \hat{n}_b \rangle) K \ . \tag{40.304}$$

for MI disappears $(\langle \hat{n}^2 \rangle - \langle \hat{n}_a \hat{n}_b \rangle)K$, for SF it becomes,

$$\begin{aligned} (\langle \hat{n}^2 \rangle - \langle \hat{n}_a \hat{n}_b \rangle) K &= \left(\frac{N^2}{M^2} - \frac{N}{M^2} + \frac{N}{M} - \frac{N^2}{M^2} + \frac{N}{M^2} \right) K \\ &= \frac{N}{M} K = N_K \ . \end{aligned} \tag{40.305}$$

The MI state does not scatter photons into resonator mode, SF state scatters a number of photons proportional to the atom number:

$$\begin{aligned} \langle a_i \rangle_{MI} &= 0 = \langle a_i \rangle_{SF} \\ \langle a_i^\dagger a_i \rangle_{MI} &= 0 \ , \ \langle a_i^\dagger a_i \rangle_{SF} = |C|^2 N_K \ . \end{aligned} \tag{40.306}$$

The mean photon number already yields information on the atomic quantum state.

40.3.7.2 Running waves

Running wave:

$$u_{0,1}(r) = \exp(\imath m k_{0,1} d) \ . \tag{40.307}$$

Then

$$\begin{aligned} A_m &= u_1^*(r_m) u_0(r_m) = e^{\imath m \alpha_-} \\ \alpha_- &= k_{0x} d \sin\Theta_0 - k_{1x} d \sin\Theta_1 \ . \end{aligned} \tag{40.308}$$

We obtain for the noise:

$$R = \langle \delta\hat{n}_a \delta\hat{n}_b \rangle \frac{\sin^2(K\alpha_-/2)}{\sin^2(\alpha_-/2)} + \left(\langle \delta\hat{n}^2 \rangle - \langle \delta\hat{n}_a \delta\hat{n}_b \rangle \right) K \ . \tag{40.309}$$

For the various states,

$$\begin{aligned} R_{MI} &= 0 \\ R_{CO} &= nK = N_K \\ R_{SF_K} &= -\frac{N}{M^2} \frac{\sin^2(K\alpha_-/2)}{\sin^2(\alpha_-/2)} + \frac{N}{M} K \ . \end{aligned} \tag{40.310}$$

Intensity of scattered light,

$$\langle \hat{D}^* \hat{D} \rangle = \langle \hat{n}_a \hat{n}_b \rangle |A|^2 + \left(\langle \hat{n}^2 \rangle - \langle \hat{n}_a \hat{n}_b \rangle \right) \sum_{i=1}^{K} |A_i|^2 \tag{40.311}$$

$$\begin{aligned} \langle \hat{D}^* \hat{D} \rangle_{MI} &= 0 \\ \langle \hat{D}^* \hat{D} \rangle_{Inc} &= K \langle \hat{n}^2 \rangle = nK \\ \langle \hat{D}^* \hat{D} \rangle_{SF} &= \left(\frac{N^2}{M^2} - \frac{N}{M^2} \right) \frac{\sin^2(K\alpha_-/2)}{\sin^2(\alpha_-/2)} + \frac{N}{M} K \ . \end{aligned}$$

MI and SF states are distinguishable in the diffraction minimum, and no distinction is possible in the maximum, because there are no fluctuations in the total number of atoms. Scattering at the maximum can be considered as a superradiance, since the intensity is proportional to N_K^2. At the minimum, scattering for MI is suppressed, scattering from SF proportional to N_K.

For even K the terms with $|A|^2$ disappear. Therefore, we only get a dependence from $\langle \hat{n}^2 \rangle - \langle \hat{n}_a \hat{n}_b \rangle$, i.e. the difference between local and non-local fluctuations. For running waves is the proportionality factor K.

40.3.7.3 Standing waves

If one of the two modes (pump or probe mode) is a standing wave in a resonator, the angular dependence of the noise becomes even stronger. We obtain new maxima in the classical diffraction (first terms in Eqs. (17, 18)) and the angular dependence of the second terms is no longer isotropic, $|A_i|^2$ returns a doubling of the lattice period or the frequency. This results in new peaks in the noise, where classically nothing is to be expected,

$$u_{0,1}(r) = \cos(m k_{0,1} d) \ . \tag{40.312}$$

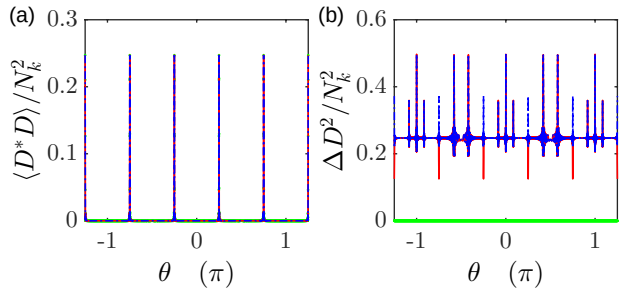

Figure 40.28: (code) For $\theta_1 = \frac{\pi}{2}$ (Probe light along lattice axis), different angles of the pump light, $P_+ = 1$ W, $\lambda_0 = \lambda_1 = 794$nm, $\lambda_G = 820$ nm. There are 150 filled lattice sites.

40.3.7.4 Questions

[871] assumes a classical incident light field, which means that the fluctuations in the Bragg-scattered light solely arise from quantum fluctuations in the atomic cloud. However, in reality the pump laser will have Poissonian fluctuations as well, $\langle \delta a_0 \rangle \neq 0$. How to treat conditional probabilities?

Binomial distribution,

$$P_n^{(m)} = \binom{m}{n} p^n (1-p)^{m-n} \ . \tag{40.313}$$

Poisson distribution,

$$P_n = \frac{\lambda^n}{n!} e^{-\lambda} \tag{40.314}$$

for large n small p we have $B_k^{(n)} \simeq P_k$ with $\lambda = np$. Thermal distribution,

$$P_n = \frac{\bar{n}^n}{(1+\bar{n})^{1+n}} \ . \tag{40.315}$$

Thermal distribution,

$$P_n = \frac{e^{\hbar\omega(n+1/2)k_B T}}{\sum_n e^{\hbar\omega(n+1/2)k_B T}} \ . \tag{40.316}$$

Photon noise at non-Bragg angles should disappear for $K \to \infty$?

In principle $g^{(2)}(\tau)$ can be determined in two ways: 1. Autocorrelation of a time-dependent intensity $I(t)$, 2. Normalized histogram of coincidences in a Hanbury-Brown-Twiss type experiment. In the first case, intensity trace can be gathered by a photon detector in current (i.e. integration) mode or by photon counting and summing up all counts within predefined time-intervals. This method is suitable to detect classical correlations or technical noise. However this method deletes the most interesting part of the information, which is photon statistics at short times. Furthermore, a photon counter has a finite bandwidth (in our case $\tau_{bw}^{-1} = 5\,\mathrm{MCnts/s}$). A single trace can thus only reproduce correctly the statistics of photons separated by $\tau_{dist} > \tau_{bw}$. If the coherence time τ_{coh} is shorter, quantum effects like antibunching will not become visible. This is why Hanbury-Brown-Twiss is needed [1171].

It is possible to generate arbitrary $g^{(2)}(\tau)$ by tailoring the waiting time distribution between photons. We have a 5 ns resolution photon arrival time trace (SR430) or a 5 μs resolution photon arrival time histogram (single-photon detector). In an experiment, we may couple the probe light leaking out of a cavity mirror through a fiber into a single-photon detector. A multi channel scaler counts the numbers of photons n_{ph} detected in subsequent time-intervals of given length τ. Now what is the noise Δn_{ph}? Is it the width of the histogram $H(n_{ph})$?

Maximum count rate: 5 counts/ µs. Time scale for CARL dynamics: 1 µs. Photon number in cavity for $P_+ = 1\,\mathrm{W}$ is $n_+ = 10^9$ and for $P_- = 1\,\mathrm{mW}$ is $n_- = 10^6$. Outcoupled power is $P_{out,-} = P_- \times 2\,\mathrm{ppm}$. Outcoming photons per second $n_{out,-} = P_-/\hbar\omega \times 1\,\mathrm{s} \simeq 10^{10}$.

Experimentally, superfluid lattices may correspond to condensates in shallow standing waves, where atoms can tunnel form site to site. Arrays of uncorrelated condensates in deep lattice would then be described by coherent states. What are the real quantum correlations in the cavity? What correlations does the CARL instability generate?

[871] assumes perfect ordering, even for the superfluid case. Superfluidity for him only means perfect mobility of the atoms between discrete, well-localized lattice sites. In practice however we will have a finite Debye-Waller factor. Can this have an impact on the quantum statistics of the scattered light?

[871] assumes the scattered light be stored in a cavity. Does the fact that we look at the outcoupled light modify the quantum statistics?

Is it possible to monitor the quantum correlations developing during CARL using the Bragg scattering noise analysis? Imagine we run a CARL experiment in high finesse and observe the superradiant ringing on a 100 µs time scale. We could use a weak collinear probe laser in low finesse to couple into the cavity short pulses (not limited by the cavity decay time). Hence, the CARL is quasi in steady state, when we detect the response of the Bragg scattering of the probe. The probe may be separated from other overlapping beams $\langle a_1 \rangle$ through homodyning, $\langle a_1^* a_1 \rangle$. The Bragg angle can be tuned by changing the wavelength.

The treatment only holds for optically dilute clouds, otherwise the scattering rate saturates. This means that only a small fraction of photons is scattered only the Bragg angles.

The portion of photons scattered into the cavity has to be integrated over the solid angle of the cavity mode. Far from the Rayleigh length we have $\tan\alpha \simeq \alpha = w(z)/w_0 = \lambda/\pi/w_0 \approx 0.13°$.

How about light Rayleigh-scattered out of the incidence plane?

40.4 Interaction of atoms with surfaces

40.4.1 Local density of states for atoms near surfaces

In the following sections we consider two-level atoms interacting with meta-materials. An atom consists of a discrete set of levels between which electric or magnetic transitions characterized by dipole moments $\mathbf{d}$ can be excited via vectorial laser light. The meta-material medium is defined by its spatially and frequency dependent relative

permittivity, $\varepsilon(\mathbf{r};\omega)$ and relative permeability, $\mu(\mathbf{r};\omega)$ [9].

The way how the atom and the medium interact can be understood introducing the notion of the photonic local density of states (LDOS). The medium shapes, via ε and μ, the LDOS for any radiation field the medium can sustain, assuming that the atom itself does not modify the LDOS. To calculate the density of states one must solve Maxwell equations and obtain the Green function $\mathcal{G}(\mathbf{r},\mathbf{r}';\omega)$, which completely describes the material. The density of states is proportional to the imaginary part of Green function. Furthermore, the Green function permits to calculate easily the propagation of an incident light field through the medium [10], and hence the local radiation intensity $\vec{\mathcal{E}}(\mathbf{r};\omega)$.

After this, one has to set up the Hamiltonian for the atom located at position $\mathbf{r}_a$ near the dielectric and solve, with a suitable ansatz, the Schrödinger equation. This yields the time evolution of the atomic state excitation probabilities [682, 41].

40.4.1.1 Density of states from Maxwell's equations

The density of states (DOS), the group velocity, and the distribution function are necessary for calculating various macroscopic quantities like specific heat, thermal conductivity, energy density, and radiation intensity. The local density of states (LDOS) is a generalization of the DOS and, unlike the DOS, a position dependent quantity. Like the DOS, the LDOS depends on the type of carrier - electron, phonon, or photon. It is generally related to the Green's function of the appropriate governing equation (Schrödinger equation for electrons, wave equation for long wavelength phonons, and Maxwell's equation for photons) and boundary conditions. Here, we are concerned with the photonic or electromagnetic LDOS [946].

The electromagnetic LDOS is related to the dyadic Green's function (DGF) of the vector Helmholtz equation. In free space the electric field and the magnetic field contributions are equal in the absence of scatterers. In other circumstances, however, there is a contribution to the LDOS from the magnetic field energy, and it is related to the magnetic DGF. Since the pioneering work of *Purcell* it is well known that the spontaneous emission rate of molecules is strongly affected by their vicinity to macroscopic objects. The LDOS (both electric and magnetic) also plays an important role in *Casimir* forces between objects. The Maxwell stress tensor in vacuum at thermal equilibrium can be expressed compactly in terms of the electric and magnetic DGF.

The spectral electric and magnetic fields are governed by the macroscopic Maxwell's equations (18.194). These equations can be converted to the vector Helmholtz equation for electric and magnetic fields (18.195). To invert these equations and express the electric and magnetic fields as integrals over the source regions, we make use of the dyadic Green's function (DGF) which also obeys the dyadic version of the vector Helmholtz equation (18.197). The electric field is obtained as a convolution integral (18.196).

[9] Note that the assumption of Drude type function is often a good one.

[10] Note that even without incident radiation the medium influences the atomic dynamics via the LDOS.

40.4.1.2 Local density of states (LDOS) and the decay rate

The concepts of density of states (DOS) and local density of states (LDOS) can be introduced starting from the situation of a non-absorbing and non-dispersive medium, $\varepsilon(\mathbf{r};\omega) = \varepsilon(\mathbf{r}) \in R^{>0}$, embedded in a closed cavity with volume $V = L^3$ assuming that $L \ll \lambda$, λ being the wavelength in vacuum). Then, a discrete set of eigenmodes of the vector Helmholtz equation can be obtained solving the eigenvalue equation [235],

$$\nabla \times \nabla \times \mathbf{e}_n(\mathbf{r}) = \varepsilon(\mathbf{r}) \frac{\omega_n^2}{c^2} \mathbf{e}_n(\mathbf{r}) \ , \tag{40.317}$$

yielding the eigenvalues ω_n/c as well as the eigenfunctions $\mathbf{e}_n(\mathbf{r})$. Since the differential operator is Hermitian, the eigenfunctions are orthogonal,

$$\int \varepsilon(\mathbf{r}) \mathbf{e}_m^*(\mathbf{r}) \cdot \mathbf{e}_n(\mathbf{r}) d^3r = \delta_{mn} \ . \tag{40.318}$$

The DOS $\rho(\omega)$ at a frequency ω counts the number of eigenmodes in an infinitely small frequency range and is defined as,

$$\rho(\omega) = \tfrac{1}{V} \sum_n \delta(\omega - \omega_n) \ . \tag{40.319}$$

This DOS is a global quantity that characterizes the spectral density of eigenmodes of the medium as a whole. A local quantity $\rho(\mathbf{r},\omega)$ (LDOS) can be introduced through a summation weighted by the amplitude of the eigenmodes at point $\mathbf{r}$,

$$\boxed{\rho(\mathbf{r},\omega) = \sum_n |\hat{\mathbf{e}}_n(\mathbf{r})|^2 \delta(\omega - \omega_n)} \ . \tag{40.320}$$

This relation defines the LDOS in the particular case of a medium for which a discrete set of eigenmodes can be introduced.

The (electric) LDOS (40.320) can be reformulated in terms of the electric Green function $\mathcal{G}(\mathbf{r},\mathbf{r}',\omega)$ being the solution of the vector Helmholtz equation (18.197) setting $\mu_r(\mathbf{r},\omega) = 1$. The solution can be cast into the shape,

$$\boxed{\mathcal{G}(\mathbf{r},\mathbf{r}',\omega) = c^2 \sum_n \hat{\mathbf{e}}_n^*(\mathbf{r}') \otimes \hat{\mathbf{e}}_n(\mathbf{r}) \left[\mathcal{PV}\left(\frac{1}{\omega_n^2 - \omega^2} \right) + \frac{\imath\pi}{2\omega_n} \delta(\omega - \omega_n) \right]} \ . \tag{40.321}$$

With this result, the LDOS can be written,

$$\begin{aligned} \rho(\mathbf{r},\omega) &= \frac{2\omega}{\pi c^2} \mathfrak{Im} \ \mathrm{Tr} \ \mathcal{G}(\mathbf{r},\mathbf{r},\omega) \qquad (40.322) \\ &= \frac{2\omega}{\pi c^2} \mathrm{Tr} \ c^2 \sum_n \mathbf{e}_n^*(\mathbf{r}) \otimes \mathbf{e}_n(\mathbf{r}) \frac{\pi}{2\omega_n} \delta(\omega - \omega_n) = \sum_n \mathbf{e}_n^*(\mathbf{r}) \cdot \mathbf{e}_n(\mathbf{r}) \delta(\omega - \omega_n) \ . \end{aligned}$$

This result shows that shows that the correct counting of eigenmodes is implicit in the Green function, although the latter can be computed by solving the Helmholtz equation without referring to any set of eigenmodes. In particular, the expression (40.322) even holds for lossy media, when a basis of eigenmodes cannot be defined [235].

40.4.1.3 Power radiated by a classical dipole

The Green tensor defined by (18.199) permits the calculation of the electric field generated by a current density according to (18.196).

For a classical point-dipole the solution can be given explicitly (see example 108). The radiated power is simply,

$$P = -\tfrac{1}{2}\mathfrak{Re} \int \mathbf{j}^*(\mathbf{r}) \cdot \vec{\mathcal{E}}(\mathbf{r}) d^3r \ . \tag{40.323}$$

With the current density parametrized as $\mathbf{j}(\mathbf{r}) = \dot{\mathbf{d}}_{eg}\delta(\mathbf{r}-\mathbf{r}_s) = -\imath\omega\mathbf{d}_{eg}\delta(\mathbf{r}-\mathbf{r}_s)$ we get,

$$P = \frac{\omega}{2}\mathfrak{Im}\ [\mathbf{d}_{eg}^* \cdot \vec{\mathcal{E}}(\mathbf{r}_s)] \ . \tag{40.324}$$

From (40.323) we obtain,

$$P = \frac{\mu_0\omega^3}{2}|\mathbf{d}_{eg}|^2\mathfrak{Im}\ [\hat{\mathbf{e}}_d\ \mathcal{G}(\mathbf{r},\mathbf{r}',\omega)\ \hat{\mathbf{e}}_d] \ , \tag{40.325}$$

where $\hat{\mathbf{e}}_d$ is the unit vector along the dipole. In this expression we assume that the source point $\mathbf{r}_s$ is located in vacuum, but the Green function $\mathcal{G}(\mathbf{r},\mathbf{r}_s,\omega)$ can describe an arbitrary environment surrounding the emitter. In particular, the emitted power calculated in this way accounts both for far-field radiation and absorption in the environment.

In the case of a dipole with a fixed orientation $\hat{\mathbf{e}}_d$, we can define a projected LDOS (sometimes called partial LDOS),

$$\rho_{\mathbf{d}}(\mathbf{r}_s,\omega) = \frac{2\omega}{\pi c^2}\mathfrak{Im}\ [\hat{\mathbf{e}}_d\ \mathcal{G}(\mathbf{r}_s,\mathbf{r}_s,\omega)\ \hat{\mathbf{e}}_d] \tag{40.326}$$

so that the full LDOS is,

$$\rho(\mathbf{r}_s,\omega) = \sum_{\hat{\mathbf{e}}_{dx},\hat{\mathbf{e}}_{dy},\hat{\mathbf{e}}_{dz}} \rho_{\mathbf{d}}(\mathbf{r}_s,\omega) = \frac{2\omega}{\pi c^2}\mathfrak{Im}\ \mathrm{Tr}\ \mathcal{G}(\mathbf{r}_s,\mathbf{r}_s,\omega) \ . \tag{40.327}$$

The projected LDOS accounts for radiation by an electric dipole with a given orientation,

$$\boxed{P = \frac{\pi\omega^2}{4\varepsilon_0}|\mathbf{d}_{eg}|^2\rho_{\mathbf{d}}(\mathbf{r}_s,\omega)} \ . \tag{40.328}$$

Example 247 (*LDOS in free space*): In the particular case of a dipole placed in 3D free space, the power transferred to the environment equals the power radiated to far-field radiation. It can be obtained from the free-space dyadic Green function $\mathcal{G}_0(\mathbf{r},\mathbf{r}_s,\omega)$, whose imaginary part at $\mathbf{r}=\mathbf{r}_s$ is obtained from the Green tensor (18.207)calculated for a bulk medium by setting $\mathbf{r}=\mathbf{r}'=\mathbf{r}_s$,

$$\mathfrak{Im}\ \mathcal{G}^{(0)}(\mathbf{r}_s,\mathbf{r}_s,\omega) = \frac{k_0}{6\pi}\mathbb{I} \ . \tag{40.329}$$

With this, the projected LDOS (40.326) along $\hat{\mathbf{e}}_d$ becomes,

$$\rho_{\mathbf{d}}^{(0)}(\mathbf{r}_s,\omega) = \frac{\omega^2}{3\pi^2c^3} \ , \tag{40.330}$$

and the full LDOS (40.327),

$$\rho^{(0)}(\mathbf{r}_s,\omega) = \frac{\omega^2}{\pi^2 c^3} \ . \tag{40.331}$$

The emitted power becomes,

$$P^{(0)} = \frac{\omega^4}{12\pi\varepsilon_0 c^3}|\mathbf{d}_{eg}|^2 \ . \tag{40.332}$$

40.4.1.4 Spontaneous emission by a quantum emitter in the weak coupling regime

In (18.126) we established a relationship between the power emitted by a classical radiator and a spontaneous emission by a quantized two-level system. The spontaneous emission rate can be evaluated in perturbation theory from Fermi's golden rule,

$$\frac{P}{\hbar\omega} \longrightarrow \frac{\pi\omega^2}{4\varepsilon_0}|\mathbf{d}|^2\rho_{\mathbf{d}}(\mathbf{r}_s,\omega) = \frac{\pi\omega_{eg}}{\hbar\varepsilon_0}|\hat{\mathbf{d}}_{eg}|^2\rho_{\mathbf{d}}(\mathbf{r}_s,\omega_{eg}) = \Gamma \ . \tag{40.333}$$

The correction factor comes from the fact that in quantum mechanics, unlike in in classical mechanics, positive and negative frequency components are treated separately as absorption resp. stimulated emission.

In free space, with the formula (40.330) we calculate for the relationship between spontaneous emission rate and the induced dipole moment,

$$\boxed{\Gamma^{(0)} = \frac{\omega_{eg}^3}{3\pi\hbar\varepsilon_0 c^3}|\mathbf{d}_{eg}|^2} \ , \tag{40.334}$$

which coincides with the expression (34.41).

40.4.1.5 Purcell factor and Lamb shift

The Purcell factor is defined as the ratio between the decay rates in the presence and in the absence of boundary conditions. It can this be evaluated from the expression (40.333) as,

$$\frac{\Gamma}{\Gamma^{(0)}} = \frac{\rho_{\mathbf{d}}(\mathbf{r}_s,\omega)}{\rho^{(0)}_{\mathbf{d}}(\mathbf{r}_s,\omega)} = \frac{6\pi c}{\omega_{eg}}\mathfrak{Im}\ \hat{\mathbf{e}}_d\ \mathcal{G}(\mathbf{r}_s,\mathbf{r}_s,\omega)\ \hat{\mathbf{e}}_d \ . \tag{40.335}$$

40.4.2 Interaction between atomic dipoles

Until now we concentrated on simple dipole in the environment of dielectric boundaries. We will now extend the formalism to interacting dipoles located at positions $\mathbf{r}_i$ and $\mathbf{r}_j$ continuing the discussion of Sec. 18.3.1.

Intermolecular energy transfer can occur through two mechanisms, namely, radiationless short-range transfer, also called *Förster transfer*, and radiative long-range transfer [399, 1151]. In the former the distance R between donor and acceptor is small compared with the electronic-energy-transfer wavelength $R \ll \lambda_A$. The free-space transfer rate behaves as R^{-6}, which can be explained by the instantaneous (longitudinal)

Coulomb interaction between the two molecules. In the latter the intermolecular distance substantially exceeds the transition wavelength, $R \gg \lambda_A$. The observed R^{-2} dependence of the transfer rate can be regarded as being the result of emission and reabsorption of real (transverse) photons, see Sec. 40.2.1 and example 240.

The Purcell factor (40.335) allows us to calculate the modification of the decay rate in the presence of a Green tensor. In the absence of boundaries we use the bulk medium Green tensor (18.214),

$$\begin{aligned}\Gamma_{ij}^{(b)} &= 3\lambda\Gamma^{(0)}\hat{\mathbf{e}}_d^* \,\mathfrak{Im}\, \mathcal{G}_b(\mathbf{r}_i,\mathbf{r}_j,\omega)\, \hat{\mathbf{e}}_d \\ &= \tfrac{3}{2}\Gamma^{(0)}\left[(1-(\hat{\mathbf{e}}_d\cdot\hat{\mathbf{e}}_R)^2)\frac{\sin kR}{kR} + (1-3(\hat{\mathbf{e}}_d\cdot\hat{\mathbf{e}}_R)^2)\left(\frac{\cos kR}{k^2R^2}-\frac{\sin kR}{k^3R^3}\right)\right] ,\end{aligned} \tag{40.336}$$

where $k^2=(\omega/c)^2\varepsilon\mu$ and $\mathbf{R}\equiv\mathbf{r}_i-\mathbf{r}_j$.

Similarly, the Lamb shift can be calculated,

$$\begin{aligned}\Delta_{ij}^{(b)} &= -\tfrac{3}{2}\lambda\Gamma^{(0)}\hat{\mathbf{e}}_d^* \,\mathfrak{Re}\, \mathcal{G}_b(\mathbf{r}_i,\mathbf{r}_j,\omega)\, \hat{\mathbf{e}}_d \\ &= \tfrac{3}{4}\Gamma^{(0)}\left[(1-(\hat{\mathbf{e}}_d\cdot\hat{\mathbf{e}}_R)^2)\frac{\cos kR}{kR} - (1-3(\hat{\mathbf{e}}_d\cdot\hat{\mathbf{e}}_R)^2)\left(\frac{\sin kR}{k^2R^2}+\frac{\cos kR}{k^3R^3}\right)\right]\end{aligned} \tag{40.337}$$

Again, the second line is obtained for free space using (18.214).

At long distances, $kR>1$, the results (40.336) and (40.337) simplify to,

$$\boxed{\begin{array}{rcl}\Delta_{ij}^{(b)} &\simeq& \tfrac{3}{4}\Gamma^{(0)}[1-(\hat{\mathbf{e}}_d\cdot\hat{\mathbf{e}}_R)^2]\frac{\cos kR}{kR}\\ \Gamma_{ij}^{(b)} &\simeq& \tfrac{3}{2}\Gamma^{(0)}[1-(\hat{\mathbf{e}}_d\cdot\hat{\mathbf{e}}_R)^2]\frac{\sin kR}{kR}\end{array}} , \tag{40.338}$$

and at very long distances, $kR\gg 1$, $\Delta_{ij}\to 0 \leftarrow \Gamma_{ij}$. This atomic dipole-dipole interaction interaction will play a role in the generation of interatomic correlations studied in Sec. 41.3.2. Do the Exc. 40.4.4.1.

40.4.2.1 Derivation of the Hamiltonian

First for one atom interacting with a dielectric then for two atoms,

$$\hat{H} = \int d^3r \int_0^\infty d\omega\hbar\omega\hat{\mathbf{f}}^\dagger(\mathbf{r},\omega)\hat{\mathbf{f}}(\mathbf{r},\omega) + \sum_{i=0}^{N}\hbar\omega_i\hat{\sigma}_i^+\hat{\sigma}_i - \sum_{i=0}^{N}\int_0^\infty d\omega\left[\hat{\mathbf{d}}_i\cdot\vec{\mathcal{E}}(\mathbf{r}_i,\omega)+H.c.\right] . \tag{40.339}$$

Here, $\hat{\mathbf{f}}(\mathbf{r},\omega)$ are polaritonic bosonic operators associated with the annihilation of the corresponding matter-light elementary excitations. The field operator is [474, 1211],

$$\vec{\mathcal{E}}(\mathbf{r},\omega) = i\vec{\epsilon}\sqrt{\frac{\hbar}{\pi\varepsilon_0}}\frac{\omega^2}{c^2}\int\sqrt{\mathfrak{Im}\;\varepsilon_r(\mathbf{r}',\omega)}\mathcal{G}(\mathbf{r},\mathbf{r}',\omega)\hat{\mathbf{f}}(\mathbf{r}',\omega)d^3r' . \tag{40.340}$$

40.4.3 Metamaterials

Ray optics (lenses, shadows, ..) for $a\gg\lambda$, photonic crystals for $a\simeq\lambda$, optical crystals and metamaterials for $a\ll\lambda$ [1190, 1045].

The permittivity ϵ and the permeability μ at *optical frequencies* are in general very different from the static values. E.g. for vacuum and electrically inactive media $\epsilon = 1$, for metals $\epsilon < 0$. For vacuum and magnetically inactive media $\mu = 1$, for resonant ferromagnets and antiferromagnets $\mu < 0$.

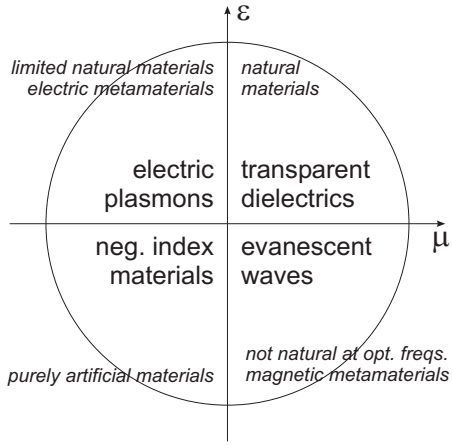

Figure 40.29: Metamaterials.

At low frequencies, conductors/metals are good as metamaterials, because they strongly respond to electromagnetic fields. At *optical frequencies* only the electric dipolemoment interacts with matter. Magnetic interaction is suppressed by the factor $(2\mu_B/ea_B)^2 = \alpha^2$. Therefore, resonant enhancement of optical magnetism is necessary, e.g. nanostructured $L-C$-circuits of wavelength-sized $\vec{\mathcal{E}}$ and $\vec{\mathcal{H}}$ guiding oscillations of a propagating light wave.

40.4.4 Exercises

40.4.4.1 Ex: Coupled dipoles model near dielectrics

Develop the vectorial coupled dipoles model in the vicinity of a dielectric using the Green tensor formalism.

Solution: *In free space the vectorial coupled dipoles model can be written (see Eq. (39.26)),*

$$\boxed{\frac{d\beta_i}{dt} = \sum_j \left(\delta_{ij}\imath\Delta - K_{ij}\right)\beta_j - \frac{\imath\Omega}{2}e^{\imath\mathbf{k}\cdot\mathbf{r}_i}} \ , \tag{40.341}$$

where the kernel is given by the projection of the Green tensor $\mathcal{G}(\mathbf{r}_i, \mathbf{r}_j, \omega_0)$ on the dipoles $\hat{\mathbf{e}}_{di}$ and $\hat{\mathbf{e}}_{dr}$ respectively located at $\mathbf{r}_i$ and $\mathbf{r}_j$,

$$K_{ij} = -\frac{3\pi\imath\Gamma}{k}\hat{\mathbf{e}}^*_{di}\ \mathcal{G}(\mathbf{r}_i, \mathbf{r}_j, \omega)\ \hat{\mathbf{e}}_{dj} \ . \tag{40.342}$$

In the absence of boundaries the Green tensor is simply the one derived for bulk media $\mathcal{G}_b(\mathbf{r}_i, \mathbf{r}_j, \omega_0)$ given by the expression (18.206). Let us first concentrate on this case.

Decomposing the kernel into real and imaginary parts,

$$K_{ij}^{(b)} = \frac{\Gamma_{ij}^{(b)}}{2} + \imath\Delta_{ij}^{(b)} = \frac{3\lambda\Gamma^{(0)}}{2}\hat{\mathbf{e}}_{di}^{*}\left[\mathfrak{Im}\ \mathcal{G}_b(\mathbf{r}_i,\mathbf{r}_j,\omega) - \imath\mathfrak{Re}\ \mathcal{G}_b(\mathbf{r}_i,\mathbf{r}_j,\omega)\right]\hat{\mathbf{e}}_{dj}\ . \quad (40.343)$$

We also find,

$$\Gamma_{ii}^{(b)} = \tfrac{3}{2}\Gamma^{(0)} \qquad \textit{and} \qquad \Delta_{ii}^{(b)} = 0\ . \quad (40.344)$$

Note, that in the scalar approximation the Green tensor reduces to the well known formula,

$$\mathcal{G}_b(\mathbf{r}_i,\mathbf{r}_j,\omega_0) \simeq \mathbb{I}\frac{e^{\imath k|\mathbf{r}_i-\mathbf{r}_j|}}{4\pi|\mathbf{r}_i-\mathbf{r}_j|}\ , \quad (40.345)$$

so that,

$$K_{ij}^{(b)} \simeq \frac{3\Gamma}{4}\frac{e^{\imath k|\mathbf{r}_i-\mathbf{r}_j|}}{\imath k|\mathbf{r}_i-\mathbf{r}_j|} \longrightarrow \frac{\Gamma}{2}e^{-\imath\mathbf{k}\cdot(\mathbf{r}_j-\mathbf{r}_m)}\frac{e^{\imath k|\mathbf{r}_j-\mathbf{r}_m|}}{\imath k|\mathbf{r}_j-\mathbf{r}_m|}\ . \quad (40.346)$$

Now, the only thing we need to do to account for boundaries is to generalize the Green tensor,

$$\mathcal{G} = \mathcal{G}_b + \mathcal{G}_d\ , \quad (40.347)$$

where G_d accounts for the presence of a dielectric. Then,

$$\frac{d\beta_i}{dt} = \left[\delta_{ij}\imath\Delta - \sum_j(K_{ij}^{(b)} + K_{ij}^{(d)})\right]\beta_j - \frac{\imath\Omega}{2}e^{\imath\mathbf{k}\cdot\mathbf{r}_i} \quad (40.348)$$

$$= \left[\imath(\Delta-\Delta_{ii}^{(d)}) - \left(\tfrac{\Gamma_{ii}^{(b)}}{2} + \tfrac{\Gamma_{ii}^{(d)}}{2}\right)\right]\beta_i - \sum_{j\neq i}\left(\tfrac{\Gamma_{ij}^{(b)}}{2} + \tfrac{\Gamma_{ij}^{(d)}}{2} + \imath\Delta_{ij}^{(b)} + \imath\Delta_{ij}^{(d)}\right)\beta_j - \tfrac{\imath\Omega}{2}e^{\imath\mathbf{k}\cdot\mathbf{r}_i}\ . \quad (40.349)$$

In particular, without dielectric,

$$\frac{d\beta_i}{dt} = \left(\imath\Delta - \frac{\Gamma_{ii}^{(b)}}{2}\right)\beta_i - \sum_{j\neq i}K_{ij}^{(b)}\beta_j - \frac{\imath\Omega}{2}e^{\imath\mathbf{k}\cdot\mathbf{r}_i}\ . \quad (40.350)$$

With a dielectric but for only a single atoms,

$$\frac{d\beta_i}{dt} = \left[\imath(\Delta-\Delta_{ii}^{(d)}) - \left(\frac{\Gamma_{ii}^{(b)}}{2} + \frac{\Gamma_{ii}^{(d)}}{2}\right)\right]\beta_i - \frac{\imath\Omega}{2}e^{\imath\mathbf{k}\cdot\mathbf{r}_i}\ . \quad (40.351)$$

40.4.4.2 Ex: Scattering Green tensor above a dielectric surface

In this exercise we calculate the Green tensor for two atomic dipoles above a homogeneous dielectric filling the $z < 0$ half space.
a. Formulate the problem.
b. Simplify the scattering Green tensor obtained by [682] for that situation.

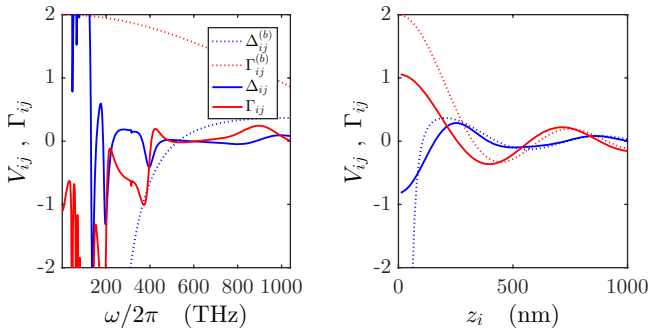

Figure 40.30: Scattering Green tensor for region-wise homogeneous dielectrics.

c. Simplify the Green tensor by assuming all atoms aligned along the y-axis at equal height from the dielectric.
d. Assume the atomic dipole moment to be aligned along the z-axis.
e. Derive the Green tensor for a single atom above the dielectric.

Solution: *a. We assume the environment composed of regions characterized by different locally homogeneous permittivities,*

$$\epsilon(\mathbf{r},\omega) = \epsilon(z,\omega) = \Theta(z) + \epsilon(\omega)\Theta(-z) = 1 + \chi_\varepsilon(\omega)\Theta(-z) \tag{40.352}$$
$$\mu(\mathbf{r},\omega) = 1 \ .$$

Supposing that the dipole sits in the region $z > 0$, the Green tensor is then,

$$\mathcal{G}(\mathbf{r},\mathbf{r}',\omega) = \begin{cases} \mathcal{G}_b(\mathbf{r},\mathbf{r}',\omega) + \mathcal{G}_d(\mathbf{r},\mathbf{r}',\omega) & \text{for} \quad z,z' > 0 \\ \mathcal{G}_d(\mathbf{r},\mathbf{r}',\omega) & \text{for} \quad z > 0 > z' \end{cases} \tag{40.353}$$

The bulk Green tensor $\mathcal{G}_b$ has been calculated in (18.206) under the assumption that whole space is homogeneous with permittivity $\epsilon(\omega) = 1$. $\mathcal{G}_d$ is scattering Green tensor. Now, we need to solve the inhomogeneous Helmholtz equation,

$$\left[\nabla_{\mathbf{r}} \times \nabla_{\mathbf{r}} \times -\tfrac{\omega^2}{c^2}\epsilon(\mathbf{r},\omega)\right](\mathcal{G}_b(\mathbf{r},\mathbf{r}',\omega) + \mathcal{G}_d(\mathbf{r},\mathbf{r}',\omega)) = \delta^{(3)}(\mathbf{r}-\mathbf{r}')\mathbb{I} \ . \tag{40.354}$$

Using (18.199) the bulk Green function can be removed and, for $\mathbf{r},\mathbf{r}' \in$ region 1, we are left with the scattering part of the Green function, which needs to satisfy the homogeneous Helmholtz equation [1313, 210],

$$\left[\nabla_{\mathbf{r}} \times \nabla_{\mathbf{r}} \times -\tfrac{\omega^2}{c^2}\chi_\varepsilon(\omega)\Theta(-z)\right]\mathcal{G}_d(\mathbf{r},\mathbf{r}',\omega) = 0 \ . \tag{40.355}$$

To deduce the Green tensor for a stratified background, it is convenient to expand it into plane waves. The Fourier transform of the Green tensor for a bulk medium (18.206) leads to [1002],

$$\mathcal{G}_b(\mathbf{r}_i,\mathbf{r}_j,\omega) = \frac{1}{(2\pi)^3 k^2}\int \frac{\mathbb{I}k^2 - \mathbf{k}'\otimes\mathbf{k}'}{k'^2 - k^2} e^{\imath\mathbf{k}'\cdot\mathbf{r}} d^3k' \ . \tag{40.356}$$

Exploiting the translational invariance of the system in the (x, y) plane, the expression can be simplified to,

$$\mathcal{G}_b(\mathbf{r}_i, \mathbf{r}_j, \omega) = \frac{\imath}{8\pi^2 k^2} \int \frac{\mathbb{I}k^2 - \mathbf{k}'\mathbf{k}'}{k'_z} e^{\imath \mathbf{k}' \cdot \mathbf{r}} dk'_x dk'_y - \frac{\hat{\mathbf{e}}_z \otimes \hat{\mathbf{e}}_z}{k^2} \delta^{(3)}(\mathbf{r}) \ , \tag{40.357}$$

using

$$k = \omega/c \quad , \quad k'_z \equiv \sqrt{k^2 - k'^2_x - k'^2_y} \quad , \quad \mathbf{k}' \equiv k'_x \hat{\mathbf{e}}_x + k'_y \hat{\mathbf{e}}_y + k'_z [\Theta(z) - \Theta(-z)] \hat{\mathbf{e}}_z \ . \tag{40.358}$$

We introduce a new coordinate system,

$$\hat{\mathbf{e}}_k \equiv \frac{\mathbf{k}'}{k'} \quad , \quad \hat{\mathbf{e}}_s \equiv \frac{\mathbf{k}' \times \hat{\mathbf{e}}_z}{|\mathbf{k}' \times \hat{\mathbf{e}}_z|} \quad , \quad \hat{\mathbf{e}}_p \equiv \hat{\mathbf{e}}_k \times \hat{\mathbf{e}}_l \ , \tag{40.359}$$

such that the direction $\hat{\mathbf{e}}_s$ corresponds to s-polarization and $\hat{\mathbf{e}}_p$ to p-polarization. Using $\mathbb{I} = \hat{\mathbf{e}}_x\hat{\mathbf{e}}_x + \hat{\mathbf{e}}_y\hat{\mathbf{e}}_y + \hat{\mathbf{e}}_z\hat{\mathbf{e}}_z = \hat{\mathbf{e}}_k\hat{\mathbf{e}}_k + \hat{\mathbf{e}}_s\hat{\mathbf{e}}_s + \hat{\mathbf{e}}_p\hat{\mathbf{e}}_p$, we find,

$$\mathcal{G}_b(\mathbf{r}_i, \mathbf{r}_j, \omega) = \frac{\imath}{8\pi^2} \int \frac{\hat{\mathbf{e}}_s\hat{\mathbf{e}}_s + \hat{\mathbf{e}}_p\hat{\mathbf{e}}_p}{k'_z} e^{\imath \mathbf{k}' \cdot \mathbf{r}} dk'_x dk'_y - \frac{\hat{\mathbf{e}}_z\hat{\mathbf{e}}_z}{k^2} \delta^{(3)}(\mathbf{r}) \ . \tag{40.360}$$

Now, we put the dielectric in the lower half space and extend the Green tensor. According to [1313, 1002, 210, 682] the scattering Green tensor for two dipole located above a homogeneous dielectric filling the $z < 0$ half space is given by,

$$\mathcal{G}_d(\mathbf{r}_i, \mathbf{r}_j, \omega) = \frac{\imath}{4\pi} \int_0^\infty \frac{k_\rho}{k_z} \left(\mathcal{G}^s(\rho, \phi, z_i, z_j, k_\rho, k_z) - \frac{k_z^2}{k^2} \mathcal{G}^p(\rho, \phi, z_i, z_j, k_\rho, k_z) \right) dk_\rho \ , \tag{40.361}$$

where $\rho \equiv \sqrt{x_{ij}^2 + y_{ij}^2}$, $\cos\phi \equiv x_{ij}/\rho$, and $k^2 = k_\rho^2 + k_z^2 \equiv k_x^2 + k_y^2 + k_z^2$.
b. The task can be performed by simply setting $\mu_i = \mu_{II} = 1$ and $\varepsilon_i = 1$ in the formulas presented by [682]. The Green tensor for s-polarization is then given by,

$$\mathcal{G}^s = \frac{r^s e^{\imath k_z (z_i + z_j)}}{2} \left[J_0(k_\rho \rho) \begin{pmatrix} 1 & 0 & 0 \\ 0 & 1 & 0 \\ 0 & 0 & 0 \end{pmatrix} + J_2(k_\rho \rho) \begin{pmatrix} \cos 2\phi & -\sin 2\phi & 0 \\ -\sin 2\phi & -\cos 2\phi & 0 \\ 0 & 0 & 0 \end{pmatrix} \right] \ . \tag{40.362}$$

For p-polarization,

$$\begin{aligned} \mathcal{G}^p = \frac{r^p e^{\imath k_z (z_i + z_j)}}{2} & \left[J_0(k_\rho \rho) \begin{pmatrix} 1 & 0 & 0 \\ 0 & 1 & 0 \\ 0 & 0 & -2k_\rho^2/k_z^2 \end{pmatrix} \right. \\ & \left. + \frac{2\imath k_\rho}{k_z} J_1(k_\rho \rho) \begin{pmatrix} 0 & 0 & \cos\phi \\ 0 & 0 & \sin\phi \\ -\cos\phi & -\sin\phi & 0 \end{pmatrix} + J_2(k_\rho \rho) \begin{pmatrix} -\cos 2\phi & \sin 2\phi & 0 \\ \sin 2\phi & \cos 2\phi & 0 \\ 0 & 0 & 0 \end{pmatrix} \right] \end{aligned} \tag{40.363}$$

with the Fresnel factors,

$$r^p = \frac{\varepsilon(\omega) k_z - k_z^d}{\varepsilon(\omega) k_z + k_z^d} \quad , \quad r^s = \frac{k_z - k_z^d}{k_z + k_z^d} \ , \tag{40.364}$$

and

$$k_z^d \equiv \sqrt{\varepsilon(\omega)k^2 - k_\rho^2} \qquad \textit{such that} \qquad \mathfrak{Re}\; k_z^d > 0\;, \tag{40.365}$$

and a suitable Drude-Lorentz model for $\varepsilon(\omega)$. Note that both matrices composing $\mathcal{G}^s$ describe a projection onto the xy-plane. The second matrix additionally describes a an azimuthal rotation around the z-axis. The first matrix composing $\mathcal{G}^p$ describes a stretching of the z-coordinate, the second ???, and the third is identical to the second component of $\mathcal{G}^s$.

c. Assuming all atoms aligned along the y-axis, we may set $\phi = 0$. The Green tensors then simplify to,

$$\mathcal{G}^s = \frac{r^s e^{2\imath k_z z_i}}{2} \begin{pmatrix} J_0(k_\rho\rho) + J_2(k_\rho\rho) & 0 & 0 \\ 0 & J_0(k_\rho\rho) - J_2(k_\rho\rho) & 0 \\ 0 & 0 & 0 \end{pmatrix} \tag{40.366}$$

$$\mathcal{G}^p = \frac{r^p e^{2\imath k_z z_i}}{2} \begin{pmatrix} J_0(k_\rho\rho) - J_2(k_\rho\rho) & 0 & \frac{2\imath k_\rho}{k_z} J_1(k_\rho\rho) \\ 0 & J_0(k_\rho\rho) + J_2(k_\rho\rho) & 0 \\ -\frac{2\imath k_\rho}{k_z} J_1(k_\rho\rho) & 0 & -\frac{2k_\rho^2}{k_z^2} J_0(k_\rho\rho) \end{pmatrix} .$$

d. Furthermore, if the dipoles are oriented long $\hat{\mathbf{e}}_d = d\hat{\mathbf{e}}_z$,

$$\hat{\mathbf{e}}_z^*\; \mathcal{G}^s\; \hat{\mathbf{e}}_z = 0 \qquad \textit{and} \qquad \hat{\mathbf{e}}_z^*\; \mathcal{G}^p\; \hat{\mathbf{e}}_z = -\frac{k_\rho^2}{k_z^2} r^p e^{2\imath k_z z_i} J_0(k_\rho\rho)\;. \tag{40.367}$$

e. The result is simply obtain from (40.353) and (40.354) by setting $\mathbf{r}_i = \mathbf{r}_j$ and

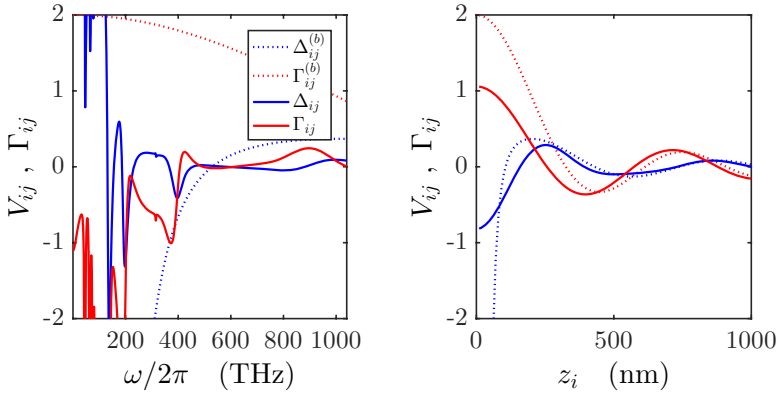

Figure 40.31: (code) Lamb-shift and Purcell factor.

using $J_0(0) = 1$ and $J_\nu(0) = 0$.

40.5 Further reading

A.N. Poddubny et al., *Microscopic model of Purcell enhancement in hyperbolic metamaterials* [1041]DOI

Wenlong Gao et al., *Topological Photonic Phase in Chiral Hyperbolic Metamaterials* [483]DOI

Haibin Wu et al., *Observation of Intracavity Electromagnetically InducedTransparency and Polariton Resonances in a Doppler-Broadened Medium* [1392]DOI

Xiaodong Zeng et al., *Spontaneous emission interference enhancement with a μ-negative metamaterial slab* [1425]DOI

Xiaodong Zeng et al., *Enhancement of the vacuum Rabi oscillation via surface plasma modes in single-negative metamaterials* [1424]DOI

F. Dubin et al., *Photon Correlation versus Interference of Single-Atom Fluorescence in a Half-Cavity* [392]DOI

U. Dorner et al., *Laser-driven atoms in half-cavities* [386]DOI

P. Lambropoulos et al., *Fundamental quantum optics in structured reservoirs* [771]DOI

40.5.1 on cavities

B. Yurke et al., *Quantum network theory* [1418]DOI

C.W. Gardiner et al., *A multimode quantum theory of a degenerate parametric amplifier in a cavity* [489]DOI

D.J. Heinzen et al., *Enhanced and Inhibited Visible Spontaneous Emission by Atoms in a Confocal Resonator* [596]DOI

D.J. Heinzen et al., *Vacuum Radiative Level Shift and Spontaneous-Emission Linewidth of an Atom in an Optical Resonator* [598]DOI

Chapter 41

Correlated atoms, entanglement and quantum gates

In Chps. 34 to 38 we concentrated on understanding the interaction of *single* atoms with light fields. In particular, we introduced the Rabi and the Jaynes-Cummings model. In Chp. 39 we introduced the coupled dipoles model for the interaction of many atoms with a single photon. In the following chapters, we will extend these models to several and many atoms and many photons [1].

model	RWA	symmetry	atom #	photon #	section
Rabi	no	$\mathcal{P}$	1	n	34.4
Jaynes-Cummings	yes	$U(1)$	1	n	35.4
Dicke	no	$\mathcal{P}$	>1	n	41.1
Tavis-Cummings	yes	$U(1)$	>1	n	41.2.2, 41.3.3

It does not come as a surprise that totally new phenomena arise from the collective interaction of several atoms with a single light mode. For instance, the atomic cloud can evolve toward a spin-squeezed or an entangled state, or it can emit light in a super- and subradiant way. The interplay between collective processes and processes favoring an individualization of the atom-light interaction is subtle, and the different models used to understand the processes only grasp partial aspects. The difficulty arises from the complexity of the task of describing the dynamics of N evolving in a Hilbert space of dimension 2^N. Approximations used to reduce the complexity of the Hilbert space come at the price of eventually loosing some interesting features. On the other hand, they may also help to crystallize fundamental symmetries, which allow us to deepen our intuition on the collective behavior of the many-body system.

Famous models used in the description of collective scattering are (among others) the Dicke model and the Tavis-Cummings model (see table above). The Dicke model (presented in Sec. 41.1) assumes a total indistinguishability of the atoms, the

[1] Other models, such as the Ising model, the Heisenberg model, or the Bose-Hubbard model are not treated here.
$\mathcal{P}$ is the parity operator defined in Eq. (41.79). The unitary group $U(1)$ corresponds to the circle group consisting of all complex numbers with absolute value 1 under multiplication.

Tavis-Cummings (discussed in Sec. 41.4 and used for the purpose of quantum computation) makes use of the rotating-wave approximation. Both models are based on the assumption of non-interacting atoms, neither by ground state collisions nor via radiation exchange, which certainly is a good assumption in the case of dilute atomic samples. On the other hand, we saw in the discussion of the coupled dipoles model in Chp. 39 that already the presence of a single photon in an atomic cloud leads noticeable interatomic interaction effects. In Sec. 41.3 we will extend the Dicke model to interacting atoms.

Finally, new phenomena arise from the presence of optical cavities shaping the spatial and spectral distribution of electromagnetic vacuum modes (see Chp. ??) and from the consideration of photonic recoil (see Chp. 42).

41.1 The Dicke model in the mean-field approximation

As we have seen in Sec. 23.3.9, the Hilbert space increases exponentially with the numbers of particles considered, the dimension of the Hilbert space of N particles being 2^N. This obviously presents a problem for numerical simulations, and simplifying models are needed. One of them is the *Dicke model*, where the N atoms are described as spin-$\frac{1}{2}$ particles and their collective interaction with a *single mode* light field via a single collective spin $\mathbf{S}$ with $S = N/2$. In this model, the dimension of the Hilbert space only scales polynomially as $2S + 1$.

In the next sections, we will introduce this model detailing its advantages and limitations and emphasizing its relations to super- and subradiance, spin squeezing and entanglement. In particular we will show that, when the coupling between the light and matter crosses a critical value, the Dicke model shows a mean-field phase transition to a superradiant phase.

41.1.1 Dicke states

The Hilbert space of the Dicke model [366, 610] is given by (the tensor product of) the states of the cavity and of the two-level atoms [2]. The Hilbert space of the cavity can be spanned by Fock states $|n\rangle$. Choosing the basis $|+\rangle \equiv \binom{0}{1}$ and $|-\rangle \equiv \binom{1}{0}$, the states of each two-level atom $j = 1, 2, .., N$ are defined through the spin operators $\hat{\mathbf{s}}_j = (\hat{s}_j^x, \hat{s}_j^y, \hat{s}_j^z)$ acting only an individual atom [3],

$$\begin{aligned} \hat{s}_j^x|... \pm ...\rangle &= \tfrac{1}{2}|... \mp ...\rangle \\ \hat{s}_j^y|... \pm ...\rangle &= \pm\imath\tfrac{1}{2}|... \mp ...\rangle \\ \hat{s}_j^z|... \pm ...\rangle &= \pm\tfrac{1}{2}|... \pm ...\rangle \ , \end{aligned} \tag{41.1}$$

and satisfying the spin algebra,

$$[\hat{s}_j^x, \hat{s}_k^y] = \imath\hat{s}_j^z\delta_{j,k} \ , \tag{41.2}$$

[2] Dicke states can also be introduced in the context of the Jaynes-Cummings model (see Sec. 41.1.1).

[3] Note, that here and in the following we set $\hbar \equiv 0$ for simplicity.

and related to the *Pauli spin matrices* (23.47) via,

$$\hat{\mathbf{s}} = \tfrac{1}{2}\vec{\hat{\sigma}} \quad , \quad \hat{s}^{\pm} = \hat{s}^x \pm \imath \hat{s}^y = \tfrac{1}{2}(\hat{\sigma}_x \pm \imath\hat{\sigma}_y) = \hat{\sigma}^{\pm} \ . \tag{41.3}$$

The Hamiltonian of the Dicke model is,

$$\hat{H} = -\Delta_c \hat{a}^\dagger \hat{a} + \sum_{j=1}^{N} \left(-\Delta_a \hat{s}_j^z + 2g(\hat{a} + \hat{a}^\dagger)\hat{s}_j^x + 2\imath g(\hat{a} - \hat{a}^\dagger)\hat{s}_j^y \right) \ . \tag{41.4}$$

Sometimes in literature the single-atom coupling strength (or half the single-atom single-photon Rabi frequency) is normalized to the atom number, $g \equiv \lambda/\sqrt{N}$. The coupling can be written as the sum of two terms: a co-rotating term that conserves the number of excitations and is proportional to $\hat{a}\hat{\sigma}^+ + \hat{a}^\dagger\hat{\sigma}^-$ and a counter-rotating term proportional to $\hat{a}\hat{\sigma}^- + \hat{a}^\dagger\hat{\sigma}^+$.

The above Hamiltonian assumes that all the spins are identical, i.e. they have the same transition frequency, they do not interact with each other, and they equally couple to the radiation field (e.g. a cavity mode). For the simple system of only two not mutually interacting spins, $\mathbf{s}_1$ and $\mathbf{s}_2$, simultaneously coupling to the same radiation field, the Dicke model has been introduced in Sec. 25.4.2. There, we have shown that the spin operators can be added, $\hat{\mathbf{S}} = \hat{\mathbf{s}}_1 + \hat{\mathbf{s}}_2$, and the total system be represented in a coupled basis, where $[\hat{s}_1 \cdot \hat{s}_2, \hat{\mathbf{S}}^2] = 0 = [\hat{s}_1 \cdot \hat{s}_2, \hat{S}_z^2]$. This concept can be generalized to an arbitrary number of spins, that is, under the above assumption, one can define macroscopic collective spin operators,

$$\hat{S}_\alpha \equiv \sum_{j=1}^{N} \hat{s}_j^\alpha \qquad \text{with} \qquad [\hat{S}_x, \hat{S}_y] = \imath \hat{S}_z \ , \tag{41.5}$$

and $\alpha = x, y, z$. Using these operators, one can rewrite the above Hamiltonian as

$$\boxed{\hat{H} = -\Delta_c \hat{a}^\dagger \hat{a} - \Delta_a \hat{S}_z + 2g\hat{a}_r \hat{S}_x - 2g\hat{a}_i \hat{S}_y} \tag{41.6}$$

with $\hat{a} = \hat{a}_r + \imath\hat{a}_i$, and it is easy to see that,

$$[\hat{H}, \hat{\mathbf{S}}^2] = 0 \neq [\hat{H}, \hat{S}_z] \ . \tag{41.7}$$

That is, the Dicke Hamiltonian preserves the spin $\langle \hat{\mathbf{S}}^2 \rangle$, but interaction with a light field can change the projection $\langle \hat{S}_z \rangle$. We will see in the following that this fact as important consequences for interaction dynamics of atomic ensembles coupled to a single light mode.

> **Example 248 (*Conservation of total spin under coherent interaction*):** More generally, a coherent interaction described by a Hamiltonian that only depends on collective spin components, $H = H(\hat{S}_x, \hat{S}_y, \hat{S}_z)$, cannot change the total spin $|\mathbf{S}|$. This is easy to see by doing a Taylor expansion of the Hamiltonian in the spin components and using $[\hat{\mathbf{S}}, \hat{\mathbf{S}}^2] = 0$. As a consequence a coherent (superradiant) spin state will stay coherent forever, unless individual atom-light interactions or decay processes occur.

41.1.1.1 Degeneracies of Dicke states

Let us now look at states having the same number N of energy packets counting free photons n and atomic excitations $N-n$. For example with $N=2$, the following states are possible. The normalization factors are simply the Clebsch-Gordan coefficients.

$\|S,M\rangle$ $\|n\rangle$	$\|\frac{N}{2},M\rangle$ $\#=1$	$\|\frac{N}{2}-1,M\rangle$ $\#=1$
0	$\|1,1\rangle = \|++\rangle$	
1	$\|1,0\rangle = \frac{1}{\sqrt{2}}(\|+-\rangle + \|-+\rangle)$	$\|0,0\rangle = \frac{1}{\sqrt{2}}(\|+-\rangle - \|-+\rangle)$
2	$\|1,-1\rangle = \|--\rangle$	

The right column of the above table contains a singlet state, which decouples from the triplet states (center column). The fact that it decouples from the deexcited triplet state makes the singlet state stable or *subradiant* [4]. See also Fig. 41.10.

For example with $N=3$ (see also Exc. 25.4.5.14),

$\|S,M\rangle$ n	$\|\frac{N}{2},M\rangle$ $\#=1$	$\|\frac{N}{2}-1,M\rangle$ $\#=2$
0	$\|\frac{3}{2},\frac{3}{2}\rangle = \|+++\rangle$	
1	$\|\frac{3}{2},\frac{1}{2}\rangle \sim \|++-\rangle + \|+-+\rangle + \|-++\rangle$	$\|\frac{1}{2},\frac{1}{2}\rangle$
2	$\|\frac{3}{2},-\frac{1}{2}\rangle \sim \|+--\rangle + \|-+-\rangle + \|--+\rangle$	$\|\frac{1}{2},-\frac{1}{2}\rangle$
3	$\|\frac{3}{2},-\frac{3}{2}\rangle = \|---\rangle$	

Example with N arbitrary,

$\|S,M\rangle$ $\|n\rangle$	$\|\frac{N}{2},M\rangle$ $\#=1$	$\|\frac{N}{2}-1,M\rangle$ $\#=N-1$	$\|\frac{N}{2}-2,M\rangle$ $\#=\frac{N(N-3)}{2}$
0	$\|\frac{N}{2},\frac{N}{2}\rangle = \|+++...\rangle$		
1	$\|\frac{N}{2},\frac{N}{2}-1\rangle \sim \sum_{perm.} \|-++...\rangle$	$\|\frac{N}{2}-1,\frac{N}{2}-1\rangle$	
2	$\|\frac{N}{2},\frac{N}{2}-2\rangle \sim \sum_{perm.} \|--+...\rangle$	$\|\frac{N}{2}-1,\frac{N}{2}-2\rangle$	$\|\frac{N}{2}-2,\frac{N}{2}-1\rangle$
$\vdots$	$\vdots$	$\vdots$	
N	$\|\frac{N}{2},-\frac{N}{2}\rangle = \|----..\rangle$		

We see that the Dicke states are not made to unambiguously label degenerate states. States $|S,M\rangle$ with $S<|M|$ are largely degenerate. The degeneracy of a Dicke state with $S\leq\frac{N}{2}$, that is, the number of states $|+\rangle^{N_+}|-\rangle^{N_-}$ composing a single Dicke state labeled by $|S,M\rangle$ is [492],

$$\# = \frac{(2S+1)N!}{(\frac{N}{2}+S+1)!(\frac{N}{2}-S)!}\ . \tag{41.8}$$

Transitions between energetically degenerate states $|S,M\rangle$ and $|S,M'\rangle$ with $M=M'$ but $S\neq S'$ are prohibited.

[4] Note that, while superradiance as well as subradiance can be explained by classical radiator models, such as the coupled dipoles model.

41.1.1.2 Mean-field approximation and light field elimination

The *mean-field approximation* consists in replacing the photonic operators by their expectation values, i.e. assuming classical light. This allows us to remove the light energy term from the Hamiltonian and replace the coupling strength by the n-photon Rabi frequency, $\Omega = 2g\sqrt{n}$. The Hamiltonian then becomes just a generalization of the semiclassical one-atom Hamiltonian (34.166) to large spins,

$$\boxed{\hat{H} = \hat{\mathbf{S}} \cdot \mathbf{G} = -\Delta_a \, \hat{S}_z + \mathfrak{Re}\, \Omega \, \hat{S}_x + \mathfrak{Im}\, \Omega \, \hat{S}_y} \,, \tag{41.9}$$

allowing for complex Rabi frequencies.

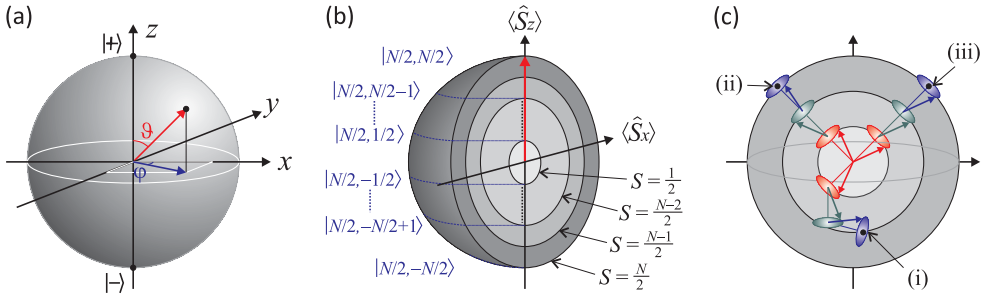

Figure 41.1: (a) Illustration of the Bloch sphere. (b) Bloch spheres of the various super/subradiant states with $N = 5$ atoms. (c) Illustration of (i) a subradiant state, (ii) a fully stretched coherent spin state, and (iii) a spin-correlated state for $N = 3$ atoms.

In the absence of spontaneous emission, any pure *single-atom* state is given by,

$$|\psi\rangle = |\vartheta, \varphi\rangle = \cos\tfrac{\vartheta}{2}|+\rangle + e^{\imath\varphi} \sin\tfrac{\vartheta}{2}|-\rangle \,, \tag{41.10}$$

where the angles ϑ and φ point to a location on the Bloch sphere characterizing the state of the atom. For example, a single initially deexcited atom having been subject to a $\frac{\pi}{2}$-pulse ends up in the state $|\frac{\pi}{2}, 0\rangle$. The expectation value of the spin operator in this state is simply obtained from,

$$\begin{aligned} \langle\vartheta,\varphi|\hat{S}_z|\vartheta,\varphi\rangle &= \cos^2\tfrac{\vartheta}{2}\langle+|\hat{S}_z|+\rangle + \sin^2\tfrac{\vartheta}{2}\langle-|\hat{S}_z|-\rangle = \tfrac{1}{2}\cos\vartheta \\ \langle\vartheta,\varphi|\hat{S}_+|\vartheta,\varphi\rangle &= e^{\imath\varphi}\sin\tfrac{\vartheta}{2}\cos\tfrac{\vartheta}{2}\langle+|\hat{S}_+|-\rangle = \tfrac{1}{2}e^{\imath\varphi}\sin\vartheta \,, \end{aligned} \tag{41.11}$$

yielding,

$$\langle\vartheta,\varphi|\hat{\mathbf{S}}|\vartheta,\varphi\rangle = \tfrac{1}{2}\begin{pmatrix} \cos\varphi\sin\vartheta \\ \sin\varphi\sin\vartheta \\ \cos\vartheta \end{pmatrix} \,. \tag{41.12}$$

We will also denote the probability of finding the system in state $|\pm\rangle$ by,

$$p_+ = \langle\hat{P}_\pm\rangle = |\langle+|\psi\rangle|^2 = \cos^2\tfrac{\vartheta}{2} = 1 - p_- \,. \tag{41.13}$$

41.1.1.3 Collective spin states

Let us now study the system obeying the Hamiltonian (41.9) in detail. The spin operators $\hat{\mathbf{S}}$ satisfy a SU(2) algebra explained in Sec. 25.3.2, i.e. $\hat{\mathbf{S}} \times \hat{\mathbf{S}} = \imath\hat{\mathbf{S}}$. The common eigenstates of $\hat{\mathbf{S}}^2$ and $\hat{S}_z$ are denoted by $|S, M\rangle$,

$$\begin{aligned} \hat{S}_z &= \hat{S}_+\hat{S}_- - \hat{S}_-\hat{S}_+ \qquad \text{with} \qquad \hat{S}_z|S,M\rangle = M|S,M\rangle \\ \hat{N}_\pm &\equiv \tfrac{1}{2}(N\mathbb{I} \pm \hat{S}_z) \qquad \text{with} \qquad \hat{N}_\pm|S,M\rangle = \tfrac{1}{2}(N \pm M)|S,M\rangle \ . \end{aligned} \tag{41.14}$$

From this we conclude that $S = N/2$ is half the number of atoms and M the inversion.

We consider an ensemble of $N = N_+ + N_-$ two-level atoms excited by a definite number of M photons, such that,

$$N = N_+ + N_- \qquad \text{and} \qquad 2M = N_+ - N_- \ . \tag{41.15}$$

Hence, $N_\pm = \frac{N}{2} \pm M$ is the number of atoms in each of the two states. The N atoms can occupy 2^N different collective states. However, when the atoms are identical and couple uniformly to the same light mode, all states where the same number of atoms is excited are energetically degenerate, and the total energy available to the system is,

$$E = M\omega_c \ . \tag{41.16}$$

The degeneracy of each many-body state with a given inversion M is given by the binomial coefficient,

$$\# = \binom{N}{\frac{N}{2}+M} = \binom{N}{N_+} = \binom{N}{N_-} \qquad \text{such that} \qquad \sum_{N_+=0}^{N} \binom{N}{N_+} = 2^N \ . \tag{41.17}$$

Therefore, we may set,

$$\boxed{|S,M\rangle \equiv |+\rangle^{N_+}|-\rangle^{N_-}} \ . \tag{41.18}$$

These states are called *Dicke states* [5].

For the special case $N = 2$ the transformation from the basis $|+\rangle^{N_+}|-\rangle^{N_-}$, used in the *Tavis-Cummings model*, to the basis $|S, M\rangle$, used in the Dicke model, is a unitary transformation. It has been extensively discussed in Sec. 25.4 at the example of two spins, whose complete Hilbert space can be expanded in the uncoupled or in the coupled basis. For $N > 2$ the situation is more complicated, since the degeneracies of both models are different. It is important to be aware that S is not simply half the atom number, but runs over $S = \frac{N}{2}, \frac{N}{2} - 1, ...$, depending on how the individual spins couple together. The degeneracy of an angular momentum state $|S, M\rangle$ with a specific inversion M but undefined orbital momentum S is determined by the condition $0 \leq S \leq M$, and given by,

$$\# = \tfrac{N}{2} - |M| + 1 \ . \tag{41.19}$$

[5] In Sec. 25.4.3 we used for the coupling of two spins the notation $|(s_1, s_2)s, m\rangle$. For coupling N spins, we should write in analogy,

$$|(\overbrace{\tfrac{1}{2}, .., \tfrac{1}{2}}^{N}), S, M\rangle \equiv |N, S, M\rangle \ .$$

Mostly, we will however drop the (constant) number N.

For example, for $N = 2$ the possible spin states are given by $|s_1 - s_2| \leq S \leq s_1 + s_2$, that is, $S = 0, 1$. And for $N = 5$, $M = \frac{3}{2}$ is supported by $S = \frac{3}{2}$ and $\frac{5}{2}$. Obviously, the degeneracy (41.19) is lower than (41.17) except for $N = 2$. Dicke states may be represented as vectors pointing to the surface of a so-called Bloch sphere of radius,

$$\|\langle N, S, M|\hat{\mathbf{S}}^2|N, S, M\rangle\| = S(S+1) \ , \tag{41.20}$$

as illustrated in Fig. 41.1(b).

41.1.1.4 Dicke Hamiltonian for 2 atoms from the Tavis-Cummings model

We start from the collective Dicke Hamiltonian (41.4) for two atoms assuming $\omega_{a1} = \omega_{a2}$ and $g_1 = g_2$, that is, both atoms are identical and inside the mode volume of the field to which they couple with equal strength, and apply the rotating wave approximation. The Hamiltonian then factorizes into a diagonal matrix of 4 by 4 blocks characterized by a given number of total excitations,

$$\hat{H}_n = \begin{pmatrix} (n+1)\omega_c - \omega_a & g\sqrt{n} & g\sqrt{n} & 0 \\ g\sqrt{n} & n\omega_c & 0 & g\sqrt{n} \\ g\sqrt{n} & 0 & n\omega_c & g\sqrt{n} \\ 0 & g\sqrt{n} & g\sqrt{n} & (n-1)\omega_c + \omega_a \end{pmatrix} . \tag{41.21}$$

Each block has two degenerate non-shifted eigenvalues and two non-degenerate shifted eigenvalues,

$$E = n\omega_c \quad \text{and} \quad E = n\omega_c \pm \varpi_n \quad \text{with} \quad \varpi_n \equiv \sqrt{(\omega_c + \omega_a)^2 - 4g^2 n} \ . \tag{41.22}$$

The description of the dynamics can be simplified by reducing the order of the matrix by calculating the average of the lines 2 and 3,

$$\hat{H}_D = \begin{pmatrix} (n+1)\omega_c - \omega_a & g\sqrt{2n} & 0 \\ g\sqrt{2n} & n\omega_c & g\sqrt{2n} \\ 0 & g\sqrt{2n} & (n-1)\omega_c + \omega_a \end{pmatrix} , \tag{41.23}$$

and opting for a new base defined by,

$$|\psi\rangle = \sum_n \begin{pmatrix} c_{22\ n-1} \\ c_{12\ n} \\ c_{11\ n+1} \end{pmatrix} |n\rangle \ , \tag{41.24}$$

with $c_{12\ n} = c_{21\ n}$. The new Hamiltonian (41.23) has exactly the same eigenvalues as the complete one (41.23), $\lambda = n\omega_c, n\omega_c \pm \varpi_n$, but without degeneracies. If we assume furthermore that the excitation is resonant, $\omega_c = \omega_a$, with high intensity, $n = |\alpha|^2$ for all n, defining the Rabi frequency $\Omega \equiv 2g\sqrt{n}$ our matrix becomes,

$$\hat{H}_D \simeq \begin{pmatrix} |\alpha|\omega & \frac{\Omega}{\sqrt{2}} & 0 \\ \frac{\Omega}{\sqrt{2}} & |\alpha|\omega & \frac{\Omega}{\sqrt{2}} \\ 0 & \frac{\Omega}{\sqrt{2}} & |\alpha|\omega \end{pmatrix} , \tag{41.25}$$

with the eigenvalue matrix,

$$E_n = U_n^\dagger \hat{H}_D U_n \simeq \begin{pmatrix} |\alpha|\omega - \Omega & & \\ & |\alpha|\omega & \\ & & |\alpha|\omega + \Omega \end{pmatrix} , \tag{41.26}$$

and the eigenvector matrix,

$$U_n \simeq \tfrac{1}{2} \begin{pmatrix} -1 & \sqrt{2} & 1 \\ \sqrt{2} & 0 & -\sqrt{2} \\ 1 & -\sqrt{2} & -1 \end{pmatrix} . \tag{41.27}$$

With this we can derive the propagator,

$$\begin{aligned} e^{-\imath \hat{H}_n t} =& \tfrac{1}{2} e^{-\imath \alpha^2 \omega \mathbf{t}} \begin{pmatrix} 1+\cos\alpha\Omega t & -\sqrt{2}\imath \sin\alpha\Omega t & -1+\cos\alpha\Omega t \\ -\sqrt{2}\imath\sin\alpha\Omega t & 2\cos\alpha\Omega t & -\sqrt{2}\imath\sin\alpha\Omega t \\ -1+\cos\alpha\Omega t & -\sqrt{2}\imath\sin\alpha\Omega t & 1+\cos\alpha\Omega t \end{pmatrix} \\ \overset{\alpha\Omega t=\pi/2}{\longrightarrow}& \tfrac{1}{2} e^{-\imath\pi/2\cdot\alpha\omega/\Omega} \begin{pmatrix} 1 & -\sqrt{2}\imath & -1 \\ -\sqrt{2}\imath & 0 & -\sqrt{2}\imath \\ -1 & -\sqrt{2}\imath & 1 \end{pmatrix} . \end{aligned}$$

The generalization to three atoms or N atoms is straightforward and will be left to Exc. 41.1.6.2.

41.1.2 Coherent spin states

By the fact that the individual spins are additive and the Hamiltonian linear in the spin operators, $\hat{H} \propto \hat{S}_z$, we know that the Schrödinger equation will be satisfied by *product states*,

$$|\Psi_N\rangle = \prod_{k=1}^{N} |\vartheta_k, \varphi_k\rangle_k , \tag{41.28}$$

where $|\vartheta_k, \varphi_k\rangle_k$ is the state of the k-the atom given by (41.10).

Coherent spin states now consist of N atoms, all being in the same state. In Exc. 41.1.6.3 we present another equivalent definition. Since the atoms are indistinguishable by the radiation field, we may as well drop the labeling index k,

$$|\Psi_N\rangle = |\vartheta, \varphi\rangle^N = \sum_{k=0}^{N} \sqrt{\binom{N}{k}} \cos^{N-k}\tfrac{\vartheta}{2} |+\rangle^{N-k} \, e^{\imath k\varphi} \sin^k \tfrac{\vartheta}{2} |-\rangle^k , \tag{41.29}$$

in agreement with (36.58), or equivalently, using the Dicke state notation (41.18),

$$\boxed{|\vartheta, \varphi\rangle^N = \sum_{k=0}^{2S} \sqrt{\binom{2S}{k}} \cos^{2S-k}\tfrac{\vartheta}{2} \, e^{\imath k\varphi} \sin^k \tfrac{\vartheta}{2} |S, S-k\rangle} . \tag{41.30}$$

Hence, similarly to the coherent state of a harmonic oscillator, which consists of a Poissonian distribution of number states, the coherent spin state consists of a binomial distribution of N_+ atoms in one state and $N - N_+$ in the other. Note also, that by construction, the coherent spin states are **stretched**, $S = N/2$. That is, they can be represented by a vector of length N equal to the radius of the (generalized) Bloch sphere [6]. In other words, S is a conserved quantum number as already shown in (41.7), and this feature does not change under the influence of the Hamiltonian (41.9). These states are called superradiant. Nevertheless, other states $|S, M\rangle$ are possible with $S \leq \frac{N}{2}$. These are squeezed, subradiant, or entangled states.

In the following we will study some of the properties of the coherent spin states. For instance, in Exc. 41.1.6.4(a) we calculate the expectation values of coherent spin states,

$$\langle \vartheta, \varphi|^N \hat{\mathbf{S}} |\vartheta, \varphi\rangle^N = S \begin{pmatrix} \cos\varphi \sin\vartheta \\ \sin\varphi \sin\vartheta \\ \cos\vartheta \end{pmatrix} . \tag{41.31}$$

Hence, the spin evolves on the surface of a Bloch sphere with radius,

$$\|\langle \vartheta, \varphi|^N \hat{\mathbf{S}} |\vartheta, \varphi\rangle^N\| = S \qquad \text{while still} \qquad \|\langle \vartheta, \varphi|^N \hat{\mathbf{S}}^2 |\vartheta, \varphi\rangle^N\| = S(S+1) . \tag{41.32}$$

For the number of atoms in each state we expect,

$$\langle \hat{N}_+ \rangle = \tfrac{N}{2} + \tfrac{1}{2}\langle \hat{S}_z \rangle = N \cos^2 \tfrac{\vartheta}{2} = N p_+ = N(1 - p_-) = N - \langle N_- \rangle . \tag{41.33}$$

41.1.3 Rotations, spin excitation and precession

We learn in quantum mechanics how to use Pauli matrices to describe rotations in the Bloch vector space (see Exc. 23.3.10.5). We will now extend this formalism to our collective spin space. A useful rule for the subsequent calculations, proved in Exc. 41.1.6.5, is the following,

$$e^{\imath F(\hat{S}_z)} \hat{S}_+ e^{-\imath F(\hat{S}_z)} = \hat{S}_+ e^{\imath[F(\hat{S}_z + \mathbb{I}) - F(\hat{S}_z)]} , \tag{41.34}$$

where F is an arbitrary function. For $F(\hat{S}_z) \equiv \phi \hat{S}_z$ the unitary transform $e^{\imath F(\hat{S}_z)}$ denotes a rotation about the z-axis, which we will study in the example below. For $F(\hat{S}_z) \equiv \zeta \hat{S}_z^2$ it generates squeezing along the z-axis, which we will study in the next section. Furthermore, we define the rotation matrices about the Cartesian axis,

$$R_x(\gamma) \equiv \begin{pmatrix} 1 & 0 & 0 \\ 0 & \cos\gamma & -\sin\gamma \\ 0 & \sin\gamma & \cos\gamma \end{pmatrix} , \qquad R_y(\gamma) \equiv \begin{pmatrix} \cos\gamma & 0 & -\sin\gamma \\ 0 & 1 & 0 \\ \sin\gamma & 0 & \cos\gamma \end{pmatrix} ,$$
$$R_z(\gamma) \equiv \begin{pmatrix} \cos\gamma & -\sin\gamma & 0 \\ \sin\gamma & \cos\gamma & 0 \\ 0 & 0 & 1 \end{pmatrix} , \tag{41.35}$$

for which it is possible to show (with $\alpha = x, y, z$),

$$\boxed{R_\alpha(\gamma) \hat{\mathbf{S}} = e^{\imath\gamma \hat{S}_\alpha} \hat{\mathbf{S}} e^{-\imath\gamma \hat{S}_\alpha}} . \tag{41.36}$$

[6] An illustration of the generalized Bloch sphere is attempted in Fig. 41.29.

Example 249 (*Rotation about* $\hat{S}_z$): Defining $F(\hat{S}_z) \equiv \phi \hat{S}_z$ the relationship (41.34) tells us,

$$e^{\imath\phi\hat{S}_z}\hat{S}_+ e^{-\imath\phi\hat{S}_z} = \hat{S}_+ e^{\imath\phi} \ ,$$

and consequently,

$$e^{\imath\phi\hat{S}_z}\hat{\mathbf{S}}e^{-\imath\phi\hat{S}_z} = \begin{pmatrix} \frac{1}{2}(e^{\imath\phi}\hat{S}_+ + e^{-\imath\phi}\hat{S}_-) \\ \frac{1}{2\imath}(e^{\imath\phi}\hat{S}_+ - e^{-\imath\phi}\hat{S}_-) \\ \hat{S}_z \end{pmatrix} = \begin{pmatrix} \cos\phi & -\sin\phi & 0 \\ \sin\phi & \cos\phi & 0 \\ 0 & 0 & 1 \end{pmatrix} \hat{\mathbf{S}} \equiv R_z(\phi)\hat{\mathbf{S}} \ .$$

Furthermore,

$$\begin{aligned} e^{-\imath\phi\hat{S}_z}|\vartheta,\varphi\rangle^N &= \sum_{k=0}^{2S} \sqrt{\binom{2S}{k}} \cos^{N-k}\tfrac{\vartheta}{2} e^{\imath k\varphi} \sin^k\tfrac{\vartheta}{2} e^{-\imath\phi(S-k)}|S,S-k\rangle \\ &= e^{-\imath\phi S}\left(e^{-\imath\phi}\cos\tfrac{\vartheta}{2}|+\rangle + e^{\imath(\varphi+\phi)}\sin\tfrac{\vartheta}{2}|-\rangle\right)^N = e^{-\imath\phi S}|\vartheta,\varphi+\phi\rangle^N \ . \end{aligned}$$

We also find,

$$\langle\vartheta,\varphi|^N R_z(\phi)\hat{\mathbf{S}}|\vartheta,\varphi\rangle^N = \tfrac{N}{2}\begin{pmatrix} \cos(\varphi+\phi)\sin\vartheta \\ \sin(\varphi+\phi)\sin\vartheta \\ \cos\vartheta \end{pmatrix} = \langle\vartheta,\varphi+\phi|^N\hat{\mathbf{S}}|\vartheta,\varphi+\phi\rangle^N \ .$$

To vary the polar angle ϑ of a coherent spin state $|\vartheta,\varphi\rangle$, we first rotate the coordinate system about the z-axis until $\varphi = 0$, then rotate about the y-axis by the desired angle θ, and finally rotate back about the z-axis to reach the initial azimuth φ,

$$\langle\vartheta,\varphi|^N R_z(\varphi)R_y^{-1}(\theta)R_z^{-1}(\varphi)\hat{\mathbf{S}}|\vartheta,\varphi\rangle^N = \tfrac{N}{2}\begin{pmatrix} \cos\varphi\sin(\theta+\vartheta) \\ \sin\varphi\sin(\theta+\vartheta) \\ \cos(\theta+\vartheta) \end{pmatrix} = \langle\vartheta+\theta,\varphi|^N\hat{\mathbf{S}}|\vartheta+\theta,\varphi\rangle^N \ .$$

The rotation about the x-axis is derived in Exc. 41.1.6.6, and in Exc. 41.1.6.7 we write down the explicit rotation matrix for two atoms.

Rotations such as the ones described by $R_\alpha(\gamma)$ are generated by the Dicke Hamiltonian (41.9), since the solution of the Schrödinger equation is,

$$\boxed{|\Psi(t)\rangle = e^{-\imath\hat{H}t}|\Psi(0)\rangle = e^{-\imath t\hat{S}_x\mathfrak{Re}\ \Omega_x - \imath t\hat{S}_y\mathfrak{Im}\ \Omega_y - \imath t\hat{S}_z\Delta}|\Psi(0)\rangle} \ . \tag{41.37}$$

That is, the Dicke Hamiltonian generates rotations $R_x(\mathfrak{Re}\ \Omega_x t)$, $R_y(\mathfrak{Im}\ \Omega_y t)$, and $R_z(\Delta t)$. This confirms that rotations do only transform coherent states into each other. Nevertheless, there are other unitary operations that transform coherent states into states that cannot be represented by coherent states. One example for this is squeezing.

41.1.3.1 Rotation algebra

The example 249 shows that rotations from an initial towards an arbitrary coherent spin states can be parametrized by a pair of Euler angles. Using (23.200) [328],

$$\begin{aligned} &U_{rt}(\vartheta,\varphi) = e^{\imath\varphi\hat{S}_z}e^{\imath\vartheta\hat{S}_y} = e^{-\imath\vartheta\hat{\mathbf{e}}_\varphi\cdot\hat{\mathbf{S}}} = e^{-\imath\vartheta(-\hat{S}_x\sin\varphi+\hat{S}_y\cos\varphi)} = e^{-\frac{\vartheta}{2}(\hat{S}_+e^{-\imath\varphi}-\hat{S}_-e^{\imath\varphi})} \\ &R(\vartheta,\varphi)\hat{\mathbf{S}} \equiv U_{rt}^\dagger(\vartheta,\varphi)\hat{\mathbf{S}}U_{rt}(\vartheta,\varphi) \end{aligned} \tag{41.38}$$

with $\hat{\mathbf{e}}_\varphi = -\hat{\mathbf{e}}_x \sin\varphi + \hat{\mathbf{e}}_y \cos\varphi$. With this we find,

$$|\vartheta,\varphi\rangle^N = U_{rt}(\vartheta,\varphi)|S,S\rangle \ . \tag{41.39}$$

41.1.4 Uncertainties, quantum projection noise and spin squeezing

Measuring the population of a coherently excited two-level system by projecting it onto an energy eigenstate introduces *quantum projection noise*. Although this inherent noise spoils the determination of the resonance frequency, it can to some extent be surpassed by *spin squeezing* [1380]. The projection noise limit has been observed with ions [653, 642] and with atomic clouds [1143]. The reduction of the noise by spin squeezing has been observed with ions [1127], micromasers [1074], and atomic clouds [572, 763]. Also, a weakly entangled state of two modes was observed for continuous spin variables [689]. Very strong squeezing spin can be obtained in a *Mott insulator* state, as demonstrated by [537].

First, we want to show that the Heisenberg uncertainty of a coherent spin state is nothing else than the quantum projection noise studied in Sec. 36.3.2. On one hand, we have,

$$\begin{aligned}
\langle\vartheta,\varphi|^N(\Delta\hat{S}_z)^2|\vartheta,\varphi\rangle^N &= \langle\vartheta,\varphi|^N\hat{S}_z^2|\vartheta,\varphi\rangle^N - (\langle\vartheta,\varphi|^N\hat{S}_z|\vartheta,\varphi\rangle^N)^2 \\
&= \sum_{k=0}^{N}\binom{N}{k}(\tfrac{N}{2}-k)^2 p_+^{N-k}p_-^k - \left(\sum_{k=0}^{N}\binom{N}{k}(\tfrac{N}{2}-k)p_+^{N-k}p_-^k\right)^2 \\
&= \left(\tfrac{N^2}{4} - N^2 p_+p_- + Np_+p_-\right) - \left(\tfrac{N}{2}(p_+-p_-)\right)^2 = Np_+p_- \ .
\end{aligned} \tag{41.40}$$

On the other hand, we have seen in (36.57) that this results corresponds to the variance of quantum projection noise,

$$\begin{aligned}
(\Delta r)^2 &= \sum_{r=0}^{N}(r-Np_\pm)^2 P_{N,r,\pm} \\
&= \sum_{k=0}^{N}(\tfrac{N}{2}-k+\tfrac{N}{2}(p_+-p_-))^2\binom{N}{k}p_+^{N-k}p_-^k = Np_+p_- \ .
\end{aligned} \tag{41.41}$$

The Heisenberg uncertainty relation (23.91) applied to angular momentum operator satisfying $[\hat{S}_x,\hat{S}_y] = \imath\hat{S}_z$ states,

$$\Delta\hat{S}_x\Delta\hat{S}_y \geq \tfrac{1}{2}|\hat{S}_z| \ . \tag{41.42}$$

Since there are no quantum correlations between the particles, the uncertainty of coherent spin states is additive (see Exc. 25.3.4.5),

$$(\Delta\hat{S}_\alpha)^2 = \sum_{k=0}^{N}(\Delta\hat{s}_k^\alpha)^2 \ . \tag{41.43}$$

For a coherent spin state we can calculate explicitly [see Exc. 41.1.6.4(b)],

$$\langle\vartheta,\varphi|^N \begin{pmatrix} \Delta\hat{S}_x^2 \\ \Delta\hat{S}_y^2 \\ \Delta\hat{S}_z^2 \end{pmatrix} |\vartheta,\varphi\rangle^N = \tfrac{N}{4} \begin{pmatrix} 1-\sin^2\vartheta\cos^2\varphi \\ 1-\sin^2\vartheta\sin^2\varphi \\ \sin^2\vartheta \end{pmatrix} . \tag{41.44}$$

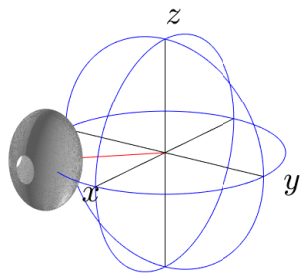

Figure 41.2: Illustration of the uncertainty of the spin components of a coherent spin state.

Example 250 (*Uncertainty of a coherent spin state after a $\frac{\pi}{2}$-pulse*): A $\frac{\pi}{2}$-pulse applied to a cloud in the collective ground state generates the state $|\vartheta,\varphi\rangle = |\frac{\pi}{2},0\rangle$. This is somewhat analogous to the beam splitting of a photonic Fock state discussed in Sec. 35.8. Interestingly, a Fock state seems more natural for an atomic cloud, while the Glauber state is more natural for a photonic mode. For example, for the particular state $|\frac{\pi}{2},0\rangle$ we find from (41.44),

$$(\Delta\hat{S}_x)^2 = 0 \qquad \text{and} \qquad (\Delta\hat{S}_y)^2 = (\Delta\hat{S}_z)^2 = \tfrac{S}{2} .$$

Note, that spin squeezing along the z-axis could be obtained by quantum non-demolition measurement of the inversion, that is, by measuring $\hat{S}_z$ without influencing the populations of the ground and excited state.

41.1.4.1 Spin squeezing by one-axis twisting

We have seen in the last section, that rotations influence the distribution of the uncertainty among the Cartesian coordinates in a specific way. It is, however, possible to manipulate the uncertainty distribution without rotating the collective spin state. An example with great practical importance is the concept of spin squeezing. It consists in establishing appropriate quantum correlations are between the individual spins, such as to partly cancel out fluctuations in one direction augmenting them in the other direction.

Squeezing of spin is not as straightforward as squeezing of bosons, since the uncertainty relations are essentially different [724]. To study spin-squeezing along the z-axis let as analyze the unitary transformation,

$$\boxed{Q_z(\zeta)\hat{\mathbf{S}} \equiv e^{\imath\zeta\hat{S}_z^2}\hat{\mathbf{S}}e^{-\imath\zeta\hat{S}_z^2}} . \tag{41.45}$$

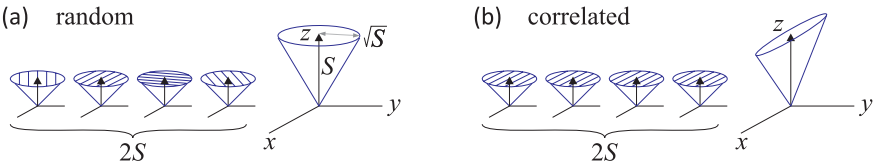

Figure 41.3: Illustration of the uncertainty in (a) a coherent state and (b) a spin-squeezed state.

Specifying the rule (41.34) for the particular case $F(\hat{S}_z) \equiv \zeta \hat{S}_z^2$, we get,

$$e^{\imath\zeta\hat{S}_z^2}\hat{S}_+ e^{-\imath\zeta\hat{S}_z^2} = \hat{S}_+ e^{2\imath\zeta(\hat{S}_z+1/2)} \ , \tag{41.46}$$

and hence,

$$Q_z(\zeta)\hat{\mathbf{S}} = e^{\imath\zeta\hat{S}_z^2}\hat{\mathbf{S}}e^{-\imath\zeta\hat{S}_z^2} = \begin{pmatrix} \frac{1}{2}(\hat{S}_+ e^{2\imath\zeta(\hat{S}_z+1/2)} + e^{-2\imath\zeta(\hat{S}_z+1/2)}\hat{S}_-) \\ \frac{1}{2\imath}(\hat{S}_+ e^{2\imath\zeta(\hat{S}_z+1/2)} - e^{-2\imath\zeta(\hat{S}_z+1/2)}\hat{S}_-) \\ \hat{S}_z \end{pmatrix} \ . \tag{41.47}$$

Let us now apply the *squeezing operator* to the state $|\frac{\pi}{2}, 0\rangle$. In Exc. 41.1.6.8 we show that,

$$\langle\tfrac{\pi}{2}, 0|^N e^{\imath\zeta\hat{S}_z^2}\hat{\mathbf{S}}e^{-\imath\zeta\hat{S}_z^2}|\tfrac{\pi}{2}, 0\rangle^N = \begin{pmatrix} 1 \\ 0 \\ 0 \end{pmatrix} \tfrac{N}{2}\cos^{N-1}\zeta \tag{41.48}$$

$$\langle\tfrac{\pi}{2}, 0|^N e^{\imath\zeta\hat{S}_z^2}\begin{pmatrix} \hat{S}_x^2 \\ \hat{S}_y^2 \\ \hat{S}_z^2 \end{pmatrix} e^{-\imath\zeta\hat{S}_z^2}|\tfrac{\pi}{2}, 0\rangle^N = \begin{pmatrix} N+1 \\ N+1 \\ 2 \end{pmatrix} \tfrac{N}{8} + \begin{pmatrix} 1 \\ -1 \\ 0 \end{pmatrix} \tfrac{N(N-1)}{8}\cos^{N-2} 2\zeta \ .$$

The dependencies of the uncertainties as a function of the squeezing parameter are plotted in Fig. 41.4. We see that the uncertainties never get smaller than the unsqueezed value. The reason is that, since the unitary transform $e^{\imath\zeta\hat{S}_z^2}$ commutes with $\hat{S}_z$, the prescription (41.45) does not immediately lead to squeezing along the z-axis.

Nevertheless, the prescription does generate quantum correlations in $\hat{S}_x$ and $\hat{S}_y$, which can be transformed to squeezing by subsequently rotating the collective spin about the x-axis [724]. As shown in Exc. 41.1.6.9, a rotation by an angle ν does not modify the x-component,

$$\begin{aligned} &\langle\tfrac{\pi}{2}, 0|^N e^{\imath\nu\hat{S}_x} e^{\imath\zeta\hat{S}_z^2}\Delta\hat{S}_x^2 e^{-\imath\zeta\hat{S}_z^2} e^{-\imath\nu\hat{S}_x}|\tfrac{\pi}{2}, 0\rangle^N \\ &\qquad = \tfrac{N(N+1)}{8} + \tfrac{N(N-1)}{8}\cos^{N-2} 2\zeta - \tfrac{N^2}{4}\cos^{2N-2}\zeta \ , \end{aligned} \tag{41.49}$$

but it modifies the other ones,

$$\begin{aligned} &\langle\tfrac{\pi}{2}, 0|^N e^{\imath\nu\hat{S}_x} e^{\imath\zeta\hat{S}_z^2}\Delta\hat{S}_{y,z}^2 e^{-\imath\zeta\hat{S}_z^2} e^{-\imath\nu\hat{S}_x}|\tfrac{\pi}{2}, 0\rangle^N \\ &\qquad = \tfrac{N}{4}\{1 + \tfrac{N-1}{4}[A \pm \sqrt{A^2+B^2}\cos(2\nu + \arctan\tfrac{B}{A})]\} \ , \end{aligned} \tag{41.50}$$

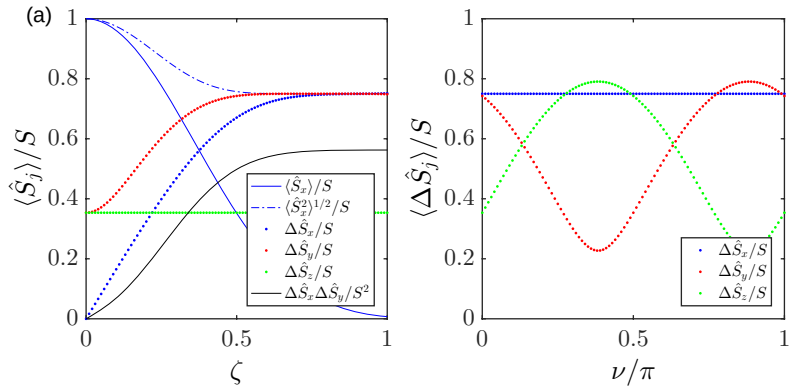

Figure 41.4: (code) (a) Uncertainties calculated in (41.48) as a function of the squeezing parameter. (b) Uncertainties after application of squeezing operator as a function of the rotation angle ν about the x-axis.

with $A \equiv 1 - \cos^{N-2} 2\zeta$ and $B \equiv 4 \sin\zeta \cos^{N-2}\zeta$. We study spin squeezing in Exc. 41.1.6.10 to 41.1.6.13. In Exc. 41.1.6.14 we investigate, whether double Fock states can lead to Heisenberg-limited interferometry, and in Exc. 41.1.6.15 we study entanglement witnesses with coherent spin states.

Obviously, since squeezed states are obtained from coherent states by unitary transform, they are still normalized,

$$\langle\vartheta,\varphi|^N e^{-\imath\zeta\hat{S}_z^2} e^{\imath\zeta\hat{S}_z^2} |\vartheta,\varphi\rangle^N = 1 \; . \tag{41.51}$$

Example 251 (*Conditional spin-squeezing by non-demolition measurement*): Technically, spin-squeezed states can be generated in experiments by quantum non-demolition measurements [163, 309, 1135]. Another idea would be to arrange for totally uniform spin-spin coupling, since this generates terms like,

$$H_{ss} = \sum_{i,j\neq i}^{N} \kappa_{ij} \hat{s}_i^z \hat{s}_j^z \simeq \kappa \sum_{i,j\neq i}^{N} \hat{s}_i^z \hat{s}_j^z = \kappa \hat{S}_z^2 \; . \tag{41.52}$$

In a cloud this latter idea is not realizable, because the interatomic coupling strength depends on the distance between the atoms, but if the atoms are coupled via their interaction with a common mode of an optical cavity it should be feasible.

41.1.5 Bosonic modes: Analogy between harmonic oscillators and collective spin states

Owing to the equidistant spectrum of their excitation levels, harmonic oscillator modes and collective spin states share many particularities, which will allow us to transfer various notions from the well-known harmonic oscillator studied in Sec. 24.6 to the spin ensembles. Respectively expanded on Fock states and Dicke states, the oscillator operators and the spin operators are approximately linked by the Holstein-Primakoff prescription, which will be worked out below. Also, we appreciated in

Sec. 35.2 the utility of quasi-probability distributions for the estimation of quantum correlations in light modes, which we will apply to spin systems below. Light fields and spin systems are examples of what is called a *bosonic mode*.

41.1.5.1 Mapping Fock and Dicke states

The operators $\hat{a}, \hat{a}^\dagger$ contain all information on a light mode. Similarly, $\hat{S}_+, \hat{S}_-, \hat{S}_z$ contain all information on a collective spin state. In the Heisenberg picture their unitary evolution under some operation (displacement, rotation, squeezing, etc.) is obtained from,

$$\hat{a}^\pm(t) = U(t)\hat{a}^\pm(0)U^\dagger(t) \qquad \text{versus} \qquad \hat{\mathbf{S}}(t) = U(t)\hat{\mathbf{S}}(0)U^\dagger(t) \; . \tag{41.53}$$

While the state of a light mode is given by an expectation value corresponding to a point in an infinite two-dimensional quadrature phase space, the state of a spin ensemble is represented as a vector in a generalized Bloch sphere,

$$\alpha(t) = \langle\psi(0)|\hat{a}^\pm(t)|\psi(0) \qquad \text{versus} \qquad \mathbf{S}(t) = \langle\Psi_N(0)|\hat{\mathbf{S}}(t)|\Psi_N(0)\rangle \; . \tag{41.54}$$

By the fact that the light mode is represented by a 2D complex plane, the commutation rule involves two field operators, while for the Bloch sphere, which is embedded in 3D space, with respect to a fixed coordinate system the commutation rule involves three field operators,

$$[\hat{a}, \hat{a}^\dagger] = 1 \qquad \text{versus} \qquad [\hat{S}_+, \hat{S}_-] = 2\hat{S}_z \; . \tag{41.55}$$

This has consequences for the uncertainty relations,

$$[\hat{x}, \hat{p}^\dagger] \geq \tfrac{1}{2} \qquad \text{versus} \qquad [\hat{S}_x, \hat{S}_y] \geq \tfrac{1}{2}|\langle S_z\rangle| \; . \tag{41.56}$$

On the other hand, as long as we are only interested in coherent evolutions, as shown in the example 248, the total angular momentum is a constant of motion. This means that an initially fully stretched collective spin state is restricted to evolve on the outer (superradiant) shell of the generalized Bloch sphere, which is a two-dimensional surface,

$$|\alpha\rangle = |\mathfrak{Re}\ \alpha, \mathfrak{Im}\ \alpha\rangle \qquad \text{versus} \qquad |\Psi_N\rangle = |\vartheta, \varphi\rangle^N \; . \tag{41.57}$$

As shown in Sec. 41.1.3, rotations do not influence any spin correlations. Therefore, we may as well introduce a local Cartesian coordinate system, rotated such that $\hat{S}_z$ is diagonal on this basis, and calculate its expectation value $\langle S_z\rangle = M$. We immediately see that the commutation rules (41.55) then become equivalent,

$$[\hat{a}, \hat{a}^\dagger] = 1 \qquad \text{versus} \qquad [\hat{S}_+, \hat{S}_-] = 2M \; , \tag{41.58}$$

as well as the corresponding uncertainty relations. In this basis the correlations can be expanded on a 2D phase space parametrized by the angles ϑ and φ.

41.1.5.2 The Holstein-Primakoff prescription

In the limit of large atom numbers the Dicke Hamiltonian can be approximated by a system of two coupled quantum oscillators. The mapping is done via the so-called *Holstein-Primakoff transformation*. The transformation is a mapping of the spin operators to boson creation and annihilation operators, effectively truncating their infinite-dimensional Fock space to finite-dimensional subspaces. Let us consider a spin operator $\hat{\mathbf{S}}$ defined by its commutation behavior $[\hat{S}_x, \hat{S}_y] = \imath \hat{S}_z$ and characterized by its eigenvectors $|S, M\rangle$,

$$\hat{\mathbf{S}}^2|S, M\rangle = S(S+1)|S, M\rangle \quad , \quad \hat{S}_z|S, M\rangle = M|S, M\rangle \ , \tag{41.59}$$

with the projection quantum number $M = -S, -S+1, \ldots, S-1, S$. We consider a single particle of spin S and take the state $|S, M = +S\rangle$ as a vacuum for a set of boson operators, and each subsequent state with lower projection quantum number as a boson excitation of the previous one,

$$|S, S-n\rangle \mapsto \frac{1}{\sqrt{n!}}(\hat{b}^\dagger)^n|0\rangle \ . \tag{41.60}$$

Each additional boson then corresponds to a decrease of M in the spin projection. Thus, the spin raising and lowering operators $\hat{S}_\pm = \hat{S}_x \pm \imath \hat{S}_y$ satisfying so that $[\hat{S}_+, \hat{S}_-] = 2\hat{S}_z$ correspond to bosonic annihilation and creation operators, respectively. The precise relations between the operators must be chosen to ensure the correct commutation relations for the spin operators. The resulting Holstein-Primakoff transformation can be written as,

$$\boxed{\hat{S}_+ = \sqrt{2S}\sqrt{1 - \tfrac{\hat{b}^\dagger \hat{b}}{2S}}\ \hat{b} \quad , \quad \hat{S}_- = \sqrt{2S}\ \hat{b}^\dagger \sqrt{1 - \tfrac{\hat{b}^\dagger \hat{b}}{2S}} \quad , \quad \hat{S}_z = (S - \hat{b}^\dagger \hat{b})} \ . \tag{41.61}$$

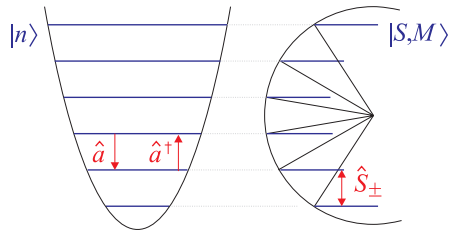

Figure 41.5: Illustration of the Holstein-Primakoff transformation.

The transformation is particularly useful in the case where S is large, when the square roots can be expanded as Taylor series, to give an expansion in decreasing powers of S [1278, 145]. We will verify the commutation relations in Exc. 41.1.6.16. The Holstein-Primakoff approximation allows us to rewrite the Hamiltonian (41.6)

as,

$$\begin{aligned}\hat{H}_{HP} &= -\Delta_c \hat{a}^\dagger \hat{a} - \Delta_a \hat{S}_z + 2g(\hat{a}+\hat{a}^\dagger)\hat{S}_x \\ &= -\Delta_c \hat{a}^\dagger \hat{a} - \Delta_a (S - \hat{b}^\dagger \hat{b}) + 2g(\hat{a}+\hat{a}^\dagger)\sqrt{2S}\left(\sqrt{1-\tfrac{\hat{b}^\dagger\hat{b}}{2S}}\;\hat{b} + \hat{b}^\dagger\sqrt{1-\tfrac{\hat{b}^\dagger\hat{b}}{2S}}\right) \\ &\simeq -\Delta_c \hat{a}^\dagger \hat{a} - \tfrac{1}{2}\Delta_a \hat{b}^\dagger\hat{b} + 2g_N(\hat{a}+\hat{a}^\dagger)(\hat{b}+\hat{b}^\dagger)\ ,\end{aligned} \tag{41.62}$$

with the collective coupling strength $g_N \equiv g\sqrt{N}$. The Hamiltonian (41.62) describes two coupled quantum oscillators without rotating-wave approximation [426] [7], a system which has already been discussed in Sec. 35.8.8 in the context of beamsplitters.

41.1.5.3 Quasi-probability distributions on the Bloch sphere

The operators contain all information on possible quantum correlations, and it is now interesting to quantify and illustrate the formation of such correlations under some manipulation. This is the purpose of the quasi-probability distributions.

The evolution of collective states and operators of a harmonic oscillator (resp. spin system) under the influence of a Hamiltonian is conveniently calculated by expanding them on a Fock (resp. Dicke) basis and evaluating propagators via unitary transformations, as in Eq. (41.53). On the other hand, quantum correlations become more visible on a Glauber (resp. coherent spin state) basis.

Now, the close analogy between harmonic oscillators and spin systems allows us to apply concepts elaborated for the harmonic oscillator to collective spin states. One example is the notion of quasi-probability distributions introduced in Sec. 35.2 for Glauber states, which we will apply to collective spin states below. In quantum optics a frequently used distribution function is the Wigner function $W_\rho(\alpha,\alpha^*)$ characterizing a light mode via an expansion into a coherent states basis $|\alpha\rangle$ spanning the complex quadrature plane. The purpose of this section is to derive an analogous function for collective spin states $W_\rho(\vartheta,\varphi)$.

We proceed by expanding an arbitrary state of a light mode on the Fock basis (24.115), which is similar to expanding coherent spin states on the Dicke basis (41.30),

$$|\psi\rangle = \sum_{n=0}^{\infty} c_n |n\rangle \qquad \text{versus} \qquad |\Psi_N\rangle = \sum_{M=+S,..,-S} c_{S,M}|S,M\rangle \tag{41.63}$$

with

$$c_n(t) = \langle n|e^{-\imath\hat{H}t}\psi(0)\rangle \qquad \text{versus} \qquad c_{S,M}(t) = \langle n|e^{-\imath\hat{H}t}\Psi_N(0)\rangle\ . \tag{41.64}$$

In particular for coherent states (resp. spin states),

$$|\alpha\rangle = \sum_{n=0}^{\infty} \frac{e^{-|\alpha|^2/2}\alpha^n}{\sqrt{n!}}|n\rangle \tag{41.65}$$

$$\text{versus} \qquad |\vartheta,\varphi\rangle^N = \sum_{M=+S,..,-S}\sqrt{\binom{N}{S+M}}\cos^{S-M}\tfrac{\vartheta}{2}e^{\imath(S+M)\varphi}\sin^{S+M}\tfrac{\vartheta}{2}|S,M\rangle\ .$$

[7] The Jaynes-Cummings model describes coupling of an atom to a harmonic oscillator mode [426]. In contrast (see 4.4).

We note that both Fock and Dicke states have no phase in phase space. Phases are generated by summing Fock (resp. Dicke) states with different dynamical phase factors corresponding to their energies.

For numerical simulations we also expand operators on the Fock (resp. Dicke) basis,

$$\begin{aligned} \hat{a} &= \sum_{n,n'=0}^{\infty} \delta_{n',n-1}\sqrt{n}|n'\rangle\langle n| \quad , \quad \hat{a}^\dagger = \sum_{n,n'=0}^{\infty} \delta_{n',n+1}\sqrt{n+1}|n'\rangle\langle n| \\ \text{versus} \quad \hat{S}_\pm &= \sum_{M,M'=+S,..,-S} \delta_{M',M\pm1}\sqrt{S(S+1)-M(M\pm1)}|S,M'\rangle\langle S,M| \\ \hat{S}_z &= \sum_{M,M'=+S,..,-S} \delta_{M',M} M|S,M'\rangle\langle S,M| \ . \end{aligned} \tag{41.66}$$

In the case of light modes, any point in phase space is reached via a displacement operator (see Eq. (24.111)). Similarly, any point on the Bloch sphere is reached via rotations about two axes [732, 328],

$$\begin{aligned} |\alpha\rangle &= D(\alpha)|0\rangle \qquad \text{versus} \quad |\vartheta,\varphi\rangle^N &= U_{rt}(\vartheta,\varphi)|S,-S\rangle \\ &= e^{\alpha\hat{a}^\dagger-\alpha^*\hat{a}}|0\rangle &= e^{\imath\varphi\hat{S}_z}e^{\imath\vartheta\hat{S}_y}|0,0\rangle^N \ . \end{aligned} \tag{41.67}$$

The Fock (resp. Dicke) basis may not the best one to reveal the existence of quantum correlations. The purpose of quasi-probability distributions defined on a basis of Glauber (resp. coherent spin) states is to provide a better characterization, in particular, on non-Gaussian collective states.

Example 252 (*Distributions for Gaussian spin states (coherent and squeezed)*): Let us now define proper quasi-probability distributions in analogy to those introduced for Glauber space in Sec. 35.2 [8]. In analogy to the example 207 we may, based on the rotation operator $R(\vartheta,\varphi)|S,S\rangle = e^{\imath\vartheta(\hat{S}_x\sin\varphi-\hat{S}_y\cos\varphi)}|S,S\rangle|\vartheta,\varphi\rangle^N$ introduced in (41.38) and the parity operator for rotations given by [732],

$$M_s = \frac{1}{R}\sum_{\ell=0}^{2S}\sqrt{\frac{2\ell+1}{4\pi}}(\gamma_\ell)^{-s}\mathbf{T}_{\ell 0} \qquad \text{with} \qquad \gamma_\ell = \frac{R\sqrt{4\pi}(2S)!}{\sqrt{(2S+\ell+1)!}\sqrt{(2S-\ell)!}} \tag{41.68}$$

$$\text{and} \qquad \mathbf{T}_{\ell m} = \sqrt{\frac{2\ell+1}{2S+1}}\sum_{M,M'=-S}^{S}\begin{pmatrix} S & \ell & S \\ M' & m & M \end{pmatrix}|S,M'\rangle\langle S,M|$$

with $R=\sqrt{S/2\pi}$ define a generalized probability distribution,

$$X_\rho(\vartheta,\varphi,s) = \text{Tr}\ \hat{\rho}U_{rt}(\vartheta,\varphi)M_sU_{rt}^\dagger(\vartheta,\varphi) \longrightarrow \langle\Psi_N|U_{rt}(\vartheta,\varphi)M_sU_{rt}^\dagger(\vartheta,\varphi)|\Psi_N\rangle \ , \tag{41.69}$$

where the second expression holds for pure states. The displacement operator from (35.56) is here replaced by a rotation parametrized by two Euler angles. From (41.69) the usual probability distributions follow as,

$$Q_\rho(\vartheta,\varphi) \equiv X_\rho(\vartheta,\varphi,-1) \quad , \quad W_\rho(\vartheta,\varphi) \equiv X_\rho(\vartheta,\varphi,0) \quad , \quad P_\rho(\vartheta,\varphi) \equiv X_\rho(\vartheta,\varphi,1) \tag{41.70}$$

[8] Compare (35.65) to (24.142).

The parity operator is expanded on the Dicke basis according to the recipe (41.68). To visualize a distribution function, we evaluate (41.69) for every point (ϑ, φ) of the Bloch sphere.
With increasing spin number S, the parity operators M_s converge to the infinite-dimensional operators Π_s of (35.57), while rotations transform into translations along the tangent of a sphere. For pure states the Wigner function is thus given by a rotation of the parity operator.

41.1.5.4 Expansion of non-Gaussian spin states

As long as a collective spin state can be expanded on a collective Dicke basis of superradiant states or reached by coherent evolution from such a state, it remains pure and can be represented by a probability distribution using the procedure outlined in the example 252. The states $|S,S\rangle$, $|S,M\rangle$, the $|\mathrm{W}\rangle$-state, and $|\vartheta,\varphi\rangle^N$ are illustrated in Fig. 41.6. Other non-Gaussian spin states can be reached, and are also shown, e.g. the $|\mathrm{N00N}\rangle$-state, the Greenberger-Horne-Zeilinger state $|\mathrm{GHZ}\rangle$, or the generalized spin cat state $|\mathrm{cat}\rangle$,

$$
\begin{aligned}
|\mathrm{W}\rangle &= |S,S-1\rangle \qquad (41.71)\\
|\mathrm{GHZ}\rangle &= \tfrac{1}{\sqrt{2}}(|\uparrow\rangle^{2S}|\downarrow\rangle^0 + |\uparrow\rangle^0|\downarrow\rangle^{2S}) = \tfrac{1}{\sqrt{2}}(|S,S\rangle + |S,-S\rangle)\\
|\mathrm{N00N}\rangle &= \tfrac{1}{\sqrt{2}}(|\uparrow\rangle^{2S}|\downarrow\rangle^0 + e^{\imath N\vartheta}|\uparrow\rangle^0|\downarrow\rangle^{2S}) = \tfrac{1}{\sqrt{2}}(|S,S\rangle + e^{\imath 2S\vartheta}|S,-S\rangle)\\
|\mathrm{cat}\rangle &= \cos\tfrac{\vartheta}{2}|S,S\rangle + e^{\imath\varphi}\sin\tfrac{\vartheta}{2}|S,-S\rangle\\
|\mathrm{squeezed}\rangle &= e^{-\imath\zeta\hat{S}_y^2/2}|S,S\rangle\ .
\end{aligned}
$$

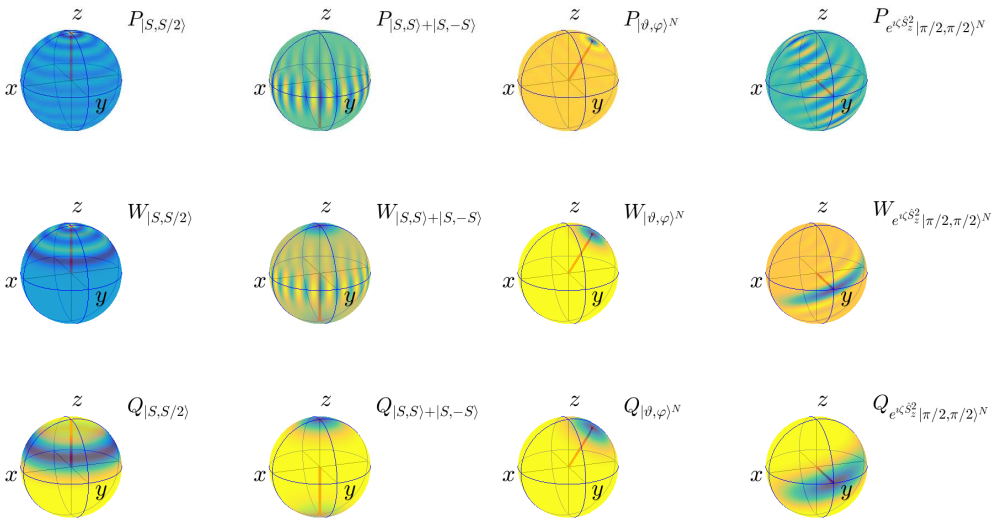

Figure 41.6: (code) P, W, and Q-distributions on the Bloch sphere for various states.

41.1.5.5 Continuous variable quantum information

Continuous variable quantum information is the area of quantum information science that makes use of physical observables with continuous spectra, like the strength of an electromagnetic field. Continuous-variable quantum computation is performed on infinite-dimensional Hilbert spaces and may be called "analog", while qubit quantum computation is performed on finite-dimensional Hilbert spaces (2^N with N the number of qubits) and may be called "digital".

Bosonic modes are examples of systems being studied for the implementation of continuous-variable quantum information. By modeling each mode of the electromagnetic field as a quantum harmonic oscillator with its associated field operators, one defines a canonically conjugate pair of variables for each mode, the so-called *quadratures*, which span a phase space on which Wigner quasi-probability distributions can be defined. Quantum measurements on such a system can be performed using homodyne and heterodyne detectors. Interestingly, qubits can be encoded into a continuous variable [530]. The procedure is easily understood at the example of a two-level atom dispersively interacting with a cavity mode studied within the Jaynes-Cummings model in Sec. 35.4.2 and illustrated in Fig. ?? and in the Exc. 35.4.5.6. See also Sec. 41.5.1.

In all approaches to quantum computing, it is important to know whether a task under consideration can be carried out efficiently by a classical computer. An algorithm might be described in the language of quantum mechanics, but upon closer analysis, reveals to be implementable using only classical resources [529], even if making use of quantum entanglement. When the Wigner quasi-probability representations of all the quantities (states, time evolutions and measurements) involved in a computation are non-negative, then they can be interpreted as ordinary probability distributions, indicating that the computation can be modeled as an essentially classical one [876].

41.1.6 Exercises

41.1.6.1 Ex: Dicke states and Clebsch-Gordan coefficients

Discuss the relationship between coherent Dicke states and Clebsch-Gordan coefficients at the example of two coupled spins.

Solution: *Note, that only fully stretched Dicke states are considered. For $N = 2 = 2S$, we have in the coupled basis,*

$$\begin{aligned}|\vartheta,\varphi\rangle^2 &= (\cos\tfrac{\vartheta}{2}|+\rangle + e^{\imath\varphi}\sin\tfrac{\vartheta}{2}|-\rangle)^2 \\ &= \cos^2\tfrac{\vartheta}{2}|+\rangle|+\rangle + e^{2\imath\varphi}\sin^2\tfrac{\vartheta}{2}|-\rangle|-\rangle + e^{\imath\varphi}\cos\tfrac{\vartheta}{2}\sin\tfrac{\vartheta}{2}(|+\rangle|-\rangle + |-\rangle|+\rangle)\ ,\end{aligned}$$

and in the uncoupled basis,

$$\begin{aligned}|\vartheta,\varphi\rangle^2 &= \sum_{k=0}^{N}\sqrt{\binom{2}{k}}\cos^{N-k}\tfrac{\vartheta}{2}e^{\imath k\varphi}\sin^k\tfrac{\vartheta}{2}|S,S-k\rangle \\ &= \cos^2\tfrac{\vartheta}{2}|1,1\rangle + \sqrt{2}e^{\imath\varphi}\cos\tfrac{\vartheta}{2}\sin\tfrac{\vartheta}{2}|1,0\rangle + e^{2\imath\varphi}\sin^2\tfrac{\vartheta}{2}|1,-1\rangle\ .\end{aligned}$$

Comparing both basis for $\varphi = 0$,

$$\begin{aligned}
&\cos^2\tfrac{\vartheta}{2}|+\rangle|+\rangle + \sin^2\tfrac{\vartheta}{2}|-\rangle|-\rangle + \cos\tfrac{\vartheta}{2}\sin\tfrac{\vartheta}{2}(|+\rangle|-\rangle + |-\rangle|+\rangle) \\
&= |\vartheta, 0\rangle^2 \\
&= \cos^2\tfrac{\vartheta}{2}|1,1\rangle + \sqrt{2}\cos\tfrac{\vartheta}{2}\sin\tfrac{\vartheta}{2}|1,0\rangle + \sin^2\tfrac{\vartheta}{2}|1,-1\rangle \ ,
\end{aligned}$$

and for $\vartheta = 0, \frac{\pi}{2}, \pi$,

$$\begin{aligned}
|+\rangle|+\rangle &= |0,0\rangle^2 = |1,1\rangle \\
\tfrac{1}{2}|+\rangle|+\rangle + \tfrac{1}{2}|-\rangle|-\rangle + \tfrac{1}{2}(|+\rangle|-\rangle + |-\rangle|+\rangle) &= |\tfrac{\pi}{2}, 0\rangle^2 = \tfrac{1}{2}|1,1\rangle + \tfrac{1}{\sqrt{2}}|1,0\rangle + \tfrac{1}{2}|1,-1\rangle \\
|-\rangle|-\rangle &= |\pi, 0\rangle^2 = |1,-1\rangle \ ,
\end{aligned}$$

from which we deduce,

$$\begin{pmatrix} |+,+\rangle \\ \frac{1}{\sqrt{2}}(|-,+\rangle + |+,-\rangle) \\ |-,-\rangle \end{pmatrix} = \begin{pmatrix} |1,1\rangle \\ |1,0\rangle \\ |1,-1\rangle \end{pmatrix} \ .$$

The same relationship is obtained by eliminating the singlet state from the unitary Clebsch-Gordan transformation between basis vectors from a coupled and an uncoupled basis,

$$\begin{pmatrix} |+,+\rangle \\ |-,+\rangle \\ |+,-\rangle \\ |-,-\rangle \end{pmatrix} = U_{CGC} \begin{pmatrix} |1,1\rangle \\ |1,0\rangle \\ |0,0\rangle \\ |1,-1\rangle \end{pmatrix} \quad \textit{with} \quad U_{CGC} = (U_{CGC}^\dagger)^{-1} = \begin{pmatrix} 1 & 0 & 0 & 0 \\ 0 & \frac{1}{\sqrt{2}} & \frac{1}{\sqrt{2}} & 0 \\ 0 & \frac{1}{\sqrt{2}} & -\frac{1}{\sqrt{2}} & 0 \\ 0 & 0 & 0 & 1 \end{pmatrix} .$$

41.1.6.2 Ex: Dicke Hamiltonian for 3 atoms

Generalize the Dicke Hamiltonian (41.23) to 3 atoms.

Solution:

41.1.6.3 Ex: Coherent spin states

Show that the coherent spin state is an eigenstate of the operator $\hat{S}_{\vartheta,\varphi} \equiv \hat{S}_x \sin\vartheta\cos\varphi + \hat{S}_y \sin\vartheta\sin\varphi + \hat{S}_z\cos\vartheta$.

Solution: *Using,*

$$\langle\vartheta,\varphi|^N \hat{\mathbf{S}} |\vartheta,\varphi\rangle^N = \tfrac{N}{2}\begin{pmatrix} \sin\vartheta\cos\varphi \\ \sin\vartheta\sin\varphi \\ \cos\vartheta \end{pmatrix} \ ,$$

we immediately see,

$$\begin{aligned}\langle\vartheta,\varphi|^N \hat{S}_{\vartheta,\varphi}|\vartheta,\varphi\rangle^N &= \langle\vartheta,\varphi|^N \left(\hat{S}_x \sin\vartheta\cos\varphi + \hat{S}_y \sin\vartheta\sin\varphi + \hat{S}_z\cos\vartheta\right)|\vartheta,\varphi\rangle^N \\ &= \tfrac{N}{2}\langle\vartheta,\varphi|^N|\vartheta,\varphi\rangle^N = \tfrac{N}{2}\ .\end{aligned}$$

41.1.6.4 Ex: Collective spin of a coherent spin state

a. Calculate the expectation values for all spin components of the collective spin $\hat{\mathbf{S}}$ in a coherent spin state see also Exc. 25.3.4.8.
b. Calculate the uncertainties for all spin components of the collective spin $\hat{\mathbf{S}}$ in a coherent spin state and check the uncertainty relation.

Solution: *a. Let us first remember,*

$$\begin{aligned}&\hat{S}_x = \tfrac{1}{2}(\hat{S}_+ + \hat{S}_-) \quad , \quad \hat{S}_y = \tfrac{1}{2\imath}(\hat{S}_+ - \hat{S}_-) \quad , \quad \hat{S}_z = \tfrac{1}{2}[\hat{S}_+, \hat{S}_-] \\ &\hat{S}_x^2 = \tfrac{1}{4}(\hat{S}_+^2 + \hat{S}_-^2 + \hat{S}_+\hat{S}_- + \hat{S}_-\hat{S}_+) \quad , \quad \hat{S}_y^2 = -\tfrac{1}{4}(\hat{S}_+^2 + \hat{S}_-^2 - \hat{S}_+\hat{S}_- - \hat{S}_-\hat{S}_+)\ .\end{aligned}$$

For the sake of notational compactness we introduce the abbreviations,

$$p_+ \equiv \cos^2\tfrac{\vartheta}{2} \quad \textit{and} \quad p_- \equiv \sin^2\tfrac{\vartheta}{2} \quad \textit{so that} \quad \sqrt{p_+p_-} = \tfrac{1}{2}\sin\vartheta\ .$$

With the expression (41.31) for a coherent spin state we calculate, with a little help from MAPLE,

$$\begin{aligned}\langle\vartheta,\varphi|^N \hat{S}_+|\vartheta,\varphi\rangle^N &= \sum_{k,l=0}^{2S}\sqrt{\binom{2S}{l}\binom{2S}{k}}p_+^{2S-l/2-k/2}e^{-\imath(l-k)\varphi}p_-^{l/2+k/2}\langle S, S-l|\hat{S}_+|S, S-k\rangle \\ &= e^{\imath\varphi}\sum_{k=0}^{2S}\binom{2S}{k}k\cos^{4S-2k+1}\tfrac{\vartheta}{2}\sin^{2k-1}\tfrac{\vartheta}{2} = N\sqrt{p_+p_-} = Se^{\imath\varphi}\sin\vartheta\ ,\end{aligned}$$

and analogously,

$$\langle\vartheta,\varphi|^N \hat{S}_z|\vartheta,\varphi\rangle^N = \sum_{k=0}^{N}\binom{N}{k}(S-k)p_+^{2S-k}p_-^k = \tfrac{N}{2} - Np_- = S\cos\vartheta\ .$$

Hence, as expected, the total spin is just the sum of the individual spins calculated in 25.3.4.8,

$$\langle\Psi_N|\hat{\mathbf{S}}|\Psi_N\rangle = \langle\vartheta,\varphi|^N\hat{\mathbf{S}}|\vartheta,\varphi\rangle^N = S\begin{pmatrix}\cos\varphi\sin\vartheta\\ \sin\varphi\sin\vartheta\\ \cos\vartheta\end{pmatrix}\ .$$

b. Now, we calculate the higher orders,

$$\begin{aligned}\langle\vartheta,\varphi|^N\hat{S}_+^2|\vartheta,\varphi\rangle^N &= \overline{\langle\vartheta,\varphi|^N\hat{S}_-^2|\vartheta,\varphi\rangle^N}\\ &= \sum_{k,l=0}^{N}\sqrt{\binom{N}{l}\binom{N}{k}}p_+^{N-k/2-l/2}e^{\imath(k-l)\varphi}p_-^{k/2+l/2}\langle S,S-l|\hat{S}_+^2|S,S-k\rangle\\ &= \sum_{k,l=0}^{N}\sqrt{\binom{N}{l}\binom{N}{k}}\sqrt{k(2S-k+1)(k-1)(2S-k+2)}p_+^{N-k/2-l/2}e^{\imath(k-l)\varphi}p_-^{k/2+l/2}\delta_{l,k-2}\\ &= e^{2\imath\varphi}\sum_{k=0}^{N}\frac{N!p_+^{N-k+1}p_-^{k-1}}{(k-2)!(N-k)!} = e^{2\imath\varphi}(N-1)Np_+p_- \ ,\end{aligned}$$

and

$$\begin{aligned}\langle\vartheta,\varphi|^N\hat{S}_+\hat{S}_-|\vartheta,\varphi\rangle^N &= \sum_{k,l=0}^{N}\sqrt{\binom{N}{l}\binom{N}{k}}p_+^{N-k/2-l/2}e^{\imath(k-l)\varphi}p_-^{k/2+l/2}\langle S,S-l|\hat{S}_+\hat{S}_-|S,S-k\rangle\\ &= \sum_{k,l=0}^{N}\sqrt{\binom{N}{l}\binom{N}{k}}(2S+2Sk-k^2-k)p_+^{N-k/2-l/2}e^{\imath(k-l)\varphi}p_-^{k/2+l/2}\delta_{l,k}\\ &= \sum_{k=0}^{N}\binom{N}{k}(N+Nk-k^2-k)p_+^{N-k}p_-^k = Np_+^2+N^2p_+p_- \ ,\end{aligned}$$

and

$$\begin{aligned}\langle\vartheta,\varphi|^N\hat{S}_-\hat{S}_+|\vartheta,\varphi\rangle^N &= \sum_{k,l=0}^{N}\sqrt{\binom{N}{l}\binom{N}{k}}p_+^{N-k/2-l/2}e^{\imath(k-l)\varphi}p_-^{k/2+l/2}\langle S,S-l|\hat{S}_-\hat{S}_+|S,S-k\rangle\\ &= \sum_{k,l=0}^{N}\sqrt{\binom{N}{l}\binom{N}{k}}(2Sk-k^2+k)p_+^{N-k/2-l/2}e^{\imath(k-l)\varphi}p_-^{k/2+l/2}\delta_{l,k}\\ &= \sum_{k=0}^{N}\binom{N}{k}(Nk-k^2+k)p_+^{N-k}p_-^k = Np_-^2+N^2p_+p_- \ .\end{aligned}$$

From this we cross-check,

$$\langle\vartheta,\varphi|^N\hat{S}_z|\vartheta,\varphi\rangle^N = \tfrac{1}{2}\langle\vartheta,\varphi|^N\hat{S}_+\hat{S}_- - \hat{S}_-\hat{S}_+|\vartheta,\varphi\rangle^N = \tfrac{N}{2}(p_+^2-Np_-^2) = \tfrac{N}{2}\cos\vartheta \ .$$

Also,

$$\begin{aligned}\langle\vartheta,\varphi|^N\hat{S}_z^2|\vartheta,\varphi\rangle^N &= \sum_{k,l=0}^{N}\sqrt{\binom{N}{l}\binom{N}{k}}p_+^{N-k/2-l/2}e^{\imath(k-l)\varphi}p_-^{k/2+l/2}\langle S,S-l|\hat{S}_z^2|S,S-k\rangle\\ &= \sum_{k,l=0}^{N}\sqrt{\binom{N}{l}\binom{N}{k}}(\tfrac{N}{2}-k)^2p_+^{N-k/2-l/2}e^{\imath(k-l)\varphi}p_-^{k/2+l/2}\langle S,S-l|S,S-k\rangle\\ &= \sum_{k=0}^{N}\binom{N}{k}(\tfrac{N}{2}-k)^2p_+^{N-k}p_-^k = \tfrac{N^2}{4}+N(1-N)p_+p_- \ ,\end{aligned}$$

and

$$\begin{aligned}\langle\vartheta,\varphi|^N\hat{S}_x^2|\vartheta,\varphi\rangle^N &= \langle\vartheta,\varphi|^N\tfrac{1}{4}\left[\hat{S}_+\hat{S}_- + \hat{S}_-\hat{S}_+ + \hat{S}_+^2 + (\hat{S}_+^2)^\dagger\right]|\vartheta,\varphi\rangle^N \\ &= \tfrac{1}{4}[Np_+^2 + Np_-^2 + 2N^2p_+p_- + 2N(N-1)p_+p_-\cos 2\varphi] \\ &= \tfrac{1}{4}[N + N(N-1)\sin^2\vartheta\cos^2\varphi]\ ,\end{aligned}$$

and

$$\begin{aligned}\langle\vartheta,\varphi|^N\hat{S}_y^2|\vartheta,\varphi\rangle^N &= \langle\vartheta,\varphi|^N\tfrac{1}{4}\left[\hat{S}_+\hat{S}_- + \hat{S}_-\hat{S}_+ - \hat{S}_+^2 - (\hat{S}_+^2)^\dagger\right]|\vartheta,\varphi\rangle^N \\ &= \tfrac{1}{4}[Np_+^2 + Np_-^2 + 2N^2p_+p_- - 2N(N-1)p_+p_-\cos 2\varphi] \\ &= \tfrac{1}{4}[N + N(N-1)\sin^2\vartheta\sin^2\varphi]\ .\end{aligned}$$

In summary,

$$\begin{aligned}\langle\vartheta,\varphi|^N\hat{S}_x^2|\vartheta,\varphi\rangle^N &= \tfrac{1}{4}[N + N(N-1)\sin^2\vartheta\cos^2\varphi] \\ \langle\vartheta,\varphi|^N\hat{S}_y^2|\vartheta,\varphi\rangle^N &= \tfrac{1}{4}[N + N(N-1)\sin^2\vartheta\sin^2\varphi] \\ \langle\vartheta,\varphi|^N\hat{S}_z^2|\vartheta,\varphi\rangle^N &= \tfrac{1}{4}[N^2 - N(N-1)\sin^2\vartheta]\ ,\end{aligned}$$

confirming,

$$\langle\vartheta,\varphi|^N\hat{S}_x^2 + \hat{S}_y^2 + \hat{S}_z^2|\vartheta,\varphi\rangle^N = \tfrac{N(N+1)}{4} = S(S+1)\ .$$

Also,

$$\begin{aligned}\langle\vartheta,\varphi|^N\Delta\hat{S}_x^2|\vartheta,\varphi\rangle^N &= \tfrac{1}{4}[N + N(N-1)\sin^2\vartheta\cos^2\varphi] - \tfrac{N^2}{4}\sin^2\vartheta\cos^2\varphi = \tfrac{N}{4}[1 - \sin^2\vartheta\cos^2\varphi] \\ \langle\vartheta,\varphi|^N\Delta\hat{S}_y^2|\vartheta,\varphi\rangle^N &= \tfrac{1}{4}[N + N(N-1)\sin^2\vartheta\sin^2\varphi] - \tfrac{N^2}{4}\sin^2\vartheta\sin^2\varphi = \tfrac{N}{4}[1 - \sin^2\vartheta\sin^2\varphi] \\ \langle\vartheta,\varphi|^N\Delta\hat{S}_z^2|\vartheta,\varphi\rangle^N &= \tfrac{1}{4}[N^2 - N(N-1)\sin^2\vartheta] - \tfrac{N^2}{4}\cos^2\varphi = \tfrac{N}{4}\sin^2\vartheta = N\sin^2\tfrac{\vartheta}{2}\cos^2\tfrac{\vartheta}{2}\ .\end{aligned}$$

Interestingly, we find, $\Delta\hat{S}_x^2 + \Delta\hat{S}_y^2 + \Delta\hat{S}_z^2 = \frac{N}{2}$. *Finally,*

$$\begin{aligned}\langle\vartheta,\varphi|^N\Delta\hat{S}_x^2|\vartheta,\varphi\rangle^N\langle\vartheta,\varphi|^N\Delta\hat{S}_y^2|\vartheta,\varphi\rangle^N &= \tfrac{N^2}{16}\left(1 - \sin^2\vartheta\cos^2\varphi\right)\left(1 - \sin^2\vartheta\sin^2\varphi\right) \\ &= \tfrac{N^2}{16}\left(\cos^2\vartheta + \sin^4\vartheta\cos^2\varphi\sin^2\varphi\right)\ ,\end{aligned}$$

which is obviously larger than $(\langle\vartheta,\varphi|^N\frac{1}{2}\hat{S}_z|\vartheta,\varphi\rangle^N)^2$.

41.1.6.5 Ex: Unitary spin transformations

Prove the relationship $e^{\imath F(\hat{S}_z)}\hat{S}_+e^{-\imath F(\hat{S}_z)} = \hat{S}_+e^{\imath[F(\hat{S}_z+\mathbb{I})-F(\hat{S}_z)]}$.

Solution: *First we remember* ($\hbar = 1$),

$$\begin{aligned}[\hat{S}_z,\hat{S}_+] = [\hat{S}_z,\hat{S}_x + \imath\hat{S}_y] &= \hat{S}_x + \imath\hat{S}_y = \hat{S}_+ \\ [\hat{S}_z,[\hat{S}_z,\hat{S}_+]] &= \hat{S}_+\ .\end{aligned}$$

keeping in mind, that $[\hat{S}_+,[\hat{S}_z,\hat{S}_+]]=0\neq[\hat{S}_z,[\hat{S}_z,\hat{S}_+]]$. *First choosing* $F(\hat{S}_z)\equiv t\hat{S}_z$, *we apply the transformation* $U=e^{-\imath t\hat{S}_z}$ *to the rising ladder operator,*

$$\begin{aligned}U^\dagger\hat{S}_+U&=e^{\imath t\hat{S}_z}\hat{S}_+e^{-\imath t\hat{S}_z}=\hat{S}_++(\imath t)[\hat{S}_z,\hat{S}_+]+\tfrac{(\imath t)^2}{2!}[\hat{S}_z,[\hat{S}_z,\hat{S}_+]]+...\\&=\hat{S}_++(\imath t)\hat{S}_++\tfrac{(\imath t)^2}{2!}\hat{S}_++...\\&=\hat{S}_+\sum_{k=0}^{\infty}\tfrac{(\imath t)^k}{k!}\mathbb{I}^k=\hat{S}_+e^{\imath t\mathbb{I}}=\hat{S}_+e^{\imath t[\hat{S}_z+\mathbb{I}-\hat{S}_z]}\ .\end{aligned}$$

Second, we can show that,

$$\begin{aligned}[\hat{S}_z^2,\hat{S}_+]&=\hat{S}_z\hat{S}_++\hat{S}_+\hat{S}_z=\hat{S}_+(\mathbb{I}+2\hat{S}_z)\\[\hat{S}_z^2,[\hat{S}_z^2,\hat{S}_+]]&=[\hat{S}_z^2,\hat{S}_+](\mathbb{I}+2\hat{S}_z)\ .\end{aligned}$$

Now, choosing $F(\hat{S}_z)\equiv t\hat{S}_z^2$, *we apply the transformation* $U=e^{-\imath t\hat{S}_z^2}$ *to the rising ladder operator,*

$$\begin{aligned}U^\dagger\hat{S}_+U&=e^{\imath t\hat{S}_z^2}\hat{S}_+e^{-\imath t\hat{S}_z^2}=\hat{S}_++(\imath t)[\hat{S}_z^2,\hat{S}_+]+\tfrac{(\imath t)^2}{2!}[\hat{S}_z^2,[\hat{S}_z^2,\hat{S}_+]]+...\\&=\hat{S}_++\imath t\hat{S}_+(\mathbb{I}+2\hat{S}_z)+\tfrac{(\imath t)^2}{2!}\hat{S}_+(\mathbb{I}+2\hat{S}_z)(\mathbb{I}+2\hat{S}_z)+...\\&=\hat{S}_+\sum_{k=0}^{\infty}\tfrac{(\imath t)^k}{k!}(\mathbb{I}+2\hat{S}_z)^k=\hat{S}_+e^{\imath t(\mathbb{I}+2\hat{S}_z)}=\hat{S}_+e^{\imath t[(\hat{S}_z+\mathbb{I})^2-\hat{S}_z^2]}\ .\end{aligned}$$

Third, we can show,

$$\begin{aligned}[\hat{S}_z^n,\hat{S}_+]&=\hat{S}_+\hat{S}_z^{n-1}+\hat{S}_z[\hat{S}_z^{n-1},\hat{S}_+]=\sum_{k=1}^{n}\hat{S}_z^{k-1}\hat{S}_+\hat{S}_z^{n-k}\\[\hat{S}_z^n,[\hat{S}_z^n,\hat{S}_+]]&=...\ .\end{aligned}$$

Now, choosing $F(\hat{S}_z)\equiv t\hat{S}_z^n$, *we apply the transformation* $U=e^{-\imath t\hat{S}_z^n}$ *to the rising ladder operator,*

$$\begin{aligned}U^\dagger\hat{S}_+U&=e^{\imath t\hat{S}_z^n}\hat{S}_+(0)e^{-\imath t\hat{S}_z^n}=\hat{S}_++\imath t[\hat{S}_z^n,\hat{S}_+]+\tfrac{(\imath t)^2}{2!}[\hat{S}_z^n,[\hat{S}_z^n,\hat{S}_+]]+...\\&=...\ .\end{aligned}$$

41.1.6.6 Ex: Rotation about the x-axis

How does the collective spin transform under rotation about the x-axis?

Solution: *First we remember,*

$$\begin{aligned}&[\hat{S}_x,\hat{S}_+]=-\hat{S}_z\quad,\quad[\hat{S}_x,[\hat{S}_x,\hat{S}_+]]=\imath\hat{S}_y\quad,\quad[\hat{S}_x,[\hat{S}_x,[\hat{S}_x,\hat{S}_+]]]=-\hat{S}_z\\&[\hat{S}_x,\hat{S}_y]=\imath\hat{S}_z\quad,\quad[\hat{S}_x,[\hat{S}_x,\hat{S}_y]]=\hat{S}_y\quad,\quad[\hat{S}_x,[\hat{S}_x,[\hat{S}_x,\hat{S}_y]]]=\imath\hat{S}_z\\&[\hat{S}_x,\hat{S}_z]=-\imath\hat{S}_y\quad,\quad[\hat{S}_x,[\hat{S}_x,\hat{S}_z]]=\hat{S}_z\quad,\quad[\hat{S}_x,[\hat{S}_x,[\hat{S}_x,\hat{S}_z]]]=-\imath\hat{S}_y\ .\end{aligned}$$

With this,

$$R_x(\theta)\hat{S}_\alpha \equiv e^{\imath\theta\hat{S}_x}\hat{S}_\alpha e^{-\imath\theta\hat{S}_x} = \hat{S}_+ + (\imath\theta)[\hat{S}_x,\hat{S}_\alpha] + \frac{(\imath\theta)^2}{2!}[\hat{S}_x,[\hat{S}_x,\hat{S}_\alpha]] + ...$$

$$R_x(\theta)\hat{S}_+ \equiv \hat{S}_+ - (\imath\theta)\hat{S}_z + \frac{(\imath\theta)^2}{2!}\imath\hat{S}_y + ... = \hat{S}_x + \imath\hat{S}_y\cos\theta - \imath\hat{S}_z\sin\theta$$

$$e^{\imath\theta\hat{S}_x}\hat{\mathbf{S}}e^{-\imath\theta\hat{S}_x} = \begin{pmatrix} \hat{S}_x \\ \hat{S}_y\cos\theta - \hat{S}_z\sin\theta \\ \hat{S}_y\sin\theta + \hat{S}_z\cos\theta \end{pmatrix} = \begin{pmatrix} 1 & 0 & 0 \\ 0 & \cos\theta & -\sin\theta \\ 0 & \sin\theta & \cos\theta \end{pmatrix}\hat{\mathbf{S}} \equiv R_x(\theta)\hat{\mathbf{S}}\ .$$

41.1.6.7 Ex: Spin operators for two atoms

Calculate explicitly for the case of two atoms the rotation matrices $e^{\imath\gamma\hat{S}_\alpha}$ for $\alpha = x, y, z$. Check the relationship $e^{\imath\gamma\hat{S}_\alpha}\hat{\mathbf{S}}e^{-\imath\gamma\hat{S}_\alpha} = R_\alpha(\gamma)\hat{\mathbf{S}}$ by explicit calculation.

Solution: *In the case of two atoms we have $S = 1$. The spin ladder operators are explicitly,*

$$\hat{S}_+ = \begin{pmatrix} 0 & 1 & 0 \\ 0 & 0 & 1 \\ 0 & 0 & 0 \end{pmatrix} \quad , \quad \hat{S}_- = \begin{pmatrix} 0 & 0 & 0 \\ 1 & 0 & 0 \\ 0 & 1 & 0 \end{pmatrix} \ ,$$

so that the spin matrices become,

$$\hat{S}_x = \tfrac{1}{2}\begin{pmatrix} 0 & 1 & 0 \\ 1 & 0 & 1 \\ 0 & 1 & 0 \end{pmatrix} \quad , \quad \hat{S}_y = \tfrac{1}{2}\begin{pmatrix} 0 & -\imath & 0 \\ \imath & 0 & -\imath \\ 0 & \imath & 0 \end{pmatrix} \quad , \quad \hat{S}_z = \tfrac{1}{2}\begin{pmatrix} 1 & 0 & 0 \\ 0 & 0 & 0 \\ 0 & 0 & -1 \end{pmatrix} \ ,$$

and their squares,

$$\hat{S}_x^2 = \tfrac{1}{4}\begin{pmatrix} 1 & 0 & 1 \\ 0 & 2 & 0 \\ 1 & 0 & 1 \end{pmatrix} \quad , \quad \hat{S}_y^2 = \tfrac{1}{4}\begin{pmatrix} 1 & 0 & -1 \\ 0 & 2 & 0 \\ -1 & 0 & 1 \end{pmatrix} \quad , \quad \hat{S}_z^2 = \tfrac{1}{4}\begin{pmatrix} 1 & 0 & 0 \\ 0 & 0 & 0 \\ 0 & 0 & 1 \end{pmatrix} \ .$$

The transformation matrix $e^{\imath\gamma\hat{S}_z}$ is easy to calculate,

$$e^{\imath\gamma\hat{S}_z} = \begin{pmatrix} e^{\imath\gamma/2} & 0 & 0 \\ 0 & 1 & 0 \\ 0 & 0 & e^{-\imath\gamma/2} \end{pmatrix} \ .$$

For the other transformations we need to diagonalize the spin operators. For $e^{\imath\gamma\hat{S}_x}$ the eigenvalue and eigenvector matrices are,

$$U_x = \begin{pmatrix} \frac{1}{2} & -\frac{1}{\sqrt{2}} & \frac{1}{2} \\ \frac{1}{\sqrt{2}} & 0 & -\frac{1}{\sqrt{2}} \\ \frac{1}{2} & \frac{1}{\sqrt{2}} & \frac{1}{2} \end{pmatrix} \quad , \quad \hat{E}_x = \begin{pmatrix} \frac{1}{\sqrt{2}} & 0 & 0 \\ 0 & 0 & 0 \\ 0 & 0 & -\frac{1}{\sqrt{2}} \end{pmatrix}$$

$$e^{\imath\gamma\hat{S}_x} = U_x e^{\imath\gamma\hat{E}_x} U_x^{-1} = \frac{1}{2}\begin{pmatrix} \cos\frac{\gamma}{\sqrt{2}}+1 & \imath\sqrt{2}\sin\frac{\gamma}{\sqrt{2}} & \cos\frac{\gamma}{\sqrt{2}}-1 \\ \imath\sqrt{2}\sin\frac{\gamma}{\sqrt{2}} & 2\cos\frac{\gamma}{\sqrt{2}} & \imath\sqrt{2}\sin\frac{\gamma}{\sqrt{2}} \\ \cos\frac{\gamma}{\sqrt{2}}-1 & \imath\sqrt{2}\sin\frac{\gamma}{\sqrt{2}} & \cos\frac{\gamma}{\sqrt{2}}+1 \end{pmatrix} .$$

and for $e^{\imath\gamma\hat{S}_y}$,

$$U_y = \begin{pmatrix} -\frac{1}{2} & \frac{1}{\sqrt{2}} & -\frac{1}{2} \\ -\frac{\imath}{\sqrt{2}} & 0 & \frac{\imath}{\sqrt{2}} \\ \frac{1}{2} & \frac{1}{\sqrt{2}} & \frac{1}{2} \end{pmatrix} \quad , \quad \hat{E}_y = \begin{pmatrix} \frac{1}{\sqrt{2}} & 0 & 0 \\ 0 & 0 & 0 \\ 0 & 0 & -\frac{1}{\sqrt{2}} \end{pmatrix}$$

$$e^{\imath\gamma\hat{S}_y} = U_y e^{\imath\gamma\hat{E}_y} U_y^{-1} = \frac{1}{2}\begin{pmatrix} \cos\frac{\gamma}{\sqrt{2}}+1 & \sqrt{2}\sin\frac{\gamma}{\sqrt{2}} & -\cos\frac{\gamma}{\sqrt{2}}+1 \\ -\sqrt{2}\sin\frac{\gamma}{\sqrt{2}} & 2\cos\frac{\gamma}{\sqrt{2}} & \sqrt{2}\sin\frac{\gamma}{\sqrt{2}} \\ -\cos\frac{\gamma}{\sqrt{2}}+1 & -\sqrt{2}\sin\frac{\gamma}{\sqrt{2}} & \cos\frac{\gamma}{\sqrt{2}}+1 \end{pmatrix} .$$

We check the relationship by showing that,

$$e^{\imath\gamma\hat{S}_z}\hat{S}_x e^{-\imath\gamma\hat{S}_z} = \frac{1}{2}\begin{pmatrix} 0 & e^{\imath\gamma/2} & 0 \\ e^{-\imath\gamma/2} & 0 & e^{\imath\gamma/2} \\ 0 & e^{-\imath\gamma/2} & 0 \end{pmatrix} = \hat{S}_x\cos\gamma - \hat{S}_y\sin\gamma = [R_z(\gamma)\hat{\mathbf{S}}]_x \ ,$$

and analogously for the other components.

41.1.6.8 Ex: Spin squeezing

a. Calculate $\langle\frac{\pi}{2},0|^N e^{\imath\zeta\hat{S}_z^2}\hat{\mathbf{S}}e^{-\imath\zeta\hat{S}_z^2}|\frac{\pi}{2},0\rangle^N$.
b. Calculate $\langle\frac{\pi}{2},0|^N e^{\imath\zeta\hat{S}_z^2}\Delta\hat{S}^2_{x,y,z}e^{-\imath\zeta\hat{S}_z^2}|\frac{\pi}{2},0\rangle^N$.

Solution: *a. We calculate,*

$$\begin{aligned}
&\langle\tfrac{\pi}{2},0|^N e^{\imath\zeta\hat{S}_z^2}\hat{S}_x e^{-\imath\zeta\hat{S}_z^2}|\tfrac{\pi}{2},0\rangle^N \\
&= \tfrac{1}{2^{2S}}\sum_{k,l=0}^{2S}\sqrt{\binom{2S}{l}\binom{2S}{k}}\langle S,S-l|\tfrac{1}{2}\left(\hat{S}_+ e^{2\imath\zeta(\hat{S}_z+1/2)} + e^{-2\imath\zeta(\hat{S}_z+1/2)}\hat{S}_-\right)|S,S-k\rangle \\
&= \tfrac{1}{2}\tfrac{1}{2^{2S}}\sum_{k,l=0}^{2S}\begin{pmatrix} \sqrt{\binom{2S}{l}\binom{2S}{k}}\sqrt{S(S+1)-(S-k)(S-k+1)}e^{2\imath\zeta(S-k+1/2)}\delta_{l,k-1} \\ +\sqrt{\binom{2S}{l}\binom{2S}{k}}e^{-2\imath\zeta(S-k-1+1/2)}\sqrt{S(S+1)-(S-k)(S-k-1)}\delta_{l,k+1}\end{pmatrix} \\
&= \tfrac{1}{2^{N+1}}\sum_{k=0}^{N}\left(\frac{N!e^{\imath\zeta(N-2k+1)}}{(k-1)!(N-k)!} + \frac{N!e^{-\imath\zeta(N-2k-1)}}{k!(N-k-1)!}\right) = \tfrac{N}{2}\cos^{N-1}\zeta \ .
\end{aligned}$$

Analogously,

$$\langle\tfrac{\pi}{2},0|^N e^{\imath\zeta\hat{S}_z^2}\hat{S}_y e^{-\imath\zeta\hat{S}_z^2}|\tfrac{\pi}{2},0\rangle^N = \tfrac{-\imath}{2^{N+1}}\sum_{k=0}^{N}\left(\frac{N!e^{\imath\zeta(N-2k+1)}}{(k-1)!(N-k)!}-\frac{N!e^{-\imath\zeta(N-2k-1)}}{k!(N-k-1)!}\right)=0\ ,$$

and,

$$\langle\tfrac{\pi}{2},0|^N e^{\imath\zeta\hat{S}_z^2}\hat{S}_z e^{-\imath\zeta\hat{S}_z^2}|\tfrac{\pi}{2},0\rangle^N = \langle\tfrac{\pi}{2},0|^N\hat{S}_z|\tfrac{\pi}{2},0\rangle^N = 0\ .$$

b. Now, from (41.47) we have,

$$\hat{\mathbf{S}}' \equiv e^{\imath\zeta\hat{S}_z^2}\hat{\mathbf{S}}e^{-\imath\zeta\hat{S}_z^2} = \begin{pmatrix} \frac{1}{2}\left(\hat{S}_+e^{2\imath\zeta(\hat{S}_z+1/2)}+e^{-2\imath\zeta(\hat{S}_z+1/2)}\hat{S}_-\right)\\ \frac{1}{2\imath}\left(\hat{S}_+e^{2\imath\zeta(\hat{S}_z+1/2)}-e^{-2\imath\zeta(\hat{S}_z+1/2)}\hat{S}_-\right)\\ \hat{S}_z\ . \end{pmatrix}$$

The square of the x-component is, using $[\hat{S}_+\hat{S}_-,\hat{S}_z]=0$,

$$\hat{S}_x'^2 = \tfrac{1}{4}\left(\hat{S}_+e^{2\imath\zeta(\hat{S}_z+1/2)}\hat{S}_+e^{2\imath\zeta(\hat{S}_z+1/2)}+e^{-2\imath\zeta(\hat{S}_z+1/2)}\hat{S}_-e^{-2\imath\zeta(\hat{S}_z+1/2)}\hat{S}_-+\hat{S}_+\hat{S}_-+\hat{S}_-\hat{S}_+\right)\ .$$

Evaluating it for an atomic cloud having suffered a $\frac{\pi}{2}$-pulse,

$$\langle\tfrac{\pi}{2},0|^N\hat{S}_x'^2|\tfrac{\pi}{2},0\rangle^N = \tfrac{1}{2^{2S+2}}\sum_{k,l=0}^{2S}\sqrt{\binom{2S}{k}\binom{2S}{l}}\langle S,S-l|\hat{S}_x'^2|S,S-k\rangle$$

$$= \tfrac{1}{2^{2S+2}}\sum_{k,l=0}^{2S}\sqrt{\binom{2S}{k}\binom{2S}{l}}\begin{pmatrix}\langle S,S-l|\hat{S}_+e^{2\imath\zeta(\hat{S}_z+1/2)}\hat{S}_+e^{2\imath\zeta(\hat{S}_z+1/2)}|S,S-k\rangle\\ +\langle S,S-l|e^{-2\imath\zeta(\hat{S}_z+1/2)}\hat{S}_-e^{-2\imath\zeta(\hat{S}_z+1/2)}\hat{S}_-|S,S-k\rangle\\ +\langle S,S-l|\hat{S}_+\hat{S}_-+\hat{S}_-\hat{S}_+|S,S-k\rangle\end{pmatrix}$$

$$= \tfrac{1}{2^{N+2}}\sum_{k=0}^{N}\begin{pmatrix}e^{2\imath\zeta(N-2k+2)}\sqrt{\frac{N!}{k!(N-k)!}\frac{N!}{(k-2)!(N-k+2)!}}\sqrt{k-1}\sqrt{N-k+2}\sqrt{k}\sqrt{N-k+1}\\ +e^{-2\imath\zeta(N-2k-2)}\sqrt{\frac{N!}{k!(N-k)!}\frac{N!}{(k+2)!(N-k-2)!}}\sqrt{k+2}\sqrt{N-k-1}\sqrt{k+1}\sqrt{N-k}\\ +\frac{N!}{k!(N-k)!}(k+1)(N-k)+\frac{N!}{k!(N-k)!}k(N-k+1)\end{pmatrix}$$

$$= \tfrac{1}{2^{N+2}}\sum_{k=0}^{N}\left(\frac{e^{4\imath\zeta}N!x^ky^{N-k}}{(k-2)!(N-k)!}+\frac{e^{4\imath\zeta}N!y^kx^{N-k}}{k!(N-k-2)!}+\frac{N!(k+1)}{k!(N-k-1)!}+\frac{N!(N-k+1)}{(k-1)!(N-k)!}\right)$$

$$= \tfrac{e^{4\imath\zeta}}{2^{N+2}}(N-1)Nx^2(x+y)^{N-2}\times 2+\tfrac{N(N+1)}{8}\ ,$$

where we used the abbreviations $x\equiv e^{-2\imath\zeta}$ and $y\equiv e^{2\imath\zeta}$. Now,

$$\langle\tfrac{\pi}{2},0|^N\hat{S}_x'^2|\tfrac{\pi}{2},0\rangle^N = \tfrac{N(N+1)}{8}+\tfrac{N(N-1)}{8}\cos^{N-2}2\zeta\ .$$

For $\zeta=0$ we recover the result from Exc. 41.1.6.4,

$$\langle\vartheta,\varphi|^N\hat{S}_x^2|\vartheta,\varphi\rangle^N = \tfrac{1}{4}\left[N+N(N-1)\sin^2\tfrac{\pi}{2}\cos^2 0\right] = \tfrac{N^2}{4}\ .$$

Analogously, we find,

$$\langle\tfrac{\pi}{2},0|^N\hat{S}_y'^2|\tfrac{\pi}{2},0\rangle^N = \tfrac{N(N+1)}{8}-\tfrac{N(N-1)}{8}\cos^{N-2}2\zeta\ .$$

41.1.6.9 Ex: Rotation of spin squeezed states

Calculate $\langle \frac{\pi}{2},0|^N e^{\imath\nu\hat{S}_x} e^{\imath\zeta\hat{S}_z^2} \Delta\hat{S}^2_{x,y,z} e^{-\imath\zeta\hat{S}_z^2} e^{-\imath\nu\hat{S}_x} |\frac{\pi}{2},0\rangle^N$.

Solution: *For the x-coordinate the calculation is easy, because,*

$$\langle \tfrac{\pi}{2},0|^N e^{\imath\nu\hat{S}_x} e^{\imath\zeta\hat{S}_z^2} \Delta\hat{S}^2_{x} e^{-\imath\zeta\hat{S}_z^2} e^{-\imath\nu\hat{S}_x} |\tfrac{\pi}{2},0\rangle^N = \langle \tfrac{\pi}{2},0|^N e^{\imath\zeta\hat{S}_z^2} \Delta\hat{S}^2_{x} e^{-\imath\zeta\hat{S}_z^2} |\tfrac{\pi}{2},0\rangle^N \ ,$$

where we can exploit the result of Exc. 41.1.6.8, yielding,

$$\langle \tfrac{\pi}{2},0|^N e^{\imath\nu\hat{S}_x} e^{\imath\zeta\hat{S}_z^2} \Delta\hat{S}^2_{x} e^{-\imath\zeta\hat{S}_z^2} e^{-\imath\nu\hat{S}_x} |\tfrac{\pi}{2},0\rangle^N = \tfrac{N(N+1)}{8} + \tfrac{N(N-1)}{8} \cos^{N-2} 2\zeta - \tfrac{N^2}{4} \cos^{2N-2}\zeta \ .$$

For the x- and y-coordinates, we note,

$$\langle \tfrac{\pi}{2},0|^N e^{\imath\nu\hat{S}_x} e^{\imath\zeta\hat{S}_z^2} \hat{S}_{y,z} e^{-\imath\zeta\hat{S}_z^2} e^{-\imath\nu\hat{S}_x} |\tfrac{\pi}{2},0\rangle^N = 0 \ .$$

Hence, we get for the y-coordinate,

$$\begin{aligned}
&\langle \tfrac{\pi}{2},0|^N e^{\imath\nu\hat{S}_x} e^{\imath\zeta\hat{S}_z^2} \Delta\hat{S}^2_{y} e^{-\imath\zeta\hat{S}_z^2} e^{-\imath\nu\hat{S}_x} |\tfrac{\pi}{2},0\rangle^N = \langle \tfrac{\pi}{2},0|^N e^{\imath\nu\hat{S}_x} e^{\imath\zeta\hat{S}_z^2} \Delta\hat{S}^2_{y} e^{-\imath\zeta\hat{S}_z^2} e^{-\imath\nu\hat{S}_x} |\tfrac{\pi}{2},0\rangle^N \\
&= \langle \tfrac{\pi}{2},0|^N e^{\imath\nu\hat{S}_x} e^{\imath\zeta\hat{S}_z^2} \hat{S}^2_{y} e^{-\imath\zeta\hat{S}_z^2} e^{-\imath\nu\hat{S}_x} |\tfrac{\pi}{2},0\rangle^N \\
&= \langle \tfrac{\pi}{2},0|^N e^{\imath\nu\hat{S}_x} \tfrac{-1}{4} \left(\hat{S}_+ e^{2\imath\zeta(\hat{S}_z+1/2)} - e^{-2\imath\zeta(\hat{S}_z+1/2)} \hat{S}_- \right)^2 e^{-\imath\nu\hat{S}_x} |\tfrac{\pi}{2},0\rangle^N \\
&= \tfrac{-1}{4} \langle \tfrac{\pi}{2},0|^N e^{\imath\nu\hat{S}_x} \left(e^{2\imath\zeta\hat{S}_z} \hat{S}_+ e^{2\imath\zeta\hat{S}_z} \hat{S}_+ e^{2\imath\zeta\hat{S}_z} + e^{-2\imath\zeta\hat{S}_z} e^{-2\imath\zeta\hat{S}_z} \hat{S}_- e^{-2\imath\zeta\hat{S}_z} \hat{S}_- - 2\hat{\mathbf{S}}^2 - 2\hat{S}_z^2 \right) e^{-\imath\nu\hat{S}_x} |\tfrac{\pi}{2},0\rangle^N \\
&= \tfrac{-1}{4} \langle \tfrac{\pi}{2},0|^N e^{\imath\nu\hat{S}_x} \left(\hat{S}_+^2 e^{6\imath\zeta(\hat{S}_z+1)} + e^{-6\imath\zeta(\hat{S}_z+1)} \hat{S}_-^2 - 2\hat{\mathbf{S}}^2 - 2\hat{S}_z^2 \right) e^{-\imath\nu\hat{S}_x} |\tfrac{\pi}{2},0\rangle^N
\end{aligned}$$

??? .

And for the z-coordinate,

$$\begin{aligned}
&\langle \tfrac{\pi}{2},0|^N e^{\imath\nu\hat{S}_x} e^{\imath\zeta\hat{S}_z^2} \Delta\hat{S}^2_{z} e^{-\imath\zeta\hat{S}_z^2} e^{-\imath\nu\hat{S}_x} |\tfrac{\pi}{2},0\rangle^N = \langle \tfrac{\pi}{2},0|^N e^{\imath\nu\hat{S}_x} \hat{S}^2_{z} e^{-\imath\nu\hat{S}_x} |\tfrac{\pi}{2},0\rangle^N \\
&= \langle \tfrac{\pi}{2},0|^N e^{\imath\nu\hat{S}_x} \hat{S}_z e^{-\imath\nu\hat{S}_x} e^{\imath\nu\hat{S}_x} \hat{S}_z e^{-\imath\nu\hat{S}_x} |\tfrac{\pi}{2},0\rangle^N = \langle \tfrac{\pi}{2},0|^N (\hat{S}_y \sin\nu + \hat{S}_z \cos\nu)^2 |\tfrac{\pi}{2},0\rangle^N \\
&= \frac{1}{2^{2S}} \sum_{k,l=0}^{N} \sqrt{\binom{N}{k}\binom{N}{l}} \langle S, S-l| \left(\tfrac{1}{2\imath} \hat{S}_+ \sin\nu - \tfrac{1}{2\imath} \hat{S}_- \sin\nu + \hat{S}_z \cos\nu \right)^2 |S, S-k\rangle \\
&= \frac{1}{2^N} \sum_{k,l=0}^{N} \sqrt{\binom{N}{k}\binom{N}{l}} \begin{pmatrix} -\frac{\sin^2\nu}{4} \sqrt{k-1}\sqrt{2S-k+2}\sqrt{k}\sqrt{2S-k+1}\delta_{l,k-2} \\ +\frac{\sin^2\nu}{4}(k+1)(2S-k)\delta_{l,k} + \frac{\sin^2\nu}{4} k(2S-k+1)\delta_{l,k} \\ -\frac{\sin^2\nu}{4} \sqrt{k+2}\sqrt{2S-k-1}\sqrt{k+1}\sqrt{2S-k}\delta_{l,k+2} \\ +\cos^2\nu (S-k)^2 \delta_{l,k} \end{pmatrix} ,
\end{aligned}$$

discarding all imaginary terms. Carrying out the calculations,

$$\langle \tfrac{\pi}{2},0|^N e^{\imath\nu\hat{S}_x} e^{\imath\zeta\hat{S}_z^2} \Delta\hat{S}^2_{z} e^{-\imath\zeta\hat{S}_z^2} e^{-\imath\nu\hat{S}_x} |\tfrac{\pi}{2},0\rangle^N = \tfrac{N}{4} \ .$$

41.1.6.10 Ex: Spin squeezing with two atoms

a. For a system of two atoms, write down the coherent state $|\vartheta,\varphi\rangle^2 = |\frac{\pi}{2},0\rangle^2$ in the Tavis-Cummings basis and in the Dicke state basis.
b. Derive the matrix representation for the squeezing operator along the z-axis and apply this operator to the above coherent spin state.
c. Compare spin squeezing with entanglement.

Solution: *a. We get in the Tavis-Cummings basis,*

$$\begin{aligned}|\vartheta,\varphi\rangle^2 &= \left(\cos\tfrac{\vartheta}{2}|+\rangle + e^{\imath\varphi}\sin\tfrac{\vartheta}{2}|-\rangle\right)^2 \\ &= \cos^2\tfrac{\vartheta}{2}|++\rangle + e^{\imath\varphi}\sin\tfrac{\vartheta}{2}\cos\tfrac{\vartheta}{2}(|+-\rangle + |+-\rangle) + e^{2\imath\varphi}\sin^2\tfrac{\vartheta}{2}|--\rangle\ ,\end{aligned}$$

such that,

$$|\tfrac{\pi}{2},0\rangle^2 = \tfrac{1}{2}(|+\rangle + |-\rangle)^2 = \tfrac{1}{2}(|++\rangle + |+-\rangle + |-+\rangle + |--\rangle)\ ,$$

while in the Dicke state basis, using

$$\begin{aligned}|\vartheta,\varphi\rangle^2 &= \sum_{k=0}^{N}\sqrt{\binom{N}{k}}\cos^k\tfrac{\vartheta}{2}e^{\imath(N-k)\varphi}\sin^{N-k}\tfrac{\vartheta}{2}|S,M\rangle \qquad \textit{with} \qquad N=2 \\ &= \cos^2\tfrac{\vartheta}{2}|1,1\rangle + 2e^{\imath\varphi}\sin\tfrac{\vartheta}{2}\cos\tfrac{\vartheta}{2}|1,0\rangle + e^{2\imath\varphi}\sin^2\tfrac{\vartheta}{2}|1,-1\rangle\ ,\end{aligned}$$

such that,

$$|\tfrac{\pi}{2},0\rangle = \tfrac{1}{2}|1,1\rangle + |1,0\rangle + \tfrac{1}{2}|1,-1\rangle\ . \tag{41.72}$$

b. Using the matrix representation of the spin operator,

$$\hat{S}_z = \begin{pmatrix}\frac{1}{2} & 0 & 0\\ 0 & 0 & 0\\ 0 & 0 & -\frac{1}{2}\end{pmatrix} \qquad \textit{and} \qquad \hat{S}_z^2 = \begin{pmatrix}\frac{1}{4} & 0 & 0\\ 0 & 0 & 0\\ 0 & 0 & \frac{1}{4}\end{pmatrix}\ ,$$

we find,

$$e^{\imath\zeta\hat{S}_z^2} = \begin{pmatrix}e^{\imath\zeta/4} & 0 & 0\\ 0 & 1 & 0\\ 0 & 0 & e^{\imath\zeta/4}\end{pmatrix}$$

Applying this operator to the coherent spin state, we get,

$$e^{\imath\zeta\hat{S}_z^2}|\vartheta,\varphi\rangle^N = \sum_{k=0}^{N}\sqrt{\binom{N}{k}}\cos^k\tfrac{\vartheta}{2}e^{\imath(N-k)\varphi}\sin^{N-k}\tfrac{\vartheta}{2}e^{\imath\zeta(S-k)^2}|S,S-k\rangle\ ,$$

such that,

$$\begin{aligned}e^{\imath\zeta\hat{S}_z^2}|\tfrac{\pi}{2},0\rangle^2 &= e^{\imath 2\varphi+\imath\zeta}\sin^2\tfrac{\vartheta}{2}|1,1\rangle + \sqrt{2}\cos\tfrac{\vartheta}{2}e^{\imath\varphi}\sin\tfrac{\vartheta}{2}|1,0\rangle + \cos^2\tfrac{\vartheta}{2}e^{\imath\zeta}|1,-1\rangle \\ &= \tfrac{e^{\imath\zeta}}{2}|1,1\rangle + \tfrac{1}{\sqrt{2}}|1,0\rangle + \tfrac{e^{\imath\zeta}}{2}|1,-1\rangle\ .\end{aligned}$$

Obviously, this state cannot be represented by a (stretched) coherent state (41.72).
c. In the Tavis-Cummings basis we calculate,

$$\hat{S}_z = \begin{pmatrix} 1 & & & \\ & 0 & & \\ & & 0 & \\ & & & -1 \end{pmatrix} \quad , \quad \hat{S}_z^2 = \begin{pmatrix} 1 & & & \\ & 0 & & \\ & & 0 & \\ & & & 1 \end{pmatrix} \quad , \quad e^{\imath\zeta\hat{S}_z^2} = \begin{pmatrix} e^{\imath\zeta} & & & \\ & 1 & & \\ & & 1 & \\ & & & e^{\imath\zeta} \end{pmatrix} .$$

Hence,

$$e^{\imath\zeta\hat{S}_z^2}\tfrac{1}{2}\begin{pmatrix} 1 \\ 1 \\ 1 \\ 1 \end{pmatrix} = \tfrac{1}{2}\begin{pmatrix} e^{\imath\zeta} \\ 1 \\ 1 \\ e^{\imath\zeta} \end{pmatrix} ,$$

only the stretched states are influenced by the squeezing operator. In a Ramsey interferometer this may be exploited to generate entanglement, $|++\rangle + |--\rangle$.

41.1.6.11 Ex: Mølmer-Sørensen gate

Derive the matrix representation for the two-qubit Mølmer-Sørensen gate $e^{\imath\zeta\hat{S}_x^2}$.

Solution: *With the definition (25.77),*

$$\hat{S}_k = \tfrac{1}{2}(\hat{\sigma}_k \otimes \mathbb{I}_2 + \mathbb{I}_2 \otimes \hat{\sigma}_k)$$

we can verify,

$$\hat{S}_x = e^{-\imath\pi\hat{S}_y/2}\hat{S}_z e^{\imath\pi\hat{S}_y/2} .$$

Using (24.153),

$$e^{\imath\zeta\hat{S}_x^2} = e^{\imath\zeta e^{-\imath\pi\hat{S}_y/2}\hat{S}_z e^{\imath\pi\hat{S}_y/2} e^{-\imath\pi\hat{S}_y/2}\hat{S}_z e^{\imath\pi\hat{S}_y/2}} = e^{e^{-\imath\pi\hat{S}_y/2}\imath\zeta\hat{S}_z^2 e^{\imath\pi\hat{S}_y/2}} = e^{-\imath\pi\hat{S}_y/2} e^{\imath\zeta\hat{S}_z^2} e^{\imath\pi\hat{S}_y/2}$$

$$= \left[\tfrac{1}{2}\begin{pmatrix} 1 & 1 & 1 & 1 \\ -1 & 1 & -1 & 1 \\ -1 & -1 & 1 & 1 \\ 1 & -1 & -1 & 1 \end{pmatrix}\right]^{-1} \begin{pmatrix} e^{\imath\zeta} & 0 & 0 & 0 \\ 0 & 0 & 0 & 0 \\ 0 & 0 & 0 & 0 \\ 0 & 0 & 0 & e^{\imath\zeta} \end{pmatrix} \tfrac{1}{2}\begin{pmatrix} 1 & 1 & 1 & 1 \\ -1 & 1 & -1 & 1 \\ -1 & -1 & 1 & 1 \\ 1 & -1 & -1 & 1 \end{pmatrix}$$

$$= \tfrac{1}{2} e^{\imath\zeta}\begin{pmatrix} 1 & 0 & 0 & 1 \\ 0 & 1 & 1 & 0 \\ 0 & 1 & 1 & 0 \\ 1 & 0 & 0 & 1 \end{pmatrix} .$$

Alternatively, we can search the eigenvalue matrix $\hat{E}$ and the eigenvector matrix U of the operator $\hat{S}_x^2 = U^{-1}EU$ and calculate $e^{\imath\zeta\hat{S}_x^2} = e^{\imath\zeta U^{-1}EU} = U^{-1}e^{\imath\zeta E}U$, which yields the same result. Applying the gate to the two-qubit ground state we generate the fully entangled EPR state.

41.1.6.12 Ex: Spin-squeezing via one-axis twisting

For a Dicke state with $N = 8$ atoms, program the matrix representations of the operators $\hat{S}_\pm$, $\hat{\mathbf{S}}$, $R_\alpha(\theta)$, and $Q_\alpha(\zeta)$ for $\alpha = x, y, z$ defined in the script, as well as the vector representation of the state $|\vartheta, \varphi\rangle$.
a. Starting from the ground state $|\vartheta, \varphi\rangle = |0, 0\rangle$, simulate the following time evolution: (i) $\frac{\pi}{2}$-pulse with the Hamiltonian $\hat{H} = \Omega \hat{S}_x$, where Ω is the Rabi frequency, (ii) interaction-free precession with the Hamiltonian $\hat{H} = \Delta \hat{S}_z$ where Δ is the detuning during a time T, (iii) $\frac{\pi}{2}$-pulse with the Hamiltonian $\hat{H} = \Omega \hat{S}_x$, (iv) projection of the energy axis. Plot the time evolution of the expectation values $\langle \hat{S}_\alpha \rangle$ and $\Delta \hat{S}_\alpha$.
b. Starting from the ground state $|\vartheta, \varphi\rangle = |0, 0\rangle$, simulate the following time evolution: (i) $\frac{\pi}{2}$-pulse with the Hamiltonian $\hat{H} = \Omega \hat{S}_y$, where Ω is the Rabi frequency, (ii) squeezing pulse along the z-axis with the squeezing parameter $\zeta = 0.6$, (iii) $\frac{\pi}{2}$-pulse with the Hamiltonian $\hat{H} = \Omega \hat{S}_x$. Plot the time evolution of the expectation values $\langle \hat{S}_\alpha \rangle$ and $\Delta \hat{S}_\alpha$. A movie can be seen at (watch movie).

Solution: *a. See plots of Fig. 41.7.*

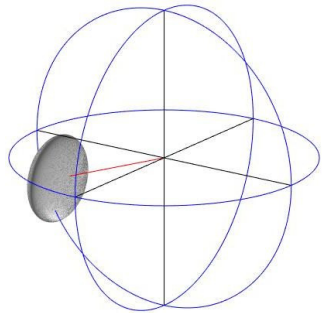

Figure 41.7: (code) Ramsey sequence.

b. See plots of Fig. 41.8.

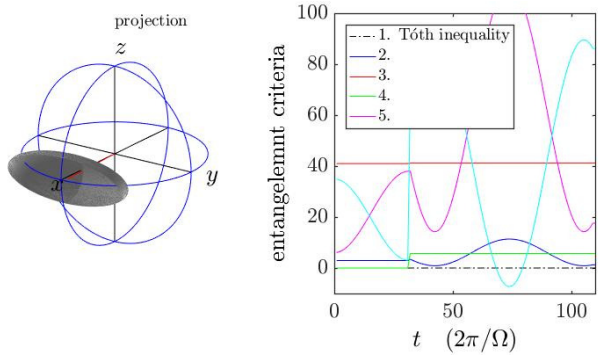

Figure 41.8: (code) Squeezing sequence.

41.1.6.13 Ex: Two-axis countertwisting

Study the Hamiltonian,

$$\hat{H} = \zeta(\hat{S}^2_{\pi/2,\pi/4} - \hat{S}^2_{\pi/2,-\pi/4}) = \tfrac{\zeta}{2\imath}(\hat{S}^2_+ - \hat{S}^2_-)$$

with $\hat{S}_{\vartheta,\varphi}$ defined in Exc. 41.1.6.3 in view of its squeezing features of an initial coherent spin state $|0,\varphi\rangle$ [724].

Solution: *The squeezing propagator generated by the Hamiltonian,*

$$\hat{H} = \zeta(\hat{S}_x + \imath\hat{S}_y)^2 - (\hat{S}_x - \imath\hat{S}_y)^2 = \zeta(\hat{S}_x\hat{S}_y + \hat{S}_y\hat{S}_x)$$

is

$$Q_z(\zeta) = e^{\imath\hat{H}t} = e^{\imath\zeta t(\hat{S}_x\hat{S}_y + \hat{S}_y\hat{S}_x)}$$

and we want to know

$$\langle\vartheta,\varphi|^N e^{\imath\zeta t(\hat{S}_x\hat{S}_y+\hat{S}_y\hat{S}_x)}\Delta\hat{S}^2_{x,y,z}e^{-\imath\zeta t(\hat{S}_x\hat{S}_y+\hat{S}_y\hat{S}_x)}|\vartheta,\varphi\rangle^N \ .$$

Note also,

$$\begin{aligned}\hat{S}_x\hat{S}_y, \hat{S}_y\hat{S}_x] &= \hat{S}_x\hat{S}_y[\hat{S}_y,\hat{S}_x] + [\hat{S}_x,\hat{S}_y]\hat{S}_x\hat{S}_y = 0\\ e^{\imath\zeta t(\hat{S}_x\hat{S}_y+\hat{S}_y\hat{S}_x)} &= e^{\imath\zeta t\hat{S}_x\hat{S}_y}e^{\imath\zeta t\hat{S}_y\hat{S}_x}\\ \hat{S}^2_x - \hat{S}^2_y &= \imath[\hat{S}_z,\hat{S}_x\hat{S}_y] \ .\end{aligned}$$

41.1.6.14 Ex: Interferometry with double Fock states

Discuss numerically whether, assuming as the initial state a double spin Fock state of the form $|+\rangle^{N_1}|-\rangle^{N_2}$, Heisenberg limited interferometry can be done within the Dicke model [184].

Solution: *Here, we want to study a product of two coherent spin states (in analogy to the superposition of two Glauber modes),*

$$\begin{aligned}|\psi\rangle = |\psi_1\rangle|\psi_2\rangle &= |\vartheta_1,\varphi_1\rangle^{N_1}|\vartheta_2,\varphi_2\rangle^{N_2} = (p_{1+}|+\rangle + p_{1-}|-\rangle)^{N_1}(p_{1+}|+\rangle + p_{1-}|-\rangle)^{N_1}\\ &= \sum_{k=0}^{2S_1}\sqrt{\binom{2S_1}{k}}p_{1+}^{S_1-k/2}p_{1-}^{k/2}\sum_{l=0}^{2S_2}\sqrt{\binom{2S_2}{l}}p_{2+}^{S_2-l/2}p_{2-}^{l/2}|S_1,M_1;S_2,M_2\rangle \ .\end{aligned}$$

Now, we construct operators acting on the whole Hilbert space,

$$|\psi\rangle \equiv |\psi_1\rangle\otimes|\psi_2\rangle \qquad , \qquad \hat{J}_\alpha \equiv \hat{S}^{(1)}_\alpha \oplus \hat{S}^{(2)}_\alpha = (\hat{S}^{(1)}_\alpha\otimes\mathbb{I}) + (\mathbb{I}\otimes\hat{S}^{(2)}_\alpha) \ ,$$

for all $\alpha = x,y,z,\pm$. The partial operators themselves are sums,

$$\hat{S}^{(\mu)}_\alpha = \sum_{k=1}^{N}\hat{S}^{(1)}_{k,\alpha} \ ,$$

with $\mu = 1, 2$. E.g. for two particles, one in each group μ, defining the basis $\{|--\rangle, |-+\rangle, |+-\rangle, |++\rangle\}$, we have,

$$\hat{J}_x = (\hat{S}_x \otimes \mathbb{I}) + (\mathbb{I} \otimes \hat{S}_x)$$
$$\hat{J}_x^2 = (\hat{S}_x \otimes \mathbb{I})^2 + (\mathbb{I} \otimes \hat{S}_x)^2 + (\hat{S}_x \otimes \mathbb{I})(\mathbb{I} \otimes \hat{S}_x) + (\hat{S}_x \otimes \mathbb{I})(\mathbb{I} \otimes \hat{S}_x) \ .$$

For the general case,

$$\begin{aligned}\hat{J}_\pm|S_1, M_1; S_2, M_2\rangle &= \sqrt{S_1(S_1+1) - M_1(M_1 \pm 1)}|S_1, M_1 \pm 1; S_2, M_2\rangle \\ &+ \sqrt{S_2(S_2+1) - M_2(M_2 \pm 1)}|S_1, M_1; S_2, M_2 \pm 1\rangle \\ \hat{J}_z|S_1, M_1; S_2, M_2\rangle &= M_1|S_1, M_1; S_2, M_2\rangle + M_2|S_1, M_1; S_2, M_2\rangle \ .\end{aligned}$$

The linear expectation values are easy to calculate,

$$\begin{aligned}&\langle\vartheta_1, \varphi_1|^{N_1}\langle\vartheta_2, \varphi_2|^{N_2}\hat{J}_+|\vartheta_1, \varphi_1\rangle^{N_1}|\vartheta_2, \varphi_2\rangle^{N_2} \\ &\qquad = \langle\vartheta_1, \varphi_1|^{N_1}\hat{S}_+^{(1)}|\vartheta_1, \varphi_1\rangle^{N_1} + \langle\vartheta_2, \varphi_2|^{N_2}\hat{S}_+^{(2)}|\vartheta_2, \varphi_2\rangle^{N_2} \\ &\qquad = S_1 e^{\imath\varphi_1}\sin\vartheta_1 + S_2 e^{\imath\varphi_2}\sin\vartheta_2 \ ,\end{aligned}$$

and so on. However, the situation is more complicated for higher momenta, such as,

$$\langle\vartheta_1, \varphi_1|^{N_1}\langle\vartheta_2, \varphi_2|^{N_2}\hat{J}_+^2|\vartheta_1, \varphi_1\rangle^{N_1}|\vartheta_2, \varphi_2\rangle^{N_2} \ ,$$

which have to be calculated numerically.
We consider the initial state,

$$|+\rangle^{N_1}|-\rangle^{N_2} = |N_1, S_1, M_1; N_2, S_2, M_2\rangle = |N_1, \tfrac{N_1}{2}, -\tfrac{N_1}{2}; N_2, \tfrac{N_2}{2}, +\tfrac{N_2}{2}\rangle \ .$$

It's like making a $\frac{\pi}{2}$-pulse and doing a complete spin-squeezing by measuring the atom number difference. The resulting state is NOT a coherent spin state, and the one-cloud Dicke model does not apply. This is analogous to combining two photonic Fock states at a beamsplitter and may be an example of sub SQL without entanglement [191]. See plots of Fig. 41.9.

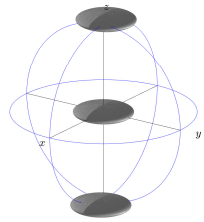

Figure 41.9: (code) Heisenberg-limited interferometry with two initial Fock states.

41.1.6.15 Ex: Entanglement criteria

A sufficient entanglement criterion for an N-qubit state is, that it violates one of the following inequalities [1315, 1316],

$$\begin{aligned}
\frac{\langle\Delta\hat{S}_z^2\rangle}{\langle\hat{S}_x\rangle^2+\langle\hat{S}_y\rangle^2} &\geq \frac{1}{N}\\
\langle\hat{S}_x^2\rangle+\langle\hat{S}_y^2\rangle+\langle\hat{S}_z^2\rangle &\leq \tfrac{N(N+2)}{4}\\
\langle\Delta\hat{S}_x^2\rangle+\langle\Delta\hat{S}_y^2\rangle+\langle\Delta\hat{S}_z^2\rangle &\geq \tfrac{N}{2}\\
\langle\hat{S}_k^2\rangle+\langle\hat{S}_m^2\rangle-\tfrac{N}{2} &\leq (N-1)\langle\Delta\hat{S}_n^2\rangle\\
(N-1)[\langle\Delta\hat{S}_k^2\rangle+\langle\Delta\hat{S}_m^2\rangle] &\geq \langle\hat{S}_k^2\rangle+\tfrac{N(N-2)}{4}\ ,
\end{aligned}$$

for $(kmn)=(123)$. Verify that, according to these criteria, coherent Dicke states are not entangled.

Solution: *With the results of Excs. 41.1.6.3 and 41.1.6.4 we find for coherent Dicke states immediately,*

$$\begin{aligned}
\frac{\langle\Delta\hat{S}_z^2\rangle}{\langle\hat{S}_x\rangle^2+\langle\hat{S}_y\rangle^2} &= \frac{1}{N\sin^2\varphi}\geq\frac{1}{N}\\
\langle\hat{S}_x^2\rangle+\langle\hat{S}_y^2\rangle+\langle\hat{S}_z^2\rangle &= \tfrac{N}{2}+\tfrac{N^4}{4}\\
\langle\Delta\hat{S}_x^2\rangle+\langle\Delta\hat{S}_y^2\rangle+\langle\Delta\hat{S}_z^2\rangle &= \tfrac{N}{2}\\
\langle\hat{S}_x^2\rangle+\langle\hat{S}_y^2\rangle-\tfrac{N}{2}-(N-1)\langle\Delta\hat{S}_z^2\rangle &= -\tfrac{N}{2}+\tfrac{N}{4}\sin^2\vartheta\leq 0\\
(N-1)[\langle\Delta\hat{S}_x^2\rangle+\langle\Delta\hat{S}_y^2\rangle]-\langle\hat{S}_z^2\rangle-\tfrac{N(N-2)}{4} &= 0\ .
\end{aligned}$$

41.1.6.16 Ex: Consistency of the Holstein-Primakoff transform

Verify that the relations (41.61) satisfy $[\hat{S}_+,\hat{S}_-]\simeq 2\hat{S}_z$ and $[\hat{S}_x,\hat{S}_y]\simeq\frac{\imath}{2}\hat{S}_z$.

Solution: *Using* $[\hat{b},\hat{b}^\dagger]=1$ *we find,*

$$\begin{aligned}
[\hat{S}_+,\hat{S}_-] &= 2S\left[\sqrt{1-\tfrac{\hat{b}^\dagger\hat{b}}{2S}}\ \hat{b},\hat{b}^\dagger\sqrt{1-\tfrac{\hat{b}^\dagger\hat{b}}{2S}}\right]\simeq 2S\left[\left(1-\tfrac{\hat{b}^\dagger\hat{b}}{4S}\right)\hat{b},\hat{b}^\dagger\left(1-\tfrac{\hat{b}^\dagger\hat{b}}{4S}\right)\right]\\
&= 2\left(S-\hat{b}^\dagger\hat{b}+\tfrac{1}{16S}\left[\hat{b}^\dagger\hat{b}\hat{a},\hat{b}^\dagger\hat{b}^\dagger\hat{b}\right]\right)\simeq 2\hat{S}_z\ ,
\end{aligned}$$

and

$$[\hat{S}_x,\hat{S}_y]=\left[\tfrac{1}{2}(\hat{S}_++\hat{S}_-),\tfrac{1}{2\imath}(\hat{S}_+-\hat{S}_-)\right]=\tfrac{-1}{4\imath}[\hat{S}_+,\hat{S}_-]\simeq\tfrac{\imath}{2}\hat{S}_z\ .$$

41.1.6.17 Ex: Dicke model of Bloch oscillations in the two-mode approximation

In the limit where Bloch oscillations can be modeled by a two-level system [1139] we may try a representation within the Dicke model and illustrate the dynamics on a Bloch sphere [1135]. The gravitational acceleration corresponds to a modification of kinetic energy without modification of the momentum state populations and without excitation of quantum coherences between them. Since the kinetic energy is represented by the vertical axis of the Bloch sphere, we may visualize acceleration via a rotation of the Bloch sphere, e.g. about the y-axis. The interpretation of the rotated Bloch sphere remains the same: the xy-plane shows the coherences and the z-axis the populations. Once this works, we can treat the thermal atomic cloud as a coherent spin state, e.g. squeeze it [724] or simulate trajectory of individual atoms inhomogeneously [345] [9,10].

Solution: *Assuming that, at any time, at most two discrete momentum states n and $n+1$ are coupled, the Hamiltonian (26.70) becomes,*

$$\begin{aligned}\tilde{H} &= 4\hbar\omega_{rec}n^2|2n\hbar k\rangle\langle 2n\hbar k| + 4\hbar\omega_{rec}(n+1)^2|2(n+1)\hbar k\rangle\langle 2(n+1)\hbar k| \\ &\quad + \tfrac{V_0}{4}\left(|2(n+1)\hbar k\rangle\langle 2n\hbar k| + |2n\hbar k\rangle\langle 2(n+1)\hbar k|\right) \ .\end{aligned}$$

Introducing spin operators for every single motional two-level atom,

$$\begin{aligned}\hat{\sigma}^+ &\equiv |p+2\hbar k\rangle\langle p| \quad , \quad \hat{\sigma}^x \equiv \hat{\sigma}^+ + \hat{\sigma}^- \quad , \quad \hat{\sigma}^z \equiv [\hat{\sigma}^+, \hat{\sigma}^-]_- \\ 2\hat{\sigma}^+\hat{\sigma}^- &= |p+2\hbar k\rangle\langle p+2\hbar k| = [\hat{\sigma}^-, \hat{\sigma}^+]_+ - [\hat{\sigma}^-, \hat{\sigma}^+]_- = \mathbb{I} + \hat{\sigma}^z \\ 2\hat{\sigma}^-\hat{\sigma}^+ &= |p\rangle\langle p| = [\hat{\sigma}^-, \hat{\sigma}^+]_+ + [\hat{\sigma}^-, \hat{\sigma}^+]_- = \mathbb{I} - \hat{\sigma}^z \ ,\end{aligned}$$

we get,

$$\begin{aligned}\tilde{H} &= 4\hbar\omega_{rec}n^2\hat{\sigma}^-\hat{\sigma}^+ + 4\hbar\omega_{rec}(n+1)^2\hat{\sigma}^+\hat{\sigma}^- + \tfrac{V_0}{4}(\hat{\sigma}^+ + \hat{\sigma}^-) \\ &= 8\hbar\omega_{rec}(n+\tfrac{1}{2})\hat{\sigma}^z + 8\hbar\omega_{rec}(n^2+n+\tfrac{1}{2}) + \tfrac{V_0}{4}\hat{\sigma}^x \ .\end{aligned}$$

Finally, we go to the collective Dicke Hamiltonian,

$$\hat{H} = \sum_j \tilde{H}_j = 8\hbar\omega_{rec}(n+\tfrac{1}{2})\hat{S}^z + 8\hbar\omega_{rec}(n^2+n+\tfrac{1}{2}) + \tfrac{V_0}{4}\hat{S}^x \ .$$

41.1.6.18 Ex: Uncertainty relation in different bases

In Exc. 41.1.6.4 the principal axes of the uncertainty ellipsoid of a coherent spin state have been derived for a fixed Cartesian coordinate system. Now, express the uncertainty ellipsoid in a local Cartesian basis anchored to spherical coordinates by $\hat{\mathbf{e}}'_x = \hat{\mathbf{e}}_r$, $\hat{\mathbf{e}}'_y = \hat{\mathbf{e}}_\theta$, and $\hat{\mathbf{e}}'_z = \hat{\mathbf{e}}_\phi$. Why is the radial projection onto the surface of the

[9] Note that, In order to simulate a series of Bloch oscillations, we must change the basis by hand after each Bragg reflection.

[10] An interesting question is, whether the Dicke picture can be extended to CARL (see Sec. 42.3.5).

generalized Bloch sphere invariant upon rotation? Interprete the projection of the uncertainty ellipsoid onto the radial axis and its dependency on rotation.

Solution: *According to Exc. 25.3.4.8 the commutation rules for an angular momentum satisfying* $[\hat{S}_x, \hat{S}_y] = \imath\hat{S}_z$ *is xxx. If now the system is in an eigenstate of* $\hat{S}_z$*, xxx. That is, the uncertainty relation describes a 2D disk tangential to the surface of the Bloch sphere, very similar to the situation in a 2D phase space, e.g. of a 1D harmonic oscillator.*

41.2 Super- and subradiance in open systems

The abstract spin formalism developed in the last sections revealed propagators allowing us to rotate and squeeze coherent spin states, but it did not tell us how to implement them physically. For this, we need to solve equations of motion derived from Hamiltonians realizable in the laboratory. In the following sections, we will set up the fundamental equations of motion (master or Heisenberg-Liouville) for open systems of N atoms subject to spontaneous emission collectively interacting with a single light mode subject to cavity decay and pumped by an external source.

We will discuss constants of motion of the Dicke and of the Tavis-Cummings model and phase transitions to superradiant states in the mean-field and in the Holstein-Primakoff approximation. Finally, we will present recent experimental realizations of Dicke phase transitions, namely superradiant self-ordering and superradiant lasing.

41.2.1 Models for open systems and phase transitions

We have already seen, that the spin quantum number S is preserved under the effect of the Dicke Hamiltonian (41.6). The spherical harmonics $|S, M\rangle$ are orthonormal and the spin operators $\hat{S}_\pm$ and $\hat{S}_{x,y,z}$ or their combinations do not allow for transitions between states with different S,

$$[\hat{H}, \hat{\mathbf{S}}^2] = 0 \quad \text{with} \quad \hat{\mathbf{S}}^2 = \tfrac{1}{2}(\hat{S}_+\hat{S}_- + \hat{S}_-\hat{S}_+) + \hat{S}_z^2 \tag{41.73}$$
$$\text{but} \quad [\hat{H}, \hat{S}_z] = \imath(\mathfrak{Im}\ \Omega\ \hat{S}_x - \mathfrak{Re}\ \Omega\ \hat{S}_y) \neq 0\ .$$

Hence, under the effect of the Dicke Hamiltonian an initial state $|N, S, M\rangle$ can only change its magnetic quantum number $|N, S, M\rangle \longrightarrow |N, S, M'\rangle$, and the manifolds with a given S form closed sub-spaces (see Exc. 41.2.4.1). In other words, once we start in a superradiant state $|N, S, M\rangle = |N, \frac{N}{2}, +\frac{N}{2}\rangle$, spin conservation excludes subradiant states, which allowed us to restrict to the superradiant Dicke subspace. Transitions between Dicke subspaces are only possible via physical processes that act on individual atoms, e.g. decay or phase fluctuation processes, as we will see later [498, 1429].

41.2.1.1 The generalized open Dicke model

In the presence of spontaneous decay or dephasing, superradiant spin conservation is no longer guaranteed. Let us have a look at the master equation for a set of N atoms

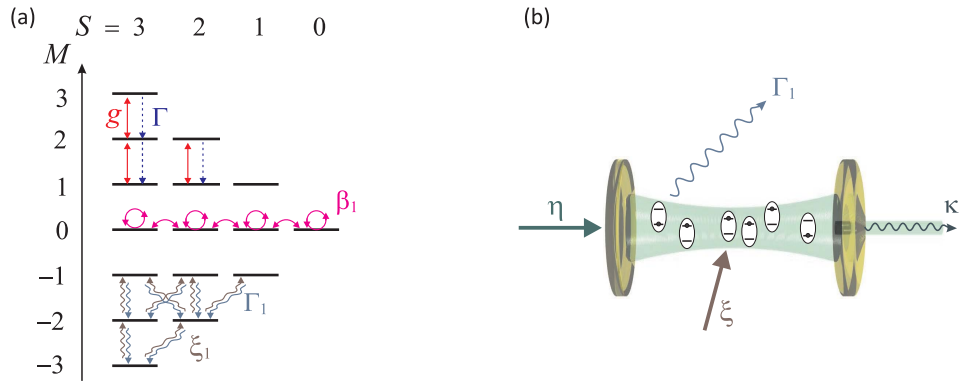

Figure 41.10: (a) Illustration of the Dicke states for $N = 6$. Hamiltonian interactions are in depicted in red. Superradiant decay occurs through a cascade from state $M = S$ to state $M = -S$. Spontaneous emission and phase noise leads to transitions along the blue arrows. The lowest states in each S subspace are dark and can only decay through a (subradiant) dark states cascade. (b) Scheme of the Dicke model.

coupled with the strength g to the mode of a cavity and additionally pumped by a classical laser field η [137, 723] (see (36.48)). After transformation into the rotating frame we have,

$$\boxed{\begin{aligned}
&\dot{\hat{\rho}} = \imath[\hat{\rho}, \hat{H}_{gD}] + \textstyle\sum_\gamma \mathcal{L}_{\gamma,\hat{L}}\hat{\rho} \qquad \text{or} \qquad \dot{\hat{A}} = -\imath[\hat{A}, \hat{H}_{gD}] + \textstyle\sum_\gamma \mathcal{L}^\dagger_{\gamma,\hat{L}}\hat{A} \\
&\hat{H}_{gD} = -\Delta_c \hat{a}^\dagger\hat{a} - \Delta_a \hat{S}_z + g(\hat{a}\hat{S}_+ + \hat{S}_-\hat{a}^\dagger) + g'(\hat{a}\hat{S}_- + \hat{S}_+\hat{a}^\dagger) - \imath\eta(\hat{a} - \hat{a}^\dagger) \\
&\text{and} \quad \mathcal{L}_{\gamma,\hat{L}}\hat{\rho} \equiv \gamma(2\hat{L}\hat{\rho}\hat{L}^\dagger - \hat{L}^\dagger\hat{L}\hat{\rho} - \hat{\rho}\hat{L}^\dagger\hat{L}) \\
&\text{and} \quad \mathcal{L}^\dagger_{\gamma,\hat{L}}\hat{A} \equiv \gamma(2\hat{L}^\dagger\hat{A}\hat{L} - \hat{L}^\dagger\hat{L}\hat{A} - \hat{A}\hat{L}^\dagger\hat{L})
\end{aligned}} \,. \tag{41.74}$$

The different coupling strengths g and g' allow us to isolate the counter-rotating terms, in order to discuss their relevance. The usual *open Dicke model* is obtained from the generalized Dicke Hamiltonian $\hat{H}_{gD}$ by setting $g' \equiv g$, while the rotating wave approximation is done by setting $g' \equiv 0$. The rates γ describe possible decay processes to which the degrees of freedom $\hat{L}$ are subject. The most relevant decay processes are listed in the following table:

decay rate γ	dissipative operator $\hat{L}$	physical process
κ	$\hat{a}$	cavity decay
ϕ	$\hat{a}^\dagger\hat{a}$	cavity phase jitter
$\gamma = \Gamma/2$	$\hat{S}_- = \sum_j \hat{s}_j^-$	collective (superradiant) atomic decay
$\gamma_1 = \Gamma_1/2$	$\hat{s}_j^-$	(transverse) single-atom decay
ξ_1	$\hat{s}_j^+$	single-atom optical pumping
β_1	$\hat{s}_j^z$	single-atom dephasing

$\Gamma = 2\gamma$ is the collective longitudinal atomic decay, κ and ϕ describe collective decay respectively collective phase noise of the cavity, while $\Gamma_1 = 2\gamma_1$, ξ_1, and β_1 stand for spontaneous emission, optical pumping via higher-lying levels, and phase fluctuation of individual atoms. The latter decay processes are described by sums of Lindbladians over all atoms. In Exc. 41.2.4.2 we derive the Heisenberg equations for the relevant degrees of freedom,

$$\begin{aligned}
\dot{\hat{a}} &= (\imath\Delta_c - \kappa - \phi)\hat{a} - \imath(g\hat{S}_- + g'\hat{S}_+) + \eta \\
\dot{\hat{S}}_- &= (\imath\Delta_a - \gamma_1 - \xi_1 - \beta_1 + \Gamma\hat{S}_z)\hat{S}_- + 2\imath\hat{S}_z(g\hat{a} + g'\hat{a}^\dagger) \\
\dot{\hat{S}}_z &= -\imath\hat{S}_+(g\hat{a} + g'\hat{a}^\dagger) + \imath(g\hat{a}^\dagger + g'\hat{a})\hat{S}_- - \Gamma\hat{S}_+\hat{S}_- - N(\gamma_1 - \xi_1)\mathbb{I} - 2(\gamma_1 + \xi_1)\hat{S}_z \\
\dot{\hat{s}}_j^- &= (\imath\Delta_a - \gamma_1 - \xi_1 - \beta_1)\hat{s}_j^- + 2\imath(g\hat{a} + g'\hat{a}^\dagger)\hat{s}_j^z \\
\dot{\hat{s}}_j^z &= -\imath(g\hat{a} + g'\hat{a}^\dagger)\hat{s}_j^+ + \imath(g\hat{a}^\dagger + g'\hat{a})\hat{s}_j^- - \gamma_1(\mathbb{I} - 2\hat{s}_j^z) + \xi_1(\mathbb{I} + 2\hat{s}_j^z) \ .
\end{aligned} \tag{41.75}$$

In Exc. 41.2.4.3 we verify that these equations of motion do not change the spin $\hat{\mathbf{S}}$. Neglecting all dissipation processes but Γ, the Eqs. (41.75) can be rewritten in terms of observables as,

$$\dot{\hat{\mathbf{S}}} = \begin{pmatrix} (g+g')(\hat{a}+\hat{a}^\dagger) \\ \imath(g-g')(\hat{a}-\hat{a}^\dagger) \\ -\Delta_a \end{pmatrix} \times \hat{\mathbf{S}} + \tfrac{\Gamma}{2} \begin{pmatrix} -\hat{S}_x + \{\hat{S}_x, \hat{S}_z\} \\ -\hat{S}_y + \{\hat{S}_y, \hat{S}_z\} \\ -2\hat{S}_z - 2\hat{S}_x^2 - 2\hat{S}_y^2 \end{pmatrix} \ . \tag{41.76}$$

Only the terms $\mathcal{L}_{\gamma_1}$, $\mathcal{L}_{\xi_1}$, and $\mathcal{L}_{\beta_1}$ can change $\hat{\mathbf{S}}^2$. The $\hat{\mathbf{S}}^2$ and $\hat{S}_z$ eigenvalues determine the coupling strength of the many-atom (Dicke) state to the cavity mode and the coherent, external drive. This coupling determines the rate of cavity photon generation as well as the pumping strength. The magnitude of the coupling strength distinguishes between superradiance and subradiance. For superradiant states the coupling strength scales superlinear in N, while for subradiant states the scaling is sublinear in N, and some subradiant states are dark. Dark means that the collective coupling to the cavity and the coherent, external drive of these states vanishes, meaning these states cannot decay via collective interactions e.g. by creating a cavity photon. However these states still decay into other states via the decay and dephasing processes $\mathcal{L}_{\gamma_1}$ and $\mathcal{L}_{\beta_1}$ acting individually on the emitters, see Fig. 41.10. Hence, spontaneous decay is an individualization process [498]. Generally, the spin preserving contributions in the master equation (41.78) generate quantum correlations leading to collective behavior (both super- and subradiance are collective effects) and the non-preserving terms destroy correlations leading to individualization (all properties scale exactly linear in N). However only the spin non-preserving contributions introduce coupling between superradiant and subradiant states, thus in order to prepare subradiant states an interplay of collectivity and individualization is necessary. Based on these considerations, we may distinguish between collective versus individual behavior and superradiant versus subradiant behavior. The latter are special cases of collective behavior. This twofold distinction seems crucial when investigating super- and subradiance in the presence of dephasing and individual decay. In Exc. 41.2.4.4 we study superradiant decay.

41.2.1.2 Symmetries of the Dicke and the Tavis-Cummings model

The total number of excitations,

$$\hat{N}_{ex} \equiv \hat{a}^\dagger \hat{a} + \hat{S}_z \tag{41.77}$$

is a constant of motion only for the Tavis-Cummings Hamiltonian, i.e. the Dicke Hamiltonian with RWA, $g' = 0$, and in the absence of pumping, $\eta = 0$,

$$[\hat{H}_{gD}, \hat{N}_{ex}] = \eta(\hat{a} - \hat{a}^\dagger) + 2g'(\hat{S}_- \hat{a} - \hat{S}_+ \hat{a}^\dagger) \ . \tag{41.78}$$

That is, the Dicke Hamiltonian preserves the excitation number, except for the counter-rotating terms, which can only change the excitation number by ± 2.

The Dicke model without RWA, $g' = g$, has one global symmetry [11],

$$\mathcal{P} : (\hat{a}, \hat{\sigma}^\pm) \to (-\hat{a}, -\hat{\sigma}^\pm) \ . \tag{41.79}$$

Because $\mathcal{P}$ squares to unity, it has two eigenvalues, 1 and -1. This symmetry is associated with a conserved quantity: the parity of the total number of excitations, $\mathcal{P} = (-1)^{N_{ex}}$. This parity conservation is a consequence of the preserved excitation number. A state of the Dicke model is said to be normal when this symmetry is preserved, and superradiant when this symmetry is spontaneously broken.

41.2.2 Superradiant Dicke phase transition

The interesting feature of the set of equations (41.75) is, that the degrees of freedom are macroscopically populated, yet, they follow the rules of quantum mechanics. For instance, we may expect them to behave as order parameters for macroscopic phase transitions. We will study one such example in the following.

41.2.2.1 Equilibrium Dicke phase transition

The Dicke model predicts a phase transition to a superradiant state, when the coupling strength g exceeds a certain critical value. To see this we simplify the Hamiltonian (41.6) by the mean-field approximation,

$$\omega_c \hat{a}^\dagger \hat{a} = \omega_c \alpha^2 \ , \tag{41.80}$$

where the field amplitude α is a real number, and calculate the free energy as a function of α,

$$\begin{aligned} F(\alpha) \equiv -\tfrac{1}{\beta} \ln Z(\alpha) \qquad \text{with} \qquad & Z(\alpha) = \mathrm{Tr}\ e^{-\beta \hat{H}} \\ \text{and} \qquad & \hat{H} = \omega_c \alpha^2 + \sum\nolimits_j \hat{h}_j \\ \text{and} \qquad & \hat{h}_j = \omega_a \hat{s}_j^z + 4g\alpha \hat{s}_j^x \ . \end{aligned} \tag{41.81}$$

[11] For a Dicke picture of CARL see Exc. 42.5.7.1.

$Z(\alpha)$ is the partition function, $\hat{h}_j$ the single-atom Hamiltonian, and $\beta \equiv 1/k_B T$. Carried out in Exc. 41.2.4.5, the calculation results in,

$$F(\alpha) = \omega_c \alpha^2 - \tfrac{N}{\beta} \ln(2 \cosh \beta E) \tag{41.82}$$

$$\text{where} \qquad \pm E \equiv \langle \hat{h}_j \rangle = \pm \sqrt{\left(\tfrac{\omega_a}{2}\right)^2 + (g\alpha)^2}$$

are the single-atom energy eigenvalues. The minimum of the free energy as a function of the field amplitude, $F'(\alpha) = 0$, yields a critical coupling strength g_c,

$$g_c \sqrt{N} = \tfrac{1}{2} \sqrt{\omega_c \omega_a \coth \tfrac{\beta \omega_a}{2}} \ , \tag{41.83}$$

Below g_c the free energy minimizes for $\alpha = 0$, and beyond g_c it minimizes for $\alpha > 0$, as seen in Fig. 41.11.

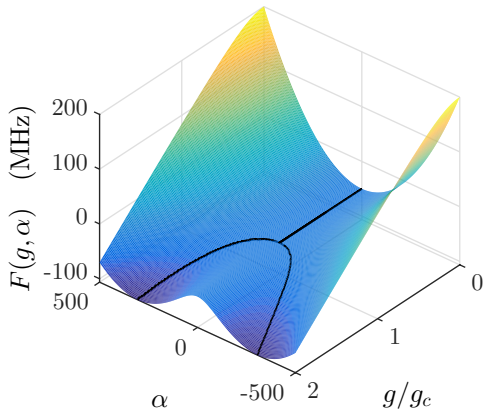

Figure 41.11: (code) Free energy as a function of coupling strength and photon number. Beyond the critical coupling strength g_c the minimum of the free energy splits opening the way for two possible equilibrium states of the mean-field phase.

Note that the critical coupling smoothly evolves down to zero temperature ($\beta \to 0$), where one obtains $g_c = \sqrt{\omega_c \omega_a / 2N}$ [12].

41.2.3 Beyond mean-field

We already applied the mean-field approximation in the derivation of the semiclassical Dicke Hamiltonian (41.9) and the Dicke phase transition (41.80). Some effects, however, are intrinsically to the existence of interatomic correlations, as for example, superradiant lasing [13]

[12] Note, that in the thermodynamic limit, $N \to \infty$, the operators can be replaced by [723]:

$$\hat{S}_x \overset{N\to\infty}{\longrightarrow} \tfrac{1}{2} \hat{N} \cos\hat{\varphi} \qquad \text{and} \qquad \hat{S}_y \overset{N\to\infty}{\longrightarrow} \tfrac{1}{2} \hat{N} \sin\hat{\varphi} \ .$$

In this case, the operators commute $[\hat{S}_x, \hat{S}_y] \to 0$.

[13] Interestingly, spin-squeezing, which is also based on interatomic correlations, can be described within the mean-field approximation.

41.2.3.1 Cumulant expansion

Often we are interested in quantum correlations rather than in the mean-field behavior of an operator. The *cumulant expansion* allows to study higher-order correlations by gradually removing lower-order ones. We introduce the correlation or cumulant expectation value between operators $\hat{A}$ and $\hat{B}$ [756, 1140],

$$\begin{aligned} \langle \hat{A} \rangle &\equiv \langle \hat{A} \rangle_c \\ \langle \hat{A}\hat{B} \rangle &\equiv \langle \hat{A} \rangle \langle \hat{B} \rangle + \langle \hat{A}\hat{B} \rangle_c \\ \langle \hat{A}\hat{B}\hat{C} \rangle &\equiv \langle \hat{A} \rangle \langle \hat{B} \rangle \langle \hat{C} \rangle + \langle \hat{A} \rangle \langle \hat{B}\hat{C} \rangle_c + \langle \hat{B} \rangle \langle \hat{A}\hat{C} \rangle_c + \langle \hat{C} \rangle \langle \hat{A}\hat{B} \rangle_c + \langle \hat{A}\hat{B}\hat{C} \rangle_c \ . \end{aligned} \tag{41.84}$$

The lowest order mean-field approximation consists in neglecting $\langle \hat{A}\hat{B} \rangle_c \simeq 0$.

Example 253 (*Superradiant lasing*): In a conventional laser amplification and optical phase coherence are established by stimulated photon emission from a population-inverted medium. This results in the Schawlow-Townes spectral linewidth, proportional to the square of the cavity decay width and inversely proportional to the photon number in the cavity. As Dicke showed, the coherence can also be stored in the emitters that constitute the gain medium provided they interact collectively with common radiation field modes [341]. If the spontaneous decay rate is much smaller than the cavity decay rate very narrow emission bandwidths far below the cavity decay width can be achieved. In Exc. 41.2.4.6 we study *superradiant lasing* in the Dicke model [868]. Cavity-mediated superradiance can also be described within the *Tavis-Cummings model* [226]. It represents an extension of the Jaynes-Cummings model for several atoms. We discussed such systems in Sec. 41.5.

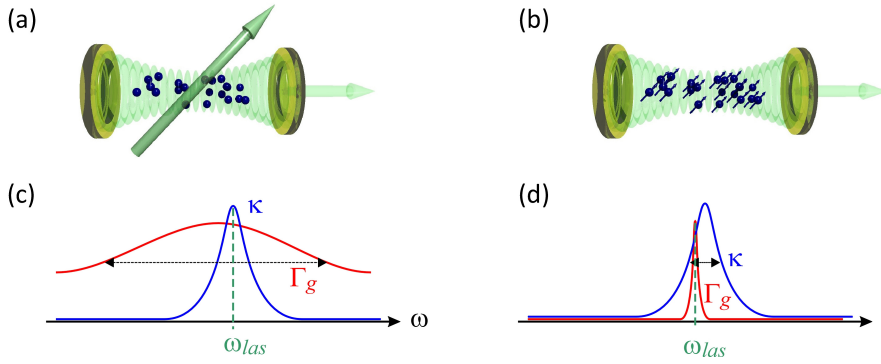

Figure 41.12: (a) Principle scheme of standard lasing. Here, the coherence is stored in the cavity field. The gain profile is much larger than the cavity width (good-cavity limit, $\kappa \ll \frac{1}{2}\Gamma_g$), as shown in (c). The laser frequency follows any (technical) cavity fluctuation: $\omega_{las} = \omega_{cav} + \omega_g \frac{2\kappa}{\Gamma_g}$. (b) *Superradiant lasing*. Here, the coherence is stored in the gain. We are in the bad-cavity limit, $\kappa \gg \Gamma_g$, as shown in (d). The laser frequency is robust to cavity fluctuations: $\omega_{las} = \omega_g + \omega_{cav} \frac{\Gamma_g}{2\kappa}$.

41.2.3.2 Superradiant lasing in the Holstein-Primakoff approximation

The superradiant phase transition was originally predicted by the Dicke model [366, 610]. It occurs when the strength of the interaction between the atoms and the field is greater than the energy of the non-interacting part of the system [14]. The collective Lamb shift, relating to the system of atoms interacting with the vacuum fluctuations, becomes comparable to the energies of atoms alone, and the vacuum fluctuations cause the spontaneous self-excitation of matter.

The transition can be readily understood by the use of the Holstein-Primakoff transformation applied to an ensemble of two-level atoms, as shown in Sec. ??, as a result of which the atoms become harmonic oscillators with frequencies equal to the difference between the energy levels. If the interaction between the atomic and the field oscillator is so strong that the system collapses in a ferroelectric-like phase transition. In Exc. 41.2.4.8 we will derive the Heisenberg equations for the open Dicke model in the Holstein-Primakoff approximation.

Example 254 (*Finding instabilities via retarded Green's functions*): Let us consider a set of linear Heisenberg equations,

$$\dot{v}_i(t) = M_{ij} v_j(t) \qquad \text{and} \qquad \dot{v}_i^\dagger(t) = M_{ij}^\dagger v_j^\dagger(t) \ .$$

The retarded *Green's function* is defined by,

$$G_{ij}(t) \equiv -\imath \langle [v_i(t), v_j^\dagger(0)] \rangle \theta(t) \ .$$

Its time derivative is,

$$\dot{G}_{ij}(t) \equiv -\imath \langle [v_i(t), v_j^\dagger(0)] \rangle \delta(t) - \imath \langle \dot{v}_i(t) v_j^\dagger(t) \rangle \theta(t) + \imath \langle v_j^\dagger(t) \dot{v}_i(t) \rangle \theta(t) \ .$$

Defining the equal-time correlation function by,

$$S_{ij} \equiv \langle [v_i(0), v_j^\dagger(0)] \rangle \ ,$$

we get,

$$\begin{aligned} \dot{G}_{ij}(t) &= -\imath S_{ij} \delta(t) - \imath M_{ik} \langle v_k(t) v_j^\dagger(t) \rangle \theta(t) + \imath M_{ik} \langle v_j^\dagger(t) v_k(t) \rangle \theta(t) \\ &= -\imath S_{ij} \delta(t) - \imath M_{ik} \langle [v_k(t), v_j^\dagger(t)] \rangle \theta(t) = -\imath S_{ij} \delta(t) + M_{ik} G_{kj}(t) \ . \end{aligned}$$

With the Fourier transform $f(\omega) = \int_{-\infty}^{\infty} dt e^{\imath \omega t} f(t)$ we finally get,

$$G(\omega) = (M + \imath \omega \mathbb{I})^{-1} \imath S \ .$$

For example, we may consider the system of two coupled oscillators studied in Sec. 35.8.8. In this case,

$$\mathbf{v} \equiv \begin{pmatrix} \hat{a} \\ \hat{a}^\dagger \\ \hat{b} \\ \hat{b}^\dagger \end{pmatrix} \qquad \text{such that} \qquad S = \text{diag}\ (1, -1, 1, -1) \ .$$

[14] This is similar to the case of superconductivity in ferromagnetism, which leads to the dynamic interaction between ferromagnetic atoms and the spontaneous ordering of excitations below the critical temperature.

In Exc. ?? we have shown that (setting $\Omega' \equiv \Omega$),

$$M = \begin{pmatrix} -\imath\omega - \kappa_a & 0 & -\frac{\imath\Omega}{2} & -\frac{\imath\Omega}{2} \\ 0 & \imath\omega - \kappa_a & \frac{\imath\Omega}{2} & \frac{\imath\Omega}{2} \\ -\frac{\imath\Omega}{2} & -\frac{\imath\Omega}{2} & -\imath\omega - \kappa_b & 0 \\ \frac{\imath\Omega}{2} & \frac{\imath\Omega}{2} & 0 & \imath\omega - \kappa_b \end{pmatrix} .$$

Thus,

$$G^R(\omega)^{-1} = S^{-1}(\omega\mathbb{I} - \imath M) = \begin{pmatrix} \omega - \omega_a + \imath\kappa_a & 0 & -\frac{\Omega}{2} & -\frac{\Omega}{2} \\ 0 & -\omega - \omega_a - \imath\kappa_a & -\frac{\Omega}{2} & -\frac{\Omega}{2} \\ -\frac{\Omega}{2} & -\frac{\Omega}{2} & \omega - \omega_b + \imath\kappa_b & 0 \\ -\frac{\Omega}{2} & -\frac{\Omega}{2} & 0 & -\omega - \omega_b - \imath\kappa_b \end{pmatrix} .$$

The superradiant transition corresponds to the requirement that one of the eigenvalues of M goes to zero [341, 723], or equivalently,

$$0 = \det G^R(\omega)^{-1} = \omega_a^2\omega_b^2 + \omega_a^2\kappa_b^2 - \omega_a\Omega^2\omega_b + \kappa_a^2\omega_b^2 + \kappa_a^2\kappa_b^2 ,$$

yielding,

$$\Omega = \sqrt{\frac{(\omega_a^2 + \kappa_a^2)(\omega_b^2 + \kappa_b^2)}{\omega_a\omega_b}} .$$

Example 255 (*Dicke phase transition with a superfluid gas in an optical cavity*): [105]

41.2.4 Exercises

41.2.4.1 Ex: Relationship between super- and subradiance and cooperativity

a. Discuss whether super- and subradiant states can be transformed into each other via unitary transformations.
b. Seek an interpretation of super- and subradiance as a modification of the structure factor by cooperativity.

Solution:

41.2.4.2 Ex: Heisenberg equation for the open Dicke model

Derive the Heisenberg equation for the open Dicke model.

Solution: *We start from the generalized Dicke Hamiltonian and the general form of the Lindbladian (41.74) to derive the Heisenberg equation,*

$$\frac{d}{dt}\hat{A} = -\imath[\hat{A}, \hat{H}_{gH}] + \mathcal{L}^\dagger_{\kappa,\hat{a}}\hat{A} + \mathcal{L}^\dagger_{\Gamma,\hat{S}_-}\hat{A} + \mathcal{L}^\dagger_{\gamma_1,\hat{s}^-}\hat{A} + \mathcal{L}^\dagger_{\xi_1,\hat{s}^+}\hat{A} + \mathcal{L}^\dagger_{\beta_1,\hat{s}^z}\hat{A} ,$$

considering the dissipation processes,

$$\begin{aligned}
\mathcal{L}^\dagger_{\kappa,\hat{a}}\hat{A} &= \kappa(\hat{a}^\dagger[\hat{A},\hat{a}] + [\hat{a}^\dagger,\hat{A}]\hat{a}) \\
\mathcal{L}^\dagger_{\phi,\hat{a}^\dagger\hat{a}}\hat{A} &= \phi(\hat{a}^\dagger\hat{a}[\hat{A},\hat{a}^\dagger\hat{a}] + [\hat{a}^\dagger\hat{a},\hat{A}]\hat{a}^\dagger\hat{a}) \\
\mathcal{L}^\dagger_{\Gamma,\hat{S}_-}\hat{A} &= \Gamma(\hat{S}_+[\hat{A},\hat{S}_-] + [\hat{S}_+,\hat{A}]\hat{S}_-) \\
\mathcal{L}^\dagger_{\gamma_1,\hat{s}^-}\hat{A} &= \gamma_1 \sum\nolimits_j (\hat{s}_i^+[\hat{A},\hat{s}_i^-] + [\hat{s}_i^+,\hat{A}]\hat{s}_i^-) \\
\mathcal{L}^\dagger_{\xi_1,\hat{s}^+}\hat{A} &= \xi_1 \sum\nolimits_j (\hat{s}_i^-[\hat{A},\hat{s}_i^+] + [\hat{s}_i^-,\hat{A}]\hat{s}_i^+) \\
\mathcal{L}^\dagger_{\beta_1,\hat{s}^z}\hat{A} &= \beta_1 \sum\nolimits_j (\hat{s}_i^z[\hat{A},\hat{s}_i^z] + [\hat{s}_i^z,\hat{A}]\hat{s}_i^z) \ ,
\end{aligned}$$

describing respectively the decay and phase jitter of the cavity field and superradiant decay, which are collective processes, and the single atom processes spontaneous decay, optical pumping, and phase noise. Using the commutation rules,

$$[\hat{s}_i^z,\hat{s}_j^\pm] = \pm\hat{s}_j^\pm\delta_{ij} \qquad \textit{and} \qquad [\hat{s}_i^+,\hat{s}_j^-] = 2\hat{s}_j^z\delta_{ij} \ ,$$

and the relationships $\hat{s}^{x,y,z} = \frac{1}{2}\hat{\sigma}^{x,y,z}$ *and* $\hat{s}^\pm = \hat{\sigma}^\pm$*, yielding,*

$$\hat{s}_j^z\hat{s}_j^\pm = \tfrac{1}{2}[\hat{s}_j^+,\hat{s}_j^-]\hat{s}_j^+ = \pm\tfrac{1}{2}\hat{s}_j^\pm = -\hat{s}_j^\pm\hat{s}_j^z \qquad \textit{and} \qquad \hat{s}_j^\pm\hat{s}_j^\mp = \tfrac{1}{2}(\mathbb{I} \mp 2\hat{s}_j^z) \ ,$$

we find,

$$\begin{aligned}
\dot{\hat{a}} &= -\imath[\hat{a},\hat{H}_{gH}] + \mathcal{L}^\dagger_{\kappa,\hat{a}}\hat{a} + \mathcal{L}^\dagger_{\phi,\hat{a}^\dagger\hat{a}}\hat{a} \\
&= \imath\Delta_c[\hat{a},\hat{a}^\dagger]\hat{a} - 2\imath g[\hat{a},\hat{a}^\dagger]\hat{S}_- - 2\imath g'\hat{S}_+[\hat{a},\hat{a}^\dagger] \\
&\qquad + \eta[\hat{a},\hat{a}^\dagger] + \kappa(\hat{a}^\dagger[\hat{a},\hat{a}] + [\hat{a}^\dagger,\hat{a}]\hat{a}) + \phi(\hat{a}^\dagger\hat{a}[\hat{a},\hat{a}^\dagger]\hat{a} + [\hat{a}^\dagger,\hat{a}]\hat{a}\hat{a}^\dagger\hat{a}) \\
&= (\imath\Delta_c - \kappa - \phi)\hat{a} - 2\imath(g\hat{S}_- + g'\hat{S}_+) + \eta \ ,
\end{aligned}$$

and,

$$\begin{aligned}
\dot{\hat{S}}_- &= -\imath[\hat{S}_-,\hat{H}_{gH}] + \mathcal{L}^\dagger_{\Gamma,\hat{S}_-}\hat{S}_- + \mathcal{L}^\dagger_{\gamma_1,\hat{s}^-}\hat{S}_- + \mathcal{L}^\dagger_{\xi_1,\hat{s}^+}\hat{S}_- + \mathcal{L}^\dagger_{\beta_1,\hat{s}^z}\hat{S}_- \\
&= \imath\Delta_a[\hat{S}_-,\hat{S}_z] - 2\imath g[\hat{S}_-,\hat{S}_+]\hat{a} - 2\imath g'[\hat{S}_-,\hat{S}_+]\hat{a}^\dagger + \Gamma[\hat{S}_+,\hat{S}_-]\hat{S}_- \\
&\qquad + \gamma_1\sum\nolimits_j[\hat{s}_j^+,\hat{s}_j^-]\hat{s}_j^- + \xi_1\sum\nolimits_j \hat{s}_j^-[\hat{s}_j^-,\hat{s}_j^+] + \beta_1\sum\nolimits_j(\hat{s}_i^z[\hat{s}_j^-,\hat{s}_i^z] + [\hat{s}_i^z,\hat{s}_j^-]\hat{s}_i^z) \\
&= (\imath\Delta_a - \gamma_1 - \xi_1 - \beta_1 + 2\Gamma\hat{S}_z)\hat{S}_- + 4\imath\hat{S}_z(g\hat{a} + g'\hat{a}^\dagger) \ .
\end{aligned}$$

and,

$$\begin{aligned}
\dot{\hat{S}}_z &= -\imath[\hat{S}_z,\hat{H}_{gH}] + \mathcal{L}^\dagger_{\Gamma,\hat{S}_-}\hat{S}_z + \mathcal{L}^\dagger_{\gamma_1,\hat{s}^-}\hat{S}_z + \mathcal{L}^\dagger_{\xi_1,\hat{s}^+}\hat{S}_z + \mathcal{L}^\dagger_{\beta_1,\hat{s}^z}\hat{S}_z \\
&= -2\imath g[\hat{S}_z,\hat{S}_+]\hat{a} - 2\imath g\hat{a}^\dagger[\hat{S}_z,\hat{S}_-] - 2\imath g'\hat{a}[\hat{S}_z,\hat{S}_-] - 2\imath g'[\hat{S}_z,\hat{S}_+]\hat{a}^\dagger + \Gamma(\hat{S}_+[\hat{S}_z,\hat{S}_-] + [\hat{S}_+,\hat{S}_z]\hat{S}_-) \\
&\qquad + \gamma_1\sum\nolimits_j(\hat{s}_j^+[\hat{s}_j^z,\hat{s}_j^-] + [\hat{s}_j^+,\hat{s}_j^z]\hat{s}_j^-) + \xi_1\sum\nolimits_j(\hat{s}_j^-[\hat{s}_j^z,\hat{s}_j^+] + [\hat{s}_j^-,\hat{s}_j^z]\hat{s}_j^+) \\
&\qquad + \beta_1\sum\nolimits_j(\hat{s}_j^z[\hat{s}_j^z,\hat{s}_j^z] + [\hat{s}_j^z,\hat{s}_j^z]\hat{s}_j^z) \\
&= -2\imath\hat{S}_+(g\hat{a} + g'\hat{a}^\dagger) + 2\imath(g\hat{a}^\dagger + g'\hat{a})\hat{S}_- - 2\Gamma\hat{S}_+\hat{S}_- - 2\sum\nolimits_j(\gamma_1\hat{s}_j^+\hat{s}_j^- - \xi_1\hat{s}_j^-\hat{s}_j^+) \\
&= -2\imath\hat{S}_+(g\hat{a} + g'\hat{a}^\dagger) + 2\imath(g\hat{a}^\dagger + g'\hat{a})\hat{S}_- - 2\Gamma(\hat{S}_+^2 - \hat{S}_z^2 + \hat{S}_z) - N(\gamma_1 - \xi_1)\mathbb{I} - 2(\gamma_1 + \xi_1)\hat{S}_z \ .
\end{aligned}$$

and,

$$\begin{aligned}\dot{\hat{s}}_j^- &= -\imath[\hat{s}_j^-, \hat{H}_{gH}] + \mathcal{L}^\dagger_{\Gamma,\hat{S}_-}\hat{s}_j^- + \mathcal{L}^\dagger_{\gamma_1,\hat{s}^-}\hat{s}_j^- + \mathcal{L}^\dagger_{\xi_1,\hat{s}^+}\hat{s}_j^- + \mathcal{L}^\dagger_{\beta_1,\hat{s}^z}\hat{s}_j^- \\ &= \Delta_a\imath[\hat{s}_j^-, \hat{s}_j^z] - 2\imath g\hat{a}[\hat{s}_j^-, \hat{s}_j^+] - 2g'\imath[\hat{s}_j^-, \hat{s}_j^+]\hat{a}^\dagger - \gamma_1[\hat{s}_j^+, \hat{s}_j^-]\hat{s}_j^- + \xi_1\hat{s}_j^-[\hat{s}_j^-, \hat{s}_j^+] \\ &\quad + \beta_1(\hat{s}_j^z[\hat{s}_j^-, \hat{s}_j^z] + [\hat{s}_j^z, \hat{s}_j^-]\hat{s}_i^z) \\ &= (\imath\Delta_a - \gamma_1 - \xi_1 - \beta_1)\hat{s}_j^- + 4\imath(g\hat{a} + g'\hat{a}^\dagger)\hat{s}_j^z \ ,\end{aligned}$$

and,

$$\begin{aligned}\dot{\hat{s}}_j^z &= -\imath[\hat{s}_j^z, \hat{H}_{gH}] + \mathcal{L}^\dagger_{\Gamma,\hat{S}_-}\hat{s}_j^z + \mathcal{L}^\dagger_{\gamma_1,\hat{s}^-}\hat{s}_j^z + \mathcal{L}^\dagger_{\xi_1,\hat{s}^+}\hat{s}_j^z + \mathcal{L}^\dagger_{\beta_1,\hat{s}^z}\hat{s}_j^z \\ &= -2\imath g(\hat{a}[\hat{s}_j^z, \hat{s}_j^+] + [\hat{s}_j^z, \hat{s}_j^-]\hat{a}^\dagger) - 2\imath g'(\hat{a}[\hat{s}_j^z, \hat{s}_j^-] + [\hat{s}_j^z, \hat{s}_j^+]\hat{a}^\dagger) + \gamma_1(\hat{s}_j^+[\hat{s}_j^z, \hat{s}_j^-] - [\hat{s}_j^+, \hat{s}_j^z]\hat{s}_j^-) \\ &\quad + \xi_1(\hat{s}_j^-[\hat{s}_j^z, \hat{s}_j^+] - [\hat{s}_j^-, \hat{s}_j^z]\hat{s}_j^+) + \beta_1(\hat{s}_j^z[\hat{s}_j^z, \hat{s}_j^z] + [\hat{s}_j^z, \hat{s}_j^z]\hat{s}_i^z) \\ &= -2\imath(g\hat{a} + g'\hat{a}^\dagger)\hat{s}_j^+ + 2\imath(g\hat{a}^\dagger + g'\hat{a})\hat{s}_j^- - 2\gamma_1\hat{s}_j^+\hat{s}_j^- + 2\xi_1\hat{s}_j^-\hat{s}_j^+ \\ &= -2\imath(g\hat{a} + g'\hat{a}^\dagger)\hat{s}_j^+ + 2\imath(g\hat{a}^\dagger + g'\hat{a})\hat{s}_j^- - \gamma_1(\mathbb{I} - 2\hat{s}_j^z) + \xi_1(\mathbb{I} + 2\hat{s}_j^z) \ .\end{aligned}$$

41.2.4.3 Ex: Spin conservation in the open Dicke model

a. Show that the Dicke Hamiltonian (41.74) with $g' = g$ preserves the spin $\hat{\mathbf{S}}^2$.
b. Show that the Dicke Hamiltonian (41.74) with $g' = 0$ preserves the spin $\hat{\mathbf{S}}^2$.
c. Verify whether the dissipative terms of the open Dicke model preserve the spin $\hat{\mathbf{S}}^2$.

Solution: *a. For the coherent part of the Dicke Hamiltonian with $g' = g$ it is easy to see,*

$$-\imath[\hat{\mathbf{S}}, \hat{H}] = -\imath[\hat{\mathbf{S}}, \omega_a\hat{S}_z + 4g(\hat{a} + \hat{a}^\dagger)\hat{S}_x] = \begin{pmatrix} -\omega_a\hat{S}_y \\ \omega_a\hat{S}_x - 4g(\hat{a} + \hat{a}^\dagger)\hat{S}_z \\ 4g(\hat{a} + \hat{a}^\dagger)\hat{S}_y \end{pmatrix} \ ,$$

so that $\frac{d}{dt}\hat{\mathbf{S}}^2 = \dot{\mathbf{S}}\cdot\hat{\mathbf{S}} + \hat{\mathbf{S}}\cdot\dot{\mathbf{S}} = 0$.
b. For the coherent part of the Dicke Hamiltonian with $g' = 0$ it is easy to see,

$$-\imath[\hat{\mathbf{S}}, \hat{H}] = -\imath[\hat{\mathbf{S}}, \omega_a\hat{S}_z + 2g(\hat{a}\hat{S}_+ + \hat{a}^\dagger S_-)] = \begin{pmatrix} -\omega_a\hat{S}_y + 2\imath g(\hat{a} - \hat{a}^\dagger)\hat{S}_z \\ \omega_a\hat{S}_x - 2g(\hat{a} + \hat{a}^\dagger)\hat{S}_z \\ 2g(\hat{a} + \hat{a}^\dagger)\hat{S}_y - 2\imath g(\hat{a} - \hat{a}^\dagger)\hat{S}_x \end{pmatrix} \ ,$$

so that $\frac{d}{dt}\hat{\mathbf{S}}^2 = \dot{\mathbf{S}}\cdot\hat{\mathbf{S}} + \hat{\mathbf{S}}\cdot\dot{\mathbf{S}} = 0$. The results are expected, since we know that $[\hat{\mathbf{S}}^2, \hat{H}] = 0$ for both Hamiltonians.
c. Using the results of Exc. 41.2.4.2,

$$\mathcal{L}\hat{\mathbf{S}} = \begin{pmatrix} \frac{1}{2}\mathcal{L}\hat{S}_+ + \frac{1}{2}\mathcal{L}\hat{S}_- \\ \frac{1}{2\imath}\mathcal{L}\hat{S}_+ - \frac{1}{2\imath}\mathcal{L}\hat{S}_- \\ \mathcal{L}\hat{S}_z \end{pmatrix} = \begin{pmatrix} \Gamma(\hat{S}_+\hat{S}_z + \hat{S}_z\hat{S}_-) \\ -\imath\Gamma(\hat{S}_+\hat{S}_z - \hat{S}_z\hat{S}_-) \\ -2\Gamma\hat{S}_+\hat{S}_- \end{pmatrix} \ ,$$

Finally, we find after elementary algebra,

$$\tfrac{d}{dt}\hat{\mathbf{S}}^2 = \mathcal{L}\hat{\mathbf{S}}\cdot\hat{\mathbf{S}} + \hat{\mathbf{S}}\cdot\mathcal{L}\hat{\mathbf{S}} = -2\Gamma(\hat{S}_+\hat{S}_- + 2\hat{S}_z^2) \neq 0 \ .$$

Note, that for a single atom, $\hat{S}_z = 1$, we get $\mathcal{L}\hat{\mathbf{S}}^2 = 0$.

41.2.4.4 Ex: Superradiant enhancement

For the open Dicke model consider the Heisenberg equations (41.75) without coherent mean-field, $\hat{a} = 0$, and disregarding single-atom decoherence, $\gamma_1 = \xi_1 = \beta_1 = 0$. Solve the equation of motion for the collective spin projection $\hat{S}_z$ for an arbitrary coherent spin state $|S, M\rangle$ and discuss the collective decay rate as a function of the collective inversion $\langle\hat{S}_z\rangle$.

Solution: *The equation of motion is,*

$$\dot{\hat{S}}_z = -2\Gamma\hat{S}_+\hat{S}_- \ .$$

Hence,

$$\begin{aligned}\langle\dot{S}_z\rangle &= -2\Gamma\langle S, M|\hat{S}_+\hat{S}_-|S, M\rangle \\ &= -2\Gamma\sqrt{(S-M+1)(S+M)}\sqrt{(S+M)(S-M+1)} \\ &= -2\Gamma(S+M)(S-M+1) \ .\end{aligned}$$

Hence, the decay rate depends on the instantaneous collective inversion $\langle\hat{S}_z\rangle = M$,

$$\begin{aligned}\langle S, S|\dot{S}_z|S, S\rangle &= -2N\Gamma \\ \langle S, 0|\dot{S}_z|S, 0\rangle &= -(\tfrac{N^2}{2} + N)\Gamma \\ \langle S, -S|\dot{S}_z|S, -S\rangle &= -2\Gamma(S-S)(S+S+1) = 0 \ .\end{aligned}$$

It is superradiantly enhanced when $M = 0$.

41.2.4.5 Ex: Equilibrium phase transition

a. Calculate the free energy of the Hamiltonian (41.6) in the mean-field approximation.
b. Minimize the free energy as a function of the field amplitude α for various coupling strengths g. **Help:** Expand the expression for $F'(\alpha)$ for small values of α. Derive the expression for the critical coupling strength.

Solution: *a. We perform the mean-field approximation via,*

$$\omega_c\hat{a}^\dagger\hat{a} = \omega_c\alpha^2 \ ,$$

where α is a real variational parameter. The Hamiltonian then reads,

$$\hat{H} = \omega_c\alpha^2 + \sum_j \hat{h}_j \qquad \textit{with} \qquad \hat{h}_j = \omega_a\hat{s}_j^z + 4g\alpha\hat{s}_j^x \ .$$

The matrix representation of the single-particle Hamiltonian is,

$$\langle s', m'|\hat{h}_j|s, m\rangle = \omega_a\langle\tfrac{1}{2}, m'|\hat{s}_j^z|\tfrac{1}{2}, m\rangle + 2g\alpha\langle\tfrac{1}{2}, m'|\hat{s}_j^+ + \hat{s}_j^-|\tfrac{1}{2}, m\rangle = \begin{pmatrix} \frac{1}{2}\omega_a & 2g\alpha \\ 2g\alpha & -\frac{1}{2}\omega_a \end{pmatrix} ,$$

with the eigenvalues,

$$E_\pm = \pm\sqrt{\tfrac{\omega_a^2}{4} + 4g^2\alpha^2} \equiv E ,$$

and the trace of the propagator,

$$Tr\; e^{-\beta\hat{h}_j} = \sum_{j=\pm}\langle j|e^{-\beta\hat{h}_j}|j\rangle = \langle +|e^{-\beta\hat{h}}|+\rangle + \langle -|e^{-\beta\hat{h}}|-\rangle = e^{-\beta E} + e^{\beta E} = 2\cosh\beta E .$$

The partition function is now,

$$Z(\alpha) = Tr\; e^{-\beta\hat{H}} = e^{-\beta\omega_c\alpha^2}\left(Tr\; e^{-\beta\hat{h}_j}\right)^N = e^{-\beta\omega_c\alpha^2}(2\cosh\beta E)^N ,$$

and the free energy,

$$\begin{aligned} F(\alpha) &\equiv -\tfrac{1}{\beta}\ln Z(\alpha) = \omega_c\alpha^2 - \tfrac{N}{\beta}\ln(2\cosh\beta E) \\ &= \omega_c\alpha^2 - \tfrac{N}{\beta}\ln\left(2\cosh\sqrt{\left(\tfrac{\beta\omega_a}{2}\right)^2 + (2\beta g\alpha)^2}\right) . \end{aligned}$$

b. The minimum of the free energy is obtained via,

$$\begin{aligned} 0 \stackrel{!}{=} F'(\alpha) &= 2\omega_c\alpha - N\beta\alpha(2g)^2\frac{\tanh\sqrt{\left(\frac{\beta\omega_a}{2}\right)^2 + (2\beta g\alpha)^2}}{\sqrt{\left(\frac{\beta\omega_a}{2}\right)^2 + (2\beta g\alpha)^2}} \\ &\simeq 2\omega_c\alpha - 2N\beta\alpha(2g)^2\frac{\tanh\beta\omega_a}{\beta\omega_a} , \end{aligned}$$

after a Taylor expansion in α. Hence, resolving for the critical coupling strength g_c,

$$g_c\sqrt{N} = \frac{1}{2}\sqrt{\omega_a\omega_c\coth\tfrac{\beta\omega_a}{2}} .$$

41.2.4.6 Ex: Superradiant lasing

a. Consider the generalized open Dicke model Hamiltonian (41.74) neglecting counter-rotating terms, $g' \equiv 0$, as well as pumping and phase fluctuations of the cavity modes, $\eta = \phi \equiv 0$. Derive the Heisenberg equations for the operators $\hat{a}$, $\hat{s}_j^-$, $\hat{s}_j^z$, $\hat{a}^\dagger\hat{s}_j^-$, $\hat{s}_i^+\hat{s}_j^-$, and $\hat{a}^\dagger\hat{a}$.
b. Calculate the expectation values of the equations of motion for all degrees of freedom and for the products specified in (a) assuming that all atoms are equal. Now, assume that the phase-invariance is not broken, $\langle\hat{a}\rangle = \langle\hat{a}^\dagger\rangle = \langle\hat{s}_1^\pm\rangle = 0$, and apply a

cumulant expansion up to second order.
c. Assuming the system to be in steady state solve the system of equations for the operators and products specified in (a) analytically. Assume $\gamma_1 \ll g \ll \kappa$ and plot $\hat{a}^\dagger\hat{a}$ as a function of the atom number N and the optical pumping rate ξ_1.
d. In which parameter regimes do you observe superradiant lasing?
e. Express $\langle \hat{\mathbf{S}}^2 \rangle$ and $\langle S_z \rangle$ in terms of single particle spin operators.
f. Evaluating $\langle \mathbf{S}^2 \rangle$ and $\langle S_z \rangle$ via the solution of the equations of motion, we find the steady-state quantum numbers always around $M \simeq \pm S$ [341]. Explain how this fact can induce squeezing, once $\langle S_z \rangle > 0$.

Solution: *a. For the specified case the Dicke Hamiltonian is [868, 341],*

$$\hat{H} = -\Delta_c \hat{a}^\dagger\hat{a} - \Delta_a \hat{S}_z + 2g(\hat{a}\hat{S}_+ + \hat{S}_-\hat{a}^\dagger) \ .$$

The equations of motion for the degrees of freedom are simply obtained from (41.75),

$$\begin{aligned}
\dot{\hat{a}} &= (\imath\Delta_c - \kappa)\hat{a} - 2\imath g \Sigma_j \hat{s}_j^- \\
\dot{\hat{s}}_j^- &= (\imath\Delta_a - \gamma_1 - \xi_1 - \beta_1)\hat{s}_j^- + 4\imath g \hat{a}\hat{s}_j^z \\
\dot{\hat{s}}_j^z &= -\gamma_1(\mathbb{I} - 2\hat{s}_j^z) + \xi_1(\mathbb{I} + 2\hat{s}_j^z) - 2\imath g \hat{a}\hat{s}_j^+ + 2\imath g \hat{a}^\dagger \hat{s}_j^- \ .
\end{aligned}$$

For the operator products we get,

$$\begin{aligned}
\frac{d}{dt}(\hat{a}^\dagger\hat{a}) &= \hat{a}^\dagger\dot{\hat{a}} + \dot{\hat{a}}^\dagger\hat{a} \\
&= \hat{a}^\dagger[(\imath\Delta_c - \kappa - \phi)\hat{a} - 2\imath g\Sigma_j \hat{s}_j^-] + [(-\imath\Delta_c - \kappa - \phi)\hat{a}^\dagger + 2\imath g \Sigma_j \hat{s}_j^+]\hat{a} \\
&= 2\kappa \hat{a}^\dagger\hat{a} + 2\imath g \Sigma_j (\hat{s}_j^+\hat{a} - \hat{a}^\dagger \hat{s}_j^-) \ ,
\end{aligned}$$

and,

$$\begin{aligned}
\frac{d}{dt}(\hat{a}^\dagger\hat{s}_j^-) &= \hat{a}^\dagger\dot{\hat{s}}_j^- + \dot{\hat{a}}^\dagger\hat{s}_j^- \\
&= \hat{a}^\dagger\left[(\imath\Delta_a - \gamma_1 - \xi_1 - \beta_1)\hat{s}_j^- + 4\imath g\hat{a}\hat{s}_j^z\right] + \left[(-\imath\Delta_c - \kappa)\hat{a}^\dagger + 2\imath g\Sigma_i \hat{s}_i^+\right]\hat{s}_j^- \\
&= (\imath\Delta_a - \gamma_1 - \xi_1 - \beta_1 - \imath\Delta_c - \kappa)\hat{a}^\dagger\hat{s}_j^- + 2\imath g\left[2\hat{a}^\dagger\hat{a}\hat{s}_j^z + \tfrac{1}{2}(N\mathbb{I} - 2\Sigma_i\hat{s}_z) + \Sigma_{i\neq j}\hat{s}_i^+\hat{s}_j^-\right] \ ,
\end{aligned}$$

and with $i \neq j$,

$$\begin{aligned}
\frac{d}{dt}(\hat{s}_i^+\hat{s}_j^-) &= \hat{s}_i^+\dot{\hat{s}}_j^- + \dot{\hat{s}}_i^+\hat{s}_j^- \\
&= \hat{s}_i^+\left[(\imath\Delta_a - \gamma_1 - \xi_1 - \beta_1)\hat{s}_j^- + 4\imath g\hat{a}\hat{s}_j^z\right] + \left[(-\imath\Delta_a - \gamma_1 - \xi_1 - \beta_1)\hat{s}_i^+ - 4\imath g\hat{s}_i^z\hat{a}^\dagger\right]\hat{s}_j^- \\
&= -2(\gamma_1 + \xi_1 + \beta_1)\hat{s}_i^+\hat{s}_j^- + 4\imath g(\hat{s}_i^+\hat{s}_j^z\hat{a} - \hat{a}^\dagger\hat{s}_i^z\hat{s}_j^-) \ .
\end{aligned}$$

b. The expectation values of the above equations are, assuming that all atoms are equal, $\langle \hat{s}_j \rangle = \langle \hat{s}_1 \rangle$, and setting for simplicity the cavity on resonance with the atoms,

$\Delta_c = \Delta_a = 0$,

$$
\begin{aligned}
\langle \dot{\hat{a}} \rangle &= -\kappa \langle \hat{a} \rangle - 2\imath g N \langle \hat{s}_1^- \rangle = 0 \\
\langle \dot{\hat{s}}_1^- \rangle &= -(\gamma_1 + \xi_1 + \beta_1) \langle \hat{s}_j^- \rangle + 4\imath g \langle \hat{a} \hat{s}_1^z \rangle = 0 \\
\langle \dot{\hat{s}}_1^z \rangle &= \xi_1 - \gamma_1 + 2(\xi_1 + \gamma_1) \langle \hat{s}_1^z \rangle - 4g \Im\mathrm{m}\ \langle \hat{a}^\dagger \hat{s}_1^- \rangle \\
\partial_t \langle \hat{a}^\dagger \hat{a} \rangle &= -2\kappa \langle \hat{a}^\dagger \hat{a} \rangle + 4Ng \Im\mathrm{m}\ \langle \hat{a}^\dagger \hat{s}_1^- \rangle \\
\partial_t \Im\mathrm{m}\ \langle \hat{a}^\dagger \hat{s}_1^- \rangle &= -(\gamma_1 - \xi_1 + \beta_1 + \kappa) \Im\mathrm{m}\ \langle \hat{a}^\dagger \hat{s}_j^- \rangle + 2g[2\langle \hat{s}_j^z \hat{a}^\dagger \hat{a} \rangle + \tfrac{1}{2}(N - 2\Sigma_i \langle \hat{s}_z \rangle) + (N-1)\langle \hat{s}_2^+ \hat{s}_1^- \rangle] \\
\partial_t \langle \hat{s}_2^+ \hat{s}_1^- \rangle &= -2(\gamma_1 + \xi_1 + \beta_1) \langle \hat{s}_2^+ \hat{s}_1^- \rangle + 4\imath g (\langle \hat{s}_2^+ \hat{a} \hat{s}_1^z \rangle - \langle \hat{s}_2^z \hat{a}^\dagger \hat{s}_1^- \rangle) \ .
\end{aligned}
$$

Now we apply the cumulant expansion (41.84) setting $\langle \hat{a} \rangle = \langle \hat{a}^\dagger \rangle = \langle \hat{s}_1^\pm \rangle = 0$ *and neglecting third-order correlations, e.g.* $\langle \hat{s}_i^z \hat{s}_i^+ \hat{s}_j^- \rangle = 0$. *That is,*

$$
\langle \hat{s}_j^z \hat{a}^\dagger \hat{a} \rangle_c = \langle \hat{s}_j^z \rangle \langle \hat{a}^\dagger \hat{a} \rangle_c \qquad \textit{and} \qquad \langle \hat{s}_i^z \hat{s}_j^+ \hat{a} \rangle_c = \langle \hat{s}_i^z \rangle \langle \hat{s}_j^+ \hat{a} \rangle_c \ .
$$

c. Postulating the system to be in steady state we set all derivatives $= 0$. *Then above system of equations can then be solved analytically. If* $N \simeq N - 1$,

$$
\begin{aligned}
4g \Im\mathrm{m}\ \langle \hat{a}^\dagger \hat{s}_1^- \rangle_c &= \xi_1 (1 - 2\langle \hat{s}_1^z \rangle) - \gamma_1 (1 + 2\langle \hat{s}_1^z \rangle) \\
2Ng \Im\mathrm{m}\ \langle \hat{a}^\dagger \hat{s}_1^- \rangle_c &= \kappa \langle \hat{a}^\dagger \hat{a} \rangle_c \\
(\beta_1 + \kappa + \xi_1 + \gamma_1) \Im\mathrm{m}\ \langle \hat{a}^\dagger \hat{s}_1^- \rangle_c &= g \left[1 + 2(1 + 2\langle \hat{a}^\dagger \hat{a} \rangle_c) \langle \hat{s}_1^z \rangle + 2N \langle \hat{s}_2^+ \hat{s}_1^- \rangle_c \right] \\
8g \langle \hat{s}_1^z \rangle_c \Im\mathrm{m}\ \langle \hat{a}^\dagger \hat{s}_1^- \rangle_c &= 2(\xi_1 + \beta_1 + \gamma_1) \langle \hat{s}_1^+ \hat{s}_2^- \rangle_c \ .
\end{aligned}
$$

Introducing the abbreviations $d_0 \equiv \frac{\xi_1 - \gamma_1}{\xi_1 + \gamma_1}$ *and* $n_c \equiv \frac{\kappa}{2Ng} \langle \hat{a}^\dagger \hat{a} \rangle_c$,

$$
\begin{aligned}
\Im\mathrm{m}\ \langle \hat{a}^\dagger \hat{s}_1^- \rangle_c &= n_c \qquad \textit{from (ii)} \\
2\langle \hat{s}_1^z \rangle &= d_0 - \frac{4g}{\xi_1 + \gamma_1} n_c \qquad \textit{from (i)} \\
\langle \hat{s}_1^+ \hat{s}_2^- \rangle_c &= \frac{4g}{\xi_1 + \beta_1 + \gamma_1} \langle \hat{s}_1^z \rangle_c \Im\mathrm{m}\ \langle \hat{a}^\dagger \hat{s}_1^- \rangle_c \\
&= \frac{2g}{\xi_1 + \beta_1 + \gamma_1} \left(d_0 - \frac{4g}{\xi_1 + \gamma_1} n_c \right) n_c \qquad \textit{from (iv)} \\
\frac{\beta_1 + \kappa + \xi_1 + \gamma_1}{g} n_c &= 1 + 2 \left(1 + 2 \frac{2Ng}{\kappa} n_c \right) \langle \hat{s}_1^z \rangle + 2N \langle \hat{s}_2^+ \hat{s}_1^- \rangle_c \qquad \textit{from (iii)} \ .
\end{aligned}
$$

Inserting the first three expressions into the last equation,

$$
0 = -\frac{\beta_1 + \kappa + \xi_1 + \gamma_1}{g} n_c + 1 + \left(1 + \frac{4Ng}{\kappa} n_c + \frac{4Ng}{\xi_1 + \beta_1 + \gamma_1} n_c \right) \left(d_0 - \frac{4g}{\xi_1 + \gamma_1} n_c \right) \ ,
$$

we obtain a quadratic equation in n_c, *namely* $0 = An_c^2 + Bn_c + C$, *with the coefficients,*

$$
\begin{aligned}
A &= -\frac{16Ng^2}{\xi_1 + \gamma_1} \left(\frac{1}{\kappa} + \frac{1}{\xi_1 + \beta_1 + \gamma_1} \right) \\
B &= -\frac{\beta_1 + \kappa + \xi_1 + \gamma_1}{g} - \frac{4g}{\xi_1 + \gamma_1} + 4Ngd_0 \left(\frac{1}{\kappa} + \frac{1}{\xi_1 + \beta_1 + \gamma_1} \right) \\
C &= 1 + d_0 \ .
\end{aligned}
$$

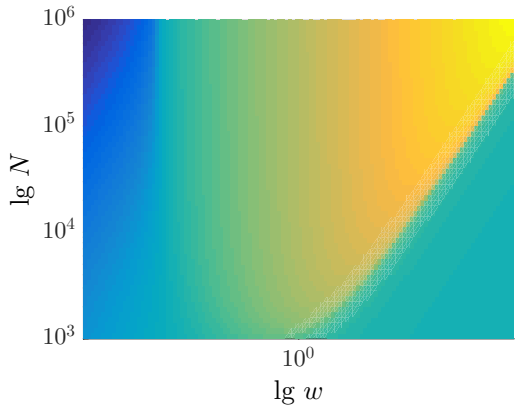

Figure 41.13: Superradiant lasing for the parameters $g = (2\pi)\ 3\,\mathrm{Hz}$, $\kappa = (2\pi)\ 150\,\mathrm{kHz}$, $\gamma_1 = (2\pi)\ 1.6\,\mathrm{mHz}$, $\beta_1 = (2\pi)\ 0.16\,\mathrm{Hz}$, and $\Delta_c = \Delta_a$.

Fig. 41.13 plots the intracavity photon number $\hat{a}^\dagger\hat{a}$ as a function of the atom number N and the optical pumping rate ξ_1. d. The superradiant laser spectrum can be calculated as the Fourier transform of the first-order correlation from,

$$\frac{d}{dt}[\hat{a}^\dagger(t)\hat{a}(0)] = \left[-\kappa\hat{a}^\dagger(t) + 2\imath g\Sigma_j \hat{s}_j^+(t)\right]\hat{a}(0)$$
$$\frac{d}{dt}[\hat{s}_j^+(t)\hat{a}(0)] = \left[-\beta_1\hat{s}_j^+(t) - 4\imath g\hat{s}_j^z(t)\hat{a}^\dagger(t) + 2\gamma_1\hat{s}_j^+(t)\hat{s}_j^z(t) - 2\xi_1\hat{s}_j^z(t)\hat{s}_j^+(t)\right]\hat{a}(0)\ .$$

Neglecting higher than second-order correlations, we get the expectation values,

$$\frac{d}{dt}\begin{pmatrix}\langle\hat{a}^\dagger(t)\hat{a}(0)\rangle\\ \langle\hat{s}_j^+(t)\hat{a}(0)\rangle\end{pmatrix} \simeq \begin{pmatrix}-\kappa & 2\imath Ng\\ -4\imath g\langle\hat{s}_j^z(t)\rangle & -\beta_1 - 2\gamma_1 - 2\xi_1\end{pmatrix}\begin{pmatrix}\langle\hat{a}^\dagger(t)\hat{a}(0)\rangle\\ \langle\hat{s}_j^+(t)\hat{a}(0)\rangle\end{pmatrix}\ .$$

e. We find,

$$\mathbf{S}^2 = \tfrac{1}{4}\sum_{i,j=1}^{N}\hat{\vec{\sigma}}_i\cdot\hat{\vec{\sigma}}_j = \tfrac{1}{4}\sum_{j=1}^{N}\hat{\vec{\sigma}}_j^2 + \tfrac{1}{4}\sum_{i\neq j}^{N}(\hat{\sigma}_i^x\hat{\sigma}_j^x + \hat{\sigma}_i^y\hat{\sigma}_j^y + \hat{\sigma}_i^z\hat{\sigma}_j^z)$$
$$= \tfrac{N}{4}\hat{\vec{\sigma}}_1^2 + \tfrac{1}{4}\sum_{i\neq j}^{N}[(\hat{\sigma}_i^+ + \hat{\sigma}_i^-)(\hat{\sigma}_j^+ + \hat{\sigma}_j^-) - (\hat{\sigma}_i^+ - \hat{\sigma}_i^-)(\hat{\sigma}_j^+ - \hat{\sigma}_j^-) + \hat{\sigma}_i^z\hat{\sigma}_j^z]$$
$$= \tfrac{N}{4}\left[(\hat{\sigma}^x)^2 + (\hat{\sigma}^y)^2 + (\hat{\sigma}^z)^2\right] + \tfrac{1}{4}\sum_{i\neq j}^{N}(4\hat{\sigma}_i^-\hat{\sigma}_j^+ + \hat{\sigma}_i^z\hat{\sigma}_j^z) = \tfrac{N}{4}3I + \sum_{i\neq j}^{N}(\hat{s}_i^-\,\hat{s}_j^+ + \hat{s}_i^z\hat{s}_j^z)\ .$$

Hence,

$$S(S+1) = \langle\mathbf{S}^2\rangle = \tfrac{3N}{4} + \sum_{i\neq j}^{N}\langle\hat{s}_i^-\,\hat{s}_j^+\rangle + \langle\hat{s}_i^z\hat{s}_j^z\rangle \qquad \textit{and} \qquad M = \langle S_z\rangle = \sum_{j=1}^{N}\langle\hat{s}_j^z\rangle\ .$$

Evaluating $\langle\mathbf{S}^2\rangle$ and $\langle S_z\rangle$ via the solution of the equations of motion, we the steady-state quantum numbers always around $M \simeq \pm S$ [341].

f. Upon superradiant lasing [1429, 341] finds strong optical pumping to subradiant states, in particular $|S,\pm S\rangle$. This is similarly to [263], only that the interatomic coupling is mediated by a cavity rather than interatomic interaction. Assuming the bulk part of the population in $|S,\pm S\rangle$ we may simplify the problem. From,

$$\hat{S}_\pm|S,M\rangle = \sqrt{S(S+1)-M(M\pm 1)}|S,M\pm 1\rangle$$

for dominating subradiant states $|S_{\simeq|M|},M\rangle$ for $M\simeq S\geq 0$,

$$\hat{S}_+|S,M\rangle = 0 \quad \textit{and} \quad \hat{S}_-|S,M\rangle = \sqrt{|M|(|M|+1)-M(M-1)}|S,M{-}1\rangle \simeq \sqrt{2S}|S,M{-}1\rangle \ ,$$

and for $M\simeq -S\leq 0$

$$\hat{S}_-|S,M\rangle = 0 \quad \textit{and} \quad \hat{S}_+|S,M\rangle = \sqrt{|M|(|M|+1)-M(M+1)}|S,M{+}1\rangle \simeq \sqrt{2S}|S,M{+}1\rangle \ .$$

That is, when the atoms are individually pumped to $M=-S\leq 0$ states $|S,-S\rangle$, subsequent coherent coupling may only drive transitions to higher states $|S,S+1\rangle$. Hence, we may define a Holstein-Primakoff approximation using $|S,-S\rangle$ as the ground state from which higher-lying oscillator states can be reached via creation operators,

$$\hat{S}_+ = \sqrt{2S}\hat{b}^\dagger \ .$$

In contrast, when the atoms are individually pumped to $M=S\geq 0$ states $|S,S\rangle$ subsequent coherent coupling may only drive transitions to lower states $|S,S-1\rangle$, so that the corresponding Holstein-Primakoff approximation uses $|S,S\rangle$ as the ground state from which lower-lying oscillator states can be reached via creation operators,

$$\hat{S}_- = \sqrt{2S}\hat{b}^\dagger \ .$$

Therefore, the Hamiltonian can be simplified as,

$$\hat{H} = g(\hat{a}^\dagger\hat{S}_- + \hat{a}\hat{S}_+) = \begin{cases} g(\hat{a}^\dagger\hat{b}^\dagger + \hat{a}\hat{b}) & \textit{for } M\geq 0 \\ g(\hat{a}^\dagger\hat{b} + \hat{a}\hat{b}^\dagger) & \textit{for } M\leq 0 \end{cases}$$

For $M\geq 0$ the Hamiltonian describes squeezing.

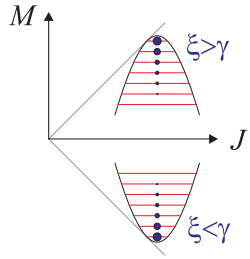

Figure 41.14: Illustration of the normal (below) and inverted (above) population of the harmonic oscillator levels in the Holstein Primakoff approximation (see also Sec. 36.2.4).

41.2.4.7 Ex: Superradiant lasing and the Schawlow-Townes limit

Discuss whether superradiant lasing beats the Schawlow-Townes limit.

Solution:

41.2.4.8 Ex: Heisenberg equation for the open Dicke model in the Holstein-Primakoff approximation

Derive the Heisenberg equations for the open Dicke model in the Holstein-Primakoff approximation.

Solution: *Starting from the Hamiltonian,*

$$\hat{H}_{HP} = -\Delta_c \hat{a}^\dagger \hat{a} - \Delta_a \hat{b}^\dagger \hat{b} + 2g_N(\hat{a} + \hat{a}^\dagger)(\hat{b} + \hat{b}^\dagger)$$

we readily derive,

$$\dot{\hat{a}} = \imath\Delta_c \hat{a} - 2\imath g_N(\hat{b} + \hat{b}^\dagger) \qquad \textit{and} \qquad \dot{\hat{b}} = \imath\Delta_a \hat{b} - 2\imath g_N(\hat{a} + \hat{a}^\dagger) \ .$$

41.3 Interacting atoms

When two atoms excited to an internal level of energy hc/λ are so close together that the range of their dipole moments overlap without forming a molecular bonding, $a_B \ll R \ll \lambda$, they may exhibit cooperative relaxation. The atoms are coupled via the radiation that they are susceptible to emit into the same continuum. The coupled atomic dipoles oscillate and decay in phase. The decays is accelerated one leads to an intense burst of coherent and spatially directional radiation. This phenomenon is termed *superradiance* [366, 1085]. We may view superradiance as destructive interference of the dipolar radiation patterns of all atoms in all but one direction of space triggered by the first spontaneous decay. The superradiant enhancement is largest when half of the atoms are deexcited. The correlated atoms can be in a Dicke state (then the total dipole moment is always zero) or in a product state (then the net dipole moment is non-zero at half-deexcitation). In the second case, we also talk about *superfluorescence*. In this case, an excited initially incoherent sample develops correlations due to the emission process. One can also imagine the case that the emission patterns pairwise cancel, and the decay is thus inhibited. This is called *subradiance*. Superradiance has been used in the microwave domain as a spectroscopic method in the observation of photon echoes.

Correlated quantum jumps are, in a sense, the few-atoms precursors of superradiance. Accelerated spontaneous decay has been predicted for atoms whose distance is shorter than the wavelength of the decaying transition [1174, 797]. Super- and subradiance has been observed in a system of two ion trapped in a Paul trap [364].

41.3.1 Rydberg blockade

Rydberg atoms (i.e. atoms in excited Rydberg states) exhibit huge polarizabilities inducing large interaction energies even at relatively modest densities. These can be so strong, that the presence of a single Rydberg-excited atom can drive out of resonance the frequencies of transitions connected to the Rydberg state for several neighboring atoms once the exciting laser is sufficiently narrow-band. This effect called *Rydberg blockade* can be described by the following interaction Hamiltonian [1110, 1243],

$$\hat{H}_{Rydberg} = \sum_{i>j} \kappa_{ij} \tfrac{1}{2}(\hat{\sigma}_i^z - 1)\tfrac{1}{2}(\hat{\sigma}_j^z - 1) \qquad \text{with} \qquad \kappa_{ij}/2\pi = \frac{C_6}{r_{ij}^6} \,, \tag{41.85}$$

where $\frac{1}{2}(\hat{\sigma}_i^z - 1) = |e\rangle_i\langle e|$ is the probability of finding the i-th atom in an excited state and C_6 interatomic van der Waals interaction coefficient of the transition.

Example 256 (*Two interacting Rydberg atoms*): In this example we study Rydberg blockade for two interacting Rydberg atoms. In this case, the Hamiltonian can be cast into the matrix form,

$$\hat{H} = -\Delta_a \hat{S}_z + \Omega \hat{S}_+ + \Omega^* \hat{S}_- + \hat{H}_{Rydberg} = \begin{pmatrix} \Delta_a & \frac{1}{2}\Omega & \frac{1}{2}\Omega^* & 0 \\ \frac{1}{2}\Omega^* & 0 & 0 & \frac{1}{2}\Omega^* \\ \frac{1}{2}\Omega & 0 & 0 & \frac{1}{2}\Omega \\ 0 & \frac{1}{2}\Omega & \frac{1}{2}\Omega^* & -\Delta_a + \kappa_{12} \end{pmatrix} .$$

The master equation can be numerically solved using the procedure outlined in example 257. The result of such a simulation is shown in Fig. 41.15. Comparing

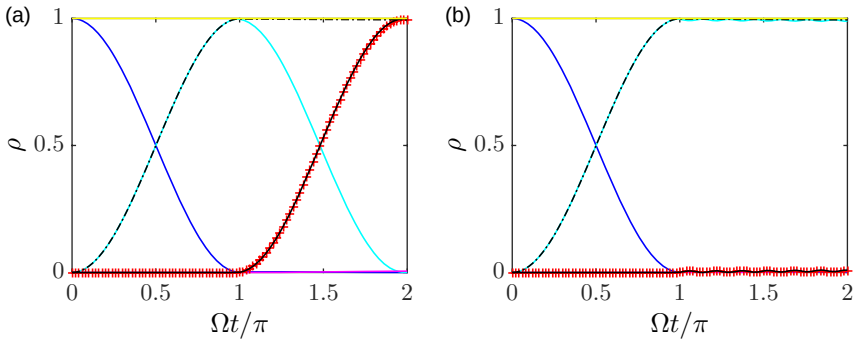

Figure 41.15: (code) Populations in a system of two two-level atoms interaction via van der Waals forces. Initially ($\Omega t < \pi$) only one atom is driven, after that only the other. We assume $\Omega \gg \Gamma$ and $C_6 = 4 \cdot 10^7$. The interatomic distance is (a) $kr_{12} = 0.5$, respectively, (a) $kr_{12} = 5$. (blue) $\rho_{11,11}$, (cyan) $\rho_{12,12}$, (magenta) $\rho_{21,21}$, (red) $\rho_{22,22}$, (black dotted) $\rho_{22}^{(1)}$, and (black) $\rho_{22}^{(2)}$.

the evolutions calculated in Fig. 41.15 for large and small interatomic distances, we see that the excitation of the first atom impedes the excitation of the second one when the interaction is strong.

Note, that an interesting situation occurs when the coupling is completely uniform (e.g. mediated by a cavity), $\kappa_{ij} \simeq \kappa$,

$$\hat{H}_{Rb} \simeq \tfrac{1}{8}\kappa(\hat{S}_z^2 - 2\hat{S}_z + 1) \ , \tag{41.86}$$

as pointed out in Eq. (41.52). Such Hamiltonians may be interesting for the generation of spin-squeezing.

41.3.2 Dipole-dipole interactions in the non-linear optics regime

The mean-field Dicke model totally neglects interactions between the atoms due to the exchange of real or virtual photons, i.e. neither resonant dipole-dipole interactions nor van der Waals interactions are considered [50, 137, 383, 416, 1099, 1110, 1197]. That is, interaction terms such as,

$$\hat{H}_{Ising} = -\sum_{i,j\neq i}^{N} \Delta_{ij}\hat{\sigma}_j^+\hat{\sigma}_i^- \tag{41.87}$$

are absent from the Hamiltonian. Spin-spin interactions are studied in the so-called *Ising model*, which is interesting in the context of (anti-)*ferromagnetism* [479, 480, 499, 723, 1434]. The negligence of interaction was, of course, the reason for the simplicity of the Dicke model and its manageability for large atom numbers. On the other hand, in Sec. 39.1.2 we have studied dipole-dipole interactions in the linear optics regime allowing for at most a single photon to interact with the cloud.

In this section, we will consider dipole-dipole interactions in very small dilute clouds interacting with an arbitrary number of photons. The possibility for the cloud of storing as many photons as there are atoms is common to the Dicke model. Here, we will call it the *non-linear optics* regime, as several photons may team up to excite higher Dicke excitations states. In particular, we will study two interacting atoms as done by the milestone experiment of DeVoe and Brewer [364]. Do the Exc. 41.3.4.1.

The starting point is the collective many-atoms Hamiltonian (39.9) of the scalar coupled dipoles model. After tracing over the vacuum modes, one obtains the master equation [15] [1090],

$$\boxed{\begin{aligned}
\hat{H} &= \tfrac{1}{2}\textstyle\sum_j \left[\Omega(\mathbf{r}_j)\hat{\sigma}_j^+ + h.c.\right] - \sum_{i,j}\Delta_{ji}\hat{\sigma}_j^+\hat{\sigma}_i^- \\
\mathcal{L}[\hat{\rho}] &= \tfrac{1}{2}\textstyle\sum_{i,j}\Gamma_{ij}\left(2\hat{\sigma}_j^-\hat{\rho}\hat{\sigma}_i^+ - \hat{\sigma}_i^+\hat{\sigma}_j^-\hat{\rho} - \hat{\rho}\hat{\sigma}_i^+\hat{\sigma}_j^-\right) \\
\mathcal{L}^\dagger[\hat{A}] &= \tfrac{1}{2}\textstyle\sum_{i,j}\Gamma_{ij}\left(2\hat{\sigma}_i^+\hat{A}\hat{\sigma}_j^- - \hat{\sigma}_i^+\hat{\sigma}_j^-\hat{A} - \hat{A}\hat{\sigma}_i^+\hat{\sigma}_j^-\right) \\
\Delta_{i\neq j} &\equiv -\tfrac{3\lambda\Gamma}{2}\,\hat{\mathbf{e}}_d^*\,\mathfrak{Re}\,G(\mathbf{r}_i,\mathbf{r}_j,\omega_0)\,\hat{\mathbf{e}}_d \quad \text{and} \quad \Delta_{jj}\equiv\Delta_a \\
\Gamma_{i\neq j} &\equiv 3\lambda\Gamma\,\hat{\mathbf{e}}_d^*\,\mathfrak{Im}\,G(\mathbf{r}_i,\mathbf{r}_j,\omega_0)\,\hat{\mathbf{e}}_d \quad \text{and} \quad \Gamma_{jj}\equiv\Gamma
\end{aligned}} \tag{41.88}$$

The expression for the line shifts Δ_{ij} and the decay rates Γ_{ij} have been derived in Sec. 40.4.1 from the bulk Green's tensor in free space. Assuming $\Delta_{ji} = 0 = \Gamma_{ji}$

[15] In return, the equations of motion (39.26) for the excitation amplitude should follow as the Heisenberg equation with the above Hamiltonian.

and $\Omega(\mathbf{r}_j) = \Omega$ we recover the mean-field Dicke model, where interaction terms are completely neglected,

$$\hat{H} = \tfrac{1}{2}\Omega \sum_j (\hat{\sigma}_j^+ + h.c.) - \Delta_a \sum_j \hat{\sigma}_j^+ \hat{\sigma}_j^- \ . \tag{41.89}$$

With (41.88) we set up either the master or the Heisenberg-Liouville equations,

$$\begin{aligned} \dot{\hat{\rho}} &= -\imath[\hat{H}, \hat{\rho}] + \mathcal{L}[\hat{\rho}] \\ \dot{\hat{A}} &= -\imath[\hat{A}, \hat{H}] + \mathcal{L}^\dagger[\hat{A}] \ . \end{aligned} \tag{41.90}$$

Note that in principle, the collective many-atom system (41.88) can be mapped to a single-atom multilevel system,

$$\frac{d}{dt}\vec{\hat{\varrho}} = \mathcal{M}\vec{\varrho} \ , \tag{41.91}$$

which is more amenable to numeric simulation using the methods presented in Sec. 34.7. However, analytically this is only simple to do in the case of two atoms, which can be mapped to a four-level system. This will be shown in Exc. 41.3.4.2.

Example 257 (*Diagonalizing collective decay*): The Lindbladian describing collective decay in (41.88) can be recast into a standard form by diagonalizing the real matrix $\mathbf{\Gamma} \equiv (\Gamma_{ij})$ [1090], that is, we define a unitary transformation $T = (T^\intercal)^{-1} \equiv (T_{jk})$,

$$D = T^\intercal \mathbf{\Gamma} T \Longrightarrow \tilde{\Gamma}_k \delta_{kj} = \sum_j T^\intercal_{ik} \Gamma_{ij} T_{jk}$$

$$\text{or} \qquad \mathbf{\Gamma} = T D T^\intercal \Longrightarrow \Gamma_{ij} = \sum_k T_{jk} \tilde{\Gamma}_k \delta_{kj} T^\intercal_{jk} \ .$$

Note that all coefficients not ornamented by a 'hat' can be moved around freely. Now, substituting the Γ_{ij},

$$\mathcal{L}[\hat{\rho}] = \tfrac{1}{2} \sum_{k,i,j} \left[2\hat{\sigma}_i^- T_{ik} \tilde{\Gamma}_k \delta_{ki} T^\intercal_{jk} \hat{\rho} \hat{\sigma}_j^+ - \hat{\sigma}_i^+ T_{ik} \tilde{\Gamma}_k \delta_{ki} T^\intercal_{jk} \hat{\sigma}_j^- \hat{\rho} - \hat{\rho} \hat{\sigma}_i^+ T_{ik} \tilde{\Gamma}_k \delta_{ki} T^\intercal_{jk} \hat{\sigma}_j^- \right] \ .$$

Now, defining new composite decay channels,

$$\hat{\Pi}_k^- = \sum_j T_{kj} \hat{\sigma}_j^- \qquad , \qquad \hat{\Pi}_k^+ = \sum_j \hat{\sigma}_j^+ T^\intercal_{kj} \ ,$$

we find,

$$\mathcal{L}[\hat{\rho}] = \tfrac{1}{2} \sum_k \tilde{\Gamma}_k [2\hat{\Pi}_k^+ \hat{\rho} \hat{\Pi}_k^- - \hat{\Pi}_k^+ \hat{\Pi}_k^- \hat{\rho} - \hat{\rho} \hat{\Pi}_k^+ \hat{\Pi}_k^-] \ .$$

Single-atom spontaneous emission simply follows from the assumption that $\Gamma_{ij} = \Gamma_1 \delta_{ij}$,

$$\mathcal{L}[\rho] = \tfrac{1}{2} \sum_j \Gamma [2\hat{\sigma}_j^- \hat{\rho} \hat{\sigma}_j^+ - \hat{\sigma}_j^+ \hat{\sigma}_j^- \hat{\rho} - \hat{\rho} \hat{\sigma}_j^+ \hat{\sigma}_j^-] \ .$$

On the other hand, Dicke superradiance follows from the assumption that $\Gamma_{ij} = \Gamma$. Introducing the collective spin operator, $\hat{S}^\pm \equiv \sum_j \hat{\sigma}_j^\pm$,

$$\begin{aligned} \mathcal{L}[\rho] &= \tfrac{1}{2} \sum_{i,j} \Gamma [2\hat{\sigma}_i^- \hat{\rho} \hat{\sigma}_j^+ - \hat{\sigma}_i^+ \hat{\sigma}_j^- \hat{\rho} - \hat{\rho} \hat{\sigma}_i^+ \hat{\sigma}_j^-] \\ &= \tfrac{1}{2} \Gamma [2\hat{S}^- \hat{\rho} \hat{S}^+ - \hat{S}^+ \hat{S}^- \hat{\rho} - \hat{\rho} \hat{S}^+ \hat{S}^-] \ . \end{aligned}$$

The uniform all-to-all coupling required for Dicke superradiance can be realized, when the atoms are localized in an area of space smaller than λ^3 or in a cavity.

41.3.2.1 Equations of motion in the presence of dipole-dipole coupling

We start from the Hamiltonian and jump operators (41.88) and derive the Heisenberg-Liouville equation (41.90),

$$\begin{aligned}\dot{\hat{\sigma}}_k^- &= -\imath[\hat{\sigma}_k^-, \hat{H}] + \mathcal{L}[\hat{\sigma}_k^-] \\ &= \tfrac{\imath}{2}\Omega(\mathbf{r}_k)\hat{\sigma}_k^z - \imath\Delta_a\hat{\sigma}_k^z\hat{\sigma}_k^- - \imath\sum_{j\neq k}^{N}\Delta_{kj}\hat{\sigma}_k^z\hat{\sigma}_j^- + \tfrac{\Gamma}{2}\hat{\sigma}_k^z\hat{\sigma}_k^- + \sum_{j\neq k}^{N}\tfrac{\Gamma_{kj}}{2}\hat{\sigma}_k^z\hat{\sigma}_j^- \ .\end{aligned} \tag{41.92}$$

Now, we assume low atomic excitation, $\langle\hat{\sigma}_k^z\rangle \simeq -1$, that is, most atoms are in the ground state. Then we may neglect correlations and find,

$$\dot{\hat{\sigma}}_k^- \simeq \left(\imath\Delta_a - \tfrac{\Gamma}{2}\right)\hat{\sigma}_k^- - \tfrac{\imath}{2}\Omega(\mathbf{r}_k) + \sum_{j\neq k}^{N}\left(\imath\Delta_{kj} - \tfrac{\Gamma_{kj}}{2}\right)\hat{\sigma}_j^- \tag{41.93}$$

or taking the expectation values,

$$\boxed{\dot{\beta}_k \simeq \left(\imath\Delta_a - \tfrac{\Gamma}{2}\right)\beta_k - \tfrac{\imath}{2}\Omega(\mathbf{r}_k) + \sum_{j\neq k}^{N}\left(\imath\Delta_{kj} - \tfrac{\Gamma_{kj}}{2}\right)\beta_j} \ . \tag{41.94}$$

These are just the equations of motion of the coupled dipoles model derived in Sec. 39.1.2. Evaluation of the coeffficients (41.88)(iv-v) yields the exponential kernel postulated in (39.29).

In Exc. 41.3.4.3 we derive them from the linear optics scalar coupled dipoles model,

$$\Delta_{j\neq i} \equiv -\frac{\Gamma\cos kr_{ji}}{kr_{ji}} \qquad \text{and} \qquad \Gamma_{j\neq i} \equiv \frac{\Gamma\sin kr_{ji}}{kr_{ji}} \tag{41.95}$$

with $r_{ji} = |\mathbf{r}_j - \mathbf{r}_i|$. These terms arise from the so-called scalar approximation of (40.338), where we neglect $1/R^2$ and $1/R^3$ terms and set $(\hat{\mathbf{e}}_d \cdot \hat{\mathbf{e}}_R) = 0$.

Example 258 (*Two atoms with dipole-dipole interactions*): For the case of only two atoms located at $\mathbf{r}_j$, using the basis defined in (25.75), we find the Hamiltonian [263],

$$\hat{H} = \begin{pmatrix} 0 & \frac{1}{2}\Omega^*(\mathbf{r}_2) & \frac{1}{2}\Omega^*(\mathbf{r}_1) & 0 \\ \frac{1}{2}\Omega(\mathbf{r}_2) & -\Delta_a & \frac{1}{2}\Delta_{21} & \frac{1}{2}\Omega^*(\mathbf{r}_1) \\ \frac{1}{2}\Omega(\mathbf{r}_1) & \frac{1}{2}\Delta_{12} & -\Delta_a & \frac{1}{2}\Omega^*(\mathbf{r}_2) \\ 0 & \frac{1}{2}\Omega(\mathbf{r}_1) & \frac{1}{2}\Omega(\mathbf{r}_2) & -2\Delta_a \end{pmatrix} , \tag{41.96}$$

with $\Omega(\mathbf{r}) = \Omega_0 e^{\imath\mathbf{k}\cdot\mathbf{r}_j}$. For two atoms the master equations (41.88) can easily be solved numerically by setting [16],

$$\hat{\sigma}_1^{\pm} = \hat{\sigma}^{\pm} \otimes \mathbb{I} \qquad \text{and} \qquad \hat{\sigma}_2^{\pm} = \mathbb{I} \otimes \hat{\sigma}^{\pm} \ , \tag{41.97}$$

as usual and,

$$\langle i, j|\hat{\rho}|m, n\rangle = \rho_{ij,mn} \ , \tag{41.98}$$

[16] Remember, that the formal solution of coherent part of the master equation can be written as $\hat{\rho}(t) = \mathcal{L}(t)\hat{\rho}(0) = e^{-\imath\hat{H}t}\hat{\rho}(0)e^{\imath\hat{H}t}$.

where the indices $i, m = 1, 2$ refer to the first atom and the indices $j, n = 1, 2$ to the second. The populations of the Dicke states $|11\rangle$, $|12\rangle$, $|21\rangle$, and $|22\rangle$ are then given by $\rho_{ij,ij}$, and the populations of the (anti-)symmetric states $|\psi\rangle^{(s,a)} = \frac{1}{\sqrt{2}}(|1,2\rangle \pm |2,1\rangle)$ are calculated via,

$$\langle\psi|^{(s,a)}\hat{\rho}|\psi\rangle^{(s,a)} = \tfrac{1}{2}(\rho_{12,12} \pm \rho_{12,21} \pm \rho_{21,12} + \rho_{21,21}) \ . \tag{41.99}$$

The temporal evolution of the populations in one and two atom systems, initially driven by a laser field which is then suddenly switched off, is shown in Fig. 41.16. Note that super and subradiance do occur for $\Delta_{12} = 0 = \Delta_a$ but necessitate $\Gamma_{ij} \neq 0$.

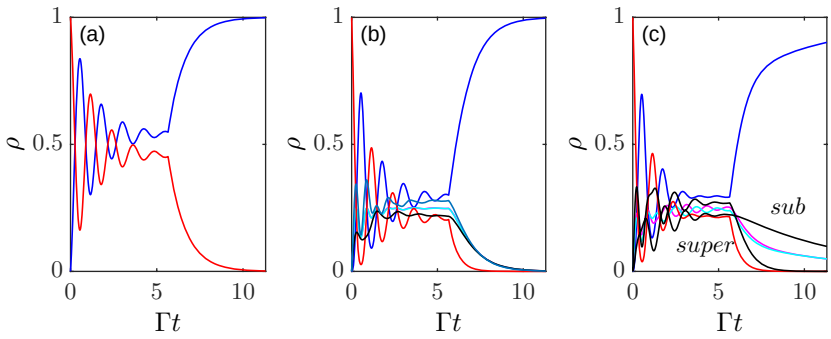

Figure 41.16: (code) (a) Response of a single two-level atom driven by a laser light with $\Omega = 5\Gamma$, $\Delta = -\Gamma$. The curves show (blue) the ground state and (red) the excited state populations. The light is switched off at $\Gamma t = 0.5$. (b) Response of two atoms $j = 1, 2$ located at $kz_j = \pm 5$ driven by the same laser light as in (a). (cyan and magenta) populations of the states $|eg\rangle$ and $|ge\rangle$. The two black lines show the populations of the (anti-)symmetric states $\frac{1}{\sqrt{2}}(|eg\rangle \pm |ge\rangle)$. (c) Same as (c) but with $kz_j = \pm 0.5$.

In Excs. 41.3.4.4 to 41.3.4.6 we study the impact of dipole-dipole interactions on super- and subradiance. In Exc. 41.3.4.7 we study three interacting two-level atoms, and in Exc. 41.3.4.8 we study two non-interacting three-level atoms.

Example 259 (*Blackbody radiation-induced superradiance*): In Exc. 34.6.7.9 we studied blackbody radiation-induced transitions in a single atom. The procedure can be generalized to several atoms [1359]. For two atoms the Liouvillean reads,

$$\begin{aligned}\dot{\hat{\rho}} &= \mathcal{L}_{bb}\hat{\rho} \\ &= -\tfrac{1}{2}\sum_{i,j=1,2}\Gamma_{ij}\left([\hat{\rho}\hat{\sigma}_i, \hat{\sigma}_j^\dagger] + [\hat{\sigma}_i, \hat{\sigma}_j^\dagger\hat{\rho}]\right) - \tfrac{1}{2}\sum_{i,j=1,2}(\Gamma_{ij} + \gamma\delta_{ij})\left([\hat{\rho}\hat{\sigma}_j^\dagger, \hat{\sigma}_i] + [\hat{\sigma}_j^\dagger, \hat{\sigma}_i\hat{\rho}]\right) \ ,\end{aligned}$$

with $\Gamma_{ij}\delta(t-t') \propto \langle\hat{E}_i(t)\hat{E}_j(t')\rangle$ containing both the real and the virtual photon exchange.

41.3.3 Cavity-mediated spin-exchange interactions

In the preceding sections we got to know two fundamentally different types of interatomic interactions, that is, Rydberg and dipole-dipole type interactions. Both are

generally nearest neighbor interactions and thus inhomogeneous. Let us nevertheless make the assumption of uniform coupling to simplify the discussion. Then the Rydberg blockade term (41.85) reads,

$$\hat{H} = \tfrac{1}{2}\sum_{i\neq j}\kappa_{ij}\hat{\sigma}_j^z\hat{\sigma}_i^z \simeq \kappa\hat{S}_z^2 \ , \tag{41.100}$$

and the Ising interaction term (41.87) becomes,

$$\hat{H}_{Ising} = -\sum_{i\neq j}\Delta_{ij}\hat{\sigma}_j^+\hat{\sigma}_i^- \simeq -\Delta_{Ising}\hat{S}_+\hat{S}_- \ . \tag{41.101}$$

A way of achieving uniform coupling consists in coupling all atoms with the same strength to the same cavity mode. This is what we will discuss in the next subsection. Do the Exc. 41.3.4.9.

In the full open system Dicke model κ and, Γ_1 describe physical processes, namely cavity decay and atomic spontaneous emission, while Γ is introduced as a mere collective decay rate, not rooted in a physical process. In reality, collective decay processes may be caused by interatomic contact interactions, but as we will see in the following, they can also be induced by coupling of the atoms to a common light mode.

Indeed, in the bad cavity limit, upon adiabatic elimination of the light mode, the cavity parameters Δ_c and κ are replaced by U_c and κ_c, which take over the role of a collective shift and decay process. This is seen in the Hamiltonian and the Lindbladian, after adiabatic elimination of the light mode, by the fact that the terms depending on κ_c have exactly the same structure as those for which collective decay at a rate Γ had been postulated in the full open Dicke model.

The systems do not differ in concept, but only in details: uniform coupling versus nearest neighbors, inhomogeneities of the light field versus disordered clouds, etc..

41.3.3.1 Adiabatic elimination of the modes of a bad high-finesse cavity

The collective Jaynes-Cummings Hamiltonian for a linear cavity (see Exc. 40.2.9.5),

$$\hat{H}_{JC} = -\Delta_c\hat{a}^\dagger\hat{a} - \imath\eta(\hat{a}-\hat{a}^\dagger) + \sum_{i=1}^{N}\left[-\tfrac{\Delta_a}{2}(\mathbb{I}_2+\hat{\sigma}_i^z) + g\sin kz_i(\hat{\sigma}_i^+\hat{a}+\hat{a}^\dagger\hat{\sigma}_i^-)\right] \ , \tag{41.102}$$

becomes in the case of perfect bunching, $z_i = z$, introducing the abbreviation $g \longrightarrow g\sin kz$,

$$\boxed{\hat{H}_{JC} = -\Delta_c\hat{a}^\dagger\hat{a} - \imath\eta(\hat{a}-\hat{a}^\dagger) - \Delta_a(\tfrac{N}{2}\mathbb{I}_2+\hat{S}_z) + g(\hat{S}_+\hat{a}+\hat{a}^\dagger\hat{S}_-)} \ , \tag{41.103}$$

where we introduced collective operators, $\hat{S}_\alpha \equiv \frac{1}{2}\sum_{i=1}^N\hat{\sigma}_i^\alpha$ for $\alpha = x, y, z$. Disregarding collective decay, $\Gamma = 0$, the Heisenberg equations become,

$$\begin{aligned}
\dot{\hat{a}} &= (\imath\Delta_c - \kappa)\hat{a} - \imath g\hat{S}_- + \eta \\
\dot{\hat{S}}_- &= (\imath\Delta_a - \tfrac{\Gamma_1}{2})\hat{S}_- + 2\imath g\hat{S}_z\hat{a} \\
\dot{\hat{S}}_z &= -\Gamma_1(\tfrac{N}{2}\mathbb{I}_2+\hat{S}_z) - \imath g(\hat{S}_+\hat{a}-\hat{a}^\dagger\hat{S}_-) \ .
\end{aligned} \tag{41.104}$$

Using $\eta \equiv \eta_r + \imath\eta_i$ we can reshape (41.104) in a real notation,

$$\begin{aligned}
\dot{\hat{a}}_r &= \tfrac{1}{2}(\dot{\hat{a}} + \dot{\hat{a}}^\dagger) &&= -\kappa\hat{a}_r - \Delta_c\hat{a}_i - g\hat{S}_y + \eta_r \\
\dot{\hat{a}}_i &= \tfrac{1}{2\imath}(\dot{\hat{a}} - \dot{\hat{a}}^\dagger) &&= -\kappa\hat{a}_i + \Delta_c\hat{a}_r - g\hat{S}_x + \eta_i \\
\dot{\hat{S}}_x &= \tfrac{1}{2}(\dot{\hat{S}}_- + \dot{\hat{S}}_+) &&= -\tfrac{\Gamma_1}{2}\hat{S}_x + \Delta_a\hat{S}_y - g\{\hat{a}_i, \hat{S}_z\} - \imath g[\hat{a}_r, \hat{S}_z] \\
\dot{\hat{S}}_y &= \tfrac{\imath}{2}(\dot{\hat{S}}_- - \dot{\hat{S}}_+) &&= -\tfrac{\Gamma_1}{2}\hat{S}_y - \Delta_a\hat{S}_x - g\{\hat{a}_r, \hat{S}_z\} + \imath g[\hat{a}_i, \hat{S}_z] \\
\dot{\hat{S}}_z &= \partial_t\tfrac{1}{2}[\hat{S}_+, \hat{S}_-] &&= -\Gamma_1(\tfrac{N}{2}\mathbb{I}_2 + \hat{S}_z) + g(\{\hat{a}_i, \hat{S}_x\} + \{\hat{a}_r, \hat{S}_y\} + \imath[\hat{a}_r, \hat{S}_x] - \imath[\hat{a}_i, \hat{S}_y])
\end{aligned} \tag{41.105}$$

The equations are equivalent to those derived by [805].

Example 260 (*Simplification for independent $\hat{a}$ and $\hat{\mathbf{S}}$*): As long as $\hat{a}$ and $\hat{\mathbf{S}}$ are independent, we may simply set $\{\hat{a}, \hat{\mathbf{S}}\} = 2\hat{a}\hat{\mathbf{S}}$ and $[\hat{a}, \hat{\mathbf{S}}] = 0$. The equations (41.105) can then be written in compact matrix notation,

$$\dot{\hat{\mathbf{S}}} = -\imath[\hat{\mathbf{S}}, \hat{H}] + \mathcal{L}_{\Gamma_1/2}\hat{\mathbf{S}} = \begin{pmatrix} -\frac{1}{2}\Gamma_1 & \Delta_a & -2g\hat{a}_i \\ -\Delta_a & -\frac{1}{2}\Gamma_1 & -2g\hat{a}_r \\ 2g\hat{a}_r & 2g\hat{a}_i & -\Gamma_1 \end{pmatrix} \begin{pmatrix} \hat{S}_x \\ \hat{S}_y \\ \hat{S}_z \end{pmatrix} - \begin{pmatrix} 0 \\ 0 \\ \Gamma_1\frac{N}{2}\mathbb{I}_2 \end{pmatrix} \tag{41.106}$$

$$= \begin{pmatrix} 2g\hat{a}_r \\ -2g\hat{a}_i \\ -\Delta_a \end{pmatrix} \times \begin{pmatrix} \hat{S}_x \\ \hat{S}_y \\ \hat{S}_z \end{pmatrix} - \Gamma_1 \begin{pmatrix} \frac{1}{2}\hat{S}_x \\ \frac{1}{2}\hat{S}_y \\ \frac{N}{2}\mathbb{I}_2 + \hat{S}_z \end{pmatrix} .$$

The equations (41.105) are just the Heisenberg-Liouville equations (41.76) derived from the open Dicke model and the open Tavis-Cummings model Hamiltonian, restricting to many immobile atoms and a single cavity mode. In the bad cavity limit, $\kappa \gg g$, the cavity field is effectively slaved to the internal atomic dynamics. Hence, we may assume $\dot{\hat{a}} \equiv 0$ and adiabatically eliminate the field. Setting $\dot{\hat{a}}_r = 0 = \dot{\hat{a}}_i$ in Eq. (41.105)(i-ii) we calculate,

$$\begin{aligned}
\hat{\Omega}_r &\equiv 2g\hat{a}_r = 2U_c(\hat{S}_x - \eta_i/g) - 2\kappa_c(\hat{S}_y - \eta_r/g) \\
\hat{\Omega}_i &\equiv 2g\hat{a}_i = -2\kappa_c(\hat{S}_x - \eta_i/g) - 2U_c(\hat{S}_y - \eta_r/g) \ ,
\end{aligned} \tag{41.107}$$

where we introduced the abbreviations,

$$U_\kappa \equiv U_c - \imath\kappa_c \qquad \text{with} \qquad U_c \equiv \frac{g^2\Delta_c}{\Delta_c^2 + \kappa^2} \qquad \text{and} \qquad \kappa_c \equiv \frac{g^2\kappa}{\Delta_c^2 + \kappa^2} \ . \tag{41.108}$$

U_c is the cooperative cavity Lamb-shift and κ_c is the Purcell-enhanced atomic decay

rate. Substituting (41.107) in the Eqs. (41.105)(iii-v) leads to [17],

$$\boxed{\begin{aligned}
\dot{\hat{S}}_x &= -(\tfrac{\Gamma_1}{2}+\kappa_c)\hat{S}_x + (\Delta_a - U_c)\hat{S}_y - 2(U_c\tilde{\eta}_r + \kappa_c\tilde{\eta}_i)\hat{S}_z + \kappa_c\{\hat{S}_x,\hat{S}_z\} + U_c\{\hat{S}_y,\hat{S}_z\} \\
\dot{\hat{S}}_y &= -(\Delta_a - U_c)\hat{S}_x - (\tfrac{\Gamma_1}{2}+\kappa_c)\hat{S}_y + 2(U_c\tilde{\eta}_i - \kappa_c\tilde{\eta}_r)\hat{S}_z - U_c\{\hat{S}_x,\hat{S}_z\} + \kappa_c\{\hat{S}_y,\hat{S}_z\} \\
\dot{\hat{S}}_z &= 2(\kappa_c\tilde{\eta}_i + U_c\tilde{\eta}_r)\hat{S}_x - 2(U_c\tilde{\eta}_i - \kappa_c\tilde{\eta}_r)\hat{S}_y - \Gamma_1(\tfrac{N}{2}\mathbb{I} + \hat{S}_z) - 2\kappa_c\hat{S}_z - 2\kappa_c(\hat{S}_x^2 + \hat{S}_y^2)
\end{aligned}} \quad . \tag{41.109}$$

Assuming $[\hat{S}_k, \hat{S}_l] = 0$ these equations simplify to the form (41.106). The number of intracavity photons is found via,

$$\hat{n} = \tfrac{1}{2g}(\hat{\Omega}_r^2 + \hat{\Omega}_i^2) = 2|U_\kappa/g|^2[(g\hat{S}_x - \eta_i)^2 + (g\hat{S}_y - \eta_r)^2] \; . \tag{41.110}$$

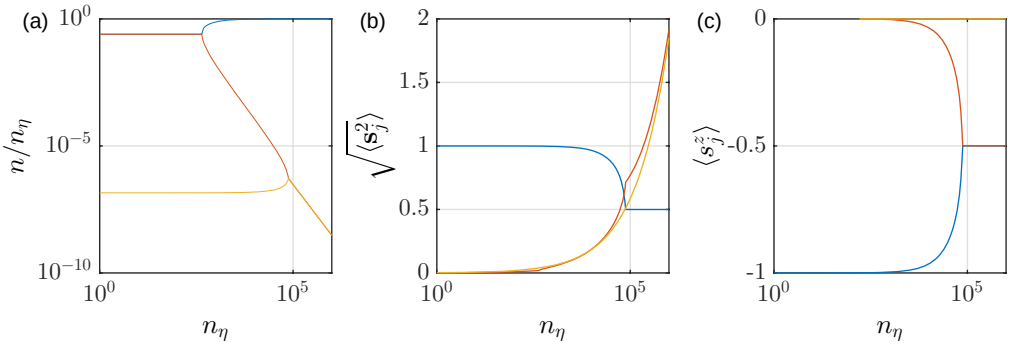

Figure 41.17: (code) Pump power dependence of (a) the intracavity photon number, (b) the total atomic spin, and (c) its projection onto the population axis.

It is interesting to consider some special cases. For example, for small $\hat{S}_{x,y} \ll \eta$, the collective dynamics will be externally controlled and the atomic spins may be considered as decorrelated. Close to the cavity resonance, $\Delta_c \ll \kappa$, Eq. (41.107) becomes,

$$\begin{aligned}
\hat{\Omega}_r &\simeq \tfrac{2}{g}(\kappa_c\eta_r - U_c\eta_i) = \frac{2g(\kappa_c\eta_r - \Delta_c\eta_i)}{\Delta_c^2 + \kappa^2} \longrightarrow \frac{2g\eta_r}{\kappa} \\
\hat{\Omega}_i &\simeq \tfrac{2}{g}(\kappa_c\eta_i + U_c\eta_r) = \frac{2g(\kappa\eta_i + \Delta_c\eta_r)}{\Delta_c^2 + \kappa^2} \longrightarrow \frac{2g\eta_i}{\kappa} \; .
\end{aligned} \tag{41.111}$$

I.e. the operators $\hat{\Omega}_{r,i}$ become real and the *cavity feedback* disappears. such that we recover the linear collective Dicke model.

[17] Equivalently, in complex notation,

$$\begin{aligned}
\Delta_\kappa\hat{a} &= g\hat{S}_- + \imath\eta \\
(\partial_t + \tfrac{\Gamma_1}{2})\dot{\hat{S}}_- &= \imath\Delta_a\hat{S}_- + 2U_\kappa(\imath\hat{S}_- - \tfrac{1}{g}\eta)\hat{S}_z \\
(\partial_t + \Gamma_1)S_z &= -\Gamma_1\tfrac{N}{2}I_2 - \kappa_c\{\hat{S}_+,\hat{S}_-\} + \tfrac{1}{g}\eta U_\kappa\hat{S}_+ + \tfrac{1}{g}\eta^* U_\kappa^*\hat{S}_- \; .
\end{aligned}$$

41.3.3.2 Hamiltonian for the Tavis-Cummings model after adiabatic elimination of the modes

Alternatively, we can try to derive a simplified Hamiltonian from which the Heisenberg-Liouville equations under adiabatic elimination of the cavity mode can be derived directly.

We have seen in Sec. 34.5.3, using the effective Hamiltonian approach, that the Heisenberg equation decomposes in a commutator and an anti-commutator. The complete Heisenberg-Liouville equation reads,

$$\boxed{\begin{aligned} \dot{\hat{\mathbf{S}}} &= -\imath[\hat{\mathbf{S}}, \hat{H}] + \mathcal{L}_{\kappa_c,\hat{S}_-}\hat{\mathbf{S}} + \sum_j \mathcal{L}_{\Gamma_1/2,\hat{s}_j^-}\hat{\mathbf{S}} \\ \text{with} \quad \hat{H} &= -2\Im\mathfrak{m}\,(\tilde{\eta}U_\kappa)\hat{S}_x - 2\Re\mathfrak{e}\,(\tilde{\eta}U_\kappa)\hat{S}_y - \Delta_a\hat{S}_z + U_c\hat{S}_+\hat{S}_- \end{aligned}} \quad . \tag{41.112}$$

As shown in Exc. 41.3.4.10, we recover exactly the equations of motion (41.109). The complete absence of the field from the equations of motion shows that, in the bad cavity limit, any coherence of the coupled atom-cavity system is entirely contained in the atomic cloud.

Comparing this model to the one of the open system Dicke model (41.74), we notice that the cavity decay plays the role of a collective decay mechanism.

41.3.3.3 The XX-Heisenberg model

Without pumping and neglecting spontaneous emission, $\eta = \Gamma_1 = 0$, we obtain the simplified Hamiltonian of the Tavis-Cummings model (41.76) with RWA, $g' = 0$,

$$\hat{H}_{TC} = -\Delta_a\hat{S}_z + U_c\hat{S}_+\hat{S}_- \ , \tag{41.113}$$

also known as the effective Hamiltonian of the *XX-Heisenberg model*. For large $N \gg 1$ the second term can safely be approximated by $\frac{1}{2}U_c\{\hat{S}_+, \hat{S}_-\}$ [956]. The Heisenberg-Liouville equations can then be written,

$$\dot{\hat{\mathbf{S}}} = \begin{pmatrix} 2U_c\hat{S}_x - 2\kappa_c\hat{S}_y \\ 2U_c\hat{S}_y + 2\kappa_c\hat{S}_x \\ -\Delta_a \end{pmatrix} \times \hat{\mathbf{S}} \ . \tag{41.114}$$

Analogously, inserting (41.107) into the above Heisenberg-Liouville equations of the Dicke model (41.76) without RWA, $g' = g$, we obtain neglecting $\eta = \Gamma = 0$,

$$\dot{\hat{\mathbf{S}}} = \begin{pmatrix} 4U_c\hat{S}_x - 4\kappa_c\hat{S}_y \\ 0 \\ -\Delta_a \end{pmatrix} \times \hat{\mathbf{S}} \ . \tag{41.115}$$

Example 261 (*One-axis twisting in the XX-Heisenberg model*): The coupling strength $\sqrt{N_+N_-} \leq \frac{N}{2}$ between the cavity mode and the atoms depends on the inversion. Hence, this leads to an inversion-dependent frequency shift known as *one-axis twisting* [18]. In the mean field treatment we simply replace

[18] This is somewhat analogous to the photon number-dependent phase shift observed in dispersive interaction in the Jaynes-Cummings model.

the operators by their expectation values. Setting $\Delta_a = 0$ in the Heisenberg-Liouville equations (41.114) and neglecting terms $\dot{\hat{S}}_z \propto \hat{S}_z$, we get,

$$\dot{\hat{\mathbf{S}}} \simeq \begin{pmatrix} 2(\kappa_c \hat{S}_x + U_c \hat{S}_y)\hat{S}_z \\ 2(\kappa_c \hat{S}_y - U_c \hat{S}_x)\hat{S}_z \\ -2\kappa_c(\hat{S}_x^2 + \hat{S}_y^2) \end{pmatrix} .$$

Starting from the initial condition, $\vec{S} = (0, 0, N/2)$, we see that the instantaneous collective dipole moment $\hat{S}_x^2 + \hat{S}_y^2$ determines the decay of the inversion, while the inversion $\hat{S}_z$ twists the dipole moment [868, 835, 959, 957, 956]. Collective decay occurs at a rate $\hat{S}_- \sqrt{\kappa_c/2}$. It is easy to see that $\partial_t \hat{\mathbf{S}}^2 = \hat{\mathbf{S}} \cdot \dot{\hat{\mathbf{S}}} + \dot{\hat{\mathbf{S}}} \cdot \hat{\mathbf{S}} = 0$.

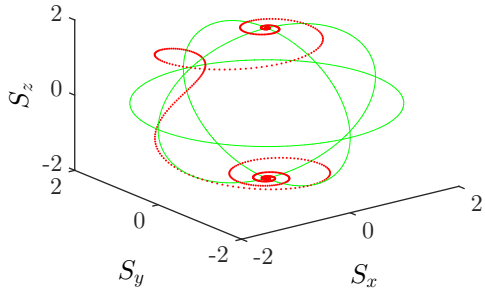

Figure 41.18: (code) One-axis twisting.

41.3.4 Exercises

41.3.4.1 Ex: Calculating with collective operators

The collective spin operators for an ensemble of J atoms with M internal levels are defined as,

$$\hat{S} = \sum_{j=1}^{J} \hat{\sigma}_j = \hat{\sigma} \otimes \mathbb{I}_M \otimes \mathbb{I}_M \otimes ... + \mathbb{I}_M \otimes \hat{\sigma} \otimes \mathbb{I}_M \otimes + ... \ ,$$

or more explicitly,

$$\hat{S}_{kl} = \sum_{j=1}^{J} \hat{\sigma}_j^{kl} = |k\rangle\langle l| \otimes \mathbb{I}_M \otimes \mathbb{I}_M \otimes ... + \mathbb{I}_M \otimes |k\rangle\langle l| \otimes \mathbb{I}_M \otimes + ... \ ,$$

with the spin matrices satisfying,

$$\hat{\sigma}_j^{kl}\hat{\sigma}_j^{mn} = \delta_{lm}\hat{\sigma}_j^{kn} \quad \text{and} \quad [\hat{\sigma}_i^{kl}, \hat{\sigma}_j^{mn}] = \delta_{ij}(\delta_{lm}\hat{\sigma}_j^{kn} - \delta_{kn}\hat{\sigma}_j^{ml})$$

$$\textstyle\sum_{m=1}^{M} \hat{\sigma}_j^{mm} = \mathbb{I}_M \quad \text{and} \quad \sum_{j=1}^{J}\sum_{m=1}^{M} \hat{\sigma}_j^{mm} = N\mathbb{I}_M \ .$$

Verify that for the case of atoms subject to spin-spin interaction,

$$\hat{H} \neq \sum_{j,m} \hat{\sigma}_j^{mm} \hat{H} \hat{\sigma}_j^{mm} \ .$$

Solution: *We calculate,*

$$\hat{S}_{kl}\hat{S}_{mn} = \sum_{i,j}\hat{\sigma}_i^{kl}\hat{\sigma}_j^{mn} = \sum_j \delta_{lm}\hat{\sigma}_j^{kn} + \sum_{i\neq j}\hat{\sigma}_i^{kl}\hat{\sigma}_j^{mn} = \delta_{lm}\hat{S}_{kn} + \sum_{i\neq j}\hat{\sigma}_i^{kl}\hat{\sigma}_j^{mn}$$
$$[\hat{S}_{kl},\hat{S}_{mn}] = \sum_{i,j}[\hat{\sigma}_i^{kl},\hat{\sigma}_j^{mn}] = \sum_{i,j}\delta_{ij}(\delta_{lm}\hat{\sigma}_j^{kn} - \delta_{kn}\hat{\sigma}_j^{ml}) = \delta_{lm}\hat{S}_{kn} - \delta_{kn}\hat{S}_{ml} \ .$$

A Hamiltonian with spin-spin interactions is generally composed of a sum of terms such as,

$$\hat{H} = a\hat{\sigma}_k^{mn} + b\hat{\sigma}_k^{mn}\hat{\sigma}_l^{pq} \ .$$

With this,

$$\begin{aligned}\sum_{j,r}\hat{\sigma}_j^{rr}\hat{H}\hat{\sigma}_j^{rr} &= a\sum_{j,r}\hat{\sigma}_j^{rr}\hat{\sigma}_k^{m,n}\hat{\sigma}_j^{rr} + b\sum_{j,r}\hat{\sigma}_j^{rr}\hat{\sigma}_k^{m,n}\hat{\sigma}_l^{p,q}\hat{\sigma}_j^{rr}\\ &= a\hat{\sigma}_k^{m,n}\delta_{kj} + a\sum_j\hat{\sigma}_k^{m,n}(1-\delta_{kj}) + b\sum_{j,r}\hat{\sigma}_j^{rr}\hat{\sigma}_k^{m,n}\hat{\sigma}_l^{p,q}\hat{\sigma}_j^{rr}\\ &\neq a\hat{\sigma}_k^{m,n} + b\hat{\sigma}_k^{mn}\hat{\sigma}_l^{pq} \ .\end{aligned}$$

41.3.4.2 Ex: Liouvillean for two dipole-coupled atoms

a. From the master equation (41.88) set up the Liouvillean $\mathcal{M}$ for a system of two atoms coupled via dipolar radiation allowing to write the master equation as $\dot{\vec{\varrho}} = \mathcal{M}\vec{\varrho}$.
b. Discuss the Lindblad term in the limit, $kr_{12} \to 0$.
c. We have seen in Exc. 34.6.7.9, how to write down the master equation for a two-level atom whose levels are coupled by blackbody radiation. Extend the procedure to two dipole-coupled two-level atoms whose levels are only coupled by blackbody radiation.

Solution: *a. We have already introduced master equations for two- and three-level systems in Secs. 34.5.2 and 34.7.1. This concept can be extended to two coupled two-level systems [110], which can be mapped as a four-level system. We start from the master equation,*

$$\frac{d\hat{\rho}}{dt} = -\imath[\hat{H},\hat{\rho}] + \mathcal{L}_{incoh}\hat{\rho} \quad \text{with} \quad \mathcal{L}_{incoh}\hat{\rho} = \tfrac{1}{2}\sum_{i,j=1}^{2}\Gamma_{ij}(2\hat{\sigma}_j^-\rho\hat{\sigma}_i^+ - \hat{\sigma}_i^+\hat{\sigma}_j^-\hat{\rho} - \hat{\rho}\hat{\sigma}_i^+\hat{\sigma}_j^-) \ ,$$

first concentrating on the coherent part,

$$\mathcal{L}_{coh}\hat{\rho} = -\imath[\hat{H},\hat{\rho}] \ .$$

The Hamiltonian and the density operator are given by,

$$\hat{H} = \begin{pmatrix}\Delta_a & \frac{1}{2}\Omega & \frac{1}{2}\Omega^* & 0\\ \frac{1}{2}\Omega^* & 0 & \frac{1}{2}\Delta_{21} & \frac{1}{2}\Omega^*\\ \frac{1}{2}\Omega & \frac{1}{2}\Delta_{12} & 0 & \frac{1}{2}\Omega\\ 0 & \frac{1}{2}\Omega & \frac{1}{2}\Omega^* & -\Delta_a\end{pmatrix} \quad \textit{and} \quad \hat{\rho} = \hat{\rho}^\dagger = \begin{pmatrix}\rho_{11,11} & \rho_{11,12} & \rho_{11,21} & \rho_{11,22}\\ \rho_{12,11} & \rho_{12,12} & \rho_{12,21} & \rho_{12,22}\\ \rho_{21,11} & \rho_{21,12} & \rho_{21,21} & \rho_{21,22}\\ \rho_{22,11} & \rho_{22,12} & \rho_{22,21} & \rho_{22,22}\end{pmatrix} \ ,$$

with the abbreviations,

$$\Delta_{12} = \Delta_{21} \equiv -\Gamma \frac{\cos kr_{12}}{kr_{12}} \qquad \textit{and} \qquad \Gamma_{12} = \Gamma_{21} \equiv \Gamma \frac{\sin kr_{12}}{kr_{12}} \qquad \textit{and} \qquad \Gamma_{11} = \Gamma_{22} = \Gamma \ ,$$

Thus, we have 16 equations to describe the evolutions of the 16 components of the total density matrix (ρ_{ij})*. After rearranging the density operator like,*

$$\begin{aligned}\hat{\vec{\varrho}} = (&\rho_{11,11} \ , \ \rho_{11,12} \ , \ \rho_{11,21} \ , \ \rho_{11,22} \ , \ \rho_{12,11} \ , \ \rho_{12,12} \ , \ \rho_{12,21} \ , \ \rho_{12,22} \ , \ \cdots \\ &\cdots \ , \ \rho_{21,11} \ , \ \rho_{21,12} \ , \ \rho_{21,21} \ , \ \rho_{21,22} \ , \ \rho_{22,11} \ , \ \rho_{22,12} \ , \ \rho_{22,21} \ , \ \rho_{22,22}) \ ,\end{aligned}$$

the coherent Liouvillean can be cast into the form (see also Sec. 34.7.1),

$$\boxed{\mathcal{L}_{coh}\hat{\rho} = -\imath[\hat{H},\hat{\rho}] \ \triangleq \ -\imath(\hat{H}\otimes\mathbb{I}_4 - \mathbb{I}_4\otimes\hat{H}^*)\hat{\vec{\varrho}} = \mathcal{M}_{coh}\hat{\vec{\varrho}}} \ ,$$

or explicitly,

$$\mathcal{M}_{coh} = -\imath \begin{pmatrix} -\hat{H}^* + \Delta_a\mathbb{I}_4 & \frac{1}{2}\Omega\mathbb{I}_4 & \frac{1}{2}\Omega^*\mathbb{I}_4 & 0 \\ \frac{1}{2}\Omega^*\mathbb{I}_4 & -\hat{H}^* & \frac{1}{2}\Delta_{12}\mathbb{I}_4 & \frac{1}{2}\Omega^*\mathbb{I}_4 \\ \frac{1}{2}\Omega\mathbb{I}_4 & \frac{1}{2}\Delta_{12}\mathbb{I}_4 & -\hat{H}^* & \frac{1}{2}\Omega\mathbb{I}_4 \\ 0 & \frac{1}{2}\Omega\mathbb{I}_4 & \frac{1}{2}\Omega^*\mathbb{I}_4 & -\hat{H}^* - \Delta_a\mathbb{I}_4 \end{pmatrix} \ .$$

For the incoherent part, where the two spins operators are,

$$\hat{\sigma}_1^{\pm} \equiv \sigma^{\pm}\otimes\mathbb{I} \qquad \textit{and} \qquad \hat{\sigma}_2^{\pm} \equiv \mathbb{I}\otimes\hat{\sigma}^{\pm} \ .$$

we express the Lindblad operator,

$$\begin{aligned}\mathcal{L}_{incoh}\hat{\rho} &= \tfrac{1}{2}\Gamma\left(2\sigma_1^-\hat{\rho}\hat{\sigma}_1^+ - \hat{\sigma}_1^+\sigma_1^-\hat{\rho} - \hat{\rho}\hat{\sigma}_1^+\sigma_1^-\right) + \tfrac{1}{2}\Gamma\left(2\sigma_2^-\hat{\rho}\hat{\sigma}_2^+ - \hat{\sigma}_2^+\sigma_2^-\hat{\rho} - \hat{\rho}\hat{\sigma}_2^+\sigma_2^-\right) \\ &\quad + \tfrac{1}{2}\Gamma_{12}\left(2\sigma_2^-\hat{\rho}\hat{\sigma}_1^+ - \hat{\sigma}_1^+\sigma_2^-\hat{\rho} - \hat{\rho}\hat{\sigma}_1^+\sigma_2^-\right) + \tfrac{1}{2}\Gamma_{12}\left(2\sigma_1^-\hat{\rho}\hat{\sigma}_2^+ - \hat{\sigma}_2^+\sigma_1^-\hat{\rho} - \hat{\rho}\hat{\sigma}_2^+\sigma_1^-\right) \\ &= \mathcal{L}_{\Gamma} + \mathcal{L}_{\Gamma_{12}} \ ,\end{aligned}$$

with

$$\mathcal{L}_{\Gamma} \equiv \tfrac{\Gamma}{2}\begin{pmatrix} 2\rho_{21,21}+2\rho_{12,12} & 2\rho_{21,22}-\rho_{11,12} & 2\rho_{12,22}-\rho_{11,21} & -2\rho_{11,22} \\ 2\rho_{22,21}-\rho_{12,11} & 2\rho_{22,22}-2\rho_{12,12} & -2\rho_{12,21} & -3\rho_{12,22} \\ 2\rho_{22,12}-\rho_{21,11} & -2\rho_{21,12} & -2\rho_{21,21}+2\rho_{22,22} & -3\rho_{21,22} \\ -2\rho_{22,11} & -3\rho_{22,12} & -3\rho_{22,21} & -4\rho_{22,22} \end{pmatrix} \ ,$$

and

$$\mathcal{L}_{\Gamma_{12}} \equiv \tfrac{\Gamma_{12}}{2}\begin{pmatrix} 2\rho_{12,21}+2\rho_{21,12} & 2\rho_{12,22}-\rho_{11,21} & 2\rho_{21,22}-\rho_{11,12} & 0 \\ 2\rho_{22,12}-\rho_{21,11} & -\rho_{12,21}-\rho_{21,12} & 2\rho_{22,22}-\rho_{12,12}-\rho_{21,21} & -\rho_{21,22} \\ 2\rho_{22,21}-\rho_{12,11} & 2\rho_{22,22}-\rho_{12,12}-\rho_{21,21} & -\rho_{12,21}-\rho_{21,12} & -\rho_{12,22} \\ 0 & -\rho_{22,21} & -\rho_{22,12} & 0 \end{pmatrix} \ ,$$

as

$$\mathcal{M}_{incoh} = \begin{pmatrix} \mathcal{G} & \mathcal{F}_1 & \mathcal{F}_2 & 0 \\ 0 & \mathcal{G} - \frac{1}{2}\Gamma\mathbb{I}_4 & -\frac{1}{2}\Gamma_{12}\mathbb{I}_4 & \mathcal{F}_2 \\ 0 & -\frac{1}{2}\Gamma_{12}\mathbb{I}_4 & \mathcal{G} - \frac{1}{2}\Gamma\mathbb{I}_4 & \mathcal{F}_1 \\ 0 & 0 & 0 & \mathcal{G} - \Gamma\mathbb{I}_4 \end{pmatrix} \quad with \quad \mathcal{G} = -\frac{1}{2}\begin{pmatrix} 0 & 0 & 0 & 0 \\ 0 & \Gamma & \Gamma_{12} & 0 \\ 0 & \Gamma_{12} & \Gamma & 0 \\ 0 & 0 & 0 & 2\Gamma \end{pmatrix}$$

$$with \quad \mathcal{F}_1 = \begin{pmatrix} 0 & \Gamma & \Gamma_{12} & 0 \\ 0 & 0 & 0 & \Gamma_{12} \\ 0 & 0 & 0 & \Gamma \\ 0 & 0 & 0 & 0 \end{pmatrix} \quad and \quad \mathcal{F}_2 = \begin{pmatrix} 0 & \Gamma_{12} & \Gamma & 0 \\ 0 & 0 & 0 & \Gamma \\ 0 & 0 & 0 & \Gamma_{12} \\ 0 & 0 & 0 & 0 \end{pmatrix} .$$

The master equation is now solved as,

$$\vec{\varrho}(t) = e^{(\mathcal{M}_{coh}+\mathcal{M}_{incoh})t}\vec{\varrho}(0) \ .$$

b. In the limit $kr_{12} \to 0$ we get for the Lindblad term,

$$\mathcal{M} = -i[\hat{H}, \vec{\rho}] = -\imath\times$$

$$\begin{pmatrix}
\rho_{11,11} & \rho_{11,12} & \rho_{11,21} & \rho_{11,22} & \rho_{12,11} & \rho_{12,12} & \rho_{12,21} & \rho_{12,22} & \rho_{21,11} & \rho_{21,12} & \rho_{21,21} & \rho_{21,22} & \rho_{22,11} & \rho_{22,12} & \rho_{22,21} & \rho_{22,22} & \\
0 & -\frac{1}{2}\Omega^* & 0 & \frac{1}{2}\Omega & \Gamma & \Gamma_{12} & 0 & \frac{1}{2}\Omega^* & \Gamma_{12} & \Gamma & 0 & 0 & 0 & 0 & 0 & \rho_{11,11} \\
-\frac{1}{2}\Omega & \Delta_a - \frac{1}{2}\Gamma & -\frac{1}{2}\Delta_{12} - \frac{1}{2}\gamma & -\frac{1}{2}\Omega & 0 & \frac{1}{2}\Omega & \Gamma_{12} & \Gamma & 0 & \frac{1}{2}\Omega^* & 0 & \Gamma & 0 & 0 & 0 & 0 & \rho_{11,12} \\
-\frac{1}{2}\Omega & -\frac{1}{2}\Delta_{12} - \frac{1}{2}\gamma & \Delta_a - \frac{1}{2}\Gamma & -\frac{1}{2}\Omega^* & 0 & 0 & \frac{1}{2}\Omega & \Gamma & 0 & 0 & \frac{1}{2}\Omega^* & \Gamma_{12} & 0 & 0 & 0 & 0 & \rho_{11,21} \\
0 & -\frac{1}{2}\Omega^* & -\frac{1}{2}\Omega & 2\Delta_a - \Gamma & 0 & 0 & 0 & \frac{1}{2}\Omega & 0 & 0 & 0 & \frac{1}{2}\Omega^* & 0 & \Gamma_{12} & \Gamma & 0 & \rho_{11,22} \\
\frac{1}{2}\Omega^* & 0 & 0 & 0 & -\Delta_a - \frac{1}{2}\Gamma & -\frac{1}{2}\Omega^* & -\frac{1}{2}\Omega & 0 & \frac{1}{2}\Delta_{12} - \frac{1}{2}\Gamma_{12} & 0 & 0 & 0 & \frac{1}{2}\Omega^* & 0 & 0 & \Gamma & \rho_{12,11} \\
0 & \frac{1}{2}\Omega^* & 0 & 0 & -\frac{1}{2}\Omega & -\Gamma & -\frac{1}{2}\Delta_{12} - \frac{1}{2}\Gamma_{12} & -\frac{1}{2}\Omega & 0 & \frac{1}{2}\Delta_{12} - \frac{1}{2}\Gamma_{12} & 0 & 0 & 0 & \frac{1}{2}\Omega^* & 0 & \Gamma_{12} & \rho_{12,12} \\
0 & 0 & \frac{1}{2}\Omega^* & 0 & -\frac{1}{2}\Omega^* & -\frac{1}{2}\Delta_{12} - \frac{1}{2}\Gamma_{12} & -\Gamma & -\frac{1}{2}\Omega^* & 0 & 0 & \frac{1}{2}\Delta_{12} - \frac{1}{2}\Gamma_{12} & 0 & 0 & 0 & \frac{1}{2}\Omega^* & 0 & \rho_{12,21} \\
0 & 0 & 0 & \frac{1}{2}\Omega^* & 0 & -\frac{1}{2}\Omega & -\frac{1}{2}\Omega & \Delta_a - \frac{1}{2}\Gamma & 0 & 0 & 0 & \frac{1}{2}\Delta_{12} - \frac{1}{2}\Gamma_{12} & 0 & 0 & \Gamma & \Gamma_{12} & \frac{1}{2}\Omega^* & \rho_{12,22} \\
\frac{1}{2}\Omega & 0 & 0 & 0 & \frac{1}{2}\Delta_{12} - \frac{1}{2}\Gamma_{12} & 0 & 0 & 0 & -\Delta_a & -\frac{1}{2}\Omega^* & -\frac{1}{2}\Omega & 0 & \frac{1}{2}\Omega & 0 & 0 & \Gamma_{12} & \rho_{21,11} \\
0 & \frac{1}{2}\Omega & 0 & 0 & 0 & \frac{1}{2}\Delta_{12} - \frac{1}{2}\Gamma_{12} & 0 & 0 & -\frac{1}{2}\Omega & -\Gamma & -\frac{1}{2}\Delta_{12} - \frac{1}{2}\Gamma_{12} & -\frac{1}{2}\Omega & 0 & \frac{1}{2}\Omega & 0 & \Gamma & \rho_{21,12} \\
0 & 0 & \frac{1}{2}\Omega & 0 & 0 & \frac{1}{2}\Delta_{12} - \frac{1}{2}\Gamma_{12} & 0 & 0 & -\frac{1}{2}\Omega^* & -\frac{1}{2}\Delta_{12} - \frac{1}{2}\Gamma_{12} & -\Gamma & -\frac{1}{2}\Omega^* & 0 & 0 & \frac{1}{2}\Omega & 0 & \rho_{21,21} \\
0 & 0 & 0 & \frac{1}{2}\Omega & 0 & 0 & \frac{1}{2}\Delta_{12} - \frac{1}{2}\Gamma_{12} & 0 & 0 & -\frac{1}{2}\Omega^* & -\frac{1}{2}\Omega & \Delta_a - \frac{1}{2}\Gamma & 0 & 0 & \frac{1}{2}\Omega & 0 & \rho_{21,22} \\
0 & 0 & 0 & 0 & \frac{1}{2}\Omega & 0 & 0 & 0 & \frac{1}{2}\Omega^* & 0 & 0 & 0 & -2\Delta_a - \Gamma & -\frac{1}{2}\Omega^* & -\frac{1}{2}\Omega & 0 & \rho_{22,11} \\
0 & 0 & 0 & 0 & 0 & \frac{1}{2}\Omega & 0 & 0 & 0 & \frac{1}{2}\Omega^* & 0 & 0 & -\frac{1}{2}\Omega & -\Delta_a - \frac{3}{2}\Gamma & -\frac{1}{2}\Delta_{12} - \frac{1}{2}\Gamma_{12} & -\frac{1}{2}\Omega & \rho_{22,12} \\
0 & 0 & 0 & 0 & 0 & 0 & \frac{1}{2}\Omega & 0 & 0 & 0 & \frac{1}{2}\Omega^* & 0 & -\frac{1}{2}\Omega^* & -\frac{1}{2}\Delta_{12} - \frac{1}{2}\Gamma_{12} & -\Delta_a - \frac{3}{2}\Gamma & -\frac{1}{2}\Omega^* & \rho_{22,21} \\
0 & 0 & 0 & 0 & 0 & 0 & 0 & \frac{1}{2}\Omega & 0 & 0 & 0 & \frac{1}{2}\Omega^* & 0 & -\frac{1}{2}\Omega^* & -\frac{1}{2}\Omega & -2\Gamma & \rho_{22,22}
\end{pmatrix}$$

Figure 41.19: Liouvillean for two dipole-coupled atoms.

$$\Gamma_{12} \to \Gamma \qquad and \qquad |\Delta_{12}| \to \infty \ ,$$

and consequently,

$$\begin{aligned}\mathcal{L}_{incoh}\hat{\rho} &= \tfrac{1}{2}\Gamma\left[2(\hat{\sigma}_1^- + \hat{\sigma}_2^-)\hat{\rho}(\hat{\sigma}_1^+ + \hat{\sigma}_2^+) - (\hat{\sigma}_1^+ + \hat{\sigma}_2^+)(\hat{\sigma}_1^- + \hat{\sigma}_2^-)\hat{\rho} - \hat{\rho}(\hat{\sigma}_1^+ + \hat{\sigma}_2^+)(\hat{\sigma}_1^- + \hat{\sigma}_2^-)\right] \\ &= \Gamma[2\hat{S}^-\hat{\rho}\hat{S}^+ - \hat{S}^+\hat{S}^-\hat{\rho} - \hat{\rho}\hat{S}^+\hat{S}^-] \ .\end{aligned}$$

That is, in this limit the single-atom decay mentioned in (41.74) turns into a collective decay.
c. The master equation is [1359],

$$\begin{aligned}\frac{d\hat{\rho}}{dt} &= \mathcal{L}_{bb}\hat{\rho} \\ &= -\tfrac{1}{2}\sum_{i,j=1,2}\left(\Gamma_{ij} + R_{ij}\right)\left([\hat{\rho}\hat{\sigma}_j^+, \hat{\sigma}_i^-] + [\hat{\sigma}_j^+, \hat{\sigma}_i^-\hat{\rho}]\right) - \tfrac{1}{2}\sum_{i,j=1,2} R_{ij}\left([\hat{\rho}\hat{\sigma}_j^-, \hat{\sigma}_i^+] + [\hat{\sigma}_j^-, \hat{\sigma}_i^+\hat{\rho}]\right) \ ,\end{aligned}$$

with $R_{ij}\delta(t-t') \propto \langle \hat{E}_i(t)\hat{E}_j(t')\rangle$ containing both the real and the virtual photon exchange. With $\Gamma = \Gamma_{ii}$, $\Gamma_{12} = \Gamma_{21}$, $R = R_{ii}$, and $R_{12} = R_{21}$, we find,

$$\begin{aligned}\dot{\hat{\rho}} &= \tfrac{\Gamma}{2}\sum_{i=1,2}\left(2\hat{\sigma}_i^-\hat{\rho}\hat{\sigma}_i^+ - \hat{\rho}\hat{\sigma}_i^+\hat{\sigma}_i^- - \hat{\sigma}_i^+\hat{\sigma}_i^-\hat{\rho}\right) + \tfrac{\Gamma_{12}}{2}\sum_{i\neq j}\left(2\hat{\sigma}_j^-\hat{\rho}\hat{\sigma}_i^+ - \hat{\rho}\hat{\sigma}_i^+\hat{\sigma}_j^- - \hat{\sigma}_i^+\hat{\sigma}_j^-\hat{\rho}\right)\\ &+ R\sum_{i=1,2}\left(\hat{\sigma}_i^+\hat{\rho}\hat{\sigma}_i^- + \hat{\sigma}_i^-\hat{\rho}\hat{\sigma}_i^+ - \hat{\rho}\right) + \tfrac{R_{12}}{2}\sum_{i\neq j}\left(2\hat{\sigma}_i^+\hat{\rho}\hat{\sigma}_j^- + 2\hat{\sigma}_j^-\hat{\rho}\hat{\sigma}_i^+ - \hat{\rho}\{\hat{\sigma}_j^-,\hat{\sigma}_i^+\} - \{\hat{\sigma}_j^-,\hat{\sigma}_i^+\}\hat{\rho}\right)\\ &= \mathcal{L}_\Gamma + \mathcal{L}_{\Gamma_{12}} + \mathcal{L}_R + \mathcal{L}_{R_{12}}\ .\end{aligned}$$

with $\mathcal{L}_\Gamma$ and $\mathcal{L}_{\Gamma_{12}}$ derived in part (b) and

$$\mathcal{L}_R = R\begin{pmatrix}\rho_{12,12}-\rho_{11,11}+\rho_{21,21} & \rho_{21,22}-\rho_{11,12} & \rho_{12,22}-\rho_{11,21} & -\rho_{11,22}\\ \rho_{22,21}-\rho_{12,11} & \rho_{11,11}-\rho_{12,12}+\rho_{22,22} & -\rho_{12,21} & -\rho_{12,22}+\rho_{11,21}\\ \rho_{22,12}-\rho_{21,11} & -\rho_{21,12} & \rho_{11,11}-\rho_{21,21}+\rho_{22,22} & \rho_{11,12}-\rho_{21,22}\\ -\rho_{22,11} & -\rho_{22,12}+\rho_{21,11} & \rho_{12,11}-\rho_{22,21} & \rho_{12,12}+\rho_{21,21}-\rho_{22,22}\end{pmatrix},$$

and

$$\mathcal{L}_{R_{12}} = R_{12}\begin{pmatrix}\rho_{21,12}+\rho_{12,21} & \rho_{12,22}-\rho_{11,21} & \rho_{21,22}-\rho_{11,12} & 0\\ \rho_{22,12}-\rho_{21,11} & -\rho_{12,21}-\rho_{21,12} & \rho_{11,11}+\rho_{22,22}-\rho_{12,12}-\rho_{21,21} & \rho_{11,12}-\rho_{21,22}\\ \rho_{22,21}-\rho_{12,11} & \rho_{11,11}+\rho_{22,22}-\rho_{12,12}-\rho_{21,21} & -\rho_{12,21}-\rho_{21,12} & \rho_{11,21}-\rho_{12,22}\\ 0 & \rho_{12,11}-\rho_{22,21} & \rho_{21,11}-\rho_{22,12} & \rho_{21,12}+\rho_{12,21}\end{pmatrix}.$$

41.3.4.3 Ex: Super- and subradiant linewidth and decay rates from the coupled dipoles model

Calculate super- and subradiance linewidth and lineshifts for two atoms interacting via dipole-dipole interaction using the linear optics scalar coupled dipoles model culminating in Eq. (39.26) using the exponential kernel (39.29).

Solution: *We consider two atoms located next to each other at positions $\pm\frac{r_{12}}{2}$ of the z-axis, i.e. [1090],*

$$\mathbf{r}_1 = \tfrac{r_{12}}{2}\hat{\mathbf{e}}_z \quad , \quad \mathbf{r}_2 = -\tfrac{r_{12}}{2}\hat{\mathbf{e}}_z \quad \text{with} \quad |\mathbf{r}_1-\mathbf{r}_2| = r_{12} \ll \lambda\ .$$

We also set $\hat{\mathbf{e}}_z \perp \mathbf{k}_0$. Then, the Rabi frequencies $\Omega(\mathbf{r}_j) = \Omega_0 e^{\imath\mathbf{k}_0\cdot\mathbf{r}_j}$ at the atomic positions can be written,

$$\Omega(\mathbf{r}_1) = \Omega_0 e^{\imath k r_{12}/2} = \Omega^*(\mathbf{r}_2) \simeq \Omega_0\ .$$

Using the linear optics ansatz (39.11) yields for the amplitudes $\beta_j = \langle j|\psi\rangle$ and $\beta_j = \bar{\beta}_j e^{-\imath\Delta_0 t+\imath\mathbf{k}_0\cdot\mathbf{r}_j}$ the equation of motion (39.26),

$$\frac{d}{dt}\bar{\beta}_j = \left(\imath\Delta_0 - \frac{\Gamma}{2}\right)\bar{\beta}_j - \frac{\imath\Omega_0}{2} - \frac{\Gamma}{2}\sum_{m\neq j} e^{-\imath\mathbf{k}_0\cdot(\mathbf{r}_j-\mathbf{r}_m)}\frac{e^{\imath k_0|\mathbf{r}_j-\mathbf{r}_m|}}{\imath k_0|\mathbf{r}_j-\mathbf{r}_m|}\bar{\beta}_m\ ,$$

which for the case of two atoms reads, for $\hat{\mathbf{e}}_z \parallel \mathbf{k}_0$,

$$\frac{d}{dt}\bar{\beta}_1 = \left(\imath\Delta_0 - \frac{\Gamma}{2}\right)\bar{\beta}_1 - \frac{\imath\Omega_0}{2} - \Gamma\frac{1}{\imath k_0 r_{12}}\bar{\beta}_2\ ,$$

and for $\hat{\mathbf{e}}_z \perp \mathbf{k}_0$,

$$\begin{aligned}\frac{d}{dt}\bar{\beta}_1 &= \left(\imath\Delta_0 - \frac{\Gamma}{2}\right)\bar{\beta}_1 - \frac{\imath\Omega_0}{2} - \Gamma\frac{e^{\imath k_0 r_{12}}}{\imath k_0 r_{12}}\bar{\beta}_2 \\ &= \left(\imath\Delta_0 - \frac{\Gamma}{2}\right)\bar{\beta}_1 - \frac{\imath\Omega_0}{2} - \Gamma\left(\frac{\cos k_0 r_{12}}{\imath k_0 r_{12}} + \frac{\sin k_0 r_{12}}{k_0 r_{12}}\right)\bar{\beta}_2 \ .\end{aligned}$$

That is,

$$\begin{aligned}&\frac{d}{dt}\begin{pmatrix}\bar{\beta}_1\\ \bar{\beta}_2\end{pmatrix} = \imath\hat{H}_{eff}\begin{pmatrix}\bar{\beta}_1\\ \bar{\beta}_2\end{pmatrix} - \frac{\imath\Omega_0}{2} \\ &\textit{with} \qquad \hat{H}_{eff} = \begin{pmatrix}\Delta_0 + \frac{\imath\Gamma}{2} & \imath\Gamma\left(\frac{\cos k_0 r_{12}}{\imath k_0 r_{12}} + \frac{\sin k_0 r_{12}}{k_0 r_{12}}\right) \\ \imath\Gamma\left(\frac{\cos k_0 r_{12}}{\imath k_0 r_{12}} + \frac{\sin k_0 r_{12}}{k_0 r_{12}}\right) & \Delta_0 + \frac{\imath\Gamma}{2}\end{pmatrix} \ .\end{aligned}$$

The eigenvalues of the effective Hamitonian are then,

$$E = \Delta_0 \pm \Gamma\frac{\cos k_0 r_{12}}{k_0 r_{12}} + \imath\Gamma\left(\frac{1}{2} \pm \frac{\sin k_0 r_{12}}{k_0 r_{12}}\right) \ .$$

Hence, for $r_{12} \ll \lambda$ *the super/sub-radiant lifetimes and energy shifts are,*

$$\Gamma_\pm = \Gamma\left(1 \pm \frac{\sin kr_{12}}{kr_{12}}\right) \gtrless \Gamma \qquad \textit{and} \qquad \Delta_\pm = \pm\Gamma\frac{\cos kr_{12}}{2kr_{12}} \ .$$

41.3.4.4 Ex: Super- and subradiance in a two atom system

Calculate the temporal behavior of the (anti-)symmetric states $\rho_{S,A} = \frac{1}{2}(\rho_{12,12} + \rho_{21,21} \pm \rho_{12,21} \pm \rho_{21,12})$ from the master equation (41.88) or the Liouville equation (41.90). Consider in particular the case of absent driving, $\Omega = 0$.

Solution: *With the Rabi frequency,* $\Omega = \Omega_0 e^{\imath kr_{12}/2}$ *and the abbreviations,*

$$\begin{aligned}&\Omega_+ \equiv \sqrt{2}\Omega_0\cos\tfrac{kr_{12}}{2} \qquad \textit{and} \qquad \Omega_- \equiv \sqrt{2}\Omega_0\sin\tfrac{kr_{12}}{2} \\ &\textit{and} \qquad \Gamma_\pm \equiv \Gamma \pm \Gamma_{12} = \Gamma\left(1 \pm \tfrac{\sin kr_{12}}{r_{12}}\right) \ ,\end{aligned}$$

we obtain for the antisymmetric state,

$$\begin{aligned}2\frac{d}{dt}\rho_A &= \frac{d}{dt}(\rho_{12,12} + \rho_{21,21} - \rho_{12,21} - \rho_{21,12}) \\ &= \Omega_0\sin\tfrac{kr_{12}}{2}(-\rho_{11,12} - \rho_{12,11} + \rho_{11,21} + \rho_{21,11} - \rho_{22,12} - \rho_{12,22} + \rho_{22,21} + \rho_{21,22}) \\ &\quad + \imath(\Gamma - \Gamma_{12})(\rho_{12,12} + \rho_{21,21} - \rho_{12,21} - \rho_{21,12} + \rho_{22,22}) \\ &= \sqrt{2}\Omega_-\mathfrak{Re}\,(-\rho_{11,12} + \rho_{11,21} - \rho_{22,12} + \rho_{22,21}) + \imath\Gamma_-(2\rho_A + \rho_{22,22})\end{aligned}$$

and for the symmetric state,

$$\begin{aligned}
2\frac{d}{dt}\rho_S &= \frac{d}{dt}(\rho_{12,12}+\rho_{21,21}+\rho_{12,21}+\rho_{21,12}) \\
&= -\imath\Omega_0\cos\tfrac{kr_{12}}{2}(\rho_{11,12}-\rho_{12,11}+\rho_{11,21}-\rho_{21,11}+\rho_{22,12}-\rho_{12,22}+\rho_{22,21}-\rho_{21,22}) \\
&\quad +\imath(\Gamma+\Gamma_{12})(\rho_{12,12}+\rho_{12,21}+\rho_{21,12}+\rho_{21,21}-\rho_{22,22}) \\
&= \sqrt{2}\Omega_+\,\mathfrak{Im}\,(\rho_{11,12}+\rho_{11,21}+\rho_{22,12}+\rho_{22,21})+\imath\Gamma_+(2\rho_S-\rho_{22,22})\ .
\end{aligned}$$

Hence, after switching off the light, $\Omega=0$,

$$\frac{d}{dt}\rho_{S,A}=\imath\Gamma_\pm(\rho_{S,A}\mp\tfrac{1}{2}\rho_{22,22})\ .$$

41.3.4.5 Ex: Two-atom toy model for super- and subradiance

Calculate the eigenvalues and eigenvectors of the Hamiltonian (41.100) for two two-level atoms located at $\mathbf{r}_j=\pm\frac{r_{12}}{2}\hat{\mathbf{e}}_z$ with $r_{ji}=|\mathbf{r}_j-\mathbf{r}_i|\ll\lambda$ [364]. Consider the limits (a) absent coupling, $\Delta_{12}=0$, (b) resonant driving, $\Delta_a=0$, and (c) absent driving, $\Omega=0$. (d) Analyze the full Hamiltonian.

Solution: *The two atoms are subject to the Rabi frequencies,* $\Omega(\mathbf{r}_1)=\Omega_0 e^{\imath kr_{12}/2}=\Omega^*(\mathbf{r}_2)$*, so that,*

$$\hat{H}'\equiv\hat{H}-\Delta_a\mathbb{I}=\begin{pmatrix}\Delta_a & \frac{1}{2}\Omega & \frac{1}{2}\Omega^* & 0\\ \frac{1}{2}\Omega^* & 0 & \frac{1}{2}\Delta_{12} & \frac{1}{2}\Omega^*\\ \frac{1}{2}\Omega & \frac{1}{2}\Delta_{12} & 0 & \frac{1}{2}\Omega\\ 0 & \frac{1}{2}\Omega & \frac{1}{2}\Omega^* & -\Delta_a\end{pmatrix}\ , \tag{41.116}$$

with $\Delta_{12}=-\Gamma\frac{\cos kr_{12}}{kr_{12}}$.
a. In the limit of absent coupling, $\Delta_{12}=0$*, we obtain,*

$$\hat{H}'\equiv\hat{H}-\Delta_a\mathbb{I}=\begin{pmatrix}\Delta_a & \frac{1}{2}\Omega & \frac{1}{2}\Omega^* & 0\\ \frac{1}{2}\Omega^* & 0 & 0 & \frac{1}{2}\Omega^*\\ \frac{1}{2}\Omega & 0 & 0 & \frac{1}{2}\Omega\\ 0 & \frac{1}{2}\Omega & \frac{1}{2}\Omega^* & -\Delta_a\end{pmatrix}\ .$$

The eigenvalue and the eigenvector matrices are, with the abbreviations $G\equiv\sqrt{\Delta_a^2+|\Omega|^2}$*,*

$$\hat{E}'\equiv\hat{E}+\Delta_a=\begin{pmatrix}-G & 0 & 0 & 0\\ 0 & 0 & 0 & 0\\ 0 & 0 & 0 & 0\\ 0 & 0 & 0 & G\end{pmatrix}\quad\textit{and}\quad U=\begin{pmatrix}\frac{-G+\Delta_a}{\Omega} & 0 & 1 & \frac{G+\Delta_a}{\Omega}\\ \frac{\Omega^*}{\Omega} & -\frac{\Omega^*}{\Omega} & -\frac{2\Delta_a}{\Omega} & \frac{\Omega^*}{\Omega}\\ 1 & 1 & 0 & 1\\ \frac{-G-\Delta_a}{\Omega} & 0 & -1 & \frac{G-\Delta_a}{\Omega}\end{pmatrix}\ .$$

We easily verify $U\hat{E}'U^{-1} = H'$ *and propagate* $Ue^{\imath\hat{E}'t}U^{-1}$ *numerically.*
b. On resonance, $\Delta_a = 0$*, and additionally assuming* $\Omega = \Omega^*$ *we obtain,*

$$\hat{H} - \Delta_a \mathbb{I} \simeq \begin{pmatrix} 0 & \frac{1}{2}\Omega & \frac{1}{2}\Omega & 0 \\ \frac{1}{2}\Omega & 0 & \frac{1}{2}\Delta_{12} & \frac{1}{2}\Omega \\ \frac{1}{2}\Omega & \frac{1}{2}\Delta_{12} & 0 & \frac{1}{2}\Omega \\ 0 & \frac{1}{2}\Omega & \frac{1}{2}\Omega & 0 \end{pmatrix} ,$$

with the eigenvalues, $E_1 = -\frac{1}{2}\Delta_{12}$*,* $E_2 = 0$*, and* $E_{3,4} = \frac{1}{4}\Delta_{12} \pm \frac{1}{4}\sqrt{16\Omega^2 + \Delta_{12}^2}$*.*
c. In the absence of driving, $\Omega = 0$*, we obtain,*

$$\hat{H} - \Delta_a \mathbb{I} \simeq \begin{pmatrix} \Delta_a & 0 & 0 & 0 \\ 0 & 0 & \frac{1}{2}\Delta_{12} & 0 \\ 0 & \frac{1}{2}\Delta_{12} & 0 & 0 \\ 0 & 0 & 0 & -\Delta_a \end{pmatrix} .$$

The eigenvalue and the eigenvector matrices are,

$$\hat{E}' \equiv \hat{E} + \Delta_a = \begin{pmatrix} \Delta_a & 0 & 0 & 0 \\ 0 & \frac{1}{2}\Delta_{12} & 0 & 0 \\ 0 & 0 & -\frac{1}{2}\Delta_{12} & 0 \\ 0 & 0 & 0 & -\Delta_a \end{pmatrix} \quad \textit{and} \quad U = \begin{pmatrix} 1 & 0 & 0 & 0 \\ 0 & \frac{1}{\sqrt{2}} & -\frac{1}{\sqrt{2}} & 0 \\ 0 & \frac{1}{\sqrt{2}} & \frac{1}{\sqrt{2}} & 0 \\ 0 & 0 & 0 & 1 \end{pmatrix} . \tag{41.117}$$

d. Applying the unitary transformation (41.117) to the full Hamiltonian (41.116), we find,

$$U^{-1}(\hat{H} - \Delta_a \mathbb{I})U = \begin{pmatrix} \Delta_a & \frac{1}{2}\Omega_+ & -\frac{\imath}{2}\Omega_- & 0 \\ \frac{1}{2}\Omega_+ & \frac{1}{2}\Delta_{12} & 0 & \frac{1}{2}\Omega_+ \\ -\frac{\imath}{2}\Omega_- & 0 & -\frac{1}{2}\Delta_{12} & -\frac{\imath}{2}\Omega_- \\ 0 & \frac{1}{2}\Omega_+ & -\frac{\imath}{2}\Omega_- & -\Delta_a \end{pmatrix} ,$$

introducing the effective Rabi frequencies for the two single-excitation modes,

$$\Omega_+ \equiv \sqrt{2}\Omega_0 \cos\tfrac{kr_{12}}{2} \qquad \textit{and} \qquad \Omega_- \equiv \sqrt{2}\Omega_0 \sin\tfrac{kr_{12}}{2}$$
$$\textit{and} \qquad \Delta_\pm \equiv \mp\tfrac{1}{2}\Delta_{12} = \pm\Gamma\tfrac{\cos kr_{12}}{2r_{12}} .$$

Hence, we see that the dipole-dipole interaction generates two collective 0,1,2-photon eigenstates $|gg\rangle$*,* $|\pm\rangle = \frac{1}{\sqrt{2}}(|eg\rangle \pm |ge\rangle)$*, and* $|ee\rangle$*. The pump efficiently couples to the superradiant state, but only very weakly to the long-lived (subradiant) state. The steady-state population of the long-lived mode then presents three typical regimes, depending on the pump strength. First, for the lowest intensities (linear-optics regime), the population of* $|ee\rangle$ *is negligible and the single-excitation modes* $|\pm\rangle$ *are driven only directly from the pump, so one obtains the following scaling for their population:*

$$P_\pm \simeq \tfrac{s_\pm}{2} \propto s \qquad \textit{with} \qquad s_\pm = \frac{2\Omega_\pm^2}{\Gamma_\pm^2 + 4(\Delta_a \mp \frac{1}{2}\Delta_\pm)^2}$$

the effective saturation parameter for each mode, and

$$s_0 = \frac{2\Omega_0^2}{\Gamma^2 + 4\Delta_a^2} \ ,$$

the single-atom one. This single-excitation regime holds for $s_\pm \ll 1$, i.e. $\Omega_+ \ll \Delta$. As the drive strength is increased, the doubly-excited state $|ee\rangle$ is substantially populated thanks to the strong coupling of the drive to the superradiant state:

$$P_+ \simeq \tfrac{s_+}{2} \propto s \qquad \text{and} \qquad P_{ee} \propto s^2 \ .$$

Then, the $|-\rangle$ state gets an additional population by decay from $|ee\rangle$, at rate Γ_-, leading to a long-lived population that grows quadratically with the saturation parameter: $P_{ee} \propto s^2$. Finally, for the largest values of the saturation parameter, i.e. with a Rabi frequency such that the dynamics of each atom is dominated by the drive ($\Omega_0 \gg \Delta \gg \Gamma, |\Delta_\pm|$), the system is cast into a separable state described by the density matrix,

$$\hat{\rho} = \tfrac{1}{2} \bigotimes_{j=1,2} \left(|g_j\rangle\langle g_j| + |e_j\rangle\langle e_j| \right) \ .$$

This mixed state projects equally on the states $|gg\rangle$, $|+\rangle$, $|-\rangle$, and $|ee\rangle$, resulting in $P_- \simeq \frac{1}{4}$. Hence, the strong pump overcomes the weak coupling of subradiant modes which, in the linear-optics regime, prevents one to populate them efficiently. The present mechanism is analogous to optical pumping, where an excited state (here $|ee\rangle$) is directly driven by the laser, and induces a population in the long-lived state (here $|-\rangle$) by incoherent decay.

41.3.4.6 Ex: Impact of dipole-dipole interactions on super- and subradiance

Here, we use the two-atom toy model studied in Fig. 41.16 to demonstrate the emergence of subradiant modes as a consequence of dipole-dipole interaction [364]. Calculate numerically the anti-symmetric state population $\hat{\rho}_A$ given in Eq. (41.99) at very long times as a function of the saturation parameter s and the interatomic distance kr_{ij}. Interpret the results.

Solution: *Fig. 41.20 shows the dependence of the decay rate of the subradiant anti-symmetric states of two atoms interacting via dipole-dipole coupling on the saturation parameter $s = \frac{2\Omega_0^2}{\Gamma^2+4\Delta^2}$ and their distance.*

41.3.4.7 Ex: Three interacting atoms

Numerically integrate the master equation (41.88) for three atoms.

Solution: *We simply extend the procedure demonstrated in the example 257 to three atoms,*

$$\hat{\sigma}_1^\pm = \hat{\sigma}^\pm \otimes \mathbb{I} \otimes \mathbb{I} \quad , \quad \hat{\sigma}_2^\pm = \mathbb{I} \otimes \hat{\sigma}^\pm \otimes \mathbb{I} \quad , \quad \hat{\sigma}_3^\pm = \mathbb{I} \otimes \mathbb{I} \otimes \hat{\sigma}^\pm \ .$$

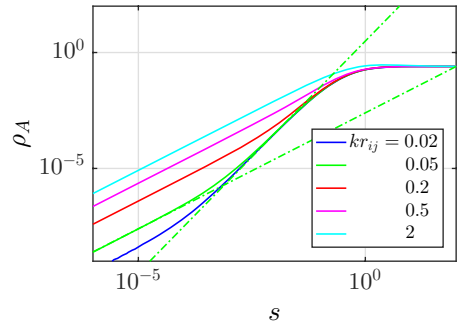

Figure 41.20: (code) Dependence of the population of the subradiant anti-symmetric state of two atoms interacting via dipole-dipole coupling on the saturation parameter and their distance.

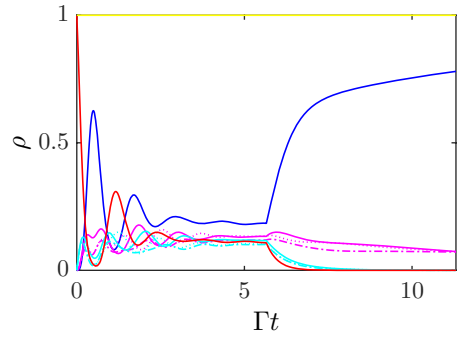

Figure 41.21: (code) Populations in a system of three interacting two-level atoms.

The result of such a simulation is shown in Fig. 41.21.

41.3.4.8 Ex: Two non-interacting three-level atoms

Extend the two two-level atoms toy model of example 257 to two non-interacting three level atoms $|1\rangle$-$|2\rangle$-$|3\rangle$ in cascade configuration.
a. Write down the total Hamiltonian and its matrix representation chosing an appropriate basis.
b. Write down the Lindbladian and numerically solve the master equation.

Solution: *a. The total Hamiltonian is,*

$$\hat{H} = \sum_{j=1,2} \left[-\Delta_a \hat{\sigma}_j^{22} + \tfrac{1}{2}\Omega_a(\hat{\sigma}_j^{12} + \hat{\sigma}_j^{21}) - \Delta_b \hat{\sigma}_j^{32}\hat{\sigma}_j^{23} + \tfrac{1}{2}\Omega_s(\hat{\sigma}_j^{23} + \hat{\sigma}_j^{32}) \right] \ .$$

Choosing the one-atom basis as,

$$|1\rangle = \begin{pmatrix} 1 \\ 0 \\ 0 \end{pmatrix} \quad , \quad |2\rangle = \begin{pmatrix} 0 \\ 1 \\ 0 \end{pmatrix} \quad , \quad |3\rangle = \begin{pmatrix} 0 \\ 0 \\ 1 \end{pmatrix}$$

the single-atom Hamiltonian can be expressed as,

$$\hat{h} = \begin{pmatrix} 0 & \frac{1}{2}\Omega_a & 0 \\ \frac{1}{2}\Omega_a & -\Delta_a & \frac{1}{2}\Omega_b \\ 0 & \frac{1}{2}\Omega_b & -\Delta_b \end{pmatrix} .$$

The collective operators can be constructed via,

$$\hat{\sigma}_1^{mn} = |m\rangle\langle n| \otimes \mathbb{I}_3 \quad , \quad \hat{\sigma}_2^{mn} = \mathbb{I}_3 \otimes |m\rangle\langle n|$$
$$\rho_1^{kk} = \rho^{k\cdot,k\cdot}(\rho^{\cdot 1,\cdot 1} + \rho^{\cdot 2,\cdot 2} + \rho^{\cdot 3,\cdot 3}) \quad , \quad \rho_2^{kk} = (\rho^{1\cdot,1\cdot} + \rho^{2\cdot,2\cdot} + \rho^{3\cdot,3\cdot})\rho^{\cdot k,\cdot k} ,$$

yielding the two-atom collective Hamiltonian,

$$\hat{H} = \hat{H}_1 + \hat{H}_2 = \hat{h} \otimes \mathbb{I}_3 + \mathbb{I}_3 \otimes \hat{h}$$
$$= \begin{pmatrix} 0 & \frac{1}{2}\Omega_a & 0 & \frac{1}{2}\Omega_a & 0 & 0 & 0 & 0 & 0 \\ \frac{1}{2}\Omega_a & -\Delta_a & \frac{1}{2}\Omega_b & 0 & \frac{1}{2}\Omega_a & 0 & 0 & 0 & 0 \\ 0 & \frac{1}{2}\Omega_b & -\Delta_b & 0 & 0 & \frac{1}{2}\Omega_a & 0 & 0 & 0 \\ \frac{1}{2}\Omega_a & 0 & 0 & -\Delta_a & \frac{1}{2}\Omega_a & 0 & \frac{1}{2}\Omega_b & 0 & 0 \\ 0 & \frac{1}{2}\Omega_a & 0 & \frac{1}{2}\Omega_a & -\Delta_a - \Delta_a & \frac{1}{2}\Omega_b & 0 & \frac{1}{2}\Omega_b & 0 \\ 0 & 0 & \frac{1}{2}\Omega_a & 0 & \frac{1}{2}\Omega_b & -\Delta_a - \Delta_b & 0 & 0 & \frac{1}{2}\Omega_b \\ 0 & 0 & 0 & \frac{1}{2}\Omega_b & 0 & 0 & -\Delta_b & \frac{1}{2}\Omega_a & 0 \\ 0 & 0 & 0 & 0 & \frac{1}{2}\Omega_b & 0 & \frac{1}{2}\Omega_a & -\Delta_a - \Delta_b & \frac{1}{2}\Omega_b \\ 0 & 0 & 0 & 0 & 0 & \frac{1}{2}\Omega_b & 0 & \frac{1}{2}\Omega_b & -\Delta_b - \Delta_b \end{pmatrix} .$$

b. With the Lindbladian,

$$\mathcal{L}\hat{\rho} = \tfrac{1}{2}\Gamma_{12} \sum_{j=1,2} (2\hat{\sigma}_j^{12}\hat{\rho}\hat{\sigma}_j^{21} - \hat{\sigma}_j^{21}\hat{\sigma}_j^{12}\hat{\rho} - \hat{\rho}\hat{\sigma}_j^{21}\hat{\sigma}_j^{12}) + \tfrac{1}{2}\Gamma_{13}(2\hat{\sigma}_j^{23}\hat{\rho}\hat{\sigma}_j^{32} - \hat{\sigma}_j^{32}\hat{\sigma}_j^{23}\hat{\rho} - \hat{\rho}\hat{\sigma}_j^{32}\hat{\sigma}_j^{23}) ,$$

the extended master equation is readily set up and can be numerically solved using the procedure outlined in example 257. The result of such a simulation is shown in Fig. 41.22.

41.3.4.9 Ex: Rydberg blockade versus spin-spin interaction

a. Direct interactions (e.g. dipole-dipole coupling or van der Waals interaction) generate collective energy shifts Δ_{ij} and collective decay Γ_{ij} (see Sec. 41.3.2 or examples 257 and 258). Discuss why these terms are not observed in Hamiltonians describing Rydberg blockade.
b. Verify whether the operators $\hat{S}_z\hat{S}_z$ or $\hat{S}_+\hat{S}_-$ generate anti-diagonal terms in the Hamiltonian [956].

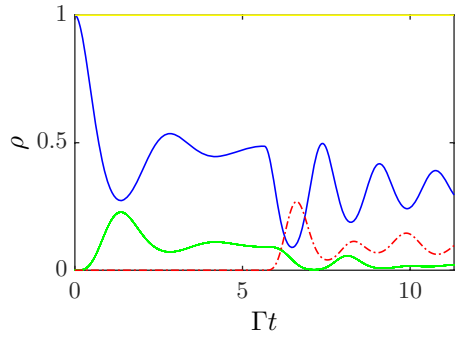

Figure 41.22: (code) Populations in a system of two interacting three-level atoms.

Solution: *Spin-spin interactions introduce collective energy shifts Δ_{ij} in the Hamiltonian and collective decay terms Γ_{ij} in the Lindbladian, which come additionally to single-atom detunings Δ and spontaneous emission Γ. Spin-spin interaction terms typically have the shape,*

$$\hat{H} \propto \hat{\sigma}_1^m \hat{\sigma}_2^n = \hat{\sigma}^m \otimes \hat{\sigma}^n = (\hat{\sigma}^m \oplus \mathbb{I})(\mathbb{I} \oplus \hat{\sigma}^n)$$
$$= \begin{pmatrix} \sigma_1^{11}\sigma_2^{11} & \sigma_1^{11}\sigma_2^{12} & \sigma_1^{12}\sigma_2^{11} & \sigma_1^{12}\sigma_2^{12} \\ \sigma_1^{11}\sigma_2^{21} & \sigma_1^{11}\sigma_2^{22} & \sigma_1^{12}\sigma_2^{21} & \sigma_1^{12}\sigma_2^{22} \\ \sigma_1^{21}\sigma_2^{11} & \sigma_1^{21}\sigma_2^{12} & \sigma_1^{22}\sigma_2^{11} & \sigma_1^{22}\sigma_2^{12} \\ \sigma_1^{21}\sigma_2^{21} & \sigma_1^{21}\sigma_2^{22} & \sigma_1^{22}\sigma_2^{21} & \sigma_1^{22}\sigma_2^{22} \end{pmatrix},$$

where,

$$\hat{\sigma}_1^m = \begin{pmatrix} \sigma_1^{11} & \sigma_1^{12} \\ \sigma_1^{21} & \sigma_1^{22} \end{pmatrix} \qquad \textit{and} \qquad \hat{\sigma}_2^n = \begin{pmatrix} \sigma_2^{11} & \sigma_2^{12} \\ \sigma_2^{21} & \sigma_2^{22} \end{pmatrix}$$

can be arbitrary Pauli matrices. The Hamiltonians for Rydberg blockade do not provide anti-diagonal terms *in contrast to spin-spin interactions,*

$$\hat{H} \propto \hat{\sigma}_1^m + \hat{\sigma}_2^n = \hat{\sigma}^m \oplus \hat{\sigma}^n = (\hat{\sigma}^m \oplus \mathbb{I}) + (\mathbb{I} \oplus \hat{\sigma}^n)$$
$$= \begin{pmatrix} \sigma_1^{11} + \sigma_2^{11} & \sigma_2^{12} & \sigma_1^{12} & 0 \\ \sigma_2^{21} & \sigma_1^{11} + \sigma_2^{22} & 0 & \sigma_1^{12} \\ \sigma_1^{21} & 0 & \sigma_1^{22} + \sigma_2^{11} & \sigma_2^{12} \\ 0 & \sigma_1^{21} & \sigma_2^{21} & \sigma_1^{22} + \sigma_2^{22} \end{pmatrix}.$$

The main difference is, however, that van der Waals interactions are essentially coherent, while dipole-dipole coupling generates correltaions via spontaneous decay Γ_{ij}.

b. We find (see also Sec. 41.3.3),

$$\hat{S}_z^2 = (\hat{\sigma}_1^z + \hat{\sigma}_2^z)(\hat{\sigma}_1^z + \hat{\sigma}_2^z) = (\hat{\sigma}^z \otimes \mathbb{I} + \mathbb{I} \otimes \hat{\sigma}^z)(\hat{\sigma}^z \otimes \mathbb{I} + \mathbb{I} \otimes \hat{\sigma}^z)$$
$$= \begin{pmatrix} 1 & 0 & 0 & 0 \\ 0 & 0 & 0 & 0 \\ 0 & 0 & 0 & 0 \\ 0 & 0 & 0 & 1 \end{pmatrix} ,$$

but

$$\hat{S}_+\hat{S}_- = (\hat{\sigma}_1^+ + \hat{\sigma}_2^+)(\hat{\sigma}_1^- + \hat{\sigma}_2^-) = (\hat{\sigma}^+ \otimes \mathbb{I} + \mathbb{I} \otimes \hat{\sigma}^+)(\hat{\sigma}^- \otimes \mathbb{I} + \mathbb{I} \otimes \hat{\sigma}^-)$$
$$= \hat{\mathbf{S}}^2 - \hat{S}_z^2 - \hat{S}_z = \begin{pmatrix} 0 & 0 & 0 & 0 \\ 0 & 1 & 1 & 0 \\ 0 & 1 & 1 & 0 \\ 0 & 0 & 0 & 2 \end{pmatrix} .$$

41.3.4.10 Ex: Adiabatic elimination of the cavity mode, general case

Derive the equations of motion (41.109) for a system consisting of many atoms interacting with a single cavity mode after adiabatic elimination of the cavity mode.

Solution: *We start from the Heisenberg-Liouville equation (41.112) including collective and single-atom decay,*

$$\dot{\hat{\mathbf{S}}} = -\imath[\hat{\mathbf{S}}, \hat{H}] + \mathcal{L}_{\kappa_c, \hat{S}_-}\hat{\mathbf{S}} + \tfrac{1}{2}(\mathcal{L}_{\Gamma_1/2, \hat{S}_+} + \mathcal{L}_{\Gamma_1/2, \hat{S}_-})\hat{\mathbf{S}} \ , \tag{41.118}$$

with the Hamiltonian ($\tilde{\eta} \equiv \eta/g$),

$$\hat{H} = -2\mathfrak{Im}\ (\tilde{\eta}U_\gamma)\hat{S}_x - 2\mathfrak{Re}\ (\tilde{\eta}U_\gamma)\hat{S}_y - \Delta_a\hat{S}_z + U_c\hat{S}_+\hat{S}_- \ , \tag{41.119}$$

where

$$\begin{aligned} \mathfrak{Re}\ \tilde{\eta}U_\gamma &= \mathfrak{Re}\ (\tilde{\eta}_r + \imath\tilde{\eta}_i)(U_c - \imath\kappa_c) = U_c\tilde{\eta}_r + \kappa_c\tilde{\eta}_i \\ \mathfrak{Im}\ \tilde{\eta}U_\gamma &= \mathfrak{Re}\ (\tilde{\eta}_r + \imath\tilde{\eta}_i)(U_c - \imath\kappa_c) = U_c\tilde{\eta}_i - \kappa_c\tilde{\eta}_r \ , \end{aligned} \tag{41.120}$$

with $U_\kappa \equiv U_c - \imath\kappa_c$. To prepare the calculations we first set up tables of useful expressions. The Heisenberg equation $\dot{\hat{S}}_\alpha = -\imath[\hat{S}_\alpha, \hat{H}]$ leads to the following relationships

between Hamiltonian terms and equations of motion:

$\hat{H}=$	$-\imath[\hat{S}_x,\hat{H}]=$	$-\imath[\hat{S}_y,\hat{H}]=$	$-\imath[\hat{S}_z,\hat{H}]=$	$-\imath[\hat{S}_+,\hat{H}]=$	$-\imath[\hat{S}_-,\hat{H}]=$
$\hat{S}_x$	0	$-\hat{S}_z$	$\hat{S}_y$	$-\imath\hat{S}_z$	$\imath\hat{S}_z$
$\hat{S}_y$	$\hat{S}_z$	0	$-\hat{S}_x$	$\hat{S}_z$	$\hat{S}_z$
$\hat{S}_z$	$-\hat{S}_y$	$\hat{S}_x$	0	0	0
$\hat{S}_x^2$	0	$-\{\hat{S}_x,\hat{S}_z\}$	$\{\hat{S}_x,\hat{S}_y\}$	$-\imath\{\hat{S}_x,\hat{S}_z\}$	$\imath\{\hat{S}_x,\hat{S}_z\}$
$\hat{S}_y^2$	$\{\hat{S}_y,\hat{S}_z\}$	0	$-\{\hat{S}_x,\hat{S}_y\}$	$\{\hat{S}_x,\hat{S}_z\}$	$\{\hat{S}_x,\hat{S}_z\}$
$\hat{S}_z^2$	$-\{\hat{S}_y,\hat{S}_z\}$	$\{\hat{S}_x,\hat{S}_z\}$	0	0	0
$\hat{S}_x\hat{S}_y$	$\hat{S}_x\hat{S}_z$	$-\hat{S}_z\hat{S}_y$	$\hat{S}_y^2-\hat{S}_x^2$	$\hat{S}_-\hat{S}_z-\hat{S}_x$	$\hat{S}_+\hat{S}_z+\hat{S}_x$
$\hat{S}_y\hat{S}_x$	$\hat{S}_z\hat{S}_x$	$-\hat{S}_y\hat{S}_z$	$\hat{S}_y^2-\hat{S}_x^2$		
$\hat{S}_x\hat{S}_z$	$-\hat{S}_x\hat{S}_y$	$\hat{S}_x^2-\hat{S}_z^2$	$\hat{S}_y\hat{S}_z$	$\imath(\hat{S}_x^2-\hat{S}_z^2)-\hat{S}_x\hat{S}_y$	$\imath(\hat{S}_z^2-\hat{S}_x^2)-\hat{S}_x\hat{S}_y$
$\hat{S}_z\hat{S}_x$	$-\hat{S}_y\hat{S}_x$	$\hat{S}_x^2-\hat{S}_z^2$	$\hat{S}_z\hat{S}_y$		
$\hat{S}_y\hat{S}_z$	$\hat{S}_z^2-\hat{S}_y^2$	$\hat{S}_y\hat{S}_x$	$-\hat{S}_x\hat{S}_z$		
$\hat{S}_z\hat{S}_y$	$\hat{S}_z^2-\hat{S}_y^2$	$\hat{S}_x\hat{S}_y$	$-\hat{S}_z\hat{S}_x$		
$\hat{S}_+$	$\imath\hat{S}_z$	$-\hat{S}_z$	0	0	$\imath\hat{S}_z$
$\hat{S}_-$	$-\imath\hat{S}_z$	$-\hat{S}_z$	0	$-\imath\hat{S}_z$	0
$\hat{\mathbf{S}}^2$	0	0	0	0	0
$\hat{S}_+\hat{S}_-$	$\{\hat{S}_y,\hat{S}_z\}-\hat{S}_y$	$\hat{S}_x-\{\hat{S}_y,\hat{S}_z\}$	0	$-2\imath\hat{S}_+\hat{S}_z$	$-2\imath\hat{S}_z\hat{S}_-$

(41.121)

Exploiting the rules (41.121) and,

$$\hat{S}_\pm=\hat{S}_x\pm\imath\hat{S}_y\quad,\quad \hat{S}_+\hat{S}_-=\hat{S}_x^2+\hat{S}_y^2+\hat{S}_z\quad,\quad \hat{\mathbf{S}}^2=\hat{S}_x^2+\hat{S}_y^2+\hat{S}_z^2\ , \tag{41.122}$$

for the coupled atom-cavity system we arrive at,

$$-\imath[\hat{\mathbf{S}},\hat{H}]=\begin{pmatrix}0\\ 2(U_c\tilde{\eta}_i-\kappa_c\tilde{\eta}_r)\hat{S}_z\\ -2(U_c\tilde{\eta}_i-\kappa_c\tilde{\eta}_r)\hat{S}_y\end{pmatrix}+\begin{pmatrix}-2(U_c\tilde{\eta}_r+\kappa_c\tilde{\eta}_i)\hat{S}_z\\ 0\\ 2(U_c\tilde{\eta}_r+\kappa_c\tilde{\eta}_i)\hat{S}_x\end{pmatrix}+\begin{pmatrix}(\Delta_a-U_c)\hat{S}_y\\ (U_c-\Delta_a)\hat{S}_x\\ 0\end{pmatrix}+\begin{pmatrix}U_c\{\hat{S}_y,\hat{S}_z\}\\ -U_c\{\hat{S}_x,\hat{S}_z\}\\ 0\end{pmatrix}\ . \tag{41.123}$$

On the other hand, the Lindbladian $\mathcal{L}_{\hat{L}}\hat{X}=\hat{L}^\dagger[\hat{X},\hat{L}]+[\hat{L}^\dagger,\hat{X}]\hat{L}$ applied to collective spin operator yields:

$\hat{L}=$	$\mathcal{L}_{\hat{L}}\hat{S}_x=$	$\mathcal{L}_{\hat{L}}\hat{S}_y=$	$\mathcal{L}_{\hat{L}}\hat{S}_z=$	$\mathcal{L}_{\hat{L}}\hat{S}_+=$	$\mathcal{L}_{\hat{L}}\hat{S}_-=$
$\hat{S}_+$	$-\{\hat{S}_x,\hat{S}_z\}-\hat{S}_x$	$-\{\hat{S}_y,\hat{S}_z\}-\hat{S}_y$	$2\hat{S}_-\hat{S}_+$	$-\{\hat{S}_+,\hat{S}_z\}-\hat{S}_+$	$-\{\hat{S}_-,\hat{S}_z\}-\hat{S}_-$
$\hat{S}_-$	$\{\hat{S}_x,\hat{S}_z\}-\hat{S}_x$	$\{\hat{S}_y,\hat{S}_z\}-\hat{S}_y$	$-2\hat{S}_+\hat{S}_-$	$\{\hat{S}_+,\hat{S}_z\}-\hat{S}_+$	$\{\hat{S}_-,\hat{S}_z\}-\hat{S}_-$
$\hat{S}_z$	$-\hat{S}_x$	$-\hat{S}_y$	0	$-\hat{S}_+$	$-\hat{S}_-$

(41.124)

Exploiting the rules (41.123) and,

$$\mathcal{L}_{\hat{L}}(\hat{X}+\hat{Y})=\mathcal{L}_{\hat{L}}\hat{X}+\mathcal{L}_{\hat{L}}\hat{Y}\ , \tag{41.125}$$

we arrive at,

$$\mathcal{L}_{\hat{S}_+}\hat{\mathbf{S}} = \begin{pmatrix} -\{\hat{S}_x,\hat{S}_z\} - \hat{S}_x \\ -\{\hat{S}_y,\hat{S}_z\} - \hat{S}_y \\ 2\hat{S}_-\hat{S}_+ \end{pmatrix} \quad , \quad \mathcal{L}_{\hat{S}_-}\hat{\mathbf{S}} = \begin{pmatrix} \{\hat{S}_x,\hat{S}_z\} - \hat{S}_x \\ \{\hat{S}_y,\hat{S}_z\} - \hat{S}_y \\ -2\hat{S}_+\hat{S}_- \end{pmatrix} \quad , \quad \mathcal{L}_{\hat{S}_z}\hat{\mathbf{S}} = \begin{pmatrix} -\hat{S}_x \\ -\hat{S}_y \\ 0 \end{pmatrix} , \tag{41.126}$$

and consequently, for the coupled atom-cavity system,

$$\mathcal{L}_{\kappa_c,\hat{S}_-}\hat{\mathbf{S}} = \kappa_c \begin{pmatrix} \{\hat{S}_x,\hat{S}_z\} - \hat{S}_x \\ \{\hat{S}_y,\hat{S}_z\} - \hat{S}_y \\ -2\hat{S}_+\hat{S}_- \end{pmatrix} \quad , \quad \tfrac{1}{2}\sum_j (\mathcal{L}_{\Gamma_1/2,\hat{s}_j^-} + \mathcal{L}_{\Gamma_1/2,\hat{s}_j^+})\hat{\mathbf{S}} = \tfrac{\Gamma_1}{2} \begin{pmatrix} -\hat{S}_x \\ -\hat{S}_y \\ -(N\mathbb{I}_2 + 2\hat{S}_z) \end{pmatrix} . \tag{41.127}$$

Putting everything together we obtain the equations of motion,

$$\begin{aligned} \dot{\hat{\mathbf{S}}} = & \begin{pmatrix} -\kappa_c - \frac{\Gamma_1}{2} & \Delta_a - U_c & -2\kappa_c\tilde{\eta}_i - 2U_c\tilde{\eta}_r) \\ U_c - \Delta_a & -\kappa_c - \frac{\Gamma_1}{2} & 2U_c\tilde{\eta}_i - 2\kappa_c\tilde{\eta}_r \\ 2\kappa_c\tilde{\eta}_i + 2U_c\tilde{\eta}_r & -2U_c\tilde{\eta}_i + 2\kappa_c\tilde{\eta}_r & -2\kappa_c - \frac{\Gamma_1}{2} \end{pmatrix} \begin{pmatrix} \hat{S}_x \\ \hat{S}_y \\ \hat{S}_z \end{pmatrix} \\ & + 2U_c \begin{pmatrix} \{\hat{S}_y,\hat{S}_z\} \\ \{\hat{S}_x,\hat{S}_z\} \\ 0 \end{pmatrix} + 2\kappa_c \begin{pmatrix} \{\hat{S}_x,\hat{S}_z\} \\ \{\hat{S}_y,\hat{S}_z\} \\ -2(\hat{S}_x^2 + \hat{S}_y^2) \end{pmatrix} - \tfrac{\Gamma_1}{2} \begin{pmatrix} 0 \\ 0 \\ N\mathbb{I}_2 \end{pmatrix} . \end{aligned} \tag{41.128}$$

Approximating $\{\hat{S}_\alpha,\hat{S}_\beta\} \simeq 2\hat{S}_\alpha\hat{S}_\beta$,

$$\dot{\hat{\mathbf{S}}} \simeq \begin{pmatrix} -\frac{\Gamma_1}{2} & \Delta_a & -\hat{\Omega}_i \\ -\Delta_a & -\frac{\Gamma_1}{2} & -\hat{\Omega}_r \\ \hat{\Omega}_i & \hat{\Omega}_r & -\Gamma_1 \end{pmatrix} \begin{pmatrix} \hat{S}_x \\ \hat{S}_y \\ \hat{S}_z \end{pmatrix} - \begin{pmatrix} 0 \\ 0 \\ \Gamma_1 \frac{N}{2}\mathbb{I}_2 \end{pmatrix} , \tag{41.129}$$

with the abbreviations,

$$\begin{aligned} \hat{\Omega}_r &\equiv 2g\hat{a}_r = 2U_c(\hat{S}_x - \eta_i/g) - 2\kappa_c(\hat{S}_y - \eta_r/g) \\ \hat{\Omega}_i &\equiv 2g\hat{a}_i = -2\kappa_c(\hat{S}_x - \eta_i/g) - 2U_c(\hat{S}_y - \eta_r/g) \ , \end{aligned} \tag{41.130}$$

41.4 Quantum correlations and entanglement

The concept of *entanglement* arose in quantum mechanics by Einstein, Podolski and Rosen's famous Gedankenexperiment, today called the *EPR paradox* [411]. In his Gedankenexperiment, Einstein tried to prove the necessity of hidden variables for quantum mechanics to be a complete theory. Consequently, we begin this chapter by introducing the notion of entangled particles and recapitulating the discussion of the EPR paradox.

Since Feynman discovered the utility of entangled states for quantum computation [1009, 268], this area of research exploded with thousands of theoretical researchers, but few experiments, due to the enormous technical difficulties of creating and controlling these states. On the other side, states of entangled photons already play an

important role in *quantum cryptography* [123]. And in the context of metrology, *spin-squeezed* correlated quantum states offer the possibility of quantum noise reduction in frequency standards [1380].

Among the various systems proposed for the realization of entangled states and quantum computing gates we will only discuss one idea, which is based on the mutual coupling of atoms through a Jaynes-Cummings-like interaction mediated by an optical mode.

41.4.1 The EPR paradox and GHZ states

Let us imagine two maximally correlated particles produced by a suitable source, which fly freely without interaction in opposite directions along the y-axis toward two detectors a and b. The particles have an internal degree of freedom (spin) $|\pm\rangle_{a,b}$, which can be measured in various directions, for example, z or x by operators $\hat{\sigma}_z^{a,b}$ or $\hat{\sigma}_x^{a,b}$. Since the particles are completely entangled, the result of a measurement on the first particle $\hat{\sigma}_z^a$ allows the prediction of the result of another measurement $\hat{\sigma}_z^b$ performed on the second particle, and similarly for $\hat{\sigma}_x^a$ and $\hat{\sigma}_x^b$. Why is that?

The theory of *hidden variables* proposed by Einstein, Podolsky and Rosen [411] postulates, that the total state describing the two particles contains all information about the way, how the particles should behave at the detectors. The information was imprinted on each one of the two particle's when they were created in the source, i.e. the total state must be of the type,

$$|\psi\rangle = \begin{pmatrix} \pm_z^a & \pm_z^b \\ \pm_x^a & \pm_x^b \end{pmatrix} , \tag{41.131}$$

where the notation should be read as a decision table.

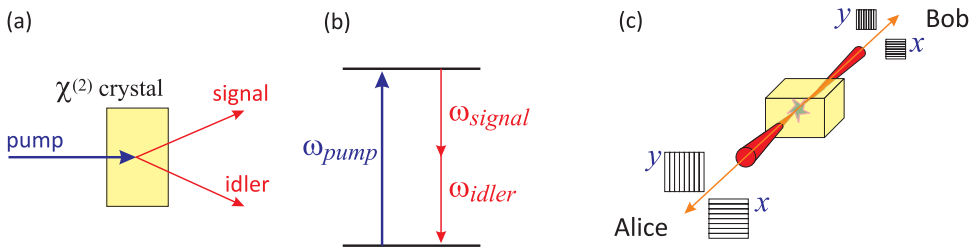

Figure 41.23: (a) Generation of entangled photon via parametric down-conversion. (b) Energy conservation upon parametric down-conversion. (c) Illustration of the EPR paradox.

On the other hand, quantum mechanics postulates that the reduction of the wavepacket describing the particle at detector a decides *spontaneously* on the result of the measurement at detector b. This decision *has no physical cause*. If the particles move with the speed of light, this decision is not restricted by *local causality* [601]. The state, also called *Bell state*, can be given in the form,

$$|\psi\rangle = |+_a \ +_b\rangle + |-_a \ -_b\rangle \ . \tag{41.132}$$

In Exc. 41.4.4.1 we check that this state cannot be expressed as a product state. Let us have a closer look at the EPR state (41.132) and imagine that particle 'a' (the one

that will later be analyzed by detector a) is embarked with Alice on a starship, while particle 'b' flies with Bob in opposite direction.

We introduce a basis choosing z as the quantization axis, that is, the basis vectors

$$|+\rangle_z = \begin{pmatrix} 1 \\ 0 \end{pmatrix} \quad , \quad |-\rangle_z = \begin{pmatrix} 0 \\ 1 \end{pmatrix} \tag{41.133}$$

are eigenvectors of the Pauli matrix $\hat{\sigma}_z$. On the other hand,

$$|+\rangle_x = \tfrac{1}{\sqrt{2}} \begin{pmatrix} 1 \\ 1 \end{pmatrix} \quad , \quad |-\rangle_x = \tfrac{1}{\sqrt{2}} \begin{pmatrix} 1 \\ -1 \end{pmatrix} \tag{41.134}$$

are eigenvectors of the Pauli matrix $\hat{\sigma}_x$. Quantum mechanics now tells us that, before any measurement, the wavefunction is in a superposition of states $|+\rangle$ and $|-\rangle$. That is, in the z-basis, using the tensor notation, we may write the entangled state (41.132) as,

$$\boxed{|\psi\rangle = \tfrac{1}{\sqrt{2}} \left(|+\rangle_z \otimes |+\rangle_z + |-\rangle_z \otimes |-\rangle_z \right)} \, . \tag{41.135}$$

But we can also express it in the x-basis,

$$\begin{aligned} |\psi\rangle &= \tfrac{1}{\sqrt{2}} \left(\tfrac{|+\rangle_x + |-\rangle_x}{\sqrt{2}} \otimes \tfrac{|+\rangle_x + |-\rangle_x}{\sqrt{2}} + \tfrac{|+\rangle_x - |-\rangle_x}{\sqrt{2}} \otimes \tfrac{|+\rangle_x - |-\rangle_x}{\sqrt{2}} \right) \\ &= \tfrac{1}{2\sqrt{2}} \begin{pmatrix} |+\rangle_x \otimes |+\rangle_x + |+\rangle_x \otimes |-\rangle_x + |-\rangle_x \otimes |+\rangle_x + |-\rangle_x \otimes |-\rangle_x \\ +|+\rangle_x \otimes |+\rangle_x - |+\rangle_x \otimes |-\rangle_x - |-\rangle_x \otimes |+\rangle_x + |-\rangle_x \otimes |-\rangle_x \end{pmatrix} \\ &= \tfrac{1}{\sqrt{2}} \left(|+\rangle_x \otimes |+\rangle_x + |-\rangle_x \otimes |-\rangle_x \right) \, . \end{aligned} \tag{41.136}$$

A generalization of this calculation to arbitrary rotations of the detector will be studied in Exc. 41.4.4.2.

After some time, Alice measures her spin in z-direction, i.e. performs a measurement of $\hat{\sigma}_z$. Her measurement not only collapses the wavefunction of Alice's spin a in either one of the states $|\pm\rangle_z$, but it instantaneously also collapses the wavefunction of Bob's spin along the z-direction,

$$|\psi\rangle \curvearrowright \begin{cases} |+\rangle_z \otimes |+\rangle_z = |+\rangle_z \otimes \frac{|+\rangle_x + |-\rangle_x}{\sqrt{2}} \\ |-\rangle_z \otimes |-\rangle_z = |+\rangle_z \otimes \frac{|+\rangle_x - |-\rangle_x}{\sqrt{2}} \end{cases} \tag{41.137}$$

Hence, if Bob measures along the z-axis, his measurement will be predefined by Alice's measurement. On the other hand, if tries to measure along the x-axis, he will find a random result with a probability of $\frac{1}{2}$ for each outcome [19]. That is, the direction of measurement in Alice's experiment fixes the quantization axis for Bob's experiment.

Two hypotheses have been put forward: The first one is that Alice's experiment sends information to Bob's experiment. Alice's particle told Bob's particle which spin

[19] Due to Bob's measurement along the x-axis Alice's wavefunction should collapse along the x-axis, as well. But according to quantum mechanics, Alice should be unable to know the spin value in x-direction, since she already knows the spin the z-direction, which is not allowed by the commutation rules,

$$[\hat{\sigma}_z^a, \hat{\sigma}_x^a] = \imath\hbar\hat{\sigma}_y^a \quad , \quad [\hat{\sigma}_z^b, \hat{\sigma}_x^b] = \imath\hbar\hat{\sigma}_y^b \, .$$

state he should be in. But this hypothesis violates the locality requirement of special relativity claiming that information cannot travel faster than light. Einstein called it 'spooky action at a distance'. The second hypothesis is to assume that quantum mechanics does not violate locality, but that the particles carry with them 'local hidden variables' [20] (like a proper DNA) whose values would be set right from the moment of the separation of the particles and which would determine the outcomes of any future spin measurement. Then, quantum mechanics would not be a complete theory, because it has nothing to say about these hidden variables.

41.4.1.1 Bell's inequality

In 1964 John S. Bell suggested an experimental test for the EPR paradox [114]. He proposed a theorem formulated as an inequality, the famous *Bell's inequality*, stating that *if the local hidden variables hypothesis proposed by Einstein is correct, then the inequality must be satisfied by experiment.*

There are many versions of Bell's inequality, all of them are equivalent. Let us follow Bell's argumentation and assume Alice and Bob to use Stern-Gerlach magnets oriented in arbitrary directions $\mathbf{a} \equiv \hat{\mathbf{e}}_{\vartheta,\varphi}$, respectively, $\mathbf{b} \equiv \hat{\mathbf{e}}_{\vartheta',\varphi'}$ to measure the expectation values,

$$\langle\psi|\hat{\vec{\sigma}}\cdot\mathbf{a}\otimes\mathbb{I}|\psi\rangle \qquad \text{and} \qquad \langle\psi|\mathbb{I}\otimes\hat{\vec{\sigma}}\cdot\mathbf{b}|\psi\rangle \tag{41.138}$$

respectively, on an anti-symmetric entangled two-spin state [21],

$$\boxed{|\psi\rangle = \tfrac{1}{\sqrt{2}}(|+\rangle_z\otimes|-\rangle_z - |+\rangle_z\otimes|-\rangle_z)} \; . \tag{41.139}$$

Let us first do the quantum calculation. Using the rules for Pauli matrices and the anti-symmetry of the entangled state,

$$\hat{\sigma}_x|\pm\rangle_z = |\mp\rangle_z \quad , \quad \hat{\sigma}_y|\pm\rangle_z = \pm\imath|\mp\rangle_z \quad , \quad \hat{\sigma}_z|\pm\rangle_z = \pm|\pm\rangle_z \; , \tag{41.140}$$

we derive in Excs. 41.4.4.3 and 41.4.4.4 the general relationship,

$$\langle\psi|\hat{\vec{\sigma}}\cdot\mathbf{a}\otimes\hat{\vec{\sigma}}\cdot\mathbf{b}|\psi\rangle = -\mathbf{a}\cdot\mathbf{b} \; , \tag{41.141}$$

which is the quantum mechanical correlation function for a joined measurement of Alice and Bob.

On the other hand, if local hidden variables exist, Alice's measurement is determined by the orientation $\mathbf{a}$ of her magnets and a (set of) hidden variable(s) λ, which are also available to Bob, whose measurement is determined by the orientation $\mathbf{b}$ of his magnets,

$$A(\mathbf{a},\lambda) \equiv \langle\psi|\hat{\vec{\sigma}}\cdot\mathbf{a}\otimes\mathbb{I}|\psi\rangle = \pm 1 \qquad \text{and} \qquad B(\mathbf{b},\lambda) \equiv \langle\psi|\mathbb{I}\otimes\hat{\vec{\sigma}}\cdot\mathbf{b}|\psi\rangle = \pm 1 \; , \tag{41.142}$$

with the crucial assumption that A does not depend on $\mathbf{b}$ and B not $\mathbf{a}$. Let us assume a probability distribution $\rho(\lambda)$ for the hidden variable satisfying $\int \rho(\lambda)d\lambda = 1$. Then the

[20] Note the difference to *non-local hidden variables* assumed by de Broglie and David Bohm in their formulation of quantum mechanics.

[21] The anti-symmetric state is chosen here for symmetry reasons facilitating the quantum calculation, but the arguments hold for any entangled state.

joint probability distribution $P(\mathbf{a},\mathbf{b})$ should coincide with the quantum mechanical correlation function,

$$P(\mathbf{a},\mathbf{b}) = \int A(\mathbf{a},\lambda)B(\mathbf{b},\lambda)\rho(\lambda)d\lambda = \langle\psi|\hat{\vec{\sigma}}\cdot\mathbf{a}\otimes\hat{\vec{\sigma}}\cdot\mathbf{b}|\psi\rangle \geq -1 \ . \tag{41.143}$$

For example, let the hidden variable now be unit vector $\vec{\lambda}$ with uniform probability distribution over all directions, such that,

$$A(\mathbf{a},\lambda) = \text{sign}(\mathbf{a}\cdot\vec{\lambda}) \qquad \text{and} \qquad B(\mathbf{b},\lambda) = -\text{sign}(\mathbf{b}\cdot\vec{\lambda}) \ . \tag{41.144}$$

Then,

$$\begin{aligned} P(\mathbf{a},\mathbf{b}) &= -\int \text{sign}(\cos\vartheta_{a\lambda})\text{sign}(\cos\vartheta_{b\lambda})\rho(\vartheta_\lambda)d\vartheta_\lambda \\ &= -\int_{\vartheta_a}^{\vartheta_b} \text{sign}(\cos\vartheta_\lambda)d\vartheta_\lambda = -1 + \tfrac{2}{\pi}\angle(\mathbf{a},\mathbf{b}) \ . \end{aligned} \tag{41.145}$$

This probability distribution clearly deviates from the quantum prediction, in particular at angles $\angle(\mathbf{a},\mathbf{b}) = \frac{\pi}{2}$, as seen in Fig. 41.24(a).

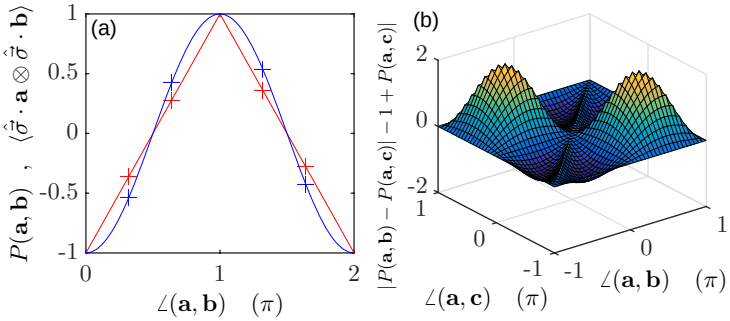

Figure 41.24: (code) (a) Joint probability distribution $P(\mathbf{a},\mathbf{b})$ in local hidden variables theory (red) and correlation function $\langle\psi|\vec{\sigma}\cdot\mathbf{a}\otimes\vec{\sigma}\cdot\mathbf{b}|\psi\rangle$ in quantum mechanics (blue). (b) Verification of Bell's inequality.

Let us finally derive Bell's inequality. Because of (41.142) for the anti-symmetric state we have the relation $B(\mathbf{b},\lambda) = -A(\mathbf{b},\lambda)$ and $A(\mathbf{a},\lambda) = A(\mathbf{a},\lambda)^{-1}$ allowing us to derive,

$$\begin{aligned} P(\mathbf{a},\mathbf{b}) - P(\mathbf{a},\mathbf{c}) &= -\int \left[A(\mathbf{a},\lambda)A(\mathbf{b},\lambda) - A(\mathbf{a},\lambda)A(\mathbf{c},\lambda)\right]\rho(\lambda)d\lambda \\ &= \int A(\mathbf{a},\lambda)A(\mathbf{b},\lambda)\left[A(\mathbf{b},\lambda)A(\mathbf{c},\lambda) - 1\right]\rho(\lambda)d\lambda \ , \end{aligned} \tag{41.146}$$

and

$$|P(\mathbf{a},\mathbf{b}) - P(\mathbf{a},\mathbf{c})| \leq \int |A(\mathbf{a},\lambda)A(\mathbf{b},\lambda)\left[A(\mathbf{b},\lambda)A(\mathbf{c},\lambda) - 1\right]|\rho(\lambda)d\lambda \tag{41.147}$$
$$\leq \int [1 - A(\mathbf{b},\lambda)A(\mathbf{c},\lambda)]\rho(\lambda)d\lambda$$
$$= \int \rho(\lambda)d\lambda + \int A(\mathbf{b},\lambda)B(\mathbf{c},\lambda)\rho(\lambda)d\lambda = 1 + P(\mathbf{b},\mathbf{c}) \ .$$

This inequality derived from the local hidden variables assumption is violated by quantum mechanics, since,

$$|\langle\hat{\vec{\sigma}}\cdot\mathbf{a}\otimes\hat{\vec{\sigma}}\cdot\mathbf{b}\rangle - \langle\hat{\vec{\sigma}}\cdot\mathbf{a}\otimes\hat{\vec{\sigma}}\cdot\mathbf{c}\rangle| = |-\mathbf{a}\cdot\mathbf{b} + \mathbf{a}\cdot\mathbf{c}| \tag{41.148}$$
$$\leq 1 - \mathbf{b}\cdot\mathbf{c} = 1 + \langle\hat{\vec{\sigma}}\cdot\mathbf{b}\otimes\hat{\vec{\sigma}}\cdot c\rangle$$

is not satisfied for arbitrary choices of $\mathbf{a}$, $\mathbf{b}$, and $\mathbf{c}$. To see this we plot in Fig. 41.24(b),

$$1 - \cos\angle(\mathbf{b},\mathbf{c}) - |\cos\angle(\mathbf{a},\mathbf{b}) - \cos\angle(\mathbf{a},\mathbf{c})| \ , \tag{41.149}$$

finding that this quantity becomes negative for some choices of the projection vectors.

Example 262 (*EPR paradox using GHZ states*): Here, we show a modified version of the EPR experiment proposed by Greenberger, Horne and Zeilinger (GHZ) based on the *GHZ state* [535]. They imagined a source creating three correlated non-interacting spin $\frac{1}{2}$ particles labeled a, b, and c flying toward three Stern-Gerlach type magnetic detectors, which measure the spins in x or in y-direction. The correct state is either quantum,

$$|\psi\rangle = |+_a \ +_b \ +_c\rangle_z - |-_a \ -_b \ -_c\rangle_z \ , \tag{41.150}$$

or

$$\boxed{|\psi\rangle = |+\rangle_z\otimes|+\rangle_z\otimes|+\rangle_z - |-\rangle_z\otimes|-\rangle_z\otimes|-\rangle_z} \ , \tag{41.151}$$

in tensor notation, or it contains hidden variables, that is, instructions telling the detectors which measurement result to exhibit upon arrival of a particle,

$$|\psi\rangle = \begin{pmatrix} \pm_x^a \ \pm_x^b \ \pm_x^c \\ \pm_y^a \ \pm_y^b \ \pm_y^c \end{pmatrix} . \tag{41.152}$$

Now, using the quantum mechanical rules (41.140), we obtain,

$$\hat{\sigma}_x\otimes\hat{\sigma}_x\otimes\hat{\sigma}_x|\psi\rangle \equiv \hat{\sigma}_x^a\hat{\sigma}_x^b\hat{\sigma}_x^c|\psi\rangle = -|\psi\rangle \ , \tag{41.153}$$

but also,

$$\hat{\sigma}_x^a\hat{\sigma}_y^b\hat{\sigma}_y^c|\psi\rangle = \hat{\sigma}_y^a\hat{\sigma}_x^b\hat{\sigma}_y^c|\psi\rangle = \hat{\sigma}_y^a\hat{\sigma}_y^b\hat{\sigma}_x^c|\psi\rangle = |\psi\rangle \ . \tag{41.154}$$

Hidden variables in a state $|\psi\rangle$ that *is not a coherent superposition* should at least be able to predict how each particle will behave in its respective detector, when we measure each one of the two spin components. From all possible combination only eight combinations can satisfy the requirement (41.154) written as,

$$\langle\hat{\sigma}_x^a\rangle\langle\hat{\sigma}_y^b\rangle\langle\hat{\sigma}_y^c\rangle = \langle\hat{\sigma}_y^a\rangle\langle\hat{\sigma}_x^b\rangle\langle\hat{\sigma}_y^c\rangle = \langle\hat{\sigma}_y^a\rangle\langle\hat{\sigma}_y^b\rangle\langle\hat{\sigma}_x^c\rangle = 1 \ . \tag{41.155}$$

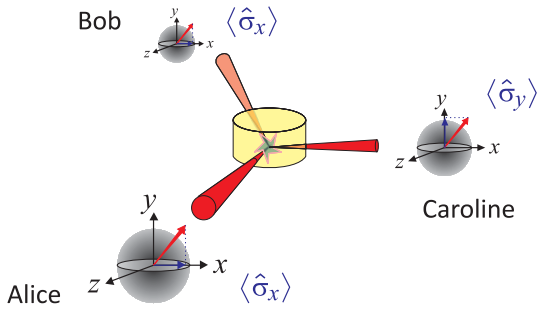

Figure 41.25: Scheme of the EPR experiment proposed by Greenberger, Horne and Zeilinger.

These are,

$$\begin{pmatrix} \langle\sigma_x^a\rangle & \langle\sigma_x^b\rangle & \langle\sigma_x^c\rangle \\ \langle\sigma_y^a\rangle & \langle\sigma_y^b\rangle & \langle\sigma_y^c\rangle \end{pmatrix} = \tag{41.156}$$
$$\begin{pmatrix} +++ \\ +++ \end{pmatrix}\begin{pmatrix} +-- \\ +-- \end{pmatrix}\begin{pmatrix} -+- \\ -+- \end{pmatrix}\begin{pmatrix} --+ \\ --+ \end{pmatrix}\begin{pmatrix} +++ \\ --- \end{pmatrix}\begin{pmatrix} +-- \\ -++ \end{pmatrix}\begin{pmatrix} -+- \\ +-+ \end{pmatrix}$$

but none of them satisfies (41.153) written as,

$$\langle\hat{\sigma}_x^a\rangle\langle\hat{\sigma}_x^b\rangle\langle\hat{\sigma}_x^c\rangle = -1 \ . \tag{41.157}$$

Therefore, the local hidden variables assumption is incompatible with quantum mechanics, and the EPR critique of quantum mechanics regarding its incompleteness must be refuted [22].

Which one of the two pictures is correct, the local hidden variables assumption or quantum mechanics, can actually be tested by Wheeler's *delayed choice* experiment. It consists of using pairs of correlated photons emitted in different directions, where they are expected by photodetectors. Polarizers located in front of the detectors fix the quantization axis to $\hat{\mathbf{e}}_x$ or $\hat{\mathbf{e}}_y$, but the choice of the axis is made only after the photons were created by the source, in order to avoid possible backactions of the polarizers on the source [23]. Bell's inequality condition [114] predicts a statistics for the results of repeated measurements where the orientation of the polarizers is randomly varied. The experiment run by Aspect [56, 54] showed that the assumption of local hidden variables violates *local realism* and thus confirmed quantum mechanics as being a complete theory.

[22] Note that the coupling of different degrees of freedom *is not* an entanglement, but it is the *condition* for being able to generate entanglement.

[23] We note that first attempts to demonstrate wave-particle duality with single photons in dilute laser beams are not really conclusive, because the attenuation of a coherent state does NOT result in a single photon states (non-classical Fock state). Even if on average only less than one photon is in the interferometer, this may still be a Glauber state. Nonetheless, real single photon experiments involving the deexcitation of individual atoms by emission of two photons, produced the same result.

41.4.2 Information entropy

According to von Neumann, we can define the *von Neumann entropy*, also called quantum *information entropy* as,

$$\boxed{S \equiv -\langle \log_2 \hat{\rho} \rangle = \mathrm{Tr}\ (\hat{\rho} \log_2 \hat{\rho}) = -\sum_n \hat{\rho}_n \log_2 \hat{\rho}_n} \ , \tag{41.158}$$

where $\rho_n \equiv \langle n|\hat{\rho}|n\rangle$. For statistically independent systems the density operator is $\hat{\rho} = \hat{\rho}_1 \otimes \hat{\rho}_2$ and the entropy is additive $S = S_1 + S_2$. The entropy is observable, that is, independent of the basis and invariant with respect to unitary transformations. Therefore, $\hat{\rho}$ can be diagonalized and can be assumed diagonal in the following examples. For N independent qubits the density operator $\hat{\rho}^{(N)}$ and the entropy $S^{(N)}$ are:

$$\begin{aligned}
&\hat{\rho}^{(0)} = |+\rangle\langle+| && , \quad S^{(0)} = 0 \text{ bit} \\
&\hat{\rho}^{(1)} = \tfrac{1}{2}(|+\rangle\langle+| + |-\rangle\langle-|) && , \quad S^{(1)} = 1 \text{ bits} \\
&\hat{\rho}^{(2)} = \tfrac{1}{4}(|++\rangle\langle++| + |+-\rangle\langle+-| + |-+\rangle\langle-+| + |--\rangle\langle--|) && , \quad S^{(2)} = 2 \text{ bits} \\
&\hat{\rho}^{(N)} = \tfrac{1}{2^N}(|++...\rangle\langle++...| + ...) && , \quad S^{(N)} = N \text{ bits} \ .
\end{aligned} \tag{41.159}$$

The set is canonical and the entropy maximal. On the other hand, if the states are entangled, the entropy is always less than $S^{(N)} = N$ bits. For the state of maximally entangled spins, we have,

$$\rho^{(N)}_{corr} = \tfrac{1}{2^N}(|++...+\rangle\langle++...+| + |--...-\rangle\langle--...-|) \quad , \quad S^{(N)}_{corr} = 1 \text{ bit} \ . \tag{41.160}$$

Entropy is a measure for the degree of entanglement of a system. For a Dicke state $|J, M\rangle$ the entropy is,

$$S_{JM} = -\log_2 \binom{2J}{J+M} \ . \tag{41.161}$$

For beam splitters, the information entropy is calculated as follows: A Fock state $|N\rangle = |+\rangle^N$ divided by a beam splitter is described by,

$$\begin{aligned}
2^{-N/2}(|+\rangle + |-\rangle)^N &= \tfrac{1}{2^{N/2}} \sum_{n=0}^{N} \binom{N}{n} |+\rangle^{N-n}|-\rangle^n \\
\rho^{(N)}_{split} &= \tfrac{1}{2^N} \sum_{n,m=0}^{N} \binom{N}{n}\binom{N}{m} |+\rangle^{N-n}|-\rangle^n\langle+|^{N-m}\langle-|^m \\
\rho^{(N)}_{split} &= \tfrac{1}{2^N} \sum_{n=0}^{N} \binom{N}{n}\binom{N}{n} |+\rangle^{N-n}|-\rangle^n\langle+|^{N-n}\langle-|^n \ .
\end{aligned} \tag{41.162}$$

For the information entropy, we obtain,

$$S^{(N)}_{split} = N + \tfrac{1}{2^N} \sum_{n=0}^{N} \binom{N}{n} \log_2 \binom{N}{n} \ . \tag{41.163}$$

The division of a beam is an incoherent process in the sense that it increases the entropy. The process is *irreversible*. The divided beams can not be recombined by a coherent process. For example, an interferometer always has two output ports. However, the phase is preserved.

The *quantum information content* is defined by the deviation from maximum entropy,

$$Q = S_{mx} - S_{actual} \ . \tag{41.164}$$

If the system is in a mixed state, the entropy measures deviations from a pure state behavior [99].

41.4.3 Classical and quantum correlations

Correlation is described by a system of coupled differential equations, each one describing another degree of freedom. The correlation between a degree of freedom and the rest of the system is lost, if their dynamics decouples. In quantum mechanics, this translates into the impossibility of factorizing the full density matrix of the correlated states. The *correlation index* is defined as the informational content of the correlation between two systems,

$$\begin{aligned} I &= Q - (Q_a + Q_b) \\ &= S_{mx,tot} - S_{actual,tot} - (S_{mx,a} - S_{actual,a} + S_{mx,b} - S_{actual,b}) \\ &= S_{actual,a} + S_{actual,b} - S_{actual,tot} \ . \end{aligned} \tag{41.165}$$

Classical correlations are those which are allowed by a local realistic theory, whereas quantum correlations are incompatible with the classical notion of local realism [99].

A measure for the entanglement of two modes is the *cross-correlation* of their intensity at equal times,

$$g^{(2)}_{a,b}(0) = \frac{\langle \hat{a}^\dagger(t)\hat{a}(t)\hat{b}^\dagger(t)\hat{b}(t)\rangle}{\langle \hat{a}^\dagger(t)\hat{a}(t)\rangle\langle \hat{b}^\dagger(t)\hat{b}(t)\rangle} \ . \tag{41.166}$$

The *Cauchy-Schwartz relation*,

$$g^{(2)}_{a,b}(\tau) \leq \sqrt{g^{(2)}_{a,a}(\tau)}\sqrt{g^{(2)}_{b,b}(\tau)} \tag{41.167}$$

only applies to classical states. Quantum states satisfy,

$$g^{(2)}_{a,b}(\tau) \leq \sqrt{\left[g^{(2)}_{a,a}(\tau) + \frac{1}{I_a(\tau)}\right]}\sqrt{\left[g^{(2)}_{b,b}(\tau) + \frac{1}{I_b(\tau)}\right]} \ , \tag{41.168}$$

where $I_k(\tau) = \langle \hat{k}^\dagger(t)\hat{k}(t)\rangle$.

Example 263 (*Classical versus quantum correlations*): A simple example for a *classical correlation* is the following: Imagine a white and a red billiard ball. Both are put in black boxes and embarked on star-ships heading off at light speed in opposite directions without letting the commanders know their color. When after one year of travel they open the boxes and verify the color of

their respective balls, they immediately know the color of the ball on the other star-ship. This 'measurement' is not limited by the speed of light, which would take two years to pass information between the star-ships.
A *quantum correlation* is more tricky than that. To get closer to the essence of quantum correlations, let us refine the classical example: Now, we assume that the billiard balls are made of different materials, so that we have one *heavy* white or red ball and one *light* white or red ball. Again they are embarked on star-ships. The commanders are now advised to open the boxes and EITHER sense the weights of the balls OR look at them to acknowledge their colors.
The difference of the quantum world begin here already: If the billiard balls were quantum particles, e.g. photons, the measurements of their properties would be exclusive.
Now, assume furthermore that instead of one box the star-ships embark 10 boxes, each one receiving one of two balls.

41.4.4 Exercises

41.4.4.1 Ex: Bell states

Show that the Bell states cannot be written as products of two states.

Solution: *In the product state,*

$$(c_+|+\rangle + c_-|-\rangle)^2 = c_+^2|++\rangle + c_-^2|--\rangle + c_+c_-|+-\rangle + c_-c_+|-+\rangle$$

the coefficients must satisfy $c_+c_- = 0$ *in order to have a Bell state, which is only possible if either* c_+ *or* c_- *is zero.*

41.4.4.2 Ex: Behavior of entanglement upon rotation of the quantization axis

Show that the anti-symmetric entangle Bell state remains entangled upon rotation of the quantization axis, that is,

$$|+\rangle_{\vartheta,\varphi} \otimes |-\rangle_{\vartheta,\varphi} - |-\rangle_{\vartheta,\varphi} \otimes |+\rangle_{\vartheta,\varphi} \;\propto\; |+\rangle_z \otimes |-\rangle_z - |-\rangle_z \otimes |+\rangle_z \;,$$

where $|\pm\rangle_{\vartheta,\varphi}$ are the eigenstates of the Pauli spin operator $\hat{\vec{\sigma}}$.

Solution: *Choosing the eigenstates of the rotated basis as,*

$$\begin{aligned}
|+\rangle_{\vartheta,\varphi} &\equiv |\vartheta,\varphi\rangle = \cos\tfrac{\vartheta}{2}|+\rangle_z + e^{\imath\varphi}\sin\tfrac{\vartheta}{2}|-\rangle_z \\
|-\rangle_{\vartheta,\varphi} &\equiv |\pi-\vartheta,\varphi+\pi\rangle = \sin\tfrac{\vartheta}{2}|+\rangle_z - e^{\imath\varphi}\cos\tfrac{\vartheta}{2}|-\rangle_z \;.
\end{aligned}$$

we see,

$$\begin{aligned}
|\psi\rangle &= \tfrac{1}{\sqrt{2}}\left[|\vartheta,\varphi\rangle \otimes |\pi-\vartheta,\varphi+\pi\rangle - |\pi-\vartheta,\varphi+\pi\rangle \otimes |\vartheta,\varphi\rangle\right] \\
&= \tfrac{1}{\sqrt{2}}\Big[\big(\cos\tfrac{\vartheta}{2}|+\rangle_z + e^{\imath\varphi}\sin\tfrac{\vartheta}{2}|-\rangle_z\big) \otimes \big(\sin\tfrac{\vartheta}{2}|+\rangle_z - e^{\imath\varphi}\cos\tfrac{\vartheta}{2}|-\rangle_z\big) \\
&\qquad - \big(\sin\tfrac{\vartheta}{2}|+\rangle_z - e^{\imath\varphi}\cos\tfrac{\vartheta}{2}|-\rangle_z\big) \otimes \big(\cos\tfrac{\vartheta}{2}|+\rangle_z + e^{\imath\varphi}\sin\tfrac{\vartheta}{2}|-\rangle_z\big)\Big] \\
&= -\tfrac{-e^{\imath\varphi}}{\sqrt{2}}\left[|+\rangle_z \otimes |-\rangle_z - |-\rangle_z \otimes |+\rangle_z\right] \;.
\end{aligned}$$

41.4.4.3 Ex: Rotations with Pauli matrices

a. Verify,

$$e^{-\imath(\pi/4)\hat{\sigma}_k}\hat{\sigma}_m e^{\imath(\pi/4)\hat{\sigma}_k} = \epsilon_{kmn}\hat{\sigma}_n + \delta_{km}\hat{\sigma}_k \qquad \text{with} \qquad (kmn) = (xyz) \ .$$

b. Prove,

$$|\vartheta,\varphi\rangle = e^{-\imath\varphi(\hat{\sigma}_z - I)/2}e^{-\imath\vartheta\hat{\sigma}_y/2}|0,0\rangle = e^{\imath\varphi/2}e^{-\imath\varphi\hat{\sigma}_z/2}e^{-\imath\vartheta\hat{\sigma}_y/2}|+\rangle \ .$$

c. Solve the eigenvalue equations,

$$\hat{\vec{\sigma}}\cdot\hat{\mathbf{e}}_z|\vartheta,\varphi\rangle = m|\vartheta,\varphi\rangle \qquad \text{and} \qquad \hat{\vec{\sigma}}\cdot\hat{\mathbf{e}}_\rho|\vartheta,\varphi\rangle = m|\vartheta,\varphi\rangle \ ,$$

with $\hat{\mathbf{e}}_\rho \equiv \hat{\mathbf{e}}_x\cos\phi + \hat{\mathbf{e}}_y\sin\phi$.

Solution: *a. This follows as a generalization of Exc. 23.3.10.5 with the definition of the Pauli matrices.*
b. We show,

$$|\vartheta,\varphi\rangle = \cos\tfrac{\vartheta}{2}|+\rangle + e^{\imath\varphi}\sin\tfrac{\vartheta}{2}|-\rangle = ...$$

c. The eigenvalue equation for polar quantization axis is,

$$\begin{aligned}\vec{\sigma}\cdot\hat{\mathbf{e}}_z|\vartheta,\varphi\rangle = \hat{\sigma}_z|\vartheta,\varphi\rangle &= \begin{pmatrix}1 & 0\\ 0 & -1\end{pmatrix}\left(\cos\tfrac{\vartheta}{2}|+\rangle + e^{\imath\varphi}\sin\tfrac{\vartheta}{2}|-\rangle\right)\\ &= \cos\tfrac{\vartheta}{2}|+\rangle - e^{\imath\varphi}\sin\tfrac{\vartheta}{2}|-\rangle \equiv m\left(\cos\tfrac{\vartheta}{2}|+\rangle + e^{\imath\varphi}\sin\tfrac{\vartheta}{2}|-\rangle\right) \ ,\end{aligned}$$

which can only be true for $m = 1$ with $|\vartheta,\varphi\rangle = |0,\varphi\rangle = |+\rangle$ or $m = -1$ with $|\vartheta,\varphi\rangle = |\pi,\varphi\rangle = |-\rangle$. Hence,

$$P_{m=1} = \langle\vartheta,\varphi|0,\varphi\rangle\langle 0,\varphi|\vartheta,\varphi\rangle = \tfrac{1}{2} = \langle\vartheta,\varphi|\pi,\varphi\rangle\langle\pi,\varphi|\vartheta,\varphi\rangle = P_{m=-1}$$
$$\langle\vartheta,\varphi|\vec{\sigma}\cdot\hat{\mathbf{e}}_z|\vartheta,\varphi\rangle = \cos\vartheta = \pm 1 = m \ .$$

For the azimuthal quantization axis,

$$\begin{aligned}\vec{\sigma}\cdot\hat{\mathbf{e}}_\rho|\vartheta,\varphi\rangle = (\hat{\sigma}_x\cos\phi + \hat{\sigma}_y\sin\phi)|\vartheta,\varphi\rangle &= \begin{pmatrix}0 & e^{-\imath\phi}\\ e^{\imath\phi} & 0\end{pmatrix}\left(\cos\tfrac{\vartheta}{2}|+\rangle + e^{\imath\varphi}\sin\tfrac{\vartheta}{2}|-\rangle\right)\\ &= e^{\imath\phi}\cos\tfrac{\vartheta}{2}|-\rangle + e^{-\imath\phi}e^{\imath\varphi}\sin\tfrac{\vartheta}{2}|+\rangle \equiv m\left(\cos\tfrac{\vartheta}{2}|+\rangle + e^{\imath\varphi}\sin\tfrac{\vartheta}{2}|-\rangle\right) \ ,\end{aligned}$$

which can only be true for $m = 1$ with $|\vartheta,\varphi\rangle = |\frac{\pi}{2},\phi\rangle$ or $m = -1$ with $|\vartheta,\varphi\rangle = |\frac{\pi}{2},\pi+\phi\rangle$. Hence,

$$P_{m=1} = \langle\vartheta,\varphi|\tfrac{\pi}{2},\phi\rangle\langle\tfrac{\pi}{2},\phi|\vartheta,\varphi\rangle = \tfrac{1}{2} = \langle\vartheta,\varphi|\tfrac{\pi}{2},\pi+\phi\rangle\langle\tfrac{\pi}{2},\pi+\phi|\vartheta,\varphi\rangle = P_{m=-1}$$
$$\langle\vartheta,\varphi|\vec{\sigma}\cdot\hat{\mathbf{e}}_\rho|\vartheta,\varphi\rangle = \cos(\varphi-\phi)\sin\vartheta = \pm 1 = m \ .$$

41.4.4.4 Ex: Projections of single-atom spins and their correlations

a. Calculate explicitly $\langle\vartheta,\varphi|\hat{\vec{\sigma}}|\vartheta,\varphi\rangle$ and $\langle\vartheta',\varphi'|\hat{\vec{\sigma}}\cdot\hat{\mathbf{e}}_{\vartheta,\varphi}|\vartheta',\varphi'\rangle$, where $|\vartheta,\varphi\rangle$ are the states defined in (41.10), using the basis ${}_z\langle+| = (1\ 0)$ and ${}_z\langle-| = (0\ 1)$.
b. For the anti-symmetric entangled two-atom spin state defined in (41.139) calculate the spin projection correlations $\langle\psi|\hat{\vec{\sigma}}\cdot\hat{\mathbf{e}}_{\vartheta,\varphi}\otimes\hat{\vec{\sigma}}\cdot\hat{\mathbf{e}}'_{\vartheta,\varphi}|\psi\rangle$.

Solution: *Using the rules (41.140) for Pauli matrices on the anti-symmetric entangled two-spin state, we can readily show,*

$$\langle\psi|\hat{\sigma}_x\otimes\hat{\sigma}_x|\psi\rangle = \langle\psi|\hat{\sigma}_y\otimes\hat{\sigma}_y|\psi\rangle = \langle\psi|\hat{\sigma}_z\otimes\hat{\sigma}_z|\psi\rangle = -1$$
$$\langle\psi|\hat{\sigma}_x\otimes\hat{\sigma}_y|\psi\rangle = \langle\psi|\hat{\sigma}_y\otimes\hat{\sigma}_z|\psi\rangle = \langle\psi|\hat{\sigma}_z\otimes\hat{\sigma}_x|\psi\rangle = 0\ .$$

a. The choice of the basis sets z as the quantization axis for which the Pauli matrices are defined. We consider an arbitrary projection axis given by the vector $|\vartheta,\varphi\rangle$. From now on dropping the subscript z, using the Pauli matrix rules, it is easy to see,

$$\langle\vartheta,\varphi|\hat{\vec{\sigma}}|\vartheta,\varphi\rangle = R_z(\varphi)R_y(\vartheta)\hat{\mathbf{e}}_z = \begin{pmatrix}\sin\vartheta\cos\varphi\\ \sin\vartheta\sin\varphi\\ \cos\vartheta\end{pmatrix} = \hat{\mathbf{e}}_{\vartheta,\varphi}\ .$$

Likewise,

$$\begin{aligned}&\langle\vartheta',\varphi'|\hat{\vec{\sigma}}\cdot\hat{\mathbf{e}}_{\vartheta,\varphi}|\vartheta',\varphi'\rangle\\ &= \left(\cos\tfrac{\vartheta'}{2}\langle+| + e^{-\imath\varphi'}\sin\tfrac{\vartheta'}{2}\langle-|\right)(\hat{\sigma}_x\sin\vartheta\cos\varphi + \hat{\sigma}_y\sin\vartheta\sin\varphi + \hat{\sigma}_z\cos\vartheta)\left(\cos\tfrac{\vartheta'}{2}|+\rangle + e^{\imath\varphi'}\sin\tfrac{\vartheta'}{2}|-\rangle\right)\\ &= \hat{\mathbf{e}}_{\vartheta,\varphi}\cdot\hat{\mathbf{e}}_{\vartheta',\varphi'}\ .\end{aligned}$$

Also,

$$|\pi-\vartheta,-\varphi\rangle = \cos\tfrac{\pi-\vartheta}{2}|+\rangle + e^{-\imath\varphi}\sin\tfrac{\pi-\vartheta}{2}|-\rangle = \sin\tfrac{\vartheta}{2}|+\rangle + e^{-\imath\varphi}\cos\tfrac{\vartheta}{2}|-\rangle = e^{-\imath\varphi}\hat{\sigma}_x|\vartheta,\varphi\rangle\ ,$$

and,

$$\hat{\sigma}_z\hat{\sigma}_y\hat{\sigma}_x|\vartheta,\varphi\rangle = \hat{\sigma}_z\hat{\sigma}_y\hat{\sigma}_x\left(\cos\tfrac{\vartheta}{2}|+\rangle + e^{\imath\varphi}\sin\tfrac{\vartheta}{2}|-\rangle\right) = -\imath|\vartheta,\varphi\rangle\ .$$

b. The correlations are,

$$\begin{aligned}&\langle\psi|\hat{\vec{\sigma}}\cdot\hat{\mathbf{e}}_{\vartheta,\varphi}\otimes\hat{\vec{\sigma}}\cdot\hat{\mathbf{e}}'_{\vartheta,\varphi})|\psi\rangle\\ &= \langle\psi|\begin{pmatrix}\hat{\sigma}_x\otimes\hat{\sigma}_x\sin\vartheta\cos\varphi\sin\vartheta'\cos\varphi' + \hat{\sigma}_x\otimes\hat{\sigma}_y\sin\vartheta\cos\varphi\sin\vartheta'\sin\varphi'\\ +\hat{\sigma}_x\otimes\hat{\sigma}_z\sin\vartheta\cos\varphi\cos\vartheta' + \hat{\sigma}_y\otimes\hat{\sigma}_x\sin\vartheta\sin\varphi\sin\vartheta'\cos\varphi'\\ +\hat{\sigma}_y\otimes\hat{\sigma}_y\sin\vartheta\sin\varphi\sin\vartheta'\sin\varphi' + \hat{\sigma}_y\otimes\hat{\sigma}_z\sin\vartheta\sin\varphi\cos\vartheta'\\ +\hat{\sigma}_z\otimes\hat{\sigma}_x\cos\vartheta\sin\vartheta'\cos\varphi' + \hat{\sigma}_z\otimes\hat{\sigma}_y\cos\vartheta\sin\vartheta'\sin\varphi'\\ +\hat{\sigma}_z\otimes\hat{\sigma}_z\cos\vartheta\cos\vartheta'\end{pmatrix}|\psi\rangle\\ &= -\begin{pmatrix}\sin\vartheta\cos\varphi\\ \sin\vartheta\sin\varphi\\ \cos\vartheta\end{pmatrix}\begin{pmatrix}\sin\vartheta'\cos\varphi'\\ \sin\vartheta'\sin\varphi'\\ \cos\vartheta'\end{pmatrix} = -\hat{\mathbf{e}}_{\vartheta,\varphi}\cdot\hat{\mathbf{e}}'_{\vartheta,\varphi} = -\cos\measuredangle(\hat{\mathbf{e}}_{\vartheta,\varphi},\hat{\mathbf{e}}'_{\vartheta,\varphi})\ .\end{aligned}$$

41.4.4.5 Ex: Entanglement

Upon detecting the polarization of one photon in an entangled photon pair the polarization of the other photon gets determined. Does this lead to a faster than light communication? Justify your answer. How would you demonstrate the no-cloning theorem from the assumption that relativistic causality should prevail.

Solution:

41.4.4.6 Ex: Entanglement

Three photon are prepared in the GHZ state defined as,

$$|\psi\rangle = \tfrac{1}{\sqrt{3}}\left(|h\rangle_1|h\rangle_2|h\rangle_3 + |v\rangle_1|v\rangle_2|v\rangle_3\right) \ .$$

Show that, when the components of polarization are measured along the axes that have an angle of 45° with respect to the original axes, corresponding to the states,

$$|h'\rangle = \tfrac{1}{\sqrt{2}}(|h\rangle + |v\rangle) \qquad \text{and} \qquad |v'\rangle = \tfrac{1}{\sqrt{2}}(|h\rangle - |v\rangle) \ ,$$

one gets necessarily an even number of photons with vertical polarization v'.

Solution: *Inserting the basis transform,*

$$|h\rangle = \tfrac{1}{\sqrt{2}}(|h'\rangle + |v'\rangle) \qquad , \qquad |v\rangle = \tfrac{1}{\sqrt{2}}(|h'\rangle - |v'\rangle)$$

in to the GHZ state, we get,

$$\begin{aligned}|\psi\rangle &= \tfrac{1}{\sqrt{3}}\tfrac{1}{\sqrt{2}^3}\left[(|h'\rangle + |v'\rangle)\otimes(|h'\rangle + |v'\rangle)\otimes(|h'\rangle + |v'\rangle) + (|h'\rangle - |v'\rangle)\otimes(|h'\rangle - |v'\rangle)\otimes(|h'\rangle - |v'\rangle)\right] \\ &= \tfrac{1}{\sqrt{6}}\left[|h'\rangle\otimes|h'\rangle\otimes|h'\rangle + |h'\rangle\otimes|v'\rangle\otimes|v'\rangle + |v'\rangle\otimes|v'\rangle\otimes|h'\rangle + |v'\rangle\otimes|h'\rangle\otimes|v'\rangle\right] \ ,\end{aligned}$$

which confirms the assertion.

41.4.4.7 Ex: NOON state

A *NOON state* is a quantum-mechanical many-body entangled state:

$$|\psi_{\text{NOON}}\rangle = \frac{|N\rangle_a|0\rangle_b + e^{\imath N\theta}|0\rangle_a|N\rangle_b}{\sqrt{2}} \ , \tag{41.169}$$

which represents a superposition of N particles in mode a with zero particles in mode b, and vice versa. Usually, the particles are photons, but in principle any bosonic field can support NOON states.
Two-photon NOON states, where $N = 2$, can be created deterministically from two identical photons and a 50:50 beam splitter. This is called the Hong-Ou-Mandel effect in quantum optics. Three- and four-photon NOON states cannot be created deterministically from single-photon states, but they have been created probabilistically via post-selection using spontaneous parametric down-conversion.

Solution: *NOON states are an important concept in quantum metrology and quantum sensing for their ability to make precision phase measurements when used in an optical interferometer. For example, consider the observable,*

$$A = |N,0\rangle\langle 0,N| + |0,N\rangle\langle N,0| \ , \tag{41.170}$$

The expectation value of A for a system in a NOON state switches between $+1$ and -1 when the phase changes from 0 to π/N. Moreover, the error in the phase measurement becomes,

$$\Delta\theta = \frac{\Delta A}{|d\langle A\rangle/d\theta|} = \frac{1}{N} \ . \tag{41.171}$$

This is the so-called Heisenberg limit, and gives a quadratic improvement over the standard quantum limit.

41.5 Creating quantum correlations

Since the experimental verification of *Bell's inequality* [57] numerous ideas were proposed for the creation and application of correlated states in distant particles. Realistic proposals on how to create such states are often based on a Jaynes-Cummings type coupling between states of atomic excitation and the degrees of freedom of a harmonic oscillator. The Jaynes-Cummings dynamics has been extensively studied in micromasers, where the non-resonant interaction of an atomic transition with the TEM_{00} mode of a stored radiation field generates quantum coherences. In very high finesse cavities, light field states with sub-Poissonian photon statistics can be generated and stored for macroscopic times, and schemes for the creation of Fock states and Schrödinger cat states were proposed and tested. Furthermore, the electronic excitation states of atoms successively traversing a micromaser can be correlated under suitable conditions. The availability of fundamental techniques motivated proposals for the investigation of phenomena such as EPR correlations, quantum teleportation, and quantum switching [382]. On the other hand, quantum coherences are very fragile to dissipation and rapidly decay when exposed to perturbations.

Jaynes-Cummings type dynamics can also be realized with a single ion stored in a Paul trap, where the interaction of its mechanical motion with an electronic transition [157] can induce very stable quantum coherences in the vibrational degrees of freedom. Schrödinger cat states have already been demonstrated in this system [866], as well as fundamental parts of a quantum computer, the quantum *controlled not gate* [866] and the quantum *phase gate* [1320]. In Sec. 41.5.1 we present a possible extension of these ideas to several atoms in a collective Jaynes-Cummings type interaction (also called Tavis-Cummings model) with a single harmonic oscillator mode.

In order to correlate particles, they must be able to exchange information, that is, they must interact in some way. One method uses ions trapped in a linear Paul trap, where they form a straight chain, individually driven by laser beams and coupled to each other via their vibrational degrees of freedom mediated through Coulomb repulsion [268]. We present this idea in Sec. 41.5.2. Such scenarios have been implemented

to create the first quantum computers. Another way consists in trapping neutral atoms in a dual optical lattice and let them undergo *controlled collisions* [661], as will be discussed in Sec. 41.5.3.

Alternative approaches to realizing quantum gates use dipole-dipole interactions [194], conditional Raman adiabatic passages by laser-induced excitation of interatomic dipole-dipole interactions [823], or interactions between permanent dipoles of atoms in Rydberg states [662] [24]

41.5.1 Correlating atoms in the Jaynes-Cummings model

In Sec. 35.4 we showed already that the Jaynes-Cummings model is able to perform coherent operations on a two-level system –which from now on we will call *qubit*–, such as the *population inversion* (NOT-gate) and the controlled dephasing of an excited dipole moment (phase gate). These operations are fundamental for applications in quantum information, however, we still lack essential ingredients allowing us to entangle states of two, three or more qubits in order to perform a *quantum register* of *qubits*. Once these register are realized, we must define coherent quantum operations called *quantum gates*.

41.5.1.1 Tavis-Cummings model for 2 atoms

In Sec. 35.4 we showed, how a Jaynes-Cummings interaction between an atom and a radiation field can exchange quantum correlations. It is reasonable to expect that, when we have two (or more) atoms interacting with the same radiation field, we can exchange correlations between atoms via the field. This would allow the implementation of entanglement protocols and quantum gates. We will disregard spontaneous processes, such that all couplings are then coherent and the processes reversible.

In Sec. 23.3.9 we learned, how to span a Hilbert space of various particles. We will now apply these notions in the scope of generalizing the Jaynes-Cummings model to *two atoms interacting with the same optical mode*, without spontaneous decay processes considered. The system is often referred to as the *Tavis-Cummings model*. The Hamiltonian of the system, which consists of two non-interacting atoms, both coupled in the same optical mode, is,

$$\boxed{\hat{H} = \omega \hat{a}^\dagger \hat{a} + \sum_{i=1,2} \omega_{ai} (\hat{\sigma}_i^+ \hat{\sigma}_i^- - \tfrac{1}{2}) + \sum_{i=1,2} \tfrac{1}{2} g_i(t) (\hat{a}\hat{\sigma}_i^+ + \hat{a}^+ \hat{\sigma}_i^-)} \,. \tag{41.172}$$

The suffix denotes the individual atoms. Note that the coupling constant $g_i(t)$ can be considered as time dependent, which may be useful for modeling radiation pulse envelopes. In matrix representation the Hamiltonian acting on the subspace of n photons is,

$$|\psi\rangle = \sum_n \begin{pmatrix} c_{11\ n+1} \\ c_{12\ n} \\ c_{21\ n} \\ c_{22\ n-1} \end{pmatrix} |n\rangle \qquad \text{where} \qquad c_{ij} \equiv_1 \langle j|_2 \langle i|\langle n|\psi\rangle \tag{41.173}$$

[24] A system to create quantum correlations is the *optical parametric oscillator* (OPO).

for example, $\langle n| \otimes \langle 1| \otimes \langle 1| = \langle n|(1\ 0\ 0\ 0)$, $\langle n| \otimes \langle 2| \otimes \langle 1| = \langle n|(0\ 1\ 0\ 0)$, and so on. The atomic transition operators are generalized to,

$$\hat{\sigma}_1^- = \sum_n |n\rangle\hat{\sigma}^- \otimes \mathbb{I}\langle n| = \sum_n |n\rangle \begin{pmatrix} & & 1 & \\ & & & 1 \\ 0 & & & \\ & 0 & & \end{pmatrix} \langle n| \tag{41.174}$$

$$\hat{\sigma}_2^- = \sum_n |n\rangle\mathbb{I} \otimes \hat{\sigma}^- \langle n| = \sum_n |n\rangle \begin{pmatrix} & 1 & & \\ 0 & & & \\ & & & 1 \\ & & 0 & \end{pmatrix} \langle n| \quad , \text{etc. .}$$

The Hamiltonian is, on this basis,

$$\hat{H} = \sum_n |n\rangle \begin{pmatrix} n\omega - \frac{\omega_{a1}}{2} - \frac{\omega_{a2}}{2} & & & \\ & n\omega - \frac{\omega_{a1}}{2} + \frac{\omega_{a2}}{2} & & \\ & & n\omega + \frac{\omega_{a1}}{2} - \frac{\omega_{a2}}{2} & \\ & & & n\omega + \frac{\omega_{a1}}{2} + \frac{\omega_{a2}}{2} \end{pmatrix} \langle n| + \sum_n |n-1\rangle\sqrt{n} \begin{pmatrix} 0 & & & \\ g_2 & & & \\ g_1 & & & \\ 0 & g_1 & g_2 & 0 \end{pmatrix} \langle n| + \sum_n |n+1\rangle\sqrt{n+1} \begin{pmatrix} 0 & g_2 & g_1 & 0 \\ & & & g_1 \\ & & & g_2 \\ & & & 0 \end{pmatrix} \langle n| \ . \tag{41.175}$$

Now, we can rearrange the subspaces and finally get,

$$\hat{H} = \sum_n |n\rangle \begin{pmatrix} (n+1)\omega - \frac{\omega_{a1}}{2} - \frac{\omega_{a2}}{2} & g_1\sqrt{n} & g_2\sqrt{n} & \\ g_1\sqrt{n} & n\omega + \frac{\omega_{a1}}{2} - \frac{\omega_{a2}}{2} & & g_2\sqrt{n+1} \\ g_2\sqrt{n} & & n\omega - \frac{\omega_{a1}}{2} + \frac{\omega_{a2}}{2} & g_1\sqrt{n+1} \\ & g_2\sqrt{n+1} & g_1\sqrt{n+1} & (n-1)\omega + \frac{\omega_{a1}}{2} + \frac{\omega_{a2}}{2} \end{pmatrix} \langle n| \ . \tag{41.176}$$

The density operator for the subspace is,

$$\hat{\rho} = \begin{pmatrix} |n+1\rangle|1\rangle_1|1\rangle_2\ {}_1\langle 1|_2\langle 1|\langle n+1| & |n+1\rangle|1\rangle_1|1\rangle_2\ {}_1\langle 1|_2\langle 2|\langle n| & \dots \\ |n\rangle|1\rangle_2|1\rangle_2\ {}_1\langle 1|_2\langle 1|\langle n+1| & \dots & \\ |n\rangle|2\rangle_1|2\rangle_2\ {}_1\langle 1|_2\langle 1|\langle n+1| & \dots & \\ |n-1\rangle|2\rangle_1|2\rangle_2\ {}_1\langle 1|_2\langle 1|\langle n+1| & \dots & \end{pmatrix} , \tag{41.177}$$

if the basis is again defined by equation (41.174).

41.5.1.2 Resonant excitation

To discuss the case of resonant excitation, $\Delta_1 = \Delta_2 = 0$, let us assume identical atoms, $\omega_{a1} = \omega_{a2} \equiv \omega_0$, and equal Rabi frequencies, $g_1 = g_2 \equiv g$. Assuming dipolarly

forbidden strongly saturated transition, $n = \alpha^2$ for all n, the Hamiltonian simplifies considerably,

$$\hat{H}_n = \begin{pmatrix} n\omega & g\sqrt{n} & g\sqrt{n} & \\ g\sqrt{n} & n\omega & & g\sqrt{n} \\ g\sqrt{n} & & n\omega & g\sqrt{n} \\ & g\sqrt{n} & g\sqrt{n} & n\omega \end{pmatrix} ,$$

the eigenvalues can be calculated and the time evolution matrix becomes, using the abbreviation $\varphi \equiv gt\sqrt{n}$,

$$\boxed{e^{-\imath\hat{H}_n t} = e^{-\imath\hat{H}_n^{A1}t} e^{-\imath\hat{H}_n^{A2}t} = \begin{pmatrix} \cos^2\varphi & \imath\sin\varphi\cos\varphi & \imath\sin\varphi\cos\varphi & -\sin^2\varphi \\ \imath\sin\varphi\cos\varphi & \cos^2\varphi & -\sin^2\varphi & \imath\sin\varphi\cos\varphi \\ \imath\sin\varphi\cos\varphi & -\sin^2\varphi & \cos^2\varphi & \imath\sin\varphi\cos\varphi \\ -\sin^2\varphi & \imath\sin\varphi\cos\varphi & \imath\sin\varphi\cos\varphi & \cos^2\varphi \end{pmatrix}} . \tag{41.178}$$

For a π-pulse, we get,

$$e^{-\imath\hat{H}_n t} \xrightarrow{\pi/2} \frac{1}{2}\begin{pmatrix} 1 & \imath & \imath & -1 \\ \imath & 1 & -1 & \imath \\ \imath & -1 & 1 & \imath \\ -1 & \imath & \imath & 1 \end{pmatrix} . \tag{41.179}$$

It is interesting to note that some superposition states completely separate from the optical mode,

$$e^{-\imath\hat{H}_n t}\begin{pmatrix} 0 \\ 1 \\ -1 \\ 0 \end{pmatrix} = \begin{pmatrix} 0 \\ 1 \\ -1 \\ 0 \end{pmatrix} \quad \text{and} \quad e^{-\imath\hat{H}_n t}\begin{pmatrix} 1 \\ 0 \\ 0 \\ -1 \end{pmatrix} = \begin{pmatrix} 1 \\ 0 \\ 0 \\ -1 \end{pmatrix} . \tag{41.180}$$

41.5.1.3 Dispersive excitation

In the dispersive limit, $\Delta_i \gg n^{1/2} g_i$, the dynamic evolution can be evaluated from a first order perturbative approach, analogous to the one already made for the standard JCM model. In this approach, the off-diagonal matrix elements (41.176) generate a light-shift of the energy levels appearing on the diagonal of the approximated matrix. Using the abbreviation $\Lambda_i \equiv g_i^2/\Delta_i$, the temporal evolution matrix $e^{-\imath\hat{H}_n t}$ can now be evaluated from,

$$\hat{H}_n = -\frac{\Delta_1 + \Delta_2}{2}\mathbb{I}_4 + \begin{pmatrix} n\Lambda_1 + n\Lambda_2 & & & \\ & -n\Lambda_1 + (n+1)\Lambda_2 & & \\ & & (n+1)\Lambda_1 - n\Lambda_2 & \\ & & & -(n+1)\Lambda_1 - (n+1)\Lambda_2 \end{pmatrix} . \tag{41.181}$$

We now assume that the light field only interacts with the upper level, as in the case of the dual resonance configuration studied in Exc. 35.4.5.4. This can be taken into account, neglecting those terms in the matrix (41.180) rotating with a positive Rabi frequency. Letting, moreover, $\Delta_1 = \Delta_2$ and $\Omega_1 = \Omega_2$, we obtain,

$$\hat{H}_n^{(1)} = \begin{pmatrix} 0 & & & \\ & -n\Lambda & & \\ & & -n\Lambda & \\ & & & -2(n+1)\Lambda \end{pmatrix} . \tag{41.182}$$

Thus, the temporal evolution is,

$$\boxed{e^{-\imath \hat{H}_n t} = \begin{pmatrix} 1 & & & \\ & e^{-n\Lambda} & & \\ & & e^{-n\Lambda} & \\ & & & e^{-2(n+1)\Lambda} \end{pmatrix}} . \tag{41.183}$$

For $\Lambda = \pi$,

$$e^{-\imath \hat{H}_n t} \xrightarrow{\pi} \begin{pmatrix} 1 & & & \\ & -1 & & \\ & & -1 & \\ & & & 1 \end{pmatrix} . \tag{41.184}$$

41.5.1.4 Bloch vector and the Q-function in the JC model with 2 atoms

Despite the more complex structure of the Hilbert space, the Bloch vectors of the individual atoms and the Q-function can be evaluated in analogy to Sec. 35.4.2. The Bloch vector is,

$$\vec{\rho}_{A1} = \frac{1}{\sqrt{2}} \begin{pmatrix} \sqrt{2}\ \mathfrak{Re}\ \rho_{12(A1)} \\ \sqrt{2}\ \mathfrak{Im}\ \rho_{12(A1)} \\ \rho_{22(A1)} - \rho_{11(A1)} \end{pmatrix} \qquad \text{where} \qquad \rho_{ij(A1)} = \mathrm{Tr}\ |i\rangle_1\langle j|\psi\rangle\langle\psi| \ . \tag{41.185}$$

In particular we have,

$$\begin{aligned} \rho_{22(A1)} &= \sum_{i,j,n} {}_2\langle j|_1\langle i|\langle n|1\rangle_1\langle 2|\psi\rangle\langle\psi|n\rangle|i\rangle_1|j\rangle_2 \qquad (41.186) \\ &= \sum_{j,n} {}_2\langle j|_1\langle 2|\langle n|\psi\rangle\langle\psi|n\rangle|1\rangle_1|j\rangle_2 \\ &= \sum_{n,m,m'} \langle n| \left(c_{2,1,m}|m\rangle\langle m'+1|c^*_{1,1,m'+1} + c_{2,2,m}|m'-1\rangle\langle m'|c^*_{1,2,m'}\rangle \right) |n\rangle \\ &= \sum_n (c^*_{1,1,n}c_{2,1,n} + c^*_{1,2,n}c_{2,2,n}) \ . \end{aligned}$$

Summarizing,

$$\begin{array}{lcl} \rho_{12(Ai\neq Aj)} & = & \sum_n (c^*_{1,1,n}c_{j,i,n} + c^*_{i,j,n}c_{2,2,n}) \\ \rho_{11(Ai\neq Aj)} & = & \sum_n (|c_{1,1,n}|^2 + |c_{i,j,n}|^2) \\ \rho_{22(Ai\neq Aj)} & = & \sum_n (|c_{j,i,n}|^2 + |c_{2,2,n}|^2) \end{array} \quad . \tag{41.187}$$

The function $Q(\alpha)$ for the JC dynamics of 2 atoms is,

$$\begin{aligned} Q(\alpha) &= \tfrac{1}{\pi}\langle\alpha|\hat{\rho}_{field}|\alpha\rangle = \tfrac{1}{\pi}\langle\alpha|\sum_{i,j} {}_2\langle j|_1\langle i|\psi\rangle\langle\psi|i\rangle_1|j\rangle_2|\alpha\rangle \qquad (41.188)\\ &= \tfrac{1}{\pi}\langle\alpha|\sum_{m,n}(c^*_{2,2,m-1}c_{2,2,n-1}|n-1\rangle\langle m-1| + c^*_{1,2,m}c_{1,2,n}|n\rangle\langle m| \\ &+ c^*_{2,1,m}c_{2,1,n}|n\rangle\langle m| + c^*_{1,1,m+1}c_{1,1,n+1}|n+1\rangle\langle m+1|)|n\rangle|\alpha\rangle \\ &= e^{-|\alpha|^2}\left[\left|\sum_n c_{2,2,n-1}\frac{\alpha^n}{\sqrt{n!}}\right|^2 + \left|\sum_n c_{1,2,n}\frac{\alpha^n}{\sqrt{n!}}\right|^2 + \left|\sum_n c_{2,1,n}\frac{\alpha^n}{\sqrt{n!}}\right|^2 + \left|\sum_n c_{2,2,n+1}\frac{\alpha^n}{\sqrt{n!}}\right|^2\right] . \end{aligned}$$

41.5.1.5 Correlating 2 atoms in the JC model

The investigations of the last section can be applied to describe the transfer of quantum coherence from one atom to another. The size of our system is now increased by the additional degrees of freedom, provided by internal states of the second atom. A suitable basis was defined in equation (23.124). Now, we imagine the following Gedankenexperiment: Starting from the initial condition that two adjacent atoms are in their respective electronic ground states, we assume a microwave $\pi/2$-pulse to create *simultaneously, but independently* on both atoms, a superposition of the HFS levels. Then, a non-resonant optical π-pulse interacts with the upper HFS level of the first atom $|1\rangle_{A1}$, and afterward the second atom $|2\rangle_{A2}$. Instead of reducing the atomic states and preparing a Schrödinger cat state in the optical field, (as we did in Sec. 35.4), we now project the field state onto the coherent state $|\beta\rangle$ and leave the atoms in a correlated state. The total procedure can be resumed by tracing the evolution of the whole state in the following suggestive way [64, 509]:

$$\begin{pmatrix} |\beta\rangle \\ 0 \\ 0 \\ 0 \end{pmatrix} \overset{\pi/2 \text{ microwave}}{\curvearrowright} \tfrac{1}{4}\begin{pmatrix} 1 \\ \imath \\ \imath \\ -1 \end{pmatrix}|\beta\rangle \overset{\pi \text{ opt+atom1}}{\curvearrowright} \tfrac{1}{4}\begin{pmatrix} |\beta\rangle \\ -\imath|-\beta\rangle \\ \imath|\beta\rangle \\ |-\beta\rangle \end{pmatrix} \overset{\pi \text{ opt+atom2}}{\curvearrowright} \tfrac{1}{4}\begin{pmatrix} |\beta\rangle \\ -\imath|-\beta\rangle \\ -\imath|-\beta\rangle \\ -|\beta\rangle \end{pmatrix}$$

$$\overset{\pi/2 \text{ microwave}}{\curvearrowright} \tfrac{1}{4}\begin{pmatrix} 1 \\ 0 \\ 0 \\ 1 \end{pmatrix}|\beta\rangle + \frac{1}{4}\begin{pmatrix} 1 \\ 0 \\ 0 \\ -1 \end{pmatrix}|-\beta\rangle \overset{\text{reduction}}{\curvearrowright} \tfrac{1}{2}\begin{pmatrix} 1 \\ 0 \\ 0 \\ -1 \end{pmatrix}|\beta\rangle \ . \tag{41.189}$$

If this procedure is extended to an arbitrary number of atoms, obviously all atoms being excited by the same optical mode before its projection in a coherent state $|\beta\rangle$

are included in the entangled state,

$$|\psi\rangle = \tfrac{1}{4}\begin{pmatrix}1\\:\\1\end{pmatrix}|\beta\rangle + \tfrac{1}{4}\begin{pmatrix}1\\:\\-1\end{pmatrix}|-\beta\rangle\ . \tag{41.190}$$

Finally, the correlation of the spin orientation of the atoms must be probed with additional laser light fields, which are selectively irradiated onto the atoms and resonantly tuned to a rapidly decaying optical transition. The states correlated in this way show a relatively low order entanglement, the von Neumann information entropy only being $S' = -\langle \log_2 \rho\rangle = N - 1$.

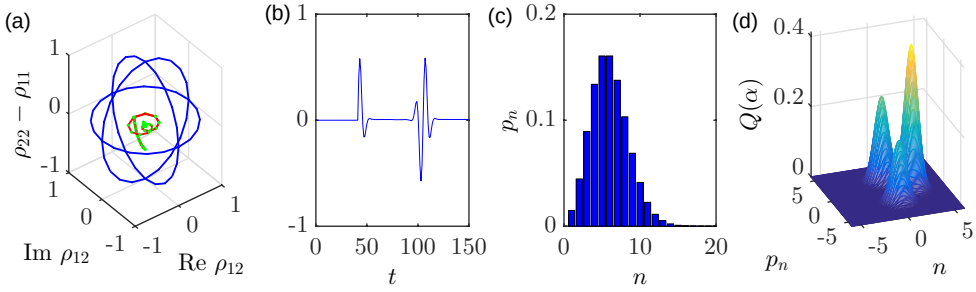

Figure 41.26: (code) Evolution of the state during a Jaynes-Cummings interaction with 2 atoms: (a) Bloch vector for the two atoms, (b) time evolution of the coherence ρ_{12} showing the phenomenon of collapse and revival, (c) distribution of photons, and (d) $Q(\alpha)$-function.

In a matricial notation the entangling gate can be expressed defining the state,

$$\begin{aligned}\langle\psi| &= \begin{pmatrix} c_{+\beta 11} & c_{+\beta 12} & c_{+\beta 21} & c_{+\beta 22} & c_{-\beta 11} & c_{-\beta 12} & c_{-\beta 21} & c_{-\beta 22}\end{pmatrix} \\ &= \langle\beta| \otimes \langle \text{atom}_1| \otimes \langle \text{atom}_2|\ .\end{aligned} \tag{41.191}$$

In this basis, the dispersive π-pulse is represented by,

$$U_{disp} \equiv \begin{pmatrix} 1 & & & & & & & \\ & & & & -1 & & & \\ & & & & & -1 & & \\ & & & 1 & & & & \\ & & & & 1 & & & \\ & -1 & & & & & & \\ & & -1 & & & & & \\ & & & & & & & 1 \end{pmatrix}\ . \tag{41.192}$$

A resonant $\pi/2$-pulse acting on the *both atoms simultaneously* does,

$$U_{reson} \equiv \mathbb{I} \otimes U^{(2)}_{\pi/2} \otimes \mathbb{I} = \frac{1}{\sqrt{2}} \begin{pmatrix} 1 & \imath & \imath & -1 & & & & \\ \imath & 1 & -1 & \imath & & & & \\ \imath & -1 & 1 & \imath & & & & \\ -1 & \imath & \imath & 1 & & & & \\ & & & & 1 & \imath & \imath & -1 \\ & & & & \imath & 1 & -1 & \imath \\ & & & & \imath & -1 & 1 & \imath \\ & & & & -1 & \imath & \imath & 1 \end{pmatrix} . \tag{41.193}$$

Now, concatenating and projecting on the Glauber state $|\beta\rangle$ we obtain, a posteriori, a unitary entangling gate,

$$U_{entangl} \equiv \mathrm{Tr}_\beta \; |\beta\rangle\langle\beta| U_{reson} U_{disp} U_{reson} |\beta\rangle\langle\beta| = \frac{1}{\sqrt{2}} \begin{pmatrix} 1 & 0 & 0 & -1 \\ 0 & -1 & -1 & 0 \\ 0 & -1 & -1 & 0 \\ -1 & 0 & 0 & 1 \end{pmatrix} \tag{41.194}$$

$$\text{such that} \quad \begin{pmatrix} 1 \\ 0 \\ 0 \\ -1 \end{pmatrix} = U_{entangl} \begin{pmatrix} 1 \\ 0 \\ 0 \\ 0 \end{pmatrix} .$$

41.5.2 Phononic quantum gate

The normal mode coupling can be used to create *quantum entanglement*. A suggested procedure to correlate two atoms '1' and '2' is shown in Fig. 41.27 [269, 606]. The atoms are regarded as qubits with the possible states of excitation $|g\rangle$ and $|e\rangle$. Additionally, the atoms are trapped (either they are ions in a linear ion trap or atoms in standing light wave sustained by a ring cavity). The are assumed to be cooled to the vibrational ground state $|0\rangle$, from which they can be coherently excited to the second collective vibrational mode $|1\rangle$ by means of a Raman transition, as illustrated in Fig. 41.27.

The sequence reads,

$$\begin{array}{cccccccc} |g_1\rangle|g_2\rangle|0\rangle & & |g_1\rangle|g_2\rangle|0\rangle & & |g_1\rangle|g_2\rangle|0\rangle & & |g_1\rangle|g_2\rangle|0\rangle \\ |g_1\rangle|e_2\rangle|0\rangle & \overset{\text{step 1}}{\curvearrowright} & |g_1\rangle|e_2\rangle|0\rangle & \overset{\text{step 2}}{\curvearrowright} & |g_1\rangle|e_2\rangle|0\rangle & \overset{\text{step 3}}{\curvearrowright} & |g_1\rangle|e_2\rangle|0\rangle \\ |e_1\rangle|g_2\rangle|0\rangle & & -\imath|g_1\rangle|g_2\rangle|1\rangle & & +\imath|g_1\rangle|g_2\rangle|1\rangle & & |e_1\rangle|g_2\rangle|0\rangle \\ |e_1\rangle|e_2\rangle|0\rangle & & -\imath|g_1\rangle|e_2\rangle|1\rangle & & -\imath|g_1\rangle|e_2\rangle|1\rangle & & -|e_1\rangle|e_2\rangle|0\rangle \end{array} . \tag{41.195}$$

Using the tensor notation $|\psi\rangle \otimes |\psi\rangle \equiv |\psi_1\rangle|\psi_2\rangle$ and introducing a matrix notation by

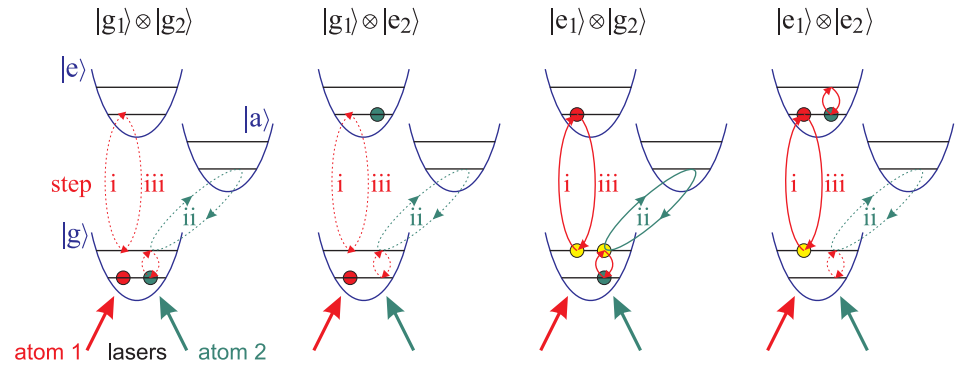

Figure 41.27: Scheme for an XOR-gate in an ion trap or a ring-cavity (see text for explanation). The four possible initial collective states respond differently to a predefined laser pulse sequence. Possible transitions are represented by solid lines, impossible transitions by dashed lines. $|a\rangle$ is an auxiliary excited level.

defining a basis as,

$$|g\rangle\otimes|g\rangle=\begin{pmatrix}1\\0\\0\\0\end{pmatrix}\ ,\ |g\rangle\otimes|e\rangle=\begin{pmatrix}0\\1\\0\\0\end{pmatrix}\ ,\ |e\rangle\otimes|g\rangle=\begin{pmatrix}0\\0\\1\\0\end{pmatrix}\ ,\ |e\rangle\otimes|e\rangle=\begin{pmatrix}0\\0\\0\\1\end{pmatrix}\ , \quad (41.196)$$

we can set up the truth table for this gate, also known as Cirac-Zoller gate, as,

$\|\psi\rangle$	$\|\psi\rangle$	$\|\psi\rangle\otimes\|\psi\rangle$	
$\|g\rangle$	$\|g\rangle$	$\|g\rangle\otimes\|g\rangle$	1
$\|g\rangle$	$\|e\rangle$	$\|g\rangle\otimes\|e\rangle$	1
$\|e\rangle$	$\|g\rangle$	$\|e\rangle\otimes\|g\rangle$	1
$\|e\rangle$	$\|e\rangle$	$-\|e\rangle\otimes\|e\rangle$	-1

$$\Longrightarrow \qquad U_{CZ}=\begin{pmatrix}1&0&0&0\\0&1&0&0\\0&0&1&0\\0&0&0&-1\end{pmatrix}\ . \quad (41.197)$$

We now define a new basis for the second atom only via $|a_2\rangle=\frac{1}{\sqrt{2}}(|g_2\rangle+|e_2\rangle)$ and $|b_2\rangle=\frac{1}{\sqrt{2}}(|g_2\rangle-|e_2\rangle)$. The basis transform corresponds to,

$$\begin{pmatrix}|g\rangle\otimes|a\rangle\\|g\rangle\otimes|b\rangle\\|g\rangle\otimes|a\rangle\\|g\rangle\otimes|b\rangle\end{pmatrix}=\tfrac{1}{\sqrt{2}}\mathbb{I}\otimes H\begin{pmatrix}|g\rangle\otimes|g\rangle\\|g\rangle\otimes|e\rangle\\|g\rangle\otimes|g\rangle\\|g\rangle\otimes|e\rangle\end{pmatrix}\quad\text{where}\quad \mathbb{I}\otimes H=\tfrac{1}{\sqrt{2}}\begin{pmatrix}1&1&0&0\\1&-1&0&0\\0&0&1&1\\0&0&1&-1\end{pmatrix} \quad (41.198)$$

is the Hadamard gate applied to the second qubit. Finally, we obtain the *controlled NOT* gate,

$$U_{XOR}=(\mathbb{I}\otimes H)U_{CZ}(\mathbb{I}\otimes H)^{-1}=\begin{pmatrix}1&0&0&0\\0&1&0&0\\0&0&0&1\\0&0&1&0\end{pmatrix}\ . \quad (41.199)$$

In particular, if $|\psi_1\rangle$ is initially in a superposition state, the states $|\psi_1\rangle$ and $|\psi_2\rangle$ end up entangled,

$$U_{XOR}(|g\rangle + |e\rangle) \otimes \mathbb{I} = \tfrac{1}{\sqrt{2}}(|g\rangle \otimes |g\rangle + |e\rangle \otimes |e\rangle) \ . \tag{41.200}$$

41.5.3 Quantum gates via controlled collisions

The proposed conditional quantum operation is based on a conditional collisional phase shift, the condition being that the atoms are in a particular state of excitation. In a suggestive notation for the Bloch vector of a particle subject to a resonant radiation pulse, the interaction is described by,

$$|\downarrow\rangle \xrightarrow{\pi/2} |\downarrow\rangle + \imath|\uparrow\rangle \xrightarrow{\pi/2} |\uparrow\rangle \xrightarrow{\pi/2} |\downarrow\rangle - \imath|\uparrow\rangle \xrightarrow{\pi/2} |\downarrow\rangle \ . \tag{41.201}$$

Jaksch demonstrated the following *phase gate*,

$$\begin{matrix} \downarrow\downarrow \\ \uparrow\downarrow \\ \downarrow\uparrow \\ \uparrow\uparrow \end{matrix} \longrightarrow \begin{matrix} \downarrow\downarrow \\ -\downarrow\uparrow \\ \uparrow\downarrow \\ \uparrow\uparrow \end{matrix} \ . \tag{41.202}$$

This gate is equivalent to the *XOR* port for the qubits defined by $\downarrow$ and $\downarrow \pm \uparrow$, since,

$$\begin{matrix} \downarrow(\downarrow \pm \uparrow) \\ \uparrow(\downarrow \pm \uparrow) \end{matrix} \longrightarrow \begin{matrix} \downarrow(\downarrow \mp \uparrow) \\ \uparrow(\downarrow \pm \uparrow) \end{matrix} \ . \tag{41.203}$$

41.5.4 Exercises

41.5.4.1 Ex: Generating a Bell state

Show that the operation $\overset{c}{X}_{01}(H_0 \otimes \mathbb{I})$, where H_0 is the Hadamard gate acting on the first qu-bit and $\overset{c}{X}_{01}$ the controlled NOT acting on the second qubit, applied to the 2-qubit ground state generates entanglement.

Solution: *We find,*

$$\overset{c}{X}_{01}(H_0 \otimes \mathbb{I}) = \begin{pmatrix} 1 & 0 & 0 & 0 \\ 0 & 1 & 0 & 0 \\ 0 & 0 & 0 & 1 \\ 0 & 0 & 1 & 0 \end{pmatrix} \left[\tfrac{1}{\sqrt{2}} \begin{pmatrix} 1 & 1 \\ 1 & -1 \end{pmatrix} \otimes \begin{pmatrix} 1 & 0 \\ 0 & 1 \end{pmatrix} \right] \begin{pmatrix} 1 \\ 0 \\ 0 \\ 0 \end{pmatrix} = \tfrac{1}{\sqrt{2}} \begin{pmatrix} 1 \\ 0 \\ 0 \\ 1 \end{pmatrix} \ .$$

41.6 Quantum gates

In *quantum information* we use the notions introduced in the preceding sections and formalize the calculation. In this section, we present a brief formal introduction to

the field of *quantum computation with qubit matrices*. The formalism is abstract, but we may keep in mind a chain of entangled ions confined in a linear Paul trap. We will show how the electronic states of the ions are correlated to form a single collective state, and how quantum gates can be realized on such correlated particles. With three ions, an arbitrary quantum gate can be implemented, which includes and generalizes the three-bit Toffoli gate.

> **Example 264 (*Boolean versus linear algebra*):** The mathematical formalism underlying *classical computing* is the *Boolean algebra*, while the formalism underlying *quantum computing* is the *linear algebra*. It is important to stress that *everything you can do on a classical computer, can you do on a quantum computer, and vice versa*. The question is simply whether you can do it in due time.

To construct a quantum gate, we need at least two qubits spanning a 4-dimensional Hilbert space, since $\mathcal{H}^2 \otimes \mathcal{H}^2$ and $\mathcal{H}^1 \otimes \mathcal{H}^4$ are isomorph, that is,

$$\begin{aligned} |\varepsilon\rangle_0|\mu\rangle_1 &= (|0\rangle_0 + \imath|1\rangle_0)(|0\rangle_1 + \imath|1\rangle_1) &&= \begin{pmatrix} |0\rangle_0|0\rangle_1 \\ \imath|0\rangle_0|1\rangle_1 \\ \imath|1\rangle_0|0\rangle_1 \\ -|1\rangle_0|1\rangle_1 \end{pmatrix} \\ \triangleq \quad |0\rangle_0|\varepsilon\mu\rangle_1 &= |00\rangle_1 + \imath|01\rangle_1 + \imath|10\rangle_1 - |11\rangle_1 &&= \begin{pmatrix} |00\rangle_1 \\ \imath|01\rangle_1 \\ \imath|10\rangle_1 \\ -|11\rangle_1 \end{pmatrix} . \end{aligned} \tag{41.204}$$

A presentation on the subject is available at (watch talk). See also the websites IBM Circuit Composer, Qiskit, Cirq, and Pennylane.

41.6.1 The qubit

As we have seen above, the two principle ways a light mode acts on a two-level system are the resonant interaction and the dispersive interaction. From the Jaynes-Cummings model (35.125) and (35.132),

$$\begin{aligned} R(\tau) &\equiv \begin{pmatrix} \cos\frac{\pi}{2}\tau & \imath\sin\frac{\pi}{2}\tau \\ \imath\sin\frac{\pi}{2}\tau & \cos\frac{\pi}{2}\tau \end{pmatrix} \overset{\tau\to 1}{\longrightarrow} \begin{pmatrix} & \imath \\ \imath & \end{pmatrix} , \\ D(\tau) &\equiv \begin{pmatrix} e^{\imath\pi\tau} & 0 \\ 0 & 1 \end{pmatrix} \overset{\tau\to 1}{\longrightarrow} \begin{pmatrix} -1 & \\ & 1 \end{pmatrix} . \end{aligned} \tag{41.205}$$

These two gates are particular cases of the most fundamental single qubit quantum gate, which can be written as,

$$\boxed{U_3(\vartheta,\varphi,\lambda) = \begin{pmatrix} \cos\frac{\vartheta}{2} & -e^{\imath\lambda}\sin\frac{\vartheta}{2} \\ e^{\imath\varphi}\sin\frac{\vartheta}{2} & e^{\imath\lambda+\imath\varphi}\cos\frac{\vartheta}{2} \end{pmatrix}} , \tag{41.206}$$

which is a unitary operation since $\det U_3(\vartheta,\varphi,\lambda) = e^{\imath(\lambda+\varphi)}$. Special cases are the *Hadamard gate*,

$$H \equiv U_3(\tfrac{\pi}{2},0,\pi) = \tfrac{1}{\sqrt{2}}\begin{pmatrix} 1 & 1 \\ 1 & -1 \end{pmatrix} , \tag{41.207}$$

and the *phase gate*,

$$U_1(\varphi) \equiv U_3(0,\varphi,0) = \begin{pmatrix} 1 & 0 \\ 0 & e^{\imath\varphi} \end{pmatrix} . \tag{41.208}$$

Phase rotations about particular angles receive specific names. For example,

$$\boxed{Z \equiv -\hat{\sigma}_z = U_1(\pi)} = |-q_0\rangle\langle q_0| , \tag{41.209}$$

is simply the negative Pauli z-matrix defined in (23.47). The *negation* in the Hilbert space $\mathcal{H}^2$,

$$\boxed{X \equiv \hat{\sigma}_x = U_3(\pi,0,\pi) = |\bar{q_0}\rangle\langle q_0|} , \tag{41.210}$$

is simply the Pauli x-matrix.

The general state of a qubit is a quantum superposition in the Hilbert space $\mathcal{H}^2$,

$$|\varepsilon\rangle = \alpha|0\rangle + \imath\beta|1\rangle = \begin{pmatrix} \alpha \\ \imath\beta \end{pmatrix} . \tag{41.211}$$

The possible outcomes of a measurement of its state are represented by a classical truth table,

$$\begin{matrix} |q_0\rangle \\ |0\rangle \\ |1\rangle \end{matrix} \quad \text{, for example} \quad |01\rangle = \begin{pmatrix} 0 \\ 1 \end{pmatrix} . \tag{41.212}$$

The only difference is, that now the possible values are not restricted to the binaries 0 or 1, but can be anything between 0 and 1, provide the total wavefunction stays normalized.

Analogously to to classical logic circuits, which can be represented by concatenated symbols, quantum circuits can be composed by concatenations of unitary operations. This is illustrated in Fig. 41.28.

41.6.2 Quantum gates of 2 qubits, the 'controlled NOT' gate

We can generalize the single-qubit algebra to arbitrary registers using the *direct* sum and the *external product* defined in (23.124) and (23.126),

$$\begin{matrix} |q_1 & q_0\rangle \\ |0 & 0\rangle \\ |0 & 1\rangle \\ |1 & 0\rangle \\ |1 & 1\rangle \end{matrix} \quad \text{, for example} \quad |01\rangle = \begin{pmatrix} 0 \\ 1 \\ 0 \\ 0 \end{pmatrix} . \tag{41.213}$$

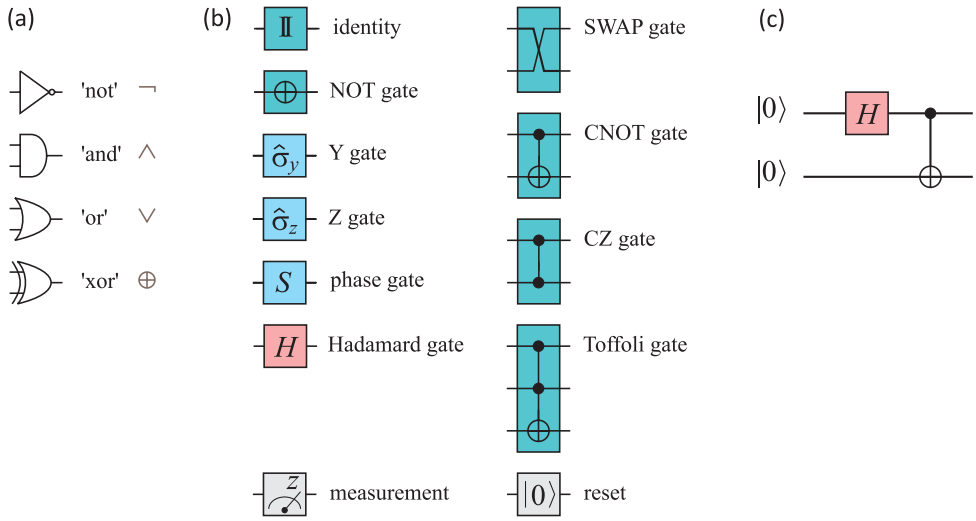

Figure 41.28: (a) Common symbols for fundamental classical gates and (b) for quantum gates. (c) Example of a quantum circuit generating Bell type entanglement.

Single qubit gates can be embedded in multi qubit registers. For example, the *negation* of 'NOT' gate in $\mathcal{H}^4$ can be applied either to the first or the second qubit [25],

$$\boxed{\begin{aligned} X_0 &\hat{=} \mathbb{I} \otimes \hat{X} = |q_1, \bar{q_0}\rangle\langle q_1, q_0| \\ X_1 &\hat{=} \hat{X} \otimes \mathbb{I} = |\bar{q_1}, q_0\rangle\langle q_1, q_0| \end{aligned}} \,. \tag{41.214}$$

The most interesting two-qubit quantum gate is the 'controlled NOT' gate or *antivalence*, which we will now discuss in detail. This gate is originally defined on $\mathcal{H}^2 \otimes \mathcal{H}^2$. The quantum operation is implemented by first going to the Hilbert space $\mathcal{H}^1 \otimes \mathcal{H}^4$, applying the unitary transform,

$$\mathbb{I} \oplus X = \begin{pmatrix} \mathbb{I}_2 & \\ & X \end{pmatrix} \,, \tag{41.215}$$

where X has been defined in Eq. (41.210), and finally returning to $\mathcal{H}^2 \otimes \mathcal{H}^2$:

$$\begin{aligned} |\varepsilon\rangle_0|\mu\rangle_1 \;\triangleq\; |0\rangle_0|\varepsilon\mu\rangle_1 \;\xrightarrow{\hat{N}}\; \delta_{\varepsilon=0}|\varepsilon\rangle_0|\mu\rangle_1 + \delta_{\varepsilon=1}|\varepsilon\rangle_1 \begin{pmatrix} 1 & \imath \\ \imath & 1 \end{pmatrix}^2 |\mu\rangle_1 \;\triangleq\; |\varepsilon\rangle_0|\varepsilon \oplus \mu\rangle_1 \\ \begin{pmatrix} |0\rangle_0|0\rangle_1 \\ \imath|0\rangle_0|1\rangle_1 \\ \imath|1\rangle_0|0\rangle_1 \\ -|1\rangle_0|1\rangle_1 \end{pmatrix} \triangleq \begin{pmatrix} |00\rangle_1 \\ \imath|01\rangle_1 \\ \imath|10\rangle_1 \\ -|11\rangle_1 \end{pmatrix} \xrightarrow{\hat{N}} \begin{pmatrix} |00\rangle_1 \\ \imath|01\rangle_1 \\ \imath|11\rangle_1 \\ -|10\rangle_1 \end{pmatrix} \triangleq \begin{pmatrix} |0\rangle_0|0\rangle_1 \\ \imath|0\rangle_0|1\rangle_1 \\ \imath|1\rangle_0|1\rangle_1 \\ -|1\rangle_0|0\rangle_1 \end{pmatrix} \end{aligned} \,. \tag{41.216}$$

[25] Note that we call 'first' the rightmost qubit.

The short-hand notation of the 'controlled NOT' operation on $\mathcal{H}^4$ can be written as,

$$\boxed{\begin{array}{lll} \overset{c}{X}_{10} & \hat{=}\, \mathbb{I}\oplus X & = |q_1, q_1\oplus q_0\rangle\langle q_1, q_0| \\ \overset{c}{X}_{01} & \hat{=}\, \mathbb{S}(\mathbb{I}\oplus X)\mathbb{S} & = |q_0\oplus q_1, q_0\rangle\langle q_1, q_0| \end{array}} \quad . \tag{41.217}$$

where the 'SWAP' operator $\mathbb{S}$ has been defined in (23.130). When the qubits addressed by a gate are not identified from their position in the tensor product, an index at the gate symbol indicates which qubits are involved. For example, X_0 inverts the first qubit q_0, and $\overset{c}{X}_{0\to 1} = \overset{c}{X}_{01}$ controls the state of the second qubit q_1 by the first one.

Example 265 (*Controlled NOT gate*): We can easily verify,

$$\begin{aligned} \overset{c}{X}_{10} &= |0\rangle\langle 0|\otimes\mathbb{I} + |1\rangle\langle 1|\otimes X \\ &= \begin{pmatrix} 1 & 0 \\ 0 & 0 \end{pmatrix}\otimes\begin{pmatrix} 1 & 0 \\ 0 & 1 \end{pmatrix} + \begin{pmatrix} 0 & 0 \\ 0 & 1 \end{pmatrix}\otimes\begin{pmatrix} 0 & 1 \\ 1 & 0 \end{pmatrix} = \begin{pmatrix} \mathbb{I} & 0 \\ 0 & X \end{pmatrix} , \end{aligned} \tag{41.218}$$

and

$$\begin{aligned} \overset{c}{X}_{01} &= \mathbb{I}|\otimes|0\rangle\langle 0| + X\otimes|1\rangle\langle 1| \\ &= \begin{pmatrix} 1 & 0 \\ 0 & 1 \end{pmatrix}\otimes\begin{pmatrix} 1 & 0 \\ 0 & 0 \end{pmatrix} + \begin{pmatrix} 0 & 1 \\ 1 & 0 \end{pmatrix}\otimes\begin{pmatrix} 0 & 0 \\ 0 & 1 \end{pmatrix} = S\overset{c}{X}_{10}S . \end{aligned} \tag{41.219}$$

41.6.3 Fundamental and universal quantum gates of 3 qubits and more

We now consider three qubits in $\mathcal{H}^8 \equiv \mathcal{H}^2\otimes\mathcal{H}^2\otimes\mathcal{H}^2$. The *truth table* has the shape,

$$\begin{array}{ccc|c} |q_2 & q_1 & q_0\rangle & \\ |0 & 0 & 0\rangle & \\ |0 & 0 & 1\rangle & \\ |0 & 1 & 0\rangle & \\ |0 & 1 & 1\rangle & \text{, for example} \\ |1 & 0 & 0\rangle & \\ |1 & 0 & 1\rangle & \\ |1 & 1 & 0\rangle & \\ |1 & 1 & 1\rangle & \end{array} \qquad |010\rangle = \begin{pmatrix} 0 \\ 0 \\ 1 \\ 0 \\ 0 \\ 0 \\ 0 \\ 0 \end{pmatrix} . \tag{41.220}$$

We choose $\mathbb{I}_8$ as the basis of $\mathcal{H}^8$. We assume that the number represented by the state $|q_2, q_1, q_0\rangle$ is $[q_2q_1q_0]_{binary} = [2^2q_2 + 2^1q_1 + 2^0q_0]_{decimal}$.

The unitary transform implemented by a quantum gate can be understood as a permutation of the basis vectors in the truth table. We can generalize the permutation rules (23.130) to 3D Hilbert spaces $\mathcal{H}^2\otimes\mathcal{H}^2\otimes\mathcal{H}^2$, where $M\otimes N\otimes R = \mathbb{S}_{01}(N\otimes M\otimes R)\mathbb{S}_{01} = \mathbb{S}_{12}(M\otimes R\otimes N)\mathbb{S}_{12} = \mathbb{S}_{01}(R\otimes N\otimes M)\mathbb{S}_{02}$, with the transformation matrices,

$$\mathbb{S}_{01} = \mathbb{I}\otimes\mathbb{S} \quad , \quad \mathbb{S}_{12} = \mathbb{S}\otimes\mathbb{I} \quad , \quad \mathbb{S}_{02} = \mathbb{S}_{01}\mathbb{S}_{12}\mathbb{S}_{01} , \tag{41.221}$$

where the operator $\mathbb{S}$ has again been taken from (23.130). In Exc. 41.6.6.4 we derive the explicit matricial forms of $\mathbb{S}_{ij}$.

Examples of fundamental three-qubits gates are, in short notation, the *negation* in $\mathcal{H}^8$,

$$\begin{aligned} X_0 &\hat{=} \mathbb{I}\otimes\mathbb{I}\otimes X = |q_2,q_1,\bar{q_0}\rangle\langle q_2,q_1,q_0| \\ X_1 &\hat{=} \mathbb{I}\otimes X\otimes\mathbb{I} = |q_2,\bar{q_1},q_0\rangle\langle q_2,q_1,q_0| \\ X_2 &\hat{=} X\otimes\mathbb{I}\otimes\mathbb{I} = |\bar{q_2},q_1,q_0\rangle\langle q_2,q_1,q_0| \ , \end{aligned} \tag{41.222}$$

the *antivalence*,

$$\begin{aligned} \overset{c}{X}_{10} &\equiv \mathbb{I}\otimes(\mathbb{I}\oplus X) &&= |q_2,q_1,q_1\oplus q_0\rangle\langle q_2,q_1,q_0| \\ \overset{c}{X}_{01} &\equiv \mathbb{S}_{01}\overset{c}{X}_{10}\mathbb{S}_{01} &&= |q_2,q_0\oplus q_1,q_0\rangle\langle q_2,q_1,q_0| \\ \overset{c}{X}_{02} &\equiv \mathbb{S}_{12}\overset{c}{X}_{01}\mathbb{S}_{12} &&= |q_0\oplus q_2,q_1,q_0\rangle\langle q_2,q_1,q_0| \\ \overset{c}{X}_{20} &\equiv \mathbb{S}_{02}\overset{c}{X}_{02}\mathbb{S}_{02} &&= |q_2,q_1,q_2\oplus q_0\rangle\langle q_2,q_1,q_0| \\ \overset{c}{X}_{21} &\equiv \mathbb{S}_{02}\overset{c}{X}_{01}\mathbb{S}_{02} &&= |q_2,q_2\oplus q_1,q_0\rangle\langle q_2,q_1,q_0| \\ \overset{c}{X}_{12} &\equiv \mathbb{S}_{12}\overset{c}{X}_{21}\mathbb{S}_{12} &&= |q_1\oplus q_2,q_1,q_0\rangle\langle q_2,q_1,q_0| \ , \end{aligned} \tag{41.223}$$

from which we get explicitly, as verified in Exc. 41.6.6.5,

$$\overset{c}{X}_{10} = \begin{pmatrix} \mathbb{I} & & & \\ & X & & \\ & & \mathbb{I} & \\ & & & X \end{pmatrix} \quad , \quad \overset{c}{X}_{20} = \begin{pmatrix} \mathbb{I} & & & \\ & \mathbb{I} & & \\ & & X & \\ & & & X \end{pmatrix} \quad , \quad \overset{c}{X}_{21} = \begin{pmatrix} \mathbb{I} & & & \\ & \mathbb{I} & & \\ & & & X\otimes\mathbb{I} \end{pmatrix} . \tag{41.224}$$

It is possible to show that all quantum logic gates can be reduced to a universal so-called *Toffoli gate* [95],

$$\begin{aligned} \mathcal{H}^8 &\xrightarrow{U} \mathcal{H}^8 \\ |q_2,q_1,q_0\rangle &\xrightarrow{U} |q_2,q_1,(q_2\wedge q_1)\oplus q_0\rangle \\ \mathbb{I}_8 &\xrightarrow{U} U \ , \end{aligned} \tag{41.225}$$

or in short-hand notation,

$$\boxed{\overset{cc}{X}_{210} = \mathbb{I}\oplus\mathbb{I}\oplus X = |q_2,q_1,(q_2\wedge q_1)\oplus q_0\rangle\langle q_2,q_1,q_0| = \begin{pmatrix} \mathbb{I}_6 & \\ & \hat{\sigma}_x \end{pmatrix}} \ , \tag{41.226}$$

as will be shown in Exc. 41.6.6.6 and 41.6.6.7.

Obviously, to perform quantum calculations, we need at least two qubits and operations acting simultaneous on both. Do the Excs. 41.6.6.8 to 41.6.6.9.

gate	symbol	matrix
identity	$\mathbb{I}$	$U_3(0,0,0)$
inversion	$X = \texttt{NOT}$	$\hat{\sigma}_x = U_3(\pi, 0, \pi)$
Pauli Y	Y	$\hat{\sigma}_y = U_3(\pi, \frac{\pi}{2}, \frac{\pi}{2})$
Pauli Z	Z	$\hat{\sigma}_z = U_1(\pi)$
S gate	S	$\hat{\sigma}_z = U_1(\frac{\pi}{2})$
T gate	T	$\hat{\sigma}_z = U_1(\frac{\pi}{4})$
Hadamard gate	H	$\frac{1}{\sqrt{2}}\begin{pmatrix} 1 & 1 \\ 1 & -1 \end{pmatrix}$
swap gate	$\mathbb{S} = \texttt{SWAP}$	$\begin{pmatrix} 1 & 0 & 0 & 0 \\ 0 & 0 & 1 & 0 \\ 0 & 1 & 0 & 0 \\ 0 & 0 & 0 & 1 \end{pmatrix}$
controlled X	$\overset{c}{X} = \texttt{CX}$	$\mathbb{I} \oplus \hat{\sigma}_x = \begin{pmatrix} \mathbb{I}_2 & 0 \\ 0 & \hat{\sigma}_x \end{pmatrix}$
controlled Z	$\overset{c}{Z} = \texttt{CZ}$	$\mathbb{I} \oplus \hat{\sigma}_z = \begin{pmatrix} \mathbb{I}_2 & 0 \\ 0 & \hat{\sigma}_z \end{pmatrix}$
controlled H	$\overset{c}{H} = \texttt{CH}$	$\mathbb{I} \oplus H = \begin{pmatrix} \mathbb{I}_2 & 0 \\ 0 & H \end{pmatrix}$
Toffoli	$\overset{cc}{X} = \texttt{CCX}$	$\mathbb{I} \oplus \mathbb{I} \oplus \hat{\sigma}_x = \begin{pmatrix} \mathbb{I}_6 & \\ & \hat{\sigma}_x \end{pmatrix}$

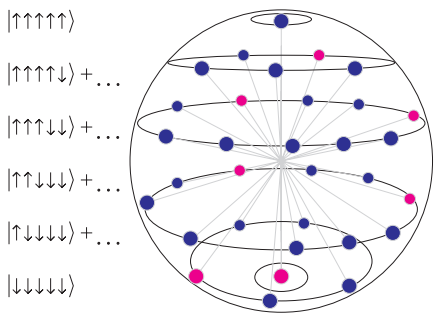

Figure 41.29: Illustration of the possible states of a 5-qubit system.

Until now, we restricted to pure states $|\psi_f\rangle = \bigotimes_k [\alpha_k|0\rangle_k + \beta_k|1\rangle_k]$ generated from an initial eigenstate $|\psi_i\rangle = \bigotimes_k |0\rangle_k$ by reversible quantum computing. The density operator can then be written,

$$\boxed{\hat{\rho} = |\psi_f\rangle\langle\psi_f| = U|\psi_i\rangle\langle\psi_i|U^\dagger} \,. \tag{41.227}$$

In the next section, following up on Sec. 34.3.3, we will discuss how projective measurements introduce irreversibility into the evolution of the density operator.

41.6.4 State propagation and projective measurements

The measurement of a qubit projects the Hilbert space on its two possible outcomes. For example, measuring the first out of three qubits means,

$$\mathcal{H}\otimes\mathcal{H}\otimes\mathcal{H}\overset{measure}{\longrightarrow}\begin{cases}|0\rangle\otimes\mathcal{H}\otimes\mathcal{H}\\ |1\rangle\otimes\mathcal{H}\otimes\mathcal{H}\end{cases}. \tag{41.228}$$

We consider a density matrix $\hat{\rho}$ operating on the entire Hilbert space and define projectors,

$$\hat{P}_j^{(n)}=\mathbb{I}\otimes...\otimes|n\rangle_j\langle n|\otimes...\otimes\mathbb{I}\qquad\text{with}\qquad n=0,1\ . \tag{41.229}$$

that, applied to a specific qubit q_j, project its state onto the eigenstate $|0\rangle$ or $|1\rangle$, respectively. A projective measurement of the j-th qubit with two possible outcomes $|q_j\rangle=|0\rangle,|1\rangle$ with the respective probabilities $p_j^{(0)},p_j^{(1)}$, generates the mixed states reduced density operator,

$$\boxed{\hat{\rho}_j^{red}=\sum_{n=0,1}p_j^{(n)}\frac{\hat{P}_j^{(n)}\hat{\rho}\hat{P}_j^{(n)}}{\text{Tr }\hat{\rho}\hat{P}_j^{(n)}}}\ . \tag{41.230}$$

Note that, a priori, $\hat{\rho}_j^{red}$ has the same rank as $\hat{\rho}$, but a more diagonal structure, since some coherences have been traced out.

41.6.4.1 Quantum state tomography

Any density operator of a pure or mixed state of an individual qubit can be expanded as,

$$\hat{\rho}_j=\tfrac{1}{2}\left(\mathbb{I}+a_j\hat{\sigma}_j^x+b_j\hat{\sigma}_j^y+c_j\hat{\sigma}_j^z\right)=\tfrac{1}{2}\begin{pmatrix}1+c_j & a_j-\imath b_j\\ a_j+\imath b_j & 1-c_j\end{pmatrix}\ , \tag{41.231}$$

where,

$$\hat{\sigma}_j^k=\mathbb{I}\otimes...\otimes\hat{\sigma}^k\otimes...\otimes\mathbb{I}\ , \tag{41.232}$$

and $\hat{\sigma}^k$ are the Pauli matrices. The parameters a_j, b_j, and c_j can be determined by measurements,

$$\boxed{\langle\hat{\vec{\sigma}}_j\rangle=\text{Tr }\hat{\rho}\hat{\vec{\sigma}}_j=\begin{pmatrix}a_j\\ b_j\\ c_j\end{pmatrix}}\ , \tag{41.233}$$

where $\hat{\rho}$ is the density matrix of the whole system.

41.6.4.2 Measurements on a single qubit

A single qubit $|\psi\rangle=\alpha|0\rangle+\beta|1\rangle$, normalized as $|\alpha|^2+|\beta|^2=1$, is described by the density operator,

$$\hat{\rho}=\begin{pmatrix}\rho_{00} & \rho_{01}\\ \rho_{10} & \rho_{11}\end{pmatrix}=|\psi\rangle\langle\psi|=\begin{pmatrix}|\alpha|^2 & \alpha\beta^*\\ \alpha^*\beta & |\beta|^2\end{pmatrix}\ . \tag{41.234}$$

A projective measurement of the qubit with two possible outcomes, $|q\rangle = |0\rangle, |1\rangle$ with the respective probabilities $p^{(0)} = |\alpha|^2$ and $p^{(1)} = |\beta|^2$, generates the mixed states reduced density operator,

$$\hat{\rho}^{red} = p^{(0)} \frac{|0\rangle\langle 0|\hat{\rho}|0\rangle\langle 0|}{\text{Tr}\ \hat{\rho}|0\rangle\langle 0|} + p^{(1)} \frac{|1\rangle\langle 1|\hat{\rho}|1\rangle\langle 1|}{\text{Tr}\ \hat{\rho}|1\rangle\langle 1|} = |\alpha|^2|0\rangle\langle 0| + |\beta|^2|1\rangle\langle 1| \ . \tag{41.235}$$

Some physical processes may not only project the density operator onto a specific basis, but onto a particular eigenstate,

$$\hat{\rho} \longrightarrow \hat{\rho}^{prj} = |0\rangle\langle 0|\hat{\rho}|0\rangle\langle 0| \ . \tag{41.236}$$

Example 266 (*Quantum Zeno effect on a single qubit*): As an example, let us express the quantum Zeno effect in quantum computing language. Starting from a two-level system in its ground state,

$$\hat{\rho}^{in} = \begin{pmatrix} 1 & 0 \\ 0 & 0 \end{pmatrix} \quad , \quad U_3(\vartheta, 0, 0) = \begin{pmatrix} \cos\vartheta & -\sin\vartheta \\ \sin\vartheta & \cos\vartheta \end{pmatrix} \ ,$$

we perform small rotations,

$$\hat{\rho}^{rot} = U_3(\vartheta,0,0)\hat{\rho}^{in}U_3(\vartheta,0,0)^\dagger = \begin{pmatrix} \cos^2\vartheta & \cos\vartheta\sin\vartheta \\ \cos\vartheta\sin\vartheta & \sin^2\vartheta \end{pmatrix} \begin{pmatrix} 1 & 0 \\ 0 & 0 \end{pmatrix} \ ,$$

before measuring the system,

$$\hat{\rho}^{red} = \cos^2\vartheta \frac{|0\rangle\langle 0|\hat{\rho}^{rot}|0\rangle\langle 0|}{\text{Tr}\ \hat{\rho}^{rot}|0\rangle\langle 0|} + \sin^2\vartheta \frac{|1\rangle\langle 1|\hat{\rho}^{rot}|1\rangle\langle 1|}{\text{Tr}\ \hat{\rho}^{rot}|1\rangle\langle 1|} = \begin{pmatrix} \cos^2\vartheta & 0 \\ 0 & \sin^2\vartheta \end{pmatrix} \ .$$

Discarding the possibility that the system be excited, we project it system onto the ground state,

$$\hat{\rho}^{fin} = |0\rangle\langle 0|\hat{\rho}^{red}|0\rangle\langle 0| = |0\rangle\langle 0|U_3(\vartheta,0,0)\hat{\rho}^{in}U_3(\vartheta,0,0)^\dagger|0\rangle\langle 0| = \begin{pmatrix} \cos^2\vartheta & 0 \\ 0 & 0 \end{pmatrix} \ .$$

On the other hand, repeating the procedure n times with $\vartheta = \frac{\pi}{2n}$ and $n \to \infty$, we find,

$$\hat{\rho}^{fin} = \lim_{n\to\infty} \left(|0\rangle\langle 0|U_3(\tfrac{\pi}{2n},0,0)\hat{\rho}^{in}U_3(\tfrac{\pi}{2n},0,0)^\dagger|0\rangle\langle 0| \right)^n = \begin{pmatrix} \lim_{n\to\infty}\cos^{2n}\frac{\pi}{2n} & 0 \\ 0 & 0 \end{pmatrix} = \hat{\rho}^{in} \ .$$

That is, the evolution of the system is frozen by too many measurements.

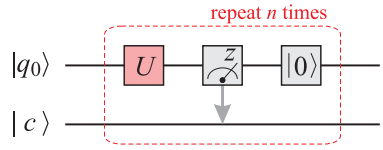

Figure 41.30: Quantum Zeno effect on a single qubit.

41.6.4.3 Measurements in two qubit systems

Let us now consider a two-qubit system $q_1 \otimes q_0$ described by the initial density matrix,

$$\hat{\rho} = \hat{\rho}_1 \otimes \hat{\rho}_0 = \begin{pmatrix} |\alpha_1|^2 & \alpha_1\beta_1^* \\ \alpha_1^*\beta_1 & |\beta_1|^2 \end{pmatrix} \otimes \begin{pmatrix} |\alpha_0|^2 & \alpha_0\beta_0^* \\ \alpha_0^*\beta_0 & |\beta_0|^2 \end{pmatrix} \tag{41.237}$$

$$= \begin{pmatrix} (\rho_1)_{00} & (\rho_1)_{01} \\ (\rho_1)_{10} & (\rho_1)_1 \end{pmatrix} \otimes \begin{pmatrix} (\rho_0)_{00} & (\rho_0)_{01} \\ (\rho_0)_{10} & (\rho_0)_1 \end{pmatrix} = \begin{pmatrix} \rho_{00\otimes 00} & \rho_{00\otimes 01} & \rho_{10\otimes 00} & \rho_{01\otimes 01} \\ \rho_{00\otimes 10} & \rho_{00\otimes 11} & \rho_{01\otimes 10} & \rho_{01\otimes 11} \\ \rho_{10\otimes 00} & \rho_{10\otimes 01} & \rho_{11\otimes 00} & \rho_{11\otimes 01} \\ \rho_{10\otimes 10} & \rho_{10\otimes 11} & \rho_{11\otimes 10} & \rho_{11\otimes 11} \end{pmatrix},$$

where we defined $\rho_{kl\otimes mn} \equiv (\rho_1)_{kl}(\rho_0)_{mn}$. Projective measurements of qubit q_1 with two possible outcomes, $|q_1\rangle = |0\rangle, |1\rangle$, with the respective probabilities $p^{(0)} = |\alpha_1|^2$ and $p^{(1)} = |\beta_1|^2$, yields the reduced density operator,

$$\hat{\rho}_1^{red} = p^{(0)} \frac{[|0\rangle\langle 0| \otimes \mathbb{I}]\hat{\rho}[|0\rangle\langle 0| \otimes \mathbb{I}]}{\text{Tr } \hat{\rho}[|0\rangle\langle 0| \otimes \mathbb{I}]} + p^{(1)} \frac{[|1\rangle\langle 1| \otimes \mathbb{I}]\hat{\rho}[|1\rangle\langle 1| \otimes \mathbb{I}]}{\text{Tr } \hat{\rho}[|1\rangle\langle 1| \otimes \mathbb{I}]} \tag{41.238}$$

$$= \frac{|\alpha_1|^2}{\rho_{00\otimes 00} + \rho_{01\otimes 01}} \begin{pmatrix} \rho_{00\otimes 00} & \rho_{00\otimes 01} & 0 & 0 \\ \rho_{01\otimes 00} & \rho_{01\otimes 01} & 0 & 0 \\ 0 & 0 & 0 & 0 \\ 0 & 0 & 0 & 0 \end{pmatrix} + \frac{|\beta_1|^2}{\rho_{10,10} + \rho_{11,11}} \begin{pmatrix} 0 & 0 & 0 & 0 \\ 0 & 0 & 0 & 0 \\ 0 & 0 & \rho_{10\otimes 10} & \rho_{10\otimes 11} \\ 0 & 0 & \rho_{11\otimes 10} & \rho_{11\otimes 11} \end{pmatrix}.$$

The inversion of qubit q_1 is,

$$\langle \hat{\sigma}_1^z \rangle = \text{Tr } \hat{\rho}\,[\hat{\sigma}^z \otimes \mathbb{I}] = \rho_{00,00} + \rho_{01,01} - \rho_{10,10} - \rho_{11,11}\ . \tag{41.239}$$

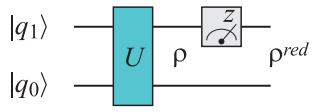

Figure 41.31: Projective measurement. After an operation U, two qubits remain in an entangled state $\hat{\rho}$. Measurement of qubit q_1 reduces the state to $\hat{\rho}^{red}$, while transferring the information to a classical channel c.

Example 267 (*Measurements on disentangled qubits*): As a particular case, let us first consider two disentangled qubits $|\psi\rangle = |q_1\rangle \otimes |q_0\rangle = [\alpha_1|0\rangle + \beta_1|1\rangle] \otimes [\alpha_0|0\rangle + \beta_0|1\rangle]$, such that,

$$\hat{\rho} = \begin{pmatrix} \alpha_1\alpha_0 \\ \alpha_1\beta_0 \\ \beta_1\alpha_0 \\ \beta_1\beta_0 \end{pmatrix} \begin{pmatrix} \alpha_1^*\alpha_0^* & \alpha_1^*\beta_0^* & \beta_1^*\alpha_0^* & \beta_1^*\beta_0^* \end{pmatrix} \tag{41.240}$$

$$= \begin{pmatrix} |\alpha_1|^2|\alpha_0|^2 & |\alpha_1|\alpha_0^*\beta_0^* & \alpha_1\beta_1^*|\alpha_0|^2 & \alpha_1\beta_1^*\alpha_0\beta_0^* \\ |\alpha_1|^2\alpha_0^*\beta_0 & |\alpha_1|^2|\beta_0|^2 & \alpha_1\beta_1^*\alpha_0^*\beta_0 & \alpha_1\beta_1^*|\beta_0|^2 \\ \alpha_1^*\beta_1|\alpha_0|^2 & \beta_1\alpha_1^*\alpha_0\beta_0^* & |\beta_1|^2|\alpha_0|^2 & |\beta_1|^2\alpha_0\beta_0^* \\ \alpha_1^*\beta_1\alpha_0^*\beta_0 & \alpha_1^*\beta_1|\beta_0|^2 & |\beta_1|^2\alpha_0^*\beta_0 & |\beta_1|^2|\beta_0|^2 \end{pmatrix}.$$

A projective measurements of qubit q_1 with two possible outcomes, $|q_1\rangle = |0\rangle_1, |1\rangle_1$ with the respective probabilities $p_0 = |\alpha_1|^2$ and $p_1 = |\beta_1|^2$, yields the reduced density operator,

$$\hat{\rho}_1^{red} = p^{(0)} \frac{[|0\rangle\langle 0| \otimes \mathbb{I}]\hat{\rho}[|0\rangle\langle 0| \otimes \mathbb{I}]}{\text{Tr } \hat{\rho}[|0\rangle\langle 0| \otimes \mathbb{I}]} + p^{(1)} \frac{[|1\rangle\langle 1| \otimes \mathbb{I}]\hat{\rho}[|1\rangle\langle 1| \otimes \mathbb{I}]}{\text{Tr } \hat{\rho}[|1\rangle\langle 1| \otimes \mathbb{I}]} \tag{41.241}$$

$$= |\alpha_1|^2 \begin{pmatrix} |\alpha_0|^2 & \alpha_0\beta_0^* & 0 & 0 \\ \alpha_0^*\beta_0 & |\beta_0|^2 & 0 & 0 \\ 0 & 0 & 0 & 0 \\ 0 & 0 & 0 & 0 \end{pmatrix} + |\beta_1|^2 \begin{pmatrix} 0 & 0 & 0 & 0 \\ 0 & 0 & 0 & 0 \\ 0 & 0 & |\alpha_0|^2 & \alpha_0\beta_0^* \\ 0 & 0 & \alpha_0^*\beta_0 & |\beta_0|^2 \end{pmatrix}$$

$$= [|\alpha_1|^2|0\rangle\langle 0| + |\beta_1|^2|1\rangle\langle 1|] \otimes \hat{\rho}_0 \ .$$

The inversion of qubit q_1 is,

$$\langle \hat{\sigma}_1^z \rangle = |\alpha_1|^2 - |\beta_1|^2 \ . \tag{41.242}$$

That is, we are left with a mixture of two product states, $|0\rangle \otimes [\alpha_0|0\rangle + \beta_0|1\rangle]$ or $|1\rangle \otimes [\alpha_0|0\rangle + \beta_0|1\rangle]$. Analogically, a projective measurements of qubit q_0 yields,

$$\hat{\rho}_0^{red} = |\alpha_0|^2\hat{\rho}_1 \otimes |0\rangle\langle 0| + |\beta_0|^2\hat{\rho}_1 \otimes |1\rangle\langle 1| \tag{41.243}$$

and $\langle \hat{\sigma}_0^z \rangle = |\alpha_0|^2 - |\beta_0|^2$.

Example 268 (*Measurements on entangled qubits*): Now, we consider two entangled qubits $|\psi\rangle = \alpha[|0\rangle \otimes |0\rangle] + \beta[|1\rangle \otimes |1\rangle]$, with $|\alpha|^2 + |\beta|^2 = 1$, such that,

$$\hat{\rho} = \begin{pmatrix} \alpha \\ 0 \\ 0 \\ \beta \end{pmatrix} \begin{pmatrix} \alpha^* & 0 & 0 & \beta^* \end{pmatrix} = \begin{pmatrix} |\alpha|^2 & 0 & 0 & \alpha\beta^* \\ 0 & 0 & 0 & 0 \\ 0 & 0 & 0 & 0 \\ \alpha^*\beta & 0 & 0 & |\beta|^2 \end{pmatrix} \ . \tag{41.244}$$

Projective measurements of qubit q_1 with two possible outcomes yields in both of the two cases, $|q_1\rangle = |0\rangle, |1\rangle$, the reduced density operator,

$$\hat{\rho}_1^{red} = p^{(0)} \frac{[|0\rangle\langle 0| \otimes \mathbb{I}]\,\hat{\rho}[|0\rangle\langle 0| \otimes \mathbb{I}]}{\text{Tr } \hat{\rho}[|0\rangle\langle 0| \otimes \mathbb{I}]} + p_1 \frac{[|1\rangle\langle 1| \otimes \mathbb{I}]\hat{\rho}[|1\rangle\langle 1| \otimes \mathbb{I}]}{\text{Tr } \hat{\rho}[|1\rangle\langle 1| \otimes \mathbb{I}]} \tag{41.245}$$

$$= \begin{pmatrix} |\alpha|^2 & 0 & 0 & 0 \\ 0 & 0 & 0 & 0 \\ 0 & 0 & 0 & 0 \\ 0 & 0 & 0 & |\beta|^2 \end{pmatrix} = |\alpha|^2[|0\rangle\langle 0| \otimes |0\rangle\langle 0|] + |\beta|^2[|1\rangle\langle 1| \otimes |1\rangle\langle 1|] \ .$$

A projective measurements of qubit q_1 would yield exactly the same result.

41.6.5 The field of quantum information

The possibility to experimentally control, manipulate and read out individual qubits gave birth to a new field of physics in the past two decades now called *quantum information*. This fields includes the more specific areas of *quantum processing* (which itself splits into the subareas of *quantum computing* and *quantum simulation*), *quantum communication*, and *quantum sensing* (see Sec. 36.5).

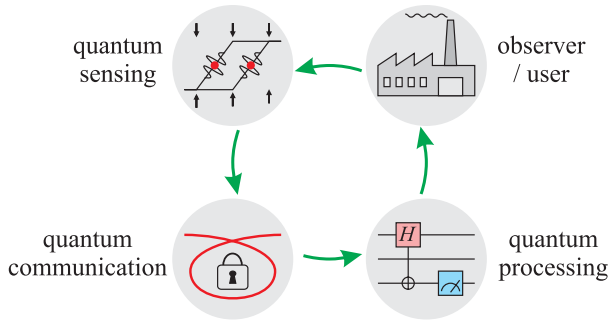

Figure 41.32: Key technologies of the second quantum revolution.

The fundamental epitomic systems on which the quantum information technologies are based are listed in the table below. Although the correspondence is oversimplified, it gives a coarse idea of the involved areas of quantum mechanics. Technological revolutions have often been triggered by paradigmatic 'paradoxes' which, in fact, were mostly dramatized juxtapositions of classical and innovative concepts and stop being paradoxical, once they have been resolved by a more complete theory. The table also lists the cornerstone paradoxes of quantum information technologies.

area	quantum computing	communication	sensing
system	two-level atom / spin	harmonic oscillator	propagation of free atom
device	qubit	photon	interferometer
phenomenon	quantum entanglement		superposition & measurement
paradox	EPR paradox		Schrödinger cat

41.6.5.1 Physical implementation of quantum computers

Quantum entanglement and information processing protocols for quantum computing have been implemented with various technologies (see table below for a non-exhaustive list), some of them pursued by private companies. Every approach has its advantages and disadvantages, the main figures of merit being the *qubit number*, the *qubit connectivity*, and the *gate fidelity*. Other important factors are *scalability*, *qubit homogeneity*, and *ease of fabrication and use*.

physical system	description	companies	publications
ions	trapped ion array	IonQ, AQT	[915, 840]
neutral atoms	optical lattice	-	[28]
transmons	superconducting JJ arrays	IBM, Google, ...	[49]
molecules	NMR on bonds in molecules	-	[1401]
NV centers	color centers in diamond	-	[1025]
quantum dots	quantum dots arrays	diraq	[814]
photons	polarization or timing	-	[1268]

Example 269 (*Quantum volume of perfect processor*): The *quantum volume* of an N-qubit quantum processor is a metric invented by IBM that characterizes the largest random quantum circuit that the device can efficiently

simulate. The formula for quantum volume is given by:

$$\text{quantum volume} = N^2 \times \text{maximal depth} \ . \tag{41.246}$$

In the case of a perfect N-qubit processor, the maximal depth is equal to N since each gate can be applied in parallel on all qubits, and there are N such layers. Therefore, the quantum volume of a perfect N-qubit processor is quantum volume $= N^3$. This means that a perfect N-qubit quantum processor can efficiently simulate random quantum circuits of up to N^3 gates. However, in reality, quantum processors suffer from errors due to various sources such as decoherence and imperfect gate operations, and as a result, their quantum volume is typically much lower than this theoretical limit.

41.6.5.2 Quantum sensing 2.0

Many sensors are based on interferometry, as explained in Sec. 36.5.3. The circuit exhibited in Fig. 41.33 visualizes the basic principle of an interferometer. The two Hadamard gates correspond to Ramsey pulses, and the controlled U gate realizes the interaction, which transfers information from the U gate to the sensing qubit.

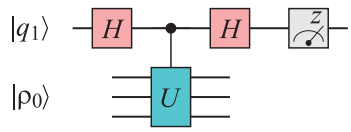

Figure 41.33: Quantum interferometry.

As mentioned in Sec. 36.3.2 and in Sec. 41.1.4, the sensitivity of interferometers can be enhanced when correlated particles are used. In Exc. 41.6.6.13 we show how the interferometer of Fig. 41.33 can be modified in order to benefit from correlated particles.

41.6.5.3 Quantum Fourier transform

The *quantum Fourier transform* (QFT) is a linear transformation on qubits and the quantum analogue of the inverse discrete Fourier transform. The quantum Fourier transform is a part of many quantum algorithms, notably Shor's algorithm for factoring and computing the discrete logarithm or the quantum phase estimation algorithm for estimating the eigenvalues of a unitary operator.

The quantum Fourier transform can be performed efficiently on a quantum computer, with a particular decomposition into a product of simpler unitary matrices. Using a simple decomposition, the discrete Fourier transform on 2^n amplitudes can be implemented as a quantum circuit consisting of only $O(n^2)$ Hadamard gates and controlled phase shift gates, where n is the number of qubits. This can be compared with the classical discrete Fourier transform, which takes $O(2^n)$ gates, which is exponentially more than in the classical case. However, the quantum Fourier transform acts on a quantum state, whereas the classical Fourier transform acts on a vector, so not every task that uses the classical Fourier transform can take advantage of this exponential speedup.

The quantum Fourier transform is the classical discrete Fourier transform applied to the vector of amplitudes of a quantum state, where we usually consider vectors of length $N = 2^n$. The classical Fourier transform acts on a vector $(x_0, x_1, \ldots, x_{N-1}) \in \mathbb{C}^N$ and maps it to the vector $(y_0, y_1, \ldots, y_{N-1}) \in \mathbb{C}^N$ according to the formula:

$$\boxed{y_k = \frac{1}{\sqrt{N}} \sum_{n=0}^{N-1} x_n \omega_N^{\mp kn} \ ,} \tag{41.247}$$

where $k = 0, 1, \ldots, N-1$ and $\omega_N = e^{2\pi\imath/N}$ and ω_N^n is an N^{th} root of unity. The lower sign holds for the *inverse* FT.

Similarly, the quantum Fourier transform acts on a quantum state $|x\rangle = \sum_{i=0}^{N-1} x_i |i\rangle$ and maps it to a quantum state $\sum_{i=0}^{N-1} y_i |i\rangle$ according to the same formula (41.247). In case that $|x\rangle$ is a basis state, the quantum Fourier Transform can also be expressed as the map,

$$|x\rangle \mapsto \frac{1}{\sqrt{N}} \sum_{k=0}^{N-1} \omega_n^{xk} |k\rangle \ . \tag{41.248}$$

Equivalently, the quantum Fourier transform can be viewed as a unitary matrix (or a quantum gate, similar to a Boolean logic gate for classical computers) acting on quantum state vectors, where the unitary matrix is given by,

$$F_N = \frac{1}{\sqrt{N}} \begin{pmatrix} 1 & 1 & 1 & 1 & \cdots & 1 \\ 1 & \omega & \omega^2 & \omega^3 & \cdots & \omega^{N-1} \\ 1 & \omega^2 & \omega^4 & \omega^6 & \cdots & \omega^{2(N-1)} \\ 1 & \omega^3 & \omega^6 & \omega^9 & \cdots & \omega^{3(N-1)} \\ \vdots & \vdots & \vdots & \vdots & & \vdots \\ 1 & \omega^{N-1} & \omega^{2(N-1)} & \omega^{3(N-1)} & \ldots & \omega^{(N-1)(N-1)} \end{pmatrix} \tag{41.249}$$

where $\omega = \omega_N$. Do the Excs. 41.6.6.10 and 41.6.6.11.

The QFT is unitary,

$$\boxed{FF^\dagger = \mathbb{I} \ ,} \tag{41.250}$$

and can be efficiently performed on a quantum computer. The quantum gates used in the circuit are the Hadamard gate and the controlled phase gate R_m,

$$H = \tfrac{1}{\sqrt{2}} \begin{pmatrix} 1 & 1 \\ 1 & -1 \end{pmatrix} \qquad \text{and} \qquad R_m = \begin{pmatrix} 1 & 0 \\ 0 & e^{2\pi\imath/2^m} \end{pmatrix} \ , \tag{41.251}$$

with $e^{2\pi\imath/2^m} = \omega_{(2^m)}$ the primitive 2^m-th root of unity. The circuit is composed of H gates and the controlled version of R_m.

All quantum operations must be linear, so it suffices to describe the function on each one of the basis states and let the mixed states be defined by linearity. This is in contrast to how Fourier transforms are usually described. We normally describe Fourier transforms in terms of how the components of the results are calculated on an arbitrary input. This is how you would calculate the path integral or show BQP is

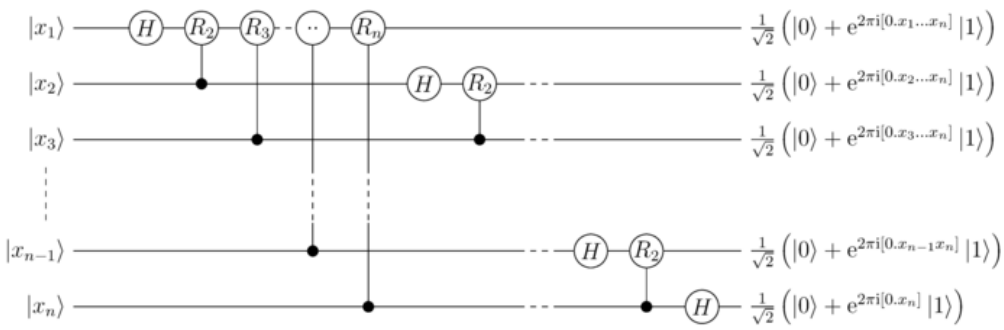

Figure 41.34: Quantum circuit for QFT with n qubits (without rearranging the order of output states).

in PP. But it is much simpler here (and in many cases) to just explain what happens to a specific arbitrary basis state, and the total result can be found by linearity.

The quantum Fourier transform can be approximately implemented for any N; however, the implementation for the case where N is a power of 2 is much simpler. As already stated, we assume $N = 2^n$. We have the orthonormal basis consisting of the vectors $|0\rangle, \ldots, |2^n - 1\rangle$. The basis states enumerate all the possible states of the qubits, $|x\rangle = |x_1 x_2 \ldots x_n\rangle = |x_1\rangle \otimes |x_2\rangle \otimes \cdots \otimes |x_n\rangle$, where $|x_j\rangle$ indicates that qubit j is in state x_j, with x_j either 0 or 1. By convention, the basis state index x orders the possible states of the qubits lexicographically, i.e. by converting from binary to decimal in this way:

$$x = x_1 2^{n-1} + x_2 2^{n-2} + \cdots + x_n 2^0 \ . \tag{41.252}$$

It is also useful to borrow fractional binary notation:

$$[0.x_1 \ldots x_m] = \sum_{k=1}^{m} x_k 2^{-k} \ . \tag{41.253}$$

For instance, $[0.x_1] = \frac{x_1}{2}$ and $[0.x_1 x_2] = \frac{x_1}{2} + \frac{x_2}{2^2}$. With this notation, the action of the quantum Fourier transform can be expressed in a compact manner:

$$\begin{aligned} \mathrm{QFT}(|x_1 x_2 \ldots x_n\rangle) = \frac{1}{\sqrt{N}} \left(|0\rangle + e^{2\pi\imath\ [0.x_n]}|1\rangle\right) \otimes \left(|0\rangle + e^{2\pi\imath\ [0.x_{n-1}x_n]}|1\rangle\right) \otimes \cdots \\ \otimes \left(|0\rangle + e^{2\pi\imath\ [0.x_1 x_2 \ldots x_n]}|1\rangle\right) \ , \end{aligned} \tag{41.254}$$

where we have used $[0.x_1 x_2 ... x_m] = [x_1 x_2 ... x_n]/2^m$. This can be seen by rewriting the formula for the Fourier transform in the binary expansion:

$$\mathrm{QFT}(|x\rangle) = \frac{1}{\sqrt{N}} \sum_{k=0}^{2^n-1} \omega_n^{xk} |k\rangle = \ldots = \frac{1}{\sqrt{N}} \bigotimes_{j=1}^{n} \left(|0\rangle + \omega_n^{x 2^{n-j}}|1\rangle\right) \ . \tag{41.255}$$

Now, we have $\omega_n^{x2^{n-j}} = e^{\frac{2\pi\imath}{2^n}x2^{n-j}} = e^{2\pi\imath(x2^{-j})}$. Let,

$$f(j) = x2^{-j} = 2^{-j}\sum_{r=1}^{n} x_r 2^{n-r} = \sum_{r=1}^{n} x_r 2^{n-j-r} \tag{41.256}$$
$$= \sum_{r=1}^{n-j} x_r 2^{n-j-r} + \sum_{r=n-j+1}^{n} x_r 2^{n-j-r} = a(j) + b(j) \ .$$

then $a(j) \in \mathbb{N}_0$, because $2^{n-j-r} \geq 0$, for $n-j-r \geq 0$, and $b(j) = 0.x_{n-j+1}x_{n-j+2}\dots x_n$, thus the (2) becomes:

$$e^{2\pi\imath f(j)} = e^{2\pi\imath(a(j)+b(j))} = e^{2\pi\imath a(j)} \cdot e^{2\pi\imath b(j)} = e^{2\pi\imath[0.x_{n-j+1}x_{n-j+2}\cdots x_n]} \ , \tag{41.257}$$

since $e^{2\pi\imath a(j)} = 1$ for all j. Then we can write:

$$\mathrm{QFT}(|x_1x_2\dots x_n\rangle) = \frac{1}{\sqrt{N}}\bigotimes_{j=1}^{n}\left(|0\rangle + \omega_n^{x2^{n-j}}|1\rangle\right) \tag{41.258}$$
$$= \frac{1}{\sqrt{N}}\bigotimes_{j=1}^{n}\left(|0\rangle + e^{2\pi\imath[0.x_{n-j+1}x_{n-j+2}\dots x_n]}|1\rangle\right)$$
$$= \frac{1}{\sqrt{N}}\left(|0\rangle + e^{2\pi\imath[0.x_n]}|1\rangle\right)\otimes\left(|0\rangle + e^{2\pi\imath[0.x_{n-1}x_n]}|1\rangle\right)\otimes\cdots\otimes\left(|0\rangle + e^{2\pi\imath[0.x_1x_2\dots x_n]}|1\rangle\right) \ .$$

To obtain this state from the circuit depicted above, a swap operations of the qubits must be performed to reverse their order. After the reversal, the n-th output qubit will be in a superposition state of $|0\rangle$ and $e^{2\pi\imath\ [0.x_1\dots x_n]}|1\rangle$, and similarly the other qubits before that (take a second look at the sketch of the circuit above).

In other words, the discrete Fourier transform, an operation on n qubits, can be factored into the tensor product of n single-qubit operations, suggesting it is easily represented as a quantum circuit (up to an order reversal of the output). In fact, each of those single-qubit operations can be implemented efficiently using a Hadamard gate and controlled phase gates. The first term requires one Hadamard gate and $(n-1)$ controlled phase gates, the next one requires a Hadamard gate and $(n-2)$ controlled phase gate, and each following term requires one fewer controlled phase gate. Summing up the number of gates, excluding the ones needed for the output reversal, gives $n + (n-1) + \cdots + 1 = n(n+1)/2 = O(n^2)$ gates, which is quadratic polynomial in the number of qubits.

The QFT is useful in the simulation of Hamiltonian evolution governed by conjugate variables,

$$e^{-\hat{H}t/\hbar} \qquad \text{where} \qquad \hat{H} = \frac{\hat{p}}{2m} + \frac{m}{2}\omega^2\hat{x}^2 \ , \tag{41.259}$$

where, similar to the *time-splitting spectral algorithm*, we may replace differential operators,

$$\hat{p} = F^{-1}\ \hat{x}\ F \ . \tag{41.260}$$

41.6.5.4 Boson sampling

A qubit is not necessarily a single (quasi-)particle, such as an atom or a photon. More generally any system which can interfere, that is be in superposition states, may qualify. F.ex. a laser pulse with squeezing/polarization as the degree of freedom can be used for *boson sampling* [1, 578, 1063, 1432].

41.6.6 Exercises

41.6.6.1 Ex: Controlled Z-gate

Check that the CZ gate is invariant under spin exchange. This fact justifies the symmetry of the symbol with respect to the two coupled qubits.

Solution: *Using,*

$$Z = -\hat{\sigma}_z = \begin{pmatrix} 1 & 0 \\ 0 & -1 \end{pmatrix}$$

and the `SWAP`*-gate introduced in (23.130) we just need to show,*

$$\overset{c}{Z}_{10} = \begin{pmatrix} 1 & 0 & 0 & 0 \\ 0 & 1 & 0 & 0 \\ 0 & 0 & 1 & 0 \\ 0 & 0 & 0 & -1 \end{pmatrix} = \mathbb{S}\overset{c}{Z}_{01}\mathbb{S} \equiv \overset{c}{Z}_{01} \ .$$

41.6.6.2 Ex: Quantum computing code for spin-squeezing

Express spin-squeezing of 2, respectively, 3 qubits by a quantum circuit.

Solution: *Check [1144]!*

41.6.6.3 Ex: Two-bit SWAP gate

Represent the two-qubit SWAP gate by a succession of three CNOT gates.

Solution: *From (41.217) we know* $\overset{c}{X}_{01} = \mathbb{S}\overset{c}{X}_{10}\mathbb{S}$. *With,*

$$\overset{c}{X}_{10} = \begin{pmatrix} 1 & 0 & 0 & 0 \\ 0 & 1 & 0 & 0 \\ 0 & 0 & 0 & 1 \\ 0 & 0 & 1 & 0 \end{pmatrix} \quad , \quad \overset{c}{X}_{01} = \begin{pmatrix} 1 & 0 & 0 & 0 \\ 0 & 0 & 0 & 1 \\ 0 & 0 & 1 & 0 \\ 0 & 1 & 0 & 0 \end{pmatrix}$$

it is easy to show that,

$$\mathbb{S} = \overset{c}{X}_{01}\overset{c}{X}_{10}\overset{c}{X}_{01} = \begin{pmatrix} 1 & 0 & 0 & 0 \\ 0 & 0 & 1 & 0 \\ 0 & 1 & 0 & 0 \\ 0 & 0 & 0 & 1 \end{pmatrix} ,$$

as illustrated in Fig. 41.35.

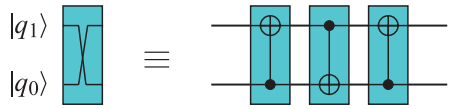

Figure 41.35: Swapping two qubits via three controlled NOT gates.

41.6.6.4 Ex: Three-bit SWAP gate

a. Convince yourself that the SWAP gates defined by (41.221) have the explicit matrix form,

$$\mathbb{S}_{ij}(k, k_{ij}) \equiv 1 \qquad \text{where} \qquad \begin{cases} k = [0, ..., 7] \\ k_{12} = [0, 1, 4, 5, 2, 3, 6, 7] \\ k_{01} = [0, 2, 1, 3, 4, 6, 5, 7] \\ k_{02} = [0, 4, 2, 6, 1, 5, 3, 7] \end{cases} ,$$

the index k indicating the column and k_{ij} the row where the matrix has an entry.
b. Verify,

$$\mathbb{S}^{-1} = \mathbb{S} \qquad , \qquad \mathbb{S}_{ij}^{-1} = \mathbb{S}_{ij} \ .$$

Solution:

41.6.6.5 Ex: Quantum gates

Verify the formulae (41.223).

Solution:

41.6.6.6 Ex: Toffoli gate

Check that the quantum circuit sketched in Fig. 41.36, which only envolves two-qubit quantum gates realizes a Toffoli gate.

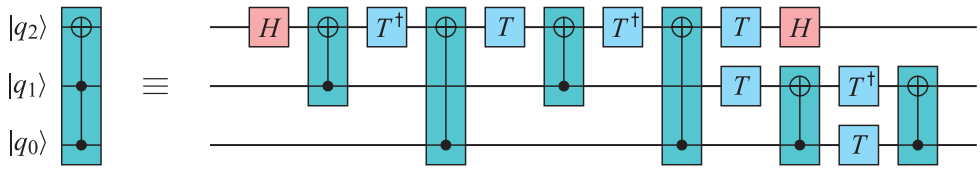

Figure 41.36: Quantum circuit realizing a Toffoli gate.

Solution: *The circuit diagram represents the operation,*

$$\overset{cc}{X}_{012} = \overset{c}{X}_{01} T_0 T_1^\dagger \overset{c}{X}_{01} T_1 H_2 T_2 \overset{c}{X}_{02} T_2^\dagger \overset{c}{X}_{12} T_2 \overset{c}{X}_{02} T_2^\dagger \overset{c}{X}_{12} H_2 = \begin{pmatrix} 1 & 0 & 0 & 0 & 0 & 0 & 0 & 0 \\ 0 & 1 & 0 & 0 & 0 & 0 & 0 & 0 \\ 0 & 0 & 1 & 0 & 0 & 0 & 0 & 0 \\ 0 & 0 & 0 & 0 & 0 & 0 & 0 & 1 \\ 0 & 0 & 0 & 0 & 1 & 0 & 0 & 0 \\ 0 & 0 & 0 & 0 & 0 & 1 & 0 & 0 \\ 0 & 0 & 0 & 0 & 0 & 0 & 1 & 0 \\ 0 & 0 & 0 & 1 & 0 & 0 & 0 & 0 \end{pmatrix},$$

or inverting the order of the significant qubits,

$$\overset{cc}{X}_{210} = S_{01} S_{12} S_{01} \overset{cc}{X}_{012} S_{01} S_{12} S_{01} = \begin{pmatrix} 1 & 0 & 0 & 0 & 0 & 0 & 0 & 0 \\ 0 & 1 & 0 & 0 & 0 & 0 & 0 & 0 \\ 0 & 0 & 1 & 0 & 0 & 0 & 0 & 0 \\ 0 & 0 & 0 & 1 & 0 & 0 & 0 & 0 \\ 0 & 0 & 0 & 0 & 1 & 0 & 0 & 0 \\ 0 & 0 & 0 & 0 & 0 & 1 & 0 & 0 \\ 0 & 0 & 0 & 0 & 0 & 0 & 0 & 1 \\ 0 & 0 & 0 & 0 & 0 & 0 & 1 & 0 \end{pmatrix}.$$

41.6.6.7 Ex: Classical and quantum logic

a. Verify $\neg(A \vee B) = \neg A \wedge \neg B$ and $A \oplus B = (\neg A \wedge B) \vee (A \wedge \neg B)$.
b. How would you realize the classical logical operations AND, OR, and XOR on a quantum computer?

Solution: *a. Trivial by comparing the truth tables.*
b. The classical logic operations AND and OR involve three bits, two at the input and one at the output. Because the corresponding quantum logic operation must be reversible, we must specify the state of all three qubits before and after the operation. That is, we are looking for a unitary transform in $\mathcal{H}^{2^3}$. *Classically, we determine the*

following truth tables,

$$|\psi\rangle_{in} = \begin{array}{c} |q_2,q_1,q_0\rangle \\ \left(\begin{array}{cc|c} 0&0&0\\ 0&0&1\\ 0&1&0\\ 0&1&1\\ 1&0&0\\ 1&0&1\\ 1&1&0\\ 1&1&1 \end{array}\right) \end{array} \quad , \quad |\psi\rangle_{out}^{AND-NOR} = \begin{array}{c} |q_2,q_1,(q_2\wedge q_1)\oplus q_0\rangle \\ \left(\begin{array}{cc|c} 0&0&0\\ 0&0&1\\ 0&1&0\\ 0&1&1\\ 1&0&0\\ 1&0&1\\ 1&1&1\\ 1&1&0 \end{array}\right) \end{array} \quad ,$$

$$|\psi\rangle_{out}^{OR-NAND} = \begin{array}{c} |q_2,q_1,(q_2\vee q_1)\oplus q_0\rangle \\ \left(\begin{array}{cc|c} 0&0&0\\ 0&0&1\\ 0&1&1\\ 0&1&0\\ 1&0&1\\ 1&0&0\\ 1&1&1\\ 1&1&0 \end{array}\right) \end{array} \quad , \quad |\psi\rangle_{out}^{XOR-NXOR} = \begin{array}{c} |q_2,q_1,(q_2\oplus q_1)\oplus q_0\rangle \\ \left(\begin{array}{cc|c} 0&0&0\\ 0&0&1\\ 0&1&1\\ 0&1&0\\ 1&0&1\\ 1&0&0\\ 1&1&0\\ 1&1&1 \end{array}\right) \end{array} \quad .$$

The classical gates are recovered by projecting the $q_0^{(out)}$ output bit on either the $q_0^{(in)} = 0$ or 1 input bit. In quantum logic, we use the relations (41.223) to construct the quantum AND (and simultaneously NOR) via the Toffoli gate,

$$U_{AND} = \overset{cc}{X}_{210} = |q_2,q_1,(q_2\wedge q_1)\oplus q_0\rangle\langle q_2,q_1,q_0| \ ,$$

or using the above defined basis,

$$\begin{array}{c} AND-NOR \\ \begin{pmatrix} |000\rangle \\ |001\rangle \\ |010\rangle \\ |011\rangle \\ |100\rangle \\ |101\rangle \\ |111\rangle \\ |110\rangle \end{pmatrix} \end{array} = \begin{pmatrix} 1&0&0&0&0&0&0&0\\ 0&1&0&0&0&0&0&0\\ 0&0&1&0&0&0&0&0\\ 0&0&0&1&0&0&0&0\\ 0&0&0&0&1&0&0&0\\ 0&0&0&0&0&1&0&0\\ 0&0&0&0&0&0&0&1\\ 0&0&0&0&0&0&1&0 \end{pmatrix} \begin{array}{c} |q_2,q_1,q_0\rangle \\ \begin{pmatrix} |000\rangle \\ |001\rangle \\ |010\rangle \\ |011\rangle \\ |100\rangle \\ |101\rangle \\ |110\rangle \\ |111\rangle \end{pmatrix} \end{array}$$

Similarly, for the quantum OR (and simultaneously NAND),

$$U_{OR} = X_2X_1X_0\overset{cc}{X}_{012}X_0X_1 = |q_2,q_1,(q_2\vee q_1)\oplus q_0\rangle\langle q_2,q_1,q_0| \ ,$$

or using the above defined basis,

$$\overset{OR-NAND}{\begin{pmatrix} |000\rangle \\ |001\rangle \\ |011\rangle \\ |010\rangle \\ |101\rangle \\ |100\rangle \\ |111\rangle \\ |110\rangle \end{pmatrix}} = \begin{pmatrix} 1 & 0 & 0 & 0 & 0 & 0 & 0 & 0 \\ 0 & 1 & 0 & 0 & 0 & 0 & 0 & 0 \\ 0 & 0 & 0 & 1 & 0 & 0 & 0 & 0 \\ 0 & 0 & 1 & 0 & 0 & 0 & 0 & 0 \\ 0 & 0 & 0 & 0 & 0 & 1 & 0 & 0 \\ 0 & 0 & 0 & 0 & 1 & 0 & 0 & 0 \\ 0 & 0 & 0 & 0 & 0 & 0 & 0 & 1 \\ 0 & 0 & 0 & 0 & 0 & 0 & 1 & 0 \end{pmatrix} \overset{|q_2,q_1,q_0\rangle}{\begin{pmatrix} |000\rangle \\ |001\rangle \\ |010\rangle \\ |011\rangle \\ |100\rangle \\ |101\rangle \\ |110\rangle \\ |111\rangle \end{pmatrix}}$$

Similarly, for the quantum XOR (and simultaneously NXOR),

$$U_{XOR} = \overset{c}{X}_{12}\overset{c}{X}_{02} = |q_2, q_1, (q_2 \oplus q_1) \oplus q_0\rangle\langle q_2, q_1, q_0| \ ,$$

or using the above defined basis,

$$\overset{XOR-NXOR}{\begin{pmatrix} |000\rangle \\ |001\rangle \\ |011\rangle \\ |010\rangle \\ |101\rangle \\ |100\rangle \\ |110\rangle \\ |111\rangle \end{pmatrix}} = \begin{pmatrix} 1 & 0 & 0 & 0 & 0 & 0 & 0 & 0 \\ 0 & 1 & 0 & 0 & 0 & 0 & 0 & 0 \\ 0 & 0 & 0 & 1 & 0 & 0 & 0 & 0 \\ 0 & 0 & 1 & 0 & 0 & 0 & 0 & 0 \\ 0 & 0 & 0 & 0 & 0 & 1 & 0 & 0 \\ 0 & 0 & 0 & 0 & 1 & 0 & 0 & 0 \\ 0 & 0 & 0 & 0 & 0 & 0 & 1 & 0 \\ 0 & 0 & 0 & 0 & 0 & 0 & 0 & 1 \end{pmatrix} \overset{|q_2,q_1,q_0\rangle}{\begin{pmatrix} |000\rangle \\ |001\rangle \\ |010\rangle \\ |011\rangle \\ |100\rangle \\ |101\rangle \\ |110\rangle \\ |111\rangle \end{pmatrix}}$$

41.6.6.8 Ex: Quantum composer

Show that the following diagrams describe identical unitary operations:

Solution: *The diagrams can easily be verified after having translated them into a matricial language as,*

a.

$$\overset{c}{X}_{01} = (\mathbb{I} \otimes H)\overset{c}{Z}_{01}(\mathbb{I} \otimes H) \ .$$

b.

$$(H \otimes H)\overset{c}{X}_{01}(H \otimes H) = \overset{c}{X}_{10} \ .$$

c.

$$(\overset{cc}{U}_{012})^2 = (\mathbb{I} \otimes \mathbb{I} \otimes \overset{c}{U}_{12})(\overset{c}{X}_{01} \otimes \mathbb{I})(\mathbb{I} \otimes \mathbb{I} \otimes (\overset{c}{U}_{12})^\dagger)(\overset{c}{X}_{01} \otimes \mathbb{I})(\mathbb{I} \otimes \mathbb{I} \otimes \overset{c}{U}_{12}) \ .$$

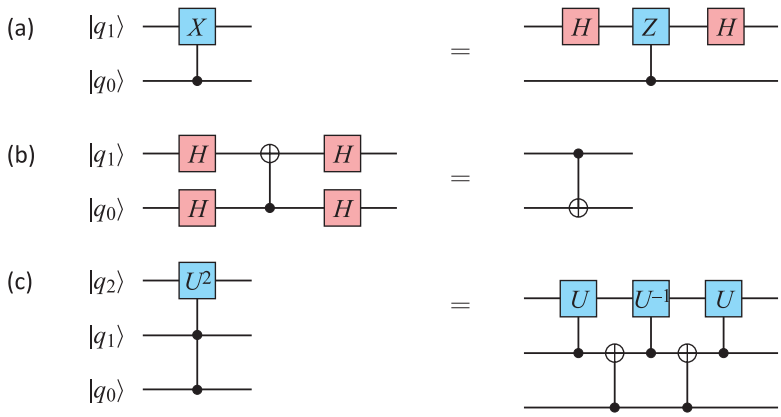

Figure 41.37:

41.6.6.9 Ex: Classical addition of two qubits

Design a quantum algorithm for the classical addition of up to 8 qubits.

Solution: *In the binary system the operation is given by the equation,*

$$\sum_{k=0}^{7} q_k = 4p_2 + 2p_1 + p_0 \ .$$

Using just XOR gates we find the scheme exhibited in Fig.41.38.

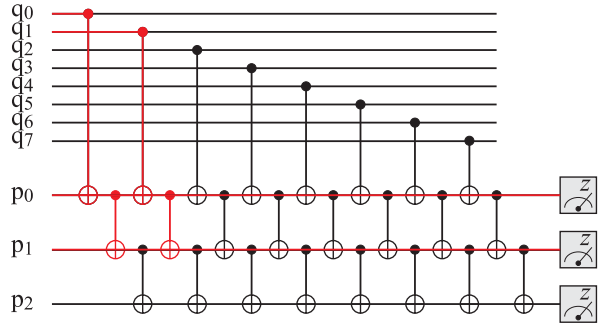

Figure 41.38: Quantum algorithm simulating the classical sum of up to 7 qubits (black lines) or up to 3 qubits (red lines).

41.6.6.10 Ex: CARL simulation on a quantum computer

Try to recast the so-called CARL Hamiltonian,

$$\hat{H} = U_0(\hat{a}_+^\dagger \hat{a}_- e^{-\imath k\hat{r}} + \hat{a}_+ \hat{a}_-^\dagger e^{\imath k\hat{r}})$$

such that it can be simulated by a sequence of quantum gates.

Solution: *We first truncate the admitted numbers of photons to some value and use the Holstein-Primakoff transformation. We must define a linear multi-qubit gate, each qubit standing for a photon. The motion is described as a 1D lattice in momentum space.*

41.6.6.11 Ex: Quantum Fourier transform on a quantum computer

Write down the QF transformation matrix for the case of $N = 4 = 2^2$ and phase $\omega = \imath$.

Solution: *The matrix reads,*

$$F_4 = \frac{1}{2}\begin{pmatrix} 1 & 1 & 1 & 1 \\ 1 & \imath & -1 & -\imath \\ 1 & -1 & 1 & -1 \\ 1 & -\imath & -1 & \imath \end{pmatrix} .$$

41.6.6.12 Ex: Three entangled qubits

a. Imagine a three-qubit quantum gate or a sequence of gates generating from the ground state the three partite states [400]:

$$|GHZ\rangle \equiv \frac{1}{\sqrt{2}}(|000\rangle + |111\rangle \qquad \text{and} \qquad |W\rangle \equiv \frac{1}{\sqrt{3}}(|001\rangle + |010\rangle + |100\rangle) .$$

b. Show how the procedure for the generation of the $|GHZ\rangle$ state can be easily extended to N entangled particles.

Solution: *a. In extension of the calculation of Exc. 41.5.4.1 it is easy to show that*

$$\overset{c}{X}_{12}\overset{c}{X}_{01}(H \otimes \mathbb{I} \otimes \mathbb{I}) \begin{pmatrix} 1 \\ 0 \\ 0 \\ 0 \\ 0 \\ 0 \\ 0 \\ 0 \end{pmatrix} = \frac{1}{\sqrt{2}} \begin{pmatrix} 1 \\ 0 \\ 0 \\ 0 \\ 0 \\ 0 \\ 0 \\ 1 \end{pmatrix}$$

generates a GHZ state. The W state is obtained via

$$X_0 \overset{c}{X}_{01} \overset{c}{X}_{12} \overset{c}{H}_{01} U_3(\arccos(-\tfrac{1}{3}), 0, 0) \begin{pmatrix} 1 \\ 0 \\ 0 \\ 0 \\ 0 \\ 0 \\ 0 \\ 0 \\ 0 \end{pmatrix} = \tfrac{1}{\sqrt{3}} \begin{pmatrix} 0 \\ 1 \\ 1 \\ 0 \\ 1 \\ 0 \\ 0 \\ 0 \\ 0 \end{pmatrix} .$$

b. We just have to continue the protocol like,

$$\overset{c}{X}_{N-1\ N} \overset{c}{X}_{N-2\ N-1} ... \overset{c}{X}_{01} (H \otimes \mathbb{I} \otimes \mathbb{I}) .$$

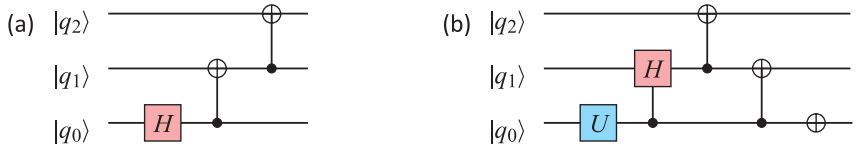

Figure 41.39: Quantum circuit generating (a) a GHZ state and (b) a W state.

41.6.6.13 Ex: Scattering circuit

a. Consider the controlled U gate given by,

$$\overset{c}{U}_{10} = |0\rangle\langle 0| \otimes \mathbb{I} + |1\rangle\langle 1| \otimes U ,$$

where U is an arbitrary unitary operation, and the quantum circuit given by,

$$M = [H \otimes \mathbb{I}] \overset{c}{U}_{10} [H \otimes \mathbb{I}]$$

and depicted in Fig. 41.33. Starting from an initial state $|0\rangle\langle 0| \otimes \hat{\rho}_0$, show, that a measurement of the first qubit $|q_1\rangle$ of the final state,

$$\hat{\rho}_f = M[|0\rangle\langle 0| \otimes \hat{\rho}_0] M^\dagger$$

yields,

$$\langle \hat{\sigma}_1^z \rangle = \mathfrak{Re}\ [\mathrm{Tr}_0\ \hat{\rho}_0 U] \qquad \text{and} \qquad \langle \hat{\sigma}_1^y \rangle = \mathfrak{Im}\ [\mathrm{Tr}_0\ \hat{\rho}_0 U] .$$

b. Calculate $\langle \vec{\hat{\sigma}}_1 \rangle$ for the case that U is a one-qubit phase gate given by (41.208).
c. Calculate $\langle \vec{\hat{\sigma}}_1 \rangle$ for the case that $U = X$ is a one-qubit `NOT` gate given by (41.210).

Solution: *a. The Hamamard gates applied to qubits q_1 and q_0 are, respectively [686],*

$$H_1 = H \otimes \mathbb{I} = \tfrac{1}{\sqrt{2}} \begin{pmatrix} \mathbb{I} & \mathbb{I} \\ \mathbb{I} & -\mathbb{I} \end{pmatrix} \qquad , \qquad H_0 = \mathbb{I} \otimes H = \tfrac{1}{\sqrt{2}} \begin{pmatrix} H & 0 \\ 0 & H \end{pmatrix} .$$

The controlled U gate is given by,

$$\overset{c}{U}_{10} = |0\rangle\langle 0| \otimes \mathbb{I} + |1\rangle\langle 1| \otimes U = \begin{pmatrix} \mathbb{I} & 0 \\ 0 & U \end{pmatrix} ,$$

so that the quantum circuit can be written as,

$$M = [H \otimes \mathbb{I}]\overset{c}{U}_{10}[H \otimes \mathbb{I}] = \tfrac{1}{2}\begin{pmatrix} \mathbb{I} & \mathbb{I} \\ \mathbb{I} & -\mathbb{I} \end{pmatrix}\begin{pmatrix} I & 0 \\ 0 & U \end{pmatrix}\begin{pmatrix} \mathbb{I} & \mathbb{I} \\ \mathbb{I} & -\mathbb{I} \end{pmatrix} = \tfrac{1}{2}\begin{pmatrix} \mathbb{I}+U & \mathbb{I}-U \\ \mathbb{I}-U & \mathbb{I}+U \end{pmatrix} .$$

Starting from an initial state

$$|0\rangle\langle 0| \otimes \hat{\rho}_0 = \begin{pmatrix} \hat{\rho}_0 & 0 \\ 0 & 0 \end{pmatrix} ,$$

we see, that the final state becomes,

$$\hat{\rho}_f = M[|0\rangle\langle 0| \otimes \hat{\rho}_0]M^\dagger = \tfrac{1}{4}\begin{pmatrix} \hat{\rho}_0 + U\rho_0 U^\dagger + (U\hat{\rho}_0 + \hat{\rho}_0 U^\dagger) & \hat{\rho}_0 - U\hat{\rho}_0 U^\dagger + (U\hat{\rho}_0 - \hat{\rho}_0 U^\dagger) \\ \hat{\rho}_0 - U\hat{\rho}_0 U^\dagger - (U\hat{\rho}_0 - \hat{\rho}_0 U^\dagger) & \hat{\rho}_0 + U\hat{\rho}_0 U^\dagger - (U\hat{\rho}_0 + \hat{\rho}_0 U^\dagger) \end{pmatrix} .$$

Tracing over the second qubit $|q_0\rangle$ yields the reduced density matrix of the probe qubit q_1,

$$\begin{aligned} \hat{\rho}^{red} = Tr_0\ \hat{\rho}_f &= \tfrac{1}{2}\begin{pmatrix} 1 + \frac{1}{2}Tr_0\ (U\hat{\rho}_0 + \hat{\rho}_0 U^\dagger) & \frac{1}{2}Tr_0\ (U\hat{\rho}_0 - \hat{\rho}_0 U^\dagger) \\ -\frac{1}{2}Tr_0\ (U\hat{\rho}_0 - \hat{\rho}_0 U^\dagger) & 1 - \frac{1}{2}Tr_0\ (U\hat{\rho}_0 + \hat{\rho}_0 U^\dagger) \end{pmatrix} \\ &= \tfrac{1}{2}\begin{pmatrix} 1 + \mathfrak{Re}\ [Tr_0\ U\hat{\rho}_0] & \imath\mathfrak{Im}\ [Tr_0\ U\hat{\rho}_0] \\ -\imath\mathfrak{Im}\ [Tr_0\ U\hat{\rho}_0] & 1 - \mathfrak{Re}\ [Tr_0\ U\hat{\rho}_0] \end{pmatrix} . \end{aligned}$$

Finally, we get for the observables of the probe qubit,

$$\begin{aligned} \langle\hat{\sigma}_1^x\rangle &= \langle 0|\hat{\rho}^{red}|1\rangle + \langle 1|\hat{\rho}^{red}|0\rangle = 0 \\ \langle\hat{\sigma}_1^y\rangle &= \imath\langle 0|\hat{\rho}^{red}|1\rangle - \imath\langle 1|\hat{\rho}^{red}|0\rangle = -\mathfrak{Im}\ [Tr_0\ \hat{\rho}_0 U] \\ \langle\hat{\sigma}_1^z\rangle &= \langle 0|\hat{\rho}^{red}|0\rangle - \langle 1|\hat{\rho}^{red}|1\rangle = \mathfrak{Re}\ [Tr_0\ \hat{\rho}_0 U] . \end{aligned}$$

b. If U is given by,

$$U = \begin{pmatrix} 1 & 0 \\ 0 & e^{\imath\varphi} \end{pmatrix} ,$$

we find,

$$\langle\vec{\hat{\sigma}}_1\rangle = \begin{pmatrix} 0 \\ \mathfrak{Im}\ (\rho_{00} + \rho_{11}e^{\imath\phi}) \\ \mathfrak{Re}\ (\rho_{00} + \rho_{11}e^{\imath\phi}) \end{pmatrix} = \begin{pmatrix} 0 \\ \rho_{11}\sin\phi \\ \rho_{00} + \rho_{11}\cos\phi \end{pmatrix} .$$

c. If $U = X$ is the inversion of a qubit, we find,

$$\langle\vec{\hat{\sigma}}_1\rangle = \begin{pmatrix} 0 \\ -\mathfrak{Im}\ (\rho_{01} + \rho_{10}) \\ \mathfrak{Re}\ (\rho_{01} + \rho_{10}) \end{pmatrix} = \begin{pmatrix} 0 \\ 0 \\ \rho_{01} + \rho_{10} \end{pmatrix} .$$

41.6.6.14 Ex: Heisenberg-limited quantum sensing

This exercise aims at showing that entangled qubits allow for phase measurements beyond the standard quantum limit. Proceed as follows:
a. Express standard Ramsey interferometry for a single qubit as a sequence of quantum gates and calculate the uncertainty of the final Bloch vector component $\Delta\hat{S}_z/||\hat{S}_z||$.
b. Repeat (a) with a product state of two qubits.
c. Plot the relative uncertainty of the inversion $(\Delta\hat{S}_z^2/\langle\hat{S}_z^2\rangle)^{1/2}$ after the Ramsey cycle as a function of the precession phase for the cases (a) and (b), as well as the spin squeezing parameter $\sqrt{N}\langle\Delta\hat{S}_y\rangle/|\langle\hat{S}_z\rangle|$ [1380, 343].
d. Repeat (b) with two entangled qubits and interpret your observations.

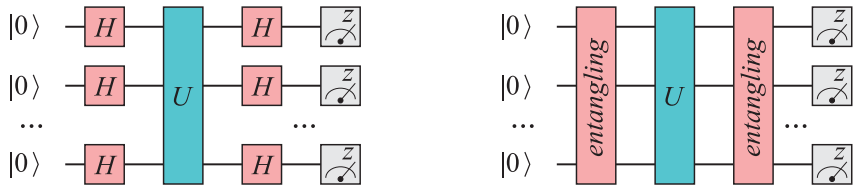

Figure 41.40: Scheme for Heisenberg-limited quantum sensing.

Solution: *a. Using the definitions of the Hadamard gate and the phase shift gate, Ramsey interferometry with a single qubit,*

$$H = \tfrac{1}{\sqrt{2}}\begin{pmatrix} 1 & 1 \\ 1 & -1 \end{pmatrix} \quad , \quad U = \begin{pmatrix} e^{\imath\varphi/2} & 0 \\ 0 & e^{-\imath\varphi/2} \end{pmatrix} \ ,$$

we easily see, with $M \equiv HUH$,

$$\hat{\rho}_f = M|0\rangle\langle 0|M^\dagger = \begin{pmatrix} \cos^2\frac{\varphi}{2} & -\imath\cos\frac{\varphi}{2}\sin\frac{\varphi}{2} \\ \imath\cos\frac{\varphi}{2}\sin\frac{\varphi}{2} & \sin^2\frac{\varphi}{2} \end{pmatrix} \ .$$

This allows us to calculate,

$$\langle\hat{\mathbf{S}}\rangle = \tfrac{1}{2}\langle\vec{\hat{\sigma}}\rangle = \tfrac{1}{2}\,Tr\,\hat{\rho}_f\begin{pmatrix}\hat{\sigma}_x \\ \hat{\sigma}_y \\ \hat{\sigma}_z\end{pmatrix} = \tfrac{1}{2}\begin{pmatrix} 0 \\ \sin\varphi \\ \cos\varphi \end{pmatrix}$$

$$\langle\hat{S}_\alpha^2\rangle = \tfrac{1}{4}\,Tr\,\hat{\rho}_f\hat{\sigma}_\alpha^2 = \tfrac{1}{4} \quad for \quad \alpha = x, y, z$$

$$\Delta\hat{S}_\alpha^2 = \tfrac{1}{4}\begin{cases} 1 & for \quad \alpha = x \\ \cos^2\varphi & for \quad \alpha = y \\ \sin^2\varphi & for \quad \alpha = z \end{cases} \ ,$$

so that $\|\langle\mathbf{S}\rangle\| = \frac{1}{2}$ *and* $\langle\hat{S}_x^2\rangle + \langle\hat{S}_y^2\rangle + \langle\hat{S}_z^2\rangle = \frac{3}{4} = S(S+1)$. *The relative uncertainty of the inversion and the spin squeezing parameter are, respectively,*

$$\sqrt{\frac{\Delta\hat{S}_z^2}{\langle\hat{S}_z^2\rangle}} = \sin\varphi \qquad and \qquad \frac{\sqrt{N}\langle\Delta\hat{S}_y\rangle}{|\langle\hat{S}_z\rangle|} = 1 \ .$$

b. For two qubits, the same calculation with $M \equiv (H \otimes H)(U \otimes U)(H \otimes H)$ *and* $\hat{\rho}_f = M|0\rangle\langle 0|M^\dagger$ *allows us to calculate (with the help of MAPLE),*

$$\langle \hat{\mathbf{S}} \rangle = \tfrac{1}{2}\langle \vec{\hat{\sigma}} \otimes \mathbb{I} + \mathbb{I} \otimes \vec{\hat{\sigma}} \rangle = \tfrac{1}{2}\, Tr\, \hat{\rho}_f \begin{pmatrix} \hat{\sigma}^x \\ \hat{\sigma}^y \\ \hat{\sigma}^z \end{pmatrix} \otimes \mathbb{I} + \tfrac{1}{2}\, Tr\, \hat{\rho}_f \mathbb{I} \otimes \begin{pmatrix} \hat{\sigma}^x \\ \hat{\sigma}^y \\ \hat{\sigma}^z \end{pmatrix} = \begin{pmatrix} 0 \\ \sin\varphi \\ \cos\varphi \end{pmatrix}$$

$$\langle \hat{S}_\alpha^2 \rangle = \tfrac{1}{4}\, Tr\, \hat{\rho}_f [\hat{\sigma}_\alpha \otimes \mathbb{I} + \mathbb{I} \otimes \hat{\sigma}_\alpha]^2 = \tfrac{1}{2} \begin{cases} 1 & for \;\; \alpha = x \\ 2 - \cos^2\varphi & for \;\; \alpha = y \\ 1 + \cos^2\varphi & for \;\; \alpha = z \end{cases}$$

$$\Delta \hat{S}_\alpha^2 = \tfrac{1}{2} \begin{cases} 1 & for \;\; \alpha = x \\ \cos^2\varphi & for \;\; \alpha = y \\ \sin^2\varphi & for \;\; \alpha = z \end{cases} ,$$

so that $\|\langle \mathbf{S} \rangle\| = 1$ *and* $\langle \hat{S}_x^2 \rangle + \langle \hat{S}_y^2 \rangle + \langle \hat{S}_z^2 \rangle = 2 = S(S+1)$. *The relative uncertainty of the inversion is,*

$$\sqrt{\frac{\Delta \hat{S}_z^2}{\langle \hat{S}_z^2 \rangle}} = \frac{\sin\varphi}{\sqrt{1 + \cos^2\varphi}} \qquad and \qquad \frac{\sqrt{N}\langle \Delta \hat{S}_y \rangle}{|\langle \hat{S}_z \rangle|} = 1 \; .$$

c. Fig. 41.41(a) shows the relative uncertainty of the inversion (dotted) for the cases (a) and (b), as well as numerical calculation for the cases of up to 4 qubits.

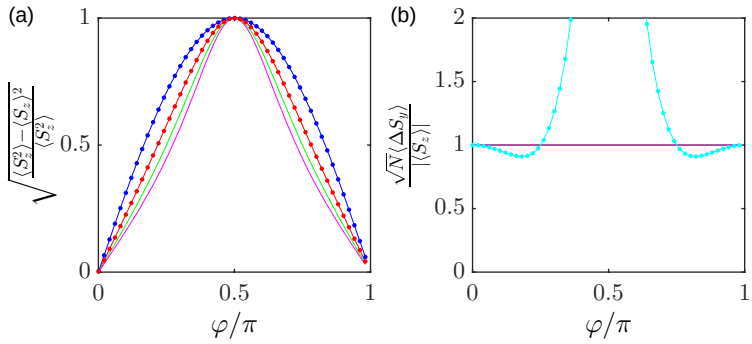

Figure 41.41: (code) (a) Relative uncertainty of the z-component as a function of the precession angle φ for various numbers of non-entangled qubits analytically (dots) and numerically (solid). (b) Metrology squeezing parameter.

d. For two entangled qubits, we replace the two-qubit Hadamard gate $H \otimes H$, *corresponding to a Ramsey pulse, by the entangling gate* $(H_1 \otimes \mathbb{I})\overset{c}{X}_{10}(H_1 \otimes \mathbb{I})$, *that is,*

$$M = (H_1 \otimes \mathbb{I})\overset{c}{X}_{10}(H_1 \otimes \mathbb{I})\; (U \otimes U)\; (H_1 \otimes \mathbb{I})\overset{c}{X}_{10}(H_1 \otimes \mathbb{I}) \; .$$

We again calculate $\hat{\rho}_f = M|0\rangle\langle 0|M^\dagger$ *and obtain,*

$$\langle \hat{\mathbf{S}} \rangle = \tfrac{1}{2}\langle \vec{\hat{\sigma}} \otimes \mathbb{I} + \mathbb{I} \otimes \vec{\hat{\sigma}} \rangle = \tfrac{1}{2}\, Tr\, \hat{\rho}_f \begin{pmatrix} \hat{\sigma}^x \\ \hat{\sigma}^y \\ \hat{\sigma}^z \end{pmatrix} \otimes \mathbb{I} + \tfrac{1}{2}\, Tr\, \hat{\rho}_f \mathbb{I} \otimes \begin{pmatrix} \hat{\sigma}^x \\ \hat{\sigma}^y \\ \hat{\sigma}^z \end{pmatrix} = \begin{pmatrix} 0 \\ \sin\varphi\cos\varphi \\ \cos\varphi \end{pmatrix}$$

$$\langle \hat{S}_\alpha^2 \rangle = \tfrac{1}{4}\, Tr\, \hat{\rho}_f [\hat{\sigma}_\alpha \otimes \mathbb{I} + \mathbb{I} \otimes \hat{\sigma}_\alpha]^2 = \tfrac{1}{2} \begin{cases} 2 - \cos^2\varphi & for \quad \alpha = x \\ 1 & for \quad \alpha = y \\ 1 + \cos^2\varphi & for \quad \alpha = z \end{cases}$$

$$\Delta \hat{S}_\alpha^2 = \tfrac{1}{2} \begin{cases} 2 - \cos^2\varphi & for \quad \alpha = x \\ 1 - 2\sin^2\varphi\cos^2\varphi & for \quad \alpha = y \\ 1 - \cos^2\varphi & for \quad \alpha = z \end{cases} .$$

The relative uncertainty of the inversion is,

$$\sqrt{\frac{\Delta \hat{S}_z^2}{\langle \hat{S}_z^2 \rangle}} = \sin\varphi \qquad and \qquad \frac{\sqrt{N}\langle \Delta \hat{S}_y \rangle}{|\langle \hat{S}_z \rangle|} = \frac{\sqrt{1 - 2\cos^2\phi \sin^2\phi}}{|\cos\phi|} .$$

In Fig. 41.41(b) we observe a reduce of the spin squeezing parameter below the classical limit. For example, for $\varphi = \pi/8$ *we get* 0.94.

41.7 Further reading

41.7.1 on collective spin states

R.H. Dicke, *Coherence in Spontaneous Radiation Processes* [366]DOI

D. Gottesman et al., *Encoding a qubit in an oscillator* [530]DOI

K. Baumann et al., *Dicke quantum phase transition with a superfluid gas in an optical cavity* [105]DOI

B.M. Garraway, *The Dicke model in quantum optics: Dicke model revisited* [492]DOI

W. Guerin, *Subradiance in a Large Cloud of Cold Atoms* [555]DOI

M. Gegg et al., *Superradiant to subradiant phase transition in the open system Dicke model: dark state cascades* [498]DOI

P. Kirton et al., *Introduction to the Dicke Model: From Equilibrium to Nonequilibrium, and Vice Versa* [723]DOI

M. Reitz et al., *Cooperative Quantum Phenomena in Light-Matter Platforms* [1090]DOI

B. Koczor et al., *Continuous phase-space representations for finite-dimensional quantum states and their tomography* [732]DOI

J. Davis et al., *Wigner negativity in spin-j systems* [328]DOI

S. Omanakuttan et al., *Spin-squeezed Gottesman-Kitaev-Preskill codes for quantum error correction in atomic ensembles* [972]DOI

41.7.2 on spin squeezing

M. Kitagawa et al., *Spin-squeezed states* [724]DOI

D.J. Wineland et al., *Squeezed atomic states and projection noise in spectroscopy* [1380]DOI

Ph. Bouyer et al., *Heisenberg-Limited Spectroscopy with Degenerate Bose-Einstein Gases* [184]DOI

G. Co et la., *Analytical and numerical analysis of the complete Lipkin-Meshkov-Glick Hamiltonian* [272]DOI

I.D. Leroux et al., *Implementation of Cavity Squeezing of a Collective Atomic Spin* [793]DOI

M. Schleier-Smith et al., *Squeezing the collective spin of a dilute atomic ensemble by cavity feedback* [1162]DOI

L. Salvi et al., *Squeezing on Momentum States for Atom Interferometry* [1135]DOI

Zilong Chen et al., *Conditional Spin Squeezing of a Large Ensemble via the Vacuum Rabi Splitting* [251]DOI

J.G. Bohnet et al., *A steady-state superradiant laser with less than one intracavity photon* [162]DOI

J.G. Bohnet et al., *Reduced spin measurement back-action for a phase sensitivity ten times beyond the standard quantum limit* [163]DOI

K. Cox et al., *Deterministic Squeezed States with Collective Measurements and Feedback* [309]DOI

B. Braverman et al., *Near-Unitary Spin Squeezing in 171Yb* [192]DOI

E. Pedrozo-Penafiel et al., *Entanglement on an optical atomic-clock transition* [940]DOI

S. Colombo et al., *Time-reversal-based quantum metrology with many-body entangled states* [286]DOI

S. Colombo et al., *Entanglement-Enhanced Optical Atomic Clocks* [287]DOI

Zeyang Li et al., *Collective Spin-Light and Light-Mediated Spin-Spin Interactions in an Optical Cavity* [799]DOI

41.7.3 on superradiant lasing

M. Tavis et al., *Exact solution for an N-molecule-radiation-field Hamiltonian* [1293]DOI

J. Krause et al., *Quantum theory of the micromaser: Symmetry breaking via off-diagonal atomic injection* [752]DOI

A.F. Huss et al., *Phase Correlation of Laser Waves with Arbitrary Frequency Spacing* [643]DOI

B.M. Peden et al., *Nondestructive cavity QED probe of Bloch oscillations in a gas of ultracold atoms* [1005]DOI

D. Meiser et al., *Prospects for a Millihertz-Linewidth Laser* [868]DOI

Th. Maier et al., *A superradiant clock laser on a magic wavelength optical lattice* [835]DOI

M.A. Norcia et al., *Strong coupling on a forbidden transition in strontium and non-destructive atom counting* [958]DOI

M.A. Norcia et al., *Superradiance on the millihertz linewidth strontium clock transition* [959]DOI

M.A. Norcia et al., *Cold-Strontium Laser in the Superradiant Crossover Regime* [957]DOI

M.A. Norcia et al., *Cavity-mediated collective spin-exchange interactions in a strontium superradiant laser* [956]DOI

Zhang Yuan et al., *Monte-Carlo simulations of superradiant lasing* [1429]DOI

K. Debnath et al., *Lasing in the superradiant crossover regime* [341]DOI

A. Bychek et al., *Superradiant lasing in inhomogeneously broadened ensembles with spatially varying coupling* [226]DOI

M. Reitz et al., *Cooperative Quantum Phenomena in Light-Matter Platforms* [1090]DOI

41.7.4 on entanglement

A. Einstein et al., *Can quantum-mechanical description of physical reality be considered complete* [411]DOI

J.S. Bell et al., *On the Einstein-Podolsky-Rosen paradox* [114]DOI

A. Aspect, *Experimental Test of Bell's Inequality Using Time-Varying Analyzers* [58]DOI

S.J. van Enk, *Single-particle entanglement* [1326]DOI

K. Gietka et al., *Quantum-enhanced interferometry with cavity QED-generated non-classical light* [509]DOI

41.7.5 on quantum information

S. Aaronson et al., *The computational complexity of linear optics* [1]DOI

H. Azuma, *Quantum computation with the Jaynes-Cummings model* [64]DOI

S.D. Bartlett et al., *Efficient Classical Simulation of Continuous Variable Quantum Information Processes* [102]DOI

M. Bindhani et al., *Quantum simulation of Jaynes-Cummings model on IBM Q-system* [145]DOI

V.K. Jain et al., *Quantum Simulation of Discretized Harmonic Oscillator on IBM Quantum Computer* [660]DOI

S. Sefi et al., *How to Decompose Arbitrary Continuous-Variable Quantum Operations* [1185]DOI

P. Sundsoy et al., *Quantum Computing, Linear optics implementations* [1278]DOI

IBM, *Quantum computing* http

Wikipedia, *Quantum Fourier transform* http

C.S. Hamilton et al., *Gaussian boson sampling* [578]DOI

N. Quesada et al., *Gaussian boson sampling using threshold detectors* [1063]DOI

Han-Sen Zhong et al., *Quantum computational advantage using photons* [1432]DOI

41.7.6 on quantum computing

I. Pogorelov et al., *Compact Ion-Trap Quantum Computing Demonstrator* [1042]DOI

T. Manovitz et al., *Trapped-Ion Quantum Computer with Robust Entangling Gates and Quantum Coherent Feedback* [840]DOI

Chapter 42

Atomic motion in optical cavities

In the preceding chapter we concentrated on the dynamics of the field modes of laser-pumped cavities. We devoted a particular attention to the role of scatterers, e.g. atoms, located in the mode volume and coupling the dynamics of counterpropagating modes. We assumed the atoms to be fixed in space, or at most subject to an external force constraining their motion. We have also seen that the coupling of counterpropagating modes critically depends on the position of the atom. Now, the cavity fields are expected to exert light forces on the atoms eventually leading to their displacement. As we will see in the following, this fact can have enormous impact on the coupling dynamics and even induce macroscopic instabilities.

We devote Sec. 42.1 to the derivation of the complete equations of motion for the case of a single atom, allowing for all degrees of freedom to be treated as quantized: the atomic excitation, the motion of its center of mass, and the radiation field in the cavity. We will provide a simple recipe for finding the suitable equations of motion depending on which degree of freedom s to be treated as quantized and which dissipation process to be taken into account. We will also show how and under which circumstances the atomic excitation may be adiabatically eliminated.

In Sec. 42.2 we generalize the equations of motion of many atoms, but treating all degrees of freedom as classical. This leads us to the paradigmatic Collective Atomic Recoil Laser (CARL), a self-organization phenomenon whose relationship to other such instabilities will be discussed in Sec. 42.3.

Finally, in Secs. 42.4 and 42.5 we will treat the light field, respectively, the atomic motion quantum mechanically and show in which sense the obtained dynamics are different.

42.1 Cavity interacting with a single atom

Here, we consider atoms interacting with the modes of an optical cavity pumped by lasers. As we saw in the previous chapter, the density of the modes in a cavity is concentrated around the optical axis, such that a scatterer located within the mode emits preferentially within the cavity, where the light is recycled. Therefore, we can in many situations treat the system as one-dimensional.

In free space, as discussed in Chp. 38, the force of light has two components: the radiation pressure, which scatters photons isotropically into space, and the dipole

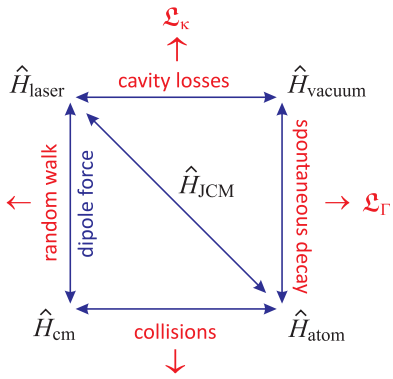

Figure 42.1: Hamiltonian in quantum optics.

force, which can be interpreted in terms of a redistribution of photons between light modes. In cavities, where the isotropic scattering is much reduced, radiative pressure can often be neglected. In contrast, if light is tuned away from atomic resonances, the atom will feel a dipole force originating from the backscattering of photons between counterpropagating modes.

42.1.1 Linear and ring cavities

We must distinguish two types of cavities with very different behaviors: The linear cavity or (*Fabry-Pérot etalon*), where counterpropagating modes form a single mode, and the ring cavity, where counterpropagating modes have independent photon budgets.

For a *linear cavity*, boundary conditions imposed by the surfaces of the cavity mirrors determine the possible spatial mode functions, which are necessarily standing waves. The amplitudes of the electric field are in second quantization (35.8),

$$\hat{\mathcal{E}}(z,t) = \hat{\mathcal{E}}^+(z,t)e^{-\imath\omega t} + \hat{\mathcal{E}}^-(z,t)e^{\imath\omega t} \qquad (42.1)$$
$$\text{with} \quad \hat{\mathcal{E}}^+(z,t) = \hat{\mathcal{E}}_1\hat{a}(t)e^{\imath kz} = (\hat{\mathcal{E}}^-(z,t))^\dagger \ .$$

with $[\hat{a},\hat{a}^\dagger] = 1$. With this we obtain, for a single atom coupled to the mode of the cavity pumped by a laser, within the dipolar approximation and the RWA [1], the following relevant contributions to the Hamiltonian ($\hbar = 1$),

$$\begin{aligned} \hat{H}_{atom} &= -\Delta_a\hat{\sigma}^+\hat{\sigma}^- + \tfrac{\hat{p}^2}{2m} \qquad (42.2)\\ \hat{H}_{cav} &= -\Delta_c\hat{a}^\dagger\hat{a} \\ \hat{H}_{atom:cav} &= g\hat{a}^\dagger\hat{\sigma}^- e^{-\imath k\hat{z}} + h.c. \\ \hat{H}_{laser:cav} &= \imath\eta\hat{a}^\dagger + h.c. \ , \end{aligned}$$

neglecting the dynamics of the pump field, which is supposed to be classical, $\eta = \delta_{fsr}\langle\hat{a}_{in}^\dagger\rangle$. Note that the propagator $e^{-\imath\hat{H}_{laser:cav}t}$ corresponds to a coherent state

[1] For the transformation into the rotating frame see the derivation of Sec. 34.4.2.

displacement operator. Δ_a is the detuning between the light and the atomic resonance, Δ_c between the light and cavity resonance and g is the light-atom coupling force, also called the single-photon Rabi frequency. Neglecting the kinetic energy term $\hat{p}^2/2m$, the photonic recoil $e^{-\imath k v \hat{z}}$, and the pumping η we recover the *Jaynes-Cummings model*. Do the Excs. 42.1.7.1 and 42.1.7.2.

For a *ring cavity*, we must distinguish the counterpropagating modes $\hat{a}_\pm$,

$$\hat{\mathcal{E}}^+(z,t) = \hat{\mathcal{E}}_1 \hat{a}_+(t) e^{\imath k z} + \hat{\mathcal{E}}_1 \hat{a}_-(t) e^{-\imath k z} = (\hat{\mathcal{E}}^-(z,t))^\dagger \ . \tag{42.3}$$

such that the total Hamiltonian $\hat{H}$ consists of the following parts [2],

$$\boxed{\begin{aligned} \hat{H}_{atom} &= \hat{H}_{electron} + \hat{H}_{motion} = -\Delta_a \hat{\sigma}^+ \hat{\sigma}^- + \frac{\hat{p}^2}{2m} \\ \hat{H}_{cav} &= -\Delta_c \hat{a}_+^\dagger \hat{a}_+ - \Delta_c \hat{a}_-^\dagger \hat{a}_- \\ \hat{H}_{atom:cav} &= g \hat{a}_+^\dagger \hat{\sigma}^- e^{-\imath k \hat{z}} + h.c. + g \hat{a}_-^\dagger \hat{\sigma}^- e^{\imath k \hat{z}} + h.c. \\ \hat{H}_{laser:cav} &= -\imath \eta_+ (\hat{a}_+ - \hat{a}_+^\dagger) - \imath \eta_- (\hat{a}_- - \hat{a}_-^\dagger) \end{aligned}} \ . \tag{42.4}$$

We identify the degrees of freedom of the system through the quantum observables appearing in the Hamiltonian: the counterpropagating modes of light with the amplitudes ($\hat{a}_\pm$), the internal degrees of freedom ($\hat{\sigma}^z, \hat{\sigma}^\pm$), and the spatial coordinates of the atom ($\hat{z}, \hat{p}$).

In contrast to linear cavities, ring cavities have the following particularities: 1. The phase of the standing wave is free to move; 2. the counterpropagating modes of the cavity have independent photon budgets, each backscattering event conserves momentum; 3. the backscattering acts on the phase of the standing wave. Atoms can be trapped by the dipole force within the cavity mode volume. The dipole force corresponds to a backscattering of photons between modes.

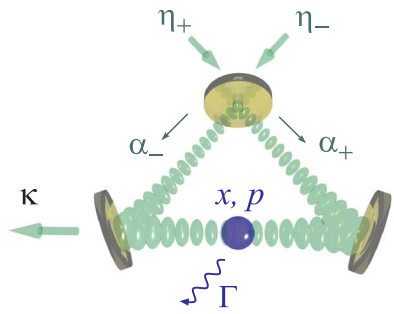

Figure 42.2: Scheme of an atom interacting with a ring cavity showing the relevant degrees of freedom ($\hat{x}$, $\hat{p}$, $\hat{a}_\pm$) and the possible decay processes (κ, Γ) for the derivation of the field equations.

[2] Throughout this chapter we will sometimes emphasize the motional degree of freedom in green color, photonic states in blue, electronic excitation states in pink.

42.1.2 Eliminating spontaneous emission and cavity decay

In fact, there are more degrees of freedom involved in the dynamics of atoms moving in a laser-pumped ring cavity, because of the atoms may scatter light into directions other than the cavity modes by spontaneous emission, and the cavity modes may decay by transmission through the mirrors. Therefore, we need to treat the respective vacuum field modes receiving the photons, $\hat{a}_{\mathbf{k}}$ and $\hat{a}_{\omega}$, quantum mechanically and include the respective Hamiltonians,

$$\begin{aligned} \hat{H}_{atom:vacuum} &= \sum_{\mathbf{k}} g_{atom:vacuum} \hat{a}^{\dagger}_{\mathbf{k}} \hat{\sigma}^{-} e^{-\imath \mathbf{k}\cdot\hat{\mathbf{r}}} + h.c. \\ \hat{H}_{cav:bath} &= \sum_{\omega} g_{cav:bath} \hat{a}^{\dagger}_{\omega} \hat{a}_{+} + g_{cav:bath} \hat{a}^{\dagger}_{\omega} \hat{a}_{-} + h.c. \ , \end{aligned} \tag{42.5}$$

in the description of the coupled dynamics. Here, $g_{atom:vacuum}$ denotes the vacuum Rabi frequency, that is, the coupling strength between the atomic dipole and the electromagnetic vacuum into which spontaneously emitted photons may escape. On the other hand, $g_{cav:bath}$ denotes the coupling strength between the cavity mode and the spectrum of electromagnetic modes into which cavity photons can escape and which we will from now on call *heat bath* to facilitate its semantic distinction from the spontaneous vacuum. The total density operator, the Hamiltonian and the equation of motion are, consequently,

$$\begin{aligned} \bar{\rho} &= \hat{\rho}_{atom} \otimes \hat{\rho}_{electron} \otimes \hat{\rho}_{cav} \otimes \hat{\rho}_{vacuum} \otimes \hat{\rho}_{bath} \\ \bar{H} &= \hat{H}_{motion} + \hat{H}_{electron} + \hat{H}_{cav} + \hat{H}_{atom:cav} + \hat{H}_{laser:cav} + \hat{H}_{atom:vacuum} + \hat{H}_{cav:bath} \\ \dot{\bar{\rho}} &= -\imath[\bar{H}, \bar{\rho}] \ . \end{aligned} \tag{42.6}$$

With the inclusion of the vacuum field modes $\hat{a}_{\omega}$ and $\hat{a}_{\mathbf{k}}$ the number of degrees of freedom to be treated literally explodes, and we have to find a way to eliminate them from the equation of motion. We do this by partially tracing the density operator over the vacuum field modes using the Weisskopf-Wigner theory,

$$\tilde{\rho} \equiv \mathrm{Tr}_{vacuum} \ \mathrm{Tr}_{bath} \ \bar{\rho} = \hat{\rho}_{atom} \otimes \hat{\rho}_{electron} \otimes \hat{\rho}_{cav} \ . \tag{42.7}$$

This allows us to reduce the Hamiltonian $\hat{H} = \bar{H} - \hat{H}_{atom:vacuum} - \hat{H}_{cav:bath}$. The price to pay is, that the equation of motion for this receives dissipative terms: The Liouville equation turns into a *master equation* with the following form,

$$\boxed{\begin{aligned} \dot{\hat{\rho}} = -\imath[\hat{H}, \hat{\rho}] \quad &+ \quad \mathcal{L}_{atom:vacuum} + \mathcal{L}_{cav:vacuum,+} + \mathcal{L}_{cav:vacuum,-} \\ \mathcal{L}_{atom:vacuum}\hat{\rho}(t) \quad &= \quad -\gamma\{\hat{\sigma}^{+}\hat{\sigma}^{-}\hat{\rho}(t) - 2\hat{\sigma}^{-}\hat{\rho}(t)\hat{\sigma}^{+} + \hat{\rho}(t)\hat{\sigma}^{+}\hat{\sigma}^{-}\} \\ \mathcal{L}_{cav:bath,\pm}\hat{\rho}(t) \quad &= \quad -\kappa\{\hat{a}^{\dagger}_{\pm}\hat{a}_{\pm}\hat{\rho}(t) - 2\hat{a}_{\pm}\hat{\rho}(t)\hat{a}^{\dagger}_{\pm} + \hat{\rho}(t)\hat{a}^{\dagger}_{\pm}\hat{a}_{\pm}\} \end{aligned}} \ , \tag{42.8}$$

where $\hat{H}$ is the Hamiltonian from (42.4). We see that each degree of freedom has its own loss mechanism. κ for the finite transmission of the resonator mirrors [283, 488] [3], Γ for the spontaneous emission, and γ_{frc}, when we exert a frictional force on the atoms.

[3] Here, we only consider cavity decay into a zero temperature reservoir without quantum phase fluctuations.

42.1.2.1 The problem with spontaneous emission in cavities

The above treatment still is incomplete, if we regard $\hat{\rho}$ as the atomic Bloch vector. The reason is that we know what the dissipative Lindbladt terms $\mathcal{L}_{vacuum}\tilde{\rho}$ generated by spontaneous emission look like for the atomic excitation $\hat{\rho}_{atom}$, but the Hamiltonian $\hat{H}_{atom:vacuum}$ also *contains the motional degree of freedom* $e^{-\imath\mathbf{k}\cdot\hat{\mathbf{r}}}$, which is intrinsically three-dimensional. That is, the dissipative terms also need to describe, how the motion diffuses in momentum space.

The inclusion of dissipative terms, however, is difficult, because unavoidable photonic recoil violates the supposed one-dimensionality of the atomic motion along the optical axis. Omnidirectional photonic recoil is also incompatible with the assumption that the momentum is quantized in multiples of $2\hbar k$ in the direction of the optical axis. And finally, if we consider degenerate matter waves, photonic recoil will eject atoms from a BEC. Even if, neglecting the emission process, we only consider absorption, we would need a quantization in multiples of $1\hbar k$ instead of $2\hbar k$. In the following, in order to keep the problem 1D, we will neglect momentum diffusion, i.e. we consider the simplified Hamiltonian $\tilde{H}$ and discard motional terms from the term $\mathcal{L}_{vacuum}\hat{\rho}$.

42.1.2.2 Quantum derivation of the CARL equations

To obtain the equations of motion we insert the Hamiltonian (42.4) into the equations for the field operators, for which the following commutation rules hold, $[\hat{a}_\pm, \hat{a}_\pm^\dagger] = 1$ and $[\hat{a}_\pm, \hat{a}_\mp^\dagger] = 0 = [\hat{a}_\pm, \hat{a}_\pm]$,

$$\begin{aligned}\dot{\hat{a}}_+ &= \imath[\hat{H}, \hat{a}_+] - \kappa\hat{a}_+ \\ &= -\imath\Delta_c[\hat{a}_+^\dagger\hat{a}_+, \hat{a}_+] + \imath g e^{-\imath k\hat{z}}\hat{\sigma}^-[\hat{a}_+^\dagger, \hat{a}_+] + \imath g e^{\imath k\hat{z}}\hat{\sigma}^+[\hat{a}_+, \hat{a}_+] + \eta_+[\hat{a}_+ - \hat{a}_+^\dagger, \hat{a}_+] - \kappa\hat{a}_+ \\ &= (-\kappa + \imath\Delta_c)\hat{a}_+ - \imath g\hat{\sigma}^- e^{-\imath kx} + \eta_+ \ ,\end{aligned} \tag{42.9}$$

and similarly for $\hat{a}_-$. For the Pauli deexcitation matrix, using the usual commutation rules for the *Pauli spin matrices* (23.47), that is $[\hat{\sigma}^+, \hat{\sigma}^-] = \hat{\sigma}_z$, $\hat{\sigma}_z\hat{\sigma}^\pm = \pm\hat{\sigma}^\pm$, and $[\hat{\sigma}^-, \hat{\sigma}^-] = 0$, we calculate,

$$\begin{aligned}\dot{\hat{\sigma}}^- &= \imath[\hat{H}, \hat{\sigma}^-] - \gamma\hat{\sigma}^- \\ &= -\imath\Delta_a[\hat{\sigma}^+\hat{\sigma}^-, \hat{\sigma}^-] + \imath g e^{\imath k\hat{z}}\hat{a}_+[\hat{\sigma}^+, \sigma^-] + \imath g e^{-\imath k\hat{z}}\hat{a}_-[\hat{\sigma}^+, \sigma^-] - \gamma\hat{\sigma}^- \\ &= (-\gamma + \imath\Delta_a)\hat{\sigma}^- + \imath g e^{\imath k\hat{z}}\hat{a}_+\hat{\sigma}_z + \imath g e^{-\imath k\hat{z}}\hat{a}_-\hat{\sigma}_z \ .\end{aligned} \tag{42.10}$$

For the Pauli inversion matrix, using the following commutation rules, $[\hat{\sigma}_z, \hat{\sigma}^+\hat{\sigma}^+] = 0$ and $[\hat{\sigma}_z, \hat{\sigma}^\pm] = \pm 2\hat{\sigma}^\pm$, we calculate,

$$\begin{aligned}\dot{\hat{\sigma}}_z &= \imath[\hat{H}, \hat{\sigma}_z] - 2\gamma - 2\gamma\hat{\sigma}_z \\ &= \imath g e^{-\imath k\hat{z}}\hat{a}_+^\dagger[\hat{\sigma}^-, \hat{\sigma}_z] + \imath g e^{\imath k\hat{z}}\hat{a}_-^\dagger[\hat{\sigma}^-, \hat{\sigma}_z] + \imath g e^{\imath k\hat{z}}\hat{a}_+[\hat{\sigma}^+, \hat{\sigma}_z] + \imath g e^{-\imath k\hat{z}}\hat{a}_-[\hat{\sigma}^+, \hat{\sigma}_z] - 2\gamma\hat{\sigma}_z \\ &= -2\gamma - 2\gamma\hat{\sigma}_z + 2\imath g e^{-\imath k\hat{z}}\hat{a}_+^\dagger\hat{\sigma}^- + 2\imath g e^{\imath k\hat{z}}\hat{a}_-^\dagger\hat{\sigma}^- - 2\imath g e^{\imath k\hat{z}}\hat{a}_+\hat{\sigma}^+ - 2\imath g e^{-\imath k\hat{z}}\hat{a}_-\hat{\sigma}^+ \ .\end{aligned} \tag{42.11}$$

Finally, we need to derive the equations governing the motion of atoms. For the position we obtain,

$$\dot{\hat{z}} = \imath[\hat{H}, \hat{z}] = \imath[\tfrac{\hat{p}^2}{2m}, \hat{z}] = \tfrac{1}{m}\hat{p} \ . \tag{42.12}$$

In order to calculate the momentum, we need to do a small auxiliary calculation. With the commutator $[\hat{z},\hat{p}] = \imath$ we derive,

$$[\hat{z}^n,\hat{p}] = \imath\frac{\delta\hat{z}^n}{\delta\hat{z}} = \imath n\hat{z}^{n-1} \tag{42.13}$$
$$[e^{\imath k\hat{z}},\hat{p}] = \sum_{n=0}^{\infty}\frac{(\imath k)^n}{n!}[\hat{z}^n,\hat{p}] = -k\sum_{n=0}^{\infty}\frac{(\imath k)^{n-1}}{(n-1)!}\hat{z}^{n-1} = -ke^{\imath k\hat{z}} \ ,$$

and with this result,

$$\begin{aligned}\dot{\hat{p}} &= \imath[\hat{H},\hat{p}] \\ &= \imath g\hat{a}_+^\dagger\hat{\sigma}^-[e^{-\imath k\hat{z}},\hat{p}] + c.c. + \imath g\hat{a}_-^\dagger\hat{\sigma}^-[e^{\imath k\hat{z}},\hat{p}] + c.c. \\ &= -\imath gk\hat{a}_+^\dagger\hat{\sigma}^-e^{-\imath k\hat{z}} + c.c. + \imath gk\hat{a}_-^\dagger\hat{\sigma}^-e^{\imath k\hat{z}} + c.c. \ .\end{aligned} \tag{42.14}$$

The *quantum Langevin equations* [283] describing the dynamics of the internal and external degrees of freedom of the atom and the field are coupled,

$$\boxed{\begin{aligned}\dot{\hat{a}}_\pm &= (-\kappa+\imath\Delta_c)\hat{a}_\pm - \imath g\hat{\sigma}^-e^{\mp\imath k\hat{z}} + \eta_\pm \\ \dot{\hat{\sigma}}^- &= (-\gamma+\imath\Delta_a)\hat{\sigma}^- + \imath g(e^{\imath k\hat{z}}\hat{a}_+ + e^{-\imath kz}\hat{a}_-)\hat{\sigma}_z \\ \dot{\hat{\sigma}}_z &= -2\gamma\hat{\sigma}_z + 2\imath g(e^{-\imath k\hat{z}}\hat{a}_+^\dagger + e^{\imath k\hat{z}}\hat{a}_-^\dagger)\hat{\sigma}^- - 2\imath g(e^{\imath k\hat{z}}\hat{a}_+ + e^{-\imath k\hat{z}}\hat{a}_-)\hat{\sigma}^+ \\ \dot{\hat{z}} &= \hat{p}/m \\ \dot{\hat{p}} &= \imath g\hbar k\hat{\sigma}^-(\hat{a}_+^\dagger e^{-\imath k\hat{z}} - \hat{a}_-^\dagger e^{\imath k\hat{z}}) + c.c.\end{aligned}} \ . \tag{42.15}$$

We may also verify,

$$\begin{aligned}\dot{\hat{n}}_+ &= \imath[\hat{H},\hat{n}_+] \\ &= \imath[-\Delta_c\hat{a}_+^\dagger\hat{a}_+ + g\hat{a}_+^\dagger\hat{\sigma}^-e^{-\imath k\hat{z}} + g\hat{a}_+\hat{\sigma}^+e^{\imath k\hat{z}} - \imath\eta_+(\hat{a}_+ - \hat{a}_+^\dagger),\hat{a}_+^\dagger\hat{a}_+] \\ &= (\eta_+ - \imath ge^{-\imath k\hat{z}}\hat{\sigma}^-)\hat{a}_+^\dagger + (\eta_+ + \imath g\hat{\sigma}^+e^{\imath k\hat{z}})\hat{a}_+ \ ,\end{aligned} \tag{42.16}$$

and hence conservation of momentum,

$$[\hat{H},\hbar k(\hat{n}_+ - \hat{n}_-) - \hat{p}] = \hbar k\eta_+(\hat{a}_+^\dagger + \hat{a}_+) - \hbar k\eta_-(\hat{a}_-^\dagger + \hat{a}_-) \ , \tag{42.17}$$

in the absence of pumping, $\eta_+ = 0 = \eta_-$.

42.1.3 Adiabatic elimination of the excited state

Under certain conditions, however, the internal and external dynamics occur at very different time scales, which allows a decoupling of the differential equations [4]. When the light fields are very detuned from atomic resonances, $\Delta_a \gg \Gamma$, the internal dynamics of the atoms is very fast, that is, the internal state adapts very rapidly to the boundary conditions defined by the external state and the state of the light field.

[4] In good cavity the limit the degrees of freedom of atomic excitation $\hat{\sigma}^\pm$ drop out of the dynamics, in the bad cavity limit, the fields $\hat{a}^\pm$ drop out of the dynamics.

Therefore, the internal state has no separate dynamics of its own, and we can adiabatically eliminate the internal degrees of freedom. Thus, we can neglect correlations between degrees of freedom, $\langle \hat{a}_\pm \hat{\sigma}^\pm \rangle = \langle \hat{a}_\pm \rangle \langle \hat{\sigma}^\pm \rangle$ etc. [1016, 481]. The adiabatic elimination of the excited state comes down to treating the atom as a classical antenna.

We obtain the stationary solutions for $t \to \infty$ in the same way as for the optical Bloch equations [see Eq. (34.188)], assuming in Eq. (42.15),

$$\dot{\hat{\sigma}}^- = 0 = \dot{\hat{\sigma}}_z \tag{42.18}$$

where $\langle \hat{\sigma}^- \rangle = \rho_{21}$. Introducing the position-dependent Rabi frequency of the atom in the standing wave [5],

$$\hat{\Omega}(z) = 2g(e^{\imath k\hat{z}}\hat{a}_+ + e^{-\imath k\hat{z}}\hat{a}_-) \ , \tag{42.19}$$

we write,

$$\begin{aligned} 0 &= (-\gamma + \imath\Delta_a)\hat{\sigma}^- + \tfrac{1}{2}\imath\hat{\Omega}\hat{\sigma}_z \\ 0 &= -2\gamma - 2\gamma\hat{\sigma}_z + \imath\hat{\Omega}^\dagger\hat{\sigma}^- - \imath\hat{\Omega}\hat{\sigma}^+ \ . \end{aligned} \tag{42.20}$$

These equations are solved by,

$$\begin{aligned} \hat{\sigma}_z(\infty) &= \frac{-2(\gamma^2 + \Delta_a^2)}{2(\gamma^2 + \Delta_a^2) + \hat{\Omega}^\dagger\hat{\Omega}} \\ \text{and} \quad \hat{\sigma}^-(\infty) &= \frac{-\imath(\gamma + \imath\Delta_a)\hat{\Omega}}{2(\gamma^2 + \Delta_a^2) + \hat{\Omega}^\dagger\hat{\Omega}} \simeq \frac{-\imath(\gamma + \imath\Delta_a)}{2\Delta_a^2}\hat{\Omega} \ . \end{aligned} \tag{42.21}$$

Inserting the approximated expression for $\hat{\sigma}^-(\infty)$ into the equation of motion (42.15) for the light modes,

$$\begin{aligned} \dot{\hat{a}}_\pm &= (-\kappa + \imath\Delta_c)\hat{a}_\pm - \imath g\hat{\sigma}^-(\infty)e^{\mp\imath k\hat{z}} + \eta_\pm \\ &= \left(-\kappa + \imath\Delta_c - \frac{g^2\gamma}{\Delta_a^2} - \frac{\imath g^2}{\Delta_a}\right)\hat{a}_\pm - \left(\frac{g^2\gamma}{\Delta_a^2} + \frac{\imath g^2}{\Delta_a}\right)e^{\mp 2\imath k\hat{z}}\hat{a}_\mp + \eta_\pm \ , \end{aligned} \tag{42.22}$$

and for the atomic momentum,

$$\begin{aligned} \dot{\hat{p}} &= \imath g\hbar k\hat{\sigma}^-(\infty)(\hat{a}_+^\dagger e^{-\imath k\hat{z}} - \hat{a}_-^\dagger e^{\imath k\hat{z}}) - \imath g\hbar k\hat{\sigma}^+(\infty)(\hat{a}_+ e^{\imath k\hat{z}} - \hat{a}_- e^{-\imath k\hat{z}}) \\ &= \frac{2\hbar k\gamma g^2}{\Delta_a^2}(\hat{a}_+^\dagger\hat{a}_+ - \hat{a}_-^\dagger\hat{a}_-) - \frac{2\imath\hbar k g^2}{\Delta_a}(e^{2\imath k\hat{z}}\hat{a}_+\hat{a}_-^\dagger - e^{-2\imath k\hat{z}}\hat{a}_+^\dagger\hat{a}_-) \ . \end{aligned} \tag{42.23}$$

Defining the light-shift U_0 caused by only one photon and the scattering rate γ_0 by,

$$U_0 \equiv \frac{g^2}{\Delta_a} \qquad \text{and} \qquad \gamma_0 \equiv \frac{\Gamma g^2}{\Delta_a^2} \ , \tag{42.24}$$

with $\Gamma = 2\gamma$, we finally get a set of equations, where the internal degree of freedom of the atom has been eliminated,

$$\boxed{\begin{aligned} \dot{\hat{a}}_\pm &= (-\kappa - \gamma_0 + \imath\Delta_c - \imath U_0)\hat{a}_\pm - (\gamma_0 + \imath U_0)e^{\mp 2\imath k\hat{z}}\hat{a}_\mp + \eta_\pm \\ \dot{\hat{p}} &= 2\hbar k\gamma_0(\hat{a}_+^\dagger\hat{a}_+ - \hat{a}_-^\dagger\hat{a}_-) + 2\imath\hbar k U_0(e^{-2\imath k\hat{z}}\hat{a}_+^\dagger\hat{a}_- - e^{2\imath k\hat{z}}\hat{a}_+\hat{a}_-^\dagger) \end{aligned}} \ . \tag{42.25}$$

[5] Note that the factor of 2 ensure consistency with previous definitions of the Rabi frequency, such as in (35.111). Note also, that $[\hat{\Omega}, \hat{\Omega}^\dagger] = 8g^2 \neq 0$, but this is negligible when the fields are large enough to be considered as classical. On the other hand the quadratic terms $\Omega^\dagger\Omega$ are negligible when they are small compared to γ^2 or Δ_a^2.

42.1.3.1 Radiation pressure and the adiabatically approximated Hamiltonian

The impact of radiation pressure should be considered when the pumping laser is close to a resonance. Then $\gamma_0 \ll U_0$ is no longer satisfied [481], and we get one more term from the equation for the atomic force: $\propto \hbar\gamma_0(|\alpha_+|^2 - |\alpha_-|^2)$.

For the adiabatically approximated Hamiltonian we get immediately from (42.4) [870],

$$\boxed{\begin{aligned}\hat{H} = \frac{\hat{p}^2}{2m} &+ \sum_{\pm}(U_0 - \Delta_c)\hat{a}_\pm^\dagger\hat{a}_\pm \\ &+ U_0(e^{-2\imath k\hat{z}}\hat{a}_+^\dagger\hat{a}_- + e^{2\imath k\hat{z}}\hat{a}_+\hat{a}_-^\dagger) - \imath\sum_{\pm}\eta_\pm(\hat{a}_\pm - \hat{a}_\pm^\dagger)\end{aligned}} \quad , \tag{42.26}$$

as shown in Exc. 42.1.7.3. Note that dissipative terms are (naturally) absent from this Hamiltonian, so that it shall not be used for the description of radiation pressure. On the other hand, all coherent terms of the equations of motion can be derived from this Hamiltonian (42.26), and we can verify momentum conservation (42.17) and deduce transformation properties. Solve the Exc. 42.1.7.4.

These equations, which we will call CARL equations for reasons that we will become clear in Sec. 42.2, describe the coupled dynamics of atoms being accelerated by the *kick* $e^{\imath k\hat{z}}$ imparted by the photonic recoil received upon scattering a photon from one mode into the counterpropagating one. In the same time, the backscattering *annihilates* a photon $\hat{a}_\pm$ in one mode and *creates* a photon $\hat{a}_\mp^\dagger$ in the counterpropagating mode. From now on we will exclusively use the CARL equations.

Finally, let us summarize, how the operators act on states and observables of the coupled system, noting that the same transformation rules as for free and trapped atoms (??) also hold for the optical lattice,

$$\boxed{\begin{array}{rclcrcl} e^{\imath k\hat{z}}|z\rangle &=& |z\rangle & , & e^{-\imath k\hat{z}}\hat{z}e^{\imath k\hat{z}} &=& \hat{z} \\ e^{\imath k\hat{z}}|p\rangle &=& |p+\hbar k\rangle & , & e^{-\imath k\hat{z}}\hat{p}e^{\imath k\hat{z}} &=& \hat{p}+\hbar k \\ \hat{a}_\pm|n\rangle &=& \sqrt{n}|n-1\rangle & , & e^{-\imath k\hat{z}}\hat{H}(\hat{z},\hat{p})e^{\imath k\hat{z}} &=& \hat{H}(\hat{z},\hat{p}-\hbar k) \\ \hat{a}_\pm^\dagger|n\rangle &=& \sqrt{n+1}|n+1\rangle & , & e^{\imath a\hat{p}/\hbar}\hat{H}(\hat{z},\hat{p})e^{-\imath a\hat{p}/\hbar} &=& \hat{H}(\hat{z}-a,\hat{p}) \end{array}} \quad . \tag{42.27}$$

For $ka = \pi$ the phase shift vanishes: $[e^{\imath\pi\hat{p}/\hbar k}, \hat{H}(\hat{z},\hat{p})] = 0$.

The dynamics is given by the time evolutions,

$$e^{-(\imath/\hbar)\hat{H}t}\hat{z}(0)e^{(\imath/\hbar)\hat{H}t} \quad , \quad e^{-(\imath/\hbar)\hat{H}t}\hat{p}(0)e^{(\imath/\hbar)\hat{H}t} \quad , \quad e^{-(\imath/\hbar)\hat{H}t}\hat{n}(0)e^{(\imath/\hbar)\hat{H}t} \; . \tag{42.28}$$

In Exc. 42.1.7.5 we calculate the photon number superposition state resulting from a kick $e^{\imath k_{kck}\hat{z}}$.

42.1.4 Adiabatic elimination of the cavity modes

We have seen in Sec. 42.1.3 how to eliminate the internal atomic degrees of freedom, once the condition $|\Delta_a| \gg \Gamma$ is satisfied. We may try an analogous treatment accounting for the limit $|\Delta_c| \gg \kappa$. In this case, the cavity fields evolve on a fast time

scale, adiabatically following the evolution of the other degrees of freedom. Hence, we set,

$$\dot{\hat{a}}_\pm = 0 \ , \tag{42.29}$$

and obtain from the first Heisenberg equation (42.15),

$$\hat{a}_\pm(\infty) = \frac{\imath g \hat{\sigma}^- e^{\mp \imath k \hat{z}} - \eta_\pm}{-\kappa + \imath \Delta_c} \ . \tag{42.30}$$

Defining,

$$U_c \equiv \frac{g^2 \Delta_c}{\kappa^2 + \Delta_c^2} \qquad \text{and} \qquad \kappa_c \equiv \frac{g^2 \kappa}{\kappa^2 + \Delta_c^2} \ , \tag{42.31}$$

we can write the position-dependent Rabi frequency (42.19) as,

$$\begin{aligned} \Omega(z) = 2g(e^{\imath k \hat{z}} \hat{a}_+ + e^{-\imath k \hat{z}} \hat{a}_-) \quad &= 2(\kappa_c + \imath U_c) \left(\frac{\eta_+ e^{\imath k \hat{z}} + \eta_- e^{-\imath k \hat{z}}}{g} - 2\imath \hat{\sigma}^- \right) \\ &\overset{\eta_\pm = 0}{\longrightarrow} -4\imath(\kappa_c + \imath U_c)\hat{\sigma}^- \ , \end{aligned} \tag{42.32}$$

in the limit of no pumping $\eta_\pm = 0$. Inserting this into the other Heisenberg equations (42.15), we immediately get,

$$\dot{\hat{\sigma}}^- = (-\gamma + \imath \Delta_a)\hat{\sigma}^- + \tfrac{\imath}{2}\Omega(z)\hat{\sigma}_z \overset{\eta_\pm = 0}{\longrightarrow} (-\gamma + \imath \Delta_a)\hat{\sigma}^- + 2(\kappa_c + \imath U_c)\hat{\sigma}^- \hat{\sigma}_z \ , \tag{42.33}$$

and

$$\dot{\hat{\sigma}}_z = -2\gamma \hat{\sigma}_z + \imath \Omega^\dagger(z)\hat{\sigma}^- - \imath \hat{\sigma}^+ \Omega(z) \overset{\eta_\pm = 0}{\longrightarrow} -2\gamma \hat{\sigma}_z - 4\kappa_c \hat{\mathbb{I}} \ , \tag{42.34}$$

as well as, $\dot{\hat{z}} = \hat{p}/m$ and

$$\dot{\hat{p}} = \imath g \hbar k \hat{\sigma}^- (e^{-\imath k \hat{z}} \hat{a}_+^\dagger - e^{\imath k \hat{z}} \hat{a}_-^\dagger) - \imath g \hbar k \hat{\sigma}^+ (e^{\imath k \hat{z}} \hat{a}_+ - e^{-\imath k \hat{z}} \hat{a}_-) \overset{\eta_\pm = 0}{\longrightarrow} 0 \ . \tag{42.35}$$

That is, in summary,

$$\boxed{\begin{array}{rcl} \dot{\hat{\sigma}}^- & = & (-\gamma - 2\kappa_c + \imath \Delta_a - 2\imath U_c)\hat{\sigma}^- \\ \dot{\hat{\sigma}}_z & = & -2\gamma \hat{\sigma}_z - 4\kappa_c \hat{\mathbb{I}} \\ \dot{\hat{p}} & = & 0 \end{array}} \ . \tag{42.36}$$

Alternatively, the coherent part of these equations can be derived by insert $\hat{a}_\pm(\infty)$ directly in the Hamiltonian (42.4). This will be done in Exc. 42.1.7.6. The equations (42.36) tell us that, in the absence of cavity decay and spontaneous emission, the atomic population will not undergo nutation, but the dipole moment will rotate with a velocity which depends on the inversion. The dynamics becomes interesting in the presence of several atoms, as studied in 41.3.3.

42.1.5 General rules for deriving equations of motion

We have, in the previous sections, derived Heisenberg equations (42.15), respectively (42.25) which, together with the Schrödinger equation for the system's state $|\psi(t)\rangle$

or the master equation for the density operator $\hat{\rho}(t)$ form an *over-complete* set. This section aims at providing a general recipe for choosing the right set of equations depending on two basic criteria for the nature of the degrees of freedom involved in the dynamics: (i) Do judge it necessary to treat the degree of freedom as quantum or may a classical description be sufficient; and (ii) Is the degree of freedom subject to dissipation (e.g. spontaneous emission of the electronic excitation, cavity decay of the field mode, or collisions messing up the center-of-mass motion), or not. The procedure, which will be applied throughout the remaining part of this chapter, leads to very different descriptions of the system depending on the specific parameter regime.

1. The procedure is generally applicable to coupled systems: We first need to *identify all relevant degrees of freedom and set up the Hamiltonian*, possibly eliminating irrelevant degrees of freedom, e.g. via adiabatic elimination or by tracing over them, if they contribute to dissipation. In the context of atoms coupled to a ring cavity, we assume our system to be in some state [6],

$$|\psi(t)\rangle = |\mathbf{r}\rangle \otimes |\alpha_+\rangle \otimes |\alpha_-\rangle \otimes |i\rangle \ , \tag{42.37}$$

   coupling the atomic motion, the light fields and the electronic excitation, although the electronic excitation $|i\rangle$ is often eliminated adiabatically. The dissipative degrees of freedom related to vacuum modes leading to spontaneous emission and cavity decay, as well as collisions between moving atoms are traced away, but may be considered in the master equation for the density operator and in the Heisenberg equations, where the corresponding decay rates are added phenomenologically.

   This first item has already been solved in the previous sections and led us to the Hamiltonian (42.4) and the corresponding Heisenberg equations (42.15), or the adiabatically approximated Hamiltonian (42.26) and the corresponding Heisenberg equations (42.25).

2. Now, we must decide which degrees of freedom B can be treated as *classical*. Typically, those are highly excited degrees of freedom (e.g. fast velocities of many photons in a mode). The corresponding operators can be substituted by their expectation value. Purely classical energy terms in the Hamiltonian can be ignored and removed. For the degrees of freedom $\hat{A}$ we want to treat as *quantum*, we chose an appropriate common basis, which can be discrete $\{|m\rangle\}$ where m is a complete set of quantum numbers. It can also be continuous $\{|\mathbf{r}\rangle\}$ or a combination of both $\{|\mathbf{r}, m\rangle\}$. Now, we need to expand all operators on the chosen basis.

3. For the quantized degrees of freedom must now decide, whether they all evolve coherently or whether they are subject to dissipation. In the first case, perform steps A4 to A7, in the second case, perform steps B4 to B7.

[6] Throughout this chapter we will denote momentum states by the Greek letters $|\mu\rangle$ or $\nu\rangle$. Photonic states will be labeled by the Latin letters $|n\rangle$ or $|m\rangle$. Electronic excitation states will be labeled by the Latin letters $|i\rangle$ or $|j\rangle$. Finally, expansion coefficients c_{ν,i,n_+,n_-} of the state or of the density matrix elements will sometimes be emphasized in red.

A4. In the case of coherent dynamics, we *expand the state* of the system $|\psi(t)\rangle$ on the whole basis. For example, expanded on a partially continuous basis, the coupled atom-ring cavity state may read,

$$|\psi(t)\rangle = \sum_{n_+,n_-,i} \int d^3r \; c_{n_+,n_-,i}(\mathbf{r},t)|\mathbf{r}\rangle \otimes |n_+\rangle \otimes |n_-\rangle \otimes |i\rangle \; , \tag{42.38}$$

where $\langle \mathbf{r}, \alpha_+, \alpha_-, i|\psi(t)\rangle = c_{n_+,n_-,i}(\mathbf{r},t)$ are the expansion coefficients depending on photon numbers $n_\pm$ in the counterpropagating light modes, the electronic excitation state i, and the atomic position $\mathbf{r}$ treated in terms of a continuous wavefunction in space [7]. When we want to treat the atomic motion as being quantized in discrete momentum states labeled by some integer number μ, we adopt the notation,

$$|\psi(t)\rangle = \sum_{\nu,n_+,n_-,i} c_{\nu,n_+,n_-,i}(t)|\nu\rangle \otimes |n_+\rangle \otimes |n_-\rangle \otimes |i\rangle \; , \tag{42.39}$$

where $\langle \nu, \alpha_+, \alpha_-, i|\psi(t)\rangle = c_{\nu,n_+,n_-,i}(t)$ are the new expansion coefficients.

A5. Next, we write down the *Schrödinger equation* for the state $|\psi(t)\rangle$, insert the expansion on the basis, and we derive a linear set of equation of motion for the expansion coefficients $\dot{c}_{\{m\}}(\mathbf{r})$. This set governs the dynamics of the quantum degrees of freedom.

A6. The dynamics of the classical degrees of freedom B is obtained by taking the expectation values of the *Heisenberg equations*. Here, we need to take care that the quantum degrees of freedom appearing in the Heisenberg equations are expressed by their expansions.

A7. The coupled set of equations for the expectation values of projectors of the system into a particular state, that is, $\dot{c}_{\{m\}}$ (respectively, $\dot{c}_{\{m\}}(\mathbf{r})$), and of observables B really represents all we need to describe the system dynamics and to simulate it numerically. Hack everything into your PC, pronto!

B4. In the case of dissipative dynamics, derive the master equation obeying commutation rules for all quantized degrees of freedom including the Lindbladt terms and expand every quantized degrees of freedom on the common basis, we do the same expansions, but,

$$\hat{\rho}(t) = |\psi(t)\rangle\langle\psi(t)| \; . \tag{42.40}$$

B5. Derive the linear set of equation of motion for the matrix elements $\dot{\rho}_{\{m\},\{n\}}$.

B6. Take the expectation values $\mathrm{Tr}\; \hat{\rho}\hat{B}$ of the Heisenberg equations for all degrees of freedom to be handled classical as expanding the quantized degrees of freedom on their basis.

B7. The coupled set of equations for $\dot{\rho}_{\{m\},\{n\}}$ and $\dot{B}$ is sufficient to describe the dynamics of the system, hack everything into your PC, pronto!

[7] Note that, in the absence of other quantum numbers, we rather use to write $c(\mathbf{r}) = \psi(\mathbf{r})$.

Let us apply the procedure to the simplest case that the electronic excitation has been adiabatically eliminated and *all* remaining degrees of freedom can be treated classical. Then we do not require a Hamiltonian, nor the Schrödinger equation. We just take the expectation value of the Heisenberg equations (42.25) for all degrees of freedom which is easy to do, because there is no quantum state to be expanded: we just can replace the operators by c-numbers,

$$\boxed{\begin{aligned} \dot{\alpha}_\pm &= (-\kappa + \imath\Delta_c - \imath U_0)\alpha_\pm - \imath U_0 e^{\mp 2\imath k z}\alpha_\mp + \eta_\pm \\ \dot{p} &= 2\imath\hbar k U_0(e^{-2\imath k z}\alpha_+^\dagger\alpha_- - e^{2\imath k z}\alpha_+\alpha_-^\dagger) \end{aligned}} \,. \tag{42.41}$$

These *totally classical* equations, called CARL equations, will be studied in the subsequent sections, while a thorough discussion of partially quantized equations of motion is postponed to Sec. 42.4.

42.1.5.1 CARL as a beam splitter

Neglecting spontaneous emission, $\gamma_0 = 0$, cavity pumping, $\eta = 0$, cavity decay, $\kappa = 0$, and cavity detuning, $\Delta_c = 0$, the CARL equations in the adiabatic approximation can be derived from the following Hamiltonian,

$$\hat{H} = \frac{\hat{p}^2}{2m} + \sum_\pm U_0\hat{a}_\pm^\dagger\hat{a}_\pm + U_0(e^{-2\imath k\hat{z}}\hat{a}_+^\dagger\hat{a}_- + e^{2\imath k\hat{z}}\hat{a}_+\hat{a}_-^\dagger) \,, \tag{42.42}$$

and read,

$$\begin{aligned} \dot{\hat{a}}_\pm &= -\imath U_0\hat{a}_\pm - \imath U_0 e^{\mp 2\imath k\hat{z}}\hat{a}_\mp \\ \dot{\hat{p}} &= 2\imath\hbar k U_0(e^{-2\imath k\hat{z}}\hat{a}_+^\dagger\hat{a}_- - e^{2\imath k\hat{z}}\hat{a}_+\hat{a}_-^\dagger) \,, \end{aligned} \tag{42.43}$$

or with the substitution $\hat{b}_\pm \equiv \hat{a}_\pm e^{\imath U_0 t}$,

$$\begin{aligned} \dot{\hat{b}}_\pm &= -\imath U_0 e^{\mp 2\imath k\hat{z}}\hat{b}_\mp \\ \ddot{\hat{b}}_\pm &= -U_0^2\hat{b}_\pm - 2k\dot{\hat{z}}U_0 e^{\mp 2\imath k\hat{z}}\hat{b}_\mp \,, \end{aligned} \tag{42.44}$$

we see that, if the motion weren't a dynamic variable, $\dot{\hat{z}} = 0$, the field amplitudes would just perform harmonic oscillations.

On the other hand, with the substitution $\hat{c} \equiv \hat{a}_+ e^{\imath k\hat{z}} + \hat{a}_- e^{-\imath k\hat{z}}$ [8], the complete Hamiltonian rephrased as,

$$\boxed{\hat{H} = \frac{\hat{p}^2}{2m} + U_0\hat{c}^\dagger\hat{c}} \,. \tag{42.45}$$

Here, we see that, if the motion described by $(\hat{z}, \hat{p})$ weren't a dynamic variable, our system would simply be a harmonic oscillator vibrating with the frequency U_0.

[8] Provided we are allowed to commute the operators $\hat{z}$ and $\hat{a}_\pm$.

42.1.5.2 Classical limit of the equations of motion

For atoms much hotter than the recoil limit and macroscopic light intensities we may replace the quantum operators by complex numbers $z \equiv \hat{z}$, $\alpha_\pm \equiv \hat{a}_\pm$ and $\rho_{21} = \hat{\sigma}^-$. The classical equations of motion (42.41) for the coupled system of a single atom confined at the position $r = z$ of the dipolar potential of a ring cavity can be cast into the form,

$$\boxed{\begin{aligned}\begin{pmatrix}\dot{\alpha}_+\\ \dot{\alpha}_-\end{pmatrix} &= \begin{pmatrix}-\kappa-\gamma_0+\imath(\Delta_c-U_0) & -(\gamma_0+\imath U_0)e^{-2\imath kz}\\ -(\gamma_0+\imath U_0)e^{2\imath kz} & -\kappa-\gamma_0+\imath(\Delta_c-U_0)\end{pmatrix}\begin{pmatrix}\alpha_+\\ \alpha_-\end{pmatrix}+\begin{pmatrix}\eta_+\\ \eta_-\end{pmatrix}\\ \dot{p} &= 2\hbar k\gamma_0(\alpha_+\alpha_+^*-\alpha_-\alpha_-^*)+2\imath\hbar kU_0(\alpha_+^*\alpha_-e^{-2\imath kz}-\alpha_+\alpha_-^*e^{2\imath kz})\end{aligned}} \,. \tag{42.46}$$

Recalling that $\alpha_\pm^*\alpha_\pm$ is the number of photons in the respective mode, we can interpret this equation as a rate equation: The number of photons in a mode α_+ changes by photon losses at a rate κ from resonator, or by gain due to backscattering from the counterpropagating mode, or by pumping with an external incident light field at rate η_+.

The equations (42.46) completely describe our coupled atom-cavity system. They are totally classical and work for both, atoms and macroscopic particles.

42.1.6 Cumulant expansion for CARL

The dynamics of quantum correlations such as $\hat{a}_+^\dagger\hat{a}_-$ or $\hat{a}_+\sigma^+$ can be derived from Heisenberg equations, as well. As an example, let us consider the adiabatically eliminated Hamiltonian (42.26) and ignore the quantized nature of the atomic motion, the relevant first-order field-field correlations are then $\hat{a}_+^2$, $\hat{a}_+^\dagger\hat{a}_+$, $\hat{a}_+^{\dagger 2}$, $\hat{a}_-^2$, $\hat{a}_-^\dagger\hat{a}_-$, $\hat{a}_-^{\dagger 2}$, $\hat{a}_+\hat{a}_-$, $\hat{a}_+\hat{a}_-^\dagger$, $\hat{a}_+^\dagger\hat{a}_-$, $\hat{a}_+^\dagger\hat{a}_-^\dagger$. From the Heisenberg equation we get, for instance,

$$\begin{aligned}\frac{d}{dt}\hat{a}_+^2 &= \imath[\hat{H},\hat{a}_+^2] \\ &= -2\imath(U_0-\Delta_c)\hat{a}_+^2+2U_0\left(e^{2\imath k\hat{z}}\hat{a}_+\hat{a}_-^\dagger-e^{-2\imath k\hat{z}}\hat{a}_+\hat{a}_-\right)-2\imath\eta_+\hat{a}_+ \,.\end{aligned} \tag{42.47}$$

This is the lowest order *cumulant expansion*. The expectation values form a system of 10 linear first order differential equations [226] from which we can calculate the steady-state of the system.

The correlation functions and spectra are obtained directly from the CARL equation for the cavity fields (42.25) using the Wiener-Khinchin theorem (35.176) and the quantum regression theorem (35.253). With the substitutions, $t \to 0$, $\hat{B} \to 1$, $\hat{A} \to d\hat{A}_k/d\tau$, and $\xi_i(\tau)\hat{A}_i(0) \to \zeta_i\hat{A}_i(\tau)$, the quantum regression theorem can be written in the form,

$$\boxed{\frac{d}{d\tau}\langle\hat{A}_k(\tau)\rangle = \sum_i \zeta_i\langle\hat{A}_i(\tau)\rangle \qquad \Longrightarrow \qquad \frac{d}{d\tau}\langle\hat{A}_k(\tau)\hat{C}(0)\rangle = \sum_i \zeta_i\langle\hat{A}_i(\tau)\hat{C}(0)\rangle} \,. \tag{42.48}$$

Applied, for example, to the correlation function (42.47), we obtain from the CARL equation (42.25), with $\gamma_0 = 0$ and $\Delta_c = 0$,

$$\frac{d}{d\tau}\langle\hat{a}_+(\tau)\hat{a}_+(0)\rangle = (-\kappa - \imath U_0)\langle\hat{a}_+(\tau)\hat{a}_+(0)\rangle - \imath U_0 e^{-2\imath k\hat{z}}\langle\hat{a}_-(0)\hat{a}_+(0)\rangle + \eta_+\langle\hat{a}_+(0)\rangle \ . \tag{42.49}$$

Repeating this calculation for the other first-order correlations functions we obtain a system of 10 linear first order differential equations, which can be solved via Laplace transform.

42.1.7 Exercises

42.1.7.1 Ex: Origin of quantum correlations

Derive the Hamiltonian (42.2) from the JCM Hamiltonian (35.111) transforming it into the co-rotating frame.

Solution: *We write the JCM Hamiltonian,*

$$\hat{H} = \omega_c\hat{a}^\dagger\hat{a} + \omega_a(\hat{\sigma}^+\hat{\sigma}^- - \tfrac{1}{2}) + \tfrac{1}{2}\Omega(\hat{a}\hat{\sigma}^+ + \hat{a}^\dagger\hat{\sigma}^-)$$

in matrix form as,

$$\hat{H}_n = \begin{pmatrix} (n-1)\omega_c & \frac{\Omega}{2}\sqrt{n} \\ \frac{\Omega}{2}\sqrt{n} & n\omega_c - \omega_a \end{pmatrix} \ .$$

Now, applying the unitary transform,

$$\hat{U} = \begin{pmatrix} e^{-\imath n\omega t} & 0 \\ 0 & e^{-\imath n\omega t} \end{pmatrix} \ ,$$

we get,

$$\tilde{H} = \hat{U}^\dagger\hat{H}\hat{U} + \imath\hbar\dot{\hat{U}}^\dagger\hat{U} = \begin{pmatrix} (n-1)(\omega_c - \omega) + \omega_a - \omega & \frac{\Omega}{2}\sqrt{n} \\ \frac{\Omega}{2}\sqrt{n} & n(\omega_c - \omega) \end{pmatrix} \ ,$$

and hence, introducing the detunings $\Delta_a \equiv \omega - \omega_a$ and $\Delta_c \equiv \omega - \omega_c$,

$$\hat{H} = -\Delta_c\hat{a}^\dagger\hat{a} - \Delta_a(\hat{\sigma}^+\hat{\sigma}^- - \tfrac{1}{2}) + \tfrac{1}{2}\Omega(\hat{a}\hat{\sigma}^+ + \hat{a}^\dagger\hat{\sigma}^-) \ .$$

42.1.7.2 Ex: Linear pumping of a cavity mode

Study how the Hamiltonian $\hat{H}_{pmp} = \imath\eta^*\hat{a} - \imath\eta\hat{a}^\dagger$, describing linear pumping of a cavity mode, fills the cavity with photons in the absence of dissipation (see also (40.2)).

Solution: *We can define a displacement operator $D(\eta t) \equiv e^{-\imath\hat{H}_{pmp}t} = e^{\eta^* t\hat{a} - \eta t\hat{a}^\dagger}$. The*

$$\begin{aligned}\langle 0|D^\dagger(\eta t)\hat{n}D(\eta t)|0\rangle &= \langle 0|D^\dagger(\eta t)\hat{a}^\dagger D(\eta t)D^\dagger(\eta t)\hat{a}D(\eta t)|0\rangle \\ &= \langle 0|(\hat{a}^\dagger + \eta^* t)(\hat{a} + \eta t)|0\rangle = \langle 0|\hat{n} + \eta^* t\hat{a} + \eta t\hat{a}^\dagger + |\eta t|^2|0\rangle = |\eta t|^2 \ .\end{aligned}$$

42.1.7.3 Ex: The adiabatically approximated Hamiltonian

a. Derive the adiabatically approximated Hamiltonian (42.26) from the total Hamiltonian (42.4).
b. Derive the CARL equations (42.25) directly from the adiabatically approximated Hamiltonian.
c. Show that, in the absence of pumping, the energy stored in the light fields is conserved separately from the mechanical energy of the atom.
d. Verify momentum conservation.

Solution: *a. With the definition of the Rabi frequency (42.19)* $\hat{\Omega} = 2g(e^{\imath k\hat{z}}\hat{a}_+ + e^{-\imath k\hat{z}}\hat{a}_-)$ *we can rewrite the Hamiltonian (42.4) as,*

$$\hat{H} = \frac{\hat{p}^2}{2m} - \Delta_a\hat{\sigma}^+\hat{\sigma}^- + \tfrac{1}{2}\hat{\Omega}^\dagger\hat{\sigma}^- + \tfrac{1}{2}\hat{\sigma}^+\hat{\Omega} - \sum_\pm \left[\Delta_c\hat{a}_\pm^\dagger\hat{a}_\pm + \imath\eta_\pm(\hat{a}_\pm - \hat{a}_\pm^\dagger)\right] ,$$

inserting the stationary solution (42.21): $\hat{\sigma}^-(\infty) = \hat{\Omega}/2\Delta_a$ *and setting* $\gamma = 0$*, we get,*

$$\begin{aligned}\hat{H} &\simeq \frac{\hat{p}^2}{2m} - \frac{\hat{\Omega}^\dagger\hat{\Omega}}{4\Delta_a} - \sum_\pm \left[\Delta_c\hat{a}_\pm^\dagger\hat{a}_\pm + \imath\eta_\pm(\hat{a}_\pm - \hat{a}_\pm^\dagger)\right] \\ &= \frac{\hat{p}^2}{2m} + \sum_\pm (U_0 - \Delta_c)\hat{a}_\pm^\dagger\hat{a}_\pm + U_0(e^{-2\imath k\hat{z}}\hat{a}_+^\dagger\hat{a}_- + e^{2\imath k\hat{z}}\hat{a}_+\hat{a}_-^\dagger) - \imath\sum_\pm \eta_\pm(\hat{a}_\pm - \hat{a}_\pm^\dagger) ,\end{aligned}$$

with $U_0 = \frac{g^2}{\Delta_a}$.
b. From this we derive,

$$\dot{\hat{a}}_+ = \imath[\hat{H}, \hat{a}_+] = (\imath\Delta_c - \imath U_0)\hat{a}_+ - \imath U_0\hat{a}_- e^{-2\imath k\hat{z}} + \eta_+ ,$$

where we used, $[\hat{a}_+^\dagger\hat{a}_+, \hat{a}_+] = -\hat{a}_+$*,* $[\hat{a}_-^\dagger\hat{a}_-, \hat{a}_+] = 0$*, and* $[\hat{a}_+^\dagger\hat{a}_-, \hat{a}_+] = -\hat{a}_-$ *and,*

$$\dot{\hat{p}} = \imath[\hat{H}, \hat{p}] = 2\imath U_0 k\left(e^{-2\imath k\hat{z}}\hat{a}_+^\dagger\hat{a}_- - e^{2\imath k\hat{z}}\hat{a}_+\hat{a}_-^\dagger\right) ,$$

where we used, $[e^{\imath k\hat{z}}, \hat{p}] = -ke^{\imath k\hat{z}}$.
c. Using the derived Hamiltonian without pumping terms and setting for simplicity $\Delta_c = 0$ *and using the commutation rules* $[\hat{a}_\pm, \hat{n}_\pm] = \hat{a}_\pm$ *and* $[\hat{a}_\pm^\dagger, \hat{n}_\pm] = -\hat{a}_\pm^\dagger$ *it is easy to show,*

$$[\hat{H}, \hat{n}_+ + \hat{n}_-] = 0 ,$$

such that kinetic energy can only be converted into potential energy,

$$[\hat{H}, \tfrac{\hat{p}^2}{2m}] = -[\hat{H}, U_0\left(\hat{a}_+^\dagger\hat{a}_- e^{-2\imath k\hat{z}} + \hat{a}_-^\dagger\hat{a}_+ e^{2\imath k\hat{z}}\right)] = 4\omega_{rec}U_0\left(\hat{a}_+^\dagger\hat{a}_- e^{-2\imath k\hat{z}} + \hat{a}_-^\dagger\hat{a}_+ e^{2\imath k\hat{z}}\right) .$$

d. Momentum conservation,

$$[\hat{H}, \hbar k(\hat{n}_+ - \hat{n}_-) - \hat{p}] = 0 .$$

42.1.7.4 Ex: Hamiltonian after adiabatic elimination of internal states for a linear cavity including counter-rotating terms

Repeat the adiabatic elimination of Sec. 42.1.4 for a linear cavity including counter-rotating terms.

Solution: *The Hamiltonian is,*

$$\begin{aligned}\hat{H} &= \frac{\hat{p}^2}{2m} - \Delta_a \hat{\sigma}^+\hat{\sigma}^- - \Delta_c \hat{a}^\dagger \hat{a} + g(\hat{a}^\dagger + \hat{a})(e^{\imath k\hat{z}} + e^{-\imath k\hat{z}})(\hat{\sigma}^- + \hat{\sigma}^+) \\ &= \frac{\hat{p}^2}{2m} - \Delta_a \hat{\sigma}^+\hat{\sigma}^- - \Delta_c \hat{a}^\dagger \hat{a} + \tfrac{\hat{\Omega}(z)}{2}(\hat{\sigma}^- + \hat{\sigma}^+) \ ,\end{aligned}$$

defining,

$$\hat{\Omega}(z) \equiv g(\hat{a}^\dagger + \hat{a}) \cos k\hat{z} = \hat{\Omega}(z)^\dagger \ .$$

The Heisenberg equations yield,

$$\begin{aligned}\dot{\sigma}^- &= -\gamma\hat{\sigma}^- + \imath[\hat{H}, \hat{\sigma}^-] = (-\gamma + \imath\Delta_a)\hat{\sigma}^- - \tfrac{\imath\Omega(z)}{2}\hat{\sigma}_z \\ \dot{\sigma}_z &= \imath[\hat{H}, \hat{\sigma}_z] - 2\gamma - 2\gamma\hat{\sigma}_z = -2\gamma - 2\gamma\hat{\sigma}_z + \imath\Omega(z)(\hat{\sigma}^+ - \hat{\sigma}^-) \ .\end{aligned}$$

In steady state,

$$\begin{aligned}\hat{\sigma}^-(\infty) &= \frac{\imath\Omega(z)}{2(-\gamma + \imath\Delta_a)}\hat{\sigma}_z(\infty) \simeq \frac{-\Omega(z)}{2\Delta_a} \\ \hat{\sigma}_z(\infty) &= \frac{-2(\gamma^2 + \Delta_a^2)}{2(\gamma^2 + \Delta_a^2) + \Omega(z)^2} \simeq -1 \\ \hat{\sigma}^+\hat{\sigma}^- &= \frac{\Omega(z)^2}{2(\gamma^2 + \Delta_a^2)} \simeq 0 \ .\end{aligned}$$

Using classical light $[\hat{a}, \hat{a}^\dagger] = 0$,

$$\hat{\Omega}^2 = g(\hat{a}^\dagger + \hat{a})^2 \cos^2 kz = 2g\hat{a}^\dagger\hat{a}\cos^2 kz + const \ ,$$

the Hamiltonian finally becomes,

$$\begin{aligned}\hat{H} &= \frac{\hat{p}^2}{2m} - \Delta_c \hat{a}^\dagger\hat{a} - \frac{\Omega(z)^2}{2\Delta_a} \\ &= \frac{\hat{p}^2}{2m} - \Delta_c \hat{a}^\dagger\hat{a} - \frac{g}{\Delta_a}\hat{a}^\dagger\hat{a}\cos^2 kz + const \ .\end{aligned}$$

42.1.7.5 Ex: Periodicity of a lattice

Assume a symmetrically pumped ring cavity in equilibrium with an atom initially at rest. What photonic states are generated in the counterpropagating light modes, when the atom is kicked by an external force imparting a sudden recoil of $\hbar k_{kck}$.

Solution:

42.1.7.6 Ex: Adiabatic elimination of the cavity modes

Derive the coherent part of the equations of motion (42.36) directly from the Hamiltonian (42.4) in the absence of pumping, $\eta_\pm = 0$, and in the limit of large cavity detunings, $|\Delta_c| \gg \kappa$.

Solution: *The Hamiltonian becomes,*

$$\hat{H}_{atom:field} = -\Delta_a \hat{\sigma}^+\hat{\sigma}^- + \frac{\hat{p}^2}{2m} - \sum_\pm \Delta_c \hat{a}_\pm^\dagger \hat{a}_\pm - \imath\eta_\pm(\hat{a}_\pm - \hat{a}_\pm^\dagger) + \tfrac{1}{2}\Omega^\dagger(z)\hat{\sigma}^- + \tfrac{1}{2}\hat{\sigma}^+\Omega(z)$$

$$\stackrel{\eta_\pm=0}{\longrightarrow} \frac{\hat{p}^2}{2m} + (2U_c - \Delta_a)\hat{\sigma}^+\hat{\sigma}^- \ .$$

Now, the equations of motion are,

$$\dot{\hat{\sigma}}^- = \imath[\hat{H}_{atom:field}, \hat{\sigma}^-] = \imath(2U_c - \Delta_a)[\hat{\sigma}^+\hat{\sigma}^-, \hat{\sigma}^-] = \imath(\Delta_a - 2U_c)\hat{\sigma}_z\hat{\sigma}^-$$
$$\dot{\hat{\sigma}}_z = \imath[\hat{H}_{atom:field}, \hat{\sigma}_z] = \imath(2U_c - \Delta_a)[\hat{\sigma}^+\hat{\sigma}^-, \hat{\sigma}_z] = 0 \ ,$$

which coincides with the coherent part of (42.36).

42.2 CARL: The collective atomic recoil laser

The *collective atomic recoil laser* (*CARL*) was first predicted in 1994 [173] as an atomic analog of FEL. The idea consists of a monochromatic homogeneous beam of moving two-level atoms (all atoms have the same velocity), a strong counterpropagating pump laser beam, and a weak copropagating probe beam tuned to the blue side of the resonance. The lasers form a standing light wave that moves in the same direction as the atoms. Atoms that are faster than the velocity of the standing wave are rejected by the maxima of the dipolar potential created by the standing wave and feel a repulsive force. Atoms that are slower than the standing wave velocity are pushed by the dipole potential maxima and feel an accelerating force. These forces can be interpreted as backscattering of photons from the pump wave into the probe wave. This redistribution of energy amplifies the contrast of the stationary wave, which in turn amplifies the backscattering efficiency, etc. Therefore, the CARL converts kinetic energy into coherent radiation (or more precisely, into an increase of the energy difference between probe and pump) mediated by atomic bunching. It is a self-amplifying mechanism. The CARL signature is a transient exponential amplification for the incident probe, which defines the frequency of the 'CARL laser'. The first experimental realization of CARL used a ring cavity [755].

42.2.1 Classical CARL equations for many mobile atoms

The preceding sections dealt with a single atom in a ring cavity. More interesting dynamics, however, emerge in the presence of several atoms, because their motion can be become correlated via their simultaneous interaction with the same two counter-propagating modes of the cavity, as illustrated in the following movie (watch movie). A talk on CARL can be assisted at (watch talk).

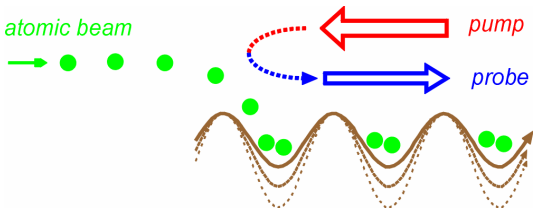

Figure 42.3: Collective atomic recoil laser.

To describe experiments dealing with many atoms, we have to extend the equations of motion (42.26) to N atoms via $z \longrightarrow z_j$ and $p \longrightarrow p_j$, where $j = 1, N$,

$$\boxed{\begin{aligned} \dot{\alpha}_\pm &= (-\kappa - \imath N U_0)\alpha_\pm - \imath U_0 \sum_{j=1}^{N} e^{\mp 2\imath k z_j}\alpha_\mp + \eta_\pm \\ \dot{p}_j &= -2\imath\hbar k U_0(\alpha_+\alpha_-^* e^{2\imath k z_j} - \alpha_-\alpha_+^* e^{-2\imath k z_j}) \end{aligned}} \quad . \tag{42.50}$$

with the kinetic and potential energies [9],

$$E_{kin} = \sum_j \frac{p_j^2}{2m} \quad , \quad E_{pot} = \sum_j U_0 |\alpha_+ e^{\imath k z_j} + \alpha_- e^{-\imath k z_j}|^2 \ . \tag{42.51}$$

If the atomic density distribution is homogeneous, the phases of randomly scattered photons destructively interfere and the quantity,

$$b \equiv \tfrac{1}{N} \sum_j e^{-2\imath k z_j} \ , \tag{42.52}$$

called *bunching parameter*, vanishes. That is, the impact of the scatterers on the light modes cancels out, as we will see in Exc. 42.2.7.1 for the case of two atoms. If on the other hand, atoms accumulate in the antinodes of the standing wave, it increases the contrast of it can spread more efficiently collectively by Bragg scattering. The particularity of the CARL is that during the temporal evolution the bunching process can amplify itself leading to an exponential growth of the counterpropagating mode, accompanied by an increasingly pronounced self-bunching.

In general, the equations can not be solved analytically, especially when the pump varies over time. A first approach consists in iterating them numerically,

$$\begin{aligned} \alpha_\pm(t+dt) &= \alpha_\pm(t) + dt\ [-(\kappa + \imath N U_0 - \imath\Delta_c)\alpha_\pm - \imath N U_0 b \alpha_\mp + \eta_\pm(t)] \\ z_j(t+dt) &= z_j + dt\ \tfrac{1}{m} p_j \\ p_j(t+dt) &= p_j - dt\ 2\imath\hbar k U_0(\alpha_+\alpha_-^* e^{2\imath k z_j} - \alpha_-\alpha_+^* e^{-2\imath k z_j}) \ . \end{aligned} \tag{42.53}$$

In Exc. 42.2.7.2 we will extend the equations (42.50) to the presence of two atomic species, and in Exc. 42.2.7.3 we will use them to describe the response of the light fields to an inertially moving atom supposing that is does not feel the CARL force.

[9] Note, that there is also a radial motion of the atom coupled to the axial movement. The coupling happens, because the axial motion influences the number of intracavity photons of the radiation field which, in turn, determines the depth of the dipole potential.

42.2.1.1 Locking of the pump laser

In practice the resonant frequency of a cavity fluctuates due to ambient noise. Hence, it is easier, experimentally, to lock the pump laser on a cavity mode, e.g. using the Pound-Drever-Hall method. This means,

$$\alpha_+ = \frac{\eta_+}{\kappa} \ . \tag{42.54}$$

In the presence of atoms, however, the resonant frequency can be shifted due to the refractive index of the atomic cloud [415]. Moreover, the shift depends on the atomic bunching and consequently varies during the dynamics of the CARL. The way the locking circuit works, is to continuously adjust the detuning between the laser and the cavity Δ_c (defined for the empty cavity) such as to maximize the amplitude of the field $|\alpha_+|$ and, hence, the transmission of the cavity filled with atoms. The dynamics of the detuning must be incorporated by an additional equation modeling the action of locking. Now that we know the effect, which an ideal lock should have, we can apply the boundary condition (42.54) and eliminate the pump mode α_+ from the dynamics of the system. That is, the following equations are usually sufficient to describe the CARL:

$$\boxed{\begin{aligned} \dot{\alpha}_- &= (-\kappa + \imath\Delta_c - \imath U_0)\alpha_- - \imath U_0 e^{-2\imath kz}\alpha_+ + \eta_- \\ m\ddot{z} &= 2\imath\hbar k U_0 \alpha_+ (\alpha_- e^{-2\imath kz} - \alpha_-^* e^{2\imath kz}) \end{aligned}} \ . \tag{42.55}$$

The frequency offset of the cavity resonances caused by the atom, U_0, can exceed the width of the cavity κ. From equation (40.146) we know,

$$|\alpha_+(\infty)|^2 = \frac{\chi\chi^*}{(\chi^2 + U_0^2)(\chi^{*2} + U_0^2)}\eta_+^2 \ .$$

The maxima of $|\alpha_+(\infty)|^2$ as a function of Δ_c give the shifted resonances of the modes.

Example 270 (*Locking on transverse modes*): We already mentioned that as the CARL accelerates, the frequency of the light which is backscattered to the probe shifts to the red until it escapes from the resonant mode. What happens if we provide another resonant mode that can receive photons? We will show in the following calculation, that CARL simply picks up the closest mode to dump the photons. The starting point is generalized CARL equations to accommodate a second reverse mode labeled β_-,

$$\begin{aligned} \dot{\alpha}_+ &= -(\kappa - \imath\Delta_c)\alpha_+ - \imath U_0(u_+^* u_+ \alpha_+ + u_+^* u_- \alpha_- + u_+^* u_\beta \beta_-) + \eta_+ \\ \dot{\alpha}_- &= -(\kappa - \imath\Delta_c)\alpha_- - \imath U_0(u_-^* u_- \alpha_- + u_-^* u_+ \alpha_+ + u_-^* u_\beta \beta_-) \\ \dot{\beta}_- &= -(\kappa - \imath\Delta_\beta)\beta_- - \imath U_0(u_\beta^* u_\beta \beta_- + u_\beta^* u_+ \alpha_+ + u_\beta^* u_- \alpha_-) \\ m\ddot{x} &= -U_0 \nabla |\alpha_+ u_+ + \alpha_- u_- + \beta_- u_\beta|^2 \ , \end{aligned} \tag{42.56}$$

com $u_\pm = e^{\pm \imath k z}$ and $u_\beta = e^{-\imath k_\beta x}$. We obtain,

$$\begin{aligned}
\dot{\alpha}_+ &= -(\kappa - \imath\Delta_c + \imath N U_0)\alpha_+ - \imath U_0 e^{-2\imath k z}\alpha_- - \imath U_1 e^{-\imath(k+k_\beta)x}\beta_- + \eta_+ \quad (42.57)\\
\dot{\alpha}_- &= -(\kappa - \imath\Delta_c + \imath N U_0)\alpha_- - \imath U_0 e^{2\imath k z}\alpha_+ - \imath U_1 e^{\imath(k-k_\beta)x}\beta_-\\
\dot{\beta}_- &= -(\kappa - \imath\Delta_\beta + \imath N U_1)\beta_- - \imath U_1 e^{\imath(k+k_\beta)x}\alpha_+ - \imath U_1 e^{-\imath(k-k_\beta)x}\beta_-\\
m\ddot{x} &= -U_0(2\imath k e^{2\imath k z}\alpha_-^*\alpha_+ - 2\imath k e^{-2\imath k z}\alpha_+^*\alpha_-)\\
&\quad - U_1(\imath(k+k_\beta)e^{\imath(k+k_\beta)x}\beta_-^*\alpha_+ - \imath(k+k_\beta)e^{-\imath(k+k_\beta)x}\alpha_+^*\beta_-)\\
&\quad - U_1(\imath(k-k_\beta)e^{\imath(k-k_\beta)x}\alpha_-^*\beta_- - \imath(k-k_\beta)e^{-\imath(k-k_\beta)x}\beta_-^*\alpha_-)\ .
\end{aligned}$$

Note that $k - k_\beta \approx 0$ and $k + k_\beta \approx 2k$. The result of the simulation is displayed in Fig. 42.4.

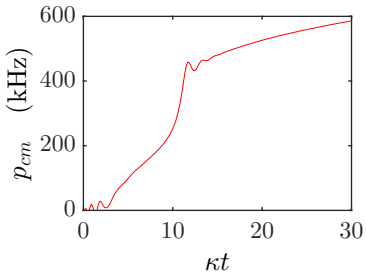

Figure 42.4: (code) The CARL locks to other modes of the cavity.

42.2.1.2 Analytic approximations for one-sided pumping and perfect bunching

Here, we will assume for simplicity, that the atoms are perfectly bunched, $z_j = z$ and $p_j = p$, i.e. they have *zero temperature*. This means that we only need to consider a single equation of motion for the atoms. However, their coupling to the cavity modes is N times stronger, which means that we have to substitute $U_0 \longrightarrow U_N \equiv N U_0$ in the equation of motion for the cavity fields.

When only one atom is in the cavity or when the atoms are perfectly bunched together, it is possible to derive analytical solutions. Particularly interesting is the following situation: We pump the cavity from one side. The pump is supposed to be dominant and locked to a resonance, such that we can neglect the feedback of the system on the pump, that is, we can assume, $\alpha_+ = \eta/\kappa$. Using the abbreviations $\chi \equiv \kappa + \imath U_0 - \imath\Delta_c$ and the photon recoil shift [481],

$$\omega_{rec} \equiv \frac{\hbar k^2}{2m}\ , \tag{42.58}$$

the equations (42.26) then become,

$$\boxed{\begin{aligned}
\dot{\alpha}_- &= -\chi\alpha_- - \imath U_N \alpha_+ e^{2\imath k z}\\
k\dot{v} &= 4\omega_{rec}\imath U_0 \alpha_+(\alpha_- e^{-2\imath k z} - \alpha_-^* e^{2\imath k z})
\end{aligned}}\ . \tag{42.59}$$

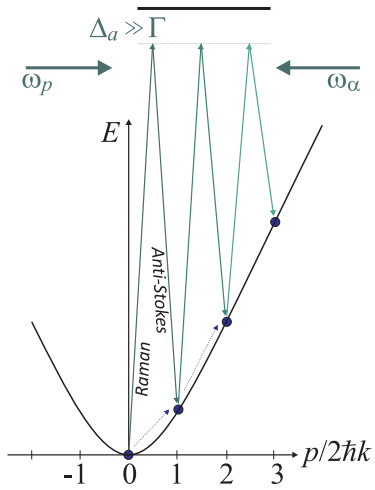

Figure 42.5: In the momentum picture the CARL acceleration process occurs as Raman-anti-Stokes processes along the free-particle dispersion relation.

We consider the stationary case (42.26). Doing the ansatz,

$$\alpha_- \equiv \beta e^{2\imath kx} \qquad \text{where} \qquad \dot{\beta} = 0 \tag{42.60}$$

we assume that the atom and the standing wave have the same velocity, that is, they move in phase. We obtain as solution,

$$\beta = \frac{-\imath U_N \alpha_+}{\kappa + 2\imath kv} \quad , \quad k\dot{v} = 8\omega_{rec} U_0^2 \alpha_+^2 \frac{2\kappa}{\kappa^2 + 4k^2 v^2} \ . \tag{42.61}$$

If $\kappa \ll 2kv$, then the differential equation is approximately solved by,

$$(kv)^3 = 3\varepsilon\kappa U_0^2 \alpha_+^2 t \ . \tag{42.62}$$

This means that the CARL frequency, that is, the frequency difference between the emitted probe wave and the incident light, increases temporarily. The frequency corresponds to the double Doppler shift. As the frequency of the probe light gradually shifts away from the cavity resonance, the probe light finally stops being amplified, and the amplitude of the probe field decreases: CARL is only a transient phenomenon. In fact, the behavior described by the equation (42.61) was observed in experiments [755].

Example 271 (*Universal scaling*): Our formula describing CARL,

$$\begin{aligned} \dot{\alpha}_- &= -\frac{\imath U_0 \eta_+}{\chi} \sum\nolimits_j e^{2\imath k z_j} - \chi \alpha_- \\ k\dot{v}_j &= -4\omega_{rec} \imath U_0 \eta_+ \left(\frac{\alpha_-}{\chi^*} e^{-2\imath k z_j} - \frac{\alpha_-^*}{\chi} e^{2\imath k z_j} \right) - \gamma_{fric} k v_j \ , \end{aligned} \tag{42.63}$$

where $\chi = \kappa + \imath N U_0 - \imath\Delta_c$, can be rewritten in terms of a universal 'scaling' if we define,

$$\tau = 4\omega_{rec}\rho t \quad \text{and} \quad \bar{\gamma} = \frac{\gamma_{fric}}{4\omega_{rec}\rho} \tag{42.64}$$
$$\theta_j = 2kz_j \quad \text{and} \quad P_j = \frac{2kv_j}{4\omega_{rec}\rho}$$
$$A = \frac{\imath|\chi|}{\chi^*\sqrt{\rho N}}\alpha_- \quad \text{and} \quad \bar{\chi} = \frac{\chi}{4\omega_{rec}\rho} \ .$$

We obtain,

$$\dot{A} = \frac{1}{N}\sum\nolimits_j e^{\imath\theta_j} - \bar{\chi}A \tag{42.65}$$
$$\dot{\theta} = P_j$$
$$\dot{P}_j = -2(A^* e^{-\imath\theta_j} + A e^{\imath\theta_j}) - \bar{\gamma}P_j \ .$$

provided that the universal scaling parameter ρ is set to,

$$\rho \equiv \left(\frac{NU_0^2\eta_+^2}{8\omega_{rec}^2|\chi|^2}\right)^{1/3} \ . \tag{42.66}$$

The meaning of the ρ parameter can be gathered by rewriting it in terms of the number of photons of the pump $|\alpha_+|^2 = \eta_+^2/\kappa^2$ and the depth of the dipolar potential $U_d = U_0|\alpha_+|^2$,

$$\rho^3 = \frac{N}{\alpha_+^2}\frac{U_d^2}{8\omega_{rec}^2} \ . \tag{42.67}$$

The ρ parameter therefore indicates the number of atoms per photon and the ratio between the depth of the dipolar trap and the photonic recoil energy.

42.2.2 Observation of CARL in ring cavities

The first observation of CARL was achieved with a cloud of 100 µK cold rubidium atoms interacting with a high finesse ring cavity [755]. In a thermal cloud the atomic motion prevents bunching, i.e. $b = 0$ so that according to Eq. (42.50) the cavity fields do not couple to the atoms. Density fluctuations that could seed CARL dynamics are rapidly washed out by thermal motion.

This problem can be circumvented by applying a robust *pre-bunching*, which can be done by subjecting the atoms to a periodic potential, e.g. via a standing wave formed by two counterpropagating cavity modes. The atoms then arrange themselves into a periodic lattice, so that the bunching parameter is initially $b \simeq 1$. If one cavity is then extinguished, a CARL dynamics can take place, until thermal motion succeeds in washing out the periodic lattice. This dynamics is illustrated in the simulation exhibited in Fig. 42.6 for the case of strontium atoms. The finite temperature of the cloud is accounted for via an initial density and momentum distribution for the atoms given by,

$$p_{0,j} = \sqrt{mk_BT}\ \zeta_j \quad \text{and} \quad z_{0,j} = \frac{\sqrt{2}}{k}\sqrt{\frac{k_BT}{U_0}}\ \zeta_j \ , \tag{42.68}$$

where ζ_j is a normally distributed random variable.

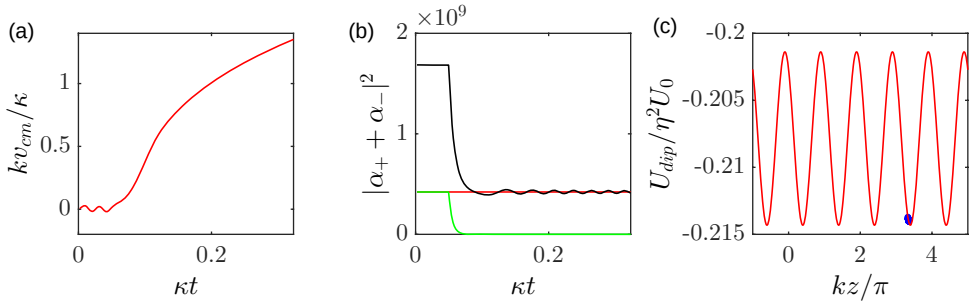

Figure 42.6: (code) Simulation for $N = 10^5$ strontium atoms at $T = 10\,\mu\text{K}$ temperature interacting via their $\Gamma = (2\pi)$ kHz narrow intercombination line at $\lambda = 689\,\text{nm}$ with a ring cavity (decay rate $\kappa = (2\pi)\ 1.7\,\text{MHz}$ and waist $w_0 = 68.4\,\mu\text{m}$). CARL dynamics is triggered by switching off one of two pump lasers whose intracavity power is $P = 1\,\text{W}$. (a) Doppler shift of the CARL-accelerated atoms, (b) interference signal between the two cavity light modes, and (c) atomic distribution in the standing wave potential.

Example 272 (*Curiosities: Atomic transport around mirrors*): Displacement of the atomic cloud in a unidirectionally pumped ring-cavity. The left and right image in Fig. 42.7 are taken for different pumping directions α. The upper cloud shows atoms trapped in the main focus of the ring-cavity. The lower traces stem from atoms transported from the focus passed the mirrors T_1 and T_2 towards the incoupling mirror located at the place where the lower traces intersect. The lower trace are imaged twice, because the imaging beam is reflected from the incoupling mirror surface, before it is sent to a photodiode.

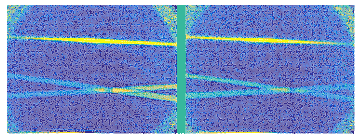

Figure 42.7: Displacement of the atomic cloud in a unidirectionally pumped ring-cavity. The left and right figures are taken for different pumping directions α. The upper cloud shows atoms trapped in the main focus of the ring-cavity. The lower traces stem from atoms transported from the focus passed the mirrors T_1 and T_2 towards the incoupling mirror located at the place where the lower traces intersect. The lower trace are imaged twice, because the imaging beam is reflected from the incoupling mirror surface, before it is sent to a photodiode.

42.2.2.1 CARL in the presence of friction forces

A feature of CARL, as it has been detected in Fig. 42.6 is, that it does not lead to a stationary state: the atoms are monotonically accelerated and the Doppler-shift of the backscattered probe light increases at the same pace. After a while, the frequency of the probe light runs out of the cavity resonance, so that the CARL dynamics starts to be suppressed. This led to a reduction of the oscillation amplitude of the interference signal observed in Fig. 42.6(b).

In order to maintain CARL strong we can think of limiting the acceleration by a friction force. How this works is illustrated in Fig. 42.8, where by subject the atoms to an optical molasses switched on at time $\kappa t = 0.3$. The friction can be incorporated into the CARl equations (42.50) via an additional force,

$$F_{frc} = -\beta_{frc} p \ . \tag{42.69}$$

We observe that the frequency shift of the backscattered light stabilizes at a lower value and that the oscillation amplitude of the interference signal is stronger than without molasses [1343].

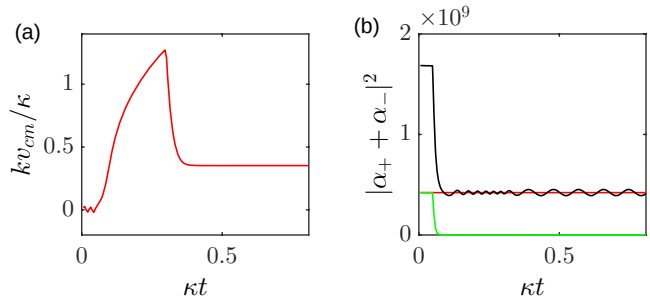

Figure 42.8: (code) Influence of an external friction force (switched on at $\kappa t = 0.3$) proportional to $\beta_{frc} = 3.8 \cdot 10^6\,\mathrm{s}^{-1}$. Other parameters are the same as in Fig. 42.6.

Let us note that, while provide a nice intuition, the description of the impact of an optical molasses force is incomplete, because it disregards heating effects caused by random photon scattering processes. The temperature of the atomic cloud is given by an equilibrium between friction and heating processes. The correct inclusion of optical molasses in the CARL dynamics will be studied in Sec. 42.6.1.

42.2.2.2 CARL in the presence of injected probe light

It is also interesting to study the impact of a weak injected probe light on the CARL dynamics. This light may have the same frequency as the pump light, $\eta_-/|\eta_-| = \eta_+/|\eta_+|$. This is for example the case, when light is backscattered from imperfection of the cavity mirror surfaces. Or may have a different frequency (provided the probe frequency is resonant to a cavity mode),

$$\eta_- = e^{\imath \Delta\nu t} \ . \tag{42.70}$$

The injected light fields η_+ and η_- create a standing light wave potential, in which the atoms move as being subject to an array of hurdles. The CARL force is too weak, the atoms will get stuck. We study this in Exc. 42.2.7.4. In Exc. 42.2.7.5 we study CARL dynamics for the case that the atoms are subject to an additional harmonic potential.

42.2.2.3 Impact of radiation pressure on CARL

CARL is a coherent force resulting from a coupling of only two counterpropagating modes of the cavity. As such, it can be derived from a potential. However, photons

may also be scattered out of the cavity and get lost for the system. These processes give rise to an additional radiation pressure force, which has been given in Eq. (42.46),

$$F_{rp} = 2\hbar k\gamma_0(\alpha_+\alpha_-^* - \alpha_-\alpha_+^*) \ . \tag{42.71}$$

But this force is weak when the laser is tuned far enough from the atomic resonance.

Fig. 42.9 shows a simulation of the impact of radiation pressure for the same system as in Fig. 42.6. For clarity the radiation pressure force has been exaggerated by a factor of 100.

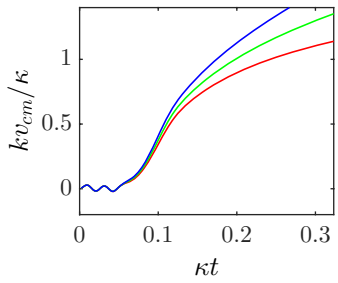

Figure 42.9: (code) Influence of radiation pressure on CARL.

42.2.3 CARL without cavity, propagation effects

Propagation effects are neglected in most treatments. An exception is [1439], who emphasize the important role of light intensity variations along the volume filled by the atomic cloud, within the SVEA, but ignoring interactions and external potentials. The approximation consists in setting $\vec{\mathcal{E}}(\mathbf{r}) = \vec{\mathcal{E}}$, i.e. assuming a uniform coupling strength $g = \frac{\Omega_1\Omega_2}{\hbar\Delta_a}$.

We assume the pump field detuning from the atomic resonance is large enough to neglect radiation pressure and to adiabatically eliminate the internal degrees of freedom. With the single-photon light shift $U_0 = \frac{g^2}{\Delta_a}$, the atomic positions z_n, the probe light field amplitude (scaled to the single-photon field amplitude) α_- and the

pump field α_+ taken as real [10],

$$\frac{\partial^2 R_n}{\partial T^2} = \frac{2\hbar k}{m}\imath U_0\alpha_+\left(\alpha_- e^{-2\imath kR_n} - \alpha_-^* e^{2\imath kR_n}\right)$$
$$\frac{\partial\alpha_-}{\partial T} + c\frac{\partial\alpha_-}{\partial Z} = -\imath U_0\alpha_+\sum_n e^{2\imath kR_n} \ .$$

In scaled units $r_n = 2kR_n$ and $p_n = P_n/\hbar k$ and $t = \omega_r T$ and $z = \omega_r Z/c$ where $\omega_r = 2\hbar k^2/m$,

$$\frac{\partial r_n}{\partial t} = p_n$$
$$\frac{\partial p_n}{\partial t} = \frac{2\imath U_0\alpha_+}{\omega_r}\left(\alpha_- e^{-\imath r_n} - \alpha_-^* e^{\imath r_n}\right)$$
$$\frac{\partial\alpha_-}{\partial t} + \frac{\partial\alpha_-}{\partial z} = -\frac{\imath U_0\alpha_+}{\omega_r}\sum_n e^{ir_n} \ .$$

Introducing the change of variables $\tau = (t-z)\sqrt{z}$ and $r_n(t) = \tilde{r}_n(\tau)$ and $p_n(t) = \sqrt{z}\tilde{p}_n(\tau)$ and $\alpha_-(t,z) = z\tilde{\alpha}_-(\tau)$, and using,

$$\frac{\tau}{2}\frac{\partial\tilde{\alpha}_-(\tau)}{\partial\tau} + \tilde{\alpha}_-(\tau) = \left(\sqrt{z} + \frac{t}{2\sqrt{z}} - \frac{3\sqrt{z}}{2}\right)z\frac{\partial\tilde{\alpha}_-(\tau)}{\partial\tau} + \tilde{\alpha}_-(\tau)$$
$$= \left(\frac{\partial\tau}{\partial t} + \frac{\partial\tau}{\partial z}\right)z\frac{\partial\tilde{\alpha}_-(\tau)}{\partial\tau} + \tilde{\alpha}_-(\tau)$$
$$= z\frac{\partial\tilde{\alpha}_-(\tau)}{\partial t} + z\frac{\partial\tilde{\alpha}_-(\tau)}{\partial z} + \tilde{\alpha}_-(\tau) = \frac{\partial\alpha_-(t,z)}{\partial t} + \frac{\partial\alpha_-(t,z)}{\partial z} \ .$$

[10] Here is a comment that Wolfgang Ketterle made on our papers [1217, 1218]:

> Regarding optical stimulation vs. atomic stimulation: There are two regimes, depending whether the atomic or optical coherences last longer. Indeed, you write: This implies that scattered photons have left the interaction volume before subsequent photons are scattered. In other terms the coherence time of the light modes is too small for the build-up of an optical interference pattern. Therefore the atomic density grating occurring in SRyS is not formed optical dipole forces but arises from the matter wave interference between different momentum states. This explains, why it is important that the thermal energy of the atoms be smaller than the recoil energy $k_BT < 2\hbar^2 2k^2/m$. Otherwise, the Doppler broadening leads to decoherence of the momentum states and consequently to a reduction of the contrast of the matter wave grating. For CARL the situation is reversed. CARL has been observed with temperatures much higher than the recoil temperature, i.e. in a regime where interferences between atoms in Raman superpositions of momentum states are smeared out by Doppler broadening. Here, the optical cavity plays a crucial role, because it stores the scattered light for such long times, that the atoms experience the force of the periodic dipole potential emerging from the interference of the probe with the pump mode. In our experiment, $c/2L = 20\,\mathrm{kHz}$, so that the lifetime is 7 orders of magnitude larger than without cavity. The gain can be varied over wide ranges, $G = 10^3 - 10^9\,\mathrm{s}^{-1}$. I disagree that you can really distinguish between optical dipole forces scattering atoms or matter wave gratings scattering light. This has confused us in earlier work, but in our 2003 Science paper (Schneble et al.) we clearly showed that even the extreme case of SRyS where the photon leaves immediately, can be described as atoms being Bragg scattered by the photons on their way out, in other words, there is a dipole force description even in this case.

it is easy to show,

$$\begin{aligned}\frac{\partial\tilde{r}_n}{\partial\tau} &= \tilde{p}_n \\ \frac{\partial\tilde{p}_n}{\partial\tau} &= \frac{2\imath U_0\alpha_+}{\omega_r}\left(\tilde{\alpha}_- e^{-\imath\tilde{r}_n} - \tilde{\alpha}_-^* e^{\imath\tilde{r}_n}\right) \\ \frac{\tau}{2}\frac{\partial\tilde{\alpha}_-}{\partial\tau} &= -\tilde{\alpha}_- - \frac{\imath N U_0\alpha_+}{\omega_r} b \ .\end{aligned}$$

In Exc. 42.2.7.6 we try a numerical approach.

42.2.4 Optical instability in ring cavities

We have until now concentrated on the regime of weak coupling, $NU_0 < 1$. If the pump laser is tuned closer to resonance, or if the number of atoms is increased, so that $NU_0 > 1$, we observe instabilities in the coupled atom-field dynamics, which critically depend on the pump intensities [942]. Imagine a sample of atoms trapped in an optical lattice formed by a symmetrically pumped ring cavity, $\eta_+ = \eta_-$. The system is stationary, the atoms are confined at the antinodes of the standing wave, the light fields are equal in strength, $\alpha_+ = \alpha_-$. At time $t = 0$ we suddenly reduce the pump rate η_- of the non-stabilized mode by only a few percent. The response of the system observed in experiment [942] is to completely break down the field α_-. The disappearance of the standing wave ejects most atoms and reduces NU_0, until the coupling gets so weak that the dynamics is essentially governed by the injected fields. The system recovers a stationary state, with much less atoms.

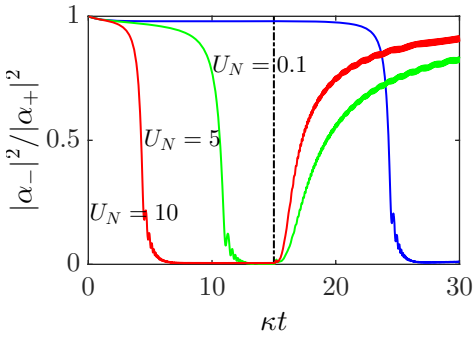

Figure 42.10: (code) Dynamics simulated with equations (42.46). At time $\kappa t = 0$ the pump rate η_- is reduced by 1%. After a certain time that depends on NU_0, the standing wave breaks down ejecting atoms from the mode volume. Here, we simulate this via an artificial linear trap loss process setting in at time $\kappa t = 15$. As a result of the diminishing NU_0 the standing wave recovers.

The physical explanation for the instability is reminiscent to the CARL behavior described in previous sections. Because atom-field coupling is strong, a small imbalance of the injected beam intensities is sufficient to displace the atoms to a location, where the light which they scatter into the reverse direction interferes destructively

with the injected light. A simple argument explains, why the standing wave is attracted towards a position where it gets unstable. We treat the imbalance $\eta_+ > \eta_-$ as if it was due to a scatterer fixed in space inside the mode volume sitting on an edge of the standing wave (corresponding to a $\pi/4$ phase shift), such that it only scatters light from α_+ into α_-, but not the other way round. Whether the phase of the standing wave adjusts itself to that of pump field or such that the scatterer sits at the bottom of the potential well depends on the ratio of the coupling to the external field (given by κ) and to the scatterer (given by U_0). If U_0 is stronger, the field is pulled towards the scatterer dragging along the atoms which are free to move. The stationary situation is therefore a displacement of the standing wave and the atoms by $\lambda/4$, which is just the position where the cavity field α_- and the injected field $\alpha_-^{(in)}$ are out of phase. The injected light is not transmitted through the cavity any more.

Note that the instability occurs in a plane wave situation, there is no need to consider the transversal motion. Furthermore, it is a single-atom effect, since we assume perfect bunching. We may therefore consider a single atom strongly coupled to the cavity and use the set of equations (42.46). In the *undepleted pump approximation* we assume $\dot{\alpha}_+ = 0$, and if the atom adiabatically follows the dynamics of the potential valley, $\ddot{x} = 0$, so that,

$$0 = -\chi\alpha_+ - \imath U_0 \sqrt{\frac{\alpha_+\alpha_-^*}{\alpha_+^*\alpha_-}}\alpha_- + \eta_+ \ , \tag{42.72}$$

$$\dot{\alpha}_- = -\chi\alpha_- - \imath U_0 \sqrt{\frac{\alpha_+^*\alpha_-}{\alpha_+\alpha_-^*}}\alpha_+ + \eta_- \ .$$

The first equation yields,

$$\alpha_+ = \frac{\eta_+}{\chi + \imath U_0 \frac{|\alpha_-|}{|\alpha_+|}} \ , \tag{42.73}$$

$$|\alpha_+| \approx \frac{\eta_+}{\chi}\left(1 - \frac{U_0^2}{2\eta_+^2}|\alpha_-|^2\right) \ .$$

Plugging this result into the second equation and assuming the laser on resonance, $\Delta_c = NU_0$, so that we may replace χ by κ, we get,

$$\dot{\alpha}_- \approx -\kappa\alpha_- - \frac{\imath U_0\eta_+}{\kappa}\frac{\alpha_-}{|\alpha_-|} + \frac{\imath U_0^3}{2\kappa\eta_+}|\alpha_-|\alpha_- + \eta_- \ . \tag{42.74}$$

This equation describes *optical bistability*.

42.2.5 Phononic coupling of atoms mediated by a ring cavity

Phonons can be understood as vibrational excitations of quantum particles (atoms) in quantized traps. When atoms are interconnected in vibrational lattices, phonons can be transferred and shared between atoms [11]. Due to the particularity of the

[11] This is similar to the situation in micromasers, where several atoms can share a single photon.

ring cavity of conserving the photonic momentum at each backscattering event, the photonic momentum can be understood as a phononic excitation, propagating in one dimension along the optical axis of the cavity.

We now consider a symmetrically pumped ring cavity [482]. The atoms are very cold and deep in the Lamb-Dicke regime. Using blue-detuned light the atoms will be trapped at the nodes of the standing wave, $kz_j = \pi/2 + kZ_j$, where Z_j are small displacements. Hence, we may expand,

$$e^{\mp 2\imath k z_j} \simeq -(1 \mp 2\imath k Z_j) \ . \tag{42.75}$$

With the abbreviation $\chi \equiv \kappa - \imath(\Delta_c - NU_0)$ and defining the center-of-mass of the small displacements, $Z_{cm} = \frac{1}{N}\sum_j Z_j$, the equation for the two field modes are,

$$\dot{\alpha}_\pm \simeq -\chi\alpha_\pm + \imath NU_0(\mp 2\imath k Z_{cm})\alpha_\mp + \eta \ . \tag{42.76}$$

Neglecting the impact of the atom on the amplitudes of the fields, we may derive the steady-state solution,

$$\alpha_\pm = \eta \frac{\chi + \imath NU_0(1 \mp 2\imath k Z_{cm})}{\chi^2 + N^2U_0^2} \ . \tag{42.77}$$

As shown in (42.28) the normalized field intensity can be written as,

$$\tfrac{1}{2\varepsilon_0 c E_1^2} I(z,t) = |\alpha_+|^2 + |\alpha_-|^2 + 2|\alpha_+||\alpha_-|\cos(2kz + 2\theta) \ , \tag{42.78}$$

provided the field amplitudes are expressed by,

$$\alpha_\pm = |\alpha_\pm| e^{\pm\imath\theta} \quad \text{such that} \quad \alpha_+\alpha_-^* = |\alpha_+||\alpha_-| e^{2\imath\theta} \quad \text{and} \quad \tan 2\theta = \frac{\mathfrak{Im}\ \alpha_+\alpha_-^*}{\mathfrak{Re}\ \alpha_+\alpha_-^*} \ . \tag{42.79}$$

Now,

$$\begin{aligned} \tan 2\theta &= \frac{\mathfrak{Im}\ [\chi + \imath NU_0(1 - 2\imath k Z_{cm})][\chi^* - \imath NU_0(1 - 2\imath k Z_{cm})]}{\mathfrak{Re}\ [\chi + \imath NU_0(1 - 2\imath k Z_{cm})][\chi^* - \imath NU_0(1 - 2\imath k Z_{cm})]} \\ &= 4NU_0 k Z_{cm} \frac{-\Delta_c + 2NU_0}{-\kappa^2 - \Delta_c^2 + 4\Delta_c NU_0 - 4N^2U_0^2 + 4N^2U_0^2(kZ_{cm})^2} \\ &\simeq \frac{4NU_0(\Delta_c - 2NU_0)}{\kappa^2 + (\Delta_c - 2NU_0)^2} k Z_{cm} \ . \end{aligned} \tag{42.80}$$

An individual atom in this optical potential feels the dipolar force,

$$\begin{aligned} m\ddot{z}_j &= [-\hbar U_0 \partial_z I]_{z=z_j} = 4\hbar k U_0 |\alpha_+||\alpha_-| \sin(2kz_j + 2\theta) \\ &= 4\hbar k U_0 \eta^2 \frac{|(\chi + iNU_0)^2 - 4N^2U_0^2(kZ_{cm})^2|}{|\chi^2 + N^2U_0^2|^2} \sin\left(2kz_j + \frac{2NU_0(\Delta_c - 2NU_0)}{\kappa^2 + (\Delta_c - 2NU_0)^2} 2kZ_{cm}\right) \\ &\simeq \frac{4\hbar k U_0 \eta^2}{\kappa^2 + \Delta_c^2} \sin\left(2kz_j + \frac{2NU_0(\Delta_c - 2NU_0)}{\kappa^2 + (\Delta_c - 2NU_0)^2} 2kZ_{cm}\right) \equiv \frac{m}{2k}\omega_0^2 \sin(2kz_j - 2\mu_j k Z_{cm}) \ , \end{aligned} \tag{42.81}$$

where,

$$m\omega_0^2 \equiv \frac{8\hbar k^2 U_0 \eta^2}{\kappa^2 + 4U_0^2} \qquad \text{and} \qquad \mu_j \equiv \frac{2NU_0|2NU_0 - \Delta_c|}{\kappa^2 + (2NU_0 - \Delta_c)^2} \ . \tag{42.82}$$

Expanding this equation around the nodes we readily obtain,

$$\boxed{k\ddot{Z}_j + \omega_0^2 \mu_j \simeq \mu_j k Z_{cm} = \frac{\mu_j}{N} \sum_j k Z_j} \ , \tag{42.83}$$

which describes the force on a single atom. Note that the harmonic force, $\omega_0^2 k Z_j$, on the atom is continuously fed by the center-of-mass force, $\omega_0^2 \mu_j k Z_{cm}$. The above equation can be rewritten as,

$$\begin{pmatrix} k\ddot{Z}_1 \\ k\dot{Z}_1 \\ k\ddot{Z}_2 \\ k\dot{Z}_2 \\ . \end{pmatrix} = \begin{pmatrix} 0 & -\omega_0^2(1-\frac{\mu_j}{N}) & 0 & -\omega_0^2\frac{\mu_j}{N} & . \\ 1 & 0 & 0 & 0 & . \\ 0 & -\omega_0^2\frac{\mu_j}{N} & 0 & -\omega_0^2(1-\frac{\mu_j}{N}) & . \\ 0 & 0 & 1 & 0 & . \\ . & . & . & . & . \end{pmatrix} \begin{pmatrix} k\dot{Z}_1 \\ kZ_1 \\ k\dot{Z}_2 \\ kZ_2 \\ . \end{pmatrix} \ . \tag{42.84}$$

The eigenvalues of the matrix are $e = \imath\omega_0, \imath\omega_0\sqrt{1-\mu_j}$. Therefore, we expect, in addition to the secular frequency ω_0, a second oscillation frequency,

$$\omega_{cm} = \omega_0\sqrt{1-\mu_j} \ . \tag{42.85}$$

We find splitting in the strong coupling regime, $g > \Gamma$, but we consider the weak coupling regime, $g < \Gamma$, to implement the phononic coupling.

Example 273 (*Two-coupled atoms*): Here we rewrite the field equations for two atoms in center-of-mass coordinates,

$$Z = \frac{z_1 + z_2}{2} \qquad \text{and} \qquad z = z_2 - z_1 \ ,$$

finding,

$$\dot{\alpha}_\pm = (-\kappa + \imath\Delta_c - 2\imath U_0)\alpha_\pm - 2\imath U_0 \alpha_\mp e^{\mp 2\imath k Z} \cos kz + \eta \ .$$

42.2.5.1 Probing the phonon spectrum

To probe the phonon spectrum, we can measure (or simulate) the oscillation of a single atom $z_j(t)$ in the presence of several atoms. The Fourier spectrum of the oscillation should reveal the frequency components of the center-of-mass motion $Z(t)$ and the relative motion.

An experimental method for observing normal modes consists in parametrically exciting the atomic motion at a modulation frequency ω_ϕ and watch out for a resonant enhancement of the vibration amplitude near the secular frequency ω and the collective frequency ω_{cm} both defined in (42.82). In practice, the atomic vibration can be excited by an external force, for example, a Bragg spectroscopic setup as it is used for driving recoil-induced resonances (RIR),

$$\dot{p}_j = 2\imath\hbar k U_0(\alpha_+^*\alpha_- e^{-2\imath k z_j} - \alpha_+\alpha_-^* e^{2\imath k z_j}) + F_{rir}\sin\omega_\phi t \ . \tag{42.86}$$

Alternatively, we may shake the intracavity standing wave by modulating the phase of the pump field,

$$\eta_\pm(t) = \eta e^{\pm \imath \phi_0 \sin \omega_\phi t} \ . \tag{42.87}$$

Fig. 42.11 shows typical resonance curves obtained by simulating the CARL equations (42.50) together with the modulation term (42.87). Being shaken for a while, the atoms suffer parametric heating visible as a noticeable increase of their kinetic energy, as seen in Fig. 42.11(a). The atomic motion, in turn, acts back on the intracavity field fields leading to a modulated photon imbalance between both.

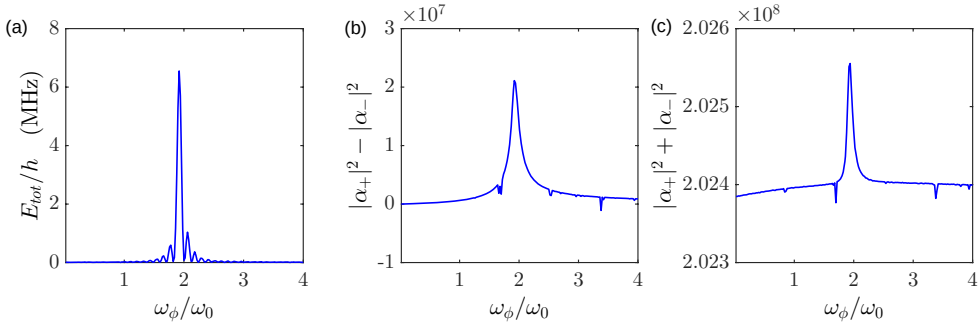

Figure 42.11: (code) Response of the cavity field to a phase modulation of the pump light. (a) Kinetic energy, (b) photon imbalance, and (c) total photon number. The simulation assumes $N = 10^6$ strontium atoms initially at $T = 1\,\mu\text{K}$ driven on the $\lambda = 689\,\text{nm}$ line and $\kappa/2\pi = 3.4\,\text{MHz}$, $\Delta_c = 2U_0$, $\eta = 10^4\kappa$, $NU_0/\kappa = -.02$, $\phi_0 = 0.01$. The calculated secular frequencies are $\omega_0 = 0.35\kappa$ and $\omega_0\sqrt{1-\mu_N} = 0.32\kappa$.

Note, that the phase modulation frequency should not exceed the cavity decay time, $\omega_\phi < \kappa$. Otherwise, even in the absence of atoms, we expect a low-pass behavior as discussed in Sec. 40.1.2, impeding that the applied phase modulation be transformed into an efficient shaking of the phase θ of the intracavity standing wave.

42.2.6 Doppler limit of cavity cooling

The interaction with an optical cavity can reduce the atomic movement. In the case of individual atoms, ... See also (watch talk).

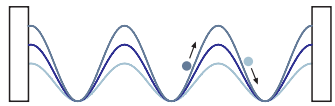

Figure 42.12: The principle of cavity cooling.

For blue detuning and strong coupling [482], the cavity backaction produces a friction force, which can be explained as follows. The field reacts to the atomic displacement with a small time-lag due to κ, which when designed properly produces a stronger deceleration when the atom moves uphill, then an acceleration when it moves

downhill. The cavity backaction thus provides a feedback mechanism to influence the atomic motion. In equilibrium with diffusion, the final temperature is given by,

$$\left(\frac{\partial E}{\partial t}\right)_{cool} = Fv = -m\beta_{fric}v^2 \tag{42.88}$$
$$\left(\frac{\partial E}{\partial t}\right)_{heat} = \frac{\hbar^2k^2}{2m}2R = \hbar\varepsilon R = \hbar\varepsilon\frac{8U_0^2\eta^2}{\kappa(\kappa^2+4U_0^2)} = \hbar\omega_0^2\frac{U_0}{\kappa} \ .$$

For strong coupling, the diffusion rate, $R = 2\frac{\eta^2}{\kappa} = 2\kappa n$, has a simple interpretation as the rate of photon losses by cavity decay. For weak coupling, $R = 8U_0^2\frac{\eta^2}{\kappa^3} = 2\kappa n\left(\frac{2U_0}{\kappa}\right)^2$, the diffusion occurs by redistribution between the cavity modes. In equilibrium,

$$k_BT = mv^2 = \frac{\hbar\varepsilon R}{\beta_{fric}} = -\hbar U_0\left(1+\frac{\kappa^2}{4U_0^2}\right) \ , \tag{42.89}$$

which is roughly on the same order as the Vuletic cooling. For example with the cavity described above and $\Delta\lambda = 0.7$ nm, so that $\Delta_a = \frac{c}{\lambda^2}\Delta\lambda = 2\pi\times 345$ GHz, we have $U_0 = 2.8\times10^{-6}\kappa$. With 10^6 atoms, we expect $T \approx 2.7\ \mu$K.

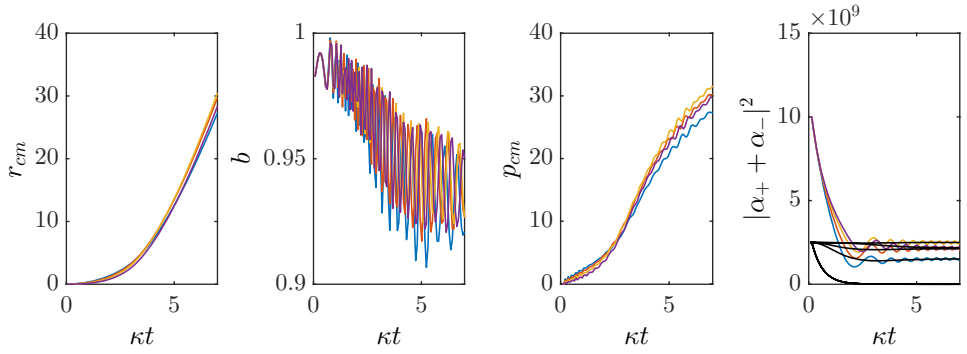

Figure 42.13: (code) Cavity cooling for various detunings.

A more rigorous treatment [482] reveals the dependence of the friction and the diffusion on the detuning,

$$\beta_{fric}^{(\Delta_c)} = \frac{32\varepsilon\eta^2U_0^2\kappa(\Delta_c-U_0)(\kappa^2-2\Delta_cU_0+\Delta_c^2)}{(\kappa^2+\Delta_c^2)^2[\kappa^2+(2U_0-\Delta_c)^2]^2} \ , \tag{42.90}$$

$$\left(\frac{\partial E}{\partial t}\right)_{heat}^{(\Delta_c)} = \hbar\varepsilon\frac{8\kappa U_0^2\eta^2}{(\kappa^2+\Delta_c^2)[\kappa^2+(2U_0-\Delta_c)^2]},$$

$$k_BT^{(\Delta_c)} = \frac{\hbar(\kappa^2+\Delta_c^2)[\kappa^2+(2U_0-\Delta_c)^2]}{4(\Delta_c-U_0)[\kappa^2-\Delta_c(2U_0-\Delta_c)]} \ .$$

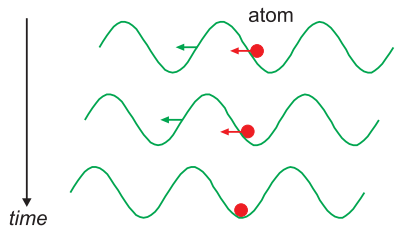

Figure 42.14: Cavity-cooling.

When the energy dissipation is made by the cavity rather than internal degrees of freedom [1349]. The cooling limit for *cavity-cooling* is than,

$$k_B T = \frac{1}{2}\hbar\kappa \left(1 + \frac{k^2 w^2}{6Q}\right) \ . \tag{42.91}$$

For a typical ring-cavity $T \approx 5\ \mu$K. The cooling power is,

$$P = \hbar\kappa.... \tag{42.92}$$

It depends a lot on the Doppler-shift of the moving atom. The capture range is limited to $kv < \kappa$.

42.2.6.1 Dissipation in cavities

We showed above that the center-of-mass motion of the atomic ensemble interacting with a symmetrically pumped ring cavity is rapidly damped. But this is not true for the motion of the individual atoms, that is, the temperature of the set is not easily reduced. To see this we look at the CARL equation (42.26) for the dipole force,

$$m\ddot{z}_j = 2\imath\hbar k U_0(\alpha_+^*\alpha_- e^{-2\imath k z_j} - \alpha_+\alpha_-^* e^{2\imath k z_j}) \ , \tag{42.93}$$

and we consider two atoms initially located in the positions $z_{1,2} = \pm z_0$. We notice that the force on the relative motion is zero,

$$m\ddot{z}_1 - m\ddot{z}_2 = 0 \ . \tag{42.94}$$

That is, the number of photons backscattered by each atom is compensated, such that the light field does not take notice of the motion of the two atoms and therefore can not dissipate its energy.

The first order fluctuations of the positions are $\langle z\rangle = 0$, but second order fluctuations, i.e. the temperature $\sim \langle z^2\rangle$, can eventually interact with the light field. Other ideas are needed to lower the temperature.

42.2.6.2 Sideband cooling in cavities

In a ring-cavity the coupling of the counter-propagating modes results in a Stark-splitting by $2U_0$ into two modes. The mode at $\Delta_c = 2U_0 < 0$ supports atoms, the one at $\Delta_c = 0$ is empty. Since $\kappa < \omega_z$, for $2U_0 \approx \omega_z$ we can do cavity sideband-cooling.

Furthermore, bunching of the atoms into the nodes modifies $\sum_k U_0 e^{-2\imath k z_k}$, which can result in self-locking. Also the laser locks automatically to the red-shifted atom-filled mode [415].

The transition can be decomposed into a spontaneous Raman transition (cavity field driven excitation followed by spontaneous emission into free space modes) and a stimulated Raman transition (cavity field driven excitation followed by cavity-stimulated emission). Let $\tilde{\Gamma}_{free} = k^3 d^2/6\pi\varepsilon_0\hbar$ be the free-space scattering rate. The scattering into a cavity mode is enhanced by $\eta_c = \tilde{\Gamma}_{cav}/\tilde{\Gamma}_{free} = 12F/\pi k^2 w^2$ [1349]. The transition between vibrational sidebands must be weighted by $\eta_{LD} = \varepsilon_{recoil}/\omega_{vib}$. If the emission takes place on a sideband which is not resonant to a cavity mode, the transition rate is reduced by the factor $\xi = (1 + (2\omega_{vib}/\kappa)^2)^{-1}$. Thus ...

42.2.7 Exercises

42.2.7.1 Ex: Anticorrelated atoms

Study the CARL equations (42.50) for the case of two fixed atoms sitting at positions $kz_1 = kz_2 - \pi$.

Solution: *For two atoms the CARL equations become,*

$$\dot{\alpha}_\pm = -\kappa\alpha_\pm - \imath U_0 e^{\mp 2\imath k z_1}\alpha_- - \imath U_0 e^{\mp 2\imath k z_2}\alpha_\mp + \eta_\pm \ .$$

Inserting the positions,

$$\dot{\alpha}_\pm = -\kappa\alpha_\pm + \eta_\pm \ ,$$

we find that the equations decouple, such that the impact of the atoms on the light modes vanishes.

42.2.7.2 Ex: Coupled motion of Rb and Cs atoms in a ring-cavity

Find out by simulation of the classical CARL equation, whether the motion of a Rb atom and a Cs atom can be coupled to the same mode of a ring cavity.

Solution: *a. For a single Rb and a single Cs atom the result is shown in the following movie (watch movie).*
b. For a rubidium and cesium cloud the result is shown in the following movie (watch movie). We how the rubidium cloud accelerates the initially resting cesium cloud.

42.2.7.3 Ex: Inertially moving atom in a ring-cavity

Illustrate by simulation of the classical CARL equation, how an inertially moving single atom pushes the wave formed by two counterpropagating modes of a ring cavity.

Solution: *The result is shown in the following movie (watch movie).*

42.2.7.4 Ex: CARL in a harmonic potential

Extend the CARL dynamics by an additional harmonic potential for the atoms and study the steady state gain as a function of cavity detuning Δ_c.

Solution: *Assuming a real and constant pump α_+ and using the abbreviation $\theta_j \equiv 2kx_j$, the fundamental equations of the CARL are [173],*

$$\dot{\alpha}_- = (-\kappa + \imath\Delta_c - \imath NU_0)\alpha_- - \imath U_0\alpha_+ \sum_j e^{-\imath\theta_j}$$
$$\ddot{\theta}_j = 8\imath\omega_{rec}U_0\alpha_+(\alpha_- e^{-\imath\theta_j} - \alpha_-^* e^{\imath\theta_j}) - \nu^2\theta_j \ .$$

Integrating the equation for the field,

$$\alpha_- = \alpha_{0-} + e^{(-\kappa+\imath\Delta_c-\imath NU_0)t}\imath U_0\alpha_+ \int_0^t d\tau e^{(\kappa-\imath\Delta_c+\imath NU_0)\tau} \sum_j e^{-\imath\theta_j(\tau)} \ .$$

Now we make the ansatz of a sinusoidal motion, $\theta_j(t) = \theta_{j0}\cos(\nu t + \phi_{j0})$, and use the expansion $e^{\imath\xi_0\sin\varphi} = \sum_n \mathcal{J}_n(\xi_0)e^{\imath n\varphi}$,

$$\begin{aligned}
\alpha_- &\simeq e^{(-\kappa-\imath U_0+\imath\Delta_c)t}\imath NU_0\alpha_+ \int_0^t d\tau e^{(\kappa+\imath NU_0-\imath\Delta_c)\tau} \sum_{j=1}^N e^{-\imath\theta_{j0}\cos(\nu\tau+\phi_{j0})} \\
&= e^{(-\kappa-\imath U_0+\imath\Delta_c)t}\imath NU_0\alpha_+ \int_0^t d\tau e^{(\kappa+\imath NU_0-\imath\Delta_c)\tau} \sum_{j=1}^N \sum_{n=-\infty}^{\infty} \mathcal{J}_n(\theta_{j0}) e^{\imath n(\nu\tau+\phi_{j0}-\pi/2)} \\
&= e^{(-\kappa-\imath U_0+\imath\Delta_c)t}\imath NU_0\alpha_+ \sum_{j=1}^N \sum_{n=-\infty}^{\infty} \mathcal{J}_n(\theta_{j0}) e^{-\imath n(\phi_{j0}-\pi/2)} \int_0^t d\tau' e^{(\kappa+\imath U_0-\imath\Delta_c-\imath n\nu)t'} \\
&= \imath NU_0\alpha_+ \sum_{j=1}^N \sum_{n=-\infty}^{\infty} \mathcal{J}_n(\theta_{j0}) e^{-\imath n(\phi_{j0}-\pi/2+\nu t)} \frac{1 - e^{(-\kappa-\imath NU_0+\imath\Delta_c+\imath n\nu)t}}{\kappa + \imath NU_0 - \imath\Delta_c - \imath n\nu} \\
&\overset{t\to\infty}{\longrightarrow} \sum_{n=-\infty}^{\infty} \sum_{j=1}^N \mathcal{J}_n(\theta_{j0}) \frac{\imath NU_0\alpha_+ e^{-\imath n(\phi_{j0}-\pi/2+\nu t)}}{\kappa + \imath NU_0 - \imath\Delta_c - \imath n\nu} \ .
\end{aligned}$$

We find [1406] that, unlike the original CARL, the system evolves to a steady state and continuously emits light. As shown in Fig. 42.15, the probe is strongly amplified when its detuning coincides with multiples of the secular frequency of harmonic potential. This effect is due to a collective response of the atomic motion to the incident pumping beam, inducing a synchronization of its oscillations in the potential.

42.2.7.5 Ex: Impact of potential barriers on CARL

Illustrate by simulation of the classical CARL equations how (a) mirror backscattering and (b) an external harmonic trapping potential influence the dynamics of an atom interacting with two counterpropagating modes of a ring cavity.

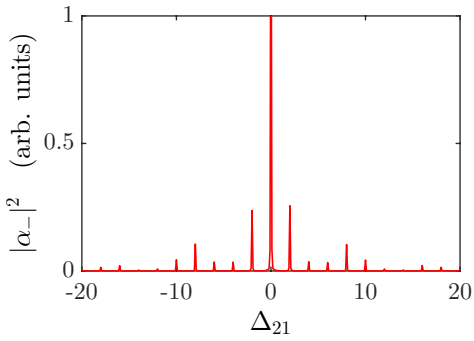

Figure 42.15: (code) Gain spectrum of the CARL confined to a harmonic potential.

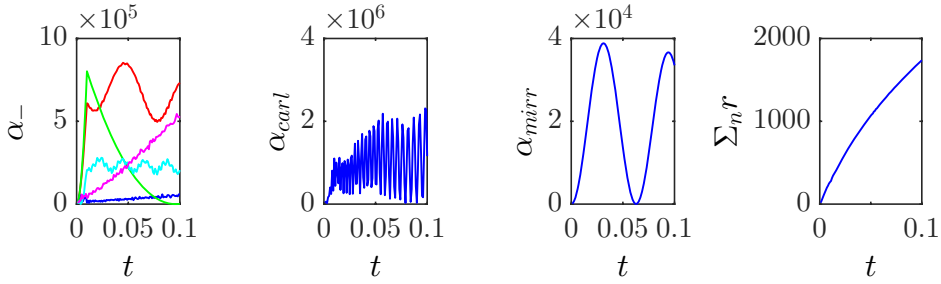

Figure 42.16: (code) Influence of mirror backscattering on CARL.

Solution: *a. The result is shown in Fig. 42.16.*
b. The result is shown in Fig. 42.17.

42.2.7.6 Ex: CARL without cavity

Discuss whether CARL can be observed without a ring-cavity.

Solution: *a. The result is shown in Fig. 42.18.*

42.2.7.7 Ex: Cavity cooling in a ring cavity

Study cavity cooling in a ring cavity as a function of (a) friction and (b) detuning.

Solution: *a. The result is shown in Fig. 42.19. b. The result is shown in Fig. 42.20.*

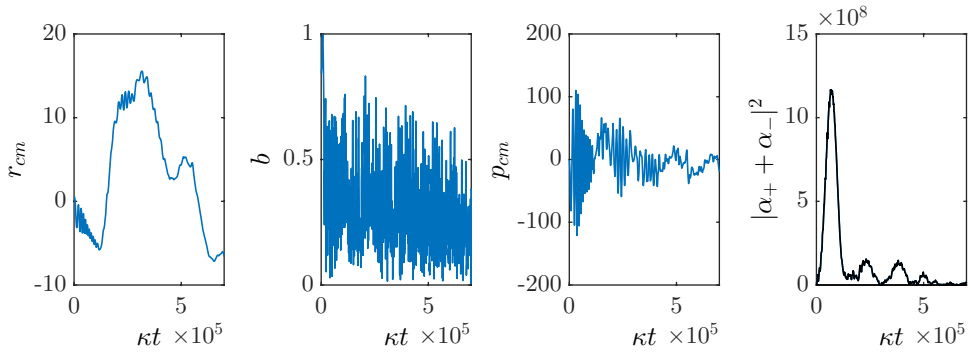

Figure 42.17: (code) Atoms in a harmonic trap irradiated by a pump laser, universally scaled version.

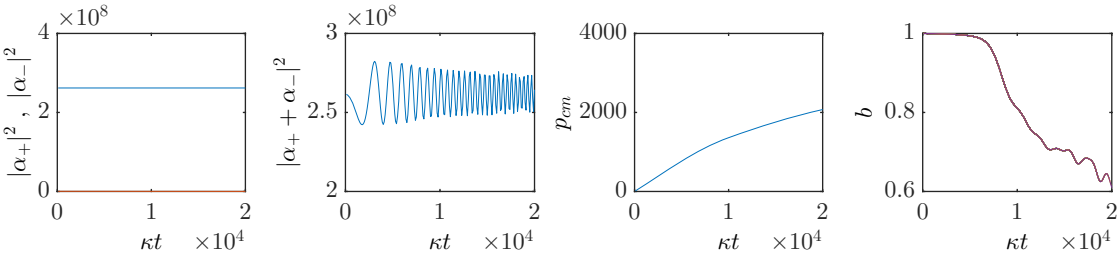

Figure 42.18: (code) One-sided switch-off experiments with/out cavity.

42.2.7.8 Ex: Motion of atoms in a ring-cavity including internal states

Motion of atoms in a ring-cavity, including internal states.

Solution: *The result is shown in Fig. 42.21.*

42.3 Phenomena related to CARL

The *collective atomic recoil laser* (CARL) unifies the principles of the FEL and LWI. Assume two-level atoms in their ground state moving against the pump beam $\mathbf{k}_2$. An (at first) weak probe beam k_1 which is blue detuned with respect to $\mathbf{k}_2$ builds a together with $\mathbf{k}_2$ a standing wave fraction moving in direction $\mathbf{v}$. This fraction gives rise to a moving dipole potential $V(\mathbf{r})$ and a light force on the atoms. If the moving standing wave is slower than the atoms (and the light frequency detuning from the atomic resonance is suitable), the atoms fall into the potential valleys by rescattering photons from the pump into the probe wave. This way they amplify the probe (they push the ponderomotive wave like the FEL), deepen the light potential valleys, are therefore further focused, etc.. We get a self-amplifying avalanche and feedback. In this process, the kinetic energy of the atoms is transformed into laser light. Or to resume: Collective recoil with self-bundeling produced by cooperative

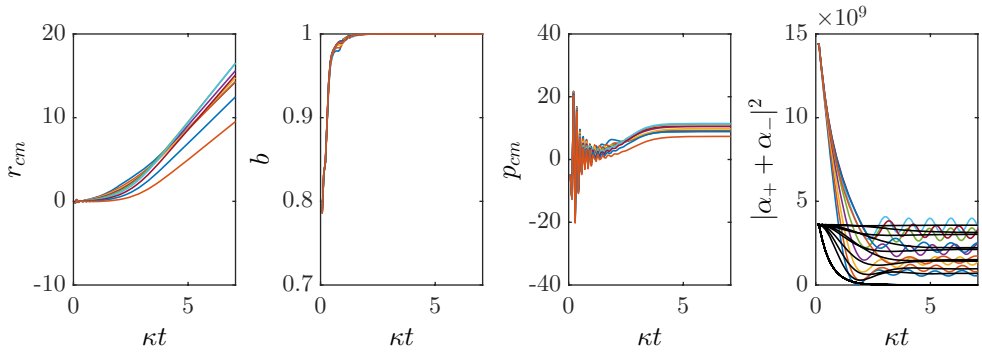

Figure 42.19: (code) Cavity cooling in a ring cavity as a function of friction.

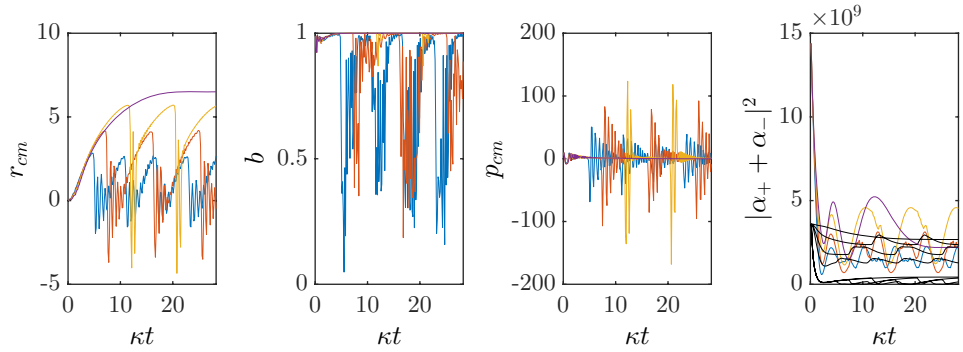

Figure 42.20: (code) Cavity cooling in a ring cavity for various detunings.

Compton-scattering generates coherent laser light [173].

The following notes first discuss the basic equations of motion in the limit of very far detuning, where the internal dynamics can be adiabatically eliminated. Then we turn our attention to some characteristic features of CARL.

42.3.1 Doppleron resonances

According to Stenholm [1262] the Raman type alternating absorption and emission can be interpreted as emission and absorption of *dopplerons*, the following conditions are equivalent,

$$\omega_0 = (l+1)(\omega + \mathbf{k}\cdot\mathbf{v}) - l(\omega - \mathbf{k}\cdot\mathbf{v}) \ . \tag{42.95}$$

The Hamiltonian is,

$$\hat{H} = \hbar\Delta\sigma^+\sigma^- + kvb^\dagger b + g/2(\sigma^+ + \sigma^-)(b^\dagger + b) \ , \tag{42.96}$$

where $\Omega \approx \sqrt{n}g$ and $b^\pm$ denotes absorption out of the wave $\omega \pm \mathbf{kv}$ or emission into the wave $\omega \mp \mathbf{k}\cdot\mathbf{v}$. Doppleron resonances can be observed experimentally.

In the experiment we sometimes observe subharmonics. The question arises whether these could be interpreted as higher-order photon scattering processes. There are

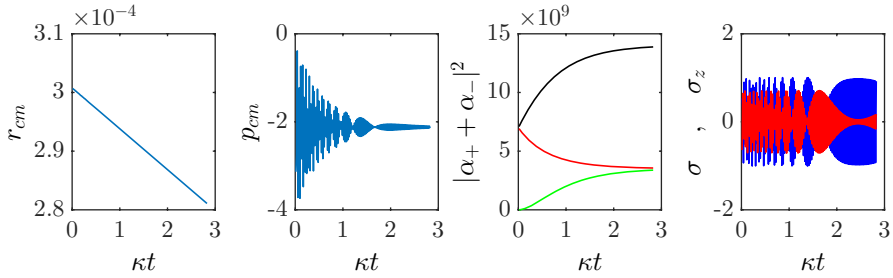

Figure 42.21: (code) Close to resonance.

two possibilities: Multiple scattering with real intermediate states or Doppleron-resonances.

Doppleron resonances are velocity-tuned resonances. The detuning of the intermediate state from the dispersion relation follows from,

$$d_1 = \omega_{pp} - \omega_{pr} - \frac{(p+2\hbar k)^2}{2m} + \frac{p^2}{2m} \qquad (42.97)$$
$$2(\omega_{pp} - \omega_{pr}) = \frac{(p+4\hbar k)^2}{2m} - \frac{p^2}{2m} \ .$$

By eliminating $\omega_{pp} - \omega_{pr}$ we find $d_1 = 2\hbar\varepsilon$. For our parameter regime $\omega_{pr} \gg \varepsilon$. Single photon $\omega_{pr} = \omega_{pp} - kv$, Doppleron $\omega_{pr} = \frac{1}{2}\omega_{pr}$ higher orders $\omega_{pr} = 2\omega_{pp} - kv - \varepsilon_1 - \varepsilon_2$.

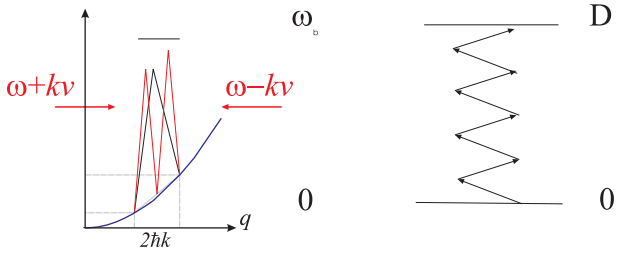

Figure 42.22: Scheme of Doppleron resonances.

42.3.2 Recoil-induced resonances

The *recoil-induced resonances* (RIR) can be explained in two complementary pictures [305]. In the Raman picture, an atomic transition stimulates Raman transitions between momentum states of the free atom without influencing the atomic excitation (the atom remains in a dark state) $\rho_{atom} \otimes |\mathbf{p}\rangle\langle\mathbf{p} + 2\hbar\mathbf{k}|$. Absorption $\Delta > 0$ or amplification $\Delta > 0$ of the probe field $\mathbf{k}_s$ by the pump field $\mathbf{k}_p$ is a result of the population imbalance. However, it is not an excitation imbalance (compare LWI) $\rho_{atom} \otimes |\mathbf{p} + 2\hbar\mathbf{k}\rangle\langle\mathbf{p} + 2\hbar\mathbf{k}| - \rho_{atom} \otimes |\mathbf{p}\rangle\langle\mathbf{p}|$. In the Rayleigh picture the RIRs are an effect of coherent backward *Bragg scattering* of the probe wave at the phase-lag

between the induced light-shift grating and the atomic density grating resulting from the periodic optical potential.

42.3.2.1 RIR-spectroscopy

Two laser beams 1 and 2 having each two different frequencies $\omega - \Delta\omega/2$ and $\omega + \Delta\omega/2$ are irradiated from two different directions enclosing a small angle θ into the atomic trap,

$$\begin{aligned} \mathcal{E}(\mathbf{r},t) &= \mathcal{E}_1 + \mathcal{E}_2 \\ &= \mathcal{E}^{(0)} \left[\cos\left(\mathbf{k}_1\cdot\mathbf{r} - (\omega - \tfrac{1}{2}\Delta\omega)t\right) + \cos(\mathbf{k}_2\cdot\mathbf{r} - \left(\omega + \tfrac{1}{2}\Delta\omega\right)t)\right] \\ &\approx 2\mathcal{E}^{(0)} \cos\left(\mathbf{K}\cdot\mathbf{r} - \omega t\right)\cos\left(\tfrac{1}{2}\mathbf{q}\cdot\mathbf{r} - \tfrac{1}{2}\Delta\omega t\right) \ , \end{aligned} \tag{42.98}$$

where $\mathbf{q} \equiv \mathbf{k}_2 - \mathbf{k}_1$ and $\mathbf{k} \equiv \frac{1}{2}(\mathbf{k}_2 + \mathbf{k}_1)$. The cycle-averaged intensities are $I_i(t) = 2\varepsilon_0 c|\mathcal{E}_i|^2 = 4\varepsilon_0 c\mathcal{E}^{(0)} \cos\left(\frac{1}{2}\mathbf{q}\cdot\mathbf{r} - \frac{1}{2}\Delta\omega t\right)$. Atoms coherently interacting with the light fields (which are tuned far from any atomic resonance) can redistribute the photons between the optical modes in a *nearly-degenerate* four-wave mixing process (4WM) thus modifying the amplitudes $\mathcal{E}_i^{(0)}$ so that a signal occurs.

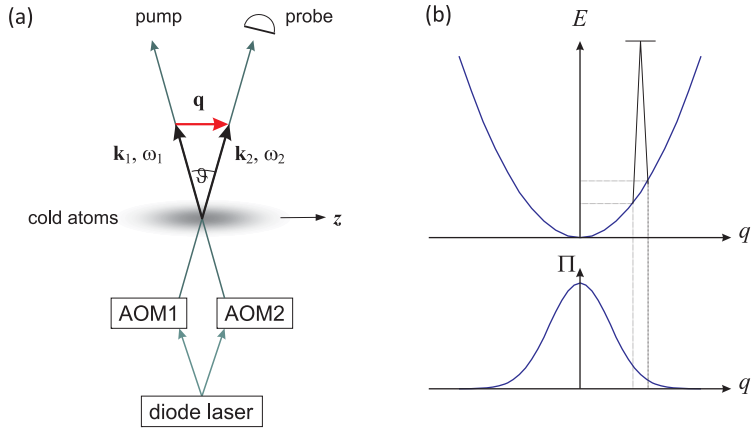

Figure 42.23: Principle scheme for RIR spectroscopy.

From symmetry considerations, it is easy to see that a homogeneous density distribution (along $\mathbf{q}$) of the motionless atoms does not give rise to a signal, neither. So let us assume that the atoms be bunched inside an optical grating according to some periodic distribution $n(z) = n_0 \sin^2 k_\lambda z$, but disregard their kinetics. The signals then generalize to,

$$\begin{aligned} \mathcal{E}_1(z,t) &= \mathcal{E}_1 + \beta n(z)\chi^{(3)}(\mathcal{E}_1 + \mathcal{E}_2)\mathcal{E}_1\mathcal{E}_2\mathcal{E}_1 + \beta n(z)\chi^{(3)}(\mathcal{E}_1 + \mathcal{E}_2)\mathcal{E}_1\mathcal{E}_2\mathcal{E}_1 \\ &= \mathcal{E}_1 + \beta n(z)\chi^{(3)}\left(2\mathcal{E}^{(0)}\cos\left(\tfrac{1}{2}qz - \tfrac{1}{2}\Delta\omega t\right)\right)\mathcal{E}_1\mathcal{E}_2\mathcal{E}_1 \end{aligned} \tag{42.99}$$

and analogous for $\mathcal{E}_2(z,t)$. Or following Lambert-Beer [748],

$$\begin{aligned} I_1(x,z,t) &= |\mathcal{E}_1|^2 \exp\left(2\imath\frac{\pi}{\lambda}\int \chi^{(3)}\left(2E^{(0)}\cos\left(\tfrac{1}{2}qz-\tfrac{1}{2}\Delta\omega t\right)\right)dy\right) \\ &= |\mathcal{E}_1|^2 \exp\left(2\imath\frac{\pi}{\lambda}\int n(x,y,z)...dy\right) \\ &= |\mathcal{E}_1|^2 \exp\left(2\imath\frac{\pi}{\lambda}n_0\sin^2 k_\lambda z\int ...dy\right) \\ I_1(t) &= \int I_1(x,z,t)dxdz\ . \end{aligned} \tag{42.100}$$

Regarding the momentum transfer, the 4WM process can be interpreted as Bragg scattering af the atoms at one of the two counterpropagating standing waves. We develop the theory if Bragg scattering in Sec. 47.2.

42.3.2.2 Temperature measurements via RIR

Temperature measurement are usually carried out by the time-of-flight method followed by absorption imaging. Alternatively, one can perform spectroscopy of RIR resonances. In the latter case, we detect intensity variations in a probe laser beam, i.e. the polarisation of the sample under the influence of *all* irradiated laser beams. In the example 200, we have seen that $\alpha \propto \mathfrak{Im}\ \chi \propto \mathfrak{Im}\ \mathcal{P} \propto \mathfrak{Im}\ \rho_{12}$. It is thus sufficient to calculate the atomic coherences, if necessary including the motional states of the atoms. Calculated by [559]

$$W(t) = \frac{\pi}{2}\frac{\Omega_1\Omega_2}{\Delta}\sqrt{\frac{mv}{k_BT}}\left[\frac{\partial}{\partial v}e^{-mv^2/2k_BT}\right]_{v=\Delta\omega(t)/q}\ . \tag{42.101}$$

42.3.2.3 RIR-spectroscopy on trapped atoms

In the case of free particles, the Raman beams interact for every detuning with a different velocity class of atoms. The atoms are almost not disturbed. In the case of trapped atoms, a coherence can be excited, and since the atoms periodically change their velocity, be read out or reexcited at a later time. The same atom can thus interact with the Raman beams at different times/detunings. If the trap is a standing wave, the situation is complicated by the fact that there are two overlapping gratings: The standing wave and the Raman grating. However, if the trap is much deeper than the Raman grating the atoms can be considered as localized.

The signature of atomic oscillation is a modulation in the RIR signal with the periodicity of the secular frequency [747, 1067].

Let us consider a standing-wave dipole-trap with $\omega_z = 2\pi \times 700\,\mathrm{kHz}$, $\omega_r = 2\pi \times 1\,\mathrm{kHz}$ and $U_{dip} = h \times 30\,\mathrm{MHz}\ = 4000 \times 2\varepsilon = 45\omega_z = 2100\omega_z$. The $100\,\mu\mathrm{K}$ cold atoms are therefore deep inside at the bottom of trap. This implies that the atomic energy levels are sharp and equally distant, and that the transitions are degenerate upon coupling by Raman-beams. If we apply a scan of $\pm 2\pi \times 300\,\mathrm{kHz}$, we will not excite the longitudinal motion. But the radial motion can be excited. As seen earlier the absorption signal is $\alpha \propto \mathfrak{Im}\ \rho_{12}$. What happens to the coherence, if the radiation is swept across a resonance depends on the scanning speed. If the scan is slow, we expect

$\alpha \propto \mathfrak{Im}\ \rho_{12}(\infty)$. We should be able to resolve the resonances [559, 561, 560] as peaks at $\pm\omega_r, \pm 2\omega_r, ...$ In contrast, if the scan is fast, as long as Δ_c is far from resonance, the population of the excited level ρ_{22} is just too small and nothing happens. When Δ_c passes through 0, the coherence ρ_{12} is excited, and can now be driven by the laser even when Δ_c is tuned far away. The coherence precesses faster and faster.

Let us compare to the situation of a laser swept across an electric dipole resonance. In analogy to the cavity response in reflection to a laser scanned across an eigenfrequency, we might expect a ringing coming from interference of the radiating electric dipole (which has been induced while the laser was close to resonance) with the original laser frequency. The radiated electric field is proportional to the excited state population. If we allow for a change of the input field, for example $\Delta_c(t)$, the Bloch-equations must be numerically integrated,

$$\rho(t + dt) = \rho(t) + dt\ M\rho(t)\ . \tag{42.102}$$

It is already clear that we should expect a ringing with exactly the time-dependent frequency $\Delta_c(t)$. Fig. 42.24 shows

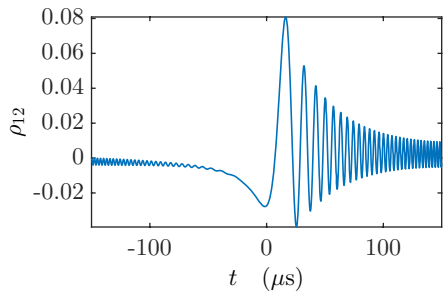

Figure 42.24: (code) Time-evolution of the atomic coherence as the driving laser frequency is swept across resonance. The parameters are $\Gamma = 2\pi \times 8\,\mathrm{kHz}$, $\Omega = 0.2\Gamma$, $\Delta = -50\Gamma..50\Gamma$ and $t = -150..150\,\mu\mathrm{s}$.

This simple mathematical model only assumes a resonance with a given width and a frequency-scanned oscillator. The physical nature of the resonance and the level splitting are not specified and the formalism should be applicable to a variety of situations. A ringing is, in fact, observed for RIR scans, if the scanning speed is too fast, in particular for atoms trapped in optical lattices. Ringing can also be generated in classical harmonic oscillators and laser-driven two-level systems as we will see in Exc. 50.1.10.5.

42.3.2.4 RIR versus CARL

The dynamics is characterized by backaction of the atomic motion onto the cavity field. In this respect there is a connection to RIR resonances in the limit investigated by [748]. While normal RIR is the action of the atomic motion on light fields, they demonstrate that in the same time the Raman-lattice influences the atomic motion. The coherence is limited by the time the photon spends in the sample (similar to the limitation of superradiant Rayleigh scattering, without photonic recycling by a

ring-cavity). Real backaction in the sense of coherent interdependence of the photonic and the kinetic degrees of freedom requires recycling of the photons.

42.3.3 FEL: the free electron laser

Normal lasers work by an inversion in the internal degrees of freedom, that is, bound electrons are excited to energetically higher orbitals, from where they can decay by emitting monochromatic light of well-defined frequency. Because, the *free electron laser* (*FEL*) works with beams of *free* electrons, they are tunable over wide frequency ranges. They have much higher efficiencies above 65%.

The principle is the following: Relativistic electrons are guided through an *undulator*, which is a device producing a magnetic field with periodically alternating polarization. Here, the electrons are subjected to a Lorentz force, $\mathbf{F} = -e\mathbf{v} \times \mathbf{B}$, forcing the electrons to oscillate with the periodicity of the undulator field. This corresponds to a dipole moment interacting with the incident light field. The transverse velocity of the electrons within the magnetic field of an incident light produces a Lorentz force in the axial direction called *ponderomotive force*. This force accelerates the electrons when they are a bit slower than the ponderomotive wave. Otherwise the electrons are decelerated. In the second case, the energy of the electrons is transmitted to the light field, which leads to a *bunching* of the atoms. Because it is a parametric process, there is a continuous energy flow between the field and the motion of the e^- (analogous to parametric Raman cooling). Thus, the FEL converts the kinetic energy of the electron beam into laser radiation. The inversion in a FEL can be interpreted as a relative displacement of the probability distributions for absorption and emission of photons in momentum space,

$$\begin{aligned} W_{abs}(\Delta) &= \operatorname{sinc}^2 \tfrac{1}{2}(\Delta + \varepsilon/2) \\ W_{abs}(\Delta) &= \operatorname{sinc}^2 \tfrac{1}{2}(\Delta - \varepsilon/2) \ , \end{aligned} \tag{42.103}$$

where $\varepsilon = \hbar k^2/2m_e$. The gain is a convolution of the difference of the above distribution with the momentum distribution of the electrons [1177].

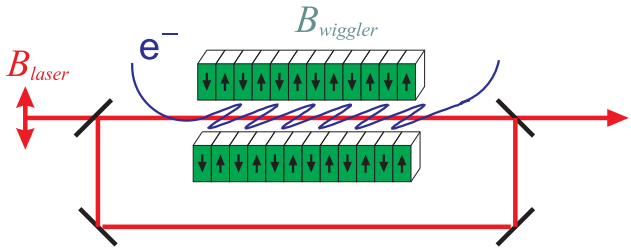

Figure 42.25: Free electron laser.

There various kinds of FELs. In stimulated Compton FELs, described by the shown Feyman graphs, the electrons are scattered by virtual (momentum transfer without energy transfer) photons of the wiggler. In Bremsstrahlungs FEL, the electrons are scattered at a static field. Virtual photons of the static field are scattered at the electrons, who then emit Bremsstrahlung an change their propagation direction. In Raman FELs very dense electron beams produce charge density oscillations,

which provides an additional effect. Free Electron Lasers already have a wide range of application ranging from biology and medicine to lithography and material science.

42.3.4 CARL in an ion storage ring

Bonifacio *et al.* [174] suggested to study collective atomic recoil lasing (CARL) with relativistic atoms. They found that using very fast atoms it should, in principle, be possible to get large CARL frequency shifts and much higher power enhancement factors than observed in free-electron lasers (FEL). Relativistic atomic velocities can be achieved in heavy ion accelerators such as the GSI heavy ion accelerator in Darmstadt and TSR ion storage ring in Heidelberg. Therefore the question arises, if CARL could be an alternative way to produce very energetic and intense UV radiation in concurrence to the FEL. In fact, CARL-based systems may prove more powerful and versatile as their electronic counterparts: Cooling techniques based on electron beams or on hybrid optical-radiofrequency friction forces are able to cool the ionic beams down to mK temperatures.

The CARL which has been predicted ten years ago by Bonifacio *et al.* [173], has recently been observed with cold atoms stored in a high-finesse ring cavity [755, 1343]. This proof of principle, now may motivate a deeper study of the figure of merit of a relativistic CARL. This short note, however, shows that a relativistic CARL is still, in my opinion, far from being realizable.

42.3.4.1 Typical heavy ion accelerator data

In his paper Bonifacio [175] suggests a ^{133}Cs beam with $E = mv^2 = 100\,\mathrm{MeV}/u$. This corresponds to a velocity of $\beta_r = c^{-1}\sqrt{2 \times 133E/m} = 0.46$ and $\gamma_r = 1.13$. The frequency is upshifted by $\omega_{pr}/\omega_{pp} = 2.4$ (from 1330 nm passing 856 nm towards 549 nm). Now ^{133}Cs is neutral, however various ionic species have been accelerated, such as $^{9}Be^{+}$ or $^{7}Li^{+}$. Bonifacio also assumes a beam density of $10^{17}\,\mathrm{m}^{-3}$ corresponding to a ion current of $I = 20\,\mathrm{A}$ and a radius of 1 mm. This current seems excessively high for state-of-the-art technologies. For comparision the following table resumes a few typical heavy ion accelerator data.

	Exper. at TSR	Exper. at GSI	Bonifacio's proposal
Ion species	$^{9}Be^{+}$	$^{7}Li^{+}$	^{133}Cs
Cooling resonance	$D2$ @ 313 nm		$D2$ @ 856 nm
Hyperfine splitting	1.3 GHz		
Ion energy $E = mv^2$	7.3 MeV		100 MeV/u
Ion velocity in β_r	0.042		0.46
Ion number N	10^7		
Circumference l	55.4 m		
Ion distance $d = l/N$	5.54 µm		
Beam diameter σ	0.4 mm		1 mm
Density $n = N/\sigma^2 l$	5×10^8 m^{-3}		10^{17} m^{-3}
Revolution time $t_{rev} = l/c\beta_r$	4.4 µs		
Ion current $I = Ne^-/t_{rev}$	0.36 µA	1 mA	20 A
Ion current density		10 A/cm^2 of 50 ns duration	
Beam temperatures	optical cooling	e^- beam cooling	
Pump laser wavelength	300 nm		1330 nm
Pump laser power			50000 W

42.3.4.2 Questions and suggestions

1. The low ion beam densities may constitute a major problem to relativistic CARL. The 20 A assumed in [175] are far from being realistic, i.e. about 7 orders of magnitude too high. For comparison: Typical electron beam densities are $n = 10^7$ cm^{-3}.

2. The assumed pump power is very high. Cavity-enhancement of the pump power could be envisaged. $P_{pump} = 100$ W seem more realistic. However, at high laser intensities higher-order nonlinear processes may happen, like multiphoton ionization.

3. The ions are passing multiple times through the interaction region. At every corner of the storage ring the quadrupole magnets induce heating by micromotion. The heating has higher-order Fourier components, and thus leads to complicated non-thermal velocity distribution. This means the ions do not stay bunched very well, at least not in momentum space. Therefore the atoms run out of phase with the pump laser after a round-trip. The question is how strong this diffusion process is compared to the CARL force.

4. Ion beams are cooled either by electron beams or optically. Electron beams exert friction forces and could be used for viscous CARL. Optical cooling is achieved by balancing the acceleration force of a copropagating laser with the counterforce exerted by an electric rf-field synchronized with the ion revolution frequency. This method might also provide optical molasses for *viscous CARL* [**?**]. According to Matthias Weidemüller only the electron beam cooling works, today. But it is connected with a strong diffusion force working against the CARL force. Fortunately, the electron beam forces only act in momentum space, i.e. one scattered electron does not noticeably modify an ion's trajectory.

5. Intrabeam scattering (IBS) by Coulomb-repulsion is a dominant heating process. Optical cooling seems to lead to a sudden Coulomb ordering, in which case IBS disappears. There is one successful crystallization experiment in a miniature non-relativistic storage ring. The ions have macroscopic distances. In a relativistic storage ring the distance would be on the order of centimeters, which is very long compared to the CARL laser wavelength. A problem which may occur is that crystallization due to Coulomb forces may perturb CARL bunching.

6. Pulsed operation may be possible. This depends on the time-scale for bunching.

7. In [175] neither the pump nor the probe laser are recycled, but the ions are. Imagine however, we could build a 10 m long high finesse ring cavity. Free spectral range $\delta = 30\,\mathrm{MHz}$. Waist $w_0 = 500\,\mathrm{mm}$. Cavity mode volume $V_{mde} = \frac{\pi}{2} L w_0^2 = 4\,\mathrm{cm}^3$. Single-photon Rabi frequency $g = (2\pi)2.3\,\mathrm{kHz}$.

42.3.4.3 Method

Talking to Matthias Weidemüller he seemed pretty reserved about the feasibility of the project at TSR. Perhaps at GSI.

Assume an atomic beam moving at $\beta_r = v/c$ with $\gamma_r = \sqrt{1-\beta_r^2}^{-1}$ irradiated by a laser beam k with a frequency ω in the lab frame. In the atomic rest frame the frequency is Doppler-shifted towards,

$$\omega' = \omega\sqrt{\frac{1-\beta_r}{1+\beta_r}} = \frac{\omega}{\gamma_r(1+\beta_r)} \ , \tag{42.104}$$

such that $\omega' \lessgtr \omega$ if $kv \gtrless 0$. Now consider two laser beams ω_{pp} and ω_{pr}. In the moving frame defined by $\omega' \equiv \omega'_{pr} = \omega'_{pp}$,

$$\omega' = \gamma_r\omega_{pp}(1+\beta_r) = \gamma_r\omega_{pr}(1-\beta_r) \ . \tag{42.105}$$

Assume there is an atomic resonance $\omega'_0 \approx \omega'$. Then the pump is red-detuned from the resonance by the same amount the probe is blue-detuned:

$$\frac{\omega_{pr}}{\omega'_0} = \frac{\omega'_0}{\omega_{pp}} \ . \tag{42.106}$$

Furthermore the atomic rest energy is,

$$E' = \gamma_r mc^2 \ . \tag{42.107}$$

The recoil energy in the rest frame is,

$$\omega'_{rec} = \frac{2\hbar k'^2}{m} = \frac{2\hbar\omega'^2_0}{mc^2} = \frac{2\hbar\omega_{pp}\omega_{pr}}{mc^2} \ . \tag{42.108}$$

42.3.4.4 Radiated power

The CARL equations are to be formulated in the rest frame [175]. The parameters which are adjusted in the lab frame have to be Lorentz-transformed properly, before being used in the CARL formalism. The coupling parameter in the moving frame is,

$$g' = \frac{d\mathcal{E}_1}{\hbar} = d\sqrt{\frac{\omega'}{\hbar\varepsilon_0 V'}} \ , \tag{42.109}$$

where $\mathcal{E}_1 = \sqrt{\hbar\omega/2\varepsilon_0 V_{mode}} \approx 3.6\,\mathrm{V/m}$. Therefore the dipole moment is just like ours $d \approx \sqrt{3\pi\varepsilon_0\hbar\Gamma/k^3} \approx 2.5\times10^{29}\,\mathrm{J/V}$. Because length is relativistically contracted, $\sqrt{V'/V} = \gamma_r$, in the lab frame,

$$g = \gamma_r^{-1/2} g' = d\sqrt{\frac{\omega'}{2\hbar\varepsilon_0\gamma_r^2 V}} \ . \tag{42.110}$$

Bonifacio's treatment yields the FEL parameter,

$$\rho = \frac{1}{1+\beta_r}\left(\frac{g^2 N S_0^2}{8\gamma_r^2 q\omega_{pp}^2}\right)^{1/3} \ , \tag{42.111}$$

where $S_0 < \frac{1}{4}$. The FEL and CARL parameter are related by the energy ratio,

$$q = \frac{\rho_c}{\rho} = \frac{E_{atom}}{E_{photon}} = \frac{\gamma_r mc^2}{\hbar\omega_{pr}} \ . \tag{42.112}$$

Using $N = nV$ the FEL parameter can also be written,

$$\rho = \frac{\gamma_r\omega_{pp}}{\omega'}\left(\frac{d^2\omega'}{\hbar\varepsilon_0\gamma_r^2 V}\frac{NS_0^2}{8\gamma_r^2\omega_{pp}^2}\frac{\hbar\omega_{pr}}{\gamma_r mc^2}\right)^{1/3} = \left(\frac{d^2 n S_0^2}{8\gamma_r\varepsilon_0 mc^2}\right)^{1/3} \ . \tag{42.113}$$

The CARL parameter is also,

$$\rho_c = \frac{1}{1+\beta_r}\left(\frac{g^2 N S_0^2}{4\gamma_r^2\omega_{pp}^2}q^2\right)^{1/3} = \frac{1}{1+\beta_r}\left(\frac{g^2 N S_0^2}{\omega_{rec}'^2}\right)^{1/3} \ , \tag{42.114}$$

which for $\beta_r \to 0$ becomes the non-relativistic CARL parameter. The energy flux density is found to be ,

$$u_{pp,pr} = |A_{pp,pr}|^2(1\mp\beta_r^2)\rho_c\hbar\omega_{pp,pr}nc \ . \tag{42.115}$$

The power is,

$$P_{in,out} = V u_{pr}\frac{1}{vt_{rev}} = |A_{pr}|^2(1\mp\beta_r^2)\rho_c\frac{\hbar\omega_{pr}}{e}\frac{Ne}{t_{rev}}\frac{c}{v} \ . \tag{42.116}$$

Assuming saturation $|A_{pr}| \approx 1$,,

$$P_{in,out}(\mathrm{W}) \approx \frac{1\mp\beta_r^2}{\beta_r}\rho_c E_{photon}(\mathrm{eV})\imath(\mathrm{A}) \ . \tag{42.117}$$

with $I = Ne^-/t_{rev}$ and at saturation $|A_{pr}|^2 \approx 1$. The gain length is,

$$l_g \approx \frac{c\beta_r\gamma_r}{2\sqrt{3}\rho\omega_0'} \ . \tag{42.118}$$

42.3.5 Matter wave superradiance

There is a close relationship between CARL and the phenomenon of *matter wave superradiance* (or *superradiant Rayleigh scattering*) [170, 1136], which will be discussed in the following sections.

In 1999 the group of W. Ketterle at the MIT made a surprising observation, when it illuminated an elongated Bose-Einstein condensate with a short linearly polarized laser pulse traversing the condensate perpendicularly to the long axis [649]. Instead of producing radiation with a dipole pattern, as we might expect for a polarized atomic cloud undergoing Rayleigh scattering, they observed emission of directional light bursts along the symmetry axis of the condensate. They also observed that some of the atoms were accelerated at angles of 45°. And these atoms could emit other generations of atoms at angles of 45°.

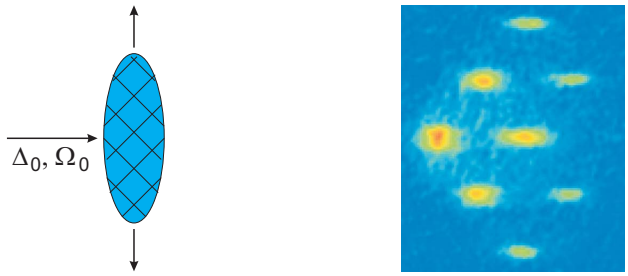

Figure 42.26: (code) Flight-of-time measurement of the atomic momentum distribution after matter wave superradiance.

The phenomenon was explained as follows. Let us imagine a first photon scattered by an atom into the direction of the long axis of the condensate. This atom will be accelerated by the photonic recoil in a direction of 135° with respect to the direction of the photon, and it will interfere with the rest of the condensate thus generating a standing matter wave of oriented in such a way, that the following photons are scattered into the same direction as the first one via Bragg scattering. This reinforces the contrast of the matter wave, etc.. We obtain an exponential gain of photons in the mode defined by the first scattered photon, as well as of the mode receiving the scattered matter wave. As the path of the gain is longer along the long axis of the condensate, this mode is favored. That is, the condensate can be considered as a cavity embracing the solid angle Ω_{sol}.

The Rayleigh scattering rate for a single atom is,

$$R_1 = \sin^2\theta\sigma(\Delta_a)\frac{I}{\hbar\omega}\frac{3\Omega_{sol}}{8\pi} \ , \tag{42.119}$$

where $\theta$is the angle between the polarization of the incident laser (intensity I) and the direction into which the light is scattered. The cross-section is $\sigma(\Delta_a) = \sigma_0\frac{\Gamma^2}{4\Delta^2+2\Omega^2+\Gamma^2}$, where $\sigma_0 = 3\frac{\lambda^2}{2\pi}$. Now, for the set of atoms, the superradiant scattering rate is not only amplified by the number of condensed atoms, N, but also by the number of atoms, N_r, already being in the mode receiving scattered atoms,

$$R_{sr} = R_1 N\frac{N_r+1}{2} \ . \tag{42.120}$$

This is the *superradiance matter wave*.

42.3.5.1 Ketterle and Dicke superradiance: The Dicke picture of CARL

At first glance there seems to be a paradox: On one hand, the collectiveness of the CARL lies in the motion, *not* in the scattering properties: Light is *localized* during the scattering process. On the other hand, superradiance means that atoms *feel* the scattering of photons by other atoms, i.e. radiatively. The relationship between Dicke superradiance and Ketterle superradiance gets clear, when we see that the momentum exchange in CARL corresponds to the same dipole-dipole force, which is at the origin of electrostriction.

The role of atoms and photons is inversed in the new understanding of cavity CARL and Ketterle superradiance: In CARL subsequent scattering processes are correlated via optical modes, in SR via atom motional coherences.

Note that quantum degeneracy is *not* essential [713]. The only property of BECs which is exploited in Ketterle's superradiance experiment is the large coherence length: Every atom is delocalized over the complete BEC. This helps! To see new effects due to quantum degeneracy, one must look at higher-order correlations, interaction-induced effects, the influence of the phonon field superimposed on the BEC.

For Ketterle's superradiant Rayleigh scattering the coherence is excited between two atomic momentum states. The correlation happens between successive scattering events, as long as atom is inside the condensate. In Dicke's idea (if atoms are closer than λ) the coherence is excited between a ground and excited electronic state. The correlation occurs between successively emitted photons, i.e. if the photons coupled to the same radiation mode. The superradiant lifetime is limited by natural decay.

What is the analogy between CARL (or Ketterle superradiance) and Dicke superradiance, exactly. Consider an ensemble of non-interacting atoms that can exist in *only two* sharp momentum states, $|k_0\rangle$ and $|k_1\rangle = |k_0 + 2q\rangle$, where $q = 2\pi/\lambda$. They interact with two counterpropagating quantized light modes, $\hat{a}_0$ and $\hat{a}_1$. We write the scattering process as $\hat{\Psi}_1^\dagger \hat{\Psi}_0 = |k_0 + 2q\rangle\langle k_0| = e^{-2iq\hat{r}}$. The Hamiltonian is then,

$$\hat{H} = \frac{k_0^2}{2m}\hat{\Psi}_0^\dagger\hat{\Psi}_0 + \frac{k_1^2}{2m}\hat{\Psi}_1^\dagger\hat{\Psi}_1 + \omega_0\hat{a}_0^\dagger\hat{a}_0 + \omega_1\hat{a}_1^\dagger\hat{a}_1 + U\hat{a}_1^\dagger\hat{a}_0\hat{\Psi}_1^\dagger\hat{\Psi}_0 + U\hat{a}_0^\dagger\hat{a}_1\hat{\Psi}_0^\dagger\hat{\Psi}_1 \ . \quad (42.121)$$

The important issue are the parametric terms $\hat{a}_1^\dagger\hat{\Psi}_1^\dagger$. For superradiance it is essential that the provenience of the emitted photons be undefined. For Dicke superradiance, photons are emitted through synchronized relaxation of the internal atomic coherence. For CARL, photons are scattered through synchronized relaxation of the motional atomic coherence. The CARL Dicke states are labeled by $|S, M\rangle$, where $2S$ is the total number of atoms and $2M$ the number of atoms in momentum state $|k_1\rangle$ minus the number of atoms in momentum state $|k_0\rangle$. Define $\hat{S}_- \equiv \hat{\Psi}_0^\dagger\hat{\Psi}_1$, and we get the usual SU(2) spin algebra,

$$\langle S, M-1|\hat{S}_-|S, M\rangle = \sqrt{S(S+1) - M(M+1)} \ . \quad (42.122)$$

the Hamiltonian

$$H = \frac{k_0^2}{2m}(S - \tfrac{1}{2}\hat{S}_z) + \frac{k_1^2}{2m}(S + \tfrac{1}{2}\hat{S}_z) + \omega_0\hat{a}_0^\dagger\hat{a}_0 + \omega_1\hat{a}_1^\dagger\hat{a}_1 + U\hat{a}_1^\dagger\hat{a}_0\hat{S}_+ + U\hat{a}_0^\dagger\hat{a}_1\hat{S}_- \ . \quad (42.123)$$

42.3.5.2 Superfluorescence as bosonic stimulation

There are two ways to understand SF. According to [366] it is *cooperative spontaneous emission* with interference of the radiation patterns. Alternatively, we may imagine that the first spontaneously scattered photon stimulates the other to emit. The scattering rate for every atom is Bose-enhanced by the presence of N other atoms by a factor $N+1$. The scattering rate for the total cloud is therefore $W \sim N(N+1) \approx N^2$. SR is [Dicke] the exponentially accelerated decay of the initial state (oscillating macroscopic dipole moment)^2, or [Ketterle] (contrast of interference pattern)^2 [172, 175].

In general, bosonic stimulation may take place by any mode taking part in the coherent scattering process, i.e. matter-wave momentum sidemodes or optical modes, as discussed by [1239, 1166].

Also interpretable as Bragg scattering of matter waves assisted by spontaneously scattered photons. The photons allow for *momentum conservation* and *irreversibilty of the gain*. Spontaneous emission is not a single-atom process, but a collective porcess, leaving atoms in a coherent superposition of ground and excited state [1216, 549].

42.3.5.3 Superfluorescence versus superradiance

It is interesting to look at Vuletic's experiment. Atoms located inside the cavity mode volume scatter light into the resonator modes. This is spontaneous emission, however modified by the mode structure of the available phase space. However, he observed higher scattering rates as expected. This is probably due to *bosonic stimulation* of the scattering process by photons which are already in the cavity. This stimulation can only be efficient, if the scattered photons are in the same mode as the stimulating ones. For Vuletic, this is satisfied because he has a large κ. In contrast we have the choice: If $kv \ll \kappa$, we may also observe SR. If $kv \gg \kappa$, only CARL. Note that Γ does not play a role, because spontaneous decay is inhibited in the cavity.

Without any symmetry breaking features, superradiance occurs in a random direction determined by the first scattered photon. In the presence of a cavity superradiance occurs in the direction of the cavity mode. If there are concurrent effects wanting to determine the direction, this only reduces the efficiency. This means for Vuletic's experiment that, since the superradiant pulse must be at 90°, the atoms must be arranged in periods such that the scattered photons interfere constructively. The spatial ordering proposed by Ritsch to explain Vuletic's observation corresponds to Inouye's BEC matter-wave grating.

If the scattered photons are in phase with the cavity, they can stimulate all the atoms having the same phase as the scattering ones $+n2\pi$.

It is all dynamical: Before the bunching is complete $|\alpha_-|^2 \lesssim N^2$. At the SR-peak, $|\alpha_-|^2 \propto N^2$.

42.3.5.4 Steady-state superradiance in a viscous CARL

Bonifacio points out [1106] the interesting fact that in the regime, where the CARL frequency does not leave the cavity resonance, the scattering amplitude is proportional

to the square of the numbers of scatterers. This behavior is typical for superradiance. The new thing is that our CARL would be a continuously superradiating system.

Consider spontaneous emission in an inverted gas. If the density is low, $n^{-1/3} \gg \lambda$, an emitted photon will leave the gas without being interacting with other photons. Otherwise, stimulated emission will occur and eventually give rise to a superradiant burst. What really counts is the *optical density*, if the emitted photon is off-resonant, it can not stimulate other atoms. What also helps is recycling of the light in a cavity: CARL is a good example, but the photons can only be rescattered if the recoiled atoms stay on resonance, $kv \ll \kappa$.

42.3.5.5 Equivalence of light and matter waves in 4WM

The exponential gain is due to a feedback. With two coupled momentum modes the matter wave is described by, $\psi \propto e^{(n+2)\imath qz} + e^{n\imath qz}$. The modes of light are, $\alpha_\pm = e^{\imath k_\pm z}$. Hence,

$$\langle \psi_2 | light | \psi_1 \rangle = \langle e^{(n+2)\imath qz} | \alpha_+^* \alpha_- | e^{n\imath qz} \rangle = \langle e^{(n+2)\imath qz} | e^{\imath(k_+ - k_-)z} | e^{n\imath qz} \rangle \qquad (42.124)$$

and,

$$\langle \alpha_2 | matter | \alpha_1 \rangle = \langle e^{\imath k_+ z} | \psi^* \psi | e^{n\imath k_- z} \rangle = \langle e^{\imath k_+ z} | e^{(n+2)\imath qz - n\imath qz} | e^{n\imath k_- z} \rangle \ . \qquad (42.125)$$

42.3.5.6 Symmetry breaking due to superradiance

For scattering between counterpropagating waves, SR is not based on bunching [1103]. Superradiance can be described classically if $k_B T > \hbar\varepsilon$, but $k_B T$ must be small enough to prevent SF to be destroyed by Doppler broadening.

The scattered power is $\propto N^2$, the scattering time is $\propto \tau/N$ or $\propto 1/kv$, the scattered energy is $\propto N^2 \times \tau/N$. Without recoil SF is symmetrical about Δ_a. With recoil it's asymmetric.

Without cavity 1. SF frequency is at ω_a, 2. no recoil-induced asymmetry, need cavity to see recoil effects on SF.

42.3.5.7 Different regimes

The relative size of kv and $\varepsilon\rho$ should delimit the classical from the quantum CARL regime.

	good cavity ($\kappa \ll kv$ or $\varepsilon\rho$)	bad cavity ($\kappa \gg kv$)
cold cloud	CARL, collective motion	SR, collective gain
warm cloud	CARL & threshold	non-collective RIR

The CARL equations in our regime read [755],

$$\beta = \frac{-iNU_0\eta_+}{\kappa\,(\kappa + 2\imath kv)} \qquad \text{and} \qquad k\dot{v} = \frac{-8\varepsilon N U_0^2 \eta_+^2}{\kappa(\kappa^2 + 4k^2v^2)} - \gamma_{frc} kv \ . \qquad (42.126)$$

Our solution for this equation for $\kappa \ll kv$ is,

$$|\beta|^2 = \frac{N^{4/3} U_0 \eta_+ \gamma_{frc}}{8\kappa^2 \varepsilon} \sim N^{4/3} \qquad \text{and} \qquad kv = \left(\frac{\varepsilon N U_0^2 \eta_+^2}{\kappa \gamma_{frc}} \right)^{1/3} \sim N^{1/3} \ . \qquad (42.127)$$

In contrast for $\kappa \gg kv$ we get from Eq. (42.126),

$$|\beta|^2 = \frac{N^2 U_0^2 \eta_+^2}{4\kappa^4} \sim N^2 \qquad \text{and} \qquad kv = \frac{-2\varepsilon N U_0^2 \eta_+^2}{\gamma_{frc}\kappa^3} \sim N \ . \tag{42.128}$$

This means we are actually in the CARL regime. If we could increase the friction such that the laser frequency would stay within the cavity resonance, we would be in the *superradiant* regime. Actually, the lowest frequency ever reached with molasses is $2kv \approx 2\pi \times 100$ kHz, which is a factor of 5 larger than the cavity linewidth. We could try to reach the superradiant regime by lowering the finesse of the cavity. Then however we also should increase U_0, i.e. reduce the detuning Δ_a, to keep staying in the coherent coupling regime. In conclusion this seems to be feasible. A major problem would however be the actual poor repeatability, i.e. shot-to-shot noise, which somewhat reduces our confidence into absolute atom number measurements.

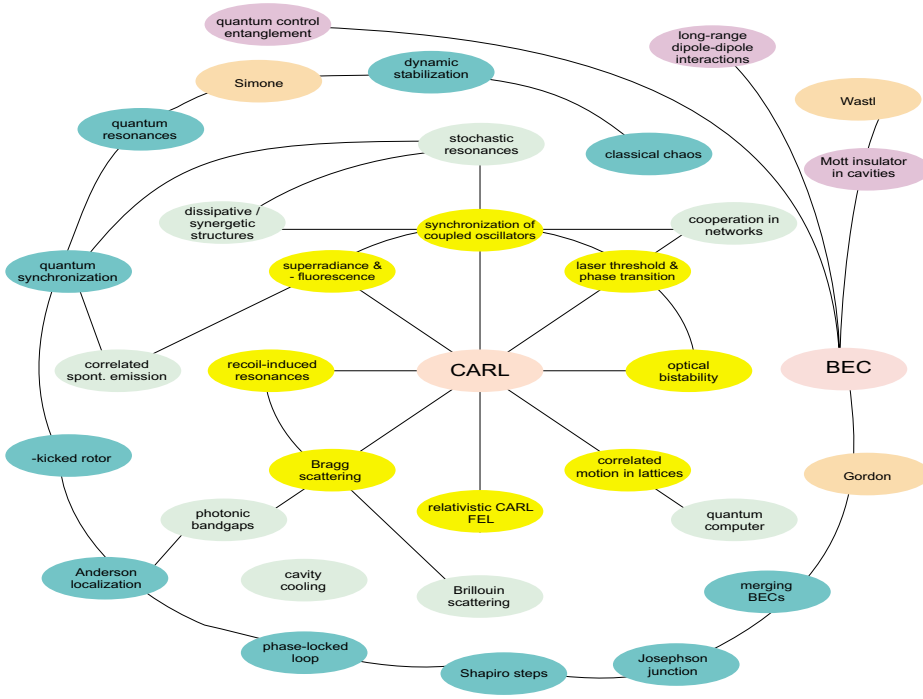

Figure 42.27: CARL and consorts.

42.3.6 Superradiance and CARL for ultracold atoms

Piovella has classified the various regimes of CARL and superradiance in the classical and the superradiant regimes. Let L be the length of the condensate or, if present, of the cavity. w is the waist and F is the finesse. We use the following definitions for the cavity decay width $\kappa = \pi c/LF$ the recoil shift $\omega_r = \hbar k^2/2m$, the dipole moment $d = \sqrt{3\pi\varepsilon_0\hbar\Gamma/k^3} = 2.5 \times 10^{-29}$ Asm and the volume of the condensate $V = \pi L w^2$. If

there is a ring cavity, V denotes the cavity mode volume. Furthermore we introduce the one-photon field strength $\mathcal{E}_1 = \sqrt{\hbar\omega_p/2\varepsilon_0 V}$, the coupling constant $\Omega_1 = d\mathcal{E}_1/\hbar$, the Rabi frequency $\Omega_I = \Omega_1|\alpha_\pm|$ and the one-photon light shift $U_1 = \Omega_1^2/\Delta_a$, where Δ_a is the atom-field detuning. We have $I/I_s = 2\Omega^2/\Gamma^2$, with $I_s = 2.5 \ \ \mathrm{mW/cm^2}$. The CARL parameter is now,

$$\rho = \left(\frac{\Omega_I}{2\Delta_a}\right)^{2/3}\left(\frac{\omega_p d^2 N}{V\hbar\varepsilon_0\omega_r^2}\right)^{1/3} = \left(\frac{NU_1^2|\alpha_\pm|^2}{2\omega_r^2}\right)^{1/3} \ , \tag{42.129}$$

where $|\alpha_\pm|^2$ is the number of photons in the cavity. Alternatively, define the coupling constant,

$$g = \frac{\Omega_I}{2\Delta_a}\left(\frac{\omega_p d^2}{2V\hbar\varepsilon_0}\right)^{1/2} = \frac{\Omega_i\Omega_1}{2\Delta_a} = \tfrac{1}{2}U_1|\alpha| = \frac{U_d}{2|\alpha|} \ . \tag{42.130}$$

Remember,

$$r_\beta = -\frac{k}{\pi w_0^2}\frac{\mathfrak{Re}\ (\alpha_{pol})}{\varepsilon_0} = \frac{U_d}{P/\hbar\omega} \ . \tag{42.131}$$

The superradiant gain is,

$$G_{sr} = \frac{2g^2 N}{\kappa} = \frac{NU_1^2|\alpha|^2}{2\kappa} \ . \tag{42.132}$$

Note that G_{sr} is exactly the width of the power broadened Rabi type coupling between the counterpropagating cavity modes. Therefore,

$$\rho^3\omega_r^2 G_{sr}\kappa\tfrac{1}{2}NU_1^2|\alpha|^2 \ . \tag{42.133}$$

We compare the Ketterle superradiance situation with our classical and our BEC ring cavity data. Early experiments [649, 1166] had been performed with ^{23}Na, but they were repeated with ^{87}Rb so that we concentrate on this latter case.

experiment		superradiant Kapitza-Dirac	superradiant Bragg	thermal cavity CARL	BEC cavity maxi(mini)
linewidth	Γ	6 MHz			
recoil shift	ω_r	3.8 kHz			
atom number	N	10^5		10^6	10^5
mode diameter	w	15 µm		130 µm	108(70) µm
mode length	L	200 µm		8.5 cm	8.7(3.4) cm
mode volume	V	$1.4 \cdot 10^{-4}$ mm^3		4.5 mm^3	3.2 mm^3
one-photon field	$\mathcal{E}_1$	320 V/m		1.8 V/m	2.1 V/m
one-photon Rabi	Ω_1	12.1 MHz		68 kHz	81 kHz
finesse	F	1		80000	160000
field decay rate	κ	120 GHz		22 kHz	10 kHz
intensity	I	63 mW/cm^2		1000 W/cm^2	100 mW/cm^2
Rabi frequency	Ω_I	26.2 MHz		3.3 GHz	33 MHz
photon number	$\lvert\alpha\rvert$	2.2		49000	408
detuning	Δ_a	420 MHz	4.4 GHz	1 THz	100 GHz
CARL parameter	ρ	1263	264	5.6	1.4
	$\omega_r\rho$	30 MHz	6.2 MHz	133 kHz	32 kHz
coupling constant	g	380 Hz	36 kHz	112 Hz	13 kHz
bandwidth	$\frac{g^2N}{\kappa}$	120 kHz	1.1 kHz	57 kHz	1.8 kHz
coupling strength	$\frac{NU_1}{\kappa}$	0.3	0.03	0.02	0.06
gain	G	$2g\sqrt{\omega_r N/\kappa}$ 43 kHz	$2g^2N/\kappa$ 2.2 kHz	$2g\sqrt{\omega_r N/\kappa}$ 29 kHz	$2g^2N/\kappa$ 3.5 kHz
CQED	?	$\Gamma, \kappa \not\ll \Omega_1 \Longrightarrow$ not CQED			
recycling	?	$g^2N/\kappa \ll \kappa \Longrightarrow$ superradiant		$g^2N/\kappa > \kappa$ $\Longrightarrow$ good cavity	$g^2N/\kappa < \kappa$ $\Longrightarrow$ bad cavity
CARL regime	?	$g^2N/\kappa \gg \omega_r$ $\Longrightarrow$ semiclassical	$g^2N/\kappa \lesssim \omega_r$ $\Longrightarrow$ quantum	$g^2N/\kappa \gg \omega_r$ $\Longrightarrow$ semiclassical	$g^2N/\kappa \lesssim \omega_r$ $\Longrightarrow$ quantum
recycling	?	$\omega_r\rho \ll \kappa$	$\omega_r\rho \ll \kappa$	$\omega_r\rho > \kappa$	$\omega_r\rho > \kappa$
CARL regime	?	$\rho \gg 1 \Longrightarrow$ semiclassical	$\rho \gg 1 \Longrightarrow$ semiclassical?	$\rho \gtrsim 1 \Longrightarrow$ semiclassical	$\rho \lesssim 1 \Longrightarrow$ quantum?

Robb [1105] has given a new interpretation to the observations by Schneble [1166].

regimes	bad cavity $\kappa \ll G$	good cavity $\kappa \gg G$
semiclass. $\omega_r < G$	MW superradiance { Kapitza-Dirac $\tau^{-1} > \omega_r$; Bragg $\tau^{-1} < \omega_r$ }	CARL
quantum $\omega_r > G$	MW superradiance { Kapitza-Dirac $\tau^{-1} > \omega_r$; Bragg $\tau^{-1} < \omega_r$ }	?

The temperature is an essential parameter. We do not need BEC, but we want $k_BT/\hbar < \kappa, \omega_r, g^2N/\kappa, \Gamma, ...$ Therefore $T \ll 480$ nK.

42.3.6.1 Raman superradiance

The SR gain can be either linear in the atom number N (single-atom or RIR gain) or non-linear (collective or CARL gain). Instabilities only occur in the collective gain regime. For a collective gain the SR mode decay rate κ and the thermal (or other type of inhomogeneous) broadening κ_R must be small compared to g^2N/κ. For Rayleigh SR the transition between the two regimes is studied by [650]. For Raman SR atom number threshold N_{thr} is too high, so that the experiments [1165, 1412, 1413] are in the linear gain regime .

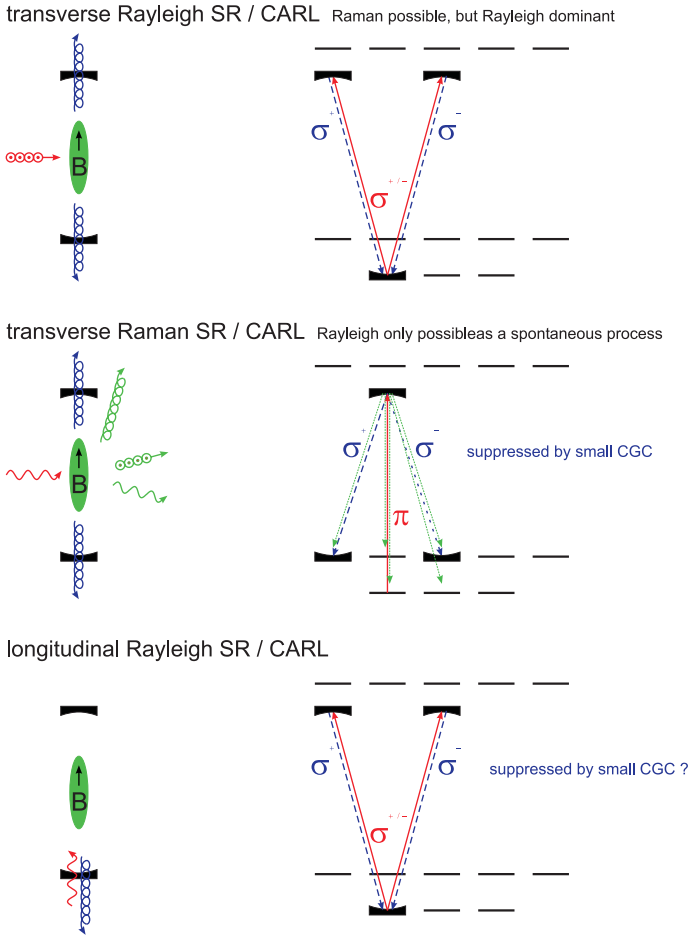

Figure 42.28: Configurations for Rayleigh and Raman CARL.

42.3.6.2 CARL

The claim [1038] is basically that CARL and superradiant Rayleigh scattering is the same process in different regimes. Both rely on collective gain, in contrast to recoil-induced resonances. Experimental signatures [649, 755] are a collective instability

resulting in bunching and directional SR light bursts. Both processes are described by the same equations (42.182). Those equations contain two free parameters: The decay rate of the optical field κ_c and the collective coupling strength ρ.

The decay rate of our ring cavity is $\kappa_c = (2\pi)$ 22 kHz, the recoil shift is $\omega_r = (2\pi)$ 14 kHz. Typical values for our experiments are $P = 1$ W, $\Delta_a = -(2\pi)$ 1 THz and $N = 10^5$. From this we derive $\eta^2 = P/(\hbar\omega\delta_{fsr}) \approx 10^9$ and $U_0 = g_1^2/\Delta_a = 3\Gamma\delta_{fsr}/k^2w^2\Delta_a \approx (2\pi)$ 340 Hz. The ρ parameter measures number round trips a photon must perform before it acquires enough Doppler shift to run out of cavity resonance,

$$\rho^3 = \frac{2NU_0^2\eta^2}{\omega_r^2} = \frac{2NU_d^2}{\eta\omega_r^2} \approx 4^3 \tag{42.134}$$

with $U_d = U_0\alpha_+^2$. For our typical conditions $\rho \gg 1$ and thus $\kappa = \kappa_c/\rho\omega_r \ll 1$. Hence, we are in the semiclassical good-cavity regime with the gain $G = \frac{1}{2}\omega_r\rho\sqrt{3} \approx (2\pi)$ 50 kHz. By reducing the collective coupling $NU_0^2\eta^2$, we may be able to reach the quantum regime $\rho < 1$. However, since $\kappa_c > \omega_r$ the quantum regime is only accessible in the superradiant limit, $\kappa > 1$. Let us assume we could reach $\rho = 0.8$. Then the gain would be $G_{SR-QT} = \frac{1}{2}\frac{\omega_r\rho^2}{\kappa} \approx (2\pi)$ 5 kHz. To reach the quantum good-cavity regime a better finesse of the cavity would be necessary; e.g. with the original finesse $F = 300000$ we would have $\kappa_c = 0.4\omega_r$. The κ - ρ phase diagram according to the above estimations is shown in Fig. 42.29.

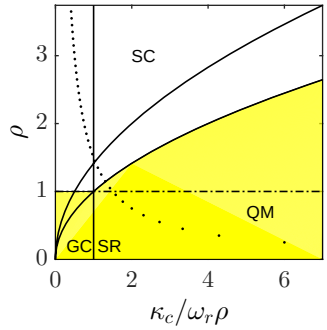

Figure 42.29: (code) Regimes of CARL. The range accessible to our experiment is denoted by the dotted line.

42.3.6.3 Cavity-enhanced superradiance

A few years ago, Ketterle and coworkers have demonstrated superradiant Rayleigh scattering from a Bose-Einstein condensate [649]. A short laser pulse shone into a BEC gave rise to motional sidemodes coupled out of the condensate, while at the same time a superradiant light pulse is emitted into the long axis of the condensate (see Fig. 42.31, left drawing). Various pictures have been stressed to explain the observations, and the close analogy to CARL has been pointed out.

In Ketterle's superradiance experiment, one may associate the part of the BEC that corresponds to atoms which have scattered a photon with an atom number

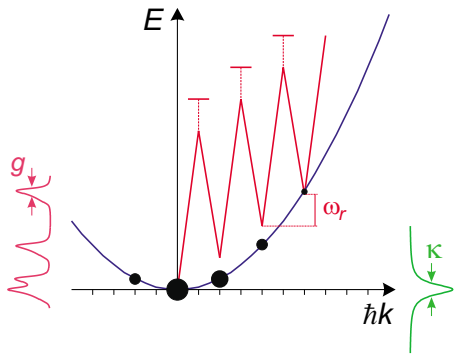

Figure 42.30: Scheme of CARL. The range accessible to our experiment is denoted by the dotted line.

N_r. The remaining part consists of N atoms. The density is modulated by interference between the two parts of the wave function, and the number of atoms that form the density modulation is $N_{mod} \propto \sqrt{NN_r}$. As for usual Bragg scattering or Dicke superradiance the number of photons n scattered at the density modulation is $n \propto N_{mod}^2 \propto N_r$. Since every scattered photon generates a recoiling atom, the number of recoiling atoms increases like $\dot{N}_r \propto n$, and we get $\dot{N}_r = GN_r$, i.e. an exponential increase of recoiling atoms with a gain factor G. This increase is mirrored by an identical increase of the number of scattered photons, which results in a gain mechanism for the scattered light mode. The incident and the scattered light mode are coherently coupled, just like in the case of CARL, so that in principle the scattered photons can be scattered back into the incident mode. Let U_0 be the Rabi frequency of the coherent mode coupling, i.e. the rate at which photons are exchanged between the modes. The collective Rabi frequency involving N atoms and n photons is then $U_0\sqrt{Nn}$. The superradiant gain corresponds to the transition rate associated with the coupling, which according to Fermi's golden rule is given by $G = U_0^2 Nn\ \rho(\omega)$.[12] Approximating the density-of-states in the vicinity of the cavity resonance by $\rho(\omega) \approx \kappa^{-1}$, where κ is the rate at which the scattered light mode decays, we see that the gain can be given the meaning of a CARL bandwidth, i.e. the width of the spectral range where the light scattering is exponentially amplified [**?**]. The prediction is to be tested.

The important point is now, that the various regimes in which CARL and superradiance may occur are characterized by the *size of the CARL gain bandwidth* as compared to the decay width κ and the recoil frequency ω_r. On one hand, we may distinguish the semiclassical regime, where the gain bandwidth is large enough to amplify many adjacent momentum states of the quantized motion, $G \gg \omega_r$ from the quantum regime, where only one momentum state can be amplified at a time, $G \ll \omega_r$. In this quantum regime the CARL interaction only couples *two momentum states* of the atomic motion.

[12]The gain bandwidth can also be understood as the power broadening of the cavity linewidth due to the collective coupling. In our CARL experiments the power broadening exceeds the cavity linewidth by more than an order of magnitude, which explains why CARL works even at very large pump-probe detunings.

In addition one has to distinguish between situations called the *good and the bad-cavity limits*. We find that conventional superradiant Rayleigh scattering from a BEC corresponds to the bad-cavity limit,[13] where the decay rate κ is much broader than the gain bandwidth. In fact, the decay width is calculated as $\kappa = c/2L$, where L is the size of the condensate along the axis into which the light is scattered. The time the scattered photons spend inside the BEC corresponds to the lifetime of a cavity. The bad-cavity limit is the regime studied by [1166]. By varying the gain bandwidth, they have been able to implement the semiclassical regime, as well as the quantum regime.[14] The various regimes of CARL are summarized in Fig. 42.31.

In contrast, our thermal CARL experiment was done in the semiclassical good-cavity limit. The field decay rate coincided with the linewidth of our ring cavity and was 7 *orders of magnitude smaller* than in the superradiance experiments. The most interesting regime can be identified by the requirement that the superradiant gain bandwidth G and the cavity field decay width κ both be smaller than the recoil shift ω_r. In terms of the parameter $\rho \equiv \sqrt[3]{G\kappa/\omega_r^2}$, which has been introduced by Bonifacio and coworkers as a universal scaling parameter for the equations of motion of the CARL system, it means that $\rho < 1$ [1106]. In this case only a single amplified momentum sideband couples to the atomic cloud. The result is a Rabi-type oscillation between the initial and the final momentum state.

Obviously for this scheme to work, the temperature of the atomic cloud must be lower than the recoil limit. By choosing appropriate parameters for our classical CARL setup we could in principle reach the quantum good-cavity regime. However, the interesting new features expected for this limit are blurred due to the high temperature. A major goal of our future research will be to study CARL with ultra-cold atoms in the yet unknown regime where $\rho < 1$. Our hope is to better understand the intricate relationship between CARL and superradiance in a regime, where the coupling between radiative and matter-wave modes is completely coherent, and for which the prospect of a robust quantum entanglement of the modes has been pointed out.

In the original superradiance experiments [649, 1166], the pulsed pump light drove a transient dynamics. The cavity in our proposed experiment will allow for much longer interaction times, and continuous superradiance will take place over a time scale at which dissipative effects due to cavity cooling will become effective.

Let us now turn to the superradiant gain experiment [649]. According to Ketterle the superradiant gain can be expressed as,

$$G = RN\frac{\Phi_s}{8\pi/3} \ , \tag{42.135}$$

where $R = \Gamma\Omega^2/(4\Delta^2 + 2\Omega^2 + \Gamma^2)$ is the single-atom Rayleigh scattering rate, with Γ being the linewidth of the atomic resonance, Δ the detuning, and Ω the Rabi

[13] Note that while the atom-field coupling constant is larger than the cavity decay width, it is much smaller than the spontaneous emission decay width of the atomic transition, so that we are still far from the cavity QED regime and may regard the light fields in our cavity as being classical.

[14] Let us add here that Schneble *et al.*[1166] gave a divergent interpretation of their observations: The bad-cavity limit was interpreted as Kapitza-Dirac scattering and the good-cavity limit as Bragg scattering scattering. As stated by Robb *et al.* [**?**] the different interpretations imply different dynamics which may be tested by experiment.

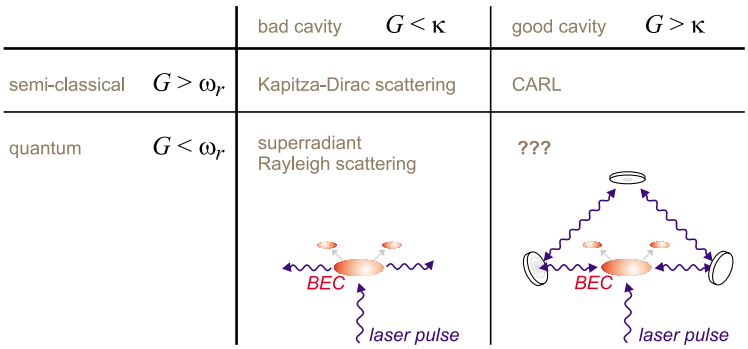

Figure 42.31: The idea of the superradiance experiment.

frequency generated by the incident laser beam. $\Phi_s \simeq \lambda^2/\frac{\pi}{4}w^2$ is the scattering solid angle, with w being the waist of the condensate. Hence, far from resonance,

$$G = \frac{\Omega^2}{\Delta^2} N \frac{3\Gamma}{2k^2 w^2} \ . \tag{42.136}$$

In Ketterle's experiments ($\Delta \simeq 100\Gamma$, $w = 15$ μm, $N = 10^5$, $\Omega \simeq 10\Gamma$) the gain is on the order of $G \simeq 170000$ kHz.

Interpreting the BEC as a cavity with finesse $F = 1$, i.e. $\kappa_c F/\pi = \delta_{fsr} = c/L$, we obtain,

$$G = \frac{\Omega^2}{2\Delta^2} \frac{\pi N}{\kappa_c} \frac{3\Gamma\delta_{fsr}}{k^2 w^2} = \frac{\Omega^2}{2\Delta} \frac{N}{\kappa_c} \frac{\Omega_{1s}}{2} 2\Delta \ , \tag{42.137}$$

where $\Omega_{1s} = 3\Gamma\delta_{fsr}/k^2w^2$ is the one-photon Rabi frequency inside the BEC cavity.

When the BEC is inside an optical cavity, the mode volumes for Ω and Ω_{1s} are equal, so that $\Omega^2 = n\Omega_{1s}^2$ and,

$$G \simeq \frac{nN_0U_0^2}{\kappa_c} = \tfrac{1}{2}\frac{\omega_r \rho^2}{\kappa} \ . \tag{42.138}$$

This is exactly the gain calculated from the above theory for the superradiant quantum regime.

Replace Γ by Γ_{sc}. For BEC decoherence is slow, so that modest gain suffices, atoms delocalized over BEC volume. At higher temperatures fast decoherence, but in cavity gain is larger, BEC coherence volume replaced by cavity volume, collectiveness transmitted differently.

Robb defines the 'gain rate',

$$g = \frac{U_0}{2}|\alpha| = \frac{\Omega}{2\Delta}\sqrt{\frac{\omega d^2}{2\hbar\varepsilon_0 V}} = \frac{\Omega}{2\Delta}\frac{dE_{1s}}{\hbar} = \frac{\Omega}{2\Delta}\Omega_{1s} \tag{42.139}$$

and the superradiant gain,

$$G = \frac{2g^2N}{\kappa} = \frac{\Omega^2}{2\Delta}\frac{N}{\kappa}\frac{\Omega_{1s}^2}{\Delta} \ . \tag{42.140}$$

Figure 42.32: Illustration of vicious circle of the CARL.

Note that g^2/κ is power broadening due to mode coupling. Typically, $g = 0.1\kappa$, so that $g^2/\kappa = 0.01\kappa \ll \omega_r$,

$$G = \frac{NU_0^2 n}{2\kappa} \ . \tag{42.141}$$

Decoherence of superradiance decreases with the delocalization of the atoms, but it does not depend on their degeneracy with other atoms. Quantum degeneracy could be interpreted as a phase-synchronized delocalization of many atoms.

Why does CARL work with (relatively) hot atoms? Thermal de Broglie wavelength at $T = 1$ μK $\lambda_{dB} = \sqrt{2\pi\hbar^2/mk_BT} \approx 200$ nm. Size of our thermal cloud $\bar{r} = \omega_r^{-1}\sqrt{k_BT/m} \approx 30$ μm and $\bar{z} \approx 8$ μm. Thomas-Fermi radii of our condensed cloud is not much different.

Note that alternative models have been stressed to describe for the various regimes of superradiant Rayleigh scattering, e.g. accounting for propagation effects (next section) [1439] and Kapitza-Dirac scattering. Superradiant pulse width $\tau_{sr} \simeq 200$ μs. Fourier width of gain profile $G = \tau_{sr}^{-1} \simeq 5000\ s^{-1}$.

42.3.6.4 Propagation effects

[1438] and [1439] developed a useful treatment for describing the Ketterle superradiance in the Raman-Nath (short strong pulse, $R \approx \omega_r$, $G \gg \omega_r$) as well as in the (long weak pulse, $R \ll \omega_r$, $G \ll \omega_r$) Bragg regime.

It is however unclear whether this treatment can be extended to account for the presence of a ring cavity. The ring cavity does more than increasing the BEC-light interaction time, $L \to \infty$. In fact, propagation effects introduce a spatial dependence of the intensity of the end-fire modes along the condensate axis. The self-injection

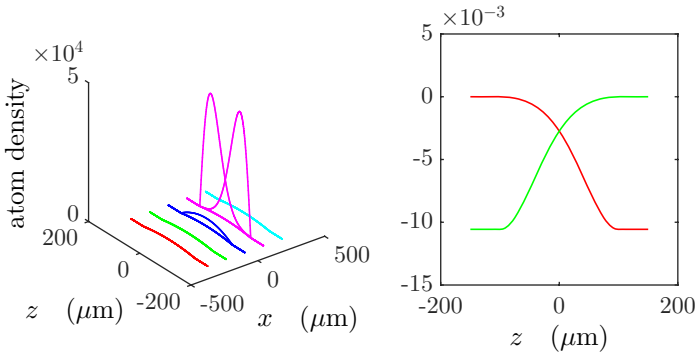

Figure 42.33: (code) Ketterle superradiance [1438].

due to photonic recycling by the ring cavity necessitates a self-organization of the spatial longitudinal mode profile.

42.3.7 Exercises

42.3.7.1 Ex: Good and bad cavity regime

What are the characteristics distinguishing the good from the bad cavity limit.

Solution:

42.3.7.2 Ex: Ringing in resonant systems

In this exercise we study ringing in (a) an excited classical harmonic oscillator and (b) in a laser-driven two-level system.

Solution: *The results are shown in Figs. 42.34.*

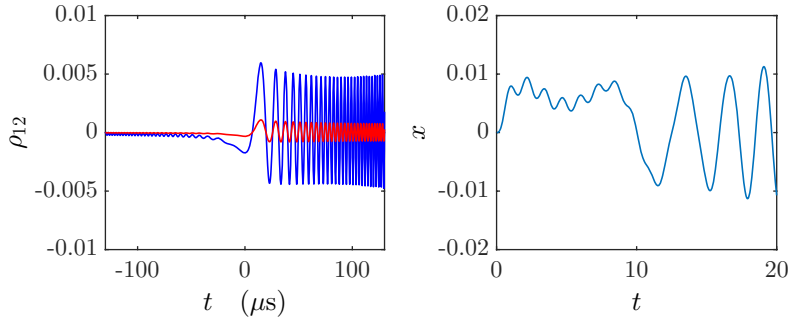

Figure 42.34: (code) Ringing in (a) an excited classical harmonic oscillator and (b) in a laser-driven two-level system.

42.4 Quantization of the atomic motion in cavities

At the beginning of this chapter we set up the complete Hamiltonian of the coupled atom-cavity system. Then tracing over dissipative degrees of freedom, we derived the master equation or derived the Heisenberg equations for the operators appearing in the remaining Hamiltonian quantum mechanically. But then for CARL we restricted to a classical treatment of the motion, as well as of the cavity modes.

Resuming the discussion started in Sec. 42.1.5 we will, in the remaining sections of this chapter, analyze effects due to the *quantization* of degrees of freedom represented by operators. The present section will (i) on a quantum description of the motion (with and without adiabatic elimination of the internal atomic dynamics and (ii) on issues arising from the presence of many atoms.

42.4.1 Quantum description of the motion

Concretely, let us analyze again the situation of a single atom interacting with a ring cavity. We assume validity of the adiabatic elimination of the internal atomic excitation and want to treat the light fields as classical. In contrast, the atomic motion is considered as quantum:

$$|\psi\rangle = |z\rangle_{motion} \otimes \cancelto{\text{classical}}{|\alpha_+\rangle \otimes |\alpha_-\rangle} \otimes \cancelto{\text{adiab.elim.}}{|i\rangle_{electron}} \to |z\rangle \ . \tag{42.142}$$

Since the motion, being the only quantum degree of freedom, is not subject to dissipation, we may use the Schrödinger equation in addition to Heisenberg equations for the light fields. Then, following the procedure outlined in Sec. 42.1.5, with z being the only quantum number, we find that the system is completely described by the dynamics of the expansion coefficients,

$$\begin{aligned} \imath\hbar \frac{d}{dt}\langle z|\psi(t)\rangle &= \langle z|\hat{H}|\psi(t)\rangle \\ \dot{\alpha}_\pm &= \langle z|\tfrac{\imath}{\hbar}[\hat{H},\hat{a}_\pm] - \kappa\hat{a}_\pm|z\rangle \ . \end{aligned} \tag{42.143}$$

Plugging in the Hamiltonian (42.26), we obtain the Schrödinger equation for the particle's motional wavefunction [15],

$$\imath\hbar \frac{d}{dt}\langle z|\psi(t)\rangle = \frac{p^2}{2m}\langle z|\psi(t)\rangle + U_0\langle z|\hat{a}_+^\dagger\hat{a}_- e^{-2\imath kz} + \hat{a}_+\hat{a}_-^\dagger e^{2\imath kz}|\psi(t)\rangle \ , \tag{42.144}$$

and the Heisenberg equations for the light fields,

$$\begin{aligned} \dot{\alpha}_\pm &= \langle z|(-\kappa + \imath\Delta_c - \imath U_0)\hat{a}_\pm + \imath U_0 e^{\mp 2\imath k\hat{z}}\hat{a}_\mp + \eta_\pm|z\rangle \\ &= (-\kappa + \imath\Delta_c - \imath U_0)\alpha_\pm + \imath U_0\alpha_\mp\langle z|\int dz|\psi(t)\rangle\langle\psi(t)|e^{\mp 2\imath k\hat{z}}|z\rangle + \eta_\pm \\ &= (-\kappa + \imath\Delta_c - \imath U_0)\alpha_\pm + \imath U_0\alpha_\mp\int dz|\psi(z,t)|^2 e^{\mp 2\imath kz} + \eta_\pm \ . \end{aligned} \tag{42.145}$$

[15] Terms of the Hamiltonian (42.26) which do not depend on z or p have been ignored, as they can be removed form the Schrödinger equation by a simple unitary transformation. Note that this can be done even though these terms depend on the field amplitudes $\alpha_\pm$.

In summary,

$$\boxed{\begin{aligned}\dot{\psi}(z) &= \frac{\imath\hbar}{2m}\frac{d^2}{dz^2}\psi(z) - \imath U_0\left(\alpha_+^\dagger\alpha_- e^{-2\imath kz} + \alpha_+\alpha_-{}^\dagger e^{2\imath kz}\right)\psi(z)\\ \dot{\alpha}_\pm &= (-\kappa + \imath\Delta_c - \imath U_0)\alpha_\pm + \imath U_0\alpha_\mp\int dz|\psi(z)|^2 e^{\mp 2\imath kz} + \eta_\pm\end{aligned}} \quad . \tag{42.146}$$

These are the new CARL equations that should be used in cases when the particle is *slower than the recoil velocity*, in which its motion must be described as a propagating matter wave. Note, that under this form, the equations can easily be generalized to apply to macroscopic wavefunctions such as a Bose-Einstein condensate.

The expectation value of the particle's position is then calculated via,

$$\begin{aligned} z(t) &= \langle\psi(0)|\hat{z}(t)|\psi(0)\rangle = \langle\psi(0)e^{-\imath\hat{H}t}|\hat{z}|e^{\imath\hat{H}t}\psi(0)\rangle \\ &= \langle\psi(t)|\hat{z}|\psi(t)\rangle = \int\langle\psi(t)|z\rangle\langle z|\hat{z}|z'\rangle\langle z'|\psi(t)\rangle dz dz' = \int z|\psi(t,z)|^2 dz \ . \end{aligned} \tag{42.147}$$

We can verify that the expectation value of the particle's position satisfies the classical equation of motion,

$$\begin{aligned} m\ddot{z} &= \langle\psi(t)|m\ddot{\hat{z}}|\psi(t)\rangle = 2\imath\hbar kU_0\left(\hat{a}_+^\dagger\hat{a}_-\langle\psi(t)|e^{-2\imath k\hat{z}}|\psi(t)\rangle - \hat{a}_+\hat{a}_-^\dagger\langle\psi(t)|e^{2\imath k\hat{z}}|\psi(t)\rangle\right) \\ &= 2\imath\hbar kU_0\left(\hat{a}_+^\dagger\hat{a}_- e^{-2\imath k\langle\psi(t)|\hat{z}|\psi(t)\rangle} - \hat{a}_+\hat{a}_-^\dagger e^{2\imath k\langle\psi(t)|\hat{z}|\psi(t)\rangle}\right) \\ &= 2\imath\hbar kU_0\left(\hat{a}_+^\dagger\hat{a}_- e^{-2\imath kz} - \hat{a}_+\hat{a}_-^\dagger e^{2\imath kz}\right) \ . \end{aligned} \tag{42.148}$$

42.4.1.1 About the origin of quantized motion

The quantization of the light field into photons is, as discussed in Chp. 35, an intrinsic property of light. In contrast, the quantization of atomic motion is less obvious, because the atoms are not confined in a trapping potential. The reason for it lies in the monochromaticity of the driving laser fields and the one-dimensional geometry of the system, which allow us to write the recoil operator (??) or (??) as,

$$\boxed{e^{2\imath k\hat{z}} = \int |p + 2\hbar k\rangle\langle p| dp} \ . \tag{42.149}$$

Inserting it into the interaction part of the CARL Hamiltonian,

$$\hat{H}_{int} = U_0(e^{-2\imath k\hat{z}}\hat{a}_+^\dagger\hat{a}_- + e^{2\imath k\hat{z}}\hat{a}_+\hat{a}_-^\dagger) \ , \tag{42.150}$$

the Schrödinger equation for the expanded wavefunction

$$|\psi\rangle = \int c(p)|p\rangle dp \tag{42.151}$$

yields,

$$\begin{aligned} \imath\hbar\frac{d}{dt}\langle p|\psi\rangle &= U_0\hat{a}_+^\dagger\hat{a}_-\langle p|e^{-2\imath k\hat{z}}|\psi\rangle + U_0\hat{a}_+\hat{a}_-^\dagger\langle p|e^{2\imath k\hat{z}}|\psi\rangle \\ = \imath\hbar\frac{d}{dt}c(p) &= U_0[\hat{a}_+^\dagger\hat{a}_- c(p + 2\hbar k) + \hat{a}_+\hat{a}_-^\dagger c(p - 2\hbar k)] \ . \end{aligned} \tag{42.152}$$

That is, if the initial momentum distribution is narrow, $\Delta p \ll 2\hbar k$, and if CARL-induced recoil due to backscattering of photons between counterpropagating modes is the only force acting on the atoms, the momentum of the atoms can only adopt discrete values in units of $2\hbar k$, *as if the atomic velocity were quantized.* That is, the quantization of the field is, in some way, imprinted on the distribution of the atomic moment, so that we may as well use a discrete notation,

$$|\psi\rangle = \sum_\nu c_\nu |\nu\rangle \ , \tag{42.153}$$

such that [16],

$$\imath\hbar \frac{d}{dt} c_\nu = U_0 \hat{a}_+^\dagger \hat{a}_- c_{\nu+1} + U_0 \hat{a}_+ \hat{a}_-^\dagger c_{\nu-1} \ . \tag{42.154}$$

Example 274 (*Analogy to the Bose-Hubbard Hamiltonian*): Interestingly the CARL Hamiltonian with quantized motion (42.150) has, in momentum space, a similar shape as the 1D Bose-Hubbard Hamiltonian in position space,

$$\begin{aligned} \hat{H} &= \sum_\nu \hbar\omega_{rec}\nu^2 + U_0 \sum_\nu \left(|\nu-1\rangle\langle\nu| \hat{a}_+^\dagger \hat{a}_- + |\nu-1\rangle\langle\nu| \hat{a}_+ \hat{a}_-^\dagger \right) \\ &= \hbar\omega_{rec} \sum_\nu \nu^2 + U_0 \hat{a}_+^\dagger \hat{a}_- \sum_\nu \hat{A}_{\nu-1}^\dagger \hat{A}_\nu + U_0 \hat{a}_+ \hat{a}_-^\dagger \sum_\nu \hat{A}_{\nu+1}^\dagger \hat{A}_\nu \ . \end{aligned}$$

Now, it is important to understand that the statement that *photonic recoil is quantized does not mean that the dipolar optical force can only be transmitted in units of* $2\hbar k$, as if the force needed to accumulate a certain amount of energy before it makes a sudden transition to a different momentum state. Rather, the probability to find an initially resting atom subject to a force in the momentum state $2\hbar k$ gradually increases with time. The atom gradually evolves into a coherent superposition of states $|0\rangle + |2\hbar k\rangle + |4\hbar k\rangle + ..$, and only when we *measure* the momentum distribution will it have to decide in which state it ended up. The expectation value of the center-of-mass momentum linearly, as long as the force is constant. A slide show on the quantized CARL can be viewed at (watch talk).

42.4.2 Discretization of the momentum states

We will now assume that, for the physical reasons described above, the motional state of the atom can only exist with momenta corresponding to multiples of twice the photonic recoil.

[16] Note that, instead of expanding the state $|\psi\rangle$, we could expand the motional wavefunction into plane waves,

$$\langle z|\tilde{\psi}\rangle = \tilde{\psi}(z) = \tfrac{1}{\sqrt{2\pi}} \sum_n c_n(t) e^{2\imath n k z} \qquad \text{normalized as} \qquad \int dz |\tilde{\psi}(z)|^2 = 1 = \sum_n |c_n(t)|^2 \ .$$

Insertion of this expansion into the quantized CARL equations (42.146) yields the same results.

42.4.2.1 Schrödinger equation approach

We basically repeat the treatment of Sec. 42.4.1, but now expanding the motion on a discrete basis of momenta labeled by an integer number ν,

$$|\psi\rangle = |\nu\rangle_{motion} \otimes \cancelto{\text{classical}}{|\alpha_+\rangle \otimes |\alpha_-\rangle} \otimes \cancelto{\text{adiab.elim.}}{|i\rangle_{electron}} \to |\nu\rangle \ . \tag{42.155}$$

Applying the recipe detailed at the beginning of Sec. 42.4, we write down the same Schrödinger equation as in (42.144) [17], but now projecting on $\langle\nu|$ rather than on $\langle z|$ and inserting the expansion (42.153) and,

$$e^{2\imath k\hat{z}} = \sum_\nu |\nu+1\rangle\langle\nu| \qquad \text{and} \qquad \hat{p} = \sum_\nu \nu 2\hbar k|\nu\rangle\langle\nu| \ . \tag{42.156}$$

We get,

$$\begin{aligned}\langle\nu|\imath\hbar\frac{d}{dt}\sum_{\nu''} c_{\nu''}|\nu''\rangle = \langle\nu|\sum_{\nu'}\frac{(\nu' 2\hbar k)^2}{2m}|\nu'\rangle\langle\nu'| \\ + U_0\left(\sum_{\nu'}|\nu'-1\rangle\langle\nu'|\hat{a}_+^\dagger\hat{a}_- + \sum_{\nu'}|\nu'+1\rangle\langle\nu'|\hat{a}_+\hat{a}_-^\dagger\right) \ .\end{aligned} \tag{42.157}$$

And from the Heisenberg equation (42.15) for light modes,

$$\langle\psi|\dot{\hat{a}}_\pm|\psi\rangle = \langle\psi|(-\kappa+\imath\Delta_c-\imath U_0)\hat{a}_\pm - \imath U_0 e^{\mp\imath 2k\hat{z}}\hat{a}_\mp + \eta_\pm|\psi\rangle \ , \tag{42.158}$$

we get,

$$\sum_{\nu',\nu''}\langle\nu'|c_\nu^*\dot{\hat{a}}_\pm c_{\nu''}|\nu''\rangle = \sum_{\nu,\nu',\nu''}\langle\nu'|c_{\nu'}^*\left[(-\kappa+\imath\Delta_c-\imath U_0)\hat{a}_\pm - \imath U_0|\nu\mp 1\rangle\langle\nu|\hat{a}_\mp+\eta_\pm\right]c_{\nu''}|\nu''\rangle \ . \tag{42.159}$$

Finally,

$$\boxed{\begin{aligned}\dot{c}_\nu &= -4\imath\omega_{rec}\nu^2 c_\nu - \imath U_0\left(\alpha_+^*\alpha_- c_{\nu+1} + \alpha_+\alpha_-^* c_{\nu-1}\right) \\ \dot{\alpha}_\pm &= (-\kappa+\imath\Delta_c-\imath U_0)\alpha_\pm - \imath U_0\alpha_\mp\sum_\nu c_{\nu\mp1}^* c_\nu + \eta_\pm\end{aligned}} \ . \tag{42.160}$$

In Exc. 42.4.7.1 and 42.4.7.2 we study the equations (42.160) in the presence of a constant external force.

42.4.2.2 Master equation approach

As in the situation under study the motion is the only quantum degree of freedom and not subject to dissipation, a master equation approach is useless, and we will show it here only for completeness.

[17] Here again, as done in Sec. 42.4.1, we ignore terms of the Hamiltonian (42.26) which do not depend on z or p.

In 42.4.7.3 we show a derivation obtained by directly inserting the adiabatically simplified Hamiltonian (42.26) into the Liouville equation (42.8). The result is,

$$\boxed{\begin{aligned}\dot{\rho}_{\mu,\nu} &= \imath(\nu-\mu)\left[(\nu+\mu)\omega_{rec}-\Delta_c\right]\rho_{\mu,\nu} \\ &\quad +\imath U_0\left[\alpha_+^*\alpha_-(\rho_{\mu,\nu-1}-\rho_{\mu+1,\nu})+\alpha_-^*\alpha_+(\rho_{\mu,\nu+1}-\rho_{\mu-1,\nu})\right] \\ \dot{\alpha}_\pm &= (-\kappa+\imath\Delta_c-\imath U_0)\alpha_\pm-\imath U_0\alpha_\mp\sum_\nu\rho_{\nu,\nu\mp1}+\eta_\pm\end{aligned}} \quad . \tag{42.161}$$

42.4.3 Quantization of the atomic motion without adiabatic elimination

So far we have discussed the quantization of the atomic motion in the CARL equations, which were obtained by adiabatic elimination of the electronically excited state. In the following, we will quantize the motion directly in the equations of motion (42.15) for the observables and in the Liouville equation for the density operator. We quantize the atomic motion along the optical z-axis simply by assuming that, in this direction, the momentum only exists in multiples of $\hbar k$, and organize up the Hilbert space like this,

$$|\psi\rangle = |\nu\rangle_{motion}\otimes|i\rangle_{electron}\otimes\cancel{|n\rangle_+\otimes|n\rangle_-}^{\text{classical}} \rightarrow |\nu,i\rangle \ , \tag{42.162}$$

that is, skipping the quantum number counting the photons, we will treat the light fields classically, $\hat{a}_\pm = \alpha_\pm$,

$$\begin{aligned}\hat{p} &= \sum_\nu \nu\hbar k|\nu\hbar k\rangle\langle\nu\hbar k|\otimes\mathbb{I} \\ e^{-\imath k\hat{z}} &= \sum_\nu |\nu\hbar k-\hbar k\rangle\langle\nu\hbar k|\otimes\mathbb{I} \\ \hat{\sigma}^+ &= \mathbb{I}\otimes|2\rangle\langle1| \\ \hat{\rho} &= |\psi\rangle\langle\psi| = \sum_{\mu,\nu,i,j} c^*_{\mu,i}c_{\nu,j}|\mu\rangle\langle\nu|\otimes|i\rangle\langle j|\end{aligned} \ , \tag{42.163}$$

where in the last equation we defined $c_{\nu,j} = \langle p,j|\psi(t)\rangle = \langle\nu\hbar k,j|\psi(t)\rangle = \langle\nu,j|\psi(t)\rangle$, such that,

$$\rho_{\mu,\nu;i,j} \equiv \langle\mu,i|\hat{\rho}|\nu,j\rangle = c^*_{\mu,i}c_{\nu,j} \ . \tag{42.164}$$

Adopting the short notation $|\nu\rangle \equiv |\nu\hbar k\rangle$ we can write the state of the system,

$$
\begin{aligned}
|\psi(t)\rangle &= \sum_\nu c_{\nu,1}|\nu\hbar k,1\rangle + c_{\nu,2}|\nu\hbar k,2\rangle \qquad (42.165)\\
\langle\psi(t)|\hat{p}|\psi(t)\rangle &= \hbar k \sum_\nu \nu(|c_{\nu,1}|^2 + |c_{\nu,2}|^2)\\
\langle\psi(t)|e^{\pm\imath k\hat{z}}|\psi(t)\rangle &= \sum_\nu (c^*_{\nu\pm1,1}c_{\nu,1} + c^*_{\nu\pm1,2}c_{\nu,2})\\
\langle\psi(t)|\hat{a}|\psi(t)\rangle &= \alpha\sum_\nu (|c_{\nu,1}|^2 + |c_{\nu,2}|^2) = \alpha\\
\langle\psi(t)|\hat{\sigma}^-|\psi(t)\rangle &= \sum_\nu c^*_{\nu,1}c_{\nu,2}\\
\langle\psi(t)|\hat{\sigma}_z|\psi(t)\rangle &= \sum_\nu (|c_{\nu,2}|^2 - |c_{\nu,1}|^2)\ .
\end{aligned}
$$

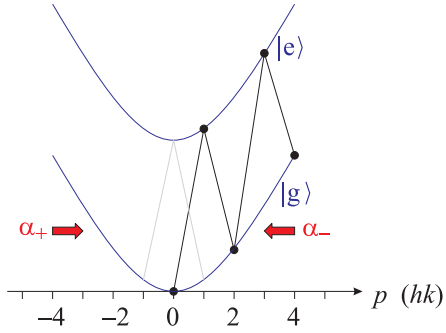

Figure 42.35: Illustration of the quantized motion.

To describe the dynamics of the system we could use the Schrödinger equation, but the Hamiltonian (42.4) does not contain spontaneous emission nor cavity decay. So, let us employ the equations of motion (42.15), which were derived from a master equation. The equation of motion for the field yields,

$$
\begin{aligned}
\dot{\alpha}_\pm &= \langle\psi(t)|\dot{\hat{a}}_\pm|\psi(t)\rangle = \langle\psi(t)|(-\kappa + \imath\Delta_c)\hat{a}_\pm - \imath g\hat{\sigma}^- e^{\mp\imath k\hat{z}} + \eta_\pm|\psi(t)\rangle \qquad (42.166)\\
&= (-\kappa + \imath\Delta_c)\alpha_\pm + \eta_\pm - \imath g\sum_\nu c^*_{\nu\mp1,1}c_{\nu,2}\\
&= (-\kappa + \imath\Delta_c)\alpha_\pm + \eta_\pm - \imath g\sum_\nu \rho_{\nu\mp1,\nu;1,2}\ .
\end{aligned}
$$

For the atomic motion we get,

$$
\dot{x} = \langle\psi(t)|\dot{\hat{x}}|\psi(t)\rangle = \frac{1}{m}\langle\psi(t)|\hat{p}|\psi(t)\rangle = \frac{\nu\hbar k}{m}\ , \qquad (42.167)
$$

and

$$\begin{aligned}\dot{p} &= \langle\psi(t)|\dot{\hat{p}}|\psi(t)\rangle \qquad (42.168)\\ &= \langle\psi(t)|\imath g\hbar k\hat{\sigma}^-\left(\hat{a}_+^\dagger e^{-\imath kz}-\hat{a}_-^\dagger e^{\imath kz}\right)-\imath g\hbar k\hat{\sigma}^+\left(\hat{a}_+e^{\imath kz}-\hat{a}_-e^{-\imath kz}\right)|\psi(t)\rangle\\ &= \sum_\nu \imath g\hbar k\left(\alpha_+^*c_{\nu-1,1}^*c_{\nu,2}-\alpha_-^*c_{\nu+1,1}^*c_{\nu,2}-\alpha_+c_{\nu+1,1}c_{\nu,2}^*+\alpha_-c_{\nu-1,1}c_{\nu,2}^*\right)\\ &= \sum_\nu \imath g\hbar k(\alpha_+^*\rho_{\nu-1,\nu;1,2}-\alpha_-^*\rho_{\nu+1,\nu;1,2}-\alpha_+\rho_{\nu,\nu+1;2,1}-\alpha_-\rho_{\nu,\nu-1;2,1})\ .\end{aligned}$$

42.4.3.1 Maxwell-Bloch equations without adiabatic elimination

Analogously to the treatment in Sec. 34.4.1, we will now derive the master equation without adiabatic elimination of the excited state (in this case called *Maxwell-Bloch equations* from the Liouville equation [first line of Eq. (42.8)] using the Hamiltonian (42.4). The coherent part is,

$$\begin{aligned}\dot{\rho}_{\mu,\nu;i,j} &\equiv \langle\mu,i|\dot{\hat{\rho}}|\nu,j\rangle = -\imath\langle\mu,i|[\hat{H},\hat{\rho}]|\nu,j\rangle \qquad (42.169)\\ &= -\imath\sum_{p,u}\langle\mu,i|\hat{H}|p,u\rangle\rho_{p,\nu;u,j}+\imath\sum_{p,u}\rho_{\mu,q;i,v}\langle p,u|\hat{H}|\nu,j\rangle\\ &= -\imath\left[\frac{(\mu\hbar k)^2}{2m}-\Delta_a\delta_{i2}-\Delta_c(|\alpha_+|^2+|\alpha_-|^2)-\imath\eta_+(\alpha_+-\alpha_+^*)-\imath\eta_-(\alpha_--\alpha_-^*)\right]\rho_{\mu,\nu;i,j}\\ &\quad-\imath g\left[\alpha_+^*\delta_{i1}\rho_{\mu+1,\nu;2,j}+\alpha_+\delta_{i2}\rho_{\mu-1,\nu;1,j}+\alpha_-^*\delta_{i1}\rho_{\mu-1,\nu;2,j}+\alpha_-\delta_{i2}\rho_{\mu+1,\nu;1,j}\right]\\ &\quad+\imath\left[\frac{(\nu\hbar k)^2}{2m}-\Delta_a\delta_{j2}-\Delta_c\left(|\alpha_+|^2+|\alpha_-|^2\right)-\imath\eta_+(\alpha_+-\alpha_+^*)-\imath\eta_-(\alpha_--\alpha_-^*)\right]\rho_{\mu,\nu;i,j}\\ &\quad+\imath g\left[\alpha_+^*\delta_{j2}\rho_{\mu,\nu-1;i,1}+\alpha_+\delta_{j1}\rho_{\mu,\nu+1;i,2}+\alpha_-^*\delta_{j2}\rho_{\mu,\nu+1;i,1}+\alpha_-\delta_{j1}\rho_{\mu,\nu-1;i,2}\right]\\ &= \left[\imath\frac{(\nu^2-\mu^2)(\hbar k)^2}{2m}+\imath\Delta_a(\delta_{i2}-\delta_{j2})\right]\rho_{\mu,\nu;i,j}\\ &\quad+\imath g\left[\alpha_+^*\left(\delta_{j2}\rho_{\mu,\nu-1;i,1}-\delta_{i1}\rho_{\mu+1,\nu;2,j}\right)+\alpha_+\left(\delta_{j1}\rho_{\mu,\nu+1;i,2}-\delta_{i2}\rho_{\mu-1,\nu;1,j}\right)\right.\\ &\qquad\left.+\left(\alpha_-^*\delta_{j2}\rho_{\mu,\nu+1;i,1}-\delta_{i1}\rho_{\mu-1,\nu;2,j}\right)+\alpha_-\left(\delta_{j1}\rho_{\mu,\nu-1;i,2}-\delta_{i2}\rho_{\mu+1,\nu;1,j}\right)\right]\ .\end{aligned}$$

The incoherent part comprises the spontaneous decay [second line of Eq. (42.8)],

$$\begin{aligned}\langle\mu,i|\mathcal{L}_{atom-vac}\hat{\rho}|\nu,j\rangle &= -\gamma\langle\mu,i|\left[\hat{\sigma}^+\hat{\sigma}^-\hat{\rho}-2\hat{\sigma}^-\hat{\rho}\hat{\sigma}^++\hat{\rho}\hat{\sigma}^+\hat{\sigma}^-\right]|\nu,j\rangle \qquad (42.170)\\ &= -\gamma\sum_{p,u}\langle\mu,i|\hat{\sigma}^+\hat{\sigma}^-|p,u\rangle\rho_{p,\nu;u,j}+2\gamma\sum_{p,u,q,v}\langle\mu,i|\hat{\sigma}^-|p,u\rangle\rho_{p,q;u,v}\langle q,v|\hat{\sigma}^+|\nu,j\rangle.\\ &\quad-\gamma\sum_{p,u}\rho_{\mu,p;i,u}\langle p,u|\hat{\sigma}^+\hat{\sigma}^-|\nu,j\rangle\\ &= -\gamma\left[\delta_{i2}\rho_{\mu,\nu;i,j}-2\delta_{i1}\delta_{j1}\rho_{\mu,\nu;2,2}+\delta_{j2}\rho_{\mu,\nu;i,j}\right]\end{aligned}$$

and the cavity decay [third line of Eq. (42.8)],

$$\langle\mu,i|\mathcal{L}_{cavity-vac,\pm}\hat{\rho}|\nu,j\rangle = -\kappa\langle\mu,i|\hat{a}_\pm^\dagger\hat{a}_\pm\hat{\rho}-2\hat{a}_\pm\hat{\rho}\hat{a}_\pm^\dagger+\hat{\rho}\hat{a}_\pm^\dagger\hat{a}_\pm|\nu,j\rangle = 0\ . \qquad (42.171)$$

Finally, using the definition of the recoil shift $\omega_{rec} = \hbar k^2/2m$ we get,

$$\boxed{\begin{aligned}
\dot{\rho}_{\mu,\nu;1,1} &= \imath(\nu^2-\mu^2)\omega_{rec}\rho_{\mu,\nu;1,1} + 2\gamma\rho_{\mu,\nu;2,2} \\
&+ \imath\hbar g\left[-\alpha_+^*\rho_{\mu+1,\nu;2,1} + \alpha_+\rho_{\mu,\nu+1;1,2} - \alpha_-^*\rho_{\mu-1,\nu;2,1} + \alpha_-\rho_{\mu,\nu-1;2,1}\right] \\
\dot{\rho}_{\mu,\nu;1,2} &= \left[\imath(\nu^2-\mu^2)\omega_{rec} - \imath\hbar\Delta_a\right]\rho_{\mu,\nu;1,2} - \gamma\rho_{\mu,\nu;1,2} \\
&+ \imath\hbar g\left[\alpha_+^*\rho_{\mu,\nu-1;1,1} - \alpha_+^*\rho_{\mu+1,\nu;2,2} + \alpha_-^*\rho_{\mu,\nu+1;1,1} - \alpha_-^*\rho_{\mu-1,\nu;2,2}\right] \\
\dot{\rho}_{\mu,\nu;2,1} &= \left[\imath(\nu^2-\mu^2)\omega_{rec} + \imath\hbar\Delta_a\right]\rho_{\mu,\nu;2,1} - \gamma\rho_{\mu,\nu;2,1} \\
&- \imath\hbar g\left[\alpha_+\rho_{\mu-1,\nu;1,1} - \alpha_+\rho_{\mu,\nu+1;2,2} + \alpha_-\rho_{\mu+1,\nu;1,1} - \alpha_-\rho_{\mu,\nu-1;2,2}\right] \\
\dot{\rho}_{\mu,\nu;2,2} &= \imath(\nu^2-\mu^2)\omega_{rec}\rho_{\mu,\nu;2,2} - 2\gamma\rho_{\mu,\nu;2,2} \\
&+ \imath\hbar g\left[\alpha_+^*\rho_{\mu,\nu-1;2,1} - \alpha_+\rho_{\mu-1,\nu;1,2} + \alpha_-^*\rho_{\mu,\nu+1;2,1} - \alpha_-\rho_{\mu+1,\nu;1,2}\right] \\
\dot{\alpha}_\pm &= (-\kappa + \imath\Delta_c - \imath U_0)\alpha_\pm + \eta_\pm - \imath g\sum_\nu \rho_{\nu\mp1,\nu;1,2}
\end{aligned}} \tag{42.172}$$

We note $\hat{\rho}_{\mu,\nu;2,1} = \hat{\rho}^*_{\nu,\mu;1,2}$.

The equations (42.172) form a set a equations to describe the quantized CARL without adiabatic elimination. And as shown in the derivation of the CARL equations (42.25), they contain radiation pressure. In Exc. 42.4.7.4 we study the quantized CARL Maxwell-Bloch equations without adiabatic elimination of the excited state for a three-level system.

42.4.4 Quantized motion with many particles

The Hamiltonian (42.144) holds for a single atom. If clouds of thermal atoms are considered, we may switch to a classical description of the motion, as done in (42.46). In the case of very cold (below the recoil limit) but still independent atoms, we may assume that they all are coherently distributed over the same momentum states. We may then apply a unique momentum state expansion for all atoms, as shown in the subsequent section.

If on the other hand quantum statistics play a role, then we need to replace the wavefunction in the Schrödinger equation (42.144) by field operators, as done in Sec. 47.5. In the following sections, we will restrict to single atoms that can be in a coherent superposition of momentum states or many atoms in a matter wave that can be treated as a c-number, e.g. a Bose-condensate without fluctuations.

42.4.4.1 Modal expansion of the motion of many independent atoms in the adiabatic approximation for one-sided pumping

Our starting point is the quantum version of the CARL equations (42.25), where we neglect spontaneous emission, $\gamma_0 = 0$. Setting $\alpha_+ = \eta_+/\kappa$ and $\eta_- = 0$ we get,

$$\boxed{\begin{aligned}
\dot{\hat{a}}_- &= (-\kappa + \imath\Delta_c - \imath U_0)\hat{a}_- - \imath U_0\tfrac{\eta_+}{\kappa}e^{-2\imath k\hat{z}_j} \\
m\ddot{\hat{z}}_j &= 2\imath\hbar k U_0(\hat{a}_+^\dagger\hat{a}_- e^{-2\imath k\hat{z}_j} - \hat{a}_+\hat{a}_-^\dagger e^{2\imath k\hat{z}_j})
\end{aligned}}, \tag{42.173}$$

where the index j runs over all atoms. For this case, the total momentum is a constant of motion for N atoms is,

$$[\hat{H}, 2\hbar k\hat{a}_-^\dagger \hat{a}_- + \sum_{j=1}^{N} \hat{p}_j] = 0 \ . \tag{42.174}$$

where the Hamiltonian is obtained from (42.26) by eliminating the mode α_+ and summing over all atoms,

$$\hat{H} = \sum_j \left[\frac{\hat{p}_j^2}{2m} + \frac{\eta_+}{\kappa} U_0 \left(e^{-2\imath k\hat{z}_j} \hat{a}_- + e^{2\imath k\hat{z}_j} \hat{a}_-^\dagger \right) \right] + (U_0 - \Delta_c)\hat{a}_-^\dagger \hat{a}_- \ . \tag{42.175}$$

To treat the motion as being quantized we define a base $|\nu\rangle_j$,

$$\hat{p}_j|\nu\rangle_j = 2\hbar k\nu|\nu\rangle_j \qquad \text{and} \qquad |\psi(z_j)\rangle = \sum_\nu c_{j,\nu}|\nu\rangle_j \ , \tag{42.176}$$

and calculate the expected value of the equations (42.173) regarding the atomic motion,

$$\begin{aligned} \frac{d\hat{a}_-}{dt} &= (-\kappa - \imath\Delta_c)\hat{a}_- - \imath U_0 \tfrac{\eta_+}{\kappa} \sum_j \langle\psi(z_j)|e^{-2\imath k\hat{z}_j}|\psi(z_j)\rangle \\ &= (-\kappa + \imath\Delta_c - \imath U_0)\hat{a}_- - \imath U_0 \tfrac{\eta_+}{\kappa} \sum_{j,\mu,\nu} c_{j,\mu}^* c_{j,\nu\, j} \langle\mu|e^{-2\imath k z_j}|\nu\rangle_j \\ &= (-\kappa + \imath\Delta_c - \imath U_0)\hat{a}_- - \imath U_0 \tfrac{\eta_+}{\kappa} \sum_{j,\nu} c_{j,\nu}^* c_{j,\nu+1} \ . \end{aligned} \tag{42.177}$$

We do not use the second equation (42.173), but instead we use the Schrödinger equation $\imath\hbar\frac{d|\psi(z_j\rangle}{dt} = \hat{H}|\psi(z_j)\rangle$, which yields,

$$\begin{aligned} \imath\hbar \sum_\nu \frac{dc_{j,\nu}}{dt}|\nu\rangle_j = \sum_\nu \frac{1}{2m} p_j^2 c_{j,\nu}|\nu\rangle_j + \hbar\Delta_c \hat{a}_-^\dagger \hat{a}_- \sum_\nu c_j(\nu)|\nu\rangle_j \\ + \hbar U_0 \eta \sum_\nu (\hat{a}_-^\dagger e^{-2\imath k z_j} + \hat{a}_- e^{2\imath k z_j}) c_{j,\nu}|\nu\rangle_j \ . \end{aligned} \tag{42.178}$$

Projecting on ${}_j\langle\mu|$, we obtain [278],

$$\boxed{\begin{aligned} \dot{c}_{j,\mu} &= -4\imath\omega_{rec}\mu^2 c_{j,\mu} - \imath\Delta_c \hat{a}_-^\dagger \hat{a}_- c_{j,\mu} - \imath U_0 \eta [\hat{a}_-^\dagger c_{j,\mu+1} + a_- c_{j,\mu-1}] \\ \dot{\hat{a}}_- &= -(\kappa + \imath\Delta_c)\hat{a} + N U_0 \eta \sum_\nu c_{j,\nu}^* c_{j,\nu+1} \end{aligned}} \ , \tag{42.179}$$

where we took the expectation value of Eq. (42.177). The equations (42.179) can be used for numerical simulations [1102].

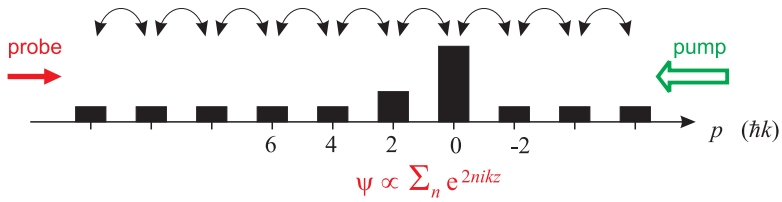

Figure 42.36: Probe light and 'bunching' when the temperature is raised.

42.4.4.2 Equations for the density matrix

The equations (42.179) allow to calculate the derivatives of the density matrix given by,

$$\varrho_{\mu,\nu} \equiv e^{-\imath(\mu-\nu)\Delta_c t}\frac{1}{N}\sum_j c_j^*(\mu)c_j(\nu)\ , \tag{42.180}$$

yielding,

$$\begin{aligned}\frac{d\varrho_{\mu,\nu}}{dt} &= e^{-\imath(\mu-\nu)\Delta_a t}N^{-1}\sum_j\left(\dot{c}^*_{j,\mu}c_{j,\nu}+c^*_{j,\mu}\dot{c}_{j,\nu}-\Delta_c c^*_{j,\mu}c_{j,\nu}\imath(\mu-\nu)\right) \\ &= e^{-\imath(\mu-\nu)\Delta_a t}N^{-1}\sum_j[\imath\omega_r(\mu^2-\nu^2)-\Delta_c\imath(\mu-\nu)]c^*_{j,\mu}c_{j,\nu}+ \\ &\quad +\imath U_0\eta\left[ac^*_{j,\mu+1}c_{j,\nu}-ac^*_{j,\mu}c_{j,\nu-1}+\hat{a}^\dagger c^*_{j,\mu-1}c_{j,\nu}-\hat{a}^\dagger c^*_{j,\mu}c_{j,\nu+1}\right]\ .\end{aligned} \tag{42.181}$$

Introducing $\tilde{a}\equiv ae^{\imath\Delta_c t}$ we finally obtain,

$$\boxed{\begin{aligned}\frac{d\varrho_{\mu,\nu}}{dt} &= \imath(\mu-\nu)[\omega_r(\mu+\nu)-\Delta_c]\varrho_{\mu,\nu} \\ &+ \imath U_0\eta\left[\tilde{a}(\varrho_{\mu+1,\nu}-\varrho_{\mu,\nu-1})+\tilde{a}^\dagger(\varrho_{\mu-1,\nu}-\varrho_{\mu,\nu+1})\right] \\ \frac{d\tilde{a}}{dt} &= -\kappa\tilde{a}-\imath NU_0\eta\sum_\nu\varrho_{\nu,\nu+1}\end{aligned}}\ . \tag{42.182}$$

These are the CARL equations for the density matrix. In 42.4.7.3 we show an alternative derivation obtained by directly inserting the adiabatically simplified Hamiltonian (42.26) into the Liouville equation (42.8).

We note, that $\sum_\nu \varrho_{\nu,\nu+1}$ is the 'bunching' and that $\varrho^*_{\mu,\nu}=\varrho_{\nu,\mu}$. The average moment is given by $\langle p\rangle=\sum_\nu \nu\varrho_{\nu,\nu}$. In the Figs. 42.37 and 42.38 we show simulations in the semi-classical regimes $\rho\gg 1$ in the 'bad-cavity' limit, $\kappa>1$, and the 'good-cavity' limit $\kappa\ll 1$.

Here are some movies illustrating the quantum CARL dynamics, simulated using the momentum state expansion (watch movie) and (watch movie). The following dynamics were calculated via direct integration of the Schrödinger equation without momentum state expansion: Bloch oscillations (watch movie), CARL dynamics (watch movie), and joint Bloch and CARL dynamics (watch movie). See also (watch talk).

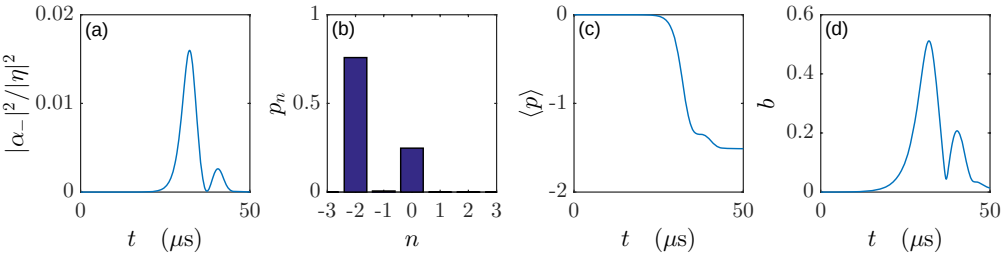

Figure 42.37: (code) Simulation of the CARL equation (42.179) in the superradiant, semi-classical, 'bad-cavity' regime for $\kappa_c = 4$, $\rho = 4$, $\Delta_c = 0$.

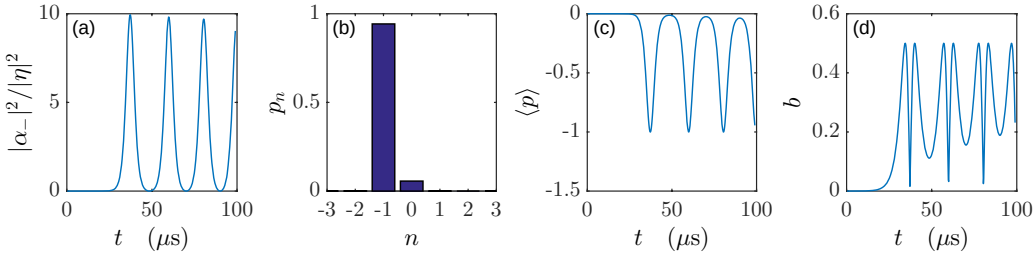

Figure 42.38: (code) Simulation of the CARL equation (42.179) in the superradiant, semi-classical, 'good-cavity' regime for $\kappa_c = 0.02$, $\rho = 4$, $\Delta_c = 0$.

42.4.5 Approximation for a bimodal momentum distribution

We observe that in the quantum regime the momentum distribution of the matter wave is bimodal, that is, only two momentum states are simultaneously populated. This justifies a simplification of the equations (42.182), assuming that at a given time, atoms must either be in a specific state $|\mu\rangle_j$ or in a superposition of this state is an adjacent state $|\mu-1\rangle_j$. Hence,

$$\begin{aligned}
\frac{d\varrho_{\mu,\mu}}{dt} &= -\imath U_0\eta(\tilde{a}\varrho_{\mu,\mu-1} - \tilde{a}^\dagger\varrho_{\mu-1,\mu}) = -\frac{d\varrho_{\mu-1,\mu-1}}{dt} \\
\frac{d\varrho_{\mu-1,\mu}}{dt} &= -\imath[(2\mu-1)\omega_r - \Delta_c]\varrho_{\mu-1,\mu} + \imath U_0\eta\tilde{a}(\varrho_{\mu,\mu} - \varrho_{\mu-1,\mu-1}) \\
\frac{d\tilde{a}}{dt} &= -\imath N U_\mu\eta\varrho_{\mu-1,\mu} - \kappa_c\tilde{a}\ .
\end{aligned} \tag{42.183}$$

Introducing the coherence $S_\mu = \varrho_{\mu-1,\mu}$ and the inversion $W_\mu = \varrho_{\mu,\mu} - \varrho_{\mu-1,\mu-1}$ and postulating the normalization $1 = \varrho_{\mu,\mu} + \varrho_{\mu-1,\mu-1}$,

$$\begin{aligned}
\frac{dW_\mu}{dt} &= -2\imath U_0\eta(\tilde{a}S_\mu^* - \tilde{a}^\dagger S_\mu) \\
\frac{dS_\mu}{dt} &= -\imath[(2\mu-1)\omega_r - \Delta_c]S_\mu + \imath U_0\eta\tilde{n}aW_\mu \\
\frac{d\tilde{a}}{dt} &= -\imath N U_0\eta S_\mu - \kappa_c\tilde{a}\ .
\end{aligned} \tag{42.184}$$

42.4.5.1 Linearization and stability analysis

We assume that the atoms are initially 'bunched' in a specific state $|\mu\rangle_j$. Only adjacent momentum states are coupled,

$$\begin{aligned}
\frac{d\varrho_{\mu+1,\mu}}{dt} &= \imath[\omega_r(2\mu+1)-\Delta_c]\varrho_{\mu+1,\mu} + \imath U_0\eta\tilde{a}^\dagger(\varrho_{\mu,\mu}-\varrho_{\mu+1,\mu+1}) \\
\frac{d\varrho_{\mu-1,\mu}}{dt} &= -\imath[\omega_r(2\mu-1)-\Delta_c]\varrho_{\mu-1,\mu} + \imath U_0\eta\tilde{a}(\varrho_{\mu,\mu}-\varrho_{\mu-1,\mu-1}) \\
\frac{d\tilde{a}}{dt} &= -\imath NU_0\eta(\varrho_{\mu,\mu+1}+\varrho_{\mu-1,\mu}) - \kappa_c\tilde{a}\ .
\end{aligned} \tag{42.185}$$

Conjugate the upper equation and build the sum and difference, $B_\mu \equiv \varrho_{\mu,\mu+1}+\varrho_{\mu-1,\mu}$ and $D_\mu \equiv \varrho_{\mu,\mu+1}-\varrho_{\mu-1,\mu}$,

$$\begin{aligned}
\frac{dB_\mu}{dt} &= \imath(\Delta_c - 2\mu\omega_r)B_\mu - \imath\omega_\mu D_\mu + \imath U_0\eta\tilde{a}(\varrho_{\mu+1,\mu+1}-\varrho_{\mu-1,\mu-1}) \\
\frac{dD_\mu}{dt} &= \imath(\Delta_c - 2\mu\omega_r)D_\mu - \imath\omega_r B_\mu - 2\imath U_0\eta\tilde{a} + \imath U_0\eta\tilde{a}(\varrho_{\mu+1,\mu+1}-2\varrho_{\mu,\mu}+\varrho_{\mu-1,\mu-1}) \\
\frac{d\tilde{a}}{dt} &= -\imath NU_0\eta B_\mu - \kappa_c\tilde{a}\ .
\end{aligned} \tag{42.186}$$

Use $\varrho_{\mu,\mu} \simeq 1$ and abbreviate $\delta_\mu \equiv 2r\omega_\mu - \Delta_c$,

$$\begin{aligned}
\frac{dB_\mu}{dt} &= -\imath\delta_\mu B_\mu - \imath\omega_r D_\mu \\
\frac{dD_\mu}{dt} &= -\imath\omega_r B_\mu - \imath\delta_r D_\mu - 2\imath U_0\eta\tilde{a} \\
\frac{d\tilde{a}}{dt} &= -\imath NU_0\eta B_\mu - \kappa_c\tilde{a}\ .
\end{aligned} \tag{42.187}$$

Seeking solution proportional to $x \equiv \bar{x}e^{\imath(\lambda-\delta_\mu)t}$,

$$\begin{aligned}
\imath\lambda\bar{B}_\mu &= -\imath\omega_\mu\bar{D}_\mu \\
\imath\lambda\bar{D}_\mu &= -\imath\omega_\mu\bar{B}_\mu - 2\imath U_\mu\eta\bar{a} \\
\imath(\lambda-\delta_\mu)\bar{a} &= -\imath NU_0\eta\bar{B}_\mu - \kappa_c\bar{a}\ .
\end{aligned} \tag{42.188}$$

Abbreviating $\Lambda_m \equiv \delta_m + \imath\kappa_c$, the characteristic equation is,

$$\det\begin{pmatrix} \lambda & \omega_r & 0 \\ \omega_r & \lambda & 2U_0\eta \\ NU_0\eta & 0 & \lambda-\Lambda_\mu \end{pmatrix} = \lambda^3 - \Lambda_\mu\lambda^2 - \omega_r^2\lambda + \omega_r^2\Lambda_\mu + 2NU_0^2\eta^2\omega_r = 0\ . \tag{42.189}$$

The gain is given by the imaginary part of λ. We have exponential amplification if $\mathrm{Im}\,\lambda < 0$. Hence, we search for solution with the lowest imaginary value.

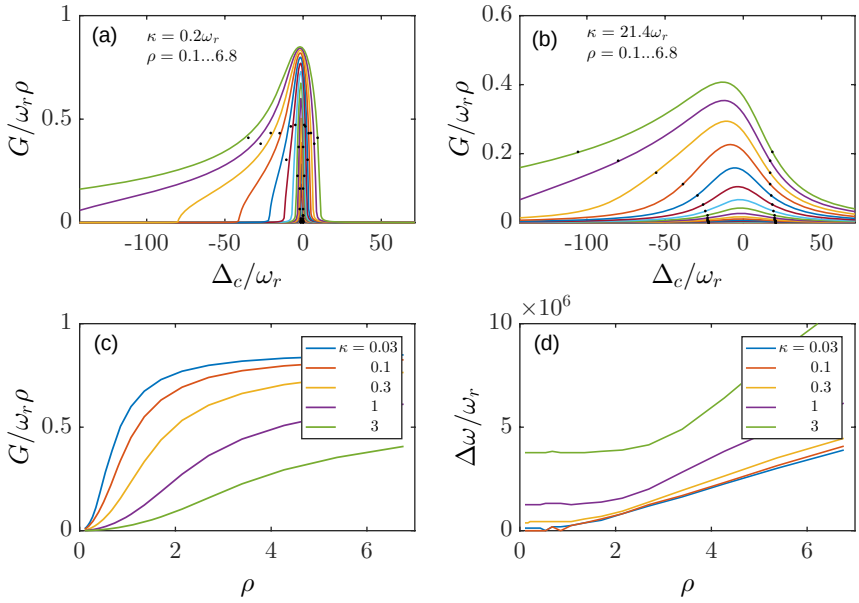

Figure 42.39: (code) Gain dependence on ρ and κ.

42.4.5.2 Universal scaling

To simplify the formulae simplify, we rescale them. We start from Eq. (42.182) and use the substitution for universal scaling,

$$\begin{aligned} \theta_j \equiv 2kz_j \quad &\text{and} \quad \bar{p}_j \equiv 2kv_j/\rho\omega_r \\ \tau \equiv \rho\omega_r t \quad &\text{and} \quad \kappa \equiv \kappa_c/\omega_r\rho \\ \bar{\lambda} \equiv \lambda/\omega_r\rho \quad &\text{and} \quad \bar{\delta}_\mu \equiv \delta_\mu/\omega_r\rho = 2\mu/\rho + \Delta_c/\omega_r\rho \\ \bar{A} \equiv (2/N\rho)^{1/2}\bar{a} \quad &\text{and} \quad \eta U_\mu \equiv \sqrt{\rho^3\omega_r^2/2N}\ . \end{aligned} \tag{42.190}$$

This reproduces the Bonifacio notation,

$$\begin{aligned} \bar{\lambda}\bar{B}_\mu + \rho^{-1}\bar{D}_\mu &= 0 \\ \bar{\lambda}\bar{D}_\mu + \rho^{-1}\bar{B}_\mu + \rho\bar{A} &= 0 \\ (\bar{\lambda} - \bar{\delta}_\mu - \imath\kappa)\bar{A} + \bar{B}_\mu &= 0\ . \end{aligned} \tag{42.191}$$

Skipping the bars, the characteristic equation reads,

$$\det \begin{pmatrix} \lambda & \rho^{-1} & 0 \\ \rho^{-1} & \lambda & \rho \\ 1 & 0 & \lambda - \delta_\mu - \imath\kappa \end{pmatrix} = (\lambda - \delta_\mu - \imath\kappa)(\lambda^2 - \rho^{-2}) + 1 = 0\ . \tag{42.192}$$

Let us first discuss the semiclassical limit, $\rho \gg 1$. In the good-cavity regime, $\kappa \simeq 0$, we may neglect the recoil shift, $2m\omega_r \to 0$, so that $\Lambda = \Delta_c$. The gain is largest

when $\Delta_c \to 0$. The characteristic equation reduces to $\lambda^3 = -1$, yielding the solutions $\lambda = 1, \frac{1}{2}(1 \pm \imath\sqrt{3})$. Hence, the gain $G = -\Im\mathfrak{m}\ \lambda$, is

$$\begin{aligned} G &= \tfrac{1}{2}\omega_r\rho\sqrt{3} \\ \Delta\omega_G &\simeq \omega_r\rho \gg \kappa_c, \omega_r\ . \end{aligned} \tag{42.193}$$

The gain bandwidth $\Delta\omega_G$ being much larger than the recoil frequency, the Bragg condition for scattering between different momentum states is approximately fulfilled for a large number of initial momenta. I.e. although the momentum transfer is quantized, $\Delta_c = n\omega_r$, the atoms can be accelerated to high velocities. From Eq. (42.186)(a) we see $|\bar{D}_\mu/\bar{B}_\mu| = \rho|\bar{\lambda}| \gg 1$, i.e. $\varrho_{\mu,\mu+1} \simeq \varrho_{\mu-1,\mu}$.

In the superradiant regime, $\kappa > 1$, of the semiclassical limit the characteristic equation reduces to $\lambda^2 = -\imath/\kappa$, i.e. $\lambda = \pm(1-\imath)/\sqrt{2\kappa}$.[18] Hence, the gain is,

$$\begin{aligned} G &= \tfrac{1}{2}\omega_r\rho\sqrt{2/\kappa} \\ \Delta\omega_G &\simeq \kappa_c = \omega_r\rho\kappa \gg \omega_r\ . \end{aligned} \tag{42.194}$$

In fact, the relative gain bandwidth is on the order of $\Delta\omega_G/\omega_r \simeq \rho \propto \left(nNU_0^2\right)^{1/3}$. Since recoil can be neglected we can have absorption or emission. The gain results from the difference bewteen the average rates of both.

Now we turn to the quantum limit, $\rho < 1$. In the good-cavity regime, $\kappa \simeq 0$, $\lambda = \rho^{-1} + \frac{1}{2}(\delta_m - \rho^{-1}) - \frac{1}{2}\sqrt{(\delta_m - \rho^{-1})^2 - 2\rho}$. Hence, the gain is,

$$\begin{aligned} G &= \tfrac{1}{2}\omega_r\rho\Im\mathfrak{m}\ \sqrt{(\delta_m - \rho^{-1})^2 - 2\rho} \simeq \tfrac{1}{2}\omega_r\rho\sqrt{2\rho} \\ \Delta\omega_G &= \omega_r\rho^{3/2} < \omega_r\ . \end{aligned} \tag{42.195}$$

In fact, the relative gain bandwidth is on the order of $\Delta\omega_G/\omega_r \simeq \rho^{3/2} \propto \sqrt{nNU_0^2}$. Here recoil plays a role so that we have emission without absorption. Gain results exclusively from emission. From Eq. ((42.186)a) we see $|\bar{D}_m/\bar{B}_m| = \rho|\bar{\lambda}| \simeq 1$, i.e. $\varrho_{m,m+1} \ll \varrho_{m-1,m}$.

In the superradiant regime, $\kappa > 1$, of the quantum limit, $\lambda = \rho^{-1} + \frac{\rho}{2}[(\delta_m - \rho^{-1}) + \imath\kappa]^{-1}$. Hence,

$$\begin{aligned} G &= \tfrac{1}{2}\omega_r\rho\frac{\rho\kappa}{(\delta_m - \rho^{-1})^2 + \kappa^2} \simeq \tfrac{1}{2}\frac{\omega_r\rho^2}{\kappa} \\ \Delta\omega_G &= \kappa_c > \omega_r\rho\ . \end{aligned} \tag{42.196}$$

The various regimes may be summarized in the following phase diagram. We will see later, that each region produces qualitatively different solutions of the full (non-linearized) equations.

[18] The assertion $\Re\mathfrak{e}\ \lambda \ll \kappa$ used to simplify the characteristic equation is compatible with the solution.

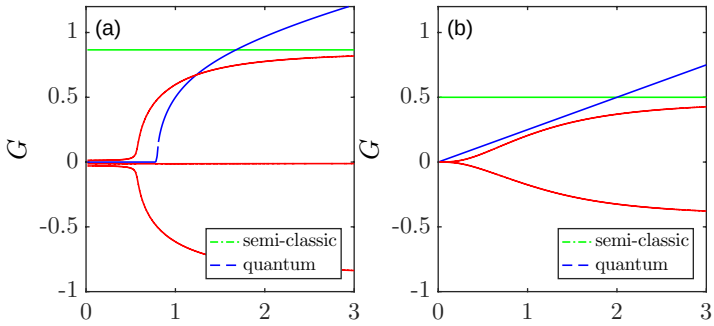

Figure 42.40: (code) Analytical approximations of the characteristic equation for the various regimes in the good-cavity limit $\kappa = 0.03$ (a) and the superradiant limit $\kappa = 2$ (b).

42.4.6 Simulation of random quantum trajectories

Spontaneous emission can induce a random walk of the atoms, which be accounted for by a proper master equation. We write the master equation for the density operator of a dissipative system, as shown in (41.74) [233, 1431],

$$\boxed{\dot{\hat{\rho}} = \imath[\hat{\rho}, \hat{H}] - \tfrac{1}{2}\sum_\mu \{\hat{\rho}, \hat{L}_\mu^\dagger \hat{L}_\mu\} + \sum_\mu \hat{L}_\mu \hat{\rho} \hat{L}_\mu^\dagger} \ . \tag{42.197}$$

The first term describes the coherent part, the second part dissipation, and the third quantum jumps. The dissipative operators $\hat{L}_\mu$ appearing in the Lindblad terms model the impact of the environment. An alternative to solving the master equation consists in simulating single trajectories of the system with a Schrödinger equation, accounting for dissipation by a non-Hermitian effective Hamiltonian and for quantum fluctuations by a stochastic noise term.

As an example, let us consider the Hamiltonian for an atom interacting with a standing wave potential,

$$\hat{H} = \frac{\hat{p}^2}{2m} + U \cos k\hat{x} \ , \tag{42.198}$$

where $\hat{p} = \hbar q \hat{\nu} = -\imath\hbar d/dx$. We define a momentum basis $|\phi(\tau_0)\rangle = \sum_\nu c_\nu |\nu\rangle$ with $\sum_\nu |c_\nu|^2 = 1$. In this basis, the momentum and the position operator can be expanded as usual,

$$\hat{p} = \hbar q \sum_{\nu=-\infty}^{\infty} \nu |\nu\rangle\langle\nu| \quad \text{and} \quad \cos k\hat{x} = \tfrac{1}{2} \sum_{\nu=-\infty}^{\infty} (|\nu+1\rangle\langle\nu| + |\nu-1\rangle\langle\nu|) \ , \tag{42.199}$$

where $\hbar q$ is the momentum transferred upon a kick. The expectation value for the momentum and the position are then,

$$\langle\hat{p}\rangle = \sum_\nu \hbar q \nu |c_\nu|^2 \qquad \text{and} \qquad \langle\cos k\hat{x}\rangle = \tfrac{1}{2}\sum_\nu (c_\nu^* c_{\nu-1} + c_\nu^* c_{\nu+1}) \ . \tag{42.200}$$

The Lindblad operators describe deceleration of the rotor. With $\mu = \pm$, we get,

$$\hat{L}_\pm = g \sum_{\nu=0}^{\infty} \sqrt{\nu+1} |\pm\nu\rangle\langle\pm\nu \pm 1| \ , \tag{42.201}$$

such that,

$$\hat{L}_\pm^\dagger \hat{L}_\pm = g^2 \sum_{\nu=0}^{\infty} \nu |\pm\nu\rangle\langle\pm\nu| \quad \text{and} \quad \hat{L}_+^\dagger \hat{L}_+ + \hat{L}_-^\dagger \hat{L}_- = g^2 \sum_{\nu=-\infty}^{\infty} |\nu|\, |\nu\rangle\langle\nu| \ . \tag{42.202}$$

Now, as we have seen in Sec. 34.5.3, we may treat the first part of the Lindblad terms in (42.197) as the dissipative part of an an *effective Hamiltonian*,

$$\boxed{\hat{H}_{eff} = \hat{H} - \tfrac{\imath}{2} \sum_\mu \hat{L}_\mu^\dagger \hat{L}_\pm} \ . \tag{42.203}$$

That is, we can attempt a *quantum Monte Carlo wavefunction simulation* of an effective Schrödinger equation.

We define the quantity $dp_\pm \equiv \langle\phi(\tau_0)|\hat{L}_\pm^\dagger \hat{L}_\pm|\phi(\tau_0)\rangle d\tau$,

$$\frac{dp_+}{d\tau} = g^2 \sum_\nu |c_\nu|^2 \quad \text{and} \quad \frac{dp_-}{d\tau} = g^2 \sum_\nu |c_{-\nu}|^2 \ . \tag{42.204}$$

To perform simulations, we start with $|\phi(\tau_0)\rangle$. After a time $d\tau$, we generate a uniform random number ζ. After infinitesimal time, we compare the random number to the accumulated probability. If $\zeta > dp_\mu$, we say that a quantum jump occurred. The new wavefunction is,

$$|\phi(\tau_0)\rangle \to \frac{\hat{L}_\pm|\phi(\tau_0)\rangle}{\|\hat{L}_\pm|\phi(\tau_0)\rangle\|} = \frac{\sum_{\nu\geq 0}\sqrt{\nu+1}c_{\pm\nu\pm1}|\nu\rangle}{\sqrt{\sum_{\nu\geq 0}\nu|c_{\pm\nu}|^2}} \ . \tag{42.205}$$

If in contrast, $\zeta < 1 - \sum_\mu dp_\mu$, then the system continues to evolve slowly. However, dissipation losses have to be compensated by renormalization,

$$|\phi(\tau_0)\rangle \to \frac{(1 - \frac{\imath}{\hbar}\hat{H}_{eff}dt)|\phi(\tau_0)\rangle}{\sqrt{1 - \sum_k dp_k}} \ , \tag{42.206}$$

where the evolution is

$$\begin{aligned}
(|\phi(dt)\rangle &= 1 - \imath\hat{H}_{eff}dt/\hbar)|\phi(\tau_0)\rangle \qquad (42.207)\\
&= \left(1 - \tfrac{\imath}{\hbar}dt\frac{\hat{p}^2}{2m} - \tfrac{\imath}{\hbar}dtU\cos k\hat{x} - \tfrac{1}{2\hbar}dt\sum_\pm \hat{L}_\pm^\dagger \hat{L}_\pm\right)\sum_\nu c_\nu|\nu\rangle\\
&= \sum_\nu c_\nu|\nu\rangle - \tfrac{\imath}{\hbar}dt\tfrac{1}{2}\sum_\nu c_\nu\hbar^2\nu^2|\nu\rangle - \tfrac{\imath}{\hbar}dt\tfrac{1}{2}\sum_\nu c_\nu U(|\nu+1\rangle + |\nu-1\rangle)\\
&\quad - \frac{g^2}{2\hbar}dt\sum_{\nu\geq 0}\nu(c_\nu|\nu\rangle + c_{-\nu}|-\nu\rangle)\\
&= |\phi(\tau_0)\rangle - \frac{\imath}{2\hbar}dt\sum_\nu c_\nu\left[\nu(\hbar^2\nu - \imath g^2)|\nu\rangle + U|\nu+1\rangle + U|\nu-1\rangle\right] \ .
\end{aligned}$$

With this we can now follow the evolution of observables, such as $\langle\phi(t)|\nu\rangle\langle\nu|\phi(t)\rangle$, $\langle\phi(t)|\hat{p}|\phi(t)\rangle$, and $\langle\phi(t)|\cos k\hat{x}|\phi(t)\rangle$, in time.

42.4.7 Exercises

42.4.7.1 Ex: Quantized CARL equations in the presence of a constant external force

a. Generalize the quantized CARL equations (42.146), respectively, (42.160) for the presence of a constant external force.
b. Now, we consider a unidirectionally pumped ring cavity, with the pump laser locked to a cavity mode, in the presence of an external periodic potential. Show that this system is equivalent to CARL in a ring cavity pumped from both sides.

Solution: *a. The procedure is analogous to [1138] when we remove the external potential, but consider the dynamics of both counterpropagating modes. We simply add the external potential to the equations of motion (42.146),*

$$\begin{aligned} \imath\hbar\frac{d}{dt}\psi(z) &= -\frac{\hbar^2}{2m}\frac{d^2}{dz^2}\psi(z) + \hbar U_0\left(\alpha_+^*\alpha_- e^{-2\imath kz} + \alpha_+\alpha_-^* e^{2\imath kz}\right)\psi(z) - maz\psi(z) \\ \dot{\alpha}_\pm &= (-\kappa + \imath\Delta_c - \imath U_0)\alpha_\pm + \imath U_0\alpha_\mp\int dz|\psi(z)|^2 e^{\mp 2\imath kz} + \eta_\pm \end{aligned} \quad .$$

With the unitary transformation $\psi = \tilde{\psi}e^{\imath maz t/\hbar}$ the Schrödinger equation simplifies to,

$$\dot{\tilde{\psi}}(z) = \frac{\imath\hbar}{2m}\left(\frac{d}{dz} + \frac{\imath mat}{\hbar}\right)^2\tilde{\psi}(z) - \imath U_0\left(\alpha_+^\dagger\alpha_- e^{-2\imath kz} + \alpha_+\alpha_-^\dagger e^{2\imath kz}\right)\tilde{\psi}(z) \ ,$$

and with the mode expansion $\tilde{\psi} = \frac{1}{\sqrt{2\pi}}\sum_\nu c_\nu(t)e^{2\imath\nu kz}$, we obtain,

$$\begin{aligned} \dot{c}_\nu &= -4\imath\omega_{rec}(\nu + \nu_{blo}t)^2 c_\nu - \imath U_0\left(\alpha_+^*\alpha_- c_{\nu+1} + \alpha_+\alpha_-^* c_{\nu-1}\right) \\ \dot{\alpha}_\pm &= (-\kappa + \imath\Delta_c - \imath U_0)\alpha_\pm - \imath U_0\alpha_\mp\sum_\nu c_{\nu\mp1}^* c_\nu + \eta_\pm \end{aligned} \quad ,$$

where,

$$\nu_{blo} \equiv \frac{ma}{2\hbar k}$$

is the so-called Bloch oscillation frequency. A simulation of such Bloch oscillations is exhibited in Figs. 42.41. See also Fig. 26.5.
b. The starting point is [1138],

$$\begin{aligned} \imath\hbar\frac{d}{dt}\psi &= -\frac{\hbar^2}{2m}\frac{d^2}{dz^2}\psi + \hbar U_0(\alpha_+^*\alpha_- e^{2\imath kz} + \alpha_+\alpha_-^* e^{-2\imath kz})\psi - maz\psi + \frac{\hbar W_0}{2}\sin(2kz+\phi)\psi \\ \alpha_+ &= \frac{\eta_+}{\kappa} \\ \dot{\alpha}_- &= -\kappa\alpha_- + NU_0\alpha_+\int|\psi|^2 e^{-2\imath kz}dz \ , \end{aligned}$$

where we used that the laser is locked to a cavity mode, $\Delta_c = U_0$. Introducing $\tilde{\alpha}_- - \alpha_- = \alpha_0 \equiv e^{2\imath\phi}W_0/4U_0$ and $\psi = \tilde{\psi}e^{\imath maz t/\hbar}$, we simplify the first and third

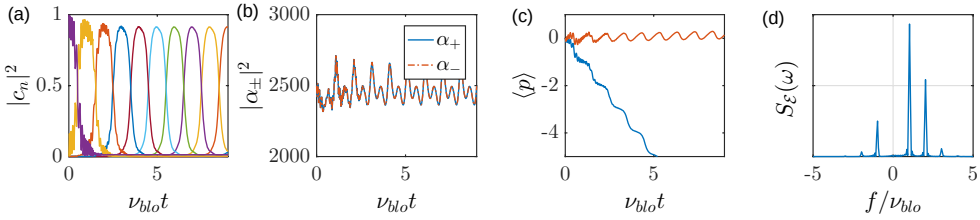

Figure 42.41: (code) Simulation of the coupled atom-ring cavity dynamics for symmetric pumping and in the presence of gravity. (a) Momentum state populations $|c_\nu|^2$, (b) photon numbers $|\alpha_\pm|^2$ in the counterpropagating cavity modes, and (c) Spectrum of the cavity modes. The parameters are $N = 20000$, $\omega_{rec} = (2\pi)\ 4.8\,\mathrm{kHz}$, $\nu_{blo} = 0.05\omega_{rec}$, $\kappa = 90\omega_{rec}$, $U_0 = -0.00035\omega_{rec}$, and $\eta_\pm = 4500\omega_{rec}$.

equation to,

$$\imath\hbar\frac{d}{dt}\tilde{\psi} = -\frac{\hbar^2}{2m}\frac{d^2}{dz^2}\tilde{\psi} + \hbar U_0(\alpha_+^*\tilde{\alpha}_- e^{2\imath kz} + \alpha_+\tilde{\alpha}_-^* e^{-2\imath kz})\tilde{\psi}$$
$$\dot{\tilde{\alpha}}_- = -\kappa(\tilde{\alpha}_- - \alpha_0) + NU_0\alpha_+\int |\tilde{\psi}|^2 e^{-2\imath kz}dz\ .$$

With the definition $\eta_- \equiv \kappa\alpha_0$, the last equation can be simplified to,

$$\dot{\tilde{\alpha}}_- = -\kappa\tilde{\alpha}_- + NU_0\alpha_+\int |\tilde{\psi}|^2 e^{-2\imath kz}dz + \eta_-\ .$$

The expansion into momentum states demonstrated in part (a) yields the final set of equations,

$$\dot{c}_\nu = -4\imath\omega_{rec}(\nu + \nu_{blo}t)^2 c_\nu - \imath U_0\frac{\eta_+}{\kappa}\left(\tilde{\alpha}_- c_{\nu+1} + \tilde{\alpha}_-^* c_{\nu-1}\right)$$
$$\dot{\tilde{\alpha}}_- = -\kappa\tilde{\alpha}_- + \imath U_0\frac{\eta_+}{\kappa}\sum_\nu c_\nu^* c_{\nu\pm1} + \eta_-\ ,$$

where the ration between the Bloch and CARL coupling strength is given by,

$$\frac{W_0}{U_0} = \frac{\eta_- e^{-2\imath\phi}}{\kappa}\ .$$

A simulation of these equations yields very similar results to the ones exhibited in Fig. 42.41, except that the cavity mode α_+ now is fixed.

42.4.7.2 Ex: Competition between CARL and Bloch oscillations

Reproduce the simulations of [1138].

Solution: *The result is exhibited in Fig. ??.*

42.4.7.3 Ex: Alternative derivation of the Maxwell-Bloch with adiabatic elimination

Derive the directly from the Liouville equation (42.8) using the Hamiltonian (42.26) in adiabatic elimination.

Solution: *Inserting the Hamiltonian into the Liouville equation we get,*

$$\begin{aligned}
\langle\mu|\dot{\hat{\rho}}|\nu\rangle &= -\imath\langle\mu|[\hat{H},\hat{\rho}]|\nu\rangle \\
&= -\imath\sum_q \langle\mu|\hat{H}|q\rangle\rho_{q,\nu} + \imath\sum_q \rho_{\mu,q}\langle q|\hat{H}|\nu\rangle \\
&= -\imath\left[\frac{(\mu\hbar k)^2}{2m} + (U_0-\Delta_c)(|\alpha_+|^2+|\alpha_-|^2) - \imath\eta_+(\alpha_+-\alpha_+^*) - \imath\eta_-(\alpha_- - \alpha_-^*)\right]\rho_{\mu,\nu} \\
&- \imath U_0\sum_q\left(\alpha_+^*\alpha_-\langle\mu|e^{-2\imath k\hat{z}}|q\rangle + \alpha_-^*\alpha_+\langle\mu|e^{2\imath k\hat{z}}|q\rangle\right)\rho_{q,\nu} \\
&+ \imath\left[\frac{(\nu\hbar k)^2}{2m} + (U_0-\Delta_c)(|\alpha_+|^2+|\alpha_-|^2) - \imath\eta_+(\alpha_+-\alpha_+^* - \imath\eta_-(\alpha_- - \alpha_-^*)\right]\rho_{\mu,\nu} \\
&+ \imath U_0\sum_q\left(\alpha_+^*\alpha_-\langle q|e^{-2\imath k\hat{z}}|\nu\rangle + \alpha_-^*\alpha_+\langle q|e^{2\imath k\hat{z}}|\nu\rangle\right)\rho_{\mu,q} \\
&= \imath(\nu^2-\mu^2)\omega_{rec}\rho_{\mu,\nu} + 2\imath U_0\left[\alpha_+^*\alpha - (\rho_{\mu,\nu-1}-\rho_{\mu+1,\nu}) + \alpha_-^*\alpha_+(\rho_{\mu,\nu+1}-\rho_{\mu-1,\nu})\right] .
\end{aligned}$$

Transforming $\tilde{\rho}_{\mu,\nu} \equiv e^{\imath(\mu-\nu)\Delta_c t}\rho_{\mu,\nu}$,

$$\begin{aligned}
\langle\mu|\dot{\tilde{\rho}}|\nu\rangle &= \langle\mu|\dot{\hat{\rho}}|\nu\rangle + \imath(\mu-\nu)\Delta_c\langle\mu|\hat{\rho}|\nu\rangle \\
&= \imath(\nu-\mu)\left[(\nu+\mu)\omega_{rec} - \Delta_c\right]\rho_{\mu,\nu} \\
&+ \imath U_0\left[\alpha_+^*\alpha_-(\rho_{\mu,\nu-1}-\rho_{\mu+1,\nu}) + \alpha_-^*\alpha_+(\rho_{\mu,\nu+1}-\rho_{\mu-1,\nu})\right] .
\end{aligned}$$

The incoherent part is,

$$\langle\mu|\mathcal{L}_{atom-vac}|\nu\rangle = 0 = \langle\mu|\mathcal{L}_{cavity-vac,\pm}|\nu\rangle .$$

42.4.7.4 Ex: Maxwell-Bloch equations without adiabatic elimination

Derive the Maxwell-Bloch equations for a three-level system coupled to a ring cavity without adiabatic elimination, but with quantized motion.

Solution: *We start from (42.15), generalize for three electronic levels, consider classical fields* $\hat{a} = \alpha$*, convert to matter wave description, and perform modal expansion,*

$$\hat{\rho}_{motion}\otimes\hat{\rho}_{atom} = |\mu\rangle\langle\nu|\otimes|\imath\rangle\langle j| \qquad with \qquad \mu,\nu\in\mathbb{Z} \qquad and \qquad i,j = 1,2,3 .$$

Expand,

$$|\psi(z,t)\rangle = \tfrac{1}{\sqrt{2\pi}}\sum_\nu c_\nu(t)e^{2\imath\nu kz}|\imath\rangle = \tfrac{1}{\sqrt{2\pi}}\sum_{\nu,i} c_{\nu,i}(t)e^{2\imath\nu kz}|\nu,\imath\rangle .$$

The only quantized degrees of freedom subject to dissipation is the atomic excitation (via spontaneous emission Γ). The optical field modes, which are also dissipated (via cavity decay κ), are treated classically. And the atomic motion is not damped. Hence, it should be sufficient to treat the atomic excitation by Bloch equations and the atomic motion by a Schrödinger equation,

42.4.7.5 Ex: Linearized quantum CARL

Analyze the quantum CARL according to [1038].

Solution: *The result is shown in Fig. 42.42.*

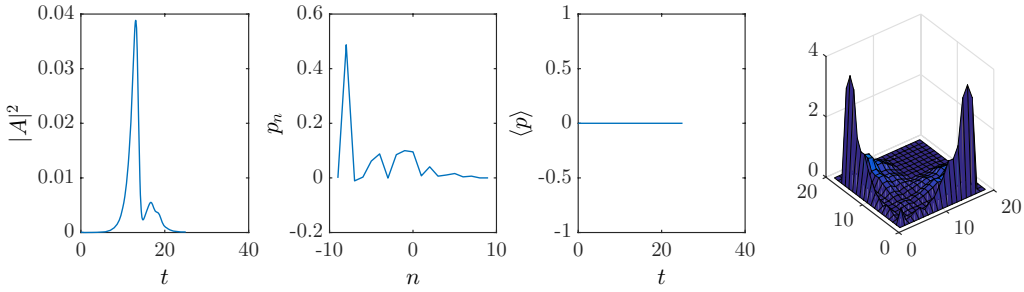

Figure 42.42: (code) Quantum CARL according to [1038].

42.5 Quantized light interacting with atoms moving in cavities

Cavity QED has been studied extensively in the context of the Jaynes-Cummings model in Sec. 35.4 and of cooperative scattering in Sec. 40.2, however, without addressing the issue of atomic motion which, via photonic recoil, inevitably influences the dynamics. We also started a discussion on the role of photonic recoil in Sec. 38.3, which will be continued in the following sections in the context of ring cavities,

$$\dot{c}_{n_+,n_-,i} = \frac{d}{dt}\langle \mathbf{r}, \alpha_+, \alpha_-, i|\psi(t)\rangle = \langle \mathbf{r}, \alpha_+, \alpha_-, i|\frac{-\imath}{\hbar}\hat{H}|\psi(t)\rangle \tag{42.208}$$
$$\dot{\alpha}_\pm = \langle\psi(t)|\dot{a}_\pm|\psi(t)\rangle = \langle\psi(t)|\tfrac{\imath}{\hbar}[\hat{H},\hat{a}_\pm] - \kappa\hat{a}_\pm|\psi(t)\rangle \ .$$

Concretely, we will be using the Hamiltonian (42.26), obtained after adiabatic elimination of the excited state.

42.5.1 QED in ring cavities

Macroscopic high-finesse ring cavities interacting with a cloud of cold atoms allowed to enter the regime of strong collective coupling. However, new interesting aspects arise from the regime of strong coupling on the level of individual atoms.

Todays research projects on cold atoms in cavities are essential divided into two classes, each class realizing an opposite regime: Cavity quantum electrodynamics (CQED) experiments as they are done by the groups of Rempe [758] and Kimble use microcavities having mode volumes so small that few photons give rise to macroscopic field strength. In such cavities the atom-field coupling is made to exceed all other decay rates. The other regime is that of cavity-cooling mainly investigated by Vuletic at the MIT and, in the case of ring cavities, of the collective atomic recoil laser (CARL) realized in the Tübingen research group. In this second regime the cavities are so large that the light fields can be considered as classical.

An interesting question is, whether the two regimes can be married to realize a system, where collective effects and entanglement between optical and atomic modes can be observed. The central idea is not to increase the coupling strength by reducing the mode volume, but to reduce the decay rates, in particular the natural linewidth of the atomic transition by choosing an atomic species that can be laser-cooled on a narrow intercombination line.

Example 275 (*CQED by reducing the ring cavity mode volume*): Technically a ring cavity design with $(w, L, F) = (30\,\mu\text{m}, 4\,\text{cm}, 200000)$ is feasible. This is enough to get below the critical atom number, but this is not sufficient to get into the CQED regime. Reducing Γ seems unavoidable.
The isotope ^{88}Sr posses a narrow transition which can be used for optical cooling. The following table compares the various systems, i.e. a CQED example taken from Rempe, the macroscopic ring cavity with rubidium used in our Tübingen CARL experiments and a cavity tuned close to the strontium intercombination line.

experiment	Rempe, Rb	Tübingen, Rb	São Carlos, Sr
Γ	$(2\pi)6$ MHz	$(2\pi)6$ MHz	$(2\pi)7.6$ kHz
F	440000	80000	200000
κ	$(2\pi)0.7$ MHz	$(2\pi)22$ kHz	$(2\pi)19$ kHz
w	29 µm	100 µm	30 µm
L	500 µm	8.5 cm	4 cm
g	$(2\pi)4$ MHz	$(2\pi)88$ kHz	$(2\pi)13$ kHz
N_{crit}	0.5	34	1.6
n_{sat}	1.1	2312	0.16

With $N = 10^4$ the cooperativity parameter N/N_{crit} is in all cases well above 1.

42.5.2 Description of quantized light fields in cavities

In order to calculate the evolution of photon distributions in the counter-propagating modes $\hat{a}_\pm$ of a ring cavity, we develop CARL in a Fock basis. For simplicity, we first consider the *motion of a single atom as classical* and fixed (i.e. not as a degree of

freedom), and we apply the adiabatic approximation. I.e. we have only two quantized degrees of freedom, which we organize like,

$$|\psi\rangle = \cancel{|\nu\rangle_{motion}}^{\text{classical}} \otimes \cancel{|i\rangle_{electron}}^{\text{adiab.elim.}} \otimes |n\rangle_+ \otimes |n\rangle_- \to |n_+, n_-\rangle \ , \quad (42.209)$$

Expanding the fields into Fock states,

$$\boxed{|\psi\rangle = \sum_{n_+,n_-} c_{n_+,n_-} |n_+, n_-\rangle} \ , \quad (42.210)$$

the field operators and the density matrix read,

$$\begin{aligned} \hat{a}_+ &= \sum_{n_+} \sqrt{n_+}|n_+ - 1\rangle\langle n_+| \otimes \mathbb{I} = \sum_{n_+,n_-} \sqrt{n_+}|n_+ - 1, n_-\rangle\langle n_+, n_-| \quad (42.211) \\ \hat{a}_- &= \mathbb{I} \otimes \sum_{n_-} \sqrt{n_-}|n_- - 1\rangle\langle n_-| = \sum_{n_+,n_-} \sqrt{n_+}|n_+ - 1, n_-\rangle\langle n_+, n_-| \\ \hat{\rho} &= |\psi\rangle\langle\psi| = \sum_{m_+,m_-,n_+,n_-} c^*_{m_+,m_-} c_{n_+,n_-} |m_+, m_-\rangle\langle n_+, n_-| \ . \end{aligned}$$

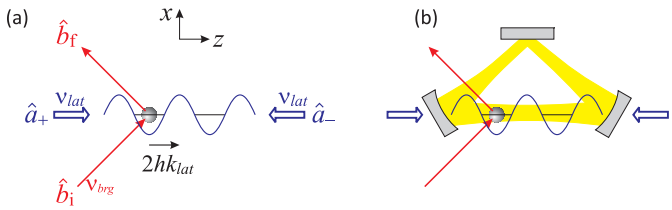

Figure 42.43: (a) Bragg scattering at a 1D optical lattice. (b) Same as in (a), but now the optical lattice is generated by the mode of an optical ring cavity.

Note that the master equation using the Lindbladt operator traces over the reservoir. Hence, the master equation only treats the cavity modes, but does not allow predictions on the quantum behavior of outcoupled fields. In order to describe e.g. quantum correlations in output field, one needs an input-output theory [283, 488].

In the case of classical motion quantum light fields,

$$\boxed{\begin{aligned} \dot{c}_{n_+,n_-} &= \imath(\Delta_c - U_0)(n_+ + n_-)\, c_{n_+,n_-} \\ &- \imath U_0 \left(e^{-2\imath kz} \sqrt{n_+(n_- + 1)}\, c_{n_+-1,n_-+1} - e^{2\imath kz} \sqrt{(n_+ + 1)n_-}\, c_{n_++1,n_--1} \right) \\ &- \eta_+ \left(\sqrt{n_+ + 1}\, c_{n_++1,n_-} - \sqrt{n_+}\, c_{n_+-1,n_-} \right) \\ &- \eta_- \left(\sqrt{n_- + 1}\, c_{n_+,n_-+1} - \sqrt{n_-}\, c_{n_+,n_--1} \right) \\ \dot{z} &= 2\imath\hbar k U_0 \sum_{n_+,n_-} \left(e^{-2\imath kz} \sqrt{(n_+ + 1)n_-}\, c^*_{n_++1,n_--1} c_{n_+,n_-} \right. \\ &\qquad \left. - e^{2\imath kz} \sqrt{n_+(n_- + 1)}\, c^*_{n_+-1,n_-+1} c_{n_+,n_-} \right) \end{aligned}} \ . \quad (42.212)$$

42.5.3 Photon backscattering for fixed atomic position

To tackle the problem of quantized light field we first assume an atom fixed in space, that is, we completely *disregard the motional degree of freedom* by setting $\hat{p} = 0$ and restricting to the Hamiltonian,

$$\hat{H} = \sum_{\pm} \omega_{\pm} \hat{a}_{\pm}^{\dagger} \hat{a}_{\pm} - \imath\eta_{\pm}(\hat{a}_{\pm} - \hat{a}_{\pm}^{\dagger}) + U_0(\hat{a}_{+}^{\dagger}\hat{a}_{-}e^{-2\imath kz} + \hat{a}_{-}^{\dagger}\hat{a}_{+}e^{2\imath kz}) \ . \tag{42.213}$$

In Exc. 42.5.7.1 we show how to cast the Hamiltonian into a matrix form using an appropriate basis already used in the discussion of the beam splitter in the photon representation in Sec. 35.8.1.

In Exc. 42.5.7.2(a) we derive the equations of motion for the components c_{n_+,n_-} of the state vector from the Schrödinger equation cavity decay. In Exc. 42.5.7.3(a) we derive the equations of motion for the components $\rho_{m_+,n_+;m_-n_-} = \langle m_+, m_-|\hat{\rho}|n_+, n_-\rangle$ of the density operator. Simulations performed based on these equations of motion are shown in Fig. 42.44).

The simulations reveal a number of interesting facts:

- The field amplitudes $|\alpha_{\pm}|^2$ execute oscillations due to CARL coupling, but with preserved Poissonian shape of the photon number distributions.
- When simulations are done with initial Fock states, they eventually relax to a Glauber state.
- The mean photon numbers and the atomic coordinates evolve in a continuous way.

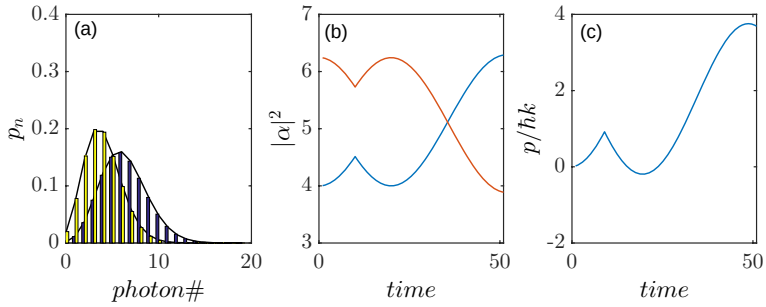

Figure 42.44: (code) Time-evolution of CARL with one classical atom and two quantized field modes. (a) Photon number distributions of two modes after some evolution time t. (b) Time-evolution of the mean photon number; at time $t = 10$, the atom is suddenly displaced. (c) Time-evolution of the (classical) atomic trajectory.

These observations are not surprising, once we understood the backscattering as a linear coupling between the modes being mediated by a beam splitter Hamiltonian of type (35.317) [19],

$$\hat{H}_{int} = U_0(\hat{a}_{+}^{\dagger}\hat{a}_{-}e^{-2\imath kz} + \hat{a}_{+}\hat{a}_{-}^{\dagger}e^{2\imath kz}) \ , \tag{42.214}$$

[19] Which itself represents a generalized displacement operator,

$$\hat{H}_{int} \simeq U_0(\alpha_{+}^{*}e^{-2\imath kz}\hat{a}_{-} + \alpha_{+}e^{2\imath kz}\hat{a}_{-}^{\dagger}) \equiv \imath\hbar\beta^{*}\hat{a}_{-} - \imath\hbar\beta\hat{a}_{-}^{\dagger} \ ,$$

for which we found the relationship (35.318),

$$\boxed{e^{-\imath\hat{H}_{int}t}\hat{a}_{\pm}e^{\imath\hat{H}_{int}t} = \hat{a}_{\pm}\cos U_0 t \pm \hat{a}_{\mp}e^{\mp 2\imath kz}\sin U_0 t} \ . \tag{42.215}$$

This means, that we expect (for a fixed location z of the atom) an oscillatory behavior of the field amplitudes $|\alpha_{\pm}|^2$ and also of the phase (encoded in $\alpha_+^*\alpha_-$), but no modification of the coherent photon statistics. On the contrary, as shown in Sec. 35.8.1, a beam splitter tends to transform sub-Poissonian states into Poissonian ones. In fact, *CARL is nothing else than a movable beam splitter.*

Non-linearity may come into play, if photonic recoil is included, i.e. if the *atomic motion itself becomes a degree of freedom.* This is the next step of our problem, that needs to be solved.

42.5.4 Quantized light fields and quantized recoil

The simulations of the preceding section show that the CARL Hamiltonian (42.214), despite the appearance of photon creation and annihilation operator, does not request recoil to be quantized: If an arbitrary momentum kick of the atom can be absorbed by the light fields, then an arbitrary dipole force can be transmitted to the atomic momentum! The momentum conservation law (42.17) does not imply quantization of photonic recoil. The question is now, how to conceal this fact with the observation of discrete momentum sidemodes [1217]. We have seen earlier, that the quantization of the motion is transferred from the quantized photon fields via the operator (42.149) to the atom: An initially resting atom can only adopt motional states with momenta equal to a multiple of $2\hbar k$.

We will now take the quantization of the atomic momentum for granted and study quantized light modes coupled by *recoiling atoms*, we extend our Hilbert space like,

$$|\psi\rangle = |\nu\rangle_{motion} \otimes \cancel{|i\rangle_{electron}}^{\text{adiab.elim.}} \otimes |n\rangle_+ \otimes |n\rangle_- \to |\nu, n_+, n_-\rangle \ , \tag{42.216}$$

Expanding the motion and fields [20],

$$\boxed{|\psi\rangle = \sum_{\nu,n_+,n_-} c_{\nu,n_+,n_-}|\nu, n_+, n_-\rangle} \ , \tag{42.217}$$

the momentum kick operator reads,

$$e^{-2\imath k\hat{z}} \otimes \mathbb{I} \otimes \mathbb{I} = \sum_{\nu} |\nu\hbar k - 2\hbar k, n_+, n_-\rangle\langle\nu\hbar k, n_+, n_-| \ . \tag{42.218}$$

since defining $\beta \equiv \frac{\imath U_0}{\hbar}\alpha_+ e^{2\imath kz}$, we find,

$$B(\beta t) = e^{-\imath\hat{H}_{int}t/\hbar} = e^{\beta^* t\hat{a}_- - \beta t\hat{a}_-^\dagger} \ .$$

[20] Note the fact, which is important for computation, that the dimension of the Hilbert space increases a lot, that is like dim $\nu \cdot$ dim $n_+ \cdot$ dim n_-, where $\nu, n_\pm$ are the numbers of states considered.

The equations of motions derived in Exc. 42.5.7.2 from the Schrödinger equation are now generalized to,

$$\begin{aligned}\dot{c}_{\nu,n_+,n_-} &= \imath(\Delta_c - U_0)(n_+ + n_-)c_{\nu,n_+,n_-} \\ &- \imath U_0\left(\sqrt{n_+(n_- + 1)}c_{\nu-1,n_+-1,n_-+1} - \sqrt{(n_+ + 1)n_-}c_{\nu+1,n_++1,m_--1}\right) \\ &- \eta_+\left(\sqrt{n_+ + 1}c_{\nu,n_++1,n_-} + \sqrt{n_+}c_{\nu,n_+-1,n_-}\right) \\ &- \eta_-\left(\sqrt{n_- + 1}c_{\nu,n_+,n_-+1} + \sqrt{n_-}c_{\nu,n_+,n_--1}\right)\end{aligned} \; . \tag{42.219}$$

Note that the general shape of fully quantized Schrödinger equations looks like,

$$\dot{c}_{\nu',n'_+,n'_-} = \begin{pmatrix} \ddots & \vdots & \\ \cdots & \mathcal{B}_{\{\nu',n'_+,n'_-\};\{\nu,n_+,n_-\}} & \cdots \\ & \vdots & \ddots \end{pmatrix} c_{\nu,n_+,n_-} \tag{42.220}$$

and for fully quantized master equations,

$$\begin{aligned}&\dot{\rho}_{\{\mu',m'_+,m'_-\};\{\nu',n'_+,n'_-\}} \\ &= \begin{pmatrix} \ddots & \vdots & \\ \cdots & \mathcal{L}_{\{\mu',m'_+,m'_-;\nu',n'_+,n'_-\};\{\mu,m_+,m_-;\nu,n_+,n_-\}} & \cdots \\ & \vdots & \ddots \end{pmatrix} \rho_{\{\mu,m_+,m_-\};\{\nu,n_+,n_-\}} \; .\end{aligned} \tag{42.221}$$

However, the mere inclusion of a third degree of freedom coupled to the other two degrees in the same linear fashion will modify the behavior of the system, which will continue to oscillate as it did before, now just involving the atomic motion in this dynamics. This behavior can only change, when we additionally consider the force equation,

$$\dot{\hat{p}} = 2\hbar k U_0(\hat{a}_+^\dagger \hat{a}_- e^{-2\imath kz} - \hat{a}_+ \hat{a}_-^\dagger e^{2\imath kz}) \; , \tag{42.222}$$

which will lead to feedback. Inserting the expansion (42.217),

$$\dot{c}_{\nu,n_+,n_-} = 2\hbar k U_0\left(c_{\nu,n_+,n_-}\sqrt{n_+(n_- + 1)} - c_{\nu,n_+,n_-}\sqrt{n_+(n_- + 1)}\right) \; . \tag{42.223}$$

Note that, in contrast to CARL equations, the fully quantized equations (42.219) *are linear*. That is, it is the 'classization' [21] of the degrees of freedom which introduces the non-linearities, which are typical for CARL, e.g. the feedback introduced by classical light fields. The process of 'classization' corresponds to *tracing* over degrees of freedom, which we want to treat classically and thus remove from the Hamiltonian.

42.5.4.1 Calculation of observables

Once the time evolution of the coefficients $c_{\nu,n_+,n_-}(t)$ has been determined by solving the differential equation (42.219) we can calculate the observables in the following

[21] As opposed to the term quantization.

way. The probability distribution for photon numbers in the mode α_+ is given by,

$$\begin{aligned} P_{n_+}(t) &= \langle\psi(t)|\mathbb{I}\otimes|n_+\rangle\langle n_+|\otimes\mathbb{I}|\psi(t)\rangle \\ &= \sum_{\nu,n_-}\langle\nu,n_+,n_-|\nu,n_+,n_-\rangle = \sum_{\nu,n_-}|c_{\nu,n_+,n_-}(t)|^2 \ , \end{aligned} \tag{42.224}$$

the mean photon number by,

$$\langle\hat{n}_+(t)\rangle = |\alpha_+(t)|^2 = \sum_{n_+} n_+ P_{n_+}(t) = \sum_{\nu,n_+,n_-} n_+|c_{\nu,n_+,n_-}(t)|^2 \ , \tag{42.225}$$

and similarly for α_-. The probability distribution for momentum states is given by,

$$P_\nu(t) = \sum_{n_+,n_-}|c_{\nu,n_+,n_-}(t)|^2 \ , \tag{42.226}$$

the mean momentum by,

$$\langle\hat{p}(t)\rangle = \sum_{\nu,n_+,n_-}\nu\hbar k|c_{\nu,n_+,n_-}(t)|^2 \ , \tag{42.227}$$

the mechanical kinetic energy by,

$$\begin{aligned} E_{kin}(t) = \frac{\langle\hat{p}^2\rangle}{2m} &= \sum_{\nu,n_+,n_-}\frac{(\nu\hbar k)^2}{2m}|c_{\nu,n_+,n_-}(t)|^2 \\ &= \sum_{\nu,n_+,n_-}\nu^2\hbar\omega_{rec}|c_{\nu,n_+,n_-}(t)|^2 \ , \end{aligned} \tag{42.228}$$

and the potential energy by,

$$\begin{aligned} E_{pot}(t) &= \hbar U_0\langle e^{-2\imath k\hat{z}}\hat{a}_+^\dagger\hat{a}_- + e^{2\imath k\hat{z}}\hat{a}_+\hat{a}_-^\dagger\rangle \\ &= \hbar U_0\sum_{\nu,n_+,n_-}\Big(c^*_{\nu+1,n_++1,n_--1}c_{\nu,n_+,n_-}\sqrt{(n_++1)n_-} \\ &\qquad + c^*_{\nu-1,n_+-1,n_-+1}c_{\nu,n_+,n_-}\sqrt{n_+(n_-+1)}\Big) \ . \end{aligned} \tag{42.229}$$

With this we can check conservation of the total photon number,

$$\langle\hat{n}_+(t)\rangle + \langle\hat{n}_-(t)\rangle = const \ , \tag{42.230}$$

of the mechanical energy,

$$E_{kin}(t) + E_{pot}(t) = const \ , \tag{42.231}$$

and of total linear momentum,

$$\hbar k[\langle\hat{n}_+(t)\rangle - \langle\hat{n}_-(t)\rangle] - \langle\hat{p}(t)\rangle = const \ . \tag{42.232}$$

42.5.4.2 Master equation for CQED with atomic recoil in the adiabatic approximation

Using the Hamiltonian (42.26) or (42.144), the expansion of the recoil operator (42.149), the expansion of the photon field operators (42.211), and the matrix representation of the density operator (34.105), that is,

$$\hat{\rho} = \sum_{\mu,\nu;m_+,n_+;m_-,n_-} |\mu, m_+, m_-\rangle \rho_{\mu,\nu;m_+,n_+;m_-,n_-} \langle \nu, n_+, n_-| \,, \tag{42.233}$$

the master equation (42.8) becomes,

$$\boxed{\langle \mu, m_+, m_-|\dot{\hat{\rho}}|\nu, n_+, n_-\rangle = -\imath\langle \mu, m_+, m_-|[\hat{H}, \hat{\rho}]|\nu, n_+, n_-\rangle + \mathcal{L}_{cavity-vac,\pm}\hat{\rho}} \,, \tag{42.234}$$

with the coherent contributions,

$$\langle \mu, m_+, m_-|[\tfrac{\hat{p}^2}{2m}, \hat{\rho}]|\nu, n_+, n_-\rangle = \omega_{rec}(\mu^2 - \nu^2)\rho_{\mu,\nu;m_+,n_+;m_-,n_-} \tag{42.235}$$

$$\langle \mu, m_+, m_-|[(U_0 - \Delta_c)\hat{a}_\pm^\dagger \hat{a}_\pm, \hat{\rho}]|\nu, n_+, n_-\rangle = (U_0 - \Delta_c) n_\pm \rho_{\mu,\nu;m_+,n_+;m_-,n_-}$$

$$\begin{aligned}
&\langle \mu, m_+, m_-|[-\imath\eta_+(\hat{a}_+ - \hat{a}_+^\dagger), \hat{\rho}]|\nu, n_+, n_-\rangle \\
&= -\imath\eta_+ \Big(\sqrt{m_+}\rho_{\mu,\nu;m_+-1,n_+;m_-,n_-} - \sqrt{m_+ + 1}\rho_{\mu,\nu;m_++1,n_+;m_-,n_-} \\
&\qquad + \sqrt{n_+}\rho_{\mu,\nu;m_+,n_+-1;m_-,n_-} - \sqrt{n_+ + 1}\rho_{\mu,\nu;m_+,n_++1;m_-,n_-} \Big)
\end{aligned}$$

$$\begin{aligned}
&\langle \mu, m_+, m_-|[-\imath\eta_-(\hat{a}_- - \hat{a}_-^\dagger), \hat{\rho}]|\nu, n_+, n_-\rangle \\
&= -\imath\eta_- \Big(\sqrt{m_-}\rho_{\mu,\nu;m_+,n_+;m_--',n_-} - \sqrt{m_- + 1}\rho_{\mu,\nu;m_+,n_+;m_-+1,n_-} \\
&\qquad + \sqrt{n_-}\rho_{\mu,\nu;m_+,n_+;m_-,n_--1} - \sqrt{n_- + 1}\rho_{\mu,\nu;m_+,n_+;m_-,n_-+1} \Big)
\end{aligned}$$

$$\begin{aligned}
&\langle \mu, m_+, m_-|[U_0 e^{-2\imath k\hat{z}}\hat{a}_+^\dagger \hat{a}_-, \hat{\rho}]|\nu, n_+, n_-\rangle \\
&= U_0 \Big(\sqrt{m_+(m_- + 1)}\rho_{\mu+1,\nu;m_+-1,n_+;m_-+1,n_-} + \sqrt{(m_+ + 1)m_-}\rho_{\mu-1,\nu;m_++1,n_+;m_--1,n_-} \Big)
\end{aligned}$$

$$\begin{aligned}
&\langle \mu, m_+, m_-|[U_0 e^{2\imath k\hat{z}}\hat{a}_+\hat{a}_-^\dagger, \hat{\rho}]|\nu, n_+, n_-\rangle \\
&= U_0 \Big(\sqrt{(n_+ + 1)n_-}\rho_{\mu,\nu-1;m_+,n_++1m_-,n_--1} + \sqrt{n_+(n_- + 1)}\rho_{\mu,\nu+1;m_+,n_+-1;m_-,n_-+1} \Big) \,,
\end{aligned}$$

and the incoherent contributions,

$$\begin{aligned}
&\langle \mu, m_+, m_-| - \kappa[\hat{a}_+^\dagger \hat{a}_+\hat{\rho} - 2\hat{a}_+\hat{\rho}\hat{a}_+^\dagger + \hat{\rho}\hat{a}_+^\dagger \hat{a}_+]|\nu, n_+, n_-\rangle \\
&\qquad = -\kappa \big(m_+\rho_{\mu,\nu;m_+,n_+;m_-,n_-} + n_+\rho_{\mu,\nu;m_+,n_+;m_-,n_-} \\
&\qquad\qquad -2\sqrt{(m_+ + 1)(n_+ + 1)}\rho_{\mu,\nu;m_++1,n_++1;m_-,n_-} \big)
\end{aligned} \tag{42.236}$$

$$\begin{aligned}
&\langle \mu, m_+, m_-| - \kappa[\hat{a}_-^\dagger \hat{a}_-\hat{\rho} - 2\hat{a}_-\hat{\rho}\hat{a}_-^\dagger + \hat{\rho}\hat{a}_-^\dagger \hat{a}_-]|\nu, n_+, n_-\rangle \\
&\qquad = -\kappa \big(m_-\rho_{\mu,\nu;m_+,n_+;m_-,n_-} + n_-\rho_{\mu,\nu;m_+,n_+;m_-,n_-} \\
&\qquad\qquad -2\sqrt{(m_- + 1)(n_- + 1)}\rho_{\mu,\nu;m_+,n_+;m_-+1,n_-+1} \big) \,.
\end{aligned}$$

42.5.5 Kicking and forcing an atom in a ring cavity

The question we want to elucidate here is, how a coupled atom-ring cavity system reacts to a kick transferring an arbitrary amount of momentum to the atom. We studied

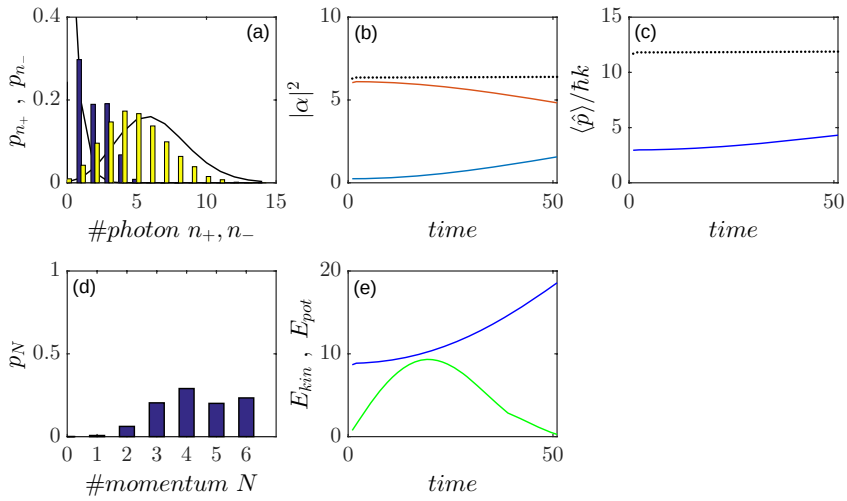

Figure 42.45: (code) Time-evolution of CARL with one classical atom and two quantized field modes. (a) Photon number distributions of two modes after some evolution time t. (b) Time-evolution of the mean photon number; at time $t = 10$, the atom is suddenly displaced. (c) Time-evolution of the (classical) atomic trajectory.

a similar question when studying the kicking of a harmonic oscillator in Sec. 24.6.2, however, the situation is quite different now because, in contrast to the harmonic oscillator, the motion of an atom subject to CARL dynamics is not localized and, hence, *not quantized*. That is, an arbitrarily kicked atom is not bound to join one of those momentum states it would populate when kicked by photonic recoil. Hence, a momentum state expansion like (42.153) is not appropriate, so that we have to go a step back and consider the Hamiltonian (42.26) again. See also (watch talk).

42.5.5.1 Kicking

Let us first describe the kick as an incoherent disruptive one time event transforming operators, the Hamiltonian and the system's state like,

$$\hat{A} \longrightarrow e^{-\imath q\hat{z}}\hat{A}e^{\imath q\hat{z}} \quad , \quad |\psi\rangle \longrightarrow e^{\imath q\hat{z}}|\psi\rangle \tag{42.237}$$

and in particular,

$$\hat{H} \longrightarrow e^{-\imath q\hat{z}}\hat{H}e^{\imath q\hat{z}} = \hat{H}(\hat{z}, \hat{p} - \hbar q) \quad , \quad \langle p|\psi\rangle \longrightarrow \langle p|e^{\imath q\hat{z}}|\psi\rangle = \langle p - \hbar q|\psi\rangle \ . \tag{42.238}$$

The Schrödinger equation tells us the system's evolution after the kick,

$$\imath\hbar\frac{d}{dt}\langle p|\psi\rangle = \frac{p^2}{2m}\langle p|\psi\rangle + U_0\left(\langle p|e^{-2\imath k\hat{z}}|\psi\rangle\hat{a}_+^\dagger\hat{a}_- + \langle p|e^{2\imath k\hat{z}}|\psi\rangle\hat{a}_+\hat{a}_-^\dagger\right) \ . \tag{42.239}$$

We remind that this equations contains CARL feedback via the simultaneous presence of $\hat{z}$ and $\hat{p}$. If we want to disregard the CARL force (assuming, for example, that the motion is totally imposed by an external force, as done in Sec. 40.2.8 in order to focus on the behavior of the light fields), we must not project the Schrödinger equation on $\langle p|$ but treat the motional degree of freedom as classical.

42.5.5.2 Forcing

Let us now describe the kick as a force $F(t) = mg\theta(t)$ being switched on at a given time, but being constant afterward,

$$\hat{H} = \frac{\hat{p}^2}{2m} + U_0 \left(e^{-2\imath k\hat{z}} \hat{a}_+^\dagger \hat{a}_- + e^{2\imath k\hat{z}} \hat{a}_+ \hat{a}_-^\dagger \right) + mg\hat{z} \ . \tag{42.240}$$

We note that with (23.167) the Hamiltonian transformed into the accelerated frame reads,

$$\begin{aligned} \hat{H} &\longrightarrow e^{-\imath mg\hat{z}t/\hbar} \hat{H} e^{\imath mg\hat{z}t/\hbar} + \imath\hbar \left(\frac{d}{dt} e^{\imath mg\hat{z}t/\hbar} \right)^\dagger e^{\imath mg\hat{z}t/\hbar} = \hat{H}(\hat{z}, \hat{p} - mgt) - mg\hat{z} \\ &= \frac{(\hat{p} - mgt)^2}{2m} + U_0 \left(e^{-2\imath k\hat{z}} \hat{a}_+^\dagger \hat{a}_- + e^{2\imath k\hat{z}} \hat{a}_+ \hat{a}_-^\dagger \right) \ . \end{aligned} \tag{42.241}$$

The Schrödinger equation for the transformed wavefunction $|\psi\rangle = |\tilde{\psi}\rangle e^{\imath mg\hat{z}t/\hbar}$, which tells us the system's evolution during the force,

$$\imath\hbar \frac{d}{dt} \langle p|\tilde{\psi}\rangle = \frac{(p - mgt)^2}{2m} \langle p|\tilde{\psi}\rangle + U_0 \left(\langle p|e^{-2\imath k\hat{z}}|\tilde{\psi}\rangle \hat{a}_+^\dagger \hat{a}_- + \langle p|e^{2\imath k\hat{z}}|\tilde{\psi}\rangle \hat{a}_+ \hat{a}_-^\dagger \right) \ , \tag{42.242}$$

has a similar shape to Eq. (42.239).

42.5.5.3 Vibrating

Another option might be to additionally confine the atom in a harmonic potential [1406],

$$\begin{aligned} \hat{H} &= \frac{\hat{p}^2}{2m} + U_0 \left(e^{-2\imath k\hat{z}} \hat{a}_+^\dagger \hat{a}_- + e^{2\imath k\hat{z}} \hat{a}_+ \hat{a}_-^\dagger \right) + \frac{m}{2} \omega^2 \hat{z}^2 \\ &= \hbar\omega (\hat{A}^\dagger \hat{A} + \tfrac{1}{2}) + U_0 \left[D^\dagger(\alpha) \hat{a}_+^\dagger \hat{a}_- + D(\alpha) \hat{a}_+ \hat{a}_-^\dagger \right] \ , \end{aligned} \tag{42.243}$$

where $D(\alpha) \equiv e^{\alpha \hat{A}^\dagger - \alpha^* \hat{A}}$ with $\alpha \equiv \frac{2\imath k a_{ho}}{\sqrt{2}}$.

42.5.5.4 Quantized equations of motion

In both cases, 'kicking' and 'forcing', we may discretize momentum space, although in the latter case we need to transform back into the lab frame after having solved the Schrödinger equation (42.219).

42.5.6 Quantum correlations

Superradiant or CARL scattering exist due to a correlation of subsequent scattering events. In the quantum regime, the emergence of quantum correlations, such as entanglement and squeezing is to be expected as a consequence of CARL dynamics [918, 1036, 1061, 1050, 1051, 1325, 279, 280, 281]. The advantage of doing CARL with BECs is the possibility to exploit the instability in the good-cavity regime to

parametrically amplify optical and matter waves, manipulate matter wave coherence properties and generate entanglement.

For the description of the dynamics of the fields, i.e. the momentum sidemodes and the cavity modes, a first-quantized treatment of the atomic motion [1038] would be sufficient. All information can be extracted from a numerical simulation of the quantum CARL equations. However, here we are also interested in quantum correlations. Hence, in a first-quantized treatment of the atomic motion, the coefficients $\hat{c}_n$ must be treated as field operators. Alternatively, we derive the basic equations rigorously from a second-quantized treatment.

42.5.6.1 Generation of squeezing and entanglement via CARL

An experiment by [1069] produces squeezing in transmission of a cavity resonantly interacting with single atoms. The effect was induced by vacuum Rabi-splitting. In our case we have a ring cavity, we operate far from equilibrium, we have classical Stark splitting. Hence, we may expect squeezing and entanglement from the CARL dynamics.

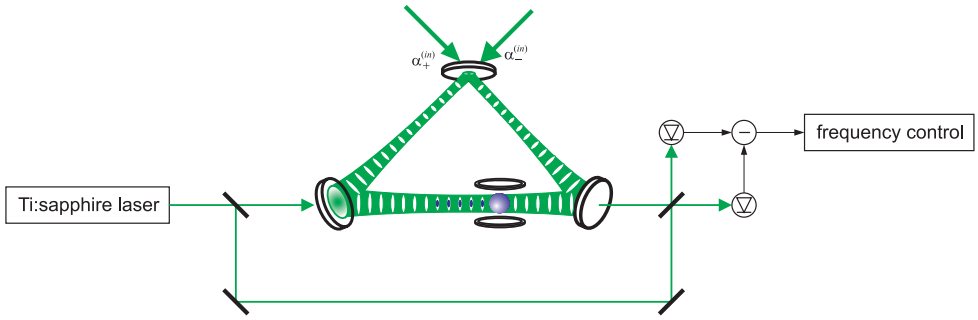

Figure 42.46: Production and detection of squeezing.

Differences between entanglement and correlation (correlations involve time or space coordinates $g(\tau)$, particles correlate across space and time, coherence).

Bragg scattering of light at an atomic grating (or simply the splitting of light at a beam splitter) is an irreversible process (see Sec. 35.8). CARL can be interpreted in terms of Bragg scattering of light at an atomic grating, which is generated itself by the Bragg scattering. Hence, the scattering of early photons influences the scattering of late photons, i.e. the scattering processes get correlated, the dynamics gets a history. The correlation between subsequent scattering processes is what preserves the coherence in CARL and superradiant Rayleigh scattering.

It is now interesting to ask how this classical correlations will behave in the quantum regime, i.e. upon 1. quantization of the motion of individual atoms and upon 2. quantization of atomic particle field. Following [918, 917, 920, 919, 1036, 1037, 1050, 1051], non-classical correlations such as entanglement of matter wave modes, and entanglement between matter-wave and optical modes is expected.

42.5.6.2 Quantum non demolition measurements with CARL

According to [1051], a ring cavity could lend itself to quantum non demolition measurements. They consider our ring cavity being pumped from both sides through an incoupling mirror. A so-called pump mode is injected with a p-polarized light field, and a probe mode with a s-polarized light field. The light of the probe mode leaking through a mirror gives information about the atoms (e.g. via the refraction index). The counterpropagating pump light gives access to higher-order moments of the atom distribution.

The problem is that the effect is based on photon exchange between the modes, and those are orthogonally polarized. Even more problematic is that, in practice, the modes have different frequencies. Other work on this subject has been done by [70, 409, 870, 872, 250].

42.5.7 Exercises

42.5.7.1 Ex: Analogy between CARL and two-atom Dicke states

a. Write the Hamiltonian (42.213) in matrix form using the basis,

$$\psi_k = \{|0,0\rangle, |0,1\rangle, |1,0\rangle, |0,2\rangle, |1,1\rangle, |2,0\rangle, ...\} \ .$$

b. Now restrict to the finite number of states $\psi_k = \{|0,0\rangle, |0,1\rangle, |1,0\rangle, |1,1\rangle\}$ and discuss the analogy between CARL and two-atom Dicke states.

Solution: *a. The Hamiltonian becomes,*

$$\hat{H} = \begin{pmatrix} 0 & -\imath\eta_- & -\imath\eta_+ & 0 & 0 & 0 & \\ \imath\eta_- & \omega_- & U & -\sqrt{2}\imath\eta_- & -\imath\eta_+ & 0 & \\ \imath\eta_+ & U & \omega_+ & 0 & -\imath\eta_- & -\sqrt{2}\imath\eta_+ & \\ 0 & \sqrt{2}\imath\eta_- & 0 & 2\omega_- & \sqrt{2}U & 0 & \\ 0 & \imath\eta_+ & \imath\eta_- & \sqrt{2}U & \omega_+ + \omega_- & \sqrt{2}U & \\ 0 & 0 & \sqrt{2}\imath\eta_+ & 0 & \sqrt{2}U & 2\omega_+ & \\ & & & & & & \ddots \end{pmatrix} .$$

b. The analogy with the two-atom Dicke Hamiltonian becomes apparent, when we restrict ourselves to the finite basis $\psi_k = \{|0,0\rangle, |0,1\rangle, |1,0\rangle, |1,1\rangle\}$,

$$\hat{H} = \begin{pmatrix} 0 & -\imath\eta_- & -\imath\eta_+ & 0 \\ \imath\eta_- & \omega_- & U & -\imath\eta_+ \\ \imath\eta_+ & U & \omega_+ & -\imath\eta_- \\ 0 & \imath\eta_+ & \imath\eta_- & \omega_+ + \omega_- \end{pmatrix} .$$

This however presupposes that coupling U and pumping $\eta_\pm$ to higher photons number states is inhibited.
Assume one photon is pumped into mode a_1. The state is then $|\psi\rangle = (0010)$. This can be written $|\psi\rangle = \frac{1}{\sqrt{2}}[(0010) + (0100)] + \frac{1}{\sqrt{2}}[(0010) - (0100)]$. The superposition

state $\frac{1}{\sqrt{2}}[(0010)+(0100)]$ *decays, but not by loss of energy, but through phase noise. How to detect state* $\frac{1}{\sqrt{2}}[(0010)-(0100)]$ *of the cavity?*
Interestingly, in the absence of pumping (and dissipation), the Hamiltonian takes the form of the Dicke Hamiltonian, where the two coupled systems are the two modes of the ring cavity. We indeed find that the singlet and triplet states $|0,1\rangle \pm |1,0\rangle$ *decouple. In analogy to Dicke states, if the modes couple to the same vacuum radiation field, there might be sub- or superradiance, or collective quantum jumps. This could be done by combining the two output ports of the ring cavity on a beam splitter. The vacuum fluctuations entering through the beam splitter ports couple simultaneously to both modes.*

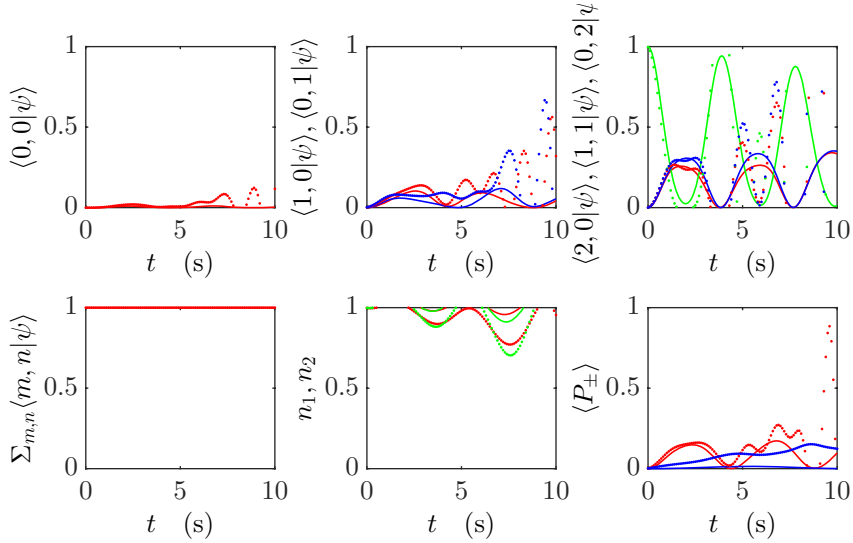

Figure 42.47: (code) Simulation of the above Hamiltonian with initial 2 photons in one mode and no pumping.

42.5.7.2 Ex: Cavity QED with Schrödinger equation

Assume a symmetrically pumped ring cavity in equilibrium with an atom at a fixed position.
a. Derive the equations of motion for the components for the probability amplitudes in a Fock state basis.
b. Express the possible initial states $|\alpha_+,\alpha_-\rangle$, $|\alpha_+,n_-\rangle$, and $|n_+,n_-\rangle$ in the Fock state basis. How to calculate the photon distribution p_{n_+}, the amplitudes of field modes $\alpha_\pm$, and the atom's position and momentum at later times of the evolution?

Solution: *a. If for simplicity we assume totally isolated cavity modes,* $\kappa = 0$*, we*

can use the Schrödinger equation,

$$\imath\hbar\frac{d}{dt}|\psi\rangle = -\hat{H}|\psi\rangle = \imath\hbar\frac{d}{dt}\sum_{n_+,n_-} c_{n_+,n_-}|n_+,n_-\rangle$$

$$= \left(\sum_{\pm}(U_0-\Delta_c)\hat{a}^\dagger_\pm\hat{a}_\pm + U_0\left(e^{-2\imath kz}\hat{a}^\dagger_+\hat{a}_- + e^{2\imath kz}\hat{a}_+\hat{a}^\dagger_-\right) - \imath\sum_{\pm}\eta_\pm(\hat{a}_\pm - \hat{a}^\dagger_\pm)\right)\sum_{n_+,n_-} c_{n_+,n_-}|n_+,n_-\rangle$$

$$= \sum_{n_+,n_-} c_{n_+,n_-}\left[(U_0-\Delta_c)(n_+ + n_-)|n_+,n_-\rangle\right.$$

$$+U_0e^{-2\imath kz}c_{n_+,n_-}\sqrt{(n_++1)n_-}|n_++1,n_--1\rangle + U_0e^{2\imath kz}c_{n_+,n_-}\sqrt{n_+(n_-+1)}|n_+-1,n_-+1\rangle$$

$$\left.-\imath\eta_+\sqrt{n_+}|n_+-1,n_-\rangle + \imath\eta_+\sqrt{n_++1}|n_++1,n_-\rangle - \imath\eta_-\sqrt{n_-}|n_+,n_--1\rangle + \imath\eta_-\sqrt{n_-+1}|n_+,n_-+1\rangle\right] .$$

Projecting the Schrödinger equation onto the state $\langle m_+,m_-|$ we get,

$$\dot{c}_{m_+,m_-} = \imath(\Delta_c-U_0)(m_++m_-)c_{m_+,m_-}$$
$$-\imath U_0e^{-2\imath kz}c_{m_+-1,m_-+1}\sqrt{m_+(m_-+1)} - \imath U_0e^{2\imath kz}c_{m_++1,m_--1}\sqrt{(m_++1)m_-}$$
$$-\eta_+c_{m_++1,m_-}\sqrt{m_++1} + \eta_+c_{m_+-1,m_-}\sqrt{m_+} - \eta_-c_{m_+,m_-+1}\sqrt{m_-+1} + \eta_-c_{m_+,m_--1}\sqrt{m_-} .$$

The motion, which is assumed to be classical, is modeled by,

$$\ddot{z} = \langle\psi|\ddot{\hat{z}}|\psi\rangle = 2\imath\hbar kU_0\left(\langle\psi|e^{-2\imath kz}\hat{a}^\dagger_+\hat{a}_-|\psi\rangle - \langle\psi|e^{2\imath kz}\hat{a}_+\hat{a}^\dagger_-|\psi>\right)$$
$$= 2\imath\hbar kU_0\sum_{n_+,n_-}\left(e^{-2\imath kz}\sqrt{(n_++1)n_-}c^*_{n_++1,n_--1}c_{n_+,n_-}\right.$$
$$\left.-e^{2\imath kz}\sqrt{n_+(n_-+1)}c^*_{n_+-1,n_-+1}c_{n_+,n_-}\right) .$$

b. Simulations of the above set of differential equations will be started from initially coherent states,

$$|\alpha_+,\alpha_-\rangle = e^{-|\alpha_+|^2/2-|\alpha_-|^2/2}\sum_{n_+,n_-}\frac{\alpha_+^{n_+},\alpha_-^{n_-}}{\sqrt{n_+!n_-!}}|n_+,n_-\rangle .$$

The other states, $|n_+,n_-\rangle$ and $|\alpha_+,n_-\rangle$ are trivial. At later times t the photon distributions can be extracted from the wavefunction via,

$$p_{n_+}(t) = \sum_{n_-}\langle n_+,n_-|\psi(t)\rangle = \sum_{n_-}c_{n_+,n_-}(t) .$$

The amplitudes of field modes follow from,

$$\alpha_\pm(t) = \sum_{n_\pm} n_\pm p_{n_\pm}(t) .$$

Finally, the position and momentum follow directly from the differential equation.

42.5.7.3 Ex: Cavity QED with density matrix

Assume a symmetrically pumped ring cavity in equilibrium with an atom at a fixed position.
a. Derive the equations of motion for the components of the density operator.
b. Write down the density operator describing two decoupled Glauber states? How to retrieve the Fock state populations from the density operator?
c. Now, assume that the atom can move. What will be the evolution of the motional state?

Solution: *a. The evolution of the density matrix* $\rho_{m_+,n_+;m_-n_-} = \langle m_+, m_-|\hat{\rho}|n_+, n_-\rangle$ *is derived from the master equation (42.8) in the adiabatic approximation inserting the Hamiltonian (42.26),*

$$\begin{aligned}
\hat{H} &= \sum_{\pm}(U_0 - \Delta_c)\hat{a}_{\pm}^{\dagger}\hat{a}_{\pm} + U_0(e^{-2\imath kz}\hat{a}_{+}^{\dagger}\hat{a}_{-} + e^{2\imath kz}\hat{a}_{+}\hat{a}_{-}^{\dagger}) - \imath\sum_{\pm}\eta_{\pm}(\hat{a}_{\pm} - \hat{a}_{\pm}^{\dagger}), \sum_{m,n} c_m^* c_n |m\rangle\langle n| \\
&= (U_0 - \Delta_c)\sum_{n_+,n_-}(n_+ + n_-)|n_+, n_-\rangle\langle n_+, n_-| \\
&\quad + U_0\sum_{n_+,n_-}\Big(e^{-2\imath kz}\sqrt{(n_+ + 1)n_-}|n_+ + 1, n_- - 1\rangle\langle n_+, n_-| \\
&\qquad + e^{2\imath kz}\sqrt{n_+(n_- + 1)}|n_+ - 1, n_- + 1\rangle\langle n_+, n_-|\Big) \\
&\quad - \imath\eta_+\sum_{n_+,n_-}\Big(\sqrt{n_+}|n_+ - 1, n_-\rangle\langle n_+, n_-| - \sqrt{n_+ + 1}|n_+ + 1, n_-\rangle\langle n_+, n_-|\Big) \\
&\quad - \imath\eta_-\sum_{n_+,n_-}\Big(\sqrt{n_-}|n_+, n_- - 1\rangle\langle n_+, n_-| - \sqrt{n_- + 1}|n_+, n_- + 1\rangle\langle n_+, n_-|\Big) \ .
\end{aligned}$$

We get for the coherent evolution,

$$\begin{aligned}
&\dot{\hat{\rho}}_{m_+,n_+;m_-n_-} \equiv \langle m_+, m_-|\dot{\rho}|n_+, n_-\rangle = -\imath\langle m_+, m_-|[\hat{H}, \hat{\rho}]|n_+, n_-\rangle \\
&= -\imath\sum_{p_+,p_-}\langle m_+, m_-|\hat{H}|p_+, p_-\rangle\hat{\rho}_{p_+,n_+;p_-,n_-} + \imath\sum_{p_+,p_-}\hat{\rho}_{m_+,p_+;m_-,p_-}\langle p_+, p_-|\hat{H}|n_+, n_-\rangle \ ,
\end{aligned}$$

giving,

$$\begin{aligned}
&\dot{\hat{\rho}}_{m_+,n_+;m_-n_-} = -\imath(U_0 - \Delta_c)(m_+ + m_- - n_+ - n_-)\hat{\rho}_{m_+,m_+;n_-,n_-} \\
&- \imath U_0 e^{-2\imath kz}\sqrt{m_+(m_- + 1)}\hat{\rho}_{m_+-1,n_+;m_-+1,n_-} - \imath U_0 e^{2\imath kz}\sqrt{(m_+ + 1)m_-}\hat{\rho}_{m_++1,n_+;m_--1,n_-} \\
&+ \imath U_0 e^{-2\imath kz}\sqrt{(n_+ + 1)n_-}\hat{\rho}_{m_+,n_++1;m_-,n_--1} + \imath U_0 e^{2\imath kz}\sqrt{n_+(n_- + 1)}\hat{\rho}_{m_+,n_+-1;m_-,n_-+1} \\
&- \eta_+\sqrt{m_+ + 1}\hat{\rho}_{m_++1,n_+;m_-,n_-} + \eta_+\sqrt{m_+}\hat{\rho}_{m_+-1,n_+;m_-,n_-} \\
&+ \eta_+\sqrt{n_+}\hat{\rho}_{m_+,n_+-1;m_-,n_-} - \eta_+\sqrt{n_+ + 1}\hat{\rho}_{m_+,n_++1;m_-,n_-} \\
&- \eta_-\sqrt{m_- + 1}\hat{\rho}_{m_+,n_+;m_-+1,n_-} + \eta_-\sqrt{m_-}\hat{\rho}_{m_+,n_+;m_--1,n_-} \\
&+ \eta_-\sqrt{n_-}\hat{\rho}_{m_+,n_+;m_-,n_--1} - \eta_-\sqrt{n_- + 1}\hat{\rho}_{m_+,n_+;m_-,n_-+1} \ .
\end{aligned}$$

For the dissipative evolution we get,

$$\mathcal{L}_{cavity-vac,\pm} = -\kappa\{\hat{a}_{\pm}^{\dagger}\hat{a}_{\pm}\hat{\rho}(t) - 2\hat{a}_{\pm}\hat{\rho}(t)\hat{a}_{\pm}^{\dagger} + \hat{\rho}(t)\hat{a}_{\pm}^{\dagger}\hat{a}_{\pm}\} \ .$$

Hence,

$$\langle m_+, m_-|\mathcal{L}_{cavity-vac,\pm}|n_+, n_-\rangle$$
$$= -\kappa \sum_{p_+,p_-} \Big(\langle m_+, m_-|\hat{a}_\pm^\dagger \hat{a}_\pm |p_+, p_-\rangle \rho_{p_+,n_+;p_-,n_-} + \rho_{m_+,p_+;m_-,p_-} \langle p_+, p_-|\hat{a}_\pm^\dagger \hat{a}_\pm |n_+, n_-\rangle \Big)$$
$$- 2\kappa \sum_{p_+,p_-,q_+,q_-} \langle m_+, m_-|\hat{a}_\pm|p_+, p_-\rangle \rho_{p_+,q_+;p_-,q_-} \langle q_+, q_-|\hat{a}_\pm^\dagger|n_+, n_-\rangle \ ,$$

and thus,

$$\mathcal{L}_{cavity-vac,+}\rho_{m_+,n_+;m_-n_-} = -2\kappa\{n_+\rho_{m_+,n_+;m_-,n_-} - \sqrt{n_+(n_++1)}\rho_{m_++1,n_++1;m_-,n_-}\}$$
$$\mathcal{L}_{cavity-vac,-}\rho_{m_+,n_+;m_-n_-} = -2\kappa\{n_-\rho_{m_+,n_+;m_-,n_-} - \sqrt{n_-(n_-+1)}\rho_{m_+,n_+;m_-+1,n_-+1}\} \ .$$

b. Simulations will be started from an initially coherent state,

$$\hat{\rho}(0) = |\alpha_+\rangle\langle\alpha_+| \otimes |\alpha_-\rangle\langle\alpha_-|$$
$$= e^{-|\alpha_+|^2-|\alpha_-|^2} \sum_{m_+,n_+,m_-,n_-} \frac{\alpha_+^{m_+}\alpha_+^{*n_+}\alpha_-^{m_-}\alpha_-^{*n_-}}{\sqrt{m_+!n_+!m_-!n_-!}} |m_+, m_-\rangle\langle n_+, n_-| \ ,$$

such that,

$$\rho_{m_+,n_+;m_-,n_-}(0) = \langle m_+, m_-|\hat{\rho}(0)|n_+, n_-\rangle = e^{-|\alpha_+|^2-|\alpha_-|^2} \frac{\alpha_+^{m_+}\alpha_+^{*n_+}\alpha_-^{m_-}\alpha_-^{*n_-}}{\sqrt{m_+!n_+!m_-!n_-!}} \ .$$

Now, we calculate the photon distributions via,

$$p_{n_+} = Tr\ \hat{\rho}|n_+\rangle\langle n_+| = \langle n_+|Tr_{n_-}\ \hat{\rho}|n_+\rangle = \sum_{n_-}\langle n_+, n_-|\hat{\rho}|n_+, n_-\rangle = \sum_{n_-}\rho_{n_+,n_+;n_-n_-} \ .$$

Of course, we expect that for separable coherent states,

$$p_{n_+} = e^{-|\alpha_+|^2}\frac{|\alpha_+|^{n_+}}{n_+!}e^{-|\alpha_-|^2}\sum_{n_-}\frac{|\alpha_-|^{n_-}}{n_-!} = e^{-|\alpha_+|^2}\frac{|\alpha_+|^{2n_+}}{n_+!} \ .$$

c. We can follow the evolution of the motional degree of freedom directly in the equation of motion of CARL,

$$\dot{\hat{p}} = 2\imath\hbar k U_0(e^{-2\imath kz}\hat{a}_+^\dagger\hat{a}_- - e^{2\imath kz}\hat{a}_+\hat{a}_-^\dagger)$$
$$= 2\imath\hbar k U_0 \sum_{n_+,n_-} \Big(e^{-2\imath kz}\sqrt{(n_++1)n_-}|n_++1, n_--1\rangle\langle n_+, n_-|$$
$$-e^{2\imath kz}\sqrt{(n_-+1)n_+}|n_+-1, n_-+1\rangle\langle n_+, n_-|\Big) \ .$$

giving,

$$\langle\psi|\dot{\hat{p}}|\psi\rangle = \sum_{m_+,m_-,n_+,n_-} c_{m_+,m_-}^* c_{n_+,n_-}\langle m_+, m_-|\dot{p}|n_+, n_-\rangle$$
$$= 2\imath\hbar k U_0 \sum_{n_+,n_-}\Big(\rho_{n_++1,n_+;n_--1,n_-}e^{-2\imath kz}\sqrt{(n_++1)n_-} - \rho_{n_+-1,n_+;n_-+1,n_-}e^{2\imath kz}\sqrt{n_+(n_-+1)}\Big) \ .$$

42.5.7.4 Ex: Photon number and momentum conservation

a. Calculate the evolution under CARL interaction, $e^{-\imath\hat{H}_{carl}t}\hat{n}_{\pm}e^{\imath\hat{H}_{carl}t}$, of the photon numbers in each mode and show that the total photon number is conserved.
b. Assuming conservation of total momentum calculate the evolution of the atomic momentum.

Solution: *a. The CARL Hamiltonian is,*

$$\hat{H}_{carl} = U_0(\hat{a}_+^\dagger \hat{a}_- e^{-2\imath k\hat{z}} + \hat{a}_+\hat{a}_-^\dagger e^{2\imath k\hat{z}}) \ .$$

With this we calculate,

$$\begin{aligned} e^{-\imath\hat{H}_{carl}t}\hat{n}_{\pm}e^{\imath\hat{H}_{carl}t} &= e^{-\imath\hat{H}_{carl}t}\hat{a}_{\pm}^\dagger e^{\imath\hat{H}_{carl}t}e^{-\imath\hat{H}_{carl}t}\hat{a}_{\pm}e^{\imath\hat{H}_{carl}t} \\ &= \left(\hat{a}_{\pm}^\dagger \cos U_0t \pm \hat{a}_{\mp}^\dagger e^{\pm 2\imath k\hat{z}} \sin U_0t\right)\left(\hat{a}_{\pm} \cos U_0t \pm \hat{a}_{\mp} e^{\mp 2\imath k\hat{z}} \sin U_0t\right) \\ &= \hat{a}_{\pm}^\dagger\hat{a}_{\pm}\cos^2 U_0t + \hat{a}_{\mp}^\dagger\hat{a}_{\mp}\sin^2 U_0t \pm \left(\hat{a}_{\pm}^\dagger\hat{a}_{\mp}e^{\mp 2\imath k\hat{z}} + \hat{a}_{\mp}^\dagger\hat{a}_{\pm}e^{\pm 2\imath k\hat{z}}\right)\sin U_0t\cos U_0t \ , \end{aligned}$$

using the result (35.318). Hence,

$$e^{-\imath\hat{H}_{carl}t}(\hat{n}_+ + \hat{n}_-)e^{\imath\hat{H}_{carl}t} = \hat{n}_+ + \hat{n}_- \ .$$

b. We also calculate,

$$\begin{aligned} &e^{-\imath\hat{H}_{carl}t}(\hat{n}_+ - \hat{n}_-)e^{\imath\hat{H}_{carl}t} \\ &\qquad = (\hat{n}_+ - \hat{n}_-)(\cos^2 U_0t - \sin^2 U_0t) + 2\left(\hat{a}_+^\dagger\hat{a}_-e^{-2\imath k\hat{z}} + \hat{a}_-^\dagger\hat{a}_+e^{2\imath k\hat{z}}\right)\sin U_0t\cos U_0t \\ &\qquad = (\hat{n}_+ - \hat{n}_-)\cos 2U_0t + \left(\hat{a}_+^\dagger\hat{a}_-e^{-2\imath k\hat{z}} + \hat{a}_-^\dagger\hat{a}_+e^{2\imath k\hat{z}}\right)\sin 2U_0t \ , \end{aligned}$$

so that,

$$e^{-\imath\hat{H}_{carl}t}\hat{p}e^{\imath\hat{H}_{carl}t} = -e^{-\imath\hat{H}_{carl}t}(\hat{n}_+ - \hat{n}_-)e^{\imath\hat{H}_{carl}t} \ .$$

42.5.7.5 Ex: Self-synchronization of Bloch oscillations

Study the Bloch-CARL dynamics for the case of a sinusoidally modulated CARL pump light intensity. Choose as the modulation frequency the expected Bloch oscillation frequency and a variable phase delay.

Solution:

42.6 Atomic self-organization in light fields

The CARL phenomenon introduced in the previous chapter raises a variety of questions, such as: How does it compare to an ordinary laser? Is there a phase transition?

Of what kind would be this transition (in the Ehrenfest or Landau classification scheme)? What are the coherence properties (measured by correlation functions)? How do these properties depend on the random motion (temperature) of the atoms? These issues will be addressed in this chapter and in the later chapter within the models of Langevin, Fokker-Planck, Vlasov, and Kuramoto.

42.6.1 The Langevin model

42.6.1.1 CARL with damping

We saw in the previous chapter that CARL is a transient phenomenon, the atoms and the phase of the light wave being continuously accelerated. However, it is possible to force stationary behavior by providing additional friction for the atoms. Such friction can be carried out by an *optical molasses* (see Sec. 43.2.1) characterized by a friction coefficient γ_{frc}. The friction force can be added to the CARL equations of motion (42.69),

$$\begin{aligned} \dot{\alpha}_- &= -\kappa\alpha_- - \imath U_0 \alpha_+ \sum_m e^{2\imath k z_m} \\ k\dot{v}_n &= 4i\omega_{rec} U_0 \alpha_+ (\alpha_- e^{-2\imath k z_n} - \alpha_-^* e^{2\imath k z_n}) - \gamma_{frc} k v_n \ . \end{aligned} \tag{42.244}$$

Now, the balance of forces happens at a well-defined atomic velocity, which incidentally corresponds to a well-defined CARL frequency. Assuming perfect 'bunching' $e^{2\imath k z_m} = e^{2\imath k z}$, and balanced forces, $\dot{v}_m = 0$ e $\alpha_- = \beta e^{2\imath k z}$ with $\dot{\beta} = 0$, we obtain for $\kappa \ll 2kv$,

$$\begin{aligned} \alpha_- &= \tfrac{-\imath N U_0 \alpha_+}{\kappa + 2\imath k v} e^{2\imath k z} \\ (kv)^3 &= \frac{2\omega_{rec}\kappa N U_0^2 \alpha_+^2}{\gamma_{fric}} \ . \end{aligned} \tag{42.245}$$

This result will be derived in Exc. 42.6.7.1.

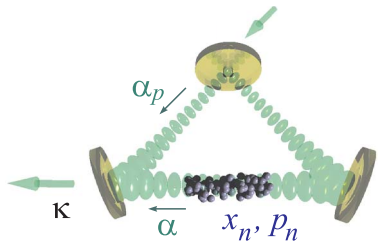

Figure 42.48: Scheme of the ring cavity.

Optical molasses obviously are subject to a cooling limit coming from the random scattering of photons. As a consequence, atoms follow a *random walk* in the momentum space, which leads to the diffusion and heating of atoms and impedes the bunching of atoms. It also turns out that a minimal grouping is required to initialize CARL. Therefore, there is a threshold behavior as a function of the equilibrium

temperature of the molasses,

$$\boxed{\begin{array}{rcl} \dot{\alpha}_- &=& -\kappa\alpha_- - \imath U_0\alpha_+ \sum_m e^{2\imath k z_m} \\ k\dot{v}_n &=& 4\omega_{rec}U_0\alpha_+(\alpha_- e^{-2\imath k z_n} - \alpha_-^* e^{2\imath k z_n}) - \gamma_{frc}kv_n + \xi_n(t) \end{array}} \ . \tag{42.246}$$

The equation corresponds to a *Langevin equation*, where the stochastic term $\xi_n(t)$ describes white noise. We can simulate this equation by a Runge-Kutta method, where the atoms are continually exposed to random momentum changes. For N atoms we need to solve $2N + 2$ Langevin equations to describe the dynamics of all degrees of freedom. The Langevin equations are associated to so-called *Fokker-Planck equations* [1343, 1106, 664, 1342]. These describe the temporal evolution of the atomic density along the optical x-axis. With these equations we replace the $2N$ trajectories of individual particles by a one-dimensional field $P(x, t)$. The *Vlasov equation* represents a different approach: Here we assume that the equilibrium between cooling and heating is achieved by a continuous thermalization process described by a single rate γ_{th} [22].

42.6.1.2 Characterization of an optical molasses

Optical molasses is discussed in Sec. 43.2.1. In Exc. 43.2.5.1 we will show how, through a linearization of the radiative pressure force, we arrive at the following approximation,

$$\mathbf{F} = -\gamma_{frc}\mathbf{v} \qquad \text{with} \qquad \gamma_{frc} \simeq -\sqrt{3}\hbar k^2 s(1+s)^{-3/2} \ , \tag{42.247}$$

where $s = I/I_s$ is the saturation parameter. This formula estimates the maximum friction force, when the lasers are tuned close to an atomic resonance [23].

A more fundamental problem is the interdependence of the molasses friction and the CARL. In fact, because the dipole potential influences the detuning of the molasses beams by light-shifting the D_2 line, the γ_{th} coefficient depends on Δ_a and η_+ (the reverse field $|\alpha_-|$ may be neglected). The threshold equations must then be solved in a self consistent way. It might however be possible to determine γ_{th} only slightly above threshold, where the modification is small, $\gamma_{th} \approx \gamma_{th}^{(thresh)}$.

42.6.1.3 Fluctuation-dissipation theorem

Trajectories of ensembles of particles subject to friction and stochastic forces can be described by *Langevin equations*. The friction and the diffusion forces are related by the *fluctuation-dissipation theorem*. This theorem states that, for a thermal sample of atoms whose coordinates θ_n follow,

$$\ddot{\theta}_n = -\gamma_{frc}\dot{\theta}_n + \xi_n(t) \ , \tag{42.248}$$

[22] Through a linearization of the CARL equations, the cavity dissipation itself is found to exert a friction force to the atoms [590, 482]. This implies the existence of diffusion and a finite equilibrium temperature even at if the atoms are initially at $T = 0$.

[23] We note that atomic species exhibiting a hyperfine structure in the ground state are subject to cooling phenomena called 'polarization gradient cooling', which can cause much higher friction coefficients.
We also note that, when the molasses is applied to atoms confined to a potential, the atomic levels can be displaced (e.g., by light-shift or the Zeeman effect). This causes an inhomogeneous effective detuning of the laser beams generating the molasses.

the Langevin force $\xi(t)$ fluctuates stochastically with,

$$\langle \xi_n(t) \rangle = 0 \qquad \text{and} \qquad \langle \xi_n(t) \xi_m(t+\tau) \rangle = 2\gamma_{frc}^2 D_T \delta_{mn} \delta(\tau) \ . \tag{42.249}$$

Here, the *diffusion coefficient*,

$$D_T = \frac{\sigma^2}{\gamma_{frc}} \tag{42.250}$$

is related to the width of the Maxwell-Boltzmann velocity distribution,

$$\sigma = 2k\sqrt{\frac{k_B T}{m}} \ . \tag{42.251}$$

42.6.1.4 Langevin simulations

The Langevin equations of CARL can be simulated, including the random term of the Langevin force, using the *Runge-Kutta method* [631]. The procedure consists in propagating a general first order differential equation,

$$\boxed{\dot{x} = f(x) + g(t)} \ , \tag{42.252}$$

subject to a deterministic force f and a stochastic noise g satisfying,

$$\langle g(t) \rangle = 0 \qquad \text{and} \qquad \langle g(t) g(t') \rangle = 2D\delta(t-t') \tag{42.253}$$

as follows,

$$\boxed{\begin{array}{rcl} x(dt) & = & x_0 + \frac{1}{2} dt [f(x_0) + f(\tilde{x})] + \zeta (2Ddt)^{1/2} \\ \text{with} \quad \tilde{x} & \equiv & x_0 + f(x_0) dt + \zeta (2Ddt)^{1/2} \end{array}} \ , \tag{42.254}$$

where ζ is a random variable distributed according to a normal (Gaussian) distribution normalized as [24],

$$\langle \zeta \rangle = 0 \qquad \text{and} \qquad \langle \zeta^2 \rangle = 1 \ . \tag{42.255}$$

42.6.1.5 Langevin simulation in the adiabatic approximation

Now, we apply this method to the CARL subject to an optical molasses. Making the adiabatic approximation $\ddot{\theta}_n = 0$, the starting point is,

$$\boxed{\begin{array}{rcll} \dot{\alpha}_- & = & -\kappa \alpha_- - \imath U_0 \alpha_+ \sum_m e^{\imath \theta_m} & \equiv B(\alpha_-, \theta_n) \\ \dot{\theta}_n & = & \frac{8i\omega_{rec} U_0 \alpha_+}{\gamma_{frc}} (\alpha_- e^{-\imath\theta_n} - \alpha_-^* e^{\imath\theta_n}) + \frac{\xi_n(t)}{\gamma_{frc}} & \equiv F(\alpha_-, \theta_n) + \frac{\xi_n(t)}{\gamma_{frc}} \end{array}} \ . \tag{42.256}$$

[24] The MATLAB random number generator satisfies this requirement: $\langle \zeta_n \rangle \triangleq sum(randn(1,N))/N = 0$ and $\langle \zeta_n^2 \rangle \triangleq sum(randn(1,N).\wedge 2)/N = 1$.

In order to apply the Runge-Kutta method (42.254), we identify the variables and functions,

$$x(t) \equiv \begin{pmatrix} \alpha_-(t) \\ \theta_n(t) \end{pmatrix} \quad , \quad f(x) \equiv \begin{pmatrix} B(\alpha_-, \theta_n) \\ F(\alpha_-, \theta_n) \end{pmatrix} \quad , \quad g(t) \equiv \begin{pmatrix} 0 \\ \xi_n(t)/\gamma_{frc} \end{pmatrix} , \tag{42.257}$$

such that,

$$\tilde{x} = \begin{pmatrix} \tilde{\alpha}_- \\ \tilde{\theta}_n \end{pmatrix} = \begin{pmatrix} \alpha_-(0) \\ \theta_n(0) \end{pmatrix} + dt \begin{pmatrix} B(\alpha_-(0), \theta_n(0)) \\ F(\alpha_-(0), \theta_n(0)) \end{pmatrix} + \begin{pmatrix} 0 \\ \zeta_n \sqrt{2D_T dt} \end{pmatrix} \tag{42.258}$$

and

$$\begin{aligned} x(dt) &= \begin{pmatrix} \alpha_-(dt) \\ \theta_n(dt) \end{pmatrix} \\ &= \begin{pmatrix} \alpha_-(0) \\ \theta_n(0) \end{pmatrix} + \frac{dt}{2} \left[\begin{pmatrix} B(\alpha_-(0), \theta_n(0)) \\ F(\alpha_-(0), \theta_n(0)) \end{pmatrix} + \begin{pmatrix} B(\tilde{\alpha}_-, \tilde{\theta}_n) \\ F(\tilde{\alpha}_-, \tilde{\theta}_n) \end{pmatrix} \right] + \begin{pmatrix} 0 \\ \zeta_n \sqrt{2D_T dt} \end{pmatrix} . \end{aligned} \tag{42.259}$$

The Langevin equation can be used to simulate the temporal evolution of CARL. Fig. 42.49 shows a simulation of the frequency and amplitude of the CARL based on prescription (42.254).

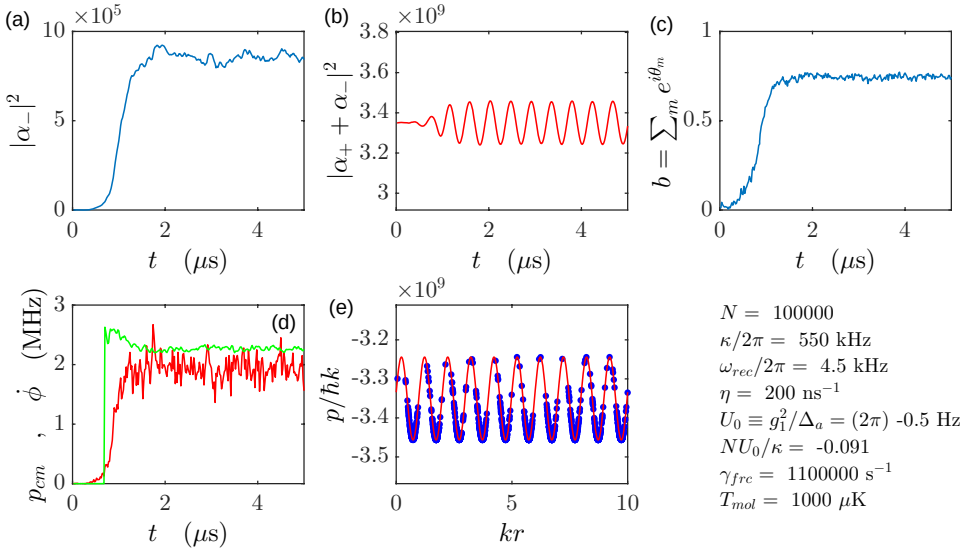

Figure 42.49: (code) Time evolution with phase transition of the viscous CARL in the adiabatic approximation. Shown are (a) the number of photons in the probe mode, (b) the beat signal, (c) the bunching, (d) the phase of the standing wave and the position of the center-of-mass of the cloud, and (e) the dipole potential calculated from (42.21) with the atomic distribution.

42.6.1.6 Langevin simulation of the full dynamics

Without adiabatic approximation, the starting point is,

$$\boxed{\begin{array}{lcll} \dot{\alpha}_- & = & \kappa\alpha_- - \imath U_0 \alpha_+ \sum_m e^{\imath\theta_m} & \equiv B(\alpha_-, \theta_n) \\ \dot{\theta}_n & = & V_n & \\ \dot{V}_n & = & 8i\omega_{rec} U_0 \alpha_+ (\alpha_- e^{-\imath\theta_n} - \alpha_-^* e^{\imath\theta_n}) - \gamma_{frc} V_n + \xi_n(t) & \equiv F(\alpha_-, \theta_n, V_n) + \xi_n(t) \end{array}} \quad . \tag{42.260}$$

In order to apply the Runge-Kutta method (42.254), we identify the variables and functions,

$$x(t) \equiv \begin{pmatrix} \alpha_-(t) \\ \theta_n(t) \\ V_n(t) \end{pmatrix} \quad , \quad f(x) \equiv \begin{pmatrix} B(\alpha_-, \theta_n) \\ V_n \\ F(\alpha_-, \theta_n, V_n) \end{pmatrix} \quad , \quad g(t) \equiv \begin{pmatrix} 0 \\ 0 \\ \xi_n(t) \end{pmatrix} \quad , \tag{42.261}$$

such that,

$$\tilde{x} = \begin{pmatrix} \tilde{\alpha}_- \\ \tilde{\theta}_n \\ \tilde{V}_n \end{pmatrix} \equiv \begin{pmatrix} \alpha_-(0) \\ \theta_n(0) \\ V_n(0) \end{pmatrix} + dt \begin{pmatrix} B\left(\alpha_-(0), \theta_n(0)\right) \\ V_n(0) \\ F\left(\alpha_-(0), \theta_n(0), V_n(0)\right) \end{pmatrix} + \begin{pmatrix} 0 \\ 0 \\ \zeta_n \sqrt{2\gamma_{frc}^2 D_T dt} \end{pmatrix} \tag{42.262}$$

and

$$\begin{aligned} x(dt) = \begin{pmatrix} \alpha_-(dt) \\ \theta_n(dt) \\ V_n(dt) \end{pmatrix} = \begin{pmatrix} \alpha_-(0) \\ \theta_n(0) \\ V_n(0) \end{pmatrix} + \frac{dt}{2} \Bigg[\begin{pmatrix} B\left(\alpha_-(0), \theta_n(0)\right) \\ V_n(0) \\ F\left(\alpha_-(0), \theta_n(0), V_n(0)\right) \end{pmatrix} \\ + \begin{pmatrix} B(\tilde{\alpha}_-, \tilde{\theta}_n) \\ \tilde{V}_n \\ F(\tilde{\alpha}_-, \tilde{\theta}_n, \tilde{V}_n) \end{pmatrix} \Bigg] + \begin{pmatrix} 0 \\ 0 \\ \zeta_n \sqrt{2\gamma_{frc}^2 D_T dt} \end{pmatrix} \quad . \end{aligned} \tag{42.263}$$

42.6.1.7 Simulation of the phase transition

The simulations of the Langevin equations shown in Figs. 42.49 and 42.50 exhibit a *temporal phase transition* due to a spontaneous self-organization of the atoms.

We can also, slowly varying some control parameter, study the threshold behavior. In Fig. 42.51, for example, we first increase and then reduce linearly the injected power α_+. We clearly observe a threshold behavior, but also a hysteresis indicating a bistability of the system. It is also interesting to note a separation of the CARL frequency and the atomic center-of-mass velocity in the green and red curves of Fig. 42.51(c).

In Fig.42.52, we increase and then reduce the temperature linearly.

The following links show simulations of the Langevin equation for CARL (watch movie) and of the Fokker-Planck equation for CARL (watch movie). Furthermore,

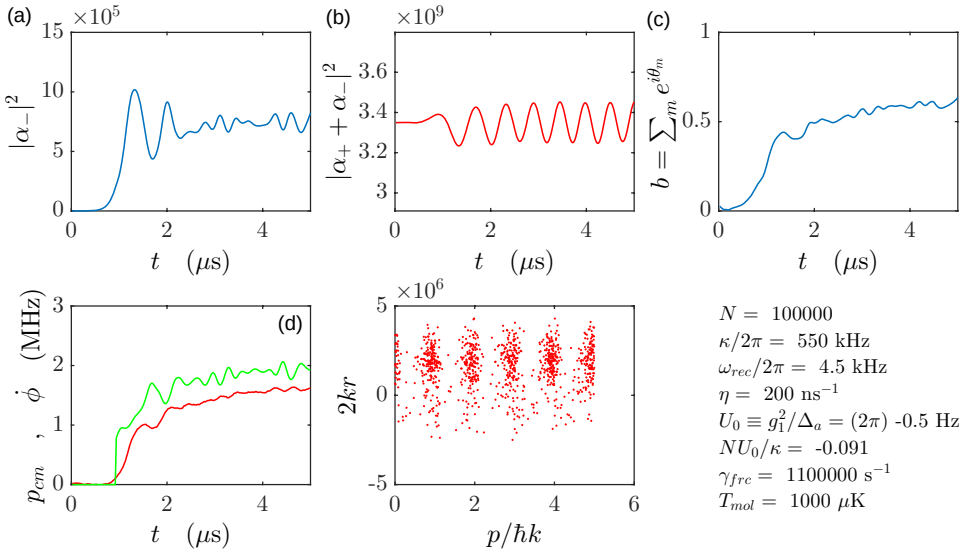

Figure 42.50: (code) Time evolution of the complete dynamics of the viscous CARL with phase transition. Same parameters as in Fig. 42.49. Shown are (a) the number of photons in the probe mode, (b) the beat signal, (c) the bunching, (d) the phase of the standing wave and the position of the center-of-mass of the cloud, and (e) the dipole potential calculated from (42.21) with the atomic distribution.

the following videos show examples of self-synchronizing systems that can be understood via the Kuramoto model: Huygens pendulum clocks (watch movie), synchronizing crickets (watch movie), buzzing mosquitoes (watch movie), singing dunes (watch movie), and the London Millenium bridge (watch movie).

42.6.2 The Fokker-Planck and the Vlasov model

The *Fokker-Planck equation* for a density distribution $Q(\mathbf{r}, t)$,

$$\frac{dQ}{dt} + Q\nabla \cdot \mathbf{v} = D\nabla^2 Q \ , \tag{42.264}$$

represents a generalization of the *continuity equation*, since with $\frac{d}{dt} \equiv \frac{\partial}{\partial t} + \mathbf{v} \cdot \nabla$, we obtain,

$$\frac{\partial Q}{\partial t} = -\nabla \cdot (\mathbf{v}Q) + D\nabla^2 Q \ . \tag{42.265}$$

If ρ is a local density, it the continuity equation reads,

$$\frac{d\rho}{dt} + \rho\nabla \cdot \mathbf{v} = 0 \ . \tag{42.266}$$

Knowing,

$$\frac{d}{dt} \equiv \frac{\partial}{\partial t} + \mathbf{v} \cdot \nabla \ , \tag{42.267}$$

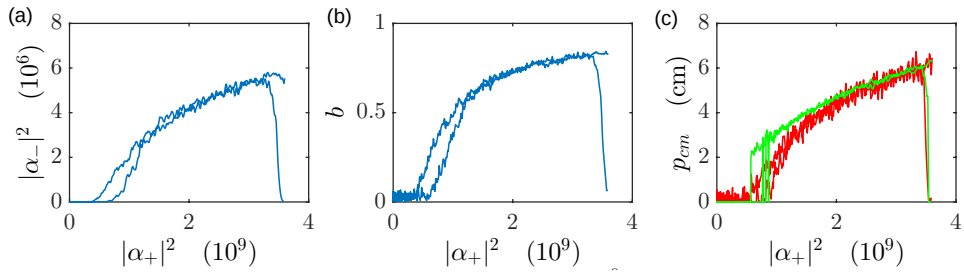

Figure 42.51: (code) (a) Number of atoms in the probe mode, (b) bunching and (c) velocity of the atoms (red) and the frequency of the CARL (green), while the pumping power is ramped.

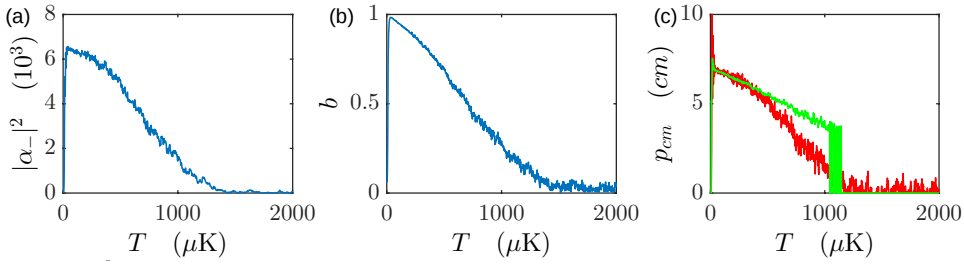

Figure 42.52: (code) Same as Fig. 42.51, but now the temperature is ramped.

we obtain,

$$\frac{\partial \rho}{\partial t} = -\nabla \cdot (\rho \mathbf{v}) \ . \tag{42.268}$$

The Fokker-Planck equation is just a generalization to include a diffusion process,

$$\frac{d\rho}{dt} + \rho \nabla \mathbf{v} = D_x \frac{\partial^2 \rho}{\partial x^2} \ , \tag{42.269}$$

or

$$\frac{\partial \rho}{\partial t} = -\nabla \cdot (\rho \mathbf{v}) + D_x \frac{\partial^2 \rho}{\partial x^2} \ . \tag{42.270}$$

42.6.2.1 Thermalization in the Fokker-Planck equation

We now apply the Fokker-Planck equation to the density distribution (42.256) of an atomic cloud subjected to the CARL force [1343, 1106]. As CARL is a one-dimensional process, we can use $\nabla \to \partial\theta$ and replace the velocity field $\mathbf{v} \to \dot{\theta}$:

$$\boxed{\begin{aligned} \dot{\alpha}_- &= -\kappa\alpha_- - \imath N U_0 \alpha_+ b \\ \frac{\partial Q}{\partial t} &= \frac{8\imath\omega_{rec} U_0 \alpha_+}{\gamma_{frc}} \frac{\partial}{\partial\theta}\left[(\alpha_- e^{-\imath\theta} - \alpha_-^* e^{\imath\theta})Q\right] + D_\theta \frac{\partial^2 Q}{\partial\theta^2} \end{aligned}} \ . \tag{42.271}$$

The position diffusion coefficient can be estimated by,

$$D_\theta = \frac{\langle k^2 v^2 \rangle}{\gamma_{frc}} \ . \tag{42.272}$$

The normalization and the 'bunching' $|b|$ are given by,

$$1 = \int_0^{2\pi} Q(\theta,t) d\theta \quad , \quad b \equiv \int_0^{2\pi} Q(\theta,t) e^{-\imath\theta} d\theta \ . \tag{42.273}$$

To simulate the equations (42.271) we expand the distribution function in spatial harmonics [1106],

$$Q(\theta,t) \equiv \sum_\nu Q_\nu(t) e^{\imath\nu\theta} \ . \tag{42.274}$$

In this expansion the normalization and the bunching become,

$$Q_0 = 1/2\pi \quad , \quad |b| = 2\pi |Q_1| \ , \tag{42.275}$$

and the equations (42.271) immediately yield,

$$\boxed{\begin{array}{rcl} \dot{\alpha}_- & = & -2\pi\imath N U_0 \alpha_+ Q_1 - \kappa \alpha_- \\ \dfrac{dQ_\nu}{dt} & = & \dfrac{8\omega_{rec} U_0 \alpha_+}{\gamma_{frc}} \nu \left(\alpha_- Q_{\nu+1} + \alpha_-^* Q_{\nu-1} \right) - \nu^2 D_\theta Q_\nu \end{array}} \ . \tag{42.276}$$

We will derive the results (42.275) and (42.276) in Exc. 42.6.7.3. Also,

$$kv = \frac{d}{dt} \arctan \frac{\mathfrak{Im}\ \alpha_-}{\mathfrak{Re}\ \alpha_-} \ , \tag{42.277}$$

and,

$$\begin{aligned} \langle \dot{\theta} \rangle &\equiv \int_0^{2\pi} \dot{Q}(\theta,t) d\theta = \sum_\nu \dot{Q}_\nu(t) \int_0^{2\pi} e^{\imath\nu\theta} d\theta \\ &= \sum_\nu \frac{8\omega_{rec} U_0 \alpha_+}{\gamma_{frc}} \nu \left(\alpha_- Q_{\nu+1} \alpha_-^* Q_{\nu-1} \right) \delta_{\nu 0} = \frac{16\omega_{rec} U_0 \alpha_+}{\gamma_{frc}} \mathfrak{Re}\ (\alpha_- Q_1^*) \ . \end{aligned} \tag{42.278}$$

These equations can be easily simulated.

Matlab simulations of the Fokker-Planck equation, shown in Fig. 42.53, reproduce quantitatively the curves previously obtained by simulations of the Langevin equations.

42.6.2.2 Bistability and instability of the viscous CARL

The threshold can be found by simulating the Fokker-Planck equation while varying a control parameter (pumping power, temperature, number of atoms) sufficiently slowly, that the system always remains in a steady state. Fig. 42.54 shows the behavior of the CARL, while the pump power is linearly reduced and then linearly increased at different velocities. We observe a bistability that slightly depends on the speed of the ramp. The behavior of the mass-center velocity kv_{cm} and the phase of the standing wave, $\dot{\phi}$, are different [1104] [25].

[25] We can expect a second phase transition when the pump power exceeds a critical value, because for $NU_0 > \kappa$, the CARL becomes unstable again: It will unlock from the self-determined frequency

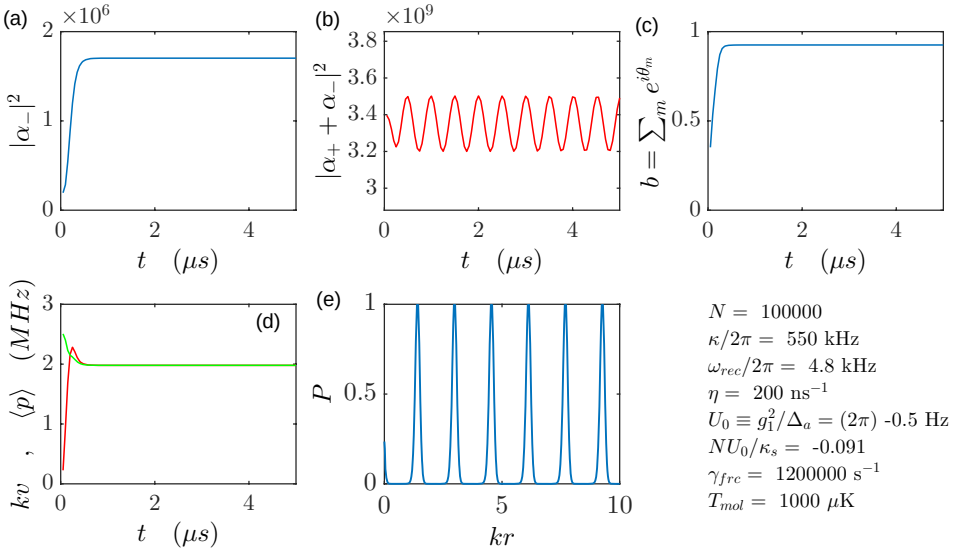

Figure 42.53: (code) Temporal evolution of the complete dynamics with phase transition of the viscous CARL. The same parameters as in Fig. 42.49. Shown are (a) the number of photons in the probe mode, (b) the beat signal, (c) the bunching, (d) the phase of the standing wave and the position of the center-of-mass of the cloud, and (e) the atomic density distribution.

42.6.3 Thermalization in the Vlasov equation

The basic equations describing our ring-cavity filled with atoms are [755],

$$\boxed{\begin{aligned} \dot{\alpha}_- &= \kappa\alpha_- - \imath U_0 \alpha_+ \sum_m e^{\imath\theta_m} \\ \dot{\theta}_n &= V_n \\ \dot{V}_n &= 8\imath\omega_{rec} U_0 \alpha_+ (\alpha_- e^{-\imath\theta_n} - \alpha_-^* e^{\imath\theta_n}) - \gamma_{frc}(V_n - V_n^{(0)}) \end{aligned}} \quad , \tag{42.279}$$

if we assume the pump mode to be stationary $\alpha_+ = \eta_+/\kappa^{-1}$ and define the atomic bunching parameter by $b = \frac{1}{N}\sum_j e^{2ikx_j}$. A non-zero steady-state temperature is reached, if we allow the steady-state velocities of the atoms $v_j^{(0)}$ to be *different* for all atoms and distributed according to a Maxwell-Gaussian velocity distribution. The assumption of a common steady-state velocity for all atoms obviously results in perfect bunching and cooling to $T = 0$.

Let us introduce a local phase space density of the atomic cloud $Q(x, p, t)$ as a two-dimensional field in phase space. The time-evolution of this quantity is given by the so-called *Vlasov equation* (or collisionless Boltzmann equation),

$$0 = \partial_t Q + v\partial_x Q + F\partial_p Q + \gamma_{th}(Q - Q_0) \ , \tag{42.280}$$

and start to oscillate strongly. However, this effect is not described by the equations used for the simulation, which suppose an adiabatic elimination of the inertia.

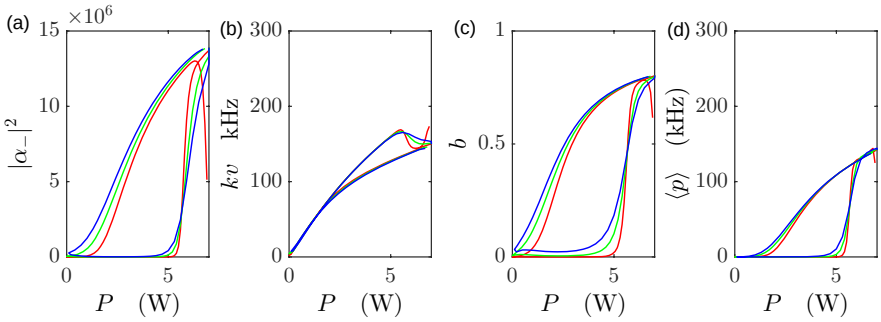

Figure 42.54: (code) Bistability of CARL near the threshold when the power is ramped at different paces.

where v and F are the center-of-mass velocity and force taken from equation (42.279) without the friction term. According to this equation the atomic cloud tends to a stationary distribution Q_0 as time goes on. Following Bonifacio *et al.* [176] and Javaloyes [665, 666, 667], we replace the friction term by an additional (Vlasov) equation:

$$\boxed{\begin{aligned} \dot{\alpha}_- &= -\imath N U_0 \alpha_+ b - \kappa \alpha_- \\ \dot{\theta} &= \omega_{rec} V \\ \dot{V} &= \imath U_0 \alpha_+ (\alpha_- e^{-\imath\theta} - \alpha_-^* e^{\imath\theta}) \\ 0 &= \partial_t Q + \dot{\theta}\partial_\theta Q + \dot{\varrho}\partial_\varrho Q + \gamma_{frc}(Q - Q_0) \end{aligned}} \quad . \tag{42.281}$$

The bunching parameter can now be rewritten in terms of

$$b = \int_0^{2\pi} d\theta \int_{-\infty}^{\infty} d\varrho \; Q(\theta, \varrho, t) \; e^{2\imath\theta} \; . \tag{42.282}$$

The equilibrium distribution is chosen to be a homogeneous cloud with a Maxwell-Boltzmann velocity distribution,

$$Q_0 = \frac{1}{2\pi}\sqrt{\frac{\sigma}{\pi}} e^{-\sigma\varrho^2} \; , \tag{42.283}$$

where $\sigma \equiv \hbar\omega_{rec}/k_B T$ with $\omega_{rec} \equiv \hbar k^2/2m$ such that $\int_0^{2\pi} d\theta \int_{-\infty}^{\infty} Q_0 d\varrho = 1$. We now perform a linear stability analysis. We expand Q around the steady state, $Q(\theta, \varrho, t) = Q_0(\varrho) + Q_1(\theta, \varrho, t)$ and retain to first order,

$$0 = \partial_t Q_1 + \dot{\theta}\partial_\theta Q_1 + \dot{\varrho}\partial_\varrho Q_0 + \gamma_{th} Q_1 \; . \tag{42.284}$$

Now we look for a time-dependent particular solution by inserting the ansatz,

$$\begin{aligned} \alpha_-(t) &= \beta_- e^{\imath\lambda t} \qquad \text{with} \qquad \dot{\beta}_- = 0 \\ Q_1(\theta, \varrho, t) &= H_1(\varrho) e^{-2\imath\theta} e^{\imath\lambda t} + c.c. \; , \end{aligned} \tag{42.285}$$

where $i\lambda \equiv \lambda_g + i\lambda_\omega$ into the field equation (42.281)a, the first order expansion of the Vlasov equation (42.284) (only retaining co-rotating terms) and into the expression for bunching (42.282). This ansatz accounts for the fact that, in steady state, we expect a fixed CARL frequency ν and a spatially modulated density distribution of the atoms. The set of equations becomes,

$$\begin{aligned} qi\lambda\beta_- &= -\kappa\beta_- - \imath N U_0 \tilde{\eta}_+ b e^{-\imath\lambda t} \\ 0 &= \imath\lambda H_1(\varrho) - 4\imath\omega_{rec}\varrho H_1(\varrho) + \imath U_0\tilde{\eta}_+\beta_-\partial_\varrho Q_0 + \gamma_{th} H_1(\varrho) \\ b &= \int_0^{2\pi} d\theta \int_{-\infty}^{\infty} d\varrho\ H_1(\varrho) e^{\imath\lambda t}\ . \end{aligned} \tag{42.286}$$

With the definition,

$$\begin{aligned} \Gamma(\sigma,\gamma_{th},\imath\lambda) &\equiv \int_{-\infty}^{\infty} \frac{d\varrho\ \partial_\varrho Q_0}{\imath\lambda - 4\imath\omega_{rec}\varrho + \gamma_{th}} \\ &= -\int_{-\infty}^{\infty} \frac{d\varrho\ 4\imath\omega_{rec} Q_0}{(\imath\lambda - 4\imath\omega_{rec}\varrho + \gamma_{th})^2}\ , \end{aligned} \tag{42.287}$$

the solution of the above set of equations is,

$$\begin{aligned} H_1(\varrho) &= \frac{-\imath U_0\tilde{\eta}_+\beta_-\partial_\varrho Q_0}{\imath\xi - 4\imath\omega_{rec}\varrho + \gamma_{th}} \\ b &= -e^{\imath\xi t}\imath U_0\tilde{\eta}_+\beta_- 2\pi\Gamma(\sigma,\gamma_{th},\imath\lambda) \\ 0 &= \left[\kappa + \imath\lambda + N U_0^2\tilde{\eta}_+^2\ 2\pi\Gamma(\sigma,\gamma_{th},\imath\lambda)\right]\ \beta_-\ . \end{aligned} \tag{42.288}$$

42.6.3.1 Calculation of the threshold

The bifurcation where the reverse field crosses the threshold to lasing occurs at $\lambda_g = 0$. We divide the field equation in real and imaginary parts,

$$\begin{aligned} \kappa + N U_0^2\tilde{\eta}_+^2\ 2\pi\mathfrak{Re}\ \Gamma(\sigma,\gamma,\imath\lambda_\omega) &= 0 \\ \nu + N U_0^2\tilde{\eta}_+^2\ 2\pi\mathfrak{Im}\ \Gamma(\sigma,\gamma,\imath\lambda_\omega) &= 0\ . \end{aligned} \tag{42.289}$$

Now the condition $\lambda_\omega \mathfrak{Re}\ \Gamma(\sigma,\gamma_{th},\imath\lambda_\omega) = \kappa\mathfrak{Im}\ \Gamma(\sigma,\gamma_{th},\imath\lambda_\omega)$ leads to,

$$\int_{-\infty}^{\infty} \frac{d\varrho\ \varrho e^{-\sigma\varrho^2}(\kappa\lambda_\omega - 2\kappa\varepsilon\varrho + \lambda_\omega\gamma_{th})}{(\lambda_\omega - 2\varepsilon\varrho)^2 + \gamma_{th}^2} = 0\ . \tag{42.290}$$

The values λ_ω where this integral is zero are inserted into one of the equations (42.289). Finally,

$$\tilde{\eta}_+^2 = \frac{-1}{N\tilde{U_0^2}\ 2\pi\mathfrak{Re}\ \kappa\Gamma(\sigma,\gamma_{th},\imath\lambda_\omega)}\ , \tag{42.291}$$

is the expression for the pump power threshold as a function of temperature σ, friction γ_{th}, cavity damping κ and coupling constant U_0. The intracavity CARL power is,

$$P_+ = \hbar\omega\delta\ \tilde{\eta}_+^2\ . \tag{42.292}$$

λ_ω is the associated CARL frequency, i.e. the frequency difference between probe and pump.

The final equations show that the threshold power drops as NU_0^2 increases. To see the dependencies of the threshold power on T and γ_{th}, we have to evaluation of the integral (42.290). Fig. 42.55 shows a numerical evaluation of Eqs. (42.290),(42.291) and (42.292) for finite T and γ_{th}.

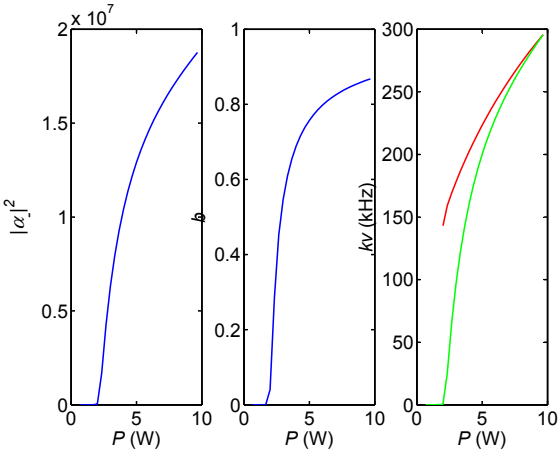

Figure 42.55: (code) Intracavity threshold power as a function of temperature and friction coefficient. The coupling strength is set to $\tilde{U}_0 = -10^{-7}$, the atom number is $N = 10^6$.

Apparently, the threshold pump power drops with vanishing friction and with low temperatures. For typical experimental situations, $T \approx 100$ μK and $\gamma_{th} \approx 10\kappa$, we expect threshold powers on the order of about $P_+ = 1$ W, corresponding to $P_+^{(out)} = 4$ μW leaking out of the cavity.

42.6.4 The Kuramoto model

Ripples on a dusty street driven by cars, rapids in a river arising spontaneously or behind an obstacle, wind blowing over a water surface spontaneously creating waves. Imagine a photon wind blowing over an atomic sea. Just like for water waves friction hinders boundless acceleration. The analogies are wind-molasses-friction, water-atoms, wind-acceleration-field, gravitation-dipole-force. The phenomenon is closely related to the *dissipative structure*. See also (watch talk) and (watch talk).

Our system has the advantage over macroscopic systems, that the hypothesis of uniform coupling is exactly satisfied, because the coupling medium, i.e. the light fields are delocalized within the cavity mode. In contrast, rapids develop exclusively behind the perturbation. There are no delay times effects and no spatial constraints due to a finite size of the individual oscillators.

The viscous CARL system is representative for of the vast class of *Kuramoto systems* [1272] introduced in Sec. ??. This can be seen most appropriately by rewriting the CARL equations in terms of phase and amplitude of individual atoms. Another approach is via the Fokker-Planck equation, for which there already exists a Kuramoto equivalence.

Why is it interesting to investigate yet another coupled oscillator system? Our

CARL is fully classical, although we deal with microscopic particle, such as atoms and photons. However, our system bears the possibility of being transferred to quantum situations, and thus to study the coupling of large ensembles of quantum oscillators. Furthermore, the coupling mechanism is well understood and controlable by experiment. Because the coupling goes through the standing wave fraction, it depends on the atom number and the coupling strength independently. Furthermore, the tunable friction force (temperature) corresponds to a variable width of the distribution of the oscillator frequencies, which we can manipulate in-situ and on-line.

Another realization of the Kuramoto model would be atoms in a ring cavity standing wave. Cold trapped atoms have the same oscillation frequencies. And thus do not need to synchronize. For hot atoms, however, the oscillation period depends on their kinetic energy.

The equation for the phases of the atoms is similar to the Kuramoto model [667],

$$\boxed{\dot{\theta}_n = \frac{K}{N}\sum_m \sin(\theta_n - \theta_m) - \xi_n(t)} \ . \tag{42.293}$$

The CARL equations which describes the dynamics of an ensemble of mean-field coupled oscillators, belong to the class of Kuramoto systems [666]. The main differences are: a Dirac-like distribution of eigenfrequencies and a mean-field self-consistently provided by a dynamical equation. Hence, in contrast to the original Kuramoto model, where the collective oscillation frequency is just the mean of the individual frequencies, the CARL frequency is self-determined and depends also on control parameters. This phenomenon is known from other systems like rhythmic applause, which only takes place by a reduction of the individual frequencies of clapping hands, towards a resonance. For this to happen the mean-field must self-adjust while the individual oscillators synchronize, e.g. the noise produce by the audience must adjust to the average desire of the audience to produce a satisfying level of noise.

In [1373] is stated: 'The essence of the problem is the competition between the intrinsic disorder (i.e. noise and diffusion) and the dynamical coupling strength. In the Kuramoto model, the disorder enters via the distribution of natural frequencies, while the effective coupling strength is set by the parameter combination $K\cos\alpha_j$.'

42.6.4.1 Phase formalism of CARL

The starting point is the CARL equations (42.50). We make ansatz,

$$\alpha_+ \equiv \alpha_1 \quad , \quad \alpha_- \equiv \alpha_2 \ e^{\imath\phi} \quad , \quad \eta_+ \equiv \eta_1 \quad , \quad \eta_- \equiv \eta_2 \ e^{\imath\Delta} \ , \tag{42.294}$$

where the quantities with numeric suffixes are real, such that,

$$|\alpha_+ + \alpha_-|^2 = \alpha_1^2 + \alpha_2^2 + 2\alpha_1\alpha_2 \ \cos\phi \ . \tag{42.295}$$

By this ansatz we assume that a pumping laser is locked to the mode α_+ of the ring cavity, such that the phases of the fields α_+ and η_+ are equal and, without loss of generality, zero. On the other hand, the phase ϕ of the probe mode is a dynamic

variable. Inserting the ansatz into the equations (42.50) we obtain,

$$\begin{aligned}
\dot{\alpha}_1 &= -(\kappa + \imath N U_0 - \imath\Delta_c)\alpha_1 - \imath U_0 \sum_n e^{-\imath\theta_n + \imath\phi}\alpha_2 + \eta_1 \ , \\
\dot{\alpha}_2 + \imath\dot{\phi}\alpha_2 &= -(\kappa + \imath N U_0 - \imath\Delta_c)\alpha_2 - \imath U_0 \sum_n e^{\imath\theta_n - \imath\phi}\alpha_1 + \eta_2 e^{\imath\Delta - \imath\phi} \ , \\
\ddot{\theta}_n &= 16\omega_{rec} U_0 \alpha_1 \alpha_2 \sin(\theta_n - \phi) \ .
\end{aligned} \tag{42.296}$$

The first two equations, which describe the dynamics of the fields, can be separated into real and imaginary parts,

$$\begin{aligned}
\dot{\alpha}_1 &= -\kappa\alpha_1 - U_0 \sum_n \sin(\theta_n - \phi)\alpha_2 + \eta_1 \\
\dot{\alpha}_2 &= -\kappa\alpha_2 + U_0 \sum_n \sin(\theta_n - \phi)\alpha_1 + \eta_2 \cos(\phi - \Delta) \ , \\
\Delta_c &= N U_0 \left(1 + N^{-1} \sum_n \cos(\theta_n - \phi)\frac{\alpha_2}{\alpha_1}\right) \ , \\
\dot{\phi} &= \Delta_c - N U_0 \left(1 + N^{-1} \sum_n \cos(\theta_n - \phi)\frac{\alpha_1}{\alpha_2}\right) - \frac{\eta_2}{\alpha_2}\sin(\phi - \Delta) \ .
\end{aligned} \tag{42.297}$$

Eliminating Δ_c, we can substitute the third and fourth equations for,

$$\dot{\phi} = U_0 \left(\frac{\alpha_2}{\alpha_1} - \frac{\alpha_1}{\alpha_2}\right) \sum_n \cos(\theta_n - \phi) - \frac{\eta_2}{\alpha_2}\sin(\phi - \Delta) \ . \tag{42.298}$$

Defining the 'bunching' parameter,

$$b \equiv |b| e^{\imath\psi} \equiv N^{-1} \sum_n e^{\imath\theta_n} \ , \tag{42.299}$$

we finally obtain, in the presence of friction and dissipation,

$$\boxed{\begin{aligned}
\dot{\alpha}_1 &= -\kappa\alpha_1 - N U_0 \alpha_2 |b| \sin(\psi - \phi) + \eta_1 \\
\dot{\alpha}_2 &= -\kappa\alpha_2 + N U_0 \alpha_1 |b| \sin(\psi - \phi) + \eta_2 \cos(\phi - \Delta) \\
\dot{\phi} &= N U_0 \left(\tfrac{\alpha_2}{\alpha_1} - \tfrac{\alpha_1}{\alpha_2}\right) |b| \cos(\psi - \phi) - \tfrac{\eta_2}{\alpha_2}\sin(\phi - \Delta) \\
\ddot{\theta}_n &= 16\omega_{rec} U_0 \alpha_1 \alpha_2 \sin(\theta_n - \phi) - \gamma_{frc}\dot{\theta}_n + \xi_n
\end{aligned}} \ . \tag{42.300}$$

A particularly interesting case is that of unidirectional pumping, $\eta_2 = 0$. Assuming that the pump mode be not affected,$\dot{\alpha}_1 = 0$, and that the probe mode be weak, $\alpha_1 \gg \alpha_2$, and making the adiabatic approximation, $\ddot{\theta}_n = 0$, of the atomic motion, we

obtain,

$$\boxed{\begin{aligned}\dot{\alpha}_2 &= -\kappa\alpha_2 + NU_0\alpha_1|b|\sin(\psi-\phi)\\ \dot{\phi} &\simeq -\frac{NU_0\alpha_1}{\alpha_2}|b|\cos(\psi-\phi)\\ \dot{\theta}_n &= \frac{\xi_n}{\gamma_{frc}} + \frac{16\omega_{rec}U_0\alpha_1\alpha_2}{\gamma_{frc}}\sin(\theta_n-\phi)\end{aligned}} \quad . \tag{42.301}$$

We note that the equation for the phases of the atoms is similar to the Kuramoto equation (42.293).

42.6.4.2 Relationship between CARL and Kuramoto

The viscous CARL described by the formulas (42.301) corresponds to the Kuramoto model [1272]. Defining $\theta_n \equiv 2kx_n$ as the position of the n^{th} atom, we assume the pump laser to be in resonance and write $\alpha_+ \equiv \eta_+/\kappa$ [755]. The diffusion in the momentum space is a process that limits the temperature in optical molasses.

We start from the Langevin equations (42.256). In addition, we assume that the standing wave propagates at a constant velocity, which is to say that for a strong viscous damping, the system quickly finds a steady state. This condition is formulated by $d_t|\alpha_-| = 0$ and $\dot{\alpha}_- = i\omega_{ca}\alpha_-$ with constant velocity ω_{ca}, which may be different from the velocity of the center of mass kv. We note that this assumption can introduce a considerable error, when used to describe temporal phase transitions, since, as shown by simulations of the complete dynamics (42.260), the mode α_- exhibits a transient behavior, as well. We obtain from the first Eq. (42.256),

$$\alpha_- = -\frac{\imath U_0\alpha_+}{\imath\omega_{ca}+\kappa}\sum_m e^{\imath\theta_m} \ . \tag{42.302}$$

Substituting Eq. (42.302) into the second equation (42.256),

$$\begin{aligned}\dot{\theta}_n &= \frac{\xi_n}{\gamma_{fr}} + \frac{8\omega_{rec}NU_0^2\alpha_+^2}{\gamma_{fr}}\frac{1}{N}\sum_m\left(\frac{e^{\imath\theta_m-\imath\theta_n}}{\imath\omega_{ca}+\kappa} + \frac{e^{-\imath\theta_m+\imath\theta_n}}{-\imath\omega_{ca}+\kappa}\right) \qquad (42.303)\\ &= \frac{\xi_n}{\gamma_{fr}} + \frac{16\omega_{rec}NU_0^2\alpha_+^2}{\gamma_{fr}(\omega_{ca}^2+\kappa^2)}\frac{1}{N}\sum_m\left[\kappa\cos(\theta_m-\theta_n)+\omega_{ca}\sin(\theta_m-\theta_n)\right] \ .\end{aligned}$$

Defining the *order parameter*,

$$b \equiv |b|e^{\imath\psi} \equiv \frac{1}{N}\sum_m e^{\imath\theta_m} \ , \tag{42.304}$$

which also implies,

$$|b|\sin(\psi-\theta_n) = \frac{1}{N}\sum_m \sin(\theta_m-\theta_n) \ , \tag{42.305}$$

we can write Eq. (42.305) as,

$$\dot{\theta}_n = \frac{\xi_n}{\gamma_{fr}} + \frac{8\varepsilon NU_0^2\alpha_+^2\kappa}{\gamma_{fr}(\omega_{ca}^2+\kappa^2)}|b|\left[\cos(\psi-\theta_n) + \frac{\omega_{ca}}{\kappa}\sin(\psi-\theta_n)\right] \ . \tag{42.306}$$

In the 'good cavity' limit, $\kappa \ll \omega$, using $(2kv)^3 = 8\varepsilon N U_0^2 \alpha_+^2 \kappa/\gamma_{fr}$ and additionally assuming small amplitude oscillations, $\psi \approx \theta_n$, that is, good 'bunching',

$$\dot{\theta}_n \approx \frac{\xi_n}{\gamma_{fr}} + \frac{(2kv)^3}{\omega_{ca}^2}|b| + \frac{(2kv)^3}{\kappa\omega_{ca}}|b|\sin(\psi - \theta_n) \; . \tag{42.307}$$

This shows that in the limit of perfect 'bunching' $\omega_{ca} = 2kv$ must be satisfied. If really $\kappa \ll \omega$ is valid, we can despise the cosine. Introducing the Kuramoto coupling constant,

$$K \equiv \frac{16\omega_{rec} N U_0^2 \alpha_+^2 \omega_{ca}}{\gamma_{fr}(\omega_{ca}^2 + \kappa^2)} \approx \frac{1}{\kappa}\left(\frac{16\omega_{rec} N U_0^2 \alpha_+^2 \kappa}{\gamma_{fr}}\right)^{2/3} = (4\omega_{rec}\rho)^2 \left(\frac{4}{\kappa\gamma_{fr}^2}\right)^{1/3} , \tag{42.308}$$

using $2\varepsilon\rho = (4\varepsilon N U_0^2 \alpha_+^2)^{1/3}$, Eq. (42.306) is precisely the one used by the *Kuramoto model* of N coupled harmonic oscillators synchronizing over time,

$$\boxed{\dot{\theta}_n \approx \frac{\xi_n}{\gamma_{fr}} + \frac{\kappa K}{\omega_{ca}}|b| + K|b|\sin(\psi - \theta_n)} \; . \tag{42.309}$$

Oscillators with $\omega_n \leq K|b|$ are locked. For a reasonable 'bunching' this is satisfied in the 'good cavity' limit.

42.6.4.3 Kuramoto model with inertial effects

It is possible to incorporate inertial effects into the Kuramoto model [3]: allowing for $\ddot{\theta}_n \neq 0$, but still assuming $d_t|\alpha_-| = 0$ and $\dot{\alpha}_- = i\omega\alpha_-$, the equation (42.303) becomes,

$$\ddot{\theta}_n = -\gamma_{fr}\dot{\theta}_n + \xi_n + \frac{16\omega_{rec} N U_0^2 \alpha_+^2}{\omega^2 + \kappa^2}\frac{1}{N}\sum_m \left[\kappa\cos(\theta_m - \theta_n) + \omega\sin(\theta_m - \theta_n)\right] \tag{42.310}$$

$$= -\gamma_{fr}\dot{\theta}_n + \xi_n + \frac{\kappa}{\omega}K|b|\cos(\psi - \theta_n) + K|b|\sin(\psi - \theta_n) \; .$$

42.6.4.4 Fokker-Planck equation

Let us write the *Kuramoto equation* including stochastic noise,

$$\dot{\theta}_n = \omega + K|b|\sin(\psi - \theta_n) + \xi_n(t) \; , \tag{42.311}$$

define the order parameter,

$$b = |b|e^{\imath\psi} \; , \tag{42.312}$$

and the Langevin-force $\langle\xi_n(t)\rangle = 0$ and $\langle\xi_n(t)\xi_m(\tau)\rangle = 2D\delta_{ij}\delta(t-\tau)$.

The Fokker-Planck equation associated to Eq. (42.311) reads,

$$\frac{\partial\rho}{\partial t} = -\frac{\partial\rho\;\left[\omega + K|b|\sin(\psi - \theta)\right]}{\partial\theta} + D\frac{\partial^2\rho}{\partial\theta^2} \; , \tag{42.313}$$

where $D = \sigma^2/\gamma_{fr}$. Inserting $\rho(\theta, t) \equiv \sum_\nu \rho_\nu(t)e^{\imath\nu\theta}$,

$$\frac{\partial\rho_\nu}{\partial t} = -(\nu^2 D + \imath\nu\omega)\rho_\nu + \tfrac{1}{2}\nu K\left(b^*\rho_{\nu-1} - b\rho_{\nu+1}\right) \; , \tag{42.314}$$

especially,

$$\int_0^{2\pi} \rho(\theta,t)d\theta = 1 \qquad \Longrightarrow \qquad \rho_0 = \tfrac{1}{2\pi} \ , \tag{42.315}$$

and we defined the bunching as $|b|$, where,

$$b \equiv \int_0^{2\pi} \rho(\theta,t)e^{-i\theta}d\theta \qquad \Longrightarrow \qquad b \equiv 2\pi\rho_1 \ . \tag{42.316}$$

42.6.4.5 Laser-type equation for CARL

Defining the displacement of the n^{th} atomic oscillator as,

$$E_n \equiv e^{\imath\theta_n} \ , \tag{42.317}$$

we can rewrite the second equation (42.256) as,

$$\dot{E}_n = \frac{\imath\xi_n}{\gamma_{fr}}E_n - \frac{8\omega_{rec}U_0\alpha_+}{\gamma_{fr}}(\alpha_- - \alpha_-^* E_n^2) \ . \tag{42.318}$$

Substituting α_- by the integral of the first equation (42.256),

$$\dot{E}_n = \frac{\imath\xi_n}{\gamma_{fr}}E_n + \frac{8\omega_{rec}\imath NU_0^2\alpha_+^2}{\gamma_{fr}}\left(\int be^{-\kappa(t-t')}dt' + E_n^2\int b^* e^{-\kappa(t-t')}dt'\right) \ . \tag{42.319}$$

In the limit $e^{-\kappa(t-t')} = \kappa^{-1}\delta(t-t')$ we obtain an equation similar to that of an ordinary laser,

$$\begin{aligned}\dot{E}_n &= \frac{\imath\xi_n}{\gamma_{fr}}E_n + \frac{8\omega_{rec}\imath NU_0^2\alpha_+^2}{\gamma_{fr}\kappa}(b + b^* E_n^2) \\ &= \frac{\imath\xi_n}{\gamma_{fr}}E_n + \frac{8\omega_{rec}\imath NU_0^2\alpha_+^2}{\gamma_{fr}\kappa}\left(\sum_m E_m + \sum_m E_m^* E_n^2\right) \ .\end{aligned} \tag{42.320}$$

42.6.5 Thermodynamics of the CARL process

There is an analogy between the laser threshold and a second-order phase transition [1184], p. 341 *ff*: '... The usual treatment of laser behavior is a self-consistent field theory. In the laser analysis each atom develops a radiating dipole in an electromagnetic field due to (i.e. emitted by) all the other atoms. The radiation field produced by an ensemble of radiating atoms is then calculated in a self-consistent fashion. (...This) suggests the identification of the laser electric field as the variable corresponding to the (...) order parameter and the atomic population inversion as that corresponding to the temperature.'

Note that numerical simulations revealed that in certain regimes the CARL corresponds to a first-order phase transition: At high temperatures the probe to pump power diagram shows bistability [665] and [1104].

The correspondence between CARL and a common laser is illustrated by the table below. A number of questions arise from the analogy:

The CARL being a laser without inversion, what is the equilibrium parameter? Is it the temperature of the atomic cloud? How to calculate the density of states?

	ferromagnet	laser
control parameter	external magnetic field H	pump intensity $\mathcal{S}$
equilibrium parameter	temperature T	population inversion σ
order parameter	magnetization $\langle M\rangle = \begin{cases} 0 & T > T_c \\ c\sqrt{\frac{T_c - T}{T}} & T < T_c \end{cases}$	electric field $\langle E\rangle = \begin{cases} 0 & \sigma > \sigma_c \\ c\sqrt{\frac{\sigma_c - \sigma}{\sigma}} & \sigma < \sigma_c \end{cases}$
probability density	$P(M) \propto e^{-F(M)/k_B T}$	P-representation $P(x,y) \propto e^{-G(x,y)/K\sigma}$
thermodyn. free energy	$F = F(T,H)$	$G(x,y)$
heat capacity	$C(T) = \frac{\partial E(T)}{\partial T}$	?

	CARL atoms	CARL light
control parameter	pump intensity η	pump intensity η
equilibrium parameter	temperature T	?
order parameter	bunching $b = \begin{cases} 0 & T > T_c \\ ? & T < T_c \end{cases}$	electric field $\langle\alpha\rangle = \begin{cases} 0 \\ ? \end{cases}$
probability density	?	?
thermody. free energy	?	?
heat capacity	?	?

42.6.6 CARL as a laser

Why is CARL a laser? What is the basic difference between CARL and an AOM or a moving Bragg mirror? CARL is essentially based on exponential self-amplification. This self-amplification is in fact observed in our switch-off experiment [755]. But a laser is normally understood as a steady-state system. For CARL to find to a steady-state we have to insert friction forces.

Gordon rewrites the CARL as a common laser: He generalizes the linear stability analysis (previous Sec.) and retains the lowest-order nonlinearity. The Fokker-Planck equations read:

$$\begin{aligned} \frac{dB_n}{d\tau} &= \imath n(aB_{n-1} + a^* B_{n+1}) - n^2 D B_n \\ \frac{da}{d\tau} &= B_1 - \kappa a \ , \end{aligned} \tag{42.321}$$

with $B_0 = 1$ and $B_{-n} = B_n^*$. Linearization means $B_{n>1} = 0$,

$$\begin{aligned} \frac{dB_1}{d\tau} &= \imath a - D B_1 \\ \frac{da}{d\tau} &= B_1 - \kappa a \end{aligned} \tag{42.322}$$

or,

$$\frac{d^2a}{d\tau^2} + (\kappa + D)\frac{da}{d\tau} + (\kappa D - \imath)a = 0 \tag{42.323}$$
$$\frac{d^2B_1}{d\tau^2} + (\kappa + D)\frac{dB_1}{d\tau} + (\kappa D - \imath)B_1 = 0$$

The determinant is,

$$\det\begin{pmatrix} -D-\lambda & \imath \\ 1 & -\kappa-\lambda \end{pmatrix} = (D+\lambda)(\kappa+\lambda) - \imath = 0 \tag{42.324}$$

Including the lowest-order nonlinear term means $B_{n>2} = 0$,

$$\frac{dB_2}{d\tau} = 2\imath a B_1 - 4DB_2 \tag{42.325}$$
$$\frac{dB_1}{d\tau} = \imath a + \imath a^* B_2 - DB_1$$
$$\frac{da}{d\tau} = B_1 - \kappa a$$

Assuming $dB_2/d\tau = 0$,

$$\frac{dB_1}{d\tau} = \imath a - \left(\frac{|a|^2}{2D} + D\right) B_1 \tag{42.326}$$
$$\frac{da}{d\tau} = B_1 - \kappa a$$

or,

$$\frac{d^2B_1}{d\tau^2} + (\kappa + D)\frac{dB_1}{d\tau} + (\kappa D - \imath)B_1 = -\frac{1}{2D}\left(\frac{d}{d\tau} + \kappa\right)|a|^2 B_1 \tag{42.327}$$
$$= -(K_1|a|^2 - K_2|a|^4)B_1$$
$$\frac{d^2a}{d\tau^2} + (\kappa + D)\frac{da}{d\tau} + (\kappa D - i)a = -\frac{|a|^2}{2D}\left(\frac{d}{d\tau} + \kappa\right)a$$

substitute $a(\tau) = A(\tau)e^{\lambda\tau}$ and Eq. (xx),

$$e^{\lambda\tau}\left(\frac{d^2}{d\tau^2} + 2\lambda\frac{d}{d\tau} + \lambda^2\right)A + e^{\lambda\tau}\left((\kappa + D)\frac{d}{d\tau} + (\kappa + D)\lambda\right)A - (\lambda^2 + D\lambda + \kappa\lambda)e^{\lambda\tau}A \tag{42.328}$$
$$= -\frac{|e^{\lambda\tau}A|^2}{2D}\left(e^{\lambda\tau}\frac{dA}{d\tau} + \lambda e^{\lambda\tau}A + \kappa e^{\lambda\tau}A\right)$$

neglect $d^2A/d\tau^2$and $|A|^2 dA/d\tau$,

$$e^{\lambda\tau}2\lambda\frac{dA}{d\tau} + e^{\lambda\tau}(\kappa + D)\frac{dA}{d\tau} = -\frac{|e^{\lambda\tau}A|^2}{2D}\left(\lambda e^{\lambda\tau}A + \kappa e^{\lambda\tau}A\right) \tag{42.329}$$

substitute back $a(\tau) = A(\tau)e^{\lambda\tau}$,

$$\begin{aligned}\frac{da}{d\tau} &= \lambda a - \frac{\lambda+\kappa}{2D(2\lambda+\kappa+D)}|a|^2 a \\ &= \lambda a - C|a|^2 a\end{aligned} \tag{42.330}$$

or,

$$\frac{d|a|^2}{d\tau} = 2|a|^2 \mathfrak{Re}\ \lambda - 2|a|^4 \mathfrak{Re}\ C \tag{42.331}$$

in steady-state,

$$0 = \lambda a - C|a|^2 a\ . \tag{42.332}$$

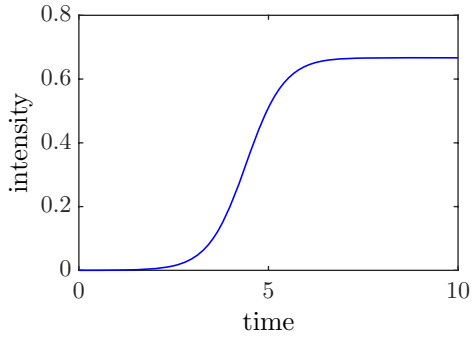

Figure 42.56: (code) Laser crossing the threshold.

According to A. Politi a general laser theory exists, there is no point in repeating this for CARL. The analogy is there and evident.

42.6.6.1 CARL as a ferromagnet

A similar treatment with $a(\tau) = A(\tau)e^{\lambda\tau}$ and $B_1(\tau) = \beta(\tau)e^{\lambda\tau}$ and $d^2\beta/d\tau^2 = 0$ and $|A|^2 d\beta/d\tau = 0$ and $\beta d|A|^2/d\tau = 0$ results in,

$$\begin{aligned}\frac{dB_1}{d\tau} &= \lambda B_1 - \frac{2\lambda+\lambda^*+\kappa}{2D(2\lambda+\kappa+D)}|a|^2 B_1 \\ &= \lambda B_1 - \tilde{C}|a|^2 B_1\ ,\end{aligned} \tag{42.333}$$

i.e. the instability comes from the field and it drives the bunching.

42.6.6.2 Out-of-equilibrium thermodynamics

Strictly speaking the above analogy is flawed. In particular the analogy between CARL bunching and ferromagnetic ordering is not good. While the ferromagnetic ordering occurs as a thermodynamic phase transition, the CARL bunching is driven by a dissipative force, which triggers spatio-temporal instabilities. Therefore viscous

CARL occurs far from thermodynamic equilibrium. This may point towards an interpretation of CARL bunching as a *dissipative structure* along the lines traced by Prigogine, who showed that *non-equilibrium may be a source of order*.

On the other hand, the laser itself is a system operating far from thermal equilibrium, since it requires a pump to emit steady-state radiation. Perhaps a comparison with *estruturas de Bénard* is better than with ferromagnets. Bénard structures occur as spontaneous breaking of translational symmetry, just like CARL. One could say that the periodicity of CARL is predefined by the pump laser wavelength, and thus not surprising. However, the size of the periodic structures is always fixed by boundary conditions in a more or less complicated way. For example, the size of the Bénard structures is fixed by the viscosity, the provided amount of heat, etc., the wavelength of surface waves can be calculated from first principles, i.e. the Navier-Stokes equations and the continuity equation for given boundary conditions. The symmetry breaking resides in the exact *place*, where the Bénard structure develops. It is the *phase*, which is broken, just like for CARL.

The Kuramoto model and the Weiss model of ferromagnetism are both mean field theories [1200]. Despite the fundamental difference that ferromagnetism is a thermodynamic feature and Kuramoto a nonequilibrium phenomenon, they are far-reaching analogies. The role of temperature in ferromagnetism is played by external noise in Kuramoto. CARL is clearly a dissipative structure: *It survives only as long as energy is fed to the system.*

42.6.6.3 Finite and infinite temperature reservoirs

The phase transition is ruled by a competition of dissipation and diffusion. If the reservoir has zero temperature $\gamma_{fric} \neq 0$ but $D = \sigma^2/\gamma_{fric} = 0$, i.e. we have dissipation without diffusion. In this case, we do not expect a threshold behavior. The Lindtbladt operator for coupling to a finite-temperature reservoir is something like $\mathcal{L} \approx \kappa(\bar{n}+1)\{...emission...\} + \kappa\bar{n}\{...absorption...\} + \eta\{...phase\ noise...\}$, where $\bar{n}$ is the mean photon number at thermal equilibrium with a given temperature $T \propto \bar{n}/(\bar{n}+1)$. The interpretation in terms of dissipation without diffusion is correct according to A. Buchleitner. There are three kinds of noises: 0 temperature noise for $\bar{n} \to 0$, ∞ temperature noise for $\bar{n} \approx \bar{n}+1$ and phase noise. Thus for $T = 0$ the energy flux goes only from the system to the reservoir. At $T > 0$ entropy may go from the reservoir to the system. The system reaches its cooling limit when the temperatures of the system and the reservoir are balanced.

But how to explain Doppler cooling or cavity-cooling? The electromagnetic vacuum is an effective $T = 0$ reservoir, but the cooling is nevertheless limited by the spontaneous decay width or the cavity linewidth, resp.. Why does coupling to a zero-temperature reservoir not cool down to zero? Apparently, the coupling is afflicted by vacuum noise. This permits coupling of degrees of freedom having different temperatures without reaching a temperature equilibrium. Examples are the limit of cavity-cooling to the cavity decay width or simply Doppler-cooling by spontaneous emission.

Interprete damping as scattering into continuum!

42.6.7 Exercises

42.6.7.1 Ex: Viscous CARL

Assuming a perfect 'bunching', $e^{2\imath kz_m} = e^{2\imath kz}$, e $\alpha_- \equiv \beta e^{2\imath kz}$ with $\dot{\beta} = 0$ and $\ddot{z} = 0$ derive the equations (42.245).

Solution: *Defining $\alpha_- \equiv \beta e^{2\imath kz}$ we transform the equation (42.244)(i) in,*

$$\dot{\beta} + 2\imath k\beta\dot{z} = -\kappa\beta - \imath N U_0 \alpha_+ \ .$$

Assuming $\dot{\beta} = 0$ the solution is,

$$\beta = \frac{-\imath U_0 \alpha_+}{\kappa + 2\imath k\dot{z}} \ .$$

The equation (42.244)(ii) gives,

$$k\ddot{z} = 4\imath\omega_{rec} U_0 \alpha_+ (\beta - \beta^*) - \gamma_{frc} k v = 4\imath\omega_{rec} U_0 \alpha_+ \left(\frac{-\imath U_0 \alpha_+}{\kappa + 2\imath k\dot{z}} - \frac{\imath U_0 \alpha_+}{\kappa - 2\imath k\dot{z}} \right) - \gamma_{frc} k\dot{z}$$

$$= \frac{8\kappa\omega_{rec} U_0^2 \alpha_+^2}{\kappa^2 + (2k\dot{z})^2} - \gamma_{frc} k\dot{z} \ .$$

Assuming $\ddot{z} = 0$ the solution is,

$$2k\dot{z}[(2k\dot{z})^2 + \kappa^2] = \frac{16\kappa\omega_{rec} U_0^2 \alpha_+^2}{\gamma_{frc}} \overset{2k\dot{z} \gg \kappa}{\longrightarrow} (2k\dot{z})^3 \ .$$

42.6.7.2 Ex: Langevin simulations

Langevin simulations

Solution: *Test of Runge-Kutta method (see program Langevin_OrnsteinUhlenbeckTest),*
Langevin simulation without adiabatic approximation (see program Langevin_CorrelationFunction),
like 'CorrelationFunction' but with an additional harmonic trap (see program Langevin_HarmonicTra
like 'CorrelationFunction' but with an additional standing wave (see program Langevin_StandingWav
without adiabatic approximation one species in a standing wave (see program Langevin_1SpeciesStand
without adiabatic approximation two species in a standing wave (see program Langevin_2SpeciesStand

42.6.7.3 Ex: Fokker-Planck equations

Derive the equations (42.275) and (42.276) from (42.273) and (42.271) applying the expansion (42.274).

Solution: *For the normalization we calculate,*

$$1 = \int_0^{2\pi} Q(\theta, t) d\theta = \sum_\nu Q_\nu(t) \int_0^{2\pi} e^{\imath\nu\theta} d\theta = \sum_\nu Q_\nu(t) 2\pi\delta_{\nu 0} = 2\pi Q_0(t) \ .$$

For the 'bunching' we calculate,

$$b = \int_0^{2\pi} Q(\theta,t)e^{-\imath\theta}d\theta = \sum_\nu Q_\nu(t)\int_0^{2\pi} e^{\imath(\nu-1)\theta}d\theta = \sum_\nu Q_\nu(t)2\pi\delta_{\nu 1} = 2\pi Q_1(t) \ .$$

For the CARL equation,

$$\sum_\nu \frac{\partial Q}{\partial t}e^{\imath\nu\theta}$$
$$= \frac{8\imath\omega_{rec}U_0\alpha_+}{\gamma_{frc}}\sum_\nu Q_\nu\left(-\imath(\nu-1)\alpha_- e^{\imath(\nu-1)\theta} - \imath(\nu+1)\alpha_-^* e^{\imath(\nu+1)\theta}\right) - \nu^2 D_\theta \sum_\nu Q_\nu e^{\imath\nu\theta} \ ,$$

and hence,

$$\frac{\partial Q}{\partial t} = \frac{8\omega_{rec}U_0\alpha_+}{\gamma_{frc}}\nu\left(Q_{\nu+1}\alpha_- + Q_{\nu-1}\alpha_-^*\right) - \nu^2 D_\theta Q_\nu \ .$$

42.6.7.4 Ex: Kuramoto simulations

Implement the Kuramoto model with pendulum clocks.

Solution: *Visualization of the Kuramoto model with pendulum clocks (see FokkerKuram_Illustration, FokkerKuram_Dissipation, FokkerKuram_Shiino).*

42.7 Coherent properties of CARL

In Sec. 42.6.1 we have demonstrated collective interaction of atoms with light fields and how the application of friction via optical molasses can lead to stationary CARL radiation at a self-determined frequency [754]. We have demonstrated that the molasses also lead to diffusion resulting in a threshold behavior and in atomic self-organization at finite temperatures [1106, 1343]. An interesting question is whether the temperature not only determines the collective behavior, but also the deviation from it. The temperature being related to the amount of random walk on top of the center-of-mass motion, we may wonder whether the viscous CARL radiation bears a signature of the atomic temperature not only in the self-determined CARL frequency, but also in the laser emission bandwidth. It is conceivable that the autocorrelation functions and the emission spectrum of the CARL are influenced by the fact that the atoms experience a random walk in momentum space due to the diffusion in the optical molasses.

In this section, we will attempt an analytical approach, present numerical simulations and discuss how to access to the informations experimentally. The Fokker-Planck approach described in Refs. [1106, 1343] is particularly well adapted to calculating collective variables. In contrast the simulation of the Langevin equation conveniently gives access to the noise properties.

42.7.1 Analytical derivation of the coherence

Our starting point are the Langevin equations (42.256) [1106, 1343] in the adiabatic limit, $\ddot{\theta}_n = 0$. The Langevin noise force is uncorrelated,

$$\langle \xi_n^*(t)\xi_m(t+\tau)\rangle \equiv \lim_{T\to\infty}\frac{1}{T}\int_0^T \xi_n^*(t)\xi_m(t+\tau)d\tau = 2D_{\dot\theta}\delta_{mn}\delta(\tau)\ , \tag{42.334}$$

where the momentum diffusion coefficient $D_{\dot\theta} = \gamma_{fr}\sigma^2$ is proportional to the atoms' equilibrium temperature, which is related to the Maxwell-Gaussian velocity spread by $\sigma \equiv 2k\sqrt{k_BT/m}$. In contrast, the trajectories of the atoms are not, because all atoms are motionally coupled by the fields, so that the noise imparted to one atom is sensed by all others. Therefore the relationship (42.335) certainly does not hold for the atomic positions,

$$\langle \theta_n^*(t)\theta_m(t+\tau)\rangle \nsim \delta_{mn}\delta(\tau)\ . \tag{42.335}$$

42.7.1.1 Single atom

So, let us first concentrate on a single atom coupled to the cavity fields. If its velocity only fluctuates a little around a mean value ω_{ca}, we may write $\theta(t) \equiv \omega_{ca}t+\varphi(t)$. The randomized position has a Gaussian statistics leading to a Brownian motion described by a Wiener-Levy stochastic process: $\langle\varphi(t)\rangle = 0$ and $\langle\varphi(t)\varphi(t+\tau)\rangle = D_\theta(2t+\tau-|\tau|)$ ([1184], p. 344),

$$R_{\dot\theta}(\tau) = \langle[\omega_{ca}+\dot\varphi(t)][\omega_{ca}+\dot\varphi(t+\tau)]\rangle = \langle\dot\varphi(t)\dot\varphi(t+\tau)\rangle = 2D_\theta\delta(\tau)\ , \tag{42.336}$$

where $D_\theta = \sigma^2/\gamma_{fr}$ is the position diffusion coefficient. Note that deterministic parts are removed from the function in order to satisfy $\langle\dot\varphi(t)\rangle = 0$. In that case the *spectral density of fluctuations of the atomic phase* is constant,

$$S_{\dot\theta}(f) = \int_{-\infty}^{\infty} R_{\dot\theta}(\tau)e^{-2\pi\imath f\tau}d\tau = 2D_\theta\ . \tag{42.337}$$

Note that $S_{\dot\theta}(f) = f^2S_\theta(f)$. The *variance of the fluctuations* for white noise is or,

$$\sigma_{\dot\theta}^2(\tau) = \langle\dot\varphi(t)^2\rangle = \frac{D_\theta}{\tau}\ . \tag{42.338}$$

Under the assumption $\dot\alpha_- = \imath\omega_{ca}\alpha_-$ and introducing the abbreviation $\alpha_0 \equiv -\imath U_0\alpha_+/(\kappa+\imath\omega_{ca})$, the first equation (42.256) takes the form $\alpha_- = \alpha_0 e^{\imath\theta}$ such that the *autocorrelation function of the field amplitude* reads,

$$\begin{aligned} R_\alpha(\tau) &\equiv \langle\alpha_-^*(t)\alpha_-(t+\tau)\rangle \\ &= |\alpha_0|^2\langle e^{\imath[\theta(t+\tau)-\theta(t)]}\rangle \\ &= |\alpha_0|^2e^{\imath\omega_{ca}\tau}\langle e^{\imath[\varphi(t+\tau)-\varphi(t)]}\rangle = |\alpha_0|^2e^{\imath\omega_{ca}\tau}\langle e^{\imath\tau\dot\varphi(t)}\rangle\ . \end{aligned} \tag{42.339}$$

In the case of a Gaussian distribution for the noise amplitude with $\dot\varphi(t) = \dot\varphi(-t)$, we

have $\langle\dot\varphi^{2k-1}\rangle/(2k-1)!=0$ and $\langle\dot\varphi^{2k}\rangle/\,(2k)!=\langle\frac{1}{2}\dot\varphi^2\rangle^k/k!$ [326, **?**, 414],

$$\begin{aligned}\langle e^{\imath\tau\dot\varphi(t)}\rangle &= \sum_k \frac{\imath^k\langle\tau^k\dot\varphi(t)^k\rangle}{k!} = \sum_k \frac{\imath^{2k}\langle\tau^{2k}\dot\varphi(t)^{2k}\rangle}{(2k)!} \\ &= \sum_k \frac{\langle-\frac{1}{2}\tau^2\dot\varphi(t)^2\rangle^k}{k!} = e^{-\frac{1}{2}\tau^2\langle\dot\varphi(t)^2\rangle}\ .\end{aligned} \tag{42.340}$$

Apparently, noise mainly affects the field's phase and not its amplitude. Note that the *first-order coherence* is just the normalized autocorrelation $g^{(1)}(\tau)\equiv R_\alpha(\tau)/R_\alpha(0)$,

$$\begin{aligned}g^{(1)}(\tau) &= e^{\imath\omega_{ca}\tau}e^{-\omega_{ca}^2\tau^2\sigma_v^2/2} \\ &= e^{\imath\omega_{ca}\tau}e^{-D_\theta|\tau|/2}\ .\end{aligned} \tag{42.341}$$

The *power spectral density* is a Lorentzian,

$$\begin{aligned}S_\alpha(\omega) &= |\alpha_0|^2\int_{-\infty}^{\infty}R_\alpha(\tau)e^{-\imath\omega\tau}d\tau \\ &= \frac{|\alpha_0|^2D_\theta^2}{(\omega-\omega_{ca})^2+D_\theta^2}\ .\end{aligned} \tag{42.342}$$

The CARL *emission bandwidth* is thus $\frac{1}{2}D_\theta$. The above results show that the CARL laser bandwidth increases linearly with temperature and reduces with the friction force. In our experiment we have $\gamma_{fr}=5\kappa$ and $\sigma=10\kappa$, so that $D_\theta=\sigma^2/\gamma_{fr}=20\kappa$. The CARL bandwidth is extremely large as compared to the CARL frequency $\omega_{ca}=5\kappa$. The reason is that we only considered a single atom. The impact of several atoms will partially compensate and reduce the linewidth.

42.7.1.2 Many atoms, hand-waving

In order to account for the combined effect of many atoms, we reconsider the Eq. (42.256). If $\dot\alpha_-=\imath\omega_{ca}\alpha_-$, we may write it like,

$$\begin{aligned}\alpha_- &= \alpha_0\sum_m e^{\imath\theta_m}\ , \\ \dot{\theta_n} &= \frac{4\varepsilon\imath U_0\alpha_+\alpha_0}{\gamma_{fr}}\sum_m\left(e^{\imath\theta_m-\imath\theta_n}+e^{-\imath\theta_m+\imath\theta_n}\right)+\frac{\xi_n}{\gamma_{fr}}\ .\end{aligned} \tag{42.343}$$

The light mode α_- appears to be a superposition of coherent waves having the same frequencies, $\alpha_m(t)=\alpha_0e^{i\omega_{ca}t+i\varphi_m(t)}$, but interrupted by random phase jumps. We may thus try an analogous argumentation as for pressure broadening,

$$\begin{aligned}\langle\alpha_-^*(t)\alpha_-(t+\tau)\rangle &= |\alpha_0|^2\int\sum_n e^{-\imath\omega_{ca}t-\imath\varphi_n(t)}\sum_m e^{\imath\omega_{ca}t+\imath\omega_{ca}\tau+\imath\varphi_n(t+\tau)}dt \\ &= |\alpha_0|^2e^{\imath\omega_{ca}\tau}\sum_{n,m}\int e^{\imath\varphi_m(t+\tau)-\imath\varphi_n(t)}dt = N\langle\alpha_n^*(t)\alpha_m(t+\tau)\rangle\delta_{nm}\ .\end{aligned}$$

Cross-terms vanish, the autocorrelation function is just the sum of the single-atom components. However, while we may view the noise impact of the atoms as coming

from a single atom, the rate of the phase jumps is much higher, than for a single atom. For one atom the probability density for encountering a coherent interval of length τ is given by $p_1(\tau)d\tau = \frac{1}{2}D_\theta e^{-D_\theta|\tau|/2}d\tau$ [816]. Thus,

$$\langle\alpha_1^*(t)\alpha_1(t+\tau)\rangle = |\alpha_0|^2 e^{\imath\omega_{ca}\tau}e^{-D_\theta|\tau|/2} = |\alpha_0|^2 e^{\imath\omega_{ca}\tau}\int_\tau^\infty p_1(\tau')d\tau' \ . \tag{42.344}$$

For N atoms we expect a probability density for encountering a coherent intervall of length τ,

$$p_N(\tau)d\tau = p_1(\tau/N)d\tau = \frac{D_\theta}{2\sqrt{N}}e^{-D_\theta|\tau|/2\sqrt{N}}d\tau \ , \tag{42.345}$$

such that $\int_0^\infty p_N(\tau')d\tau' = 1$. However this remains to prove. Thus,

$$g_N^{(1)}(\tau) = e^{\imath\omega_{ca}\tau}\int_\tau^\infty p_N(\tau')d\tau' = e^{\imath\omega_{ca}\tau - D_\theta|\tau|/2\sqrt{N}} \ . \tag{42.346}$$

The second-order correlation function is,

$$g_N^{(2)}(\tau) = 1 + |g_N^{(1)}(\tau)|^2 \ . \tag{42.347}$$

The laser bandwidth is accordingly reduced by,

$$D_N = \frac{D_\theta}{\sqrt{N}} \ . \tag{42.348}$$

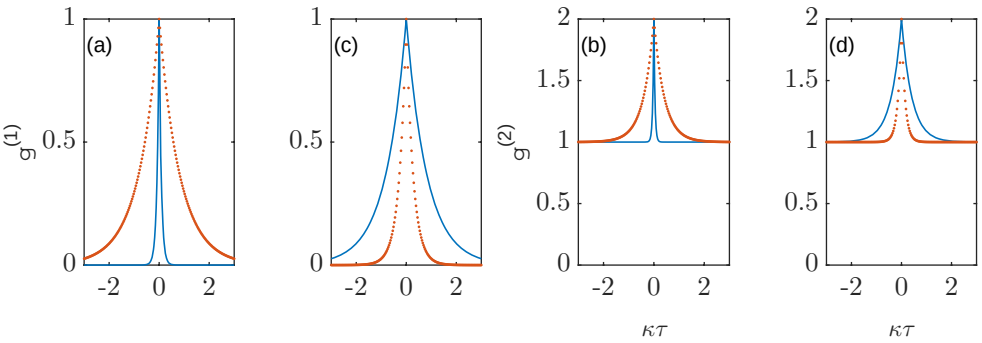

Figure 42.57: (code) First and second-order correlation functions. The solid and dotted lines in (a) and (b) are calculated for $N = 1$ and $N = 100$, resp.. The solid and dotted lines in (c) and (d) are calculated for $T = 100\,\mu\text{K}$ and $T = 300\,\mu\text{K}$, resp..

Fig. 42.57 shows the dependencies of the correlation functions on N and T. For $N = 10^6$ atoms the CARL bandwidth becomes $\beta_N = 0.01\kappa$, which is already well below any mechanical noise. The linewidth reduction with increasing atom numbers is quantitatively supported by numerical simulations (see below).

42.7.1.3 Many atoms, formal

In order to account for the combined effect of many atoms, we reconsider the Eq. (42.256). If $\dot{\alpha}_- = \imath\omega_{ca}\alpha_-$, we get,

$$\alpha_- = -\frac{\imath U_0 \alpha_+}{\kappa + \imath\omega_{ca}} \sum_m e^{\imath\theta_m} \ , \tag{42.349}$$
$$\dot{\theta_n} = \frac{4\varepsilon U_0^2 \alpha_+^2}{\gamma_{fr}\left(\kappa + \imath\omega_{ca}\right)} \sum\nolimits_m \left(e^{\imath\theta_m - \imath\theta_n} + e^{-\imath\theta_m + \imath\theta_n}\right) + \frac{\xi_n}{\gamma_{fr}} \ .$$

The autocorrelation is then,

$$R_\alpha(\tau) \equiv \langle \alpha_-^*(t)\alpha_-(t+\tau)\rangle = \frac{U_0^2\alpha_+^2}{\kappa^2+\omega_{ca}^2} \sum_{n,m} \langle e^{\imath\theta_n(t+\tau)-\imath\theta_m(t)}\rangle \tag{42.350}$$
$$= |\alpha_0|^2 e^{\imath\omega_{ca}\tau} \sum\nolimits_{n,m} \langle e^{\imath\varphi_n(t+\tau)-\imath\varphi_m(t)}\rangle = |\alpha_0|^2 e^{\imath\omega_{ca}\tau} \sum\nolimits_{n,m,k} \frac{\imath^k}{k!} \langle [\varphi_n(t+\tau)-\varphi_m(t)]^k\rangle$$
$$= |\alpha_0|^2 e^{\imath\omega_{ca}\tau} \sum\nolimits_{n,m,k} \frac{\imath^k}{k!} \sum\nolimits_{j=0}^{k} (-1)^j \binom{k}{j} \langle \varphi_n(t+\tau)^j \varphi_m(t)^{k-j}\rangle \ .$$

The main role of cavity-induced interparticle correlations is to self-consistently establish a constant center-of-mass motion ω_{ca}. We may, to first order, neglect the possibility that the coupling correlates the noise, since the noise is imprinted from the outside, i.e. the molasses. Therefore, $\langle \varphi_n(t+\tau)\varphi_m(t)\rangle \propto \delta_{nm}$,

$$\langle \varphi_n(t+\tau)^j \varphi_m(t)^{k-j}\rangle = \sum\nolimits_{all\ pairs} \langle \varphi_n(t+\tau)^2\rangle^{j/2} \langle \varphi_m(t)^2\rangle^{k/2-j/2} \tag{42.351}$$
$$= \frac{j!}{2^{j/2}(j/2)!} \frac{(k-j)!}{2^{(k-j)/2}(k/2-j/2)!} \langle \varphi_n(t+\tau)^2\rangle^{j/2} \langle \varphi_m(t)^2\rangle^{k/2-j/2}$$

so that,

$$R_\alpha(\tau) = |\alpha_0|^2 e^{\imath\omega_{ca}\tau} \sum_{n,m,k} \frac{\imath^k}{k!} \sum_{j=0}^{k} \binom{k}{j} \frac{j!}{2^{j/2}(j/2)!} \frac{(k-j)!}{2^{(k-j)/2}(k/2-j/2)!} \langle \varphi_n(t+\tau)^2\rangle^{j/2} \langle \varphi_m(t)^2\rangle^{k/2-j/2} \ , \tag{42.352}$$

where j and k are even,

$$R_\alpha(\tau) = |\alpha_0|^2 e^{\imath\omega_{ca}\tau} \sum\nolimits_{n,m,k} \frac{\imath^k}{2^{k/2}(k/2)!} \sum_{j=0}^{k} \binom{k/2}{j/2} \langle \varphi_n(t+\tau)^2\rangle^{j/2} \langle \varphi_m(t)^2\rangle^{k/2-j/2}$$
$$= |\alpha_0|^2 e^{\imath\omega_{ca}\tau} \sum_{n,m,k} \frac{1}{(k/2)!} \left(-\frac{1}{2}\langle \varphi_n(t+\tau)^2\rangle - \frac{1}{2}\langle \varphi_m(t)^2\rangle\right)^{k/2} \tag{42.353}$$
$$= |\alpha_0|^2 e^{\imath\omega_{ca}\tau} \sum_n e^{-\frac{1}{2}\langle \varphi_n(t+\tau)^2\rangle} \sum\nolimits_m e^{-\frac{1}{2}\langle \varphi_m(t)^2\rangle} = |\alpha_0|^2 N^2 e^{\imath\omega_{ca}\tau} e^{-\frac{1}{2}\langle \varphi_n(t+\tau)^2\rangle} e^{-\frac{1}{2}\langle \varphi_n(t)^2\rangle} \ .$$

42.7.1.4 Memory effects

Relax adiabaticity, $\dot{\alpha}_- \neq \imath\omega_{ca}\alpha_-$, substitute $\beta = e^{\kappa t}\alpha_-$,

$$\dot{\theta} = \frac{4\varepsilon\imath U_0\alpha_+}{\gamma_{fr}}\left(\beta e^{-\imath\theta-\kappa t} - \beta^* e^{\imath\theta-\kappa t}\right) + \frac{\xi}{\gamma_{fr}} \ , \tag{42.354}$$
$$\beta = -\imath U_0\alpha_+ \int^t e^{\imath\theta+\kappa t'}dt' \ .$$

so that,

$$\begin{aligned} R_\alpha(\tau) &\equiv \langle\alpha_-^*(t)\alpha_-(t+\tau)\rangle = \langle e^{-\kappa t}\beta^*(t)e^{-\kappa t-\kappa\tau}\beta(t+\tau)\rangle \\ &= e^{-\kappa\tau}\langle e^{-2\kappa t}\beta^*(t)\beta(t+\tau)\rangle \\ &= U_0^2\alpha_+^2 e^{-\kappa\tau}\int\int^t\int^{t+\tau} e^{\imath\theta(t'')-\imath\theta(t')+\kappa t'+\kappa t''-2\kappa t}dt''dt'dt \\ &= U_0^2\alpha_+^2 e^{-\kappa\tau}\int\int^t\int^{t+\tau} e^{\imath\omega_{ca}t''-\imath\omega_{ca}t'+\imath\varphi(t'')-\imath\varphi(t')+\kappa t'+\kappa t''-2\kappa t}dt''dt'dt \ . \end{aligned} \tag{42.355}$$

Using the representation of half the δ-distribution $\int^t e^{(\imath\omega_{ca}+\kappa)t'}dt' = \delta_{1/2} = \lim_{\kappa\to 0}\frac{1}{\kappa+\imath\omega_{ca}}$.

42.7.1.5 Schawlow-Townes limit for CARL

The ultimate limit for the spectral purity of a perfectly stable laser oscillator is the *Schawlow-Townes limit* [1150]. The origin of this limitation is the discrete nature of the light field. Similarly to quantum projection noise, which is caused by the discretisation of atomic energy levels, the optical *shot-noise* registered in photodetectors arises from the discrete repartition of electromagnetic energy in photons. With a laser power P, a cavity bandwidth κ and an interrogation time τ, the Allan variance [**?**] and the linewidth of a Schawlow-Townes limited laser are given by,

$$\sigma_{ST}(\tau) = \frac{1}{\omega/\kappa}\frac{1}{\sqrt{(P/\hbar\omega)\tau}} \ , \tag{42.356}$$
$$\beta = \kappa^2\frac{\hbar\omega}{P} \ .$$

In the case of CARL, using $P = \delta\hbar\omega|\alpha_-|^2$ the variance is $\sigma_{ST}^2(\tau) = \kappa/\tau\omega\delta|\alpha_-|^2 \approx 10^{-20}\ \mathrm{s}/\tau$. The shot-noise which limits the CARL is not the one of the CARL light itself, but the random momentum kicks imparted by molasses-cooled atoms. The CARL linewidth is $\beta = \kappa^2/\delta|\alpha_-|^2 = 10^{-14}\kappa$.

The time-lap between two scattering events for a single atom be distributed according to $p_1(\tau)d\tau = \gamma e^{-\gamma\tau}d\tau$. What is the waiting time distribution for two atoms [1154]? Schenzle related the waiting time distribution to the autocorrelation function $g^{(2)}(\tau)$.

Fig. 42.58(e-f) shows spectra of the CARL frequency obtained by Fourier-transforming the autocorrelation function of a Langevin-simulated trajectory of the CARL frequency. The width results from thermal fluctuations in the atomic motion induced by momentum diffusion in the molasses. It is clearly visible that the width is reduced when the atom number is increased, thus confirming Eq. (42.348).

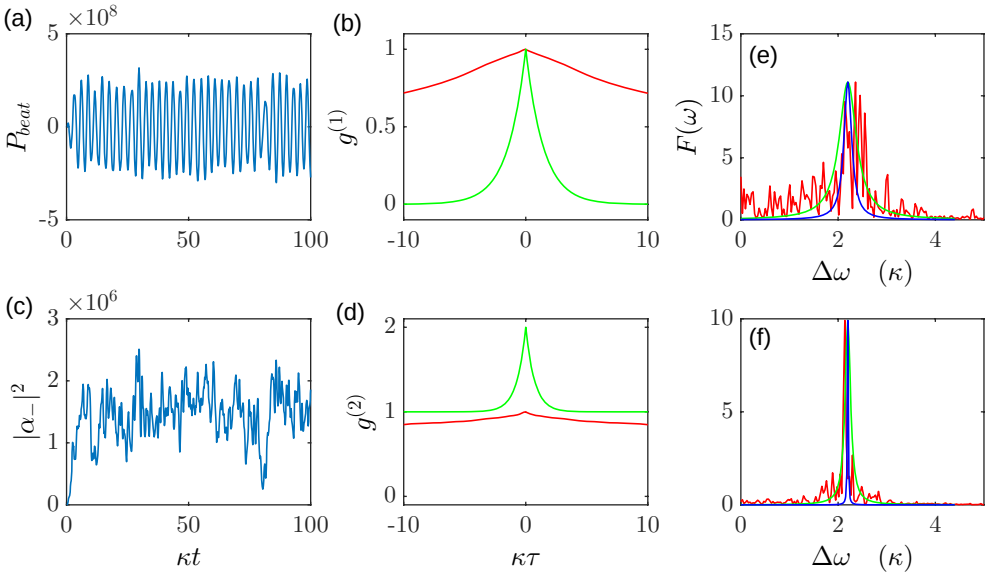

Figure 42.58: Simulated time-dependence of the (a) beat and the (b) intensity signals. Calculated (c) first and second-order correlation functions. The temperature was set to $T = 100\,\mu\text{K}$ and the atom number to $N = 40$. (e-f) Spectra of the CARL laser for (e) 4 and (f) 40 atoms. The total coupling constant NU_0 has been held constant, only the number of atoms whose trajectories are simulated is varied.

42.7.2 Measuring the coherence properties

We may also attempt to verify the predictions in experiment. Our signals are the beams transmitted through the cavity mirrors.

42.7.2.1 Homodyne signal

Ideally in order to get the full information on the the first-order coherence, we should record both the in-phase and the quadrature component of the field $\alpha_- = \mathfrak{Re}\ \alpha_- + i\mathfrak{Im}\ \alpha_-$ by homodyning it with the local oscillator α_+. Thus we need to use both ports of the beamsplitter: For the in-phase component we get,

$$\begin{aligned} P^{(ph)}_{hody} &\propto b^\dagger b - c^\dagger c \\ &= |\alpha_+\sqrt{\eta} + \alpha_-\sqrt{1-\eta}|^2 - |\alpha_+\sqrt{1-\eta} - \alpha_-\sqrt{\eta}|^2 \\ &= (1-2\eta)(|\alpha_-|^2 - |\alpha_+|^2) + 4\sqrt{\eta-\eta^2}\alpha_+\mathfrak{Re}\ \alpha_- \ . \end{aligned} \tag{42.357}$$

For a 50% beamsplitter the offsets disappear, $P^{(ph)}_{hody} \propto= 2\alpha_+\mathfrak{Re}\ \alpha_-$, which means that the homodyne signal is insensitive to intensity noise in the individual ports. Similarly we obtain for the quadrature component,

$$\begin{aligned} P^{(qu)}_{hody} &\propto |\alpha_+\sqrt{\eta} + \imath\alpha_-\sqrt{1-\eta}|^2 - |\alpha_+\sqrt{1-\eta} - \imath\alpha_-\sqrt{\eta}|^2 \\ &= -2\alpha_+\mathfrak{Im}\ \alpha_-. \end{aligned} \tag{42.358}$$

By mounting a piezo on one of the mirrors in the homodyne loop, we can influence which quadrature component to map. Is there a way how to get $\mathfrak{Im}\ \alpha_-$ and $\mathfrak{Re}\ \alpha_-$ simultaneously?

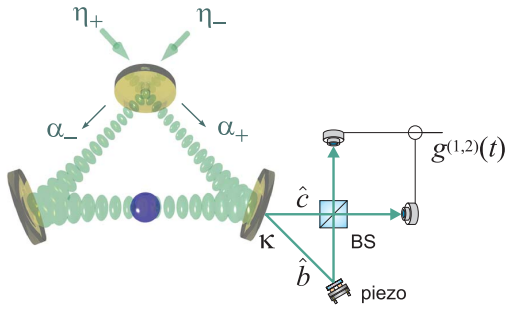

Figure 42.59: Homodyning the counterpropagating beams.

Knowing α_- we can calculate the *first order coherence*,

$$g^{(1)}(\tau) \equiv \frac{\langle \alpha^*(t)\alpha(t+\tau)\rangle}{\langle \alpha^*(t)\alpha(t)\rangle} = \frac{\int \alpha^*(t)\alpha(t+\tau)dt}{\int \alpha(t)^2 dt} \ , \tag{42.359}$$

the *second-order coherence*,

$$\begin{aligned} g^{(2)}(\tau) &\equiv \frac{\langle \alpha^*(t)\alpha^*(t+\tau)\alpha(t+\tau)\alpha(t)\rangle}{\langle \alpha^*(t)\alpha(t)\rangle^2} \\ &= \frac{\int P_-(t)P_-(t+\tau)dt}{\int P_-(t)dt} \ , \end{aligned} \tag{42.360}$$

and the *emission spectrum* (power spectral density),

$$F(\omega) = \frac{1}{\pi}\mathfrak{Re} \int g^{(1)}(\tau)e^{\imath\omega\tau}d\tau \ . \tag{42.361}$$

All these quantities can be evaluated from numerical simulations of the Langevin equations.

Example 276 (*Real Signals*): What is recorded in experiment is the probe field power P_{probe} and only one quadrature component of the beat between the probe and the pump. The probe signal is simply,

$$P_- \propto |\alpha_-|^2 \ . \tag{42.362}$$

So it may be used directly for the $g^{(2)}(\tau)$ intensity correlation function (42.360) analogous to the *Hanbury-Brown-Twiss* experiment.
In contrast, the beat signal is obtained in a *Young* type experiment,

$$P_{beat} \propto |\alpha_+ \pm \alpha_-|^2 = |\alpha_+|^2 + |\alpha_-|^2 \pm 2\alpha_+ \mathfrak{Re}\ \alpha_- \ , \tag{42.363}$$

because we may assume α_+ real. Obviously, the beat signal oscillates between the limits $\pm 2\alpha_+|\alpha_-|$. Using only one port of the beamsplitter, we miss information on the other quadrature phase. The question arises now, how to calculate

the spectrum if only the real part of the field $\mathfrak{Re}\ \alpha$ is known. The interesting quantity is $|g^{(1)}(\tau)|$, because it contains the information on the photon statistics. This function is smooth (it does not oscillate) and should in our case describe an exponential decay (42.341). Fortunately, from numerical calculation it seems that $|g^{(1)}(\tau)|$ is just the convolution of $\langle \mathfrak{Re}\ \alpha(t) \mathfrak{Re}\ \alpha(t+\tau)\rangle / \langle \mathfrak{Re}\ ^2\alpha(t)\rangle$, so that we may recover the informations. For the spectrum, which is calculated from the complex quantity $g^{(1)}(\tau)$ the question is more delicate. It comes down to asking if,

$$F(\omega) \propto \mathfrak{Re} \int \langle \mathfrak{Re}\ \alpha(t) \mathfrak{Re}\ \alpha(t+\tau)\rangle\ e^{\imath\omega\tau} d\tau \tag{42.364}$$

gives the correct spectrum (42.361).

42.7.2.2 Impact of finite time window

Technical noise may overrule the thermal noise just like in ordinary lasers. This situation may change if atom numbers are low, so that we have bad statistics, or if the collective force is strong enough to correlate the noise.

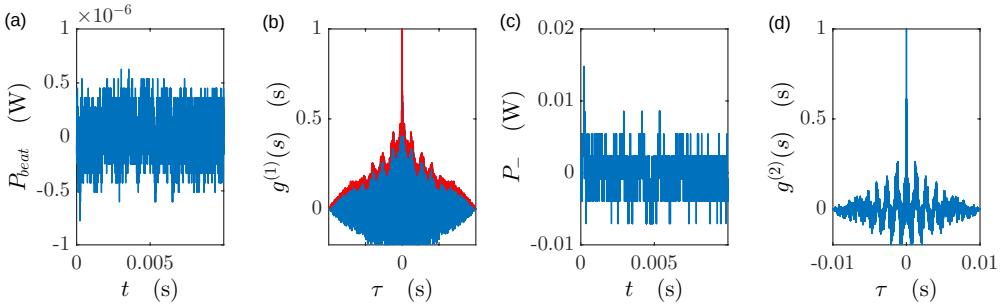

Figure 42.60: (code) Measured trajectories (a) and (b) and correlation functions (c) and (d) of the CARL laser. The coupling constant was $NU_0 = -0.1$.

The spectral width may also be limited by the finite time window $t \in [-\frac{1}{2}t_0, \frac{1}{2}t_0]$, which is taken for computing the spectrum. Even a perfect harmonic oscillation $\alpha_-(t) = \alpha_- e^{\imath\omega_{ca}t}$ will then have a finite bandwidth,

$$\begin{aligned} \mathcal{F}_{a_-}(\omega) &= \mathcal{F}[\alpha_- e^{\imath\omega_{ca}t}] \star \mathcal{F}[\chi_{[-t_0/2,t_0/2]}(t)] \\ &= \alpha_- \delta(\omega-\omega_{ca}) \star \sqrt{\frac{2}{\pi}} \frac{\sin \frac{1}{2}\omega t_0}{\omega} = \alpha_- \sqrt{\frac{2}{\pi}} \frac{\sin \frac{1}{2}(\omega-\omega_{ca})t_0}{(\omega-\omega_{ca})} \ . \end{aligned} \tag{42.365}$$

The spectrum $S_{\alpha_-}(\omega) = |\mathcal{F}_{a_-}(\omega)|^2$ has a bandwidth of $\beta = 5.6/t_0$. For example an oscillation observed for a period 100 times longer than the cavity decay time, $t_0 = 100/\kappa$, the bandwidth will be $\beta = 0.056\kappa$. Simulations are based on the Langevin equation.

42.7.3 Exercises

42.7.3.1 Ex: Autocorrelation functions

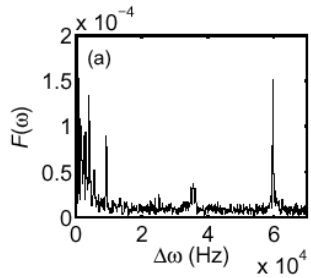

Figure 42.61: Spectrum of the CARL calculated from the first-order correlation function in Fig. 42.60(c). The coupling constant was $NU_0 = -0.1\kappa$.

Solution: *Waiting time distribution for two scatterers (see Autocorrelation0), Autocorrelation function for simple signals (see Autocorrelation1), Generate white noise as random phase jumps (see Autocorrelation2), Finite numbers of oscillations limit the resolution (see Autocorrelation3), and Finite numbers of oscillations limit the resolution (see Autocorrelation4).*

42.7.3.2 Ex: Signal-to-noise ratio of Bloch oscillations

You want to evaluate the stability of a noisy periodic signal. How many noisy oscillations do you have to observe in order to evaluate the oscillation period with a given S/N ratio [1403].

Solution: *Study width of Fourier transform? Measure other forces, e.g. magnetic field using* ^{87}Sr*?*
http://es.mathworks.com/help/signal/ug/determine-cyclic-behavior-in-data.html
http://es.mathworks.com/help/signal/ug/find-periodicity-using-autocorrelation.html

42.8 Further reading

J. Guo et al., *Recoil-induced Resonances in Non-linear Spectroscopy* [559]DOI

J.-Y. Courtois et al., *Recoil-induced Resonances in Cesium: An Atomic Analog to the Free Electron Laser* [305]DOI

P. R. Hemmer et al., *Self-Organization, Broken Symmetry, and Lasing in an Atomic Vapor: The Interdependence of Gratings and Gain* [603]DOI

G.-L. Lippi et al., *Spontaneous Generation of a Longitudinal Atomic Density Grating in Sodium Vapor* [803]DOI

D.R. Meacher et al., *Method for Velocimetry of Cold Atoms* [865]DOI

P. Verkerk et al., *Comment on "Spontaneous Generation of a Longitudinal Atomic Density Grating in Sodium Vapor"* [1333]DOI

S. Barbay et al., *Pump-probe spectroscopy of the sodium D line and the question of recoil-induced gratings in hot vapors* [89]DOI

P.R. Berman, *Comparison of recoil-induced resonances and the collective atomic recoil laser* [131]DOI

M. Vengalattore et al., *Optical bistability at low light level due to collective atomic recoil* [1332]DOI

V. Vuletic et al., *Three-dimensional cavity Doppler cooling and cavity sideband cooling by coherent scattering* [1347]DOI

M. Gangl et al., *Cold atoms in a high-Q ring cavity* [482]DOI

S. Ostermann et al., *Atomic self-ordering in a ring cavity with counterpropagating pump fields* [987]DOI

S.C. Schuster et al., *Supersolid properties of a Bose-Einstein condensate in a ring resonator* [1175]DOI

J. Léonard et al., *Supersolid formation in a quantum gas breaking continuous translational symmetry* [788]DOI

J.K. Asbóth et al., *Optomechanical coupling in a one-dimensional optical lattice* [50]DOI

G.R.M. Robb, *Dispersive optical bistability in cold atomic vapours* [1104]DOI

R. Culver et al., *Collective strong coupling of cold potassium atoms in a ring cavity* [312]DOI

S. Bux et al., *Cavity-controlled matter wave superradiance at the recoil limit* [223]DOI

R.J. Schulze et al., *Optomechanical approach to cooling of small polarizable particles in a strongly pumped ring cavity* [1173]DOI

42.8.1 on CARL

R. Bonifacio et al., *The self-consistent pendulum picture of the free electron laser revised* [169]DOI

R. Bonifacio et al., *Collective atomic recoil laser (CARL) optical gain without inversion by collective atomic recoil and self-bunching of two-level atoms* [173]DOI

R. Bonifacio et al., *A quantum model for collective recoil lasing* [171]DOI

S. Gupta et al., *Cavity Nonlinear Optics at Low Photon Numbers from Collective Atomic Motion* [563]DOI

M.S. Shahriar et al., *Ultrahigh enhancement in absolute and relative rotation sensing using fast and slow light* [1189]DOI

F. Zimmer et al., *Sagnac Interferometry Based on Ultraslow Polaritons in Cold Atomic Vapors* [1436]DOI

G.E. Stedman et al., *Ring-laser tests of fundamental physics and geophysics* [1248]DOI

Shanchao Zhang et al., *A dark-line two-dimensional magneto-optical trap of 85Rb atoms with high optical depth* [1427]DOI

42.8.2 on self-organization

J. Javaloyes et al., *Reduced Model for the Description of Radiation-Matter Interaction Including Atomic Recoil* [665]DOI

J. Javaloyes et al., *Self-Generated Cooperative Light Emission Induced by Atomic Recoil* [666]DOI

T. Griesser et al., *A Vlasov approach to bunching and selfordering of particles in optical resonators* [543]DOI

Part VII

Atom Optics

Chapter 43

Manipulation of atomic gases

The field of *atom optics* deals with the motion of atoms and its control by technical tools. At high velocities with no external forces, the atoms follow straight paths, similar to light beams in *classical optics*. At low speeds, they propagate as waves, similarly to wave optics in Maxwell's theory of *electrodynamics*. The term *atom optics* emphasizes the analogy and the duality in the behavior of microscopic particles.

The *duality principle* is one of the fundamental ideas of quantum mechanics. The appearance of an object as a wave or as a particle depends on the situation in which it is observed. While the wave nature of light was well established in classical physics since a long time, Louis de Broglie was the first in 1924 to apply the duality principle also to massive particles and to predict that particles, under certain conditions, behave like waves whose wavelengths increase as their velocity decreases. Each particle (or sample of particles) is delocalized along a distance corresponding to the 'de Broglie wavelength'. This feature of the matter was soon discovered experimentally in electron beams and is still used today in commercial devices, for example in electron microscopes.

The laser was discovered in 1956. In a laser, light particles are forced to oscillate synchronously, that is, coherently. By analogy, we can raise the question whether a similar phenomenon can occur with massive particles, and whether it is possible to construct an *atom laser*. Such a device would emit coherent matter waves just as the laser emits coherent light. When a gas is cooled to very low temperatures, the Broglie waves of the atoms become very long and, if the gas is sufficiently dense, eventually overlap. If the gas consists of a single species of bosonic particles with all atoms being in the same quantum state, their Broglie waves interfere constructively thus and form a huge wave of coherent matter. This matter wave is described by a single wavefunction exhibiting long range order and having a single phase. If this wavefunction is formed inside a trap, all atoms accumulate in its ground state. Thus, we obtain a pure quantum state of many bodies in the kinetic degree of freedom [1]. The transition of a gas from individual atoms to a degenerate mesoscopic many-body quantum state occurs as a phase transition named *Bose-Einstein condensation* (BEC) as a homage to Bose and Einstein who predicted the effect already in 1924 [181, 410].

The course begins in this chapter with a presentation of the most important experimental techniques for cooling, trapping, manipulating and detecting atomic gases. The knowledge of these techniques will allow for a better understanding of how it is possible to generate and analyze all the effects mentioned above. Chp. 45 introduces

[1] In particular, for very cold atoms whose internal excitation occurs on a very different energy scale, the corresponding degree freedom is frozen and does not influence the kinetics.

the phenomenon of Bose-Einstein condensation and the following chapters focus on the thermodynamic, superfluid, coherent and dielectric properties of condensates.

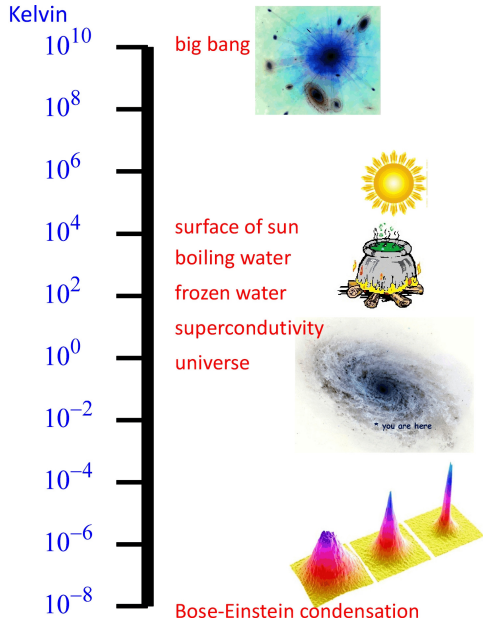

Figure 43.1: Temperature scale.

The incomparable success of atomic optics has been rewarded with 20 nobel prices in the last 25 years (Dehmelt, Paul, Ramsey, Cohen-Tannoudji, Chu, Phillips, Cornell, Wieman, Ketterle, Hänsch, Glauber, Hall, Wineland, Haroche, Ahskin) plus several indirectly related noble prices (De Gennes, Leggett, Thouless, Haldane, Kosterlitz). For review articles on BEC see [999, 319, 297, 512, 1122, 1238], [712] or check in internet sites *http://amo.phy.gasou.edu/bec.html* and *http://jila.edu/bec.html*.

In this chapter we review the basic techniques of *Atomic Optics*, emphasizing the cooling, trapping and measurement of cold atomic gases. See also (watch talk) and (watch talk).

43.1 The atomic motion

43.1.1 The atom as a matter wave

We have already emphasized that atomic optics deals with the motion of atoms in a gas, that is, we are interested only in the external degrees of freedom of the atoms. To describe the motion of a free massive particle in one dimension, we write the Hamiltonian,

$$\hat{H} = -\frac{\hbar^2}{2m}\frac{d^2}{dx^2} \ . \tag{43.1}$$

Therefore, the general solution of the stationary Schrödinger equation,

$$\hat{H}\psi(x) = E\psi(x) \ , \tag{43.2}$$

is,

$$\psi(x) = Ae^{\imath kx} + Be^{-\imath kx} \qquad \text{with} \qquad k = \sqrt{\frac{2mE}{\hbar^2}} \ . \tag{43.3}$$

Note, that the wavefunctions $e^{\imath kx}$ are not quadratically integrable. On the other hand, they do not represent real physical systems. In practice, we need to consider wavepackets or specify a finite volume for the particle.

Note also that the eigenvalue spectrum of is continuous. To warrant the interpretation of the wavefunction as a probability density we will require quadratic integrability, $\int |\psi|^2 d^3r = 1$. This means that the wavefunction can not be infinite in a finite volume, but it can be infinite in an infinitely small volume.

The description of the atomic motion by a wave equation emphasizes the fact that microscopic particles have wave properties with each atom corresponding to a velocity-dependent *de Broglie wave*,

$$\boxed{\lambda_{dB} = \frac{h}{p}} \ , \tag{43.4}$$

which describes the coherence length of the atom.

43.1.1.1 Characteristic velocities

The behavior of an atom described by the Schrödinger equation depends very much on its kinetic energy. At high velocities (or short de Broglie waves), it will behave like a classical particle with a well-defined trajectory. At low velocities (or long de Broglie waves), it will propagate like a wave and exhibit phenomena such as diffraction and interference. Therefore, it is important to highlight some characteristic velocity regimes.

Most optical cooling techniques are based on the removal of kinetic energy upon light scattering on electronic transitions. It is, therefore, interesting to compare the kinetic energy (or temperature) of an ensemble of atoms with the width Γ of the transition. The *Doppler limit* is given by (see Exc. 43.1.4.1),

$$k_B T_D = \frac{\hbar}{2}\Gamma \ . \tag{43.5}$$

We can also compare the kinetic energy with the energy transferred to an atom by the absorption of a single photon. The *photonic recoil* energy is given by,

$$k_B T_{rec} = \frac{\hbar^2 k^2}{2m} \ . \tag{43.6}$$

Atomic clouds with temperatures around $T \simeq T_D = 10..1000\,\mu\text{K}$ are called *cold*. Clouds with temperatures around and below $T \lesssim T_{rec} = 0.1..10\,\mu\text{K}$ are called *ultracold*.

In most atomic optical experiments we do not work with individual atoms (or ions), but with relatively dilute ensembles of atoms, called *clouds*. In general, clouds can not be described by a single wavefunction. Either we describe every atom by a separate and independent wavefunction (which only works when the atoms do not interact), or we describe the cloud by probability distributions (such as the 'density

matrix'). Let us now consider a thermal cloud. The *Maxwell-Boltzmann distribution* of velocities is,

$$g(\mathbf{v}) = \sqrt{\frac{m}{2\pi k_B T}}^3 e^{-m\mathbf{v}^2/2k_B T} \ . \tag{43.7}$$

This distribution is normalized, $\int g(\mathbf{v}) d^3\mathbf{v} = \int_0^\infty 4\pi v^2 g(v) dv = 1$. Average velocity is now

$$\bar{v} = \int v g(v) dv = \sqrt{\frac{k_B T}{m}} \ . \tag{43.8}$$

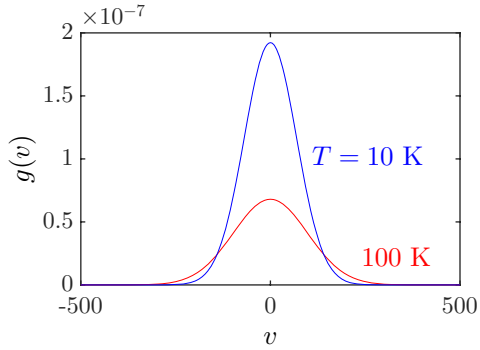

Figure 43.2: (code) Maxwell-Boltzmann distribution.

We define the *thermal de Broglie wavelength* of an atomic ensemble as,

$$\boxed{\lambda_{therm} \equiv \frac{h}{m\bar{v}} = \sqrt{\frac{2\pi\hbar^2}{mk_B T}}} \ . \tag{43.9}$$

It represents an average over the de Broglie wavelengths of all atoms of the sample. When a dense gas is sufficiently dense, so that this quantity exceeds the average distance between atoms,

$$\rho \equiv n\lambda_{therm}^3 > 1 \ , \tag{43.10}$$

where n is the atomic density, we enter a new regime, where the *Maxwell-Boltzmann law* ceases to be valid. Since $\lambda_{therm} \propto T^{-1/2}$, this regime corresponds to low temperatures. The quantity ρ is called *phase space density*. A phase space density approaching 1 means an increased probability of finding *more than one atom per elementary phase space cell*. We then enter the regime of quantum degeneracy, where the Boltzmann statistics must be replaced by the Bose-Einstein statistics, in the case of bosons, or the Fermi-Dirac statistics, in the case of fermions. We will deepen the discussion of quantum statistics of ideal gases in Chp. 44. From the condition $n\lambda_{therm}^3 \simeq 1$, we obtain

$$k_B T_c = \frac{1}{m}\left(\frac{2\pi\hbar}{\lambda_{therm}}\right)^2 = \frac{(2\pi\hbar)^2 n^{2/3}}{m} \ . \tag{43.11}$$

43.1.2 Localized atoms

To avoid perturbative influence of the environment on the atoms, they are often trapped in potentials, which suspend them in a volume distant from massive walls. The Hamiltonian of a trapped atoms is,

$$\hat{H} = -\frac{\hbar^2}{2m}\frac{d^2}{dx^2} + U(x) \ . \tag{43.12}$$

As the wavefunction is now localized, the spectrum of possible energies organizes into discrete levels, and the atoms are allocated in populations of these levels.

Often, a 3D potential can be written in the form,

$$U(x,y,z) = U_x(x) + U_y(y) + U_z(z) \ . \tag{43.13}$$

This is the case, for example, of a rectangular well characterized by $U_x(x) = U_y(y) = U_z(z) = U_0/3$ inside the well. The relationship (43.13) also holds for a harmonic potential,

$$U(\mathbf{r}) = \frac{m}{2}\left(\omega_x^2 x^2 + \omega_y^2 y^2 + \omega_z^2 z^2\right) \ . \tag{43.14}$$

In these cases, a product ansatz for the wavefunction is generally useful,

$$\psi(\mathbf{r}) = \psi_x(x)\psi_y(y)\psi_z(z) \ , \tag{43.15}$$

since its insertion into the Schrödinger equation,

$$\begin{aligned}&\left[-\frac{\hbar^2}{2m}\left(\frac{d^2}{dx^2} + \frac{d^2}{dy^2} + \frac{d^2}{dz^2}\right) + U_x(x) + U_y(y) + U_z(z)\right]\psi_x(x)\psi_y(y)\psi_z(z) \\ &= E\psi_x(x)\psi_y(y)\psi_z(z) \ ,\end{aligned} \tag{43.16}$$

separates it into three independent one-dimensional equations,

$$-\frac{\hbar^2}{2m}\frac{\psi_x''(x)}{\psi_x(x)} + U_x(x) = const. \equiv E_x \ , \tag{43.17}$$

and similarly for y and z. Since $E = E_x + E_y + E_z$, we can have the same energy for different combinations of E_x, E_y and E_z. That is, multidimensional systems are often degenerate.

43.1.3 Density-of-states of a trapping potential

The way an atomic cloud accommodates itself inside a trapping potential is governed by the density of available states. To calculate this density, we consider the Hamiltonian $H(\mathbf{r},\mathbf{p}) = \frac{\hbar^2 k^2}{2m} + U(\mathbf{r})$. For a cylindrical harmonic oscillator we write,

$$U(\mathbf{r}) = \frac{m}{2}\omega_r^2 r^2 + \frac{m}{2}\omega_z^2 z^2 \qquad \text{where} \qquad r^2 = x^2 + y^2 \ , \tag{43.18}$$

or $U(\mathbf{x}) = \frac{m}{2}\omega_r^2\rho^2$, where $\rho^2 = x^2 + y^2 + \lambda^2 z^2$ with $\lambda = \omega_z/\omega_r$. We define $\bar{\omega} = (\omega_r^2\omega_z)^{1/3} = \lambda^{1/3}\omega_r$. The single-particle levels of this Hamiltonian are, $\epsilon_{n_x n_y n_z} = \hbar\omega_x n_x + \hbar\omega_y n_y + \hbar\omega_z n_z$, where the n_j are integer numbers.

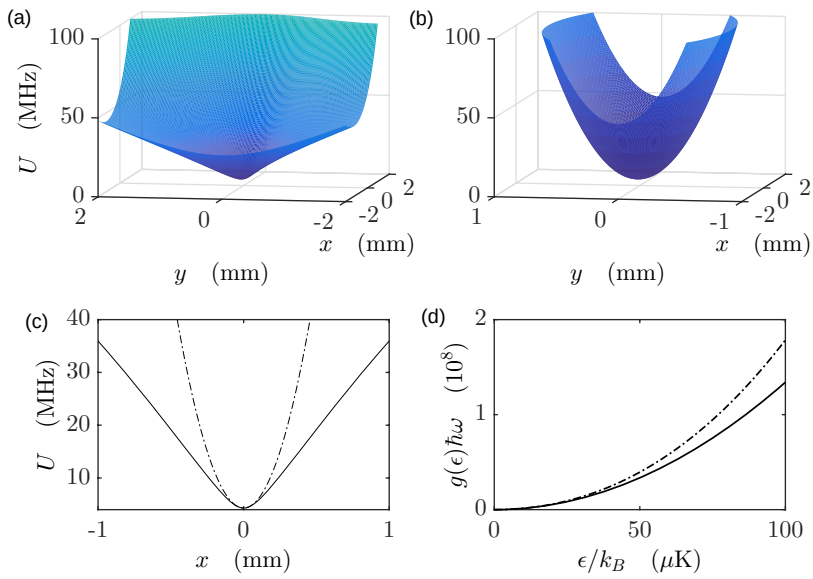

Figure 43.3: (code) (a) The figure shows two dimensions of a Ioffe-Pritchard type magnetic trapping potential (characterized by being approximately linear at large distances from the center and harmonic near the center). (b) Harmonic approximation (most experimentally feasible potentials are approximately harmonic near the center). (c) One-dimensional cut through the potential of (a,b). (d) Density of states for a harmonic (dotted line) and a Ioffe-Pritchard type potential (solid line).

We now introduce the *density of states* $\eta(\epsilon)$ for an arbitrary potential via,

$$\boxed{\int \eta(\epsilon)d\epsilon \equiv \frac{1}{(2\pi)^3}\int d^3r d^3k = \frac{(2m)^{3/2}}{(2\pi)^2\hbar^3}\int d^3r \int d\epsilon\sqrt{\epsilon - U(\mathbf{r})}} \ . \tag{43.19}$$

For the cylindrical harmonic trap defined in (43.18), we find with a little help from Dr. Bronstein [201],

$$\begin{aligned}\eta(\epsilon) &= \frac{(2m)^{3/2}}{(2\pi)^2\hbar^3}\int d^3r\sqrt{\epsilon - \frac{m}{2}\omega_r^2\rho^2} \\ &= \frac{1}{(2\pi)^2}\frac{8\epsilon^2}{(\hbar\bar{\omega})^3}\int_{-1}^{1}d\tilde{x}\int_{-\sqrt{1-\tilde{x}^2}}^{\sqrt{1-\tilde{x}^2}}d\tilde{y}\int_{-\sqrt{1-\tilde{x}^2-\tilde{y}^2}}^{\sqrt{1-\tilde{x}^2-\tilde{y}^2}}d\tilde{z}\sqrt{1-\tilde{x}^2-\tilde{y}^2-\tilde{z}^2}\ .\end{aligned} \tag{43.20}$$

The resolution of the integral gives,

$$\boxed{\eta(\epsilon) = \frac{\epsilon^2}{2(\hbar\bar{\omega})^3}} \quad \text{(harmonic potential)} \ . \tag{43.21}$$

Another example is the box potential. In this case we can simply obtain,

$$\boxed{\eta(\epsilon) = \frac{(2m)^{3/2}}{(2\pi)^2\hbar^3}\int_V d^3r\sqrt{\epsilon} = \frac{(2m)^{3/2}}{(2\pi)^2\hbar^3}V\sqrt{\epsilon}} \quad \text{(box potential)} \ . \tag{43.22}$$

A generalization is discussed in the Exc. 43.1.4.2.

43.1.4 Exercises

43.1.4.1 Ex: Fundamental temperature limits

Calculate the Doppler limit, the recoil limit, and the threshold to quantum degeneracy for an atomic cloud of density $n = 10^{14}\,\mathrm{cm}^{-3}$ for the sodium $D2$ transition ($\lambda = 590\,\mathrm{nm}$, $\Gamma/2\pi = 10\,\mathrm{MHz}$) and the rubidium $D2$ transition ($\lambda = 780\,\mathrm{nm}$, $\Gamma/2\pi = 6\,\mathrm{MHz}$).

Solution: *For sodium* $T_D = 240\,\mu\mathrm{K}$, $T_{rec} = 1.2\,\mu\mathrm{K}$, *and* $T_c = 220\,\mathrm{nK}$. *For rubidium* $T_D = 144\,\mu\mathrm{K}$, $E_R = 180\,\mathrm{nK}$, *and* $T_c = 830\,\mathrm{nK}$.

43.1.4.2 Ex: Density of states for non-harmonic potentials

Calculate the density of states for non-harmonic potentials, $\hat{H} = \frac{\hbar^2 k^2}{2m} + \left|\frac{x}{2\bar{x}}\right|^p + \left|\frac{y}{2\bar{y}}\right|^l + \left|\frac{z}{2\bar{z}}\right|^q$ using Ref. [72]. Apply the result to a quadrupolar potential.

Solution: *This reference found the following solution,*

$$\eta(\epsilon) = \frac{(2m)^{3/2}}{(2\pi)^2\hbar^3} 8\bar{x}\bar{y}\bar{z}F(p,l,q)\varepsilon^{1/p+1/q+1/l+1/2}$$
$$F(p,l,q) = \int_{-1}^{1}(1-\tilde{x}^p)^{1/2+1/q+1/l}d\tilde{x}\int_{-1}^{1}(1-\tilde{x}^l)^{1/2+1/q}d\tilde{y}\int_{-1}^{1}(1-\tilde{x}^q)^{1/2}d\tilde{z}\ .$$

For example, for a quadrupole trap,

$$F(p,l,q) = \frac{2^{10}}{105}\sqrt{2}$$
$$g(\epsilon) = \frac{2^{13}}{105}\frac{m^{3/2}}{\pi^2\hbar^3}\bar{x}\bar{y}\bar{z}\epsilon^{7/2}\ .$$

43.2 Optical cooling

As discussed in Sec. 38.2, the force exerted by a light field on an atom can be of two types: a dissipative force arising called *radiation pressure*, which is often used for optical cooling purposes, and a conservative *dipolar force* which often serves for the engineering of optical trapping potentials. Both applications of optical forces will be detailed in the following sections.

43.2.1 Optical molasses

In the *Doppler cooling* model, we treat the phenomenology of optical forces quantitatively by considering the amplitude, phase and frequency of a classical field interacting with the dipole of an atomic transition in a two-level atom. From Eq. (38.25) and previous definitions of Ω and Ω_{sat}, and with the intensity $I \propto \mathcal{E}^2$, we can write the *saturation parameter*,

$$s = \frac{I}{I_{sat}} = \frac{\Omega^2}{\Omega_{sat}^2} = \frac{\Omega^2}{\Gamma^2/2} \ , \tag{43.23}$$

and

$$\mathbf{F}_{rp} = \frac{\hbar \mathbf{k} \Gamma}{2} \frac{s}{(2\Delta/\Gamma)^2 + 1 + s} \ . \tag{43.24}$$

Now, if we consider an atom propagating in $\mp z$ direction with the velocity v_z counterpropagating to a light wave detuned by Δ from the resonance, the total detuning will be

$$\Delta \longrightarrow \Delta \mp k v_z \ . \tag{43.25}$$

where the term kv_z is the Doppler shift. The force $F_\pm$ acting on the atom will be in the direction opposite to the motion,

$$\mathbf{F}_\pm = \pm \frac{\hbar \mathbf{k} \Gamma}{2} \frac{s}{(2(\Delta \mp k v_z)/\Gamma)^2 + 1 + s} \ . \tag{43.26}$$

Supposing now, that we have two light fields propagating in directions $\pm z$, the total force will be $\mathbf{F} = \mathbf{F}_+ + \mathbf{F}_-$. If kv_z is small compared to Γ and Δ, we find through a Taylor expansion,

$$F_z \simeq 4\hbar k s \frac{k v_z (2\Delta/\Gamma)}{[1 + s + (2\Delta/\Gamma)^2]^2} \ . \tag{43.27}$$

This expression shows that, if the detuning Δ is negative (that is, on the red side of the resonance), then the cooling force will oppose the motion and be proportional to the atomic velocity. Fig. 43.4 shows this decelerating dissipative force as a function of v_z at a detuning $\Delta = -\Gamma$ with $I = I_{sat}/2$. The one-dimensional motion of the atom is thus behaving like being subject to a friction force which is proportional to the atomic velocity,

$$F_z \simeq \alpha_d v_z \qquad \text{with} \qquad \alpha_d = s \frac{-4k^2(2\Delta/\Gamma)}{1 + s + (2\Delta/\Gamma)^2} \ . \tag{43.28}$$

The proportionality factor, is just the *friction coefficient*.

However, the atom will not cool down indefinitely. At some point, the Doppler cooling rate will be balanced by the heating rate coming from the momentum fluctuations of the atom absorbing and remitting photons. The *Doppler cooling limit* is given by,

$$k_B T = \hbar \frac{\Gamma}{2} \ , \tag{43.29}$$

as we will see in Exc. 43.2.5.1. This limit is generally, for alkaline atoms, on the order of dozens of micro-Kelvin. In the early years of cooling and trapping, the Doppler limit was thought to be a real physical barrier. But in 1988, several groups

have shown that, in fact, atoms could be cooled well below the Doppler limit. The effect arises in atoms, whose ground state exhibits a hyperfine structure. We will show simplified one-dimensional models for sub-Doppler cooling in the next section. Resolve the Exc. 43.2.5.2.

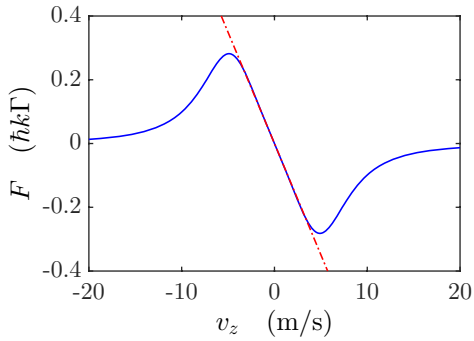

Figure 43.4: (code) Doppler force due to one-dimensional radiative pressure as a function of atomic velocity along the z-axis for red detuning $\Delta = -\Gamma$ at a light intensity of $I = 2I_{sat}$. The solid line shows the exact expression for the restoring force [Eq (43.26)]. The broken line shows the approximate linear expression of the velocity dependence according to Eq. (43.27).

43.2.2 Sub-Doppler cooling

It turns out that atoms with a hyperfine structure in the ground state can be cooled below the Doppler limit (43.5). To explain this unexpected observation, models involving a slow motion of the atoms in polarization gradients of a standing light wave have been invoked. The phenomenon is now known as *polarization gradient cooling*.

Two principal mechanisms for cooling atoms to temperatures below the Doppler limit are based on spatial polarization gradients. These two mechanisms, however, invoke very different physical processes and are distinct by the spatial dependence of the light polarization. A key point is that these sub-Doppler mechanisms only work on atoms with multiple ground state levels. Two parameters, the friction coefficient and the capture velocity, determine the importance of these cooling processes. In this section we compare the expressions for these quantities in the sub-Doppler regime to those found by the conventional one-dimensional Doppler cooling model for optical molasses.

43.2.2.1 Lin ⊥ lin molasses

In the first case, two counterpropagating light waves with orthogonal linear polarizations form a standing wave. This configuration is familiarly called lin-perp-lin. Fig. 43.5 illustrates the change of polarization every period of $\lambda/8$ from linear to circular to linear again, but rotated by 90°, and so on [323]. Along the same distance, the light-atom coupling produces a periodic energy shift (light-shift) of the ground state Zeeman levels. To illustrate the cooling mechanism, we assume the simplest case, a transition $J_g = \frac{1}{2} \longrightarrow J_e = \frac{3}{2}$. As shown in Fig. 43.5 an atom moving through

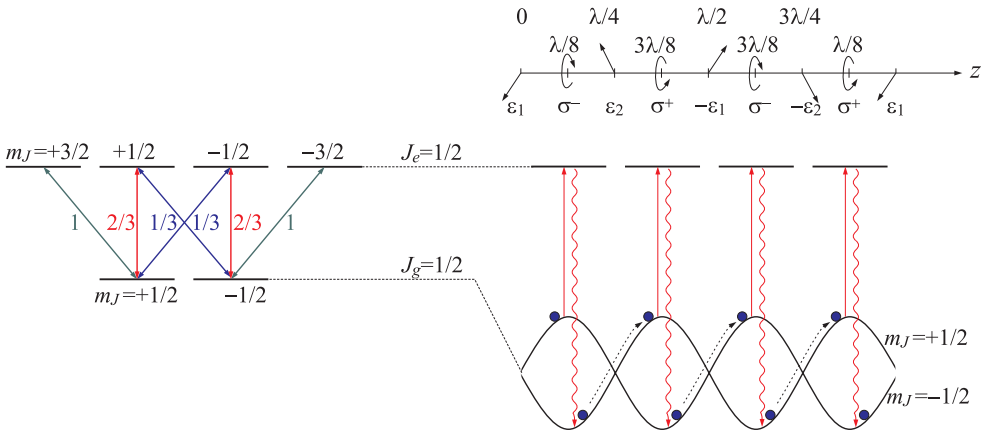

Figure 43.5: The upper line shows, how the polarization changes as a function of position (in units of a wavelength) for the 'lin-perp-lin' standing wave configuration. The figure below shows a simplified picture of the Sisyphus cooling mechanism for an atom with two levels, $J_g \leftrightarrow J_e$.

the region $z \simeq \lambda/8$, where the polarization is σ_-, will see its population pumped to $J_g = -\frac{1}{2}$. In addition, the Clebsch-Gordan coefficients that control the dipolar coupling of the $J_e = \frac{3}{2}$ require that the $J_g = -\frac{1}{2}$ couples to σ_- with a force three times larger than the $J_g = +\frac{1}{2}$ does. The difference of the coupling forces leads to the light-shift between the two fundamental states shown in Fig. 43.5. As the atom continues to move toward $+z$, the relative coupling forces are reversed near $3\lambda/8$, where the polarization is essentially σ_+. Thus, the relative energy levels of the two hyperfine fundamental states oscillate 'out of phase' when the atom moves through the standing wave.

The fundamental idea is that the optical pumping rate, which always redistributes population to the lower hyperfine level, delays the light-shift of the atom moving through the field. The result is a 'Sisyphus effect', where the atom spends most of its time in sub-levels climbing a potential hill and thus converting kinetic energy into potential energy. This accumulated potential energy is subsequently dissipated by spontaneous emission to the electromagnetic modes of the vacuum. Simultaneously, the spontaneous emission transfers the population back to the lower one of two ground state levels. The lower diagram of Fig. 43.5 illustrates the phase delay of optical pumping. For this cooling mechanism to work, the optical pumping time, which is controlled by the intensity of the light, must be sufficiently slow to give the atom enough time to climb a noticeable part of the light-shift potential. This time essentially depends on the speed of the atom. As the atom is moving slowly, having previously been cooled by the Doppler mechanism, the light field must be weak in order to decrease the optical pumping rate. Interestingly, this physical picture combines the conservative dipole optical force, whose spatial integral gives rise to the mounts and valleys of the potential on which the atom moves, and the irreversible dissipation of energy by spontaneous emission, which is necessary for any type of cooling.

We can obtain simple expressions for the friction coefficient and the capture ve-

locity after some definitions. As in the Doppler cooling model we define the friction coefficient α_{lpl} as the proportionality constant between the force F and the atomic velocity v,

$$F = -\alpha_{lpl} v \ . \tag{43.30}$$

We assume that the light field is tuned to the red of the transition J_g - J_e,

$$\Delta = \omega - \omega_0 \ , \tag{43.31}$$

and we denote the light-shifts of the levels $J_g = \pm\frac{1}{2}$ as $\Delta_\pm$, respectively. At the position $z = \lambda/8$, we find $\Delta_- = 3\Delta_+$ and at $z = 3\lambda/8$, $\Delta_+ = 3\Delta_-$. As the applied field is tuned to red, all $\Delta_\pm$ have negative values. Now, for the cooling mechanism to be efficient, the optical pumping time τ_p should be similar to the time needed for an atom with velocity v to move from the bottom to the top of the potential, $\frac{\lambda/4}{v}$,

$$\tau_p = \frac{\lambda/4}{v} \tag{43.32}$$

or

$$\Gamma' \simeq kv \ , \tag{43.33}$$

where $\Gamma' = 1/\tau_p$ and $\lambda/4 \simeq 1/k$. Now, the energy W dissipated during a cycle of escalation and spontaneous emission is essentially the average energy difference between the light-shifted ground states, $\Delta_{ls} \equiv \Delta_+ + \Delta_-$, that is $W \simeq -\hbar\Delta_{ls}$. Therefore, the rate for energy dissipation is,

$$\frac{dW}{dt} = \Gamma'\hbar\Delta_{ls} \ . \tag{43.34}$$

At the same time, every temporal energy change of a system can always be expressed as $\frac{dW}{dt} = \mathbf{F}\cdot\mathbf{v}$. Therefore, in this one-dimensional model, considering Eq. (43.31), we can write,

$$\frac{dW}{dt} = -\alpha_{lpl} v^2 = -\Gamma'\hbar\Delta_{ls} \ , \tag{43.35}$$

such that with (43.33),

$$\alpha_{lpl} = -\frac{\Gamma'\hbar\Delta_{ls}}{v^2} \simeq -kv\frac{\hbar\Delta_{ls}}{v^2} \simeq -\frac{\hbar k^2\Delta_{ls}}{\Gamma'} \ . \tag{43.36}$$

Note that since $\Delta < 0$, α_{lpl} is a positive quantity. Also note, that for large detunings, ($\Delta \gg \Gamma$) Eq. (38.24) gives,

$$\frac{U}{\hbar} = \frac{\Delta_{ls}}{4} = \frac{\Omega^2}{4\Delta} \ . \tag{43.37}$$

It is also true that for light-shifts, which are large compared to the natural width of ground state ($\Delta_{ls} \gg \Gamma'$), and for large red detunings ($\Delta \gtrsim 4\Gamma$),

$$\frac{\Gamma}{\Gamma'} \simeq \frac{\Delta^2}{4\Omega^2} \ . \tag{43.38}$$

Therefore, the sub-Doppler friction coefficient can also be written,

$$\alpha_{lpl} = -\frac{\hbar k^2\Delta}{4\Gamma} \tag{43.39}$$

Eq. (43.39) makes two remarkable predictions: Firstly, in the 'lin-perp-lin' configuration the sub-Doppler friction coefficient can be a large number in comparison to α_d. Note that from Eq. (43.28), with $I \lesssim I_{sat}$ and $\Delta \gg \Gamma$,

$$\alpha_d \simeq \hbar k^2 \left(\frac{\Gamma}{\Delta}\right)^3 , \tag{43.40}$$

and

$$\frac{\alpha_{lpl}}{\alpha_d} \simeq \left(\frac{\Delta}{\Gamma}\right)^4 . \tag{43.41}$$

Secondly, α_{lpl} is independent of the intensity of the applied field. This last result is different from the friction coefficient, which is proportional to the field intensity up to until saturation (see Eq. (43.28)). However, although α_{lpl} seems impressive, the range of atomic velocities where it can operate is constrained by the condition,

$$\Gamma' \simeq kv . \tag{43.42}$$

The ratio of the capture velocities for sub-Doppler versus Doppler cooling is therefore only,

$$\frac{v_{lpl}}{v_d} \simeq \frac{4\Delta_{ls}}{\Delta} . \tag{43.43}$$

Fig. 43.6 graphically illustrates the comparison between the Doppler and the 'lin-perp-lin' sub-Doppler cooling mechanisms. The dramatic difference of the capture ranges is evident. Note also that the slopes of the curves give the friction coefficients and that, within the capture range, the slope is much steeper for the sub-Doppler mechanism.

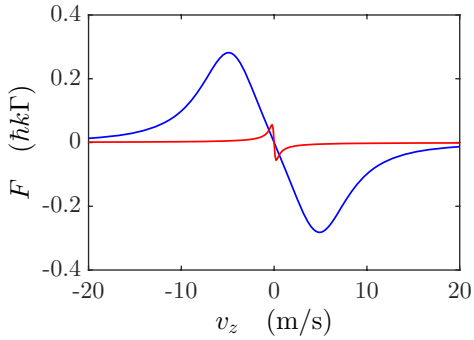

Figure 43.6: (code) Comparison of slopes, amplitudes, and capture ranges for Doppler and Sisyphus cooling.

43.2.2.2 σ^+-σ^- molasses

The second mechanism operates with two counterpropagating light beams, which are circularly polarized in opposite directions. When the two counterpropagating beams have the same amplitude, the resulting polarization is always linear and orthogonal

to the propagation axis, but the tip of the polarization vector traces a helix with a periodicity of λ [see Fig. 43.7(b)]. The physics of this sub-Doppler mechanism *does not involve hill-climbing nor spontaneous emission*, but an imbalance of the photon scattering rates by the two counterpropagating light waves as the atom moves along the z-axis. This imbalance leads to a velocity-dependent force counteracting the atomic displacement. The essential factor leading to the different scattering rates is the creation of a population orientation along the z-axis between the sub-levels of the atomic ground state. The more populated sub-levels scatter more photons. Now, considering the energy level diagram (see Fig. 43.5) and the symmetry of the Clebsch-Gordan coefficients, it is evident that transitions $J_g = \frac{1}{2} \leftrightarrow J_e = \frac{3}{2}$ coupled by linearly polarized light can not produce an orientation of the population in the ground state. In fact, the simplest system exhibiting this effect is $J_g = 1 \leftrightarrow J_e = 2$. A measure for this orientation is the magnitude of the matrix element $\langle J_z \rangle$ between the sublevels $J_{g_z} = \pm 1$. For an atom at rest at the position $z = 0$ interacting with the light polarized along the y-direction, the light-shifts Δ_0 and $\Delta_\pm$ of the three sub-levels of the ground state would be,

$$\Delta_{+1} = \Delta_{-1} = \tfrac{3}{4}\Delta_0 \ , \tag{43.44}$$

and the stationary populations would be 4/17, 4/17 e 9/17, respectively. Obviously, linearly polarized light does not produce a stationary orientation, $\langle J_z \rangle_s = 0$. But when the atom begins to move along the z-axis with velocity v, it sees a linear polarization precessing about the axis of propagation at an angle $\varphi = kz = -kvt$. This precession gives rise to a new term in the Hamiltonian, $V = kvJ_z$. Furthermore, when we transform to a rotating coordinate system, the eigenfunctions of the Hamiltonian of the atom moving in this new 'inertial' system become linear combinations of the basis functions of the resting atom. The expectation value of the stationary orientation operator J_z, is now zero in the inertial system [323],

$$\langle J_z \rangle = \frac{40}{17}\frac{\hbar k v}{\Delta_0} = \hbar(\Pi_+ - \Pi_-) \ . \tag{43.45}$$

Note that, as the expectation value of the orientation is nonzero only when the atom moves. In Eq. (43.45) we denote the populations of the sub-levels $|\pm>$ as $\Pi_\pm$, and we interpret nonzero matrix elements as a direct measure of the population difference between the ground state levels $|\pm>$. Note that, since Δ_0 is negative (red tuning), the Eq. (43.45) tells us, that the population Π_- is larger than Π_+. Now, when an atom traveling in $+z$ direction is exposed to two light waves with polarizations $\sigma_\mp$ propagating in the $\mp z$ directions, the preponderance of population in the state $|-\rangle$ will result in a higher scattering rate from the wave propagating in $-z$ direction. Therefore, the atom will be subject to a total force opposite to its movement and proportional to its velocity. The differential scattering rate is,

$$\frac{40}{17}\frac{kv}{\Delta_0}\Gamma' \ . \tag{43.46}$$

With a quantized momentum of $\hbar k$ transferred at each scattering event, the total force is,

$$F = \frac{40}{17}\frac{\hbar k^2 v \Gamma'}{\Delta_0} \ . \tag{43.47}$$

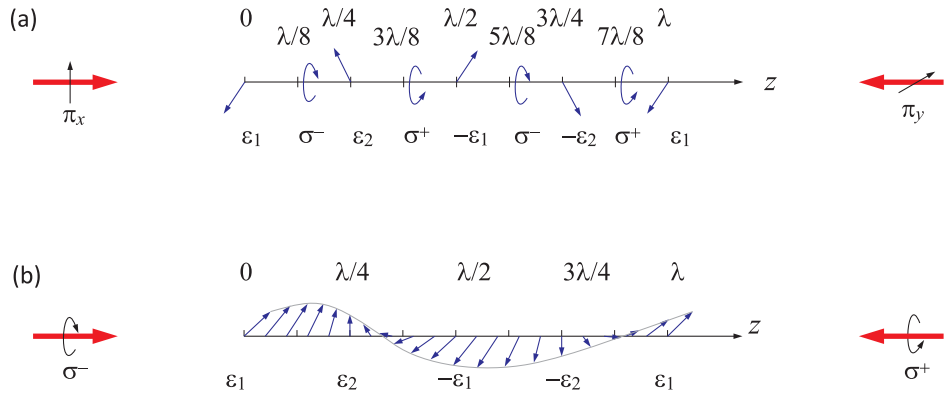

Figure 43.7: Polarization as a function of position (in units of a wavelength) for the σ^+-σ^- standing wave configuration.

The friction coefficient α_{cp} is,

$$\alpha_{cp} = -\frac{40}{17}\hbar k^2 \frac{\Gamma'}{\Delta_0} \ , \tag{43.48}$$

which is a positive quantity, since Δ_0 is negative for red detuning. Comparing α_{cp} with α_{lpl} we see, that α_{cp} must be much smaller, because we always assumed that the light shifts Δ are much larger than the linewidths Γ'. However, the heating rate due to fluctuations of the recoil is also much lower. Thus, the minimum temperatures that can be reached with the two sub-Doppler mechanisms are comparable.

Although the Doppler cooling mechanism also depends on an imbalance of scattering from counterpropagating light waves, in this case the imbalance comes from the fact that the Doppler shift experienced by the moving atoms leads to different probabilities for photon scattering. For the sub-Doppler mechanism the scattering probabilities from the two light waves are the same, but the ground state populations are not. The state with the largest population suffers the highest scattering rate.

43.2.3 Raman cooling

43.2.3.1 Optical cooling of confined particles

It is also possible to cool ions confined in a trap [1381]. The direction of their motion and their velocity change periodically with the secular frequencies ζ_r und ζ_z. For optical cooling it is sufficient to irradiate a single red-detuned running-wave light field: In a real ion trap the cylindrical symmetry cannot be realized with absolute precision so that we get different secular frequencies $\zeta_x \neq \zeta_y \neq \zeta_z$ and a coupling of the degrees of freedom for all directions of space. The cooling of the ionic motion in a single direction results in a cooling of the motion in the other directions.

In the rest system of an ion oscillating in a harmonic trap the Doppler-shift of the laser frequency changes periodically: $\mathbf{v}(t) = \mathbf{v}_0 \cos \zeta_{r,z} t$. The ion absorbs therefore in its rest system the light on a withb of sidebands whose distance and strength depend on the oscillation frequency and amplitude. The absorption profile of a transition

in such a harmonically vibrating ion follows as a convolution of the Lorentz profile $\mathcal{L}_\Gamma$, describing the naturally broadened resonance, with a function $\mathcal{S}$, describing the splitting of the absorption profile into sidebands [655]:

$$\mathcal{A}(\Delta) = (\mathcal{L}_\Gamma \star \mathcal{S})(\Delta) \quad , \quad \mathcal{S}(\Delta) = \sum_n \mathcal{J}_n(\mathbf{k}\cdot\mathbf{v}_0/\zeta_{r,z})^2 \delta(\Delta - n\zeta_{r,z}) \ . \tag{43.49}$$

$\mathcal{J}_n$ denotes the Bessel function of n^{th} order. In essence, the system is governed by three time-constants: The natural decay width of the cooling transition Γ is a measure for the inneratomic time scale, since it determines the average duration of absorption-emissions cycles. The secular frequencies $\zeta_{r,z}$ determine the time scales for changes in the external degrees of freedom, i.e. for changes of the ion's location and velocity. The Doppler-shift kv_0 of the resonance frequency in the return point of the ion motion finally, is a measure for the kinetic energy of the ion.

The relative importance of these three characteristic frequencies reveal the state of the ion in the trap. The modulation index $\mathbf{k}\mathbf{v}_0/\zeta_{r,z}$ decides on the height and the number of sidebands in the excitation spectrum. The better the ion has been cooled, the smaller the modulation index and the smaller the height and number of sidebands. The kinetic energy of the ion is,

$$E_{kin} = \frac{1}{2} m v_0^2 = \frac{1}{2} m \zeta_{r,z}^2 x_0^2 \ . \tag{43.50}$$

The modulation index $\mathbf{k}\mathbf{v}_0/\zeta_{r,z} = kx_0 = 2\pi x_0/\lambda$ is also called *Lamb-Dicke parameter*. By cooling the Lamb-Dicke parameter is so much reduced and the ion is so well localized that its motional sidebands are smaller than the wavelength of the exciting light. It then is in the so-called Lamb-Dicke regime $x_0 \ll \lambda$ [**?**] and has so small motional sidebands that they do not contribute to the line shape and do not influence the line width. Therefore the linear Doppler effect vanishes.

The quantity $\zeta_{r,z}/\Gamma$ defines the *resolution* of the sidebands. If the resolution is poor, we talk about weak confinement, else about strong confinement. Therefore the same ion can be weakly confined with respect to an allowed transition and strongly confined with respect to a forbidden transition. The cooling processes in the two cases of strong and weak trapping must be described differently. At weak confinement the oscillation frequency $\zeta_{r,z}$ is so slow that many absorption-emission cycles with the time constant Γ^{-1} can occur during one oscillation period. Cooling process and cooling limit are approximately the same as for free particles and are described by Doppler cooling.

43.2.3.2 Raman sideband cooling

In the case of strong confinement for the description of the cooling process we must consider the quantization of the motional energy in the harmonic potential. The two levels coupled by the narrow transition split into vibrational sublevels $|n_{r,z}\rangle$, which are populated in thermal equilibrium according to the Bose-Einstein distribution and have the kinetic energies E_{kin},

$$n_{r,z} = \frac{1}{e^{\hbar\zeta_{r,z}/k_B T} - 1} \quad \text{and} \quad E_{kin} = \hbar\zeta_{r,z}(n_{r,z} + \tfrac{1}{2}) \ . \tag{43.51}$$

To perform the so-called optical cooling *sideband cooling* [1381] the laser is tuned to the first lower sideband. The laser light is then scattered in a Raman-Anti-Stokes process at the excited electronic state with a vibrational quantumnumber lower by 1 $|e, n_{r,z} - 1\rangle$. The subsequent spontaneous decay occurs most probably to the same vibrational substate of the ground state $|g, n_{r,z} - 1\rangle$. The net effect of such a scattering process therefore is a transition to the next lower vibrational quantum number. The zero point energy of the ion in the trapping potential cannot be underscored by cooling, $E_{kin} > \frac{1}{2}\hbar\zeta_{r,z}$ (for the Yb^+ ion it is $E_{kin} > 2\,\mathrm{neV}$). However, the uncertainty of the kinetic energy, and the temperature T given by (43.51) have no lower limit [367].

At every absorption process, free particles carry away the momentum of the photons $\hbar k$. The recoil of a free Yb^+ ion corresponds to the frequency shift $\varepsilon/2\pi = 5.3\,\mathrm{kHz}$. On a narrow transition, it yields a resonance at the frequency ε. For trapped ions, this is not the case, because the momentum is absorbed by the whole trap (see analogy to the *Mößbauer effect*).

43.2.3.3 Stimulated Raman sideband cooling

We may use two lasers detuned far from resonance to couple two vibrational states. However, additional dissipation by optical pumping is still required.

Numerous schemes have been tested to cool neutral atoms in optical lattices. For the schemes to work, the ion should be already in the Lamb-Dicke regime. Otherwise, transitions with transfer of higher vibrational quantum numbers $n_{r,z}$ are possible during spontaneous emission. The Lamb-Dicke limit is set by $kr < 1$, or,

$$\langle n \rangle = \frac{m\omega_{trap}}{2\hbar k^2} \ . \tag{43.52}$$

This means that higher trap frequencies ease the required temperature at which sideband cooling can start to work.

43.2.4 Adiabatic cooling of an optical lattice

Adiabatic cooling by [701] in 1D. Defining the lattice constant Q_0, the Boltzmann factor $f_B \equiv e^{-\hbar\omega/k_B T}$, the initial thermal population $\pi_n = (1 - f_B) f_B^n$, the recoil energy $E_{rec} \equiv \frac{\hbar^2 k^2}{2m}$,

$$\frac{k_B T}{2} = \sum_n \frac{\pi_n}{\hbar Q_0} \int_{(n+1)^{th}\text{Bloch band}} \frac{p^2}{2m} dp = 2 \sum_n \frac{\pi_n}{\hbar Q_0} \int_{n\hbar Q_0/2}^{(n+1)\hbar Q_0/2} \frac{p^2}{2m} dp \tag{43.53}$$

$$= 2E_{rec} \left(\frac{Q_0}{k}\right)^2 \sum_{n=0}^{\infty} \pi_n \frac{3n^2 + 3n + 1}{24} = E_{rec} \left(\frac{Q_0}{k}\right)^2 \frac{1 + 4f_B + f_B^2}{12(1 - f_B)^2} \ . \tag{43.54}$$

Furthermore,

$$f_B = \frac{\bar{n}}{1 + \bar{n}} \qquad \Longleftrightarrow \qquad \bar{n} = \frac{f_B}{1 - f_B} \ .$$

43.2.5 Exercises

43.2.5.1 Ex: Optical molasses

Optical molasses are created (in one dimension) by two beams counterpropaganting lasers tuned to red of an atomic transition. Each of the laser beams exerts on the atoms the radiative pressure force $F_\pm = \hbar k \frac{\Gamma}{2} \frac{s}{[2(\Delta \pm kv)/\Gamma]^2+1+s}$. Δ is the detuning of the laser, ν is the velocity of an atom.
a. Show that for small velocities ($|kv| \ll \Gamma$ and $\Delta \leq \Gamma$) the optical molasses can be understood as a friction force and calculate the friction coefficient.
b. Heating processes caused by spontaneous emission limit the minimum temperature that can be reached in optical molasses. Calculate the laser tuning, where the temperature reaches its minimum value and specify the cooling limit.
Help: Suppose a one-dimensional molasses and assume, that the spontaneous emission only happens along this dimension. The heating rate follows from the scattering rate R through $\left(\frac{dE}{dt}\right)_{heat} = \frac{d}{dt}\frac{\langle p^2\rangle}{2m} = \frac{\hbar^2 k^2}{2m} 2R$, the cooling rate follows from $\left(\frac{dE}{dt}\right)_{cool} = Fv$.

Solution: *The force exerted on an atom is,*

$$\begin{aligned} F = F_+ - F_- &= \hbar k \Gamma s \left(\frac{1}{[2(\Delta + kv)/\Gamma]^2 + 1 + s} - \frac{1}{[2(\Delta - kv)/\Gamma]^2 + 1 + s} \right) \\ &= \hbar k \Gamma \frac{s}{2} \frac{-16 \Delta kv/\Gamma^2}{[(2\Delta/\Gamma)^2 + (2kv/\Gamma)^2 + 1 + s]^2 - (4\Delta kv/\Gamma)^2} \end{aligned}$$

A first order Taylor expansion gives,

$$\begin{aligned} F(\nu) &= F(0) + v \frac{\partial}{\partial \nu} F(0) \\ &= 0 + v \left[\hbar k \Gamma \frac{s}{2} \frac{-16 \frac{\Delta k}{\Gamma^2} \left[\left(2\frac{\Delta}{\Gamma} \right)^2 + \left(2\frac{kv}{\Gamma} \right)^2 + 1 + s \right)^2 - \left(4\frac{\delta kv}{\Gamma} \right)^2 \right] + 16 \frac{\Delta kv}{\Gamma^2} \frac{\partial}{\partial z} denominator(\nu)}{\left[\left(2\frac{\Delta}{\Gamma} \right)^2 + \left(2\frac{kv}{\Gamma} \right)^2 + 1 + s \right)^2 - \left(4\frac{\Delta kv}{\Gamma} \right)^2 \right]} \right] \\ &= -\alpha_d v \end{aligned}$$

when

$$\alpha_d = 4\hbar k^2 s \frac{2\Delta/\Gamma}{[(2\Delta/\Gamma)^2 + 1 + s]^2} \ .$$

We find the maximums of the coefficient of friction for $0 = d\alpha_d/d\Delta$ at the detunings $\Delta_m = \pm\Gamma\sqrt{\frac{1+s}{12}}$:

$$\alpha_d(\Delta_m) = \sqrt{3}\hbar k^2 s (1+s)^{-3/2} \overset{s \ll 1}{\longrightarrow} \sqrt{3}\hbar k^2 s \ .$$

b. The stationary temperature is reached when the cooling and heating rates are balanced $\left(\frac{dE}{dt}\right)_{heat} = -\left(\frac{dE}{dt}\right)_{cool}$. The cooling rate corresponds to the dissipated power,

$\left(\frac{dE}{dt}\right)_{cool} = Fv \approx -\alpha_d v^2$. *The heating rate is* $\left(\frac{dE}{dt}\right)_{heat} = \frac{d}{dt}\frac{\langle p^2\rangle}{2m} = \frac{\hbar^2k^2}{2m}2R$, *where* $R = \frac{F_+ + F_-}{\hbar k} = \Gamma\frac{I/I_s}{\left(2\frac{\Delta}{\Gamma}\right)^2+1+\frac{I}{I_s}}$ *is the scattering rate. Equalization gives,*

$$k_B T_{mi} = m v_{mi}^2 = \frac{m\left(\frac{dE}{dt}\right)_{cool}}{\alpha_d} = \frac{m\left(\frac{dE}{dt}\right)_{heat}}{\alpha_d} = \frac{m\frac{\hbar^2k^2}{2m}2R}{\alpha_d}$$
$$= \frac{m\frac{\hbar^2k^2}{2m}2\Gamma\frac{s}{[(2\Delta/\Gamma)^2+1+s]^2}}{4\hbar k^2 s\frac{2\Delta/\Gamma}{[(2\Delta/\Gamma)^2+1+s]^2}} = \hbar\Gamma\frac{(2\Delta/\Gamma)^2+1+s}{8\Delta/\Gamma} \approx \frac{\hbar\Gamma}{4}\left(\frac{2\Delta}{\Gamma}+\frac{\Gamma}{2\Delta}\right) .$$

This expression is minimized by $\Delta = \frac{1}{2}\Gamma$, *and we obtain* $k_B T_{mi} \approx \frac{1}{2}\hbar\Gamma$.

43.2.5.2 Ex: Atomic fountain

In atomic fountains atoms are accelerated upward by a 'moving optical molasses'. After the molasses has been switched off, they perform a ballistic flight in the Earth gravitational field. The moving molasses is generated by two pairs of counterpropagating laser beams intersecting at right angle and oriented both at an angle of 45° with respect to gravity. The upgoing beams are tuned to the blue, and the counterpropagating downgoing beams have the same detuning to the red side of the atomic resonance (λ = 780 nm). Supposing that the resonator is close to the position of the molasses and has with negligible length, what should be the detuning in order to achieve 1 s time period between the two passages of the atoms through the microwave resonator?

Solution: *The Doppler shift is* $\Delta = \mathbf{kv} = kv\cos 45° = \frac{2\pi\nu}{\lambda\sqrt{2}}$. *Ballistic flight is described by* $s(t) = -\frac{g}{2}t^2 + \nu(0)t$, *where* $s(t_1 = 1\ s) = 0$. *So we have...*

43.3 Optical and magneto-optical traps

43.3.1 The magneto-optical trap

An apparently fatal obstacle to the confinement of particles by optical forces is Earnshaw's optical theorem. This theorem states that, if a force is proportional to the light intensity, its divergence must be zero because the divergence of the Poynting vector expressing the directional flux of intensity is zero inside a volume without sources nor sinks of radiation. The absence of divergence precludes the possibility of a restoring force to the interior at all places of a closed surface [52]. However, Earnshaw's optical theorem can be bypassed by a clever trick. The internal degrees of freedom of the atom (i.e., its electronic energy levels) can change the proportionality between the force and the Poynting vector in a position-dependent manner, such that the optical Earnshaw's theorem does not apply. Spatial confinement is then possible using the radiative pressure force generated by counterpropagating light beams. The most common trap configuration is based on a radial magnetic field gradient produced by a quadrupolar field and three pairs of counterpropagating circularly polarized laser

beams tuned to the red of an atomic transition and intersecting at right angles at the point where the field is zero. This *magneto-optical trap* (*MOT*) uses the position-dependent Zeeman shift of the electronic levels as the atom moves in the radially increasing magnetic field. The use of circularly polarized light which is red-detuned by about Γ results in a spatially varying transition probability, whose effect is to produce a restoring force that pulls the atom back to the origin. To understand bet-

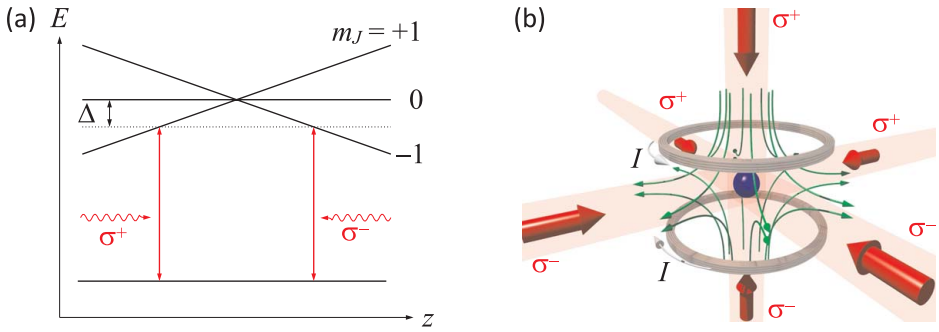

Figure 43.8: Left: Diagram of the energy level shift in an MOT, when an atom moves out of the center of the trap. A restoring force is observed around the indicated resonance positions. Right: Scheme of a typical MOT set up showing the six laser beams and the current-carrying coils in anti-Helmholtz configuration producing the quadrupolar magnetic field.

ter how the trapping scheme works, we consider a two-level atom with a transition $J = 0 \to J = 1$ moving along the z-direction. We apply a magnetic field $\mathcal{B}(z)$ growing linearly with the distance from the origin. The Zeeman shifts of the electronic levels depend on the position,

$$\Delta_{\mathcal{B}} = \frac{\mu_B g_F m_F}{\hbar} \frac{d\mathcal{B}}{dz} z \equiv \partial z \omega_{zeem} \ , \tag{43.55}$$

see Fig. 43.8. We also apply counterpropagating laser beams along the directions $\pm z$ with circular polarizations of opposite signs and tuned to the red of the atomic transition. It is clear from Fig. 43.8 that an atom moving in $\pm z$ direction will scatter $\sigma_{\mp}$ type photons at a faster rate than $\sigma_{\pm}$ type photons, because the Zeeman effect will pull the $\Delta m_J = \mp 1$ transition closer to the laser frequency. The expression for the radiation pressure force extends Eq. (43.26) to include the Doppler effect kv_z and the Zeeman effect,

$$F_{\pm z} = -\frac{\hbar k}{2} \Gamma \frac{2\Omega^2}{4(\Delta \pm k v_z \pm z \partial \omega_{zeem})^2 + 2\Omega^2 + \Gamma^2} \ . \tag{43.56}$$

The atom will, therefore, feel a restoring force which pushes it back to the origin. If the laser beams are red-detuned by an amount $\Delta = -\Gamma$, the Doppler shift of the atomic motion introduces velocity-depending term to the restoring force, such that for small displacements and velocities the total restoring force can be expressed by the sum of a term which is linear in the velocity and a term which is linear in the displacement,

$$F_{MOT} = F_{1z} + F_{2z} = -\alpha \dot{z} - \kappa z \ , \tag{43.57}$$

as we will study in Exc. 43.3.3.1. From Eq. (43.57) we can derive the equation of motion of a damped harmonic oscillator with mass m,

$$\ddot{z} + \frac{2\alpha}{m}\dot{z} + \frac{\kappa}{m}z = 0 \ . \tag{43.58}$$

The damping constant α and the spring constant κ can be written compactly in terms of atomic parameters and the field as,

$$\kappa = \frac{16\hbar k\Gamma\Omega^2\Delta\partial_z\omega_{zeem}}{4\Delta^2 + 2\cdot 6\Omega^2 + \Gamma^2} \ . \tag{43.59}$$

and

$$\alpha = \kappa\frac{k}{\partial_z\omega_{zeem}} \ . \tag{43.60}$$

Typical conditions for MOT are $\Omega = \Gamma/2$, $\Delta = -\Gamma$. For typical MOTs,

$$\alpha \simeq 2\cdot 10^{-22}\,\mathrm{Ns/m} \qquad \text{and} \qquad \kappa \simeq 3.7\cdot 10^{-19}\,\mathrm{N/m} \ . \tag{43.61}$$

We can also estimate the curvature of the MOT,

$$\omega = \sqrt{\frac{\kappa}{m}} \simeq (2\pi)\ 200\,\mathrm{Hz} \ . \tag{43.62}$$

Solve Exc. 43.3.3.2.

MOTs are realized with current-carrying coils in anti-Helmholtz configuration which generates a quadrupolar geometry potential. Near the center, the magnetic field and its absolute value are well approximated by,

$$\vec{\mathcal{B}} = q\begin{pmatrix} x \\ y \\ -2z \end{pmatrix} \qquad \text{and} \qquad |\vec{\mathcal{B}}| = q\mathcal{B}\sqrt{r^2 + 4z^2} \ , \tag{43.63}$$

with $r^2 = x^2 + y^2$ and the gradient $q \equiv \partial_r B$ is a constant, which depends only on the geometry of the coils and the current in them. Thus, the extension of the above results to three dimensions is simple if we consider the fact that the gradient of the quadrupolar field in the z-direction is twice the gradient in the radial directions x and y, such that $\kappa_z = 2\kappa_x = 2\kappa_y$.The damping term, which proportional to the velocity, implies that the kinetic energy E is dissipated from the atom (or a cloud of atoms) as,

$$E/E_0 = e^{-2\alpha t/m} \ , \tag{43.64}$$

where m is the atomic mass and E_0 the kinetic energy at the beginning of the cooling process. Therefore, the dissipative force term cools the atomic cloud and, at the same time, combines with the position-dependent term to confine it. The time constant for the damping,

$$\tau = \frac{m}{2\alpha} \tag{43.65}$$

is typically dozens of microseconds. It is important to keep in mind that a MOT is anisotropic, since the restoring force is proportional to the anisotropic field gradients.

Figure 43.9: Picture of a strontium MOT operated at 461 nm. The atomic cloud, which consists of about 10^6 atoms at 5 mK temperature is visible as a diffuse spot located inside a three-mirror ring cavity.

Because of its dissipative non-conservative nature, it is is more accurate to characterize a MOT by the maximum capture rate, rather than by a 'potential depth'.

In early experiments MOTs were loaded from a decelerated atomic beam. Later it was shown, that the low-velocity tail of the Maxwell-Boltzmann distribution provides a sufficient amount of atoms that can be captured by a MOT, so that it can be loaded directly from an atomic vapor at room temperature. Now many groups in the world use these assemblies for applications ranging from precision spectroscopy to the optical control of reactive collisions; the MOT has become the working horse of atom optics.

43.3.1.1 Density in a MOT

A typical MOT captures up to a billion atoms in a volume of a few $1\,\mathrm{mm}^3$ resulting in densities of $\sim 10^{10}\,\mathrm{cm}^{-3}$. Although a MOT works as a versatile and robust 'reaction cell' for many applications, the frequencies of the light beams must be tuned close to atomic transitions, which bears the disadvantage that a considerable fraction of atoms remains in excited states. This fact is at the origin of two processes limiting the density of a MOT: (1) losses of trapped atoms by collisions and (2) repulsive forces

between the atoms caused by reabsorption of photons scattered within the cloud. Collisional losses arise from two sources: (i) hot atoms of the residual gas inside the chamber can elastically collide with cold atoms and kick them out of the MOT, and (ii) cold atoms in excited states can undergo inelastic binary collisions. 'Photon-induced repulsion' or *radiation trapping* arises when a trapped atom spontaneously emits a photon, which is then reabsorbed by other atoms. If the optical density of the cloud is high, it can take a long time for the photon to find its way out [2]. Since any photon exchange between two atoms will increase their relative momentum by $2\hbar k$, this leads to a repulsive force, which is proportional to the absorption cross section for the incident light beam. When this repulsive force balances the confining force exerted by the MOT, any increase in the number of trapped atoms augments its size, but its density.

43.3.1.2 Dark SPOT

In order to overcome the 'radiation trapping' effect, the atoms can be optically pumped into a 'dark' hyperfine level of the ground state that does not interact with the MOT light. In a conventional MOT one usually employs an auxiliary light beam called 'repumper', copropagating with the MOT beams, but tuned to another transition between hyperfine levels of the ground and excited states. The repumper recycles the population leaking out of the (not perfectly) cyclic MOT transition. As an example, Fig. 43.10 shows the MOT and repumper transitions for sodium.

In contrast to this conventional MOT, the scheme known as the *dark spontaneous force optical trap* (dark SPOT), passes the repumping beam through a glass plate the center of which is obstructed by a small circular disk. The shadow of this disk is projected into the center of the trap in such a way that the atoms in the center are not repumped back into the cyclic transition, but spend most of their time ($\sim 99\%$) in 'dark' hyperfine levels. While the cooling and confinement force continue to operate on the periphery of MOT, its center does not feel any radiation pressure. Dark SPOTs are able to increase the density of a trapped cloud by almost *two orders* of magnitude.

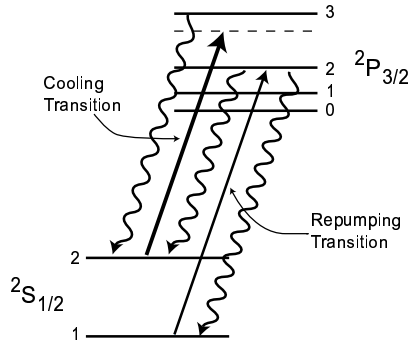

Figure 43.10: Hyperfine structure in sodium atoms showing the usual cooling, pumping, and repumping transitions.

[2] E.g. a photon at the center of the sun will take thousands of years to get out.

43.3.2 Optical dipole traps

When temporal variations are to be applied to a confinement potential, magnetic fields are not the best choice, because they are slow and of limited spatial resolution. On the other side, laser beams can be varied quickly and in localized well. The dipole force exerted by a far-detuned laser beam can be derived from the gradient of the Rabi frequency $\mathbf{F} = -\nabla(\mathbf{d}\cdot\vec{\mathcal{E}})$. Hence, it can be derived from an optical potential, which can be used for trapping. The force may be attractive (toward the intensity maximum) or repulsive.

Compared to MOTs, optical traps (*far off-resonance optical trap*, FORT) are tuned far away from resonances, where the population in excited states is insignificant and spontaneous forces are absent. Note from Eq. (38.22), that spontaneous forces fall off with the square of the detuning while the potential derived from the dipolar force only decreases linearly with the detuning. The off-resonant optical density is negligible, so that radiation trapping is not an issue. The most simple FORT consists of a single focussed, linearly polarized gaussian laser beam tuned far to the red of an atomic resonance. For large detunings and strong field gradients the Eqs. (38.24) and Eqs. (38.25) become [547],

$$\boxed{U(\mathbf{r}) \simeq \frac{\hbar\Omega(\mathbf{r})^2}{4\Delta} = \frac{3\pi c^2}{2\omega_0^3}\frac{\Gamma}{\Delta}I(\mathbf{r}) \quad \text{and} \quad \hbar\gamma_{sct}(\mathbf{r}) \simeq \sigma_a(\Delta)\frac{I(\mathbf{r})}{\omega} = \frac{3\pi c^2}{2\omega_0^3}\left(\frac{\Gamma}{\Delta}\right)^2 I(\mathbf{r})}\,, \tag{43.66}$$

using the Rabi frequency $\hbar\Omega = d_{12}\mathcal{E}$, the dipole moment $d_{12} = \sqrt{3\pi\varepsilon_0\hbar\Gamma/k^3}$, and the intensity $I = \frac{\varepsilon_0}{2}c|\mathcal{E}|^2$. This shows that the potential becomes directly proportional to the light intensity and inversely proportional to the detuning. Therefore, at large detuning but very high intensity, the depth of the FORT can be maintained, although the atoms do not absorb photons. Important advantages of FORTs as compared to MOTs are: (1) high densities ($\sim 10^{12}\,\mathrm{cm}^{-3}$) and (2) a well-defined polarization axis along which the atoms can be aligned or oriented (polarization of the spins).

Since lasers beams can easily be manipulated in position, intensity, and frequency, they can realize a large wide variety of possible geometries. For example, with a focused laser beam, one may influence the local density of a condensate and stir it around by moving the position of the laser beam. Strongly focused laser beams are often used for transporting or manipulating microscopic objects in arrangements called *optical tweezers*. And with standing light waves, it is possible to form periodic optical lattices in one, two or three dimensions (see Sec. 46.4.2).

43.3.2.1 Spin relaxation

When the atomic ground state has a hyperfine structure, another relaxation mechanism can be observed: Near-resonance Raman scattering can induce transitions between hyperfine states causing a population redistribution of between Zeeman substates called *spin relaxation*. In magnetic traps, this can lead to losses, because not all Zeeman substates are trapped.

The rate of an arbitrary scattering process starting from an initial state $|F, m\rangle$ through several possible excited states $|F'_j, m'_j\rangle$ to a final state $|F''m''\rangle$ is, according

to the formula of Kramers-Heisenberg [895],

$$\gamma_{Fm\to F'm'} \propto \left| \sum_j \frac{\alpha^{(F'_j m'_j)}_{Fm\to F'm'}}{\Delta_{F'_j m'_j}} \right|^2 . \tag{43.67}$$

Far from resonance the scattering decreases as Δ^2 for Rayleigh scattering, $Fm = F'm'$. Raman scattering, $Fm \neq F'm'$, is further suppressed by destructive interference of the different scattering paths.

In the case of rubidium, we calculate,

$$\gamma_{spin} = \frac{3c^2\omega^4}{8\pi}\frac{70}{81}\Gamma^2 \left| \left(\frac{1}{\omega_{D1}}\right)^3 \frac{1}{\Delta_{D1}} - \left(\frac{1}{\omega_{D2}}\right)^3 \frac{1}{\Delta_{D2}} \right|^2 \frac{I_0}{\hbar\omega} . \tag{43.68}$$

43.3.2.2 Potential of a Gaussian beam

The *far-off resonance optical trap* (FORT) is an example of an optical trap based on dipole forces [547]. The intensity distribution of a gaussian beam with a diameter of w_0 at its waist is [3],

$$I(\mathbf{r}) = \frac{2P}{\pi w_0^2} e^{(-2x^2-2y^2)/w_0^2} e^{-z^2/z_R^2} , \tag{43.69}$$

where P is the total power of the beam and $z_R \equiv \pi w_0^2/\lambda$ the *Rayleigh length* at a given wavelength λ. The dipolar potential is given by (43.66). Using the potential depth,

$$\boxed{U_0 \equiv \frac{3\pi c^2}{2\omega_0^3}\frac{\Gamma}{\Delta}\frac{2P}{\pi w_0^2}} , \tag{43.70}$$

which is $U_0 < 0$ for red-detuned light, we can approach the potential near its center, that is, near the optical axis, $r \ll \frac{1}{2}w_0$, and within the range of the Rayleigh length, $z \ll \pi w_0^2/\lambda$, by a harmonic potential [4],

$$\begin{aligned} U(\mathbf{r}) &\simeq U_0 e^{(-2x^2-2y^2)/w_0^2} e^{-z^2/z_R^2} \simeq U_0 \left(1 - \frac{2x^2+2y^2}{w_0^2} - \frac{z^2}{z_R^2}\right) \\ &\equiv U_0 + \frac{m}{2}\omega_r^2 r^2 + \frac{m}{2}\omega_z^2 z^2 \equiv k_B T \left(\frac{U_0}{k_B T} + \frac{r^2}{2\bar{r}^2} + \frac{z^2}{2\bar{z}^2}\right) . \end{aligned} \tag{43.71}$$

This leads to the equivalences,

$$\boxed{\begin{array}{rclcrcl} \omega_r &=& \frac{2}{w_0}\sqrt{\frac{U_0}{m}} &,& \omega_z &=& \frac{1}{z_R}\sqrt{\frac{2U_0}{m}} \\ \bar{r} &=& \frac{w_0}{2}\sqrt{\frac{k_B T}{U_0}} &,& \bar{z} &=& z_R\sqrt{\frac{k_B T}{2U_0}} \end{array}} . \tag{43.72}$$

Solve Excs. 43.3.3.3 and 43.3.3.4.

[3] See script on *Electrodynamics* (2023).

[4] The diameter of a Gaussian beam can be characterized in several ways,

$$\bar{r}_{1/\sqrt{e}\text{-radius}} = \frac{\bar{r}_{1/e^2\text{-radius}}}{\sqrt{2}} = \sqrt{2}\,\bar{r}_{1/e^2\text{-radius}} = \frac{\bar{r}_{1/2\text{-radius}}}{2\ln 2} ,$$

and $\bar{r}_{\text{-rms}} \equiv \bar{r}_{1/\sqrt{e}\text{-diam}}$ and $\bar{r}_{\text{-hwhm}} \equiv \bar{r}_{1/2\text{-diam}}$ and $\bar{r}_{\text{-diam}} = 2\bar{r}_{\text{-radius}}$.

Example 277 (*Dipole trap for rubidium*): The formulas (43.66) hold for a two-level system. In case of the $D1$- and $D2$-lines of rubidium, we must consider all contributions weighted by the respective detunings,

$$U_0 \equiv \sigma_0 \frac{\hbar\Gamma}{4}\left(\frac{1}{\Delta_{D1}} + \frac{g_{D2}/g_{D1}}{\Delta_{D2}}\right)\frac{I_0}{\hbar\omega} \simeq \frac{3\hbar\pi c^2}{2\omega^2}\frac{\Gamma}{\Delta}\frac{I_0}{\hbar\omega} \ ,$$

where $g_{D2}/g_{D1} = 2$.
Similarly, the spontaneous emission rate is,

$$\gamma_{sct} \simeq \frac{\pi c^2\Gamma^2}{2\omega^2}\left(\frac{1}{\Delta_{D1}^2} + \frac{g_{D2}/g_{D1}}{\Delta_{D2}^2}\right)\frac{I_0}{\hbar\omega} \ .$$

The spontaneous emission rate decays faster with detuning than the potential depth. Thus, heating can be avoided by working at large detunings and providing higher laser intensities. Defining the recoil temperature by,

$$T_{rec} = \frac{\hbar^2 k^2}{k_B m} \ ,$$

the *heating rate* is [547],

$$\dot{T} = \frac{1}{3}T_{rec}\gamma_{sct} = \frac{\hbar^2 k^2}{3mk_B}\gamma_{sct} \ .$$

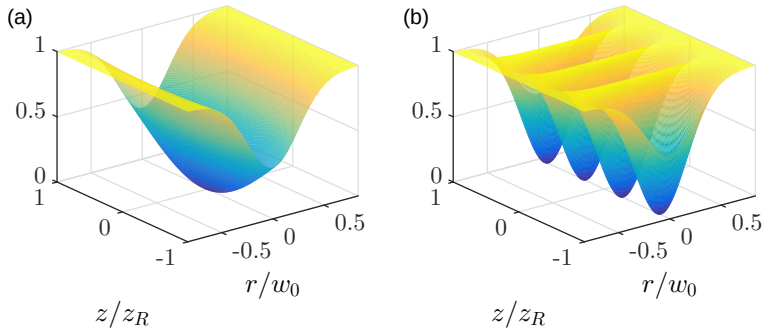

Figure 43.11: (code) (left) Dipole potential created by a Gaussian beam. (right) Dipole potential created by a stationary light wave.

43.3.2.3 Trapping in standing light waves

If both counterpropagating modes are pumped at different powers, $P_\pm$, the intensity distribution is,

$$I(\mathbf{r}) = \frac{2}{\pi w_0^2} e^{(-2x^2-2y^2)/w_0^2} e^{-z^2/z_R^2}\left|\sqrt{P_+}e^{\imath kz} + \sqrt{P_-}e^{-\imath kz}\right|^2 \ . \tag{43.73}$$

Defining the contrast of the standing wave as,

$$C_{sw} \equiv \frac{4\sqrt{P_+P_-}}{(\sqrt{P_+}+\sqrt{P_-})^2} \ , \tag{43.74}$$

we can express the potential depth by,

$$\boxed{U_0 = \frac{3\pi c^2}{2\omega_0^3}\frac{\Gamma}{\Delta}\frac{2(\sqrt{P_+}+\sqrt{P_-})^2}{\pi w_0^2} = \frac{3\pi c^2}{2\omega_0^3}\frac{\Gamma}{\Delta}\frac{8(\sqrt{P_+P_-})^2}{\pi w_0^2 C_{sw}}} \ . \tag{43.75}$$

Therefore, within the Rayleigh length, the potential is,

$$\begin{aligned} U(\mathbf{r}) &\simeq U_0 e^{(-2x^2-2y^2)/w_0^2} e^{-z^2/z_R^2} \frac{P_+ + P_- + 2\sqrt{P_+P_-}\cos kz}{P_+ + P_- + 2\sqrt{P_+P_-}} \\ &\simeq C_{sw} U_0 e^{-2\rho^2/w_0^2} \frac{P_+ + P_- + 2\sqrt{P_+P_-}\cos kz}{4\sqrt{P_+P_-}} \ . \end{aligned} \tag{43.76}$$

Neglecting terms containing higher powers of the coordinates than squared, we can also write,

$$U(\mathbf{r}) \simeq U_0 \left(1 - \frac{2x^2}{w_0^2} - \frac{2y^2}{w_0^2} - \frac{\sqrt{P_+P_-}}{(\sqrt{P_+}+\sqrt{P_-})^2}k^2z^2 + ...\right) \ . \tag{43.77}$$

This leads to the identities,

$$\boxed{\begin{array}{rclcrcrcl} \omega_r &=& \frac{2}{w_0}\sqrt{\frac{U_0}{m}} &,& \omega_z &=& \frac{1}{z_R}\sqrt{\frac{2U_0}{m}} &,& \omega_{lat} = k\sqrt{\frac{C_{sw}U_0}{2m}} \\ \bar{r} &=& \frac{w_0}{2}\sqrt{\frac{k_BT}{U_0}} &,& \bar{z} &=& \frac{\sqrt{2}}{k}\sqrt{\frac{k_BT}{U_0}} & & \end{array}} \ . \tag{43.78}$$

Solve the Excs. 43.3.3.5, 43.3.3.6, and 43.3.3.7.

43.3.3 Exercises

43.3.3.1 Ex: Linearization of the MOT

Derive the friction coefficient and the spring constant for a MOT.

Solution: *We use the following expressions,*

$$\sigma(\Delta) = \frac{\sigma_0\Gamma^2}{4\Delta^2+2\Omega^2+\Gamma^2} \quad \textit{and} \quad \sigma_0 = 3\frac{\lambda^2}{2\pi} \quad \textit{and} \quad \Omega^2 = \Gamma\sigma_0\frac{I}{\hbar\omega} \quad \textit{and} \quad \frac{I}{I_s} = \frac{2\Omega^2}{\Gamma^2} \ .$$

For strong/weak saturation,

$$\frac{I}{\hbar\omega}\sigma(\Delta) \begin{cases} \overset{\Omega\gg\Delta,\Gamma}{\longrightarrow} \frac{\Gamma}{2} \\ \overset{\Gamma\gg\Omega,\Gamma}{\longrightarrow} \frac{\Omega^2}{\Gamma} \end{cases} \ .$$

The scattering force is,

$$F = \frac{I}{\hbar\omega}\sigma(\Delta)\hbar k = \frac{\hbar k\Gamma\Omega^2}{4\Delta^2+2\Omega^2+\Gamma^2} \ .$$

The trapping force in a MOT in z-direction (and analogously in x and y-direction) is $F_s = F_z^+ + F_z^-$ *with,*

$$F_z^{\pm} \equiv \frac{\hbar k \Gamma \Omega^2 e^{-2\frac{x^2}{w^2}-2\frac{y^2}{w^2}}}{4[\Delta \pm k v_z \pm \frac{\mu_B g_F m_F}{\hbar}\ \partial_z B\ z]^2 + 2\Omega^2[2e^{-2\frac{y^2}{w^2}^2-2\frac{z^2}{w^2}} + 2e^{-2\frac{y^2}{w^2}-2\frac{z^2}{w^2}} + 2e^{-2\frac{x^2}{w^2}-2\frac{y^2}{w^2}^2}\ ] + \Gamma^2} \ .$$

In the trap center, $x = y = z = 0$*, defining* $\partial_z \omega_{zee} \equiv (\mu_B g_F m_F/\hbar)\ \partial_z B$*,*

$$F_z^{\pm} \equiv \frac{\hbar k \Gamma \Omega^2}{4[\Delta \pm k v_z \pm \partial_z \omega_{zee}\ z]^2 + 12\Omega^2 + \Gamma^2} \ .$$

Now, we linearize for small Ω*,*

$$\begin{aligned} F_z(z, v_z) &= F(0,0) + z\frac{\partial}{\partial z}F(0,0) + v_z\frac{\partial}{\partial v_z}F(0,0) + ... \\ &= 0 + z\frac{16\hbar k \Gamma \Omega^2 \Delta\ \partial_z \omega_{zee}}{(4\Delta^2 + 12\Omega^2 + \Gamma^2)^2} + v_z\frac{16\hbar k \Gamma \Omega^2 \Delta\ k}{(4\Delta^2 + 12\Omega^2 + \Gamma^2)^2} + o(z^3) \ , \end{aligned}$$

such that,

$$F_z(z, v_z) = -\kappa z - \alpha v_z$$

with

$$\kappa \equiv \frac{16\hbar k \Gamma \Omega^2 \Delta\ \partial_z \omega_{zee}}{(4\Delta^2 + 12\Omega^2 + \Gamma^2)^2} \qquad \textit{and} \qquad \alpha \equiv \kappa \frac{k}{\partial_z \omega_{zee}} \qquad \textit{and} \qquad \omega = \sqrt{\frac{\kappa}{m}} \ .$$

Using typical parameters for a Na MOT $\Gamma = (2\pi)\ 9.89\,\mathrm{MHz}$*,* $\lambda = 589\,\mathrm{nm}$*,* $w_0 = 0.64\,\mathrm{cm}$*,* $\partial_z B = 2\partial_x B = 20\,\mathrm{G/cm}$*,* $I_s = 6\,\mathrm{mW/cm^2}$*, and* $I = 60\,\mathrm{mW/cm^2}$*, we find,*

$$\begin{aligned} \kappa &= 3.7 \cdot 10^{-19}\,\mathrm{N/m} \\ \alpha &= 2.2 \cdot 10^{-22}\,\mathrm{Ns/m} \\ \omega &= (2\pi)\ 500\,\mathrm{Hz} \ . \end{aligned}$$

43.3.3.2 Ex: Design of a Zeeman slower

In this exercise we will design a 'decreasing field *Zeeman slower*' for strontium (see also Exc. 34.6.7.3).

a. Calculate the mean velocity of atoms in a strontium gas heated to 500° C. What is the Doppler shift for an atom moving at this velocity at the cooling transition at $\lambda = 461\,\mathrm{nm}$ (linewidth 30.5 MHz)?

b. Assuming you want to decelerate a fraction of 20% of the atoms flying in a particular direction, to what frequency should a counterpropagating laser (intensity $I = 20\,\mathrm{mW/cm^2}$) be tuned in order to slow down the atoms?

c. Suppose the strontium atoms were always in resonance with the counterpropagating laser light while being decelerated. What would be the evolution of their Doppler shift along their trajectory (supposed to be on a straight line antiparallel to the laser

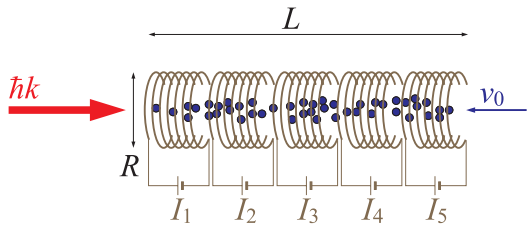

Figure 43.12: Design of a Zeeman slower.

beam).
d. In order to maintain the laser always in resonance we need to compensate for the diminishing Doppler shift along the atomic trajectory. This can be done exploiting the Zeeman shift induced by a magnetic field. We will now design a magnetic field generating an appropriate Zeeman shift. For simplicity, let us assume 5 identical radial solenoids distributed over $L = 30\,\text{cm}$ as sketched in Fig. 43.12, the only adjustable parameters being the currents in all solenoids, which need to be optimized such as to compensate the Doppler shift along the atom's trajectory.
e. Simulate the 1D trajectory of an atom cooled by the Zeeman slower.

Solution: *The results are shown in Fig. 43.13.*

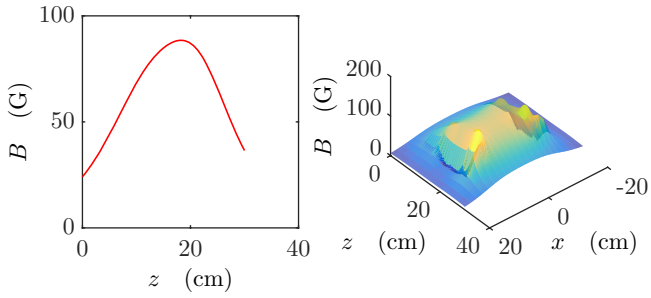

Figure 43.13: Magnetic field in a Zeeman slower.

43.3.3.3 Ex: Dipole trap near an intercombination line

a. Strontium has a strong transition ($\Gamma_{461} = (2\pi)\ 30.5\,\text{kHz}$) at 461 nm and a weak intercombination resonance ($\Gamma_{689} = (2\pi)\ 7.6\,\text{kHz}$) at 689 nm. A Gaussian laser beam with the power $P = 10\,\text{mW}$ focused to a waist of $w_0 = 100\,\mu\text{m}$ is tuned $\Delta_{689} = -(2\pi)\ 10\,\text{GHz}$ below the intercombination transition. Calculate the potential depth and the vibration frequencies for atoms trapped by this laser beam considering both resonances. What is the scattering rate on the two transitions.
b. Supposes that the trapped atomic cloud consists of $N = 10^8$ atoms at the temperature $T = 10\,\mu\text{K}$. Calculate the atomic density n_0 in the center of the cloud.

Solution: *a. Based on the formula (43.70) we find for the potential depth,*

$$U_{0,k} = \frac{3\pi c^2 \Gamma_k}{2\omega_0^3 \Delta_k} I_0 \ ,$$

with $k = 461$ *ou* $k = 689$*, such that,*

$$\frac{U_{0,461}}{U_{0,689}} = \frac{\Gamma_{461}\Delta_{689}}{\Gamma_{689}\Delta_{461}} \ .$$

The scattering rate is,

$$\gamma_{sct} = \left(\frac{\Gamma_{461}\Delta_{689}}{\Gamma_{689}\Delta_{461}}\right)^2 \ .$$

43.3.3.4 Ex: Dipole trap with a focused beam

a. Calculate the vibration frequencies of ^{87}Rb atoms confined in an optical trap consisting of a focused laser beam with the power $P = 10\,\mathrm{W}$ and the beam diameter $w_0 = 100\,\mu\mathrm{m}$. The laser beam is tuned 5 nm to the red side of the rubidium $D1$ resonance located at $\lambda = 795\,\mathrm{nm}$.
b. Assume that the trapped atomic cloud consists of $N = 10^8$ atoms at the temperature $T = 100\,\mu\mathrm{K}$. Calculate the atomic density n_0 in the center of the cloud.
c. The cross section for elastic collisions is $\sigma = 10^{-12}\,\mathrm{cm}^2$. How many times do atoms meet on average?

Solution: *a. The intensity of the beam is,*

$$I(r,z) = \frac{2P}{\pi w(z)^2} e^{-2r^2/w(z)^2} \quad with \quad w(z) = w_0\sqrt{1+\left(\frac{z}{z_R}\right)^2} \quad and \quad z_R = \frac{\pi w_0^2}{\lambda} \ ,$$

and $I_0 = \frac{2P}{\pi w_0^2} = 64000\,\mathrm{W/cm}^2$*. For rubidium we have* $\Gamma = (2\pi)\ 6\,\mathrm{MHz}$*. For* $\Delta = -2\pi\frac{c}{\lambda^2}\Delta\lambda = -2\pi \times 2300\,\mathrm{GHz}$ *we expect an optical potential of,*

$$U_0 = \frac{3\pi c^2 \Gamma}{2\omega_0^3 \Delta} I_0 = h \times 82\,\mathrm{MHz} = 4\,\mathrm{mK} \ .$$

If we approach the intensity profile harmonically, we obtain the secular radial frequency, $\omega_r = \sqrt{\frac{2U_0}{m}}\frac{\sqrt{2}}{w_0} = 2\pi \times 2$ *kHz, e axial,* $\omega_z = \sqrt{\frac{2U_0}{m}}\frac{1}{z_R} = 2\pi \times 35$ *Hz.*
b. At the specified temperature the cloud size is given by $k_B T = m\omega_r^2 r^2$*. Hence,*

$$\bar{r} = \sqrt{\frac{k_B T}{2U_0}}\frac{w_0}{\sqrt{2}} = 8\,\mu\mathrm{m} \qquad and \qquad \bar{z} = \sqrt{\frac{k_B T}{2U_0}} z_R = 2.8\,\mathrm{mm} \ .$$

The atomic density follows from the normalization condition,

$$n_0 = \frac{N}{(2\pi)^{3/2}\bar{r}^2\bar{z}} = 3.5 \times 10^{13}\,\mathrm{cm}^{-3} \ .$$

c. The collision rate is given by $\gamma_{coll} = \sigma\bar{v}n_0 = 3.5\,\mathrm{s}^{-1}$ *with* $\bar{v} = \sqrt{\frac{k_B T}{m}}$*.*

43.3.3.5 Ex: Optical lattice

A laser beam with wavelength $\lambda_{dip} = 1064\,\text{nm}$, power $P = 2\,\text{W}$, and diameter $w_0 = 50\,\mu\text{m}$ is subdivided into three retroreflected beams intersecting at right angles. With this configuration we form a cubic optical lattice for strontium atoms, whose relevant transition lies at $\lambda_{Sr} = 461\,\text{nm}$ and has a decay width of $\Gamma_{Sr} = (2\pi)\ 32\,\text{MHz}$. Calculate the potential depth and the secular frequencies.

Solution: *The dipolar potential is,*

$$U_d(\mathbf{r}) = \frac{3\pi c^2 \Gamma_{461}}{2\omega_{461}^3} \frac{1}{\omega_d - \omega_{461}} I(\mathbf{r}) \ ,$$

with a maximum intensity,

$$I_0 = \frac{2P}{\pi w_0^2} \ .$$

We expect a potential depth of,

$$U_0 = \frac{3\pi c^2 \Gamma_{461}}{2\omega_{461}^3} \frac{1}{\omega_d - \omega_{461}} I_0 \simeq k_B \cdot 20\ \mu K \ ,$$

for the given parameters and a single laser beam. For superposed laser beams, the effective intensity is the sum of all. Thus, as the laser is divided into three parts before being superposed and retroreflected, we have twice the effective intensity and twice the potential depth.
The secular frequencies depend on the geometry of the beam. Expanding the spatial distribution of a single focused beam,

$$I(r,z) = \frac{2P}{\pi w_0^2} e^{-2r^2/w(z)^2} \qquad with \qquad w(z) = \sqrt{1 - \left(\frac{z}{z_R}\right)^2} \ ,$$

near the position $r = z = 0$, we obtain,

$$\omega_r = \sqrt{\frac{2U_0}{m}} \frac{\sqrt{2}}{w_0} \simeq (2\pi)\ 276\,\text{Hz} \qquad and \qquad \omega_z = \sqrt{\frac{2U_0}{m}} \frac{1}{z_R} \simeq (2\pi)\ 0.57\,\text{Hz} \ ,$$

with $z_R = \pi w_0^2/\lambda$. For an optical lattice with lattice constant $\lambda/2$, we expand,

$$I(z) = \cos\frac{kz}{2} \ ,$$

and obtain,

$$\omega_z = \sqrt{2\frac{2U_0}{m}} k \simeq (2\pi)\ 188\,\text{kHz} \ .$$

43.3.3.6 Ex: Minimum optical lattice depth

Estimate the minimum required intensity of two counterpropagating laser beams tuned 7 GHz to the red of the strontium intercombination transition at 689 nm necessary to sustain an optical lattice exhibiting a single vibrational level.

Solution: *Approximating a lattice antinode by a harmonic potential, the condition for having a bound state is,*

$$U_0 > \frac{\hbar\omega_{lat}}{2}$$

using the results of Sec. 43.3.2,

$$U_0 = \frac{3\pi c^2}{2\omega_0^3}\frac{\Gamma}{\Delta}4I \qquad and \qquad \omega_{lat} = k\sqrt{\frac{U_0}{2m}} \ .$$

Hence,

$$U_0 > \frac{\hbar^2 k^2}{8m} = \frac{E_{rec}}{4} \ ,$$

that is,

$$I > \frac{\omega_0^3 E_{rec}}{24\pi c^2}\frac{\Delta}{\Gamma} \approx 1.6\,\mathrm{W/cm}^2 \ .$$

43.3.3.7 Ex: Ring shaped optical potential

An interesting system is the $1D$ array of annular optical potentials realized in a standing wave formed by red-detuned Gaussian beam and a counterpropagating blue-detuned doonat-mode. In general, the tight longitudinal confinement freezes out the axial motion by *quantum confinement*. It can be readily shown [1388] that in the far-off resonance case and if the potential is approximate by a harmonic potential around its minimum the eigenenergy spectrum is given by,

$$E_{pq} = U_0 + \hbar\omega(q + \tfrac{1}{2}) + \frac{\hbar^2 p^2}{2mR_0^2} \ .$$

It thus reproduces the ro-vibrational spectrum of a $2D$ artificial molecule and gives rise to two normal motions. In its ground state, we have the atom optical analog of a $2D$ rigid rotator. Gravity plays formally the same role as static electric fields for molecules. Such systems might be interesting for investigating the selection rules for transitions between ro-vibrational states involving conservation of total angular momentum of light and atoms and yield insight into the concept of orbital angular momentum of light fields.

Solution:

43.3.3.8 Ex: Time-averaged trap

For sufficiently fast periodic displacements of a far-detuned laser beam it is possible to engineer effective more complicated trapping potential. What are the conditions for modulation speed? Simulate the effective trapping potential generated by a vibrating laser beam.

Solution: *The result is shown in Fig. 43.14.*

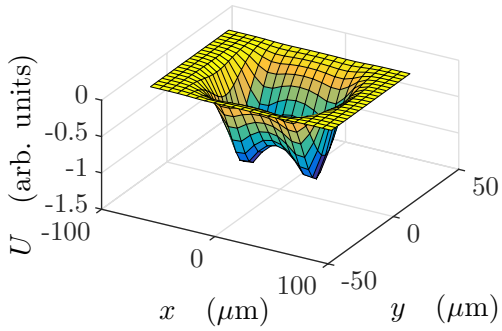

Figure 43.14: Effective potential in radial direction of a shaking dipole trap.

43.4 Magnetic traps

Purely magnetic traps are widely used in atom optics, where they served, e.g., for the first realizations of Bose-Einstein condensation (BEC). The most important feature that distinguishes magnetic traps is, that they do not need light to confine atoms. Hence, they are free of heating effects caused by photonic absorption, which turned out to be necessary condition for reaching BEC. Magnetic traps rely on the interaction of atomic spins with magnetic fields and gradients designed to contain the atoms. Depending on the sign of U and $\mathbf{F}$, atoms in states whose energy increases or decreases with the magnetic field are called 'low-field seekers' or 'high-field seekers', respectively. One might think, that it should be possible to trap atoms in any of these states, generating either a magnetic field minimum or a maximum. Unfortunately, only low-field seekers can be trapped in static magnetic fields, because in free space magnetic fields can not form maxima. Even though low-field seekers are not in the energetically lowest hyperfine levels, they can still be trapped because the rate of spontaneous emission through the magnetic dipole is $\sim 10^{-10}\,\mathrm{s}^{-1}$, and hence completely negligible. However, spin changing collisions can induce losses and limit the maximum densities. Solve Exc. 43.4.6.1.

The most basic static magnetic trap for neutral atoms is generated by a pair of current-carrying coils in anti-Helmholtz configuration (similar to the geometry used for a MOT), producing an axially symmetric qudrupolar magnetic field. Since this field configuration always has a central point, where the magnetic field disappears, non-adiabatic Majorana transitions can occur when the atom passes through the

zero point. The transitions transfers population from a low-field seeking state to a high-field seeker, which consecutively is expelled from the trap. This problem can be overcome by using a different magnetic field geometries. One example is the so-called *magnetic bottle* also called the *Ioffe-Pritchard trap*, where the minimum field amplitude has a finite value different from zero. Other methods to eliminate the zero-field point are time-varying potentials, such as the time-orbiting potential (TOP) trap, or the application of an 'optical plug', which consist in an intense dipolar optical laser beam, tuned to the blue of an atomic transition, focused into the center of a quadrupole trap where the magnetic field is zero, and repelling the atoms from this area.

43.4.1 Quadrupolar traps and Majorana spin-flips

The most basic static magnetic trap for neutral atoms is generated by a pair of current-carrying coils in anti-Helmholtz configuration producing an axially symmetric quadrupolar magnetic field, as shown in Fig. 43.15.

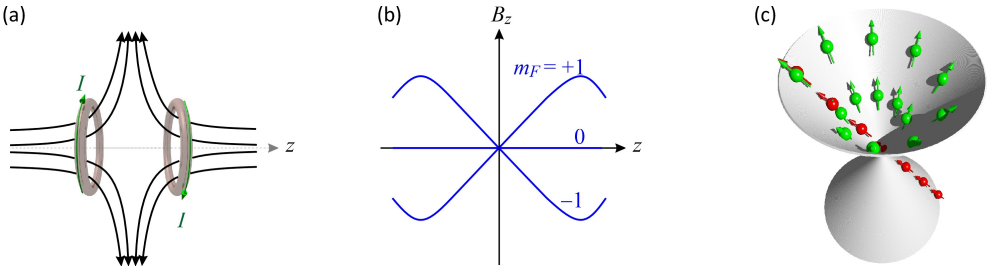

Figure 43.15: (a) Quadrupolar magnetic trap generated by a pair of current-carrying wires in anti-Helmholtz configuration. (b) Ground state energy levels of ^{23}Na, $^2S_{1/2}$, $F = 1$ as a function of axial distance from the trap center. (c) Illustration of Majorana spin-flips: The red atom passes through the hole, while the green one moves adiabatically avoiding the hole.

Close to the trap center an expansion of the magnetic field generated by anti-Helmholtz coils yields,

$$\vec{\mathcal{B}} = \begin{pmatrix} x \\ y \\ -2z \end{pmatrix} \partial_r \mathcal{B} \ , \tag{43.79}$$

where the field gradient $\partial_r B$ along radial direction $r^2 \equiv x^2 + y^2$ in the trap center depends on the applied current and the geometry of the coils. However, the 1:2 aspect ratio is generic for all quadrupolar potentials, as we will see in Exc. 43.4.6.2. We easily verify that,

$$\nabla \cdot \vec{\mathcal{B}} = 0 \qquad \text{but} \qquad \nabla |\vec{\mathcal{B}}| = \frac{\partial_r \mathcal{B}}{\sqrt{r^2 + 4z^2}} \begin{pmatrix} x \\ y \\ 4z \end{pmatrix} \ . \tag{43.80}$$

Thus, the quadrupolar magnetic potential is linear in the spatial coordinates,

$$\boxed{U(\mathbf{r}) = -|\vec{\mu}||\vec{\mathcal{B}}| = \mu_B g_J m_J \ \partial_r \mathcal{B} \ \sqrt{r^2 + 4z^2}} \ , \tag{43.81}$$

where $2\partial_r \mathcal{B} = \partial_z \mathcal{B}$.

To calculate the *rms*-radius $\bar{r}$ of a cloud of temperature T confined to this potential, we set,

$$k_B T \equiv U(\bar{r}, 0) = \mu_B \bar{r} \partial_r \mathcal{B} \ , \tag{43.82}$$

and obtain the density distribution,

$$n(\mathbf{r}) = n_0 e^{-U(\mathbf{r})/k_B T} = n_0 e^{-\sqrt{r^2+4z^2}/\bar{r}} \ . \tag{43.83}$$

Normalization requires,

$$\begin{aligned} N &= \int_{R^3} n(\mathbf{r}) \ d^3 r = n_0 \int_{-\infty}^{\infty} \int_0^{\infty} e^{-\sqrt{r^2+4z^2}/\bar{r}} 2\pi r \ dr dz \\ &= n_0 2\pi \bar{r}^2 \int_{-\infty}^{\infty} \int_{2|z|/\bar{r}}^{\infty} \xi e^{-\xi} d\xi dz = n_0 2\pi \bar{r}^2 \int_{-\infty}^{\infty} e^{-\frac{2|z|}{\bar{r}}} \left(1 + \tfrac{2|z|}{\bar{r}}\right) \ dz \\ &= n_0 2\pi \bar{r}^3 \int_0^{\infty} e^{-\zeta} (1+\zeta) \ d\zeta = n_0 4\pi \bar{r}^3 \ . \end{aligned} \tag{43.84}$$

Therefore, the effective volume is, $V_{eff} = 4\pi \bar{r}^3$. In application example is discussed in Exc. 43.4.6.3.

43.4.1.1 Majorana spin-flips

The quadrupolar trap is the simplest one that can be technically realized. Unfortunately, this trap is not stable because of the phenomenon of *Majorana spin-flips*, which expel atoms from the trapped cloud. Since this field configuration always has a central point, where the magnetic field disappears, non-adiabatic Majorana transitions can occur when the atom passes through the zero point [see Fig. 43.15(c)]. The disappearance of the field leaves the atoms disoriented, that is, ready to reorient their spins. The transitions transfer population from a low-field seeking state to a high-field seeker, which consecutively is expelled from the trap. This problem is particularly severe for hydrogen, where it can induce a so-called *relaxation explosion* [618].

From (43.82) we get the *rms*-radius,

$$\bar{r} = \frac{k_B T}{\mu_B \partial_r \mathcal{B}} \ . \tag{43.85}$$

The average velocity of an atom is,

$$\bar{v} = \sqrt{\frac{k_B T}{m}} \ . \tag{43.86}$$

In order for the atomic motion in the magnetic potential to be adiabatic [so that Eq. (43.81) applies], the *local Larmor frequency*,

$$\omega_{Larmor}(\mathbf{r}) = \frac{\mu_B}{\hbar} \sqrt{r^2 + 4z^2} \partial_r \mathcal{B} \tag{43.87}$$

must be faster, than any change the atom might experience due to its motion with velocity $\mathbf{v}$. I.e. we need [1018],

$$\omega_{Larmor}(\mathbf{r}) > \frac{\mathbf{v} \cdot \nabla |\vec{\mathcal{B}}|}{|\vec{\mathcal{B}}|} \ . \tag{43.88}$$

For a quadrupolar trap, this can not be satisfied within a certain volume located at the trap center, since the expression (43.88) divergence near the center. This ellipsoidal volume is delimited by $\mathbf{r}_{sf}$ given by the condition,

$$\omega_{Larmor}(\mathbf{r}_{sf}) \equiv \frac{\mathbf{v}\cdot\nabla|\vec{\mathcal{B}}|}{|\vec{\mathcal{B}}|} \ . \tag{43.89}$$

For our quadrupole trap,

$$\frac{\mathbf{v}\cdot\nabla|\vec{\mathcal{B}}|}{|\vec{\mathcal{B}}|} = \frac{\mathbf{v}\cdot\frac{\partial_r\mathcal{B}}{\sqrt{r_{sf}^2+4z_{sf}^2}}}{\partial_r\mathcal{B}\sqrt{r_{sf}^2+4z_{sf}^2}}\begin{pmatrix} x_{sf} \\ y_{sf} \\ 4z_{sf}\end{pmatrix} = \frac{x_{sf}v_x + y_{sf}v_y + 4z_{sf}v_z}{r_{sf}^2+4z_{sf}^2} \ . \tag{43.90}$$

Considering for simplicity only radial motion, $\mathbf{v} = v\hat{\mathbf{e}}_r$, then by equating (43.87) and (43.89),

$$\frac{\mu_B}{\hbar} r_{sf}\partial_r\mathcal{B} = \omega_{Larmor}(r_{sf}) = \frac{v}{r_{sf}} \ , \tag{43.91}$$

that is, the spin-flip volume is on the order of,

$$r_{sf} = \sqrt{\frac{\hbar v}{\mu_B\partial_r\mathcal{B}}} \ . \tag{43.92}$$

Let us now estimate the spin relaxation rate from the flow of atoms through the volume,

$$\frac{1}{\tau_{sf}} = N\frac{r_{sf}^3}{V_{eff}}\frac{\bar{v}}{r_{sf}} \ , \tag{43.93}$$

where r_{sf}^3/V_{eff} is simply the fraction of the cloud's volume overlapping with the spin-flip volume. Then,

$$\begin{aligned}\frac{1}{\tau_{sf}} &= \frac{N}{4\pi\bar{r}^3}r_{sf}^2\bar{v} = \frac{N}{4\pi\left(\frac{k_BT}{\mu_B\partial_r\mathcal{B}}\right)^3}\frac{\hbar\bar{v}}{\mu_B\partial_r\mathcal{B}}\bar{v} \\ &= \frac{N\hbar}{4\pi(k_BT)^3}(\mu_B\partial_r\mathcal{B})^2\frac{k_BT}{m} = \frac{N\hbar(\mu_B\partial_r\mathcal{B})^2}{4\pi m(k_BT)^2} \ .\end{aligned} \tag{43.94}$$

That is, the problem gets worse when the cloud is cooled to low temperatures.

43.4.2 Magnetic Ioffe-type traps

The spin-flip problem can be overcome by using a different magnetic field geometries. One example is the so-called *magnetic bottle*, also called the *Ioffe-Pritchard trap* illustrated in Fig. 43.16(a), where the minimum field amplitude has a finite value different from zero. Other methods to eliminate the zero-field point are time-varying potentials, such as the time-orbiting potential (TOP) trap illustrated in Fig. 43.16(b) and discussed in Exc. 43.4.6.4 [417, 580], or the application of an 'optical plug', which consist in an intense dipolar optical laser beam, tuned to the blue of an atomic transition, focused into the center of a quadrupole trap where the magnetic field is zero, and

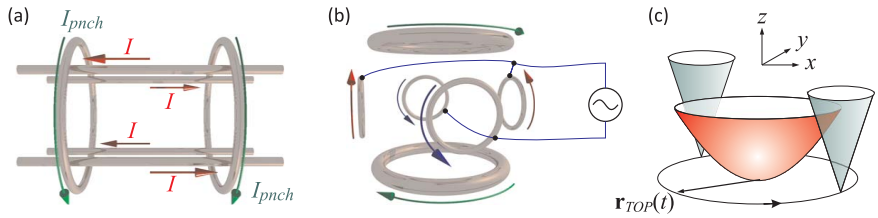

Figure 43.16: (a) Magnetic trap in Ioffe-Pritchard configuration. (b) Time-Orbiting Potential (TOP) trap. (c) Death-circle in a TOP trap.

repelling the atoms from this area (see Fig. 43.24). The advantage of Ioffe-Pritchard-type traps is that they are always harmonic sufficiently close to the trap center, which simplifies the theoretical treatment in many respects, as shown in Exc. 43.4.6.5.

Close to the trap center Ioffe-Pritchard-type traps are described by,

$$\boxed{U(\mathbf{r}) = \mu_B g_F m_F \sqrt{\mathcal{B}_0^2 + (r\partial_r \mathcal{B})^2 + (z\partial_z \mathcal{B})^2}} \,, \tag{43.95}$$

and this magnetic trapping potential can be harmonically approximated by,

$$\begin{aligned} U(\mathbf{r}) &\simeq \mu_B g_F m_F \left(\mathcal{B}_0 + \frac{(r\partial_r \mathcal{B})^2}{2B_0} + \frac{(z\partial_z \mathcal{B})^2}{2B_0} \right) \\ &\equiv const + \frac{m}{2}\omega_r^2 r^2 + \frac{m}{2}\omega_z^2 z^2 \equiv k_B T \left(const + \frac{r^2}{2\bar{r}^2} + \frac{z^2}{2\bar{z}^2} \right) \,, \end{aligned} \tag{43.96}$$

where the *rms*-radius $\bar{r} = \omega_r^{-1}\sqrt{k_B T/m}$ follow from the normalization of the density $n(\mathbf{r}) = n_0 e^{-U(\mathbf{r})/k_B T}$ to the number of atoms,

$$N = \int n(\mathbf{r}) d^3 r = n_0 \int_0^\infty e^{-r^2/2\bar{r}^2} 2\pi dr \int_{-\infty}^\infty e^{-z^2/2\bar{z}^2} dz = n_0 (2\pi)^{3/2} \bar{r}^2 \bar{z} \equiv n_0 V_{eff} \,. \tag{43.97}$$

The trap frequencies can be calculated as,

$$\omega_{r,z} = \sqrt{\frac{\mu_B (\partial_r \mathcal{B}_{r,z})^2}{m\mathcal{B}_0}} \,. \tag{43.98}$$

The Earth's gravitational field deforms the trapping potential and, in the case of a harmonic potential, causes a gravitational sag without changing the secular frequencies of the potential. Assuming the potential to be given by,

$$U = \frac{m}{2}\omega_r^2 r^2 + \frac{m}{2}\omega_z^2 z^2 - mgz = \frac{m}{2}\omega_r^2 r^2 + \frac{m}{2}\omega_z^2 (z - g/\omega_z^2)^2 - \frac{m}{2} g^2/\omega_z^2 \,, \tag{43.99}$$

the atoms sag to a height of g/ω_z^2. In time-dependent traps, gravity causes a more complex behavior [573]. Important works have been done by [261, 1030, 421, 554, 5, 327, 776, 781, 357]. We study the impact of gravitation in Exc. 43.4.6.6.

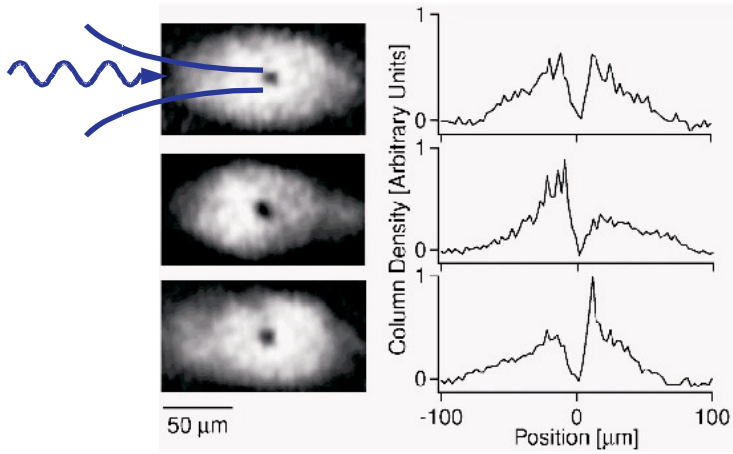

Figure 43.17: Creation of a repulsive hole by light tuned to the blue of an atomic transition.

43.4.2.1 Characterization of Ioffe-type traps

The 'time-of-flight' density distribution is,

$$r_{ToF} = \sqrt{\bar{r}^2 + \bar{v}^2 t_{ToF}^2} = \sqrt{\frac{k_B T}{m}} \sqrt{\frac{1}{\omega_r^2} + t_{ToF}^2} \simeq t_{ToF} \sqrt{\frac{k_B T}{m}} \ . \tag{43.100}$$

The *phase space density* is,

$$\rho = n_0 \lambda_{dB}^3 = \frac{N}{(2\pi)^{3/2} \bar{r}^2 \bar{z}} \left(\frac{2\pi\hbar^2}{m k_B T} \right)^{3/2} = N \omega_r^2 \omega_z \left(\frac{\hbar}{k_B T} \right)^3 = \zeta(3) \left(\frac{T_c}{T} \right)^3 \ . \tag{43.101}$$

where $\zeta(3) = 1.202$ is,

$$k_B T_c = \hbar \left(\frac{N \omega_r^2 \omega_z}{\zeta(3)} \right)^{1/3} \tag{43.102}$$

is the critical temperature. The *maximum collision rate* is,

$$\gamma_{coll} = n_0 \sigma \bar{v} = n_0 4\pi a_s^2 \sqrt{\frac{k_B T}{m}} \ . \tag{43.103}$$

The average collision rate can be obtained from,

$$\bar{\gamma}_{coll} N = \frac{1}{N} \int \gamma_{coll}(\mathbf{r}) n(\mathbf{r}) d^3 r = \frac{\int \sigma \bar{v} n^2(\mathbf{r}) d^3 \mathbf{r}}{\int n(\mathbf{r}) d^3 r} \ . \tag{43.104}$$

43.4.3 Radiative coupling and evaporative cooling

As we saw in the last section, optical cooling becomes ineffective when the density of the gas is high. Hence, we need another dissipation mechanism to cool trapped atoms. A method called *evaporation* has been proposed by Hess [616] for spin-polarized hydrogen (H↑) and was observed by Masuhara et al. [855]. Later, evaporation was used

Figure 43.18: The basic idea of evaporation consists in removing hot particles from the sample.

on alkali metals [5, 1018, 330]. A detailed review of the subject was published by Ketterle and van Druten [711].

Another collision-based cooling mechanism is *sympathetic cooling*. The technique was originally used in ion traps. Later it was applied to neutral atoms confined in magnetic traps. The idea is to get the cloud under study into thermal contact with a cold buffer gas. In some cases, the buffer gas may be optically or evaporatively cooled. Sympathetic cooling has been used in magnetic traps to create double condensates [939] and to cool fermions until the regime of quantum degeneracy [347].

43.4.4 Evaporative cooling

Evaporation always occurs when energetic particles abandon a system with finite bonding energy, removing more than their share of average energy per particle. Here, we consider the case of a finite-sized trapping potential, that is, the potential has an edge or a beak through which hot atoms, with sufficient kinetic energy to reach that region, may leave the trap. In the ideal case, this will lead to a complete truncation of the hot tail of the equilibrium Maxwell-Boltzmann velocity distribution. If the remaining system finds back to thermal equilibrium, it will do at a lower temperature. The redistribution of kinetic energy between atoms leading to *thermalization* occurs through elastic collisions.

43.4.4.1 Truncating the Boltzmann distribution

Let us first explain how the truncation leads to colder temperatures.

The objective is to calculate the Boltzmann distribution in a particular trap for a given atom number N and temperature T. The first step is to obtain the density-

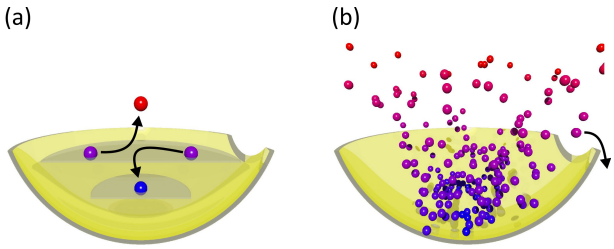

Figure 43.19: Principle of (a) rethermalization due to elastic collisions and (b) evaporation.

of-states. For an isotropic harmonic trap $\varepsilon = \frac{p^2}{2m} + V(r)$ with $V(r) = \frac{m}{2}\omega^2 r^2$, it is,

$$\eta(\varepsilon)d\varepsilon = \frac{1}{(2\pi)^3}\int_V d^3r d^3k = \frac{2\pi(2m)^{3/2}}{h^3}\int_V \sqrt{\varepsilon - V(r)}d^3r d\varepsilon = \frac{\varepsilon^2 d\varepsilon}{2(\hbar\omega)^3} \ . \quad (43.105)$$

The atom density is,

$$n(\varepsilon) = e^{(\mu-\varepsilon)/k_BT} = Ze^{-\varepsilon/k_BT} \ . \quad (43.106)$$

From these expression we obtain the atom number,

$$N = \int_0^\infty n(\varepsilon)\eta(\varepsilon)d\varepsilon = \int_0^\infty e^{(\mu-\varepsilon)/k_BT}\frac{\varepsilon^2}{2(\hbar\omega)^3}d\varepsilon = Z\frac{(k_BT)^3}{(\hbar\omega)^3} \ , \quad (43.107)$$

which we may now use to calibrate the fugacity via

$$Z = N\frac{(\hbar\omega)^3}{(k_BT)^3} \ , \quad (43.108)$$

which finally allows us to calculate the total energy,

$$E = \int_0^\infty \varepsilon n(\varepsilon)\eta(\varepsilon)d\varepsilon = \int_0^\infty \varepsilon e^{(\mu-\varepsilon)/k_BT}\frac{\varepsilon^2}{2(\hbar\omega)^3}d\varepsilon = 3Z\frac{(k_BT)^4}{(\hbar\omega)^3} = 3Nk_BT \ . \quad (43.109)$$

The evaporation consists in truncating the distribution function $n(\varepsilon)$ at some energy $\hbar\omega_{rf}$. We get with $\beta \equiv (k_BT)^{-1}$,

$$\tilde{N} = \int_0^{\hbar\omega_{rf}} n(\varepsilon)\eta(\varepsilon)d\varepsilon = N\left(1 - \frac{2 + 2\beta\hbar\omega_{rf} + (\beta\hbar\omega_{rf})^2}{2e^{\beta\hbar\omega_{rf}}}\right) \quad (43.110)$$

and

$$\tilde{E} = \int_0^{\hbar\omega_{rf}} \varepsilon n(\varepsilon)\eta(\varepsilon)d\varepsilon = E\left(1 - \frac{6 + 6\beta\hbar\omega_{rf} + 3(\beta\hbar\omega_{rf})^2 + (\beta\hbar\omega_{rf})^3}{6e^{\beta\hbar\omega_{rf}}}\right) \ . \quad (43.111)$$

As the truncation removes the hottest atoms from the cloud, we loose atom number and energy. Assuming the existence of some rethermalization mechanism, we may now use the new values for N and T to calculate the new equilibrium Boltzmann distribution starting all over from Eq. (43.106),

$$N \longleftarrow \tilde{N} \quad \text{and} \quad T \longleftarrow \frac{\tilde{E}}{3Nk_B} \quad (43.112)$$

Repeating this over and over the temperature will gradually reduce. The cooling process can be speed up by readjusting the truncation frequency to the actual temperature. This is called forced evaporation (see Fig. 43.20).

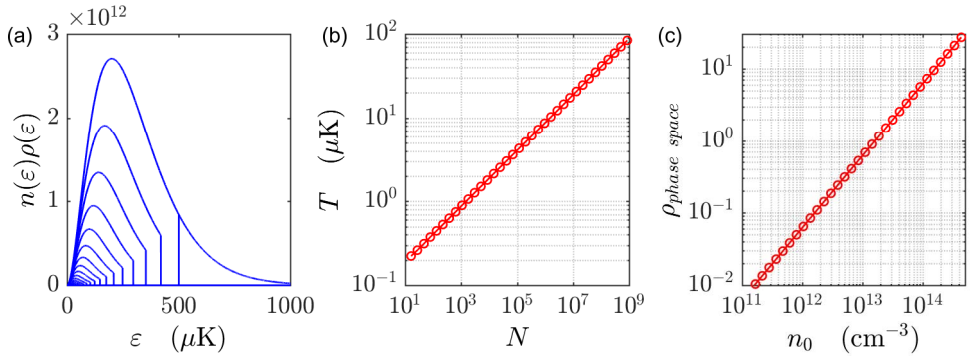

Figure 43.20: (code) (a) Forced evaporation by truncating the Boltzmann distribution over and over again. (b) Evolution of the temperature and (c) of the phase space density with number of remaining atoms.

43.4.4.2 Rethermalization

As already mentioned, rethermalization occurs due to elastic collisions. It needs more or less three collisions per atom to rethermalize a cloud [914, 1394], so that the collision rate determines the speed of the evaporation process. A large collision rate is desirable to keep the evaporation process faster than trap loss processes. Evaporation ramps between several seconds and a minute are typical.

The maximum rate of elastic collisions between trapped atoms (in the trap center) is,

$$\gamma_{coll} = n_0 \sigma_{el} \bar{v} \sqrt{2} \propto \rho^3 N^{2/3} \ , \tag{43.113}$$

where n_0 is the peak density,

$$\sigma_{el} = 8\pi a_s^2 \ , \tag{43.114}$$

is the cross-section for elastic collisions and, $\bar{v}$ being the average thermal velocity of the cloud, $\sqrt{2}\bar{v}$ is the average relative velocity between two of its atoms [710]. This formula gives the average collision rate at the *center of the cloud*, where the density is highest. To calculate the total collision rate, we need to integrate over the entire volume of the cloud,

$$\bar{\gamma}_{coll} = \tfrac{1}{N} \int \gamma_{coll}(\mathbf{r}) n(\mathbf{r}) d^3 r = \frac{\int \sigma_{el} \bar{v} n^2(\mathbf{r}) d^3 r}{\int n(\mathbf{r}) d^3 r} \ . \tag{43.115}$$

For harmonic potential we find an average rate reduced by $2\sqrt{2}$, for linear potentials by 8. We verify this in Exc. 43.4.6.7. Finally, the rate for collision events is two times smaller, as it involves two atoms at a time.

Obviously, the evaporation process slows down when the cloud cools more, unless the edge of the potential is lowered, such that the hotter atoms of the colder cloud can

be evaporated. By continually lowering the edge of the potential, while the atomic cloud keeps on rethermalizing (this procedure is called *forced evaporation*) very low temperatures in the nano-Kelvin regime can be achieved, and the phase space density can be increased by many orders of magnitude (between a MOT and a BEC there are 6 orders of magnitude) up to the threshold of Bose-Einstein condensation. Of course, this is only possible by sacrificing many hot atoms. Even with a well optimized evaporation ramp (i.e., a controlled lowering of the potential edge), usually only some 0.1% of the atoms reach the condensation phase after about 500 collisions per atom.

Two aspects should be mentioned regarding the optimization of the evaporation ramp. The first aspect is, that elastic collisions with atoms from the residual background vapor of the vacuum chamber limit the lifetime of the trap. Therefore, the evaporation must be sufficiently fast, which requires either a high rate of elastic collisions or a good vacuum. A compromise must be found between a slow but efficient evaporative cooling and a minimization of the losses, which come into play when the evaporation takes too long. The second aspect is, that the dimensionality of the evaporation surface determines the effectiveness of the cooling. In the first demonstration of evaporation, H↑ atoms of a hot cloud were ejected over a saddle point. The saddle was located a small region away from the trap center, and only atoms with sufficient kinetic energy *along a certain direction*, $E_z > U_{edge}$, could leave the trap. In such cases, evaporation is called one-dimensional. Even though ergodic redistribution due to anharmonicities of the potential will drive, sooner or later, all the atoms to this region, this effect becomes less pronounced when the cloud cools down, because the atoms accumulate at the bottom of the approximately harmonic (and therefore separable) potential. This fact has inhibited efficient evaporation of H↑ below 120 μK [466].

A second evaporative technique has been demonstrated in traps called *time-orbiting potential* (TOP) [1018]. It is a feature of TOP traps to display a spatial region called a 'death-circle', where passing atoms are ejected from the trap. This fatal circle can act as a 2-dimensional evaporation surface, provided the radius of the circle is large enough [580]. However, under the influence of gravity the dimensionality is further reduced to 1D [710].

The most successful evaporation technique implemented so far is based on a radiative coupling of confined and free states. We discuss this technique in the following sections. Publications on *evaporative cooling* are [819, 892, 1018, 1058, 127, 882, 914, 420, 425, 602, 948, 616, 855, 330, 711, 1393, 582, 848, 387, 618]. See ([297], Sec. 3.1.4) for an overview.

43.4.4.3 Adiabatic decompression

The condition for *adiabatic decompression* of a trapping potential is,

$$\frac{|\dot{\omega}_{trap}|}{\omega_{trap}} \ll \omega_{trap} \ . \tag{43.116}$$

The population of the quantized levels should not change under adiabatic decompression, $e^{\hbar\omega_i/k_BT_i} = e^{\hbar\omega_f/k_BT_f}$, and the phase space density remains unchanged,

$n_i \lambda_{dB,i} = n_f \lambda_{dB,f}$. If this is true, then the temperature and density change as,

$$\frac{\omega_f}{\omega_i} = \frac{T_f}{T_i} = \left(\frac{n_f}{n_i}\right)^{3/2} . \tag{43.117}$$

Solve Exc. 43.4.6.8.

43.4.4.4 Radiative coupling of internal state

The most successful evaporation technique implemented so far is based on a radiative coupling of confined and free states. We discuss this technique in the following sections. See ([297], Sec. 3.1.4) for an overview.

The radiative coupling technique originates from an idea proposed by Pritchard et al. [582], who have already had some experience with radiofrequency spectroscopy in magnetically trapped neutral atoms [848, 602]. The spatial dependence of the Zeeman splitting is an intrinsic feature of magnetic traps. Irradiation of a radio wave at a certain frequency couples trapped and untrapped Zeeman substates at a well-defined distance from the trap center. This gives rise to a 3D evaporation surface, where the passing atoms can undergo Landau-Zener transitions and be expelled from the trap. The technical advantages of this technique are substantial: The magnetic trapping potential does not have to be manipulated, for example, by the creation of a nozzle, and the potential edges can be easily controlled by the radiofrequency. If evaporation is forced via a continuous reduction of the radiofrequency and if the evaporation ramp is optimized, the density will increase as well as the collision rate. Rethermalization will accelerate and initiate a self-accelerated evaporation process (*run-away evaporation*). Rf-evaporation was first demonstrated by Ketterle and colleagues [330]. Solve Exc. 43.4.6.9.

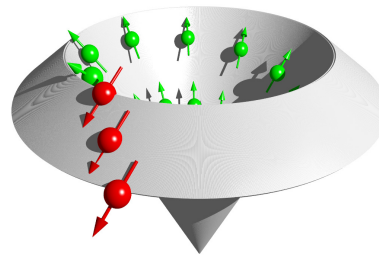

Figure 43.21: Illustration of evaporative truncation.

43.4.4.5 Adiabatic and diabatic limits of rf-induced evaporation

Rf-induced evaporation can be described within the formalism of the dressed atom [277], where the different states m_F of an atom with spin F are coupled to an rf-field [5], which we assume to be linearly polarized:

$$\mathcal{B}(t) = \mathcal{B}\hat{\mathbf{e}}_{rf} \cos \omega t \ . \tag{43.118}$$

The element of the coupling matrix between the levels, $|F, m_F\rangle$ and $|F, m_F \pm 1\rangle$ is,

$$\Omega = \frac{\mu_B g}{4\hbar} \left| \vec{\mathcal{B}}_{rf} \times \hat{\mathbf{e}}_B \right| \sqrt{F(F+1) - m_F(m_F+1)} \ , \tag{43.119}$$

where g is the atomic g-factor and $\hat{e}_B$ the orientation of the local static magnetic field.

[5] Alternatively, a *microwave* frequency may be used to couple *different hyperfine levels*.

The adiabatic potentials $U(r)$ are obtained through the eigenvalues of the atomic states dressed by the local magnetic field $\mathcal{B}(r)$. In the dressed atom picture, we consider the total energy of the atom plus the field of N radiofrequency photons. Without coupling, this simply means that $N\hbar\omega$ is added to the atomic Zeeman energies, resulting in a Zeeman pattern being vertically shifted by $N\hbar\omega$ for $N = 0, \pm 1, ...$ At positions where the rf-field is in resonance, curves with $\Delta N = 1$ intersect. Here, the coupling develops an *avoided crossing*, which determines the pattern of adiabatic energy levels [see Fig. 43.22(b)].

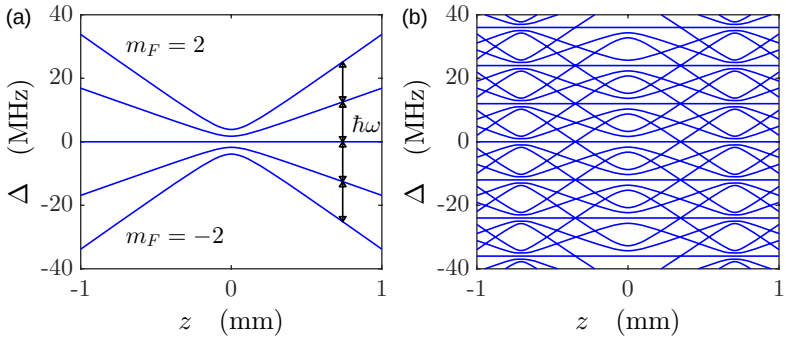

Figure 43.22: (code) (Left) Potentials due to the Zeeman structure of an atom in the ground state with $F = 1$. (Right) Adiabatic potentials resulting from the coupling of Zeeman levels via radiofrequency radiation being resonant with the difference of Zeeman levels at the position 0.7.

A slowly moving atom remains on the curve of an *adiabatic potential*. As an example, let us assume an atom in the hyperfine state $|F, F\rangle$ moving away from the center of the trap. When it comes close to resonance, the rf-field blends this state with other m_F-states, from the $|F, F-1\rangle$ down to the $|F, -F\rangle$ state, which changes the slope of the potential curve. Beyond the resonance point, the atomic state is adiabatically transformed into an untrapped high-field seeking state, and the atom is repelled from the trap. Thus, while passing the avoided crossing, the atom has emitted $2F$ rf-photons in a stimulated manner and inverted the orientation of both the electron and the nuclear spin.

In this way the radiofrequency generates an adiabatic potential surface with a depth of approximately $|m_F|\hbar(\omega - \omega_0)$, where ω_0 is the resonant rf-frequency at the center of the trap. The evaporation process corresponds, then, to the removal of the most energetic atoms out of the trap.

For this adiabatic picture to be valid, an adiabaticity condition must be fulfilled. This condition requires that the energy difference at the avoided crossover be larger than the energy uncertainty related to the limited time that an atom with velocity v spends in the resonance region. For a two-level system coupled by a matrix element V_{12} and an atom moving with velocity v along the z-axis, the transition probability P between the adiabatic curves is given by the *Landau-Zener formula* [1114],

$$P = 1 - e^{-\xi} \quad \text{with} \quad \xi = \frac{2\pi|V_{12}|^2}{\hbar g \mu_B \partial_z \mathcal{B} v} \,. \tag{43.120}$$

The Landau-Zener theory is strictly valid only for a two-level system, which we use here only for a qualitative discussion of two following limiting cases.

For a weak rf-field, $\xi \ll 1$, P is much smaller than 1, i.e., the atoms remain predominantly on the diabatic surface shown in Fig. 43.22(a). The probability for a *spin flip* transition is, $P \approx t$, which describes the diabatic limit of rf-induced evaporative cooling: The atomic energy levels are almost unperturbed, the atoms often spill across the resonance surface, and only after $1/P$ oscillations, they spin-flip from the hyperfine state $|F, F\rangle$ to the $|F, F-1\rangle$.

The adiabatic limit is clearly the ideal situation for evaporative cooling. However, the evaporation process in a trap (with oscillation time T_{osc}) saturates at a lower rf-power. The condition for saturation is $P \approx T_{osc}/\tau_{el}$, where τ_{el} is the average time between two collisions. This means that an energetic atom is evaporated before it collides again.

Only the component of the magnetic field of the rf-radiation which is *perpendicular* to the magnetic trapping field induces spin-flips. In certain geometries of the confinement potential, for example the quadrupole trap, the magnetic field covers the entire solid angle. Consequently, there are two points where the trapping field and the rf-field are parallel and the elements of the transition matrix consequently zero. Within an area around these points, the coupling is diabatic. In practice however, the rf-transition can be sufficiently saturated that this area is small and does not strongly affect the evaporation efficiency.

Note also that gravitation deforms the equipotential surfaces of the confinement potential, which can reduce the evaporation efficiency [710]. Solve Exc. 43.4.6.10.

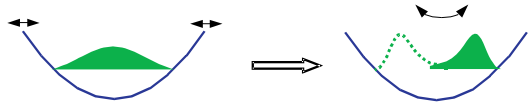

Figure 43.23: Effective potential due to a rapid modulation of the trap's location.

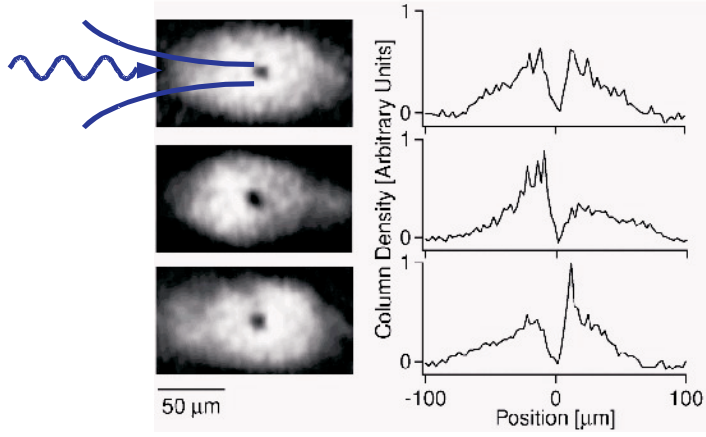

Figure 43.24: Creation of a repulsive hole by light tuned to the blue of an atomic transition.

43.4.5 Sympathetic cooling

The efficiency of evaporative cooling depends on the rate of interatomic collisions. However, there are atomic species with unfavorable, that is, small or even negative scattering lengths. Also, while at low temperatures only s-wave collisions occur (higher partial waves being frozen behind the centrifugal barrier), such collisions are prohibited for fermionic gases. Fermions or species with unfavorable scattering lengths can not be cooled by evaporation. There is, however, another technique called *sympathetic cooling* by thermal contact with another species. The additional species is, in general, actively cooled (e.g., by evaporation), while the species of interest is passively cooled via elastic collisions with atoms of the additional species. Of course, for this scheme to work the *interspecies scattering length* and the mass ratio must be adequate to ensure adequate thermal coupling.

Following [935] the transfer of kinetic energy between two colliding atoms is reduced by a factor depending on the their mass difference,

$$\xi = \frac{4m_1 m_2}{(m_1 + m_2)^2} \ . \tag{43.121}$$

Around $3/\xi$ collisions per atom on average are required for complete thermalization of a gas. For example, for the Rb-Li mixture, we have $3/\xi = 12.4$. The collision rate is,

$$\Gamma_{coll} = \sigma_{12}\bar{v} \int n_1(\mathbf{r}) n_2(\mathbf{r}) d^3r \ , \tag{43.122}$$

where the average thermal velocity is,

$$\bar{v} = \sqrt{\frac{8k_B}{\pi}\left(\frac{T_1}{m_1} + \frac{T_2}{m_2}\right)} \ . \tag{43.123}$$

The instantaneous temperature is calculated by,

$$\gamma_{therm} = -\frac{1}{\Delta T}\frac{d\Delta T}{dt} \ , \tag{43.124}$$

or via simulations: $\Delta T(t + dt) = \Delta T(t) - \Delta T(t)\gamma_{therm} dt$. Following [346] the rethermalization rate is connected to the collision rate via,

$$\boxed{\gamma_{therm} = \frac{\xi}{3}\left(\frac{\Delta E_{1\to 2}}{N_1 k_B \Delta T} + \frac{\Delta E_{2\to 1}}{N_2 k_B \Delta T}\right) = \frac{\xi}{3}\left(\frac{\Gamma_{coll}}{N_1} + \frac{\Gamma_{coll}}{N_2}\right)} \ . \tag{43.125}$$

Analytic solutions can be derived for harmonic traps. This will be studied in Excs. 43.4.6.11 and Exc. 43.4.6.12.

43.4.6 Exercises

43.4.6.1 Ex: Lack of trapping potentials for strong field seekers

Show that it is not possible to create magnetic trapping potentials for atoms in low-field seeking Zeeman states.

Solution: *Consider the potential,*

$$U(\mathbf{r}) = -\alpha|\vec{\mathcal{B}}|^2 = -\alpha(\mathcal{B}_x^2 + \mathcal{B}_y^2 + \mathcal{B}_z^2) \ .$$

Now we calculate,

$$\nabla^2|\vec{\mathcal{B}}|^2 = 2(|\nabla\mathcal{B}_x|^2 + |\nabla\mathcal{B}_y|^2 + |\nabla\mathcal{B}_z|^2 + \mathcal{B}_x\nabla^2\mathcal{B}_x + \mathcal{B}_y\nabla^2\mathcal{B}_y + \mathcal{B}_z\nabla^2\mathcal{B}_z) \ .$$

Using

$$\nabla^2\vec{\mathcal{B}} = \nabla(\nabla\cdot\vec{\mathcal{B}}) = \nabla\times(\nabla\times\vec{\mathcal{B}}) \ ,$$

and knowing, that in magnetostatics $\nabla\cdot\vec{\mathcal{B}} = 0 = \nabla\times\vec{\mathcal{B}}$*, we find,*

$$\nabla^2|\vec{\mathcal{B}}|^2 = 2(|\nabla\mathcal{B}_x|^2 + |\nabla\mathcal{B}_y|^2 + |\nabla\mathcal{B}_z|^2) > 0 \ .$$

The same argument holds for the trapping potential,

$$U(\mathbf{r}) = -\alpha|\vec{\mathcal{B}}| = -\alpha\sqrt{\mathcal{B}_x^2 + \mathcal{B}_y^2 + \mathcal{B}_z^2} \ .$$

43.4.6.2 Ex: Quadrupolar potential

Show that for a quadrupolar trap always holds $2\partial_r\mathcal{B}_{qua} = \partial_z\mathcal{B}_{qua}$.

Solution: *Maxwell's fourth equation gives,*

$$0 = \nabla\cdot\vec{\mathcal{B}} = \frac{\partial\vec{\mathcal{B}}}{\partial x} + \frac{\partial\vec{\mathcal{B}}}{\partial y} + \frac{\partial\vec{\mathcal{B}}}{\partial z} = 2\frac{\partial\vec{\mathcal{B}}}{\partial r} + \frac{\partial\vec{\mathcal{B}}}{\partial z} \ .$$

43.4.6.3 Ex: Magnetic quadrupole trap

a. Consider ^{87}Rb atoms confined in a magnetic trap with $\vec{\mathcal{B}}(x,y,z) = x \quad y \quad -2z \times 200\,\mathrm{G/cm}$. The atoms are in the state $|F=1, m_F=-1\rangle$ with the g-factor $g_F = 1/2$. Check whether it is reasonable to assume constant vibration frequencies for such traps.
b. Assume that the trapped atomic cloud consists of $N = 10^8$ atoms at temperature $T = 100\,\mathrm{K}$. Calculate the atomic density n_0 at the center of the cloud.
c. The cross section for elastic collisions is $\sigma = 10^{-12}\,\mathrm{cm}^2$. How many times do atoms meet in the middle of the trap?

Solution: *a. There are no oscillation frequencies in quadrupolar potentials.*
b. We showed in class that the maximum atomic density in a quadrupolar trap is,

$$n_0 = \frac{N}{(2\pi)^{3/2}\bar{r}^2\bar{z}} \ ,$$

hence, we find $n_0 = 3.5\times10^{13}\,\mathrm{cm}^{-3}$.
c. The collision rate is given by $\gamma_{coll} = \sigma\bar{v}n_0 = 3.5\,\mathrm{s}^{-1}$ *with* $\bar{v} = \sqrt{\frac{k_BT}{m}}$.

43.4.6.4 Ex: TOP trap

The TOP trap (time-orbiting potential) was the first design to allow for Bose-Einstein condensation in 1995. It consists of the superposition of a quadrupolar magnetic field, with the radial and axial gradients $2\partial_r \mathcal{B}_{qua} = \partial_z \mathcal{B}_{qua}$), and a homogeneous magnetic field $\mathcal{B}_{top}$ rotating in the symmetry plane of the quadrupole field. Atoms which oscillate with an amplitude beyond a given radius r_d, called the 'circle of death', undergo Majorana transitions and are expelled from the trap.
a. Calculate the radius of the death circle.
b. Plot the time-averaged 'effective' trapping potential.

Solution: *a. The death circle radius is,*

$$r_{death} = \frac{\mathcal{B}_{r,top}}{\partial_r \mathcal{B}_{r,qua}} \ .$$

The potential can be expressed as,

$$U(\mathbf{r}) = -\mu \cdot \mathcal{B}_{top} - \frac{\mu(\partial_r \mathcal{B}_{qua})^2}{4\mathcal{B}_{top}(r^2 + 8z^2)} \ ,$$

the density with,

$$n(\mathbf{r}) = n_0 e^{-(r^2+8z^2)/2\bar{r}} \ ,$$

and the actual volume as,

$$V_{eff} \equiv \frac{N}{n_0} = \pi^{3/2}\bar{r}^3 \ .$$

b. The result is shown in Fig. 43.25.

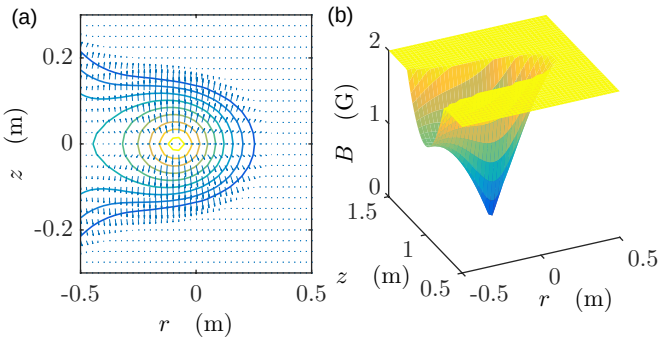

Figure 43.25: (code) Effective potential in radial direction of a shaking dipole trap.

43.4.6.5 Ex: Harmonic trap

Calculate the vibration frequencies of ^{87}Rb atoms trapped in a harmonic trap, when the atoms are in the $|F = 1, m_F = -1\rangle$ hyperfine level of the ground state.

Solution: *The potential is,*

$$U(\mathbf{r}) = -\mu_B g_F m_F |\vec{\mathcal{B}}| = \frac{m}{2}(\omega_x^2 x^2 + \omega_y^2 y^2 + \omega_z^2 z^2) = k_B T \left(\frac{x^2}{2\bar{x}^2} + \frac{y^2}{2\bar{y}^2} + \frac{z^2}{2\bar{z}^2} \right) ,$$

and the density,

$$n(\mathbf{r}) = n_0 e^{-U(\mathbf{r})/k_B T} .$$

Normalization requires,

$$N = \int n(\mathbf{r}) d^3 r = n_0 (2\pi)^{3/2} \bar{x}\bar{y}\bar{z} \equiv n_0 V_{eff} .$$

The expressions for the potential give,

$$\bar{x} = \sqrt{\frac{k_B T}{m\omega_x^2}} ,$$

etc.. If we know the magnetic field through its curvatures, B_j", that is, $|\vec{\mathcal{B}}| = \mathcal{B}"_x x^2 + \mathcal{B}"_y y^2 + \mathcal{B}"_z z^2$, we can calculate the frequencies:

$$\omega_x = \sqrt{\frac{2\mu_B g_F m_F}{m}} .$$

etc..

43.4.6.6 Ex: Gravitational sag in a trap

Consider (a) a quadrupolar trap and (b) an isotropic harmonic trap. What is the gradient, respectively the curvature of the trapping potential required to suspend a cloud of rubidium subject to gravitation? What is the sag of the cloud in the potential due to gravitation?

Solution: *a. The potential of a quadrupolar trap subject to gravitation can be written,*

$$U(r,z) = \mu \partial_r \mathcal{B} \sqrt{r^2 + 4z^2} + mgz .$$

We let $r = 0$,

$$U(0,z) = 2\mu \partial_r \mathcal{B} |z| + mgz .$$

The minimum of this potential stays at the same place $z = 0$, but the slope changes. For $2\mu\partial_r\mathcal{B} < mg$, the trap becomes unstable.
b. The potential of an isotropic harmonic trap subject to gravitation can be written,

$$U(r,z) = \tfrac{m}{2}\omega_r^2 r^2 + \tfrac{m}{2}\omega_z^2 z^2 + mgz .$$

We let $r = 0$. The position of the minimum is given by,

$$0 = \partial_z U(0,z) = m\omega_z^2 z + mg .$$

The minimum of this potential is lower by $z = g/\omega_z^2$, but for any ω_z, there is always a place, where the trap is stable. We can rewrite the potential as

$$U(r,z) = \frac{m}{2}\omega_r^2 r^2 + \frac{m}{2}\omega_z^2\left(z + \frac{g}{\omega_z^2}\right)^2 + const. \ .$$

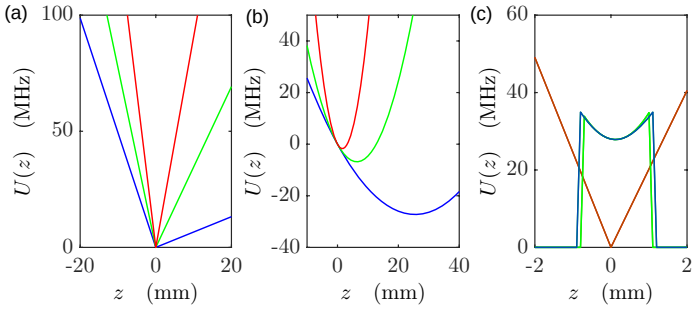

Figure 43.26: (code) Gravitational sag in a quadrupole and in a harmonic trap.

43.4.6.7 Ex: Mean collision rate

Assuming that the peak collision rate γ_{coll} is known, calculate the average collision rate (a) in a quadrupolar and (b) in a harmonic trap.

Solution: *a. As shown in Eq. (43.83) and (43.97) the density of an atomic cloud confined in a quadrupole trap is,*

$$n(\mathbf{r}) = n_0 e^{-\sqrt{r^2+4z^2}/\bar{r}}$$
$$with \qquad n_0 = \frac{N}{4\pi\bar{r}^3} \qquad and \qquad \bar{r} = \frac{k_B T}{\mu_B g_J m_J \partial_r \mathcal{B}} \qquad and \qquad N = \int n(\mathbf{r}) d^3 r \ .$$

Hence,

$$\bar{\gamma}_{coll} = \frac{1}{N}\int \sigma_{el}\bar{v} n^2(\mathbf{r}) d^3 r = \frac{\sigma_{el}\bar{v}}{N}\int \left[\frac{N}{4\pi\bar{r}^3} e^{-\sqrt{r^2+4z^2}/\bar{r}}\right]^2 d^3 r$$
$$= \frac{\sigma_{el}\bar{v}}{N}\frac{N}{4\pi\bar{r}^3}\frac{1}{8}\int \frac{N}{4\pi\bar{r}^3} e^{-\sqrt{(2r)^2+4(2z)^2}/\bar{r}} d^3(2r) = \frac{\sigma_{el}\bar{v}}{N}\frac{N}{4\pi\bar{r}^3}\frac{1}{8}N = \frac{\gamma_{coll}}{8} \ .$$

b. The density of an atomic cloud confined in a quadrupole trap is,

$$n(\mathbf{r}) = n_0 e^{-r^2/2\bar{r}^2}$$
$$with \qquad n_0 = \frac{N}{(2\pi)^{3/2}\bar{r}^3} \qquad and \qquad \bar{r} = \sqrt{\frac{k_B T}{2\mu_B g_J m_J}} \qquad and \qquad N = \int n(\mathbf{r}) d^3 r \ .$$

Hence,

$$\bar{\gamma}_{coll} = \frac{1}{N}\int \sigma_{el}\bar{v}n^2(\mathbf{r})d^3r = \frac{\sigma_{el}\bar{v}}{N}\int\left[\frac{N}{(2\pi)^{3/2}\bar{r}^3}e^{-r^2/2\bar{r}^2}\right]^2 d^3r$$
$$= \frac{\sigma_{el}\bar{v}}{N}\frac{N}{(2\pi)^{3/2}\bar{r}^3}\frac{1}{2^{3/2}}\int\frac{N}{(2\pi)^{3/2}\bar{r}^3}e^{-(\sqrt{2}r)^2/2\bar{r}^2}d^3(\sqrt{2}r) = \frac{\sigma_{el}\bar{v}}{N}\frac{N}{4\pi\bar{r}^3}\frac{1}{2^{3/2}}N = \frac{\gamma_{coll}}{2^{3/2}}\ .$$

43.4.6.8 Ex: Adiabatic compression

How does temperature change upon adiabatic compression of (a) a quadrupole trap and (b) a harmonic trap. How do density, phase space density, and elastic collision rate vary. **Help:** Define the compression for quadrupole trap as $\eta \equiv \partial_r\mathcal{B}_{r,final}/\partial_r\mathcal{B}_{r,initial}$ and for harmonic trap as $\eta \equiv \omega_{r,final}/\omega_{r,initial}$.

Solution: *a. We have already shown in a previous exercise that the e^{-1} radius $\bar{r}$ of a cloud in a quadrupole trap is,*

$$\bar{r} \equiv \frac{k_BT}{\mu_Bg_Fm_F\partial_r\mathcal{B}}$$

and the density,

$$n_0 = \frac{N}{(2\pi)^{3/2}\bar{r}^2\bar{z}}\ .$$

As the phase space density can not change when we make adiabatic variations, $\rho = n_0\lambda_{therm}^3 = const$, the density changes with the temperature as $n_0 \propto \lambda_{therm}^{-3} \propto T^{3/2}$. We also know $\bar{v} = \sqrt{k_BT/m}$, such that the collision rate is $\gamma = \sigma\bar{v}n_0 \propto \sqrt{T}T^{3/2}$. Thus, the density and temperature change with the pressure as,

$$\eta = \frac{\partial_r\mathcal{B}_{r,final}}{\partial_r\mathcal{B}_{r,initial}} = \frac{T_f\bar{r}_i}{T_i\bar{r}_f} = \frac{T_fn_f^{1/3}}{T_in_i^{1/3}} = \frac{T_f^{3/2}}{T_i^{3/2}} = \frac{n_f}{n_i} = \frac{\gamma_f^{3/4}}{\gamma_i^{3/4}}\ .$$

b. We have already shown in a previous exercise that the rms*-radius $\bar{r}$ of a harmonically trapped cloud is,*

$$\bar{r} \equiv \sqrt{\frac{k_BT}{m\omega^2}}\ ,$$

and the maximum density

$$n_0 = \frac{N}{(2\pi)^{3/2}\bar{x}\bar{y}\bar{z}}\ .$$

With the same argument of (a) we find now,

$$\eta = \frac{\omega_{r,final}}{\omega_{r,initial}} = \frac{T_f^{1/2}\bar{r}_i}{T_i^{1/2}\bar{r}_f} = \frac{T_f^{1/2}n_i^{1/3}}{T_i^{1/2}n_f^{1/3}} = \frac{T_f}{T_i} = \frac{n_f^{2/3}}{n_i^{2/3}} = \frac{\gamma_f^{1/2}}{\gamma_i^{1/2}}\ .$$

43.4.6.9 Ex: RF-antenna for radiative coupling

Calculate the Rabi frequency that can be generated by an rf-antenna consisting of a single square loop with side length $L = 2\,\mathrm{cm}$ on a cloud of trapped ^{87}Rb atoms located in the center of the loop on transitions between magnetic sublevels of the $F = 1$ ground state hyperfine structure. Assume the antenna to carry an ac-current with $I = 1\,\mathrm{A}$ amplitude.

Solution: *The first step is to calculate the magnetic field generated at the position of the cloud (assumed to be small). At rf-frequencies we can treat the magnetic field as being quasi static, i.e. we apply the the Biot-Savart law. The result of a numerical integration is shown in Fig. 43.27. We see that* $1\,\mathrm{A}$ *of current amplitude in the square loop generates a magnetic field of* $0.28\,\mathrm{G}$ *amplitude.*

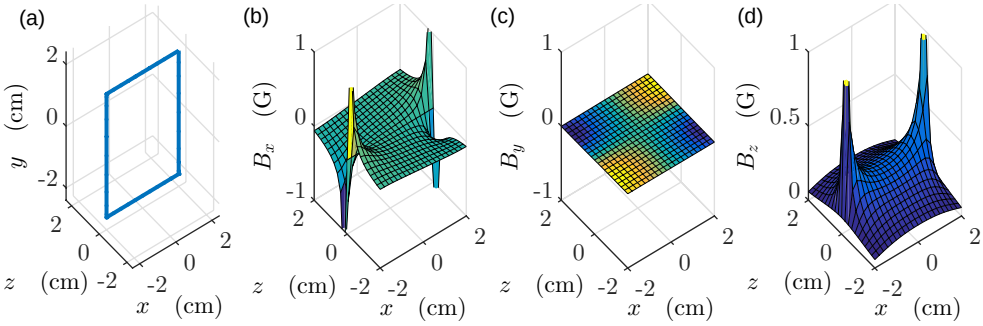

Figure 43.27: (code) RF-antenna for radiative coupling.

43.4.6.10 Ex: Landau-Zener transitions

Consider a rubidium-88 cloud in its ground state $^2S_{1/2}, F = 1, m_F = -1$ confined in an isotropic quadrupolar potential with the gradient $200\,\mathrm{G/cm}$. To initiate an efficient radiofrequency evaporation, you want atoms crossing the region where the radiofrequency couples the Zeeman states to make a transition to the untrapped Zeeman state $m_F = 0$ with 95% probability. What is the amplitude of the required magnetic field.

Solution: *When the sum of the kinetic and the potential energy of the atom is larger than* $\hbar\omega_{rf}$*, the atom can climb the potential up to the distance* R *from the center, where the Zeeman states suffer an avoided crossing. They follow the adiabatic path with the Landau-Zener transition probability,*

$$P_{LZ} = 1 - e^{-2\pi\Omega^2/\frac{\partial\Delta}{\partial R}v} \ ,$$

where the (co-rotating part of the) Rabi frequency is,

$$\Omega = \langle 1, 0|\mathbf{d}|1, -1\rangle \frac{\vec{\mathcal{B}}_{rf}}{2\hbar} \approx \frac{\mu_B \mathcal{B}_{rf}}{6\hbar} \ ,$$

and the energy splitting along the radial axis (here we have $\vec{\mathcal{B}}_{rf} \perp \vec{\mathcal{B}}_{trap}$) is,

$$\Delta = \frac{\mu_B \mathcal{B}_{trap}}{2\hbar} \ ,$$

with $\partial_r \mathcal{B}_{trap} = 200\,\mathrm{G/cm}$. The excess energy of atoms of $100\,\mu\mathrm{K}$ temperature is,

$$v = \sqrt{\frac{2E_{exc}}{m}} \ ,$$

with $E_{exc} = \frac{1}{2}k_B T$. Using these relationships we need, in order to obtain efficient cooling ($P_{LZ} > 95\%$), to fulfill,

$$\mathcal{B}_{rf} > \frac{6\hbar}{\mu_B}\sqrt{\frac{\partial_R \Delta v}{2\pi}\ln(1-P_{LZ})} \approx 0.052\,\mathrm{G} \ .$$

43.4.6.11 Ex: Damping in mixtures of species

From Eq. (43.125) derive the interspecies thermalization rate for harmonic potentials.

Solution: *With the potential $V_j(r) = \frac{1}{2}m_j\omega_{rj}^2 r^2 + \frac{1}{2}m_j\omega_{zj}^2 r^2 = k_B T_j \ \left(r^2/2\bar{r}_j^2 + z^2/2\bar{z}_j^2\right)$ the densities are $n_j(r) = n_{0j}e^{-r^2/2\bar{r}_j^2 - z^2/2\bar{z}_j^2}$, and the integral is [927],*

$$\begin{aligned}
\Gamma_{coll} &= \sigma_{12}\bar{v}n_{01}n_{02}\int e^{-r^2/2\bar{r}_1^2 - z^2/2\bar{z}_1^2 - r^2/2\bar{r}_2^2 - z^2/2\bar{z}_2^2}\ d^3\mathbf{r} \\
&= \frac{\sigma_{12}\bar{v}n_{01}n_{02}(2\pi)^{3/2}}{\sqrt{(\bar{x}_1^{-2}+\bar{x}_2^{-2})(\bar{y}_1^{-2}+\bar{y}_2^{-2})(\bar{z}_1^{-2}+\bar{z}_2^{-2})}} \\
&= \frac{\sigma_{12}\bar{v}N_1N_2}{(2\pi)^{3/2}\sqrt{(\bar{x}_1^2+\bar{x}_2^2)(\bar{y}_1^2+\bar{y}_2^2)(\bar{z}_1^2+\bar{z}_2^2)}} \ ,
\end{aligned}$$

letting $N = n_0(2\pi)^{3/2}\bar{x}\bar{y}\bar{z}$. Defining $m_2\omega_2^2 = \beta^2 m_1\omega_1^2$,

$$\Gamma_{coll} = \frac{(m_1\omega_1^2)^{3/2}\sigma_{12}\bar{v}N_1N_2}{(2\pi k_B)^{3/2}\,(T_1 + T_2\beta^{-2})^{3/2}} \ .$$

Once more, according to [346], the rethermalization rate is,

$$\gamma_{therm} = \frac{\xi(N_1+N_2)(m_1\omega_1^2)^{3/2}\sigma_{12}\sqrt{T_1/m_1 + T_2/m_2}}{3\pi^2 k_B(T_1 + T_2\beta^{-2})^{3/2}} \ .$$

For an anisotropic trap, we take the geometric mean of the trap frequencies, $\omega_1 = \sqrt{\omega_{1x}\omega_{1y}\omega_{1z}}$. The scattering length then follows from,

$$|a_{12}| = \sqrt{\sigma_{12}/4\pi} \ .$$

43.4.6.12 Ex: Damping in mixtures of species

Describe the damping in mixtures of species, and show how to use a measurement of the damping time for a determination of the interspecies the scattering length.

Solution: *The damping is described by two differential equations [439],*

$$\ddot{z}_1 = -\omega_1^2 z_1 - \frac{4}{3}\frac{m_2}{m}\frac{N_2}{N}\gamma_{therm}(\dot{z}_1 - \dot{z}_2)$$
$$\ddot{z}_2 = -\omega_2^2 z_2 - \frac{4}{3}\frac{m_1}{m}\frac{N_1}{N}\gamma_{therm}(\dot{z}_2 - \dot{z}_1) \ ,$$

or in matrix form,

$$\begin{pmatrix} \dot{y}_1 \\ \dot{z}_1 \\ \dot{y}_2 \\ \dot{z}_2 \end{pmatrix} = \begin{pmatrix} -\frac{4}{3}\frac{m_2}{m}\frac{N_2}{N}\Gamma & -\omega_1^2 & \frac{4}{3}\frac{m_2}{m}\frac{N_2}{N}\Gamma & 0 \\ 1 & 0 & 0 & 0 \\ \frac{4}{3}\frac{m_1}{m}\frac{N_1}{N} & 0 & -\frac{4}{3}\frac{m_1}{m}\frac{N_1}{N}\Gamma & -\omega_2^2 \\ 0 & 0 & 1 & 0 \end{pmatrix} \begin{pmatrix} y_1 \\ z_1 \\ y_2 \\ z_2 \end{pmatrix} \ ,$$

where $\gamma_{therm} = n_{12}\sigma_{12}v$ *with* $n_{12} = \left(\frac{1}{N_1} + \frac{1}{N_2}\right)\int n_1 n_2 d^3\mathbf{r}$. *Hence,*

$$\gamma_{therm} = \left(\frac{1}{N_1} + \frac{1}{N_2}\right)\Gamma_{coll} \ .$$

43.5 Other traps

43.5.1 Ion traps

The electric charge of ions allow for their efficient manipulation and control by electric and magnetic fields exploiting the Coulomb-Lorentz force. In fact, the control is so good, that it is possible to isolate and store individual ions or even arrays of quantum entangled ions and to perform coherent operations on them, which qualifies them as quantum registers. Two different types of traps have been investigated. In *Penning trap*s [1014], electrically charged particles are subjected to a radially attractive quadrupolar electrostatic field superimposed to an axial magnetostatic field forcing the particles into closed circular orbitals [6]. In the so-called *radiofrequency trap* or *Paul trap* –*Wolfgang Paul* received the Nobel Prize in 1989 together with Hans Dehmelt and Norman Ramsey– charged particles subjected to an alternating electric field with quadrupolar symmetry. Hyperboloidal electrode configurations produce saddle-shaped potentials, as shown in Fig. 43.29, which are, at any instant of time, parabolically repulsive in the one direction (axial or radial) and parabolically attractive in the other (radial or axial). The alternating electric field causes a periodic reorientation of the Coulomb force, which leads to a time-averaged parabolic

[6] Note that purely electrostatic fields do not lend themselves to trapping, since the necessary condition for the existence of minima in a potential, $\partial_i\partial_j\phi < 0$, does not obey the Laplace equation.

quasi-potential $\Phi(\mathbf{r}, t)$. In this potential the particles perform harmonic oscillations at characteristic frequencies, which are independent of the oscillation amplitude [1001]:

$$\Phi(r, z) = \Phi_0(t)(r^2 - 2z^2) \quad , \quad r^2 = x^2 + y^2 \ , \tag{43.126}$$

where the polarity is alternated at a radiofrequency Ω_a,

$$\Phi_0(t) = \Phi_{dc} + \Phi_{ac} \cos(\Omega_a t) \ . \tag{43.127}$$

Φ_{dc} denotes the amplitude of the *dc* part of the voltage, Φ_{ac} the amplitude of the *ac* part. The potential $\Phi(r, z, t)$ exerts, in the temporal average, a central force on the ion, if the radiofrequency field satisfies specific conditions.

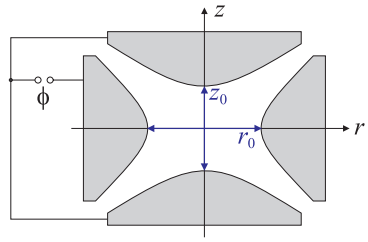

Figure 43.28: Geometry of the Paul trap.

43.5.1.1 Evaluation of the stability diagram

Paul traps do not have to have perfect quadrupolar geometry. To determine the secular frequencies of the pseudo-potential for an arbitrary geometry, we expand the potential around the position $\mathbf{r}_0$ of the potential minimum, which depends on the geometry of the electrodes and the applied voltages,

$$\begin{aligned} \Phi(\mathbf{r}) &= \Phi_a + (\mathbf{r} - \mathbf{r}_0)\nabla\Phi(\mathbf{r}_0) + \tfrac{1}{2}[(\mathbf{r} - \mathbf{r}_0)\nabla]^2\Phi(\mathbf{r}_0) + ... \\ &\equiv \Phi_a[1 + b_r(r - r_0)^2 + b_z(z - z_0)^2] \ . \end{aligned} \tag{43.128}$$

In the last step, we assume that the potential has an almost cylindrical shape. For a given geometry, the curvatures $b_{z,r}$ can be extracted from numerical simulations. From the continuity equation, we find $b_z = -2b_r$. The polarity of the electrodes is modulated with frequency Ω,

$$\Phi(\mathbf{r}, t) = \Phi(\mathbf{r})(\zeta - \cos \Omega t) \ . \tag{43.129}$$

The equations of motion are derived from $m\ddot{\mathbf{r}} = -e\nabla\phi(\mathbf{r}, t)$,

$$m\ddot{r}_j + 2e\Phi_a b_j(\zeta - \cos \Omega t) r_j = 0 \ . \tag{43.130}$$

Introducing the parameters a and q,

$$a_z = \frac{8e\phi_a b_z \zeta}{m\Omega^2} = -2a_r \quad \text{and} \quad q_z = \frac{4e\Phi_a b_z}{m\Omega^2} = -2q_r \ , \tag{43.131}$$

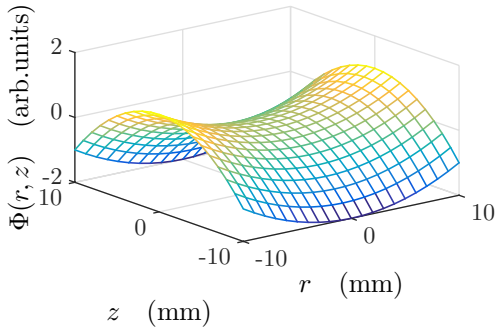

Figure 43.29: (code) Two-dimensional illustration of time-dependent potential: at each instant of time the potential has the form of a saddle. The potential rotates around the vertical axis at an appropriate pace.

we arrive at the so-called *Mathieu equation* [869, 446],

$$\ddot{r}_j + \tfrac{1}{4}\Omega^2(a_j - 2q_j\zeta\cos\Omega t)r_j = 0\ . \tag{43.132}$$

These equations predict stable orbits, provided that the parameters a and q are within the so-called stability diagram shown in Fig. 43.30.

According to these equations, the ion goes through oscillatory motions that are defined by the trap parameters a_i and q_i. For the motion of the ion to be finite, its oscillation amplitude may not exceed the boundaries defined by the electrodes. This condition imposes an allowed regime for the trap parameters called *stability diagram* [869].

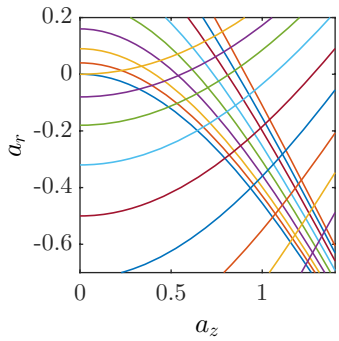

Figure 43.30: (code) Stability diagram.

In the limit $|a_i|, q_i \ll 1$ the ion travels only a short distance $s \ll r_0$ during one modulation period Ω_a. Then the ion undergoes a slow periodic motion called *macromotion* within the trapping potential with the secular frequency ζ_i. This motion is modulated by a rapid oscillation called *micromotion*, which is excited by the modulation field Ω_a. Without *dc* voltage applied between the ring and the endcaps, $a_i = 0$, the motion of the ion is described by the following simple equation:

$$r_i(t) = r_i^0\left(1 - \tfrac{1}{2}q_i\cos\Omega_a t\right)\cos\zeta_i t \quad , \quad \zeta_i = \tfrac{1}{\sqrt{8}}q_i\Omega_a \quad , \quad i = r, z\ . \tag{43.133}$$

The orbit of the ion is confined to the inner region of the trap, if its kinetic energy is less than $m\zeta_r^2 r_0^2 + M\zeta_z^2 z_0^2$. Since the trap is, at any instant of time, focusing in some directions and defocusing others, it is not a conservative potential. The oscillatory motion (disregarding micromotion) of the ion, however suggests a model, where the trap is described by a pseudo-potential [446, **?**] whose depth is,

$$D_z = \tfrac{q_z}{8} e V_{ac} = 2D_r \qquad \text{if} \qquad a_i = 0 \ . \tag{43.134}$$

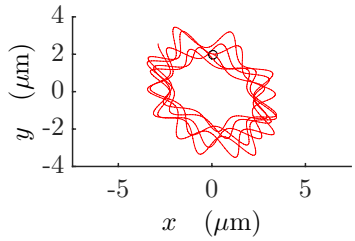

Figure 43.31: (code) Simulated micro- and macromotion of an ion.

Other geometries, deviating from the perfect quadrupole, are possible for the electrodes. These traps are also well described by equation (43.126), as long as the ion is near the trap center. For example, higher order multipolar traps have been used for trapping ion clouds [1357], as well as Paul-Straubl traps [1167] and storage rings [1350]. Particularly important for the storage of arrays of cooled ions with applications in quantum computing is the *linear Paul trap* [1055, 452, 1054], where immobilized ions are aligned on a linear chain. The advantage of the linear trap, as compared to other traps designed for many ions, is the easier optical access to individual ions by focused laser beams and the possibility of canceling the micromotion.

43.5.2 Micromotion

The motion of an ion in a Paul trap is a superposition of two vibrations with the respective oscillation frequencies Ω_a (modulation frequency) and $\zeta_{r,z}$ (secular frequencies for radial and axial direction vibrations). For an ion in thermal equilibrium (i.e., without active cooling), the mean kinetic energies of the micro- and macromotion are equal [150].

The macromotion can be reduced by cooling, in contrast to the micromotion, which is constantly excited by the modulation of the applied electric field [267]. On the other hand, the amplitude of the micromotion decreases with the distance of the ion from the trap center and, in the minimum of the pseudo potential, disappears completely. Therefore, to suppress the micromotion, it is imperative to cool the macromotion and push the ion to the trap center, if necessary, using additional static electric fields. Since the frequency of the micromotion is much higher than that of the macromotion, the dynamic sidebands can be resolved on a sufficiently narrow optical transition. When the modulation frequency Ω_a is very high, the secular frequencies of the macromotion are also high, so that even large optical transitions are able to resolve the macromotional sidebands. This is called the *strong coupling* regime.

Because of Coulomb repulsion, only a single atom can be at the center of a Paul trap, such that it is difficult to zero micromovement. One solution is to use a linear trap, where the center is smeared out over a straight line. Solve Exc. 43.5.4.1.

Example 278 (*Numerical calculation of the electric field created by a charged surface*): To calculate the trapping potential for a charged particle held on top of a planar microtrap structure, we proceed as follows. The energy of a charge in an electric field is $H = -e\Phi$. The electrostatic potential is given by Coulomb's law,

$$\Phi(\mathbf{r}) = \frac{1}{4\pi\epsilon_0}\sum_n \int_{V_n} \frac{\rho(\mathbf{r}')}{|\mathbf{r}-\mathbf{r}'|}dV' - \frac{1}{4\pi}\sum_n \int_{S_n} \Phi_n \frac{\mathbf{r}-\mathbf{r}'}{|\mathbf{r}-\mathbf{r}'|^3}d\mathbf{f}' + \frac{1}{4\pi}\sum_n \int_{S_n} \frac{\vec{\mathcal{E}}(\mathbf{r}')}{|\mathbf{r}-\mathbf{r}'|}\cdot d\mathbf{f}' \ ,$$

where ϕ_n is the voltage applied to the n-th boundary. In practice, electric fields are generated by electrodes set to specific voltages. Using the Dirichlet boundary conditions, we only retain the second term. Furthermore, to account for the planar geometry of the chip electrodes, we only consider surface boundaries in the $y' = 0$ plane,

$$\Phi(\mathbf{r}) = -\frac{1}{4\pi}\sum_n \Phi_n \int_{S_n} \frac{y dx' dz'}{\sqrt{(x-x')^2 + y^2 + (z-z')^2}^3} \ .$$

This implies that the field lines cross the chip surface orthogonally, which in reality is only true if the chip electrodes cover the whole area. Therefore, we

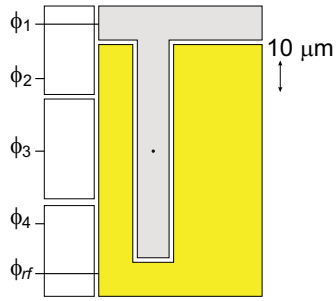

Figure 43.32: Possible design for a microchip ion trap. Φ_n are static potentials except for Φ_0, which is alternates sign with radio frequency.

only consider small gaps between the electrodes. We digitize the integral by dividing every electrode Φ_n into a number of identical surface elements Δf_m,

$$\Phi(\mathbf{r}) = -\frac{1}{4\pi}\sum_{n,m} \Phi_n \frac{y\Delta f_m}{\sqrt{(x-x_m)^2 + y^2 + (z-z_m)^2}^3} \ .$$

This formula can easily be evaluated numerically. A concrete example for a microchip ion trap is shown in Fig. 43.32.

Example 279 (*Numerical calculation of the magnetic field created by a current wire*): Current-carrying wires may exert Lorentz forces on the ions. The magnetostatic field is given by the Biot-Savart law,

$$\vec{\mathcal{B}}(\mathbf{r}) = \frac{\mu_0}{4\pi}\int_V \frac{(\mathbf{r}-\mathbf{r}')\times\mathbf{j}}{|\mathbf{r}-\mathbf{r}'|^3}dV' \ .$$

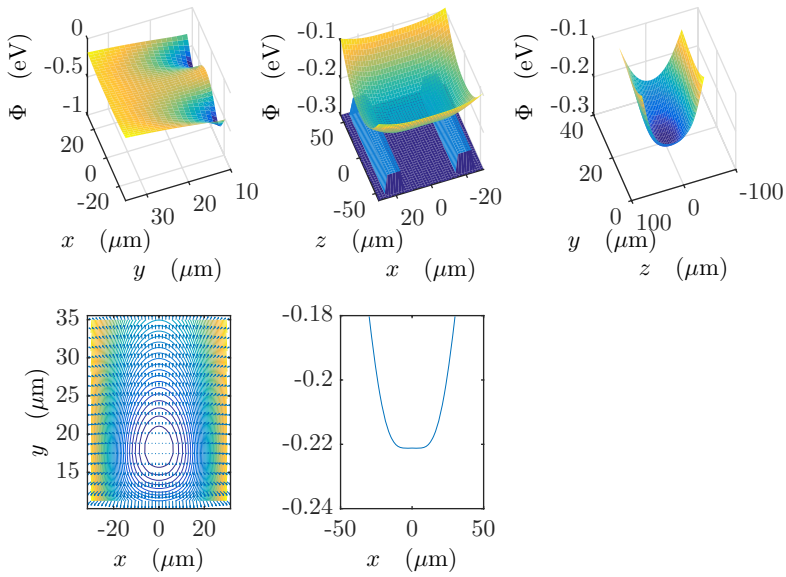

Figure 43.33: (code) Two-dimensional cuts through the electric potential generated by the microchip shown in Fig. 43.32 for $\Phi_{rf} = 100$ V and $\Phi_j = 0$.

In practice magnetic fields are created by current-carrying wires. Those can be parametrized by one-dimensional currents, $\mathbf{j} = I\delta^2 d\mathbf{s}$, so that,

$$\vec{\mathcal{B}}(\mathbf{r}) = \frac{\mu_0 I}{4\pi} \int_C \frac{d\mathbf{s}' \times (\mathbf{r} - \mathbf{r}')}{|\mathbf{r} - \mathbf{r}'|^3}$$

$$|\vec{\mathcal{B}}(\mathbf{r})| = \frac{\mu_0 I}{4\pi} \sum_n \frac{\sqrt{ds_{y,n}^2 (z - z_n)^2 + ds_{z,n}^2 (x - x_n)^2 + ds_{x,n}^2 (y - y_n)^2}}{\sqrt{(x - x_n)^2 + (y - y_n)^2 + (z - z_n)^2}^3} .$$

can immediately be numerically solved.

43.5.2.1 Electronic detection of ions

The presence of ions in the trap can be probed through the damping that they induce a coupled electronic resonance circuit [1356, 1362].

43.5.3 QUEST

Homonuclear atoms and dimers do not have a permanent electrical dipole moment, but they may have a permanent magnetic dipole moment. Therefore, homonuclear dimers must be confined by magnetic field gradients, or else an electric dipole moment must be *induced* by an oscillating electromagnetic field. In the optical regime, this was demonstrated with the quasi-electrostatic trap (*QUEST*).

In contrast, heteronuclear dimers are polar molecules with a permanent electric dipole moment, which can be quite large if the molecules are deeply bound. According to Earnshaw's theorem, there is no static magnetic field maximum in free space. Thus, no 'high-field seeking' state can be trapped. In principle, QUEST-type dipolar optical

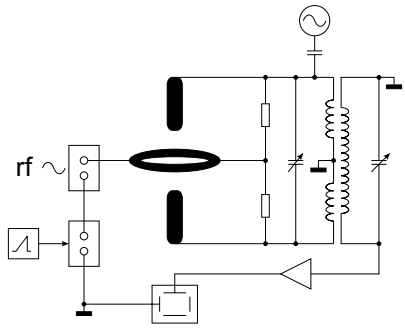

Figure 43.34: Resonance circuit for electronic ion detection. The trap is operated by a radiofrequency, while a DC voltage is scanned across the stability diagram. Simultaneously, an oscillating field is tuned near one of the trap's secular frequencies. When the stability point is such, that the secular frequency coincides with the frequency of the oscillating field, the motion of the ions is parametrically excited and the resonance circuit is damped. This damping is detected by a narrow-band amplifier.

traps can also be used for heteronuclear dimers. The problem is, however, that in contrast to homonuclear molecules, transitions between the vibrational ground state levels are possible. Thus, the light generating the QUEST also induces transitions leading to a redistribution of the population over all vibrational states.

Very far from resonance,

$$U_{dip}(\mathbf{r}) = -\alpha_{stat}\frac{I(\mathbf{r})}{2\varepsilon_0 c} \ . \tag{43.135}$$

Loosely bound homonuclear molecules are subject to the sum of the restoring forces exerted by magnetic traps on the individual atoms, $\mu_m = 2\mu_a$ and $d_m = 2d_a$. This is also true for heteronuclear molecules as long as the trapping potential is much weaker than the binding energy.

Example 280 (*Permanent electric dipole moment of LiRb*): The interaction energy of two dipoles is,

$$\hat{H}_{int} = \frac{1}{4\pi\varepsilon_0}\frac{\mathbf{p}_1\cdot\mathbf{p}_2 - 3(\mathbf{p}_1\cdot\hat{\mathbf{r}})(\mathbf{p}_2\cdot\hat{\mathbf{r}})}{r^3} \ .$$

Thus, two identical dipoles with 1 Debye $= 10^{-27}/2.998\,\mathrm{Cm} = 10^{-19}/c\,\mathrm{Cm}^2\,/\,\mathrm{s} =$ 39.36 ea_B parallel oriented at a distance $r = 1\,\mu\mathrm{m}$ have the energy,

$$\hat{H}_{int} = \frac{1}{4\pi\varepsilon_0}\frac{p^2}{r^3} \approx h \times 1.5\,\mathrm{MHz} \approx k_B \times 73\,\mu\mathrm{K} \ .$$

For example, LiRb has an electrical dipole moment of between -2 and -4.2 Debye depending on the vibrational state of the molecule.

43.5.4 Exercises

43.5.4.1 Ex: Coulomb repulsion in linear Paul trap

Coulombian repulsion prevents that two ions confined in a linear Paul trap be simultaneously in the ground state. Determine the spatial extent of the ground state

and the depth of the potential in the pseudo-potential approximation. What is the equilibrium distance of the ions?

Solution: *The size of the ground state is,*

$$a_{trap} = \sqrt{\frac{\hbar}{m\omega_{trap}}} \ .$$

The Coulomb repulsion balances the potential energy. For two ions the equilibrium distance is,

$$d_{Coul} = \sqrt{\frac{e^2}{\pi\varepsilon_0 m\omega_{trap}^2}} \ .$$

Therefore two ions can share the ground state if $a_{trap} > d_{Coul}$*. For this to happen, we find* $\omega_{trap} > 2\pi\times 10^{21}$ Hz*! Also we didn't account for micromotional heating which also will occur. Then how about linear ion traps? Obviously, in the experiments carried out thus far the ions settle down in chains and are well localized and distinguishable, i.e. not condensed in an ionic condensate. And the reason for that is certainly not fermionic statistics. The ions are apparently not in the longitudinal ground state of the linear trap, but just in the transversal.*

43.5.4.2 Ex: Motion of ions in a surface Paul trap

Programs on the motion of ions in a surface Paul trap.

Solution: *IonBecCalcs1: Coulomb potential of point charges.*
IonBecCalcs2: Dirichlet boundary problem, ion surface trap chip design.
IonBecCalcs3: Dirichlet boundary problem, ion surface trap chip design, improved chip design, calculates curvatures.
IonBecCalcs4: Dirichlet boundary problem, ion surface trap chip design, improved chip design, generates potentials and force fields.
IonBecCalcs5: Dirichlet boundary problem, ion surface trap chip design, planar waveguide, mass spectrometer.
IonBecSimul1: Motion of a single ion in a Paul trap [237].
IonBecSimul2: Motion of a single ion in a chip trap.

43.6 Analysing techniques

To analyze the kinetic state of an atomic gas and, for example, to identify the presence of a Bose-Einstein condensate, it is necessary to measure its spatial or momentum distributions. However, the only way to gather information from the atoms is to throw some kind of particles into them and to detect, where these particles are scattered. The most suitable particle to penetrate an ultra-high vacuum chamber surely is the *photon*. Therefore, apart from few exceptions where electron beams are used, all information on ultra-cold gases has been obtained so far through their reactions to incident laser beams [626, 238, 34, 670, 534].

43.6.1 Time-of-flight imaging

The most common imaging techniques measure the absorption of a laser beam by an atomic cloud after a *time-of-flight* or the dispersion of a laser beam induced by trapped cloud. The amplitude E_0 of a light wave traversing an atomic cloud of diameter L and characterized by the refractive index η is modified by a factor $e^{\imath\omega L\eta/c}$. For an inhomogeneous cloud, we have,

$$\mathcal{E} = \mathcal{E}_0 e^{\imath\omega L/c} \exp\left(\imath\frac{\omega}{c}\int_{-\infty}^{\infty}(\eta(\mathbf{r})-1)dz\right) . \tag{43.136}$$

We can approximate the refractive index by the atomic susceptibility,

$$\eta = \sqrt{1+\chi} \simeq 1+\frac{\chi}{2} \qquad \text{with} \qquad \chi = -\frac{4\pi n(\mathbf{r})}{k^3(2\Delta/\Gamma+\imath)} . \tag{43.137}$$

where $n(\mathbf{r})$ is the density distribution of the cloud. The imaginary part of the susceptibility is related to the *absorption coefficient* α and the real part to the *dispersion coefficient* δ,

$$\mathfrak{Im}\ \chi = \frac{\alpha}{\omega/c} \qquad \text{and} \qquad \mathfrak{Re}\ \chi = \frac{2\delta}{\omega/c} . \tag{43.138}$$

Now, the absorption and dispersion coefficients can be related to the optical cross-section $\sigma(\Delta)$ defined in (22.102) [816], where Δ is the detuning of light frequency from an atomic resonance, whose linewidth is Γ. This result is called the *optical theorem*,

$$\alpha = n\sigma(\Delta) \qquad \text{and} \qquad \delta = n\sigma(\Delta)\frac{\Delta}{\Gamma} , \tag{43.139}$$

Finally, we obtain the *Lambert-Beer law*,

$$\boxed{\mathcal{E} = \mathcal{E}_0 e^{\imath\omega L/c} \exp\left[\imath\sigma(\Delta)\left(\frac{\imath}{2}-\frac{\Delta}{\Gamma}\right)\int_{-\infty}^{\infty} n(\mathbf{r})dz\right] \equiv \mathcal{E}_0 e^{\imath\omega L/c} e^{-b/2} e^{\imath\varphi}} . \tag{43.140}$$

For the intensity, $I \propto |E|^2$, we get,

$$\frac{I}{I_0} = \exp\left[-\sigma(\Delta)\int_{-\infty}^{\infty} n(\mathbf{r})dz\right] \equiv e^{-b} . \tag{43.141}$$

The *absorption* b describes the loss of intensity for the laser beam due to scattering by the (disordered) atoms. It is strong near resonance, but diminished quadratically with the detuning Δ. The scattering is necessarily accompanied by radiation pressure accelerating and heating the atoms. The *dispersion* φ describes the refraction of the laser beam by the atomic density distribution (which for this purpose can be considered as continuous) [298, 458]. It disappears in resonance and diminishes slowly with increased detuning ($\propto \Delta$). It is connected to the dipole force and, thus, does not heat the atomic cloud. The coefficient φ describes the phase shift of the electromagnetic wave transmitted through the atomic cloud.

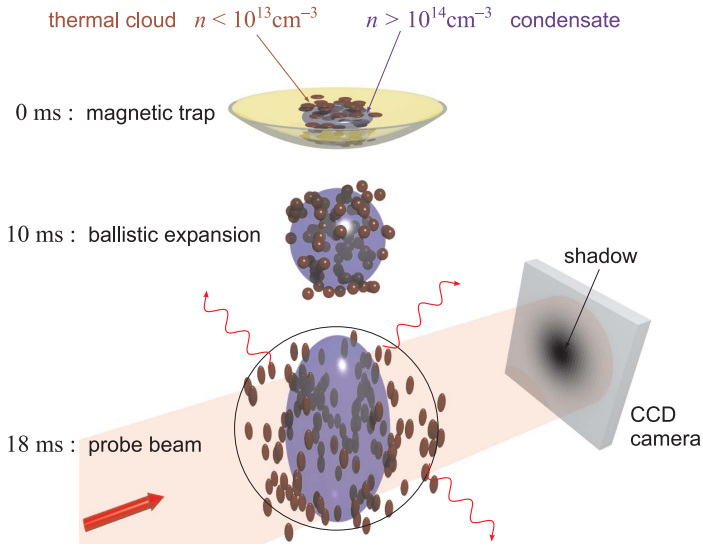

Figure 43.35: Sequence of a typical time-of-flight experiment: As soon as the trapping potential is suddenly switched off, the atomic cloud ballistically expands for 18 ms, before it is illuminated by a short resonant laser pulse. The shadow printed by the cloud onto the beam is photographed by a CCD camera.

43.6.2 Absorption imaging

Let us now detail the experimental process of *absorption imaging* (see Fig. 43.36): The trap confining the atomic cloud is suddenly turned off, thus letting the atoms, accelerated by the Earth's gravitation, fall for a flight time of a few ms. Then a pulse of a resonant laser light, whose diameter is much larger than the size of the cloud, is irradiated. The local attenuation of the beam intensity $I \sim |\mathcal{E}|^2$ can be related through the absorption b (also called *optical density* or *optical depth*) to the atomic density via,

$$-\ln \frac{I(x,y)}{I_0} = b(x,y) = \sigma(\Delta) \int n(\mathbf{r}) dz \ . \tag{43.142}$$

The shadow printed by the atomic cloud on the transverse profile of the laser beam is recorded by a CCD camera.

We have already noted that the absorption is accompanied by radiative pressure. After some scattering events, due to the photonic recoil, the atoms have accumulated a sufficiently large velocity, and therefore a sufficiently large Doppler shift, to be out of resonance with the laser beam. Subsequent photons are no longer scattered by the atoms and only contribute to increase the illumination of the CCD camera without carrying any information about the presence of atoms. Consequently, it is advantageous to use very short laser pulses. In addition, the intensity of the laser beam should not saturate the transition in order to guarantee an optical cross-section, which is independent of the intensity, and hence to guarantee the validity of the Lambert-Beer law. Finally, the laser frequency must be tuned perfectly to resonance, $\Delta = 0$. Otherwise, the interaction between the laser beam and the atomic cloud becomes

partially dispersive, which leads to a focusing or defocusing of the laser beam by refraction and a distortion of the image making it impossible to estimate the size of the cloud.

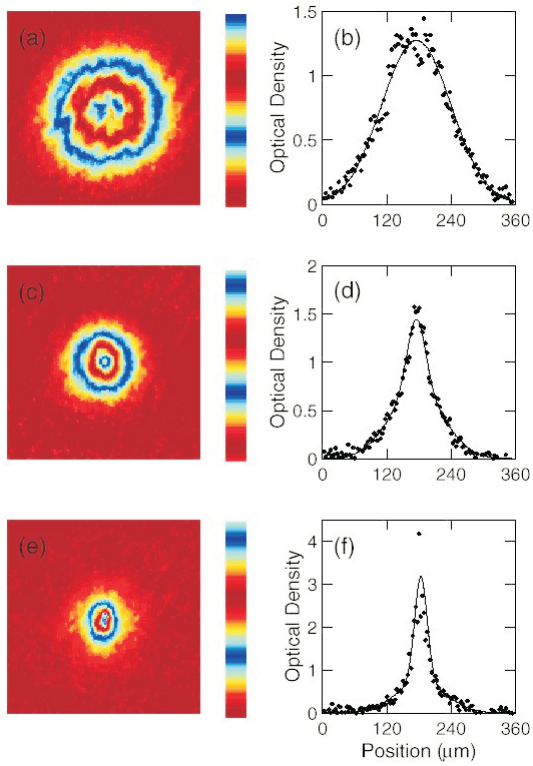

Figure 43.36: Absorption images after a time-of-flight allow to identify the presence of a Bose-condensate through its characteristic momentum distribution. Shown are images (a,b) above, (c,d) slightly below, and (e,f) well below the critical temperature for a Bose-Einstein phase transition (figures [580]).

Fig. 43.36 shows examples of absorption images of an atomic cloud taken at different stages of the evaporation process. Fig. 43.36(a,b) was taken at a temperature of 320 nK; the cloud is large and isotropic and therefore purely thermal. At 250 nK [see Fig. 43.36(c,d)] an elliptically shaped part appears in the center of the thermal cloud. And at 180 nK [see Fig. 43.36(e,f)] the thermal cloud almost completely disappeared for the benefit of the condensate. A quantitative evaluation of the condensed fraction is given in Sec. 44.1.4. Solve the Excs. 43.6.6.2 and 43.6.6.1.

43.6.3 Dispersive imaging

The absorption imaging technique is destructive, because of the involved ballistic expansion and also because of the radiative pressure exerted by the resonant imaging beam, which accelerates and heats the atomic cloud. That is, the measurement process messes up the distributions of the cloud, such that a second image taken after

the first one will give different results. However, there is a non-destructive imaging technique called *dispersive imaging* or *phase contrast imaging*. In this technique, the laser light is tuned sufficiently far from resonance, $|\Delta| \gg \Gamma$, for spontaneous emission and heating induced by random photonic recoil to be negligible [34]. This permits to take a series of consecutive images and create a *movie* of the temporal evolution of the cloud. Another advantage of this technique is the low off-resonant optical density, which allows to take pictures of very dense clouds *in situ*, that is, *while they are confined in a trap*.

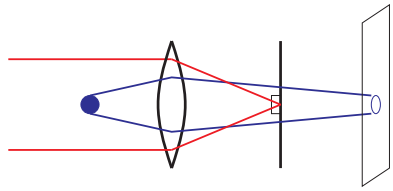

Figure 43.37: Scheme for dispersive images.

The physical quantity which is measured by this method is the local phase shift of the wavefront of the probe laser. Wavefront distortions are difficult to measure. To transform the phase profile into an intensity profile, a method known from classical optics called *Schlieren method* is used. It is based on the interference of the probe beam with its distorted wavefront and a reference plane wave. In practice, there are several possibilities. For *dark-ground imaging*, the part of the incident beam not having interacted with the atoms is blocked behind the interaction zone (see Fig. 43.37)

$$\bar{I}_{dg} = \tfrac{1}{2}|\mathcal{E} - \mathcal{E}_0|^2 = I_0 \left| e^{-b/2+\imath\varphi} - 1 \right|^2 \overset{b\to 0}{\longrightarrow} I_0 \varphi^2 = I_0 b \frac{\Delta^2}{\Gamma^2} \,. \tag{43.143}$$

The intensity signal $\bar{I}_{dg}$ is quadratic in optical density b.

For *phase contrast imaging*, the part of the beam not having interacted with the atoms receives a phase shift of $\lambda/4$ with respect to the part of the beam having interacted with the atoms:

$$\bar{I}_{pc} = \tfrac{1}{2}|\mathcal{E} - \mathcal{E}_0 + \mathcal{E}_0 e^{\pm\imath\pi/2}|^2 = I_0 \left| e^{-b/2+\imath\varphi} - 1 + e^{\pm\imath\pi/2} \right|^2 \overset{b\to 0}{\longrightarrow} I_0(\pm 1 + \varphi)^2 \simeq I_0 \left(1 \pm b\frac{\Delta}{\Gamma} \right) \,. \tag{43.144}$$

The intensity $\bar{I}_{pc}$ is linear in b and, consequently, more sensitive to weak signals. Finally, a third technique, called *polarization contrast imaging*, detects the local birefringence of the atomic cloud [188, 1125].

The imaging techniques shown so far only allow to visualize the instantaneous density distribution of the atomic cloud $n(\mathbf{r})$. If we are interested in other quantities, we have to conceive the experiment in such a way, that the desired information leaves its signatures in the density distribution. For example, to measure the excitation

frequencies of a condensate, which can perturb its shape and observe the subsequent time evolution of $n(\mathbf{r}, t)$ via dispersive imaging [674, 883, 35, 712].

43.6.4 Reconstruction of column-integrated absorption images

Assume cylindrical symmetry $n(\mathbf{r}) = n(r, z)$, with $r = \sqrt{x^2 + y^2}$. Absorption images are *column-integrated*, i.e. they are taken by integration along the x-axis,

$$\frac{I(y,z)}{I_0(y,z)} = e^{-\sigma \int n(r,z)dx} = e^{-\sigma f(y,z)} \ . \tag{43.145}$$

The radial density can be recovered by tomography [342, 389, 993],

$$n(r,z) = \frac{1}{(2\pi)^2} \int (\mathcal{F}_y f)(\kappa_y, z) J_0(\kappa_y r) d\kappa_y \ . \tag{43.146}$$

This is called *image reconstruction* or *Fourier reconstruction* or *inverse Abel transform* and will we studied in Exc. 43.6.6.3.

43.6.5 Condensable atomic species

Early work on BEC has been done by [1149, 93, 149, 248, 802]. Proposals for atomic gases withe from [592, 1275, 1269]. An appropriate BEC candidate must fulfill a few conditions: The transition wavelengths must be *accessible by laser light*, the level scheme should exhibit a *closed cycling transition* for laser cooling and have a reasonable pressure in gas phase. Furthermore, it is desirable to have a large HFS, metastable electronic state, no trapping state, large positive scattering length, Feshbach resonances. For sympathetic cooling it may be nice to have several isotopes of the same element.

The most common elements are alkalis, alkali earths and noble gases. The following gases have already been condensed ^{1}H, ^{1}He*, ^{7}Li, ^{23}Na, ^{85}Rb, and ^{87}Rb [31], [329], [189], [188], [1126], [301], [580], [585]. Investigations in ^{1}Ne*, ^{39}K, ^{133}Cs, ^{x}Sr, ^{x}Cr and ^{40}Ca are underway [1227], [556], [737], [1056], [1202], [113], [466].

43.6.6 Exercises

43.6.6.1 Ex: Lensing by cold clouds

The interaction of light with two-level atoms generates a susceptibility which gives rise to a refraction index,

$$\eta(\mathbf{r}) = \sqrt{1 - \frac{4\pi n(\mathbf{r})}{k^3(2\Delta/\Gamma + \imath)}} \ ,$$

where $n(\mathbf{r})$ is the cloud's density distribution and $\Gamma/2\pi = 30.5\,\mathrm{MHz}$ for strontium.
a. Calculate the phase-shift suffered by a light beam crossing an ultracold atomic cloud ($N = 10^5$, $T = 1\,\mu\mathrm{K}$) confined in an isotropic harmonic trap ($\omega_{trp} = (2\pi)\ 100\,\mathrm{Hz}$) as a function of detuning.
b. Estimate the focal distance of the cloud for $\Delta = -\Gamma$.

Solution: *a. The density distribution is,*

$$n(\mathbf{r}) = \frac{N}{(2\pi)^{3/2}\bar{r}^3} e^{-r^2/2\bar{r}^2} \qquad with \qquad \bar{r} = \sqrt{\frac{k_B T}{m\omega_{trp}^2}} \ .$$

The phase shift is then,

$$\varphi = \int_{-\infty}^{\infty} n(0,0,z)\sigma(\Delta)\frac{\Delta}{\Gamma}dz = \frac{3\lambda^2}{2\pi}\frac{\Gamma^2}{4\Delta^2+2\Omega^2+\Gamma^2}\frac{\Delta}{\Gamma}\frac{N}{(2\pi)^{3/2}\bar{r}^3}\int_{-\infty}^{\infty} e^{-z^2/2\bar{r}^2}dz$$
$$= \frac{3N\lambda^2}{(2\pi)^{5/2}}\frac{\Delta\Gamma}{4\Delta^2+2\Omega^2+\Gamma^2}\frac{m\omega_{trp}^2}{k_B T}\sqrt{2\pi} = \frac{3N}{k^2}\frac{\Delta\Gamma}{4\Delta^2+2\Omega^2+\Gamma^2}\frac{m\omega_{trp}^2}{k_B T} \ .$$

b. Let us assume that the phase shift is negligible for a beam passing at a distance $\bar{r}$

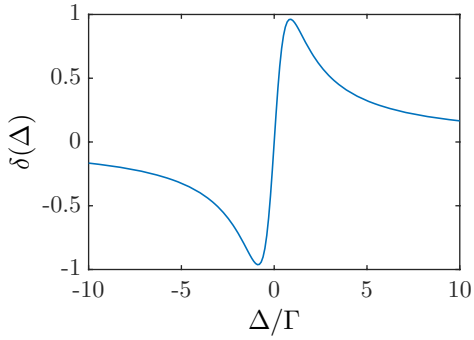

Figure 43.38: (code) Lensing.

from the cloud center. Then we estimate the focal distance f from,

$$\frac{\varphi\lambda/2}{\bar{r}} = \tan\theta \simeq \sin\theta = \frac{\bar{r}}{f}$$

as,

$$f \simeq \frac{2\bar{r}^2}{\varphi\lambda} \approx 1\,\text{mm} \ .$$

43.6.6.2 Ex: Optical density

A cloud of $N = 10^6$ ^{87}Rb atoms is prepared in a cylindrical harmonic trap characterized by the axial vibration frequencies $\omega_z = (2\pi)\ 50\,\text{Hz}$ and the radial one $\omega_r = (2\pi)\ 200\,\text{Hz}$. The experimenter takes the absorption image after 18 ms time-of-flight, as shown in Fig. 43.36(a). A pixel of the CCD camera corresponds to 5 µm in real space.
a. At what temperature is the phase transition to Bose-Einstein condensate to be expected?

b. Determine the temperature of the sample.
c. Evaluate its density distribution.
d. Evaluate the resonant optical density for the $D2$-transition at 780 nm along the symmetry axis of the trapped cloud.

Solution: *a. The critical temperature is* $T_c = \frac{\hbar(\omega_r^2\omega_z)^{1/3}}{k_B}\left(\frac{N}{1.202}\right)^{2/3}$, *giving* $T_c = 570\,\mathrm{nK}$.
b. The cloud is purely thermal, since the distribution after ballistic expansion is isotropic. From the image's rms*-diameter,* $\bar{\mathbf{r}}_{tof}$, *we calculate the* rms*-diameter of the velocity distribution,* $\bar{v} = \frac{\bar{r}_{tof}}{t_{tof}}$, *and therewith the temperature,* $T = \frac{m\bar{v}^2}{k_B}$. *This yields* $T = 17\,\mu\mathrm{K}$.
c. The thermal cloud is described by a Gaussian distribution, $n(\mathbf{r}) = n_0 e^{-U(\mathbf{r})/k_BT}$. *Normalization gives,*

$$N = \int n(\mathbf{r})d^3r = n_0 \iiint_{-\infty}^{\infty} e^{(-m\omega_r^2r^2 - m\omega_z^2z^2)/2k_BT}dxdydz = n_0\sqrt{\left(\frac{2\pi k_BT}{m}\right)^3\frac{1}{\omega_r^4\omega_z^2}}\,.$$

Or $n_0 = N\sqrt{\left(\frac{m}{2\pi k_BT}\right)^3\omega_r^4\omega_z^2}$. *This yields,* $n_0 = 4.8\cdot 10^{11}\,\mathrm{cm}^{-3}$.
d. The optical density is now,

$$b = 3\frac{\lambda^2}{2\pi}\int_{-\infty}^{\infty} n(\mathbf{r})dz = 3\frac{\lambda^2}{2\pi}n_0\int_{-\infty}^{\infty} e^{-m\omega_z^2z^2/2k_BT}dz = 3\frac{\lambda^2}{2\pi}n_0\sqrt{\frac{2\pi k_BT}{m\omega_z^2}}\,.$$

This gives $b = 44.8$.

43.6.6.3 Ex: Inverse Abel transformation

Calculate the inverse Abel transform using Bessel of an arbitrary function in 2D.

Solution: *MW_AbelTrafo1: Inverse Abel transform using Bessel of a real Fermi sphere. MW_AbelTrafo2: Inverse Abel transform using Bessel of an arbitrary function in 2D. MW_AbelTrafo3: Inverse Abel transform . MW_AbelTrafo4: Forward Abel transform, comparison with column integration and analytical formula. MW_AbelTrafo5: Forward Abel transform, comparison with column integration and analytical formula in 2D.*

43.7 Further reading

H.J. Metcalf and P. van der Straaten, *Laser cooling and trapping* [880]$_{\mathrm{ISBN}}$

Y.B. Ovchinnikov et al., *A Zeeman slower based on magnetic dipoles* [990]$_{\mathrm{DOI}}$

S.C. Bell et al., *A slow atom source using a collimated effusive oven and a single-layer variable pitch coil Zeeman slower* [115]$_{\mathrm{DOI}}$

R.A. Cline et al., *Spin relaxation of optically trapped atoms by light scattering* [271]DOI

M. Defrise et al., *Three-dimensional image reconstruction from complete projections* [342]DOI

V. Dribinski et al., *Reconstruction of Abel-transformable images: The Gaussian basis-set expansion Abel transform method* [389]DOI

P.A. Vicharelli et al., *Iterative method for computing the inverse Abel transform* [1336]DOI

Y. Castin et al., *Limit of Doppler cooling* [239]DOI

D.A. Steck et al., *Rubidium 87 D Line Data* [1245]DOI

D.A. Steck et al., *Rubidium 85 D Line Data* [1246]DOI

M.G. Raizen et al., *Stochastic cooling of atoms using lasers* [1068]DOI

Jiazhong Hu et al., *Creation of a Bose-condensed gas of* ^{87}*Rb by laser cooling* [640]DOI

43.7.1 on gravimetry

S. Abend et al., *Atom-chip fountain gravimeter* [?]DOI

G. Ferrari et al., *Long-Lived Bloch Oscillations with Bosonic Sr Atoms and Application to Gravity Measurement* [440]DOI

K. Gietka et al., *A supersolid-based gravimeter in a ring cavity* [508]DOI

43.7.2 on strontium (metrology)

D.S. Barker et al., *Enhanced magnetic trap loading for atomic strontium* [96]DOI

Y. Bidel et al., *Coherent light transport in a cold strontium cloud* [138]DOI

I. Courtillot et al., *Efficient cooling and trapping of strontium atoms* [303]DOI

E.M. Bridge et al., *A vapor cell based on dispensers for laser spectroscopy* [403]DOI

A. Brusch et al., *Hyperpolarizability Effects in a Sr Optical Lattice Clock* [205]DOI

D.E. Chang et al., *Controlling dipole-dipole frequency shifts in a lattice-based optical atomic clock* [247]DOI

L. Couturier et al., *Measurement of the strontium triplet Rydberg series by depletion spectroscopy of ultracold atoms* [306]DOI

A. Derevianko et al., *Colloquium: Physics of optical lattice clocks* [358]DOI

G. Ferrari et al., *Precision frequency measurement of visible intercombination lines of strontium* [437]DOI

G. Ferrari et al., *Cooling of Sr to high phase-space density by laser and sympathetic cooling in isotopic mixtures* [438]DOI

T. Fukuhara et al., *Degenerate Fermi Gases of Ytterbium* [476]DOI

T. Fukuhara et al., *Mott insulator of ultracold alkaline-earth-metal-like atoms* [475]DOI

S.M. Heider et al., *Hyperfine structure of ^{87}Sr in the $^3P_2$ metastable state* [595]DOI

Fachao Hu et al., *Analyzing a single-laser repumping scheme for efficient loading of a strontium magneto-optical trap* [639]DOI

T. Ido et al., *Optical clocks based on ultracold neutral strontium atoms* [646]DOI

C. Javaux et al., *Modulation-free pump-probe spectroscopy of strontium atoms* [671]DOI

H. Katori et al., *Magneto-optical trapping and cooling of strontium atoms down to the photon recoil temperature* [702]DOI

T.H. Loftus et al., *Magnetic trapping of ytterbium and the alkaline-earth metals* [808]DOI

T.H. Loftus et al., *Narrow line cooling and momentum-space crystals* [809]DOI

T.H. Loftus et al., *Narrow line cooling finite photon recoil dynamics* [810]DOI

A.D. Ludlow et al., *Ultracold strontium clock: Applications to the measurement of fundamental constant variations* [821]DOI

Y.N. Martinez de Escobar et al., *Two-photon photoassociative spectroscopy of ultracold ^{88}Sr* [336]DOI

P.G. Mickelson et al., *Repumping and spectroscopy of laser-cooled Sr atoms using the $(5s5p)^3P_2$-$(5s4d)^3D_2$ transition* [887]DOI

N.V. Morrow, *Feedback Control of Atomic Motion in an Optical Lattice* [925]DOI

T. Mukaiyama et al., *Recoil-Limited Laser Cooling of ^{87}Sr Atoms Near the Fermi Temperature* [937]DOI

S.B. Nagel et al., *Magnetic trapping of metastable $^3P_2$ atomic strontium* [941]DOI

M.A. Norcia et al., *Narrow-line laser cooling by adiabatic transfer* [955]DOI

I. Nosske et al., *Two-dimensional magneto-optical trap as a source for cold strontium atoms* [960]DOI

Y.B. Ovchinnikov et al., *A permanent Zeeman slower for Sr atomic clock* [991]DOI

J.E. Sansonetti et al., *Wavelengths, transition probabilities, and energy levels for the spectrum of neutral strontium* [1142]DOI

R. Santra et al., *High-accuracy optical clock via three-level coherence in neutral bosonic ^{88}Sr* [1145]DOI

S. Snigirev et al., *Fast and dense magneto-optical traps for strontium* [1224]$_{\text{DOI}}$

F. Sorrentino et al., *Laser cooling and trapping of atomic strontium for ultracold atoms physics, high-precision spectroscopy and quantum sensors* [1230]$_{\text{DOI}}$

S. Stellmer et al., *Detection and manipulation of nuclear spin states in fermionic strontium* [1253]$_{\text{DOI}}$

S. Stellmer et al., *Reservoir spectroscopy of 5s5p* $^3P_2$*-5snd* $^3D_{1,2,3}$ *transitions in strontium* [1256]$_{\text{DOI}}$

A.V. Taichenachev et al., *Magnetic field-induced spectroscopy of forbidden optical transitions with application to lattice-based optical atomic clocks* [1290]$_{\text{DOI}}$

Z.W. Barber et al., *Direct excitation of the forbidden clock transition in neutral* ^{174}*Yb atoms confined to an optical lattice* [90]$_{\text{DOI}}$

A. Traverso et al., *Inelastic and elastic collision rates for triplet states of ultracold strontium* [1317]$_{\text{DOI}}$

M. Yasuda et al., *Lifetime Measurement of the* $^3P_2$ *Metastable State of Strontium Atoms* [1410]$_{\text{DOI}}$

G. Verma et al., *A compact atomic beam based system for Doppler-free laser spectroscopy of Strontium atoms* [1334]$_{\text{DOI}}$

Xinye Xu et al., *Cooling and trapping of atomic strontium* [1404]$_{\text{DOI}}$

T. Zelevinsky et al., *Optical clock and ultracold collisions with trapped strontium atoms* [1423]$_{\text{DOI}}$

43.7.3 on strontium (quantum degeneracy)

B.J. DeSalvo et al., *Degenerate Fermi gas of* ^{87}*Sr* [359]$_{\text{DOI}}$

Y.N. Martinez de Escobar et al., *Bose-Einstein Condensation of* ^{84}*Sr resonance at large detuning* [337]$_{\text{DOI}}$

Meng Khoon Tey et al., *Double-degenerate Bose-Fermi mixture of strontium* [1296]$_{\text{DOI}}$

P.G. Mickelson et al., *Bose-Einstein Condensation of* ^{88}*Sr Through Sympathetic Cooling with* ^{87}*Sr* [888]$_{\text{DOI}}$

S. Stellmer et al., *Bose-Einstein condensation of strontium* [1257]$_{\text{DOI}}$

S. Stellmer et al., *Bose-Einstein condensation of* ^{86}*Sr* [1258]$_{\text{DOI}}$

S. Stellmer et al., *Creation of Ultracold* Sr_2 *Molecules in the Electronic Ground State* [1254]$_{\text{DOI}}$

S. Stellmer et al., *Laser Cooling to Quantum Degeneracy* [1255]$_{\text{DOI}}$

Chapter 44

Thermodynamics of ideal quantum gases

The journey of the quest for Bose-Einstein condensation (BEC) begins with its prediction by Bose and Einstein in 1926. The first hint, that the condensation was more than just a theoretical fantasy came from London [812], who linked the newly discovered phenomenon of superfluidity in ^{4}He to BEC. However, the interpretation of the λ-point in terms of BEC was not obvious, because strong interactions between particles concealed the role of quantum statistics, and the thermodynamic potentials exhibited divergences at the critical temperature instead of discontinuities, as expected for an ideal gas BEC. These uncertainties triggered an intense search for other systems. In 1954, Schafroth pointed out that electron pairs can be seen as composite bosons and may form Bose-Einstein condensates at low temperatures [1149]. In 1957, Bardeen, Cooper and Schrieffer developed the microscopic theory of superconductivity [93], after other researchers, including Blutt, Schaffrot, Fröhlich and Bogolubov, had suggested a relationship of this phenomenon to Bose condensation of electron pairs (nowadays called Cooper pairs).

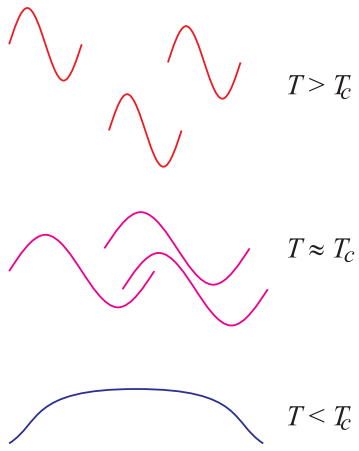

Figure 44.1: Illustration of atomic Broglie waves. From the top to the bottom the temperature of the atoms is decreasing.

Motivated by the need to test the concept of condensation of composite particles

in weakly interacting systems, in 1962 *Blatt et al.* proposed the investigation of the BEC in gases of *excitons* [149]. Excitons are bound electron-hole pairs that can form a weakly interacting gas in certain non-metallic crystals. They are interesting because their small mass allows BEC at high temperatures and gas density can be controlled over a wide range, by only modifying the intensity of the optical excitation. Being *quasi-particles*, excitons can be created and annihilated, that is their number is not conserved. Excitons were discovered in 1968, and the first evidence for Bose-Einstein of biexciton molecules in a CuCl crystal dates back to 1979 [248].

The laser as coherence phenomenon between photons shares many analogies with condensates. However, photons are quasi-particles as well, and again their number is not conserved [1]. Hence, there is no phase transition: When an optical cavity containing photonic modes is cooled, the photons prefer to disappear in the walls of the cavity instead of condensing.

Hecht [592] suggested in 1959, followed by Stwalley and Nosanow [1275] in 1976, that an atomic hydrogen gas with polarized spins would be an appropriate candidate for BEC. The advantage of this system is that interactions between atoms are weak and only give rise to a negligible quantum depletion below 1%. In 1978 Greytak and Kleppner started at the MIT intensive efforts to generate BECs in dilute hydrogen gases. In the 1990s, important advances in the cooling of atoms using laser light allowed to reach very low temperatures, and the invention of the magneto-optical trap (MOT) for neutral atoms permitted their spatial confinement and the compression of their density. These successes boosted efforts to try to create BEC in alkaline gases, which have electronic level schemes that lend themselves to optical cooling. Later, it was discovered that the phase space density in MOTs is limited by radiation trapping effects. As a solution to this problem, scientists had to learn how to trap atoms without the use of light in conservative traps, e.g. by their magnetic dipole moment, and to replace optical cooling with *evaporative cooling*. This was the crucial step that finally permitted to reach BEC in alkaline gases in 1995. Later, the hydrogen experiment, which initially stimulated the alkaline experiments, now taking advantage of their success, has been taken to BEC as well [466].

Why did it take so long to reach Bose-Einstein condensation, seven decades after its prediction by Bose and Einstein? How can we *see* when we have a condensate? What are the characteristics of a BEC accessible to observation and how to measure them? These are the answers that we will answer in the following sections. Solve

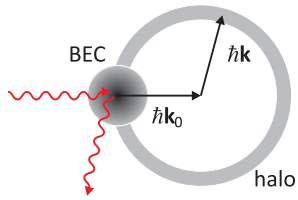

Figure 44.2: Scheme of the Broglie wave of cold atoms. From top to bottom the temperature decreases.

Exc. 44.1.5.1.

[1] The chemical potential of photons is $\mu = 0$.

44.1 Quantum statistics of an ideal Bose gas

The canonical approach to statistical mechanics begins with the probabilistic analysis of Boltzmann's velocity distribution of an ideal gas. For a gas consisting of particles of mass m at temperature T, the velocity distribution is given by the well-known *Maxwell-Boltzmann law* (MB) [641]

$$g(\mathbf{v}) = \left(\sqrt{\frac{m}{2\pi k_B T}}\right)^3 e^{-m\mathbf{v}^2/2k_B T} \ , \tag{44.1}$$

where k_B is the Boltzmann constant. Maxwell-Boltzmann's law was experimentally proven by Otto Stern in 1920, using a primitive atomic beam and a simple time-of-flight technique based on a rotating drum for selecting atomic velocities. With the advent of laser spectroscopy, the MB law and its limitations can be tested with highly improved accuracy. This law describes well the behavior of weakly interacting hot atoms. Deviations from this law are insignificant until, at low temperatures, quantum effects come into play. For this to happen the temperature must be so low that the atomic Broglie wavelengths become comparable to the average distance between particles. For a gas in thermal equilibrium the characteristic wavelength, called *thermal de Broglie wavelength*, is,

$$\boxed{\lambda_{therm} = \sqrt{\frac{2\pi\hbar^2}{mk_B T}}} \ , \tag{44.2}$$

where $\hbar = h/2\pi$ is Planck's constant. In a gas of density n, the mean distance between particles is $n^{-1/3}$. So, quantum effects are expected to emerge when $n^{-1/3} \sim \lambda_{dB}(T)$, such that the limit for this regime is defined by,

$$k_B T(n) = \frac{2\pi\hbar^2}{m} n^{2/3} \ . \tag{44.3}$$

For example, an atomic gas with density $n \sim 10^{16}\,\text{cm}^{-3}$ and temperature 900 K is certainly in the classical regime, since $n^{-1/3} \sim 10^6\,\text{cm} \gg \lambda_{dB} = 10^{-9}\,\text{cm}$. To observe quantum effects, we need relatively dense and cold clouds of atoms. In most gases, lowering the temperature or increasing the density promotes the system to liquidity before the quantum regime is reached. Well-known exceptions are spin-polarized hydrogen (H↑), which does not become liquid and helium, which exhibits quantum degeneracy effects in the liquid phase, although these effects are quite complex due to strong interparticle forces.

We have already seen that all particles in the quantum world are either *bosons* with integer spin or *fermions* with semi-integer spin. Fermions do not share a quantum state, because they must follow the *Pauli's exclusion principle*. They obey a quantum statistical distribution called *Fermi-Dirac distribution* (FD). In contrast, bosons enjoy to share a quantum state and even encourage other bosons to join them in a process called *bosonic stimulation*. Bosons obey a quantum statistical distribution called *Bose-Einstein distribution* (BE). The basic difference between the MB-statistics on one hand and the BE- or FD-quantum statistics on the other is that the former applies to identical particles which, however, are distinguishable from each other, while the

second describes identical indistinguishable particles. For the BE/FD statistics one can derive [726] the occupancy number for a non-degenerate quantum state having the energy ε when the system is kept at temperature T,

$$\boxed{w_{T,\mu} = \frac{1}{(2\pi)^3} \frac{1}{e^{\beta(\varepsilon-\mu)} \mp 1}} \,, \tag{44.4}$$

where we used the abbreviation $\beta \equiv 1/k_B T$. The upper sign refers to the BE statistics, the lower sign to the FD statistics. The chemical potential μ is an important system parameter, which helps to normalize the distribution (44.4) to the total number of particles,

$$N = \sum_{\varepsilon} w_{T,\mu}(\varepsilon) \,. \tag{44.5}$$

Similarly, the total energy of the system is given by,

$$E = \sum_{\varepsilon} \varepsilon w_{T,\mu}(\varepsilon) \,. \tag{44.6}$$

A very remarkable effect occurs in a bosonic gas at a certain characteristic *critical temperature* T_c: below this temperature a substantial fraction of the total number of particles occupies the lowest energy state, while all other states are occupied by a negligible number of particles. Above the transition temperature the macroscopic observables of the gas, such as pressure, heat capacity, etc., receive contributions of all states with a certain statistical weight, but without favoring the state of lower energy. Below the transition temperature, the observables are altered by a macroscopic occupation of the ground state, which results in dramatic changes of the thermodynamic properties. The phase transition is named after Shandrasekar Bose [181] and Albert Einstein [410] *Bose-Einstein condensation* (BEC).

44.1.1 Condensation of a free gas confined in a box potential

One of the keys to understanding BEC is the behavior of the chemical potential μ at very low temperatures. The chemical potential is responsible for the concentration of a large number of atoms in the ground state N_0. A system with a large number of non-interacting bosons condenses to the ground state when the temperature approaches zero, $N_0 \to N$. The Bose-Einstein distribution function (44.4) gives the population of the ground state, $\varepsilon = 0$, in the zero temperature limit, $N = \lim_{T\to 0}(e^{-\beta\mu} - 1)^{-1} = -1/\beta\mu$, or in terms of the *fugacity* defined by,

$$\boxed{Z \equiv e^{\beta\mu}} \,, \tag{44.7}$$

we may write, $Z \simeq 1 - 1/N$. It should be noted that the chemical potential in a bosonic system must always be less than the ground state energy in order to guarantee non-negative occupation $w_{T,\mu}(\varepsilon)$ of any state. $Z \simeq 1$ denotes macroscopic occupation of the ground state. We define the critical temperature for Bose-Einstein condensation via the occupation of the ground state. Above this temperature the occupancy of ground state is not macroscopic, below it is.

For a Bose gas of N non-interacting particles with mass m confined inside a box potential of volume $V = L^3$ the critical temperature for BEC can be calculated from equation (44.3). The boundary conditions require that the momenta satisfy $p_j = 2\pi\hbar l_j/L$, where $j = x, y$ or z and j are integers. Each state is labeled by a set of three integers (l_x, l_y, l_z). In the *thermodynamic limit*, the sum over all quantum states can be converted into an integral over a continuum of states,

$$\sum_{\mathbf{r},\mathbf{k}} \overset{N\to\infty}{\longrightarrow} \frac{1}{\hbar^3}\int d^3r d^3p = \int d^3r d^3k \ . \tag{44.8}$$

For a free gas with energy $\varepsilon = p^2/2m$ we can derive, simplifying the calculation using the *density of states* η defined by (43.19), which basically depends on the geometry of our system [2]. Using the occupation number $w_{T,\mu}(\varepsilon)$ for the Bose-Einstein distribution (44.4) in the thermodynamic limit and the density-of-states in a box potential (43.22), let us calculate the total number of particles,

$$\begin{aligned} N &= N_0 + \iint w_{T,\mu}(\varepsilon(\mathbf{r},\mathbf{k}))d^3r d^3k = N_0 + (2\pi)^3\int_0^\infty w_{T,\mu}(\varepsilon)\eta(\varepsilon)d\varepsilon \\ &= N_0 + \frac{\sqrt{2m}^3}{(2\pi)^2\hbar^3}V\int_0^\infty \frac{\varepsilon^{1/2}d\varepsilon}{e^{\beta(\varepsilon-\mu)}-1} \ , \end{aligned} \tag{44.9}$$

where the ground state population N_0 is maintained explicitly. In the process of converting the sum to an integral (44.8) the density of states disappears when we approach the ground state. This error is corrected by adding a contribution of an explicit term N_0 to the integral.

44.1.1.1 Riemann's zeta function

At this point, to help simplifying the notation, we introduce the *Bose function* and its integral representation,

$$g_\xi(Z) = \sum_{t=1}^\infty \frac{Z^t}{t^\xi} = \frac{1}{\Gamma(\xi)}\int_0^\infty \frac{x^{\xi-1}dx}{Z^{-1}e^x - 1} \ . \tag{44.10}$$

where $\Gamma(\eta)$ denotes the Gamma function. Analogically, we can define the *Fermi function* via,

$$f_\xi(Z) = \sum_{t=1}^\infty -\frac{(-Z)^t}{t^\xi} = \frac{1}{\Gamma(\xi)}\int_0^\infty \frac{x^{\xi-1}dx}{Z^{-1}e^x + 1} \ . \tag{44.11}$$

For classical particles,

$$c_\xi(Z) = \frac{1}{\Gamma(\xi)}\int_0^\infty \frac{x^{\xi-1}dx}{Z^{-1}e^x + 0} = Z \ . \tag{44.12}$$

A particular value is the *Riemann zeta-function*,

$$g_\xi(1) = \zeta(\xi) \ . \tag{44.13}$$

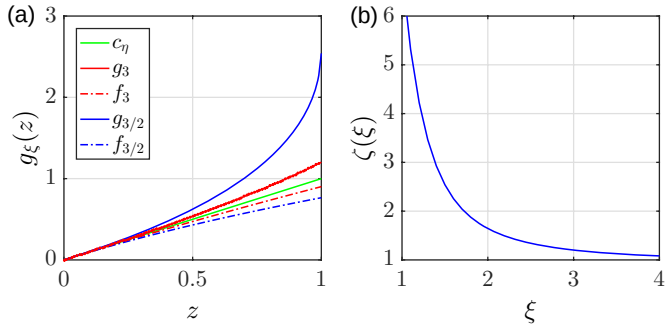

Figure 44.3: (code) (a) Bose and Fermi functions for box potentials (g_3 and f_3) and for harmonic potentials ($g_{3/2}$ and $f_{3/2}$). Also shown is the Boltzmann limit (44.12). (b) Riemann function.

With this definition and the definition of the thermal Broglie wavelength (44.2), Eq. (44.9) becomes,

$$N = N_0 + \frac{V}{\lambda_{th}^3(T)} g_{3/2}(e^{\beta\mu}) \ . \tag{44.14}$$

We can use Eq. (44.14) to calculate the critical temperature[3] $T_c^{(3/2)}$ defined for $N_0 \nearrow 0$ and $\mu \to 0$. Above the phase transition, $T > T_c^{(3/2)}$, the population is distributed over all states, each individual state being weakly populated. Below $T_c^{(3/2)}$ the chemical potential is fixed by $\mu = 0$ and the number of the particles occupying the excited states is,

$$N_{th} = \frac{V}{\lambda_{th}^3(T)} g_{3/2}(1) = N \left(\frac{T}{T_c^{(3/2)}} \right)^{3/2} \ , \tag{44.15}$$

with $g_{3/2}(1) = 2.612$. Since $N_0 + N_{th} = N$, the number of particles in the ground state is given by,

$$\boxed{\frac{N_0}{N} = 1 - \left(\frac{\min(T, T_c^{(3/2)})}{T_c^{(3/2)}} \right)^{3/2} \qquad \text{with} \qquad k_B T_c^{(3/2)} = \frac{2\pi\hbar^2}{m} \left(\frac{N}{V g_{3/2}(1)} \right)^{2/3}} \ , \tag{44.16}$$

N_0/N is the fraction of the atomic cloud which is condensed in the ground state. The abrupt occurrence of a finite occupation in a single quantum state at temperature below $T_c^{(3/2)}$ indicates a spontaneous change in the system and a thermodynamic phase transition. Solve Exc. 44.1.5.2.

[2]We must, however, keep in mind that the state density approach is an approximation not valid for experiments with a limited number of atoms.

[3]The superscript (3/2) denotes the box potential shape of the trapping potential. See 44.1.5.3 for an explanation of the notation.

44.1.2 Condensation of a harmonically confined gas

The critical temperature T_c^0 can be significantly altered, when the atoms are confined to a spatially inhomogeneous potential. The critical temperature depends on the general shape and the tightness of the potential. Let us consider N particles of an ideal Bose gas distributed over several quantum states of an arbitrary potential. The occupation number $w_{T,\mu}(\varepsilon)$ of particles at an energy level ε is still given by (44.4), the ground state energy is defined as zero. In the thermodynamic limit, the relation between the chemical potential and the total number of particles is still given by Eq. (44.9), with an adequate density of states $\eta(\varepsilon)$. The state density for an arbitrary confinement potential $U(\mathbf{r})$ can be found by generalizing the calculation to the free gas. The phase space volume between the energy surfaces ε and $\varepsilon + d\varepsilon$ is proportional to the number of states in this energy range. However, the external potential limits the space available for the gas. For a harmonic potential (43.18) with the mean secular frequency $\bar{\omega}$ the density-of-states $\eta(\varepsilon)$ has already been calculated in Eq. (43.21). With this, we can analogically to (44.9) calculate,

$$N = N_0 + \iint w_{T,\mu}(\varepsilon(\mathbf{r},\mathbf{k}))d^3r d^3k = N_0 + (2\pi)^3 \int_0^\infty w_{T,\mu}(\varepsilon)\eta(\varepsilon)d\varepsilon \tag{44.17}$$
$$= N_0 + \frac{1}{2(\hbar\bar{\omega})^3}\int_0^\infty \frac{\varepsilon^2 d\varepsilon}{e^{\beta(\varepsilon-\mu)}-1} = N_0 + \left(\frac{k_B T}{\hbar\bar{\omega}}\right)^3 g_3(Z)\ .$$

In the same way as for a potential well we find for a harmonic potential,

$$N_{th} = \left(\frac{k_B T}{\hbar\bar{\omega}}\right)^3 g_3(1) = N\left(\frac{T}{T_c^{(3)}}\right)^3\ , \tag{44.18}$$

with $g_3(1) = 1.202$. Since $N_0 + N_{th} = N$, the number of particles in the ground state is,

$$\boxed{\frac{N_0}{N} = 1 - \left(\frac{\min(T, T_c^{(3)})}{T_c^{(3)}}\right)^3 \qquad \text{with} \qquad k_B T_c^{(3)} = \hbar\bar{\omega}\left(\frac{N}{g_3(1)}\right)^{1/3}}\ . \tag{44.19}$$

The superscript (3) indicates the harmonic shape of the trap.

Fig. 44.4(left) traces the condensed fraction N_c/N measured as a function of the reduced temperature $T/T_c^{(3)}$. Experiments [580, 417] confirm Bose's ideal gas theory in the thermodynamic limit.

We note that smaller trapping volumes (or tighter potentials) increase the critical temperature T_c, thus allowing for quantum degeneracy at higher temperatures, which can be advantageous in experimentation. Also, at a given temperature, a strongly confining potential reduces the total minimum number of atoms required to reach condensation.

44.1.3 Energy and heat capacity

When the number of atoms is limited, $N < \infty$, we expect a slightly reduced critical temperature [551]. In addition, the interatomic interaction reduces the critical temperature [72]. The technical resolution of most experiments today is not sufficient to

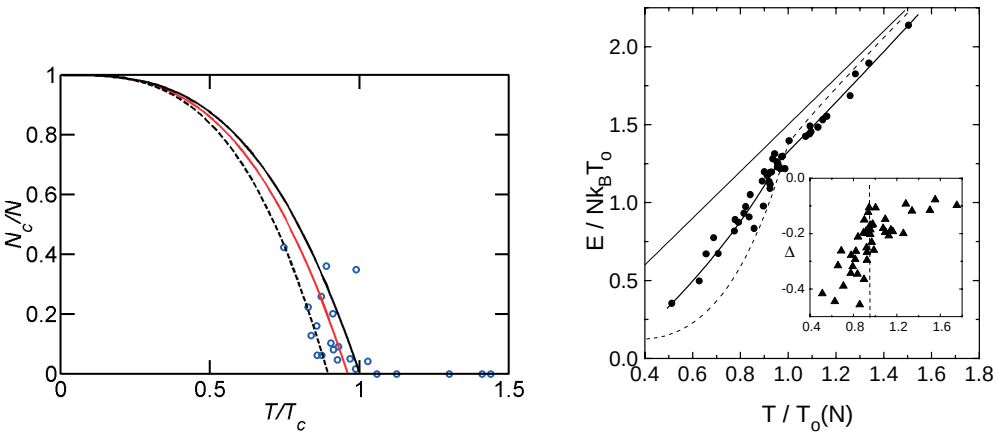

Figure 44.4: Left: Condensed fraction N_c/N as a function of reduced temperature $T/T_c^{(3)}$. The circles represent measured values. The upper solid line shows the theory for an ideal gas, the intermediate solid line shows a curve fitted to the measurements, and the lower part is a theoretical curve taking into account finite size effects and interatomic interactions. Right: Measurement of the release energy [417].

permit the study of these effects. However, measurements of other thermodynamic quantities such as energy and heat capacity [347, 417] showed significant deviations from the ideal gas behavior due to interaction effects. Therefore, although temperature being the most basic variable of the thermodynamic state, the system needs to be characterized by other quantities.

Heat is not a state variable because the amount of heat needed to raise the temperature of the system depends on how the heat is transferred. The *heat capacity* quantifies the system's ability to secure its energy. In conventional systems, the heat capacity is typically given either specified at constant volume or at constant pressure. Together with this specification, heat capacities are extensive state variables. When crossing a phase transition, the temperature-dependent heat capacity measures the degree of change in the system above and below the critical temperature and provides valuable information about the general type of phase transition.

The total energy $E/N \equiv N^{-1} \int \epsilon w d^3x d^3k$ per particle is given by,

$$\frac{E}{N} = \frac{\int \epsilon w_{T,\mu}(\mathbf{x},\mathbf{k}) d^3x d^3k}{\int w_{T,\mu}(\mathbf{x},\mathbf{k}) d^3x d^3k} = \frac{\int \epsilon \eta(\epsilon)(e^{\beta(\epsilon-\mu)}-1)^{-1} d\varepsilon}{\int \eta(\epsilon)(e^{\beta(\epsilon-\mu)}-1)^{-1} d\varepsilon} = 3k_B T \frac{g_4(Z)}{g_3(Z)} \ . \qquad (44.20)$$

For a confined gas, volume and temperature are interdependent, and the concept of pressure is somewhat vague. In this case, we can not refer to the heat capacity at constant volume or pressure. However, one can define the heat capacity for a fixed number of particles,

$$C(T) = \frac{\partial E(T)}{\partial T} \ . \qquad (44.21)$$

Recalling the implicit dependencies of the thermodynamic variables on temperature,

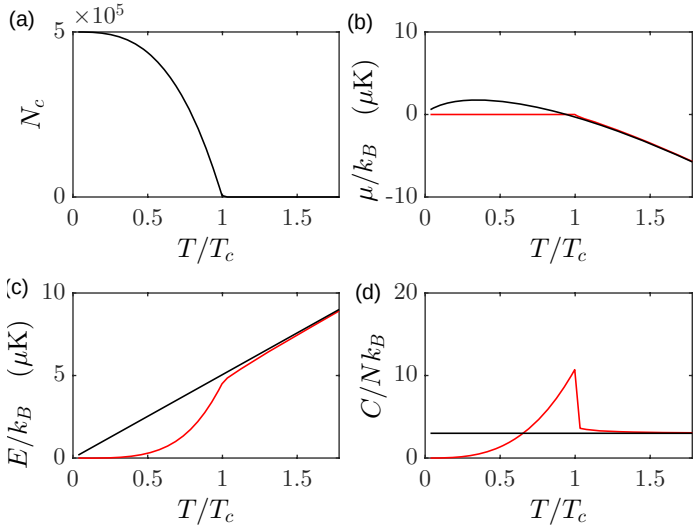

Figure 44.5: (code) Numerical calculation of thermodynamic potentials for a Bose gas as a function of temperature for a given trapping potential. (a) Chemical potential, (b) energy, (c) heat capacity per particle, and (d) total heat capacity.

we can evaluate (44.19):

$$C(T) = \beta \int_0^\infty \varepsilon f(\varepsilon)^2 \rho(\varepsilon) \left[\mu'(T) + \frac{\varepsilon - \mu}{T}\right] e^{\beta(\varepsilon-\mu)} d\varepsilon \ , \tag{44.22}$$

where the derivative of the chemical potential approaching the phase transition from above, $T \searrow T_c^0$, is

$$\mu'(T_c^+) = -\frac{1}{T} \frac{\int_0^\infty \varepsilon f(\varepsilon)^2 \rho(\varepsilon) e^{\beta\varepsilon} d\varepsilon}{\int_0^\infty f(\varepsilon)^2 \rho(\varepsilon) e^{\beta\varepsilon} d\varepsilon} \ . \tag{44.23}$$

Calculating the second moments of the distributions obtained for the same density by time-of-flight of absorption images, we obtain the kinetic energy,

$$U = \int \frac{p^2}{2m} n(\mathbf{p}) d^3\mathbf{p} \ . \tag{44.24}$$

For confined ideal gases, the virial theorem ensures $E_{kin} + E_{pot} = 2E_{kin}$. For real gases, the repulsive energy of the mean field adds to this energy, $E = E_{kin} + E_{pot} + E_{self}$. The sudden extinction of the trapping potential before time-of-flight takes away the potential energy E_{pot} non-adiabatically. The kinetic energy and the self-energy of the condensate are fully converted into kinetic energy during ballistic expansion. It is this energy, $p^2/2m = E_{kin} + E_{self}$, which is sometimes called *release energy*, which is measured after ballistic expansion [4]. Fig. 44.4(right) shows a measurement of the release energy. Solve the Exc. 44.1.5.3.

[4] It is interesting to measure the heat capacity of a partially condensed cloud near the critical point and analyze the discontinuity, because it contains important information about interatomic interactions and finite-size effects ([297], Seç. 3.4). In addition, the classification of Bose-Einstein condensation as a phase transition depends very much on the behavior of the thermodynamic potential near the critical point [772, 641].

44.1.4 Distribution functions for a Bose gas

Bose-Einstein condensates consist of atoms sharing a single quantum state. In inhomogeneous potentials, the condensate and the thermal fraction form spatially separated clouds, concentrated around the center of the potential and therefore very dense. For this reason, interatomic interaction effects generally dominate the density and momentum distribution of the condensed fraction. However, the non-condensed (or normal, or thermal) fraction is also subject to modifications due to the bosonic nature of the atoms. Since the density of the normal fraction is generally much smaller, these modifications are weak. In this section, we will only discuss these effects briefly, but we note that the calculations are analogous to the calculations for fermionic gases presented in Sec. 44.2.4.

For an ideal Bose gas the density and momentum distributions are expressed by Bose functions $g_{3/2}(z)$ [297]. For example, as will be derived in Exc. 44.1.5.4(a), the density and momentum distributions are,

$$\boxed{\begin{aligned} n(\mathbf{x}) &= \frac{1}{\lambda_{dB}^3}\, g_{3/2}(e^{-\beta[U(\mathbf{x})-\mu]}) \\ n(\mathbf{k}) &= \frac{a_{trap}^6}{\lambda_{dB}^3}\, g_{3/2}(e^{\beta(\mu-\mathbf{p}^2/2m)}) \end{aligned}} \quad \text{bosonic distribution functions .} \tag{44.25}$$

In the classical limit, we can calibrate the chemical potential by Eq. (44.14) for a box potential or by (44.17) for a harmonic potential,

$$g_{3/2}(e^{\beta\mu}) \to c_{3/2}(e^{\beta\mu}) = e^{\beta\mu} = \begin{cases} \frac{N}{V}\lambda_{th}^3 & \text{for a box potential} \\ c_3(e^{\beta\mu}) = N\left(\frac{\hbar\bar{\omega}}{k_BT}\right)^3 & \text{for a harmonic potential} \end{cases} . \tag{44.26}$$

Hence, we obtain for the classical density distribution,

$$\begin{aligned} n(\mathbf{x}) &= \frac{1}{\lambda_{th}^3} c_{3/2}(e^{-\beta[U(\mathbf{x})-\mu]}) = \frac{e^{\beta\mu}}{\lambda_{th}^3} e^{-\beta U(\mathbf{x})} \qquad (44.27) \\ &= \begin{cases} \frac{N}{V} e^{-\beta U(\mathbf{x})} & \text{for a box potential} \\ N\sqrt{\frac{m\bar{\omega}^2}{2\pi k_BT}}^3 e^{-\beta m\bar{\omega}^2 x^2/2} & \text{for a harmonic potential} \end{cases} . \end{aligned}$$

Similarly, the momentum density distribution is given by,

$$\begin{aligned} n(\mathbf{k}) &= \frac{a_{trp}^6}{\lambda_{th}^3} c_{3/2}(e^{\beta(\mu-p^2/2m)}) = \frac{a_{trp}^6 e^{\beta\mu}}{\lambda_{th}^3} e^{-\beta p^2/2m} \qquad (44.28) \\ &= \begin{cases} \frac{N}{V} a_{trp}^6 e^{-\beta U(\mathbf{x})} & \text{for a box potential} \\ N\hbar^3\sqrt{\frac{1}{2\pi m k_BT}}^3 e^{-\beta p^2/2m} & \text{for a harmonic potential} \end{cases} . \end{aligned}$$

We see that we recover the Maxwell-Boltzmann velocity distribution, as seen in Fig. 44.6,

$$n(\mathbf{v}) = n(\mathbf{k})\frac{m^3}{\hbar^3} = N\sqrt{\frac{m}{2\pi k_BT}}^3 e^{-\beta m v^2/2} . \tag{44.29}$$

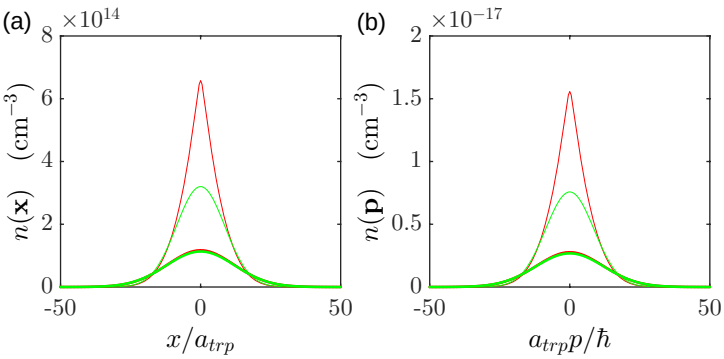

Figure 44.6: (code) (a) Density and (b) momentum distribution of a Bose gas (red) and a Boltzmann gas (green) at $T = 1.1T_c$ (solid line) and at $T = 2T_c$ (dotted line).

44.1.4.1 Ballistic expansion

To describe the density distribution of an ultracold Bose-gas after a time-of-flight we replace in the second Eq. (44.25): $\mathbf{k} = m\mathbf{r}/\hbar t_{tof}$. We obtain the density distribution,

$$n_{tof}(\mathbf{r}, t_{tof}) = \left(\frac{m}{\hbar t_{tof}}\right)^3 n(\mathbf{k} = m\mathbf{r}/\hbar t_{tof}) = \left(\frac{m}{\hbar t_{tof}}\right)^3 \frac{a_{trp}^6}{\lambda_{th}^3} g_{3/2}(e^{(\mu - mr^2/2t_{tof}^2)/k_BT})$$
$$\overset{T\to\infty}{\longrightarrow} \left(\frac{m}{\hbar t_{tof}}\right)^3 N\hbar^3 \sqrt{\frac{1}{2\pi m k_B T}}^3 e^{-mr^2/2t_{tof}^2 k_B T} = \frac{N}{(2\pi)^{3/2} r_{rms}^3} e^{-r^2/2r_{rms}^2} , \quad (44.30)$$

where we defined,

$$r_{rms} \equiv \sqrt{\frac{k_B T}{m}} t_{tof} . \quad (44.31)$$

This distribution does not directly depend on the potential $U(\mathbf{r})$, that is, the expansion is isotropic. However, the chemical potential does depend on the potential. For very long flight times (usually several 10 ms) the density resembles a Gaussian distribution [297]. In Exc. 44.1.5.4(b) we determine the time-of-flight density distribution of an ultracold Bose gas.

In a time-of-flight experiment, any deviation observed between the results (44.30) and (44.31) points towards an impact of quantum statistics. However, absorption images only record projections of the time-of-flight distribution on a plane.

44.1.4.2 Temperature and excitations

The *temperature of a Bose condensate* is given by the ratio of the numbers of condensed and thermal atoms. What about collective excitations in pure condensate? Can they be cooled? In fact, an oscillating BEC is not in thermal equilibrium. However, in the presence of some dissipation mechanism the excitations may thermalize evolving towards a steady state. Once the collective excitations have become thermal excitations, they simply increase the thermal fraction.

44.1.5 Exercises

44.1.5.1 Ex: Boson or fermion?

Whether an atom is a fermion or boson solely depends on its total spin. Half-integer spin particles are fermions, integer spin particles are bosons. For example, Rb atoms have in the ground state $J = 1/2, I = 7/2$ and F integer, and therefore are bosons. Ca^+ ions have $J = 1/2$ and no hyperfine structure, and thus are fermions. ^{6}Li has the half-integer F and is a boson.
Decide on the bosonic or fermionic nature of the following atoms/molecules:
^{85}Rb with $I = 3/2$ in the state $^2S_{1/2}$
^{88}Sr with $I = 0$ in the state $^1S_0$
^{88}Sr with $I = 0$ in the state $^3P_2$
^{87}Sr with $I = 9/2$ in the state $^1S_0$
$^{172}Yb^+$ with $I = 0$ in the state $^2S_{1/2}$
$^{171}Yb^+$ with $I = 1/2$ in the state $^2S_{1/2}$

Solution: *^{85}Rb in the state $^2S_{1/2}$ has the total spin $F = 1$ or $F = 2$ and is a boson*
^{88}Sr in the state $^1S_0$ has the total spin $F = 0$ and is a boson
^{88}Sr in the state $^3P_2$ has the total spin $F = 2$ and is a boson
^{87}Sr in the state $^1S_0$ has the total spin $F = 9/2$ and is a fermion
$^{172}Yb^+$ in the state $^2S_{1/2}$ has the total spin $F = 0$ and is a boson
$^{171}Yb^+$ in the state $^2S_{1/2}$ has the total spin $F = 0$ or $F = 1$ and is a boson

44.1.5.2 Ex: Monoatomic gas

Consider a classical monoatomic gas made up of N non-interacting atoms of mass m confined in a container of volume V, at temperature T. The Hamiltonian corresponding to an atom is given by $\hat{H} = (p_x^2 + p_y^2 + p_z^2)/2m$.
a. Show that the atomic canonical partition function is $\zeta = V/\lambda^3$, where $\lambda = h/\sqrt{2\pi m k_B T}$ is the thermal de Broglie wavelength.
b. Using ζ of the previous item, obtain the system's partition function Z and the Helmholtz free energy F. Also obtain the free energy per atom $f = F/N$ in the thermodynamic limit $N \longrightarrow \infty$, $V \longrightarrow \infty$, $v = N/V$ fixed.
c. Obtain internal energy U and the gas pressure p.
d. Calculate the chemical potential and entropy per atom in the thermodynamic limit.

Solution: *a. Be $\beta = 1/k_B T$. The atomic canonical partition function is,*

$$\zeta = \frac{1}{h^3}\int e^{-\beta H} dp_x dp_y dp_z dx dy dz = \frac{1}{h^3}\int e^{-\beta(p_x^2+p_y^2+p_z^2)/2m} dp_x dp_y dp_z dx dy dz$$
$$= \frac{V}{h^3}\left(\frac{2\pi m}{\beta}\right)^{3/2} = V\left(\frac{2\pi m k_B T}{h^2}\right)^{3/2} = \frac{V}{\lambda^3}\ .$$

b. For a sample of N atoms we have $Z = \frac{\zeta^N}{N!} = \frac{V^N}{N!\lambda^{3N}}$. With this,

$$F = -k_B T \ln Z = -k_B T \left(N \ln \frac{V}{\lambda^3} - N! \right) \ .$$

Using the Stirling formula,

$$F = -k_B T \left(N \ln \frac{V}{\lambda^3} - N \ln N + N \right) = -k_B T N \left(\ln \frac{V}{N\lambda^3} + 1 \right) \ ,$$

and

$$f = -k_B T \left(\ln \frac{v}{\lambda^3} + 1 \right) \ .$$

c. The internal energy is,

$$U = -\frac{\partial}{\partial \beta} \ln Z = -N \frac{\partial}{\partial \beta} \ln \zeta = \frac{3N}{2\beta} = \frac{3N}{2} k_B T \ .$$

The pressure is,

$$p = -\frac{\partial F}{\partial V} = k_B T \frac{\partial}{\partial V} \ln Z = k_B T \frac{N}{V} \ .$$

d. The chemical potential is,

$$\mu = \frac{\partial F}{\partial N} = -k_B T \left(\ln \frac{V}{\lambda^3} - \ln N \right) = -k_B T \ln \frac{v}{\lambda^3} \ .$$

The entropy is

$$s = \frac{\partial f}{\partial T} \ ,$$

or, using $f = u - Ts$, $u = U/N$,

$$s = \frac{u - f}{T} = k_B T \left(\ln \frac{v}{\lambda^3} + \frac{5}{2} \right) \ ,$$

which is the Sackur-Tetrode formula.

44.1.5.3 Ex: Generalization for arbitrary potentials in reduced dimensions

The calculation of the thermodynamic potentials can be generalized to arbitrary trapping potentials and dimensions [181, 410, 338, 73, 1405, 457, 74, 551, 615, 722, 711, 945, 772, 812, 417]. To do so, we consider a generic power law potential confining an ideal Bose gas in α dimensions,

$$U(\mathbf{r}) = \sum\nolimits_{i=1}^{\alpha} \left| \frac{x_i}{a_i} \right|^{t_i} \ ,$$

and define a parameter describing the confinement power of the potential,

$$\xi = \frac{\alpha}{2} + \sum\nolimits_{i=1}^{\alpha} \frac{1}{t_i} \ .$$

For example, for a three-dimensional potential, $\alpha = 3$. Now, for a 3D harmonic potential, $\xi = 3$, and for 3D box potential, $\xi = 3/2$.
a. Calculate the density of states η using the equation (43.19) employing Bose functions (44.10).
b. Prove the following expressions:

bosonic potentials

$$\begin{array}{rcl}
\frac{N_0}{N} & = & 1 - \left(\frac{\min(T,T_c)}{T_c}\right)^{\xi} \\
\frac{E}{Nk_BT} & = & \xi \frac{g_{\xi+1}(Z)}{g_\xi(Z)} \left(\frac{\min(T,T_c)}{T_c}\right)^{\xi} \\
\frac{S}{Nk_B} & = & 4\frac{g_{\xi+1}(Z)}{g_\xi(Z)} - \frac{2\mu}{k_BT} \\
\frac{C}{Nk_B} & = & \xi(\xi+1)\frac{g_{\xi+1}(Z)}{g_\xi(Z)} \left(\frac{\min(T,T_c)}{T_c}\right)^{\xi} - \xi^2 \frac{g_\xi(Z)}{g_{\eta-1}(Z)} \frac{\max(T-T_c,0)}{T-T_c} \\
\frac{C_{T>T_c}}{Nk_B} & = & \xi(\xi+1)\frac{g_{\xi+1}(Z)}{g_\xi(Z)} - \xi^2 \frac{g_\xi(Z)}{g_{\xi-1}(Z)} \quad , \quad \frac{C_{T<T_c}}{Nk_B} = \xi(\eta+1)\frac{g_{\xi+1}(1)}{g_\xi(1)} \\
\frac{\Delta C_{T_c}}{Nk_B} & = & \frac{C_{T_c^-} - C_{T_c^+}}{Nk_B} = \xi^2 \frac{g_\xi(1)}{g_{\xi-1}(1)}
\end{array} .$$

Solution: *a. The calculations are analogous to those performed for homogeneous Bose-gases, and we restrict ourselves here to give the general results for the thermodynamic quantities [72, 1405], e.g. the internal energy E and the heat capacity C. The expression for the critical temperature for N confined particles in a generic power law potential in α dimensions is,*

$$T_c^0 = k_B^{-1} \left[\frac{h^\alpha}{(2\pi m)^{\alpha/2}} \frac{N}{2^\alpha} \frac{1}{g_\eta(1) \prod_{i=1}^{\alpha} a_i \Gamma(t_i^{-1}+1)} \right]^{1/\eta} .$$

To evaluate the temperature dependence of the thermodynamic variables, we can calculate the fugacity $Z(T) = e^{\beta\mu}$ from the second of the above equations to E/Nk_BT [641]. For $T > T_c$ we derive fugacity as the root of $g_\eta(Z) = g_\eta(1)(T_c/T)^\eta$ and for $T < T_c$ the fugacity is simply $Z = 1$.
b. It is especially interesting to compare the discontinuity of the heat capacity and its a derivative $\partial C(T)/\partial T$ for several power law potentials and confinement dimensions, since this may clarify the nature of the phase transition. The thermodynamic quantities take a particularly simple form for power law potentials.
It is also interesting to note that the jump in the heat capacity at the phase transition is higher for any power law potential than for a potential well. This is due to the fact that the increase of the gas' energy requires work against the confinement potential. Steeper potentials (i.e., smaller coefficients t_i) give higher values for T_c^0. The critical temperature also depends on the confinement power of the potential,

$$\eta = -\frac{T_c^0}{N} \left(\frac{dN_0}{dT}\right)_{T=T_c^0} .$$

44.1.5.4 Ex: Time-of-flight distribution of a Bose-gas

a. Derive the formulae (44.25) describing the density and momentum distribution of an ultracold Bose-gas.
b. Calculate the time-of-flight distribution of a Bose-gas as a function of temperature (i) analytically for a harmonic potential and (ii) numerically for an arbitrary potential.

Solution: *a. To start with, we need to know the trap's geometry $V(\mathbf{r})$. Let us first assume a harmonic potential,*

$$V(\mathbf{r}) = \tfrac{m}{2}\omega_x^2 x^2 + \tfrac{m}{2}\omega_y^2 y^2 + \tfrac{m}{2}\omega_z^2 z^2 \ .$$

From the time-of-flight picture we can determine the number of atoms N. We also assume a given temperature T and proceed as follows. First we calculate the chemical potential from the normalization condition $N = \int n(e)\rho(e)de$.

44.2 Quantum statistics of an ideal Fermi gas

Atoms are fermions or bosons, or depending on their spin is integer or semi-integer. For example, ^{87}Rb atoms with their total integer spin of F are bosons, while ^{40}K atoms having a half-integer spin are fermions. At high phase space densities, atoms have to figure out how they will organize their coexistence. Bosons encourage each other to occupy the same phase space cell, in contrast to the reluctant fermions, which prefer to follow Pauli's exclusion principle. The different behavior is described by different quantum statistics that determine how the phase space (i.e., the available energy levels) has to be filled by the atoms. The Bose-Einstein distribution is valid for bosons, the distribution of Fermi-Dirac for fermions and both asymptotically approach the Boltzmann distribution at high temperatures. We have seen that bosons undergo a phase transition and condense in the ground state when the temperature is reduced below a critical threshold. On the other hand, the fermions organize their phase space, so that their energy levels are arranged like a ladder. The impact of fermionic quantum statistics on a cold cloud of atoms were observed experimentally by DeMarco and Jin [347, 966]. They cooled a two-components Fermi gas of 7×10^5 potassium atoms down to 300 nK, which corresponded to 60% of the atoms populating energy levels below the Fermi energy. The measured density distribution was found to deviate from the one expected for an ideal Boltzmann gas [5].

44.2.1 Chemical potential and Fermi radius for a harmonic trap

The phase space density for a *degenerate Fermi gas* has already been given in (44.4). In the same way as for a Bose gas, the chemical potential must satisfy the normalization

[5] We note that meanwhile ultracold two-components Fermi gas have been demonstrated to form bosonic Cooper-pairs, similarly to the phenomena known as superconductivity in some metals and as superfluidity of the fermionic ^{3}He.

condition,

$$N = \iint w_{T,\mu}(\mathbf{x},\mathbf{k}) d^3\mathbf{x} d^3k = (2\pi)^3 \int w_{T,\mu}(\varepsilon)\eta(\varepsilon) d\varepsilon \tag{44.32}$$
$$= \frac{1}{2(\hbar\bar{\omega})^3} \int_0^\infty \frac{\varepsilon^2 d\varepsilon}{e^{\beta(\varepsilon-\mu)}+1} = \left(\frac{k_B T}{\hbar\bar{\omega}}\right)^3 f_3(Z) \; .$$

In the last line, we inserted the density of the states into a harmonic potential (43.21) and used the definition of the Fermi functions (44.11).

For low temperatures, $x \equiv \mu \gg 1$, we can use the Sommerfeld expansion which in first order gives $f_\eta(e^x) \simeq x^\eta/\Gamma(\eta+1)$. From this we immediately obtain the energy, the Fermi radius and the momentum of free particles,

$$E_F = \mu(T=0) = \hbar\bar{\omega}(6N)^{1/3} \tag{44.33}$$
$$r_F = \sqrt{\frac{2E_F}{m\omega_r^2}} \quad \text{and} \quad z_F = \sqrt{\frac{2E_F}{m\omega_z^2}}$$
$$K_F = \sqrt{\frac{2mE_F}{\hbar^2}} \; .$$

Using the second order of the Sommerfeld expansion, $f_\xi(e^x) \simeq \frac{x^\xi}{\Gamma(\xi+1)}\left(1 + \frac{\pi^2\xi(\xi-1)}{6x^2} + ...\right)$, we obtain for the chemical potential the equation, $0 = \mu^3 + (\pi k_B T)^2 \mu - E_F^3$. The approximate solution of this equation, neglecting terms such as $4\pi^6 k_B^6 T^6 \ll 27 E_F^6$, is

$$\mu = E_F \left[1 - \frac{\pi^2}{3}\left(\frac{k_B T}{E_F}\right)^2\right] \; . \tag{44.34}$$

In the limit of high temperatures, $f_\eta(Z) \overset{Z\to 1}{\longrightarrow} Z$

$$N = \left(\frac{k_B T}{\hbar\bar{\omega}}\right)^3 e^{\beta\mu} = \left(\frac{k_B T}{\hbar\bar{\omega}}\right)^3 (1 + \beta\mu + ...) \; , \tag{44.35}$$
$$\mu \approx k_B T \ln N \left(\frac{\hbar\bar{\omega}}{k_B T}\right)^3 = k_B T \ln \frac{1}{6}\left(\frac{E_F}{k_B T}\right)^3 \; .$$

This means that we recover the *Boltzmann gas*, which satisfies an ideal gas equation similar to that of particles in a box potential,

$$N = \left(\frac{k_B T}{\hbar\bar{\omega}}\right)^3 \qquad \text{(Boltzmann)} \; . \tag{44.36}$$

For comparison, for bosons we have,

$$\frac{N_0}{N} = 1 - \left(\frac{T}{T_c}\right)^3 \frac{g_3(Z)}{g_3(1)} \qquad \text{(Bose)} \; . \tag{44.37}$$

The chemical potentials are calculated in Fig. 44.7(a).

44.2.2 Energy

The total energy $E_1 \equiv E/N \equiv N^{-1}\int \epsilon w d^3\mathbf{x} d^3k$ per particle is given by,

$$\begin{aligned} E_1 &= \frac{\int \epsilon w_{T,\mu}(\mathbf{x},\mathbf{k}) d^3\mathbf{x} d^3k}{\int w_{T,\mu}(\mathbf{x},\mathbf{k}) d^3\mathbf{x} d^3k} \\ &= \frac{\int \epsilon\eta(\epsilon)\left(e^{\beta(\epsilon-\mu)}+1\right)^{-1} d\varepsilon}{\int \eta(\epsilon)\left(e^{\beta(\epsilon-\mu)}+1\right)^{-1} d\varepsilon} = 3k_BT\frac{f_4(Z)}{f_3(Z)} \ . \end{aligned} \tag{44.38}$$

Again using the Sommerfeld approximation, we see that for $T \to 0$ the energy is limited by

$$\begin{aligned} E_1 &= \frac{3}{N\beta(\beta\hbar\bar{\omega})^3} f_4(e^{\beta\mu}) \\ &= \frac{3\mu^4}{4E_F^3}\left(1+\frac{2\pi^2}{(\beta\mu)^2}+...\right) \overset{T\to 0}{\longrightarrow} \frac{3}{4}E_F \qquad \text{(Fermi)} \ . \end{aligned} \tag{44.39}$$

because the atoms are forced to adopt a state of larger dynamics in the outermost regions of the trap. This implies, $E_1/E_F \overset{T\to 0}{\longrightarrow} 3/4$.

In the limit of high temperatures, $T \to \infty$, a classical gas has the energy per particle,

$$E_1 = \frac{3}{N\beta(\beta\hbar\bar{\omega})^3} f_4\left(f_3^{-1}\left(\frac{(\beta E_F)^3}{6}\right)\right) \approx 3k_BT \qquad \text{(Boltzmann)} \ , \tag{44.40}$$

which is seen by taking the high temperature limit $f_\eta(Z) \overset{Z\to 0}{\longrightarrow} Z$ and extrapolating to all Z. This implies, $E_1/E_F \overset{T\to\infty}{\longrightarrow} 3k_BT/E_F$.

Comparing with bosons,

$$E_1 = 3k_BT\frac{g_4(1)}{g_3(1)} \approx 2.7 \qquad \text{(Bose)} \ . \tag{44.41}$$

44.2.3 Entropy and heat capacity

The entropy $S = -k_B\int g(\epsilon)\left[w\ln w + (1-w)\ln(1-w)\right] d\epsilon$ per particle is,

$$S_1 = 4k_B\frac{f_4(Z)}{f_3(Z)} - \frac{\mu}{T} = \frac{4E_1}{3T} - \frac{\mu}{T} \ . \tag{44.42}$$

The heat capacity per particle $C_1 = \frac{\partial E_1}{\partial T}\big|_N$ is easily calculated using $Zf'_\eta(Z) = f_{\eta-1}(Z)$,

$$C_1 = 3k_B\frac{f_4(Z)}{f_3(Z)} - \frac{3\mu}{T}\left(1-\frac{f_4(Z)f_2(Z)}{f_3(Z)^2}\right) = \frac{E_1}{T} - \frac{3\mu}{T}\left(1-\frac{f_4(Z)f_2(Z)}{f_3(Z)^2}\right) \ . \tag{44.43}$$

For fermions well below the Fermi temperature, $T \to 0$, using the Sommerfeld approximation, we calculate,

$$C_1 \overset{T\to 0}{\longrightarrow} \frac{3\pi^2}{2}\frac{k_BT}{T_F} \qquad \text{(Fermi)} \ . \tag{44.44}$$

For high temperature T

$$C_1 \approx 3k_B \qquad \text{(Boltzmann)} \ . \tag{44.45}$$

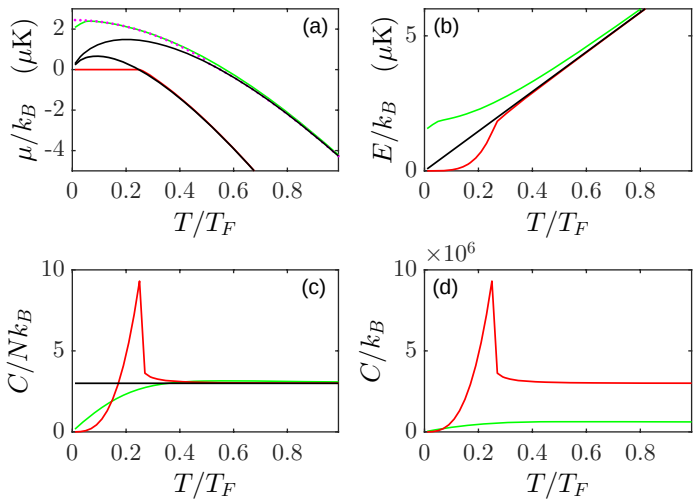

Figure 44.7: (code) Numerical calculation of thermodynamic potentials for Bose (red) and Fermi (green) gases as a function of temperature for a given harmonic trapping potential. (a) Chemical potential, (b) energy, (c) heat capacity per particle, and (d) total heat capacity. The dotted magenta line in (a) shows the chemical potential calculated from the Sommerfeld approximation.

44.2.4 Distributions of a Fermi gas

44.2.4.1 Spatial distribution

The density distribution is,

$$n(\mathbf{x}) = \int w_{T,\mu}(\mathbf{x},\mathbf{k}) d^3\mathbf{k} = \frac{1}{(2\pi)^2} \int \frac{2k^2 dk}{e^{\beta[\hbar^2 k^2/2m + U(\mathbf{x}) - \mu]} + 1} \tag{44.46}$$
$$= \frac{1}{(2\pi)^2} \left(\frac{2m}{\hbar^2}\right)^{3/2} \int \frac{\sqrt{\varepsilon} d\varepsilon}{e^{\beta[\varepsilon + U(\mathbf{x}) - \mu]} + 1} = \frac{1}{(2\pi)^2} \left(\frac{2m}{\beta\hbar^2}\right)^{3/2} \Gamma(3/2) f_{3/2}(e^{-\beta[U(\mathbf{x})-\mu]}) \ ,$$

such that,

$$\boxed{n(\mathbf{x}) = \lambda_{dB}^{-3} f_{3/2}(e^{-\beta[U(\mathbf{x})-\mu]})} \qquad \text{(Fermi)} \ . \tag{44.47}$$

At low temperatures, $T \to 0$, we can apply the Sommerfeld expansion [221], which to first order gives $\mu \to E_F$,

$$n(\mathbf{x}) \approx \frac{1}{(2\pi)^2}\frac{\Gamma(3/2)}{\Gamma(5/2)}\left(\frac{2m}{\hbar^2}\left[\mu - U(\mathbf{x})\right]\right)^{3/2} \tag{44.48}$$
$$= \frac{1}{(2\pi)^2}\frac{2}{3}\left(\frac{2m}{\hbar^2}\right)^{3/2}\left(E_F - \frac{m}{2}\omega_r^2\rho^2\right)^{3/2} = \frac{8\lambda}{\pi^2}\frac{N}{R_F^3}\left(1 - \frac{\rho^2}{R_F^2}\right)^{3/2} .$$

At high temperatures, $T \to \infty$, we should recover the Boltzmann gas situation,

$$n(\mathbf{x}) = \lambda_{dB}^{-3} f_{3/2}(e^{-\beta[U(\mathbf{x})-\mu]}) \tag{44.49}$$
$$\approx \lambda_{dB}^{-3} N\left(\beta\hbar\bar{\omega}\right)^3 e^{-\beta U(\mathbf{x})} = \left(\frac{m\beta\bar{\omega}^2}{2\pi}\right)^{3/2} N e^{-\beta m(\omega_x^2 x^2 + \omega_y^2 y^2 + \omega_z^2 z^2)/2} .$$

It's easy to check, $\int n(\mathbf{x}) d^3\mathbf{x} = N$. Introducing the peak density n_0, we obtain,

$$\boxed{n(\mathbf{x}) = n_0 e^{-m\omega^2\rho^2/2k_BT}} \quad \text{(Boltzmann)} . \tag{44.50}$$

The *rms*-radius of the distribution is $\sigma_j = \sqrt{k_BT/m\omega_j^2}$, which seems contrary to the above results, $\frac{m}{2}\omega_j^2\left\langle x_j^2\right\rangle = k_BT$. In comparison,

$$\boxed{n(\mathbf{x}) = \lambda_{dB}^{-3} g_{3/2}\left[e^{\beta(\mu - U(\mathbf{x}))}\right]} \quad \text{(Bose gas above } T_c\text{)} . \tag{44.51}$$

where $\lambda_{dB} = \sqrt{2\pi\hbar^2/mk_BT}$ e $a_{tr} = \sqrt{\hbar/m\bar{\omega}}$.

44.2.4.2 Momentum distribution

The momentum distribution is,

$$\tilde{n}(\mathbf{k}) = \int w_{T,\mu}(\mathbf{x},\mathbf{k}) d^3\mathbf{x} = \frac{1}{(2\pi)^2}\int \frac{rdrdz}{e^{\beta[\varepsilon(k) + m\omega_r^2\rho^2/2 - \mu]} + 1} \tag{44.52}$$
$$= \frac{1}{(2\pi)^3}\int \frac{4\pi\rho^2 d\rho}{e^{\beta[\varepsilon + m\omega_r^2\rho^2/2 - \mu]} + 1}$$
$$= \frac{1}{(2\pi)^2}\left(\frac{2}{\beta m\omega_r^2}\right)^{3/2}\int \frac{\sqrt{t}dt}{e^{\beta[\varepsilon + t - \mu]} + 1} = \frac{1}{(2\pi)^2}\left(\frac{2}{\beta m\omega_r^2}\right)^{3/2}\Gamma(3/2) f_{3/2}(e^{\beta(\mu-\varepsilon)}) ,$$

such that,

$$\boxed{\tilde{n}(\mathbf{k}) = \lambda_{dB}^{-3} a_{tr}^6 f_{3/2}(e^{\beta(\mu-\varepsilon)})} \quad \text{(Fermi)} . \tag{44.53}$$

At low temperatures, $T \to 0$,

$$\tilde{n}(\mathbf{k}) \approx \frac{1}{(2\pi)^2}\left(\frac{2}{\beta m\omega_r^2}\right)^{3/2}\frac{\Gamma(3/2)}{\Gamma(5/2)}\left(\beta\left[\mu - \varepsilon\right]\right)^{3/2} \tag{44.54}$$
$$\approx \frac{1}{(2\pi)^2}\left(\frac{2}{m\omega_r^2}\right)^{3/2}\frac{2}{3}\left(E_F - \frac{\hbar^2k^2}{2m}\right)^{3/2} = \frac{8}{\pi^2}\frac{N}{K_F^3}\left(1 - \frac{k^2}{K_F^2}\right)^{3/2} .$$

This can easily be integrated by dimensions,

$$\tilde{n}_{T\to 0}(k_z) = \int_{-\infty}^{\infty}\int_{-\infty}^{\infty} \tilde{n}_{cl}(\mathbf{k})dk_x dk_y = \frac{8}{\pi^2}\frac{N}{K_F^3}\int\int_{|k|\le K_F}\left(1-\frac{k^2}{K_F^2}\right)^{3/2} dk_x dk_y \tag{44.55}$$

$$= \frac{8}{\pi^2}\frac{N}{K_F^3}\int_0^{2\pi}\int_0^{\sqrt{K_F^2-k_z^2}}\left(1-\frac{k_z^2}{K_F^2}-\frac{k_\rho^2}{K_F^2}\right)^{3/2} k_\rho dk_\rho d\phi = \frac{16}{5\pi}\frac{N}{K_F}\left(1-\frac{k_z^2}{K_F^2}\right)^{5/2} .$$

It is easy to check $\int_{-\infty}^{\infty}\tilde{n}_{T\to 0}dk_z = N$, with Maple.

At high temperatures, $T\to\infty$, we should recover the Boltzmann gas situation,

$$\boxed{\tilde{n}(\mathbf{k}) \approx \left(\frac{\hbar^2\bar{\omega}^2}{2\pi m\omega_r^2}\right)^{3/2} N e^{-\beta\varepsilon}} \quad \text{(Boltzmann)} . \tag{44.56}$$

Since ε is the kinetic energy, the *rms*-radius $\sqrt{k^2}$ of this distribution is $\beta\hbar^2\langle k^2\rangle = m$. In comparison,

$$\boxed{\tilde{n}_B(\mathbf{k}) = \lambda_{dB}^{-3}a_{tr}^6\ g_{3/2}\left[e^{\beta\left(\mu-\mathbf{p}^2/2m\right)}\right]} \quad \text{(Bose gas above } T_c\text{)} . \tag{44.57}$$

Example 281 (*Integrated momentum distribution of a Fermi gas*): To integrate the momentum distribution of finite temperature Fermi gas by dimensions,

$$\tilde{n}(k_z) = \frac{1}{(2\pi)^3}\left(\frac{2}{\beta m\tilde{\omega}_{tr}^2}\right)^{3/2}\int_{-\infty}^{\infty}\int_{-\infty}^{\infty}\int_0^{\infty}\frac{4\pi\tilde{r}^2 d\tilde{r}}{e^{\beta\varepsilon-\beta\mu+\tilde{r}^2}+1}dk_y dk_x \tag{44.58}$$

$$= \frac{1}{(2\pi)^3}\left(\frac{2}{\beta m\tilde{\omega}_{tr}^2}\right)^{3/2} 2\pi\int_0^{\infty}\int_0^{\infty}\frac{4\pi\tilde{r}^2 d\tilde{r}}{e^{\beta\hbar^2k_z^2/2m+\beta\hbar^2k_\rho^2/2m-\beta\mu+\tilde{r}^2}+1}k_\rho dk_\rho$$

$$= \frac{1}{\pi}\left(\frac{2}{\beta m\tilde{\omega}_{tr}^2}\right)^{3/2}\frac{2m}{\beta\hbar^2}\int_0^{\infty}\int_0^{\infty}\frac{\tilde{k}_\rho d\tilde{k}_\rho}{e^{\beta\hbar^2k_z^2/2m-\beta\mu+\tilde{r}^2+\tilde{k}_\rho^2}+1}\tilde{r}^2 d\tilde{r}$$

$$= \frac{1}{\pi}\left(\frac{2}{\beta m\tilde{\omega}_{tr}^2}\right)^{3/2}\frac{2m}{\beta\hbar^2}\frac{1}{2}\int_0^{\infty}\tilde{r}^2\ln\frac{1}{1+e^{-\beta\hbar^2k_z^2/2m+\beta\mu-\tilde{r}^2-k_\rho^2}}\Bigg|_0^{\infty}d\tilde{r}$$

$$= \frac{2}{\pi\left(\beta\hbar\tilde{\omega}_{tr}\right)^2}\left(\frac{2}{\beta m\tilde{\omega}_{tr}^2}\right)^{1/2}\int_0^{\infty}\tilde{r}^2\ln\left(1+e^{\beta\mu-\beta\hbar^2k_z^2/2m-\tilde{r}^2}\right)d\tilde{r} .$$

44.2.4.3 Time-of-flight distribution

To describe time-of-flight images we substitute $\mathbf{k} = m\mathbf{r}/\hbar t$. We obtain the density distribution from a convolution,

$$n_{ToF}(\mathbf{x},t) = \frac{1}{(2\pi)^3}\int d^3\mathbf{x}_0 d^3\mathbf{k}\frac{\delta^3(\mathbf{x}-\mathbf{x}_0-\mathbf{p}t/m)}{e^{\beta(H(\mathbf{x}_0,\mathbf{p})-\mu)}+1} \tag{44.59}$$

$$= \frac{1}{(2\pi)^3}\int\frac{d^3\mathbf{k}}{e^{\beta(H(\mathbf{x}+\mathbf{p}t/m,\mathbf{p})-\mu)}+1}$$

$$= \frac{1}{(2\pi)^3}\int\frac{dk_x dk_y dk_z}{e^{\beta\Sigma_j\left[\hbar^2k_j^2/2m+\frac{1}{2}m\omega_j^2(x_j+\hbar k_j t/m)^2\right]}/Z+1} .$$

We rewrite the exponent,

$$\hbar^2 k_j^2/2m + \tfrac{1}{2}m\omega_j^2\left(x_j + \hbar k_j t/m\right)^2 = \hbar^2 k_j^2/2m(1+\omega_j^2 t^2) + \omega_j^2 t x_j \hbar k_j + \tfrac{1}{2}m\omega_j^2 x_j^2$$

$$= \left(\sqrt{\frac{\hbar^2 k_j^2}{2m}(1+\omega_j^2 t^2)} + \frac{\omega_j^2 t x_j \sqrt{2m}}{2\sqrt{1+\omega_j^2 t^2}}\right)^2 + \frac{m\omega_j^2 x_j^2}{2(1+\omega_j^2 t^2)} \tag{44.60}$$

$$= \xi_j + \frac{m}{2}\breve{\omega}_j^2 x_j^2 \ .$$

where we define $\breve{\omega}_i \equiv \omega_i \left(1+\omega_i^2 t^2\right)^{-1/2}$. With the substitution $d\xi_j = dk_j \sqrt{\frac{2\hbar^2}{m}\xi_j \left(1+\omega_j^2 t^2\right)}$ we obtain

$$n_{ToF}(\mathbf{x},t) = \frac{1}{(2\pi)^3}\left(\frac{mk_BT}{2\hbar^2}\right)^{3/2}\frac{1}{\prod_i\left(1+\omega_i^2 t^2\right)}\int \frac{\beta^{3/2}\left(\xi_x\xi_y\xi_z\right)^{-1/2}d\xi_x d\xi_y d\xi_z}{e^{\beta\Sigma_j\left[\xi_j+\frac{m}{2}\breve{\omega}_j^2 x_j^2\right]}/Z+1} \tag{44.61}$$

$$= \frac{1}{2^3\pi^{3/2}}\frac{1}{\lambda_{dB}^3}\frac{\tilde{\omega}^3}{\bar{\omega}^3}\int \frac{\beta^{3/2}\xi^{-3/2}4\pi\xi^2 d\xi}{e^{\beta\Sigma_j\left[\xi+\frac{m}{2}\breve{\omega}_j^2 x_j^2\right]}/Z+1} \ ,$$

where $\bar{\omega} \equiv (\omega_x\omega_y\omega_z)^{1/3}$ and $\breve{\omega} \equiv (\breve{\omega}_x\breve{\omega}_y\breve{\omega}_z)^{1/3}$.

$$\boxed{n_{ToF}(\mathbf{x},t) = \frac{1}{\lambda_{dB}^3}\frac{\breve{\omega}^3}{\bar{\omega}^3} f_{3/2}\left(e^{\beta\mu - \frac{1}{2}\beta m\Sigma_j\breve{\omega}_j^2 x_j^2}\right)} \ . \tag{44.62}$$

For long times-of-flight $t \gg \omega^{-1}$,

$$n_{ToF}(\mathbf{x},t) = \frac{1}{\lambda_{dB}^3}\frac{1}{\bar{\omega}^2 t^2} f_{3/2}\left(e^{\beta\left(\mu - m\mathbf{x}^2/2t^2\right)}\right) = \left(\frac{m}{\hbar t}\right)^3 \tilde{n}(m\mathbf{x}/t) \ . \tag{44.63}$$

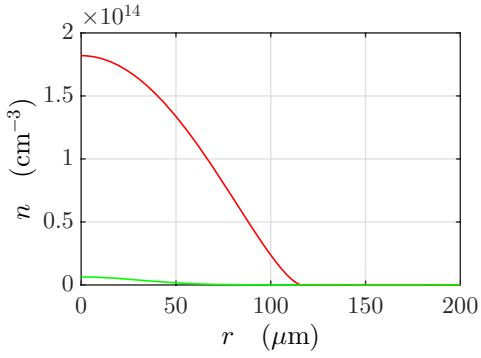

Figure 44.8: (code) Time-of-flight velocity distribution of (red) a Li Fermi gas at $T = 0$ with vanishing initial spatial distribution [221] and (green) a thermal gas at $T = T_F$.

At low temperatures,

$$n_{ToF}(\mathbf{x},t) = \left(\frac{m}{\hbar t}\right)^3 \frac{N}{K_F^3}\frac{8}{\pi^2}\left(1-\frac{(m\mathbf{x}/\hbar t)^2}{K_F^2}\right)^{3/2} = \left(\frac{m}{\hbar t}\right)^3 \frac{R_F^3}{6\pi^2\lambda}\left[1-\left(\frac{R_F m\mathbf{x}/\hbar t}{(48N\lambda)^{1/3}}\right)^2\right]^{3/2} \tag{44.64}$$

At high temperatures,

$$\begin{aligned} n_{ToF}(\mathbf{x},t) &= \frac{1}{\lambda_{dB}^3}\frac{1}{\bar{\omega}^2 t^2} f_{3/2}(e^{\beta(\mu - m\mathbf{x}^2/2t^2)}) \\ &\approx \frac{1}{\lambda_{dB}^3}\frac{1}{\bar{\omega}^2 t^2} e^{\beta(\mu - m\mathbf{x}^2/2t^2)} \\ &\approx \left(\frac{mk_BT}{2\pi\hbar^2}\right)^{3/2}\frac{1}{\bar{\omega}^2t^2}N\left(\frac{\hbar\bar{\omega}}{k_BT}\right)^3 e^{-\beta m\mathbf{x}^2/2t^2} \approx N\frac{\bar{\omega}}{t^2}\left(\frac{m}{2\pi k_BT}\right)^{3/2} e^{-\beta m\mathbf{x}^2/2t^2}\,. \end{aligned} \tag{44.65}$$

A *rms*-width is,

$$\begin{aligned} \langle r_{ToF}^2\rangle &= \int r^2 n_{ToF}(\mathbf{x},t)d^3\mathbf{x} \\ &= \frac{1}{\lambda_{dB}^3}\frac{\check{\omega}^3}{\bar{\omega}^3}\int r^2 f_{3/2}\left(e^{\beta\mu - \frac{1}{2}\beta m\Sigma_j \check{\omega}_j^2 x_j^2}\right)d^3\mathbf{x} \\ &= \frac{2}{m\check{\omega}_r^2 N}\int \frac{\varepsilon g(\varepsilon)d\varepsilon}{e^{\beta(\varepsilon-\mu)}+1} = \frac{k_BT}{m\check{\omega}_r^2}\frac{g_4(Z)}{g_3(Z)}\,. \end{aligned} \tag{44.66}$$

This shows that the width of the flight-of-time distribution can simply be obtained from the spatial distribution by substituting $\omega \to \omega/\sqrt{1+\omega^2t^2}$. Of course this does not hold for condensed gases Bose.

44.2.5 Equipartition theorem

We find for harmonic traps,

$$\begin{aligned} E_{pot,1} &= \frac{\int U(\mathbf{x})w_{T,\mu}(\mathbf{x},\mathbf{k})d^3\mathbf{x}d^3\mathbf{k}}{\int w_{T,\mu}(\mathbf{x},\mathbf{k})d^3\mathbf{x}d^3\mathbf{k}} = \frac{1}{(2\pi)^3N2}\int \frac{m\omega^2r^2d^3\mathbf{x}d^3\mathbf{k}}{e^{\beta[\hbar^2k^2/2m+m\omega^2r^2/2-\mu]}+1} \\ &= \frac{16}{\pi N\beta^4(\hbar\omega)^3}\int \frac{u^4v^2dudv}{e^{u^2+v^2}/Z+1} \\ &= \frac{1}{(2\pi)^3N2m}\int \frac{\hbar^2k^2d^3\mathbf{x}d^3\mathbf{k}}{e^{\beta[\hbar^2k^2/2m+m\omega^2r^2/2-\mu]}+1} = \frac{\int \hbar^2k^2w_{T,\mu}(\mathbf{x},\mathbf{k})d^3\mathbf{x}d^3\mathbf{k}}{2m\int w_{T,\mu}(\mathbf{x},\mathbf{k})d^3\mathbf{x}d^3\mathbf{k}} = E_{kin,1}\,. \end{aligned} \tag{44.67}$$

This confirms the *equipartition theorem* for confined particles, which postulates,

$$E = E_{kin} + E_{pot} = 2E_{kin}\,. \tag{44.68}$$

In flight time, however, E_{pot} suddenly vanishes.

44.2.5.1 Calibrating the number of atoms

Experimentally, to calibrate N, we can use either the measured value of $\langle k^2 \rangle$ at $T = 0$, which gives $\mu = E_F = 4E/3$ and consequently,

$$N = \frac{32}{3} \left(\frac{\hbar^2 \langle k^2 \rangle}{6m\hbar\bar{\omega}} \right)^3 . \tag{44.69}$$

Or we determine the temperature T_g where the Boltzmann gas turns into a Fermi gas $3\mu/4 = 3k_B T_g$,

$$N = \frac{32}{3} \left(\frac{k_B T_g}{\hbar\bar{\omega}} \right)^3 . \tag{44.70}$$

44.2.6 Density and momentum distribution for anharmonic potentials

44.2.6.1 Width of momentum distribution for anharmonic potentials

If the potential is non-harmonic, the widths of Fermi distributions must in general be calculated numerically. I.e. first $g(\epsilon)$ is determined by integrating for every value of ϵ the root $\sqrt{\epsilon - U(\mathbf{x})}$ over the entire volume, where $U(\mathbf{x}) < \epsilon$, i.e. in the case of cylindrical symmetry,

$$g(\epsilon) = \frac{(2m)^{3/2}}{2\pi\hbar^3} \int \sqrt{\epsilon - U(r,z)} r dr dz . \tag{44.71}$$

Second the chemical potential must also be calculated numerically from $N = \int g(\epsilon) \left(e^{\beta(\epsilon-\mu)} + 1 \right)^{-1} d\epsilon$ by minimizing the function,

$$o(Z) = \left| \beta N - \int \frac{g(x/\beta) dx}{e^x/Z + 1} \right| . \tag{44.72}$$

Finally, the *rms*-momentum width of a degenerate Fermi-gas is calculated from,

$$\frac{\langle k^2 \rangle}{k_F^2} = \frac{E_1}{E_F} = \frac{1}{NE_F} \int \frac{\epsilon g(\epsilon) d\epsilon}{e^{\beta(\epsilon-\mu)} + 1} . \tag{44.73}$$

It is important to note that the temperature cannot be obtained from $\hbar^2 \langle k^2 \rangle / 2m = 3Nk_B T$ any more. Rather for a given $\langle k^2 \rangle$ the parameter β in the integral (44.71) must be fitted to satisfy the equation.

Alternatively, we may assume a polynomial potential for which the density of states can be described by $g(\epsilon) \propto \epsilon^n$. Then,

$$\frac{\langle k^2 \rangle}{k_F^2} = \frac{1}{E_F} \frac{\int \epsilon g(\epsilon) \left(e^{\beta(\epsilon-\mu)} + 1 \right)^{-1} d\epsilon}{\int g(\epsilon) \left(e^{\beta(\epsilon-\mu)} + 1 \right)^{-1} d\epsilon} = \frac{T}{T_F} \frac{(n+1) f_{n+2}(Z)}{f_{n+1}(Z)} , \tag{44.74}$$

For a harmonic potential we recover the energy formula,

$$\frac{\langle k^2 \rangle}{k_F^2} = \frac{3T}{T_F} \frac{f_4(Z)}{f_3(Z)} , \tag{44.75}$$

and for hot clouds the classical limit holds,

$$\frac{\langle k^2\rangle}{k_F^2} = \frac{n+1}{\beta E_F} \ . \tag{44.76}$$

Must for a single dimension the value be divided by three? $\hbar^2\langle k_j^2\rangle = 2mk_BTf_4(Z)/f_3(Z)$ setting $\epsilon = \hbar^2k^2/m$.

For a harmonic potential $g(\epsilon) \propto \epsilon^2$ and for a linear potential $g(\epsilon) \propto \epsilon^{7/2}$. Intermediate values are possible for non isotropic traps, which are linear in some directions and harmonic in others, e.g. for a radially quadrupolar and axially harmonic trap, we expect $g(\epsilon) \propto \epsilon^3$ and thus $E = 4Nk_BT$. In general, we may have more complicated situations, where the trap becomes non-harmonic beyond a certain distance from the origin. In those cases, the density of states may be approximated by series,

$$g(\epsilon) \propto \epsilon^2 + \eta\epsilon^3 \ , \tag{44.77}$$

where η is a small parameter, so that,

$$\frac{\langle k^2\rangle}{k_F^2} = \frac{1}{E_F}\frac{\int(\epsilon^3+\eta\epsilon^4)(e^{\beta(\epsilon-\mu)}+1)^{-1}d\epsilon}{\int(\epsilon^2+\eta\epsilon^3)(e^{\beta(\epsilon-\mu)}+1)^{-1}d\epsilon} = \frac{T}{T_F}\frac{3f_4(Z)+12\eta f_5(Z)}{f_3(Z)+3\eta f_4(Z)} \ , \tag{44.78}$$

which in the classical limit gives rise to energies $E = 3..4Nk_BT$ depending on the value of η.

Such effects must be considered when the time-of-flight method is used for temperatures measurements. For example, if we underestimate $g(\varepsilon)$ by assuming a harmonic potential at all ε, although the potential is quadrupolar at large $\varepsilon \gg k_BT$, we get a wrong estimate for the temperature $T_{wrng} = E/3Nk_B$ instead of $T_{corr} = E/4Nk_B$.

44.2.6.2 Width of the density distribution for anharmonic potentials

The result also permits to calculate the *rms* spatial width,

$$\sum\nolimits_{j=1}^{3}\frac{m}{2}\omega_j^2\langle x_j^2\rangle = 3k_BT\frac{f_4(Z)}{f_3(Z)} \ . \tag{44.79}$$

Let us for simplicity assume $\omega_i = \omega_j$. So in the classical limit,

$$\frac{\langle x_j^2\rangle}{R_F^2} = \frac{\langle \mathbf{x}^2\rangle}{3R_F^2} = \frac{E_1}{3E_F} = \frac{1..1.3T}{T_F} \ . \tag{44.80}$$

If the potential is non-harmonic, the widths of Fermi distributions must in general be calculated numerically. We may use the same results for the density of states and the chemical potential as for the momentum width calculations. Then,

$$\frac{\langle x_j^2\rangle}{R_F^2} = \frac{E_1}{3E_F} = \frac{1}{3E_F}\frac{\int \epsilon g(\epsilon)\left(e^{\beta(\epsilon-\mu)}+1\right)^{-1}d\epsilon}{\int g(\epsilon)\left(e^{\beta(\epsilon-\mu)}+1\right)^{-1}d\epsilon} \ . \tag{44.81}$$

44.2.7 Classical gas

For a harmonic potential [330] the fraction of particles with energy smaller than $\eta k_B T$ is,

$$N(\eta) = \frac{1}{2N(\hbar\bar{\omega})^3}\int_0^{\eta k_B T}\frac{d\epsilon}{e^{\beta\epsilon}/Z-0} \approx 1-\frac{2+2\eta+\eta^2}{2e^\eta} \tag{44.82}$$
$$E(\eta) = \frac{1}{2N(\hbar\bar{\omega})^3}\int_0^{\eta k_B T}\frac{\epsilon^2 d\epsilon}{e^{\beta\epsilon}/Z-0} \approx 3-\frac{6+6\eta+3\eta^2+\eta^3}{6e^\eta}\ ,$$

while for a quadrupole potential,

$$N(\eta) \approx -2\sqrt{z}\frac{105+70\eta+28\eta^2+8\eta^3}{\sqrt{\pi}105e^\eta}+\mathrm{erf}(\sqrt{\eta}) \tag{44.83}$$
$$E(\eta) \approx -\frac{2}{9}\sqrt{z}\frac{945+630\eta+252\eta^2+72\eta^3+16\eta^4}{\sqrt{\pi}105e^\eta}+\frac{9}{2}\mathrm{erf}(\sqrt{\eta})\ .$$

44.2.7.1 Momentum distribution for a classical gas

For high temperatures, $T\to\infty$, we should recover the ideal Boltzmann gas situation, $f_{3/2}\to id$,

$$\tilde{n}_{T\to\infty}(\mathbf{k}) = \frac{1}{(2\pi)^3}\int\frac{4\pi\rho^2 d\rho}{e^{\beta[\varepsilon+m\omega_{tr}^2\rho^2/2-\mu]}} = \frac{1}{2\pi^2}e^{-\beta(\varepsilon-\mu)}\int e^{-\beta m\omega_{tr}^2\rho^2/2}\rho^2 d\rho \tag{44.84}$$
$$= \left(\frac{1}{2\pi\beta m\omega_{tr}^2}\right)^{3/2} e^{-\beta(\varepsilon-\mu)} = \lambda_{dB}^{-3}a_{tr}^6\ e^{\beta(\mu-\varepsilon)}\ .$$

Since the chemical potential satisfies the normalization, $\int\tilde{n}_{T\to\infty}(\mathbf{k})d^3\mathbf{k}=1$,

$$\tilde{n}_{T\to\infty}(\mathbf{k}) = \left(\frac{1}{2\pi\beta m\omega_{tr}^2}\right)^{3/2} N\left(\frac{\hbar\omega_{tr}}{k_B T}\right)^3 e^{-\beta\varepsilon} = N\sqrt{\frac{\hbar^2}{2\pi m k_B T}}^3\ e^{-\hbar^2k^2/2mk_BT}\ . \tag{44.85}$$

This is easy to integrate by dimensions, so that,

$$\tilde{n}_{T\to\infty}(k_z) = \int_{-\infty}^{\infty}\int_{-\infty}^{\infty}\tilde{n}_{T\to\infty}(\mathbf{k})dk_x dk_y = N\sqrt{\frac{\hbar^2}{2\pi m k_B T}}e^{-\hbar^2k_z^2/2mk_BT}\ . \tag{44.86}$$

The rms-width of this distribution is,

$$\Delta k_z = \frac{\sqrt{mk_BT}}{\hbar}\ . \tag{44.87}$$

44.2.7.2 Correlating fluctuations in the number of atoms

Experimentally the atom number will fluctuate. To minimize this problem we can renormalize it to a norm number N_{norm} by multiplying the measured time-of-flight

variance $\langle x_{tof}^2 \rangle$ with,

$$C_T(N) = \frac{\langle \tilde{x}_{tof}^2 \rangle}{\langle x_{tof}^2 \rangle} = \frac{N}{N_{norm}} \frac{f_4(\tilde{Z})}{f_4(Z)} \tag{44.88}$$
$$= \frac{N}{N_{norm}} \frac{f_4\left[f_3^{-1}(N_{norm}(\beta\hbar\bar{\omega})^3)\right]}{f_4\left[f_3^{-1}(N(\beta\hbar\bar{\omega})^3)\right]} \ .$$

44.2.8 Intensive and extensive parameters

The distinction between an *intensive parameter* and an *extensive parameter* is based on the concept that the system under investigation can be subdivided into smaller, identical and non-interconnected entities within which the parameter in question has the same properties, such that this parameter does not change, when the system is divided or subentities are combined [6] An intensive property is a global property, meaning that it is a physical property of a system that does not depend on the system size or the amount of material in the system. Examples of intensive properties are the temperature and the hardness of an object. No matter how small a diamond is cut, it maintains its intrinsic hardness.

By contrast, an extensive property is one that is additive for independent, non-interacting subsystems. The property is proportional to the amount of material in the system. For example, both the mass and the volume of a diamond are directly proportional to the amount that is left after cutting it from the raw mineral. Mass and volume are extensive properties, but hardness is intensive.

The ratio of two extensive properties, such as mass and volume, is scale-invariant, and this ratio, the density, is hence an intensive property.

Intensive parameter are: chemical potential, concentration, density (or specific gravity), ductility, elasticity, electrical resistivity, hardness, magnetic field, magnetization, malleability, melting point and boiling point, molar absorptivity, pressure, specific energy.

Extensive parameter are: energy, entropy, Gibbs energy, length, mass, particle number, momentum, number of moles, volume, magnetic moment, electrical charge, weight.

44.2.9 Signatures for quantum degeneracy of a Fermi gas

Whether an atom is a *fermion* or a *boson* uniquely depends on its total spin. Halfinteger spin particles are fermions, integer spin particles are bosons. E.g. Rb atoms have in the ground state $J = 1/2, I = 7/2$, integer F, and are therefore bosons. Ca^+ ions have $J = 1/2$ and no hyperfine structure so that F is halfinteger, and are therefore fermions. ^{6}Li has half-integer F and is a boson.

For a *composite particle* the quantum statistical nature may depend on the interaction strength of the partners. For weak interaction, e.g. Feshbach the total spins of the partners will couple to a total total spin, which determines the nature of the composite particle. A fermion pairing with a fermion or a boson pairing with a boson will

[6] How to derive the thermodynamic potentials from the macrocanonical partition function? How to calculate pressure and volume? [check thermodynamic derivations from Romero-Rochin [see Freddy's thesis].

be bosons. A fermion pairing with a boson will be a fermion. Composite trimers may be either bosonic or fermionic depending on the coupling scheme. Can the quantum nature change with the tightness of the binding? What is the total spin of a deeply bound molecule? [1084, 183, 513], [**?**, 622, 1020, **?**]

44.2.9.1 Optical density of a Fermi gas

With the local density of a Fermi gas,

$$n_{loc} = \frac{k_F^3}{3\pi^2} \tag{44.89}$$

the *optical density* is at $T = 0$,

$$\begin{aligned} \int \sigma n dy &= \frac{8\sigma}{\pi^2}\frac{N}{R_F^3}\int_{-R_F}^{R_F}\left(1-\frac{x^2+y^2}{R_F^2}-\frac{z^2}{Z_F^2}\right)^{3/2}dy \\ &= \frac{8\sigma}{\pi^2}\frac{N}{R_F^3}\left(1-\frac{x^2}{R_F^2}-\frac{z^2}{Z_F^2}\right)^{3/2}\int_{-R_F}^{R_F}\left(1-\frac{y^2}{R_F^2-x^2-R_F^2z^2/Z_F^2}\right)^{3/2}dy\ . \end{aligned} \tag{44.90}$$

Writing $a = R_F/\sqrt{R_F^2 - x^2 - R_F^2 z^2/Z_F^2}$,

$$\begin{aligned} \int \sigma n dy &= \frac{8\sigma}{\pi^2}\frac{N}{R_F^2 a^4}\int_{-a}^{a}(1-\tilde{y}^2)^{3/2}d\tilde{y} \\ &= \frac{2\sigma}{\pi^2}\frac{N}{R_F^2 a^4}\left(9a\sqrt{1-a^2}-2a^3\sqrt{1-a^2}+3\arcsin a\right)\ . \end{aligned} \tag{44.91}$$

In the center, $a = 1$,

$$\int \sigma n dy = \frac{3N\sigma}{\pi R_F^2} = \frac{9m\omega_r^2 N}{k_L^2 E_F}\ , \tag{44.92}$$

such that for $E_F \simeq 1\mu$K we expect $n_{loc} \simeq 4\times 10^{12}$ cm^{-3}.

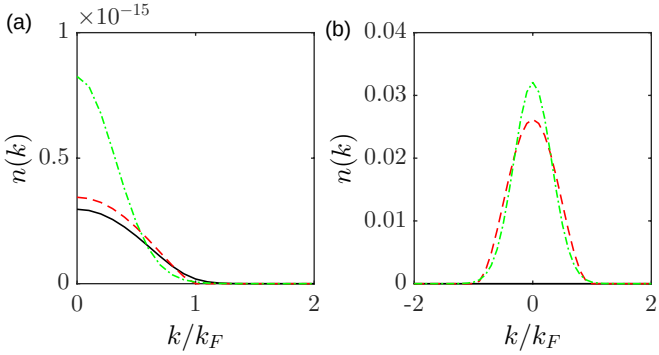

Figure 44.9: (code) (a) Radial momentum distribution and (b) distribution of momentum classes in the direction of k_z for a Fermi gas at $T/T_F = 0.2$ μK (solid), a classical gas (dash-dotted), and a Fermi gas at $T = 0$ (dashed).

44.2.9.2 'Pauli blocking' of sympathetic cooling

For a harmonic trap $U = \mu B = m\omega^2 r^2$ the *rms*-radius of a thermal cloud,

$$r_{rms} = \sqrt{\frac{2k_B T}{m\omega_r^2}} = \sqrt{\frac{k_B T}{\mu \partial_r^2 B}} \,, \tag{44.93}$$

is independent on the atomic mass. This means that a Li and a Rb cloud in the same harmonic trap at the same temperature have the same radius. This ensures good overlap. E.g. at $T = 10$ μK assuming the Rb secular frequencies $\omega_r \simeq 2\pi \times 300$ Hz and $\omega_z \simeq 2\pi \times 30$ Hz, we expect $r_{rms} = 16$ μm and $z_{rms} = 160$ μm. However below the temperature $0.5T_F$, which is $T_F \simeq 1$ μK for $N_F = 10^4$, the quantum pressure stops the reduction of the fermion cloud while cooling. This evtl. reduces the overlap with the boson cloud, disconnects the two clouds and stops the evaporative cooling. On the other hand, the interaction energy of the boson cloud also increases its size, when the Rb cloud approaches the critical temperature $T_c \simeq 0.6$ μK for $N_B = 10^6$.

The *Pauli blocking* of sympathetic cooling is a signature for the advent of quantum statistics [348, 540, 967]. It is due to a reduced mobility (or better reduced available phase space at collisions) of the atoms and not to be confused with the prohibition of s-wave collisions due to the *Pauli exlusion principle*. Furthermore, elastic collisions are suppressed [347], because atoms cannot be scattered into occupied trap levels [637, 1319, 562, 567].

44.2.9.3 Superfluid suppression of sympathetic cooling

The fermions inside the bosonic cloud can be regarded as impurities. If they travel too slow, $v < c$, and if the condensed fraction is too large, the motion will be frictionless and thermalization stops. If they travel fast, quasiparticles are excited, which can be removed by evaporation. With the typical velocity of sound in the BEC $c = \hbar\sqrt{16\pi na}/2m_B \approx 2$ mm/s, or $\frac{m}{2}c^2 \approx k_B \times 20$ nK, we see that this is no real danger.

44.2.9.4 Component separation

If the interspecies interaction h is stronger than the inter-bosonic interaction, the components may separate [965]. Otherwise a small fermionic cloud stays inside the BEC.

44.2.9.5 Excess energy modifies 2^{nd} moment

Independent on any model, just look deviation from Gaussian (interaction energy plays no role for the fermions). Also calculate the 2^{nd} moment $U = \int E_{kin}(k)n(k)dk$, where $n(k)$ is measured in time-of-flight and $E_{kin} = \hbar^2 k^2/2m$.

44.2.9.6 Modification of light scattering

The unavailability of final momentum states inhibits scattering in a similar way as the Lamb-Dicke effect. Forward scattering is suppressed, because all small momentum states are occupied. Furthermore, spontaneous emission is suppressed like in photonic

band gaps. However, here it is rather an atomic momentum band gap. Could it be that because scattering is suppressed, in-situ images of fermions are hampered?

A condition for this effect to play a role is $k_{rec} \ll k_F$. For Li the temperature must be $k_B T_F = \hbar^2 k_F^2/2m = \hbar\bar{\omega}(6N)^{1/3} \gg \hbar^2 k_L^2/2m \approx k_B \times 3\ \mu$K. I.e. we need quite large Fermi gases.

44.2.9.7 Hole heating

Loss processes that remove particles from an atom trap leave holes behind in the single particle distribution if the trapped gas is a degenerate fermion system. The appearance of holes increases the temperature, because of an increase in the energy share per particle if cold particles are removed. Heating is significant if the initial temperature is well below the Fermi temperature. Heating increases the temperature to $T > T_F/4$ after half of the systems lifetime, regardless of the initial temperature. The *hole heating* has important consequences for the prospect of observing Cooper pairing in atom traps.

44.2.10 Fermi gas in reduced dimensions

In n dimensions with the energy $\varepsilon = ap^s + br^t$ [**?**] we have to generalize the results of the last chapter,

$$N = g\frac{\Gamma\left(\frac{n}{s}+1\right)\Gamma\left(\frac{n}{t}+1\right)}{(2\hbar)^n a^{n/s} b^{n/t}\Gamma\left(\frac{n}{2}+1\right)^2}(k_B T)^{n/s+n/t} f_{n/s+n/t}(z)\ . \tag{44.94}$$

This gives for a harmonic trap where $\varepsilon = \frac{1}{2m}p^2 + \frac{m}{2}\omega^2 r^2$ and with the spin degeneracy factor $g = 1$,

$$N = \left(\frac{k_B T}{\hbar\omega}\right)^n f_n(z)\ . \tag{44.95}$$

The Fermi energy again follows from Sommerfeld's expansion,

$$E_F = (n!N)^{1/n}\hbar\omega\ . \tag{44.96}$$

We now assume a $1D$ potential $V = \frac{m}{2}\omega_z^2 r^2$ embedded in a $3D$ trap. A true $1D$ situation arises when the atoms occupy all low-lying axial levels with the lowest radial vibrational quantum number, i.e. $E_F \ll \hbar\omega_r$ which gives,

$$N \ll \frac{\omega_r}{\omega_z}\ . \tag{44.97}$$

Such quantum degenerate $1D$ fermion gases realize the so-called *Luttinger liquid*. One of the hallmarks of Luttinger liquids is *spin-charge separation*.

Example 282 (*Estimations for 1D*): Let us consider a Fermi gas in a very elongated microtrap: $\omega_r = \sqrt{\frac{87}{7}}2\pi \times 1.4$ kHz and $\omega_z = \sqrt{\frac{87}{7}}2\pi \times 15$ Hz for Rb. With $N_{Li} = 10^5$ the Fermi temperature is as high as $T_F \simeq 5\ \mu$K. However we

need $N \ll 100$ to see $1D$ features.
Assume $\varepsilon = \frac{1}{2m}p^2 + \frac{m^2}{4}b^4r^4$,

$$N = \frac{1}{(\hbar b)^n}\frac{\Gamma\left(\frac{n}{4}+1\right)}{\Gamma\left(\frac{n}{2}+1\right)}(k_BT)^{3n/4}f_{3n/4}(z)$$
$$E_F \approx (\hbar b)^{4/3}\left(N\frac{\Gamma\left(\frac{n}{2}+1\right)\Gamma(\frac{3n}{4}+1)}{\Gamma\left(\frac{n}{4}+1\right)}\right)^{4/3n} .$$

In $1D$,

$$N = \frac{1.02}{\hbar b}(k_BT)^{3/4}f_{3/4}(z)$$
$$E_F \approx 0.87(N\hbar b)^{4/3} .$$

44.2.11 Exercises

44.2.11.1 Ex: Li Fermi gas

Programs on Li Fermi gases.

Solution: *FermiBlocking1: Density distribution of a Li Fermi gas.*
FermiBlocking2: Momentum distribution of a Li Fermi gas.
FermiBlocking3: Time-of-flight distribution of a Li Fermi gas.
FermiBlocking4: Temperature dependence of the rms-size of a Li Fermi gas [221].
FermiBlocking4a: Temperature dependence of the rms-size of a Li Fermi gas [221], in the Sommerfeld approximation.
FermiBlocking4b: Temperature dependence of the rms-size of a Li Fermi gas [221], numerical integration of density of states.
FermiBlocking5: Temperature dependence of ToF sizes for various atom numbers.

44.3 Further reading

V.S. Bagnato et al., *Bose-Einstein Condensation in an External Potential* [73]$_{\text{DOI}}$

D.A. Butts et al., *Trapped Fermi gases* [221]$_{\text{DOI}}$

Chapter 45

Bose-Einstein condensation

The experimental verification of Bose and Einstein's prediction was for a long time a cherished dream of many physicists. On the one hand, several phenomena have been related to BEC in the past, for example, the phenomenon of superfluidity in liquid helium and superconductivity. On the other hand, these strongly interacting systems are not pure enough to clearly identify the role of BEC. In 1995, however, Bose-Einstein condensation of weakly interacting confined atomic gases was achieved in several laboratories [31, 331, 189, 580]. This success gave rise to a revolution in atom optics documented in an enormous amount of theoretical and experimental work. While initial work focused on the equilibrium thermodynamics of condensates near the phase transition, very soon the dynamic response of condensates to perturbations was the subject of in-depth investigations, followed by the study of superfluid characteristics, quantum transport phenomena, the interaction of condensates with light, of condensed gas mixtures [939, 1261], and the behavior of condensates in periodic potentials. To name only a few landmarks, we mention the creation of vortices [856, 833] and quantum turbulence [609], the realization of various types of atom lasers [881, 30, 154, 570] and atom interferometers with condensates [574, 746], the coherent amplification of matter waves [649, 749, 651, 354], the creation of the Mott insulating states in optical lattices [537], the study of condensates in reduced dimensions [924], the Anderson localization of atomic matter waves [245, 1101], the observation of Feshbach type collision resonances [300, 648, 1349] and Efimov states [750, 100], the creation of homonuclear molecular [538, 677, 311, 1443, 1402, 612] and heteronuclear condensates [986] and degenerate Fermi gases [347], the observation of BCS type pairing [623, 539], the observation of matter wave superradiance [649] and the interaction of condensates with optical cavities [1217, 223] and with surfaces [119].

It is clearly unthinkable to discuss all matters in this course. Let us, however, give a basic and practical introduction to atomic optics with condensates.

45.1 Bose-Einstein condensation of dilute gases

The challenge of the experimental realization of Bose-Einstein condensation is the preparation of a very dense sample of very cold atoms. In practice, the first step consists in providing an atomic gas, for example, of an alkali metal. This is done by heating the metal in an oven (or sometimes in a dispenser). The atoms being ejected from the metal and forming a hot gas are then forced through a nozzle out of the oven, where they form a hot atomic beam. Some experiments employ a *Zeeman*

slower, which is a device that decelerates the fast atoms of the beam by means of a counterpropagating laser exerting a radiative pressure force. A position-dependent magnetic field applied along the trajectory of the atoms is calculated in order to compensate for the Doppler decreasing shift of the decelerated atoms and to ensure that the laser always stays in resonance with an atomic transition (see Exc. 34.6.7.3). Velocities around 30 m/s are realistic and low enough to allow the capture of the atoms by a magneto-optical (MOT) trap. Usually, some 10^9 atoms are captured in a few seconds.

MOTs do not only trap atoms, but simultaneously cool them down to the Doppler limit of typically some 10 μK. Quasi-resonant optical traps, such as MOT, are afflicted by the problem of radiation trapping (see Sec. 43.3.1), which limits the densities of atomic clouds to typically $10^{11}\,\mathrm{cm}^3$. This corresponds (at temperatures close to the Doppler limit) to phase space densities several orders of magnitude away from the threshold to Bose-Einstein condensation. For this reason, the atoms are transferred from the MOT to a potential exempt of radiative pressure force, for example, an optical dipole potential or a magnetic trap.

Once the atoms are confined in such a conservative potential, all the light beams are turned off, and the technique of evaporative cooling is activated (see Sec. 43.4.3). That is, the effective potential is deformed (for example, by an irradiated radiofrequency) in a way to skim out hot atoms and leave behind a cooler sample. This however supposes that the atomic cloud finds back to thermal equilibrium afterwards. As the rethermalization happens by elastic collisions, a high atomic density is necessary, which is often achieved via a compression of the trapping potential. In general, 99.9% of the atoms must be sacrificed to condense the rest. Finally, the momentum distribution is imaged after a time of free expansion. This is done by irradiation of a probe laser pulse (see Fig. 43.36). The entire process of producing a condensed cloud usually takes between 10 s and 60 s.

45.1.1 Condensate of alkaline gases

The first experimental observation of Bose-Einstein condensation was done with a dilute rubidium gas by Cornell and Wieman at the Joint Institute for Laboratory Astrophysics (JILA) [31]. A group from the University of Texas [580, 301] used rubidium as well. A group led by Ketterle from the Massachusetts Institute of Technology (MIT) created the first sodium condensate. And a group led by Hulet from Rice University opted for lithium [189, 187], which has a slightly negative scattering length, $a = -27.3a_B$. In this situation, only small condensates are expected to be stable [1122, 1270], which explains the observation of a limited number of about 1400 condensed lithium atoms. Meanwhile, Bose-Einstein condensation has been achieved with many other species, such as ^{1}H [466], ^{85}Rb [293], ^{4}He* [1107], ^{133}Cs [1227], ^{39}K [1056], ^{4}Ne [113], ^{88}Sr [1257], or even molecules [1396].

45.1.2 Condensation of hydrogen

Hydrogen is a very interesting element to study condensation, because its short scattering length, $a \approx 1.23a_B$, makes it an almost ideal gas. Consequently, the three-body collision rate causing losses is weak, even at very high densities. Since the mass of

hydrogen is small, the critical temperature is high. The simplicity of its electronic structure allows precise calculations of the interaction potentials based on fundamental principles, which can thus be tested experimentally.

Twenty years after having started the project of condensing dilute hydrogen gases, Greytak and Kleppner [466] crossed the phase transition at a temperature of 50 μK with an atomic density of $5 \times 10^{15}\,\mathrm{cm}^{-3}$. The number of condensed atoms was 10^9, which corresponds to a condensed fraction below 10% [1]. The condensed cloud had a needle-like shape of 15 μm diameter and 5 mm length. It was detected by an *in situ* measurement technique of the atomic velocity distribution.

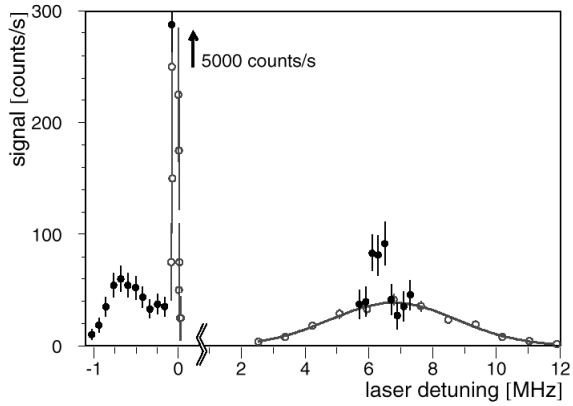

Figure 45.1: Spectrum of condensed hydrogen.

45.1.3 Recognizing Bose-Einstein condensates

'How to recognize the presence of a condensate, what are its signatures?' We have already seen in Sec. 44.1.4 that, trapped inside a confinement potential, an ultracold ideal Bose-gas has a modified density distribution when Bose-Einstein statistics come into play. Below the critical temperature the density distribution is well described by a superposition of a condensed cloud concentrated in the trap's ground state and a thermal cloud distributed over several vibrationally excited states. We thus expect distinct distribution functions for both clouds, and the same is true for the momentum distribution. The splitting of the distribution functions in two fractions occurs abruptly during the phase transition to quantum degeneracy. In a real gas, however, the interatomic collisions have a drastic influence on the distribution functions and the behavior of the gas at the phase transition, and we are obliged to develop a more general theory in order to quantitatively understand the thermodynamic properties (temperature, critical point, heat capacity, ...) through the measured static quantities (density, number of atoms, condensed fraction, ...).

'What observables can be measured in the laboratory?' In fact, with few exceptions, the only accessible quantity is the *spatial density distribution* of the atomic cloud

[1] When the condensed fraction and the density are too high, losses induced by dipolar spin-flip processes predominate over the gain due to evaporative cooling of the thermal cloud [618].

$n(\mathbf{r})$ measured after a time of ballistic expansion. Information on non-trivial properties of the condensate, for example, its dynamic behavior (excitations, superfluidity, turbulence, ...) or its coherent features (phase, correlations, ...), can only be gathered through an observation of the condensate's response to applied perturbations. Solve the Excs. 45.1.5.1 and 45.1.5.2.

45.1.4 Photon condensation

An interesting question is that of the possibility of *photon condensation* and its relationship to the laser. The relationship is not that obvious because, on one hand atomic condensates are produced by evaporating a ensemble in constant thermal equilibrium, while on the other hand the photonic laser requires inversion, which is a highly non-equilibrium situation. And under the constraint of having to reduce its energy, a photon gas trapped in an optical cavity has the simpler alternative to let photons escape into the void by annihilating them on the cavity walls, as it happens for black-body radiation. Since the number of photons in a cavity is not conserved, the chemical potential disappears, $\mu = 0$. The density of states can be written,

$$u(\nu) = \frac{8\pi V}{c^3} \frac{E^2 dE}{h^2} \ . \tag{45.1}$$

It is the same as in the Debye model. Planck's formula now follows from,

$$u(\epsilon)d\epsilon = \frac{1}{V}\epsilon f_{BE}(\epsilon)\rho(\epsilon)d\epsilon \ , \tag{45.2}$$

where f_{BE} is the Bose-Einstein distribution. Hence, the treatment of the photons as indistinguishable particles following the Bose-Einstein distribution is equivalent to assuming a Boltzmann distribution for waves with quantized energies.

Nevertheless, one can imagine a photonic gas in thermal equilibrium with an atomic gas through Compton scattering [712]. In fact, photon condensation was observed experimentally [727]. Also, there are theories about superfluid photon gases [254] [2].

[2] *Bose-Einstein condensation occurs in thermal equilibrium when entropy is maximized by putting a macroscopic population of atoms into the ground state of the system. It might appear counter-intuitive that an apparently highly ordered state as the Bose condensate maximizes entropy. However, only the particles in excited states contribute to the entropy. Their contribution is maximized at a given total energy by forming a Bose condensate in the ground state and distributing the remaining atoms among higher energy states. A macroscopic population of atoms in the ground state of the system is achieved simply by lowering the temperature of the sample. This is in contrast to the optical laser where a non-equilibrium process is necessary to place a macroscopic population of photons in a single mode of the electromagnetic field. This is due to the fact that, unlike photons, the number of atoms is conserved. For bosonic atoms, the lowest entropy state below a certain temperature includes a macroscopic population of the ground state. In contrast, when one cools down a blackbody cavity, the cavity empties. Photons do not Bose condense into the ground state of the cavity, but are absorbed by the walls. The absorbed energy leads to a larger entropy than forming a Bose condensate. The laser phenomenon requires inversion of the active medium characterized by a 'negative' temperature. In that sense, 'lasing' of atoms is a simpler phenomenon than lasing of light –all you need to do is cool a gas! However, if a photon gas would thermalize while the number of photons is conserved, it would be described by a Bose-Einstein distribution with non-zero chemical potential and could form a Bose condensate. Thermalization with number conservation is possible, for example, by Compton scattering with a thermal electron gas [712].*

45.1.5 Exercises

45.1.5.1 Ex: Condensation of ions

Discuss the possibility of creating Bose-Einstein condensates from ionic clouds.

Solution: *Assuming that we can cool the ions to the ground state of a tight trap, they will still have μm distances because of Coulomb repulsion. The de Broglie wavelength then needs to be ...*

45.1.5.2 Ex: Isobaric impurities

Discuss the possibility of creating Bose-Einstein condensates with isobaric species.

Solution:

45.2 Quantum theory

As detailed above, interatomic interactions strongly influence the properties of Bose-Einstein condensates, even their density and momentum distributions. For a correct interpretation of the experimental measurements a theoretical many-body treatment taking care of these interactions is compulsory. This is done through a description of the atomic distribution as a *scalar field of matter* called *second quantization*, where the atoms are treated as delocalized Broglie waves. However, we will leave a thorough introduction of this formalism to Chp. 50.3 or referto [1355].

45.2.1 Description of the atom as a scalar field

In position space a state with n particles can be described in a canonically quantized way by a *field operator*,

$$\hat{\Psi}(\mathbf{r}_1, ..., \mathbf{r}_n, t) = \hat{\psi}^\dagger(\mathbf{r}_1, t) \cdot ... \cdot \hat{\psi}^\dagger(\mathbf{r}_n, t)\hat{\Psi}_0 \quad , \quad \hat{\psi}(\mathbf{r})\hat{\Psi}_0 = 0 \ , \tag{45.3}$$

where Ψ_0 is the vacuum state. The field operators $\hat{\psi}(\mathbf{r}, t)$ and $\hat{\psi}^\dagger(\mathbf{r}, t)$ annihilate, respectively create, an atom at position $\mathbf{r}$ and time t. This state represents a bosonic Fock state and can be generated from the empty state by a sequence of individual particle creation operators. Applying the notions and rules developed for the harmonic oscillator in Sec. 24.6.1, we can define a coherent state of bosonic matter as,

$$|\hat{\Phi}(t)\rangle = \sum_{n=0}^{\infty} \frac{N^{n/2}}{\sqrt{n!}} |\hat{\Psi}(\mathbf{r}_1, ..., \mathbf{r}_n, t)\rangle \ . \tag{45.4}$$

The field operators for particle creation and annihilation are normalized to the number of atoms and satisfy the following commutation rules,

$$\begin{array}{llcl}
\text{(i)} & [\hat{\psi}(\mathbf{r}),\hat{\psi}(\mathbf{r}')]_- & = & 0 \\
\text{(ii)} & [\hat{\psi}(\mathbf{r}),\hat{\psi}^\dagger(\mathbf{r}')]_- & = & \delta^3(\mathbf{r}-\mathbf{r}') \quad , \quad \hat{\psi}^\dagger(\mathbf{r}) = \int d^3r'\hat{\psi}^\dagger(\mathbf{r}')\delta^3(\mathbf{r}-\mathbf{r}') \\
\text{(iii)} & [\hat{\psi}(\mathbf{r}),\hat{N}]_- & = & \hat{\psi}(\mathbf{r}) \quad , \quad \hat{N} = \int d^3r'\hat{\psi}^\dagger(\mathbf{r}')\hat{\psi}(\mathbf{r}') \\
\text{(iv)} & [\hat{\psi}(\mathbf{r}),\hat{\mathbf{p}}]_- & = & \frac{\hbar}{\imath}\nabla\hat{\psi}(\mathbf{r}) \quad , \quad \hat{\mathbf{p}} = \int d^3r'\hat{\psi}^\dagger(\mathbf{r}')(\frac{\hbar}{\imath}\nabla')\hat{\psi}(\mathbf{r}') \\
\text{(v)} & [\hat{\psi}(\mathbf{r}),\mathcal{H}]_- & = & \imath\hbar\frac{\partial}{\partial t}\hat{\psi}(\mathbf{r})
\end{array} \tag{45.5}$$

The last equation is the Heisenberg equation of motion and describes the dynamics of a system whose *many-body Hamiltonian* $\mathcal{H} \equiv \mathcal{H}_{cm} + \mathcal{H}_{self}$ for N bosons interacting within an external potential V_{trap} in second quantization is defined by [3],

$$\begin{aligned}
\mathcal{H}_{cm} &\equiv \int d^3r\hat{\psi}^\dagger(\mathbf{r})\left(-\frac{\hbar^2}{2m}\nabla^2 + V_{trap}(\mathbf{r},t)\right)\hat{\psi}(\mathbf{r}) \\
\mathcal{H}_{self} &\equiv \int d^3r\int d^3r'\hat{\psi}^\dagger(\mathbf{r})\hat{\psi}^\dagger(\mathbf{r}')V_{coll}(\mathbf{r}-\mathbf{r}')\hat{\psi}(\mathbf{r}')\hat{\psi}(\mathbf{r})
\end{aligned} \quad . \tag{45.6}$$

The equations (45.5) and (45.6) represent the foundation of the theory of ultracold bosonic gases. However, to solve the equations, we will need to apply some simplifications, which will be discussed in the following sections. For example, we will generally assume that the temperature of the sample is $T = 0$, and that all atoms are condensed. Also, in a first time, we will neglect quantum fluctuations, replacing field operators with complex numbers. And finally, we will need to handle the nonlinear term appearing in $\mathcal{H}_{self}$ and which signs responsible for collisions between atoms.

45.2.2 Quantum scattering at low temperatures

To simplify the term $\mathcal{H}_{self}$, we have to go back to Secs. 33.2.5 (and following) and study the phenomenon of the elastic collisions in the ultracold regime. For simplicity, we consider two particles without internal degrees of freedom with masses m_1 and m_2 approaching each other along the z-axis [276, 1363]. Neglecting spin-spin and spin-orbit interactions, the Schrödinger equation in the inertial center-of-mass system is given by (33.115),

$$\left(-\frac{\hbar^2}{2m^*}\nabla^2 + V_{coll}(r)\right)\hat{\psi}(\mathbf{r}) = E\hat{\psi}(\mathbf{r}) \ , \tag{45.7}$$

where $\mathbf{r} = \mathbf{r}_1 - \mathbf{r}_2$ is the momentary interatomic separation, $r = |\mathbf{r}|$, and $m_r \equiv m_1m_2/(m_1+m_2)$ is the reduced mass of atomic collision partners. We assume that the interatomic potential, $V_{coll}(r)$, is spherically symmetrical. In the asymptotic limit of large separations [4], and in the Born-approximation (33.135), the solution of

[3] Sometimes the *Kamiltonian* is used for canonical and macrocanonic ensembles. It defined by, $\mathcal{K} = \mathcal{H}_{cm} + \mathcal{H}_{self} - \int d^3\mathbf{r}\hat{\psi}^\dagger(\mathbf{r})\mu\hat{\psi}(\mathbf{r})$, where μ is the chemical potential.

[4] This means, $r \gg r_0$, where r_0 is the range of potential $V(r)$.

Eq. (45.7) can be seen as the sum of an incident plane wave and a scattered spherical wave modulated with a certain amplitude $f(\theta)$,

$$\psi(\mathbf{r}) = e^{\imath kz} + f(\theta)\frac{e^{\imath kr}}{r} \ , \tag{45.8}$$

where $k = \sqrt{2m_r E/\hbar^2}$ is the amplitude of the wavevector of the incident and scattered waves and θ the angle between r and z. The function $f(\theta)$ is called *scattering amplitude* and determines the scattering cross-section for s-wave collision through the expression [see (33.123)],

$$\frac{d\sigma}{d\Omega} = |f(\theta)|^2 \ . \tag{45.9}$$

where $d\Omega = \sin\theta d\theta d\phi$ is an element of the solid angle. To calculate the scattering amplitude, we expand the wavefunction (45.8) into spherical partial waves of orders ℓ of the angular momentum, as done in (33.136),

$$f_k(\theta) = \frac{1}{k}\sum_{\ell=0}^{\infty}(2\ell+1)P_\ell(\cos\theta)e^{\imath\delta_\ell}\sin\delta_\ell \ . \tag{45.10}$$

The collision cross section has been shown in (33.148) to be given by,

$$\sigma = \frac{4\pi}{k^2}\sum_{\ell=0}^{\infty}(2\ell+1)\sin^2\delta_\ell \ . \tag{45.11}$$

For a potential with finite range, that is, a potential falling faster than r^{-3} with the distance (interatomic potentials usually fall as r^{-6} or r^{-7}), the phase shift satisfies,

$$\delta_\ell \propto k^{2\ell+1} \tag{45.12}$$

for small k. In ultra-cold gases, the collision energy is very low and $k \to 0$. Thus the scattering will be dominated by terms with $\ell = 0$. This is the so-called limit of *s-wave scattering*. In this limit the Eqs. (45.10) can be approximated as,

$$f_k(\theta) = \frac{1}{k}e^{\imath\delta_0}\sin\delta_0 \ . \tag{45.13}$$

45.2.3 Scattering length

For $\ell = 0$, taking the limit $k \to 0$, we define the *scattering length* a_s via,

$$\frac{\mathfrak{Im}\ f_k(\theta)}{\mathfrak{Re}\ f_k(\theta)} = \tan\delta_0 \equiv -\tan ka_s \ . \tag{45.14}$$

Therefore, the scattering length and cross section are given at very low temperatures at the asymptotic boundary by,

$$\boxed{a_s = -\frac{\delta_0}{k} \qquad \text{and} \qquad \sigma = 4\pi a_s^2} \ . \tag{45.15}$$

The scattering process can be interpreted as follows: During a collision, the system's wavefunction undergoes a phase shift, δ_0, which may be positive or negative, depending on the sign of a_s. If $a_s < 0$, the phase is 'delayed' by the collision. This corresponds to an attractive interaction. In contrast, if $a_s > 0$, the phase is 'advanced' and the interaction is repulsive. Of course, the intensity of the interaction is proportional to the value of $|a_s|$. The expression for σ in Eq. (45.15) indicates, that the atoms behave like *hard spheres* with radius $|a_s|$. The specific value of a_s will depend on the interaction potential, however, the details of the potential are unimportant, as all information about the collision is already contained in a_s. Consequently, in the low-energy limit, we can assume that the collision is mediated by an effective potential $V_{coll}(\mathbf{r})$, which has the particularity,

$$\int V_{coll}(\mathbf{r}) d^3r = \frac{4\pi\hbar^2}{m} a_s \equiv g \ . \tag{45.16}$$

This has been shown in Sec. 33.1.2. Consequently, the effective interaction between two particles at positions $\mathbf{r}$ and $\mathbf{r}'$ can be considered as contact interaction given by [5],

$$V_{coll}(\mathbf{r}, \mathbf{r}') = \frac{g}{2} \delta(\mathbf{r} - \mathbf{r}') \ . \tag{45.17}$$

The interatomic interaction potential decides on the value of the scattering length a_s: A repulsive potential corresponds to a positive a_s. For a purely attractive potential that does not support bound states a_s is negative, and for an attractive potential that supports bound states a_s may be positive or negative depending on the proximity of the last bound vibrational state of the interaction potential below the dissociation limit.

45.2.4 The mean field approximation

The *mean-field theory* (MFT) or *local density approximation* (LDA) is based on the assumption of *hard sphere collision*s between atoms (as described by the potential (45.17)) propagating through a locally homogeneous mean-field potential, $\frac{g}{2}|\hat{\psi}(\mathbf{r})|^2$. The procedure is also called *regularization of the interaction*.

Thus, the mean-field energy of a condensate is proportional to the density of the gas n and to a single atomic constant, which is the scattering length a_s. Its presence in the Gross-Pitaevskii equation emphasizes its impact on shape, dynamic stability and many other properties of the condensate. For example, the mean-field interaction contributes to the broadening of a condensed wavepacket, and consequently contracts its momentum distribution in comparison with an ideal gas. Homogeneous condensates with a negative scattering length are unstable, because the attempt of such a condensate to lower its self-energy by increasing its density also increases the rate of inelastic three-body collisions until the condensate collapses.

[5] The *Hartree-Fock-Bogolubov method* (HFB) for the mean-field theory disregards corrections of higher orders, for example, due to the renormalization of the scattering length. It also neglects quantum depletion due to the correlation effects of the order of $N_{out}/N = \frac{5}{8}\sqrt{\pi}\sqrt{a^3 n_0}$. The theory mean-field supposes the validity of the *Born approximation*, that is, two-body correlations are neglected, $\hat{\psi}(\mathbf{r}') \approx \hat{\psi}(\mathbf{r})$ and $\int d^3R V_{coll}(\mathbf{R}) = \frac{g}{2}$.

45.2.5 Gross-Pitaevskii equation

The Heisenberg equation [last line of (45.5)] is equivalent to the *variational principle*, as stated by the Ehrenfest theorem,

$$\imath\hbar\frac{d\hat{\psi}}{dt} = \frac{\delta\mathcal{H}}{\delta\hat{\psi}^\dagger} \ . \tag{45.18}$$

This facilitates the derivation of the equation of motion for the atomic field. With the Hamiltonian (45.6) in the mean-field approximation,

$$\mathcal{H}_{atom} \equiv \mathcal{H}_{cm} + \mathcal{H}_{mf} \qquad \text{with} \qquad \mathcal{H}_{mf} \equiv \int d^3r\hat{\psi}^\dagger(\mathbf{r},t)\frac{g}{2}|\hat{\psi}(\mathbf{r},t)|^2\hat{\psi}(\mathbf{r},t) \ , \tag{45.19}$$

we find the *non-linear Schrödinger equation*,

$$\left[-\frac{\hbar^2}{2m}\nabla^2 + V_{trap}(\mathbf{r},t) + g|\hat{\psi}(\mathbf{r},t)|^2\right]\hat{\psi}(\mathbf{r},t) = \imath\hbar\frac{\partial}{\partial t}\hat{\psi}(\mathbf{r},t) \ . \tag{45.20}$$

Remember that, despite their symbol $\hat{\psi}$, which usually is associated to wavefunctions, and the fact that they satisfy a non-linear Schrödinger equation the field operators are represented by matrices acting of many-body states. That is, Eq. (45.20) also represents a Heisenberg equation for the field operators.

A common approximation is the *Bogolubov prescription*, where the field operators describing the condensate and its fluctuations are decomposed into a complex function, $\psi_0(\mathbf{r}) \equiv \langle\hat{\psi}(\mathbf{r})\rangle$ called *condensed wavefunction*, which can be chosen as the *order parameter* of the system, and a small perturbation, $\delta\hat{\psi}(\mathbf{r}) \equiv \hat{\psi}(\mathbf{r}) - \psi_0(\mathbf{r})$ describing *thermal excitations*. At zero temperature, we can neglect the excitations [108], and our system is completely described by a single wavefunction, $\psi_0(\mathbf{r},t)$, obeying the famous *Gross-Pitaevskii equation* (*GPE*),

$$\boxed{\left[\frac{-\hbar^2}{2m}\nabla^2 + V_{trap}(\mathbf{r},t) + g|\psi_0(\mathbf{r},t)|^2\right]\psi_0(\mathbf{r},t) = \imath\hbar\frac{\partial}{\partial t}\psi_0(\mathbf{r},t)} \ . \tag{45.21}$$

45.2.5.1 Spontaneous breaking of gauge symmetry

The description of a condensate by a single macroscopic wavefunction means that we attribute a well-defined phase to it. However, the GPE does not allow us to predict, which phase between 0 and 2π this will be, and we have to assume, that the BEC chooses its phase spontaneously when it undergoes the phase transition to quantum degeneracy. This principle is called *spontaneous breaking of gauge symmetry* [6]. In Exc. 45.2.6.2 we study the relation between the fact of having exactly N atoms in a condensate and a well-defined phase φ, knowing that these two quantities are conjugate variables having to satisfy a Heisenberg uncertainty relation.

[6] An alternative way of modeling the development of a BEC phase is based on measurement theory. See also (35.72) for an analogy to the correct state of a laser.

45.2.6 Exercises

45.2.6.1 Ex: Derivation of the non-linear Schrödinger equation

Derive the non-linear Schrödinger equation using (a) the commutator relation (45.5)(v) and (b) the variational expression (45.18).

Solution: *From the commutator relation,*

$$\imath\hbar\frac{\partial}{\partial t}\hat{\psi}(\mathbf{r}) = [\hat{\psi}(\mathbf{r}),\mathcal{H}]_- = \left[\hat{\psi}(\mathbf{r}),\int d^3r'\hat{\psi}^\dagger(\mathbf{r}')\left(-\frac{\hbar^2}{2m}\nabla'^2 + V_{trap}(\mathbf{r}',t) + \frac{g}{2}\hat{\psi}^\dagger(\mathbf{r}')\hat{\psi}(\mathbf{r}')\right)\hat{\psi}(\mathbf{r}')\right]_-$$

$$= -\frac{\hbar^2}{2m}\int d^3r[\hat{\psi}(\mathbf{r}),\hat{\psi}^\dagger(\mathbf{r}')]_-\nabla'^2\hat{\psi}(\mathbf{r}') + \int d^3r[\hat{\psi}(\mathbf{r}),\hat{\psi}^\dagger(\mathbf{r}')]_- V_{trap}(\mathbf{r}',t)\hat{\psi}(\mathbf{r}')$$

$$+ \frac{g}{2}\int d^3r[\hat{\psi}(\mathbf{r}),\hat{\psi}^\dagger(\mathbf{r}')\hat{\psi}^\dagger(\mathbf{r}')]_-\hat{\psi}(\mathbf{r}')\hat{\psi}(\mathbf{r}')$$

$$= -\frac{\hbar^2}{2m}\nabla^2\hat{\psi}(\mathbf{r}) + V_{trap}(\mathbf{r},t)\hat{\psi}(\mathbf{r}) + \frac{g}{2}\int d^3r\left\{[\hat{\psi}(\mathbf{r}),\hat{\psi}^\dagger(\mathbf{r}')]_-\hat{\psi}^\dagger(\mathbf{r}') + \hat{\psi}^\dagger(\mathbf{r}')[\hat{\psi}(\mathbf{r}),\hat{\psi}^\dagger(\mathbf{r}')]_-\right\}\hat{\psi}(\mathbf{r}')\hat{\psi}(\mathbf{r}')$$

$$= \left(-\frac{\hbar^2}{2m}\nabla^2 + V_{trap}(\mathbf{r},t) + g|\hat{\psi}(\mathbf{r})|^2\right)\hat{\psi}(\mathbf{r}) \ ,$$

using the commutation relation $[\hat{\psi}(\mathbf{r}),\hat{\psi}^\dagger(\mathbf{r})]_- = \delta(\mathbf{r}-\mathbf{r}')$.
b. From the variational expression,

$$\imath\hbar\frac{\partial}{\partial t}\hat{\psi}(\mathbf{r}) = \frac{\delta\mathcal{H}}{\delta\hat{\psi}^\dagger} = \frac{\delta}{\delta\hat{\psi}^\dagger}\int d^3r'\hat{\psi}^\dagger(\mathbf{r}')\left(-\frac{\hbar^2}{2m}\nabla'^2 + V_{trap}(\mathbf{r}',t) + \frac{g}{2}\hat{\psi}^\dagger(\mathbf{r}')\hat{\psi}(\mathbf{r}')\right)\hat{\psi}(\mathbf{r}')$$

$$= \left(-\frac{\hbar^2}{2m}\nabla^2 + V_{trap}(\mathbf{r},t) + g|\hat{\psi}(\mathbf{r})|^2\right)\hat{\psi}(\mathbf{r}) \ .$$

45.2.6.2 Ex: Spontaneous breaking of gauge symmetry

One of the primary characteristics of a condensate is its phase coherence. Now, consider a condensate with exactly N atoms. The exact knowledge of the atom number implies a totally uncertain phase of the condensate, according to Heisenberg's uncertainty relation. Explain this contradiction!

Solution: *Following Yukalov [297], the existence of a single phase is* not essential *for BECs. The question of symmetry breaking as a concept of quantum field theory only arises for homogeneous systems. If, in a phase transition, the two phases have different symmetries, the transition is accompanied by a symmetry breaking. Only continuous phase transitions may exhibit symmetry breaking. Therefore, spontaneous symmetry breaking is not expected for homogeneous condensates, but only in confined, finite or interacting systems. Gauge symmetry breaking leads to collapse and revivals due to particle number fluctuations. It was demonstrated [1115], that the theory of BEC can also be formulated without the concept of symmetry breaking. The existence of off-diagonal long-range order (ODLRO) in the density operator, which is an indicator for long-range correlations between particles, is equivalent to the presence of a condensed phase in a sample.*

45.3 Approximate solutions of the Gross-Pitaevskii equation

45.3.1 Stationary GPE

In cases where the external potential is stationary, $V_{trap}(\mathbf{r},t) = V_{trap}(\mathbf{r})$, the temporal dependency of the GPE can be removed by the ansatz,

$$\psi_0(\mathbf{r},t) = \psi_0(\mathbf{r})e^{-\imath\mu t/\hbar} \ . \tag{45.22}$$

This gives the stationary Gross-Pitaevskii equation,

$$\boxed{\left[\frac{-\hbar^2}{2m}\nabla^2 + V_{trap}(\mathbf{r}) + g|\psi_0(\mathbf{r})|^2\right]\psi_0(\mathbf{r}) = \mu\psi_0(\mathbf{r})} \ , \tag{45.23}$$

where μ is called the *chemical potential*. Solve Exc. 45.3.4.1.

45.3.2 Trapped condensates and the Thomas-Fermi limit

45.3.2.1 Free particles

The wavefunction of free particles, $V(\mathbf{r}) = 0$, can be described by a plane wave,

$$\psi(\mathbf{r}) = \sqrt{n}e^{\imath\mathbf{k}\cdot\mathbf{r}} \ , \tag{45.24}$$

also called the Hartree solution. Inserted it into the equation of Gross-Pitaevskii equation,

$$E(k) = \frac{\hbar^2k^2}{2m} + gn \ , \tag{45.25}$$

we observe a *gap* in the energy spectrum due to the interaction.

45.3.2.2 Ideal gas in a harmonic potential

Most experiments apply non-isotropic (often cylindrical) potentials, which are additionally distorted by the mean-field. Hence, the non-linear term of the GPE is important, and the spatial coordinates can not be separated. However, assuming an ideal gas and a harmonic potential, the dimensions could be separated, as demonstrated in Sec. 24.5.5, even when the potential is not isotropic. It is then sufficient to consider one-dimensional problems with $g = 0$,

$$\left[-\frac{\hbar^2}{2m}\frac{\partial^2}{\partial x^2} + \frac{m}{2}\omega_x^2\hat{x}^2\right]\psi_n = \mu_n\psi_n \ . \tag{45.26}$$

In this limit, the GPE is nothing more than the usual Schrödinger equation, which has the well-known spectrum (24.110) and the solutions (24.109).

45.3.2.3 Ideal gas in an isotropic potential

In the case of an ideal gas trapped in a spherically symmetric potential, as shown in (25.34), the Schrödinger equation can be reduced to its radial component,

$$\left[\frac{\partial^2}{\partial r^2} + \frac{2}{r}\frac{\partial}{\partial r} - \frac{l(l+1)}{r^2} + V_{trap}(r)\right] f_{nlm}(r) = \mu_{nl} f_{nlm}(r) \ , \tag{45.27}$$

with the solution (25.18),

$$\psi_n(r,\vartheta,\varphi) = \sum_{l,m} f_{nlm}(r) Y_{lm}(\vartheta,\varphi) \tag{45.28}$$

The differential equation (45.27) can be solved numerically by Runge-Kutta type methods,

$$\begin{pmatrix} f'' \\ f' \end{pmatrix} = \begin{pmatrix} \frac{2}{r} & \mu + \frac{l(l+1)}{r^2} - V_{trap}(r) \\ 1 & 0 \end{pmatrix} \begin{pmatrix} f' \\ f \end{pmatrix} \ . \tag{45.29}$$

45.3.2.4 Thomas-Fermi limit for strong interactions

In the case of strong interactions, the kinetic energy term can be neglected, at least in the center of the cloud, where the mean-field energy is stronger. For this case, called *Thomas-Fermi limit*, the GPE solution is easy,

$$|\psi_0(\mathbf{r})|^2 = \frac{\mu - V_{trap}}{g} \ . \tag{45.30}$$

The chemical potential follows from the normalization condition,

$$N = \int_{n(\mathbf{r})>0} n(\mathbf{r}) d^3\mathbf{r} \ . \tag{45.31}$$

In the case of an cylindrical harmonic oscillator potential, $V_{trap}(r,z) = \frac{m}{2}(\omega_r^2 r^2 + \omega_z^2 z^2)$, the chemical potential is,

$$\mu = \left(\frac{15Ng}{8\pi}\right)^{2/5} \left(\frac{m}{2}(\omega_r^2\omega_z)^{2/3}\right)^{3/5} \ . \tag{45.32}$$

The radial size σ of the condensate follows from $n(r_{hw},0) = \frac{n(0,0)}{2}$,

$$r_{hw} = \sqrt{\frac{\mu}{m\omega_r^2}} \ . \tag{45.33}$$

Solve the Excs. 45.3.4.2 and 45.3.4.3.

45.3.3 Variational treatment of the GPE

The many-body Hamiltonian (45.19) can be used as an *energy functional*,

$$E[\psi_0] \equiv \langle \mathcal{H}[\psi_0] \rangle = \int d^3r \left[\frac{\hbar^2}{2m}|\nabla\psi_0|^2 + V_{trap}(\mathbf{r})|\psi_0|^2 + \frac{g}{2}|\psi_0|^4\right] \ , \tag{45.34}$$

from which, using the variational condition (45.18), we have derived the Gross-Pitaevskii equation (45.21). Hence, the wavefunction ψ_0 minimizes the functional [378]. By inserting an ansatz for the wavefunction with adjustable parameters, the functional provides conditions to optimize these parameters.

The *variational method* is useful e.g. for finding the ground state wavefunction of a condensate in an arbitrarily shaped trap or to perform a stability analysis of a condensate with attractive interatomic forces.

45.3.3.1 Finding the fundamental state of the GPE

This problem of finding the ground state wavefunction of a condensate consists in finding the ψ for which the energy $\mathcal{H}[\psi]$ goes to a minimum. In general, the functional has the form $\mathcal{H}[\psi] = \int f[\psi, \nabla\psi] d^3r$. The fastest way to the minimum is to reduce the energy by varying ψ in that direction, where the gradient $\delta\mathcal{H}/\delta\psi^*$ is largest, that is,

$$\begin{aligned} \mathcal{H} &\to \mathcal{H}[\psi + \tau \, \tfrac{\delta\mathcal{H}}{\delta\psi^*}] \\ \psi &\to \psi + \tau \tfrac{\delta\mathcal{H}}{\delta\psi^*} \ , \end{aligned} \tag{45.35}$$

with the boundary condition, that the normalization must be preserved. Formally, this problem is similar to a time-dependent Gross-Pitaevskii equation, but with *imaginary time*. Physically, the procedure, called the *steepest descent method*, can be interpreted as applying a heavily 'overdamped' friction force,

$$\frac{\partial\psi}{\partial\tau} = \frac{\delta\mathcal{H}}{\delta\psi^*} \ . \tag{45.36}$$

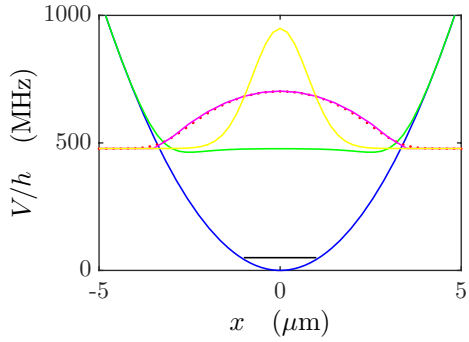

Figure 45.2: (code) Calculation of the BEC wavefunction by the steepest descent method (red dots). Also shown are the ideal gas approximation (yellow line) and the Thomas-Fermi approximation (magenta line), as well as the ground state energy (black line) and the chemical potential (green line).

In practice, the procedure is as follows: we start with a trial wavefunction, for example, the exact solution of the interaction-free case. This function is now propagated in imaginary time, using the complete Hamiltonian including the non-linear term, and then renormalized:

$$\hbar\frac{\partial}{\partial t}\psi(\mathbf{r}, t) = \mathcal{H}(\mathbf{r})\psi(\mathbf{r}, t) \ . \tag{45.37}$$

Substituting the imaginary unit i in the time-dependent Gross-Pitaevskii equation (45.21) by -1, we obtain,

$$\psi(\mathbf{r}, t + dt) = [1 - \hbar^{-1}\mathcal{H}(\mathbf{r})dt]\psi(\mathbf{r}, t) \tag{45.38}$$
$$\psi'(\mathbf{r}, t) \equiv \frac{\psi(\mathbf{r}, t + dt)}{|\psi(\mathbf{r}, t + dt)|} \to \psi(\mathbf{r}, t) \ .$$

This procedure is repeated until the function converges. Since this method is derived from a variational principle, it only serves to find the ground state of the trapping potential. It can not be used for excited states (with the exception of vortex states, where in cylindrical coordinates the Hamiltonian differs by an additional centrifugal term).

45.3.3.2 Collapse and stabilization of condensates with attractive interactions

Attractive interactions destabilize a Bose-Einstein condensate. Since the interaction energy, $4\pi\hbar^2 a_s n/m$, of a condensate with negative scattering length decreased with increasing density n, the condensate attempts to lower its interaction energy by increasing its density until it succumbs to inelastic two-body spin-changing collisions of to three-body collisions leading to the formation of molecules [1270]. Strictly speaking, this only holds true for homogeneous condensates. In the presence of a trapping potential, however, the zero-point energy exerts a kinetic pressure, which counteracts the *condensate collapse* to a certain extent, such that small condensates are stabilized. This can be verified by inserting a Gaussian wavefunction $\psi_0 \propto e^{-r^2/2\bar{r}^2}$ into the energy functional (45.34). Varying the radius $\bar{r}$ of the condensate, we find a local minimum where the condensate is stable. Calculations for spherical traps predict [1122, 319],

$$N_{min} \simeq 0.575 \frac{a_{trp}}{|a_s|} \ , \tag{45.39}$$

where $a_{trp} = \sqrt{\hbar/m\omega_{trp}}$.

The atomic species ^{7}Li has a slightly negative scattering length $a_s = -27.3a_B$. As can be seen in Fig. 45.3, small condensates can survive in a confining trap, since the energy functional has a local minimum [189, 187, 1124]. Solve Exc. 45.3.4.4.

45.3.4 Exercises

45.3.4.1 Ex: GPE in dimensionless units

Use the following abbreviations to rewrite the Gross-Pitaevskii equation and its solution for a harmonic isotropic potential in dimensionless units,

$$\begin{array}{llll} V_1 & \equiv V_{trap}/\hbar\omega_{trp} & V_{trap} & = \frac{m}{2}\omega_{trp}^2 r^2 \\ \mathbf{r}_1 & \equiv \mathbf{r}/a_{trp} & a_{trp} & = \sqrt{\hbar/m\omega_{trp}} \\ \mu_1 & \equiv \mu/\hbar\omega_{trp} & T_1 & \equiv k_B T/\hbar\omega_{trp} \\ \psi_1 & \equiv \psi/a_{trp}^{3/2} & p_1 & \equiv a_{trp}p/\hbar \\ g & \equiv 4\pi\hbar^2 a/m & g_1 & \equiv 8\pi N_0 a/a_{trp} \end{array}$$

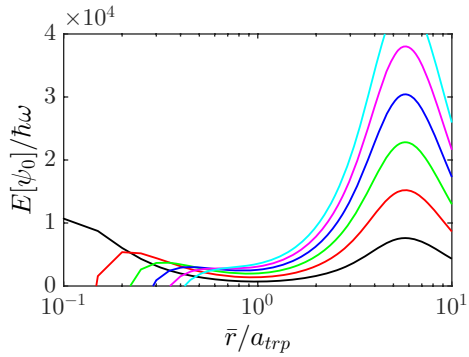

Figure 45.3: (code) Energy of a ^{7}Li condensate in a harmonic isotropic potential with $\omega_{trp} = (2\pi)$ 50 Hz with $N = 500$ atoms (linha inferior) up to $N = 3000$ (linha superior) when the radius $\bar{r}$ of the condensate is varied.

Solution: *In* 3 *dimensions the GPE becomes,*

$$\left(\nabla_1^2 + r_1^2 + g_1|\psi_1|^2\right)\psi_1 = \mu\psi_1 \ .$$

45.3.4.2 Ex: Interacting gas in an isotropic potential

Consider the potential $V(\mathbf{r}) = V(r)$, such that the wavefunction will have radial symmetry, $\psi(\mathbf{r}) = \frac{\phi(r)}{r}$. Rewrite the Gross-Pitaevskii equation for the function ϕ [626].

Solution: *The Gross-Pitaevskii equation is,*

$$\imath\hbar\frac{\partial\psi(\mathbf{r})}{\partial t} = \left(-\frac{\hbar^2}{2m}\nabla^2 + V_{trap}(r) + g|\psi(\mathbf{r})|^2\right)\psi(\mathbf{r})$$

or [626],

$$\mu\frac{\phi(r)}{r} = \left(-\frac{\hbar^2}{2m}\left[\frac{1}{r}\frac{\partial^2}{\partial r^2}r + \frac{1}{r^2\sin\vartheta}\frac{\partial}{\partial\vartheta}\left(\sin\vartheta\frac{\partial}{\partial\vartheta}\right) + \frac{1}{r^2\sin^2\vartheta}\frac{\partial^2}{\partial\varphi^2}\right] + V_{trap}(r) + g\left|\frac{\phi(r)}{r}\right|^2\right)\frac{\phi(r)}{r}$$

$$\mu\phi(r) = \left(-\frac{\hbar^2}{2m}\frac{\partial^2}{\partial r^2} + V_{trap}(r) + g\frac{|\phi(r)|^2}{r^2}\right)\phi(r) \ ,$$

with

$$\int|\psi(\mathbf{r})|^2 d^3r = 4\pi\int_0^\infty|\psi(\mathbf{r})|^2 r^2 dr = 4\pi\int_0^\infty|\phi(\rho,z)|^2 dr = 1 \ .$$

45.3.4.3 Ex: Interacting gas in a cylindrical potential

Consider the potential $V(\mathbf{r}) = V(\rho, z)$, such that the wavefunction will have rotational symmetry, $\psi(\rho, z, \varphi) = \frac{\phi(\rho,z)}{\rho}$. Rewrite the Gross-Pitaevskii equation for the function ϕ [626].

Solution: *The Gross-Pitaevskii equation is,*

$$i\hbar\frac{\partial}{\partial t}\frac{\phi(\rho,z)}{\rho} = \left(-\frac{\hbar^2}{2m}\left[\frac{1}{\rho}\frac{\partial}{\partial\rho}\left(\rho\frac{\partial}{\partial\rho}\right) + \frac{1}{\rho^2}\frac{\partial^2}{\partial\varphi^2} + \frac{\partial^2}{\partial z^2}\right] + V_{trap}(\rho,z) + g\left|\frac{\phi(\rho,z)}{\rho}\right|^2\right)\frac{\phi(\rho,z)}{\rho}$$

$$i\hbar\frac{\partial\phi(\rho,z)}{\partial t} = -\frac{\hbar^2}{2m}\left[\frac{\partial^2}{\partial\rho^2} - \frac{1}{\rho}\frac{\partial}{\partial\rho} + \frac{1}{\rho^2} + \frac{\partial^2}{\partial z^2}\right]\phi(\rho,z) + V_{trap}(\rho,z)\phi(\rho,z) + g\frac{|\phi(\rho,z)|^2}{\rho^2}\phi(\rho,z) \ .$$

Often we have a harmonic trap at least in the radial direction, $\rho_1 \equiv \rho/a_\rho$. An appropriate scale is then,

$$\imath\frac{\partial\phi(\rho,z)}{\partial\omega_\rho t} = -\frac{1}{2}\left[\frac{\partial^2}{\partial\rho_1^2} - \frac{1}{\rho_1}\frac{\partial}{\partial\rho_1} + \frac{1}{\rho_1^2} + \frac{\partial^2}{\partial(z/a_\rho)^2}\right]\phi(\rho,z) + \frac{V_{trap}(\rho,z)}{\hbar\omega_\rho}\phi(\rho,z) + \frac{4\pi\hbar a_s|\phi(\rho,z)|^2}{\rho_1^2}\phi(\rho,z) \ ,$$

with

$$\int|\psi(\mathbf{r})|^2 d^3r = 2\pi\int_{-\infty}^{\infty}\int_0^{\infty}|\psi(\mathbf{r})|^2\rho d\rho dz = 2\pi\int_{-\infty}^{\infty}\int_0^{\infty}\frac{|\phi(\rho,z)|^2}{\rho}d\rho dz = 1 \ .$$

45.3.4.4 Ex: Collapse of condensate with attractive interactions

A Bose-Einstein condensate of ^{7}Li may become unstable due to attractive interatomic forces, the scattering length being $a_s = -27.3a_B$. Consider the radial Gross-Pitaevskii Hamiltonian with an external harmonic potential with the oscillation frequency $\omega_{trp}/(2\pi) = 50$ Hz. Using the variational method, determine the maximum number of atoms allowing for a stable condensate. (Note that the derived minimization condition must be evaluated numerically.)

Solution: *We want to minimize the radial Gross-Pitaevskii Hamiltonian,*

$$\hat{H}_\alpha = -\frac{\hbar^2}{2m}\frac{d^2}{dr^2} + \frac{m}{2}\omega^2 r^2 + \frac{g|\phi_\alpha(r)|^2}{r^2} \ ,$$

with $\psi_\alpha(\mathbf{r}) = \frac{\phi_\alpha(r)}{r}$ e $g = N\frac{4\pi\hbar^2 a_s}{m}$ making the ansatz $\psi_\alpha(\mathbf{r}) = Ae^{-\alpha r^2}$. Normalization requires,

$$1 = \langle\psi_\alpha|\psi_\alpha\rangle = 4\pi\int_0^{\infty}|\psi_\alpha(\mathbf{r})|^2 r^2 dr = 4\pi\int_0^{\infty}|\phi_\alpha(r)|^2 dr = 4\pi\int_0^{\infty}A^2 e^{-2\alpha r^2}r^2 dr = A^2\sqrt{\frac{\pi}{2\alpha}}^3 \ .$$

Hence, $A^2 = \sqrt{2\alpha/\pi}^3$. The ground state energy is now,

$$\begin{aligned}
\mu_\alpha &= \langle\phi_\alpha|\hat{H}_\alpha|\phi_\alpha\rangle = 4\pi\int_0^\infty \phi_\alpha(r)\hat{H}_\alpha\phi_\alpha(r)dr \\
&= 4\pi A^2\int_0^\infty re^{-\alpha r^2}\left[-\tfrac{\hbar^2}{2m}(-6\alpha+4r^2\alpha^2)+\tfrac{m}{2}\omega^2r^2+gA^2e^{-2\alpha r^2}\right]re^{-\alpha r^2}dr \\
&= \tfrac{4\pi A^2}{\alpha\sqrt{\alpha}}\tfrac{6\hbar^2\alpha}{2m}\int_0^\infty\zeta^2e^{-2\zeta^2}d\zeta+\tfrac{4\pi A^2}{\alpha^2\sqrt{\alpha}}\left(-\tfrac{4\hbar^2\alpha^2}{2m}+\tfrac{m\omega^2}{2}\right)\int_0^\infty\zeta^4e^{-2\zeta^2}d\zeta+\tfrac{4\pi A^2}{\alpha\sqrt{\alpha}}gA^2\int_0^\infty\zeta^2e^{-4\zeta^2}d\zeta \\
&= \tfrac{4\pi A^2}{\alpha\sqrt{\alpha}}\tfrac{6\hbar^2\alpha}{2m}\tfrac{1}{8}\sqrt{\tfrac{\pi}{2}}+\tfrac{4\pi A^2}{\alpha^2\sqrt{\alpha}}\left(-\tfrac{4\hbar^2\alpha^2}{2m}+\tfrac{m\omega^2}{2}\right)\tfrac{3}{32}\sqrt{\tfrac{\pi}{2}}+\tfrac{4\pi A^2}{\alpha\sqrt{\alpha}}gA^2\tfrac{\sqrt{\pi}}{32} = \tfrac{3\hbar^2\alpha}{2m}+\tfrac{m\omega^2}{2\alpha}+g\left(\tfrac{\alpha}{\pi}\right)^{3/2} .
\end{aligned}$$

Minimizing,

$$0 = \frac{\partial\mu_\alpha}{\partial\alpha} = \frac{\partial}{\partial\alpha}\left[\frac{3\hbar^2\alpha}{2m}+\frac{m\omega^2}{2\alpha}+g\left(\frac{\alpha}{\pi}\right)^{3/2}\right] = \frac{3\hbar^2\alpha^2-m^2\omega^2+3\pi^{-3/2}g\alpha^{\frac{5}{2}}m}{2m\alpha^2}$$

we obtain,

$$0 = 3\hbar^2\alpha^2-m^2\omega^2+3\pi^{-3/2}g\alpha^{\frac{5}{2}}m \ .$$

This equation must be evaluated numerically.

45.4 Elementary excitations

The dynamics of Bose-Einstein condensates is usually studied by observing the change of their shape in response to temporal variations in the trapping potential. The simplest variation surely consists in suddenly removing the trapping potential altogether. Consequently, the first experiment performed with a BEC was the study of its ballistic expansion [31, 420, 238] (see Sec. 45.7.1).

On the other hand, the temporal variation of the potential can also be a small oscillatory or pulsed perturbation, for example, a small modification of the amplitude of the trapping field, a displacement or a local anisotropy induced by the dipole force of a laser beam tuned far away from resonance. It is even conceivable to manipulate the self-energy of the condensate or to irradiate electromagnetic waves, which couples internal atomic excitation levels or states of the atomic motion [108, 33, 1241, 674, 883, 1210, 406, 1271, 675, 976, 1240, 501]. The response of the condensate to such small perturbations can be understood by a linearized model of the Gross-Pitaevskii equation, which we will present in the following sections.

45.4.1 Bogolubov spectrum of excitations

To analyze the spectrum of a condensate's response to small perturbations, let us follow Bogolubov's treatment of the time-dependent Gross-Pitaevskii equation [1238]. We start by substituting Eq. (45.20) [405],

$$\hat{\psi}(\mathbf{r},t) \longrightarrow \hat{\psi}(\mathbf{r},t)e^{-\imath\mu t/\hbar} \ , \tag{45.40}$$

which gives us,

$$\left[-\frac{\hbar^2}{2m}\nabla^2+V_{trap}(\mathbf{r})+g|\hat{\psi}(\mathbf{r},t)|^2\right]\hat{\psi}(\mathbf{r},t) = \left[\mu+i\hbar\frac{\partial}{\partial t}\right]\hat{\psi}(\mathbf{r},t) \ . \tag{45.41}$$

The *Bogolubov prescription* now consists in approximating the field operators of the condensate by a sum of the equilibrium wavefunction, which is interpreted as a complex number, and a small perturbation, which conserves its operator character,

$$\hat{\psi}(\mathbf{r},t) \simeq \psi_0(\mathbf{r}) + \delta\hat{\psi}(\mathbf{r},t) \ . \tag{45.42}$$

This treatment assumes that most atoms are condensed, $N - N_0 \ll N_0$, and only a few thermal atoms are left out.

Applying the *Bogolubov transform*,

$$\boxed{\delta\hat{\psi}(\mathbf{r},t) \equiv \sum_{\mathbf{k}} u_{\mathbf{k}}(\mathbf{r})\hat{a}_{\mathbf{k}}(t) + v^*_{\mathbf{k}}(\mathbf{r})\hat{a}_{\mathbf{k}}(t)^\dagger} \ , \tag{45.43}$$

the perturbation is expressed as a superposition of amplitudes for annihilation and creation of non-interacting *quasi-particles*. By inserting this ansatz into the Gross-Pitaevskii equation, we obtain a linear system of equations called *Bogolubov-de Gennes equations*.

45.4.1.1 Semi-classical approximation

To simplify the equations, let us neglect the operator character of the quasi-particle by doing the substitutions,

$$\hat{a}_{\mathbf{k}} \to e^{-\imath\omega_{\mathbf{k}}t} \qquad \text{and} \qquad \hat{a}^\dagger_{\mathbf{k}} \to e^{\imath\omega_{\mathbf{k}}t} \ . \tag{45.44}$$

That is, we insert the ansatz (45.42) with,

$$\delta\hat{\psi}(\mathbf{r},t) \equiv u_{\mathbf{k}}(\mathbf{r})e^{-\imath\omega_{\mathbf{k}}t} + v^*_{\mathbf{k}}(\mathbf{r})e^{\imath\omega_{\mathbf{k}}t} \ , \tag{45.45}$$

into the Gross-Pitaevskii equation (45.41), we look for the lowest order,

$$\left(-\frac{\hbar^2}{2m}\nabla^2 + V_{trap} + g|\psi_0|^2\right)\psi_0 = \mu\psi_0 \ , \tag{45.46}$$

and we collect the terms of first order in $e^{\pm i\omega_{\mathbf{k}}t}$, neglecting terms of order $u^2_{\mathbf{k}}, v^{*2}_{\mathbf{k}}$ or higher,

$$\begin{aligned} -\frac{\hbar^2}{2m}\nabla^2 u_{\mathbf{k}} + V_{trap}u_{\mathbf{k}} + 2g\psi_0^2 u_{\mathbf{k}} - g\psi_0^2 v^*_{\mathbf{k}} &= \mu u_{\mathbf{k}} + \hbar\omega_{\mathbf{k}}u_{\mathbf{k}} \\ \frac{\hbar^2}{2m}\nabla^2 v_{\mathbf{k}} - V_{trap}v_{\mathbf{k}} - 2g\psi_0^2 v_{\mathbf{k}} + g\psi_0^2 u^*_{\mathbf{k}} &= -\mu v_{\mathbf{k}} + \hbar\omega_{\mathbf{k}}v_{\mathbf{k}} \ . \end{aligned} \tag{45.47}$$

Introducing the abbreviations $n = \psi_0^2$ and,

$$\mathcal{L} \equiv \frac{-\hbar^2\nabla^2}{2m} + V_{trap} + 2gn - \mu \ , \tag{45.48}$$

we can write

$$\begin{pmatrix} \mathcal{L} - \hbar\omega_{\mathbf{k}} & gn \\ gn & \mathcal{L} + \hbar\omega_{\mathbf{k}} \end{pmatrix} \begin{pmatrix} u_{\mathbf{k}} \\ v_{\mathbf{k}} \end{pmatrix} = \left[\begin{pmatrix} \mathcal{L} & gn \\ gn & \mathcal{L} \end{pmatrix} - \hbar\omega_{\mathbf{k}}\hat{\sigma}_z \right] \phi_k = 0 \ , \tag{45.49}$$

with $\hat{\sigma}_z$ being the third Pauli matrix. The solution of Eq. (45.49) is given by the requirement, that the determinant of the matrix be 0,

$$\hbar\omega_{\mathbf{k}} = \sqrt{\mathcal{L}^2 - (gn)^2} \ . \tag{45.50}$$

The object

$$\phi_{\mathbf{k}} \equiv \begin{pmatrix} u_k(\mathbf{r}) \\ v_k(\mathbf{r}) \end{pmatrix} \tag{45.51}$$

is called a *normal mode* of the condensate. The normal modes (45.50) are orthonormal,

$$\langle \phi_{\mathbf{k}} | \phi_{\mathbf{k}'} \rangle = \int d\mathbf{r} \phi^\dagger_{\mathbf{k}}(\mathbf{r}) \hat{\sigma}_z \phi_{\mathbf{k}'}(\mathbf{r}) = \delta_{\mathbf{k},\mathbf{k}'} \ , \tag{45.52}$$

which means that *the modes do not interact*, that is, the quasi-particles *do not collide*.

For homogeneous systems or at the interior of a large condensate with strong interactions, we can assume that the potential is approximately constant, $V_{trap} \to 0$, and kinetic energy negligible compared to the self-energy, and Eq. (45.41) shows us, $\mu \to gn$. Assuming plane waves,

$$u_{\mathbf{k}}(\mathbf{r}) \equiv u e^{\imath \mathbf{k}\cdot\mathbf{r}} \qquad \text{and} \qquad v_{\mathbf{k}}(\mathbf{r}) \equiv v e^{\imath \mathbf{k}\cdot\mathbf{r}} \ , \tag{45.53}$$

we obtain the *Bogolubov spectrum* of elementary excitations,

$$\boxed{\hbar\omega_{\mathbf{k}} = \sqrt{\frac{\hbar^2\mathbf{k}^2}{2m}\left(\frac{\hbar^2\mathbf{k}^2}{2m} + 2\mu\right)}} \ . \tag{45.54}$$

which corresponds to a *dispersion relation* for Bose-Einstein condensates. For an interacting gas, the collective modes are distortions of the condensate, caused by restoring forces originating in the finite compressibility of the gas.

45.4.1.2 Phonon- and particle-like excitations

The coefficients u and v describe the annihilation and u^* and v^* the creation of *quasi-particle*s called *fonon*s or *elementary excitation*s. Two limits are interesting. In the low energy limit, $\frac{\hbar^2\mathbf{k}^2}{2m} \ll gn(\mathbf{r})$, we create *phonon-like excitation*s. The Bogolubov spectrum becomes,

$$\hbar\omega^{ph}_{\mathbf{k}} \simeq c_s \hbar k \qquad \text{with} \qquad c_s \equiv \sqrt{\frac{ng}{m}} \ . \tag{45.55}$$

Here is c_s the *sound velocity* inside the condensate. The fact that, comparing (45.54) and (45.55), we find,

$$\hbar\omega_{\mathbf{k}} > \hbar\omega^{ph}_{\mathbf{k}} \tag{45.56}$$

for all $\mathbf{k}$ is the *Landau criterion* for the superfluidity of the condensate. It means that, for an object being dragged through the condensate with a velocity less than c_s, it does not become energetically favorable to produce excitations, see Fig. 45.4. Therefore, the object will move without dissipation, which is an important characteristic of superfluids. Experiments demonstrated this manifestation of superfluidity by slowly

stirring a strongly focused blue-detuned laser through a condensate. We will come back to this in Sec. 46.1.1.

In the high energy limit, $\frac{\hbar^2\mathbf{k}^2}{2m} \gg gn(\mathbf{r})$, we create *particle-like excitations*. The Bogolubov spectrum becomes,

$$\hbar\omega_{\mathbf{k}}^{pa} = \frac{\hbar^2\mathbf{k}^2}{2m} \ . \tag{45.57}$$

In this limit, we recover the quadratic dispersion relation of free particles, as seen in Fig. 45.4.

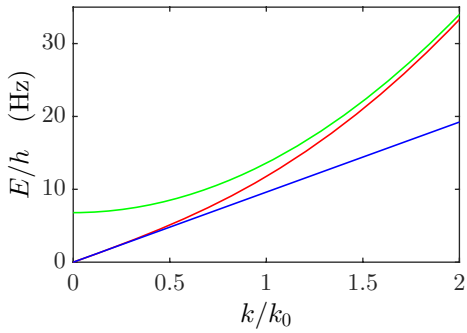

Figure 45.4: (code) Bogolubov spectrum (red), phonon limit (blue line) and particle limit (green line).

Experimentally, the complete Bogolubov spectrum (45.54) can be measured by Bragg spectroscopy [1260, 1239] (see Sec. 47.2). Solve Exc. 45.4.3.1.

45.4.2 Excitation of normal modes

In the simplest case, we generate a perturbation as a weak additional potential in the Gross-Pitaevskii equation (45.41),

$$\left[\mathcal{L} - gn + f_+(\mathbf{r})e^{-\imath\omega_p t} + f_-(\mathbf{r})e^{\imath\omega_p t}\right]\hat{\psi} = i\hbar\frac{\partial}{\partial t}\hat{\psi}(\mathbf{r},t) \ . \tag{45.58}$$

After the Bogolubov transform (45.45) we now have,

$$\left[\begin{pmatrix}\mathcal{L} & gn\\ gn & \mathcal{L}\end{pmatrix} - \hbar\omega_{\mathbf{k}}\sigma_3\right]\begin{pmatrix}u(\mathbf{r})\\ v(\mathbf{r})\end{pmatrix} = -\begin{pmatrix}f_+(\mathbf{r})\psi_0(\mathbf{r})\\ f_-^*(\mathbf{r})\psi_0^*(\mathbf{r})\end{pmatrix} \ . \tag{45.59}$$

The solution of this equation is found by expanding the amplitudes $u(\mathbf{r})$ and $v(\mathbf{r})$ into normal modes,

$$\begin{pmatrix}u(\mathbf{r})\\ v(\mathbf{r})\end{pmatrix} = \sum_{\mathbf{k}} c_{\mathbf{k}}\phi_{\mathbf{k}}(\mathbf{r}) \qquad \text{and} \qquad \begin{pmatrix}f_+(\mathbf{r})\psi_0(\mathbf{r})\\ f_-^*(\mathbf{r})\psi_0^*(\mathbf{r})\end{pmatrix} = \sum_{\mathbf{k}} g_{\mathbf{k}}\phi_{\mathbf{k}}(\mathbf{r}) \ , \tag{45.60}$$

where $g_{\mathbf{k}}$ is given by the overlap integral,

$$g_{\mathbf{k}} = \int d\mathbf{r}\phi_{\mathbf{k}}^\dagger(\mathbf{r})\sigma_3\begin{pmatrix}f_+(\mathbf{r})\psi_0(\mathbf{r})\\ f_-^*(\mathbf{r})\psi_0^*(\mathbf{r})\end{pmatrix} \ . \tag{45.61}$$

To calculate the response of the condensate to a given perturbation $f_{\pm}(\mathbf{r})$, we must first calculate the normal mode spectrum $\phi_{\mathbf{k}}(\mathbf{r})$ from the Bogolubov equation (45.49). After that, we can calculate the coefficients (45.61). Inserting the expansions into the Eq. (45.59), we obtain the response of the condensate,

$$\begin{pmatrix} u(\mathbf{r}) \\ v(\mathbf{r}) \end{pmatrix} = -\sum_{\mathbf{k}} \frac{g_{\mathbf{k}}/\hbar}{\omega_{\mathbf{k}} - \omega} \phi_{\mathbf{k}} \ . \tag{45.62}$$

The deviation, which is observed for resonant excitation, is due to the neglected losses and non-linear effects.

45.4.2.1 Classification of normal modes

BECs often have cylindrical symmetry, $\psi(\mathbf{r}) = \psi_0(r, z)$. In this case, similar calculations to those shown above, result in analytical expressions for the frequencies of the elementary excitations. These frequencies were derived by [318] [7]. The modes can be classified by their main quantum numbers n_r and by their multipolar moment ℓ. Examples are the *surface excitation* or *shape oscillation* ($n_r = 0$) and the *compression oscillation* ($n_r \neq 0$). Special cases are called *shaking mode*, *breathing mode* ($n_r = 1, \ell = 0$), and *swirling mode*. In the case of cylindrical symmetry, the projection of the angular momentum onto the symmetry axis m is the relevant quantum number. The dispersion relations are,

$$\begin{aligned}
&\omega(\ell, \mp m = \ell) = |m|\omega_r^2 \\
&\omega(\ell, \mp m = \ell - 1) = |m|\omega_r^2 + \omega_z^2 \\
&\omega(\ell, \mp m = \ell - 2) = \omega_r^2 \left[2|m| + 2 + \tfrac{3}{2}\lambda^2 \mp \sqrt{(|m| + 2 - \tfrac{3}{2}\lambda^2)^2 + 2\lambda^2(|m| + 1)} \right] \\
&\omega(\ell, \mp m = \ell - 3) = \omega_r^2 \left[2|m| + 2 + \tfrac{7}{2}\lambda^2 \mp \sqrt{(|m| + 2 - \tfrac{5}{2}\lambda^2)^2 + 6\lambda^2(|m| + 1)} \right] \ ,
\end{aligned} \tag{45.63}$$

where λ is the aspect ratio $\lambda = \omega_z/\omega_r$. Obviously, higher excitation orders depend on the trap geometry. Moreover, we can easily see, that occasional degeneracies must arise for specific aspect ratios. For example, when $\omega_+(2,0) = 2\omega(2,2)$, we derive from (45.63) the condition $\lambda = \sqrt{16/7}$, and when $\omega_+(2,0) = 2\omega_-(2,0)$, we derive $\lambda = \frac{1}{6}\sqrt{77 + 5\sqrt{145}}$.

45.4.2.2 Quantum depletion

Following Bogolubov's theory the *quantum depletion* is given by,

$$\frac{\delta N}{N} = \frac{1}{N} \sum_{\mathbf{k}} \int d^3r |v_{\mathbf{k}}(\mathbf{r})|^2 \ . \tag{45.64}$$

[7] It is worth mentioning that the linearized theory applies to *small perturbations*. Strong disturbances render the dynamics chaotic, since the energy is coupled to many modes of excitation.

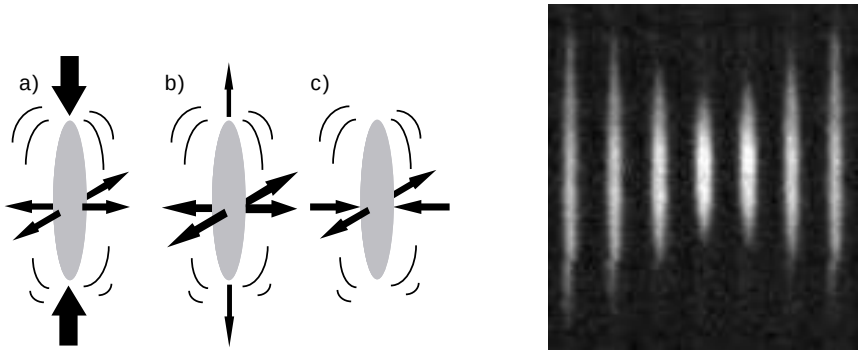

Figure 45.5: Normal modes of a BEC. (a) Shape oscillation, (b) breathing oscillation, and (c) quadrupole oscillation. (d) Non-destructive measurements of quadrupolar vibrations of a BEC [1240].

45.4.2.3 Fluctuations in BECs

Fluctuations in condensates are reduced as compared to thermal ensembles. Non-linearities are always very sensitive to fluctuations (see the laser). Therefore, we have to look at closer at collisions. For 3-body decay in a thermal source, $\langle\rho(\mathbf{r})^3\rangle \sim 6\langle\rho(\mathbf{r})\rangle^3$, and in a coherent source: $\langle\rho(\mathbf{r})^3\rangle \sim \langle\rho(\mathbf{r})\rangle^3$ [217, 1227].

45.4.3 Exercises

45.4.3.1 Ex: Sound velocity in the Thomas-Fermi regime

Consider a condensate of $N = 10^5$ ^{87}Rb atoms confined to an isotropic harmonic potential with secular frequency $\omega_{trp} = (2\pi)\ 50$ Hz. Remember $a_s = 110a_B$ and use the Thomas-Fermi approximation.
a. Evaluate the chemical potential.
b. Calculate the sound velocity at the center of the condensate.

Solution: *a. In the Thomas-Fermi limit the density distribution is given by,*

$$n(\mathbf{r}) = \tfrac{1}{g}\left(\mu - \tfrac{m}{2}\omega_{trp}^2 r^2\right) .$$

Normalization gives,

$$N = \int n(\mathbf{r})d^3r = \tfrac{1}{g}\int_0^{\sqrt{2\mu/m\omega_{trp}^2}} \left(\mu - \tfrac{m}{2}\omega_{trp}^2 r^2\right) 4\pi r^2 dr = \frac{8\pi\mu}{15g}\sqrt{\frac{2\mu}{m\omega_{trp}}} .$$

Hence,

$$\mu = \left(\frac{15Ng}{8\pi}\right)^{2/5}\left(\frac{m}{2}\omega_{trp}^2\right)^{3/5} .$$

This gives $\mu = h \cdot 796$ Hz.
b. The density at the center of the condensate now is,

$$n_0 = \frac{\mu}{g} .$$

The velocity of sound at the center is given by,

$$c_s = \sqrt{\frac{gn_0}{m}} = \sqrt{\frac{\mu}{m}} \ .$$

Hence, we find $c_s = 1.9$ *mm/s.*

45.5 Hydrodynamics and the propagation of sound

The question arises how the elementary excitations relate to the phenomenon of *sound*, well known from the hydrodynamic theory of superfluid ^{4}He proposed by Landau [772]. The *hydrodynamic regime* is characterized by the dominance of collisions [8]. On the other hand, Bogolubov's theory describes elementary excitations in the *collisionless regime*, where *quasi-particles* do not interact [9]. There is, therefore, a great motivation to study excitations with condensates in a very dense regime, where one can expect to recover predictions of hydrodynamic theory.

The hydrodynamic regime is reached, when the *free path* of the particles is smaller than the wavelength of the sound, that is [10],

$$l_{mfp} < \lambda/2\pi \ . \tag{45.65}$$

45.5.1 Zero, first and second sound

The occurrence of several types of sound was related by Tisza and London to the existence of superfluid and normal components in ^{4}He [954]. The *second sound* is a quantum phenomenon, where the heat transfer occurs as an *wave-like motion* instead of being diffusive. Heat takes the place of pressure in normal sound waves called *first sound*. This induces a very high thermal conductivity. At temperatures below the λ-point, ^{4}He has the highest known conductivity of all materials (a few hundred times higher than copper).

The *zero sound* was introduced by Landau to name quantum vibrations in Fermi quantum liquids. This sound can not be seen as a simple wave of compression and rarefaction. In gaseous condensates, the zero sound corresponds to the elementary excitation called *phonon-like*.

Finally, the excitation called *particle-like* or *ballistic*, observed in gaseous condensates has no correspondence in dense superfluids, since the mean free path there is too short. The various regimes accessible in condensed gasses are listed in the following table [33, 35, 544, 704, 1198, 1241, 1240, 456]:

[8] Collisions prevent condensation, because they localize the particles. This is the reason for the large quantum depletion, which in ^{4}He is of the order of 10% and hides effects of quantum statistics. Quantum depletion prevents any form of long-range order, as this requires delocalization.

[9] Bogolubov's theory assumes that the only impact of collisions is to deform the dispersion relationship, keeping the collective modes orthogonal.

[10] Note the similarity to the Ioffe-Regel criterion.

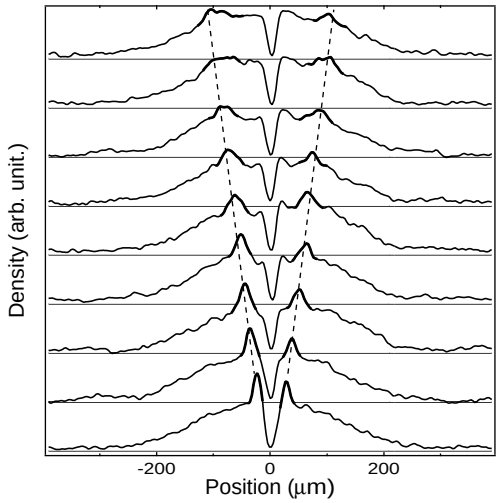

Figure 45.6: (code) Consecutive measurements of the BEC density profile showing the propagation of zero sound. The sound was excited by a blue-detuned laser tuned focused into the middle of the BEC (lower curve). The other curves show how the perturbation propagates towards the edges of the BEC.

regime	range scale	energy range	condensate	thermal cloud
collision-less	$k^{-1} < \xi < l_{mfp}$	$\frac{\hbar^2}{2ml^2_{mfp}} < gn_0 < \frac{\hbar^2 k^2}{2m}$	ballistic	ballistic
collision-less	$\xi < k^{-1} < l_{mfp}$	$\frac{\hbar^2}{2ml^2_{mfp}} < \frac{\hbar^2 k^2}{2m} < gn_0$	zero sound	ballistic
hydrodynamic	$\xi < l_{mfp} < k^{-1}$	$\frac{\hbar^2 k^2}{2m} < \frac{\hbar^2}{2ml^2_{mfp}} < gn_0$	second sound	first sound

(45.66)

normal modes			$qR \ll 1$
macroscopic			$qa \ll 1$
beyond Bogolubov			$qa > 1$
superfluid (TF limit, LDA)	$E_{self} \gg E_{kin}$	$8\pi Na \gg a_{ho}$	$a_{ho} \gg \xi$
???	$E_{self} \ll E_{kin}$	$8\pi Na \ll a_{ho}$	$a_{ho} \ll \xi$
collision-less	$\gamma_{coll} \ll \frac{\hbar q^2}{2m}$		$ql_{mfp} \ll 1$
hydrodynamic	$\gamma_{coll} > \frac{\hbar q^2}{2m}$		$ql_{mfp} > 1$

(45.67)

With $l_{mfp} \simeq 1/n_{th}\sigma$. Typical values are,

$$\begin{array}{ll} a = 0..1000 a_B & = 0..50\,\text{nm} \\ n^{-1/3} & = 20..200\,\mu\text{m} \\ 2\pi/q & = 0.2..\infty\,\mu\text{m} \\ \xi = \sqrt{8\pi n a}^{-1} & = 0.03..30\,\mu\text{m} \\ a_{ho} = \sqrt{\hbar/m\omega_{tr}} & = 0.1..3\,\mu\text{m} \\ 2\pi/k_F = 2\pi a_{ho}(48N)^{-1/6} & = 30..70\,\mu\text{m} \end{array} \tag{45.68}$$

The various regimes of sound are distinguished by frequency shifts and damping rates of the collective modes, which depend on the density (determining the mean-field energy and the mean free path) and the temperature (controlling the ratio between condensed and normal fraction). The quantity

$$\xi \equiv \frac{1}{\sqrt{8\pi a_s n}} \,, \tag{45.69}$$

is called *healing length*.

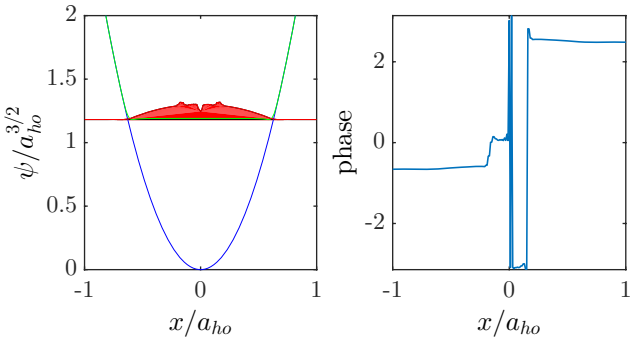

Figure 45.7: Simulation of the propagation of sound toward the edges of the condensate.

45.6 Momentum representation

We showed in Sec. 23.3.7, that the wavefunctions can be represented in the spatial or the momentum domain. These notions can be extended to the second quantization procedure by generalizing the equations (23.104),

$$\boxed{\hat{a}_{\mathbf{k}} \equiv \frac{1}{\sqrt{(2\pi)^3 V}} \int \hat{\psi}(\mathbf{r}) e^{-\imath \mathbf{k}\cdot\mathbf{r}} d^3 r \quad , \quad \hat{\psi}(\mathbf{r}) \equiv \sqrt{\frac{V}{(2\pi)^3}} \int \hat{a}_{\mathbf{k}} e^{\imath \mathbf{k}\cdot\mathbf{r}} d^3 k} \,. \tag{45.70}$$

Differently from (23.104) we chose here a normalization, which leaves the field operators $a_{\mathbf{k}}$ without unit.

45.6.1 Confined particles

In the case of confined atoms, $\mathcal{H} = \mathcal{H}_{cm} + V_{trap}(\mathbf{r}) + \mathcal{H}_{self}$, we get sharp eigenvalues,

$$\hat{a}_{\mathbf{k}} = \frac{1}{V} \sum_{\mathbf{k}'} \hat{a}_{\mathbf{k}'} \delta^{(3)}(\mathbf{k} - \mathbf{k}') \ . \tag{45.71}$$

We insert this in equation (45.70),

$$\begin{aligned} \hat{\psi}(\mathbf{r}) &= \sqrt{\tfrac{1}{(2\pi)^3 V}} \sum_{\mathbf{k}'} \hat{a}_{\mathbf{k}'} \int \delta^{(3)}(\mathbf{k} - \mathbf{k}') e^{\imath \mathbf{k}\cdot\mathbf{r}} d^3k \\ &= \sqrt{\tfrac{1}{(2\pi)^3 V}} \sum_{\mathbf{k}'} \hat{a}_{\mathbf{k}} e^{\imath \mathbf{k}\cdot\mathbf{r}} = \sum_{\mathbf{k}} u_{\mathbf{k}}(\mathbf{r}) \hat{a}_{\mathbf{k}} \ , \end{aligned} \tag{45.72}$$

thus making an expansion of the condensate into plane waves,

$$u_{\mathbf{k}}(\mathbf{r}) = \tfrac{1}{\sqrt{(2\pi)^3 V}} e^{\imath \mathbf{k}\cdot\mathbf{r}} \ , \tag{45.73}$$

which is particularly adapted to the 3D box potential, $V_{trap}(\mathbf{r}) \equiv \infty$ se $r > R$. Also, we calculate,

$$\hat{a}_{\mathbf{k}} = \sqrt{\tfrac{1}{(2\pi)^3 V}} \int \hat{\psi}(\mathbf{r}) e^{-\imath \mathbf{k}\cdot\mathbf{r}} d^3r = \int \hat{\psi}(\mathbf{r}) u^*_{\mathbf{k}}(\mathbf{r}) d^3\mathbf{r} \ . \tag{45.74}$$

We obtain the observable commutation rules from (45.5),

$$[\hat{a}_{\mathbf{k}}, \hat{a}^\dagger_{\mathbf{k}'}] = \delta_{\mathbf{k}\mathbf{k}'} \quad , \quad [\hat{a}_{\mathbf{k}}, \hat{a}_{\mathbf{k}'}] = 0 \quad , \quad \hat{N} = \sum_{\mathbf{k}} \hat{a}^\dagger_{\mathbf{k}} \hat{a}_{\mathbf{k}} \ . \tag{45.75}$$

Using the following mathematical relationships,

$$\tfrac{1}{(2\pi)^3 V} \sum_{\mathbf{k}} e^{-\imath \mathbf{k}\cdot(\mathbf{r}-\mathbf{r}')} = \delta^3(\mathbf{r} - \mathbf{r}') \quad \text{and} \quad \tfrac{1}{(2\pi)^3 V} \int d^3\mathbf{r} e^{\imath(\mathbf{k}'-\mathbf{k})\cdot\mathbf{r}} = \delta_{\mathbf{k},\mathbf{k}'} \ , \tag{45.76}$$

and easy to show for plane waves,

$$\sum_{\mathbf{k}} u^*_{\mathbf{k}}(\mathbf{r}) u_{\mathbf{k}}(\mathbf{r}') = \delta^3(\mathbf{r} - \mathbf{r}') \quad \text{and} \quad \int u^*_{\mathbf{k}}(\mathbf{r}) u_{\mathbf{k}'}(\mathbf{r}) d^3\mathbf{r} = \delta_{\mathbf{k}\mathbf{k}'} \ . \tag{45.77}$$

In Exc. 45.6.4.1 we will check the validity of the commutation rules (45.75), and in Exc. 45.6.4.2 we derive the following representation of the Hamiltonian:

$$\boxed{\begin{aligned} \mathcal{H} &= \int d^3r \hat{\psi}^\dagger(\mathbf{r}) \left(-\frac{\hbar^2}{2m} \nabla^2 + V_{trap}(\mathbf{r}) \right) \hat{\psi}(\mathbf{r}) \\ &\quad + \frac{g}{2} \int d^3r \int d^3r' \hat{\psi}^\dagger(\mathbf{r}) \hat{\psi}^\dagger(\mathbf{r}') \delta(\mathbf{r} - \mathbf{r}') \hat{\psi}(\mathbf{r}') \hat{\psi}(\mathbf{r}) \\ &= \sum_{\mathbf{k}} \frac{\hbar^2 \mathbf{k}^2}{2m} \hat{a}^\dagger_{\mathbf{k}} \hat{a}_{\mathbf{k}} + \sum_{\mathbf{k},\mathbf{k}'} \hat{a}^\dagger_{\mathbf{k}} V_{\mathbf{k},\mathbf{k}'} \hat{a}_{\mathbf{k}'} + \frac{g}{2} \sum_{\mathbf{k},\mathbf{k}',\mathbf{k}''} \hat{a}^\dagger_{\mathbf{k}} \hat{a}^\dagger_{\mathbf{k}'} \hat{a}_{\mathbf{k}''} \hat{a}_{\mathbf{k}+\mathbf{k}'-\mathbf{k}''} \end{aligned}} \ , \tag{45.78}$$

with the abbreviation,

$$V_{\mathbf{k},\mathbf{k}'} = \int u^*_{\mathbf{k}}(\mathbf{r}) V_{trap}(\mathbf{r}) u_{\mathbf{k}'}(\mathbf{r}) d^3\mathbf{r} = \tfrac{1}{(2\pi)^3} \int V_{trap}(\mathbf{r}) e^{\imath(\mathbf{k}'-\mathbf{k})\mathbf{r}} d^3\mathbf{r} \ . \tag{45.79}$$

The equation of motion for the momentum wavefunction now becomes,

$$\imath\hbar \frac{\partial}{\partial t} \hat{a}_{\mathbf{k}} = [\hat{a}_{\mathbf{k}}, \mathcal{H}] = \frac{\hbar^2 \mathbf{k}^2}{2m} \hat{a}_{\mathbf{k}} + \sum_{\mathbf{k}'} V_{\mathbf{k},\mathbf{k}'} \hat{a}_{\mathbf{k}'} + g \sum_{\mathbf{k}',\mathbf{k}''} \hat{a}^\dagger_{\mathbf{k}'} \hat{a}_{\mathbf{k}''} \hat{a}_{\mathbf{k}+\mathbf{k}'-\mathbf{k}''} \ . \tag{45.80}$$

45.6.1.1 Harmonically confined particles

In harmonic traps, $V_{trap}(r) = \frac{m}{2}\omega^2_{trp} r^2$, the motion can be canonically quantized,

$$\hat{a} = \frac{1}{\sqrt{2}} \left(\frac{\hat{r}}{a_{trp}} \mp i a_{trp} \hat{p} \right) \qquad , \qquad \mathcal{H}_{cm} = \sum_{\mathbf{k}} \hbar\omega_{trp} \hat{a}^\dagger_{\mathbf{k}} \hat{a}_{\mathbf{k}} \ , \tag{45.81}$$

with the size of the ground state,

$$a_{trp} \equiv \sqrt{\frac{\hbar}{m\omega_{trp}}} \ . \tag{45.82}$$

As an alternative notation we could introduce,

$$|\mathbf{r}\rangle \equiv \hat{\psi}^\dagger(\mathbf{r}) \qquad \text{and} \qquad |\mathbf{k}\rangle \equiv \hat{a}^\dagger_{\mathbf{k}} \ . \tag{45.83}$$

Hence, just considering the ground state of the trap, that is, assuming that the atomic motion be frozen, our Hamiltonian becomes:

$$\mathcal{H}_{cm} + \mathcal{H}_{self} = \hbar\omega_{trp} \hat{a}^\dagger \hat{a} + \frac{g}{2} \hat{a}^\dagger \hat{a}^\dagger \hat{a} \hat{a} \ . \tag{45.84}$$

45.6.2 Thomas-Fermi limit

In the limit of negligible kinetic energy (that is, in the middle of a large condensate) with the analytical form of the condensate wavefunction,

$$\hat{\psi}(\mathbf{r}) \propto \sqrt{n_0} \left(1 - \frac{\mathbf{r}^2}{\mathbf{r}_0^2} \right) \ , \tag{45.85}$$

the transformation (45.70) allows us to derive an expression for the momentum distribution,

$$|a(\mathbf{k})| \propto \frac{J_1(\mathbf{k} \cdot \mathbf{r}_0)}{(\mathbf{k} \cdot \mathbf{r}_0)^2} \ . \tag{45.86}$$

45.6.2.1 Width of the momentum distribution

It is interesting to compare the size of an ideal gas condensate with the size of an interacting condensate. We can express the Thomas-Fermi radius as,

$$\Delta r_{TF} = a_{trp} \sqrt{\frac{\mu}{\hbar\omega_{trp}}} \ . \tag{45.87}$$

The Heisenberg limit requires,

$$\Delta p_{TF} = \frac{\hbar}{\Delta r_{TF}} \ . \tag{45.88}$$

Since $\sqrt{\mu/\hbar\omega_{trp}} > 1$, the interaction increases the volume of the condensate, but restricts the distribution of its velocities. For a hypothetical thermal Boltzmann gas having the same temperature,

$$\Delta r_{th} = a_{trp}\sqrt{\frac{k_B T}{\hbar\omega_{trp}}} \qquad \text{and} \qquad \Delta p_{th} = \frac{\hbar}{a_{trp}}\sqrt{\frac{k_B T}{\hbar\omega_{trp}}} \ . \tag{45.89}$$

The thermal cloud *is not at the Heisenberg limit*, because $\sqrt{k_B T/\hbar\omega_{trp}} > 1$.

These relationships were experimentally confirmed [1260] by measurements of the velocity distributions of condensates using a Bragg spectroscopy technique (see Sec. 47.2). It is interesting to note that the measured widths of velocity distributions were *lower than the photonic recoil limit*, $\hbar k/m \simeq 30$ mm/s for ^{87}Rb.

45.6.3 Master equation approach

The Hamiltonian that describes a BEC in second quantization in an orthonormal set of energy eigenfunctions reads:

$$\begin{aligned} \mathcal{H} &= \sum\nolimits_{i,j} \mathcal{H}^{(ij)}_{atom} \hat{a}^\dagger_i \hat{a}_j + \sum_{i,j,k,l} \tfrac{1}{2} W^{(ijkl)} \hat{a}^\dagger_i \hat{a}^\dagger_j \hat{a}_k \hat{a}_l \\ \mathcal{H}^{(ij)}_{atom} &= \langle \phi_i | \tfrac{1}{2m}\mathbf{p}^2 + V_{trap}(\mathbf{r}) | \phi_j \rangle \\ W^{(ijkl)} &= g \int \phi_i(\mathbf{r})\phi_j(\mathbf{r})\phi_k(\mathbf{r})\phi_l(\mathbf{r}) d^3 r \ . \end{aligned} \tag{45.90}$$

The inclusion of spontaneous processes (one-body-loss, dephasing) requires a master equation including a *Lindblad term* within a density matrix formalism. The von Neumann equation for the density operator reads:

$$\begin{aligned} \frac{d}{dt}\hat{\rho} &= -\imath[V, \hat{\rho}] + \mathcal{L}\hat{\rho} \\ \mathcal{L}_{one-body\ loss} &\equiv \kappa(2\hat{a}\hat{\rho}\hat{a}^\dagger - \hat{a}^\dagger\hat{a}\hat{\rho} - \hat{\rho}\hat{a}^\dagger\hat{a}) \\ \mathcal{L}_{one-body\ feeding} &\equiv \kappa(2 + 2\hat{a}^\dagger\hat{\rho}\hat{a} - \hat{a}\hat{a}^\dagger\hat{\rho} - \hat{\rho}\hat{a}\hat{a}^\dagger) \\ \mathcal{L}_{two-body\ loss} &\equiv \kappa\left(2\hat{a}^2\hat{\rho}\hat{a}^{\dagger 2} - \hat{a}^{\dagger 2}\hat{a}^2\hat{\rho} - \hat{\rho}\hat{a}^{\dagger 2}\hat{a}^2\right) \ . \end{aligned} \tag{45.91}$$

45.6.4 Exercises

45.6.4.1 Ex: Commutators in momentum space

Demonstrate the validity of the commutation rules (45.75).

Solution: *It holds,*

$$\delta^3(\mathbf{r}-\mathbf{r}') = [\hat{\psi}(\mathbf{r}), \hat{\psi}^\dagger(\mathbf{r}')] = \tfrac{1}{(2\pi)^3 V} \sum_{\mathbf{k},\mathbf{k}'} e^{-\imath\mathbf{k}\cdot\mathbf{r}+\imath\mathbf{k}'\cdot\mathbf{r}'} [\hat{a}_{\mathbf{k}}, \hat{a}^\dagger_{\mathbf{k}'}] = \tfrac{1}{(2\pi)^3 V} \sum_{\mathbf{k},\mathbf{k}'} e^{-\imath\mathbf{k}\cdot\mathbf{r}+i\mathbf{k}'\cdot\mathbf{r}'} [\hat{a}_{\mathbf{k}}, \hat{a}^\dagger_{\mathbf{k}'}] \ .$$

This is valid when $[\hat{a}_{\mathbf{k}}, \hat{a}^\dagger_{\mathbf{k}'}] = \delta_{\mathbf{k},\mathbf{k}'}$. *Also holds,*

$$0 = [\hat{\psi}(\mathbf{r}), \hat{\psi}(\mathbf{r}')] = \tfrac{1}{(2\pi)^3 V} \sum_{\mathbf{k},\mathbf{k}'} e^{\imath \mathbf{k}\cdot\mathbf{r} + \imath \mathbf{k}'\cdot\mathbf{r}'} [\hat{a}_{\mathbf{k}}, \hat{a}_{\mathbf{k}'}] = \tfrac{1}{(2\pi)^3 V} \sum_{\mathbf{k},\mathbf{k}'} e^{\imath \mathbf{k}\cdot\mathbf{r} + \imath \mathbf{k}'\cdot\mathbf{r}'} [\hat{a}_{\mathbf{k}}, \hat{a}_{\mathbf{k}'}] \ ,$$

This is valid when $[\hat{a}_{\mathbf{k}}, \hat{a}^\dagger_{\mathbf{k}'}] = 0$. *We can also express,*

$$\hat{N} = \int d^3\mathbf{r} \hat{\psi}^\dagger(\mathbf{r}) \hat{\psi}(\mathbf{r}) = \tfrac{1}{(2\pi)^3 V} \sum_{\mathbf{k},\mathbf{k}'} \int d^3\mathbf{r} e^{\imath(\mathbf{k}-\mathbf{k}')\cdot\mathbf{r}} \hat{a}^\dagger_{\mathbf{k}'} \hat{a}_{\mathbf{k}} = \sum_{\mathbf{k},\mathbf{k}'} \hat{a}^\dagger_{\mathbf{k}'} \hat{a}_{\mathbf{k}} \delta_{\mathbf{k},\mathbf{k}'} = \sum_{\mathbf{k}} \hat{a}^\dagger_{\mathbf{k}} \hat{a}_{\mathbf{k}} \ .$$

45.6.4.2 Ex: Commutators in momentum space

Derive the representation (45.78) of the Hamiltonian.

Solution: *The energy can also be calculated by,*

$$\begin{aligned}
\mathcal{H} &= \int d^3\mathbf{r} \hat{\psi}^\dagger(\mathbf{r}) \left(-\frac{\hbar^2}{2m} \nabla^2 + V_{trap}(\mathbf{r}) \right) \hat{\psi}(\mathbf{r}) + \tfrac{g}{2} \int d^3\mathbf{r} \int d^3\mathbf{r}' \hat{\psi}^\dagger(\mathbf{r}) \hat{\psi}^\dagger(\mathbf{r}') \delta(\mathbf{r}-\mathbf{r}') \hat{\psi}(\mathbf{r}') \hat{\psi}(\mathbf{r}) \\
&= ... + \tfrac{g}{2} \int d^3\mathbf{r} \int d^3\mathbf{r}' \sum_{\mathbf{k}} u^*_{\mathbf{k}}(\mathbf{r}) \hat{a}^\dagger_{\mathbf{k}} \sum_{\mathbf{k}} u^*_{\mathbf{k}}(\mathbf{r}') \hat{a}^\dagger_{\mathbf{k}} \delta(\mathbf{r}-\mathbf{r}') \sum_{\mathbf{k}} u_{\mathbf{k}}(\mathbf{r}') \hat{a}_{\mathbf{k}} \sum_{\mathbf{k}} u_{\mathbf{k}}(\mathbf{r}) \hat{a}_{\mathbf{k}} \\
&= ... + \tfrac{g}{2} \sum_{\mathbf{k},\mathbf{k}',\mathbf{k}'',\mathbf{k}'''} \hat{a}^\dagger_{\mathbf{k}} \hat{a}^\dagger_{\mathbf{k}'} \hat{a}_{\mathbf{k}''} \hat{a}_{\mathbf{k}'''} (2\pi)^{-6} \int d^3\mathbf{r} \int d^3\mathbf{r}' e^{-\imath \mathbf{k}\cdot\mathbf{r}} e^{-\imath \mathbf{k}'\mathbf{r}'} \delta(\mathbf{r}-\mathbf{r}') e^{\imath \mathbf{k}''\mathbf{r}'} e^{\imath \mathbf{k}'''\mathbf{r}} \\
&= ... + \tfrac{g}{2} \sum_{\mathbf{k},\mathbf{k}',\mathbf{k}'',\mathbf{k}'''} \hat{a}^\dagger_{\mathbf{k}} \hat{a}^\dagger_{\mathbf{k}'} \hat{a}_{\mathbf{k}''} \hat{a}_{\mathbf{k}'''} (2\pi)^{-6} \int d^3\mathbf{r} e^{-\imath \mathbf{k}\cdot\mathbf{r}} e^{-\imath \mathbf{k}'\mathbf{r}} e^{\imath \mathbf{k}''\mathbf{r}} e^{\imath \mathbf{k}'''\mathbf{r}} \\
&= \sum_{\mathbf{k}} \frac{\hbar^2 \mathbf{k}^2}{2m} \hat{a}^\dagger_{\mathbf{k}} \hat{a}_{\mathbf{k}} + \sum_{\mathbf{k},\mathbf{k}'} \hat{a}^\dagger_{\mathbf{k}} V_{\mathbf{k},\mathbf{k}'} \hat{a}_{\mathbf{k}'} + \frac{g}{2} \sum_{\mathbf{k},\mathbf{k}',\mathbf{k}''} \hat{a}^\dagger_{\mathbf{k}} \hat{a}^\dagger_{\mathbf{k}'} \hat{a}_{\mathbf{k}''} \hat{a}_{\mathbf{k}+\mathbf{k}'-\mathbf{k}''} \ ,
\end{aligned}$$

where we defined,

$$V_{\mathbf{k},\mathbf{k}'} = \int u^*_{\mathbf{k}}(\mathbf{r}) V_{trap}(\mathbf{r}) u_{\mathbf{k}'}(\mathbf{r}) d^3\mathbf{r} = \tfrac{1}{(2\pi)^3} \int V_{trap}(\mathbf{r}) e^{\imath(\mathbf{k}'-\mathbf{k})\mathbf{r}} d^3\mathbf{r} \ .$$

45.7 Condensates at finite temperature

45.7.1 Ballistic expansion of a bosonic gas

As discussed in Sec. 43.6, the atomic density distributions are revealed through their interaction with a laser beam. The problem with imaging a confined condensate is, on the one hand, its very high optical density, which inhibits the penetration of resonant light and, on the other hand, its very small size, which is often below the diffraction limit and prevents its optical resolution. As discussed in Sec. 43.6, both

problems can be avoided by the time-of-flight imaging technique, which consists in quickly switching off the trap and dropping the atomic cloud (see Fig. 43.35). If the switching-off process is fast enough, the potential energy is lost, but in the course of ballistic expansion, the self-energy is transformed into kinetic energy. Both the self-energy transformed to kinetic energy and the inherent initial kinetic energy contribute to blow up the size of the atomic cloud, so that the density rapidly decreases. After a few 10 ms, when the optical density is sufficiently low (on the order of 1), the cloud can be imaged via its absorption of a resonant laser beam. The condensate, which is about 10 times denser than the thermal cloud, has a much larger repulsive self-energy. When the condensate is suddenly released from its trap, its explosion is accelerated by this self-energy, and the acceleration is faster in those directions, where the confining potential was stronger [626, 238]. Therefore, the aspect ratio of the condensate's shape is inverted during the flight time [712, 238]. In contrast, the self-energy of the thermal cloud is relatively insignificant. Therefore, its spatial density after a time of free expansion reflects the pure velocity distribution of the atomic cloud while it was trapped. This allows the interpretation of the spatial distribution of the expanded cloud in terms of a *temperature* of the trapped cloud.

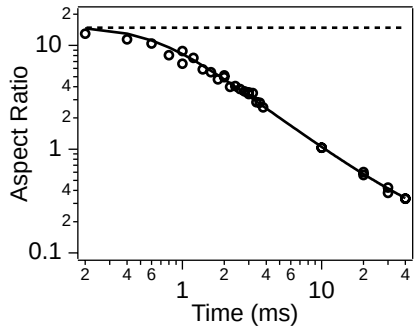

Figure 45.8: Inversion of aspect ratio during time-of-flight. The frequencies of the harmonic trap were $\omega_r = (2\pi) \cdot 248$ Hz and $\omega_r = (2\pi) \cdot 16$ Hz [712].

45.7.1.1 Popov approximation

The Popov decomposition separates the condensed part, described by a c-number $\phi \equiv \langle \hat{\psi} \rangle$ and normalized to the number of condensed atoms N_0 from the thermal part

$\tilde{\psi} \equiv \hat{\psi} - \phi$, which keeps track of the quantum nature of the Bose-gas [380],

$$\begin{aligned}
\mathcal{K} &= \mathcal{K}_0 + \mathcal{K}_1 + \mathcal{K}_1^\dagger + \mathcal{K}_2 \qquad (45.92)\\
\mathcal{K}_0 &= \int d^3\mathbf{r}\phi^*(\mathbf{r}) \left(-\frac{\hbar^2}{2m}\nabla^2 + V_{trap}(\mathbf{r}) + \frac{g}{2}|\phi|^2 - \mu \right) \phi(\mathbf{r})\\
\mathcal{K}_1 &= 0 \quad \text{if} \quad [\mathcal{L} - gn_0(\mathbf{r})]\phi(\mathbf{r}) = 0\\
\mathcal{K}_2 &= \int d^3r \left[\tilde{\psi}^+(\mathbf{r})\mathcal{L}\tilde{\psi}(\mathbf{r}) + \frac{g}{2}\left(\phi(\mathbf{r})^2\tilde{\psi}^+(\mathbf{r})\tilde{\psi}^+(\mathbf{r}) + \phi^*(\mathbf{r})^2\tilde{\psi} + (\mathbf{r})\tilde{\psi}(\mathbf{r}) \right) \right]\\
\mathcal{L} &\equiv -\frac{\hbar^2}{2m}\nabla^2 + V_{trap}(\mathbf{r}) - \mu + 2gn(\mathbf{r})\\
n(\mathbf{r}) &= n_0(\mathbf{r}) + n_T(\mathbf{r}) = |\phi(\mathbf{r})|^2 + \langle \tilde{\psi}^\dagger(\mathbf{r})\tilde{\psi}(\mathbf{r}) \rangle \ .
\end{aligned}$$

We perform the Bogolubov transform to the diagonalized Hamiltonian,

$$\begin{aligned}
\mathcal{K}_{Popov} &= \mathcal{K}_0 + \sum\nolimits_j \varepsilon_j \hat{b}_j^+ \hat{b}_j \qquad (45.93)\\
\tilde{\psi}(\mathbf{r}) &= \sum\nolimits_j u_j(\mathbf{r})\hat{b}_j - v_j^*(\mathbf{r})\hat{b}_j^+\\
\delta_{jk} &= \int d^3r \left(u_j u_k^* - v_j v_k^* \right)\\
\delta_{jk} &= [\hat{b}_j, \hat{b}_k^+] \ .
\end{aligned}$$

This yields a set of equations for elementary excitations (quasi-particle excitations in a diagonalized energy space),

$$\begin{aligned}
N_j &= \left[\exp(\varepsilon_j/k_BT) - 1 \right]^{-1} \qquad (45.94)\\
n_T(\mathbf{r}) &= \sum\nolimits_j \left[\left(|u_j|^2 + |v_j|^2 \right) N_j + |v_j|^2 \right]\\
\mathcal{L}u_j(\mathbf{r}) - gn_0(\mathbf{r})v_j(\mathbf{r}) &= \varepsilon_j u_j(\mathbf{r}) \ ,\\
\mathcal{L}v_j(\mathbf{r}) - gn_0(\mathbf{r})u_j(\mathbf{r}) &= -\varepsilon_j v_j(\mathbf{r}) \ .
\end{aligned}$$

The quantum depletion at $T = 0$ [last term in the density $n(\mathbf{r})$] may be neglected. In this zero-temperature limit, the equations simplify to yield the Gross-Pitaevskii equation. We may separate these equations using auxiliary functions [645],

$$\begin{aligned}
\tilde{\psi}_j^{(\pm)}(\mathbf{r}) &\equiv u_j(\mathbf{r}) \pm v_j(\mathbf{r}) \qquad (45.95)\\
\hat{h}_0 &\equiv \mathcal{L} - gn_0(\mathbf{r})\\
\hat{h}_0\tilde{\psi}_j^{(+)}(\mathbf{r}) &= E_j\tilde{\psi}_j^{(-)}(\mathbf{r}) \ .
\end{aligned}$$

The eigenvalue equations that one gets after substituting (III.2.5) into (III.2.4) may be solved by expanding in a set of eigenfunctions of $\hat{h}_0$:

$$\begin{aligned}
\tilde{\psi}_j^{(\pm)}(\mathbf{r}) &\equiv \sum\nolimits_\alpha c_\alpha^{(j)}\phi_\alpha(\mathbf{r}) \qquad (45.96)\\
\hat{h}_0\phi_\alpha(\mathbf{r}) &\equiv \varepsilon_\alpha\phi_\alpha(\mathbf{r})\\
\sum\nolimits_\beta (M_{\alpha\beta} + \varepsilon_\alpha\delta_{\alpha\beta})\varepsilon_\beta c_\alpha^{(j)} &= E_j^2 c_\alpha^{(j)}\\
M_{\alpha\beta} &= 2g\int \phi_\alpha^*(\mathbf{r})n_0(\mathbf{r})\phi_\beta(\mathbf{r})d^3r \ .
\end{aligned}$$

45.7.2 Hartree-Fock approach

45.7.2.1 Two-gas model for $T > 0$

The two phases of a condensate above $T = 0$ have a specific interdependence, which makes it possible to treat the problem with an approximation, where only the condensed part influences the non-condensed and not vice versa [379]. The HFB equation (III.2.11) is solved for the condensed part alone, assuming $n_{th} = 0$. The condensate wavefunction and the chemical potential are derived from that, *f.e.* using numerical methods like the method of steepest descent. The effective potential for the thermal cloud in the presence of a condensate is:

$$V_{1,eff}(\mathbf{r}_1) = V_{1,trap}(\mathbf{r}_1) + g_1|\psi_1(\mathbf{r}_1)|^2 \ . \tag{45.97}$$

Next, we diagonalize the Schrödinger equation:

$$[-\nabla_1^2 + V_{1,eff}(\mathbf{r}_1)]\psi_{1,j}(\mathbf{r}_1) = 2E_{1,j}\psi_{1,j}(\mathbf{r}_1) \ , \tag{45.98}$$

maintaining the normalization,

$$1 = \int |\psi_{1,j}(\mathbf{r}_1)|^2 d^3\mathbf{r}_1 \ . \tag{45.99}$$

This provides us with the energy eigenvalues of the excited trap states and their eigenfunctions. One can f.e. guess an eigenvalue and numerically solve the Schrödinger equation using Runge-Kutta integration routines. The eigenfunction will probably diverge. In this case, we vary the eigenvalue until the solution converges.

Finally, we can calculate the thermal density distribution:,

$$\begin{aligned} N_j &\equiv [\exp((E_{1,j} - \mu_1)/k_B T_1) - 1]^{-1} \\ n_{th}(\mathbf{r}_1) &= \sum\nolimits_j N_j |\psi_{1,j}(\mathbf{r}_1)|^2 \ , \end{aligned} \tag{45.100}$$

and all thermodynamic potentials, as shown in Sec. 44.1.2.

A more sophisticated method uses self-consistent recursion [645]. Here, the thermal density is plugged back into the HFB equation, and the whole procedure is repeated until it converges.

45.7.2.2 Hartree-Fock approximation

We have already seen that, inside a trap the condensate occupies the lowest vibrational level, whereas the atoms of the thermal gas are distributed among all levels. The trapping potential is often harmonic, $U_{trp}(\mathbf{r}) = \frac{m}{2}\omega_r^2 r^2$, with secular frequencies ω_r typically on the order of several tens or hundreds of Hz. The spatial (radial) extent of the vibration levels varies a lot with their quantum number, $r_j = \sqrt{(2j+1)\hbar/m\omega_r}$. This naturally produces a *separation of the thermal (or normal) and condensate fractions* at $T > 0$, which does not exist for a homogeneous gas and which allows (up to a certain degree) an individual treatment of the two fractions. The details of the interaction between the two fractions are very complicated and are still under intense theoretical investigation. However, to understand the shape of a trapped atomic cloud and other characteristics, we can use a simple approximate model [**?**, 645], assuming

that the condensate is only weakly disturbed by the thermal cloud. In contrast, the presence of the condensate dramatically modifies the potential for the thermal atoms. Therefore, we must *first* calculate the density of the condensate $n_0(\mathbf{r})$, *before* calculating that of the thermal cloud. If this procedure is applied iteratively, it is called *Hartree-Fock method*:

i. We start with $n_{th}(\mathbf{r}) = 0$;

ii. we solve the GPE $\left(-\frac{\hbar^2}{2m}\Delta + V_{trap}(\mathbf{r}) - \mu + g\left[|\psi(\mathbf{r})|^2 + n_{th}(\mathbf{r})\right]\right)\psi(\mathbf{r})$ numerically with the steepest descent method, we derive μ and ψ, and also $n(\mathbf{r}) = |\psi(\mathbf{r})|^2 + n_{th}(\mathbf{r})$;

iii. assuming that collisions between atoms of the thermal cloud, the density of which is weak, can be neglected, we can view the cloud as an ideal gas in a potential modified by the strongly anharmonic mean field of the condensate, $V_{trap}(\mathbf{r}) + 2gn(\mathbf{r})$, we calculate the thermal density $n'_{th}(\mathbf{r}) = \lambda_{dB}^{-3} g_{3/2}\left(\exp\frac{V_{trap}(\mathbf{r})-\mu+2gn(\mathbf{r})}{k_B T}\right)$;

iv. we start over at (ii) using the new thermal density.

We can now calculate the total energy,

$$U = \int d^3r \left(\psi(\mathbf{r})\frac{-\hbar^2\nabla^2}{2m}\psi(\mathbf{r}) + V_{trap}(\mathbf{r})n(\mathbf{r}) + \frac{g}{2}[2n(\mathbf{r})^2 - n_0(\mathbf{r})] + h^{-3}\int d^3k \frac{-\hbar^2k^2}{2m} n(\mathbf{r},\mathbf{k})\right) \tag{45.101}$$

$$= \int d^3\mathbf{r} \left(\psi(\mathbf{r})\frac{-\hbar^2\nabla^2}{2m}\psi(\mathbf{r}) + V_{trap}(\mathbf{r})n(\mathbf{r}) + \frac{g}{2}[2n(\mathbf{r})^2 - n_0(\mathbf{r})] + \frac{3k_BT}{2\lambda_{dB}^3} g_{3/2}\left[\exp\frac{V_{trap}(\mathbf{r})-\mu+2gn(\mathbf{r})}{k_BT}\right]\right)$$

and other thermodynamic quantities.

45.7.3 Ideal gas limit

Consider the ideal gas in an isotropic harmonic potential. The excitation spectrum then takes the form:

$$f(\mathbf{k},\mathbf{r}) = n(\mathbf{k},\mathbf{r}) \tag{45.102}$$
$$\varepsilon_{HF}(\mathbf{k},\mathbf{r}) = \mathcal{L}(\mathbf{k},\mathbf{r}) = \frac{\hbar^2\mathbf{k}^2}{2m} + V(\mathbf{r}) - \mu \ .$$

We can immediately calculate:

$$
\begin{aligned}
g &\longrightarrow 0 \\
\mu &\overset{g\to 0}{\longrightarrow} \tfrac{3}{2}\hbar\omega \\
\phi(\mathbf{r}) &\overset{g\to 0}{\longrightarrow} \tfrac{\sqrt{N_0}}{\pi^{3/4}a_{trap}^{3/2}} \exp(-\frac{\mathbf{r}^2}{2a_{trap}^2}) \\
E_{kin} &= \int \phi(\mathbf{r}) \frac{-\hbar^2\Delta}{2m} \phi(\mathbf{r}) d^3r = -\tfrac{9}{4} N_0 \hbar\omega \\
n_{th}(\mathbf{r}) \overset{g\to 0}{\longrightarrow} \int f(\mathbf{r}\cdot\mathbf{k}) d^3\mathbf{k} &= \frac{1}{\lambda_{dB}^3} g_{3/2}\left[\exp\left(\tfrac{V_{trap}(\mathbf{r})-\mu}{k_B T}\right)\right] \\
N_{th} \overset{g\to 0}{\longrightarrow} \int n_{th}(\mathbf{r}) d^3\mathbf{r} &= \left(\frac{k_B T}{\hbar\omega}\right)^3 g_3\left[\exp\left(\tfrac{\mu}{k_B T}\right)\right] \\
U \overset{g\to 0}{\longrightarrow} \int \varepsilon_{HF} f(\mathbf{r}\cdot\mathbf{k}) d^3\mathbf{r}\cdot\mathbf{d}^3k &= 3k_B T \left(\frac{k_B T}{\hbar\omega}\right)^3 g_4\left[\exp\left(\tfrac{\mu}{k_B T}\right)\right] \ .
\end{aligned}
\tag{45.103}
$$

45.7.4 Exercises

45.7.4.1 Ex: Ballistic expansion of a condensate

Calculate the ballistic expansion of a ^{87}Rb BEC initially confined in a cylindrically symmetric trap with secular frequencies $\omega_z = 20\,\text{Hz}$ and $\omega_r = 100\,\text{Hz}$.

Solution: *The result is shown in Fig. 45.9.*

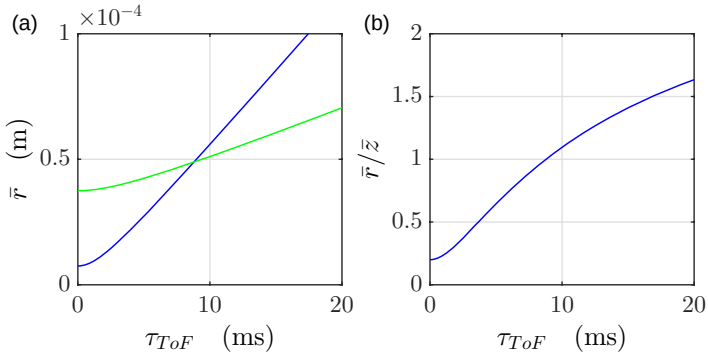

Figure 45.9: (code) Ballistic expansion of a condensate.

45.8 Numerical simulations of the Gross-Pitaevskii equation

To simulate the one-dimensional evolution of a wavepacket following the Gross-Pitaevskii equation,

$$\imath\hbar\frac{\partial}{\partial t}\psi(z,t) = \left[\frac{-\hbar^2}{2m}\frac{d^2}{dz^2} + V_{trap}(z) + |\psi(z,t)|^2\right]\psi(z,t) \ . \tag{45.104}$$

we solve iteratively [1046],

$$\psi(z,t+dt) = \psi(z,t) + dt\dot{\psi}(z,t) \ . \tag{45.105}$$

As initial state we choose, $\psi(z,0) = e^{-z^2/2\bar{z}^2}e^{\imath kz}$, where $k \equiv \sqrt{2mE}/\hbar$ is the wavevector.

The numerical propagation is conveniently performed using the *time-splitting spectral algorithm* [85, 84, 83, 486], which can be easily extended to two dimensions.

45.8.1 Crank-Nicholson-Crout algorithm

45.8.1.1 Crank-Nicholson-Crout algorithm for the time-dependent Schrödinger equation

The *Crank-Nicholson algorithm* goes as follows. The time-dependent Schrödinger equation in one dimension,

$$\frac{\partial}{\partial t}\psi(x,t) = \frac{\imath\hbar}{2m}\frac{\partial^2}{\partial x^2}\psi(x,t) - \frac{\imath V(x)}{\hbar}\psi(x,t) \tag{45.106}$$

is a parabolic partial differential equation. We usually seek a solution on an interval $x \in [a,b]$ and $t > 0$. The solution is uniquely determined from boundary conditions: $\psi(a,t) = \psi(b,t) = 0$ and $\psi(x,0) = g(x)$. One method for numerical solution solves for the values of the wavefunction on a regular grid of dimension $h = (b-a)/N_x$ in x and τ in t:,

$$\psi_j^k = \psi(a+jh, k\tau) \ . \tag{45.107}$$

The derivatives are replaced by simple finite differences. The r.h.s. of the equation at the grid point (i,j) is then,

$$\frac{\imath\hbar}{2mh^2}\left(\psi_{j+1}^k - 2\psi_j^k + \psi_{j-1}^k\right) - \frac{iV(a+jh)}{\hbar}\psi_j^k = \sum_{m=0}^{N} iH_{jm}\psi_j^k \ , \tag{45.108}$$

where H is a real symmetric tridiagonal matrix (provided $V(x)$ is real). The l.h.s. of the equation can be replaced either by a forward or backward difference,

$$\frac{\psi_j^{k+1} - \psi_j^k}{\tau} \quad \text{or} \quad \frac{\psi_j^k - \psi_j^{k-1}}{\tau} \ , \tag{45.109}$$

which, when combined with the r.h.s. gives the explicit algorithm,

$$\psi^{k+1} = (1 + iH\tau)\psi^k \quad \text{or} \quad \psi^k = (1 - \imath H\tau)\psi^{k+1} \ . \tag{45.110}$$

The Crank Nicholson Algorithm averages both,

$$(1 - \imath H\tau/2)\psi^{k+1} = (1 + \imath H\tau/2)\psi^k \ . \tag{45.111}$$

This method is a second order algorithm in t, i.e. the discretization error decreases as τ^2. The finite difference representation of the second derivative d^2/dx^2 is also good to second order in h^2. The Crank-Nicholson Algorithm also gives a unitary evolution in time. That is especially useful for quantum mechanics where unitarity assures that the normalization of the wavefunction is unchanged over time. The algorithm steps the solution forward in time by one time unit, starting from the initial wavefunction at $t = 0$. According to the Crank-Nicholson scheme, the time stepping process is half explicit and half implicit. The implicit part involves solving a tridiagonal system. That solution is accomplished by Crout reduction, a direct method related to Gaussian elimination and LU decomposition.

To simplify the algorithm we have chosen units in which the Planck constant $\hbar = 1$, time step $\tau = 1$ and the spatial separation $h = 1$. This can always be arranged by an appropriate redefinition of mass and potential: $m = m_{SI}\ h^2/\tau\hbar$ and $V = V_{SI}\ \tau/h$.

45.8.1.2 Crank-Nicholson algorithm for the time-dependent Gross-Pitaevskii equation

The Crank-Nicholson algorithm [7],

$$\begin{aligned}\frac{\imath\left(\varphi_j^{n+1} - \varphi_j^n\right)}{\Delta} &= -\frac{\varphi_{j+1}^{n+1} - 2\varphi_j^{n+1} + \varphi_{j-1}^{n+1} + \varphi_{j+1}^n - 2\varphi_j^n + \varphi_{j-1}^n}{2h^2} \\ &+ \frac{1}{2}\left(\frac{c(x_j)^2}{4} + n\frac{|\varphi_j^n|^2}{(x_j)^2}\right)\left(\varphi_j^{n+1} + \varphi_j^n\right) \ .\end{aligned} \tag{45.112}$$

Introducing abbreviations,

$$B(\varphi_j^{n+1} - \varphi_j^n) = -A\left(\varphi_{j+1}^{n+1} - 2\varphi_j^{n+1} + \varphi_{j-1}^{n+1} + \varphi_{j+1}^n - 2\varphi_j^n + \varphi_{j-1}^n\right) + C_j^n\left(\varphi_j^{n+1} + \varphi_j^n\right) \ . \tag{45.113}$$

Can be rewritten as,

$$A\varphi_{j+1}^{n+1} + \left(-2A + B - C_j^n\right)\varphi_j^{n+1} + A\varphi_{j-1}^{n+1} = -A\varphi_{j+1}^n + \left(2A + B + C_j^n\right)\varphi_j^n - A\varphi_{j-1}^n = X_j^n \ . \tag{45.114}$$

The set of equations,

$$\begin{pmatrix} -2A - B - C_1^n & A & 0 & \cdots & 0 \\ A & -2A - B - C_2^n & A & \cdots & 0 \\ 0 & A & -2A - B - C_3^n & \ddots & 0 \\ \vdots & \vdots & \ddots & \ddots & \vdots \\ 0 & 0 & \cdots & A & -2A - B - C_j^n \end{pmatrix} \begin{pmatrix} \varphi_1^{n+1} \\ \varphi_2^{n+1} \\ \varphi_3^{n+1} \\ \vdots \\ \varphi_j^{n+1} \end{pmatrix} = \begin{pmatrix} X_1^n \\ X_2^n \\ X_3^n \\ \vdots \\ X_j^n \end{pmatrix} \tag{45.115}$$

can be solved by inverting tridiagonal matrix. Set $\varphi_0^{n+1} = \varphi_{J+1}^{n+1} = 0$. Run a loop $j = 1, .., J$. Assume given $\varphi_1^{n+1} = \varphi_j^{n+1}$,

$$\varphi_{j+1}^{n+1} = \frac{X_j^n}{A} + \frac{2A - B + C_j^n}{A}\varphi_j^{n+1} - \varphi_{j-1}^{n+1} \ . \tag{45.116}$$

45.8.2 Time-splitting spectral algorithm: Coherent propagation

We write the one-dimensional GPE in the form,

$$\imath\hbar\frac{\partial\psi(x,t)}{\partial t} = -\frac{\hbar^2}{2m}\nabla^2\psi(x,t) + V(x)\psi(x,t) + \frac{4\pi\hbar^2 a_s}{m(2r_h)^2}|\psi(x,t)|^2\psi(x,t) \qquad (45.117)$$

for $a < x < b$. Choose periodic boundary conditions, $\psi(a,t) = \psi(b,t)$ and $\psi_x(a,t) = \psi_x(b,t)$. Various methods are known to solve the GPE numerically, such as the *Crank-Nicholson algorithm*. The *time-splitting spectral algorithm* (TSSA) consists in solving the first and the second of the following equations in two distinct steps [85, 84, 83, 486],

$$\frac{\partial\psi(x,t)}{\partial t} = -\imath\frac{V(x)}{\hbar}\psi(x,t) - \imath\frac{g_{1D}}{\hbar}|\psi(x,t)|^2\psi(x,t) \qquad (45.118)$$
$$\frac{\partial\psi(x,t)}{\partial t} = i\frac{\hbar}{2m}\psi_{xx}(x,t)\ ,$$

i.e. we discretize in space using $x = a + j(b-a)/M$ and $k = 2\pi l/(b-a)$ such that $k\,(x-a) = 2\pi lj/M$. We propagate half the way, $\Delta t/2$, in time,

$$\varphi_x \equiv e^{-\frac{\imath}{\hbar}(V(x)+g_{1D}|\psi(x,t)|^2)\frac{\Delta t}{2}}\psi(x,t) \qquad (45.119)$$

for $j = 0, .., M-1$. Now we propagate the spectral components, $(\mathcal{F}\varphi)_k \equiv \sum_{j=0}^{M-1}\varphi_x e^{-2\pi ilj/M}$, in momentum space and transform back, $(\mathcal{F}^{-1}\varphi)_x \equiv M^{-1}\sum_{l=-M/2}^{M/2-1}\varphi_k e^{2\pi ilj/M}$,

$$\phi_x \equiv \mathcal{F}^{-1}\left[e^{\imath\frac{\hbar}{2m}k^2\Delta t}(\mathcal{F}\varphi)_k\right]\ . \qquad (45.120)$$

for $l = -M/2, .., M/2-1$. Finally, we propagate the remaining time, $\Delta t/2$,

$$\psi(x,t+dt) = e^{-\frac{\imath}{\hbar}(V(x)+g_{1D}|\phi_x|^2)\frac{\Delta t}{2}}\phi_x\ . \qquad (45.121)$$

Compared to the Crank-Nicholson algorithm time-splitting spectral algorithm has several advantages:

- TSSA is much much faster, especially, for large arrays;
- No divergence, perfect reversibility;
- Imaginary version yields same density shape as steepest descent.

But there are problems:

- The coherent version changes shape, maybe it's due to ifft(fft(x))!=x;
- The imaginary version mixes up real and imag parts;
- Don't know how to generalize to coupled GPEs.

45.8.2.1 Time-splitting spectral algorithm for coupled GPEs

Write the one-dimensional GPE in the form,

$$\begin{aligned} \imath\hbar\frac{\partial\psi_1(x,t)}{\partial t} &= -\frac{\hbar^2}{2m}\nabla^2\psi_1(x,t) + V(x)\psi_1(x,t) + \frac{4\pi\hbar^2 a_s}{m(2r_h)^2}|\psi_1(x,t)|^2\psi_1(x,t) \\ &+ \frac{\hbar}{2}\Omega_{mw}\psi_2(x,t) + \hbar\Delta_{mw}\psi_1(x,t) \\ \imath\hbar\frac{\partial\psi_2(x,t)}{\partial t} &= -\frac{\hbar^2}{2m}\nabla^2\psi_2(x,t) + V(x)\psi_2(x,t) + \frac{4\pi\hbar^2 a_s}{m(2r_h)^2}|\psi_2(x,t)|^2\psi_2(x,t) \\ &+ \frac{\hbar}{2}\Omega_{mw}\psi_1(x,t) \end{aligned} \tag{45.122}$$

for $a < x < b$. Choose periodic boundary conditions, $\psi(a,t) = \psi(b,t)$ and $\psi_x(a,t) = \psi_x(b,t)$. We generalize the *time-splitting spectral algorithm*,

$$\begin{aligned} \frac{\partial\psi_1(x,t)}{\partial t} &= -\frac{\imath}{\hbar}V(x)\psi_1(x,t) - \frac{\imath}{\hbar}g_{1D}|\psi_1(x,t)|^2\psi_1(x,t) - \imath\Delta_{mw}\psi_1(x,t) - \frac{\imath}{2}\Omega_{mw}\psi_2(x,t) \\ \frac{\partial\psi_2(x,t)}{\partial t} &= -\frac{\imath}{\hbar}V(x)\psi_2(x,t) - \frac{\imath}{\hbar}g_{1D}|\psi_2(x,t)|^2\psi_2(x,t) - \frac{\imath}{2}\Omega_{mw}\psi_1(x,t) \\ \frac{\partial\psi_1(x,t)}{\partial t} &= i\frac{\hbar}{2m}\psi_{xx1}(x,t) \\ \frac{\partial\psi_2(x,t)}{\partial t} &= i\frac{\hbar}{2m}\psi_{xx2}(x,t)\ , \end{aligned} \tag{45.123}$$

i.e. we discretize in space and propagate half the way, $\Delta t/2$, in time,

$$\begin{aligned} \varphi_{x1} &\equiv \psi_1(x,t) - \left[\left(\frac{\imath}{\hbar}V(x) + \frac{\imath}{\hbar}g_{1D}|\psi_1(x,t)|^2 + i\Delta_{mw}\right)\psi_1(x,t) - \frac{\imath}{2}\Omega_{mw}\psi_2(x,t)\right]\frac{\Delta t}{2} \\ \varphi_{x2} &\equiv \psi_1(x,t) - \left[\left(\frac{\imath}{\hbar}V(x) + \frac{\imath}{\hbar}g_{1D}|\psi_2(x,t)|^2\right)\psi_2(x,t) - \frac{\imath}{2}\Omega_{mw}\psi_1(x,t)\right]\frac{\Delta t}{2}\ . \end{aligned} \tag{45.124}$$

Since we here use the first order Taylor expansion of the exponential function, we introduce an error that we have to keep low by renormalizing the wavefunction after each step. Now we propagate the spectral components in momentum space and transform back,

$$\begin{aligned} \phi_{x1} &\equiv \mathcal{F}^{-1}\left[e^{\imath\frac{\hbar}{2m}k^2\Delta t}(\mathcal{F}\varphi_{x1})_k\right] \\ \phi_{x2} &\equiv \mathcal{F}^{-1}\left[e^{\imath\frac{\hbar}{2m}k^2\Delta t}(\mathcal{F}\varphi_{x2})_k\right]\ , \end{aligned} \tag{45.125}$$

for $l = -M/2, .., M/2-1$. Finally, we propagate the remaining time, $\Delta t/2$,

$$\begin{aligned} \psi_1(x,t+dt) &= \phi_{x1} - \left[\left(\frac{\imath}{\hbar}V(x) + \frac{\imath}{\hbar}g_{1D}|\phi_{x1}|^2 + \frac{\imath}{2}\Delta_{mw}\right)\phi_{x1} - \frac{\imath}{2}\Omega_{mw}\phi_{x2}\right]\frac{\Delta t}{2} \\ \psi_2(x,t+dt) &= \phi_{x1} - \left[\left(\frac{\imath}{\hbar}V(x) + \frac{\imath}{\hbar}g_{1D}|\phi_{x2}|^2\right)\phi_{x2} - \frac{\imath}{2}\Omega_{mw}\phi_{x1}\right]\frac{\Delta t}{2}\ . \end{aligned} \tag{45.126}$$

45.8.2.2 Spinor notation

It may be possible to simplify the notation by writing the wavefunction as a spinor, $\vec{\psi} \equiv \begin{pmatrix} \psi_1 \\ \psi_2 \end{pmatrix}$. Now the non-kinetic part of the coupled GPE can be written,

$$\frac{\partial \vec{\psi}(x,t)}{\partial t} = M\vec{\psi}(x,t) \ , \tag{45.127}$$

with the matrix,

$$M = \begin{pmatrix} -\frac{\imath}{\hbar}V(x) - \frac{\imath}{\hbar}g_{1D}|\psi_1(x,t)|^2 - \imath\Delta_{mw} & -\frac{\imath}{2}\Omega_{mw} \\ -\frac{\imath}{2}\Omega_{mw} & -\frac{\imath}{\hbar}V(x) - \frac{\imath}{\hbar}g_{1D}|\psi_2(x,t)|^2 \end{pmatrix} \ , \tag{45.128}$$

and the solution,

$$\vec{\psi}(x,t) = e^{Mt}\vec{\psi}(x,0) \ . \tag{45.129}$$

Let us now abbreviate the matrix by,

$$M = \begin{pmatrix} A & B \\ B & D \end{pmatrix} \ . \tag{45.130}$$

The matrix is diagonalized with the unitary transforms,

$$U = \frac{1}{\sqrt{2\Delta}} \begin{pmatrix} \frac{A-D}{2B} + \Delta & \frac{A-D}{2B} - \Delta \\ 1 & 1 \end{pmatrix} \quad \text{and} \quad U^{-1} = \frac{1}{\sqrt{2\Delta}} \begin{pmatrix} 1 & -\frac{A-D}{2B} + \Delta \\ -1 & \frac{A-D}{2B} + \Delta \end{pmatrix} \ . \tag{45.131}$$

The eigenvalue matrix is,

$$U^{-1}MU = \begin{pmatrix} E_1 & 0 \\ 0 & E_2 \end{pmatrix} \tag{45.132}$$

with $E_{1,2} = \frac{1}{2}A + \frac{1}{2}D \pm B\Delta$. Here we used the abbreviation $\Delta = \sqrt{\left(\frac{D-A}{2B}\right)^2 + 1}$. The formal solution now reads,

$$\vec{\psi}(x,t) = \exp\left[U \begin{pmatrix} E_1 & 0 \\ 0 & E_2 \end{pmatrix} U^{-1} t\right] \vec{\psi} = U \begin{pmatrix} e^{E_1 t} & 0 \\ 0 & e^{E_2 t} \end{pmatrix} U^{-1}\vec{\psi}(x,0) \ . \tag{45.133}$$

This formula can easily be computed, because the block matrices of transform U are diagonal in x.

45.8.3 Wavepacket propagation

45.8.3.1 1D simulations

We want to describe the one-dimensional evolution of an atomic wavepacket according to the Schrödinger equation. The problem is fully described by [1046],

$$\imath\hbar\frac{\partial}{\partial t}\psi(z,t) = \frac{-\hbar^2}{2m}\frac{d^2}{dz^2}\psi(z,t) + V(z)\psi(z,t) \ . \tag{45.134}$$

Numerically the Schrödinger equation is integrated via,

$$\psi(z,t+dt) = \psi(z,t) + dt\dot{\psi}(z,t) \ . \tag{45.135}$$

The initial state of the wavepacket is set to $\psi(z,0) = e^{-z^2/2\bar{z}^2} e^{\imath kz}$, where $k \equiv \sqrt{2mE}/\hbar$ is its wavevector.

The numerical propagation is conveniently done with the time-splitting spectral algorithm [85, 84, 83, 486].

The flux is,

$$\psi \nabla \psi = 0 \ . \tag{45.136}$$

45.8.3.2 2D simulations

We want to describe the two-dimensional evolution of an atomic wavepacket according to the Schrödinger equation. The problem is fully described by,

$$\frac{-\hbar^2}{2m}\left(\frac{d^2}{dx^2} + \frac{d^2}{dz^2}\right)\Psi(x,z,t) + V(x,z)\Psi(x,z,t) = i\hbar\frac{\partial}{\partial t}\Psi(x,z,t) \ . \tag{45.137}$$

Since the potential is conservative, we separate the time-evolution,

$$\Psi(x,z,t) = \psi(x,z)e^{-\imath Et/\hbar} \tag{45.138}$$

The initial shape of the wavefunction moving along the y coordinate could be a Gaussian,

$$\psi(x,z) = \psi_x(x,0)\psi_z(0,z) = (2\pi\sigma_x\sigma_z)^{-1/2}\, e^{-x^2/4\sigma_x^2 - z^2/4\sigma_y^2} \ . \tag{45.139}$$

We can assume $\sigma_z \gg \sigma_x$ and obtain an effectively one-dimensional model, $E = E_{kz}$. Set,

$$\psi(x,z,0) = \phi(x,z)e^{-\imath k_z z} \tag{45.140}$$

and,

$$-\frac{d^2}{dz^2}\phi(x,z) + 2\imath k_z \frac{d}{dz}\phi(x,z) = \frac{d^2}{dx^2}\phi(x,z) + \left[\frac{2m}{\hbar^2}E_{kz} - \frac{2m}{\hbar^2}V(x,z) - k_z^2\right]\phi(x,z) \ , \tag{45.141}$$

and,

$$\begin{aligned}
\frac{d}{dz}\phi(x,z) &= \frac{d^2}{dx^2}\phi(x,z) - \frac{2m}{\hbar^2}V(x,z)\phi(x,z) \qquad (45.142)\\
\frac{d}{dz}\phi(x,z) &= \frac{1}{2\imath k_z}\frac{1}{dx^2}[\phi(x-dx,z) - 2\phi(x,z) + \phi(x+dx,z)] - \frac{m}{\imath k_z \hbar^2}V(x,z)\phi(x,z) \ .
\end{aligned}$$

Discretize in steps dz.

45.8.3.3 Reflection from a potential barrier

Now we allow for a change of direction. We assume that a matter wave with wavevector $\mathbf{k}_0 = k_{0x}\hat{\mathbf{e}}_x + k_{0y}\hat{\mathbf{e}}_y = k_0\hat{\mathbf{e}}_x \sin\alpha + k_{0y}\hat{\mathbf{e}}_y \cos\alpha$, runs towards a potential step. If

the step is sharp, $V(x) = V_1\theta(-x) + V_2\theta(x)$, the following ansatz is reasonable,

$$\begin{aligned}\psi_0(x,y) &= e^{\imath x k_x + \imath y k_y} \\ \psi_1(x,y) &= re^{-\imath x k_x + \imath y k_y} \\ \psi_2(x,y) &= te^{\imath x k'_x + \imath y k_y}\end{aligned} \tag{45.143}$$

and we have to solve the equations,

$$\begin{aligned}\frac{-\hbar^2}{2m}\left(\frac{d^2}{dx^2}+\frac{d^2}{dy^2}\right)(\psi_0+\psi_1) &= (E-V_1)(\psi_0+\psi_1) \\ \frac{-\hbar^2}{2m}\left(\frac{d^2}{dx^2}+\frac{d^2}{dy^2}\right)\psi_2 &= (E-V_2)\psi_2\ .\end{aligned} \tag{45.144}$$

In the step is smooth, $V(x\to-\infty) = V_1 < V_2 = V(x\to\infty)$, the situation is more complicated. Let us set $V(x) = (V_1 - V_2)\frac{1}{\pi}\arctan x + \frac{1}{2}(V_1+V_2)$.

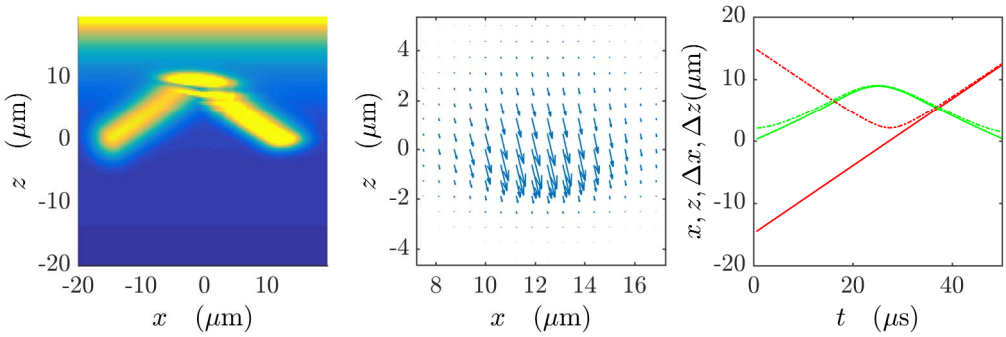

Figure 45.10: (code) Reflection of a wavepacket at a potential barrier. Do evanescent matter waves propagate along the barrier? Is there an atomic analogue to the Goos-Hänchen shift?

45.8.4 Exercises

45.8.4.1 Ex: Propagation of wavefunctions

Programs on the propagation of wavefunctions.

Solution: *BecAdjust1 harmonic potential, comparison to Thomas-Fermi, correct norm, physical units.*
BecAdjust1b harmonic potential, comparison to Thomas-Fermi, correct norm, physical units, negative potential.
BecAdjust2 harmonic potential, real-time propagation of a soliton, correct norm, dimensionless scaling.
BecAdjust3 harmonic potential, sudden phase-shift of half the condensate, wrong norm, dimensionless scaling.
BecAdjust4 real-time propagation of merging double-well BECs, wrong norm, dimensionless scaling.

BecAdjust5 real-time propagation of 2 adjacent ballistically expanding BECs, wrong norm, dimensionless scaling.
BecAdjust6 ground state of an adiabatic potential, sudden displacement.
BecTwoDim1 2 dimensions, switching from double-well to single-well.
BecTwoDim1b 2 dimensions, switching from double-well to single-well.
BecTwoDim1c 2 dimensions, switching from double-well to single-well.
BecTwoDim2 Two-gas description of finite Temperature BECs, first the method of Steepest Descent, second solving the thermal gas Schrödinger equation for T¿0.
BecTwoDim3 2 dimensions, switching from double-well to single-well.
TimeSplitSpectralProp1 Compares Runge-Kutta or Crank-Nicholson-finite-difference (CNFD)-like algorithm with time-splitting spectral algorithm (TSSA) based on standard Strang splitting [Bao02,03,04].
TimeSplitSpectralProp2 Try coupled GPEs with TSSP, second method, no work???
TimeSplitSpectralProp3 Single GPE, yet another version.
TimeSplitSpectralProp4 Rescaled version.
TimeSplitSpectralProp5 Rescaled version, steepest descent using TSSP with sine-fft, no work???
BecMomentum1 Integrating the GPE by the method of steepest descent in Fourier space, harmonic potential, no interaction.

45.8.4.2 Ex: Programs on wavepackets reflected from potential barriers

Programs on wavepackets reflected from potential barriers.

Solution: *WavepacketPropagation1 2D, Runge-Kutta, evanescent wave potential.*
WavepacketPropagation2 2D, time-splitting spectral method, hard wall potential.
WavepacketPropagation3 1D, Wavepacket propagation integrating the Schrödinger equation, Runge-Kutta.
WavepacketPropagation4 1D, time-splitting spectral algorithm.

45.9 Further reading

E.A. Cornell, *Very Cold Indeed: The Nanokelvin Physics of Bose-Einstein Condensation* [291]DOI

F. Dalfovo et al., *Theory of Bose-Condensation in Trapped Gases* [319]DOI

Ph.W. Courteille et al., *Bose-Einstein Condensation of Trapped Atomic Gases* [297]DOI

A.J. Leggett, *Bose-Einstein condensation in the alkali gases Some fundamental concepts* [785]DOI

C.J. Myatt et al., *Production of Two Overlapping Bose-Einstein Condensates by Sympathetic Cooling* [939]DOI

W. Ketterle et al., *Making, probing and understanding Bose-Einstein condensates* [712]DOI

Chapter 46

Superfluid and coherent properties of Bose-Einstein condensates

Superfluid liquids or gases are distinguished by their ability to sustain flow without dissipation, i.e. flow which is free of viscous damping. The phenomenon of superfluidity is a well-known property of liquid ^{4}He, but the relationship between superfluidity and Bose-Einstein condensation in this strongly interacting system is not trivial. The situation is much simpler in weakly interacting Bose gases, where the superfluid fraction is almost identical with the condensed fraction and the normal phase of the fluid with the thermal fraction. The availability of dilute gas Bose-Einstein condensates now offers the unique opportunity to study the complicated interdependence between superfluidity and condensation.

46.1 Superfluidity in quantum gases

The *superfluidity* of a gaseous condensate, which is one of its most apparent properties, is intrinsically linked to interatomic collisions. To characterize this phenomenon, it is useful to define some parameters. In the local-density approximation, the *homogeneity* of a gas of N atoms with the thermal de Broglie wavelength (43.9) confined inside a harmonic trap with the ground state size defined by (24.85), is characterized by,

$$\frac{k_B T}{\hbar \omega_{trp}} = \frac{2\pi a_{trp}^2}{\lambda_{therm}^2} \ . \tag{46.1}$$

For a typical experimental situation, $k_B T/\hbar\omega_{trp} \approx N^{1/3} \approx 100$. This shows that the assumption of a locally homogeneous gas is generally a good approximation. With the definition of the *healing length* (45.69), the degree of superfluidity of a condensate with density n can be cast into the form,

$$\frac{gn}{\hbar \omega_{trp}} = \frac{a_{trp}^2}{\xi^2} \ . \tag{46.2}$$

For a typical experimental situation, $a_{trp}^2/\xi^2 \approx 100$. A parameter that well characterizes the importance of interatomic forces within a condensate is the gas *dilution*,

$$na_s^3 = \frac{a_s^2}{8\pi\xi^2} \ . \tag{46.3}$$

The typical numerical value $na_s^3 \approx 10^{-5}$ shows, that atomic gases are usually very dilute, although interatomic forces play an important role in the dynamics of condensates. In contrast, three-body collisions can be totally neglected, because the probability to have three atoms close to each other is even lower than the probability for two atoms.

There are several manifestations of phenomena linked to superfluidity, such as the behavior of collective elementary excitations, superfluid flow of non-circulating topological modes, quantized flux in vortices and matter wave solitons, which will be discussed in the following sections.

46.1.1 Landau's criterion for superfluidity

According to Landau, the phenomenon of superfluidity is rooted in the particular character of the Bogolubov spectrum of elementary excitations (45.54). Let us consider a bosonic fluid at a given temperature moving with velocity v. A macroscopic obstacle in the path of the superfluid can generate elementary excitations. That is, a fraction of the kinetic energy of the fluid is transferred to these excitations, thereby decelerating the fluid and causing *viscosity*. With the excitation energy $\mathcal{E}(p)$ and the momentum $\mathbf{p}$, the total energy of the fluid interacting with the obstacle is,

$$E = \mathcal{E}(p) + \frac{(\mathbf{p}+M\mathbf{v})^2}{2M} = \mathcal{E}(p) + \mathbf{p}\cdot\mathbf{v} + \tfrac{1}{2}Mv^2 + \frac{p^2}{2M} \simeq \mathcal{E}(p) + \mathbf{p}\cdot\mathbf{v} + \tfrac{1}{2}Mv^2 \ , \tag{46.4}$$

where M is the total mass of the superfluid. Since the term $Mv^2/2$ is the initial kinetic energy of the fluid, $\mathcal{E}(p) + \mathbf{p}\cdot\mathbf{v}$ represents the excitation energy. And since the kinetic energy of the superfluid can only be diminished by the excitation, we need $\mathcal{E}(p) + \mathbf{p}\cdot\mathbf{v} < 0$. Finally, as $\mathcal{E}(p)$ must be positive, the condition for generating elementary excitations is,

$$\mathcal{E}(p) \leq pv \ , \tag{46.5}$$

where $\mathbf{p}$ and $\mathbf{v}$ are antiparallel.

Therefore, there is a relative *minimum velocity* between the fluid and the obstacle, called *critical Landau velocity*, for creating excitations,

$$v_c = \min\left(\frac{\mathcal{E}(p)}{p}\right) \ . \tag{46.6}$$

For velocities below v_c, it is impossible to generate excitations, and there is no mechanism to decrease the kinetic energy of the fluid. As a result, the system becomes superfluid [772].

The spectrum of elementary excitations for a weakly interacting condensate, is the Bogolubov spectrum (45.54). The graph Fig. 46.1 shows, that for velocities below the sound velocity given by (45.56), $v < c_s$, the curve representing the propagation of the

perturbation does not cross the Bogolubov spectrum. That is, the perturbation can not be converted into excitations, which is only possible when $v > c_s$.

In an ideal condensate without interactions, $a_s = 0$, the Bogolubov spectrum reduces to the quadratic dispersion relation of free particles, which means that there is no critical velocity, $v_c = c_s$. Consequently, it is always possible to excite the condensate, that is, an ideal condensate can not be superfluid, and, as first pointed out by Landau: *superfluidity and Bose-Einstein condensation are different phenomena.*

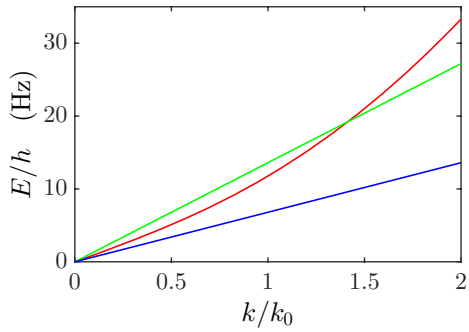

Figure 46.1: (code) Landau's criterion for superfluidity. Slow perturbations (blue line) do not cross the Bogolubov spectrum (red line) and do not generate excitations. Rapid perturbations (green line) cross the spectrum and can be dissipated.

46.1.2 Impurity scattering

A first hint for the superfluid nature of Bose-Einstein condensates is the fact that the hydrodynamic theory of superfluidity describes well the collective excitations (see Sec. 45.5). Moreover, several experiments provided direct evidence for the superfluid nature of condensates. For example, via a calorimetric measurement [1071]: A condensate, stirred around by a rotating far blue-detuned laser beam, dissipated atoms to the thermal fraction of the atomic cloud, provided the stirring velocity exceed a certain *critical velocity* v_c: At lower velocities, the perturbation did not lead to dissipation. At higher velocities, phonons were excited and the cloud was heated. In a subsequent experiment, perturbation-induced density fluctuations were observed *in vivo* and *in situ* [978]. When the stirring speed was below the critical velocity, the density was almost homogeneous, thus indicating superfluid flow. When, however, the stirring speed exceeded v_c, atoms piled up in front of the stirring beam, and the resulting pressure gradients led to a turbulent flow around the perturbation and to dissipation.

The critical velocity v_c found in the stirring experiments was about ten times smaller than the local sound velocity c_s,

$$c_s \equiv \sqrt{\frac{gn}{m}} = \frac{\hbar}{\sqrt{2}m\xi} \ . \tag{46.7}$$

In fact, while the onset of dissipation is accelerated by turbulence around the *macroscopic object* traversing the superfluid, the local sound velocity (46.8) is derived for

a *microscopic object*. Puzzled by this discrepancy, Chikkatur *et al.* [255] studied the motion of microscopic atomic impurities through a condensate. The *impurity* was created by transferring a few atoms out of the original BEC from the trapped state $|F = 1, m_F = -1\rangle$ to the free state $|F = 1, m_F = 0\rangle$ via induced Raman transitions. The initial velocity was adjusted by the laser beams exciting the Raman transition (polarization, incident angle and relative detuning) to satisfy the Bragg condition (see Sec. 47.2). After the free impurity passed through the BEC, the trap was switched off, a Stern-Gerlach magnetic field gradient was pulsed to separate atoms in different Zeeman states, and finally the atoms were detected via time-of-flight imaging (see Sec. 43.6.1). When the initial velocity of the impurity was well above a critical value given by the local velocity of sound, ultracold s-wave collisions between impurity atoms and the stationary condensate distributed the momenta of the collision partners uniformly. In TOF images this appeared as a *circular halo* centered around the center-of-mass momentum of the collision partners (see Fig. 46.2). When, however, the initial velocity of the impurity was reduced, its collision rate with the stationary condensate was suppressed and the trajectory became superfluid.

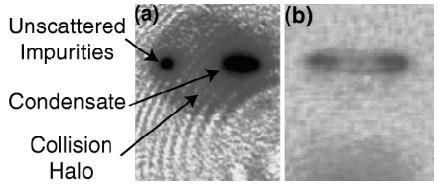

Figure 46.2: (a) Scattering of impurities at velocities above the critical velocity. The presence of a halo indicates the occurrence of collisions between the impurity and the condensate dissipating the relative kinetic energy. (b) For velocities below the critical velocity the halo disappears.

46.1.3 Hydrodynamic theory of superfluidity

For the description of superfluidity a hydrodynamic theory is adequate. Therefore, we will rewrite the time-dependent Gross-Pitaevskii equation (45.21). We consider the general case, in which the external potential $V_{trp}(\mathbf{r}, t)$ depends on time. The wavefunction can be written by defining the density and the velocity fields,

$$\phi(\mathbf{r}, t) = \sqrt{n_0(\mathbf{r}, t)} e^{i\theta(\mathbf{r},t)} \tag{46.8}$$

$$\mathbf{v}_s(\mathbf{r}, t) = \frac{\mathbf{j}(\mathbf{r}, t)}{n_0(\mathbf{r}, t)} = \frac{1}{2im} \frac{1}{n(\mathbf{r}, t)} \left[\phi^*(\mathbf{r}, t)\nabla\phi(\mathbf{r}, t) - \nabla\phi^*(\mathbf{r}, t)\phi(\mathbf{r}, t)\right] .$$

This gives,

$$\mathbf{v}_s(\mathbf{r}, t) = \tfrac{\hbar}{m}\nabla\theta(\mathbf{r}, t) . \tag{46.9}$$

From the GPE we derive the continuity and the Navier-Stokes equations:

$$\frac{\partial n}{\partial t} + \nabla(\mathbf{v}_s n) = 0 \tag{46.10}$$

$$m\frac{\partial \mathbf{v}_s}{\partial t} + \nabla\left(V_{trp} + gn - \frac{\hbar^2 a}{2m\sqrt{n}}\nabla^2\sqrt{n} - \mu + \frac{m}{2}\mathbf{v}_s^2\right) = 0 .$$

We can see that the hydrodynamic behavior of a BEC depends greatly on the quantum phase θ. When the kinetic pressure is small compared to the mean-field energy,

$$m\frac{\partial \mathbf{v}_s}{\partial t} + \nabla\left(V_{trp} + gn + \frac{m}{2}\mathbf{v}_s^2\right) = 0 \ . \tag{46.11}$$

This is the *Euler equation* for a fluid with a potential flow. This equation and the *continuity equation* have the typical structure of equations describing superfluids at $T = 0$. This is due 1. to the presence of a Bose-Einstein condensate allowing us to formulate an equation for a complex *order parameter*, and 2. to the presence of interactions, included via the pressure term in the Euler equation, which are necessary condition for superfluidity.

At zero temperature, the entire fluid is superfluid. Moreover, in the Gross-Pitaevskii approximation, the whole fluid is condensed. Therefore, $\mathbf{v}_s(\mathbf{r}, t)$ is the velocity flow of the superfluid [1].

46.2 Topological modes

Significant manifestations of superfluidity are associated with rotational phenomena. An example is the occurrence of *scissor mode*s [557], which are excited, when an angular momentum is suddenly applied to a condensate confined in an anisotropic trap. This can be done via a sudden reorientation of the symmetry axis of the trap [843, 842]. The condensate responds to this perturbation by an oscillation of its inclination implemented by an *irrotational superfluid flow*. The excitation spectrum reflects the strong reduction of the inertial momentum for superfluids.

The most rigorous manifestation of superfluidity, however, is the occurrence of a quantized and persistent current, called *quantized vortex*. In contrast to the elementary excitations, which must be created by perturbations, the vortex is a *stationary* (or *topological mode*) solution of the Gross-Pitaevskii equation Eq. (45.21).

Work on vortices has been done by [857, 833, 1071, 978, 255, 557, 843, 834, 253, 29, 1113, 377, 658, 222, 1420].

46.2.1 Vortices

From Eq. (46.9) it is easy to see, that the superfluid is non-rotational, that is,

$$\nabla \times \mathbf{v}_s(\mathbf{r}, t) = 0 \ . \tag{46.12}$$

This raises the question, how vortices are possible. The solution to this apparent contradiction is, that Eq. (46.12) does not apply, when the phase exhibits a singularity. Consider, for example, a closed loop C around the singularity. In a vortex, the superfluid current is pulled by the phase gradient, $\mathbf{v} = \frac{\hbar}{m}\nabla\theta$. For the condensate wavefunction to be well defined, the phase variation $\Delta\theta$ around the loop must be a multiple of 2π, that is,

$$\Delta\theta = \oint_C \nabla\theta \cdot d\mathbf{l} = 2\pi\ell \ . \tag{46.13}$$

[1] This is not the case for strongly interacting superfluids, such as superfluid helium, where the normal fluid fraction is considerable.

where ℓ is an integer. Therefore, we can calculate the *circulation* Γ around the closed loop, that is,

$$\Gamma = \oint_C \mathbf{v}_s(\mathbf{r},t)\cdot d\mathbf{l} = \frac{h}{m}\ell \ . \tag{46.14}$$

Apparently, the superfluid circulation is quantized in units of $\hbar/m$. The parameter ℓ is called *charge of the vortex* and measures, in unit of h, the quantized angular momentum of the vortex.

In addition, the flow must be persistent, because its circulation can only be changed in a discontinuous way, by overcoming a discrete energy barrier, which requires energy coming e.g. from thermal excitations. Clearly, the normal (thermal) fraction of a gas can also have a circular flow. However, the disordered microscopic motion of each individual particle causes a viscous drag that prevents the persistence of the flow in the absence of a torque. This is in contrast to superfluid flow, which persists even without external torque. The issues of vortex stability, formation, and topology were addressed in recent experiments [856, 833, 834, 253, 29]. Solve the Excs. 46.2.6.1 and 46.2.6.2.

The kinetic energy per unit vortex length can be estimated from a semi-classical approach. First, we define as the mass density ρ_m of the superfluid. If n is the particle density, $\rho_m = nm$. The kinetic energy of a flux line at the radius r is,

$$\mathcal{E}_{kin} = \tfrac{1}{2}\rho_m v_s^2 = \frac{\hbar^2\ell^2}{2m}\frac{n}{r^2} \ . \tag{46.15}$$

To obtain the kinetic energy per unit length, we integrate the expression (46.21) over a plane perpendicular to the vortex axis. Note, however, that the velocity field is $v_s \propto r^{-1}$ and, therefore, can not be integrated from zero. Instead, we begin the integration at a radius given by the *healing length* ξ, which represents a measure of the vortex core size. Now, the kinetic energy per unit length is,

$$E_{semi} = \int_0^{2\pi}\int_\xi^R \mathcal{E}_{kin}(\mathbf{r}) r dr d\theta = \pi n \frac{\hbar^2\ell^2}{m}\ln\frac{R}{\xi} \ . \tag{46.16}$$

Note, that a multiply charged vortex carrying the entire angular momentum $\ell = \ell_0$ of the superfluid is energetically less favorable than an ensemble of ℓ_0 vortices with unit charge $\ell = 1$. Therefore, a multiply charged vortex is unstable and may decay to several single charge vortices.

To calculate exactly the energy of a vortex, we do the following ansatz,

$$\Phi_0(\mathbf{r}) = \phi(r,z)e^{i\ell\vartheta} \ , \tag{46.17}$$

we then solve the Gross-Piatevskii equation (45.21) numerically, and calculate the expectation value of the energy of the vortex through the expression,

$$\langle\Phi_0|\hat{H}|\Phi_0\rangle = \int d^3\mathbf{r}\left[\tfrac{\hbar^2}{2m}|\nabla\Phi_0(r,z)|^2 + V_{trp}|\phi(r,z)|^2 + g|\phi(r,z)|^4\right] \ , \tag{46.18}$$

where $\hat{H}$ is the Gross-Pitaevskii Hamiltonian.

The calculation yields for energy per unit length of a single charge vortex in a uniform cylindrical condensate [1017],

$$E_{unif} = \pi n\tfrac{\hbar^2}{m}\ln\left(1.464\tfrac{R}{\xi}\right) \ , \tag{46.19}$$

which is very close to our semi-classical prediction. Although the wavefunction $|\phi(r,z)|$ has no analytic form, it can be shown by a variational approach, that the trial wavefunction,

$$|\phi(r,z)| = \frac{nr}{\sqrt{2\ell^2\xi^2 + r^2}} \tag{46.20}$$

is a good approximation [1017]. Note that the healing length ξ characterizes the size of the vortex. For a superfluid, we can calculate the total energy of the vortex exactly, because the fluid is confined in all directions,

$$E_{tot} = \frac{4\pi n_0}{3}\frac{\hbar}{m}\ln\left(0.671\frac{R_r}{\xi_0}\right) \ , \tag{46.21}$$

where n_0 and ξ_0 are, respectively, the density and healing length at the center of the fluid. R_z and R_r are, respectively, the extensions of the cloud along the axial and radial directions within the Thomas-Fermi approximation.

46.2.1.1 Creation and detection of vortices

The first superfluid vortex was observed 1979 in ^{4}He [1409]. For gaseous condensates, two approaches have been employed to produce vortices. Either one stirs the atomic cloud in order to impart an angular momentum to it. This can be done by rotating the (anisotropic) trap during the process of forced evaporation with time-orbiting magnetic fields or with an optical spoon. The vortex state is formed when the critical temperature for condensation is crossed. An alternative method is to imprint a 2π circular phase gradient into a previously created condensate. Indeed, the local phase of a matter wave can be manipulated via a local modification of the potential depth, which can be achieved by a Stark shift induced by a far-detuned laser beam [377]. Focused into a tiny spot which is moved across the condensate, the laser beam will create a phase gradient, which in turn will cause a velocity flow. It is important to force the local density at the center of the vortex to zero, which can be achieved via a proper design of the trapping potential (e.g., a Mexican hat-shaped potential), and let the BEC then relax to the vortex state.

A variation of this method [1378] avoids the need for relaxation processes. In this configuration the phase gradient is created through a *local* Raman coupling between two internal atomic states (for example, in ^{87}Rb the two trappable Zeeman states $|F, m_F\rangle = |1,-1\rangle$ to $|2,1\rangle$). At the spots, where the focused Raman beams hit the condensate, atoms were dynamically converted from the ground state to the excited state. The circular trajectory of the spots and the rotation speed were calculated such as to generate a toroidal topology for the adiabatic population transfer. The process was coherent and allowed to directly construct and shape the vortex wave function. We study this experiment in more detail in the Exc. 46.2.6.3.

In confined single-species condensates the diameter of the vortex core is on the order of the healing length, 2ξ. With typical values of $2\xi \approx 0.4$ μm it is thus way too small to be imaged *in situ*, and ballistic expansion times of several 10 ms are necessary. On the other hand, in double condensates formed by two repelling species (e.g. the two states $|2,1\rangle$ and $|1,-1\rangle$ in ^{87}Rb), one of the species can form a vortex around the second. In this case, the diameter of the vortex core, is determined by the diameter of the condensate of the second species and, hence, much larger. When

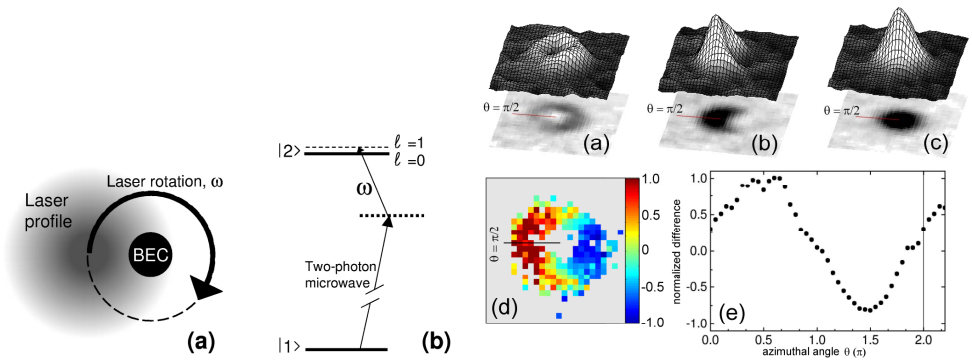

Figure 46.3: (Left) Scheme of the experiment [856]. (Medium) Level system used. (Right) Density distribution of a vortex state: (a) (the visible atoms are in the upper hyperfine state), (b) after a $\pi/2$-pulse and (c) after a π-pulse (the visible atoms are in the lower hyperfine state). The images (d) and (e) visualize the phase slip around the vortex.

the second species is selectively removed (e.g. by the radiative pressure exerted by a resonant laser), and the vortex in the first species can be studied by *in situ* imaging of the confined density distribution [857].

A particularly smart detection method for vortices is based on matter wave interferometry (see Sec. 46.3.3). Here, two matter waves, that is, the vortex state in $|2,1\rangle$ and a (reference) ground state BEC in $|1,-1\rangle$ are coherent mixed via a resonant two-photon radiofrequency $\pi/2$-pulse. The resulting matter wave interference patterns reveals the phase profile of the vortex (see Fig. 46.3).

46.2.1.2 Stability

In a topologically 'singly-connected' trap, for example a potential harmonic, vortices do not represent the lowest energy eigenstate, and they must decay to the ground state. If the mean-field energy of the condensate is weak compared to the kinetic energy, $gn_0/\hbar\omega_z \ll 1$, the healing length will exceed the size of the BEC, $\xi \gg a_{trp}$, and the vortex rapidly decays by dissipating its excess energy to thermal excitation. Such BECs can not be considered superfluid. If the mean-field interaction is strong, the vortex spontaneously breaks azimuthal symmetry, moves away from the center and exits the condensate on a spiral-shaped trajectory [1113]. Nevertheless, the decay time may be quite long.

On the other hand, a vortex can be the ground state of a 'multiply-connected' trap (for example, a toroidal potential). Such a potential can be realized as the temporal average of a harmonic potential with a small rotating anisotropy [833]. In such geometries vortices are extremely stable.

46.2.1.3 Vortex precession

A radial force acting on a vortex results in a radial displacement and a precession about the symmetry axis. The effect, known as *Magnus effect* [658], is due to pressure

imbalances on the vortex surface. A radial force naturally arises, when the core is displaced from the center, because local pressure gradients will force the vortex out of the center toward regions with lower densities. Experimentally, a slow precession ($\sim$ 1 Hz) spiraling the vortex toward the rim of the condensate has been observed [29] by taking a succession of nondestructive images.

46.2.2 Vortex lattices

Superfluid ^{4}He in a rotating bucket spontaneously develops symmetrically organized vortex patterns. Similar phenomena can be observed, when a dilute gas Bose-Einstein condensate is forced to rotate [222] at a given frequency Ω. The energy in the rotating system receives an additional contribution from the centrifugal term, $U_{rot}(\mathbf{r}) = U_{trp}(\mathbf{r}) - \Omega L_z$, where $L_z = \hbar N l_z$, and $l_z = i(y\partial_x - x\partial_y)$ is the angular momentum of the individual atoms. If the rotation is slow, the energy ΩL_z is too small to force the condensed wavefunction to rotate. If the rotation frequency is beyond a critical value Ω_c, the *time-averaged* potential, $U_{rot}(\mathbf{r})$ eventually develops a local minimum in the center, thus adopting the toroidal shape. For non-interacting gases, the critical frequency coincides with the radial secular frequency, $\Omega_c = \omega_r$. Then the radial restoring force of the trap does not balance the centrifugal force, such that atoms can escape from the trap. However, for superfluid gases the critical frequency is reduced, $\Omega_c < \omega_r$. Between the rotation frequencies $\Omega = \Omega_c$ and $\Omega = \omega_r$, the state with the lowest energy in the toroidal potential is the vortex, whose filament is pinned to the symmetry axis. For even higher rotation frequencies, we could expect a single vortex with a larger winding number (more than the phase winding of 2π for a single turn). However, individual multiple-order vortices in harmonic traps are unstable. Instead, vortex lattices [222] called *Abricosov lattice*s will form. For a given trapping potential and mean-field energy, the symmetry of the lattice and the number of vortices depend on the rotation frequency Ω. Counter-intuitively, the angular momentum of individual particles l_z *is not quantized*. When we vary Ω, regimes of forbidden l_z (i.e. when no vortex pattern is formed) alternate with allowed regimes. The discontinuous transition from one vortex pattern to another is a first-order phase transition, which spontaneously breaks one symmetry to form another. An upper limit for the rotation speed is given by the equilibrium between the centrifugal force and the radial restoring force of the trapping potential at $\Omega = \omega_r$.

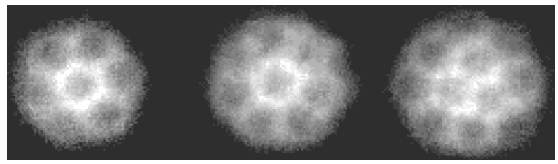

Figure 46.4: Abricosov vortex lattice.

These patterns of vortex lattices were observed in experiments using the *stirring method*, which consists in brushing a far-detuned focused laser ('optical spoon') around the rim of a condensate [833] at a certain frequency Ω. In this experiment, the ratio of the mean-field energy to the kinetic energy was $gn_0/\hbar\omega_z = a_{trp}^2/2\xi^2 > 100$. Beyond a certain critical rotation frequency, $\Omega_c \approx 2\pi \times 150$ Hz, a single central vortex

was formed. At even higher frequency, a symmetrical vortex lattice appeared in a transverse plane (see Fig. 46.4). Finally, at rotation frequencies near the radial trap frequency ω_r, the condensate wavefunction became turbulent and finally disappeared. As soon as the optical spoon was removed, the vortex lattice gradually decayed losing the vortices one by one.

46.2.3 Solitons

Work on solitons has been done by [1416, 1377, 856, 1378, 921, 1089, 657, 938, 218, 69, 397, 212, 356].

46.2.3.1 Dark solitons

Solitons are non-singular solutions of any equation satisfying,

$$|\psi(\mathbf{r},t)| = |\psi(\mathbf{r}-\mathbf{v}t)| \ . \tag{46.22}$$

Solitons are well known to occur in non-linear optical media, for example in optical fibers, when dispersion is counterbalanced by self-phase modulation, such that optical signals propagate without spreading. The Gross-Pitaevskii equation is another example for a nonlinear wave equation supporting soliton-like solutions. States called *dark soliton* or *twisted state* with a dynamically stable density dip are expected in condensates with repulsive interactions [921, 1089, 657, 938]. In contrast to topologically stable states, for example, vortices, dark solitons are pseudo-defects, the decay of which, even though it may be slow, is topologically trivial. Due of the greater freedom of movement of their wavefunctions, solitons can be distorted by complex deformations [218]. Soliton-like matter wave states were initially observed in superfluid ^{3}He-B [69]. In dilute gases, the size of the solitons is of the order of healing length.

The first dark solitons in dilute gases were created by applying an inhomogeneous phase shift to a condensate [212, 356]. One half of the condensate was irradiated by a far-detuned laser pulse (detuning Δ, Rabi frequency Ω, duration $\tau \ll \hbar/gn_0$) in order to advance the phase of this part of the condensate by $\varphi = \Omega^2\tau/4\Delta$. When the phase shift was set to π, an abrupt phase gradient developed at the boundary delimiting the two halves. The condensate reacted to the phase gradient by developing a deep density minimum all along the boundary corresponding to a soliton (see Fig. 46.5). The phase distribution can also be imaged by interferometric techniques based on Bragg diffraction (see Sec. 47.2). In one dimension, the density dip of the soliton corresponds to a node of the dipolar topological mode [1378, 921, 938].

The abrupt phase gradient at the boundary plane exerts a force trying to increase the gap, while repulsive interactions work to heal it. At zero temperature, this balance ensures the dynamic stability of the soliton. While a perfect dark soliton should be stationary, experiments [212, 356] revealed that solitons with finite contrast propagate along the direction of the plane's normal vector with a velocity, which must always be less than the local sound velocity,

$$v_{sol} = c_s\sqrt{\frac{n_{sol}}{n}} \ , \tag{46.23}$$

where n is the peak density of the condensate and n_{sol} the density at the bottom of the dark soliton [1089, 657]. Fig. 46.5 shows that the soliton develops a curvature

when it propagates. One reason for this is a slower sound velocity, $c_s = \sqrt{gn_0/m}$, on the edges of the condensate, where the density is lower. The second reason is, that the density in the dip, n_{sol}, goes to zero at the edges. In the presence of a thermal cloud, dissipation reduces the contrast of the density dip and accelerates the soliton, until it reaches the sound velocity c_s and finally disappears.

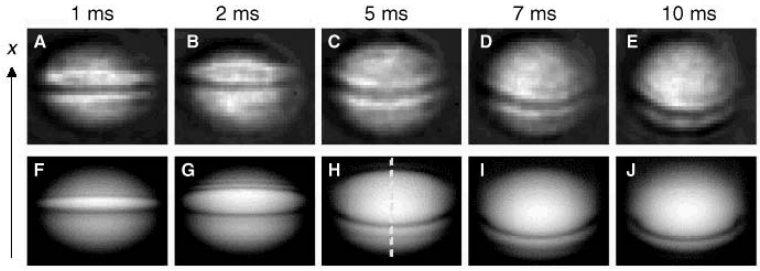

Figure 46.5: Solitons.

46.2.3.2 Bright solitons

In condensates with attractive interactions *bright solitons* have been observed, as well [715, 695].

46.2.4 Description of general topological modes

A coherent *topological mode* is a stationary solution of the *Gross-Pitaevskii equation*,

$$\left[-\frac{\hbar^2}{2m}\nabla^2 + U_{tr}(\mathbf{r}) + \frac{4\pi\hbar^2 a_s}{m}N|\phi_n|^2\right]\phi_n(\mathbf{r}) = E_n\Phi(\mathbf{r}) \ . \tag{46.24}$$

These modes can be calculated using an *optimized perturbation theory* [297]. We separate the Hamiltonian into an unperturbed part and a perturbed part, $\hat{H} = \hat{H}_0 + \Delta\hat{H}$, where the unperturbed part now depends on variational parameters,

$$\hat{H} = \hat{H}_0(u, v, ..) + \Delta H \ . \tag{46.25}$$

As usual, the first-order energy correction is,

$$E_n^{(1)}(u, v, ..) = E_n^{(0)}(u, v, ..) + \langle\Phi_n^{(0)}|\Delta\hat{H}|\Phi_n^{(0)}\rangle \ , \tag{46.26}$$

where the $\Phi_n^{(0)} = \Phi_n^{(0)}(u, v, ..)$ are the solutions of the unperturbed Hamiltonian $\hat{H}_0$. Once the energies are found, we must minimize them in terms of the variational parameters,

$$\frac{\partial E_n}{\partial u} = 0 \quad , \quad \frac{\partial E_n}{\partial v} = 0... \ . \tag{46.27}$$

With these parameters, we obtain the energies and the wavefunctions [2].

[2] Excited modes can be understood stationary matter waves with the trap serving as a cavity.

46.2.4.1 Creation of topological modes

One possibility of creating topological modes is to apply a temporal modulation to the trapping potential [1416]. The modulation frequency must be resonant with the energy difference between the excited mode and the ground state. Another possibility is to vary the interaction energy via a modulation of the scattering length in the vicinity of a *Feshbach resonance* [301].

The steady-state situation of a cloud in a stationary trap is *thermal equilibrium*, that is, inversion is not possible. At a time-dependent (e.g. shaking) potential however, for example, transitions to excited vibrational levels can be driven. These can generate inversion, provided collision-induced relaxation is not too fast [3].

46.2.5 Turbulence

The issue of turbulence is one of the most important problems of classical physics yet to be solved [442]. In superfluids, restrictions imposed by quantum mechanics constrain the emergence of turbulence, which is then called *quantum turbulence*. On the other hand, the study of quantum turbulence can improve our understanding of *classical turbulence* [384]. Recently, the study of the dynamics of a ensemble of vortices in a Bose-Einstein condensate allowed the identification of signatures of quantum turbulence [609, 584].

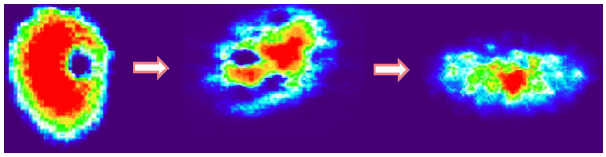

Figure 46.6: Turbulence.

46.2.6 Exercises

46.2.6.1 Ex: Comparison between the quantum and the classical vortex

Consider a vortex around a straight line along the z-axis at $r = 0$. Compare the radial velocity variation of a quantum vortex with that of a classical one.

Solution: *Because of symmetry, the flux lines around the axis are concentric. Therefore,* $\mathbf{v}_s(\mathbf{r}) = v_s(\mathbf{r})\hat{\theta}$. *Choosing the loop* C *as a centered circle of radius* r*, we get*

$$\Gamma = \int_0^{2\pi} v_s(\mathbf{r},t)\hat{\theta}\cdot(\hat{\theta}rd\theta) = 2\pi r v_s(\mathbf{r},t) = \frac{\hbar}{m}\ell \ .$$

Therefore, the velocity field of the superfluid is a quantized vortex,

$$\mathbf{v}_s(\mathbf{r},t) = \ell\frac{\hbar}{mr}\hat{\theta} \ .$$

[3] The dynamics of atoms trapped in a harmonic potential is similar to the Jaynes-Cummings dynamics of an optical mode. However, the non-linear condensate self-interaction changes the situation and makes the collisions being collective.

This is in contrast to classical fluids, where vortices generally satisfy the rotational field $\mathbf{v} = \mathbf{\Omega} \times \mathbf{r}$*, where* Ω *is the angular velocity. In this case, instead of decreasing, the amplitude of the velocity field increases with the radius.*

46.2.6.2 Ex: Singularity in vortices

Show for the above simple example,

$$\nabla \times \mathbf{v}_s(\mathbf{r}, t) = \hat{\mathbf{z}} \frac{\ell h}{m} \delta(x)\delta(y) \ .$$

Solution: *The rotation reads in cylindrical coordinates* (r, θ, z)*:*

$$\nabla \times \mathbf{v}_s = \left(\frac{1}{r} \frac{\partial}{\partial \theta} v_z - \frac{\partial}{\partial z} v_\theta \right) \hat{\mathbf{r}} + \left(\frac{\partial}{\partial z} v_r - \frac{\partial}{\partial r} v_z \right) \hat{\theta} + \left(\frac{1}{r} \frac{\partial}{\partial r} (r v_\theta) - \frac{1}{r} \frac{\partial}{\partial \theta} v_r \right) \hat{\mathbf{z}} \ .$$

For our case,

$$\nabla \times \mathbf{v} = \left(\frac{1}{r} \frac{\partial}{\partial r} (r v_\theta) \right) \hat{\mathbf{z}} = \ell \frac{\hbar}{mr} \ .$$

46.2.6.3 Ex: Phase-engineering of a vortex state

The first vortex in a dilute gas was created at the JILA [857]. Study the paper and explain in detail, how the vortex was created.

Solution: *Beginning with a standard BEC of* ^{87}Rb *in the fundamental state* $|1, -1\rangle$ *confined to a harmonic potential, the hyperfine state* $|2, 1\rangle$ *was coupled by microwave-radiofrequency two-photon radiation. The sum of the frequencies has been tuned* $\Delta_{rf}/2\pi = 94$ *Hz out of resonance. The radiation intensity was adjusted to a Rabi frequency of* $\Omega_{rf} = (2\pi)35$ *Hz, causing the Bloch vector of the effective two-level system to precede with a generalized Rabi frequency* $G_{rf} = (\Omega_{rf}^2 + \Delta_{rf}^2)^{1/2} = (2\pi)100$ *Hz. Spatial and temporal control over the conversion rate between the hyperfine states was obtained by an additional laser beam focused into the BEC (*$P = 10$ *nW,* $w_0 = 180$ *μm) and rotating with frequency* ω_{rot} *about the symmetry axis of the trap. The laser was tuned* $\Delta_l = (2\pi)800$ *MHz to the blue of the D2 line, thus causing an inhomogeneous and time-varying dynamic Stark shift* $\Omega_l(\mathbf{r}, t)^2/4\Delta_l$*, where* Ω_l *is the Rabi frequency at the D2 transition. While ground state atoms located at the trap center did not feel the Stark shift modulation, atoms located at a distance* r_{rot} *of the center were subjected to the total contrast of the modulation and, therefore, to the microwave radiation through the two modulation sidebands located in* $\Delta_{rf} \pm \omega_{rot}$*. To satisfy the resonance condition for one of the sidebands and excite transitions from the ground state to the state* $|2, 1\rangle$*, the rotation frequency was synchronized with the precession frequency,* $|\omega_{rot}| = G_{rf}$*. This is equivalent to accommodating the precession phase of the Bloch vector,* $G_{rf}t$*, with the azimuthal Broglie phase of the atoms created in the state* $|2, 1\rangle$*,* $\omega_{rot}t$*, ensuring a unique de Broglie phase along the rotation path. The*

phase gradient of the matter wave then generated a circular flow and formed a vortex.

46.3 Atom optics

Unlike the photons [770], there is no doubt about the fact that atoms are particles. On the other hand, the deep analogy between light and matter, resulting from the particle-wave duality, prompted de Broglie in 1924 to ascribe a *wave* to each massive particle, whose wavelength would be a function of the particle's momentum. Whether an atom behaves more like a particle or a wave depends on the specific experimental situation. For example, interferometers emphasize its wave nature: Atoms are able to interfere with *themselves*, when their Broglie wavelength is coherently split and then recombined. (Bosonic) atoms are able to interfere with other atoms, if their de Broglie wavelengths are greater than their distances. For this to happen, it requires high densities and very low temperatures, that is, high phase space densities. When the phase space densities are so high that the Broglie waves come into contact, effects of quantum statistics begin to influence the dynamics of the atoms, and fermions will behave differently from bosons.

Analogously to the distinction between classical and laser optics, we can separate the area of conventional atomic optics working with individual, mutually incoherent atoms, from the area of coherent atomic optics working with Bose-Einstein condensates. Unlike for the study of phenomena related to superfluidity, gases with weak interatomic interactions are generally more useful for the study of the coherent properties of condensates and for application in atomic optics. Nevertheless, interatomic collisions increase the complexity of the dynamics of matter waves interacting with atom optical devices, by introducing non-linarities analogous to those known from nonlinear optics and thus raising the field of *nonlinear atom optics*.

46.3.1 Atomic optical tools

The basic equipment of an atomic optics laboratory [904, 6, 1032, 463, 1060] comprises atomic beams, atom traps, lenses and waveguides, various types of mirrors and resonators, Stern-Gerlach type matter wave polarizers, de Broglie wave phase shifters based on Bragg diffraction, and a multitude of atomic beam gratings. Obviously, gratings allow the construction of atom interferometers, which are used in experiments and high precision devices, for example, atomic gyroscopes and gravimeters. Other applications for atomic beams controlled by atom optical elements are in atomic holography for the projection of complex pattern into integrated semiconductor circuits [923], in lithography [1309], and in microscopy [376].

An important feature of atoms (as compared to light) is the existence of a rich internal structure providing a wealth of additional degrees of freedom, whose dynamics (of the Bloch vector) is frequently entangled with the motional dynamics (of the de Broglie wave). This allows to monitor (e.g. in matter wave interferometers) the evolution of the motional state of the matter wave via an observation of the internal excitation. Moreover, in some interferometers, the de Broglie wave is not even split, and one does interferometry with completely immobile atoms or ions [642].

The epitome of a coherent light source is the laser, and we may ask whether there is a material analogue, which would be a source of coherent matter [1386, 179, 1231, 625, 933, 730] serving for *coherent atom optics*. In fact, we may already consider a trapped condensate as a stationary *atom laser* pulse with the trapping potential playing the role of the laser resonator. While most atom optical devices (including conventional atomic interferometers) do not require mutual coherence of atoms, certain applications take advantage of an intense, highly directional, monochromatic, and coherent atom source. In this respect, atom lasers are much superior to thermal atomic beams. While a thermal beam contains about 10^{-12} atoms per mode and a magneto-optical trap about 10^{-6}, a condensed mode may contain more than 10^6 atoms. Condensates offer the advantage of large de Broglie wave amplitudes and de Broglie wavelengths as long as their actual size (which can be much longer than optical wavelengths). And for an atom laser, the coherence length can even be longer than that of the condensate from which it emerged. This obviously has a major impact on the sensitivity and resolution of atom optical elements, in particular those, where atomic coherence is important, for example, atom interferometers. Without doubt atom lasers will replace conventional atomic beams in precision measurement of fundamental constants and tests of fundamental symmetries ([Phys. World (mar,97) p.43]). Finally, atom lasers are crucial for nonlinear optics.

Also of interest are the references [1229, 923, 1072, 774, 1121, 80, 608, 390, 1059, 355, 620, 1092, 656, 1156, 133, 376, 1366].

46.3.2 The atom laser

A large number of techniques for making an *atom laser* has already been developed [881, 36, 890, 30, 154, 570, 849] and theories on atom lasers have been formulated [565, 931, 1384, 1353, 644]. The following sections are devoted to explaining, why the term atom laser is justified. For the reasoning we will let as guide by the optical laser.

We already mentioned the *trapping potential* (replacing the resonator in lasers) as a major ingredients of an atom laser [4]. Another necessary feature would be the availability of an *output coupling* mechanism, which we still need to discuss in the following. Apart from these more practical aspects, we need to prove, that atom lasers are indeed *phase-coherent*, and we have to clarify the role of *bosonic stimulation* and of *irreversibility* in the production process of a BEC.

46.3.2.1 Bosonic stimulation and irreversibility

The gain mechanism for optical lasers is photonic stimulation of atoms inciting them to emit other photons into the stimulating mode. The atomic laser operates in a similar way. Atoms trapped in a potential constitute a thermal reservoir. Binary collisions redistribute the atoms among the vibrational energy levels of the potential. If a vibrational level already contains an atomic population, Bose-Einstein quantum statistics will encourage atoms involved in a collision process to join this level. Ultimately, this comes down to an irreversible pumping of a single level, where the atoms accumulate to build a single degenerate quantum state. Bose condensation is always

[4] Coherent reflection of atom laser beams has been demonstrated [167, 45, **?**], and an atom laser cavity with efficient transverse focusing has been built [156]

the result of *bosonic stimulation*. However, the dynamics and time scale for the formation of a condensate have been controversially discussed, until some experiments [890] could directly visualize *in vivo* the process of nucleation and the exponential amplification at the center of a thermal cloud (see Fig. 46.7).

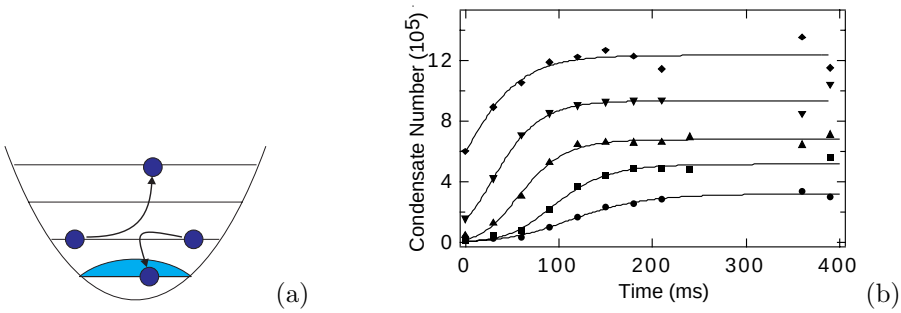

Figure 46.7: (a) Illustration of the idea of bosonic stimulation. (b) The curves show the growth of a condensate toward thermal equilibrium for different initial numbers of condensed atoms.

The very high concentration of population in a single phase space cell during the creation of a condensate represents a dramatic reduction of entropy. Since the total entropy can not decrease, the condensate must be coupled to a thermal reservoir receiving the excess entropy. This coupling is necessarily irreversible. In practice, the reservoir is the cloud of thermal atoms, whose energy is spread over many vibrational states. Irreversibility is introduced by collisions and the subsequent removal of the hottest atoms.

46.3.2.2 Phase of a condensate and first and higher-order coherences

First-order coherence and long-range order are necessary conditions for assigning a single global phase to the condensate. The existence of a single phase, and the possibility of measuring it, were questioned in the past. Certainly, the phase of a BEC is not observable *by itself*, but only *the relative phase* of two condensates.

The intrinsic phase-coherence of condensates has demonstrated in many experiments. An early example [575] employed internal state interferometry by splitting and remixing ^{87}Rb condensates trapped in the different Zeeman states $|F, m_F\rangle = |1, -1\rangle$ and $|2, 1\rangle$. They found that the phase was remembered for times longer than 150 ms. In another experiment [33, 712, 1353], illustrated in Fig. 46.8, a condensate was spatially split in two halves and then recombined. The interpenetration of the two halves at a well-defined relative velocity gave rise to a clear matter wave interference pattern. This ability of ballistically expanding condensates to interfere demonstrated the absence of a random phase lag during the expansion process and that the preservation of the condensates' long range order. However, under the repulsive influence of the mean-field energy, the phase profile of a released condensate evolves in a non-uniform but well-defined manner [1209].

The homogeneity of the phase of a *confined* condensate was also confirmed experimentally [1259, 569, 155] through interferometric techniques based on Bragg diffrac-

tion (see Sec. 47.2.2). The spatial coherence of an output coupled atom laser has been verified with a double-slit experiment [155]. And the temporal coherence of an atom laser beam was shown to be Fourier-limited by the finite output coupling time [**?**].

Similar to Young's double slit experiment in optics, the observation of matter wave interference only indicates first-order coherence, i.e. amplitude fluctuations in the matter field. Signatures for the presence of higher-order coherences in condensates were discovered in other experiments: The second-order correlation function, which represents a measure for intensity fluctuations (number of particles) in the matter field, was derived from measurements of the condensate's release energy [714]. And the third-order coherence can be deduced from a comparison of the three-body recombination rates for condensed and thermal clouds [217].

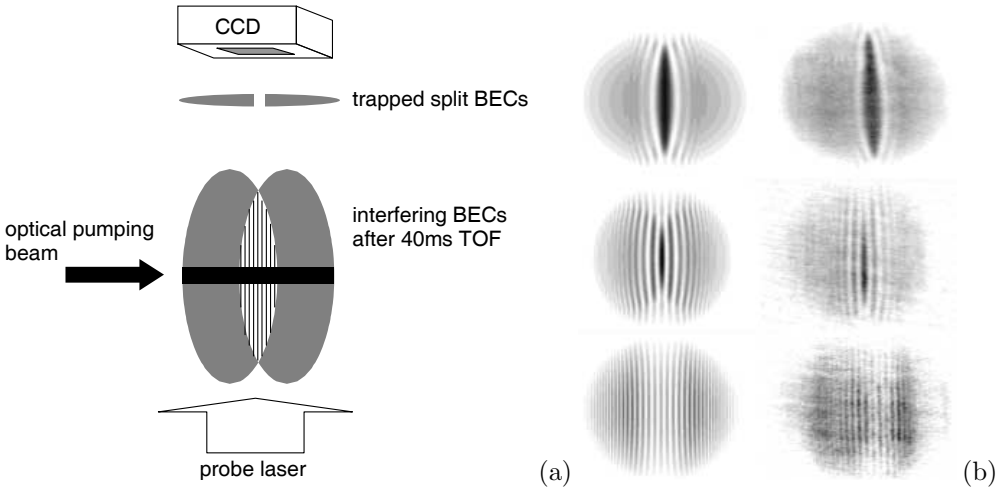

Figure 46.8: (a) Scheme for observation of matter wave interference. (b) Interference fringes.

A reliable characterization of atom number fluctuations and matter wave phase fluctuations in condensates is important for the simple reason, that these fluctuations will limit ultimately the resolution of atom interferometers, analogous to the *Schawlow-Townes limit* in lasers.

46.3.2.3 Output coupling

The *output coupler* for a trapped condensate plays a role similar to that of the partially reflecting mirror of a laser resonator. It transfers a fraction of condensed atoms out of the trapping potential through a coherent coupling to untrapped states. The coupling can be conveniently implemented via adiabatic potentials (see 38.1.3 and 43.4.3) generated by radiation (e.g. radiofrequency pulses [881] or continuous radiofrequency [154]). Also, pairs of laser beams in Raman configuration can create a coherent quasi-continuous and well-collimated atomic beam [570] and tunneling can give rise to a pulsed mode-locked atom laser (*mode-locked laser*) [30].

A trapped condensate represents a *finite reservoir* from which an atom laser can

be fed. For a really cw atom laser, an incoherent pumping mechanism, continuously feeding the BEC, while it delivers atoms to the atom laser, is still lacking [838].

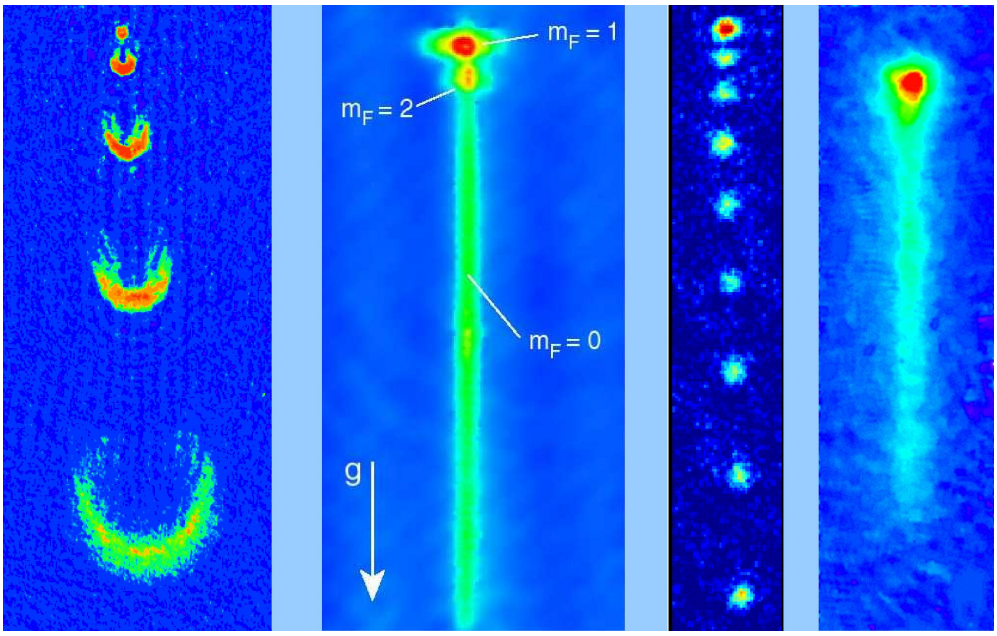

Figure 46.9: Several types of atomic lasers realized, from left to right at the MIT in 1997, in Munich in 1999, at Yale in 1998, and at NIST in 1999. The vertical sizes of the images are, from left to right: 5, 2, 0.5, and 1 mm.

46.3.3 Atomic interferometry with Bose-Einstein condensates

The most obvious use of an atom laser is within an atomic interferometer [1260, 1237, 168, 569, 155, 1209, 714, 217, 992, 353, 900, 926]. Many types of interferometers have been developed over the years. First of all, we note that the interferometric idea can be realized in the spatial domain (e.g. an atomic beam passing through a light wave) or in the time domain (e.g. a trapped atomic cloud or an immobile trapped ion irradiated by a pulsed light) [178, 642, 1073, 511].

Furthermore, depending on the involved degree of freedom (kinetic or internal excitation), we may distinguish two types of interferometers. Matter wave interferometers operating with the kinetic degree of freedom often use beam splitters based on Bragg diffraction [746, 992, 569, 1209]. Matter wave interferometers involving internal degrees of freedom generally couple two species of condensates, that is, two condensates in different states of internal excitation, for example, in different Zeeman [1261], hyperfine [939, 575, 900], or dressed states [780]. The phases of two BECs in different internal states, which we will call $|\pm\rangle$, evolve according to their respective chemical potentials, $\varphi_{|\pm\rangle}(t) = \mu_{|\pm\rangle}t$. The accumulated phases are not directly observable, but their difference, $\Delta\varphi(t)$, can be measured by *Ramsey interferometry*.

46.3.4 Non-linear atomic optics

In classical nonlinear optics, the interaction between matter (e.g. dilute gases) and light is described by Maxwell's equations. The electromagnetic field $\mathbf{E}$ creates a macroscopic polarization,

$$\mathbf{P}(\mathbf{r},t) = \chi(\mathbf{E})\mathbf{E}(\mathbf{r},t) = \chi^{(1)}\cdot\mathbf{E} + \chi^{(3)} : \mathbf{EEE} + \dots \,. \tag{46.28}$$

which in turn acts back onto the field. Higher-order processes, such as *self-focusing*, *second-harmonic generation*, *four-wave mixing*, etc. are described by the non-linear susceptibility $\chi^{(3)}$. These processes require the presence of a non-linear medium (the vacuum polarization itself being too small [696, 553]).

The role of binary collisions in coherent matter wave optics, as described by the nonlinear term in the Gross-Pitaevskii equation (45.21), is very similar to the role of the third-order nonlinear susceptibility in quantum optics [787, 746, 354, 518, 1318, 697, 586, 700, 792, 318, 591]. For example, if the atomic interaction is repulsive, the nonlinear term tries to increase the size of the condensate as much as possible within the limits imposed by the trapping potential. This behavior is analogous to the phenomenon of *self-defocusing* known in non-linear optics.

Small-amplitude elementary oscillations are well described by the *Bogolubov-de Gennes equations*, which are a linearized version of the Gross-Pitaevskii equation [297]. On the other hand, large-amplitude oscillations, which are sensitive to the nonlinear mean-field interaction [1222], showed a splitting of the frequency for quasi-particle excitation, in analogy with the generation of the second-harmonic (*SHG*) in quantum optics [591].

Other phenomena, such as matter wave *phase conjugation* and four waves mixing (*4WM*) [518] have been observed in experiments [354]. The three matter wave modes for the nonlinear mixing were produced out of a single condensate by applying two short consecutive sequences of Bragg diffraction pulses. The condensates are created in the same spatial region, but at different times. The nonlinear mixing during the process of spatial separation was observed by time-of-flight images.

The geometry of the laser beams is shown in Fig. 46.10(a) in the laboratory system. A first standing wave light pulse is generated by lasers $\mathbf{k}_1$ and $\mathbf{k}_2$ detuned from each other by an amount, such that the Bragg condition is satisfied and the momentum $\mathbf{p}_2 = \hbar\mathbf{k}_1 - \hbar\mathbf{k}_2$ is transmitted to the diffracted atoms. Then, a second standing wave light pulse formed by lasers $\mathbf{k}_1$ and $\mathbf{k}_3 = -\mathbf{k}_1$ transmits to the diffracted atoms the momentum $\mathbf{p}_3 = 2\hbar\mathbf{k}_1$. The duration and intensity of the standing waves are adjusted such as to create an approximately equal distribution of N_j^0 atoms in all three condensate momentum modes, each mode having a different momentum, $\mathbf{p}_1 = 0$, $\mathbf{p}_2$, and p_3. Initially, the three wavepackets $\hat{\psi}_j \equiv \hat{\psi}_0(\mathbf{r})\mathrm{e}^{i\mathbf{p}_j\mathbf{r}/\hbar}$ overlap. The nonlinear term in the Gross-Pitaevskii equation mixes the wavepackets while they separate to form other wavepackets, $\hat{\psi}_4 \sim g\hat{\psi}_j^+\hat{\psi}_m\hat{\psi}_n\mathrm{e}^{i\mathbf{p}_4\cdot\mathbf{r}/\hbar}$, where,

$$\begin{aligned} N_4 &= -N_j + N_j^0 = N_m - N_m^0 = N_n - N_n^0 = \sum\nolimits_{\kappa=1}^{3}(N_\kappa^0 - N_\kappa) \\ \mathbf{p}_4 &= -\mathbf{p}_j + \mathbf{p}_m + \mathbf{p}_n \\ p_4^2 &= -p_j^2 + p_m^2 + p_n^2 \,. \end{aligned} \tag{46.29}$$

To produce the new momenta, $\mathbf{p}_4 \neq \mathbf{p}_1, \mathbf{p}_2, \mathbf{p}_3$, the corresponding wavepackets must gather atoms from all three initial packets $\mathbf{p}_1 \neq \mathbf{p}_2 \neq \mathbf{p}_3$.

The experimental observation of a newly emerging wavepacket $\hat{\psi}_4$ has two complementary interpretations: In the inertial system defined by $\mathbf{p}_1 = -\mathbf{p}_3$ [see Fig. 46.10(b)], the wavepackets $\hat{\psi}_1$ and $\hat{\psi}_3$ suffer elastic collisions. The direction in which the condensates are scattered is, a priori, isotropic. The injection of a third condensate $\hat{\psi}_2$ bosonically stimulates the formation of a forth one, $\hat{\psi}_4$, in a predefined direction $\mathbf{p}_4 = -\mathbf{p}_2$. The laws of conservation for the particle numbers, momenta, and energies (46.29) only allow processes, which can be interpreted as degenerate 4WM in this inertial system. Each of the wavepackets $\hat{\psi}_1$ and $\hat{\psi}_3$ sacrifice N_4 atoms to create a new wavepacket $\hat{\psi}_4$ and to amplify the wavepacket $\hat{\psi}_2$. The redistribution of atoms is a coherent process.

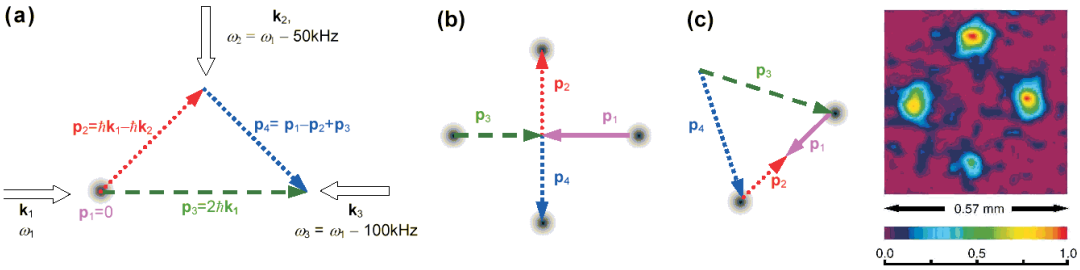

Figure 46.10: Matter wave 4WM can be illustrated (a) in the laboratory system, or (b) in the inertial system defined by $p_1 = -p_3$, or (c) in the system defined by $p_1 = -p_2$. In each system the process has a different physical interpretation (see text). The right image shows the experimental result.

The second interpretation becomes clear in the inertial system, in which $\mathbf{p}_1 = -\mathbf{p}_2$ [see Fig. 46.10(c)]. The conservation of energy only allows scattering products satisfying $p_4 = p_3$, that is, $\hat{\psi}_1^+ \hat{\psi}_2 \hat{\psi}_3$ and $\hat{\psi}_2^+ \hat{\psi}_1 \hat{\psi}_3$. In this system, the process can be interpreted as Bragg diffraction of the wavepacket $\hat{\psi}_3$ by the matter wave lattice formed by $\hat{\psi}_1$ and $\hat{\psi}_2$. The wavepacket $\hat{\psi}_4$ is nothing more than the first diffraction order. Unlike the Bragg diffraction in an optical lattice (see Sec. 47.2), the Bragg diffraction by a matter wave lattice requires nonlinear mixing through binary atomic collisions. Thus, the number of redistributed atoms depends on parameters such as the interatomic interaction strength, the size of the condensate, and the collision time between the wavepackets, i.e. the time that the wavepackets spend together before separating.

Despite the similarity with the optical counterpart, matter wave 4WM is fundamentally different: The number of particles must be conserved and the energy-momentum dispersion relation is not linear. Furthermore, while photons require the presence of a nonlinear medium in order to participate in higher-order processes, atomic matter waves mix through binary collisions.

46.4 Quantum atom optics

When describing a condensate by the Gross-Pitaevskii equation, we specify a phase and an atom number. However, both are conjugate quantities, which can not be specified without uncertainty. So, what does the BEC really look like: a Glauber state or rather a Fock state? We need to be careful. Certainly, it makes no sense talking about the absolute phase of a single BEC. Only the *relative phase* between *two* BECs matters. The condition for interference is, that we do not know, from which condensate the interfering atom came $\Delta N \Delta\varphi \geq 1$. So, the relative atom number must be uncertain.

46.4.1 Quantum transport

Now, let us imagine two BECs in a double-well potential. Atoms may be move between the wells via *Josephson tunneling*, even if the height of the barrier is higher than the atomic energy. Hence, the motion is a type of *quantum transport*. Be $\psi(\mathbf{r},t) = \psi_1(\mathbf{r})e^{i\mu_1 t/\hbar} + \psi_2(\mathbf{r})e^{i\mu_2 t/\hbar}$. In elongated traps the Josephson current is obtained as the expectation value of the *flux operator*,

$$I(z,t) = \frac{i\hbar}{2m}\int\left(\psi(\mathbf{r},t)\frac{d}{dz}\psi^*(\mathbf{r},t) - c.c.\right)dxdy\ . \tag{46.30}$$

One obtains,

$$I(z,t) = \frac{i\hbar}{2m}\int\left(\psi_1\frac{d\psi_1^*}{dz} + \psi_1\frac{d\psi_1^*}{dz} + \psi_1\frac{d\psi_1^*}{dz}e^{i(\mu_1-\mu_2)t/\hbar} + \psi_1\frac{d\psi_1^*}{dz}e^{i(\mu_1-\mu_2)t/\hbar} - c.c.\right)dxdy\ . \tag{46.31}$$

Choosing the original phase of the two condensates equal to zero, the time-independent terms are real and cancel each other, leaving,

$$\begin{aligned} I(z,t) &= \frac{i\hbar}{2m}\int\left(\psi_1\frac{d\psi_2}{dz} - \psi_2\frac{d\psi_1}{dz}\right)2i\sin\frac{(\mu_1-\mu_2)t}{\hbar}dxdy \\ &\equiv I_0\sin\frac{(\mu_1-\mu_2)t}{\hbar}\ . \end{aligned} \tag{46.32}$$

This shows that the current oscillates in time. This feature is well-known for *Josephson junction* in superconductors.

The question is now, what will be the steady-state of the two BECs [982]. Experiments have shown, that the BECs will gradually evolve into a superposition of number states, until they are coherent. The time scale is set by Josephson tunneling. The same interference pattern would result from BECs initially having well-defined phases [5,6]

[5] Also, a *spin-squeezed state* i.e. a state with sub-Poissonian number statistics approaching pure number states have been compared to coherent states. Superposition of the first ones exhibited no interference while superposition of the second ones lead to observable interference.

[6] If two Josephson-coupled BECs are initially in Fock-states, the current must initially be a quantum superposition of all currents corresponding to all possible atom number differences. This quantum superposition decoheres rapidly, leaving behind a semi-classical oscillation.

46.4.2 Optical lattices and the Mott insulator

We have already pointed out in Sec. 43.3.2, that laser beams tuned far away from resonances serve to construct trapping potentials for atoms. Laser beams incident on the atomic cloud under various angles allow the engineering of a large diversity of geometries for attractive potentials (with red tuned lasers) or repulsive potentials (with blue tuned lasers). Various cooling methods can be combined with dipolar traps, for example, Doppler cooling [647], Raman cooling [579], evaporative cooling [5], or gravitational Sisyphus cooling [948]. A particularly interesting geometry is that of are optical lattice, which we will discuss in the following sections.

46.4.2.1 Bragg scattering from optical lattices

In solid state physics the structure of crystal is studied by Bragg or von Laue scattering with X-ray radiation. Similar techniques can be used in optical lattices [146, 1157, 1360, 1361, 1217]. Under certain conditions, we can even expect to open a *photonic band gap* [37, 361, 1158], which draws an analogy between optical lattices and *photonic crystal*.

A great advantage of optical lattices is the possibility of directly visualizing the momentum distribution of the confined atoms, that is, the distribution of atoms over the *Brillouin zone*.

46.4.2.2 Bloch bands with mean field interaction

The Gross-Pitaevski equation is,

$$H\psi = \frac{-\hbar^2}{2m}\frac{d^2}{dx^2} + v\cos Kx + c|\psi|^2 = \mu\psi \ . \tag{46.33}$$

We have a periodic potential, $U(x) = U(x+X)$. In the following, we restrict ourselves to $1D$. Assume e.g. a sine wave potential,

$$U(x) = U_0\cos(2Kx) \ . \tag{46.34}$$

The Gross-Pitaevskii equation is rescaled via $k/K \to k$, $2Kx \to x$, $4\varepsilon t \to t$, $\psi/\sqrt{n} \to \psi$ and $C = \pi n a_s/K^2$. All frequencies are scaled like $U/4\varepsilon \to U$. Then,

$$-\tfrac{1}{2}\frac{\partial^2\psi}{\partial x^2} + (U\cos x - U)\ \psi + C|\psi|^2\psi = \mu\psi \ . \tag{46.35}$$

The Bloch-theorem says that the Schrödinger equation be solved by any Bloch state. Those are superpositions of plane-wave momentum states [**?**],

$$\psi(x) = e^{\imath kx}u_k(x) \ , \tag{46.36}$$

with $u_k(x) = u_k(x+X)$. We obtain,

$$-\tfrac{1}{2}\left(\frac{\partial}{\partial x} + \imath k\right)^2 u_k + U\cos x\ u_k + C|u_k|^2u_k = [\mu(k) + U]u_k \ . \tag{46.37}$$

Inserting the plane-wave expansions $u_k(x) = \sum_{q=-N}^{N} a_q(k) e^{iqx}$ into the Schrödinger equation, we get,

$$\sum_{q=-N}^{N} \Big[\tfrac{1}{2}(q+k)^2 a_q e^{\imath qx} + \tfrac{1}{2} U a_q (e^{\imath(q+1)x} + e^{\imath(q-1)x}) + C \sum_{m,n=-N}^{N} a_m a_n^* a_q e^{\imath(m-n+q)x} - [\mu(k)+U] a_q e^{\imath qx} \Big] = 0 \tag{46.38}$$

$$\tfrac{1}{2}(q+k)^2 a_q + \tfrac{1}{2} U(a_{q-1} + a_{q+1}) + C a_q \sum_{n=-N}^{N} |a_n|^2 - [\mu(k)+U] a_q = 0 \ .$$

We choose a cut-off q_0 so that $a_{q>q_0} = 0$. For a given k the coefficients a_q and the chemical potential μ, and thus the Bloch wave $u_k(x)$ can easily be calculated by minimizing the left hand side of the above equation. Note that for $C = 0$ we have we linear set of differential equation that can be solved as an eigenvalue problem (see Sec. 26.2.2).

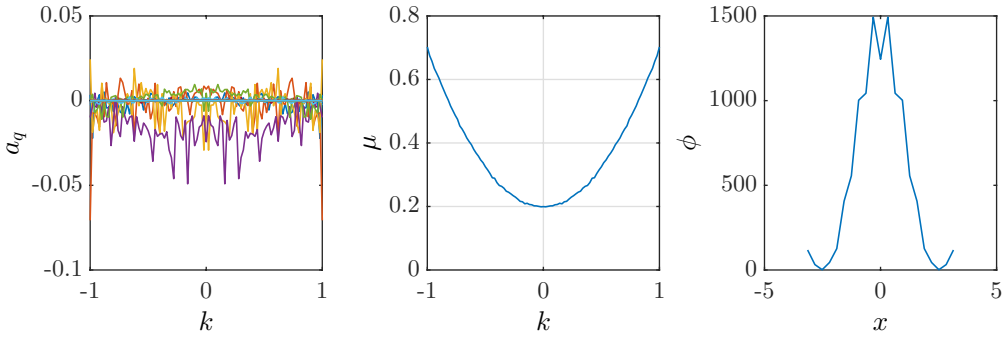

Figure 46.11: (code) Nonlinear interaction matrix finds just one minimum, dependence on k, [1389, 1391].

If we only consider the two lowest Bloch bands

$$u_k(x) = e^{\imath kx} a(x) + e^{\imath(k-K)x} b(x) \tag{46.39}$$

with $|a|^2 + |b|^2 = 1$, so that

$$|u_k|^2 = \left(e^{\imath kx} a + e^{\imath(k-K)x} b \right) \left(a e^{\imath kx} + b e^{\imath(k-K)x} \right) = 1 + 2ab \cos Kx \ , \tag{46.40}$$

and insert this into the Gross-Pitaevski equation Eq. (46.37), we find that the system of differential equations Eq. (46.38) simplifies to,

$$\begin{pmatrix} \frac{\hbar^2 k^2}{2m} + c & \frac{v}{2} + abc \\ \frac{v}{2} + abc & \frac{\hbar^2 (k-K)^2}{2m} + c \end{pmatrix} \begin{pmatrix} a \\ b \end{pmatrix} = \mu \begin{pmatrix} a \\ b \end{pmatrix} \ . \tag{46.41}$$

For $-2ab = \frac{v}{c}$ the off-diagonal elements vanish, and because the interacting BEC shields the potential. Since $|2ab| \leq 1$, this is only possible for $c \geq v$.

If we substitute $\mu = \tilde{\mu} + \frac{1}{2}\frac{\hbar^2 k^2}{2m} + \frac{1}{2}\frac{\hbar^2 (k-K)^2}{2m} + \frac{3}{2}c$, multiply the first row with b, the second with a and add both rows, we obtain,

$$2\tilde{\mu} = \frac{v}{2ab} \ . \tag{46.42}$$

Example 283 (*Estimations*): Estimated radial BEC size $r_t \simeq 10\ \mu m$, estimated number of atoms per antinode $n_{1D} \simeq 1000\ \mu\mathrm{m}^{-1}$,

$$\omega_r = \frac{\hbar k^2}{2m} = 2\pi \cdot 3.8\,\mathrm{kHz} \tag{46.43}$$

$$g_{1D} = \frac{4\pi\hbar^2 a_s}{m r_t^2} \tag{46.44}$$

$$g_{1D} n_{1D} = h \cdot 77\,\mathrm{Hz} \tag{46.45}$$

Since we need at least two Bloch bands to see interesting effects, we must arrange for much stronger mean fields.

46.4.2.3 The Mott insulator

In the Mott insulating state, the atoms are *localized* at individual sites of an optical lattice. On one hand, the localization impedes any phase relation between atoms at different sites, that is, at a given site the phase uncertainty $\Delta\phi$ is complete. But at the same time, there is a perfect correlation of the atom number at each site known as *spin squeezing* [7], because (in a homogeneous lattice) every site contains exactly the same number of atoms, that is, the atom number uncertainty ΔN tends to zero. At a given lattice site, the number of atoms and the phase of the wavefunction can not be simultaneously fixed: $\Delta N \Delta\phi > 1$.

The absence of relative coherence between different sites and of the ability to interfere prohibits the description of the system by a single global wavefunction and the use of the Gross-Pitaevskii equation. Nevertheless, the Mott insulating state is not equivalent to a completely randomized sample. On the contrary, the coherence only changes its character [8].

The *Mott transition* of a condensate from a superfluid state and to state of a *Mott insulator* occurs as a *quantum phase transition*, because it is driven by quantum fluctuations rather than of thermal noise. Therefore, it is a direct result of Heisenberg's uncertainty relation.

46.4.2.4 The Bose-Hubbard model

The *Bose-Hubbard model* gives an approximate description of the physics of interacting *bosons* in a lattice. The model is closely related to the fermionic Hubbard model, used in solid state physics for the description of superconducting systems and the hopping of electrons between the atoms of a solid crystalline lattice.

[7] The spin squeezing feature makes the Mott insulator interesting for spectroscopy at the *Heisenberg limit* and for quantum computation.

[8] Remember, that the Fock state is a complicated superposition of Glauber states. The disappearance and reappearance of coherence is reminiscent to the phenomenon of collapse and revival in the Jaynes-Cummings model.

The Bose-Hubbard model starts from the following Hamiltonian [982, 537],

$$\hat{H} = -J \sum_{(i,j)} \hat{a}_i^\dagger \hat{a}_j + \sum_i \varepsilon_i \hat{n}_i + \tfrac{1}{2} U \sum_i \hat{n}_i(\hat{n}_i - 1) \ , \tag{46.46}$$

where

$$J \equiv \int d^3\mathbf{x} \ w^*(\mathbf{x} - \mathbf{x}_i) \left[-\tfrac{\hbar}{2m} \nabla^2 + V_0(\mathbf{x}) \right] w^*(\mathbf{x} - \mathbf{x}_i) \ , \tag{46.47}$$

and

$$U \equiv \frac{4\pi a_s \hbar^2}{m} \int d^3\mathbf{x} \ |w^*(\mathbf{x})|^4 \ , \tag{46.48}$$

with $\varepsilon_i \equiv \frac{4\pi a_s \hbar^2}{m} \int d^3\mathbf{x} \ V_{trap}(\mathbf{x}) |w(\mathbf{x} - \mathbf{x}_i)|^2 \approx V_{trap}(\mathbf{x})$ and $w(\mathbf{x}) = w(x)w(y)w(z)$ are the *Wannier functions* for an individual particle. We assume for the moment a homogeneous condensate.

The Hilbert space dimension of the Bose-Hubbard model grows exponentially with the number of atoms N and the number of sites L,

$$D_b = \frac{(N_b + L + 1)!}{N_b!(L-1)!} \ . \tag{46.49}$$

For the Fermi-Hubbard model, the Pauli exclusion principle leads to the Hilbert space dimension,

$$D_f = \binom{L}{N_f} \ . \tag{46.50}$$

In three dimensional lattices the Hilbert space grows even faster. Therefore, it is a difficult computational task to model or simulate such systems, and generally not possible fro more than 20 atoms and 20 lattice sites.

At zero temperature, the Bose-Hubbard model (in the absence of disorder) predicts the atomic ensemble to be an a Mott insulating state (MI) when $J \ll U$, a superfluid state (SF) when $J \gg U$, or a *supersolid phase* (SS), where both solid and superfluid phases (diagonal and off-diagonal) coexist. Mott insulation phases are characterized by integer site occupation numbers, by the existence of an energy gap for particle-hole excitations, and zero compressibility. In the presence of disorder, a third phase, the *Bose glass* exists. This phase is insulation because of the Anderson localization effects. Bose glass is characterized by a finite compressibility, the absence of a gap, and an infinite superfluid susceptibility [449]. See also (watch talk).

In the limit of strong tunneling and weak interactions, $J \gg U$, the matter wave function looks like a *Bloch state*,

$$|\psi_{SF}\rangle \sim \left(\sum_{i=1}^{M} \hat{a}_i^\dagger \right)^N |0\rangle \ . \tag{46.51}$$

The variance of the number of particles per site is Poissonian, $\sigma_{SF} \sim \sqrt{N_i}$, that is, the wavefunction per lattice site is (quasi)-coherent. However, the total wavefunction is delocalized over all lattice sites, the local wavefunctions have a rigid phase relationship

and no long-range coherence. Otherwise, the matter wave function is an independent product of *Fock states*,

$$|\psi_{MI}\rangle \sim \prod_{i=1}^{M} (\hat{a}_i^\dagger)^n |0\rangle \ . \tag{46.52}$$

The momentum distribution in terms of Wannier functions is [558, 1390],

$$n(\mathbf{k}) = |w(\mathbf{k})|^2 \sum_{i,j} e^{i\mathbf{k}(\mathbf{r}_i - \mathbf{r}_j)} \langle \hat{a}_i^\dagger \hat{a}_j \rangle \ . \tag{46.53}$$

46.4.3 Schrödinger cats

Ruostekoski *et al.* [1120] proposed a double BEC system consisting of two momentum sidemodes and a far-off resonance laser beam that constantly spontaneously redistributes the atoms between the sidemodes. Homodyne detection of the scattered photons established *relative phase* information in such a way, that the relative number information is blurred in such a way that both sidemodes evolve into a simultaneous superposition of phase and number states. They disregard thermal excitations and two-body collisions. The cats are very sensitive to decoherence.

Cirac *et al.* [266] and Gordon *et al.* [524] consider Josephson double species condensates. The relative atom numbers Rabi flop. Mediated by the mean-field the systems may evolve into cats. The proposals have been reexamined by Dalvit *et al.* [324]. Other contributions come from [517, 617, 1127, 1074, 661]. First experiments on spin-squeezed states have been made by [982].

46.4.4 Exercises

46.4.4.1 Ex: Superfluid to Mott insulator transition

Consider a condensate trapped in a 3D *simple cubic* optical lattice with lattice spacing l. The Hamiltonian can be written as,

$$\hat{H} = -J \sum_{i,j} \delta_{ij}^{(1)} \hat{a}_i^\dagger \hat{a}_j + \tfrac{U}{2} \sum_i \hat{a}_i^\dagger \hat{a}_i^\dagger \hat{a}_i \hat{a}_i \ ,$$

where $\hat{a}_i$ ($\hat{a}_i^\dagger$) is the operator annihilating (creating) one boson in the lattice site i; $\delta_{ij}^{(1)} = 1$ only when i and j are nearest neighbors, otherwise it is zero. Assume a total of $M \gg 1$ sites, periodic boundary conditions in the x, y, and z directions, and $U > 0$. On this lattice we consider the construction operator $\hat{b}_s^\dagger$ defined in the following way:

$$\hat{b}_s^\dagger = \tfrac{1}{\sqrt{M}} \sum_i \hat{a}_i^\dagger \ .$$

a. Describe the action of this construction operator.
b. Derive the commutation relation,

$$[\hat{a}_\alpha, \hat{b}_s^\dagger] = \tfrac{1}{\sqrt{M}} \ .$$

c. Derive the commutation relation,

$$[\hat{a}_\alpha, (\hat{b}_s^\dagger)^N] = \tfrac{N}{\sqrt{M}} (\hat{b}_s^\dagger)^{N-1} \ .$$

d. Suppose that the following N-atom state exists:

$$|N, SF\rangle \equiv \tfrac{1}{\sqrt{N!}}(\hat{b}_s^\dagger)^N|0\rangle \ ,$$

where SF stands for a name label (and not for quantum numbers). Show that for $N = M$ we have $\hat{a}_\alpha|N, SF\rangle = |N-1, SF\rangle$.
e. Define the density operator for the site i as $\hat{n}_i = \hat{a}_i^\dagger \hat{a}_i$. Calculate the density fluctuation,

$$\Delta n_i = \sqrt{\langle \hat{n}_i^2\rangle - \langle \hat{n}_i\rangle^2}$$

of the state $|N, SF\rangle$ with $N = M$.
f. Calculate the total energy $\langle H\rangle$ with the state $|N, SF\rangle$.
g. Next consider the state,

$$|N, MI\rangle \equiv \prod_j \hat{a}_j^\dagger|0\rangle \ .$$

Calculate $\langle \hat{a}_i^\dagger \hat{a}_j\rangle$ and the density fluctuations Δn_i for this state.
h. Calculate the total energy $\langle H\rangle$ with the state $|N, MI\rangle$.
i. Discuss the energy for the states $|N, SF\rangle$ and $|N, MI\rangle$. Which one is the ground state? How to make a ground state change from $|N, SF\rangle$ to $|N, MI\rangle$?

Solution:

46.5 Further reading

M.R. Matthews et al., *Vortices in a Bose-Einstein Condensate* [857]DOI

K.M. Mertes et al., *Nonequilibrium Dynamics and Superfluid Ring Excitations in Binary Bose-Einstein Condensates* [879]DOI

I. Bloch, *Ultracold quantum gases in optical lattices* [153]DOI

J. Estève et al., *Squeezing and entanglement in a Bose-Einstein condensate* [427]DOI

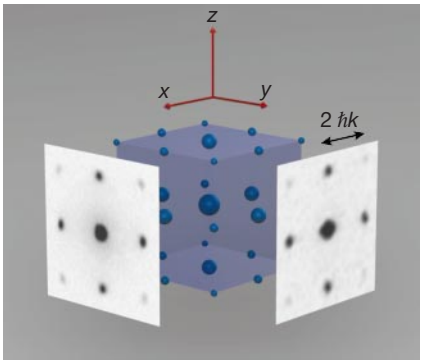

Figure 1 Schematic three-dimensional interference pattern with measured absorption images taken along two orthogonal directions. The absorption images were obtained after ballistic expansion from a lattice with a potential depth of $V_0 = 10E_r$ and a time of flight of 15 ms.

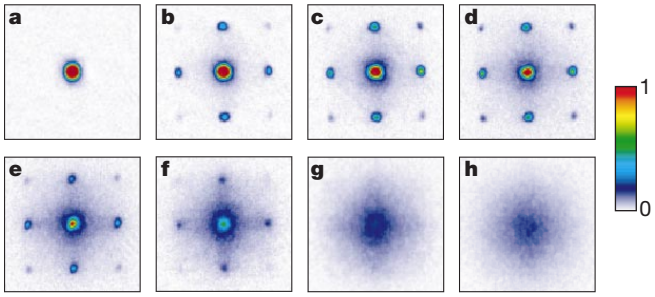

Figure 2 Absorption images of multiple matter wave interference patterns. These were obtained after suddenly releasing the atoms from an optical lattice potential with different potential depths V_0 after a time of flight of 15 ms. Values of V_0 were: **a**, 0 E_r; **b**, 3 E_r; **c**, 7 E_r; **d**, 10 E_r; **e**, 13 E_r; **f**, 14 E_r; **g**, 16 E_r; and **h**, 20 E_r.

Figure 46.12: Signature of the Mott phase.

Chapter 47

Interaction of Bose-Einstein condensates with light

Light can essentially be used in two ways for the manipulation of matter waves: 1. Tuned *far from resonance*, light serves to create conservative optical dipole potentials (see Secs. 43.3.2 and 46.4.2). In such circumstances the states of internal atomic excitation can be adiabatically eliminated from the description of the center-of-mass dynamics. 2. *Close to resonance* the situation is quite different, but even then, the coherent excitation of internal states may allow for a controlled manipulation of the atomic motion. Among the examples discussed in the following sections are the adiabatic sweeps, the Raman output coupler, Bragg pulses, photoassociation, and matter wave superradiance (see Fig. 47.1).

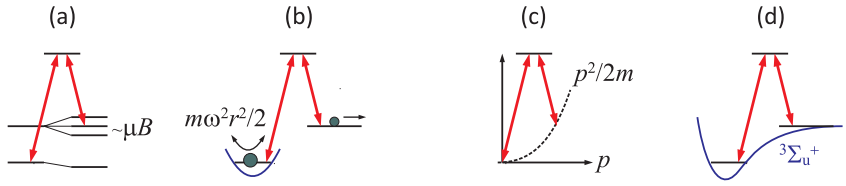

Figure 47.1: Different types of coherent coupling: (a) coherent coupling of hyperfine levels, (b) coupling from a confined state to the continuum of free states, (c) mutual coupling of different velocity states of an atom, and (d) coupling between a (collisional) state of two free atoms with a bound molecular state.

47.1 Scattering of light by degenerate gases

47.1.1 The structure factor for degenerate quantum gases

We introduced in Sec. 39.1.1 the notion of the structure factor, where it was used to characterize the scattering of light by thermal distributions of atoms. To characterize the scattering of matter waves, we must generalize the notion of the structure factor. We wrote in (39.3) the Fourier transform of the density distribution, which now becomes, after inserting $\hat{n}(\mathbf{r}) = \hat{\psi}^\dagger(\mathbf{r})\hat{\psi}(\mathbf{r})$ and the plane wave expansion (45.70),

$$\hat{\rho}^\dagger(\mathbf{q}) = \int \hat{\psi}^\dagger(\mathbf{r})\hat{\psi}(\mathbf{r})e^{\imath\mathbf{q}\cdot\mathbf{r}}d^3r = \tfrac{V}{(2\pi)^3}\iiint \hat{a}^\dagger_{\mathbf{k}'}\hat{a}_{\mathbf{k}}e^{\imath(\mathbf{k}-\mathbf{k}'+\mathbf{q})\cdot\mathbf{r}}d^3k'd^3kd^3r\ . \qquad (47.1)$$

With (45.76) and assuming sharp momenta (45.71),

$$\hat{\rho}^\dagger(\mathbf{q}) = V^2 \iint \hat{a}^\dagger_{\mathbf{k}'} \hat{a}_{\mathbf{k}} \delta_{\mathbf{k}',\mathbf{k}+\mathbf{q}} d^3k' d^3k = \sum_{\mathbf{k}',\mathbf{k}} \hat{a}^\dagger_{\mathbf{k}'} \hat{a}_{\mathbf{k}} \delta_{\mathbf{k}',\mathbf{k}+\mathbf{q}} \ . \tag{47.2}$$

Finally,

$$\boxed{\hat{\rho}^\dagger(\mathbf{q}) = \sum_{\mathbf{k}} \hat{a}^\dagger_{\mathbf{k}+\mathbf{q}} \hat{a}_{\mathbf{k}} = \sum_{\mathbf{k}} |\mathbf{k}+\mathbf{q}\rangle\langle\mathbf{k}|} \ . \tag{47.3}$$

Hence, $\hat{\rho}^\dagger(\mathbf{q})$ describes the scattering of an atom with the momentum $\mathbf{k}$ to $\mathbf{k}+\mathbf{q}$. We also find,

$$\hat{\rho}^\dagger(\mathbf{q}) = \hat{\rho}(-\mathbf{q}) \ . \tag{47.4}$$

Understanding the fundamental state $|g\rangle$ as the state without excitations, we define the *static structure factor* (39.5) now normalized to the number of particles [1237],

$$\boxed{S(\mathbf{q}) \equiv \tfrac{1}{N}\langle g|\hat{\rho}(\mathbf{q})\hat{\rho}^\dagger(\mathbf{q})|g\rangle} \ , \tag{47.5}$$

as a generalization of the classical structure factor. The static structure factor describes the probability to excite a condensate by creating a quasi-particle with momentum $\mathbf{k}$. We will need these notions in the Sec. 47.2.3.

The *dynamic structure factor* is obtained from $S(\mathbf{q}) = \int S(\mathbf{q},\omega)d\omega$ and measures the density of correlations in the ground state with 0 momentum. The formula describes, how an atom probes its environment by scattering quasi-particles back and forth,

$$S(\mathbf{q},\omega) = \tfrac{1}{N}\sum_f \langle g|\hat{\rho}(\mathbf{q})|f\rangle\langle f|\hat{\rho}(\mathbf{q})|g\rangle \hbar\delta(\hbar\omega - E_f + E_g) \ . \tag{47.6}$$

Solve the Excs. 47.1.6.1 to 47.1.6.5.

Example 284 (*Spatial coherence and the correlation function*): The *spatial coherence* can be defined by [CCT & Aspect],

$$\boxed{F(\mathbf{x}) \equiv \int \langle \mathbf{r}|\hat{\rho}|\mathbf{r}+\mathbf{x}\rangle d^3r = \int e^{\imath\mathbf{k}\cdot\mathbf{x}}\langle\mathbf{k}|\hat{\rho}|\mathbf{k}\rangle d^3k} \ . \tag{47.7}$$

We will demonstrate this relationship in Exc. 47.1.6.6. The *coherence length* ξ is given by $F(\xi) = \frac{1}{e}F(0) = \frac{1}{e}$. A *second order correlation function* is defined by,

$$\boxed{\begin{aligned} g^{(2)}(\mathbf{r}_1,\mathbf{r}_2) &= \frac{\langle\hat{\psi}^\dagger(\mathbf{r}_1)\hat{\psi}^\dagger(\mathbf{r}_2)\hat{\psi}(\mathbf{r}_2)\hat{\psi}(\mathbf{r}_1)\rangle}{\langle\hat{n}(\mathbf{r}_1)\rangle\langle\hat{n}_2(\mathbf{r})\rangle} \\ g^{(2)}(\mathbf{r}) &\equiv g^{(2)}(\mathbf{r}_1,\mathbf{r}_1+\mathbf{r}) \end{aligned}} \ .$$

47.1.2 The structure factor in Bragg spectroscopy

47.1.2.1 The Hamiltonian of the Rayleigh scattering process

In Sec. 23.5.3 we saw the Galilei-boost (??),

$$|\mathbf{k}+\mathbf{q}\rangle = e^{\imath\mathbf{q}\cdot\hat{\mathbf{r}}}|\mathbf{k}\rangle \ . \tag{47.8}$$

In the second quantization we generalize to,

$$|\mathbf{k}+\mathbf{q}\rangle = \int \hat{\psi}^\dagger(\mathbf{r}) e^{\imath \mathbf{q}\cdot\mathbf{r}} \hat{\psi}(\mathbf{r}) d^3r |\mathbf{k}\rangle = \hat{\rho}^\dagger(\mathbf{q})|\mathbf{k}\rangle \ . \tag{47.9}$$

Thus, we can implement the second quantization by simply replacing $e^{\imath \mathbf{q}\cdot\mathbf{r}}$ by $\hat{\rho}^\dagger(\mathbf{q})$. Now, the Hamiltonian for the process of a photon absorption from the mode $\hat{c}_{\mathbf{k}_i}$, taking into account the photonic recoil, was introduced in (38.6),

$$\hat{H}_{int} = \hbar\Omega(\hat{\mathbf{r}}) e^{-\imath \mathbf{k}_i\cdot\hat{\mathbf{r}}} \hat{c}_{\mathbf{k}_i} \hat{\sigma}^+ + c.c. \ . \tag{47.10}$$

If the process is followed by the reemission of a photon to the mode $\hat{c}_{\mathbf{k}_f}$,

$$\boxed{\hat{H}_{int} = \hbar\Omega(\hat{\mathbf{r}}) e^{\imath(\mathbf{k}_f-\mathbf{k}_i)\cdot\mathbf{r}} \hat{c}^\dagger_{\mathbf{k}_f} \hat{c}_{\mathbf{k}_i}} \ . \tag{47.11}$$

Going to second quantization, as done in (47.9), and doing the Fourier transform [1],

$$\tilde{H}_{int} = C \sum_{\mathbf{p}_f,\mathbf{p}_i} \hat{c}^\dagger_{\mathbf{k}_f} \hat{c}_{\mathbf{k}_i} \hat{a}^\dagger_{\mathbf{p}_f} \hat{a}_{\mathbf{p}_i} \delta_{\mathbf{k}_f-\mathbf{k}_i+\mathbf{p}_f-\mathbf{p}_i} \ . \tag{47.12}$$

We assume here, that the light modes $\mathbf{k}_i$ and $\mathbf{k}_f$ are predefined, but the velocities $\mathbf{p}_i$ are distributed. Otherwise, in the expression (47.12), we must also sum over light modes [2],

$$\boxed{\tilde{H}_{int} = C \sum_{\mathbf{k}_i,\mathbf{k}_f,\mathbf{p}_i,\mathbf{p}_f} \hat{c}^\dagger_{\mathbf{k}_f} \hat{c}_{\mathbf{k}_i} \hat{a}^\dagger_{\mathbf{p}_f} \hat{a}_{\mathbf{p}_i} \delta_{\mathbf{k}_f-\mathbf{k}_i+\mathbf{p}_f-\mathbf{p}_i}} \ , \tag{47.13}$$

where C is a normalization constant. This Hamiltonian describes the elementary scattering process as a process of four wave mixing (4WM) [712, 1238]. The light and the atoms are treated on equal footings as modes which can receive (quasi-)particle populations, and the scattering corresponds to a redistribution of populations between the modes [3].

The Hamiltonian (47.13) can be applied to various situations, such as spontaneous or stimulated Rayleigh scattering or Bragg scattering, depending on which ones of the modes $\mathbf{k}_f$, $\mathbf{k}_i$, $\mathbf{p}_f$, and $\mathbf{p}_i$ are populated or filtered by imposed boundary conditions.

Using momentum conservation $\mathbf{q} \equiv \mathbf{k}_f - \mathbf{p}_i = -\mathbf{p}_f + \mathbf{p}_i$, we obtain the cross section,

$$\left(\frac{d\sigma}{d\Omega}\right)_{\mathbf{k}_i\to\mathbf{k}_f} = C^2 \sum_f |\langle f|\hat{H}_{int}|i\rangle|^2 = C^2 \sum_f |\langle f| \sum_{\mathbf{p}_i} \hat{c}^\dagger_{\mathbf{k}_i+\mathbf{q}} \hat{c}_{\mathbf{k}_i} \hat{a}^\dagger_{\mathbf{p}_i-\mathbf{q}} \hat{a}_{\mathbf{p}_i} |i\rangle|^2 \ , \tag{47.14}$$

Example 285 (*Description of Bragg scattering via the structure factor*): In this example we irradiate two plane waves in directions $\mathbf{k}_1$ and $\mathbf{k}_2$ into a Bose-Einstein condensate. The total intensity will be,

$$I_{mod}(\mathbf{r},t) = I\cos(\mathbf{q}\cdot\mathbf{r} - \omega t) \qquad \text{with} \qquad \mathbf{q} = \mathbf{k}_1 - \mathbf{k}_2 \ . \tag{47.15}$$

[1] $\hat{a}_{\mathbf{p}}$ and $\hat{a}^\dagger_{\mathbf{p}}$ are the operators of the quantized atomic field, while $\hat{c}_{\mathbf{k}}$ and $\hat{c}^\dagger_{\mathbf{k}}$ are the operators of the light fields.

[2] Note the different form of this Hamiltonian as compared to (39.10).

[3] This is analogous to the way, in which a 'collision' redistributes atomic populations between momentum modes. We will discuss this general concept of 4WM in Secs. 47.3.4 and 46.3.4.

and the optical potential,

$$V_{mod} = \frac{\hbar\Gamma^2}{8\Delta} I \cos(\mathbf{q}\cdot\mathbf{r} - \omega t) = \frac{\hbar\Gamma^2}{8\Delta}\frac{I}{2I_{sat}}(e^{\imath\mathbf{q}\cdot\mathbf{r}-\imath\omega t} + e^{-\imath\mathbf{q}\cdot\mathbf{r}+\imath\omega t}) \qquad (47.16)$$
$$\rightarrow \hat{V}_{mod} = \frac{V}{2}[\hat{\rho}^\dagger(\mathbf{q})e^{-\imath\omega t} + \hat{\rho}^\dagger(-\mathbf{q})e^{\imath\omega t}] \ .$$

Now, the transition rate is [1238],

$$\frac{W}{N} = 2\pi\Omega_R^2 S(\mathbf{q},\omega) = \frac{2\pi}{N\hbar}\left(\frac{V}{2}\right)^2 \sum_f |\langle f|\hat{\rho}^\dagger(\mathbf{q})|g\rangle|^2 \delta(\hbar\omega - (E_f - E_g)) \ , \quad (47.17)$$

with $\frac{V}{2} = \hbar\Omega_R$.

Resolve Exc. 47.1.6.7.

47.1.3 Bosonic stimulation

We assume in the following weak light intensities (and hence a negligible contribution of the Mollow fluorescence spectrum). That is, without cooperative effects the light would be elastically scattered by Rayleigh scattering. Now, we adopt a notation labeling the multimodal state by the numbers of photons and atoms distributed over the available light and momentum modes. That is, the initial state consists of $n_{\mathbf{p}}$ atoms distributed over momentum atomic states $\mathbf{p}$ and $N_{\mathbf{k}}$ photons distributed over wave vector modes $\mathbf{k}$ denoted by $|...N_{\mathbf{k}}...\rangle_{rad} \otimes |...n_{\mathbf{p}}...\rangle_{at}$:

$$|i\rangle \equiv |...n_{\mathbf{p}_i}...n_{\mathbf{p}_f}...\rangle_{at} \ \otimes |...N_{\mathbf{k}_i}...N_{\mathbf{k}_f}...\rangle_{rad} \equiv \left|\begin{matrix}...n_{\mathbf{p}_i}...n_{\mathbf{p}_f}... \\ ...N_{\mathbf{k}_i}...N_{\mathbf{k}_f}...\end{matrix}\right\rangle \ , \qquad (47.18)$$

where we introduced the vector-like notation for notational compactness.

A particular scattering process can be treated like a 'collision' by redistributing the initial populations to final populations:

$$|f\rangle = \left|\begin{matrix}...n_{\mathbf{p}_i} - 1...n_{\mathbf{p}_f} + 1... \\ ...N_{\mathbf{k}_i} - 1...N_{\mathbf{k}_f} + 1...\end{matrix}\right\rangle \ . \qquad (47.19)$$

We write the matrix element,

$$\langle f|\hat{H}_{int}|i\rangle \propto \left\langle\begin{matrix}...n_{\mathbf{p}_i''}...n_{\mathbf{p}_f''}... \\ ...N_{\mathbf{k}_i''}...N_{\mathbf{k}_f''}...\end{matrix}\right| C \sum_{\mathbf{k}_i',\mathbf{k}_f',\mathbf{p}_i',\mathbf{p}_f'} \hat{c}^\dagger_{\mathbf{k}_f'}\hat{c}_{\mathbf{k}_i'}\hat{a}^\dagger_{\mathbf{p}_f'}\hat{a}_{\mathbf{p}_i'}\delta_{\mathbf{k}_f'-\mathbf{k}_i'+\mathbf{p}_f'-\mathbf{p}_i'} \left|\begin{matrix}...n_{\mathbf{p}_i}...n_{\mathbf{p}_f}... \\ ...N_{\mathbf{k}_i}...N_{\mathbf{k}_f}...\end{matrix}\right\rangle \ . \qquad (47.20)$$

Assuming that all modes are not degenerate, such that $[\hat{a}_{\mathbf{p}_f}, \hat{a}^\dagger_{\mathbf{p}_i}] = \delta_{\mathbf{p}_f,\mathbf{p}_i}$, that is, $\hat{a}^\dagger_{\mathbf{p}_f}$ and $\hat{a}_{\mathbf{p}_f}$ only act on the mode $|n_{\mathbf{p}_f}\rangle_{at}$, etc.,

$$\sum_{\mathbf{p}_i'} \hat{a}_{\mathbf{p}_i'}|...n_{\mathbf{p}_i}...\rangle_{at} = \sum_{\mathbf{p}_i} \sqrt{n_{\mathbf{p}_i}}|...n_{\mathbf{p}_i} - 1...\rangle_{at} \qquad (47.21)$$
$$\text{and} \quad \sum_{\mathbf{p}_f'} \hat{a}^\dagger_{\mathbf{p}_f'}|...n_{\mathbf{p}_f}...\rangle_{at} = \sum_{\mathbf{p}_f} \sqrt{n_{\mathbf{p}_f}+1}|...n_{\mathbf{p}_f}+1...\rangle_{at} \ ,$$

as well as,

$$\sum_{\mathbf{k}'_i} \hat{c}_{\mathbf{k}'_i} |...N_{\mathbf{k}_i}...\rangle_{rad} = \sum_{\mathbf{k}_i} \sqrt{N_{\mathbf{k}_i}} |...N_{\mathbf{k}_i} - 1...\rangle_{rad} \tag{47.22}$$

$$\text{and} \quad \sum_{\mathbf{k}'_f} \hat{c}^\dagger_{\mathbf{k}'_f} |...N_{\mathbf{k}_f}...\rangle_{rad} = \sum_{\mathbf{k}_f} \sqrt{N_{\mathbf{k}_f}+1} |...N_{\mathbf{k}_f}+1...\rangle_{rad} \ .$$

Let us now assume for a moment, that the photon is scattered to the vacuum, that is, the final mode of light is initially empty, $N_{\mathbf{k}_f} = 0$ [4],

$$\begin{aligned} &\langle f|\hat{H}_{int}|i\rangle_{inel} \qquad (47.23)\\ &\propto \left\langle \begin{matrix} ...n_{\mathbf{p}''_i}...n_{\mathbf{p}''_f}... \\ ...N_{\mathbf{k}''_i}...N_{\mathbf{k}''_f}... \end{matrix} \middle| \sum_{\mathbf{p}_f,\mathbf{p}_i,\mathbf{k}_f,\mathbf{k}_i} \sqrt{N_{\mathbf{k}_i}}\sqrt{n_{\mathbf{p}_f}+1}\sqrt{n_{\mathbf{p}_i}} \middle| \begin{matrix} ...n_{\mathbf{p}_i}-1...n_{\mathbf{p}_f}+1... \\ ...N_{\mathbf{k}_i}-1...1_{\mathbf{k}_f}... \end{matrix} \right\rangle \\ &= \sum_{\mathbf{p}_f,\mathbf{p}_i,\mathbf{k}_f,\mathbf{k}_i} \sqrt{N_{\mathbf{k}_i}}\sqrt{n_{\mathbf{p}_f}+1}\sqrt{n_{\mathbf{p}_i}} \delta_{N_{\mathbf{k}''_i},N_{\mathbf{k}_i}-1}\delta_{N_{\mathbf{k}''_f},N_{\mathbf{k}_f}+1}\delta_{n_{\mathbf{p}''_i},n_{\mathbf{p}_i}-1}\delta_{n_{\mathbf{p}''_f},n_{\mathbf{p}_f}+1} \\ &= \sqrt{N_{\mathbf{k}_i}}\sqrt{n_{\mathbf{p}_f}+1}\sqrt{n_{\mathbf{p}_i}} \ . \end{aligned}$$

Obviously, the differential scattering cross-section,

$$\boxed{\left(\frac{d\sigma}{d\Omega}\right)_{inel} \propto N_{\mathbf{k}_i}(n_{\mathbf{p}_f}+1)n_{\mathbf{p}_i}} \ . \tag{47.24}$$

depends, in addition to the numbers of provided photons $N_{\mathbf{k}_i}$ and atoms $n_{\mathbf{p}_i}$ in the initial mode, also on the *number of atoms in the final mode* $n_{\mathbf{p}_f}$. This amplification of the probability of the scattering process is called *bosonic stimulation*.

Now, we consider the degenerate case, where the initial atomic momentum mode coincides with the final mode, $n_{\mathbf{p}_f} = n_{\mathbf{p}_i}$. In this case,

$$\sum_{\mathbf{p}'_f=\mathbf{p}'_i} \hat{a}^\dagger_{\mathbf{p}'_f}\hat{a}_{\mathbf{p}'_i}|...n_{\mathbf{p}_i}...n_{\mathbf{p}_f}...\rangle_{at} = \sum_{\mathbf{p}'_i} \hat{a}^\dagger_{\mathbf{p}'_i}\hat{a}_{\mathbf{p}'_i}|...n_{\mathbf{p}_i}...n_{\mathbf{p}_i}...\rangle_{at} = \sum_{\mathbf{p}_i} n_{\mathbf{p}_i}|...n_{\mathbf{p}_i}...n_{\mathbf{p}_i}...\rangle_{at} \ , \tag{47.25}$$

and a calculus analogous to (47.23) yields,

$$\langle f|\hat{H}_{int}|i\rangle_{el} \propto \left\langle \begin{matrix} ...n_{\mathbf{p}''_i}...n_{\mathbf{p}''_f}... \\ ...N_{\mathbf{k}''_i}...N_{\mathbf{k}''_f}... \end{matrix} \middle| \sum_{\mathbf{p}_i,\mathbf{k}_f,\mathbf{k}_i} \sqrt{N_{\mathbf{k}_i}} n_{\mathbf{p}_i} \middle| \begin{matrix} ...n_{\mathbf{p}_i}...n_{\mathbf{p}_i}... \\ ...N_{\mathbf{k}_i}-1...1_{\mathbf{k}_f}... \end{matrix} \right\rangle \tag{47.26}$$

$$= \sum_{\mathbf{p}_i,\mathbf{k}_f,\mathbf{k}_i} \sqrt{N_{\mathbf{k}_i}} n_{\mathbf{p}_i} \ {}_{rad}\langle ...N_{\mathbf{k}''_i}...N_{\mathbf{k}''_f}...|...N_{\mathbf{k}_i}-1...1_{\mathbf{k}_f}...\rangle_{rad} \ {}_{at}\langle ...n_{\mathbf{p}''_i}...n_{\mathbf{p}''_f}...|...n_{\mathbf{p}_i}...n_{\mathbf{p}_i}...\rangle_{at}$$

$$= \sum_{\mathbf{p}_i,\mathbf{k}_f,\mathbf{k}_i} \sqrt{N_{\mathbf{k}_i}} n_{\mathbf{p}_i} \delta_{N_{\mathbf{k}''_i},N_{\mathbf{k}_i}-1}\delta_{N_{\mathbf{k}''_f},N_{\mathbf{k}_f}+1}\delta_{n_{\mathbf{p}''_i},n_{\mathbf{p}_i}}\delta_{n_{\mathbf{p}''_f},n_{\mathbf{p}_i}} = \sqrt{N_{\mathbf{k}_i}} n_{\mathbf{p}_i} \ .$$

Now, the differential scattering cross-section,

$$\boxed{\left(\frac{d\sigma}{d\Omega}\right)_{el} \propto N_{\mathbf{k}_i} n^2_{\mathbf{p}_i}} \ , \tag{47.27}$$

[4] We will discuss later the case, where the scattering is (bosonically) stimulated by the number of photons already present in the final mode prior to the scattering process.

only depends on the number of provided photons $N_{\mathbf{k}_i}$ and the number of atoms $n_{\mathbf{p}_i}$ in the initial mode.

47.1.3.1 Elastic and inelastic scattering

The interpretation of the result is the following: Light can be scattered in two ways: (i) with or (ii) without change of atomic moment distribution. The event of a photon scattering (47.19) then it consists of two terms (47.24) and (47.27) [1044],

$$\frac{d\sigma}{d\Omega} = \left(\frac{d\sigma}{d\Omega}\right)_{el} + \left(\frac{d\sigma}{d\Omega}\right)_{inel} . \tag{47.28}$$

The first term of (47.28) occurs when the momentum of the scattering atom does not change, $\mathbf{p} = \mathbf{q}$, that is, when the populations of the momentum states $n_{\mathbf{p}}$ and $n_{\mathbf{q}}$ do not change. The corresponding term (47.27) describes elastic Rayleigh scattering. This process is coherent, that is, the phase relationship between the incident wave and the outgoing wave is fixed, because the photon emission is self-stimulated. I.e. it decays to the original mode via *forward scattering* within the angle defined by the *phase matching condition* $\vartheta < \lambda/d$, where d is the size of the atomic sample [712]. This contribution is dispersive, reversible, and conservative, and it is at the origin of the dipole force.

The second term of (47.28) is the inelastic part of Rayleigh scattering, where an atom with the initial momentum $n_{\mathbf{p}}$ is scattered to the momentum state $n_{\mathbf{q}}$. This term is absorptive, dissipative, and spontaneous. The frequency of the photons is shifted, a momentum is imparted to the atom, such that the process is incoherent. Hence, a suggestive way of expressing the differential scattering cross-section (47.19) is,

$$\frac{d\sigma}{d\Omega} \propto \left| \sum_i n_i \langle i|\hat{H}_{int}|i\rangle \right|^2 + \sum_{i\neq f} n_i(1+n_f)|\langle i|\hat{H}_{int}|f\rangle|^2 , \tag{47.29}$$

where $|i\rangle$ and $|f\rangle$ denote momentum states of the atomic sample.

The bosonic stimulation of inelastic Rayleigh scattering represents a way to overcome, on one hand the restrictive phase matching condition, and on the other the incoherence of the scattering into large angles. For non-interacting systems of localized bosons $S(\mathbf{q},\omega)$ can be expressed using single particle states $|i\rangle$ with energy E_i and population N_i [see (39.3) and (39.6)],

$$S(\mathbf{q},\omega) = N \left| \sum_i n_i \langle i|\hat{H}_{int}|i\rangle \right|^2 \delta(\omega) + N \sum_{i\neq f} |\langle f|\hat{H}_{int}|i\rangle|^2 n_i(n_f+1)\delta[\omega-(E_f-E_i)/\hbar] , \tag{47.30}$$

with $S_0(\mathbf{q}) = |\langle\hat{\rho}^\dagger(\mathbf{q})\rangle|^2 = \left|\sum_i n_i\langle i|\hat{H}_{int}|i\rangle\right|^2$.

47.1.4 Playing with bosonic and fermionic states

Here, we want to address the question, whether scattering processes are influenced by bosonic stimulation or cooperative enhancement. Let us consider the case of N atoms (bosons or fermions) generated from vacuum by operators $\hat{a}_m^\dagger(\mathbf{q})|0\rangle$, where m

indicates some additional quantum number (for example, the vibrational state of a loose trapping potential) helping us to enumerate fermionic states, and $\mathbf{q}$ indicates the momentum (considered independent from the trapping potential for short enough times). The operators respect the rules,

$$\begin{aligned} &[\hat{a}_m(\mathbf{0}), \hat{a}_n(\mathbf{q})]_\mp = 0 = [\hat{a}_m^\dagger(\mathbf{0}), \hat{a}_n^\dagger(\mathbf{q})]_\mp \\ \text{and} \quad &[\hat{a}_m(\mathbf{0}), \hat{a}_n^\dagger(\mathbf{q})]_\mp = \delta_{m,n}\delta_{\mathbf{0},\mathbf{q}} \quad \text{and} \quad \hat{a}_m(\mathbf{q})|0\rangle = 0 \ , \end{aligned} \tag{47.31}$$

where upper signs hold for bosons and lower signs for fermions. Initially the N atoms are in the bosonic, respectively, fermionic many-body state [919],

$$\boxed{|\Psi_b^{(N)}(\mathbf{0})\rangle = \tfrac{1}{\sqrt{N!}}\hat{a}_0^\dagger(\mathbf{0})^N|0\rangle \quad \text{resp.} \quad |\Psi_f^{(N)}(\mathbf{0})\rangle = \prod_{n=0}^{N-1}\hat{a}_n^\dagger(\mathbf{0})|0\rangle} \ . \tag{47.32}$$

Note that $|\Psi_b^{(N)}(\mathbf{0})\rangle = |N\rangle$ is a Fock state satisfying $\langle\Psi_b^{(N)}(\mathbf{0})|\Psi_b^{(N)}(\mathbf{0})\rangle = 1$, while $|\Psi_f^{(N)}(\mathbf{0})\rangle$ is a product state being normalized as well, $\langle\Psi_f^{(N)}(\mathbf{0})|\Psi_f^{(N)}(\mathbf{0})\rangle = 1$.

Probing the number of atoms in a many-body state is done by,

$$N = \langle\Psi|\hat{N}|\Psi\rangle \quad \text{where} \quad \hat{N} = \int \hat{\psi}^\dagger(\mathbf{r})\hat{\psi}(\mathbf{r})d^3r = \sum_{m,\mathbf{k}}\hat{a}_m^\dagger(\mathbf{k})\hat{a}_m(\mathbf{k}) \ , \tag{47.33}$$

or if we are only interested in a particular momentum state $\mathbf{k}$ and vibrational state m,

$$\langle\Psi|\hat{N}_m(\mathbf{k})|\Psi\rangle = \langle\Psi|\hat{a}_m^\dagger(\mathbf{k})\hat{a}_m(\mathbf{k})|\Psi\rangle = \|\hat{a}_m(\mathbf{k})|\Psi\rangle\|^2 \ . \tag{47.34}$$

Other possible many-body states are bosonic or fermionic product states,

$$\boxed{|\Psi^{(N_1)}(\mathbf{0})\rangle|\Psi^{(N_2)}(\mathbf{q})\rangle} \ . \tag{47.35}$$

We will see in 47.1.6.9 that product states are normalized if the partial states are normalized. Explicitly,

$$\begin{aligned} |\Psi_b^{(N_1)}(\mathbf{0})\rangle|\Psi_b^{(N_2)}(\mathbf{q})\rangle &= \frac{1}{\sqrt{N_1!N_2!}}\hat{a}_0^\dagger(\mathbf{0})^{N_1}\hat{a}_0^\dagger(\mathbf{q})^{N_2}|0\rangle \\ |\Psi_f^{(N_1)}(\mathbf{0})\rangle|\Psi_f^{(N_2)}(\mathbf{q})\rangle &= \prod_{n=0}^{N_1-1}\hat{a}_n^\dagger(\mathbf{0})\prod_{n=0}^{N_2-1}\hat{a}_n^\dagger(\mathbf{q})|0\rangle \ . \end{aligned} \tag{47.36}$$

Note, that product states in the same mode need renormalization when merged,

$$|\Psi_b^{(N_1)}(\mathbf{0})\Psi_b^{(N_2)}(\mathbf{0})\rangle = \frac{1}{\sqrt{N_1!N_2!}}\hat{a}_0^\dagger(\mathbf{0})^{N_1+N_2}|0\rangle = \sqrt{\binom{N_1+N_2}{N_1}}|\Psi_b^{(N_1+N_2)}(\mathbf{0})\rangle \ , \tag{47.37}$$

for example, $|\Psi_b^{(N)}(\mathbf{0})\Psi_b^{(1)}(\mathbf{0})\rangle = \sqrt{N+1}|\Psi_b^{(N+1)}(\mathbf{0})\rangle$.

A $\pi/2$-Bragg pulse has the faculty to transfer 50% of the atoms into a momentum mode $\mathbf{q}$, thus creating a new state where every single atom lives in a coherent

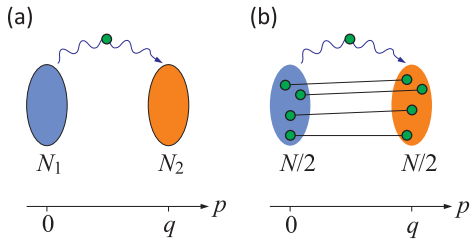

Figure 47.2: Cartoon of (a,b) bosonic stimulation and (c,d) cooperative enhancement.

superposition of two momenta,

$$\boxed{\begin{aligned} |\Psi_b^{(brgg,N)}(\mathbf{0},\mathbf{q})\rangle &= \frac{[\hat{a}_0^\dagger(\mathbf{0})+\hat{a}_0^\dagger(\mathbf{q})]^N}{\sqrt{2^N N!}}|0\rangle = \sum_{n=0}^{N}\binom{N}{n}\frac{\hat{a}_0^\dagger(\mathbf{0})^N\hat{a}_0^\dagger(\mathbf{q})^{N-n}}{\sqrt{2^N N!}}|0\rangle \\ |\Psi_f^{(brgg,N)}(\mathbf{0},\mathbf{q})\rangle &= \prod_{n=0}^{N-1}\frac{[\hat{a}_n^\dagger(\mathbf{0})+\hat{a}_n^\dagger(\mathbf{q})]}{\sqrt{2^N}}|0\rangle \end{aligned}} \quad . \tag{47.38}$$

In the following, we will study scattering processes, that is, fluctuations, in the presence of the states (47.35) or (47.38).

47.1.4.1 Bosonic stimulation versus cooperative enhancement by a Bragg grating

Now, we scatter a photon, whose fate is not of interest here, but which triggers possible transitions of an atom sitting together with N_1 atoms in the momentum state $\mathbf{0}|0\rangle$ towards another momentum state $\mathbf{q}|0\rangle$ initially populated with N_2 atoms via the operator,

$$\hat{H} = \sum_m \hat{a}_m^\dagger(\mathbf{k})\hat{a}_m(\mathbf{0}) \ , \tag{47.39}$$

which in fact is nothing else than the static structure factor. Applying this process to bosonic or fermionic clouds, as defined in (47.32), we find *bosonic stimulation* only in the case of bosons,

$$\boxed{\langle\Psi^{(N_1-1)}(\mathbf{0})\Psi^{(N_2)}(\mathbf{q})|\hat{H}|\Psi^{(N_1)}(\mathbf{0})\Psi^{(N_2-1)}(\mathbf{q})\rangle = \delta_{\mathbf{k},\mathbf{q}}\begin{cases}\sqrt{N_1 N_2} & \text{for bosons}\\ 1 & \text{for fermions}\end{cases}} \ , \tag{47.40}$$

as will be shown in Exc. 47.1.6.10(a). The transition probabilities are then,

$$\frac{d\sigma}{d\Omega} = |\langle f|\hat{H}|i\rangle|^2 = \delta_{\mathbf{k},\mathbf{q}}\begin{cases}N_1 N_2 & \text{for bosons}\\ 1 & \text{for fermions}\end{cases} \ . \tag{47.41}$$

Note, that these results does not change in the presence of a Bragg grating not participating in the dynamics:

$$\langle\Psi_b^{(M-1)}(\mathbf{0})\Psi_b^{(brgg,N+1)}(\mathbf{0},\mathbf{q})|\hat{H}|\Psi_b^{(M)}(\mathbf{0})\Psi_b^{(brgg,N)}(\mathbf{0},\mathbf{q})\rangle = 1 \ . \tag{47.42}$$

However, applying the same scattering process between a BEC with M atoms and the Bragg state defined in (47.38) consisting of N atoms, we identify two interesting possibilities for which we find,

$$\boxed{\begin{array}{lcl}\langle\Psi_b^{(M-1)}(\mathbf{0})\Psi_b^{(brgg,N)}(\mathbf{0},\mathbf{q})|\hat{H}|\Psi_b^{(M)}(\mathbf{0})\Psi_b^{(brgg,N-1)}(\mathbf{0},\mathbf{q})\rangle & = & (\delta_{\mathbf{k},\mathbf{0}}+\delta_{\mathbf{k},\mathbf{q}})\sqrt{MN}\\ \langle\Psi_b^{(M)}(\mathbf{q})\Psi_b^{(brgg,N-1)}(\mathbf{0},\mathbf{q})|\hat{H}|\Psi_b^{(M-1)}(\mathbf{q})\Psi_b^{(brgg,N)}(\mathbf{0},\mathbf{q})\rangle & = & \delta_{\mathbf{k},\mathbf{q}}\sqrt{MN}\end{array}} \,. \tag{47.43}$$

Interestingly, we find the same expression for bosons and for fermions,

$$\boxed{\langle\Psi_{b,f}^{(brgg,N-1)}(\mathbf{0},\mathbf{q})\Psi_{b,f}^{(1)}(\mathbf{q})|\hat{H}|\Psi_{b,f}^{(brgg,N)}(\mathbf{0},\mathbf{q})\rangle = \sqrt{\tfrac{N}{2}}\left[\delta_{\mathbf{k},\mathbf{0}} \pm \tfrac{N-1}{2}(\delta_{\mathbf{k},\mathbf{0}}+\delta_{\mathbf{k},\mathbf{q}})\right]} \,. \tag{47.44}$$

as will be shown in Exc. 47.1.6.10(b). The transition probabilities are then for boson and for fermions,

$$\frac{d\sigma}{d\Omega} = |\langle f|\hat{H}|i\rangle|^2 = \delta_{\mathbf{k},\mathbf{q}}\frac{N}{2}\frac{(N-1)^2}{4} \,. \tag{47.45}$$

This means that, if $\mathbf{k}=\mathbf{0}$ or $\mathbf{k}=\mathbf{q}$, the scattering is subject to *cooperative enhancement* by a factor of $N/2$ (which is the number of atoms in each of the momentum state $\mathbf{0}$ and $\mathbf{q}$) independently on the quantum nature of the atom (boson or fermion). That is, the probability that the scattered atoms joins one of the two momentum goes, for large N, like N^2, but for $N=1$ there is no enhancement possible. Do Exc. 47.1.6.11.

47.1.4.2 Interpretation of bosonic stimulation as cooperative enhancement

The distinction between spontaneous and stimulated processes is not always obvious, as there is a whole world of cooperative processes in between those two concepts, for instance, superradiance, Bragg scattering, and enhanced spontaneous emission into a resonant cavity. All those processes have in common that they are amplified by fluctuations.

Example 286 (*Stimulated emission versus spontaneous emission: Cooperativity in a cavity*): Let us first discuss the case of a cavity. Vacuum fluctuations (VF) are structured by a cavity (finesse F) leading to a modified DOS becoming anisotropic and developing spectral resonances. In resonance the VFs are enhanced (we get a standing wave of VFs), while off resonance they are suppressed. Therefore, an excited atom placed inside a cavity will suffer 'spontaneous stimulation' to decay into the cavity mode. Alternatively, we may say that the atom not only reacts to the local VFs but to all VFs reflected F times by the cavity mirrors provided these VFs are in phase (which is the case when the cavity is resonant). That is, *cavity-enhanced VFs amplify scattering into cavity modes* and, as we argued in Sec. 40.1.4 the VFs are measured by the structure factor (40.44).
Note, that the presence of photons in the cavity does not stimulate 'additionally', because stimulated emission and absorption are reversible processes.

Example 287 (*Bragg scattering: Cooperativity in a lattice*):

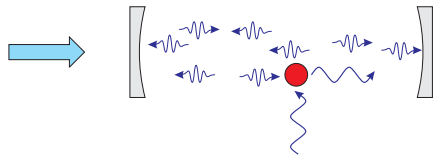

Figure 47.3: Cartoon of cooperative enhancement in a cavity.

Example 288 (*Matter wave superradiance and CARL: Cooperativity in a BEC*): We have seen that the stimulated processes mentioned above do not rely on quantum statistics, but rather on symmetry and coherence. Let us start with a naive picture of bosonic stimulation, a concept which can be applied to matter waves [713]. The physical process behind bosonically stimulated scattering is, that the presence of a macroscopically occupied state increases the density fluctuations of the system, and bosonically enhanced scattering is simply the diffraction of particles from these density fluctuations measured by $S(\mathbf{q},\omega)$.

47.1.5 Collective scattering for condensates with interactions

Until now we totally disregarded interactions between particles. Correlations are introduced in a BEC by interactions between the atoms. Therefore, collective scattering effects are influenced by interactions, while on the other hand an ideal gas ($gn \to 0$) scatters like an ultra-cool non-degenerate thermal cloud. In this sense, particle-like excitations ($\mathbf{p}^2/2m \gg gn$) in an interacting BEC behave like thermal atoms. The mean-field energy can be seen as resulting from excitations of phonon pairs. These pairwise excitations populate the momentum modes, which modify the scattering of light via bosonic stimulation. That is, an interacting condensate ($gn > 0$) gives a collective response to an incident light beam. Note that $\mu > 0$ is possible when $V(\mathbf{r}) \neq 0$ and $gn \neq 0$ even if $T \to 0$, which is the case here considered.

What is the nature of the collective behavior? 1. The Bogolubov spectrum is modified. In the phononic regime, the absence of dispersion allows the definition of a speed of sound. 2. The scattering of light can be suppressed by excitation of phonon pairs. This effect is anisotropic and more pronounced in forward direction. That is, the resonance at which the light is scattered is shifted and broadened. The latter effect is understood via destructive interference of two processes: Scattering from a BEC to the momentum mode $\mathbf{k}$ and from the momentum mode $-\mathbf{k}$ to a BEC.

It is important to be aware that the notion of *bosonic stimulation* $\sim n_i(1+n_f)$ and *fermionic inhibition* $\sim n_i(1-n_f)$ also has its limitations, when interatomic interactions are not negligible, that is, when the quantum depletion is remarkable [527, 862]. The effect of interatomic collisions can be taken into account as contributions of pair correlations to the ground state of the BEC,

$$|\psi_0, n_0\rangle = |n_0, 0, 0\rangle - \sum_{\mathbf{k}} (v_{\mathbf{k}}^2/u_{\mathbf{k}}^2)|n_0-2, 1, 1\rangle + \sum_{\mathbf{k}} (v_{\mathbf{k}}^2/u_{\mathbf{k}}^2)^2 |n_0-4, 2, 2\rangle - \dots , \quad (47.46)$$

where $|n_0, n_{\mathbf{k}}, n_{-\mathbf{k}}\rangle$ denotes the state with n_0 atoms in the trap's ground state and $n_{\pm\mathbf{k}}$ atoms in the momentum mode $\mathbf{k}$, where $v_{\mathbf{k}}^2$ is the average population of momentum

mode $\mathbf{k}$. The populated recoil modes result in a increase of spontaneous emission by a factor of $v_{\mathbf{k}}^2 = 1 + u_{\mathbf{k}}^2$. We can also understand the modification of the scattering rate as resulting from small scale inhomogeneities generated by pair correlations. The effect is strongest at small scattering angles, that is in forward direction.

47.1.6 Exercises

47.1.6.1 Ex: Sum rules for the dynamic structure factor

Derive the following sum rules for the norm, the kinetic energy, and the compressibility,

$$\begin{aligned} S(\mathbf{q}) &= \int S(\mathbf{q},\omega)d\omega \\ \frac{\hbar^2 q^2}{2m} &= \int \hbar\omega S(\mathbf{q},\omega)d\omega \\ \frac{\kappa^2}{2} &= \int \frac{S(\mathbf{q},\omega)}{\hbar\omega}d\omega\Big|_{\mathbf{q}\to 0} \end{aligned} .$$

Solution: *According to [877] ...*

47.1.6.2 Ex: Interaction energy of a condensate via spatial coherence

Show that the total energy of a condensate is given by $\langle U\rangle = \frac{1}{2}\int n(\mathbf{r}_1)U(\mathbf{r}_1 - \mathbf{r}_2)g^{(2)}(\mathbf{r}_1,\mathbf{r}_2)n(\mathbf{r}_2)d^3r_1 d^3r_2$.

Solution: *The interaction energy expressed by the correlation function is,*

$$\langle U\rangle = \tfrac{1}{2}\int n(\mathbf{r}_1)U(\mathbf{r}_1-\mathbf{r}_2)g^{(2)}(\mathbf{r}_1,\mathbf{r}_2)n(\mathbf{r}_2)d^3r_1 d^3r_2 \simeq \frac{2\pi\hbar^2}{m}a g^{(2)}(0)\tfrac{1}{2}\int n(\mathbf{r})^2 d^3r \ .$$

47.1.6.3 Ex: Structure factor of a condensate in the local density approximation

Calculate the structure factor of a condensate in the local density approximation (LDA) [204, 1237].

Solution: *With* $E_r = \frac{\hbar^2 q^2}{2m}$ *and* $\mu = \frac{\hbar^2}{2m\xi^2}$, *where* $\xi = (8\pi na)^{-1/2}$, *using the Bogolubov expression,*

$$S(\mathbf{q},\omega) = \frac{\hbar^2 q^2}{2m\epsilon(\mathbf{q})}\delta(\omega - \epsilon(\mathbf{q})/\hbar)$$

inserting the Bogolubov dispersion relation $\epsilon(\mathbf{q}) = \sqrt{\frac{\hbar^2 q^2}{2m}\left(\frac{\hbar^2 q^2}{2m} + gn(\mathbf{r})\right)}$ *and calculating the average over the Thomas-Fermi profile,* $n(\mathbf{r}) = g^{-1}[\mu - V_{ext}(\mathbf{r})]$*, we obtain,*

$$S_{LDA}(\mathbf{q},\omega) = \frac{15\pi}{8}\frac{\hbar^2\omega^2 - E_r^2}{E_r\mu^2}\left(1 - \frac{\hbar^2\omega^2 - E_r^2}{2E_r\mu}\right)^{1/2} .$$

This holds for $q\xi < 1$*, where for contrapropagating waves* $q = 2\cdot 2\pi/\lambda$*. Alternatively*

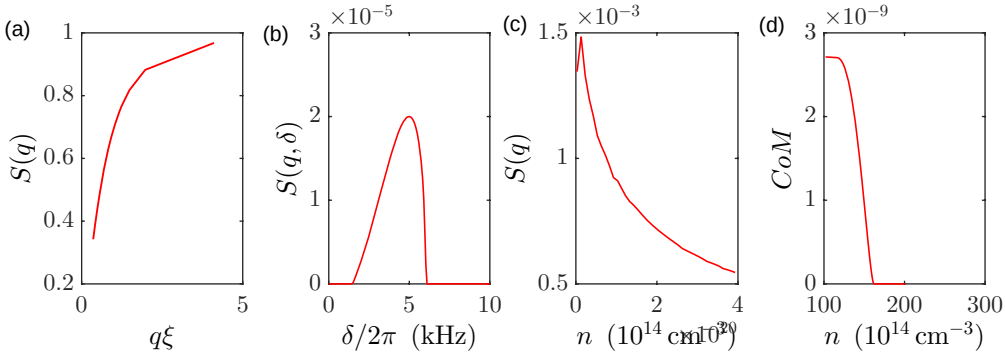

Figure 47.4: (code) (a) Static structure factor. (b) Dynamic structure factor. (c) Integrated dynamic structure factor. (d) Center-of-mass momentum.

[527, 861, 862],

$$S(q) = (u_q - v_q)^2 = (\cosh\phi_q - \sinh\phi_q)^2$$
$$\tanh 2\phi_q = \frac{\mu}{E_r(q) + \mu}$$
$$E_r(q) = \frac{\hbar^2 q^2}{2m} .$$

47.1.6.4 Ex: Structure structure of a Fermi gas

Calculate the structure factor for Bragg scattering on a Fermi gas.

Solution: *We calculate the Bragg scattering profile using the two-level model in addition to the Schrödinger equation and construct the sum of the density distributions at* $0\hbar q$ *and* $2\hbar q$*. Then, we calculate the axial center-of-mass momentum as a function of* ω*,*

$$p_{cm}(q,\omega) = \int n_{q,\omega}(z)dz .$$

On the other hand, the center-of-mass momentum is related to the dynamic structure factor via [1331],

$$p_{cm}(q,\omega) = \frac{\hbar\Omega_{br}^2}{2}\, S(q,\omega) \star \frac{1 - \cos(\omega t_{br})}{\omega^2} .$$

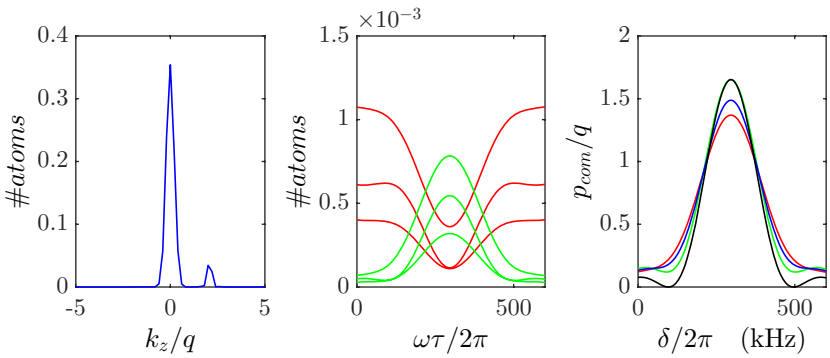

Figure 47.5: (code) (a) Density distribution after Bragg diffraction. (b) Diffraction efficiency as a function of Bragg detuning. (c) Center-of-mass momentum after Bragg diffraction.

In a Fermi gas the atoms are not correlated, so that the structure factor is $S(q,\omega) = \delta(\omega - \omega_R)$. *The center-of-mass momentum is thus approximately,*

$$p_{cm}(q,\omega) = \frac{\hbar\Omega_{br}^2}{2} \frac{1-\cos[(\omega-\omega_R)]t_{br})}{(\omega-\omega_R)^2} .$$

However, the inhomogeneity of the gas causes.
Alternatively, with $N(\mathbf{k}) = \theta(k_F - k)$,

$$\begin{aligned} S_{fermi}(\mathbf{q}) &= \int d\mathbf{k} N(\mathbf{k})[1 - N(\mathbf{k}+\mathbf{q})] \\ &= \int d\phi d\vartheta dk \; k^2 \sin\vartheta \; \theta(k_F - k) \left[1 - N(k_F - |\mathbf{k}+\mathbf{q}|)\right] \\ &= ??? \\ &= \left\{ \begin{pmatrix} \frac{3q}{4k_F} - \frac{q^3}{16k_F^3} & for & 0 < q < 2k_F \\ 1 & for & 2k_F < q \end{pmatrix} \right. \end{aligned}$$

47.1.6.5 Ex: Structure factor of a heteronuclear mixture

In this exercise we discuss the structure factor of a heteronuclear mixture (specifically contemplating ^{6}Li mixed with ^{87}Rb) generalizing the available theory for Li spin mixtures to heteronuclear mixtures [288, 472, 473, 1331]. The total dynamic structure factor is,

$$S(q,\omega) = S_{87,87}(q,\omega) + S_{6,6}(q,\omega) + S_{6,87}(q,\omega) + S_{87,6}(q,\omega) .$$

Exciting the Bragg resonance for Li, the Rb cloud would stay unaffected,the such that around $\omega/2\pi = 295$ kHz, $S_{87,87}(q,\omega) = 0$, as well as, $S_{6,87}(q,\omega) = S_{87,6}(q,\omega) = 0$. For Fermi gas $S_{6,6}(q,\delta) \to 1$, except if Bose gas induces Li-Li correlations, as in the case of BCS-pairing of phonon-mediated Efimov states.

How does Rb influence the Bragg scattering of Li? Via a variation of the apparent mass as a displacement of the Bragg resonance or as a second peak appearing at a specific detuning of the Bragg beams at $\omega_{6,6} * 6/(6+87)$?

Solution: *We have,*

$$p_{cm}(q,\omega) = \frac{\hbar\Omega_{br}^2}{2}\ S(q,\delta) \star \frac{1-\cos(\omega t_{br})}{\omega^2}\ .$$

and

	symbol &definition	*Bose gas at $T=0$*	*Fermi gas at $T=0$*
momentum population	$N(\mathbf{k})=$	?	$\theta(k_F-k)$
weighting factor		$F_b^{sp}=1+N_b(k_L)$	$F_f^{sp}=1-N_f(k_L)$
for spontaneous emisssion		$=\cosh^2\left(\frac{1}{2}\tanh^{-1}\frac{k_s^2}{k_L^2/2+k_s^2}\right)$	$=\theta(k_L-k_F)$
static structure factor	$S(\mathbf{q})=\int S(\mathbf{q},\omega)d\omega$	?	$\int d\mathbf{k}\ N(\mathbf{k})[1-N(\mathbf{k}+\mathbf{q})]$ $=\left(\frac{3q}{4k_F}-\frac{q^3}{16k_F^3}\right)(q\leq 2k_F)$ -
weighting factor for Rayleigh scattering	$F^{Ry}=$	?	?
dynamic structure factor	$S(\mathbf{q},\omega)=$	?	?
autocorrelation function	$g_2(\mathbf{r})=1+\frac{2}{N}\sum_{\mathbf{q}}[S(\mathbf{q})-1]e^{-\imath\mathbf{q}\cdot\mathbf{r}}$	$g_{2,f}(\mathbf{r})=$	$1-\frac{9}{(k_Fr)^4}\left[\frac{\sin k_Fr}{k_Fr}-\cos k_Fr\right]$
crosscorrelation function		–	–

47.1.6.6 Ex: Spatial coherence of a condensate

Derive the relationship (47.7).

Solution: *Using the expression (23.101), that is,*

$$\langle\mathbf{r}|\mathbf{k}\rangle = \tfrac{1}{(2\pi)^{3/2}}e^{\imath\mathbf{k}\cdot\mathbf{r}}\ ,$$

we calculate,

$$\begin{aligned}\int\langle\mathbf{r}|\hat{\rho}|\mathbf{r}+\mathbf{x}\rangle d^3r &= \iiint\langle\mathbf{r}|\mathbf{k}\rangle\langle\mathbf{k}|\hat{\rho}|\mathbf{k}'\rangle\langle\mathbf{k}'|\mathbf{r}+\mathbf{x}\rangle d^3kd^3k'd^3r\\ &= \tfrac{1}{(2\pi)}\iiint e^{\imath\mathbf{k}\cdot\mathbf{r}}\langle\mathbf{k}|\hat{\rho}|\mathbf{k}'\rangle e^{\imath\mathbf{k}'\cdot(\mathbf{r}+\mathbf{x})}d^3kd^3k'd^3r\\ &= \iint\langle\mathbf{k}|\hat{\rho}|\mathbf{k}'\rangle e^{\imath\mathbf{k}'\cdot\mathbf{x}}\delta^{(3)}(\mathbf{k}-\mathbf{k}')d^3kd^3k' = \int\langle\mathbf{k}|\hat{\rho}|\mathbf{k}\rangle e^{\imath\mathbf{k}\cdot\mathbf{x}}d^3k\ .\end{aligned}$$

47.1.6.7 Ex: Structure factor for Bragg scattering

Demonstrate the following relationships,

$$\frac{dp_{cm}(\mathbf{q},\omega)}{dt} = -m\omega_z^2 z_{cm} + \hbar q\frac{\Omega_{br}^2}{2}\int d\delta'[S(\mathbf{q},\omega')-S(-\mathbf{q},-\omega')]\frac{\sin(\omega-\omega')t_{br}}{\omega-\omega'}$$

$$\ddot{p}_{cm}(q,\omega)+\omega_z^2 p_{cm} = \hbar q\frac{\Omega_{br}^2}{2}\int d\omega'[S(\mathbf{q},\omega')-S(-\mathbf{q},-\omega')]\cos(\omega-\omega')t_{br}\longrightarrow 0\ .$$

Solution:

47.1.6.8 Ex: Commutation expressions for bosons and fermions

Verify the following useful commutation relations:
a. For bosons,

$$\hat{a}_m(\mathbf{k})\hat{a}_n^\dagger(\mathbf{q})^N = N\delta_{m,n}\delta_{\mathbf{k},\mathbf{q}}\hat{a}_n^\dagger(\mathbf{q})^{N-1} + \hat{a}_n^\dagger(\mathbf{q})^N\hat{a}_m(\mathbf{k}) \ , \tag{47.47}$$

which can be generalized to,

$$\begin{aligned}&\hat{a}_m(\mathbf{k})[\hat{a}_n^\dagger(\mathbf{q}_1) + \hat{a}_n^\dagger(\mathbf{q}_2)]^N \\ &\quad = N\delta_{m,n}\left(\delta_{\mathbf{k},\mathbf{q}_1} + \delta_{\mathbf{k},\mathbf{q}_2}\right)[\hat{a}_n^\dagger(\mathbf{q}_1) + \hat{a}_n^\dagger(\mathbf{q}_2)]^{N-1} + [\hat{a}_n^\dagger(\mathbf{q}_1) + \hat{a}_n^\dagger(\mathbf{q}_2)]^N\hat{a}_m(\mathbf{k}) \ .\end{aligned} \tag{47.48}$$

b. For fermions do not support macroscopic populations of the type $\hat{a}_n^\dagger(\mathbf{q})^N$. Performing a number P of permutations of the operators and assuming that one fermion of the product state is in the internal state n, we calculate,

$$\hat{a}_n(\mathbf{k})\prod_{m=0}^{N-1}\hat{a}_m^\dagger(\mathbf{q}) = (-1)^P\left[\delta_{\mathbf{k},\mathbf{q}}\prod_{m\neq n}^{N-1}\hat{a}_m^\dagger(\mathbf{q}) - \prod_{m=0}^{N-1}\hat{a}_m^\dagger(\mathbf{q})\hat{a}_n(\mathbf{k})\right] \ . \tag{47.49}$$

If none of the fermions of the product state is in state n the first part of the sum simply vanishes. This expression can also be generalized to,

$$\begin{aligned}&\hat{a}_n(\mathbf{k})\prod_{m=0}^{N-1}[\hat{a}_m^\dagger(\mathbf{q}_1) + \hat{a}_m^\dagger(\mathbf{q}_2)] = (-1)^P\prod_{m\neq n}^{N-1}[\hat{a}_m^\dagger(\mathbf{q}_1) + \hat{a}_m^\dagger(\mathbf{q}_2)]\hat{a}_n(\mathbf{k})[\hat{a}_n^\dagger(\mathbf{q}_1) + \hat{a}_n^\dagger(\mathbf{q}_2)] \\ &= (-1)^P\left[(\delta_{\mathbf{k},\mathbf{q}_1} + \delta_{\mathbf{k},\mathbf{q}_2})\prod_{m\neq n}^{N-1}[\hat{a}_m^\dagger(\mathbf{q}_1) + \hat{a}_m^\dagger(\mathbf{q}_2)] - \prod_{m=0}^{N-1}[\hat{a}_m^\dagger(\mathbf{q}_1) + \hat{a}_m^\dagger(\mathbf{q}_2)]\hat{a}_n(\mathbf{k})\right] \ .\end{aligned} \tag{47.50}$$

Solution: *a. For bosons the subsequent arguments the following side calculation will be useful,*

$$\begin{aligned}\hat{a}_m(\mathbf{k})\hat{a}_n^\dagger(\mathbf{q})^N &= \delta_{m,n}\delta_{\mathbf{k},\mathbf{q}}\hat{a}_n^\dagger(\mathbf{q})^{N-1} + \hat{a}_n^\dagger(\mathbf{q})\hat{a}_m(\mathbf{k})\hat{a}_n^\dagger(\mathbf{q})^{N-1} \\ &= ... = N\delta_{m,n}\delta_{\mathbf{k},\mathbf{q}}\hat{a}_n^\dagger(\mathbf{q})^{N-1} + \hat{a}_n^\dagger(\mathbf{q})^N\hat{a}_m(\mathbf{k}) \ .\end{aligned}$$

b. For fermions do not support macroscopic populations of the type $\hat{a}_n^\dagger(\mathbf{q})^N$. Performing a number P of permutations of the operators and assuming that one fermion of the product state is in the internal state n, we calculate,

$$\begin{aligned}\hat{a}_n(\mathbf{k})\prod_{m=0}^{N-1}\hat{a}_m^\dagger(\mathbf{q}) &= (-1)^P\prod_{m\neq n}^{N-1}\hat{a}_m^\dagger(\mathbf{q})\hat{a}_n(\mathbf{k})\hat{a}_n^\dagger(\mathbf{q}) = (-1)^P\prod_{m\neq n}^{N-1}\hat{a}_m^\dagger(\mathbf{q})[\delta_{\mathbf{k},\mathbf{q}} - \hat{a}_n^\dagger(\mathbf{q})\hat{a}_n(\mathbf{k}) \\ &= (-1)^P\left[\delta_{\mathbf{k},\mathbf{q}}\prod_{m\neq n}^{N-1}\hat{a}_m^\dagger(\mathbf{q}) - \prod_{m=0}^{N-1}\hat{a}_m^\dagger(\mathbf{q})\hat{a}_n(\mathbf{k})\right] \ .\end{aligned}$$

If none of the fermions of the product state is in state n the first part of the sum simply vanishes.

47.1.6.9 Ex: Extracting the atom number from many-body states

Verify the normalization of (a) the bosonic Fock state (47.32), (b) the fermionic product state (47.32), (c) the bosonic product state (47.35), (d) the bosonic Bragg grating state (47.37), and (e) the fermionic Bragg grating state (47.37). **Help:** Speed up the calculations by using the results of 47.1.6.8.

Solution: *a. For the BEC Fock state we have,*

$$\begin{aligned}\langle\Psi_b^{(N)}(\mathbf{0})|\hat{N}_m(\mathbf{k})|\Psi_b^{(N)}(\mathbf{0})\rangle &= \tfrac{1}{N!}\langle 0|\hat{a}_0(\mathbf{0})^N\hat{a}_m^\dagger(\mathbf{k})\hat{a}_m(\mathbf{k})\hat{a}_0^\dagger(\mathbf{0})^N|0\rangle\\ &= \tfrac{1}{N!}\left\|N\delta_{m,0}\delta_{\mathbf{k},\mathbf{q}}\hat{a}_n^\dagger(\mathbf{0})^{N-1}|0\rangle\right\|^2\\ &= N\delta_{m,0}\delta_{\mathbf{k},\mathbf{q}}\||\Psi_b^{(N-1)}\rangle\|^2 = N\delta_{m,0}\delta_{\mathbf{k},\mathbf{q}}\ ,\end{aligned}$$

yielding $\langle\Psi_b^{(N)}(\mathbf{0})|\hat{N}|\Psi_b^{(N)}(\mathbf{0})\rangle = \sum_{m,\mathbf{k}}\langle\Psi_b^{(N)}(\mathbf{0})|\hat{N}_m(\mathbf{k})|\Psi_b^{(N)}(\mathbf{0})\rangle = N$.
b. For the Fermi sea state we have,

$$\begin{aligned}\langle\Psi_f^{(N)}(\mathbf{0})|\hat{N}_m(\mathbf{k})|\Psi_f^{(N)}(\mathbf{0})\rangle &= \langle 0\left|\prod_{n'=0}^{N-1}\hat{a}_{n'}(\mathbf{0})\hat{a}_m^\dagger(\mathbf{k})\hat{a}_m(\mathbf{k})\prod_{n=0}^{N-1}\hat{a}_n^\dagger(\mathbf{0})\right|0\rangle\\ &= \|\hat{a}_m(\mathbf{k})\hat{a}_m^\dagger(\mathbf{0})\prod_{n\neq m}^{N-1}\hat{a}_n^\dagger(\mathbf{0})|0\rangle\|^2 = \delta_{\mathbf{0},\mathbf{k}}\|\Psi_f^{(N-1)}(\mathbf{0})\|^2 = \delta_{\mathbf{0},\mathbf{k}}\ ,\end{aligned}$$

yielding $\langle\Psi_f^{(N)}(\mathbf{0})|\hat{N}|\Psi_f^{(N)}(\mathbf{0})\rangle = N$.
c. For the bosonic product state we have,

$$\begin{aligned}&\langle\Psi_b^{(N_1)}(\mathbf{0})\Psi_b^{(N_2)}(\mathbf{q})|\hat{N}_0(\mathbf{k})|\Psi_b^{(N_1)}(\mathbf{0})\Psi_b^{(N_2)}(\mathbf{q})\rangle\\ &\quad= \frac{1}{N_1!N_2!}\langle 0|\hat{a}_0(\mathbf{q})^{N_2}\hat{a}_0(\mathbf{0})^{N_1}\hat{a}_0^\dagger(\mathbf{k})\hat{a}_0(\mathbf{k})\hat{a}_0^\dagger(\mathbf{0})^{N_1}\hat{a}_0^\dagger(\mathbf{q})^{N_2}|0\rangle\\ &\quad= \frac{1}{N_1!N_2!}\|N_1\delta_{\mathbf{k},\mathbf{0}}\hat{a}_0^\dagger(\mathbf{0})^{N_1-1}\hat{a}_0^\dagger(\mathbf{q})^{N_2}|0\rangle + \hat{a}_0^\dagger(\mathbf{0})^{N_1}\hat{a}_0(\mathbf{k})\hat{a}_0^\dagger(\mathbf{q})^{N_2}|0\rangle\|^2\\ &\quad= \frac{1}{N_1!N_2!}\left(N_1^2\delta_{\mathbf{k},\mathbf{0}}\|\hat{a}_0^\dagger(\mathbf{0})^{N_1-1}\hat{a}_0^\dagger(\mathbf{q})^{N_2}|0\rangle\|^2 + N_2^2\delta_{\mathbf{k},\mathbf{q}}\|\hat{a}_0^\dagger(\mathbf{0})^{N_1}\hat{a}_0^\dagger(\mathbf{q})^{N_2-1}|0\rangle\|^2\right)\\ &\quad= N_1\delta_{\mathbf{k},\mathbf{0}} + N_2\delta_{\mathbf{k},\mathbf{q}}\ ,\end{aligned}$$

yielding $\langle\Psi_b^{(N_1)}(\mathbf{0})\Psi_b^{(N_2)}(\mathbf{q})|\hat{N}|\Psi_b^{(N_1)}(\mathbf{0})\Psi_b^{(N_2)}(\mathbf{q})\rangle = \sum_{\mathbf{k}}(N_1\delta_{\mathbf{k},\mathbf{0}} + N_2\delta_{\mathbf{k},\mathbf{q}}) = N_1 + N_2$.
d. To probe the number of bosons of the Bragg-state being in momentum state $\mathbf{k}$*, we do,*

$$\begin{aligned}&\langle\Psi_b^{(brgg,N)}(\mathbf{0},\mathbf{q})|\hat{N}(\mathbf{k})|\Psi_b^{(brgg,N)}(\mathbf{0},\mathbf{q})\rangle\\ &\qquad= \tfrac{1}{2^N N!}\langle 0|[\hat{a}_0(\mathbf{0}) + \hat{a}_0(\mathbf{q})]^N\hat{a}_0^\dagger(\mathbf{k})\hat{a}_0(\mathbf{k})[\hat{a}_0^\dagger(\mathbf{0}) + \hat{a}_0^\dagger(\mathbf{q})]^N|0\rangle\\ &\qquad= \tfrac{1}{2^N N!}\|N(\delta_{\mathbf{k},\mathbf{0}} + \delta_{\mathbf{k},\mathbf{q}})[\hat{a}_0^\dagger(\mathbf{0}) + \hat{a}_0^\dagger(\mathbf{q})]^{N-1}|0\rangle\|^2\\ &\qquad= \tfrac{N^2}{2N}(\delta_{\mathbf{k},\mathbf{0}} + \delta_{\mathbf{k},\mathbf{q}})\||\Psi_{b,N-1}^{(sctt)}\rangle\|^2 = \tfrac{N}{2}(\delta_{\mathbf{k},\mathbf{0}} + \delta_{\mathbf{k},\mathbf{q}})\ ,\end{aligned}$$

yielding $\langle\Psi_b^{(brgg,N)}(\mathbf{0},\mathbf{q})|\hat{N}|\Psi_b^{(brgg,N)}(\mathbf{0},\mathbf{q})\rangle = N$.
e. For fermions we get analogously,

$$\begin{aligned}\langle\Psi_f^{(brgg,N)}(\mathbf{0},\mathbf{q})|\hat{N}_m(\mathbf{k})|\Psi_f^{(brgg,N)}(\mathbf{0},\mathbf{q})\rangle &= \|\tfrac{1}{\sqrt{2^N}}\hat{a}_m(\mathbf{k})\prod_{n=0}^{N-1}[\hat{a}_n^\dagger(\mathbf{0})+\hat{a}_n^\dagger(\mathbf{q})]|0\rangle\|^2\\ &= \tfrac{1}{2^N}[\delta_{\mathbf{k},\mathbf{0}}+\delta_{\mathbf{k},\mathbf{q}}]\|\prod_{n\neq m}^{N-1}[\hat{a}_n^\dagger(\mathbf{0})+\hat{a}_n^\dagger(\mathbf{q})]|0\rangle\|^2\\ &= \tfrac{1}{2}(\delta_{\mathbf{k},\mathbf{0}}+\delta_{\mathbf{k},\mathbf{q}})\||\Psi_b^{(brgg,N-1)}(\mathbf{0},\mathbf{q})\rangle\|^2 = \tfrac{1}{2}(\delta_{\mathbf{k},\mathbf{0}}+\delta_{\mathbf{k},\mathbf{q}})\ ,\end{aligned}$$

also yielding $\langle\Psi_f^{(brgg,N)}(\mathbf{0},\mathbf{q})|\hat{N}|\Psi_f^{(brgg,N)}(\mathbf{0},\mathbf{q})\rangle = \frac{N}{2}$.

47.1.6.10 Ex: Bosonic stimulation and cooperative enhancement by lattices of bosons and fermions

Compare bosons and fermions with respect to (a) bosonic stimulation and (b) cooperative enhancement.

Solution: *a. To discuss bosonic stimulation we study the Rayleigh scattering of a single atom out of a matter wave populated with* N_1 *atoms into another one populated with* N_2 *atoms,*

$$|\Psi_b^{(N_1)}(\mathbf{0})\rangle|\Psi_b^{(N_2-1)}(\mathbf{q})\rangle \overset{\hat{H}}{\curvearrowright} |\Psi_b^{(N_1-1)}(\mathbf{0})\rangle|\Psi_b^{(N_2)}(\mathbf{q})\rangle\ ,$$

mediated by the scattering Hamiltonian $\hat{H} \equiv \sum_m \hat{a}_m^\dagger(\mathbf{k})\hat{a}_m(\mathbf{0})$, *with* $\mathbf{k}\neq\mathbf{0}$. *For bosonic clouds we get,*

$$\begin{aligned}&\langle\Psi_b^{(N_1-1)}(\mathbf{0})\Psi_b^{(N_2)}(\mathbf{q})|\hat{H}|\Psi_b^{(N_1)}(\mathbf{0})\Psi_b^{(N_2-1)}(\mathbf{q})\rangle\\ &\quad= (\delta_{\mathbf{k},\mathbf{0}}+\delta_{\mathbf{k},\mathbf{q}})\frac{\langle 0|\hat{a}_0(\mathbf{0})^{N_1-1}\hat{a}_0(\mathbf{q})^{N_2}|\hat{a}_0^\dagger(\mathbf{k})\hat{a}_0(\mathbf{0})|\hat{a}_0^\dagger(\mathbf{0})^{N_1}\hat{a}_0^\dagger(\mathbf{q})^{N_2-1}|0\rangle}{\sqrt{N_1!N_2!(N_1-1)!(N_2-1)!}}\\ &\quad= 0+\delta_{\mathbf{k},\mathbf{q}}\sqrt{N_1N_2}\ ,\end{aligned}$$

using

$$\hat{a}_0(\mathbf{q})^{N_2}\hat{a}_0^\dagger(\hat{a}(\mathbf{q})^{N_2-1}|0\rangle = (N_2-1)\hat{a}_0(\mathbf{q})^{N_2-1}\hat{a}_0^\dagger(\mathbf{q})^{N_2-2}|0\rangle = ... = (N_2-1)!\hat{a}_0(\mathbf{q})|0\rangle = 0\ .$$

For fermionic clouds we get,

$$\begin{aligned}&\langle\Psi_f^{(N_1-1)}(\mathbf{0})\Psi_f^{(N_2)}(\mathbf{q})|\hat{H}|\Psi_f^{(N_1)}(\mathbf{0})\Psi_f^{(N_2-1)}(\mathbf{q})\rangle\\ &\quad= \langle 0|\prod_{m_1'=0}^{N_1-2}\hat{a}_{m_1'}(\mathbf{0})\prod_{m_2'=0}^{N_2-1}\hat{a}_{m_2'}(\mathbf{q})|\hat{a}_n^\dagger(\mathbf{q})\hat{a}_n(\mathbf{0})|\prod_{m_1=0}^{N_1-1}\hat{a}_{m_1}^\dagger(\mathbf{0})\prod_{m_2=0}^{N_2-2}\hat{a}_{m_2}^\dagger(\mathbf{q})|0\rangle\\ &\quad= \langle 0|\prod_{m_2'\neq n}^{N_2-2}\hat{a}_{m_2'}(\mathbf{q})\hat{a}_n(\mathbf{q})\hat{a}_n^\dagger(\mathbf{q})\prod_{m_2=0}^{N_2-2}\hat{a}_{m_2}^\dagger(\mathbf{q})\prod_{m_1'=0}^{N_1-2}\hat{a}_{m_1'}(\mathbf{0})\hat{a}_n(\mathbf{0})\hat{a}_n^\dagger(\mathbf{0})\prod_{m_1\neq n}^{N_1-2}\hat{a}_{m_1}^\dagger(\mathbf{0})|0\rangle\\ &\quad= \langle 0|\hat{a}_n(\mathbf{0})\hat{a}_n^\dagger(\mathbf{0})|0\rangle = 1\ .\end{aligned}$$

This shows that, in contrast to bosons, the scattering of fermions is not bosonically enhanced.

b. We study the two processes,

$$|\Psi_b^{(M)}(\mathbf{0})\Psi_b^{(brgg,N)}(\mathbf{0},\mathbf{q})\rangle \overset{\hat{H}}{\curvearrowright} |\Psi_b^{(M-1)}(\mathbf{0})\Psi_b^{(brgg,N+1)}(\mathbf{0},\mathbf{q})\rangle$$
$$|\Psi_b^{(M)}(\mathbf{q})\Psi_b^{(brgg,N)}(\mathbf{0},\mathbf{q})\rangle \overset{\hat{H}}{\curvearrowright} |\Psi_b^{(M+1)}(\mathbf{q})\Psi_b^{(brgg,N-1)}(\mathbf{0},\mathbf{q})\rangle \ ,$$

For the first one we find,

$$\begin{aligned}
&\langle\Psi_b^{(M-1)}(\mathbf{0})\Psi_b^{(brgg,N+1)}(\mathbf{0},\mathbf{q})|\hat{a}_0^\dagger(\mathbf{k})\hat{a}_0(\mathbf{0})|\Psi_b^{(M)}(\mathbf{0})\Psi_b^{(brgg,N)}(\mathbf{0},\mathbf{q})\rangle \\
&= \frac{\langle 0|\hat{a}_0(\mathbf{0})^{M-1}[\hat{a}_0(\mathbf{0})+\hat{a}_0(\mathbf{q})]^{N+1}\hat{a}_0^\dagger(\mathbf{k})\hat{a}_0(\mathbf{0})\hat{a}_0^\dagger(\mathbf{0})^M[\hat{a}_0^\dagger(\mathbf{0})+\hat{a}_0^\dagger(\mathbf{q})]^N|0\rangle}{\sqrt{2^{N+1}(N+1)!2^{M-1}(M-1)!2^N N!2^M M!}} \\
&= \frac{\langle 0|\hat{a}_0(\mathbf{0})^{M}[\hat{a}_0(\mathbf{0})+\hat{a}_0(\mathbf{q})]^{N+1}\hat{a}_0^\dagger(\mathbf{k})\hat{a}_0^\dagger(\mathbf{0})^M[\hat{a}_0^\dagger(\mathbf{0})+\hat{a}_0^\dagger(\mathbf{q})]^N|0\rangle}{(M-1)!N!2^{M+N}\sqrt{M(N+1)}} + 0 \\
&= \frac{\left\langle 0 \left| \begin{array}{c} \hat{a}_0(\mathbf{0})^M(N+1)(\delta_{\mathbf{k},\mathbf{0}}+\delta_{\mathbf{k},\mathbf{q}})[\hat{a}_0(\mathbf{0})+\hat{a}_0(\mathbf{q})]^N\hat{a}_0^\dagger(\mathbf{0})^M[\hat{a}_0^\dagger(\mathbf{0})+\hat{a}_0^\dagger(\mathbf{q})]^N \\ +\hat{a}_0(\mathbf{0})^M\hat{a}_0^\dagger(\mathbf{k})[\hat{a}_0(\mathbf{0})+\hat{a}_0(\mathbf{q})]^{N+1}\hat{a}_0^\dagger(\mathbf{0})^M[\hat{a}_0^\dagger(\mathbf{0})+\hat{a}_0^\dagger(\mathbf{q})]^N \end{array} \right| 0 \right\rangle}{(M-1)!N!2^{M+N}\sqrt{M(N+1)}} \\
&= \frac{(N+1)(\delta_{\mathbf{k},\mathbf{0}}+\delta_{\mathbf{k},\mathbf{q}})M!N!2^{M+N}\left\langle \Psi_b^{(M)}(\mathbf{0})\Psi_b^{(brgg,N)}(\mathbf{0},\mathbf{q})|\Psi_b^{(M)}(\mathbf{0})\Psi_b^{(brgg,N)}(\mathbf{0},\mathbf{q})0\right\rangle}{(M-1)!N!2^{M+N}\sqrt{M(N+1)}} \\
&= (\delta_{\mathbf{k},\mathbf{0}}+\delta_{\mathbf{k},\mathbf{q}})\sqrt{M(N+1)} \ ,
\end{aligned}$$

and for the second one,

$$\begin{aligned}
&\langle\Psi_b^{(M+1)}(\mathbf{q})\Psi_b^{(brgg,N-1)}(\mathbf{0},\mathbf{q})|\hat{a}_0^\dagger(\mathbf{k})\hat{a}_0(\mathbf{0})|\Psi_b^{(M)}(\mathbf{q})\Psi_b^{(brgg,N)}(\mathbf{0},\mathbf{q})\rangle \\
&= \frac{\langle 0|\hat{a}_0(\mathbf{q})^{M+1}[\hat{a}_0(\mathbf{0})+\hat{a}_0(\mathbf{q})]^{N-1}\hat{a}_0^\dagger(\mathbf{k})\hat{a}_0(\mathbf{0})\left[\hat{a}_0^\dagger(\mathbf{0})+\hat{a}_0^\dagger(\mathbf{q})\right]^N\hat{a}_0^\dagger(\mathbf{q})^M|0\rangle}{\sqrt{2^{N-1}(N-1)!2^{M+1}(M+1)!2^N N!2^M M!}} \\
&= \frac{\delta_{\mathbf{k},\mathbf{q}}\langle 0|\hat{a}_0(\mathbf{q})^{M+1}[\hat{a}_0(\mathbf{0})+\hat{a}_0(\mathbf{q})]^{N-1}\hat{a}_0^\dagger(\mathbf{q})^{M+1}N[\hat{a}_0^\dagger(\mathbf{0})+\hat{a}_0^\dagger(\mathbf{q})]^{N-1}|0\rangle}{M!(N-1)!2^{M+N}\sqrt{N(M+1)}} \\
&= \frac{\delta_{\mathbf{k},\mathbf{q}}N(N-1)!(M+1)!2^{M+N}\left\langle \Psi_b^{(M+1)}(\mathbf{0})\Psi_b^{(brgg,N-1)}(\mathbf{0},\mathbf{q})|\Psi_b^{(M+1)}(\mathbf{0})\Psi_b^{(brgg,N-1)}(\mathbf{0},\mathbf{q})0\right\rangle}{M!(N-1)!2^{M+N}\sqrt{N(M+1)}} \\
&= \delta_{\mathbf{k},\mathbf{q}}\sqrt{N(M+1)} \ .
\end{aligned}$$

For fermions we get analogously,

$$\begin{aligned}
\langle\Psi_f^{(brgg,N-1)}(\mathbf{0},\mathbf{q})\Psi_f^{(1)}(\mathbf{k})|\Psi_f^{(brgg,N)}(\mathbf{0},\mathbf{q})\rangle &= \sum_m \|\tfrac{1}{\sqrt{2^N}}\hat{a}_m^\dagger(\mathbf{k})\hat{a}_m(\mathbf{0})\prod_{n=0}^{N-1}[\hat{a}_n^\dagger(\mathbf{0})+\hat{a}_n^\dagger(\mathbf{q})]|0\rangle\|^2 \\
&= \tfrac{1}{2^N}\sum_m \|\hat{a}_m^\dagger(\mathbf{k})\prod_{n\neq m}^{N-1}[\hat{a}_n^\dagger(\mathbf{0})+\hat{a}_n^\dagger(\mathbf{q})]|0\rangle\|^2 \\
&\simeq N\left\|\hat{a}_0^\dagger(\mathbf{k})|\tfrac{1}{\sqrt{2}}\Psi_f^{(brgg,N-1)}(\mathbf{0},\mathbf{q})\rangle\right\|^2 \\
&= \tfrac{N}{2}\langle\Psi_f^{(brgg,N-1)}(\mathbf{0},\mathbf{q})|1-\hat{N}(\mathbf{k})|\Psi_f^{(brgg,N-1)}(\mathbf{0},\mathbf{q})\rangle \\
&= \tfrac{N}{2}\left[1-\tfrac{N-1}{2}(\delta_{\mathbf{0},\mathbf{k}}+\delta_{\mathbf{0},\mathbf{q}})\right] \ .
\end{aligned}$$

47.1.6.11 Ex: Cooperative enhancement versus bosonic stimulation

CARL amplification comes from cooperativity not from bosonic stimulation [919, 713, 1166], that is, it should work for fermions and boltzons. To demonstrate this proceed as follows:
a. Set up the single-atom Hamiltonian for a 3D harmonic potential in which the atoms (bosons or fermions) are initially placed allowing for the possibility of momentum recoil by photon scattering. This disregards the trap's inhomogeneity, but is a good assumption for short times. What are the eigenfunction of this Hamiltonian? Calculate the expectation value for the density distribution. Express the field operators in momentum space. Express the lowest energy states for a bosonic/fermionic cloud in momentum representation.
b. Now apply a $\pi/2$-Bragg-pulse imparting the recoil $\mathbf{K}$ to the cloud. What is the resulting state? Recalculate the expectation value for the density distribution.
c. Now, assume the presence of another free (test) atom (or photon). Write down the Hamiltonian and the wavefunction for this atom. It is supposed to interact with the atomic cloud via the (perturbatively treated) interaction potential,

$$\hat{V} = \lambda \int d^3r \hat{\psi}_1^\dagger(\mathbf{r})\hat{\psi}_2^\dagger(\mathbf{r})\hat{\psi}_2(\mathbf{r})\hat{\psi}_1(\mathbf{r}) \ .$$

Calculate the probability that the atom is scattered at a particular wavevector, i.e. determine the cooperative enhancement factor.
d. Is cooperative enhancement possible with just one atom?
e. How about cooperative enhancement in a cavity, when cooperativity is ensured by a single atom plus all its mirror images?

Solution: *a. Following [919] we consider a field $\hat{\psi}_1(\mathbf{r})$ containing N identical bosons or fermions in a harmonic trap,*

$$\hat{H}_{ho} = \hbar\omega_m(\hat{n} + \tfrac{1}{2}) \ ,$$

with the single particle orbitals $\varphi_m(\mathbf{r}) = X_{m_x}(x)Y_{m_y}(y)Z_{m_z}(z)$. The Hamiltonian of the harmonic oscillator plus recoil and the corresponding eigenfunctions are,

$$\hat{H}_1\varphi_m(\mathbf{r})e^{\imath\mathbf{k}\cdot\mathbf{r}} = \left(\frac{\mathbf{p}_1^2}{2M} + \hbar\omega_m\right)\varphi_m(\mathbf{r})e^{\imath\mathbf{k}\cdot\mathbf{r}} = \left(\hbar\omega_{rec}(\mathbf{k}) + \hbar\omega_m\varphi_m(\mathbf{r})e^{\imath\mathbf{k}\cdot\mathbf{r}}\right) = E_1\varphi_m(\mathbf{r})e^{\imath\mathbf{k}\cdot\mathbf{r}} \ ,$$

with the recoil shift $\omega_{rec}(\mathbf{k}) = \hbar\mathbf{k}^2/2M$. For example, the density distribution for bosons is,

$$n_b(\mathbf{r}) = \langle\hat{n}_b(\mathbf{r})\rangle = \langle\hat{\psi}_1^\dagger(\mathbf{r})\hat{\psi}_1(\mathbf{r})\rangle = N|\varphi_0(\mathbf{r})|^2 \qquad with \qquad \int |\varphi_0(\mathbf{r})|^2 d^3r = 1 \ . \quad (47.51)$$

Let us now define the field operators in momentum space,

$$\hat{a}_m^\dagger(\mathbf{k}) \equiv \int d^3r\varphi_m(\mathbf{r})e^{\imath\mathbf{k}\cdot\mathbf{r}}\hat{\psi}_1^\dagger(\mathbf{r}) \qquad , \qquad \varphi_m(\mathbf{r})\hat{\psi}_1^\dagger(\mathbf{r}) \equiv \int d^3k\hat{a}_m^\dagger(\mathbf{k})e^{-\imath\mathbf{k}\cdot\mathbf{r}} \ . \quad (47.52)$$

In momentum space the initial states for bosonic or fermionic clouds are,

$$|\phi_b(0)\rangle = \frac{1}{\sqrt{N!}}\hat{a}_0^\dagger(0)^N|0\rangle \quad , \quad |\phi_f(0)\rangle = \prod_{m=0}^{N-1}\hat{a}_m^\dagger(0)|0\rangle \ .$$

b. After the Bragg pulse the many-body state will be,

$$|\psi_b(\tau_{brgg})\rangle = \frac{1}{\sqrt{2^N N!}}[\hat{a}_0^\dagger(0)+\hat{a}_0^\dagger(\mathbf{K})]^N|0\rangle \quad , \quad |\psi_f(\tau_{brgg})\rangle = \frac{1}{\sqrt{2^N}}\prod_{m=0}^{N-1}[\hat{a}_0^\dagger(0)+\hat{a}_0^\dagger(\mathbf{K})]|0\rangle \ .$$

We see that the 50/50-Bragg pulse transforms every atom independently from the other into a superposition of momentum states. To calculate the new density distribution it is thus sufficient to substitute in Eq. (47.52),

$$\tfrac{1}{\sqrt{2}}\hat{a}_0^\dagger(0) \curvearrowright \tfrac{1}{\sqrt{2}}[\hat{a}_0^\dagger(0)+\hat{a}_0^\dagger(\mathbf{K})] = \tfrac{1}{\sqrt{2}}\int d^3r\varphi_0(\mathbf{r})\left(1+e^{\imath\mathbf{K}\cdot\mathbf{r}}\right)\hat{\psi}_1^\dagger(\mathbf{r}) \ ,$$

and repeat the calculation of (47.51),

$$n_b(\mathbf{r}) = \left|\varphi_0(\mathbf{r})\tfrac{1}{\sqrt{2}}\left(1+e^{\imath\mathbf{K}\cdot\mathbf{r}}\right)\hat{\psi}_1^\dagger(\mathbf{r})\right|^2 = N\varphi_0(\mathbf{r})|^2(1+1\cos\mathbf{K}\cdot\mathbf{r}) \ .$$

c. The wavefunction of the additional atom be $\hat{\psi}_2(\mathbf{r})$. The free-atom Hamiltonian and the corresponding eigenfunctions are,

$$\hat{H}_2\tfrac{1}{\sqrt{V}}e^{\imath\mathbf{k}\cdot\mathbf{r}} = \frac{\mathbf{p}_2^2}{2M}\tfrac{1}{\sqrt{V}}e^{\imath\mathbf{k}\cdot\mathbf{r}} = \hbar\omega_2(\mathbf{k})\tfrac{1}{\sqrt{V}}e^{\imath\mathbf{k}\cdot\mathbf{r}} = E_2\tfrac{1}{\sqrt{V}}e^{\imath\mathbf{k}\cdot\mathbf{r}} \ .$$

d.

47.2 Bragg diffraction

An important technique for manipulating the atomic motion is by *Bragg diffraction* [5]. It allows the coherent transfer of atoms to other states of motion or to superpositions of motional states, and is extremely useful for applications, such as the realization of matter wave beamsplitters [746] and atomic lasers, or for the targeted excitation of quasi-particles [746, 1259, 1237].

To implement Bragg diffraction, we consider two laser pulses with different frequencies and propagation directions $\omega, \mathbf{k}_\omega$ and $\omega-\Delta\omega, \mathbf{k}_{\omega-\Delta\omega}$, detuned from an atomic resonance and intersecting at the position of atoms under an angle ϑ, as shown in Fig. 47.6(a). The superposition of the electric fields of the light beams,

$$\begin{aligned} E &= E_0e^{\imath(\mathbf{k}_\omega\cdot\mathbf{r}-\omega t)} + E_0e^{\imath[\mathbf{k}_{\omega-\Delta\omega}\cdot\mathbf{r}-(\omega-\Delta\omega)t]} = E_0e^{\imath(\mathbf{k}_\omega\cdot\mathbf{r}-\omega t)}\left(1+e^{-\imath(\mathbf{q}\cdot\mathbf{r}-\Delta\omega t)}\right) \\ &= 2E_0e^{\imath(\mathbf{k}_\omega\cdot\mathbf{r}-\omega t)}e^{-\frac{\imath}{2}(\mathbf{q}\cdot\mathbf{r}-\Delta\omega t)}\cos\tfrac{\mathbf{q}\cdot\mathbf{r}-\Delta\omega t}{2} \ , \end{aligned} \tag{47.53}$$

[5] The idea is analogous to the manipulation of the **k**-vector of light waves by acousto-optic modulators.

where $\mathbf{q} \equiv \mathbf{k}_\omega - \mathbf{k}_{\omega-\Delta\omega}$, produces a standing light wave with an intensity proportional to,

$$|E|^2 = 4E_0^2 \cos^2 \tfrac{\mathbf{q}\cdot\mathbf{r}-\Delta\omega t}{2} = 2E_0^2[1 + \cos(\mathbf{q}\cdot\mathbf{r} - \Delta\omega t) \ , \tag{47.54}$$

with which the atoms interact.

The Bragg diffraction technique has proven extremely efficient: up to 100% of the atoms can be transferred to well-defined momentum sidemodes. In general, the components of a cloud with different momentum modes overlap during the time scale of the Bragg pulses. They only separate spatially after a ballistic flight time, which then allows their identification via absorption imaging.

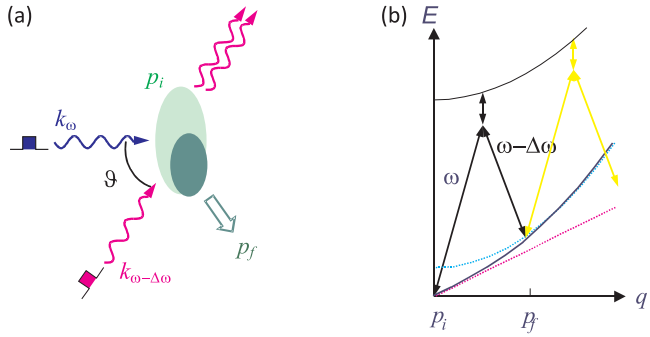

Figure 47.6: Bragg scattering of atoms at a standing light wave. (a) Geometric layout: Short pulses of two laser beams in Raman configuration enclosing an angle of ϑ and detuned from each other by $\Delta\omega$ are simultaneously irradiated into the cloud. (b) Bogolubov dispersion relation for interacting condensates (blue line). The quadratic dispersion relation (cyan) holds for free particles, and the linear dispersion relation (magenta) for phonon excitations.

47.2.1 Interpretations of the Bragg diffraction process

Bragg's diffraction can be treated within the formalism developed in Sec. 47.1.2, as will be shown later, in Sec. 47.2.3. But before that, let us present a simplified approach and several simple pictures illustrating the dynamics of Bragg diffraction.

47.2.1.1 Bragg diffraction picture

The *first interpretation* of this phenomenon is as *matter wave Bragg diffraction* at a standing light wave (i.e. an one-dimensional optical lattice) formed by two crossing pulsed laser beams [6]. We consider atoms initially at rest exposed to the standing wave (47.53) with $\Delta\omega = 0$ and $\mathbf{q} \equiv q\hat{\mathbf{e}}_z$, such that the dipolar potential $U \propto |E|^2$ is, with (47.54),

$$U(z) = U_0 \cos^2 \tfrac{qz}{2} \ . \tag{47.55}$$

[6]Note, that the initial population of the recoil mode should be small. Otherwise, since Bragg diffraction is a coherent and thus reversible process, atoms initially in the recoil mode are transferred back to the original matter wave mode.

Assuming a given finite interaction time τ, the modulation of the local phase of the atoms becomes [7],

$$\boxed{\psi_\tau(z) = \psi_0(z) e^{\imath U(z)\tau/\hbar} = \psi_0(z) e^{\frac{\imath}{2\hbar} U_0 \tau(\cos qz + 1)} = \psi_0(z) e^{\imath U_0 \tau/2\hbar} \sum_n \imath^n J_n(\tfrac{U_0\tau}{2\hbar}) e^{inqz}} \ , \tag{47.56}$$

where J_n are the Bessel functions of the first kind [8].

Example 289 (*Bragg diffraction after a time-of-flight*): To calculate the density distribution after a certain flight time t_{ToF}, we construct the Fourier transform of $\psi_\tau(z)$,

$$\tilde{\psi}_\tau(q) = \tilde{\psi}_0(q) \star \sum_n J_n^2(U_0\tau/2\hbar)\delta(q - nk) \ , \tag{47.57}$$

and we evaluate it via $\tilde{z} \equiv t_{ToF}\hbar q/m$,

$$\tilde{\psi}_\tau(\tilde{z}) = \tilde{\psi}_0(\tilde{z}) \star \sum_n J_n^2(U_0\tau/2\hbar)\delta(\tilde{z} - nt_{ToF}\hbar k/m) \ . \tag{47.58}$$

The density distribution of the expanded condensate $\rho_0(\tilde{z}) = |\tilde{\psi}_0(\tilde{z})|^2 = e^{-(\tilde{z}/2r_{ToF})^2}$, where $r_{ToF} = t_{ToF}\sqrt{k_B T/m}$, is,

$$\rho(\tilde{z}) = \sum_n \rho_0(\tilde{z} - nt_{ToF}\hbar k/m)|J_n(U_0\tau/2\hbar)|^2 \ . \tag{47.59}$$

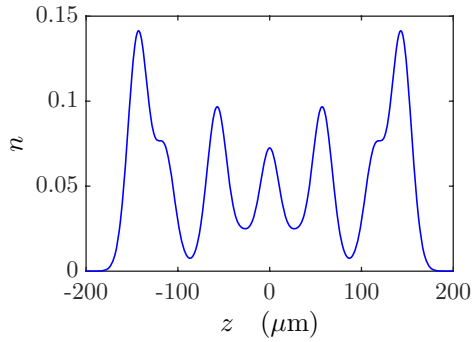

Figure 47.7: (code) Density distribution after time-of-flight.

The condensed wavefunction evolves into a superposition of motional modes, which correspond to the diffraction orders of Bragg scattering and their amplitudes through the Bessel functions J_n. The diffraction efficiency increases with laser intensity and with time.

Now, we need to generalize this result to the propagating standing wave of the expression (47.54). The intensity generates a dipole potential,

$$U(z,t) \approx U_0 \cos^2 \tfrac{q_z z - \Delta\omega t}{2} \ , \tag{47.60}$$

[7] Using the Jacobi-Anger expansion, $e^{\imath\beta\cos x} = \sum_n \imath^n J_n(\beta) e^{\imath nx}$.
[8] Andreas got $\psi_0(z)\sum_n J_n^2(U_0\tau/2\hbar)e^{inqz/2}$.

so that the condensate now evolves according to,

$$\psi(z,t) = \psi_0(z) e^{\imath/\hbar \int_{t_0}^{t_0+\tau} U(z,t)dt} = \psi_0(z) e^{\imath/\hbar \int_{t_0}^{t_0+\tau} U_0 \cos^2 \frac{q_z z - \Delta\omega t}{2} dt} \ . \tag{47.61}$$

For short interaction times, $\tau \ll 2\pi/\Delta\omega$, ...

47.2.1.2 Compton scattering picture

The *second interpretation* is that of *Compton scattering*: Spontaneous Rayleigh scattering of a photon from a mode $\mathbf{k}_\omega$ into a solid angle around $\mathbf{k}_{\omega-\Delta\omega}$ leaves an atom with the recoil momentum $\hbar\mathbf{q} \equiv \mathbf{p}_f \cdot \mathbf{p}_i$. Of course, one can *stimulate* the Rayleigh scattering process by providing the laser mode $\mathbf{k}_\omega - \Delta\omega$ at the entrance. By replacing the spontaneous output mode with a stimulated input mode, we increase the probability for an atomic recoil in the momentum mode $\hbar\mathbf{q}$, which is thus pre-selected by the choice of $\mathbf{k}_{\omega-\Delta\omega}$. Since the elementary scattering process must conserve energy and total momentum,

$$\begin{aligned} \hbar\omega + \frac{p_i^2}{2m} &= \hbar(\omega - \Delta\omega) + \frac{p_f^2}{2m} \\ \hbar\mathbf{k}_i + \mathbf{p}_i &= \hbar\mathbf{k}_f + \mathbf{p}_f \ , \end{aligned} \tag{47.62}$$

we obtain the *Bragg condition*,

$$\boxed{E = \Delta\omega = \frac{p_f^2}{2m} - \frac{p_i^2}{2m} = \frac{(\mathbf{p}_f - \mathbf{p}_i)^2}{2m} + \frac{(\mathbf{p}_f - \mathbf{p}_i)\cdot\mathbf{p}_i}{m} = \frac{q^2}{2m} + \frac{\mathbf{q}\cdot\mathbf{p}_i}{m}} \ . \tag{47.63}$$

Expressed by the Bragg angle, the condition reads,

$$q = \sqrt{(\mathbf{p}_f - \mathbf{p}_i)^2} = \sqrt{\hbar^2\mathbf{k}_i^2 + \hbar^2\mathbf{k}_f^2 - 2\hbar^2\mathbf{k}_i\mathbf{k}_f} \simeq \hbar\mathbf{k}_i\sqrt{2 - 2\cos\theta} = 2\hbar k_i \sin\vartheta/2 \ . \tag{47.64}$$

The efficiency for transferring atoms to the recoil mode depends on the fulfillment of this condition. The Bragg condition can be employed to select higher diffraction orders.

47.2.1.3 Stimulated Raman scattering picture

A *third interpretation* is as *stimulated Raman scattering* between two different kinetic states of the atom [see 47.6(b)]. In fact, the momentum modes $\mathbf{p}_i$ and $\mathbf{p}_f$ have different energies, which, for a condensate, are determined by the Bogolubov spectrum [512]. By varying the angle ϑ in the Bragg condition (47.63), we can choose the amount of energy to be transferred and thus probe the spectrum, i.e. measure the excitation energy $E(\mathbf{q},\mu)$ as a function of the momentum $\mathbf{q}$ and the chemical potential μ in the particle regime $\mathbf{q}^2/2m \gg \mu$, as well as in the phonon regime $\mathbf{q}^2/2m \ll \mu$. On the other hand, varying the detuning $\Delta\omega$ in the Bragg condition (47.63), we selectively address different velocity classes of a gas or condensate, which allows us to probe its velocity distribution. This procedure is called spectroscopy of *recoil-induced resonances* (RIR) [305, 1259]. RIR spectroscopy also provides detailed information on the mean-field energy and the (inhomogeneous) density distribution of a condensate. Note, finally, that Bragg scattering is closely related to *Kapitza-Dirac* scattering of atomic beams, well-known in conventional atom optics [693, 531].

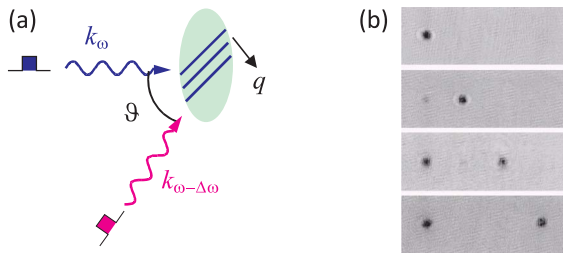

Figure 47.8: Bragg scattering of atomic clouds. (a) Geometric layout as in 47.6. Here, we assume $p_i = 0$. (b) Experiment showing coherent splitting by a Bragg pulse.

47.2.1.4 Coherent splitting

There is a general interest in the possibility of dividing phase space by coherent coupling of otherwise independent modes. We are talking, of course, about double slits or beamsplitters, which represent an essential tool of quantum mechanics. Bragg diffraction realizes a beamsplitter for atomic clouds analogous to the optical beamsplitter. In fact, Bragg diffraction has been used for the realization of output couplers for atom lasers and for atom interferometers. A suggestion that is sometimes made is the following: 'A condensate is a macroscopically populated momentum mode. The Bragg beamsplitter divides the phase space into two entangled output modes. Shouldn't it be possible to generate a macroscopic superposition of two condensates, i.e. a really macroscopic Schrödinger cat?' of the type

$$(|\Psi_+\rangle + |\Psi_-\rangle) \ . \tag{47.65}$$

Their is an obvious fundamental interest to study such states and the mechanisms leading to their decoherence (see Sec. 36.1.1).

To clarify the situation, we first have to say, what we mean by *Schrödinger cat*. A Schrödinger cat is a quantum superposition of many-body states. A perfect cat made of N two-level atoms can be expressed as $|++...\rangle \pm |--...\rangle$. The Einstein-Podolsky-Rosen (EPR) and the Greenberger-Horne-Zeilinger states (GHz) belong to this category. The degree of entanglement of the cat is measured by the information entropy defined as $S = -\langle \log_2 \hat{\rho} \rangle$, where $\hat{\rho}$ is the density operator. The information entropy measures the amount of classical information that can be encoded in the quantum state. For example, the entropy of a perfect cat state is $S = 1$ bit, because if we find one of the atoms in the state $|+\rangle$, we know that all others are in the same state.

Second, we have to explain, what we mean by a *beamsplitter*. Subject to a beam splitting process, every individual atom has the choice between one of two output ports. However, if the process is coherent, every atom will evolve into a coherent superposition, but it does so independently from the other atoms. That is, we can write the state of the atomic cloud as a product state of *Schrödinger kittens* $(|+\rangle \pm |-\rangle)^N$, but no real cat. The information entropy is $S = N$ bit, as for independent atoms. *Clearly, the state (47.65) is NOT the state generated by a beamsplitter!* Nevertheless, the beamsplitter creates a certain correlation between the two modes (see Sec.35.8).

It may come as a surprise, that a condensate composed of totally delocalized atoms coherently interacting with a homogeneous light field (the photons of the Bragg

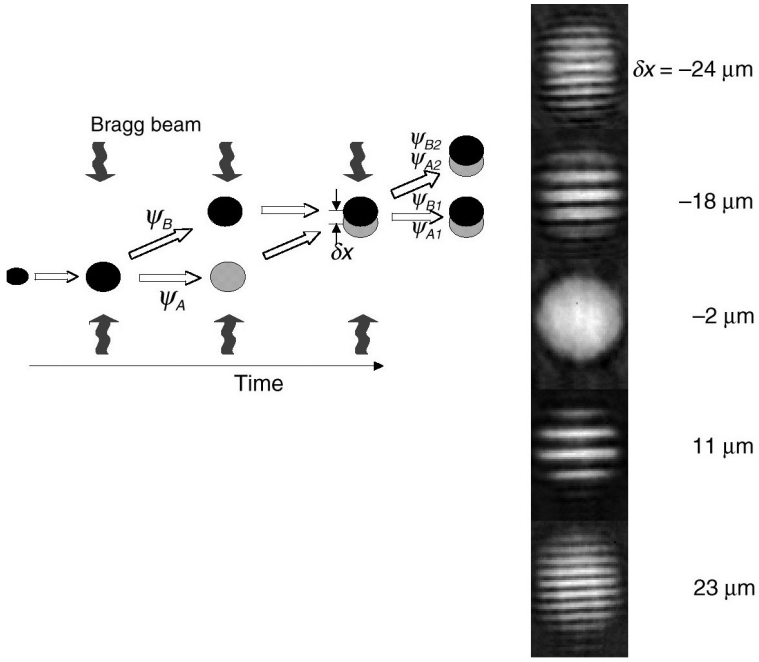

Figure 47.9: Bragg interferometer.

beams are totally delocalized over the field mode including the condensate volume) increases its entropy from 1 to N bits. This argument, however, would be the same for a non-condensed *thermal* cloud being sufficiently cold that the thermal de Broglie wavelengths exceeds the size of the cloud. That is, even in condensates the photons are scattered by individual atoms. The interaction with the light *localizes* one atom in the condensate before removing it from there by recoil. Nevertheless, cooperative interaction of several atoms with a light mode is possible, e.g. in superradiance or when the photons are recycled by means of an optical cavity, as in the Jaynes-Cummings model.

47.2.2 Bragg interferometry of a thermal gas

Even above the critical temperature the momentum distribution of a dilute thermal gas is (slightly) modified by quantum statistics, i.e. by the classical, bosonic or fermionic nature of the gas. The momentum distributions have been calculated in Chp. 44. We have already emphasized that Bragg interferometry can be used to measure the momentum distribution of a gas via RIR spectroscopy, whether the gas is condensed or thermal. Now, let us discuss Bragg interferometry on a thermal gas, based on the articles [853] and [344].

47.2.2.1 Free evolution of a thermal cloud

To describe the Bragg scattering process quantitatively, we interpret it as a *Raman transition between discrete atomic momentum states governed by a Schrödinger equa-*

tion. On the other hand, as long as no radiation is incident the atomic center-of-mass wavefunctions evolve freely or under the constraint of an external potential. That is, both processes concern the same motional degree of freedom. In order to derive a complete quantum model, let us first develop the formalism for the description of the free evolution of a thermal cloud, then we explain how a resonant radiation can be included.

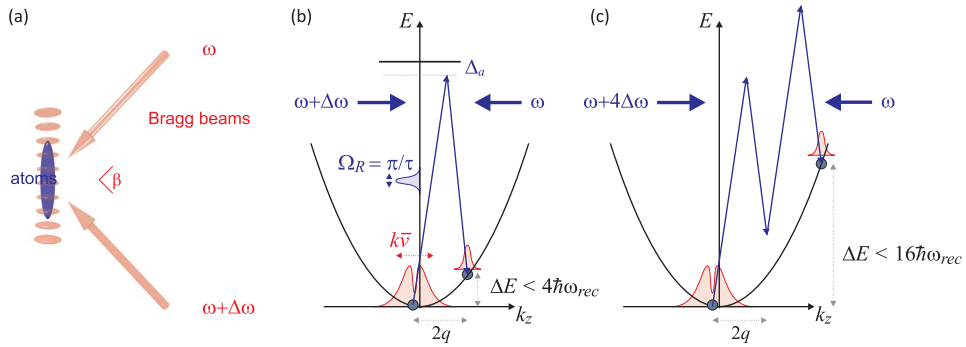

Figure 47.10: (a) Geometry for Bragg diffraction. (b) Illustration of a Raman transition between two points of the free-particle dispersion curve, when the atoms are initially thermally distributed. (c) Same as (a), but now the detuning $\Delta\omega$ is adjusted for second-order Bragg diffraction.

We consider a thermal atomic cloud initially distributed over many momentum classes according to the Maxwell-Boltzmann velocity distribution,

$$D(k_z) = \frac{\hbar}{(2\pi m k_B T)^{1/2}} e^{-\hbar^2 k_z^2/2mk_BT} = \frac{e^{-\pi k_z^2/k_{therm}^2}}{k_{therm}} , \tag{47.66}$$

using $k_{therm} \equiv 2\pi/\lambda_{therm}$ and (43.9). Because of the inhomogeneity of the distribution, any evolution of atoms belonging to specific momentum classes caused by velocity-selective radiation pulses, must be calculated with individual atoms. The final momentum distribution (e.g. after a pulse sequence) can then be obtained by weighing with the individual evolution with the initial momentum distribution [9].

We describe the quantum state of a thermal atom $|\psi\rangle$ as a plane wave, $\langle z|\psi\rangle \propto e^{\imath k_z z}$, which in momentum space corresponds to a Dirac distribution, $\langle k_z|\psi\rangle \propto \delta(z - z_0)$. Without radiative coupling, we describe the evolution in momentum space by the solution of the Schrödinger equation (or propagator),

$$\langle k_z|\psi(t)\rangle = e^{\imath \hat{H} t/\hbar} \langle k_z|\psi(0)\rangle . \tag{47.67}$$

In free space, with the Hamiltonian $\hat{H}_{free} = \hbar^2 k_z^2/2m$, the wavefunction is obviously constant.

In order to couple two intervals of momentum distribution by resonant radiation, we first need to duplicate the Hilbert space,

$$a_{i,k_z}(t) \equiv \langle i|\psi_{k_z}(t)\rangle = \langle i|\langle k_z|\psi(t)\rangle \tag{47.68}$$

[9] The procedure neglects interatomic interactions, which is always a good presumption, for example, for an ultracold Fermi gas [347] or for ^{88}Sr atoms, which have a very small scattering length.

with $i = 1, 2$. Note that, in this case, the Hilbert spaces are not disjunct.

To obtain the atomic momentum distribution after the application of a pulse sequence, we calculate the evolution of the amplitudes a_{j,k_z} for a variety of initial momenta and weigh the final populations of the momentum states with the distribution function $D(k_z)$. The number of atoms expected in the zeroth and first Bragg diffraction order is, therefore,

$$N_j(t) = \int D(k_z)|a_{j,k_z}(t)|^2 dk_z \ . \tag{47.69}$$

47.2.2.2 Bragg scattering and RIR

For large momentum distributions, $T \gg T_{rec}$, the atomic cloud occupies many momentum states, such that the Bragg scattering produces a RIR-like signal. That is, the scattering probability is proportional to the *population difference* of the initial and final momentum states, as discussed in Sec. 42.3.2. The number of scattered atoms/photons is, therefore,

$$\dot{N}_{brg} \propto \Omega_R \left.\frac{\partial D(k_z)}{\partial k_z}\right|_{k_z=\hbar m\Delta\nu/q} \ . \tag{47.70}$$

where,

$$\Omega_R = \frac{\Omega_1\Omega_2}{2\Delta_a} = \frac{1}{\Delta_a}\frac{3\lambda^2}{4\pi}\frac{\Gamma}{\hbar\omega}\sqrt{I_1 I_2} = \frac{3\pi c^2 I}{\hbar\omega^3}\frac{\Gamma}{\Delta_a} \tag{47.71}$$

is the two-photon Rabi frequency. For very narrow momentum distributions, $T \ll T_{rec}$, we may assume the atomic cloud to occupy only a single momentum state,

$$\dot{N}_{brg} \propto \Omega_R D(k_z) \ . \tag{47.72}$$

The transition rate per atom is then given by [1238],

$$\frac{W}{N} = \frac{2\pi\hbar}{N}\Omega_R^2 \sum_f |\langle f|\hat{\rho}^\dagger(\mathbf{k})|g\rangle|^2 \delta(\hbar\nu - E_f + E_g) \equiv 2\pi\Omega_R^2 S(\mathbf{k}, \nu) \ . \tag{47.73}$$

As illustrated in Fig. 47.10, to scatter an atom with the initial wavevector k_z to the next higher momentum state $k_z + 2q$, the Bragg condition requires,

$$\Delta\nu_R = \nu_{R2} - \nu_{R1} = \frac{\hbar(k_z + 2q)^2}{2m} - \frac{\hbar k_z^2}{2m} = \frac{2\hbar q}{m}(k_z + q) \ . \tag{47.74}$$

If we tune $\Delta\nu(\pm\Delta k_z)$ until the Bragg signal $\dot{N}_{brg}$ drops to $e^{-1/2}$,

$$\Delta\nu_R(\Delta k_z) - \Delta\nu_R(-\Delta k_z) = \frac{4\hbar\Delta k_z q}{m} = \frac{4\hbar q}{m}\frac{\sqrt{m k_B T}}{\hbar} = 4q\sqrt{\frac{k_B T}{m}} \ . \tag{47.75}$$

47.2.2.3 Bragg scattering by free atoms

Let us first assume that during the Bragg pulse only two discrete atomic momentum states $j = 0, 1$ are coupled [699, 148, 853, 344], and that trapping potentials are absent or can be neglected. This is justified for Bragg pulse sequences much shorter

than an oscillation period of the trap. We denote the probability amplitudes for the two momentum states by momentum space wavefunctions a_{j,k_z}. They correspond to atoms with initial momenta $\hbar k_z$ that are coupled to states with momentum $\hbar k_z' = \hbar(k_z + 2q)$. The temporal evolution of the amplitudes under the action of the Bragg light is given by the solutions of the Schrödinger equation [853, 344],

$$\begin{pmatrix} a_{0,k_z}(t) \\ a_{1,k_z}(t) \end{pmatrix} = e^{-\imath \hat{H}_R t/\hbar} \begin{pmatrix} a_{0,k_z}(0) \\ a_{1,k_z}(0) \end{pmatrix} , \tag{47.76}$$

with the Hamiltonian,

$$\boxed{\hat{H}_R = \begin{pmatrix} \frac{\hbar^2}{2m}k_z^2 & \frac{1}{2}\hbar\Omega_R \\ \frac{1}{2}\hbar\Omega_R & \frac{\hbar^2}{2m}k_z'^2 - \hbar\delta \end{pmatrix}} , \tag{47.77}$$

where $\Delta = 2\hbar q^2/m - \delta$ is the detuning of the Bragg lasers from the recoil shift. When the Bragg light is switched off, the Hamiltonian simplifies to,

$$\hat{H}_{free} = \begin{pmatrix} \frac{\hbar^2}{2m}k_z^2 & 0 \\ 0 & \frac{\hbar^2}{2m}k_z'^2 - \delta \end{pmatrix} . \tag{47.78}$$

Concatenating temporal evolutions described by $e^{-\imath \hat{H}_R t/\hbar}$ and $e^{-\imath \hat{H}_{free} t/\hbar}$, the phase evolution of individual atoms in momentum state superpositions can be calculated for arbitrary sequences of pulses separated by intervals of free evolution, for example, Ramsey-type sequences.

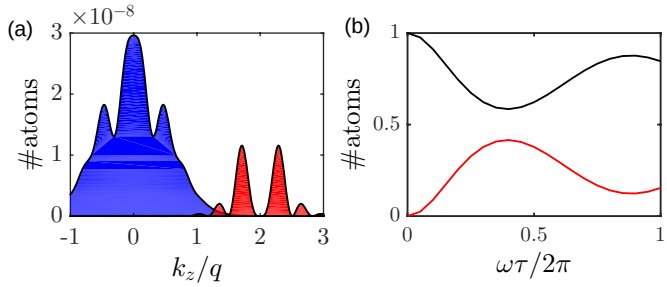

Figure 47.11: (code) (a) Distribution of momentum classes in the direction of k_z after irradiation of a 2π Bragg pulse. The width of the structure is determined by the power broadening of the Raman transition. (b) Temporal evolution of the populations of the momentum states 0 and $2q$.

47.2.2.4 Bragg scattering by trapped particles

When trapped atoms are considered, the problem arises that the Hilbert space of momentum states is simultaneously coupled by two interactions: a moving optical lattice (generated by the Bragg lasers) and the (harmonic) trap. However, the situation gets simpler if a separation of the scales is possible. In general, the duration of a pulse

is very short, $\tau \ll 2\pi/\omega_z$. In contrast, the duration of a free evolution period Δt (e.g. in a Ramsey cycle) may be such, that it is no more negligible compared to a trap oscillation period, so that we need to account for the action of the trapping potential explicitly.

As the trap couples the atomic momenta with the atomic positions ($E_{kin} + E_{pot} = const$), the initial spatial distribution of the atoms must now be considered. For simplicity, we describe it as a thermal Gaussian, similarly to what has been done in Eq. (47.66) for the momentum distribution,

$$G(z) = \sqrt{\frac{m\omega_z^2}{2\pi k_B T}} e^{-m\omega_z^2 z^2/2k_B T} = \frac{e^{-\pi z^2/a_z^4 k_{therm}^2}}{a_z^2 k_{therm}} \ . \tag{47.79}$$

Beginning with the positions z and initial momenta k_z, after a diffraction pulse transferring the recoil $2q$ to part of the atoms and being short enough not to change their positions, the atoms follow classical trajectories. The atomic momenta (now depending on time) are simply the solution of the equation of motion $\hbar \dot{k}_z = -m\omega_z^2 z$ with the initial conditions $z(0) = z$ and $k_z(0) = k_z$, respectively, $k'_z(0) = k_z + 2q$,

$$\begin{aligned} \tilde{k}_z(t) &= k_z \cos\omega_z t - \frac{m\omega_z}{\hbar} z \sin\omega_z t \\ \tilde{k}'_z(t) &= (k_z + 2q)\cos\omega_z t - \frac{m\omega_z}{\hbar} z \sin\omega_z t \ , \end{aligned} \tag{47.80}$$

where the first expression holds for non-diffracted atoms and the second for diffracted atoms. These momenta are substituted for k_z and k'_z, respectively, in the Hamiltonians (47.77) and (47.78). As the Bragg pulses are short compared to the oscillation period, $\tau \ll 2\pi/\omega_z$, the effect of the trapping potential may be neglected during Bragg scattering. This means that the Hamiltonian $\hat{H}_R$ depends on $\tilde{k}_z(t)$, but can be treated as time-independent for the short intervals τ. In contrast, the Hamiltonian for free propagation $\hat{H}_{free}$ depends on the time, if Δt is long. In this case, the phase evolution of the atoms in both coupled states can be described by the time evolution operator as,

$$\boxed{e^{-\imath \hat{H}_{free} t/\hbar} = \begin{pmatrix} \exp\left(-\imath \int_0^t dt \frac{\hbar}{2m} \tilde{k}_z^2(t)\right) & 0 \\ 0 & \exp\left(-\imath \int_0^t dt \left[\frac{\hbar}{2m} \tilde{k}_z'^2(t) - \delta\right]\right) \end{pmatrix}} \ . \tag{47.81}$$

Since the amplitudes a_{j,z,k_z} now also depend on the initial atomic positions, the final populations of the momentum states must be additionally weighted with the initial spatial distribution. Therefore, the Eq. (47.69) for the expected the numbers of diffracted and non-diffracted atoms must be replaced by,

$$N_j(t) = \iint D(k_z) G(z) \left|a_{j,z,k_z}(t)\right|^2 dk_z dz \ . \tag{47.82}$$

In practice, however, it might be a good approximation to assume small displacements around a δ-shaped position distribution. Note, that the transformation (47.80) must be repeated for every free evolution pulse of a sequence.

Example 290 (*Approximation for small displacements*): In practice, we may neglect the displacements, $z \simeq 0$. Then the equations (47.80) simplify to,

$$\tilde{k}_z(t) = k_z \cos\omega_z t \qquad \text{and} \qquad \tilde{k}'_z(t) = (k_z + 2q)\cos\omega_z t \ .$$

Inserting them in (47.81) we obtain for the propagator,

$$e^{-\imath \hat{H}_{free} t/\hbar}$$
$$= \exp\left(-\frac{\imath\hbar k_z^2}{4m\omega_z}(\cos\omega_z t \sin\omega_z t + \omega_z t)\right)\begin{pmatrix} 1 & 0 \\ 0 & \exp\left(-\frac{\imath\hbar q k_z}{2m\omega_z}(\cos\omega_z t \sin\omega_z t + \omega_z t)\right)\end{pmatrix} .$$

In Exc. 47.2.4.1 we will study the behavior of an ultracold atomic cloud subject to a gravitational potential during a Ramsey-Bordé sequence.

47.2.2.5 Bloch equations approach

Experimentally, we observe decoherence of the dynamics described above on a very slow time scale. This phenomenon can be included in a description based on Bloch equations,

$$\frac{d}{dt}\vec{\rho}_{k_z}(\tau) = M_j \vec{\rho}_{k_z}(\tau) \ , \tag{47.83}$$

with

$$\vec{\rho}_{k_z}(\tau) = \begin{pmatrix} \rho_{00,k_z}(\tau) \\ \rho_{01,k_z}(\tau) \\ \rho_{10,k_z}(\tau) \\ \rho_{11,k_z}(\tau) \end{pmatrix} \qquad \text{and} \qquad M_j = \begin{pmatrix} 0 & \Gamma & \frac{\imath}{2}\Omega_R & -\frac{\imath}{2}\Omega_R \\ 0 & -\Gamma & -\frac{\imath}{2}\Omega_R & \frac{\imath}{2}\Omega_R \\ \frac{\imath}{2}\Omega_R & -\frac{\imath}{2}\Omega_R & -\gamma - \imath\Delta_j & 0 \\ -\frac{\imath}{2}\Omega_R & \frac{\imath}{2}\Omega_R & 0 & -\gamma + \imath\Delta_j \end{pmatrix} \tag{47.84}$$

with the solution,

$$\vec{\rho}_{k_z}(\tau) = e^{M_3 t} e^{M_2 t} e^{M_1 t} \vec{\rho}_{k_z}(0) \tag{47.85}$$

with,

$$\Delta_1 = \frac{\hbar}{2m}(k_z + 2q)^2 - \Delta\nu - \frac{\hbar}{2m}k_z^2 \tag{47.86}$$
$$\Delta_3 = \frac{\hbar}{2m}\left[(k_z + 2q)\cos\omega_{tr}\tau\right]^2 - \frac{\hbar}{2m}\left[(k_z + 2q)\cos\omega_{tr}\tau - 2q\right]^2 - \Delta\nu \ .$$

We weigh populations with the initial momentum distribution,

$$N_j(\tau) \equiv \int D(k_z)\rho_{jj,k_z}(\tau)dk_z \ . \tag{47.87}$$

47.2.2.6 Kapitza-Dirac scattering

An atomic beam with longitudinal de Broglie wavelength $\lambda_{dB} = h/p$ diffracted by a solid periodic grating with a slit distance of d receives a transverse amplitude modulation. In the far field, this generates focuses at angles defined by $n\lambda_{dB}/d = \sin\vartheta$.

Alternatively, the grating may consist of a standing light wave detuned from resonances. The standing wave will create a periodic optical potential, which imprints a transverse phase modulation on the atomic beam. In the far field, the result will be the same as for the solid grating. Each atom will evolve into a superposition of momentum sidemodes $\pm n2\hbar k$, without any momentum having been transferred to the atoms. The diffraction angle is again $\sin\vartheta = \pm n2\hbar k/p = \pm n\lambda_{dB}/(\lambda/2)$, where $\lambda/2 = d$ is the periodicity of the standing light wave. However, this is only true if the phase shift is much smaller than π. This scheme is called the *Raman-Nath regime* or the regime of *Kapitza-Dirac scattering*. An equivalent condition for this regime is, that the interaction time is less than a period of oscillation in the optical potential, $\tau \ll \sqrt{\hbar/\omega_{rec}/U}$, or $v_{trans}\tau \ll \lambda$.

The Raman-Nath regime is realized by a very focused optical standing wave. A wave that is not plane can be considered a superposition of many spatial modes. Since (off-resonant) scattering (absorption followed by induced emission) corresponds to a photon redistribution between spatial modes, in a tight waist the phase matching condition is somewhat relaxed and minor corrections to the energy balance are possible. In a certain sense, Kapitza-Dirac scattering is the inverse process of 'forward scattering' of a laser beam passing through an atomic cloud: the roles of light and atoms are exchanged. The requirement that the interaction time be short implies, that the light grating is 'optically dilute' for the atomic beam [10].

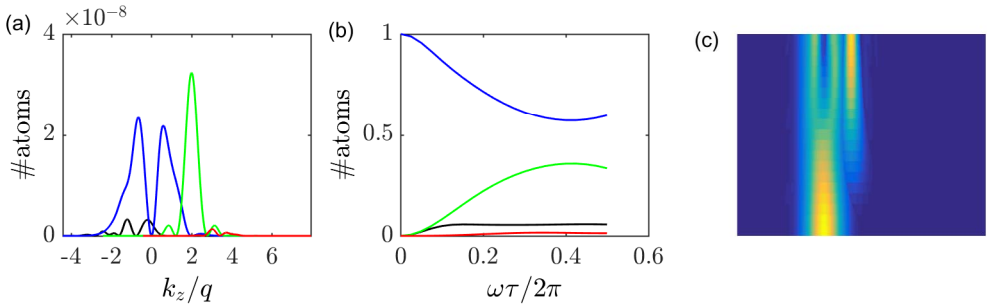

Figure 47.12: (code) (a) Distribution of momentum classes in the direction of k_z after irradiation of a π Bragg pulse. (b,c) Temporal evolution of the populations of the momentum states nq.

For larger Rabi frequencies,

$$\Omega_R \gg \frac{2\hbar q\sigma_{k_z}}{m} , \tag{47.88}$$

with $\sigma_{k_z} = \sqrt{mk_BT/\hbar^2}$ being the width of the momentum distribution, the Doppler broadening is dominated by power broadening, meaning that Bragg diffraction occurs all over the atomic cloud. At some point, however, the Rabi frequency becomes comparable to the energy difference between adjacent momentum states, and Kapitza-Dirac scattering sets in. According to [148] the scattering will stay two-state like as

[10] Note, that we usually employ the term of *optical diluteness* the other way round, i.e. an atomic cloud can be optically dilute (or dense) for a laser beam.

long as the Rabi frequency fulfills the condition,

$$\Omega_R \ll \frac{\hbar}{m}(4q^2 - 2q\sigma_{k_z}) \; . \tag{47.89}$$

In the Kapitza-Dirac regime, the large energy uncertainty, connected with the fast coupling rate, allows several momentum states to be coupled simultaneously. In particular the Bragg Hamiltonian is replaced by,

$$\hat{H}_\tau = \begin{pmatrix} \ddots & \ddots & & & \\ \ddots & \frac{\hbar(k_z-2q)^2}{2m} + \delta & \frac{\Omega_R}{2} & & \\ & \frac{\Omega_R}{2} & \frac{\hbar k_z^2}{2m} & \frac{\Omega_R}{2} & \\ & & \frac{\Omega_R}{2} & \frac{\hbar(k_z+2q)^2}{2m} - \delta & \ddots \\ & & & \ddots & \ddots \end{pmatrix} \; . \tag{47.90}$$

The crossover from the Bragg-diffraction regime to Kapitza-Dirac scattering is a smooth transition. As we will see below, for intermediate Rabi frequencies (here $1\,\mathrm{MHz} > \Omega_R/2\pi > 100\,\mathrm{kHz}$) the neighboring diffraction states, corresponding to momentum shifts of $4\hbar q$ and $-2\hbar q$ (second and minus first order), are scarcely populated. For higher and higher Rabi frequencies, $\Omega_R/2\pi > 1\,\mathrm{MHz}$, the scattering populates more and more diffraction orders.

47.2.2.7 Higher-order Bragg scattering

Higher-order Bragg scattering is possible as well. Then the $2n$-photon Rabi frequency must be calculated and inserted in the second diagonal of (47.90).

47.2.3 Bragg spectroscopy of a condensate

To measure the Bogolubov spectrum, we need to excite perturbations in a condensate and study its reaction [1238].

Let us now imagine that the potential has the form of a standing wave. Technically this can be done by two laser beams having the same frequency crossing at the position of the atoms,

$$V_{trap}(\mathbf{r}, t) \equiv \tfrac{V}{2} e^{\imath \mathbf{q}_1 \cdot \mathbf{r} - \imath\omega t} + \tfrac{V}{2} e^{\imath \mathbf{q}_2 \cdot \mathbf{r} - \imath\omega t} \; . \tag{47.91}$$

Choosing the coordinate system such that, $\mathbf{q}_1 \equiv (k_x, 0, k_z)$ and $\mathbf{q}_1 \equiv (k_x, 0, -k_z)$,

$$V_{trap}(\mathbf{r}, t) = \tfrac{V_x}{2} e^{\imath k_z z - \imath\omega t} + \tfrac{V_x}{2} e^{-\imath k_z z + \imath\omega t} \; , \tag{47.92}$$

with $V_x \equiv V e^{ik_x x}$. With this weak perturbation applied to the atoms, we make the ansatz,

$$\psi(\mathbf{r}, t) = e^{-\imath\mu t/\hbar} \left(\psi_0(\mathbf{r}, t) + u(t) e^{\imath k_z z - \imath\omega t} - v(t) e^{-\imath k_z z + \imath\omega t} \right) \; , \tag{47.93}$$

where the amplitudes of the perturbation, $u(t)$ and $v(t)$, only vary slowly in time. Assuming that ψ_0 is fairly homogeneous, i.e. $\langle \psi_0 | \nabla_z | \psi_0 \rangle \simeq 0$, the momentum transferred to the BEC is,

$$\langle \psi(\mathbf{r}, t) | - \imath\hbar\nabla_z | \psi(\mathbf{r}, t) \rangle = \hbar k_z (|u|^2 - |v|^2) \; . \tag{47.94}$$

We can now solve the Gross-Pitaevskii equation (45.20) in the same way as in Sec. 45.4.1 inserting the ansatz (47.93). The terms proportional to $e^{\imath k_z z - \imath\omega t}$ are,

$$\frac{\hbar^2\mathbf{k}_z^2}{2m}u+\frac{V}{2}\psi_0+g\left(|\psi_0|^2+|u|^2+|v|^2\right)u+g\psi_0^2 v+g|v|^2u+g|\psi_0|^2u=\left(\imath\hbar\frac{\partial}{\partial t}+\hbar\omega+\mu\right)u\,, \tag{47.95}$$

and the analogously for $e^{-\imath k_z z+\imath\omega t}$. Using $\mu = gn = g|\psi_0|^2$ and assuming that the perturbation is weak, $|u|, |v| \ll |\psi_0|$, we obtain,

$$\begin{aligned}\left(\frac{\hbar^2k^2}{2m}+gn\right)u+\frac{V}{2}\psi_0-gnv&=\left(\imath\hbar\frac{\partial}{\partial t}+\hbar\omega\right)u\\ -\left(\frac{\hbar^2k^2}{2m}+gn\right)v-\frac{V}{2}\psi_0+gnu&=\left(-\imath\hbar\frac{\partial}{\partial t}+\hbar\omega\right)v\,.\end{aligned} \tag{47.96}$$

This effect is called *Bragg diffraction* of atoms by a standing light wave.

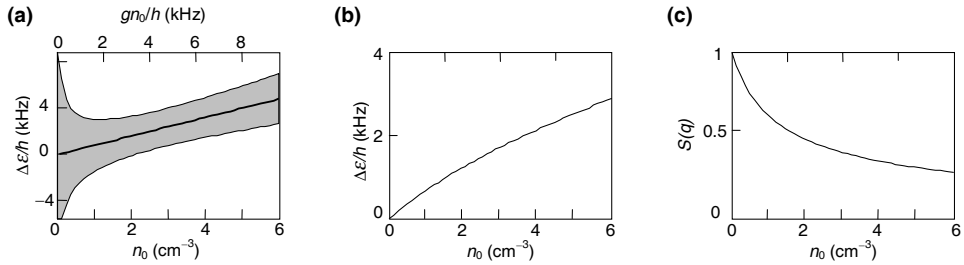

Figure 47.13: Spectrum of elementary excitations.

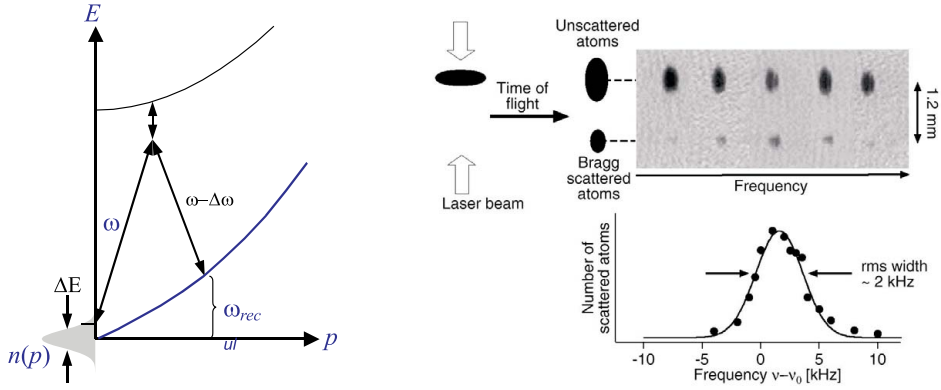

Figure 47.14: Spectrum of elementary excitations.

Using $\mathcal{L} \equiv \frac{\hbar^2\mathbf{k}^2}{2m} + V_{trap} + 2gn - \mu - \imath\hbar\frac{\partial}{\partial t}$, we can write,

$$\begin{pmatrix}\mathcal{L}-\hbar\omega_{\mathbf{k}} & -gn\\ -gn & \mathcal{L}+\hbar\omega_{\mathbf{k}}\end{pmatrix}\begin{pmatrix}u\\ v^*\end{pmatrix}=0\,. \tag{47.97}$$

These equations can be decoupled using the Bogolubov transform.

We calculate the momentum transferred to the BEC, assuming ψ_0 to be fairly homogeneous,

$$\langle\psi(\mathbf{r},t)|-\imath\hbar\nabla|\psi(\mathbf{r},t)\rangle=\hbar\mathbf{q}(|u|^2-|v|^2)\ . \tag{47.98}$$

47.2.4 Exercises

47.2.4.1 Ex: Bragg diffraction in a Ramsey-Bordé interferometer

Simulate the behavior of a cold atomic cloud subject to a gravitational potential during a Ramsey-Bordé sequence using the formalism developed in Sec. 47.2.2.

Solution: *We just need to modify the equations (47.80). The atomic momenta depending on time are now simply the solution of the equation of motion $\hbar\dot{k}_z=mg$ with the initial conditions $z(0)=z$ and $k_z(0)=k_z$, respectively, $k_z(0)=k_z+2q$,*

$$\tilde{k}_z(t)=k_z+\frac{mg}{\hbar}t\qquad\text{and}\qquad\tilde{k}'_z(t)=k_z+2q+\frac{mg}{\hbar}t\ ,$$

and the free space propagator (47.81) becomes,

$$e^{-\imath\hat{H}_{free}t/\hbar}=\begin{pmatrix}\exp\left(-\frac{\imath\hbar}{2m}\int_0^t\left[k_z+\frac{mg}{\hbar}t\right]^2dt\right)&0\\0&\exp\left(-\frac{\imath\hbar}{2m}\int_0^t\left[k_z+2q+\frac{mg}{\hbar}t\right]^2dt+\imath\delta t\right)\end{pmatrix}$$
$$=\exp\left(-\imath\left[\frac{\hbar k_z^2}{2m}t+\frac{g}{2}k_zt^2+\frac{mg^2}{6\hbar}t^3\right]\right)\begin{pmatrix}1&0\\0&\exp\left(-\imath\left[\frac{\hbar qk_z}{m}t+\frac{2mgq}{\hbar}t^2\right]-\imath\Delta t\right)\end{pmatrix}\ .$$

See also Excs. 23.5.6.2 and 23.5.6.3. We can now use this propagator to simulate a Ramsey-Bordé interferometer type sequence in a gravitational field, assuming resonant Bragg pulses, $\delta=2\hbar q^2/m$. It consists of the following sequence:
(i) First $\frac{\pi}{2}$-Bragg pulse,

$$\psi^{(1)}_{k_z}(t=\tfrac{\pi}{2\Omega_R})=e^{-\imath\pi\hat{H}_R/2\hbar\Omega_R}\psi_{k_z}(0)\ ,$$

(ii) free evolution,

$$\psi^{(2)}_{k_z}(t=\tau)=e^{-\imath\hat{H}_{free}(\tilde{k}_z,\tilde{k}'_z)\tau/\hbar}\psi^{(1)}_{k_z}(0)\qquad\text{with}\qquad\left\{\begin{array}{l}\tilde{k}_z(t)=k_z+\frac{mg}{\hbar}t\\\tilde{k}'_z(t)=k_z+2q+\frac{mg}{\hbar}t\end{array}\right.\ ,$$

(iii) π-pulse,

$$\psi^{(3)}_{k_z}(t=\tfrac{\pi}{\Omega_R})=e^{-\imath\pi\hat{H}_R/\hbar\Omega_R}\psi^{(2)}_{k_z}(0)\ ,$$

(iv) free evolution,

$$\psi^{(2)}_{k_z}(t=\tau)=e^{-\imath\hat{H}_{free}(\tilde{\tilde{k}}_z,\tilde{\tilde{k}}'_z)\tau/\hbar}\psi^{(1)}_{k_z}(0)\qquad\text{with}\qquad\left\{\begin{array}{l}\tilde{\tilde{k}}_z(t)=\tilde{k}'_z-2q+\frac{mg}{\hbar}t=k_z+\frac{2mg}{\hbar}t\\\tilde{\tilde{k}}'_z(t)=\tilde{k}_z+2q+\frac{mg}{\hbar}t=k_z+2q+\frac{2mg}{\hbar}t\end{array}\right.\ ,$$

(v) and second $\frac{\pi}{2}$-pulse,

$$\psi^{(3)}_{k_z}(t=\tfrac{\pi}{2\Omega_R})=e^{-\imath\pi\hat{H}_R/2\hbar\Omega_R}\psi^{(2)}_{k_z}(0)\ .$$

Note, that the model is only good for short sequences, $mg\Delta t\ll\hbar q$.

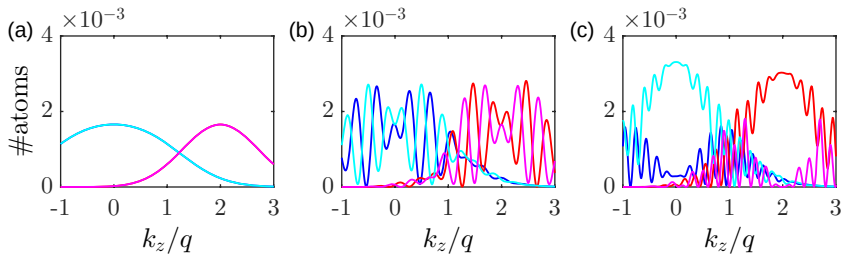

Figure 47.15: (code) Momentum distributions during a Ramsey-Bordé pulse sequence with $N = 10^5$ strontium atoms of temperature $T = 800\,\mathrm{nK}$ subject to Bragg pulses at $\lambda_{brg} = 461\,\mathrm{nm}$ under 60° angle (a) after the first $\frac{\pi}{2}$-pulse, (b) after the π-pulse, and (c) after the second $\frac{\pi}{2}$-pulse. Blue and red line are calculated with $g = 9.81\,\mathrm{m/s^2}$, cyan and magenta lines with $(1 + 7 \cdot 10^{-10})g$. The Rabi frequency is $\Omega_R = (2\pi)\ 30\,\mathrm{kHz}$ and the free evolution time $\tau = 100\,\mu\mathrm{s}$.

47.3 Matter wave superradiance

47.3.1 Classical superradiance

The Bragg beam splitter introduced in the last section does not give rise to collective scattering, even when the atoms are as strongly correlated as in a condensate. On the other hand, collective scattering is known to occur in a classical gas: When two atoms excited to an internal energy level, $\sim hc/\lambda$, are separated by a distance R too large to form a molecule, but smaller than the wavelength of the excited transition, $a_B \ll R \ll \lambda$, the atoms are coupled to the electromagnetic continuum by the same radiation that they emit (see Fig. 47.16). The dipole moments of the atoms stimulate each other to emit, and we observe a synchronized and accelerated relaxation, resulting in a coherent and directional burst of radiation [366, 1085]. The directionality of the radiation is due to a destructive interference of the dipolar radiation patterns emitted by the atoms in all directions except the direction chosen by the first emitted photon. This direction is random (except when bosonically stimulated). The atomic sample evolves, during this time, to a state of coherent superposition, until all the atoms are deexcited. This phenomenon is called *Dicke superradiance*. A similar effect exists for matter waves, and will be discussed in the following sections [649].

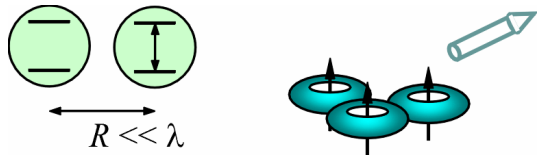

Figure 47.16: Superradiance assumes small interatomic distances compared to the wavelength of the excited dipole. Toroidal interference patterns interfering constructively in only one direction.

47.3.2 Matter wave superradiance & CARL

We consider the process of Rayleigh scattering from a condensate. The scattering rate obviously depends on the number of atoms and the laser intensity. The crucial point now is, that this rate can be stimulated by populations in the output modes, that is, the modes of scattered light and the atomic recoil modes. Matter and light participate in the scattering process as equal partners. In Sec. 47.2.1 we showed that Bragg scattering can be interpreted as *optical stimulation of matter wave scattering*. By analogy, it is possible to imagine a process of *wave matter stimulation of light scattering*. We will now discuss such a process, called *superradiant Rayleigh scattering* or *matter wave superradiance* (MWSR) [649], with the help of the small cartoon shown in Fig. 47.17. See also (watch talk).

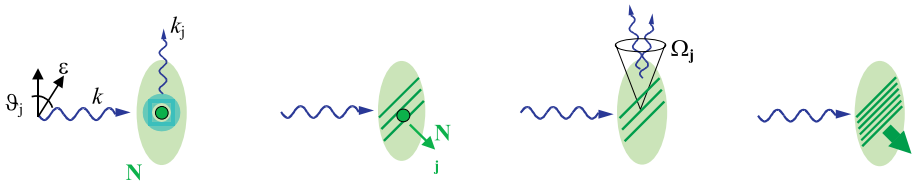

Figure 47.17: Cartoon for MWSR (see text).

Let us imagine an elongated condensate, subject to a magnetic field directed along its long axis and illuminated perpendicularly to the long axis by a linearly polarized laser beam. The scattered light is emitted into a (toroidal) dipolar radiation pattern. The fraction of the light scattered into the solid angle Ω_j, which is inclined by angle ϑ_j with respect to the polarization of the incident laser is $\Omega_j \sin^2\vartheta_j/(8\pi/3)$. Of course, the number of scattered photons also depends on the optical cross section σ and the number of scattering atoms N_0. When an atom, recoiling due to the transfer of one unit of photonic momentum, moves with a speed of a few centimeters per second through the condensate, it interferes with other atoms of the condensate, thus forming a wave matter grating. The grating, the lifetime of which is long in comparison to the scattering rate, now stimulates subsequent photons to follow the same path Ω_j and receives, in turn, the scattering atoms. In other words, the bosonic stimulation of the scattering process by the N_j atoms already populating the recoil mode amplifies the photon scattering rate by a factor of $N_j + 1$. The differential optical cross section (power P_j scattered into the direction Ω_j divided by the laser intensity I) is [649],

$$\frac{d\sigma}{d\Omega_j} = \frac{P_j}{I} = \frac{\Omega_j \sin^2\vartheta_j}{8\pi/3}\sigma N_0(N_j+1)\ . \tag{47.99}$$

Each scattering event of a photon into the mode Ω_j transfers an atom to the recoil mode N_j:

$$\dot{N}_j = P_j/\hbar\omega \equiv G_j N_j \qquad \text{where} \qquad G_j = \frac{I}{\hbar\omega}\sigma\frac{\Omega_j \sin^2\vartheta_j}{8\pi/3}N_0\ . \tag{47.100}$$

The phase matching condition is satisfied for a solid angle of approximately $\Omega_j = \lambda^2/A_j$, where A_j is the cross-sectional area of the condensate. If l_j is the length of

condensate, we can write,

$$G_j = \frac{I}{\hbar\omega}\sigma\frac{\sin^2\vartheta_j}{8\pi/3}n_0\lambda^2 l_j \ . \tag{47.101}$$

With the atomic density $n_0 = N_0/(A_j l_j)$, the factor $n_0\lambda^2 l_j$ describes the optical density of the BEC in the direction of the scattering. Therefore, we obtain *exponential gain* for the atom number N_j, that is, the process is self-amplifying.

Using the terms of the *dressed atom* picture, we would say that the excited state of our system is formed by the BEC and the laser mode. This state relaxes to a state formed by the recoiled atoms and the scattered photons. The exponential gain occurs, when this system exhibits inversion. The inversion is maintained, until the BEC is completely transferred to the momentum recoil modes [11].

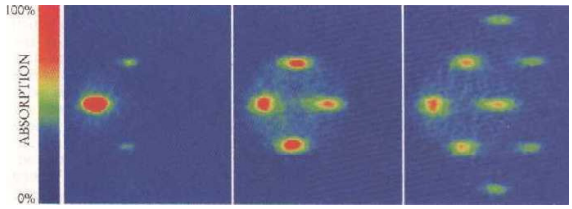

Figure 47.18: Observation of matter wave superradiance.

It is instructive to compare Dicke superradiance and matter wave superradiance. Dicke superradiance is induced by an electronic coherence between adjacent atoms. It requires a sufficiently long coherence time for the atomic dipoles. On the other hand, MWSR is a coherence effect between two states of the atomic center-of-mass motion, i.e. the condensed state and a momentum sidemode. A long lifetime of this coherence is necessary to allow for correlations between successive scattering events. The coherence lifetime corresponds to a coherence length, which for a condensate is equal to its physical size, whereas for a thermal cloud, it only corresponds to its thermal Broglie wavelength. This explains why it is difficult to observe MWSR with non-condensed atomic clouds.

Since the scattered photons quickly leave the BEC, there is no feedback or bosonic stimulation by the optical output mode. This can be interpreted as a fast decaying cavity mode, and the regime is called the *bad cavity limit*. Let us now imagine, that the photons were recycled, for example, via an optical cavity constructed around the BEC and reflecting back the photons emitted in the solid angle Ω_j [12]. The mirrors of the cavity create reflection images of the radiating atoms, which increase the *density of states*, the scattering rate, and the gain G_j increase by a factor of $8F/\pi$. An

[11] Superradiant scattering is due to a nonlinear coupling between two matter waves and two optical waves in a *four-wave mixing* process (4WM) interpreted as scattering of light *from* a wave matter *stimulated* by a wave matter mode. The process does not require nonlinearity due to collisions, but it works with an ideal gas, $g \to 0$. This distinguishes it from the 4WM of four matter waves, studied in Sec. 46.3.4 and interpreted as a scattering of atoms by a matter wave stimulated by matter wave mode, and 4WM in quantum optics involving four photons. But in all cases bosonic stimulation is crucial.

[12] Alternatively, we may imagine a scheme decelerating of the group velocity of the light pulse.

interesting question now is, what happens in the limit $F \to \infty$. If the decay of the cavity mode, and therefore the removal of photons from the coherent interaction zone (which is precisely the volume occupied by the BEC) is slow, the MWSR process seems to be doubly stimulated, optically and atomically. However, in this case we also expect the inverse process, where photons are scattered back to the original mode, to occur and to be stimulated by the number of atoms N_0 in the condensate. We see that the simple picture of bosonic stimulation does not work in this case, and a more complete model including the possibility of Rabi oscillations amplified by stimulated emission is necessary [13].

47.3.3 Amplification of matter and light waves

The feedback-induced exponential gain giving rise to the phenomenon of MWSR can be used to construct a phase-coherent amplifier of matter and light waves. After all, the momentum side modes observed in the MWSR process [649] already represent amplified vacuum fluctuations. To experimentally realize a *coherent matter wave amplifier* [749, 651], it is sufficient to replace the vacuum fluctuations of the original MWSR experiment with a small *seed condensate*: $\sim 0.1\%$ of the 'mother condensate' proved sufficient to stimulate the matter wave amplifier. The seed condensate was created by Bragg diffraction transferring atoms from the mother BEC to another momentum state (see Sec. 47.2). The matter wave grating formed by interference of the seed condensate and the mother BEC was subsequently amplified by a MWSR pulse. The gain for the atom number in the seed condensate was 10 to 100 depending on the intensity and duration of the MWSR pulse. Finally, the coherence of the amplification process was demonstrated by *active atom interferometry* using the Ramsey scheme: One of the interferometer arms consisted of the amplified seed condensate and the other of a reference condensate (local oscillator) especially created by Bragg diffraction from the mother condensate. The observation of interference between these two matter waves proved the coherence of the amplification process and the existence of a well-defined phase relationship between the input and the output of the matter wave amplifier.

In analogy to electronics, we may consider the coherent matter wave amplifier as an *active device* complementing the atom optical toolbox of *passive device*s (see Sec. 46.3.1).

47.3.4 Four-wave mixing of optical and matter waves

We will now make an attempt to categorize the various scattering processes involving condensates. Let us first return to the radiation pressure [Fig. 47.20(a)], where an incident photon is spontaneously scattered into a random direction. The isotropy of

[13] The phenomenon of the matter wave superradiance can be understood without quantization of the atomic motion [**?**] and, in particular, without quantum degeneracy. A cold and dense thermal cloud can show the phenomenon of MWSR [1413]. The scattered light forms together with the pump light, a propagating standing light wave, from which the atoms are scattered by Bragg diffraction. Atoms are accelerated by the CARL effect [305, 173, 775, 918, 917, 749, 651, 650] through a coherent redistribution of photons between the pump and scattered modes. However, as was shown later-on, the different recoil modes of the condensate exhibit phase-coherence, which is not explained by a theories treating the atomic motion semi-classically.

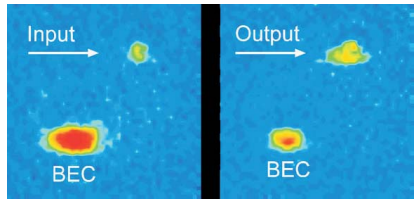

Figure 47.19: Matter wave amplification of a 'seed condensate' at the expense of a 'mother condensate'. Time-of-flight imaging visualizes the condensate's momentum distribution.

the scattering process can, however, be broken when certain directions (i.e. spatial modes) are favored by bosonic stimulation. The symmetry of the roles of matter wave modes and light modes allows us to treat both on the same footing, for example, we can stimulate scattered modes either by matter of light waves.

Let us first have a look at stimulation by optical modes [Fig. 47.20(b) and (c)]. Fig. (b) describes optical four-wave mixing (4WM) in nonlinear optical media, i.e. *optically stimulated scattering of photons* from a standing light wave, which is a 4WM process of 4 photons. Fig. (c) describes Bragg scattering, i.e. an *optically stimulated scattering of atoms* by a standing light wave, which is a 4WM process of 2 photons and 2 atoms.

Similarly, a scattering process can also be stimulated by a macroscopic number of atoms in a recoil mode [Fig. 47.20(d) and (f)]. Fig. (d) describes superradiant Rayleigh scattering and matter wave amplification, i.e. scattering of photons *stimulated by a de Broglie wave*, which again corresponds to 4WM of 2 photons and two atoms. Fig. (e) describes amplification of a laser pulse by superradiant Rayleigh scattering, i.e. scattering of photons in a matter wave with *double stimulation by light waves and de Broglie waves*, which once again is a 4WM process of 2 photons and 2 atoms. Finally, Fig. (f) describes the basic process of nonlinear atom optics, i.e. the scattering of atoms by a matter wave *stimulated by de Broglie waves*, which is a 4WM process of 4 atoms.

47.4 Condensates in electronically excited states

The interaction between condensates and light has, so far, been treated in the limit where the *population of excited states can be neglected or adiabatically eliminated.* An example was the coherent coupling of different kinetic states of an atom by a method called *Bragg diffraction* discussed in Sec. 47.2.

On the other hand, atoms can have metastable excited states, which can introduce new degrees of freedom, and a whole world of new problems emerges that need to be addressed: How do condensed atoms move, when they are in different states of internal excitation (or superposition of states), and how do atoms in different states interact with each other? We will now turn our attention to coherent coupling of internal states [14].

[14] We will disregard, for the moment, possible effects due to inhomogeneous broadening caused by the finite volume of the cloud inside the potential (Zeeman shift in magnetic traps or dynamic Stark shift optical traps) or effects due to interatomic interactions. But we have to keep in mind, that

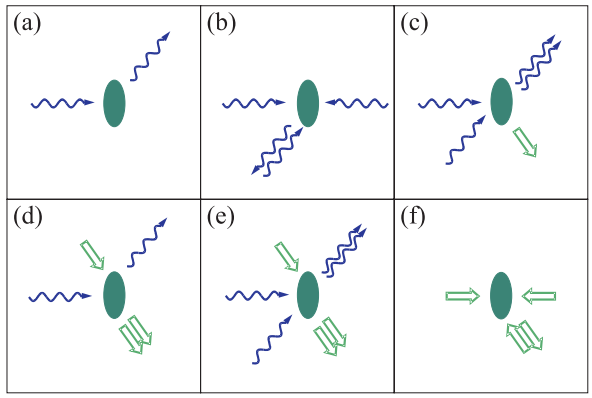

Figure 47.20: Schematic comparison of 4WM processes between light and matter wave modes. (a) Spontaneous emission, (b) classical 4WM of light modes, (c) Bragg scattering, (d) superradiant Rayleigh scattering, respectively, matter wave amplification, (e) optical amplification, and (f) 4WM of matter waves.

In Sec. 47.4.1 we will show how to generalize the second-quantized formalism introduced in 45.2.1 in order to deal with coupled condensates in different states of internal excitation.

In Sec. 47.4.2 we will discuss examples of how coherent coupling of two states can be accomplished either by radiofrequency/microwave radiation or by two laser beams in Raman configuration. In order to avoid spontaneous relaxation, we often choose state with low excitation energy, for example, within the hyperfine structure ($\hat{H} \sim \mathbf{I}\cdot\mathbf{J}$) or the Zeeman structure ($\hat{H} \sim \mu \cdot B$) of the electronic ground state. But one can also consider the coupling between different *kinetic states* of free atoms $\hat{H} \sim \mathbf{p}^2/2m$, or the *output coupling* of atoms confined to a trapping potential ($\hat{H} \sim \frac{m}{2}\omega^2\mathbf{r}^2$), or even a chemical coupling between a vibrational state of two atoms bound together to form a molecular and a state, where the same two atoms are free and involved in an elastic collision.

Finally, in Sec. 47.4.3 we will show how to harness the forces induced by atom-light coupling in order to design new geometries of trapping potentials.

47.4.1 Theory of the interaction of condensates with light

Let us consider two Bose-Einstein condensates in the mean-field approximation consistent of atoms in two different internal excitation states, ψ_1 and ψ_2, separated by the energy $\hbar\omega_0$. We illuminate the BEC by a plane wave of monochromatic light with the frequency ω. The formal procedure consists of constructing the Hamiltonian of

interatomic interaction can have a big impact on the dynamics, because the chemical potential of each condensate depends on its number of atoms. Thus, in view of the inhomogeneity of the trapping potential, the transfer of atoms can excite oscillations and sound waves in the condensates.

individual atoms, as done in Eq. (38.2), and then quantizing the field of matter [1036],

$$\hat{H}_{atom} = |1\rangle \hat{H}^{(1)}_{cm} \langle 1| + |2\rangle (\hat{H}^{(2)}_{cm} + \hbar\omega_0)\langle 2| \qquad \text{where} \qquad \hat{H}^{(j)}_{cm} = \frac{\hat{\mathbf{p}}^2}{2m} + V^{(j)}_{trap}(\hat{\mathbf{r}}) \ , \tag{47.102}$$

where we allow for the fact that the trapping potentials can be different for the two excitation states. We assume that atoms in different states of excitation are distinguishable, such that their respective wavefunctions commute:

$$\hat{\psi}_j(\mathbf{r}) \equiv |j\rangle\langle j|\hat{\psi}(\mathbf{r}) \quad , \quad [\hat{\psi}_j(\mathbf{r}), \hat{\psi}_{j'}(\mathbf{r})] = \delta_{jj'}\delta^3(\mathbf{r}-\mathbf{r}') \ . \tag{47.103}$$

However, we need to consider interatomic collisions which, in the mean-field approximation (45.19) are described by,

$$\hat{H}^{(j)}_{mf} = \int \hat{\psi}^\dagger_j(\mathbf{r}) \frac{2\pi\hbar^2 a_s}{m} \hat{\psi}_j(\mathbf{r}) d^3r \ . \tag{47.104}$$

The total atomic Hamiltonian is then a generalization of the many-body Hamiltonian (45.6),

$$\boxed{\mathcal{H}_{atom} = \int \hat{\psi}^\dagger_1(\mathbf{r}) \left(\hat{H}^{(1)}_{cm} + \hat{H}^{(1)}_{mf}\right) \hat{\psi}_1(\mathbf{r}) d^3r + \int \hat{\psi}^\dagger_2(\mathbf{r}) \left(\hat{H}^{(2)}_{cm} + \hat{H}^{(2)}_{mf} + \hbar\omega_0\right) \hat{\psi}_2(\mathbf{r}) d^3r} \ . \tag{47.105}$$

47.4.1.1 Interaction with a single light mode

The normalized annihilation operator for a photon in mode $\mathbf{k}$ is,

$$\vec{\mathcal{E}}^+(\mathbf{r}) = \sqrt{\tfrac{\hbar\omega}{2\varepsilon_0 V}} \vec{\epsilon} \hat{a} e^{\imath \mathbf{k}\cdot\mathbf{r}} \ . \tag{47.106}$$

The semi-classical Hamiltonian (the light not being quantized) of individual particles is, in the rotating wave approximation,

$$\hat{H}_{field} = \hbar\omega \hat{a}^\dagger \hat{a} \qquad \text{and} \qquad \hat{H}_{int} = -\hat{\mathbf{d}} \cdot \hat{\vec{\mathcal{E}}} = -|2\rangle \hat{\mathbf{d}}^+ \cdot \hat{\vec{\mathcal{E}}}^+ \langle 1| - |1\rangle \hat{\mathbf{d}}^- \cdot \hat{\vec{\mathcal{E}}}^- \langle 2| \ . \tag{47.107}$$

For a condensate we still need to second-quantize the interaction part of the Hamiltonian which, disregarding collisions gives [15],

$$\boxed{\mathcal{H} = \hat{H}_{field} + \mathcal{H}_{atom} - \int \left(\hat{\mathbf{d}}^+ \cdot \hat{\vec{\mathcal{E}}}^+ \hat{\psi}^\dagger_2(\mathbf{r}) \hat{\psi}_1(\mathbf{r}) + \hat{\mathbf{d}}^- \cdot \hat{\vec{\mathcal{E}}}^- \hat{\psi}^\dagger_1(\mathbf{r}) \hat{\psi}_2(\mathbf{r})\right) d^3r} \ . \tag{47.108}$$

With the Hamiltonian (47.108) we derive the Heisenberg equations for the condensate respecting the commutation rules (47.103) [16],

$$\begin{aligned} \dot{\hat{\psi}}_2 &= -\tfrac{\imath}{\hbar}(\hat{H}_{cm} + \hbar\omega_0)\hat{\psi}_2 + \tfrac{\imath}{\hbar}\hat{\mathbf{d}}^+ \cdot \hat{\vec{\mathcal{E}}}^+ \hat{\psi}_1 \\ \dot{\hat{\psi}}_1 &= -\tfrac{\imath}{\hbar}\hat{H}_{cm}\hat{\psi}_1 + \tfrac{\imath}{\hbar}\hat{\mathbf{d}}^- \cdot \hat{\vec{\mathcal{E}}}^- \hat{\psi}_2 \ . \end{aligned} \tag{47.109}$$

[15] Or, by defining the Rabi frequency g_1 generated by a single photon, $\mathcal{H}_{int} = -\imath\hbar g_1 \hat{a} \int d^3\mathbf{r} \hat{\psi}^\dagger_2(\mathbf{r}) e^{\imath\mathbf{k}\cdot\mathbf{r}} \hat{\psi}_1(\mathbf{r}) + h.c.$.

[16] In the first quantization, these equations would simply be the equations of motion for the amplitudes of the fundamental and excited states.

We transform to the non-rotating coordinate system by $\tilde{\psi}_2 \equiv \psi_2 e^{\imath\omega t}$ and $\tilde{\vec{\mathcal{E}}}^+ \equiv \hat{\vec{\mathcal{E}}}^+ e^{\imath\omega t}$ introducing the detuning $\Delta \equiv \omega - \omega_0$:

$$\partial_t \tilde{\psi}_2 = \imath(\Delta - \tfrac{1}{\hbar}\hat{H}_{cm})\tilde{\psi}_2 + \tfrac{\imath}{\hbar}\hat{\mathbf{d}}^+ \cdot \tilde{\vec{\mathcal{E}}}^+ \tilde{\psi}_1 \ . \tag{47.110}$$

Making the adiabatic approximation $\partial_t \tilde{\psi}_2 = 0$ and disregarding the external degree of freedom, $\hat{H}_{cm} = 0$, we obtain,

$$\tilde{\psi}_2 = \frac{\imath \hat{\mathbf{d}}^+ \cdot \tilde{\vec{\mathcal{E}}}^+}{\hbar\Delta} \tilde{\psi}_1 \ . \tag{47.111}$$

47.4.1.2 Heisenberg equation for the light field

Similarly, we can write the Heisenberg equation for the light mode,

$$\frac{d\hat{a}}{dt} = \frac{\imath}{\hbar}[\mathcal{H}, \hat{a}] = -\imath\omega\hat{a} + \imath\sqrt{\tfrac{\omega}{2\varepsilon_0 V}} \int \hat{\mathbf{e}}_{\mathbf{k}} e^{-\imath\mathbf{k}\cdot\mathbf{r}} \cdot \left(\hat{\mathbf{d}}^+ \hat{\psi}_2^\dagger \hat{\psi}_1 + \hat{\mathbf{d}}^+ \hat{\psi}_1^\dagger \hat{\psi}_2\right) d^3r \ . \tag{47.112}$$

The integration of this gives the distribution of the fields (incident and scattered), such that,

$$\tilde{\vec{\mathcal{E}}}^+(\mathbf{r}) = \tilde{\vec{\mathcal{E}}}^+_{in}(\mathbf{r}) + \int K(\mathbf{d}, \mathbf{r} - \mathbf{r}') \hat{\psi}_1^+(\mathbf{r}') \hat{\psi}_1(\mathbf{r}') d^3\mathbf{r}' \ , \tag{47.113}$$

with the kernel:

$$K(\mathbf{d}, \mathbf{r}) = \frac{1}{4\pi\varepsilon_0} \left[k^2 (\mathbf{R} \times \mathbf{d}) \times R \frac{e^{\imath kR}}{R} + [3\mathbf{R}(\mathbf{R}\cdot\mathbf{d} - \mathbf{d})] \left(\frac{1}{R^3} - \frac{\imath k}{R^2} \right) e^{\imath kR} \right] \ . \tag{47.114}$$

We focus on the first term dominating in the far-field, and neglect the second term by letting $R \approx r - \hat{\mathbf{e}}_R \cdot \mathbf{r}'$ and $\hat{R} \approx r$. We also define $\mathbf{k}_s \equiv k\hat{\mathbf{e}}_R$, and we only retain the term of order $1/R$. In this Born approximation for optically thin media, we obtain,

$$K(\mathbf{d}, \mathbf{r}) \simeq \frac{1}{4\pi\varepsilon_0} \frac{e^{ikR}}{r} k^2 (\mathbf{r} \times \mathbf{r}) \times \mathbf{d} e^{-\imath\mathbf{k}_s \mathbf{r}'} \ . \tag{47.115}$$

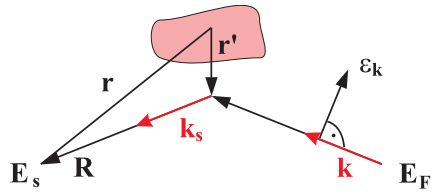

Figure 47.21: Scheme for the light scattering off a condensate.

47.4.1.3 Incident plane waves

When we now excite the condensate by a plane wave,

$$\hat{\vec{\mathcal{E}}}^+_{in}(\mathbf{r}) = \tfrac{1}{2}\vec{\epsilon} e^{\imath\mathbf{k}\cdot\mathbf{r}} \ , \tag{47.116}$$

we derive in the Born approximation of the equation (47.113):

$$\tilde{\vec{\mathcal{E}}}_s^+(\mathbf{r}) = \frac{1}{4\pi\varepsilon_0}\frac{e^{\imath kR}}{r}k^2\mathbf{r}\times(\mathbf{r}\times\hat{\mathbf{d}}^-)\int e^{-\imath\mathbf{k}_s\mathbf{r}'}\hat{\psi}_1^\dagger(\mathbf{r}')\hat{\psi}_2(\mathbf{r}')d^3r' \ , \tag{47.117}$$

and from this the fluorescence spectrum.

47.4.2 STIRAP & adiabatic sweep

A frequent problem for experimenters is the need to transfer a magnetically trapped atomic cloud from one Zeeman or hyperfine state to another. We will present here two techniques called STImulated Raman Adiabatic Passage and *adiabatic sweep*.

47.4.2.1 Adiabatic sweep

To discuss the adiabatic sweep, we consider the example of a ^{87}Rb cloud trapped in the state $|F, m_F\rangle = |2, -2\rangle$. The application of resonant radiofrequency radiation to the transition $|2, -2\rangle$-$|2, -1\rangle$ also couples all other m_F states and causes a diffusion of the atomic populations toward an uncontrollable mixture of states. An alternative is the application of a ramp sweeping the radiofrequency from red to blue (or vice versa). Such a ramp is able to transfer the entire population toward the opposite Zeeman state $|2, +2\rangle$. To see this, we solve the Schrödinger equation, $|\psi(t + dt)\rangle = e^{\imath H\ dt}|\psi(t)\rangle$, iteratively,

$$H = \begin{pmatrix} 0 & \frac{1}{2}\Omega & 0 & 0 & 0 \\ \frac{1}{2}\Omega & -\Delta & \frac{1}{2}\Omega & 0 & 0 \\ 0 & \frac{1}{2}\Omega & -2\Delta & \frac{1}{2}\Omega & 0 \\ 0 & 0 & \frac{1}{2}\Omega & -3\Delta & \frac{1}{2}\Omega \\ 0 & 0 & 0 & \frac{1}{2}\Omega & -4\Delta \end{pmatrix} . \tag{47.118}$$

The initial population distribution is $|\psi(t)\rangle = \begin{pmatrix} 1 & 0 & 0 & 0 & 0 \end{pmatrix}^t$. Ω is the Rabi frequency generated by the radiofrequency, $\Delta(t)$ is the instantaneous detuning. The curves of Fig. 47.22 show the temporal evolution of populations $|\langle k|\psi(t)\rangle|^2$.

The disadvantage of this method is that only the external (fully stretched) states $|m_F| = F$ can be interconverted.

47.4.2.2 Sweep through a dark resonance

To discuss STIRAP, let us think of how to transfer atoms from the state $|1\rangle \equiv |2, 2\rangle$ to $|2\rangle \equiv |2, 1\rangle$. The general idea consists in applying two radiation fields with Rabi frequencies Ω_{13} and Ω_{23}, tuned a bit out of resonance with an intermediate state $|3\rangle$, $\Delta_{13} = \Delta_{23} \neq 0$, in a counterintuitive pulse sequence. That is, the field Ω_{23} is applied first and then adiabatically turned down, while the field Ω_{13} is ramped up. This method is capable of transferring all atoms.

Considering the example of the preceding section, we will discuss here another option (see Fig. 47.23). We consider continuous microwave fields with fixed tunings Δ_{13} to the red of the state $|3\rangle \equiv |1, 1\rangle$ state. Now, we apply a ramp to the second

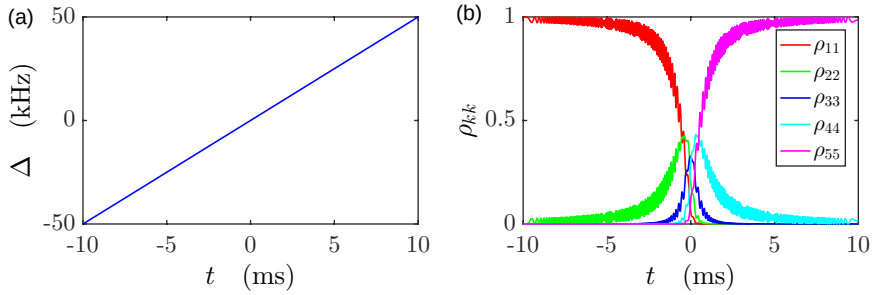

Figure 47.22: (code) Adiabatic sweep through the ground state ^{87}Rb $F = 2$. The Rabi frequency is $\Omega = (2\pi)8$ kHz. The frequency ramp is $\Delta(t) = \frac{t}{t_m}\,(2\pi)50$ kHz with $t_m = 10$ ms. The red line shows the evolution of the population in the state $|2,-2\rangle$, the green line of state $|2,+2\rangle$, and the blue line is the sum of the populations of all other states.

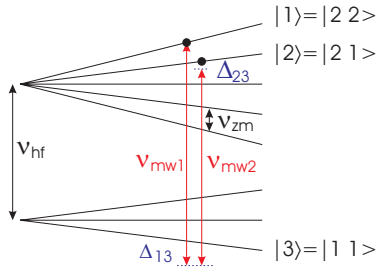

Figure 47.23: STIRAP.

microwave field Δ_{23}, such that the two radiation fields, at some point, cross the Raman resonance, for example,

$$\nu_{mw1} = \nu_{hf} + 3\nu_{zm} + \Delta_{13} \qquad \text{and} \qquad \nu_{mw2}(t) = \nu_{hf} + 2\nu_{zm} + \Delta_{23}(t)\ . \tag{47.119}$$

The evolution of the populations can be simulated by iterative solution of the Schrödinger equation, $|\psi(t+dt)\rangle = e^{iH\ dt}|\psi(t)\rangle$ with,

$$\hat{H} = \begin{pmatrix} 0 & 0 & \frac{1}{2}\Omega_{13} \\ 0 & \Delta_{23} - \Delta_{12}(t) & \frac{1}{2}\Omega_{23} \\ \frac{1}{2}\Omega_{13} & \frac{1}{2}\Omega_{23} & \Delta_{23} \end{pmatrix}\ . \tag{47.120}$$

The initial population distribution is $|\psi(t)\rangle = \begin{pmatrix} 1 & 0 & 0 \end{pmatrix}^t$. The curves of Fig. 47.24 show the temporal evolution of the populations $|\langle k|\psi(t)\rangle|^2$.

47.4.3 Condensate in adiabatic potentials

Adiabatic potentials have already been introduced in Secs. 38.1.3 and 43.4.3. Here, we will focus on the dynamics of condensed atoms in different states of electronic excitation, when these states are subject to different potentials and radiation fields

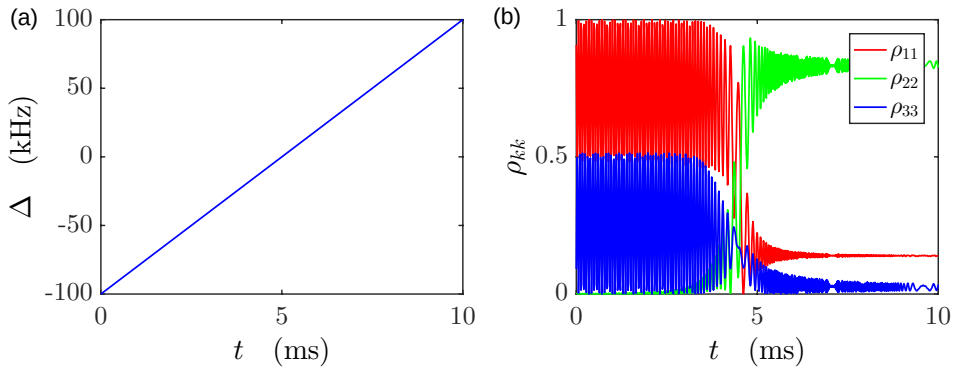

Figure 47.24: (code) STIRAP ramp through a dark resonance. Here, the Rabi frequencies are $\Omega_{13} = \Omega_{23} = 2\pi 10$ kHz. The frequency of the first microwave is $\Delta_{13} = (2\pi)10$ kHz and the frequency ramp of the second microwave is given by $\Delta_{23}(t) = \frac{2t-t_m}{t_m}\ (2\pi)100$ kHz, where $t_m = 10$ ms.

that can induce transitions between the states. In particular, we consider paramagnetic atoms in different Zeeman states placed in inhomogeneous static magnetic fields and subject to single-mode or multi-mode radiofrequency radiation fields [299]. To simplify the problem, let us concentrate on two-level systems, e.g. a system with the total spin $F = \frac{1}{2}$ [1437], and only consider the one-dimensional case.

47.4.3.1 Coupled Gross-Pitaevskii equations

For a single atom the Hamiltonian is the one given in (38.13),

$$\hat{H}(\mathbf{r}) = |1\rangle \left(\tfrac{1}{2}\mu_B g_F B(\mathbf{r}) - \tfrac{1}{2}\hbar\omega\right) \langle 1| + |2\rangle \left(-\tfrac{1}{2}\mu_B g_F B(\mathbf{r}) + \tfrac{1}{2}\hbar\omega\right) \langle 2| + |1\rangle \tfrac{1}{2}\hbar\Omega \langle 2| + |2\rangle \tfrac{1}{2}\hbar\Omega \langle 1| \,. \tag{47.121}$$

With the definition,

$$\hat{\psi}_k(\mathbf{r}) \equiv \langle k|\hat{\psi}(\mathbf{r})\rangle \ , \tag{47.122}$$

and the abbreviation $\hbar\Delta(\mathbf{r}) \equiv \mu_B g_F B(\mathbf{r}) - \hbar\omega(\mathbf{r})$ we proceed to the second quantization via,

$$\boxed{\begin{aligned} \mathcal{H} &= \sum_{k\neq m} \int d^3r\ \hat{\psi}_k^\dagger \left[\frac{-\hbar^2\nabla^2}{2m} + \tfrac{1}{2}u_{kk}\hat{\psi}_k^\dagger\hat{\psi}_k + \tfrac{1}{2}u_{k,m}\psi_m^\dagger\hat{\psi}_m\right]\hat{\psi}_k \\ &+ \left[(-1)^k\tfrac{\hbar}{2}\Delta(\mathbf{r})\hat{\psi}_k^\dagger\hat{\psi}_k + \tfrac{\hbar}{2}\Omega(\mathbf{r})(\hat{\psi}_k^\dagger\hat{\psi}_m + \psi_m^\dagger\hat{\psi}_k)\right] \end{aligned}} \ . \tag{47.123}$$

The total energy of the system is the sum of the energies of the individual condensates (kinetic, potential, and collisional interaction) *plus* the interspecies collisional interaction energy. The coefficients $u_{kl} = 4\pi\hbar^2 a_{kl}/m$ with the scattering lengths a_{kl} govern the impact of the collisions.

The interaction with the radiofrequency field leads to Rabi oscillations with fre-

quency Ω [17] The tuning of the radiofrequency depends on the position, due to the non-homogeneous Zeeman shift Δ. Also, to simplify the model, we assume $u_{kl} = 0$ for $k \neq l$,

$$\hat{H} = \sum_{k \neq m} \int d^3r \, \hat{\psi}_k^\dagger \left[\frac{-\hbar^2 \nabla^2}{2m} + \tfrac{1}{2} u_{kk} \hat{\psi}_k^\dagger \psi_k \right] \psi_k + \left[(-1)^k \tfrac{\hbar}{2} \Delta(\mathbf{r}) \hat{\psi}_k^\dagger \hat{\psi}_k + \tfrac{\hbar}{2} \Omega \left(\hat{\psi}_k^\dagger \psi_m + \hat{\psi}_m^\dagger \hat{\psi}_k \right) \right] . \tag{47.124}$$

From the Heisenberg equations of motion for the field operators of the matter wave and the light, we obtain [1437],

$$\imath \dot{\hat{\psi}}_1 = -\tfrac{1}{\hbar}[\hat{H}, \hat{\psi}_1] = \frac{\delta \hat{H}}{\hbar \delta \hat{\psi}_1^\dagger} = \left(\frac{-\hbar^2 \nabla^2}{2m} + u_{11} \hat{\psi}_1^\dagger \hat{\psi}_1 - \tfrac{\hbar}{2} \Delta(\mathbf{r}) \right) \hat{\psi}_1 + \tfrac{\hbar}{2} \Omega \hat{\psi}_2 \tag{47.125}$$

$$\imath \dot{\hat{\psi}}_2 = -\tfrac{1}{\hbar}[\hat{H}, \hat{\psi}_2] = \frac{\delta \hat{H}}{\hbar \delta \hat{\psi}_2^\dagger} = \left(\frac{-\hbar^2 \nabla^2}{2m} + u_{22} \hat{\psi}_2^\dagger \hat{\psi}_2 + \tfrac{\hbar}{2} \Delta(\mathbf{r}) \right) \hat{\psi}_2 + \tfrac{\hbar}{2} \Omega \hat{\psi}_1 .$$

The adiabatic potentials follow from a point-wise diagonalization of the Hamiltonian, assuming that the atomic movement evolves in sufficiently small steps.

47.4.3.2 One-dimensional case

The reduction of the dimensionality of the Gross-Pitaevskii equation is shown in Sec. 48.1. Applying this to our case, we consider a one-dimensional potential $V(\mathbf{r}) = V(z)$ and assume condensates being radially homogeneous within the radial diameter r_h. In this case, we can neglect the radial kinetic energy. As normalization then requires,

$$\int_{-r_h}^{r_h} \int_{-r_h}^{r_h} \int_{-\infty}^{\infty} |\hat{\psi}(\mathbf{r})|^2 d^3r = (2r_h)^2 \int_{-\infty}^{\infty} |\hat{\psi}(z)|^2 dz = 1 , \tag{47.126}$$

replacing $\hat{\psi}(\mathbf{r}) = \frac{\hat{\phi}(z)}{2r_h}$ and $g_{kk} = \frac{u_{kk}}{(2r_h)^2}$, the Gross-Pitaevskii equation and the normalization condition adopt a particularly simple form,

$$\imath\hbar \frac{\partial}{\partial t} \hat{\phi}(z) = \left(-\frac{\hbar^2}{2m} \frac{\partial^2}{\partial z^2} + V_{trap}(z) + N g_{1D} |\hat{\phi}(z)|^2 \right) \hat{\phi}(z) . \tag{47.127}$$

The coupled equations are now,

$$\imath \dot{\hat{\phi}}_1 = \left(\frac{-\partial_z^2}{2m} + g_{11} \hat{\phi}_1^\dagger \hat{\phi}_1 - \frac{m}{4} \omega_z^2 z^2 - \tfrac{1}{2} \Delta_0 \right) \hat{\phi}_1 + \tfrac{1}{2} \Omega \phi_2 \tag{47.128}$$

$$\imath \dot{\hat{\phi}}_2 = \left(\frac{-\partial_z^2}{2m} + g_{22} \hat{\phi}_2^\dagger \hat{\phi}_2 + \frac{m}{4} \omega_z^2 z^2 + \tfrac{1}{2} \Delta_0 \right) \hat{\phi}_2 + \tfrac{1}{2} \Omega \hat{\phi}_1 .$$

with,

$$\int_{-\infty}^{\infty} |\hat{\phi}_1(z)|^2 + |\hat{\phi}_2(z)|^2 dz = 1 . \tag{47.129}$$

This set of equations can be solved numerically by first identifying the ground state using the 'steepest descent' method and then propagating it in real time while slowly varying $\Delta(\mathbf{r}, t)$ or $\Omega(t)$.

[17] We are neglecting the possibility, that the coupling force may, in principle, be inhomogeneous, if the orientation of the magnetic field is not uniform.

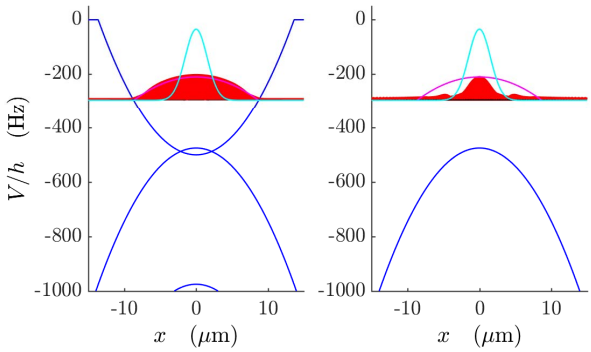

Figure 47.25: (code) Two coupled condensates.

47.4.3.3 Damping

A heuristic way of introducing damping could be as follows: We write down the condensate velocity field as,

$$m\mathbf{v}(\mathbf{r},t) = \hbar \frac{\hat{\phi}^*(\mathbf{r},t)\nabla\hat{\phi}(\mathbf{r},t) - \nabla\hat{\phi}^*(\mathbf{r},t)\hat{\phi}(\mathbf{r},t)}{2\imath n(\mathbf{r},t)} \ , \tag{47.130}$$

and subject it to a friction force,

$$E_{fr} = -\gamma r v \ . \tag{47.131}$$

The problem with the coupled GPE approach is that in the absence of damping any even small modification of the coupling triggers collective oscillations, so that the ground state is not found. A numerical method to minimize the total energy cannot be used, because the minimum is the untrapped state, so that all atoms are lost. It seems that a master equation approach is necessary to introduce damping. An alternative (but cheap) way is the following. The coupled GPEs were written in the dressed states basis. Thus, if the Rabi frequency is strong enough to completely decouple the dressed states, the dressed states represent good quantum numbers, and the GPEs are appropriately written in a diagonal basis, i.e. the GPEs decouple on adiabatic potentials [18],

$$V_{ad,k}(z) = -(-1)^k \frac{1}{2}\sqrt{\hbar^2\Omega^2 + [\mu_B g_F B(z) - \hbar\omega]^2} \ , \tag{47.132}$$

and we obtain,

$$\imath\dot{\hat{\phi}}_k = \left(\frac{-\partial_z^2}{2m} + V_{ad,k}(z) + g_{kk}\hat{\phi}_k^\dagger\hat{\phi}_k\right)\hat{\phi}_k \ . \tag{47.133}$$

47.4.3.4 Observations

An interesting question is, whether BECs trapped at different antinodes will synchronize their phases. Traditionally, BECs mutually influence their de Broglie waves

[18] Gravitation can be included by $V_{ad,k}(z) \to V_{ad,k}(z) + mgz$.

either by colliding or by some kind of coherent coupling, e.g. Josephson tunneling or radiative coupling of internal or motional states. Sound propagation through a standing wave requires tunneling. It cannot propagate if the potential is too deep. Then excitations stay local. Is it possible to translate the ring cavity coupling mechanism to the quantum regime of Bose-condensates confined to different antinodes? By analogy to the classical situation, one expects the de Broglie wave to correlate. In the matter wave language we would say, that the BEC wavefunctions transfer their excitations via the standing wave, i.e. they share a common excitation energy via the exchange of phonons. In the presence of a dissipation mechanism (e.g. via cavity cooling, by friction with a thermal cloud, etc.), which carries away the excess entropy, the excitations will damp [632]. This means the condensates mutually adjust and synchronize their phases. It is worth noticing, that the BEC will merge although they might be trapped at very distant locations, were coupling by tunneling is prohibited. Cavity-mediated cooling in ring cavities is known to damp essentially the center-of-mass motion. The relative motion of the trapped particles is damped on a much longer time-scale. In the case of BECs, however, the situation is different from the single-particle case: The strong motional correlations within a BEC, we have to treat them like a single particle. Since BECs trapped at different antinodes are likely to have different sizes, they also have different collective secular frequencies. Therefore the center-of-mass motion and the relative motion of different BECs periodically exchange kinetic energy, which leads to an indirect cooling also of the relative motion. TOF interference experiments can reveal phase differences [663].

47.4.3.5 Microwave and radio frequency spectra

For an irradiated magnetic field $B_{rf}(t) = B_{rf}\hat{\mathbf{e}}_{rf}\cos\omega t$ the coupling matrix element is,

$$\hbar\Omega = \frac{1}{4}\mu_B g_F(\mathbf{B}_{rf}\times\hat{\mathbf{e}}_z)\sqrt{F(F+1)-m_F(m_F\pm 1)}\ . \tag{47.134}$$

With $P_{in} = 35$ dBm coupled into the microwave, typically $P_{out} = 200$ W are radiated [385]. At the atomic location, at a distance of $r = 30$ cm, we get $B_{rf} = \sqrt{\mu_0 P/4\pi c r^2} = 8.6$ mG, and thus expect $\Omega \lesssim (2\pi)$ 1 kHz. Typical measured Rabi frequencies are 7.6 kHz. Let us count with the 5 kHz in the following. For an irradiated power of +27 dBm we may get some $\Omega = 2\pi \times xxx$ kHz.

To estimate the *chemical potential*, we use the Thomas-Fermi approximation,

$$2\mu = \hbar\omega_{ho}\left(\frac{15Na}{a_{ho}}\right)^{2/5}\ , \tag{47.135}$$

where $\omega_{ho} \equiv (\omega_r^2\omega_z)^{1/3}$ and $a_{ho} = \sqrt{\hbar/m\omega_{ho}}$ is the size of the ground state of the Ioffe trap. For $N = 1\times 10^5$ condensed atoms, we expect $2\mu \approx 20\hbar\omega_{ho} \approx h\times 8$ kHz. The Thomas-Fermi radius is $R_{tf} = \sqrt{2\mu/m\omega_{trap}^2} \approx 4.5$ μm. Note that this is not too far from a $1D$ situation defined by $\omega_r \ll \mu \ll \hbar\omega_z$ (or equivalently $a_z \gg \xi \gg a_r$). The radio frequency ω_{rf} is resonant over the range from $\mu_B B_0/\hbar$ to $\mu_B B_0/\hbar + \mu$. The radio frequency is resonant in the range $\hbar\omega = U(\frac{g}{\omega_x^2} \pm R_{tf}, 0)$, i.e. over an interval $\hbar\Delta\omega = 2mgR_{tf} \approx h\times 20$ kHz [154].

47.4.4 Exercises

47.4.4.1 Ex: Output coupler for trap extraction applications

Write down, in second quantization, the Hamiltonian of a condensate trapped in a harmonic potential and couple it to a free condensate. Simulate the coupled GPEs.

Solution:

47.4.4.2 Ex: Gravitational acceleration in radio frequency combs

The first scenario is to observe Bloch oscillations in a radio frequency lattice due to gravitational acceleration. In order to obtain an equidistant lattice, we chose small magnetic offset fields leading to steep constant gradients. For example for $\omega_{n+1}-\omega_n = 2\pi\times 4\,\mathrm{kHz}$, $B_0 = 0.16\,\mathrm{G}$, $\nabla_x B = 140\,\mathrm{G/cm}$ and $\Omega = 2\pi\times 1\,\mathrm{kHz}$, we get $d \approx 0.6\,\mu\mathrm{m}$ and $V_{ad} = h\times 1\,\mathrm{kHz} \approx 0.7E_r$ [299]. The velocity acquired by gravitational acceleration

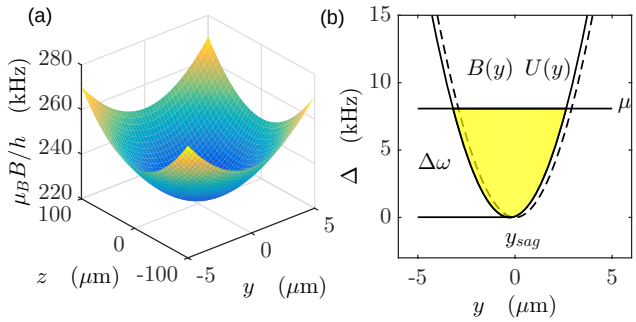

Figure 47.26: (code) (a) Two-dimensional cut through a Ioffe trapping potential with $B_0 = 0.16\,\mathrm{G}$, $\omega_r/2/\pi = 950\,\mathrm{Hz}$, and $\omega_z/2/\pi = 50\,\mathrm{Hz}$. (b) Vertical cut through the Ioffe trap without (dashed line) and with gravity (solid line). The range over which the BEC can be excited is the shaded area, the upper limit of which corresponds to the chemical potential $\mu/h = 4\,\mathrm{kHz}$ with $N = 10^6$ condensed atoms.

in a field-free case along one lattice period is $v_{gr} = dt = \sqrt{2ad} \approx 3.5\,\mathrm{mm/s}$. The atoms are Bragg-reflected when the acquired velocity matches the Bragg condition $v_{brg} \approx 7.5\,\mathrm{mm/s}$, which occurs after a time $t = v_{brg}/a \approx 0.8\,\mathrm{ms}$. The secular frequency of the potential sites is,

$$\omega_{ho} = \frac{2\mu_B g_F b_y}{\sqrt{2m\hbar\Omega}} \ . \tag{47.136}$$

For $b_y = 140\,\mathrm{G/cm}$ and $\Omega = 2\pi\times 1\,\mathrm{kHz}$ we expect $\omega_{ho} \approx 2\pi\times 6.3\,\mathrm{kHz}$.

Solution: *The gravitational potential difference over a single lattice period, $\Delta E_{grav} = mgd \approx h\times 2.1\,\mathrm{kHz}$, is on the same order of magnitude as the first Bloch band [30]. The solid state approach introduces Bloch bands [cf. Fig. 47.28(a)], If the Bloch states are characterized by $|n, q(t)\rangle$. The mean velocity is,*

$$\langle v\rangle_n(q(t)) = \frac{1}{\hbar}\frac{dE_n(q(t))}{dq} \tag{47.137}$$

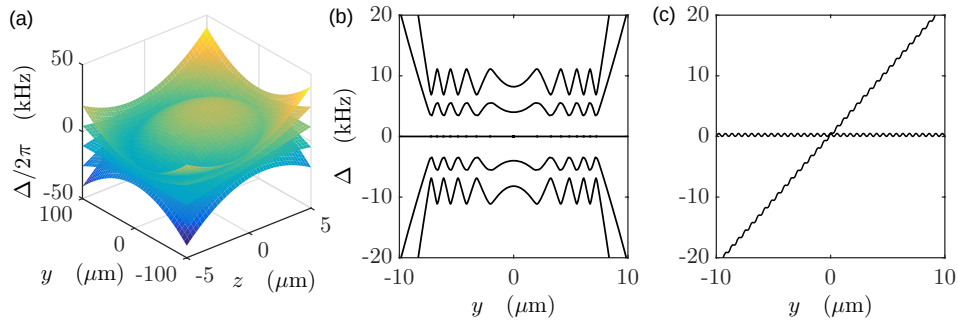

Figure 47.27: (code) (a) Adiabatic potentials for the $F = 2$ hyperfine state without gravity. Two frequencies are irradiated at $\omega_n/2\pi = 30, 90\,\mathrm{kHz}$ with $\Omega/2\pi = 1\,\mathrm{kHz}$. (b) Upper adiabatic potential without and with gravity and $\omega_n/2\pi = (6+3n)\,\mathrm{kHz}$ with $\Omega/2\pi = 1\,\mathrm{kHz}$. (c) Periodic potential with the lattice constant d and the modulation depth V_{ad}. The different shape of the lattice comes from the fact that in (a,b) we are still in the flat harmonic part of the potential.

with

$$q(t) = q(0) + mat/\hbar\ , n \tag{47.138}$$

where $a = g$. The velocity thus exhibits an oscillatory time dependence shown in Fig. 47.28(b). Our goal is to observe these oscillations in a radio frequency lattice in order to use them as a tool for probing and characterizing this lattice. For this purpose we produce a ^{87}Rb BEC, keep the rf-shield on. Irradiate additional rf- or mw-radiation and wait for a time t. Then we switch off the magnetic field and do time-of-flight imaging. We expect periodic change of the velocity acquired during the irradiation time. This velocity $v_n(t)$ influences the falling distance at time-of-flight,

$$s(t, t_{tof}) = \frac{a}{2} t_{tof}^2 + v_n(t) t_{tof}\ . \tag{47.139}$$

For small velocities $v_n(t) \approx 1$ mm/s, the displacement $v_n(t)t_{tof}$ may be barely visible. There are however problems: 1. High loss rates due to collisions and Majorana spin-flips limit the lifetime. 2. The fast down-ramping makes that the BEC is not in equilibrium. We observe interference fringes, which do not result from rf. 3. Switch-off problems giving rise to Majorana losses, when a magnetic zero is swept across the BEC. This makes nice Stern-Gerlach pictures. Nevertheless, we see BEC pulses outcoupled by rf, falling the gravitational field. The critical point of the experiment is probably the adiabatic transfer of the atoms into the lattice. It is possible to ramp the rf power, but not the frequency. In exchange, we can ramp the magnetic field offset which allows us to tune the resonant locations. The grating should be switched on or ramped in slowly to guarantee that the BEC completely goes to the lowest band.

47.4.4.3 Ex: Egg-shell trap and frustrated outcoupling

It is at first sight counterintuitive that non-resonant frequency components, i.e. frequency components which would not couple the atoms to other Zeeman states, never-

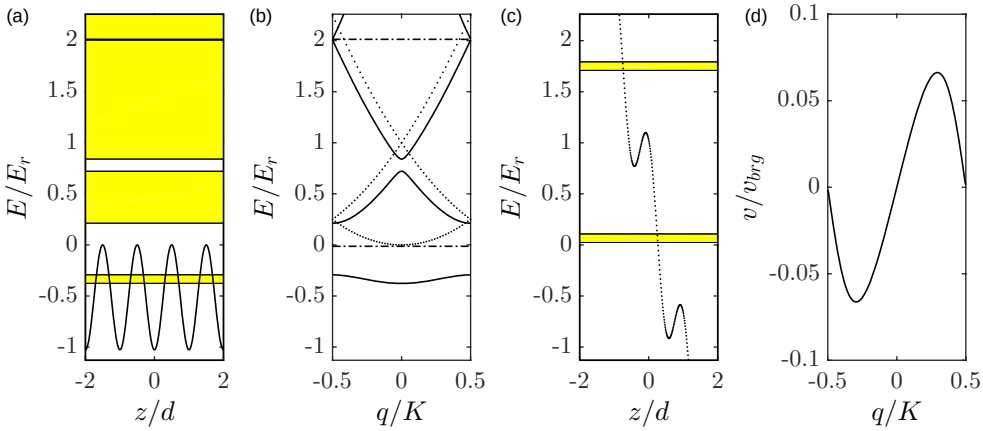

Figure 47.28: (code) (a) Lattice potential without gravity. The shaded areas denote the Bloch bands in position space. The parameters are taken from Fig. 47.27. The corresponding lattice constant is $d = 0.6$ μm and the potential depth is $V_{ad} = 1.2E_r$. (b) Bloch bands in momentum space (solid lines). The dotted lines represent expected energy levels in the harmonic approximation. The dashed line show the free particle case. (c) Mean velocity. (d) Bloch bands in momentum space (solid lines). The dotted lines represent expected energy levels in the harmonic approximation. The dashed line show the free particle case.

theless contribute to generate an adiabatic potential. In order to test this, we image the following second scenario. This scenario is to make an rf-knife as for evaporation or atom lasing. Then irradiate rf component slightly higher then the first one. In the adiabatic picture the outcoupling should be stopped. On the other hand, if the frequencies are too close (like degenerate) this picture cannot be true. Where is the limit? This is an additional limitation for the smallness of the lattice constant: $V_{Stark,1} \ll |\mu_B g_F B - \hbar\omega_2|$. States should couple unperturbed potentials to avoid interferences, i.e. ???

Solution: *The radiofrequency is ramped from -40 kHz (red) to $+40$ kHz (blue), then a Stern-Gerlach experiment is performed, and finally time-of-flight images are taken. To understand the observed images, we have to proceed in several steps. 1. The Rabi frequency is estimated by comparing the speed with which other Zeeman states are populated with Schrödinger equation simulations of an adiabatic transfer due to the frequency ramp. It is $\Omega \approx 2\pi \times 1$ kHz. 2. The time-of-flight duration is easily calibrated by comparison with in-situ images. 3. The Stern-Gerlach force is easily calibrated by comparing the behavior of $m_F = 0$ and $m_F \geq 1$ atoms. The impact of gravity during the trapping period is seen by comparing the behavior of $m_F = 0$ and $m_F \geq 1$ atoms. As soon as $m_F \leq -1$ atoms are produced, these anti-trapped atoms are accelerated away from the Ioffe trap, which we describe as $B = \sqrt{B_0^2 + b_y^2 y^2}$, with the force $-\partial_y \mu_B g_F m_F B(y) = -\mu_B g_F m_F b_y^2 y / \sqrt{B_0^2 + b_y^2 y^2}$, where $b_y = 140\,\mathrm{G/cm}$ plus*

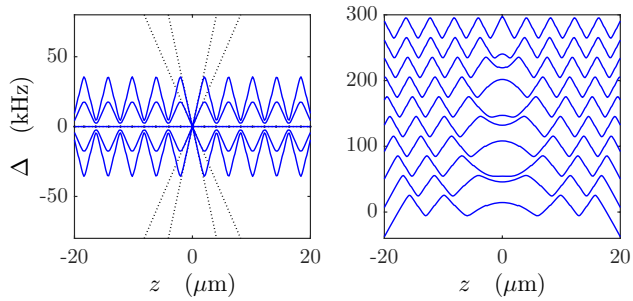

Figure 47.29: (code) (a) Adiabatic potentials. (b) Downramping B_0.

gravity. We thus have to solve the differential equation,

$$\dot{y} = v \tag{47.140}$$
$$\dot{v} = \frac{-\mu_B g_F m_F b_y^2 y}{m\sqrt{B_0^2 + b_y^2 y^2}} + g \ .$$

for different atoms labelled k produced at time t_k with the initial conditions $y(t_k) \approx 0$

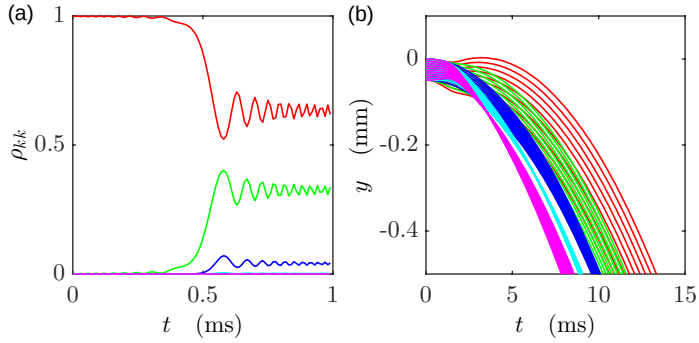

Figure 47.30: (code) (a) Evolution of the populations of the five Zeeman states. The adiabatic ramp is performed in 1 ms.

and $\dot{y}(t_k) = 0$. 2. The Stern-Gerlach acceleration is due to residual magnetic field gradients during the trap switch off. Therefore, the direction of the Stern-Gerlach force, $-\nabla\mu_B g_F m_F B_{SG}(y,z) = -\mu_B g_F m_F \mathbf{b}_{SG}$, is not controlled (but nevertheless reproducible). The final values of the Ioffe trap acceleration period are used as starting conditions for the equation,

$$\dot{y} = v \tag{47.141}$$
$$\dot{v} = \frac{-\mu_B g_F m_F b_{SG,y}}{m} \ .$$

4. And finally, time-of-flight,

$$s = \frac{g}{2} t_{ToF}^2 + v t_{ToF} \ . \tag{47.142}$$

The easiest way to handle these equations is numerical iteration.

47.4.4.4 Ex: Optical dipole trap with $1D$ gradients from Ioffe wires

The third scenario consists in the generation of steep $1D$ magnetic field gradients is most convenient with microtraps [1348]. On the other hand, we wish to expose an elongated atomic cloud to a $1D$ periodic potential. To separate the trapping potential from periodic potential to be probed by the atoms, let us consider 1 μK cold ^{87}Rb atoms stored in an optical dipole trap with radial secular frequencies of $\omega_r = (2\pi)\ 1\,\text{kHz}$ and an axial frequency of $\omega_r = (2\pi)\ 10\,\text{Hz}$. The thermal cloud is then $\bar{z} = \sqrt{k_B T/m\omega_z} \approx 160\,\mu\text{m}$ long and has a radial size of $\bar{z} \approx 1.6\,\mu\text{m}$. Let us also assume that the magnetic field gradient is provided by two parallel current-carrying wires running perpendicularly to the dipole trap axis (see scheme of Fig. 47.31).

Solution: *We simulate,*

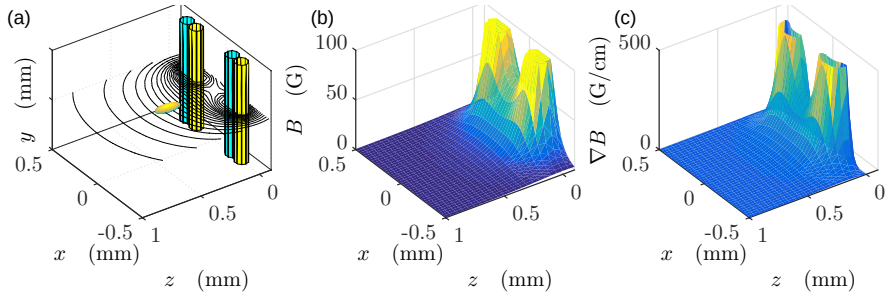

Figure 47.31: (code) (a) Scheme of dipole trap and magnetic fields. (b) Magnetic field. (c) Gradient.

47.4.4.5 Ex: Multiple BECs coupled by radiation via GPEs

Programs on multiple BECs coupled by radiation via GPEs.

Solution: *Before doing GPE simulations, do adiabatic ramp to check appropriate parameters. Some literature [316, 1007, 30, 155, 154, 295, 625, 988, 850, 284, 1437, 1438]. Look up Numerical Recipes Chapter 16.1.*

- *AdiabaticBecCoupled: coupling with anti-trapped state.*
- *AdiabaticBecCoupled1: phase separation of two-species BECs due to repulsive interaction.*
- *AdiabaticBecCoupled2: trapped BECs, Euler agorithm.*
- *AdiabaticBecCoupled2b:trapped BECs, 4th order Runge-Kutta algorithm.*

- *AdiabaticBecCoupled2c:atom laser, compare pure and dressed states.*
- *AdiabaticBecCoupled3: with gravity, watching dressed and bare states.*
- *AdiabaticBecCoupled4: five level system.*

Comments: Runge-Kutta does not improve a lot. Seems like the way Ψ converges for $r \to \infty$ makes the change; take larger intervals or suppress Ψ at ∞.

47.5 Interaction between condensates and optical cavities

In 47.4.1 we have set up the many-body Hamiltonian (47.108) describing the interaction of a matter wave (treated in mean-field approximation) with an incident light field. We emphasized the role of photonic recoil in (47.231). In the following sections we aim at applying this theory to the particular case of atoms interacting with two counterpropagating modes of an optical ring cavity. The system has already been studied in Chp. 42 in the context of CARL, where the atomic motion, as well as the light fields, have mostly been treated classically.

CARL is based on a coherent redistribution of photons between the two counterpropagating modes of a moving standing light wave mediated by atoms which are located in the mode volume. Cooperative Compton scattering induces a collective atomic recoil and a self-bunching of the atoms, which results in an exponential gain for the optical mode receiving the scattered photons. The recent observation of the MWSR [649] in a BEC raises the question about an ultra-cold version of CARL [918, 617]. In MWSR the long coherence time of a BEC establishes a strong correlation between subsequent elastic Rayleigh scattering events mediated by very stable quasi-particle excitations. The feedback of these excitations on the laser creates an *exponential* gain for the optical mode receiving the scattered photons [650, 305, 173, 775, 918, 917, 749, 651, 650].

We have discussed the classical CARL earlier in the superradiant as well as the good-cavity regime. We have also generalized the problem to the case of quantized atomic motion (see Sec. ??) and to quantized radiation fields (see Sec. ??). The internal states were always adiabatically eliminated. In the following, we will fully quantize the bosonic atomic particle field.

The advantages of this second quantization is that interatomic interactions, quantum fluctuations, and decoherence of the matter wave can be taken into account. Various proposals have been made focusing on either one of the above three aspects. Fundamental aspects of the BEC-in-a-cavity-system lead into two directions: 1. quantum synchronization and 2. quantum correlations.

The system under consideration is a BEC of two-level atoms with transition resonance frequency ω_0 trapped in an external magnetic trap, located inside the mode volume of a ring cavity and interacting with its light modes. The atomic field operators obey the commutation relations,

$$\begin{aligned} [\hat{\psi}_k(\mathbf{r}), \hat{\psi}_m^\dagger(\mathbf{r}')] &= \delta_{km}\delta^{(3)}(\mathbf{r}, \mathbf{r}') \\ [\hat{\psi}_k(\mathbf{r}), \hat{\psi}_m(\mathbf{r}')] &= 0 = [\hat{\psi}_k^\dagger(\mathbf{r}), \hat{\psi}_m^\dagger(\mathbf{r}')] \ , \end{aligned} \tag{47.143}$$

where $k, m = 1, 2$ label the internal state of the atoms. In general, the light field consists of only *two* counterpropagating monochromatic modes with Rabi frequencies $2g\hat{a}_\pm^\dagger \hat{a}_\pm$. Choosing the coordinate system properly, we can set the wavevectors of the modes as $\mathbf{k}_+ \cdot \hat{\mathbf{e}}_r = k\hat{z} = -\mathbf{k}_- \cdot \hat{\mathbf{e}}_r$. The second-quantized Hamiltonian is a generalization of (42.4),

$$\mathcal{H} = \mathcal{H}_{atom} + \mathcal{H}_{atom-atom} + \mathcal{H}_{atom-cav} + \hat{H}_{cav} + \hat{H}_{laser-cav} \ , \tag{47.144}$$

where,

$$\boxed{\begin{aligned}
\mathcal{H}_{atom} &= \int d^3r \hat{\psi}_1^\dagger(\mathbf{r}) \left(\frac{\hat{p}^2}{2m} + V_1(\mathbf{r}) \right) \hat{\psi}_1(\mathbf{r}) \\
&\quad + \int d^3r \hat{\psi}_2^\dagger(\mathbf{r}) \left(\frac{\hat{p}^2}{2m} + V_2(\mathbf{r}) - \Delta_a \right) \hat{\psi}_2(\mathbf{r}) \\
\mathcal{H}_{atom-atom} &= \textstyle\sum_{i=1,2} \int d^3r \hat{\psi}_i^\dagger(\mathbf{r}) \hat{\psi}_i^\dagger(\mathbf{r}) \frac{u_{ii}}{2} \hat{\psi}_i(\mathbf{r}) \hat{\psi}_i(\mathbf{r}) \\
&\quad + \int d^3r \hat{\psi}_1^\dagger(\mathbf{r}) \hat{\psi}_2^\dagger(\mathbf{r}) \frac{u_{12}}{2} \hat{\psi}_2(\mathbf{r}) \hat{\psi}_1(\mathbf{r}) \\
\mathcal{H}_{atom-cav} &= \textstyle\sum_\pm g\hat{a}_\pm \int d^3r \hat{\psi}_2^\dagger(\mathbf{r}) e^{\pm \imath kz} \hat{\psi}_1(\mathbf{r}) + h.c. \\
\hat{H}_{cav} &= -\textstyle\sum_\pm \Delta_c \hat{a}_\pm^\dagger \hat{a}_\pm \\
\hat{H}_{laser-cav} &= -\textstyle\sum_\pm \imath\eta_\pm (\hat{a}_\pm - \hat{a}_\pm^\dagger)
\end{aligned}} \ , \tag{47.145}$$

with $u_{ij} \equiv 4\pi\hbar^2 a_{s,ij}/m$.

Various approximations can be made depending on the subject of interest. For example, if only one cavity mode, $\hat{a}_\pm$, is strongly pumped, such that the field becomes intense, we may remove the term $\hat{H}_{laser-cav}$ and describe the field mode classically by a Rabi frequency Ω. The interaction between the pump mode and the cavity is then, $\hat{H}_{atom-pump} = \frac{\hbar\Omega}{2} e^{-\imath\omega_2 t} \int d^3r \hat{\psi}_2^\dagger(\mathbf{r}) e^{\imath k\hat{z}} \hat{\psi}_1(\mathbf{r}) + h.c.$.

A talk on this subject is available at (watch talk).

47.5.1 Ideal gas Hamiltonian after adiabatic elimination

Assuming the light fields to be tuned far from resonance we disregard spontaneous emission, as explained in Sec. 42.1.2, and adiabatically eliminate the internal states, as shown in Sec. 42.1.3 [1051, 278]. On the other hand, we treat the light field and the atomic motion in second quantization. The canonical way to describe a BEC interacting with *two* optical modes $\hat{a}_\pm$ is to second-quantize the single-particle Hamiltonian (42.26),

$$\boxed{\begin{aligned}
\mathcal{H} &\simeq \int d^3r \hat{\psi}^\dagger(\mathbf{r}) \left(\frac{\hat{\mathbf{p}}^2}{2m} + V_{trap}(\mathbf{r}) + \frac{u}{2}\hat{N}(\mathbf{r}) \right) \hat{\psi}(\mathbf{r}) + (\hat{N}U_0 - \Delta_c) \sum_\pm \hat{a}_\pm^\dagger \hat{a}_\pm \\
&+ U_0 \hat{a}_+^\dagger \hat{a}_- \int d^3r \hat{\psi}^\dagger(\mathbf{r}) e^{-2\imath kz} \hat{\psi}(\mathbf{r}) + h.c. - \imath \sum_\pm \eta_\pm (\hat{a}_\pm - \hat{a}_\pm^\dagger)
\end{aligned}} \ , \tag{47.146}$$

where $\hat{\psi}(\mathbf{r})$ is now the ground-state wave function of the matter wave, $u = 4\pi\hbar^2 a_s/m$ in the *mean-field approximation* and,

$$U_0 = \frac{g^2}{\Delta_a} \ , \tag{47.147}$$

when the mode to mode coupling strength. This adiabatically approximated Hamiltonian looks very similar to (42.26).

47.5.2 Expansion into momentum states

It is useful to convert the Hamiltonian to momentum space via a plane wave expansion of the BEC according to (45.70),

$$\hat{\psi}(\mathbf{r}) = \sqrt{\tfrac{V}{(2\pi)^3}} \int \hat{c}_{\mathbf{q}} e^{\imath \mathbf{q}\cdot\mathbf{r}} d^3q \qquad \text{with} \qquad [\hat{a}_{\mathbf{q}}, \hat{a}_{\mathbf{q}'}] = \delta_{\mathbf{q},\mathbf{q}'} \ . \tag{47.148}$$

The conversion of that Hamiltonian part $\mathcal{H}_{bec}$ to momentum space has been demonstrated in (45.78),

$$\mathcal{H}_{bec} = \sum_{\mathbf{q}} \frac{\mathbf{q}}{2m} \hat{c}^\dagger_{\mathbf{q}} \hat{c}_{\mathbf{q}} + \sum_{\mathbf{q},\mathbf{q}'} \hat{c}'^\dagger_{\mathbf{q}} V_{\mathbf{q}',\mathbf{q}} \hat{c}_{\mathbf{q}} + \frac{u}{2} \sum_{\mathbf{q},\mathbf{q}',\mathbf{q}''} \hat{c}^\dagger_{\mathbf{q}} \hat{c}'^\dagger_{\mathbf{q}} \hat{c}''_{\mathbf{q}} \hat{c}_{\mathbf{q}} + \mathbf{q}' - \mathbf{q}'' \ . \tag{47.149}$$

The light field part $\hat{H}_{cav}$ remains unchanged and the atom-light interaction becomes using (47.3),

$$\begin{aligned} \mathcal{H}_{bec-cav} &= U_0 \int \hat{\psi}^\dagger(\mathbf{r}) \hat{a}^\dagger_+ \hat{a}_- e^{-\imath(\mathbf{k}_+ - \mathbf{k}_-)\cdot\mathbf{r}} \hat{\psi}(\mathbf{r}) d^3r + h.c. \qquad (47.150) \\ &= \imath\hbar U_0 \hat{a}^\dagger_+ \hat{a}_- V \int\int \hat{c}^\dagger(\mathbf{q}') \hat{c}(\mathbf{q}) \delta^3(\mathbf{q} - \mathbf{q}' - 2k\hat{\mathbf{e}}_z) d^3q d^3q' = U_0 \hat{a}^\dagger_+ \hat{a}_- \sum_{\mathbf{q}} \hat{c}^\dagger_{\mathbf{q}-2\mathbf{k}} \hat{c}_{\mathbf{q}} \ . \end{aligned}$$

All in all,

$$\boxed{\begin{aligned} \mathcal{H} &= \sum_{\mathbf{q}} \frac{\mathbf{q}^2}{2m} \hat{c}^\dagger_{\mathbf{q}} \hat{c}_{\mathbf{q}} + \sum_{\mathbf{q},\mathbf{q}'} \hat{c}^\dagger_{\mathbf{q}'} V_{\mathbf{q}',\mathbf{q}} \hat{c}_{\mathbf{q}} + \frac{u}{2} \sum_{\mathbf{q},\mathbf{q}',\mathbf{q}''} \hat{c}^\dagger_{\mathbf{q}} \hat{c}^\dagger_{\mathbf{q}'} \hat{c}_{\mathbf{q}''} \hat{c}_{\mathbf{q}+\mathbf{q}'-\mathbf{q}''} \\ &+ (\hat{N}U_0 - \Delta_c) \sum_{\pm} \hat{a}^\dagger_\pm \hat{a}_\pm + U_0 \hat{a}^\dagger_+ \hat{a}_- \sum_{\mathbf{q}} \hat{c}^\dagger_{\mathbf{q}-2\mathbf{k}} \hat{c}_{\mathbf{q}} - \imath \sum_{\pm} \eta_\pm (\hat{a}_\pm - \hat{a}^\dagger_\pm) \end{aligned}} \ . \tag{47.151}$$

The BEC-CARL equations of motion are readily obtained from the Heisenberg equations,

$$\begin{aligned} \imath \frac{d\hat{c}_{\mathbf{p}}}{dt} &= [\hat{c}_{\mathbf{p}}, \mathcal{H}] = \frac{q^2}{2m} \hat{c}_{\mathbf{p}} + \sum_{\mathbf{q}} V_{\mathbf{p},\mathbf{q}} \hat{c}_{\mathbf{q}} + u \sum_{\mathbf{q},\mathbf{q}'} \hat{c}^\dagger_{\mathbf{q}} \hat{c}_{\mathbf{q}'} \hat{c}_{\mathbf{q}-\mathbf{q}'+\mathbf{p}} + U_0 \hat{a}^\dagger_+ \hat{a}_- \hat{c}_{\mathbf{p}+2\mathbf{k}} + h.c. \\ \imath \frac{d\hat{a}_\pm}{dt} &= [\hat{a}_\pm, \mathcal{H}] = (\hat{N}U_0 - \Delta_c) \hat{a}_\pm + U_0 \hat{a}_\mp \sum_{\mathbf{q}} \hat{c}^\dagger_{\mathbf{q}\mp 2\mathbf{k}} \hat{c}_{\mathbf{q}} + \imath\eta_\pm \ . \end{aligned} \tag{47.152}$$

47.5.2.1 Discretization of the momentum space

Assuming the BEC to be initially at rest with 0 temperature, its momentum state can be written as $\hat{c}_{\mathbf{0}}$. And if the dynamics only involves the z-axis, then all momentum states are separated by multiples of $2\hbar k$, such that we may replace the labeling by integer numbers: $\hat{c}_{\mathbf{q}} \to \hat{c}_n$. We get,

$$\begin{aligned}\mathcal{H} = &\sum_n \frac{n^2 q^2}{2m}\hat{c}_n^\dagger \hat{c}_n + \sum_{n,n'} \hat{c}_{n'}^\dagger V_{n',n}\hat{c}_n + \frac{u}{2}\sum_{n,n',n''} \hat{c}_n^\dagger \hat{c}_{n'}^\dagger \hat{c}_{n''}\hat{c}_{n+n'-n''} \\ &+ \sum_\pm \left(\hat{N}U_0 - \Delta_c\right)\hat{a}_\pm^\dagger \hat{a}_\pm + U_0 \hat{a}_+^\dagger \hat{a}_- \sum_n \hat{c}_{n-1}^\dagger \hat{c}_n + h.c. - \imath\eta_\pm(\hat{a}_\pm - \hat{a}_\pm^\dagger) \ .\end{aligned} \tag{47.153}$$

Neglecting the external trapping potential and collisions the Heisenberg equations for the field and the atomic motion now read,

$$\begin{aligned}\frac{d\hat{c}_n}{dt} &= -\imath[\hat{c}_n, \mathcal{H}] = -\imath\frac{n^2k^2}{2m}\hat{c}_n + U_0\hat{a}_+^\dagger \hat{a}_- \hat{c}_{n+1} + h.c. \\ \frac{d\hat{a}_\pm}{dt} &= -\imath[\hat{a}_\pm, \mathcal{H}] = (\hat{N}U_0 - \Delta_c)\hat{a}_\pm + U_0\hat{a}_\mp \sum_n \hat{c}_{n\mp 1}^\dagger \hat{c}_n + \imath\eta_\pm \ .\end{aligned} \tag{47.154}$$

These equations look identical to those found in (42.160).

47.5.3 Damping of BECs in cavities

Horak et al. [634] treat the BEC as an entity, as if is was located at a single antinode. They find that excitations can be damped. Local phase shifts in a BEC give rise to excitations. How about if the phase shift occurs only at a spatially well-defined location, i.e. at a specified antinode? Following [632, 633] in the Lamb-Dicke limit only low-lying modes are damped. Higher-order modes are damped via self-interaction and trap anharmonicity.

47.5.3.1 Self-consistent ground state

There is no entanglement if the field is too strong $|\alpha|^2 \gg 1$. If the internal states can be adiabatically eliminated, the basic equations now read (use $U_N \equiv NU_0$) with $u = 4\pi\hbar^2 a_s/m$,

$$\begin{aligned}\frac{d}{dt}\alpha_\pm(t) &= -[\kappa - \imath\Delta_c + \imath U_N]\alpha_\pm(t) - \imath U_N\langle e^{\mp 2\imath k\hat{z}}\rangle\alpha_\mp(t) + \eta_\pm \\ \imath\hbar\frac{d}{dt}\psi(z,t) &= \left[\frac{\hat{p}^2}{2m} + \hbar U_0\left|\alpha_+(t)e^{\imath kz} + \alpha_-(t)e^{-\imath kz}\right|^2 + u|\psi(z,t)|^2\right]\psi(z,t) \ ,\end{aligned} \tag{47.155}$$

where $\langle e^{\mp\imath k\hat{z}}\rangle = \int \psi^*(z,t)e^{\mp\imath k\hat{z}}\psi(z,t)dz$. The wavefunction is scaled such that $\int |\psi|^2 d^3z = N$.

If we assume that the cavity field adiabatically follows the BEC, $\dot{\alpha}_\pm = 0$,

$$\alpha_\pm(t) = \eta_\pm \frac{\kappa - \imath\Delta_c + \imath U_N - \imath U_N\langle e^{-2\imath k\hat{z}}\rangle}{(\kappa - \imath\Delta_c + \imath U_N)^2 + N^2U_0^2\langle e^{2\imath k\hat{z}}\rangle\langle e^{\mp\imath k\hat{z}}\rangle} \ . \tag{47.156}$$

The equations are solved self-consistently, i.e. we start from trial field and wavefunction,

$$\alpha_\pm(0) \equiv \eta_\pm \quad , \quad \psi(0) \equiv \frac{e^{-x^2}}{|e^{-x^2}|} \ . \tag{47.157}$$

Then the potential is calculated, for example,

$$V = \begin{cases} U_0 |\alpha e^{\imath kx} + \beta e^{-\imath kz}|^2 & \text{for} \quad |z| < z_{max} \\ 2\eta^2 & \text{for} \quad |z| > z_{max} \end{cases} \tag{47.158}$$

Then the groundstate wavefunction ψ is found by iterating Eq. (47.155)(b) with the method of steepest descent,

$$H = -\frac{\hbar^2}{2m}\nabla^2 + V + Nu|\psi|^2 \tag{47.159}$$
$$\psi(t+dt) = \frac{\psi(t)(1-\hbar^{-1}H\ dt)}{|\psi(t)(1-\hbar^{-1}H\ dt)|} \ .$$

The solution is used to calculate $\langle e^{\mp \imath k\hat{z}} \rangle$ and $\alpha_\pm$. If the laser is locked to resonance, we can use $\Delta_c = U_N$. And now $\alpha_\pm$ is used to calculate the potential in the GPE again. This procedure is repeated until convergence.

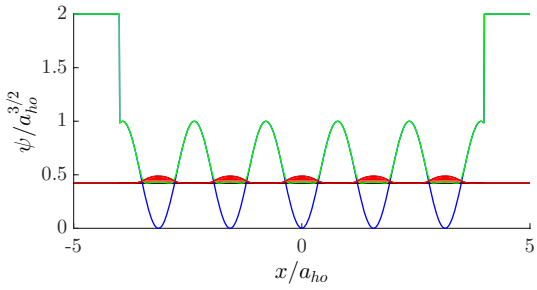

Figure 47.32: (code) BEC in a periodic potential. Shown is the potential $V(x)$ and the wavefunction $\psi(x)$ with an offset corresponding to $min(H)$. The normalization is $z = z/a_{ho}$, $(\psi/a_{ho})^{3/2}$.

Horak et al. [632] seem to believe that a BEC falling through a cavity field is adiabatically transferred to the ground state. If the trap is deep, this must result in trapping along the axial cavity direction.

Example 291 (*Optimum cavity-finesse*): Size in the Thomas-Fermi limit $V = 3 \times 3 \times 20\,\mu\text{m}^3$. The chemical potential is $\mu = h \times 3\,\text{kHz}$. The atom number $N = 10^5$. Near the D_2 line about 50 antinodes are filled with BEC.
In a simulation for cavity-damping Horak et al. [634] assumed $N = 10^5$, $\kappa = 100\omega_r = 50\varepsilon$, $NU_0 = 10\kappa$, $\eta^2 = 20\kappa N\omega_r$. With these parameters we expect for

our system,

$$\kappa/2\pi = 700\,\mathrm{kHz} \qquad \text{or} \qquad F = 2400 \tag{47.160}$$
$$\Delta_a = \frac{Ng^2}{10\kappa} = 2\pi \times 1.4\,\mathrm{GHz}$$
$$\alpha_+ = \frac{\eta}{\kappa} = \sqrt{20000} \qquad \text{or} \qquad P = 17\,\mu\mathrm{W}$$
$$\gamma_{scat} = \frac{g^2\Gamma}{\Delta_a^2}\alpha_+^2 = 600\,\mathrm{s}^{-1}$$
$$U = \hbar U_0 4\alpha_+^2 = \hbar\frac{10\kappa}{10^5}80000 = 800\hbar\omega_r\ .$$

This is about two orders of magnitude too short.

As soon as the ground state is found, one may propagate the equations (47.155) in *real time* with the Hamiltonian,

$$H = \frac{\hat{p}^2}{2m} + U_0|\alpha_\pm(t)e^{\imath kx} + \alpha_\mp(t)e^{-\imath kx}|^2 + Nu|\psi(x,t)|^2 \tag{47.161}$$

in the usual way. However, the subsystems may evolve on very different time-scales, so that a scale separation, as done for (47.156) may be appropriate.

47.5.4 BECs in two internal states coupled by a cavity

A lossy cavity can act as an effective *zero temperature reservoir*. One possible implementation [663] realizes a three-level cycling scheme, with two BECs in two ground states $|g_1\rangle$ and $|g_2\rangle$ coherently coupled by a two-photon transition (Raman-lasers or microwave-radiofrequency combination). The ground states are additionally coupled by an irreversible Raman transition via an intermediate spontaneously decaying level $|e\rangle$. One transition is not driven but stimulated by a ring cavity mode $\hat{a}$.

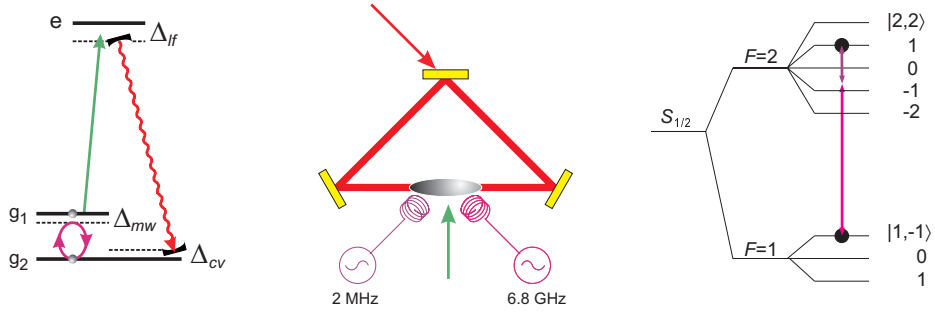

Figure 47.33: (code) (a) Level scheme with a microwave-driven hyperfine structure, a laser-driven optical transition, and a cavity-enhanced Raman deexcitation. (b) Ring cavity used for the experiment. (c) Scheme for coupling the Zeeman states $|2,1\rangle$ and $|1,-1\rangle$ with a two-photon transition in a magnetic trap.

The Hamiltonian consists of three parts, the BEC energy $\mathcal{H}_{bec}$, the interaction energy with the coherent coupling assumed to be classical $\mathcal{H}_{cpl}$ and the interaction

with the mode of a ring cavity $\mathcal{H}_{cav}$ treated quantum mechanically ($\hbar = 1$),

$$\begin{aligned}\mathcal{H} &= \mathcal{H}_{bec} + \mathcal{H}_{cpl} + \mathcal{H}_{cav} \qquad (47.162)\\ &= \int d^3r\ \hat{\psi}_1^\dagger \left(\tfrac{-\nabla^2}{2m} + V + \tfrac{u_{11}}{2}\hat{\psi}_1^\dagger\hat{\psi}_1 + \tfrac{u_{12}}{2}\hat{\psi}_2^\dagger\hat{\psi}_2 \right)\hat{\psi}_1 +\\ &+ \int d^3r\ \hat{\psi}_2^\dagger \left(\tfrac{-\nabla^2}{2m} + V + \tfrac{u_{12}}{2}\hat{\psi}_1^\dagger\hat{\psi}_1 + \tfrac{u_{22}}{2}\hat{\psi}_2^\dagger\hat{\psi}_2 \right)\hat{\psi}_2 +\\ &+ \int d^3r\ \left(-\Delta_{mw}\hat{\psi}_1^\dagger\hat{\psi}_1 + \tfrac{\Omega_{mw}}{2}\hat{\psi}_1^\dagger\hat{\psi}_2 + h.c. \right) + \int d^3r\ \left(g_{cv}\hat{a}\hat{\psi}_1^\dagger\hat{\psi}_2 + h.c. \right) - \Delta_{cv}\hat{a}^\dagger\hat{a}\ .\end{aligned}$$

The BEC energy consists of the two energies (kinetic, potential, self) of the individual BECs and the cross-species interaction proportional to $u_{kl} = 4\pi\hbar^2 a_{kl}/m$. The interaction energy with the classical microwave frequency (mostly we will assume $\Delta_{mw} = 0$) leads to Rabi flopping with frequency Ω_{mw}. Finally, the incident light field is treated classically with a Rabi frequency Ω_{lf} and a detuning Δ_{lf}, while the cavity field is treated quantum mechanically with a coupling constant Ω_{cv} and a detuning Δ_{cv}. The irreversible coupling leads to an energy contribution where $g_{cv} \equiv \Omega_{lf}\Omega_{cv}/2\Delta_{lf}$ is the two-photon Rabi-frequency if the auxiliary state is adiabatically eliminated. From the Heisenberg equations of motion for the matter wave and the optical field operators we obtain,

$$\begin{aligned}\dot{\hat{\psi}}_1 &= \imath[H, \hat{\psi}_1] = -\imath\frac{\delta H}{\delta\hat{\psi}_1^\dagger} \qquad (47.163)\\ &= -\imath\left(\frac{-\nabla^2}{2m} + V + u_{11}|\hat{\psi}_1|^2 + u_{12}|\hat{\psi}_2|^2 \right)\hat{\psi}_1 - \imath\left(\tfrac{\Omega_{mw}}{2} + g_{cv}\hat{a} \right)\hat{\psi}_2 - \imath\Delta_{mw}\hat{\psi}_1\ ,\\ \dot{\hat{\psi}}_2 &= \imath[\hat{H}, \hat{\psi}_2] = -\imath\frac{\delta H}{\delta\hat{\psi}_2^\dagger}\\ &= -\imath\left(\frac{-\nabla^2}{2m} + V + u_{12}|\hat{\psi}_1|^2 + u_{22}|\hat{\psi}_2|^2 \right)\hat{\psi}_2 - \imath\left(\tfrac{\Omega_{mw}}{2} + g_{cv}\hat{a}^\dagger \right)\hat{\psi}_1\ ,\\ \dot{\hat{a}} &= \imath[\hat{H}, \hat{a}] - \tfrac{\kappa}{2}\hat{a} = -\imath\frac{\delta H}{\delta\hat{a}^\dagger} - \tfrac{\kappa}{2}\hat{a}\\ &= -\imath\int d^3r\ g_{cv}\hat{\psi}_1\hat{\psi}_2^\dagger - \left(\imath\Delta_{cv} + \tfrac{\kappa}{2} \right)\hat{a}\ .\end{aligned}$$

Example 292 (*Single atoms in two states interacting with a cavity*): As a first example, we start from the matter wave Hamiltonian (47.162) for two coupled BECs and neglect the center-of-mass motion (and consequence the condensate part, i.e. self-interaction, kinetic energy and the external potential). Furthermore, we assume $\hat{\psi}_i(\mathbf{r}) = \hat{c}_i\delta^3(\mathbf{r})$,

$$\begin{aligned}\mathcal{H} &= \mathcal{H}_{bec} + \mathcal{H}_{clp} + \mathcal{H}_{cav} \qquad (47.164)\\ &= -\Delta_{mw}\hat{c}_1^\dagger\hat{c}_1 + \tfrac{\Omega_{mw}}{2}\hat{c}_1^\dagger\hat{c}_2 + g_{cv}\hat{a}\hat{c}_1^\dagger\hat{c}_2 + h.c. - \Delta_{cv}\hat{a}^\dagger\hat{a}\ .\end{aligned}$$

Consequently, the Heisenberg equations of motion are simply,

$$\begin{aligned}\dot{\hat{c}}_1 &= -\imath\left(\tfrac{\Omega_{mw}}{2} + g_{cv}\hat{a} \right)\hat{c}_2 - \imath\Delta_{mw}\hat{c}_1 \qquad (47.165)\\ \dot{\hat{c}}_2 &= -\imath\left(\tfrac{\Omega_{mw}}{2} + g_{cv}\hat{a}^\dagger \right)\hat{c}_1\\ \dot{\hat{a}} &= -\imath g_{cv}\hat{c}_1\hat{c}_2^\dagger - \left(\imath\Delta_{cv} + \tfrac{\kappa}{2} \right)\hat{a}\ .\end{aligned}$$

Obviously, since the matter wave degree of freedom is ignored, the dynamics only concerns the Bloch vector. Simulations of these equations are exhibited in Fig. 47.34 and in movies that can be watched under (watch movie) and (watch movie).

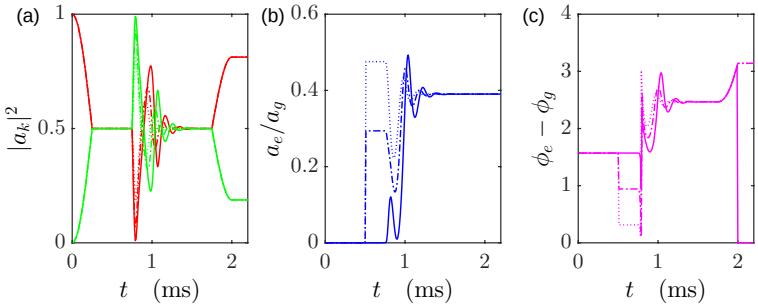

Figure 47.34: (code) Bloch vector phase stabilization in the cavity. (a) Populations and (b) coherences.

47.5.4.1 Phase description

If we replace all field operator $\hat{\psi}_k$ and $\hat{c}$ in the Eqs. (47.163) by c-numbers, we obtain a set of three equations that can be simulated by numerical procedures. Obviously, the equations then do not allow for quantum fluctuations and correlations. Furthermore, by setting,

$$\psi_k(\mathbf{r},t) \equiv \sqrt{N_k(t)}\varphi(\mathbf{r})e^{\imath\Phi_k} \ , \tag{47.166}$$

where $k = 1, 2$ and φ is invariable and normalized to $1 = \int d^3r \ |\varphi|^2$, we assume the condensates can only vary global phases and atom numbers and not their shape or local phases. Then, defining the chemical potentials as,

$$\mu_k \equiv \int d^3r \ \varphi \left(\frac{-\nabla^2}{2m} + V + u_{kk}N_k|\varphi|^2 + u_{kl}N_L|\varphi|^2 \right) \varphi \ , \tag{47.167}$$

and introducing new variables via $\Phi \equiv \Phi_1 - \Phi_2$ and $P_\Phi \equiv \frac{1}{2}(N_2 - N_1)$ we arrive at,

$$\boxed{\begin{array}{rcl} \dot{\Phi} & = & \mu_2 - \mu_1 - \Delta_{mw} - \dfrac{2P_\Phi}{\sqrt{N_1N_2}} \ \mathfrak{Re} \ \left(\frac{1}{2}\Omega_{mw} + g_{cv}c\right) e^{-\imath\Phi} \\ \dot{P}_\Phi & = & -2\sqrt{N_1N_2} \ \mathfrak{Im} \ \left(\frac{1}{2}\Omega_{mw} + g_{cv}c\right) e^{-\imath\Phi} \\ \dot{c} & = & -\imath g_{cv}\sqrt{N_1N_2}e^{\imath\Phi} - \left(\imath\Delta_{cv} + \frac{1}{2}\kappa\right) c \end{array}} \ , \tag{47.168}$$

as shown in 47.5.5.6.

47.5.4.2 Thomas-Fermi approximation

With $N = N_1 + N_2$ and $u_{12} - u_{11} \approx u_{22} - u_{12}$ difference of the self-energies is,

$$\begin{aligned}(\mu_2 - \mu_1) &= [(u_{12} - u_{11})N_1 + (u_{22} - u_{12})N_2] \int d^3r \ |\varphi|^4 \\ &\simeq (u_{12} - u_{11})N \int d^3r \ |\varphi|^4 \ .\end{aligned} \tag{47.169}$$

The integral is on the order of 1, but to be more accurate, we integrate the square of the Thomas-Fermi profile. This is an approximation, because the shape of the Thomas-Fermi profile depends on the number of condensed atoms. On the other hand, the approximation should be good when the mean-field energy is dominant. The density distribution of a BEC with N atoms in the Thomas-Fermi approximation is,

$$n = \frac{1}{u}\left(\mu - \frac{m}{2}\omega_\rho^2\rho^2 - \frac{m}{2}\omega_z^2 z^2\right) \ , \tag{47.170}$$

where $u = 4\pi\hbar^2 a_s/m$ and $2\mu = \left(\frac{15u}{4\pi}Nm^{3/2}\omega_\rho^2\omega_z\right)^{2/5}$. The BEC shape function is normalized. Hence,

$$\int d^3r \ |\varphi|^4 = \frac{1}{N^2}\int d\mathbf{r} \ n^2 = \frac{15}{4Nu_s(\hbar\mu)^{5/2}}\int(\hbar\mu\tilde{\rho}^2 - \tilde{z}^2)^2\tilde{\rho}d\tilde{\rho}d\tilde{z} = \frac{4\mu}{7Nu} \ . \tag{47.171}$$

Now, the equations to be simulated read,

$$\begin{aligned}\dot{\Phi} &= \frac{u_{12} - u_{11}}{7u\hbar}4\mu - \Delta_{mw} - \frac{4P_\Phi}{\sqrt{N^2 - 4P_\Phi^2}}\mathfrak{Re}\ \left(\tfrac{1}{2}\Omega_{mw} + g_{cv}c\right)e^{-\imath\Phi} \\ \dot{P}_\Phi &= -\sqrt{N^2 - 4P_\Phi^2}\,\mathfrak{Im}\ \left(\tfrac{1}{2}\Omega_{mw} + g_{cv}c\right)e^{-\imath\Phi} \\ \dot{c} &= -\tfrac{\imath}{2}g_{cv}\sqrt{N^2 - 4P_\Phi^2}e^{\imath\Phi} - (\imath\Delta_{cv} + \tfrac{1}{2}\kappa)c \ .\end{aligned} \tag{47.172}$$

Example 293 (*Interpretation of the ultracold fusion via analogy with two-level system*): The chemical potential of the BECs in both states shifts the energy levels up depending on the inversion, $\mu_2 - \mu_1 \propto N_2 - N_1$. If the inversion oscillates the spontaneous Raman cycle periodically meets resonance, and takes place. Note that, since atomic motion is not considered, the energy gap due to the finite cavity detuning can only be bridged in resonance, $\mu_2 - \mu_1 = \kappa$. Oscillation simulates Doppler shift of thermal motion in Doppler cooling. Raman scattering takes the role of spontaneous emission in the cooling process. The only role of the cavity is to introduce irreversibility. Raman scattering is only supported in one direction: However, it is not relevant to have a ring cavity.

47.5.4.3 Basic Josephson junction (case i)

To gain an understanding of the Eqs. (47.168), let us treat some special cases. Let us first assume the absence of a driven auxiliary level, $\Omega_{lf}, \Omega_{cv}, g_{cv} = 0$. If $\sqrt{N_1 N_2} \simeq \frac{1}{2}N$,

the last equations read,

$$\begin{aligned}\dot\Phi &= \mu_2 - \mu_1 - \Delta_{mw} - \frac{2\Omega_{mw}}{N} P_\Phi \cos\Phi \\ \dot P_\Phi &= \frac{N\Omega_{mw}}{2}\sin\Phi\ .\end{aligned} \tag{47.173}$$

To be able to draw an analogy between our system and the equations describing Josephson Junctions we set $u_{11} = u_{22}$. This assumption is questionable as in reality $u_{11} < u_{12} < u_{22}$ and thus $\mu_2 - \mu_1 \propto N$ rather than $\mu_2 - \mu_1 \propto N_2 - N_1$. All conclusions based on this approximation should be taken with great caution.

Setting $\sqrt{N_1 N_2} \approx \frac{1}{2}N$ so that $\mu_2 - \mu_1 = (u_{11} - u_{12})(N_2 - N_1)\int d\mathbf{r}\,|\varphi^4(\mathbf{r})| = 2\hbar U P_\Phi$ and furthermore assuming $\Delta_{cv} = 0$ and $P_\Phi \ll N$,

$$\dot\Phi = 2UP_\Phi \quad , \quad \dot P_\Phi = \frac{N\Omega}{2}\sin\Phi\ . \tag{47.174}$$

These equations are formally identical to those describing a *Josephson junction* in a superconductor, if we interpret Φ as the voltage across the junction and P_Φ as the Josephson current.

47.5.4.4 Resistively shunted Josephson junction (case ii)

With the same approximations as above, but now including a driven auxiliary level, $\Omega_{lf}, \Omega_{cv}, g_{cv} \neq 0$,

$$\begin{aligned}\dot\Phi &= 2UP_\Phi - \frac{4P_\Phi}{N}\mathfrak{Re}\ \left(\tfrac{1}{2}\Omega_{mw} + g_{cv}c\right)e^{-\imath\Phi} \approx 2UP_\Phi \\ \dot P_\Phi &= -N\mathfrak{Im}\ \left(\tfrac{1}{2}\Omega_{mw} + g_{cv}c\right)e^{-\imath\Phi}\ , \\ \dot c &= -\tfrac{\imath}{2}g_{cv}Ne^{\imath\Phi} - \left(\imath\Delta_{cv} + \tfrac{1}{2}\kappa\right)c\ .\end{aligned} \tag{47.175}$$

We adiabatically eliminate c to second order, i.e. $\ddot c = 0$,

$$\begin{aligned}\ddot c &= \tfrac{1}{2}g_{cv}N\dot\Phi e^{\imath\Phi} - \left(\imath\Delta_{cv} + \tfrac{1}{2}\kappa\right)\left[-\tfrac{\imath}{2}g_{cv}Ne^{\imath\Phi} - \left(\imath\Delta_{cv} + \tfrac{1}{2}\kappa\right)c\right] = 0 \\ c &= \frac{-\imath g_{cv}Ne^{\imath\Phi}}{2\imath\Delta_{cv} + \kappa} - \frac{2g_{cv}N\dot\Phi e^{\imath\Phi}}{\left(2\imath\Delta_{cv} + \kappa\right)^2}\ .\end{aligned} \tag{47.176}$$

Finally,

$$\frac{1}{2U}\ddot\Phi = \dot P_\Phi = \frac{N\Omega_{mw}}{2}\sin\Phi + \frac{g_{cv}^2N^2\kappa}{4\Delta_{cv}^2 + \kappa^2} - \frac{8g_{cv}^2N^2\Delta_{cv}\kappa}{(4\Delta_{cv}^2 + \kappa^2)^2}\dot\Phi \tag{47.177}$$

defining a fictive mass M, a friction coefficient a_r and a force F_d by,

$$M = \frac{1}{2U} \quad , \quad a_r = \frac{8\Delta_{cv}g_{cv}^2N^2\kappa}{(\kappa^2 + 4\Delta_{cv}^2)^2} \quad , \quad F_d = \frac{g_{cv}^2N^2\kappa}{\kappa^2 + 4\Delta_{cv}^2}\ , \tag{47.178}$$

we obtain

$$M\ddot\Phi + a_r\dot\Phi - \tfrac{1}{2}\Omega_{mw}N\sin\Phi = F_d\ . \tag{47.179}$$

This equation describes the motion of a fictitious phase particle. Another application of this equation is a pendulum driven by a tangential force, subject to friction and to gravitation. It is also used to describe a phase-locked loop or a resistively shunted Josephson junction. In the absence of the inertial term, i.e. in the overdamped case we obtain the so-called Adler equation. The force can be derived from a potential. One can also write down the kinetic and potential energies,

$$E_{kin} = \frac{P_\Phi^2}{2M} = U\dot{\Phi}^2 \quad , \quad V = F_d\Phi + \frac{\Omega_{mw}N}{2}\cos\Phi \ . \tag{47.180}$$

The washboard type potential is shown in Fig. 47.35(d). Hence, from the Hamiltonian $H = E_{kin} + E_{pot}$, we recover the equation of motion (without dissipation) using the Ehrenfest correspondences,

$$\dot{\Phi} = \frac{\partial H}{\partial P_\Phi} = P_\Phi/M \quad , \quad \dot{P}_\Phi = -\frac{\partial H}{\partial \Phi} = F_d - \tfrac{1}{2}\Omega_{mw}N\sin\Phi \ . \tag{47.181}$$

With $P_\Phi = -\imath\partial/\partial\Phi$ we find the commutator,

$$[\Phi, P_\Phi] = \imath \ . \tag{47.182}$$

Stationary solutions, $\dot{\Phi} = 0$, occur at the phases,

$$\Omega_{mw}\sin\Phi = -\frac{2F_d}{N} \ . \tag{47.183}$$

Fig. 47.35(b) shows the range of possible Ω for which stable phases exist. In order to check if the solutions are stable, we expand $\Phi \equiv \Phi_0 + \Phi_1$ with $\dot{\Phi} = 0$ and $\sin(\Phi_0 + \Phi_1) \approx \sin\Phi_0 + \Phi_1\cos\Phi_0$, and get in first order

$$a_r\dot{\Phi}_1 - \frac{\Omega_{mw}N}{2}\Phi_1\cos\Phi_0 = 0 \ . \tag{47.184}$$

The solution $\Phi_1 \sim e^{\varepsilon t}$ with $\varepsilon = \Omega N/2a_r\ \cos\Phi_0$ is stable only if $\varepsilon < 0$, which requires $\Phi_0 < 3\pi/2$ and excludes the upper half of the branch. For simulations,

$$\begin{aligned} \dot{\Phi} &= \Psi \\ \dot{\Psi} &= \Omega_{mw}NU\sin\Phi - 2Ua_r\Psi + 2UF_d \\ c &= \frac{-igNe^{\imath\Phi}}{2i\nu + \kappa} - \frac{2gN\dot{\Phi}e^{\imath\Phi}}{(2i\nu+\kappa)^2} \ . \end{aligned} \tag{47.185}$$

47.5.4.5 Stationary solutions of full model (case iii)

We now come back to the Eqs. (47.168). They read at steady-state using $c = |c|e^{\imath\Phi_C}$,

$$\begin{aligned} \frac{\mu_1 - \mu_2}{\hbar} + \Delta_{mw} &= \frac{-2P_\Phi}{\sqrt{N_1N_2}}\mathfrak{Re}\ \left(\tfrac{1}{2}\Omega_{mw} + g_{cv}|c|e^{\imath\Phi_C}\right)e^{-\imath\Phi} \\ 0 &= \mathfrak{Im}\ \left(\tfrac{1}{2}\Omega_{mw} + g_{cv}|c|e^{\imath\Phi_C}\right)e^{-\imath\Phi} \\ \left(\imath\Delta_{cv} + \tfrac{1}{2}\kappa\right)|c| &= -ig_{cv}\sqrt{N_1N_2}e^{\imath(\Phi-\Phi_C)} \ . \end{aligned} \tag{47.186}$$

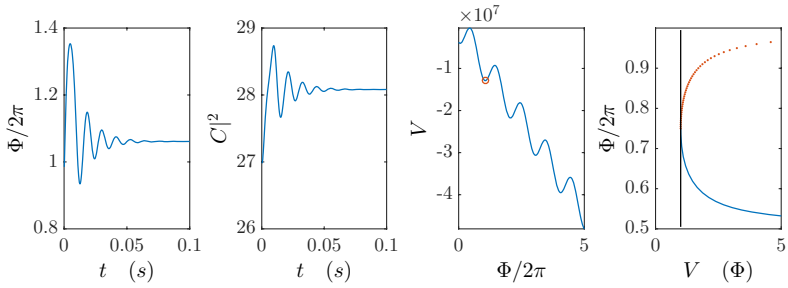

Figure 47.35: (code) Simulation of the shunted JJ model Eq. (47.179). (a) Damping of the phase difference. (b) Stable branch from a linear stability analysis. (c) Photon number in the cavity from Eq. (47.172)(c). (d) Washboard potential for the fictitious phase particle.

Setting $\Delta_{mw} = 0$ and evaluating real parts and imaginary parts separately, we arrive at,

$$\begin{aligned}
\frac{\mu_1 - \mu_2}{\hbar} &= \frac{-2P_\Phi}{\sqrt{N_1 N_2}} \left(\tfrac{1}{2}\Omega_{mw} \cos\Phi + g_{cv}|c| \cos(\Phi_C - \Phi) \right) \\
0 &= -\tfrac{1}{2}\Omega_{mw} \sin\Phi + g_{cv}|c| \sin(\Phi_C - \Phi) \\
\tfrac{1}{2}\kappa|c| &= g_{cv}\sqrt{N_1 N_2} \sin(\Phi - \Phi_C) \\
\Delta_{cv}|c| &= -g_{cv}\sqrt{N_1 N_2} \cos(\Phi - \Phi_C)
\end{aligned} \tag{47.187}$$

and

$$\begin{aligned}
\frac{\mu_1 - \mu_2}{\hbar} &= \frac{-2P_\Phi}{\sqrt{N_1 N_2}} \left(\tfrac{1}{2}\Omega_{mw} \cos\Phi - \frac{\Delta_{cv}|c|^2}{\sqrt{N_1 N_2}} \right) \\
\kappa|c|^2 &= -\Omega_{mw}\sqrt{N_1 N_2} \sin\Phi \\
\left(\Delta_{cv}^2 + \tfrac{1}{4}\kappa^2\right)|c|^2 &= g_{cv}^2 N_1 N_2
\end{aligned} \tag{47.188}$$

yielding

$$\Omega_{mw} \sin\Phi = -\frac{4F_d\sqrt{N_1 N_2}}{N^2} \quad , \quad |c|^2 = \frac{4F_d N_1 N_2}{\kappa N^2} \tag{47.189}$$

and

$$\begin{aligned}
\Omega_{mw} \cos\Phi &= -\frac{\sqrt{N_1 N_2}}{P_\Phi} \frac{(\mu_1 - \mu_2)}{\hbar} + \frac{2\Delta_{cv}|c|^2}{\sqrt{N_1 N_2}} \\
\Omega^2 &= \left(\frac{4F_d\sqrt{N_1 N_2}}{N^2} \right)^2 + \left(2\sqrt{N_1 N_2}U + \frac{8\Delta_{cv}\sqrt{N_1 N_2}F_d}{\kappa N^2} \right)^2
\end{aligned} \tag{47.190}$$

identify a bistable region

This yields if initially $N_1 = N_2 = \frac{1}{2}N$ and $\Delta = 0$,

$$\begin{aligned}
\Omega \sin\Phi &= -\frac{2F_d}{N} \quad , \quad |c|^2 = \frac{F_d}{\kappa} \\
\Omega^2 &= \left(\frac{2F_d}{N} \right)^2 + \left(NU + \frac{4\Delta_{cv}F_d}{\kappa N} \right)^2 ,
\end{aligned} \tag{47.191}$$

which confirms Eq. (47.184).

47.5.4.6 Paradox with fixed atom numbers

According to Pitaevskii a phase synchronization requires the exchange of atoms. If we knew the exact atom number in each well, the relative phases had to be uncertain. This is how the Mott-Insulator works. If no atoms are exchanged by Josephson tunneling, we could measure N_j, and due to cavity coupling still know that the phases are fixed. *Probably* Pitaevskii is right: It makes no sense talking of the de Broglie phases of BECs at different antinodes, if the BECs are not coherently coupled. The cavity mode do not couple the de Broglie phases. If this is true, then a cavity standing wave can support two ground state BECs without a fixed relationship between them. Any phase difference between them turn into excitations *only as soon as the BECs are directly coupled*.

How about there is some coherence in the atom numbers (spin squeezing) like in the Mott insulator. Then coherence would reappear as the BECs are melted.

On the other hand, if the BEC would decouple, sound could not propagate. Is N_j the right quantum number, shouldn't we rather consider atom-photon correlations, polaritons, or what? Also the notion of well-known or fixed atom numbers has to be clarified, because their location may change due to the displacement of the standing wave. For example, we could say: *fixed atom number at a given location*, having in mind a device that constantly and non-destructively measures the number of atoms within a well-defined area of space. Or we could say: *fixed atom number in a given antinode* and imagine a system, which tracks the antinodes' location and constantly and non-destructively measures the number of atoms within this antinode. Also we can imagine a Gedankenexperiment were exactly two BECs produced in different vacuum chambers are trapped in different antinodes of the same ring cavity standing wave.

47.5.4.7 Simulation of the 1D coupled GPE equations

Our goal is to directly simulate the complete set of coupled GPEs (47.166). We will however assume that the intermediate state of the two-photon coupling can be adiabatically eliminated and we will restrict ourselves to one dimension.

In order to go to 1D, we first calculate the chemical potential of a cylindrically symmetric BEC. In the Thomas-Fermi limit,

$$n(\mathbf{r}) = \frac{\mu - U(\mathbf{r})}{u} \ , \tag{47.192}$$

The chemical potential follows from the normalization condition,

$$N = \int_{n(\mathbf{r})>0} n(\mathbf{r}) d^3r = \frac{4\pi}{u} \frac{4}{15} \frac{\sqrt{2}\mu^{5/2}}{m^{3/2}\omega_r^2\omega_z} \ . \tag{47.193}$$

We obtain,

$$\mu = \left(\frac{15Nu}{\sqrt{2}16\pi} m^{3/2}\omega_r^2\omega_z \right)^{2/5} \ , \tag{47.194}$$

with $u \equiv 4\pi\hbar^2 a_s/m$. The radial size of the BEC follows from $n(r_{hw}, 0) = \frac{n(0,0)}{2}$ and reads,

$$r_{hw} = \sqrt{\frac{\mu}{m\omega_r^2}} \ . \tag{47.195}$$

Often it is a good approximation to assume condensates which are *radially homogeneous* two-dimensional condensates over a width r_{hw}. This may be the case for pancake shape traps. In this case we may neglect the radial kinetic energy. Since the normalization then requires,

$$\int_{-r_h}^{r_h}\int_{-r_h}^{r_h}\int_{-\infty}^{\infty}|\psi(\mathbf{r})|^2 d^3r = (2r_{hw})^2\int_{-\infty}^{\infty}|\psi(z)|^2 dz = 1 \ , \tag{47.196}$$

by substituting $\psi(\mathbf{r}) = \frac{\phi(z)}{2r_{hw}}$ and $u_{1D} = \frac{u}{(2r_{hw})^2}$, the GPE and the normalization condition adopts a particularly simple form,

$$\imath\hbar\frac{\partial}{\partial t}\phi(z) = \left(-\frac{\hbar^2}{2m}\frac{\partial^2}{\partial z^2} + V_{trap}(z) + N\ u_{1D}|\phi(z)|^2\right)\phi(z) \ . \tag{47.197}$$

Now applying the Thomas-Fermi approximation for a harmonic potential, we get,

$$|\phi(z)|^2 = \frac{\mu - \frac{m}{2}\omega_z^2 z^2}{N\ u_{1D}} \ . \tag{47.198}$$

with,

$$\mu = \left(\tfrac{9}{32}u_{1D}^2 N^2 m\omega_z^2\right)^{1/3} \ . \tag{47.199}$$

47.5.4.8 Finding the ground state with steepest descent

Characteristic length scale $z \in [-7\,\mu\text{m}, 7\,\mu\text{m}]$, radial trap frequency $\omega_z = 2\pi\cdot 40\,\text{Hz}$, potential,

$$V_1 = V_2 = \frac{m}{2}\omega_z^2 z^2 \ . \tag{47.200}$$

We start with Gaussian density distribution assuming that all atoms are inthe ground state,

$$\psi = \frac{e^{-z^2/2z_{ho}^2}}{\sqrt{\int e^{-z^2/z_{ho}^2}dz}} \ , \tag{47.201}$$

with $z_{ho} = \sqrt{\hbar/m\omega_z}$.

In reality the BEC is rather in the Thomas-Fermi limit. To calculate this, we propagate the one-dimensional GPE,

$$\left[\frac{-\hbar^2}{2m}\nabla^2 + V(z) + Nu_{1D}|\psi|^2\right]\psi = \imath\hbar\frac{d}{dt}\psi \tag{47.202}$$

in imaginary time in order to find the ground state. Here $u_{1D} = \frac{\pi\hbar^2 a_s}{m r_{hw}^2}$. The resulting wavefunction is our starting point for all subsequent simulations.

47.5.4.9 Coupled condensates with cavity, Runge-Kutta method

The interaction strengths for the states $|2,1\rangle$ and $|1,-1\rangle$ are $(u_{11}, u_{12}, u_{22}) = (0.97, 1, 1.03)u_{1D}$. We take the equations of [663]. Defining the following spinor,

$$\Psi \equiv \begin{pmatrix}\psi_1\\ \psi_2\\ c\end{pmatrix} \ , \tag{47.203}$$

and writing the coupled GPE equations like,

$$K[\Psi] \equiv -\frac{\imath}{\hbar} dt \begin{pmatrix} \left(\frac{-\hbar^2}{2m}\nabla^2 + V_1 + Nu_{11}|\psi_1|^2 + Nu_{12}|\psi_2|^2\right)\psi_1 + \hbar\left(\frac{\Omega_{mw}}{2} + g_{cv}c\right)\psi_2 + \hbar\Delta_{mw}\psi_1 \\ \left(\frac{-\hbar^2}{2m}\nabla^2 + V_1 + Nu_{22}|\psi_2|^2 + Nu_{12}|\psi_1|^2\right)\psi_2 + \hbar\left(\frac{\Omega_{mw}}{2} + g_{cv}c^*\right)\psi_1 \\ \hbar\int g_{cv}\psi_1\psi_2^* dz + \hbar\left(\Delta_{cv} - \imath\frac{\kappa}{2}\right)c \end{pmatrix} , \tag{47.204}$$

we can employ the forth-order Runge-Kutta method via,

$$\begin{aligned} \delta\psi_a &= K[\Psi] \quad , \quad \delta\psi_1 = K\left[\Psi + \tfrac{1}{2}\delta\psi_a\right] \quad , \\ \delta\psi_C &= K\left[\Psi + \tfrac{1}{2}\delta\psi_1\right] \quad , \quad \delta\psi_d = K\left[\Psi + \delta\psi_C\right] \\ \Psi &= \psi_1 + \frac{\delta\psi_{1a}}{6} + \frac{\delta\psi_{1b}}{3} + \frac{\delta\psi_{1c}}{3} + \frac{\delta\psi_{1d}}{6} \ . \end{aligned} \tag{47.205}$$

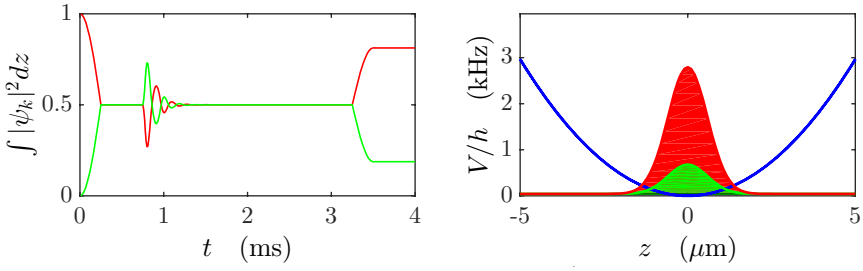

Figure 47.36: (code) Ramsey cycle with intermediate cavity damping.

Even though better than the Euler method, the Runge-Kutta method diverges too fast, and especially the calculation of the gradient is too slow.

47.5.4.10 Coupled condensates without cavity, time-splitting spectral algorithm

An alternative method is the *time-splitting spectral algorithm*, which is more robust for trap oscillation, because it accepts periodic boundary conditions. Write the one-dimensional GPE in the form,

$$\imath\hbar\frac{\partial\psi(x,t)}{\partial t} = -\frac{\hbar^2}{2m}\Delta\psi(x,t) + V(x)\psi(x,t) + N\frac{4\pi\hbar^2 a_s}{m(2r_{hw})^2}|\psi(x,t)|^2\psi(x,t) \tag{47.206}$$

for $a < x < b$. Choose periodic boundary conditions, $\psi(a,t) = \psi(b,t)$ and $\psi_x(a,t) = \psi_x(b,t)$. Various methods are known to solve the GPE numerically, such as the *Crank-Nicholson algorithm*. The time-splitting spectral algorithm consists in solving the first and the second of the following equations in two distinct steps [85, 84, 83, 486],

$$\begin{aligned} \frac{\partial\psi(x,t)}{\partial t} &= -\imath\frac{V(x)}{\hbar}\psi(x,t) - \imath N\frac{u_{1D}}{\hbar}|\psi(x,t)|^2\psi(x,t) \\ \frac{\partial\psi(x,t)}{\partial t} &= \imath\frac{\hbar^2}{2m}\psi_{xx}(x,t) \ , \end{aligned} \tag{47.207}$$

i.e. we discretize in space using $x = a + j(b-a)/M$ and $k = 2\pi l/(b-a)$ such that $k(x-a) = 2\pi lj/M$. We propagate half the way, $\Delta t/2$, in time,

$$\varphi_x \equiv e^{-\frac{\imath}{\hbar}(V(x)+u_{1D}|\psi(x,t)|^2)\frac{\Delta t}{2}}\psi(x,t) \tag{47.208}$$

for $j = 0, .., M-1$. Now we propagate the spectral components, $(\mathcal{F}\varphi)_k \equiv \sum_{j=0}^{M-1}\varphi_x e^{-2\pi\imath lj/M}$, in momentum space and transform back, $\left(\mathcal{F}^{-1}\varphi\right)_x \equiv M^{-1}\sum_{l=-M/2}^{M/2-1}\varphi_k e^{2\pi\imath lj/M}$,

$$\phi_x \equiv \mathcal{F}^{-1}\left[e^{\imath\frac{\hbar}{2m}k^2\Delta t}(\mathcal{F}\varphi)_k\right] \ . \tag{47.209}$$

for $l = -M/2, .., M/2-1$. Finally, we propagate the remaining time, $\Delta t/2$,

$$\psi(x, t+dt) = e^{-\frac{\imath}{\hbar}(V(x)+u_{1D}|\phi_x|^2)\frac{\Delta t}{2}}\phi_x \ . \tag{47.210}$$

Now we just have to generalize this method to coupled GPEs. We simplify the notation by writing the wavefunction as a spinor, $\vec{\psi} \equiv \begin{pmatrix}\psi_1\\ \psi_2\end{pmatrix}$. Now the non-kinetic part of the coupled GPE can be written,

$$\frac{\partial\vec{\psi}(x,t)}{\partial t} = M\vec{\psi}(x,t) \tag{47.211}$$

with the matrix,

$$M = \begin{pmatrix} -\frac{\imath}{\hbar}V(x) - \frac{\imath}{\hbar}u_{1D}|\psi_1(x,t)|^2 - \imath\Delta_{mw} & -\frac{\imath}{2}\Omega_{mw} \\ -\frac{\imath}{2}\Omega_{mw} & -\frac{\imath}{\hbar}V(x) - \frac{\imath}{\hbar}u_{1D}|\psi_2(x,t)|^2 \end{pmatrix} \tag{47.212}$$

and the solution

$$\vec{\psi}(x,t) = e^{Mt}\vec{\psi}(x,0) \ . \tag{47.213}$$

Let us now abbreviate the matrix by,

$$M = \begin{pmatrix} A & B \\ B & D \end{pmatrix} \ . \tag{47.214}$$

The matrix is diagonalized with the unitary transforms,

$$U = \frac{1}{\sqrt{2\Delta}}\begin{pmatrix} \frac{A-D}{2B} + \Delta & \frac{A-D}{2B} - \Delta \\ 1 & 1 \end{pmatrix} \quad \text{and} \quad U^{-1} = \frac{1}{\sqrt{2\Delta}}\begin{pmatrix} 1 & -\frac{A-D}{2B} + \Delta \\ -1 & \frac{A-D}{2B} + \Delta \end{pmatrix} \ . \tag{47.215}$$

The eigenvalue matrix is,

$$U^{-1}MU = \begin{pmatrix} E_1 & 0 \\ 0 & E_2 \end{pmatrix} \tag{47.216}$$

with $E_{1,2} = \frac{1}{2}A + \frac{1}{2}D \pm B\Delta$. Here we used the abbreviation $\Delta = \sqrt{\left(\frac{D-A}{2B}\right)^2 + 1}$. The formal solution now reads,

$$\vec{\psi}(x,t) = \exp\left[U\begin{pmatrix} E_1 & 0 \\ 0 & E_2 \end{pmatrix}U^{-1}t\right]\vec{\psi} = U\begin{pmatrix} e^{E_1 t} & 0 \\ 0 & e^{E_2 t} \end{pmatrix}U^{-1}\vec{\psi}(x,0) \ . \tag{47.217}$$

This formula can easily be computed, because the block matrices of transform U are diagonal in x.

The next step is to propagate the spectral components in momentum space independently for both states and transform back,

$$\phi_{x1} \equiv \mathcal{F}^{-1}\left[e^{\imath\frac{\hbar}{2m}k^2\Delta t}\left(\mathcal{F}\varphi_{x1}\right)_k\right] \tag{47.218}$$
$$\phi_{x2} \equiv \mathcal{F}^{-1}\left[e^{\imath\frac{\hbar}{2m}k^2\Delta t}\left(\mathcal{F}\varphi_{x2}\right)_k\right] \ .$$

Finally, we propagate the remaining time, $\Delta t/2$, using the same procedure as above.

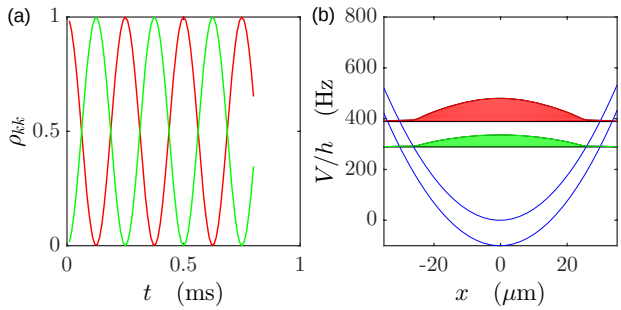

Figure 47.37: (code) Rabi flopping with oscillating BEC.

47.5.4.11 Experimental realization

To implement the proposed scheme, we need two stable ground states, e.g. hyperfine states coupled by a microwave radiation. The low field seeking states of ^{87}Rb, $|2,2\rangle$ and $|1,-1\rangle$, cannot be coupled by a microwave single-photon transition, nor by an optical two-photon transition. Furthermore, those states have different magnetic trapping strength, which would reduce the spatial overlap of the clouds. There are two options to circumvent the problem. Either, we transfer the atoms into an optical trap and apply a magnetic offset field. In this case we could use for example the $|2,-1\rangle$ and $|1,-1\rangle$ states and couple them by a microwave single photon transition. Or we transfer the atoms to a superposition of the low field seeking states $|2,1\rangle$ and $|1,-1\rangle$. These states must then be resonantly coupled with a two-photon transition, i.e. combination of a microwave and a radiofrequency. This is the option pursued in our approach.

47.5.4.12 Preparation of the system

We start from an experimental setup used for the first studies of condensates interacting with resonators [1217]. Atoms are trapped and precooled in magneto-optical traps and then transferred via several intermediate traps to a Ioffe type magnetic trap. Here a cloud of typically $N = 2 \cdot 10^5$ ^{87}Rb atoms is Bose-condensed by forced evaporation in the $|2,2\rangle$ hyperfine state.

Trap frequencies for atoms in the $|m_F| = 2$ states are measured to be in radial direction $\omega_r = 2\pi \cdot 281$ Hz and in axial direction $\omega_z = 2\pi \cdot 41.3$ Hz. In $|m_F| = 1$ states they are smaller by a factor of $\sqrt{2}$.

47.5.4.13 Transfer of the atoms to the cavity mode

Due to a misalignment of the Ioffe wires with respect to the cavity mode a large transverse homogeneous magnetic field must be applied ... compensation coils ... current stabilization of Agilent supply. A TEM_{00} mode of the cavity is permanently driven by a light field. In order to minimize heating and losses due to Rayleigh scattering [224], the BEC is moved around, between and into the center of the lobes of the TEM_{00} intensity distribution.

47.5.4.14 Transfer from $|2,2\rangle$ to $|2,1\rangle$

The atoms are transferred via the intermediate $|1,1\rangle$ state by means of two successive adiabatic microwave sweeps. The duration of both sweeps is $\Delta t = 600$ μs. Their frequency span is $\Delta\nu = 800$ kHz. The efficiency for the transfer is about 80% and heats the atomic cloud considerably. The populations of the various Zeeman states are probed using the Stern-Gerlach technique.

The Rabi frequency of the microwave is determined by varying the sweep time, measuring the transfer efficiency and fitting a Landau-Zener formula. The resulting microwave Rabi frequency is $\Omega_{mi} = 2\pi \cdot 72$ kHz. The adiabatic transfer achieved with the frequency sweeps can be described and simulated with three-level Bloch and Schrödinger equations.

47.5.4.15 Two-photon coupling $|2,1\rangle$ to $|1,-1\rangle$

We label the interesting states $|2\rangle \equiv |2,1\rangle$ and $|1\rangle \equiv |1,-1\rangle$. The hyperfine structure splitting is $\nu_{hf} = 6\ 834\ 682\ 610.904\ 30$ Hz, Zeeman-shift of the resonance frequency according to the Breit-Rabi formula $\nu_{zm} = -4$ kHz. The resonance frequency is at $\nu_{eg} = \nu_{hf} + \nu_{zm}$.

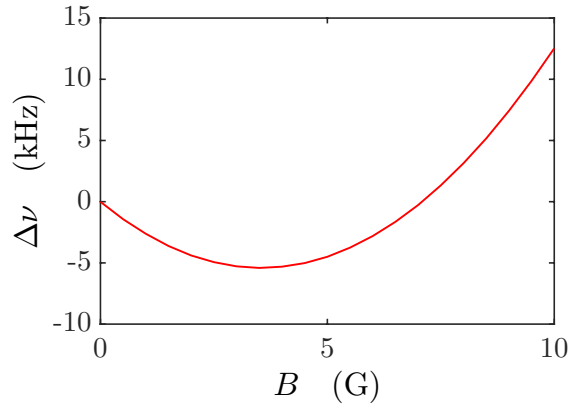

Figure 47.38: (code) (a) Frequency difference between $|2,1\rangle$ and $|1,-1\rangle$ as a function of magnetic field.

The two-photon transition uses $|i\rangle \equiv |2,0\rangle$ as an intermediate state. The detuning from this intermediate state is typically $\Delta_{is} = \pm 2\pi \cdot 200$ kHz. The measured total

Rabi frequency is then $\Omega_{mw} = \frac{\Omega_{mi}\Omega_{rf}}{2\Delta_{is}} = 2\pi \cdot 720$ Hz. From this we derive the radiofrequency Rabi frequency, $\Omega_{rf} = 2\pi \cdot 4$ kHz.

47.5.4.16 Imaging

The populations of both states are measured independently by time-of-flight absorption imaging. First, a vertical probe beam resonant to the transition between the $S_{1/2}, F = 2$ levels and the $P_{1/2}, F' = 3$ levels records the population in state $|e\rangle$. Then, a laser beam resonant to the repumping transition from $S_{1/2}, F = 1$ to $P_{1/2}, F' = 2$ pumps the $|1\rangle$ atoms into the $S_{1/2}, F = 2$ levels, where they are imaged by a horizontal probe beam. This allows us to measure the populations $N_k/(N_e + N_g)$ with low noise. Purging pulse???

47.5.4.17 Rabi flopping and excitation spectra

With three-level Bloch or Schrödinger equations we can simulate the Rabi flopping of the populations and the excitation spectra. However, we experimentally observe damping of the coherence that is not understood within the three-level model. They do not arise from the presence of the intermediate state $|i\rangle$, which is not populated during the interaction. To understand the damping we have to take into account spatial inhomogeneities and interatomic interaction in the condensate.

47.5.4.18 Collapse and revival

We observe collapse and revivals.

47.5.4.19 Mean-field effects

The triplet scattering length of ^{87}Rb is $a_s = 99a_B$. The scattering lengths for the useful low field seeking hyperfine states are $a_{|1,-1\rangle} = 1.03a_s$, $a_{|1,-1\rangle|2,1\rangle} = a_s$, and $a_{|2,1\rangle} = 0.97a_s$. Because $a_{|1,-1\rangle|2,1\rangle}/\sqrt{a_{|1,-1\rangle}a_{|2,1\rangle}} \approx 1.0005 > 1$ the BECs in the two hyperfine states tend to demix [575].[19]

Raised questions:

1. Why is it important that the chemical potential and any magnetic field fluctuations are small compared to the cavity linewidth, $\mu, \Delta B(t) \ll \kappa$?

2. The large impact of the ring cavity seems surprising in view of the poor cavity to free space ratio?

3. Why does it have to be a "ring" cavity? Only to prevent the spatial structuring of the BEC at the antinodes?

4. There are two phases, the de Broglie phase of the atomic motion (external degree) of freedom and the Bloch vector phase of the electronic motion (internal degree of freedom). Which one synchronizes? Both? Cool the atomic motion via dissipation of internal energy.

[19] Note that Jaksch et al. assume $a_{11} = a_{22} = 103a_B$.

47.5.4.20 Laser locking scheme

The cloud can be overlapped with the modes of a ring cavity with finesse $F = 150000$, which corresponds to the cavity linewidth $\kappa = 2\pi \times 10$ kHz. The cavity has the coupling strength $g_{cv} = 2\pi \times 80$ kHz.

An antenna couples a microwave frequency ω_{mw} into the cloud. The frequency is adjusted to resonance with the Zeeman-shifted hyperfine splitting, such that $\omega_{mw} = \omega_{hf} + \omega_{zm} = \omega_{|2\ 1\rangle} - \omega_{|1\ -1\rangle} + \frac{1}{2}\mu_B B_{offset}$. A titanium-sapphire laser at $\lambda = 797$ nm with frequency ω_{11} is tightly phase-locked to a TEM_{11} mode using the Pound-Drever-Hall method. This laser continuously probes the cavity during a whole experimental cycle. An AOM driven with a radiofrequency ω_{ao} shifts the laser frequency to $\omega_{pp} = \omega_{11} + \omega_{ao}$. This frequency pumps the atoms transversally to the ring cavity's optical axis. The AOM frequency is chosen such, that the Raman condition is fulfilled with the next but one cavity mode, i.e. $\omega_{pr} + \delta_\kappa = \omega_{11} + 2\delta_{fsr} = \omega_{mw} + \omega_{pp}$. Additionally, the pump frequency is modulated creating sidebands at the frequency $\omega_{eo} = \omega_{pr} + \delta_\kappa$, which are resonant with the next but one cavity mode in order to probe right detuning.

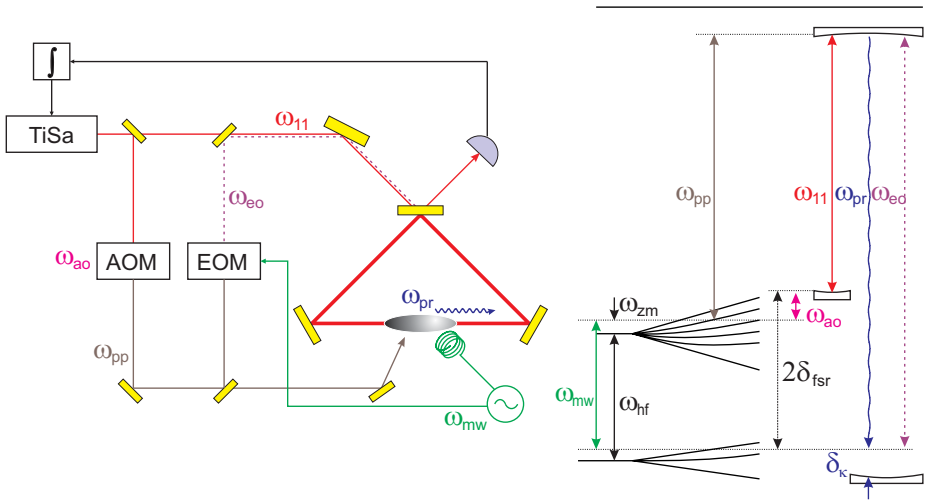

Figure 47.39: (code) (a) Laser locking scheme for ring cavity-assisted cycling. (b) Level scheme.

The Rabi frequency of the Raman laser ω_{pp} can be tuned over wide ranges, as well as its detuning from the auxiliary level. For example with $\Omega_{lf} = \Gamma = 2\pi \times 6$ MHz and $\Delta_{lf} = 10\Gamma = 2\pi \times 30$ GHz the light-shift is $g = \Omega_{lf}\Omega_{cv}/2\Delta_{1f} = 2\pi \times 10$ Hz. Consequently, the Raman coupling strength is $\sqrt{N}g$.

47.5.4.21 Time sequence

Let us now design the sequence and timing of a possible experiment. 1. Preparation of a BEC inside the Ioffe wire trap. 2. Transfer to $|21\rangle$ via $|11\rangle$. 3. Irradiation of a two-photon microwave $\pi/2$ pulse coupling the $|21\rangle$ and $|1-1\rangle$ states. 4. Attenuated

irradiation of the two-photon microwave frequency and transversal irradiation of an external light field. 5. Phase-interferometry.

47.5.4.22 Phase measurement

To prove the fusion of the two BECs, it is necessary to measure the evolution of their relative phase under the influence of the ring cavity-assisted cycling scheme. Internal state Ramsey interferometer with BECs have been demonstrated [574]. We use the definition of the two-species one-body density matrix,

$$\rho_{kl}(\mathbf{x},\mathbf{x}') \equiv \langle \hat{\psi}_l^\dagger(\mathbf{x}')\hat{\psi}_k(\mathbf{x})\rangle \simeq \sqrt{N_l N_k}\varphi^*(\mathbf{x}')\varphi(\mathbf{x})e^{\imath\Phi_k-\imath\Phi_l} \tag{47.219}$$

and at $\mathbf{x}=0$,

$$\begin{aligned}\rho_{12}(0,0) &= \sqrt{N_1N_2}|\varphi(0)|^2 e^{\imath\Phi} \\ \rho_{kk}(0,0) &= N_k|\varphi(0)|^2 \ .\end{aligned} \tag{47.220}$$

The fringe visibility is,

$$v(\mathbf{x}) = \frac{2|\rho_{12}(\mathbf{x},\mathbf{x})|}{\rho_{11}(\mathbf{x},\mathbf{x})+\rho_{22}(\mathbf{x},\mathbf{x})} \tag{47.221}$$

and at $\mathbf{x}=0$,

$$v(0) = \frac{2\sqrt{N_lN_2}}{N_l+N_2} = \sqrt{1-\frac{4P_\Phi^2}{N^2}} \ . \tag{47.222}$$

Probably one has to average over several initial phase randomly distributed over $[0,2\pi]$ [663].

47.5.4.23 Undamped Josephson coupling

The basic equations for a Josephson type coupling of a BEC in two states are [1377],

$$\imath\begin{pmatrix}\dot\Psi_1\\ \dot\Psi_2\end{pmatrix} = \begin{pmatrix}H_2^0+H_2^{MF}-\frac{\delta}{2} & \Omega\\ \Omega & H_1^0+H_1^{MF}+\frac{\delta}{2}\end{pmatrix}\begin{pmatrix}\Psi_2\\ \Psi_1\end{pmatrix} \ . \tag{47.223}$$

From this follows with $N_{ij}=\int dz\Psi_i^*(z)\Psi_j(z)$,

$$\begin{aligned}\dot N_2 &= -\imath\Omega(N_{21}-N_{12}) \\ \dot N_1 &= +\imath\Omega(N_{21}-N_{12}) \\ \dot N_{21} &= -\imath\delta N_{21}+\imath\Lambda(t)-\imath\Omega(N_2-N_1) \ .\end{aligned} \tag{47.224}$$

Here,

$$\Lambda(t) = \underbrace{-2z_0\int dz\ z\Psi_2^*(z)\Psi_1(z)}+\underbrace{\int dz(H_2^{MF}-H_1^{MF})\Psi_2^*(z)\Psi_1(z)} \ . \tag{47.225}$$

The first term in $\Lambda(t)$ comes from the different positions of the two condensates and is neglected here. The second term results from the mean-field energy difference. It would vanish, when the scattering lengths would be the same for both states, because

$$H_2^{MF}-H_1^{MF} = (\lambda_{22}-\lambda_{21})|\Psi_2|^2-(\lambda_{11}-\lambda_{21})|\Psi_1|^2 \ . \tag{47.226}$$

We now make the ansatz,

$$\Psi_j(z,t) = \sqrt{N_i(t)}e^{\imath\phi_i(t)}\Phi_i(z) \ . \tag{47.227}$$

Here, we allow the phase and the atom number to evolve in time, while the spatial evolution is separated. In Ref. [**?**] this spatial modulation is neglected!

By plugging into (1) we obtain the following equation of motion,

$$\begin{aligned}\dot{\eta} &= -k(1-\eta^2)^{1/2}\sin\phi \\ \dot{\phi} &= -[(\mu_2-\mu_1)-\delta] + k\eta(1-\eta^2)^{-1/2}\cos\phi \ .\end{aligned} \tag{47.228}$$

with

$$\begin{aligned}\eta &= \frac{N_2-N_1}{N} = \frac{2}{N}P_\Phi \\ \phi &= \phi_2-\phi_1 \\ k &= 2\Omega\underbrace{\int dz\Phi_2(z)\Phi_1(z)}_{1} = 2\Omega \ .\end{aligned} \tag{47.229}$$

Comparison with Ref. [**?**] yields (setting the cavity coupling to zero, $g=0$):

$$\begin{aligned}\frac{2}{N}\dot{P}_\Phi &= -2\Omega(1-\frac{4}{N^2}P_\Phi^2)^{1/2}\sin\phi \\ \dot{P}_\Phi &= -(N^2-4P_\Phi^2)^{1/2}\mathfrak{Im}\ (\frac{1}{2}\Omega e^{-\imath\phi}) \ .\end{aligned} \tag{47.230}$$

This coincides except for a factor of $-\frac{1}{2}$,

$$\begin{aligned}\dot{\phi} &= -[(\mu_2-\mu_1)-\delta] + k\eta(1-\eta^2)^{-1/2}\cos\phi \\ \dot{\phi} &= -[\mu_2-\mu_1-\delta] + 4\Omega\frac{P_\Phi}{\sqrt{N^2-4P_\Phi^2}}\cos\phi \\ \dot{\phi} &= \mu_2-\mu_1-\delta - \frac{4P_\Phi}{\sqrt{N^2-4P_\Phi^2}}\mathfrak{Re}\ (\frac{1}{2}\Omega e^{-\imath\phi}) \ .\end{aligned} \tag{47.231}$$

This coincides except for a factor of $-\frac{1}{2}$ in the last term.

47.5.4.24 Analytic estimations

Using Eq. (47.179) we calculate the friction coefficient $a_r = 56$, the force $F_d = 1125\omega$ and the critical Rabi frequency $2F_d/N = 0.38\omega$. Let us pick a point out of the stable branch in Fig. 47.35(b), for $\Phi = 1.25\omega$ we obtain from Eq. (47.184) $\Omega = -2F_d\sin\Phi/N = 0.27\omega$. The stationary photon number in the cavity is then obtained from the first Eq. (47.188), $|c|^2 = F_d/\kappa = 28$.

For an atom number $N = 6000$ and a mean density of $n = 1.8\times10^{14}$ cm^3 the selfenergy is $NU = 0.2\omega \approx h\times 44$ Hz and the mass of the phason is $M = (2U)^{-1} = 15000\omega^{-1}$. The real atom number will probably be 50 times higher.

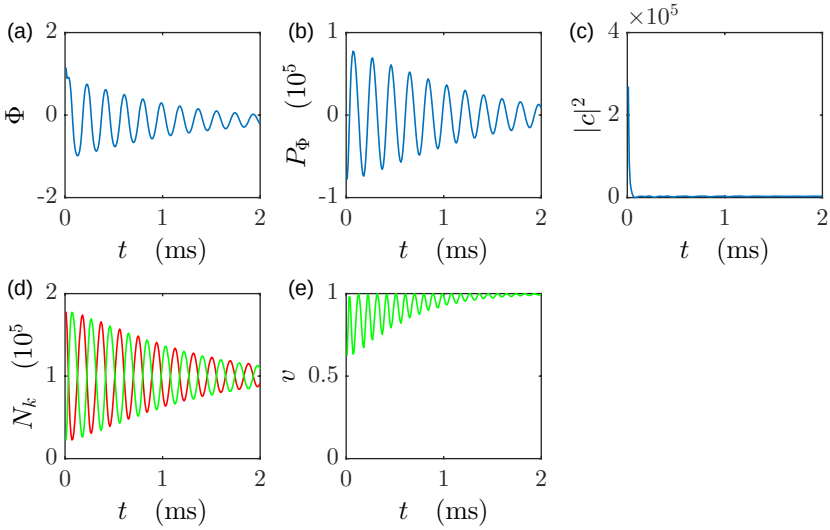

Figure 47.40: (code) Numerical simulation of the semiclassical two-mode model (47.172). Time-dependence of (a) the relative phase, (b) the particle number difference, (c) the light in the resonant cavity mode, and (d) the particle numbers in both modes. The parameters are $\Delta_{mw} = 0$, $\Omega_{mw} = 2\pi\times 5$ kHz, $\Delta_{lf} = -2\pi\times 20$ GHz, $\Omega_{lf} = 2\pi\times 6$ MHz, and $\Delta_{cv} = \Delta_{mw} - \kappa/2$. (e) Fringe visibility.

47.5.4.25 Arrays of coupled Josephson junctions

One-dimensional arrays of coupled Josephson junctions have been realized with standing wave dipole beams [240]. By combining this idea and the internal states JJs it may be possible to realize two-dimensional arrays of couples JJs. Is this useful for quantum computing?

Imagine a standing wave, where one or more antinodes are filled each one with two BEC species, i.e. BECs in different hyperfine levels. We couple the two levels with Raman beams. The question is now, whether the ring cavity damping mechanism allows to unite the BECs *within every well*. The idea of [663] of coupling via an auxiliary level is replaced by the ring cavity cooling mechanism?

47.5.5 Exercises

47.5.5.1 Ex: BEC damping in cavities

Programs on BEC damping in cavities.

Solution: *BecStandingWave1: periodic potential, steepest descent, then free expansion.*
BecStandingWave2: periodic potential, shifted after some time, shows Blochbands.
BecCavity0: Horak et al. PRA 61, 033609.
BecCavity1: steepest descent self-consistent with two stationary ring-cavity field modes.
BecCavity2: steepest descent self-consistent with two stationary ring-cavity field modes,

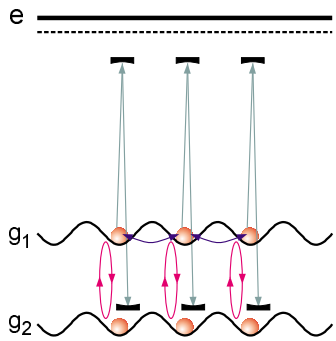

Figure 47.41: (a) Idea for a possible implementation of a $2D$ network of Josephson junctions.

correct norm, correct scaling.
BecCavity3: steepest descent followed by real-time propagation self-consistent with two stationary ring-cavity field modes.
BecCavity4: steepest descent propagation self-consistent with two time-dependent ring-cavity field modes.
BecCavity5: steepest descent self-consistent with two stationary ring-cavity field modes, correct norm, correct scaling to wavelength.
BecCavity5b: real-time self-consistent with two stationary ring-cavity field modes, correct norm, correct scaling to wavelength.

47.5.5.2 Ex: Second-quantized CARL equations

Calculate the commutators $[\hat{\psi}_j(\mathbf{r}), \mathcal{H}]$ and $[\hat{a}_\pm, \mathcal{H}]$, where $\mathcal{H}$ is the Hamiltonian (47.145) and $\hat{\psi}_1$ and $\hat{\psi}_2$ the ground and excited state wave functions, respectively.

Solution: *Using the commutation rules (47.143) we immediately find, ignoring collisions,*

$$
\begin{aligned}
[\hat{\psi}_1(\mathbf{r}), \mathcal{H}_{bec}] &= \left(\frac{-\nabla^2}{2m} + V_1(\mathbf{r}) \right) \hat{\psi}_1(\mathbf{r}) \\
[\hat{\psi}_2(\mathbf{r}), \mathcal{H}_{bec}] &= \left(\frac{-\nabla^2}{2m} + V_2(\mathbf{r}) - \Delta_a \right) \hat{\psi}_2(\mathbf{r}) \\
[\hat{\psi}_1(\mathbf{r}), \mathcal{H}_{atom-cav}] &= \sum_\pm g \hat{a}_\pm^\dagger \hat{\psi}_2(\mathbf{r}) e^{\mp \imath kz} \\
[\hat{\psi}_2(\mathbf{r}), \mathcal{H}_{atom-cav}] &= \sum_\pm g \hat{a}_\pm \hat{\psi}_1(\mathbf{r}) e^{\pm \imath kz} \\
[\hat{a}_\pm, \mathcal{H}_{atom-cav}] &= g \int d^3 r \hat{\psi}_2(\mathbf{r}) e^{\mp \imath kz} \hat{\psi}_1^\dagger(\mathbf{r}) \\
[\hat{a}_\pm, \mathcal{H}_{cav}] &= -\Delta_c \hat{a}_\pm \\
[\hat{a}_\pm, \mathcal{H}_{laser-cav}] &= \imath \eta_\pm \ .
\end{aligned}
$$

47.5.5.3 Ex: Second-quantized adiabatically approximated CARL Hamiltonian

a. Derive the adiabatically approximated CARL Hamiltonian in second quantization.
b. Derive the CARL equations of motion from the adiabatically approximated Hamiltonian in second quantization.
c. Show that the derived Hamiltonian simplifies to (42.26) in the single atom limit.

Solution: *a. With the results derived in Exc. 47.5.5.2 the Heisenberg equation of motion for the excited state field operator reads,*

$$\begin{aligned} 0 \stackrel{!}{=} \imath\frac{d\hat{\psi}_2(\mathbf{r})}{dt} &= [\hat{\psi}_2(\mathbf{r}), \mathcal{H}] \\ &= \left(\frac{-\nabla^2}{2m} + V_2(\mathbf{r}) - \Delta_a\right)\hat{\psi}_2(\mathbf{r}) + \sum_{\pm} g\hat{a}_{\pm}\hat{\psi}_1(\mathbf{r})e^{\pm\imath\mathbf{k}_{\pm}\cdot\mathbf{r}} \ . \end{aligned}$$

We neglect the kinetic and potential energy of the center-of-mass motion, which are small compared to Δ_a, and resolve for $\hat{\psi}_2$,

$$\hat{\psi}_2(\mathbf{r},\infty) = \frac{g}{\Delta_a}\left(\hat{a}_+\hat{\psi}e^{\imath kr} + \hat{a}_-\hat{\psi}e^{-\imath kr}\right) \ ,$$

where we simplified the notation by setting $\hat{\psi} \equiv \hat{\psi}_1$. We insert this result into the contributions to the Hamiltonian (47.145) containing $\hat{\psi}_2$,

$$\begin{aligned} \mathcal{H}_{atom} &= \int d^3r\hat{\psi}^\dagger(\mathbf{r}')\left(\frac{p^2}{2m} + V(\mathbf{r})\right)\hat{\psi}(\mathbf{r}') + \int d^3r\hat{\psi}_2^\dagger(\mathbf{r}')\left(\frac{p^2}{2m} + V(\mathbf{r}) - \Delta_a\right)\hat{\psi}_2(\mathbf{r}') \\ &\simeq H_{bec} + \frac{g^2}{\Delta_a^2}\int d^3r\left(\hat{a}_+^\dagger\hat{\psi}^\dagger e^{-\imath kr} + \hat{a}_-^\dagger\hat{\psi}^\dagger e^{\imath kr}\right)(-\Delta_a)\left(\hat{a}_+\hat{\psi}e^{\imath kr} + \hat{a}_-\hat{\psi}e^{-\imath kr}\right) \\ &= \mathcal{H}_{bec} - NU_0\left(\hat{a}_+^\dagger\hat{a}_+ + \hat{a}_-^\dagger\hat{a}_-\right) - U_0^\dagger\hat{a}_+\hat{a}_-\int d^3r\hat{\psi}^\dagger e^{-2\imath kr}\hat{\psi} - U_0\hat{a}_+\hat{a}_-^\dagger\int d^3r\hat{\psi}^\dagger e^{2\imath kr}\hat{\psi} \ , \end{aligned}$$

and

$$\begin{aligned} \mathcal{H}_{atom-cav} &= g\int d^3r\hat{\psi}_2^\dagger(\mathbf{r}')e^{\imath kr}\hat{\psi}(\mathbf{r}')a_+ + g\int d^3r\hat{\psi}_2^\dagger(\mathbf{r}')e^{-\imath kr}\hat{\psi}(\mathbf{r}')\hat{a}_- + h.c. \\ &= U_0\int d^3r\left(\hat{a}_+^{\dagger\hat{\psi}^\dagger}\hat{\psi} + \hat{a}_-^\dagger\hat{\psi}\dagger e^{2\imath kr}\hat{\psi}\right)\hat{a}_+ + U_0\int d^3r\left(\hat{a}_+^{\dagger\hat{\psi}^\dagger}e^{-2\imath kr}\hat{\psi} + \hat{a}_-^\dagger\hat{\psi}\dagger\hat{\psi}\right)\hat{a}_- + h.c. \\ &= NU_0\left(\hat{a}_+^\dagger\hat{a}_+ + \hat{a}_-^\dagger\hat{a}_-\right) + U_0\hat{a}_+^\dagger\hat{a}_-\int d^3r\hat{\psi}^\dagger e^{-2\imath kr}\hat{\psi} + U_0\hat{a}_+\hat{a}_-^\dagger\int d^3r\hat{\psi}^\dagger e^{2\imath kr}\hat{\psi} + h.c. \\ &= 2NU_0\left(\hat{a}_+^\dagger\hat{a}_+ + \hat{a}_-^\dagger\hat{a}_-\right) + 2U_0a_+^\dagger\hat{a}_-\int d^3r\hat{\psi}^\dagger e^{-2\imath kr}\hat{\psi} + 2U_0\hat{a}_+\hat{a}_-^\dagger\int d^3r\hat{\psi}^\dagger e^{2\imath kr}\hat{\psi} \ . \end{aligned}$$

Finally,

$$\begin{aligned}\mathcal{H} &= \mathcal{H}_{atom} + \mathcal{H}_{atom-cav} + H_{cav} + H_{laser-cav} \\ &\simeq H_{bec} + (\hat{N}U_0 - \Delta_c)\left(\hat{a}_+^\dagger \hat{a}_+ + \hat{a}_-^\dagger \hat{a}_-\right) \\ &\quad + U_0 \hat{a}_+^\dagger \hat{a}_- \int d^3r \hat{\psi}^\dagger e^{-2\imath kz}\hat{\psi} + U_0 \hat{a}_+ \hat{a}_-^\dagger \int d^3r \hat{\psi}^\dagger e^{2\imath kz}\hat{\psi} - \imath \sum_\pm \eta_\pm(\hat{a}_\pm - \hat{a}_\pm^\dagger) \ .\end{aligned}$$

This adiabatically approximated Hamiltonian looks very similar to (42.26).
b. The Heisenberg equations yield,

$$\begin{aligned}\imath \frac{d\hat{\psi}(\mathbf{r})}{dt} &= [\hat{\psi}(\mathbf{r}), \mathcal{H}] \\ &= \left(\frac{\hat{\mathbf{p}}^2}{2m} + V(\mathbf{r}) + u\hat{n}(\mathbf{r}) + U_0(\hat{a}_+^\dagger \hat{a}_+ + \hat{a}_-^\dagger \hat{a}_-) + \hat{a}_+\hat{a}_- e^{-2\imath kz} + \hat{a}_+\hat{a}_- e^{2\imath kz}\right)\hat{\psi}(\mathbf{r}) \ ,\end{aligned}$$

and

$$\imath \frac{d\hat{a}_\pm}{dt} = [\hat{a}_\pm, \mathcal{H}] = (NU_0 - \Delta_c)\hat{a}_\pm + U_0 \hat{a}_\mp \int \hat{\psi}^\dagger(\mathbf{r}) e^{\mp 2\imath kz}\hat{\psi}(\mathbf{r}) d^3r + \imath\eta_\pm \ ,$$

c. The single atom limit can be expressed by $\int d^3r \hat{\psi}^\dagger(\mathbf{r})\hat{\psi}(\mathbf{r}) = 1$.

47.5.5.4 Ex: BEC-CARL equations from the adiabatically approximated CARL Hamiltonian

Derive the BEC-CARL equations from the adiabatically approximated CARL Hamiltonian (47.148).

Solution: *The BEC-CARL equations are,*

$$\begin{aligned}\imath\hbar \frac{d\hat{\psi}(\mathbf{r})}{dt} &= [\hat{\psi}(\mathbf{r}), \mathcal{H}] \\ &= \left(\frac{-\hbar^2\nabla^2}{2m} + V_1(\mathbf{r}) + \imath\hbar U_0(\hat{a}_-^\dagger e^{-\imath\mathbf{k}\cdot\mathbf{r}} - \hat{a}_- e^{\imath\mathbf{k}\cdot\mathbf{r}}) + \hbar(\hat{a}_+^\dagger \hat{a}_+ + \hat{a}_-^\dagger \hat{a}_-)U_0\right)\hat{\psi}(\mathbf{r}) \\ \imath\hbar \frac{d\hat{a}}{dt} &= [\hat{a}, \mathcal{H}] \\ &= -\hbar\delta + \imath U_0 \int d^3r \hat{\psi}_1^\dagger(\mathbf{r}) e^{-\imath\mathbf{k}\cdot\mathbf{r}}\hat{\psi}_1(\mathbf{r}) \ ,\end{aligned}$$

where $U_0 \equiv g^2/\Delta_a$.

47.5.5.5 Ex: Origin of quantum correlations

The BEC-CARL Hamiltonian has been shown to generate quantum correlations between optical and matter wave modes [918, 1036]. Discuss whether they are a many-body effect (bosonic stimulation) or just due to coherences between motional states

of single atoms.

Solution: *CARL is not conditioned to bosonic stimulation and even works with fermions. ???*

47.5.5.6 Ex: Ultracold fusion

Derive from Eqs. (47.165) using the definitions (47.167) and (47.168) the Eqs. (47.168).

Solution: *Substituting the definitions (47.167) into (47.165) we find,*

$$\begin{aligned}
\sqrt{N_1}\varphi\imath\dot{\Phi}_1 e^{\imath\Phi_1} + \frac{\dot{N}_1}{2\sqrt{N_1}}\varphi e^{\imath\Phi_1} &= -\imath\left(\frac{-\nabla^2}{2m} + V + u_{11}N_1\varphi^2 + u_{12}N_2\varphi^2 + \hbar\Delta_{mw}\right)\sqrt{N_1}\varphi e^{\imath\Phi_1} \\
&\quad - \imath\left(\frac{\Omega_{mw}}{2} + g_{cv}a\right)\sqrt{N_2}\varphi e^{\imath\Phi_2} \qquad (47.232) \\
\sqrt{N_2}\varphi\imath\dot{\Phi}_2 e^{\imath\Phi_2} + \frac{\dot{N}_2}{2\sqrt{N_2}}\varphi e^{\imath\Phi_2} &= -\imath\left(\frac{-\nabla^2}{2m} + V + u_{22}N_2\varphi^2 + u_{12}N_1\varphi^2\right)\sqrt{N_2}\varphi e^{\imath\Phi_2} \\
&\quad - \imath\left(\frac{\Omega_{mw}}{2} + g_{cv}a^*\right)\sqrt{N_1}\varphi e^{\imath\Phi_1} \\
\dot{a} &= -\imath\int d^3r\; g_{cv}\sqrt{N_1N_2}\varphi^2 e^{\imath(\Phi_1-\Phi_2)} - (\imath\Delta_{cv} + \tfrac{\kappa}{2})a\;.
\end{aligned}$$

We may eliminate the normalized wavefunction φ by multiplication it with φ and integration $\int d^3r$. Exploiting the definition of the chemical potential, we get,

$$\begin{aligned}
N_1\imath\dot{\Phi}_1 + \tfrac{1}{2}\dot{N}_1 &= -\imath\left(\frac{\mu_1}{\hbar} + \Delta_{mw}\right)N_1 - \imath\left(\tfrac{1}{2}\Omega_{mw} + g_{cv}a\right)\sqrt{N_1N_2}e^{\imath(\Phi_2-\Phi_1)} \\
-N_2\imath\dot{\Phi}_2 + \tfrac{1}{2}\dot{N}_2 &= \imath\frac{\mu_2}{\hbar}N_2 + \imath\left(\tfrac{1}{2}\Omega_{mw} + g_{cv}a\right)\sqrt{N_1N_2}e^{-\imath(\Phi_1-\Phi_2)} \\
\dot{a} &= -\imath g_{cv}\sqrt{N_1N_2}e^{\imath(\Phi_1-\Phi_2)} - \left(\imath\Delta_{cv} + \tfrac{1}{2}\kappa\right)a\;. \qquad (47.233)
\end{aligned}$$

The real parts of the sum $\frac{1}{\imath N_1}$(47.233)(a)+$\frac{1}{\imath N_2}$(47.233)(b) and of the difference (47.233)(b)−(47.233)(a) yield introducing $\Phi \equiv \Phi_1 - \Phi_2$, $P_\Phi \equiv \frac{1}{2}(N_2 - N_1)$,

$$\begin{aligned}
\dot{\Phi} &= \frac{\mu_2 - \mu_1}{\hbar} - \Delta_{mw} - \frac{2P_\Phi}{\sqrt{N_1N_2}}\mathfrak{Re}\;\left(\tfrac{1}{2}\Omega_{mw} + g_{cv}c\right)e^{-\imath\Phi}\;, \qquad (47.234) \\
\dot{P}_\Phi &= -2\sqrt{N_1N_2}\mathfrak{Im}\;\left(\tfrac{1}{2}\Omega_{mw} + g_{cv}c\right)e^{-\imath\Phi} \\
\dot{c} &= -\imath g_{cv}\sqrt{N_1N_2}e^{\imath\Phi} - \left(\imath\Delta_{cv} + \tfrac{1}{2}\kappa\right)c\;.
\end{aligned}$$

47.6 Further reading

47.6.1 on Ramsey-Bordé interferometry

F. Riehle, *Optical Ramsey Spectroscopy in a Rotating Frame: Sagnac Effect in a Matter-Wave Interferometer* [1095]DOI

M. Kasevich et al., *Atomic Interferometry Using Stimulated Raman Transitions* [698]DOI

M. Kasevich, *Measurement of the Gravitational Acceleration of an Atom with a Light-Pulse Atom Interferometer* [699]DOI

47.6.2 on BEC-light interaction

H.D. Politzer, *Light incident on a Bose-condensed gas* [1043]DOI

A. Görlitz et al., *Enhancement and Suppression of Spontaneous Emission and Light Scattering by Quantum Degeneracy* [527]DOI

P.C. Bons et al., *Quantum Enhancement of the Index of Refraction in a Bose-Einstein Condensate* [177]DOI

O. Zobay et al., *Dynamics of matter-wave and optical fields in superradiant scattering from Bose-Einstein condensates* [1438]DOI

Y. Yoshikawa et al., *Observation of Superradiant Raman Scattering in a Bose-Einstein Condensate* [1412]DOI

Y. Yoshikawa et al., *Superradiant light scattering from thermal atomic vapors* [1413]DOI

M.M. Cola et al., *Theory of Collective Raman Scattering from a Bose-Einstein Condensate* [282]DOI

M.M. Cola et al., *Robust Generation of Entanglement in Bose-Einstein Condensates by Collective Atomic Recoil* [279]DOI

M.M. Cola et al., *A Condensate in a Lossy Cavity: Collective Atomic Recoil and Generation of Entanglement* [280]DOI

M.M. Cola et al., *Entanglement in a Bose-Einstein condensate by collective atomic recoil* [281]DOI

D.M. Stamper-Kurn et al., *Spinor Condensates and Light Scattering from Bose-Einstein Condensates* [1238]DOI

D. Schneble et al., *The Onset of Matter-Wave Amplification in a superradiant Bose-Einstein-Condensate* [1166]DOI

M.G. Moore et al., *Quantum optics of a Bose-Einstein condensate coupled to a quantized light field* [920]DOI

M.G. Moore et al., *Atomic Four-Wave Mixing Fermions versus Bosons* [919]DOI

M.G. Moore et al., *Optical control and entanglement of atomic Schroedinger fields* [918]DOI

W. Ketterle et al., *Does Matter Wave Amplification Work for Fermions* [713]DOI

N. Piovella et al., *Quantum fluctuations and entanglement in the collective atomic recoil laser using a Bose-condensate* [1036]DOI

D. Jaksch et al., *Uniting Bose-Einstein condensates in optical resonators* [663]DOI

S. Ritter et al., *Dynamical Coupling between a Bose-Einstein Condensate and a Cavity Optical Lattice* [**?**]DOI

D. Schneble et al., *Raman amplification of matter waves* [1165]DOI

G.A. Prataviera et al., *Trap environnement effects over quantum statistics and atom-photon correlations in the collective-atomic-recoil laser* [1050]DOI

S.A. Gardiner et al., *Cavity-assited quasiparticle damping in a Bose-Einstein Condensate* [490]DOI

P. Horak et al., *Coherent Dynamics of Bose-Einstein Condensates in High-finesse Optical Cavities* [632]DOI

P. Horak et al., *Dissipative Dynamics of Bose Condensates in Optical Cavities* [633]DOI

W. Ketterle et al., *Collective Enhancement and Suppression in Bose-Einstein Condensates* [709]DOI

W. Ketterle et al., *Does Matter Wave Amplification Work for Fermions?* [713]DOI

W. Ketterle, *Comment on 'Electromagnetic Wave Dynamics in Matter-Wave Superradiant Scattering'* [708]DOI

Chapter 48

Bosons and fermions in optical lattices and reduced dimensions

48.1 Condensation in reduced dimensions

In highly anisotropic trapping potentials the behavior of condensates can be dramatically altered by freezing inaccessible dimensions. We consider, for example, a condensate with the chemical potential μ trapped in the harmonic potential,

$$V_{trp} = \sum_{k=1,2,3} \tfrac{m}{2}\omega_k^2 x_k^2 \ . \tag{48.1}$$

If one of the secular frequencies exceeds the chemical potential, $\omega_k \gg \mu$, the corresponding degree of freedom is inaccessible to elementary excitations of the condensate and can be regarded as frozen. We discuss, in the following, the cases of condensates in one- and two-dimensional potentials.

48.1.1 Condensation in $1D$

We first consider the case $\omega_x, \omega_y \gg \omega_z$, such that the condensate is strongly compressed in the radial direction (x and y), such that the condensate takes the shape of a *cigar*. Then, deeply in the Thomas-Fermi regime, we can assume a *radially homogeneous* density distribution, that is, we can make ansatz,

$$\hat{\psi}(\mathbf{r}) \equiv C\hat{\phi}(z) \ , \tag{48.2}$$

where the constant is fixed by,

$$\int_{\mathbb{R}^3} |\hat{\psi}(\mathbf{r})|^2 d^3r = C^2 2\pi r_\perp^2 \int_{-\infty}^{\infty} |\phi(z)|^2 dz = 1 \ . \tag{48.3}$$

Requiring that the new one-dimensional wavefunction be normalized also, we conclude $C = (2\pi r_\perp^2)^{-1/2}$. Inserting the ansatz (48.2) into the stationary Gross-Pitaevskii equation we find immediately,

$$\boxed{\left(-\frac{\hbar^2}{2m}\frac{d}{dz} + V_{trp}(z) + N g_{1D}|\hat{\phi}(z)|^2\right)\hat{\phi}(z) = \mu\hat{\phi}(z)} \ , \tag{48.4}$$

where we introduced the abbreviation,

$$g_{1D} \equiv \frac{g}{(2r_h)^2} \ . \tag{48.5}$$

This GPE describes a condensate called *one-dimensional*.

Now applying the Thomas-Fermi approximation to a harmonic potential, we obtain,

$$|\hat{\phi}(z)|^2 = \frac{\mu - \frac{m}{2}\omega_z^2 z^2}{g_{2D}} \ . \tag{48.6}$$

with

$$\mu = \left(\tfrac{9}{32} g_{2D}^2 m \omega_z^2\right)^{1/3} \ . \tag{48.7}$$

48.1.2 Condensation in $2D$

Now, we consider the case $\omega_x, \omega_y \ll \omega_z$, such that the condensate is strongly compressed in the axial direction (x and y), such that the condensate takes the shape of a*panqueca*. Then, deeply in the Thomas-Fermi regime, we can assume a *axially homogeneous* density distribution, that is, we can make ansatz,

$$\hat{\psi}(\mathbf{r}) \equiv C\hat{\phi}(x,y) \ , \tag{48.8}$$

where the constant is fixed by,

$$\int_{\mathbb{R}^3} |\hat{\psi}(\mathbf{r})|^2 d^3r = C^2 2z_\perp \int_{\mathbb{R}^2} |\phi(x,y)|^2 dz = 1 \ . \tag{48.9}$$

Requiring that the new one-dimensional wavefunction be normalized also, we concludes $C = (2z_\perp)^{-1/2}$. Inserting the ansatz (48.2) into the stationary Gross-Pitaevskii equation we find immediately,

$$\boxed{\left(-\frac{\hbar^2}{2m}\frac{d}{dx} - \frac{\hbar^2}{2m}\frac{d}{dy} + V_{trp}(x,y) + N g_{2D}|\hat{\phi}(x,y)|^2\right)\hat{\phi}(x,y) = \mu\hat{\phi}(x,y)} \ , \tag{48.10}$$

where we introduced the abbreviation,

$$g_{2D} \equiv \frac{g}{2z_\perp} \ . \tag{48.11}$$

This GPE describes a condensate called *two-dimensional*.

Now applying the Thomas-Fermi approximation to a harmonic potential, we obtain,

$$|\phi(x,y)|^2 = \frac{\mu - \frac{m}{2}\omega_r^2 r^2}{g_{2D}} \ . \tag{48.12}$$

with

$$\mu = \left(\frac{g_{2D}}{\pi} m \omega_r^2\right)^{1/2} \ . \tag{48.13}$$

We show a slightly stricter derivation of the results (48.4) and (48.10) in the Exc. 48.1.4.1.

48.1.3 Interacting gas in a cylindrical potential

Within a cylindrical potential $V(\mathbf{r}) = V(\rho, z)$ the wavefunction will be rotationally symmetrical. With the replacement,

$$\psi(\rho, z, \varphi) \equiv \frac{\phi(\rho, z)}{\rho} \ , \tag{48.14}$$

the Gross-Pitaevskii equation can be written in cylindrical coordinates as follows [626],

$$i\hbar \frac{\partial \phi(\rho,z)}{\partial t} = -\frac{\hbar^2}{2m}\left[\frac{\partial^2}{\partial \rho^2} - \frac{1}{\rho}\frac{\partial}{\partial \rho} + \frac{1}{\rho^2} + \frac{\partial^2}{\partial z^2}\right]\phi(\rho,z) + V_{trap}(\rho,z)\phi(\rho,z) + g\frac{|\phi(\rho,z)|^2}{\rho^2}\phi(\rho,z) \ , \tag{48.15}$$

with the normalization,

$$\int |\psi(\mathbf{r})|^2 d^3r = 2\pi \int_{-\infty}^{\infty}\int_0^{\infty} |\psi(\mathbf{r})|^2 \rho d\rho dz = 2\pi \int_{-\infty}^{\infty}\int_0^{\infty} \frac{|\phi(\rho,z)|^2}{\rho} d\rho dz = 1 \ . \tag{48.16}$$

48.1.4 Exercises

48.1.4.1 Ex: Derivation of the Gross-Pitaevskii equation in reduced dimensions

In general, due to the nonlinear term in the Gross-Pitaevskii equation, the wavefunction can not be factorized. However, when the potential is extremely anisotropic, we note that the dimensions of the wavefunction decouple: in the case of a cigar-shaped condensate, the radial diameter does not depend on z and in the case of a pancake-shaped condensate, the axial thickness does not depend on ρ.
Use this argument to derive the 1D and 2D Gross-Pitaevskii equations for cylindrical harmonic potentials.

Solution: *The Gross-Pitaevskii equation is in spherical coordinates,*

$$\left[-\frac{\hbar^2}{2m}\left(\frac{1}{\rho}\frac{\partial}{\partial \rho}\left(\rho\frac{\partial}{\partial \rho}\right) + \frac{1}{\rho^2}\frac{\partial^2}{\partial \varphi^2} + \frac{\partial^2}{\partial z^2}\right) + V(\rho,z) + g|\hat{\psi}(\rho,z)|^2\right] = \mu\hat{\phi}(\rho,z) \ .$$

With the given argument, we can make a separation ansatz,

$$\hat{\psi}(\mathbf{r}) \equiv \hat{\phi}_\rho(\rho)\phi_z(z) \ .$$

With this ansatz the GPE is,

$$-\frac{\hbar^2}{2m}\frac{1}{\phi_\rho(\rho)}\frac{1}{\rho}\frac{\partial}{\partial \rho}\left(\rho\frac{\partial}{\partial \rho}\right)\phi_\rho(\rho) + \frac{m}{2}\omega_\rho^2\rho^2 - \frac{\hbar^2}{2m}\frac{1}{\phi_z(z)}\frac{\partial^2}{\partial z^2}\phi_z(z) + \frac{m}{2}\omega_z^2 z^2 + g|\phi_\rho(\rho)\phi_z(z)|^2 = \mu \ .$$

48.2 Tonks-Girardeau gas in $1D$ potentials

Preliminary investigations have been carried out on two-step condensation and reversible condensation [**?**]. Normal condensates in $3D$ have so strong interactions and are trapped in so weak traps that $\hbar\omega_{trap} \ll \mu$, which is equivalent to $a_{trap} \gg \xi$. One may however realize very anisotropic traps where the above conditions are not satisfied in some dimensions of space, for example in $1D$ one could think of $\hbar\omega_z \ll \mu \ll \hbar\omega_\perp$. For $n = 10^{14}$ cm^{-3} a typical values for the chemical potential is $\mu = gn = 2\pi\hbar\times 800$ Hz. Contrary to thermal gases which are always isotropic, the condensate freezes out of the strongly confining dimensions [971, 1022, 536, 527, 200], i.e. the radial motion is tightly confined to zero point oscillations.

One can define a $1D$ scattering length by,

$$a_{1D} = -\frac{d_\perp^2}{2a}\left(1 - C\frac{a}{d_\perp}\right) , \tag{48.17}$$

where $C = -\zeta(\frac{1}{2}) \simeq 1.4603...$ and $d_\perp = \sqrt{\hbar/m\omega_\perp}$,

$$g_{1D} = -\frac{2\hbar^2}{ma_{1D}} = \frac{g}{\pi d_\perp^2\,(1 - Ca/d_\perp)} , \tag{48.18}$$

where $g = 4\pi\hbar^2 a/m$. Introducing an effective scattering length $a_{eff} \equiv a(1-Ca/d_\perp)^{-1}$, we may write,

$$g_{1D} = \frac{4\hbar^2 a_{eff}}{md_\perp^2} . \tag{48.19}$$

Or alternatively defining a $1D$ density via $n_{1D} \equiv \pi d_\perp^2 n$, we may write,

$$n_{1D}g_{1D} = \frac{gn}{1 - Ca/d_\perp} . \tag{48.20}$$

Such system are interesting for studying new phenomena like the expected phase domains in *quasi-condensates*, the continuous cross-over of bosons to fermions in *Tonks-Girardeau gas* [1312, 997, 998, 720]. Furthermore, some topological excitations are predicted to be more stable in lower dimensions such as solitons ind $1D$ and vortices in $2D$.

Homogeneous BECs only exist in $3D$. In $1D$ there is no finite transition temperature. In trapped BECs however condensation can take place. For a $1D$ Bose gas the degree of correlation depends on the ratio between the repulsive energy of uncorrelated atoms, $E_{unc} = g_{1D}n_{1D}$, and the quantum kinetic energy needed to correlate atoms by localizing them with respect to each other within the mean interparticle distance $d = n_{1D}^{-1}$, i.e. $E_{cor} = \hbar^2/2md^2$:

$$\gamma \equiv \frac{E_{unc}}{4E_{cor}} = \frac{mg_{1D}}{2n_{1D}\hbar^2} . \tag{48.21}$$

Or using the above relations,

$$\gamma = \frac{2a_{eff}}{n_{1D}d_\perp^2} = \frac{2a_{eff}}{\pi n d_\perp^4} \tag{48.22}$$

according to the *Lieb-Liniger model*. When $\gamma \gg 1$ the correlations overwhelm; it is the Tonks-Girardeau regime or the regime of *impenetrable bosons* or *fermionization*. In the other limit, $\gamma \ll 1$, the mean-field regime, the GP equation is good.

For our lithium experiment, we have in the micro-trap for rubidium, $\omega_\perp = 2\pi \times 5$ kHz and $\omega_\parallel = 2\pi \times 10\,\text{Hz}$. Thus $a_\perp = 0.15a_B$ with $a = 3.4a_B$ and $a_{eff} \simeq 1.06a$ and $\gamma \simeq 0.07$ for $n = 10^{14}\,\text{cm}^{-3}$.

48.2.1 Kosterlitz-Thouless transition in $2D$ potentials

bosonization, *Luttinger liquid*

Homogeneous BECs only exist in $3D$. In $2D$ occurs a *Kosterlitz-Thouless transition* into a superfluid state. This proves that noncondensed superfluid exist. On the other hand, nonsuperfluid condensates also exist, e.g. the Bose glass.

48.2.2 Mott insulator, Bose-Hubbard model

For a condensate in a periodic lattice superposed to an external potential V_{trap} (taking account of possible intensity gradients of the lattice beams) the *Bose-Hubbard model* predicts the following Hamiltonian [982, 537],

$$H = -J\sum_{(i,j)} \hat{a}_i^\dagger \hat{a}_j + \sum_i \varepsilon_i \hat{n}_i + \tfrac{1}{2}U\sum_i \hat{n}_i(\hat{n}_i - 1)\ , \tag{48.23}$$

where $J \equiv \int d^3\mathbf{x}\, w^*(\mathbf{x}-\mathbf{x}_i)\left[-\frac{\hbar}{2m}\Delta + V_0(\mathbf{x})\right] w^*(\mathbf{x}-\mathbf{x}_i)$ and $U \equiv \frac{4\pi a_s\hbar^2}{m}\int d^3\mathbf{x}\,|w^*(\mathbf{x})|^4$ and $\varepsilon_i \equiv \frac{4\pi a_s\hbar^2}{m}\int d^3\mathbf{x}\, V_{trap}(\mathbf{x})|w(\mathbf{x}-\mathbf{x}_i)|^2 \approx V_{trap}(\mathbf{x})$ and $w(\mathbf{x}) = w(x)w(y)w(z)$ are single-particle Wannier functions. Let us assume for now a homogeneous condensate. In the limit of strong tunneling and weak interactions, $J \gg U$, the matterwave function resembles a *Bloch state*,

$$|\psi_{SF}\rangle \sim \left(\sum_{i=1}^M \hat{a}_i^\dagger\right)^N |0\rangle\ . \tag{48.24}$$

The on-site particle number variance is Poissonian, $\sigma_{SF} \sim \sqrt{N_i}$, i.e. the on-site wavefunction is (quasi-)coherent. The total wavefunction is delocalized over all sites of the lattice, the (sub-)BECs have a rigid phase relation and there is long-range phase coherence. In the invers case, the matterwave function is a product of independent *Fock states*,

$$|\psi_{MI}\rangle \sim \prod_{i=1}^M (\hat{a}_i^\dagger)^n |0\rangle\ . \tag{48.25}$$

The atoms are localized in individual sites and there is a perfect correlation of the particle number in each site, known as *spin-squeezed state*, i.e. the variance tends to zero, $\sigma_{MI} \to 0$. The Mott transition is characterized by $\sigma = \frac{1}{2}$. In a given site, the

atom number and the phase of the wavefunction cannot be known simultaneously: $\Delta N \Delta\phi < 1$. Therefore, the on-site wavefunction loose their relative coherence and capability to interfere. They cannot be described by a single global wavefunction and do not follow the Gross-Pitaevskii equation. However, this state is not equivalent to a completely randomized ensemble. Rather the *coherence is transferred from inter-site correlations to inner-site correlations* (keep in mind that a Fock state is a complicated superposition of Glauber states). This is somehow analogous to collaps and revival in the Jaynes-Cummings model.

The Mott transition between the superfluid and the *Mott insulator* phase is a *quantum phase transition*, since it is driven by quantum fluctuations rather than themal noise. Thus it is a direct result of Heisenberg's incertainty relation.

These features make optical lattices in the Mott insulating phase interesting for spectroscopy at the *Heisenberg limit* and quantum computing.

Momentum distribution in terms of Wannier functions,

$$n(\mathbf{k}) = |w(\mathbf{k})|^2 \sum_{i,j} e^{i\mathbf{k}(\mathbf{r}_i - \mathbf{r}_j)} \langle \hat{a}_i^\dagger \hat{a}_j \rangle \ . \tag{48.26}$$

Practical Aspects Normal MOT loaded $3D$ lattices have filling factors of $1/10$ per site. Sophisticated Raman-sideband cooling schemes are necessary (*evtl.* aided by collisional cooling of optically uncooled dimensions). Alternatively, one may fill $1D$ or $3D$ lattices from a BEC, which offers low temperatures and high densities, so large filling factors, but quantum generacy is not a requirement (what matters is that only the lowest band is populated).

We may go to $1D$ configurations. In order to get good signal contrast despite the small number of sites, large filling factors are necessary. Even though spin-squeezing is possible, the weak lateral confinement makes it hard to reach the Mott insulating regime. An improvement could be the use of $1D$ arrays of annular traps, because of the tighter lateral confinement. Alternatively, we may fill a $3D$ lattice with 1 to 3 atoms per site and some 150000 sites. Low atom numbers make it easier to resolve the Mott transition. Typical numbers are $\nu_{trap} \approx 50$ Hz, $\nu_{Gauss} \approx 60$ Hz, $\nu_{lattice} \approx 30$ kHz $\approx 22 E_{recoil}$.

For quantum gate application, spin squeezing is important since the entangling pulse area depends on the on-site interaction energy $\frac{4\pi a_s \hbar^2}{m} n$, but it is not necessary to have only a single atom per site. What is the deeper relationship of the Mott spin-squeezing and the entanglement achievable by quantum gates [661]?

Probing is simply done by free expansion and observation of the interference patterns as the image of the momentum space distribution. The periodic structure of the density distribution causes a periodic pattern in momentum space, and since in the superfluid phase the ....

For inhomogeneous systems, superfluid and Mott insulating phases with different (integral atom number) populations may coexist. The Mott insulating phase is characterized by a gap in the excitation spectrum (precisely the one that inhibits the atomic mobility). This may be probed by applying potential gradients designed to overcome the gap.

The Mott insulating phase is not equivalent to random dephasing in the sites. The latter one causes a broadening of the interference patterns. If all atoms at all sites had

the same phase (which is possible in a single realization, but highly unlikely, because such a state cannot be generated on purpose since this would violate the uncertainty principle) they could constructively interfere.

An important signature of is the *incompressibility of a Mott insulator*. This distinguishes it from a superfluid. Even more fundamental [502] is the fact that particle-hole pairs are localized. The $\mu - J/U$ phase diagram is most significant...

48.3 Bose- and Anderson glasses

The Mott insulator *gap* plays quite a similar role as the photonic band gap. The collectivity (or long-range correlation) resides in the fact that the band gap is global. The particularity of Anderson localization and Bose glasses is that the *gapless localization* [325, 1093].

In the presence of disorder the superfluid to Mott-insulator transition is supplemented by additional insulating phases called *Bose glass* and *Anderson glass* [782, 877, 325]. It may also allow the study of *Anderson localization*. Note that there are links with Raizen's dynamical localization of chaos and strong localization in photonic bandgaps.

48.3.1 Condensates in speckle potentials

To generate disordered potentials optical speckles can be imaged into the trapping region. Alternatively, one may consider using the fragmentation observed close to microtraps. In any case the disordered potential must satisfy some conditions to make localization interesting. In particular their should be global correlations. I.e. either the atoms are condensed and form a coherent matter-wave; for example, $\mu > \langle V_{spckl} \rangle$. Then interesting effects occur for when the healing length exceeds the characteristic length of the disorder, $\langle z_{spckl} \rangle < \xi$ [829, 270]. Or the atoms are localized, $\mu < \langle V_{spckl} \rangle$, but exhibit long-range number correlations [782, 877, 325]. Than interesting effects are expected when the tunneling rate is sufficiently strong.

Let us first discuss the first case. The disorder is characterized in terms of an average potential depth $\langle V_{spckl} \rangle = \left(2\Gamma^2/6\delta\right)(\sigma_I/I_S)$ and the correlation length is of course diffraction limited $\langle z_{spckl} \rangle = 1.22\lambda l/D$, as compared to the chemical potential $\mu = (\hbar\omega_{trp}/2)\left(15N_0 a/a_{trp}\right)^{2/5}$ and the healing length, $\xi = (8\pi na)^{-1/2} = \hbar/\sqrt{2m\mu}$, respectively. In the experiment [270] a magnetically trapped BEC with $\mu = 5$ kHz and $\xi = 0.11$ μm is suddenly released into a $\langle V_{spckl} \rangle = 0..0.7\mu$ deep speckle. As the BEC expands it reduces its μ until the atoms get localized as soon as $\mu < \langle V_{spckl} \rangle$. Since the speckle is too coarse, $\langle z_{spckl} \rangle = 50\xi$, tunneling is not possible; this localization is thus not Anderson localization. The situation may be more interesting when the kinetic energy dominates the chemical potential.

A BEC in a pure deep speckle potential is not Bose glass: A Bose glass is not just *several uncorrelated BECs*, but rather *several uncorrelated BECs despite the presence of tunneling*, or *despite a large healing length*, where the tunnelling is compromised by interference, which because of disorder is destructive. The process must be reversible, since $T = 0$. Just like Mott insulator.

48.3.2 Bose glasses in mixtures of species

A possible realization implies double species: One species is trapped in a $3D$ optical lattice, the other one is weakly trapped in a magnetic potential. For example, we could load a cold ^{6}Li gas in a lattice and study transport phenomena and localization in a ^{87}Rb Bose gas, i.e. Bose glasses. Or the transport of a ^{6}Li Fermi gas in a ^{87}Rb lattice in analogy to solids [985].

In the case of Bose glass studies, to minimize the impact on ^{87}Rb, the lattice beams should be tuned close and red to the ^{6}Li line and be weak. The lattice will be blue-detuned for ^{87}Rb, so that they will be kept away from the ^{6}Li, if the potential modulation is too deep. This is not desired, especially because the interspecies scattering length is small. The scheme will not work when the ^{87}Rb chemical potential is lower than the trap depth. It might then be necessary to use a Feshbach resonance.

Concretely, we start cooling ^{6}Li and ^{87}Rb to a few μK. Then we load ^{6}Li into a $2D$ or $3D$ lattice produced at 680 nm. Estimate beam waists, powers, potential depths. Think about acustic noise. Calculate interspecies collision rates (time scale of the experiment), find signatures (interference with a reference BEC, inhibited transport....).

Using the quadrupolar magnetic fields it might be possible to address individual lattice sites [24], which is useful to create disorder.

The following experiments will provide signatures:

1. Let the ^{87}Rb BEC exposed to the ^{6}Li lattice interfere with a non exposed BEC [829, 270, 1093, 985].

2. Measure suppression of transport: Inhibited expansion (switch off magnetic trap for Rb), or inhibited displacement (shift the trap sideways).

Some ideas:

1. Load ^{6}Li into a 3D optical lattice, make it a band insulator or not, compare the behavior of the ^{87}Rb BEC for both cases.

48.3.3 Disorder in Mott-insulators

A more straightforward approach may thus be to directly localize the atoms, but nevertheless ensure global correlations. To sort out the various superfluid-insulator transitions, let us imagine a double potential $V = V_{lttc} + V_{spckl}$. The generalized Bose-Hubbard Hamiltonian reads,

$$H = -\sum_{(i,j)} \left(J_0^{lttc} + \delta J_{ij}^{spckl} \right) \hat{a}_i^\dagger \hat{a}_j + \tfrac{1}{2} U_0 \sum_i \hat{n}_i(\hat{n}_i - 1) + \sum_i \varepsilon_i \hat{n}_i \ , \qquad (48.27)$$

with $\varepsilon_i \equiv \frac{4\pi a_s \hbar^2}{m} \int d^3\mathbf{x}\ V_{spckl}(\mathbf{x}) |w(\mathbf{x} - \mathbf{x}_i)|^2$ and $\left\langle \delta J_{ij}^{spckl} \right\rangle = 0$ can be neglected. The dynamics is governed by the interplay between hopping (tunneling), J, interactions, U, and disorder, ε. Let us call CF the condensed fraction and SF the superfluid fraction. The onset of a small perturbation of the lattice potential may induce a dynamical quantum phase transition from a superfluid to a Bose or Anderson glass. This is studied [325] by preparing an ordinary superfluid BEC, transfering it into a regular optical lattice such as to drive it to the Mott phase, where in principle, $CF = SF \to 0$. However, chosing small (or non-integer) filling factors, $\Upsilon < 1$, there will be a fraction of atoms hopping around. Let's call this a pseudo-Mott insulator (Note that this prohibits the use of strong confining potentials, which support

the formation of various Mott insulator domains filled by different, but everywhere integer numbers of atoms.) This mobility corresponds to a delocalization and thus a superfluid fraction, $1 > CF = SF > 0$. This is the ideal situation to study the impact of additional disorder. With disorder both, the condensed and the superfluid fraction are dramatically reduced, however while SF tends to zero, CF stays finite, $0 \neq CF > SF \to 0$. This is what is interesting: Localization despite phase-coherence. In such Bose glasses interactions and disorder both work to localize.

	Mott insulator	pseudo Mott insulator	Bose glass
Hamiltonian	Bose-Hubbard		generalized Bose-Hubba
filling factor	$\Upsilon = 1, 2, ..$	$\Upsilon < 1$, (non-integer)	Υ
regime	$U_0 \gg J_0 > J_{ij}^{spckl}, V_{spckl} \to 0$		$U_0 \gg J_0 > J_{ij}^{spckl}, V_{spckl}$
behavior for $V_{lttc} \to \infty$	$CF = SF \to 0$	$1 > CF = SF > 0$	$0 \neq CF > SF \to 0$
potential	V_{lttc}, U_0		U_0 with V_{spckl}
excitation spectrum	gap		no gap
analogy	Fock states		

Two basic concepts must be distinguished: 1. Bose-condensation is understood as phase-coherence, i.e. the capability of matter wave interference. Condensates have a broken gauge symmetry, and thus a global phase. 2. Superfluidity is understood as mobility, i.e. delocalization. All localizing effects reduce the superfluid fraction. The two concepts are *not equivalent*. This is seen in the fact that there are non-condensed superfluids in reduced dimensions, and non-superfluid condensates. A Bose glass is such a non-superfluid condensate; it has a gapless excitation spectrum. A Mott-insulator is neither a condensate nor a superfluid; it has a gap in the excitation spectrum.

48.4 Fermi gases in optical lattices and reduced dimensions

48.4.1 Band insulator, Fermi-Hubbard model

The Pauli principle gives rise to an energy gap in a Fermi gas and makes it a *band insulator* [735], *antiferromagnetic phases*.

48.4.1.1 Fermi gas in an optical lattice

Transfer a pure Fermi gas in an optical lattice [624].

48.4.2 Fermionic superfluidity in polarized samples

In solids, mixtures of spin states tend to adjust their respective chemical potentials, e.g. at pn-junction or for Pauli paramagnetism [see Sec. 16.1.6]. In contrast, in polarized gases where the collisions are elastic, no spin-flips occur and a chemical potential imbalance can survive. Such polarized fermionic samples exhibit interesting superfluid effects such as phase separation [1441, 1000]. This is not possible in superconductors because of the Meissner effect for charged particles.

Experimentally one creates an unbalanced mixture of ^{6}Li $|1/2, \pm 1/2\rangle$ states. Above a critical polarization $P \propto (P_+ - P_-)(P_+ + P_-)$, the excess cloud forms a polarized shell around an unpolarized core of paired atoms. This occurs as a quantum phase transition between a homogeneous superfluid and a phase-separated superfluid-normal state.

The scattering length is (besides the polarization) a second important control parameter and can be varied via a Feshbach resonance. On the BEC side of the resonance (tight binding regime), $k_F a \gg 1$, the superfluid phase may coexist with the polarized normal phase. On the BCS side (highly correlated multiparticle system beyond mean-field) a Fermi sea is needed to stabilize the superfluid. There is a strong repulsion between atoms and molecules leading to a phase separation. The pairing gap Δ prevents unpaired atoms from entering the superfluid. However, even further on the BCS side, $\Delta < |\mu_2 - \mu_1|$ the gap reduces

Unpaired atoms can perturb and disrupt the BCS state, once $\Delta < |\mu_2 - \mu_1|$.

48.4.3 Luttinger liquids in $1D$ optical lattices

Strong correlated systems, may exhibit their atomic quantum optics features beyond mean-field physics better in reduced dimensions. The Kondo effect is in close relationship to a *Luttinger liquid* and the *Anderson model*.

A Luttinger liquid is a paramagnetic one-dimensional metal without Landau quasiparticle excitations [1341]. All physical properties can be calculated, e.g. by *bosonization*. The elementary excitations are collective charge and spin modes, leading to *charge-spin separation*. Although charge-spin separation has been observed in semiconductors [740], some particularities have been elusive in solid state systems. Luttinger liquids have been realized in ultracold gases [924, 1064]. This dilute system might be suitable to probe above particularities.

$1D$ BEC $\longrightarrow$ Luttinger liquid $\longrightarrow$ Lieb-Liniger, $V = 0$, or Mathieu, $g = 0$, or Tonks-Girardeau, $g = \infty$ [1077]. Repulsive interactions between the spin states of a two-component Fermi gas are treated by [1400, 1397]. For attractive interactions one obtains a *Luther-Emery liquid* characterized by atomic density waves through spin pairing [1399]. The complete phase diagram for a Fermi gas in a $1D$ optical lattice contains metallic, Mott insulating and band insulating phases [687, 1096, 688]. Disorder influences phase transitions [1398].

48.4.3.1 Bose metals

Superconductivity obtains when all Cooper pairs lock into a single quantum state. There are two cases: 1. The radius of gyration of the Cooper pairs is smaller than the interpair spacing. The pairs are then bosons, whose condensation is possible. The resulting phase coherence thwarts localization. Superconductivity can be thought of as BEC. 2. The Cooper pair radius is larger than the interpair spacing. The mapping of Cooper pairs and bosons then breaks down, nonetheless phase coherence exists.

A *metal* is characterized by mobile non-paired fermions. Theory predicts, [1029, 1172], that when fermions pair to bosons they loose their mobility, except if they condense and form a superfluid. The *Bose metal* remains elusive.

48.4.4 Kondo physics

The *Kondo effect* is known from solid state physics. It may also be investigated in optical gratings [1076, 997]. Take two $1D$ BECs, one is a quantum liquid, the other is in an optical lattice. Assume $a_s \ll a_{ho} = \sqrt{\hbar/m\omega}$. Then $g_{\beta\beta'} = 2\pi a_{\beta\beta'}/a_{ho}$. The grating trapped atoms are then immersed in a magnetically trapped Bose-liquid. Just like quantum dots immersed in a superconducting current of electrons.

48.4.5 Born-Oppenheimer systems

Keywords: ultracold *Born-Oppenheimer gas*, *gaseous solid*.

Idea: Mulding of a solid state consistent of bosons or fermions. Their quantum nature does not matter, because the distance is large and the interatomic interaction is strong. The crystal atoms are trapped in an optical lattice, evtl. a Mott insulator phase to control the lattice populations.

Let a gaseous atomic Fermi gas flow around the atoms. This should hold the atoms trapped together. Even if the optical lattice is turned down. There should form a self-determined self-consistent lattice structure.

To make the problem treatable, one must be able to make the Born-Oppenheimer approximation: $m_e \ll m_{latt}$. LiRb could be a good toy model for metals $m_{Li} \ll m_{Rb}$.

Which type of crystals will form? With an optical we may easily form not fcc, but bcc or sc cubes [Ashcroft and Mermin, "Solid states physics", p. 67] [1021, 798].

48.4.5.1 List of programs on thermalization of atomic clouds

- AtomicClouds1: Density in a harmonic potential.
- AtomicClouds2: Density in a quadrupole trap.
- AtomicClouds3: Sum and product density of two clouds in a quadrupole trap.
- AtomicClouds4: Thermalization of two clouds in a quadrupole trap.
- AtomicClouds5: Thermalization of two clouds in a quadrupole trap, collision rate depends on overlap.
- AtomicClouds6: Thermalization of two clouds in a the real LiRb Ioffe trap.

48.5 Further reading

G.A. Prataviera et al., *Trap environnement effects over quantum statistics and atom-photon correlations in the collective-atomic-recoil laser* [1050]DOI

Chapter 49

Multicomponent BECs, mixed species and fermionic superfluids

49.1 Mixtures of boson condensates

49.1.1 Two-mode model

A quantum field can be composed of several distinguishable species, that is, species with different internal states, for example, hyperfine or Zeeman substates [939, 1261, 214, 858, 574, 573, 891, 1239, 775]. These states may be coupled by different means, for example, lasers in Raman configuration, microwaves, Feshbach resonances, Josephson tunneling, etc.. The Rabi frequency λ describes such coupling:

$$\imath\hbar\frac{\partial}{\partial t}\vec{\Psi}(\mathbf{r},t) = \hat{H}_\delta\vec{\Psi}(\mathbf{r},t) \qquad \text{with} \qquad \vec{\Psi} \equiv \begin{pmatrix}\psi_a\\ \psi_b\end{pmatrix}, \tag{49.1}$$

with the Hamiltonian,

$$\hat{H} = \frac{-\hbar^2\Delta}{2m} + V_{trap}(\mathbf{r}) + Ng\left[|\psi_a(\mathbf{r},t)|^2 + |\psi_b(\mathbf{r},t)|^2\right] \tag{49.2}$$

$$\text{where} \qquad \hat{H}_\delta = \begin{pmatrix}H & \lambda/2\\ \lambda/2 & H-\delta\end{pmatrix}.$$

Individual BECs or mixtures of uncoupled BECS called *spinors* exhibit U(1) symmetry (infinite cylinder). The components may interpenetrate, overlap and tunnel through each other. In contrast, BECs with many coupled species exhibit SU(2) (sphere) symmetry. This is important for creating vortices, since it is necessary to first implement a SU(2) symmetry.

49.1.2 Spinores

To observe *ferromagnetism*: prepare a $m_F = -1, 0$ BEC using B-field gradients and observe how they change positions.

At long distance the total spins of the two atoms couple as $(f_1 f_2)f$. The interaction potential, therefore, is

$$V(\mathbf{r}_1-\mathbf{r}_2)=\delta(\mathbf{r}_1-\mathbf{r}_2)\sum_{f=0,f\ \text{even}}^{f_1+f_2} g_f\hat{P}_f \tag{49.3}$$

$$\mathbf{f}_1\mathbf{f}_2=\sum_{f=0,f\ \text{even}}^{f_1+f_2}\frac{1}{2}\left[f(f+1)-f_1(f_1+1)-f_2(f_2+1)\right]\hat{P}_f\ ,$$

with $g_f=4\pi\hbar^2 a_f/m$ e $\sum_{f\ \text{even}}\hat{P}_f=1$ and $\hat{P}_f=|f\rangle\langle f|$.

With the Zeeman states [775]

$$V(\mathbf{r}_1-\mathbf{r}_2)=\delta(\mathbf{r}_1-\mathbf{r}_2)\sum_{f=0,f\text{even}}^{f_1+f_2} g_f\sum_{m_f=-f}^{f}\hat{P}_{f,m_f}\ . \tag{49.4}$$

49.1.2.1 $f=1$-states

For $f_j=1$

$$1=\hat{P}_0+\hat{P}_2 \tag{49.5}$$
$$\mathbf{f}_1\mathbf{f}_2=-2\hat{P}_0+\hat{P}_2\ .$$

we can express,

$$V(\mathbf{r}_1-\mathbf{r}_2)=\delta(\mathbf{r}_1-\mathbf{r}_2)\left(g_0\hat{P}_0+g_2\hat{P}_2\right) \tag{49.6}$$
$$=\frac{4\pi\hbar^2}{m}\delta(\mathbf{r}_1-\mathbf{r}_2)\left[\bar{a}+\mathbf{f}_1\mathbf{f}_2\Delta a\right]\ .$$

defining $\bar{a}=\frac{1}{3}(2a_2+a_0)$ and $\Delta a=\frac{1}{3}(a_2-a_0)$. Therefore, the many-body Hamiltonian is,

$$H=\int d^3\mathbf{r}\,()\ . \tag{49.7}$$

Elastic and inelastic scattering [1238]

$$\begin{aligned}
g_{|1,\pm 1t\rangle+|1,\pm 1\rangle}&=g_2 \quad , \quad a_{|1,\pm1\rangle+|1,\pm1\rangle}=\bar{a}+\Delta a \\
g_{|1,0\rangle+|1,0\rangle}&=\tfrac{1}{3}(2g_2+g_0) \quad , \quad a_{|1,0\rangle+|1,0\rangle}=\bar{a} \\
g_{|1,\pm1\rangle+|1,\mp1\rangle}&=\tfrac{1}{6}(g_2+2g_0) \quad , \quad a_{|1,\pm1\rangle+|1,\mp1\rangle}=\bar{a}-\Delta a \\
g_{|1,\pm1\rangle+|1,0\rangle}&=\tfrac{1}{2}g_2 \quad , \quad a_{|1,\pm1\rangle+|1,0\rangle}=\bar{a}+\Delta a \\
g_{|1,+1\rangle|1,-1\rangle\leftrightarrow|1,0\rangle|1,0\rangle}&=\tfrac{1}{3}(g_2-g_0) \quad , \quad a_{|1,+1\rangle|1,-1\rangle\leftrightarrow|1,0\rangle|1,0\rangle}=\Delta a\ .
\end{aligned} \tag{49.8}$$

49.1.2.2 $f=2$-states

Para $f_j=2$

$$1=\hat{P}_0+\hat{P}_2+\hat{P}_4 \tag{49.9}$$
$$\mathbf{f}_1\mathbf{f}_2=-6\hat{P}_0-3\hat{P}_2+4\hat{P}_4$$
$$(\mathbf{f}_1\mathbf{f}_2)^2=36\hat{P}_0+9\hat{P}_2+16\hat{P}_4\ .$$

$$\hat{P}_0 = -\frac{2}{15} - \frac{1}{90}\mathbf{f}_1\mathbf{f}_2 + \frac{1}{90}(\mathbf{f}_1\mathbf{f}_2)^2 \tag{49.10}$$
$$\hat{P}_2 = -\frac{8}{21} - \frac{8}{63}\mathbf{f}_1\mathbf{f}_2 - \frac{1}{63}(\mathbf{f}_1\mathbf{f}_2)^2$$
$$\hat{P}_4 = \frac{53}{35} + \frac{29}{210}\mathbf{f}_1\mathbf{f}_2 + \frac{1}{210}(\mathbf{f}_1\mathbf{f}_2)^2 \ .$$

we can express,

$$V(\mathbf{r}_1 - \mathbf{r}_2) = \delta(\mathbf{r}_1 - \mathbf{r}_2)\left(g_0\hat{P}_0 + g_2\hat{P}_2 + g_4\hat{P}_4\right) \tag{49.11}$$
$$= \frac{4\pi\hbar^2}{m}\delta(\mathbf{r}_1 - \mathbf{r}_2)\left[\left(-\frac{2}{15}a_0 - \frac{8}{21}a_2 + \frac{53}{35}a_4\right) + ..\right] \ .$$

49.2 Fermion-boson mixtures

Two-Species Mixture of Quantum Degenerate Bose and Fermi Gases [568]
Degenerate Atom-Molecule Mixture in a Cold Fermi Gas [736]
Mixture of ultracold lithium and cesium atoms in an optical dipole trap [928]
Quasi-pure Bose-Einstein Condensate Immersed in a Fermi Sea [1168]

49.2.1 Sympathetic cooling

According to [935] the reduction factor due to the mass difference of the collision partners is,

$$\xi = \frac{4m_1m_2}{(m_1+m_2)^2} \ . \tag{49.12}$$

About $3/\xi$ collisions per atom are needed for complete thermalization of a gas. For the *Rb-Li* combination this gives $3/\xi = 12.4$. The collision rate,

$$\Gamma_{coll} = \sigma_{12}\bar{v}\int n_1(\mathbf{r})n_2(\mathbf{r})d^3\mathbf{r} \ , \tag{49.13}$$

where the mean thermal relative velocity is,

$$\bar{v} = \sqrt{\frac{8k_B}{\pi}\left(\frac{T_1}{m_1} + \frac{T_2}{m_2}\right)} \ . \tag{49.14}$$

The instantaneous temperature is calculated via,

$$\gamma_{therm} = -\frac{1}{\Delta T}\frac{d\Delta T}{dt} \ , \tag{49.15}$$

or for simulations: $\Delta T(t+dt) = \Delta T(t) - \Delta T(t)\gamma_{therm}dt$. According to [346] the rethermalization rate is connected to the collision rate via,

$$\gamma_{therm} = \frac{\xi}{3}\left(\frac{\Delta E_{1\to2}}{N_1k_B\Delta T} + \frac{\Delta E_{2\to1}}{N_2k_B\Delta T}\right) = \frac{\xi}{3}\left(\frac{\Gamma_{coll}}{N_1} + \frac{\Gamma_{coll}}{N_2}\right) \ . \tag{49.16}$$

For an isotropic harmonic trap we can derive analytic solutions. With the potentials $V_j(r) = \frac{1}{2}m_j\omega_{rj}^2r^2 + \frac{1}{2}m_j\omega_{zj}^2r^2 = k_BT_j\ \left(r^2/2\bar{r}_j^2 + z^2/2\bar{z}_j^2\right)$ the densities read

$n_j(r) = n_{0j} e^{-r^2/2\bar{r}_j^2 - z^2/2\bar{z}_j^2}$, and the integral becomes [927],

$$\begin{aligned}\Gamma_{coll} &= \sigma_{12}\bar{v} n_{01} n_{02} \int e^{-r^2/2\bar{r}_1^2 - z^2/2\bar{z}_1^2 - r^2/2\bar{r}_2^2 - z^2/2\bar{z}_2^2}\, d^3r \\ &= \frac{\sigma_{12}\bar{v} n_{01} n_{02} (2\pi)^{3/2}}{\sqrt{(\bar{x}_1^{-2} + \bar{x}_2^{-2})(\bar{y}_1^{-2} + \bar{y}_2^{-2})(\bar{z}_1^{-2} + \bar{z}_2^{-2})}} \\ &= \frac{\sigma_{12}\bar{v} N_1 N_2}{(2\pi)^{3/2}\sqrt{(\bar{x}_1^2 + \bar{x}_2^2)(\bar{y}_1^2 + \bar{y}_2^2)\,(\bar{z}_1^2 + \bar{z}_2^2)}}\ ,\end{aligned} \tag{49.17}$$

setting $N = n_0(2\pi)^{3/2}\bar{x}\bar{y}\bar{z}$. Defining $m_2\omega_2^2 = \beta^2 m_1\omega_1^2$,

$$\Gamma_{coll} = \frac{(m_1\omega_1^2)^{3/2}\sigma_{12}\bar{v} N_1 N_2}{(2\pi k_B)^{3/2}(T_1 + T_2\beta^{-2})^{3/2}}\ . \tag{49.18}$$

Again according to [346] the rethermalization rate becomes,

$$\gamma_{therm} = \frac{\xi(N_1 + N_2)(m_1\omega_1^2)^{3/2}\sigma_{12}\sqrt{T_1/m_1 + T_2/m_2}}{3\pi^2 k_B (T_1 + T_2\beta^{-2})^{3/2}}\ . \tag{49.19}$$

For an anisotropic trap take $\omega_1 = \sqrt{\omega_{1x}\omega_{1y}\omega_{1z}}$ the geometric mean of the trap frequencies. Then the scattering length follows from,

$$|a_{12}| = \sqrt{\sigma_{12}/4\pi}\ . \tag{49.20}$$

49.2.1.1 Damped oscillations with two species

Damping is decribed by two coupled differential equations [439],

$$\begin{aligned}\ddot{z}_1 &= -\omega_1^2 z_1 - \frac{4}{3}\frac{m_2}{m}\frac{N_2}{N}\gamma_{therm}(\dot{z}_1 - \dot{z}_2) \\ \ddot{z}_2 &= -\omega_2^2 z_2 - \frac{4}{3}\frac{m_1}{m}\frac{N_1}{N}\gamma_{therm}(\dot{z}_2 - \dot{z}_1)\end{aligned} \tag{49.21}$$

or in matrix form,

$$\begin{pmatrix}\dot{y}_1 \\ \dot{z}_1 \\ \dot{y}_2 \\ \dot{z}_2\end{pmatrix} = \begin{pmatrix}-\frac{4}{3}\frac{m_2}{m}\frac{N_2}{N}\Gamma & -\omega_1^2 & \frac{4}{3}\frac{m_2}{m}\frac{N_2}{N}\Gamma & 0 \\ 1 & 0 & 0 & 0 \\ \frac{4}{3}\frac{m_1}{m}\frac{N_1}{N} & 0 & -\frac{4}{3}\frac{m_1}{m}\frac{N_1}{N}\Gamma & -\omega_2^2 \\ 0 & 0 & 1 & 0\end{pmatrix}\begin{pmatrix}y_1 \\ z_1 \\ y_2 \\ z_2\end{pmatrix}\ , \tag{49.22}$$

where $\gamma_{therm} = n_{12}\sigma_{12}v$ with $n_{12} = \left(\frac{1}{N_1} + \frac{1}{N_2}\right)\int n_1 n_2 d^3\mathbf{r}$. Thus,

$$\gamma_{therm} = \left(\frac{1}{N_1} + \frac{1}{N_2}\right)\Gamma_{coll}\ . \tag{49.23}$$

49.2.1.2 Gravitational sag

The potential force for a species is $|\mu|/\mu_B = g_F m_F$. For ${}^{87}Rb,{}^2S_{1/2}, |2,2\rangle$ we get 1, for $|1,-1\rangle$ we get $\frac{1}{2}$, for ${}^6Li,{}^2S_{1/2}, |\frac{3}{2},\frac{3}{2}\rangle$ we get 1, and for $|\frac{1}{2},-\frac{1}{2}\rangle$ we get $\frac{1}{3}$. The *gravitational sag* for a harmonic trap is,

$$\Delta y = g/\omega_y^2\ . \tag{49.24}$$

49.2.1.3 Heating

Trap loss rate,

$$\dot{N} = L - \gamma N - \beta \int n^2 d^3r - \beta_3 \int n^3 d^3r \ . \tag{49.25}$$

49.2.2 Cooling strategies

The Fermi exclusion principle introduces a cooling barrier at low temperatures between identical fermions. One strategies that circumvents the problem is the use of fermionic spin mixtures [347] such as ^{6}Li-^{7}Li or ^{40}K-^{41}K. Cooling of fermions in different HFS levels is limited to ~1 μK: If all states in the Fermi see are populated there are no more unoccupied states necessary for rethermalizing collisions!

49.2.2.1 Sympathetic cooling

Another method for cooling fermions is *sympathetic cooling* with an actively cooled bosonic cloud. Important issues are the optimum evaporation path, loss processes, ...

The *Fermi temperature* scales like the critical temperature, $T_c \propto T_F$, with,

$$T_F = \frac{\hbar\tilde{\omega}}{k_B}(6N_F)^{1/3} \qquad \text{and} \qquad T_c = \frac{\hbar\bar{\omega}}{k_B}\left(\frac{N_B}{g_3(1)}\right)^{1/3} \ , \tag{49.26}$$

where $g_3(1) = 1.202$. The secular frequencies for Li and Rb scale like $\tilde{\omega} = \bar{\omega}\sqrt{87/6}$ where $\bar{\omega} = (\omega_x\omega_y\omega_z)^{1/3}$. This means that the temperatures can only be tuned by controlling the relative atom numbers.

49.2.2.2 Degrading heat capacity

To reach the Fermi regime with sympathetic cooling several conditions must be satisfied: 1. The spatial overlap must be good. Large mass ratios lead to different cloud sizes and different gravitational sagging. 2. The interspecies collision rate must be high. 3. The Bose cloud should not be condensed, $T_F \gg T_c$. 4. The Bose cloud should have a much higher heat capacity than the Fermi cloud, $C_{87} \gg 0.1C_6$ [202].

In a magnetic trap the secular frequencies $\tilde{\omega}$ and $\bar{\omega}$ have a fixed ratio so that condition 3. implies,

$$\frac{T_F}{T_c} = \sqrt{87/6}\left(6g_3(1)\frac{N_6}{N_{87}}\right)^{1/3} \gg 1 \ , \tag{49.27}$$

or $400N_6 \gg N_{87}$. In contrast in optical traps the secular frequencies depend on the detuning from atomic resonances, and may be tuned.

How to achieve very low temperatures via sympathetic cooling [977], [1052], [202], [295]?

49.2.2.3 Losses

To quantitatively study the impact of $|2,1\rangle$ atoms on the Li cloud lifetime, we write,

$$\dot{n}_6 = -G_{inel} n_6 n_{87,|2,1\rangle} \tag{49.28}$$

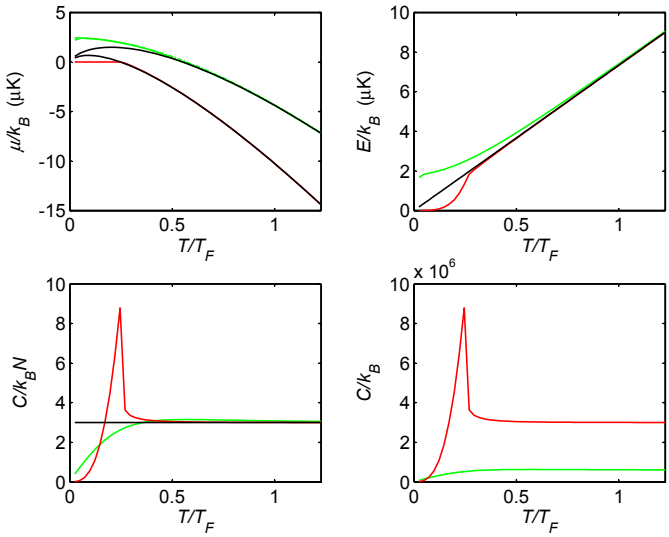

Figure 49.1: Density of states and chemical potential for a harmonic (dashed lines) and a Ioffe-Pritchard trap.

with the constraint $N_{87,|2,1\rangle} - N_{6,|3/2,3/2\rangle} = const$, we obtain the spin relaxation rate coefficient $G_{inel} = 1.2(3) \times 10^{-15}$ cm^2/s. Spin-relaxation, the only allowed collision-induced transitions are,

$$
\begin{aligned}
|2,1\rangle + |3/2,3/2\rangle &\rightarrow |2,2\rangle + |3/2,1/2\rangle \\
|2,1\rangle + |3/2,3/2\rangle &\rightarrow |2,2\rangle + |1/2,1/2\rangle + \nu_{6,hf} \\
|2,1\rangle + |3/2,3/2\rangle &\rightarrow |1,1\rangle + |3/2,3/2\rangle + \nu_{87,hf}
\end{aligned}
\tag{49.29}
$$

$$
\begin{aligned}
|1,-1\rangle + |3/2,3/2\rangle &\rightarrow |1,0\rangle + |3/2,1/2\rangle + \nu_{87,rf} + \nu_{6,rf} \\
|1,-1\rangle + |3/2,3/2\rangle &\rightarrow |1,0\rangle + |1/2,1/2\rangle + \nu_{87,rf} + \nu_{6,hf} \ .
\end{aligned}
$$

Three-body recombination,...

49.2.2.4 Dipolar relaxation of fully stretched ^{87}Rb

The dipolar relaxation of the $^{87}Rb, |2,2\rangle$ state is on the order of $G_{dip} = 2\times10^{-15}$ cm^3/s [159]. We establish the following rate equations,

$$
\begin{aligned}
\dot{N}_{|2,2\rangle} &= -G_{dip} \int n^2_{|2,2\rangle} d^3\mathbf{r} - G_{inel} \int n_{|2,2\rangle} n_{|2,1\rangle} d^3r \\
\dot{N}_{|2,1\rangle} &= G_{dip} \int n^2_{|2,2\rangle} d^3\mathbf{r} - G_{inel} \int n_{|2,2\rangle} n_{|2,1\rangle} d^3r \ .
\end{aligned}
\tag{49.30}
$$

Using $n_j = n_{0j} e^{-U_j/k_B T}$ with $U_{|2,2\rangle} = \frac{m}{2}\omega_r^2 r^2 + \frac{m}{2}\omega_z^2 z^2$ and $U_{|2,1\rangle} = \frac{1}{2}U_{|2,2\rangle}$, we get,

$$N_{|2,2\rangle} = \int n_{|2,2\rangle} d^3r = n_{0|2,2\rangle} \int e^{-m\omega_x^2 x^2/2k_B T} d^3r = n_{0|2,2\rangle} \sqrt{\frac{2\pi k_B T}{m\tilde{\omega}^2}}^3 \tag{49.31}$$

$$N_{|2,1\rangle} = \int n_{|2,1\rangle} d^3r = n_{0|2,1\rangle} \int e^{-m\omega_x^2 x^2/4k_B T} d^3r = n_{0|2,1\rangle} \sqrt{\frac{4\pi k_B T}{m\tilde{\omega}^2}}^3$$

$$\int n_{|2,2\rangle}^2 d^3r = \left(\frac{1}{2}\right)^{3/2} n_{0|2,2\rangle} N_{|2,2\rangle}$$

$$\int n_{|2,2\rangle} n_{|2,1\rangle} d^3r = \left(\frac{1}{3}\right)^{3/2} n_{0|2,2\rangle} N_{|2,1\rangle}$$

finally,

$$\dot{N}_{|2,2\rangle} = -G_{dip} \left(\frac{m\tilde{\omega}^2}{4\pi k_B T}\right)^{3/2} N_{2,2}^2 - G_{inel} \left(\frac{m\tilde{\omega}^2}{6\pi k_B T}\right)^{3/2} N_{2,2} N_{2,1} \tag{49.32}$$

$$\dot{N}_{|2,1\rangle} = G_{dip} \left(\frac{m\tilde{\omega}^2}{4\pi k_B T}\right)^{3/2} N_{2,2}^2 - G_{inel} \left(\frac{m\tilde{\omega}^2}{6\pi k_B T}\right)^{3/2} N_{2,2} N_{2,1} \ .$$

49.2.3 Mixed species experiments

The studied fermionic species are ^{40}K and ^{6}Li in combination with various other fermionic or bosonic species to allow for cooling. Both species exhibit Feshbach resonances: ^{40}K has one between $|9/2, -9/2\rangle$ and $|9/2, -7/2\rangle$ at 202 G [1081]. ^{6}Li has a broad $|1/2, \pm 1/2\rangle$ interstate Feshbach resonance at 850 G [679, 311].

49.2.3.1 Bragg scattering at BECs in the Lamb-Dicke limit

Make very deep traps such as [1168] or optical confinement, such that $\omega_{vib} \gg \varepsilon$. Bragg scattering off such BECs should not destroy them. How steep can we make the lithium surface trap? Everybody goes to the lower states: ^{7}Li, $|1, -1\rangle$-^{6}Li, $|1/2, -1/2\rangle$ or ^{23}Na, $|1, -1\rangle$-^{6}Li, $|1/2, -1/2\rangle$. How can we do this? Temperature determined from spatial extend of bosonic cloud in-situ.

49.2.4 Collapse and demixing of mixed species

49.2.4.1 Collapse

The collisional properties of ultracold K-Rb mixtures may lead to the collapse of a degenerate Fermi Gas [439, 905, 8, 262]. Until now we have neglected mean-field interactions between fermions and bosons. With interspecies interaction $g_{mx} = 2\pi\hbar^2 a_{mx}/m_{rd}$ where $m_{rd}^{-1} = m_6^{-1} + m_{87}^{-1}$ the GPEs read,

$$\left[-\frac{\hbar^2\nabla^2}{2m_{87}} + V_{87}(\mathbf{r}) + g|\phi_{87}|^2 + g_{mx}|\phi_6|^2\right]\phi_{87} = \mu_{87}\phi_{87} \tag{49.33}$$

$$\left[-\frac{\hbar^2\nabla^2}{2m_6} + V_6(\mathbf{r}) + g_{mx}|\phi_{87}|^2\right]\phi_6 = \mu_6\phi_6 \ .$$

The solution of the fermionic density distribution at $T \to 0$ is now,

$$\begin{aligned} n_6 &= \kappa \left(\mu_6 - V_6 - g_{mx} n_{87}\right)^{3/2} \ , \\ |\nabla \phi_6|^2 &= k_6^2 = \left(6\pi^2 n_6\right)^{2/3} \ . \end{aligned} \tag{49.34}$$

with $\kappa = 2^{1/2} m_6^{3/2}/3\pi^2\hbar^3$. To get a temperature dependence [262] use the Sommerfeld approximation. According to this the effective bosonic Hamiltonian including boson-fermion interaction at $T \to 0$,

$$\begin{aligned} H_{eff} &= \int d\mathbf{r} \left\{ \frac{\hbar^2}{2m_{87}} |\nabla \phi_{87}|^2 + (V_{87}(\mathbf{r}) - \mu_{87})|\phi_{87}|^2 + \frac{g}{2}|\phi_{87}|^4 + (V_6(\mathbf{r}) - \mu_6)|\phi_6|^2 + g_{mx}|\phi_{87}|^2|\phi_6|^2) \right. \\ &= \int d\mathbf{r} \left\{ \frac{\hbar^2}{2m_{87}} |\nabla \phi_{87}|^2 + (V_{87}(\mathbf{r}) - \mu_{87})|\phi_{87}|^2 + \frac{g}{2}|\phi_{87}|^4 - \kappa^{-2/3} n_6^{5/3}) \right\} \ . \end{aligned} \tag{49.35}$$

We assume now that both species of atoms experience the same potential $V(\mathbf{r}) \equiv V_j(\mathbf{r}) = \frac{m_j}{2}\omega_{j,z}^2 z^2 + \frac{m_j}{2}\omega_{j,r}^2 \rho^2 = \frac{m_j}{2}\omega_j^2 \left(\lambda^2 z^2 + \rho^2\right)$. To find out the condition for collapse we first determine μ_6 via the normalization condition $N_6 = \int d\mathbf{r}\ n_6(\mathbf{r})$. This is done by numerically integration Eq. (49.40). μ_{87} gives an offset and may be set to zero. We now insert the ansatz of the wavefunction,

$$\begin{aligned} \phi_{87} &= \left(\frac{N_B \lambda}{w^3 a^3 \pi^{3/2}}\right)^{1/2} \exp\left(-\frac{\rho^2 + \lambda^2 z^2}{2w^2 a^2}\right) \\ |\nabla \phi_{87}|^2 &= \frac{\rho^2 + \lambda^4 z^2}{w^4 a^4} |\phi_{87}|^2 \end{aligned} \tag{49.36}$$

using $a = \sqrt{\hbar/m_{87}\omega_{87}}$ and a variational parameter w and integrate Eq. (49.41) numerically.

49.2.4.2 Demixing

While collapse occurs for $g_{mx} < 0$, for $g_{mx} > 0$ the components may demix. For homogeneous systems the condition for demixing is [232],

$$g_{mx}^2 > g_{87} g_{FF} \qquad \text{with} \qquad g_{FF} = \frac{2}{3\kappa^{2/3} n_6^{1/3}} \ , \tag{49.37}$$

so that,

$$\frac{g_{mx}}{g_{87}} > \left(\frac{\pi m_{87}}{2m_6 (6\pi^2 n_6)^{1/3} a}\right)^{1/2} \ . \tag{49.38}$$

49.2.5 Fermion-boson collapse and demixing of ^{7}Li-^{87}Rb

49.2.5.1 Analytic estimation

An expansion of the interaction term in g_{mx} up to third order,

$$g_{mx}|\phi_{87}|^2|\phi_6|^2 = \kappa(\mu_6 - V)^{3/2} g_{mx} n_{87} - \frac{3}{2}\kappa(\mu_6 - V)^{1/2} g_{mx}^2 n_{87}^2 + \frac{3}{8}\frac{\kappa}{(\mu_6 - V)^{1/2}} g_{mx}^3 n_{87}^3 \tag{49.39}$$

$$\approx -\frac{3}{2}\kappa\mu_6^{1/2} g_{mx}^2 n_{87}^2 + \frac{3\kappa}{8\mu_6^{1/2}} g_{mx}^3 n_{87}^3 \ ,$$

yields,

$$H_{eff} \equiv C + \int d\mathbf{r} \left\{ \frac{\hbar^2}{2m_{87}}|\nabla\phi_{87}|^2 + (V_{eff} - \mu_B)|\phi_{87}|^2 + \frac{g_{eff}}{2}|\phi_{87}|^4 + \frac{\kappa}{8\mu_6^{1/2}} g_{mx}^3 |\phi_{87}|^6 \right\} , \tag{49.40}$$

where we used the definition $V_{eff}(\mathbf{r}) \equiv V(\mathbf{r})\left(1 - \frac{3}{2}\kappa\mu_6^{1/2} g_{mx}\right)$ and $g_{eff} \equiv g_{87} - \frac{3}{2}\kappa\mu_6^{1/2} g_{mx}^2$. There is a problem with factor 3 in the last term as compared to [262]. This is due to the fact that they go back from $(\mu_6 - V_6 - g_{mx} n_{87})^{3/2}$ to $-\frac{5}{2}(\mu_6 - V_6 - g_{mx} n_{87})^{5/2}$ before doing the expansion and then neglect the zeroth order. We now insert the ansatz of the wavefunction (49.42),

$$H_{eff} = \frac{2N_{87}\lambda}{\pi^{1/2}} \int_0^\infty d\rho \int_{-\infty}^\infty dz \ \rho \left\{ \frac{\hbar^2}{2m_{87}} \frac{\rho^2 + \lambda^4 z^2}{w^2 a^2} e^{-\rho^2 - \lambda^2 z^2} + (V_{eff} - \mu_{87}) e^{-\rho^2 - \lambda^2 z^2} \right. \tag{49.41}$$

$$\left. + \frac{N_6\lambda}{w^3 a^3 \pi^{3/2}} \frac{g_{eff}}{2} e^{-2\rho^2 - 2\lambda^2 z^2} + \left(\frac{N_{87}\lambda}{w^3 a^3 \pi^{3/2}}\right)^2 \frac{\kappa}{8\mu_6^{1/2}} g_{mx}^3 e^{-3\rho^2 - 3\lambda^2 z^2} \right\} \ .$$

All integrals can be solved exactly, so that we get,

$$\frac{H_{eff}}{N_{87}\hbar\omega_{87}} = \frac{2+\lambda}{4w^2} + \frac{3}{4}\frac{V_{eff}}{V} w^2 - \frac{\mu_{87}}{\hbar\omega_{87}} + \frac{g_{eff}}{2} \frac{\lambda}{(2\pi)^{3/2}\hbar\omega_{87} a^3} \frac{N_{87}}{w^3} + \frac{\kappa}{8\mu_6^{1/2}} g_{mx}^3 \frac{\lambda^2}{3^{3/2}\pi^3 \hbar\omega_{87} a^6} \frac{N_{87}^2}{w^6} \ . \tag{49.42}$$

Using ^{40}K with $a_s = 99.2 a_B$ and $a_{mx} = -410 a_B$ and $\omega_{87,r} = 2\pi \times 215$ Hz and $N_{87} = 50000$ and $N_6 \to N_{40} = 20000$ this reproduces the results of [262]. For ^{6}Li with $N_{87} = 50000$ and $N_6 = 20000$, we expect instability for $a_{mx} < -240 a_B$.

49.2.6 Ions in BECs

The hybrid system consistent of individual ions and Bose-condensed clouds of neutral atoms opens up new horizons. Many novel phenomena, such as controlled atom-ion collisions, charge transfer processes, polarization and structuring of an ultracold atomic cloud by ions, etc. can be studied.

During elastic collisions between ions ant atoms electrons can be exchanged between the collision partners. This may lead to interesting effects, in particular when

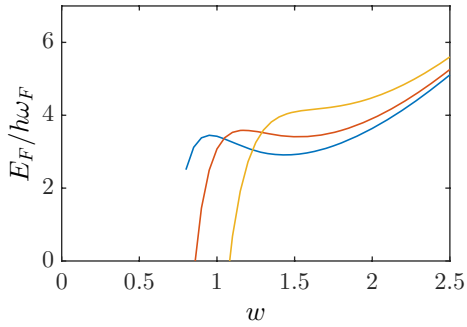

Figure 49.2: (code) Density of states and chemical potential for a harmonic (dashed lines) and a Ioffe-Pritchard trap.

the atoms are delocalized in a Bose-condensate. The ions polarize their surrounding atoms and induce an isotropic potential $\propto 1/r^4$, which has a much longer range than the $\propto 1/r^6$ interatomic van der Waals potential. Atoms are attracted by an ion and may be bound and form a giant *molecular atom*, whose nucleus is a single localized ion and whose shell is a Bose-condensate of several 100 neutral atoms.

49.2.7 Exercises

49.2.7.1 Ex: Instable fermion-boson mixtures

Solution: *InstableFermionBoson1: Analytic approximation from [Chui04] for 40-K.*
InstableFermionBoson1b: Analytic approximation from [Chui04] for 6-Li.
InstableFermionBoson2: Numerical integration, naive Hamiltonian.
InstableFermionBoson2b: Numerical integration, numerical integration, Hamiltonian from [Molmer98].
InstableFermionBoson2c: Numerical integration, numerical integration, Hamiltonian from [Capuzzi03].
InstableFermionBoson3: Numerical integration, instable 7-Li BEC.
InstableFermionBoson4: Numerical integration, repulsive mixtures.

49.3 Molecular BECs

49.3.1 Thermodynamics of trapped molecules

We consider a mixture of atomic fermions coupled to bosonic thermal molecules and condensed molecules via a Feshbach resonance. The molecular distribution function,

$$g_m(\epsilon) = \frac{1}{e^{\beta_m(\epsilon+\epsilon_{res}-\mu_m)}-1} \ , \tag{49.43}$$

takes into account the Feshbach-tunable internal energy of the molecules. It is now possible to set up a coupled thermodynamics and to calculate the atomic, molecular and condensed fractions as a function of ϵ_{res} and T [1379]. It also possible to determine trajectories in the phase diagrams for changes of ϵ_{res} starting at some given initial temperature T_i. The treatment of [1379] is however limited to ideal gases and probably will fails to quantitatively describe the BCS physics. The treatment is however useful to predict the conversion efficiency from a cold Fermi gas to molecules. This efficiency depends on the magnetic field ramp. *Adiabatic ramps* of ϵ_{res} are characterized by a constant total entropy, *sudden changes* conserve total energy. The conversion efficiency upon adiabatic ramps is much higher. Hence, the fact that molecular BECs have also been produced using fast ramps has been interpreted as a proof for the preexistence of BCS pairs before the ramp [1444, 1080, 1442].

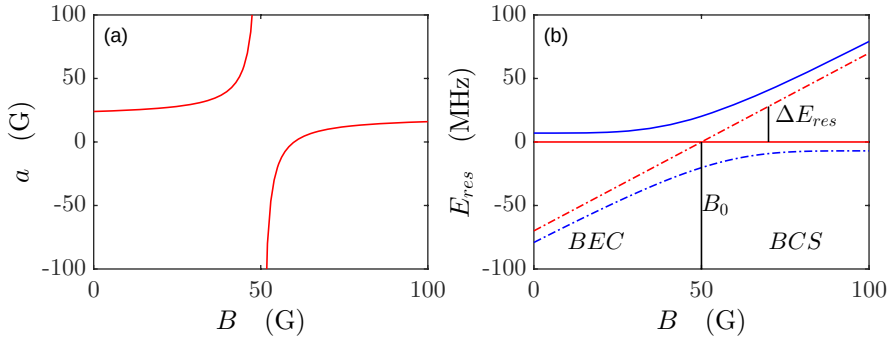

Figure 49.3: (code) (a) Scattering length as a function of magnetic field strength near a Feshbach resonance. (b) Energies of the bound state (solid) and the free channel (dashed). An avoided crossing introduces a pairing gap.

In contrast, [431]Phys Rev Lett/PRL92,130401 claims that the total wave function has molecular character even at detunings $\delta \gtrsim 0$. For $a(B) > 0$ the molecular binding energy is,

$$\epsilon_m \simeq \hbar^2/ma(B)^2 \ . \tag{49.44}$$

Cooper pairing and the *BCS transition*, analogous to electrons in solids, may be studied in optical traps. Long lifetimes up to 3 min can be achieved with careful control of the laser intensity [347, 966]. The absence of Coulomb interactions makes atomic systems very pure. But the transition temperatures are low. Currently, $T_{BCS} \simeq 0.2T_F$.

Note that a *molecular BEC* is unlike a *BCS pair*: in a molecular BEC, $k_F a < 1$, the molecules are delocalized in the BEC, but the atoms are localized within the molecule. For Cooper-pairs the two atoms forming the pair are delocalized within the BEC [1080, 1079].

49.3.2 Production of homonuclear BECs

Jin's group [538, 1081]. Using the Feshbach resonance on fermions, aided by the Pauli exclusion principle preventing relaxation, e.g. $^{40}K_2$ has a relaxation of only 0.5 s.

Production of Li_2 BECs, almost simultaneous detected at ENS, Innsbruck and MIT [678, 311, 1443].

Na_2 BECs were detected at MIT [1402] and Cs_2 BECs at Innsbruck [612].

49.3.3 Molecular solitons in BECs

While the self-interaction in BECs $\hat{\psi}_a^+\hat{\psi}_a^+\hat{\psi}_a\hat{\psi}_a$ corresponds to third-order nonlinearities $\chi^{(3)}$ in quantum optics, the second-harmonic generation of molecules $\hat{\psi}_m^+\hat{\psi}_a\hat{\psi}_a$ from atoms corresponds to second-order nonlinearities $\chi^{(2)}$. The single-species Gross-Pitaevski equation cannot produce solitons in three dimensions [391]. The free-bound coupling of atoms and molecules at low densities is particle-like and only forms individual dressed molecules similar to Cooper-pairs. At high densities, $\chi^{(3)}$ and $\chi^{(2)}$ interplay in such a way to make a coherent coupling between two BECs at the base of strong, coherent, non-linear and interactions giving rise to a *soliton matter wave*.

49.4 Cooper pairing mechanisms and transition temperatures

Valuable contribution to BCS theory for atomic Fermi gases have been made by [93, 92, 87, 995, 160, 627, 600, 88, 599, 899, 408, 86, 1234, 431, 1023, 369, 564, 1015, 719, 1288]. See also Sec. 21.4.

Dynamics of the BCS-BEC Crossover in a degenerate Fermi Gas, experimental work comes from [623, 539, 1078].

There are various options for Cooper pairing avoiding the Pauli principle:

49.4.1 BEC-BCS transition

The phenomena of superconductivity and superfluidity have fascinated physicists since the 20th century. In 1911, superconductivity was discovered when resistance of mercury was observed to vanish below a certain critical temperature [974]. In 1957 Bardeen, Cooper and Schrieffer (BCS) formulated the theory on superconductivity [93, 94], which predicts that, in fermionic systems below a certain temperature, there is formation of a *gap* of minimal excitation energy in the conductor. With this theory, many properties of superfluids and superconductors can be explained, as we will see in the following sections.

49.4.1.1 Pairing in a gas of fermionic atoms

Superfluids are fundamentally associated with the quantum properties of bosons. Therefore, to create a superfluid from a fermionic system, it is necessary to pair the fermions. The simplest way to imagine a pairing of fermions is to create a two-body bound state of two fermions. For example, two paired fermionic spin-1/2 particles form a single bosonic integer-spin particle. In recent experiments studying the BCS-BEC transition, the fermionic particles are atoms (e.g. ^{40}K) forced to form a diatomic molecule. These diatomic molecules, below a critical temperature, will form a BEC [1080]. Fig. 49.4(a) illustrates a superfluid containing such pairs.

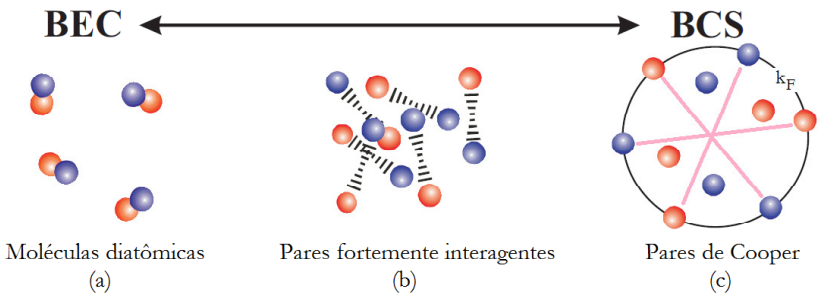

Figure 49.4: Illustration of fermion pairing in the BCS-BEC transition. The two colors represent fermions in two different spins states. Two states are required if the fermions are paired through s-wave ($\ell = 0$) interaction.

In the other pairing process, the Cooper pairing, the basic nature of the fermionic system is much more apparent. Cooper considered the problem of two fermions with equal-sized but and opposite momenta outside a perfect *Fermi sea* [290] [1] and noted that due to the Pauli exclusion principle, these two fermions are prevented from occupying momentum states inside the so-called Fermi sea, that is $k < k_F$ where k_F is the Fermi wavevector. This fermion pair, which is prevented from penetrating the Fermi sphere is called *Cooper pair*.

Now if only one electron pair were free to pair outside the Fermi sea, this would not lead to superconductivity, since all fermions must be allowed to participate in the pairing process. The superconductivity theory of Bardeen-Cooper-Schrieffer (BCS) was able to link the many-body theory to this problem and succeeded in describing the phenomenon of superconductivity [93, 94].

Qualitatively the BCS state results from a loss of correlations between fermions on the Fermi surface in momentum space [see Fig. 49.4(c)]. Spatially, the pairs are highly overlapping and can not simply be considered as bosons. Close to the BCS limit the momentum distribution only changes to the usual Fermi sea, that is, an exponentially small region near the Fermi surface.

It is interesting to consider what happens if diatomic molecules become increasingly weakly bound, that is, when the binding energy E_b of the molecules becomes smaller than the Fermi energy E_F. We may also consider the increase in the interaction energy of a Cooper-paired state up to E_F. The essence of the BCS-BEC transition is that these two possibilities describe the same physical state. As the interaction between fermions is increased, there will be a continuous change (or transition) between a BCS state of a BEC state of diatomic molecules. The point where two fermions in vacuum would have zero binding energy is considered the apex of the transition. The pairing of such a state is represented in Fig. 49.4(b). These pairs share some properties with diatomic molecules and some properties with Cooper pairs.

[1] The energy of the two fermions turns out to be smaller than the expected value of $2E_F$ for attractive and weak interactions. This finding contrasts with the behavior of two fermions in vacuum; in this case, a bound state can not exist until the interaction strength reaches a certain value. The main difference between the two situations arises from Pauli's exclusion principle which, in the case of Cooper pairs prevents the two fermions from occupying momentum states $k < k_F$.

49.4.1.2 Varying the interaction strength

It is instructive to consider a physical situation that allows for the pairing (see Fig. 49.5). Suppose that we start with an attractive potential between two atomic fermions in vacuum, e.g. a hard-core potential with characteristic length r_0 shown in Fig. 49.5. If this potential is very shallow, there will be a weak attractive interaction between the fermions. As we deepen the potential, the interaction between the fermions becomes stronger and, when the attraction is strong enough, a bound molecular state will appear. This molecule will become increasingly tightly bound as the potential becomes deeper.

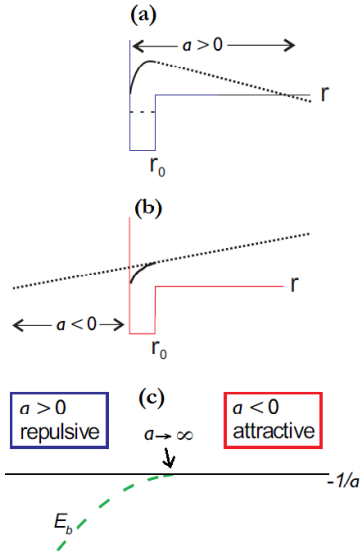

Figure 49.5: Scattering wavefunction in the presence of an attractive potential (b) and a deeper attractive potential (a) in the regime where the potential of the bound state (dashed line) is close to the *threshold*. Note that the scattering length changes sign when the bound state moves through the threshold.

The interaction in this system can be characterized by the scattering length a. The sign of a determines whether the interaction is attractive ($a < 0$) or repulsive ($a > 0$). The quantity a is related to the collision cross-section through $\sigma = 4\pi a^2$. Figs. 49.5(a) and 49.5(b) show a pictorial representation of a. Before the bound state appears, a is large and negative, which corresponds to a strong attractive interaction. As the bound state passes through the threshold the value of a diverges and, beyond the threshold, becomes larger and positive, which corresponds to a strong repulsive interaction. When a is much greater than r_0, the interaction independs on the shape of the potential, and when $a > 0$, it is related to the two-body binding energy through $E_b = \frac{\hbar^2}{ma^2}$, where m is the mass of one fermion [1129].

Now, if we consider an ensemble of many fermions under the situation depicted in Fig. 49.5, we have a system that can be changed from BCS to BEC, by simply tuning the attractive potential. To the far right of Fig. 49.5(c) we have a small and negative a and, hence, we are in a BCS state. On the opposite side of the figure, we

have an ensemble of diatomic molecules and therefore a BEC state. It is important to note that although the interaction between fermion pairs is stronger in the BEC limit, from the point of view of collisions in molecular gas, the BEC boundary is weakly interacting because the molecule-molecule interaction is weak.

49.4.1.3 Simplified theory

The BCS theory was originally applied to the regime where the interaction energy is extremely small compared to the Fermi energy. In this case, the chemical potential μ can be set to E_F, which simplifies the calculations reasonably. Leggett pointed out that, examining the equation describing the BCS gap upon varying μ, this equation becomes precisely the Schrödinger equation for a diatomic molecule in the limit where μ dominates [784].

Let us consider a homogeneous Fermi system at $T = 0$ in three dimensions consistent of a mixture with the same quantity of atoms in the two states. Applying the usual BCS theory results in an equation for the *gap*,

$$\Delta_k = -\sum_{\mathbf{k}'} U_{kk'} \frac{\Delta_{k'}}{2E_{k'}} \ , \tag{49.45}$$

where $E_k = \sqrt{\xi_k^2 + \Delta^2}$, $\xi_k = \epsilon_k - \mu$, and $\epsilon_k = \frac{\hbar^2 k^2}{2m}$. $U_{kk'} < 0$ is the attractive interaction for the scattering of fermions with momenta k' and $-k'$ to momenta k and $-k$. We can also obtain the equation for the total number of fermions in both states, N_{tot},

$$\langle N_{tot} \rangle = \sum_{\mathbf{k}} \left(1 - \frac{\xi_k}{E_k} \right) \ . \tag{49.46}$$

To solve Eq. (49.45) in the BCS limit the standard approach is to assume that the potential is constant with a value $U < 0$, which means that the gap is constant, i.e., $\Delta_k = \Delta$. In this case, the equation of the gap (49.45) becomes,

$$-\frac{1}{U} = \sum_{\mathbf{k}} \frac{1}{2E_k} \ . \tag{49.47}$$

We can see that this equation may diverge. In the BCS limit we also have $\mu = E_F$ and, given that there is the Debye energy limit $\hbar\omega_D \ll E_F$, the density of states is constant with the value $N(\xi = 0)$. The equation for the gap now becomes,

$$-\frac{1}{N(0)U} = \int_{-\hbar\omega_D}^{\hbar\omega_D} \frac{d\xi}{2\sqrt{\xi_k^2 + \Delta^2}} \ . \tag{49.48}$$

Solving Eq. (49.48) we produce the BCS result: $\Delta \approx 2\hbar\omega_D e^{-1/N(0)|U|}$.

Extending this calculation to the transition in atomic systems, we can no longer apply the cut-off $\hbar\omega_D$. The solution to the divergence problem, in this case, is not trivial and requires a renormalization procedure, which can be found in the reference [**?**].

The result of this procedure is a renormalized equation for the gap:

$$-\frac{m}{4\pi\hbar^2 a} = \frac{1}{V} \sum_{\mathbf{k}} \left(\frac{1}{2E_k} - \frac{1}{2\epsilon_k} \right) \ , \tag{49.49}$$

where the interaction is now described by the s-wave scattering length a instead of U, and V is the volume of the system. In addition, for the transition we can not assume $\mu = E_F$; instead, we must solve simultaneously the equation of the gap (49.49) and the equation of the number (49.46) in order to get μ and the gap Δ. This can be done resolving as a function of the dimensionless parameter $k_F a$, where $\hbar k_F = \sqrt{2mE_F}$, as done in Ref. [846].

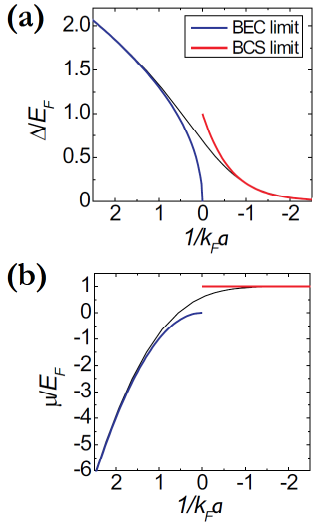

Figure 49.6: The gap, Δ, and the chemical potential, μ, of a homogeneous Fermi gas at $T = 0$, as determined via the NSR theory. The red and blue lines show the BCS and BEC theory. Note that the theories only deviate significantly from the complete theory inside the interval $-1 < \frac{1}{k_F a} < 1$ [1082].

The black lines in Fig. 49.6 show the result of the calculations of Δ and μ. Also are plotted the values of these two parameters calculated in the BCS and BEC limits, where we find that the BCS-BEC transition occurs in a relatively small region of the parameter $1/k_F a$, that is, between $-1 < \frac{1}{k_F a} < 1$. In typical experiments studying this transition (with ^{40}K or ^{6}Li) this interval corresponds to a ranging from $-2000a_0$, crossing the divergence ($a \to \infty$), until $2000a_0$, where a_0 is the Bohr radius.

It is useful to understand explicitly the value and meaning of both Δ and μ in these two limits. μ is equal to E_F in the BCS limit and equal to $-E_b/2 = -(\frac{1}{k_F a})^2 E_F$ in the BEC limit. Δ is equal to $E_F e^{-\frac{\pi}{k_F |a|}}$ in the BCS limit and equal to $E_F \sqrt{\frac{16}{3\pi} \frac{1}{k_F a}}$ in the BEC limit [846].

49.4.1.4 Beyond $T = 0$

A very important parameter for any superfluid system is the so-called phase transition temperature T_c. In the BCS-BEC transition T_c increases as the interaction is increased, that is, it is lower in the BCS regime and higher in the BEC regime. For a homogeneous system in the BCS regime $T_c/T_F = \frac{8}{\pi} e^{\gamma - 2} e^{-\frac{\pi}{2k_F |a|}}$, where $\gamma = 0.58$

[588]. In the BEC regime $T_c/T_F = 0.22$ [1017]. Note that in the BCS regime T_c can be extremely small due to the exponential dependence on $1/k_F a$.

In the BCS regime pairing and phase transition to a superfluid state occur at the same temperature. In the BEC regime this is not the case. It is natural to expect that there should be a cross-over between these two behaviors in the BCS-BEC transition, i.e. there should be a point in the transition, where the pairing temperature T^* is distinct from T_c, but not much different.

The above discussions and calculations, while providing a basic introduction to the BCS-BEC transition theory, are far from the current situation of this theory. For example, the result for the chemical potential at the singularity (where $1/k_F a = 0$) is significantly different from the result of more accurate calculations based on Monte Carlo simulations [234, 59]. Thus, it is clear that the addition of higher order correlations in the theory of the BCS-BEC transition theory is required.

The BCS-BEC transition was studied in laboratory [1083] using ^{40}K as the fermionic sample, prepared in two hyperfine states $|F = 9/2, m_F = 9/2\rangle$ and $|F = 9/2, m_F = 7/2\rangle$. Other group also studied this transition in different fermionic species. Many studies involving the BCS-BEC transition have been made, such as studies on the change of momentum distribution in this transition [1078], studies of collective oscillations [428], the modification of the expansion of ultracold clouds [1426], and the change of the critical velocity of the superfluid flow throughout the transition [894].

49.4.2 s- and p-wave pairing

Cooper pairing can occur between two fermions being in different spin states [87, 160]. For pure two-component Fermi systems the critical temperature follows to first order from [995, 600],

$$g_F \int_0^\infty \frac{p^2 dp}{2\pi^2\hbar^3} \frac{1}{\varepsilon_p} \frac{1}{e^{\varepsilon_p/k_B T^0_{BCS}} + 1} = 1 \ , \tag{49.50}$$

with $\varepsilon_p = p^2/2m_F - \mu$ i.e.,

$$k_B T^0_{BCS} = \frac{e^{C_E}}{\pi} \frac{8}{e^2} \varepsilon_F \exp\left(-\frac{\pi}{2k_F|a_s|}\right) \ . \tag{49.51}$$

However, spin- and density fluctuations in the Fermi cloud mediate an interaction between the fermions, which reduces T^0_{BCS} by a factor 2.2 in the case of two components and increases T^0_{BCS} for several components. The critical temperature is then,

$$k_B T_{BCS} \simeq 0.3\varepsilon_f \exp\left(-\frac{\pi}{2k_F|a_s|}\right) \ , \tag{49.52}$$

where $\varepsilon_F = \hbar^2 k_F^2/2m$. Therefore transfer half the population into an different Zeeman state, e.g. state ^{6}Li, $|1/2, 1/2\rangle|1/2, -1/2\rangle$ or ^{40}K, $|9/2, -9/2\rangle|9/2, -7/2\rangle$. This is only possible with optical traps. The s-wave scattering length for ^{6}Li is $a_s \simeq -2160 a_B$, even in this channel.

Use p-wave collisions as pairing mechanism [408]. The critical temperature is then,

$$k_B T_{BCS} \simeq \varepsilon_F \exp\left(-\frac{\pi}{2(k_F|a_p|)^3}\right) \ . \tag{49.53}$$

The p-wave scattering length for ^{6}Li is $a_p \simeq -35 a_B$.

49.4.3 Resonance superfluidity and boson-induced interactions

In general $k_F|a| \ll 1$, so that the pairing temperature is way too low. There are however two approaches to rise the critical temperature:

1. Increase the s-wave or the p-wave scattering length by a Feshbach resonance [1426, 1084] (see also Sec. 33.4.2).

2. For a Fermi gas embedded in a Bose condensate, there can be boson-mediated interaction, similar to phonon-mediated interaction in ^{3}He-^{4}He [144, 600]. This can give rive to an effective fermion-fermion scattering length, i.e. a Rb Bose gas may catalyse an enhancement of ^{6}Li-^{6}Li interactions. For a discussion on how to reach very cold temperatures via sympathetic cooling see Sec. 49.2.2.

All experiments used s-wave pairing of spin-mixtures enhanced by Feshbach resonances. BCS pairing has been observed in experiments by various methods: 1. Radio frequency spectroscopy probes the excitations spectrum [539], which should show a pairing gap [101, 256]. 2. Superfluidity is seen as the occurrence of vortices in a Fermi gas [1444].

49.5 Controlling the interatomic interaction

Collisions play an important role in all areas of atomic physics. By *elastic collisions*, an atom exchanges only kinetic energy, which is important, for example, for the thermalization of atomic clouds upon evaporative cooling. During a collision, the interatomic forces deform the electronic orbitals and displace energy levels and resonances. This is a hindrance to applications in frequency standards (such as atomic fountains), where the accuracy of the measurement of narrow resonances is limited by these effects. On the other hand, *controlled* elastic collisions are the essential ingredient of some quantum computer schemes [661]. An *inelastic collision* involves the internal degree of freedom of atoms, that is, the atoms modify their excitation levels. The excess excitation energy is transferred to the atomic motion as kinetic energy, which in turn, provided it is sufficiently high, can expel the atoms out of the trap.

Collisions can be classified by their energy: A *cold collision* is characterized by an interaction time, which is so long, that absorption and photon emission processes can occur during this period. This allows the manipulation of the collisions by irradiation of resonant laser beams [1279]. A collision is called *ultra-cold collision*, when the kinetic energy of the atoms lies below the photon recoil limit. At these temperatures, only partial s-waves contribute to the collision. In general, ultra-cold collisions are influenced by quantum statistics (bosonic or fermionic), whereas 'cold only' collisions can often be treated by classical theory.

49.5.1 Detection of Feshbach resonances

The spin structure of alkaline atoms is complex and results from a combination of electron-exchange energy, hyperfine spin coupling and Zeeman interactions. This gives rise to a multiplicity of energy levels, which increases the likelihood of an occurrence of Feshbach resonances. There are several ways to detect a Feshbach resonance. An

experiment done at the University of Texas at Austin used *photoassociation spectroscopy with resolved Zeeman structure* to prove the first Feshbach resonance in a thermal cloud of ^{85}Rb atoms [300]. An alternative method measures the influence of the Feshbach resonance on the elastic collision section [1108]. A third detection method, which proves the impact of a Feshbach resonance on a BEC, has been used for ^{23}Na [648]. Other Feshbach resonances were later found in ^{133}Cs [1349] and many other species or combinations of species [**?**].

49.5.2 Free-bound coupling by Feshbach resonances

First theoretical studies have been carried out by [1308, 391, 627]. The simplistic image of the scattering length (see Sec. **??**) is a good approximation for isolated atoms, very diluted clouds or condensates far away from a Feshbach resonance, $B - B_{FB} \to \infty$. However, the divergence of the condensate's mean field energy at $B \to B_{FB}$ is not a realist concept. In fact, the molecular state represents a separate species of particles and a new thermodynamic fraction which, when the Feshbach resonance is excited in a BEC, is expected to form a *molecular condensate* [1308]. The atomic BEC and the molecular BEC are coupled by tunneling of atom pairs between them. This coupling is described by the following contribution to the Hamiltonian:

$$H \sim \hat{\psi}^2_{atom}\hat{\psi}^\dagger_{mol} + (\hat{\psi}^\dagger_{atom})^2\hat{\psi}_{mol} \ . \tag{49.54}$$

The signature of this new type of quantum tunneling can be observed in Josephson-like oscillations as a response to an abrupt modification of the scattering length induced by a sudden change of the magnetic field.

One problem with the mixed atomic-molecular system is the rapid relaxation of the molecular states. In fact, bound states have high vibrational energy and can easily relax by inelastic collisions with atoms or other molecules. Relaxation may make it difficult to detect molecular condensates.

The coherent free-bound coupling has been studied in a series of theoretical and experimental publications [1314, 668, 391, 1307, 1308, 648, 1108, 1349, 293]. The chemical potential of a BEC in the Thomas-Fermi approximation depends on the scattering length via $\mu = gn$. The relationship may be useful to (a) study the collapse of BECs and to make BECs with new species, (b) to study the phase separation of BECs in different internal states tuning between miscible and non-miscible BECs, (c) to study Josephson oscillations adjusting the difference of the chemical potentials of two species, and (d) to study the dynamics of BECs.

But the physics of the BECs are considerably richer than that of a modified scattering length, due to the possibility of a free-bound coupling to a vibrational molecular state. Josephson oscillations far away from resonance between states of molecular and atomic BECs can be excited in response to an abrupt change of detuning. Near resonance, the production of molecules induces a self-stabilization and a minimum in energy dependence of the density. Consequently, the density is self-determined, which is a property of *rarefied liquid*s. Gases and liquids are both fluid. Their viscosity is much lower than that of a solid. Gases are distinguished from liquids by their self-diffusion and much greater compressibility, gases do not form surfaces. For liquids we have almost $(\partial n_{lq}/\partial P) \approx 0$, or in harmonic traps $(\partial n_{lq}/\partial \omega_{trap}) \approx 0$.

The treatment of the free-bound coupling introduced in the preceding section leads to non-physical phenomena when applied in BECs. Therefore, we reformulate the many-body problem allowing for the emergence of a separate molecular condensate coherently coupled to the atomic one:

$$
\begin{aligned}
H &= \int_{R^3} u(\mathbf{r}) d^3\mathbf{r} \ , \qquad (49.55)\\
n(\mathbf{r}) &= |\hat{\psi}_a|^2 + \tfrac{1}{2}|\hat{\psi}_m|^2, \\
u_{kin}(\mathbf{r}) &= \hat{\psi}_a^+ \left(\tfrac{-\hbar^2}{2M}\Delta + V_a(\mathbf{r}) \right) \hat{\psi}_a + \hat{\psi}_m^+ \left(\tfrac{-\hbar^2}{4M}\Delta + V_m(\mathbf{r}) + \Delta E \right) \hat{\psi}_m \ , \\
u_{self}(\mathbf{r}) &= \hat{\psi}_a^+ \left(g_{aa}|\hat{\psi}_a|^2 \right) \hat{\psi}_a + \hat{\psi}_m^+ \left(g_{mm}|\hat{\psi}_m|^2 \right) \hat{\psi}_m \ , \\
u_{mutual}(\mathbf{r}) &= g_{am}|\hat{\psi}_a|^2|\hat{\psi}_m|^2 \ , \\
u_{conv}(\mathbf{r}) &= \frac{\alpha}{\sqrt{2}} \left(\hat{\psi}_a^2 \hat{\psi}_m^\dagger + (\hat{\psi}_a^\dagger)^2 \hat{\psi}_m \right) \ ,
\end{aligned}
$$

where M denotes the atomic mass, α the atom-molecule coupling $\alpha\delta_{\mathbf{K},\mathbf{k}+\mathbf{k}'} = \sqrt{\Omega}\langle \mathbf{K}, m|V_{hfs}|\mathbf{k},\mathbf{k}'\rangle$. The contribution u_{conv} can be interpreted as *second harmonic generation* (SHG). With the commutation rules:

$$
\begin{aligned}
\left[\hat{\psi}_j^\dagger(\mathbf{r},t), \hat{\psi}_k(\mathbf{r}',t)\right] &= \delta_{jk}\delta^3(\mathbf{r}-\mathbf{r}') \ , \qquad (49.56)\\
\left[\hat{\psi}_j(\mathbf{r},t), \hat{\psi}_k(\mathbf{r}',t)\right] &= 0 \ ,
\end{aligned}
$$

and the Heisenberg equations,

$$
\left[H, \hat{\psi}_j(\mathbf{r},t)\right] = i\hbar\partial_t \hat{\psi}_j^+(\mathbf{r},t) \ , \qquad (49.57)
$$

we can calculate the dynamics of this coupled system.

The equilibrium situation is described by the atomic and molecular chemical potentials to be balanced, $\mu = \mu_a = \mu_m$. Expressing the BEC as a c-number and defining $n \equiv \phi^2$:

$$
\begin{aligned}
\mu\phi_a(\mathbf{r}) &= \left[\tfrac{-\hbar^2}{2M_a}\Delta + V_a(\mathbf{r}) + g_{aa}n_a(\mathbf{r}) + g_{am}n_m(\mathbf{r}) \right] \phi_a(\mathbf{r}) + \sqrt{2}\alpha\phi_m(\mathbf{r})\phi_a(\mathbf{r}) \ , \qquad (49.58)\\
2\mu\phi_m(\mathbf{r}) &= \left[\tfrac{-\hbar^2}{4M_m}\Delta + V_m(\mathbf{r}) + g_{mm}n_m(\mathbf{r}) + g_{am}n_a(\mathbf{r}) \right] \phi_m(\mathbf{r}) + \tfrac{1}{\sqrt{2}}\alpha\phi_a^2(\mathbf{r}) \ .
\end{aligned}
$$

49.5.2.1 Bose-Einstein condensation of ^{85}Rb

The scattering length of the isotope ^{85}Rb in the ground state $F = 2, m_F = -2$ is negative, $a_{|2,-2\rangle} \approx -400a_B$, which prevents the formation of stable condensates with this atomic species. However, in the vicinity of a Feshbach resonance, the scattering length is very sensitive to ambient magnetic fields B (see Fig. 33.30), and can change its amplitude and even its sign.

Consequently, quantum degeneration was reached with ^{85}Rb [293] operating in a region, where the scattering length is positive. The evaporative cooling of a gas

from this isotope is troubled by a minimum in the temperature dependence of the cross section for elastic collisions around 350 μK, which is a peculiarity of ^{85}Rb. In addition, inelastic two- or three-body collisions of are very common in some regimes of the scattering length. Nevertheless, these difficulties can be avoided [293] using relatively weak confinement potential to reduce the density of the atomic cloud. Also, via a temporal control of the scattering length through a magnetic field $a(B(t))$, it is possible to design a sophisticated evaporation trajectory avoiding the critical regimes.

The active control of the scattering length also allows to push a ^{85}Rb condensate into the ideal gas regime, $a(B) \to 0$, or toward the Thomas-Fermi limit of a strongly interacting gas, $a(B) > 10000 a_B$, where the assumption of a very dilute gas, (46.3), starts to fail and effects beyond the mean field approximation are expected. Since the volume and shape of a condensate depend on its self-energy, their measurement yields information about the actual value of the scattering length.

Near a Feshbach resonance, at an amplitude of the magnetic field of $B = 166.8$ G, the scattering length changes from positive to negative (see Fig. 33.30). Crossing this point, we observe a catastrophic dynamic behavior [1109]: The BEC tries to reduce its self-energy by compressing its density until it succumbs emitting a jet of hot atoms.

49.5.2.2 Production of molecules inside condensates

The complicated ro-vibrational structure of molecules prevents their efficient cooling by optical means. Nevertheless, some alternative techniques, such as supersonic expansion, cryogenic cooling [387] and magnetic trapping [1365] managed to cool molecular samples to temperatures around one Kelvin.

Photoassociation (PA) can be used [82] as a tool to convert a large number of atoms to ultra-cold molecules. Based on this technique, molecules were synthesized in the rotational ground state at temperatures of 100 μK, but distributed over a large number of highly excited vibrational states [445]. Alternatively, it is possible to consider a coupling of atomic states to a single ro-vibrational molecular state using two lasers in Raman configuration. This scheme is known as *two-photon photoassociation* (see Fig. 49.7). In equilibrium, the production of molecules by this method depends on the entropies of the coupled system [668]. In a thermal atomic gas, the (quasi-[2]) continuum of dissociated atomic states has a much greater entropy than the discrete spectrum of bound vibrational molecular states. The equilibrium of the free-bound coherent coupling, therefore, is biased toward the side of the continuum, that is, molecules dissociate faster than they associate, and the molecular production is negligible. However, when the atomic cloud approaches the quantum degeneracy regime, the phase space is considerably reduced (a condensate has zero entropy), and the free-bound coherent coupling can transform a considerable amount of condensed atoms to a *molecular condensate*. The formation of molecules within a condensate can be interpreted as a chemical process, where bosonic stimulation plays the role of a catalyst. The dynamics of this process is induced by quantum statistics rather than chemical forces between atoms.

The experimental procedure for synthesizing ^{87}Rb is quite simple: A condensate of some 10^5 atoms in the electronic ground state $^2S_{1/2}$ ($f = 1, m_f = -1$) and two laser

[2]The atoms are still confined to the trapping potential.

beams in the Raman configuration are irradiated for some 100 ms. As shown on the left side of Fig. 49.7, the first laser excites the transition between the ground state of free atoms and a vibrational state of the excited interatomic interaction potential 0_g^-. Its frequency is tuned $\Delta_1 = -150$ MHz below resonance. The second laser couples the molecular state of the interatomic ground state potential (in this case, it is the second vibrational state below the ionization threshold, $v = -2, \ell = 0$) and the excited molecular state of the 0_g^- potential (chosen for its large Franck-Condon overlap with the molecular ground state). This laser is tuned to $\Delta_2 = \Delta_1 + 636\,\text{MHz}$. Since the two frequencies are derived from a single laser using an acousto-optical modulator, their phases are coherent, that is, the Raman frequency $\Delta_1 - \Delta_2$ is sufficiently stable to couple only a single ro-vibrational state connected through a dark resonance to the collision channel. The molecules are not directly detected, but at the end of the Raman laser pulse, condensate losses due to the formation of molecules are measured by time-of-flight imaging. The dark resonance is detected by repeating the sequence with different laser detunings.

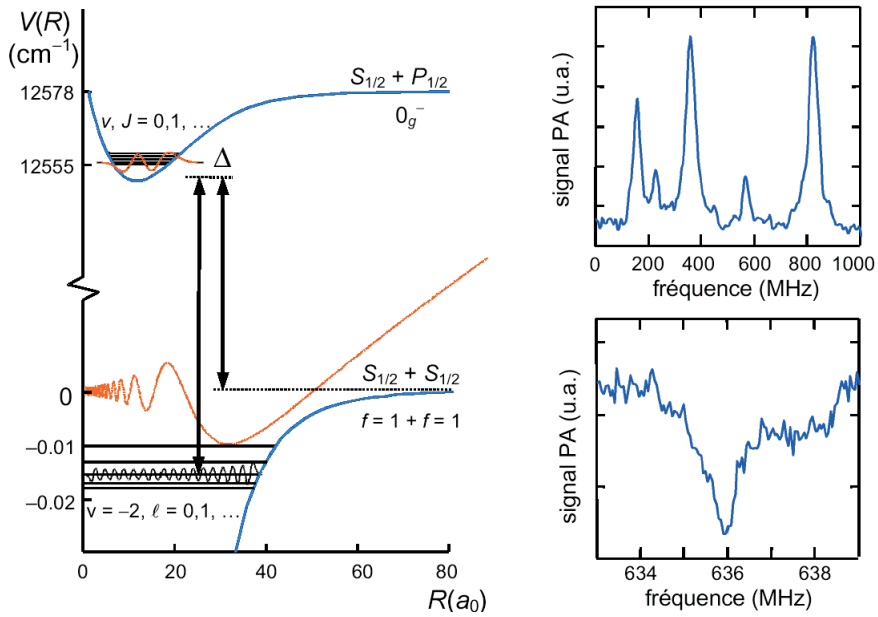

Figure 49.7: Free-bound-bound two-photon photoassociation in ^{87}Rb. During the collision of two atoms in their lower hyperfine level of the ground state, $^2S_{1/2}, f = 1, m_f = -1$, collide, they undergo a photoassociative Raman transition to the bound vibrational state $v = -2, l = 0, F = 2, m_F = -2$ located 636.0094 MHz below the ionization threshold. The intermediate excited state is $v, J = 0$ at $12555\,\text{cm}^{-1}$ of the 0_g^- potential connecting to the asymptote $^2S_{1/2} - ^2P_{1/2}$. The levels are chosen for their large Franck-Condon overlap.

While in a thermal cloud, two-photon photoassociation resonances have widths of some MHz (see Fig. 49.7 top right), the dark resonances measured in BECs have widths less than 2 kHz, which clearly shows the coherence of the coupling in the latter case. The narrowness of the dark resonance allows to measure the ionization energy of

the molecular ground state, $E = 2\pi\hbar \times 636.0094$ MHz, with unprecedented resolution, only limited by the spatially inhomogeneous distribution of the condensate's self-energy. Molecules are created in a specific state and preselected: They are at rest because the Raman process does not transfer momentum, the molecular state chosen in this experiment [1396] has no rotation, but the energy of the vibrational excitation is large (Rydberg's molecular states).

It is natural to ask in what situation the molecules should form an molecular condensate. In principle, for each ro-vibrational molecular state the lowest molecular state of the confining potential can accommodate a molecular BEC. However, the width of the dark resonance should be lower than the secular frequencies of the trap, to selectively populate a single (fundamental) motional state. In addition, the molecules should be reasonably stable. Unfortunately, molecules with highly excited vibrations undergo inelastic collisions with atoms (or other molecules if their density is high), which converts the vibrational excitation energy to kinetic energy for the atom and the molecule resulting in losses for the confined cloud [77]. Fast inelastic relaxation toward lower vibrational states limits the lifetime of the molecular Rydberg states to some 100 μs [1396]. We might think of coupling lower vibrational states of the molecular potential, provided the Franck-Condon overlap is sufficient. However, the energies of these vibrational levels are so far apart, that the frequencies of the Raman beams must be produced by different lasers. These lasers must be extremely stable, that is, their spectral emission bandwidth must be less than the desired resolution of the dark resonance.

49.6 Feshbach resonances in BECs

The equilibrium situation is described by the atomic and molecular chemical potentials being balanced $\mu = \mu_a = \mu_m$. If we express the BECs as c-numbers defining $n \equiv \phi^2$:

$$\mu\phi_a(\mathbf{r}) = \left[\tfrac{-\hbar^2}{2M_a}\Delta + V_a(\mathbf{r}) + g_{aa}n_a(\mathbf{r}) + g_{am}n_m(\mathbf{r})\right]\phi_a(\mathbf{r}) + \sqrt{2}\alpha\phi_m(\mathbf{r})\phi_a(\mathbf{r}) \ , \tag{49.59}$$

$$2\mu\phi_m(\mathbf{r}) = \left[\tfrac{-\hbar^2}{4M_m}\Delta + V_m(\mathbf{r}) + g_{mm}n_m(\mathbf{r}) + g_{am}n_a(\mathbf{r})\right]\phi_m(\mathbf{r}) + \tfrac{1}{\sqrt{2}}\alpha\phi_a^2(\mathbf{r}) \ .$$

49.6.1 Thomas-Fermi limit

For weak coupling strength $\alpha \to 0$, the contributions of a *single* atom and a *single* molecule to the total energy are:

$$1H = \int_{R^3} \left(U_a(\mathbf{r})n_a(\mathbf{r}) + U_m(\mathbf{r})n_m(\mathbf{r})\right) d^3\mathbf{r} \ , \tag{49.60}$$

$$1U_a(\mathbf{r}) = \tfrac{-\hbar^2}{2M_a}\Delta + V_a(\mathbf{r}) + g_{aa}n_a(\mathbf{r}) + g_{am}n_m(\mathbf{r}) \ ,$$

$$U_m(\mathbf{r}) = \tfrac{-\hbar^2}{2M_m}\Delta + V_m(\mathbf{r}) + g_{mm}n_m(\mathbf{r}) + g_{am}n_a(\mathbf{r}) \ .$$

For small molecular condensates, in the Thomas-Fermi limit:

$$U_a(\mathbf{r}) = V_a(\mathbf{r}) + g_{aa} n_a(\mathbf{r}) \ , \tag{49.61}$$
$$U_m(\mathbf{r}) = V_m(\mathbf{r}) + g_{am} n_a(\mathbf{r}) \ .$$

The elastic cold collision of two particles, atoms or molecules, $i, j = a, m$, can be described by the real part of the scattering length $a_{ij} = a'_{ij} - i a''_{ij}$, which is related to the interparticle interaction strength $g_{ij} = 4\pi\hbar^2 a'_{ij}/M_{ij}$, where we used the reduced mass $M_{ij}^{-1} = M_i^{-1} + M_j^{-1}$ of particle pairs, i.e. $M_{aa} = M/2$, $M_{am} = 2M/3$ and $M_{mm} = M$. Similarly, inelastic collisions are described by the imaginary part $K_{ij}^{(inel)} = 4\pi\hbar^2 a''_{ij}/M_{ij}$. Additionally we have the interspecies coupling strength α.

49.6.2 Off-resonant and resonant limit

Far from the Feshbach resonance, $\Delta E \longrightarrow \infty$, in the Thomas-Fermi limit, $g \equiv 2g_a \equiv g_m$. The minimum energy density is,

$$u_{\min} = \phi_a^+ \left(\tfrac{g_a}{2} - \tfrac{\alpha^2}{\Delta E} \right) n \phi_a \ , \tag{49.62}$$

and the equations (49.58) reduce to the well-known single-species GPE where the scattering has changed to,

$$a_{eff} = a_0 - \frac{M}{4\pi\hbar^2} \frac{2\alpha^2}{2\mu_a - \mu_m} \frac{1}{B - B_{FB}} \ . \tag{49.63}$$

Tuning a from *positive side* into resonance, i.e. driving the scattering length from positive values to 0 reduces the self-energy $4\pi\hbar^2 a/M \cdot n_a \longrightarrow 0$, so that the BEC must collaps according to the a_{eff} description, unless it is stabilized by a confining trap allowing a certain maximum n_a. However, in the correct two-species description, the atoms can tunnel into molecular states thus reducing n_a to a number that can actually be balanced by the confining trap. This effect stabilizes the BEC.

The a_{eff} description also suggests unphysical divergences.

49.6.2.1 Decay

Collisions will induce a fast relaxation of highly excited *molecular Rydberg states*. We have two competing time scales. Fast relaxation of high vibrational states by inelastic (molecule-atom) 3-body collisions typically happens for $n = 10^{14}$ cm^{-3} and $\Gamma_{typical}$ within $\tau_{relax} = 1$ μs..1 ms. The condensate dynamics governed by self-energy $i\hbar\partial_t\psi = \frac{4\pi\hbar^2 1}{m} n\psi$ which happens within τ_{cond} =several 100 ms. It seems, that adiabatic tuning into FBR may be barely feasible.

The decay gives rise to an irreversibility and thus to a dependence of the state on history which is not included in the a_{eff} description.

49.7 Raman photoassociation in BECs

49.7.1 Molecule production

Complicated ro-vibrational structure of molecules inhibits efficient laser cooling. Supersonic expansion internally cold but translationally hot, cryogenic cooling [387] and

magnetic trapping [1365] works down to K. Incoherent photoassociation has produced molecules rotationally as cold as 100 μK, but still populates many excited vibrational states and has a large energy spread [445]. Other work has been done by [82], [690], [832], [669], [1396], [638].

In a BEC we can state-selectively (here: no rotation, high vibration, weakly bound) create ^{87}Rb molecules at rest (no motion). Raman dark resonance width of 1.5 kHz influenced by molecule- atomic BEC interactions. The molecular binding energy is precisely measurable $\varepsilon = 2\pi \times 636.0094$ MHz. Is useful for determining the potentials even more accurately.

Procedure is very simple: Make a BEC of a few 10^5 atoms in the ground state ^{87}Rb $5^2S_{1/2}(f = 1, m_f = -1)$ with variable densities $n_0 = 0.8...2.7$ cm^{-3}. Then irradiate a collinear pair of laser beams for $\tau = 150...550$ ms with $\Delta_1 = 2\pi \times -150$ MHz and detuned from an upper 0_g^- long range molecular state and $\Delta_2 = \Delta_1 + 636$ MHz phase coherent to Δ_1 within 1 kHz. The momentum transfer is neglegible, because $\mathbf{k}_1 \approx \mathbf{k}_2$. Neighboring atoms interact via $V_g(R)$, the Raman beams couple the free collisional channel via a dark resonance to a single ro-vibrational bound state. Finally measure the losses $N(\tau)/N_0$ from the BEC via fluorescence TOF. The dark resonance is probe by repeating the sequence with various detunings.

The width and shift of the resonance depends on the laser intensities I_1 and I_2 and detuning Δ_1 and on the peak density of the condensate. AC-Stark shift and *power*-broadening due to spontaneous Raman scattering of molecules removing them from the BEC. The dependence on the laser parameter can be removed by extrapolation to 0.

The Doppler broadening is not important, because $E_{kin} \approx 6$ nK and $E_{pot} \approx 100$ nK. Zeeman brodening is neglegible, because $\vec{\mu}_{mol} = 2\vec{\mu}_{atom}$ so that it is smaller than1.5 kHz/G. No radiative decay? In the Thomas-Fermi limit the energy width of the atomic BEC is strongly reduced, because of the large coordinate distribution and the uncertainty relation. The resonance width is therefore attributed to molecule-atom interactions.

To treat the problem, we can use equations (49.58), and set $u_{kin} \to 0$ and $u_{conv} \to 0$. In analogy to equation (49.60), we get,

$$\begin{aligned} H &= \int_{R^3} \left(U_a(\mathbf{r})n_a(\mathbf{r}) + U_m(\mathbf{r})n_m(\mathbf{r})\right) d^3\mathbf{r} \qquad (49.64) \\ U_a(\mathbf{r}) &= V_a(\mathbf{r}) + g_{aa}n_a(\mathbf{r}) = const \\ U_m(\mathbf{r}) &= V_m(\mathbf{r}) + g_{am}n_a(\mathbf{r}) \ , \end{aligned}$$

where $g_{aa} = 4\pi\hbar^2 a'_{aa}/M$ and $g_{am} = 3\pi\hbar^2 a'_{am}/M$ and $V_m(\mathbf{r}) = 2V_a(\mathbf{r})$. We know from earlier experiments that $a'_{aa} = 104a_B$ and $a''_{aa} \approx 0$. When converting a pair of atoms into a molecule, we have to cross the energy gap $\Delta U(\mathbf{r}) \equiv U_m(\mathbf{r}) - 2U_a(\mathbf{r}) = (g_m - 2g_a)n_a(\mathbf{r})$. The coordinate dependence broadens the transition. A crude model for the photoassociative loss rate $\dot{n}_a(\mathbf{r}, t)$ permits a rough estimate of $a'_{am} \approx -180a_B$ and $a''_{am} < 110a_B$, or equivalently g_{am} and $K_{am}^{(inel)} < 8 \cdot 10^{-11}$cm^3/s. That means that at $n_a(0) = 10^{14}$cm^3 peak density the lifetime of the molecules lies at about $\tau_{inel} = 0.1...0.5$ms and much faster than the trap secular frequency, so that the molecules can be considered at rest during the whole process. For longer vibrational lifetimes, the inhomogeneous broadening transforms into an oscillator spectrum which

could be resolved by the Raman transition. The lowest trap oscillation level for each vibrational state can, in principle, accommodate a molecular ground state BEC.

Vibrationally excited molecules collide inelastically with atoms (or other molecules if the density is high enough) converting their vibrational energy into kinetic energy for the atom and the molecule resulting in trap loss. This process is very strong for high vibrational excitation [77]. This process is also the reason for the observed strong inelastic losses near Feshbach resonances. The analogy to Feshbach resonances comes from the fact that they can be interpreted as coming from a transient intermediate molecular state in a 2-atom collision. Both schemes of controlled molecule production may be useful only if the lowest vibrational levels are populated or a level with inhibited decay.

However, if the lifetime of the vibrational state τ_{vib} is long enough, both schemes are not simply collision resonances (resonant modification of the scattering length), but a separate population of the molecular state builds up and the *cm-* degree of freedom interacts with the atomic BEC.

Outlook on reversible creation of molecular BECs with exotic phenomena provided the vibrational relaxation by molecule-atom and molecule-molecule collisions can be overcome. Molecular laser may be feasible by choosing laser geometries different from parallel beams, so that the momentum transfer expulses the molecules from the atomic BEC.

49.8 Production of heteronuclear molecules

Our main goal is the production of LiRb molecules. Two ways are possible: Using Feshbach resonances or via Raman-Photoassociation. Stability issues: They might be much more unstable then fermionic species molecules. Molecules may be short-lived due to inelastic or *reactive losses* [315].

49.8.1 General production schemes

49.8.1.1 Photoassociation

Mixed species collisions have no resonant dipole-dipole interaction [707, 837]. Therefore excited state collisions of different species are purely short-ranged. This makes free-bound *photoassociation* more difficult, but enhanced bound-bound transitions towards deeply bound vibrational states. For reasonable rates laser intensities on the order of 100 W/cm^2 are required. High densities more than 10^{11} cm^{-3} are desired. The lowest fine structure dissociation limit is good to prevent predissociation [706]: Li($2s$)-Rb($5p_{1/2}$).

The ground state $^3\Sigma$ potential supports around 60 vibrational levels. It is 300 cm^{-1} deep (or 20 nm at 795 nm).

49.8.1.2 Two-color photoassociation

For a coherent coupling via *stimulated Raman photoassociation* of those states stable lasers are necessary. Phase-locked stabilization either requires photonic fibres or locking to a common cavity. The free-bound laser must be very strong.

49.8.1.3 Feshbach resonance

Proposal for heteronuclear molecules via Feshbach resonances stem from [738, 1274]. Also *heteronuclear Feshbach resonance* has been observed for ^{6}Li^{7}Li [1327], ^{6}Li^{23}Na, [1242], and ^{40}K^{87}Rb [**?**].

49.8.2 LiRb molecules

The LiRb sytem is interesting for its large permanent electric dipole moment. Also, the combination LiRb has been shown advantageous for reaching low temperatures due to the large mass difference (see Sec. 49.2.2). E.g. try boson-mediated s-wave or p-wave Cooper pairing without no ^{6}Li^{6}Li Feshbach resonance enhancement. In contrast, the ^{6}Li^{87}Rb interaction can be tuned by an interspecies Feshbach resonance (tuning both resonances simultaneously does not work anyway). The predicted pairing temperatures are very low [408], $T \ll 1$ nK for $a_{bf} \gg 200a_B$ and $n_f \gg 10^{14}$ cm^{-3}.

The idea for their production is to cool ^{6}Li and ^{87}Rb atoms down, excite a Feshbach resonance and simultaneously a Raman transition.

49.8.2.1 Production scheme for LiRb molecules

- Step 1: Transfer atoms from the triplet scattering channel $|2,-2\rangle|3/2,3/2\rangle$ towards $|1,-1\rangle|1/2,-1/2\rangle$ via a combination of microwave pulses driving the hyperfine resonance and adiabatic radiofrequency sweeps, carefully designed to populate the desired states.

- Step 2: The colliding channel is coupled to a low-lying bound vibrational level via a Raman transition. An appropriate scheme has to be found, satisfying the selection rules for radiative transitions, maximizing the Franck-Condon overlaps and working at convenient transition wavelengths. The Raman transition must be driven by a stabilized system of two lasers; their relative stability should be high enough to allow for a resolution of the secular frequencies of the trapping potential [3].

- Exciting Raman transitions, Scheme 1: The atoms collide in their fully stretched $|2,2\rangle|3/2,3/2\rangle$ channel which only connects to the $a^3\Sigma^+$ potential. The amplitude of the scattering wavefunction is enhance by a Feshbach resonance. A laser at 1700 nm excites close to the outer turning point a level of the $(1)^3\Pi$ potential, which mixes via spin-orbit coupling with the $(2)^1\Sigma^+$ potential to give rise to a 0^+ level structure. The inner turning point has a good Franck-Condon overlap with low-lying vibrational levels of the $X^1\Sigma^+$ ground state potential.

- Exciting Raman transitions, Scheme 2: The atoms collide in a channel which has admixtures of the $X^1\Sigma^+$ ground state potential.

[3] Is PA coupling strong enough even in presence of spontaneous decay? What are the selection rules for bound-bound transitions to deeply bound levels?

49.8.3 Stability of LiRb Rydberg molecules

The heteronuclear ^{6}Li^{87}Rb molecules will be unstable against collisions with Li and in particular bosonic Rb atoms, whose density is very high. However sufficiently deep bound LiRb molecules are fermionic and thus stable against ultra-slow inelastic collisions. In contrast, this is not true for highly excited vibrational states. Close to dissociation the quantum statistics of the constituents is expected to dominate the collision process, which leads to accelerated decay. How deep must the binding be for stable LiRb clouds? What loss mechanisms are possible [44]?

49.8.3.1 Tuning the binding energy

There are two contradictory pictures. In a 'single-channel picture', close to a FR the bound states of potential V_b interacts with the collisional channel of another potential V_c. This interaction deepens (or flattens) V_c and causes a continuum state of V_c to move into a bound state of V_c. The binding energy then increases with the detuning.

In a two-channel picture, have [1242].

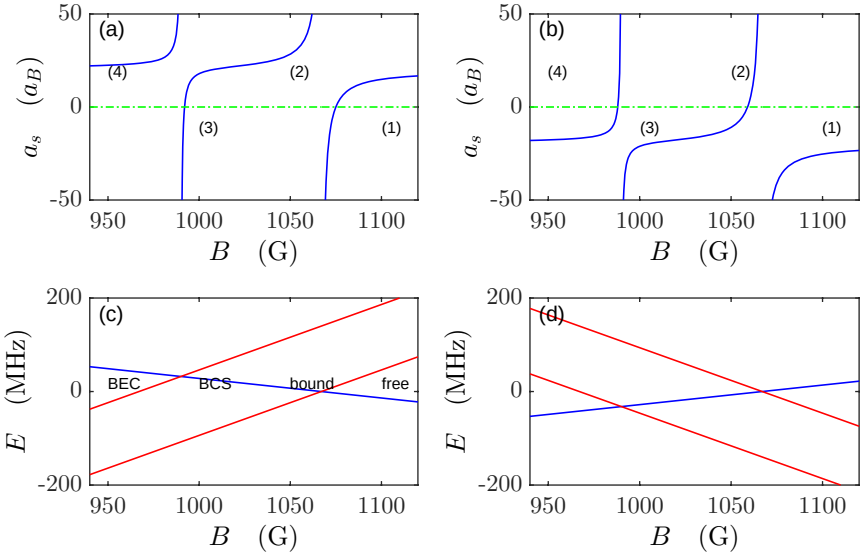

Figure 49.8: (code) Tuning of scattering length (a,b) and bound state energies (c) near Feshbach resonances for (a) $a_s(0) > 0$, (b) $a_s(0) < 0$. Here (1,3) $a_s > 0$, (2,4) $a_s < 0$.

49.8.4 Removing Li and Rb molecules

Nocif Li and Rb atoms can be removed by *Stern-Gerlach separation*. This may work if the goal is separate imaging of atoms and molecules. It may however be too slow to prevent collisions. Another option is resonant excitation of the atoms. But this requires GHz far-detuned lasers.

We want to separate Rb atoms and LiRb molecules in time-of-flight. The clouds are 7 µK hot. We want to apply a $b = 40\,\mathrm{G/cm}$ gradient force for less than $\Delta t = 500\,\mu\mathrm{s}$.

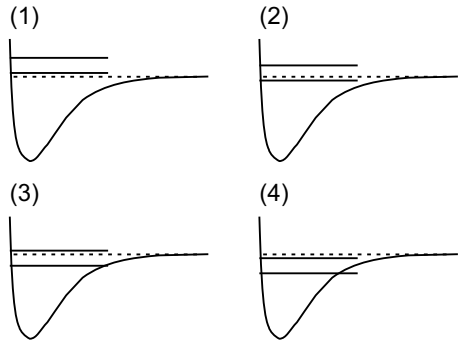

Figure 49.9: (code) (1,3) $a_s < 0$, (2,4) $a_s > 0$.

Hence, the thermal expansion velocity,

$$\bar{v} = \sqrt{\frac{k_B T}{m_{87}}} \simeq \sqrt{\frac{k_B T}{m_{93}}} \simeq 2.5\,\mathrm{cm/s} \tag{49.65}$$

must be smaller than the separation velocity,

$$\Delta v = \int \frac{F_{87}}{m_{87}} dt - \int \frac{F_{93}}{m_{93}} dt \simeq 2\frac{F_{87}}{m_{87}}\Delta t \simeq 2\frac{\mu_B b}{m_{87}}\Delta t \simeq 2.6\,\mathrm{cm/s}\ . \tag{49.66}$$

49.8.4.1 Optical transitions in the Paschen-Goudsmith regime

There are cycling transitions out of the absolute ground state in the Paschen-Back regime. For ^{87}Rb the $^2S_{1/2}$ ground state $|F = 1, m_F = 1\rangle$ connects to $|m'_J = -\frac{1}{2}, m'_I = \frac{3}{2}\rangle$. From here laser light can reach the excited $^2P_{3/2}$ state $|m'_J = -\frac{3}{2}, m'_I = \frac{3}{2}\rangle$, which connects to $|F' = 0, m'_F = 0\rangle$. For ^{6}Li the $^2S_{1/2}$ ground state $|F = \frac{1}{2}, m_F = \frac{1}{2}\rangle$ connects to $|m'_J = -\frac{1}{2}, m'_I = 1\rangle$. From here laser light can reach the excited $^2P_{3/2}$ state $|m'_J = -\frac{3}{2}, m'_I = 1\rangle$, which connects to $|F' = \frac{1}{2}, m'_F = -\frac{1}{2}\rangle$. Note the latter transitions would be forbidden in the Zeeman regime, because $\Delta > 1$.

49.8.5 Detecting molecules

49.8.5.1 Ramping through a Feshbach resonance

A procedure could be

1. Create an ultracold mixture of atomic Li and Rb.
2. Quickly tune the magnetic field to 1080 nm above the Feshbach resonance at 1070 nm.
3. Ramp the magnetic field across the Feshbach resonance to 1060 nm such that the binding energy ΔE_B is increased, thus creating up to 40000 LiRb molecules.

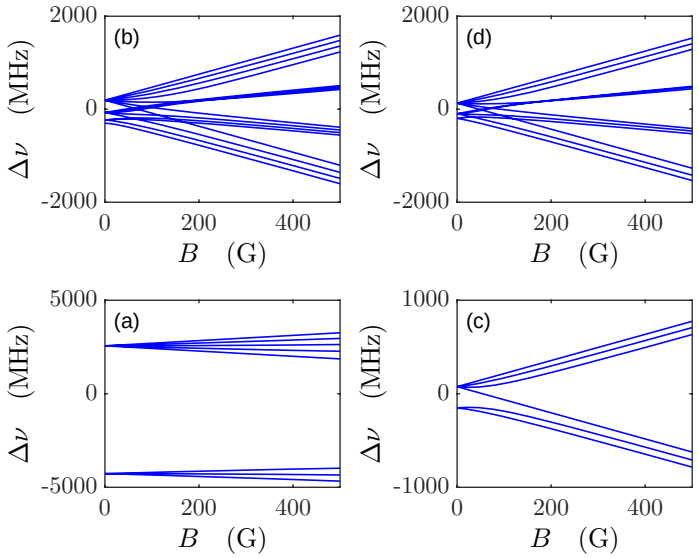

Figure 49.10: Zeeman splitting in the Paschen-Back regime. (a) ^{87}Rb $^2S_{1/2}$, (b) ^{87}Rb $^2P_{3/2}$, (c): ^{6}Li $^2S_{1/2}$, and (c): ^{6}Li $^2P_{3/2}$. The cycling transitions are marked by thick lines.

4. Immediately switch off the dipole trap to reduce the density and diminish the collision rate between LiRb molecules and Rb atoms.

5. Ramp the homogeneous magnetic field back through the Feshbach resonance to 1080 nm, thus reconverting the molecules into atoms.

6. Switch off the homogeneous magnetic field.

7. Immediately absorption image the Li atoms. The visible Li atoms are those that have been bound to Rb atoms previously.

8. Repeat the sequence 1. to 7. now skipping step 5. In this case no Li atoms should be visible, because they are all bound to Rb atoms.

If the Li signal is too weak because the steps 5. and 6. take too much time, it may be possible to watch the Rb cloud. In order to separate those Rb atoms which have not been bound to a Li atom from those who have, one could apply a gradient field to Stern-Gerlach separate LiRb from Rb. In this case the following sequence might work:

1.-4. as above.

5. Apply a gradient field. It can be superposed to the homogeneous field provided both are chosen collinear.

6. Ramp the homogeneous magnetic field back through the Feshbach resonance to 1080 nm, thus reconverting the molecules into atoms.

7. Switch off all magnetic fields.

8. Immediately absorption image the Rb atoms. A bimodal distribution of Rb atoms should be visible [402].

49.8.5.2 Radiofrequency spectroscopy of molecules

Following [983] we could try to excite molecular resonances without any hope of detecting them. It's just an additional loss channel. It could reveal precious information on the size of the scattering length.

How to predict the location of the binding energy peak? If we assume that the measure trap loss width corresponds to the real width of the Feshbach resonance, we can calculate the profile of the scattering length and the binding energy from $E_b = \frac{\hbar^2}{2ma_s^2}$.

1. Transfer Li atoms into $|1/2, -1/2\rangle$ state (i.e. $|m_J, m_I\rangle = |1/2, -1/2\rangle$).
2. Tune close to the Feshbach resonance of the $|1/2, 1/2\rangle$ state.
3. Populate the $|1/2, 1/2\rangle$ state by rf-spectroscopy.
4. Near the Feshbach resonance a second peak blue-detuned from the resonant energy for the population transfer should appear due to the formation of molecules with a certain binding energy.
5. Image the atoms remaining in the $|1/2, 1/2\rangle$ state.
6. Image the atoms in the $|1/2, -1/2\rangle$ state together with the molecules.
7. The molecular decay is expected to be fast leading to important losses in the image 6.. In contrast, it should not matter for the image 5.

The transition frequency is about 50 MHz. Note that the $\Delta m_I \neq 0$ transition may be very weak. Alternatively, one could probe from the ^{6}Li$|F = 3/2, m_F = 3/2\rangle$ state with a transition frequency of 500 MHz or from the ^{87}Rb$|F = 2, m_F = 2\rangle$ state with a frequency of 6.8 GHz.

49.8.6 Binding energy in the harmonic trap

One expects resonances of trap-assisted binding [219, 983, 360]. However, our weak scattering length and the (relatively) weak trap mitigates this behavior. The spectrum is given by,

$$\frac{\Gamma(-E_b/2\hbar\omega_{ho} + 3/4)}{\Gamma(-E_b/2\hbar\omega_{ho} + 1/4)} = \frac{a_{ho}}{2a_s} \ , \tag{49.67}$$

where $a_{ho} = \sqrt{\hbar/m\omega_{ho}}$. Making use of $\lim_{x\leftarrow\infty} \frac{\Gamma(-x+3/4)}{\Gamma(-x+1/4)} \to \sqrt{x}$, we find for large scattering lengths,

$$-E_b = \frac{\hbar}{2\mu a_s} \ . \tag{49.68}$$

Within the Feshbach resonance $|B - B_0| \ll \Delta B$,

$$E_b = -\frac{\hbar^2}{2ma_{bg}^2 \left(1 - \frac{\Delta B}{B - B_0}\right)^2} \simeq -\frac{\hbar^2}{2ma_{bg}^2} \left(\frac{B - B_0}{\Delta B}\right)^2 \ . \tag{49.69}$$

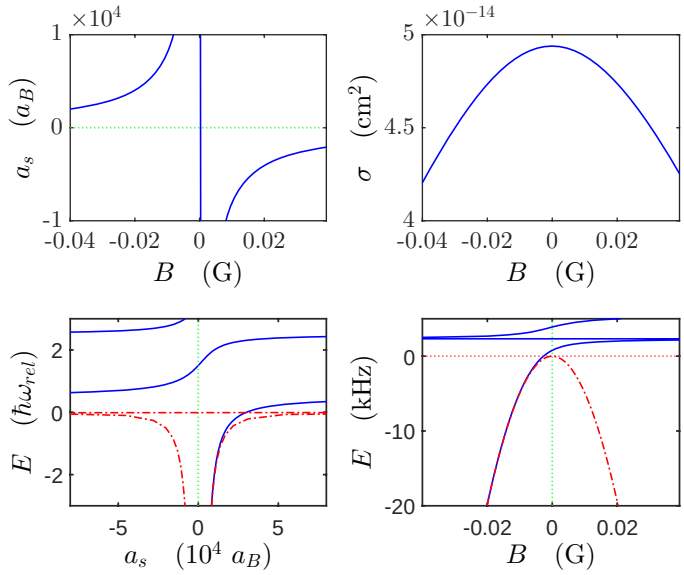

Figure 49.11: Trap binding.

E.g. let us choose a detuning of $B - B_0 = -0.1\Delta B$, where $E_b = h \times 8$ MHz. Then a magnetic field noise of $dB \approx 1$ mG causes an inhomogeneous broadening of the transition by $dE_b \simeq -\frac{\hbar^2}{ma_{bg}^2}\frac{B-B_0}{\Delta B^2}dB \approx h \times 20$ kHz. The broadening increases linearly with detuning.

Thermal broadening may reduce the production efficiency of LiRb atoms. At 7 μK the broadening is 146 kHz. It is recommended to have at least one species condensed [623, 996].

49.8.7 Dipolar relaxation and three-body decay in mixed species

The rate equations for the collisional decay of a Li-Rb mixture are,

$$\dot{N}_6 = \int d^3\mathbf{r}\ \left(-\gamma_6 n_6 - G_{6,6}n_6^2 - G_{6,87}n_6 n_{87} - K_{6,6,6}n_6^3 - K_{6,6,87}n_6^2 n_{87} - K_{6,87,87}n_6 n_{87}^2\right) \tag{49.70}$$

$$\dot{N}_{87} = \int d^3\mathbf{r}\ \left(-\gamma_{87} n_{87} - G_{87,87}n_{87}^2 - G_{6,87}n_6 n_{87} - K_{87,87,87}n_{87}^3 - K_{6,87,87}n_6 n_{87}^2 - K_{6,6,87}n_6^2 n_{87}\right)\ .$$

For a harmonic trap the densities are Gaussian function, $n_j = n_{0,j}e^{-U_j/k_BT_j}$ with $U_j = \frac{m_j}{2}\omega_{r,j}^2 r^2 + \frac{m_j}{2}\omega_{z,j}^2 z^2$. The masses, the trapping potentials and the temperatures for the clouds may differ. We will however assume that the trap have identical shapes, $\omega_{r,87}/\omega_{z,87} = \omega_{r,6}/\omega_{z,6}$, so that the traps may be decribed by isotropic potentials with an averaged secular frequencies, $U_j = \frac{m_j}{2}\omega_j^2 x^2$ with $\omega_j = \left(\omega_{r,j}^2\omega_{z,j}\right)^{1/3}$. We define $\xi \equiv m_6\omega_6^2 T_{87}/m_{87}\omega_{87}^2 T_6$ and the effective volumes $V_{87} \equiv \left(\frac{2\pi k_B T_{87}}{m_{87}\tilde{\omega}_{87}^2}\right)^{3/2} = \xi^{3/2}V_6$. The

integrals can analytically be evaluated,

$$N_j = \int n_j d^3\mathbf{r} = n_{0,j} \int e^{-m_j\omega_j^2 x^2/2k_B T_j} d^3\mathbf{r} = n_{0,j} \sqrt{\frac{2\pi k_B T_j}{m_j\omega_j^2}}^3 = n_{0,j} V_j \tag{49.71}$$

$$\int n_j^k d^3\mathbf{r} = k^{-3/2} n_{0,j}^k V_j$$

$$\int n_{87}^k n_6^l d^3\mathbf{r} = (k + l\xi)^{-3/2} n_{0,87}^k n_{0,6}^l V_{87}$$

finally,

$$\frac{\dot{N}_6}{N_6} = -\gamma_6 - \frac{G_{6,6}}{2^{3/2}}\frac{N_6}{V_6} - \frac{\xi^{3/2} G_{6,87}}{(1+\xi)^{3/2}}\frac{N_{87}}{V_{87}} - \frac{K_{6,6,6}}{3^{3/2}}\frac{N_6^2}{V_6^2} - \frac{\xi^{3/2} K_{6,6,87}}{(1+2\xi)^{3/2}}\frac{N_{87}N_6}{V_{87}V_6} - \frac{\xi^{3/2} K_{6,87,87}}{(2+\xi)^{3/2}}\frac{N_{87}^2}{V_{87}^2} \tag{49.72}$$

$$\frac{\dot{N}_{87}}{N_{87}} = -\gamma_{87} - \frac{G_{87,87}}{2^{3/2}}\frac{N_{87}}{V_{87}} - \frac{G_{6,87}}{(1+\xi)^{3/2}}\frac{N_6}{V_6} - \frac{K_{87,87,87}}{3^{3/2}}\frac{N_{87}^2}{V_{87}^2} - \frac{K_{6,87,87}}{(2+\xi)^{3/2}}\frac{N_{87}N_6}{V_{87}V_6} - \frac{K_{6,6,87}}{(1+2\xi)^{3/2}}\frac{N_6^2}{V_6^2} .$$

Trap loss due to collisions with the background gas is negligible, $\gamma \approx 0$. Two-body relaxation is impossible in the energetic ground state, $G_{x,y} \simeq 0$. $K_{x,y,z}$ are the rate coefficients for losses due to collisions involving atoms of species xyz. The Rb density is overwhelming, $n_6 \ll n_{87}$. Hence the rate equations can be simplified. The terms in $K_{6,6,87}n_6^2$ are explicitly retained, although they are small, in order to permit a modeling of a resonant enhancement of $K_{6,6,87}$ near a ^{6}Li p-wave Feshbach resonance. Else we may set $K_{6,6,87} = 0$. Approximating $V \simeq 3{\times}10^{-15}$ m^3. Setting the initial atom numbers to $N_6 = 50000$ and $N_{87} = 200\,000$ and assuming $K_{87-87-87} \simeq K_{87-87-6} \approx 2.8 \times 10^{-28}$ cm^6/s [984], we get the following curves,

$$\dot{N}_6 V_{87}^2 = -\frac{\xi^3 K_{6,6,6}(B)}{3^{3/2}} N_6^3 - \frac{\xi^3 K_{6,6,87}(B)}{(1+2\xi)^{3/2}} N_{87} N_6^2 - \frac{\xi^{3/2} K_{6,87,87}(B)}{(2+\xi)^{3/2}} N_{87}^2 N_6 \tag{49.73}$$

$$\dot{N}_{87} V_{87}^2 = -\frac{K_{87,87,87}(B)}{3^{3/2}} N_{87}^3 - \frac{\xi^3 K_{6,6,87}(B)}{(1+2\xi)^{3/2}} N_{87} N_6^2 - \frac{\xi^{3/2} K_{6,87,87}(B)}{(2+\xi)^{3/2}} N_{87}^2 N_6 .$$

Now we develop full rate equation model considering all possible processes, try the ansatz $K_{6,6,87} \simeq 10\hbar/m\ a_{6,6}^{8/3} a_{6,87}^{4/3}$ and $K_{6,87,87} \simeq 10\hbar/m\ a_{6,6}^{4/3} a_{6,87}^{8/3}$, calculate rate equations across Feshbach resonances,

$$\dot{N}_6 = -\frac{10\hbar\ a_{6,6}^{8/3} a_{6,87}^{4/3}}{mV^2} N_6^2 N_{87} - \frac{10\hbar\ a_{6,6}^{4/3} a_{6,87}^{8/3}}{mV^2} N_6 N_{87}^2 \tag{49.74}$$

$$\dot{N}_{87} = -\frac{10\hbar\ a_{87,87}^{4}}{mV^2} N_{87}^3 - \frac{10\hbar\ a_{6,6}^{4/3} a_{6,87}^{8/3}}{mV^2} N_6 N_{87}^2 - \frac{10\hbar\ a_{6,6}^{8/3} a_{6,87}^{4/3}}{mV^2} N_6^2 N_{87} .$$

49.8.8 ^{6}Li^{87}Rb $X^1\Sigma^+(v = 0)$ ground state molecules

According to [1274] it should be possible to with heteronuclear dimers to convert free atoms via a Feshbach resonance to a molecular BEC of weakly bound $a^3\Sigma^+$ molecules.

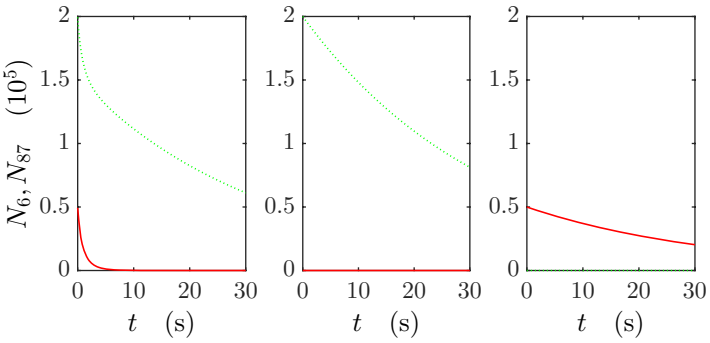

Figure 49.12: (a) Simultaneous decay of Li and Rb, (b) decay of Rb when Li is absent from the trap, (c) and decay of Li when Rb is absent from the trap.

Those are then excited to the outer turning point of the $(1)^3\Pi$ level, which mixes with the $A^1\Sigma^+$ level to form a 0^+ potential, which has 4 turning points. The molecules are then deexcited at the inner turning point towards the absolute ground state $X^1\Sigma^+$. Unfortunately, the laser wavelengths are difficult. For the pump at 1700 nm and for the dump at 830 nmm (Fig. 49.13, left) or 693 nm and 495 nm (Fig. 49.13, right).

Other more sophisticated transitions towards higher levels or using more intermediate steps are possible.

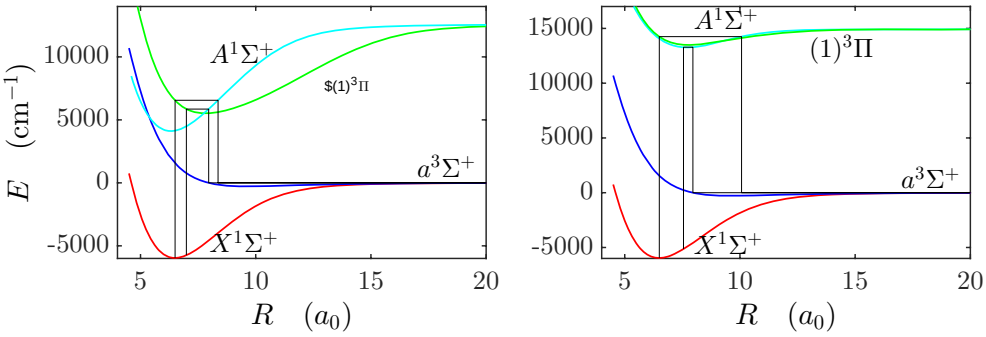

Figure 49.13: Scheme for deexciting ^{6}Li^{87}Rb molecules to low-lying vibrational states. Left: $\lambda_{pump} = 1707.592$ nm and $\lambda_{dump} = 862.4407$ nm. Right: $\lambda_{pump} = 701.7544$ nm and $\lambda_{dump} = 500.2802$ nm.

49.9 Further reading

J. R. Abo-Shaeer et al., *Coherent Molecular Optics Using Ultracold Sodium Dimers* [2]DOI

Zhao-Qing Zhang et al., *Transition from an atomic to a molecular Bose-Einstein condensate* [1430]DOI

49.9.1 on Fermi degeneracy

B. DeMarco et al., *Onset of Fermi-Degeneracy in a Trapped Atomic Gas* [347]DOI

, *Pauli Blocking of Collisions in a Quantum Degenerate Atomic Fermi Gas* [348]DOI

Chapter 50

Quantum theory of non-relativistic fields

50.1 Quantizing the scalar field

50.1.1 States of individual atoms in a gas

To introduce the physical situation, we consider an external potential $U(\mathbf{r})$ representing a cubic box of length L and volume $V = L^3$. Introducing periodic boundary conditions, $\phi(x+L, y+L, z+L) = \phi(x, y, z)$, the Schrödinger equation for the spatial motion of a single atom in the box can be written as,

$$-\frac{\hbar^2}{2m}\nabla^2\phi_{\mathbf{k}}(\mathbf{r}) = \varepsilon_{\mathbf{k}}\phi_{\mathbf{k}}(\mathbf{r}) \ , \tag{50.1}$$

where the eigenfunctions and corresponding eigenvalues are given by

$$\phi_{\mathbf{k}}(\mathbf{r}) = \tfrac{1}{\sqrt{V}}e^{\imath\mathbf{k}\cdot\mathbf{r}} \qquad \text{and} \qquad \varepsilon_{\mathbf{k}} = \frac{\hbar^2k^2}{2m} \ . \tag{50.2}$$

The wavefunctions $\phi_k(\mathbf{r})$ represent *plane wave solutions*, normalized to the volume of the box, with $\mathbf{k}$ the wave vector of the atom, $k = |\mathbf{k}| = 2\pi/\lambda_{dB}$ the wave number, and λ_{dB} the de Broglie wavelength. The periodic boundary conditions give rise to a discrete set of wavenumbers, $k_\alpha = (2\pi/L)n_\alpha$ with $n_\alpha \in \{0, \pm1, \pm2, ...\}$ and $\alpha \in \{x, y, z\}$.

50.1.2 Wave functions for pairs

The Hamiltonian for the motion of two atoms with interatomic interaction $\mathcal{V}(\mathbf{r}_{12})$ and confined by the cubic box potential $\mathcal{U}(\mathbf{r})$ defined above is given by

$$\mathcal{H} = \sum_{i=1,2}\left(-\frac{\hbar^2}{2m_i}\nabla_i^2 + \mathcal{U}(\mathbf{r}_i)\right) + \mathcal{V}(\mathbf{r}_{12}) \ . \tag{50.3}$$

When the cubic box $\mathcal{U}(\mathbf{r})$ is macroscopically large, the pair is in the extreme collisionless limit and the dynamics may be described accurately by neglecting the interaction $\mathcal{V}(\mathbf{r}_{12})$, i.e., the Schrödinger equation takes the form

$$\left(-\frac{\hbar^2}{2m_1}\nabla_1^2 - \frac{\hbar^2}{2m_2}\nabla_2^2\right)\psi_{\mathbf{k}_1,\mathbf{k}_2}(\mathbf{r}_1, \mathbf{r}_2) = E_{\mathbf{k}_1,\mathbf{k}_2}\psi_{\mathbf{k}_1,\mathbf{k}_2}(\mathbf{r}_1, \mathbf{r}_2) \ . \tag{50.4}$$

In this limit we have complete separation of variables so that the pair solution can be written in the form of a product wavefunction

$$\psi_{\mathbf{k}_1,\mathbf{k}_2}(\mathbf{r}_1,\mathbf{r}_2) = \tfrac{1}{V} e^{i\mathbf{k}_1\cdot\mathbf{r}_1} e^{i\mathbf{k}_2\cdot\mathbf{r}_2} \ , \tag{50.5}$$

with $\mathbf{k}_i$ the wavevector of atom i, quantized as $k_{i\alpha} = \frac{2\pi}{L} n_{i\alpha}$ with $n_{i\alpha} \in \{0, \pm 1, \pm 2, ...\}$. This wavefunction is normalized to unity (one pair). The energy eigenvalues are

$$E_{\mathbf{k}_1,\mathbf{k}_2} = \frac{\hbar^2 k_1^2}{2m_1} + \frac{\hbar^2 k_2^2}{2m_2} \ . \tag{50.6}$$

Note that in this case

$$E_{\mathbf{k}_1,\mathbf{k}_2} \neq E_{\mathbf{k}_2,\mathbf{k}_1} \qquad \text{for} \qquad \mathbf{k}_1 \neq \mathbf{k}_2 \ . \tag{50.7}$$

Importantly, only for pairs of *unlike* atoms the product wavefunctions (7.5) represent uniquely defined quantum mechanical eigenstates for the eigenvalues $E_{\mathbf{k}_1,\mathbf{k}_2}$. By unlike we mean that the atoms may be distinguished from each other because they are of different species. For *identical* atoms, i.e., atoms of the same isotopic species, the situation is fundamentally different. In this case the product wavefunctions (7.5) are degenerate with pair wavefunctions in which the atoms are exchanged,

$$E_{\mathbf{k}_1,\mathbf{k}_2} = E_{\mathbf{k}_2,\mathbf{k}_1} \qquad \text{also for} \qquad \mathbf{k}_1 \neq \mathbf{k}_2 \ . \tag{50.8}$$

This implies that any linear combination of the type

$$\psi_{\mathbf{k}_1,\mathbf{k}_2}(\mathbf{r}_1,\mathbf{r}_2) = \frac{1}{V}\frac{1}{|c_1|^2+|c_2|^2} c_1 e^{i\mathbf{k}_1\cdot\mathbf{r}_1} e^{i\mathbf{k}_2\cdot\mathbf{r}_2} + c_2 e^{i\mathbf{k}_2\cdot\mathbf{r}_2} e^{i\mathbf{k}_1\cdot\mathbf{r}_1} \tag{50.9}$$

represents a properly normalized energy eigenstate of the pair. This is called *exchange degeneracy*. As we shall see in the next section, this degeneracy gives rise to *quantum correlations* in the motion of the atoms that depend on the quantum statistical nature of the atoms as well as on their internal state.

50.1.3 Identical particles and exchange operator

Before starting the subject of many-body wavefunctions, we first recall the consequences of the indistinguishability of identical particles in quantum mechanics. Particles are called identical if there is no physical way to establish whether or not two particles have been exchanged. To describe the exchange we introduce the *exchange operator* $\mathcal{P}$. For two identical particles in an arbitrary pair state $\psi(\mathbf{r}_1,\sigma_1;\mathbf{r}_2,\sigma_2)$ the operator $\mathcal{P}$ is defined by

$$\mathcal{P}\psi(\mathbf{r}_1,\sigma_1;\mathbf{r}_2,\sigma_2) \equiv \psi(\mathbf{r}_2,\sigma_2;\mathbf{r}_1,\sigma_1) \ , \tag{50.10}$$

where $\mathbf{r}_1$ and $\mathbf{r}_2$ are the *position coordinates* and σ_1 and σ_2 the *spin coordinates* of the particles 1 and 2, respectively. The effect of this operator is to exchange the particle labels. Because $\mathcal{P}$ is a norm-conserving operator, $\langle\psi|\mathcal{P}^\dagger\mathcal{P}|\psi\rangle = 1$, we have

$$\mathcal{P}^\dagger\mathcal{P} = 1 \ . \tag{50.11}$$

Furthermore, exchanging the particles twice must leave the pair state unchanged. Therefore, we have

$$\mathcal{P}^2 = 1 \ . \tag{50.12}$$

and writing $\mathcal{P} = \mathcal{P}^\dagger \mathcal{P}\mathcal{P} = \mathcal{P}$, we see that $\mathcal{P}^\dagger$ is *hermitian*, i.e., the eigenvalues are real and have to ± 1 for the norm to be conserved.

Any pair state $\psi(\mathbf{r}_1, \sigma_1; \mathbf{r}_2, \sigma_2)$ can be written as the sum of a *symmetric* $(+)$ and an *antisymmetric* $(-)$ part (see Problem 7.1). Therefore, the eigenstates of $\mathcal{P}$ span the full Hilbert space of the pair and $\mathcal{P}$ is not only hermitian but also an *observable*. Remarkably, in nature particles of a given species are found to show always the same symmetry under exchange, corresponding to *only one* of the eigenvalues of $\mathcal{P}$. This important observation means that for *identical* particles the pair wavefunction *must* be an eigenfunction of the exchange operator. In other words: linear combinations of symmetric and antisymmetric pair wavefunctions (like the simple product wavefunction) violate experimental observation. When the wavefunction is symmetric under exchange of two particles the particles are called *bosons*, when antisymmetric the particles are called *fermions*. We do not enter in the relation between spin and statistics except from mentioning that the bosons turn out to have *integral* total spin and the fermions *half-integral* total spin.

> **Example 294 (*Symmetry of wavefunctions*):** Any pair wavefunction can be written as the sum of a part symmetric under exchange and a part antisymmetric under exchange of the pair. To see this we write a pair wavefunction as $|\psi\rangle = \frac{1}{2}(1+\mathcal{P})|\psi\rangle + \frac{1}{2}(1-\mathcal{P})|\psi\rangle$, where $\mathcal{P}$ is the exchange operator, $\mathcal{P}^2 = 1$. The first term is symmetric, $\mathcal{P}(1+\mathcal{P})|\psi\rangle = (\mathcal{P}+\mathcal{P}^2)|\psi\rangle = (1+\mathcal{P})|\psi\rangle$, and the second term is antisymmetric, $\mathcal{P}(1-\mathcal{P})|\psi\rangle = (\mathcal{P}-\mathcal{P}^2)|\psi\rangle = -(1-\mathcal{P})|\psi\rangle$.

50.1.4 Fermions and Pauli principle

Let us turn to the case of two fermions in the pair state $\psi(\mathbf{r}_1, \sigma_1; \mathbf{r}_2, \sigma_2)$. As we are dealing with fermions we know that P must have the eigenvalue -1,

$$\mathcal{P}\psi(\mathbf{r}_1, \sigma_1; \mathbf{r}_2, \sigma_2) = -\psi(\mathbf{r}_1, \sigma_1; \mathbf{r}_2, \sigma_2) \ . \tag{50.13}$$

Combining with the definition (7.10) we obtain the condition

$$\psi(\mathbf{r}_2, \sigma_2; \mathbf{r}_1, \sigma_1) = -\psi(\mathbf{r}_1, \sigma_1; \mathbf{r}_2, \sigma_2) \ . \tag{50.14}$$

For fermions in the same spin state ($\sigma_1 = \sigma_2 = \sigma$) and at the same position ($\mathbf{r}_1 = \mathbf{r}_2 = \mathbf{r}$) this condition can only be satisfied if $\psi(\mathbf{r}, \sigma; \mathbf{r}, \sigma) = -\psi(\mathbf{r}, \sigma; \mathbf{r}, \sigma)$. Hence, two fermions in the same spin state have *zero probability* to be found at the same position. Therefore, the fermions show correlated motion. Importantly, these *kinematic correlations* occur irrespective of the presence or absence of forces between the particles.

As the fermions are identical particles the pair hamiltonian $\mathcal{H}$ is invariant under exchange of the two particles, i.e., the exchange operator $\mathcal{P}$ commutes with the hamiltonian and $\mathcal{P}$ and $\mathcal{H}$ share a complete set of eigenstates. Thus also the eigenfunctions of the hamiltonian must be antisymmetric under exchange of the fermions.

We first look at the symmetry of the spin states. With a $(s_1 \times s_1)$ Clebsch-Gordan decomposition,

$$|S, M_S\rangle = \sum_{m_{S_1}, m_{S_2}} |s_1, m_{s_1}; s_2, m_{s_2}\rangle\langle s_1, m_{s_1}; s_2, m_{s_2}|S, M_S \tag{50.15}$$

we find for the case $(1/2 \times 1/2)$, i.e., for two $s = 1/2$ fermions the spin states,

$$\left.\begin{array}{l} |1,+1\rangle = |\uparrow\uparrow\rangle \\ |1,0\rangle = \frac{1}{2}(|\uparrow\downarrow\rangle + |\downarrow\uparrow\rangle) \\ |1,-1\rangle = |\downarrow\downarrow\rangle \end{array}\right\} \quad (S=1)$$
$$|0,0\rangle = \frac{1}{2}(|\uparrow\downarrow\rangle - |\uparrow\downarrow\rangle) \qquad (S=0) \tag{50.16}$$

Hence, presuming the fermion to be in a symmetric spin state, for instance the state $|1,1\rangle$, the orbital wavefunction must be antisymmetric,

$$\psi^-_{\mathbf{k}_1,\mathbf{k}_2}(\mathbf{r}_1,\mathbf{r}_2) = \frac{1}{V}\sqrt{\frac{1}{2}}(e^{i\mathbf{k}_1\cdot\mathbf{r}_1}e^{i\mathbf{k}_2\cdot\mathbf{r}_2} - e^{i\mathbf{k}_1\cdot\mathbf{r}_2}e^{i\mathbf{k}_2\cdot\mathbf{r}_1})|\uparrow\uparrow\rangle \ . \tag{50.17}$$

If the fermions are in different orbital states ($\mathbf{k}_1 \neq \mathbf{k}_2$) this gives rise to the above mentioned *kinematic correlations*. For two fermions in the same orbital state ($\mathbf{k}_1 = \mathbf{k}_2 = \mathbf{k}$) Eq. (7.17) yields identically zero,

$$\psi^-_{\mathbf{k},\mathbf{k}}(\mathbf{r}_1,\mathbf{r}_2)|1,1\rangle \equiv 0 \ . \tag{50.18}$$

Table 7.1: In the ortho and para isomers of the hydrogen and deuterium molecule the distribution over the rotational levels is affected by quantum statistics (only even or odd levels).

			symmetry				
species	J	I	ψ_{nucl}	ψ_{rot}	ψ_{vib}	$^1\Sigma_g^+$	ψ_{tot}
ortho-H_2	1,3,5,..	1	S	A	S	A	S
ortho-D_2	0,2,4,..	1	A	S	S	A	A
para-H_2	0,2,4,..	0	A	S	S	A	S
para-D_2	1,3,5,..	0,2	S	A	S	A	A

(50.19)

Thus, also its norm $|\psi^-_{\mathbf{k},\mathbf{k}}(\mathbf{r}_1,\mathbf{r}_2)|^2$ is zero. Apparently two (identical) fermions cannot occupy the same state; such a coincidence is *entirely* destroyed by interference. Hence, the Pauli exclusion principle, holds for all fermionic particles and not only for fermions. Starting from an anti-symmetric spin state the orbital part should symmetric. An example is given by the state

$$\psi^-_{\mathbf{k}_1,\mathbf{k}_2}(\mathbf{r}_1,\mathbf{r}_2)|0,0\rangle = \frac{1}{V}\sqrt{\frac{1}{2}}e^{i\mathbf{k}_1\cdot\mathbf{r}_1}e^{i\mathbf{k}_2\cdot\mathbf{r}_2}(|\uparrow\downarrow\rangle - |\downarrow\uparrow\rangle) \ . \tag{50.20}$$

In this case no restriction is found for the relative positions of the fermions.

We found that the quantum mechanical *indistinguishability* of *identical* particles affects the distribution of particles over the single-particle states. For fermions this is

made explicit by the Pauli principle. Also the distribution in configuration space is affected. Remarkably, these kinematic correlations happen in the complete absence of forces between the particles: it is a purely quantum statistical effect. A consequence of such correlations can be observed in the rotational properties of homonuclear diatomic molecules: depending on the total spin of the molecules either the even or the odd rotational levels are observed. This is illustrated in Table 7.1 for the ortho and para isomers of hydrogen (bosonic atoms) and deuterium (fermionic atoms).

50.1.5 Spinorbitals and Slater determinants

Eq. (7.17) can be written in the form of a determinant,

$$\psi^-_{\mathbf{k}_1,\mathbf{k}_2}(\mathbf{r}_1,\mathbf{r}_2)|1,1\rangle = \sqrt{\frac{1}{2}}\begin{vmatrix}\phi_{\mathbf{k}_1\uparrow}(1) & \phi_{\mathbf{k}_2\uparrow}(1)\\ \phi_{\mathbf{k}_1\uparrow}(2) & \phi_{\mathbf{k}_2\uparrow}(2)\end{vmatrix}\,, \tag{50.21}$$

where,

$$\phi_{\mathbf{k}_j\uparrow}(i) = \tfrac{1}{V^{1/2}}e^{i\mathbf{k}_1\cdot\mathbf{r}_i}\chi_\uparrow(\sigma_i) \tag{50.22}$$

are called *spin orbitals*. Similarly, the symmetric spin state $|1,0\rangle$ in combination with the antisymmetric orbital state $\psi^-_{\mathbf{k}_1,\mathbf{k}_2}(\mathbf{r}_1,\mathbf{r}_2)$ can be written as the sum of two determinants,

$$\psi^-_{\mathbf{k}_1,\mathbf{k}_2}(\mathbf{r}_1,\mathbf{r}_2)|1,0\rangle = \frac{1}{2}\begin{vmatrix}\phi_{\mathbf{k}_1\uparrow}(1) & \phi_{\mathbf{k}_2\downarrow}(1)\\ \phi_{\mathbf{k}_1\uparrow}(2) & \phi_{\mathbf{k}_2\downarrow}(2)\end{vmatrix} + \frac{1}{2}\begin{vmatrix}\phi_{\mathbf{k}_1\downarrow}(1) & \phi_{\mathbf{k}_2\uparrow}(1)\\ \phi_{\mathbf{k}_1\downarrow}(2) & \phi_{\mathbf{k}_2\uparrow}(2)\end{vmatrix}\,, \tag{50.23}$$

where $\phi_{\mathbf{k}_j\downarrow}(i) = \phi_{\mathbf{k}_j}(i)\chi_\downarrow(\sigma_i)$ with $i = 1, 2$. The two-body state (7.19) consisting of an antisymmetric spin state and a symmetric orbital state ($\mathbf{k}_1 = \mathbf{k}_2$) takes the form

$$\psi^-_{\mathbf{k}_1,\mathbf{k}_2}(\mathbf{r}_1,\mathbf{r}_2)|0,0\rangle = \sqrt{\frac{1}{2}}\begin{vmatrix}\phi_{\mathbf{k}_1\uparrow}(1) & \phi_{\mathbf{k}_2\uparrow}(1)\\ \phi_{\mathbf{k}_1\uparrow}(2) & \phi_{\mathbf{k}_2\uparrow}(2)\end{vmatrix}\,. \tag{50.24}$$

Indeed, the property of determinants to vanish when two columns or two rows are equal assures that the wavefunction vanishes when two fermions are in the same state α or share the same (position and spin) coordinates $(i) = (\mathbf{r}_i, \sigma_i)$, while exchanging two rows or two columns yields the minus sign required for anti-symmetric wavefunctions. One can easily show that any two-body fermion state can be expressed as a linear combination of determinantal spin-orbital states.

Slater generalized this approach to antisymmetrize N-fermion systems,

$$\psi_\alpha(\mathbf{r}_1,\sigma_1;...;\mathbf{r}_N,\sigma_N) = \sqrt{\frac{1}{N!}}\begin{vmatrix}\phi_{\alpha_1}(\mathbf{r}_1,\sigma_1) & \cdots & \phi_{\alpha_N}(\mathbf{r}_1,\sigma_1)\\ \vdots & \ddots & \vdots\\ \phi_{\alpha_1}(\mathbf{r}_N,\sigma_N) & \cdots & \phi_{\alpha_N}(\mathbf{r}_N,\sigma_N)\end{vmatrix}\,. \tag{50.25}$$

In this form the determinant is called a *Slater determinant*. It is the simplest generalization of the product wavefunction with the proper symmetry under interchange of any two fermions and consistent the Pauli principle. It is a true milestone

in many-body physics. In Dirac notation the antisymmetrized form of N fermions in states $\alpha_1, ..., \alpha_N$ is given by

$$|\alpha_1, ..., \alpha_N\rangle \equiv \tfrac{1}{N!} \sum_P (-1)^p P|\alpha_1, ...\alpha_N) \ , \tag{50.26}$$

where $|\alpha_1, ..., \alpha_N) \equiv |\alpha_1\rangle_1 \otimes |\alpha_2\rangle_2 \otimes ...|\alpha_N\rangle_N$ is the N-body product state of the single-particle states $|\alpha_\kappa\rangle_i$, where $\kappa = 1, .., N$ is the *state index* and $i = 1, .., N$ is the *particle index*. The sum runs over all permutations P of the particles, p being the *parity* (number of transpositions; i.e., binary interchanges) required to realize the permutation starting from an initial ordering fixed by convention. As the sum runs over all permutations, it makes no difference whether we permute all particles or permute all states of the particles. We choose the permutation operator P to *act on the state index* (κ) *and not on the particle index* (i). With this choice, the interchange of the states of particles 1 and 2 is written as

$$P|\alpha_1, ...\alpha_N) = |\alpha_1, ...\alpha_N) = |\alpha_1\rangle_1 \otimes ...|\alpha_N\rangle_N \ . \tag{50.27}$$

To assure a uniquely defined sign of the Slater determinants we shall adopt the standard ordering convention of atomic configurations (see below). The state labeling $\alpha_1, ...\alpha_N$ represents both the orbital and the spin quantum numbers, e.g. $\phi_{\alpha_\kappa}(\mathbf{r}_i, \sigma_i) = \phi_{\mathbf{k}_1\uparrow}(\mathbf{r}_i, \sigma_i)$. These functions are called *spinorbitals*.

50.1.6 Bosons and normalization

For bosons the energy eigenfunctions must be symmetric under exchange of the atoms. For spinless bosons (like ^{4}He atoms) or boson in symmetric spin states this suggests to use Eq.(7.9) in the form

$$\Psi_{\mathbf{k}_1,\mathbf{k}_2}(\mathbf{r}_1, \mathbf{r}_2) = \tfrac{1}{V}\sqrt{\tfrac{1}{2!}}(e^{i\mathbf{k}_1\cdot\mathbf{r}_1}e^{i\mathbf{k}_2\cdot\mathbf{r}_2} + e^{i\mathbf{k}_1\cdot\mathbf{r}_2}e^{i\mathbf{k}_2\cdot\mathbf{r}_1}) \ . \tag{50.28}$$

For $\mathbf{k}_1 \neq \mathbf{k}_2$ this form is appropriate because it is symmetric and also has the proper normalization of unity, $\langle\mathbf{k}_1, \mathbf{k}_2|\mathbf{k}_1, \mathbf{k}_2\rangle = 1$ (cf. Problem 7.2). For $\mathbf{k}_1 = \mathbf{k}_2 = \mathbf{k}$ the situation is different. Eq. (7.28) yields norm 2 rather than the physically required value unity. In this case the properly symmetrized and normalized wavefunction is the product wavefunction

$$\Psi_{\mathbf{k},\mathbf{k}}(\mathbf{r}_1, r_2) = \tfrac{1}{V}e^{i\mathbf{k}_1\cdot\mathbf{r}_1}e^{i\mathbf{k}_2\cdot\mathbf{r}_2} \ , \tag{50.29}$$

with $\langle\mathbf{k}, \mathbf{k}|\mathbf{k}, \mathbf{k}\rangle = 1$. Explicit symmetrization is superfluous because the product wavefunction is symmetrized to begin with. The general form (7.28) may still be used *provided the normalization is corrected for the degeneracy of occupation* (in this case we have to divide by an extra factor $\sqrt{2}$). For bosons in antisymmetric spin states we require the motional wavefunction to be also antisymmetric. Like in the fermion case this gives rise to kinematic correlations.

Example 295 (): Show that Eq. (7.28) has unit normalization for $\mathbf{k}_1 \neq \mathbf{k}_2$,

$$\mathcal{N} = \sqrt{\tfrac{1}{2}}\langle\mathbf{k}_1, \mathbf{k}_2|\mathbf{k}_1, \mathbf{k}_2\rangle = 1 \ .$$

By definition the norm is given by

$$\mathcal{N} = \sqrt{\tfrac{1}{2}}\{(\mathbf{k}_1,\mathbf{k}_2| + (\mathbf{k}_2,\mathbf{k}_1|\}\sqrt{\tfrac{1}{2}}\{|\mathbf{k}_1,\mathbf{k}_2) + |\mathbf{k}_2,\mathbf{k}_1)\}$$
$$= \tfrac{1}{2}\{(\mathbf{k}_1,\mathbf{k}_2|\mathbf{k}_1,\mathbf{k}_2) + (\mathbf{k}_1,\mathbf{k}_2|\mathbf{k}_2,\mathbf{k}_1) + (\mathbf{k}_2,\mathbf{k}_1|\mathbf{k}_1,\mathbf{k}_2) + (\mathbf{k}_2,\mathbf{k}_1|\mathbf{k}_2,\mathbf{k}_1)\} = 1 \ .$$

Here we used $(\mathbf{k}_1,\mathbf{k}_2|\mathbf{k}_2,\mathbf{k}_1) = 0 = (\mathbf{k}_2,\mathbf{k}_1|\mathbf{k}_1,\mathbf{k}_2)$ because $k_1 \neq \mathbf{k}_2$. Further we have $(\mathbf{k}_1,\mathbf{k}_2|\mathbf{k}_1,\mathbf{k}_2) = 1 = (\mathbf{k}_2,\mathbf{k}_1|\mathbf{k}_2,\mathbf{k}_1)$.

50.1.7 Generalization of the symmetrization to many-body states

We found from the analysis of two-body systems that the quantum mechanical *indistinguishability* of identical particles affects the distribution of particles over the single-particle states. For fermions (antisymmetric under exchange) this is made explicit by the Pauli principle, which excludes double occupation of the same state. For bosons (symmetric under exchange) double occupation affects the normalization of the state. In both cases the distribution in configuration space is affected; kinematic correlations happen between the particles in the complete absence of interatomic forces: it is a purely quantum statistical phenomenon. The analysis of systems of two identical particles can be extended to many-body systems of identical particles.

For each particle i we can define a Hilbert space $\mathcal{H}_i$ spanned by a basis consisting of a complete orthonormal set of states $\{|\mathbf{k}_s\rangle_i\}$,

$$_i\langle\mathbf{k}_{s'}|\mathbf{k}_s\rangle_i = \delta_{\mathbf{k}_s,\mathbf{k}_{s'}} \qquad \text{and} \qquad \sum_{\mathbf{k}_s} |\mathbf{k}_s\rangle_{ii}\langle\mathbf{k}_s| = 1 \ . \tag{50.30}$$

where $s \in \{1,...,N\}$ is the state index and $i \in \{1,...,N\}$ the particle index. In principle $|\mathbf{k}_s\rangle_i$ stands for the full description of the eigenstates of the particle i, including the internal state (for instance the hyperfine state in the case of atoms). The wavefunctions of the Schrödinger picture areobtained as the probability amplitude to find the particle at position $\mathbf{r}_i$,

$$\psi_{\mathbf{k}_s}(\mathbf{r}_i) = \langle\mathbf{r}_i|\mathbf{k}_s\rangle \equiv \langle\mathbf{r}_i|\mathbf{k}_s\rangle_i \ . \tag{50.31}$$

For spinless particles (like ^{4}He atoms) in the box potential $U(\mathbf{r})$ introduced earlier, these wavefunctions are best chosen to be the plane waves given by Eq. (7.2); for harmonic trapping potentials they will be harmonic oscillator eigenstates; for electrons in the Coulomb field of the nucleus they are the atomic spinorbitals, etc.. Also in the presence of interactions such wavefunctions remain a good basis set but the simple interpretation as single-particle eigenstates is lost.

For the N-body system we can define a Hilbert space as the tensor product space

$$\mathbf{H}^N = \mathbf{H}_1 \otimes \mathbf{H}_2 \otimes ... \otimes \mathbf{H}_N \tag{50.32}$$

of the N single-particle Hilbert spaces Hi and represented by the orthonormal basis $\{|\mathbf{k}_1,...,\mathbf{k}_N)\}$ where

$$\{|\mathbf{k}_1,...,\mathbf{k}_N)\} \equiv |\mathbf{k}_1\rangle_1 \otimes |\mathbf{k}_2\rangle_2 \otimes ... \otimes |\mathbf{k}_N\rangle_N \tag{50.33}$$

is the N-body tensor product state of the single-particle states $|\mathbf{k}_s\rangle i$ with normalization condition $(\mathbf{k}'_1, ..., \mathbf{k}'_N|\mathbf{k}_1, ..., \mathbf{k}_N) = \delta_{\mathbf{k}_1,\mathbf{k}'_1}...\delta_{\mathbf{k}_N,\mathbf{k}'_N}$ and closure,

$$\sum_{\mathbf{k}_1,...,\mathbf{k}_N} |\mathbf{k}_1, ..., \mathbf{k}_N)(\mathbf{k}_1, ..., \mathbf{k}_N| = \prod_{i=1}^{N} \left(\sum_{\mathbf{k}_s} |\mathbf{k}_s\rangle_i i\langle \mathbf{k}_s| \right) = 1 \ . \tag{50.34}$$

The notation of curved brackets $|\mathbf{k}_1, ..., \mathbf{k}_N)$ is reserved for unsymmetrized many-body states; i.e. product states written with the convention of referring always in the same order from left to right to the states of particle 1 through N. Sometimes we shall use an implicit definition of the N-body state $|N_\gamma)$ by specifying the index γ as an array of state indices,

$$|N_\gamma) = |\mathbf{k}_1, ..., \mathbf{k}_N) \qquad \text{for} \qquad \gamma = \{1, ..., N\} \ . \tag{50.35}$$

To deal with the indistinguishability of particles in the many-body case, we argue that all dynamical properties must remain unchanged under an arbitrary permutation P of these particles. This means that all operators representing a dynamical variable of the system must be invariant under these permutations. This holds in particular for the Hamilton operator and implies that P commutes with the hamiltonian, just as we found for the exchange operator in the two-body case. This is of course not surprising because any permutation can be realized by a sequence of binary interchanges of particles. A many-body state $|\psi^{(S)}\rangle$ is called symmetric (bosonic) if it is invariant under all permutations P,

$$P|\psi^{(S)} = |\psi^{(S)} \ . \tag{50.36}$$

Similarly, a many-body state $|\psi^{(A)}\rangle$ is called antisymmetric (fermionic) if it satisfies the property,

$$P|\psi^{(A)} = (-)^p|\psi^{(A)} \ . \tag{50.37}$$

where $(-)^p = 1$ for all even permutations and $(-)^p = -1$ for all odd permutations, p being the number of binary interchanges required to realize the permutation. We thus can identify two orthogonal subspaces within the product space $\mathcal{H}^{(N)}$: the symmetric subspace $\mathcal{H}^{(S)}$ (for bosons) and the antisymmetric subspace $\mathcal{H}^{(A)}$ (for fermions),

$$\mathcal{H}^{(A)} \oplus \mathcal{H}^{(A)} \in \mathcal{H}^{(A)} \ . \tag{50.38}$$

50.1.7.1 Fermions

For identical fermions in states $\mathbf{k}_1, ..., \mathbf{k}_N$ the N-body state has to be antisymmetrized. This is done by summing over all permutations using a plus sign for all even permutations and a minus sign for all odd permutations,

$$|\mathbf{k}_1, ..., \mathbf{k}_N\rangle \equiv \sqrt{\frac{1}{N!}} \sum_P (-1)^p P|\mathbf{k}_1, ..., \mathbf{k}_N\rangle \ . \tag{50.39}$$

Note that this expression represents a Slater determinant and therefore satisfies the condition (7.36). As the sum runs over all permutations, it makes no difference whether we permute all particles or permute all states of the particles. We choose the permutation operator P *to act on the state index (s) and not on the particle index*

(i) as this allows us to conserve the *ordering convention of the particle index*. With this choice, the interchange of the states of particles 1 and 2 is written as,

$$\mathcal{P}|\mathbf{k}_1, \mathbf{k}_2, ..., \mathbf{k}_N\rangle = |\mathbf{k}_2, \mathbf{k}_1, ..., k_N\rangle = -|\mathbf{k}_2\rangle_1 \otimes |\mathbf{k}_1\rangle_2 \otimes .. \otimes |\mathbf{k}_N\rangle_N\rangle \ . \tag{50.40}$$

To assure a uniquely defined sign of the Slater determinants we need to define the non-permuted state by adopting an *ordering convention of the states*. The quantity

$$\mathcal{A} \equiv \sqrt{\frac{1}{N!}} \sum_P (-1)^p P \tag{50.41}$$

can be interpreted as the antisymmetrization operator that projects an arbitrary unsymmetrized state $|\mathbf{k}_1, ..., \mathbf{k}_N\rangle$ onto the antisymmetric subspace $\mathcal{H}^{(A)}$.

50.1.7.2 Bosons

For identical bosons the N-body state has to be symmetrized. This is done by summing over all permutations while correcting for the degeneracy of occupation (just like in the two-body case) in order to maintain unit normalization. For a N-body system with n_1 particles in state $\mathbf{k}_1$, n_2 particles in state $\mathbf{k}_2$, ... and n_l particles in state $\mathbf{k}_l$ we obtain [1],

$$|\mathbf{k}_1, \mathbf{k}_1, ..., \mathbf{k}_N\rangle \equiv \sqrt{\frac{1}{N! n_1! ... n_l!}} \sum_P P|\mathbf{k}_1, \underset{n_1}{\mathbf{k}_2}, ..., \underset{n_2}{\mathbf{k}_2}, ..., \underset{n_l}{...}, \mathbf{k}_N\rangle \ , \tag{50.42}$$

where $N = n_1 + n_2 + ... + n_l$. In view of the symmetric form, in the bosonic case there is no significance in the order in which the states are written. The quantity,

$$\mathcal{S} \equiv \sum_P P \tag{50.43}$$

can be interpreted as the symmetrization operator that projects an arbitrary unsymmetrized state $|\mathbf{k}_1, ..., \mathbf{k}_N)$ onto the symmetric N-body subspace $\mathcal{H}^{(S)}$.

As an example we consider the special case of N bosons in the same state, $|\mathbf{k}_s, ..., \mathbf{k}_s)$. Here all $N!$ permutations leave the unsymmetrized wavefunction unchanged and we obtain $N!$ identical terms with normalization coefficient $1/N!$, reflecting the feature that the wavefunction was symmetrized to begin with; i.e. $|\mathbf{k}_s, ..., \mathbf{k}_s\rangle = |\mathbf{k}_s, ..., \mathbf{k}_s)$.

Problem 7.3. Show that for $N > 2$,

$$\mathcal{S} + \mathcal{A} \neq \mathcal{I} \ .$$

50.1.7.3 Anderson's orthogonality theorem

Consider a system of N fermions in its ground state; i.e., all single-particle levels are occupied up to the highest level (Fermi level). Let us denote the states of the

[1] We use the convention in which all classically defined permutations are included in the summation. In an alternative convention the permutations of atoms in identical states are omitted. This results in a different normalization factor in the definition of the same symmetrized state.

fermions by $|\alpha_i\rangle$, with $i \in \{1, ..., N\}$. Next we introduce an impurity in the system. This changes both the energies and the wavefunctions of all the fermions. These distorted wavefunctions are denoted by $|\beta_i\rangle$. Anderson pointed out that the many-body states $|\varphi_\alpha\rangle = |\alpha_1, ..., \alpha_N\rangle$ and $|\varphi_\beta\rangle = |\beta_1, ..., \beta_N\rangle$ are essentially orthogonal; i.e., $\langle\varphi_\alpha|\varphi_\beta\rangle \ll 1$ *irrespective of the strength of the perturbation.* This feature is fundamental because it represents a situation where perturbation theory works at the two-body level but fails at the many-body level.

To demonstrate the validity of this theorem, we start by expressing the symmetrized states in terms of the unsymmetrized states,

$$\langle\varphi_\alpha|\varphi_\beta\rangle = \frac{1}{N!}\sum_{P_\alpha}(-1)^{p_\alpha}P_\alpha\sum_{P_\beta}(-1)^{p_\beta}P_\beta(\alpha_1, ..., \alpha_N|\beta_1, ..., \beta_N) \ , \tag{50.44}$$

where P_α and P_β are the permutation operators of the bra and ket states, respectively, To evaluate this expression we note that the perturbed states $|\beta_i\rangle_n$ of particle n, with $n \in \{1, ..., N\}$, can be decomposed with respect to the unperturbed basis $\{|\beta_i\rangle_n\}$,

$$|\beta_i\rangle_n = \sum_i |\alpha_i\rangle_n \ {}_n\langle\alpha_i|\beta_j\rangle_n \ , \tag{50.45}$$

where the states $|\alpha_i\rangle_n$, with $i \leq N$, correspond to the occupied levels. Taking this into account and using the orthonormality of the basis $\{|\alpha_i\rangle\}$, we find,

$$(\alpha_1, ..., \alpha_N|\beta_1, ..., \beta_N) = \sum_{i_1=1}^{N}\cdots\sum_{i_N=1}^{N}(\alpha_1, ..., \alpha_N|\alpha_{i_1}, ..., \alpha_{i_N})\langle\alpha_{i_1}|\beta_1\rangle_1...\langle\alpha_{i_N}|\beta_N\rangle_N = \langle\alpha_1|\beta_1\rangle...\langle\alpha_N|\beta \tag{50.46}$$

Note that the particle indices have been eliminated because the inner products are independent of the particle considered. Thus, the inner product $\langle\varphi_\alpha|\psi_\beta\rangle$ can be written as,

$$\langle\varphi_\alpha|\varphi_\beta\rangle = \frac{1}{N!}\sum_{P_\alpha}(-1)^{p_\alpha}P_\alpha\sum_{P_\beta}(-1)^{p_\beta}P_\beta\langle\alpha_1|\beta_1\rangle...\langle\alpha_N|\beta_N\rangle \ . \tag{50.47}$$

Importantly, as the particle index has been removed the result of the second summation is not affected by the action of the operator $(-1)^{p_\alpha}P_\alpha$. Hence, as there $N!$ possible permutations, the expression for $\langle\varphi_\alpha|\psi_\beta\rangle$ simplifies to,

$$\langle\varphi_\alpha|\varphi_\beta\rangle = \sum_{P_\beta}(-1)^{p_\beta}P_\beta\langle\alpha_1|\beta_1\rangle...\langle\alpha_N|\beta_N\rangle \ , \tag{50.48}$$

which can be written as the determinant of the single-particle overlap matrix,

$$\langle\varphi_\alpha|\psi_\beta\rangle = \begin{vmatrix} \langle\alpha_1|\beta_1\rangle & \cdots & \langle\alpha_1|\beta_N\rangle \\ \vdots & \ddots & \vdots \\ \langle\alpha_N|\beta_1\rangle & \cdots & \langle\alpha_N|\beta_N\rangle \end{vmatrix} \ . \tag{50.49}$$

Specializing to the case $|\alpha_i\rangle = |\beta_i\rangle$ and using the orthonormality of the basis $\{|\alpha_i\rangle\}$ we readily verify the normalization of the many-body state $|\varphi_\alpha\rangle$,

$$\langle\varphi_\alpha|\varphi_\alpha\rangle = \begin{vmatrix} 1 & \cdots & 0 \\ \vdots & \ddots & \vdots \\ 0 & \cdots & 1 \end{vmatrix} = 1 \ . \tag{50.50}$$

On the other hand, if the two states are only approximately equal, $|\alpha_i\rangle \simeq |\beta_i\rangle$; we have $\langle\alpha_i|\beta_i\rangle = 1 - \varepsilon$ with $\varepsilon \ll 1$, and $\langle\alpha_i|\beta_i\rangle \ll 1$. In this case $\langle\varphi_\alpha|\psi_\beta\rangle \longrightarrow 0$ for $N \longrightarrow \infty$.

50.1.8 Occupation number representation

50.1.8.1 Introduction

The notation of the previous section calls for simplification. This is realized by introducing construction operators which satisfy an algebra that enforces the quantum statistics. The first construction operators were introduced by Paul Dirac in 1927 [371]. Starting from Maxwell's equations, Dirac quantized the electromagnetic field by treating the eigenmodes of the field as independent harmonic oscillators. The excitation level of the oscillator represents the mode occupation of the field. The raising (lowering) operators of the oscillator serve to construct the field by creation (annihilation) of photons, the quanta of the radiation field, which occupy the modes. The commutation relations between the operators define the algebra that enforces the Bose statistics of the field. This marks the start of quantum field theory. In the same year Pascual Jordan and Oskar Klein showed that the method could be extended to describe quantum many-body systems of bosons satisfying the Schrödinger equation [683]. Adapting the algebra, Jordan and Wigner further extended the method to describe quantum many-body systems of interacting fermionic particles [684]. The above sequence of seminal papers is not complete without the name of Vladimir Fock, who emphasized in 1932 the use of field operators (construction operators for configuration space) [459]. This approach leads to an operator identity resembling the Schrödinger equation, which explains the unfortunate name second quantization for the construction operator formalism. In following sections we give a concise introduction in the construction operator formalism for quantum many-body systems. For a systematic introduction the lecture notes of Jan de Boer are recommended [335].

50.1.8.2 Number states in the N-body Hilbert space

The notation of the properly symmetrized states can be further compacted by listing only the occupations of the states,

$$|\tilde{n}_\gamma\rangle = |n_1, n_2, ..., n_l\rangle \equiv |\underbrace{\mathbf{k}_1, \mathbf{k}_1, ...}_{n_1}, \underbrace{\mathbf{k}_2, \mathbf{k}_2, ...}_{n_2}, \underbrace{..., \mathbf{k}_l}_{n_l}\rangle \ , \tag{50.51}$$

where $\gamma = \{1, 1, ..., 2, 2, ..., n_l\}$ with $l \lesssim N$. In this way the states take the shape of *number states*, which are the basis states of the occupation number representation (see next section). For the case of N bosons in the same state $|\mathbf{k}_s\rangle$ the number state

is given by $|n_s\rangle \equiv |\mathbf{k}_s, ..., \mathbf{k}_s\rangle$; for a single particle in state $|\mathbf{k}_s\rangle$ we have $|1_s\rangle \equiv |\mathbf{k}_s\rangle$. Note that the Bose symmetrization procedure puts no restriction on the value or order of the occupations $n_1, ..., n_l$ as long as they add up to the total number of particles, $n_1 + n_2 + ... + n_l = N$. For fermions the notation is the same but because the wavefunction changes sign under permutation the order in which the occupations are listed becomes subject to convention (for instance in order of growing energy of the states). Up to this point and in view of Eqs. (50.42) and (50.40) the number states (50.51) have normalization,

$$\langle n_1', n_2', ...|n_1, n_2, ...\rangle = \delta_{n_1', n_1}\delta_{n_2', n_2}... \tag{50.52}$$

and closure

$$\sum_{n_1, n_2, ...}{}' |n_1, n_2, ...\rangle\langle n_1, n_2, ...| = \mathbb{I} \ , \tag{50.53}$$

where the prime indicates that the sum over all occupations equals the total number of particles, $n_1 + n_2 + ... + n_l = N$. This is called closure within $\mathcal{H}^N$.

50.1.8.3 Number states in Grand Hilbert space - construction operators

An important generalization of number states is obtained by interpreting the occupations $n_s, n_t, ...$ as the eigenvalues of number operators $\hat{n}_s, \hat{n}_t, ...$ defined by

$$\hat{n}_s|n_s, n_t, ..., n_l\rangle = n_s|n_s, n_t, ..., n_l\rangle \ . \tag{50.54}$$

With this definition the expectation value of $\hat{n}_s$ is exclusively determined by the occupation of state $|s\rangle$; it is independent of the occupation of all other states. Therefore, the number operators may be interpreted as acting in a Grand Hilbert space, also known as Fock space, which is the direct sum of the Hilbert spaces of all possible atom number states of a gas cloud, including the vacuum,

$$\mathcal{H}^{Gr} = \mathcal{H}^0 \oplus \mathcal{H}^1 \oplus ... \oplus \mathcal{H}^N \oplus ... \ . \tag{50.55}$$

By adding an atom we shift from $\mathcal{H}^N$ to $\mathcal{H}^{N+1}$, analogously we shift from $\mathcal{H}^N$ to $\mathcal{H}^{N-1}$ by removing an atom. As long as this does not affect the occupation of the single-particle state $|s\rangle$ the operator $\hat{n}_s$ yields the same result. Hence, the *number states* $|n_s, n_t, ..., n_l\rangle$ from $\mathcal{H}^N$ may be reinterpreted as number states $|n_s, n_t, ..., n_l, 0_a, 0_b, ..., 0_z\rangle$ within $\mathcal{H}^{Gr}$ by specifying — in principle — the occupations

50.1.9 Field operators

Let us write the total number operator (7.98) in the position representation. Using the closure relation $\mathbb{I} = \int dr|\mathbf{r}\rangle\langle\mathbf{r}|$ we obtain,

$$\hat{N} = \int d^3r \sum_{s,s'} \hat{a}_{s'}^\dagger \langle s'|\mathbf{r}\rangle\langle\mathbf{r}|s\rangle\hat{a}_s = \int d^3r \sum_{s'} \phi_{s'}^*(\mathbf{r})\hat{a}_{s'}^\dagger \sum_{s,s'} \phi_s(\mathbf{r})\hat{a}_s \ , \tag{50.56}$$

where the $\mathbf{r}|s\rangle = \psi_s(\mathbf{r})$ are the wavefunctions of an arbitrary single-particle basis $\{|s\rangle\}$. With this transformation we introduced two operator densities,

$$\hat{\psi}(\mathbf{r}) \equiv \sum_s \psi(\mathbf{r})\hat{a}_s \qquad \text{and} \qquad \hat{\psi}^\dagger(\mathbf{r}) \equiv \sum_s \psi^*(\mathbf{r})\hat{a}_s^\dagger \ , \tag{50.57}$$

which are called field operators in view of their dependence on position. In terms of these field operators the total number operator takes the form,

$$\hat{N} = \int d^3r \hat{\psi}^\dagger(\mathbf{r})\hat{\psi}(\mathbf{r}) = \int d^3r \hat{n}(\mathbf{r}) \ , \tag{50.58}$$

where we defined the density operator $\hat{n}(\mathbf{r})$ as the diagonal part of the density matrix operator. The field operators are construction operators that create or annihilate particles at a given position. Let us demonstrate this for $\hat{\psi}(\mathbf{r})$: This field operator is a creation operator because it is defined in terms of creation operators,

$$\hat{\psi}^\dagger(\mathbf{r})|0\rangle = \sum_s \psi_s^*(\mathbf{r})\hat{a}_s^\dagger|0\rangle = \sum_s |s\rangle\langle s|\mathbf{r}\rangle = |\mathbf{r}\rangle \ . \tag{50.59}$$

Using the closure relation, we found that $\hat{\psi}^\dagger(\mathbf{r})$ creates from the vacuum a particle in state $|\mathbf{r}\rangle$; i.e., a particle at position $\mathbf{r}$. Similarly we can show that $\hat{\psi}(\mathbf{r})$ is the corresponding annihilation operator,

$$\hat{\psi}(\mathbf{r})|0\rangle = |0\rangle \ . \tag{50.60}$$

The field operators are important quantities because (at least in principle) the positions of the particles can be measured to arbitrary accuracy in any many-body system, also when the concept of stationary single-particle states has lost meaning due to coupling by the interactions.

50.1.9.1 Position representation

50.1.10 Exercises

50.1.10.1 Ex: Atom-field coupling

We determine here the coupling Hamiltonian for an atom in a classical field under two equivalent forms (we have only considered the quantum case in the course). We consider the case of the simplest hydrogen atom, with a single electron (reduced mass m, charge $q = -e$) bound to a proton by the Coulomb potential U. This atom interacts also with a laser wave, whose potential and scalar vectors are $\mathbf{V}(\mathbf{r}, t)$ and $\mathbf{A}(\mathbf{r}, t)$.

1. Derive the complete classical Hamiltonian of the atom from the standard form of the classical Lagrangian of a charge in a field: $L = T - q(V + U) + q\mathbf{v} \cdot \mathbf{A}$. What is the link between the electron's velocity and its momentum (conjugate with its position)?

2. Show that the quantum hamiltonian is thus:

$$H = \frac{1}{2m}(\mathbf{P} - q\mathbf{A}(\mathbf{R}, t))^2 + qU(\mathbf{R}) + qV(\mathbf{R}) \ .$$

3. Show that in the Coulomb gauge, $\nabla \cdot \mathbf{A} = 0$, V can be set to zero without loss of generality.

4. Show that in the Coulomb gauge, $\mathbf{A} \cdot \mathbf{P} = \mathbf{P} \cdot \mathbf{A}$. Develop accordingly the full Hamiltonian.

5. Under which hypotheses does H reduce to $H = H_0 - (q/m)\mathbf{P} \cdot \mathbf{A}(0, t)$, where H_0 is the free atomic Hamiltonian?// We now transform the Hamiltonian under the more

standard dipole form using the Göppert-Mayer transformation. We restart from the full Hamiltonian, with all terms including $V(\mathbf{r}, t)$.
6. We neglect the terms quadratic in $\mathbf{A}$. The atom being small compared to the optical wavelength, give the Hamiltonian obtained by expanding $\mathbf{A}$ and $\mathbf{V}$ to the lowest relevant order. Use the notation $\mathbf{D} = q\mathbf{R}$.
7. Show that a proper gauge transformation cancels $\mathbf{A}(0, t)$.
8. Show that in this new gauge, the Hamiltonian reads $H = H_0 - \mathbf{D} \cdot \mathbf{E}(0)$. Is this result gauge-dependent?

Solution: *1. From classical dynamics (see Landau or Goldstein):*

$$L = T - q(V + U) + q\mathbf{v} \cdot \mathbf{A} \ ,$$

where $V + U$ is the total scalar potential seen by the electron. We use the standard analytical mechanics approach to derive the Hamliltonian. The momentum is defined as

$$\mathbf{p} = \nabla_v L = m\mathbf{v} + q\mathbf{A} \ ,$$

and the Hamiltonian as:

$$H = \mathbf{v} \cdot \nabla_v L - L = \tfrac{m}{2} v^2 + q(V + U) = \tfrac{1}{2m}(\mathbf{p} - q\mathbf{A})^2 + q(U + V) \ .$$

2. The quantum Hamiltonian follows by replacing all positions and momenta by non-commuting operators.
3. Follows directly from the properties of the Fourier-transformed fields,

$$\mathbf{A}(r, t) = \frac{1}{4\pi} \int \mathcal{A}(\mathbf{k}, \omega) e^{i(\mathbf{k}\cdot\mathbf{r} - \omega t)} d\mathbf{k} d\omega \ .$$

Longitudinal and transverse potentials w.r.t. k:

$$\mathcal{A}(\mathbf{k}, \omega) = \mathcal{A}(\mathbf{k}, \omega)_{\|} + \mathcal{A}_{\perp} \qquad \textit{hence} \qquad \mathbf{A}(\mathbf{r}, t) = \mathbf{A}_{\|} + \mathbf{A}_{\perp} \ .$$

The Fourier transform of $\mathbf{r} \cdot \mathbf{A}$ is $i\mathbf{k} \cdot \mathcal{A}$ hence $\mathbf{A}_{\|} = 0 = \mathcal{A}_{\|}$. The electric field is transverse also and hence $V = 0$ since ∇V is longitudinal (proportional to $\mathbf{k}$ in Fourier space).
4. We have,

$$[P_i, f(\mathbf{R})] = -i \frac{\partial f}{\partial R_i} \qquad \textit{for} \qquad i \in x, y, z$$

$$\sum_i [P_i, A_i] = -i\hbar \sum_i \frac{\partial A_i}{\partial R_i} = -i\hbar \nabla \cdot \mathbf{A} = 0$$

$$\mathbf{P} \cdot \mathbf{A} = \sum_i P_i A_i = \sum_i A_i P_i = \mathbf{A} \cdot \mathbf{P} \ .$$

And finally,

$$H = \frac{p^2}{2m} + qU(\mathbf{R}) - \frac{q}{m} \mathbf{P} \cdot \mathbf{A} + \frac{q^2}{2m} \mathbf{A} \cdot \mathbf{A} \ .$$

5. Hypotheses:

- *Weak field (much lower than atomic field unit, 10^{11} V/m), A $\mathbf{A}\cdot\mathbf{A}$ quadratic term negligible compared to first order contribution.*
- *Radiation wavelength: about 1μ m; Atomic size: about 100 pm : Neglect spatial variation of the vector potential across atomic orbit: $\mathbf{A}(\mathbf{R},t)=\mathbf{A}(0,t)$ (dipole approximation),*

$$H = H_0 - \frac{q}{m}\mathbf{P}\cdot\mathbf{A}(0,t)\ .$$

6. Restart from full Hamiltonian

$$H = \frac{1}{2m}(\mathbf{P}-q\mathbf{A}(\mathbf{R},t))^2 + qU(\mathbf{R}) + qV(\mathbf{R},t)\ ,$$

and perform dipole approximation first. For the vector potential

$$\mathbf{A}(\mathbf{R},t) = \mathbf{A}(0,t)\ ,$$

and (keeping first order)

$$V = V(0,t) + \mathbf{R}\cdot\nabla V(0,t)\ ,$$

The space-independent term in V has no effect

$$H = H_0 - \frac{q}{m}\mathbf{P}\cdot\mathbf{A}(0,t) + \mathbf{D}\cdot\nabla V(0,t)\ ,$$

with

$$\mathbf{D} = q\mathbf{R}\ .$$

7. Perform a gauge transformation:

$$\mathbf{A}\to\mathbf{A}' = \mathbf{A}+\nabla\chi(\mathbf{r},t)$$
$$V\to V' = V - \frac{\partial\chi}{\partial t}$$

and choose

$$\chi(\mathbf{r},t) = -\mathbf{r}\cdot\mathbf{A}(0,t)\ ,$$

so that $\mathbf{A}'(0,t)=0$. Then

$$V' = V + \mathbf{r}\cdot\frac{\partial\mathbf{A}(0,t)}{\partial t}$$
$$\nabla V'(0) = V(0) + \frac{\partial\mathbf{A}(0,t)}{\partial t} = -\mathbf{E}(0)\ .$$

8. We got,

$$H = H_0 - \mathbf{D}\cdot\mathbf{E}(0)\ .$$

50.1.10.2 Ex: Atom and classical field

We consider a two-level atom coupled to a classical field $\mathbf{E} = \mathbf{E}_0 exp[-i(\omega t + \phi)]$. We examine the Rabi oscillation and the Ramsey separated oscillatory field spectroscopic method. We use the two-level atom model (ground state $|g\rangle$ and excited state $|e\rangle$) with a transition angular frequency ω_{eg} and the Pauli matrices notations. We note $\Delta \equiv \omega_{eg} - \omega$. The atom is initially in $|g\rangle$.
1. Show that the atom-field Hamiltonian is $H = H_0 + H_1$, where $H_0 = \hbar\omega_0\sigma_z/2$ is the free Hamiltonian and $H_1 = -\hbar\Omega\cos(\omega t+\phi)\sigma_x$, where the Rabi frequency $\Omega = \mathbf{d}\cdot\mathbf{E}_0/\hbar$ is assumed real.
2. Switch to an interaction representation with respect to $H_0' = \hbar\omega\sigma_z/2$. Show that the Hamiltonian contains four terms and that two of them are negligible (RWA approximation).
3. Show finally that the new Hamiltonian is $H = \frac{\hbar\Omega'}{2}\sigma_{\mathbf{n}}$, where $\mathbf{n}$ is a unit vector whose expression will be given.
4. Show that H generates a rotation of the Bloch vector around $\mathbf{n}$. Discuss the interesting limit cases. Give at resonance the probability p_e for finding the atom in $|e\rangle$ as a function of time.
5. Give the atomic state transformations performed by a resonant $\pi/2$-pulse such that $t = \pi/2\Omega$.
6. The atom is submitted to two very short nearly resonant $\pi/2$-pulses both with a duration τ a phase $\phi = -\pi/2$, separated by a long time interval T. In which condition can we assume that these pulses are resonant?
7. Show that at the end of the second pulse, $p_e = (1 + \cos\Delta T)/2$. Comment.
8. We assume that the detection noise is only of statistical origin. Show that two ω values can be distinguished provided their angular frequency difference obeys $\delta > \frac{\sqrt{2}}{T\sqrt{N}}$, where N is the total number of atoms detected.

Solution:

50.1.10.3 Ex: Optical Bloch equations

We consider the interaction of a damped two-level atom with a classical field. Show that the evolution equations for the atomic density matrix read:

$$\frac{d\rho_{ee}}{dt} = \frac{d}{\hbar}\text{Im}\ (\rho_{eg}E_1^*) - \Gamma\rho_{ee}$$
$$\frac{d\rho_{eg}}{dt} = -i\Delta\rho_{eg} - \frac{d}{2\hbar}E_1(\rho_{ee} - \rho_{gg}) - \gamma'\rho_{eg}\ ,$$

where Γ is the spontaneous emission rate, $\gamma' = \gamma + \Gamma/2$, γ being the transverse relaxation rate and $E_1 = E_0 e^{-i\phi}$ (plus the notations of the previous exercise). Deduce the evolution equations for the coordinates x, y and z of the Bloch vector. Give the steady state solution of these equations in the simple situation when E_1 is real and atom and field are at resonance for an atom initially in $|g\rangle$. Consider simple limit cases.

Solution:

50.1.10.4 Ex: Field algebra

We demonstrate here a few simple properties of the annihilation and creation operators, as well as of the coherent state. In the following, $f(N)$ (e.g. $\sin(N)$ or $\sqrt{N}$) represents an operator function of the photon number operator. We assume that f can always be expanded in a power series. Results of questions 1-4 are used in the problem.
1. Show that the eigenstates of $f(N)$ are the Fock states $|n\rangle$ with eigenvalues $f(n)$.
2. Show that $\frac{1}{N}\hat{a}^\dagger|n\rangle = |n+1\rangle$.
3. Show that $\hat{a}\frac{1}{N}\hat{a}|n\rangle = |n-1\rangle$.
4. Show that $\hat{a}f(N) = f(N+1)\hat{a}$ and $f(N)\hat{a}^\dagger = a^\dagger f(N+1)$.
5. Show that the coherent states are an overcomplete basis of the single mode Hilbert space: $\mathbb{1} = \frac{1}{\pi}\int d^2\alpha\ |\alpha\rangle\langle\alpha|$. **Hint:** Use Fock state expansion and integration in polar coordinates.
6. We couple a classical current at frequency ω with a field mode a frequency ω_0. Give the amplitude of the created coherent field as a function of time.

Solution:

50.1.10.5 Ex: Phase space distributions

1. Compute the three characteristic functions for the coherent state $\alpha\rangle$. 2. Show that $Q^{[\rho]}(\alpha) = \frac{1}{\pi}\langle 0|D(-\alpha)\rho D(\alpha)|0\rangle = \frac{1}{\pi}\mathrm{Tr}[|0\rangle\langle 0|D(-\alpha)\rho D(\alpha)|0\rangle]$. **Hint:** use linearity of the trace, the closure relations of coherent states.
3. Compute the Q function of a coherent state and of a Fock state.
4. **Difficult:** Show that $W(x,p) = \frac{1}{\pi}\int du\langle\frac{u}{2}|D(-\alpha)\rho D(\alpha)\mathcal{P}|\frac{u}{2}\rangle = \frac{2}{\pi}\mathrm{Tr}[D(-\alpha)\rho D(\alpha)\mathcal{P}]$.

Solution:

50.1.10.6 Ex: Construction operators and occupation number representation

Many body quantum systems are described by symmetrized or antisymmetrized wavefunctions. To keep the calculations manageable this is done in the occupation number representation. Below follows a series of questions with regard to the properties of construction operators. Nota bene: With $\{a,b\}$ we refer to anticommutator of a and b. We presume that the standard ordering is represented by the alphabetic ordering of the state indices.
1. For an arbitrary normalized one-body eigenstate $|s\rangle$, i.e. $\langle s'|s\rangle = \delta_{s,s'}$, we have by definition $|s\rangle \equiv |1_s\rangle \equiv |\bar{1}_s\rangle = \hat{a}_s^\dagger|0\rangle$. Comment of the differences of notation.
2. Give the definition of the creation operator $\hat{a}_s^\dagger$ acting on the number state $|n_s, n_t, ..., n_l\rangle$ for bosons.

3. Give the definition of the annihilation operator $\hat{a}_s$ acting on the number state $|n_s, n_t, ..., n_l\rangle$ for bosons.
4. Evaluate $\hat{a}_s^\dagger|0_q, 0_s, ...\rangle$ for fermions.
5. Evaluate $\hat{a}_s^\dagger|1_q, 0_s, ...\rangle$ for fermions.
6. Evaluate $\hat{a}_s^\dagger|1_q, 1_s, ...\rangle$ for fermions.
7. Show that also the vacuum state $|0\rangle$ is normalized.
8. Calculate the norm $\langle 2_s|2_s\rangle$ for bosons and fermions without using the fermion rule $\hat{a}_s^\dagger|1_q, 1_s, ...\rangle = 0$.
9. Derive $[\hat{a}_q^\dagger, \hat{a}_s^\dagger] = 0$ for bosons.
10. Derive $\{\hat{a}_q^\dagger, \hat{a}_s^\dagger\} = 0$ for fermions.
11. Derive $\{\hat{a}_q, \hat{a}_s^\dagger\} = \delta_{q,s}$ for fermions.
12. Show that $[\hat{n}_q, \hat{a}_s^\dagger] = +\hat{a}_s^\dagger\delta_{q,s}$ for both bosons and fermions.

Solution: *1. By the ket $|1_s\rangle$ one means the number state in which one particle occupies the state $|s\rangle$. By the ket $|\tilde{1}_s\rangle$ one means the number state in Grand Hilbert space consisting of only a single particle, a particle in state $|s\rangle$.*
2. The definition of the creation operator is $\hat{a}_s^\dagger|n_s, n_t, ..., n_l\rangle \equiv \sqrt{n_s+1}|n_s{+}1, n_t, ..., n_l\rangle$.
3. The definition of the annihilation operator is $\hat{a}_s|n_s, n_t, ..., n_l\rangle \equiv \sqrt{n_s}|n_s{-}1, n_t, ..., n_l\rangle$.
4. $\hat{a}_s^\dagger|0_q, 0_s, ...\rangle = |0_q, 1_s, ...\rangle$.
5. $\hat{a}_s^\dagger|1_q, 0_s, ...\rangle = -|0_q, 1_s, ...\rangle$.
6. $\hat{a}_s^\dagger|1_q, 1_s, ...\rangle = 0$.
7. The normalization of the vacuum state is $\langle 0|0\rangle = \langle 1_s|\hat{a}_s^\dagger\hat{a}_s|1_s\rangle = \langle 1_s|\hat{n}_s|1_s\rangle = \langle 1_s|1_s\rangle = \langle s|s\rangle = 1$.
8. The normalization of the state $\langle 2_s|2_s\rangle$ is for bosons:

$$\langle 2_s|2_s\rangle = \tfrac{1}{2}\langle 1_s|\hat{a}_s\hat{a}_s^\dagger|1_s\rangle = \tfrac{1}{2}\langle 1_s|\hat{a}_s^\dagger\hat{a}_s + 1|1_s\rangle = \tfrac{1}{2}\langle 1_s|\hat{n}_s + 1|1_s\rangle = \langle 1_s|1_s\rangle = 1 \ .$$

For fermions (not using the fermion rule $\hat{a}_s^\dagger|1_q, 0_s, ...\rangle = 0$):

$$\langle 2_s|2_s\rangle = \tfrac{1}{2}\langle 1_s|\hat{a}_s\hat{a}_s^\dagger|1_s\rangle = \tfrac{1}{2}\langle 1_s|\hat{a}_s^\dagger\hat{a}_s - 1|1_s\rangle = \tfrac{1}{2}\langle 1_s|\hat{n}_s - 1|1_s\rangle = 0 \ .$$

9. First we consider $q \neq s$:

$$[\hat{a}_q^\dagger, \hat{a}_s^\dagger]|n_s, n_q, ..., n_l\rangle = ...$$

Next we consider the case $q = s$:

$$[\hat{a}_q^\dagger, \hat{a}_s^\dagger]|n_s, n_q, ..., n_l\rangle = ...$$

10. First we consider $q \neq s$. The creation operators can only yield a nonzero result if $n_s = 0$ and $n_q = 0$. Thus we have:

$$\{\hat{a}_q^\dagger, \hat{a}_s^\dagger\}|0\rangle = ...$$

In the case $q = s$ the anwer is trivially zero because no two fermions can occupy the same state.
11. 12.

50.1.10.7 Ex: Important commutation relations for boson field operators

Consider a many-body system of particles confined by on external potential $\mathcal{U}(\mathbf{r})$. At sufficiently low densities this system may be described by the hamiltonian for a pairwise interacting system,

$$\mathcal{H} = \sum_i \mathcal{H}^{(i)} + \tfrac{1}{2}\sum_{i,j} \mathcal{H}^{(i,j)} \ ,$$

where

$$\mathcal{H}^{(i)} = \frac{\mathbf{p}_i^2}{2m} + \mathcal{U}(\mathbf{r}_i)$$

is the free particle contribution of particle i and $\mathcal{H}^{(i,j)} = \mathcal{V}(\mathbf{r}_i, \mathbf{r}_j)$ represents the potential energy of interaction between the particles i and j. At sufficiently low temperatures this potential may be approximated by the expression

$$\mathcal{V}(\mathbf{r}_i, \mathbf{r}_j) = g\delta(\mathbf{r}_i - \mathbf{r}_j) \ ,$$

where $g = (4\pi\hbar^2/m)a$ and a is called the s-wave scattering length. In the occupation number representation for a system of identical particles the hamiltonian takes the form

$$\hat{H} = \hat{H}^{(1)} + \hat{H}^{(2)} \ ,$$

where

$$\hat{H}^{(1)} = \sum_{s,s'} \hat{a}^\dagger_{s'} \langle s'|\mathcal{H}^{(1)}|s\rangle \hat{a}_s \ ,$$

and

$$\hat{H}^{(2)} = \tfrac{1}{2}\sum_{t,t'}\sum_{s,s'} \hat{a}^\dagger_{s'}\hat{a}^\dagger_{t'}\langle s', t'|\mathcal{H}^{(1,2)}|s,t\rangle \hat{a}_t\hat{a}_s \ ,$$

Here $|s\rangle, |s'\rangle \in \{|s\rangle\}$, and $|t\rangle, |t'\rangle \in \{|t\rangle\}$ represent single particle eigenstates of the Hamiltonians $\mathcal{H}^{(1)}$ and $\mathcal{H}^{(2)}$, respectively. Rewriting the hamiltonian in terms of field operators we obtain

$$\hat{H}^{(1)} = \int d\mathbf{r}\hat{\psi}^\dagger(\mathbf{r})\mathcal{H}_0\hat{\psi}(\mathbf{r})$$

with $\mathcal{H}_0 = p^2/2m + \mathcal{U}(\mathbf{r})$ and

$$\hat{H}^{(2)} = \tfrac{1}{2}\int d\mathbf{r}d\mathbf{r}'\hat{\psi}^\dagger(\mathbf{r})\hat{\psi}^\dagger(\mathbf{r}')\mathcal{V}(\mathbf{r},\mathbf{r}')\hat{\psi}(\mathbf{r}')\hat{\psi}(\mathbf{r}) \ .$$

Here $\mathbf{r}$ is the position coordinate of a single particle and $\mathbf{r}, \mathbf{r}'$ are the position coordinates of a pair of particles. The total number operator is defined as the integral over the density operator

$$\hat{N} = \int d\mathbf{r}\hat{n}(\mathbf{r}) \ .$$

Three commutation relations for boson field operators are crucial for the understanding of the ground state of an interacting bosonic superfluid:

$$[\hat{\psi}(\mathbf{r}), \hat{H}^{(1)}] = \mathcal{H}_0(\mathbf{p}, \mathbf{r})\hat{\psi}(\mathbf{r})$$
$$[\hat{\psi}(\mathbf{r}), \hat{H}^{(2)}] = g\hat{n}(\mathbf{r})\hat{\psi}(\mathbf{r})$$
$$[\hat{\psi}(\mathbf{r}), \hat{N}] = \hat{\psi}(\mathbf{r}) \ .$$

Derive the above commutation relations.

Solution: *a. First we recall* $\hat{N} = \int d\mathbf{r}' \hat{n}(\mathbf{r}')$ *and write the commutator in the form,*

$$[\hat{\psi}(\mathbf{r}), \hat{N}] = \int d\mathbf{r}' [\hat{\psi}(\mathbf{r}), \hat{n}(\mathbf{r}')] \ ,$$

where $\hat{n}(\mathbf{r}')$ *is the number-density operator. Using the commutation relation* $[\hat{n}(\mathbf{r}), \hat{\psi}(\mathbf{r}')] = -\hat{\psi}(\mathbf{r}')\delta(\mathbf{r} - \mathbf{r}')$ *we find by integration over* $\mathbf{r}'$*,*

$$\int d\mathbf{r}' [\hat{\psi}(\mathbf{r}), \hat{n}(\mathbf{r}')] = \int d\mathbf{r}' \hat{\psi}(\mathbf{r}')\delta(\mathbf{r} - \mathbf{r}') = \hat{\psi}(\mathbf{r}) \ .$$

b. First we write the commutator in the form,

$$[\hat{\psi}(\mathbf{r}), \hat{H}^{(2)}] = \int d\mathbf{r}' [\hat{\psi}(\mathbf{r}), \hat{H}^{(2)}(\mathbf{r}')] \ ,$$

where $\hat{H}^{(2)}(\mathbf{r}') = \frac{g}{2}\hat{\psi}^\dagger(\mathbf{r}')\hat{(}\mathbf{r}')\hat{\psi}(\mathbf{r}')$ *is the construction operator density for the two-body interaction* $\mathcal{V}(\mathbf{r}_1, \mathbf{r}_2) = g\delta(\mathbf{r}_1 - \mathbf{r}_2)$*. Using the commutation relations* $[\hat{\psi}(\mathbf{r}), \hat{\psi}^\dagger(\mathbf{r}')] = \delta(\mathbf{r} - \mathbf{r}')$*,* $[\hat{\psi}(\mathbf{r}), \hat{\psi}(\mathbf{r}')] = 0$*, and* $[\hat{n}(\mathbf{r}), \hat{\psi}(\mathbf{r}')] = -\hat{\psi}(\mathbf{r}')\delta(\mathbf{r} - \mathbf{r}')$ *we find after integration over* $\mathbf{r}'$*,*

$$\begin{aligned}
\int d\mathbf{r}' [\hat{\psi}(\mathbf{r}), \hat{H}^{(2)}(\mathbf{r}')] &= \tfrac{g}{2} \int d\mathbf{r}' [\hat{\psi}(\mathbf{r})\hat{\psi}^\dagger(\mathbf{r}')\hat{n}(\mathbf{r}')\hat{\psi}(\mathbf{r}') - \hat{\psi}^\dagger(\mathbf{r}')\hat{n}(\mathbf{r}')\hat{\psi}(\mathbf{r}')\hat{\psi}(\mathbf{r})] \\
&= \tfrac{g}{2} \int d\mathbf{r}' [\hat{\psi}^\dagger\hat{\psi}(\mathbf{r})(\mathbf{r}')\hat{n}(\mathbf{r}')\hat{\psi}(\mathbf{r}') - \hat{\psi}^\dagger(\mathbf{r}')\hat{\psi}(\mathbf{r})\hat{n}(\mathbf{r}')\hat{\psi}(\mathbf{r}') + 2\delta(\mathbf{r} - \mathbf{r}')\hat{n}(\mathbf{r}')\hat{\psi}(\mathbf{r}')] \\
&= g\hat{n}(\mathbf{r})\hat{\psi}(\mathbf{r}) \ .
\end{aligned}$$

50.1.10.8 Ex: Amplitude and phase of the order parameter

To analyze the deviations from the stationary state we write the order parameter in a form separating the fluctuations of the amplitude from those of the phase,

$$\Psi(\mathbf{r}, t) = |\Psi(\mathbf{r}, t)|e^{-i\mu t/\hbar + i\Phi(\mathbf{r},t)} \ .$$

Using the Bogolubov ansatz the amplitude takes the form

$$|\Psi(\mathbf{r}, t)| = \sqrt{n_0(\mathbf{r}, t)} \ .$$

The overall phase $\phi(\mathbf{r}, t)$ is a real quantity defined as

$$\phi(\mathbf{r}, t) \equiv \mu t - \Phi(\mathbf{r}, t) \ .$$

The phase $\Phi(\mathbf{r}, t)$ is called the *fluctuating phase* and represents the *deviation* from the dynamical phase evolution $\mu t/\hbar$ of the stationary state $\Psi_0(\mathbf{r}, t)$. The current density is defined as

$$\mathbf{j}(\mathbf{r}, t) = \frac{i\hbar}{2m}(\Psi\nabla\Psi^* - \Psi^*\nabla\Psi) \ .$$

a. Derive the following expression for the current density,

$$\mathbf{j}(\mathbf{r},t) = \frac{\hbar}{m} n_0(\mathbf{r},t)\nabla\Phi(\mathbf{r},t) \ .$$

b. Show that the time dependence of the phase of the order parameter can be expressed in the form,

$$-\hbar\frac{\partial\phi}{\partial t} = \frac{\hbar^2}{2m}(\nabla\Phi)^2 + \mathcal{U}(\mathbf{r}) + g|\Psi|^2 - \frac{\hbar^2}{2m}\frac{1}{|\Psi|}\nabla^2|\Psi| \ .$$

Hint: Use the difference of time-dependent GP equation and its complex conjugate.

Solution:

50.2 Quantum statistics

To describe the time evolution of an isolated quantum gas, in principle, all we need to know is the many-body wavefunction plus the hamiltonian operator. Of course, in practice, these quantities will be known only to limited accuracy. Therefore, just as in the case of classical gases, we have to rely on statistical methods to describe the properties of a quantum gas. This means that we are interested in the occupation probability of quantum many-body states. In view of the convenience of the occupation number representation we ask in particular for the occupation probability P_γ of the number states $|\tilde{n}_\gamma\rangle$. The canonical ensemble introduced in Section 1.2.4 is not suited for this purpose because it presumes a fixed number of atoms N, whereas the ensemble of number states $\{|\tilde{n}_\gamma\rangle\}$ is defined in Grand Hilbert space in which the number of atoms is not fixed. This motivates us to introduce an important variant of the canonical ensemble which is known as the grand canonical ensemble.

50.2.1 Grand canonical distribution

In the grand canonical approach we consider a small system which can exchange not only heat but also atoms with a large reservoir. Like in the canonical case a small system is split off as a part of a one-component gas of N_{tot} identical atoms at temperature T (total energy $_{tot}$). We can visualize the situation as a cloud of trapped atoms connected asymptotically to a homogeneous gas at very low density, a bit reminiscent of the conditions for evaporative cooling (see Section 1.4.1). We are interested in conditions in which the quantum resolution limit is reached in the center of the cloud and the cloud has to be treated as an interacting quantum many-body system. In the reservoir the density can be made arbitrarily low, so the reservoir atoms may be treated quasi-classically.

According to the statistical principle, the probability $P_0(E,N)$ that the trapped gas (the subsystem) has total energy between E and $E+\delta E$ and consists of a number of trapped atoms between N and $N+\delta N$ is proportional to the number $\Omega^{(0)}(E,N)$ of

states accessible to the total system in which the subsystem matches the conditions for E and N,

$$P_0(E,N) = C_0\Omega^{(0)}(E,N) \ , \tag{50.61}$$

where C_0 is a normalization constant. Because the atoms of the subsystem do not interact with the atoms of the reservoir (except for a vanishingly fraction of the atoms near the edge of the trap) the probability $P_0(E,N)$ can be written as the product of the number of quantum mechanical N-body states $\Omega_N(E)$ with energy near E with the number of microstates $\Omega(E^*,N^*)$ with energy near $E^* = E_{tot} - E$ accessible to the $N^* = N_{tot} - N$ atoms of the rest of the gas,

$$P_0(E,N) = C_0\Omega(E,N)\Omega(E_{tot}-E, N_{tot}-N) \ , \tag{50.62}$$

If the total number of atoms is very large ($N_{tot} \gg 1$) the trapped number will always be much smaller than the number in the remaining gas, $N \lll N^*$. Similarly, the amount of heat involved is small, $E \lll E^*$. Thus the distribution $P_0(E,N)$ can be calculated by treating the remaining gas as both a heat reservoir and a particle reservoir for the small system. The ensemble of subsystems with energy near E and atom number near N is called the grand canonical ensemble.

The probability P_γ that the small system is in a specific, properly symmetrized, many-body energy eigenstate $|\tilde{n}_\gamma\rangle$ is given by

50.2.2 Bose-Einstein condensation

50.3 Further reading

L. Amico et al., *Quantum Many Particle Systems in Ring-Shaped Optical Lattices* [27]DOI

S. Beattie et al., *Atom-interferometric studies of light scattering* [109]DOI

J.M. Bendickson et al., *Analytic expressions for the electromagnetic mode density in finite, one-dimensional, photonic* [121]DOI

P.R. Berman et al., *Quantum-information storage A Schrödinger-picture approach* [132]DOI

Y. Bromberg et al., *Bloch Oscillations of Path-Entangled Photons* [198]DOI

Y. Bromberg et al., *Control of coherent backscattering by breaking optical reciprocity* [199]DOI

D.E. Chang et al., *Self-Organization of Atoms along a Nanophotonic Waveguide* [246]DOI

J.J. Choquette et al., *Superradiance subradiance and suppressed superradiance of dipoles near a metal interface* [259]DOI

R. Corrêa et al., *Quantum Interference of Force* [294]DOI

J.H. Eberly, *Emission of one photon in an electric dipole transition* [404]DOI

D. Farina et al., *Hamiltonian analysis of the transition to the high-gain regime* [433]DOI

M. Fleischhauer, *Spontaneous emission and level shifts in absorbing disordered dielectrics and dense atomic gases: A Green's-function approach* [453]DOI

Ya.A. Fofanov et al., *Spatial distribution of optically induced atomic excitation in a dense and cold atomic ensemble* [460]DOI

A. Gaëtan et al., *Observation of collective excitation of two individual atoms in the Rydberg blockade regime* [477]DOI

A. García-Etxarri et al., *Strong magnetic response of submicron Silicon particles in the infrared* [484]DOI

Ch. Grossert et al., *Phase dependent loading of Bloch bands and Quantum simulation of relativistic wave equation predictions with ultracold atoms in variably shaped optical lattice potentials* [550]DOI

L. Karpa et al., *A Stern-Gerlach experiment for slow light* [694]DOI

T. Kinoshita et al., *A quantum Newton's cradle* [721]DOI

A.F. Kockum et al., *Ultrastrong coupling between light and matter* [731]DOI

M. Lebugle et al., *Experimental observation of N00N state Bloch oscillations* [779]DOI

J. Léonard et al., *Supersolid formation in a quantum gas breaking continuous translational symmetry* [788]DOI

Ch. Maschler et al., *Cold Atom Dynamics in a Quantum Optical Lattice Potential* [854]DOI

F. Mivehvar et al., *Driven-Dissipative Supersolid in a Ring Cavity* [903]DOI

J. Ruostekoski, *Optical Kagome Lattice for Ultracold Atoms with Nearest Neighbor Interactions* [1116]DOI

J. Ruostekoski et al., *Emergence of correlated optics in one-dimensional waveguides for classical and quantum atomic gases* [1117]DOI

A. Narayanaswamy et al., *Dyadic Green's functions and electromagnetic local density of states* [946]DOI

B. Olmos et al., *Long-Range Interacting Many-Body Systems with Alkaline-Earth-Metal Atoms* [970]DOI

M. Sukharev et al., *Numerical studies of the interaction of an atomic sample with the electromagnetic field in two dimensions* [1276]DOI

A. Rai et al., *Possibility of coherent phenomena such as Bloch oscillations with single photons via W states* [1066]DOI

M. Reza Bakhtiari et al., *Nonequilibrium Phase Transition of Interacting Bosons in an Intra-Cavity Optical Lattice* [76]$_{\text{DOI}}$

G.A. Prataviera et al., *Continuous measurement of atom-number moments of a Bose-Einstein condensate by photodetection* [1051]$_{\text{DOI}}$

Part VIII

Instrumentation of a Quantum Optics Lab

Chapter 51

Gaussian optics and the polarization of light

The objective of this part of the course is to introduce the student into the basics of *Gaussian optics* and *polarizations optics*. The student will learn how to transform the diameter and the divergence of a Gaussian beam using lenses and telescopes and to analyze and manipulate the polarization of a laser beam.

51.1 Some more basic notions

51.1.1 Definition of photometric quantities

The *radiant energy* W is the total energy emitted from a source. The *radiant power* P (or radiant flux) is the total energy emitted per second. The *radiance* $L(\Omega)$ is defined as the power radiated (emitted, reflected, transmitted or received) under an angle θ through a surface element $d\mathbf{A}$ into a solid angle element $d\Omega = \sin\theta d\theta d\phi$. It is a directional quantity indicating how much of the power will be received by an optical system looking at that surface from a specified angle of view,

$$\boxed{P = \int L(\Omega) dA_n d\Omega} \,. \tag{51.1}$$

Spectral densities are denoted by an index ν, e.g. $P = \int P_\nu(\nu) d\nu$. In (51.1), $dA_n \equiv \hat{\mathbf{n}} \cdot d\mathbf{A} = dA \cos\theta$ is the projection of the surface element onto the surface normal. The quantity,

$$I^* = \int L(\Omega) d\Omega \tag{51.2}$$

is called *radiant intensity*.

> **Example 296 (*Angular distribution of thermal radiation*):** In a blackbody in thermal equilibrium with its surroundings (e.g the walls of a cavity) the radiation is isotropic with a spectral energy distribution given by Planck's law. This means that at any point of the volume of the blackbody radiator an imaginary volume element radiates energy in all directions of space, such that the radiance into a specific solid angle element is,
>
> $$L(\Omega) = \bar{u} \frac{c}{4\pi} \,. \tag{51.3}$$

Radiation passing under an angle θ through a hole of size $dA = dA_n/\cos\theta$ into a specific solid angle element $d\Omega$ generates the radiance,

$$\frac{\partial^2 P}{\partial\Omega\partial A} = L(\Omega)\cos\theta \ . \tag{51.4}$$

In *any* direction we get,

$$\frac{\partial P_\nu}{\partial A} = \int_{\text{half sphere}} L_\nu(\Omega)\cos\theta d\Omega = \bar{u}\frac{c}{4\pi}\int_0^{2\pi} d\phi \int_0^{\pi/2} \cos\theta\sin\theta d\theta = \frac{c\bar{u}}{4} \ . \tag{51.5}$$

Summing up over all surface elements of a sphere of radius R,

$$P = \int \frac{\partial P}{\partial A} dA = \frac{c\bar{u}}{4} R^2 \int_0^{2\pi} d\phi \int_0^{\pi} \sin\theta d\theta = \pi R^2 c\bar{u} \ . \tag{51.6}$$

Accordingly, the spectral distribution is, using Planck's law,

$$P_\nu = P\frac{8\pi h\nu^3}{c^3}\frac{1}{e^{\beta\hbar\omega}-1} = \frac{8\pi^2 R^2 h\nu^3}{c^2}\frac{1}{e^{\beta\hbar\omega}-1} \ . \tag{51.7}$$

A detector covers itself a finite solid angle $d\Omega = \frac{dA'\cos\theta'}{r^2}$. The radiant flux for $r^2 \gg dA, dA'$ can then be expressed as,

$$d\Phi = L(\Omega)dA\cos\theta d\Omega = L(\Omega)dA\cos\theta\frac{dA'\cos\theta'}{r^2} \tag{51.8}$$

$$\text{that is} \qquad \Phi = \int_A\int_{A'} \frac{L(\Omega)}{r^2}\cos\theta\cos\theta' dA dA' \ .$$

Note that for isotropic sources (51.8) is symmetric upon interchanging emitter and detector with regard to θ and θ' or dA and dA'. Furthermore, the formula demonstrates that the radiant flux emitted into the unit solid angle is proportional to $\cos\theta$ (Lambert's law). An example for such a source is a hole with the area dA in a blackbody radiation cavity (see Fig. 51.1). Solve Excs. 51.1.2.1 and 51.1.2.2.

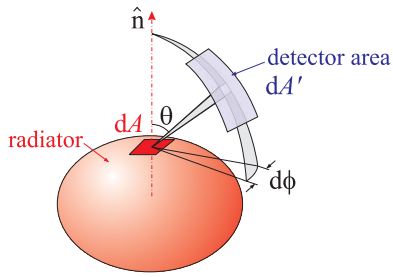

Figure 51.1: Illustration of the radiance.

Note that it is impossible to increase the radiance of a source by any sophisticated imaging optics [352]. This means that the image dA^* of a radiation source dA never has a larger radiance than the source itself. It is true that the flux density can be increased by focussing the radiation. The solid angle, however, into which radiation

from the image dA^* is emitted is also increased by the same factor. Therefore, the radiance does not increase. In fact, because of inevitable reflection, scattering, and absorption losses of the imaging optics, the radiance of the image dA^* is, in practice, always less than that of the source. A strictly parallel light beam would be emitted into the solid angle $d\Omega = 0$. With a finite radiant power this would imply an infinite radiance L, which is impossible. This illustrates that such a light beam cannot be realized. The radiation source for a strictly parallel beam anyway has to be a point source in the focal plane of a lens. Such a point source with zero surface cannot emit any power.

Example 297 (*Radiance of the sun*): An area $A = 1\,\mathrm{m}^2$ of the Earth's surface receives at normal incidence from the sun about $P/A = 1.35\,\mathrm{kW/m}^2$ of intensity. Since the sun covers an angle of $\theta = 0.53°$ seen from the Earth, we can estimate the sun's radiance as,

$$L = \frac{P}{A\Omega} = \frac{P}{A\int_0^{2\pi}\int_0^{\theta}\sin\theta d\theta d\phi} \simeq \frac{P}{A\pi\theta^2} \approx 2\cdot 10^4\,\mathrm{kW\ m^{-2}\ ster^{-1}}\ .$$

The total power received by the Earth is $\frac{P}{A}\pi R_{Earth}^2$. The total power emitted by the sun is $\frac{P}{A}4\pi d_{sun-Earth}^2$.

Example 298 (*Radiance of a HeNe laser*): We consider a HeNe laser emitting $P = 1\,\mathrm{mW}$ of power from a $w_0 = 1\,\mathrm{mm}$ beam waist into an angle of $2\theta = 0.067°$. With a typical emission bandwidth of $\Delta\nu = 1\,\mathrm{MHz}$ the spectral radiance is,

$$L_\nu = \frac{P_\nu}{A\Omega} \simeq \frac{P}{\pi w_0^2\ \pi\theta^2\ \Delta\nu} \approx 1\,\mathrm{kWsm^{-2}\ ster^{-1}}\ .$$

For comparison, the sun's radiance at it's surface ($T = 6000\,\mathrm{K}$) at the same wavelength as the HeNe laser is,

$$L_\nu = \frac{Lu_\nu}{\bar{u}} \approx 5\,\mathrm{nWsm^{-2}\ ster^{-1}}\ .$$

51.1.2 Exercises

51.1.2.1 Ex: Emission of an argon laser

The angular divergence of the output from a $P = 1\,\mathrm{W}$ argon laser is assumed to be $\alpha = 4\cdot 10^{-3}\,\mathrm{rad}$.
a. Calculate the radiance L and the radiant intensity I_1 of the laser beam and the irradiance I (intensity) at a surface 1 m away from the output mirror, when the laser beam diameter at the mirror is $2w_s = 2\,\mathrm{mm}$.
b. What is the spectral power density $u(\nu)$ if the laser bandwidth is 1 MHz?

Solution: *a. The spot size on the output mirror is* $A = \pi w_s^2 \approx 3.1\cdot 10^{-2}\,\mathrm{cm}^2$. *The radiant intensity at the mirror is then,*

$$I_1 = \frac{P}{A} \approx 32\,\mathrm{W/cm}^2\ .$$

The solid angle Ω into which the laser beam is emitted is,

$$\Omega = \int d\Omega = \int_0^{2\pi} \int_0^{\alpha} \sin\theta d\theta d\phi = 2\pi(1-\cos\alpha) \simeq \pi\alpha^2 \ .$$

The radiance L of the laser is then,

$$L = \frac{P}{A\Omega} = \frac{P}{\pi w_s^2 \ \pi\alpha^2} \approx 6.4 \cdot 10^9 \, \mathrm{Wm^{-2}} \ \mathrm{sr^{-1}} \ .$$

At a surface a distance $z = 1$ m from the mirror, the spot size is:

$$A_2 = dA + z^2 d\Omega \approx 0.53 \, \mathrm{cm}^2 \ .$$

The intensity at the surface is:

$$I_2 = \frac{P}{A_2} \approx 1.9 \, \mathrm{W/cm}^2 \ .$$

b. For a spectral width $\Delta\nu = 1\,\mathrm{MHz}$, the spectral power density at the distant surface is:

$$u_2(\nu) = \frac{I_2/c}{\Delta\nu} \approx 6.3 \cdot 10^{-11} \, \mathrm{Ws}^2 \ \mathrm{m}^3 \ .$$

This should be compared with the visible part of the solar radiation on Earth ($I \approx 10^3 \, \mathrm{W/m}^2$ and $\Delta\nu \approx 3 \cdot 10^{16} \, \mathrm{s^{-1}}$), yielding $u_{RS}(\nu) = 10^{-22} \, \mathrm{Ws}^2/\mathrm{m}^3$, which is smaller by 13 orders of magnitude.

51.1.2.2 Ex: Photosynthetically active radiation

The photon flux density and the photosynthetically active radiation (PAR) are defined as,

$$\eta_{photon} \equiv \frac{\int_{\lambda_1}^{\lambda_2} u(\lambda,T) \frac{\lambda}{hcN_A} d\lambda}{\int_{\lambda_1}^{\lambda_2} u_{Pl}(\lambda,T) d\lambda} \qquad \text{and} \qquad \eta_{PAR} = \frac{\int_{\lambda_1}^{\lambda_2} u(\lambda,T) d\lambda}{\int_0^{\infty} u(\lambda,T) d\lambda} \ ,$$

where $\lambda_1 = 400\,\mathrm{nm}$ and $\lambda_2 = 700\,\mathrm{nm}$ delimit the range, where photosynthesis takes place. Calculate both quantities for a blackbody at $T = 5800\,\mathrm{K}$ temperature. Plot them as a function of temperature in the range $T = 300..6000\,\mathrm{K}$.

Solution: *The photon energy density in the case of blackbody radiation is,*

$$u_{Pl}(\lambda,T)d\lambda = -\frac{8\pi ch}{\lambda^5} \frac{1}{e^{\beta hc/\lambda} - 1} d\lambda \ .$$

With this we find $\beta h\nu_1 \approx 5.99$, and $\beta h\nu_2 \approx 3.43$, and,

$$\eta_{photon} = \frac{\int_{\lambda_1}^{\lambda_2} u_{Pl}(\lambda,T) \frac{\lambda}{hcN_A} d\lambda}{\int_{\lambda_1}^{\lambda_2} u_{Pl}(\lambda,T) d\lambda} = \frac{\beta}{N_A} \frac{\int_{\beta h\nu_1}^{\beta h\nu_2} \frac{x^2}{e^x - 1} dx}{\int_{\beta h\nu_1}^{\beta h\nu_2} \frac{x^3}{e^x - 1} dx} \approx 0.394 \, \mathrm{mol/(day \ W)} \ .$$

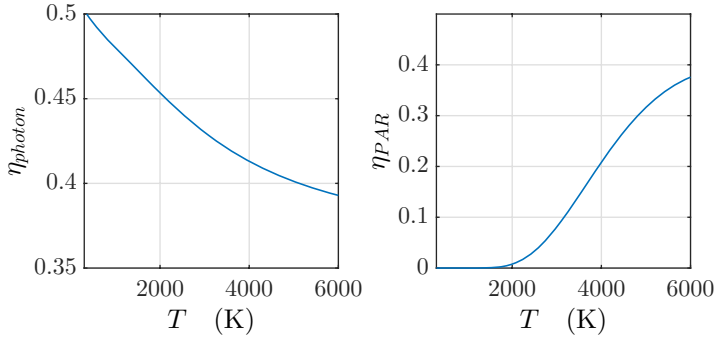

Figure 51.2: Temperature dependence of photosynthetically active radiation.

Now,

$$\eta_{PAR} = \frac{\int_{\lambda_1}^{\lambda_2} u_{Pl}(\lambda,T)d\lambda}{\int_0^{\infty} u_{Pl}(\lambda,T)d\lambda} = \frac{\int_{\beta h\nu_1}^{\beta h\nu_2} \frac{x^2}{e^x-1}dx}{\int_0^{\infty} \frac{x^3}{e^x-1}dx} = \frac{15}{\pi^4}\int_{\beta h\nu_1}^{\beta h\nu_2} \frac{x^2}{e^x-1}dx \approx 0.0878 \ .$$

The graphs are shown in Fig. 51.2.

51.2 Introduction to Gaussian optics

51.2.1 Wave equation and beam parameters

At first sight, one might think that the propagation of laser light is well described by the laws of geometrical optics. On closer inspection it turns out, however, that laser beams behave in many respects more like plane waves with their energy is concentrated near an optical axis. The electro-magnetic fields satisfy the *wave equation*,

$$k^2 u + \nabla^2 u = 0 \ . \tag{51.9}$$

For waves propagating in z direction, $u = \psi(x,y,z)e^{-\imath kz}$, one obtains a Schrödinger-like equation [734],

$$2\imath k\frac{\partial\psi}{\partial z} - \frac{\partial^2\psi}{\partial x^2} - \frac{\partial^2\psi}{\partial y^2} = 0 \ , \tag{51.10}$$

where $\partial^2\psi/\partial z^2$ has been neglected.

To describe a *Gaussian beam*, we choose an exponential ansatz and introduce two parameters, which can vary along the propagation axis z: $P(z)$ is a complex phase shift and $q(z)$ a complex parameter, whose imaginary part describes the diameter of the beam. The ansatz,

$$\psi = e^{-\imath\left[P(z)+k(x^2+y^2)/2q(z)\right]} \tag{51.11}$$

leads to [1],

$$0 = (q'-1)\frac{\imath k(x^2+y^2)}{q^2} - 2\imath P' + \frac{2}{q} \ . \tag{51.12}$$

[1] See script on *Electrodynamics* (2023), Sec. 7.4.2..

In order for Eq. (51.12) to hold for all x and y, we need $q' = 1$ and $P' = \frac{-\imath}{q}$. Integrating q', we find

$$q = q_0 + z \ . \tag{51.13}$$

It is useful to introduce real beam parameters,

$$\frac{1}{q} \equiv \frac{1}{R} - \imath \frac{\lambda}{\pi w^2} \ . \tag{51.14}$$

Inserting these into Eq. (51.10),

$$\psi = e^{-\imath P - \imath \frac{k(x^2+y^2)}{2R} - \frac{(x^2+y^2)}{w^2}} \ , \tag{51.15}$$

it becomes clear that $R(z)$ is the radius of curvature and $w(z)$ the beam diameter. Evaluating q_0 at the position of the focus (waist of the beam), where $R = \infty$, we obtain from (51.13) and (51.14)

$$w^2(z) = w_0^2 \left[1 + \left(\frac{\lambda z}{\pi w_0^2} \right)^2 \right] \qquad \text{and} \qquad R(z) = z \left[1 + \left(\frac{\pi w_0^2}{\lambda z} \right)^2 \right] \ . \tag{51.16}$$

Normalizing the intensity to the total power, we may write the radial intensity distributions as,

$$I_z(x,y) = \frac{2P}{\pi w(z)^2} e^{-2(x^2+y^2)/w(z)^2} \ . \tag{51.17}$$

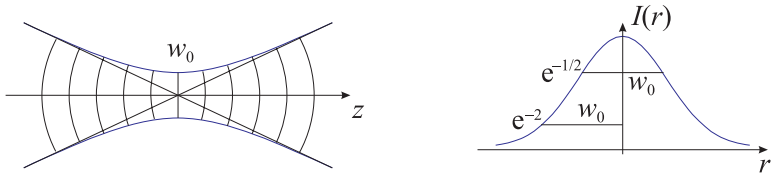

Figure 51.3: (Left) Propagation of the beam along the optical axis. (Right) Cross section of a Gaussian laser beam.

51.2.2 Transfer matrices

For the practical work with Gauss beams it is helpful to introduce transfer matrices, which describe the transformation of a Gauss beam through optical components along the optical axis. The matrix

$$\mathbf{M} = \begin{pmatrix} a & b \\ c & d \end{pmatrix} \tag{51.18}$$

transforms the beam parameter q in the following way:

$$q(z) = \frac{aq(0) + b}{cq(0) + d} \ . \tag{51.19}$$

Transfer matrices allow to calculate, how the parameters R and w transform along the optical axis across the optical elements or in free space. The most common optical elements are lenses, crystals, prisms, mirrors and cavities. For example, the matrix for propagation in free space of a beam over a distance d is,

$$\mathbf{M} = \begin{pmatrix} 1 & d \\ 0 & 1 \end{pmatrix} \tag{51.20}$$

and the matrix for transformation through a thin lens with focal distance f,

$$\mathbf{M} = \begin{pmatrix} 1 & 0 \\ -1/f & 1 \end{pmatrix} . \tag{51.21}$$

It is interesting to note that the transfer matrices are the same as those, which in classical beam optics transform the vector, whose components are the distance of the beam from the optical axis y and its divergence $y'(z)$:

$$\begin{pmatrix} y(z) \\ y'(z) \end{pmatrix} = \mathbf{M} \begin{pmatrix} y(0) \\ y'(0) \end{pmatrix} . \tag{51.22}$$

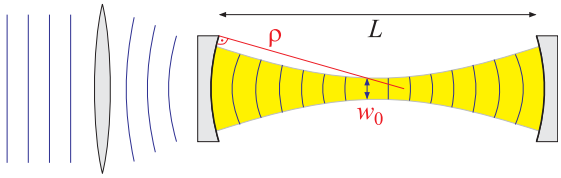

Figure 51.4: Coupling a Gaussian beam of light into cavity requires matching of the phase fronts.

Fig. 51.4 shows that coupling a Gaussian beam of light into a cavity requires matching of the phase fronts. Solve the Excs. 51.2.3.1 to 51.2.3.16 [352, 734, 1364].

51.2.3 Exercises

51.2.3.1 Ex: Imaging through a thin lens

In classical ray optics the equations describing the focusing of a thin lens are given by,

$$\frac{1}{f} = \frac{1}{g} + \frac{1}{b} \quad \text{and} \quad \frac{b}{g} = \frac{B}{G} ,$$

where f is the focal distance of the lens, g the distance between the object and the lens, b the distance between the image and the lens, G the size of the object, and B the size of the image.
At what distance from an object of size $G = 1$ mm do you have to place a thin lens with focal distance $f = 100$ mm in order to obtain a ten times larger image? Test your result in practice.

Solution: *From the lens equations,*

$$\frac{1}{f} = \frac{1}{g} + \frac{1}{b} = \frac{1}{g} + \frac{G}{B}\frac{1}{g} = \frac{1}{g} + \frac{1}{10g} = \frac{11}{10g} \ .$$

Hence, $g = 1.1f$.

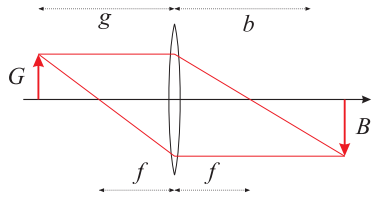

Figure 51.5: Ray optics.

51.2.3.2 Ex: Image of a convex lens

Show that with a convex lens of focal distance f the smallest distance between object and image should be $s = 4f$.

Solution: *The lens equation postulates,*

$$\frac{1}{f} = \frac{1}{b} + \frac{1}{g} \ ,$$

such that

$$b + g = b + \frac{1}{\frac{1}{f} - \frac{1}{b}} = \frac{b^2}{b - f} \ .$$

Minimizing the distance between object and image,

$$0 = \frac{\partial(b+g)}{\partial b} = \frac{\partial}{\partial b}\frac{b^2}{b-f} = b\frac{b-2f}{(b-f)^2} \ ,$$

we get $b = 2f = g$ *and hence,* $b + g > 4f$.

51.2.3.3 Ex: Telescope with ray optics

In classical optics the transfer matrix for the propagation of a beam through free space and through a thin lens are given, respectively, by

$$M_{free} = \begin{pmatrix} 1 & d \\ 0 & 1 \end{pmatrix} \qquad \text{and} \qquad M_{lens} = \begin{pmatrix} 1 & 0 \\ -1/f & 1 \end{pmatrix} \ .$$

The transfer between a point z_0 of the optical axis and a point z_1 is described by

$$\begin{pmatrix} y(z_1) \\ y'(z_1) \end{pmatrix} = M_{free} \begin{pmatrix} y(z_0) \\ y'(z_0) \end{pmatrix} \ .$$

Here, y is the distance of a beam ray from the optical axis and $y' = \frac{dy}{dx}$ its divergence. Use this formalism to design a 3 times magnifying telescope with two lenses have, respectively, the focal lengths $f_1 = 100\,\text{mm}$ and $f_2 = 300\,\text{mm}$.

Solution: *The total optical system is a concatenation of 3 matrices,*

$$M_{tot} = M_{lens,2} M_{free} M_{lens,1} = \begin{pmatrix} 1 & 0 \\ -1/f_2 & 1 \end{pmatrix} \begin{pmatrix} 1 & d \\ 0 & 1 \end{pmatrix} \begin{pmatrix} 1 & 0 \\ -1/f_1 & 1 \end{pmatrix} = \begin{pmatrix} 1 - \frac{d}{f_1} & d \\ \frac{d}{f_1 f_2} - \frac{1}{f_1} - \frac{1}{f_2} & 1 - \frac{d}{f_2} \end{pmatrix} .$$

The variable parameter is the distance d between the two lenses, the condition of a telescope is that a coaxial input ray, $y'(z_0) = 0$, is transformed into a coaxial output ray, $y'(z_1) = 0$. Hence,

$$\begin{pmatrix} y(z_1) \\ 0 \end{pmatrix} = M_{tot} \begin{pmatrix} y(z_0) \\ 0 \end{pmatrix} = \begin{pmatrix} \left(1 - \frac{d}{f_1}\right) y(z_0) \\ \left(\frac{d}{f_1 f_2} - \frac{1}{f_1} - \frac{1}{f_2}\right) y(z_0) \end{pmatrix} .$$

This can only be true if

$$d = f_1 + f_2 \ .$$

The magnification is then

$$\frac{y(z_1)}{y(z_0)} = 1 - \frac{d}{f_1} = \frac{f_2}{f_1} \ .$$

51.2.3.4 Ex: Ray tracing

Simulate the trajectory of a ray of light traversing under an angle a layer of a material with a refraction index characterized by a Gaussian profile.

Solution: *The simulation is shown in Fig. 51.6.*

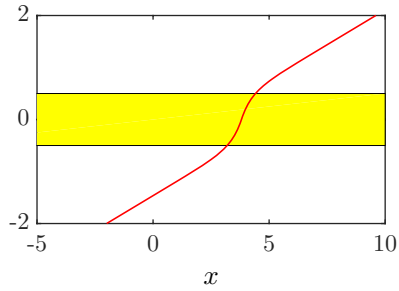

Figure 51.6: (code) Trajectory of a ray of light with 15° angle of incidence.

51.2.3.5 Ex: The eye

The effective distance between the cornea and the lens of the eye is 2.5 cm, and the lens is in contact with the eye. To resolve two very close points, their images on the retina must be on two non-adjacent cone cells (i.e. there must be at least one non-activated cone cell between the images). The cone cells are about 1 μm apart.
a. What is the smallest angle ϵ under which two points are still separately perceptible? Assume that the direct beams P, P' are not refracted.
b. How close can the two points P_1 and P_2 be, at a distance of 20 m from the eye, so that they are still separately perceptible?

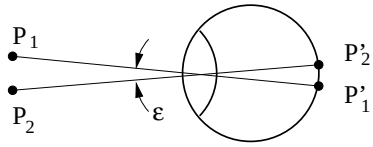

Figure 51.7: The eye.

Solution:

51.2.3.6 Ex: Microscope

A simple homemade microscope consists of two convex lenses, each one with a diffractive power of 20 dpt, fixed at the extremities of a 30 cm long tube.
a. Wie groß ist die Tubuslänge dieses Mikroskops?
b. Wie groß ist der Abbildungsmaßstab des Mikroskops?
c. Welche Vergrößerung erreicht das Mikroskop? Gehen Sie davon aus, dass die deutliche Sehweite 25 cm beträgt.
d. Wie weit muss sich der Gegenstand vor dem Objektiv befinden, damit er im Auge des Betrachters scharf abgebildet wird?

Solution:

51.2.3.7 Ex: Classical cloaking with four lenses

Can you design a system of four lenses (focal distances f_1, f_2, $f_3 = f_2$, and $f_4 = f_1$) separated by three distances $t_1 = f_1 + f_2$, t_2, and $t_3 = t_1$, such that the system appears to be invisible for an observer looking through the lenses [258]?

Solution: *The transfer matrix of this system is,*

$$M = \begin{pmatrix} 1 & 0 \\ -\frac{1}{f_1} & 1 \end{pmatrix} \begin{pmatrix} 1 & f_1+f_2 \\ 0 & 1 \end{pmatrix} \begin{pmatrix} 1 & 0 \\ -\frac{1}{f_2} & 1 \end{pmatrix} \begin{pmatrix} 1 & t_2 \\ 0 & 1 \end{pmatrix} \begin{pmatrix} 1 & 0 \\ -\frac{1}{f_2} & 1 \end{pmatrix} \begin{pmatrix} 1 & f_1+f_2 \\ 0 & 1 \end{pmatrix} \begin{pmatrix} 1 & 0 \\ -\frac{1}{f_1} & 1 \end{pmatrix}$$
$$= \begin{pmatrix} 1 & -f_1 \frac{2f_1f_2+2f_2^2-t_2f_1}{f_2^2} \\ 0 & 1 \end{pmatrix} .$$

In order to obtain, that this matrix is equal to,

$$M = \begin{pmatrix} 1 & L \\ 0 & 1 \end{pmatrix} ,$$

with $L = t_1 + t_2 + t_3$, the distance t_2 be chosen such that,

$$t_2 = 2f_2 \frac{f_1+f_2}{f_1-f_2} .$$

Choosing, for instance, $2f_2 = f_1$ we get $t_2 = 3f_1$.
Comment: *Works in practice with $f_1 = 2f_2 = 2f_3 = f_4 = 50\,\mathrm{mm}$, $t_1 = t_3 = 75\,\mathrm{mm}$, and $t_2 = 150\,\mathrm{mm}$. However, lens aberrations spoil the visibility of the effect.*

51.2.3.8 Ex: Diameter of a Gaussian beam

You are blocking part of a laser beam with a razor blade mounted on a translation stage allowing you to vary the horizontal position. At the same time, you observe the transmitted power P. You observe that, for varying the power between 16% and 84%, you need to vary the translation by 140 µm. What is the diameter of the Gaussian beam?

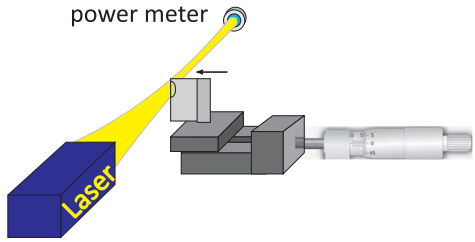

Figure 51.8: Diameter of a Gaussian beam.

Solution: *We calculate,*

$$\frac{\tilde{P}(\tilde{x})}{P} = \int_{-\infty}^{\tilde{x}} \int_{-\infty}^{\infty} \frac{2}{\pi w_0^2} e^{-2r^2/w_0^2} dx dy = \frac{1}{\pi} \int_{-\infty}^{\infty} e^{-\theta^2} d\theta \int_{-\infty}^{\tilde{\xi}} e^{-\xi^2} d\xi = \tfrac{1}{2} \operatorname{erf}\left(\tfrac{\tilde{x}\sqrt{2}}{w_0}\right) + \tfrac{1}{2} .$$

Hence, $\tilde{P}(-w_0/2) = P \cdot 16\%$ and $\tilde{P}(w_0/2) = P \cdot 84\%$, which means that the value of the translation corresponds precisely to the waist.

51.2.3.9 Ex: Diffraction of a Gaussian beam at a slit

a. Determine the power loss suffered by a Gaussian beam passing through a one-dimensional slit, assuming that the beam hits the slit in its center.
b. Calculate the diffraction pattern produced by the slit.
c. A laser beam ($\lambda = 633\,\text{nm}$) looses 50% of its power after being passed through a slit. At a distance of $L = 1\,\text{m}$ behind the slit appear diffraction patterns exhibiting first minima at $\Delta x = 1\,\text{mm}$ to both sides of the central peak. Determine the diameter of the Gaussian beam.

Solution: *a. We have,*

$$P_{tr} = \int_{-\infty}^{\infty}\int_{-d/2}^{d/2} I(x,y)dxdy = \int_{-\infty}^{\infty}\int_{-d/2}^{d/2} \frac{2P}{\pi w^2} e^{(-2x^2-2y^2)/w^2} dxdy = P\,erf\left(\frac{d}{w\sqrt{2}}\right) .$$

b. We let the slit be oriented in x-direction. The field is then obtained by Fourier transformation,

$$u(\theta_x,\theta_y) \propto F[\chi_{[-d/2,d/2]}] = \int_{-\infty}^{\infty}\int_{-d/2}^{d/2} dxdy e^{\imath k_x x + \imath k_y y} = 2\pi\delta(k_y)\frac{2}{k_x}\sin\frac{k_x d}{2} ,$$

where the diffraction angle is, $\theta_x \simeq \sin\theta_x = \frac{k_x}{k}$. *The intensity is just the square,*

$$I(\theta_x) = \left(2\pi d \frac{\sin\frac{kd}{2}\theta_x}{\frac{kd}{2}\theta_x}\right)^2 .$$

We normalize via,

$$\int I(\theta_x)d\theta_x = \int \left(2\pi d \frac{\sin\frac{kd}{2}\theta_x}{\frac{kd}{2}\theta_x}\right)^2 d\theta_x = (2\pi d)^2 \frac{2}{kd}\int_{-\infty}^{\infty}\frac{\sin^2 x}{x^2}dx = (2\pi d)^2\frac{2}{kd}\pi ,$$

such that

$$I(\theta_x,\theta_y) = \frac{I_0}{(2\pi d)^2\frac{2}{kd}\pi}\left(2\pi d\frac{\sin\frac{kd}{2}\theta_x}{\frac{kd}{2}\theta_x}\right)^2 = I_0\frac{kd}{2\pi}\left(\frac{\sin\frac{kd}{2}\theta_x}{\frac{kd}{2}\theta_x}\right)^2 .$$

c. From

$$\frac{P_{tr}}{P} = 50\% = \text{erf}(0.477) = \text{erf}\left(\tfrac{d}{w\sqrt{2}}\right) ,$$

we get

$$w = \frac{d}{0.477\sqrt{2}} .$$

The diameter of the slit can be determined by observing the interference fringes. The first minimum is observed under the diffraction angle $\theta_x \simeq \tan\theta_x = \frac{\Delta x}{L}$, *corresponding to a zero passage of the diffraction function at* $\frac{kd}{2}\theta_x = \pi$. *Hence,*

$$w = \frac{d}{0.477\sqrt{2}} = \frac{1}{0.477\sqrt{2}}\frac{2\pi}{k\theta_x} = \frac{1}{0.477\sqrt{2}}\frac{\lambda}{\Delta x}L \approx 938\,\mu\text{m} .$$

51.2.3.10 Ex: Diffraction of a Gaussian beam at a pinhole

a. Determine the power loss suffered by a Gaussian beam passing through the center of a a pinhole of radius R.
b. A laser beam ($\lambda = 633\,\text{nm}$) looses 50% of its power after being passed through a slit. At a distance of $L = 1\,\text{m}$ behind the slit appear diffraction patterns exhibiting a first minimum at a distance $\Delta b = 1\,\text{mm}$ from the optical axis. Determine the diameter of the Gaussian beam. Help: The first ring of destructive interference occurs under an angle of $\sin\theta = 1.22\frac{\lambda}{2R}$.

Solution: *a. For a pinhole,*

$$P_{tr} = 2\pi \int_0^R I(x,y) r dr = 2\pi \int_0^R \frac{2P}{\pi w^2} e^{-2r^2/w^2} r dr = P(1 - e^{-2R^2/w^2}) \ .$$

b. From

$$\frac{P_{tr}}{P} = 50\% = 1 - e^{-2R^2/w^2}$$

we get,

$$w = R\sqrt{\frac{-2}{\ln\left(1 - \frac{P_{tr}}{P}\right)}} = 1.7R \ .$$

With $R = \frac{1.22\lambda}{2\sin\theta} \simeq \frac{1.22\lambda}{2\theta}$ *we get,*

$$w = 1.7 \cdot \frac{1.22\lambda}{2\theta} = 1.7 \cdot \frac{1.22\lambda L}{2\Delta b} = 656\,\mu\text{m} \ .$$

51.2.3.11 Ex: Focusing a HeNe laser

The output beam from an HeNe laser with a confocal resonator ($\rho = L = 30\,\text{cm}$) is focused by a lens of $f = 30\,\text{cm}$, 50 cm away from the output mirror. Calculate the location of the focus, the Rayleigh length, and the beam waist in the focal plane.

Solution: *The transfer matrix for half a round trip in a confocal cavity,* $\rho = L$, *starting from the waist is,*

$$\mathcal{M}_{cav} = \begin{pmatrix} 1 & L/2 \\ 0 & 1 \end{pmatrix} \begin{pmatrix} 1 & 0 \\ -2/\rho & 1 \end{pmatrix} \begin{pmatrix} 1 & L/2 \\ 0 & 1 \end{pmatrix} = \begin{pmatrix} 0 & L/2 \\ -2/L & 0 \end{pmatrix} \ .$$

Self-consistency of the beam parameter $\frac{1}{q_0} = \frac{1}{R_0} - \imath\frac{\lambda}{\pi w_0^2} = -\imath/z_{R0}$ *requires,*

$$\imath z_{R0} = q_0 = \frac{M_{11}q_0 + M_{12}}{M_{21}q_0 + M_{22}} = -\frac{L}{2} - \frac{L^2}{4q(0)} = -\frac{L}{2} - \frac{L^2}{4\imath z_{R0}} \ .$$

The imaginary part of this equation yields the waist and Rayleigh length,

$$w_0 = \sqrt{\frac{\lambda L}{2\pi}} \approx 174\,\mu\text{m} \qquad \textit{and} \qquad z_{R0} = \frac{\pi w_0^2}{\lambda} \approx 15\,\text{cm} \ .$$

The beam diameter at the surfaces of the laser mirrors is,

$$w_{mir} = w_0\sqrt{1+\left(\frac{\lambda z}{\pi w_0^2}\right)^2} \approx 246\,\mu\text{m} \ .$$

To obtain the beam parameters at the location of the exterior focus we set up the transfer matrix,

$$\mathcal{M}_{ext} = \begin{pmatrix} 1 & d_2 \\ 0 & 1 \end{pmatrix}\begin{pmatrix} 1 & 0 \\ -1/f & 1 \end{pmatrix}\begin{pmatrix} 1 & d_1 \\ 0 & 1 \end{pmatrix} = \begin{pmatrix} 1-d_2/f & d_1 - d_1d_2/f + d_2 \\ -1/f & 1-d_1/f \end{pmatrix} \ ,$$

with $d_1 = z_1 + L/2$ where $z_1 = 50\,\text{cm}$. The beam parameter is now,

$$q_2 = \frac{M_{11}q_0 + M_{12}}{M_{21}q_0 + M_{22}} = \frac{(f-d_2)q_0 + fd_1 - d_1d_2 + fd_2}{-q_0 + f - d_1} = \frac{(f-d_2)\imath z_{R0} + fd_1 - d_1d_2 + fd_2}{\imath z_{R0} + f - d_1} \ ,$$

with the real part,

$$0 = \mathfrak{Re}\ q_2 = \frac{(f-d_2)\imath z_{R0}\imath z_{R0} + (fd_1 - d_1d_2 + fd_2)(f-d_1)}{z_{R0}^2 + (f-d_1)^2}$$
$$\Longrightarrow d_2 = f\frac{z_{R0}^2 + d_1(d_1-f)}{z_{R0}^2 + (d_1-f)^2} \approx 51.72\,\text{cm} \ ,$$

and the imaginary part,

$$z_{R2} = \mathfrak{Im}\ q_2 = \frac{1}{\imath}\frac{(f-d_2)\imath z_{R0}(f-d_1) + (fd_1 - d_1d_2 + fd_2)\imath z_{R0}}{z_{R0}^2 + (f-d_1)^2} = \frac{f^2 z_{R0}}{z_{R0}^2 + (f-d_1)^2} \approx 9.3\,\text{cm}$$
$$\Longrightarrow w_2 = \sqrt{\frac{\lambda z_{R2}}{\pi}} \approx 137\,\mu\text{m} \ .$$

Note that classical ray optics would have predicted,

$$0 \simeq \frac{1}{d_1} + \frac{1}{d_2} - \frac{1}{f} \qquad \textit{and} \qquad w_2 \simeq w_1\frac{d_2}{d_1} \ ,$$

giving with $d_1 = z_1 + L/2$,

$$d_2 \simeq \frac{1}{\frac{1}{f} - \frac{1}{z_1 + L/2}} \approx 55.7\,\text{cm} \qquad \textit{and} \qquad w_2 = w_1\sqrt{\frac{d_2 - f}{d_1 - f}} \simeq w_1\frac{d_2}{d_1} \approx 149\,\mu\text{m}$$
$$\textit{and} \qquad z_R = \frac{\pi w_2^2}{\lambda} \approx 11\,\text{cm} \ .$$

51.2.3.12 Ex: Spatial filtering

A nearly parallel Gaussian beam with $\lambda = 500\,\text{nm}$ is expanded by a telescope with two lenses of focal lengths $f_1 = 1\,\text{cm}$ and $f_2 = 10\,\text{cm}$, illustrated in the figure. The

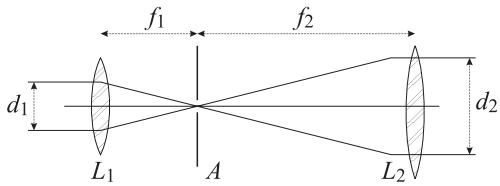

Figure 51.9: Beam-expanding telescope with an aperture in the focal plane.

spot size at the entrance lens is $w = 1\,\text{mm}$.
a. Why does an aperture in the focal plane improve the quality of the wave fronts in the expanded beam by eliminating perturbations due to diffraction effects by dust and other imperfections on the lens surfaces?
b. What is the diameter of this aperture, if 95% of the intensity is transmitted?

Solution: *a. Dust particles on the lens L_1 cause scattering of light in all directions. This light is not focused by L_1, and therefore only a tiny fraction can pass through the aperture. The same is true for imperfections of lenses or mirror surfaces. Without the aperture the superposition of scattered light or light with deformed wavefronts with the incident light causes interference patterns. The aperture therefore 'cleans' the Gaussian laser beam.*
b. The beam waist at the focus is

$$w_0 = \frac{f\lambda}{\pi w} = 1.59\,\mu\text{m} \ .$$

The power transmitted through the aperture with radius a is $P_t = P_i(1 - e^{-2a^2/w_0^2})$. For $P_t/P_i = 0.95$ we obtain $a = 1.95\,\mu\text{m} = 1.22 w_0$.

51.2.3.13 Ex: Transverse mode selection in an Ar laser

An argon laser oscillating at $\lambda = 488\,\text{nm}$ with resonator length $d = 100\,\text{cm}$ and two mirrors with radius $R_1 = \infty$ and $R_2 = 400\,\text{cm}$ has an intracavity circular aperture close to the spherical mirror to prevent oscillation on transversal modes. Estimate the maximum diameter of the aperture that introduces losses $\gamma_{diffr} < 1\%$ for the TEM_{00} mode, but prevents oscillation of higher transverse modes, which without the aperture have a net gain of 10%.

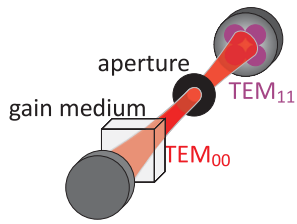

Figure 51.10: Transverse mode selection in an Ar laser.

Solution: *The transfer matrix for the resonator,*

$$\mathcal{M} = \begin{pmatrix} 1 & d \\ 0 & 1 \end{pmatrix} \begin{pmatrix} 1 & 0 \\ -2/\rho & 1 \end{pmatrix} \begin{pmatrix} 1 & d \\ 0 & 1 \end{pmatrix} = \begin{pmatrix} 1 - \frac{2d}{\rho} & 2d\left(1 - \frac{d}{\rho}\right) \\ -\frac{2}{\rho} & 1 - \frac{2d}{\rho} \end{pmatrix}$$

transforms the beam parameter like,

$$q(0) = \frac{M_{11}q(0) + M_{12}}{M_{21}q(0) + M_{22}} = \frac{\left(1 - \frac{2d}{\rho}\right)\imath z_{R0} + 2d\left(1 - \frac{d}{\rho}\right)}{-\frac{2}{\rho}\imath z_{R0} + 1 - \frac{2d}{\rho}} = \imath z_{R0} = \imath\frac{\pi w_0^2}{\lambda} \ .$$

The imaginary part of this equation yields,

$$z_{R0}^2 = \rho d\left(1 - \frac{d}{\rho}\right)$$

or

$$w_0 = \sqrt{\frac{\lambda}{\pi}\sqrt{\rho d\left(1 - \frac{d}{\rho}\right)}} \approx 519\,\mu\text{m}$$

for the beam waist. The beam diameter at the exit mirror is then,

$$w_1 = w_0\sqrt{1 + \left(\frac{\lambda z}{\pi w_0^2}\right)^2} \approx 599\,\mu\text{m} \ .$$

The power transmitted through an aperture located at the exit mirror is,

$$P_{tr} = \int_0^{r_0} 2\pi I(r) r dr = 2\pi\frac{2P}{\pi w_1^2}\int_0^{r_0} e^{-2r^2/w_1^2} r dr = P\left(1 - e^{-2r_0^2/w_1^2}\right) \equiv P \cdot 99\% \ .$$

This gives $r_0 > w_1\sqrt{-\frac{1}{2}\ln 0.01} \approx 909\,\mu\text{m}$. *According to Demtröder, Fig. 5.12 the Fresnel number* N_F *should be smaller than* 0.8, *in order to increase the losses of the* TEM_{10} *mode above 10%. The Fresnel number is defined as,*

$$N_F = \frac{1}{\pi}\frac{\pi a^2}{\pi w_s^2} \ ,$$

where w_s *is the beam waist of the fundamental mode. Therefore,*

$$a^2 < 0.8 \cdot \pi w_s^2 \ ,$$

Yielding $a \leq 944\,\mu\text{m}$. *The radius of the aperture therefore must lie between* $a \in [904, 944]\,\mu\text{m}$.

51.2.3.14 Ex: Anamorphic prism

A prism can be used for expansion of a laser beam if the incident beam is nearly parallel to the prism surface. Calculate the angle of incidence α for which a laser beam transmitted through a rectangular glass prism with an $\varepsilon = 45°$ base angle is expanded tenfold.

Solution: *From the figure we see,*

$$\cos\varepsilon = \frac{d_2}{D} \qquad \textit{and} \qquad \cos\alpha = \frac{d_1}{D} \ .$$

Hence,

$$\frac{d_2}{d_1} = \frac{\cos\varepsilon}{\cos\alpha} \equiv 10 \ ,$$

or, for $\varepsilon = 45°$*,*

$$\alpha = \arccos\frac{\cos\varepsilon}{10} \approx 85.9° \ .$$

The incident beam has an angle of $90° - \alpha$ *against the prism surface. From this we can infer the required refractive index must be,*

$$n_{rfr} = \frac{\sin\alpha}{\sin\varepsilon} \approx 1.41 \ .$$

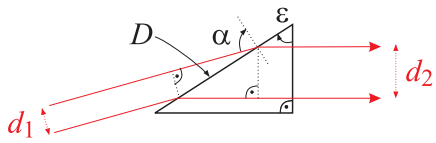

Figure 51.11: Beam expanding prism.

51.2.3.15 Ex: Anamorphic prism pair

An *anamorphic prism* pair is a setup consisting of two prisms through which a laser beam is passed under specific angles. The angles can be chosen such as to change the beam diameter only in the p-plane.
a. Calculate, for a single prism with refractive index $n = 1.5$, the beam expansion for an incidence angle of $\theta_1 = 57°$ and an exit angle of $0°$. How large must the base angle β of the prism be for this to be possible?
b. How must the second prism be aligned in order for the beam transmitted to this second prism to remain parallel to the incident beam? Note, that an anamorphic prism pair does not allow to correct for astigmatism. This requires cylindrical lenses.

Solution: *a. From Snell's law,*

$$n_{rfr} = \frac{\sin\theta_1}{\sin\theta_2} \ ,$$

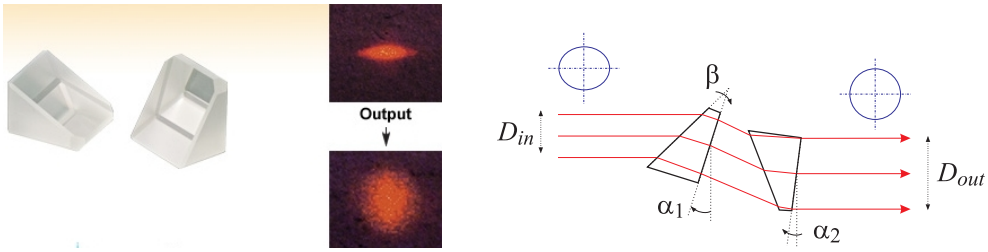

Figure 51.12: (Left) Anamorphic prisms (Thorlabs, PS870). (Right) Geometry of the beam transformation. The entrance side of a prism is often chosen close to the Brewster angle, while the exit side treated carries an anti-reflexion coating.

we derive,

$$\frac{d_2}{d_1} = \frac{\cos\theta_2}{\cos\theta_1} = \frac{\sqrt{1-\sin^2\theta_1/n_{rfr}^2}}{\sqrt{1-\sin^2\theta_1}} \approx 1.5 \ .$$

The base angle under the given condition should be,

$$\beta = \theta_2 = \arcsin(\sin\theta_1/n_{rfr}) \approx 34^\circ \ ,$$

which can be derived geometrically.
b. The incidence angle on the second (identical) prism is,

$$\theta_1' = 90^\circ - \alpha_2 - \beta \ .$$

From this xxx.

51.2.3.16 Ex: Beam steering with two wedged substrates

The wavevector of a laser beam is generally aligned with one or more adjustable reflective mirrors. Alternatively, one may use a pair of rotatable transmissive wedged substrates. Calculate the wave vector of a laser beam after its transmission through two $\epsilon = 3^\circ$ wedged, 2 mm thick, AR-coated substrates with the refraction index $n_{rfr} = 1.5134$ at 689 nm, each one rotated by $\theta_{1,2}$ from some normal position.

Solution: *We assume the incident beam parallel to the optical axis,* $\mathbf{k}_0 = k\hat{\mathbf{e}}_z$. *The normal vectors of the wedges (wedge angle* $\varepsilon = 3^\circ$*) are,*

$$\hat{\mathbf{e}}_{\perp 1} = \begin{pmatrix} \cos\theta_1 & \sin\theta_1 & 0 \\ -\sin\theta_1 & \cos\theta_1 & 0 \\ 0 & 0 & 1 \end{pmatrix} \begin{pmatrix} \cos\varepsilon & 0 & \sin\varepsilon \\ 0 & 1 & 0 \\ -\sin\varepsilon & 0 & \cos\varepsilon \end{pmatrix} \begin{pmatrix} 0 \\ 0 \\ -1 \end{pmatrix} = \begin{pmatrix} -\sin\varepsilon\cos\theta_m \\ \sin\varepsilon\sin\theta_m \\ -\cos\varepsilon \end{pmatrix}$$

and $\hat{\mathbf{e}}_{\perp 2} = \begin{pmatrix} -\sin\varepsilon\cos\theta_2 \\ \sin\varepsilon\sin\theta_2 \\ \cos\varepsilon \end{pmatrix}$.

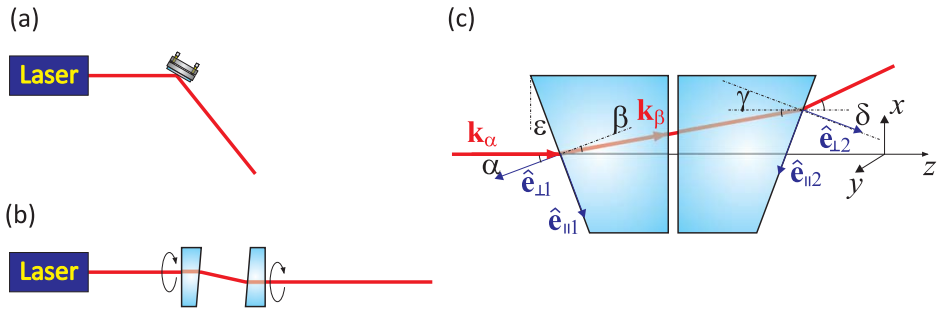

Figure 51.13: Beam steering with two rotatable wedged substrates (see Thorlabs, PS810).

We also define normal vectors in the direction where the refraction plane cuts the wedge surface,

$$\hat{\mathbf{e}}_{\parallel 1} = \frac{\hat{\mathbf{e}}_{\perp 1} \times (\hat{\mathbf{e}}_{\perp 1} \times \mathbf{k}_\alpha)}{|\hat{\mathbf{e}}_{\perp 1} \times (\hat{\mathbf{e}}_{\perp 1} \times \mathbf{k}_\alpha)|} \qquad \textit{and} \qquad \hat{\mathbf{e}}_{\parallel 2} = \frac{\hat{\mathbf{e}}_{\perp 2} \times (\hat{\mathbf{e}}_{\perp 2} \times \mathbf{k}_\gamma)}{|\hat{\mathbf{e}}_{\perp 2} \times (\hat{\mathbf{e}}_{\perp 2} \times \mathbf{k}_\gamma)|} \ .$$

The refraction of a wavevector at a tilted interface between air and a dielectric with

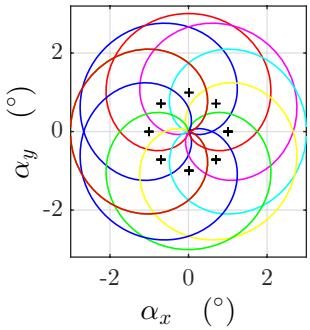

Figure 51.14: (code) Refraction angles that can be reached.

refractive index n_{rfr} follows Snell's law,

$$n_{rfr} = \frac{\sin\alpha}{\sin\beta} = \frac{\sin\delta}{\sin\gamma} \ ,$$

where the angles are given by,

$$\begin{aligned} \mathbf{k}_\alpha \cdot \hat{\mathbf{e}}_{\perp 1} &= -k\cos\alpha \quad , \quad \mathbf{k}_\beta \cdot \hat{\mathbf{e}}_{\perp 1} = -k\cos\beta \\ \mathbf{k}_\gamma \cdot \hat{\mathbf{e}}_{\perp 2} &= k\cos\gamma \quad , \quad \mathbf{k}_\delta \cdot \hat{\mathbf{e}}_{\perp 2} = k\cos\delta \ . \end{aligned}$$

With this we can derive coordinate-free notation,

$$\mathbf{k}_\beta = -\hat{\mathbf{e}}_{\perp 1} k\cos\beta - \hat{\mathbf{e}}_{\parallel 1} k\sin\beta \qquad \textit{where} \qquad \sin\beta = \frac{\sin\alpha}{n_{rfr}} = \frac{1}{n_{rfr}}\sqrt{1 - \frac{(\mathbf{k}_\alpha \cdot \hat{\mathbf{e}}_{\perp 1})^2}{k^2}} \ .$$

Concatenating two wedges by $\mathbf{k}_\gamma = \mathbf{k}_\beta$ *and,*

$$\mathbf{k}_\delta = -\hat{\mathbf{e}}_{\perp 2} k \cos\delta + \hat{\mathbf{e}}_{\parallel 2} k \sin\eta_2 \qquad \textit{where} \qquad \sin\delta = n_{rfr}\sin\gamma \equiv n_{rfr}\sqrt{1 - \frac{(\mathbf{k}_\gamma \cdot \hat{\mathbf{e}}_{\perp 2})^2}{k^2}}\,.$$

Fig. 51.14 shows the angles that can be reached after the first wedge by rotating θ_1 *(black curve) and after the second wedge by rotating* $\theta_{1,2}$ *(colored curves).*

51.2.4 *Experiment: Measuring the diameter of a Gaussian laser beam*

Most laser beams exhibit a Gaussian shape transverse intensity distribution, as we will study in this experiment.

1. Measure the phase profile of a helium-neon laser. To this end fix a razor blade on a translation stage and move it sideways into the beam. From the power of the partially blocked beam $\int_F I(x,y)dxdy$, where F is the cross section of the unblocked part of the beam, $w(z)$ can be determined (see Excs. 51.2.3.8 to 51.2.3.10).

Example 299 (*LOGaussian01*): Example for the experimental determination of a Gaussian beam. We fit the integral,

$$\frac{\tilde{P}}{P} = \int_{-\infty}^{\tilde{x}}\int_{-\infty}^{\infty} \frac{2}{\pi w(z)^2} e^{-2r^2/w(z)^2}\,dxdy \qquad (51.23)$$
$$= \frac{2}{\sqrt{\pi}w(z)^2}\int_{-\infty}^{\tilde{x}\sqrt{2}/w(z)} e^{-\xi^2}\,d\xi = \tfrac{1}{2}\left[\mathrm{erf}\left(\tfrac{\tilde{x}\sqrt{2}}{w(z)}\right)+1\right]$$

to the measured data by varying only $w(z)$.

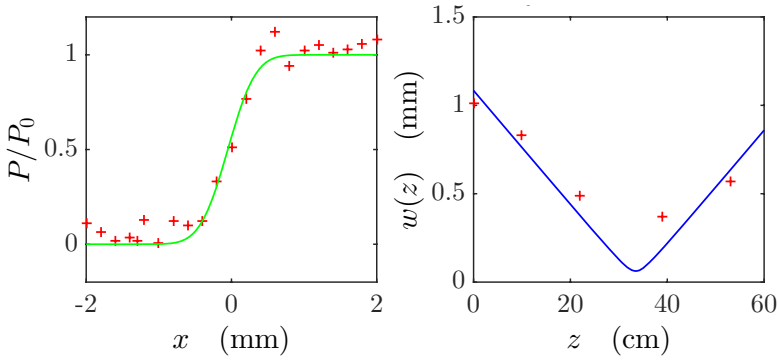

Figure 51.15: (code) (a) Adjustment of an error function for a measured beam profile. (b) Adjustment of a laser beam propagation using Gaussian optics.

51.2.5 *Experiment: Measuring the parameters of a Gaussian laser beam*

Once a Gaussian beam has been characterized at a given position z, the transfer matrix formalism allows us to calculate its shape at any position along the optical axis. In this experiment, we will study the propagation of a Gaussian beam through free space [see Eqs. (51.16)] and its transformation through a thin lens with focal distance f. For the latter one, we obtain directly after the lens,

$$\frac{1}{R(z \searrow 0)} = \frac{1}{R(z \nearrow 0)} - \frac{1}{f} \,. \tag{51.24}$$

1. Focus the beam with a lens. Measure the beam diameter at 3 different locations. Compare with the prediction of Gaussian optics.

2. Set up a 1:3 telescope and verify that the outgoing beam is collimated.

51.2.6 *Experiment: Spatial filtering with a pinhole*

Laser light emitted from diode lasers is often astigmatic and has an irregular beam profile. The beam profile can be purified by passing it through an optical fiber or a pinhole, however, at the price of losing power.

1. Focus the beam of a HeNe laser with a lens of $f = 100\,\text{mm}$ focal distance onto a pinhole. Observe the interference fringes and, from their distance from the optical axis, infer the diameter of the pinhole.

2. Remove the higher-order diffraction rings with an iris and compare the beam profile with that of a Gaussian beam. What are the divergence and the waist of the spatially filtered beam (see Exc. 51.2.3.10)?

51.3 Introduction to polarization optics

A laser usually has a well-defined polarization, e.g. , linear or circular. The polarizations can be transformed into one another through a *quarter waveplate* ($\lambda/4$) or a *half waveplate* ($\lambda/2$) by a Fresnel rhomb or other birefringent elements. Superpositions of polarizations can be separated by a *polarizing beam splitter*.

Waveplates consist of thin sheets of *birefringents crystal*s, which are transparent material characterized by anisotropic refraction indices. Cut in a particular way, a birefringent crystal can exhibit a polarization-dependent refraction index, allowing to control the retardation of a light beam as a function of its polarization. The thickness of a waveplate determines the retardation of one polarization axis with respect to the other.

In practice, the degree of freedom of polarization is often used for separating counterpropagating light fields, e.g. in ring lasers, by means of elements called *optical diode* or *optical isolator*, which consist of a Faraday rotator and $\lambda/2$ waveplate. Another practical example is the use of $\lambda/4$ in double passage. An incoming beam can be separated from a returning beam by using a $\lambda/4$ waveplate and a polarizing beam splitter.

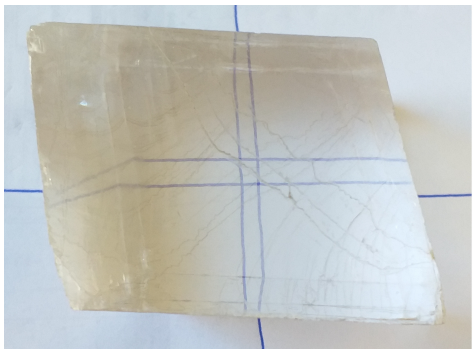

Figure 51.16: (Left) Transmission through a birefringent crystal. (Right) $\lambda/2$-waveplate mounted in a rotation stage.

51.3.1 Jones matrices

The term *polarization* is defined in relation to a fixed coordinate system, while the term *helicity* denotes the direction of rotation of the polarization vector with respect to the direction of propagation of the light beam. The polarization of a beam propagating in z-direction can easily be expressed by a vector of complex amplitude,

$$\vec{\mathcal{E}}(\mathbf{r},t) = \begin{pmatrix} a \\ b \\ 0 \end{pmatrix} e^{\imath kz - \imath\omega t} = \begin{pmatrix} 1 \\ e^{-\imath\phi}|b|/|a| \\ 0 \end{pmatrix} |a| e^{\imath kz - \imath\omega t} \ . \tag{51.25}$$

The angle $\phi = \arctan \frac{\mathfrak{Im}\ ab^*}{\mathfrak{Re}\ ab^*}$ determines the polarization of the light beam. A polarization is linear when $\phi = 0$ and circular when $\phi = \pi/2$. $|b|/|a|$ is, hence, the degree of ellipticity. A polarization rotator for linearly polarized light (e.g., a sugar solution) is described by the following *Jones matrix* (we will restrict to the x-y-plane)

$$M_{rotator}(\phi) = \begin{pmatrix} \cos\phi & \sin\phi \\ -\sin\phi & \cos\phi \end{pmatrix} \ , \tag{51.26}$$

where ϕ is the rotation angle. For the Faraday rotator the sign of the rotation angle depends on the propagation direction of the laser beam. A *polarizer* projects the polarization onto a specific axis. In the case of the x-axis Jones matrix is,

$$M_{polarizer} = \begin{pmatrix} 1 & 0 \\ 0 & 0 \end{pmatrix} \ . \tag{51.27}$$

If the rotation angle is ϕ,

$$M_{polarizer}(\phi) = \begin{pmatrix} \cos\phi & \sin\phi \\ -\sin\phi & \cos\phi \end{pmatrix} \begin{pmatrix} 1 & 0 \\ 0 & 0 \end{pmatrix} \begin{pmatrix} \cos\phi & \sin\phi \\ -\sin\phi & \cos\phi \end{pmatrix}^{-1} \ . \tag{51.28}$$

Other components, such as electro-optical modulators or phase plates are birefringent crystals, which act only on one of the two optical axes. If only the y axis is optically

active, the Jones' matrix is,

$$M_{\theta\text{-waveplate}} = \begin{pmatrix} 1 & 0 \\ 0 & e^{\imath\theta} \end{pmatrix} . \tag{51.29}$$

For $\theta = 2\pi/n$ we obtain a λ/n-waveplate. When we rotate the waveplate and therefore the optically inactive axis to an angle ϕ, the Jones matrices are,

$$\begin{aligned} M_{\theta\text{-waveplate}}(\phi) &= \begin{pmatrix} \cos\phi & \sin\phi \\ -\sin\phi & \cos\phi \end{pmatrix} \begin{pmatrix} 1 & 0 \\ 0 & e^{\imath\theta} \end{pmatrix} \begin{pmatrix} \cos\phi & \sin\phi \\ -\sin\phi & \cos\phi \end{pmatrix}^{-1} \\ &= \begin{pmatrix} \cos^2\phi + e^{\imath\theta}\sin^2\phi & -\sin\phi\cos\phi + e^{\imath\theta}\sin\phi\cos\phi \\ -\sin\phi\cos\phi + e^{\imath\theta}\sin\phi\cos\phi & \sin^2\phi + e^{\imath\theta}\cos^2\phi \end{pmatrix} . \end{aligned} \tag{51.30}$$

In most cases, we use quarter waveplates $\lambda/4$,

$$M_{\lambda/4}(\phi) = \begin{pmatrix} \cos^2\phi + \imath\sin^2\phi & (-1+\imath)\sin\phi\cos\phi \\ (-1+\imath)\sin\phi\cos\phi & \sin^2\phi + \imath\cos^2\phi \end{pmatrix} \tag{51.31}$$

and half waveplates $\lambda/2$,

$$M_{\lambda/2}(\phi) = \begin{pmatrix} \cos 2\phi & -\sin 2\phi \\ -\sin 2\phi & -\cos 2\phi \end{pmatrix} . \tag{51.32}$$

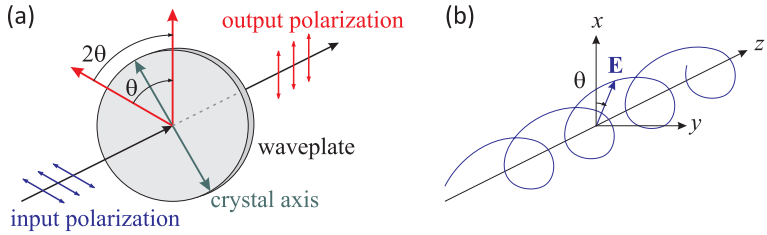

Figure 51.17: (a) Rotation of the polarization by a birefringent waveplate. (b) Illustration of a circularly polarized light wave.

Combinations of $\lambda/2$ waveplates and *Faraday rotator*s are used as *optical isolator*, also called *optical diode*.

51.3.2 Fresnel formulae

Reflection and transmission of a beam of light at a surface depend on the polarization of the light and the angle of incidence. They are described by the *Fresnel formula*:

$$\begin{aligned}
\left(\frac{I_{0t}}{I_{0i}}\right)_s &= T_s = \left(\frac{2\sin\theta_t\cos\theta_i}{\sin(\theta_i+\theta_t)}\right)^2 \\
\left(\frac{I_{0r}}{I_{0i}}\right)_s &= R_s = \left(-\frac{\sin(\theta_i-\theta_t)}{\sin(\theta_i+\theta_t)}\right)^2 \\
\left(\frac{I_{0t}}{I_{0i}}\right)_p &= T_p = \left(\frac{2\sin\theta_t\cos\theta_i}{\sin(\theta_i+\theta_t)\cos(\theta_i-\theta_t)}\right)^2 \\
\left(\frac{I_{0r}}{I_{0i}}\right)_p &= R_p = \left(\frac{\tan(\theta_i-\theta_t)}{\tan(\theta_i+\theta_t)}\right)^2 .
\end{aligned} \tag{51.33}$$

The angles of incidence and transmission are related by Snell's law: $n_1\sin\theta_i = n_2\sin\theta_t$.

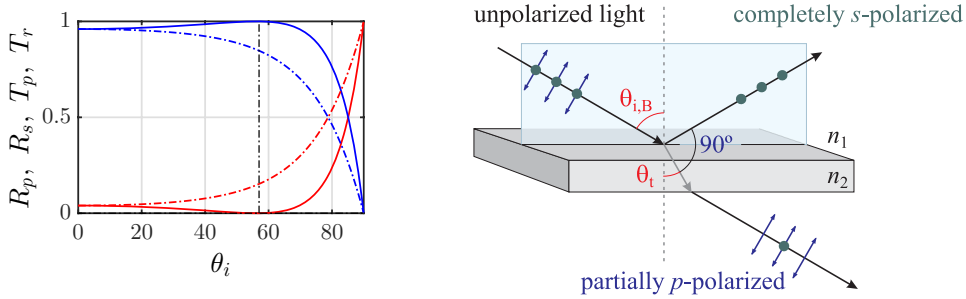

Figure 51.18: (code) (Left) Fresnel formulae showing the angular dependence of t_s (red solid), r_s (green dash-dotted), t_p (blue dashed), and r_p (cyan dotted) for reflection from and transmission through a piece of glass-air interface. (Right) Interfaces between optical media with different reflection indices can act like polarizers: Light reflected from a glas surface under the Brewster angle is completely s-polarized, while the transmitted light is partially p-polarized. The notation s comes from *senkrecht*, i.e. perpendicular to the plane spanned by the incident and reflected light beams, while p means *parallel* to this plane.

The *Brewster angle* $\theta_{i,B}$ is reached, when $\theta_{i,B}+\theta_t = 90°$, i.e., when following Snell's law,

$$n_1\sin\theta_{i,B} = n_2\sin(90°-\theta_{i,B}) = n_2\cos\theta_{i,B} . \tag{51.34}$$

Hence, the Brewster angle is given by,

$$\tan\theta_{i,B} = \frac{n_2}{n_1} . \tag{51.35}$$

Resolve the exercises 51.3.4.1 to 51.3.4.5.

51.3.3 Stokes parameters

In quantum mechanics the *Stokes parameters* of a light beam with horizontal and vertical polarizations, $\hat{a}_h$ and $\hat{a}_v$, satisfying,

$$[\hat{a}_k, \hat{a}_m^\dagger] = \delta_{km} \ , \tag{51.36}$$

with $k, m = h, v$ are defined by,

$$\boxed{\begin{aligned} \hat{S}_0 &\equiv \hat{a}_h^\dagger \hat{a}_h + \hat{a}_v^\dagger \hat{a}_v \\ \hat{S}_1 &\equiv \hat{a}_h^\dagger \hat{a}_h - \hat{a}_v^\dagger \hat{a}_v \\ \hat{S}_2 &\equiv \hat{a}_h^\dagger \hat{a}_v e^{\imath\theta} + \hat{a}_v^\dagger \hat{a}_h e^{-\imath\theta} \\ \hat{S}_3 &\equiv -\imath(\hat{a}_h^\dagger \hat{a}_v e^{\imath\theta} - \hat{a}_v^\dagger \hat{a}_h e^{-\imath\theta}) \end{aligned}} \ . \tag{51.37}$$

The Stokes parameters exhaustively describe the polarization state of a light beam. It is interesting, that the vector $\hat{\mathbf{S}}$ with components S_j with $j = 1, 2, 3$ satisfies the SU(2) spin algebra,

$$[\hat{S}_k, \hat{S}_m] = 2\imath\epsilon_{kmn}\hat{S}_n \qquad \text{and} \qquad \hat{\mathbf{S}}^2 = \hat{S}_0^2 + 2\hat{S}_0 \ , \tag{51.38}$$

as will be shown in Exc. 51.3.4.6. It is conveniently pictured on a Poincaré sphere or as a polarization ellipse. In the classical limit we get,

$$\begin{aligned} \hat{S}_0 &= I \\ \hat{S}_1 &= Ip\cos 2\psi \cos 2\chi \\ \hat{S}_2 &= Ip\sin 2\psi \cos 2\chi \\ \hat{S}_3 &= Ip\sin 2\chi \ , \end{aligned} \tag{51.39}$$

with I the light intensity (eventually normalized to the single-photon light intensity), the degree of polarization p. Obviously,

$$\hat{S}_1^2 + \hat{S}_2^2 + \hat{S}_3^2 = p^2 \hat{S}_0^2 \ . \tag{51.40}$$

51.3.4 Exercises

51.3.4.1 Ex: Light power control using polarization optics

The power of a laser beam can be regulated by a combination of a half-wave plate and a polarizing beam splitter. By how many degrees do you have to rotate the waveplate in order to reduce the light power by a factor of 2? Use the Jones matrices to justify your response. **Advice:** Look up the Jones matrices (51.32) and (51.27). Test your result in practice.

Solution: *The action of the optical components on the polarization is described by,*

$$\begin{pmatrix} E_x(z_1) \\ E_y(z_1) \end{pmatrix} = M_{pol} M_{\lambda/2}(\phi) \begin{pmatrix} E_x(z_0) \\ E_y(z_0) \end{pmatrix}$$
$$= \begin{pmatrix} 1 & 0 \\ 0 & 0 \end{pmatrix} \begin{pmatrix} \cos 2\phi & -\sin 2\phi \\ -\sin 2\phi & -\cos 2\phi \end{pmatrix} \begin{pmatrix} E_x(z_0) \\ E_y(z_0) \end{pmatrix} = \begin{pmatrix} \cos 2\phi & -\sin 2\phi \\ 0 & 0 \end{pmatrix} \begin{pmatrix} E_x(z_0) \\ E_y(z_0) \end{pmatrix} .$$

We assume an initially linear polarization $\mathbf{E}(z_0) = E_x(z_0)\hat{\mathbf{e}}_x$*, so that the initial intensity is* $I(z_0) \propto E_x(z_0)^2$*,*

$$\begin{pmatrix} E_x(z_1) \\ E_y(z_1) \end{pmatrix} = \begin{pmatrix} \cos 2\phi & -\sin 2\phi \\ 0 & 0 \end{pmatrix} \begin{pmatrix} E_x(z_0) \\ 0 \end{pmatrix} = \begin{pmatrix} E_x(z_0)\cos 2\phi \\ 0 \end{pmatrix} .$$

The final intensity is $I(z_1) = E_x^2(z_1) + E_y^2(z_1)$*. Hence,*

$$\frac{I(z_1)}{I(z_0)} = \cos^2 2\phi \equiv \frac{1}{2} ,$$

gives $\phi = 22.5°$*.*

51.3.4.2 Ex: Jones matrices

Consider a linearly polarized laser beam passing twice through a $\lambda/4$, first in direction of the optical axis, the second time in opposite direction. Calculate the final polarization.

Solution: *The propagation direction of the beam doesn't matter for the retardation. We can show* $M_{\lambda/4}(\phi)^2 = M_{\lambda/2}(\phi)$ *and* $M_{\lambda/4}(\pi/4) = \begin{pmatrix} 0 & -1 \\ -1 & 0 \end{pmatrix}$.

51.3.4.3 Ex: Intensity transmitted through a polarizer

Unpolarized light of intensity I_0 is transmitted through a polarizer with thickness $d = 1\,\text{mm}$. Calculate the transmitted intensity when the absorption coefficients for the two polarizations are $\alpha_\parallel = 100\,\text{cm}^{-1}$ and $\alpha_\perp = 5\,\text{cm}^{-1}$.

Solution: *Using the Lambert-Beer law,* $I = I_0 e^{-\alpha d}$*, we have* $I_\parallel \approx 4.5 \cdot 10^{-5} I_0$ *and* $I_\perp \approx 0.6 I_0$*.*

51.3.4.4 Ex: Thickness of a half-waveplate

A birefringent quartz crystal is characterized by different refraction indices of the ordinary beam $n_o = 1.544$ and the extraordinary beam $n_e = 1.553$. Calculate the necessary thickness of a quartz waveplate to be used as a $\lambda/2$ retarder at 633 nm. Choose an appropriate waveplate from the Thorlabs catalogue. How thick would a

calcite waveplate ($n_o = 1.658$, $n_e = 1.486$)?

Solution: *The phase difference is,*

$$\phi = \frac{2\pi d(n_o - n_e)}{\lambda} \stackrel{!}{=} \pi \ .$$

Hence for quartz,

$$d = \frac{\lambda}{2(n_o - n_e)} \approx 35.2\,\mu\text{m} \ .$$

The waveplate WPHSM05-633 would be a good choice. For calcite we would have,

$$d = \frac{\lambda}{2(n_o - n_e)} \approx 1.84\,\mu\text{m} \ .$$

51.3.4.5 Ex: Faraday isolator

A Faraday rotator is a device exploiting the Faraday effect to rotate the polarization of a light beam according to the Jones matrix,

$$M_{Faraday}(\phi) = \begin{pmatrix} \cos\phi & -\mathbf{k}\cdot\hat{\mathbf{e}}_z \sin\phi \\ \mathbf{k}\cdot\hat{\mathbf{e}}_z \sin\phi & \cos\phi \end{pmatrix} \ , \tag{51.41}$$

where $\mathbf{k}$ is the wavevector of the light beam. An optical diode is composed by a $\phi = 45°$ Faraday rotor sandwiched between two polarizers rotated by $\phi = 45°$ with respect to each other.
a. How is the polarization of a light beam changed after a double passage (back and forth) through a Faraday rotator?
b. Calculate what happens to a light beam upon a single passage through a Faraday rotator in either direction $\mathbf{k}$ and $-\mathbf{k}$?

Solution: *a. The polarization is unchanged, since,*

$$\begin{pmatrix} \cos\phi & -\mathbf{k}\cdot\hat{\mathbf{e}}_z \sin\phi \\ \mathbf{k}\cdot\hat{\mathbf{e}}_z \sin\phi & \cos\phi \end{pmatrix} \begin{pmatrix} \cos\phi & \mathbf{k}\cdot\hat{\mathbf{e}}_z \sin\phi \\ -\mathbf{k}\cdot\hat{\mathbf{e}}_z \sin\phi & \cos\phi \end{pmatrix} \begin{pmatrix} a \\ b \end{pmatrix} = \begin{pmatrix} a \\ b \end{pmatrix} \ .$$

b. We assume the entrance polarizer oriented along the $\hat{\mathbf{e}}_x$ axis and the exit polarizer rotated by 45°,

$$M_{in} = \begin{pmatrix} 1 & 0 \\ 0 & 0 \end{pmatrix} \qquad with \qquad M_{rot}(\phi) = \begin{pmatrix} \cos\phi & -\sin\phi \\ \sin\phi & \cos\phi \end{pmatrix} \ ,$$

such that,

$$M_{out} = M_{rot}(\tfrac{\pi}{4}) M_{in} M_{rot}(\tfrac{\pi}{4})^{-1} = \begin{pmatrix} \frac{1}{2} & \frac{1}{2} \\ \frac{1}{2} & \frac{1}{2} \end{pmatrix} \ .$$

Without loss of generality we assume the light to be initially polarized as $\hat{\varepsilon} = \hat{\mathbf{e}}_x$ *and the entrance polarizer transmissive. Then for a propagation in* $\mathbf{k}$*-direction,*

$$M_{out}M_{Faraday}M_{in}\begin{pmatrix}1 & 0\end{pmatrix} = \begin{pmatrix}\frac{1}{2} & \frac{1}{2}\\ \frac{1}{2} & \frac{1}{2}\end{pmatrix}\begin{pmatrix}\cos\frac{\pi}{4} & -\sin\frac{\pi}{4}\\ \sin\frac{\pi}{4} & \cos\frac{\pi}{4}\end{pmatrix}\begin{pmatrix}1 & 0\\ 0 & 0\end{pmatrix}\begin{pmatrix}1\\ 0\end{pmatrix} = \begin{pmatrix}\frac{1}{\sqrt{2}}\\ \frac{1}{\sqrt{2}}\end{pmatrix} .$$

And for a propagation in $-\mathbf{k}$*-direction,*

$$M_{in}M_{Faraday}^{-1}M_{out}\begin{pmatrix}a\\ b\end{pmatrix} = \begin{pmatrix}1 & 0\\ 0 & 0\end{pmatrix}\begin{pmatrix}\cos\frac{\pi}{4} & \sin\frac{\pi}{4}\\ -\sin\frac{\pi}{4} & \cos\frac{\pi}{4}\end{pmatrix}\begin{pmatrix}\frac{1}{2} & \frac{1}{2}\\ \frac{1}{2} & \frac{1}{2}\end{pmatrix}\begin{pmatrix}a\\ b\end{pmatrix} = \begin{pmatrix}0\\ 0\end{pmatrix} .$$

51.3.4.6 Ex: Stokes parameters

For the Stokes parameters defined in (51.43) prove the following relationships,

$$[\hat{S}_k, \hat{S}_m] = 2\imath\epsilon_{kmn}\hat{S}_n \qquad \text{and} \qquad \hat{\mathbf{S}}^2 = \hat{S}_0^2 .$$

Solution: *We calculate using* $[\hat{a}_h, \hat{a}_h^\dagger] = 1 = [\hat{a}_v, \hat{a}_v^\dagger]$ *and* $[\hat{a}_v, \hat{a}_h^\dagger] = 0$*,*

$$\begin{aligned}[\hat{S}_1, \hat{S}_2] &= (\hat{a}_h^\dagger\hat{a}_h - \hat{a}_v^\dagger\hat{a}_v)(\hat{a}_h^\dagger\hat{a}_v e^{\imath\theta} + \hat{a}_v^\dagger\hat{a}_h e^{-\imath\theta}) - (\hat{a}_h^\dagger\hat{a}_v e^{\imath\theta} + \hat{a}_v^\dagger\hat{a}_h e^{-\imath\theta})(\hat{a}_h^\dagger\hat{a}_h - \hat{a}_v^\dagger\hat{a}_v)\\ &= \hat{a}_h^\dagger(\hat{a}_h\hat{a}_h^\dagger - \hat{a}_h^\dagger\hat{a}_h)\hat{a}_v e^{\imath\theta} + (\hat{a}_h^\dagger\hat{a}_h - \hat{a}_h\hat{a}_h^\dagger)\hat{a}_h\hat{a}_v^\dagger e^{-\imath\theta}\\ &\quad + \hat{a}_h^\dagger\left(\hat{a}_v\hat{a}_v^\dagger - \hat{a}_v^\dagger\hat{a}_v\right)\hat{a}_v e^{\imath\theta} + \hat{a}_h\hat{a}_v^\dagger e^{-\imath\theta}(\hat{a}_v^\dagger\hat{a}_v - \hat{a}_v\hat{a}_v^\dagger)\\ &= 2\hat{a}_h^\dagger\hat{a}_v e^{\imath\theta} - 2\hat{a}_h\hat{a}_v^\dagger e^{-\imath\theta} = 2\imath\hat{S}_3 ,\end{aligned}$$

and similarly for the other commutators. Also,

$$\begin{aligned}\hat{\mathbf{S}}^2 &= (\hat{a}_h^\dagger\hat{a}_h - \hat{a}_v^\dagger\hat{a}_v)^2 + (\hat{a}_h^\dagger\hat{a}_v e^{\imath\theta} + \hat{a}_v^\dagger\hat{a}_h e^{-\imath\theta})^2 - (\hat{a}_h^\dagger\hat{a}_v e^{\imath\theta} - \hat{a}_v^\dagger\hat{a}_h e^{-\imath\theta})^2\\ &= (\hat{a}_h^\dagger\hat{a}_h - \hat{a}_v^\dagger\hat{a}_v)^2 + 2\hat{a}_h^\dagger\hat{a}_v\hat{a}_v^\dagger\hat{a}_h + 2\hat{a}_v^\dagger\hat{a}_h\hat{a}_h^\dagger\hat{a}_v\\ &= (\hat{a}_h^\dagger\hat{a}_h + \hat{a}_v^\dagger\hat{a}_v)^2 + 2\hat{a}_h^\dagger\hat{a}_h + 2\hat{a}_v^\dagger\hat{a}_v = \hat{S}_0^2 + 2\hat{S}_0 .\end{aligned}$$

51.3.5 *Experiment: Polarization of a helium-neon laser*

We will now analyze and manipulate the polarization of a laser beam in practice.

1. Pass the beam of a helium-neon laser through a polarizer and a quarter- resp. half-waveplate. Analyze the polarization using a rotatable second polarizer for various rotation angles of the waveplate. Sketch the transmitted intensity as a function of the rotation angle of the beamsplitter in a polar diagram. How good can you achieve linear and circular polarization?

2. Characterize the polarization of a helium-neon laser by sketching the transmitted intensity through a polarizing beamsplitter as a function of the rotation angle of the beamsplitter in a polar diagram. Now couple the laser beam to a Fabry-Pérot interferometer. What do you observe? Place a quarter-waveplate at the output of the helium-neon laser and characterize again the polarization. What do you observe at the Fabry-Pérot interferometer?

3. Use a quarter-waveplate to separate a beam of light from a counterpropagating beam according to Fig. 51.19.

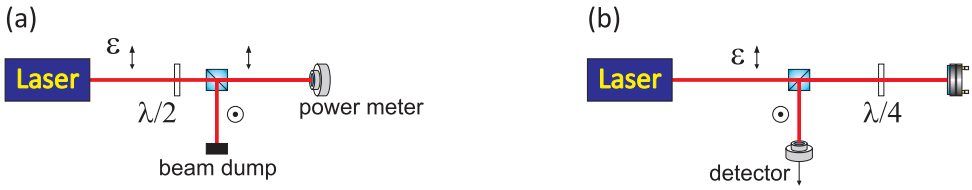

Figure 51.19: (a) Power control of a light beam and (b) separation of counterpropagating beams through polarization optics.

4. Characterize an optical insulator. Optimize its extinction.

51.3.6 *Experiment: Measuring the Brewster angle*

Any interface between two transparent materials with different refraction indices reflects a part of incident light depending on the polarization and the angle of incidence, as predicted by Fresnels formulae (51.33).

1. Measure the transmission by a glass plate as a function of the angle of incidence for two orthogonal polarizations and determine the Brewster angle.

2. Mirrors can change the polarization of a light beam and, for example, transform a linear polarization into elliptical. Determine the degree of ellipticity for a given mirror.

3. How does a mirror transform the polarization and the helicity of a reflected laser beam?

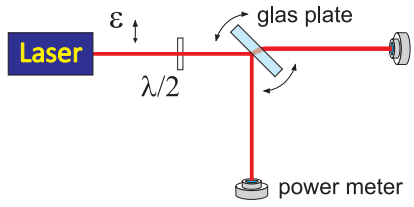

Figure 51.20: Measuring the Brewster angle by varying the tilt of a glas plate.

51.3.7 *Experiment: Pockels cell*

Pockels cells are birefringent crystals allowing to manipulate the polarization of a laser beam by application of a voltage.

1. Prepare a laser beam by passing it through a polarizer followed by a half-waveplate and a second polarizer. Observe the intensity transmitted and reflected through the last polarizer as a function of the rotation angle of the half-waveplate.

2. Use the EOM as a Pockels cell by placing it between the half-waveplate and the second polarizer. Supply a voltage between 0 V and 350 V to the EOM. Measures the intensity of reflected and transmitted light as a function of the supplied voltage and prepare a diagram. What do you observe when you rotate either the half-waveplate or the EOM?

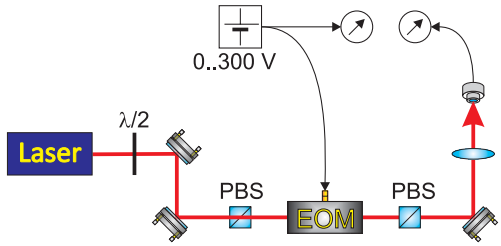

Figure 51.21: Scheme for using an EOM as a Pockels cell.

51.4 Laguerre-Gaussian light modes

Light beams not only possess polarization, but can also have orbital angular momentum. This property of light can impressively demonstrated at the so-called *Laguerre-Gaussian mode*s.

These modes can be produced by means of masks resembling *Fresnel zone plate*. Fresnel zone plates are masks consisting of concentric sequences of bright (transmitting) and dark (absorbing) rings. The diameters of the rings are selected in such a way that the diameters of the rings defined by the bright rings interfere constructively at a certain distance f_1 on the optical axis and form a 'focus' there. For this purpose, the distance d_n of the n^{th} ring must satisfy the condition,

$$d_n = \sqrt{(f_1 + n\lambda)^2 - f_1^2} \simeq \sqrt{2 f_1 n \lambda}\ . \tag{51.42}$$

For a given zone plate there are other focuses at smaller distances,

$$f_k = \frac{d_n^2 - k^2 n^2 \lambda^2}{2kn\lambda} \simeq \frac{d_n^2}{2kn\lambda} = \frac{f_1}{k}\ . \tag{51.43}$$

In order to separate the beams diffracted by the zone plate into a given focus from those diffracted into other focuses or not being diffracted at all, we pass the beam

through an iris diaphragm localized at the desired focus and recollimate the beam by means of a lens, as shown in Fig. 51.22.

The phase profile of the beam can be viewed interferometrically (see Fig. 51.22) by overlapping a plane wave laser beam. With a *neutral density filter* the intensities of the overlapping beams can be adjusted to maximize the contrast.

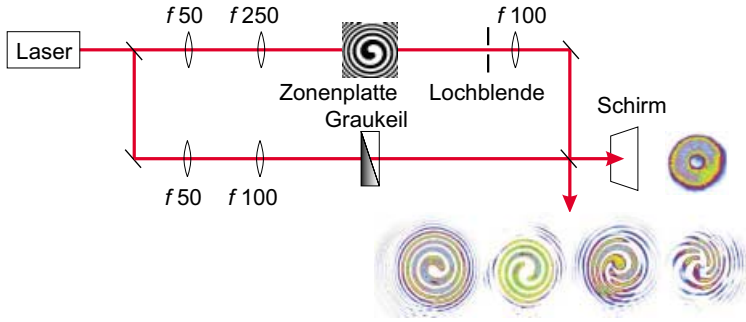

Figure 51.22: Creation of Laguerre-Gaussian modes.

Now, for realizing Laguerre-Gaussian light modes, we use Fresnel zone plates with spiral patterns, instead of concentric rings. In contrast to the Gaussian mode, the Laguerre-Gauß modes exhibit an intensity minimum on the optical axis (doonat mode). Their phase profiles can be viewed by interferometry [21].

51.4.1 *Experiment: Generating a Laguerre-Gaussian mode*

In this experiment, we will...

1. Construct the interferometer sketched in Fig. 51.22 using adequate Fresnel zone plates. What do you observe in the diffracted beam and in the interferogram, when instead of filtering the principal focus f_1 you filter a higher order focus?

2. Pass a Laguerre-Gauß laser beam through a $\lambda/2$ waveplate. How does the angular orbital momentum change when you change the rotation? What happens upon reflection from a mirror?

3. Slightly misalign the mode-matching between the Laguerre-Gauß beam and the Gaussian reference beam until you observe multiple fringes. What do you observe?

51.5 Further reading

M. Born, *Principles of Optics* [180]$_{\text{ISBN}}$

H. Kogelnik et al., *Laser Beams and Resonators* [734]$_{\text{DOI}}$

W. Demtröder, *Atoms, Molecules and Photons: An Introduction to Atomic, Molecular, and Quantum Physics* [352]$_{\text{ISBN}}$

J. Weiner et al., *Light-matter interaction, Fundamentals and applications* [1364]DOI

G.A. Fowles, *Introduction to Modern Optics* [464]ISBN

J.S. Choi et al., *Paraxial ray optics cloaking* [258]DOI

51.5.1 on Stokes parameters

W.P. Bowen et al., *Polarization Squeezing of Continuous Variable Stokes Parameters* [185]DOI

51.5.2 on Laguerre-Gauss modes

L. Allen et al., *Orbital Angular Momentum of Light and the Transformation of Laguerre-Gaussian Laser Modes* [21]DOI

Chapter 52

Electronics and radiofrequency

For the control and regulation of important quantum optical devices, such as EOMs, AOMs, laser diodes, photodiodes, piezos etc., *electronic circuit*s are necessary. The aim of this chapter is to provide practical know-how in the basics of electronics.

52.1 Introduction to electronic circuits

52.1.1 Passive electronic components

Electronic components which are characterized by a fixed impedance are called *passive*. The most common devices are resistors, capacitors, and inductances. For their handling, it is useful to be able to identify their impedance from their labeling.

The values of the resistances of resistors are generally codified by colored rings. The first ring to be considered is the one closest to a terminal. In case of 4 rings, the first two rings are to be considered as digits, the third ring gives the exponent 10. With five rings, the first three are digits and the forth gives the exponent of 10. The last ring, in both cases specifies the tolerance of the value of the resistance.

There are various types of capacitors depending on the employed materials for the dielectric medium (paper, ceramics, polyester, electrolyte made of aluminum and electrolyte made of tantalum). Electrolyte capacitors have a defined polarity, and an reversion of their voltage supply can result in their explosion. The value of the capacitance is generally written on their body, as well as their maximum allowed operating voltage. Also the polarity of electrolyte capacitors is always indicated (although there can be some confusion with regard to the physical and technical direction of the current flow). Ceramic and polyester capacitors can have their values either written in letters or color coded. The color code sequence is similar to that of resistors, with the first two digits devoted to the digits, the third to the multiplier exponent, the forth to the tolerance, and the fifth for the maximum voltage. In case of printed numbers, the first two numbers represent the first two digits, and the third one represents the numbers of 0 before the decimal point. In all cases (colors or digits), the value is given in picoFarads. With more modern serigraphic techniques, some capacitors have their values printed directly in Farads (micro, nano and pico). In these cases, the letter denoting the unit also serves to mark the decimal point. For example, 2n2 means 2.2 nF.

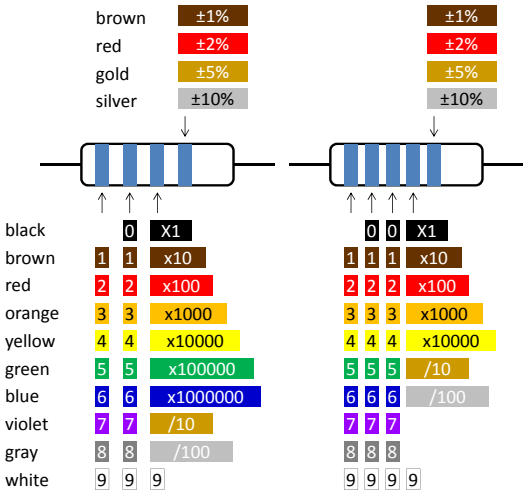

Figure 52.1: Color code for resistors with 4 and 5 rings.

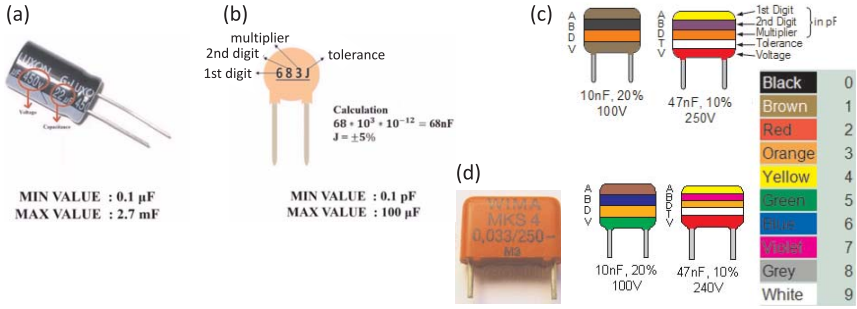

Figure 52.2: (Left) Electrolyte aluminum capacitors. (Center) Polyester capacitor and color code. (Right) Ceramic capacitor.

52.1.2 Active electronic components and the *pn*-junction

Diodes, transistors, photodiodes, operational amplifiers are called *active components*, because their current-to-voltage curve is non-linear, their response $I = I(U)$ cannot be described by a single constant value, but depends on the applied voltage.

During this course we will work a lot with *operational amplifiers* (OpAmp), which are integrated circuits designed to amplify input signals with characteristics that are entirely determined by external components. This feature makes them easy to use and extremely versatile.

OpAmps are generally found encapsulated in DIL type housings (dual in line), which means that they have two lines of 4 pins. The sequence of pins is numerated in counter-clockwise orientation, and they have a mark on the side of pin 1. It is always recommend to obtain the datasheet of the OpAmp since, despite a usual pin compatibility ensured by the various OpAmp manufacturers, deviations are frequent.

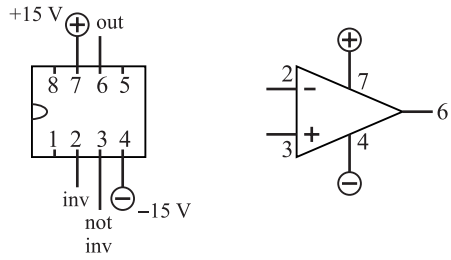

Figure 52.3: (Left) Schematic symbol of an OpAmp; (Right) Pin layout of a standard OpAmp.

52.1.3 Electronic circuits

Amplification or control circuits are nowadays mostly realized with *operational amplifiers* (*OpAmp*). The advantage of an OpAmp compared to circuits based on transistors is, that their properties are almost independent of their internal structure. Hence, their properties can be personalized via an external feedback realized with external components. The input of an OpAmp does not require current. OpAmps amplify the voltage difference between the non-inverting input (+) and the inverting (-). For most practical matters we can assume, that the OpAmp has infinite amplification and negligible input impedance.

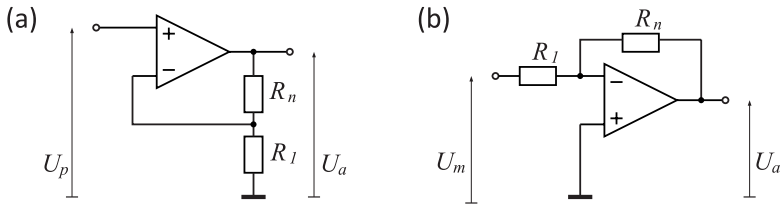

Figure 52.4: (Left) Principle scheme of a standard OpAmp. (Center) Non-inverting amplifier. (Right) Inverting amplifier.

OpAmps can be used as *inverting amplifiers* or *non-inverting amplifiers*. Using *Kirchhoff's rules* for the *loops* and *nodes* of the circuit, we find for a non-inverting amplifier,

$$\frac{U_e}{R_1} = -\frac{U_a}{R_1 + R_n} \quad , \quad G = 1 + \frac{R_n}{R_1} \; . \tag{52.1}$$

This becomes clear noting that, since no voltage is dropped between the inputs (+) and (-), the input voltage must be equal to the voltage drop at R_1. And since the non-inverting input does not deliver current, the currents traversing the resistances R_n and R_1 must be equal. For the inverting amplifier, we find,

$$\frac{U_a}{R_n} = -\frac{U_e}{R_1} \quad , \quad G = -\frac{R_n}{R_1} \; . \tag{52.2}$$

This becomes clear noting that, since the input (-) does not drag current, the currents traversing the resistances R_n and R_1 must cancel each other.

Changing the resistances R to inductances L or capacitances C, it becomes possible to influence the frequency response of the amplifying circuit. The impedance are,

$$Z_L = \imath L\omega \quad , \quad Z_C = \frac{1}{\imath C\omega} \ . \tag{52.3}$$

For the calculation of the amplification wit complex impedances, we just take the absolute value of the gain G.

52.1.4 The thermoelectric effect

52.1.4.1 Seebeck effect

The Seebeck effect is a classic example of an electromotive force (EMF) and leads to measurable currents or voltages in the same way as any other EMF. The local current density is given by,

$$\mathbf{J} = \sigma(-\nabla V + \mathbf{E}_{emf}) \ , \tag{52.4}$$

where V is the local voltage, and σ is the local conductivity. In general, the Seebeck effect is described locally by the creation of an electromotive field,

$$\mathbf{E}_{emf} = -S\nabla T \ , \tag{52.5}$$

where S is the Seebeck coefficient (also known as thermopower), a property of the local material, and ∇T is the temperature gradient.

The Seebeck coefficients generally vary as function of temperature and depend strongly on the composition of the conductor. For ordinary materials at room temperature, the Seebeck coefficient may range in value from $-100\,\mu\text{V/K}$ to $+1000\,\mu\text{V/K}$.

If the system reaches a steady state, where $\mathbf{J} = 0$, then the voltage gradient is given simply by the emf:

$$-V = S\Delta T \ . \tag{52.6}$$

This simple relationship, which does not depend on conductivity, is used in the thermocouple to measure a temperature difference; an absolute temperature may be found by performing the voltage measurement at a known reference temperature. A metal of unknown composition can be classified by its thermoelectric effect if a metallic probe of known composition is kept at a constant temperature and held in contact with the unknown sample that is locally heated to the probe temperature. It is used commercially to identify metal alloys. Thermocouples in series form a *thermopile*. Thermoelectric generators are used for creating power from heat differentials.

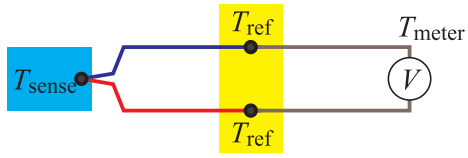

Figure 52.5:

52.1.4.2 Peltier effect

When an electric current is passed through a circuit of a thermocouple, heat is evolved at one junction and absorbed at the other junction. This is known as Peltier Effect and is named after a physicist. The Peltier effect is the presence of heating or cooling at an electrified junction of two different conductors. When a current is made to flow through a junction between two conductors, A and B, heat may be generated or removed at the junction. The Peltier heat generated at the junction per unit time is,

$$\dot{Q} = (\Pi_A - \Pi_B)I \ , \tag{52.7}$$

where Π_A and Π_B are the Peltier coefficients of conductors A and B, and I is the electric current (from A to B). The total heat generated is not determined by the Peltier effect alone, as it may also be influenced by Joule heating and thermal-gradient effects (see below).

The Peltier coefficients represent how much heat is carried per unit charge. Since charge current must be continuous across a junction, the associated heat flow will develop a discontinuity if Π_A and Π_B are different. The Peltier effect can be considered as the back-action counterpart to the Seebeck effect (analogous to the back-EMF in magnetic induction): if a simple thermoelectric circuit is closed, then the Seebeck effect will drive a current, which in turn (by the Peltier effect) will always transfer heat from the hot to the cold junction. The close relationship between Peltier and Seebeck effects can be seen in the direct connection between their coefficients [635, 1306]:

$$\Pi = TS \ . \tag{52.8}$$

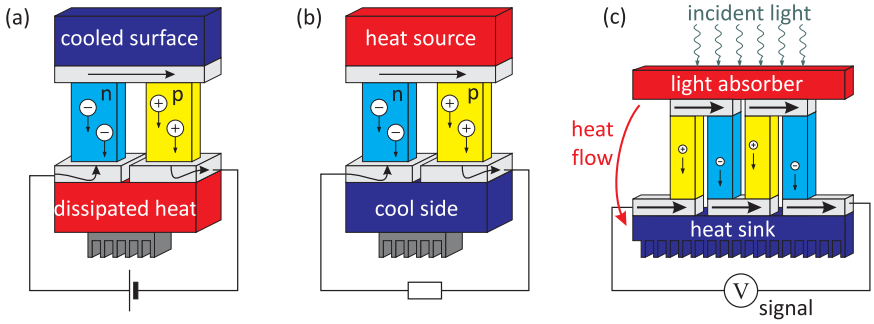

Figure 52.6: (a) Peltier cooler, (b) voltage generator or heat sensor, and (c) heat or radiation sensor with thermocouples connected in parallel.

52.1.5 Exercises

52.1.5.1 Ex: Integrator with operational amplifier

Based on the two golden rules for operational amplifiers, (1) $I_+ = I_- = 0$ A and (2) $U_+ = U_-$, show that the output voltage U_a at the integrated circuit shown in the figure is: $U_a = \frac{1}{RC} \int U_e dt$.

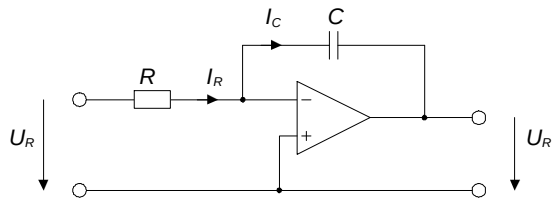

Figure 52.7: Integrator with operational amplifier.

Solution: *Using the golden rule, we get:*

$$U_e = RI_R \qquad \textit{and} \qquad I_R = I_C \qquad \textit{and} \qquad U_a = \frac{1}{C}\int I_C \; dt \; .$$

From this follows,

$$U_a = \frac{1}{RC}\int U_e \; dt \; .$$

52.1.5.2 Ex: Low-pass filter using an OpAmp

Using an inverting operational amplifier design a simple low-pass filter with a constant amplification of 10 at low frequencies and diminishing gain above 10 kHz. Calculate the Bode diagram (i.e. the frequency-dependent gain and phase-shift of your circuit. What is the gain reduction per octave?

Solution: *Choosing a circuit like in Fig. 52.3(b) with an impedance in parallel* $R_n = R_2 \parallel 1/\imath C\omega$*, we find a gain curve of,*

$$G(\omega) = -\frac{1}{\frac{1}{R_2} + \imath C\omega}\frac{1}{R_1} \; ,$$

that is,

$$|G(\omega)| = \frac{R_2}{R_1}\sqrt{\frac{1}{1+(R_2C\omega)^2}} \qquad \textit{and} \qquad \arctan\phi = \frac{\mathrm{Im}\;\; G(\omega)}{\mathrm{Re}\;\; G(\omega)} = -R_2C\omega \; .$$

The reduction per octave is,

$$\left|\frac{G(2\omega)}{G(\omega)}\right| = \sqrt{\frac{1+(2\omega R_2C)^2}{1+(\omega R_2C)^2}} \overset{\omega\to\infty}{\longrightarrow} 3\,\mathrm{dB} \; .$$

52.1.6 *Experiment: Amplifiers and active filters*

Here, we will learn how to use OpAmps: We will start mounting a 10-fold inverting amplifier on a breadboard and then modify the external passive components, such as to build a low-pass filter.

1. Assemble on a breadboard a simple inverting amplifier using an OpAmp. Use 10 kΩ resistors at the input aim for an amplification factor of 10.

2. Test the circuit with a frequency generator and an oscilloscope.

3. Modify the circuit such as to obtain a low-pass filter with $f_g = 50$ kHz bandwidth and test the circuit again.

52.1.7 *Experiment: Peltier element and thermistor*

Here, we will learn how to use a Peltier element and a thermistor. A *thermistor* is nothing else than a well-calibrated resistor with temperature-dependent resistance (see Fig. 52.9).

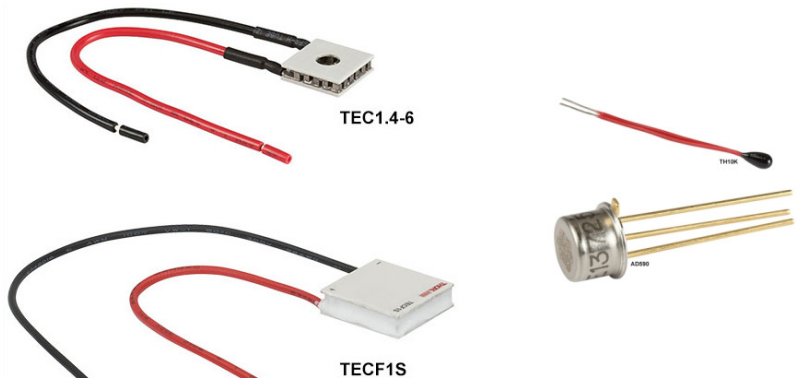

Figure 52.8: Pictures of Peltier elements, a thermistor, and an AD590 temperature transducer.

1. Connect a Peltier element to a 1 A current source and bring one of the two surfaces of the Peltier element into thermal contact with a heat sink. What do you observe?

2. Bring a 10 kΩ thermistor in thermal contact with either of the two surfaces of the Peltier element and measure its resistance. What do you observe?

3. Can you imagine a feedback logic evaluating the measured resistance in order to control the current applied to the Peltier element such as to maintain constant the temperature of the surface not connected to the heat sink.

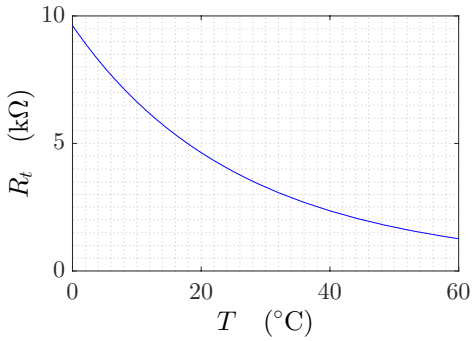

Figure 52.9: Calibration curve for a 10 kΩ thermistor from Thorlabs.

52.2 Detectors

52.2.1 Photodiodes

Most active components are many of *semiconductor* characterized by a relatively large band gap between the valence band and the conduction band. By appropriate doping of the material with donors (p-type) or acceptors (n-type) a semiconductor can be made conductive. The most basic semiconductor element, which is the *diode* consists of a junction of two types of semiconductors, as shown in Fig. 52.10.

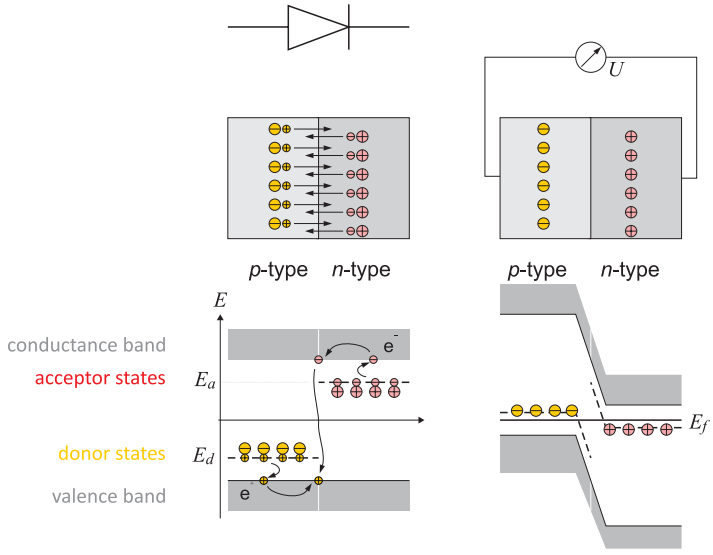

Figure 52.10: Joining a p-type and a n-type doped semiconductor (left) one observes a charge carrier redistribution across the pn transition (right).

Our first task will be to construct a *photo detector*. The central part of a photodetector is the photodiode. We have at our disposal silicium *pin*-photodiodes of the type C30822E of the company Perkin Elmer and of the type FFD100.

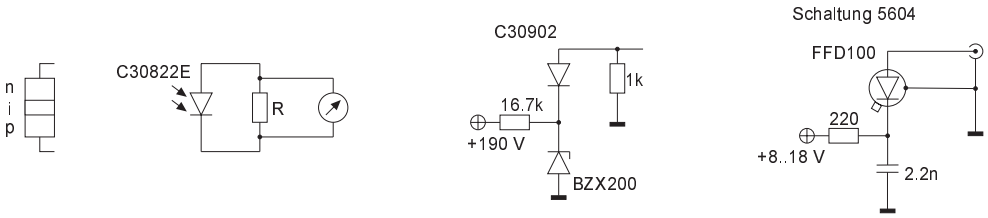

Figure 52.11: Circuit with photodiode.

Photodiodes exploit an intrinsic photoeffect of semiconductor *pn*-junctions. In the transition region, free electrons of the *n*-type semiconductor and excess holes of the *p*-type semiconductor are drifting into the respective opposite semiconductor, where they recombine. The consequence is a transition zone with a charge carrier depletion, which acts as a barrier and has an intrinsic capacitance. The charge carrier imbalance gives rise to an electric field across the junction. The energy liberated during the recombination process can be dissipated via emission of light.

The reverse process is also possible: Via the intrinsic photoeffect, light irradiated into the *pn*-junction can lift electrons from the valence into the conduction band, thus generating pairs of charge carriers. Under the influence of the electric field across the junction, the holes flow to the edge of the p domain and the electrons flow to the n domain. This part of the current is called *drift current*. A smaller part, called the *diffusion current*, has its origin in the diffusion of the electron-hole pairs formed in the edge regions. Since these minority charge carriers have only a limited lifetime before they recombine, only the part of the current generated within a few units of the diffusion lengths near the charge carrier zone contributes. This results in an external photovoltaic voltage at the electrodes of the photodiode. If the photodiode is connected to a load, a photocurrent will flow, which is composed, as mentioned above, by the drift current of the charge carrier zone and the diffusion current from its edges.

The principal scheme of a pin diode is illustrated in Fig. 52.12(left): A weakly doped intrinsic layer separates the p and the n conductor. This reduces the capacity of the barrier. The current at short circuit is proportional to the light power. A photodiode is always operated in blocking direction. A negative offset voltage reduces the capacity of the *pn*-junction.

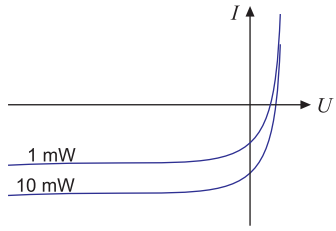

Figure 52.12: (code) U-I dependence of a photodiode.

Despite all measures the *pn*-junction capacity remains finite. One can model the impact of the *pn*-junction capacity via a replacement diagram. The voltage drop is

$$\frac{U(\omega)}{U_0} = \frac{R_L||\frac{1}{\imath\omega C}}{R_i + \left(R_L||\frac{1}{\imath\omega C}\right)} = \frac{\frac{R_i||R_L}{R_i}}{1+\imath\omega C(R_i||R_L)} \ . \tag{52.9}$$

For high load resistances the frequency response obviously becomes load-independent. For small loads, $R_L < R_i$, the band width of the photodiode is dramatically increased to $\omega_g = 1/R_L C$. In the same time, however, the amplification drops to $V = R_L/R_i$.

52.2.2 Exercises

52.2.2.1 Ex: Photomultiplier

The anode of a photomultiplier tube is connected by a resistor of $R = 1\,\mathrm{k\Omega}$ to ground. The stray capacitance is 10 pF, the current amplification 10^6, and the anode rise time 1.5 ns. What is the peak amplitude and the halfwidth of the anode output pulse produced by a single photoelectron? What is the dc output current produced by 10^{-12} W cw radiation at $\lambda = 500\,\mathrm{nm}$, if the quantum efficiency of the cathode is $\eta = 0.2$ and the anode resistor $R = 10^6\,\Omega$? Estimate the necessary voltage amplification of a preamplifier (a) to produce 1 V pulses for single-photon counting; and (b) to read 1 V on a dc meter of the cw radiation?

Solution: *The anode voltage pulse is,*

$$U_a(t) = \frac{Q(t)}{C} = \left(\frac{1}{C}\int_0^{\Delta t} i_{ph}(t)dt\right)\cdot e^{-t/RC} \ .$$

a. The time constant $\tau = RC = 10^{-8}\,\mathrm{s}$, which governs the decay of the voltage at C, is long compared with the rise time $\Delta t = 1.5\,\mathrm{ns}$. Therefore we can neglect the decay during the rise time and obtain for the pulse maximum,

$$U_a = \frac{1}{C}\cdot 10^6 e = \frac{1}{C}\cdot 1.6\cdot 10^{-13}\,\mathrm{C}$$

with $C = 10^{-11}\,\mathrm{F}$ we obtain $U_a(t) = 1.6\cdot 10^{-2}\cdot e^{-t\cdot 10^8}\,\mathrm{V}$. The peak amplitude is $U_{max} = 16\,\mathrm{mV}$. The halfwidth of the pulse is obtained from $e^{-10^8 t} = \frac{1}{2}$, yielding $\Delta t_1 = 6.9\cdot 10^{-9}\,\mathrm{s}$.
b. For $P = 10^{-12}\,\mathrm{W}$ cw radiation power at $\lambda = 500\,\mathrm{nm}$, the number of photoelectrons per second is,

$$n_{PE} = \eta\frac{P}{h\nu} = 4.5\cdot 10^5\,\mathrm{s^{-1}} \ .$$

With an amplification factor M, the anode current is: $i_a = n_{PE}\cdot e\cdot M$. The voltage across the anode resistor R is $U_a = i_a R = R n_{PE} e M = 72\,\mu\mathrm{V}$. Note that for cw measurements, a larger resistance of $R \approx 1\,\mathrm{M\Omega}$ is used, because the time resolution is not important here. For $R = 10^6\,\Omega$, we get $U_a = 72\,\mathrm{mV}$. In order to produce 1 V output pulses for single photoelectrons, an amplification of $M_2 \approx 62$ of the preamplifier is required.

52.2.2.2 Ex: Optical image intensifier

A manufacturer of a two-stage optical image intensifier states that incident intensities of $10^{-17}\,\mathrm{W}$ at $\lambda = 500\,\mathrm{nm}$ can still be 'seen' on the phosphor screen of the output state. Estimate the minimum intensity amplification, if the quantum efficiency of the cathodes and the conversion efficiency of the phosphor screens are both 0.2 and the collection efficiency of light emitted by the phosphor screens is 0.1. The human eye needs at least 20 photons/s to observe a signal.

Solution: *For* $10^{-17}\,\mathrm{W}$ *at* $\lambda = 500\,\mathrm{nm}$, $25\,\mathrm{photons/s}$ *fall onto the first cathode. The human eye can see* $20\,\mathrm{photons/s}$, *which corresponds to* $8 \cdot 10^{-18}\,\mathrm{W}$. *With a collection efficiency of* 0.1 *the last phosphor screen has to emit at least* $8 \cdot 10^{-17}\,\mathrm{W}$. *With a conversion efficiency of 0.2, the intensity amplification has to be*

$$V_I = \frac{8 \cdot 10^{-17}}{1 \cdot 10^{-17} \cdot 0.23} = 1000 \ .$$

52.2.2.3 Ex: Photovoltaic detector

Estimate the maximum output voltage of an open photovoltaic detector at room temperature under $10\,\mu\mathrm{W}$ irradiation when the photocurrent of the shortened output is $50\,\mu\mathrm{A}$ and the dark current is $50\,\mathrm{nA}$.

Solution: *With* $I_{ph} = 50\,\mu\mathrm{A}$ *and* $I_d = 50\,\mathrm{nA}$ *we get,*

$$U_{ph}(I = 0) = \frac{k_B T}{e}\left[\ln\left(\frac{I_{ph}}{I}\right) + 1\right] = 0.2\,\mathrm{V} \ .$$

52.2.3 *Experiment: Taking the response function of a photodiode*

In this part of the lab course, we will learn to solder and set up simple electronic circuits. We will also learn how to identify the connections of a photodiode and mount into a case with BNC connectors. Finally, we will characterize the photodiode for use in future applications. Initially, we will work without offset voltage, later we will apply a voltage and identify its impact [1].

1. Connect an LED to a function generator and make it blink at low frequencies adjusting the offset and the amplitude of the output voltage. Shine the light onto your photodiode and monitor the signal on an oscilloscope. Explain your observations.

[1] Datasheet for the Photodiode FFD100 see appendix Fig. 56.21,
data sheet for the Photodiode C30822E see appendix Fig. 56.22.

2. Reduce the amplitude and adjust the offset until you observe a sinusoidal signal. Increase the frequency and explain your observations. (Note that the response of LEDs is extremely fast (MHz).) Determine the bandwidth of your detector.

3. Measure the current at short circuit. Connect a $R = 10\,\mathrm{k\Omega}$ resistive load in parallel to the photodiode output and measure the voltage drop into this load.

4. Characterize the photodetector with respect to its sensitivity (in A/W) by varying the load.

5. How is the frequency response of the photodiode modified by the load? Measure bandwidth as a function of the load. Adjust the load until the detector (circuit including photodiode and resistor) has a bandwidth of 10 kHz (which is sufficient for many applications).

6. Apply a 10 V voltage in reverse direction and analyze again the sensitivity and the bandwidth of your photodetector. Note that the blinking LED can be replaced by a rotating chopper wheel.

Example of a measured characterization of a photodiode.

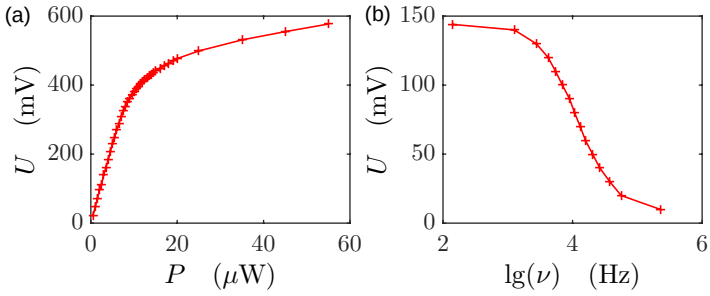

Figure 52.13: (a) Calibration of a photodiode, measured voltage as a function of the incident light power. (b) Low-pass behavior of a resistive charge of 90 kΩ.

52.3 Introduction to radiofrequency components

52.3.1 VCOs and the generation of rf-sidebands

Voltage-controlled oscillators (*VCO*) serve to generate variable radiofrequencies. They are the basis for most function generators. A useful particularity of VCOs is the possibility modulate the frequency and phase of an optical carrier wave by modulating the control voltage of a VCO at low frequency.

The modulation of the carrier wave generates sidebands. This can be seen by expanding the signal which carries the phase modulation into a Fourier series,

$$Ae^{\imath\omega t+\imath\beta\sin\Omega t} = Ae^{\imath\omega t}\sum_{k=-\infty}^{\infty} J_k(\beta)e^{\imath k\Omega t} \simeq Ae^{\imath\omega t} + J_1(\beta)Ae^{\imath\omega t+\imath\Omega t} + J_{-1}(\beta)Ae^{\imath\omega t-\imath\Omega t} \tag{52.10}$$

when the *modulation index* β is small. Here, $J_{-k}(\beta) = (-1)^k J_k(\beta)$ are the Bessel functions. This is in contrast to amplitude modulation, which is described by only two symmetric sidebands,

$$A(1 + \beta \sin \Omega t)e^{\imath\omega t} = Ae^{\imath\omega t}\left(1 + \frac{\beta}{2\imath}(e^{\imath\Omega t} - e^{-\imath\Omega t})\right) . \tag{52.11}$$

For *amplitude modulation* (*AM*) the beat signals between the carrier frequency and the two sidebands are in phase, i.e.,

$$\left|e^{\imath\omega t} + e^{\imath(\omega\pm\Omega)t}\right|^2 = 2 + e^{\imath\Omega t} + e^{-\imath\Omega t} . \tag{52.12}$$

For *phase modulation* (*PM*) the beat signal are in counter-phase, i.e.,

$$\left|e^{\imath\omega t} + e^{\imath(\omega\pm\Omega)t+\imath\pi/2}\right|^2 = 2 + \imath e^{\pm\imath\Omega t} - \imath e^{\mp\imath\Omega t} . \tag{52.13}$$

In the case of AM, the amplitude is blurred, but the phase at zero-crossing is well defined. In the case of PM, the amplitude in the antinode is sharp, but the phase of the zero-crossing is blurred.

It is not easy to transform AM into PM, and vice versa. In fact, the phase between carrier and sidebands can be varied, for example by adding an AC voltage, $\sqrt{2}e^{\imath\omega t+3\imath\pi/4}$ to the signal; however, it is not easy to transform synchronized phases into opposite phases.

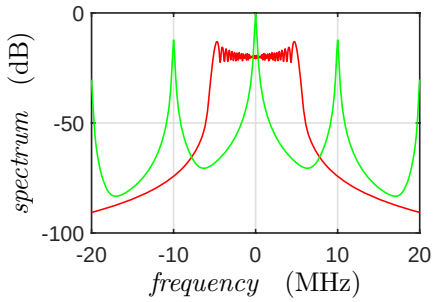

Figure 52.14: (code) Frequency spectra of a phase-modulated carrier frequency for $\Delta\omega = 5\,\text{MHz}$ modulation excursion and (red) $\omega = 100$ kHz modulation frequency ($\beta = \frac{\Delta\omega}{\Omega} = 50$) and (green) $\omega = 10\,\text{MHz}$ modulation frequency ($\beta = 0.5$). Furthermore, a $\gamma = 100\,\text{kHz}$ resolution linewidth is assumed.

As shown in Eq. (52.10), the spectrum of a signal with phase modulation (PM) consists of discrete lines, called sidebands, whose amplitudes are given by Bessel functions,

$$S(\omega) = \sum_{k=-\infty}^{\infty} |A\mathcal{J}_k(\beta)|^2 \delta(\omega + k\Omega) . \tag{52.14}$$

In real systems, the sidebands have finite widths γ due to frequency noise or the finite resolution of the detectors. In the case of Lorentzian line profiles, we have,

$$S(\omega) = \sum_{k=-\infty}^{\infty} |A\mathcal{J}_k(\beta)|^2 \frac{\beta^2}{(\omega - k\Omega)^2 + \beta^2} . \tag{52.15}$$

52.3.2 Mixers

A *frequency mixer* is a nonlinear electrical circuit that creates new frequencies from two input signals, e.g. the sum and difference of the input frequencies. A device that has a non-linear (e.g. exponential) characteristic can act as a mixer. Passive mixers use one or more diodes and rely on their non-linear relation between voltage and current. Active mixers use an amplifying device (such as a transistor) to increase the strength of the product signal.

Mixers may be classified by their topology: An unbalanced mixer, in addition to producing a product signal, allows both input signals to pass through and appear as components in the output. A single-balanced mixer is arranged with one of its inputs applied to a balanced (differential) circuit so that either the local oscillator (LO) or signal input (RF) is suppressed at the output, but not both. A double-balanced mixer has both its inputs applied to differential circuits, so that neither of the input signals and only the product signal appears at the output. Double balanced mixers are more complex and require higher drive levels than unbalanced and single-balanced designs.

In practice, mixers are widely used to shift signals from one frequency range to another, a process known as *heterodyning*, in order to facilitate signal transmission or further signal processing. Frequency mixers are also used to modulate a carrier signal in radio transmitters, as product detectors, phase detectors, or frequency multipliers.

52.3.2.1 Diode

The non-linearity (or non-Ohmic behavior) of a diode can be used to create a simple unbalanced mixer producing the original frequencies as well as their sum and their difference. The current I through an ideal diode as a function of the voltage U across it is given by an exponential function,

$$I = I_0(e^{qU/k_BT} - 1) \ . \tag{52.16}$$

The exponential can be expanded as $e^x - 1 \simeq x + \frac{x^2}{2}$. Suppose that the sum of the two input signals $U_1 + U_2$ is applied to a diode, and that an output voltage is generated that is proportional to the current through the diode [e.g. by providing the voltage that is present across a resistor in series with the diode, as shown in Fig. 52.15(a)]. Then, disregarding the constants in the diode equation, the output voltage will have the form,

$$\begin{aligned} U_0 &= (U_1 + U_2) + \tfrac{1}{2}(U_1 + U_2)^2 + ... \\ &= (U_1 + U_2) + \tfrac{1}{2}(U_1^2 + 2U_1U_2 + U_2^2) + ... \ . \end{aligned} \tag{52.17}$$

The ellipsis represents all the higher powers of the sum which we assume to be negligible for small signals.

Suppose that two input sinusoids of different frequencies, $U_1 = \sin\omega_1 t$ and $U_2 = \sin\omega_2 t$ are fed into the diode. The signal U_0 becomes:

$$U_0 = (\sin\omega_1 t + \sin\omega_2 t) + \tfrac{1}{2}(\sin^2\omega_1 t + 2\sin\omega_1 t \sin\omega_2 t + \sin^2\omega_2 t) + ... \ . \tag{52.18}$$

Ignoring all terms except for the $\sin\omega_1 t \sin\omega_2 t$ term we get,

$$U_0 = 2\sin\omega_1 t \sin\omega_2 t + ... = \cos(\omega_1 t - \omega_2 t) - \cos(\omega_1 t + \omega_2 t) + ... \ , \tag{52.19}$$

demonstrating how new frequencies are created from the mixer.

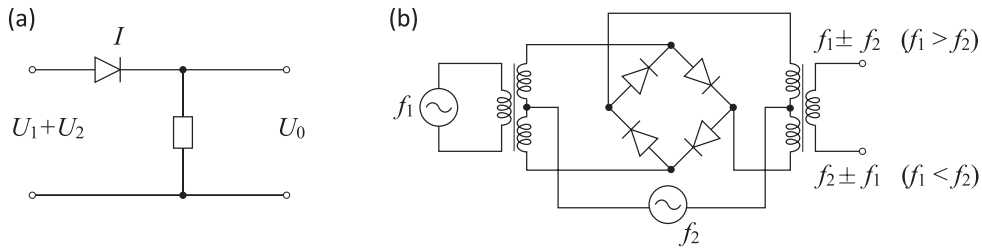

Figure 52.15: (a) Mixing two signal at a diode. (b) Schematic diagram of a double-balanced passive diode mixer (also known as a ring modulator). There is no output unless both f_1 and f_2 inputs are present, though f_2 (but not f_1) can be DC.

52.3.2.2 Switching

Another form of mixer operates by switching, with the smaller input signal being passed inverted or non-inverted according to the phase of the local oscillator (LO). This would be typical of the normal operating mode of a packaged double balanced mixer, with the local oscillator drive considerably higher than the signal amplitude.

The aim of a switching mixer is to achieve linear operation over the signal level by means of hard switching, driven by the local oscillator. Mathematically, the switching mixer is not much different from a multiplying mixer. Instead of the LO sine wave term, we would use the signum function. In the frequency domain, the switching mixer operation leads to the usual sum and difference frequencies, but also to further terms, e.g. $\pm 3f_{LO}$, $\pm 5f_{LO}$, etc.. The advantage of a switching mixer is that it can achieve (with the same effort) a lower noise figure and larger conversion gain. This is because the switching diodes or transistors act either like a small resistor (switch closed) or large resistor (switch open), and in both cases only a minimal noise is added. From the circuit perspective, many multiplying mixers can be used as switching mixers, just by increasing the LO amplitude.

52.3.2.3 Modulation and demodulation

Mixers are often used for modulation or demodulation purposes. Suppose we have on one hand a *carrier* signal, $U_{carrier} = \cos \omega t$, also called *local oscillator*. This may be a constant radiofrequency emitted by an antenna or a microwave. On the other hand, we have a reference signal which we want to transport somewhere else, $U_{ref} = \cos \Omega t$. Used as a modulator the mixer will simple multiply,

$$U_{mod} = U_{carrier} U_{ref} = \cos \omega t \cos \Omega t = \tfrac{1}{2} \cos[(\omega - \Omega)t] + \tfrac{1}{2} \cos[\omega + \Omega)t] \; . \qquad (52.20)$$

Thus the mixer output contains two frequencies, the sum and the difference. Supposing that ω is a frequency in a range that can be radiated by antenna and Ω an acoustic frequency, both frequency components $\omega \pm \Omega \simeq \omega$ will be radiated.

On the side of the receiver, who also has access to a synthesizer generating a signal $U_{carrier} = \cos \omega t$, we will use the mixer as a demodulator,

$$U_{demod} = U_{carrier} U_{mod} = \cos^2 \omega t \cos \Omega t = \tfrac{1}{2}(\cos 2\omega t + 1) \cos \Omega t \; . \qquad (52.21)$$

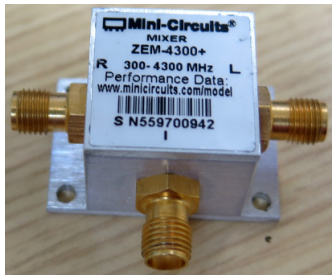

Figure 52.16: Picture of a radiofrequency mixer.

If $\omega \gg \Omega$, the carrier oscillation can easily be removed by a low-pass filter,

$$U_{filtered} = \tfrac{1}{2}\cos\Omega t \propto U_{ref} \ . \tag{52.22}$$

That is, we recover the original information. And this holds even when the reference signal is (slowly) varying in amplitude or frequency, such as in the case of an acoustic signal [2]. Resolve Exc. 52.3.3.1.

52.3.2.4 Filtering with a mixer

Suppose we have a signal containing many frequency components (which may vary slowly in time), $U_{noisy}(t) = \sum_n A(\omega_n)e^{\imath\omega_n t}$ in complex notation, and that the signal we are interested in is an amplitude at a known particular frequency ω_0. By demodulating,

$$U_{sig}(t) = U_{noisy}(t)e^{-\imath\omega_0 t} = \sum_n A(\omega_n)e^{\imath\omega_n t}e^{-\imath\omega_0 t} = \sum_n A(\omega_n)e^{\imath(\omega_n-\omega_0)t} \ , \tag{52.23}$$

and low-pass filtering the lowest frequency component, i.e. $\omega_n - \omega_0 \simeq 0$,

$$U_{filtered} = A(\omega_0) \ . \tag{52.24}$$

This even holds for continuous noise spectra, $U_{noisy}(t) = \int A(\omega)e^{\imath\omega t}d\omega$, since,

$$U_{sig}(t) = U_{noisy}(t)e^{-\imath\omega_0 t} = \int_{-\infty}^{\infty} A(\omega)e^{\imath\omega t}e^{-\imath\omega_0 t}d\omega = \int_{-\infty}^{\infty} A(\omega+\omega_0)e^{\imath\omega t}d\omega \ , \tag{52.25}$$

and low-pass filtering with a filter bandwidth $\Delta\omega$,

$$U_{filtered} = \int_{-\Delta\omega}^{\Delta\omega} A(\omega+\omega_0)e^{\imath\omega t}d\omega \simeq A(\omega_0)2\Delta\omega \ . \tag{52.26}$$

Such techniques are widely used in lock-in amplifiers (see Sec. 52.4.3).

[2] In complex notation, $U_{in} = e^{\imath\omega t}$, $U_{mod} = U_{in}e^{\imath\Omega t} = e^{\imath(\omega+\Omega)t}$, $U_{demod} = U_{mod}e^{-\imath\omega t} = e^{\imath\Omega t}$.

52.3.3 Exercises

52.3.3.1 Ex: Phase modulation

a. Show that it is not possible to construct a periodic phase modulation function such that the signal has only two sidebands.
b. Compare the spectra $\sum_{k=-\infty}^{\infty} J_k(M)e^{\imath k\Omega t} = e^{\imath M\sin\Omega t}$ and $\sum_{k=-\infty}^{\infty}|J_k(M)|e^{\imath k\Omega t}$. Can you detect phase modulation of a photodetector signal on a spectrum analyzer? How about amplitude modulation?

Solution: *a. The question is whether there is a periodic function $f(t)$ such that,*

$$e^{\imath\omega t+\imath f(t)} = e^{\imath\omega t} + Me^{\imath(\omega+\Omega)t} - Me^{\imath(\omega-\Omega)t}$$

or equivalently $e^{if(t)} = 1 + 2\imath M\sin\Omega t$. Such a function would have to satisfy,

$$1 = |1 + 2\imath M\sin\Omega t|^2 = 1 + 4M^2\sin^2\Omega t \ ,$$

which only holds for $M = 0$. In contrast, a sinusoidal phase modulation satisfies,

$$1 = |e^{\imath M\sin\Omega t}|^2 = \left|\sum_{k=-\infty}^{\infty} J_k(M)e^{\imath k\Omega t}\right|^2 = \sum_{k,m=-\infty}^{\infty} J_k(M)J_m(M)e^{\imath(k-m)\Omega t} = \sum_{k=-\infty}^{\infty}|J_k(M)|^2 \ .$$

b. Phase modulation cannot be seen by a spectrum analyzer, simply because the signal recorded by a photodetector is,

$$|E_{pm}|^2 = |e^{\imath\omega t+\imath M\sin\Omega t}|^2 = 1 \ .$$

On the other hand, amplitude modulation is visible, since,

$$|E_{am}|^2 = |(1 + M\cos\Omega t)e^{\imath\omega t}|^2 = 1 + \tfrac{M^2}{2} + 2M\cos\Omega t + \tfrac{M^2}{2}\cos 2\Omega t \ .$$

52.3.4 *Experiment: Creating sidebands on a radiofrequency*

In this exercise, we will understand the origin of sidebands as we'll see them emerge from a modulation spectrum when we gradually increase the modulation index [3].

1. Take a VCO, for example, ZOS-100+ from MiniCircuits. Study the datasheet and drive the VCO with an AC voltage. Vary the amplitude and the frequency of the voltage and observe the output signal of the VCO on a spectrum analyzer.

2. Try to understand the spectrum observing the limiting cases $\Omega \gg \Delta\omega$ and $\Omega \ll \Delta\omega$. How can you read Ω and Δf from the spectra in both cases?

3. Write a MATLAB program to simulate the spectrum.

[3] Datasheet for the VCO see appendix Fig. 56.16,
data sheet for the variable attenuator see appendix Fig. 56.17,
data sheet for the mixer see appendix data sheet Fig. 56.19.

52.4 Measurement instrumentation

52.4.1 Sample-and-hold circuit

sample-and-hold circuit Solder on euroboard

52.4.2 Box-car integrator

box-car integrator Solder on euroboard

52.4.3 Lock-in amplifier

An *lock-in amplifier* (also called a phase-sensitive rectifier or *mixer*) is an amplifier that can measure a weak electrical signal by modulating the signal by a reference signal with a known frequency and phase. The device represents a bandpass filter with an extremely narrow bandwidth and, therefore, improves the signal-to-noise ratio (SNR). DC or AC noise components are efficiently filtered.

Download an illustration of the working principle of a *lock-in amplifier* here.

52.4.4 *Experiment: Building a lock-in amplifier*

Let's now build a lock-in amplifier. The principle is illustrated in Fig. 52.17(a). The sinusoidal signal discriminated at a non-linear line is switched on and off in the lock-in by a switch. At the same time, the inverted signal (i.e., phase shifted by 180°) is turned off and on. Both signals are combined and low-pass filtered. As Fig. 52.17(b) shows, the sign of the filtered signal depends on the phase between the discriminator and the TTL signal controlling the switch [4]

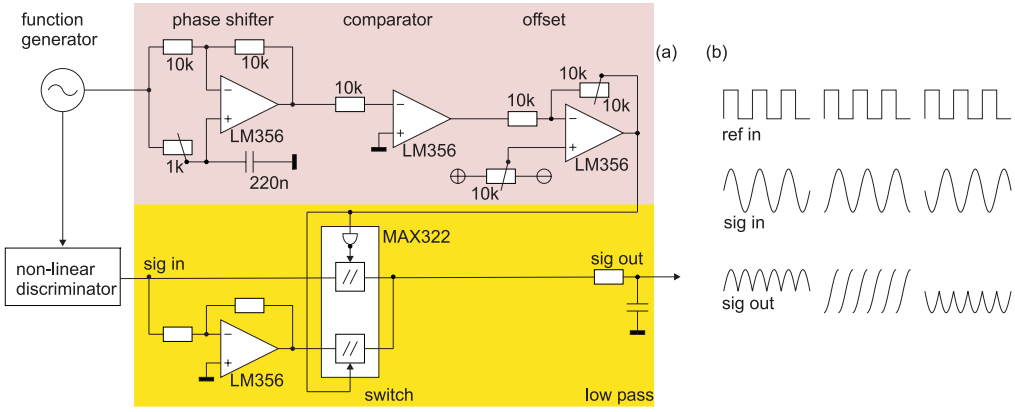

Figure 52.17: (a) Principal scheme of a lock-in amplifier. (b) Mode of operation.

[4] Datasheets for the operational amplifier see appendix Fig. 56.24, data sheet for the switch see appendix Fig. 56.23.

1. Create the circuit sketched in Fig. 52.17(a) on a circuit board and test it by varying the phase between the modulated output signal and the TTL signal provided by a function generator.

52.5 Further reading

P. Horowitz et al., *The art of electronics* [635]$_{\text{DOI}}$

U. Tietze et al., *Halbleiterschaltungstechnik* [1306]$_{\text{DOI}}$

Chapter 53

Quantum optics and optical interferometry

The objective of this chapter is to introduce the basics of optical *interferometry*. We will see, how to match the light modes in optical cavities and fibers, and to phase-match the wavefronts of two laser beams in order to detect their frequency beating with a photodetector. Furthermore, he will learn how to handle essential tools of *quantum electronics*, such as a piezo-electric transducer, an electro-optic modulator, and an acousto-optic modulator, used in interferometry, as discussed in Secs. 53.4.1 to 53.4. Interferometers have versatile applications such as 1. for the detection of very small length variations (as for example caused by gravitational waves), 2. as vibration and inertial sensors, or in 3. the transmission of information (radio).

53.1 Introduction to interferometry

53.1.1 Beam splitter

The essential component of any interferometer is the (non-polarizing) *beam splitter*.

We consider a classical lossless beam splitter with electric fields incident at both its inputs. The two output fields E_c and E_d are linearly related to the inputs through

$$\begin{pmatrix} \mathcal{E}_c \\ \mathcal{E}_d \end{pmatrix} = \begin{pmatrix} r_{ac} & t_{bc} \\ t_{ad} & r_{bd} \end{pmatrix} \begin{pmatrix} \mathcal{E}_a \\ \mathcal{E}_b \end{pmatrix} , \tag{53.1}$$

where the 2×2 element is the beam splitter matrix. r and t are the reflectance and transmittance along a particular path through the beam splitter, that path being indicated by the subscripts.

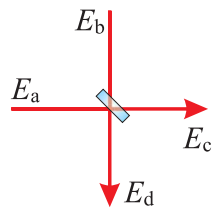

Figure 53.1: Beam splitter.

Assuming the beam splitter removes no energy from the light beams, the total output energy can be equated with the total input energy, reading

$$|\mathcal{E}_c|^2 + |\mathcal{E}_d|^2 = (|r_{ac}||\mathcal{E}_a| + |t_{bc}|\mathcal{E}_b|)^2 + (|t_{ad}||\mathcal{E}_a| + |r_{bd}||\mathcal{E}_b|)^2 = |\mathcal{E}_a|^2 + |\mathcal{E}_b|^2 \ . \quad (53.2)$$

This can only be true for any field amplitudes, if the following relationships between reflectance and transmittance are satisfied,

$$|r_{ac}|^2 + |t_{ad}|^2 = 1 = |r_{bd}|^2 + |t_{bc}|^2 \quad \text{and} \quad r_{ac}t^*_{bc} + t_{ad}r^*_{bd} = 0 \ . \quad (53.3)$$

We write each r and t as a complex number having an amplitude and phase factor accounting for possible phase shifts of a beam as it reflects or transmits at the beam splitting surface. From the second equation (53.3) we obtain,

$$\frac{|r_{ac}|}{|t_{ad}|} = -\frac{|r_{bd}|}{|t_{bc}|} e^{\imath(\phi_{ad}-\phi_{bd}+\phi_{bc}-\phi_{ac})} \quad (53.4)$$

which is true when $\phi_{ad} - \phi_{bd} + \phi_{bc} - \phi_{ac} = \pi$. Squaring both sides of the expression (53.4) and comparing this with the first equation (53.3) we obtain the result

$$|t_{ad}| = |t_{bc}| \equiv \sqrt{T} \quad \text{and} \quad |r_{ac}| = |r_{bd}| \equiv \sqrt{R} \ . \quad (53.5)$$

It follows that

$$\boxed{R + T = 1} \ . \quad (53.6)$$

The above result holds for any type of beam splitting device. For beam splitting at dielectric interfaces in particular we know that the electric field amplitude does not suffer phase shifts upon transmission and no phase shifts upon reflection at an optical more dilute medium. But it suffers a 180° phase shift upon reflection at an optical denser medium. For the situation depicted in Fig. 53.1, we conclude $\phi_{ac} = \phi_{bd} = \phi_{bc} = 0$ and $\phi_{ad} = \pi$. With this constraints the matrix describing a lossless beam splitter reads,

$$\boxed{\begin{pmatrix} \mathcal{E}_c \\ \mathcal{E}_d \end{pmatrix} = \begin{pmatrix} \sqrt{R} & \sqrt{T} \\ -\sqrt{T} & \sqrt{R} \end{pmatrix} \begin{pmatrix} \mathcal{E}_a \\ \mathcal{E}_b \end{pmatrix}} \ . \quad (53.7)$$

53.1.2 Piezo-electric actuator

The piezo-electricity effect describes the reciprocal action between mechanical pressure (from Greek: piézein - press) and electrical voltage in solids. It is based on the phenomenon that occurs in the regular deformation of certain piezoelectric materials: at the surface occur displacements of electric charges creating microscopic dipoles inside the unit cells. The sum over all the unit cells of the crystal leads to a macroscopically measurable electrical voltage. The deformation should be directed, which means, that the pressure is not applied from all sides on the crystal, but for example only on opposite sides.

On the other hand, by applying an electric voltage, a crystal (or piezo-ceramic element) may be deformed. Like any other solid body, piezo-electric crystals can execute mechanical vibrations. In a *piezo-electric actuator* (or piezo transducer PZT), these vibrations can be electrically excited. The frequency of the vibrations depend

only on the speed of sound (which is a constant of the material) and the dimensions of the actuator. Therefore, actuators are also suitable for realizing oscillators (for example, quartz crystals). The piezo-electric effect can only occur in non-conductive materials (e.g., lead titanate zirconate).

When a voltage is applied to the piezo-ceramic in the direction of polarization, we observe an expansion in this direction and a perpendicular contraction. Depending on the employed material and the coefficient for piezo-electric strain d, stretches up to $\Delta l/l = 0.15\%$ can be obtained:

$$\Delta l = d\mathcal{E} l_0 \ , \tag{53.8}$$

where l_0 is the length of the actuator and $E = U/l_0$ the amplitude of the electric field. The elongation effect is therefore proportional to the field strength and the overall length of the actuator. To achieve large stretches with manageable electrical voltages, actuator discs are often stacked (mechanical circuit in series and electric circuit in parallel).

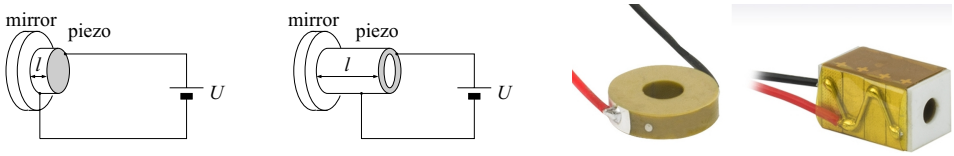

Figure 53.2: (Left) Scheme of mirrors mounted on a piezo actuator having the shape of a disc or a ring. (Right) Photos of a ring piezo and a piezo stack.

Negative voltages with respect to the orientation of the discs cause a contraction. However, negative voltages can also cause a change in the polarization state of the piezo and should therefore be avoided! In electrical circuits, piezoelectric actuators introduce a capacitance with a relative dielectric constant between 600 and 5000 and an internal resistance of about $10^8\ \Omega$ depending on the material. See Exc. 53.1.10.1.

53.1.3 Michelson and Mach-Zehnder interferometer

Interferometry is a technique exploiting the interference of waves coherently split and recombined by beam splitters. Sufficiently stable interferometers allow to visualize variations of the path lengths of two or more partial waves following different pathways as an alteration of constructive and destructive interference.

The two most common types of interferometers are the *Michelson interferometer* and the *Mach-Zehnder interferometer* are depicted in Fig. 53.3. The advantages of the Michelson interferometer are an easy alignment and the need of only one beamsplitter. The advantage of the Mach-Zehnder interferometer is a direct optical access to both output ports of the interferometer. The following treatment applies to both types.

The field amplitude of a laser beam, $\mathcal{E}_i$, with frequency, $\omega = ck$, is divided by a beam splitter (reflectivity $\sqrt{R}$) into a transmitted $\mathcal{E}_t$ and a reflected beam $\mathcal{E}_r$,

$$\mathcal{E}_r = \sqrt{R_1}\mathcal{E}_i \qquad \text{and} \qquad \mathcal{E}_t = \sqrt{1-R_1}\mathcal{E}_i \ , \tag{53.9}$$

where we disregard possible phase-shifts upon reflection at optically dilute interface. The energy is obviously conserved, $|\mathcal{E}_r|^2 + |\mathcal{E}_t|^2 = \mathcal{E}_i^2$.

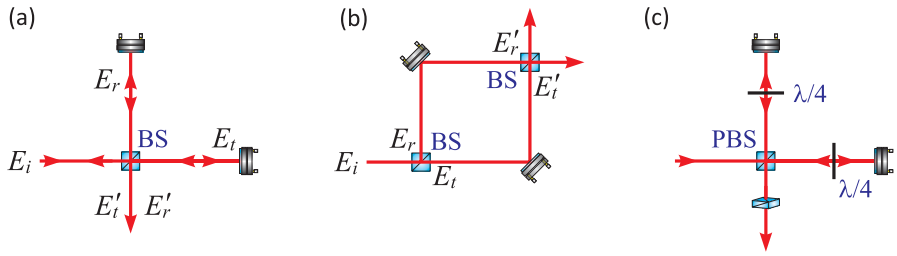

Figure 53.3: Principle of a two-beam interferometer: (a) Michelson interferometer and (b) Mach-Zehnder interferometer using non-polarizing beamsplitters. (c) Michelson interferometer using a polarizing beamsplitter.

We consider the Mach-Zehnder interferometer sketched in Fig. 53.3 with one arm of length L_r, which can be varied by a piezo, and the other arm of length L_t,

$$\mathcal{E}_r' = \mathcal{E}_r e^{2\imath k L_r} \qquad \text{and} \qquad \mathcal{E}_t' = \mathcal{E}_t e^{2\imath k L_t} \ . \tag{53.10}$$

The beams are recombined on a second beam splitter and sent to a photodetector, whose signal is,

$$\begin{aligned} I &\propto |\sqrt{R_2}\mathcal{E}_r' + \sqrt{1-R_2}\mathcal{E}_t'|^2 \\ &= |\sqrt{R_2}\sqrt{R_1}e^{2\imath k L_r} + \sqrt{1-R_2}\sqrt{1-R_1}e^{2\imath k L_t}|^2 \mathcal{E}_i^2 \ . \end{aligned} \tag{53.11}$$

Hence,

$$I \propto R_2 R_1 + (1-R_2)(1-R_1) + 2\sqrt{R_2}\sqrt{R_1}\sqrt{1-R_2}\sqrt{1-R_1}\cos[2k(L_t - L_r)] \ . \tag{53.12}$$

For reflectivities of $R_1 = R_2 = 50\%$, we get,

$$\boxed{I \propto \tfrac{1}{2} + \tfrac{1}{2}\cos[2k(L_t - L_r)]} \ . \tag{53.13}$$

It is important to realize that, while superpositions of light field amplitudes in the same mode interfere, *superpositions of light field amplitudes in different modes do not*. For example, the superposition of two plane waves with equal frequency and polarization interferes,

$$\left| \begin{pmatrix} \mathcal{E}_1 + \mathcal{E}_2 \\ 0 \end{pmatrix} \right|^2 = |\mathcal{E}_1 + \mathcal{E}_2|^2 \ , \tag{53.14}$$

while the superposition of two plane waves with equal frequency but different polarizations does not,

$$\left| \begin{pmatrix} \mathcal{E}_1 \\ 0 \end{pmatrix} + \begin{pmatrix} 0 \\ \mathcal{E}_2 \end{pmatrix} \right|^2 = |\mathcal{E}_1|^2 + |\mathcal{E}_2|^2 \ . \tag{53.15}$$

Solve the Excs. 53.1.10.2 to 53.1.10.4.

53.1.4 Coherence and spectrum of a light field

We have seen above that interferometers probe the electric field amplitude rather than the intensity. For this reason, they are suited to measure the first-order correlation function $g^{(1)}(\tau)$ and the emission spectrum, which are defined by,

$$g^{(1)}(\tau) \equiv \frac{\langle \mathcal{E}^-(t)\mathcal{E}^+(t+\tau)\rangle}{\langle \mathcal{E}^-(t)\mathcal{E}^+(t)\rangle} \qquad \text{and} \qquad S_{\mathcal{E}}(\omega) \equiv \mathcal{F}[g^{(1)}(\tau)] \ . \tag{53.16}$$

As an example, Fig. 53.4 shows the aurocorrelation function and spectrum of a simultaneously amplitude- and phase-modulated laser beam, $\mathcal{E}(t) = (1+n\cos\omega_n t)e^{\imath m \sin\omega_m t}$.

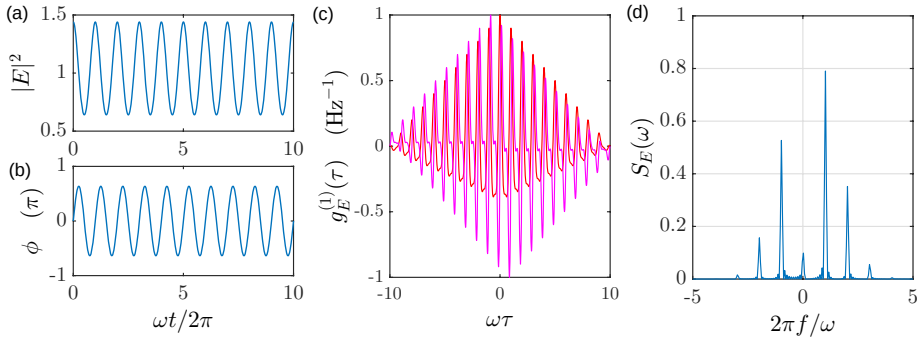

Figure 53.4: (code) (a) Amplitude and (b) phase of the electric field, with $n = 0.2$, $m = 1$, and $\omega_n = \omega_m = (2\pi)\ 1\,\mathrm{Hz}$. (c) Aurocorrelation function and (d) spectrum of the light field.

53.1.5 Birefringent interferometer

A *birefringent interferometer* or *Lyot filter* consists of one or more birefringent crystals mounted onto a rotation frame between two polarizers. Let n_o and $n_e = n_o + \Delta n$ be the refractive indices of the normal and the extraordinary axis, respectively. The corresponding Jones matrix is then,

$$\mathcal{M} = \begin{pmatrix} 1 & 0 \\ 0 & 0 \end{pmatrix} \begin{pmatrix} \cos\phi & \sin\phi \\ -\sin\phi & \cos\phi \end{pmatrix} \begin{pmatrix} e^{\imath k_0 L} & 0 \\ 0 & e^{\imath k_e L} \end{pmatrix} \begin{pmatrix} \cos\phi & -\sin\phi \\ \sin\phi & \cos\phi \end{pmatrix} \begin{pmatrix} 1 & 0 \\ 0 & 0 \end{pmatrix} , \tag{53.17}$$

Such that,

$$\begin{pmatrix} \mathcal{E}_{out} \\ 0 \end{pmatrix} = \mathcal{M} \begin{pmatrix} \mathcal{E}_{in} \\ 0 \end{pmatrix} = \begin{pmatrix} \left(e^{\imath k_0 L}\cos^2\phi + e^{\imath k_e L}\sin^2\phi\right)\mathcal{E}_{in} \\ 0 \end{pmatrix} . \tag{53.18}$$

By trigonometric transformations it is possible to show, that the transmission $T \equiv |\mathcal{E}_{out}/\mathcal{E}_{in}|^2$ is,

$$\boxed{T(\lambda,\phi) = |e^{\imath k_0 L}\cos^2\phi + e^{\imath k_e L}\sin^2\phi|^2 = 1 - \sin^2 2\phi \sin^2\tfrac{\pi L\Delta n}{\lambda}} \ . \tag{53.19}$$

For $\phi = 45°$ the transmission becomes simply,

$$T(\lambda, \tfrac{\pi}{4}) = \cos^2 \tfrac{\pi L \Delta n}{\lambda} \ . \tag{53.20}$$

In practice Lyot filters are often used, placed under the Brewster angle inside ring cavity lasers, as frequency selective elements. Frequently, birefringent plates of different thicknesses are stacked,

$$T(\lambda) = T_1(\lambda) T_2(\lambda) \ , \tag{53.21}$$

in order to increase the frequency selectivity. Furthermore, when the axis of the birefringent plates are rotated by fixed angles $\Delta\alpha$ with respect to each other,

$$T(\lambda, \alpha) = T_1(\lambda, \alpha) T_2(\lambda, \alpha + \Delta\alpha) \ , \tag{53.22}$$

the frequency of maximum transmission can be tuned by simply rotating the stack as a whole by an angle α. See 53.1.10.5.

A Lyot filter can be considered an interferometer, because it splits and recombines the polarization vector of a light beam in two parts following the ordinary and the extraordinary axis of the birefringent crystal. This is somewhat analogous to the Michelson interferometer depicted in Fig. 53.3(c).

53.1.6 Optical resonators

Optical cavities consist of an arrangement of mirrors reflecting the light beams in such a way, that they form a closed path. Since light that entered the cavity is performing there many round trips before it is transmitted again or absorbed, the light power is considerably enhanced, i.e. cavities can store light.

Light which is to resonate in the cavity must satisfy the boundary condition, that the mirror surfaces coincide with standing wave nodes. Therefore, in a cavity with length L only a discrete spectrum of wavelengths $N\frac{\lambda}{2} = L$ can be resonantly amplified, where N is a natural number. Because of this property, cavity are often used as frequency filters or optical spectrum analyzers: Only frequencies $\nu = N\delta_{fsr}$ are transmitted, where

$$\boxed{\delta_{fsr} = c/2L} \tag{53.23}$$

is the free spectral range of the cavity.

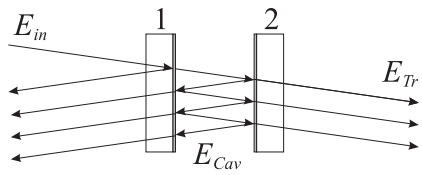

Figure 53.5: Multiple interference in an optical cavity.

Cavities are characterized on one hand by their geometry, i.e. the curvature and the distance of their mirrors, and on the other hand by their finesse, which is given by the reflectivity of their mirrors. Let us first study the finesse. Regarding the cavity as a multipass interferometer [351], we can derive expressions for the reflected and

transmitted intensity as a function of frequency [1]. The so-called *Airy formula* for transmission and reflection are,

$$\frac{\mathcal{E}_{refl}}{\mathcal{E}_{in}} = r_1 - \frac{t_1^2 r_2 e^{2\imath kL}}{1 - r_1 r_2 e^{2\imath kL}} \quad \text{and} \quad \frac{\mathcal{E}_{trns}}{\mathcal{E}_{in}} = \frac{t_1 t_2 e^{\imath kL}}{1 - r_1 r_2 e^{2\imath kL}} \ . \tag{53.24}$$

In terms of intensity, assuming identical mirrors, $r_1 = r_2 = \sqrt{R}$ and $t_1 = t_2 = \sqrt{T}$, and neglecting possible absorptive losses, $A = 1 - R - T = 0$,

$$\boxed{\frac{I_{refl}}{I_{in}} = \frac{(\frac{2F}{\pi})^2 \sin^2 \frac{\Delta}{2\delta_{fsr}}}{1 + (\frac{2F}{\pi})^2 \sin^2 \frac{\Delta}{2\delta_{fsr}}} \quad \text{and} \quad \frac{I_{trns}}{I_{in}} = \frac{1}{1 + (\frac{2F}{\pi})^2 \sin^2 \frac{\Delta}{2\delta_{fsr}}}} \ , \tag{53.25}$$

where R is the reflectivity of a mirror and $\delta = 4\pi L/\lambda = 2\pi\nu/\delta_{fsr}$. The transmission curve of a cavity has a finite transmission bandwidth $\Delta\nu$, which depends on the reflectivity of the mirrors. The finesse of a cavity is defined by

$$\boxed{F \equiv \frac{2\pi\delta_{fsr}}{\kappa} = \frac{\pi\sqrt{R}}{1-R}} \ . \tag{53.26}$$

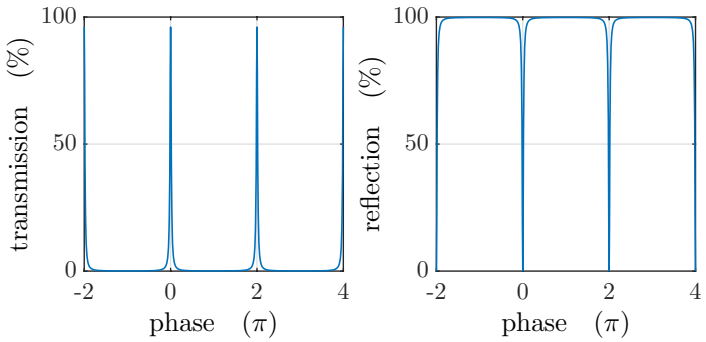

Figure 53.6: (code) Transmission and reflection through a resonator.

Note that factors others than the finite reflectivity may degrade the finesse of a cavity. For example, an imperfect mirror flatness (commonly specified as λ/F_{surf}) reduces the finesse to [351],

$$F_{tot} = \left(\frac{1}{F} + \frac{1}{F_{surf}} \right)^{-1} \ . \tag{53.27}$$

.

The geometry of a cavity must satisfy certain conditions, in order to be stable [734]. Besides the main longitudinal modes a cavity possesses transverse modes of the order TEM_{mn}, whose frequencies are given by [2],

$$\nu/\delta_{fsr} = (q+1) + \frac{m+n+1}{\pi} \arccos \sqrt{\left(1 - \frac{L}{\rho_1}\right)\left(1 - \frac{L}{\rho_2}\right)} \ . \tag{53.28}$$

[1] See script on *Electrodynamics* (2023), Exc. 7.3.6.16.
[2] See script on *Electrodynamics* (2023), Sec. 7.4.2.2.

A *confocal cavity* with degenerate transverse modes, $\rho_1 = \rho_2 = L$, is particularly suited as optical spectrum analyzer.

The diameter of the beam waist in the cavity is,

$$w_0 = \sqrt[4]{\left(\frac{\lambda}{\pi}\right)^2 \frac{L(\rho_1 - L)(\rho_2 - L)(\rho_1 + \rho_2 - L)}{(\rho_1 + \rho_2 - 2L)^2}} \,. \tag{53.29}$$

For an optimal coupling of the light into the cavity the Gaussian laser beam must be matched to the cavity's geometry of the cavity, i.e. diameter and divergence of the laser beam must be adapted to the cavity mode with a suitable arrangement of lenses [352, 734]. See Excs. 53.1.10.6 to 53.1.10.11.

53.1.7 Dielectric mirrors and filters

Dielectric mirrors and filters are multiple beam interferometers in a similar sense as Fabry-Pérot cavities. They consist of stacks of thin dielectric layers with alternating refraction indices [3].

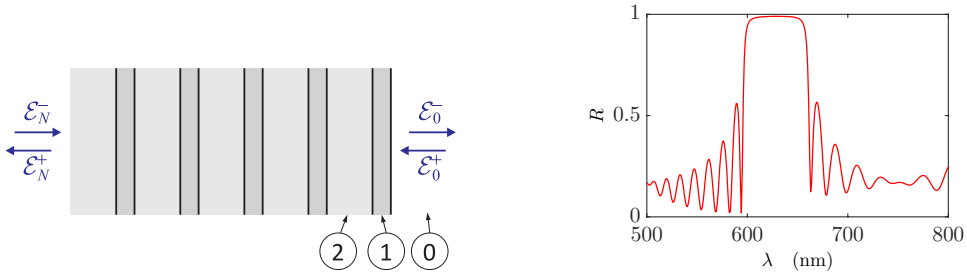

Figure 53.7: (code) Reflection by a high reflecting mirror made of 10 layers with $n_1 = 2.4$ and $\Delta z_1 = 80\,\text{nm}$ alternating with 10 layers with $n_2 = 1.5$ and $\Delta z_2 = 500\,\text{nm}$. The absorption coefficient for each layer is supposed to be $\alpha = 0.2\%$. The beam impinges from vacuum, $n_0 = 1$.

Reflections of $R = 99.999\%$ can be reached which, applied of superpolished mirrors, allow for the construction of cavities with finesse $F > 300000$. On the other anti-reflection coatings can be applied to surfaces reducing their reflections to below $R = 0.1\%$. See Excs. 53.1.10.12 and 53.1.10.13 [352, 800].

53.1.8 Optical fibers

An *optical fiber* is a waveguide in which light is guided by internal total reflection. The total reflection occurs between layers with different refractive indices called *fiber core* and *fiber cladding*. The core is the central region of the optical fiber where the light is guided. In order to create guiding conditions, the refractive index of the core must be higher than the one of the cladding. The cladding diameter is typically 8 to 10 times the *mode field diameter* (MFD) of the fundamental mode. In general, MFD

[3] See script on *Electrodynamics* (2023), Sec. 7.1.7.

is greater than the physical diameter of the fiber core, which means that some optical power is always guided by the fiber cladding as an evanescent wave.

The *cut-off wavelength* λ_{co} of an optical fiber is the wavelength above which a guided mode of a waveguide ceases to exist. For wavelength longer than λ_{co} an optical fiber becomes single-mode. At wavelengths shorter than λ_{co} several optical modes may propagate and the fiber becomes multi-mode. The cut-off wavelength is directly related to the core diameter of the fiber $\lambda_{co} \propto \emptyset$. For

$$\frac{\lambda}{2} < \emptyset < \lambda \qquad \text{or equivalently} \qquad \emptyset < \lambda < 2\emptyset \tag{53.30}$$

the fiber is single-mode. For $\lambda > 2\emptyset$ no guided mode exists and for $\emptyset > \lambda$ the fiber becomes multimode.

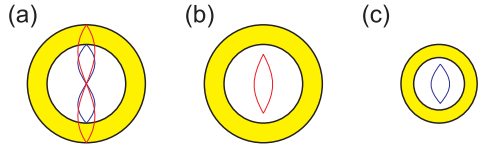

Figure 53.8: Mono-mode waveguiding by optical fibers.

The *numerical aperture* is a measure of the acceptance angle of the fiber. It is very important because it determines how strongly a fiber guides light, and so how resistant it is to bend-induced losses. The numerical aperture can be defined by the acceptance angle of the fiber, though as this is highly diverging in space it is rather complicated to reach a simple definition. It is most convenient to define the NA in terms of the relative indices of core and cladding glass forming the fiber waveguide:

$$NA = \sin\tfrac{\theta_a}{2} = \sqrt{n_{core}^2 - n_{clad}^2} \simeq \sqrt{2n_{core}^2 \delta n}\ , \tag{53.31}$$

where δn is the index difference between the core and cladding. An optical fiber with 'high' numerical aperture will confine light more strongly in the core, and so support guidance further above cut-off. This attribute has two important effects: (a) it will be single-mode over a greater range of wavelengths than is possible with a fiber with a 'low' numerical aperture fiber and (b) it will still guide a single-mode when coiled or bent to a smaller diameter.

53.1.8.1 Multi-mode, mono-mode, and polarization maintaining fibers

Many types of fibers are currently available for a large variety of applications.

53.1.9 Laser gyroscope and the Sagnac effect

Gyroscopes are based on the *Sagnac effect*. They are based on a ring cavity mounted on a rotating stage, as shown in Fig. 53.10(a). Let us, for simplicity first consider a circular path for the light beam (e.g. a fiber-based ring cavity) rotating at an angular velocity Ω. Then the time needed for the light beam to travel in either one of the two directions is,

$$t_\pm = \frac{(2\pi \pm \Omega t_\pm)r}{c} = \frac{2\pi r}{c \mp \Omega r}\ , \tag{53.32}$$

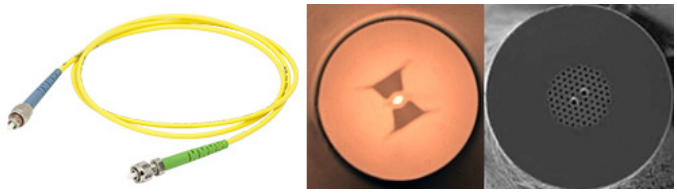

Figure 53.9: (Left) Fiber patch cord, (center) cross section of a bow-tie polarization maintaining fiber, and (right) cross section of a photonic crystal fiber.

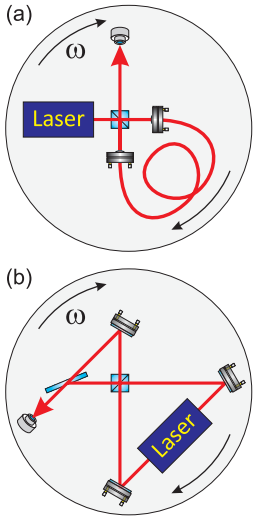

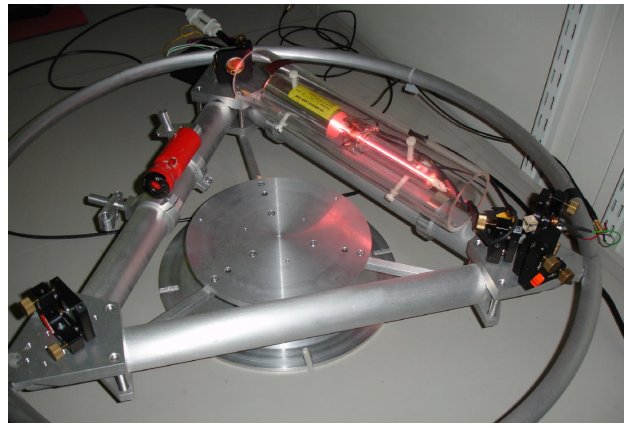

Figure 53.10: (a) Principle scheme of a fiber-based Sagnac interferometer. (b,c) Laser gyroscope realized with a HeNe gain tube.

that is,

$$\Delta t \equiv t_+ - t_- = \frac{4\pi r^2 \Omega}{c^2 - \Omega^2 r^2} \simeq \frac{4\pi r^2 \Omega}{c^2} \equiv \frac{4A\Omega}{c^2} \ , \tag{53.33}$$

where A is the area enclosed by the path. This formula can be generalized to arbitrary paths.

For example, assuming an interferometer with $A = 1\,\mathrm{m}^2$ at rest in an Earth-based system, $\Omega \simeq 2\pi/24\,\mathrm{h}$, the time difference for light propagating along the two directions is $\Delta t \approx 3 \cdot 10^{-21}\,\mathrm{s}$ and the path difference $\Delta L = c\Delta t \approx 100\,\mathrm{fm}$. The frequency shift is,

$$\boxed{\Delta v = k(v_+ - v_-) = k(2\Omega r) = \frac{\sqrt{4\pi A}\Omega}{\lambda}} \ , \tag{53.34}$$

yielding for the given example of an Earth-based interferometer $\Delta\nu \approx 400\,\mathrm{Hz}$.

53.1.10 Exercises

53.1.10.1 Ex: Characterizing a piezo actuator

In order to characterize a recently purchased piezo actuator (Thorlabs, TA0505D024W) a Scientific Initiation student sets up a Michelson interferometer driven by a HeNe laser beam. Scanning the voltage applied to the piezo through the entire permitted range, he observes 8.8 oscillations of the interference fringes. What is the piezo displacement per volt?

Solution: *The allowed voltage range is* $\Delta U = 0 \,..\, 75\,\mathrm{V}$. *With* N *the number of observed oscillations, the piezo displacement per volt is,*

$$\frac{\Delta z}{\Delta U} = \frac{N\lambda/2}{\Delta U} = 37.3\,\mathrm{nm/V} \ .$$

53.1.10.2 Ex: Michelson interferometer

The figure 53.11 shows a Michelson interferometer containing in one arm an airtight 5 cm long cell with glass windows. Light with wavelength $\lambda = 500\,\mathrm{nm}$ is used. After the cell has been evacuated, the interference pattern shifts by 60 fringes. Use this information to calculate the refractive index of air at atmospheric pressure. With what accuracy can you determine the refractive index with this method?

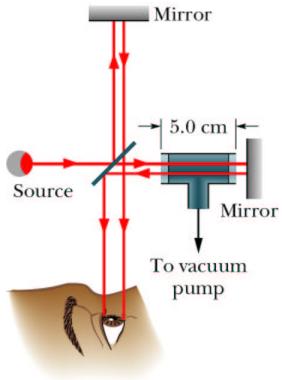

Figure 53.11:

Solution: *The variation of the path length of the interferometer arm containing the cell due to the refractive index is, after the passage of* $N = 60$ *fringes,*

$$N\frac{\lambda}{2} = n_{refr}L - L \ .$$

Hence,

$$n_{refr} - 1 = \frac{N\pi}{kL} \approx 3 \cdot 10^{-4} \ .$$

Assuming that the uncertainty of $\Delta N = 1$ fringe, the refractive index can be measured with an precision of,

$$\Delta n_{refr} = \frac{\partial n_{refr}}{\partial N}\Delta N = \frac{\pi}{kL} \approx 5 \cdot 10^{-6} \ .$$

53.1.10.3 Ex: Michelson interferometer

Assume that a signal-to-noise ratio of 50 has been achieved in measuring the fringe pattern of a Michelson interferometer with one continuously moving mirror. Estimate the minimum path length ΔL that the mirror has to travel in order to reach an accuracy of $\Delta\lambda = 10^{-4}\,\mathrm{nm}$ in the measurement of a laser wavelength at $\lambda = 600\,\mathrm{nm}$.

Solution: *The spectral resolution is,*

$$\frac{\lambda}{\Delta\lambda} = 50\frac{\Delta L}{\lambda}$$

yields $\Delta L = 7.2\,\mathrm{cm}$.

53.1.10.4 Ex: Rotating the polarization with a Mach-Zehnder interferometer

Using the Jones matrix formalism demonstrate how to use the Mach-Zehnder interferometer setup sketched in the figure to rotate the polarization of a linearly polarized laser beam in an electronically controlled way using a piezo actuator mounted in ones of the interferometer arms.

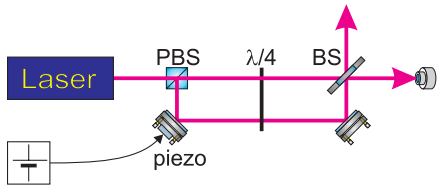

Figure 53.12:

Solution: *We assume initially linearly polarized light,* $\begin{pmatrix}1\\1\end{pmatrix}$. *The x and y-components, having been separated by a PBS and passed through the same $\lambda/4$-plate, yield contrary circular polarizations $\sigma^{\pm}$. If one of the polarizations is phase-shifted by a piezo, the recombined field reads,*

$$\begin{pmatrix}1\\ \imath\end{pmatrix} + \begin{pmatrix}1\\ -\imath\end{pmatrix} e^{\imath\phi} = 2e^{\imath\phi/2}\begin{pmatrix}\cos\phi\\ \sin\phi\end{pmatrix} \ .$$

The fact that the polarization vector is purely real shows that the polarization is linear and can be rotated by simply varying the piezo voltage.

53.1.10.5 Ex: Lyot filter

Consider a Lyot filter with two plates ($L_1 = 1\,\text{mm}$ and $L_2 = 4\,\text{mm}$) with the refraction indices $n_o = 1.40$ in the fast axis and $n_e = 1.45$ in the slow axis.
a. Calculate the transmission peaks of the Lyot filter as a function of λ for the rotation angle $\phi = 45°$.
b. Determine the transmitted intensity $I(\phi)$ as a function of the rotation angle ϕ for a fixed wavelength λ. What is the contrast of the transmitted intensity for arbitrary values of λ if the absorption losses are 2%?

Solution: *a. From (53.20) we have for* $\phi = 45°$,

$$T(\lambda) = T_0 \cos^2 \frac{\pi \Delta n L_1}{\lambda} \cos^2 \frac{\pi \Delta n L_2}{\lambda} \ ,$$

with 2% absorption losses $T_0 = 0.98$. *Transmission peaks appear for the condition,*

$$\frac{\pi \Delta n L_1}{\lambda} = m_1 \pi \qquad \textit{and} \qquad \frac{\pi \Delta n L_2}{\lambda} = m_2 \pi \ ,$$

with $m_1, m_2 \in \mathbb{N}$. *For* $\lambda = 500\,\text{nm}$ *we obtain* $m_1 = 100$ *and* $m_2 = 400$. *For* $m_1 = 101$ *we get* $\lambda = 495\,\text{nm}$, *such that the thin plate has a free spectral range* $\Delta\lambda_{fsr} = 5\,\text{nm}$. *For* $m_2 = 401$ *we get* $\lambda = 498.75\,\text{nm}$, *such that the thick plate has* $\Delta\lambda_{fsr} = 1.25\,\text{nm}$.
b. From (53.19) we have,

$$T(\phi, \lambda) = T_0 \left[1 - \sin^2 \left(\frac{2\pi}{\lambda} \Delta n L \right) \sin^2 2\phi \right] \ ,$$

where $\lambda = 2\Delta nL/m$ m *is the first factor 0 and* $T(\phi, \lambda_{max})$ *has a maximum transmission* T_0, *independent of* ϕ. *For* $\lambda = 2\Delta nL/(m + \frac{1}{2})$ *this factor becomes 1 and the transmission is* $T(\phi) = T_0(1 - \sin^2 2\phi)$. *The contrast is then:*

$$\frac{T_{max}}{T_{min}} = \frac{1}{1 - \sin^2 2\phi} \ .$$

53.1.10.6 Ex: Wedge-shaped etalon

A beam of light of wavelength $\lambda = 683\,\text{nm}$ with large diameter is incident perpendicularly on the first of two quadratic plates. Each plate has the edge length 120 mm; at the left edge the plates touch each other, at the right edge they are separated by a wire of $d_w = 0.048\,\text{mm}$ in diameter. The air between the plates acts as a thin layer.
a. How many interference fringes does an observer see from above this arrangement?
b. Now suppose that the incident light be white. Will the interference pattern at the far left be bright or dark?

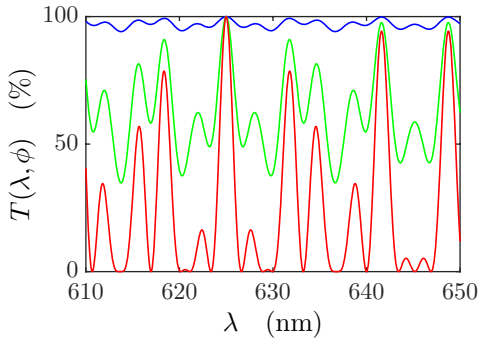

Figure 53.13: Transmission curve of a Lyot filter for (blue) $\alpha = 5^\circ$, (green) $\alpha = 20^\circ$, and (red) $\alpha = 45^\circ$.

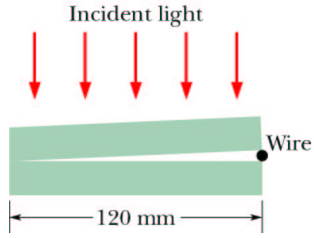

Figure 53.14:

c. Starting from the left edge there will be a series of interference minima, whose position depend on the wavelength of the light. For what light color (blue or red) will the minimum be closer to the edge?

Solution: *a. Light is only transmitted when the distance between the plates (as a function of the x-position) is close to* $d(z) \simeq N\frac{\lambda}{2}$. *Therefore, we see in reflection alternating as a function of z, between 0 and* $N_{max} = 2\frac{d_w}{\lambda} \approx 140$ *fringes.*
b. At the left end, where the distance is less than $\lambda/2$, *the reflection has a minimum, because 5% of the light (in case of a glas-air surface) are reflected at the interface upper plate-gap with no phase-shift and another* $95\% \times 5\%$ *at the interface gap-lower plate with* 180° *phase shift. If the distance between the reflective layers is much smaller than* $\lambda/2$, *the two reflected beams will interfere destructively. However, the contrast will not be perfect, because the two reflected intensities are not exactly equal. In any case, at least* $95\%^2$ *of the intensity are transmitted at any distance fro the edge.*
c. For blue light, the first minimum is closer to the edge.
Note added:
This can be calculated explicitly using the transfer matrix formalism [4]. *The T-matrix* $M_{inter}(n_0, n_1)$ *for transfer through an interface between two layers with different refractive indices* n_0 *and* n_1 *and the T-matrix* $M_{prop}(n_1)$ *for propagation within a*

[4] See script on *Electrodynamics* (2023), Sec. 7.1.7.

medium with a given refractive index n_1 are,

$$M_{inter}(n_0,n_1)=\frac{1}{2n_1}\begin{pmatrix}n_1+n_0 & n_1-n_0\\ n_1-n_0 & n_1+n_0\end{pmatrix}\quad and\quad M_{prop}(n_1)=\begin{pmatrix}e^{\imath n_1 kL} & 0\\ 0 & e^{-il\not{\Lambda}kL}\end{pmatrix}\ .$$

In our case, we have two layers $n_2=n_0$ separated by an air-gap $n_1=1$. Hence,

$$\begin{aligned}M_{total}&=\frac{1}{2n_0}\begin{pmatrix}n_0+1 & n_0-1\\ n_0-1 & n_0+1\end{pmatrix}\begin{pmatrix}e^{\imath kL} & 0\\ 0 & e^{-\imath kL}\end{pmatrix}\frac{1}{2}\begin{pmatrix}1+n_0 & 1-n_0\\ 1-n_0 & 1+n_0\end{pmatrix}\\ &=\frac{1}{n_0}\begin{pmatrix}n_0\cos kL+(1+n_0^2)\frac{\imath}{2}\sin kL & -\frac{\imath}{2}(n_0^2-1)\sin kL\\ \frac{\imath}{2}(n_0^2-1)\sin kL & n_0\cos kL-(1+n_0^2)\frac{\imath}{2}\sin kL\end{pmatrix}\ ,\end{aligned}$$

yielding the reflection,

$$R=\frac{\mathcal{E}_0^-}{\mathcal{E}_0^+}=-\frac{M_{21}}{M_{22}}=\frac{\imath(1-n_0^2)\sin kL}{2n_0\cos kL-(1+n_0^2)\imath\sin kL}\overset{kL\to 0}{\longrightarrow}0\ .$$

53.1.10.7 Ex: Fabry-Perot interferometer

The dielectric coatings of each plate of a Fabry-Perot interferometer have the following specifications: $R=98\%$, $A=0.3\%$. The flatness of the surfaces is $\lambda/100$ at $\lambda=500\,\text{nm}$.
a. Estimate the finesse from (53.24) and (53.27), the maximum transmission, and the spectral resolution of the FPI for a plate separation of 5 mm.
b. Show that, for a given absorption, the transmitted intensity decreases with increasing reflectivity. Explain why. **Note:** A trade-off between high finesse and high transmission at a given absorption $A>0$, called *impedance matching*, is reached by maximizing the intracavity intensity. For a symmetric cavity, it can be shown that impedance matching is reached for $A=T$.

Solution: *a. The field transmitted through the two mirrors of the cavity is,*

$$\mathcal{E}_{trns}=\mathcal{E}_{in}\frac{t_1t_2e^{\imath kL}}{1-r_1r_2e^{2\imath kL}}\ .$$

Assuming $r_1=r_2$ and $t_1=t_2$ and $T=t_1t_2=1-R-A$, the transmitted intensity is,

$$\frac{I_{trns}}{I_{in}}=\left|\frac{\mathcal{E}_{trns}}{\mathcal{E}_{in}}\right|^2=\frac{(1-R-A)^2}{1+R^2-2R\cos 2kL}\overset{kL=n\pi}{\longrightarrow}\frac{(1-R-A)^2}{(1-R)^2}\ .$$

With $R=0.98$, $A=0.003$, we get $I_{trns}/I_{in}=0.72$. The reflectivity finesse is $F_R=\frac{\pi\sqrt{R}}{1-R}=155.5$. The flatness finesse per mirror is: $F_f=100$. The total finesse is,

$$F_{tot}=\left(\frac{1}{F_R}+\frac{1}{F_f}\right)^{-1}\approx 60.9\ .$$

The cavity line width is,

$$\frac{\kappa}{2\pi} = \frac{\delta_{fsr}}{F} = \frac{1}{F}\frac{c}{2L} = 492\,\mathrm{MHz} \ .$$

Hence, for $d = 5$ nm and we get the spectral resolution,

$$\frac{\kappa}{2\pi\nu} = \frac{\kappa\lambda}{2\pi c} = \frac{\lambda}{F2L} \approx 8.2 \cdot 10^{-7} \ .$$

b. Absorption eats intensity upon each reflection. As the number of cavity round trip with reflections increases with R, the intensity eaten by absorption increases with R, as well.

53.1.10.8 Ex: Confocal and concentric cavities

a. Calculate the spectrum of longitudinal and transverse modes for (i) a confocal cavity ($\rho_a = \rho_b = L$) and (ii) a concentric cavity ($\rho_a = \rho_v = L/2$). Interpret the results. b. Assuming radii of curvature $\rho_a = \rho_b = 5$ cm and a finesse of $F = 500$ for the cavity, how precise must the length of the cavity be adjusted in order to observe only longitudinal modes in the transmission spectrum?

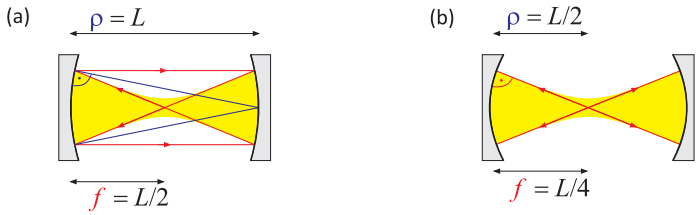

Figure 53.15: (a) Confocal cavity and (b) concentric cavity.

Solution: *a. For the case (i) the formula (53.28) gives,*

$$\frac{\nu}{\delta_{fsr}} = N + 1 + \frac{m+n+1}{\pi}\frac{\pi}{2} \ .$$

For the case (ii) the formula (53.28) gives,

$$\frac{\nu}{\delta_{fsr}} = N + 1 + \frac{m+n+1}{\pi}\,0 \ .$$

In case (i) an additional semi-integer mode appears. It is due to the fact that in this geometry, the complete 'round-trip' is doubled.
b. From (53.28) we derive the longitudinal and transverse spectrum of a symmetric cavity,

$$\nu = \delta_{fsr}\left[(q+1) + \tfrac{1}{\pi}(m+n+1)\arccos\left(1 - \tfrac{L}{\rho}\right)\right] \ .$$

We now ask, how much we may vary L in order for the frequency shift of the transverse mode TEM_{01} with respect to any (half-)longitudinal mode to be smaller than κ.

Expanding the arccos term for small deviations of $L = \rho + \Delta L$ from ρ we obtain for case (i):

$$\frac{\kappa}{2\pi} > \frac{2\delta_{fsr}}{\pi} \arccos\left(1 - \frac{\rho + \Delta L}{\rho}\right) \simeq \delta_{fsr}\left(1 + \frac{2\Delta L}{\pi\rho}\right) ,$$

that is,

$$\Delta L < \frac{\kappa}{4\delta_{fsr}}\rho = \frac{\pi}{2F}\rho \approx 160\,\mu\text{m} .$$

And for case (ii) expanding the arccos term for small deviations of $L = \rho/2 + \Delta L$ from $\rho/2$ we obtain:

$$\frac{\kappa}{2\pi} > \frac{2\delta_{fsr}}{\pi} \arccos\left(1 - \frac{2\rho + \Delta L}{\rho}\right) \simeq \delta_{fsr}\frac{2}{\pi}\sqrt{\frac{2\Delta L}{\rho}} ,$$

that is,

$$\Delta L < \frac{\rho}{2}\left(\frac{\kappa}{4\delta_{fsr}}\right)^2 = \frac{\pi^2\rho}{8F^2} \approx 25\,\mu\text{m} .$$

53.1.10.9 Ex: Thermal drift of a laser cavity

Estimate the frequency drift of a laser oscillating at $\lambda = 500\,\text{nm}$ because of thermal expansion of the resonator at a temperature drift of $1^\circ\,\text{C/h}$, when the resonator mirrors are mounted on distance-holder rods a. made of invar and b. made of fused quartz.

Solution: *We have,*

$$\frac{\Delta\nu}{\nu} = \frac{\Delta d}{d} = \alpha T .$$

A temperature drift of $1\,\text{C/h}$ gives, for invar rods ($\alpha = 1.2 \cdot 10^{-6}\,\text{K}^{-1}$), a frequency drift per hour of $\frac{\Delta\nu}{\nu} = 1.2 \cdot 10^{-6}$. For $\nu = c/\lambda = 6 \cdot 10^{14}\,\text{s}^{-1}$, hence $\Delta\nu = 720\,\text{MHz/h}$. For fused quartz ($\alpha = 0.4 - 0.5 \cdot 10^{-6}\,\text{K}^{-1}$ the drift is three times smaller, while for Zerodur it is more than 12 times smaller.

53.1.10.10 Ex: Stability of a supercavity

Consider a non-confocal optical cavity of 10 cm length whose spacer is made of (i) aluminum, (ii) stainless steel, (iii) invar steel, (iv) fused quartz, (v) Zerodur, and (vi) ULE. The cavity is maintained at constant temperature with a precision of 0.001 C. What maximum drift do you estimate for its resonance frequency at 633 nm?

Solution: *The resonance frequency is a multiple of the FSR, $\nu = N\delta_{fsr} = Nc/2L$. Hence, it depends on length variations like,*

$$\Delta\nu = \frac{\partial\nu}{\partial L}\Delta L = -\frac{Nc}{2L^2}\Delta L = -\frac{\nu}{L}\Delta L ,$$

which in turn depend on temperature variation like,

$$\Delta L = L\alpha\Delta T \ ,$$

where α is the thermal expansion coefficient. Hence,

$$\Delta\nu = -\nu\alpha\Delta T \ .$$

The thermal expansion coefficients for the specified materials are:

material	α $[10^{-6}\,\mathrm{K}^{-1}]$	$\Delta\nu$
Al	23.1	11 MHz
steel	11.0..13.0	≈ 5.7 MHz
invar	1.2	570 kHz
fused quartz	0.59	280 kHz
Zerodur	0.007..0.1	3.3..47 kHz
ULE	0	0

53.1.10.11 Ex: Fabry-Perot interferometer as optical spectrum analyzer

A confocal FPI shall be used as optical spectrum analyzer, with a free spectral range of $\delta_{fsr} = 3\,\mathrm{GHz}$. Calculate the mirror separation L and the finesse that is necessary to resolve spectral features in the laser output within $\Delta\nu = 10\,\mathrm{MHz}$. What is the minimum reflectivity R of the mirrors, if the surface finesse is $F_S = 500$?

Solution: *For a radius of curvature much smaller than the radius of the mirror $\rho \ll r$ the free spectral range of a confocal cavity is $\Delta\nu = c/4L$, hence,*

$$L = \frac{c}{4\delta_{fsr}} \approx 2.5\,\mathrm{cm} \ .$$

From this we obtain the total finesse,

$$F^* = \frac{\delta\nu}{\Delta\nu} \approx 300 \ ,$$

and with,

$$\frac{1}{F^{*2}} = \frac{1}{F_R^2} + \frac{1}{F_S^2} \ ,$$

the reflectivity finesse becomes, $F_R = 375$. Finally, the reflectivity must be chosen $R > 1 - \pi/F^* \approx 99.16\%$.

53.1.10.12 Ex: Interference and colors filters

Strontium atoms resonantly driven by two lasers at 461 nm and 689 nm emit fluorescence light at both wavelengths. Because the red transition is 5000 times narrower than the blue one, the red fluorescence is much weaker and difficult to detect. Find

a suitable low-pass filter in the Thorlabs® catalogue suppressing the blue light sufficiently to be sure that any fluorescence recorded after the filter must be resulting from the red transition. What signal ratios can you achieve with a single filter? Consider interference filters as well as color filters.

Solution: *Our best choice would be the model FELH0650 long pass filter at* 650 nm *with 0.0000872186% transmission at* 461 nm *and 96.5242% transmission at* 689 nm.

53.1.10.13 Ex: Interference filter

An interference filter shall be designed with peak transmission at $\lambda = 550\,\text{nm}$ and a bandwidth of 5 nm. Estimate the reflectivity R of the dielectric coatings and the thickness of the etalon, if no further transmission maximum is allowed between 350 and 750 nm.

Solution: *The free spectral range must be chosen such that* $2\Delta\lambda_{fsr} > 750\,\text{nm} - 350\,\text{nm}$. *Hence,*

$$\Delta\lambda_{fsr} \geq 200\,\text{nm} \ .$$

This corresponds to a free spectral range of,

$$\delta_{fsr} = \frac{c}{2L} = \frac{\partial\nu}{\partial\lambda}\Delta\lambda_{fsr} = -\frac{c}{\lambda^2}\Delta\lambda_{fsr} = -198\,\text{THz} \ ,$$

or to an etalon thickness of $L \leq 756\,\text{nm}$. *If the bandwidth is* $\Delta\lambda = 5\,\text{nm}$, *the finesse must be* $F = \delta_{fsr}/\Delta\nu = |\Delta\lambda_{fsr}/\Delta\lambda| = 40$. *If the finesse is solely determined by the reflectivity* R, *then,*

$$F = \frac{\pi\sqrt{R}}{1-R} \ ,$$

that is, $R = 0.9245$.

53.1.10.14 Ex: Cut-off wavelength of a single-mode fiber

You want to transport 461 nm light via a polarization maintaining single-mode fiber. How do you need to choose the cut-off wavelength of the fiber? Assuming a 50% coupling efficiency, how much power can you get through the 5 nm long fiber? Choose a model from the Thorlabs catalog and justify your choice.

Solution: *The cut-off wavelength must be somewhere between* $\lambda/2$ *and* λ *in order to prevent the formation of a transverse standing wave other than the fundamental mode* $\lambda/2$. *In our case,* $\lambda_{co} = 230..460\,\text{nm}$.
A possible model would be 'P1-405B-FC-5', Single Mode Patch Cable, $405 - 532\,\text{nm}$, *FC/PC,* $\emptyset 3\,\text{mm}$ *Jacket,* 5 m *Long.*
The typical insertion loss (connector to connector) is specified as 2.5 dB, *the attenuation is something like* 40 dB/km. *Hence, we expect* $(2.5 + 0.2)\,\text{dB}$ *total loss. However, the free space to fiver coupling is generally less efficient.*

53.1.10.15 Ex: Exc Numerical aperture of a fiber

Calculate the numerical aperture of a step-index fiber with core refraction index n_{core} and cladding refraction index $n_{cladding}$ considering the scheme 53.16.

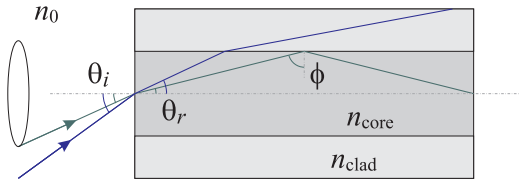

Figure 53.16:

Solution: *The numerical apertures is defined by,*

$$NA = \sin\theta_i \ .$$

Snell's law hold for the incoupled beam,

$$\frac{\sin\theta_i}{\sin\theta_r} = \frac{n_{core}}{n_0} = n_{core} \ .$$

Total internal reflection occurs between core and cladding,

$$\frac{\sin 90^\circ}{\sin\phi} = \frac{n_{core}}{n_{cladding}} \ .$$

With $\sin\theta_r = \cos\phi$ *we finally get,*

$$NA = n_{core}\sin\theta_r = n_{core}\cos\phi = n_{core}\sqrt{1-\sin^2\phi} = \sqrt{n_{cladding}^2 - n_{core}^2} \ .$$

53.1.10.16 Ex: Tuning by tilting an etalon

a. It is a common method to tune an etalon (or dielectric mirror or waveplate) to a certain transmission wavelength by tilting it as a whole with respect to the optical axis (without changing its intrinsic alignment. Does the tilt increase or decrease the wavelengths of the transmission peaks? Justify your answer. What is the implication for a dielectric mirror to be used under a non-normal angle of incidence?
b. A narrow band interference filter consisting of a glas plate coated on both surfaces has the following characteristics: thickness $L = 0.5\,\text{mm}$, refractive index $n_{rfr} = 1.45$, central wavelength $\lambda_{eff} = 706\,\text{nm}$, and bandwidth $\Delta\lambda = 0.3\,\text{nm}$. Considering the filter as Fabry-Pérot etalon, calculate its free spectral range, its finesse, and the reflectivity of its surfaces.
c. Assuming that the filter of part (b) can be tilted from normal incidence up to an angle $\theta_{max} = 35^\circ$, how far will the center frequency shift. Prepare a graph showing

λ_{eff} as a function of θ.

Solution: *a. A seemingly plausible but wrong argument is, that tilting makes the beam path longer, and that this must be compensated by a longer wavelength. A closer look shows, where the above argument is wrong. Following a ray from one layer to the next one under some angle, and back to the first layer along a 'reflected' beam, we actually don't get back to the place where we started, but rather to some offset position. But it doesn't make sense to compare the phases of two beams as measured at two different positions. A correct way to understand the issue is to consider the phase shift along a direction perpendicular to the coating layers, which is obviously reduced for tilted incidence, as illustrated in Fig. 53.17(a).*
Dielectric multilayer mirrors can be highly reflecting only in a limited spectral bandwidth. When such a mirror, designed for use with normal incidence of the light, is tilted against an incident beam, the reflection features are shifted toward shorter wavelengths.
b. From the given characteristics we calculate,

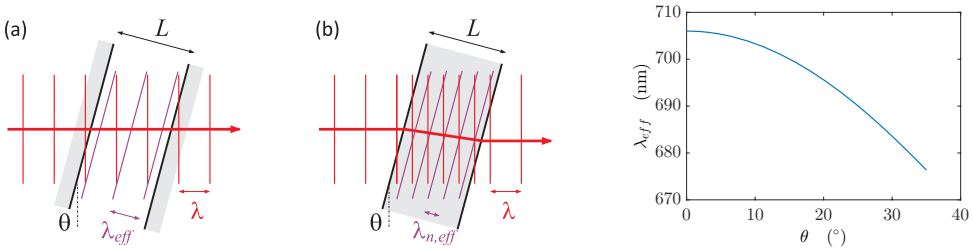

Figure 53.17: (a) Reducing the effective phase shift in a tilted air-spaced etalon. (b) Reducing the effective phase shift in a tilted dielectric etalon. (c) Tuning range of a tilted interference filter.

$$\delta_{fsr} = \frac{c}{2Ln_{refr}} \approx 207\,\mathrm{GHz} \quad , \quad \frac{\kappa}{2\pi} = \frac{c\Delta\lambda}{\lambda^2} \approx 190\,\mathrm{GHz} \quad , \quad F = \frac{2\pi\delta_{fsr}}{\kappa} = 1.1 = \frac{\pi\sqrt{R}}{1-R} \,,$$

from which we get $R = 10\%$.
c. By geometry the effective resonant wavelength of a tilted etalon is reduced. For an air-spaced etalon, $\lambda_{eff} = \lambda\cos\theta$, as seen in Fig. 53.17(b) For a dielectric etalon, we have to take into account Snell's law,

$$n_{rfr} = \frac{\sin\theta}{\sin\beta} = \frac{\lambda}{\lambda_n} \,.$$

Hence, we expect the tuning curve exhibited in Fig. 53.17(c), and parametrized by,

$$\begin{aligned}\lambda_{eff} = \lambda_n\cos\theta &= \frac{\lambda}{n_{rfr}}\cos\left(\arcsin\frac{\sin\theta}{n_{rfr}}\right) \\ &= \frac{\lambda}{n_{rfr}}\sqrt{1-\sin^2\left(\arcsin\frac{\sin\theta}{n_{rfr}}\right)} = \lambda_{max}\sqrt{1-\frac{\sin^2\theta}{n_{rfr}^2}} \,.\end{aligned}$$

53.1.10.17 Ex: Double MZI as a model for Coherent Back-Scattering

Consider the setup shown in Fig. 53.18 and calculate the signal observed on the photodetector for arbitrary phase shifts ϕ and arbitrary rotation angles α by the $\lambda/2$-waveplate.

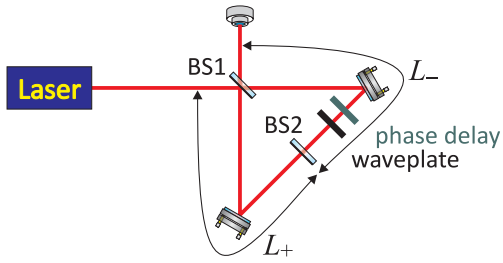

Figure 53.18: Double Mach-Zehnder interferometer.

Solution: *The electric field reaching the detector is the superposition of 4 paths. Without waveplate ($\alpha = 0$),*

$$\begin{aligned}\frac{\mathcal{E}_d}{\mathcal{E}_0} &= \sqrt{1-R_1}e^{\imath kL_+}(-\sqrt{R_2})e^{\imath kL_+}(-\sqrt{R_1}) \\ &\quad + \sqrt{R_1}e^{\imath kL_-}\sqrt{1-R_2}e^{\imath kL_+}(-\sqrt{R_1}) \\ &\quad + \sqrt{1-R_1}e^{\imath kL_+}\sqrt{1-R_2}e^{\imath kL_-}\sqrt{1-R_1} \\ &\quad + \sqrt{R_1}e^{\imath kL_-}\sqrt{R_2}e^{\imath kL_-}\sqrt{1-R_1} \\ &= e^{\imath kL}\left[2\sqrt{1-R_1}\sqrt{R_1}\sqrt{R_2}\cos 2k\Delta L + (1-2R_1)\sqrt{1-R_2}\right]\end{aligned}$$

introducing the abbreviation $L_\pm \equiv L/2 \pm \Delta L$. In particular, for $R_1 = 50\%$ we get,

$$\frac{E_d}{E_0} = \sqrt{R_2}e^{ikL}\cos 2k\Delta L \ .$$

For $R_2 = 0$ the double MZI is a model for CBS, because all the light reflected from the setup is going into backward direction.
With the $\lambda/2$-waveplate described by the Jones-matrix,

$$M_{\lambda/2}(\alpha) = \begin{pmatrix} \cos 2\alpha & -\sin 2\alpha \\ -\sin 2\alpha & -\cos 2\alpha \end{pmatrix} \qquad \textit{with} \qquad M_{\lambda/2}(\alpha)^2 = \mathbb{I} \ ,$$

we can generalize the ansatz:

$$\begin{aligned}
\begin{pmatrix}\mathcal{E}_\perp\\ \mathcal{E}_\parallel\end{pmatrix} &= \sqrt{1-R_1}e^{\imath kL_+}(-\sqrt{R_2})e^{\imath kL_+}(-\sqrt{R_1})\begin{pmatrix}\mathcal{E}_{0\perp}\\ \mathcal{E}_{0\parallel}\end{pmatrix}\\
&\quad+\sqrt{R_1}e^{\imath kL_-}M_{\lambda/2}(\alpha)e^{\imath\phi}\sqrt{1-R_2}e^{\imath kL_+}(-\sqrt{R_1})\begin{pmatrix}\mathcal{E}_{0\perp}\\ \mathcal{E}_{0\parallel}\end{pmatrix}\\
&\quad+\sqrt{1-R_1}e^{\imath kL_+}\sqrt{1-R_2}e^{\imath\phi}M_{\lambda/2}(\alpha)e^{\imath kL_-}\sqrt{1-R_1}\begin{pmatrix}\mathcal{E}_{0\perp}\\ \mathcal{E}_{0\parallel}\end{pmatrix}\\
&\quad+\sqrt{R_1}e^{\imath kL_-}M_{\lambda/2}(\alpha)e^{\imath\phi}\sqrt{R_2}e^{\imath\phi}M_{\lambda/2}(\alpha)e^{\imath kL_-}\sqrt{1-R_1}\begin{pmatrix}\mathcal{E}_{0\perp}\\ \mathcal{E}_{0\parallel}\end{pmatrix}\\
&= e^{\imath kL+\imath\phi}\begin{pmatrix}E_\perp\\ E_\parallel\end{pmatrix}\left[2\sqrt{1-R_1}\sqrt{R_1}\sqrt{R_2}\cos(2k\Delta L-\phi)+(1-2R_1)\sqrt{1-R_2}M_{\lambda/2}(\alpha)\right] .
\end{aligned}$$

In particular, for $R_1 = 50\%$ the setup becomes insensitive on the polarization of the waveplate:

$$\begin{pmatrix}E_\perp\\ E_\parallel\end{pmatrix} = e^{\imath kL+\imath\phi}\sqrt{R_2}\cos(2k\Delta L-\phi)\begin{pmatrix}E_{0\perp}\\ E_{0\parallel}\end{pmatrix} .$$

53.1.11 *Experiment: Mach-Zehnder interferometer*

The Mach-Zehnder interferometer and the Michelson interferometer are the two most common two-beam interferometers. For the realization of the following project prior knowledge of 1. Gaussian beams (see Sec. 51.2), 2. photodetectors (see Sec. 52.2.1), and 3. piezo-electric transducers (see Sec. 53.1.2) is required.

1. Set up a Mach-Zehnder interferometer with a piezo in one of the arms according to Fig. 53.3(a). Optimize the phase matching of the two beams onto a photodetector and the rotation of the $\lambda/2$-waveplates until you obtain visible interference patterns.

2. Vary the length of one arm of the interferometer using the piezo. Measure the contrast of the interference fringes and discuss from which parameters it depends and how it can be maximized.

3. Rotate the first $\lambda/2$-waveplate (behind the laser). What do you observe? Explain the observation!

4. Remove the PBS in front of the photodetector. What do you observe? Explain the observation!

5. If a piezo is used, vary the voltage applied to the piezo-electric actuator and measure the voltage expansion coefficient d.

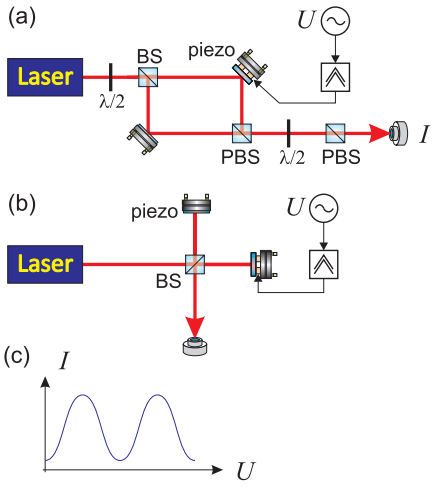

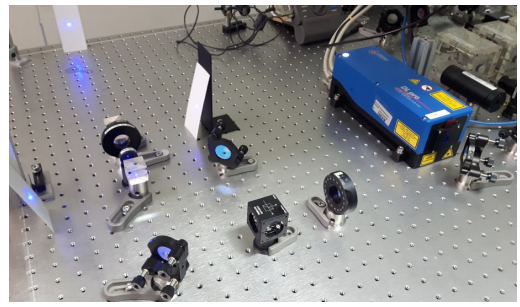

Figure 53.19: Setup for (a) a Mach-Zehnder interferometer or (b) a Michelson interferometer. (BS) non-polarizing beamsplitter, (PBS) polarizing beamsplitter. (c) Signal on the photodetector as a function of the length variation of an arm of the interferometer.

53.1.12 *Experiment: Fabry-Pérot cavity*

A Fabry-Pérot cavity is a typical multi-beam interferometer.

1. Set up a Fabry-Pérot cavity according to Fig. 53.20 and mode-match a laser beam into the cavity. Scan the cavity length using a piezo and observe the transmitted spectrum on an oscilloscope. What do you observe?

2. If an ECDL is used, vary the current and the temperature of the laser diode. What do you observe? Vary the frequency of the diode laser by scanning the piezo transducer of the laser cavity. Observe the mode spectrum of the laser in the transmission signal of the cavity. Measure its free spectral range, the transmission linewidth, and the finesse of the cavity.

Optical cavities are frequently used as *optical spectrum analyzers*. For this application, it is helpful to simplify the intrinsic mode spectrum of the cavity by using a confocal design, where all transerse modes are degenerated. We will now set up an optical cavity and characterize it by its free spectral range and its finesse. Then we will analyze its mode spectrum and modify its geometry to make it confocal.

1. Couple a laser beam into a cavity as shown in Fig. 53.20. The cavity provided by this tinker course consists of a plane incoupler ($\rho_1 = \infty$, $R_1 = 98\%$) and a high reflector ($\rho_2 = 25\,\text{mm}$, $R_2 = 99.8\%$). Position the mirror at a distance L, where the cavity is stable. Calculate the free spectral range, the finesse, the diameter of the beam waist.

2. Optimize the phase-matching of the laser beam to the cavity. In order to do this, (a) measure the diameter of the diode laser beam, (b) determine the lens

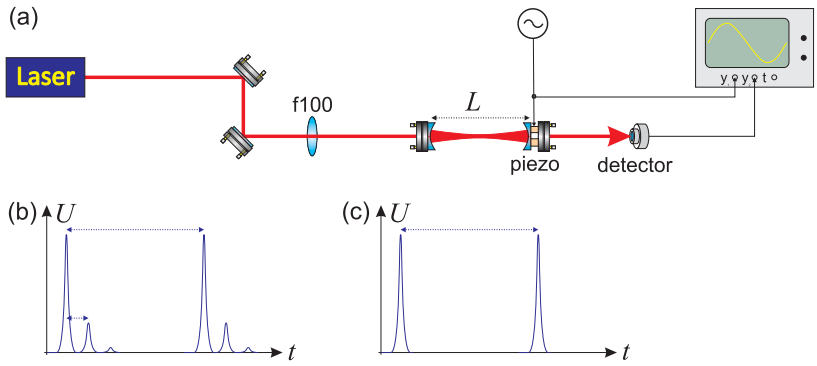

Figure 53.20: (a) Setup for aligning a confocal resonator. (b) Transmission spectrum of the cavity for non-confocal alignment. (c) Same as (b) but for the case of confocal alignment.

which can be used to focus down to the beam waist of the cavity. How does the transmission spectrum change upon the beam matching?

53.1.13 *Experiment: Fizeau interferometer*

A *Fizeau interferometer* is a device allowing to analyze the rugosity of surfaces.

1. Set up a Fizeau interferometer according to Fig. 53.20.

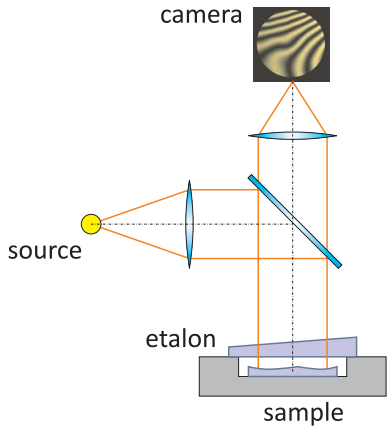

Figure 53.21: Principle of operation of a Fizeau interferometer.

53.1.14 *Experiment: Coupling light into an optical fiber*

Coupling a laser beam into an optical fiber is a delicate task, requiring a good collimation optics and full control over the 6 degrees of freedom defining a laser beam: horizontal and vertical position, horizontal and vertical tilt, beam diameter and divergence.

1. Redirect the light of a HeNe laser via two adjustable mirrors into a fiber collimator in such a way that the beam is not deviated from the optical axis by the collimator.

2. Now connect (a) a multimode fiber and (b) a single mode fiber to the collimator. Optimize the coupling by walking the laser beam and by adjusting the focus of the fiber collimator. What differences do you observe for multi- and single mode fibers?

53.2 Conventional light sources and lasers

For the first half of the 20-th century these assumptions matched the available light sources, usually incandescent, arc or plasma discharge lamps. After the invention of the laser in 1958, single mode and pulsed lasers quickly replaced the lamps as a source for optical excitation. These new light sources initiated a revolution in optical science, the consequence of which continue to reverberate through modern sciences and applied technologies. The characteristics of laser sources are far superior to the old lamps in all respects. They are intense, collimated, spectrally narrow and phase coherent. The laser gave rise to a multitude of new spectroscopic techniques and new disciplines, such as quantum electronics, the study of statistical properties of light in quantum optics, optical cooling and trapping of microscopic particles, the control of chemical reactivity, and new technologies for imaging and high resolution microscopy. The impact the laser had on technology is only comparable to that of to the invention of the transistor. See also (watch talk).

The laser produces light through an optical quantum amplification process based on the stimulated emission of electromagnetic radiation. The term 'laser' is an acronym for 'Light Amplification by Stimulated Emission of Radiation'. A laser differs from other light sources in that it emits *coherent* light. Its spatial coherence allows the light to be focused on a very tiny spot, where the concentration of energy is sufficient for applications such as laser cutting and lithography. The spatial coherence also allows it to collimate a laser beam over large distances, that is, the light forms a concentrated beam propagating in a straight line. Lasers can also have a very high temporal coherence, which corresponds to a very narrow spectrum, that is, lasers usually emit a single very well defined color of light. The extreme temporal coherence can be used to produce pulses of light as short as a femtosecond. In addition, laser light is polarized.

In 1917, Albert Einstein established the theoretical foundations of the laser in an article 'Zur Quantentheorie der Strahlung' through a rederivation of Max Planck's radiation law. He proposed a mechanism explaining how light is absorbed and emitted from atoms. The fundamental ingredient is that the photon can be emitted in two different ways, by spontaneous emission, an indeterministic process that occurs without physical reason, or by stimulated emission. This latter emission process occurs because of stimulation by light, which is already present in the system and represents the fundamental mechanism of the laser. In the following decade German and American researchers experimentally confirmed the phenomena of stimulated emission and negative absorption, that is, gain. In 1950, Alfred Kastler (French physicist and No-

bel Prize in Physics of 1966) proposed the method of optical pumping, confirmed experimentally two years later by other French physicists.

In 1953, Charles Townes produced the first microwave amplifier called *maser*, a device that operates similarly to the laser but amplifies microwave radiation instead of visible or infrared radiation. However, Townes' maser was unable to emit light continuously. In 1955, in the Soviet Union, Nikolay Basov and Aleksandr Prokhorov solved the problem of continuous operation using atoms with more than two energy levels. These level systems were able to sustain a permanent population inversion of an energetic level decaying to a less energetic system by releasing light via stimulated emission. Despite the fact that several prominent physicists, including Niels Bohr, John von Neumann, and Isidor Rabi, argued that the maser violates Heisenberg's uncertainty principle and therefore could not work, in 1964, Charles Townes, Nikolay Basov and Aleksandr Prokhorov shared the Nobel Prize in Physics for fundamental work in the field of quantum electronics that led to the realization of oscillators and amplifiers based on the maser principle.

In 1957, Charles Townes and Arthur Schawlow, from the Bell labs, began to seriously study feasibility of an 'optical maser'. In 1958, the Bell labs submitted a patent proposing a scheme for optical radiation, and Schawlow and Townes presented a scientific paper. Simultaneously, at the Columbia University, the PhD student Gordon Gould was working on the energy levels of excited thallium. In 1957-8, Gould and independently Prokhorov, Schawlow and Townes proposed the use of an open resonator, which later became an essential component of the laser. Gould also proposed several possible applications for a laser, such as spectrometry, interferometry, the radar, and nuclear fusion. He continued to develop the idea, and filed a patent application in April 1959. The United States Patent Office dismissed his application, and granted a patent to the Bell Labs in 1960. Gould won his first minor patent in 1977 after a 28-year fight, and it took him until 1987 to win his first significant process in the struggle, when a federal judge ordered the United States Patent Office to issue to Gould patents for optical pumping and the invention of a laser based on the principle of electrical gas discharge.

It was Theodore Maiman, who on May 16, 1960, operated the first working laser at the Hughes Research Laboratories, Malibu, California, evincing several other research teams, including the ones of Townes at Columbia University, of Schawlow at Bell Labs, and Gould at the company TRG (Technical Research Group). Maiman's laser used a synthetic solid-state ruby crystal pumped by a flash lamp to produce red laser light at 694 nm wavelength; however, the device was only capable of pulsed operation due to its three-level pumping scheme. Later in 1960, the first gas laser was built, using a helium-neon mixture, which was capable of continuous operation in the infrared spectrum. Basov and Javan proposed the concept of a semiconductor laser diode. In 1962, the first laser diode device, made of gallium arsenide, was realized emitting near-infrared light. Nowadays, laser diodes are available in various spectral regimes up to the UV.

Interestingly, despite many attempts, it has not yet been possible to manufacture yellow or green laser diodes.

Figure 53.22: First suggested application in 1964 of a (left) HeNe laser and (right) a diode laser.

53.2.1 Features and operation of lasers

To understand how a laser operates, we consider the process of absorption and emission of light by an atom. Following Bohr's model an absorbed photon raises an electron from a lower orbit to a higher orbit, and when the electron returns back to the ground state, it re-emits a photon in an arbitrary direction.

When we illuminate a sample of N atoms, N_1 atoms of which are in the ground state, by a radiation field, the absorption rate depends on the field intensity $I(\nu)$ and a constant B_{12}, which is characteristic for the transition,

$$R_{abs} \propto B_{12} I(\nu) N_1 \ . \tag{53.35}$$

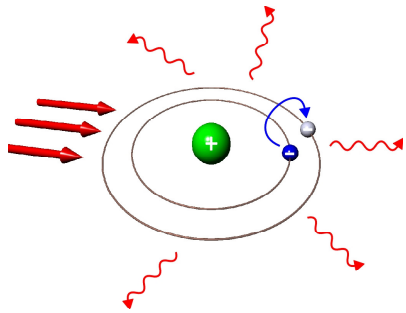

Figure 53.23: Bohr's model of photon absorption.

The emission rate depends on the number of atoms N_2 in the excited state, such that,

$$R_{sp} \propto A_{21} N_2 \ . \tag{53.36}$$

As the excited state has more energy, it can decay by itself (i.e. spontaneously) to a lower energy state. Einstein's brilliant idea now was to postulate a third process, which he called stimulated emission,

$$R_{st} \propto B_{21} I(\nu) N_2 \ . \tag{53.37}$$

In this process, an incident photon stimulates an excited atom to transfer the electron to a lower orbit. The released energy is then used to form a second photon, which is in all respects identical to the first. This process is necessary to ensure that, in thermal equilibrium, the population of the states follows Boltzmann's law.

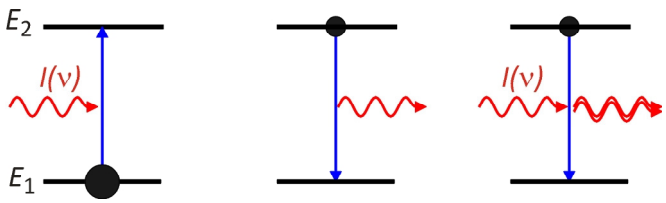

Figure 53.24: Einstein's model of absorption and spontaneous and stimulated emission.

Obviously, absorption decreases the intensity of a light beam crossing the atomic sample, while stimulated emission amplifies it. In order to amplify incident light, the gain in intensity must overcome the losses. Therefore, we need the absorption processes to be less frequent than the stimulated emission processes, i.e. the number of atoms in the excited state N_2 must exceed the number of atoms in the ground state $N_1 < N_2$.

We can easily write the rate equation,

$$\frac{dN_2}{dt} = -A_{21}N_2 - B_{21}I(\nu)N_2 + B_{21}I(\nu)N_1 = -\frac{dN_1}{dt} \ , \tag{53.38}$$

with $N = N_1 + N_2$. It is easy to solve this equation. The result is,

$$N_2 = \frac{I(\nu)B_{21}N}{A + 2B_{21}I(\nu)}[1 - e^{-(A_{21}+2B_{21}I(\nu))t}] < N_1 \ . \tag{53.39}$$

The graphical representation 53.25 shows the temporal behavior of the populations

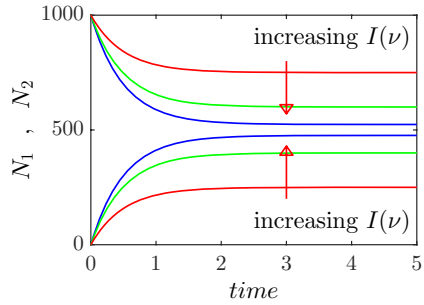

Figure 53.25: (code) Impossibility of achieving inversion in a two-level system.

N_1 (in green in the figure) and N_2 (in blue), reaching a state of equilibrium after a certain time. By increasing the intensity of the incident light, we observe that the curves approach each other but never cross. That is, in a two-level system, we always get $N_1 > N_2$ and the populations are never inverted. Therefore, amplification of light as in the laser does not happen.

Fortunately, we can resort to a trick by inserting a third level. Ensuring that the decay rate of the (metastable) state E_3 is much slower than the optical pumping to this state via the driven transition $E_1 \rightarrow E_2$ followed by a rapid decay $E_2 \rightarrow E_3$, we can reach the situation $N_3 > N_1$. Now it is possible to amplify light, which is resonant with the transition $E_2 \rightarrow E_3$.

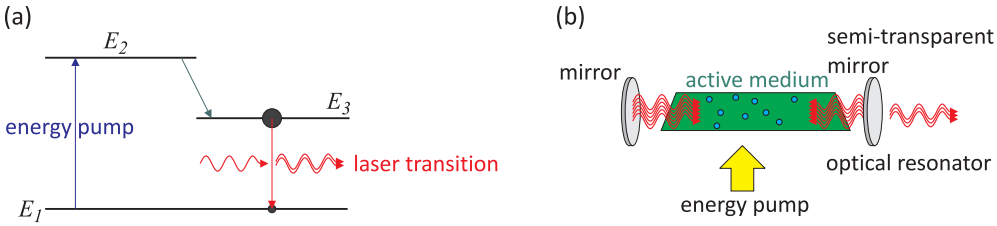

Figure 53.26: Basics of a laser: (a) Level system and (b) principle scheme.

What are the minimum requirements for the realization of a laser? The first condition is that the *pumping cycle is irreversible* to ensure that the processes of stimulated emission and absorption do not compensate. Spontaneous emission is irreversible and can be incorporated into a three-level system.

The second condition is the existence of a *stimulated emission process*, because we want the amplified photon to be an exact copy of the incident photon.

The third requirement is a *feedback mechanism* that synchronizes the amplification processes by different atoms in a disordered environment, such as a gas. Mirrors are ideal because they increase the effective gain path, i.e. the distance within which inverted atoms can amplify light. Also, the mirrors define the phase of the light wave, since the standing wave formed by the counterpropagating light fields must have nodes on the surfaces of the mirrors.

53.2.1.1 Threshold condition

According to the *Lambert-Beer law* the intensity of a monochromatic laser beam evolves, on its way through a gas of two-level atoms with energies $E_2 - E_1 = \hbar\omega_0$ like,

$$I(z,\nu) = I(0,\nu)e^{-\alpha(\nu)z} \ , \tag{53.40}$$

where the frequency-dependent absorption coefficient,

$$\boxed{\alpha(\nu) = [N_1 - \tfrac{g_1}{g_2}N_2]\sigma(\nu)} \ , \tag{53.41}$$

is determined by the absorption cross section $\sigma(\nu)$ for the transition and by the inversion,

$$\Delta N \equiv \tfrac{g_1}{g_2}N_2 - N_1 \ , \tag{53.42}$$

which determines whether stimulated emission prevails or absorption: For $\Delta N > 0$, the absorption coefficient $\alpha(\nu)$ becomes negative and the incident wave is amplified instead of attenuated [351].

If the active medium is placed between two mirrors [Fig. 53.26(b)], the wave is reflected back and forth, and traverses the amplifying medium many times, which

increases the total amplification. With the length L of the active medium the total gain factor per single round-trip without losses is,

$$G(\nu) = \frac{I(\nu, 2L)}{I(\nu, 0)} = e^{-2\alpha(\nu)L} \ . \tag{53.43}$$

A mirror with reflectivity R reflects only the fraction R of the incident intensity. The wave therefore suffers at each reflection a fractional reflection loss of $(1 - R)$. Furthermore, absorption in the windows of the cell containing the active medium, diffraction by apertures, and scattering due to dust particles in the beam path or due to imperfect surfaces introduce additional losses. When we summarize all these losses by a loss coefficient γ, which gives the fractional energy loss $\Delta W/W$ per round-trip time T, the intensity I decreases without an active medium per round-trip as,

$$I(2d, \nu) = I(0, \nu)e^{-\gamma} \ . \tag{53.44}$$

Including the amplification by the active medium with length L, we obtain for the intensity after a single round-trip through the resonator with length d, which may be larger than L:

$$I(2d, \nu) = I(0, \nu)e^{-2\alpha(\nu)L-\gamma} \ . \tag{53.45}$$

The wave is amplified if the gain overcomes the losses per round-trip. This implies that,

$$-2L\alpha(\nu) = 2L\Delta N\sigma(\nu) > \gamma \ , \tag{53.46}$$

which yields the threshold condition for the population difference,

$$\Delta N > \Delta N_{thr} = \frac{\gamma}{2L\sigma(\nu)} \ . \tag{53.47}$$

If the inverted population difference ΔN of the active medium is larger than ΔN_{thr}, a wave that is reflected back and forth between the mirrors will be amplified in spite of losses, therefore its intensity will increase.

The wave is initiated by spontaneous emission from the excited atoms in the active medium. Those spontaneously emitted photons that travel into the right direction (namely, parallel to the resonator axis) have the longest path through the active medium and therefore the greater chance of creating new photons by induced emission. Above the threshold they induce a photon avalanche, which grows until the depletion of the population inversion by stimulated emission just compensates the repopulation by the pump. Under steady-state conditions the inversion decreases to the threshold value ΔN_{thr}, the saturated net gain is zero, and the laser intensity limits itself to a finite value I_L. This laser intensity is determined by the pump power, the losses γ, and the gain coefficient $\alpha(\nu)$.

The frequency dependence of the gain coefficient $\alpha(\nu)$ is related to the line profile $g(\nu - \nu_0)$ of the amplifying transition. Without saturation effects (i.e. for small intensities), $\alpha(\nu)$ directly reflects this line shape, for homogeneous as well as for inhomogeneous profiles. According to (53.41) and (22.87) we obtain with the Einstein coefficient B_{ik},

$$\alpha(\nu) = \Delta N\sigma(\nu) = -\Delta N(h\nu/c)B_{12}(\nu - \nu_0) \ , \tag{53.48}$$

which shows that the amplification is largest at the line center ν_0. For high intensities, saturation of the inversion occurs, which is different for homogeneous and for inhomogeneous line profiles.

The loss factor γ also depends on the frequency ν because the resonator losses are strongly dependent on ν. The frequency spectrum of the laser therefore depends on a number of parameters.

53.2.1.2 Applications of lasers in industry and fundamental research

Among their many applications, lasers are nowadays used in compact disc players, laser printers, and bar code scanners, optical fibers and optical communication, laser surgery and skin treatments, welding, cutting and machining, military devices, distance and velocity measurements, projectors, laser pointers, etc..

In fundamental research (in particular on atomic gases, metamaterials, etc.), the laser plays elementary roles in the areas of photonics, quantum computers, metrology, frequency combs, and atomic clocks (laser-based clocks are up to 1000 times more stable than the best state-of-the-art microwave clocks).

We all know that light is a wave. With the invention of the laser we found a process and a device to make this light coherent. On the other hand, since de Broglie's assertion we know that *matter is a wave, as well.* Is it conceivable to construct a matter laser? Yes, it is! The first coherent matter wave was in fact observed in 1995. This state of matter, also called Bose-Einstein condensate, was predicted by Bose and Einstein in 1924. To create a Bose-Einstein condensate, we need, similarly to the laser, that the matter waves interfere constructively in a way that they amplify each other. For this, the Broglie wavelength of the particles, which constitute the matter, must be longer than the distance between them. Assuming a typical average distance on the order of µm, this corresponds to an average velocity of the particles of mm/s or a temperature of some 100 nK.

53.2.2 HeNe laser

HeNe lasers are gas lasers, whose gain medium consists of a mixture of 90% helium and 10% neon at a total pressure of about 1 Torr excited by a small electrical discharge. The most widely used transition wavelength is at 632.8 nm.

Fig. 53.27(a) shows the principle scheme of a commercial HeNe laser. The distance between the high-reflecting mirror (R_{hr}) and the output coupler (R_{oc}) determines the free spectral range δ_{fsr}. Typically, a HeNe laser operates on two or three longitudinal modes separated by δ_{fsr}. As illustrated in Fig. 53.27(b), the numbers of lasing modes above threshold depends on the ratio of gain-to-loss. Fig. 53.27(c) shows the optical pumping scheme to reach inversion on three of the lasing transitions at 632.8 nm, 1.15 µm, and 3.39 µm.

53.2.3 Diode laser

A laser diode is electrically a *pin*-diode. The active region of the laser diode is in the intrinsic (i) region, and the carriers (electrons and holes) are pumped into that depletion region from the n- and p-doped regions respectively. The depletion region, devoid of any charge carriers, forms as a result of the difference in electrical potential

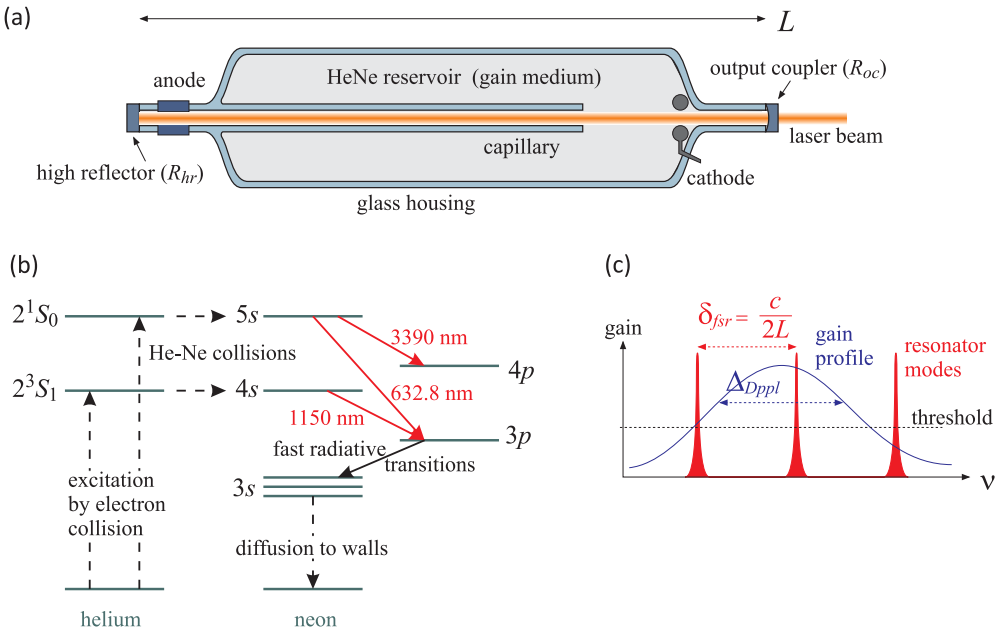

Figure 53.27: (a) Construction scheme of a HeNe laser. (b) Gain and emission profile. (c) Optical pumping scheme.

between n- and p-type semiconductors wherever they are in physical contact. Unlike a regular diode, the goal for a laser diode is to recombine all carriers in the i region, and produce light.

Figure 53.28: (Left) Laser diode with protective housing removed, e.g. using a can opener. (Right) Laser diode collimator.

53.2.3.1 Generation of light

Electrons and holes present in the same region may recombine or 'annihilate' by spontaneous emission of photons with energy equal to the difference between the electron's original state and hole's state (see Fig. 52.10). This is in contrast to a conventional semiconductor junction diode, where the energy released from the recombination is carried away as phonons, i.e. lattice vibrations. Spontaneous emission below the lasing

threshold is the operating mode of an LED. While spontaneous emission is necessary to initiate laser oscillation, it contributes to reduce the efficiency of a laser operating above threshold.

One condition for lasing is that, in the absence of stimulated emission, electrons and holes may coexist in proximity to one another without recombining immediately. For typical diode laser materials the 'upper-state lifetime' or 'recombination time' is on the order of a nanosecond. A nearby photon with energy equal to the recombination energy can cause recombination by stimulated emission. This generates another photon of the same frequency, polarization, and phase, traveling in the same direction as the first photon. In this way stimulated emission will cause gain for an optical wave in the injection region, and the gain increases as the number of electrons and holes injected across the junction increases.

53.2.3.2 Optical cavity and laser modes

As in other lasers, the gain region needs to be surrounded by an optical cavity providing optical feedback. In its simplest form, a laser diode is made in the shape of a narrow optical waveguide on a the surface of a crystal. The two ends of the crystal are cleaved to form perfectly smooth, parallel edges, forming a Fabry-Pérot resonator. Emitted photons will travel along the waveguide, be amplified by stimulated emission and reflected several times from each end face before exiting. If the losses due to absorption and incomplete reflection from the end facets are smaller than the gain, the diode begins to 'lase'.

Important properties of laser diodes are determined by the geometry of the optical cavity. If the waveguide is thick compared to the wavelength of the light, it can support higher-order transverse optical modes. The laser is then called 'multi-mode'. These transversely multi-mode lasers are adequate for application where high power is needed, for example, in printing, activating chemicals, or pumping other types of lasers.

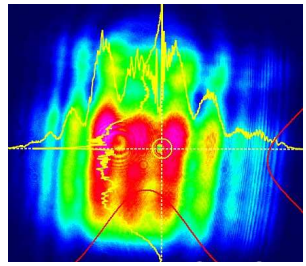

Figure 53.29: Typical beam profile of a multimode laser diode (Thorlabs, L450P1600MM.

For applications requesting small focused beams the waveguide must be made narrow, on the order of the optical wavelength, such that only a single transverse mode is supported, and one ends up with a diffraction-limited beam. Such single spatial mode devices are used for optical storage, laser pointers, and fiber optics. Note that these lasers may still support multiple longitudinal modes, and thus can lase simultaneously at multiple wavelengths. The wavelength emitted is a function of the band-gap of the semiconductor material and the modes of the optical cavity. In

general, the maximum gain will occur for photons with energy slightly above the band-gap energy, and the modes nearest the peak of the gain curve will lase most strongly. The width of the gain curve will determine the number of additional 'side modes' that may also lase, depending on the operating conditions. Single spatial mode lasers that can support multiple longitudinal modes are called Fabry-Pérot (FP) lasers. A FP laser will lase at multiple cavity modes within the gain bandwidth of the lasing medium. The number of lasing modes in an FP laser is usually unstable, and can fluctuate due to changes in current or temperature.

Single spatial mode diode lasers can be designed so as to operate on a single longitudinal mode. These single frequency diode lasers exhibit a high degree of stability, and are used in spectroscopy and metrology, and as frequency references. Single frequency diode lasers are classed as either distributed feedback (DFB) lasers or distributed Bragg reflector (DBR) lasers.

Due to diffraction, the beam diverges (expands) rapidly after leaving the chip, typically at 30 degrees vertically by 10 degrees laterally. A lens must be used in order to form a collimated beam like that produced by a laser pointer. If a circular beam is required, cylindrical lenses and other optics are used. For single spatial mode lasers, using symmetrical lenses, the collimated beam ends up being elliptical in shape, due to the difference in the vertical and lateral divergences.

53.2.3.3 Distributed Bragg reflector lasers and distributed feedback lasers

The simple diode described above has been heavily modified in recent years to accommodate modern technology, resulting in a variety of types of laser diodes. One example is the distributed Bragg reflector laser (DBR). It consists of a monolithic single frequency laser diode, characterized by an optical cavity consisting of an electrically or optically pumped gain region between two mirrors to provide feedback. One of the mirrors is a broadband reflector and the other mirror is wavelength selective so that gain is favored on a single longitudinal mode, resulting in lasing at a single resonant frequency. The broadband mirror is usually coated with a low reflectivity coating to allow emission. The wavelength selective mirror is a periodically structured diffraction grating with high reflectivity. The diffraction grating is etched into the semiconductor within a non-pumped, or passive region of the cavity.

A distributed feedback laser (DFB) is a monolithic single frequency laser diode with a diffraction grating etched close to the *pn*-junction of the diode aiming at stabilizing the lasing wavelength. This grating acts like an optical filter, causing a single wavelength to be fed back to the gain region and lase. Since the grating provides the feedback that is required for lasing, reflection from the facets is not required. Thus, at least one facet of a DFB is anti-reflection coated. The DFB laser has a stable wavelength that is set during manufacturing by the pitch of the grating, and can only be tuned slightly with temperature. DFB lasers are widely used in optical communication applications, where a precise and stable wavelength is critical.

53.2.3.4 ECDL

An *extended-cavity diode laser* (*ECDL*) is an optical setup based on a laser diode chip, which typically has one end anti-reflection (AR) coated, and the laser resonator is completed with a collimating lens and a mirror, as shown in Fig. 53.30(a). The

extended external laser resonator introduces various new features and options: Compared to a standard laser diode, the longer resonator increases the damping time of the intracavity light according to Eq. (53.26), and thus allows for lower phase noise and a smaller emission linewidth (in single-frequency operation). Furthermore, it opens the way for inserting frequency-selective optical components into the extended laser resonator, such as narrow-band Fabry-Pérot etalons or diffraction gratings, which can further *reduce the linewidth* and even allow to *tune and control the frequency* of the laser.

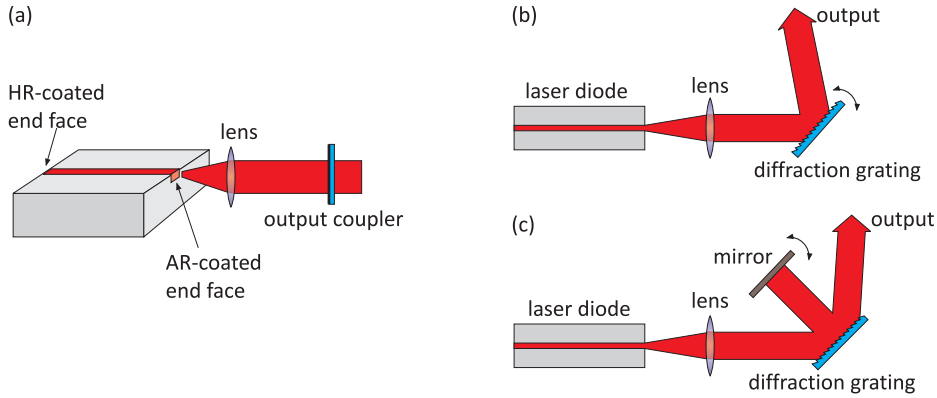

Figure 53.30: (a) ECDL with an AR-coated laser diode and an external mirror. (b) Littrow configuration. (c) Littmann configuration.

Tunable ECDLs based on diffraction grating as the wavelength-selective element are also called grating-stabilized diode lasers. The common Littrow configuration Fig. 53.30(b) generates optical feedback to the laser diode chip by retro-reflecting the first-order diffracted beam from the grating. The emission wavelength can be tuned by slightly tilting the diffraction grating. A disadvantage of this configuration is, that the tilt also changes the direction of the output beam, which is inconvenient for many applications.

In the Littman-Metcalf configuration Fig. 53.30(c), the grating angle is held fixed, and an additional mirror is used to reflect the first-order beam back into the laser diode. The wavelength can be tuned by rotating that mirror. This configuration offers a fixed direction of the output beam, and also tends to exhibit a smaller linewidth, as the wavelength selectivity is stronger, because the wavelength-dependent diffraction occurs twice per resonator round trip. A disadvantage is that the zero-order reflection of the beam reflected by the tuning mirror is lost, so that the output power is lower than that of a Littrow laser.

New concepts have recently become popular, such as the so-called *cat-eye laser* [75, 510, 124], where the frequency-selective element is an extremely narrow-band (0.3 nm) optical filter [5].

By adjusting the tilt angle of a grating or a narrow-band filter by means of a piezo an extremely fine tuning of the emission frequency is possible, while coarse tuning of the frequency over a range of several nanometers is typically achieved by changing

[5] Available from Semrock or Laseroptik.

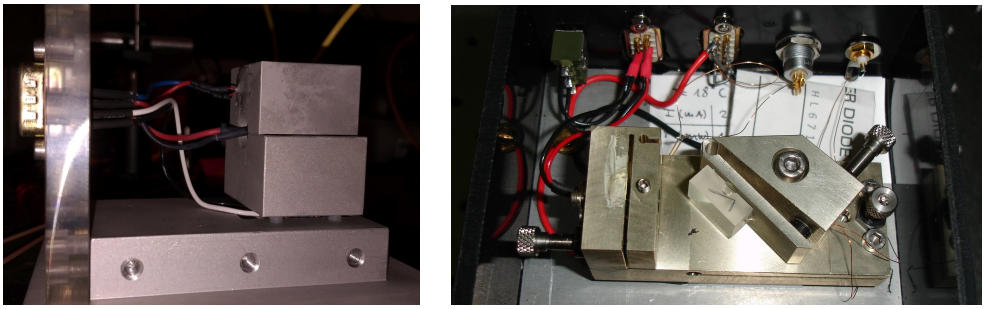

Figure 53.31: (Left) Side view of a 'free-running' laser diode mounted in a collimator (Thorlabs, LT110P-B) clamped in an aluminum block cooled by a Peltier element (Thorlabs, TEC3-6) and whose temperature is measured by a thermistor (Thorlabs, TH10K). (Right) Top view of a home-built ECDL laser in Littrow configuration. The diode collimator is clamped into the left mount. a holographic grating (Newport, 10HG2000-475-1) is glued to the right mount, whose angle can be adjusted mechanically and via a piezo. The whole setup is cooled by a Peltier element mounted on the bottom of the base plate.

the temperature and the laser current. Typical linewidths of free-running ECDLs are well below 5 MHz. Controlling the laser temperature, current, and piezo voltage by active feedback circuits (e.g. within a Pound-Drever-Hall servo electronics) emission bandwidths in the milliHertz range have been achieved, which corresponds to quality factors of the laser oscillator of up to 10^{18}.

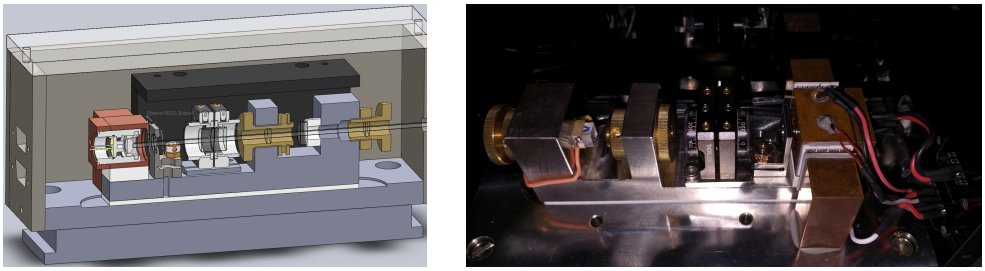

Figure 53.32: (Left) Construction plan of a home-built ECDL lasers in cat-eye configuration. (Right) Side view of the cat-eye laser.

In comparison to other laser types, a *diode laser* exhibits, the advantage of a very small size and a compact design. They are, in general, easy to handle and can be controlled conveniently via current and temperature. However, they also have the disadvantage of a large beam divergence and a broad emission spectrum. The beam divergence can be compensated by a collimation optics in front of the laser diode.

The temperature has an impact on the band structure of the *pn*-transition of the laser diode and hence on the frequency. Therefore, it is stabilized via a Peltier element, which is mounted underneath the laser diode holder. The degree of freedom is used for tuning the laser frequency in wide steps.

53.2.3.5 Pulsed diode lasers

Diode lasers can be used for generating ultrashort pulses either with various techniques of mode locking or with gain switching. Typically, pulses with durations between 0.5 and 5 ps and pulse repetition rates between 1 GHz and hundreds of giga-Hertz are generated with mode locking. In extreme cases, the repetition rate can even be above 1 THz. The main application of ultrafast diode lasers is in optical fiber communications systems, where such lasers function as pulse sources of fast data transmitters or for all-optical signal processing.

Common techniques for mode locking of diode lasers are active ore passive mode locking. Active mode locking can be accomplished with an optical modulator in the laser resonator. This is usually either an electro-absorption modulator in the form of an unpumped region with some modulated voltage, or an amplifying section where the drive current is modulated. Passive mode locking relies on a saturable absorber in the resonator. This can simply be an unpumped section of the device. It is common to apply an electrical bias for adjusting the absorber properties. However, the recovery time of that kind of absorber is fairly long. Shorter recovery times are achieved e.g. by implanting nitrogen (N^+ or N_2^+) ions from one facet. This introduces crystal defects, where carriers can recombine. The absorber is often placed at a resonator end, but it can also be placed somewhere within the resonator so that different pulses can meet in the absorber (colliding pulse mode locking).

For pulse repetition rates roughly below 10 GHz, an external cavity setup is usually required, as a monolithic device would become too long. The extended cavity may be an ECDL setup. Another technical approach is to incorporate the semiconductor chip into a ring laser resonator made of optical single-mode fiber. In the latter case, the resonator is typically much longer, and allows the use of fiber-optic components. The semiconductor device may then be a fiber-coupled semiconductor optical amplifier (SOA).

External-cavity lasers have various advantages: The pulse repetition rate can be chosen in a wide range, and can easily be tuned e.g. by moving the end mirror, or with a fiber resonator by stretching a piece of fiber with a piezo transducer. It is possible to insert an optical filter for fixing the emission wavelength, or use a diffraction grating as the end mirror (Littrow configuration; see the article on external-cavity diode lasers). Even for higher pulse repetition rates, where harmonic mode locking is required, external-cavity devices can be advantageous, because they have a potential for lower laser noise, e.g. in the form of timing jitter. Therefore, mode-locked external-cavity diode lasers sometimes compete with mode-locked fiber lasers in areas where monolithic laser diodes would not be suitable. On the other hand, a monolithic setup with fundamental mode locking can be very compact, much cheaper to manufacture, and can exhibit very robust pulse emission.

On the other hand, mode-locked diode lasers are subject to various limitations, which do not allow them to reach the full performance potential of, e.g., mode-locked fiber lasers: The pulse energy is fairly limited often far below 1 pJ. Average output powers are often below 1 mW. Due to the short upper-state lifetime, ultrafast semiconductor lasers are generally not suitable for lower repetition rates of e.g. well below 1 GHz, except with synchronous pumping. Although the gain bandwidth of semiconductors would be compatible with pulse durations of a few tens of femtoseconds, the pulse durations achieved are usually much longer at least hundreds of femtoseconds,

and often picoseconds. The pulse formation dynamics are relatively complicated, e.g. due to nonlinear phase changes associated with gain saturation, and difficult to optimize. The pulse quality is normally not as good as e.g. for mode-locked fiber lasers. In particular, there are often additional satellite pulses, caused e.g. by imperfections of the anti-reflection coating. Also, the pulses are often chirped, i.e. they are not bandwidth-limited. The timing jitter and the noise of other pulse parameters are higher than for other mode-locked lasers. This is partly a consequence of the low power level.

53.2.3.6 Tapered amplifiers and injection locking

Other ways to amplify a the power of a laser without altering its coherence properties are using a *tapered amplifier* or via *injection locking* also called *master-slave locking* [208, 807] (see Fig. 53.33).

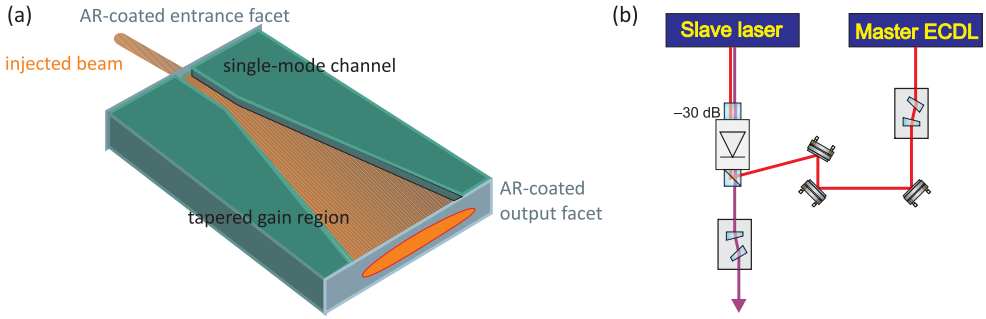

Figure 53.33: (a) Tapered amplifiers are available e.g. from Eagleyard. (b) Principle of injection locking.

The description presented here uses semi-classical laser rate equations [806]. Assuming that the master and the slave laser field are given by, respectively,

$$E_{inj} = A_{inj} e^{-\imath\omega_{inj} t} e^{\imath\phi_{inj}(t)} \quad \text{and} \quad E = A e^{-\imath\omega_s t} e^{\imath\phi_s(t)} \,, \tag{53.49}$$

The phase difference between the both fields is denoted by $\phi(t) = \phi_s(t) - \phi_m(t)$. Now, Considering the semi-classical laser rate equations we can describe the impact of the master laser field in the slave laser,

$$\begin{aligned} \frac{dA(t)}{dt} &= \frac{1}{2} g[N(t) - N_{th}]A(t) + \kappa A_{inj} \cos\phi(t) \\ \frac{d\phi(t)}{dt} &= \frac{\alpha}{2}[N(t) - N_{th}] - \kappa \frac{A_{inj}}{A(t)} \sin\phi(t) - \Delta\omega \\ \frac{dN(t)}{dt} &= J - \gamma_N N(t) - [\gamma_p + g[N(t) - N_{th}]A(t)^2 \,, \end{aligned} \tag{53.50}$$

where $A(t)$ is the field amplitude normalized as $A^2(t) = S(t)$, and $S(t)$ is the photon number. $N(t)$ is the number of carriers in the slave laser, and the other parameters are g laser gain coefficient, N_{th} threshold carrier number, κ coupling coefficient, α linewidth enhancement factor, γ_p photon decay rate, N carrier recombination rate,

J pump current normalized by electron charge, $\Delta\omega$ frequency difference between the master and the free running slave $\omega_m - \omega_s$. The parameter κ describes the rate at which the photons of the master laser enter into the slave laser cavity and is given in terms of the cavity quality factor,

$$\kappa = \frac{\omega_s}{2Q} \ . \tag{53.51}$$

From the steady state solutions of above equations, we can obtain the frequency locking range,

$$-\kappa\sqrt{(1+\alpha^2)}\sqrt{\frac{P_{inj}}{P_s}} < \Delta\omega < \kappa\sqrt{\frac{P_{inj}}{P_s}} \ , \tag{53.52}$$

where P_{inj}/P_s is the master laser fraction power used for the injection locking and P_s is the power of slave laser. From equation 4.25 we can see that the locking range is determined by the amplitude ratio between the fields and by the cavity quality factor since $\kappa \propto Q^{-1}$. Therefore, lasers with low Q are easier to lock. On the other hand, this leads to increased laser linewidth that reduces the phase noise performance of the injection locking systems. For higher injection ratio P_{inj}/P_s also results in a large locking range, which also makes the lock easier to achieve.

53.2.4 Exercises

53.2.4.1 Ex: Conventional light sources and lasers

Compare the properties of an incandescent light and a laser.

Solution:

53.2.4.2 Ex: Threshold inversion for lasing 1

Calculate the necessary threshold inversion of a gas laser transition at $\lambda = 500\,\text{nm}$ with the transition probability $A_{ik} = 5{\cdot}10^7\,\text{s}^{-1}$ and a homogeneous linewidth $\Delta\nu_{hom} = 20\,\text{MHz}$. The active length is $L = 20\,\text{cm}$ and the resonator losses per round-trip are $\gamma = 5\%$.

Solution: *The inversion n_{thr} is the density of excited atoms producing gain by stimulated emission. According to (53.46), this inversion is at threshold, when the gain along the optical path equalizes the losses,*

$$2Ln_{thr}\sigma = \gamma \ ,$$

where $2L$ is the round trip length. The absorption cross-section is related to the Einstein coefficient B_{ik} by Eq. (22.87),

$$B_{ik} = \frac{c}{h\nu}\int \sigma d\nu \simeq \frac{c}{h\nu}\bar{\sigma}\Delta\nu_{hom} \ ,$$

With $B_{ik} = \frac{c^3}{8\pi h\nu^3}A_{ik}$ we obtain,

$$\bar{\sigma} = \frac{h\nu}{c\Delta\nu_{hom}}B_{ik} = \frac{\lambda^2}{8\pi\Delta\nu_{hom}}A_{ik} \ ,$$

and finally,

$$n_{thr} = \frac{8\pi\Delta\nu_{hom}\gamma}{2\lambda^2 L A_{ik}} \approx 5 \cdot 10^6\,\mathrm{cm}^{-3} \ .$$

53.2.4.3 Ex: Threshold inversion for lasing 2

A laser medium has a Doppler-broadened gain profile of halfwidth $\delta\nu = 2\,\mathrm{GHz}$ and central wavelength $\lambda = 633\,\mathrm{nm}$. The homogeneous width is 50 MHz, and the transition probability $A_{ik} = 10^8\,\mathrm{s}^{-1}$. Assume that one of the resonator modes ($L = 40\,\mathrm{cm}$) coincides with the center frequency ν_0 of the gain profile. What is the threshold inversion for the central mode, and at which inversion does oscillation start on the two adjacent longitudinal modes if the resonator losses are 10%?

Solution: *The spacing of the longitudinal modes is,*

$$\delta_{fsr} = \frac{c}{2L} = 375\,\mathrm{MHz} \ .$$

The population density due to thermal broadening is,

$$n(v_z) = n(v_z = 0)e^{-(\nu-\nu_0)^2/\delta\nu^2} \ .$$

At $\nu = \nu_0 \pm \delta_{fsr}$ the population density for the adjacent modes has decreased to $n_1 = 0.83 n_0$. We already verified in Exc. 53.2.4.2 that the threshold inversion is,

$$\Delta n_{thr} = \frac{8\pi\nu_{hom} fsr\gamma}{2\lambda^2 L A_{ik}} \approx 3.9 \cdot 10^6\,\mathrm{cm}^{-3} \ .$$

Oscillation begins at the adjacent modes if threshold is reached for this mode. Then the inversion at the central mode is (without saturation) $n_0 = n_1/0.83$.

53.2.4.4 Ex: Mode pulling in an active resonator

The frequency of a passive resonator mode ($L = 15\,\mathrm{cm}$) lies $0.5\Delta\nu_D$ away from the center of the Gaussian gain profile of a gas laser at $\lambda = 632.8\,\mathrm{nm}$. Estimate the mode pulling if the cavity resonance width is 2 MHz and $\Delta\nu_D = 1\,\mathrm{GHz}$.

Solution: *The mode pulling is weighed with the quality factors of the resonances $\Delta\nu_{cav}/\Delta\nu_{gain}$ and the distance between the centers of the resonator mode and the gain curve:*

$$\nu_{pulled} = \nu_{cav} + \frac{\Delta\nu_{cav}}{\Delta\nu_{gain}}(\nu_{cav} - \nu_{gain}) = \nu_{cav} + \frac{\Delta\nu_{cav}}{\Delta\nu_{gain}} 0.5\Delta\nu_D \approx \nu_{cav} + 1\,\mathrm{MHz} \ .$$

53.2.4.5 Ex: Spatial hole-burning

Assume a laser transition with a homogeneous width of 100 MHz, while the inhomogeneous width of the gain profile is 1 GHz. The resonator length is $d = 200\,\text{cm}$ and the active medium with length $L \ll d$ is placed $a = 20\,\text{cm}$ from one end mirror. Estimate the spacing of the spatial hole-burning modes. How many modes can oscillate simultaneously if the unsaturated gain at the line center exceeds the losses by 10%?

Solution: *We have,*

$$\delta\nu_{spa} = \frac{2L}{ap}\delta_{fsr} \ ,$$

with $p = 2, 3, 4, ..$ *and* $\delta_{fsr} = c/2d = 150\,\text{MHz}$. *Hence, for* $p = 2$ *we expect* $\delta\nu_{spa} = 1.5\,\text{MHz}$. *For* $p = 3$ *we get* $\delta\nu_{spa} = 1.0\,\text{GHz}$. *For a Doppler width of* $\delta\nu_D = 1\,\text{GHz}$ *the gain at the first adjacent spatial hole burning mode is* $g = g_0 e^{-1/0.36} = 0.06 g_0$. *This mode does not reach the threshold. The adjacent resonator mode is* 150 MHz *away from the line center. Its unsaturated gain is* $g = g_0 e^{-0.15^2/(0.36\cdot 1)} = 0.94 g_0$. *Here, the net gain is* $0.94 \cdot 1.1 = 1.03$ *without mode competition. The two adjacent resonator modes reach the threshold. Therefore three longitudinal modes can oscillate.*

53.2.4.6 Ex: Optimizing the transmission of laser output mirrors

Estimate the optimum transmission of the laser output mirror if the unsaturated gain per round trip is 2 and the internal resonator losses are 10%.

Solution: *The total output intensity of a laser with unsaturated gain* g_0, *internal cavity losses* γ_0, *length* L *of the active medium, and mirror losses* $T + A = 1 - R = \gamma_M$ *is:*

$$I_{out} = \gamma_M \left[\frac{2g_0 L}{\gamma + \gamma_M} - 1\right] \frac{I_{sat}}{2} \ .$$

Differentiating gives,

$$\frac{dI_{out}}{d\gamma_M} = \left[\left(\frac{2g_0 L}{\gamma + \gamma_M} - 1\right) - \gamma_M \frac{2g_0 L}{(\gamma + \gamma_M)^2}\right] \frac{I_{sat}}{2} = 0 \ .$$

This yields,

$$\gamma_M^{opt} = \sqrt{2g_0 L \gamma_0} - \gamma_0 \ .$$

With $\gamma_0 = 0.1$ *and* $2g_0 L = 2$ *follows,*

$$\gamma_M^{opt} = 34.7\% = 1 - R \ .$$

The output mirror should have a reflectivity of $R = 65.3\%$.

53.2.4.7 Ex: Mode selection in a HeNe laser

A HeNe laser with an unsaturated gain of $G(\nu_0) = 1.3$ per round trip at the center of the Gaussian gain profile with halfwidth $\Delta\nu_D = 1.5\,\text{GHz}$ has a resonator length

of $d = 50\,\text{cm}$ and total losses of 4%. Single-mode operation at ν_0 is achieved with a coated tilted etalon inside the resonator. Design the optimum combination of etalon thickness and finesse.

Solution: *The axial modes are separated by* $\delta_{fsr} = c/2L = 300\,\text{MHz}$. *The gain factor G follows the Doppler profile,*

$$G(\nu) = G(\nu_0)e^{-(\nu-\nu_0)^2/(0.36\Delta\nu_D^2)} \ .$$

such that at $\nu_1 = \nu \pm \delta_{fsr}$ *the gain is* $G(\nu_1) = 0.896G(\nu_0) = 1.16$. *With 4% losses the net gain at* ν_1 *is reduced to 1.12. Hence, the losses of the etalon at* ν_1 *must be at least 12% in order to prevent laser oscillation. The transmission of the etalon with thickness t and refractive index* $n_{refr} = 1.4$ *is,*

$$T = \frac{1}{1 + F\sin^2\frac{\phi}{2}} \ ,$$

with $\phi = \frac{2\pi\nu\Delta s}{c} = \frac{2\pi\nu}{c}2n_{refr}t$. *For* $\nu = \nu_0$ *we get* $T = 1$ *and* $\phi/2 = m\pi = \frac{2\pi\nu_0}{c}n_{refr}t$. *For* $\nu = \nu_1$ *we get* $T \leq 0.88$ *and* $\sin\frac{\phi_1}{2} \geq \sqrt{0.12/F}$. *We have* $\phi_1 = \phi_0 + \Delta\phi$ *or* $\Delta\phi = \frac{1}{c}4\pi(\nu_1 - \nu_0) = 2\pi \cdot 10^{-4}n_{refr}t$. *The thickness t of the etalon should be small in order to minimize walk-off losses by the tilted etalon. If we assume as a reasonable number* $t = 0.5\,\text{cm}$, *we get,* $\Delta\phi = 2.5°$. *Hence,* $\sin\frac{\Delta\phi}{2} = \sin\frac{\phi_1}{2} = 0.044$ *and* $F \geq \frac{0.12}{0.044^2} = 63$. *With* $F^* = \frac{\pi}{2}\sqrt{F}$, *we obtain for the necessary finesse* F^* *the relation* $F \geq 12.5$. *Since* $F^* = \frac{\pi\sqrt{R}}{1-R}$, *web get* $R_E \geq 0.78$, *i.e. the etalon reflectivity should be larger than 78%.*

53.2.4.8 Ex: Mode hopping in a HeNe laser

A single-mode HeNe laser with resonator length $L = 15\,\text{cm}$ is tuned by moving a resonator mirror mounted on a piezo. Estimate the maximum tuning range before a mode hop will occur, assuming an unsaturated gain of 10% at the line center and resonator losses of 3%. What voltage has to be applied to the piezo (expansion 1 nm/V) for this tuning range?

Solution: *The free spectral range is* $\delta_{fsr} = c/2L = 10^9\,\text{GHz}$, *so that only one mode can oscillate if this mode is close to the center of the gain profile. The unsaturated gain at* ν_0 *is 10%. With losses of 3% the net gain is 7%, hence,* $G(\nu_0) = 1.07$. *When tuning away from the gain center, the net gain factor should always be* > 1. *Hence,*

$$G = 1.1 \cdot e^{-(\nu-\nu_0)^2/(0.36\Delta\nu_D^2)} - 0.03 \leq 1 \ .$$

With $\Delta\nu_D = 1.5\,\text{GHz}$ *we estimate* $\nu - \nu_0 \leq 213\,\text{MHz}$. *The maximum tuning range is from* $\nu_0 - 213\,\text{MHz}$ *up to* $\nu_0 + 213\,\text{MHz}$. *In order to tune over one free spectral range, the mirror separation must change by* $\Delta L = \lambda/2$ *Hence,*

$$\Delta L = \frac{\lambda}{2}\frac{2(\nu - \nu_0)}{\delta_{fsr}} = 135\,\text{nm}$$

at 633 nm. *The required voltage is,*

$$\Delta U = \frac{dU}{dx}\Delta x = 135\,\mathrm{V} \ .$$

53.2.4.9 Ex: Mode selection with an intracavity etalon

Mode selection in an argon laser is often accomplished with an intracavity etalon. What is the frequency drift of the transmission maximum
a. for a solid fused quartz etalon with thickness $d = 1$ cm due to a temperature change of 2° C?
b. For an air-space etalon with $d = 1$ cm due to an air pressure change of 4 mbar?
c. Estimate the average time between two mode hopes (cavity length $L = 100$ cm) for a temperature drift of 1° C/h or a pressure drift of 2 mbar/h.

Solution: *a. For the solid etalon* ($n_{refr} = 1.4$, $\alpha = 4 \cdot 10^{-7}\,\mathrm{K^{-1}}$*), we estimate,*

$$\frac{\Delta\nu}{\nu} = \frac{\Delta d}{d} + \frac{\Delta n_{refr}}{n_{refr}} \ .$$

The second term is small and can be neglected,

$$\Delta\nu = \nu\alpha\Delta T \approx 4.9 \cdot 10^7\,\mathrm{Hz} \ .$$

b. For an air-spaced etalon we can neglect the first term if the spacers are made of Zerodur or the distance is temperature-compensated. The optical path due to air at a pressure p is, for a length d equal to $s = nd$ *with* n_{refr}*(air at* $p = 1$ *bar)=1.00028. The change in s is,*

$$\Delta s = (n-1)d\frac{\Delta p}{p} \ .$$

Hence,

$$\left|\frac{\Delta\nu}{\nu}\right| = \frac{\Delta s}{s} = \frac{n_{refr}-1}{n_{refr}}\frac{\Delta p}{p} = 1.12 \cdot 10^{-6} \ .$$

For $\nu = 6 \cdot 10^{14}\,\mathrm{s^{-1}}$ *follows* $\Delta\nu = 6.72 \cdot 10^8\,\mathrm{s^{-1}} = 672$ MHz. *This illustrates that an air-spaced etalon is less stable than a solid etalon.*
c. With $L = 100$ cm *the mode spacing is* $\delta\nu = 150$ MHz. *For a temperature drift of* 1° /h *the solid etalon has a frequency drift of* 336 MHz/h.

53.2.4.10 Ex: Frequency and intensity noise of a laser

A single-mode laser is frequency stabilized onto the slope of the transmission maximum of an external reference Fabry-Perot interferometer made of invar with a free spectral range of 8 GHz. Estimate the frequency stability of the laser
a. against temperature drifts, if the FPI is temperature stabilized within 0.01°C,
b. against acoustic vibrations of the mirror distance L in the FPI with amplitudes of

100 nm.
c. Assume that the intensity fluctuations are compensated to 1% by a difference amplifier. Which frequency fluctuations are still caused by the residual intensity fluctuations, if a FPI with a free spectral range of 10 GHz and a finesse of 50 is used for frequency stabilization at the slope of the FPI transmission peak?

Solution: *The length of the etalon is,*

$$L = \frac{c}{2\delta_{fsr}} \approx 1.8\,\mathrm{cm} \ .$$

a. The change of L with temperature is for invar ($\alpha = 1.2 \cdot 10^{-6}\,\mathrm{K^{-1}}$),

$$\Delta L = d\alpha\Delta T \ ,$$

hence,

$$\left|\frac{\Delta\nu}{\nu}\right| = \frac{\Delta L}{L} = 1.2 \cdot 10^{-8} \ .$$

For $\nu = 5 \cdot 10^{14}\,\mathrm{s^{-1}}$ ($\lambda = 600\,\mathrm{nm}$) we get $\Delta\nu = 6\,\mathrm{MHz}$.
b. If L changes by 1 nm due to acoustic vibrations,

$$\frac{\Delta L}{L} = 5.8 \cdot 10^{-8} = \left|\frac{\Delta\nu}{\nu}\right| \ .$$

Hence, $\Delta\nu = 28\,\mathrm{MHz}$.
c. With a free spectral range $\delta\nu_{FPI} = 10\,\mathrm{GHz}$ of the FPI and a finesse $F^* = 50$, the full halfwidth of the transmission peak is $\Delta\nu_{FPI} = \delta\nu_{FPI}/F^* = 200\,\mathrm{MHz}$. The transmitted intensity is,

$$I_t = I_0 T = I_0 \frac{1}{1 + F\sin^2\frac{\phi}{2}} \ ,$$

with $F = (\frac{2}{\pi}F^*)^2 = 1000$. The stabilization system interprets an intensity change of 1% as a transmission change ΔT, i.e., a change $\Delta\phi$ of ϕ, and because $\phi = \frac{2\pi}{\lambda}\Delta s$ we get $\Delta\phi = \frac{2\pi}{c}\Delta s\Delta\nu$ also as a change of ν. A rough estimation of $\Delta\nu$ goes as follows. A frequency change of 100 MHz changes (at a fixed plate separation $L = 0.5\Delta s$) the transmission by 100% from 0 to 1. A transmission change of 1% therefore corresponds to a frequency change of $0.01 \cdot 100\,\mathrm{MHz} = 1\,\mathrm{MHz}$. A more elaborate calculation uses the relation,

$$\Delta T = \frac{dT}{d\phi}\Delta\nu \ ,$$

because $\Delta T = 0.01$. Now, we just need,

$$\frac{dT}{d\phi} = \frac{F\sin\frac{\phi}{2}\cos\frac{\phi}{2}}{(1 + F\sin^2\frac{\phi}{2})^2} \qquad \textit{and} \qquad \frac{d\phi}{d\nu} = \frac{2\pi\Delta s}{c} \ .$$

53.2.5 *Experiment: Analyzing the mode structure of a HeNe laser*

Here we will analyze the mode structure of a HeNe laser via (i) an optical spectrum analyzer and (ii) a radiofrequency spectrum analyzer. We will also try to unravel the polarization of the laser light.

1. Couple the light of a HeNe laser simultaneously into an optical spectrum analyzer and a radiofrequency spectrum analyzer. What do you observe when you slightly heat the laser housing? Calculate from your observations the length of the laser cavity.

2. Pass the light through a $\lambda/4$-plate and then through a polarizing beam splitter. What do you observe in the two output ports of the PBS?

53.2.6 *Experiment: Adjusting the threshold of an ECDL laser*

Here we will construct a diode laser in Littmann configuration.

1. Take a laser diode, a Peltier cooler, a thermistor, a piezo transducer, and a diffraction grating. Put everything together.

2. Optimize the threshold. Analyze the emission spectrum with an optical spectrum analyzer.

53.3 Introduction to optical phase and frequency modulation

53.3.1 Acousto-optic modulator

The *acousto-optic modulator AOM* permits fast frequency and amplitude variations of a laser beam. Because it does not incorporate mechanical parts, it works without fatigue. AOMs are used, for instance, in laser printers, where the gray tone of a pixel can be adjusted via the intensity of the laser beam, while its position (rows and columns) is varied by a rotating mirror and the drum propagating the paper sheet. In quantum optics labs they are frequently used for fast (down to μs) switching on and off, intensity control, and super-fine frequency-tuning of laser beams. The angular deflection of the first-order diffracted beam upon frequency tuning, which is often perceived as an inconvenience, can be circumvented by double-passage through the AOM.

The acousto-optic modulator consists of a piece of crystal (or glass) excited by an acoustic wave with frequency f produced by a piezo-electric transducer (see Sec. 53.3.1) mounted perpendicularly to propagation direction of the laser beam. The sound waves propagate through the crystal as density fluctuations periodically changing the refraction index n. The incident light is diffracted through Brillouin scattering at the spatial modulation of the refraction index. In a wave picture, the process can be interpreted as Bragg scattering of a light wave (with its wavelength inside the crystal

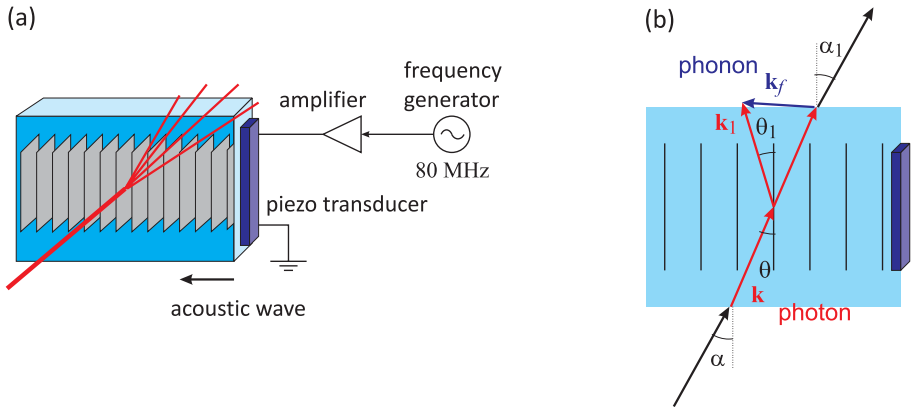

Figure 53.34: (a) Principle of the acousto-optic modulator. (b) Scheme of the diffraction in an acousto-optic modulator: A photon with wavevector k is scattered by a phonon with wavevector k_1 resulting in a photon with wavevector k_f.

$\lambda_n = 2\pi/k_n = c/n\nu$) from a density grating. c/n is the propagation velocity of light inside the crystal. Since phonons (with their wavelength $\lambda_f = 2\pi/k_f = c_f/f$, where c_f is the sound velocity in the crystal) are quantized and can only be emitted and absorbed entirely, the frequency of the first-order diffraction is $\nu_1 = \nu + f$. In case of an ideal adjustment of the Bragg angle, the *Bragg condition* results in $\theta_1 = \theta$ (see Fig. 53.34),

$$\sin\theta = \frac{k_f}{2k} = \frac{f\lambda_n}{2c_f} \ . \tag{53.53}$$

Since the laser beam is refracted when it enters the crystal, the relation between the incidence and exit angle is given by *Snell's law*, $\sin\alpha = n\sin\theta$. With this, the Bragg condition can be written,

$$\boxed{\sin\alpha = \frac{f\lambda}{2c_f}} \ . \tag{53.54}$$

The angle between the 0^{th} and the 1^{st} order is, hence, 2α.

In a corpuscular picture, the process can be understood as a *four-wave mixing* (*4WM*) between photons and phonons. The deflection of the laser beam is a consequence of momentum, $\mathbf{k}_1 = \mathbf{k} + \mathbf{k}_f$. The frequency shift corresponds exactly to the Doppler shift induced by the Brillouin scattering (absorption and reemission of a phonon in reverse direction), and we obtain a relationship that is equivalent to the Bragg condition,

$$f = \nu_1 - \nu = 2\nu\frac{c_f\sin\theta}{c/n} \ . \tag{53.55}$$

From the Bragg condition, knowing the deflection angle and the (fixed) frequency shift, we can calculate the sound velocity. A typical value is $c_f \simeq 4200$ m/s [6]

An AOM works best (highest diffraction efficiency in to the first Bragg order, which may reach more than 90%) at a specific radiofrequency, which typically is located

[6]The result (53.55) can be derived from conservations laws for energy $\omega_1 = \omega + \omega_f$ and momentum

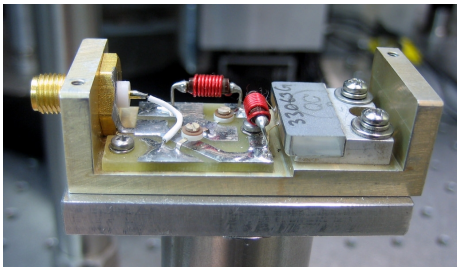

Figure 53.35: Image of an AOM without cover.

somewhere in the range $f = 40...800\,\mathrm{MHz}$, the most common one being 80 MHz. Deviations from this 'center frequency' are possible within a range of typical $\pm 10\%$ of the center frequency.

53.3.2 Electro-optic modulator

An *electro-optic modulator* is an optical device with which, by an applied voltage, the phase, frequency, amplitude or direction of a light beam can be modulated. Modulation bandwidths in the GHz regime are possible. In the simplest case, the EOM consists of a crystal (e.g., lithium niobate), whose refractive index depends on the amplitude of the local electric field. That is, when a lithium niobate crystal is exposed to an electric field the speed of light propagation is reduced. One can thus control the phase of a light beam at the output of a crystal by inserting it into a plate capacitor and applying a voltage. The phase shift of the light depends linearly on the applied voltage.

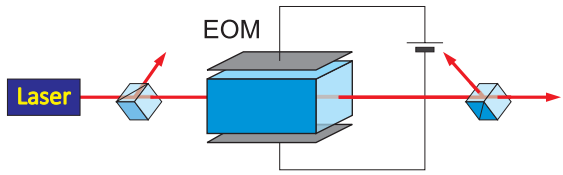

Figure 53.36: Electro optic modulator.

EOMs are often used to generate sidebands in a monochromatic laser beam. They are also used as *Pockels cell*, i.e., as a voltage-controlled phase-plate. The Pockels effect produces in a medium a *birefringence*, which depends linearly on the applied electric field. This is in contrast to the *Kerr effect*, in which the birefringence depends in a quadratic form of the electric field.

$\mathbf{k}_1 = \mathbf{k} + \mathbf{k}_f$. Defining $\omega \equiv 2\pi\nu$, $\omega_1 \equiv 2\pi\nu_1$ and $\omega_f \equiv 2\pi f$ we find,

$$\frac{\omega_f^2}{c_f} = \mathbf{k}_f^2 = (\mathbf{k}_1 - \mathbf{k})^2 = k_1^2 + k^2 - 2\mathbf{k}_1 \cdot \mathbf{k} = \frac{\omega_1^2}{c_n^2} + \frac{\omega^2}{c_n^2} - \frac{2\omega\omega_1}{c_n^2}\cos(2\theta) \simeq \frac{4\omega\omega_1}{c_n^2}\sin^2\theta \ .$$

With $\omega_1 \simeq \omega$ we reproduce the result [1407, 1408].

Suppose the optically inactive axis is x. In this case, the influence of EOM on the polarization of a laser beam is described by

$$\mathcal{M}_{EOM}(\theta) = \begin{pmatrix} 1 & 0 \\ 0 & e^{\imath\theta} \end{pmatrix} . \tag{53.56}$$

For operation as a Pockels cell, the EOM is inserted between two crossed polarizers oriented, e.g., along the x and y axis. The EOM itself is rotated by an angle ϕ,

$$\begin{aligned} \mathcal{M}_{Pockels}(\theta,\phi) &= \begin{pmatrix} 0 & 0 \\ 0 & 1 \end{pmatrix} \begin{pmatrix} \cos\phi & \sin\phi \\ -\sin\phi & \cos\phi \end{pmatrix} \begin{pmatrix} 1 & 0 \\ 0 & e^{\imath\theta} \end{pmatrix} \begin{pmatrix} \cos\phi & -\sin\phi \\ \sin\phi & \cos\phi \end{pmatrix} \begin{pmatrix} 1 & 0 \\ 0 & 0 \end{pmatrix} \\ &= 2\imath e^{\imath\theta/2} \sin\tfrac{\theta}{2} \sin\phi\cos\phi \begin{pmatrix} 0 & 0 \\ 1 & 0 \end{pmatrix} , \end{aligned} \tag{53.57}$$

For $\phi = \pi/4$ we get,

$$\mathcal{M}_{Pockels}(\theta, \tfrac{\pi}{4}) = \imath e^{\imath\theta/2} \sin\tfrac{\theta}{2} \begin{pmatrix} 0 & 0 \\ 1 & 0 \end{pmatrix} . \tag{53.58}$$

That is, an incident beam of light, $\mathbf{E} = E\hat{\mathbf{e}}_x$, linearly polarized in x-direction is rotated into the y-direction and, depending on the phase shift θ, it is completely blocked or transmitted through the Pockels cell [see Fig. 53.37(a)],

$$I_{tr} = I_0 \sin^2\tfrac{\theta}{2} . \tag{53.59}$$

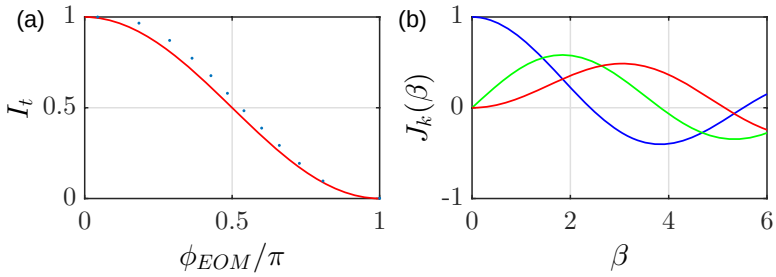

Figure 53.37: (code) (a) Effect of a Pockels cell. The solid line was calculated with the Eq. (53.57), the dotted was measured experimentally. (b) Lowest-order Bessel functions.

53.3.3 Optical phase modulation

The frequency and the phase of a laser beam can be influenced and modulated similarly to radiofrequency signals. We can therefore use the calculation of Sec. 52.3.1 completely, only changing the carrier frequency to be the frequency of the light: The

Fourier expansion of a complex-valued periodic function $s(x)$ into a series is defined as,

$$s_N(x) = \sum_{k=-N}^{N} c_k e^{\imath kx} \qquad \text{where} \qquad c_k = \frac{1}{2\pi}\int_{2\pi} s(x) e^{-\imath kx} dx \ . \tag{53.60}$$

Applying this to the modulated phase shift factor $s(\Omega t) = e^{\imath\theta(t)}$ with $\theta(t) \equiv \beta \sin \Omega t$, we get,

$$s_N(\Omega t) = \sum_{k=-\infty}^{\infty} c_k e^{\imath k\Omega t} \qquad \text{where} \qquad c_k = \frac{1}{2\pi}\int_{-\pi}^{\pi} e^{\imath\beta \sin \Omega t} e^{-\imath k\Omega t} d\Omega t \ , \tag{53.61}$$

but the Fourier coefficients are nothing else than the integral definition of the k-th order Bessel function,

$$J_k(\beta) \equiv \frac{1}{2\pi}\int_{-\pi}^{\pi} e^{\imath(\beta \sin \tau - k\tau)} d\tau \ , \tag{53.62}$$

where $J_{-k}(\beta) = -J_k(\beta)$. Hence, we may write the electric field,

$$\boxed{\begin{aligned} E(t) &= e^{\imath[kz-\omega t+\imath\theta(t)]} = e^{\imath(kz-\omega t)} \sum_{k=-\infty}^{\infty} J_k(\beta) e^{\imath k\Omega t} \\ &\simeq J_0(\beta) e^{\imath\omega t} + J_1(\beta) e^{\imath\omega t+\imath\Omega t} + J_{-1}(\beta) e^{\imath\omega t-\imath\Omega t} \end{aligned}} \ . \tag{53.63}$$

For small modulation indices β only the lowest-order Bessel function contribute noticeable amplitudes, as illustrated in Fig. 53.37(b).

The interpretation of this is, that *phase modulation* imprints sidebands onto a monochromatic laser beam. These sidebands are independent modes which can be resolved, e.g. with an optical spectrum analyzer, as illustrated in Fig. 53.38.

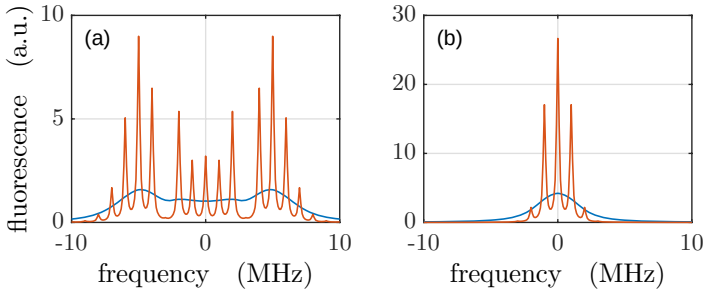

Figure 53.38: (code) Phase modulation sidebands with high (left) and low (right) modulation index resolved by a narrow (red) or broad (blue) filter.

Technically the phase can be modulated by means of an electro-optical modulator, as shown in Fig. 53.39(b). Alternatively, one may apply a periodic modulation of the current which controls a diode laser, as shown in Fig. 53.39(a), which can be done e.g. by inductive coupling using a *bias-T*.

From (53.63) we immediately see that phase modulation remains invisible for a photodetector measuring $|E(t)|^2$. Imagine, however, that the light passes through a

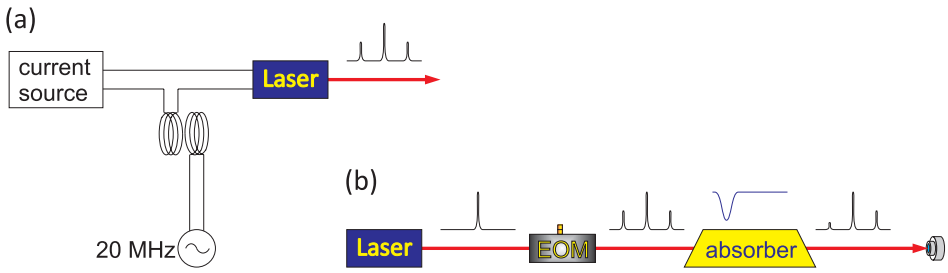

Figure 53.39: (a) Scheme for phase modulation of a diode laser by modulating the drive current. (b) Phase modulation with an external EOM followed by frequency-selective absorption of the lower sideband.

frequency-selective absorber, as illustrated in Fig. 53.39(b), such that the sidebands suffer unequal losses. Then the photodetector will record (apart from a constant offset) a signal oscillating at the frequency Ω,

$$\begin{aligned} |E(t)|^2 &= \left|J_0(\beta)e^{\imath\omega t} + aJ_1(\beta)e^{\imath\omega t+\imath\Omega t} + bJ_{-1}(\beta)e^{\imath\omega t-\imath\Omega t}\right|^2 \\ &= J_0(\beta)^2 + (a+b)J_1(\beta)^2 + (a-b)J_0(\beta)J_1(\beta)2\cos\Omega t + \dots \ . \end{aligned} \tag{53.64}$$

This idea is at the heart of powerful spectroscopic techniques, such as *frequency modulation spectroscopy*, *modulation transfer spectroscopy*, and the *Pound-Drever-Hall* frequency stabilization technique.

53.3.4 Exercises

53.3.4.1 Ex: Response time of an AOM

A beam of light at 689 nm focused to a waist of 100 µm passes through the crystal of an 80 MHz AOM, characterized by a sound velocity of $c_s = 4200\,\mathrm{m/s}$.
a. By how much the first diffraction order is deflected by the AOM? Regarding the beam divergence of the Gaussian beam, will it be possible to spatially separate the diffraction orders?
b. An experimentalist ramps the driving frequency between 70 and 90 MHz by means of a voltage-controlled oscillator. What is the range of diffraction angles covered?
c. Estimating the response time of the AOM by the time that the traveling sound wave needs to cover a distance corresponding to the focus of the light beam, how fast can the experimentalist switch off the light beam by suddenly interrupting the driving signal? What is the modulation bandwidth of the AOM?
d. The light beam passes through the AOM at a distance of $d = 2\,\mathrm{mm}$ from the piezo transducer generating the sound wave. How will this fact limit response time?

Solution: *a. The deflection angle is given by,*

$$\sin\alpha = \frac{f\lambda}{2c_f} \approx 0.376^\circ \ .$$

The divergence angle of the Gaussian beam is,

$$\frac{w_0}{z_R} = \frac{\lambda}{\pi w_0} \approx 0.126^\circ \ .$$

Hence, the beams can still be separated.
b. The deflection angle varies between 0.329° *and* 0.423°.
c. The response time would be,

$$\tau = \frac{w_0}{c_f} \approx 23.8\,\text{ns} \ ,$$

and the bandwidth correspondingly $\tau^{-1} \approx 42\,\text{MHz}$.
d. The response time would be then limited to,

$$\tau = \frac{d}{c_f} \approx 476\,\text{ns} \ .$$

53.3.4.2 Ex: Intensity stabilization with a Pockels cell

Assume that the output power of a laser shows random fluctuations of about 5%. Intensity stabilization is accomplished by a Pockels cell with a halfwave voltage of 600 V. Estimate the ac output voltage of the amplifier driving the Pockels cell that is necessary to stabilize the transmitted intensity if the Pockels cell is operated around the maximum slope of the transmission curve.

Solution: *The Jones matrix for the Pockels cell is,*

$$\begin{pmatrix} E_x \\ E_y \end{pmatrix} = (1 - e^{\imath\theta}) \begin{pmatrix} 1 & -1 \\ 1 & -1 \end{pmatrix} \begin{pmatrix} E_{x0} \\ E_{y0} \end{pmatrix} = (1 - e^{\imath\theta})(E_{x0} - E_{y0}) \begin{pmatrix} 1 \\ 1 \end{pmatrix} \ .$$

Hence, the transmitted intensity is,

$$\begin{aligned} I = |E_x \hat{\mathbf{e}}_x + E_y \hat{\mathbf{e}}_y|^2 &= 2(E_{x0} - E_{y0})^2 (1 - e^{\imath\theta})(1 - e^{-\imath\theta}) \\ &= 4(E_{x0} - E_{y0})^2 (1 - \cos\theta) = 8(E_{x0} - E_{y0})^2 \sin^2 \frac{\theta}{2} \ . \end{aligned}$$

The transmission of the Pockels cell is,

$$T = T_0 \cos^2 aU \ ,$$

where V *is the applied voltage and* a *is a constant which depends on the electro-optic coefficient and the dimensions of the modulator. If for* $U_0 = 0$ *we have total transmission,* $T(U_0) = T_0$*, and for* $U_m = 600\,\text{V}$ *zero transmission,* $T(U_m) = 0$*, then* $aV = \pi/2$*. The system should operate at the maximum slope of* dT/dV*. Then,*

$$\Delta T = \frac{\partial T}{\partial U} \Delta U = -2aT_0 \cos aU \sin aU \Delta U \ .$$

For a fluctuation in intensity of 5% the transmission must change by $\Delta T = -0.05T_0$ in order to compensate for the fluctuations. Hence,

$$\Delta U = \frac{0.05}{2a\cos aU \sin aU} \ .$$

The maximum slope is realized for $aV = 45°$. Hence, $U = 19\,\mathrm{V}$.

53.3.4.3 Ex: Generating sidebands with an EOM

An EOM (e.g. Thorlabs, EO-PM-NR-C1) characterized by a half-wave voltage of $U_{hwv} = 230\,\mathrm{V}$ at 689 nm is to be used to generate optical sidebands at 20 MHz.
a. Estimate numerically, how much voltage amplitude at what frequency a frequency generator must provide in order to generate optical sidebands having half the light power as the carrier?
b. How high must the finesse of a 5 cm confocal Fabry-Pérot spectrum analyzer be in order to resolve the sidebands.

Solution: *a. The height of the sidebands is given by the Bessel functions. The ratio between the first-order sidebands and the carrier is given by,*

$$\left|\frac{J_1(\beta)}{J_0(\beta)}\right|^2 \stackrel{!}{=} \frac{1}{2} \ ,$$

with the modulation index $\beta = U/U_{hwv}$ where U is the voltage provided by the frequency generator. Numerically one finds that $\beta \approx 1.16$ solves the above condition. This corresponds to,

$$U = \beta U_{hwv} \approx 267\,\mathrm{V} \ .$$

b. The free spectral range of the etalon being $\delta_{fsr} = c/2L$, the resolution must be,

$$20\,\mathrm{MHz} > \frac{\kappa}{2\pi} = \frac{\delta_{fsr}}{F} \ .$$

Hence, $F > 150$.

53.3.4.4 Ex: Reflection of a phase-modulated signal from an optical cavity

A phase-modulated light beam (modulation frequency $f = 20\,\mathrm{MHz}$) is reflected from an optical cavity and recorded by a fast photodetector, whose bandwidth is larger than f. Using the Airy formulae for the electric field of a light beam reflected from a cavity (53.24) calculate the reflection spectrum, that is, the intensity of reflected light as a function of detuning $\Delta = \omega - \omega_c$, where ω is the frequency of the light and ω_c a resonant frequency of the cavity. What frequency components does the photodetector signal contain.

Solution: *See Sec. 55.3.3.*

53.3.5 *Experiment: Characterizing an AOM*

Fig. 53.40 illustrates the setup, use, and test of an AOM. It is recommended familiarizing with the operation principle of a *voltage-controlled oscillator* (*VCO*) (see Sec. 52.3.1) and a voltage-controlled *variable attenuator*. We will also learn how to use a spectrum analyzer [7].

1. Optimize a diffraction efficiency of the AOM. What are the impacts of the Bragg angle, the radiofrequency power, and the laser beam diameter.

2. Measure the deflection angle as a function of the applied radiofrequency. Based on this result, calculate the sound velocity in the crystal.

3. Measure the diffraction efficiency as a function of the applied radiofrequency power at a fixed Bragg angle. Repeat the measurement optimizing the Bragg angle for every value of the radiofrequency.

4. Reduce the radiofrequency power using the variable voltage-controlled attenuator. Determine the diffraction efficiency as a function of radiofrequency power.

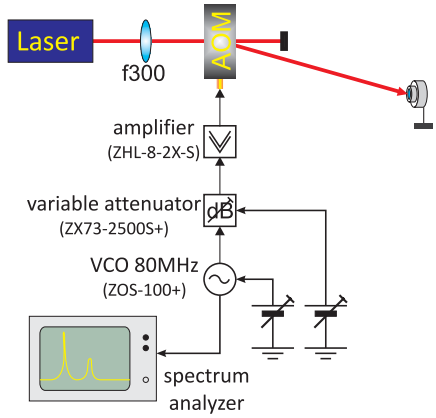

Figure 53.40: Setup for testing an acousto-optic modulator.

See Fig. 53.41.

53.3.6 *Experiment: EOM in a Mach-Zehnder interferometer*

Here we will learn to operate an EOM as Pockels cell and as phase modulator.

1. Align a laser beam through an electro-optic modulator. Supply a voltage between 0 V and 500 V to the EOM. Test its operation by beating the ordinary with the extraordinary beam. Modulate the supply voltage at a low frequency.

[7] Data sheet for the VCO see appendix Fig. 56.16,
data sheet for the AOM see appendix Fig. 56.20

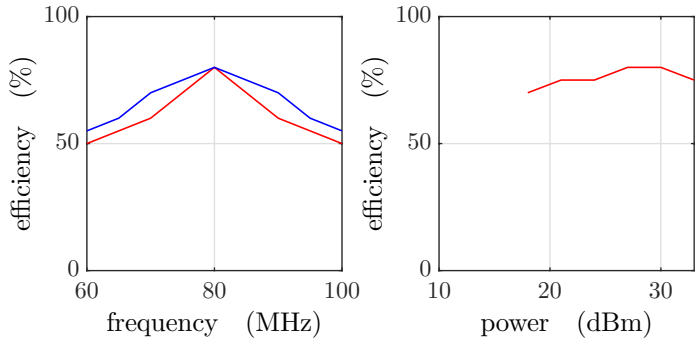

Figure 53.41: Example of measured efficiency curves.

2. Set up a Mach-Zehnder interferometer by phase-matching the exit beam of the EOM with a part of the input beam.

3. The interferometer provides a mean to convert a phase modulation into an amplitude modulation. Describe this feature theoretically using the Eqs. (52.12) and (52.13).

4. Use the EOM as a Pockels cell. Rotate the EOM by 45° around the optical axis. Probe the polarization of the outgoing beam with a polarization filter.

5. Modulate the EOM and show that the light acquires sidebands.

53.3.7 *Experiment: Creating sidebands with an EOM*

EOMs can be used to generate optical sidebands [8].

1. Apply the required voltages to a VCO (MiniCircuits, ZOS100), until it generates a variable frequency between 40 and 60 MHz. Attenuate the power with a variable attenuator up to −20 dBm. Check the amplitude and frequency with a spectrum analyzer.

2. Add a bias-T to the power supply of a laser diode. Observe the transmission spectrum of a Fabry-Pérot cavity for various frequencies and modulation amplitudes. Determine the modulation index. Use the known distance of the sidebands to estimate the finesse of the Fabry-Pérot cavity.

53.4 Radiofrequency techniques and the transfer of information

It often happens that information is coded within a frequency band corresponding to wavelengths which are not easily transported to other locations. For example, audio

[8] Datasheet for the VCO see appendix Fig. 56.16,
data sheet for the power divider see appendix Fig. 56.18,
data sheet for the mixer see appendix Fig. 56.19

frequencies (speech or music), ones they are converted to electromagnetic vibrations, correspond to wavelengths of hundreds of kilometers. Such waves are very difficult to radiate and are subject to diffraction.

For this reason, audio frequencies are often used to *modulate* so-called carriers, which in turn are chosen in frequency ranges which are easy to radiate by antennas. This is the basic idea of the radio, where the carrier frequencies are typically chosen in the MHz regime. But information can as well be encoded into laser beams, as illustrated in Fig. 53.42.

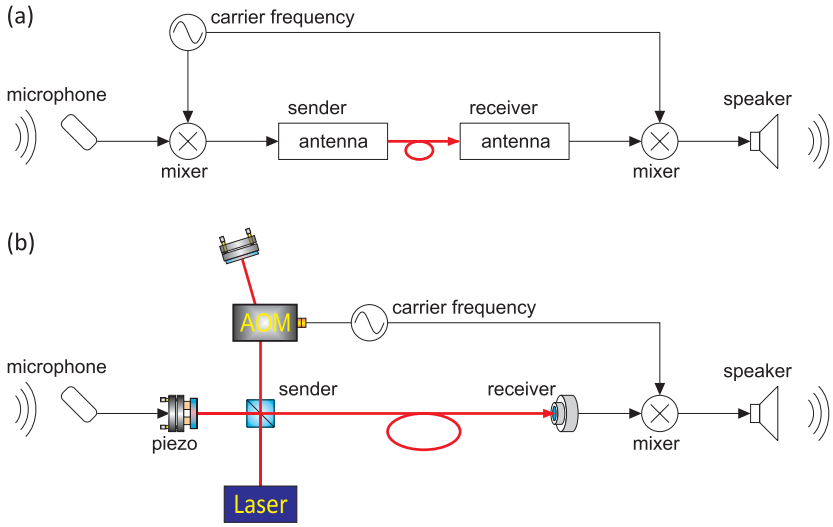

Figure 53.42: Analogy between radio transmission (a) and heterodyne techniques with a laser (b).

53.4.1 Measurement of a frequency beat

Interferometry is always based on the splitting and recombination of a wave, e.g., a laser beam or a matter wave. The recombination of laser beams is always a little technical challenge, as it requires a perfect phase matching of the Gaussian laser modes. Let us consider two plane waves $\mathcal{E}_1 = Ae^{\imath\omega_1 t}$ and $\mathcal{E}_2 = Ae^{\imath\omega_2 t}$ impinging on a photodiode. We suppose that they are phase-matched, such that their wavevectors are parallel. The photodiode then generates a *beat signal*,

$$\boxed{I = |\mathcal{E}_1 + \mathcal{E}_2|^2 = AB[2 + 2\cos(\omega_1 - \omega_2)t]} \,. \tag{53.65}$$

In practice, laser beams are usually not plane waves, but have a finite diameter and radius of curvature. In order to get a high contrast signal, a good phase-matching of the beams is important in order to obtain a strong photodiode signal.

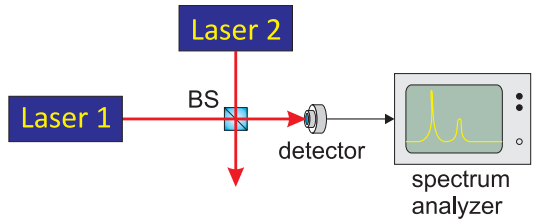

Figure 53.43: Principle of a beat frequency measurement.

53.4.2 Homodyne method

For the *homodyne method* the field amplitude of a laser beam, E_i, with frequency, $\omega = ck$, is divided by a beam splitter (reflectivity $R = |\eta|^2 \simeq 50\%$) into a reference beam (reflection at an optically dilute medium) and a probe beam, exactly as we have done for the Michelson interferometer in Sec. 53.1.3, when we obtained the formula (53.13) [9],

$$I \propto 1 + \cos[k(L_t - L_r)] \; . \tag{53.66}$$

However, we will now modulate the path length of one interferometer arm, e.g. using an EOM, $L_r = L_r(t)$. The modulation can, but does not need to be sinusoidal. In fact it may be an arbitrary radiofrequency signal, e.g. generated by acoustic sound. Restricting to small modulation amplitudes, $kL_r \ll \pi$, and choosing the length of the interferometer arms such that,

$$\boxed{I(t) \propto \sin kL_r \simeq kL_r(t)} \; , \tag{53.67}$$

we see, that the photodetector signal will reproduce the modulation signal. In other words, we encoded information on a laser beam, which carries it (e.g. through an optical fiber) to another place.

53.4.3 Heterodyne method

The *heterodyne method* is similar to the homodyne one, except that the probe beam is frequency-shifted (e.g., by the passage through an AOM operated at frequency Ω),

$$\mathcal{E}'_t = \mathcal{E}_t e^{\imath kL_t + \imath\Omega t} \; . \tag{53.68}$$

The photodetector signal generated by the beams after their recombination at the beam splitter is,

$$\begin{aligned} I &\propto \left|(1-\eta)\mathcal{E}_r e^{\imath kL_r} + \eta\mathcal{E}_t e^{\imath kL_t + \imath\Omega t}\right|^2 \\ &= \left|-(1-\eta)\eta\mathcal{E}_i e^{\imath kL_r} + \eta(1-\eta)\mathcal{E}_i e^{\imath kL_t + \imath\Omega t}\right|^2 \\ &= \left|(1-\eta)\eta\mathcal{E}_i\right|^2 \left|-e^{2\imath kL_r} + e^{\imath kL_t + \imath\Omega t}\right|^2 \; . \end{aligned} \tag{53.69}$$

[9] Here, we call $L_{t,r}$ the total length of the interferometer arm (back and forth for Michelson, one-way for Mach-Zehnder).

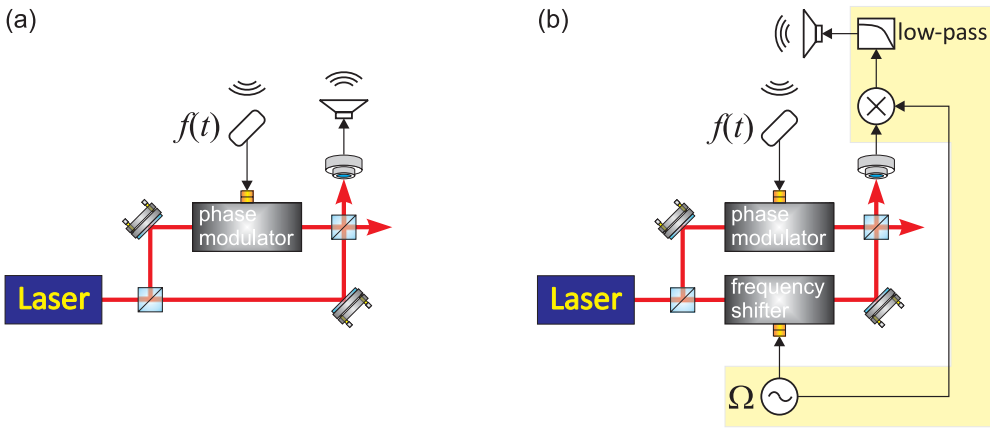

Figure 53.44: Principle scheme of the (a) homodyning and (b) heterodyning technique at the example of a Mach-Zehnder interferometer. The components in the yellow area of (b) constitute a Lock-In amplifier.

This signal is now demodulated with the AOM frequency,

$$Ie^{\imath\Omega t} \propto \left|-e^{\imath kL_r} + e^{\imath kL_t + \imath\Omega t}\right|^2 e^{i\Omega t} = e^{2\imath\Omega t} - e^{\imath k(L_t-L_r)+2\imath\Omega t} - e^{-\imath k(L_t-L_r)} \ . \quad (53.70)$$

A low-pass filter cuts all ac-components of the signal,

$$\boxed{I_{filtered}(t) \propto -e^{-\imath k(L_t-L_r)} \simeq -1 + \imath k[L_t - L_r(t)]} \ , \quad (53.71)$$

for small signal amplitudes $L_r(t)$.

53.4.4 Measuring the quadrature components of an electric field

Photodetectors measure intensities $I \propto |\vec{\mathcal{E}}|^2$. Sometimes, however, we are interested in the electric field itself, for example, when we want to get the correlation function $g^{(1)}(\tau)$ and the spectrum $S_{\mathcal{E}}(\omega)$ of a signal. A frequently used procedure consists in beating the signal of interest with a frequency-shifted local oscillator and demodulating the *quadrature components* of the beat signal.

Let us consider a signal of interest $\mathcal{E}_{sig}(t) = |\mathcal{E}_{sig}|e^{\imath\phi(t)}$ with information encoded in the temporal behavior of the phase $\phi(t)$. The first step consists in beating this signal on a photodetector with a frequency-shifted local oscillator $\mathcal{E}_{lo}(t) = |\mathcal{E}_{lo}|e^{\imath\omega_{lo}t}$, yielding a photocurrent,

$$S \propto |\mathcal{E}_{sig} + \mathcal{E}_{lo}|^2 = |\mathcal{E}_{sig}|^2 + |\mathcal{E}_{lo}|^2 + 2|\mathcal{E}_{lo}||\mathcal{E}_{sig}|\cos[\omega_{lo}t - \phi(t)] \ . \quad (53.72)$$

Now, demodulating this signal simultaneously with the local oscillator frequencies $\cos\omega_{lo}t$ and $\sin\omega_{lo}t$, we get,

$$\begin{aligned} U_c &= S\cos\omega_{lo}t = |\mathcal{E}_{lo}||\mathcal{E}_{sig}|\cos\phi(t) + \text{oscillating terms} \quad (53.73)\\ U_s &= S\sin\omega_{lo}t = |\mathcal{E}_{lo}||\mathcal{E}_{sig}|\sin\phi(t) + \text{oscillating terms} \ , \end{aligned}$$

where the oscillating terms can be removed by a low-pass filtering. Finally, we calculate,

$$|\mathcal{E}_{sig}| = \frac{\sqrt{U_c^2+U_s^2}}{|E_{lo}|} \qquad \text{and} \qquad \tan\phi(t) = \frac{U_s}{U_c} \ , \tag{53.74}$$

and obtain the electric field via,

$$\boxed{\mathcal{E}_{sig} = |\mathcal{E}_{sig}|e^{\imath\phi(t)} = \frac{\sqrt{U_c^2+U_s^2}}{|\mathcal{E}_{lo}|}e^{\imath \arctan\frac{U_s}{U_c}}} \ . \tag{53.75}$$

53.4.5 Exercises

53.4.5.1 Ex: Pound-Drever-Hall signal

Consider the photodetector signal of Exc. 53.3.4.4. What signal do you observe when demodulating the signal with an oscillation of frequency f? Calculate the derivative of the signal close to resonance; from which parameters does the slope depend, and how must you choose the modulation index to maximize it?

Solution: *As shown in Sec. 55.3.3, the reflection profile of a cavity is (ω in radians and δ_{fsr} in Hertz),*

$$\mathcal{E}_r(\omega) = \mathcal{E}_{in}(\omega)\sqrt{R}\frac{1-e^{\imath 2kL}}{1-Re^{\imath 2kL}} = \mathcal{E}_{in}(\omega)\sqrt{R}\frac{1-e^{\imath\Delta/\delta_{fsr}}}{1-Re^{\imath\Delta/\delta_{fsr}}} \ ,$$

where $\omega = N2\pi\delta_{fsr}$ and $kL = \frac{kc}{2\delta_{fsr}} = \frac{\omega}{2\delta_{fsr}} = \pi N + \frac{\Delta}{2\delta_{fsr}}$. The sideband spectrum,

$$e^{\imath(\omega t+\beta\sin\Omega t)} \simeq e^{\imath\omega t}\left[J_0(\beta)+J_1(\beta)e^{\imath\Omega t}+J_{-1}(\beta)e^{-\imath\Omega t}\right]$$

reflected from the cavity generates in the photodetector, among others, frequency components oscillating with $e^{-\imath\Omega t}$,

$$|\mathcal{E}_r|^2 = e^{-\imath\Omega t}J_0(\beta)J_1(\beta)\mathcal{E}_r(\omega)\mathcal{E}_r^*(\omega+\Omega) + e^{-\imath\Omega t}J_0(\beta)J_{-1}(\beta)\mathcal{E}_r^*(\omega)\mathcal{E}_r(\omega-\Omega) + ...$$

Demodulation with $e^{\imath\Omega t+\imath\theta}$ yields,

$$\begin{aligned} S \equiv c|\mathcal{E}_r|^2 e^{\imath\Omega t+\imath\theta} &\simeq Re\ e^{\imath\theta}J_0(\beta)J_1(\beta)\left[\mathcal{E}_r(\omega)\mathcal{E}_r^*(\omega+\Omega)-\mathcal{E}_r^*(\omega)\mathcal{E}_r(\omega-\Omega)\right] \\ &= \mathfrak{Re}\ e^{\imath\theta}J_0(\beta)J_1(\beta)\mathcal{E}_{in}(\omega)R\times \\ &\times\left(\frac{1-e^{\imath\Delta/\delta_{fsr}}}{1-Re^{\imath\Delta/\delta_{fsr}}}\frac{1-e^{-\imath(\Delta+\Omega)/\delta_{fsr}}}{1-Re^{-\imath(\Delta+\Omega)/\delta_{fsr}}} - \frac{1-e^{-\imath\Delta/\delta_{fsr}}}{1-Re^{-\imath\Delta/\delta_{fsr}}}\frac{1-e^{\imath(\Delta-\Omega)/\delta_{fsr}}}{1-Re^{\imath(\Delta-\Omega)/\delta_{fsr}}}\right) \end{aligned}$$

close to resonance we expand the exponential,

$$\frac{1-e^{\imath\Delta/\delta_{fsr}}}{1-Re^{\imath\Delta/\delta_{fsr}}} \simeq \frac{-\imath\Delta/\delta_{fsr}}{1-R-\imath R\Delta/\delta_{fsr}} = \frac{1}{R+\imath T\delta_{fsr}/\Delta} \ .$$

Hence, approximating $R \simeq 1$, we get,

$$
\begin{aligned}
S &= \mathfrak{Re}\ e^{\imath\theta} J_0(\beta) J_1(\beta) \mathcal{E}_{in}(\omega) R \times \\
&\times \left(\frac{1}{R + \imath T\delta_{fsr}/\Delta} \frac{1}{R - \imath T\delta_{fsr}/(\Delta+\Omega)} - \frac{1}{R - \imath T\delta_{fsr}/\Delta} \frac{1}{R + \imath T\delta_{fsr}/(\Delta-\Omega)} \right) \\
&\simeq \mathfrak{Re}\ e^{\imath\theta} J_0(\beta) J_1(\beta) \mathcal{E}_{in}(\omega) \left(\frac{1}{\imath T\delta_{fsr}/\Delta} \frac{1}{1 - \imath T\delta_{fsr}/\Omega} - \frac{1}{-\imath T\delta_{fsr}/\Delta} \frac{1}{1 + \imath T\delta_{fsr}/(-\Omega)} \right) \\
&= Re\ e^{\imath\theta} J_0(\beta) J_1(\beta) \mathcal{E}_{in}(\omega) \frac{\Delta}{\imath T\delta_{fsr}} \frac{2}{1 - \imath T\delta_{fsr}/\Omega} \ .
\end{aligned}
$$

Choosing $\theta = \pi/2$ and using $T\delta_{fsr} = \kappa/2$, we finally get,

$$
S \simeq J_0(\beta) J_1(\beta) \mathcal{E}_{in}(\omega) \frac{\Delta}{\kappa/2} \frac{2}{1 + \kappa^2/4\Omega^2} \simeq J_0(\beta) J_1(\beta) \mathcal{E}_{in}(\omega) \frac{4\Delta}{\kappa} \ .
$$

Therefore, the slope of the PDH error signal is simply the inverse cavity linewidth.

53.4.6 *Experiment: Beating two lasers*

In this exercise, we will ...

1. Take two independent lasers operating at nearly the same frequency (within $\sim 1\,\mathrm{GHz}$) and overlap them at a (non-polarizing) beam splitter.
2. Focus one of the ports of the beam splitter on a photodetector with large band width ($\sim 1\,\mathrm{GHz}$).
3. Analyze the beat signal on a spectrum analyzer.
4. Focus a helium-neon laser onto a fast photodetector and determine the free spectral range of the laser resonator.

53.4.7 *Experiment: Homo- and heterodyning with a Michelson interferometer*

In this exercise, we will ...

1. Set up a Michelson interferometer.

53.5 Further reading

C.J. Buczek et al., *Laser injection locking* [208]DOI

Zhixin Liu et al., *Optical Injection Locking: From Principle to Applications* [807]DOI

H. Kogelnik et al., *Laser Beams and Resonators* [734]DOI

A. Yariv, *Quantum Electronics* [1407]DOI

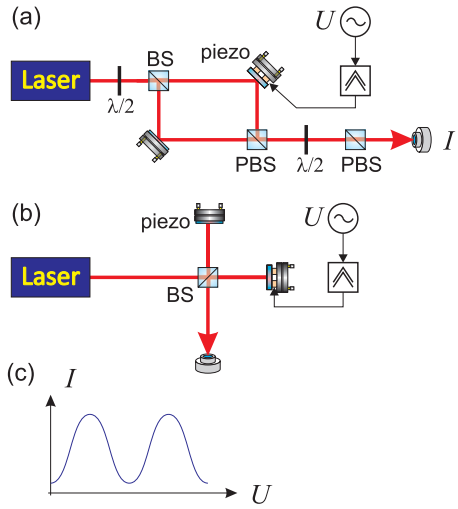

Figure 53.45: Homo- and heterodyning with a Michelson interferometer.

A. Yariv et al., *Optical waves in crystals* [1408]DOI

W. Demtröder, *Atoms, Molecules and Photons: An Introduction to Atomic- Molecular- and Quantum Physics* [352]DOI

W. Lichten, *Precise Wavelength Measurements and Optical Phase Shifts: I. General Theory* [800]DOI

W.W. Chow, *The ring laser gyro* [260]DOI

Chapter 54

Optical spectroscopy

Modern 'optics' is to be understood as 'physics of light-matter interaction' in the optical energy regime. In this sense, this area of physics comprises quantum optics, photonics, atomic physics, and atom optics. Since the invention of the laser the field of optics has seen a huge technological progress leading to the development of extremely powerful and precise tool for investigating and manipulating matter. The femtosecond laser, the frequency comb, atomic interferometers and clocks, and Bose-Einstein condensation are just a few examples.

Spectroscopy is the art of taking and interpreting spectra, i.e. frequency-dependent response functions. The variety of spectroscopic techniques is so overwhelming that a survey is hopeless. As the course also aims at familiarizing the student with applications, a major part of this course will concentrate on techniques employed and available in quantum optics labs. These techniques are mostly oriented toward ultra-high resolution spectroscopy and techniques of manipulating the motion of atoms.

In Sec. 54.1 to 54.4.3, we will try various spectroscopic techniques applied to atomic or cavity resonances.

54.1 Spectrometer and monochromator

Typical dispersive devices are *prisms* and *gratings*.

- lateral displacement as a function of λ
- spectral resolving power $R = |\lambda/\Delta\lambda| = |\nu/\Delta\nu|$
- Rayleigh criterion

54.1.1 Prism spectrometer

For a symmetrical arrangement ($\alpha_1 = \alpha_2 = \alpha$) it is easy to see from Fig. 54.1 that, $\beta = \frac{1}{2}\epsilon$ and $\theta = 2(\alpha - \beta)$. Snell's law the yields,

$$n = \frac{\sin\alpha}{\sin\beta} = \frac{\sin\frac{1}{2}(\theta+\epsilon)}{\sin\frac{1}{2}\epsilon} \ . \tag{54.1}$$

Hence,

$$\frac{dn}{d\theta} = \frac{1}{2}\frac{\cos\frac{1}{2}(\theta+\epsilon)}{\sin\frac{1}{2}\epsilon} \ , \tag{54.2}$$

or

$$\frac{d\theta}{dn} = \frac{\sin\frac{1}{2}\epsilon}{1 - n^2 \sin\frac{1}{2}\epsilon} \ . \tag{54.3}$$

The angular dispersion is therefore,

$$\frac{d\theta}{d\lambda} = \frac{\sin\frac{1}{2}\epsilon}{1 - n^2 \sin\frac{1}{2}\epsilon} \frac{dn}{d\lambda} \ . \tag{54.4}$$

The spectral dispersion of typical transparent materials is on the order of $-dn/d\lambda \approx 10^{-4}$.

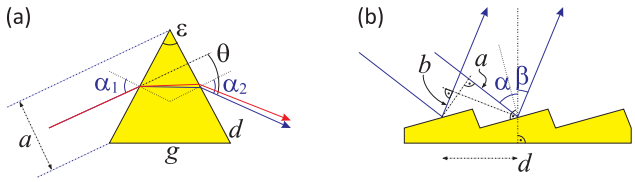

Figure 54.1: Illustration of (a) the prism spectrometer and (b) the grating spectrometer.

Example 300 (*Prism spectrometer*): We calculate the angular dispersion for an equilateral prism ($\sin\frac{1}{2}\epsilon = 0.5$) made of BK7 for two superposed wavelength $\lambda_1 = 461\,\text{nm}$ ($n_{\lambda_1} = 1.5243$) and $\lambda_2 = 633\,\text{nm}$ (with $n_{\lambda_2} = 1.5151$) to be,

$$d\theta = \frac{1}{\sqrt{1 - (n/2)^2}} dn \approx 0.8^\circ \ .$$

The resolving power can be calculated, once we have expressed the limiting aperture $a = d\cos\alpha$ where $d = g/(2\sin\frac{\epsilon}{2})$,

$$\left|\frac{\lambda}{\Delta\lambda}\right| = a\frac{d\theta}{d\lambda} = \frac{g\cos\alpha}{1 - n^2\sin\frac{1}{2}\epsilon}\frac{dn}{d\lambda} = g\frac{dn}{d\lambda} \ . \tag{54.5}$$

Solve Exc. 51.2.3.14.

54.1.2 Grating spectrometer

Destructive interference occurs for,

$$\Delta s = m\lambda = a - b = d\sin\alpha - d\sin\beta \ . \tag{54.6}$$

Frequently used is the so-called *Littrow configuration* for which $\alpha = -\beta$.

The grating represents a multiple beam interferometer, because the beams reflected from every groove of the grating are phase-shifted by amounts (setting $\alpha = 0$,

$$\delta = \tfrac{2\pi}{\lambda}\Delta s = -2\pi\frac{d}{\lambda}\sin\beta \ . \tag{54.7}$$

The sum of the reflections from N grooves of an incident plane wave $E_{in} = E_0 e^{\imath(\mathbf{k}\cdot\mathbf{r}-\omega t}$ is therefore,

$$\mathcal{E}_r = \sqrt{R}\mathcal{E}_0 \sum_{m=0}^{N} e^{\imath \mathbf{k}_r\cdot\mathbf{r}-\omega t} e^{\imath m\delta} = \sqrt{R}E_0 e^{\imath \mathbf{k}_r\cdot\mathbf{r}-\omega t} \frac{1-e^{\imath N\delta}}{1-e^{\imath\delta}} \ . \tag{54.8}$$

Consequently, the intensity is,

$$I_r = RI_0 \frac{\sin^2 \frac{N}{2}\delta}{\sin^2 \frac{1}{2}\delta} \ . \tag{54.9}$$

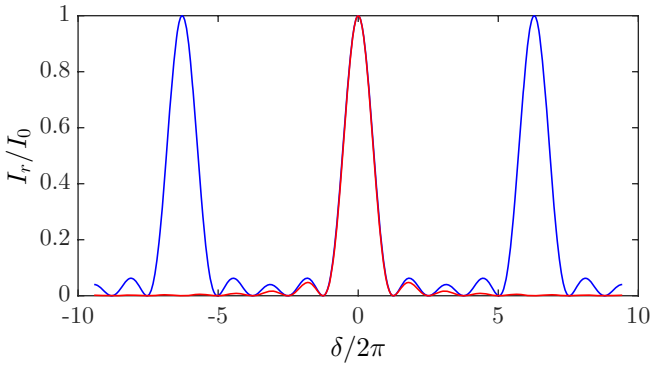

Figure 54.2: (code) Reflection curve of a diffraction grating.

The angular dispersion is, using Eqs. (54.7) and (54.6),

$$\frac{d\beta}{d\lambda} = \left(\frac{d\lambda}{d\beta}\right)^{-1} = -\frac{m}{d\cos\beta} = -\frac{\sin\alpha - \sin\beta}{\lambda\cos\beta} \ . \tag{54.10}$$

The resolving power is,

$$\left|\frac{\lambda}{\Delta\lambda}\right| = \frac{Nd(\sin\alpha - \sin\beta)}{\lambda} = mN \ . \tag{54.11}$$

Solve Exc. 54.1.3.1, 54.1.3.2, and 54.1.3.3.

54.1.3 Exercises

54.1.3.1 Ex: Resolution of a grating spectrometer

Calculate the spectral resolution of a grating spectrometer with an entrance slit width of 10 µm, focal lengths $f_1 = f_2 = 2\,\mathrm{m}$ of the mirrors M1 and M2, a grating with 1800 grooves/mm and an angle of incidence $\alpha = 45°$. What is the useful minimum slit width if the size of grating is $100 \times 100\,\mathrm{mm}^2$?

Solution: *From the equation*

$$\frac{\lambda}{\Delta\lambda} = mN$$

we obtain with $N = 1800 \cdot 100$ *and* $m = 1$, $\lambda/\Delta\lambda = 1.8 \cdot 10^5$. *However, this does not take into account the finite width* b *of the entrance slit* s_1. *The two spectral lines at* λ_1 *and* λ_2 *can be resolved if the images* $s_2(\lambda_1)$ *and* $s_2(\lambda_2)$ *can be resolved. The width of these slit images is*

$$\Delta s_2 = f_2\lambda/a + bf_2/f_1 \ .$$

For $a = 10\,\mathrm{cm}$, $f_2 = f_1 = 2\,\mathrm{m}$, *hence* $\Delta s_2 = 20\lambda + 10\,\mu\mathrm{m}$. *For* $\lambda = 500\,\mathrm{nm}$, *hence* $\Delta s_2 = 20\,\mu\mathrm{m}$. *The separation of* $s_2(\lambda_1)$ *and* $s_2(\lambda_2)$ *is:*

$$\Delta s_2 = f_2 \frac{d\beta}{d\lambda}\Delta\lambda$$

with β *being the diffraction angle. From the grating equation for* $m = 1$*:* $d(\sin\alpha + \sin\beta) = \lambda$ *we get,*

$$\frac{d\beta}{d\lambda} = \left(\frac{d\lambda}{d\beta}\right)^{-1} = \frac{1}{d\cos\beta} \ .$$

Now $\cos\beta = \sqrt{1-\sin^2\beta} = \sqrt{1-\left(\frac{\lambda}{d} - \sin\alpha\right)^2}$, *such that,*

$$\Delta s_2 = \frac{f_2\Delta\lambda}{d\cos\beta} \geq \Delta s_2 \qquad or \qquad \Delta\lambda \geq \frac{\Delta s_2 d\cos\beta}{f^2} \ .$$

For $\alpha = 45°$, $\lambda = 500\,\mathrm{nm}$, $d = (1/18000)\,\mathrm{cm} = 0.56\,\mu\mathrm{m}$, $\cos\beta = 0.9825$, *we get* $\beta = 11°$. *Now,* $\Delta\lambda \geq 1.1 \cdot 10^{-11}\,\mathrm{m}$, *that is* $\frac{\lambda}{\Delta\lambda} = \frac{500\cdot 10^{-9}}{1.1\cdot 10^{-11}} = 4.5 \cdot 10^4$. *This is three times smaller than mN. The useful minimum entrance slit width is given by,*

$$b_{min} = \frac{2f_1}{d}\lambda = \frac{2}{0.1} \cdot 5 \cdot 10^{-7}\,\mathrm{m} = 10\,\mu\mathrm{m} \ .$$

54.1.3.2 Ex: Grating spectrometer

The spectrometer in Exc. 54.1.3.1 shall be used in first order for a wavelength range around 500 nm. What is the optimum blaze angle, if the geometry of the spectrometer allows an angle of incidence α about 20°?

Solution: *The optimum blaze angle is* $\theta = (\alpha - \beta)/2$. *With* $\alpha = 20°$, $\lambda = 500\,\mathrm{nm}$, β *can be obtained from the grating equation with* $m = 1$*:*

$$d(\sin\alpha + \sin\beta) = \lambda \ .$$

With $d = 1/18000\,\mathrm{cm}$ *we get* $\beta = -33.5°$ *and then* $\theta = 26.7°$.

54.1.3.3 Ex: Littrow grating

Calculate the number of grooves/mm for a Littrow grating for a 25° incidence at $\lambda = 488\,\mathrm{nm}$ (i.e., the first diffraction order is being reflected back into the incident beam at an angle $\alpha = 25°$ to the grating normal).

Solution: *The condition for a Littrow grating to first order is:*

$$2d \sin \alpha = \lambda \ ,$$

from which $d = 580.9\,\mathrm{nm}$. *Hence, the number of grooves is* $1721\,/\mathrm{mm}$.

54.1.3.4 Ex: Combining spectrometers

A fluorescence spectrum shall be measured with a spectral resolution of $10^{-2}\,\mathrm{nm}$. The experimenter decides to use a crossed arrangement of grating spectrometer (linear dispersion: $0.5\,\mathrm{nm/mm}$) and FPI of Exc. 53.1.10.7. Estimate the optimum combination of spectrometer slit width and FPI plate separation.

Solution: *For* $\Delta\lambda = 10^{-2}\,\mathrm{nm}$ *and* $\lambda = 500\,\mathrm{nm}$ *the spectral resolution has to be at least:*

$$\frac{\lambda}{\Delta\lambda} \geq 5 \times 10^4 \ .$$

The effective finesse of the FPI in Exc. 53.1.10.7 is $F^*_{total} = 47.6$. *The plate separation then has to be,*

$$d = \tfrac{1}{2}\Delta s = \frac{1}{2}\frac{\lambda^2}{\Delta\lambda}F^* = 0.26\,\mathrm{mm} \ .$$

The free spectral range is $\Delta\nu = c/2d$, *hence,*

$$|\delta\lambda| = +\frac{c}{\nu^2}|\delta\nu| = \frac{\lambda^2}{2d} = 0.38\,\mathrm{nm} \ .$$

The spectral interval $\delta\lambda$ *transmitted by the spectrograph should be smaller than* $\delta\nu$ *in order to avoid the overlap of different orders. This means that the spectral resolution of the spectrograph* $\delta\lambda = d\lambda/dx\ \Delta s \leq 0.38\,\mathrm{nm}$ *with a linear dispersion of* $d\lambda/dx = 5 \times 10^{-2}\,\mathrm{nm/mm}$. *Therefore,* $\Delta s \leq 0.38\,\mathrm{mm}\,/5 \times 10^{-1} = 0.76\,\mathrm{mm}$.

54.1.4 *Experiment: Separating bichromatic light by prisms and gratings*

In this experiment we will study the dispersive power of a prism and a grating.

1. Combine the beams of a helium-neon laser and a laser at 461 nm via a beam-splitter. Pass this combination through a prism and quantify the dispersion.
2. Calculate the minimum angle between the two beams.
3. Shine the combination onto a reflection grating and quantify the dispersion.

54.1.5 *Experiment: Thorlabs optical spectrum analyzer*

CCS175, characterization, Thorlabs ® tour.
Czerny-Turner CCD spectrometer

1. Irradiate light on OSA and observe the spectrum.

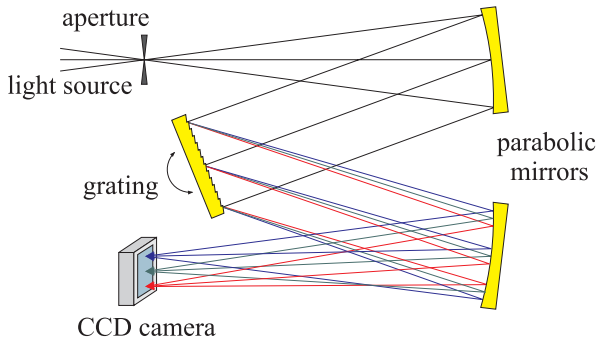

Figure 54.3: Principle of operation of a Czerny-Turner monochromator.

54.1.6 *Experiment: HighFinesse wavemeter*

Wavemeters measure the wavelength of monochromatic light sources by interference. One type of wavemeter is based on a Michelson interferometer, where the length of one interferometer arm is uniformly increased while the interference fringes are counted. Counting the fringes of a known reference laser simultaneously and comparing the counts of the unknown and the reference laser, the wavelength of the unknown laser can be determined with high precision (down to 2 MHz resolution).

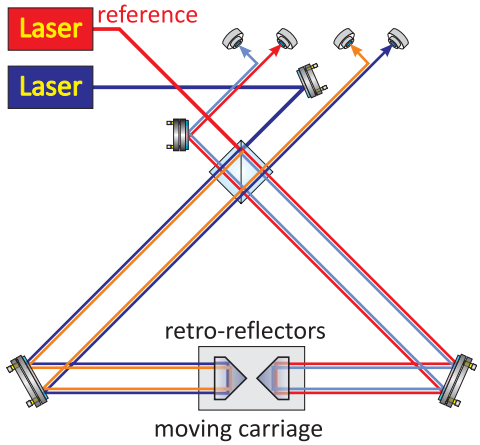

Figure 54.4: Principle of operation of a Michelson-type wavemeter.

1. HighFinesse WSU30, characterization.

54.2 Fluorescence, excitation, and absorption spectroscopy

Depending on the information we want to extract from a sample and on the available instrumentation various types of spectroscopic techniques are possible, which will be discussed on the following sections.

54.2.1 Classification of spectroscopic methods

It is important to distinguish *fluorescence spectra* from *excitation spectra*: Fluorescence spectra are taken by processing the light emitted from a radiator in a monochromator. That is, the light is shone onto a spectral band filter, which only transmits a narrow fraction of the fluorescence spectrum. The power of the transmitted light is measured with a detector. Upon changing the center frequency of the band filter, different components of the fluorescence spectrum are measured, thus yielding a curve $u(\nu)$, which represents the spectral energy density of the radiator [see Fig. 54.5(a,d)].

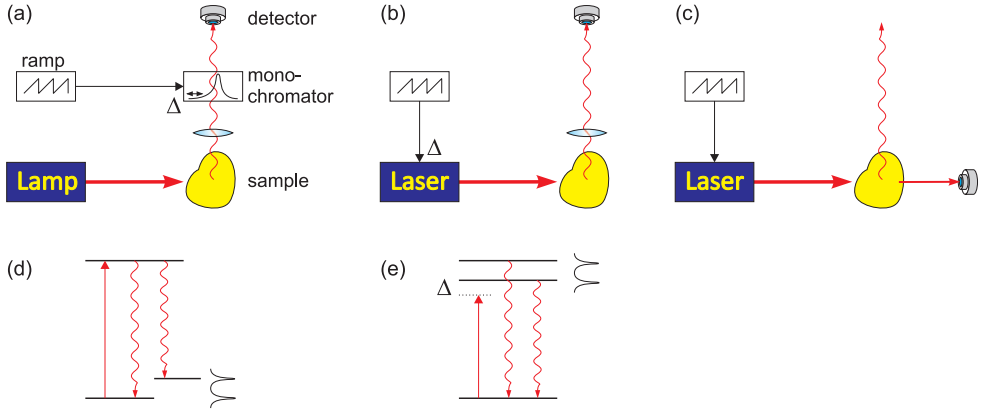

Figure 54.5: (a) Taking a fluorescence spectrum, (b) an excitation spectrum, and (c) an absorption spectrum. Typical level schemes for (d) fluorescence spectroscopy and (e) excitation or absorption spectroscopy.

In contrast to fluorescence spectroscopy, excitation or absorption spectra are taken by varying the frequency of the light exciting a sample. The reemitted light is then measured by a detector without discriminating its frequency components. Obviously, both method yield very different information about the scatterer [see Fig. 54.5(b,c,e)]. Depending on whether the scattered of the transmitted light is detected, we speak of excitation and absorption spectroscopy.

54.2.2 Saturated absorption spectroscopy

One of the most popular spectroscopic technique is *saturation spectroscopy*, as it is simple, robust, and allows to avoid Doppler-broadening. There are, however, many

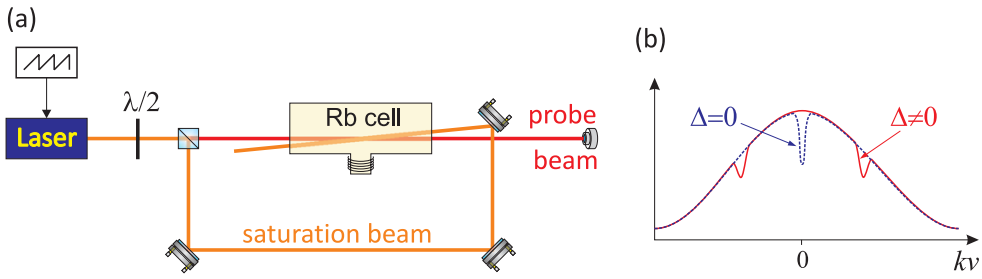

Figure 54.6: (a) Experimental scheme for saturated absorption spectroscopy. (b) Spectral hole burning by the counter-propagating saturation and probe beams for (red) detuned and (blue) resonant light.

possible implementations of saturation spectroscopy, f.ex. *frequency modulation spectroscopy* or *modulation transfer spectroscopy*, which we will present in the following.

54.2.2.1 Calculation of the Lamb-dip

The scheme known as *Lamb-dip spectroscopy* and which is illustrated in Fig. 54.6(a), consists in a cell filled with a gas [for example, atomic rubidium whose resonance frequency is $\omega_0 = ck = 2\pi c/780\,\text{nm}$ and decay rate is $\Gamma = (2\pi)\ 6\,\text{MHz}$] and two laser beams with the same frequency ω, but propagating in opposite directions. One is called the saturating beam, the other probe beam.

The basic idea is that, if the laser frequency is detuned from resonance, $\omega \neq \omega_0$, the counter-propagating beams will interact with different velocity classes (i.e. atomic velocities projected on the optical axis, $v = \mathbf{v}\cdot\hat{\mathbf{e}}_\mathbf{k}$), which results in two distinct 'holes' in the excitation profile [red curve in Fig. 54.6(b)]. Only for resonant light, $\omega = \omega_0$, will the counter-propagating beams interact with the same velocity class (i.e. atomic velocities with $v = 0$). The 'holes' in the excitation profile then overlap thus leading to a deeper depression called Lamb-dip [blue curve in Fig. 54.6(b)].

For a quantitative description of the Lamb-dip we consider Maxwell's one-dimensional and normalized velocity distribution,

$$\rho(v)dv = \sqrt{\frac{m}{2\pi k_B T}} e^{-mv^2/2k_B T} dv \ . \tag{54.12}$$

As an example, we consider a gas at $T = 300\,\text{K}$ temperature, where the partial pressure of rubidium is about $P = 10^{-1}\,\text{mbar}$, such that the particle density is,

$$n(T) = \frac{P}{k_B T} \ . \tag{54.13}$$

We also assume a cell length of $L = 10\,\text{cm}$.

The probe laser intensity is below saturation, such that the optical cross section for an atom moving with velocity v, is,

$$\sigma(v) = \frac{6\pi}{k^2} \frac{\Gamma^2}{4(\omega - \omega_0 - kv)^2 + \Gamma^2} \ , \tag{54.14}$$

where we considered the fact that the atoms moving with the velocity v along the optical axis perceive the probe laser beam as Doppler-shifted by an amount kv.

The saturating laser now has high intensity. Let us suppose here, $\Omega \equiv 10\Gamma$, where Ω is the Rabi frequency caused by the saturating laser. In this way, it creates a population of N_e atoms in the excited state. Since this population is missing in the ground state, $N_g = N - N_e$, the absorption is reduced for the probe beam by a factor,

$$\frac{N_e}{N} = \frac{\Omega^2}{4(\omega - \omega_0 + kv)^2 + 2\Omega^2 + \Gamma^2} \ . \tag{54.15}$$

In contrast to (54.14), we now have to consider saturation broadening.

We will now calculate the spectrum of the optical density for the probe laser, $O_D(\omega)$, and the light intensity transmitted through the cell, $\frac{I}{I_0} = e^{-O_D}$, according to the Lambert-Beer law.

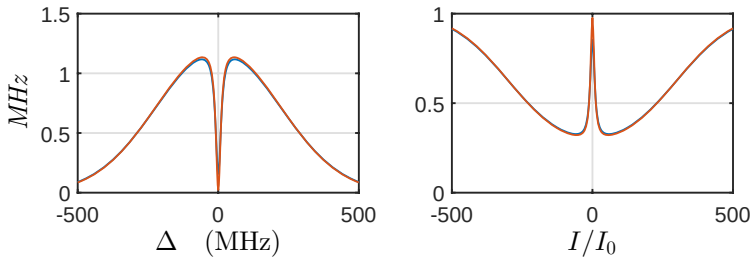

Figure 54.7: (code) (a) Optical density and (b) absorption. (Blue) Integral formula and (green) approximation for high temperature and high saturation.

The optical density with Doppler broadening is,

$$O_D(T,\omega) = Ln(T) \int_{-\infty}^{\infty} \tfrac{N_g - N_e}{N} \sigma(v)\rho(v) dv \tag{54.16}$$

$$= L\frac{P}{k_B T}\sqrt{\frac{m}{2\pi k_B T}}\frac{6\pi}{k^2}\int_{-\infty}^{\infty}\left(1 - \frac{2\Omega^2}{4(\Delta + kv)^2 + 2\Omega^2 + \Gamma^2}\right)\frac{\Gamma^2}{4(\Delta - kv)^2 + \Gamma^2} e^{-mv^2/2k_B T} dv \ ,$$

with $\Delta \equiv \omega - \omega_0$ and substituting $N_g - N_e = N - 2N_e$. The widths of the three distribution functions are, respectively,

$$\begin{aligned}
\delta\nu_{sat} &= \sqrt{\tfrac{1}{2}\Omega^2 + \tfrac{1}{4}\Gamma^2} \approx (2\pi)\ 68\,\text{MHz} && \text{for the saturating beam} \\
\delta\nu_{Dpp} &= k\sqrt{\tfrac{k_B T}{m}} \approx (2\pi)\ 217\,\text{MHz} && \text{for the Doppler broadening} \\
\delta\nu_{prb} &= \tfrac{1}{2}\Gamma \approx (2\pi)\ 3\,\text{MHz} && \text{for the probe beam}
\end{aligned} \tag{54.17}$$

where $\bar{v} = \sqrt{k_B T/m}$ is the mean atomic velocity (or the *rms* width) of Maxwell's distribution. Since the spectral width of the probe laser spectrum is much smaller, we can replace it by a δ-function,

$$\frac{\Gamma^2}{4(\Delta - kv)^2 + \Gamma^2} \longrightarrow \frac{\pi\Gamma}{2}\delta(\Delta - kv) \ , \tag{54.18}$$

which gives,

$$O_D(T,\omega) \simeq L\frac{P}{k_BT}\sqrt{\frac{m}{2\pi k_BT}}\frac{6\pi}{k^3}\int_{-\infty}^{\infty}\left(1-\frac{2\Omega^2}{4(\Delta+kv)^2+2\Omega^2+\Gamma^2}\right)\times \quad (54.19)$$
$$\times\frac{\pi\Gamma}{2}\delta(\Delta-kv)e^{-mv^2/2k_BT}dkv$$
$$= L\frac{P}{k_BT}\sqrt{\frac{m}{2\pi k_BT}}\frac{6\pi}{k^3}\frac{\pi\Gamma}{2}\left(1-\frac{2\Omega^2}{8\Delta^2+2\Omega^2+\Gamma^2}\right)e^{-m(\Delta/k)^2/2k_BT}\,.$$

The *Lamb dip* is the narrow (Doppler-free) feature in the center of the the spectrum exhibited in Fig. 54.7. Lamb-dip spectra are commonly serve as frequency references for laser frequency stabilization schemes.

54.2.3 Frequency modulation and modulation transfer spectroscopy

Variations of the saturation spectroscopic idea are the *frequency modulation spectroscopy* (FMS) and the *modulation transfer spectroscopy* (MTS). The basic scheme of those techniques is shown in Fig. 54.8. As in saturation spectroscopy, two counterpropagating beams interact with the same atoms of a molecular gas, but now one of the beams is frequency-modulated (e.g. using an electro-optic modulator). In the FMS configuration, the probe beam is modulated, and the sidebands are discriminated at the spectral feature generated by the saturation beam in a very similar way as for the Pound-Drever-Hall technique. The profile of the FMS signal is calculated in Exc. 54.2.4.3 [795, 147, 576, 1225, 692, 231, 393, 1201, 1153, 628, 831].

In the MTS configuration, the saturation beam is modulated, and the sidebands are transferred to the probe beam via nonlinear four-wave mixing processes. In both cases, the sidebands are demodulated with the local oscillator frequency driving the EOM.

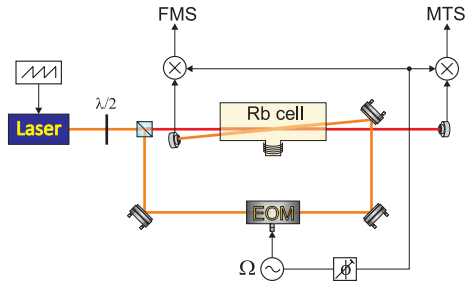

Figure 54.8: Schemes of frequency-modulation and modulation transfer spectroscopy.

The advantages of both techniques is, that they generate dispersive Doppler-free lineshapes. The FMS signal appears as a sharp feature on top of a large Doppler background (similarly to the Lamb-dip). In contrast, the MTS signal is free from

Doppler background. The MTS signal recorded by the photodetector is given by,

$$I(\Delta) = \sum_{a,b} \frac{\mu_{ab}^2}{\gamma_j + \imath\delta} \left(\frac{1}{\gamma_{ab} + \imath(\Delta + \delta/2)} - \frac{1}{\gamma_{ab} + \imath(\Delta + \delta)} + \frac{1}{\gamma_{ab} - \imath(\Delta - \delta)} - \frac{1}{\gamma_{ab} - \imath(\Delta - \delta/2)} \right) , \tag{54.20}$$

where a and b denote the lower and upper levels, μ_{ab}^2 is the electric dipole moment, γ_{ab} is the optical relaxation rate, γ_j is the decay of the energy level j of the molecule, and δ is the modulation frequency. Behind the mixer we see the electric signal,

$$S(\Delta, \vartheta) = \mathrm{Re}\,[I(\Delta) e^{-\imath\varphi}] , \tag{54.21}$$

where ϑ is the demodulation phase [830]. The curves are shown in Fig. 54.8.

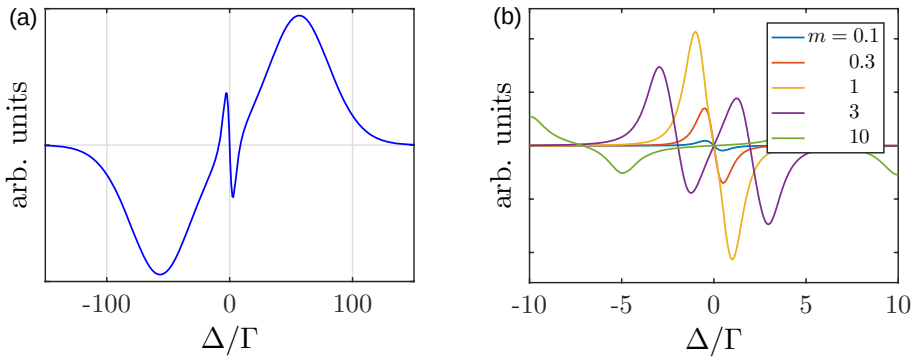

Figure 54.9: (code) (a) Calculated FMS signals and (b) MTS signals as a function of detuning for various modulation indices.

Example 301 (*Modulation transfer spectroscopy*): Modulation transfer spectroscopy is caused by four-wave mixing (4WM) processes, which have the general form $P(\omega+\Omega) = \chi^{(3)}(\omega+\Omega)E_s(\omega_s)E_p(\omega_s)E_s^*(\omega_s-\Omega)$, or similar. When the beams ω and ω_s are counter-propagating, and the atoms are moving, their resonances shift toward $\omega \mp \mathbf{k}\cdot\mathbf{v}$, respectively in the atomic rest system. Resonant enhancement of 4WM occurs, when one of the intermediate levels coincides with ω_0:

$$\begin{aligned} &\omega - \mathbf{k}\cdot\mathbf{v} = \omega_0 \\ &(\omega - \mathbf{k}\cdot\mathbf{v}) - (\omega + \mathbf{k}\cdot\mathbf{v} - \Omega) = 0 \\ &(\omega - \mathbf{k}\cdot\mathbf{v}) - (\omega + \mathbf{k}\cdot\mathbf{v} - \Omega) + (\omega + \mathbf{k}\cdot\mathbf{v}) = \omega_0 \\ &(\omega - \mathbf{k}\cdot\mathbf{v}) - (\omega + \mathbf{k}\cdot\mathbf{v} - \Omega) + (\omega + \mathbf{k}\cdot\mathbf{v}) - (\omega - \mathbf{k}\cdot\mathbf{v} + \Omega) = 0 . \end{aligned}$$

Assuming $\omega = \omega_s = \omega - 0$, these resonances reduced to,

$$\mathbf{k}\cdot\mathbf{v} = 0, \pm\Omega ,$$

and similarly for the other 4WM processes. This means, that the saturation beam burns holes in the velocity distribution at $\mathbf{k}\cdot\mathbf{v} = 0, \pm\frac{1}{2}\Omega, \pm\Omega$, which modulate the probe beam.

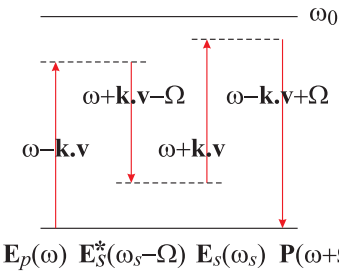

Figure 54.10: Levels involved in 4WM upon MTS.

54.2.4 Exercises

54.2.4.1 Ex: Width of the absorption band

The resonator of a dye laser with a large emission bandwidth additionally contains an absorbing (dense) gas. The absorption spectrum of the gas is Lorentzian with a width of 3 GHz, and the absorption coefficient has, in the middle of the absorption line (at 600 nm), the value of 0.2. What are the maximum and minimum relative spectral distances $\Delta f/\Delta f_0$ of the axial modes within the spectral range of the absorption, compared to the distances Δf_0 of the empty resonator?

Solution: *The susceptibility of the absorption line can also be described as complex refractive index,*

$$n = n' + \imath n'' = 1 + C\left[\frac{(\nu_0-\nu)\frac{1}{2}\Delta\nu}{(\nu_0-\nu)^2+\left(\frac{1}{2}\Delta\nu\right)^2} + \imath\frac{\left(\frac{1}{2}\Delta\nu\right)^2}{(\nu_0-\nu)^2+\left(\frac{1}{2}\Delta\nu\right)^2}\right] ,$$

where n' is the dispersion and n'' the absorption. In resonance the dispersion disappears, therefore $C = 0.2$ is the absorption. The real part of the refraction index gives the dispersion, such that the distances of the modes is, $\nu_{n+1} - \nu_n = \frac{c}{n2L}$. The relationship between the mode distances in the full resonator and the empty resonator is $\frac{\Delta f}{\Delta f_0} = \frac{1}{n}$.

54.2.4.2 Ex: Lorentz and Gaussian profiles

At which detuning is a Doppler-broadened line dominated by Lorentzian profile of the transition?

Solution: *We consider a cell of length L at temperature T. With the optical cross section,*

$$\sigma = \frac{6\pi}{k^2}\frac{\Gamma^2}{4(\omega-\omega_0-kv)^2+2\Omega^2+\Gamma^2}$$

and the Maxwell-Boltzmann distribution,

$$\rho dv = \sqrt{\frac{m}{2\pi k_B T}}e^{-mv^2/2k_BT}dv$$

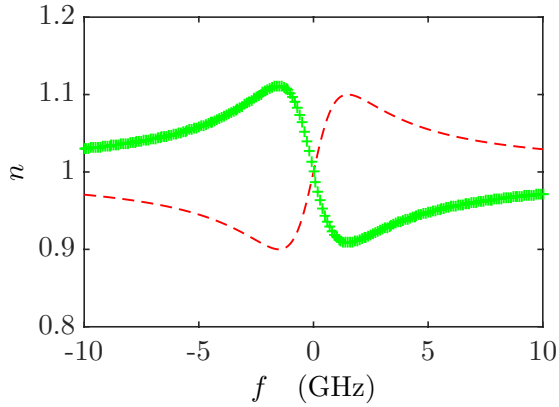

Figure 54.11: (code) Refraction index (red,–) and mode distance (green, +) as a function of the detuning.

the optical density is,

$$O_D(T,\omega) = L\frac{P}{k_BT}\sqrt{\frac{m}{2\pi k_BT}}\frac{6\pi}{k^2}\int_{-\infty}^{\infty} e^{-mv^2/2k_BT}\frac{\Gamma^2}{4(\omega-\omega_0-kv)^2+2\Omega^2+\Gamma^2}dv \ .$$

We consider the normalized spectra,

$$\sigma = \frac{a/\pi}{x^2+a^2} \qquad \textit{and} \qquad \rho = \frac{1}{b\sqrt{\pi}}e^{-x^2/b^2} \ .$$

54.2.4.3 Ex: Frequency-modulation spectroscopy

Calculate the FMS spectrum for a rubidium gas (describing the atoms as a two-level system) under the conditions specified in Sec. 54.2.2 and assuming a modulation frequency of $f = 10\,\mathrm{MHz}$ and a modulation index of $\beta = 1$.

Solution: *The optical density derived in (54.19),*

$$O_D(\Delta) = C\left(1-\eta\frac{2\Omega^2}{8\Delta^2+2\Omega^2+\Gamma^2}\right)e^{-\Delta^2/2\delta_{Dpp}^2} \ ,$$

describes the Lamb-dip spectrum, where we now additionally account for imperfections in the saturation (misalignment, time-of-flight broadening, etc.) by a factor $\eta \in [0,1]$. The probe beam is now frequency-modulated,

$$E_{prb,0}(\Delta) = J_0(\beta)e^{\imath\Delta t} + J_1(\beta)e^{\imath(\Delta+f)t} + J_{-1}(\beta)e^{\imath(\Delta-f)t} \ ,$$

and transmitted through the cell, counter-propagating to the (unmodulated) saturation beam, where the sidebands suffer different frequency-dependent attenuations,

$$E_{prb}(\Delta) = E_{prb,0}(\Delta)e^{-\frac{1}{2}O_D(\Delta)} \ .$$

The photodetector records the signal,

$$\begin{aligned} I_{prb}(\Delta) &= |E_{prb}(\Delta)|^2 \\ &= |J_0(\beta)e^{-\frac{1}{2}O_D(\Delta)}e^{\imath\Delta t} + J_1(\beta)e^{-\frac{1}{2}O_D(\Delta+f)}e^{\imath(\Delta+f)t} + J_{-1}(\beta)e^{-\frac{1}{2}O_D(\Delta-f)}e^{\imath(\Delta-f)t}|^2 \\ &= J_0(\beta)^2 e^{-O_D(\Delta)} + J_0(\beta)J_1(\beta)e^{-\frac{1}{2}O_D(\Delta)-\frac{1}{2}O_D(\Delta+f)}(e^{\imath ft} + e^{-\imath ft}) \\ &\qquad + J_0(\beta)J_{-1}(\beta)e^{-\frac{1}{2}O_D(\Delta)-\frac{1}{2}O_D(\Delta-f)}(e^{\imath ft} + e^{-\imath ft}) + \dots \ . \end{aligned}$$

The demodulated signal is,

$$S(\Delta) = I_{prb}(\Delta)e^{-\imath ft+\imath\varphi} \ ,$$

which, after low-pass filtering, becomes,

$$S(\Delta) = J_0(\beta)J_1(\beta)e^{\imath\varphi}e^{-O_D(\Delta/2)}\left[e^{-\frac{1}{2}O_D(\Delta+f)} - e^{-\frac{1}{2}O_D(\Delta-f)}\right] \ .$$

The FMS spectrum is shown in Fig. 54.9(a).

54.2.5 *Experiment: Rubidium Lamb-dips*

In this exercise, we will spectroscopically identify the various lines of the rubidium D_2-transition of the isotopes ^{87}Rb and ^{85}Rb. The hyperfine splittings of the ground and excited states are reproduced in Fig. 54.12.

1. Set up the optics for a Lamb-dip spectroscopy as shown in Fig. 54.12.

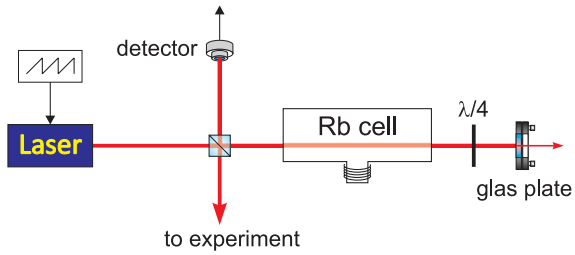

Figure 54.12: Saturation spectroscopy.

2. Fig. 54.13 shows a typical spectrum recorded with a rubidium gas cell. Find an interpretation for the various lines of the spectrum.

54.3 Polarization spectroscopy

The *Hänsch-Couillaud technique* uses the *birefringence* of certain materials, devices, or gases.

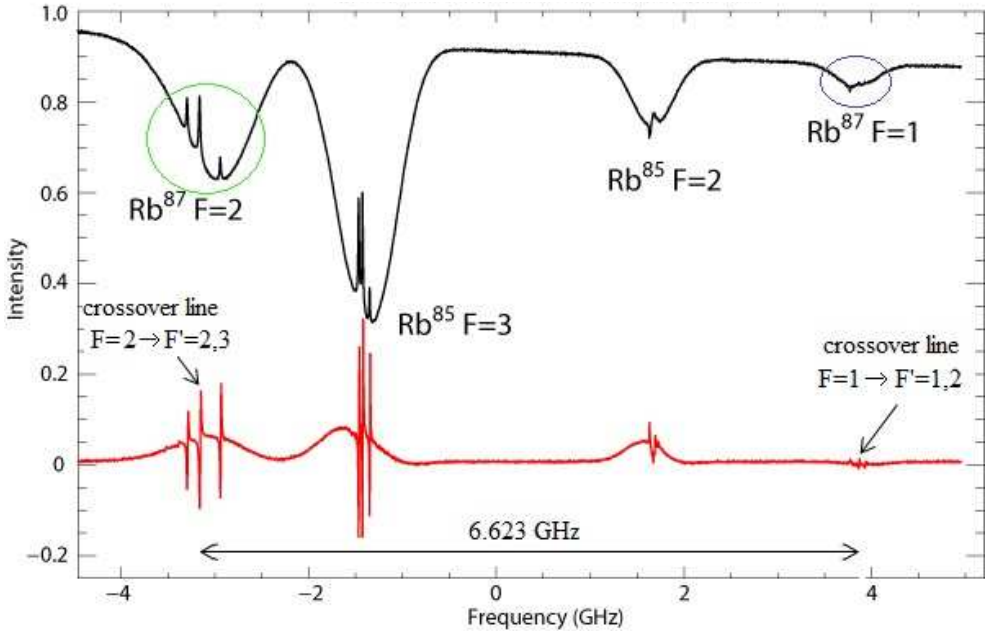

Figure 54.13: (Black) Lamb-dip spectroscopy of a rubidium gas (natural isotope mixture of ^{85}Rb and ^{87}Rb) showing the hyperfine structure transitions of the D2-line. (Red) Derivative of the spectrum in (a).

54.3.1 Birefringent cavity

We consider a birefringent cavity exhibiting slightly different path lengths for two axis that we will call, respectively, *ordinary* and*extraordinary*. Fig. 54.14(a) shows the optical setup. The detector signals may be calculated via a concatenation of the Jones matrices for a $\lambda/2$-plate, the transmissive response of the cavity, another $\lambda/2$-plate, and finally a polarizing beam splitter,

$$\begin{pmatrix} E_o \\ E_e \end{pmatrix} = M \begin{pmatrix} 1 \\ 0 \end{pmatrix} \qquad with \tag{54.22}$$

$$M \equiv \begin{pmatrix} \cos\beta & \sin\beta \\ -\sin\beta & \cos\beta \end{pmatrix} \begin{pmatrix} \frac{T}{1-Re^{2\imath k_o L}} & 0 \\ 0 & \frac{T}{1-Re^{2\imath k_e L}} \end{pmatrix} \begin{pmatrix} \cos\alpha & \sin\alpha \\ -\sin\alpha & \cos\alpha \end{pmatrix} . \tag{54.23}$$

For the particular polarization angles $\alpha = \frac{\pi}{4}$ and $\beta = 0$, we derive the difference of the photodetector signals,

$$\Delta I = |E_o|^2 - |E_e|^2 = \frac{T^2}{2} \left[\frac{1}{1 - R^2 - 2R\cos 2k_o L} - \frac{1}{1 - R^2 - 2R\cos 2k_e L} \right] . \tag{54.24}$$

As Fig. 54.14(b) demonstrates, the spectra corresponding to the axis, obtained by ramping the laser frequency are slightly shifted with respect to each other. Their subtraction leads to a dispersive lineshape that suits for laser locking purposes in the so-called *Hänsch-Couillaud* stabilization.

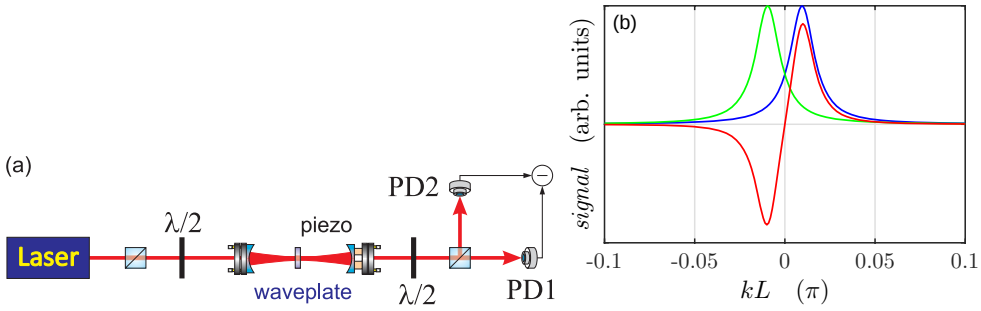

Figure 54.14: (code) (a) Generating a Hänsch-Couillaud error signal by transmission of a birefringent linear cavity. (b) Signals recorded by the two photodetectors (blue and green) and their difference (red).

54.3.2 *Experiment: Birefringence of a ring cavity*

Birefringence automatically occurs in a ring cavities. In this exercise, we will analyze the birefringence observed in reflection of a such a ring cavity. In a *ring cavity*, the resonance frequencies of the s-polarized and the p-polarized modes are slightly shifted from one another due to the different penetration depth of the s- and p-polarized light modes into the layers of the dielectric mirrors. For a moderate finesse of the cavity (say $\mathcal{F} = 2000$), the modes actually overlap. This leads to a birefringence used in the

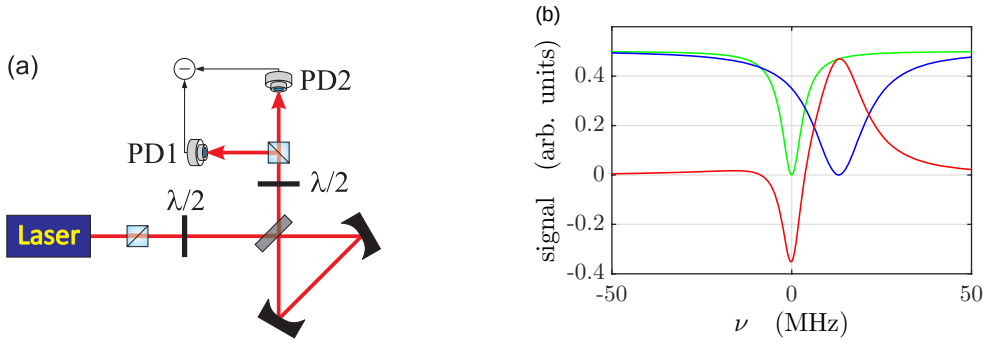

Figure 54.15: (code) (a) Generating a Hänsch-Couillaud error signal by (a) reflection from a ring cavity and (b) transmission of a linear cavity containing a Brewster plate. (b) Signals recorded by the two photodetectors (blue and green) and their difference (red). (a) Reflection signals $|E_s|^2$ and $|E_p|^2$ from a birefringent cavity with $\delta_{fsr} = 8.2\,\mathrm{GHz}$, $\varphi_s = 0$, $R_{hr,s} = 99.97\%$, $R_{ic,s} = 99.74\%$, $F_s = \pi(R_{hr,s}^2 R_{ic,s})^{1/6}/[1-(R_{hr,s}^2 R_{ic,s})^{1/3}]$, $\varphi_p = 0.01$, $R_{hr,p} = 99.92\%$, $R_{ic,p} = 99.34\%$, and $F_p = \pi(R_{hr,p}^2 R_{ic,p})^{1/6}/[1-(R_{hr,p}^2 R_{ic,p})^{1/3}]$. (b) Difference $|E_s|^2 - |E_p|^2$.

famous Hänsch-Couillaud locking scheme. The detector signal in the scheme shown in the figure may calculated via a concatenation of the Jones matrices for a $\lambda/2$-plate, the reflective response of the ring cavity, another $\lambda/2$-plate, and finally a polarizing

beam splitter,

$$\begin{pmatrix} E_s \\ E_p \end{pmatrix} = M \begin{pmatrix} 1 \\ 0 \end{pmatrix} \quad with \tag{54.25}$$

$$M \equiv \begin{pmatrix} \cos\beta & \sin\beta \\ -\sin\beta & \cos\beta \end{pmatrix} \begin{pmatrix} \frac{1-e^{-2\pi\imath\omega/\delta_{fsr}+\imath\phi_s}}{1-R_s e^{-2\pi\imath\omega/\delta+\imath\phi_s}} & 0 \\ 0 & \frac{1-e^{-2\pi\imath\omega/\delta_{fsr}+\imath\phi_p}}{1-R_p e^{-2\pi\imath\omega/\delta+\imath\phi_p}} \end{pmatrix} \begin{pmatrix} \cos\alpha & \sin\alpha \\ -\sin\alpha & \cos\alpha \end{pmatrix} .$$

Calculating $|E_s|^2$ and $|E_p|^2$ as a function of the laser frequency ω reproduces the curves plotted in Fig. 54.15(a).

1. x

54.4 Other spectroscopic techniques

54.4.1 Mode-locked femtosecond laser

Mode-locking is a technique in optics by which a laser can be made to produce pulses of light of extremely short duration, down to the order of femtoseconds. The basis of the technique is to induce a fixed-phase relationship between the longitudinal modes of the laser's resonant cavity. Constructive interference between these modes can cause the laser light to be produced as a train of pulses.

In a simple laser, each of these cavity modes amplified within the bandwidth of the gain medium oscillates independently, with no fixed relationship between each other. The individual phase of the light waves in each mode is not fixed, and may vary randomly due to such things as thermal changes in materials of the laser. In lasers with only a few oscillating modes, interference between the modes can cause beating effects in the laser output, leading to fluctuations in intensity; in lasers with many thousands of modes, these interference effects tend to average to a near-constant output intensity.

If instead of oscillating independently, each mode operates with a fixed phase relation to the other modes. Instead of a random or constant output intensity, the modes of the laser will periodically constructively interfere with one another, producing an intense burst or pulse of light. Such a laser is said to be *mode-locked* or *phase-locked*. These pulses occur separated in time by $\tau = 2L/c$, where τ is the laser cavity round trip time and corresponds to the cavity's inverse free spectral range.

54.4.1.1 Active mode-locking

The most common active mode-locking technique places a standing wave electro-optic modulator (EOM) into the laser cavity. When driven with a sinusoidal electrical signal, this produces an amplitude modulation of the light in the cavity. Considering this in the frequency domain, if a mode has optical frequency ν, and is amplitude-modulated at a frequency f, the resulting signal has sidebands at optical frequencies $\nu \pm f$. The modulation frequency is now chosen to coincide with the cavity's free spectral range, $f = \delta_{fsr}$, and since the sidebands are driven in-phase, the central mode and the adjacent modes will be phase-locked together. Further operation of the

modulator on the sidebands produces phase-locking of the $\nu \pm 2f$ modes, and so on until all modes in the gain bandwidth are locked.

This process can also be considered in the time domain. The amplitude modulator acts as a weak 'shutter' to the light bouncing between the mirrors of the cavity, attenuating the light when it is 'closed', and letting it through when it is 'open'. If the modulation rate f is synchronized to the cavity round-trip time τ, then a single pulse of light will bounce back and forth in the cavity. The actual strength of the modulation does not have to be large; a modulator that attenuates 1% of the light when 'closed' will mode-lock a laser, since the same part of the light is repeatedly attenuated as it traverses the cavity.

Related to this amplitude modulation (AM), active mode-locking is frequency modulation (FM) mode-locking, which uses a modulator device based on the acousto-optic effect. This device, when placed in a laser cavity and driven with an electrical signal, induces a small, sinusoidally varying frequency shift in the light passing through it. If the frequency of modulation is matched to the round-trip time of the cavity, then some light in the cavity sees repeated upshifts in frequency, and some repeated downshifts. After many repetitions, the upshifted and downshifted light is swept out of the gain bandwidth of the laser. The only light which is unaffected is that which passes through the modulator when the induced frequency shift is zero, which forms a narrow pulse of light.

The third method of active mode-locking is synchronous mode-locking, or synchronous pumping. In this, the pump source (energy source) for the laser is itself modulated, effectively turning the laser on and off to produce pulses.

54.4.1.2 Passive mode-locking

Passive mode-locking techniques are those that do not require a signal external to the laser to produce pulses. Rather, they use the light in the cavity to cause a change in some intracavity element, which will then itself produce a change in the intracavity light. A commonly used device to achieve this is a saturable absorber.

A saturable absorber is an optical device that exhibits an intensity-dependent transmission. For passive mode-locking, ideally a saturable absorber will selectively absorb low-intensity light, and transmit light which is of sufficiently high intensity. When placed in a laser cavity, a saturable absorber will attenuate low-intensity constant wave light (pulse wings). However, because of the somewhat random intensity fluctuations experienced by an un-mode-locked laser, any random, intense spike will be transmitted preferentially by the saturable absorber. As the light in the cavity oscillates, this process repeats, leading to the selective amplification of the high-intensity spikes, and the absorption of the low-intensity light. After many round trips, this leads to a train of pulses and mode-locking of the laser.

Considering this in the frequency domain, if a mode has optical frequency ν, and is amplitude-modulated at a frequency nf, the resulting signal has sidebands at optical frequencies $\nu \pm nf$ and enables much stronger mode-locking for shorter pulses and more stability than active mode-locking, but has startup problems.

Saturable absorbers are commonly liquid organic dyes, but they can also be made from doped crystals and semiconductors. Semiconductor absorbers tend to exhibit very fast response times ($\sim$100 fs), which is one of the factors that determines the

final duration of the pulses in a passively mode-locked laser. In a colliding-pulse mode-locked laser the absorber steepens the leading edge while the lasing medium steepens the trailing edge of the pulse.

There are also passive mode-locking schemes that do not rely on materials that directly display an intensity dependent absorption. In these methods, nonlinear optical effects in intracavity components are used to provide a method of selectively amplifying high-intensity light in the cavity, and attenuation of low-intensity light. One of the most successful schemes is called Kerr-lens mode-locking (KLM), also sometimes called 'self mode-locking'. This uses a nonlinear optical process, the optical Kerr effect, which results in high-intensity light being focussed differently from low-intensity light. By careful arrangement of an aperture in the laser cavity, this effect can be exploited to produce the equivalent of an ultra-fast response time saturable absorber.

54.4.2 Frequency comb

In optics, a frequency comb is a laser source whose spectrum consists of a series of discrete, equally spaced frequency lines. Frequency combs can be generated by a number of mechanisms, including periodic modulation (in amplitude and/or phase) of a continuous-wave laser, four-wave mixing in nonlinear media, or stabilization of the pulse train generated by a mode-locked laser. The invention of the *frequency comb* represents a breakthrough in ultrahigh resolution spectroscopy, which was honored with the Nobel price attributed to Theodor Hänsch in 2005 [1411, 681, 629, 630, 934, 11, 1294].

The frequency domain representation of a perfect frequency comb is a series of delta functions spaced according to,

$$f_n = f_{ceo} + n f_{rep} \ , \tag{54.26}$$

where n is an integer, f_{rep} is the comb tooth spacing (equal to the mode-locked laser's repetition rate or, alternatively, the modulation frequency), and f_{ceo} is the carrier offset frequency, which is less than f_{rep}. Combs spanning an octave in frequency (i.e., a factor of two) can be used to directly measure (and correct for drifts in) f_{ceo}. Thus, octave-spanning combs can be used to steer a piezoelectric mirror within a carrier-envelope phase-correcting feedback loop. Any mechanism by which the combs' two degrees of freedom (f_{rep} and f_{ceo}) are stabilized generates a comb that is useful for mapping optical frequencies into the radio frequency for the direct measurement of optical frequency.

54.4.2.1 Spectrum of a frequency comb

The field emitted by a pulsed laser characterized by its pump laser frequency ν, the *repetition rate* f_{rep}, and the pulse width T, can be given as a temporal sequence of Gaussian shaped pulses. The repetition is mathematically described as a convolution of the Gaussian profile with a sum of temporal δ-functions displaced in time,

$$\boxed{E(t) = \cos 2\pi\nu t \left(\sum_n \delta(t - \tfrac{n}{f_{rep}}) \star e^{-t^2/T^2} \right) = \cos 2\pi\nu t \sum_n e^{-(t-\frac{n}{f_{rep}})^2/T^2}} \ . \tag{54.27}$$

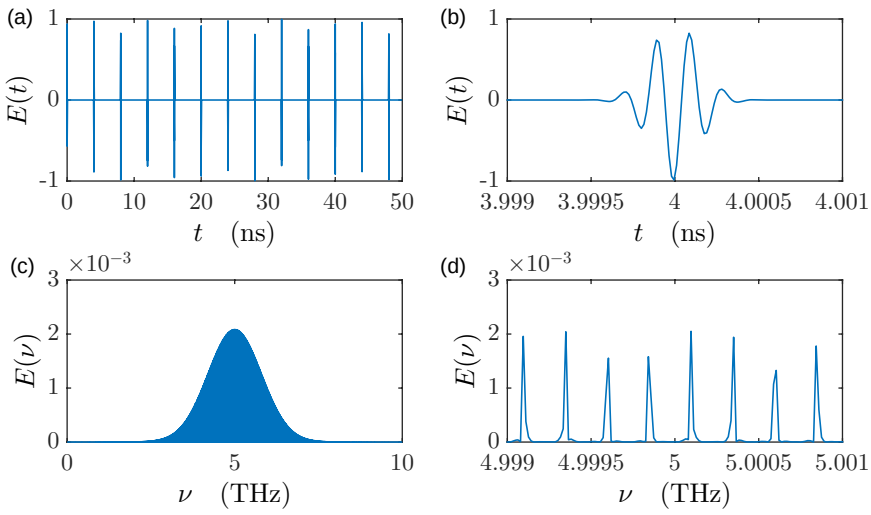

Figure 54.16: (code) Pulse train (a,b) and spectrum (b,c).

The carrier under each pulse is phase-shifted with respect to the adjacent pulse, except when the laser is mode-locked, that is, when,

$$\cos 2\pi\nu t = \cos 2\pi\nu(t + \tfrac{1}{f_{rep}}) \ . \tag{54.28}$$

The Fourier transform of the laser field (54.27) is,

$$\begin{aligned} \mathcal{F}[E(t)] &= \int_{-\infty}^{\infty} e^{-\imath\omega t} \cos 2\pi\nu t \sum_n e^{-(t-n/f_{rep})^2/T^2} dt \\ &= \tfrac{1}{2} \sum_n \int_{-\infty}^{\infty} e^{-\imath(\omega-2\pi\nu)t} e^{-(t-n/f_{rep})^2/T^2} dt \ , \end{aligned} \tag{54.29}$$

where neglect negative frequency components. Using the rules,

$$\mathcal{F}[f(t)e^{\imath\Omega t}] = \int_{-\infty}^{\infty} e^{-\imath\omega t} f(t) e^{\imath\Omega t} dt = (\mathcal{F}f)(\omega - \Omega) \tag{54.30}$$

$$\text{and} \qquad \mathcal{F}[f(t-T)] = \int_{-\infty}^{\infty} e^{-\imath\omega t} f(t-T) dt = e^{-\imath\omega T}(\mathcal{F}f)(\omega)$$

$$\text{and} \qquad \mathcal{F}[e^{-t^2/T^2}] = \int_{-\infty}^{\infty} e^{-\imath\omega t} e^{-t^2/T^2} dt = T\sqrt{\pi} e^{-T^2\omega^2/4}$$

we get,

$$E(\omega) = \mathcal{F}[E(t)] = \tfrac{1}{2} T\sqrt{\pi} e^{-T^2(\omega-2\pi\nu)^2/4} \sum_n e^{-\imath(\omega-2\pi\nu)n/f_{rep}} \ . \tag{54.31}$$

We now write the pump laser frequency as,

$$\nu \equiv m f_{rep} + f_{ceo} \ , \tag{54.32}$$

where we set $m \in \mathbb{N}$ and call $|f_{ceo}| < f_{rep}$ the *carrier envelope offset*. We also express the Fourier frequency by,

$$\omega \equiv 2\pi(\eta f_{rep} + f_{ceo}) \ , \tag{54.33}$$

firstly *without* specifying that η be an integer number. The spectrum is,

$$|E(\omega)|^2 = \tfrac{1}{4}\pi T e^{-T^2(\omega-2\pi\nu)^2/2} \left| \sum_n e^{-2\pi i n(\eta-m)} \right|^2 \ , \tag{54.34}$$

which only gives contributions for,

$$\eta = \frac{\omega - 2\pi f_{ceo}}{2\pi f_{rep}} \in \mathbb{N} \ . \tag{54.35}$$

I.e. the spectrum of comb frequencies is,

$$\boxed{|E(\omega)|^2 = \tfrac{1}{4}\pi T e^{-T^2(\omega-2\pi\nu)^2/2} \sum_n \delta[\omega - (n f_{rep} + f_{ceo})]} \ . \tag{54.36}$$

The δ-function comes from the fact that the sum of (54.35) over many oscillations $e^{-2\pi i n(\eta-m)}$ vanishes by destructive interference, except when they are *in phase*, which is just the case when $\omega = n f_{rep} + f_{ceo}$.

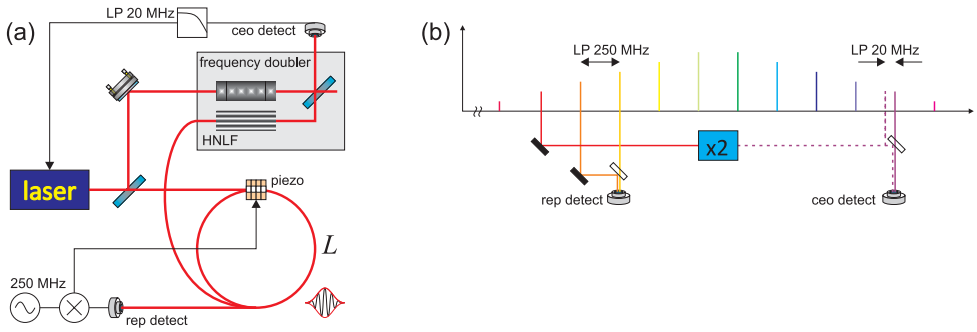

Figure 54.17: (a) Scheme and (b) operation principle of a frequency comb with control of the repetition rate and the carrier envelope offset.

54.4.2.2 Mode-locking of a frequency comb

From Eq. (54.28) we see that *mode-locking* is achieved when,

$$\frac{\nu}{f_{rep}} = m + \frac{f_{ceo}}{f_{rep}} \in \mathbb{N} \ , \tag{54.37}$$

which implies $f_{ceo} = 0$. Eq. (54.36) then becomes,

$$|E(\omega)|^2 = \frac{\pi T}{4} e^{-T^2(\omega-2\pi\nu)^2/2} \sum_n \delta(\omega - n f_{rep}) \ , \tag{54.38}$$

which means that all comb frequencies are locked.

54.4.2.3 Referencing radio and optical frequencies

In a frequency comb f_{rep} is easy to measure, as one just has to filter the beat of the comb light with a low pass filter cutting off frequency components higher than f_{rep}, as illustrated in Fig. 54.17. In contrast, measuring f_{ceo} is more complicated. Unless we have an octave spanning frequency comb, i.e. there are two frequencies in the comb,

$$\nu_1 = m_1 f_{rep} + f_{ceo} \quad \text{and} \quad \nu_2 = m_2 f_{rep} + f_{ceo} \ , \tag{54.39}$$

such that $\nu_2 = 2\nu_1 + \Delta\nu$ with $|\Delta\nu| < |f_{ceo}|$, i.e. $m_2 = 2m_1$. We get,

$$m_2 f_{rep} + f_{ceo} = 2m_1 f_{rep} + 2f_{ceo} + \Delta\nu \ , \tag{54.40}$$

or,

$$f_{ceo} = -\Delta\nu \ . \tag{54.41}$$

54.4.2.4 Dual comb spectroscopy

Optical sensors are based on the interaction of light with matter and are often implemented like some kind of spectrometer. The ideal sensor should detect a given substance with great sensitivity, identify it (especially in the presence of many other substances or a noisy background) and quantify it. Add to these features the ability to perform measurements in real time, if possible remotely, in a compact and easy-to-use assembly at affordable price, and we have an absolutely non-trivial problem. Broadband sources allow to detect multiple substances, but have limitations in resolution, calibration or acquisition time. Monochromatic sources allow good resolution, but in general have limitations on tunability and spectral coverage. The sensitivity can be increased by increasing the optical path of interaction, requiring multi-pass cells or resonant optical cavities, which augment the complexity of the setup. Finally, the detection method places limits on the acquisition rate and also on the sensitivity. Particularly the Fourier transform spectroscopy uses broadband incoherent light sources and the time of acquisition and resolution are limited by the speed of translation of a mechanical stage, as well as the range of its displacement. Here, the use of optical frequency combs replacing the incoherent sources, combined with *dual comb spectroscopy*, brings important advantages [1337, 613].

54.4.3 Multi-photon spectroscopy

54.4.4 Raman spectroscopy

Raman spectroscopy is a spectroscopic technique typically used to determine vibrational modes of molecules, although rotational and other low-frequency modes of systems may also be observed. Raman spectroscopy is commonly used in chemistry to provide a structural fingerprint by which molecules can be identified. Raman spectroscopy relies upon inelastic scattering of photons, known as Raman scattering. A source of monochromatic light, usually from a laser in the visible, near infrared, or near ultraviolet range is used, although X-rays can also be used. The laser light interacts with molecular vibrations, phonons or other excitations in the system, resulting in the energy of the laser photons being shifted up or down. The shift in energy

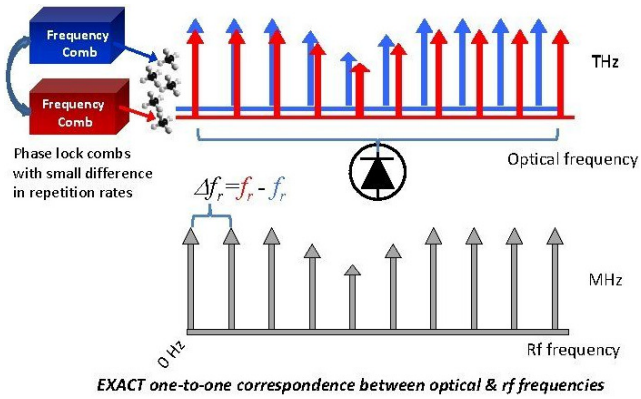

Figure 54.18: Principle of dual comb spectroscopy.

gives information about the vibrational modes in the system. Infrared spectroscopy typically yields similar, complementary, information.

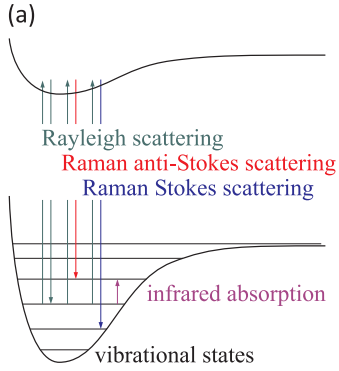

Figure 54.19: Energy-level diagram showing the states involved in Raman spectra.

Typically, a sample is illuminated with a laser beam. Electromagnetic radiation from the illuminated spot is collected with a lens and sent through a monochromator. Elastic scattered radiation at the wavelength corresponding to the laser line (Rayleigh scattering) is filtered out by either a notch filter, edge pass filter, or a band pass filter, while the rest of the collected light is dispersed onto a detector.

Spontaneous Raman scattering is typically very weak; as a result, for many years the main difficulty in collecting Raman spectra was separating the weak inelastically scattered light from the intense Rayleigh scattered laser light (referred to as 'laser rejection'). Historically, Raman spectrometers used holographic gratings and multiple dispersion stages to achieve a high degree of laser rejection. In the past, photomultipliers were the detectors of choice for dispersive Raman setups, which resulted in long acquisition times. However, modern instrumentation almost universally employs notch or edge filters for laser rejection. Dispersive single-stage spectrographs, for example Czerny-Turner (CT) monochromators (see Sec. 54.1.5), paired with CCD

detectors are common.

The name 'Raman spectroscopy' typically refers to vibrational Raman using laser wavelengths which are not absorbed by the sample. Raman spectroscopy is used in chemistry to identify molecules and study chemical bonding and intramolecular bonds. Because vibrational frequencies are specific to a molecule's chemical bonds and symmetry (the fingerprint region of organic molecules is in the wavenumber range $500 - 1500\,\mathrm{cm}^{-1}$, Raman provides a fingerprint to identify molecules.

In solid-state physics, Raman spectroscopy is used to characterize materials, measure temperature, and find the crystallographic orientation of a sample. As with single molecules, a solid material can be identified by characteristic phonon modes. Information on the population of a phonon mode is given by the ratio of the Stokes and anti-Stokes intensity of the spontaneous Raman signal. Raman spectroscopy can also be used to observe other low frequency excitations of a solid, such as plasmons, magnons, and superconducting gap excitations. Distributed temperature sensing (DTS) uses the Raman-shifted backscatter from laser pulses to determine the temperature along optical fibers.

54.4.5 Time-resolved spectroscopy

pump-probe spectroscopy

54.5 Further reading

G.C. Bjorklund, *Frequency-Modulation Spectroscopy: A new Method for Measuring Weak Absorptions and Dispersions* [147]DOI

J.L. Hall et al., *Optical Heterodyne Saturation Spectroscopy* [576]DOI

J.J. Snyder et al., [1225]DOI

R.K. Kaj et al., *High-Frequency Optically Heterodyned Saturation Spectroscopy via Resonant Degenerate Four-Wave Mixing* [692]DOI

G. Camy et al., *Heterodyne Saturation Spectroscopy through Frequency Modulatiof the Saturating Beam* [231]DOI

M. Ducloy et al., *Theory of Degenerate Four-Wave Mixing in Resonant Doppler-Broadened Media II* [393]DOI

J.H. Shirley, *Modulation Transfer Processes in Optical Heterodyne Saturation Spectroscopy* [1201]DOI

A. Schenzle et al., *Phase Modulation Laser Spectroscopy* [1153]DOI

L. Hollberg et al., *Measurement of the shift of Rydberg energy levels incuded by blackbody radiation* [628]DOI

L.S. Ma et al., *Optical Heterodyne Spectroscopy Enhanced by an External Optical Cavity: Toward Improved Working Standards* [831]DOI

L.S. Ma et al., *Spectroscopy of Te2 with Modulation Transfer Reference Lines for Precision Spectroscopy in Yb* [830]$_{\text{DOI}}$

Chapter 55

Locking circuits

In a laboratory we are often confronted with the need to control the value of a physical parameter, f.ex., room temperature, currents and voltages, or the frequency and intensity of laser beams. The physical discipline dealing with the fundamental concepts of this field is called *control theory* and its application to development of automatic control systems is called *control engineering*.

In this chapter, after a brief introduction into *control theory*, we will design and construct a few automatic control systems, which are common in quantum optics labs.

55.1 Introduction to control theory

The minimum ingredients of a control system are 1. a *sensor* measuring the actual value of the parameter to be controlled (e.g., a thermometer), 2. an *actuator* capable of correcting the value (e.g., a heater or cooler), and 3. a suitable *controller* (*servo system*) linking sensor and actuator thus providing a feedback.

The controller comprises a *comparator* comparing the measured value with a reference and delivers the difference to a controller, which may be implemented electronically by proportional control, *PID control*, bistable hysteretic control, or programmable logic control. Older controller units have been mechanical, as in a carburetor. Finally, the value computed by the controller is delivered to an actuator, which manipulates and changes a variable in the controlled system (or *plant*).

55.1.1 Open- and closed-loop control

Fundamentally, there are two types of control loop: *open loop* control, and *closed loop* (feedback) control.

In open loop control, the control action from the controller is independent of the 'process output' (or 'controlled process variable'). An example of this is a central heating boiler controlled only by a timer, so that heat is applied for a constant time, regardless of the temperature of the building. The control action is the switching on/off of the boiler. The process output is the building temperature.

In closed loop control, the control action from the controller is dependent on the process output. In the case of the boiler analogy, this would include a thermostat to monitor the building temperature, and thereby feed back a signal to ensure the controller maintains the building at the temperature set on the thermostat. A closed loop controller therefore has a feedback loop which ensures the controller exerts a

control action to give a process output the same as the 'reference input' or 'set point'. For this reason, closed loop controllers are also called feedback controllers.

The definition of a closed loop control system is *a control system capable of canceling the deviation of a system variable from a reference value by means of a feedback signal computed from a measured value of the variable and used to act on the system in a controlled way* [1249]. Automatic feedback control has revolutionized all areas of human activities.

To overcome the limitations of the open-loop controller, control theory introduces *feedback*. A closed-loop controller uses feedback to control states or outputs of a dynamical system. Its name comes from the information path in the system: process inputs (e.g. voltage applied to an electric motor) have an effect on the process outputs (e.g. speed or torque of the motor), which is measured with sensors and processed by the controller; the result (the control signal) is 'fed back' as input to the process, closing the loop.

Closed-loop controllers have the following advantages over open-loop controllers:

- disturbance rejection (such as hills in the cruise control example above)
- guaranteed performance even with model uncertainties, when the model structure does not match perfectly the real process and the model parameters are not exact
- unstable processes can be stabilized
- reduced sensitivity to parameter variations
- improved reference tracking performance

In some systems, closed-loop and open-loop control are used simultaneously. In such systems, the open-loop control is termed feedforward and serves to further improve reference tracking performance.

55.1.1.1 Closed-loop transfer function

Due to noise the variables of the system become time-dependent. The output of the system $y(t)$ is fed back through a sensor measurement F to a comparison with the reference value $r(t)$. The controller C then takes the error $e(t)$ (difference) between the reference and the output to change the inputs $u(t)$ to the system under control P. This is shown in the figure. This kind of controller is a closed-loop controller or feedback controller. We will restrain here to *single-input-single-output control* systems (SISO) disregarding the possibility of having multiple and interdependent inputs and outputs.

If we assume the controller C, the plant P, and the sensor F are linear and time-invariant (i.e. elements of their transfer function $C(s)$, $P(s)$, and $F(s)$ do not depend on time), the systems above can be analyzed using the Laplace transform on the variables, $U(s) = \mathcal{L}u(t)$, $Y(s) = \mathcal{L}y(t)$, and $R(s) = \mathcal{L}r(t)$. Here,

$$s \equiv \imath f \tag{55.1}$$

is an abbreviation for the imaginary Fourier frequency component f of the noise. In the following sections we will, however, characterize the transfer functions in terms

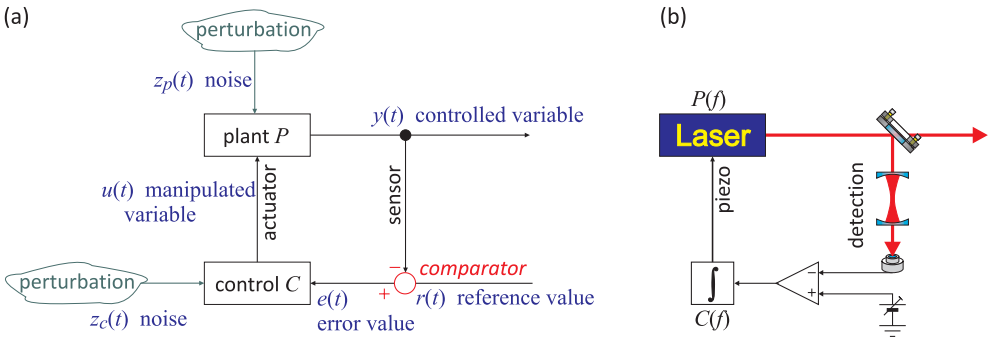

Figure 55.1: (a) General schematic diagram of a feedback loop. (b) Possible implementation for the frequency stabilization of a laser to a cavity resonance,

of real Fourier frequencies. The theoretical foundation of Linear Time-Independent (LTI) systems is outsourced to Sec. 56.2.

For a control to work, it needs to know in which direction to act and when the control point is reached. Therefore, each control needs a slope (*discriminator*) crossing zero. This can be implemented by comparing the signal $Y(f)$ delivered by the detector (for simplicity assumed to be frequency-independent) with a reference signal R. The error signal $E(f) = R(f) - Y(f)$ is then processed by a controller C, and the control signal $U(f)$ is passed, via an actuator (for simplicity assumed to be frequency-independent), to the controlled device P. The controlled device (and obviously all other components of the circuit) are subject to perturbations Z. The transfer functions form a closed control circuit described by the following relations:

$$Y(f) = P(f)U(f) \quad \text{and} \quad U(f) = C(f)E(f) \quad \text{and} \quad E(f) = R(f) - Y(f)\,. \tag{55.2}$$

Solving the system of equations (55.2) for $Y(f)$ in terms of $R(f)$ gives,

$$\boxed{Y(f) = \frac{P(f)C(f)}{1 + P(f)C(f)}\, R(f) \equiv H(f)R(f)}\,. \tag{55.3}$$

$H(s)$ is referred to as the closed-loop transfer function of the system. The numerator $V(f) \equiv P(f)C(f)$ is called the *forward gain* (*open-loop gain*) from R to Y, and the denominator is one plus the gain in going around the feedback loop, the so-called *loop gain*. If $|P(f)C(f)| \gg 1$, i.e. it has a large norm with each value of f, and then $Y(f) \simeq R(f)$ and the output closely tracks the reference input.

55.1.1.2 Noise reduction via feedback circuits

We have seen that the idea of *locking*, whether mechanical or electronic, is to bring a given physical signal Y to a predetermined value R and lock it there, which is the role of the control circuit or *regulator*. Now, considering a possible perturbation of the plant (see Fig. 55.1) by noise Z_p and also of the regulator by noise Z_c, the result (55.3) must be generalized,

$$Y(f) = \frac{P(f)C(f)}{1 + P(f)C(f)} R(f) + \frac{P(f)C(f)}{1 + P(f)C(f)} Z_c(f) + \frac{1}{1 + P(f)C(f)} Z_p(f)\,, \tag{55.4}$$

or,

$$\boxed{Y(f) = \frac{1}{1+V(f)^{-1}}[R(f)+Z_c(f)] + \frac{1}{1+V(f)}Z_p(f)} \,. \tag{55.5}$$

This shows that, provided the open loop gain is high enough, perturbations affecting the plant can be efficiently be neutralized. In contrast, noise entering via the control cannot be suppressed, and this fact is independent on the chosen controller transfer function: *Perturbations entering between the measurement point and the input of the regulator are not eliminated*! Consequently, the detector (which generally works with very low signals) should not introduce or let penetrate noise, because this affects the variable to be controlled: Any variation of the steering variable at the regulator will be transmitted 1 to 1.

In the following, we will discuss the most common controller called PID-servo.

55.1.2 PID feedback control

A *PID controller* continuously calculates an error value $e(t)$ as the difference between a desired setpoint and a measured process variable and applies a correction based on proportional, integral, and derivative terms. PID is an acronym for Proportional-Integral-Derivative, referring to the three terms operating on the error signal to produce a control signal.

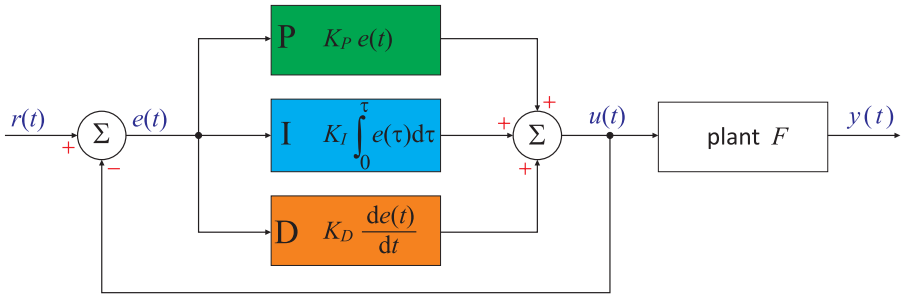

Figure 55.2: A block diagram of a PID controller in a feedback loop, $r(t)$ is the desired process value or 'set point', and $y(t)$ is the measured process value. A proportional-integral-derivative controller (PID controller) is a control loop feedback mechanism control technique widely used in control systems.

The theoretical understanding and application dates from the 1920s, and they are implemented in nearly all analogue control systems; originally in mechanical controllers, and then using discrete electronics and latterly in industrial process computers. The PID controller is probably the most-used feedback control design.

If $u(t)$ is the control signal sent to the system, $y(t)$ is the measured output and $r(t)$ is the desired output, and tracking error $e(t) = r(t) - y(t)$, a PID controller has the general form,

$$\boxed{u(t) = K_P e(t) + K_I \int e(\tau)d\tau + K_D \frac{de(t)}{dt}} \,. \tag{55.6}$$

The desired closed loop dynamics is obtained by adjusting the three parameters K_P, K_P, and K_I, often iteratively by 'tuning' and without specific knowledge of a plant model. Stability can often be ensured using only the proportional term. The integral term permits the rejection of a step disturbance (often a striking specification in process control). The derivative term is used to provide damping or shaping of the response [1].

Applying Laplace transformation results in the transformed PID controller equation,

$$\boxed{U(f) = \left(K_P + K_I \frac{1}{\imath f} + K_D \imath f\right) E(f) \equiv C(f)E(f)}\,, \tag{55.7}$$

defining the PID controller transfer function $C(f)$.

From equations (55.6) or (55.7) we immediately see that the PID transfer functions can readily be implement in electronic circuits using resistors (P), capacitors (I), and inductances (D).

Example 302 (*Comparing servo controllers*): We now assume a low-pass behavior for the plant,

$$P(f) = \frac{1}{1 + \imath f/f_c}\,,$$

and analyze the feedback circuit for four cases.

- The first one is that of a proportional servo, $C(f) = K_P$. Then, Eq. (55.5) reads,

$$Y = \frac{K_P}{1 + \imath f/f_c + K_P}(R + Z_c) + \frac{1 + \imath f/f_c}{1 + \imath f/f_c + K_P} Z_p$$
$$\begin{cases} \stackrel{s\to 0}{\longrightarrow} \frac{K_P}{1+K_P}(R + Z_c) + \frac{1}{1+K_P} Z_p \\ \stackrel{s\to\infty}{\longrightarrow} \frac{K_P f_c}{\imath f}(R + Z_c) + Z_p \end{cases}.$$

  We see that, for limited open-loop gain, noise affecting the plant Z_p is not eliminated at low frequencies. Additionally, at high frequencies, the gain for the error signal R drops like -6dB/oct.

- The second case is that of an integral servo $C(f) = K_I/\imath f$. Then Eq. (55.5) reads,

$$Y = \frac{K_I/\imath f}{1 + \imath f/f_c + K_I/\imath f}(R + Z_c) + \frac{1 + \imath f/f_c}{1 + \imath f/f_c + K_I/\imath f} Z_p$$
$$\begin{cases} \stackrel{f\to 0}{\longrightarrow} R + Z_c + \frac{\imath f}{K_I} Z_p \\ \stackrel{\to\infty}{\longrightarrow} \frac{K_I f_c}{(\imath f)^2}(R + Z_c) + Z_p \end{cases}.$$

  Apparently, the noise Z_p is now eliminated at low frequencies. However, the gain for R drops even faster at high frequencies.

[1] PID controllers are the most well established class of control systems: however, they cannot be used in several more complicated cases, especially if MIMO systems are considered.

- The third case is that of a PI-servo, $C(f) = K_P + K_I/\imath f$. Then Eq. (55.5) reads,

$$Y = \frac{K_P + K_I/\imath f}{1 + \imath f/f_c + K_P + K_I/\imath f}(R + Z_c) + \frac{1 + \imath f/f_c}{1 + \imath f/f_c + K_P + K_I/\imath f} Z_p$$
$$\begin{cases} \stackrel{f\to 0}{\longrightarrow} R + Z_c + \frac{\imath f}{K_I} Z_p \\ \stackrel{f\to\infty}{\longrightarrow} \frac{f_c K_P}{\imath f}(R + Z_c) + Z_p \end{cases},$$

  which represents a viable compromise, since it has the same low-frequency behavior as the I-servo, but at high frequencies the gain for R drops only like -6dB/oct.

- Finally, the forth case is that of a PID-servo, $C(f) = K_D \imath f + K_P + K_I/\imath f$. Then Eq. (55.5) reads,

$$Y = \frac{K_D \imath f + K_P + K_I/\imath f}{1 + \imath f/f_c + K_D \imath f + K_P + K_I/\imath f}(R + Z_c) + \frac{1 + \imath f/f_c}{1 + K_D \imath f + K_P + K_I/\imath f} Z_p$$
$$\begin{cases} \stackrel{f\to 0}{\longrightarrow} R + Z_c + \frac{\imath f}{K_I} Z_p \\ \stackrel{f\to\infty}{\longrightarrow} \frac{1}{1+1/f_c K_d}(R + Z_c) + \frac{1}{f_c K_D} Z_p \end{cases}.$$

  The low-frequency behavior remains still the same, but at high frequencies the gain for R stays constant.

A time domain analysis shows that P regulators have little phase lag, but the controlled variable can not be zeroed. On the other hand, I regulators have finite control bandwidth, but the controlled variable can be zeroed. PI regulators (parallel circuit of P and I regulators) have a reaction time $T_n = K_P/K_I$; that is, the jump response is advanced by T_n in comparison to the regulator I.

In the time domain we can summarize that regulators

- D are characterized by the absence of memory, but they are very fast,
- P have no idea of the strength of their impact,
- I increase their impact in time until the error disappears.

For practical PID controllers, a pure differentiator is neither physically realizable nor desirable due to amplification of noise and resonant modes in the system. Therefore, a phase-lead compensator type approach is used instead, or a differentiator with low-pass roll-off [635, 461, 462, 1306]. See Excs. 55.2.3.1 and 55.2.3.2.

Like any real system, the controlled device behaves as a low-pass for manipulations or perturbations at high frequency. In other words, the device can only respond to external perturbations with finite speed. This delay of the response leads to a phase shift that can reverse the sign of the error signal $E(f)$ and transform a negative feedback into a positive feedback. Now, in the case that there are high frequency perturbations, for which the amplification of the closed control circuit is > 1, these perturbations can be amplified to form oscillations. These oscillations, which occur at the bandwidth of the closed loop gain are called *servo oscillations*.

Fig. 55.3 illustrates the necessity of optimizing the gain and the frequency response of the servo circuit: A proportional servo simply providing a frequency-independent gain $C(f) = K_P$ will lead to a forward gain $R(f) \propto P(f)$ exhibiting a low-pass behavior, i.e. a phase-shift $\phi = -\pi/2$ transforming negative to positive feedback. The gain at the frequency where this happens need to be lower than 1, otherwise the feedback servo will generate servo-oscillations, i.e. it will oscillate at the lowest Fourier frequencies where noise is amplified. A PI-servo alleviates this problem by a phase shift in opposite direction.

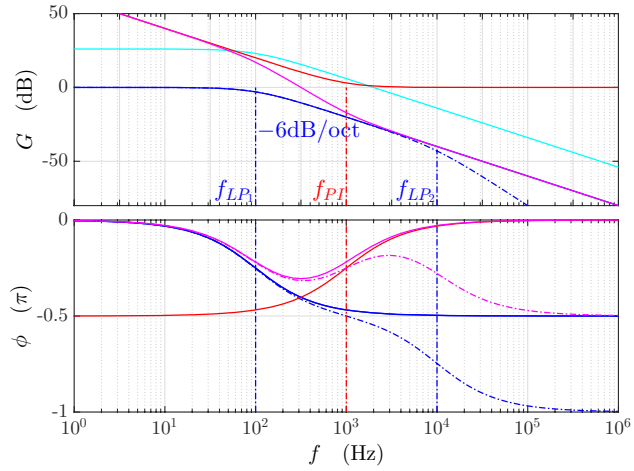

Figure 55.3: (code) Bode diagram for a plant subject to low-pass behavior and for a PI-servo. (blue solid) Low-pass filter with 100 Hz bandwidth; (blue dash-dotted) another low-pass filter at 100 kHz; (cyan) same as blue, but amplified by 20 dB; (red) PI-servo; (magenta) open-loop amplification.

55.1.3 Noise transfer in feedback loops

In order to develop a model for noise transfer we must understand what noise is and how it can be measured. This is not a simple task and we therefore outsourced a proper discussion to Sec. 56.3. Here, we will only use the information that noise affecting a signal $y(t)$ is quantified by a *spectral noise density* defined as the Fourier transform of the signal's autocorrelation function (56.59),

$$S_y(f) \equiv \mathcal{F}[\overline{y^*(t)y(t+\tau)}] \; . \tag{55.8}$$

Now, we can see how noise is transmitted through an LTI device $P(f)$:

$$\boxed{Y(f) = P(f)X(f) \quad \Rightarrow \quad S_y(f) = |P(f)|^2 S_x(f)} \; . \tag{55.9}$$

This result can be applied to our formula (55.5) describing a feedback loop,

$$\boxed{S_y(f) = \left|\frac{1}{1+V(f)^{-1}}\right|^2 S_c(f) + \left|\frac{1}{1+V(f)}\right|^2 S_p(f)} \; . \tag{55.10}$$

This formula describes how a servo control shapes the noise spectrum of a feedback-controlled variable $y(t)$.

Example 303 (*Noise reduction by feedback*): As an example, let us study the control circuit for stabilizing a laser to a cavity mode depicted in Fig. 55.1(b) using the following additional background information: The laser frequency ω be perturbed by $1/f$ noise described by the power spectral density,

$$S_p(f) \equiv 2 \cdot 10^{-24}/f \ .$$

This noise enters the feedback loop via the fluctuations $z_p(t)$ depicted in

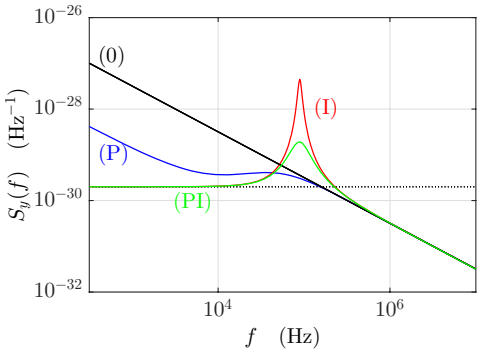

Figure 55.4: (code) Spectral density of frequency fluctuations of the servo system exhibited in Fig. 55.2. Shown is the spectral noise density $S_y(f)$ of the laser light for 4 different feedback gain curves: (black solid) no feedback control $C(f) = 0$, (blue) P-regulator with $C(f) = 4$, (red) I-regulator with $C(f) = 5 \cdot 10^6/\imath f$, and (green) PI-regulator $C(f) = 4 + 5 \cdot 10^6/\imath f$.

Fig. 55.1(a). The black solid line in Fig. 55.4 traces the noise spectrum $S_p(f)$, which is also the noise expected for the laser without feedback loop. Furthermore the optical cavity, which constitutes the essential part of the regulator, is itself afflicted by acoustic noise and thermal drifts which, for simplicity, we describe by a white Fourier frequency spectrum given by,

$$S_c(f) \equiv 2 \cdot 10^{-30}\,\mathrm{Hz}^{-1} \ ,$$

and represented by the black dotted line in Fig. 55.4. As we have seen, servos systems always have a finite bandwidth beyond which noise is fully coupled to the system. For example in laser frequency locks, the weakest point of a servo chain is often the small bandwidth of a piezo transducer used to correct the length of the laser cavity. We describe this behavior by a low-pass filter for the transfer function of the laser,

$$P(f) = \frac{1}{1 + \imath f/f_c}$$

with a bandwidth of $f_c = 10\,\mathrm{kHz}$.
Fig. 55.4 demonstrates how the $1/f$ noise $S_p(f)$ can be efficiently suppressed at frequencies below the low-pass filter cut-off f_c to a value limited by the white noise $S_c(f)$ entering through the regulator. As predicted by the formula (55.10), the suppression of the noise $S_p(f)$becomes all the better, as the open-loop gain

$V(f)$ gets higher. However, with the amplification of the controller, also the gain of the closed control circuit increases, and this necessarily causes phase shifts, which lead to (servo-)oscillations in the circuit appearing as a strong peak of strong noise around a certain Fourier frequency f_{bw} characterizing the bandwidth of the closed loop servo system. Note that high-frequency noise, to which the cavity might be subject, is not coupled to the laser, because it is filtered by the low-pass filter $P(f)$ to the same extend as the error signal itself.

The next example, exhibited in Fig. 55.5, shows the experimental characterization of a dye laser locked via the Pound-Drever-Hall technique (see Sec. 55.3.3) to an optical cavity.

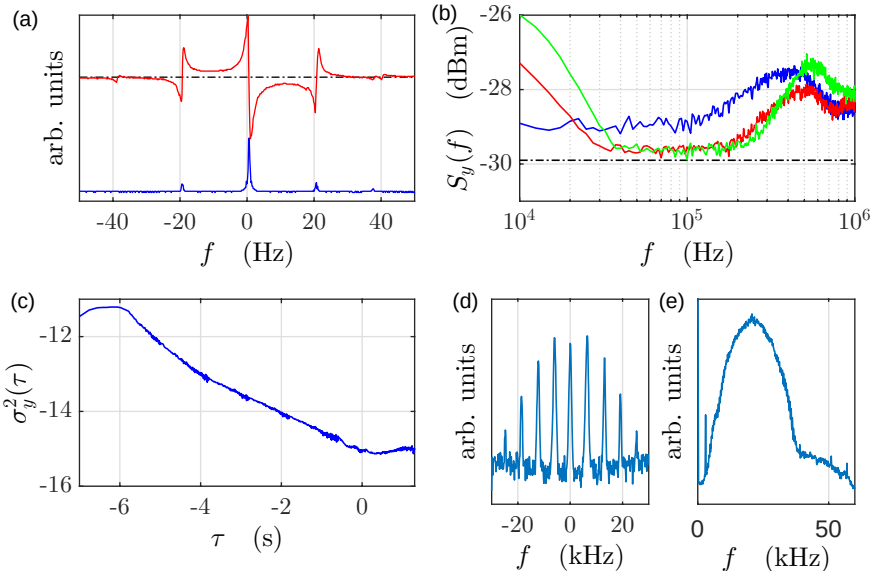

Figure 55.5: Characterization of a Pound-Drever-Hall stabilization of a dye laser. (a) PDH error signal (red) and cavity transmission signal (blue), (b) spectral density of frequency fluctuations, (c) Allan variance. (d-e) Beat signals of Mach-Zehnder interferometers. In (d) one interferometer arm is passed through an optical fiber attached to a piezo transducer to which a sinusoidal 5 kHz modulation of is applied. This demonstrates the sensitivity of optical fibers to acoustic noise. In (e) one interferometer arm is send to another optical table and back. This demonstrates how mechanical vibrations of optical components in the beam path can broaden the spectrum of a laser field.

55.2 Amplitude stabilization circuits

55.2.1 Laser intensity stabilization with an AOM

The light emitted from lasers is generally subject to *frequency fluctuations* and *intensity fluctuations*, which are unacceptable for many applications. In this section we will construct an *intensity stabilization* for a laser beam.

One way of stabilizing the light intensity of a laser beam consists in using the an acousto-optic modulator, as shown in Fig. 55.6. The first Bragg diffraction order (see Sec. 53.3.1) is focused onto a photodiode. Intensity fluctuations of the light recorded by the photodiode are converted into voltage fluctuations, processed by an electronic circuit fed back to the AOM. The intensity of light diffracted into the first order can be controlled via the power of the radiofrequency alimenting the AOM. The control circuit can now be conceived such as to neutralize the intensity fluctuations recorded by the photodiode.

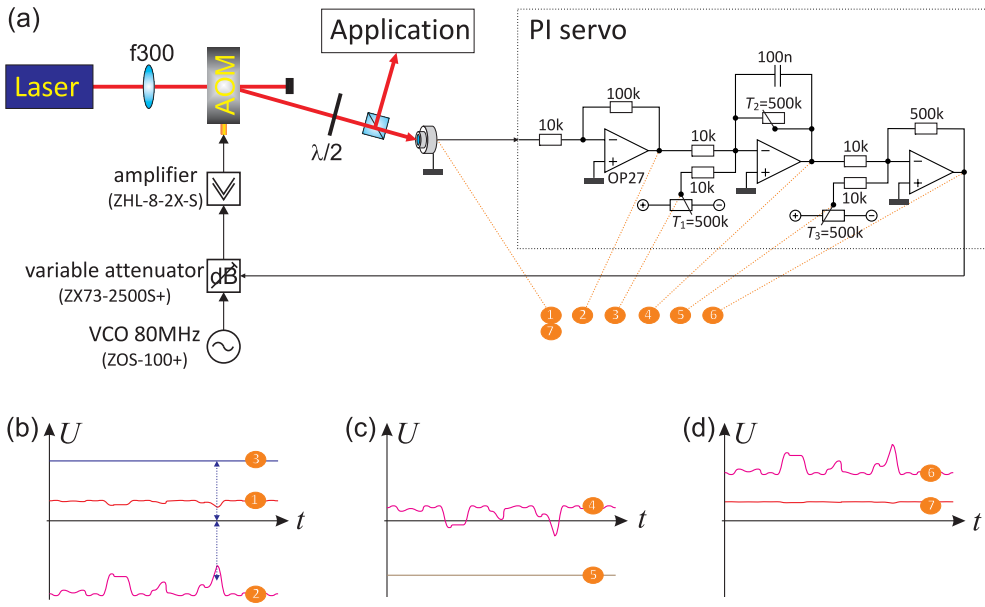

Figure 55.6: (a) Layout of the intensity control. The variable attenuator controls the amplitude of the radiofrequency driving the AOM: low voltage (0 V) increases the attenuation, high voltage (+16 V) reduces it. The sketched control circuit realizes a negative feedback, when the photodetector produces a positive signal. (b-d) Signals recorded at the test points of the circuits shown in (a). See text for explanations.

55.2.1.1 Operation principle and adjustment procedure

The idea of the intensity stabilization is illustrated in Fig. 55.6(b-d): The laser intensity scattered into the first diffraction order is recorded by a photodiode (test point 1 in the figure). The signal is then amplified (and inverted) by a first OpAmp (test point 2). The trimmer T_1 (test point 3) is now adjusted to a positive voltage compensating the DC part of the signal (2), i.e., the sum (2+3) after being inverted and amplified by the second OpAmp (test point 4), should be around zero DC. The signal (2+3) is called *error signal*, since it is this signal which tells us in which direction the control circuits has to work to counteract the power fluctuation. In the present design, the second OpAmp also incorporates the PI servo (see Sec. 55.1), which can be adjusted via the amplification of the trimmer T_2 and the capacity C.

It is now important to realize, that the variable attenuator works best around a given control voltage, which is provided by adding via the trimmer T_3 (test point 5) and a third OpAmp an appropriate offset. Furthermore, we note that variable attenuator reduces its attenuation with increasing control voltage. Thus, the control signal (test point 6) works to enhance the efficiency of the AOM, when the photodiode signals a power drop, and vice versa. As a result, the light power in the first diffraction order is stabilized, however, at a level inferior to the unstabilized power [1306, 462].

The trimmers of the servo circuits can be adjusted using the following procedure:

1. Observe the light intensity and its fluctuations at test point (1), set test point (4) to ground (e.g. short-circuiting the trimmer T_2), and adjust trimmer T_3 until the light intensity level is at bit lower than the lowest fluctuations.

2. Reconnect test point (4) to the circuit and adjust trimmer T_1 until the voltage at test point (4) cancels to zero.

55.2.2 PI servo for a current stabilization

Many applications in quantum optics require very stable high currents, for instance, in coils generating magnetic field for atomic trapping potentials. Here, we will construct a *PI servo* to para realize a *current stabilization*.

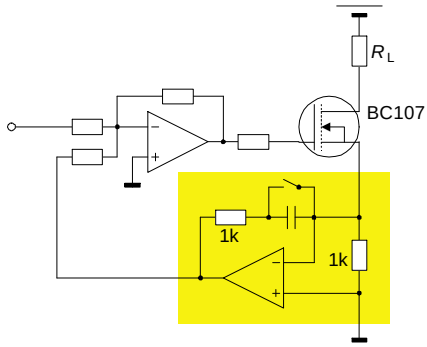

Figure 55.7: Current stabilization.

55.2.3 Exercises

55.2.3.1 Ex: Integrator

Determine the transfer function of the circuit depicted in Fig. 55.8. What kind of control circuit is it?

Solution: *The transfer function is that of a PI-servo,*

$$G(\omega) = -\frac{1}{R_1}\left(R_n + \frac{1}{\imath f C}\right) .$$

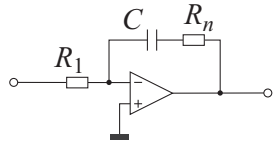

Figure 55.8:

55.2.3.2 Ex: PID controller

Consider the PID controller transfer function in series,

$$C(f) = K\left(1 + \frac{1}{\imath f T_I}\right)(1 + \imath f T_D) \ ,$$

a first-order low-pass filter in the feedback loop,

$$F(f) = \frac{1}{1 + \imath f T_F} \ ,$$

and a linear actuator with low-pass behavior,

$$P(f) = \frac{A}{1 + \imath f T_P} \ .$$

How do you have to choose the various time constants in order to let the closed-loop transfer function be $H(f) = 1$.

Solution: *Insert the components C, F, and P into the expression for closed-loop transfer function $H(f)$, then tuning is very easy simply choosing,*

$$K = \frac{1}{A} \quad , \quad T_I = T_F \quad , \quad T_D = T_P$$

and get $H(f) = 1$ identically.

55.2.4 *Experiment: Development of an intensity stabilization*

We will now set up up an intensity stabilization. For the realization of the project prior knowledge of 1. photodetectors (see Sec. 52.2.1), 2. acousto-optic modulators (AOM) (see Sec. 53.3.1), 3. electronic circuits (see Sec. 52.1.3), and 4. control circuits (see Sec. 55.1) is required.

1. Realize the optical setup illustrated in Fig. 55.6. Optimize the alignment of the AOM (in particular, the focus and the Bragg angle) in order to maximize the efficiency of the AOM. Take care not to saturate the photodiode, if necessary adapt the load resistance (see Sec. 52.1.). Study the data sheet of the variable attenuator.

2. Derive and plot the transfer function for ac-signals of the electronic circuit. What kind of control circuit is it?

3. Set up the electronic circuit exhibited in Fig. 55.6. Test it by observing the signals at the six test points marked in the circuit diagram. Understand and interprete the roles of the three adjustable parameters: input offset, amplification, and output offset.

4. Incorporate the servo circuit into the optical setup as shown in Fig. 55.6. How to make sure the circuit is operating properly? [2].

55.2.5 *Experiment: PI servo for a current stabilization*

How to control high currents? How to dramatically increase the switching speed despite inductive loads and eddy currents?

1. Connect a resistive charge to a voltage source. Insert a *MOSFET* into the circuit and a small resistor. Control the gate of the MOSFET with a voltage and measure the current of the circuit via the voltage drop at the small resistor as a function of the gate voltage.

2. Now control the gate voltage via the voltage measured at the small resistor and measure again the dependency voltage-to-current.

55.3 Frequency stabilization circuits

Although lasers are often monochromatic, they generally have a poor intrinsic frequency stability, that is, the frequency of the light field $E(t) = \sin \omega t$ drifts in time, $\omega = \omega(t)$ on a time scale, which is slow in comparison to the oscillation period $1/\omega$. The reasons for these drifts are typically acoustic noise or thermal drifts to which the laser device is subject and which are difficult to avoid.

Often it is much easier to guarantee the mechanical and thermal stability of a passive device exhibiting resonances, such as an optical cavity. Furthermore, nature provides intrinsically stable resonances, such as narrow atomic transitions. These resonances can be used to actively stabilize the frequency of lasers via feedback servo circuits. In the following sections we will present a few common techniques.

55.3.1 Side-of-fringe stabilization to/of a Fabry-Pérot cavity

Resonances are generally characterized by peaked profiles symmetrically centered about a resonance frequency ω_0. Excited by a laser field of frequency ω, they respond by an oscillation whose amplitude depends on the detuning $\omega - \omega_0$. Unfortunately, the amplitude of the response signal does not tell us, whether the detuning is positive

[2] Datasheet for the VCO see appendix Fig. 56.16,
data sheet for the variable attenuator see appendix Fig. 56.17,
data sheet for the amplifier see appendix Fig. 56.15.

or negative. We have to invent techniques allowing us to extract this information from the response signal and to generate a true error signal.

One of these techniques is the *side-of-fringe stabilization* technique illustrated in Fig. 55.9. Here, the laser tuned to one side of the optical resonance such that, when the laser frequency drifts, the response signal increases or decreases correspondingly. Technically, this is achieved by comparing (i.e. subtracting) the response signal with a stable reference signal.

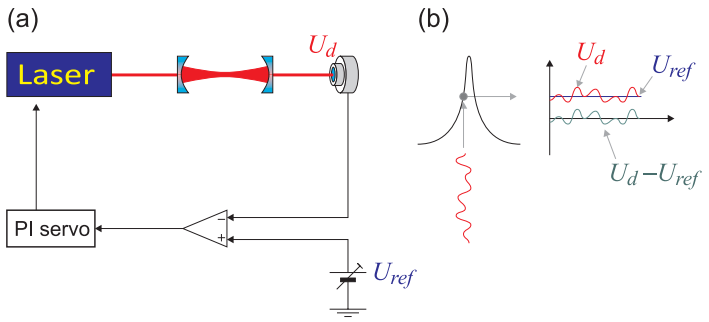

Figure 55.9: (a) Frequency stabilization to a cavity using the side-of-fringe method. (b) The laser is tuned to rising (or falling) slope of a transmission curve of a Fabry-Pérot cavity. The error signal is compared with reference voltage.

55.3.2 Lock-in method for frequency stabilizing to/of a cavity

One method of stabilizing a laser on a resonator consists in modulating the frequency slightly and then demodulating the transmission signal of the resonator at the same frequency. This is the so-called *lock-in method*. Frequency modulation of the laser beam can be done by modulating the laser diode feed current, the piezo of the extended laser cavity or using an AOM. Fig. 55.10 shows the layout of the optical assembly.

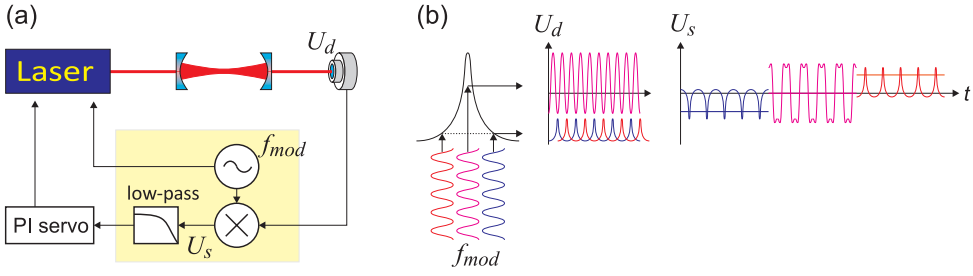

Figure 55.10: (a) Frequency stabilization to a cavity using the lock-in method. (b) Frequency-modulated signals applied to a resonance suffer a period doubling, when the signal frequency is close to resonance. By demodulating the signals discriminated at the resonance profile, we obtain, after averaging over a period, a DC voltage that is proportional to the frequency detuning. The yellow area denotes the components constituting the lock-in amplifier.

The principle of control through modulation is explained in Fig. 55.10(a). A laser beam passes twice (round-trip) through an *acousto-optic modulator* fed by a radiofrequency voltage with modulated frequency, $\omega(t) = \omega_c + M \cos ft$. Here, the modulation frequency is much lower than its amplitude (or frequency excursion), $f \ll M$. The laser beam is now injected into an optical cavity and the frequency of the laser tuned near a resonance of the cavity. The dependence of the transmission on the frequency is described in good approximation of the *Airy formula* by a Lorentzian,

$$I(\omega) = \frac{\gamma^2}{4(\omega - \omega_0)^2 + \gamma^2} \ . \tag{55.11}$$

The signal transmitted through the cavity [see Fig. 55.10(b)],

$$U_d(t) = I(\omega(t)) = \frac{\gamma^2}{4\left(\omega_c + M \cos ft - \omega_0\right)^2 + \gamma^2} \ , \tag{55.12}$$

is demodulated by a lock-in amplifier [see Fig. 55.10(c)],

$$U_s(t) = U_d(t) \cos(ft + \phi) \ , \tag{55.13}$$

integrated with a locking electronics [see Fig. 55.10(d)]

$$\bar{U}_s(t) = \frac{1}{T} \int_0^T U_s(t) dt \ . \tag{55.14}$$

and used to control the piezo of the laser's extended cavity.

55.3.3 Pound-Drever-Hall stabilization

When the frequency of a carrier wave ω is modulated by a frequency Ω [3], the spectrum consists of sidebands the frequencies and phases of which can be calculated from an expansion of the wave in Bessel functions. Let N be the modulation excursion and $J_k(x)$ the Bessel function of the order k. Higher-order sidebands $k > 1$ are usually dropped in the calculation,

$$e^{\imath(\omega t + N \sin \Omega t)} = e^{\imath\omega t}[-J_1(N)e^{\imath\Omega t} + J_0(N) + J_1(N)e^{-\imath\Omega t}] \ . \tag{55.15}$$

From the latter expression, it can be seen that the spectrum of sidebands is formed

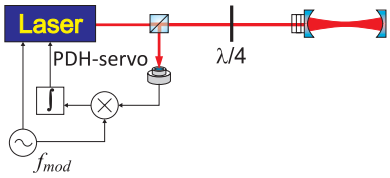

Figure 55.11: Frequency stabilization to a cavity using the Pound-Drever-Hall method.

by the frequencies ω and $\omega \pm \Omega$. A resonator responds to a field of incident light

[3] Remember that we specify all frequencies except the free spectral range δ_{fsr} in radians.

$E_0(\omega)$ oscillating with frequency ω by reflecting the field (R: reflectivity of mirrors, δ_{fsr}: free spectral range)

$$E_r(\omega) = E_0(\omega)\sqrt{R}\frac{1-e^{-\imath\omega/\delta_{fsr}}}{1-R\ e^{-\imath\omega/\delta_{fsr}}}\ , \tag{55.16}$$

where the amplitude and the phase of the reflected light field follow from the relation $E_r(\omega) = |E_r(\omega)|e^{\imath\phi(\omega)}$. Obviously the field of the reflected light is strong only, when the laser frequency is close to one mode of the resonator (when ω/δ is an integer number). By inserting Eq. (55.16) into Eq. (55.15), we obtain the response of the resonator to a field containing sidebands as a function of the frequency of light ω, of the modulation frequency Ω, and of the cavity finesse,

$$\begin{aligned}|E_{tot}|^2 &= |e^{\imath\omega t}[J_1(N)E_r(\omega+\Omega)e^{\imath\Omega t} + J_0(N)E_r(\omega) - J_1(N)E_r(\omega-\Omega)e^{-\imath\Omega t}]|^2 \\ &= J_0(N)J_1(N)E_r(\omega+\Omega)e^{\imath\Omega t} + J_0(N)J_1(N)E_r^*(\omega-\Omega)e^{\imath\Omega t} + ... + c.c.\ .\end{aligned} \tag{55.17}$$

The contributions of the reflected field to the current in the photodetector, $|E_r|^2$, oscillating with frequency Ω and extracted by the alternating current $e^{-i\Omega t+i\theta}$ (θ is an arbitrarily chosen phase angle), are

$$\begin{aligned}S_{PDH} &= |E_{tot}|^2 e^{-i\Omega t+i\theta} \\ &= J_0(N)J_1(N)\mathfrak{Re}\ \{e^{\imath\theta}[E_r^*(\omega)E_r(\omega+\Omega) - E_r(\omega)E_r^*(\omega-\Omega)]\} + ...\ .\end{aligned} \tag{55.18}$$

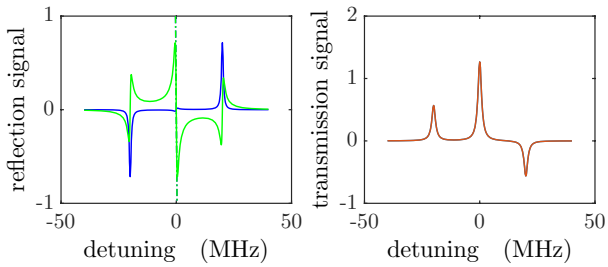

Figure 55.12: (code) (Left) Pound-Drever-Hall reflection signal for $\theta = 0, \pi/2$. (Right) Transmission signal.

By a suitable choice of the modulation index, the pre-factor containing Bessel functions (and therefore the signal amplitude) can be maximized. That is the case, for $M \simeq 1.1$ (see Exc. 53.4.5.1). Each of the two parts of the summation in the above equation is the result of a beating of the carrier $E_r(\omega)$ with one of the sidebands $E_r(\omega \pm \Omega)$. Only those optical sidebands being close to a mode of the resonator provide, along with the radiofrequency sidebands, contributions to the reflection signal

The dependence of the reflection signal S_{PDH} on the frequency ω is shown in Fig. 55.12(a). The antisymmetric shape and the zero-crossing slope are ideal for use as a discriminator generating an *error signal* for a frequency stabilization. This method is called *Pound-Drever-Hall method*.

55.3.4 Phase stabilization of standing waves

For the stabilization of the phase of a standing wave one can use the following scheme. It is similar to the homodyne method used with the Michelson interferometer with the difference that laser beam separation and recombination are done at different beam splitters.

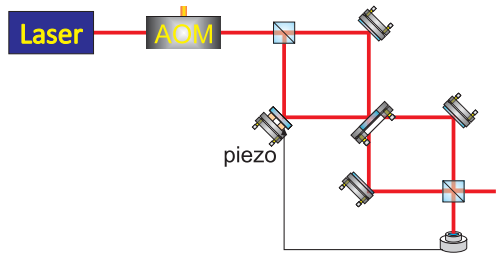

Figure 55.13: Phase stabilization.

55.3.5 Frequency-offset locking with phase-locked loops

Many application in spectroscopy require two stable lasers emitting at different but well-defined and tunable frequencies. Examples are stimulated Raman transitions, or the spectroscopy of atoms interacting with optical cavities [224]. In the following we will discuss and compare different approaches to locking one laser to another laser using a phase-locked loop (PLL). See also (watch talk).

55.3.5.1 VCO and mixing

In a *phase-locked loop* one tries to synchronize a self-sustained oscillator, in general realized by a VCO, with a local oscillator. The VCO generates an ac-voltage U_{rf}, whose frequency is tuned via a dc-control-voltage U_{ct} around a center frequency ω_0, as shown in Fig. 55.14(a). It can be modeled by,

$$\boxed{U_{rf}(t) = 2B\cos\phi(t) \qquad \text{with} \qquad \frac{d\phi}{dt} = \omega_0 + KU_{ct}(t)} \; . \tag{55.19}$$

The local oscillator produces an ac-voltage, $U_{lo}(t) = A\sin\phi_{lo}(t)$. A mixer multiplies both signals,

$$U_d(t) = AB\left(\sin[\phi_{lo}(t) - \phi(t)] + \sin[\phi_{lo}(t) + \phi(t)]\right) \; . \tag{55.20}$$

See also Exc. 55.3.7.1.

55.3.5.2 Low-pass filtering

The multiplied signal U_d contains all information about frequency deviations of the VCO from the LO. To extract them, we *low-pass filter* this signal, cutting off all high frequency components, i.e. apply the filter transfer function,

$$F(f) = (1 + sRC)^{-1} \; . \tag{55.21}$$

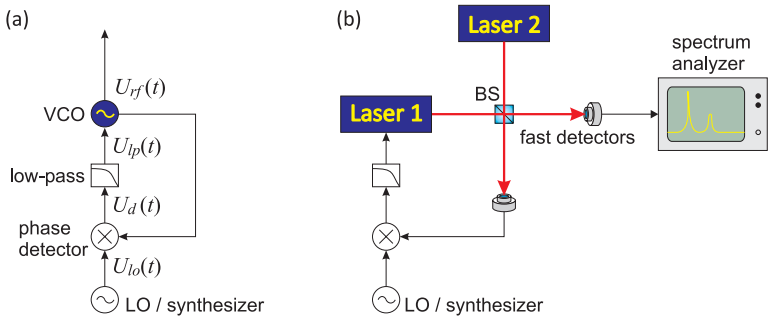

Figure 55.14: (a) PLL to lock a VCO to a reference oscillator LO. (b) PLL to lock the difference frequency of two lasers to a LO.

The signal of the filter is $U_{lp}(f) \equiv F(f)U_d(f)$. In time domain, which is obtained by a Laplace transform, $F(t) = (RC)^{-1}\theta(t)e^{-t/RC}$, such that

$$U_{lp}(t) = F \star U_d(t) = \int_{-\infty}^{\infty} F(t-\tau)U_d(\tau)d\tau = \frac{e^{-t/RC}}{RC}\int_{-\infty}^{t} e^{\tau/RC}U_d(\tau)d\tau \ . \quad (55.22)$$

The derivative is obviously,

$$\frac{dU_{lp}}{dt} + \frac{U_{lp}}{RC} = \frac{U_d(t)}{RC} = \frac{AB}{RC}\sin\left[\phi_{lo}(t) - \phi(t)\right] \ , \quad (55.23)$$

inserting the above expression for U_d. Note, that we would have obtained the same result using control theory (see Sec. 55.1).

55.3.5.3 Phase synchronization

The phase synchronization servo is closed by setting $U_{ct} = U_{lp}$. Thus we may substitute $U_{lp}(t)$ and define $\psi \equiv \phi - \phi_{lo}$,

$$\frac{d^2\psi}{dt^2} + \frac{1}{RC}\frac{d\psi}{dt} + \frac{KAB}{RC}\sin\psi = -\frac{d^2\phi_{lo}}{dt^2} - \frac{1}{RC}\left(\frac{d\phi_{lo}}{dt} - \omega_0\right) \ . \quad (55.24)$$

In most cases the LO frequency varies slowly, so that we may assume $\dot{\phi_{lo}} = \omega_{lo}$,

$$\frac{d^2\psi}{dt^2} + \frac{1}{RC}\frac{d\psi}{dt} + \frac{KAB}{RC}\sin\psi = -\frac{1}{RC}\left(\omega_{lo} - \omega_0\right) \ . \quad (55.25)$$

Hence, a PLL generates a signal $U_{rf}(t)$ having approximately the same (time-dependent) frequency as the local oscillator $U_{lo}(t)$. The equation is identical to that of an overdamped rotator or a resistively shunted Josephson junction [1031].

We observe that the PLL is locking to servo oscillations. The spectrum of signal produced by the VCO exhibits sidebands as soon as the loop is closed. Their amplitude depends on the gain, their frequency varies with the offset voltage controlling the VCO.

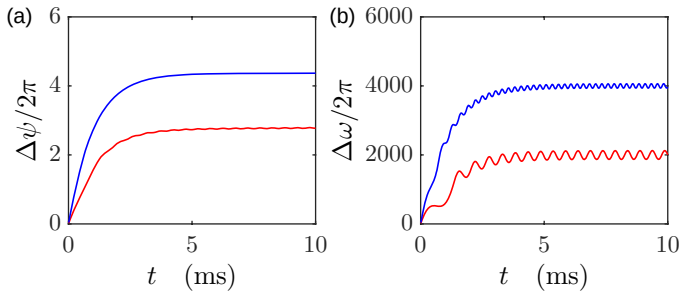

Figure 55.15: (code) Simulation of (a) the phase and (b) frequency difference in a PLL for (red) $\omega_{lo} - \omega_0 = (2\pi)$ 2 kHz and (blue) 4 kHz.

55.3.6 Frequency-offset locking using transfer cavities

Sometimes we want to take a ultra-high resolution spectrum in a frequency region, where there is no reference frequency available nearby. By nearby we mean frequency regimes which can be reached by PLLs based on frequency beats on fast photodetectors, as studied in Sec. 55.3.5. A possible method consists in the use of an optical *transfer cavity*.

Here, a reference laser stabilized to a known frequency ω_{ref}, e.g. via a saturation spectroscopy to an atomic transition, is used to lock a piezo-tunable optical cavity (called transfer cavity), as shown in Fig. 55.16. The cavity in turn is used to lock the spectroscopy laser $\omega_{blu-las}$, e.g. via the Pound-Drever-Hall method.

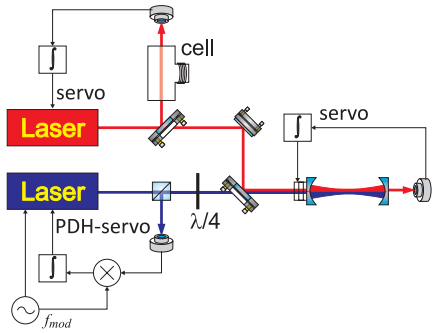

Figure 55.16: Schematic view of a transfer cavity locking system involving three cascaded servo systems for (i) the stabilization of the reference laser to a known frequency; (ii) of the transfer cavity to the reference laser, and (iii) of the spectroscopy laser to the transfer cavity.

Two issues need to be considered when using the transfer cavity scheme:

- The scheme does not permit tuning of the spectroscopy laser; this feature must be included using, e.g. AOMs (see Sec. 53.3.1) of PLL offset locks (see Sec. 55.3.5).

- The use of piezo in the transfer cavity is incompatible with its high-level thermal and mechanical stabilization. This means that special care must be taken in

the design of the reference laser in order to avoid degradation of the stability of the transfer cavity via the servo lock.

The whole locking scheme consists of three cascaded servo loops (see Fig. 55.16). To model the transfer of stability from the reference to the spectroscopy laser, we write down the following relations,

$$\begin{aligned} \omega_{red-las} &= H_{sat}(f)\omega_{ref} \\ N_{red-trns}\delta_{fsr} &= H_{trns}(f)\omega_{red-las} \\ \omega_{blu-las} &= H_{pdh}(f)N_{blu-trans}\delta_{fsr} \ . \end{aligned} \tag{55.26}$$

In the absence of noise or for perfect servos, $H_x \to 1$, we get,

$$\omega_{blu-las} = \frac{N_{blu-trans}}{N_{red-trans}}\omega_{red-las} \ . \tag{55.27}$$

We assume specific transfer functions for the closed-loop gains of the three servos and describe the impact of noise by adding frequency deviations $\Delta\omega$ entering at various points.

55.3.7 Exercises

55.3.7.1 Ex: Schemes for laser tuning

Discuss the two PLL-setups shown in Fig. 55.17.

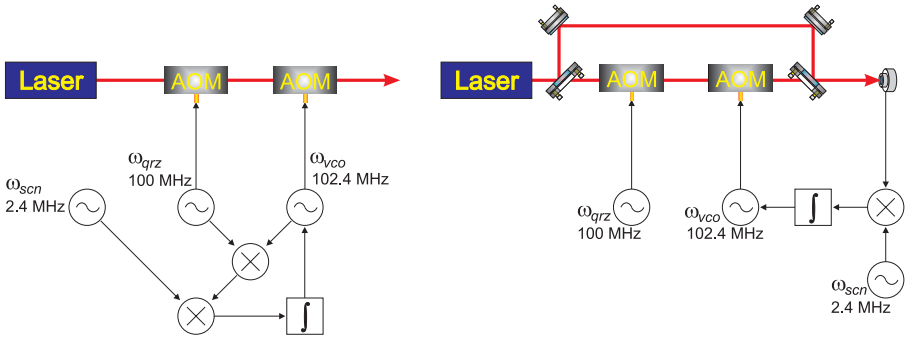

Figure 55.17: Two schemes for laser tuning.

Solution:

55.3.8 *Experiment: Stabilizing a laser to a cavity*

Here is, how we are going to stabilize a laser to a cavity:

1. Stabilize a helium-neon laser to a Fabry-Pérot cavity, generating a frequency modulation by modulating the laser diode current or the piezo of the extended

cavity. Choose a modulation frequency in the range of $f \simeq 1\,\text{kHz}$ and a modulation amplitude in the range of $M \simeq 5$ MHz. Adjust the reference voltage of the control electronics until the error signal is symmetrical.

2. If you do not have a lock-in amplifier available, construct one following the project Sec. 52.4.3.

3. Now, do the opposite, stabilizing the optical cavity to the laser frequency using the resonator piezo as control element.

4. Vary the optical setup now modulating the frequency using an AOM (see Fig. 55.18).

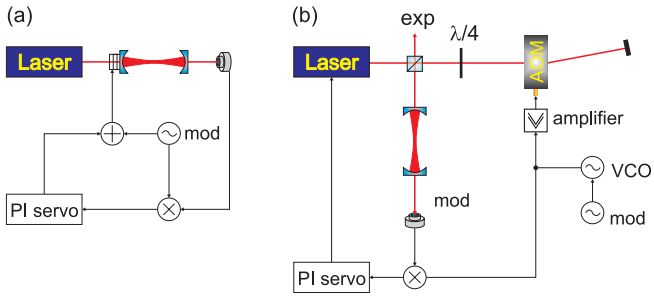

Figure 55.18: Variations on the same theme: (a) Frequency stabilization of a cavity to a laser frequency using the lock-in method. This method is often used for spectral filtering of a laser beam by a transmission etalon. (b) Frequency stabilization of a laser to a cavity using an AOM. The advantage of using an AOM compared to the scheme shown in Fig. 55.10 is, that only the beam injected into the cavity is modulated, but not the beam used for the main experiment.

55.3.9 *Experiment: Pound-Drever-Hall locking*

Now we will stabilize a laser to a cavity using the Pound-Drever-Hall technique [180, 388]:

1. Consider the reflected signal. To do this, separate the beam injected into the resonator from the reflected beam by means of a $\lambda/4$ waveplate and a polarizing beam splitter.

2. Now analyze the reflected signal with a fast photodetector at a spectrum analyzer.

3. Demodulate the signal with the modulation frequency. Vary the length of the cables. Optimize the slope of the error signal by a suitable choice of frequency and modulation excursion [4].

[4] Datasheet for the VCO see appendix Fig. 56.16,
data sheet for the power splitter see appendix Fig. 56.18,
data sheet for the mixer see appendix Fig. 56.19.

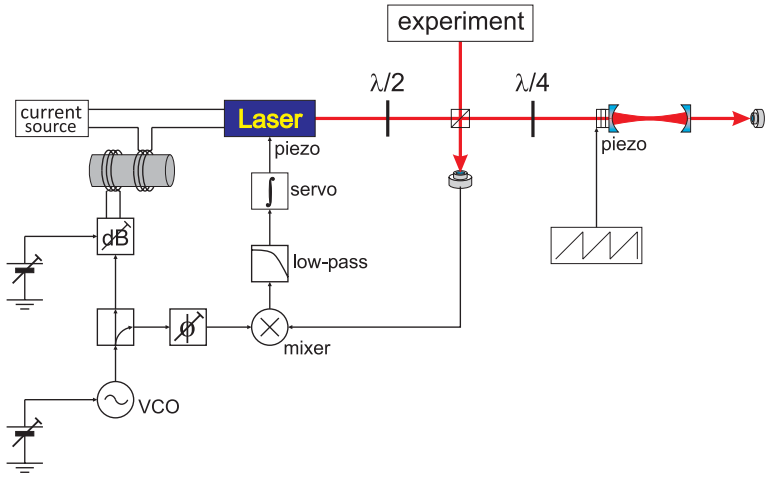

Figure 55.19: Setup of a frequency regulator following Pound-Drever-Hall. VCO: Voltage-Controlled Oscillator, LT: power splitter, dB: variable attenuator, LP: low-pass filter.

55.4 Further reading

55.4.1 on frequency noise description

D.W. Allan, *Statistics of atomic frequency standards* [18]DOI

J.A. Barnes et al., *Characterization of frequency stability* [97]DOI

J.L. Stewart, *The power spectrum of a carrier frequency modulated by Gaussian noise* [1264]DOI

D.S. Elliott et al., *Extracavity laser band-shape and bandwidth modification* [414]DOI

L.S. Cutler, *Some Aspects of the Theorv and Measurement of Frequency Fluctuations in Frequency Standards* [314]DOI

D.B. Sullivan et al., *Characterization of Clocks and Oscillators* [1277]ISBN

G. Di Domenico et al., *Simple approach to the relation between laser frequency noise and laser line shape* [381]DOI

J. Appel et al., *A versatile digital GHz phase lock for external cavity diode lasers* [40]DOI

L. Ricci et al., *A compact grating-stabilized diode laser system for atomic physics* [1094]DOI

G. Ritt et al., *Laser frequency offset locking using a side of filter technique* [1100]DOI

A.S. Arnold et al., *A simple extended-cavity diode laser* [46]DOI

E.C. Cook et al., *High passive-stability diode-laser design for use in atomic-physics experiments* [289]DOI

C.J. Hawthorn et al., *Littrow configuration tunable external cavity diode laser with fixed direction output beam* [589]DOI

Huanqian Loh et al., *Influence of grating parameters on the linewidths of external-cavity diode lasers* [811]DOI

Y. Shimada et al., *A simplified 461-nm laser system using blue laser diodes and a hollow cathode lamp for laser cooling of Sr* [?]DOI

55.4.2 on laser stabilization

J. Alnis et al., *Stable diode lasers for hydrogen precision spectroscopy* [?]DOI

J. Alnis et al., *Subhertz linewidth diode lasers by stabilization to vibrationally and thermally compensated ultralow-expansion glass Fabry-Pérot cavities* [?]DOI

L. Couturier et al., *Laser frequency stabilization using a commercial wavelength meter* [?]DOI

K. Huang et al., *Microcontroller-based locking in optics experiments* [?]DOI

Shun Wu et al., *Direct fiber comb stabilization to a gas-filled hollow-core photonic crystal fiber* [?]DOI

Y.N. Zhao et al., *Sub-Hertz frequency stabilization of a commercial diode laser* [?]DOI

R.W.P. Drever et al., *Laser Phase and Frequency Stabilization Using an Optical Resonator* [388]DOI

D. Budker et al., *Obtaining frequency markers of variable separation with a spherical mirror Fabry-Perot interferometer* [209]DOI

55.4.3 on control theory

U. Tietze et al., *Halbleiterschaltungstechnik* [1306]ISBN

O. Föllinger et al., *Regelungstechnik: Einführung in die Methoden und ihre Anwendung* [462]ISBN

Chapter 56

Appendices to 'Instrumentation of a Quantum Optics Lab'

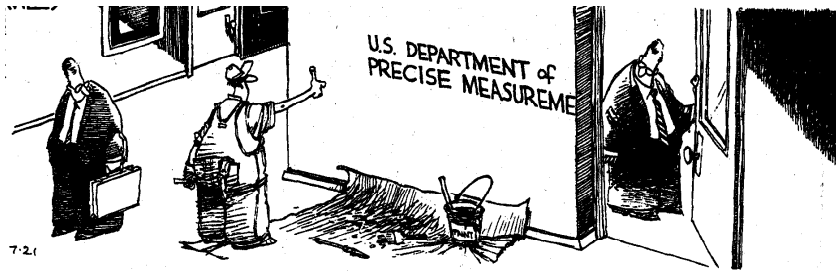

Figure 56.1: At the National Institute for Standards and Technology (NIST).

56.1 Calculating the uncertainty of measured quantities

56.1.1 Mean value and standard deviation

Mean value and *standard deviation* are defined by,

$$\bar{x} \equiv \frac{1}{N}\sum_k x_k \qquad \text{and} \qquad \sigma_{\bar{x}} \equiv \sqrt{\frac{1}{N-1}\sum_k (x_k - \bar{x})^2}\ . \tag{56.1}$$

The standard deviation can be weighed by a confidence parameter,

$$\bar{x} \equiv \frac{\sum_k w_k x_k}{\sum_k w_k} \qquad \text{and} \qquad \sigma_{\bar{x}} \equiv \frac{1}{\sqrt{\sum_k w_k}} \tag{56.2}$$

Weighing by individual standard deviation,

$$w_k \equiv \frac{1}{\sigma_k^2} \qquad \text{for} \qquad \sigma_k = \sigma_0 \tag{56.3}$$

gives,

$$\bar{x} \equiv \frac{\sum_k \frac{x_k}{\sigma_k^2}}{\sum_k \frac{1}{\sigma_k^2}} = \sigma_{\bar{x}}^2 \sum_k \frac{x_k}{\sigma_k^2} \overset{\sigma_k=\sigma_0}{\longrightarrow} \frac{1}{N}\sum_k x_k \quad \text{with} \quad \sigma_{\bar{x}} \equiv \frac{1}{\sqrt{\sum_k \frac{1}{\sigma_k^2}}} \overset{\sigma_k=\sigma_0}{\longrightarrow} \frac{\sigma_0}{\sqrt{N}} \tag{56.4}$$

or,

$$\hat{\sigma}_{\bar{x}} \equiv \sigma_{\bar{x}}\chi_v \overset{\sigma_k=\sigma_0}{\longrightarrow} \sqrt{\frac{1}{N-1}\sum_k (x_k - \bar{x})^2} \tag{56.5}$$

$$\chi_v = \sqrt{\frac{1}{N-1}\sum_k \frac{(x_k-\bar{x})^2}{\sigma_i^2}} \; .$$

From error propagation

$$\Delta\bar{x} \equiv \sqrt{\frac{1}{N}\sum_k \Delta x_k^2} \; . \tag{56.6}$$

56.1.1.1 χ^2-fit

The χ^2-fit of a constant of a function $y = f(x)$ to a measured data set (x_k, y_k) is,

$$\chi^2 = \frac{1}{N(N-1)}\sum_k [f(x_k) - y_k]^2 \; . \tag{56.7}$$

The above formula suggest that, increasing the number of measurements $N \to \infty$ we could pull the error to zero. This, however, is NOT TRUE. If the standard deviation is smaller than the precision Δ of the measurement tool, the error will be limited by Δ,

$$\bar{y} \pm \max(\sigma, \Delta) \; . \tag{56.8}$$

56.1.2 Error propagation

The *error propagation* for a function $f(x_1, x_2, ..)$ is given by,

$$\Delta f = \sqrt{\left(\frac{\partial f}{\partial x_1}\right)^2 \Delta x_1^2 + \left(\frac{\partial f}{\partial x_2}\right)^2 \Delta x_2^2 + ...} < \left|\frac{\partial f}{\partial x_1}\right| \Delta x_1 + \left|\frac{\partial f}{\partial x_2}\right| \Delta x_2 + ... \; . \tag{56.9}$$

Calculations can often be simplified by noting that the four fundamental operations, $f = x_1 \pm x_2$, $f = x_1 x_2$, and $f = \frac{x_1}{x_2}$ allow us to simply add the relative errors,

$$\frac{\Delta f}{f} = \frac{\Delta x_1}{x_1} + \frac{\Delta x_2}{x_2} \; . \tag{56.10}$$

Alternatively, we may use the following quick rules,

$$\begin{array}{rrcrl}
\textit{sum}: & f \pm \Delta f = & (x \pm \Delta x) + (y \pm \Delta y) & = & (x+y) \quad \pm (\Delta x + \Delta y) \\
\textit{subtraction}: & f \pm \Delta f = & (x \pm \Delta x) - (y \pm \Delta y) & = & (x-y) \quad \pm (\Delta x + \Delta y) \\
\textit{multiplication}: & f \pm \Delta f = & (x \pm \Delta x)\cdot(y \pm \Delta y) & = & (x\cdot y) \quad \pm (x\Delta y + y\Delta x) \\
\textit{division}: & f \pm \Delta f = & \frac{x\pm\Delta x}{y\pm\Delta y} & = & \frac{x}{y} \quad \pm \frac{1}{y^2}(x\Delta y + y\Delta x) \\
\textit{power}: & f \pm \Delta f = & (x \pm \Delta x)^n & = & x^n \quad \pm n x^{n-1}\Delta x
\end{array} \; . \tag{56.11}$$

Example 304 (*Error propagation*): Let us study the following example,

$$f = \frac{x_1}{x_2 + a}$$
$$\Longrightarrow \Delta f = f\frac{\Delta x_1}{x_1} + f\frac{\Delta(x_2+a)}{x_2+a} = f\frac{\Delta x_1}{x_1} + f\frac{\Delta x_2}{x_2+a} \ .$$

56.1.3 Fitting a curve

We start defining the following prescription to calculate mean values,

$$\bar{x} \equiv \frac{1}{N}\sum_{k=1}^{N} x_k \quad , \quad \overline{xy} \equiv \frac{1}{N}\sum_{k=1}^{N} x_k y_k \ . \tag{56.12}$$

For a *fit* of a *linear curve* $f(x) = ax + b$ to a data set $\{x_k, y_k\}_{k\in[1,N]}$, we calculate (see also Exc. 27.2.3.3),

$$\boxed{f(x) = ax + b \quad , \quad a = \frac{\overline{xy} - \bar{x}\,\bar{y}}{\overline{x^2} - \bar{x}^2} = \frac{\overline{(x-\bar{x})y}}{\overline{(x-\bar{x})^2}} \quad , \quad b = \frac{\bar{y}\,\overline{x^2} - \overline{xy}\,\bar{x}}{\overline{x^2} - \bar{x}^2} = \bar{y} - a\bar{x}} \ . \tag{56.13}$$

The uncertainties are obtained via,

$$\Delta y = \sqrt{\frac{N}{N-2}\overline{(ax+b-y)^2}} \quad , \quad \Delta a = \Delta y\sqrt{\frac{1}{N\ (\overline{x^2} - \bar{x}^2)}} = \frac{\Delta y}{\sqrt{N\ \overline{x-\bar{x}}}} \tag{56.14}$$
$$, \quad \Delta b = \Delta y\sqrt{\frac{\overline{x^2}}{N\ \overline{x^2} - \bar{x}^2}} = \Delta y\sqrt{\frac{\overline{x^2}}{N\ \overline{x-\bar{x}}}} \ .$$

To fit an *exponential curve* $f(x) = \beta e^{\alpha x}$, we simply convert the data set $\{x_k, v_k\} \equiv \{x_k, \lg y_k\}$, calculate the mean values of the decadal logarithm using the recipe (56.12), and fit a linear curve $\tilde{f}(x) = \lg f(x) = \frac{\alpha}{\ln 10}x + \lg\beta \equiv ax + b$ in a semi-logarithmic scale to the data set $\{x_k, v_k\}$. This gives,

$$\boxed{f(x) = \beta e^{\alpha x} \quad , \quad \frac{\alpha}{\ln 10} = a = \frac{\overline{x\lg y} - \bar{x}\ \overline{\lg y}}{\overline{x^2} - \bar{x}^2} \quad , \quad \lg\beta = b = \frac{\overline{\lg y}\ \overline{x^2} - \overline{x\lg y}\ \bar{x}}{\overline{x^2} - \bar{x}^2}} \ . \tag{56.15}$$

To fit a *power law curve* $f(x) = \beta x^\alpha$, we simply convert the data set $\{u_k, v_k\} \equiv \{\lg x_k, \lg y_k\}$, calculate the mean values of the decadal logarithm using the recipe (56.12), and fit the linear curve $\tilde{f}(x) = \lg f(x) = \alpha\lg x + \lg\beta \equiv ax + b$ in a double-logarithmic scale to the data set $\{u_k, v_k\}$. This gives,

$$\boxed{f(x) = \beta x^\alpha \quad , \quad \alpha = a = \frac{\overline{\lg x\lg y} - \overline{\lg x}\ \overline{\lg y}}{\overline{\lg x^2} - \overline{\lg x}^2} \quad , \quad \lg\beta = b = \frac{\overline{\lg y}\ \overline{\lg x^2} - \overline{\lg x\lg y}\ \overline{\lg x}}{\overline{\lg x^2} - \overline{\lg x}^2}} \ . \tag{56.16}$$

56.1.4 Probability density

Consider a function $P(x)$ having the meaning of a *probability* depending on a variable $x \in [-\infty, \infty]$. The *probability density* $\rho(x)$ is defined as its derivative, $\rho(x) = P'(x)$, such that,

$$P(x) = \int_{-\infty}^{\infty} \rho(t)dt \qquad \text{with} \qquad P(-\infty) = 0 \qquad \text{and} \qquad P(\infty) = 1 \ . \tag{56.17}$$

Every probability must have the same likeliness, i.e.,

$$P(x) = \zeta_n \ , \tag{56.18}$$

where $\zeta_n \in [0, 1]$ is a uniformly distributed *random variable*. In order to numerically generate a *stochastic distribution*, we have to invert the distribution function, i.e. when ζ_n is generated by a computer, then

$$\boxed{x_n = P^{-1}(\zeta_n)} \tag{56.19}$$

is the distribution of the random variable x_n. In other words, a histogram of x_n reproduces the probability density $\rho(x)$.

Let us, for example, consider the Boltzmann distribution,

$$P(x) \equiv 1 - e^{-\beta x} \ . \tag{56.20}$$

Probing the probability with a random number, as in (56.18), we obtain the random variable via (56.19),

$$x_n = P^{-1}(\zeta_n) = -\frac{1}{\beta} \ln(1 - \zeta_n) \ . \tag{56.21}$$

The histogram of this random variable x_n can directly be compared with the probability density $\rho(x)$ given by,

$$\rho(x) = P'(x) = \beta e^{-\beta x} \ . \tag{56.22}$$

This is illustrated in Fig. 56.2(a).

Example 305 (*Probability density of a Gaussian distribution*): Another example is the *error function* given by,

$$\mathrm{erf}(x) \equiv \frac{2}{\sqrt{\pi}} \int_0^x e^{-t^2} dt \ .$$

By define the probability function,

$$P(x) \equiv \frac{1}{2}[\mathrm{erf}(x) - \mathrm{erf}(-\infty)] = \frac{1}{\sqrt{\pi}} \int_{-\infty}^x e^{-t^2} dt \ .$$

Probing the probability with a random number, as in (56.18), we obtain the random variable via (56.19),

$$x_n = P^{-1}(\zeta_n) = \mathrm{erf}^{-1}(2\zeta_n - 1) \ .$$

The histogram of this random variable x_n can directly be compared with the probability density $\rho(x)$, which is nothing else than the Gauss function,

$$\rho(x) = P'(x) = \frac{1}{\sqrt{\pi}} e^{-x^2} = 2\mathrm{erf}'(x) \ .$$

This is illustrated in Fig. 56.2(b).

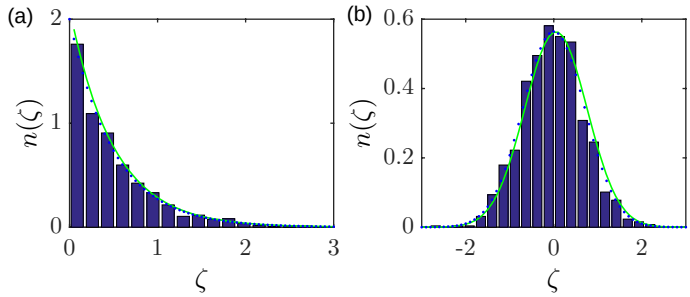

Figure 56.2: (code) (a) Boltzmann distribution simulated by random numbers (histogram). The numerical derivative of this distribution is shown as a blue dotted line, and the probability density as a green solid line. (b) Error function probability distribution simulated by random numbers (histogram). The numerical derivative of the error function is shown as a blue dotted line, and the Gauss function as a green solid line.

56.2 Deepening control theory

The variation of a physical quantity (e.g., a voltage or a temperature) in time is called *signal*. In a specific environment or technical device, such a variation may cause other physical quantities to change as well. For example, the rise in temperature of an optical cavity may modify its length and its resonance frequency, while the inverse is not true. This feature is illustrated by a block diagram as shown in Fig. 56.3, where $x(t)$ denotes the variation of a physical quantity (called *input*) that causes the variation of another quantity $y(t)$ (called *output*). The precise way how $y(t)$ depends on $x(t)$ depends on the particularities of the device, which is labeled by a symbol $\mathcal{T}$ called transfer function. $\mathcal{T}$ is in fact an operator acting on functions and transforming input signals into output signals.

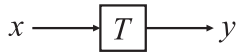

Figure 56.3: Transfer and modification of a time-dependent signal.

While we have described above the transfer of (time-varying) signals, the same feature can be treated in frequency domain via Fourier or Laplace-transforms. This script is not the right place to recapitulate the mathematics of these transforms, and we will restrict ourselves to reproducing some on the most fundamental results, as we may need them in the following.

56.2.1 Analysis techniques - frequency domain and time domain

Mathematical techniques for analyzing and designing control systems fall into two different categories:

Frequency domain: In this type the values of the state variables, the mathematical variables representing the system's input, output and feedback are represented

as functions of frequency. The input signal and the system's transfer function are converted from time functions to functions of frequency by a transform such as the Fourier transform, Laplace transform, or Z transform. The advantage of this technique is that it results in a simplification of the mathematics; the differential equations that represent the system are replaced by algebraic equations in the frequency domain which are much simpler to solve. However, frequency domain techniques can only be used with linear systems, as mentioned above.

Time-domain state space representation: In this type the values of the state variables are represented as functions of time. With this model the system being analyzed is represented by one or more differential equations. Since frequency domain techniques are limited to linear systems, time domain is widely used to analyze real-world nonlinear systems. Although these are more difficult to solve, modern computer simulation techniques such as simulation languages have made their analysis routine.

In contrast to the frequency domain analysis of the classical control theory, modern control theory utilizes the time-domain state space representation, a mathematical model of a physical system as a set of input, output and state variables related by first-order differential equations. To abstract from the number of inputs, outputs and states, the variables are expressed as vectors and the differential and algebraic equations are written in matrix form (the latter only being possible when the dynamical system is linear). The state space representation (also known as the 'time-domain approach') provides a convenient and compact way to model and analyze systems with multiple inputs and outputs. With inputs and outputs, we would otherwise have to write down Laplace transforms to encode all the information about a system. Unlike the frequency domain approach, the use of the state-space representation is not limited to systems with linear components and zero initial conditions. 'State space' refers to the space whose axes are the state variables. The state of the system can be represented as a point within that space.

56.2.1.1 Signal transfer through LTI systems without delay

For an operator $\mathcal{T}$ transforming a temporal signal $x(t)$ into a signal $y(t)$,

$$y(t) = \mathcal{T}x(t) \ , \tag{56.23}$$

to be *linear* and time-independent, we require,

$$\begin{aligned} \mathcal{T}[\alpha x_1(t) + \beta x_2(t)] &= \alpha\mathcal{T}[x_1(t)] + \beta\mathcal{T}[x_2(t)] \\ \mathcal{T}[x(t-\tau)] &= \mathcal{T}[x(t)] \star \delta(t-\tau) \ , \end{aligned} \tag{56.24}$$

where the $\star$ denotes a convolution,

$$(f \star g)(t) = \int_{-\infty}^{\infty} f(\tau)g(t-\tau)d\tau \ . \tag{56.25}$$

Such system are called *Linear Time-Independent LTI* systems [1].

[1] To be more general, also the derivative and integral of the output signal must be included (see later sections).

56.2.1.2 Laplace transform

We define the *Laplace transform* $\mathcal{L}$ as a linear operator acting on a signal $x(t)$ defined through,

$$\mathcal{L}... \equiv \int_{-\infty}^{0} ...e^{st}d\tau \ . \tag{56.26}$$

The frequency variable is denoted by the imaginary quantity $s = \imath f$. The question is now, what is the meaning of the Laplace operator?

To answer this question, we start introducing the pulse response $h(t)$ via

$$h(t) = \mathcal{T}[\delta(t)] \tag{56.27}$$

as the reaction of a system $\mathcal{T}$ to a pulse $\delta(t)$. Now, it is easy to see, that the operator $\mathcal{P}$ defined as,

$$\mathcal{P}... \equiv h(t) \star ... \ , \tag{56.28}$$

and which describes the convolution of an arbitrary input signal with the pulse response, satisfies the above linearity condition. Now calculating,

$$\mathcal{P}e^{st} = h(t) \star e^{st} = \int_{-\infty}^{0} h(\tau)e^{s(t-\tau)}d\tau = \mathcal{L}[h(t)] \cdot e^{st} = (\mathcal{L}h)(s) \cdot e^{st} \ , \tag{56.29}$$

we find that the functions e^{st} are eigenfunctions of the operator $\mathcal{P}$ with the eigenvalues $\mathcal{L}[h(t)]$, which are just the Laplace transforms of the pulse response.

We can now expand arbitrary functions $x(t)\theta(t)$ in a Laplace series and obtain,

$$\mathcal{L}[h(t) \star x(t)] = \int_{-\infty}^{0} h(t) \star e^{st} \ x(t)dt = (\mathcal{L}h)(s) \int_{-\infty}^{0} e^{st}x(t)dt = (\mathcal{L}h)(s) \cdot (\mathcal{L}x)(s) \ . \tag{56.30}$$

The convolution on the left-hand side is in time domain, while the product on the right-hand side is in frequency domain.

56.2.1.3 Pulse and jump response from a transfer function

The transmission of a signal by an element of a control loop can be described in the temporal or spectral domain [462, 496, 839], and we can switch from one representation to another via Laplace transformation. Operators of LTI systems $\mathcal{T}$ are represented by products with spectral functions in frequency-domain, $\tilde{F}(s)\cdot... = (\mathcal{L}F)(s)\cdot...$ or convolutions with time-varying functions in time-domain, $F(t) \star ...$,

$$\begin{aligned} y(t) &= \mathcal{T}x(t) \\ &\overset{Laplace}{\longrightarrow} \tilde{y}(s) = \tilde{F}(s) \cdot \tilde{x}(s) \\ &\overset{inverse\ Laplace}{\longrightarrow} y(t) = F(t) \star x(t) \ . \end{aligned} \tag{56.31}$$

In practice, the function $\tilde{F}(f)$ can be determined by feeding a sinusoidal signal with amplitude $x(s)$ into the system, measuring $y(s)$ (which is a complex number) [2],

[2] From now on, we will drop the tilde $\sim$ on transfer functions and amplitudes, when it is clear that we are in frequency-domain.

and calculating

$$F(s) = \frac{y(s)}{x(s)} \ . \tag{56.32}$$

The transitory behavior $F(t)$ can in practice be extracted via an adequate choice of the test function, f.ex., the response to a pulse:

$$\begin{aligned} x(t) &= \delta(t) \\ \overset{Laplace}{\longrightarrow} \ y(s) &= F(s) \\ \overset{inverse\ Laplace}{\longrightarrow} \ y(t) &= F(t) \ , \end{aligned} \tag{56.33}$$

or to a sudden jump:

$$\begin{aligned} x(t) &= \theta(t) \\ \overset{Laplace}{\longrightarrow} \ y(s) &= F(s)/s \\ \overset{inverse\ Laplace}{\longrightarrow} \ y(t) &= \int_0^t F(\tau) d\tau \ . \end{aligned} \tag{56.34}$$

Here, $\theta(t)$ denotes the Heavyside function, which is 1 for $t > 0$ and 0 else. The time-dependent function, which describes the pulse response is often used as a symbol for a specific control loop element.

The pulse response works in a similar way as the Green's function procedure: Wanting to know how a loop control element F transforms a given input signal $x(t)$ into an output signal $y(t)$, i.e., $y(t) = F(t) \star x(t)$, we produce a rapid pulse leading to the output,

$$y_\delta(t) = F(t) \star \delta(t) = F(t) \ . \tag{56.35}$$

Now, once we know $F(t)$, the response to arbitrary input signals can be computed via,

$$y(t) = y_\delta(t) \star x(t) \ . \tag{56.36}$$

56.2.1.4 Bode diagram and polar diagram

The *Bode diagram* illustrates the transfer function in the spectral domain on a bilogarithmic scale separating the amplitude spectrum from the phase spectrum [see Fig. 56.4(a-b)]. Frequency regions, where $|F(s)|$ or $\varphi(s)$ vary particularly strongly are nicely emphasized in the polar representation [see Fig. 56.4(c-d)].

For LTI systems $F(s)$ is always a rational function and can, hence, be represented by its poles and zeros in the complex plane,

$$F(s) = A \frac{(s-a_1)(s-a_2)...(s-a_n)}{(s-b_1)(s-b_2)...(s-b_n)} \ . \tag{56.37}$$

With this, $F(s)$ is analytical and conform, i.e., multiple curves in the s-plane are represented in an isogonal way in the $F(s)$-plane. In order to avoid that the eigenfunctions e^{st} oscillate and diverge, it is necessary that all the poles and zeros are in the left halfplane.

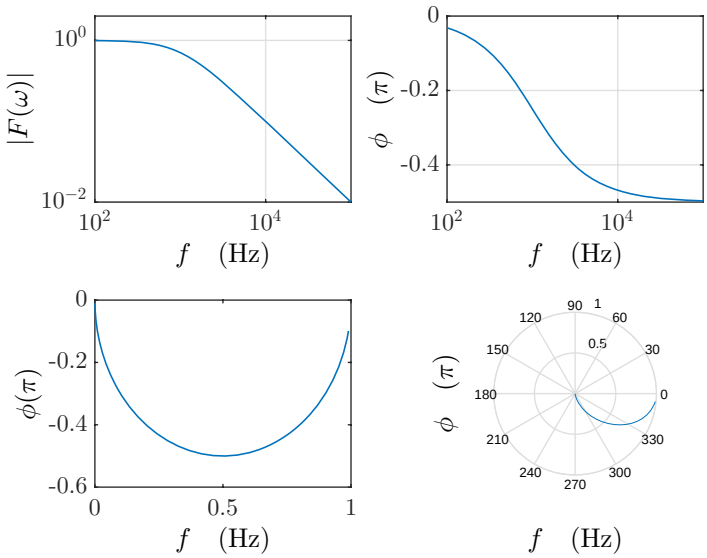

Figure 56.4: (code) Bode diagram.

56.2.2 Algebra of transfer circuits

A technical realization of a signal transfer circuit is illustrated by a signal flux diagram, which itself corresponds to the formalism of linear operators. As shown in Fig. 56.5, signals can be

- (a) added $(f_1 + f_2)(t) \equiv f_1(t) + f_2(t)$,
- (b) multiplied $(f_1 \cdot f_2)(t) \equiv f_1(t) \cdot f_2(t)$,
- (c) combined $f_1(t) = f_2(t)$,
- (d) transformed $f_2(t) = F[f_1](t) \equiv F(f_1(t))$,
- (e) connected in parallel $(F_1 + F_2)[f(t)] \equiv F_1[f(t)] + F_2[f(t)]$,
- (f) connected in series $(F_1 \circ F_2)[f(t)] \equiv F_1[F_2[f(t)]]$,

Mathematically, the functions $f(t)$ form a *vector space* and the operators $F[f]$ a *ring*. The linear operators generally are defined implicitly by a system of differential equations. The particular case of linear systems is considerably simpler. The general circuit shown in Fig. 56.5(g) corresponds to the differential equation,

$$0 = F[x_1, .., x_k, \partial_t x_1, .., \partial_t x_k, y_1, .., y_j] \ . \tag{56.38}$$

The linearity $F[\lambda f_1 + \mu f_2] = \lambda F[f_1] + \mu F[f_2]$ warrants that this equation becomes,

$$0 = [1 + \partial_t + ... + \int dt + ...]y_k = [1 + \partial_t + ... + \int dt + ...]x_j \ . \tag{56.39}$$

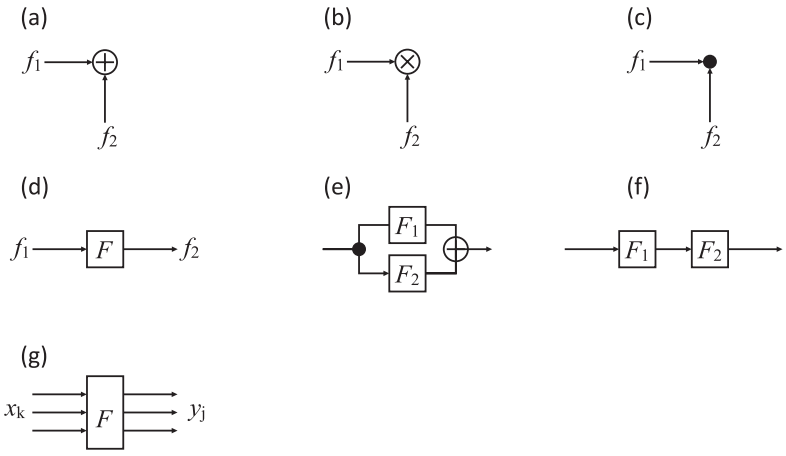

Figure 56.5: LTI circuits.

Note that the multiplication, the derivation, and the integration are linear operators in the same sense as the Fourier and the Laplace transformation.

Linear differential equations can be Laplace transformed. The corresponding transfer function is,

$$F(s) = F(-\delta + \imath\omega) \equiv \frac{\mathcal{L}y(t)}{\mathcal{L}x(t)} \ . \tag{56.40}$$

In the Laplace-transformed space the operations multiplication, derivation, and integration are all replaced by multiplications:

$$\mathcal{L}[\lambda + \partial_t + ... + \int dt + ...] = \lambda + s + ... + \frac{1}{s} \ . \tag{56.41}$$

With this, the control loop elements and the additive nodes can be used to completely represent a control circuit.

The characteristic responses of components are frequently non-linear (e.g. transistor). For small signal amplitudes, these response functions, and also multiplication points (e.g. mixers) can be linearized by Taylor expansion up to first order,

$$\begin{aligned} y_0 + \Delta y &= F[x_{01} + \Delta x_1, ..., x_{0k} + \Delta x_k] \\ &= F[x_{01}, ..., x_{0k}] + \left(\frac{\partial F}{\partial x_1}\right)_0 \Delta x_1 + ... + \left(\frac{\partial F}{\partial x_k}\right)_0 \Delta x_k \ , \end{aligned} \tag{56.42}$$

with $y_0 = 0 = F[x_{01}, ..., x_{0k}]$ giving,

$$\Delta y = \left(\frac{\partial F}{\partial x_1}\right)_0 \Delta x_1 + ... + \left(\frac{\partial F}{\partial x_k}\right)_0 \Delta x_k \ . \tag{56.43}$$

For example for a multiplication point,

$$\Delta y = K_1 \Delta x_1 + K_2 \Delta x_2 \ . \tag{56.44}$$

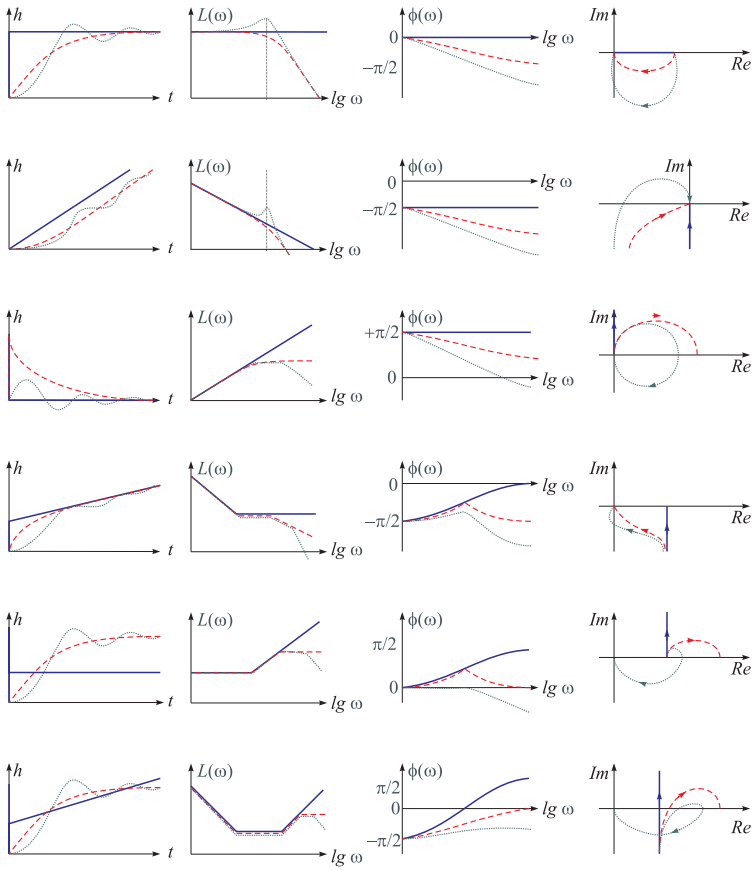

Figure 56.6: Transfer function $h(t) = \frac{y(t)}{x_w}$, Bode diagram amplitude $L(\omega) = 20 \lg |F_R|$ and phase $\varphi = \arctan \frac{\Im \mathfrak{m} \ F_R}{\Re \mathfrak{e} \ F_R}$, and polar representation $F(i\omega) = \Re \mathfrak{e} \ F_R + i \Im \mathfrak{m} \ F_R$ of the most common regulators. With delay time (—), $T_2 = T_1 = 0$, first order with delay time (- - -), $T_2 = 0 \neq T_1$, and second order $(\cdots)$, $T_2 \neq 0 \neq T_1$. From top to bottom, the diagrams show the regulators P, I, D, PI, PD, and PID, described by the equations (56.45) and (56.46).

56.2.2.1 Regulators

For many circuits, it is sufficient to restrict to combinations of resistive (proportional), capacitive (integral), and inductive (differential) circuits. Then, the general case of a control regulator is that of a $PID - T_1 ... T_n$-element, meaning that:

$$T_2^2 \ddot{y} + T_1 \dot{y} + y = K_D \dot{x} + K_P x + K_I \int dt x = K_P \left(x + T_v \dot{x} + \frac{1}{T_n} \int dt x \right) \ , \quad (56.45)$$

corresponding to the transfer function,

$$F(s) = \frac{K_D s + K_P + K_I / s}{1 + T_1 s + T_2^2 s^2} = \frac{(1 + T_v s + 1/T_n s)}{1 + T_1 s + T_2^2 s^2} \ . \quad (56.46)$$

In literature, two notations are used for the constants. They are linked via: $K_D \equiv K_P T_v$ and $K_I \equiv K_P / T_n$. The stationary behavior is obtained setting the delays to

zero: $T_n \equiv 0$.

Example 306 (*PID regulators*): For example, for a *proportional regulator*, we have,

$$y = K_P x_w \qquad \text{and} \qquad F_R = K_P \ , \tag{56.47}$$

for an *integral regulator* with time delay T_1, we have,

$$T_1 \dot{y} + y = K_I \int x_w dt \qquad \text{and} \qquad F_R = \frac{K_I}{s(1+sT_1)} \ , \tag{56.48}$$

or for a *PID regulator* without delay, we have,

$$y = K_P x_w + K_D \dot{x}_w + K_I \int x_w dt \qquad \text{and} \qquad F_R = K_P + \frac{K_I}{s} + K_D s \ . \tag{56.49}$$

Since there are three basic operations (multiplication with 1, s and $1/s$), in the end, all rational circuit elements can be reduced to an addition and concatenation of proportional $F(s) = K_P$, integral $F(s) = K_I/s$, and differentials elements, $F(s) = K_D s$. In particular, $PID{-}T_1 ... T_n$ circuits can be constructed by putting in parallel P, I, and D regulators concatenated with delay elements T_1. The possibility of feedback opens other possibilities [see Fig. 56.7(a)].

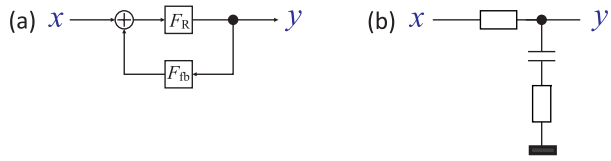

Figure 56.7: (a) Circuit with feedback, (b) low-pass filter circuit.

Example 307 (*Low-pass filter and time delays*): We consider the example of a low-pass filter exhibited in Fig. 56.7(b) and described by the equation,

$$F(\imath\omega) = \frac{R + \imath\omega L + 1/\imath\omega C}{R_i + R + \imath\omega L + 1/\imath\omega C} \ . \tag{56.50}$$

I.e., we have a $PID - T_1 T_2$ circuit.
Another example, is the dead time circuit,

$$y(t) = x(t - T_t) \quad \text{and} \quad F(s) = e^{-sT_t} \ . \tag{56.51}$$

We have,

$$F(\imath\omega) = e^{-\imath\omega T_t} F_0 \quad \text{and} \quad |F(\imath\omega)| = F_0 \quad \text{and} \quad \varphi(\imath\omega) = -\omega T_t \ . \tag{56.52}$$

Hence, dead time circuits produce phase shifts, which are proportional to the dead time interval T_t.

56.2.2.2 Heuristic rules for the Bode diagram

Any deviation of the amplitude spectrum from $n \cdot 6$dB/octave to $(n+1) \cdot 6$dB/octave causes a retardation in the phase spectrum of 90°. At the cut-off frequency, where the inclination changes its behavior, the phase shift is just 45°. A deviation to higher/lower inclinations shifts the phase by ±90°. (This does not hold for some phase-shifting circuits).

56.2.2.3 Transfer function of feedback circuits

Fig. 56.7 shows the idea underlying the feedback,

$$F(s) = \frac{1}{1/F_R - F_{fb}} \ . \tag{56.53}$$

For example, for $F_R = 1/T_1 s$ and $F_{fb} = -1$ we have,

$$F(s) = \frac{1}{1 + T_1 s} \ , \tag{56.54}$$

which corresponds to a delay element (or high-pass filter).

For F_r being a proportional element, we say that the feedback rigid, for F_r being differential, the feedback is anticipating, and for F_r being integral, the feedback is delaying.

56.2.3 Stability of feedback circuits

As discussed above, the transfer function of the feedback circuit is,

$$H(s) = \frac{F(s)}{1 + F(s)F_{fb}(s)} \ . \tag{56.55}$$

The *open loop gain* is $V(s) = F(s)F_{fb}(s)$. The circuit is stable, when for all the eigenfunctions e^{st}, that do not decay with $Re\ s \geq 0$, the transfer function of the feedback circuit is finite, $H(s) < \infty$.

An equivalent criterion is the *Nyquist criterion*: *The curve $V(i\omega)$ to $\omega \in [0; \infty[$ must always bypass the point of instability at $Re\ s = -1$ leaving it on the left side. That is, considering negative frequencies, the curve should not circle this point.* Fig. 56.9 shows an example.

56.2.4 Further topics in control theory

56.2.4.1 Nonlinear control theory

Linear control theory applies to systems made of devices which obey the superposition principle, which means roughly that the output is proportional to the input. They are governed by linear differential equations. A major subclass is systems which in addition have parameters which do not change with time, called linear time invariant (LTI) systems. These systems are amenable to powerful frequency domain mathematical techniques of great generality, such as the Laplace transform, Fourier transform, Z transform, Bode plot, root locus, and Nyquist stability criterion. These lead to a description of the system using terms like bandwidth, frequency response, eigenvalues, gain, resonant frequencies, poles, and zeros, which give solutions for system response and design techniques for most systems of interest.

Nonlinear control theory covers a wider class of systems that do not obey the superposition principle, and applies to more real-world systems, because all real control systems are nonlinear. These systems are often governed by nonlinear differential equations. If only solutions near a stable point are of interest, nonlinear systems can often be linearized by approximating them by a linear system using perturbation theory, and linear techniques can be used.

P-servo with rigid feedback	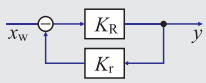	*P*	$K_P = \frac{K_R}{1+K_r K_R} \xrightarrow{K_P \to \infty} \frac{1}{K_r}$
P-servo with yielding feedback	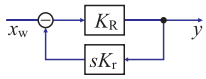	*P*-T_1	$K_P = K_R \;,\; T_1 = K_R K_r$ for $K_R \ll \infty$
		I	$K_I = K_r^{-1}$ for $K_R \to \infty$
P-servo with yielding feedback	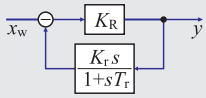	*PD*-T_1	$K_P = K_R \;,\; T_v = T_r \;,\; T_1 = T_r + K_r K_R$ for $K_R \ll \infty$
		PI	$K_P = T_r/K_r \;,\; T_n = T_r$ for $K_R \to \infty$
P-servo with delayed feedback	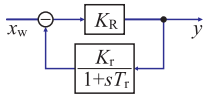	*PD*-T_1	$K_P = \frac{K_R}{1+K_r K_R} \;,\; T_v = T_r \;,\; T_1 = \frac{T_r}{1+K_r K_R}$ for $K_R \ll \infty$
		PD	$K_P = 1/K_r \;,\; T_v = T_r$ for $K_R \to \infty$
P-servo with delayed yielding feedback	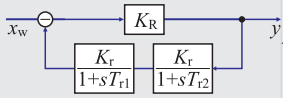	*PID*	$K_P = \frac{T_{r1}+T_{r2}}{K_{r1}K_{r2}} \;,\; T_v = \frac{T_{r1}T_{r2}}{T_{r1}+T_{r2}} \;,\; T_n = T_{r1}+T_{r2}$ for $K_R \to \infty$
P-servo with two delay circuits in the feedback	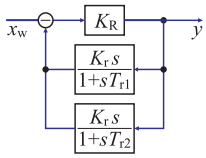	*PID*	$K_P = \frac{T_{r1}+T_{r2}}{K_{r1}(T_{r1}-T_{r2})} \;,\; T_v = \frac{T_{r1}T_{r2}}{T_{r1}+T_{r2}} \;,\; T_n = T_{r1}+T_{r2}$ for $K_R \to \infty$ and $T_{r1} > T_{r2}$
I-servo with rigid feedback	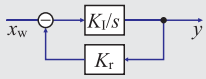	*P*-T_1	$K_P = \frac{1}{K_r} \;,\; T_1 = \frac{1}{K_I K_r}$
I-servo with yielding feedback	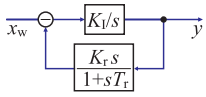	*PI*-T_1	$K_P = \frac{K_I T_r}{1+K_I K_r} \;,\; T_n = T_r \;,\; T_1 = \frac{T_r}{1+K_I K_r}$

Figure 56.8: Some examples for feedback regulators. The columns show from left to right: the nomenclature, the circuit diagram, the behavior, and the constants of the LTI system.

56.2.4.2 MIMO control systems

In this script we restrict to *single-input single-output control systems* (*SISO*), which is the simplest and most common type, in which one output is controlled by one control signal. Examples are the temperature control or an audio system, in which the control input is the input audio signal and the output is the sound waves from the speaker.

In contrast, *multiple-input multiple-output control systems* (*MIMO*) are found in more complicated systems. For example, modern large telescopes such as the Keck and MMT have mirrors composed of many separate segments each controlled by an actuator. The shape of the entire mirror is constantly adjusted by a MIMO active optics control system using input from multiple sensors at the focal plane, to compensate for changes in the mirror shape due to thermal expansion, contraction, stresses as it is rotated and distortion of the wavefront due to turbulence in the atmosphere.

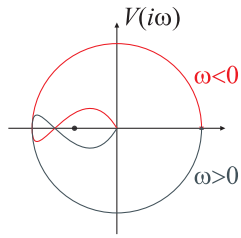

Figure 56.9: Illustration of the Nyquist criterion.

Another example are ultra-stable laser systems stabilized by combinations of fast actuators with low dynamic range and slow actuators with large dynamic range.

56.2.5 Exercises

56.2.5.1 Ex: Step response

Calculate the step response of a low-pass filter using the Laplace transform formalism.

Solution:

56.3 Characterization of stability

The quality factor of a resonance measured with an oscillator in its function as a measuring apparatus for the resonance frequency is named *precision*. The precision also includes the perturbations to which the controlled oscillator is exposed and can be understood as the standard deviation of the frequency realized by the standard. The temporal or spectral behavior of precision, i.e. the stability can e.g. measured directly by comparing similar but independent standards. The reciprocal of the spread of the frequency realizations of an ensemble of similar standards is called *reproducibility*. The term reproducibility is also used to compare the frequencies of an individual standard before and after readjustment of all its technical parameters.

The *accuracy* is defined as the degree of agreement between the frequency realized by the standard and the defined standard frequency, i.e. the frequency that would be displayed in the fault-free ideal case [3]. The accuracy is always less than the quality of the resonance and the certainty of it center frequency. It includes the precision and limits the reproducibility [19]. The fact that the accuracy is related to the ideal case of absent errors implies that it cannot be measured directly. It must be inferred indirectly through model assumptions regarding the measuring apparatus estimating the probability for presumed or possible errors. We then speak of the *uncertainty* of the measured value [275].

The temporal or spectral behavior of *accuracy* is called *stability*. It is measurable and is quantified in the frequency domain by the *spectral density of fluctuations*

[3] For example, when a measurement apparatus for the constant π provided the value $x = 3.141\ 59\ (12)$, then the accuracy is $x - \pi$ and the precision 0.000 12.

and in the time domain best by the *Allan variance*. The noise is now the physical phenomenon that manifests itself as a deviation from the optimal stability.

The stability that an ideal frequency standard can achieve in principle is proportional to quality factor of the resonance $\omega/(\Delta\omega_{nat}+\Delta\omega_{broaden})$ and the signal-to-noise ratio of the control signal S/N. Hence, the stability can be optimized by choosing atomic transitions with small spontaneous decay rates $\Delta\omega_{nat}$. Appropriate techniques for the experimental preparation of the resonance limit the influence of line broadening mechanisms $\Delta\omega$. According to the Fourier theorem, the resolution of narrow lines requires long observation times. Now, the control signal of a feedback regulator can only be determined after a whole observation period. This means that the apparatus already must have an intrinsic stability good enough that the frequency does not leave the control range during a period of observation. Furthermore, a better signal-to-noise ratio can improve the precision with which the line center of the resonance can be determined.

Ultimately, the most promising way to increase the accuracy of a frequency standard seems to be to choose the highest possible transition frequencies ω, provided that the oscillations can still be counted electronically, or be linked in a phase-coherent way to oscillators generating countable oscillations, e.g. using frequency combs. The requirement of phase coherence at optical frequencies puts the laser in the focus of interest in metrology.

56.3.1 Quantifying frequency fluctuations

The following sections deal with perturbation-induced fluctuations of the laser frequency, i.e. frequency noise. To characterize the behavior of an oscillator (especially when used as a frequency standard), it is necessary to introduce some concepts that allow the quantitative description of the noise. The most important are reproducibility, stability, spectral density of fluctuations, Allan variance, and emission bandwidth. The basic work on this has been carried out at the National Bureau of Standards (NBS) in Boulder, Co, USA [18, 19, 97, 314].

56.3.1.1 Stability in the frequency domain, spectral fluctuation density

The instantaneous amplitude of an oscillator, e.g. the electric field of a laser radiation, can be written,

$$\mathcal{E}(t) = \mathcal{E}_0(t)e^{\imath\phi(t)} \ . \tag{56.56}$$

noise afflicts phase and amplitude. In the following we will neglect amplitude noise, $\mathcal{E}_0(t) = \mathcal{E}_0$, and if the frequency fluctuations only deviate slightly from a mean value, $\omega_0 \gg |\dot{\varphi}(t)|$, we may write,

$$\phi(t) \equiv \omega_0 t + \varphi(t) \ . \tag{56.57}$$

In the following, we will often consider normalized frequency fluctuations,

$$y(t) = \dot{\varphi}(t)/\omega_0 \ . \tag{56.58}$$

When measuring stability, one must differentiate between *deterministic fluctuations* and *stochastic noise*. Deterministic fluctuations are usually due to inadequate control of equipment parameters. They generate systematic errors and slow drifts

$y_{sys}(t)$ which, if one recognizes them as such in time domain measurements (measure for sufficiently long times!), can be subtracted and disregarded. Stochastic noise, however, is stationary:

$$\overline{y_{sto}(t)} = \overline{y(t) - y_{sys}(t)} = 0 \qquad \text{defining} \qquad \overline{y(t)} \equiv \lim_{T\to\infty} \frac{1}{T} \int_0^T y(t)dt \tag{56.59}$$

as the time average. In the following only stationary stochastic fluctuations are considered.

Let us take a look at the *autocorrelation function* of the phase defined as,

$$\boxed{R_y(\tau) \equiv \overline{y^*(t)y(t+\tau)} = \lim_{T\to\infty} \frac{1}{T} \int_0^T y^*(t)y(t+\tau)\rangle d\tau} \tag{56.60}$$

and the *spectral density of phase fluctuations* which, according to the *Wiener-Khintchine theorem*, can be obtained as the Fourier transform of the autocorrelation function,

$$\boxed{S_y(f) \equiv \mathcal{F}R_y(\tau) = \int_{-\infty}^{\infty} R_y(\tau)e^{-2\pi\imath f\tau}d\tau} \ . \tag{56.61}$$

The normalized density of frequency fluctuations $S_y(f)$ is a spectral quantity with the unit 1/Hz. Frequency and phase fluctuations are linked by:

$$S_{\dot{x}}(f) = f^2 S_x(f) \ , \tag{56.62}$$

as will be shown in Exc. 56.3.3.1. Also,

$$S_{ax}(f) = a^2 S_x(f) \ , \tag{56.63}$$

If the integral of the spectral fluctuation density is finite it corresponds, according to the definition (56.62), to the noise power or the mean square deviation of a measured variable:

$$\int_0^\infty S_y(f)df = R_y(0) = \overline{|y(t)|^2} < \infty \ . \tag{56.64}$$

56.3.1.2 Model of noise

Measurements seem to confirm today that stochastic fluctuations in frequency standards can be traced back to a few additive noise processes with different physical origins and different frequency responses [18]:

$$\boxed{S_y(f) = \sum_{\beta=-2}^{2} h_\beta f^\beta} \ . \tag{56.65}$$

The table below lists the most common ones.

This noise model is based on the assumption that the noise processes it describes operate in all Fourier frequency ranges, which violates the requirement (56.64). The dilemma does not arise in experiment, since the integration over an unlimited Fourier

noise type	$S_y(f)$	$\sigma_y^2(\tau)$
white phase noise	$h_2 f^2$	$\propto \frac{h_2}{\tau^2}$
flicker phase noise	$h_1 f^1$	$\propto \frac{h_1}{\tau^2}$
white frequency noise	$h_0 f^0$	$\frac{h_0}{2\tau}$
flicker frequency noise	$h_{-1} f^{-1}$	$h_{-1} 2 \ln 2$
random walk frequency drifts	$h_{-2} f^{-2}$	$h_{-2} \frac{(2\pi)^2}{6} \tau$

Table 56.1: *Spectral fluctuation density and Allan-variance for common noise processes [97].*

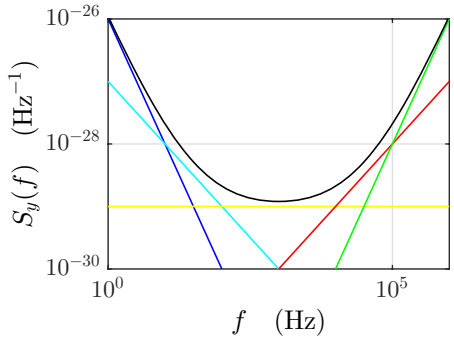

Figure 56.10: Noise model according to (56.65).

frequency range is not a realistic concept in that each measurement only takes a finite time τ, so that very low frequencies below a cut-off frequency $f_{min} = 2\pi/\tau$ are not perceived. In addition, every real data acquisition system has a low-pass behavior with a cut-off frequency f_{max}, so that high frequencies also do not contribute to the integral. These bandwidth constraints enforce the condition (56.64) for the five noise processes assumed by (56.65) [794]. The measure for the noise power in any case has the form: $\int_{f_{min}}^{f_{max}} S_y(f) df$.

56.3.1.3 Description of stability in the time domain, Allan variance

Temporal frequency fluctuations of an oscillator can be measured by *discriminating the frequency fluctuations at the dispersive profile of a resonance* (or error signal) and convert it into voltage fluctuations. It is just the curve exhibited by a spectrum analyzer to which the error signal is fed, as illustrated by the left setup of Fig. 56.12.

Like any physical quantity, frequency fluctuations can only be measured as an average over an *integration time interval* τ imposed by the measuring apparatus. The k-th measurement of the quantity y at the time t_k results in the measured value:

$$y_k(\tau) = \frac{1}{\tau} \int_{t_k}^{t_k+\tau} y(t) dt \ . \tag{56.66}$$

Assuming that the dead time of the measuring apparatus is negligible (if necessary, technical precautions must be taken to meet this requirement approximately), the variance of stochastic noise can be expressed as follows:

$$\sigma_y^2(\tau) = \frac{1}{N-1}\sum_{k=1}^{N} y_k^2 \qquad \text{where} \qquad \overline{y_k} = 0 \ . \tag{56.67}$$

The variance is a direct measure of the stability of an oscillator in time domain. It is measured from a discrimination of the error signal in a similar way as the fluctuation density $S_y(f)$. However, as illustrated by the left setup of Fig. 56.12, the discriminated signal is recorded in time domain, e.g. by an oscilloscope.

The variance can be linked to the spectral density of frequency fluctuations in frequency domain by Fourier transformation. With the Heaviside step function Θ the following relationship can be given [314, 18, 61],

$$\sigma_y^2(\tau) = \int_0^\infty S_y(f)|\mathcal{F}\zeta_1(f)|^2 df \qquad \text{where} \qquad \zeta_1(t) = \frac{1}{\tau}\Theta_{[-\tau,0]}(t) \ , \tag{56.68}$$

is the area-normalized jump function, which models the duration of the integration time τ. Its Fourier-transform is the transfer function of the equivalent filter.

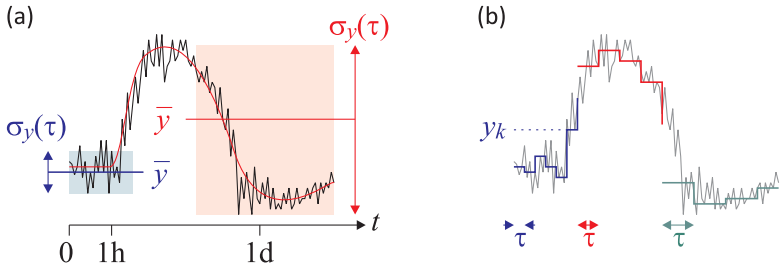

Figure 56.11: (a) Noise can exhibit very different short and long time behavior. (b) Any measurement needs a minimum integration time.

It turns out that the variance for $1/f$ noise and for stochastic drifts ($1/f^2$ noise) diverges at the lower limit, i.e. this variance is not useful for practical applications. The divergence comes from the fact that for longer and longer measurements ($N \to \infty$), respectively, smaller and smaller Fourier frequencies ($f \to 0$), longer and longer periodic fluctuations can be identified as such, while for shorter measurements they appear as linear drifts. One way out is to calculate the variance for a limited number k of measurement data and to average the variances of M of such data sets of length k. This variance converges for a larger number of noise processes. This so-called pair variance ($k = 2$) or *Allan variance* is widely used:

$$\boxed{\sigma_y^2(\tau) = \frac{1}{2M}\sum_{j=1}^{M}(y_{2j} - y_{2j-1})^2} \ . \tag{56.69}$$

Like the normal variance, the Allan variance can also be related to the spectral density

of frequency fluctuations:

$$\sigma_y^2(\tau) = \int_0^\infty S_y(f)|\mathcal{F}\zeta_2(f)|^2 df \qquad \text{where} \qquad \zeta_2(t) \equiv \tfrac{1}{\sqrt{2}}[\zeta_1(t) - \zeta_1(-t)] \ . \tag{56.70}$$

The Fourier transforms of the step functions $\zeta_1(t)$ and $\zeta_2(t)$ will be calculated in Exc. 56.3.3.2, as well as the variances for white noise.

56.3.2 Power spectral density

It is important not to confuse the spectral density of frequency fluctuations with the power spectral density of the oscillator defined via the *autocorrelation function of the field amplitude* [4],

$$\boxed{R_{\mathcal{E}}(\tau) \equiv \langle \mathcal{E}^*(t)\mathcal{E}(t+\tau)\rangle = \mathcal{E}_0^2 \langle e^{\imath[\phi(t+\tau)-\phi(t)]}\rangle = \mathcal{E}_0^2 e^{\imath\omega_0\tau}\langle e^{\imath[\varphi(t+\tau)-\varphi(t)]}\rangle} \ , \tag{56.71}$$

as its Fourier transform,

$$\boxed{S_{\mathcal{E}}(\omega) = \mathcal{F}R_{\mathcal{E}}(\tau)} \ . \tag{56.72}$$

The power spectral density is typically measured as the beat frequency of two independent oscillators. It is just the curve exhibited by a spectrum analyzer to which the beat signal is fed, as illustrated in the right setup of Fig. 56.12.

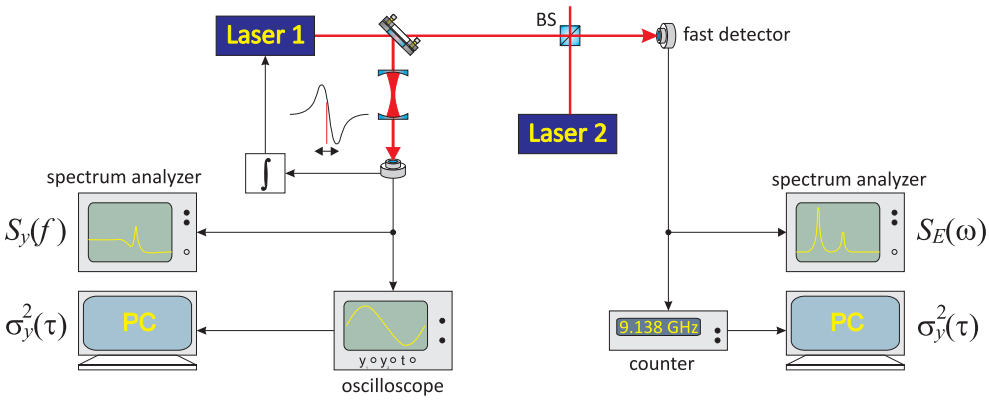

Figure 56.12: (left) Setup for measuring the spectral density of frequency fluctuations $S_y(f)$ and the Allan variance $\sigma_y^2(\tau)$ of laser 1 discriminating it at the slope of transmission signal of an optical cavity. (right) The power spectral density $S_{\mathcal{E}}(\omega)$ can be found as the beat signal between two lasers and either be exhibited on a spectrum analyzer $S_{\mathcal{E}}(\omega)$ or counted and processed to an Allan variance $\sigma_y^2(\tau)$.

The beat spectrum is the convolution of the emission bandwidth of the two oscillators,

$$S_{\mathcal{E}}(\omega) = S_{\mathcal{E},laser1}(\omega) * S_{\mathcal{E},laser2}(\omega) \ . \tag{56.73}$$

[4] Note that the *first-order coherence* is just the normalized autocorrelation,

$$g^{(1)}(\tau) \equiv \frac{\langle \mathcal{E}^*(t)\mathcal{E}(t+\tau)\rangle}{\langle \mathcal{E}^*(t)\mathcal{E}(t)\rangle} = \frac{R_{\mathcal{E}}(\tau)}{R_{\mathcal{E}}(0)} \ .$$

.

In particular, for the case that we have good reasons to believe that one laser is much narrower than the other, the power spectral density $S_{\mathcal{E}}(\omega)$ will reflect the emission spectrum of just the broader laser. Note that the power spectral density derived from a beat of two independent (uncorrelated) oscillators gives us information on their true emission bandwidths, which is relevant e.g. for resolving narrow atomic transitions. On the other hand, the stability measures $S_y(f)$ and $\sigma_y^2(\tau)$ derived from a discriminated error signal (left setup in Fig. 56.12) only tell us the stability of an oscillator with respect to the reference from which the error signal was derived, e.g. the transmission slope of an optical cavity.

56.3.2.1 Spectral noise power density in the case of white noise

The spectral noise power density $S_{\mathcal{E}}(\omega)$ of the field $\mathcal{E}(t)$ of an oscillator can, in the case of white frequency noise, be related to the spectral density of its frequency fluctuations. In the case of a laser oscillator, the half-width half maximum of the spectral noise power density, i.e. the emission bandwidth, is often specified. We will, in the following, derive the emission spectrum for the case of white Gaussian noise [1264, 414, 381].

In Exc. 56.3.3.3 we show that for a *Gaussian noise process* holds [326, 414],

$$\left\langle e^{-\imath[\varphi(t)-\varphi(t+\tau)]} \right\rangle = e^{-\left\langle [\varphi(t)-\varphi(t+\tau)]^2 \right\rangle/2} \,. \tag{56.74}$$

Now we set $\varphi(t) = \omega_0 \int_0^t y(t')dt'$ using (56.58) and obtain,

$$\begin{aligned} \left\langle [\varphi(t)-\varphi(t+\tau)]^2 \right\rangle &= \left\langle \omega_0^2 \left[\int_0^\tau y(t')dt' \right]^2 \right\rangle = \omega_0^2 \int_0^\tau \int_0^\tau \langle y(t')y(t'') \rangle \, dt'dt'' \\ &= \omega_0^2 \int_0^\tau \int_0^\tau R_y(t'-t'')dt'dt'' = 2\omega_0^2 \int_0^\tau (\tau - t) R_y(t)dt \,. \end{aligned} \tag{56.75}$$

Using (56.61), we now substitute the autocorrelation function by its Fourier transform, the spectral fluctuation density, $R_y(t) = \int_0^\infty S_y(f) e^{2\pi\imath f t} df$:

$$\begin{aligned} \left\langle [\varphi(t)-\varphi(t+\tau)]^2 \right\rangle &= 2\omega_0^2 \int_0^\infty S_y(f) \int_0^\tau (\tau - t) e^{2\pi\imath f t} dt df \\ &= 2\omega_0^2 \int_0^\infty S_y(f) \left(\frac{\sin \pi f \tau}{2\pi f} \right)^2 df + \text{imaginary part} \,. \end{aligned} \tag{56.76}$$

We neglect the imaginary part.

For Markovian white noise the phase fluctuations are δ-distributed, which means,

$$R_y \equiv \langle y^*(t) y(t+\tau) \rangle = h_0 \delta(\tau) \qquad \text{and} \qquad S_y(f) = h_0 = const. \tag{56.77}$$

I.e. the so-called *white noise* is characterized by a constant spectral density of phase fluctuations. Carrying on the calculation (56.76) for the case of white frequency noise we get,

$$\left\langle [\varphi(t)-\varphi(t+\tau)]^2 \right\rangle = \frac{h_0 \omega_0^2 |\tau|}{\pi} \int_0^\infty \left(\frac{\sin x}{x} \right)^2 dx = \frac{h_0 \omega_0^2 |\tau|}{2} \,. \tag{56.78}$$

With this result, we can undertake to calculate the autocorrelation function of the field amplitude (56.71),

$$R_{\mathcal{E}}(\tau) = \mathcal{E}_0^2 e^{\omega_0 \tau} e^{-h_0 \omega_0^2 |\tau|/2} \ . \tag{56.79}$$

The resulting *power spectral density* (56.72) is [5]:

$$\boxed{S_{\mathcal{E}}(\omega) = \mathcal{E}_0^2 \int_{-\infty}^{\infty} R_{\mathcal{E}}(\tau) e^{-\imath(\omega-\omega_0)\tau} d\tau = \frac{2h_0\omega_0^2}{4\Delta^2 + (h_0\omega_0^2/2)^2}} \ , \tag{56.80}$$

where $\Delta \equiv \omega - \omega_0$ is the deviation of the oscillator frequency from the center frequency ω_0. Thus, the the emission spectrum for the case of white Gaussian noise is a Lorentzian profile with the *laser emission bandwidth*,

$$\boxed{\beta = \tfrac{1}{2} h_0 \omega_0^2} \ . \tag{56.81}$$

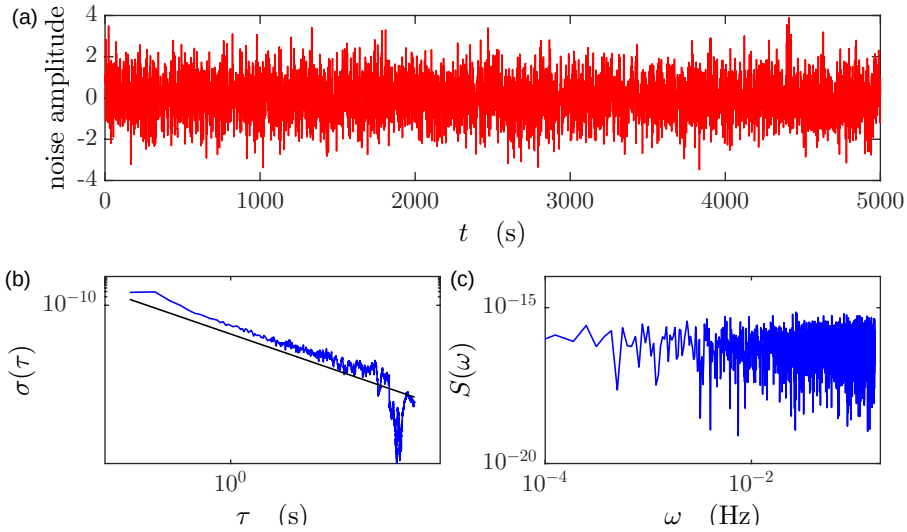

Figure 56.13: (code) Allan variance (b) and spectral density of frequency fluctuations (c) calculated from a randomly generated data set (a).

The Lorentz shape of the emission profile of an oscillator or a resonance always indicates white noise of the underlying frequency fluctuation density. In this sense, the Lorentz form of the natural broadening of an atomic resonance can also be traced back to the white noise of the vacuum fluctuations. Here, the emission bandwidth has to be replaced by the natural linewidth. The Allan variance in this case is:

$$\sigma_y^2(\tau) = \frac{h_0}{2\tau} = \frac{1}{Q^2} \frac{1}{\Gamma} \frac{1}{\tau} \ . \tag{56.82}$$

with the linewidth (FWHM) $\Gamma = h_0\omega_0^2/2$ and $Q = \omega_0/\Gamma$ and indicates the maximum achievable stability for a frequency standard that is coupled to the resonance ω_0.

[5] Using $\mathcal{F}[e^{-a|x|}] = \int_{-\infty}^{\infty} e^{-a|t|} e^{-\imath\omega t} dt = \frac{2a}{a^2+\omega^2}$.

56.3.2.2 Spectral noise power density in case of periodic phase perturbation

The momentary deflection of the oscillator can be described in the case of a harmonic phase disturbance by equation (56.60) with the additional condition: $\phi(t) = N \sin \Omega t$. The frequency fluctuation density and the Allan variance are obtained in this case:

$$S_y(f) = \left(\frac{fN}{2\omega_0}\right)^2 \delta(f-\Omega) \qquad \text{resp.} \qquad \sigma_y^2(\tau) = \left(\frac{\Omega N}{2\omega_0}\right)^2 \frac{\sin^2 \Omega\tau/2}{\Omega\tau/2} \ . \tag{56.83}$$

The spectral noise power density consists of a discrete spectrum of sidebands, the number and height of which is given by the modulation index N:

$$\boxed{S_{\mathcal{E}}(\omega) = \sum_{n=-\infty}^{\infty} |J_n(N)|^2 \delta(\omega - \omega_0 - \Omega)} \ . \tag{56.84}$$

A full width at half maximum of the spectral noise power density cannot be specified. However, as a measure of the emission bandwidth of the oscillator, the frequency spacing of the sideband of the highest order can be understood, the height of which corresponds to at least half the height of the carrier frequency ω_0.

56.3.3 Exercises

56.3.3.1 Ex: Spectral density of frequency fluctuations

Prove the relationship $S_{\dot{x}}(f) = f^2 S_x(f)$.

Solution: *We start showing* $(\mathcal{F}f')(\omega) = 2\pi\imath\omega(\mathcal{F}f)(\omega)$. *First we define* $u = e^{-2\pi\imath\omega t}$ *and* $v = f(t)$ *such that* $du = -2\pi\imath\omega e^{-2\pi\imath\omega t}dt$ *and* $dv = f'(t)dt$. *Then we integrate by parts,*

$$\begin{aligned}(\mathcal{F}f')(\omega) &= \int_{-\infty}^{\infty} f'(t)e^{-2\pi\imath\omega t}dt = f(t)e^{-2\pi\imath\omega t}\big|_{-\infty}^{\infty} - \int_{-\infty}^{\infty}(-2\pi\imath\omega)e^{-2\pi\imath\omega t}f(t)dt \\ &= 2\pi\imath\omega \int_{-\infty}^{\infty} e^{-2\pi\imath\omega t}f(t)dt = 2\pi\imath\omega(\mathcal{F}f)(\omega) \ .\end{aligned}$$

Furthermore,

$$[\mathcal{F}(f'g')](\omega) = [(Ff') * (Fg')](\omega) = (2\pi\imath\omega)^2[\mathcal{F}(fg)](\omega) \ .$$

Now, writing spectrum as,

$$\begin{aligned}S_{\dot{x}}(f) &= \int R_{\dot{x}}(\tau)e^{-2\pi i f\tau}d\tau = \int \left[\lim_{T\to\infty}\frac{1}{T}\int_0^T \dot{x}(t)\dot{x}(t+\tau)dt \ e^{-2\pi i f\tau}\right]d\tau \\ &= \lim_{T\to\infty}\frac{1}{T}\int_0^T \left[\int \dot{x}(t)\dot{x}(t+\tau)e^{-2\pi i f\tau}d\tau\right]dt \ ,\end{aligned}$$

and identifying $f(t) \equiv \dot{x}(t)$ *and* $g(t) \equiv \dot{x}(t+\tau)$ *we get,*

$$S_{\dot{x}}(f) = f^2 S_x(f) \ .$$

56.3.3.2 Ex: Allan variance for white noise

a. Calculate the Fourier transform of step function $\zeta_1(t)$ and the one-point variance for white noise from its definition (56.68).
b. Repeat the calculation for the step function $\zeta_2(t)$ and the Allan variance as defined in (56.70).

Solution: *a. The Fourier transform of step function* $\zeta_1(t) = \frac{\Theta_{[-\tau,0]}(t)}{\tau}$ *is,*

$$(\mathcal{F}\zeta_1)(f) = \int_{-\infty}^{\infty} \zeta_1(t) e^{2\pi\imath f t} dt = \frac{1}{\tau}\int_{-\tau}^{0} e^{2\pi\imath f t} dt = \frac{1 - e^{-2\pi\imath f\tau}}{2\pi i f\tau} \ ,$$

such that,

$$|(\mathcal{F}\zeta_1)(f)|^2 = \frac{\sin^2 \pi f\tau}{(\pi f\tau)^2} \ .$$

The one-point variance is now,

$$\sigma_y^2(\tau) = \int_0^{\infty} S_y(\tau) |\mathcal{F}\zeta_1(f)|^2 df = h_0 \int_0^{\infty} \frac{\sin^2 \pi f\tau}{(\pi f\tau)^2} df = \frac{h_0}{2|\tau|} \ .$$

b. The Fourier transform of the step function $\zeta_2(t) = \frac{\zeta_1(t) - \zeta_1(-t)}{\sqrt{2}}$ *is,*

$$(\mathcal{F}\zeta_2)(f) = \int_{-\infty}^{\infty} \zeta_2(t) e^{2\pi\imath f t} dt = \frac{1}{\sqrt{2}} \left(\frac{1 - e^{-2\pi\imath f\tau}}{2\pi\imath f\tau} - \frac{e^{2\pi\imath f\tau} - 1}{2\pi\imath f\tau} \right) \ .$$

such that,

$$|(\mathcal{F}\zeta_2)(f)|^2 = 2\frac{\sin^4 \pi f\tau}{(\pi f\tau)^2} \ .$$

The Allan variance is now,

$$\sigma_y^2(\tau) = \int_0^{\infty} S_y(\tau) |\mathcal{F}\zeta_2(f)|^2 df = h_0 \int_0^{\infty} \frac{2\sin^4 \pi f\tau}{(\pi f\tau)^2} df = \frac{h_0}{2|\tau|} \ .$$

56.3.3.3 Ex: Gaussian noise process

Prove the relationship (56.75) for a *Gaussian noise process* characterized by,

$$\frac{\langle A^{2n} \rangle}{(2n)!} = \frac{\langle A^2 \rangle^n}{2^n n!} \qquad \text{and} \qquad \langle A^{2n-1} \rangle = 0 \ .$$

Solution: *We calculate,*

$$\begin{aligned} \left\langle e^{-\imath[\varphi(t) - \varphi(t+\tau)]} \right\rangle &= \sum_n \frac{1}{(2n)!} \left\langle -\imath^{2n} [\varphi(t) - \varphi(t+\tau)]^{2n} \right\rangle \\ &= \sum_n \frac{1}{n!} \left\langle -\tfrac{1}{2} [\varphi(t) - \varphi(t+\tau)]^2 \right\rangle^n = e^{-\left\langle [\varphi(t) - \varphi(t+\tau)]^2 \right\rangle / 2} \ . \end{aligned}$$

56.4 Data sheets

The following pages contain the data sheets of the main components used in this course.

HL6722G

AlGaInP Laser Diode

opnext
Powered by HITACHI

ODE-208-220E (Z)

Rev.5
Mar. 2005

Description

The HL6722G is a 0.67 µm band AlGaInP index-guided laser diode with a multi-quantum well (MQW) structure. It is suitable as a light source for bercode scanner, and various other types of optical equipment. Hermetic sealing of the package assures high reliability.

Features

- Visible light output at wavelengths up to 680 nm
- Single longitudinal mode
- Continuous operating output: 5 mW CW
- Low voltage operation: 2.7 V Max
- Low current operation: 32 mA Typ
- Built-in monitor photodiode

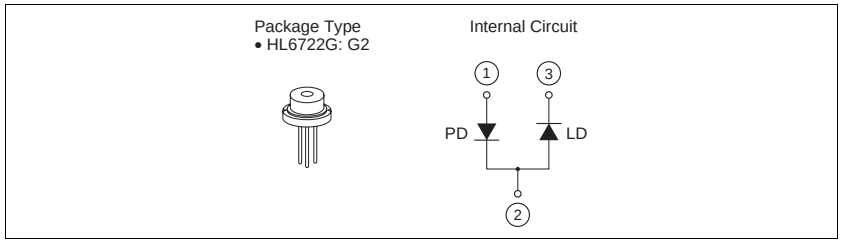

opnext
Powered by HITACHI

Figure 56.14: Data sheet for the diode laser from Thorlabs, model Hitachi HL6722G.

Coaxial

Amplifier

ZHL-2-8

50Ω Medium High Power 10 to 1000 MHz

ZHL-2-8X

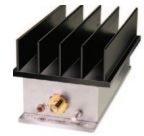

ZHL-2-8

SMA version shown

Features

- wideband, 10 to 1000 MHz
- high IP3, +38 dBm typ.
- medium high power, 29 dBm min.

Applications

- VHF/UHF
- test equipment
- cellular
- instrumentation
- laboratory

CASE STYLE: T34

Connectors	Model	Price	Qty.
BNC	ZHL-2-8	$525.00 ea.	(1-9)
BNC	ZHL-2-8X	$515.00 ea.	(1-9)
SMA	ZHL-2-8-S	$535.00 ea.	(1-9)
SMA	ZHL-2-8X-S	$525.00 ea.	(1-9)

Electrical Specifications

MODEL NO.	FREQ. (MHz)		GAIN (dB)			MAXIMUM POWER OUTPUT (dBm)		DYNAMIC RANGE		VSWR (:1) Max.		DC POWER	
	f_L	f_U	Min.	Typ.	Flatness Max.	(1 dB Compr.) Min.	Input (no damage)	NF (dB) Typ.	IP3 (dBm) Typ.	In	Out	Volt (V) Nom.	Current (A) Max.
ZHL-2-8	10	1000	31	35	±1.0	+29	+5	10.0	+38	2.0	2.0	24	0.6
ZHL-2-8X*	10	1000	31	35	±1.0	+29	+5	10.0	+38	2.0	2.0	24	0.6

* Heat sink not included
Open load is not recommended, potentially can cause damage.
With no load derate max input power by 20 dB

To order without heat sink, add suffix X to model number. Alternative heat sinking and heat removal must be provided by the user to limit maximum temperature to 65°C, in order to ensure proper performance. For reference, this requires thermal resistance of user's external heat sink to be 1.35°C/W Max.

Maximum Ratings

Operating Temperature	-20°C to 65°C
Storage Temperature	-55°C to 100°C
DC Voltage	+25V Max.

Permanent damage may occur if any of these limits are exceeded.

Outline Drawing

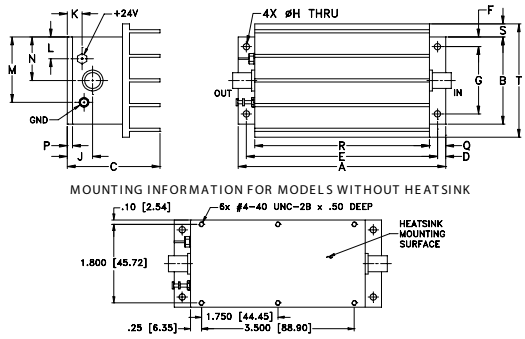

Figure 56.15: Data sheet for the rf-amplifier from MiniCircuits, model ZHL-2-8.

Coaxial

Voltage Controlled Oscillator ZOS-100+

Dual Output 50 to 100 MHz

Features

- octave bandwidth
- linear tuning, 4.5 MHz/V typ.
- excellent harmonic suppression, -29 dBc typ.
- rugged shielded case
- protected by US Patent, 6,943,629

Applications

- auxiliary output freq. monitoring
- load insensitive source

CASE STYLE: BR386

Connectors	Model	Price	Qty.
SMA	ZOS-100+	$119.95	(1-9)

+ RoHS compliant in accordance with EU Directive (2002/95/EC)

The +Suffix has been added in order to identify RoHS Compliance. See our web site for RoHS Compliance methodologies and qualifications.

Electrical Specifications

FREQUENCY (MHz)		POWER OUTPUT (dBm) Typ.		TUNING VOLTAGE (V)		PHASE NOISE (dBc/Hz) SSB at offset frequencies: Typ.			PULLING (MHz) pk-pk (open/short)	PUSHING (MHz/V)	TUNING SENSITIVITY (MHz/V)	HARMONICS (dBc)		3 dB MODULATION BANDWIDTH (MHz)	DC OPERATING POWER	
Min.	Max.	Main	Aux.	Min.	Max.	10 kHz	100 kHz	1 MHz	Typ.	Typ.	Typ.	Typ.	Max.	Typ.	Vcc (volts)	Current (mA) Max.
50	100	+9	-12	1	16	-111	-131	-143	0.026	0.25	4.5	-29	-20	0.1	12	140

Maximum Ratings

Operating Temperature	-55°C to 85°C
Storage Temperature	-55°C to 100°C
Absolute Max. Supply Voltage (Vcc)	+16V
Absolute Max. Tuning Voltage (Vtune)	+18V

all specifications: 50 ohm system
Permanent damage may occur if any of these limits are exceeded.

electrical schematic

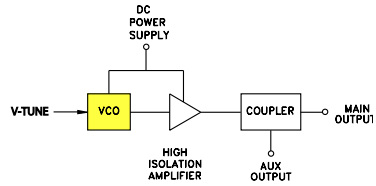

Outline Drawing

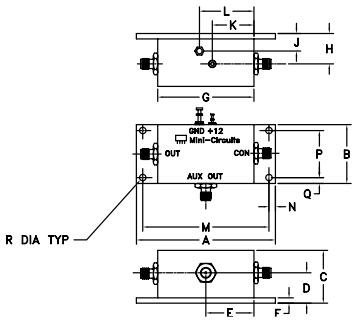

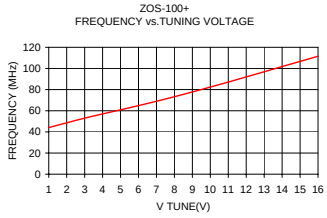

Outline Dimensions (inch / mm)

A	B	C	D	E	F	G	H	J	K	L	M	N	P	Q	R	wt
3.25	1.38	1.25	.71	1.13	.125	2.25	.71	.41	.98	1.28	2.950	.15	1.100	.14	.150	grams
82.55	35.05	31.75	18.03	28.70	3.18	57.15	18.03	10.41	24.89	32.51	74.93	3.81	27.94	3.56	3.81	180

Figure 56.16: Data sheet for the Voltage-Controlled Oscillator (VCO) from Minicircuits, model ZOS-100+.

Coaxial

Voltage Variable Attenuator

ZX73-2500+

50Ω 10 to 2500 MHz

FEMALE SMA shown

CASE STYLE: GD958

SMA	Connectors	Model	Price	Qty.	Case
INPUT	**OUTPUT**				
FEMALE	**FEMALE**	ZX73-2500-S+	$49.95	(1-9)	GD958
MALE	**FEMALE**	ZX73-2500M-S+	$49.95	(1-9)	GD1163

+ RoHS compliant in accordance with EU Directive (2002/95/EC)

The +Suffix has been added in order to identify RoHS Compliance. See our web site for RoHS Compliance methodologies and qualifications.

Maximum Ratings

Operating Temperature	-55°C to 85°C
Storage Temperature	-55°C to 85°C
Absolute Max. Supply Voltage (V+)	12V
Absolute Max. Control Voltage (Vcrtl)	20V
Absolute Max. RF Input Level	+20 dBm

Permanent damage may occur if any of these limits are exceeded.

Features

- Broadband, 10-2500 MHz
- IP3, +43 dBm typ.
- 40 dB attenuation @ 1500 MHz
- Good VSWR at in /out ports over attenuation range
- No external bias and RF matching network required
- Shielded case
- Protected by US Patent 6,790,049

Applications

- Variable gain amplifier
- Power level control
- Feed-forward amplifiers
- ALC circuits

Outline Drawing (GD958)

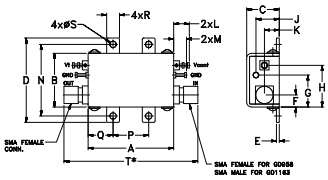

Outline Dimensions (inch / mm)

A	B	C	D	E	F	G	H	J
1.20	**.75**	**.46**	**1.18**	**.04**	**.17**	**.45**	**.59**	**.33**
30.48	19.05	11.68	29.97	1.02	4.32	11.43	14.99	8.38

K	L	M	N	P	Q	R	S	T	wt.
.21	**.22**	**.18**	**1.00**	**.50**	**.35**	**.18**	**.106**	**1.88**	**grams**
5.33	5.59	4.57	25.40	12.70	8.89	4.57	2.69	47.75	35.0

Note:

* T dimension is 2.05 inch (52.07 mm) for GD1163 Case Style.

Electrical Specifications (T_{AMB}= 25°C)

FREQ. (MHz)		MIN. INSERTION LOSS, dB (+15V)		MAX. ATTENUATION dB (0V)		INPUT POWER (dBm)	CONTROL Voltage (V)	CONTROL Current (mA)	IP3 (dBm)	RETURN LOSS[1] (dB)	POWER SUPPLY Voltage (V)	POWER SUPPLY Current (mA)
Min.	Max.	Typ.	Max.	Typ.	Min.	Max.		Max.	Typ.	Typ.		Max.
10	500	3.0	4.6	55	41	+20	0 - 17	30	43	20	+3 to +5	5
500	1500	3.3	5.0	40	30	+20	0 - 17	30	43	20	+3 to +5	5
1500	2500	4.0	6.2	37	25	+20	0 - 17	30	44	20	+3 to +5	5

Notes:
Rise/Fall time: 14μSec/25μSec Typ.
Switching Time, turn on/off: 14μSec/25μSec Typ.
[1] Improved R. Loss in/out performance can be achieved at certain frequencies by choosing a V+ between +3V to +5V

Equivalent Schematic

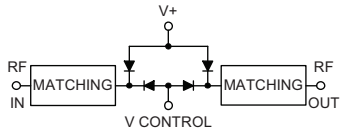

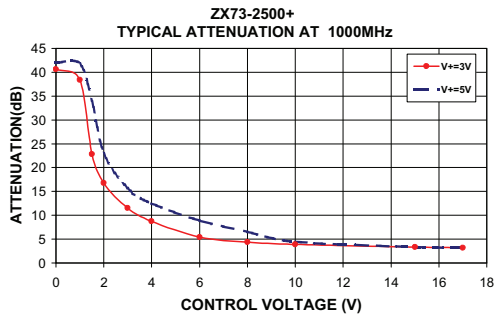

Figure 56.17: Data sheet for the voltage-controlled variable attenuator from Minicircuits, model ZX73-2500+.

Plug-In

Power Splitter/Combiner

PSC-2-1+
PSC-2-1

2 Way-0° 50Ω 0.1 to 400 MHz

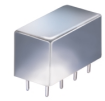

CASE STYLE: A01
PRICE: $14.20 ea. QTY. (1-9)

+ RoHS compliant in accordance with EU Directive (2002/95/EC)

The +Suffix identifies RoHS Compliance. See our web site for RoHS Compliance methodologies and qualifications.

Maximum Ratings

Operating Temperature	-55°C to 100°C
Storage Temperature	-55°C to 100°C
Power Input (as a splitter)	1W max.
Internal Dissipation	0.125W max.

Pin Connections

SUM PORT	1
PORT 1	5
PORT 2	6
GROUND	2,3,4,7,8
CASE GROUND	2,3,4,7,8

Features

- wideband, 0.1 to 400 MHz
- low insertion loss, 0.4 dB typ.
- rugged welded construction

Applications

- VHF/UHF
- federal & defense communications

Outline Drawing

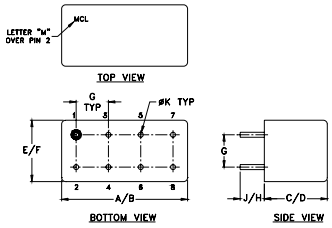

Outline Dimensions (inch / mm)

A	B	C	D	E	F
.770	.800	.385	.400	.370	.400
19.56	20.32	9.78	10.16	9.40	10.16
G	H	J	K		wt
.200	.20	.14	.031		grams
5.08	5.08	3.56	0.79		5.2

Electrical Specifications

FREQ. RANGE (MHz)	ISOLATION (dB)						INSERTION LOSS (dB) ABOVE 3.0 dB						PHASE UNBALANCE (Degrees)			AMPLITUDE UNBALANCE (dB)		
	L		M		U		L		M		U		L	M	U	L	M	U
f_L-f_U	Typ.	Min	Typ.	Min	Typ.	Min	Typ.	Max.	Typ.	Max.	Typ.	Max.	Max.	Max.	Max.	Max.	Max.	Max.
0.1-400	20	15	25	20	25	20	0.2	0.6	0.4	0.75	0.6	1.0	2.0	3.0	4.0	0.15	0.2	0.3

L = low range [f_L to 10 f_L] M = mid range [10 f_L to f_U/2] U= upper range [f_U/2 to f_U]

Typical Performance Data

Frequency (MHz)	Insertion Loss (dB)		Amplitude Unbalance (dB)	Isolation (dB)	Phase Unbalance (deg.)	VSWR S	VSWR 1	VSWR 2
	S-1	S-2						
0.10	3.23	3.23	0.00	24.82	0.01	1.16	1.37	1.37
5.00	3.14	3.14	0.00	35.64	0.01	1.10	1.11	1.11
20.00	3.18	3.17	0.00	35.33	0.03	1.11	1.10	1.10
40.00	3.18	3.18	0.00	34.39	0.02	1.12	1.10	1.10
60.00	3.22	3.22	0.00	33.16	0.02	1.12	1.09	1.09
80.00	3.24	3.24	0.00	31.85	0.04	1.13	1.09	1.09
100.00	3.24	3.24	0.00	30.68	0.05	1.13	1.09	1.09
150.00	3.28	3.27	0.00	28.37	0.04	1.14	1.08	1.08
175.00	3.31	3.30	0.01	27.46	0.07	1.14	1.07	1.07
200.00	3.32	3.31	0.01	26.72	0.05	1.15	1.07	1.07
225.00	3.32	3.31	0.01	26.14	0.02	1.15	1.06	1.06
250.00	3.37	3.36	0.01	25.65	0.05	1.15	1.06	1.06
300.00	3.41	3.38	0.03	24.88	0.10	1.15	1.06	1.06
350.00	3.47	3.44	0.03	24.40	0.06	1.16	1.08	1.07
400.00	3.50	3.46	0.04	23.86	0.05	1.18	1.10	1.09

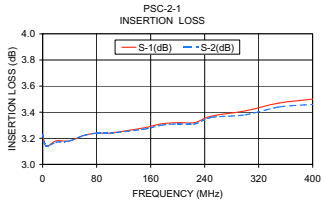

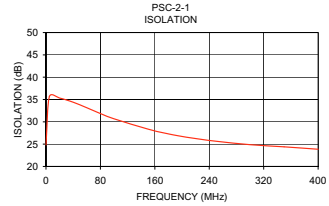

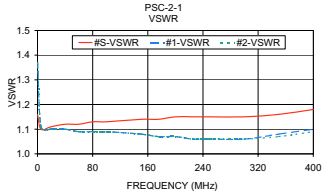

electrical schematic

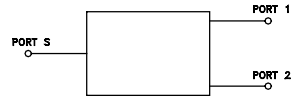

Mini-Circuits®
ISO 9001 ISO 14001 CERTIFIED

ALL NEW minicircuits.com

REV. A
M98898
PSC-2-1
HY/TD/CP
070202

P.O. Box 350166, Brooklyn, New York 11235-0003 (718) 934-4500 Fax (718) 332-4661 For detailed performance specs & shopping online see Mini-Circuits web site
The Design Engineers Search Engine Provides ACTUAL Data Instantly From MINI-CIRCUITS At: www.minicircuits.com

Figure 56.18: Data sheet for the power divider from Minicircuits, model PSC-2-1.

Plug-In

Frequency Mixer

SRA-2CM+

Level 7 (LO Power +7 dBm) 5 to 1000 MHz

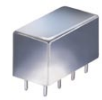

CASE STYLE: A01
PRICE: $18.20 ea. QTY (1-9)

+ RoHS compliant in accordance with EU Directive (2002/95/EC)

The +Suffix has been added in order to identify RoHS Compliance. See our web site for RoHS Compliance methodologies and qualifications.

Maximum Ratings

Operating Temperature	-55°C to 100°C
Storage Temperature	-55°C to 100°C
RF Power	50mW
IF Current	40mA

Pin Connections

LO	8
RF	1
IF	3,4^
GROUND	2,5,6,7
CASE GROUND	2,5,6,7

^ *pins must be connected together externally*

Features

- excellent conversion loss, 5.27 dB typ.
- good L-R isolation, 35 dB typ. L-I isolation, 30 dB typ.
- rugged welded construction
- hermetic

Applications

- VHF/UHF
- cellular
- defense & federal communications
- ISM/GSM

Outline Drawing

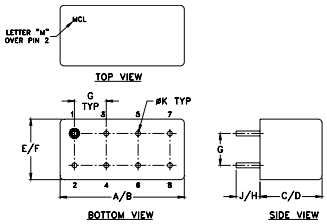

Outline Dimensions (inch / mm)

A	B	C	D	E	F
.770	.800	.385	.400	.370	.400
19.56	20.32	9.78	10.16	9.40	10.16
G	H	J	K		wt
.200	.20	.14	.031		grams
5.08	5.08	3.56	0.79		5.2

Electrical Specifications

FREQUENCY (MHz)		CONVERSION LOSS (dB)				LO-RF ISOLATION (dB)						LO-IF ISOLATION (dB)					
		Mid-Band m			Total Range	L		M		U		L		M		U	
LO/RF f_L-f_U	IF	$\bar{X}$	σ	Max.	Max.	Typ.	Min.	Typ.	Min.	Typ.	Min.	Typ.	Min.	Typ.	Min.	Typ.	Min.
5-1000	DC-1000	5.27	.04	7.0	8.5	60	50	35	30	30	25	50	45	30	25	25	20

1 dB COMP.: +1 dBm typ.

L = low range [f_L to 10 f_L] m= mid band [2f_L to f_U/2] M = mid range [10 f_L to f_U/2] U = upper range [f_U/2 to f_U]

Typical Performance Data

Frequency (MHz)		Conversion Loss (dB)	Isolation L-R (dB)	Isolation L-I (dB)	VSWR RF Port (:1)	VSWR LO Port (:1)
RF	LO	LO +7dBm	LO +7dBm	LO +7dBm	LO +7dBm	LO +7dBm
5.00	35.00	7.36	67.00	67.00	5.03	4.09
38.13	68.13	5.59	54.82	53.34	1.40	3.04
71.27	41.27	5.30	49.15	48.13	1.31	2.99
137.53	107.53	5.33	46.10	45.22	1.27	2.83
200.00	170.00	5.35	42.68	41.91	1.24	2.82
236.93	206.93	5.27	41.09	40.29	1.24	2.72
303.20	273.20	5.28	39.42	38.94	1.24	2.76
336.33	306.33	5.42	39.72	36.88	1.26	2.77
402.60	372.60	5.63	38.13	35.49	1.30	2.85
468.86	438.86	5.62	37.15	35.09	1.37	2.84
535.13	505.13	5.87	35.49	32.57	1.45	2.97
568.26	538.26	6.01	35.26	31.27	1.50	2.96
634.53	604.53	6.17	36.03	29.46	1.61	3.10
700.79	670.79	6.68	38.00	30.29	1.70	3.21
767.06	737.06	6.49	38.00	29.92	1.85	3.09
800.19	770.19	6.11	39.26	28.34	2.01	3.03
833.33	803.33	6.37	39.87	27.52	2.08	3.08
899.59	869.59	6.80	40.23	26.99	2.32	3.39
965.86	935.86	6.86	42.61	25.65	2.53	3.58
1000.00	969.00	7.10	44.90	24.17	2.76	3.76

Electrical Schematic

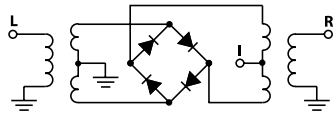

Figure 56.19: Data sheet for the mixer from Minicircuits, model SRA-2CM+.

SPECIFICATIONS				
AO Medium				TeO2
Acoustic Velocity				4.2 mm/μs
Active Aperture*	2.5	mm 'L' X	1	mm 'H'
Center Frequency (Fc)				80 MHz
RF Bandwidth	20 MHz @	-10 dB	Return Loss	
Input Impedance				50 Ohms Nominal
VSWR @ Fc				1.3 :1 Max
Wavelength				442-633 nm
Insertion Loss				4 % Max
Reflectivity per Surface				1 % Max
Anti-Reflection Coating				MIL-C-48497
Optical Power Density				250 W/mm^2
Contrast Ratio				1000 :1 Min
Polarization			90 ° To Mounting Plane	

PERFORMANCE VS WAVELENGTH				
Wavelength (nm)	**442**	**488**	**515**	**633**
Saturation RF Power (W)	0.27	0.33	0.36	0.55
Bragg Angle (mr)	4.2	4.6	4.9	6
Beam Separation (mr)	8.4	9.2	9.8	12

PERFORMANCE VS BEAM DIAMETER			
Beam Diameter (μm)	**200**	**300**	**500**
at Wavelength (nm)	633	633	633
Diffraction Efficiency (%)	80	83	85
Rise Time (nsec)	34	49	80
	15.9	10.6	6.3
	10	5	1

Figure 56.20: Data sheet for the acousto-optic modulator (AOM) from Crystal Technologies, model AOMO 3080-120.

Silicon PIN Photodiodes - Large Area, Fast Response Time – 400 nm to 1100 nm

The FFD series devices are high-quality, large-area, high-speed, N-type Si PIN photodiodes in hermetically sealed TO packages designed for the 400 nm to 1100 nm wavelength range. The FND-100Q has a quartz window to enhance UV responsivity.

Preamplifiers

Preamplifier modules incorporating these photodiodes are available on a custom basis.

Si PINs – Large Area, Fast Response

Typical Characteristics @ T = 22º C

Part #	Standard Package	Photo Sens. Diam. (mm)	Resp. @ 900 nm (A/W)	Dark Current Id (nA)	Spect. Noise Curr. Dens. In (fW/√Hz)	Cap. @ 100 kHz Cd (pF)	Response Time tr (ns)	NEP @ 900 nm (fW/√Hz)	Bias Volt (V)
FFD-040B	Y	1	0.58	1	18	1.8	2	31	15
FFD-100	B	2.5	0.58	2	25	8.5	3.5	44	15
FFD-200	C3	5.1	0.58	4	36	30	5	62	15
FND-100Q	B	2.5	0.58	10	60	8.5	2	100	90

Typical Applications

Laser detection systems, fast pulse detection, instrumentation, and high-speed switching.

Figure 56.21: Data sheet for the photo diode from Perkin Elmers FDD100.

Detectors

Silicon Epitaxial PIN Photodiodes - High Speed – 400 nm to 1100 nm

The C30736 series of high-speed epitaxial silicon PIN photodetectors provide fast response and good quantum efficiency in the spectral range between 400 nm and 1100 nm. These devices are optimized for high-speed, high volume and low cost applications. Standard sizes include 0.25 mm, 0.5 mm, 1.0 mm, 1.5 x 1.5 mm, and custom sizes can be accomodated depending on volume required. Available in plastic surface mount packages and in chip form.

Silicon Epitaxial PIN Photodiodes

Typical Characteristics @ T = 22º C

Part #	Standard Package	Photo Sens. Diam. (mm)	Resp. @ 870 nm (A/W)	Dark Current @2V Id (nA)	Spect. Noise Curr. Dens. In (fW/√Hz)	Cap. @ 100 kHz Cd (pF)	Response Time tr (ns)	NEP @ 870 nm (fW/√Hz)	Bias Volt (V)
C30736-1	Chip form	0.20	0.55	0.05	6	0.75	0.3	11	2
C30736-2	Chip form	0.50	0.55	0.10	10	1.5	0.5	18	2
C30736-3	Chip form	1.5 x 1.5	0.55	0.50	50	14	0.3	91	2

Silicon PIN Photodiodes - Standard N-Type – 400 nm to 1100 nm

The C308XX series devices are high-quality N-type Si PIN photodiodes in hermetically sealed TO packages designed for the 400 nm to 1100 nm wavelength region.

Si PINs – Standard N-Type

Typical Characteristics @ T = 22º C

Part #	Standard Package	Photo Sens. Diam. (mm)	Resp. @ 900 nm (A/W)	Dark Current Id (nA)	Spect. Noise Curr. Dens. (fA/√Hz)	Cap. @ 100 kHz Cd (pF)	Response Time tr (ns)	NEP @ 900 nm (fW/√Hz)	Bias Volt (V)
C30807E	A	1	0.6	1	18	2.5	3	30	45
C30808E	B	2.5	0.6	3	31	6	5	52	45
C30822E	C	5	0.6	5	40	17	7	67	45
C30809E	C3	8	0.6	7	47	35	10	79	45
C30810E	D	11.4	0.6	30	98	70	12	163	45

Typical Applications

Laser detection systems, photometry, data transmission, instrumentation, and high-speed switching.

Silicon PIN Photodiodes - Large Area, Fast Response Time – 400 nm to 1100 nm

The FFD series devices are high-quality, large-area, high-speed, N-type Si PIN photodiodes in hermetically sealed TO packages designed for the 400 nm to 1100 nm wavelength range. The FND-100Q has a quartz window to enhance UV responsivity.

Preamplifiers

Preamplifier modules incorporating these photodiodes are available on a custom basis.

Si PINs – Large Area, Fast Response

Typical Characteristics @ T = 22º C

Part #	Standard Package	Photo Sens. Diam. (mm)	Resp. @ 900 nm (A/W)	Dark Current Id (nA)	Spect. Noise Curr. Dens. In (fW/√Hz)	Cap. @ 100 kHz Cd (pF)	Response Time tr (ns)	NEP @ 900 nm (fW/√Hz)	Bias Volt (V)
FFD-040B	Y	1	0.58	1	18	1.8	2	31	15
FFD-100	B	2.5	0.58	2	25	8.5	3.5	44	15
FFD-200	C3	5.1	0.58	4	36	30	5	62	15
FND-100Q	B	2.5	0.58	10	60	8.5	2	100	90

Typical Applications

Laser detection systems, fast pulse detection, instrumentation, and high-speed switching.

6

Figure 56.22: Data sheet for the photo diode from Perkin Elmers C30822E.

19-0350; Rev 0; 12/94

MAXIM

Precision, Dual-Supply, SPST Analog Switches

General Description

The MAX320/MAX321/MAX322 are precision, dual, SPST analog switches designed to operate from ±3V to ±8V dual supplies. The MAX320 has two normally open (NO) switches and the MAX321 has two normally closed (NC) switches. The MAX322 has one NO and one NC switch. Low power consumption (1.25mW) makes these parts ideal for battery-powered equipment. They offer low leakage currents (100pA max) and fast switching speeds (t_{ON} = 150ns max, t_{OFF} = 100ns max).

The MAX320 series, powered from ±5V supplies, offers 35Ω max on-resistance (R_{ON}), 2Ω max matching between channels, and 4Ω max R_{ON} flatness.

These switches also offer 5pC max charge injection and a minimum of 2000V ESD protection per Method 3015.7.

For equivalent devices specified for single-supply operation, see the MAX323/MAX324/MAX325 data sheet. For quad versions of these switches, see the MAX391/MAX392/MAX393 data sheet.

Applications

Battery-Operated Systems	Sample-and-Hold Circuits
Heads-Up Displays	Guidance and Control Systems
Audio and Video Switching	Military Radios
Test Equipment	Communications Systems
±5V DACs and ADCs	PBX, PABX

Features

- **Low On-Resistance, 35Ω max (16Ω typical)**
- **R_{ON} Matching Between Channels <2Ω**
- **R_{ON} Flatness <4Ω**
- **Guaranteed Charge Injection <5pC**
- **Bipolar Supply Operation (±3V to ±8V)**
- **Low Power Consumption, <1.25mW**
- **Low Leakage Current Over Temperature, <2.5nA at +85°C**
- **Fast Switching, t_{ON} <150ns, t_{OFF} <100ns**
- **Guaranteed Break-Before-Make (MAX322 only)**

Ordering Information

PART	TEMP. RANGE	PIN-PACKAGE
MAX320CPA	0°C to +70°C	8 Plastic DIP
MAX320CSA	0°C to +70°C	8 SO
MAX320CUA	0°C to +70°C	8 µMAX
MAX320C/D	0°C to +70°C	Dice*
MAX320EPA	-40°C to +85°C	8 Plastic DIP
MAX320ESA	-40°C to +85°C	8 SO
MAX320EJA	-40°C to +85°C	8 CERDIP**
MAX320MJA	-55°C to +125°C	8 CERDIP**

Ordering Information continued at end of data sheet.

** Contact factory for dice specifications.*

*** Contact factory for availability.*

Pin Configurations/Functional Diagrams/Truth Tables

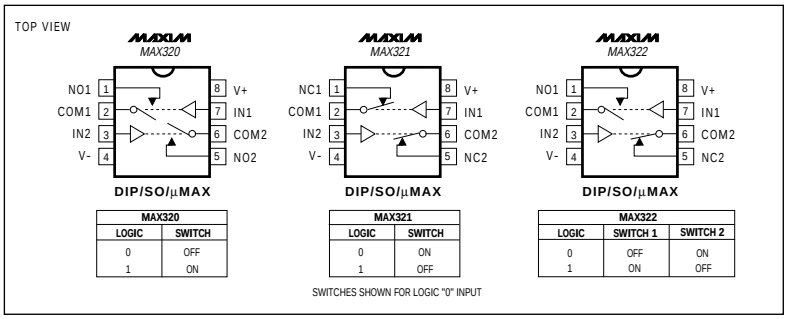

MAX320	
LOGIC	SWITCH
0	OFF
1	ON

MAX321	
LOGIC	SWITCH
0	ON
1	OFF

MAX322		
LOGIC	SWITCH 1	SWITCH 2
0	OFF	ON
1	ON	OFF

SWITCHES SHOWN FOR LOGIC "0" INPUT

Figure 56.23: Data sheet for the digital switch MAX322 from Maxim.

National Semiconductor

August 2000

LM741
Operational Amplifier

General Description

The LM741 series are general purpose operational amplifiers which feature improved performance over industry standards like the LM709. They are direct, plug-in replacements for the 709C, LM201, MC1439 and 748 in most applications.

The amplifiers offer many features which make their application nearly foolproof: overload protection on the input and output, no latch-up when the common mode range is exceeded, as well as freedom from oscillations.

The LM741C is identical to the LM741/LM741A except that the LM741C has their performance guaranteed over a 0˚C to +70˚C temperature range, instead of −55˚C to +125˚C.

Features

Connection Diagrams

Metal Can Package

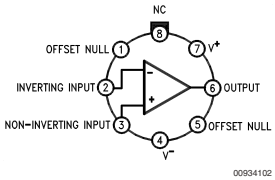

Note 1: LM741H is available per JM38510/10101

Order Number LM741H, LM741H/883 (Note 1), **LM741AH/883 or LM741CH**
See NS Package Number H08C

Dual-In-Line or S.O. Package

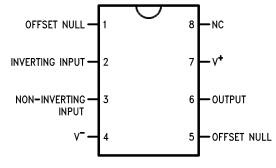

Order Number LM741J, LM741J/883, LM741CN
See NS Package Number J08A, M08A or N08E

Ceramic Flatpak

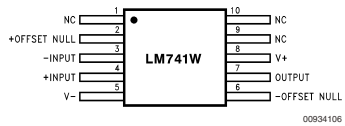

Order Number LM741W/883
See NS Package Number W10A

Typical Application

Offset Nulling Circuit

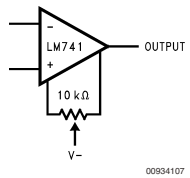

 DS009341

Figure 56.24: Data sheet for the operational amplifier LM741 from National Semiconductor.

ANALOG DEVICES

Low-Noise, Precision Operational Amplifier

OP27

FEATURES

Low Noise: 80 nV p-p (0.1 Hz to 10 Hz), 3 nV/$\sqrt{\text{Hz}}$
Low Drift: 0.2 μV/°C
High Speed: 2.8 V/μs Slew Rate, 8 MHz Gain Bandwidth
Low V_{OS}: 10 μV
Excellent CMRR: 126 dB at V_{CM} of ±11 V
High Open-Loop Gain: 1.8 Million
Fits 725, OP07, 5534A Sockets
Available in Die Form

GENERAL DESCRIPTION

The OP27 precision operational amplifier combines the low offset and drift of the OP07 with both high speed and low noise. Offsets down to 25 μV and drift of 0.6 μV/°C maximum make the OP27 ideal for precision instrumentation applications. Exceptionally low noise, e_n = 3.5 nV/$\sqrt{\text{Hz}}$, at 10 Hz, a low 1/f noise corner frequency of 2.7 Hz, and high gain (1.8 million), allow accurate high-gain amplification of low-level signals. A gain-bandwidth product of 8 MHz and a 2.8 V/μsec slew rate provides excellent dynamic accuracy in high-speed, data-acquisition systems.

A low input bias current of ±10 nA is achieved by use of a bias-current-cancellation circuit. Over the military temperature range, this circuit typically holds I_B and I_{OS} to ±20 nA and 15 nA, respectively.

The output stage has good load driving capability. A guaranteed swing of ±10 V into 600 Ω and low output distortion make the OP27 an excellent choice for professional audio applications.

(Continued on page 7)

PIN CONNECTIONS

TO-99
(J-Suffix)

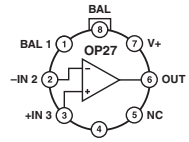

8-Pin Hermetic DIP
(Z-Suffix)
Epoxy Mini-DIP
(P-Suffix)
8-Pin SO
(S-Suffix)

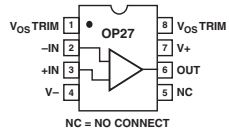

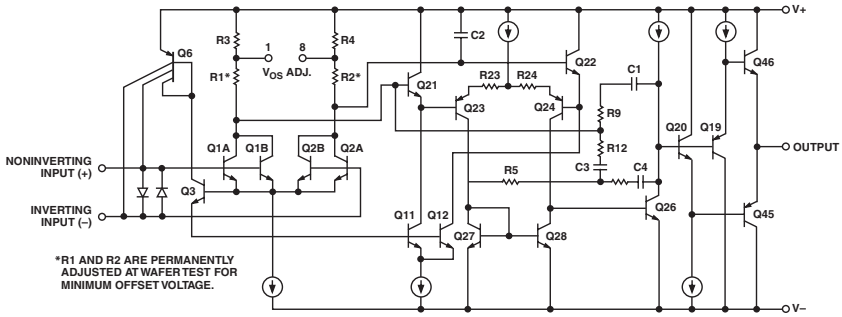

Figure 1. Simplified Schematic

Figure 56.25: Data sheet for the operational amplifier OP27 from Analog Devices.

Bibliography

[1] S. Aaronson and A. Arkhipov, *The computational complexity of linear optics*, ePrints (2010), arXiv1011.3245, ⊙.

[2] J. R. Abo-Shaeer, D. E. Miller, J. K. Chin, K. Xu, T. Mukaiyama, and W. Ketterle, *Coherent molecular optics using ultracold sodium dimers*, Phys. Rev. Lett. **94** (2005), 040405, ⊙DOI.

[3] J. A. Acebrón, L. L. Bonilla, and R. Spigler, *Synchronization in populations of globally coupled oscillators with inertial effects*, Phys. Rev. E **62** (2000), 3437, ⊙DOI.

[4] J. R. Ackerhalt and B. W. Shore, *Rate equations versus Bloch equations in multiphoton ionization*, Phys. Rev. A] **16** (1977), 277, ⊙.

[5] C. S. Adams, H. J. Lee, N. Davidson, M. Kasevich, and S. Chu, *Evaporative cooling in a crossed dipole trap*, Phys. Rev. Lett. **74** (1995), 3577, ⊙.

[6] C. S. Adams, M. Sigel, and J. Mlynek, *Atom optics*, Phys. Rep. **240** (1994), 143.

[7] S. K. Adhikari, *Coupled Bose-Einstein condensate: Collapse for attractive interaction*, Phys. Rev. A **63** (2001), 043611, ⊙.

[8] ———, *Mean-field description of a dynamical collapse of a fermionic condensate in a trapped boson-fermion mixture*, Phys. Rev. A **70** (2004), 043617, ⊙DOI.

[9] G. S. Agarwal, *Vacuum-field Rabi splitting in a microwave absorption by Rydberg atoms in a cavity*, Phys. Rev. Lett. **53** (1984), 1732, ⊙.

[10] G. S. Agarwal, M. O. Scully, and H. Walther, *Inhibition of decoherence due to decay in a continuum*, Phys. Rev. Lett. **86** (2001), 4271, ⊙DOI.

[11] B. Agate, B. Stormont, A. J. Kemp, C. T. A. Brown, U. Keller, and W. Sibbett, *Simplified cavity designs for efficient and compact femtosecond cr:lisaf lasers*, Opt. Comm. **205** (2002), 207.

[12] Y. Aharonov and J. Anandan, *Phase change during cyclic evolution*, Phys. Rev. Lett. **58** (1987), 1593, ⊙.

[13] Y. Aharonov and D. Bohm, *Significance of electromagnetic potentials in the quantum theory*, Phys. Rev. **115** (1959), 485, ⊙DOI.

[14] Y. Aharonov, D. Falkoff, E. Lerner, and H. Pendleton, *A quantum characterization of classical radiation*, Ann. Phys. (N.Y.) **39** (1966), 498.

[15] E. Akkermans, A. Gero, and R. Kaiser, *Photon localization and Dicke superradiance in atomic gases*, Phys. Rev. Lett. **101** (2008), 103602, ⊙DOI.

[16] F. Albarelli, A. Ferraro, M. Paternostro, and M. G. A. Paris, *Nonlinearity as a resource for nonclassicality in anharmonic systems*, Phys. Rev. A **93** (2016), 032112.

[17] R. Alicki, *The markov master equations and the Fermi golden rule*, International journal of Theoretical Physics (1977).

[18] D. W. Allan, *Statistics of atomic frequency standards*, Proc. of the IEEE **54** (1966), 221.

[19] D. W. Allan, J. H. Shoaf, and D. Halford, *Statistics of time and frequency data analysis*, NBS Monographs **140** (1974), 151.

[20] L. Allen, M. Babiker, W. K. Lai, and V. E. Lembessis, *Atom dynamics in multiple laguerre-gaussian beams*, Phys. Rev. A **54** (1996), 4259, ⊙.

[21] L. Allen, M. W. Beijersbergen, R. J. C. Spreeuw, and J. P. Woerdman, *Orbital angular momentum of light and the transformation of laguerre-gaussian laser modes*, Phys. Rev. A **45** (1992), 8185, ⊙.

[22] L. Allen, V. E. Lembessis, and M. Babiker, *Spin-orbit coupling in free-space laguerre-gaussian light beams*, Phys. Rev. A **53** (1996), R2937, ⊙.

[23] L. Allen and M. J. Padgett, *The poynting vector in laguerre-gaussian beams and the interpretation of their angular momentum density*, Opt. Comm. **187** (2000), 67, ⊙.

[24] W. Alt, D. Schrader, S. Kuhr, M. Müller, V. Gomer, and D. Meschede, *Single atoms in a standing-wave dipole trap*, Phys. Rev. A **67** (2003), 033403.

[25] T. P. Altenmüller and A. Schenzle, Phys. Rev. A **49** (1994), 2016.

[26] A. Alù and N. Engheta, *Pairing an epsilon-negative slab with a mu-negative slab resonance, tunneling and transparency*, IEEE Transactions Antennas and propagation **51** (2003), 2558, ⊙DOI.

[27] L. Amico, A. Osterloh, and F. Cataliotti, *Quantum many particle systems in ring-shaped optical lattices*, Phys. Rev. Lett. **95** (2005), 063201, DOI.

[28] M. Anderlini, P. J. Lee, B. L. Brown, J. Sebby-Strabley, W. D. Phillips, and J. V. Porto, *Controlled exchange interaction between pairs of neutral atoms in an optical lattice*, Nature **448** (2007), 452, ⊙DOI.

[29] B. P. Anderson, P. C. Haljan, C. E. Wieman, and E. A. Cornell, *Vortex precession in Bose-Einstein condensates: Observations with filled and empty cores*, Phys. Rev. Lett. **85** (2000), 2857, ⊙.

[30] B. P. Anderson and M. A. Kasevich, *Macroscopic quantum interference from atomic tunnel arrays*, Science **282** (1998), 1686, ⊙.

[31] M. H. Anderson, J. R. Ensher, M. R. Matthews, C. E. Wieman, and E. A. Cornell, *Observation of Bose-Einstein condensation in a dilute atomic vapor*, Science **269** (1995), 198, ⊙.

[32] A. André, L.-M. Duan, and M. D. Lukin, *Coherent atom interactions mediated by dark-state polaritons*, Phys. Rev. Lett. **88** (2002), 243602, ⊙.

[33] M. R. Andrews, D. M. Kurn, H.-J. Miesner, D. S. Durfee, C. G. Townsend, S. Inouye, and W. Ketterle, *Propagation of sound in a Bose-Einstein condensate*, Phys. Rev. Lett. **79** (1997), 0553, ⊙.

[34] M. R. Andrews, M. O. Mewes, N. J. Van Druten, D. S. Durfee, D. M. Kurn, and W. Ketterle, *Direct, non-destructive observation of a bose condensate*, Science **273** (1996), 84.

[35] M. R. Andrews, D. M. Stamper-Kurn, H. J. Miesner, D. S. Durfee, C. G. Townsend, S. Inouye, and W. Ketterle, *Erratum: Propagation of sound in a Bose-Einstein condensate*, Phys. Rev. Lett. **80** (1997), 2967.

[36] M. R. Andrews, C. G. Townsend, H.-J. Miesner, D. S. Durfee, D. M. Kurn, and W. Ketterle, *Observation of interference between two bose condensates*, Science **275** (1997), 637, ⊙.

[37] M. Antezza and Y. Castin, *Fano-hopfield model and photonic band gaps for an arbitrary atomic lattice*, Phys. Rev. A **80** (2009), 013816, ⊙DOI.

[38] _____, *Spectrum of light in a quantum fluctuating periodic structure*, ePrints (2009), 0903.0765, ⊙.

[39] _____, *Photonic band gap in an imperfect atomic diamond lattice: Penetration depth and effects of finite size and vacancies*, Phys. Rev. A **88** (2013), 033844, ⊙DOI.

[40] J. Appel, P. J. Windpassinger, D. Oblak, U. B. Hoff, N. KjÃ¦rgaard, and E. S. Polzik, *Mesoscopic atomic entanglement for precision measurements beyond the standard quantum limit*, Proceedings of the National Academy of Sciences **43** (2009), 753.

[41] M. O. Araújo, J. Carlos de A. Carvalho, and A. Laliotis, *Suppression of super- and subradiant emission for a line of cs atoms interacting with a resonant plane sapphire surface*, draft **65** (2023), 1345.

[42] F. T. Arecchi and R. Bonifacio, IEEE J. Quantum Electron. **1** (1965), 169.

[43] E. Arimondo, M. Inguscio, and P. Violino, *Experimental determination of the hyperfine structure in the alkali atoms*, Rev. Mod. Phys. **49** (1977), 31.

[44] M. Arndt, M. BenDahan, D. Guéry-Odelin, M. W. Reynolds, and J. Dalibard, *Observation of a zero-enery resonance in cs-cs collisions*, Phys. Rev. Lett. **79** (1997), 625, ⊙.

[45] A. S. Arnold, C. MacCormick, and M. G. Boshier, *An adaptive inelastic magnetic mirror for Bose-Einstein condensates*, ePrints (2001), cond–mat/0103586, ⊙.

[46] A. S. Arnold, J. S. Wilson, and M. G. Boshier, *A simple extended-cavity diode laser*, Rev. Sci. Instr. **69** (1998), 1236, ⊙.

[47] M. Artoni and G. La Rocca, *Optically tunable photonic stop bands in homogeneous absorbing media*, Phys. Rev. Lett. **96** (2006), 073905, ⊙.

[48] M. Artoni, G. La Rocca, and F. Bassani, *Resonantly absorbing one-dimensional photonic crystals*, Phys. Rev. E **72** (2005), 046604, ⊙.

[49] F. Arute, K. Arya, R. Babbush, D. Bacon, and et al., *Quantum supremacy using a programmable superconducting processor*, Nature **574** (2019), 505.

[50] J. K. Asbóth, P. Domokos, H. Ritsch, and A. Vukics, *Self-organization in a cavity field: Threshold, bistability, and scaling laws*, Phys. Rev. A **72** (2005), 053417, ⊙DOI.

[51] A. Ashkin, *Trapping of atoms by resonance radiation pressure*, Phys. Rev. Lett. **40** (1978), 729, ⊙DOI.

[52] A. Ashkin and J. P. Gordon, *Stability of radiation-pressure particle traps: an optical earnshaw theorem*, Opt. Lett. **8** (1978), 511, ⊙DOI.

[53] N. W. Ashkroft and D. N. Mermin, *Solid state physics*, Hartcourt College publishers, 1976, ISBN.

[54] A. Aspect, Ph. Grangier, and G. Roger, *Experimental realization of Einstein-podolski-rosen-bohm gedankenexperiment: A new violation of bell's inequalities*, Phys. Rev. Lett. **49** (1982), 91, ⊙.

[55] A. Aspect, R. Kaiser, N. Vansteenkiste, P. Vignolo, and C. I. Westbrook, *Nondestructive detection of atoms bouncing on an evanescent wave*, Phys. Rev. A **52** (1995), 4704.

[56] Alain Aspect, J. Dalibard, and J. Roger, *Experimental test of bell's inequality using time-varying analyzers*, Phys. Rev. Lett. **49** (1982), 1804, ⊙.

[57] Alain Aspect, P. Grangier, and G. Roger, Opt. Lett. **8** (1981), 511.

[58] ———, *Experimental test of bell's inequality using time-varying analyzers*, Phys. Rev. Lett. **47** (1982), 460, ⊙DOI.

[59] G. E. Astrakharchik, J. Boronat, J. Casulleras, and S. Giorgini, *Equation of state of a Fermi gas in the BEC-BCS crossover: A quantum monte carlo study*, Phys. Rev. Lett. **93** (2004), 200404, ⊙.

[60] P. W. Atkins and R. S. Friedman, *Molecular quantum mechanics*, Oxford University Press, 1997, ISBN.

[61] C. Audoin, *Frequency metrology*, Rendiconti della Scuola Intern. di Fisica ?Enrico Fermi? **LIVIII or LXVIII** (1980), 169.

[62] Koray Aydin, Irfan Bulu, and Ekmel Ozbay, *Focusing of electromagnetic waves by a left-handed metamaterial flat lens*, Opt. Exp. **13** (2005), 08753.

[63] M. Aymar and O. Dulieu, *Calculation of accurate permanent dipole moments of the lowest 1,3 s+ states of heteronuclear alkali dimers using extended basis sets*, J. Chem. Phys. **122** (2005), 204302, ⊙.

[64] H. Azuma, *Quantum computation with the Jaynes-Cummings model*, Progr. Theor. Phys. **126** (2008), 369.

[65] M. Babiker, W. L. Power, and L. Allen, *Light-induced torque on moving atoms*, Phys. Rev. Lett. **73** (1994), 1239, ⊙.

[66] R. Bachelard, H. Bender, Ph. W. Courteille, N. Piovella, C. Stehle, C. Zimmermann, and S. Slama, *Role of mie scattering in the seeding of matter-wave superradiance*, Phys. Rev. A **86** (2012), 043605.

[67] R. Bachelard, Ph. W. Courteille, R. Kaiser, and N. Piovella, *Resonances in mie scattering by an inhomogeneous atomic cloud*, Europhys. Lett. **97** (2012), 14004.

[68] R. Bachelard, N. Piovella, W. Guerin, and R. Kaiser, *Collective effects in the radiation pressure force*, Phys. Rev. A **94** (2016), 033836.

[69] S. Backhaus, S. Pereverzev, R. W. Simmonds, A. Loshak, J. C. Davis, and R. E. Packard, *Discovery of a metastable pi-state in a superfluid he-3 weak link*, Nature **392** (1998), 687.

[70] S. N. Bagayev, V. S. Egorov, I. B. Mekhov, P. V. Moroshkin, I. A. Chekhonin, E. M. Davliatchine, and E. Kindel, *Resonant nonstationary amplification of polychromatic laser pulses and conical emission in an optically dense ensemble of neon metastable atoms*, Phys. Rev. A **68** (2003), 043812, ⊙.

[71] V. S. Bagnato, N. P. Bigelow, G. I. Surdutovich, and S. C. Zilio, *Dynamical stabilization: A new model for supermolasses*, J. Opt. Soc. Am. B **19** (1994), 1568.

[72] V. S. Bagnato, G. P. Lafyatis, A. G. Martin, E. L. Raab, R. N. Ahmad-Bitar, and D. E. Pritchard, *Continuous stopping and trapping of neutral atoms*, Phys. Rev. Lett. **58** (1987), 2194.

[73] V. S. Bagnato, D. E. Pritchard, and D. Kleppner, *Bose-Einstein condensation in an external potential*, Phys. Rev. A **35** (1987), 4354, ⊙DOI.

[74] Vanderlei S. Bagnato, *Simple calculation of the spatial evolution of atoms in a trap during occurance of Bose-Einstein condensation*, Phys. Rev. A **54** (1996), 1726, ⊙DOI.

[75] X. Baillard, A. Gauguet, S. Bize, P. Lemonde, Ph. Laurent, A. Clairon, and P. Rosenbusch, *Interference-filter-stabilized external-cavity diode lasers*, Opt. Commun. **266** (2006), 609, ⊙.

[76] M. Reza Bakhtiari, A. Hemmerich, H. Ritsch, and M. Thorwart, *Nonequilibrium phase transition of interacting bosons in an intra-cavity optical lattice*, Phys. Rev. Lett. **114** (2014), 123601, ⊙DOI.

[77] N. Balakrishnan, R. C. Forrey, and A. Dalgarno, *Threshold phenomena in ultra-cold atom-molecule collisions*, Chem. Phys. Lett. **280** (1997), 1.

[78] N. L. Balazs, *The energy-momentum tensor of the electromagnetic field inside matter*, Phys. Rev. **91** (1953), 408, ⊙DOI.

[79] V. C. Ballenegger and T. A. Weber, *The ewald-oseen extinction theorem and extinction lengths*, Am. Assoc. Phys. Teachers **67** (1998), 599.

[80] V. I. Balykin, V. S. Letokhov, Yu. B. Ovchinnikov, and A. I. Sidorov, *Quantum-state selective mirror reflection of atoms by laser light*, Phys. Rev. Lett. **60** (1988), 2137, ⊙.

[81] A. Bambini and S. Geltman, *Feshbach resonances in cold collisions of potassium atoms*, Phys. Rev. A **65** (2002), 062704, ⊙.

[82] Y. B. Band and P. S. Julienne, *Ultra-cold molecule production by laser-cooled atom photoassociation*, Phys. Rev. A **51** (1995), R4317, ⊙.

[83] Weizhu Bao and Qiang Du, *Computing the ground state solution of a Bose-Einstein condensates by a normalized gradient flow*, SIAM J. Sci. Comput. **25** (2004), 1674, ⊙.

[84] Weizhu Bao, D. Jaksch, and P. A. Markowich, *Numerical solution of the Gross-Pitaevskii equation for Bose-Einstein condensation*, J. Comp. Phys. **187** (2003), 318, ⊙.

[85] Weizhu Bao, Shi Jin, and P. A. Markowich, *On time-splitting spectral approximations for the schrödinger equation in the semiclassical regime*, J. Comp. Phys. **175** (2002), 487, ⊙.

[86] M. A. Baranov, M. S. Marénko, Val. S. Rychkov, and G. V. Shlyapnikov, *Superfluid pairing in a polarized dipolar Fermi gas*, Phys. Rev. A **66** (2002), 013606, ⊙.

[87] M. A. Baranov and D. S. Petrov, *Critical temperature and Ginzburg-Landau equation for a trapped Fermi gas*, Phys. Rev. A **58** (1998), R801, ⊙.

[88] ———, *Low-energy collective excitations in a superfluid trapped Fermi gas*, Phys. Rev. A **62** (2000), 041601, ⊙.

[89] S. Barbay, G. Fabre, and G. L. Lippi, *Pump-probe spectroscopy of the sodium d line and the question of recoil-induced gratings in hot vapors*, Opt. Commun. **165** (1999), 119.

[90] Z. W. Barber, C. W. Hoyt, C. W. Oates, L. Hollberg, A. V. Taichenachev, and V. I. Yudin, *Direct excitation of the forbidden clock transition in neutral ^{174}yb atoms confined to an optical lattice*, Phys. Rev. Lett. **96** (2006), 083002, ⊙DOI.

[91] A. Barchielli, L. Lanz, and G. M. Prosperi, *A model for the macroscopic description and continual observations in quantum mechanics*, Il Nuovo Cimento **72** (1982), 79.

[92] J. Bardeen, G. Baym, and D. Pines, *Interactions between he3 atoms in dilute solutions of he3 in superfluid he4*, Phys. Rev. Lett. **17** (1966), 372, ⊙.

[93] J. Bardeen, L. N. Cooper, and J. R. Schrieffer, *Microscopic theory of superconductivity*, Phys. Rev. **106** (1957), L162, ⊙.

[94] ———, *Theory of superconductivity*, Phys. Rev. **108** (1957), 1175, ⊙.

[95] A. Barenco, C. H. Bennett, R. Cleve, D. P. DiVincenzo, N. Margolus, P. Shor, T. Sleator, J. A. Smolin, and H. Weinfurter, *Elementary gates for quantum computation*, Phys. Rev. A **52** (1995), 3457.

[96] D. S. Barker, B. J. Reschovsky, N. C. Pisenti, and G. K. Campbell, *Enhanced magnetic trap loading for atomic strontium*, Phys. Rev. A **92** (2015), 043418, ⊙DOI.

[97] J. A. Barnes, L. S. Cutler, and et al., *Characterization of frequency stability*, IEEE Trans. Instr. Meas. **20** (1971), 105.

[98] S. M. Barnett, *Resolution of the Abraham-Minkowski dilemma*, Phys. Rev. Lett. **104** (2010), 070401, ⊙.

[99] S. M. Barnett and S. J. D. Phoenix, *Information theory, squeezing and quantum correlations*, Phys. Rev. A **44** (1991), 535, ⊙.

[100] G. Barontini, C. Weber, F. Rabatti, J. Catani, G. Thalhammer, M. Inguscio, and F. Minardi, *Observation of heteronuclear atomic Efimov resonances*, ePrints **09014584** (2009), ⊙.

[101] M. Bartenstein, A. Altmeyer, S. Riedl, S. Jochim, C. Chi, J. Hecker Denschlag, , and R. Grimm, *Collective excitations of a degenerate gas at the BEC-BCS crossover*, Phys. Rev. Lett. **92** (2004), 203201, ⊙.

[102] S. D. Bartlett, B. C. Sanders, S. L. Braunstein, and K. Nemoto, *Efficient classical simulation of continuous variable quantum information processes*, Phys. Rev. Lett. **88** (2002), 097904.

[103] J. P. Bartolotta, S. B. Jäger, J. T. Reilly, M. A. Norcia, J. K. Thompson, G. Smith, and M. J. Holland, *Entropy transfer from a quantum particle to a classical coherent light field*, ePrints **arXiv:2105.03780v1** (2021).

[104] G. R. Barwood and et al., *Frequency measurements on optically narrowed rb-stabilized laser diodes at 780 nm and 795 nm*, Appl. Phys. B **53** (1991), 142, ⊙.

[105] K. Baumann, C. Guerlin, F. Brennecke, and T. Esslinger, *Dicke quantum phase transition with a superfluid gas in an optical cavity*, Nature **464** (2010), 1301, ⊙DOI.

[106] C. Baxter, M. Babiker, and R. Loudon, *Canonical approach to photon pressure*, Phys. Rev. A **47** (1993), 1278, ⊙.

[107] C. Baxter and R. Loudon, *Canonical approach to photon pressure*, J. Mod. Opt. **57** (2010), 830, ⊙DOI.

[108] G. Baym and C. J. Pethick, *Ground-state properties of magnetically trapped Bose-condensed rubidium gas*, Phys. Rev. Lett. **76** (1996), 6, ⊙.

[109] S. Beattie, B. Barrett, I. Chan, C. Mok, I. Yavin, and A. Kumarakrishnan, *Atom-interferometric studies of light scattering*, Phys. Rev. A **80** (2009), 013618, DOI.

[110] L. Béguin, A. Vernier, R. Chicireanu, T. Lahaye, and A. Browaeys, *Direct measurement of the van derwaals interaction between two Rydberg atoms*, Phys. Rev. Lett. **110** (2013), 263201, ⊙.

[111] G. Behinaein, V. Ramareddy, P. Ahmadi, and G. S. Summy, *Exploring the phase space of the quantum delta kicked accelerator*, ePrints (2006), physics/0609203, ⊙.

[112] A. Beige and G. C. Hegerfeldt, *Projection postulate and atomic quantum zeno effect*, Phys. Rev. A **53** (1996), 53.

[113] H. C. W. Beijerinck, E. D. J. Vredenbregt, R. J. W. Stas, M. R. Doery, and J. G. C. Tempelaars, *Prospects for Bose-Einstein condensation of metastable neon atoms*, Phys. Rev. A **61** (2000).

[114] J. S. Bell, *On the Einstein-podolsky-rosen paradox*, Physics Physique Fizika **1** (1964), 195, DOI.

[115] S. C. Bell, M. Junker, M. Jasperse, L. D. Turner, Y.-J. Lin, I. B. Spielman, and R. E. Scholten, *A slow atom source using a collimated effusive oven and a single-layer variable pitch coil zeeman slower*, Rev. Sci. Instr. **81** (2010), 013105, ⊙DOI.

[116] F. Bello, *Negative index of refraction in a four-level system with magnetoelectric cross coupling and local field corrections*, Phys. Rev. A **84** (2011), 013803.

[117] C. M. Bender, S. Boettcher, and P. N. Meisinger, *Pt-symmetric quantum mechanics*, J. Math. Phys. **40** (1999), 2201, ⊙.

[118] C. M. Bender, Brody, and P. N. Jones, *Complex extension of quantum mechanics*, Phys. Rev. Lett. **89** (2002), 270401, ⊙.

[119] H. Bender, Ph.W. Courteille, C. Marzok, C. Zimmermann, and S. Slama, *Direct measurement of intermediate-range casimir-polder potentials*, Phys. Rev. Lett. **104** (2010), 083201.

[120] H. Bender, C. Stehle, S. Slama, R. Kaiser, N. Piovella, C. Zimmermann, and Ph.W. Courteille, *Observation of cooperative mie scattering from an ultracold atomic cloud*, Phys. Rev. A **82** (2011), 011404(R).

[121] J. M. Bendickson, J. P. Dowling, and M. Scalora, *Analytic expressions for the electromagnetic mode density in finite, one-dimensional, photonic band-gap structures*, Phys. Rev. E **53** (1996), 4107, ⊙DOI.

[122] T. B. Benjamin and F. Ursell, Proc. R. Soc. London A **225** (1954), 505.

[123] C. H. Bennett, *Quantum information and quantum computation*, Phys. Today Okt 1995 (1995), 25.

[124] Sh. Bennetts, G. D. McDonald, K. S. Hardman, J. E. Debs, C. C. N. Kuhn, J. D. Close, and N. P. Robins, *External cavity diode lasers with 5khz and 200nm tuning range at 1.55 um and for linewidth measurement*, Opt. Exp. **22** (2014), 10642.

[125] M. J. Berg, C. M. Sorensen, and A. Chakrabarti, *Patterns in mie scattering: evolution when normalized by the rayleigh cross section*, Appl. Opt. **44** (2005), 7487, ⊙.

[126] ———, *A new explanation of the extinction paradox*, J. Quant. Spectrosc. Rad. Transfer **112** (2011), 1170, ⊙DOI.

[127] T. Bergeman, G. Erez, and H. J. Metcalf, *Magneto-static trapping fields for neutral atoms*, Phys. Rev. A **35** (1987), 1535, ⊙DOI.

[128] T. Bergeman, A. J. Kerman, J. Sage, S. Sainis, and D. DeMille, *Prospects for production of ultracold $x^1\sigma^+$ rbcs molecules*, Eur. Phys. J. D **31** (2004), 179, ⊙.

[129] T. Bergeman, M. G. Moore, and M. Olshanii, *Atom-atom scattering under cylindrical harmonic confinement: Numerical and analytic studies of the confinement induced resonance*, Phys. Rev. Lett. **91** (2003), 163201.

[130] J. Bergquist, R. G. Hulet, W. M. Itano, and D. J. Wineland, *Observation of quantum jumps in a single atom*, Phys. Rev. Lett. **57** (1986), 1699.

[131] P. R. Berman, *Comparison of recoil-induced resonances and the collective atomic recoil laser*, Phys. Rev. A **59** (1999), 585, ⊙.

[132] ———, *Optical faraday rotation*, Am. J. Phys. **78** (2009), 270, ⊙.

[133] S. Bernet, M. K. Oberthaler, R. Abfalterer, J. Schmiedmayer, and A. Zeilinger, *Coherent frequency shift of atomic matter waves*, Phys. Rev. Lett. **77** (1996), 5160.

[134] M. V. Berry, *Quantal phase factors accompanying adiabatic changes*, Proc. R. Soc. Lond. A **392** (1984), 45, ⊙DOI.

[135] H. A. Bethe and R. Jackiw, *Intermediate quantum mechanics*, Taylor & Francis, 1997, ISBN.

[136] Hans A. Bethe and Edwin E. Salpether, *Quantum mechanics of one- and two-electron atoms*, Springer-Verlag, 1 ed., Berlin, 1957, ISBN.

[137] M. J. Bhaseen, J. Mayoh, B. D. Simons, and J. Keeling, *Dynamics of nonequilibrium Dicke models*, Phys. Rev. A **85** (2012), 013817, ⊙DOI.

[138] Y. Bidel, B. Klappauf, J. C. Bernard, D. Delande, G. Labeyrie, C. Miniatura, D. Wilkowski, and R. Kaiser, *Coherent light transport in a cold strontium cloud*, Phys. Rev. Lett. **88** (2002), 203902, ⊙DOI.

[139] T. Bienaimé, R. Bachelard, J. Chabé, M. T. Rouabah, L. Bellando, Ph. W. Courteille, N. Piovella, and R. Kaiser, *Interplay between radiation pressure force and scattered light intensity in the cooperative scattering by cold atoms*, J. Mod. Opt. **61** (2014), 18.

[140] T. Bienaimé, R. Bachelard, N. Piovella, and R. Kaiser, *Cooperativity in light scattering by cold atoms*, Fortschr. Phys. **61** (2012), 377.

[141] T. Bienaimé, S. Bux, E. Lucioni, Ph. W. Courteille, N. Piovella, and R. Kaiser, *Observation of cooperative radiation pressure in presence of disorder*, Phys. Rev. Lett. **104** (2010), 183602.

[142] T. Bienaimé, M. Petruzzo, D. Bigerni, N. Piovella, and R. Kaiser, *Atom and photon measurement in cooperative scattering by cold atoms*, J. Mod. Opt. **58** (2011), 1942, ⊙DOI.

[143] T. Bienaimé, N. Piovella, and R. Kaiser, *Controlled Dicke subradiance from a large cloud of two-level systems*, Fortschr. Phys. **108** (2012), 123602.

[144] M. J. Bijlsma, E. Zaremba, and H. T. C. Stoof, *Condensate growth in trapped bose gases*, (2000), cond-mat/0001323.

[145] M. Bindhani, B. K. Behera, and P. K. Panigrahi, *Quantum simulation of Jaynes-Cummings model on ibm q-system*, (2020), ⊙.

[146] G. Birkl, M. Gatzke, I. H. Deutsch, S. L. Rolston, and W. D. Phillips, *Bragg sccattering from atoms in optical lattices*, Phys. Rev. Lett. **75** (1995), 2823, ⊙.

[147] G. C. Bjorklund, *Frequency-modulation spectroscopy: A new method for measuring weak absorptions and dispersions*, Opt. Lett. **5** (1980), 15.

[148] P. B. Blakie and R. J. Ballagh, *Mean-field treatment of bragg scattering from a Bose-Einstein condensate*, J. Phys. B **33** (2000), 3961, ⊙.

[149] M. Blatt, K.W. Boër, and W. Brandt, *Bose-Einstein condensation of excitons*, Phys. Rev. **126** (1962), 1691.

[150] R. Blatt, P. Zoller, G. Holzmüller, and I. Siemers, *Brownian motion of a parametric oscillator: A model for ion confinement in radio frequency traps*, Z. Phys. D **4** (1986), 121.

[151] G. Blatter, *Quantenmechanik*, http://www.itp.phys.ethz.ch/research/condmat/vortex/lectu Zürich, 2005.

[152] D. Bloch and M. Ducloy, *Atom-wall interaction*, physics/0503146 (2005), ⊙.

[153] I. Bloch, *Ultracold quantum gases in optical lattices*, Nature Physics **1** (2005), 23, ⊙.

[154] I. Bloch, T. W. Hänsch, and T. Esslinger, *Atom laser with a cw output coupler*, Phys. Rev. Lett. **82** (1999), 3008, ⊙.

[155] I. Bloch, Th. W. Hänsch, and T. Esslinger, *Measurement of the spatial coherence of a trapped Bose-gas at the phase transition*, Nature **403** (2000), 166, ⊙.

[156] I. Bloch, M. Köhl, M. Greiner, T. W. Hänsch, and T. Esslinger, *Optics with an atom laser beam*, Phys. Rev. Lett. **87** (2001), 030401, ⊙.

[157] C. A. Blockley, D. F. Walls, and H. Risken, *Quantum collapses and revivals in a quantized trap*, Europhys. Lett. **17** (1992), 509.

[158] G. Boedecker and C. Henkel, *All-frequency effective medium theory of a photonic crystal*, Opt. Exp. **270** (2003), 1901, ⊙DOI.

[159] H. M. J. M Boesten, A. Moerdijk, and B. J. Verhaar, *Dipolar decay in two recent Bose-Einstein condensation experiments*, Phys. Rev. A **54** (1996), R29, ⊙.

[160] J. L. Bohn, *Cooper pairing in ultracold k-40 using Feshbach resonances*, Phys. Rev. A **61** (2000), 053409, ⊙.

[161] J. L. Bohn and P. S. Julienne, *Prospects for influencing scattering lengths with far-off-resonance light*, Phys. Rev. A **56** (1997), 1486, ⊙.

[162] J. G. Bohnet, Z. Chen, J. M. Weiner, D. Meiser, M. J. Holland, and J. K. Thompson, *A steady-state superradiant laser with less than one intracavity photon*, Nature **484** (2012), 78, ⊙DOI.

[163] J. G. Bohnet, K. C. Cox, M. A. Norcia, J. M. Weiner, Z. Chen, and J. K. Thompson, *Reduced spin measurement back-action for a phase sensitivity ten times beyond the standard quantum limit*, Nature Phot. **8** (2014), 731, ⊙DOI.

[164] C. F. Bohren and D. R. Huffman, *Absorption and scattering of light by small particles*, John Wiley and Sons, New York, 1981, ISBN.

[165] P. Boissel and F. Kerherve, *Absorption de lumière par des atomes dans une onde évanescente*, Opt. Comm. **37** (1981), 397, ⊙.

[166] J. J. Bollinger, W. M. Itano, D. J. Wineland, and D.J.Heinzen, *Optimal frequency measurements with maximally correlated states*, Phys. Rev. A **54** (1996), 4649, ⊙.

[167] K. Bongs, S. Burger, G. Birkl, K. Sengstock, W. Ertmer, K. Rzazewski, A. Sanpera, and M. Lewenstein, *Coherent evolution of bouncing Bose-Einstein condensates*, Phys. Rev. Lett. **83** (1999), 3577, ⊙.

[168] K. Bongs, S. Burger, S. Dettmer, J. Arlt, W. Ertmer, and K. Sengstock, *A waveguide for Bose-Einstein condensates*, Phys. Rev. Lett. **63** (2000), 031602, ⊙.

[169] R. Bonifacio, F. Casagrande, and A. Airoldi, *The self-consistent pendulum picture of the free electron laser revised*, Opt. Comm. **80** (1991), 370, ⊙DOI.

[170] R. Bonifacio, F. S. Cataliotti, M. Cola, L. Fallani, C. Fort, N. Piovella, and M. Inguscio, *Superradiant light scattering from a moving Bose-Einstein condensate*, Opt. Comm. **233** (2004), 155, ⊙.

[171] R. Bonifacio, M. M. Cola, N. Piovella, and G. R. M. Robb, *A quantum model for collective recoil lasing*, Europhys. Lett. **69** (2005), 55, ⊙DOI.

[172] R. Bonifacio and L. A. Lugiato, *Superfluorescence in a cavity*, Opt. Comm. **47** (1983), 79, ⊙DOI.

[173] R. Bonifacio and L. De Salvo, *Collective atomic recoil laser (carl) optical gain without inversion by collective atomic recoil and self-bunching of two-level atoms*, Nucl. Instrum. Methods A **341** (1994), 360, DOI.

[174] R. Bonifacio, L. De Salvo, and W. A. Barletta, *Relativistic theory of the collective atomic recoil laser*, Nucl. Instr. Methods in Phys. Research A **384** (1997), 337, ⊙.

[175] R. Bonifacio, L. De Salvo, and G. R. M. Robb, *Propagation effects in a collective atomic recoil laser*, Opt. Commun. **137** (1997), 276, ⊙DOI.

[176] R. Bonifacio and Ph. Verkerk, Opt. Commun. **124** (1996), 469, ⊙.

[177] P. C. Bons, R. de Haas, D. de Jong, A. Groot, and P. van der Straten, *Quantum enhancement of the index of refraction in a Bose-Einstein condensate*, Phys. Rev. Lett. **116** (2016), 173602, ⊙DOI.

[178] Ch. J. Bordé, *Atom interferometry with internal state labeling*, Phys. Lett. A **140** (1989), 10, ⊙.

[179] ———, *Amplification of atomic fields by stimulated emission of atoms*, Phys. Lett. A **204** (1995), 217, ⊙.

[180] M. Born, 1980, ISBN.

[181] Satyendra N. Bose, *Plancks gesetz und lichtquantenhypothese*, Z. Phys. **26** (1924), 178.

[182] I. Bouchoule, H. Perrin, A. Kuhn, M. Morinaga, and C. Salomon, *Neutral atoms prepared in fock states of a one-dimensional harmonic potential*, Phys. Rev. A **59** (1999), R8, ⊙.

[183] T. Bourdel, J. Cubizolles, L. Khaykovich, K. M. F. Magalhaes, S. J. J. M. F. Kokkelmans, G. V. Shlyapnikov, and C. Salomon, *Measurement of the interaction energy near a Feshbach resonance in a ^{6}li Fermi gas*, Phys. Rev. Lett. **91** (2003), 020402, ⊙.

[184] Ph. Bouyer and M. A. Kasevich, *Heisenberg-limited spectroscopy with degenerate Bose-Einstein gases*, Phys. Rev. A **56** (1997), R1083, ⊙DOI.

[185] W. P. Bowen, R. Schnabel, H.-A. Bachor, and Ping Koy Lam, *Polarization squeezing of continuous variable stokes parameters*, Phys. Rev. Lett. **88** (2002), 093601, ⊙DOI.

[186] E. Braaten and H.-W. Hammer, *Universality in few-body systems with large negative scattering length*, Phys. Rep. **428** (2006), 259, ⊙.

[187] C. C. Bradley, C. A. Sackett, and R. G. Hulet, *Analysis of in situ images of Bose-Einstein condensates of lithium*, Phys. Rev. A **55** (1997), 3951, ⊙.

[188] ———, *Bose-Einstein condensation of lithium: Observation of limited condensate number*, Phys. Rev. Lett. **78** (1997), 985, ⊙.

[189] C. C. Bradley, C. A. Sackett, J. J. Tolett, and R. G. Hulet, *Evidence of Bose-Einstein condensation in an atomic gas with attractive interactions*, Phys. Rev. Lett. **75** (1995), 1687, ⊙.

[190] B. H. Bransden and C. J. Joachain, *Physics of atoms and molecules*, 1983, ISBN.

[191] D. Braun, G. Adesso, F. Benatti, R. Floreanini, U. Marzolino, M. W. Mitchell, and S. Pirandola, *Quantum-enhanced measurements without entanglement*, Rev. Mod. Phys. **90** (2018), 035006, ⊙DOI.

[192] B. Braverman, A. Kawasaki, E. Pedrozo-Pe nafiel, S. Colombo, Chi Shu, Zeyang Li, E. Mendez, M. Yamoah, L. Salvi, D. Akamatsu, Yanhong Xiao, and V. Vuletic, *Near-unitary spin squeezing in* ^{171}*yb*, Phys. Rev. Lett. **122** (2019), 223203, ⊙DOI.

[193] F. Brennecke, T. Donner, S. Ritter, T. Bourdel, M. Köhl, and T. Esslinger, *Cavity QED with a Bose-Einstein condensate*, Nature **250** (2007), 268, ⊙.

[194] G. K. Brennen, C. M. Caves, P. S. Jessen, and I. H. Deutsch, *Quantum logic gates in optical lattices*, Phys. Rev. Lett. **82** (1999), 1060, ⊙.

[195] F. Bretenaker, A. Le Floch, and L. Dutriaux, *Direct measurement of the optical Goos-Hänchen effect in lasers*, Phys. Rev. Lett. **68** (1992), 931, ⊙.

[196] I. Brevik and S. A. Ellingsen, *Possibility of measuring the abraham force using whispering gallery modes*, Phys. Rev. A **81** (2010), 063830, ⊙DOI.

[197] Léon Brillouin, *La mécanique ondulatoire de schrödinger: une méthode générale de resolution par approximations successives*, Comptes Rendus de l'Academie des Sciences **183** (1926), 24.

[198] Y. Bromberg, Y. Lahini, and Y. Silberberg, *Bloch oscillations of path-entangled photons*, Phys. Rev. Lett. **105** (2010), 263604, ⊙DOI.

[199] Y. Bromberg, B. Redding, S. M. Popoff, and H. Cao, *Control of coherent backscattering by breaking optical reciprocity*, Phys. Rev. Lett. **86** (2016), 1402, ⊙DOI.

[200] J. C. Bronski, L. D. Carr, B. Deconinck, and J. N. Kutz, *Bose-Einstein condensates in standing waves: The cubic nonlinear schrödinger equation with a periodic potential*, Phys. Rev. Lett. **86** (2001), 1402, ⊙.

[201] I. N. Bronstein and K. A. Semandjajew, *Taschenbuch der mathematik*, Thun und Franfurt, Main, 1978, ISBN.

[202] M. Brown-Hayes and R. Onofrio, *Optimal cooling strategies for magnetically trapped fermi-bose mixtures*, Phys. Rev. A **70** (2004), 063614, ⊙.

[203] M. Brune, S. Haroche, J. M. Raimond, L. Davidovich, and N. Zagury, *Manipulation of photons in a cavity by dispersive atom-field coupling: Quantum-nondemolition measurement and generation of "schrödinger cat" states*, Phys. Rev. A **45** (1992), 5192, ⊙.

[204] A. Brunello, F. Dalfovo, L. Pitaevskii, S. Stringari, and F. Zambelli, *Momentum transferred to a trapped Bose-Einstein condensate by stimulated light scattering*, **64** (2001), 063614, ⊙.

[205] A. Brusch, R. Le Targat, X. Baillard, M. Fouché, and P. Lemonde, *Hyperpolarizability effects in a sr optical lattice clock*, Phys. Rev. Lett. **96** (2006), 103003, ⊙DOI.

[206] A. Buchleitner, M. B. d'Arcy, S. Fishman, S. A. Gardiner, I. Guarneri, Z.-Y. Ma, L. Rebuzzini, and G. S. Summy, *Quantum accelerator modes from the farey tree*, Phys. Rev. Lett. **96** (2006), 164101, ⊙.

[207] W. Buckel, *Supraleitung, grundlagen und anwendungen*, 1977, ISBN.

[208] C. J. Buczek, R. J. Freiberg, and M. L. Skolnic, *Laser injection locking*, Proc. IEEE **61** (1973), 1411.

[209] D. Budker, S. M. Rochester, and V. V. Yashchuk, *Obtaining frequency markers of variable separation with a spherical mirror fabry-perot interferometer*, Rev. Sci. Instr. **71** (2000), 2984.

[210] S. Y. Buhmann, *Dispersion forces ii*, Springer Tracts in Modern Physics 248, 287, Springer-Verlag Berlin Heidelberg, 2012, ⊙ISBNDOI.

[211] I. Bulu, H. Caglayan, and E. Ozbay, *Experimental demonstration of labyrinth-based left-handed metamaterials*, Opt. Exp. **13** (2005), 10238.

[212] S. Burger, K. Bongs, S. Dettmer, W. Ertmer, K. Sengstock, A. Sanpera, G. V. Shlyapnikov, and M. Lewenstein, *Dark solitons in Bose-Einstein condensates*, Phys. Rev. Lett. **83** (1999), 5198, ⊙.

[213] J. P. Jr. Burke, *Theoretical investigation of cold slkali atom collisions*, PhD thesis (1999).

[214] J. P. Jr. Burke, J. L. Bohn, B. D. Esry, and C. H. Greene, *Impact of the 87rb singlet scattering length on suppressing inelastic collisions*, Phys. Rev. A **55** (1997), R2511, ⊙.

[215] ———, *Prospects of mixed-isotope Bose-Einstein condensates in rubidium*, Phys. Rev. Lett. **80** (1998), 2097, ⊙.

[216] K. Burnett, *An intimate gathering of bosons*, Science **267** (1996), 0182, ⊙.

[217] E. A. Burt, R. W. Ghrist, C. J. Myatt, M. J. Holland, E. A. Cornell, and C. E. Wieman, *Coherence, correlations, and collisions: What one learns about Bose-Einstein condensates from their decay*, Phys. Rev. Lett. **79** (1997), 337, ⊙.

[218] Th. Busch and J. R. Anglin, *Wave-function monopoles in Bose-Einstein condensates*, Phys. Rev. A **60** (1999), 2669, ⊙.

[219] Th. Busch, J. I. Cirac, V. M. Pérez-García, and P. Zoller, *Stability and collective excitations of a two-component Bose-Einstein condensed gas: A moment approach*, Phys. Rev. A **56** (1997), 2978.

[220] P. N. Butcher and D. Cotter, Cambridge University Press, 1991, ISBN.

[221] D. A. Butts and D. S. Rokhsar, *Trapped Fermi gases*, Phys. Rev. A **55** (1997), 4346, ⊙DOI.

[222] ———, *Predicted signatures of rotating Bose-Einstein condensates*, Nature **397** (1999), 327, ⊙.

[223] S. Bux, Ch. Gnahm, R. A. Maier, C. Zimmermann, and Ph. W. Courteille, *Cavity-controlled matter wave superradiance at the recoil limit*, Phys. Rev. Lett. **106** (2011), 203601.

[224] S. Bux, G. Krenz, S. Slama, C. Zimmermann, and Ph.W. Courteille, *Ultra-cold atoms in an optical cavity: Two-mode laser locking avoiding radiation pressure*, Appl. Phys. B **89** (2007), 181.

[225] S. Bux, E. Lucioni, H. Bender, T. Bienaimé, K. Lauber, C. Stehle, C. Zimmermann, S. Slama, Ph. W. Courteille, N. Piovella, and R. Kaiser, *Cooperative scattering by cold atoms*, J. Mod. Opt. **57** (2010), 1841.

[226] A. Bychek, Ch. Hotter, D. Plankensteiner, and H. Ritsch, *Superradiant lasing in inhomogeneously broadened ensembles with spatially varying coupling*, ePrints (2021), arXiv2105.11023, ⊙DOI.

[227] B. Cabrera, *First results from a superconductive detector for moving magnetic monopoles*, Phys. Rev. Lett. **48** (1982), 1378.

[228] K. E. Cahill and R. J. Glauber, *Density operators and quasiprobability distributions*, Phys. Rev. **177** (1969), 1882.

[229] A. Campa, *The study of the equilibrium and of the dynamical properties of long-range interacting systems*, AIP Conf. Proc. **970** (2008), 3, ⊙.

[230] G. K. Campbell, A. E. Leanhardt, J. Mun, M. Boyd, E. W. Streed, W. Ketterle, and D. E. Pritchard, *Photon recoil momentum in dispersive media*, Phys. Rev. Lett. **94** (2005), 170403.

[231] G. Camy, Ch. J. Bordé, and M. Ducloy, *Heterodyne saturation spectroscopy through frequency modulation the saturating beam*, Opt. Comm. **41** (1982), 325, ⊙.

[232] P. Capuzzi, A. Minguzzi, and M. P. Tosi, *Collective excitations of a trapped boson-fermion mixture across demixing*, Phys. Rev. A **67** (2003), 053605.

[233] G. G. Carlo, G. Benenti, and D. L. Shepelyansky, *Dissipative quantum chaos: Transition from wave packet collapse to explosion*, Phys. Rev. Lett. **95** (2005), 164101, ⊙.

[234] J. Carlson, S.-Y. Chang, V. R. Pandharipande, and K. E. Schmidt, *Superfluid Fermi gases with large scattering length*, Phys. Rev. Lett. **91** (2003), 050401, ⊙.

[235] R. Carminati, A. Cazé, D. Cao, F. Peragut, V. Krachmalnicoff, R. Pierrat, and Y. De Wilde, *Electromagnetic density of states in complex plasmonic systems*, Surf. Sci. Rep. **70** (2015), 1, ⊙DOI.

[236] L. D. Carr and et al., *Cold and ultracold molecules: science, technology and applications*, New J. Phys. **11** (2009), 055009, ⊙.

[237] R. Casdorff and R. Blatt, *Ordered structures and statistical properties of ion clouds stored in a paul trap*, Appl. Phys. B **45** (1988), 175, ⊙.

[238] Y. Castin and R. Dum, *Bose-Einstein condensates in time dependent traps*, Phys. Rev. Lett. **77** (1996), 5315, ⊙.

[239] Y. Castin, H. Walls, and J. Dalibard, *Limit of doppler cooling*, J. Opt. Soc. Am. B **6** (1989), 2046, ⊙DOI.

[240] F. S. Cataliotti, S. Burger, C. Fort, P. Maddaloni, F. Minardi, A. Trombettoni, A. Smerzi, and M. Inguscio, *Josephson junction arrays with Bose-Einstein condensates*, Science **293** (2001), 843, ⊙DOI.

[241] C. M. Caves, *Quantum-mechanical noise in an interferometer*, Phys. Rev. D **23** (1981), 1693, ⊙DOI.

[242] C. M. Caves and G. J. Milburn, *Quantum mechanics of measurements distributed in time ii*, Phys. Rev. A **36** (1987), 5543.

[243] E. Cedra and E. Tirapegui, Phys. Rev. Lett. **78** (1997), 859.

[244] Jr. Ch. P. Poole, H. A. Farach, and R. J. Creswick, *Superconductivity*, 2007, ISBN.

[245] J. Chabé, G. Lemarie, B. Grémaud, D. Delande, P. Szriftgiser, and J. C. Garreau, *Experimental observation of the anderson metal-insulator transition with atomic matter waves*, Phys. Rev. Lett. **101** (2008), 255702, ⊙.

[246] D. E. Chang, J. I. Cirac, and H. J. Kimble, *Self-organization of atoms along a nanophotonicwaveguide*, Phys. Rev. Letters **110** (2013), 113606, ⊙DOI.

[247] D. E. Chang, Jun Ye, and M. D. Lukin, *Controlling dipole-dipole frequency shifts in a lattice-based optical atomic clock*, Phys. Rev. A **69** (2004), 023810, ⊙DOI.

[248] L. L. Chase, N. Peyghambarian, G. Grynberg, and A. Mysyrowicz, *Evidence for Bose-Einstein condensation of biexcitons in CuCl*, Phys. Rev. Lett. **42** (1979), 1231.

[249] Qijin Chen, J. Stajic, Shina Tan, and K. Levin, *Shapiro steps observed in a dc superconducting quantum interference device with multiple junctions in each arm*, Appl. Phys. Lett. **80** (2002), 1025, ⊙.

[250] W. Chen, D. Meiser, and P. Meystre, *Cavity QED determination of atomic number statistics in optical lattices*, Phys. Rev. A **75** (2007), 23812, ⊙DOI.

[251] Zilong Chen, Ju. G. Bohnet, S. R. Sankar, Jiayan Dai, and J. K. Thompson, *Conditional spin squeezing of a large ensemble via the vacuum Rabi splitting*, Phys. Rev. Lett. **106** (2011), 133601, ⊙DOI.

[252] Qiang Cheng and Tie Jun Cui, *High-power generation and transmission in a left-handed planar waveguide excited by an electric dipole*, Opt. Exp. **13** (2005), 10230.

[253] F. Chevy, K. Madison, and J. Dalibard, *Measurement of the angular momentum of a rotating Bose-Einstein condensate*, Phys. Rev. Lett. **85** (2000), 2223, ⊙.

[254] R. Y. Chiao and J. Boyce, *Bogoliubov dispersion relation and the possibility of superfluidity for weakly-interacting photons in a 2d photon fluid*, Phys. Rev. A (1999), quant-ph/9905001.

[255] A. P. Chikkatur, A. Görlitz, D. M. Stamper-Kurn, S. Inouye, S. Gupta, and W. Ketterle, *Suppression and enhancement of impurity scattering in a Bose-Einstein condensate*, Phys. Rev. Lett. **85** (2000), 483, ⊙.

[256] C. Chin, M. Bartenstein, A. Altmeyer, S. Riedl, S. Jochim, J. Hecker Denschlag, and R. Grimm, *Observation of the pairing gap in a strongly interacting Fermi gas*, Science **305** (2004), 1128, ⊙.

[257] C. Chin, R. Grimm, P. Julienne, and E. Tiesinga, *Feshbach resonances in ultracold gases*, Rep. Mod. Phys. **82** (2010), 1225, ⊙DOI.

[258] J. S. Choi and J. C. Howell, *Paraxial ray optics cloaking*, Opt. Exp. **22** (2014), 29465, ⊙DOI.

[259] J. J. Choquette, K.-P. Marzlin, and B. C. Sanders, *Superradiance, subradiance, and suppressed superradiance of dipoles near a metal interface*, Phys. Rev. A **82** (2010), 023827, ⊙DOI.

[260] W. W. Chow, J. Gea-Banacloche, L. M. Pedrotti, V. E. Sanders, W. Schleich, and M. O. Scully, *The ring laser gyro*, Rev. Mod. Phys. **57** (1985), 61, DOI.

[261] Steve Chu, J. E. Bjorkholm, A. Ashkin, and A. Cable, *Experimental observation of optically trapped atoms*, Phys. Rev. Lett. **57** (1986), 314.

[262] S. T. Chui, V. N. Ryzhov, and E. E. Tareyeva, *Stability of the bose system in Bose-Fermi mixture with attraction between bosons and fermions*, JETP Lett. **80** (2004), 274.

[263] A. Cipris, N. A. Moreira, T. S. do Espirito Santo, P. Weiss, C. J. Villas-Boas, R. Kaiser, W. Guerin, and R. Bachelard, *Subradiance with saturated atoms: Population enhancement of the long-lived states*, Phys. Rev. Lett. **126** (2021), 103604, ⊙DOI.

[264] J. I. Cirac, R. Blatt, A. S. Parkins, and P. Zoller, *Quantum collapse and revival in the motion of a single trapped ion*, Phys. Rev. A **49** (1994), 1202, ⊙.

[265] J. I. Cirac, R. Blatt, P. Zoller, and W. D. Phillips, *Laser cooling of trapped ions in a standing wave*, Phys. Rev. A **46** (1992), 2668, ⊙.

[266] J. I. Cirac, M. Lewenstein, K. Molmer, and P. Zoller, *Quantum superpositions states of Bose-Einstein condensates*, Phys. Rev. A **57** (1998), 1208.

[267] J. I. Cirac, M. Lewenstein, and P. Zoller, *Quantum dynamics of a laser-cooled ideal gas*, Phys. Rev. A **50** (1994), 3409, ⊙.

[268] J. I. Cirac and P. Zoller, *Decoherence, continuous observation, and quantum computing: A cavity QED model*, Phys. Rev. Lett. **75** (1995), 3788, ⊙.

[269] ———, *Quantum computation with cold trapped atoms*, Phys. Rev. Lett. **74** (1995), 4091, ⊙DOI.

[270] D. Clément, A. F. Varón, M. Hugbart, J. A. Retter, P. Bouyer, L. Sanchez-Palencia, and D. M. Gangardt, *Suppression of transport of an interacting elongated Bose-Einstein condensate in a random potential*, Phys. Rev. Lett. **95** (2005), 170409, ⊙.

[271] R. A. Cline, J. D. Miller, M. R. Matthews, and D. J. Heinzen, *Spin relaxation of optically trapped atoms by light scattering*, Opt. Lett. **19** (1994), 207.

[272] G. Co and S. De Leo, *Analytical and numerical analysis of the complete lipkin-meshkov-glick hamiltonian*, ePrints **arXiv:1805.12442v1** (2018), ⊙DOI.

[273] N. V. Cohan, D. Pugh, and R. H. Tredgold, *Band structure of diamond*, Proc. Phys. Soc. **82** (1963), 65, ⊙.

[274] E. Cohen, H. Larocque, F. Bouchard, F. Nejadsattari, Y. Gefen, and E. Karimi, *Geometric phase from aharonov-bohm to pancharatnam-berry and beyond*, Nature Rev. **1** (2019), 437, ⊙DOI.

[275] E. R. Cohen, *Uncertainty and error in physical measurements*, Rendiconti della Scuola Intern. di Fisica 'Enrico Fermi' **CX** (1992), 11.

[276] C. Cohen-Tannoudji, B. Diu, and F. Lao, *Quantum mechanics*, 1, vol. 1 & 2, 1977, ISBN.

[277] C. Cohen-Tannoudji, J. Dupont-Roc, and G. Grynberg, *Photons and atoms: Introduction to quantum electrodynamics*, John Wiley and Sons New York, 1992, ISBN.

[278] M. M. Cola, *Collective atomic recoil in ultracold atoms: Advances and applications*, Dissertation Milano (2003).

[279] M. M. Cola, M. G. A. Paris, and N. Piovella, *Robust generation of entanglement in Bose-Einstein condensates by collective atomic recoil*, Phys. Rev. A **70** (2004), 43809, ⊙DOI.

[280] M. M. Cola, M. G. A. Paris, N. Piovella, and R. Bonifacio, *A condensate in a lossy cavity: Collective atomic recoil and generation of entanglement*, J. Mod. Opt. **51** (2004), 1043, ⊙DOI.

[281] ———, *Entanglement in a Bose-Einstein condensate by collective atomic recoil*, J. Phys. B **37** (2004), S187, ⊙DOI.

[282] M. M. Cola and N. Piovella, *Theory of collective Raman scattering from a Bose-Einstein condensate*, Phys. Rev. A **70** (2004), 45601, ⊙.

[283] M. J. Collett and C. W. Gardiner, *Squeezing of intracavity and travelling-wave light fields produced in parametric amplification*, Phys. Rev. A **30** (1984), 1386, ⊙.

[284] Y. Colombe, E. Knyazchyan, O. Morizot, B. Mercier, V. Lorent, and H. Perrin, *Ultracold atoms confined in rf-induced two-dimensional trapping potentials*, Europhys. Lett. **67** (2004), 593, ⊙.

[285] Y. Colombe, T. Steinmetz, G. Dubois, F. Linke, D. Hunger, and J. Reichel, *Strong atom field coupling for bose Einstein condensates in an optical cavity on a chip*, Nature **250** (2005), 272, ⊙.

[286] S. Colombo, E. Pedrozo-Pe nafiel, A. F. Adiyatullin, Zeyang Li, E. Mendez, Chi Shu, and V. Vuletic, *Time-reversal-based quantum metrology with many-body entangled states*, Nature Phys. **18** (2022), 925, ⊙DOI.

[287] S. Colombo, E. Pedrozo-Pe nafiel, and V. Vuletic, *Entanglement-enhanced optical atomic clocks*, ePrints **arXiv:2209.00471v3** (2022), ⊙DOI.

[288] R. Combescot, S. Giorgini, and S. Stringari, *Molecular signatures in the structure factor of an interacting Fermi gas*, Europhys. Lett. **75** (2006), 695, ⊙.

[289] E. C. Cook, P. J. Martin, T. L. Brown-Heft, J. C. Garman, and D. A. Steck, *High passive-stability diode-laser design for use in atomic-physics experiments*, Rev. Sci. Instr. **83** (2010), 043101, ⊙.

[290] L. N. Cooper, *Bound electron pairs in a degenerate fermi-gas*, Phys. Rev. **104** (1956), 1189.

[291] E. A. Cornell, *Very cold indeed: The nanokelvin physics of Bose-Einstein condensation*, J. Res. Natl. Inst. Stand. Tech. **101** (1996), 419.

[292] A. Corney, *Atom and laser-spectroscopy*, Oxford Scientific Publications at the Clarendon Press, 1977, ISBN.

[293] S. L. Cornish, N. R. Claussen, J. L. Roberts, E. A. Cornell, and C. E. Wieman, *Stable 85rb Bose-Einstein condensates with widely tunable interactions*, Phys. Rev. Lett. **85** (2000), 1795, ⊙.

[294] R. Corrêa, M. F. B. Cenni, and P. L. Saldanha, *Quantum interference of force*, Quantum **2** (2018), 112, ⊙DOI.

[295] R. Côté, R. Onofrio, and E. Timmermans, *Sympathetic cooling route to Bose-Einstein condensate/fermi-liquid mixtures*, Phys. Rev. A **72** (2005), 041605, ⊙.

[296] R. Côté, B. Segev, and M. G. Raizen, *Retardation effects on quantum reflection from an evanescent-wave atomic mirror*, Phys. Rev. A **58** (1998), 3999, ⊙.

[297] Ph. W. Courteille, V. S. Bagnato, and V. I. Yukalov, *Bose-Einstein condensation of trapped atomic gases*, Laser Phys. **11** (2001), 659–800.

[298] Ph. W. Courteille, S. Bux, E. Lucioni, K. Lauber, T. Bienaimé, R. Kaiser, and N. Piovella, *Modification of radiation pressure due to cooperative scattering of light*, Euro. Phys. J. D **58** (2010), 69.

[299] Ph. W. Courteille, B. Deh, J. Fortágh, A. Günther, S. Kraft, C. Marzok, S. Slama, and C. Zimmermann, *Highly versatile atomic micro traps generated by multifrequency magnetic field modulation*, J. Phys. B **39** (2006), 1055.

[300] Ph. W. Courteille, R. S. Freeland, D. J. Heinzen, F. A. van Abeelen, and B. J. Verhaar, *Observation of a Feshbach resonance in cold atom scattering*, Phys. Rev. Lett. **81** (1998), 69.

[301] Ph. W. Courteille, D. J. Han, R. H. Wynar, and D. J. Heinzen, *New observation of Bose-Einstein condensation of ^{87}rb atoms in a magnetic top trap*, Proc. of SPIE **3270** (1998), 116.

[302] J. Courtial, D. A. Robertson, K. Dholakia, L. Allen, and M. J. Padgett, *Rotational frequency shift of a light beam*, Phys. Rev. Lett. **81** (1998), 4828, ⊙.

[303] I. Courtillot, A. Quessada, R. P. Kovacich, J-J. Zondy, A. Landragin, A. Clairon, and P. Lemonde, *Efficient cooling and trapping of strontium atoms*, Opt. Lett. **28** (2003), 468, ⊙DOI.

[304] J.-Y. Courtois, J.-M. Courty, and S. Reynaud, *Quantum nondemolition measurements using a crossed kerr effect between atomic and light fields*, Phys. Rev. A **52** (1995), 1507.

[305] J.-Y. Courtois, G. Grynberg, B. Lounis, and P. Verkerk, *Recoil-induced resonances in cesium: An atomic analog to the free electron laser*, Phys. Rev. Lett. **72** (1994), 3017, ⊙.

[306] L. Couturier, I. Nosske, F. Hu, C. Tan, C. Qiao, Y. H. Jiang, P. Chen, and M. Weidemüller, *Measurement of the strontium triplet Rydberg series by depletion spectroscopy of ultracold atoms*, Phys. Rev. A **99** (2019), 022503, ⊙DOI.

[307] J. J. Cowan and B. Anicin, *Longitudinal and transversal displacements of a bounded microwave beam at total internal reflection*, J. Opt. Soc. Am. **67** (1977), 1307.

[308] J. M. Cowley, *Diffraction physics*, 1981, ISBN.

[309] K. C. Cox, G. P. Greve, J. M. Weiner, and J. K. Thompson, *Deterministic squeezed states with collective measurements and feedback*, Phys. Rev. Lett. **116** (2016), 093602, ⊙DOI.

[310] A. D. Cronin, J. Schmiedmayer, and D. E. Pritchard, *Optics and interferometry with atoms and molecules*, Rev. Mod. Phys. **81** (2009), 1051, ⊙DOI.

[311] J. Cubizolles, T. Bourdel, S. J. J. M. F. Kokkelmans, G. V. Shlyapnikov, and C. Salomon, *Production of long-lived ultracold li_2 molecules from a Fermi gas*, Phys. Rev. Lett. **91** (2003), 240401, ⊙.

[312] R. Culver, A. Lampis, B. Megyeri, K. Pahwa, L. Mudarikwa, M. Holynski, Ph. W. Courteille, and J. Goldwin, *Collective strong coupling of cold potassium atoms in a ring cavity*, New J. Phys. **18** (2016), 113043.

[313] M. O. Terra Cunha, J. A. Dunningham, and V. Vedral, *Entanglement in single-particle systems*, Proc. R. Soc. **463** (2007), 2277, ⊙DOI.

[314] L. S. Cutler and C.L. Searle, *Some aspects of the theory and measurement of frequency fluctuations in frequency standards*, Proc. of the IEEE **54** (1966), 136.

[315] M. T. Cvitas, P. Soldan, J. M. Hutson, P. Honvault, and J.-M. Launay, *Ultracold collisions involving heteronuclear alkali metal dimers*, Phys. Rev. Lett. **94** (2005), 200402, ⊙.

[316] M. Ben Dahan, E. Peik, Y. Castin, and C. Salomon, *Bloch oscillations of atoms in an optical potential*, Phys. Rev. Lett. **76** (1996), 4508, ⊙.

[317] J. P. Dahl and M. Springborg, *The morse oscillator in position space, momentum space, and phase space*, J. Chem. Phys. **88** (1988), 4535.

[318] F. Dalfovo, S. Giorgini, M. Guillemas, L. Pitaevski, and S. Stringari, *Collective and single particle excitations of a trapped Bose-Einstein condensate*, Phys. Rev. A **56** (1997), 3840, ⊙.

[319] F. Dalfovo, S. Giorgini, L. P. Pitaevskii, and S. Stringari, *Theory of Bose-condensation in trapped gases*, Rev. Mod. Phys. **71** (1999), 463, cond-mat/9806038.

[320] F. Dalfovo and S. Stringari, *Bosons in anisotropic traps: Ground state and vortices*, Phys. Rev. A **53** (1996), 2477, ⊙.

[321] J. Dalibard, Y. Castin, and K. Molmer, *Wave-function approach to dissipative processes in quantum optics*, Phys. Rev. Lett. **68** (1992), 580, ⊙DOI.

[322] J. Dalibard and C. Cohen-Tannoudji, *Dressed-atom approach to atomic motion in laser light: The dipole force revisited*, J. Opt. Soc. Am. B **2** (1985), 1707.

[323] ———, *Laser cooling below the doppler limit by polarization gradients: Simple theoretical studies*, J. Opt. Soc. Am. B **6** (1989), 2023.

[324] D. A. R. Dalvit, J. Dziarmaga, and W. H. Zurek, *Decoherence in Bose-Einstein condensates: Towards bigger and better schroedinger cats*, Phys. Rev. A **62** (2000), 13607, ⊙.

[325] B. Damski, J. Zakrzewski, L. Santos, P. Zoller, and M. Lewenstein, *Atomic bose and anderson glasses in optical lattices*, Phys. Rev. Lett. **91** (2003), 080403, ⊙.

[326] W. B. Davenport and W. L. Root, *An introduction to the theory of random signals and noise*, 1958, ISBN.

[327] N. Davidson, H. J. Lee, C. S. Adams, M. Kasevich, and S. Chu, *Long atomic coherence times in an optical dipole trap*, Phys. Rev. Lett. **74** (1995).

[328] J. Davis, M. Kumari, R. B. Mann, and S. Ghose, *Wigner negativity in spin- j systems*, Phys. Rev. Res. **3** (2021), 033134, ⊙DOI.

[329] K. B. Davis, M.-O. Mewes, M. R. Andrews, N. J. van Druten, D. S. Durfee, D.M. Kurn, and W. Ketterle, *Bose-Einstein condensation in an gas of sodium atoms*, Phys. Rev. Lett. **75** (1995), 3969, ⊙.

[330] K. B. Davis, M.-O. Mewes, M. A. Joffe, M. R. Andrews, and W. Ketterle, *Evaporative cooling of sodium atoms*, Phys. Rev. Lett. **74** (1995), 5202, ⊙.

[331] K. B. Davis, M.-O. Mewes, and W. Ketterle, *An analytical model for evaporative cooling of atoms*, Appl. Phys. B **60** (1995), 155, ⊙.

[332] D. A. Dawson, J. Stat. Phys. **31** (1983), 29.

[333] J. O. Day, E. Brekke, and T. G. Walke, *Dynamics of low-density ultracold Rydberg gases*, Phys. Rev. A **75** (2008), 052712, ⊙DOI.

[334] O. Costa de Beauregard, *Translational internal spin effect with moving particles*, Phys. Rev. **134** (1964), ⊙.

[335] J. de Boer and G. E. Uhlenbeck, *Construction operator formalism for many particle systems*, In Studies in Statistical Mechanics, J. de Boer and G.E. Uhlenbeck (Eds.), (North Holland, 1965)] **III** (1996), 212.

[336] Y. N. Martinez de Escobar, P. G. Mickelson, P. Pellegrini, S. B. Nagel, A. Traverso, M. Yan, R. Côté, and T. C. Killian, *Two-photon photoassociative spectroscopy of ultracold 88sr*, Phys. Rev. A **78** (2008), 062708, DOI.

[337] Y. N. Martinez de Escobar, P. G. Mickelson, M. Yan, B. J. DeSalvo, S. B. Nagel, and T. C. Killian, *Bose-Einstein condensation of 84sr resonance at large detuning*, Phys. Rev. Lett. **103** (2009), 200402, ⊙DOI.

[338] S. R. de Groot, G. J. Hooyman, and C. A. Ten Deldam, Proc. R. Soc. Lond. A **203** (1950), 266.

[339] R. L. de Matos Filho and W. Vogel, *Second-sideband laser cooling and nonclassical motion of trapped ions*, Phys. Rev. **50** (1994), R1988.

[340] F. A. de Oliveira, M. S. Kim, P. L. Knight, and V. Buek, *Properties of displaced number states*, Phys. Rev. A **41** (1990), 2645.

[341] K. Debnath, Y. Zhang, and K. Mølmer, *Lasing in the superradiant crossover regime*, Phys. Rev. A **98** (2018), 063837, ⊙DOI.

[342] M. Defrise, D. W. Townsend, and R. Clack, *Three-dimensional image reconstruction from complete projections*, Phys. Med. Biol. **34** (1989), 573, ⊙DOI.

[343] C. L. Degen, F. Reinhard, and P. Cappellaro, *Quantum sensing*, Rev. Mod. Phys. **89** (2017), 035002, ⊙DOI.

[344] B. Deh, C. Marzok, S. Slama, C. Zimmermann, and Ph. W. Courteille, *Bragg spectroscopy and Ramsey interferometry with an ultracold Fermi gas*, Appl. Phys. B **97** (2009), 387, ⊙DOI.

[345] B. Deh, C. Marzok, C. Zimmermann, and Ph. W. Courteille, *Feshbach resonances in mixtures of quantum degenerate ^{6}li and ^{87}rb gases*, Phys. Rev. A **77** (2008), 010701(R), DOI.

[346] G. Delannoy, S. G. Murdoch, V. Boyer, V. Josse, P. Bouyer, and A. Aspect, *Understanding the production of dual Bose-Einstein condensation with sympathetic cooling*, Phys. Rev. A **63** (2001), 051602, ⊙.

[347] B. DeMarco and D. S. Jin, *Onset of fermi-degeneracy in a trapped atomic gas*, Science **285** (1999), 1703, ⊙DOI.

[348] B. DeMarco, S. B. Papp, and D. S. Jin, *Pauli blocking of collisions in a quantum degenerate atomic Fermi gas*, Phys. Rev. Lett. **86** (2001), 5409, ⊙DOI.

[349] D. DeMille, *Quantum computation with trapped polar molecules*, Phys. Rev. Lett. **88** (2002), 067901, ⊙.

[350] D. Demille, *Using molecules to measure nuclear spin-dependent parity violation*, Phys. Rev. Lett. **100** (2008), 023003, ⊙.

[351] W. Demtröder, *Laser spectroscopy*, 1988, ⊙ISBN.

[352] ———, *Atoms, molecules and photons: An introduction to atomic- molecular- and quantum physics*, Springer, 2006.

[353] L. Deng, E. W. Hagley, J. Denschlag, J. E. Simsarian, M. Edwards, C. W. Clark, K. Helmerson, S. L. Rolston, and W. D. Phillips, *Temporal matter-wave-dispersion talbot effect*, Phys. Rev. Lett. **83** (1999), 5407.

[354] L. Deng, E. W. Hagley, J. Wen, M. Trippenbach, Y. Band, P. S. Julienne, J. E. Simsarian, K. Helmerson, S. L. Rolston, and W. D. Phillips, *Four-wave mixing with matter waves*, Nature **398** (1999), 218, ⊙.

[355] J. Denschlag, D. Cassettari, and J. Schmiedmayer, *Guiding neutral atoms with a wire*, Phys. Rev. Lett. **82** (1999), 201.

[356] J. Denschlag, J. E. Simsarian, D. L. Feder, Charles W. Clark, L. A. Collins, J. Cubizolles, L. Deng, E. W. Hagley, K. Helmerson, W. P. Reinhardt, S. L. Rolston, B. I. Schneider, and W. D. Phillips, *Generating solitons by phase engineering of a Bose-Einstein condensate*, Science **287** (2000), 97.

[357] M. T. DePue, C. McCormick, S. L. Winoto, S. Oliver, and D. S. Weiss, *Unity occupation of sites in a 3d optical lattice*, Phys. Rev. Lett. **82** (1999), 2262, ⊙DOI.

[358] A. Derevianko and H. Katori, *Colloquium: Physics of optical lattice clocks*, Rev. Mod. Phys. **83** (2011), 331, ⊙DOI.

[359] B. J. DeSalvo, M. Yan, P. G. Mickelson, Y. N. Martinez de Escobar, and T. C. Killian, *Degenerate Fermi gas of 87sr*, ePrints **arXiv:1005.0668** (2010), ⊙DOI.

[360] F. Deuretzbacher, K. Plassmeier, D. Pfannkuche, F. Werner, C. Ospelkaus, S. Ospelkaus, K. Sengstock, and K. Bongs, *Heteronuclear molecules in an optical lattice: Theory and experiment*, ePrints (2007), cond–mat/0703322, ⊙.

[361] I. Deutsch, Barenco, and Ekert, Proc. Roy. Soc. Lond. **x** (1995), 669.

[362] I. H. Deutsch and P. S. Jessen, *Quantum state control in optical lattices*, Phys. Rev. A **57** (1995), 1972, ⊙.

[363] I. H. Deutsch, R. J. C. Spreeuw, S. L. Rolston, and W. D. Phillips, *Photonic band gaps in optical lattices*, Phys. Rev. A **52** (1995), 1394, ⊙DOI.

[364] R. G. DeVoe and R. G. Brewer, *Observation and superradiant and subradiant spontaneous emission of two trapped ions*, Phys. Rev. Lett. **76** (1996), 2049, ⊙DOI.

[365] P. G. S. Dias, M. Frometa, P. H. N. Magnani, , K. R. B. Theophilo, M. Hugbart, Ph. W. Courteille, and R. C. Teixeira, *Mirror-assisted backscattering interferometry to measure the first-order correlation function of the light emitted by quantum scatterers*, Phys. Rev. A **104** (2021), 053716, ⊙DOI.

[366] R. H. Dicke, *Coherence in spontaneous radiation processes*, Phys. Rev. **93** (1954), 99, ⊙DOI.

[367] F. Diedrich, J.C. Bergquist, W.I. Itano, and D.J. Wineland, *Laser cooling to the zero-point energy of motion*, Phys. Rev. Lett. **62** (1989), 403, ⊙.

[368] C. M. Tokarsky Dieguez, L. V. Montanheiro, L. Berbeka Cleto, M. J. C. Bonfim, and C. A. Dartora, *Os fundamentos quânticos da ressonância magnética nuclear*, Rev. Bras. Ens. Fís. **40** (2018), e1310, ⊙DOI.

[369] R. B. Diener and Tin-Lun Ho, *Projecting fermion pair condensates into molecular condensates*, ePrint (2004), ⊙.

[370] Yi S. Ding and Ruo-Peng Wang, *Possible realization of negative refraction in Bose-Einstein condensates*, Phys. Rev. B **84** (2011), 045107.

[371] P. A. M. Dirac, *The quantum theory of the emission and absorption of radiation*, Proc. Roy. Soc. A **114** (1927), 243.

[372] ———, *Quantized singularities in the electromagnetic field*, Proc. Roy. Soc. A **133** (1931), 60.

[373] ———, *The cosmological constants*, Nature **139** (1937), 323.

[374] ———, *The principles of quantum mechanics*, Oxford University Press, 4th ed., 1947, ISBN.

[375] A B. Djurisic and E. H. Li, *Modeling the index of refraction of insulating solids with a modified lorentz oscillator model*, Appl. Opt. **37** (1998), 5291, ⊙DOI.

[376] R. B. Doak, R. E. Grisenti, D. S. Rehbein, G. Schmahl, J. P. Toennies, and Ch. W"oll, *Towards realization of an atomic de broglie microscope: Helium atoms focussing using fresnel zone plates*, Phys. Rev. Lett. **83** (1999), Atom Optics.

[377] L. Dobrek, M. Gajda, M. Lewenstein, K. Sengstock, G. Birkl, and W. Ertmer, *Optical generation of vortices in trapped Bose-Einstein condensates*, Phys. Rev. A **60** (1999), 3381, ⊙.

[378] R. J. Dodd, *Approximate solutions of the nonlinear schrödinger equation for ground and excited states of Bose-Einstein condensates*, J. Res. Natl. Inst. Stand. Tech. **101** (1996), 545.

[379] R. J. Dodd, M. Edwards, and C. W. Clark, *Two-gas description of dilute Bose-Einstein condensates at finite temperature*, J. Phys. B: At. Mol. Opt. Phys. **32** (1999), 4107, ⊙DOI.

[380] R. J. Dodd, M. Edwards, C. W. Clark, and K. Burnett, *Collective excitations of Bose-Einstein condensed gases at finite temperatures*, Phys. Rev. A **57** (1998), R32, ⊙.

[381] G. Di Domenico, St. Schilt, and P. Thomann, *Simple approach to the relation between laser frequency noise and laser line shape*, Appl. Opt. **49** (2010), 4801, DOI.

[382] P. Domokles, J. M. Raimond, M. Brune, and S. Haroche, Phys. Rev. A **52** (1995), 3554.

[383] P. Domokos and H. Ritsch, *Collective cooling and self-organization of atoms in a cavity*, Phys. Rev. Lett. **89** (2002), 253003, ⊙DOI.

[384] R. Donelly and C. Swanson, *Quantum turbulence*, J. Fluid Mech. **173** (1986), 387, ⊙.

[385] T. Donner, *Erzeugung ultrakalter gemische aus fermionischen und bosonischen atomen*, Diplomarbeit Tübingen (2004), ⊙.

[386] U. Dorner and P. Zoller, *Laser-driven atoms in half-cavities*, Phys. Rev. A **66** (2002), 023816.

[387] J. M. Doyle, B. Friederich, J. Kim, and D. Patterson, *Buffer-gas loading of atoms and molecules into a magnetic trap*, Phys. Rev. A **52** (1995), ⊙.

[388] R. W. P. Drever, J. L. Hall, F. V. Kowalski, J. Hough, G. M. Ford, A. J. Munley, and H. W. Ward, *Laser phase and frequency stabilization using an optical resonator*, Appl. Phys. B **31** (1983), 97, ⊙.

[389] V. Dribinski, A. Ossadtchi, V. A. Mandelshtam, and H. Reislera, *Reconstruction of abel-transformable images: The gaussian basis-set expansion abel transform method*, Rev. Sci. Instrum. **73** (2002), 2634, ⊙DOI.

[390] M. Drndic, W. D. Phillips, A. Aspect, and et al., *Properties of microelectromagnet mirrors as reflectors of cold rb atoms*, Phys. Rev. A **60** (1999), 4012, ⊙.

[391] P. D. Drummond, K. V. Kheruntsyan, and H. He, *Coherent molecular solitons in Bose-Einstein condensates*, Phys. Rev. Lett. **81** (1998), 3055, ⊙.

[392] F. Dubin, D. Rotter, M. Mukherjee, C. Russo, J. Eschner, and R. Blatt, *Photon correlation versus interference of single-atom fluorescence in a half-cavity*, Phys. Rev. Lett. **98** (2007), 183003, ⊙.

[393] M. Ducloy and D. Bloch, *Theory of degenerate four-wave mixing in resonant doppler-broadened media II*, J. Physique **43** (1982), 57.

[394] G. J. Duffy, S. Parkins, T. Müller, M. Sadgrove, R. Leonhardt, and A. C. Wilson, *Experimental investigation of early-time diffusion in the quantum kicked rotor using a Bose-Einstein condensate*, Phys. Rev. E **70** (2004), 056206, ⊙.

[395] O. Dulieu and P. S. Julienne, *Coupled channel bound states calculations for alkali dimers using the fourier grid method*, J. Chem. Phys. **103** (1995), 60, ⊙.

[396] R. Dum, A. S. Parkins, P. Zoller, and C.W. Gardiner, *Monte carlo simulation of master equations in quantum optics for vacuum, thermal, and squeezed reservoirs*, Phys. Rev. A **46** (1992), 4382, ⊙.

[397] R. Dum, A. Sanpera, K.-A. Suominen, M. Brewczyk, M. Kus, K. Rzazewski, and M. Lewenstein, *Wave packet dynamics with Bose-Einstein condensates*, Phys. Rev. Lett. **80** (1998), 3899, ⊙.

[398] Ho Trung Dung, S. Y. Buhmann, L. Knöll, D.-G. Welsch, S. Scheel, and J. Kästel, *Electromagnetic-field quantization and spontaneous decay in left-handed media*, Phys. Rev. A **68** (2003), 043816, ⊙DOI.

[399] Ho Trung Dung, L. Knöll, and D.-G. Welsch, *Intermolecular energy transfer in the presence of dispersing and absorbing media*, Phys. Rev. A **65** (2002), 043813, ⊙DOI.

[400] W. Dür, G. Vidal, and J. I. Cirac, *Three qubits can be entangled in two inequivalent ways*, Phys. Rev. A **62** (2000), 062314, ⊙DOI.

[401] J. Durnin, J. J. Miceli, and J. H. Eberly, *Diffraction-free beams*, Physical Review Letters **58** (1987), 1499.

[402] S. Dürr, T. Volz, and G. Rempe, *Dissociation of ultracold molecules with Feshbach resonances*, Phys. Rev. A **70** (2004), 031601.

[403] C. S. Adams E. M. Bridge, J. Millen and M. P. A. Jones, *A vapor cell based on dispensers for laser spectroscopy*, Rev. Sci. Instrum. **80** (2008), 013101, DOI.

[404] J. H. Eberly, *Emission of one photon in an electric dipole transition of one among n atoms*, J. Phys. B: At. Mol. Opt. Phys. **39** (2006), ⊙DOI.

[405] M. Edwards, R. J. Dodd, C. W. Clark, and K. Burnett, *Zero-temperature, mean-field theory of atomic Bose-Einstein condensates*, J. Res. Natl. Inst. Stand. Tech. **101** (1996), 553.

[406] M. Edwards, P. A. Ruprecht, K. Burnett, R. J. Dodd, and C. W. Clark, *Collective excitations of atomic Bose-Einstein condensates*, Phys. Rev. Lett. **77** (1996), 1671, ⊙.

[407] V. Efimov, *Energy levels arising from resonant two-body forces in a three-body system*, Phys. Lett. B **33** (1970), 563, ⊙.

[408] D. V. Efremov and L. Viverit, *p-wave cooper pairing of fermions in mixtures of dilute Fermi and bose gases*, Phys. Lett. B **65** (2002), 13519, ⊙.

[409] V. S. Egorov, V. N. Lebedev, I. B. Mekhov, P. V. Moroshkin, I. A. Chekhonin, and S. N. Bagayev, *Coherent interaction of laser pulses in a resonant optically dense extended medium under the regime of strong field-matter coupling*, Phys. Rev. A **69** (2004), 033804, ⊙.

[410] A. Einstein, *Quantentheorie des einatomigen idealen gases*, S. B. Kgl. Preuss. Akad. Wiss. **35** (1924).

[411] A. Einstein, B. Podolsky, and N. Rosen, *Can quantum-mechnical description of physical reality be considered complete?*, Phys. Rev. **47** (1935), 777, ⊙.

[412] J. Eiselt and H. Risken, *Quasiprobability distributions for the Jaynes-Cummings model with cavity damping*, Phys. Rev. A **43** (1991), 346.

[413] A. C. Elitzur and L. Vaidman, *Quantum mechanical interaction-free measurements*, Found. Phys. **23** (1993), 987, ⊙DOI.

[414] D. S. Elliott, Rajarshi Roy, and S. J. Smith, *Extracavity laser bandshape and bandwidth modification*, Phys. Rev. A **26** (1982), 12, ⊙.

[415] Th. Elsässer, B. Nagorny, and A. Hemmerich, *Collective sideband cooling in an optical ring cavity*, Phys. Rev. A **67** (2003), 051401(R), ⊙.

[416] C. Emary and T. Brandes, *Quantum chaos triggered by precursors of a quantum phase transition: The Dicke model*, Phys. Rev. Lett. **90** (2003), 044101, ⊙DOI.

[417] J. R. Ensher, D. S. Jin, M. R. Matthews, C. E. Wieman, and E. A. Cornell, *Bose-Einstein condensation in a dilute gas: Measurement of energy and ground-state occupation*, Phys. Rev. Lett. **77** (1996), 4984, ⊙.

[418] T. Erber, P. Hammerling, G. Hockney, M. Porrati, and S. Putterman, *Resonance fluorescence and quantum jumps in single atoms: Testing the randomness of quantum mechanics*, Ann. Phys. **190** (1989), 254.

[419] Ph. T. Ernst, S. Götze, J. S. Krauser, K. Pyka, D.-S. Lühmann, D. Pfannkuche, and K. Sengstock, *Probing superfluids in optical lattices by momentum-resolved bragg spectroscopy*, Nature Phys. **06** (2009), 56, ⊙DOI.

[420] U. Ernst, A. Marte, F. Schreck, J. Schuster, and G. Rempe, *Bose-Einstein condensation in a pure ioffe-pritchard field configuration*, Europhys. Lett. **41** (1997), 1, ⊙.

[421] W. Ertmer, R. Blatt, J. L. Hall, and M. Zhu, *Laser manipulation of atomic beam velocities: Demonstration of stopped atoms and velocity reversal*, Phys. Rev. Lett. **54** (1985), 996.

[422] J. Eschner, G. Morigi, F. Schmidt-Kaler, and R. Blatt, *Laser cooling of trapped ions*, J. Opt. Soc. Am. B **20** (2003), 1003, ⊙.

[423] J. Eschner, Ch. Raab, F. Schmidt-Kaler, and R. Blatt, *Light interference from single atoms and their mirror images*, Nature **413** (2001), 495, ⊙.

[424] B. D. Esry, Ch. H. Greene, and H. Suno, *Threshold laws for three-body recombination*, Phys. Rev. A **65** (2001), 10705(R), ⊙.

[425] T. Esslinger, I. Bloch, and T. W. Hänsch, *Bose-Einstein condensation in a quadrupople-ioffe configuration trap*, Phys. Rev. A **58** (1998), R2664.

[426] L. E. Estes, Th. H. Keil, and L. M. Narducci, *Quantum-mechanical description of two coupled harmonic oscillators*, Phys. Rev. **175** (1968), 286, ⊙DOI.

[427] J. Estève, C. Gross, A. Weller, S. Giovanazzi, and M. K. Oberthaler, *Squeezing and entanglement in a Bose-Einstein condensate*, Nature **455** (2008), 1216, ⊙DOI.

[428] A. Altmeyer et al., *Precision measurements of collective oscillations in the BEC-BCS crossover*, Phys. Rev. Lett. **98** (2007), 040401, ⊙.

[429] M. J. Everitt, T. D. Clark, P. B. Stiffell, J. F. Ralph, A. R. Bulsara, and C. J. Harland, *Persistent entanglement in the classical limit*, New J. Phys. **7** (2005), 64.

[430] C. Fabre, R. G. DeVoe, and R. G. Brewer, *Ultrahigh-finesse optical cavities*, Opt. Lett. **6** (1986), 365.

[431] G. M. Falco and H. T. C. Stoof, *Crossover temperature of Bose-Einstein condensation in an atomic Fermi gas*, Phys. Rev. Lett. **92** (2004), 130401, ⊙.

[432] M. Faraday, Phil. Trans. R. Soc. London A **52** (1831), 319.

[433] D. Farina, F. Casagrande, U. Colombo, and R. Pozzoli, *Hamiltonian analysis of the transition to the high-gain regime in a compton free-electron-laser amplifier*, Phys. Rev. E **49** (1994), 1603, DOI.

[434] S. Fauve and et Al., Phys. Rev. Lett. **68** (1992), 3160.

[435] P. O. Fedichev, Yu Kagan, G. V. Shlyapnokov, and J. T. M. Walraven, *Influence of nearly resonant light on the scattering length in low-temperature atomic gases*, Phys. Rev. Lett. **77** (1996), 2913, ⊙.

[436] E. Fermi, *Motion of neutrons in hydrogenous substances*, Ricerca Scientifica **7** (1936), 13.

[437] G. Ferrari, P. Cancio, R. Drullinger, G. Giusfredi, N. Poli, M. Prevedelli, C. Toninelli, and G. M. Tino, *Precision frequency measurement of visible intercombination lines of strontium*, Phys. Rev. Lett. **91** (2003), 243002, ⊙DOI.

[438] G. Ferrari, R. E. Drullinger, N. Poli, F. Sorrentino, and G. M. Tino, *Cooling of sr to high phase-space density by laser and sympathetic cooling in isotopic mixtures*, Phys. Rev. A **73** (2006), 023408, ⊙DOI.

[439] G. Ferrari, M. Inguscio, W. Jastrzebski, G. Modugno, G. Roati, and A. Simoni, *Collisional properties of ultracold k-rb mixtures*, Phys. Rev. Lett. **89** (2002), 053202, ⊙.

[440] G. Ferrari, N. Poli, F. Sorrentino, and G. M. Tino, *Long-lived Bloch oscillations with bosonic sr atoms and application to gravity measurement at the micrometer scale*, Phys. Rev. Lett. **97** (2006), 060402, ⊙DOI.

[441] H. Feshbach, *Unified theory of nuclear reactions*, Annals of Physics **5** (1958), 357.

[442] R. P. Feynman, *Application of quantum mechanics to liquid helium*, Prog. Low Temp. Phys. **1** (1955), 17.

[443] Z. Ficek, T. Tanas, and S. Kielich, *Effect of interatomic interactions on resonance fluorescence of two atoms coherently driven by strong resonant laser field*, Opt. Acta **30** (1983), 713.

[444] M. Fichet, F. Schuller, D. Bloch, and M. Ducloy, *van der waals interactions between excited-state atoms and dispersive dielectric surfaces*, Phys. Rev. A **51** (1995), 1553, ⊙DOI.

[445] A. Fioretti, D. Comparat, A. Crubellier, and O. Dulieu, *Formation of cold cs2 molecules through photoassociation*, Phys. Rev. Lett. **80** (1998), 4402, ⊙.

[446] E. Fischer, *Dreidimensionale stabilisierung von ladungsträger in einem vierpolfeld*, Z. Phys. **156** (1959), 1.

[447] W. Fischer and I. Lieb, *Funktionentheorie*, Vieweg Studium, Aufbaukurs Mathematik, 1983.

[448] G. P. Fisher, *The electric dipole moment of a moving magnetic dipole*, Am. J. Phys. **39** (1971), 1528.

[449] M. P. A. Fisher, P. B. Weichman, G. Grinstein, and D. S. Fisher, *Boson localization and the superfluid-insulator transition*, Phys. Rev. B **40** (1989), 546.

[450] S. Fishman, D. R. Grempel, and R. E. Prange, *Chaos, quantum recurrences, and anderson localization*, Phys. Rev. Lett. **49** (1982), 509, ⊙.

[451] S. Fishman, I. Guarneri, and L. Rebuzzini, *Stable quantum resonances in atom optics*, Phys. Rev. Lett. **89** (2002), 084101, ⊙.

[452] P. T. Fisk, M. A. Lawn, and C. Coles, *Laser cooling of 171yb+ ions a linear paul trap*, Appl. Phys. B **57** (1993), 287.

[453] M. Fleischhauer, *Spontaneous emission and level shifts in absorbing disordered dielectrics and dense atomic gases: A green's-function approach*, Phys. Rev. A **60** (1999), 2434, ⊙DOI.

[454] M. Fleischhauer, A. Imamoglu, and J. P. Marangos, *Electromagnetically induced transparency, optics in coherent media*, Rev. Mod. Phys. **77** (2005), 633, ⊙DOI.

[455] M. Fleischhauer and M. D. Lukin, *Dark-state polaritons in electromagnetically induced transparency*, Phys. Rev. Lett. **84** (2000), 5094, ⊙.

[456] M. Fliesser and R. Graham, *Hidden symmetry of collisionless sound of bose condensates in anisotropic traps*, Phys. Rev. A **59** (1999), R27, ⊙.

[457] DOIVanderlei S. Bagnato and Daniel Kleppner, *Bose-Einstein condensation in low-dimensional traps*, Phys. Rev. A **44** (1991), 7439, ⊙.

[458] DOIR. Bachelard and N. Piovella and Ph. W. Courteille, *Cooperative scattering and radiation pressure force in dense atomic clouds*, Phys. Rev. A **84** (2011), 013821.

[459] V. Fock, *Konfigurationsraum und zweite quantelung*, Zeitschrift für Physik **75** (1932), 622.

[460] Ya. A. Fofanov, A. S. Kuraptsev, I. M. Sokolov, and M. D. Havey, *Spatial distribution of optically induced atomic excitation in a dense and cold atomic ensemble*, Phys. Rev. A **87** (2013), 063839, DOI.

[461] O. Föllinger, *Regelungstechnik*, 1985.

[462] ———, *Regelungstechnik: Einführung in die methoden und ihre anwendung*, Hütig, 2008.

[463] C. J. Foot, H. Wu, E. Arimondo, and G. Morigi, *Optical elements for interferometry of atoms with j-greater-than-1*, J. de Physique **4** (1993), 1913.

[464] G. R. Fowles, *Introduction to modern optics*, Dover Publications, 1989, ⊙ISBN.

[465] R. S. Freeland, *Photoassociation spectroscopy of ultracold and Bose-condensed atomic gases*, PhD thesis (2001).

[466] D. G. Fried, T. C. Killian, L. Willmann, D. Landhuis, S. C. Moss, D. Kleppner, and T. J. Greytak, *Bose-Einstein condensation of atomic hydrogen*, Phys. Rev. Lett. **81** (1998), 3811, ⊙.

[467] R. Friedberg, S. R. Hartmann, and J. T. Manassah, *Frequency shifts in emission and absorption by resonant systems of two-level atoms*, Phys. Rep. **7** (1973), 101, DOI.

[468] R. Friedberg and J. T. Manassah, *Effects of including the counterrotating term and virtual photons on the eigenfunctions and eigenvalues of a scalar photon collective emission theory*, Phys. Lett. A **372** (2008), 2514, ⊙DOI.

[469] ———, *Reply to: Comment on: Effects of including the counterrotating term and virtual photons on the eigenfunctions and eigenvalues of a scalar photon collective emission theory; phys. lett. a 372 (2008) 2514; phys. lett. a 372 (2008) 5732*, Phys. Lett. A **372** (2008), 5734, ⊙DOI.

[470] ———, *Cooperative lamb shift in an ellipsoid*, Phys. Rev. A **81** (2010), 063822, ⊙DOI.

[471] H. Friedrich, *Theoretische atomphysik*, Springer, 1990, ISBN.

[472] J. Fuchs, G. J. Duffy, G. Veeravalli, P. Dyke, M. Bartenstein, C. J. Vale, P. Hannaford, and W. J. Rowlands, *Molecular Bose-Einstein condensation in a versatile low power crossed dipole trap*, J. Phys. B **40** (2007), 4109, ⊙.

[473] J. Fuchs, C. Ticknor, P. Dyke, G. Veeravalli, E. Kuhnle, W. Rowlands, P. Hannaford, and C. J. Vale, *Binding energies of 6 li p-wave Feshbach molecules*, Phys. Rev. A **77** (2008), 053616, ⊙.

[474] S. Fuchs and S. Y. Buhmann, *Purcell-dicke effect for an atomic ensemble near a surface*, Europhys. Lett. **124** (2018), 34003, ⊙DOI.

[475] T. Fukuhara, S. Sugawa, M. Sugimoto, S. Taie, and Y. Takahashi, *Mott insulator of ultracold alkaline-earth-metal-like atoms*, Phys. Rev. A **79** (2009), 041604(R), ⊙DOI.

[476] T. Fukuhara, Y. Takasu, M. Kumakura, and Y. Takahashi, *Degenerate Fermi gases of ytterbium*, Phys. Rev. Lett. **98** (2007), 030401, ⊙DOI.

[477] A. Gaëtan, Y. Miroshnychenko, T. Wilk, A. Chotia, . Viteau, D. Comparat, P. Pillet, A. Browaeys, and Ph. Grangier, *Observation of collective excitation of two individual atoms in the Rydberg blockade regime*, Nature Phys. **84** (2009), 2814, DOI.

[478] E. J. Galvez, P. R. Crawford, H. I. Sztul, M. J. Pysher, P. J. Haglin, and R. E. Williams, *Geometric phase associated with mode transformations in optical beams bearing orbital angular momentum*, Phys. Rev. Lett. **90** (2003), 203901, ⊙.

[479] S. Gammelmark and K. Molmer, *Phase transitions and Heisenberg limited metrology in an ising chain interacting with a single-mode cavity field*, New J. Phys. **13** (2011), 053035, ⊙DOI.

[480] ———, *Interacting spins in a cavity: Finite-size effects and symmetry-breaking dynamics*, Phys. Rev. A **85** (2012), 042114, ⊙DOI.

[481] M. Gangl and H. Ritsch, *3d dissipative motion of atoms in a strongly coupled driven cavity*, Eur. Phys. J. D **8** (2000), 29, ⊙.

[482] ———, *Cold atoms in a high-q ring cavity*, Phys. Rev. A **61** (2000), 043405, ⊙.

[483] Wenlong Gao, M. Lawrence, Biao Yang, Fu Liu, Fengzhou Fang, B. BÃ©ri, J. Li, and Shuang Zhang, *Topological photonic phase in chiral hyperbolic metamaterials*, Phys. Rev. Lett. **114** (2015), 037402.

[484] A. García-Etxarri, R. Gómez-Medina, L. S. Froufe-Pérez, C. López, L. Chantada, F. Scheffold, J. Aizpurua, M. Nieto-Vesperinas, and J. J. Sáenz, *Strong magnetic response of submicron silicon particles in the infrared*, Opt. Exp. **19** (2011), 4815, ⊙DOI.

[485] J. C. García-Melgarejo, N. Lozano-Crisóstomo, J. J. Escobedo-Alatorre, K. J. Sánchez-Pérez, M. Torres-Cisneros, E. S. Arroyo-Rivera, and R. Guzmán-Cabrera4, *A numerical perspective on the Jaynes-Cummings model wigner function*, Computacíon y Sistemas **23** (2019), 1125.

[486] J. J. García-Ripoll and V. M. Pérez-García, *Optimizing schrödinger functionals using sobolev gradients: Application to quantum mechanics and nonlinear optics*, SIAM J. Sci. Comput. **23** (2001), 1316, ⊙.

[487] C. W. Gardiner, *Quantum noise*, Springer-Verlag, Berlin, 1991, ISBN.

[488] C. W. Gardiner and M. J. Collett, *Input and output in damped quantum systems: Quantum stochastic differential equations and the master equation*, Phys. Rev. A **31** (1985), 3761, ⊙.

[489] C. W. Gardiner and C. M. Savage, *A multimode quantum theory of a degenerate parametric amplifier in a cavity*, Opt. Comm. **50** (1984), 173, ⊙.

[490] S. A. Gardiner, K. M. Gheri, and P. Zoller, *Cavity-assited quasiparticle damping in a Bose-Einstein condensate*, Phys. Rev. A **63** (2001), 051603(R), ⊙DOI.

[491] J. R. Gardner, R. A. Cline, J. D. Miller, D. J. Heinzen, H. M. J. M. Boesten, and B. J. Verhaar, *Collisions of doubly spin-polarized ultracold 85 rb atoms*, Phys. Rev. Lett. **74** (1995), 3764, ⊙.

[492] B. M. Garraway, *The Dicke model in quantum optics: Dicke model revisited*, Phil. Trans. R. Soc. A **369** (2011), 1137, ⊙DOI.

[493] B. M. Garraway, P. L. Knight, and J. Steinbach, *Dissipation of quantum superpositions*, Appl. Phys. B **60** (1995), 63.

[494] W. R. Garrett, R. C. Hart, J. E. Wray, I. Datskou, and M. G. Payne, *Large multiple collective line shifts observed in three-photon excitations of xe*, Phys. Rev. Lett. **64** (1995), 1717, DOI.

[495] J. C. Garrison and R. Y. Chiao, *Canonical and kinetic forms of the electromagnetic momentum in an ad hoc quantization scheme for a dispersive dielectric*, Phys. Rev. A **70** (1995), 053826.

[496] J. D. Gaskill, *Linear systems, fourier transforms and optics*, John Wiley & sons, 1978, ISBN.

[497] S. Gasparinetti, J.-C. Besse, M. Pechal, R. D. Buijs, Ch. Eichler, H. J. Carmichael, and A. Wallraff, *Two-photon resonance fluorescence of a ladder-type atomic system*, Phys. Rev. A **100** (2019), 033802, ⊙DOI.

[498] M. Gegg, A. Carmele, A. Knorr, and M. Richter, *Superradiant to subradiant phase transition in the open system Dicke model: dark state cascades*, New J. Phys. **20** (2018), 013006, ⊙DOI.

[499] J. Gelhausen, M. Buchhold, A. Rosch, and P. Strack, *Quantum-optical magnets with competing short- and long-range interactions: Rydberg-dressed spin lattice in an optical cavity*, SciPost Phys. **1** (2016), 004, ⊙DOI.

[500] M. Gell-Mann and J. B. Hartle, *Decoherent histories quantum mechanics and copenhagen quantum mechanics*, ePrints (2021), ⊙.

[501] S. D. Gensemer and D. S. Jin, *Transition from collisionless to hydrodynamic behavior in an ultracold atomic gas*, Phys. Rev. Lett. **87** (2001), 173201, ⊙.

[502] F. Gerbier, A. Widera, S. Fölling, O. Mandel, T. Gericke, and I. Bloch, *Phase coherence of an atomic mott insulator*, Phys. Rev. Lett. **95** (2005), 050404, ⊙.

[503] R. Gerritsma, G. Kirchmair, F. Zähringer, E. Solano, R. Blatt, and C. F. Roos, *Quantum simulation of the dirac equation*, Nature Lett. **463** (2010), 68, ⊙.

[504] Ch. Gerry and P. L. Knight, *Introductory quantum optics*, Cambridge, 2005, ⊙ISBN.

[505] I. Giaver, *Detection of the ac josephson effect*, Phys. Rev. Lett. **14** (1965), 904.

[506] A. F. Gibson, M. F. Kimmitt, and A. C. Walker, *Photon drag in germanium*, Appl. Phys. Lett. **17** (1970), 75.

[507] H. Gießen, J. D. Berger, G. Mohs, P. Meystre, and S. F. Yelin, *Cavity-modified spontaneous emission: From Rabi oscillations to exponential decay*, Phys. Rev. A **53** (1996), 2816.

[508] K. Gietka, F. Mivehvar, and H. Ritsch, *A supersolid-based gravimeter in a ring cavity*, Phys. Rev. Lett. **122** (2018), 190801, ⊙DOI.

[509] K. Gietka, T. Wasak, J. Chwedeńczuk, F. Piazza, and H. Ritsch, *Quantum-enhanced interferometry with cavity QED-generated non-classical light*, Eur. J. Phys. D **71** (2017), 0273, ⊙DOI.

[510] M. Gilowski, Ch. Schubert, M. Zaiser, W. Herr, T. Wuebena, T. Wendrich, T. Mueller, E. M. Rasel, and W. Ertmer, *Narrow bandwidth interference filter-stabilized diode laser systems for the manipulation of neutral atoms*, Opt. Commun. **280** (2007), 443.

[511] D.M. Giltner, Phys. Rev. Lett. **75** (1995), 2638.

[512] S. Giorgini, L.P. Pitaevskii, and S. Stringari, *Thermodynamics of a trapped Bose-condensed gas*, J. Low Temp. Phys. **109** (1997), 309, ⊙.

[513] S. Giovanazzi, A. Görlitz, and T. Pfau, *Tuning the dipolar interaction in quantum gases*, Phys. Rev. Lett. **89** (2002), 130401, ⊙.

[514] S. Giovanazzi, D. O'Dell, and G. Kurizki, *Density modulations of Bose-Einstein condensates via laser-induced interactions*, Phys. Rev. Lett. **88** (2002), 130402, ⊙.

[515] R. J. Glauber, *Coherent and incoherent states of the radiation field*, Phys. Rev. **131** (1963), 2766, ⊙.

[516] ———, *The quantum theory of optical coherence*, Phys. Rev. **130** (1963), 2529.

[517] E. V. Goldstein, M. G. Moore, and P. Meystre, *Non-linear manipulation and control of matter waves*, Laser Phys. (1999), quant-ph/9906088.

[518] E. V. Goldstein, K. Plättner, and P. Meystre, *Atomic phase-conjugation from a bose condensate*, J. Res. Natl. Inst. Stand. Technol. **101** (1996), 583.

[519] H. Goldstein, *Klassische mechanik*, Akademische Verlagsgesellschaft Wiesbaden, 1983.

[520] H. Goldstein, C. P. Poole, and J. L. Safko, *Classical mechanics*, Addison Wesley, 2000, ISBN.

[521] J. W. Goodman, *Introduction to fourier optics*, McGraw-Hill physical and quantum electronics series, W. H. Freeman, 1996, ISBN.

[522] F. Goos and H. Hänchen, *Ein neuer und fundamentaler versuch zur totalreflektion*, Ann. Physik (Leipz.) **1** (1947), 333.

[523] F. Goos and H. Lindberg-Hänchen, *Neumessung des strahlversetzungeffectes bei totalreflexion*, Ann. Physik (Leipz.) **5** (1949), 251.

[524] D. Gordon and C. M. Savage, *Creating macroscopic superpositions with Bose-Einstein condensates*, Phys. Rev. A **59** (1999), 4623, ⊙.

[525] J. P. Gordon, *Radiation forces and moment in dielectric media*, Phys. Rev. A **8** (1973), 14, ⊙DOI.

[526] J. P. Gordon and A. Ashkin, *Motion of atoms in a radiation trap*, Phys. Rev. A **21** (1980), 1606, ⊙DOI.

[527] A. Görlitz, A. P. Chikkatur, and W. Ketterle, *Enhancement and suppression of spontaneous emission and light scattering by quantum degeneracy*, Phys. Rev. A **63** (2001), R041601, ⊙DOI.

[528] A. Görlitz, M. Weidemüller, T. W. HÃ¤nsch, and A. Hemmerich, *Observing the position spread of atomic wave packets*, Phys. Rev. Lett. **78** (1997), 2096, ⊙DOI.

[529] D. Gottesman, *The heisenberg representation of quantum computers*, ePrints **arXiv:quant-ph/9807006** (1998), ⊙.

[530] D. Gottesman, A. Kitaev, and J. Preskill, *Encoding a qubit in an oscillator*, Phys. Rev. A **64** (2001), 012310, ⊙DOI.

[531] P. L. Gould, G. A. Ruff, and D. E. Pritchard, *Diffraction of atoms by light: The near-resonant kapitza-dirac effect*, Phys. Rev. Lett. **56** (1986), 827.

[532] I. S. Gradshteyn and I.M. Ryzhik, *Table of integrals, series, and products*, Elsevier, 2007, ISBN.

[533] R. Graham, M. Schlautmann, and D. L. Shepelyansky, *Dynamical localization in josephson junctions*, Phys. Rev. Lett. **67** (1991), 255, ⊙.

[534] R. Graham and D. Walls, *Spectrum of light scattered from a weakly interacting Bose-Einstein condensed gas*, Phys. Rev. Lett. **76** (1996), 1774.

[535] D. M. Greenberger, M. A. Horne, A. Shimony, and A. Zeilinger, *Bell's theorem without inequalities*, Am. J. Phys. **58** (1990), 1131.

[536] M. Greiner, I. Bloch, O. Mandel, T. W. Hänsch, and T. Esslinger, *Exploring phase coherence in a 2d lattice of Bose-Einstein condensates*, Phys. Rev. Lett. **87** (2001), 160405, ⊙.

[537] M. Greiner, O. Mandel, T. Esslinger, T. W. Hänsch, and I. Bloch, *Quantum phase transition from a superfluid to a mott insulator in a gas of ultracold atoms*, Nature **415** (2002), 39, ⊙.

[538] M. Greiner, C. A. Regal, and D. S. Jin, *Emergence of a molecular Bose-Einstein condensate from a Fermi gas*, Nature **426** (2003), 537, ⊙.

[539] ———, *Probing the excitation spectrum of a Fermi gas in the BCS-BEC crossover regime*, Phys. Rev. Lett. **94** (2005), 070403, ⊙.

[540] M. Greiner, C. A. Regal, C. Ticknor, J. L. Bohn, and D. S. Jin, *Detection of spatial correlations in an ultracold gas of fermions*, Phys. Rev. Lett. **92** (2004), 150405, ⊙.

[541] W. Greiner, *Relativistic quantum mechanics: Wave equations*, Springer, 2nd ed., 1987, ISBN.

[542] G. F. Gribakin and V. V. Flambaum, *Calculation of the scattering length in atomic collisions using the semiclassical approximation*, Phys. Rev. A **48** (1993), 546, ⊙.

[543] T. Griesser, H. Ritsch, M. Hemmerling, and G. R. M. Robb, *A vlasov approach to bunching and selfordering of particles in optical resonators*, Eur. J. Phys. **58** (2010), 349.

[544] A. Griffin and E. Zaremba, *First and second sound in a uniform bose gas*, Phys. Rev. A **56** (1997), 4839, ⊙.

[545] D. J. Griffiths, *Introduction to electrodynamics*, Prentiss-Hall, 1989, ⊙ISBN.

[546] _____, *Introduction to quantum mechanics*, Pearson Prentice Hall, New Jersey, 2005, ⊙ISBN.

[547] R. Grimm, M. Weidemüller, and Y. B. Ovchinnikov, *Optical dipole traps for neutral atoms*, Adv. At. Mol. Opt. Phys. **42** (2000), 95, ⊙.

[548] F. Gross, *Relativistic quantum mechanics and field theory*, Wiley, 2nd ed., 1999, ISBN.

[549] M. Gross and S. Haroche, *Superradiance: An essay on the theory of collective spontaneous emission*, Phys. Rep. **93** (1982), 301, ⊙DOI.

[550] Ch. Grossert, M. Leder, and M. Weitz, *Phase dependent loading of Bloch bands and quantum simulation of relativistic wave equation predictions with ultracold atoms in variably shaped optical lattice potentials*, J. Mod. Opt. **63** (2015), 1805, ⊙DOI.

[551] S. Grossmann and M. Holthaus, *On Bose-Einstein condensation in harmonic traps*, Phys. Lett. A **208** (1995), 188, ⊙.

[552] G. Gründler, *Electrical charges in gravitational fields and Einstein's equivalence principle*, ePrints (2015), 1509.08757, ⊙.

[553] G. Grynberg and J.-Y. Courtois, *Sur la possibilité d'observer la non-linéarité du vide par conjugaison de phase optique*, C.R. Acacd. Sci. Paris **311** (1990), 1149.

[554] G. Grynberg, B. Lounis, P. Verkerk, J.-Y. Courtois, and C. Salomon, *Quantized motion of cold cesium atoms in two- and three-dimensional optical potentials*, Phys. Rev. Lett. **70** (1993), 2249, ⊙.

[555] W. Guerin, M. Araújo, and R. Kaiser, *Subradiance in a large cloud of cold atoms*, Phys. Rev. Lett. **116** (2016), 083601.

[556] D. Guéry-Odelin, J. Söding, P. Desbiolles, and J. Dalibard, *Is Bose-Einstein condensation of atomic cesium possible?*, Europhys. Lett. **44** (1998), 25.

[557] D. Guéry-Odelin and S. Stringari, *Scissors mode and superfluidity of a trapped Bose-Einstein condensed gas*, Phys. Rev. Lett. **83** (1999), 4452, ⊙.

[558] L. Guidoni and P. Verkerk, *Optical lattices: Cold atoms ordered by light*, J. Opt. B: Quantum Semiclass. Opt. **1** (1999), R23, ⊙DOI.

[559] J. Guo, P. R. Berman, H. Dubetsky, and G. Grynberg, *Recoil-induced resonances in non-linear spectroscopy*, Phys. Rev. A **46** (1992), 1426, ⊙.

[560] Jun Guo, *Contribution of energy continuum states to probe absorption signal of atoms in one-dimensional optical molasses*, Phys. Rev. A **49** (1994), 3934, ⊙DOI.

[561] Jun Guo and P. R. Berman, *Recoil-induced resonances in pump-probe spectroscopy*, Phys. Rev. A **47** (1993), 4128.

[562] S. Gupta, Z. Hadzibabic, M. W. Zwierlein, B. J. Verhaar, and W. Ketterle, *Radio-frequency spectroscopy of ultracold fermions*, Sciencexpress (2003), 1, ⊙.

[563] S. Gupta, K. L. Moore, K. W. Murch, and D. M. Stamper-Kurn, *Cavity nonlinear optics at low photon numbers from collective atomic motion*, Phys. Rev. Lett. **99** (2005), 213601.

[564] V. Gurarie, L. Radzihovsky, and A. V. Andreev, *Quantum phase transitions across a p-wave Feshbach resonance*, ePrint (2004), ⊙.

[565] A. M. Guzman, M. Moore, and P. Meystre, *Theory of a coherent atomic-beam generator*, Phys. Rev. A **53** (1996), 977.

[566] B. Hacker, S. Welte, S. Daiss, A. Shaukat, S. Ritter, Lin Li, and G. Rempe, *Deterministic creation of entangled atom-light schrÃ¶dinger-cat states*, Nature Phot. **13** (2019), 110, DOI.

[567] Z. Hadzibabic, S. Gupta, C. A. Stan, C. H. Schunck, M. W. Zwierlein, K. Dieckmann, and W. Ketterle, *Fiftyfold improvement in the number of quantum degenerate fermionic atoms*, Phys. Rev. Lett. **91** (2003), 160401, ⊙.

[568] Z. Hadzibabic, C. A. Stan, K. Dieckmann, S. Gupta, M. W. Zwierlein, A. Görlitz, and W. Ketterle, *Two-species mixture of quantum degenerate bose and Fermi gases*, Phys. Rev. Lett. **88** (2002), 160401, ⊙.

[569] E. W. Hagley, L. Deng, M. Kozuma, M. Trippenbach, Y. B. Band, M. Edwards, M. Doery, P. S. Julienne, K. Helmerson, S. L. Rolston, and W. D. Phillips, *Measurement of the coherence of a Bose-Einstein condensate*, Phys. Rev. Lett. **83** (1999), 3112, ⊙.

[570] E. W. Hagley, L. Deng, M. Kozuma, J. Wen, K. Helmerson, S. L. Rolston, and W. D. Phillips, *A well-collimated quasi-continuous atom laser*, Science **283** (1999), 1706, ⊙.

[571] H. Haken, *Synergetics. an introduction. nonequilibrium phase transitions in physics, chemistry and biology*, 3 ed., Synergetics, vol. 1, Springer-Verlag, 1983, ISBN.

[572] J. Hald, J. L. Sorensen, C. Schori, and E. S. Polzik, *Spin squeezed atoms: A macroscopic entangled ensemble created by light*, Phys. Rev. Lett. **83** (1999), 1319, ⊙.

[573] D. S. Hall, J. R. Ensher, D. S. Jin, and et al., *Recent experiments with Bose-condensed gases at JILA*, Proc. SPIE **3270** (1998), 98, cond-mat/9903459.

[574] D. S. Hall, M. R. Matthews, J. R. Ensher, C. E. Wieman, and E. A. Cornell, *Dynamics of component separation in a binary mixture of Bose-Einstein condensates*, Phys. Rev. Lett. **81** (1998), 1539, ⊙.

[575] D. S. Hall, M. R. Matthews, C. E. Wieman, and E. A. Cornell, *Measurements of relative phase of two-component Bose-Einstein condensates*, Phys. Rev. Lett. **81** (1998), 1543, ⊙.

[576] J. L. Hall, L. Hollberg, T. Baer, and H. G. Robinson, *Optical heterodyne saturation spectroscopy*, Appl. Phys. Lett. **39** (1981), 680.

[577] D. Halliday, R. Resnick, and J. Walker, *Fundamentals of physics*, 7 ed., John Wiley and sons, 2005, ISBN.

[578] C. S. Hamilton, R. Kruse, L. Sansoni, S. Barkhofen, Ch. Silberhorn, and I. Jex, *Gaussian boson sampling*, Phys. Rev. Lett. **119** (2017), 170501, ⊙.

[579] D.-J. Han, S. Wolf, S. Oliver, C. McCormick, M. T. DePue, and D. S. Weiss, *3d Raman sideband cooling of cesium atoms at high density*, Phys. Rev. Lett. **85** (2000), 724, ⊙.

[580] D. J. Han, R. H. Wynar, Ph. W. Courteille, and D. J. Heinzen, *Bose-Einstein condensation of large numbers of atoms in a magnetic time-averaged orbiting potential trap*, Phys. Rev. A **57** (1998), R4114.

[581] T. W. Hänsch and A. L. Schawlow, *Cooling of gases by laser radiation*, Opt. Comm. **13** (1975), 68, ⊙DOI.

[582] S. Haroche, J. C. Gay, and G. Grynberg (eds.), *Atom traps*, World Scientific, 1989.

[583] T. Hartmann, F. Keck, H. J. Korsch, and S. Mossmann, *Dynamics of Bloch oscillations*, New J. Phys. **6** (2004), 2.

[584] J. A. Seman Harutiniam, *Study of excitations in a Bose-Einstein condensate*, Ph.D. thesis, Universidade de São Paulo, 2011.

[585] L. V. Hau, B. D. Busch, Ch. Liu, Z. Dutton, M. M. Burns, and J. A. Golovchenko, *Near-resonant spatial images of a confined Bose-Einstein condensates in a 4-dee magnetic bottle*, Phys. Rev. A **58** (1998), R54, ⊙.

[586] L. V. Hau, S. E. Harris, Z. Dutton, and C. H. Behroozi, *Light speed reduction to 17 metres per second in an ultracold atomic gas*, Nature **397** (1999), 594, ⊙DOI.

[587] M. P. Haugan and F. V. Kowalski, *Spectroscopy of atoms and molecules in gases: Corrections to the doppler-recoil shift*, Phys. Rev. A **25** (1982), 2102, ⊙.

[588] R. Haussman, *Properties of Fermi liquid at the superfluid transition in the crossover region between bcs superconductivity and Bose-Einstein condensation*, Phys. Rev. B **49** (1994), 12975, ⊙.

[589] C. J. Hawthorn, K. P. Weber, and R. E. Scholten), *Littrow configuration tunable external cavity diode laser with fixed direction output beam*, ePrints (2001), 4477, ⊙.

[590] G. Hechenblaikner, M. Gangl, P. Horak, and H. Ritsch, *Cooling an atom in a weakly driven high-q cavity*, Phys. Rev. A **58** (1998), 3030.

[591] G. Hechenblaikner, O. M. Maragò, E. Hodby, J. Arlt, S. Hopkins, and C. J. Foot, *Observation of harmonic generation and nonlinear coupling in the collective dynamics of a Bose-Einstein condensate*, Phys. Rev. Lett. **85** (2000), 692, ⊙.

[592] C. E. Hecht, *The possible superfluid behaviour of hydrogen atom gases and liquids*, Physica **25** (1959), 1159.

[593] N. R. Heckenberg, R. McDuff, C. P. Smith, and A.G. White, *Generation of optical phase singularities by computer-generated holograms*, Opt. Lett. **17** (1992), 221.

[594] G. C. Hegerfeldt and M. B. Plenio, *Spectral structures induced by electron shelving*, Phys. Rev. A **52** (1995), 3333, ⊙.

[595] S. M. Heider and G. O. Brink, *Hyperfine structure of* ^{87}sr *in the* $^3p_2$ *metastable state*, Phys. Rev. A **16** (1977), 1371, ⊙DOI.

[596] D. J. Heinzen, J. J. Childs, J. E. Thomas, and M. S. Feld, *Enhanced and inhibited visible spontaneous emission by atoms in a confocal resonator*, Phys. Rev. Lett. **58** (1987), 1320, ⊙DOI.

[597] ———, *Errata*, Phys. Rev. Lett. **58** (1987), 2153, ⊙DOI.

[598] D. J. Heinzen and M. S. Feld, *Vacuum radiative level shift and spontaneous-emission linewidth of an atom in an optical resonator*, Phys. Rev. Lett. **59** (1987), 2623, ⊙DOI.

[599] H. Heiselberg, *Fermi systems with long scattering lengths*, Phys. Rev. A **63** (2001), 043606, ⊙.

[600] H. Heiselberg, C. J. Pethick, H. Smith, and L. Viverit, *Influence of induced interactions on the superfluid transition in dilute Fermi gases*, Phys. Rev. Lett. **85** (2000), 2418, ⊙.

[601] W. Heisenberg, *Physik und philosophie*, S. Hirzel Verlag, 6. Auflage, Stuttgart, 2000, ISBN.

[602] K. Helmerson, A. Martin, and D. E. Pritchard, *Laser and rf spectroscopy of magnetically trapped neutral atoms*, J. Opt. Soc. Am. B **9** (1992), 483.

[603] P. R. Hemmer, N. P. Bigelow, D. P. Katz, M. S. Shahriar, L. DeSalvo, and R. Bonifacio, *Self-organization, broken symmetry, and lasing in an atomic vapor: The interdependence of gratings and gain*, Phys. Rev. Lett. **77** (1996), 1468, ⊙.

[604] A. Hemmerich, Phys. Rev. Lett. **68** (1992).

[605] ———, Phys. Rev. Lett. **72** (1994).

[606] ———, *Quantum entanglement in dilute optical lattices*, Phys. Rev. A **60** (1999), 943, ⊙.

[607] A. Hemmerich and T. W. Hänsch, *Two-dimensional atomic crystal bound by light*, Phys. Rev. Lett. **70** (1993).

[608] C. Henkel, C. I. Westbrook, and A. Aspect, *Quantum reflection: Atomic matter wave optics in an attractive exponential potential*, J. Opt. Soc. Am. B **13** (1996), 233, ⊙.

[609] E. A. L. Henn, J. A. Seman, G. Roati, K. M. F. Magalh aes, and V. S. Bagnato, *Emergence of turbulence in an oscillating Bose-Einstein condensate*, Phys. Rev. Lett. **103** (2009), 045301, ⊙.

[610] K. Hepp and E. Lieb, *On the superradiant phase transition for molecules in a quantized radiation field: the Dicke maser model*, Annals of Phys. **76** (1973), 360, ⊙DOI.

[611] J. Herb, P. Meerwald, M. J. Moritz, and H. Friedrich, *Quantum-mechanical deflection function*, Phys. Rev. A **60** (1999), 853, ⊙.

[612] J. Herbig, T. Kraemer, M. Mark, T. Weber C. Chin, H.-C. Nägerl, and R. Grimm, *Preparation of a pure molecular quantum gas*, Science **301** (2003), 1510, ⊙.

[613] D. I. Herman, C. Weerasekara, L. C. Hutcherson, F. R. Giorgetta, and K. C. Coss, *Precise multispecies agricultural gas flux determined using broadband open-path dual-comb spectroscopy*, Science Advances **7** (2021), eabe9765.

[614] G. Herzberg, *Molecular spectra and molecular structure. i - spectra of diatomic molecules*, Springer, 1950, ISBN.

[615] C. Herzog and M. Olshanii, *Trapped bose gas: The canonical versus grand canonical statistics*, Phys. Rev. A **55** (1997), 3254, ⊙.

[616] H. F. Hess, *Evaporative cooling of magnetically trapped spin-polarized hydrogen*, Phys. Rev. B **34** (1986), 3476.

[617] J. Heurich, M. G. Moore, and P. Meystre, *Cavity atom optics and the 'free atom laser'*, Opt. Commun. **179** (2000), 549, ⊙.

[618] T. W. Hijmans, Yu. Kagan, and G. V. Shlyapnikov, *Bose condensation and relaxation explosion in magnetically trapped atomic hydrogen*, Phys. Rev. B **48** (1993), 12886, ⊙.

[619] E. A. Hinds and St. M. Barnett, *Momentum exchange between light and a single atom: Abraham or minkowski?*, Phys. Rev. Lett. **102** (2009), 050403, ⊙DOI.

[620] E. A. Hinds, M. G. Boshier, and I. G. Hughes, *Magnetic waveguide for trapping cold atom gases in two dimensions*, Phys. Rev. Lett. **80** (1998), 645, ⊙.

[621] K. M. Ho, C. T. Chan, and C. M. Soukoulis, *Existence of a photonic gap in periodic dielectric structures*, Phys. Rev. Lett. **65** (1990), 3152, ⊙.

[622] Tin-Lun Ho and E. J. Mueller, *High temperature expansion applied to fermions near Feshbach resonance*, Phys. Rev. Lett. **92** (2004), 160404, ⊙.

[623] E. Hodby, S. T. Thompson, C. A. Regal, M. Greiner, A. C. Wilson, D. S. Jin, E. A. Cornell, and C. E. Wieman, *Production efficiency of ultracold Feshbach molecules in bosonic and fermionic systems*, Phys. Rev. Lett. **94** (2005), 120402, ⊙.

[624] W. Hofstetter, J. I. Cirac, P. Zoller, E. Demler, and M. D. Lukin, *High-temperature superfluidity of fermionic atoms in optical lattices*, Phys. Rev. Lett. **89** (2002), 220407, ⊙.

[625] M. J. Holland and J. Cooper, *Expansion of a Bose-Einstein condensate in a harmonic potential*, Phys. Rev. A **53** (1996), R1954, ⊙.

[626] M. J. Holland, D. S. Jin, M. L. Ciafalo, and J. Cooper, *Emergence of interaction effects in Bose-Einstein condensation*, Phys. Rev. Lett. **78** (1997), 3801, ⊙.

[627] M. J. Holland, J. Park, and R. Walser, *Formation of pairing fields in resonantly coupled Bose-Einstein condensates*, Phys. Rev. Lett. **86** (2000), 1915, ⊙.

[628] L. Hollberg, L. S. Ma, M. Hohenstatt, and J. L. Hall, *Precision measurement by optical heterodyne techniques*, Proc. SPIE **426** (1983), 91.

[629] R. Holzwarth, Th. Udem, T. W. Hänsch, J. C. Knight, W. J. Wadsworth, and P. St. J. Russell, *Optical frequency synthesizer for precision spectroscopy*, Phys. Rev. Lett. **85** (2000), 2264.

[630] R. Holzwarth, M. Zimmermann, Th. Udem, T. W. Hänsch, P. Russbüldt, K. Gäbel, R. Poprawe, J. C. Knight, W. J. Wadsworth, and P. St. J. Russell, *White-light frequency comb generation with a diode-pumped cr:lisaf laser*, Opt. Lett. **26** (2000), 1376.

[631] Rebecca L. Honeycutt, *Stochastic runge-kutta algorithms, i. white noise*, Phys. Rev. A **45** (1992), 600, ⊙.

[632] P. Horak, S. M. Barnett, and H. Ritsch, *Coherent dynamics of Bose-Einstein condensates in high-finesse optical cavities*, Phys. Rev. A **61** (2000), 033609, ⊙DOI.

[633] P. Horak and H. Ritsch, *Dissipative dynamics of bose condensates in optical cavities*, Phys. Rev. A **63** (2001), 023603, ⊙.

[634] _____, *Manipulating a Bose-Einstein condensate with a single photon*, Eur. Phys. J. D **13** (2001), 279, ⊙.

[635] P. Horowitz and W. Hill, *The art of electronics*, Cambridge Universty Press, 2001, ISBN.

[636] Ch. Hotter, D. Plankensteiner, and H. Ritsch, *Continuous narrowband lasing with coherently driven v-level atoms*, New J. Phys. **22** (2020), 113021, ⊙DOI.

[637] M. Houbiers, H. T. C. Stoof, W. I. McAlexander, and R. G. Hulet, *Elastic and inelastic collisions of li-6 atoms in magnetic and optical traps*, Phys. Rev. A **57** (1998), R1497, ⊙.

[638] Bambi Hu and Le-Man Kuang, *Tunneling dynamics of Bose-Einstein condensates with Feshbach resonances*, Phys. Rev. A **62** (2000), 023610, ⊙.

[639] Fachao Hu, I. Nosske, L. Couturier, C. Tan, C. Qiao, P. Chen, Y. H. Jiang, Bing Zhu, and M. Weidemüller, *Analyzing a single-laser repumping scheme for efficient loading of a strontium magneto-optical trap*, Phys. Rev. A **99** (2019), 033422, ⊙DOI.

[640] Jiazhong Hu, A. Urvoy, Z. Vendeiro, V. CrÃ©pel, W. Chen, and V. Vuletic, *Creation of a Bose-condensed gas of ^{87}rb by laser cooling*, Science **358** (2017), 1078, ⊙DOI.

[641] K. Huang, *Statistical mechanics*, John Wiley and Sons, 1987, ISBN.

[642] R. Huesmann, Ch. Balzer, Ph. W. Courteille, W. Neuhauser, and P. E. Toschek, *Single-atom interferometry*, Phys. Rev. Lett. **82** (1999), 1611.

[643] A. F. Huss, R. Lammegger, C. Neureiter, E. A. Korsunsky, and L. Windholz, *Phase correlation of laser waves with arbitrary frequency spacing*, Phys. Rev. Lett. **93** (2004), 223601, ⊙.

[644] D. A. W. Hutchinson, *Self-consistent effects of continuous wave output coupling of atoms from a Bose-Einstein condensate*, Phys. Rev. Lett. **82** (1999), 6, ⊙.

[645] D. A. W. Hutchinson, E. Zaremba, and A. Griffin, *Finite temperature excitations of a trapped bose gas*, Phys. Rev. Lett. **78** (1997), 1842, ⊙.

[646] Tetsuya Ido, M. Boyd, A. Ludlow, T. Zelevinsky, S. Foreman, S. Blatt, M. Notcutt, and J. Ye, *Optical clocks based on ultracold neutral strontium atoms*, ESA Proceedings (2005), ⊙DOI.

[647] Tetsuya Ido, Yoshitomo Isoya, and Hidetoshi Katori, *Optical-dipole trapping of sr atoms at a high phase-space density*, Phys. Rev. A **61** (2000), 061403(R), ⊙.

[648] S. Inouye, M. R. Andrews, J. Stenger, H.-J. Miesner, D. M. Stamper-Kurn, and W. Ketterle, *Observation of Feshbach resonances in a Bose-Einstein condensate*, Nature **392** (1998), 151, ⊙DOI.

[649] S. Inouye, A. P. Chikkatur, D. M. Stamper-Kurn, J. Stenger, D. E. Pritchard, and W. Ketterle, *Superradiant rayleigh scattering from a Bose-Einstein condensate*, Science **285** (1999), 571, ⊙DOI.

[650] S. Inouye, R. F. Löw, S. Gupta, T. Pfau, A. Görlitz, T. L. Gustavson, D. E. Pritchard, and W. Ketterle, *Amplification of light and atoms in a Bose-Einstein condensate*, Phys. Rev. Lett. **85** (2000), 4225, ⊙.

[651] S. Inouye, T. Pfau, S. Gupta, A. P. Chikkatur, A. Görlitz, D. E. Pritchard, and W. Ketterle, *Phase-coherent amplification of atomic matter-waves*, Nature **402** (1999), 641, ⊙DOI.

[652] K. Ishizaki, M. Koumura, K. Suzuki, K. Gondaira, and S. Noda, *Realization of three-dimensional guiding of photons in photonic crystals*, Nature Phot. **7** (2013), 133, ⊙DOI.

[653] W. M. Itano, J. C. Bergquist, J. J. Bollinger, J. M. Gilli-Gans, D. J. Heinzen, F. L. Moore, M. G. Raizen, and D. J. Wineland, *Quantum projection noise: Population fluctuations in two-level systems*, Phys. Rev. A **47** (1993), 3554, ⊙DOI.

[654] W. M. Itano, J. J. Bollinger, and D. J. Wineland, *Quantum zeno effect*, Phys. Rev. A **41** (1990), 2295, ⊙.

[655] W. M. Itano and D. J. Wineland, *Laser cooling of ions stored in harmonic and penning traps*, Phys. Rev. A **25** (1982), 35, ⊙.

[656] H. Ito, T. Nakata, K.Sakaki, M. Ohtsu, K. I. Lee, and W. Jhe, *Laser-spectroscopy of atoms guided by evanescent waves in micron-sized hollow optical fibers*, Phys. Rev. Lett. **76** (1996), 4500.

[657] A. D. Jackson, G. M. Kavoulakis, and C. J. Pethick, *Solitary waves in clouds of Bose-Einstein condensates*, Phys. Rev. A **58** (1998), 2417, ⊙.

[658] B. Jackson, J. F. McCann, and C. S. Adams, *Vortex line and ring dynamics in trapped Bose-Einstein condensates*, Phys. Rev. A **61** (2000), 013604.

[659] J. D. Jackson, *Classical electrodynamics*, John Wiley and Sons, 1999, ISBN.

[660] V. K. Jain, B. K. Behera, and P. K. Panigrahi, *Quantum simulation of discretized harmonic oscillator on ibm quantum computer*, (2020).

[661] D. Jaksch, J.-J. Briegel, J. I. Cirac, C. W. Gardiner, and P. Zoller, *Entanglement of atoms via cold controlled collisions*, Phys. Rev. Lett. **82** (1998), 1975, ⊙.

[662] D. Jaksch, J. I. Cirac, P. Zoller, S. L. Rolston, R. Côté, and M. D. Lukin, *Fast quantum gates for neutral atoms*, Phys. Rev. Lett. **85** (2000), 2208, ⊙.

[663] D. Jaksch, S. A. Gardiner, K. Schluze, J. I. Cirac, and P. Zoller, *Uniting Bose-Einstein condensates in optical resonators*, Phys. Rev. Lett. **86** (2001), 4733, ⊙.

[664] J. Javaloyes, Ph. W. Courteille, M. Perrin, G.-L. Lippi, and A. Politi, *Spontaneous ordering in cold atomic clouds*, Opt. Phot. News **16, (12) and 22 (2005)** (2005).

[665] J. Javaloyes, G. L. Lippi, and A. Politi, *Reduced model for the description of radiation-matter interaction including atomic recoil*, Phys. Rev. A **68** (2003), 033405, ⊙.

[666] J. Javaloyes, M. Perrin, G.-L. Lippi, and A. Politi, *Self-generated cooperative light emission induced by atomic recoil*, Phys. Rev. A **70** (2004), 23405, ⊙.

[667] J. Javaloyes, M. Perrin, and A. Politi, *Collective atomic recoil laser as a synchronization transition*, Phys. Rev. E **78** (2008), 11108, ⊙.

[668] J. Javanainen and M. Yu. Ivanov, *Splitting a trap containing a Bose-Einstein condensate: Atom number fluctuations*, Phys. Rev. A **60** (1999), 2351, ⊙.

[669] J. Javanainen and M. Mackie, *Coherent photoassociation of a Bose-Einstein condensate*, Phys. Rev. A **59** (1999), R3186, ⊙.

[670] J. Javanainen and J. Ruostekoski, *Off-resonance light scattering from low-temperature bose and Fermi gases*, Phys. Rev. A **52** (1995), 3033, ⊙.

[671] C. Javaux, I. G. Hughes, G. Locheada, J. Millen, and M. P. A. Jones, *Modulation-free pump-probe spectroscopy of strontium atoms*, Eur. Phys. J. D **57** (2002), 151, DOI.

[672] E. T. Jaynes and F. W. Cummings, *Comparison of quantum and semiclassical radiation theories with application to the beam maser*, Proc. IEEE **51** (1963), 89.

[673] P. S. Jessen and I. H. Deutsch, *Optical lattices*, Adv. At. Mol. Opt. Phys. **37** (1996), 95, ⊙.

[674] D. S. Jin, J. R. Ensher, M. R. Matthews, C. E. Wieman, and E. A. Cornell, *Collective excitations of a Bose-Einstein condensate in a dilute gas*, Phys. Rev. Lett. **77** (1996), 420, ⊙.

[675] D. S. Jin, M. R. Matthews, J. R. Ensher, C. E. Wieman, and E. A. Cornell, *Temperature-dependent damping and frequency shifts in collective excitations of a dilute Bose-Einstein condensate*, Phys. Rev. Lett. **78** (1997), 764, ⊙.

[676] J. D. Joannopoulos, S. G. Johnson, J. S. Winn, and R. D. Meade, *Photonic crystals: Molding the flow of light*, Princeton University Press, 2011, ISBN.

[677] S. Jochim, M. Bartenstein, A. Altmeyer, G. Hendl, C. Chin, J. Hecker Denschlag, and R. Grimm, *Pure gas of optically trapped molecules created from fermionic atoms*, Phys. Rev. Lett. **91** (2003), 240402, ⊙.

[678] S. Jochim, M. Bartenstein, A. Altmeyer, G. Hendl, S. Riedl, C. Chin, J. Hecker Denschlag, and R. Grimm, *Bose-Einstein condensation of molecules*, Science **302** (2003), 2101, ⊙.

[679] S. Jochim, M. Bartenstein, G. Hendl, J. Hecker Denschlag, R. Grimm, A. Mosk, and M. Weidemüller, *Magnetic field control of elastic scattering in a cold gas of fermionic lithium atoms*, Phys. Rev. Lett. **89** (2002), 273202, ⊙.

[680] S. John and Tran Quang, *Localization of superradiance near a photonic band-gap*, Phys. Rev. Lett. **74** (1995), 3419, ⊙.

[681] D. J. Jones, S. A. Diddams, J. K. Ranka, A. Stentz, R. S. Windeler, J. L. Hall, and S. T. Cundiff, *Carrier-envelope phase control of femtosecond mode-locked lasers and direct optical frequency synthesis*, Science **288** (2000), 635.

[682] R. Jones, J. A. Needham, I. Lesanovsky, F. Intravaia, and B. Olmos, *Modified dipole-dipole interaction and dissipation in an atomic ensemble near surfaces*, Phys. Rev. A **97** (2018), 053841, ⊙DOI.

[683] P. Jordan and O. Klein, *Zum mehrkörperproblem der quantentheorie*, Zeitschrift für Physik **45** (1927), 751.

[684] P. Jordan and E. Wigner, *über das paulische äquivalenzverbot*, Zeitschrift für Physik **47** (1928), 631.

[685] B. D. Josephson, *Possible new effects in superconductive tunneling*, Phys. Lett. **1** (1962), 251.

[686] C. Raitz Jr., *Implementação experimental de um termómetro quântico usando ressonância magnética nuclear*, Ph.D. thesis, Centro Brasileiro de Pesquisas Físicas, Rio de Janeiro, 2015.

[687] V. L. Campo jr. and K. Capelle, *Phase diagram of harmonically confined one-dimensional fermions with attractive and repulsive interactions*, Phys. Rev. A **72** (2005), 061602(R), ⊙.

[688] V. L. Campo Jr, K. Capelle, J. Quintanilla, and C. Hooley, *Quantitative determination of the hubbard model phase diagram from optical lattice experiments by two-parameter scaling*, Phys. Rev. Lett. **99** (2007), 240403, ⊙.

[689] B. Juisgaard, A. Kozhekin, and E. S. Polzik, *Experimental long-lived entanglement of two macroscopic objects*, Nature **413** (2001), 400, ⊙.

[690] P. S. Julienne, K. Burnett, Y. B. Band, and W.C. Stwalley, *Stimulated Raman molecule production in Bose-Einstein condensates*, Phys. Rev. A **58** (1998), R797, ⊙.

[691] R. Kaiser, *Quantum multiple scattering*, J. Mod. Opt. **56** (2009), 2082, ⊙DOI.

[692] R. K. Kaj, D. Bloch, J. J. Snyder, G. Camy, and M. Ducloy, *High-frequency optically heterodyned saturation spectroscopy via resonant degenerate four-wave mixing*, Phys. Rev. Lett. **44** (1982), 1251.

[693] P. L. Kapitza and P. A. M. Dirac, *The deflection of electrons from standing light waves*, Proc. Roy. Soc. Lond. (1933), 297.

[694] L. Karpa and M. Weitz, *A stern-gerlach experiment for slow light*, Nature Phot. **2** (2006), 332, DOI.

[695] T. Karpiuk, M. Brewczyk, S. Ospelkaus-Schwarzer, K. Bongs, M. Gajda, and K. Rzazÿewski, *Soliton trains in Bose-Fermi mixtures*, Phys. Rev. Lett. **93** (2004), 100401, ⊙.

[696] R. Karplus and M. Neumann, *The scattering of light by light*, Phys. Rev. **83** (1950), 776.

[697] A. Kasapi, M. Jain, G. Y. Jin, and S. E. Harris, *Electromagnetically induced transparency: Propagation dynamics*, Phys. Rev. Lett. **74** (1995), 2447, ⊙.

[698] M. Kasevich and S. Chu, *Atomic interferometry using stimulated raman transitions*, Phys. Rev. Lett. **67** (1991), 181.

[699] ———, *Measurement of the gravitational acceleration of an atom with a light-pulse atom interferometer*, Appl. Phys. B **54** (1992), 321, ⊙DOI.

[700] M. M. Kash, V. A. Sautenkov, A. S. Zibrov, L. Hollberg, G. R. Welch, M. D. Lukin, Y. Rostovtsev, E. S. Fry, and M. O. Scully, *Ultraslow group velocity and enhanced nonlinear optical effects in a coherently driven hot atomic gas*, Phys. Rev. Lett. **82** (1999), 5229, ⊙.

[701] A. Kastberg, W. D. Phillips, S. L. Rolston, R. J. C. Spreeuw, and P. S. Jessen, *Adiabatic cooling of cesium to 700nk in an optical lattice*, Phys. Rev. Lett. **74** (1995), 1542, ⊙.

[702] H. Katori, T. Ido, Y. Isoya, and M. Kuwata-Gonokami, *Magneto-optical trapping and cooling of strontium atoms down to the photon recoil temperature*, Phys. Rev. Lett. **82** (1999), 1116, DOI.

[703] G. W. Kattawar and G. N. Plass, *Electromagnetic scattering from absorbing spheres*, Appl. Opt. **6** (1967), 1377, ⊙.

[704] G. M. Kavoulakis and C. J. Pethick, *Quasi-one-dimensional character of sound propagation in elongated Bose-Einstein condensed clouds*, Phys. Rev. A **58** (1998), 1563.

[705] J. Keaveney, A. Sargsyan, U. Krohn, I. G. Hughes, D. Sarkisyan, and C. S. Adams, *Cooperative lamb shift in an atomic vapor layer of nanometer thickness*, Phys. Rev. Lett. **108** (2012), 173601, DOI.

[706] A. J. Kerman, J. M. Sage, S. Sainis, T. Bergeman, and D. DeMille, *Production and state-selective detection of ultracold RbCs molecules*, Phys. Rev. Lett. **92** (2004), 153001, ⊙.

[707] ———, *Production of ultracold, polar RbCs molecules via photoassociation*, Phys. Rev. Lett. **92** (2004), 033004, ⊙.

[708] W. Ketterle, *Comment on 'electromagnetic wave dynamics in matter-wave superradiant scattering'*, Phys. Rev. Lett. **106** (2011), 118901, ⊙DOI.

[709] W. Ketterle, A. P. Chikkatur, and C. Raman, *Collective enhancement and suppression in Bose-Einstein condensates*, **551** (2000), 337, ⊙DOI.

[710] W. Ketterle and N. J. Van Druten, *Bose-Einstein condensation of a finite number of particles trapped in one or three dimensions*, Phys. Rev. A **54** (1996), 656.

[711] ———, *Evaporative cooling of trapped atoms*, Adv. At. Mol. Opt. Phys. **37** (1996), 181, ⊙.

[712] W. Ketterle, D. S. Durfee, and D. M. Stamper-Kurn, *Making, probing and understanding Bose-Einstein condensates*, Proc. Int. School of Phys. Enrico Fermi **CXL** (1999), 67, ⊙.

[713] W. Ketterle and Shin Inouye, *Does matter wave amplification work for fermions?*, Phys. Rev. Lett. **86** (2001), 4203, ⊙DOI.

[714] W. Ketterle and H.-J. Miesner, *Coherence properties of bose condensates and atom lasers*, Phys. Rev. A **56** (1997), 3291, ⊙.

[715] A. Kevin, E. Strecker, Guthrie, B. Partridge, Andrew, G. Truscott, and Randall G. Hulet, *Formation and propagation of matter-wave soliton trains*, Nature **417** (2002), 150.

[716] W. F. Kielhorn, *A technique for measurement of vector and tensor polarization in solid spin one polarized targets*, Ph.D. thesis, University of Texas at Austin, 1991, ⊙DOI.

[717] A. H. Kiilerich and et al., Phys. Rev. A **92** (2015), 032124.

[718] H. J. Kimble and L. Mandel, *Resonance fluorescence with excitation of finite bandwidth*, Phys. Rev. A **15** (1977), 689, ⊙.

[719] J. Kinnunen, M. Rodríguez, and P. Törmä, *Pairing gap and in-gap excitations in trapped fermionic superfluids*, Science **305** (2005), 1131, ⊙.

[720] T. Kinoshita, T. Wenger, and D. S. Weiss, *Observation of a one-dimensional Tonks-Girardeau gas*, Science **305** (2004), 1125.

[721] ———, *A quantum newton's cradle*, Nature **440** (2006), 900, DOI.

[722] K. Kirsten and D. J. Toms, *Bose-Einstein condensation of atomic gases in a general harmonic-oscillator confining potential trap*, Phys. Rev. A **54** (1996), 4188.

[723] P. Kirton, M. M. Roses, J. Keeling, and E. G. Dalla Torre, *Introduction to the Dicke model: From equilibrium to nonequilibrium, and vice versa*, Adv. Quantum Technol. **2** (2019), 1800043, ⊙DOI.

[724] M. Kitagawa and M. Ueda, *Squeezed spin states*, Phys. Rev. A **47** (1993), 5138, ⊙DOI.

[725] J. Kitching, S. Knappe, and E. A. Donley, *Atomic sensors - a review*, IEEE Sensors J. **11** (2011), 1749, ⊙DOI.

[726] C. Kittel, *Elementary statistical physics*, John Wiley and Sons, 1976, ISBN.

[727] J. Klaers, J.Schmitt, F. Vewinger, and M. Weitz, *Bose-Einstein condensation of photons in an optical microcavity*, eprints **1007.4088** (1999), ⊙.

[728] B. G. Klappauf, W. H. Oskay, D. A. Steck, and M. G. Raizen, *Observation of noise and dissipation effects on dynamical localization*, Phys. Rev. Lett. **81** (1998), 1203.

[729] ———, *Quantum chaos with cesium atoms: pushing the boundaries*, Physica D **131** (1999), 78, ⊙.

[730] B. Kneer, T. Wong, K. Vogel, W. P. Schleich, and D. F. Walls, *Generic model of an atom laser*, Phys. Rev. A **58** (1998), 4841, ⊙.

[731] A. F. Kockum, A. Miranowicz, S. De Liberato, S. Savastra, and F. Nori, *Ultrastrong coupling between light and matter*, Nature Rev. Phys. **1** (2019), 19, ⊙DOI.

[732] B. Koczor, R. Zeier, and S. J. Glaser, *Continuous phase-space representations for finite-dimensional quantum states and their tomography*, Phys. Rev. A **101** (2020), 022318, ⊙DOI.

[733] A. F. Koenderink and W. L. Vos, *Light exiting from real photonic band gap crystals is diffuse and strongly directional*, Phys. Rev. Lett. **91** (2003), 213902.

[734] H. Kogelnik and X. Y. Li, *Laser beams and resonators*, Appl. Opt. **5** (1966), 1550, DOI.

[735] M. Köhl, H. Moritz, T. Stöferle, K. Günter, and T. Esslinger, *Fermionic atoms in a three dimensional optical lattice: Observing Fermi surfaces, dynamics, and interactions*, Phys. Rev. Lett. **94** (2005), 080403, ⊙.

[736] S. J. J. M. F. Kokkelmans, G. V. Shlyapnikov, and C. Salomon, *Degenerate atom-molecule mixture in a cold Fermi gas*, Phys. Rev. A **69** (2004), 031602R, ⊙.

[737] S. J. J. M. F. Kokkelmans, B. J. Verhaar, and K. Gibble, *Prospects for Bose-Einstein condensation in cesium*, Phys. Rev. Lett. **81** (1998), 951, ⊙.

[738] S. J. J. M. F. Kokkelmans, H. M. J. Vissers, and B. J. Verhaar, *Formation of a bose condensate of stable molecules via a Feshbach resonance*, Phys. Rev. A **63** (2001), 031601(R), ⊙.

[739] V. Kokoouline, O. Dulieu, R. Kosloff, and F. Masnou-Seeuws, *Mapped fourier methods for long-range molecules: Application to perturbations in the $Rb_2(0_u^+)$ photoassociation spectrum*, J. Chem. Phys. **110** (1999), 9865, ⊙.

[740] C. Kollath, , and U. Schollwöck, *Cold Fermi gases: a new perspective on spin-charge separation*, New J. Phys. **8** (2006), 220, ⊙.

[741] K. Kopitzky, *Einführung in die festkörperphysik*, Teubner, 1986, ISBN.

[742] S. A. Koppell, Y. Israel, A. J. Bowman, B. B. Klopfer, and M. A. Kasevich, *Transmission electron microscopy at the quantum limit*, Appl. Phys. Lett. **120** (2021), 190502, ⊙DOI.

[743] M. Korek, A. R. Allouche, M. Kobeissi, A. Chaalan, M. Dagher, K. Fakherddin, and M. Aubert-Frécon, Chem. Phys. **256** (2000), 1.

[744] S. Kotochigova, P. S. Julienne, and E. Tiesinga, *Ab initio calculation of the KRb dipole moments*, Phys. Rev. A **68** (2003), 022501.

[745] S. Kotochigova, E. Tiesinga, and P. S. Julienne, *Photoassociative formation of ultracold polar krb molecules*, Eur. Phys. J. D **31** (2004), 189, ⊙.

[746] M. Kozuma, L. Deng, E. W. Hagley, J. Wen, R. Lutwak, K. Helmerson, S. L. Rolston, and W. D. Phillips, *Coherent splitting of Bose-Einstein condensed atoms with optically induced bragg diffraction*, Phys. Rev. Lett. **82** (1999), 871.

[747] M. Kozuma, Y. Imai, K. Nakagawa, and M. Ohtsu, *Observation of transient response of recoil-induced resonance: A method for the measurement of atomic motion in an optical standing wave*, Phys. Rev. A **52** (1995), R3421, ⊙.

[748] M. Kozuma, K. Nakagawa, W. Jhe, and M. Ohtsu, *Observation of temporal behavior of an atomic wavepacket localized in an optical potential*, Phys. Rev. Lett. **76** (1996), 2428, ⊙.

[749] M. Kozuma, Y. Suzuki, Y. Torii, T. Saguira, T. Kaga, E. W. Hagley, and L. Deng, *Phase-coherent amplification of matter-waves*, Science **286** (1999), 2309, ⊙.

[750] T. Kraemer, M. Mark, P. Waldburger, J. G. Danzl, C. Chin, B. Engeser, A. D. Lange, K. Pilch, A. Jaakkola, H.-C. Nägerl, and R. Grimm, *Evidence for Efimov quantum states in an ultracold gas of cesium atoms*, Nature **428** (2005), 155.

[751] Hendrik A. Kramers, *Wellenmechanik und halbzählige quantisierung*, Zeitschrift für Physik **39** (1926), 828.

[752] J. Krause, M. O. Scully, and H. Walther, *Quantum theory of the micromaser: Symmetry breaking via off-diagonal atomic injection*, Phys. Rev. A **34** (1986), 2032.

[753] H. N. S. Krishnamoorthy, Z. Jacob, E. Narimanov, I. Kretzschmar, and V. M. Menon, *Topological transitions in metamaterials*, Science **336** (2012), 205.

[754] D. Kruse, M. Ruder, J. Benhelm, C. von Cube, C. Zimmermann, Ph. W. Courteille, B. Nagorny, Th. Elsässer, and A. Hemmerich, *Cold atoms in a high-q ring-cavity*, Phys. Rev. A **67** (2003), 051802(R).

[755] D. Kruse, C. von Cube, C. Zimmermann, and Ph. W. Courteille, *Observation of lasing mediated by collective atomic recoil*, Phys. Rev. Lett. **91** (2003), 183601.

[756] R. Kubo, *Generalized cumulant expansion method*, J. Phys. Soc. Jap. **17** (1962), 1100, ⊙DOI.

[757] T. Kuga, Y. Torii, N. Shiokawa, T. Hirano, Y. Shimizu, and H. Sasada, *Novel optical trap of atoms with a doughnut beam*, Phys. Rev. Lett. **78** (1997), 4713, ⊙.

[758] A. Kuhn, M. Hennrich, and G. Rempe, *Deterministic single-photon source for distributed quantum networking*, Phys. Rev. Lett. **89** (2002), 067901.

[759] K. Kumar, Proc. R. Soc. London A **452** (1996), 1113.

[760] G. Kurizki and A. Z. Genack, *Suppression of molecular interactions in periodic dielectric structures*, Phys. Rev. Lett. **61** (1988), 2269.

[761] G. Kurizki, M. O. Scully, and C. Keitel, *Free-electron lasing without inversion by interference of momentum states*, Phys. Rev. Lett. **70** (1993), 1433, ⊙.

[762] A. Kuzmich, A. Dogariu an L. J. Wang, D. W. Milonni, and R. Y. Chiao, *Signal velocity, causality, and quatum noise in superluminal light pulse propagation*, Phys. Rev. Lett. **86** (2001), 3925, ⊙.

[763] A. Kuzmich, L. Mandel, and N. P. Bigelow, *Generation of spin squeezing via continuous quantum nondemolition measurement*, Phys. Rev. Lett. **85** (2000), 1594, ⊙DOI.

[764] P. Kwiat, H. Weinfurter, Th. Herzog, A. Zeilinger, and M. A. Kasevich, *Interaction-free measurement*, Phys. Rev. Lett. **74** (1995), 4763, ⊙DOI.

[765] P. Kwiat, A. G. White, J. R. Mitchell, O. Nairz, G. Weihs, H. Weinfurter, and A. Zeilinger, *High-efficiency quantum interrogation measurements via the quantum zeno effect*, Phys. Rev. Lett. **83** (1999), 4725, ⊙DOI.

[766] C. C. Kwong, T. Yang, M. S. Pramod, K. Pandey, D. Delande, R. Pierrat, and D. Wilkowski, *Cooperative emission of a coherent superflash of light*, Phys. Rev. Lett. **113** (2014), 223601, ⊙DOI.

[767] G. Labeyrie, C. Miniatura, and R. Kaiser, *Large faraday rotation of resonant light in a cold atomic cloud*, Phys. Rev. A **64** (2000), 033402, quant-ph/0103045.

[768] G. Labeyrie, C. A. Müller, D. S. Wiersma, Ch. Miniatura, and R. Kaiser, *Observation of coherent backscattering of light by cold atoms*, J. Opt. B **2** (2000), 672, ⊙.

[769] A. Lakhtakia, *Positive and negative Goos-Hänchen shifts and negative phase-velocity mediums (alias left-handed materials)*, ePrints:Physics0305133 (2003), ⊙.

[770] W. E. Jr. Lamb, *Anti-photon*, Appl. Phys. B **60** (1995), 77, ⊙DOI.

[771] P. Lambropoulos, G. M. Nikolopoulo, T. R. Nielsen, and S. Bay, *Fundamental quantum optics in structured reservoirs*, Rep. Progr. Phys. **63** (1966), 455, ⊙DOI.

[772] L. D. Landau, Butterworth-Heinemann, 1937, ISBN.

[773] R. Landauer, *Inadequacy of entropy and entropy derivatives in characterizing the steady state*, Phys. Rev. A **12** (1975), 636.

[774] A. Landragin, G. Labeyrie, R. Kaiser, N. Vansteenkiste, C. I.Westbrook, and A. Aspect, *Specular versus diffuse reflection of atoms from an evanescent wave from mirror*, Opt. Lett. **21** (1996), 1591.

[775] C. K. Law and N. P. Bigelow, *Amplifying an atomic wave signal using a Bose-Einstein condensate*, Phys. Rev. A **58** (1998), 4791.

[776] J. Lawall, S. Kulin, B. Saubamea, N. Bigelow, M. Leduc, and C. Cohen-Tannoudji, *Three-dimensional laser cooling of helium beyond the single-photon recoil limit*, Phys. Rev. Lett. **75** (1995), 4194.

[777] M. Lax, W. H. Louisell, and W. B. McKnight, *From maxwell to paraxial wave optics*, Phys. Rev. A **11** (1975), 1365, ⊙.

[778] L. J. LeBlanc, M. C. Beeler, K. Jiménez-García, A. R. Perry, S. Sugawa, R. A. Williams, and I. B. Spielman, *Direct observation of zitterbewegung in a Bose-Einstein condensate*, New. J. Phys. **15** (2013), 073011, ⊙.

[779] M. Lebugle, M. Gräfe, R. Heilmann, A. Perez-Leija, S. Nolte, and A. Szameit, *Experimental observation of n00n state Bloch oscillations*, Nature Comm. **6** (2015), 8273, ⊙DOI.

[780] E. S. Lee, C. Geckeler, J. Heurich, A. Gupta, K.-I. Cheong, S. Secrest, and P. Meystre, *Dark states of dressed Bose-Einstein condensates*, Phys. Rev. A **60** (1999), 4006, ⊙.

[781] H. J. Lee, C. S. Adams, M. Kasevich, and S. Chu, *Raman cooling of atoms in an optical dipole trap*, Phys. Rev. Lett. **76** (1996), 2658, ⊙.

[782] Ji-Woo Lee, Min-Chul Cha, and Doochul Kim, *Phase diagram of a disordered boson Hubbard model in two dimensions*, Phys. Rev. Lett. **87** (2001), 247006, ⊙.

[783] P. J. Lee, M. Anderlini, B. L. Brown, J. Sebby-Strabley, W. D. Phillips, and J. V. Porto, *Sublattice addressing and spin-dependent motion of atoms in a double-well lattice*, Phys. Rev. Lett. **99** (2007), 020402, ⊙DOI.

[784] A. J. Leggett, *Cooper pairing in spin-polarized Fermi systems*, J. Phys. C (Paris) **41** (1980), 7.

[785] ———, *Bose-Einstein condensation in the alkali gases: Some fundamental concepts*, Rev. Mod. Phys. **73** (2001), 307.

[786] R. H. Lehmberg, *Radiation from an n-atom system. i. general formalism*, Phys. Rev. A **3** (1970), 883, ⊙DOI.

[787] G. Lenz, P. Meystre, and E. M. Wright, *Non-linear atom optics*, Phys. Rev. Lett. **71** (1993), 3271, ⊙.

[788] J. Léonard, A. Morales, Ph. Zupancic, T. Esslinger, and T. Donner, *Supersolid formation in a quantum gas breaking continuous translational symmetry*, Nature **543** (2016), 87, ⊙DOI.

[789] U. Leonhardt, *Quantum physics of simple optical instruments*, Rep. Progr. Phys. **66** (2003), 1207, ⊙DOI.

[790] ———, *Optical conformal mapping*, Science **312** (2006), 1777, ⊙.

[791] U. Leonhardt and H. Paul, *Measuring the quantum state of light*, Prog. Quant. Electr. **19** (1995), 89, ⊙.

[792] U. Leonhardt and P. Piwnicki, *Relativistic effects of light in moving media with extremely low group velocity*, Phys. Rev. Lett. **85** (2000), 822, ⊙.

[793] I. D. Leroux, M. H. Schleier-Smith, and V. Vuletic, *Implementation of cavity squeezing of a collective atomic spin*, Phys. Rev. Lett. **104** (2010), 073602, ⊙DOI.

[794] P. Lesage and C. Au doin, *Characterization and measurement of time and frequency stability*, Radio Science (1979).

[795] M. D. Levenson and G. L. Eesley, *Polarization selective optical heterodyne detection for dramatically improved sensitivity in laser spectroscopy*, Appl. Phys. **19** (1979), 1.

[796] I.N. Levine, *Quantum chemistry 5th ed.*, Prentice-Hall Of India Pvt. Limited, 2006, ISBN.

[797] M. Lewenstein and Juha Javanainen, *Cooperative quantum jumps with two atoms*, Phys. Rev. Lett. **59** (1987), 1289, ⊙.

[798] M. Lewenstein, L. Santos, M. A. Baranov, and H. Fehrmann, *Atomic Bose-Fermi mixtures in an optical lattice*, Phys. Rev. Lett. **92** (2004), 50401, ⊙.

[799] Zeyang Li, B. Braverman, S. Colombo, Chi Shu, A. Kawasaki, A. F. Adiyatullin, E. Pedrozo-Penafiel, E. Mendez, and V. Vuletic, *Collective spin-light and light-mediated spin-spin interactions in an optical cavity*, Phys. Rev. X **3** (2022), 020308, ⊙DOI.

[800] W. Lichten, *Precise wavelength measurements and optical phase shifts: I. general theory*, J. Opt. Soc. Am. A **2** (1985), 1869, ⊙.

[801] T. K. Lim, S. K. Duffy, and W. C. Damert, *Efimov states in the 4he trimer*, Phys. Rev. Lett. **38** (1977), 341, ⊙.

[802] Jia Ling Lin and J. P. Wolfe, *Bose-Einstein condensation of paraexcitons in stressed Cu2O*, Phys. Rev. Lett. **71** (1993), 1222, ⊙.

[803] G.-L. Lippi, G. P. Barozzi, S. Barbay, and J. R. Tredicce, *Spontaneous generation of a longitudinal atomic density grating in sodium vapor*, Phys. Rev. Lett. **76** (1996), 2452, ⊙.

[804] Ch. Lisdat, O. Dulieu, H. Knöckel, and E. Tiemann, *Inversion analysis of k2 coupled electronic states with the fourier grid method*, Eur. Phys. J. D **17** (2001), 319, ⊙.

[805] Haonan Liu, S. B. Jäger, Xianquan Yu, S. Touzard, A. Shankar, M. J. Holland, and T. L. Nicholson, *Rugged mhz-linewidth superradiant laser driven by a hot atomic beam*, Phys. Rev. Lett. **125** (2020), 253602.

[806] Zhixin Liu and R. Slávik, *Optical injection locking: From principle to applications*, J. Lightwave Techn. **38** (2020), 43.

[807] Zhixin Liu and Radan Slavík, *Optical injection locking: From principle to applications*, J. Lightwave Tech. **38** (2020), 43.

[808] T. Loftus, J. R. Bochinski, and T. W. Mossberg, *Magnetic trapping of ytterbium and the alkaline-earth metals*, Phys. Rev. A **66** (2002), 013411, ⊙DOI.

[809] T. H. Loftus, T. Ido, M. M. Boyd, A. D. Ludlow, and Jun Ye, *Narrow line cooling and momentum-space crystals*, Phys. Rev. A **70** (2004), 063413, ⊙DOI.

[810] _____, *Narrow line cooling finite photon recoil dynamics*, Phys. Rev. Lett. **93** (2004), 073003, ⊙DOI.

[811] Huanqian Loh, Yu-Ju Lin, I. Teper, M. Cetina, J. Simon, J. K. Thompson, and V. Vuletic, *Influence of grating parameters on the linewidths of external-cavity diode lasers*, Appl. Opt. **45** (2008), 9191, ⊙.

[812] F. London, *On the Bose-Einstein condensation*, Nature **54** (1938), 947.

[813] P. Longo and J. Evers, *Far-field signatures of a two-body bound state in collective emission from interacting two-level atoms on a lattice*, Phys. Rev. Lett. **112** (2014), 193601.

[814] D. Loss and D. P. DiVincenzo, *Quantum computation with quantum dots*, Phys. Rev. A **57** (1998), 120, ⊙DOI.

[815] H. K. Lotsch, *Beam displacement at total reflection: The Goos-Hänchen effect*, Optik **2** (1970), 116.

[816] R. Loudon, *The quantum theory of light*, Clarendon Press Oxford, 1982, ISBN.

[817] R. Loudon, S. M. Barnett, and C. Baxter, *Radiation pressure and momentum transfer in dielectrics: The photon drag effect*, Phys. Rev. A **71** (2005), 063802, ⊙.

[818] R. Loudon and P. L. Knight, *Squeezed light*, J. Mod. Opt. **34** (1987), 709.

[819] R. V. E. Lovelace, C. Mehanian, T. J. Tommila, and D. M. Lee, *Magnetic confinement of a neutral gas*, Nature **318** (1985), 30.

[820] W. T. Lu and S. Sridhar, *Flat lens without optical axis: Theory of imaging*, Opt. Exp. **13** (2005), 10673.

[821] A. D. Ludlow, S. Blatt, T. Zelevinsky, G. K. Campbell, M. J. Martin, J. W. Thomsen, M. M. Boyd, and J. Ye, *Ultracold strontium clock: Applications to the measurement of fundamental constant variations*, Eur. Phys. J. Special Topics **163** (2008), 9, ⊙DOI.

[822] L. A. Lugiato, A. Gatti, and E. Brambilla, *Quantum imaging*, J. Opt. B: Quantum Semiclass. Opt. **4** (2002).

[823] M. D. Lukin and P. R. Hemmer, *Quantum entanglement via optical control of atom-atom interactions*, Phys. Rev. Lett. **84** (2000), 2818, ⊙.

[824] Chiyan Luo, S. G. Johnson, and J. D. Joannopoulos, *All-angle negative refraction in a three-dimensionally periodic photonic crystal*, Appl. Phys. Lett. **81** (2002), 2352, ⊙.

[825] Chiyan Luo, S. G. Johnson, J. D. Joannopoulos, and J. B. Pendry, *All-angle negative refraction without negative effective index*, Phys. Rev. B **65** (2002), 201104(R), ⊙.

[826] ———, *Negative refraction without negative index in metallic photonic crystals*, Opt. Exp. **11** (2003), 00746, ⊙.

[827] ———, *Subwavelength imaging in photonic crystals*, Phys. Rev. B **68** (2003), 045115, ⊙.

[828] T. Luu and A. Schwenk, *Three-fermion problems in optical lattices*, Phys. Rev. Lett. **98** (2007), 103202, ⊙.

[829] J. E. Lye, L. Fallani, M. Modugno, D. Wiersma, C. Fort, and M. Inguscio, *A Bose-Einstein condensate in a random potential*, (2004), cond-mat/0412167.

[830] L. S. Ma, Ph. W. Courteille, G. Ritter, W. Neuhauser, and R. Blatt, *Spectroscopy of te_2 with modulation transfer: Reference lines for precision spectroscopy in yb*, Appl. Phys. B **57** (1993), 159.

[831] L. S. Ma and J. L. Hall, *Optical heterodyne spectroscopy enhanced by an external optical cavity: Toward improved working standards*, IEEE J. Quant. Electr. **26** (1990), 2006.

[832] M. Mackie, X. Kowalski, and J. Javanainen, *Bose-stimulated Raman adiabatic passage in photoassociation*, Phys. Rev. Lett. **84** (2000), 3803, ⊙.

[833] K. M. Madison, F. Chevy, W. Wohlleben, and J. Dalibard, *Vortex formation in a stirred Bose-Einstein condensate*, Phys. Rev. Lett. **84** (1999), 806, ⊙.

[834] ———, *Vortex lattices in a stirred Bose-Einstein condensate*, (1999), cond-mat/0004037.

[835] Th. Maier, S. Kraemer, L. Ostermann, and H. Ritsch, *A superradiant clock laser on a magic wavelength optical lattice*, Opt. Exp. **22** (2014), 13269, ⊙DOI.

[836] J. T. Manassah, *The dynamical cooperative lamb shift in a system of two-level atoms*, Phys. Rev. A **81** (2009), 063822, ⊙DOI.

[837] M. W. Mancini, G. D. Telles, A. R. L. Caires, V. S. Bagnato, and L. G. Marcassa, *Observation of ultracold ground-state heteronuclear molecules*, Phys. Rev. Lett. **92** (2004), 133203.

[838] E. Mandonnet, R. Dum, A. Minguzzi, I. Carusotto, Y. Castin, and J. Dalibard, *Evaporative cooling of an atomic beam*, Eur. Phys. J. D **10** (2000), 9.

[839] H. Mann, H. Schiffelgen, and R. Froriep, *Einführung in die regelungstechnik*, Hanser-Verlag München, 2009, ISBN.

[840] T. Manovitz, Yotam Shapira, Lior Gazit, Nitzan Akerman, and Roee Ozeri, *Trapped-ion quantum computer with robust entangling gates and quantum coherent feedback*, Phys. Rev. X Quantum **3** (2022), 010347, ⊙DOI.

[841] M. Mansuripur, *Resolution of the abrahamï¿½minkowski controversy*, Opt. Comm **283** (2010), 1997.

[842] O. M. Maragò, G. Hechenblaikner, E. Hodby, and C. J. Foot, *Temperature dependence of damping and frequency shifts of the scissors mode of a trapped Bose-Einstein condensate*, Phys. Rev. Lett. **86** (2001), 3938, ⊙.

[843] O. M. Maragò, S. A. Hopkins, J. Arlt, E. Hodby, G. Hechenblaikner, and C. J. Foot, *Observation of the scissors mode and evidence for superfluidity of a trapped Bose-Einstein condensed gas*, Phys. Rev. Lett. **84** (2000), 2056, ⊙.

[844] M. Marinescu, *Computation of the scattering length and effective range in molecular physics*, Phys. Rev. A **50** (1994), 3177, ⊙.

[845] M. Marinescu and H. R. Sadeghpour, *Long-range potentials for two-species alkali-metal atoms*, Phys. Rev. A **59** (1999), 390, ⊙.

[846] M. Marini, F. Pistolesi, and G. C. Strinati, *Evolution from bcs superconductivity to bose condensation: Analytic results for the crossover in three dimensions*, Eur. Phys. J. B **1** (1998), 151, ⊙.

[847] C. Clay Marston and G. G. Balint-Kurti, *The fourier grid hamiltonian method for bound state eigenvalues and eigenfunctions*, J. Chem. Phys. **91** (1989), 3571, ⊙.

[848] A. G. Martin, K. Helmerson, V. S. Bagnato, G. P. Lafyatis, and D. E. Pritchard, *Rf spectroscopy of trapped neutral atoms*, Phys. Rev. Lett. **61** (1988), 2431, ⊙.

[849] J. L. Martin, C. R. McKenzie, N. R. Thomas, J. C. Sharpe, D. M. Warrington, P. J. Manson, W. J. Snadle, and A. C. Wilson, *Output coupling of a Bose-Einstein condensate formed in a top trap*, J. Phys. B. **32** (1999), 3065.

[850] P. J. Martin, B. G. Oldaker, A. H. Miklich, and D. E. Pritchard, *Bragg scattering of atoms from a standing light wave*, Phys. Rev. Lett. **60** (1988), 515.

[851] N. Marzari, A. A. Mostofi, J. R. Yates, I. Souza, and D. Vanderbilt, *Maximally localized wannier functions: Theory and applications*, Rev. Mod. Phys. **84** (2012), 1419, DOI.

[852] K.-P. Marzlin, Weiping Zhang, and Barry C. Sanders, *Creation of skyrmions in a spinor Bose-Einstein condensate*, Phys. Rev. A **62** (2000), 13602, ⊙.

[853] C. Marzok, B. Deh, S. Slama, C. Zimmermann, and Ph. W. Courteille, *In situ Ramsey interferometry and diffraction echo with an ultracold Fermi gas*, Phys. Rev. A **78** (2008), 021602(R), ⊙DOI.

[854] Ch. Maschler and H. Ritsch, *Cold atom dynamics in a quantum optical lattice potential*, Phys. Rev. Lett. **95** (2005), 260401, DOI.

[855] N. Masuhara, J. M. Doyle, J. C. Sandberg, D. Kleppner, T. J. Greytak, H. F. Hess, and G. P. Kochanski, *Evaporative cooling of spin-polarized atomic hydrogen*, Phys. Rev. Lett. **61** (1988).

[856] M. R. Matthews, B. P. Anderson, P. C. Haljan, D. S. Hall, M. J. Holland, J. E. Williams, C. E. Wieman, and E. A. Cornell, *Watching a superfluid untwisting itself*, Phys. Rev. Lett. **83** (1999), 3358, ⊙.

[857] M. R. Matthews, B. P. Anderson, P. C. Haljan, D. S. Hall, C. E. Wieman, and E.A. Cornell, *Vortices in a Bose-Einstein condensate*, Phys. Rev. Lett. **83** (1999), 2498, ⊙.

[858] M. R. Matthews, D. S. Hall, D. S. Jin, J. R. Ensher, C. E. Wieman, E. A. Cornell, F. Dalfovo, C. Minnitti, and S. Stringari, *Dynamical response of a Bose-Einstein condensate to a discontinuous change in internal state*, Phys. Rev. Lett. **81** (1998), 243, ⊙.

[859] C. E. Máximo, N. Piovella, Ph. W. Courteille, R. Kaiser, and R. Bachelard, *Spatial and temporal localization of light in two dimensions*, Phys. Rev. A **92** (2015), 062702.

[860] T. Mayer-Kuckuk, *Atomphysik*, Teubner Studienbücher, 1985, ISBN.

[861] I. E. Mazets, *Ground state of a Bose-Einstein condensate which scatters coherently laser radiation*, Euro. Phys. J. D **8** (2000), 371.

[862] ———, *Incoherent scattering of light by a Bose-Einstein condensate of interacting atoms*, (2000), quant-ph/0003126.

[863] D. McGloin and K. Dholakia, *Bessel beams: Diffraction in a new light*, Contemporary Physics **46** (2005), 15.

[864] A. R. McGurn, K. T. Christensen, F. M. Mueller, and A. A. Maradudin, *Anderson localization in one-dimensional randomly disordered optical systems that are periodic on average*, Phys. Rev. B **47** (1993), 13120, ⊙.

[865] D. R. Meacher, D. Boiron, H. Metcalf, C. Salomon, and G. Grynberg, *Method for velocimetry of cold atoms*, Phys. Rev. A **50** (1994), R1992, ⊙.

[866] D. M. Meekhof, C. Monroe, B. E. King, W. M. Itano, and D. J. Wineland, *Generation of nonclassical motional states of a trapped atom*, Phys. Rev. Lett. **76** (1996), 1797, ⊙.

[867] S. Y. T. Meerakker and et. al., *Direct measurement of the radiative lifetime of vibrationally excited oh radicals*, Phys. Rev. Lett. **95** (2005), 013003, ⊙.

[868] D. Meiser, Jun Ye, D. R. Carlson, and M. J. Holland, *Prospects for a millihertz-linewidth laser*, Phys. Rev. Lett. **102** (2009), 163601, ⊙DOI.

[869] J. Meixner and F.W. Schäfke, *Mathieu'sche funktionen und sphäroidfunktionen*, Springer-Verlag Berlin (1954).

[870] I. B. Mekhov, V. S. Egorov, V. N. Lebedev, P. V. Moroshkin, I. A. Chekhonin, and S. N. Bagayev, *Strong light-matter coupling: parametric interactions in a cavity and free-space*, quant-ph/0607033 (2006), ⊙.

[871] I. V. Mekhov, C. Maschler, and H. Ritsch, *Cavity-enhanced light scattering in optical lattices to probe atomic quantum statistics*, Phys. Rev. Lett. **98** (2007), 100402, ⊙DOI.

[872] ———, *Light scattering from ultracold atoms in optical lattices as an optical probe of quantum statistics*, Phys. Rev. A **76** (2007), 053618, ⊙DOI.

[873] ———, *Probing quantum phases of ultracold atoms in optical lattices by transmission spectra in cavity quantum electrodynamics*, Nature Physics **3** (2007), 319, ⊙DOI.

[874] I. V. Mekhov and H. Ritsch, *Quantum nondemolition measurements and state preparation in quantum gases by light detection*, Phys. Rev. Lett. **102** (2008), 020403, ⊙.

[875] C. R. Menegatti, *Trap loss in a rubidium crossed dipole trap by short-range photoassociation*, Phys. Rev. A **87** (2013), 053404, ⊙.

[876] N. C. Menicucci, P. van Loock, M. Gu, C. Weedbrook, T. C. Ralph, and M. A. Nielsen, *Universal quantum computation with continuous-variable cluster states*, Phys. Rev. Lett. **97** (2006), 110501, ⊙DOI.

[877] C. Menotti, M. Krämer, OL. Pitaevskii, and S. Stringari, *Dynamic structure factor of a Bose-Einstein condensate in a one-dimensional optical lattice*, Phys. Rev. A **67** (2002), 053609, ⊙.

[878] C. Menotti and S. Stringari, *Collective oscillations in a one-dimensional trapped Bose-Einstein gas*, Phys. Rev. A **66** (2002), 043610, ⊙.

[879] K. M. Mertes, J. W. Merrill, R. Carretero-González, D. J. Frantzeskakis, P. G. Kevrekidis, and D. S. Hall, *Nonequilibrium dynamics and superfluid ring excitations in binary Bose-Einstein condensates*, Phys. Rev. Lett. **99** (2007), 190402, ⊙.

[880] H. J. Metcalf and P. Van der Straten, *Laser cooling and trapping*, Springer, 1999.

[881] M.-O. Mewes, M. R. Andrews, D. M. Kurn, D. S. Durfee, C. G. Townsend, and W. Ketterle, *Output coupler for Bose-Einstein condensed atoms*, Phys. Rev. Lett. **78** (1997), 582, ⊙.

[882] M.-O. Mewes, M. R. Andrews, N. J. van Druten, D. M. Kurn, D. S. Durfee, and W. Ketterle, *Bose-Einstein condensation in a tightly confining dc magnetic trap*, Phys. Rev. Lett. **77** (1996), 416, ⊙.

[883] M.-O. Mewes, M. R. Andrews, N. J. van Druten, D. M. Kurn, D. S. Durfee, C. G. Townsend, and W. Ketterle, *Collective excitations of a Bose-Einstein condensation in a magnetic trap*, Phys. Rev. Lett. **77** (1996), 988, ⊙.

[884] R. Meyer, *Trigonometric interpolation method for one-dimensional quantum-mechanical problems*, J. Chem. Phys. **52** (1969), 2053.

[885] V. Meyer, M. A. Rowe, D. Kielpinski, C. A. Sackett, W. M. Itano, C. Monroe, and D. J. Wineland, *Experimental demonstration of entanglement-enhanced rotation angle estimation using trapped ions*, Phys. Rev. Lett. **86** (2001), 5870, ⊙.

[886] P. Meystre and M. Sargent III, *Elements of quantum optics*, 2 ed., Springer-Verlag, Berlin Heidelberg, 1990, ISBN.

[887] P. G. Mickelson, Y. N. Martinez de Escobar, P. Anzel, B. J. DeSalvo, S. B. Nagel, A. J. Traverso, M. Yan, and T. C. Killian, *Repumping and spectroscopy of laser-cooled sr atoms using the $(5s5p)^3p_2$-$(5s4d)^3d_2$ transition*, J. Phys. B: At. Mol. Opt. Phys. **42** (2009), 235001, ⊙DOI.

[888] P. G. Mickelson, Y. N. Martinez de Escobar, M. Yan, B. J. DeSalvo, and T. C. Killian, *Bose-Einstein condensation of ^{88}sr through sympathetic cooling with ^{87}sr*, Phys. Rev. A **81** (2010), 051601(R), ⊙DOI.

[889] F. H. Mies, C. J. Williams, P. S. Julienne, and M. Krauss, *Estimating bounds on collisional relaxation rates of spin-polarized ^{87}Rb atoms at ultracold temperatures*, J. Res. Natl. Inst. Stand. Tech. **101** (1996), 521.

[890] H.-J. Miesner, D. M. Stamper-Kurn, M. R. Andrews, D. S. Durfee, S. Inouye, and W. Ketterle, *Bosonic stimulation in the formation of a Bose-Einstein condensate*, Science **279** (1998), 1005, ⊙.

[891] H.-J. Miesner, D. M. Stamper-Kurn, J. Stenger, S. Inouye, A. P. Chikkatur, and W. Ketterle, *Observation of metastable states in spinor Bose-Einstein condensates*, Phys. Rev. Lett. **82** (1999), 2228, ⊙.

[892] A. L. Migdall, J. V. Prodan, W. D. Phillips, T. H. Bergman, and H. J. Metcalf, *First observation of magnetically trapped neutral atoms*, Phys. Rev. Lett. **54** (1985), 2596.

[893] G. Milburn, *Intrinsic decoherence in quantum mechanics*, Phys. Rev. A **44** (1991), 5401, ⊙.

[894] D. E. Miller, *Critical velocity for superfluid flow across the BEC-BCS crossover*, Phys. Rev. Lett. **99** (2007), 070402, ⊙.

[895] J. D. Miller, R. A. Cline, and D. J. Heinzen, *Far-off-resonance optical trapping of atoms*, Phys. Rev. A **47** (1993), R4567, ⊙.

[896] Randell L. Mills, *The grand unified theory of classical quantum mechanics*, ISBN.

[897] P. W. Milonni, *The quantum vacuum: An introduction to quantum electrodynamics*, Academic, San Diego, 1994, ISBN.

[898] P. W. Milonni and R. W. Boyd, *Momentum of light in a dielectric medium*, Adv. Opt. Phot. **2** (2010), 519, ⊙.

[899] J. N. Milstein, S. J. J. M. F. Kokkelmans, and M. J. Holland, *Resonance theory of the cross-over from bardeen-cooper-schrieffer superfluidity to Bose-Einstein condensation in a dilute Fermi gas*, Phys. Rev. A **66** (2002), 043604, ⊙.

[900] F. Minardi, C. Fort, P. Maddaloni, M. Modugno, and M. Inguscio, *Time-domain atom interferometry across the threshold for Bose-Einstein condensation*, ePrints (2001), cond–mat/0103602, ⊙.

[901] Z. K. Minev, S. O. Mundhada, S. Shankar, P. Reinhold, R. Gutiérrez-JÃ¡uregui, R. J. Schoelkopf, M. Mirrahimi, H. J. Carmichael, and M. H. Devoret, *To catch and reverse a quantum jump mid-flight*, Nature **570** (2019), 200, ⊙DOI.

[902] B. Misra and E. C. G. Sudarshan, *The zeno paradox in quantum theory*, J. Math. Phys. **18** (1977), 756.

[903] F. Mivehvar, S. Ostermann, F. Piazza, and H. Ritsch, *Driven-dissipative supersolid in a ring cavity*, Phys. Rev. Lett. **120** (2018), 123601, ⊙DOI.

[904] J. Mlynek, V. Balykn, and P. Meystre, *"topical review"*, Appl. Phys. B **54** (1992).

[905] G. Modugno, G. Roati, F. Riboli, F. Ferlaino, R. J. Brecha, and M. Inguscio, *Collapse of a degenerate Fermi gas*, Science **297** (2002), 2240, ⊙.

[906] A. J. Moerdijk, B. J. Verhaar, and A. Axelsson, *Resonances in ultracold collisions of 6li, 7li, and 23na*, Phys. Rev. A **51** (1995), 4852, ⊙.

[907] A. J. Moerdijk, B. J. Verhaar, and T. M. Nagtegaal, *Collisions of dressed ground-state atoms*, Phys. Rev. A **53** (1996), 4343, ⊙.

[908] D. Mogilevtsev, F. A. Pinheiro, R. R. dos Santos, S. B. Cavalcanti, and L. E. Oliveira2, *Light propagation and anderson localization in disordered superlattices containing dispersive metamaterials effects of correlated disorder*, Phys. Rev. B **84** (2011), 094204, ⊙.

[909] M. Mohammad, Eunjong Kim, Xueyue Zhang, A. Sipahigil, P. B. Dieterle, A. J. Keller, A. Asenjo-Garcia, D. E. Chang, and O. Painter, *Cavity quantum electrodynamics with atom-like mirrors*, Nature **569** (2019), 692, ⊙DOI.

[910] B. R. Mollow, *Power spectrum of light scattered by two-level systems*, Phys. Rev. A **188** (1969), 1969.

[911] _____, *Stimulated emission and absorption near resonance for driven systems*, Phys. Rev. A **5** (1972), 2217.

[912] _____, *Pure-state analysis of resonant light scattering: Radiative damping, saturation, and multiphoton effects*, Phys. Rev. A **12** (1975), 1919.

[913] K. Mølmer, Y. Castin, and J. Dalibard, *Monte-carlo wave-function method in quantum optics*, J. Opt. Soc. Am. B **10** (1993), 524, ⊙DOI.

[914] C. Monroe, E. A. Cornell, C. A. Sackett, C. J. Myatt, and C. E. Wieman, *Measurement of cs-cs elastic scattering at t=30uk*, Phys. Rev. Lett. **70** (1993), 414, ⊙.

[915] Th. Monz, Ph. Schindler, J. T. Barreiro, M. Chwalla, D. Nigg, W. A. Coish, M. Harlander, W. Hänsel, M. Hennrich, and R. Blatt, *14-qubit entanglement: Creation and coherence*, Phys. Rev. Lett. **106** (2011), 130506, ⊙DOI.

[916] F. L. Moore, J. C. Robinson, C. F. Bharucha, B. Sundaram, and M. G. Raizen, *Atom optics realization of the quantum δ-kicked rotor*, Phys. Rev. Lett. **75** (1995), 4598, ⊙.

[917] M. G. Moore and P. Meystre, *Optical control and entanglement of atomic schrödinger fields*, Phys. Rev. A **59** (1999), 1754, ⊙DOI.

[918] _____, *Theory of superradiant scattering of laser light from Bose-Einstein condensates*, Phys. Rev. Lett. **83** (1999), 5202, ⊙.

[919] _____, *Atomic four-wave mixing: Fermions versus bosons*, Phys. Rev. Lett. **86** (2001), 4199, ⊙DOI.

[920] M. G. Moore, O. Zobay, and P. Meystre, *Quantum optics of a Bose-Einstein condensate coupled to a quantized light field*, Phys. Rev. A **60** (1999), 1491, ⊙DOI.

[921] S. A. Morgan, R. J. Ballagh, and K. Burnett, *Solitary-wave solutions to nonlinear schrödinger equations*, Phys. Rev. A **55** (1997), 4338, ⊙.

[922] O. Morice, Y. Castin, and J. Dalibard, *Refraction index of a dilute bose gas*, Phys. Rev. A **51** (1995), 3896.

[923] M. Morinaga, M. Yasuda, T. Kishimoto, F. Shimizu, J.-I. Fujita, and S. Matsui, *Holographic manipulation of a cold atom beam*, Phys. Rev. Lett. **77** (1996), 802, ⊙.

[924] H. Moritz, T. Stöferle, K. Günter, M. Köhl, and T. Esslinger, *Confinement induced molecules in a 1d Fermi gas*, Phys. Rev. Lett. **94** (2005), 210401, ⊙.

[925] N. V. Morrow, S. K. Dutta, and G. Raithel, *Feedback control of atomic motion in an optical lattice*, Phys. Rev. Lett. **88** (2002), 093003, ⊙DOI.

[926] O. Morsch, J. H. Müller, M. Cristiani, and E. Arimondo, *Coherent acceleration and Landau-Zener tunneling of Bose-Einstein condensates in 1-d optical lattices*, ePrints (2001), cond–mat/0103466, ⊙.

[927] A. Mosk, S. Jochim, H. Moritz, Th. Elsässer, and M. Weidemüller, *Resonator-enhanced optical dipol trap for fermionic lithium atoms*, Opt. Lett. **26** (2001), 1837.

[928] A. Mosk, S. Kraft, M. Mudrich, K. Singer, W. Wohlleben, R. Grimm, and M. Weidemüller, *Mixture of ultracold lithium and cesium atoms in an optical dipole trap*, Appl. Phys. B **73** (2001), 791, ⊙.

[929] N.F. Mott and H. S. W. Massey, *The atomic theory of atomic collisions i and ii*, Oxford Scientific Publications at the Clarendon Press, 1965, ISBN.

[930] M. Movre and G. Pichler, *Resonance interaction and self-broadening of alkali resonance lines i. adiabatic potential curves*, J. Phys. B **10** (1977), 2631, ⊙.

[931] G. M. Moy, J. J. Hope, and C. M. Savage, *Atom laser based on Raman transitions*, Phys. Rev. A **55** (1997), 3631.

[932] ———, *Born and markov approximations for atom lasers*, Phys. Rev. A **59** (1999), 667.

[933] G. M. Moy and C. M. Savage, *Output coupling for an atom laser by state change*, Phys. Rev. A **56** (1997), R1087.

[934] O. D. Mücke, R. Ell, A. Winter, Jung-Won Kim, J. R. Birge, L. Matos, and F. X. Kärtner, *Self-referenced 200 mhz octave-spanning ti:sapphire laser with 50 attosecond carrier-envelope phase jitter*, Opt. Exp. **13** (2005), 5163, ⊙.

[935] M. Mudrich, S. Kraft, K. Singer, R. Grimm, A. Mosk, and M. Weidemüller, *Sympathetic cooling with two atomic species in an optical trap*, Phys. Rev. Lett. **88** (2002), 253001.

[936] H. W. Mueller and et al., Phys. Rev. Lett. **78** (1997), 2357.

[937] T. Mukaiyama, H. Katori, T. Ido, Ying Li, and M. Kuwata-Gonokami, *Recoil-limited laser cooling of ^{87}sr atoms near the Fermi temperature*, Phys. Rev. Lett. **90** (2003), 113002, ⊙DOI.

[938] A. E. Muryshev, H. B. Van Linden Van Den Heuvell, and G. V. Shlyapnikov, *Stability of standing matter waves in a trap*, Phys. Rev. A **60** (1999), 2665, ⊙.

[939] C. J. Myatt, E. A. Burt, R. W. Ghrist, E. A. Cornell, and C. E. Wieman, *Production of two overlapping Bose-Einstein condensates by sympathetic cooling*, Phys. Rev. Lett. **78** (1997), 586, ⊙DOI.

[940] E. Pedrozo-Pe nafiel, S. Colombo, Chi Shu, A. F. Adiyatullin, Zeyang Li, E. Mendez, B. Braverman, A. Kawasaki, D. Akamatsu, Yanhong Xiao, and V. Vuletic, *Entanglement on an optical atomic-clock transition*, Nature **414** (2016), 588, ⊙DOI.

[941] S. B. Nagel, C. E. Simien, S. Laha, P. Gupta, V. S. Ashoka, and T. C. Killian, *Magnetic trapping of metastable $^3p_2$ atomic strontium*, Phys. Rev. A **67** (2003), 011401(R), ⊙DOI.

[942] B. Nagorny, Th. Elsässer, and A. Hemmerich, *Collective atomic motion in an optical lattice formed inside a high finesse cavity*, Phys. Rev. Lett. **91** (2003), 153003, ⊙.

[943] W. Nagourney, J. Sandberg, and H. G. Dehmelt, *Shelved optical electron amplifier: Observation of quantum jumps*, Phys. Rev. Lett. **56** (1986), 2797.

[944] K. Nakayama, Y. Yoshikawa, H. Matsumoto, Y. Torii, and T. Kuga, *Precise intensity correlation measurement for atomic resonance fluorescence from optical molasses*, Opt. Exp. **18** (2010), 6604.

[945] R. Napolitano, J. De Luca, V. S. Bagnato, and G. C. Marques, *Effect of finite numbers in the Bose-Einstein condensation of a trapped gas*, Phys. Rev. A **55** (1997), R3954, ⊙.

[946] A. Narayanaswamy and G. Chen, *Dyadic green's functions and electromagnetic local density of states*, J. Quant. Spectr. Rad. Transfer **111** (2009), 12, ⊙DOI.

[947] L. M. Narducci, H. M. Doss, P. Ru, M. O. Scully, S. Y. Zhu, and C. Keitel, *A simple model of a laser without inversion*, Opt. Comm. **81** (1991), 379, ⊙.

[948] N. R. Newbury, C. J. Myatt, E. A. Cornell, and C. E. Wieman, *Gravitational sisyphus cooling of 87rb in a magnetic trap*, Phys. Rev. Lett. **74** (1995), 2196, ⊙.

[949] Hyunchul Nha, Young-Tak Chough, and Kyungwon An, *A high phase-space-density gas of polar molecules*, Phys. Rev. A **62** (2000), 021801(R), ⊙DOI.

[950] G. Nicolis, G. Dewel, and P. Turner (Eds.) (eds.), *Can broken symmetry occur in driven systems?*, Order and Fluctuations in Equilbirium and Non-Equilibirum Statistical Mechanics, 2000.

[951] G. Nicolis and I. Prigogine, *Self-organization in non-equilibrium systems*, Wiley, 1977, ISBN.

[952] G. Nienhuis, *Theory of quantum jumps in three-level-atoms*, Phys. Rev. A **35** (1987), 4639, ⊙.

[953] G. Nienhuis, F. Schuller M., and Ducloy, *Nonlinear selective reflection from an atomic vapor at arbitrary incidence angle*, Phys. Rev. A **38** (1988), 5197, ⊙.

[954] T. Nikuni and A. Griffin, *Landau-khalatnikov two-fluid hydrodynamics of a trapped bose gas*, Phys. Rev. A **63** (2001), 033608.

[955] M. A. Norcia, J. R. K. Cline, J. P. Bartolotta, M. J. Holland, and J. K. Thompson, *Narrow-line laser cooling by adiabatic transfer*, New J. Phys. **20** (2018), 023021, ⊙DOI.

[956] M. A. Norcia, R. J. Lewis-Swan, J. R. K. Cline, Bihui Zhu, A. M. Rey, and J. K. Thompson, *Cavity-mediated collective spin-exchange interactions in a strontium superradiant laser*, Science **361** (2018), 259, ⊙DOI.

[957] M. A. Norcia and J. K. Thompson, *Cold-strontium laser in the superradiant crossover regime*, Phys. Rev. X **6** (2016), 011025, ⊙DOI.

[958] ———, *Strong coupling on a forbidden transition in strontium and nondestructive atom counting*, Phys. Rev. A **93** (2016), 023804, ⊙DOI.

[959] M. A. Norcia, M. N. Winchester, J. R. K. Cline, and J. K. Thompson, *Superradiance on the millihertz linewidth strontium clock transition*, Sci. Adv. **2** (2016), e:1601231, DOI.

[960] I. Nosske, L. Couturier, F. Hu, C. Tan, C. Qiao, J. Blume, Y. H. Jiang, Peng Chen, and M. Weidemüller, *Two-dimensional magneto-optical trap as a source for cold strontium atoms*, Phys. Rev. A **96** (2017), 053415, ⊙DOI.

[961] H. M. Nussenzveig, *Curso de física básica: Mecânica - vol 1*, 7 ed., Edgar Blucher, 2013, ISBN.

[962] ———, *Curso de física básica: Fluidos, oscilações e ondas, calor - vol 2*, 7 ed., Edgar Blucher, 2014, ISBN.

[963] ———, *Curso de física básica: Eletromagnetismo - vol 3*, 7 ed., Edgar Blucher, 2015, ISBN.

[964] ———, *Curso de física básica: ótica, relatividade e física quântica - vol 4*, 7 ed., Edgar Blucher, 2016, ISBN.

[965] N. Nygaard and K. Mølmer, *Component separation in harmonically trapped boson-fermion mixtures*, Phys. Rev. A **59** (1999), 2974, ⊙.

[966] K. M. OHara, S. R. Granade, M. E. Gehm, T. A. Savard, S. Bali, C. Freed, and J. E. Thomas, *Ultrastable co_2 laser trapping of lithium fermions*, Phys. Rev. Lett. **82** (1999), 4204.

[967] K. M. OHara, S. L. Hemmer, M. E. Gehm, S. R. Granade, and J. E. Thomas, *Observation of a strongly interacting degenerate Fermi gas of atoms*, Science **298** (2002), 2179, ⊙.

[968] M. Ö. Oktel and Ö. E. Müstecaplýoglu, *Electromagnetically induced left-handedness in a dense gas of three-level atoms*, Phys. Rev. A **70** (2004), 053806, ⊙DOI.

[969] H. Okuda and H. Sasada, *Huge transverse deformation in nonspecular reflection of a light beam possessing orbital angular momentum near critical incidence*, Opt. Exp. **14** (2006), 8393, ⊙.

[970] B. Olmos, D. Yu, Y. Singh, F. Schreck, K. Bongs, and I. Lesanovsky, *Long-range interacting many-body systems with alkaline-earth-metal atoms*, Phys. Rev. Lett. **110** (2013), 143602, ⊙DOI.

[971] M. Olshanii, *Atomic scattering in the presence of an external confinement and a gas of impenetrable bosons*, Phys. Rev. Lett. **81** (1998), 938, ⊙.

[972] S. Omanakuttan and T. J. Volkoff, *Spin-squeezed gottesman-kitaev-preskill codes for quantum error correction in atomic ensembles*, Phys. Rev. A **108** (2023), 022428, ⊙DOI.

[973] A. T. OŃeil, I. MacVicar, L. Allen, and M. J. Padgett, *Intrinsic and extrinsic nature of the orbital angular momentum of a light beam*, Phys. Rev. Lett. **88** (2002), 053601, ⊙.

[974] H. K. Onnes, *On the sudden rate at which the resistance of mercury disappears*, Akad. van Wetenschappen **14** (1911), 818.

[975] M. Onoda, S. Murakami, and N. Nagaosa, *Hall effect of light*, Phys. Rev. Lett. **93** (2004), 083901, ⊙.

[976] R. Onofrio, D. S. Durfee, C. Raman, M. Köhl, C. E. Kuklewicz, and W. Ketterle, *Surface excitations in a Bose-Einstein condensate*, Phys. Rev. Lett. **84** (2000), 810, ⊙.

[977] R. Onofrio and C. Presilla, *Reaching Fermi degeneracy in two-species optical dipole traps*, Phys. Rev. Lett. **89** (2002), 100401, ⊙.

[978] R. Onofrio, C. Raman, J. M. Vogels, J. Abo-Shaeer, A. P. Chikkatur, and W. Ketterle, *Observation of superfluid flow in a Bose-Einstein condensed gas*, Phys. Rev. Lett. **85** (2000), 2228, ⊙.

[979] P. P. Orth, R. Hennig, Ch. H Keitel, and J. Evers, *Negative refraction with tunable absorption in an active dense gas of atoms*, New J. Phys. **15** (2013), 013027, ⊙DOI.

[980] L. Ortiz-Gutiérrez, R. C. Teixeira, A. Eloy, D. Ferreira da Silva, R. Kaiser, R. Bachelard, and M. Fouché, *Mollow triplet in cold atoms*, New J. Phys. **21** (2019), 093019, ⊙DOI.

[981] ———, *Mollow triplet in cold atoms*, New J. Phys. **21** (2019), 093019, ⊙DOI.

[982] C. Orzel, A. K. Tuchman, M. L. Fenselau, M. Yasuda, and M. A. Kasevich, *Squeezed states in a Bose-Einstein condensate*, Science **291** (2001), 2386, ⊙.

[983] C. Ospelkaus, S. Ospelkaus, L. Humbert, P. Ernst, K. Sengstock, and K. Bongs, *Ultracold heteronuclear molecules in a 3d optical lattice*, Phys. Rev. Lett. **97** (2006), 120402, ⊙.

[984] C. Ospelkaus, S. Ospelkaus, K. Sengstock, and K. Bongs, *Interaction-driven dynamics of 40 k / 87 rb fermi-bose gas mixtures in the large particle number limit*, Phys. Rev. Lett. **96** (2005), 020401, ⊙.

[985] S. Ospelkaus, C. Ospelkaus, O. Wille, M. Succo, P. Ernst, K. Sengstock, and K. Bongs, *Localization of bosonic atoms by fermionic impurities in a 3d optical lattice*, Phys. Rev. Lett. **96** (2006), 180403, ⊙.

[986] S. Ospelkaus, A. Pe'er, K.-K. Ni, J. J. Zirbel, and B. Neyenhuis, *Ultracold dense gas of deeply bound heteronuclear molecules*, ePrints (2003), 0802.1093, ⊙.

[987] S. Ostermann, T. Griesser, and H. Ritsch, *Atomic self-ordering in a ring cavity with counterpropagating pump fields*, Europhys. Lett. **109** (2015), 43001.

[988] H. Ott, E. de Mirandes, F. Ferlaino, G. Roati, G. Modugno, and M. Inguscio, *Collisionally induced transport in periodic potentials*, Phys. Rev. Lett. **92** (2004), 160601, ⊙.

[989] H. Ouerdane and M. J. Jamieson, *Scattering parameters for cold lirb and narb collisions derived from variable phase theory*, Phys. Rev. A **70** (2004), 022712, ⊙.

[990] Yu. B. Ovchinnikov, *A zeeman slower based on magnetic dipoles*, Opt. Comm. **276** (2007), 261, ⊙DOI.

[991] ———, *A permanent zeeman slower for sr atomic clock*, Eur. J. Phys. ST **163** (2008), 95, ⊙DOI.

[992] Yu. B. Ovchinnikov, J. H. Müller, M. R. Doery, M. J. R. Vredenbregt, K. Helmerson, S. L. Rolston, and W. D. Phillips, *Diffraction of a released Bose-Einstein condensate by a pulsed standing light wave*, Phys. Rev. Lett. **83** (1999), 284, ⊙.

[993] R. Ozeri, J. Steinhauer, N. Katz, and N. Davidson, *Direct observation of the phonon energy in a Bose-Einstein condensate by tomographic imaging*, Phys. Rev. Lett. **88** (2002), 220401, ⊙.

[994] G. Y. Panasyuk, J. C. Schotland, and V. A. Markel, *Short-distance expansion for the electromagnetic half-space green's tensor: general results and an application to radiative lifetime computations*, J. Phys. A: Math. Theor. **42** (2009), 275203, ⊙DOI.

[995] T. Papenbrock and G. F. Bertsch, *Pairing in low-density Fermi gases*, Phys. Rev. C **59** (1999), 2052, ⊙.

[996] S. B. Papp and C. E. Wieman, *Observation of heteronuclear Feshbach molecules from a ^{85}rb-^{87}rb gas*, Phys. Rev. Lett. **97** (2006), 180404, ⊙.

[997] B. Paredes, C. Tejedor, and J. I. Cirac, *Fermionic atoms in optical superlattices*, ePrints (2003), cond–mat/0306497, ⊙.

[998] B. Paredes, A. Widera, V. Murg, O. Mandel, S. Fölling, I. Cirac, G. V. Shlyapnikov, Th. W. Hänsch, and I. Bloch, *Tonks-Girardeau gas of ultracold atoms in an optical lattice*, Nature **429** (2004), 277, ⊙.

[999] A. S. Parkins and D. F. Walls, *The physics of trapped dilute gas Bose-Einstein condensates*, Phys. Rep. **303** (1998), 1.

[1000] G. B. Partridge, Wenhui Li, R. I. Kamar, Yean an Liao, and R. G. Hulet, *Pairing and phase separation in a polarized Fermi gas*, Science **311** (2006), 503, ⊙.

[1001] W. Paul, O. Osberghaus, and E. Fischer, *Ein Ionenkäfig*, Forschungsberichte des Wirtschafts- und Verkehrsministerium Nordrhein-Westfalen, Westdeutscher Verlag Köln-Opladen (1958).

[1002] M. Paulus, Ph. Gay-Balmaz, and O. J. F. Martin, *Accurate and efficient computation of the green's tensor for stratified media*, Phys. Rev. E **62** (2000), 5797, ⊙DOI.

[1003] D. Pavolini, A. Crubellier, P. Pillet, L. Cabaret, and S. Liberman, *Experimental evidence for subradiance*, Phys. Rev. Lett. **54** (1985), 1917.

[1004] J. P. Paz and W. H. Zurek, *Environnement-induced decoherence and the transition from quantum to classical*, Lect. notes in Phys. **587** (2002), 77, ⊙.

[1005] B. M. Peden, D. Meiser, M. L. Chiofalo, and M. J. Holland, *Nondestructive cavity QED probe of Bloch oscillations in a gas of ultracold atoms*, Phys. Rev. A **80** (2009), 043803, ⊙DOI.

[1006] J. Pedlosky, *Geophysical fluid dynamics*, 2007, ISBN.

[1007] E. Peik, M. Ben Dahan, I. Bouchoule, Y. Castin, and C. Salomon, *Bloch oscillations of atoms, adiabatic rapid passage, and monokinetic atomic beams*, Phys. Rev. A **55** (1997), 2989, ⊙DOI.

[1008] B. Pelle, A. Hilico, G. Tackmann, Q. Beaufils, and F. Pereira dos Santos, *State-labeling wannier-stark atomic interferometers*, Phys. Rev. A **83** (2013), 023601.

[1009] T. Pellizzari, S. A. Gardiner, J. I. Cirac, and P. Zoller, Phys. Rev. Lett. **75** (1995), 3788.

[1010] J. Pendry, *Playing tricks with light*, Science **285** (1999), 1687, ⊙.

[1011] J. B. Pendry, *Negative refraction makes a perfect lens*, Phys. Rev. Lett. **85** (2000), 3966, ⊙.

[1012] ———, *A chiral route to negative refraction*, Science **306** (2004), 1353, ⊙DOI.

[1013] ———, *Negative refraction*, Cont. Phys. **45** (2004), 191, ⊙.

[1014] F. M. Penning, *Die glimmentladung bei niedrigem druck zwischen koaxialen zylindern in einem axialen magnetfeld*, Physica **3** (1936), 873.

[1015] A. Perali, P. Pieri, and G. C. Strinati, *Extracting the condensate density from projection experiments with Fermi gases*, ePrint (2005), ⊙.

[1016] M. Perrin, G.-L. Lippi, and A. Politi, *Phase-transition in a radiation-matter interaction with recoil and collisions*, Phys. Rev. Lett. **86** (2001), 4520, ⊙.

[1017] C. Pethick and H. Smith, *Bose-Einstein condensation in dilute gases*, Cambridge University Press, 2002, ISBN.

[1018] W. Petrich, M. H. Anderson, J. R. Ensher, and E. A. Cornell, *Stable, tightly confining trap for evaporative cooling of neutral atoms*, Phys. Rev. Lett. **74** (1995), 3352, ⊙.

[1019] D. Petrosyan, *Tunable photonic band gaps with coherently driven atoms in optical lattices*, Phys. Rev. A **84** (2007), 2551, ⊙DOI.

[1020] D. S. Petrov, *Three-boson problem near a narrow Feshbach resonance*, Phys. Rev. Lett. **93** (2004), 143201, ⊙.

[1021] D. S. Petrov, G. E. Astrakharchik, D. J. Papoular, C. Salomon, and G. V. Shlyapnikov, *Crystalline phase of strongly interacting Fermi mixtures*, (2007), ⊙.

[1022] D. S. Petrov, M. Holzmann, , and G. V. Shlyapnikov, *Bose-Einstein condensation in quasi-2d trapped gases*, Phys. Rev. Lett. **84** (2000), 2551, ⊙.

[1023] D. S. Petrov, C. Salomon, and G. V. Shlyapnikov, *Weakly bound dimers of fermionic atoms*, Phys. Rev. Lett. **93** (2004), 090404, ⊙.

[1024] K. I. Petsas, A. B. Coates, and G. Grynberg, *Crystallography of optical lattices*, Phys. Rev. A **50** (1994), 5173, ⊙.

[1025] S. Pezzagna and J. Meijera, *Quantum computer based on color centers in diamond*, Appl. Phys. Rev. **8** (2021), 011308, ⊙DOI.

[1026] L. Pezze, A. Smerzi, M. K. Oberthaler, R. Schmied, and Ph. Treutlein, *Quantum metrology with nonclassical states of atomic ensembles*, Rev. Mod. Phys. **90** (2018), 035005, ⊙DOI.

[1027] R. N. C. Pfeifer, T. A. Nieminen, N. R. Heckenberg, and H. Rubinsztein-Dunlop, *Colloquium: Momentum of an electromagnetic wave in dielectric media*, Rev. Mod. Phys. **79** (2007), 1197.

[1028] E. Pfleghaar, A. Marseille, and A. Weis, *Quantitative investigation of the effect of resonant absorbers on the Goos-Hänchen shift*, Phys. Rev. Lett. **70** (1993), 2281, ⊙.

[1029] P. Phillips and D. Dalidovich, *The elusive bose metal*, Science **302** (2003), 243, ⊙.

[1030] William D. Phillips and Harold Metcalf, *Laser deceleration of an atomic beam*, Physical Review Letters **48** (1982), 596.

[1031] A. Pikovsky, M. Rosenblum, and J. Kurths, *Synchronization: A universal concept in nonlinear sciences*, Cambridge, University press (2001).

[1032] Pierre Pillet Ed., *Optics and interferometry with atoms*, J. Physique II **4** (1994), 1877.

[1033] F. Pillon, H. Gilles, and S. Girard, *Experimental observation of the Imbert-Fedorov transverse displacement after a single total reflection*, Appl. Opt. **43** (2004), 1863.

[1034] F. Pillon, H. Gilles, S. Girard, M. Laroche, R. Kaiser, and A. Gazibegovic, *Goos-Hänchen and Imbert-Fedorov shifts for leaky guided modes*, J. Opt. Soc. Am. B **22** (2005), 1290.

[1035] N. Piovella, R. Bachelard, and Ph. W. Courteille, *Fluid description of the cooperative scattering of light by spherical atomic clouds*, J. Plasma Phys. **79** (2013), 413.

[1036] N. Piovella, M. Cola, and R. Bonifacio, *Quantum fluctuations and entanglement in the collective atomic recoil laser using a Bose-Einstein condensate*, Phys. Rev. A **67** (2003), 013817, ⊙.

[1037] ———, *Classical and quantum regimes in the collective atomic recoil laser from a Bose-Einstein condensate*, J. Mod. Opt. **51** (2004), 1019.

[1038] N. Piovella, M. Gatelli, and R. Bonifacio, *Quantum effects in the collective light scattering by coherent atomic recoil in a Bose-Einstein condensate*, Opt. Commun. **194** (2001), 167, ⊙.

[1039] D. Plankensteiner, Ch. Hotter, and H. Ritsch, *Quantumcumulants.jl: A julia framework for generalized mean-field equations in open quantum systems*, Quantum **6** (2021), 617, ⊙DOI.

[1040] A. Poddubny, I. Iorsh, P. Belov, and Y. Kivshar, *Hyperbolic metamaterials*, Nature Phot. **7** (2013), 958.

[1041] A. N. Poddubny, P. A. Belov, P. Ginzburg, A. V. Zayats, and Y. S. Kivshar, *Microscopic model of purcell enhancement in hyperbolic metamaterials*, Phys. Rev. B **86** (2012), 035148, ⊙DOI.

[1042] I. Pogorelov, T. Feldker, Ch. D. Marciniak, L. Postler, G. Jacob, O. Krieglsteiner, V. Podlesnic, M. Meth, V. Negnevitsky, M. Stadler, B. Höfer, C. Wächter, K. Lakhmanskiy, R. Blatt, P. Schindler, and T. Monz, *Compact ion-trap quantum computing demonstrator*, Phys. Rev. X **2** (2021), 020343, ⊙DOI.

[1043] H. D. Politzer, *Light incident on a Bose-condensed gas*, Phys. Rev. A **43** (1991), 6444.

[1044] ———, *Bose-stimulated scattering off a cold atom trap*, Phys. Rev. A **55** (1997), 1140, ⊙.

[1045] A. K. Popov and V. M. Shalaev, *Negative-index metamaterials: second-harmonic generation, manley-rowe relations and parametric amplification*, Appl. Phys. B **84** (2006), 131, ⊙.

[1046] U. V. Poulsen and K. Mølmer, *Atomic reflection from a magnetic mirror: Beyond the adiabatic approximation*, Eur. Phys. J. D **11** (2000), 151, ⊙.

[1047] E. A. Power, *Effect on the lifetime of an atom undergoing a dipole transition due to the presence of a resonating atom*, J. Chem. Phys. **46** (1967), 4297, ⊙.

[1048] W. L. Power, L. Allen, M. Babiker, and V. E. Lembessis, *Atomic motion in light beams possessing orbital angular momentum*, Phys. Rev. A **52** (1995), 479.

[1049] S. Prasad and R. J. Glauber, *Coherent radiation by a spherical medium of resonant atoms*, Phys. Rev. A **82** (2010), 063805, ⊙DOI.

[1050] G. A. Prataviera, *Trap environnement effects over quantum statistics and atom-photon correlations in the collective-atomic-recoil laser*, Phys. Rev. A **67** (2003), 045602, ⊙.

[1051] G. A. Prataviera and M. C. de Oliveira, *Continuous measurement of atom-number moments of a Bose-Einstein condensate by photodetection*, Phys. Rev. A **70** (2004), 011602(R), ⊙DOI.

[1052] C. Presilla and R. Onofrio, *Cooling dynamics of ultracold two-species Fermi bose mixtures*, Phys. Rev. Lett. **90** (2003), 030404, ⊙.

[1053] J. Preskill, *Magnetic monopole*, Ann. Rev. Nucl. Part. **34** (1984), 461, ⊙.

[1054] J. D. Prestage, G. J. Dick, and L. Maleki, *New ion trap for frequency standard applications*, J. Appl. Phys. **66** (1989), 1013.

[1055] J. D. Prestage, R. L. Tjoelker, R. T. Wang, G. J. Dick, and L. Maleki, *Hg+ trapped ion standard with the superconducting cavity maser oscillator*, IEEE Trans. Instr. and Meas. **42** (1993), 200.

[1056] M. Prevedelli, F. S. Cataliotti, E. A. Cornell, J. R. Ensher, C. Fort, L. Ricci, G. M. Tino, and M. Inguscio, *Trapping and cooling of potassium isotopes in a double-magneto-optical-trap apparatus*, Phys. Rev. A **59** (1999), 886, ⊙.

[1057] I. Prigogine, *Non-equilibrium statistical mechanics*, Monographs in Statistical Physics, vol. 1, John Wiley and Sons, 1973, ISBN.

[1058] D. E. Pritchard, *Cooling neutral atoms in a magnetic trap for precision spectroscopy*, Phys. Rev. Lett. **51** (1983), 1336, ⊙.

[1059] D. E. Pritchard, R. A. Rubenstein, A. Dhirani, D. A. Kokorowski, E. T. Smith, T. D. Hammond, and B. Rohwedder, *Longitudinal atom optics using localized oscillating fields: A fully quantum-mechanical treatment*, Phys. Rev. A **59** (1999), 4641.

[1060] A. M. Eds. Prokhorov et al., *Laser cooling and trapping*, Laser Physics **4** (1994), 829.

[1061] Han Pu, Weiping Zhang, and P. Meystre, *Wave mixing of optical pulses and Bose-Einstein condensates*, Phys. Rev. Lett. **91** (2003), 150407, ⊙.

[1062] Ravinder Puri, *Mathematical methods of quantum optics*, Springer Series in Optical Sciences (2000).

[1063] N. Quesada, J. M. Arrazola, and N. Killoran, *Gaussian boson sampling using threshold detectors*, Phys. Rev. A **98** (2018), 062322, ⊙.

[1064] S. De Palo R. Citro, E. Orignac and M. L. Chiofalo, *Evidence of luttinger-liquid behavior in one-dimensional dipolar quantum gases*, Phys. Rev. A **75** (2007), 051602(R), ⊙.

[1065] E. L. Raab, M. Prentiss, A. Cable, S. Chu, and D. E. Prichard, *Trapping of neutral sodium atoms with radiation pressure*, Phys. Rev. Lett. **59** (1987), 2631, ⊙FndDoi10.1103/PhysRevLett.59.2631.

[1066] A. Rai and G. S. Agarwal, *Possibility of coherent phenomena such as Bloch oscillations with single photons via w states*, Phys. Rev. A **79** (2009), 053849, ⊙DOI.

[1067] G. Raithel, G. Birkl, W. D. Phillips, and S. L. Rolston, *Compression and parametric driving of atoms in optical lattices*, Phys. Rev. Lett. **78** (1997), 2928, ⊙.

[1068] M. G. Raizen, J. Koga, B. Sundaram, Y. Kishimoto, H. Takuma, and T. Tajima, *Stochastic cooling of atoms using lasers*, Phys. Rev. A **58** (1998), 4757, ⊙DOI.

[1069] M. G. Raizen, R. J. Thompson, R. J. Brecha, H. J. Kimble, and H. J. Carmichael, *Normal-mode splitting and linewidth averaging for two-state atoms in an optical cavity*, Phys. Rev. Lett. **63** (1989), 240.

[1070] A. D. Rakic, A. B. Djurisic, J. M. Elazar, and M. L. Majewski, *Optical properties of metallic films for vertical-cavity optoelectronic devices*, Appl. Opt. **37** (1998), 5271, ⊙DOI.

[1071] C. Raman, M. Köhl, R. Onofrio, D. S. Durfee, C. E. Kuklewicz, Z. Hadzibabic, and W. Ketterle, *Evidence for a critical velocity in a Bose-Einstein condensed gas*, Phys. Rev. Lett. **83** (1999), 2502, ⊙.

[1072] N. Ramsey, *A new molecular beam method*, Phys. Rev. **76** (1949), 996.

[1073] E. M. Rasel, M. K. Oberthaler, H. Batelaan, J. Schmiedmayer, and A. Zeilinger, *Atom wave interferometry with diffraction gratings of light*, Phys. Rev. Lett. **75** (1995), 2633.

[1074] A. Rauschenbeutel, G. Nogues, S. Osnaghi, P. Bertet, M. Brune, J.-M. Raimond, and S. Haroche, *Step-by-step engineering of multiparticle entanglement*, Science **288** (2000), 2024.

[1075] F. Ravndal, *Symmetric and conserved energy-momentum tensors in moving media*, Europhys. Lett. **99** (2012), 50002, ⊙DOI.

[1076] A. Recati, P. O. Fedichev, W. Zwerger, J. Von Delft, and P. Zoller, *Dissipative spin-boson model and kondo effect in low dimensional quantum gases*, ePrints (2002), cond–mat/0212413, ⊙.

[1077] A. Recati, P. O. Fedichev, W. Zwerger, and P. Zoller, *Spin-charge separation in ultracold quantum gases*, Phys. Rev. Lett. **90** (2003), 020401, ⊙.

[1078] C. A. Regal, M. Greiner, S. Giorgini, M. Holland, and D. S. Jin, *Momentum distribution of a Fermi gas of atoms in the BCS-BEC crossover*, ePrint (2005), ⊙.

[1079] C. A. Regal, M. Greiner, and D. S. Jin, *Lifetime of molecule-atom mixtures near a Feshbach resonance in 40*, Phys. Rev. Lett. **92** (2004), 083201, ⊙.

[1080] ———, *Observation of resonance condensation of fermionic atom pairs*, Phys. Rev. Lett. **92** (2004), 040403, ⊙.

[1081] C. A. Regal and D. S. Jin, *Measurement of positive and negative scattering lengths in a Fermi gas of atoms*, Phys. Rev. Lett. **90** (2003), 230404, ⊙.

[1082] ———, *Experimental realization of the BCS-BEC crossover with a Fermi gas of atoms*, Adv. At. Mol. Opt. Phys. **54** (2007), 1, ⊙.

[1083] C. A. Regal, C. Ticknor, J. L. Bohn, and D. S. Jin, *Creation of ultracold molecules from a Fermi gas of atoms*, Nature **424** (2003), 047, ⊙.

[1084] ———, *Tuning p-wave interactions in an ultracold Fermi gas of atoms*, Phys. Rev. Lett. **90** (2003), 053201, ⊙.

[1085] N. E. Rehler and J. H. Eberly, Phys. Rev. A **3** (1971), 1735, ⊙DOI.

[1086] M. Reich, U. Sterr, and W. Ertmer, *Scheme for measuring a berry-phase in an atom interferometer*, Phys. Rev. A **47** (1993), 2518, ⊙.

[1087] M. D. Reid, *Quantum theory of optical bistability without adiabatic elimination*, Phys. Rev. A **37** (1988), 4792, ⊙.

[1088] ———, *Demonstration of the Einstein-podolsky-rosen paradox using nondegenerate parametric amplification*, Phys. Rev. A **40** (1989), 913.

[1089] W. P. Reinhardt and C. W. Clark, *Soliton dynamics in the collisions of Bose-Einstein condensates: An analogue of the josephson effect*, J. Phys. B **30** (1997), L785.

[1090] M. Reitz, Ch. Sommer, and C. Genes, *Cooperative quantum phenomena in light-matter platforms*, Phys. Rev. X **3** (2022), 010201, ⊙DOI.

[1091] R. H. Renard, *Total reflection: A new evaluation of the Goos-Hänchen shift*, J. Opt. Soc. Am. **54** (1964), 1190.

[1092] M. J. Renn, D. Montgomery, O. Vdovin, D. Z. Anderson, C. E. Wieman, and E. A. Cornell, *Laser-guided atoms in hollow optical fibers*, Phys. Rev. Lett. **75** (1995), 3253.

[1093] J. A. Retter, A. F. Varón, D. Clément, M. Hugbart, P. Bouyer, L. Sanchez-Palencia, D. Gangardt, G. V. Shlapnikov, and A. Aspect, *Inhibition of transport of a Bose-Einstein condensate in a random potential*, ePrints (2005), cond–mat/0509605, ⊙.

[1094] L. Ricci, M. Weidemüller, T. Esslinger, A. Hemmerich, C. Zimmermann, V. Vuletic, W. König, and T. W. Hänsch, *A compact grating-stabilized diode laser system for atomic physics*, Opt. Comm. **117** (1995), 541.

[1095] F. Riehle, T. Kisters, A. White, J. Helmecke, and C. J. Bordé, *Optical ramsey spectroscopy in a rotating frame: Sagnac effect in a matter-wave interferometer*, Phys. Rev. Lett. **67** (1991), 177.

[1096] M. Rigol, R. T. Scalettar, P. Sengupta, and G. G. Batrouni, *Time-of-flight variables and the formation of mott domains of fermions and bosons on optical lattices*, Phys. Rev. B **73** (2006), 121103, ⊙.

[1097] W. Rindler, *Relativity and electromagnetism: The force on a magnetic monopole*, Am. J. Phys. **57** (1989), 993, ⊙.

[1098] J. Ringot, P. Szriftgiser, J. C. Garreau, and D. Delande, *Experimental evidence of dynamical localization and delocalization in a quasiperiodic driven system*, Phys. Rev. Lett. **85** (2000), 2741, ⊙.

[1099] H. Ritsch, P. Domokos, F. Brennecke, and T. Esslinger, *Cold atoms in cavity-generated dynamical optical potentials*, Rev. Mod. Phys. **85** (2013), 553, ⊙DOI.

[1100] G. Ritt, G. Cennini, C. Geckeler, and M. Weitz, *Laser frequency offset locking using a side of filter technique*, Appl. Phys. B **79** (2004), 363, ⊙.

[1101] G. Roati, C. D'Errico, L. Fallani, M. Fattori, C. Fort, M. Zaccanti, G. Modugno, M. Modugno, and M. Inguscio, *Anderson localization of a non-interacting Bose-Einstein condensate*, Nature **453** (2008), 0895, ⊙.

[1102] G. R. M. Robb and B. W. J. McNeil, *Four-wave mixing with self-phase matching due to collective atomic recoil*, Phys. Rev. Lett. **94** (2005), 023901, ⊙.

[1103] G. R. M. Robb, B. W. J. McNeil, and R. Bonifacio, *Recoil-induced symmetry breaking in superfluorescence*, Phys. Rev. A **61** (2000), 031801, ⊙.

[1104] G. R. M. Robb, B. W. J. McNeil, R. Bonifacio, and N. Piovella, *Dispersive optical bistability in cold atomic vapours*, Opt. Commun. **194** (2001), 151.

[1105] G. R. M. Robb, N. Piovella, and R. Bonifacio, *The semiclassical and quantum regimes of superradiant light scattering from a Bose-Einstein condensate*, J. Opt. B: Quantum Semiclassical Opt. **7** (2005), 93, ⊙.

[1106] G. R. M. Robb, N. Piovella, A. Ferraro, R. Bonifacio, Ph. W. Courteille, and C. Zimmermann, *Collective atomic recoil lasing including friction and diffusion effects*, Phys. Rev. A **69** (2004), 041403(R).

[1107] A. Robert, O. Sirjean, A. Browaeys, J. Poupard, S. Nowak, D. Boiron, C. I. Westbrook, and A. Aspect, *A Bose-Einstein condensate of metastable atoms*, Science **292** (2001), 461.

[1108] J. L. Roberts, N. R. Claussen, J. P. Jr. Burke, C. H. Greene, E. A. Cornell, and C. E. Wieman, *Resonant magnetic field control of elastic scattering in cold 85rb*, Phys. Rev. Lett. **81** (1998), 5109, ⊙.

[1109] J. L. Roberts, N. R. Claussen, S. L. Cornish, E. A. Donley, E. A. Cornell, and C. E. Wieman, *Controlled collapse of a Bose-Einstein condensate*, ePrints (2001), cond–mat/0102116, ⊙.

[1110] F. Robicheaux and J. V. Hernández, *Many-body wave function in a dipole blockade configuration*, Phys. Rev. A **72** (2005), 063403, ⊙DOI.

[1111] R. Röhlsberger, K. Schlage, B. Sahoo, S. Couet, and R. Rï¿½ffer, *The collective lamb shift in nuclear c-ray superradiance*, J. Mod. Opt. **328** (2010), 1248, ⊙DOI.

[1112] ———, *Collective lamb shift in single-photon superradiance*, Science **328** (2010), 1248, ⊙DOI.

[1113] D. S. Rokhsar, *Vortex stability and persistent currents in trapped bose gases*, Phys. Rev. Lett. **79** (1997), 2164, ⊙.

[1114] J. R. Rubbmark, M. M. Kash, M. G. Littman, and D. Kleppner, *Dynamical effects at avoided level crossings: A study of the Landau-Zener effect using Rydberg atoms*, Phys. Rev. A **23** (1981), 3107.

[1115] A. E. Ruckenstein, *Bose condensation without broken symmetries*, (2001), cond-mat/0104010.

[1116] J. Ruostekoski, *Optical kagome lattice for ultracold atoms with nearest neighbor interactions*, Phys. Rev. Lett. **103** (2009), 080406, ⊙DOI.

[1117] ———, *Emergence of correlated optics in one-dimensional waveguides for classical and quantum atomic gases*, Phys. Rev. Lett. **117** (2016), 143602, ⊙DOI.

[1118] J. Ruostekoski and J. Javanainen, *Lorentz-lorentz shift in a Bose-Einstein condensate*, Phys. Rev. A **56** (1997), 2056, ⊙DOI.

[1119] ———, *Quantum field theory of cooperative atom response: Low light intensity*, Phys. Rev. A **55** (1997), 513, ⊙.

[1120] J. Ruostekoski and D. F. Walls, *Bose-Einstein condensate in a double-well potential as an open quantum system*, Phys. Rev. A **58** (1998), R50, ⊙.

[1121] P. A. Ruprecht, M. J. Holland, and K. Burnett, *Dynamical effects in atom optics*, Phys. Rev. A **49** (1994), 4726.

[1122] P. A. Ruprecht, M. J. Holland, K. Burnett, and M. Edwards, *Time-dependent solutions of the nonlinear schrödinger equation for Bose-condensed trapped neutral atoms*, Phys. Rev. A **51** (1995), 4704.

[1123] S. M. Rytov, *Electromagnetic properties of a finely stratified medium*, Sov. Phys. JETP **2** (1954), 466, ⊙.

[1124] C. A. Sackett, C. C. Bradley, and R. G. Hulet, *Bose-Einstein condensation in lithium*, Appl. Phys. B **65** (1997), 433.

[1125] C. A. Sackett, C. C. Bradley, M. Welling, and R. G. Hulet, *Bose-Einstein condensation of lithium*, Bra. J. Phys. **27** (1997), 154, ⊙.

[1126] C. A. Sackett, J. M. Gerton, M. Welling, and R. G. Hulet, *Measurements of collective collapse in a Bose-Einstein condensate with attractive interactions*, Phys. Rev. Lett. **82** (1999), 876, ⊙.

[1127] S. A. Sackett, D. Kielpinski, B. E. King, C. Langer, V. Meyer, C. J. Myatt, M. Rowe, Q. A. Turchette, W. M. Itano, D. J. Wineland, and C. Monroe, *Experimental entanglement of four particles*, Nature **404** (2000), 256.

[1128] J. D. Sakurai and J. J. Napolitano, *Modern quantum mechanics*, John Wiley and Sons, 1999, ISBN.

[1129] J. J. Sakurai, *Advanced quantum mechanics*, Pearson Education India, 1967.

[1130] P. L. Saldanha, *Division of the energy and of the momentum of electromagnetic waves in linear media into electromagnetic and material parts*, Opt. Comm. **284** (2011), 2653, ⊙DOI.

[1131] ———, *Quantum analysis of the direct measurement of light waves*, New J. of Phys. **16** (2014), 013021.

[1132] P. L. Saldanha and J. S. Oliveira Filho, *Hidden momentum and the abraham-minkowski debate*, Phys. Rev. A **95** (2017), 043804.

[1133] ———, *Inconsistency of a realistic interpretation of quantum measurements: a simple example*, Bras. J. Phys. **95** (2020), 043804, ⊙DOI.

[1134] P. L. Saldanha and C. H. Monken, *Interaction between light and matter: a photon wave function approach*, New J. of Phys. **13** (2011), 073015, ⊙DOI.

[1135] L. Salvi, N. Poli, V. Vuletić, and G. M. Tino, *Squeezing on momentum states for atom interferometry*, Phys. Rev. Lett. **120** (2018), 033601, ⊙DOI.

[1136] L. De Salvo, R. Saers, S. Bartalini, F.S. Cataliotti, L. Fallani, C. Fort, I. Herrera, and M. Inguscio, *From superradiant rayleigh scattering to bragg scattering*, Eur. Phys. J. D (2004), ⊙.

[1137] M. Samoylova, N. Piovella, R. Bachelard, and Ph. W. Courteille, *Microscopic theory of photonic bandgaps in optical lattices*, Opt. Comm. **312** (2014), 94.

[1138] M. Samoylova, N. Piovella, M. Holynski, Ph.W. Courteille, and R. Bachelard, *One-dimensional photonic band gaps in optical lattices*, Annual Review of Cold Atoms and Molecules **2** (2014), 193.

[1139] M. Samoylova, N. Piovella, G. Robb, R. Bachelard, and Ph. W. Courteille, *Synchronisation of Bloch oscillations by a ring cavity*, Opt. Exp **23** (2015), 14823.

[1140] M. Sánchez-Barquilla, R. E. F. Silva, and J. Feist, *Cumulant expansion for the treatment of light-matter interactions in arbitrary material structures*, J. Chem. Phys. **152** (2020), 034108, ⊙DOI.

[1141] L. Sanchez-Mondragon, N. B. Narozhny, and J. H. Eberly, *Theory of spontaneous emission line shape in an ideal cavity*, Phys. Rev. Lett. **51** (1983), 550, ⊙.

[1142] J. E. Sansonetti and G. Nave, *Wavelengths, transition probabilities, and energy levels for the spectrum of neutral strontium*, J. Phys. Chem. Ref. Data **39** (2010), 033103, ⊙DOI.

[1143] G. Santarelli, Ph. Laurent, P. Lemonde, A. Clairon, A. G. Mann, S. Chang, A. N. Luiten, and C. Salomon, *Quantum projection noise in an atomic fountain: A high stability cesium frequency standard*, Phys. Rev. Lett. **82** (1999), 4619, ⊙.

[1144] G. Ch. Santra, F. Jendrzejewski, Ph. Hauke, and D. J. Egger, *Squeezing and quantum approximate optimization*, ePrints **arXiv:2205.10383** (2005), ⊙DOI.

[1145] R. Santra, E. Arimondo, T. Ido, Ch. H. Greene, and Jun Ye, *High-accuracy optical clock via three-level coherence in neutral bosonic* ^{88}*sr*, Phys. Rev. Lett. **94** (2005), 173002, ⊙DOI.

[1146] W. Saslow, T. K. Bergstresser, and M. L. Cohen, *Band structure and optical properties of diamond*, Phys. Rev. Lett. **16** (1966), 0354, ⊙.

[1147] Th. Sauter, R. Blatt, W. Neuhauser, and P.E. Toschek, *Observation of quantum jumps*, Phys. Rev. Lett. **57** (1986), 1696, ⊙.

[1148] ———, *Quantum jumps observed in the fluorescence of a single ion*, Opt. Comm. **60** (1986), 287, ⊙.

[1149] M. R. Schafroth, *Theory of superconductivity*, Phys. Rev. **96** (1954), 1442.

[1150] A. L. Schawlow and C.H. Townes, *Infrared and optical masers*, Phys. Rev. **112** (1958), 1940.

[1151] S. Scheel and S. Y. Buhmann, *Macroscopic quantum electrodynamics - concepts and applications*, Acta Physcia Slovaca **5** (2008), 675, ⊙DOI.

[1152] A. Schenzle and R.G. Brewer, *Macroscopic quantum jumps in a single atom*, Phys. Rev. A **34** (1986), 3127, ⊙.

[1153] A. Schenzle, R. G. Devoe, and R. G. Brewer, *Phase modulation laser spectroscopy*, Phys. Rev. A **25** (1982), 2606, ⊙.

[1154] A. Schenzle, R. G. DeVoe, and R. G. Brewer, *Possibility of quantum jumps*, Phys. Rev. A **33** (1986), 2127, ⊙.

[1155] L. I. Schiff, *Quantum mechanics*, McGraw Hill Book Company, 1968.

[1156] M. Schiffer, M. Rauner, S. Kuppens, M. Zinner, K. Sengstock, and W. Ertmer, *Guiding, focusing, and cooling of atoms in a strong dipole potential*, Appl. Phys. B **67** (1998), 705.

[1157] A. Schilke, C. Zimmermann, Ph. W. Courteille, and W. Guerin, *Photonic band gaps in one-dimensionally ordered cold atomic vapors*, Phys. Rev. Lett. **106** (2011), 223903.

[1158] ———, *Optical parametric oscillation with distributed feedback in cold atoms*, Nature Phot. **6** (2012), 101 letter.

[1159] S. Schiller, *Hydrogenlike highly charged ions for tests of the time independence of fundamental constants*, Phys. Rev. Lett. **98** (2007), 180801, ⊙.

[1160] W. Schleich, *Quantum optics in phase space*, Wiley-VCH, 2001, ISBN.

[1161] W. Schleich and M. O. Scully, *Quantum-noise quenching in the correlated spontaneous-emission laser as a multiplicative noise process. i. a geometrical argument*, Phys. Rev. A **37** (1988), 1261.

[1162] M. H. Schleier-Smith, I. D. Leroux, and V. Vuletic, *Squeezing the collective spin of a dilute atomic ensemble by cavity feedback*, Phys. Rev. A **81** (2010), 021804(R), ⊙DOI.

[1163] S. Schlunk, M. B. d'Arcy, S. A. Gardiner, and G. S. Summy, *Experimental observation of high-order quantum accelerator modes*, Phys. Rev. Lett. **90** (2003), 124002, ⊙.

[1164] D. T. Schmithey, M. Beck, M. G. Raymer, and A. Faridani, *Measurement of the wigner distribution and the density matrix of a light mode using optical homodyne tomography: Application to squeezed state and the vacuum*, Phys. Rev. Lett. **70** (1993), 1244.

[1165] D. Schneble, G. K. Campbell, E. W. Streed, M. Boyd, D. E. Pritchard, and W. Ketterle, *Raman amplification of matter waves*, Phys. Rev. A **69** (2004), 041601, ⊙.

[1166] D. Schneble, Y. Torii, M. Boyd, E. W. Streed, D. Pritchard, and W. Ketterle, *The onset of matter-wave amplification in a superradiant Bose-Einstein condensate*, Science **300** (2003), 475, ⊙.

[1167] C. A. Schrama, E. Peik, W. W. Smith, and H. Walther, *Novel miniature ion traps*, Opt. Comm. **101** (1993), 32.

[1168] F. Schreck, L. Khaykovich, K. L. Corwin, T. Bourdel, J. Cubizolles, and C. Salomon, *Quasipure Bose-Einstein condensate immersed in a Fermi sea*, Phys. Rev. Lett. **87** (2001), 080403, ⊙.

[1169] E. Schrödinger, Brit. Journ. f. the Philos. of Science III (1952).

[1170] M. Schubert, I. Siemers, and R. Blatt, *Line shape of three-level ions in paul traps*, Phys. Rev. A **39** (1989), 5098.

[1171] M. Schubert, I. Siemers, R. Blatt, W. Neuhauser, and P. E. Toschek, *Photon antibunching and non-poissonian fluorescence of a single three-level ion*, Phys. Rev. Lett. **68** (1992), 3016, ⊙DOI.

[1172] H. J. Schulz, *Interacting electrons in one dimension: Luttinger liquids*, Physica C **235-240** (1994), 217, ⊙.

[1173] R. J. Schulze, C. Genes, and H. Ritsch, *Optomechanical approach to cooling of small polarizable particles in a strongly pumped ring cavity*, Phys. Rev. A **81** (2010), 063820, ⊙DOI.

[1174] A. S. Schumovsky, R. Taras, and Tram Quang, *Collective jumps in a system of three-level atoms*, Opt. Comm. **64** (1987), 45.

[1175] S. C. Schuster, P. Wolf, S. Ostermann, S. Slama, and C. Zimmermann, *Supersolid properties of a Bose-Einstein condensate in a ring resonator*, Phys. Rev. Lett. **124** (2020), 143602, ⊙DOI.

[1176] M. O. Scully, *From lasers and masers to phaseonium and phasers*, Phys. Rep. **219** (1992), 191.

[1177] ———, *Fel*, Phys. Rev. Lett. **70** (1993), 1433.

[1178] ———, *Condensation of n bosons and the laser phase transition analogy*, Phys. Rev. Lett. **82** (1999), 3927, ⊙.

[1179] ———, *Collective lamb shift in single photon Dicke superradiance*, Phys. Rev. Lett. **102** (2009), 143601, ⊙DOI.

[1180] M. O. Scully, E. S. Fry, C. H. Raymond Ooi, and K. Wodkiewicz, *Directed spontaneous emission from an extended ensemble of n atoms: Timing is everything*, Phys. Rev. Lett. **96** (2006), 010501, ⊙DOI.

[1181] ———, *The effects of the n atom collective lamb shift on single photon superradiance*, Phys. Lett. A **373** (2009), 1283, ⊙DOI.

[1182] M. O. Scully and A. A. Svidzinsky, *The super of superradiance*, Science **325** (2009), 1510, ⊙DOI.

[1183] ———, *The lamb shift-yesterday, today, and tomorrow*, Science **328** (2010), 1239, ⊙DOI.

[1184] M. O. Scully and M. S. Zubairy, *Quantum optics*, Cambridge University Press, 1997, ISBN.

[1185] S. Sefi and P. van Loock, *How to decompose arbitrary continuous-variable quantum operations*, Phys. Rev. Lett. **107** (2011), 170501.

[1186] J. Seke, *The counter-rotating terms in the superradiance*, Il Nuove Cimente **7** (1986), 447, ⊙.

[1187] I. V. Shadrivov, A. A. Sukhorukov, and Y. S. Kivshar, *Complete band gaps in one-dimensional left-handed periodic structures*, Phys. Rev. Lett. **95** (2005), 193903.

[1188] E. Shahmoon, D. S. Wild, M. D. Lukin, and S. F. Yelin, *Cooperative resonances in light scattering from two-dimensional atomic arrays*, Phys. Rev. Lett. **118** (2017), 113601, ⊙DOI.

[1189] M. S. Shahriar, G. S. Pati, R. Tripathi, V. Gopal, M. Messall, and K. Salit, *Ultrahigh enhancement in absolute and relative rotation sensing using fast and slow light*, Phys. Rev. A **75** (2007), 053807.

[1190] V. M. Shalaev, *Optical negative-index metamaterials*, Nature Photonics **1** (2006), 41, ⊙.

[1191] Weilong She, Jianhui Yu, and Raohui Feng, *Observation of a push force on the end face of a nanometer silica filament exerted by outgoing light*, Phys. Rev. Lett. **101** (2008), 243601, ⊙.

[1192] P. Shekhar and Z. Jacob, *Strong coupling in hyperbolic metamaterials*, Phys. Rev. B **90** (2014), 045313, ⊙DOI.

[1193] R. A. Shelby, D. R. Smith, and S. Schultz, *Experimental verification of a negative index of refraction*, Science **292** (2001), 77.

[1194] Jian Qi Shen, *Negatively refracting atomic vapour*, J. Mod. Opt. **53** (2006), 2195, ⊙.

[1195] Jian Qi Shen, J. Almlöf, and S. He, *Negative permeability in a λ-type three level atomic vapor*, Appl. Phys. A **87** (2006), 291, ⊙DOI.

[1196] Jian-Qi Shen, Zhi-Chao Ruan, and Sailing He, *How to realize a negative refractive index material at the atomic level in an optical frequency range*, J. Zhejiang University SCIENCE **5** (2004), 1322, ⊙DOI.

[1197] Jiteng Sheng, Yuanxi Chao, Santosh Kumar, Haoquan Fan, J. Sedlacek, and J. P. Shaffer, *Intracavity Rydberg-atom electromagnetically induced transparency using a high-finesse optical cavity*, Phys. Rev. A **96** (2017), 033813, ⊙DOI.

[1198] V. B. Shenoy and Tin-Lun Ho, *First and second sound modes of a Bose-Einstein condensate in a harmonic trap*, Phys. Rev. Lett. **80** (1998), 3895.

[1199] D. L. Shepelyanski, *Localization of diffusive excitation in multi-level systems*, Physica D **28** (1987), 103.

[1200] Masatoshi Shiino, *Dynamic behavior of of stochastic systems of infinitely many coupled nonlinear oscillators exhibiting phase transitions of mean-field-type: H theorem on asymptotic approach to equilibrium and critical slowing down of order parameter*, Phys. Rev. A **36** (1987), 2393, ⊙.

[1201] J. H. Shirley, *Modulation transfer processes in optical heterodyne saturation spectroscopy*, Opt. Lett. **7** (1982), 537.

[1202] G. V. Shlyapnikov, J. T. M. Walraven, U. M. Rahmanov, and M. W. Reynolds, *Decay-kinetics and Bose-condensation in a gas of spin-polarized triplett helium*, Phys. Rev. Lett. **73** (1994), 3247.

[1203] A. E. Siegman, J. Opt. Soc. Am. A **2** (1985), 1793.

[1204] ———, *Lasers*, 1986, ISBN.

[1205] D. E. Sikes and D. D. Yavuz, *Negative refraction using Raman transitions and chirality*, Phys. Rev. A **84** (2011), 053836, ⊙DOI.

[1206] P. Simoneau, S. Le Boiteaux, C. B. De Araujo, D. Bloch, J.R. Rios Leite, and M. Ducloy, *Doppler-free evanescent wave spectroscopy*, Opt. Comm. **59** (1986), 103, ⊙.

[1207] A. Simoni, F. Ferlaino, G. Roati, G. Modugno, and M. Inguscio, *Magnetic control of the interaction in ultracold k-rb mixtures*, Phys. Rev. Lett. **90** (2003), 163202, ⊙.

[1208] N. B. Simpson, K. Dhokalian, L. Allan, and M. J. Padt, *Mechanical equivalence of spin and orbital angular momentum of light: An optical spanner*, Opt. Lett. **22** (1997), 52.

[1209] J. E. Simsarian, J. Denschlag, M. Edwards, C. W. Clark, L. Deng, E. W. Hagley, K. Helmerson, S. L. Rolston, and W. D. Phillips, *Imaging the phase of an evolving Bose-Einstein condensate wavefunction*, Phys. Rev. Lett. **85** (2000), 2040, ⊙.

[1210] K. G. Singh and D. S. Rokshar, *Collective excitations of a confined Bose-Einstein condensate*, Phys. Rev. Lett. **77** (1996), 1667, ⊙.

[1211] K. Sinha, B. Prasanna Venkatesh, and P. Meystre, *Collective effects in casimir-polder forces*, Phys. Rev. Lett. **121** (2018), 183605.

[1212] J. Sinova, S. O. Valenzuela, J. Wunderlich, C. H. Back, and T. Jungwirth, *Spin hall effects*, Rev. Mod. Phys. **87** (2015), 1213.

[1213] S. E. Skipetrov and J. H. Page, *Red light for anderson localization*, New J. Phys. **18** (2015), 021001, ⊙DOI.

[1214] S. E. Skipetrov and I. M. Sokolov, *Magnetic-field-driven localization of light in a cold-atom gas*, Phys. Rev. Lett. **114** (2015), 053902, ⊙.

[1215] S. E. Skipetrov and I.M. Sokolov, *Absence of anderson localization of light in a random ensemble of point scatterers*, Phys. Rev. Lett. **112** (2014), 023905, ⊙DOI.

[1216] N. Skribanowitz, I. P. Hermann, J. C. MacGilliwray, and M. S. Feld, *Observation of Dicke superradiance in optically pumped HF gas*, Phys. Rev. Lett. **30** (1973), 309, ⊙.

[1217] S. Slama, S. Bux, G. Krenz, C. Zimmermann, and Ph. W. Courteille, *Superradiant rayleigh scattering and collective atomic recoil lasing in a ring cavity*, Phys. Rev. Lett. **98** (2007), 053603.

[1218] S. Slama, G. Krenz, S. Bux, C. Zimmermann, and Ph. W. Courteille, *Cavity-enhanced superradiant rayleigh scattering with ultracold and Bose-Einstein condensed atoms*, Phys. Rev. A **75** (2007), 063620.

[1219] S. Slama, C. von Cube, B. Deh, A. Ludewig, C. Zimmermann, and Ph. W. Courteille, *Phase-sensitive detection of bragg-scattering at 1d optical lattices*, Phys. Rev. Lett. **94** (2005), 193901.

[1220] S. Slama, C. von Cube, M. Kohler, C. Zimmermann, and Ph. W. Courteille, *Multiple reflections and diffuse scattering in bragg scattering at optical lattices*, Phys. Rev. A **73** (2006), 023424.

[1221] S. Slama, C. von Cube, A. Ludewig, M. Kohler, C. Zimmermann, and Ph. W. Courteille, *Dimensional crossover in bragg scattering from optical lattices*, Phys. Rev. A **72** (2005), 031402(R).

[1222] A. Smerzi and S. Fantoni, *Large amplitude oscillations of a bose condensate*, Phys. Rev. Lett. **78** (1997), 3589, ⊙.

[1223] M. J. Snadden, A. S. Bell, R. B. M. Clarke, E. Riis, and D. H. McIntyre, *Doughnut mode magneto-optical trap*, J. Opt. Soc. Am. B **14** (1997), 544, ⊙.

[1224] S. Snigirev, A. J. Park, A. Heinz, I. Bloch, and S. Blatt, *Fast and dense magneto-optical traps for strontium*, Phys. Rev. A **99** (2019), 063421, ⊙DOI.

[1225] J. J. Snyder, R. K. Kaj, D. Bloch, and M. Ducloy, *High-sensitivity nonlinear spectrocopy using a frequency-offset pump*, Opt. Lett. **5** (1980), 163.

[1226] I. I. Sobelman, *Introduction to the theory of atomic spectra*, Pergamon Press Oxford (1972), ISBN.

[1227] J. Söding, D. Guéry-Odelin, P. Desbiolles, F. Chevy, H. Inamori, and J. Dalibard, *Three-body decay of a rubidium Bose-Einstein condensate*, Appl. Phys. B **69** (1999), 257, ⊙.

[1228] C. M. Sorensen and D. J. Fischbach, *Patterns in mie scattering*, Opt. Comm. **173** (2000), 145, ⊙.

[1229] A. V. Soroko, *Creation of an intended atomic wave using laser radiation*, J. Phys. B **30** (1997), 5621.

[1230] F. Sorrentino, G. Ferrari, N. Poli, R. Drullinger, and G. M. Tino, *Laser cooling and trapping of atomic strontium for ultracold atoms physics, high-precision spectroscopy and quantum sensors*, Modern Physics Letters B **20** (2006), 1287, ⊙DOI.

[1231] R. J. C. Spreeuw, T. Pfau, U. Janicke, and M. Wilkens, *Laser-like scheme for atomic-matter waves*, Europhys. Lett. **32** (1995), 469.

[1232] M. D. Srinivas and E. B. Davies, *Photon counting probabilities in quantum optics*, Optica Acta **28** (1981), 981.

[1233] A. A. Stahlhofen and G. Nimtz, *Evanescent modes are virtual photons*, Europhys. Lett. **76** (2006), 189, ⊙.

[1234] J. Stajic, J. N. Milstein, Qijin Chen, M. L. Chiofalo, M. J. Holland, K. Levin, M. D. Srinivas, and E. B. Davies, *The nature of superfluidity in ultracold Fermi gases near Feshbach resonances*, ePrints (2003), cond–mat/0309329, ⊙.

[1235] Y. Stalgies, I. Siemers, B. Appasamy, T. Altevogt, and P. E. Toschek, *The spectrum of single-atom resonance fluorescence*, Europhys. Lett. **35** (1996), 259, ⊙DOI.

[1236] Y. Stalgies, I. Siemers, B. Appasamy, and P. E. Toschek, *Light shift and fano resonances in a single cold ion*, J.Opt. Soc. Am. **15** (1998), 2505.

[1237] D. M. Stamper-Kurn, A. P. Chikkatur, A. Görlitz, S. Inouye, S. Gupta, D. E. Pritchard, and W. Ketterle, *Excitation of phonons in a Bose-Einstein condensate by light scattering*, Phys. Rev. Lett. **83** (1999), 2876, ⊙.

[1238] D. M. Stamper-Kurn and W. Ketterle, *Spinor condensates and light scattering from Bose-Einstein condensates*, Proc. Les Houches Summer School, Session LXXII (2000), ⊙.

[1239] D. M. Stamper-Kurn, H.-J. Miesner, A. P. Chikkatur, S. Inouye, J. Stenger, and W. Ketterle, *Quantum tunneling across spin domains in a BEC*, Phys. Rev. Lett. **83** (1999), 661, ⊙.

[1240] D. M. Stamper-Kurn, H.-J. Miesner, S. Inouye, M. R. Andrews, and W. Ketterle, *Collisionless and hydrodynamic excitations of a Bose-Einstein condensate*, Phys. Rev. Lett. **81** (1998), 500, ⊙.

[1241] ———, *Excitations of a Bose-Einstein condensate at non-zero temperature: A study of zero, first, and second sound*, ePrints: cond-mat/9801262 (1998), ⊙.

[1242] C. A. Stan, M. W. Zwierlein, C. H. Schunck, S. M. F. Raupach, and W. Ketterle, *Observation of Feshbach resonances between two different atomic species*, Phys. Rev. Lett. **93** (2004), 143001, ⊙.

[1243] J. Stanojevic and R. Côté, *Many-body Rabi oscillations of Rydberg excitation in small mesoscopic samples*, Phys. Rev. A **80** (2009), 033418, ⊙DOI.

[1244] J. Stare and G. G. Balint-Kurti, *Fourier grid hamiltonian method for solving the vibrational schrödinger equation in internal coordinates: Theory and test applications*, J. Phys. Chem. A **107** (2003), 7204, ⊙.

[1245] D. A. Steck, *Rubidium 87 d line data*, unpublished (2003), ⊙.

[1246] ———, *Rubidium 85 d line data*, unpublished (2008), ⊙.

[1247] D. A. Steck, K. Jacobs, H. Mabuchi, T. Bhattacharya, and S. Habib, *Quantum feedback control of atomic motion in an optical cavity*, Phys. Rev. Lett. **92** (2003), ⊙.

[1248] G. E. Stedman, *Ring-laser tests of fundamental physics and geophysics*, Rep. Mod. Phys. **60** (1997), 615.

[1249] J. J. Di Steffano, A. R. Stubberud, and I. J. Williams, *Feedback and control systems*, Schaums outline series, McGraw-Hill, 1967.

[1250] D. L. Stein, *Dissipative structures, broken symmetry, and the theory of equilibrium phase transitions*, J. Chem. Phys. **72** (2000), 2869.

[1251] I. Steiner and P. E. Toschek, *Quenching phase noise: Correlated spontaneous emission versus phase locking*, Phys. Rev. Lett. **74** (1995), 4639, ⊙.

[1252] J. I. Steinfeld, *Molecules and radiation*, MIT Press, Cambridge, 2005, ISBN.

[1253] S. Stellmer, R. Grimm, and F. Schreck, *Detection and manipulation of nuclear spin states in fermionic strontium*, Phys. Rev. A **84** (2011), 043611, ⊙DOI.

[1254] S. Stellmer, B. Pasquiou, R. Grimm, and F. Schreck, *Creation of ultracold sr_2 molecules in the electronic ground state*, Phys. Rev. Lett. **109** (2012), 115302, ⊙DOI.

[1255] ———, *Laser cooling to quantum degeneracy*, Phys. Rev. Lett. **110** (2013), 263003, ⊙DOI.

[1256] S. Stellmer and F. Schreck, *Reservoir spectroscopy of 5s5p $^3p_2$-5snd $^3d_{1,2,3}$ transitions in strontium*, Phys. Rev. A **90** (2014), 022512, ⊙DOI.

[1257] S. Stellmer, M. K. Tey, Bo Huang, R. Grimm, and F. Schreck, *Bose-Einstein condensation of strontium*, Phys. Rev. Lett. **103** (2009), 200402, ⊙DOI.

[1258] S. Stellmer, Meng Khoon Tey, R. Grimm, and F. Schreck, *Bose-Einstein condensation of ^{86}sr*, Phys. Rev. A **82** (2010), 041602(R), ⊙DOI.

[1259] J. Stenger, S. Inouye, M. R. Andrews, H.-J. Miesner, D. M. Stamper-Kurn, and W. Ketterle, *Strongly enhanced inelastic collisions in a Bose-Einstein condensate near Feshbach resonances*, Phys. Rev. Lett. **82** (1999), 2422, ⊙.

[1260] J. Stenger, S. Inouye, A. P. Chikkatur, D. M. Stamper-Kurn, D. E. Pritchard, and W. Ketterle, *Bragg spectroscopy of a Bose-Einstein condensate*, Phys. Rev. Lett. **82** (1999), 4569, ⊙.

[1261] J. Stenger, S. Inouye, D. M. Stamper-Kurn, H.-J. Miesner, A. P. Chikkatur, and W. Ketterle, *Spin domains in ground state spinor Bose-Einstein condensates*, Nature **396** (1998), 345.

[1262] S. Stenholm, *Doppleron resonances*, Opt. Comm. **22** (1977), 123.

[1263] ———, *The semiclassical theory of laser cooling*, Rev. Mod. Phys. **58** (1986), 699, ⊙.

[1264] J. L. Stewart, *The power spectrum of a carrier frequency modulated by gaussian noise*, Proc. of the IRE **42** (1954), 1539.

[1265] D. Stoler, *Equivalence class of minimum uncertainty wavepackets*, Phys. Rev. D **1** (2006), 3217, ⊙.

[1266] _____, *Photon antibunching and possible ways to observe it*, Phys. Rev. Lett. **33** (2006), 1397, ⊙.

[1267] M. Stoll and T. K?hler, *Production of three-body Efimov molecules in an optical lattice*, Phys. Rev. A **72** (2005), 022714, ⊙.

[1268] Th. Stolz, H. Hegels, M. Winter, B. Röhr, Ya-Fen Hsiao, L. Husel, G. Rempe, and S. Dürr, *Quantum-logic gate between two optical photons with an average efficiency above 40%*, Phys. Rev. X **12** (2022), 021035, ⊙DOI.

[1269] H. T. C. Stoof, *Atomic bose gas with a negative scattering length*, Phys. Rev. A **49** (1995), 3824, ⊙.

[1270] H. T. C. Stoof and M. Bijlsma, *Degeneracy effects on the relaxation and recombination of adsorbed doubly polarized atomic hydrogen*, Phys. Rev. B **49** (1994), 422.

[1271] S. Stringari, *Collective excitations of a trapped Bose-condensate gas*, Phys. Rev. Lett. **77** (1996), 2360, ⊙.

[1272] S. H. Strogatz, *From kuramoto to crawford: Exploring the onset of synchronization in populations of coupled oscillators*, Physica D **143** (2000), 1, ⊙.

[1273] _____, *Exploring complex networks*, Nature **410** (2001), 268, ⊙.

[1274] W. C. Stwalley, *Efficient conversion of ultracold Feshbach-resonance-related polar molecules into ultracold ground state ($x\ ^1\sigma^+, v = 0, j = 0$) molecules*, Eur. Phys. J. D **31** (2004), 221, ⊙.

[1275] William C. Stwalley and L. H. Nosanow, *Possible new quantum systems*, Phys. Rev. Lett. **36** (1976), 910.

[1276] M. Sukharev and A. Nitzan, *Numerical studies of the interaction of an atomic sample with the electromagnetic field in two dimensions*, Phys. Rev. A **84** (2011), 043802, ⊙DOI.

[1277] D. B. Sullivan, *Characterization of clocks and oscillators*, Forgotten Books, 1990, ISBN.

[1278] P. Sundsoy and E. Fjeldberg, *Quantum computing, linear optics implementations*, ePrints: arXiv **1607.03935** (2016), ⊙.

[1279] K.-A. Suominen, *Theories for cold atomic collisions in light fields*, J. Phys. B **29** (1996), 5981, ⊙.

[1280] R. T. Sutherland and F. Robicheaux, *Collective dipole-dipole interactions in an atomic array*, Phys. Rev. A **94** (2016), 013847, ⊙DOI.

[1281] O. Svelto, *Self-focussing, self-trapping, and self-phase modulation of laser beams*, Progr. Opt. **12** (1974), 1, DOI.

[1282] A. A. Svidzinsky and Jun-Tao Chang, *Comment on: Effects of including the counterrotating term and virtual photons on the eigenfunctions and eigenvalues of a scalar photon collective emission theory; phys. lett. a 372 (2008) 2514*, Phys. Lett. **372** (2008), 5732, ⊙.

[1283] ———, *Cooperative spontaneous emission as a many-body eigenvalue problem*, Phys. Rev. A **77** (2008), 043833, ⊙DOI.

[1284] A. A. Svidzinsky, Jun-Tao Chang, and M. O. Scully, *Dynamical evolution of correlated spontaneous emission of a from a uniformly excited cloud of atoms*, Phys. Rev. Lett. **100** (2008), 160504, ⊙DOI.

[1285] ———, *Cooperative spontaneous emission of n atoms: Many-body eigenstates, the effect of virtual lamb shift processes, and analogy with radiation of n classical oscillators*, Phys. Rev. A **81** (2010), 053821, ⊙DOI.

[1286] A. A. Svidzinsky and M. O. Scully, *Evolution of collective n atom states in single photon superradiance: Effect of virtual lamb shift processes*, Opt. Comm. **282** (2009), 2894, ⊙DOI.

[1287] P. Szarek, *Electric permittivity in individual atomic and molecular systems through direct associations with electric dipole polarizability and chemical hardness*, J. Phys. Chem. C **121** (2017), 12593.

[1288] M. H. Szymańska, B. D. Simons, and K. Burnett, *Dynamics of the BCS-BEC crossover in a degenerate Fermi gas*, Phys. Rev. Lett. **94** (2005), 170402, ⊙.

[1289] J. W. R. Tabosa and D. V. Petrov, *Optical pumping of orbital angular momentum of light in cold cesium atoms*, Phys. Rev. Lett. **83** (1999), 4967, ⊙.

[1290] A. V. Taichenachev, V. I. Yudin, C. W. Oates, C. W. Hoyt, Z. W. Barber, and L. Hollberg, *Magnetic field-induced spectroscopy of forbidden optical transitions with application to lattice-based optical atomic clocks*, Phys. Rev. Lett. **96** (2006), 083001, ⊙DOI.

[1291] Zhixiang Tang, Runwu Peng, Dianyuan Fan, Shuangchun Wen, Hao Zhang, and Liejia Qian, *Absolute left-handed behaviors in a triangular elliptical-rod photonic crystal*, Opt Exp. **13** (2005), 09796.

[1292] M. Tanifuji, *Polarization phenomena in physics*, World Scientific, 2018, DOIISBN.

[1293] M. Tavis and F. W. Cummings, *Exact solution for an n-molecule-radiation-field hamiltonian*, Phys. Rev. **170** (1998), 379, ⊙.

[1294] H. R. Telle, B. Lipphardt, and J. Stenger, *Kerr-lens, mode-locked lasers as transfer oscillators for optical frequency measurements*, Appl. Phys. B **74** (2002), 1.

[1295] I. Teper, Yu-Lu Lin, and V. Vuletić, *Resonator-aided single-atom detection on a microfabricated chip*, Phys. Rev. Lett. **97** (2006), 023002.

[1296] Meng Khoon Tey, S. Stellmer, R. Grimm, and F. Schreck, *Double-degenerate Bose-Fermi mixture of strontium*, Phys. Rev. A **82** (2010), 011608(R), ⊙DOI.

[1297] M. Theis, G. Thalhammer, K. Winkler, M. Hellwig, G. Ruff, R. Grimm, and J. Hecker Denschlag, *Tuning the scattering length with an optically induced Feshbach resonance*, Phys. Rev. Lett. **93** (2004), 123001, ⊙.

[1298] W. R. Theis, *Grundzüge der Quantentheorie*, Teubner Studienbücher, 1985, ISBN.

[1299] L. H. Thomas, Nature **117** (1926), 514, ⊙.

[1300] R. J. Thompson, G. Rempe, and H. J. Kimble, *Observation of normal mode splitting for an atom in an optical cavity*, Phys. Rev. Lett. **68** (1992), 1132, ⊙.

[1301] H. R. Thorsheim, J. Weiner, and P. S. Julienne, *Laser-induced photoassociation of ultracold sodium atoms*, Phys. Rev. Lett. **58** (1987), 2420.

[1302] E. Tiesinga, A. J. Moerdijk, B. J. Verhaar, and H. T. C. Stoof, *Conditions for Bose-Einstein condensation in magnetically trapped atomic cesium*, Phys. Rev. A **46** (1992), R1167, ⊙.

[1303] E. Tiesinga, B.J. Verhaar, and H. T. C. Stoof, *Threshold and resonance phenomena in ultracold ground-state collisions*, Phys. Rev. A **47** (1993), 4114, ⊙.

[1304] E. Tiesinga, C. J. Williams, and P. S. Julienne, *Photoassociative spectroscopy of highly excited vibrational levels of alkali dimers: Green's function approach for eigenvalue solvers*, Phys. Rev. A **57** (1998), 4257, ⊙[Tiesinga98].

[1305] E. Tiesinga, C. J. Williams, P. S. Julienne, K. M. Jones, P. D. Lett, and W. D. Phillips, *A spectroscopic determination of scattering lengths for sodium atom collisions*, J. Res. Natl. Inst. Stand. Tech. **101** (1996), 505.

[1306] U. Tietze and Ch. Schenk, *Halbleiterschaltungstechnik*, ISBN.

[1307] E. Timmermans, P. Tommasini, R. Côté, M. Hussein, and A. Kerman, *Rarefied liquid properties of hybrid atom-molecular Bose-Einstein condensates*, Phys. Rev. Lett. **83** (1999), 2691, ⊙.

[1308] E. Timmermans, P. Tommasini, M. Hussein, and A. Kerman, *Feshbach resonances in atomic Bose-Einstein condensates*, Phys. Rep. **315** (1999), 199, ⊙.

[1309] G. Timp, R. E. Behringer, D. M. Tennant, J. E. Cunningham, M. Prentiss, and K. K. Berggren, *Using light as a lens for submicron, neutral-atom lithography*, Phys. Rev. Lett. **69** (1992), 1636, ⊙.

[1310] U. M. Titulaer and R. J. Glauber, *Correlation functions for coherent fields*, Phys. Rev. **140** (1999).

[1311] O. Toader, T. Y. M. Chan, and S. John, *Photonic band gap architectures for holographic lithography*, Phys. Rev. Lett. **92** (2004), 043905, ⊙.

[1312] B. Laburthe Tolra, K. M. OHara, J. H. Huckans, W. D. Phillips, S. L. Rolston, and J. V. Porto, *Observation of reduced three-body recombination in a correlated 1d degenerate bose gas*, Phys. Rev. Lett. **92** (2004), 190401, ⊙.

[1313] M. S. Tomas, *Green function for multilayers light scattering in planar cavities*, Phys. Rev. A **51** (1995), R22, ⊙DOI.

[1314] P. Tommasini, E. Timmermans, R. Cote, M. Hussein, and A. Kerman, *Inter-condensate tunneling in Bose-Einstein condensates with Feshbach resonances*, ePrints (1999), cond–mat/9805323, ⊙.

[1315] G. Tóth, C. Knapp, O. Gühne, and H. J. Briegel, *Optimal spin squeezing inequalities detect bound entanglement in spin models*, Phys. Rev. Lett. **99** (2007), 250405, ⊙DOI.

[1316] ———, *Spin squeezing and entanglement*, Phys. Rev. A **79** (2009), 042334, ⊙DOI.

[1317] A. Traverso, R. Chakraborty, Y. N. Martinez de Escobar, P. G. Mickelson, S. B. Nagel, M. Yan, and T. C. Killian, *Inelastic and elastic collision rates for triplet states of ultracold strontium*, Phys. Rev. A **79** (2009), 060702(R), ⊙DOI.

[1318] M. Trippenbach, Y. B. Band, and P. S. Julienne, *Four wave mixing in the scattering of Bose-Einstein condensates*, Opt. Exp. **3** (1999), 530.

[1319] A. G. Truscott, K. E. Strecker, W., I. McAlexander, Guthrie, B. Partridge, and R. G. Hulet, *Observation of Fermi pressure in a gas of trapped atoms*, Science **291** (2001), 2570, ⊙.

[1320] Q. A. Turchette, C. J. Hood, W. Lange, H. Mabuchi, and H. J. Kimble, *Measurement of conditional phase shifts for quantum logic*, Phys. Rev. Lett. **75** (1995), 4710, ⊙.

[1321] M. Uria, P. Solano, and C. Hermann-Avigliano, *Deterministic generation of large fock states*, Phys. Rev. Lett. **125** (1992), 093603.

[1322] L. Vaidman, *On the realization of interaction-free measurements*, Quantum Opt. **6** (1994), 119, ⊙DOI.

[1323] F. A. van Abeelen, D. J. Heinzen, and B. J. Verhaar, Phys. Rev. A **57** (1998), R4102, ⊙.

[1324] D. V. van Coevorden, R. Sprik, A. Tip, and A. Lagendijk, *Photonic band gap structure of atomic lattices*, Phys. Rev. Lett. **77** (1996), 2412, ⊙.

[1325] R. van der Stam, *Superradiant scattering of laser light from a Bose-Einstein condensater*, Dissertation (2006).

[1326] S. J. van Enk, *Single-particle entanglement*, Phys. Rev. A **72** (2005), 064306, ⊙.

[1327] E. G. M. van Kempen, B. Marcelis, and S. J. J. M. F. Kokkelmans, *Formation of fermionic molecules via interisotope Feshbach resonances*, Phys. Rev. A **70** (2004), 050701(R), ⊙.

[1328] G. Vandegrift, *The moessbauer effect explained*, Am. J. Phys. **66** (1998), 593, DOI.

[1329] J. Vanier and C. Au doin, *The quantum physics of atomic frequency standards*, Adam Hilger, Bristol and Philadelphia, 1989, ISBN.

[1330] S. Varró, N. Kroó, G. Farkas, and P. Dombi, *Spontaneous emission of radiation by metallic electrons in the presence of electromagnetic fields of surface plasmon oscillations*, J. Mod. Opt. **57** (2010), 80.

[1331] G. Veeravalli, E. Kuhnle, P. Dyke, and C. J. Vale, *Bragg spectroscopy of a strongly interacting Fermi gas*, ePrints **08092145** (2008), ⊙.

[1332] M. Vengalattore, M. Hafezi, M. D. Lukin, and M. Prentiss, *Optical bistability at low light level due to collective atomic recoil*, Phys. Rev. Lett. **101** (2008), 063901, ⊙.

[1333] P. Verkerk, N. P. Bigelow, L. De Salvo, and R. Bonifacio, *Comment on "spontaneous generation of a longitudinal atomic density grating in sodium vapor"*, Phys. Rev. Lett. **79** (1997), 3094, ⊙DOI.

[1334] G. Verma, C. Vishwakarma, C. V. Dharmadhikari, and U. D. Rapol, *A compact atomic beam based system for doppler-free laser spectroscopy of strontium atoms*, Rev. Sci. Instrum. **88** (2016), 033103, DOI.

[1335] V. G. Veselago, *The electrodynamics of substances with simultaneously negative values of ε and μ*, Sov. Phys. Uspekhi **10** (2008), 509, ⊙.

[1336] P. A. Vicharelli and W. P. Lapatovich, *Iterative method for computing the inverse abel transform*, Appl. Phys. Lett. **50** (1987), 557, ⊙DOI.

[1337] F. S. Vieira, F. C. Cruz, D. F. Plusquellic, and S. A. Diddams, *Tunable resolution terahertz dual frequency comb spectrometer*, Opt. Exp. **24** (2016), 30100, ⊙DOI.

[1338] D. G. Voelz, *Computational fourier optics: A matlab tutorial*, SPIE Press monograph, SPIE Press, 2011, ISBN.

[1339] J. M. Vogels, R. S. Freeland, C. C. Tsai, B. J. Verhaar, and D. J. Heinzen, *Coupled singlet-triplet analysis of two-color cold-atom photoassociation spectra*, Phys. Rev. A **61** (2000), 043407, ⊙.

[1340] J. M. Vogels, C. C. Tsai, R. S. Freeland, S. J. J. M. F. Kokkelmans, B. J. Verhaar, and D. J. Heinzen, *Prediction of Feshbach resonances in collisions of ultracold rubidium atoms*, Phys. Rev. A **56** (1997), R1067, ⊙.

[1341] Johannes Voit, *One-dimensional Fermi liquids*, Rep. Prog. Phys. **57** (1994), 977–1116, cond-mat/9510014.

[1342] C. von Cube, S. Slama, M. Kohler, C. Zimmermann, and Ph. W. Courteille, *Creating and probing long-range order in atomic clouds*, Fortschr. Phys. **54** (2006), 726.

[1343] C. von Cube, S. Slama, D. Kruse, C. Zimmermann, Ph. W. Courteille, G. R. M. Robb, N. Piovella, and R. Bonifacio, *Self-synchronization and dissipation-induced threshold in collective atomic recoil lasing*, Phys. Rev. Lett. **93** (2004), 083601.

[1344] J. von Neumann, *Mathematical foundations of quantum mechanics*, Princeton University Press, 1955, ISBN.

[1345] C. F. von Weizsäcker, *Einheit der natur*, München, 1971, ISBN.

[1346] ———, *Aufbau der physik*, München, 2006, ISBN.

[1347] V. Vuletic, H. W. Chan, and A. T. Black, *Three-dimensional cavity doppler cooling and cavity sideband cooling by coherent scattering*, Phys. Rev. A **64** (2001), 033405, ⊙.

[1348] V. Vuletic, Ch. Chin, A. J. Kerman, and S. Chu, *Degenerate Raman sideband cooling of trapped cesium atoms at very high atomic densities*, Phys. Rev. Lett. **81** (1998), 5768, ⊙.

[1349] V. Vuletic, A. J. Kerman, Cheng Chin, and S. Chu, *Observation of low-field Feshbach resonances in collisions of cesium atoms*, Phys. Rev. Lett. **82** (1999), 1406, ⊙.

[1350] I. Waki, S. Kassner, G. Birkl, and H. Walther, *Observation of ordered structures of laser-cooled ions in a quadrupole storage ring*, Phys. Rev. Lett. **68** (1993), 2007.

[1351] T. Walker, D. Sesko, and C. Wieman, *Collective behaviour of optically trapped neutral atoms*, Phys. Rev. Lett. **64** (1990), 408, ⊙.

[1352] S. Wallentowitz and W. Vogel, *Reconstruction of the quantum mechanical state of a trapped ion*, Phys. Rev. Lett. **75** (1995), 2932.

[1353] H. Wallis and H. Steck, *Inseparable time evolution of anisotropic Bose-Einstein condensates*, Europhys. Lett. **41** (1998), 477, ⊙.

[1354] J. Walraven, *Atomic physics*, unpublished, Amsterdam, 2018, .

[1355] ———, *Quantum gases*, unpublished, Amsterdam, 2019, .

[1356] J. Walz, (1991).

[1357] J. Walz, I. Siemers, M. Schubert, W. Neuhauser, and R. Blatt, *Motional stability of a nonlinear parametric oscillator: Ion storage in the rf octupole trap*, Europhys. Lett. **21** (1993), 183.

[1358] Changbiao Wang, *Can the Abraham light momentum and energy medium constitute a Lorentz four-vector?*, J. Mod. Phys. **4** (2013), 1123, ⊙DOI.

[1359] Tun Wang, S. F. Yelin, R. Côté, E. E. Eyler, S. M. Farooqi, P. L. Gould, M. Kostrun, D. Tong, and D. Vrinceanu, *Superradiance in ultracold Rydberg gases*, Phys. Rev. A **75** (2007), 033802, ⊙DOI.

[1360] M. Weidemüller, A. Görlitz, Th. W. Hänsch, and A. Hemmerich, *Local and global properties of light-bound atomic lattices investigated by bragg diffraction*, Phys. Rev. A **58** (1998), 4647, ⊙.

[1361] M. Weidemüller, A. Hemmerich, A. Görlitz, T. Esslinger, and Th. W. Hänsch, *Bragg diffraction in an atomic lattice bound by light*, Phys. Rev. Lett. **75** (1995), 4583, ⊙.

[1362] C. J. Weiner, J. J. Bollinger, F. L. Moore, and D. J. Wineland, *Electrostatic modes as a diagnostic*, Phys, Rev. A **49** (1994), 3842.

[1363] J. Weiner, V. S. Bagnato, S. Zilio, and P. S. Julienne, *Experiments and theory in cold and ultracold collisions*, Rev. Mod. Phys. **71** (1999), 1.

[1364] J. Weiner and P.-T. Ho, *Light-matter interaction, fundamentals and applications*, John Wiley & Sons, Hokoken, New Jersey, 2003, ⊙ISBN.

[1365] J. D. Weinstein, R. DeCarvalho, Th. Guillet, B. Friedrich, and J. M. Doyle, *Magnetic trapping of calcium monohydride molecules at millikelvin temperatures*, Nature **395** (1998), 148, ⊙.

[1366] D. S. Weiss, B.C. Young, and S. Chu, *Precision measurement of h/mcs based on photon recoil using laser-cooled atoms and atomic interferometry*, Appl. Phys. B **59** (1994), 217.

[1367] S. B. Weiss, M. Bhattacharya, and N. P. Bigelow, *Calculation of the interspecies s-wave scattering length in an ultracold na-rb vapor*, Phys. Rev. A **68** (2003), 042708, ⊙.

[1368] M. Weissbluth, *Atoms and molecules*, Students Edition Academic Press, San Diego, 1978, ISBN.

[1369] Ch. Weitenberg, P. Schauss, T. Fukuhara, M. Cheneau, M. Endres, I. Bloch, and S. Kuhr, *Coherent light scattering from a two-dimensional mott insulator*, Phys. Rev. Lett. **106** (2011), 215301, ⊙DOI.

[1370] G. Wentzel, *Eine verallgemeinerung der quantenbedingungen für die zwecke der wellenmechanik*, Zeitschrift für Physik **38** (1926), 518.

[1371] C. I. Westbrook, R. N. Watts, C. E. Tanner, S. L. Rolston, W. D. Phillips, P. D. Lett, and P. L. Gould, *Localization of atoms in a three-dimensional standing wave*, Phys. Rev. Lett. **65** (1990), 33, ⊙.

[1372] D. S. Wiersma, P. Bartolini, A. Lagendijk, and R. Righini, *Localization of light in a disordered medium*, Nature **390** (1997), 671, ⊙.

[1373] K. Wiesenfeld, P. Colet, and S. H. Strogatz, *Frequency locking in josephson arrays: Connection with the kuramoto model*, Phys. Rev. E **57** (1998), 1563, ⊙.

[1374] E. P. Wigner, *On the behavior of cross sections near thresholds*, Phys. Rev. **73** (1948), 1002.

[1375] L. R. Wilcox and W. E. Lamb Jr, Phys. Rev. **119** (1960), 1915, ⊙.

[1376] W. J. Wild and C. Lee Giles, *Goos-Hänchen shifts from absorbing media*, Phys. Rev. A **25** (1982), 2099.

[1377] J. Williams, R. Walser, J. Cooper, E. Cornell, and M. Holland, *Nonlinear josephson-type oscillations of a driven, two-component Bose-Einstein condensate*, Phys. Rev. A **59** (1999), R31, ⊙.

[1378] J. E. Williams and J. E. Holland, *Preparing topological states of a Bose-Einstein condensate*, Nature **401** (1999), 568, ⊙.

[1379] J. E. Williams, N. Nygaard, and C. W. Clark, *Phase diagrams for an ideal gas mixture of fermionic atoms and bosonic molecules*, New J. Phys. **6** (2004), 123, ⊙.

[1380] D. J. Wineland, J. J. Bollinger, W. M. Itano, and D. J. Heinzen, *Squeezed atomic states and projection noise in spectroscopy*, Phys. Rev. A **50** (1994), 67, ⊙DOI.

[1381] D. J. Wineland and H. G. Dehmelt, *Proposed* $10^{14}\delta n < n$ *laser fluorescence spectroscopy on* Tl^{+} *mono-ion oscillator*, Bull. Am. Phys. Soc. **20** (1975), 637.

[1382] D. J. Wineland and W. M. Itano, *Laser cooling of atoms*, Phys. Rev. A **20** (1979), 1521, ⊙DOI.

[1383] ———, *Laser cooling of ions stored in harmonic and penning traps*, Phys. Rev. A **25** (1982), 35, ⊙.

[1384] H. M. Wiseman, *Defining the (atom) laser*, Phys. Rev. A **56** (1997), 2068.

[1385] ———, *Light amplification without stimulated emission: Beyond the standard quantum limit to the laser linewidth*, Phys. Rev. A **60** (1999), 4083, ⊙DOI.

[1386] H. M. Wiseman and M. J. Collett, *An atom laser based on dark-state cooling*, Phys. Lett. A **202** (1995), 246, ⊙.

[1387] M. Woldeyohannes and S. John, *Coherent control of spontaneous emission near a photonic band edge*, J. Opt. B **5** (2003), R43, ⊙.

[1388] E. M. Wright and D. F. Walls, *Collapses and revivals of Bose-Einstein condensates formed in small atomic samples*, Phys. Rev. Lett. **77** (1996), 2158, ⊙.

[1389] Biao Wu, R. B. Diener, and Qian Niu, *Bloch waves and Bloch bands of Bose-Einstein condensates in optical lattices*, Phys. Rev. A **65** (2002), 025601, ⊙.

[1390] Biao Wu and Qian Niu, *Nonlinear Landau-Zener tunneling*, Phys. Rev. A **61** (2000), 023402, ⊙DOI.

[1391] ———, *Superfluidity of Bose-Einstein condensate in an optical lattice: Landau-Zener tunnelling and dynamical instability*, New journal of Phys. **5** (2003), 104, ⊙.

[1392] Haibin Wu and Min Xiao, *Observation of intracavity electromagnetically induced transparency and polariton resonances in a doppler-broadened medium*, Phys. Rev. Lett. **100** (2008), 173602, ⊙.

[1393] Huang Wu, E. Arimondo, and C. J. Foot, *Dynamics of evaporative cooling for Bose-Einstein condensation*, Phys. Rev. A **56** (1997), 560.

[1394] Huang Wu and Ch. J. Foot, *Direct simulation of evaporative cooling*, J. Phys. B **29** (1996), L321, ⊙.

[1395] Jin-Hui Wu, M. Artoni, and G. C. La Rocca, *Controlling the photonic band structure of optically driven cold atoms*, J. Opt. Soc. Am. B **25** (2008), 1840, ⊙DOI.

[1396] R. Wynar, R. S. Freeland, D. J. Han, C. Ryu, and D. J. Heinzen, *Molecules in a Bose-Einstein condensate*, Science **287** (2000), 1016.

[1397] G. Xianlong, M. Polini, R. Asgari, and M. P. Tosi, *Density-functional theory of strongly correlated Fermi gases in elongated harmonic traps*, Phys. Rev. A **73** (2005), 033609, ⊙.

[1398] G. Xianlong, M. Polini, B. Tanatar, and M. P. Tosi, *Interacting Fermi gases in disordered one-dimensional lattices*, cond-mat/0603118 (2006), ⊙.

[1399] G. Xianlong, M. Polini, M. P. Tosi, V. L. Campo jr., and K. Capelle, *Emergence of atomic density waves in a trapped Luther-Emery fermion gas*, ePrints (2005), cond–mat/0506570, ⊙.

[1400] G. Xianlong, M. Polini, M. P. Tosi, V. L. Campo jr., K. Capelle, and M. Rigol, *Emergence of atomic density waves in a trapped Luther-Emery fermion gas*, Phys. Rev. B (2006), cond-mat/0512184 (2006), ⊙.

[1401] Tao Xin, Bi-Xue Wang, Ke-Ren Li, Xiang-Yu Kong, Shi-Jie Wei, Tao Wang, Dong Ruan, and Gui-Lu Long, *Nuclear magnetic resonance for quantum computing: Techniques and recent achievements*, Chinese Physics B **27** (2018), 020308, ⊙DOI.

[1402] K. Xu, T. Mukaiyama, J. R. Abo-Shaeer, J. K. Chin, D. E. Miller, and W. Ketterle, *Formation of quantum-degenerate sodium molecules*, Phys. Rev. Lett. **91** (2003), 210402, ⊙.

[1403] Victoria Xu, M. Jaffe, C. D. Panda, S. L. Kristensen, L. W. Clark, and H. Müller, *Probing gravity by holding atoms for 20 seconds*, Science **366** (2019), 745.

[1404] Xinye Xu, T. H. Loftus, J. L. Hall, A. Gallagher, and Jun Ye, *Cooling and trapping of atomic strontium*, J. Opt. Soc. Am. B **20** (2003), 968, ⊙DOI.

[1405] Ziyun Yan, *Bose-Einstein condensation of a trapped gas in n dimensions*, Phys. Rev. A **59** (1999), 4657, ⊙.

[1406] G. J. Yang, L. Zhang, and W. Shu, *Light amplification through collective atomic recoil motion modified by a harmonic potential*, Phys. Rev. A **68** (2003), 063802, ⊙.

[1407] Amnon Yariv, *Quantum electronics*, 1967, ISBN.

[1408] Amnon Yariv and P. Yeh, *Optical waves in crystals*, 2002, ISBN.

[1409] E. J. Yarmchuk, M. J. V. Gordon, and R. E. Packard, *Observation of stationary vortex arrays in rotating superfluid helium*, Phys. Rev. Lett. **43** (1979), 214, ⊙.

[1410] M. Yasuda and H. Katori, *Lifetime measurement of the $^3p_2$ metastable state of strontium atoms*, Phys. Rev. Lett. **92** (2004), 153004, ⊙DOI.

[1411] Jun Ye, H. Schnatz, and L. W. Hollberg, *Optical frequency combs: From frequency metrology to optical phase control*, IEEE J. Sel. Top. QE **9** (2003), 1041.

[1412] Yutaka Yoshikawa, Toshiaki Sugiura, Yoshio Torii, and Takahiro Kuga, *Observation of superradiant Raman scattering in a Bose-Einstein condensate*, Phys. Rev. A **69** (2004), 41603(R), ⊙.

[1413] Yutaka Yoshikawa, Yoshio Torii, and Takahiro Kuga, *Superradiant light scattering from thermal atomic vapors*, Phys. Rev. Lett. **94** (2005), 083602, ⊙.

[1414] Deshui Yu, *Photonic band structure of the three-dimensional ^{88}sr atomic lattice*, Phys. Rev. A **84** (2011), 043833, ⊙DOI.

[1415] H. P. Yuen, *Two-photon coherent states of the radiation field*, Phys. Rev. A **13** (1976), 2226.

[1416] V. I. Yukalov, E. P. Yukalova, and V. S. Bagnato, *Non-ground-state Bose-Einstein condensates of trapped atoms*, Phys. Rev. A **56** (1997), 4845, ⊙.

[1417] B. Yurke and J. S. Denker, *Quantum network theory*, Phys. Rev. A **29** (1984), 1419, ⊙DOI.

[1418] B. Yurke and D. Stoler, *Use of cavities in squeezed-state generation*, Phys. Rev. A **29** (1984), 408, ⊙DOI.

[1419] N. A. Zaitsev, I. V. Matyushkin, and D. V. Shamonov, *Numerical solution of the thomas-Fermi equation for the centrally symmetric atom*, Russian Microelectronics, Translated from Mikroelektronika, Vol.33, Pag.372 **33** (2004), 303, ⊙DOI.

[1420] Francesca Zambelli and Sandro Stringari, *Quantized vortices and collective oscillations of a trapped Bose-Einstein condensate*, Phys. Rev. Lett. **81** (1998), 1754, ⊙.

[1421] M. Zamboni-Rached, L. A. Ambrosio, A. H. Dorrah, and M. Mojahedi, *Structuring light under different polarization states within micrometer domains: exact analysis from the maxwell equations*, Optics Express **25** (2017), 10051.

[1422] M. Zamboni-Rached and E. Recami, *Subluminal wave bullets: Exact localized subluminal solutions to the wave equations*, Phys. Rev. A **77** (2008), 033824.

[1423] T. Zelevinsky, M. M. Boyd, A. D. Ludlow, S. M. Foreman, S. Blatt, T. Ido, and J. Ye, *Optical clock and ultracold collisions with trapped strontium atoms*, Hyperfine Interactions **174** (2007), 55, DOI.

[1424] Xiaodong Zeng, Gaoxiang Li, Yaping Yang, and Shiyao Zhu, *Enhancement of the vacuum Rabi oscillation via surface plasma modes in single-negative metamaterials*, Phys. Rev. A **86** (2012), 033819.

[1425] Xiaodong Zeng, Jingping Xu, and Yaping Yang, *Spontaneous emission interference enhancement with a $\hat{I}\frac{1}{4}$-negative metamaterial slab*, Phys. Rev. A **84** (2011), 033834.

[1426] J. Zhang, E. G. M. Van Kempen, T. Bourdel, L. Khaykovich, J. Cubizolles, F. Chevy, M. Teichmann, L. Tarruell, S. J. J. M. F. Kokkelmans, and C. Salomon, *Expansion of a lithium gas in the BEC-BCS crossover*, AIP Conf. Proc. **770** (2005), ⊙.

[1427] Shanchao Zhang, J. F. Chen, Chang Liu, Shuyu Zhou, M. M. T. Loy, G. K. L. Wong, and Shengwang Dub), *A dark-line two-dimensional magneto-optical trap of 85rb atoms with high optical depth*, Rev. Sci. Instr. **83** (2012), 073102.

[1428] Wen-Zhuo Zhang, Peng Zhang, Ru-Quan Wang, and Wu-Ming Liu, *Testing the equivalence between the canonical and minkowski momentum of light with ultracold atoms*, Phys. Rev, A **85** (2012), 053604, ⊙DOI.

[1429] Yuan Zhang, Yu-Xiang Zhang, and K. Mølmer, *Monte-carlo simulations of superradiant lasing*, New J. Phys. **20** (2018), 112001, ⊙DOI.

[1430] Zhao-Qing Zhang, King-Chuen Chiu, and Daozhong Zhang, *Transition from an atomic to a molecular Bose-Einstein condensate*, Nature **592** (2021), 708, ⊙DOI.

[1431] O. V. Zhirov and D. L. Shepelyansky, *Quantum synchronization*, Eur. Phys. J. D **38** (2006), 375, ⊙.

[1432] Han-Sen Zhong and et al., *Quantum computational advantage using photons*, Science **370** (2020), 1460.

[1433] Min-Kang Zhou, Bruno Pelle, Adèle Hilico, and Franck Pereira dos Santos, *Atomic multiwave interferometer in an optical lattice*, Phys. Rev. A **88** (2013), 013604.

[1434] Bihui Zhu, J. Marino, N. Y. Yao, M. D. Lukin, and E. A. Demler, *Dicke time crystals in driven-dissipative quantum many-body systems*, Phys. Rev. Lett. **21** (2019), 073028, ⊙DOI.

[1435] S. C. Zilio and V. S. Bagnato, *Mecânica, calor, ondas*, script, 2000, .

[1436] F. Zimmer and M. Fleischhauer, *Sagnac interferometry based on ultraslow polaritons in cold atomic vapors*, Phys. Rev. Lett. **92** (2004), 253201.

[1437] O. Zobay and B. M. Garraway, *Atom trapping and two-dimensional Bose-Einstein condensates in field-induced adiabatic potentials*, Phys. Rev. A **69** (2004), 023605, ⊙.

[1438] O. Zobay and G. M. Nikolopoulos, *Dynamics of matter-wave and optical fields in superradiant scattering from Bose-Einstein condensates*, Phys. Rev. A **72** (2005), 041604(R), ⊙.

[1439] ———, *Spatial effects in superradiant rayleigh scattering from Bose-Einstein condensates*, Phys. Rev. A **73** (2006), 013620, ⊙.

[1440] P. Zoller, M. Marte, and D. F. Walls, *Quantum jumps in atomic systems*, Phys. Rev. A **35** (1987), 198, ⊙.

[1441] M. W. Zwierlein, A. Schirotzek, C. H. Schunck, and W. Ketterle, *Fermionic superfluidity with imbalanced spin populations*, Science **311** (2006), 492, ⊙.

[1442] M. W. Zwierlein, C. H. Schunck, C. A. Stan, S. M. F. Raupach, and W. Ketterle, *Formation dynamics of a fermion pair condensate*, Phys. Rev. Lett. **94** (2005), 180401, ⊙.

[1443] M. W. Zwierlein, C. A. Stan, C. H. Schunck, S. M. F. Raupach, S. Gupta, Z. Hadzibabic, and W. Ketterle, *Observation of Bose-Einstein condensation of molecules*, Phys. Rev. Lett. **91** (2003), 250401, ⊙.

[1444] M. W. Zwierlein, C. A. Stan, C. H. Schunck, S. M. F. Raupach, A. J. Kerman, and W. Ketterle, *Condensation of pairs of fermionic atoms near a Feshbach resonance*, Phys. Rev. Lett. **92** (2004), 120403, ⊙.

Index